JANUARY/FEBRUARY 1999
Volume 10, Number 1

© *Copyright 1999 by the American Chemical Society*

Bioconjugate Chemistry

EDITORIAL: Thanks to Our Reviewers

It is a pleasure to acknowledge the contributions of the reviewers of manuscripts submitted in 1998 for publication in *Bioconjugate Chemistry*. Their unselfish service has been essential in the shaping of the ninth volume of the journal. The scientific community is fortunate that its members are willing to share their time and specialized knowledge in this way. The reviewers are listed on the following page.

Claude F. Meares
Editor-in-Chief

10.1021/bc990280b CCC: $18.00 © 1999 American Chemical Society
Published on Web 01/18/1999

List of Reviewers

Eric Aboayge
Ralph Abraham
Michael J. Abrams
Abe Abuchowski
Maciej Adamczyk
Sudhir Agrawal
Toshihiro Akaike
Kazunari Akiyoshi
James Alderfer
Vernon L. Alvarez
Gordon L. Amidon
Carolyn J. Anderson
Haruhiko Aoyagi
Yasushi Arano
D. Attwood
Alexandre Avrameas
Kenneth D. Bagshawe
Kwamena E. Baidoo
James R. Baker
Robert W. Baldwin
Hagan P. Bayley
Marcel B. Bally
George Barisas
Miroslav Baudys
Serge Beaucage
Paul L. Beaumier
Jean-Paul Behr
Donald E. Bergstrom
Purshotam Bhan
Christopher Bieniarz
Gary Bignami
David C. Blakey
Forrest Blocker
Nicholas Bodor
Alexei A. Bogdanov
Philip H. Bolton
Philip N. Borer
Ronald Breslow
Donald J. Buchsbaum
Joseph Cappello
Jorge A. Carrasquillo
Paul Carter
Jonathan B. Chaires
Chien-Hsing Ken Chang
Ravi V. J. Chari
David Curiel
Valerian T. D'Souza
Masah Damha
Gary S. David
Alan Davison
G. Divita
Sally J. DeNardo
Jean F. Desreux
Richard A. Dluhy
Ruth Duncan
Richard H. Ebright
Fritz Eckstein
Michael Eisenhut
Alan L. Epstein
Ramon Eritja
Falk Fahrenholz
Mark A. Findeis
Raymond A. Firestone
Alan J. Fischman
Arthur E. Frankel
Alan R. Fritzberg
Michael J. Gait
Jean Gariépy
Gary D. Glick
William F. Goeckler
Kieran F. Geoghegan
Victor S. Goldmacher
Wayne Gombotz
David A. Goodwin
Serengulam V. Govidan
Marc M. Greenberg
Gary L. Griffiths
Stephen E. Halford
Michelle M. Hanna
J. Milton Harris
Mitsuru Hashida
Martha Hayden
John E. Hearst
Ned D. Heindel
Ilkka Hemmila
Peter Hoogerhout
Thomas Horn
J. P. Hieble
Michael G. Hill
Donald J. Hnatowich
Thomas Horn
Robert H. E. Hudson
Esther Hurwitz
Mark Hylarides
Yuji Inada
Thomas L. James
Nebojsa Janjic
Herbert P. Jennissen
Seo Young Jeong
Tae H. Ji
David K. Johnson
William T. Jones
Manfred Jung
Silvia Jurisson
Alexander V. Kabanov
Lou-Sing Kan
Arthur Karlin
Kazunori Kataoka
John A. Katzenellenbogen
Randal J. Kaufman
Akihiko Kawai
George L. Kenyon
David E. Kerr
David Kessel
Sung Wan Kim
Eiichi Kimura
Dalton King
James F. King
Hiromi Kitano
M. Kohl
Junji Konishi
Jindrich Kopecek
Eric P. Krenning
David Kukis
Hank F. Kung
John M. Lambert
Richard G. Lawton
Bernard Lebleu
Yuan C. Lee
J. Y. Legendre
John R. Lever
Shuang Liu
Joseph Loo
Timo Lovgren
Philip S. Low
Jeffry S. Mann
Stephen Marburg
Atsushi Maruyama
Kazuo Maruyama
Gary R. Matsueda
Mark Matteucci
Larry W. McLaughlin
A. J. McNally
Thomas J. Meade
Gary E. Means
Damon L. Meyer
R. G. Melton
Rich B. Meyer
Patrick Midoux
Chad Mirkin
Nabuo Monji
Deane Mosher
Veli-Matti Mukkala
Gerald Munch
Akira Murakami
John R. Murphy
Vasu Nair
Momoru Nakanishi
Peter E. Nielsen
Hiroyuki Nishimura
Robin Offord
Teruo Okano
Leslie E. Orgel
Kinam Park
William M. Pardridge
Dean Pettit
Alfred Pingoud
Richard T. Pon
Glenn D. Prestwich
Tariq M. Rana
Vic Raso
Annie C. Roche
Steven R. Roffler
Steven E. Rokita
Keith Rose
Edward J. Roy
Erik Rump
S. Scott Saavedra
W. Mark Saltzman
Andrew V. Schally
P. August Schubiger
Jody Schultz
Gary B. Schuster
Todd Sells
Peter Senter
Jonathan L. Sessler
Robert Shapiro
A. Dean Sherry
John E. Shively
Tony Siadak
Clay Siegall
Nathan Siemers
David S. Sigman
John Sommerville
E. M. Southern
Caroline J. Springer
Lloyd M. Smith
Mark Stebbins
Stanley Stein
Donald F. Steiner
Valentino Stella
Fu-min Su
Yuichi Sugiyama
Håkan P. Svensson
Brian D. Sykes
Francis C. Szoka, Jr.
Yoshinobu Takakura
H. M. Therien
David H. Thompson
H. Holden Thorp
Lutz F. Tietze
David Tirrell
Donald A. Tomalia
Vladimir P. Torchilin
Carlo Turano
Ganesan Vaidyanathan
Daniel A. Vallera
Francesco M. Veronese
Ronald E. Viola
Ellen S. Vitetta
Wynn A. Volkert
Vivekananda M. Vrudhula
Ernst Wagner
Alan Wahl
Andrew H-J. Wang
Changlin Wang
E. Sally Ward
Michael J. Waring
Andy Watson
David S. Watt
Michael J. Welch
David E. Wemmer
Ronald Wetzel
D. Scott Wilbur
Meir Wilchek
Itamar Willner
J. Wilschut
George Y. Wu
Shinji Yamashita
Cecil C. Yip
Nobuhiko Yui
Samuel Zalipsky
Michael Zalutsky
N. J. Zuidam

BC990280B

TEACHING EDITORIAL

Spacers, Probability, and Yields

Donald M. Simons

Dade Behring Inc., P.O. Box 6101, M/S 709, Newark, Delaware 19714-6101. Received June 27, 1998

Spacers (linkers and bridgers) are extensively used in the synthesis of bioconjugates. This communication is concerned with spacers of the homobifunctional type—diols, diamines, dicarboxylic acids, etc.—in which the functional groups are equally reactive and sufficiently far apart that the reaction of one does not affect the reactivity of the other. In many cases, the first reaction carried out with such molecules is intended to derivatize, or to protect, only one functional group, leaving the other free for some subsequent reaction. No matter how these reactions are carried out, however, both diderivatized and unreacted spacers are always present in the final crude reaction mixture.

It is an almost universal custom among synthetic chemists to calculate a theoretical yield for the monoderivatized spacer as if it were the only product formed and to disregard the diderivatized product completely. However, information on the relative amounts of products present can at times be useful, particularly for cases in which the isolated yield of monoderivatized spacer turns out to be substantially less than anticipated. Comparison of the observed ratio of diderivatized spacer to monoderivatized spacer (r)[1] with the expected value (EV_r) can often distinguish which of the common causes of yield deficits—mechanical loss,[2] incomplete conversion, improper technique—is the predominant factor (Table 1).

In a homogeneous system, the expected values for the amounts of products formed in the reaction of a homobifunctional spacer with a monofunctional derivatizing agent are dictated by the chosen stoichiometry and the law of binomial distribution. (The law of binomial distribution may not apply in a heterogeneous reaction system.) Calculation of these values is straightforward and is the main subject of the following communication.

HOMOGENEOUS REACTION SYSTEMS

A reaction is regarded as homogeneous if both the homobifunctional spacer and its monoderivatized product remain in solution throughout the reaction. For purpose of illustration, consider the reaction of an equimolar mixture of a diamine and an acyl halide. Here, the amount of acyl halide used is just sufficient to react with exactly half of the total amine groups present.[3] If the reaction goes to completion, the probability that any given amine group will react (p) is 0.50. Correspondingly, the probability that any given amine group will not react (q) is $1 - 0.50 = 0.50$. These two probability values, identical in this particular case, are all that is needed to calculate the expected mole fractions of unreacted diamine (UND), diderivatized diamine (DID), and the desired monoderivatized diamine (MOD) in the final reaction mixture. Thus, the mole fraction of DID is obtained by multiplying the probability that one amine group in a molecule has reacted by the probability that the second amine group has also reacted:

$$\text{mole fraction of DID} = p \times p = p^2 = (0.50)^2 = 0.25$$

In similar fashion, the mole fraction of unreacted diamine is the product of the probabilities that both amine groups in a molecule have not reacted:

$$\text{mole fraction of UND} = q \times q = q^2 = (0.50)^2 = 0.25$$

The mole fraction of the desired monoderivative (MOD) is twice the product of the probability that one amine has reacted and the probability that the other amine has not reacted:

$$\text{mole fraction of MOD} = 2pq = 2 \times 0.50 \times 0.50 = 0.50$$

(The factor 2 is necessary because MOD can be formed in two different ways, that is, acyl halide can react at

Table 1. Use of Observed Ratio of Diderivatized Spacer to Monoderivatized Spacer (r) in Diagnosis of a Yield Deficit

r	probable cause for yield deficit[a]
equal to EVr[b]	mechanical loss
less than EV_r	incomplete conversion[c]
greater than EV_r	inadequate or improper mixing

[a] These guidelines can be subverted by use of impure reactants, by weighing errors, etc. [b] EV_r = expected value for r at complete conversion. [c] Incomplete conversion can result from a loss of derivatizing agent through side reactions (hydrolysis, etc.) as well as from incomplete reaction.

[1] Suitable values for r can often be obtained by analytical chromatography, which is especially convenient when the derivative group is a good chromophore. Because r is a ratio, the extinction coefficient is not required. If the derivative group is not a chromophore, a small sample of the reaction mixture can be treated with a large excess of a second chromophoric reactant. This then provides a measure of the ratio of unreacted spacer to monoderivatized spacer, which can be used in place or r. As a specific example, picrylsulfonic acid is a useful second chromophoric reactant for spacers of the diamine type.

[2] The term "mechanical loss" covers all those inevitable losses that occur during the manipulations required for transfer, purification, and isolation of the product. Even with good workup procedures and careful attention to details, it is difficult to reduce mechanical loss much below 8−10%.

[3] It is assumed that the reactants are mixed to homogeneity before any reaction takes place, that is, that the mixing is ideal. Ideal mixing can be approximated fairly closely for slow reactions but becomes increasingly difficult to attain as the reaction rate increases. Any deviation from ideal mixing always leads to a diminished yield of the monosubstituted derivative.

10.1021/bc980071b CCC: $18.00 © 1999 American Chemical Society
Published on Web 12/24/1998

Scheme 1. Expected Values (mol) for Products from an Equimolar Reaction of a Diamine Spacer and an Acyl Halide

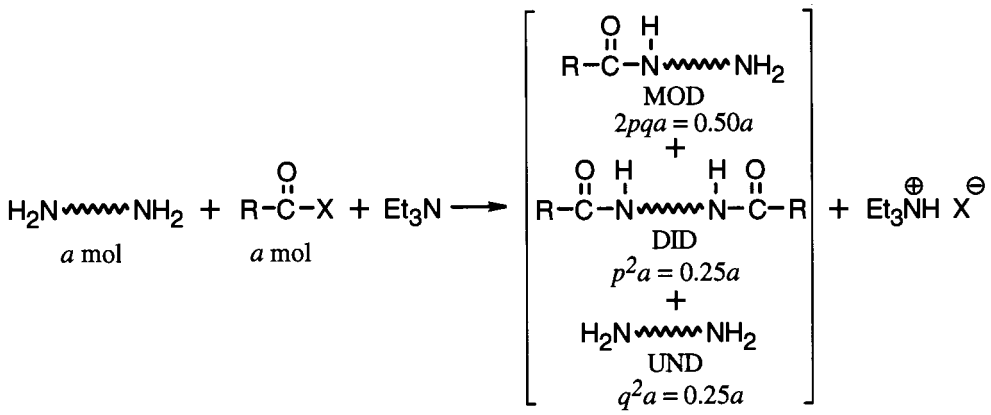


Table 2. Relationship between the Ratio of Diderivatized Spacer to Monoderivatized Spacer (*r*) and Conversion (*x*) in an Equimolar Reaction of a Homobifunctional Spacer and a Monofunctional Derivatizing Agent: $x(\%) = 400r/(1 + 2r)$[a]

r	*x* (%)
0.167	50
0.190	55
0.214	60
0.241	65
0.269	70
0.300	75
0.333	80
0.370	85
0.409	90
0.452	95
0.500	100

[a] Derivation of equation shown in footnote 4.

either of the two ends of the symmetrical diamine molecule to give the same product.) And finally, the expected value of *r* at complete conversion (EV_r) is

$$EV_r = p^2/2pq = p/2(1 - p) = 0.50$$

Multiplying each of the respective mole fractions by the initial moles of diamine actually used gives the moles of product formed (Scheme 1).

All of the above calculations are based on the assumption that the conversion of reactants to products is quantitative. Table 2 shows the relationship between the ratio of diderivatized spacer to monoderivatized spacer (*r*) and conversion (*x*). This relationship can also be expressed by the equation $x\ (\%) = 400r/(1 + 2r)$. In systems in which the reaction rate is not too fast, periodic measurement of *r* provides an elegantly simple method for following the kinetics.[4]

The true theoretical yield of monosubstituted product obtainable from the reaction of an *equimolar* mixture of a homobifunctional spacer and a monofunctional derivatizing reagent is 50 mol %. Further, one-half of the derivatizing reagent is lost through being converted to the disubstituted product. The efficiency can be increased by changing the stoichiometry, that is, by using a smaller ratio of derivatizing reagent to spacer. An example of this technique, taken from Aldenhoff et al. (*1*), describes the preparation of the monotrityl ether of triethylene glycol by reaction of trityl chloride (TrCl) with triethylene glycol (TEG):

> "To a stirred solution of triethylene glycol (75.09 g, 500.00 mmol) and 4-(dimethylamino)pyridine (0.38 g, 3.13 mmol) in 125 mL of anhydrous pyridine was added triphenylmethyl chloride (17.42 g, 63.50 mmol)[*sic*] in 10 portions during 3h. The solution was stirred for 16h under exclusion of moisture. Then, pyridine was removed (last traces were removed by coevaporation with toluene). The residue was taken up in dichloromethane and washed with saturated aqueous bicarbonate (three times) and water (three times). The organic layer was dried on magnesium sulfate, filtered, and concentrated to dryness under reduced pressure. The crude product was applied to a silica gel column. Elution with 1:1 petroleum ether/ethyl acetate afforded pure 1-(2′-O-triphenylmethylethoxy)-2-(2′-hydroxyethoxy)ethane (i.e., monotritylated triethylene glycol) as a viscous oil...yield, 20.56 g..."

(There is a minor uncertainty in the amount of trityl chloride used: 63.50 mmol requires 17.70 g instead of "17.42 g". The following calculations are based on 63.50 mmol.)

The probability that any given hydroxyl group has reacted (*p*) is numerically equal to the fraction of hydroxyl groups reacted. It is thus equal to the ratio of the equivalents of hydroxyl reacted (equal to the equivalents of trityl chloride used) to the total equivalents of hydroxyl initially present:[5]

$$p = 63.50/(2 \times 500.00) = 0.06350$$

The probability that any given hydroxyl group has not reacted (*q*) is, as always, $1 - p$:

$$q = 1 - 0.0635 = 0.9365$$

The expected mole fractions of the various products are calculated exactly as before:

[4] Derivation of $x\ (\%) = 400r/(1 + 2r)$. Consider the reaction of a homobifunctional spacer (*a* mole; 2*a* equiv) with an equimolar amount of a monofunctional derivatizing agent (MDA, *a* mole; *a* equiv). At time *t*, the conversion = *x* = the fraction of MDA reacted, and *ax* = the equivalents of MDA reacted. The value of *p* at time *t* is numerically equal to the fraction of spacer functional groups reacted. Thus, $p = ax/2a = x/2$. Substituting $x/2$ for *p* in $r = p/2(1 - p)$ gives $r = x/2(2 - x)$. Rearranging the last equation gives $x = 4r/(1 + 2r)$ or $x(\%) = 400r/(1 + 2r)$.

[5] General equations for calculation of probabilities in the reaction of *a* moles of homobifunctional spacer with *b* moles of monofunctional derivatizing agent: $p = b/2a$; $q = (1 - b/2a)$.

mole fraction of Tr-TEG-Tr $= p^2 = (0.06350)^2 =$ 0.004032

mole fraction of unreacted TEG $= q^2 = (0.9365)^2 =$ 0.8770

mole fraction of Tr-TEG $= 2\,pq = 2 \times 0.06350 \times$ 0.9365 $= 0.1189$

Scheme 2 shows a summary of the complete stoichiometry for this reaction.[6] The true theoretical yield of monotritylated triethylene glycol is 23.33 g. The actual yield reported (20.56 g) thus corresponds to 88.13% of the expected value. (If the amount of trityl chloride used was in fact 17.42 g (62.49 mmol), then the theoretical yield is 22.99 g and the recovery is 89.43%. Either way, this is obviously an excellent procedure for synthesis of the monotrityl ether of triethylene glycol.)

The foregoing calculations describe a bulk process, one in which the total amounts of the reactants are combined at the start. Aldenhoff et al. used an incremental process, adding the trityl chloride in 10 portions over a 3 h period. Both processes lead to the same final theoretical product distribution, however. A somewhat idealized summary of the incremental process is depicted in Table 3 in the form of a spreadsheet. [Instructions for reproducing the spreadsheet are given in a footnote to the table.[7]] In each step, the product distribution is calculated by applying the relevant probability values for the added increment to the products formed in the preceding step. For example, consider step 2 (The subscripts here refer to the step numbers, not row numbers or numbers of atoms or groups; the quantities are in moles):

cell F6: $\mathrm{TEG}_2 = {q_2}^2 \times \mathrm{TEG}_1$

cell G6: $\mathrm{Tr\text{-}TEG}_2 = (2 \times p_2 \times q_2 \times \mathrm{TEG}_1) + (q_2 \times \mathrm{Tr\text{-}TEG}_1)$

cell H6: $\mathrm{Tr\text{-}TEG\text{-}Tr}_2 = ({p_2}^2 \times \mathrm{TEG}_1) + (p_2 \times \mathrm{Tr\text{-}TEG}_1) + \mathrm{Tr\text{-}TEG\text{-}Tr}_1$

These equations state that the amount of Tr-TEG present at the end of step 2 is the sum of that newly formed from TEG_1 plus the residual amount—the amount *not* converted to $\mathrm{Tr\text{-}TEG\text{-}Tr}_2$—from step 1. In like fashion, the amount of Tr-TEG-Tr present at the end of step 2 is the amount newly formed from TEG_1 plus the amount formed from $\mathrm{Tr\text{-}TEG}_1$ plus the amount previously formed in Step 1 ($\mathrm{Tr\text{-}TEG\text{-}Tr}_1$). The spreadsheet format makes it easy to apply the formulas to each row in turn.

There is nothing particularly unique about the ten-step incremental process. The amount of each increment added can be decreased or increased and the table correspondingly lengthened or shortened without in any way affecting the final product distribution. It should be noted in this regard that a bulk process is an incremental process consisting of only one step.

In practical synthetic work, it is not necessary to either add increments in equal amounts nor drive the reaction to completion in any step except the last. The important factors are order of addition, reaction rate, and mixing technique. These are discussed in more detail later.

It is sometimes necessary to activate a homobifunctional spacer in order to link it to the desired reagent. Examples are the activation of a glycol with carbonyldiimidazole (CDI) followed by reaction with an amine to give a urethane, and activation of a dicarboxylic acid with isobutyl chloroformate (IBCF) followed by reaction with an amine to give an amide (mixed anhydride process) (Scheme 3). An interesting detail for reactions of this type is that the final product distribution is insensitive to the amount of activating agent used, so long as it lies in the range 1−2 mol/mol of homobifunctional spacer. First, consider the two extremes. Activation of 1 mol of a dicarboxylic acid spacer with 1 mol of isobutyl chloroformate ($p = 0.50$; $q = 0.50$) will give the expected binomial distribution: 0.25 mol of unreacted dicarboxylic acid, 0.25 mol of bis(mixed anhydride), and 0.50 mol of mono(mixed anhydride). Subsequent reaction with 1 mol of amine does not alter this distribution, thus yielding 0.25 mol of unreacted dicarboxylic acid, 0.25 mol of bisamide, and 0.50 mol of monoamide. Alternatively, activation of 1 mol of dicarboxylic acid with 2 mol of isobutyl chloroformate simply converts it to a new homobifunctional reactant; subsequent treatment with 1 mol of amine, followed by hydrolysis of excess mixed anhydride groups, will again give the same expected distribution: 0.25 mol of unreacted dicarboxylic acid, 0.25 mol of bisamide, and 0.50 mol of monoamide.

Consider now the activation of 1 mol of dicarboxylic acid with 1.5 mol of isobutyl chloroformate. Expected values for the activation step ($p = 1.5/2 = 0.750$; $q = 0.250$) are 0.0625 mol of unreacted dicarboxylic acid, 0.3750 mol of mono(mixed anhydride), and 0.5625 mol of bis(mixed anhydride). Subsequent treatment of this mixture with exactly 1 mol of amine gives the product distribution shown in Scheme 4. After hydrolysis of the excess mixed anhydride end groups, the reaction mixture contains 0.25 mol of dicarboxylic acid, 0.25 mol of bisamide, and 0.50 mol of monoamide, exactly as in the two preceding cases.

In a homogeneous system, no variation in experimental procedure can lead to a yield of monosubstituted spacer greater than that set by the stoichiometry and probability. However, procedure can drastically affect how closely the product distribution actually obtained approximates the expected values, particularly in those cases in which the reaction velocity is very fast. Order of addition is especially important. Visualize the consequences of slowly—slowly relative to the reaction rate—adding a solution of a diamine to a solution of an acyl halide. In the reactor, an excess of acyl halide over diamine will exist nearly to the point that half of the diamine has been added. Consequently, this half of the diamine becomes totally diacylated, and no more acyl halide remains to react with the second half. The final result is a mixture of diamide and unreacted diamine containing practically none of the monoacylated product. A more appropriate way to carry out this type of reaction is to add dropwise a solution of acyl halide (as dilute as possible) to a very vigorously agitated solution of diamine (as concentrated as possible, considering viscosity, solubility, etc.) at a temperature low enough to slow the rate of reaction substantially. The object again is to prevent

[6] General equations for calculation of expected values (moles) for products formed in the reaction of a moles of homobifunctional spacer with b moles of monofunctional derivatizing agent: Monosubstituted spacer $= b(1 - b/2a)$; disubstituted spacer $= b2/4a$; unreacted spacer $= (a - b + b2/4a)$. The sum of these three values is always equal to a, a detail useful for cross−checking the mass balance. When the derivatizing agent is present in excess, that is, $b > 2a$, these equations no longer have physical meaning.

[7] When set up as a spreadsheet, Table 3 is readily adaptable to any kind of addition process.

Scheme 2. Summary of Stoichiometry in the Preparation of the Monotrityl Ether of Triethylene Glycol by Reaction of Trityl Chloride (TrCl) with Triethylene Glycol (TEG)[a]

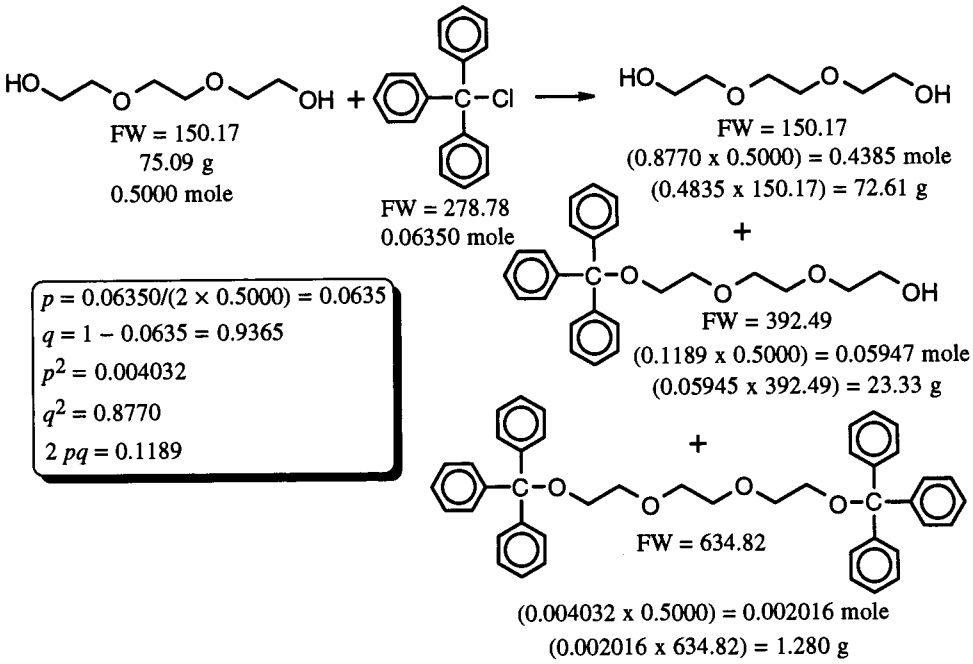


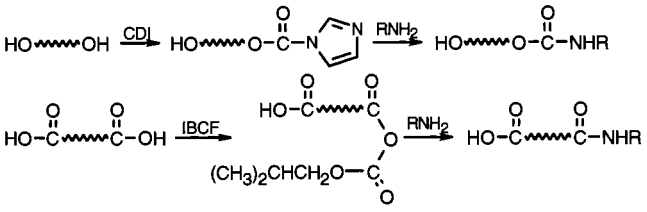
Table 3. Cumulative Change in Product Distribution following Addition of Trityl Chloride (10 Portions, 0.006 35 mol Each) to Triethylene Glycol (0.5000 mol)[a]

	A	B	C	D	E	F	G	H
1		values at beginning of each step				values at end of each step		
2		TrCl	hydroxyl	*p*	*q*	TEG	Tr-TEG	Tr-TEG-Tr
3	step	increments	(equiv)			(mol)	(mol)	(mol)
4	0	0.000 00	1.0000			0.5000	0.000 00	0.000 000
5	1	0.006 35	1.0000	0.006 35	0.993 65	0.4937	0.006 31	0.000 020
6	2	0.006 35	0.9937	0.006 39	0.993 61	0.4874	0.012 54	0.000 081
7	3	0.006 35	0.9873	0.006 43	0.993 57	0.4811	0.018 69	0.0001 81
8	4	0.006 35	0.9810	0.006 47	0.993 53	0.4749	0.024 75	0.000 323
9	5	0.006 35	0.9746	0.006 52	0.993 48	0.4688	0.030 74	0.000 504
10	6	0.006 35	0.9683	0.006 56	0.993 44	0.4626	0.036 65	0.000 726
11	7	0.006 35	0.9619	0.006 60	0.993 40	0.4565	0.042 47	0.000 988
12	8	0.006 35	0.9556	0.006 65	0.993 35	0.4505	0.048 22	0.001 290
13	9	0.006 35	0.9492	0.006 69	0.993 31	0.4445	0.053 88	0.001 633
14	10	0.006 35	0.9429	0.006 73	0.9932 7	**0.4385**	**0.059 47**	**0.002 016**
15	sum	0.063 50						

	A	B	C	D	E	F	G	H
5		0.006 35	=C4−B4	=B5/C5	=1−D5	=F4*E5∧2	=(2*D5*E5*F4)+E5*G4	=D5∧2*F4+D5*G4+H4

[a] Calculations using an Excel spreadsheet: enter the appropriate numerical values in row 4. Enter 0.006 35 in B5, select B5 and fill down to row 14 (step 10). Enter relative references in the cells of row 5 as shown. Select C5−H5 and drag fill handle to row 14. (The calculations are based on ideal mixing and quantitative reaction for each step.)

Scheme 3. Examples of Spacer Activation and Subsequent Derivatization[a]



[a] CDI = carbonyldiimidazole; IBCF = isobutyl chloroformate.

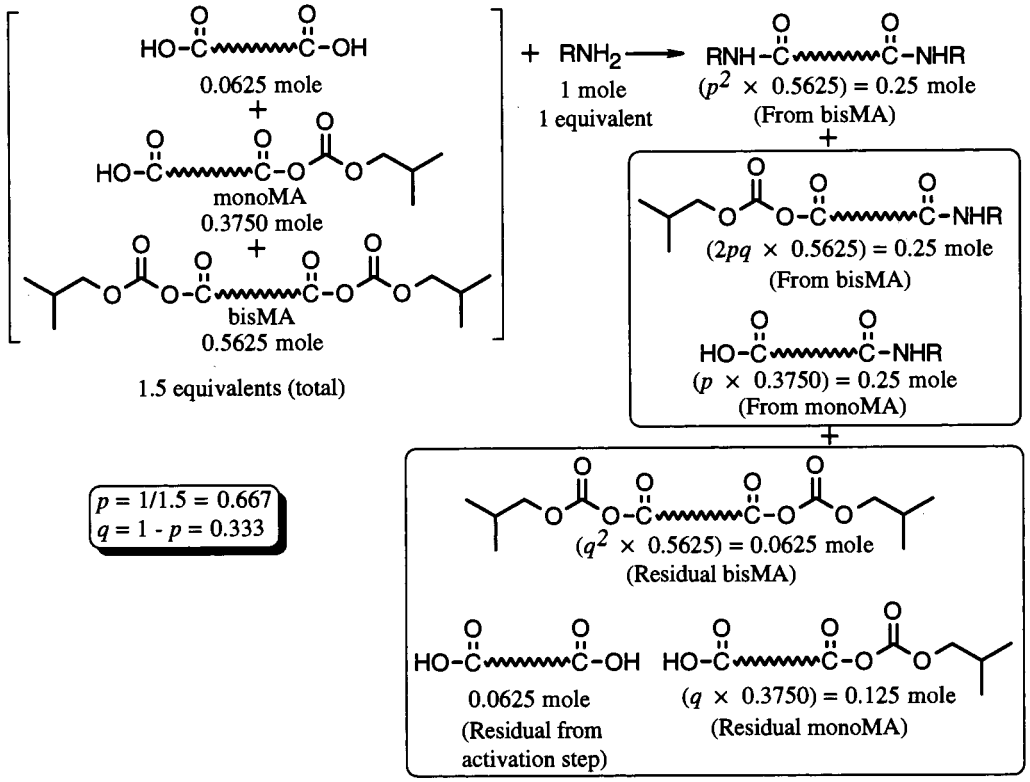
excess diacylation, since even here an excess of acyl halide over diamine can temporarily exist in the microenvironment around each newly added drop. It is therefore important that complete mixing takes place before any substantial amount of reaction has occurred.[8] An observed DID/MOD mole ratio (*r*) greater than the expected value (EV_r) is almost always the signature of a procedural problem.

HOMOTRI- AND HOMOPOLYFUNCTIONAL REACTANTS

The law of binomial distribution applies equally well to reactants with functionality greater than 2, subject again to the restriction that all the functional groups must be equally reactive. For example, the expected product distribution (mol fractions) from a reaction of equimolar quantities of a triamine and a monofunctional

[8] Depending on the case at hand, other options might include adding any catalyst, acid acceptor, etc., only after the primary reactants have been thoroughly mixed.

Scheme 4. Expected Values for the Reaction of 1 mol of Amine with 1 mol of Dicarboxylic Acid Previously Activated with 1.5 mol of Isobutyl Chloroformate[a]



[a] MA = mixed anhydride.

Table 4. Equimolar Reaction of a Homopolyfunctional Reagent (HPFR) Bearing *n* Functional Groups and a Monofunctional Derivatizing Reagent: Unreacted HPFR as a Function of *n*

n	unreacted HPFR (mole fraction)
2	0.2500
3	0.2963
4	0.3164
5	0.3277
6	0.3349
7	0.3399
8	0.3436
9	0.3464
10	0.3487
∞	0.3679

derivatizing agent are

$$p = 0.3333;\ q = 0.6667$$

$$\text{unreacted triamine} = q^3 = 0.2963$$

$$\text{monosubstituted triamine} = 3pq^2 = 0.4444$$

$$\text{disubstituted triamine} = 3p^2q = 0.2222$$

$$\text{trisubstituted triamine} = p^3 = 0.0370$$

A notable feature in the reaction of equimolar quantities of a homopolyfunctional reagent (HPFR) and a monofunctional derivatizing reagent is that the mole fraction of HPFR remaining unreacted *increases* as the number of functional groups (*n*) on the HPFR molecule increases, ultimately approaching the transcendental value 1/*e* (=0.367 879 441...) as a limit (Table 4).

Although these principles are relevant to conjugate syntheses with polyfunctional reagents such as the recently developed dendrimer reagents (*2*), they apply less well to proteins. In proteins, even functional groups of the same type possess widely differing reactivities due to the steric environment, different pK_a values, etc.

HETEROGENEOUS REACTION SYSTEMS

The above considerations apply to a homogeneous reaction, i.e., one in which both the homobifunctional spacer and its monoderivatized product remain in solution throughout the reaction. It is sometimes possible to find a solvent in which the reactants are soluble but the monoderivatized product is insoluble, precipitating as soon as it forms. Under these conditions, the law of binomial distribution no longer holds, and it is possible to get much higher yields than in a homogeneous system. A specific example of such a heterogeneous reaction system is encountered in the reaction of ethylene glycol bis(3-aminopropyl) ether [2997-01-5] with succinic anhydride in acetonitrile. The highly insoluble monoamide [144923-24-0] is obtainable in yields as high as 85% (*3*).

ACKNOWLEDGMENT

The author thanks his colleagues at Dade Behring Inc. for their many cogent comments, criticisms, and suggestions during preparation of the manuscript: Roger Bauer, William P. Bedzyk, Daniel V. Brown, Alan R. Craig, Pratap Singh, Richard W. Stout, John C. Thompson, and Chengrong Wang.

LITERATURE CITED

(1) Aldenhoff, Y. B. J., Pijpers, A. P., and Koole, L. H. (1997) Synthesis of a new photoreactive derivative of dipyridamole and its use in the manufacture of atificial surfaces with low

thrombogenicity. *Bioconjugate Chem. 8*, 296−303.

(2) Singh, P. (1998) Terminal groups in starburst dendrimers. Activation and reactions with proteins. *Bioconjugate Chem. 9*, 54−63.

(3) Obzansky, D. M., Simons, D. M., and Tseng, S. Y. T. Method for specific binding assays using a releasable ligand. U.S. Patent 5,332,679, July 26, 1994, 68 pp.

BC980071B

ARTICLES

Bis(Hydroxamamide)-Based Bifunctional Chelating Agent for ^{99m}Tc Labeling of Polypeptides

Le-Cun Xu,[†] Morio Nakayama,*[,†] Kumiko Harada,[†] Akihiko Kuniyasu,[†] Hitoshi Nakayama,[†] Seiji Tomiguchi,[‡] Akihiro Kojima,[‡] Mutsumasa Takahashi,[‡] Masahiro Ono,[§] Yasushi Arano,[§] Hideo Saji,[§] Zhengsheng Yao,[∥] Harumi Sakahara,[∥] Junji Konishi,[∥] and Yoshitaka Imagawa[⊥]

Faculty of Pharmaceutical Sciences, Kumamoto University, 5-1 Oe-Honmachi, Kumamoto 862, Japan, Department of Radiology, Kumamoto University School of Medicine, Honjo, Kumamoto 860, Japan, Department of Patho-Functional Bioanalysis, Graduate School of Pharmaceutical Sciences, Department of Nuclear Medicine and Diagnostic Imaging, Graduate School of Medicine, Kyoto University, Yoshida-Shimoadachi-cho, Sakyo-ku, Kyoto 606-01, Japan, and The Chemo-Sero Therapeutic Research Institute, Kyokushi-mura, Kikuchi-gun, Kumamoto 869-12, Japan. Received February 25, 1998; Revised Manuscript Received August 10, 1998

To develop chelating molecules that provide ^{99m}Tc-labeled polypeptides of high in vivo stability and high specific activities under mild reaction conditions, an asymmetrical bis(benzohydroxamamide) compound with an amine group, 4′-aminomethyl-*N*,*N*′-trimethylenedibenzohydroxamamide [$NH_2-C_3(BHam)_2$], was designed and synthesized. The amine residue of $NH_2-C_3(BHam)_2$ was converted to a maleimide group by reaction with *N*-succinimidyl-6-maleimidohexanoate, and the conjugation product was coupled to thiol groups of a monoclonal antibody against osteogenic sarcoma (OST7, IgG_1) pretreated with 2-iminothiolane to prepare $C_3(BHam)_2-$OST7. ^{99m}Tc radiolabeling of $C_3(BHam)_2-$OST7 was performed by the exchange reaction with [^{99m}Tc]glucoheptonate. [^{99m}Tc]$C_3(BHam)_2-$OST7 was further characterized using directly radioiodinated OST7 ([^{125}I]OST7) and [^{111}In]labeled OST7 with 1-[4-[(5-maleimidopentyl)amidobenzyl]ethylenediamine-*N*,*N*,*N*′*N*′-tetraacetic acid (EMCS−Bz-EDTA) as references. [^{99m}Tc]$C_3(BHam)_2-$OST7 was obtained with radiochemical yields of over 94% at protein concentrations as low as 0.2 mg/mL at room temperature for 1 h. [^{99m}Tc]$C_3(BHam)_2-$OST7 remained stable after incubation in freshly prepared murine plasma and in the presence of cysteine. Similar binding affinities to tumor cells were observed between [^{99m}Tc]$C_3(BHam)_2-$OST7 and [^{125}I]-OST7. When injected into normal mice, [^{99m}Tc]$C_3(BHam)_2-$OST7 exhibited radioactivity levels in the blood similar to [^{111}In]-EMCS−Bz-EDTA-OST7 up to 24 h postinjection with significantly faster elimination rate of the radioactivity from the liver. In nude mice bearing osteogenic sarcoma, no significant differences were observed in the radioactivity levels in the blood and the tumor between [^{99m}Tc]$C_3(BHam)_2-$OST7 and [^{125}I]OST7 at 24 h postinjection. These findings indicated that $C_3(BHam)_2$ provided ^{99m}Tc chelate of high stability at low concentrations even when conjugated to an intact antibody. Such characteristics render bis(hydroxamamide) compounds useful as chelating molecules for preparation of ^{99m}Tc-labeled polypeptides.

INTRODUCTION

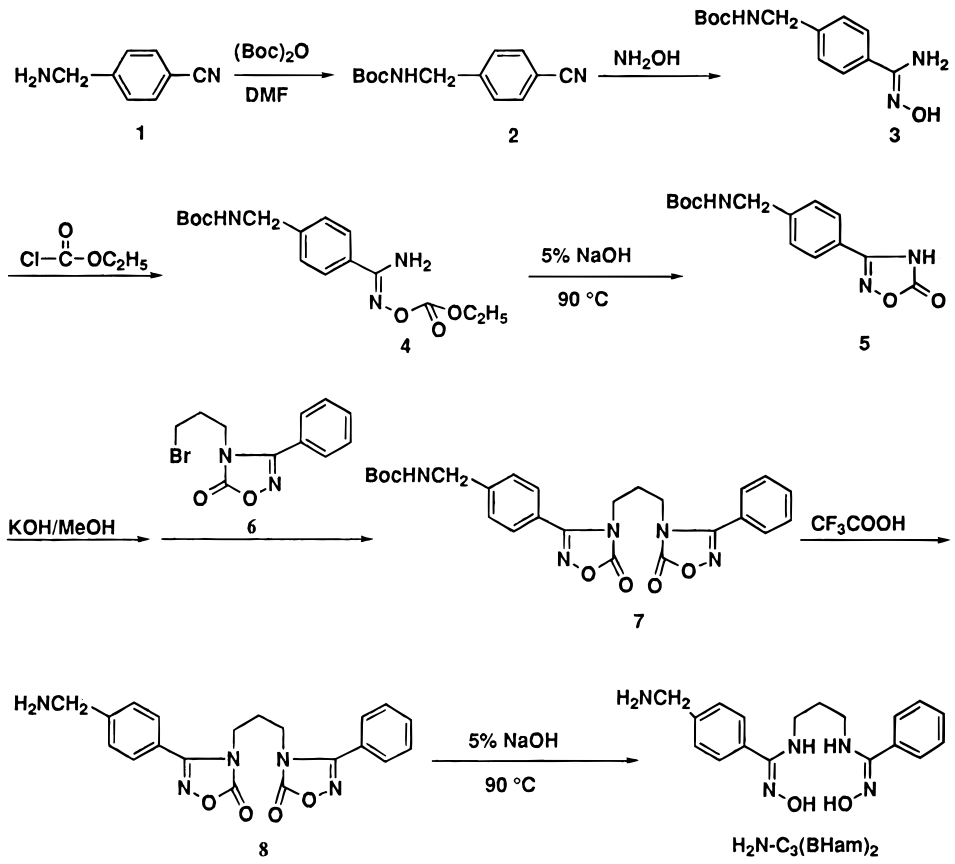
Radiopharmaceuticals derived from low molecular weight polypeptides such as single-chain Fv fragment, octreotide, and chemotactic peptide have attracted attention for imaging of the sites of tumors, infection, and thrombosis (*1*−*3*). The rapid pharmacokinetic properties of these molecules enable target visualization at early postinjection intervals using radionuclides with short half-lives. ^{99m}Tc is an ideal radionuclide for scintigraphic imaging applications due to its excellent physical properties, low cost, and ready availability (*4*). Since most polypeptides do not possess binding sites to form ^{99m}Tc chelates of high in vivo stability, appropriate chelating molecules are incorporated into polypeptide molecules to prepare ^{99m}Tc-labeled peptides for in vivo applications.

Previous efforts directed toward the conjugation of ^{99m}Tc to polypeptides include the use of tetradentate ligands with N_3S or N_2S_2 ligand systems, which contain one or two thiol groups (*5*−*9*). While the thiol groups in the molecules facilitate the formation of mononuclear ^{99m}Tc complexes with high stability, the presence of the free thiol group may restrict the conjugation reactions with polypeptides and subsequent storage of the resulting bioconjugates. Protection of a thiol group was performed to conjugate a N_3S chelating molecule to an antibody fragment, which necessitated a deprotection step before

* To whom correspondence should be addressed. Phone: 81-96-371-4358. Fax: 81-96-372-7182. E-mail: morio@gpo.kumamoto-u.ac.jp.
[†] Kumamoto University.
[‡] Kumamoto University School of Medicine.
[§] Graduate School of Pharmaceutical Sciences.
[∥] Kyoto University.
[⊥] The Chemo-Sero Therapeutic Research Institute.

10.1021/bc980024j CCC: $18.00 © 1999 American Chemical Society
Published on Web 12/22/1998

Scheme 1



^{99m}Tc complexation reaction (*9*). Exchange reactions between the free thiol groups of the chelating agents and disulfide bonds in peptides may also constitute a potential problem in the conjugation reactions. In addition, some chelating agents require harsh ^{99m}Tc complexation conditions (elevated temperatures or high pH) to prepare ^{99m}Tc chelates with high radiochemical yields (*10*−*12*). Thus, development of thiol-free chelating molecules that provide ^{99m}Tc complexes with high in vivo stability and high specific activities under mild complexation conditions would facilitate further application of ^{99m}Tc to a variety of polypeptides of interest for diagnostic nuclear medicine.

Hydrazino nicotinamide (HYNIC) is a representative thiol-free chelating agent, and applicability of this chelating agent for ^{99m}Tc labeling of polypeptides has been well demonstrated (*13*−*15*). HYNIC has been reported to act as a mono- or bidentate ligand and forms ^{99m}Tc chelates of high specific activity with high radiochemical yields in the presence of appropriate co-ligands such as glucoheptonate or tricine. We initiated a program to develop new thiol-free chelating molecules with a tetradentate ligand system. Previous studies suggested that *N*-hydroxy-carboximidamide (hydroxamamide, abbreviated as Ham)-based tetradentate ligands, bis(Ham), form ^{99m}Tc chelates with high stability and high specific activity with high radiochemical yields (*16*−*19*). These findings prompted us to design bis(Ham) derivatives with a functional group for the conjugation with polypeptides.

In the present study, an asymmetrical bis(benzohydroxamamide) compound with an amine group at the conjugation site, 4′-aminomethyl-*N*,*N*′-trimethylenedibenzohydroxamamide [$NH_2-C_3(BHam)_2$], was designed and synthesized as outlined in Scheme 1. The ability of $NH_2-C_3(BHam)_2$ as a chelating molecule for ^{99m}Tc-labeled polypeptides was estimated using a monoclonal antibody (mAb) against osteogenic sarcoma (OST7, IgG_1) as a model. For comparison, OST7 was labeled with radioiodine by direct iodination and with indium-111 (^{111}In) using 1-[4-[(5-maleimidopentyl)amidobenzyl]ethylenediamine-*N*,*N*,*N*′*N*′-tetraacetic acid (EMCS−Bz-EDTA) as the chelating agent. Chemical structures of each conjugate are illustrated in Figure 1.

MATERIALS AND METHODS

Reagents and Chemicals. Proton nuclear magnetic resonance (^{1}H NMR) spectra were recorded on a JNM-500 (500 MHz) instrument (JEOL Ltd., Tokyo, Japan). Electron impact mass spectra (EI-MS) and fast atom bombardment mass spectra (FAB-MS) were obtained with a JMS-DX303HF mass spectrometer (JEOL Ltd.). Melting points were determined with a Yanaco Micro Melting Point Apparatus and were reported uncorrected. Na[^{125}I]I was obtained from Daiichi- Kagaku (Tokyo) and diluted with phosphate buffer (PB; 0.1 M, pH 7.4) to 0.37−3.7 MBq (0.01−0.1 mCi)/μL before use. $^{111}InCl_3$ [74 MBq (2 mCi)/mL in 0.02 N HCl] was supplied by Nihon-Medi-Physics (Tokyo, Japan). [^{99m}Tc]Pertechnetate ($^{99m}TcO_4^-$) was eluted in saline solution on a daily basis from Daiichi Radioisotope Labs. generators (Chiba, Japan). 3-Phenyl-4-(3-bromopropyl)-Δ^2-1, 2, 4-oxadiazolin-5-one (compound 6 in Scheme 1) was synthesized according to the procedures described previously (*19*). Both *N*-(ϵ-maleimidocaproyloxy)succinimide (EMCS) and EMCS−Bz-EDTA were purchased from Dojindo Labs (Kumamoto, Japan). 2-Iminothiolane (2-IT) was obtained from Nacalai Tesque, Inc. Kyoto, Japan). Size-exclusion HPLC was performed using a TSK guard column SW_{XL} (6.0 × 40 mm) connected to a TSK G3000SW_{XL} (7.8 × 300 mm) column, eluted with 0.1 M PB (pH 7.0) containing 0.3 M

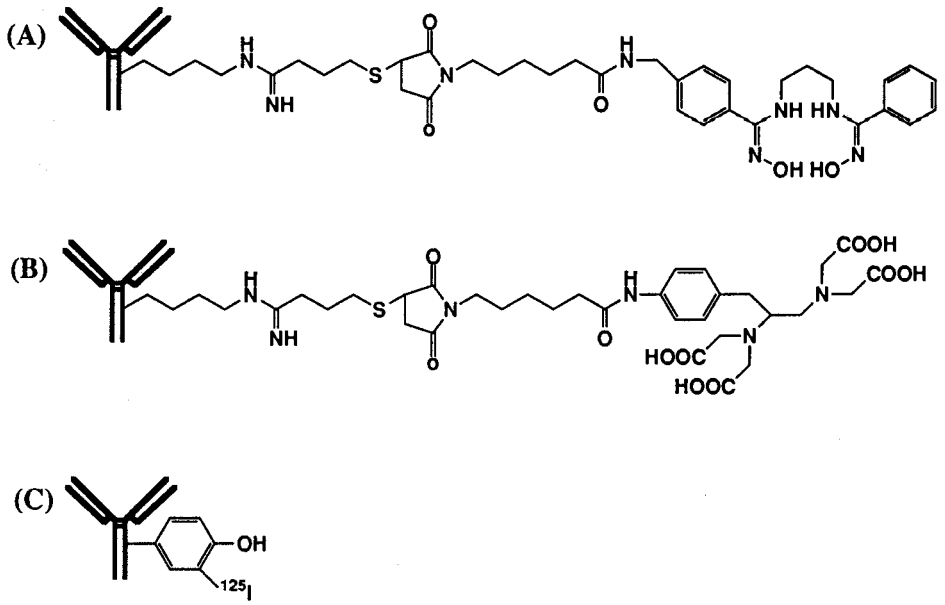


Figure 1. Chemical structures of $C_3(BHam)_2$−OST7 conjugate (A), EMCS−Bz-EDTA-OST7 conjugate (B) and ^{125}I-labeled OST7 (C).

sodium chloride at a flow rate of 0.5 mL/min. The eluent was monitored at 280 nm with an ultraviolet (UV) detector (Hitachi L-400 UV detector; Hitachi, Tokyo) and a well-type NaI (Tl) scintillation detector (Aloka PS-201; Aloka, Tokyo) coupled with a universal scalar (Aloka TCD 501). TLC analyses were performed with cellulose plates (Merck 5577) using 0.02 M phosphate-buffered saline (PBS, pH 7.0) as the developing solvent. Under these conditions, protein-bound radioactivity remained at the origin while $^{99m}TcO_4^-$ and [^{99m}Tc]cysteine moved with the solvent front. Cellulose acetate electrophoresis (CAE) was run on Separax SP (Joko, Tokyo) at a constant current of 0.8 mA/cm for 30 min in 0.072 M veronal buffer (pH 8.6). The migration distance of the antibody was determined by Ponceau 3R staining. To facilitate collection of urine and feces after administration of radiolabeled antibodies, mice were housed in metabolic cages (metabolica, MM type; Sugiyama-Gen Iriki Co. Ltd., Tokyo).

Tumor and mAb. KT005-cloned human osteosarcoma was maintained by serial subcutaneous transplantation in athymic nude mice. Female BALB/c athymic mice were implanted s.c. with 1−2 mm cubed pieces of KT005. Tumors of 0.2−0.5 g in weight at ca. 2 weeks postplantation were used in vivo study. Single-cell suspensions from xenografted tumors were used for the in vitro study *(20,21)*. The mAb against osteogenic sarcoma (OST7, IgG_1) was generated by a standard hybridoma technique, as described previously (*22*).

Synthesis of *p*-[*N*-(*tert*-Butoxycarbonyl)aminomethyl]benzonitrile (2). To a solution of *p*-(aminomethyl)benzonitrile (**1**, 10 g, 0.075 mol) in 60 mL *N,N′*-dimethyformamide (DMF) was gradually added a solution of $(Boc)_2O$ (17.4 g, 0.080 mol) in 50 mL of DMF, and the mixture was stirred at room temperature for 1 h. After removing the solvent in vacuo (30 mmHg), water (100 mL) was added to produce a white precipitate. The precipitate was collected and recrystallized from methanol−water (5:4) to produce compound **2** (17.5 g) in 99% yield. Mp 108−109 °C. ^{1}H NMR (DMSO-d_6): δ 7.479 (s, 1H, NH), 7.399−7.776 (m, 4H, aromatic H), 4.186 (s, 2H, NCH_2), 1.381 (s, 9H, $(CH_3)_3C$). EI-MS calculated for $C_{13}H_{17}N_2O_2$ (M^+): *m/z* 232. Found: 232. Anal. Calcd for $C_{13}H_{16}N_2O_2$: C, 67.22; H, 6.94; N, 12.06. Found: C, 67.46; H, 7.15; N, 11.85.

Synthesis of *p*-[*N*-(*tert*-Butoxycarbonyl)aminomethyl]benzohydroxamamide (3). A solution of free hydroxylamine was prepared by treating 13.8 g (0.20 mol) of hydroxylamine hydrochloride with 18 g (0.20 mol) of sodium bicarbonate in 100 mL of water. Compound **2** (36.8 g, 0.15 mol) in 100 mL of methanol was then added to the solution of free hydroxylamine, and the mixture was stirred at 60 °C for 8 h. After removing the solvent in vacuo, 100 mL of water was added to produce a white precipitate. Compound **3** was obtained after recrystallization of the precipitate from ethanol−water (1:1) with 94% (37.3 g) yield. Mp 152−153 °C. ^{1}H NMR (DMSO-d_6): δ 9.550 (s, 1H, OH), 7.364 (s, 1H, N*H*CH_2), 7.203−7.608 (m, 4H, aromatic H), 5.737 (s, 2H, NH_2), 4.120 (d, 2H, NHCH_2), 1.386 (s, 9H, $(CH_3)_3C$). EI-MS calculated for $C_{13}H_{20}N_3O_3$ (M^+): *m/z* 265. Found: 265. Anal. Calcd for $C_{13}H_{19}N_3O_3$: C, 58.85; H, 7.22; N, 15.84. Found: C, 59.08; H, 7.17; N, 15.70.

Synthesis of *p*-[*N*-(*tert*-Butoxycarbonyl)aminomethyl]benzamamide *O*-Ethoxycarbonyloxime (4). To a chilled solution of compound **3** (37 g, 0.14 mol) in 350 mL of dry acetone in an ice bath was slowly added 15.2 g (0.14 mol) of ethyl chlorocarbonate while maintaining the reaction temperature. A white precipitate of hydroxamamide hydrochloride was produced. While maintaining the reaction temperature at 0−4 °C, a solution of NaOH (5.7 g, 0.14 mol) in 100 mL of water was then gradually added. After stirring for 1 h at room temperature, the solvent was removed in vacuo. The solid residue was recrystallized from ethanol−water (1:1) to produce 37 g of compound **4** as white crystals (78%). Mp 109−110 °C. ^{1}H NMR (DMSO-d_6): δ 7.413 (s, 1H, N*H*CH_2), 7.270−7.631 (m, 4H, aromatic H), 6.749 (s, 2H, NH_2), 4.152 (d, 2H, NHCH_2), 4.175 (q, 2H, J = 7.32 Hz, OCH_2CH_3), 1.251 (t, 3H, J = 7.32 Hz, OCH_2CH_3), 1.386 (s, 9H, $(CH_3)_3C$). EI-MS calculated for $C_{16}H_{24}N_3O_5$ (M^+): *m/z* 337. Found: 337. Anal. Calcd for $C_{16}H_{23}N_3O_5$: C, 56.96; H, 6.87; N, 12.45. Found: C, 57.21; H, 6.96; N, 12.54.

Synthesis of 3-[*p*-(*N*-(*tert*-Butoxycarbonyl)aminomethyl)phenyl]-Δ^2-1,2,4-oxadiazolin-5-one (5). Compound **4** (36 g, 0.11 mol) was added to a solution of NaOH (17 g) in 300 mL of water, and the mixture was heated in a boiling water bath for 10 min. After the solution

became clear, the reaction mixture was cooled in an ice bath and acidified with acetic acid to produce a while precipitate. The precipitate was collected and recrystallized from ethanol−water (5:6) to yield 28 g of compound **5** as white crystal (87%). Mp 176−177 °C. ^{1}H NMR (DMSO-d_6): δ 7.441 (s, 1H, N*H*CH$_2$), 7.397−7.753 (m, 4H, aromatic H), 4.186 (d, 2H, NHC*H*$_2$), 1.385 (s, 9H, (CH$_3$)$_3$C). EI-MS calculated for $C_{14}H_{18}N_3O_4$ (M^+): *m/z* 291. Found: 291. Anal. Calcd. for $C_{14}H_{17}N_3O_4$: C, 57.72; H, 5.88; N, 14.42. Found: C, 57.61; H, 5.85; N, 14.28.

Synthesis of 3-[*p*-(*N*-(*tert*-Butoxycarbonyl)aminomethyl)phenyl]-3′-phenyl-4,4′-trimethylenedi-Δ^2-1, 2, 4-oxadiazolin-5-one (7). To a solution of compound **5** (15.5 g, 0.053 mol) in methanol (40 mL) was added a solution of KOH (3.0 g, 0.053 mol) in 50 mL of methanol. After stirring for 10 min, the solvent was removed in vacuo. The residue was dissolved in 80 mL of dry DMF, and 13.5 g (0.047 mol) of 3-phenyl-4-(3-bromopropyl)-Δ^2-1, 2, 4-oxadiazolin-5-one (*19*) was added. After 3 days of stirring at 50 °C, the precipitates were filtered off and the filtrate was evaporated in vacuo. Chloroform (30 mL) was added to the residue, and the organic phase was washed sequentially with 1.0 M NaOH and water. After drying over anhydrous $MgSO_4$, the solvent was removed in vacuo. The solid residue was crystallized from ethanol to give 14.9 g of compound **7** (57%) as white crystals. Mp 166−167 °C. ^{1}H NMR (DMSO-d_6): δ 7.415−7.699 (m, 9H, aromatic H), 4.228−4.241 (d, 2H, NH$_2$C*H*$_2$), 3.557−3.584 (m, 4H, C*H*$_2$CH$_2$C*H*$_2$), 1.746−1.774 (m, 2H, CH$_2$C*H*$_2$CH$_2$), 1.411 [s, 9H, (CH$_3$)$_3$C]. FAB-MS calculated for $C_{25}H_{28}N_5O_6$ (MH^+): *m/z* 493. Found: 493. Anal. Calcd for $C_{25}H_{27}N_5O_6$: C, 60.84; H, 5.51; N, 14.19. Found: C, 60.49; H, 5.56; N, 13.88.

Synthesis of 3-[*p*-(Aminomethyl)phenyl]-3′-phenyl-4,4′-trimethylenedi-Δ^2-1,2,4-oxadiazolin-5-one (8). Compound **7** (2.47 g, 0.005 mol) was dissolved in a mixed solution of trifluoroacetic acid (25 mL) and anisole (25 mL) at 0 °C. After stirring at room temperature for 1 h, the solvent was removed in vacuo. The residue was dissolved in water, and 1 N NaOH was added to bring the solution pH to ca. 9−10. A white precipitate was obtained after chilling the solution in an ice bath. Recrystallization of the precipitate from ethanol produced compound **8** (1.5 g, 74%). Mp 157−158 °C. ^{1}H NMR (DMSO-d_6): 7.485−7.704 (m, 9H, aromatic H), 3.551−3.584 (m, 4H, C*H*$_2$CH$_2$C*H*$_2$), 3.828 (s, 2H, NH$_2$C*H*$_2$), 1.724−1.1.783 (m, 2H, CH$_2$C*H*$_2$CH$_2$). FAB-MS calculated for $C_{20}H_{20}N_5O_4$ (MH^+): *m/z* 393. Found: 393. Anal. Calcd. for $C_{20}H_{19}N_5O_4 \cdot 1/2H_2O$: C, 59.7; H, 5.01; N, 17.4. Found: C, 59.96; H, 4.851; N, 17.17.

Synthesis of NH$_2$-C$_3$(BHam)$_2$. Compound **8** (1.0 g, 2.5 mmol) was added to 20 mL of 5% NaOH, and the mixture was heated with stirring at 90 °C for 10 min. After cooling to 0−4 °C in an ice bath, the reaction mixture was neutralized with 1 M HCl. A white precipitate was obtained after cooling the reaction solution on ice for several hours. The precipitate was collected and crystallized from ethanol to give 0.6 g (1.8 mmol) of NH$_2$−C$_3$(BHam)$_2$ as white crystals (72%). Mp 179−180 °C. ^{1}H NMR (DMSO-d_6): δ 9.705 (s, 2H, OH), 8.213 (s, 2H, N*H*$_2$-CH$_2$), 7.332−7.473 (m, 9H, aromatic H), 5.642−5.694 (m, 2H, *H*NCH$_2$CH$_2$CH$_2$N*H*), 4.037 (s, 2H, NH$_2$C*H*$_2$), 2.858−2.897 (m, 4H, HNC*H*$_2$CH$_2$C*H*$_2$NH), 1.366−1.392 (m, 2H, HNCH$_2$C*H*$_2$CH$_2$NH). FAB-MS calcd for $C_{18}H_{23}N_5O_2$ (MH^+): *m/z* 341. Found: 341. Anal. Calcd for $C_{18}H_{23}N_5O_2$: C, 63.32; H, 6.79; N, 20.51. Found: C, 63.42; H, 7.02; N, 20.28.

Preparation of C$_3$(BHam)$_2$−OST7 Conjugate. The conjugation reaction of NH$_2$−C$_3$(BHam)$_2$ with OST7 was performed according to the procedure described previously (*23*) with slight modifications as follows. To 0.5 mL of a solution of OST7 (9 mg/mL) in well-degassed 0.16 M borate buffer (pH 8.0) containing 2 mM ethylenediaminetetraacetic acid (EDTA) was added 25 μL of 2-IT (2 mg/mL) in the same buffer. After gentle agitation at room temperature for 1 h, excess 2-IT was removed by the centrifugation through gel-filtration columns packed with Sephadex G-50 (Pharmacia Biotech, Tokyo) equilibrated with 0.1 M PBS (pH 5.5) containing 2 mM EDTA. EMCS in DMF (50 μL, 40 mM) was added to an equal volume of NH$_2$−C$_3$(BHam)$_2$ (80 mM) in the same solvent. After stirring the reaction mixture for 30 min at room temperature, 20 μL of this solution was slowly added to the freshly thiolated OST7 solution (0.5 mL) and the reaction mixture was stirred gently at room temperature for 2 h. The solution was further agitated gently for 30 min after addition of iodoacetamide (20 μL, 10 mg/mL) to alkylate the unreacted thiol groups. The C$_3$(BHam)$_2$−OST7 conjugate was separated from unreacted small molecules using Sephadex G-50 column chromatography (1.5 × 37 cm) equilibrated and eluted with PBS (pH 7.0). The number of C$_3$(BHam)$_2$ chelates introduced per molecule of OST7 was estimated by measuring the number of thiol groups of OST7 before and after addition of the reaction mixture of EMCS and NH$_2$−C$_3$(BHam)$_2$ using 2,2′-dithiopyridine (*24*). C$_3$(BHam)$_2$−OST7 was characterized by SDS−PAGE using 4% stacking gels and 8% running gels according to the method of Laemmli under nonreducing conditions (*25*). After mixing with 4% SDS, the samples were immersed for 5 min in a boiling water bath and loaded on the gels at a concentration of 4.0 μg of protein per lane. Electrophoresis was performed with a current of 20 mA per gel until the bromophenol blue marker reached the bottom of the gel. After running, gels were stained with 0.02% Coomassie brilliant blue (CBB) R250 in 25% methanol/10% acetic acid, and subsequently destained by equilibrating with 5% acetic acid/2% glycerol.

^{99m}Tc Labeling of C$_3$(BHam)$_2$-OST7. C$_3$(BHam)$_2$−OST7 was labeled with ^{99m}Tc by reaction with [^{99m}Tc]-glucoheptonate. A freshly collected solution (3−4 mL) of $^{99m}TcO_4^-$ [1 mCi (37 MBq)/mL] was added to a vial containing lyophilized glucoheptonate (4 mg) and $SnCl_2$ (60 μg) under a nitrogen atmosphere and allowed to stand for 15 min at room temperature. Aliquots of this solution (200 μL) were added to the C$_3$(BHam)$_2$−OST7 solution (200 μL) of varying protein concentrations and incubated for 1 h at room temperature. Radiochemical purities of [^{99m}Tc]C$_3$(BHam)$_2$−OST7 were determined by TLC, CAE, size-exclusion HPLC, and SDS−PAGE. Autoradiography of the dried PAGE gels was carried out by placing them on X-ray film (Fuji Photo Film Inc., Tokyo, Japan) for 12 h.

Stability of ^{99m}Tc-Labeled C$_3$(BHam)$_2$-OST7. [^{99m}Tc]-C$_3$(BHam)$_2$−OST7 (0.2 mg/mL; 20 μL) was added to a tube containing 200 μL of freshly prepared murine plasma to a final protein concentration of 1.3×10^{-7} M. After incubating the solution at 37 °C for 6 and 18 h, the mixture was analyzed by CAE and TLC. Stabilities of [^{99m}Tc]C$_3$(BHam)$_2$−OST7 were also estimated in the presence of cysteine. A 10 μL aliquot of 1.2×10^{-6} M [^{99m}Tc]C$_3$(BHam)$_2$−OST7 in 0.1 M PBS (pH 7.0) was mixed with 10 μL of cysteine to make the final concentrations of cysteine in the range of 3.6×10^{-6} to 3.6×10^{-4} M. The mixture was incubated at 37 °C for 1 and 6 h and analyzed by TLC using 0.005 M PB (pH 7) as the eluent. In this TLC system, [^{99m}Tc]cysteine showed an

R_f value above 0.8, while [^{99m}Tc]C_3(BHam)$_2$−OST7 remained at the origin.

Preparation of [^{111}In]EMCS−Bz-EDTA-OST7 and [^{125}I]OST7. Conjugation of EMCS−Bz-EDTA to OST7 was performed by maleimide−thiol chemistry using 2-IT, and the conjugate was labeled with ^{111}In, as described previously (*24, 26*). The number of chelating agents attached per molecule of OST7 was 2.2 as determined by calculating the number of thiol groups per molecule of OST7 before and after conjugation with EMCS−Bz-EDTA. Radiochemical purity of [^{111}In]EMCS−Bz-EDTA-OST7 was over 92% as determined by CAE analysis. Direct radioiodination of OST7 was performed by the chloramine-T method (*27*). To 100 μL of OST7 (0.25 mg/mL) in 0.3 M phosphate buffer (pH 7.3) was added 2 μL of Na[^{125}I]I and 12.5 μL of chloramine-T solution (0.1 mg/mL) in the same buffer. After 10 of min incubation at room temperature, the reaction was terminated by addition of 3 μL of aqueous sodium bisulfite (0.7 mg/mL). [^{125}I]OST7 was purified by the centrifuged gel-filtration column method using Sephadex G-50 as described above. Radiochemical purity of the radioiodinated OST7 was over 97% as determined by CAE analysis.

Immunoreactivity Measurement. The immunoreactivities of [^{99m}Tc]C_3(BHam)$_2$−OST7 and [^{125}I]OST7 were determined as described previously (*20, 21, 23*). Single-cell suspensions from xenografted tumors [(1×10^4)−(1×10^7)] in 100 μL of Dulbecco's PBS were incubated with 100 μL of radiolabeled OST7s in microcentrifugation tubes (5.7 × 46 mm) for 2 h at 4 °C. After centrifugation at 10000*g*, the supernatant was aspirated off and the radioactivity was determined using an Aloka ARC-2000 auto-well γ system (Aloka, Tokyo).

In Vivo Studies. An aliquot of 120 μL of [^{99m}Tc]C_3(BHam)$_2$−OST7 [0.5 mCi (18.5 MBq)/0.2 mg/0.4 mL] or 50 μL of [^{111}In]EMCS−Bz-EDTA-OST7 [10 μCi (370 KBq)/40 μg/50 μL] was added to 3 mL of unmodified OST7 (0.2 mg/mL) in 0.1 M PBS (pH 7.0). The biodistribution of radioactivity after intravenous administration of each radiolabeled OST7 was monitored at 1, 3, 6, and 24 h postinjection into 5-week-old male ddY mice weighing 20−25 g (*28*). Groups of five mice each receiving ca. 20 μg of OST7 were used for the experiment (*20, 21, 23, 29*). Organs or tissues of interest were removed and weighed, and their radioactivities were determined using an Aloka ARC-2000 auto-well γ system.

An aliquot of 40 μL of [^{99m}Tc]C_3(BHam)$_2$−OST7 [0.5 mCi (18.5 MBq)/0.2 mg/0.4 mL] and 30 μL of [^{125}I]OST7 [1 μCi (37 KBq)/2.5 μg/10 μL] were added to 1 mL of unmodified OST7 (0.2 mg/mL). Athymic mice bearing osteogenic sarcoma were treated intravenously with 100 μL of the mixture. At 24 h postinjection, the animals were sacrificed and the organs or tissues of interest were removed and weighed, and the radioactivity in each organ or tissue was measured immediately for ^{99m}Tc and 3 days later for ^{125}I using an Aloka ARC-2000 auto-well γ system.

Statistical Analyses. Data are expressed as means (standard deviation) where appropriate. Results were statistically analyzed using unpaired Mann−Whitney test for in vivo studies. Differences were considered significant when p value was less than 0.05.

RESULTS

Synthesis of NH_2-C_3(BHam)$_2$. The asymmetrical bis(Ham) compound NH_2−C_3(BHam)$_2$ was synthesized according to the synthetic procedure reported previously for symmetrical bis(Ham) compounds (*19*). After protecting the amino group of *p*-(aminomethyl)benzonitrile (**1**) with Boc, the resulting compound **2** was reacted with hydroxylamine to prepare compound **3**. Treatment of compound **3** with ethyl chlorocarbonate gave compound **4**, which was cyclized to oxadiazoline derivative **5** by heating in alkaline solution. After conversion to the potassium salt, compound **5** was alkylated with compound **6** to produce an asymmetrical bis(oxadiazoline) precursor **7**. NH_2−C_3(BHam)$_2$ was obtained by deprotection of the Boc group by trifluoroacetic acid, followed by decyclization in alkaline solution. The overall yield was 19%.

Table 1. Radiochemical Yields of [^{99m}Tc]C_3(BHam)$_2$-OST7 at Different Antibody Concentrations

concentration of C_3(BHam)$_2$−OST7 conjugate (mg/mL)	labeling yields[a] (%)
2.0	98.1 ± 1.7
1.0	96.0 ± 1.5
0.5	94.5 ± 1.9
0.2	94.3 ± 1.7
unmodified OST7 (0.2 mg/mL)	<3

[a] ^{99m}Tc labeling was performed at room temperature for 1 h. Means ± s.d. of four experiments. Radiochemical yields were determined by CAE.

Preparation of ^{99m}Tc-labeled C_3(BHam)$_2$-OST7. C_3(BHam)$_2$−OST7 conjugate was prepared by converting the amine group of NH_2−C_3(BHam)$_2$ to a maleimide group with EMCS, followed by conjugation reaction of the maleimide groups with the thiol groups of 2-IT-modified OST7. The number of chelating agents attached per molecule of OST7 was estimated to be 1.9 by measuring the thiol groups of OST7 before and after the conjugation reactions (2.1 and 0.2, respectively). The amount of free thiol groups were negligible after treatment of the conjugate with iodoacetamide. The C_3(BHam)$_2$−OST7 conjugate showed a single elution profile on size-exclusion HPLC at a retention time identical to that of unmodified OST7 when measured at 280 nm (data not shown).

^{99m}Tc radiolabeling of the conjugate was performed by exchange reaction with [^{99m}Tc]glucoheptonate. Radiochemical yields of [^{99m}Tc]C_3(BHam)$_2$−OST7 at different antibody concentrations are summarized in Table 1. [^{99m}Tc]C_3(BHam)$_2$−OST7 was obtained in more than 95% radiochemical yields at antibody concentrations over 1 mg/mL. High radiochemical yields were also registered at lower antibody concentrations. Under these conditions, radioactivities associated with antibody fractions were less than 3% when unconjugated OST7 (0.2 mg/mL) was reacted with [^{99m}Tc]glucoheptonate. Figure 2 shows a CAE radioactivity profile of [^{99m}Tc]C_3(BHam)$_2$−OST7 when ^{99m}Tc labeling was performed at an antibody concentration of 0.2 mg/mL. Figure 3 shows a typical UV chromatogram of unmodified OST7 and a radiochromatogram of [^{99m}Tc]C_3(BHam)$_2$−OST7 when analyzed by size-exclusion HPLC. The radiochromatogram superimposed well on the spectrophotometric elution profile of unmodified OST7 at 280 nm.

SDS−PAGE profiles of ^{99m}Tc-labeled C_3(BHam)$_2$−OST7, C_3(BHam)$_2$−OST7 conjugate, and unmodified OST7 performed under nonreducing conditions are illustrated in Figure 4. The CBB-stained bands (B) of [^{99m}Tc]C_3(BHam)$_2$−OST7 (lane 1) and C_3(BHam)$_2$−OST7 (lane 2) showed single bands corresponding to unmodified OST7 (lane 3). The autoradiogram of [^{99m}Tc]C_3(BHam)$_2$−OST7 (A) showed a single radioactive band in the fraction identical to that of unmodified OST7.

Table 2 shows the time course of changes in antibody-bound radioactivity after incubation of [^{99m}Tc]C_3(BHam)$_2$−

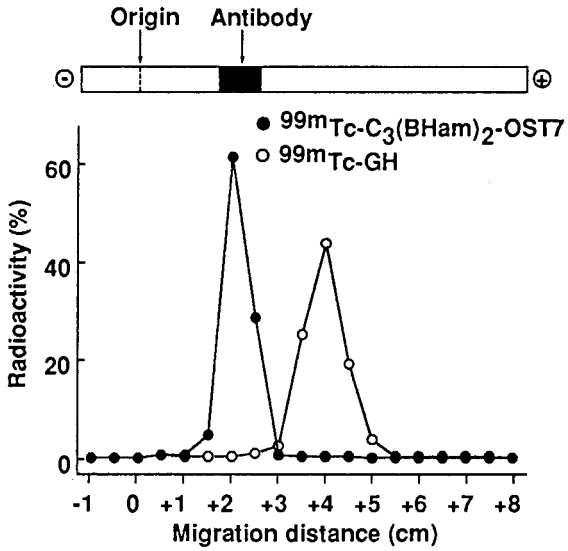


Figure 2. A typical radioactivity profile of [^{99m}Tc]C_3(BHam)$_2$−OST7 when analyzed by cellulose acetate electrophoresis.

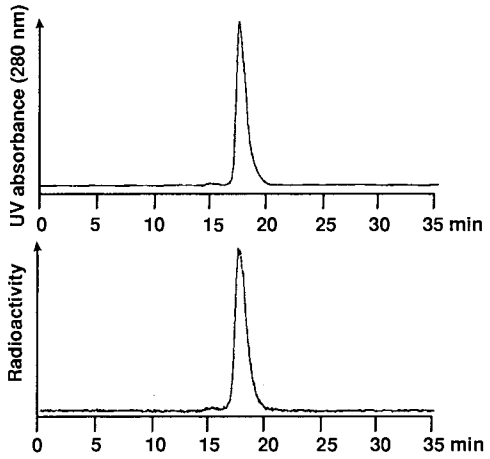


Figure 3. Size-exclusion HPLC profiles of the unmodified OST7 (UV 280 nm, top) and [^{99m}Tc]C_3(BHam)$_2$−OST7 (radioactivity, bottom).

OST7 in freshly prepared murine plasma at 37 °C. [^{99m}Tc]C_3(BHam)$_2$−OST7 showed only slight release of radioactivity after 18 h of incubation in plasma. Similar results were obtained by TLC analyses. Table 3 shows the radioactivity in the antibody fractions as a function of incubation time of [^{99m}Tc]C_3(BHam)$_2$−OST7 in buffered-solutions of different cysteine concentrations. [^{99m}Tc]C_3-(BHam)$_2$−OST7 remained stable after 6 h of incubation in the presence of 3.6×10^{-5} M cysteine. However, ca. 10% of the initial radioactivity was released from [^{99m}Tc]-C_3(BHam)$_2$−OST7 after 6 h of incubation in the presence of 3.6×10^{-4} M cysteine.

Immunoreactivity. Figure 5 shows the binding of [^{99m}Tc]C_3(BHam)$_2$−OST7 and [^{125}I]OST7 to KT005 cells as a function of cell number. No significant differences were observed in the cell-bound radioactivity between [^{99m}Tc]C_3(BHam)$_2$−OST7 and [^{125}I]OST7. No significant differences were observed in the cell-bound radioactivity between [^{99m}Tc]C_3(BHam)$_2$−OST7 and [^{125}I]OST7 when incubated with KT005 in the presence of varying concentrations of unmodified OST7 (data not shown).

In Vivo Studies. Table 4 shows the biodistribution of radioactivity after administration of [^{99m}Tc]C_3(BHam)$_2$−OST7 and [^{111}In]EDTA-Bz-EMCS−OST7 in normal mice. No significant differences were observed in the radioactivity levels of blood or spleen between [^{99m}Tc]C_3(BHam)$_2$−OST7 and [^{111}In]EDTA-Bz-EMCS−OST7 at all postinjection time points. [^{99m}Tc]C_3(BHam)$_2$−OST7 registered significantly ($p < 0.01$) lower radioactivity levels in the kidney and the liver at 24 h postinjection than those of [^{111}In]EMCS−Bz-EDTA-OST7. [^{99m}Tc]C_3(BHam)$_2$−OST7 also indicated higher levels of excretion radioactivity from the body as reflected by significantly higher amounts of radioactivity in the feces ($p < 0.01$). Low radioactivity levels were also observed in the stomach at all postinjection intervals.

Biodistributions of radioactivity after simultaneous administration of [^{99m}Tc]C_3(BHam)$_2$−OST7 and [^{125}I]-OST7 into nude mice bearing KT005 tumor cells are shown in Table 5. No significant differences were observed in radioactivity levels in the blood, lung, and the

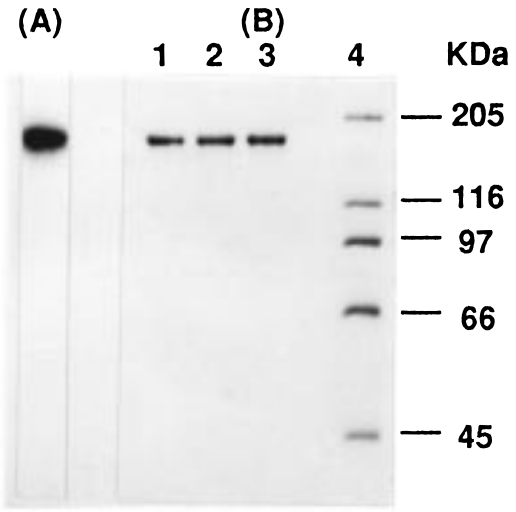


Figure 4. SDS−PAGE profiles of [^{99m}Tc]C_3(BHam)$_2$−OST7 (lane 1), C_3(BHam)$_2$−OST7 (lane 2), and unmodified OST7 (lane 3) as determined by CBB staining under nonreducing conditions. Molecular mass standards (lane 4) are myosin (205 kDa), *E. coli* β-galactosidase (116 kDa), rabbit muscle phosphorylase-*b* (97 kDa), bovine serum albumin (66 kDa), and hen egg white ovalbumin (45 kDa). The left lane (A) shows SDS−PAGE radioactivity profiles of [^{99m}Tc]C_3(BHam)$_2$−OST7 obtained by autoradiography.

Table 2. Percent Antibody-Bound Radioactivity after Incubation of [^{99m}Tc]C_3(BHam)$_2$-OST7[a] in Freshly Prepared Murine Plasma at 37 °C

incubation time (h)	antibody-bound radioactivity[b] (%)
0	94.9 (93.1−96.6)
6	93.5 (93.4−93.6)
18	91.7 (91.1−92.3)

[a] Final concentration of [^{99m}Tc]C_3(BHam)$_2$-OST7 was 1.3×10^{-7} M. [b] Means of duplicate experiments (ranges in parentheses), as determined by CAE.

Table 3. Percent Antibody-Bound Radioactivity Following Incubation of [^{99m}Tc]C_3(BHam)$_2$-OST7[a] in Cysteine Solution at 37 °C

	antibody bound radioactivity[b] (%) at the given cysteine concentration (antibody/cysteine)		
incubation time (h)	3.6×10^{-6} M (1:6)	3.6×10^{-5} M (1:60)	3.6×10^{-4} M (1:600)
0	94.3 ± 1.7	94.3 ± 1.7	94.3 ± 1.7
1	94.7 ± 2.5	94.1 ± 1.5	91.1 ± 0.9
6	93.6 ± 2.3	93.2 ± 2.7	86.0 ± 3.2

[a] Final concentration of [^{99m}Tc]C_3(BHam)$_2$-OST7 was 6.0×10^{-7} M. [b] Mean and sd of four experiments for each point.

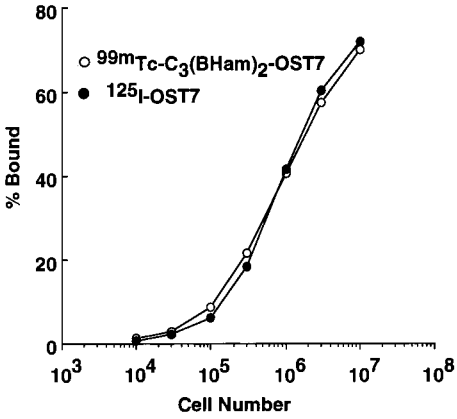


Figure 5. Reactivity of [^{99m}Tc]C_3(BHam)$_2$−OST7 and [^{125}I]-OST7 to KT005 tumor cell. Radioactivity (%) bound to the cells is plotted against cell number.

Table 4. Biodistribution of Radioactivity after Injection of [^{99m}Tc]C_3(BHam)$_2$-OST7 and [^{111}In]EMCS-Bz-EDTA-OST7 in Normal Mice[a]

organ	1 h	3 h	6 h	24 h
	[^{99m}Tc]C_3(BHam)$_2$-OST7			
blood	25.12 ± 2.46	23.51 ± 1.94	18.83 ± 1.76	12.39 ± 1.57
spleen	3.79 ± 0.44	3.74 ± 0.38	3.26 ± 0.57	2.67 ± 0.29
kidney	3.04 ± 0.42[c]	3.23 ± 0.36[d]	3.48 ± 0.51	2.30 ± 0.12[d]
liver	7.84 ± 1.23[c]	6.60 ± 1.02	4.28 ± 0.43	2.23 ± 0.59[d]
stomach[b]	0.56 ± 0.23	0.78 ± 0.21	0.62 ± 0.36	0.80 ± 0.17
intestine	3.04 ± 0.68[d]	3.61 ± 0.53[d]	2.53 ± 0.33[d]	1.08 ± 0.15[d]
urine[b]				3.91 ± 2.52[d]
feces[b]				16.70 ± 3.85[d]
	[^{111}In]EMCS-Bz-EDTA-OST7			
blood	26.59 ± 0.54	22.52 ± 0.90	17.89 ± 1.53	11.98 ± 0.59
spleen	3.63 ± 0.92	3.41 ± 0.23	3.04 ± 0.56	2.13 ± 0.29
kidney	4.25 ± 0.62	4.07 ± 0.27	3.79 ± 0.44	2.74 ± 0.15
liver	6.15 ± 0.51	5.67 ± 0.34	5.12 ± 0.70	4.27 ± 0.61
stomach[b]	0.31 ± 0.06	0.49 ± 0.19	0.58 ± 0.05	0.68 ± 0.11
intestine	1.38 ± 0.10	1.67 ± 0.15	1.74 ± 0.15	1.32 ± 0.04
urine[b]				9.40 ± 1.16
feces[b]				3.37 ± 0.53

[a] Expressed as percent injected dose per gram of wet tissue. [b] Expressed as percent injected dose per tissue. [c] Differences between [^{99m}Tc]C_3(BHma)$_2$-OST7 and [^{111}In]EMCS-Bz-EDTA-OST7 were analyzed by the unpaired Mann−Whitney test ($p < 0.05$). [d] Differences were analyzed by the unpaired Mann−Whitney test ($p < 0.01$).

tumor, although [^{99m}Tc]C_3(BHam)$_2$−OST7 showed slightly higher radioactivity levels in the liver, kidney, and intestine.

DISCUSSION

To assess the ability of tetradentate bis(Ham) ligands as chelating molecules for ^{99m}Tc labeling of polypeptides, bis(BHam) derivatives with polypeptide bindings sites were designed and synthesized. A prior study of ^{111}In labeling of antibodies using cyclic DTPA dianhydride as a chelating agent indicated that the induction of intramolecular cross-linking of antibodies interferes with ^{111}In complexation reaction with the DTPA moieties attached to antibodies and results in underestimation of the stability of ^{111}In-DTPA-labeled antibodies (*24*). For accurate estimation of bis(Ham) as a chelating molecule for ^{99m}Tc labeling of polypeptides, therefore, bis(BHam) derivatives with single polypeptide-binding sites were designed. We attempted to prepare bis(BHam) derivatives by a one-step reaction between 2-substituted 1,3-dibromopropanes with potassium 3-phenyl-Δ^2-1,2,4-oxadiazolin-5-one to introduce a functional group in the propylene backbone. However, the reaction of 2-substituted 1,3-dibromopropanes with the oxadiazoline derivative failed due to generation of propene derivative as the major product. Since the symmetrical bis(BHam) compounds can also be prepared after isolating monoalkylated hydroxamamide intermediates (*19*), similar synthetic procedures were employed for synthesis of the asymmetrical bis(BHam) derivative, NH_2−C_3(BHam)$_2$, as outlined in Scheme 1. Each intermediate compound was stable and easily purified by recrystallization. The final product, NH_2−C_3(BHam)$_2$, was a colorless crystal and was stable after storage for 1 year at 4−10 °C. The present synthetic procedure would allow versatile molecular design of asymmetrical bis(Ham) derivatives for further application to antibody fragments and peptides for diagnostic nuclear medicine.

Table 5. Biodistribution of Radioactivity at 24 h after Co-Injection of [^{99m}Tc]C_3(BHam)$_2$-OST7 and [^{125}I]OST7 in Athymic Mice Bearing Osteogenic Sarcoma[a]

	[^{99m}Tc]C_3(BHam)$_2$-OST7		[^{125}I]OST7	
tissue	% ID/ g tissue	tissue/ blood	% ID/ g tissue	tissue/ blood
blood	4.85 ± 0.61 *ns*[b]		4.23 ± 0.53	
liver	2.53 ± 0.16 $p < 0.05$[c]	0.53 ± 0.08 $p < 0.05$	1.16 ± 0.11	0.27 ± 0.02
kidney	2.24 ± 0.20 $p < 0.05$	0.47 ± 0.03 $p < 0.05$	1.30 ± 0.16	0.30 ± 0.02
intestine	0.65 ± 0.06 $p < 0.05$	0.14 ± 0.03 $p < 0.05$	0.32 ± 0.04	0.08 ± 0.00
spleen	1.40 ± 0.13 $p < 0.05$	0.29 ± 0.02 $p < 0.05$	0.98 ± 0.09	0.23 ± 0.02
lung	1.97 ± 0.28 *ns*	0.42 ± 0.03 *ns*	1.79 ± 0.24	0.42 ± 0.02
stomach[d]	0.14 ± 0.01 $p < 0.05$	*nd*[e]	0.16 ± 0.02	
tumor	11.92 ± 1.90 *ns*	2.52 ± 0.53 *ns*	10.48 ± 1.74	2.48 ± 0.53

[a] Expressed as percent injected dose per gram wet tissue. [b] Not significant. [c] Differences between [^{99m}Tc]C_3(BHam)$_2$-OST7 and [^{125}I]OST7 were analyzed by unpaired Mann−Whitney test. [d] Expressed as percent injected dose per tissue. [e] Not determined.

To estimate the ability of NH_2−C_3(BHam)$_2$ as a chelating molecule for polypeptides, stability estimation of ^{99m}Tc-labeled C_3(BHam)$_2$−OST7 should be performed using C_3(BHam)$_2$−OST7 that preserves the original immunoreactivity of the antibody. Among various procedures to conjugate amine compounds to polypeptides, we selected maleimide−thiol chemistry for lack of intra- or intermolecular cross-linking of polypeptide by this conjugation procedure (*23*, *24*, *26*, *29*). We attempted to purify the reaction product between NH_2−C_3(BHam)$_2$ and EMCS before the conjugation reaction with OST7. However, the purification of EMCS−NH_2−C_3(BHam)$_2$ from unreacted NH_2−C_3(BHam)$_2$ was found to be difficult using silica gel column chromatography due to high hydrophilic properties of the two compounds. While the reaction product of EMCS and compound **8** may be purified by column chromatography, decomposition of the maleimide group may proceed during hydrolysis of the oxadiazoline group. On the other hand, since deferoxamine was successfully conjugated to thiolated antibodies in situ without isolating the reaction product of deferoxamine and EMCS (*20*, *23*), similar procedures were employed for the preparation of C_3(BHam)$_2$−OST7. The stable linkage between OST7 and NH_2−C_3(BHam)$_2$ would also be useful to estimate the stability of ^{99m}Tc-bis(BHam) chelate in the OST7 conjugate for subsequent in vitro and in vivo studies. Since 2-IT was also utilized as a bifunctional chelating agent for ^{99m}Tc labeling of antibodies due to introduction of thiol groups *(30)*, the unreacted thiol

groups of OST7 were completely alkylated with iodoacetamide before ^{99m}Tc radiolabeling reactions. During conjugation and labeling, no fragmentation or dimerization of the antibody was observed (Figures 3 and 4). The lack of changes in immunoreactivity of OST7 was also confirmed by cell-binding studies (Figure 5).

Since $C_3(BHam)_2$ forms ^{99m}Tc complex over a wide pH range (*19*), complexation at pH of 7.0 was selected for physiological reasons. The exchange reaction with [^{99m}Tc]-glucoheptonate was selected to minimize the hydrolysis reaction of ^{99m}Tc during radiolabeling. High radiochemical yields were observed at final protein concentrations as low as 0.2 mg/mL after 1 h of incubation at room temperature as confirmed by size-exclusion HPLC and CAE analyses (Figure 3 and Table 1). Negligible amount of ^{99m}Tc incorporated into unmodified OST7 suggested selective complexation of ^{99m}Tc to $C_3(BHam)_2$ even when the chelate was covalently attached to high molecular weight polypeptides that possess endogenous ^{99m}Tc-binding sites such as imidazoles (*31*). This was supported by the selective complexation of ^{99m}Tc to bis(BHam) in the presence of an equimolar amount of IgG antibody (*19*). High stability of [^{99m}Tc]$C_3(BHam)_2$−OST7 was demonstrated by the almost unchanged antibody-bound radioactivity before and after incubation of [^{99m}Tc]$C_3(BHam)_2$−OST7 in murine plasma or in buffered-solutions containing varying amounts of cysteine (Tables 2 and 3). Although some decrease in the antibody-bound radioactivity was observed at high cysteine concentration, strong resistance of [^{99m}Tc]C_3(BHam)2-OST7 against cysteine transchelation was observed at a cysteine concentration similar to that in plasma (5×10^{-5} M). High stability of [^{99m}Tc]$C_3(BHam)_2$−OST7 in plasma and in the presence of cysteine also supported the selective complexation reaction of ^{99m}Tc to the $C_3(BHam)_2$ moiety in the $C_3(BHam)_2$−OST7 conjugate.

To further estimate in vivo stability, the biodistribution of the radioactivity after administration of [^{99m}Tc]$C_3(BHam)_2$−OST7 was compared with those of [^{111}In]-EMCS−Bz-EDTA-OST7 and [^{125}I]OST7. [^{111}In]EMCS−Bz-EDTA-OST7 was selected due to formation of ^{111}In chelate with high in vivo stability (*24, 32*) and conjugation procedure similar to those for [^{99m}Tc]$C_3(BHam)_2$−OST7. No significant differences were observed in the radioactivity levels in the blood between the two radiolabeled OST7s up to 24 h postinjection (Table 4), reinforcing the high stability of [^{99m}Tc]$C_3(BHam)_2$−OST7 in the blood. Low radioactivity levels in the stomach indicated the absence of reoxidation of ^{99m}Tc in $C_3(BHam)_2$−OST7 to $^{99m}TcO_4^-$ ion. The faster elimination rate of the radioactivity from the liver with [^{99m}Tc]$C_3(BHam)_2$−OST7 suggested that $C_3(BHam)_2$ might generate radiometabolites with much faster elimination rate from the lysosomal compartment of the liver after lysosomal proteolysis, as reflected by the higher radioactivity levels excreted from the body at 24 h postinjection. Since hepatobiliary excretion of the radioactivity was also observed after administration of [^{99m}Tc]$C_3(BHam)_2$ in mice (*19*), the rapid elimination rate of the radioactivity provides further evidence for the high in vivo stability of [^{99m}Tc]-$C_3(BHam)_2$−OST7, even after lysosomal proteolysis in the liver. The ability of $C_3(BHam)_2$ to form ^{99m}Tc chelate with high in vivo stability without impairing the biological reactivity of the parent polypeptides was confirmed by the similar tumor-to-blood ratios of the radioactivity between [^{99m}Tc]$C_3(BHam)_2$−OST7 and [^{125}I]OST7 in nude mice (Table 5). The slightly higher radioactivity levels of [^{99m}Tc]$C_3(BHam)_2$−OST7 in the liver, intestine, and kidney compared to those observed with [^{125}I]OST7 may reflect slightly slower elimination rates of radiometabolites derived from [^{99m}Tc]$C_3(BHam)_2$−OST7 than those of [^{125}I]OST7 (*32, 33*).

In conclusion, the findings in this study indicated that the newly designed $C_3(BHam)_2$ generated ^{99m}Tc-labeled antibodies with high in vivo stability at low protein concentrations with high radiochemical yields under mild reaction conditions, due to selective complexation of $C_3(BHam)_2$ with ^{99m}Tc. Such characteristics of $C_3(BHam)_2$ would render bis(Ham) derivatives useful as chelating molecules for ^{99m}Tc-labeled polypeptides. The absence of thiol groups in bis(Ham) molecules may also be advantageous for incorporation of ^{99m}Tc into peptides with disulfide bonds. Acceleration of the elimination rates from the liver and alternation of the excretion pathway from hepatobiliary to urine of [^{99m}Tc]$C_3(BHam)_2$ may constitute further program for clinical applications of the ligand system. The versatile synthetic procedure of bis(Ham) would be advantageous for such molecular design.

ACKNOWLEDGMENT

The authors are grateful to Nihon Medi-Physics Co. Ltd. Tokyo, for their kind gift of $^{111}InCl_3$. This study was supported in part by Grants-in-Aid for Developing Scientific Research (08557135, 09672279, and 05807203) from the Ministry of Education, Science, Culture and Sports of Japan.

LITERATURE CITED

(1) Pearson, D. A., Lister-James, J., McBride, W. J., Wilson, D. M., Martel, L. J., Civitello, E. R., Taylor, J. E., Moyer, B. R., and Dean, R. T. (1996) Somatostatin receptor-binding peptides labeled with technetium-99m: Chemistry and initial biological studies. *J. Med. Chem. 39,* 1361−1371.

(2) Vallabhajosula, S., Moyer, B. R., Lister-James, J., McBride, B. J., Lipszyc, H., Lee, H., Bastidas, D., and Dean, R. T. (1996) Preclinical evaluation of technetium-99m-labeled somatostatin receptor-binding peptides. *J. Nucl. Med. 37,* 1016−1022.

(3) Verhaar, M. J., Keep, P. A., Hawkins, R. E., Robson, L., Casey, J. L., Pedley, B., Boden, J. A., Begent, R. H., and Chester, K. A. (1996) Technetium-99m radiolabeling using a phage-derived single-chain Fv with a C-terminal cysteine. *J. Nucl. Med. 37,* 868−872.

(4) Fischman, A. J., Babich, J. W., and Strauss, H. W. (1993) A ticket to ride − Peptide radiopharmaceuticals. *J. Nucl. Med. 34,* 2253−2263.

(5) Arano, Y., Yokoyama, A., Furukawa, T., Horiuchi, K., Yahata, T., Saji, H., Sakahara, H., Nakashima, T., Koizumi, M., Endo, K., and Torizuka, K. (1987) Technetium-99m-labeled monoclonal antibody with preserved immunoreactivity and high in vivo stability. *J. Nucl. Med. 28,* 1027−1033.

(6) Baidoo, K. E., Scheffel, U., and Lever, S. Z. (1990) ^{99m}Tc labeling of proteins: Initial evaluation of a novel diaminedithiol bifunctional chelating agent. *Cancer Res. 50* (Suppl.), 799s−803s.

(7) Eisenhut, M., Lehmann, W. D., Becker, W., Behr, T., Elser, H., Strittmatter, W., Steinstrasser, A., Baum, R. P., Valerius, T., Repp, R., and Deo, Y. (1996) Bifunctional NHS−BAT ester for antibody conjugation and stable technetium-99m labeling: Conjugation chemistry, immunoreactivity and kit formulation. *J. Nucl. Med. 37,* 362−370.

(8) Fritzberg, A. R., Abrams, P. G., Beaumier, P. L., Kashina, S., Morgan, A. C., Rao, T. N., Reno, J. M., Sanderson, J. A., Srinivasan, A., Wilbur, D. S., and Vanderheyden, J.-L. (1988) Specific and stable labeling of antibodies with technetium-99m with a diamide dithiolate chelating agent. *Proc. Natl. Acad. Sci. U.S.A. 85,* 4025−4029.

(9) Weber, R. W., Boutin, R. H., Nedelman, M. A., Lister-James, J., and Dean, R. T. (1990) Enhanced kidney clearance with an ester-linked ^{99m}Tc-radiolabeled antibody Fab′-chelator conjugate. *Bioconjugate Chem. 1,* 431−437.

(10) Arano, Y., Yabuki, M., Yahata, T., Horiuchi, K., and Yokoyama, A. (1990) Stable and lipophilic technetium-99m dithiosemicarbazone complexes with 5-6-five-membered chelate ring structure. *Chem. Pharm. Bull. 38,* 3099−3101.

(11) Canney, D. J., Billings, J., Francesconi, L. C., Guo, Y. Z., Haggerty, B. S., Rheingold, A. L., and Kung, H. F. (1993) Dicarboxylate diamide dimercaptide (N_2S_2) technetium-99m complexes: Synthesis and biological evaluation as potential renal radiopharmaceuticals. *J. Med. Chem. 36,* 1032−1040.

(12) Frizberg, A. R. (1987) Advances in ^{99m}Tc-labeling of antibodies. *Nucl. Med. 26,* 7−12.

(13) Abrams, M. J., Juweid, M., tenKate, C., Schwartz, D. A., Hauser, M. M., Gaul, F. E., Fuccello, A. J., Rubin, R. H., Strauss, H. W., and Fischman, A. J. (1990) Technetium-99m-human polyclonal IgG radiolabeled via hydrazino nicotinamide derivative for imaging focal sites of infection in rats. *J. Nucl. Med. 31,* 2022−2028.

(14) Schwartz, D. A., Abrams, M. J., Hauser, M. M., Gaul, F. E., Larsen, S. K., Rauh, D., and Zubieta, J. A. (1991) Preparation of hydrazino-modified proteins and their use for the synthesis of ^{99m}Tc-protein conjugates. *Bioconjugate Chem. 2,* 333−336.

(15) Babich, J. W., and Fischman, A. J. (1995) Effect of "coligand" on the biodistribution of Tc-99m-labeled hydrazino nicotinic acid derivatized chemotactic peptides. *Nucl. Med. Biol. 22,* 25−30.

(16) Nakayama, M., Saigo, H., Kai, E., Koda, A., Ozaki, H., Harada, K., Sugii, A., Tomiguchi, S., Kojima, A., and Hara, M. (1992) Hydroxamamide as a chelating moiety for the preparation of ^{99m}Tc radiopharmaceuticals (I). *Nucl. Med. Commun. 13,* 445−449.

(17) Nakayama, M., Saigo, H., Koda, A., Ozeki, K., Harada, K., Sugii, A., Tomiguchi, S., Kojima, A., Hara, M., Nakashima, R., Ohyama, Y., Takahashi, M., Takata, J., and Karube, Y. (1994) Hydroxamamide as a chelating moiety for the preparation of Tc-99m radiopharmaceuticals (II). The Tc-99m complexes of hydroxamamide derivatives. *Appl. Radiat. Isot. 45,* 735−740.

(18) Nakayama, M., Xu, L. C., Koga, Y., Harada, K., Sugii, A., Nakayama, H., Tomiguchi, S., Kojima, A., Ohyama, Y., Takahashi, M., and Okabayashi, I. (1997) Hydroxamamide as a chelating moiety for the preparation of Tc-99m-radiopharmaceuticals (III). Characterization of various ^{99m}Tc-hydroxamamides. *Appl. Radiat. Isot. 48,* 571−577.

(19) Xu, L. C., Nakayama, M., Harada, K., Nakayama, H., Tomiguchi, S., Kojima, A., Takahashi, M., and Arano, Y. (1998) Synthesis and evaluation of hydroxamamide-based tetradentate ligands as a new class of thiol-free chelating molecules for ^{99m}Tc radiopharmaceuticals. *Nucl. Med. Biol. 25,* 295−303.

(20) Koizumi, M., Endo, K., Kunimatsu, M., Sakahara, H., Nakashima, T., Kawamura, Y., Watanabe, Y., Saga, T., Konishi, J., Yamamuro, T., Hosoi, S., Toyama, S., Arano, Y., and Yokoyama, A. (1988) ^{67}Ga-labeled antibodies for immunoscintigraphy and evaluation of tumor targeting of drug-antibody conjugate in mice. *Cancer Res. 48,* 1189−1194.

(21) Sakahara, H., Endo, K., Koizumi, M., Nakashima, T., Kunimatsu, M., Watanabe, Y., Kawamura, Y., Nakamura, T., Ohta, H., Kotoura, Y., Yamamuro, T., Hosoi, S., Toyama, S., and Torizuka, K. (1988) Relationship between in vitro binding activity and in vivo tumor accumulation of radiolabeled monoclonal antibodies. *J. Nucl. Med. 29,* 235−240.

(22) Hosoi, S., Nakamura, T., Higashi, S., Yamamuro, T., Toyama, S., Shinimiya, K., and Mikawa, H. (1982) Detection of human osteosarcoma-associated antigen(s) by monoclonal antibodies. *Cancer Res. 42,* 654−659.

(23) Arano, Y., Inoue, T., Mukai, T., Wakisaka, K., Sakahara, H., Konishi, J., and Yokoyama, A. (1994) Discriminated release of a hippurate-like radiometal chelate in nontarget tissues for target-selective radioactivity localization using pH-dependent dissociation of reduced antibody. *J. Nucl. Med. 35,* 326−333.

(24) Arano, Y., Uezono, T., Akizawa, H., Ono, M., Wakisaka, K., Nakayama, M., Sakahara, H., Konishi, J., and Yokoyama, A. (1996) Reassessment of diethylenetriaminepentaacetic acid (DTPA) as a chelating agent for indium-111 labeling of polypeptides using a newly synthesized monoreactive DTPA derivative. *J. Med. Chem. 39,* 3451−3460.

(25) Laemmli, U. K. (1970) Cleavage of structural proteins during the assembly of the head bacteriophase T4. *Nature 227,* 680.

(26) Arano, Y., Wakisaka, K., Ohmomo, Y., Uezono, T., Mukai, T., Motonari, H., Shiono, H., Sakahara, H., Konishi, J., Tanaka, C., and Yokoyama, A. (1994) Maleimidoethyl 3-(tri-*n*-butylstannyl)hippurate: A useful radioiodination reagent for protein radiopharmaceuticals to enhance target selective radioactivity localization. *J. Med. Chem., 37,* 2609−2618.

(27) Wilbur, D. S., Hadley, S. W., Grant, L. M., and Hylarides, M. D. (1991) Radioiodinated iodobenzoyl conjugates of a monoclonal antibody Fab fragment. in vivo comparisons with chloramine-T-labeled Fab. *Bioconjugate Chem. 2,* 111−116.

(28) Imai, S., Morimoto, J., Tsubura, T., Esaki, K., Michalides, R., Holmes, R. S., Deimling, O., and Hilgers, J. (1986) Genetic marker patterns and endogeneous mammary tumor virus genes in inbred mouse strains in Japan. *Exp. Anim. 35,* 263−273.

(29) Arano, Y., Wakisaka, K., Ohmono, Y., Uezono, T., Akizawa, H., Nakayama, M., Sakahara, H., Tanaka, C., Konishi, J., and Yokoyama, A. (1996) Assessment of radiochemical design of antibodies using an ester bond as the metabolizable linkage: Evaluation of maleimidoethyl 3-(tri-*n*-butylstannyl)-hippurate as a radioiodination reagent of antibodies for diagnostic and therapeutic applications. *Bioconjugate Chem. 7,* 628−637.

(30) Joiris, E., Bastin, B., and Thornback, J. R. (1991) A new method for labeling of monoclonal antibodies and their fragments with technetium-99m. *Nucl. Med. Biol. 18,* 353−356.

(31) Zamora, P. O., and Rhodes, B. A. (1992) Imidazoles as well as thiolates in proteins bind technetium-99m. *Bioconjugate Chem. 3,* 493−498.

(32) Arano, Y., Mukai, T., Akizawa, H., Uezono, T., Motonari, H., Wakisaka, K., Kairiyama, C., and Yokoyama, A. (1995) Radiolabeled metabolites of proteins play a critical role in radioactivity elimination from the liver. *Nucl. Med. Biol. 22,* 555−564.

(33) Arano, Y., Mukai, T., Uezono, T., Wakisaka, K., Motonari, H., Akizawa, H., Taoka, Y., and Yokoyama, A. (1994) A biological method to evaluate bifunctional chelating agents to label antibodies with metallic radionuclides. *J. Nucl. Med. 35,* 890−898.

BC980024J

Further Studies on the Protein Conjugation of Hydroxamic Acid Bifunctional Chelating Agents: Group-Specific Conjugation at Two Different Loci

Ahmad Safavy,*,† M. B. Khazaeli,‡ Marion Kirk,§ Lori Coward,§ and Donald J. Buchsbaum†

Departments of Radiation Oncology, Medicine, and Pharmacology, and Comprehensive Cancer Center, University of Alabama at Birmingham, Birmingham, Alabama 35294. Received April 30, 1998; Revised Manuscript Received October 9, 1998

A procedure utilizing an activated ester approach for conjugation of unprotected hydroxamic acids to antibodies and peptides was recently reported. Here, an alternative method with advantages over the activated ester strategy is described. This protocol utilizes the hydrazone formation between a hydrazide derivative of the trihydroxamate ligand trisuccin and either a ketone derivative of antibody or the aldehyde groups, generated by oxidation of the carbohyrate residues. Thus, the trisuccin carboxylic acid (**1**) was derivatized with *tert*-butyl carbazate to the hydrazide **2**, and the protecting groups were removed by catalytic hydrogenation and acidolysis with TFA to afford the hydroxamate hydrazide **4**. Conjugation of **4** to monoclonal antibody CC49 was effected by two approaches: attachment through the amine (e.g., lysine) residues of the antibody or oxidation of the carbohydrate residues. The extent of conjugations were monitored by MALDI, through evaluation of the increases in molecular weights of the conjugates compared to the unconjugated antibody. The first approach utilizing a ketone linker (6-oxoheptanoic acid, OHA) which served as a hydrazide anchor, is being introduced in this report as a new technique for conjugation of hydrazide derivatives to proteins. The OHA approach proved to be a superior strategy over the aldehyde approach in the ease of the procedure and yield of protein recovery. It also had the advantage of yielding more control in adjusting the ligand-to-protein ratio and was therefore selected for protocol optimization. All conjugates resulting from both approaches were radiolabeled with ^{125}I and screened for their immunoreactivity. Furthermore, the conjugates prepared through the optimized OHA protocol were radiolabeled with both ^{99m}Tc and ^{125}I for which the radiolabeling yields and immunoreactivities are reported.

INTRODUCTION

Radiometal labeling of monoclonal antibodies (MAbs),[1] antibody fragments, and peptides has found a wide range of applicability in biology and medicine (*1*−*6*). A frequently used technique is the use of a heterobifunctional chelating agent which serves as a bridge between the metallic cation and the protein. Two requirements for such a linker to qualify as a potential labeling agent are (1) it should form metal chelation with high in vitro and in vivo stability, and (2) the linker as a whole should be biologically stable. Therefore, in addition to the metal complex stability, the overall usefulness of the labeled conjugate is dependent on the stability of the linker-protein bond (*7*−*9*). Premature cleavage of this bond may result in the release of the radionuclide before the construct reaches its intended target and will result in an insufficient target radioactivity dose for imaging or therapy, and an increase in background uptake in normal tissues. In an effort to design protein radiolabeling reagents capable of meeting these two requirements, we reported on the application of hydroxamate-derived bifunctional chelating agents (BCAs) to radiometal labeling of antibodies and peptides (*1*, *10*). Although the metal chelation of the hydroxamic acids had been well established, their utilization as BCAs was a new concept which turned out to be a challenging problem, due to the interference of the hydroxamate functionalities with the conjugation chemistries used for their attachment to a protein molecule. Our original procedure connected an O-benzyl-protected trihydroxamate, trisuccin, to MAbs, followed by removal of the benzyl groups by hydrogenation of the conjugate (*10*). Recently, we reported on an improved technique using the *o*-nitrophenol (ONP) activated ester of unprotected trisuccin (*11*). In this procedure, the fully deprotected hydroxamate was activated by ONP in the presence of a carbodiimide and used for the antibody conjugation without isolation. Due to the importance of the conjugation step and its effect on the subsequent application of the constructs, we continued our search for still better techniques. Our ultimate goal was a protocol in which stable derivatives of hydroxamic acids are conveniently and efficiently conjugated to the protein via a covalent bond which is stable under most

* To whom correspondence should be addressed at the Department of Radiation Oncology, 1824 sixth Ave. S., WTI 674, Birmingham, AL 35294.

† Department of Radiation Oncology.

‡ Department of Medicine.

§ Department of Pharmacology.

[1] Abbreviations: BCA, bifunctional chelating agent; cpm, counts per minute; DCC, dicyclohexyl carbodiimide; DMAP, *N*,*N*-(dimethylamino)pyridine; DPBS, Dulbecco's PBS; HOBT, *N*-hydroxy benzotriazole; HSA, human serum albumin; ITLC, instant thin-layer chromatography; L:MAb, ligand-to-antibody ratio; MAb, monoclonal antibody; MALDI, matrix-assisted laser desorption/ionization time-of-flight mass spectrometry; OHA-NS, 6-oxoheptanoic acid, N-succinimidyl ester; ONP, *o*-nitrophenyl; PBS, phosphate-buffered saline; RY, radiolabeling yield; SD, standard deviation; SEC, size-exclusion chromatography; SOX, sugar-oxidation.

10.1021/bc980045d CCC: $18.00 © 1999 American Chemical Society
Published on Web 12/15/1998

chemical and physiological conditions. Also of importance are the selectivity and site-targeting involved in the conjugation strategy. Electrophilic covalent coupling of BCAs to antibodies has traditionally been targeted at the amino terminal ends of polypeptide chains and ϵ-amino functions of the lysine residues, with the latter probably being the major site of reaction (*12*). A mechanistically different procedure for antibody conjugation of BCAs is utilization of the oxidized carbohydrate residues through Schiff base formation (*13, 14*). It has been postulated that derivatization of antibodies through this route would result in formation of conjugates with more preserved biological activities (*15*). The latter procedure was originally used for the attachment of horseradish peroxidase to an immunoglobulin (*16*) and was later extended to the conjugation of monoclonal antibodies (*12, 15*).

We report here two new protocols for the attachment of unprotected hydroxamate hydrazides targeted at two different sites of the MAb CC49, the lysine residues residing across the immunoglobulin molecule and the carbohydrate moieties of the hinge region. Although, in the case of this antibody, our results favor the former method, the latter protocol may also be useful for other glycoproteins and molecules containing oxidizable carbohydrate residues or suitable carbonyl functions. This, in turn, will have the benefit of reaction manipulation in tailoring a desired conjugation and more control on the reaction outcome.

EXPERIMENTAL PROCEDURES

General. The benzyl-protected trisuccin, **1**, was prepared as described previously (*10*). HPLC analyses were carried out on a Bio-Rad model 5000 Titanium system (Bio-Rad, Richmond, CA) equipped with model 1806 UV−vis detector and Beckman model 170 radioisotope detector, operated by ValueChrome software (Bio-Rad). For analytical SEC, a 7.5 mm × 25 cm G3000SW column (TosoHaas, Montgomeryville, PA) was used. PBS (10 mM) containing 10 mM Na_2SO_4 at pH 6.7 was used as solvent. Preparative SEC was carried out using sephadex G-25 columns (PD-10, Pharmacia Biotech AB, Uppsala, Sweden) eluted with DPBS. Mass spectra were run on an API III triple quadrupole mass spectrometer (PE-Sciex, Toronto, Ontario) in electrospray mode and PerSeptive Biosystems (Framingham, MA) Voyager Elite MALDI instruments. Microanalyses were performed by Atlantic Microlab (Atlanta, GA). *N*-Succinimidyl 6-oxoheptanoate was provided by Biolinx, Inc. (biolinx@aol.com). Metal-free purified water was obtained from a Milli-QF system (Millipore, Bedford, MA). Sodium [^{99m}Tc]-pertechnetate was purchased from Syncor (Birmingham, AL). ITLC was carried out on silica gel-impregnated glass fiber slides (Gelman Sciences, Ann Arbor, MI).

***N*-[Tris[2-[[*N*-(benzyloxy)amino]carbonyl]ethyl]-methyl]succinic *N′*-(*tert*-butyloxycarbonyl)hydrazide, 2.** To the solution of the trisuccin carboxylic acid **1** (500 mg, 0.75 mmol) in 10 mL of dry THF was added HOBT (102 mg, 0.75 mmol) and *tert*-butyl carbazate (Aldrich, 100 mg, 0.75 mmol). The mixture was cooled in an ice bath under argon and a solution of DCC (171 mg, 0.83 mmol) was added in small portions. The reaction was allowed to reach room temperature with stirring for 18 h. The solid was separated by filtration and the filtrate was concentrated in vacuo to an oily residue. The oil was redissolved in 50 mL of ethyl acetate, and the solution was washed with 10% citric acid, water, 10% $NaHCO_3$, and water. After drying over Na_2SO_4, the solvent was distilled in vacuo and the residue was charged into a silica gel column and eluted with chloroform and a 0 to 5% methanol gradient. Pooled fractions containing the product were distilled in vacuo and triturated with ether to afford 535 mg (92%) of a white powder. An analytical sample was prepared by crystallization from toluene/2-propanol (crystalline needles): mp 99.8−101.2 °C; 1H NMR (DMSO-d_6) δ 1.38 (s, 9H), 1.8 (m, 12H), 2.30 (m, 4H), 4.75 (s, 6H), 7.23 (bs, 1H), 7.35 (m, 15H), 8.65 (bs, 1H), 9.50 (bs, 1H), 10.95 (bs, 3H). Anal. calcd for $C_{40}H_{52}N_6O_{10}$: C, 61.84%; H, 6.75%; N, 10.82%. Found: C, 61.80%; H, 6.77%; N, 10.85%; ESMS (M + H) 777.

***N*-[Tris[2-[(*N*-hydroxyamino)carbonyl]ethyl]-methyl]succinic *N′*-(*tert*-butyloxycarbonyl)hydrazide, 3.** The hydrogenation procedure reported previously was used (*11*). Briefly, the protected hydroxamate **2** (500 mg, 0.71 mmol) was dissolved in 100 mL of HPLC-grade methanol and a slurry of 10% Pd/C (41 mg, 0.039 mmol) in methanol was added. The sealed flask was evacuated for 10 min with stirring and was charged with hydrogen gas at 10 psi, and the mixture was shaken for 65 h. The solvent was partially removed in vacuo to 10% of its original volume, the catalyst was removed by an Acrodisc syringe-tip 0.2 μm filter (Gelman Sciences, Ann Arbor, MI) and the solvent was distilled in vacuo. The light yellow glass was recrystallized from 2-propanol to obtain 310 mg (95%) of a white powder. mp 91.2−91.9 °C (dec). ^{1}H NMR (DMSO-d_6) δ 1.40 (s, 9H), 1.82 (m, 12H), 2.26 (m, 4H), 7.74 (bs, 1H), 8.64 (bs, 3H), 9.50 (bs, 1H), 10.30 (bs, 1H). Anal. Calcd for $C_{19}H_{34}N_6O_{10}$: C, 45.05%; H, 6.77%; N, 16.59%. Found: C, 45.15%; H, 6.79%; N, 16.60%. ESMS (M + H) 507.

***N*-[Tris[2-[[*N*-(hydroxy)amino]carbonyl]ethyl]-methyl]succinic hydrazide, 4.** Five milliliters of a mixture of trifluoroacetic acid, thioanisole, 1,2-ethanedithiol, and anisole (90:5:3:2, v/v) was added to the blocked hydrazide **3** (300 mg, 59 mmol) under argon and the resulting solution was allowed to stand at room temperature for 1 h. The solvent was distilled in vacuo and the solid residue was washed with hot 2-propanol to afford an off-white crystalline solid. The solid was dried in a vacuum over P_2O_5 to obtain 222 mg (92.5%) of the product. mp 79.3−82.6 °C (dec). ^{1}HNMR (DMSO-d_6) δ 1.78 (m, 12H), 2.32 (m, 4H), 7.28 (bs, 1H), 8.75 (bs, 2H), 10.30 (m, 4H). ESMS (M + H) 406.

Antibody Conjugation. Method A. The solution of the MAb CC49, reactive with the TAG-72 antigen expressed in carcinomas (*17*) (50 μL, 7 mg/mL), in DPBS was added to 300 μL of a 50 mM PBS buffer at pH 8.1. The resulting solution was stirred at 0 °C and the solution of OHA-NS (5.7 μg, 23.5 nmol) in 50 μL of DMF was added. After 90 min at 0 °C, the reaction was quenched by addition of 20 μL of 2 M glycine in the PBS buffer and the mixture was purified on a PD-10 column eluted with a 100 mM acetate buffer, pH 5.5. The elution was monitored by a UV flow-through detector, and the single MAb peak was collected in a 2 mL fraction. This was concentrated to 300 μL in a Centricon-50 concentrator (Amicon, Inc., Beverly, MA). To this solution, at room temperature and with stirring, was added the solution of the hydrazide **4** (0.12−1.2 μmol) in water (5−20 μL). The reaction mixture was stirred at room temperature for 90 min at which time 20 μL of $NaCNBH_3$ solution in water was added to a final concentration of 100 mM in $NaCNBH_3$. The resulting mixture was stirred gently at room temperature for 18 h followed by purification of the conjugate on a PD-10 column eluted with DPBS. The fraction containing the conjugate was concentrated to 300 μL as described above.

Method B. The solution of the MAb CC49 (50 μL, 7 mg/mL) in DPBS was added to 400 μL of 100 mM acetate buffer at pH 4.2 containing 0.3% EDTA. To this solution was added a solution of sodium periodate in water to a final molar ratio of 1000 with respect to the MAb (32 mM in $NaIO_4$). The mixture was stirred at 5 °C in the dark for 1 h followed by purification of the oxidized MAb on a PD-10 column eluted with 50 mM acetate buffer, pH 4.2. The MAb-containing fraction was concentrated to 200 μL in a Centricon-50 concentrator. A solution of the hydrazide **4** (0.12−1.2 μmol) in 200 mM acetate buffer at pH 5.5 was added to the MAb solution at room temperature with stirring, followed after 90 min by the addition of 15 μL of $NaCNBH_3$ in water to a final concentration of 100 mM in $NaCNBH_3$. The solution was stirred at room temperature for 18 h, and the conjugate was purified by gel filtration on a PD-10 column eluted with DPBS.

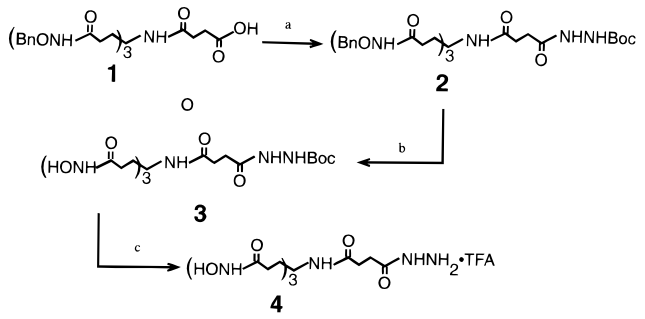
MALDI Analyses. Samples were analyzed in the positive mode on a Voyager Elite mass spectrometer with delayed extraction technology (PerSeptive Biosystems, Framingham, MA). The acceleration voltage was set at 25 kV, and 50−100 laser shots were summed. Sinapinic acid (Aldrich Chemical Co., Milwaukee, WI), dissolved in a 1:1 (v/v) mixture of acetonitrile:0.1% TFA, was used as the matrix. Bovine serum albumin (1 pmol/μL) was added as an internal standard. Equal volumes of sample and matrix were mixed on a smooth plate. The average of three measurements was used. For each reaction, the intact MAb was scanned as the control for evaluation of the following conjugation. In the OHA method, the molecular weight increase of the OHA-MAb intermediate was calculated using the unconjugated control. The molecular weight of this intermediate then served as the control to measure the increase in the molecular weight of the final product conjugate. Each difference in molecular weight was divided by the molecular weight of the corresponding linker to measure the linker:MAb ratio. For the SOX method, with no intermediate conjugate, the molecular weight difference between the final conjugate and the starting intact MAb was used.

Technetium-99m Radiolabeling. Sodium [^{99m}Tc]-pertechnetate (5 mCi in saline) was added to the solution of the MAb conjugate in DPBS. Under oxygen-free conditions, 25 μL of a 2 mg/mL solution of stannous chloride, containing 40 mg/mL of 2-hydroxy-2-methyl propionic acid, was added, and the mixture was incubated at 35 °C for 45 min. The labeled conjugate was then purified on a PD-10 column eluted with DPBS containing 0.1% HSA.

Iodine-125 Radiolabeling. A standard iodogen radiolabeling method was used (*18*). Briefly, 10 mg of iodogen was dissolved in 1 mL of chloroform, and 5 μL of this solution was dispensed into a vial containing a polystyrene bead. The bead was then dried under an argon flow. Sodium [^{125}I]-periodate (5 mCi/bead) was added, followed by 5× (v/v) of a pH 7.6 phosphate buffer. The MAb was added, the mixture was incubated for 15 min, and the labeled MAb was purified on a PD-10 column eluted with 0.1% HSA in DPBS.

Immunoreactivity Screening. Polystyrene beads (6.4 mm, specular finish) were coated with mucin (Sigma) in PBS (4.4 mg/100 mL) overnight and were washed and blocked with 0.1% HSA. For each assay, a control test tube containing no bead, as a counting standard for [^{99m}Tc]- or [^{125}I]-CC49, and a nonspecific binding tube containing the bead and 5 μL of a 5 mg/mL solution of the unlabeled MAb as a competitor of the labeled CC49, were used. Other tubes contained decreasing concentrations (1:2 to 1:200) of the unlabeled MAb. To all tubes were added 100 μL of the labeled MAb CC49 (12000−20000 cpm) followed by vortexing at room temperature for 1 h. All tubes, except the counting standard, were washed with DPBS, the beads were transferred into clean test tubes and were counted in a γ counter for 1 min. The percent of the radioactivity bound to the mucin-coated beads were calculated. The inverse of the percent binding values was plotted against the cold MAb concentrations. Extrapolation to infinite MAb concentration determined the percent immunoreactivity[2] of the labeled MAb CC49.

Scheme 1[a]



[a] (a) $BocNHNH_2$, HOBT, DCC, THF; (b) H_2, Pd/C (10%), MeOH; (c) TFA:thioanisole:ethane-dithiol:anisole, 90:5:3:2, v/v.

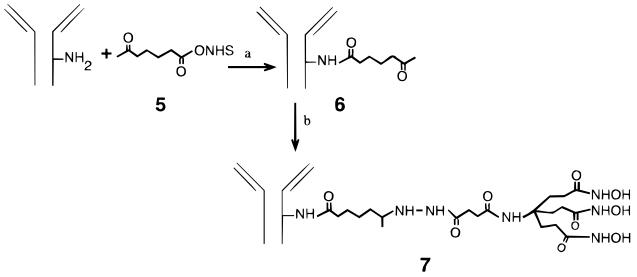
RESULTS AND DISCUSSION

Since the introduction of our first hydroxamate BCA, trisuccin (*10*), we have devoted considerable effort to develop a flexible and efficient conjugation protocol for the covalent attachment of unprotected hydroxamate ligands to proteins and peptides (*1, 11*). Our ultimate goal was establishing a protocol which uses a stable derivative of hydroxamic acids to target a specific function on the protein, generating a stable hydroxamate−protein bond with retention of both the biological activity of the protein or peptide moiety and the metal-chelating property of the hydroxamate ligand. The stability and shelf life duration of the BCA would be of importance especially for the development of a radiolabeling kit. Recently, we reported a procedure in which an *o*-nitrophenyl activated ester of the hydroxamic acid was used for conjugation to the amine residues of the MAb CC49, as well as a synthetic peptide, used as model proteins (*11*). In this report, we introduce a newer technique which utilizes a suitably functionalized yet stable derivative of trisuccin which is capable of conjugation to the same model protein under mild reaction conditions.

Synthesis. The hydrazide derivative of trisuccin was prepared in three steps from the protected carboxylic hydroxamate **1**, as shown in Scheme 1. Thus, compound **1** was coupled to *tert*-butyl carbazate by a standard DCC/HOBT reaction and the product **2** was hydrogenated to remove the benzyl protecting groups. This hydrogenation protocol had been developed previously (*11*) to minimize or eliminate the overreduction of the hydroxamate functions (*19*). All mass spectroscopic and NMR data indicated hydrogenation only to the desired extent with no overreduced products formed. Compound **3** was further deprotected by acidolysis to afford the final product **4**. All intermediates and the final product were analyzed

[2] The percent immunoreactivity refers to the fraction of the immunoreactive radiolabeled antibody as determined by its binding at infinite antigen excess.

Scheme 2[a]



[a] (a) PBS, pH 8.1; (b) **4**, acetate buffer, pH 5.5, 2-propanol, $NaCNBH_3$.

by standard techniques which identified the expected structures. The overall yield of the synthesis was 72%.

Protein Conjugation. Two methods for the conjugation of **4** to the MAb CC49 were used: a linker-mediated technique (the OHA method, A), targeting the lysine residues of the protein, and an oxidation-mediated technique (the SOX method, B), targeting the carbohydrate residues of the antibody.

The OHA Method. The linker-mediated technique is a two-step process in which a hydrazide-binding molecule is first introduced into the protein to serve as the *anchor* for the incoming BCA. In the second step, a molar excess of the hydrazide-containing BCA is added to target the ketone function of the anchor. The rationale for this approach is based on two considerations: (1) the higher rate of condensation of the of hydrazide groups with ketones at the pH range of $5 < pH < 6$, and (2) the use of a large excess of the hydrazide with respect to the available protein $-NH_2$ groups. To optimize this procedure, we first carried out a number of conjugations to assess the general trend of the reaction and then used these results to optimize the protocol. Since the selected lysine residues of MAbs are readily available for conjugation and their modification, carried out under appropriate conditions, does not result in the loss of biological activity, we selected this residue to build the hydrazide-binding scaffold on the protein as shown in Scheme 2. Thus, *N*-succinimidyl 6-oxoheptanoate (OHA-NS, **5**) was selected as the bifunctional linker due to its ability to react with the lysine ϵ-amino groups through the activated ester moiety on one end and to a hydrazide through its ketone function, on the other. The OHA-NS was conjugated to MAb CC49 through standard N-hydroxysuccinimide active ester procedures. The reactions were generally complete within an hour or less and showed high coupling efficiencies, i.e., the experimentally measured number of linkers per MAb as compared to their theoretical values. It should be noted that while the kinetics of this reaction was not quantified, we observed that the number of linkers attached to the antibody, as measured by MALDI, did not increase any further by an increase in the incubation time. These data, for different OHA-NHS:CC49 mole ratios, are shown in Table 1. In the second step of the process, the hydroxamate hydrazide **4** was reductively coupled to the OHA−protein conjugate **6** in a low-pH medium to afford the final product conjugate **7**. The low pH of this reaction provides the advantage of a selective coupling between the hydrazide function of the hydroxamic BCA and the implanted ketone group of the OHA handle. While amines undergo only very slow reactions with ketones at pH 5.0−5.5, hydrazides condense quite readily with ketones at this pH range to produce the corresponding hydrazone (*20*). This selectivity is an important feature of the hydrazide functionality, which prevents the competing reaction of the endogenous amine functions of the protein.[3] These competing reactions may complicate the outcome of the conjugation process in the form of inter- or intramolecular protein condensations. To further stabilize the conjugate, the hydrazone bond was reduced under mild conditions with sodium cyanoborohydride, to the corresponding substituted hydrazide (*21*). The final product conjugates were analyzed by MALDI to evaluate the number of ligands incorporated into the protein molecule. These results for the conjugation of trisuccin hydrazide **4** to CC49 are shown in Table 2. Under the unoptimized conditions of Table 2, even at a high OHA:MAb ratio of 9, and at **4**:MAb ratios of 20 and below, the extent of conjugation was negligible. A larger difference in the molecular weights appeared at **4**:MAb ratios of >50, where the increase continued even at a lower OHA:MAb of 3.

Table 1. Conjugation Efficiencies of 4-CC49 Formation as a Function of OHA:MAb Mole Ratios[a,b]

conjugate	OHA:MAb[c]	OHA:MAb[d]	**4**:Mab[d]
A	5	2 (0.7)[e]	0.4 (0.1)[e]
B	10	4 (0.7)	0.4 (0.1)
C	20	8 (1.0)	0.6 (0.1)
D	50	17 (1.6)	0.8 (0.2)

[a] The OHA-MAb coupling was carried out at pH 7.5. [b] A theoretical **4**:MAb ratio of 10 was used for the second step of each reaction. [c] Theoretical. [d] Experimental (MALDI). [e] ±SD ($n = 3$).

Table 2. Conjugation Efficiencies of 4-CC49 Formation as a Function of both OHA:MAb and 4:MAb Mole Ratios[a]

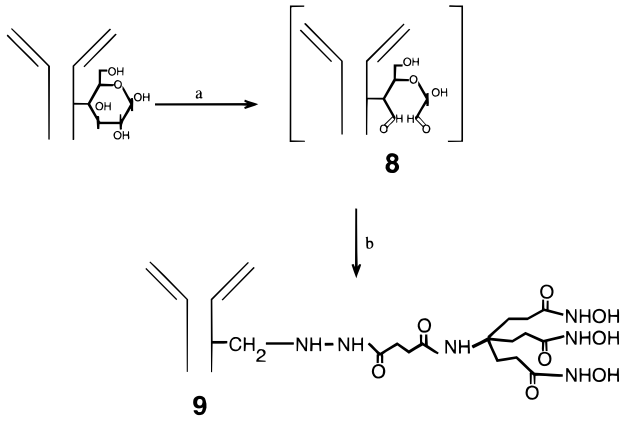
conjugate	OHA:Mab[b]	**4**:MAb[c]	**4**:Mab[d]
E	9[e]/10	5	0.5 (0.1)[g]
F	9[e]/10	10	0.6 (0.1)
G	9[e]/10	20	0.8 (0.1)
H	9[e]/10	50	1.4 (0.4)
J	3[f]/5	500	1.7 (0.3)
K	3[f]/5	1000	2.3 (0.3)

[a] The OHA-MAb coupling was carried out at pH 8.1. [b] Experimental/theoretical. [c] Theoretical. [d] Experimental. [e] ±SD = 0.9 ($n = 3$). [f] ±SD = 0.5 ($n = 3$). [g] ±SD ($n = 3$).

The SOX Method. The in situ conversion of the carbohydrate moieties of an antibody to aldehyde groups by oxidizing agents, followed by reductive amination by an NH_2-containing molecule, has been reported (*14, 16*). In our earlier approaches, we attempted without much success to apply this technique to the conjugation of an aminohydroxamate to MAbs (*11*). We ascribed this lack of reaction to the low carbohydrate content of the IgGs (*22*) and did not further pursue the strategy. Interested in the development of conjugates with highly preserved immunoreactivities, we decided to investigate the oxidation method again, this time with a hydrazide (**4**) instead of an amine. This approach is shown in Scheme 3. Thus, the Mab CC49 was oxidized with sodium periodate in a low-pH acetate buffer to prevent self-condensation of the protein. After purification of the oxidized antibody, the trisuccin hydrazide **4** was added and the pH was raised to activate the hydrazide. Several reactions at different **4**:MAb ratios were carried out, and the conjugate product (**9**, Scheme 3) was analyzed by MALDI. In contrast to

[3] Safavy, A., unpublished results. The selective hydrazide-ketone coupling reported here has also been confirmed by our work on the synthesis of a conjugate of trisuccinn hydrazide with an 8-amino acid peptide, containing an unprotected lysine residue and the OHA linker on the N-terminal. No detectable coupling of the hydrazide with the side-chain amine of lysine was observed. These results will be submitted for publication shortly.

Scheme 3[a]



[a] (a) $NaIO_4$, acetate buffer, pH 4.2; (b) **4**, acetate buffer, pH 5.5, $NaCNBH_3$.

the OHA method, the oxidation reactions generally showed lower yields of final product recovery. Closer analyses of these reactions revealed that a considerable portion of the protein was lost due to self-condensation as evidenced by the formation of an insoluble precipitate. This loss of product was found to be pH dependent: to activate the amino groups of a BCA for condensation with an aldehyde, the pH of the solution has to be raised from the pH at which the antibody was oxidized. At this stage, the native amine residues of the protein may start condensing with the newly formed aldehydes, resulting in higher molecular weight aggregates. This may explain why our earlier attempts with an amino-trisuccin (*11*) were not successful. With the hydrazide **4**, however, it was possible to use a lower pH for the condensation reaction, and we were able to isolate the desired product, albeit at a low yield. Furthermore, it was found that the oxidation step of this approach was quite sensitive toward concentration of the oxidizing agent. At $NaIO_4$ concentrations above 50 mM, the MALDI showed considerable amounts of fragmentation of the MAb. An optimized protocol for conjugation of **4** to CC49 was, however, worked out, as shown in the Experimental Procedures, which resulted in a **4**:CC49 ratio of 2.5 and an immunoreactivity of 40% for the ^{125}I-labeled conjugate.

Optimization of the Conjugation Protocol. Because no special immunoreactivity advantages were realized from the oxidation method, we chose the OHA method for optimization and evaluated further modifications accordingly. The results of Table 1 (column 3, the OHA:MAb MALDI values) show that the average efficiency[4] of the first step, conjugation of OHA to the MAb, was 38.5 ± 2.8% at a buffer pH of 7.5. Increasing the pH to 8.1 increased this yield to 80 ± 20% as shown by the OHA:MAb ratios of Table 2 (column 2). The latter pH was therefore used for all OHA couplings which consistently showed coupling yields within the same range or higher (Table 3), according to the MALDI analyses. We further considered that the 7-carbon structure of OHA may impart some degree of lipophilicity which may pull the linker deep inside of the antibody molecule due to hydrophobic forces. This hydrophobic repulsion may, in turn, "*hide*" the ketone residue from a reactive collision with the incoming hydrophilic hydrazide. To overcome this problem, we increased the organic character of the reaction medium by lowering the ionization power of the reaction buffer and introducing 2-propanol as the cosolvent. Indeed, these modifications did increase the conjugation efficiency, as shown in Table 3. The measured ratios for conjugates 50:1 and 100:1 (**L** and **M** of Table 3, respectively), for instance, are higher or comparable to those for 500:1 and 1000:1 conjugates obtained under unoptimized conditions (**J** and **K** of Table 2, respectively). Compounds **L**−**P** (Table 3) were radiolabeled with both ^{99m}Tc and ^{125}I, for evaluation of their labeling efficiencies and immunoreactivities as shown in Table 4. The use of ^{125}I instead of a radiometal has the advantage of excluding the effects of the metallic cation and associated labeling chemistries on the immunoreactivity, thus revealing the pure effect of the BCA conjugation. These would constitute reference values against which the immunoreactivity of the radiometal-linked antibody could be compared. Immunoreactivities were estimated through a modified Lindmo assay (*23*). The RYs for ^{99m}Tc labeling of the conjugates and their specific activities increased with an increase in the L:MAb ratio while the RYs for iodinations did not significantly change indicating the lack of dependence of this labeling on the number of metal-chelating ligands. Interestingly, all immunoreactivities of the ^{99m}Tc-labeled antibodies were slightly lower than those for the ^{125}I-labeled conjugates. This observation may show an expected effect of the metal on the overall structure of the protein.

Table 3. Optimized Conjugation Efficiencies of 4:CC49 Formation as a Function of both OHA:Mab and 4:Mab[a]

conjugate	OHA:Mab[b]	**4**:MAb[c]	**4**:Mab[d]
L	9.6[e]/10	50	2.1 (0.3)[f]
M	9.6[e]/10	100	2.5 (0.3)
N	9.6[e]/10	250	3.2 (0.5)
P	9.6[e]/10	500	3.5 (0.5)

[a] All **4**-CC49 couplings carried out in acetate buffer/2-propanol mixture. [b] Experimental/theoretical. [c] Theoretical. [d] Experimental. [e] ±SD = 0.6 (n = 3). [f] ±SD (n = 3).

Table 4. Radiolabeling Yields (RY) and Immunoreactivities (IR) of the ^{99m}Tc- and ^{125}I-Labeled 4-CC49 Conjugates[a]

conjugate	^{99m}Tc-RY (%)	99mTc-IR (%)	SA[b] (mCi/mg)	^{125}I-RY (%)	^{125}I-IR (%)
L	72	56	9	50	63
M	81	51	9	50	59
N	81	50	13.5	50	67
P	87	45	15.4	50	50

[a] Averages of two runs. All conjugates prepared under optimized conditions. [b] Specific activities for ^{99m}Tc−CC49 conjugates.

CONCLUSION

The work described in this report introduces two new strategies for the conjugation of unprotected hydroxamic acids to suitable proteins, peptides, and other molecules of biological and medicinal interest. The technique utilizes a new derivative of our trihydroxamate ligand, trisuccin, containing a hydrazide function and capable of forming a hydrazone with carbonyl-containing molecules. Two important advantages of this new method are (1) the use of a stable derivative of hydroxamic acids, as opposed to those with more limited stabilities (e.g., activated esters) (*11*), and (2) the chemical compatibility of the hydrazide and hydroxamate functionalities. Conjugation may be conducted through two different routes: in the ketolinker-mediated path, the hydroxamate hy-

[4] The average efficiencies (AEs) were calculated from the following equation: $AE = 100\{\sum(n, i=1)[(OHA:MAb)_E/(OHA:MAb)_T]/n\}$, where n is the number of conjugates in a series, $[OHA:MAb]_E$ and $[OHA:MAb]_T$ are the experimental and theoretical linker-to-MAb ratios, respectively.

drazide is directed to a carbonyl function, anchored on the protein molecule during a previous step; in the sugar oxidation route, the hydroxamate is directed toward the in situ generated aldehydes. These studies indicated that the former method was a more efficient technique which better preserved the structural integrity of the protein. As a whole, this new strategy may constitute a useful option in the covalent attachment of unprotected hydroxamates to molecules with biological, industrial, and synthetic applications.

ACKNOWLEDGMENT

This work was supported by NIH Grants CA62550, CA44173, and DOE DE-FG02-96ER62181. The authors acknowledge the assistance of Dr. Ramin Arani (Biostatistics Unit) for the calculation of standard deviations, the Comprehensive Cancer Center Nuclear Magnetic Resonance Shared Facilities for ^{1}H NMR spectra, and Kamellia Safavy for protein determinations and radioimmunoassays. We thank Sally Lagan for manuscript preparation.

LITERATURE CITED

(1) Safavy, A., Khazaeli, M. B., and Buchsbaum, D. J. (1997) Synthesis of bombesin analogues for radiolabeling with Rhenium-188. *Cancer 80* (Suppl.), 2354−2359.

(2) Yarranton, G. (1997) Antibodies as carriers for drugs and radioisotopes. In *Antibody Therapeutics* (W. J. Harris and J. R. Adair, Eds.) pp 53−72, CRC Press, Boca Raton.

(3) Govindan, S. N., Goldenberg, D. M., Grenbenau, R. C., Hansen, H. J., and Griffiths, G. L. (1996) Thiolations, ^{99m}Tc labelings, and animal in vivo biodistributions of divalent monoclonal antibody fragments. *Bioconjugate Chem. 7*, 290−297.

(4) Kotts, C. E., Su, F. M., Leddy, C., Dodd, T., Scates, S., Shalaby, M. R., Wirth, C. M., Giltinan, D., Schroff, R. W., Fritzberg, A. R., Shepard, H. M., Slamon, D. J., and Hutchins, B. M. (1996) ^{186}Re-labeled antibodies to p185^{HER2} as HER2-targeted radioimmunopharmaceutical agents: Comparison of physical and biological characteristics with ^{125}I and ^{131}I-labeled counterparts. *Cancer Biother. Radiopharm. 11*, 133−144.

(5) Fischman, A. J., Babich, J. W., and Strauss, H. W. (1993) A ticket to ride: Peptide radiopharmaceuticals. *J. Nucl. Med. 34*, 2253−2263.

(6) Liu, S., Edwards, D. S., and Barrett, J. A. (1997) ^{99m}Tc labeling of highly potent small peptides. *Bioconjugate Chem. 8*, 621−636.

(7) Arano, Y., Wakisaka, K., Mukai, T., Uezono, T., Motonari, H., Akizawa, H., Kairiyama, C., Ohmomo, Y., Tanaka, C., Ishiyama, M., Sakahara, H., Konishi, J., and Yokoyama, A. (1996) Stability of a metabolizable ester bond in radioimmunoconjugates. *Nucl. Med. Biol. 23*, 129−136.

(8) DeNardo, S. J., Zhong, G.-R., Salako, Q., Li, M., DeNardo, G. L., and Meares, C. F. (1995) Pharmacokinetics of chimeric L6 conjugated to indium-111- and yttrium-90-DOTA-peptide in tumor-bearing mice. *J. Nucl. Med. 36*, 829−836.

(9) Ultee, M. E., Bridger, G. J., Abrams, M. J., Longley, C. B., Burton, C. A., Larsen, S. K., Henson, G. W., Padmanabhan, S., Gaul, F. E., and Schwartz, D. A. (1997) Tumor imaging with technetium-99m-labeled hydrazinonicotinamide-Fab′ conjugates. *J. Nucl. Med. 38*, 133−138.

(10) Safavy, A., Buchsbaum, D. J., and Khazaeli, M. B. (1993) Synthesis of N-[tris[2-[[N−(benzyloxy)amino]carbonyl]ethyl]-methyl]succinamic acid, trisuccin. Hydroxamic acid derivatives as a new class of bifunctional chelating agents. *Bioconjugate Chem. 4*, 194−198.

(11) Safavy, A., Sanders, A., Qin, H., and Buchsbaum, D. J. (1997) Conjugation of unprotected trisuccin, *N*-[tris[2-[(*N*-hydroxyamino)carbonyl]ethyl]methyl]succinamic acid, to monoclonal antibody CC49 by an improved active ester protocol. *Bioconjugate Chem. 8*, 766−771.

(12) Brinkley, M. (1993) A brief survey of methods for preparing protein conjugates with dyes, haptens, and cross-linking reagents. In *Perspectives in Bioconjujate Chemistry* (C. F. Meares, Ed.) pp 59−70, American Chemical Society, Washington, DC.

(13) Tijsen, P., and Kurstack, E. (1984) Highly efficient and simple methods for the preparation of peroxidase and active peroxidase-antibody conjugates for immunoassays. *Anal. Biochem. 136*, 451−457.

(14) Chamow, S. M., Kogan, T. P., Peers, D. H., Hastings, R. C., Byrn, R. A., and Ashkenazi, A. (1992) Conjugation of soluble CD4 without loss of biological activity via a novel carbohydrate-directed cross-linking reagent. *J. Biol. Chem. 267*, 15916−15922.

(15) Rodwell, J. D., Alvarez, V. L., Lee, C., Lopes, A. D., Goers, J. W. F., King, H. D., Powsner, H. J., and McKern, T. J. (1986) Site specific covalent modification of monoclonal antibodies: In vitro and in vivo evaluations. *Proc. Natl. Acad. Sci. U.S.A. 83*, 2632−2636.

(16) Nakane, P. K., and Kawaoi, A. (1974) Peroxidase-labeled antibody. A new method of conjugation. *J. Histochem. Cytochem. 22*, 1084−1091.

(17) Muraro, R., Kuroki, M., Wunderlich, D., Poole, D. J., Colcher, D., Thor, A., Greiner, J. W., Simpson, J. F., Molinolo, A., Noguchi, P., and Schlom, J. (1988) Generation and characterization of B72.3 second generation monoclonal antibodies reactive with the tumor-associated glycoprotein 72 antigen. *Cancer Res. 48*, 4588−4596.

(18) Fraker, P. J., and Speck, J. C. (1978) Protein and cell membrane iodinations with a sparingly soluble chloroamide, 1,3,4,6-tetrachloro-3α,6α-diphenylglycoluril. *Biochem. Biophys. Res. Commun. 80*, 849−857.

(19) Bergeron, R. J., McManis, J. S., Phanstiel, O., IV, and Vinson, J. R. T. (1995) A versatile synthesis of deferrioxamine B. *J. Org. Chem. 60*, 109−114.

(20) Shao, J., and Tam, J. P. (1995) Unprotected peptides as building blocks for the synthesis of peptide dendrimers with oxime, hydrazone, and thiazolidine linkages. *J. Am. Chem. Soc. 117*, 3893−3899.

(21) Jentoft, N., and Dearborn, D. G. (1979) Labeling of proteins by reductive methylation using sodium cyanoborohydride. *J. Biol. Chem. 254*, 4359−4365.

(22) Goding, J. W. (1986) Production and applications of monoclonal antibodies in cell biology, biochemistry and immunology. *Monoclonal Antibodies: Principles and Practice,* pp 5−58, Academic Press, Orlando.

(23) Lindmo, T., Boven, E., Cuttitta, F., Fedorko, J., and Bunn, P. A., Jr. (1984) Determination of the immunoreactive fraction of radiolabeled monoclonal antibodies by linear extrapolation to binding at infinite antigen excess. *J. Immunol. Methods. 72*, 77−89.

BC980045D

Conjugation of Dipeptide to Fluorescent Dyes Enhances Its Affinity for a Dipeptide Transporter (PEPT1) in Human Intestinal Caco-2 Cells

Hiroshi Abe,[†] Momoko Satoh,[†] Seiji Miyauchi,[†] Satoshi Shuto,[‡] Akira Matsuda,[‡] and Naoki Kamo*[,†]

Laboratory of Biophysical Chemistry and Medicinal Chemistry, Graduate School of Pharmaceutical Sciences, Hokkaido University, Sapporo, 060-0812 Japan. Received May 22, 1998;
Revised Manuscript Received November 5, 1998

Dipeptide transporters in small intestine have a very wide substrate specificity, so that the transporter sometimes serves as a carrier for peptide-like compounds. We have synthesized dipeptide analogues conjugated at an ϵ-amino group of Lys in Val-Lys or Lys-Sar with fluorescent compounds such as fluorescein isothiocyanate and coumarin-3-carboxylic acid. Uptakes of these peptide analogues were examined by measuring intracellular accumulations into monolayers of the human intestinal epithelial cell line Caco-2 expressing the dipeptide transporter PEPT1. Kinetic analysis and effects of addition either of uncoupler (protonophore) or by Gly-Sar, one of the good substrates of PEPT1, revealed that fluorescent dipeptides were taken up by passive diffusion. In contrast, these analogues remarkably inhibited the Gly-Sar uptake by Caco-2 cells. Among the fluorescent analogues synthesized in this paper, Val-Lys(Flu) was the most potent competitive inhibitor against the Gly-Sar uptake with an inhibition constant of 5 μM. This value is the smallest among those ever reported: Val-Lys(Flu) has the highest affinity for PEPT1 among chemicals ever reported. The importance of the hydrophobic part of the substrate was pointed out.

INTRODUCTION

Dipeptide transporters in small intestine play an important role in the efficient absorption of small peptides following the digestion of dietary proteins (*1*). Due to the structural diversity of these oligopeptides, the peptide transporter is believed to have very broad substrate specificity. In some cases, this transporter serves as a carrier for pharmacological-active peptide-like compounds, which are exemplified by oral β-lactam antibiotics (*2*−*4*), the anti-neoplastic agent bestatin (*5*), and angiotensin-converting enzyme (ACE) inhibitors (*6*, *7*).

From a study on structure−activity relationship, Kramer et al. (*4*) proposed the essential structure of a substrate that is recognized and transported by the intestinal dipeptide/oligopeptide transporter. The requisite structure has the peptide core with a free negatively charged C-terminal group; a large extent of bulkiness of the side chain of the C-terminal amino acid is allowed, as exemplified by one of the substrates having high affinity, ACE inhibitor captopril (*6*, *7*). An N-terminal amino group or a weakly basic group at the N-terminals also seems essential (*8*); a wide variety in chemical structure or bulkiness of the side chain is allowed as true of the C-terminal.

The dipeptide transporter with large capacity and broad specificity could be used as a shuttle system to increase intestinal absorption of poorly absorbable drugs by conjugation of these drugs to a dipeptide or tripeptide core. On the basis of this idea, we synthesized conjugated dipeptide analogues: the ϵ-amino group of Lys in Val-Lys or Lys-Sar was conjugated with fluorescent dyes such as fluorescein isothiocyanate (FITC, abbreviated as Flu) or coumarin-3-carboxylic acid (Coum).[1] We chose these two peptides as a dipeptide core, since they might not be digested by peptidase in the intestine (*9*). The reason for our choice of Lys is the existence of an amino group at the ϵ-position to which we could easily add the fluorescent dye, a model of a poorly absorbing drug. The fluorescence of the bioconjugate allows easy assay of the accumulation of these peptide analogues into cells.

Unfortunately, contrary to our expectations, these fluorescent peptide analogues were not transported by PEPT1 in Caco-2 cells. Quite interestingly, however, the affinity of these analogues to PEPT1 was very high; Val-Lys(Flu) competitively inhibited the Gly-Sar uptake by Caco-2 cells with an inhibition constant of 5 μM. This figure is the smallest of all reported values for inhibitors and substrates of PEPT1: this fluorescent peptide analogue has the highest affinity for PEPT1 among chemicals ever reported.

MATERIALS AND METHODS

Materials. Carbonyl cyanide *m*-chlorophenylhydrazone (CCCP), Coum, and glycylsarcosine were purchased from Sigma Chemical Co. (St. Louis, MO). [^{14}C]glycylsarcosine ([^{14}C]Gly-Sar) (1.78 GBq/mmol) was purchased from Daiichi Pure Chemicals Co., Ltd. (Ibaraki, Japan).

* Corresponding author. Fax +81-11-706-4989. E-mail, nkamo@pharm.hokudai.ac.jp.
[†] Laboratory of Biophysical Chemistry.
[‡] Laboratory of Medicinal Chemistry.

[1] Abbreviations: CCCP, carbonyl cyanide *m*-chlorophenylhydrazone; Coum, coumarin-3-carboxylic acid; FITC, fluorescein isothiocyanate; Flu, fluorescein; Gly-Sar, glycylsarcosine; HEPES, *N*-2-hydroxyethylpiperazine-*N*′-2-ethanesulfonic acid; MES, 2-(*N*-morpholino)ethanesulfonic acid; Tris, Tris(hydroxymethyl)aminomethane; WSCD, water-soluble carbodiimide [1-ethyl-3-(3-dimethylaminopropyl)carbodiimide].

10.1021/bc980049i CCC: $18.00 © 1999 American Chemical Society
Published on Web 12/31/1998

The culture medium (RPMI 1640) and fetal bovine serum (FBS) were purchased from GIBCO BRL Life Technologies (Grand Island, NY). THF was purchased as a dehydrated solvent from Kanto Chemical Co. Inc. (Tokyo, Japan). DMF was distilled from CaH_2 at reduced pressure. Toluene and Et_2O were distilled from sodium metal/benzophenone ketyl. Unless otherwise stated, starting materials were obtained from commercial suppliers and were used without further purification. All amino acids used were L-isomer. Boc-Val and Boc-Lys(Cbz) were purchased from Peptide Institute, Inc. (Osaka, Japan). Lys(Cbz)-O*t*-Bu, Lys(Cbz)-OMe and Sar-O*t*-Bu were purchased from Kokusan Chemical Co. Inc. (Tokyo). FITC was purchased from Molecular Probes Inc. (Eugene, OR). Other chemicals used were of highest purity available.

Synthesis. *General Procedures.* ^{1}H NMR spectra were obtained on a JEOL EX270 or Bruker ARX500 and are given in parts per million (δ) relative to either tetramethylsilane or the solvent signal as internal reference ($CHCl_3$, 7.27 ppm; DMSO, 2.49 ppm). Splitting patterns are designated as follows: s, singlet; d, doublet; t, triplet; q, quartet; m, multiplet; br, broad. Analytical thin-layer chromatography was carried out on silica gel 60 (Merck, 70−230 mesh or 230−400 mesh). All reactions were performed under a nitrogen atmosphere, unless stated otherwise.

Synthesis of Dipeptide Analogues. Boc-Val-Lys(Cbz)-Ot-Bu (5). A mixture of Boc-Val (3.26 g, 15 mmol), Lys(Cbz)-O*t*-Bu·HCl (5.05 g, 15 mmol), HOBt (6.19 g, 30 mmol), and DMAP (1.83 g, 15 mmol) in DMF (120 mL) were stirred at 0 °C for 15 min; then WSCD·HCl (2.93 g, 15.3 mmol) was added. After 30 min, the reaction mixture was warmed to room temperature and stirred for a further 2 h. The mixture was diluted with EtOAc (300 mL) and washed successively with 0.6 M citric acid (150 mL), H_2O (150 mL), aqueous saturated $NaHCO_3$ (150 mL), H_2O (150 mL), and brine (100 mL), then dried (Na_2SO_4) and concentrated. The resulting residue was purified by column chromatography (SiO_2, 75:1 $CHCl_3$-MeOH) to give **5** (7.02 g, 87% as a white amorphous powder). ^{1}H NMR ($CDCl_3$, 270 MHz): 0.84 (3 H, d, J = 6.6 Hz, Val-CH_3), 0.93 (3 H, d, J = 6.6 Hz, Val-CH_3), 1.20−1.87 (24 H, m, Lys β, γ, δ −CH_2, 2 × *t*-Bu), 2.06−2.11 (1 H, m, Val β-CH), 3.11−3.25 (2 H, m, Lys ϵ-CH_2), 4.00 (1 H, dd, J = 6.2 Hz, Val α-CH), 4.44 (1 H, ddd, J = 3.8, 7.6, 8.7 Hz, Lys α-CH), 5.09 (2 H, s, PhCH_2), 5.21 (1 H, m, Val α-NH), 5.34 (1 H, br s, Lys ϵ-NH), 6.64 (1 H, d, J = 7.6 Hz, Lys α-NH), 7.35−7.38 (5 H, m, Ph).

*Boc-Val-Lys-Ot-Bu·HCl (**6**).* A solution of **5** (6.3 g, 11.8 mmol) in AcOH (250 mL) containing 10% Pd/C (500 mg) was stirred under atmospheric pressure of hydrogen for 4 h. The catalyst was filtered off by Celite filtration. The filtrate was diluted with toluene and concentrated until no AcOH remained. The crude oil was dissolved in MeOH−H_2O (10:1, 100 mL), and the solution was put on a Diaion WA-30 resin column (HCl form), which was developed with MeOH−H_2O (10:1). The eluent was concentrated, and the resulting residue was azeotroped with toluene (×2) to give **6** (5.0 g, 100% as a white solid). ^{1}H NMR ($CDCl_3$, 270 MHz): 0.93 (3 H, d, J = 6.6 Hz, Val-CH_3), 1.00 (3 H, d, J = 6.6 Hz, Val-CH_3), 1.14−1.89 (24 H, m, Lys β, γ, δ-CH_2, 2× *t*-Bu), 2.08−2.15 (1 H, m, Val β-CH), 3.07 (2 H, br, Lys ϵ-CH_2), 4.24 (1 H, dd, J = 5.3, 8.6 Hz, Val α-CH), 4.37−4.39 (1 H, m, Lys α-CH), 5.58 (1 H, d, J = 9.9 Hz, Val α-NH), 7.74 (1 H, d, J = 7.3 Hz, Lys α-NH), 8.27 (3 H, br, Lys ϵ-NH_3).

*Boc-Val-Lys(Flu)-Ot-Bu (**9a**).* FITC (269 mg, 0.690 mmol) was added to a solution of **6** (308 mg, 0.726 mmol) in DMF (20 mL), followed by Et_3N (101 μL, 0.724 mmol) at 0 °C, and the mixture was stirred at the same temperature for 15 min and then at room temperature for 30 min. The reaction mixture was diluted with EtOAc (50 mL) and washed successively with 0.6 M citric acid (40 mL), H_2O (30 mL), and brine (20 mL), then dried (Na_2SO_4) and concentrated. The resulting residue was purified by column chromatography (SiO_2 15:1:0.08 $CHCl_3$-MeOH−AcOH) to give **9a** (525 mg, 96% as a yellow powder). ^{1}H NMR (DMSO-d_6, 500 MHz): 0.83 (3 H, d, J = 6.9 Hz, Val-CH_3), 0.87 (3 H, d, J = 6.9 Hz, Val-CH_3), 1.23−1.77 (24 H, m, Lys β, γ, δ −CH_2, 2× *t*-Bu), 1.94 (1 H, m, Val β-CH), 3.51 (2 H, br, Lys ϵ-CH_2), 3.85 (1 H, dd, J = 7.9 Hz, Val α-CH), 4.14 (1 H, dd, J = 7.9, 13.4 Hz, Lys α-CH), 6.57 (2 H, dd, J = 2.0, 8.7 Hz, xanthene H-2′, H-7′), 6.60 (1 H, d, J = 8.8 Hz, Val α-NH), 6.61 (2 H, d, J = 8.7 Hz, xanthene H-1′, H-8′), 6.68 (2 H, d, J = 2.0 Hz, xanthene H-4′, H-5′), 7.18 (1 H, d, J = 8.3 Hz, H-3), 8.05 (2 H, m, Lys α-NH, Lys ϵ-NH_3), 8.24 (1 H, br, H-6), 9.85 (1 H, br, NH), 10.11 (2 H, s, 2× OH). FAB−HRMS calcd for $[C_{41}H_{50}N_4O_{10}S + H]^+$: 791.3325. Found: 791.3307.

*Val-Lys(Flu)·HCl (**10a**).* A mixture of **9a** (467 mg, 0.591 mmol) in THF (5 mL) and 4 M HCl/dioxane solution (30 mL) was stirred at room temperature for 30 min and evaporated under reduced pressure. The resulting residue was triturated with Et_2O and dried in vacuo to give **10a** (397 mg, 100% as an orange powder). ^{1}H NMR (CD_3OD, 270 MHz): 1.09 (3 H, d, J = 7.3 Hz, Val-CH_3), 1.12 (3 H, d, J = 7.3 Hz, Val-CH_3), 1.47−2.03 (6 H, m, Lys β, γ, δ −CH_2), 2.26 (1 H, m, Val β-CH), 3.66 (2 H, m, Lys ϵ-CH_2), 3.82 (1 H, d, J = 5.5 Hz, Val α-CH), 4.47 (1 H, m, Lys α-CH), 7.20 (2 H, dd, J = 2.2, 9.1 Hz, xanthene H-2′, H-7′), 7.34 (2 H, d, J = 2.2 Hz, xanthene H-4′, H-5′), 7.40 (1 H, d, J = 8.3 Hz, Ar H-3), 7.61 (2 H, d, J = 9.1 Hz, xanthene H-1′, H-8′), 8.12 (1 H, dd, J = 2.2, 8.3 Hz, Ar H-4), 8.57 (1 H, d, J = 2.2 Hz, Ar H-6). FAB−HRMS calcd for $[C_{32}H_{34}N_4O_8S + H]^+$: 574.3128. Found: 574.3143.

*Boc-Val-Lys(Coum)-Ot-Bu (**9b**).* WSCD·HCl (150 mg, 0.783 mmol) was added to a mixture of **6** (316 mg, 0.745 mmol), coumarin-3-carboxylic acid (149 mg, 0.783 mmol), and HOBt (300 mg, 1.49 mmol) in DMF (15 mL) at 0 °C. After 10 min, Et_3N (103 μL, 0.745 mmol) was added, and the mixture was stirred at the same temperature for 30 min. After the reaction mixture was stirred at room temperature for 2 h, it was diluted with EtOAc (40 mL) and washed successively with 0.6 M citric acid (30 mL), H_2O (20 mL), and brine (20 mL), then dried (Na_2SO_4) and concentrated. The residue was purified by column chromatography (SiO_2, 40:1 $CHCl_3$-MeOH) to give **9b** (394 mg, 92% as a white amorphous). ^{1}H NMR ($CDCl_3$ 270 MHz): 0.93 (3 H, d, J = 6.7 Hz, Val-CH_3), 0.98 (3 H, d, J = 6.7 Hz, Val-CH_3), 1.33−1.95 (24 H, m, Lys β, γ, δ −CH_2, 2 × *t*-Bu), 2.16 (1 H, m, Val β-CH), 3.46 (2 H, br, Lys ϵ-CH_2), 4.05 (1 H, m, Val α-CH), 4.40 (1 H, m, Lys α-CH), 5.18 (1 H, d, J = 8.6 Hz, Val α-NH), 6.68 (1 H, d, J = 7.3 Hz, Lys α-NH), 7.35−7.41 (2 H, m, H-8, H-6), 7.66 (1 H, m, H-7), 7.77 (1 H, m, H-5), 8.87 (1 H, m, Lys ϵ-NH_2), 8.96 (1 H, s, H-4). FAB−HRMS calcd for $[C_{30}H_{43}N_3O_8 + H]^+$: 574.3128. Found: 574.3143.

*Val-Lys(Coum)·HCl (**10b**).* The desired product **10b** (243 mg, 100% as a white powder) was obtained from **9b** (308 mg, 0.662 mmol) in a similar manner as described for the synthesis of **10a**. ^{1}H NMR (CD_3OD, 270 MHz): 1.07 (3 H, d, J = 7.1 Hz, Val-CH_3), 1.11 (3 H, d, J = 7.1 Hz, Val-CH_3), 1.50−2.01 (6 H, m, Lys β, γ, δ −CH_2), 2.23 (1 H, m, Val β-CH), 3.44 (2 H, m, Lys ϵ-CH_2), 3.74 (1 H, d, J = 5.5 Hz, Val α-CH), 4.46 (1 H, dd, Lys α-CH), 7.41−7.47 (2 H, m, H-6, H-8), 7.75 (1 H, ddd, J = 1.6, 7.1, 8.7 Hz, H-7), 7.85 (1 H, dd, J = 1.6, 7.9 Hz, H-5), 8.84 (1 H,

s, H-4), 9.05 (1 H, m, Lys α-NH). FAB−HRMS calcd for $[C_{21}H_{27}N_3O_6 + H]^+$: 418.1978. Found: 418.1976.

*Boc-Lys(Cbz)-Sar-Ot-Bu (**7**).* Compound **7** was prepared from Boc-Lys(Cbz) (2.2 g, 5.78 mmol) and Sar-O*t*-Bu·HCl (1.0 g, 5.5 mmol) using the procedure described for the synthesis of **5**. The crude product was purified by column chromatography (SiO_2, 10:1 $CHCl_3$-MeOH) to give **7** (2.79 g, 100% as a white solid). ^{1}H NMR ($CDCl_3$, 270 MHz) 1.13−1.89 (24 H, m, Lys *β*, *γ*, *δ* $-CH_2$, 2× *t*-Bu), 2.90−3.30 (5 H, m, Lys *ϵ*-CH_2, N−CH_3), 3.54−4.38 (2 H, m, Sar-CH_2), 4.39−4.75 (1 H, m, Lys α-CH), 5.00−5.20 (3 H, m, PhC*H*$_2$, Lys *ϵ*-NH), 5.24−5.49 (1 H, m, Lys α-NH), 7.26−8.06 (5 H, m, Ph).

*Boc-Lys-Sar-Ot-Bu·HCl (**8**).* The desired product **8** (2.10 g, 100% as a yellow oil) was obtained from **7** (2.6 g, 5.13 mmol) in a similar manner as described for the synthesis of **6**. ^{1}H NMR (DMSO-d_6, 270 MHz): 1.16−1.76 (24 H, m, Lys *β*, *γ*, *δ* −CH2, 2 × *t*-Bu), 2.73 (2 H, m, Lys *ϵ*-CH2), 2.81, 3.06 (3 H, m, N−CH_3), 3.62−4.18 (2 H, m, Sar-CH_2), 4.23−4.47 (1 H, m, Lys α-CH), 6.77−7.06 (1 H, m, Lys α-NH), 7.11−7.27 (5 H, m, Ph), 8.02 (3 H, br, NH_3).

*Boc-Lys(Flu)-Sar-Ot-Bu (**11a**).* Compound **11a** was prepared from **8** (1.1 g, 2.68 mmol) and FITC (954 mg, 2.45 mmol) using the procedure described for the synthesis of **9a**. The crude product was purified by column chromatography (SiO_2, 15:1:0.016 $CHCl_3$-MeOH−AcOH) to give **11a** (1.32 g, 71% as a yellow powder). ^{1}H NMR (DMSO-d_6, 500 MHz) 1.20−1.70 (24 H, m, Lys *β*, *γ*, *δ* $-CH_2$, 2 × *t*-Bu), 2.83, 3.09, 3.18 (3 H, m, N−CH_3), 3.49 (2 H, m, Lys *ϵ*-CH_2), 3.76−4.20 (2 H, m, Sar α-CH2), 4.42 (1 H, m, Lys α-CH), 6.54 (2 H, dd, J = 1.7, 8.9 Hz, xanthene H-2′, H-7′), 6.61 (2 H, d, J = 1.7 Hz, xanthene H-4′, H-5′), 6.67 (2 H, d, J = 8.9 Hz, xanthene H-1′, H-8′), 6.95 (1 H, m, Lys α-NH), 7.15 (1 H, d, J = 8.3 Hz, H-3), 7.75 (1 H, d, J = 7.9 Hz, H-4), 8.29 (1 H, s, H-6), 8.46 (1 H, m, Lys *ϵ*-NH), 10.27 (1 H, br, Ar−NH); FAB−HRMS calcd for $[C_{39}H_{46}N_4O_{10}S + H]^+$ 763.3012, found 763.3011.

*Lys(Flu)-Sar·HCl (**12a**).* The desired product **12a** (97 mg, 100% as an orange powder) was obtained from **11a** (122 mg, 160 *μ*mol) in a similar manner as described for the synthesis of **10a**. ^{1}H NMR (DMSO-d_6, 270 MHz): 1.35−1.85 (6 H, m, Lys *β*, *γ*, *δ* $-CH_2$), 2.89, 3.10 (3 H, m, N−CH_3), 3.50 (2 H, m, Lys *ϵ*-CH_2), 3.94−4.23 (2 H, m, Sar-CH_2), 4.43 (1 H, m, Lys α-CH), 6.48−6.67 (4 H, m, xanthene H-1′, H-8′, H-2′, H-7′), 6.74 (2 H, d, J = 1.7 Hz, xanthene H-4′, H-5′), 7.19 (1 H, d, J = 8.3 Hz, H-3), 7.86 (1 H, dd, J = 1.7, 8.3 Hz, H-4), 8.24 (3 H, br s, NH_3), 8.42 (1 H, s, H-6), 8.68 (1 H, br s, Lys *ϵ*-NH), 10.8 (1 H, br s, Ar−NH). FAB−HRMS calcd for $[C_{30}H_{30}N_4O_8S + H]^+$: 607.1862. Found: 607.1870.

*Boc-Lys(Coum)-Sar-Ot-Bu (**11b**).* Compound **11b** was prepared from **8** (702 mg, 1.71 mmol) and coumarin-3-carboxylic acid (341 mg, 1.79 mmol) using the procedure described for the synthesis of **9b.** The crude product was purified by column chromatography (SiO_2, 40:1 $CHCl_3$-MeOH) to give **11b** (790 mg, 85% as a white amorphous powder). ^{1}H NMR ($CDCl_3$, 270 MHz): 1.42−1.90 (24 H, overlapping m, Lys *β*, *γ*, *δ* $-CH_2$, 2 × *t*-Bu), 2.97, 3.13 (3 H, m, N−CH_3), 3.46 (2 H, m, Lys *ϵ*-CH2), 3.73−4.29 (2 H, m, Sar-CH_2), 4.41−4.69 (1 H, m, Lys α-CH), 5.31 (1 H, m, Lys α-NH), 7.33−7.41 (2 H, overlapping m, H-8, H-6), 7.63−7.70 (2 H, m, H-7, H-5), 8.81 (1 H, m, Lys *ϵ*-NH), 8.90 (1 H, s, H-4). FAB−HRMS calcd for $[C_{28}H_{39}N_3O_8 + H]^+$: 546.2815. Found: 546.2804.

*Lys(Coum)-Sar·HCl (**12b**).* The desired product **12b** (260 mg, 100% as a white powder) was obtained from **11b** (333.7 mg, 6.12 mmol) in a similar manner as described for the synthesis of **10a**. ^{1}H NMR (DMSO-d_6, 270 MHz): 1.53−1.79 (6 H, m, Lys *β*, *γ*, *δ* $-CH_2$), 2.88, 3.09 (3 H, m, N−CH_3), 3.39−3.30 (2 H, m, Lys *ϵ*-CH_2), 3.94, 4.18 (2 H, m, Sar-CH_2), 4.41 (1 H, m, Lys α-CH), 7.45 (1 H, ddd, J = 1.0, 7.6, 7.9 Hz, H-6), 7.52 (1 H, dd, J = 1.0, 8.6 Hz, H-8), 7.76 (1 H, ddd, J = 1.3, 7.6, 8.6 Hz, H-7), 8.00 (1 H, dd, J = 1.3, 7.6, 8.6 Hz, H-5), 8.71 (1 H, m, Lys *ϵ*-NH), 8.86 (1 H, s, H-4). FAB−HRMS calcd for $[C_{19}H_{23}N_3O_6 + H]^+$: 390.1665. Found: 390.1671.

*Boc-Val-Lys(Cbz)-OMe (**15**).* A mixture of Boc-Val (6.67 g, 30.7 mmol), Lys(Cbz)-OMe·HCl (8.47 g, 25.6 mmol), HOBt (10.5 g, 50.9 mmol), and 4-methylmorpholine (2.81 mL, 25.6 mmol) in DMF (170 mL) was stirred at 0 °C for 15 min. Then, WSCD·HCl (6.38 g, 33.3 mmol) was added to the solution. After 30 min, the reaction mixture was warmed to room temperature and stirred for 10 h. It was diluted with EtOAc (350 mL) and washed successively with 0.6 M citric acid (200 mL), H_2O (150 mL), aqueous saturated $NaHCO_3$ (200 mL), H_2O (150 mL), and brine (100 mL), dried (Na_2SO_4), and concentrated. The resulting residue was purified by column chromatography (SiO_2, 80:1 $CHCl_3$-MeOH) to give **15** (10.56 g, 83.7%) as white solid. ^{1}H NMR (DMSO-d_6, 500 MHz) 0.75 (3 H, d, J = 6.7 Hz, Val-CH_3), 0.79 (3 H, d, J = 6.7 Hz, Val-CH_3), 1.15−1.70 (15 H, Lys *β*, *γ*, *δ* $-CH_2$, *t*-Bu), 1.85 (1 H, m, Val *β*-CH), 2.90 (2 H, m, Lys *ϵ*-CH2), 3.53 (3H, s, CO_2CH_3), 3.75 (1 H, dd, J = 9.0 Hz, Val α-CH), 4.14 (1 H, dt, J = 5.9, 7.2 Hz, Lys α-CH), 5.53 (2 H, s, PhC*H*$_2$), 6.52 (1 H, d, J = 9.0 Hz, Val α-NH), 7.14 (1 H, t, J = 5.0 Hz, Lys *ϵ*-NH), 7.22−7.35 (5 H, m, Ph), 8.07 (1 H, d, J' = 7.2 Hz, Lys α-NH).

*Boc-Val-Lys-OMe (**16**).* A solution of **15** (4.96 g, 10.06 mmol) in MeOH (80 mL) containing 10% Pd/C (500 mg) was stirred under atmospheric pressure of hydrogen for 2 h. The catalyst was filtered off by Celite filtration. The filtrate was concentrated to give **16** (3.61 g, 100% as a white amorphous). ^{1}H NMR (DMSO-d_6, 500 MHz): 0.75 (3 H, d, J = 6.7 Hz, Val-CH_3), 0.79 (3 H, d, J = 6.7 Hz, Val-CH_3), 1.15−1.64 (15 H, m, Lys *β*, *γ*, *δ* $-CH_2$, *t*-Bu), 1.85 (1 H, m, Val *β*-CH), 3.00 (2 H, m, Lys *ϵ*-CH2), 3.54 (3 H, s, CO_2CH_3), 3.75 (1 H, dd, J = 8.0 Hz, Val α-CH), 4.16 (1 H, dt, J = 8.3 Hz, Lys α-CH), 6.56 (1 H, m, Val α-NH), 8.11 (1 H, m, Lys α-NH).

*Boc-Val-Lys(Flu)-OMe (**17a**).* Compound **17a** was prepared from **16** (2.80 g, 7.80 mmol) and FITC (3.04 g, 7.81 mmol) using the procedure described for the synthesis of **9a**. The crude product was purified by column chromatography (SiO_2, 13:1:0.14 $CHCl_3$-MeOH−AcOH) to give **17a** (4.13 g, 70.7% as a yellow amorphous): ^{1}H NMR (CD_3OD, 500 MHz) 0.93 (3 H, d, J = 6.7 Hz, Val-CH_3), 0.97 (3 H, d, J = 6.7 Hz, Val-CH_3), 1.38−1.94 (15 H, m, Lys *β*, *γ*, *δ* -CH_2, *t*-Bu), 2.02 (1 H, m, Val *β*-CH), 3.61 (2 H, br s, Lys *ϵ*-CH_2), 3.69 (3 H, s, CO_2CH_3), 3.91 (1 H, d, J = 6.9 Hz, Val α-CH), 4.45 (1 H, m, Lys α-CH), 6.54 (2 H, dd, J = 2.3, 8.7 Hz, xanthene H-2′, H-7′), 6.68 (2 H, m, xanthene H-1′, H-8′), 7.08−7.21 (3 H, m, Ar H-3, xanthene H-4′, H-5′), 7.75 (1 H, m, Ar H-4), 8.14 (1 H, br s, Ar H-6). $[C_{38}H_{44}N_4O_{10}S + H]^+$: 749.2856. Found: 749.2812.

*Val-Lys(Flu)-OMe·HCl (**18a**).* The desired product **18a** (445 mg, 94% yellow powder) was obtained from **17a** (500 mg, 0.668 mmol) in a similar manner as described for the synthesis of **10a**. ^{1}H NMR (CD_3OD, 270 MHz): 1.09 (3 H, d, J = 6.9 Hz, Val-CH_3), 1.11 (3 H, d, J = 6.9 Hz, Val-CH_3), 1.35−2.10 (6 H, m, Lys *β*, *γ*, *δ*-CH2), 3.39 (1 H, m, Val *β*-CH), 3.65 (3 H, s, CO_2CH_3), 3.70 (2 H, m, Lys *ϵ*-CH_2), 3.83 (1 H, d, J = 5.7 Hz, Val α-CH), 4.50 (1 H, m, Lys α-CH), 7.19 (2 H, dd, J = 2.3, 9.2 Hz, xanthene H-2′, H-7′), 7.33 (2 H, d, J = 2.3 Hz, xanthene H-4′, H-5′), 7.39 (1 H, d, J = 8.3 Hz, Ar H-3), 7.59 (2 H, d, J = 9.2 Hz, xanthene H-1′, H-8′), 8.12 (1 H, dd, J = 2.1, 8.3 Hz,

Ar H-4), 8.58 (1 H, d, $J = 2.1$ Hz, Ar H-6). FAB−HRMS calcd for $[C_{33}H_{36}N_4O_8S + H]^+$: 649.2332. Found: 649.2343.

*Boc-Val-Lys(Flu) (**19a**).* NaOH (5 M, 0.44 mL) was added dropwise to a solution of **17a** (1.5 g, 2.0 mmol) in MeOH/dioxane (8/2 mL) at 0 °C, and the mixture was stirred at room temperature for 2 h. The reaction mixture was diluted with EtOAc (200 mL) and washed successively with 0.6 M citric acid (150 mL), H_2O (100 mL), and brine (80 mL), dried (Na_2SO_4), and concentrated. The resulting residue was purified by flash silica gel column chromatography (4.5:1:0.1 $CHCl_3$-MeOH−AcOH) to give **19a** (1.3 g, 88% as a yellow powder). ^{1}H NMR (CD_3OD, 270 MHz): 0.92 (3 H, d, $J = 6.6$ Hz, Val-CH_3), 0.97 (3 H, d, $J = 6.6$ Hz, Val-CH_3), 1.28−2.06 (16 H, m, Lys β, γ, δ−CH_2, *t*-Bu, Val β-CH) 3.63 (2 H, m, Lys ϵ-CH_2), 3.94 (1 H, d, $J = 6.8$ Hz, Val α-CH), 4.43 (1 H, m, Lys α-CH), 6.54 (2 H, dd, $J = 2.4$, 8.7 Hz, xanthene H-2′, H-7′), 6.66 (1 H, m, Ar H-3), 6.68 (2 H, d, $J = 1.9$ Hz, xanthene H-4′, H-5′), 7.14 (2 H, d, $J = 8.2$ Hz, xanthene H-1′, H-8′), 7.76 (1 H, m, Ar H-4), 8.14 (1 H, br, Ar H-6). FAB−HRMS calcd for $[C_{37}H_{42}N_4O_8S + H]^+$: 735.2699. Found: 735.2723.

Cell Culture. Caco-2 cells (ATCC HTB-37) at passage 28 were purchased from the American Type Culture Collection. They were passaged in 75 cm^2 culture flasks (FALCON, Becton Dickinson and Co., Lincoln Park, NJ) in culture medium consisting of RPMI 1640 supplemented with FBS (15%), HEPES (5 mM), and $NaHCO_3$ (2 g/L) without antibiotics. The cells were maintained at 37 °C in an atmosphere of 5% CO_2. Cells between the 30th and 40th passage were used in this study. At approximately 80% confluence, cells were seeded using 0.02% EDTA and 0.05% trypsin at a density of 53 000 cells/cm^2 on 60 mm plastic culture dishes. The cells were fed fresh medium every 3 days and were used between the 14th and 16th day for the transport studies.

Uptake Experiments in Monolayer Caco-2 Cells. The uptake of [^{14}C]Gly-Sar by Caco-2 cells was measured. The composition of the incubation medium was 140 mM NaCl, 3 mM KCl, 1 mM $CaCl_2$, 1 mM $MgCl_2$, 5 mM D-glucose, 5 mM MES (pH 6.0), or HEPES (pH 7.4). After removal of the culture medium, each dish was washed once with 5 mL of the incubation medium (pH 7.4) prewarmed at 37 °C and incubated with 2 mL of the same medium for 10 min at 37 °C. The cells were then incubated with 2 mL of incubation medium (pH 6.0) containing [^{14}C]Gly-Sar in the absence or the presence of inhibitors for a designated period at 37 °C. The medium was then aspirated off, and the dishes were rapidly rinsed twice with ice-cold incubation medium (pH 7.4). The cells were solubilized in 1 mL of 1 M NaOH followed by neutralization by 1 mL of 1 M HCl. The cell-associated radioactivity was determined in an ACSII scintillation counting cocktail (Amersham, Buckinghamshire England) by a liquid scintillation counter (LSC 2500, Packard).

The uptake of fluorescent dipeptide analogues was measured, unless otherwise indicated, in a similar manner as described above. The cells were solubilized in 1.5 mL of 1 M NaOH using a rubber policeman and neutralized by 1.5 mL of 1 M HCl. The extracted solution was centrifuged in a tabletop microfuge (Hitachi, Tokyo). The supernatant was diluted with 25 mM Tris-buffer (pH 9.6). The fluorescent intensity due to cell accumulation of fluorescein derivatives was determined with a Hitachi MPF-1 fluorometer (Hitachi, Tokyo) with emission at 520 ± 5 nm and excitation at 489 ± 5 nm. The fluorescent intensity by coumarin-3-carboxy derivatives was determined with emission at 410 ± 5 nm and excitation at 320 ± 5 nm. When the uptake of drugs was measured in the presence of CCCP, the cells were preincubated for 30 min at 37 °C with 1.5 mL of incubation medium (pH 6.0) containing 40 μM CCCP, and then incubated for the designated period at 37 °C with 1.5 mL of the incubation medium (pH 6.0) containing various drugs with 40 μM CCCP. The cells were then treated as described above.

The uptake of cepharosporins (cefadroxil and cephradine) was measured, unless otherwise indicated, in a similar manner as described above. The accumulation of cepharosporins was linear within 15 min, then the uptake rates were estimated from the slope. The cells were scraped with a rubber policeman into 1 mL of extraction solution (30 mM phosphate buffer pH 7.0/methanol, 50:50) and maintained for 1 h at room temperature. The extraction solution was centrifuged at 15 000 rpm in a tabletop microfuge (Hitachi, Tokyo Japan) for 15 min, and the supernatant was passed through a Millipore filter (SJGVL, 0.22 μm). The concentrations of cepharosporins in the filtrate were determined by a high-performance liquid chromatography L-6000 (Hitachi, Tokyo Japan) equipped with an UV detector L4000 (Hitachi Co.). The HPLC conditions were column, ERC ODS 6.0 mm inside diameter × 100 mm (ERC Inc., Saitama Japan); mobile phase, 50 mM phosphate buffer (pH 7.0)/methanol, 90:10 for cefadroxil and 70:30 for cephradine; flow rate, 0.8 mL/min; wavelength, 262 nm; injection volume, 20 μL; room temperature.

In all uptake measurements, unless otherwise indicated, values were corrected for the protein content. The protein content of the cell monolayers solubilized in 1.0 mL of 1 M NaOH was determined using a Bio-Rad protein assay kit (Bio-Rad Laboratories, Richmond, CA) with bovine serum albumin as a standard.

Kinetic Analysis of Gly-Sar Uptake. The uptake data of Gly-Sar were fitted to a Michaelis−Menten type equation with a nonsaturable component by an iterative nonlinear least-squares method using a MULTI program (*12*),

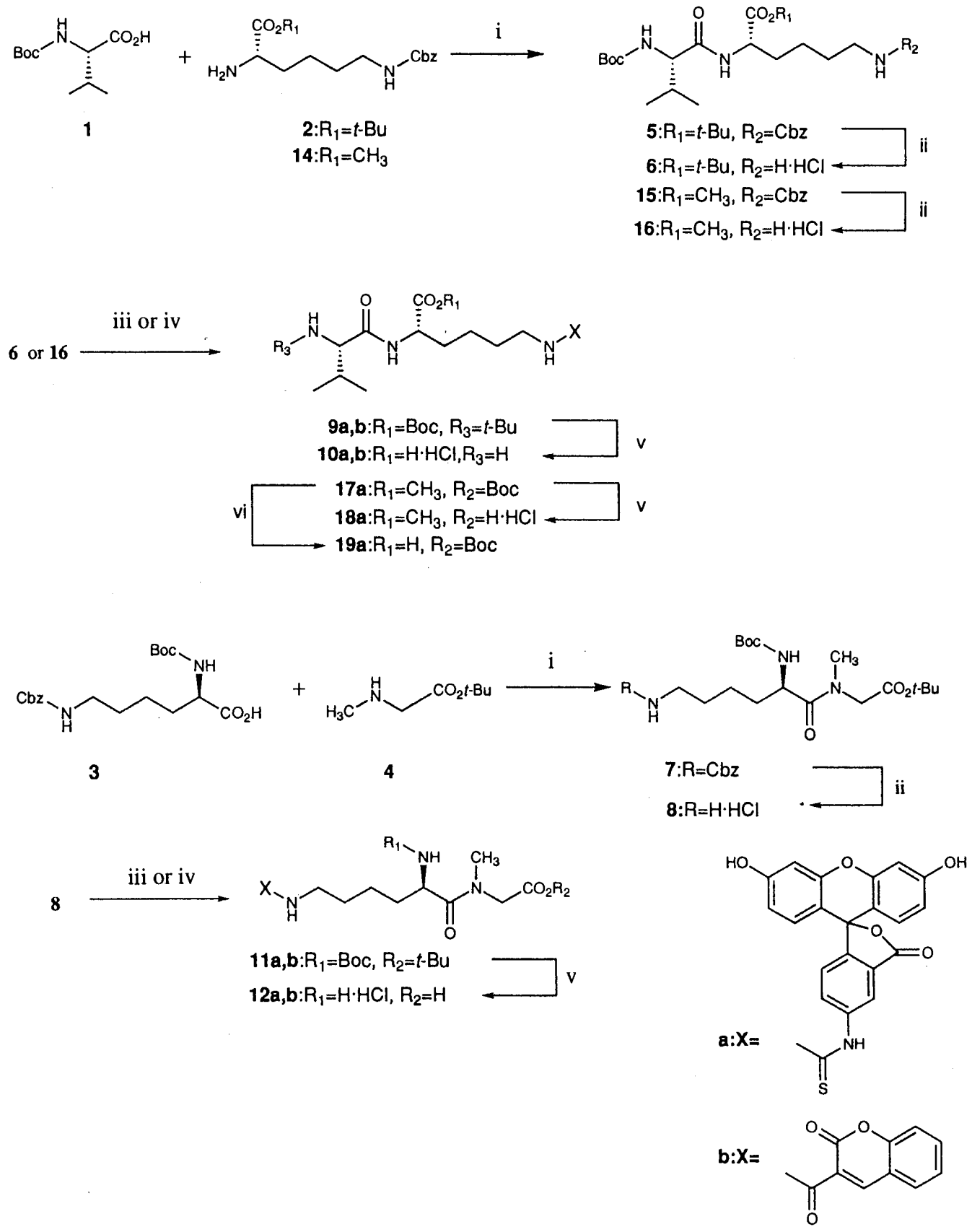
$$v_0 = \frac{V_{max}[S]}{K_m + [S]} + K_d[S] \quad (1)$$

where v_0 represents the initial uptake rate of Gly-Sar; V_{max}, the maximum uptake velocity; [s], the concentration of Gly-Sar; K_m, Michaelis constant; K_d, the coefficient of passive diffusion.

RESULTS AND DISCUSSION

Synthesis of the Fluorescent Dipeptide Analogues. Kramer et al. (*4*) reported that the minimum requirement of the chemical structure of substrates for recognition by the dipeptide transporter is the existence of the peptide bond, a free carboxyl group, and an α-amino group in N-terminal. Considering these structural requirements and the ease of preparing bioconjugates as described in the Introduction, Val-Lys and Lys-Sar were selected as the core of the dipeptide analogues, although recently it is shown that the existence of the peptide bond is not essential (*13*, *14*). It is also expected that these dipeptides are highly resistant to hydrolysis by peptidase owing to the bulky group of Val and to methylated amino groups of Sar. The strategy of the synthesis of fluorescent dipeptide analogues was conjugation of a fluorescent dye to ϵ-amino group of the dipeptides (see Scheme 1). Here, **a** represents FITC (Flu), and **b**, Coum. These fluorescent dyes were selected from the point that FITC is relatively large in the molecular size and Coum, small.

Scheme 1[a]



[a] Reagents: i, WSCD·HCl, HOBt, DMAP, DMF; (ii), 10% Pd/C, AcOH, then ion exchanger resin; iii, FITC, Et_3N, DMF; iv, Coumarin-3-carboxylic acid, WSCD·HCl, HOBt, Et_3N, DMF; v, 4 M HCl/dioxane.

Using proptected amino acids which are commercially available, desired products **10a**, **10b**, **12a**, **12b**, **18a**, and **19a** were synthesized by the usual reactions of peptide condensation and deprotection. Overall yield was **10a**, 84%; **10b**, 80%; **12a**, 71%; **12b**, 85%; **18a**, 56%; **19a**, 52%. It is noted that for removal of Cbz-protecting group from

5, **7**, and **15**, we chose acetic acid as a reaction solvent since the resulting product was unstable in a neutral solution and led to an undesired reaction of isomerization. After removal of Cbz-protecting group, the product was applied to a weakly acidic ion-exchange resin column to obtain **6**, **8**, and **16** as a hydrochloride salt. Protected Val-Lys(Flu), **18a**, and **19a** were synthesized to investigate the effect of amino or carbonyl group in Val-Lys(Flu) on the recognition by the dipeptide transporter.

Since the high purity of compounds **10a**, **10b**, **12a**, **12b**, **18a**, and **19a** was confirmed by NMR analysis, these compounds were used in the transport experiment without further purification. Fluorescein (Flu) is strongly fluorescent either in the conjugated or nonconjugated state. Although Coum itself has a little fluorescence, conjugation to dipeptide enhanced the quantum yield.

The fluorescent dipeptide analogues of Val-Lys(Flu) and (Flu)Lys-Sar were digested in the presence of cytosolic enzymes in Caco-2 cells, and analysis with aid of their fluorescence showed that the hydrolysis of Val-Lys or Lys-Sar occurred. The half-time was about 25 min for both. These analogues showed their inhibition on Gly-Sar uptake when they were added (see below): not the digested products but the analogues themselves exerted the inhibition.

Accumulation of Fluorescent Dipeptide Analogues by Caco-2 Cells. The uptake of (Flu)Lys-Sar and Val-Lys(Flu) was linear with respect to time within 20 min (data not shown); the rate of uptake was estimated by the accumulation in 15 min. (Coum)Lys-Sar and Val-Lys(Coum), on the other hand, were rapidly degraded to coumarin-3-carboxylic acid inside cells. We therefore were unable to determine the initial uptake of Coum analogues.

The kinetics of the Flu analogues was measured. The uptake of (Flu)Lys-Sar and Val-Lys(Flu) increased linearly and showed no saturation up to 2 mM with the increase in concentration: for (flu)Lys-Sar, uptake (pmol/mg/15 min) = (0.624 ± 0.016) × (concn in μM), $R = 0.996$, and for Val-Lys(Flu), uptake (pmol/mg/15 min) = (0.521 ± 0.02) × (concn in μM), R = 0.993. In Caco-2 cells, dipeptide is taken up by a symporter (co-transporter) with H^+ that is energized by an inwardly electrochemical potential difference of proton. If these Flu analogues are accumulated by the symporter, the uptake should cease or at least decrease with the addition of an uncoupler that dissipates the proton electrochemical potential. On the contrary, however, CCCP, the uncoupler, did not decrease the accumulation (see Figure 1). Gly-Sar is a substrate of a dipeptide transporter, PEPT1, that is expressed in Caco-2 cells (*10*, *11*). Gly-Sar did not inhibit the uptake of these analogues (see Figure 1). These three observations imply that (Flu)Lys-Sar and Val-Lys(Flu) are accumulated into cells via a passive diffusion. Figure 1 shows that addition of CCCP and Gly-Sar increased the accumulation of (Flu)Lys-Sar and Val-Lys(Flu). A plausible reason for this increase will be discussed later.

Kinetic Analysis of Active Gly-Sar Accumulation by Caco-2 Cells. Although Gly-Sar is known to be a substrate of PEPT1, we ourselves characterized Gly-Sar uptake by Caco-2 cells. The initial uptake rates were estimated by the slope of the total accumulation vs time; this slope was constant up to 15 min. Analysis with eq 1 gave the following values: V_{max} = 2.4 nmol/h/mg of protein, K_m = 0.86 mM, and K_d = 1.2 nmol/h/mg of protein. These values were consistent with those reported by others (*15*). Figure 1 shows that CCCP decreased the uptake of Gly-Sar, implying that this uptake requires a proton electrochemical potential. It is worth noting that

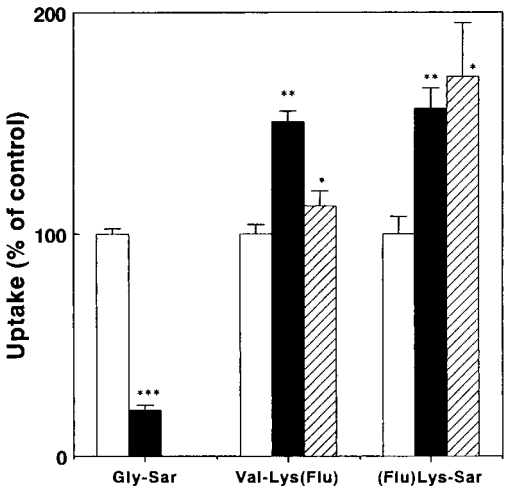


Figure 1. Effect of Gly-Sar and CCCP on the uptake of Val-Lys(Flu) and (Flu)Lys-Sar by Caco-2 cells. (*Leftmost columns*) Uptake of 100 μM Gly-Sar was measured in the absence (unfilled column) or presence (filled column) of 40 μM CCCP. (*Middle and rightmost columns*) Uptake of 200 μM Val-Lys(Flu) or (Flu)Lys-Sar was measured in the absence (unfilled column) or the presence(filled column) of 40 μM CCCP or of 10 mM Gly-Sar (striped column). The uptake was determined in 15 min incubation, then normalized by that for the value of corresponding control experiments. Each column represents the mean ± S. E. of three experiments. (***) $P < 0.005$; (**) $P < 0.01$; (*) $P < 0.05$, significant differences from the control using Student's *t*-test.

a single Michaelis−Menten term is enough to describe the uptake kinetics aside from the passive diffusion term. This would suggest the existence of only one transporter that transports Gly-Sar. This is consistent with the reported fact that Caco-2 cells functionally express PEPT1 as the only dipeptide transporter revealed by the Northern blot analysis (*16*).

Remarkable Inhibition of Gly-Sar Uptake by the Fluorescent Dipeptide Analogues. As described above, the fluorescent dipeptide analogues were not taken up by any transporters although these have a peptide bond. We next examined whether these analogues are recognized by the dipeptide transporter PEPT1 whose substrate is Gly-Sar. Inhibition of Gly-Sar uptake by these fluorescent dipeptide analogues was measured, and results (Figure 2) showed that these analogues strongly inhibited the uptake. It is noted that 1 mM Val-Lys(Flu) completely inhibited the Gly-Sar uptake. Cefalexin and cefadroxil are known to be transported by PEPT1 (*11*, *16*, *17*), but their inhibition was much weaker than the analogues.

To evaluate the kinetic type of inhibition by fluorescent dipeptide analogues, we performed Dixon plot analysis of Gly-Sar uptake by Val-Lys(Flu). Results are detailed in Figure 3 where the three lines cross at one point, indicating the competitive inhibition of Gly-Sar by Val-Lys(Flu) (*18*, *19*). The inhibition constant (K_i) was calculated to be 5 μM, which is the smallest value reported so far. The values of K_i or K_m reported for various peptide transport systems are in the range 1−10 mM (*17*, *20*, *21*). In other words, this compound has the highest affinity for PEPT1 among both inhibitors and substrates that have ever been reported.

We do not yet know the molecular mechanism of the inhibition by fluorescent analogues; do the analogues inhibit the binding of Gly-Sar or its intraprotein translocation? Two facts that (1) fluorescent analogues are transported by a passive diffusion mechanism and (2)

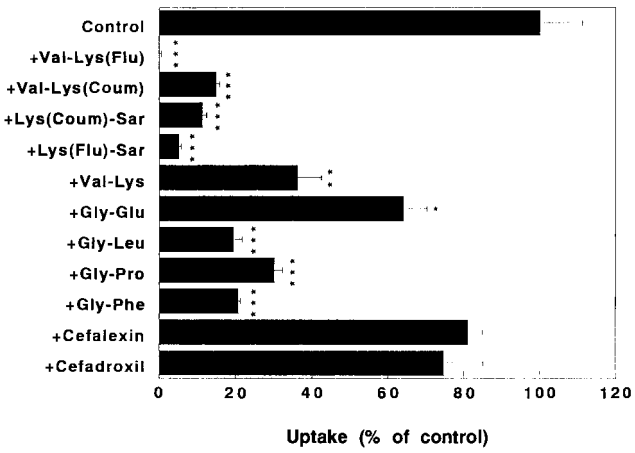


Figure 2. Effect of various fluorescent dipeptide-analogues, dipeptides or antibiotics on the uptake of Gly-Sar, a substrate of PEPT1. Uptake rate of 100 μM Gly-Sar was measured in the absence or the presence of 1 mM various fluorescent dipeptide-analogues, dipeptides or antibiotics. Initial uptake rates were determined using a linear regression of the linear portion in Gly-Sar uptake (measured at 5, 10, and 15 min). The uptake rate was normalized by that for the absence of fluorescent dipeptide-analogues. Each column represents the mean ± SE of three experiments. (***) $P < 0.005$; (**) $P < 0.01$; (*) $P < 0.05$, significant differences from the control using Student's *t*-test.

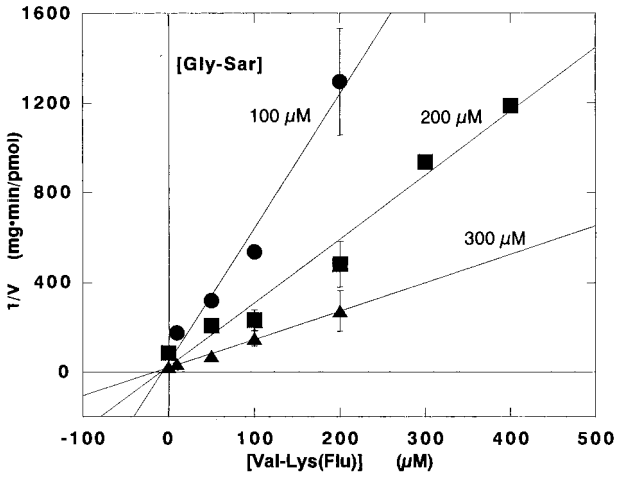


Figure 3. Dixon-Webb plot analysis for the inhibition of Gly-Sar uptake by Val-Lys(Flu) . The experiments were performed as described in the legend to Figure 1 in the presence of various concentrations of Val-Lys(Flu). Circles, squares and triangles represent 100, 200, and 300 μM Gly-Sar uptake rate, respectively. These rates were corrected for the passive diffusion (see eq 1). The inhibition of Gly-Sar upatake by Val-Lys(Flu) was analyzed by Dixon-Webb plot, showing the competitive inhibition. The K_i value was determined to be 5 μM from the intersection of the three lines. Each point represents the mean ± SE of three experiments.

inhibition is competitive suggest that these analogues strongly inhibit the binding of Gly-Sar to the transporter: the fluorescent analogues can bind the binding site of the transporter but they are not transported owing to their bulkiness. In this respect, Otto et al. (*22*) reported that a fluorescent dipeptide β-Ala-Lys-Nϵ-AMCA (AMCA is 7-amino-4-methylcoumarin-3-acetic acid) is transported by a dipeptide transporter of adenohypophysial folliculostellate cells. The reason that this fluorescent dipeptide is transported and our fluorescent dipeptide is not transported is not known.

What Chemical Features Enhance the Recognition by PEPT1? Inhibition of Gly-Sar uptake by several

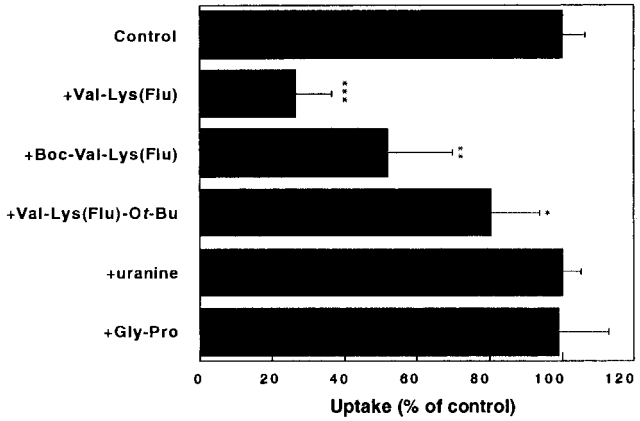


Figure 4. Effect of modification of the amino or carboxyl group in Val-Lys(Flu) on the Gly-Sar uptake. The experiments were performed as described in the legend to Figure 1. The uptake rate of 20 μM Gly-Sar was measured in the presence of 100 μM of each compound and was corrected for the passive diffusion. The uptake rate was normalized by that obtained in the absence of compounds. Each column represents the mean ± SE of three experiments. (***) $P < 0.01$; (**) $P < 0.05$; (*) $P < 0.1$, significant differences from the control using Student's *t*-test.

derivatives of Val-Lys(Flu) or related compounds was measured. The fluorescein (uranine) itself had no effect on the uptake, indicating that the peptide core of Val-Lys(Flu) is recognized by PEPT1. Figure 2 shows that an inhibition of Gly-Sar by Val-Lys is about 35% while the conjugation of Val-Lys to Flu inhibited it appreciably. Why does this conjugation increase the affinity although Flu is not recognized at all? The answer to this remains unclear. We can only point out the importance of the hydrophobicity of the dipeptide analogues. This tendency seems to appear in Figure 2; among Gly-X peptides, the order of inhibition by X is Phe > Leu > Pro > Glu, an order corresponding to hydrophobicity, although the differences are small. An experiment on the importance of hydrophobicity is now in progress in this laboratory.

We prepared two derivatives from Val-Lys: N-terminal-modulated Boc-Val-Lys(Flu) and C-terminal-modulated Val-Lys(Flu)-O*t*-Bu. As seen in Figure 4, the order of the inhibition is Val-Lys(Flu) > Boc-Val-Lys(Flu) > Val-Lys(Flu)-O*t*-Bu. This means that the carboxyl group might be more essential in the recognition by the peptide transporter than the amino group. This is consistent with the study on the intestinal absorption of cefixime and aminocephalosporin that do not have an α-amino group (*23*).

Possible Use of This Strong Inhibitor. We described here our successful preparation of a strong inhibitor of PEPT1. The inhibition constant is the smallest of those yet reported. The primary use of this strong inhibitor is to examine the possibility that some drugs can be transported via PEPT1. Our preliminary experiments were the initial uptake rate of 1 mM cefadroxil was 0.218 ± 0.004 nmol/min/mg of protein (mean ± SE, $n = 3$) and the addition of 200 and 500 μM Val-Lys(Flu) reduced 0.079 ± 0.001 (36.4% of the control) and 0.047 ± 0.001 (22.5%) nmol/min/mg of protein, respectively. Similarly, the rate of 1 mM cephradine was 0.200 ± 0.003 nmol/min/mg of protein (mean ± SE, $n = 3$) and the addition of 200 and 500 μM Val-Lys(Flu) reduced 0.091 ± 0.002 (45%) and 0.067 ± 0.001 (30%) nmol/min/mg of protein, respectively. These suggest that the present fluorescent analogue is the useful tool for this purpose. Second, the high affinity of the dipeptide analogues synthesized is applicable to the resin of the affinity chromatography; results in Figure 4 suggest that the

N-terminal should be linked to the resin. The high affinity of these analogues is also a powerful tool for purification of the dipeptide transporter.

Plausible Reasons Why CCCP Increases the Uptake of These Analogues. Figure 1 shows that CCCP increases the uptake of Val-Lys(Flu) and (Flu)Lys-Sar. If the uptake process requires energy, CCCP should show the reverse effect. There is no reason for the enhancement except the following: Val-Lys(Flu) is expelled by an energy-requiring efflux transporter in Caco-2 cells; the existence of an efflux transporter has been suggested (*24*, *25*). Results of Figure 1 suggest the high affinity of Val-Lys(Flu) to the efflux transporter, because this analogue is transported by passive diffusion so that its intracellular concentration might not be large. The reason Gly-Sar increases the uptake of Val-Lys(Flu) and (Flu)Lys-Sar is not yet clear. We are now analyzing this efflux transporter.

CONCLUDING REMARKS

We conjugated the dipeptide to fluorescent dyes. The resulting conjugates showed the highest affinity to the dipeptide transporter among those reported to date, although the conjugates are not transported by the transporter. Use of the high affinity of the analogues might help to characterize the transporter. As one reason for the high affinity, we pointed out the hydrophobicity; we should determine on a molecular basis whether this hypothesis is correct. We unfortunately failed to synthesize here the conjugated drugs that are transported by the transporter, and further study is needed to synthesize such chemicals which can improve the poor absorption in intestine.

ACKNOWLEDGMENT

We thank Dr. M. Sugawara in Department of Pharmacy, Hokkaido University Hospital for his guidance of HPLC experiments and Miss R. Tateoka for her assistance. This investigation was supported in part by a Grant-in-Aid from the Ministry of Education, Science, Sports and Culture of Japan.

LITERATURE CITED

(1) Adibi, S. A., and Mercer, D. W. (1973) Protein digestion in human intestine as reflected in luminal, mucosal, and plasma amino acid concentrations after meals. *J. Clin. Invest. 52*, 1586−1594.

(2) Okano, T., Inui, K., Maegawa, H., Takano, M., and Hori, R. (1986) H^+ uphill transport of aminocephalosporins via the dipeptide transport system in rabbit intestinal brush-border membranes. *J. Biol. Chem. 261*, 14130−14134.

(3) Tsuji, A., Terasaki, T., Tamai, I., and Hirooka, H. (1987) H^+ gradient-dependent and carrier-mediated transport of cefixime, a new cephalosporin antibiotic, across brush-border membrane vesicles from rat small intestine. *J. Pharmacol. Exp. Ther. 241*, 594−601.

(4) Kramer, W., Dechent, C., Girbig, F., Gutjahr, U., and Neubauer, H. (1990) Intestinal uptake of dipeptides and β-lactam antibiotics. I. The intestianl uptake system for dipeptides and β-lactam antibiotics is not part of a brush border membrane peptidase. *Biochim. Biophys. Acta 1030*, 41−49.

(5) Inui, K., Tomita Y., Katsura, T., Okano, T., Takano, M., and Hori, R. (1992) H^+ coupled active transport of bestatin via the dipeptide transport system in rabbit intestinal brush-border membranes. *J. Pharmacol. Exp. Ther. 260,* 482−486.

(6) Hu, M., and Amidon, G. L. (1988) Passive and carrier-mediated intestinal absorption components of captopril. *J. Pharm. Sci. 77,* 1007−1011.

(7) Swaan, P. W., Stehouwer, M. C., and Tukker, J. J. (1995) Molecular mechanism for the relative binding affinity to the intestinal peptide carrier. Comparison of three ACE-inhibitors: enalapril, enalaprilat and lisinopril. *Biochim. Biophys. Acta 1236*, 31−38.

(8) Taylor M. D., and Amidon G. L., Eds. (1995) in *Peptide-based Drug Design: Controlling Transport and Metabolism*, pp 1−567, American Chemical Society, Washington, DC.

(9) Woodley, J. F. (1994) Enzymatic barriers for GI peptide and protein delivery. *Crit. Rev. Ther. Drug Carrier Syst. 11*, 61−95.

(10) Dantzig, A. H., and Bergin, L. (1990) Uptake of the cephalosporin, cephalexin, by a dipeptide transport carrier in the human intestinal cell line, Caco-2. *Biochim. Biophys. Acta 1027*, 211−217.

(11) Inui, K., Yamamoto, M., and Saito, H. (1992) Transepithelial transport of oral cephalosporins by monolayers of intestinal epithelial cell line Caco-2: Specific transport systems in apical and basolateral membranes. *J. Pharmacol. Exp. Ther. 261,* 195−201.

(12) Yamaoka, K., Tanigawara, Y., Nakagawa, T., and Uno T. (1981) A pharmacokinetic analysis program (MULTI) for microcomputer. *J. Pharmacobio-Dyn. 4*, 879−885.

(13) Ganapathy, M. E., Huang, W., Wang, H., Ganapathy V., and Leibach, F. H. (1998) Valacyclovir: A substrate for the interstinal and renal peptide transporters PEPT1 and PEPT2. *Biochem. Biophys. Res. Commun. 246*, 470−475.

(14) Enjoh, M., Hashimoto, K, Arai, S., and Shimizu, M. (1996) Inhibitory effect of arphamenin A on intestinal dipeptide transort. *Biosci. Biotechnol. Biochem. 60*, 1893−1895.

(15) Brandsch, M., Miyamoto, Y., Ganapathy, V., and Leibach, F. H. (1994) Expression and protein kinase C-dependent regulation of peptide/H^+ co-transport system in the Caco-2 human colon carcinoma cell line. *Biochem. J. 299*, 253−260.

(16) Ganapathy, M. E., Brandsch, M., Prasad, D., Ganapathy V., and Leibach, F. H. (1995) Differential recognition of β-lactam antibiotics by intestinal and renal peptide transporters, PEPT1 and PEPT2. *J. Biol. Chem. 270*, 25672−25677.

(17) Dantzig, A. H., Tabas, L. B., and Bergin, L. (1992) Cefaclor uptake by the proton-dependent dipeptide transport carrier of human intestinal Caco-2 cells and comparison to cephalexin uptake. *Biochim. Biophys. Acta 1112*, 167−173.

(18) Dixon, M. (1953) The determination of enzyme inhibitor constants. *Biochem. J. 55*, 170−171.

(19) Bornish-Bowden, A. (1974) A simple graphical method for determining the inhibition constants of mixed, uncompetitive and noncompetitive inhibitors. *Biochem. J. 137,* 143−144.

(20) Ganapathy, V., Burckhardt, G., and Leibach, F. H. (1984) Characteristics of glycylsarcosine transport in rabbit intestinal brush-border membrane vesicles. *J. Biol. Chem. 259*, 8954−8959.

(21) Dantzig, A. H., Duckworth, D. C., and Tabas, L. B. (1994) Transport mechanism responsible for the absorption of loracarbef, cefixime, and cefuroxime exetil into human intestinal Caco-2 cells. *Biochim. Biophys. Acta 1191*, 7−13.

(22) Otto, C., Dieck, S., and Bauer, K. (1996) Dipeptide uptake by adenohypophysial folliculostellate cells. *Am. J. Physiol. 271*, C210−C217.

(23) Bai, P. F., Subramanian, P., Mosberg, H. I., and Amidon, G. L. (1991) Structural requirements for the intestinal mucosal-cell peptide transporter: the need for N-terminal α-amino group. *Pharm. Res. 8*, 593−599.

(24) Elferink, R. P. L., Bakker, C. T. M., and Jansen, P. L. M. (1993) Glutathione-conjugate transport by human colon adenocarcinoma cells (Caco-2 cells). *Biochem. J. 290*, 756−764.

(25) Collington, G. K., Hunter, J., Allen, C. N., Simmons, N. L., and Hirst, B. H. (1992) Polarized efflux of 2,7-bis(2-carboxyethyl)-5(6)-carboxyfluorescein from cultured epithelial cell monolayers. *Biochem. Pharm. 44*, 417−424.

BC980049I

Retention of Biologic Activity of Human Epidermal Growth Factor Following Conjugation to a Blood-Brain Barrier Drug Delivery Vector via an Extended Poly(ethylene glycol) Linker

Yoshiharu Deguchi, Atsushi Kurihara, and William M. Pardridge*

Department of Medicine, UCLA School of Medicine, Los Angeles, California 90095-1682. Received May 23, 1998; Revised Manuscript Received September 15, 1998

Human brain gliomas overexpress the receptor for epidermal growth factor (EGF), and radiolabeled EGF is a potential peptide radiopharmaceutical for imaging human brain tumors, should this peptide be made transportable through the blood-brain barrier (BBB) in vivo. Peptide drug delivery to the brain may be facilitated by conjugating peptide radiopharmaceuticals to BBB drug delivery vectors such as the OX26 monoclonal antibody (MAb), which undergoes receptor-mediated transcytosis through the BBB via the brain capillary endothelial transferrin receptor. EGF was biotinylated with NHS-XX-biotin, where NHS = *N*-hydroxysuccinimide and -XX- = bis (aminohexanoyl) spacer arm. The [^{125}I]EGF-XX-biotin rapidly bound to C6 rat glioma cells transfected with the human EGF receptor. However, no binding to the C6 EGF receptor was detected when the [^{125}I]EGF-XX-biotin was bound to a conjugate of streptavidin (SA) and the OX26 MAb. An alternative linker strategy using poly(ethylene glycol) (PEG) of 3400 Da molecular mass (PEG^{3400}) was evaluated, wherein EGF was monobiotinylated with NHS-PEG^{3400}-biotin. Attachment of the [^{125}I]EGF-PEG^{3400}-biotin to the OX26/SA conjugate did not impair binding of the construct to the EGF receptor in C6 glioma cells. The length of the -PEG- spacer arm and the -XX- spacer arm was >200 atoms and 14 atoms, respectively. These studies demonstrate that the use of the extended PEG linker releases steric hindrance of MAb transport vectors on binding of EGF to its cognate receptor on glioma cells. Attachment of EGF peptide radiopharmaceuticals to BBB drug delivery systems such as the OX26 MAb using extended PEG linkers allows for retention of the bifunctionality of the conjugate with binding to both EGF and transferrin receptors.

INTRODUCTION

Human gliomas overexpress the epidermal growth factor (EGF) receptor (*1*). Therefore, radiolabeled EGF is a potential peptide radiopharmaceutical that could be used to image human brain tumors (*2*), using standard external detection modalities such as single photon emission computed tomography (SPECT). However, EGF does not cross the blood-brain barrier (BBB) (*3*). The BBB is intact in the early stages of brain tumor growth and at the margins of the tumor (*4*), especially to larger molecular weight molecules such as peptides or antibodies (*5*). Therefore, the use of EGF as a peptide radiopharmaceutical for imaging human brain tumors will require a BBB drug delivery system.

Peptide drug delivery to the brain is facilitated by conjugation of a nontransportable peptide therapeutic to a BBB delivery vector (*6*). The latter is comprised of a modified protein or receptor-specific monoclonal antibody (MAb) that undergoes receptor-mediated transcytosis through the BBB in vivo. Peptide pharmaceuticals have been delivered through the BBB in rats using an anti-transferrin receptor MAb (*7*) and in Rhesus monkeys using an anti-insulin receptor MAb (*8*). However, it is possible that once a peptide radiopharmaceutical is conjugated to a BBB drug delivery system, the peptide will no longer bind with high affinity to its cognate receptor on brain cells. In this event, prior studies have used a cleavable (disulfide) linker for attachment of the peptide pharmaceutical to the BBB delivery vector (*9*). However, in this case, release of the peptide from the delivery vector requires cleavage of the disulfide to activate the peptide pharmaceutical. Since most disulfide reductase activity may be within the cytosol of cells (*10*), the use of a cleavable disulfide linker requires that the BBB delivery system contain an endosomal release function. A different conjugation strategy, which is examined in the present studies, is to employ an extended, poly(ethylene glycol) (PEG) linker between the peptide radiopharmaceutical and the BBB transport vector, in this case the OX26 MAb which is specific for the rat transferrin receptor. The use of the extended PEG linker increases the length of the linker from 14 atoms, which is the case for the conventional bis (aminohexanoyl) spacer arm, to >200 atoms, in the case of a PEG linker of 3400 Da.

EXPERIMENTAL PROCEDURES

Materials. Na[^{125}I] was supplied by Amersham (Arlington Heights, IL). Biotin-XX-NHS was supplied by Cal Biochem (San Diego, CA), where XX = bis (aminohexanoyl) spacer arm and NHS = *N*-hydroxysuccinimide. NHS-PEG^{3400}-biotin was obtained from Shearwater Polymers (Huntsville, AL). Chloramine T was purchased from MCB Reagents (Cincinnati, OH). Recombinant streptavidin (SA), recombinant human epidermal growth factor (EGF), and all other reagents were obtained from Sigma

* To whom correspondence should be addressed. Tel: (310) 825-8858. Fax: (310) 206-5163. E-mail: wpardrid@med1.medsch.ucla.edu.

10.1021/bc9800522 CCC: $18.00 © 1999 American Chemical Society
Published on Web 12/09/1998

Chemical Co. (St. Louis, MO). Vydac C4 (10 × 250 mm) reversed-phase HPLC columns were obtained from Separations Group (Hesperia, CA). TSK-gel G2000 SW_{XL} HPLC columns (7.8 × 300 mm) were obtained from TosoHaas (Montgomeryville, PA). High-Trap copper affinity columns (1 mL) and 1 × 30 cm Superose 12HR columns were obtained from Pharmacia (Piscataway, NJ). Centricon-30 microconcentrators were obtained from Amicon Corp. (Beverly, MA). C6 rat glioma cells transfected with the gene for the human EGF receptor (*2*) were kindly provided by Dr. Robert Fenstermaker of the Roswell Park Cancer Institute (Buffalo, NY), and these cells are designated C6EGFRp.

Preparation of [^{125}I]EGF-XX-biotin. NHS-XX-biotin (65 nmol in 10 μL of 100% dimethyl sulfoxide) was added in an 8:1 molar ratio to 50 μL of EGF (8.3 nmol in 0.05 M $NaHCO_3$, pH 8.3) and this mixture was incubated at room temperature for 60 min. The biotin-XX-EGF was directly iodinated by adding 6 μL (5 μg) to 20 μL of 0.3 M Na_2HPO_4, pH 7.0, followed by the addition of 2 mCi of ^{125}I and 10 μL (0.8 μg) of chloramine T. Following incubation at room temperature for 60 s, an additional 10 μL aliquot (0.8 μg) of chloramine T was added followed 60 s later by the addition of 50 μL (65 nmol) of sodium metabisulfite to terminate the iodination reaction. The mixture was then applied to a Sephadex G-25 gel filtration column followed by elution in 0.1 M Na_2HPO_4/0.15 M NaCl/pH 7.4/0.1% bovine serum albumin (BSA). The [^{125}I]EGF-XX-biotin was labeled to a specific activity of 548 μCi/nmol.

Preparation of [^{125}I]EGF-PEG^{3400}-biotin. NHS-PEG^{3400}-biotin (65 nmol in 100 μL of 0.05 M $NaHCO_3$) was added in an 8:1 molar ratio to 50 μg of EGF (8.0 nmol in 100 μL of 0.05 M $NaHCO_3$, pH 8.3) followed by incubation at room temperature for 60 min. Of this mixture, 20 μL was added to 20 μL of 0.3 M NaH_2PO_4 (pH 7.0) followed by the addition of 2 mCi of ^{125}I and 10 μL (0.8 μg) of chloramine T. After a 60 s incubation, an additional 10 μL (0.8 μg) of chloramine T was added, and 60 s later, the reaction was terminated by the addition of 50 μL (65 nmol) of sodium metabisulfite. Buffer A [0.05 M NaH_2PO_4/0.5 M NaCl/pH 7.0] was added to a volume of 1 mL and the mixture was then applied to a 1 mL High-Trap copper affinity column (*11*). The column was initially washed with 5 mL of water and charged with 0.5 mL of 0.1 M $CuSO_4$ followed by washing with 5 mL of water, followed by application of the sample. The column was washed with 10 mL of buffer A and the [^{125}I]EGF-PEG^{3400}-biotin was eluted with 5 mL of 50 mM imidazole in buffer A; 1 mL of this eluate (250 μCi) was added to a Centricon-3 microconcentrator and the volume was reduced to 200 μL by centrifugation at 7500 rpm (7500 g) for 40 min at room temperature. An aliquot of this fraction was then injected on the gel filtration HPLC column (see below) to determine the mobility of [^{125}I]EGF-PEG^{3400}-biotin. An aliquot was also injected into 2 Superose 12HR gel filtration columns in series and eluted with 0.01 M Na_2HPO_4/0.15 M NaCl/pH 7.4 at 0.5 mL/min, and 0.5 mL fractions were collected and detected at A_{220} by fast protein liquid chromatography (FPLC). The chemical identity of the EGF-[PEG-biotin]$_n$, where n = the number of PEG-biotin moieties per EGF, was determined by matrix assisted-laser desorption ionization mass spectrometry (MALDI). EGF-[PEG-biotin]$_3$ eluted at fractions 54−55 and constituted 7% of the total; EGF-[PEG-biotin]$_2$ and EGF-[PEG-biotin]$_1$ eluted at fractions 58−59 and 63−64 and constituted 35% and 43% of the total, respectively, and unconjugated EGF eluted at fractions 75−76 and comprised 15% of the total.

Preparation of EGF and OX26 MAb Conjugates. The conjugate of the OX26 MAb and recombinant streptavidin (SA) was prepared with a thiol-ether linkage as described previously (*12*). Briefly, 17 mg of OX26 MAb was thiolated with a 10:1 molar ratio of 2-iminothiolane; 7 mg of recombinant SA was activated with a 20:1 molar ratio of *m*-maleimidobenzoyl *N*-hydroxysuccinimide ester (MBS). The OX26/SA conjugate was labeled with 2.5 μCi of [^{3}H]biotin and was purified on a 2.6 × 92 cm column of Sephacryl S300HR (Pharmacia) followed by elution in 0.01 M Na_2HPO_4/0.15 M NaCl/pH 7.4/0.05% Tween-20 at 30 mL/h, and 3 mL fractions were collected. The conjugate peak was separated from either aggregates, unconjugated OX26 MAb, or unconjugated SA. The number of biotin-binding sites per OX26/SA conjugate was 3.3 ± 0.3, as determined with the [^{3}H]biotin binding assay (*12*).

The conjugate of OX26/SA and [^{125}I]EGF-PEG^{3400}-biotin was prepared by mixing 1 mL of the imidazole eluate from the High-Trap column containing 200 μCi of [^{125}I]EGF-PEG^{3400}-biotin (0.6 nmol) and 400 μg of OX26/SA (2.0 nmol). This volume was reduced to 0.2 mL with a Centricon-30 microconcentrator by centrifugation at 6300 rpm (5000 g) for 20 min at room temperature. The entire mixture was then applied to a TSK-gel G2000 SW_{XL} HPLC gel filtration column, followed by elution in 0.01 M Na_2HPO_4/0.15 M NaCl/pH 7.4/0.05% Tween-20 at a flow rate of 0.5 mL/min for 40 min, and 0.5 mL fractions were collected and counted for ^{125}I radioactivity. The conjugate of [^{125}I]EGF-PEG^{3400}-biotin bound to OX26/SA eluted at 7.0 mL from the column and this conjugate was subsequently used in the radioreceptor assays described below.

The conjugate of OX26/SA and [^{125}I]EGF-XX-biotin was prepared by mixing [^{125}I]EGF-XX-biotin (0.4 nmol) eluted from the Sephadex G-25 column with 60 μg of OX26/SA (0.30 nmol), followed by injection on the TSK G2000 SW_{XL} gel filtration HPLC column and elution as described above. The [^{125}I]EGF-XX-biotin bound to OX26/SA eluted at 7.0 mL from this column and was well separated from nonbiotinylated [^{125}I]EGF, which eluted at 11−12 mL.

C6EGFRp Radioreceptor Assays. C6EGFRp cells were grown in Dulbecco's modified Eagle medium (DMEM) with 4.5 g/L D-glucose, 4 mM glutamine, 10% fetal bovine serum, and 250 μg/mL G418, used as a selection agent, in 24-well cluster dishes. At 24 h prior to the radioreceptor assays, the medium was changed to DMEM with 4.5 g/L D-glucose, 1% fetal bovine serum, and 1 μM dexamethasone to induce expression of the EGF receptor (*2*). The assay was terminated by aspiration of medium, and washing wells with 0.01 M HEPES/0.15 M NaCl/pH 7.4 (HBS buffer). Radioreceptor assays were performed in the 24-well cluster dishes at 23 °C with 200 μL of final volume in the HBS buffer with 0.1% BSA. The wells contained 0.1 μCi/mL (0.18 nM) of [^{125}I]EGF conjugate and varying concentrations of unlabeled recombinant EGF ranging from 0.1 nM to 1 μM. Experimental incubations were performed from 15 to 120 min. The cell monolayer was solubilized by the addition of 0.5 mL of 1 N NaOH and incubated at 55 °C for 30 min or overnight at room temperature followed by counting for ^{125}I radioactivity and measurement of cell protein with the bicinchoninic acid (BCA) protein assay (Pierce Chemical Co.). Binding was expressed as percent of medium counts bound per milligram of cell protein and represents both surface bound and internalized ligand. Binding of the OX26/SA conjugate to C6 cells was confirmed by adding [^{3}H]biotin complexed to OX26/SA to cultured C6 cells; binding increased linearly with incubation time and was 4−5%/mgp at 60 min of incubation.

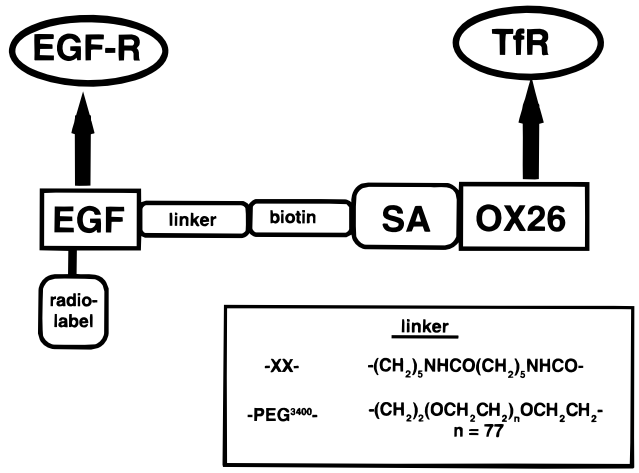


Figure 1. Structure of conjugate of EGF attached to the OX26 MAb using either a bis (aminohexanoyl) spacer arm (-XX-) or a 3400 Da poly(ethylene glycol) (PEG) spacer arm. The stable thioether linkage between OX26 and streptavidin (SA) is prepared in parallel with monobiotinylation of EGF using either NHS-XX-biotin or NHS-PEG^{3400}-biotin. The construct is prepared to ensure retention of the bifunctionality of the conjugate with binding to both the EGF receptor (EGF-R) via the EGF moiety or to the transferrin receptor (TfR) via the OX26 MAb moiety. The EGF is radiolabeled by iodination of EGF tyrosine residues. The length of the -XX- linker is 14 atoms and the length of the -PEG^{3400}- linker is >200 atoms.

RESULTS

The structure of the EGF/OX26 conjugate using a biotin/streptavidin linker is shown in Figure 1 for either the -XX- linker or the -PEG^{3400}- linker. The -XX- linker is 14 atoms long and the -PEG^{3400}- linker is >200 atoms long (Figure 1).

The binding of [^{125}I]EGF-XX-biotin to the C6EGFRp cells was avid and reached equilibrium by 60 min of incubation (Figure 2A) and was completely saturated by unconjugated EGF (Figure 2B). In contrast, conjugation of [^{125}I]EGF-XX-biotin to OX26/SA resulted in a more than 5-fold inhibition of binding of the EGF to the C6 cells (Figure 2A) and this binding was independent of unlabeled EGF added to the medium (Figure 2B). These results indicated that biotinylation, per se, of EGF did not impair binding to the EGF receptor, but attachment of EGF-XX-biotin to the OX26/SA drug delivery system essentially eliminated binding of the conjugate to the EGF receptor. Therefore, binding of the conjugate to the EGF receptor was assessed following the use of a PEG linker coupling EGF to OX26/SA.

The [^{125}I]EGF-PEG^{3400}-biotin eluted from TSK gel filtration HPLC column at a volume of 13.5 mL (Figure 3). However, after conjugation to OX26/SA, the [^{125}I]EGF-PEG^{3400}-biotin eluted at 7.0−7.5 mL from the column (Figure 3). Conjugation of EGF-PEG^{3400}-biotin to OX26/SA increased the molecular mass of the EGF construct from approximately 10 000 Da (Experimental Procedures) to 210 000 Da, since the OX26/SA has a size of 200 000 Da. The binding of [^{125}I]EGF-PEG^{3400}-biotin to the C6EGFRp cells was high (Figure 4A) and was comparable to the binding of the [^{125}I]EGF-XX-biotin (Figure 2A). The binding of [^{125}I]EGF-PEG^{3400}-biotin to the C6 cells was nearly completely displaced by the addition of unlabeled EGF to the medium, and the ED_{50} of this inhibition was approximately 1 nM (Figure 4B). This ED_{50} of EGF inhibition of the binding of [^{125}I]EGF-PEG^{3400}-biotin to the C6 cells approximates the ED_{50} of EGF inhibition of the binding [^{125}I]EGF-XX-biotin to these cells (Figure 2B). The conjugation of [^{125}I]EGF-PEG^{3400}-biotin to OX26/SA did not impair the binding of the EGF construct to the C6 cells (Figure 4A), and approximately 50% of the binding was inhibited by unlabeled EGF added to the medium (Figure 4B). The [^{125}I]EGF-XX-biotin or the [^{125}I]EGF-PEG^{3400}-biotin was metabolically stable during all radioreceptor assay incubations as the trichloroacetic acid (TCA) precipitability of medium ^{125}I radioactivity was >98% at all time points.

DISCUSSION

Human brain tumors frequently overexpress the EGF receptor (*13*, *14*). Radiolabeled monoclonal antibodies (MAb) to the EGF receptor have been used to image human gliomas in vivo (*15*). However, MAbs do not cross the BBB (*6*) and can image human brain tumors only when there is preexisting BBB disruption. For example, radiolabeled nonspecific MAbs image advanced human gliomas just as well as EGF receptor-specific MAbs, especially in patients with prior radiation therapy to the brain tumor (*15*), which causes BBB disruption (*16*). In the early stage of growth of a human brain tumor in an untreated patient, even metastatic tumors to brain (*17*),

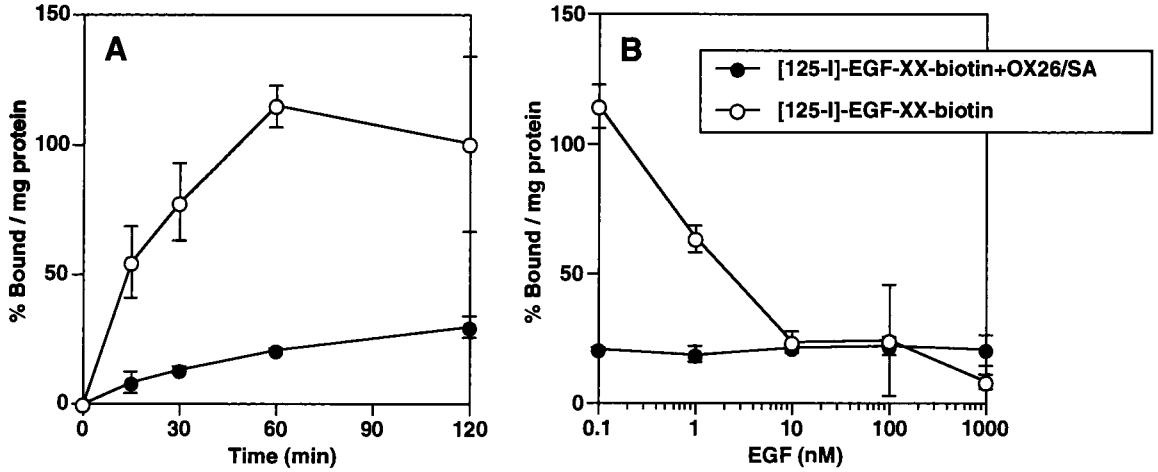


Figure 2. Radioreceptor assay showing binding of either [^{125}I]EGF-XX-biotin conjugated to OX26/SA (closed circles) or binding of [^{125}I]EGF-XX-biotin (open circles) to C6 rat glioma cells transfected with the human EGF receptor. Data are mean ± SE (n = 3 replicas at each point). (A) Time course of binding of either construct to the cells. (B) Saturation analysis was performed at 60 min incubations by adding varying concentrations of unlabeled recombinant EGF to the medium.

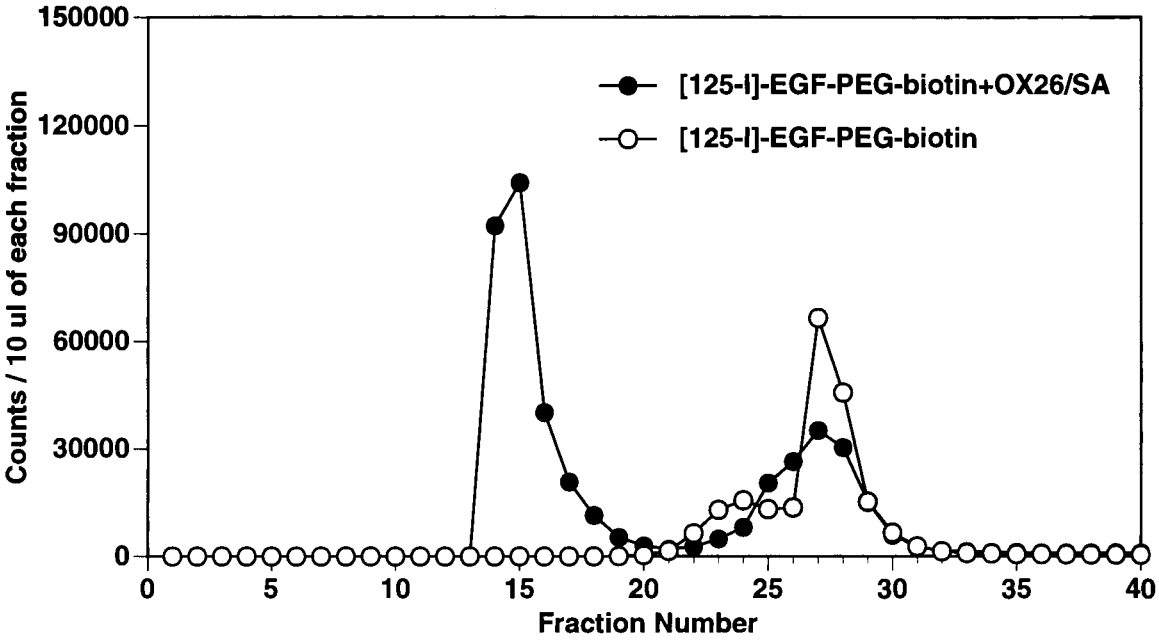


Figure 3. Elution of either [^{125}I]EGF-PEG^{3400}-biotin (open circles) or [^{125}I]EGF-PEG^{3400}-biotin conjugated to OX26/SA (closed circles) from a TSK-gel G2000 SW_{XL} gel filtration HPLC column. Each fraction was 0.5 mL and was accounted for ^{125}I radioactivity.

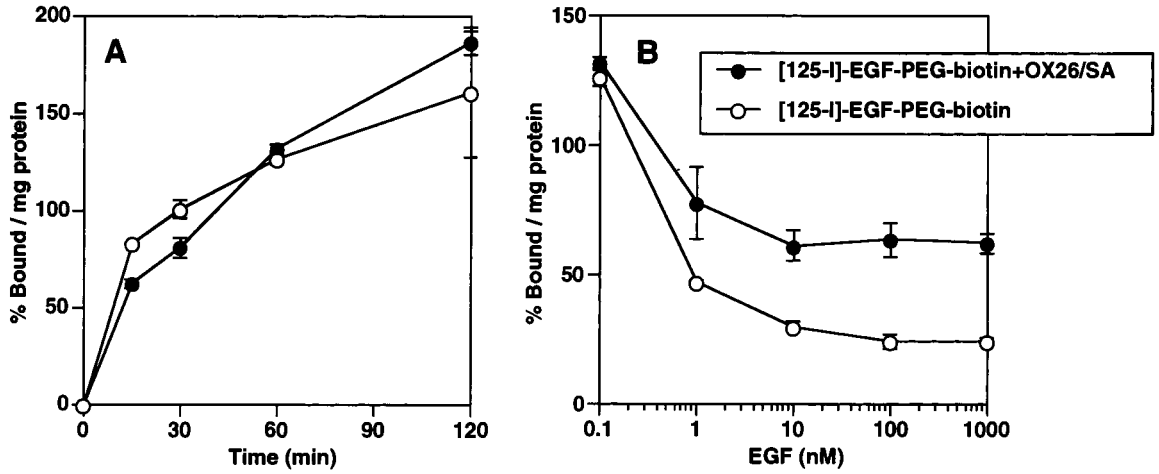


Figure 4. Radioreceptor assay showing binding of either [^{125}I]EGF-PEG^{3400}-biotin conjugated to OX26/SA (closed circles) or binding of [^{125}I]EGF-PEG^{3400}-biotin (open circles) to C6 rat glioma cells transfected with the human EGF receptor. Data are mean ± SE (n = 3 replicas at each point). (A) Time course of binding of either construct to the cells. (B) Saturation analysis was performed at 60 min incubations by adding varying concentrations of unlabeled recombinant EGF to the medium.

the BBB is intact, and it is at this stage that imaging and diagnosis of nascent brain tumors is most needed. Imaging of early brain tumors where the BBB is intact with either MAbs or peptide radiopharmaceuticals such as EGF requires the attachment of the tumor imaging agent to a BBB drug delivery system. The present studies make an initial evaluation of the molecular formulation required to attach EGF to a BBB transport vector in such a way that binding of the peptide to the EGF receptor is retained following conjugation to the delivery vector.

The results of these studies are consistent with the following conclusions. First, human EGF can be biotinylated with succinimide esters of biotin to target the ϵ-amino groups of lysine residues, with retention of ligand affinity for the EGF receptor. Second, when EGF-XX-biotin is conjugated to OX26/SA, the EGF no longer binds to the EGF receptor (Figure 2). Third, substitution of the 14 atom bis(aminohexanoyl) spacer arm between the biotin moiety and the EGF with a >200 atom extended poly(ethylene glycol) linker restores affinity of EGF for its cognate receptor despite conjugation of the peptide to the BBB delivery vector, OX26/SA (Figure 4).

Biotinylation of EGF with NHS-XX-biotin targets the ϵ-amino moiety of surface lysine residues. Murine EGF lacks internal lysine residues, but human EGF has 2 lysine residues at positions 28 and 48 (*18*, *19*). Although the amino terminus is also a target for biotinylation with succinimide esters, the biotinylation was performed at pH 8.3, which preferentially exposes the ϵ-amino moieties of lysine residues to the succinimide ester (*20*). The EGF-XX-biotin still binds to the human EGF receptor in transfected C6 rat glioma cells as EGF inhibits this binding with an ED_{50} of approximately 1 nM (Figure 2). The total binding of either [^{125}I]EGF-XX-biotin or [^{125}I]EGF-PEG^{3400}-biotin, expressed as percent bound per $(\text{milligram})_p$, is nearly identical to the total binding of unconjugated [^{125}I]EGF to the C6-$EGFR_p$ cells (*2*), indicating that neither biotinylation nor pegylation, per se, impairs ligand binding to the human EGF receptor. These results are consistent with earlier immunocytochemistry experi-

ments showing that biotinylated EGF binds to the EGF receptor in frozen sections of human glioma cells in vitro (*1*). Moreover, EGF-biotin detects the EGF receptor on human glioma cells immunocytochemically with a greater sensitivity than that achieved with monoclonal antibodies to the EGF receptor (*1*). The retention of ligand affinity for its cognate receptor following biotinylation on lysine residues, and the fact that mouse EGF lacks internal lysine residues (*18*, *19*), suggests that the lysine residues at positions 28 or 48 of human EGF do not participate in binding to the EGF receptor. However, when the OX26 MAb is conjugated to streptavidin via a stable thioether linkage and this complex is then bound to EGF-XX-biotin, the EGF no longer binds to the EGF receptor (Figure 2). These observations suggest that binding of EGF-XX-biotin to OX26/SA causes significant steric hindrance of binding of EGF to its cognate receptor. Although a vasoactive intestinal peptide (VIP) analogue has been successfully attached to OX26/SA with the biotin-XX-linker, and with retention of peptide affinity for the cognate receptor (*12*), the attachment of opioid peptides to OX26/SA with this linker eliminates peptide affinity for the opioid receptor (*9*). In the event that the non-cleavable (amide) -XX- linker eliminates ligand and receptor binding following attachment of the peptide to the delivery vector, previous studies have employed a cleavable (disulfide) -SS- linker between the biotin moiety and the therapeutic peptide. In this case, the peptide becomes biologically active with restoration of affinity for its cognate receptor following cleavage of the disulfide bond and release of the peptide from the OX26/SA delivery system (*9*). However, if the majority of the disulfide reductase resides in the cytosol of brain cells (*10*), it is necessary for the vector-SS-peptide conjugate to undergo release from the intracellular endosomal compartment following receptor-mediated endocytosis into the brain cell. In the absence of an obligatory endosomal release function built into the delivery system, the exposure of the conjugate to the cytoplasmic disulfide reductase may be minimal.

Given the potential limitations of either the noncleavable (amide) -XX- linker or the cleavable (disulfide) -SS- linker, there is a need for a third approach for conjugating peptide therapeutics to MAb-based BBB delivery systems that allows for retention of receptor affinity of the peptide therapeutic but does not require a disulfide cleavage. These requirements are satisfied with the use of an extended PEG linker between the biotin moiety and the peptide therapeutic. The radioreceptor assays in Figure 4 show that EGF-PEG^{3400}-biotin binds with high affinity to the EGF receptor, and the ED_{50} of EGF inhibition of this binding is 1 nM, which is identical to ED_{50} of EGF inhibition of EGF-XX-biotin binding to the EGF receptor (Figure 2). Therefore, the placement of the 3400 Da PEG moiety on a surface lysine residue of EGF does not impair peptide binding to the EGF receptor. When the EGF-PEG^{3400}-biotin is conjugated to OX26/SA, there is no impairment in the binding of the EGF to its cognate receptor on C6 glioma cells (Figure 4). The time course of EGF-PEG^{3400}-biotin binding to C6 glioma cells is identical with or without attachment to OX26/SA (Figure 4A). In addition, more than 50% of the binding of [^{125}I]-EGF-PEG^{3400}-biotin conjugated to OX26/SA is displaced by native EGF in the medium (Figure 4B). In the presence of saturating concentrations of EGF (>10 nM) there is still significant binding of [^{125}I]EGF-PEG^{3400}-biotin conjugated to OX26/SA (Figure 4B), and this residual binding is a result of conjugate binding to the transferrin receptor on the C6 glioma cells.

In summary, these studies describe the molecular formulation of an EGF peptide radiopharmaceutical that is conjugated to the OX26 MAb BBB drug delivery system, using an extended poly(ethylene glycol) linker between EGF and the biotin moiety. In contrast to a short bis(aminohexanoyl) -XX- linker, the PEG linker allows for retention of EGF binding to its cognate receptor on rat glioma cells. Many human brain gliomas overexpress the EGF receptor (*1*, *13*, *14*), and EGF peptide radiopharmaceuticals are potential imaging agents for detection of these tumors (*2*). However, EGF does not cross the BBB (*3*), which is consistent with the absence of EGF receptors on endothelial cells (*21*). An optimal use of EGF peptide radiopharmaceuticals to image human brain tumors may require a molecular reformulation of the peptide that involves conjugation to a BBB drug delivery vector.

ACKNOWLEDGMENT

Dr. Deguchi was supported by the Department of Biopharmacy, School of Pharmaceutical Sciences, University of Shizuoka, Shizuoka, Japan, and Dr. Kurihara was supported by Sankyo Co., Ltd., Tokyo, Japan. This work was supported in part by a grant from the Department of Energy.

LITERATURE CITED

(1) Torp, S. H., Helseth, E., Dalen, A., and Unsgaard, G. (1991) Epidermal growth factor receptor expression in human gliomas. *Cancer Immunol. Immunother. 33*, 61−64.

(2) Fenstermaker, R. A., Capala, J., Barth, R. F., Hujer, A., Kung, H.-J., and Kaetzel, D. M. (1995) The effect of epidermal growth factor receptor (EGFR) expression on in vivo growth of rat C6 glioma cells. *Leukemia 9* (Suppl. 1), S106−S112.

(3) Nave, K. A., Probstmeier, R., and Schachner, M. (1985) Epidermal growth factor does not cross the blood-brain barrier. *Cell Tissue Res. 241*, 453−457.

(4) Blasberg, R. G., and Groothuis, D. R. (1986) Chemotherapy of brain tumors: physiological and pharmacokinetic considerations. *Sem. Oncol. 13*, 70−82.

(5) Inamura, T., and Black, K. L. (1994) Bradykinin selectively opens blood-tumor barrier in experimental brain tumors *J. Cereb. Blood Flow Metabol. 14*, 862−870.

(6) Pardridge, W. M. (1991) *Peptide Drug Delivery to the Brain*, pp 1−357, Raven Press, New York.

(7) Bickel, U., Yoshikawa, T., Landaw, E. M., Faull, K. F., and Pardridge, W. M. (1993) Pharmacologic effects in vivo in brain by vector-mediated peptide drug delivery. *Proc. Natl. Acad. Sci. 90*, 2618−2622.

(8) Wu, D., Yang, J., and Pardridge, W. M. (1997) Drug targeting of a peptide radiopharmaceutical through the primate blood-brain barrier in vivo with a monoclonal antibody to the human insulin receptor. *J. Clin. Invest. 100*, 1804−1812.

(9) Bickel, U., Kang, Y.-S., and Pardridge, W. M. (1995) In vivo cleavage of a disulfide-based chimeric opioid peptide in rat brain. *Bioconjugate Chem. 6*, 211−218.

(10) Papini, E., Rappuoli, R., Murgia, M., and Montecucco, C. (1993) Cell penetration of diptheria toxin. *J. Biol. Chem. 268*, 1567−1574.

(11) Sakane, T., and Pardridge, W. M. (1997) Carboxyl-directed pegylation of brain-derived neurotrophic factor markedly reduces systemic clearance with minimal loss of biologic activity. *Pharm. Res. 14*, 1085−1091.

(12) Wu, D., and Pardridge, W. M. (1996) CNS pharmacologic effect in conscious rats after intravenous injection of a biotinylated vasoactive intestinal peptide analogue coupled to a blood-brain barrier drug delivery system. *J. Pharmacol. Exp. Ther. 279*, 77−83.

(13) Libermann, T. A., Nusbaum, H. R., Razon, N., Kris, R., Lax, I., Soreq, H., Whittle, N., Waterfield, M. D., Ullrich, A., and Schlessinger, J. (1984) Amplification, enhanced expres-

sion and possible rearrangement of EGF receptor gene in primary human brain tumours of glial origin. *Nature 313*, 144−147.
(14) Wong, A. J., Bigner, S. H., Bigner, D. D., Kinzler, K. W., Hamilton, S. R., and Vogelstein, B. (1987) Increased expression of the epidermal growth factor receptor gene in malignant gliomas is invariably associated with gene amplification. *Proc. Natl. Acad. Sci. U.S.A. 84*, 6899−6903.
(15) Kalofonos, H. P., Pawlikowska, T. R., Hemingway, A., Courtenay-Luck, N., Dhokia, B., Snook, D., Sivolapenko, G. B., Hooker, G. R., McKenzie, C. G., Lavender, P. J., Thomas, D. G. T., and Epenetos, A. A. (1989) Antibody guided diagnosis and therapy of brain gliomas using radiolabeled monoclonal antibodies against epidermal growth factor receptor and placental alkaline phosphatase. *J. Nucl. Med. 30*, 1636−1645.
(16) Rubin, P., Gash, D. M., Hansen, J. T., Nelson, D. F., and Williams, J. P. (1994) Disruption of the blood-brain barrier as the primary effect of CNS irradiation. *Radiother. Oncol. 31*, 51−60.
(17) Zhang, R.-d., Price, J. E., Fujimaki, T., Bucana, C. D., and Fidler, I. J. (1992) Differential permeability of the blood-brain barrier in experimental brain metastases produced by human neoplasms implanted into nude mice. *Am. J. Pathol. 141*, 1115−1124.
(18) Hommel, U., Harvey, T. S., Driscoll, P. C., and Campbell, I. D. (1992) Human epidermal growth factor: high-resolution solution structure and comparison with human transforming growth factor α. *J. Mol. Biol. 227*, 271−282.
(19) Remy, S., Reilly, R. M., Sheldon, K., and Gariepy, J. (1995) A new radioligand for the epidermal growth factor receptor: ^{111}In labeled human epidermal growth factor derivatized with a bifunctional metal-chelating peptide. *Bioconjugate Chem. 6*, 683−690.
(20) Ralph, L. D., Ransone, C. M., Treuheit, M., Lauren, S., Katta, V., and Litzinger, D. C. (1995) Site-specific conjugation of diethylenetriaminepentaacetic acid to recombinant human granulocyte-colony-simulating factor: preservation of protein structure and function. *Biochemistry 34*, 4889−4897.
(21) Gospodarowicz, D., Brown, K. D., Birdwell, C. R., and Zetter, B. R. (1978) Control of proliferation of human vascular endothelial cells. *J. Cell Biol. 77*, 774−788.

BC9800522

Antibody-Directed Enzyme Prodrug Therapy with the T268G Mutant of Human Carboxypeptidase A1: In Vitro and in Vivo Studies with Prodrugs of Methotrexate and the Thymidylate Synthase Inhibitors GW1031 and GW1843

L. A. Wolfe, R. J. Mullin, R. Laethem, T. A. Blumenkopf, M. Cory, J. F. Miller, B. R. Keith, J. Humphreys, and G. K. Smith*

Glaxo Wellcome Research and Development Inc., Five Moore Drive, Research Triangle Park, North Carolina 27709. Received May 27, 1998; Revised Manuscript Received November 4, 1998

Antibody-directed enzyme prodrug therapy (ADEPT) is a technique to increase antitumor selectivity in cancer chemotherapy. Our approach to this technology has been to design a mutant of human carboxypeptidase A (hCPA1-T268G) which is capable of hydrolyzing in vivo stable prodrugs of MTX and targeting this enzyme to tumors on an Ep-CAM1-specific antibody, ING1. Through the use of this >99% human enzyme which is capable of catalyzing a completely nonhuman reaction, we hope to increase ADEPT selectivity while decreasing overall immunogenicity of the enzyme−antibody conjugate. In the current report, prodrugs of the thymidylate synthase inhibitors GW1031 and GW1843 and the dihydrofolate reductase inhibitor methotrexate were studied for their wild-type and mutant hCPA enzyme hydrolysis, their in vivo stability, and their use in therapy. Prodrugs with high k_{cat}/K_m ratios for mutated versus wild-type hCPA1 were examined in vitro for their stability in human pancreatic juice, and in vivo for their stability in mouse plasma and tissues. In addition, targeting and in vivo enzyme activity studies were performed with an ING1 antibody conjugate of the mutant enzyme (ING1-hCPA1-T268G). Finally, in vivo therapy studies were performed with LS174T tumors to demonstrate proof of principle. Results indicate that prodrugs can be synthesized that are selective and efficient substrates of hCPA1-T268G and not substrates of the endogenous CPA activities; this leads to excellent in vivo stability for these compounds. In vivo conjugate targeting studies showed that the antibody−enzyme conjugate was targeted to the tumor and enzyme was initially active in vivo at the site. Unfortunately therapeutic studies did not demonstrate tumor reduction. Experiments to determine reasons for the lack of antitumor activity showed that the enzyme activity decreased as a result of enzyme instability. The results offer encouragement for additional novel mutant enzyme improvements and additional in vivo studies on this unique approach to ADEPT.

INTRODUCTION

One of the problems associated with cancer chemotherapy is the lack of selectivity of drug for neoplastic cells over normal proliferating cells, and the resulting systemic toxicity (*1*, *2*). In an attempt to circumvent these problems, investigators have examined the potential of using monoclonal antibodies (mAbs)[1] that bind to tumor-selective antigens localized on the surface of neoplastic cells. This binding specificity can be exploited for tumor-specific delivery of materials conjugated to a targeting antibody. Cytotoxic drugs have been coupled to mAbs (*3*, *4*), and the resulting conjugates are more selective for tumor cells than are drugs alone. Toxicity also is reduced, allowing more drug to be used without affecting highly sensitive normal cells. However, low drug delivery is a problem generally associated with this approach. Efficient drug delivery is compromised by (a) the limitation caused by the number of drug molecules that can be attached to the antibody, (b) antigen density, (c) the limited diffusibility of conjugates compared to drugs alone due to differences in their sizes, and (d) poor internalization of conjugate. Because of these problems, investigators continue to look for alternate modes of therapy.

ADEPT has been proposed as a means to solve these problems (*5*−*10*). This technology involves selectively delivering an activating enzyme to the tumor site by conjugating it to a targeting antibody. This activating enzyme is then used to convert systemically administered

* Correspondence should be addressed to this author at the Department of Molecular Biochemistry, Glaxo Wellcome Research and Development, Venture 300, Research Triangle Park, NC 27709. Phone: (919) 483-1502. Fax: (919) 483-4320. Email: gks39645@glaxowellcome.com.

[1] Abbreviations: GW1031, *N*-(2-fluoro-4(((1,2-dihydro-3-methyl-1-oxobenzo(*f*)quinazolin-9-yl)methyl)amino)benzoyl)-L-glutamic acid, 1031U89; GW1843, (*S*)-2-(5-(((1,2-dihydro-3-methyl-1-oxobenzo(*f*)quinazolin-9-yl)methyl)amino)-1-oxo-2-isoindolinyl)glutaric acid, 1843U89; mtx, methotrexate; mAbs, monoclonal antibodies; ADEPT, antibody-directed enzyme prodrug therapy; CPA, carboxypeptidase type A; CPG2, carboxypeptidase type G2; CPA1, carboxypeptidase type A1; HPA, hippuryl-L-phenylalanine; HPL, hippuryl-D,L-phenyllactate; HPLC, high-performance liquid chromatography; CPG, carboxypeptidase type G; HOAc, acetic acid; FBS, fetal bovine serum; sc, subcutaneous; PBS, Dulbecco's phosphate-buffered saline; ip, intraperitoneal; iv, intravenous; SIP, small intestine/pancreas; HCl, hydrochloric acid; MTD, maximum tolerated dose; DHFR, dihydrofolate reductase; TS, thymidylate synthase.

10.1021/bc980057z CCC: $18.00 © 1999 American Chemical Society
Published on Web 01/18/1999

prodrug to drug at the tumor site. The catalytic potential of a targeted enzyme and the high potential prodrug concentration may overcome the low drug delivery problem. The toxic drug would be concentrated around the tumor, and its comparatively low molecular weight should allow for better tumor penetration than antibody−drug conjugates. In addition, this regional tumor-specific activation should lower systemic toxicity. An important decision that needs to be made with this type of therapy is what types of prodrugs and enzymes are to be employed. Although the need to find new active drugs still exists, it would also be of benefit to look at prodrugs of drugs currently used in the clinic since their toxicity and efficacy profiles are already understood. Enzymes that have been considered for ADEPT include both endogenous and nonendogenous types (*11*). One endogenous enzyme being investigated is alkaline phosphatase for the hydrolysis of phosphorylated prodrugs of phenol mustard (*12*), etoposide (*13*−*15*), and mitomycin C (*14*). Another enzyme is carboxypeptidase A for the hydrolysis of methotrexate prodrugs (*16*). Some nonendogeneous enzymes being used include cytosine deaminase for the conversion of 5-fluorocytosine to 5-fluorouracil (*17*) and the bacterial enzyme CPG2 for the cleavage of the glutamic acid moiety from prodrugs of alkylating agents (*18*).

The ADEPT approach is not without its problems. Use of endogenous enzymes may result in the hydrolysis of prodrugs at sites distal to the tumor site, thus increasing toxicity. By contrast, nonendogenous enzymes may generate an immune response which would interfere with multiple rounds of therapy. To address these problems, we recently reported an alternate approach to ADEPT. This strategy in its most generalized form uses an endogenous enzyme mutated at the active site to perform an otherwise nonendogenous reaction to convert an in vivo stable prodrug to active drug only at the targeted tumor. In our prototype example of the concept, the "novel endogenous enzyme" was based upon human CPA1. Binding pocket mutations were introduced into hCPA1 to alter the substrate specificity of the enzyme to allow for hydrolysis of novel prodrugs that were not substrates for wild-type hCPA (*19*). This "novel endogenous enzyme" should be less immunogenic than nonendogenous enzymes, and prodrug hydrolysis at sites distal to tumors should be better controlled than in systems based upon endogenous activities. Simultaneously we have attempted to match mutant enzyme constructs with prodrugs of methotrexate (*19*) and two promising active drugs, GW1031 (*20*) and GW1843 (*20*−*25*). In the current report, the most promising of the previously reported MTX prodrugs and novel prodrugs of two thymidylate inhibitors were studied in vitro and in vivo to determine the therapeutic potential of this approach.

MATERIALS AND METHODS

Chemicals. GW1031, GW1843, and all prodrugs were synthesized at Glaxo Wellcome Inc., Research Triangle Park, NC. ING1-TMT was obtained from Sterling Winthrop Immunoconjugates (Philadelphia, PA). ^{90}Y was purchased from Dupont NEN (Milford, MA). Methotrexate, HPA, trypsin, HPL, and L-glutamine were purchased from Sigma Chemical Co. (St. Louis, MO). RPMI-1640 tissue culture medium was purchased from Gibco BRL (Grand Island, NY), and FBS was purchased from JRH Biosciences (Lenexa, KY). Human serum was prepared in house from blood donors.

Kinetic Assays. Determination of the activity of hCPA1 and hCPA1-T268G on prodrugs was done by kinetic assays. Kinetic assays either were performed spectrophotometrically as described by Smith et al. (*19*) or were HPLC-based. HPLC assays were carried out in 0.5 mL reactions at 25 °C in assay buffer (25 mM Tris-HCl, 100 mM NaCl, pH 7.4). Reactions with varying concentrations of prodrug in buffer were preincubated at 25 °C for 3 min before reactions were initiated by addition of a known amount of human CPA enzyme. Aliquots (75 μL) of the reaction were withdrawn at predetermined times and stopped by the addition of 75 μL of 1 M perchloric acid. An aliquot of the acidified reaction (20 μL) was injected onto a Waters Nova-Pak C18 column, and the prodrug and drug were resolved with the following step gradient (solvent A = 0.1% aqueous trifluoroacetic acid, solvent B = 0.1% trifluoroacetic acid in acetonitrile): 18% B for 3 min, 18−50% B over 0.1 min, and 50% B for 3.9 min. Kinetic rates were determined from the linear portion of product vs time plots.

HPLC Analysis. HPLC analysis of in vivo samples consisted of using a 715 WISP autoinjector (Waters, Milford, MA), a constaMetric 4100 solvent delivery system (LDC Analytical, Riviera Beach, FL), a variable-wavelength spectroMonitor D detector (LDC) set at the absorbance maximum of each individual prodrug, and a 3.9 × 300 mm C18, 4 μm Nova-Pak or a C18, 10 μm μBondapak HPLC column equipped with a C18 guard column. Data acquisition and analysis were performed with a DS-80 microcomputer (Digital Specialities, Chapel Hill, NC). Prodrugs of GW1031 and GW1843 and the MTX prodrug 2-carboxyPhe were injected onto the Nova-pak column equilibrated at 5−20% acetonitrile containing 2% HOAc, pH 3.0, and run at a flow rate of 1 mL/min. A linear gradient was immediately run over 25−35 min to a final concentration of 50% acetonitrile, 2% HOAc, pH 3.0. Absorbance was monitored at 259−266 nm. All other prodrugs were injected onto the μBondapak column equilibrated with 16% acetonitrile, 5 mM Pic A, 10 mM $NH_4H_2PO_4$. A linear gradient of 16−50% acetonitrile was run over 30 min at 1 mL/min, and compounds were detected at 307 nm.

Stability in Human Pancreatic Fluid. Prodrugs were evaluated for their stability in activated human pancreatic fluid as described by Smith et al. (*19*). Briefly, prodrug stability was determined in diluted activated pancreatic fluid. After selected incubation times, prodrug hydrolysis was determined by HPLC.

Animals and Cell Lines. CD-1 nu/nu female mice (4−6 weeks old, 20−24 g) were purchased from Charles River Laboratories (Wilmington, MA). CB17 and Swiss nude female mice were purchased from Taconic Farms, Inc. (Germantown, NY). Mice were housed in microisolator cages (Lab Products Inc., Rockville, MD) in groups of up to four mice per cage. The human colon adenocarcinoma cell lines (WiDr and LS174T) were purchased from the American Type Culture Collection (Rockville, MD). Wein-133 cells, a B-cell lymphoma, were kindly provided by Dr. John Tite (The Wellcome Research Laboratories, Beckenham, U.K.). WiDr cells were grown in RPMI 1640, low-folate media supplemented with 10% charcoal-dialyzed FBS and with 10 nM calcium leucovorin (Glaxo Wellcome Inc., RTP, NC). Wein-133 cells were grown in RPMI 1640 containing 10% FBS with an additional 2.05 mM L-glutamine added.

Tumor Implantation. WiDr cells were implanted sc as a 0.15 mL solution of 1.5 × 10^6 cells in PBS. LS174T and Wein-133 cells were implanted as a 0.20 mL solution of 2 × 10^6 cells in 50% low-endotoxin matrigel (Col-

laborative Biomedical Products, Bedford, MA) in PBS. Wein-133 cells were implanted into 400 rad irradiated nude mice (Gammacell 40 irradiator, Nordion International Inc., Ontario, Canada). Tumors were allowed to grow to approximately 200−400 mg before animals were used for study.

In Vivo Drug Stability and Biodistribution. Mice bearing either WiDr, Wein-133, or LS174T tumors were dosed ip bolus or iv at 50 mg/kg by injecting 0.01 mL/g mouse with a 5 mg/mL solution of prodrug in PBS, pH 6−8. Animals were sacrificed after 30 min and 2 h, and the plasma, liver, kidney, small intestine and pancreas, large intestine, spleen, cecum, feces, and tumor tissues were collected. Plasma was frozen at −70 °C, and tissues were snap-frozen in liquid nitrogen and stored at −70 °C. Duplicate animals were sacrificed for each time point. Plasma was prepared for extraction by dilution (4-fold) with ice-cold 0.1 N HCl. Tissues were prepared for extraction by homogenization with a Polytron (Brinkmann Instruments, Westbury, NY) equipped with a PTA 7 generator in 5 volumes of ice-cold 0.1 N HCl. Drugs were subsequently extracted by adding 5 volumes of −20 °C acetonitrile to 2 volumes of the HCl homogenate. After a 5 min incubation on ice, samples were centrifuged at 12400*g* for 15 min. Supernatants were collected and diluted 3.57-fold with PBS to reduce the final acetonitrile concentration to 20%. Diluted supernatants were then analyzed by HPLC as described above. To account for drug recovery, control homogenates were spiked with drug, prodrug, or PBS prior to the acetonitrile extraction step. After correction for recovery of these standards, the levels of drug and prodrug and the stability of the prodrug were calculated.

Toxicity of MTX and Prodrugs in Mice. MTX prodrugs demonstrating good kinetic and in vivo stability profiles were compared to MTX for toxicity. Prodrugs were dosed iv into mice for 5 days, and a prodrug was considered toxic if weight loss exceeded 15%. CD-1 nu/nu female mice were dosed with MTX (2, 4, or 6 mg/kg), MTX-Phe (5, 15, or 45 mg/kg), MTX-2-cyclopentylPhe, MTX-3-cyclopentylPhe, or MTX-3-cyclopentylPhe (10, 20, or 40 mg/kg). Swiss nude mice were dosed with MTX (2.5, 4, or 5.5 mg/kg), MTX-cyclopentylTyr, or MTX-3-cyclobutylPhe (30, 40, or 50 mg/kg).

Radiolabeling of ING1 Antibody. ^{90}Y-Antibody conjugate, [^{90}Y]-TMT-ING1, was prepared from TMT-ING1 as follows. Using metal-free containers and pipets throughout, 3.8 μL of ^{90}Y (0.075 mCi, diluted with Ultrex water) was combined with 50 μL of ING1-TMT at 5 mg/mL (250 μg). The reaction was mixed and allowed to stand 60 min at 25 °C; 5 μL of 10 mM diethylenetriaminepentaacetic acid (DTPA) was added, mixed, and allowed to stand another 30 min. The reaction was purified through two 1 mL Biospin 30 columns (Biorad) equilibrated with Dulbecco's phosphate-buffered saline. Quality control was determined by thin-layer chromatography of a small aliquot on silica gel 60 (0.2 mm thickness; catalog no. 5735; E. Merck; mobile phase 5 g of ammonium acetate, 50 mL of H_2O, and 50 mL of methanol). The percent of the Biospin-purified material as chelate was typically over 95%. The purified material was diluted into 4.9 mL of 5 mg/mL ascorbate. Animals were dosed with 200 μL of ascorbate-diluted material.

Conjugation of Mutant hCPA to ING1. Antibody−enzyme conjugate ING1-hCPA1-T268G was prepared as described previously (*19*). Briefly, the process was carried out in three steps.

(A) Enzyme Modification. Four milligrams of mutant carboxypeptidase A was combined with 0.15 mg of Sulfo-SMCC (Pierce Chemical Co.) in 400 μL of PBS and was stirred for 45 min at 25 °C. The modified enzyme was then purified through a 1 × 13 cm G-25 medium column equilibrated with PBS.

(B) Antibody Modification. The full-length IgG_1 antibody ING1 was modified with the amine-reactive reagent 2-iminothiolane; 1.8 mg of antibody was combined with 0.22 mg of 2-iminothiolane in 1.3 mL of 50:50 PBS/0.1 M triethanolamine hydrochloride, 2 mM EDTA, pH 8.0, under anaerobic conditions. This was allowed to react with stirring for 1 h and 45 min, and the modified antibody was purified through a 1 × 13 cm G-25 medium column equilibrated with 0.02 M sodium acetate, 0.1 M NaCl, pH 5.8, bubbled with and maintained under a He atmosphere.

(C) Coupling of Modified Antibody with Modified Enzyme. The modified antibody was collected directly from the G-25 column into the solution of the modified carboxypeptidase A. The resulting mixture was then adjusted to pH 7.4 with NaOH, made anaerobic, and allowed to react with stirring at 4 °C for 18 h. After treatment with 0.3 mM mercaptoethanolamine at room temperature for 1 h, the conjugate was then concentrated to 1 mL on an Amicon PM10 membrane and then purified on Superose 12 HR 10/30.

In Vivo Targeting Studies. Targeting studies were done with radiolabeled antibody (ING1) alone and with antibody−enzyme conjugate (ING1-hCPA1-T268G). CB17 SCID female mice bearing LS174T tumors sc were dosed iv with 10 μg of [^{90}Y]-TMT-ING1. At 24, 48, 72, or 144 h after antibody administration, 100 mg tissue fragments were dissolved in 1 mL of Solvable tissue solubilizer solution (NEN Research Products, Boston, MA) at 55 °C for 48 h, followed by counting in 20 mL of Formula 989 scintillation cocktail (NEN). The second targeting experiment was designed to assay targeted CPA activity in tissues. Swiss nude female mice bearing LS174T tumors sc were dosed iv with 300 μg of ING1-hCPA1-T268G conjugate. At 6, 24, 48, or 72 h following dosing, plasma and tissues were collected and snap-frozen in liquid N_2 and stored at −80 °C. Plasma and tissues were diluted or homogenized in assay buffer and incubated (without centrifugation) in 20 μM MTX-3-cyclopentylTyr for varying times. Reactions were stopped with the addition of perchloric acid, and supernatants were analyzed by HPLC.

In Vivo Therapy Studies. Swiss nu/nu female mice bearing LS174T sc implants were dosed with 300 μg of ING1-hCPA1-T268G. After 24, 48, or 72 h, mice were dosed iv for 5 days with 30 mg/kg MTX-3-cyclopentylTyr. Mice were monitored for tumor regression.

Conjugate Activity (Post-Tumor Injection). Swiss nude female mice bearing LS174T tumors were dosed with 300 μg of ING1-hCPA1-T268G conjugate at three sites directly into the tumor. Mice were then dosed iv with 100 mg/kg MTX-3-cyclopentylTyr 30 min prior to sacrificing at 0.5, 6, 24, 48, or 96 h post-conjugate administration. Plasma and tumor were extracted and frozen in liquid N_2 and stored −80 °C. Samples were processed for prodrug and drug levels as described above.

In Vitro HCPA1 And Hcpa1-T268G Stability Studies. Wild type (hCPA1) and mutant (hCPA1-T268G) enzymes were studied for their stability at 0.1 mg/mL in PBS or human serum. Blood was collected from a healthy, normal volunteer. Serum was generated at room temperature, collected by centrifugation, and stored as aliquots at −70 °C. Enzyme was diluted from 1 mg/mL stocks (in 50 mM Tris, pH 7.4) directly into PBS, or

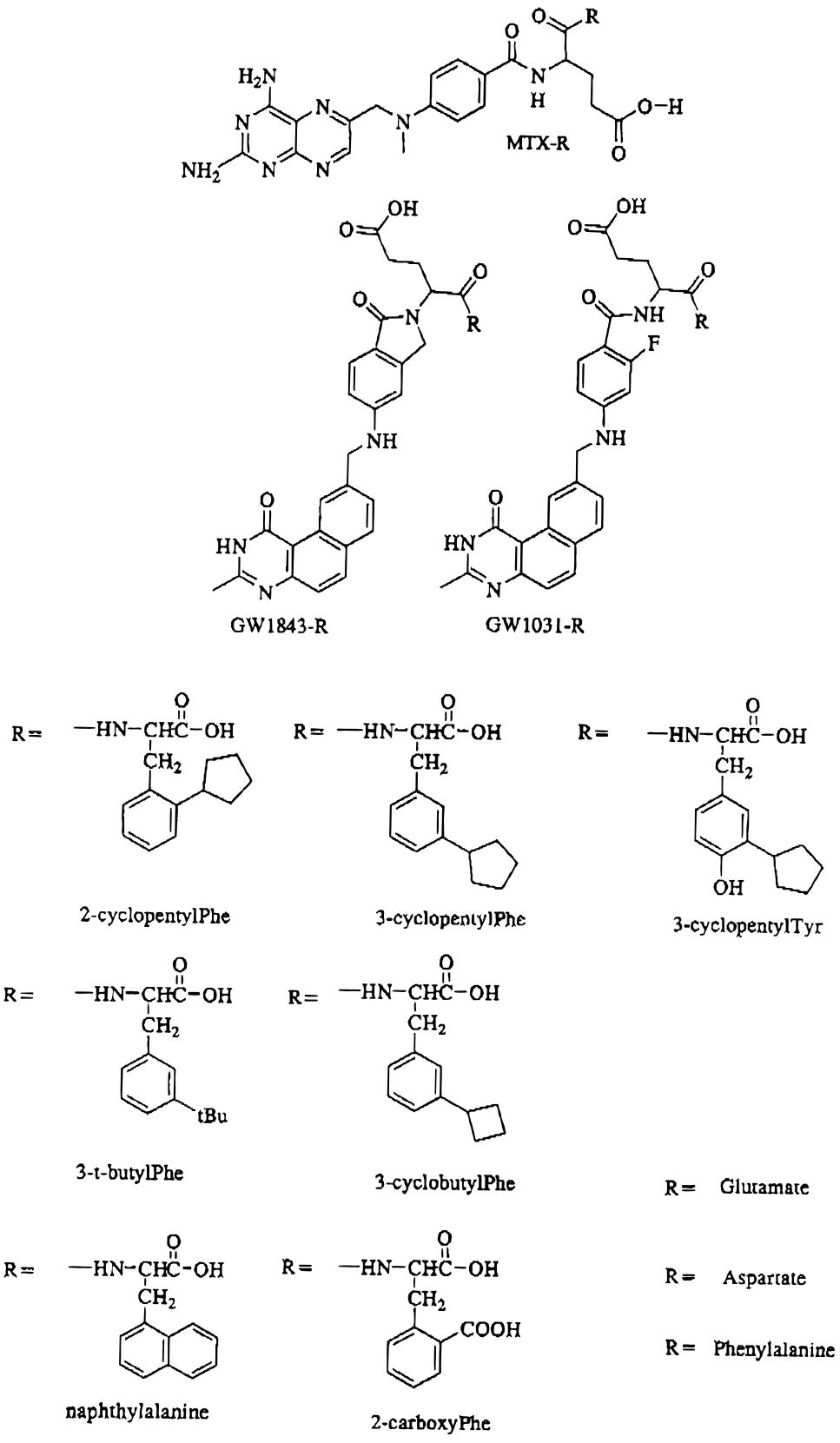


Figure 1. Prodrug structures.

human serum. Samples were then sterile-filtered into sterile screw cap centrifuge tubes for denaturation reactions. Sterility was maintained throughout the experiment. At specified times, samples were removed and assayed for CPA activity with hippurylphenylalanine as described previously (*19*).

RESULTS

Prodrugs under investigation were classified into four catagories (Figure 1 and Table 1). Class I prodrugs have natural, nonpolar amino acids and are substrates for wild-type CPA1. Class II prodrugs have natural, acidic amino acids. Class III prodrugs have nonnatural, bulky,

Table 1. Kinetics of Prodrug Hydrolysis by wt-hCPA1, wt-hCPA2, and hCPA1-T268G Compared to Stability in Human Pancreatic Juice

		k_{cat}/K_m (s^{-1} M^{-1})			
prodrug[a]	class[b]	wt-hCPA1	wt-hCPA2	T268G-hCPA1	pancreatic juice[c]
MTX-Phe	I	441000	89400	7350000	1
GW1031-Phe	I	335000	nd[3]	nd	2
GW1843-Phe	I	690	nd	12600	630
GW1031-Glu	II	120	nd	90	nd
MTX-Glu	II	170	0	120	830
MTX-Asp	II	80	0	60	1410
GW1031-naphthylAla	III	260	nd	171000	5
MTX-naphthylAla	III	1400	1400000	1360000	2
MTX-3-cyclobutylPhe[e]	III	0	260	1800000	2100
MTX-2-cyclopentylPhe	III	200	771	157000	680
MTX-3-cyclopentylPhe	III	0	25	92400	21400
MTX-3-*tert*-butylPhe	III	0	79	384000	4170
MTX-3-cyclopentylTyr	III	0	0	158000	50000
MTX-2-carboxyPhe	IV	3	nd	680	>50000
GW1031-2-carboxyPhe	IV	0.2	nd	180	7500

[a] All data from MTX prodrugs are reproduced from Smith et al. (*19*) and included here for comparison with in vivo data. [b] Class I: prodrugs with natural, nonpolar amino acids (substrates for wild-type CPA1). Class II: prodrugs with natural, acidic amino acids (substrates for wt carboxypeptidase G). Class III: prodrugs with nonnatural, bulky, aromatic amino acids (substrates for larger pocket mutants). Class IV: prodrugs with nonnatural, acidic, aromatic amino acids. [c] Pancreatic juice: numbers represent stability relative to MTX-Phe. [d] nd: not determined. [e] In Phe and Tyr prodrugs, position 2 = ortho and position 3 = meta.

aromatic amino acids and were designed to be substrates for larger-pocket hCPA mutants. Class IV prodrugs have nonnatural, acidic, aromatic amino acids and were designed as substrates for positively charged mutant carboxypeptidases.

Kinetic Assays. k_{cat} and K_m values for prodrugs of MTX were reported previously (*19*). Here, kinetic constants for the prodrugs of GW1031 and GW1843 were measured using wild-type (hCPA1) and mutant human CPA1 (hCPA1-T268G). Values were compared to those of MTX-Phe, a prodrug suggested by Vitols et al. (*26*) to have good potential in ADEPT. An ADEPT prodrug should show resistance to hydrolysis by endogenous enzymes such as wild-type hCPA1 and be easily hydrolyzed by an activating enzyme such as hCPA1-T268G. Therefore, desirable substrates for ADEPT would have much lower k_{cat}/K_m ratios with hCPA1 than that with hCPA1-T268G. In addition, a poor k_{cat}/K_m for hCPA2 also is needed (*19*). Our data (Table 1) indicate that while MTX-Phe demonstrated a extremely high k_{cat}/K_m ratio for hCPA1-T268G, it was also a very good substrate for hCPA1 and hCPA2. GW1031-Phe also had a similarly high k_{cat}/K_m for the wild-type enzyme, but GW1843-Phe was not hydrolyzed by either enzyme as efficiently as the other class I prodrugs. These data indicate that the class I prodrugs MTX-Phe and GW1031-Phe would not likely be good candidates in ADEPT since premature prodrug hydrolysis would likely occur in vivo. The other class I prodrug, GW1843-Phe, and all class II prodrugs tested were poor substrates for either the hCPA1 or the hCPA1-T268G enzyme. This poor hydrolysis with hCPA1-T268G in addition to the lack of specificity for the mutant enzyme over the wild-type enzyme indicates that these compounds are poor substrates in ADEPT with hCPA1-T268G. Class III prodrugs gave kinetic profiles where the k_{cat}/K_m for the mutant enzyme was much better than that observed with the wild-type enzyme. GW1031-naphthylAla, like MTX-naphthylAla reported previously (*19*), is a poor hCPA1 substrate but is an excellent hCPA1-T268G substrate. However, MTX-naphthylAla is an excellent substrate for hCPA2 as well, and therefore would be a poor ADEPT prodrug. With the exception of the naphthylAla prodrugs and MTX-2-cyclopentylPhe, class III prodrugs had no observed turnover of prodrug with hCPA1 (*19*). All class III MTX prodrugs showed some turnover with hCPA2, except MTX-3-cyclopentylTyr. However, observed turnover was modest with the exception of MTX-naphthylAla. The very high k_{cat}/K_m and specificity of class III prodrugs for hCPA1-T268G indicate that class III prodrugs show potential for ADEPT. The kinetic data from class IV prodrugs resembled that of class II prodrugs in that there was poor enzyme activity with both enzymes (*19*). Therefore, class IV prodrugs are not likely candidates for ADEPT with hCPA1-T268G. Based on the kinetic data, the top four prodrugs (all class III) are rank-ordered for stability versus the hCPA enzymes as MTX-3-cyclopentylTyr > MTX-3-cyclopentylPhe > MTX-3-*tert*-butylPhe > MTX-3-cyclobutylPhe.

Pancreatic Fluid Assays. In an attempt to model their in vivo stability, selected prodrugs were analyzed for their stability in activated human pancreatic fluid (*19*). MTX-Phe, a prodrug previously reported in the literature as having potential in ADEPT, was chosen as the prodrug with which others were compared. Higher relative stabilities in pancreatic fluid should correlate to an increase in in vivo prodrug stability. Results (Table 1) from the pancreatic fluid assay correlated fairly well with the kinetic data shown in the same table. Higher relative stability in pancreatic fluid paralleled resistance to hydrolysis by wild-type hCPA1 and hCPA2 in our kinetic assays (*19*). Based on the pancreatic fluid assays, the three best prodrugs are rank-ordered for stability as MTX-3-cyclopentylTyr > MTX-3-cyclopentylPhe > GW1031-2-carboxyPhe. The latter, which belongs to class IV, would not be a good prodrug with T268G. If more weight is given to the pancreatic fluid assay, which should be a better indication of in vivo stability than the kinetic assays, then the data indicate that MTX-3-cyclopentylTyr > MTX-3-cyclopentylPhe > MTX-3-cyclobutylPhe, MTX-3-*tert*-butylPhe. If a correlation of the pancreatic juice stability and the in vivo stability could be found, it would point to the former as a useful primary screen for in vivo stability of compounds. In vivo experiments were conducted to test this.

In Vivo Stability and Biodistribution. Fourteen prodrugs were examined for their stability (Table 2) and biodistribution in mice (Table 3). The compound suggested by Vitols et al. (MTX-Phe) showed poor stability

Table 2. In Vivo Prodrug Stability (% of Prodrug to Prodrug + Drug)[a]

Prodrug[b]	time (h)	plasma	liver	kidney	Lg. Int[c]	SIP[d]	spleen	cecum	feces	tumor[e]
MTX-Phe	0.5	31	95	100	65	17	81			65
	2	3	8	nd[f]	22	0	nd			nd
GW1031-Phe	0.5	80	45	75	67		39			63
GW1843-Phe	0.5	100				91				
	2	93				47				
GW1031-Glu	0.5	99	98	98	93	83	100			96
	2	100	97	97	100	68	100			76
MTX-Asp	0.5	100	97	98	100	86	70	63	21	82
	2	100	93	98	65	54	0	48	52	59
GW1031-naphthylAla	0.5	93	87	89	94	10	100			
	2	48	90	74	87	1	100			
MTX-naphthylAla	0.5	66	59			2				
	2	nd	nd			0				
MTX-2-cyclopentylPhe	0.5	95	90	84	93	77	98	75	71	
	2	90	76	81	57	35	100	56	55	
MTX-3-cyclobutylPhe	0.5	97	81	83	74	87	96	100	92	100
	2	nd	73	82	85	68	nd	100	68	88
MTX-3-cyclopentylPhe	0.5	100	83	100	100	97	100	100	97	
	2	nd	94	100	100	93	nd	99	94	
MTX-3-*tert*-butylPhe	0.5	100	91	53	nd	91	nd	100		
	2	100	89	22	67	67	nd	81		
MTX-3-cyclopentylTyr	0.5	100	100	100	100	100	100	100	100	
	2	100	100	100	100	100	100	100	100	
MTX-2-carboxyPhe	0.5	100	100	100	100	100	100			100
	2	100	89	100	100	97	100			100
GW1031-2-carboxyPhe	0.5	100	99	100	100	99	99			100
	2	99	98	99	100	98	nd			100

[a] CD-1 nu/nu female mice were dosed ip or iv with 50 mg/kg of prodrug. After 0.5 or 2 h, plasma and tissues were removed. Plasma was frozen at −70 °C, and tissues were snap-frozen in liquid N_2, and stored at −70 °C. Samples were diluted or homogenized in 0.1 N HCl. Prodrug and drug were extracted in acetonitrile, and supernatants were analyzed by HPLC as a percentage of prodrug to prodrug + drug. [b] Prodrug: MTX-Asp, MTX-2-cyclopentylPhe, MTX-3-cyclobutylPhe, MTX-3-cyclopentylPhe, MTX-3-*tert*-butylPhe, and MTX-3-cyclopentylTyr dosed iv; all others dosed ip. [c] Lg.Int: large intestine. [d] SIP: small intestine and pancreas. [e] Tumor: LS174T for MTX-3-cyclobutylPhe; WiDr for MTX-Phe; GW1031-Phe, GW1031-Glu, and Wein-133 for all others. [f] nd = no drug or prodrug detected.

Table 3. In Vivo Prodrug Biodistribution (nmol of Prodrug/g of Tissue)[a]

prodrug[b]	time (h)	plasma	liver	kidney	Lg.Int[c]	SIP[d]	spleen	cecum	feces	tumor[e]
MTX	0.5	13.7	634.5	15.2	6.8	199.8	0	11.7	554.7	
	2	0.6	29.0	8.5	55.0	87.2	0	255.9	1380.0	
MTX-Phe	0.5	17.8	335.1	26.9	19.3	17.3	19.9			3.0
	2	1.1	0.6	0	1.1	nd[f]	nd			nd
GW1031-Phe	0.5	32.0	79.7	6.7	17.9		7.8			2.6
GW1843-Phe	0.5	22.1				170.2				
	2	0.3				17.6				
GW1031-Glu	0.5	41.5	770.3	175.8	12.2	48.2	23.4			6.0
	2	4.2	579.8	70.3	1.0	55.6	1.8			1.2
MTX-Asp	0.5	46.7	287.8	93.4	5.7	21.3	3.4	8.5	4.2	7.5
	2	2.0	161.6	12.6	19.4	14.2	0	35.8	207.0	0.8
GW1031-naphthylAla	0.5	32.4	135.3	29.2	14.9	27.7	30.9			
	2	2.8	371.2	4.0	1.1	1.8	1.5			
MTX-naphthylAla	0.5	8.0	49.8			7.5				
	2	nd	nd			nd				
MTX-2-cyclopentylPhe	0.5	28.5	113.5	5.6	5.2	364.5	1.4	6.8	150.2	
	2	1.1	43.9	3.2	27.3	31.7	1.1	235.1	646.2	
MTX-3-cyclobutylPhe	0.5	22.2	53.8	7.3	2.7	301.3	2.7	4.5	426.8	4.8
	2	nd	47.8	3.0	4.4	140.0	nd	0.8	389.8	2.4
MTX-3-cyclopentylPhe	0.5	1.1	54.3	6.8	2.6	377.9	8.4	4.1	1104.0	
	2	nd	126.2	1.3	6.2	211.0	nd	108.3	1506.0	
MTX-3-*tert*-butylPhe	0.5	2.6	58.6	2.2	nd	550.8	nd	16.3	880.0	
	2	0.7	39.5	0.2	14.7	44.9	nd	402.3	1226.0	
MTX-3-cyclopentylTyr	0.5	3.3	47.7	3.7	7.9	373.8	0.6	14.4	665.9	
	2	0.6	110.1	0.5	12.5	322.2	0.2	4.8	738.4	
MTX-2-carboxyPhe	0.5	51.4	171.9	55.4	12.1	127.4	12.4			6.9
	2	0.2	7.5	3.8	91.8	24.1	1.0			1.5
GW1031-2-carboxyPhe	0.5	71.4	343.4	94.5	25.3	188.1	30.9			6.7
	2	1.4	33.3	14.5	45.4	69.1	nd			1.3

[a] Mice were dosed and samples processed as described in Table 2. Plasma and tissue prodrug levels were determined. Values are in nmol/g for tissue and μM for plasma. [b] Prodrug:MTX, MTX-Asp, MTX-2-cyclopentylPhe, MTX-3-cyclobutylPhe, MTX-3-cyclopentylPhe, MTX-3-*tert*-butylPhe, and MTX-3-cyclopentylTyr dosed iv; all others dosed ip. [c] Lg.Int: large intestine. [d] SIP: small intestine and pancreas. [e] Tumor: LS174T for MTX-3-cyclobutylPhe; WiDr for MTX-Phe; GW1031-Phe, GW1031-Glu, and Wein-133 for all others. [f] nd = no drug or prodrug detected.

in vivo, as expected, based on the kinetic and pancreatic fluid assay data. MTX-Phe was completely converted to drug in the small intestine and pancreas by 2 h (*19*). One other class I prodrug, GW1031-Phe, was similarly unstable, and the other, GW1843-Phe, was somewhat more stable than MTX-Phe in vivo, consistent with their CPA

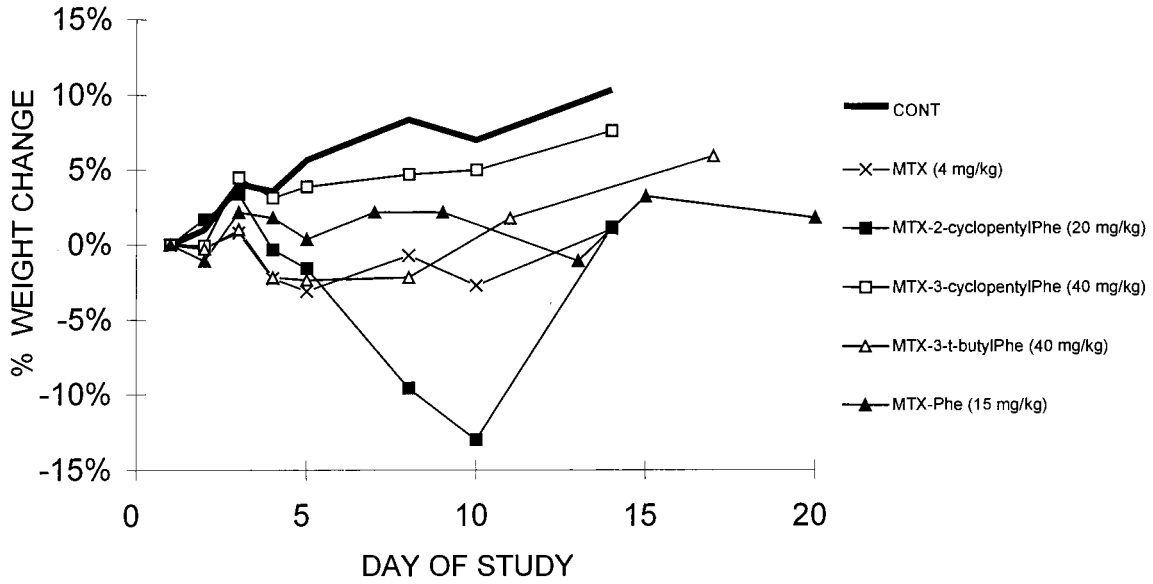


Figure 2. Toxicity of MTX and prodrugs in CD-1 nu/nu mice. CD-1 nu/nu female mice were dosed iv for 5 days with varying concentrations of MTX or selected class III prodrugs. A prodrug was deemed toxic if a 15% weight loss occurred. Doses shown for MTX and MTX-2-cyclopentylPhe were at the limit of toxicity. Doses for MTX-3-cyclopentylPhe and MTX-3-*tert*-butylPhe were the highest doses tested. Data are represented as percent weight change as a function of time.

substrate activity and pancreatic fluid stability. The two prodrugs tested in vivo from class II, GW1031-Glu and MTX-Asp, were more stable, again consistent with their stability from hCPA1 hydrolysis. Hydrolysis of these compounds was observed, however, particularly in tissues taken from the gut, where concentrations of CPA are the highest. Class III prodrugs generally gave better in vivo stability results than class I and class II. The exception was MTX-naphthylAla which is a substrate for wild-type hCPA2 and gave a profile similar to those of class I. The rest of the class III prodrugs are rank-ordered for stability as MTX-3-cyclopentylTyr > MTX-3-cyclopentylPhe > MTX-3-cyclobutylPhe > MTX-3-*tert*-butylPhe > MTX-2-cyclopentylPhe. Class IV prodrugs had similar stability profiles to MTX-3-cyclopentylTyr, the most stable class III prodrug. The biodistributions of class I, class II, and class IV prodrugs and the naphthylAla class III prodrugs indicate that the liver is the primary site of initial prodrug accumulation. The other class III prodrugs were found more in the small intestine and pancreas than the liver at the earliest time point tested. In all studies where feces were analyzed, the prodrug concentration in the feces after 2 h was higher than any tissue studied. This generally was the case after 30 min as well. All prodrug classes demonstrated rapid plasma clearance. This rapid biliary excretion was similar to that observed for MTX (*27*). Based upon kinetic data, pancreatic juice assays, and the in vivo stability and biodistribution results in mice, five prodrugs (MTX-Phe, MTX-2-cyclopentylPhe, MTX-3-cyclopentylPhe, MTX-3-*tert*-butylPhe, and MTX-3-cyclopentylTyr) were selected for mouse toxicity studies and compared to MTX.

Toxicity of MTX and Prodrugs in Mice. Selected prodrugs were evaluated in vivo for toxicity and compared to MTX (Figures 2 and 3). Toxicity was defined as death and/or a greater than 15% weight loss. In Figure 2, doses shown for MTX (4 mg/kg), MTX-Phe (15 mg/kg), and MTX-2-cyclopentylPhe (20 mg/kg) were at the limit of toxicity, and consistent with this, each produced a significant delay in weight increase at this dose. MTX-Phe resulted in 4 of 4 deaths at the dose above this limit (45 mg/kg). Doses for MTX-3-cyclopentylPhe (40 mg/kg) and MTX-3-*tert*-butylPhe (40 mg/kg) were the highest

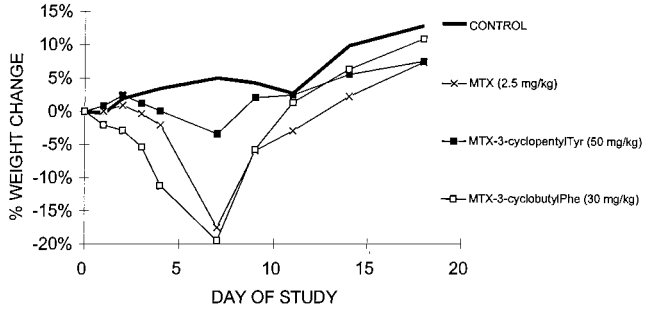


Figure 3. Toxicity of MTX and prodrugs in Swiss nude mice. Swiss nude female mice were dosed as described in Figure 2. The dose shown for MTX-3-cyclopentylTyr was the highest dose tested. The dose for MTX-3-cyclobutylPhe was the lowest dose tested and resulted in 2 of 3 deaths. The dose for MTX was the highest dose tested without toxicity. Data are represented as described in Figure 2.

doses tested; the latter compound produced a delay in weight increase. In Figure 3, the dose shown for MTX-3-cyclobutylPhe (30 mg/kg) was the lowest dose tested and resulted in 2 of 3 deaths. The dose for MTX (2.5 mg/kg) was the highest dose tested without toxicity. The dose for MTX-3-cyclopentylTyr (50 mg/kg) was the highest dose tested and had no toxicity. The data indicate that the in vivo stable prodrugs MTX-3-cyclopentylPhe, MTX-3-*tert*-butylPhe, and MTX-3-cyclopentylTyr could be safely dosed at 10−20 times the MTX maximum tolerated dose while the less stable prodrugs MTX-Phe, MTX-2-cyclopentylPhe, and MTX-3-cyclobutylPhe were toxic. These unstable and toxic prodrugs therefore would be less useful ADEPT prodrugs.

In Vivo Targeting Studies. Targeting studies were done to determine if an antibody−enzyme conjugate, ING1-hCPA1-T268G, which targets Ep-CAM-1 (*28*) on LS174T tumors, could be shown to target the tumor in vivo and if the enzyme moiety of the conjugate retained its catalytic activity in vivo. Desired results would be an accumulation of antibody−enzyme conjugate only at the tumor with a concurrent drop of plasma levels of conjugate. In vivo targeting studies were first done with ^{90}Y-labeled antibody to verify that ING1 targets LS174T. The data indicated that dosing with 10 μg of ING1 does target

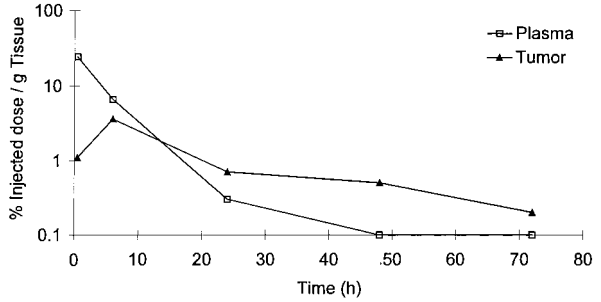


Figure 4. In vivo targeting of ING1-hCPA1-T268G in mice. Swiss nude female mice bearing LS174T tumors sc were dosed iv with 300 μg of ING1-hCPA1-T268G conjugate. At 6, 24, 48, or 72 h following dosing, plasma and tissues were collected and snap-frozen in liquid N_2 and stored −80 °C. Plasma and tissues were diluted or homogenized in assay buffer and incubated (without centrifugation) in 20 μM MTX-3-cyclopentylTyr for varying times. Reactions were stopped with the addition of perchloric acid, and supernatants were analyzed by HPLC. Data are reported as % injected dose/g of tissue as a function of time.

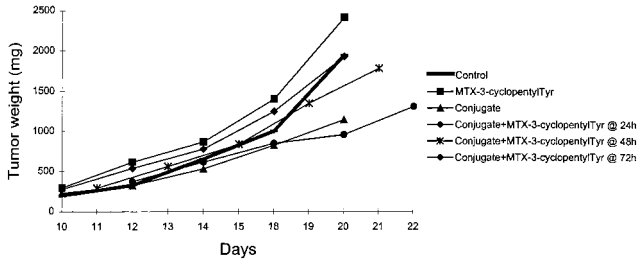


Figure 5. In vivo therapy study. Swiss nu/nu female mice bearing LS174T sc implants were dosed with 300 μg of ING1-hCPA1-T268G. After 24, 48, or 72 h, mice were dosed iv for 5 days with 30 mg/kg MTX-3-cyclopentylTyr. Mice were monitored for tumor growth using electronic caliper measurements.

LS174T with levels approaching 30% ID/g of tissue at 48 h while antibody levels in the liver were only 7% (data not shown). All other tissues studied (plasma, kidney, bone, and spleen) had less accumulation of antibody than tumor. Tumor-to-blood ratios were 1.0, 1.9, 4.4, and 19.6 at 24 h, 48 h, 72 h, and 144 h, respectively. Thus, ING1 targeted tumor and was cleared from circulation. A second targeting study was then performed by dosing with 300 μg of the ING1-hCPA1-T268G antibody−enzyme conjugate. Targeting studies with ING1-hCPA1-T268G (Figure 4) gave tumor-to-blood ratios of 2.7 at 24 h. As expected, conjugate levels in the blood dropped rapidly while levels in the tumor showed a much slower rate of decrease. The level of active conjugate found in tumor was approximately 1% ID/g of tissue. These data were encouraging, and an in vivo therapy study was designed.

In Vivo Therapy Study. An in vivo therapy study in Swiss nude mice bearing LS174T was performed using a single 300 μg dose of ING1-hCPA1-T268G followed by five daily doses of 30 mg/kg MTX-3-cyclopentylTyr. Prodrug dosing was commenced at 24, 48, or 72 h post-conjugate dose. Mice were monitored for tumor growth inhibition and compared to untreated mice. Results (Figure 5) indicate that under these conditions, the ADEPT was not efficacious.

Conjugate Activity (Post-Tumor Injection). In an attempt to determine why the therapy studied failed, the activity of ING1-hCPA1-T268G conjugate was studied as a function of time after direct injection into LS174T tumors. In this experiment, conjugate was injected into the tumor. Then immediately or 6, 24, 48, or 96 h later MTX-3-cyclopentylTyr was dosed systemically as in the therapy experiment. After another 30 min, animals were killed, and MTX and MTX-3-cyclopentylTyr levels were determined in tumor and plasma as described in the in vivo drug stability section. This protocol allowed determination of hCPA1-T268G activity. The results (Table 4) show absolute levels of these compounds as well as the inferred percent conversion of prodrug to drug at that site. It can be seen that prodrug was found in both the tumor and plasma at all time points. In addition, drug (MTX) was also found in the tumors at the early time points. The targeted enzyme converted 42.9, 30.1, and 0% of MTX-3-cyclopentylTyr to MTX at 0.5, 6, and 24 h, respectively. No MTX was found in the plasma at any time point. This indicates that the MTX found in the tumors was generated exclusively via the tumor-localized enzyme. In addition, since MTX was not found in tumors from (control) animals that were not dosed with conjugate, the prodrug was synthesized specifically by the targeted enzyme. This experiment then clearly shows that active enzyme was localized to the tumor by the ING1-hCPA1-T268G conjugate, and the activity was capable of producing MTX in situ. However, enzyme activity targeted to the tumor was lost by 24 h. Therefore, the result explains the lack of response in the in vivo therapy study since the earliest prodrug was dosed for therapy 24 h after conjugate administration. By then, conjugate activity would of been lost.

Table 4. Activity of ING1-T268G-CPA1 after Direct Injection into LS174T Tumors (% Conversion of MTX-3-cyclopentylTyr)[a]

time[b] (h)	plasma [MTX][c]	plasma [prodrug]	plasma % conv	tumor [MTX]	tumor [prodrug]	tumor % conv
CTL[d]	0	18.6	0	0	5.2	0
0.5	0	18.5	0	2.2	2.8	44.0
6	0	25.9	0	2.0	5.0	28.6
24	0	5.83	0	0	9.6	0
48	0	23.2	0	0	7.7	0
96	0	24.3	0	0	9.8	0

[a] Swiss nude female mice bearing LS174T tumors were dosed with 300 μg of ING1-hCPA1-T268G conjugate at 3 sites directly into the tumor. Mice were then dosed iv with 100 mg/kg MTX-3-cyclopentylTyr at 0.5, 6, 24, 48, or 96 h post-conjugate administration. Mice were sacrificed 30 min following prodrug administration. Plasma and tumor were extracted and snap-frozen in liquid N_2 and stored at −80 °C. Samples were processed and analyzed by HPLC for prodrug concentration and stability (% conversion of MTX-3-cyclopentylTyr). [b] Time: time between conjugate dose and tissue extraction. [c] Concentration in μM (plasma) or nmol/g of tissue (tumor). [d] CTL: no conjugate control.

In Vitro Conjugate Stability Studies. We have reported that hCPA1-T268G is relatively stable at 37 °C (*19*). Therefore the complete loss of activity by 24 h was surprising. One possible explanation for the loss of conjugate activity in the therapy study is that serum factors may inactivate the enzyme. To test this, an in vitro 37 °C stability study was performed on both hCPA1 and hCPA1-T268G in PBS and in human serum. Results in Figure 6 show that, as we reported previously, the half-life for the wt hCPA1 was significantly longer in PBS than was that of hCPA1-T268G. This loss of stability upon mutation may derive from the destabilizing effect that cavity-creating mutations can produce (*29*). Surprisingly, however, the half-life of hCPA1 was reduced dramatically from 140 h in PBS to ∼24 h in human serum. The half-life of the hCPA1-T268G was also reduced by human serum, but not as dramatically, from 24 to ∼15 h. This inactivation of the enzyme in human serum resulted in 70% loss of hCPA1-T268G activity by 24 h and 90% loss of activity by 72 h. Thus, serum factors do inactivate the enzyme and can probably account for

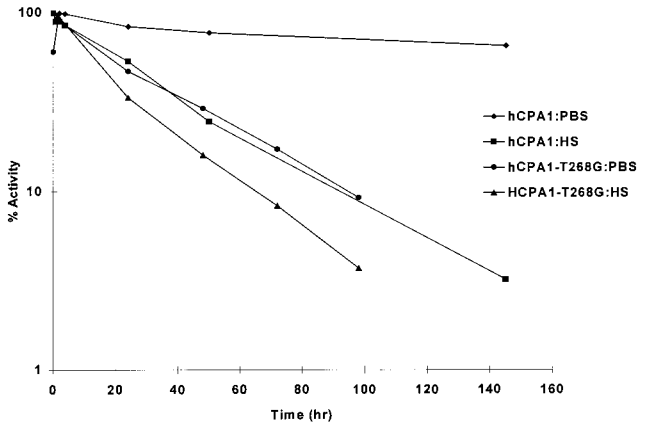


Figure 6. Stability of hCPA1 and hCPA1-T268G at 37 °C in vitro in PBS or human serum (HS). Wild-type (hCPA1) and mutant (hCPA1-T268G) enzymes were studied for their stability at 0.1 mg/mL in PBS or human serum. Enzyme was diluted directly into PBS or human serum. At specified times, samples were removed and assayed for CPA activity with hippurylphenylalanine. Data are shown as percent enzyme activity as a function of time.

some of the activity loss in vivo. However, since 30% activity remained at 24 h, the serum denaturation studies may not account for loss of all detectable activity in vivo at the tumor by 24 h. The stability of the enzyme under in vivo relevant conditions clearly warrants further study.

DISCUSSION

Our approach to ADEPT is to overcome the problem of enzyme selectivity vs immunogenicity by mutating a human enzyme to provide it with a nonendogenous activity, thereby minimizing immunogenicity and maximizing selectivity. The objectives of the current study were to examine the stability of four classes of prodrugs which would be suitable substrates for the novel mutant human enzyme hCPA1-T268G but would not be substrates for the wild-type hCPA1. The short-term biodistribution of these prodrugs was also determined in this effort. Selected prodrugs were then evaluated in vivo for their toxicity, elimination, and pharmacokinetic profiles. Finally targeting studies were done with antibody and antibody−enzyme conjugate in preparation for an in vivo therapy study.

Three assays were developed to examine prodrug stability. For a primary screen, kinetic assays were performed to generate k_{cat} and K_m values. The in vivo stabilities of prodrugs were then determined in mice. Compounds with both high and low k_{cat}/K_m ratios were studied in vivo to demonstrate a correlation between the kinetic and in vivo data. A third assay, human pancreatic fluid stability, was later developed as a simpler and perhaps more relevant reflection of prodrug stability in humans. This last assay was eventually used as a secondary screen prior to the more time-consuming in vivo study. Promising MTX prodrugs were dosed in mice up to 20 times the MTD of MTX to determine if a MTD of prodrug could be obtained. Targeting studies were done to demonstrate that our antibody was selective by targeting tumor better than normal tissue and that our antibody−enzyme conjugate was both selective and active. Finally, an in vivo therapy study was done.

The data indicate that we were able to generate very stable prodrugs of both the DHFR inhibitor MTX and the TS inhibitor GW1031 (MTX-3-cyclopentylTyr, MTX-carboxyPhe, GW1031-2-carboxyPhe, and MTX-3-cyclopentylPhe). The pancreatic fluid and in vivo screens produced the same trends for stability. It was expected that the stability of prodrugs in vivo or in pancreatic fluid would be predicted from the k_{cat}/K_m for the prodrug with hCPA1 and hCPA2. Generally, the hCPA1 kinetics alone were enough to predict in vivo and pancreatic fluid stabilities. The naphthylalanyl prodrugs of GW1031 and MTX, however, were much less stable in both the in vivo and pancreatic fluid assays than predicted from the kinetic data of hCPA1 alone. The lack of stability of these compounds in vivo, particularly in the small intestine and pancreas, seemed to suggest the presence of carboxypeptidases other than CPA1 in both mice and humans. Another CPA, CPA2, has been identified in rat (*30*) and human (*31*) but has yet to be reported in the cow (*32*). This enzyme prefers bulkier amino acids than CPA1. Indeed, we have shown previously that the MTX-naphthylalanine prodrug is hydrolyzed 1000 times more efficiently by hCPA2 than hCPA1 (*19*, *31*). We assume that CPA2 is the activity in mice and human pancreatic juice responsible for the hydrolysis of the naphthylalanyl prodrugs of GW1031 and MTX (*19*), and when it was included in the analysis, the stabilities of all compounds in vivo or in pancreatic fluid were readily predicted (*19*).

The highest in vivo stability, along with high hCPA1-T268G activity, was observed with the nonnatural, bulky, aromatic amino acid prodrug MTX-3-cyclopentylTyr, a class III prodrug. With the exception of the naphthylalanyl prodrugs as discussed above, this class in general showed the most promise for ADEPT with good in vivo stability and high hCPA1-T268G activity. Prodrugs of class IV, those with a nonnatural, acidic, aromatic amino acid substituent, and which were designed as substrates for mutant carboxypeptidases with positively charged active sites, also showed excellent in vivo stability. These compounds were, however, not good substrates for hCPA1-T268G, and efforts to produce an enzyme with an active site positive charge have thus far been unsuccessful (Table 1 and ref *19*). Nonetheless, their in vivo properties make them of continued interest. Compounds of class II, those prodrugs with an aspartate or glutamate substituent, were less stable in vivo, but considerably more stable than those of class I. As such they too may have utility if an appropriate enzyme can be produced. Finally, compounds of class I, those with a natural, nonpolar amino acid attached and which are substrates for wild-type CPA1, had low stability in vivo. These compounds would appear to have the lowest probable utility for ADEPT.

It is possible that semistable prodrugs could be used in ADEPT. Obviously, very stable prodrugs such as MTX-3-cyclopentylTyr would be best; however, prodrugs with partial degradation may still be useful if systemic toxicity can be avoided. For example, Senter et al. (*14*) using an alkaline phosphatase catalyzed system observed better antitumor activity with etoposide phosphate than etoposide, even though they observed prodrug hydrolysis in the absence of antibody−enzyme conjugate. In our case, the maximum tolerated dose of stable and semistable methotrexate prodrugs in mice was determined to ascertain how much endogenous degradation would be acceptable. Toxicity studies indicated that stable prodrugs such as MTX-3-cyclopentylTyr, MTX-3-cyclopentylPhe, and MTX-3-*tert*-butylPhe could be dosed at least 10−20 times the maximum tolerated dose of MTX. Semistable prodrugs such as MTX-2-cyclopentylPhe, as expected, were more toxic than our most stable prodrugs but less toxic than MTX alone.

Vitols et al. (*33*) reported the class I prodrug metho-

trexate-phenylalanine and showed in vitro that UCLA-P3 growth inhibition (ID_{50} values) of the prodrug in the presence of their CPA−mAb conjugate approached that of methotrexate. From these data, they inferred that methotrexate-phenylalanine would be an optimal ADEPT prodrug. However, our data indicate that class I prodrugs including methotrexate-phenylalanine are highly susceptible to in vivo degradation by endogenous enzymes, like CPA, and that using class I prodrugs designed for these enzymes would give unsatisfactory results. It is worthy of note, though, that although MTX-Phe was rapidly hydolyzed in vivo and as a result more toxic than the more in vivo stable prodrugs, its toxicity was still less than that of MTX, which may provide it some utility in ADEPT with hCPA1 or hCPA1-T268G.

Pharmacokinetic analysis showed that for all compounds, prodrug levels decreased rapidly in the plasma between 30 min and 2 h and followed this trend in almost all the tissues studied. The exceptions to this trend can probably be attributed to the variations typically seen between animals. Initial prodrug levels were high in the liver. This might be expected since the liver functions as a drug detoxification organ. The rapid biliary excretions of MTX and MTX prodrugs are responsible for the high prodrug levels in feces and small intestine and pancreas. This rapid excretion may be species-specific since the principle route of MTX clearance in humans is via the urine (*27*). The levels of prodrug found in tumor, while low, are consistent with the levels of methotrexate found in murine leukemias following ip dosage with the maximum tolerated dose of 3 mg/kg of methotrexate (*34*).

Metabolic cage studies were employed to monitor biliary excretion of class III prodrugs (data not shown). These studies indicated that class III prodrugs exhibit rapid fecal excretion with a small percentage of prodrug found in the urine. This fecal excretion is consistent with that of MTX (*27*).

We have previously demonstrated that ADEPT using a mutated human enzyme and novel prodrugs works in cell culture (*19*). In that study, HT-29 cells were exposed to varying levels of antibody−enzyme conjugate followed by varying concentrations of MTX-3-cyclopentylTyr. IC_{50}'s were determined and compared to MTX alone. The data demonstrated the efficacy of this variation on ADEPT in vitro. The current work extends those data further by including targeting studies and an in vivo therapy study.

ING1, an antibody that recognizes an epitope on Ep-CAM1 (*28*) on human colorectal carcinomas, was dosed into mice to determine antibody specificity. Data indicated a time-dependent drop in percent ID in all tissues studied. After plasma clearance, the levels were highest in the tumor, followed by spleen, liver, kidney, and bone. At 144 h, the latest time point tested, the tumor-to-blood ratio was 19. The in vivo targeting of the antibody−enzyme conjugate also showed an encouraging tumor-to-plasma ratio. At 24 h, a ratio of 2.7 was observed with ~1% ID/g of tumor found.

A possible explanation for the lack of a tumor response in vivo to therapy was instability of the conjugate. To test this hypothesis, a study was set up where conjugate was directly injected into the tumor, followed by a bolus dose of MTX-3-cyclopentylTyr. Then enzyme activity as a function of time postinjection was determined by monitoring percent prodrug hydrolysis 30 min after each prodrug injection time. The data suggested that the conjugate does suffer a time-dependent drop in activity in vivo. While there was in vivo enzyme activity present at up to 6 h post-conjugate injection, there was no detectable activity in vivo 24 h after injection. This explains the lack of antitumor activity in the in vivo therapy study since the earliest prodrug was dosed 24 h after conjugate administration. As shown in Figure 6, both wt- and T268G-hCPA1 were inactivated by human serum. Thus, a partial explanation for the loss of conjugate activity in vivo is inactivation by serum elements. (Preliminary experiments indicate that 5 mM mercaptoethanolamine in PBS can also accelerate denaturation of both wt- and T268G-hCPA1, resulting in loss of 50 and 75% activity by 18 h, respectively, which suggests that the serum factors may include thiols.) However, there appear to be additional features as well since at 37 °C in human serum, 30% of T268G-hCPA1 remained at 24 h and 10% remained at 72 h. Continued studies of this enzyme and its properties are warranted to enhance this promising approach to ADEPT. Further study using a different tumor model also may aid in determining if ADEPT works in vivo. In the current study, the human colon adenocarcinoma cell line LS174T was chosen based on the targeting ability of our ING1 antibody to it. Previous studies indicate that MTX, at nontoxic doses, only delays growth of LS174T tumors. Since one of the goals of ADEPT is to avoid the systemic toxicity seen during therapy while maintaining or improving efficacy, studies using a tumor model that responds better to MTX would help in determining the utility of ADEPT.

The development of mAbs represents an additional mode of cancer therapy and has led to the emergence of ADEPT. The novel approach we have taken, in which a mutant human enzyme is used for the conversion of stable prodrugs to their toxic form, appears to offer a high potential of success. This approach addresses two of the hurdles facing ADEPT. The use of a human enzyme should minimize the immunogenicity. The active site mutation will allow for the development of an exogenous enzymatic activity allowing for increased prodrug stability. The development of an antibody with better specificity in combination with a more stable antibody−enzyme conjugate would be beneficial and should give better antitumor results with MTX prodrugs in mice. Antitumor studies in mice using the other two antifolates, GW1031 and GW1843, are difficult because they exert their effect by inhibiting thymidylate synthase. This inhibition cannot take place in the presence of high circulating thymidine levels as observed in mice (*35*). For this reason, mouse antitumor studies were not done with prodrugs of these two antifolates.

LITERATURE CITED

(1) Zubrod, C. G. (1982) Principles of chemotherapy. in *Cancer Medicine* (Holland, J. F., and Frei, E., Eds.) pp 627−632, Lea & Febiger, Philadelphia.

(2) Mihich, E., and Creaven, P. J. (1982) Principles of pharmacology and toxicology. in *Cancer Medicine* (Holland, J. F., and Frei, E., Eds.) pp 685−715, Lea & Febiger, Philadelphia.

(3) Hellstrom, K. E., Hellstrom, I., and Goodman, G. E. (1987) Antibodies for drug delivery. in *Controlled Drug Delivery, Fundamentals and Applications* (Robinson, J. R., and Lee, V. H. L., Eds.) 2nd ed., pp 623−653, Marcel Dekker, New York.

(4) Smyth, M. J., Pietersz, G. A., Classon, B. J., and McKenzie, I. F. C. (1986) Specific targeting of chlorambucil to tumors with the use of monoclonal antibodies. *J. Natl. Cancer Inst. 76*(3), 503−510.

(5) Senter, P. D. (1990) Activation of prodrugs by antibody−enzyme conjugates: a new approach to cancer therapy. *FASEB J. 4*, 188−193.

(6) Bagshawe, K. D., Springer, C. J., Searle, F., Antoniw, P., Sharma, S. K., Melton, R. G., and Sherwood, R. F. (1988) A

cytotoxic agent can be generated selectively at cancer sites. *Br. J. Cancer 58*, 700−703.
(7) Bagshawe, K. D. (1989) Towards generating cytotoxic agents at cancer sites. *Br. J. Cancer 60*, 275−281.
(8) Hellstrom, K. E., and Senter, P. D. (1991) Activation of prodrugs by targeted enzymes. *Eur. J. Cancer 27*(11), 1342−1343.
(9) Philpott, G. W., Bower, R. J., Parker, K. L., Shearer, W. T., and Parker, C. W. (1974) Affinity cytotoxicity of tumor cells with antibody−glucose oxidase conjugates, peroxidase, and arsphenamine. *Cancer Res. 34*, 2159−2164.
(10) Philpott, G. W., Bower, R. J., and Parker, C. (1973) Selective iodination and cytotoxicity of tumor cells with an antibody−enzyme conjugate. *Surgery (St. Louis) 74*(1), 51−58.
(11) Senter, P. D., Wallace, P. M., Svensson, H. P., Kerr, D. E., Hellstrom, I., and Hellstrom, K. E. (1991) Activation of prodrugs by antibody−enzyme conjugates. in *Immunobiology of proteins and peptides VI* (Atassi, M. Z., Ed.) pp 97−105, Plenum Press, New York.
(12) Wallace, P. M., and Senter, P. D. (1991) In vitro and in vivo activities of monoclonal antibody−alkaline phosphatase conjugates in combination with phenol mustard phosphate. *Bioconjugate Chem. 2*(5), 349−352.
(13) Haisma, H. J., Boven, E., van Muijen, M., De Vries, R., and Pinedo, H. M. (1992) Analysis of a conjugate between anti-carcinoembryonic antigen monoclonal antibody and alkaline phosphatase for specific activation of the prodrug etoposide phosphate. *Cancer Immunol. Immunother. 34*, 343−348.
(14) Senter, P. D., Schreiber, G. J., Hirschberg, D. L., Ashe, S. A., Hellstrom, K. E., and Hellstrom, I. (1989) Enhancement of the in vitro and in vivo antitumor activities of phosphorylated mitomycin C and etoposide derivatives by monoclonal antibody−alkaline phosphatase conjugates. *Cancer Res. 49*, 5789−5792.
(15) Senter, P. D., Saulnier, M. G., Schreiber, G. J., Hirschberg, D. L., Brown, J. P., Hellstrom, I., and Hellstrom, K. E., (1988) Anti-tumor effects of antibody−alkaline phosphatase conjugates in combination with etoposide phosphate. *Proc. Natl. Acad. Sci. U.S.A. 85*, 4842−4846.
(16) Haenseler, E., Esswein, A., Vitols, K. S., Montejano, Y., Mueller, B. M., Reisfeld, R. A., and Huennekens, F. M. (1992) Activation of methotrexate-α-alanine by carboxypeptidase A−monoclonal antibody conjugate. *Biochemistry 31*, 891−897.
(17) Senter, P. D., Su, P. C. D., Katsuragi, T., Sakai, T., Cosand, W. L., Hellstrom, I., and Hellstrom, K. E., (1991) Generation of 5-fluorouracil from 5-fluorocytosine by monoclonal antibody−cytosine deaminase conjugates. *Bioconjugate Chem. 2*, 447−451.
(18) Springer, C. J., Bagshawe, K. D., Sharma, S. K., Searle, F., Boden, J., Antoniw, P., et al. (1991) Ablation of human choriocarcinoma xenografts in nude mice by antibody-directed enzyme prodrug therapy (ADEPT) with three novel compounds. *Eur. J. Cancer 27*(11), 1361−1366.
(19) Smith, G. K., Banks, S., Blumenkopf, T. A., Cory, M., Humphreys, J., Laethem, R. M., Miller, J., Moxham, C. P., Mullin, R., Ray, P. H., Walton, L. M., and Wolfe, L. A. (1997) Toward Antibody-directed enzyme prodrug therapy with the T268G mutant of human carboxypeptidase A1 and novel in vivo stable prodrugs of MTX. *J. Biol. Chem. 272*(25), 15804−15816.
(20) Pendergast, W., Dickeerson, S. H., Dev, I. K., Ferone, R., Duch, D. S., and Smith, G. K. (1994) Benzo[*f*]quinazoline inhibitors of thymidylate synthase: Methyleneamino-linked aroylglutamate derivitives. J. Med. Chem. 37(6), 838−844.
(21) Duch, D. S., Banks, S., Dev, I. K., Dickerson, S. H., Ferone, R., Heath, L. S., Humphreys, J., Knick, V., Pendergast, W., Singer, S., Smith, G. K., Waters, K., and Wilson, H. R. (1993) Biochemical and cellular pharmacology of 1843U89, a novel benzoquinazoline inhibitor of thymidylate synthase. *Cancer Res. 53*, 810−818.
(22) Smith, G. K., Amyx, H., Boytos, C. M., Duch, D. S., Ferone, R., and Wilson, H. R. (1995) Enhanced antitumor activity for the thymidylate synthase inhibitor for 1843U89 through decreased host toxicity with oral folic acid. *Cancer Res. 55*, 6117−6125.
(23) Pendergast, W., Dickerson, S., Dev, I., Ferone, R., Duch, D., and Smith, G. (1992) Benzoquinazoline inhibitors of thymidylate synthase: effect on cytotoxicity and thymidylate synthase activity of variation of side chain structure and C3 substitution. *Proc. Am. Assoc. Cancer Res. 33*, 407.
(24) Banks, S. D., Waters, K. A., Barrett, L. L., and Smith, G. K. (1992) Destruction of WiDr multicellular tumor spheroids with novel thymidylate synthase inhibitor at physiological thymidine concentrations. *Proc. Am. Assoc. Cancer Res. 33*, 407.
(25) Wilson, H. R., Heath, L. S., Knick, V. C., Koszalka, G. W., and Ferone, R. (1992) In vivo antitumor activity of GW1843, a new antifolate thymidylate synthase inhibitor. *Proc. Am. Assoc. Cancer Res. 33*, 407.
(26) Vitols, K. s., Haag-Zeino, B., Baer, T., Montejano, Y. D., and Huennekens, F. M. (1995) Methotrexate-α-phenylalanine: Optimization of methotrexate prodrug for activation by carboxypeptidase A−monoclonal antibody conjugate. *Cancer Res. 55*, 478−481.
(27) Rosenberg, I. H., and Selhub, J. (1986) Intestinal Absorption of Folates. in *Folates and Pterins* (Blakley, R. L., and Whitehead, V. M., Eds.) Vol. 3, pp 148−176, Wiley-Interscience, New York.
(28) Lituinov, S. V., Velders, M. P., Bakker, H. A., Fleuren, G. J., and Warnaar, S. O. (1994) Ep-CAM: a human epithelial antigen is a homophilic cell−cell adhesion molecule. *J. Cell Biol. 125*(2), 437−446.
(29) Kidera, A., Inaka, K., Matsushima, M., Go, N. (1994) Response of dynamic structure to removal of a disulfide bond: normal mode refinement of C77A/C95A mutant of human lysozyme. *Protein Sci. 3* (1), 92−102.
(30) Gardell, S. J., Craik, C. S., Clauser, E., Goldsmith, E. J., Stewart, C. B., Graf, M., and Rutter, W. J. (1988) A novel rat carboxypeptidase, CPA2: characterization, molecular cloning, and evolutionary implications on substrate specificity in the carboxypeptidase gene family. *J. Biol. Chem. 263*(33), 17828−17836.
(31) Laethem, R. M., Blumenkopf, T. A., Cory, M., Elwell, L., Moxham, C. P., Ray, P. H., Walton, L. M., and Smith, G. (1996) Expression and characterization of human pancreatic preprocarboxypeptidase A1 and preprocarboxypeptidase A2. *Arch. Biochem. Biophys. 332*, 8−18.
(32) Cueni, L. B., Bazzone, T. J., Riordan, J. F., and Vallee, B. L. (1980) Affinity chromatographic sorting of carboxypeptidase A and its chemically modified derivatives. *Anal. Biochem. 107*, 341−349.
(33) Vitols, K. S., Hanseler, E., Montejano, Y., Muller, B. M., Reisfeld, R. A., and Huennekens, F. M. (1992) Enhanced cytotoxicity of methotrexate alpha-peptide prodrugs for UCLA-P3 cells treated with enzyme-conjugated monoclonal antibody KS1/4. *Antibody, Immunoconjugates, Radiopharm. 5*(1), 140.
(34) Sirotnak, F. M., DeGraw, J. I. (1984) Selective antitumor action of folate analogues. in *Folate Antagonist as Therapeutic Agents* (Sirotnak, F. M., Burchall, J. J., Ensminger, W. B., and Montgomery, J. A., Eds.) Vol 2, pp 47−54, Academic Press, Inc., Orlando.
(35) Jackman, A. L., Taylor, G. A., Calvert, A. H., and Harrap, K. R. (1984) Modulation of anti-metabolite effects: Effects of thymidine on the efficacy of the quinazoline-based thymidylate synthetase inhibitor, CB3717. *Biochem. Pharmacol. 33*, 3269−3275.

BC980057Z

Coupling of Nuclear Localization Signals to Plasmid DNA and Specific Interaction of the Conjugates with Importin α

Carole Ciolina, Gerardo Byk, Francis Blanche,† Vincent Thuillier,† Daniel Scherman, and Pierre Wils*

UMR 133 CNRS/Rhône-Poulenc Rorer and Rhône-Poulenc Rorer Gencell, Centre de Recherche de Vitry Alfortville, B.P.14, 13 quai Jules Guesde, 94403 Vitry-sur-Seine Cedex, France. Received June 5, 1998; Revised Manuscript Received October 23, 1998

The nuclear localization signal (NLS) of the SV40 large T antigen efficiently induces nuclear targeting of proteins. We have developed a chemical strategy for covalent coupling of NLS peptides to plasmid DNA. A *p*-azido-tetrafluoro-benzyl-NLS peptide conjugate was synthesized. This conjugate was used to covalently associate NLS peptides to plasmid DNA by photoactivation. Reporter gene was expressed after transfection of the plasmid−NLS conjugates in NIH 3T3 cells. The conjugates interacted specifically with the NLS-receptor importin α, but plasmid−NLS conjugates were not detected in the nucleus, by fluorescence microscopy, after cytoplasmic microinjection.

INTRODUCTION

Plasmids used for nonviral gene therapy are generally delivered as a complex with a variety of chemical or biochemical vectors to obtain maximal transfection efficiency. Among the various chemical vectors developed for gene transfer, cationic lipids are the most widely used (*1*). Nonviral gene transfer with cationic lipids can be divided into several steps (*2*): internalization of the DNA could occur via fusion at the cellular membrane or via endocytosis (*3*), then the plasmid diffuses to the nuclear enveloppe and enters the nucleus probably through the pore complexes. One of the steps limiting nonviral gene transfer efficiency is the entry of plasmid DNA from the cytoplasm into the nucleus (*2*, *4*−*6*).

The role of signal sequences for protein import into the nucleus is well documented (*7*, *8*). Proteins larger than 60 kDa are excluded from the nucleus unless they harbor a nuclear localization signal (NLS).[1] The NLSs usually comprise highly basic stretches of amino acids (*7*). Among the different NLSs, the NLS of the simian virus 40 (SV40) large T antigen has been extensively studied. This short peptide possesses five basic amino acids and efficiently induces nuclear targeting when conjugated to a nonkaryophilic protein of molecular mass up to 465 kDa (*9*). Moreover, nuclear import is increased when several independent SV40 large T antigen NLS peptides are conjugated to a protein (*10*). Karyopherin α is involved in nuclear protein import through association with nuclear localization signals in the cytoplasm, then binding to the nuclear pore complex (*11*, *12*). The 58 kDa mouse karyopherin α (called importin α or *m*-importin) binds to NLS sequence and then interacts with karyopherin *β* (also called importin *β*). The resulting complex binds to the nuclear pore (*13*) and is translocated through the pore in a mechanism involving the small GTPase Ran (*14*) and other proteins.

We developed a new methodology to covalently associate NLS peptides to DNA in which cationic NLS peptides are covalently bound to plasmid DNA by photoactivation. We report here the synthesis and characterization of these conjugates and demonstrate that they specifically interact with the NLS-receptor importin α.

EXPERIMENTAL PROCEDURES

Analytical and Semipreparative HPLC. Analytical and semipreparative HPLC were performed on a Merck-Hitachi gradient pump equipped with a AS-2000A autosampler, an L-6200A intelligent pump, and a UV−vis detector L-4000.

Method 1. For analytical separations, we used a column C18 Vydac 218 TP54 (Interchim, Montluçon, France) using a gradient of acetonitrile/water 0.1% TFA (from 0 to 41% acetonitrile in 25 min) with a flow rate of 1 mL/min during 25 min. For semipreparative separation, we used a column C18 Vydac-218 TP 1022 (10 mm) using a gradient of acetonitrile/water 0.1% TFA (from 5 to 50% acetonitrile in 40 min) with a flow rate of 7 mL/min during 40 min. Detection was by UV absorbance at 254 nm.

Method 2. The HPLC system used a 250 × 4.6 mm C8 Vydac column and a gradient of 5 to 50% acetonitrile over 40 min in 0.1 M triethylammonium acetate, pH 7.5 (flow rate = 1 mL/min). Detection was by UV absorbance at 250 nm.

Peptide Synthesis. The following peptides were synthesized: peptide *β*ACGAGPKKKRKV containing wild-type SV40 large T NLS (NLS) or peptide *β*ACGAGPKNKRKV containing mutant SV40 large T NLS (mNLS) or peptide CYGGPDEVKRKKKP containing SV40 large T NLS reverse sequence. Peptides were synthesized on Applied Biosystems 431A automatic synthesizer using a Rink amide resin as solid support and Fmoc strategy for amino acid assembly. A fluorescent molecular probe, Lissamine rhodamine B, was coupled manually in a separate flask at the N-terminal position of the NLS or mNLS peptides with a solution of dichloromethane containing 10 mol/equiv excess of Lissamine rhodamine B sulfonyl chloride (mixture of two isomers purchased from Aldrich), diisopropylethylamine (DIEA-pH 10), and

* To whom correspondence should be addressed. E-mail: pierre.wils@rp-rorer.fr. Phone: 33 1 55 71 37 33. Fax: 33 1 55 71 37 96.

† Rhône-Poulenc Rorer Gencell.

[1] Abbreviations: NLS, nuclear localization signal; SV40, Simian virus 40; TFPAM-6, *N*-(4-azido-2,3,5,6-tetrafluorobenzyl)-6-maleimidylhexanamide; GST, glutathione *S*-transferase.

10.1021/bc980061a CCC: $18.00 © 1999 American Chemical Society
Published on Web 12/17/1998

a catalytic amount of dimethylaminopyridine (DMAP). The peptides were cleaved from the Rink resin as usual and purified by HPLC. Analytical and semipreparative HPLC were performed as described above (method 1). The final purified products were analyzed by mass spectroscopy.

Lissamine-SO_2-βACGAGPKKKRKVNH_2 (HPLC, analytical, $R_t = 26.9$ min; semipreparative, $R_t = 28-31$ min; MH^+, 1782); Lissamine-SO_2-βACGAGPKNKRKVNH_2 (HPLC, analytical, $R_t = 25$ min; semipreparative, $R_t = 26-34$ min; MH^+, 1767).

Preparation of *p*-Azido-tetrafluoro-benzyl-peptide Conjugates. Lyophilized *N*-(4-azido-2,3,5,6-tetrafluorobenzyl)-6-maleimidylhexanamide [TFPAM-6 (Molecular Probes, Eugene, OR)] was dissolved in dimethyl sulfoxide (DMSO) at a concentration of 1 mg/mL. Lyophilized peptides were dissolved in 100 mM triethylammonium acetate, pH 7.5, at a concentration of 1 mg/mL. Equimolar quantities of TFPAM-6 and peptide were mixed at room temperature. The reaction was monitored by HPLC, and, after 2 h, the conjugate was purified by HPLC as described above (method 2). The conjugate was analyzed by mass spectroscopy. *p*-Azido-tetrafluoro-benzyl-lissamine-SO_2-βACGAGPKKKRKVNH_2 (HPLC, $R_t = 36$ min; MH^+, 2195); *p*-azido-tetrafluoro-benzyl-lissamine-SO_2-βACGAGPKNKRKVNH_2 (HPLC, $R_t = 38.9$ min; MH^+, 2181); *p*-azido-tetrafluoro-benzyl-CYGGPDEVKRKKKP (HPLC, $R_t = 26$ min; MH^+, 2018).

Covalent Coupling of Peptide Conjugates to ds-DNA. Plasmid pCMVLacZ (7257 bp) carries a cassette containing the enhancer-promoter from the immediate-early gene of cytomegalovirus (CMV) and the gene coding β-galactosidase. Plasmid DNA was purified using Wizard Megaprep kit (Promega, Madison, WI). *p*-Azido-tetrafluoro-benzyl-peptide conjugate was mixed with dsDNA (final concentration 0.3 μg/μL) at various molar excess depending on the assay. The mixture was cooled in an ice−water bath below a sun lamp (Rad Free UV lamp-365 nm, Schleicher and Schuell, Ecquevilly, France) and illuminated for 15 min in the dark. Excess *p*-azido-tetrafluoro-benzyl-peptide conjugate was removed by ion-exchange chromatography (PCR Purification kit, Qiagen, Hilden, Germany). The average number of fluorescent peptides attached to the DNA was determined with a Titertek Fluoroskan II Spectrofluorimeter with free and illuminated *p*-azido-tetrafluoro-benzyl-peptide conjugate for calibration curve (excitation, 544 nm; emission, 590 nm).

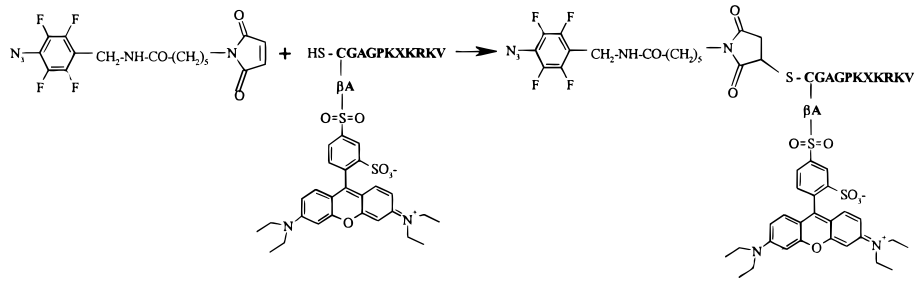
Preparation of Recombinant Importin α-GST Protein. Mouse importin α was cloned into pGEX-2T to produce a GST fusion protein: importin α-GST (*11*). The plasmid encoding the fusion protein was kindly provided by Dr. Y. Yoneda (Osaka University Medical School, Osaka, Japan). Importin α-GST was overexpressed in *Escherichia coli* strain BL21 grown in 1 L of LB medium, as previously described (*11*). Cells were harvested by centrifugation, washed with 100 mL of PBS and resuspended in 20 mL of buffer A [50 mM Tris-HCl, pH 8.3, 1 mM EDTA, 2 mM dithiotreitol, 0.5 M NaCl, and 200 μM Pefabloc (Boehringer, Manheim, Germany)]. Cells were disrupted by sonication at 4 °C during 30 min. The extract was clarified by centrifugation (15000*g*, 1 h). The recombinant protein was purified by affinity chromatography on glutathione-Sepharose 4B (Pharmacia, Uppsala, Sweden) equilibrated in buffer A. Glutathione-Sepharose 4B (8 mL) was cast in a HR10/10 column (Pharmacia, Uppsala, Sweden) connected to an HPLC system (Gilson 305). The clarified cell extract was loaded on the column at 0.5 mL/min. The column was washed with buffer B (20 mM HEPES-NaOH pH 7.3, 2 mM dithiotreitol, 1 mg/L leupeptin, 1 mg/L pepstatin, and 1 mg/L aprotinin). The column was incubated 10 min in buffer B containing 20 mM glutathione, after which the recombinant protein was eluted at 0.5 mL/min. The protein fractions are desalted on disposable Sephadex G-25 M columns (PD-10, Pharmacia, Uppsala, Sweeden) and eluted with 50 mM HEPES-NaOH, pH 7. Protein concentration was 0.6 mg/mL. The purity of the recombinant protein was assessed by denaturing polyacrylamide gel electrophoresis and Coomasie staining. Its identity was checked by Western blotting and probing with a polyclonal antiserum raised against the internal peptide: SEGYTFQVQDGAPGTFBF. The N-terminus of importin α-GST was also sequenced.

Importin α Binding Assay. All assays were performed using importin α-GST recombinant protein. Binding to importin α was performed according to Rexach and Blobel (*15*), with the following modifications: all assays were performed in binding buffer (20 mM HEPES, pH 6.8, 150 mM potassium acetate, 2 mM magnesium acetate, and 2 mM and 100 μg/mL bovine serum albumin). The GST fusion protein was incubated with glutathione-sepharose beads (Pharmacia Biotech, Uppsala, Sweden). Importin α-GST fusion protein (1 μg per 10 μL of beads) was incubated with beads in 0.5 mL of binding buffer for 30 min at room temperature. The beads were collected by centrifugation at 2000*g* for 30 s and were washed five times with 0.5 mL of binding buffer. Washed beads were resuspended in binding buffer with 1 vol of buffer/vol of beads.

The bead slurry (80 μL) was incubated with 2 μg of peptide−DNA conjugate, in 0.5 mL of binding buffer, for 30 min at room temperature. The beads were collected by centrifugation at 2000*g* for 30 s. The supernatant was removed and 30 μL was used to analyze the presence of the unbound DNA (this fraction is called the unbound fraction). The beads were washed five times with 0.5 mL of binding buffer and centrifugated at 2000*g* for 30 s. Finally, beads, corresponding to the bound fraction, were resuspended with 15 μL of electrophoresis loading buffer (0.05% bromophenol blue, 40% sucrose, 0.1 M EDTA pH 8, 0.5% sodium lauryl sulfate). The bound and unbound fractions were analyzed by electrophoresis on 0.8% agarose gel and DNA was stained with ethidium bromide for qualitative determination. Quantitative DNA evaluation in the unbound and bound fractions was obtained by resuspending beads in 160 μL of binding buffer and peptide−plasmid conjugate and dsDNA were measured according to the Picogreen ds DNA quantitation kit (Molecular Probes, Eugene, OR).

Transgene Expression Studies. NIH 3T3 cells were obtained from the American Type Culture Collection (ATCC CRL-1658). The cells were grown in Dulbecco's modified Eagle's medium (DMEM, Gibco, Grand Island, NY) containing 4.5 g/L glucose, supplemented with 2 mM glutamine, 100 units/mL penicillin, 100 μg/mL streptomycin, and 10% foetal bovine serum. Cells were grown at 37 °C in a 5% CO_2/air incubator. One day before the transfection assay, 24-well culture plates were seeded with 50 000 cells/well. Cationic lipid RPR 120535 (*16*) was used for the transfection assays. Plasmids were diluted in 150 mM NaCl at 20 ng/μL concentration, then mixed with a cationic lipid solution (0.12 mM). The DNA/cationic lipid complex was diluted in culture medium (Dulbecco's modified Eagle's medium) in the absence of serum and then added to the cells (0.5 μg of DNA and 3 nmol lipid/well). After 2 h at 37 °C in a 5% CO_2/air incubator, 10% foetal bovine serum was added to the cells. The cells were incubated for 48 h at 37 °C in a 5% CO_2/air incu-

Scheme 1: Synthesis of *p*-Azido-tetrafluoro-benzyl-peptide Conjugates. The Peptide Contains either the NLS Sequence (X = K) or the Mutant Sequence (X = N)



TFPAM-6 Lissamine rhodamine B labeled peptide p-azido-tetrafluoro-benzyl-peptide conjugate

bator. The cells were washed twice with PBS and lysed with 250 μL of cell culture lysis reagent (Promega, Madison, WI). β-Galactosidase expression was measured according to the Lumigal β-Galactosidase genetic reporter system (Clontech, Palo Alto, CA). Light emission was measured by integration over 10 s using a Lumat LB9501 luminometer (EG and G, Berthold, Evry, France). Light emission was normalized to the protein concentration determined using the Pierce BCA assay (Pierce, Rockford, IL).

Microinjection Studies. CV-1 cells were kindly provided by Dr. S. Koutouzov (INSERM U25, Paris, France). Cells were cultured in Minimum Essential medium (MEM, Gibco, Grand Island, NY) supplemented with 2 mM glutamine, 100 units/mL penicillin, 100 μg/mL streptomycin, and 10% foetal bovine serum. Cells were grown at 37 °C in a 5% CO_2/air incubator on CELLocate microgrid coverslips (Eppendorf, Hamburg, Germany). The solution of DNA was injected into the cells via glass micropipets having tip diameters ranging from 0.3 to 0.7 μm (Femtotips, Eppendorf, Hamburg, Germany) at 1 μg/μL concentration. Injections were carried out under visual control on a fixed stage of an inverted phase contrast microscope (Axiovert 135, Zeiss, Le Pecq, France) using a Micromanipulator 5171 and Microinjector 5242 (Eppendorf, Hamburg, Germany). The average volume (0.1−0.2 pL) injected into each cell was determined by injecting [^{35}S]dATPαS into cells and measuring the radioactive content (*6*). These corresponded to an average of 6000−12000 plasmid molecules/cell. Following injection, the cells were incubated for 30 min to 6 h at 37 °C in a 5% CO_2/air incubator. The cells were washed three times with PBS, fixed for 20 min in 3% paraformaldehyde in PBS, and washed three times with PBS. Nuclei were then stained with 4,6-diamidino-2-phenylindole (DAPI), at a concentration of 0.1 μg/mL, for 15 min, and washed with PBS. The cells were mounted in Mowiol for examination. Slides were examined with a Zeiss Axiophot fluorescence microscope, with a 100× objective lens, coupled to a cooled CCD camera (Hamamatsu) and a Samba imaging software (Unilog, Meylan, France).

RESULTS

Preparation of *p*-Azido-tetrafluoro-benzyl-peptide Conjugates. Peptides containing wild-type SV40 large T NLS sequence (NLS) or mutant SV40 large T NLS (mNLS) were used. Introduction of a point mutation in the NLS sequence (asparagine instead of lysine) induces loss of NLS targeting activity (*9*). Scheme 1 illustrates the chemistry used to prepare *p*-azido-tetrafluoro-benzyl-peptide conjugates. The coupling step involves reaction of TFPAM-6 bearing a maleimide group with a peptide bearing a nucleophilic thiol residue (*17*). Equimolar quantities of the two reagents were used. Since TFPAM-6 absorbs at 250 nm, the conjugation chemistry was easily monitored by reversed-phase HPLC. After 2 h, the reaction was complete as shown by the disappearance of TFPAM-6 and of the starting peptide (Figure 1). The final product was analyzed by mass spectroscopy, which confirmed the disappearance of starting reagents, and the experimental mass was similar to the calculated mass. The yield of this reaction was

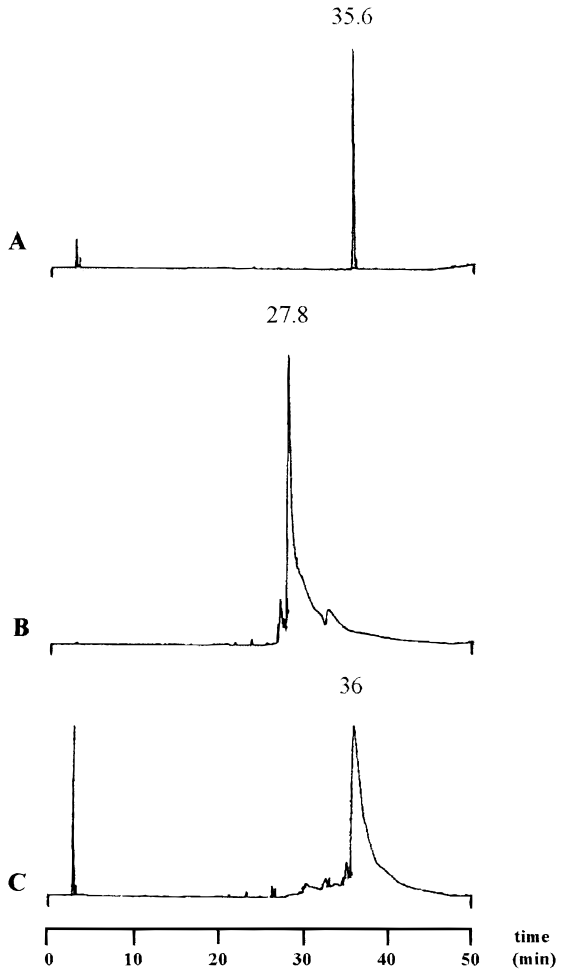


Figure 1. HPLC chromatograms of *p*-azido-tetrafluoro-benzyl-peptide conjugates. HPLC profiles of starting material and conjugate obtained after 2 h of reaction are shown. The molecules were analyzed by reversed phase HPLC using method 2 described in the experimental procedures (absorption wavelength = 250 nm). (A) TFPAM-6; (B) NLS peptide; (C) *p*-azido-tetrafluoro-benzyl-NLS peptide conjugate after 2 h of incubation.

90%. The peptides used were labeled with a fluorescent molecule, lissamine rhodamine B. The conjugate had the same fluorescent properties as the starting peptide (data not shown).

Covalent Attachment of Peptides to dsDNA. The *p*-azido-tetrafluoro-benzyl-peptide conjugates bearing either NLS or mNLS sequence were used to covalently modify plasmids by photoactivation. *p*-Azido-tetrafluoro-benzyl-peptide conjugates were mixed with dsDNA at peptide/DNA molar ratios varying between 5 and 1000 and illuminated at 365 nm. After purification on ion-exchange columns, the average number of peptide linked to the DNA could be measured by taking advantage of the peptide fluorescent labeling: by varying the *p*-azido-tetrafluoro-benzyl-peptide/DNA molar ratio during the coupling step, conjugates bearing an average number of 1 peptide/plasmid molecule to 300 peptides/plasmid (7257 bp) were obtained. During the last coupling step, 20% of the added *p*-azido-tetrafluoro-benzyl-peptide conjugates were found covalently linked with plasmid DNA after purification. For example, with a molar excess (NLS peptide/plasmid) of 500, the average number of NLS peptides linked per plasmid DNA was 100 ± 28 (six experiments). Plasmids modified with NLS and mNLS peptides are referred to as plasmid−NLS and plasmid−mNLS, respectively.

Characterization of Peptide−Plasmid Conjugates. Peptide−plasmid conjugates were analyzed by agarose gel electrophoresis as described in the Experimental Procedures. With 1−100 peptides/plasmid DNA molecule, there was no visible modification of plasmid DNA migration, and peptide−plasmid conjugates appeared on gels as supercoiled DNA. With higher numbers of peptides per plasmid DNA molecule, plasmid DNA migration delay was observed. No delay was observed when plasmid DNA was mixed with nonilluminated NLS peptides (data not shown).

The reporter gene expression was studied after transfection of NIH3T3 cells. Modified plasmids with 3−43 NLS peptides/plasmid DNA molecule expressed β-galactosidase. The increase of expression obtained with 3 NLS peptides/plasmid DNA is not significant. The expression was decreased by 60% with plasmids bearing 43 NLS peptides (Figure 2). Similar results were obtained with mNLS peptides (data not shown).

Importin α Binding Assay. Binding of the modified plasmids to importin α was studied on a importin α-GST fusion protein, using glutathione-sepharose beads, followed by agarose gel electrophoresis. Plasmid−NLS was detected in the bound fraction (interacting with the importin α-GST-beads) whereas nonmodified plasmid was all recovered in the supernatant (Figure 3). The same result was obtained with plasmid−mNLS instead of nonmodified plasmid (data not shown).

Double-stranded DNA in the fraction bound to importin α-GST was quantified using either the intrinsic fluorescence of the lissamine rhodamine B or, for higher sensitivity, using an intercalating fluorescent molecule, Picogreen reagent. Plasmid−NLS bound significantly more to importin α-GST beads than either plasmid-mNLS, nonmodified plasmid, or plasmid conjugated to reverse NLS peptide (VKRKKKP) (Figure 4A and data not shown). Moreover, no specific binding to importin α-GST was detected using neither plasmid prepared by mixing with *p*-azido-tetrafluoro-benzyl-NLS peptide conjugates, without further UV irradiation, nor plasmid prepared by mixing with a *p*-azido-tetrafluoro-benzyl-NLS peptide that had been irradiated prior to contact with DNA (Figure 4B). Hence, the binding of plasmid−

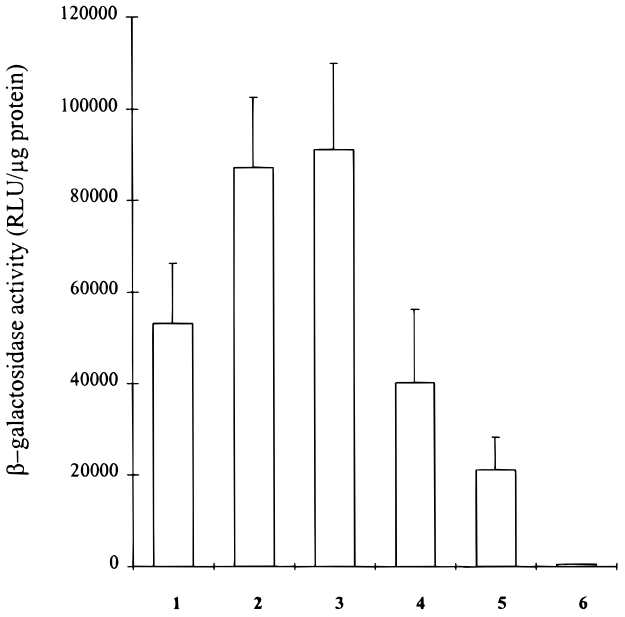


Figure 2. Transgene expression after transfection of plasmid−NLS conjugates. Nonmodified plasmid and plasmid−NLS conjugates were used for transfecting NIH3T3 cells with cationic RPR 120535. The β-galactosidase expression was evaluated after 24 h of incubation. (1) Nonmodified plasmid; plasmid−NLS with the following NLS peptide/plasmid molar ratio: (2) 3; (3) 8; (4) 16; (5) 43; (6) no plasmid. Values are means ± SD (n = 3).

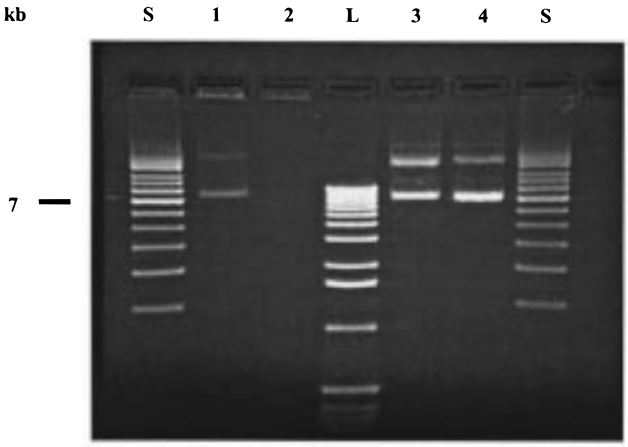


Figure 3. Interaction between importin α-GST and plasmid−NLS conjugates. Beads-immobilized importin α-GST (2 μg) was incubated for 30 min at room temperature with a plasmid conjugated to 66 NLS peptides (1 μg) (1 and 3) or nonmodified plasmid (1 μg) (2 and 4). Bound (1 and 2) and unbound (3 and 4) fractions were analyzed by 0.8% agarose gel electrophoresis and ethidium bromide staining. L = molecular weight marker for linear DNA fragments (1 kb ladder). S = molecular weight marker for supercoiled DNA fragments (1 kb ladder).

NLS to importin α is mediated by the specific interaction of nonmodified NLS peptide covalently bound to DNA and its receptor.

By increasing the ratio of *p*-azido-tetrafluoro-benzyl-NLS peptide, 2−26 NLS peptides were covalently attached to dsDNA. Plasmid interaction with importin α-GST increased with increasing number of peptides per plasmid (Figure 4C). By increasing this number up to 45 and 100, the quantity of dsDNA interacting with 2 μg importin α-GST fusion protein was 30 and 60 ng, respectively (data not shown).

Microinjection Studies. NLS-modified plasmids were microinjected into the cytoplasm of CV-1 cells. Plasmids with 100 NLS peptides/plasmid molecule were used. Cells

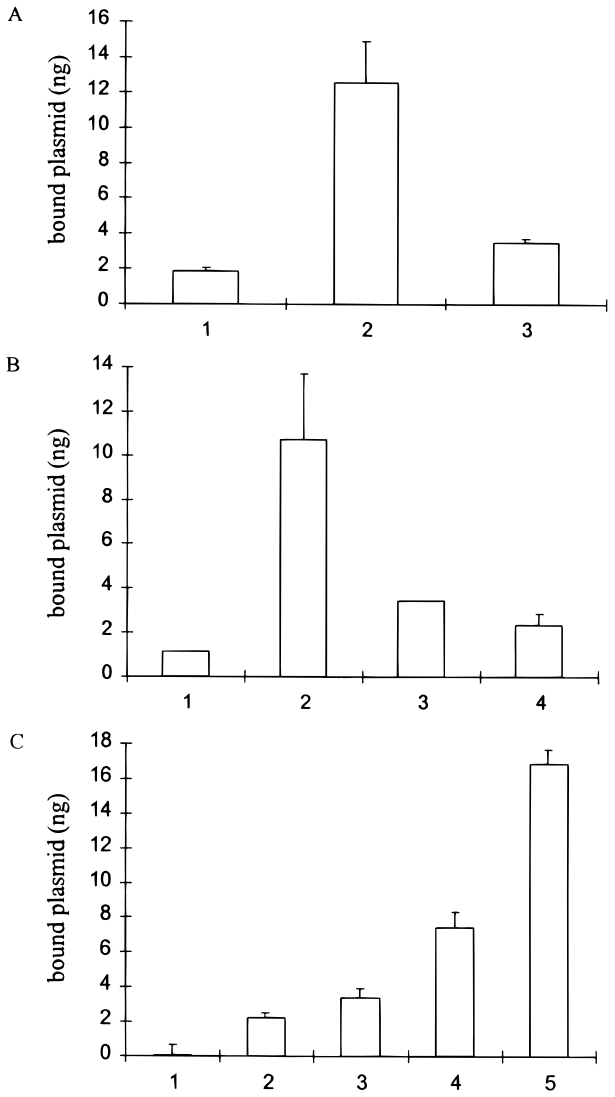


Figure 4. Quantitative analysis of plasmid−NLS conjugates binding to importin α-GST. Immobilized importin α-GST (2 μg) was incubated for 30 min at room temperature with the different conjugates (1 μg). DNA in the bound fractions was measured as described in the Experimental Procedures. (A) Nonmodified plasmid (1); plasmid conjugated to 18 NLS peptides (2); plasmid conjugated to 26 mNLS peptides (3). (B) Nonmodified plasmid (1); plasmid conjugated to 18 NLS peptides (2); plasmid prepared with *p*-azido-tetrafluoro-benzyl-NLS peptide, without UV illumination (3); plasmid mixed with *p*-azido-tetrafluoro-benzyl-NLS peptide UV illuminated before coupling (4). (C) Nonmodified plasmid (1); plasmid−NLS conjugate with 2 NLS/plasmid (2); plasmid−NLS conjugate with 6 NLS/plasmid (3); plasmid−NLS conjugate with 12 NLS/plasmid (4); plasmid−NLS conjugate with 26 NLS/plasmid (5). Data represent means of two determinations, with error bars indicating the maximal experimental value.

were fixed after 30 min, 2 or 6 h, and nuclei were stained with DAPI. An intense cytoplasmic fluorescence was observed 30 min after microinjection into the cytoplasm, indicating that DNA could only be detected in the cytoplasm (Figure 5A). Cytoplasmic microinjection of NLS-conjugated BSA in the same conditions gave a high nuclear staining (data not shown). The DNA fluorescence pattern evolved 2 h after microinjection into the cytoplasm (Figure 5C): half of the stained cells showed the same intense fluorescent pattern observed at 30 min and the rest exhibited a single fluorescent spot in the cytoplasm. After 6 h, nearly all cells had only one residual fluorescent spot in the cytoplasm (Figure 5E).

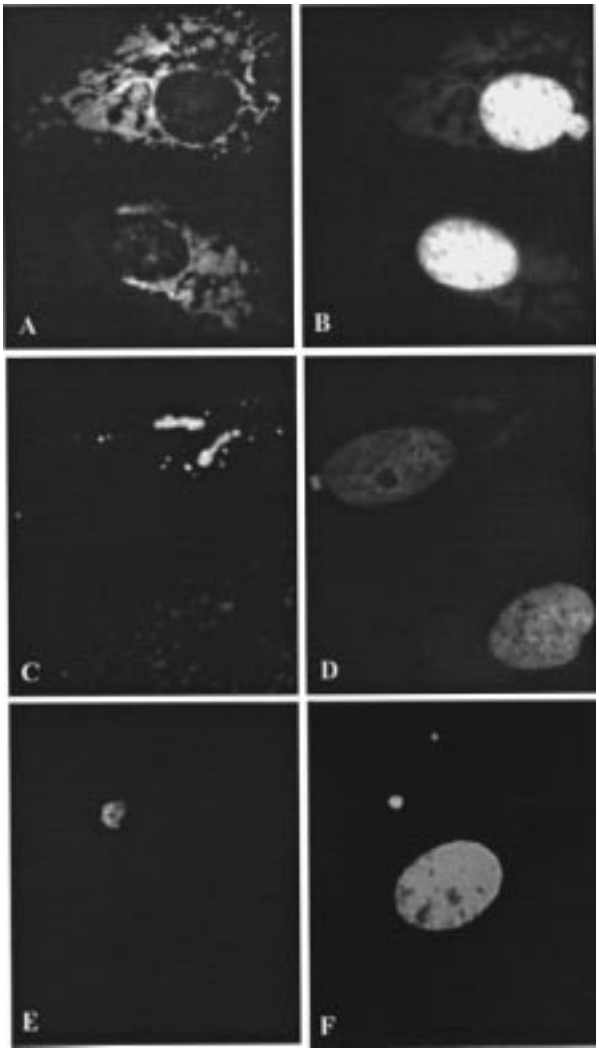


Figure 5. Cytoplasmic microinjection of plasmid−NLS conjugate. CV-1 cells were cytoplasmically microinjected with plasmid−NLS (100 NLS peptides/plasmid DNA molecule) and fixed after 30 min (A and B), 2 h (C and D), or 6 h (E and F). Fluorescent microscopy of plasmid−NLS (A, C, and E) and nuclei staining with 4,6-diamidino-2-phenylindole (B, D, and F) are shown.

DISCUSSION

Several methods for covalent attachment of molecules to nucleic acids have been developed and reported so far (*18*−*20*). Among them, the use of photoactive molecules, such as tetrafluorophenylazido groups, leads to an efficient photomodification of DNA (*21*). We have conjugated a cationic peptide, NLS from SV40 large T antigen, to a photoactive tetrafluorophenylazido-containing molecule. The NLS peptide had a sulfhydryl reactive group and the photoactive molecule, TFPAM-6, a maleimide group which reacted to give a photoactive NLS peptide. The peptide used had a fluorescent moiety, making it possible to follow the conjugation to plasmid DNA, to quantify the average number of peptides bound to DNA and to study the intracellular fate of the conjugates. Moreover, we found that the molecules labeled with lissamine rhodamine B are easier to purify and more chemically stable than those labeled with another fluorophore such as tetramethylrhodamine.

Covalent coupling of ligands to the DNA could cause transcriptional inactivation. According to a study on the expression of a biotinylated plasmid prepared with a similar photomodification chemistry, a plasmid with up

to 40 biotins coupled/plasmid retained 40% biological activity (*19*). Plasmids conjugated to NLS peptides by covalent coupling using a cyclopropapyrroloindole group were modified with 24−101 peptides/1 kb (*22*). With this number of peptides per plasmid, transgene expression was abolished. With the photoactive *p*-azido-tetrafluorobenzyl-peptide conjugates, lower levels of modification were obtained and the modified plasmids were still biologically active. With up to 43 peptides per plasmid DNA (7 kb), modified plasmids remained biologically functional. This result is in agreement with transgene expression data previously reported (*19*). It is also important to notice that plasmid−NLS conjugates appeared on gels as supercoiled DNA.

Using a binding assay, we showed that NLS peptides attached to dsDNA interacted with the NLS-binding protein, importin α. This interaction was specific and depended on the number of peptides conjugated to dsDNA. Our results show that NLS peptides are recognized despite the plasmid electrostatic properties. Plasmids associated to NLS peptides by covalent coupling were studied in digitonin-permeabilized cells (*22*). Nuclear accumulation of the plasmid DNA was observed and was dependent on the number of NLS peptides: peptide−plasmid conjugates bearing less than approximately 40 NLS/1 kb did not accumulate in the nucleus. In our experiments, we chose to couple a low number of peptides (less than 10 peptides/1 kb) in order to maintain a certain amount of transgene expression. Nuclear accumulation of plasmid DNA was also obtained in isolated male pronuclei with NLS peptides associated to plasmid DNA by electrostatic interactions (*23*).We demonstrate here that NLS peptides bound to DNA interact with their receptor: this recognition step is a prerequisite for import via the classical NLS-dependent pathway.

However, after microinjection in the cytoplasm, plasmid−NLS conjugates were not detected in the nucleus. These results are in agreement with microinjection data previously reported (*22*). Our microscopic studies suggest that microinjected plasmid−NLS conjugates are progressively degraded in the cytoplasm, since the staining observed gradually decreased with time. After 6 h, only one spot of fluorescent plasmid−NLS was detected, which probably corresponded to the site of injection. This suggests that the bulk of microinjected plasmid did not readily diffuse from the site of injection. It is possible that part of plasmid−NLS molecules could be sequestered in the cytoplasm as observed for naked DNA injected in myotubes (*5*).

In conclusion, we have designed a novel simple chemistry for coupling by photoactivation peptides to plasmid DNA. This technology allows the control of the number of peptides linked to DNA which is determinant for maintaining plasmid integrity and expression. Moreover, we show in the present work that a conjugate between a targeting NLS−peptide and plasmid−DNA is recognized by importin α NLS receptor. The present strategy could thus be used for coupling other ligands to plasmid DNA, study plasmid−ligand conjugate interaction with receptors. Since a fluorescent peptide could be coupled, the technology also allows to follow intracellular fate of the peptide−DNA conjugate.

ACKNOWLEDGMENT

This work was supported by a grant from the French Ministry of Research. We thank Dr François F. Clerc and his staff for peptide synthesis and Dr. Marc Vuilhorgne and his staff from the Structural Analysis Department of Rhône-Poulenc Rorer for mass spectroscopy analysis. We thank D.Bisch for importin α-GST purification.

LITERATURE CITED

(1) Ledley, F. D. (1995) Non viral gene therapy: the promise of genes as pharmaceutical products. *Hum. Gene Ther. 6*, 1129−1144.

(2) Zabner, J., Fasbender, A. J., Moninger, T., Poellinger, K. A., and Welsh, M. J. (1995) Cellular and molecular barriers to gene transfer by a cationic lipid. *J. Biol. Chem. 270*, 18997−19007.

(3) Escriou, V., Ciolina, C., Lacroix, F., Byk, G., Scherman, D., and Wils, P. (1998) Cationic lipid-gene transfer: effect of serum on cellular uptake and intracellular fate of polyamine/DNA complexes. *Biochim. Biophys. Acta 1368*, 276−288.

(4) Mirzayans, R., Remy, A. A., and Malcolm, P. C. (1992) Differential expression and stability of foreign genes introduced into human fibroblasts by nuclear versus cytoplasmic microinjection. *Mutat. Res. 281*, 115−122.

(5) Dowty, M. E., Williams, P., Zhang, G., Hagstrom, J. E., and Wolff, J. A. (1995) Plasmid DNA entry into postmitotic nuclei of primary rat myotubes. *Proc. Natl. Acad. Sci. U.S.A. 92*, 4572−4576.

(6) Escriou, V., Ciolina, C., Helbling-Leclerc, A., Wils, P., and Scherman, D. (1998) Cationic lipid-mediated gene transfer: analysis of cellular uptake and nuclear import of plasmid DNA. *Cell Biol. Toxicol. 14*, 95−104.

(7) Garcia-Bustos, J., Heitman, J., and Hall, M. N. (1991) Nuclear protein localization. *Biochim. Biophys. Acta 1071*, 83−101.

(8) Yoneda, Y. (1997) How proteins are transported from cytoplasm to the nucleus. *J. Biochem. Tokyo 121*, 811−817.

(9) Lanford, R. E., Kanda, P., and Kennedy, R. C. (1986) Induction of nuclear transport with a synthetic peptide homologous to th SV40 T Antigen transport signal. *Cell 46*, 575−582.

(10) Dworetzky, S. I., Lanford, R. E., and Feldherr, C. M. (1988) The effects of variations in the number and sequence of targeting signals on nuclear uptake. *J. Cell. Biol. 107*, 1279−1287.

(11) Imamoto, N., Schimamoto, T., Takao, T., Tachibana, T., Kose, S., Matsubae, M., Sekimoto, T., Shimonishi, Y., and Yoneda, Y. (1995) In vivo evidence for involvement of a 58kDa component of nuclear pore-targeting complex in nuclear protein import. *EMBO J. 14*, 3617−3626.

(12) Nadler, S. G., Tritschler, D., Haffar, O. K., Blake, J., Bruce, A. G., and Cleaveland, J. S. (1997) Differential expression and sequence-specific interaction of karyopherin α with nuclear localization sequences. *J. Biol. Chem. 272*, 4310−4315.

(13) Görlich, D., Vogel, F., Mills, A. D., Hartmann, E., and Laskey, R. A. (1995) Distinct functions for the two importin subunits in nuclear protein import. *Nature 377*, 246−248.

(14) Moore, M. S., and Blobel, G. (1993) The GTP-binding protein Ran/TC4 is required for protein import into the nucleus. *Nature 365*, 661−663.

(15) Rexach, M., and Blobel, G. (1995) Protein import into nuclei: association and dissociation reactions involving transport substrate, transport factors, and nucleoporins. *Cell 83*, 683−692.

(16) Byk, G., Dubertret, C., Escriou, V., Frederic, M., Jaslin, G., Rangara, R., Pitard, B., Crouzet, J., Wils, P., Schwartz, B., and Scherman, D. (1998) Synthesis, activity, and structure−activity relationship studies of novel cationic lipids for DNA transfer. *J. Med. Chem. 41*, 224−235.

(17) Aggeler, R., Chicas-Cruz, K., Cai, S., Keana, J. F. W., and Capaldi, R. A. (1992) Introduction of reactive residues in the ϵ subunit of *Escherichia coli* ATPase, modification of these sites with tetrafluorophenyl azide-maleimides and examination of changes in the binding of the ϵ subunit when different nucleotides are in catalytic sites. *J. Biochem. Tokyo 31*, 2986−2961.

(18) Forster, A. C., McInnes, J. L., Skingle, D. C., and Symons, R. H. (1985) Nonradioactive hybridization probes prepared

by the chemical labeling of DNA and RNA with a novel reagent, photobiotin. *Nucleic Acids Res. 13*, 745−761.
(19) Leahy, P., Carmichael, G. G., and Rossomando, E. F. (1996) Novel biotinylated plasmid expression vectors retain biological function and can bind streptavidin. *Bioconjugate Chem. 7*, 545−551.
(20) Geselowitz, D. A., and Neumann, R. D. (1995) Quantitation of triple-helix formation using a photocross-linkable aryl azide/biotin/oligonucleotide conjugate. *Bioconjugate Chem. 6*, 502−506.
(21) Levina, A. S., Tabatadze, D. R., Dobrikov, M. I., Shishkin, G. V., and Zarytova, V. P. (1996) Sequence-specific photomodification of single-stranded and double-stranded DNA fragments by oligonucleotide perfluoroazide derivative. *Antisense Nucleic Acid Drug Dev. 6*, 127−132.
(22) Sebestyén, M. G., Ludtke, J. J., Bassik, M. C., Zhang, G., Budker, V., Lukhtanov, E. A., Hagstrom, J. E., and Wolff, J. A. (1998) DNA vector chemistry: the covalent attachment of signal peptides to plasmid DNA. *Nat. Biotech. 16*, 80−85.
(23) Collas, P., and Aleström, P. (1996) Nuclear localization signal of SV40 T antigen directs import of plasmid DNA into sea urchin male pronuclei in vitro. *Mol. Reprod. Dev. 45*, 431−438.

BC980061A

A Fluorescent Radioiodinated Oligonucleotidic Photoaffinity Probe for Protein Labeling: Synthesis and Photolabeling of Thrombin

Catherine Berens,[†,‡] Pierre J. Courtoy,[‡] and Etienne Sonveaux*[,†]

Laboratoire de Chimie Thérapeutique et de Radiopharmacie, UCL 7340, 73 Avenue Emmanuel, Mounier, B-1200 Bruxelles, Belgium, and Unité de Biologie Cellulaire, UCL 7541, Christian de Duve Institute of Cellular Pathology, 75 Avenue Hippocrate, B-1200 Bruxelles, Belgium. Received June 10, 1998; Revised Manuscript Received October 1, 1998

To study the interactions between oligonucleotides and proteins, an original photoaffinity radiolabeling probe has been synthesized. Starting with a 5′-pyridyldithio-3′-amino-oligonucleotide, the photophore benzophenone was first coupled to the 3′ end, through acylation by an activated ester of benzoylbenzoic acid. A fluorescein molecule was grafted by alkylation of the free 5′-SH. This compound was finally radiolabeled with ^{125}I using IodoBeads. The selective photolabeling of thrombin in a complex protein mixture by the radioiodinated probe validates this strategy to identify oligonucleotide-binding proteins.

INTRODUCTION

The potential of oligodeoxyribonucleotides (ODNs) as antigene or antisense agents to inhibit protein expression, or as direct aptamers to proteins, is investigated increasingly. The best known examples of protein-binding ODNs are phosphodiester (PO) ODNs, featuring a G quartet, that inhibit the serine protease thrombin, a key blood-coagulation enzyme and, accordingly, a major target for anticoagulant therapy (Bock et al., 1992, Wang et al., 1993, Padmanabhan et al., 1993, Macaya et al., 1995, Shaw et al., 1995, Tsiang et al., 1995). Depending on their length and secondary structure (Tasset et al., 1997), G-quartet ODNs can bind either to the fibrinogen recognition or to the heparin-binding exosite of thrombin. Phosphorothioates (PS) ODNs, selected for their metabolic stability, avidly bind to various proteins such as recombinant soluble CD4 receptor, HIV-1 envelope glycoprotein gp120, HIV-1 reverse transcriptase, basic fibroblast growth factor (bFGF), acidic FGF, FGF-4, platelet-derived growth factor, vascular endothelial growth factor, laminin [reviewed by Stein (1995)] and more trivially, albumin (Greig et al., 1995). The sequence requirement for affinity is far less stringent for phosphorothioates than for phosphodiesters. In other words, PO−ODNs appear as unstable, but selective agents while PS−ODNs are more stable but less selective. 3′-Modified phosphodiester ODNs, resistant to 3′-exonuclease (the major serum nucleasic activity), probably feature a better compromise between stability and selectivity (Tidd and Warenius, 1989; Shaw et al., 1991).

The study of protein−ODN interactions was however not the initial focus in nucleic acid drug research. The major goal of ODNs is the antisense effect, i.e., the specific inhibition of translation of a (pre)mRNA, induced by a sequence-selective hybridization by Watson−Crick pairing with the antisense ODN. Nevertheless, whatever the nature of ODN backbone (be it PO, PS, or 3′-modified PO), an absolute requirement for an antisense effect is the cellular penetration of the ODN that presumably depends on receptor-mediated endocytosis, a process for which protein−ODN interactions are major determinants (Loke et al., 1989; Yakubov et al., 1989; Beltinger et al., 1995).

As protein−ODN interactions are so ubiquitous, we aimed at devising a standard procedure to synthesize ODN-affinity probes that would allow for specific and efficient labeling of target proteins. A photo-cross-linkable probe was favored because it could enable one to study in situ time-dependent phenomena such as the cellular penetration of ODNs. This tool would in particular prove valuable to characterize the series of protein associations of an antisense ODN on its journey from the cellular surface to the endosomes (early or late), and from the cytosol to the nucleus [reviewed by Akhtar and Juliano (1992)].

This report describes the synthesis, characterization, and radioiodination of an ODN coupled to the photophore benzophenone. This probe was further evaluated in vitro by photolabeling human and bovine thrombin. In cell biological experiments, this fluorescent ODN appears suitable for time-resolved (by flashing at different times) and space-resolved (by using confocal microscopy) chemoselective studies (by affinity labeling).

EXPERIMENTAL PROCEDURES

General. Unless otherwise stated, all reagents used for this study were of analytical grade. All buffers were made with milliQ water (Millipore). The 5′-pyridyldithio-3′-amino-oligonucleotide (ODN1, see Figure 1) was obtained by the method of Arar et al. (1995). The disulfide phosphoramidite building block and the suitably derivatized glass beads required for 5′ and 3′ modifications respectively are available from Glen Research (VA, Thiol Modifier C6 S−S and 3′-Amino-Modifier C7 CPG). High-performance liquid chromatography was performed on a Spectra Physics apparatus, using reversed-phase C18 columns (BioSil C18 HL 90-5S from Bio-Rad, or Adsorbosphere from AllTech) at a flow rate of 1 mL/min and a linear gradient of eluent B (triethylammonium acetate (TEAA) 0.1 M pH 7.0 in CH_3CN:H_2O, 60/40) in eluent A

* To whom correspondence should be addressed. Phone: 32.2.764.54.61. Fax: 32.2.764.73.63. E-mail: sonveaux@cmfa.ucl.ac.be.

[†] Laboratoire de Chimie Thérapeutique et de Radiopharmacie.

[‡] Unité de Biologie Cellulaire.

10.1021/bc980065f CCC: $18.00 © 1999 American Chemical Society
Published on Web 12/11/1998

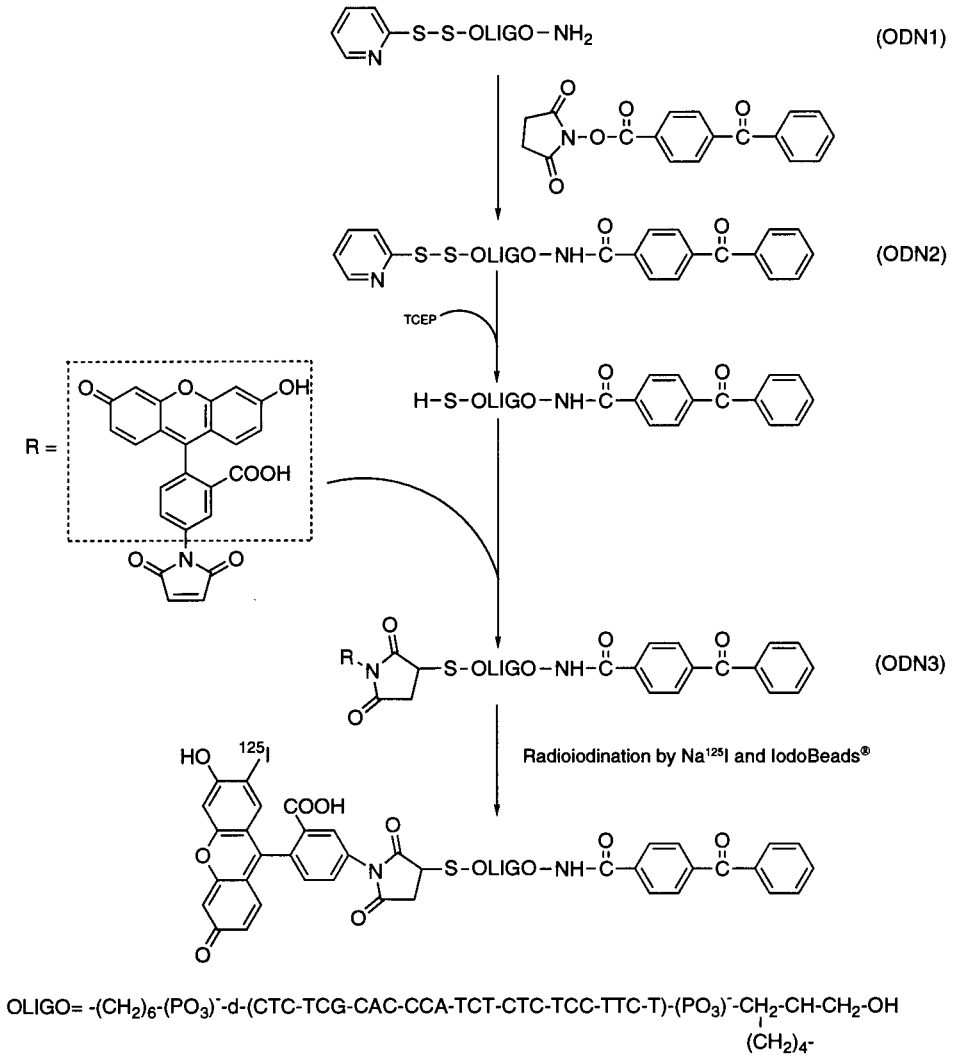
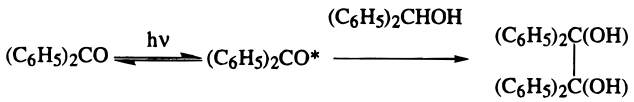


Figure 1. Structures and synthesis of ODNs. [TCEP is tris(2-carboxyethyl)phosphine].

(0.1 M TEAA, pH 7.0, in H_2O:CH_3CN, 95/5) from 0 to 100% over 60 min. Aqueous solutions were evaporated without heating on a Speed Vac centrifugal evaporator (Savant). The concentrations of purified ODNs were determined by UV spectroscopy at the maximum absorbance of the ODN (269 nm), using extinction coefficients calculated as described by Brown and Brown (1991).

For photo-cross-linking experiments, samples were exposed in open Petri dishes to illumination with three lamps (total power of 60 W, 30 W from above, 2 × 15 W lateral; Vilber Lourmat, Marne la Vallée, France, λ_{max} at 365 nm, no emission below 300 nm) at a distance of ~10 cm, or with only one 8 W lamp. To verify that the energy absorbed by the sample was sufficient to give a significant yield of cross-linking, a control reaction was used, based on the coupling, in a closed quartz cuvette, of 4.4 mM benzophenone with 0.1 M diphenylmethanol in benzene (quantum yield of ~0.5−1.0 in degassed solutions; Moore et al., 1961).



In these conditions, and using the 60 W lamp system, the half-life of benzophenone was ca. 18 min.

Synthesis of the ODN1−Benzophenone Conjugate (ODN2). ODN1 (30.3 nmol) was dissolved in 180 μL of 0.2 M borate buffer, pH 9. Two milligrams of 4-benzoylbenzoic acid *N*-hydroxysuccinimidyl ester (Sigma; total excess 200×) was solubilized in 20 μL of dry dimethylformamide (distilled on P_2O_5). Five aliquots (4 μL each) of this DMF solution were successively added to the stirred ODN solution, at 30 min intervals. The suspension was stirred for another 3 h after the last 4-benzoylbenzoic acid *N*-hydroxysuccinimidyl ester addition (total reaction time 5 h), centrifuged, and the supernatant filtered on a Nylon Acrodisc filter (0.45 μm, Gelman Sciences). This solution was precipitated with ethanol and the insoluble material redissolved in 200 μL of water. Pure ODN2 was isolated from this solution by HPLC (retention time = 25.5 min; yield 63%).

Synthesis of the Fluorescein−ODN2 Conjugate (ODN3). ODN2 (9.5 nmol) was dissolved in degassed phosphate buffer (100 mM, pH 7, 95 μL). A solution of tris(2-carboxyethyl)phosphine hydrochloride (TCEP, Sigma) in the same buffer (27.2 μg in 5 μL, 95 nmol, total excess 10×) was added to the ODN solution, and the stirred mixture was allowed to react in the dark under an argon atmosphere for 1 h. Nucleic acids were then precipitated by ethanol in order to eliminate the excess of unreacted TCEP, and the solid phase was dissolved in degassed phosphate buffer (180 μL). A solution of fluorescein-5-maleimide (Molecular Probes, 0.406 mg, 950

nmol, total excess 100×) in acetonitrile:water (1:1; 20 μL) was added to the solution of the reduced ODN2, and the mixture was stirred in the dark under an argon atmosphere for 30 min. ODN3 was first precipitated by ethanol and then purified by HPLC (retention time = 21.5 min; yield = 73%).

Radiolabeling of ODN3. Two IodoBeads (Pierce) were placed in an Eppendorf SafeLock tube, washed with phosphate buffer (0.1 M, pH 7.4, 3 × 1 mL), and covered with the same buffer (390 μL). A $Na^{125}I$ solution (10 μL, 1 mCi, Amersham) was carefully added to this suspension under a well-ventilated hood and allowed to react for 5 min. A solution of ODN3 (2.0 nmol) in phosphate buffer (0.1 M, pH 7.4, 100 μL) was then added. After 30 min of reaction, the supernatant was removed and mixed with a solution (500 μL) containing NaI (4.5 mg/mL) and $Na_2S_2O_3$ (4 mg/mL). The excess of radioiodine was eliminated by gel filtration on Sephadex G-25 (NAP-10, Pharmacia). After a concentration step (partial evaporation of the solution in a Speed Vac), an ethanol precipitation allowed one to obtain the radiolabeled ODN3 with a radiochemical purity of nearly 100% [paper chromatography assay on Whatman Chromatography Paper 1, 87 g/m^2, 0.16 mm thickness; mobile phase, methanol/water (7:3)].

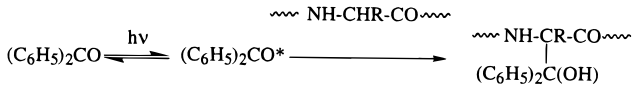
Photo-Cross-Linking of ODN3 to Human Thrombin. Human thrombin (176 pmol, ~3000 NIH units/mg of protein, Sigma) was dissolved in PBS−Ca^{2+} buffer (pH 7.4, 578 μL). An aqueous solution of radiolabeled ODN3 (22 μL, 176 pmol) was added. Half of this sample was exposed at 4 °C to UV irradiation in a Petri dish at a total power of 60 W. The other half was incubated in the dark (without being submitted to any UV irradiation). Aliquots submitted to both conditions were taken at different times ranging from 15 to 60 min. These aliquots were analyzed by a 5−15% SDS−PAGE (total amount of thrombin loaded per well = 100 ng). The gel was dried, exposed to a PhosphorImager intensifying screen, and read on a PhosphorImager apparatus (Molecular Dynamics, 410 A model) or autoradiographed.

Determination of the Photo-Cross-Linking Yield Using a Thrombin Aptamer. We used in this experiment Tasset's aptamer 60-18[29] [5′-AGT CCG TGG TAG GGC AGG TTG GGG T*GA CT-3′; K_d = 0.5 nM; Tasset et al. (1997)], which bears near the 3′ end an amino-modified T (indicated by an asterisk (*); Amino-Modifier C6 dT, Glen Research), to which a benzophenone moiety was coupled by the protocol used to obtain ODN2 (see above). Two parallel assays were conducted, involving (i) the 3′-amino aptamer 60−18[29] as a negative control and (ii) the 3′-benzophenone-derivatized aptamer 60-18[29]. Either 1.12 nmol of the 3′-amino aptamer 60-18[29] (solubilized in 10 μL of binding buffer, total excess 5×) or the same amount of the 3′-benzophenone-derivatized aptamer 60-18[29] was added to 7.5 μg of human thrombin (224 pmol, ~3000 NIH units/mg of protein, Sigma) solubilized in 740 μL of binding buffer (20 mM Tris acetate, pH 7.4, 140 mM NaCl, 5 mM KCl, 1 mM $CaCl_2$, 1 mM $MgCl_2$; Bock et al., 1992; Macaya et al., 1995). Half of both mixtures was exposed at 4 °C to 60 W UV irradiation in Petri dishes, while the other halves were incubated at 4 °C in the dark. Aliquots were taken at time intervals ranging 15−120 min. These aliquots were analyzed by 5−15% SDS−PAGE (total amount of thrombin loaded per well = 500 ng) and revealed by silver staining.

Binding Selectivity of ODN3 for Bovine Thrombin. An aqueous solution of radiolabeled ODN3 (9.2 μL, 73.5 pmol) was added to bovine thrombin (7.3 nmol, ~75 NIH units/mg of protein, Sigma) dissolved in PBS-Ca^{2+} buffer (pH 7.4, 40.8 μL) and incubated at 4 °C in the dark for 2 h, before UV irradiation at 8 W for 15 min. An aliquot of this solution (containing 10 μg of thrombin) was analyzed by a 5−15% SDS−PAGE, and the gel was treated as above.

RESULTS AND DISCUSSION

Engineering of the Probe. To generate an appropriate probe to study ODN−protein interactions, a benzophenone−ODN conjugate was selected for several reasons [reviewed by Dorman and Prestwich (1994)]. (i) Benzophenone is excited at a wavelength (333 nm) that does not affect proteins. (ii) Benzophenone has a broad reactivity: its easily accessible n,π* diradicaloid triplet state is able to cross-link with amino acids residues, one typical reaction being the insertion into the α C−H bond as illustrated below [for a detailed discussion, see Deseke et al. (1998)]:



(iii) Since its unreacted triplet state simply returns to the ground state and does not react with water, benzophenone can be repeatedly excited. Contrary to the irreversibly destructed photophores such as azides, benzophenone derivatives can thus repeatedly absorb photons, until a productive reaction takes place. This property considerably facilitates experiments since benzophenone derivatives can be manipulated in subdued day light without problem. (iv) High yields of photo-cross-linking are usually obtained. Typical photo-cross-linking yields are 40−80% (Williams and Coleman, 1982; Mahmood et al., 1987; Shoelson et al., 1993; Thiele and Fahrenholz, 1993; Chaudhary and Prestwich, 1997). Such clear advantages make benzophenone a molecule of choice in engineering photo-cross-linking ODNs.

The ODN chosen for this study was a PO−ODN 25-mer complementary to the AUG initiation site of the *gag* gene of HIV-1 (Lisziewicz et al., 1994). Its sequence contains only one dG, and the ODN should have no more affinity for thrombin than a random 25-mer. This ODN was further selected because of the wealth of biological information available on its PS counterpart, the gene-expression modulator 91 (GEM 91), an anti HIV-1 former drug candidate from Hybridon (Lisziewicz et al., 1994). We indeed intended to use the probe for subsequent experiments on cells.

The radiolabeling procedure was of course a critical aspect. A standard 5′-^{32}P labeling using T4 polynucleotide kinase was not considered, because phosphatases are known to easily remove this label (Shaw et al., 1991). Tritium labeling (Graham et al., 1993) was also disregarded, because of the long exposure times needed to reveal this β-emitting radionuclide. Fluorescein is a phenolic compound able to incorporate the ^{125}I γ-emitting radionuclide in high yield. Moreover, a fluorescein appendage allows one to use confocal microscopy in experiments involving whole cells (Pichon et al., 1997). The 3′-end of the ODN being reserved for the grafting of benzophenone, fluorescein was attached at its 5′-end. Both 5′- and 3′-ends of our ODN were thus capped by unnatural residues. This protects the sequence against exonuclease degradation (Arar et al., 1995).

Synthesis and Radiolabeling of the Probe (Figure 1). The 5′-pyridyl-dithio-3′-amino PO−ODN (ODN1) was obtained by a standard solid-support synthesis. A practi-

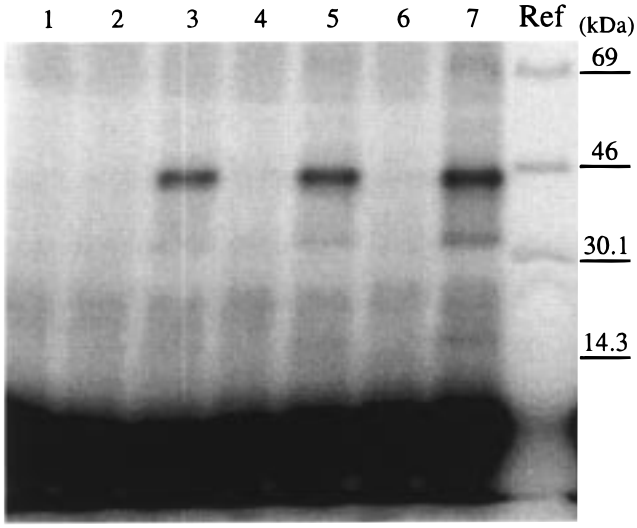


Figure 2. Photo-cross-linking of radioiodinated ODN3 to purified human thrombin. [^{125}I]ODN3 was incubated with thrombin without preincubation as explained in the text. Lane 1: starting time (0 min, no irradiation performed). Lanes 2, 4, and 6: incubation for 15, 30, and 60 min without irradiation. Lanes 3, 5 and 7: UV irradiation for 15, 30, and 60 min, respectively. Irradiation is necessary for photo-cross-linking to occur. The thrombin-ODN3 complex formed features a M_r of ca. 43 kDa, which corresponds to the sum of the MW of thrombin and ODN3.

cal way to monitor the reactions leading to ODN2 and ODN3 was reversed-phase HPLC. The coupling of ODN1, first with a benzophenone derivative and then with a fluorescein derivative, was in both cases associated with large changes in retention times, allowing for an easy recovery of the pure modified ODNs by semipreparative HPLC.

The grafting of benzophenone on the 3′-NH_2 of ODN1 was performed with a suspension of the insoluble 4-benzoylbenzoic acid N-hydroxysuccinimyl ester in an aqueous solution of the ODN. Assays of couplings in several binary solvents were unsuccessful. The chromatogram of the crude mixture was obscured by the presence of several byproducts derived from the acylating agent, but an ethanol precipitation greatly simplified the HPLC trace. Unreacted ODN1 (t_R = 18.1 min) and benzophenone-coupled ODN2 (t_R = 25.5 min, 63%) only subsisted.

The 5′-pyridyldithio moiety of ODN2 was reduced by a water-soluble phosphine. The 5′-HS−ODN was isolated by ethanol precipitation and immediately alkylated by fluorescein-5-maleimide. A new ethanol precipitation was necessary to remove the excess of the alkylating agent. The HPLC trace then showed only a low molecular weight contaminant (t_R = 18.7 min) followed by ODN3 (t_R = 21.5 min, baseline separation). The yield of the synthesis of ODN3 from ODN2 was 73%.

The radioiodination method used in this study was safe and efficient, reaching a specific radioactivity of 16 μCi/μg ODN (160.000 Ci/mol ODN or 18 × 10^{10} cpm/μmol ODN). For comparison, a specific radioactivity of the order of 12 × 10^7 cpm/μmol ODN would have been obtained if ODN3 had been tritiated by Graham's method (specific radioactivity accessible with Graham's protocol: ca. 4 × 10^7 cpm/μmol of purine; Graham et al., 1993). Sodium thiosulfate was added after radioiodination to quench any remaining electrophilic halogen species. Cold sodium iodide was also added to displace radioactive iodide anions possibly associated to the biopolymer by weak forces. A gel exclusion chromatography, followed by an ethanol precipitation, was then performed.

Photoaffinity Labeling of Human Thrombin. As long as no G-quartet is involved in the structure of ODN3, the dissociation constant of its complex with thrombin is estimated to be in the micromolar range or higher: K_d = 8.3 μM for a random library of 96-mers and 5.0 μM for

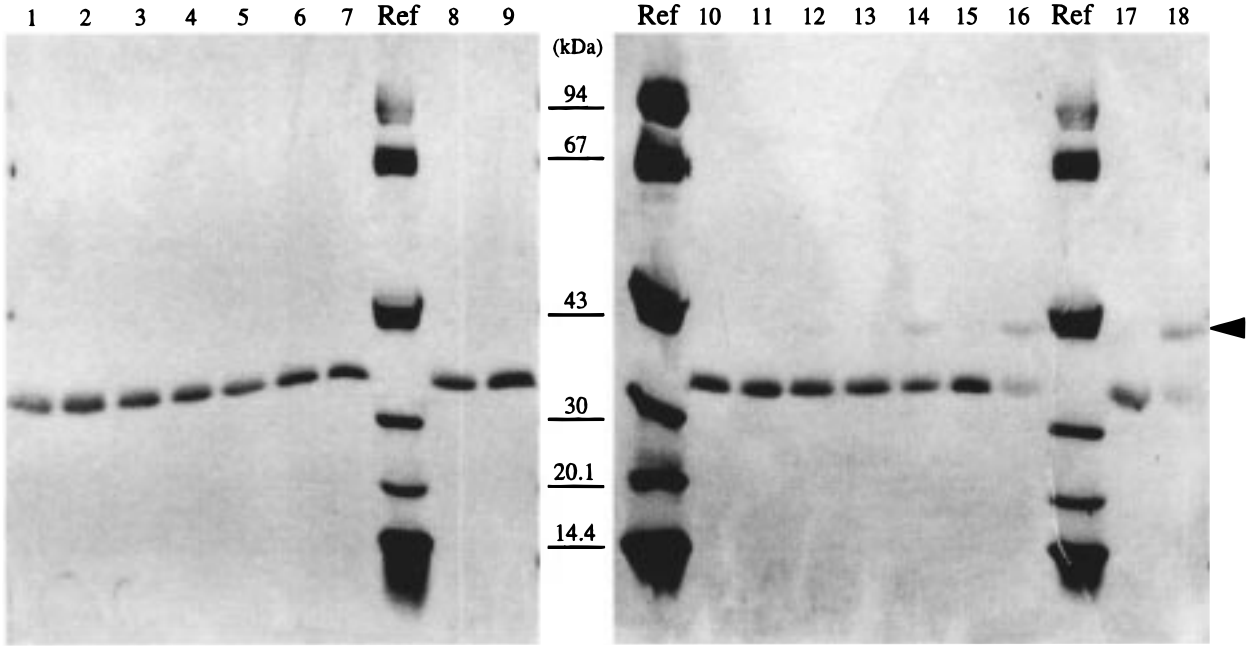


Figure 3. Silver-stained PAGE: yield of photo-cross-linking and necessity of a benzophenone residue for the photo-cross-linking to occur. Thrombin aptamer 60−18[29] was incubated with purified human thrombin, without preincubation as explained in the text. On the left, this aptamer was only 3′-protected by an amino function. On the right, the aptamer was bearing a 3′ benzophenone residue. Lanes 1 and 10: starting time (0 min, no irradiation performed). Lanes 2, 4, 6, 8, 11, 13, 15, and 17: incubation for 15, 30, 60 and 120 min without irradiation. Lanes 3, 5, 7, 9, 12, 14, 16, and 18: UV irradiation for 15, 30, 60, and 120 min, respectively. The presence of benzophenone and irradiation were necessary for the photo-cross-linking to occur (the product of which is indicated by an arrowhead at right). The yield of photo-cross-linking, measured by gel scanning, increased from 15% after 15 min of irradiation to 70% after 120 min.

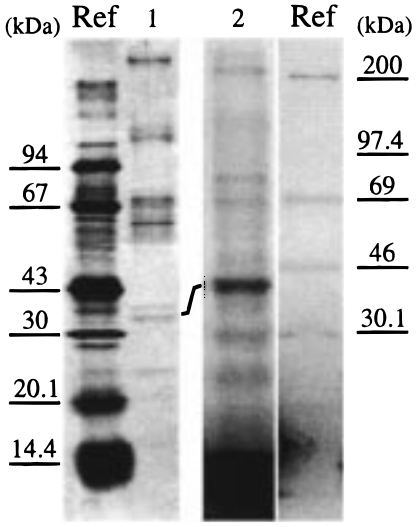


Figure 4. Binding selectivity of radioiodinated ODN3 for bovine thrombin in a crude preparation. Lane 1 is a silver staining of 400 ng of a crude bovine thrombin sample. Lane 2 is the PhosphorImager analysis of its photo-cross-linking with [^{125}I]ODN3. Markers for silver staining (from Pharmacia Biotech) are shown at left. Radiomarkers (from Amersham) are shown at right. The twisted bar between the two gels indicates band shift upon formation of a covalent complex.

a random library of 66-mers (Tasset et al., 1997); $K_d = 1$ μM for a 24-mer having a low propensity to form a G-quartet (ODN ***5*** of Macaya et al., 1995). The photo-cross-linking conditions used in this experiment were thus rather demanding as the complexed fraction of the ODN was probably as low as a few percent.

Figure 2 shows the results of the photolabeling of the purest commercially available human thrombin. No labeling was observed without irradiation. The maximum labeling yield was reached within 1 h. The intensity of the thrombin band decreased thereafter (data not shown), probably due to the photohydrolysis of the carbon−iodine bond releasing $^{125}I^-$ iodide anions (Wolf and Kharasch, 1961; Tejedor and Ballesta, 1983; Boule et al., 1984). As expected, the photo-cross-linking of thrombin increased its apparent molecular mass, from ca. 33.5 kDa to ca. 43 kDa, corresponding to the sum of the molecular masses of thrombin and ODN3. The association of ODN3 with thrombin was relatively rapid as a preincubation in the dark before irradiation had no effect on the intensity of the shifted band (data not shown).

Determination of the Photo-Cross-Linking Yield Using a High-Affinity Thrombin Aptamer. The irradiation of a dilute equimolar mixture of human thrombin with [^{125}I]ODN3 gave a low yield of labeled thrombin, as indicated by the ratio of the protein-associated radioactivity to the radioactivity migrating at the front of the PAGE (assumed to represent unreacted [^{125}I]ODN3; Figure 2). This could be due either to the very low equilibrium concentration of the thrombin−ODN3 complex, or to the inefficacy of the coupling reaction. The second hypothesis seemed unlikely, since yields are usually described as excellent. We nevertheless determined the efficacy of photo-cross-linking, using a conjugate of benzophenone with an aptamer featuring a high affinity for thrombin. Tasset's aptamer 60-18[29], whose K_d for thrombin is about 0.5 nM (Tasset et al., 1997), was coupled to a benzophenone molecule, and a mixture of thrombin with an excess of this conjugate was irradiated (in this case, human thrombin was calculated to be practically 100% in the form of its complex). We detected by silver staining on PAGE both unreacted thrombin and the thrombin−ODN covalent complex (Figure 3). The photo-cross-linking yield at a given irradiation time was determined as the amount of complex formed versus the total amount of thrombin. This yield increased with the irradiation time from 15% after 15 min to 70% after 2 h. The efficacy of the photochemical reaction was thus high, as expected.

A benzophenone moiety was necessary for the cross-linking to occur: even under irradiation, the underivatized aptamer formed no detectable SDS-stable complex with thrombin.

Binding Selectivity of ODN3 for Bovine Thrombin. As can be seen in Figure 4, ODN3 showed a chemoselectivity for bovine thrombin: despite this protein being only a minor constituent in a crude preparation, the major band observed resulted from the association of ODN3 with bovine thrombin.

Conclusion and Perpectives. We reported in this communication an efficient synthesis of a multipurpose ODN derivative. This probe was able to selectively photolabel a low-affinity protein using mild irradiation conditions after such a short time as 15 min. The probe was designed for time-resolved and space-resolved experiments on whole cells. We are currently using this tool for deciphering the process of ODN entry into mammalian cells.

ACKNOWLEDGMENT

C.B. was Aspirant of the Belgian Fonds National de la Recherche Scientifique. This work was supported by the French Agence Nationale de Recherche sur le SIDA, the Fonds des Sciences of the UCL (fellowship to C.B.), Fonds National de la Recherche Scientifique and the Belgian Federal Office for Scientific, Technical, and Cultural Affairs (Concerted Actions 172-94/99). The authors wish to thank Prof. M. Monsigny for a gift of ODN1 as well as for advice in synthesis, and Prof. Bernard Gallez for counseling in the radioiodination experiments.

LITERATURE CITED

Akhtar, S., and Juliano, R. L. (1992) Cellular uptake and intracellular fate of antisense oligonucleotides. *Trends Cell Biol. 2*, 139−144.

Arar, K., Aubertin, A.-M., Roche, A.-C., Monsigny, M., and Mayer, R. (1995) Synthesis and antiviral activity of peptide−oligonucleotide conjugates prepared by using N_α-bromoacetyl peptides. *Bioconjugate Chem. 6*, 573−577.

Beltinger, C., Saragovi, H. U., Smith, R. M., LeSauteur, L., Shah, N., DeDionisio, L., Christensen, L., Raible, A., Jarett, L., and Gewirtz, A. M. (1995) Binding, uptake, and intracellular trafficking of phosphorothioate-modified oligodeoxynucleotides. *J. Clin. Invest. 95*, 1814−1823.

Bock, L. C., Griffin, L. C., Latham, J. A., Vermaas, E. H., and Toole, J. J. (1992) Selection of single-stranded DNA molecules that bind and inhibit human thrombin. *Nature 355*, 564−566.

Boule, P., Guyon, C., and Lemaire, J. (1984) Photochemistry and environment VI. Direct phototransformation of chlorophenols and interactions with phenol on UV exposure in aqueous solution. *Toxicol. Environ. Chem. 7*, 97−110.

Brown, T., and Brown, D. J. S. (1991) Modern machine-aided methods of oligodeoxyribonucleotide synthesis. in *Oligonucleotides and Analogues. A Practical Approach* (F. Eckstein, Ed.) pp 1−24, IRL Press at Oxford University Press, Oxford.

Chaudhary, A., and Prestwich, G. D. (1997) Photoaffinity analogue for the antiinflammatory drug α-trinositol: synthesis and identification of putative molecular targets. *Bioconjugate Chem. 8*, 680−685.

Deseke, E., Nakatani, Y., and Ourisson G. (1998) Intrinsic reactivities of amino acids towards photoalkylation with benzophenone. A study preliminary to photolabeling of the transmembrane protein glycophorin A. *Eur. J. Org. Chem. 2*, 243−251.

Dorman, G., and Prestwich, G. D. (1994) Benzophenone photophores in biochemistry. *Biochemistry 33*, 5661−5673.

Graham, M. J., Freier, S. M., Crooke, R. M., Ecker, D. J., Maslova, R. N., and Lesnik, E. A. (1993) Tritium labeling of antisense oligonucleotides by exchange with tritiated water. *Nucleic Acids Res. 21*, 3737−3743.

Greig, M. J., Gaus, H., Cummins, L. L., Sasmor, H., and Griffey, R. H. (1995) Measurement of macromolecular binding using electrospray mass spectrometry. Determination of dissociation constants for oligonucleotide-serum albumin complexes. *J. Am. Chem. Soc. 117*, 10765−10766.

Lisziewicz, J., Sun, D., Weichold, F. F., Thierry, A. R., Lusso, P., Tang, J., Gallo, R. C., and Agrawal, S. (1994) Antisense oligodeoxynucleotide phosphorothioate complementary to Gag mRNA blocks replication of human immunodeficiency virus type 1 in human peripheral blood cells. *Proc. Natl. Acad. Sci. U.S.A. 91*, 7942−7946.

Loke, S. L., Stein, C. A., Zhang, X. H., Mori, K., Nakanishi, M., Subasinghe, C., Cohen, J. S., and Neckers, L. M. (1989) Characterization of oligonucleotide transport into living cells. *Proc. Natl. Acad. Sci. U.S.A. 86*, 3474−3478.

Macaya, R. F., Waldron, J. A., Beutel, B. A., Gao, H., Joesten, M. E., Yang, M., Patel, R., Bertelsen, A. H., and Cook, A. F. (1995) Structural and functional characterization of potent antithrombotic oligonucleotides possessing both quadruplex and duplex motifs. *Biochemistry 34*, 4478−4492.

Mahmood, R., Cremo, C, Nakamaye, K. L., and Yount, R. G. (1987) The interaction and photolabeling of myosin subfragment 1 with 3′(2′)-O-(4-benzoyl)benzoyl-adenosine 5′-triphosphate. *J. Biol. Chem. 262*, 14479−14486.

Moore, W. M., Hammond, G. S., and Foss, R. P. (1961) Mechanisms of photoreactions in solutions. I. Reduction of benzophenone by benzhydrol. *J. Am. Chem. Soc. 83*, 2789−2794.

Padmanabhan, K., Padmanabhan, K. P., Ferrara, J. D., Sadler, J. E., and Tulinsky, A. (1993) The structure of α-thrombin inhibited by a 15-mer single-stranded DNA aptamer. *J. Biol. Chem. 268*, 17651−17654.

Pichon, C., Arar, K., Stewart, A. J., Duc Dodon, M., Gazzolo, L., Courtoy, P. J., Mayer, R., Monsigny, M., and Roche, A.-C. (1997) Intracellular routing and inhibitory activity of oligonucleopeptides containing a KDEL motif. *Mol. Pharmacol. 51*, 431−438.

Shaw, J.-P., Kenneth, K., Bird, J., Fishback, J., and Froehler, B. (1991) Modified deoxyoligonucleotides stable to exonuclease degradation in serum. *Nucleic Acids Res. 19*, 747−750.

Shaw, J.-P., Fishback, J. A., Cundy, K. C., and Lee, W. A. (1995) A novel oligodeoxynucleotide inhibitor of thrombin. I. In vitro metabolic stability in plasma and serum. *Pharm. Res. 12*, 1937−1942.

Shoelson, S. E., Lee, J., Lynch, C. S., Backer, J. M., and Pilch, P. F. (1993) Bpa^{B25} insulins. photoactivatable analogues that quantitatively cross-link, radiolabel and activate the insulin receptor. *J. Biol. Chem. 268*, 4085−4091.

Stein, C. A. (1995) Does antisense exist? *Nat. Med. 1*, 1119−1121.

Tasset, D. M., Kubick, M. F., and Steiner, W. (1997) Oligonucleotide inhibitors of human thrombin that bind distinct epitopes. *J. Mol. Biol. 272*, 688−698.

Tejedor, F., and Ballesta, J. P. G. (1983) Iodination of *p*-nitrophenyl ethers used as photolabels. *Anal. Biochem. 128*, 115−120.

Thiele, C., and Fahrenholz, F. (1993) Photoaffinity labeling of central cholecystokinin receptors with high efficiency. *Biochemistry 32*, 2741−2746.

Tidd, D. M., and Warenius H. M. (1989) Partial protection of oncogene, anti-sense oligodeoxynucleotides against serum nuclease degradation using terminal methylphosphonate groups. *Br. J. Cancer 60*, 343−350.

Tsiang, M., Jain, A. K., Dunn, K. E., Rojas, M. E., Leung, L. L. K., and Gibbs, C. S. (1995) Functional mapping of the surface residues of human thrombin. *J. Biol. Chem. 270*, 16854−16863.

Wang, K. Y., Krawczyk, S. H., Bischofberger, N., Swaminathan, S., and Bolton, P. H. (1993) The tertiary structure of a DNA aptamer which binds to and inhibits thrombin determines activity. *Biochemistry 32*, 11285−11292.

Williams, N., and Coleman, P. S. (1982) Exploring the adenine nucleotide binding sites on mitochondrial F_1-ATPase with a new photoaffinity probe, 3′-O-(4-Benzoyl)-benzoyl adenosine 5′-triphosphate. *J. Biol. Chem. 257*, 2834−2841.

Wolf, W., and Kharasch, N. (1961) Photolysis of aromatic iodo compounds as a synthetic tool. *J. Org. Chem. 26*, 283−284.

Yakubov, L. A., Deeva, E. A., Zarytova, V. F., Ivanova, E. M., Ryte, A. S., Yurchenko, L. V., and Vlassov, V. V. (1989) Mechanism of oligonucleotide uptake by cells: Involvement of specific receptors? *Proc. Natl. Acad. Sci. U.S.A. 86*, 6454−6458.

BC980065F

Poly(ethylene glycol)-*block*-poly(L-lysine) Dendrimer: Novel Linear Polymer/Dendrimer Block Copolymer Forming a Spherical Water-Soluble Polyionic Complex with DNA

Joon Sig Choi, Eun Jung Lee, Young Hun Choi, Yong Joo Jeong, and Jong Sang Park*

Department of Chemistry, Seoul National University, San 56-1, Shillim-dong, Kwanak-ku, Seoul, 151-742, Korea. Received June 20, 1998; Revised Manuscript Received September 17, 1998

Methoxypoly(ethylene glycol)-*block*-poly(L-lysine) dendrimer was designed to form a water-soluble complex with plasmid DNA. The copolymer was synthesized by the liquid-phase peptide synthesis method. It was characterized by ^{1}H NMR and matrix-assisted laser desorption ionization-time-of-flight (MALDI-TOF) mass spectrum. Agarose gel electrophoresis and DNase I protection assay proved that this linear polymer/dendrimer block copolymer assembled spontaneously with plasmid DNA, forming a water-soluble complex which increased the stability of the complexed DNA. Atomic force microscopy of the complex was evaluated at various charge ratios showing that the copolymer/DNA complex was like a globular shape.

Block copolymers containing poly(ethylene glycol) (PEG) have been used in various drug delivery systems (*1*). PEG is a very attractive polymer in some aspects. The polymer is nontoxic, nonimmunogenic, and effective in solubilizing other hydrophobic polymers coupled to it (*2*). PEG has been conjugated linearly to polycationic polymers such as poly(L-lysine) (PLL) (*3*) and polyspermine (*4*) in order to improve solubility and gene transfer efficiency. Also, we have demonstrated that PEG-*graft*-PLL, a comb-shaped copolymer, showed improved cell viability and transfection efficiency in comparison with PLL (*5*).

The physicochemical characteristics of the methoxypoly(ethylene glycol) (mPEG)-*block*-PLL copolymer/nucleic acid complex have been recently studied. The shape and size distributions of the complex were reported to be dependent on the nature of PLL and/or the nucleic acid. In the case of the mPEG-*b*-PLL (10 kDa) complexed with plasmid DNA, a large size exceeding 100 nm was observed, forming a extended toroidal structure (*3*). In comparison, the mPEG-*b*-PLL (20 mer)/salmon testes DNA complex demonstrated that a smaller sized complex was dominant with a small fraction of secondary aggregates (*6*). Also, the mPEG-*b*-PLL (18 mer) was analyzed to form a small spherical nanoassociate with antisense oligonucleotide (ca. 60 nm) by the dynamic light-scattering method (*7*).

Many synthetic polycationic polymers were synthesized and tested for their potential utility in the field of gene therapy. Among them, dendrimers—hyperbranched macromolecules—were distinctive due to their defined structure and large number of surface amino groups. Polycationic dendrimers are capable of electrostatic interaction with polyanions, such as nucleic acids. Therefore, some dendrimers were introduced for the transfer of antisense (*8*) or plasmid DNA (*9*) in vitro and showed remarkable efficiency.

In keeping with the polymers mentioned above, we report herein a conceptually new approach that is designed to conjugate linear PEG with a dense globular macromolecule, PLL dendrimer. We present the characteristics of the complex formed by plasmid DNA and this linear polymer/dendrimer block copolymer that is composed of biocompatible mPEG and L-lysine.

We synthesized the mPEG-*b*-PLL dendrimer in which 16 surface amines were present (generation 4, Figure 1A). mPEG-amine (Sigma, St. Louis, MO) was used as the polymeric supporter, and the PLL dendrimer was prepared by repeated liquid-phase peptide synthesis (*10*) using fluoren-9-ylmethoxycarbonyl (Fmoc) chemistry. mPEG-amine (M_w = 5757, M_n = 5697, M_w/M_n = 1.01, determined by MALDI-TOF mass spectrum) was stirred with 4 equiv of *N*-hydroxybenzotriazole (HOBt), 2-(1H-benzotriazole-1-yl)-1,1,3,3-tetramethyluronium hexafluorophosphate (HBTU), *N*-α-*N*-ϵ-di-Fmoc-L-lysine (AnaSpec, Inc., San Jose, CA), and *N*,*N*-diisopropylethylamine (DIPEA), respectively, in anhydrous *N*,*N*-dimethylformamide (DMF). After the coupling reaction reached completion, the mixture was precipitated with 10-fold excess of cold ether and further washed two times with ether. Piperidine (30%) was used for deprotection of the Fmoc group of lysine. The reaction mixture was precipitated and washed with cold ether as mentioned above. From the reaction mixture, only mPEG-coupled products were precipitated in cold ether, and other byproducts were removed by washing with excess ether. To remove small traces of excess reagents, the precipitate was recrystalized in pure ethanol. The precipitates were dried in vacuo and prepared for further coupling reaction. The coupling and deprotection reactions were repeated four times. The amounts of *N*-α-*N*-ϵ-di-Fmoc-L-lysine, HOBt, HBTU, and DIPEA were doubled in each coupling reaction to meet the 4 equiv. Each reaction progress was monitored by ninhydrin test and ^{1}H NMR until completed.[1] The copolymer was dialyzed for 1 day against water using Spectra/Por dialysis membrane (molecular weight cutoff = 6000−8000, Spectrum, Los Angeles, CA) and collected by freeze drying. This linear polymer/dendrimer block copolymer was further characterized by MALDI-TOF

* To whom correspondence should be addressed. Tel: +82 2 880 6660. Fax: +82 2 889 1568. E-mail: pfjspark@plaza.snu.ac.kr.

[1] ^{1}H NMR (D_2O): δ 1.64 [br m, $(CH_2)_3$], 3.08 (br m, CH_2−N), 3.39 (s, CH_3−O), 3.68 (s, CH_2CH_2−O), 4.25 (br m, COCH−N).

10.1021/bc9800668 CCC: $18.00 © 1999 American Chemical Society
Published on Web 12/31/1998

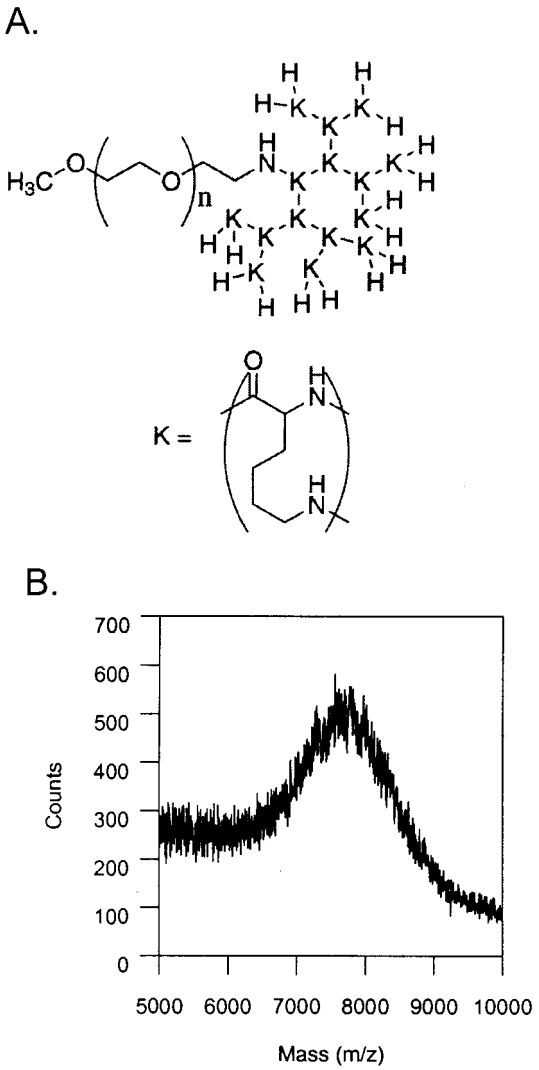


Figure 1. (A) Structural formula of mPEG-*b*-PLL dendrimer. (B) MALDI-TOF mass spectrum of the copolymer. The spectrum was obtained on a PerSeptive Biosystems instrument in the linear mode at 20 kV. The sample was dissolved in water containing 2,5-dihydroxybenzoic acid as a matrix.

mass spectrum (PerSeptive Biosystems, Inc., Framingham, MA) (Figure 1B). The M_w and M_n values of this copolymer were 7594 and 7553, respectively (M_w/M_n = 1.01).[2]

Figure 2 shows the agarose gel electrophoresis data of the copolymer/plasmid DNA associates. Complexes were formed at different charge ratios between the copolymer and pSV-β-gal plasmid DNA (Promega, Madison, WI) by incubation in 15 mM HEPES buffer (0.15 M NaCl, pH 7.4) at room temperature for 30 min. Each sample was then analyzed by electrophoresis on a 0.7% agarose gel containing ethidium bromide (0.5 μg/mL of gel). As the quantity of mPEG-*b*-PLL dendrimer increased, inhibition of migration into the agarose gel increased. At a cationic/anionic charge ratio of 2, complete retardation occurred (lane 3).

The shape and particle size distributions of the copolymer/plasmid complex at various charge ratios were examined by atomic force microscopy (NanoScope IIIa system, Digital Instruments, Inc., Santa Barbara, CA) under the same condition as reported previously with

[2] The M_w and M_n values of the product based on its structural formula were calculated to be 7678 and 7618, respectively.

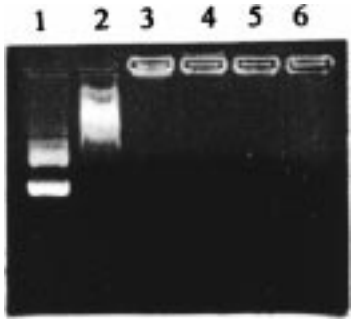


Figure 2. Analysis of complex formation at various charge ratios by agarose gel electrophoresis. pSV-β-gal plasmid DNA (1.0 μg) only (lane 1), charge ratio of copolymer/DNA = 1, 2, 3, 5, and 6 (lanes 2, 3, 4, 5, and 6, respectively). A total of 1.89×10^{15} negative charges are present per 1.0 μg of plasmid DNA, whereas the copolymer has 1.26×10^{15} charges/1.0 μg.

some modification (*3*). From the aqueous complex solution, 1−2 μL containing a final 10 μg/mL of plasmid DNA was deposited onto the surface of freshly split mica. After 1−2 min for adsorption, excess solution was removed by filter paper. The mica was further dried in room temperature and prepared for imaging. When the copolymer was mixed below the charge ratio enough to neutralize DNA, partially associated particles were observed (charge ratio of copolymer/DNA = 1, Figure 3A) as already shown in agarose gel electrophoresis (Figure 2, lane 2). Globular complexes were predominant in the case of charge ratio of copolymer/DNA = 2 (Figure 3B). When the charge ratio was raised to 4, even though a few further associated aggregates between some complexes were observed, most of the complexes were like globular shapes (Figure 3C). In both cases when the charge ratio of copolymer/DNA = 2 or 4, the size range was from ~50 to 250 nm. The average diameter was calculated to be 105 ± 67 nm (copolymer/DNA = 2, n = 30). It could be thought that the complex composed of the mPEG-*b*-PLL dendrimer/pSV-β-gal DNA forms an apparent globular structure, in contrast to the extended toroidal structures of the mPEG-*b*-PLL block copolymer/DNA complex (*3*). It was supposed that PLL dendrimer contained more condensed surface amines in a spatial arrangement than linear PLL and that the dendrimer behaved as a nondraining globular biopolymer (*11*), which led to the ability of this linear polymer/dendrimer block copolymer to form a spherical complex with plasmid DNA.

Nuclease resistance of the complexed DNA was examined at different charge ratios. After adding the copolymer to 4.0 μg of plasmid DNA at various charge ratios from 0 to 4 in 50 μL of 20 mM HEPES buffer (0.15 M NaCl, pH 7.4), the mixtures were incubated for 30 min at room temperature. After incubation, the mixtures were further incubated in the presence of 8.9 units of DNase I (Sigma, St. Louis, MO) for 20 min at room temperature. A total of 75 μL of stop solution (4 M ammonium acetate, 20 mM EDTA, and 2 mg/mL glycogen) was added to each mixture, which was kept in ice. After addition of 37 μL of 1% SDS, DNA was extracted with TE-saturated phenol/chloroform and precipitated by ethanol. The DNA was analyzed by 0.7% agarose gel electrophoresis (Figure 4). In the case of low charge ratios (lanes 2, 3, and 4), plasmid DNA was fragmented and linearized. The position of linearized plasmid DNA was compared with the molecular weight marker. But, nuclease resistance of the complexed DNA was improved much as the charge ratio of the copolymer/DNA increased up to 2 or 4 (lanes 5 and 6). No fragmentation was observed, and both supercoiled and open circular forms of plasmid DNA were obtained.

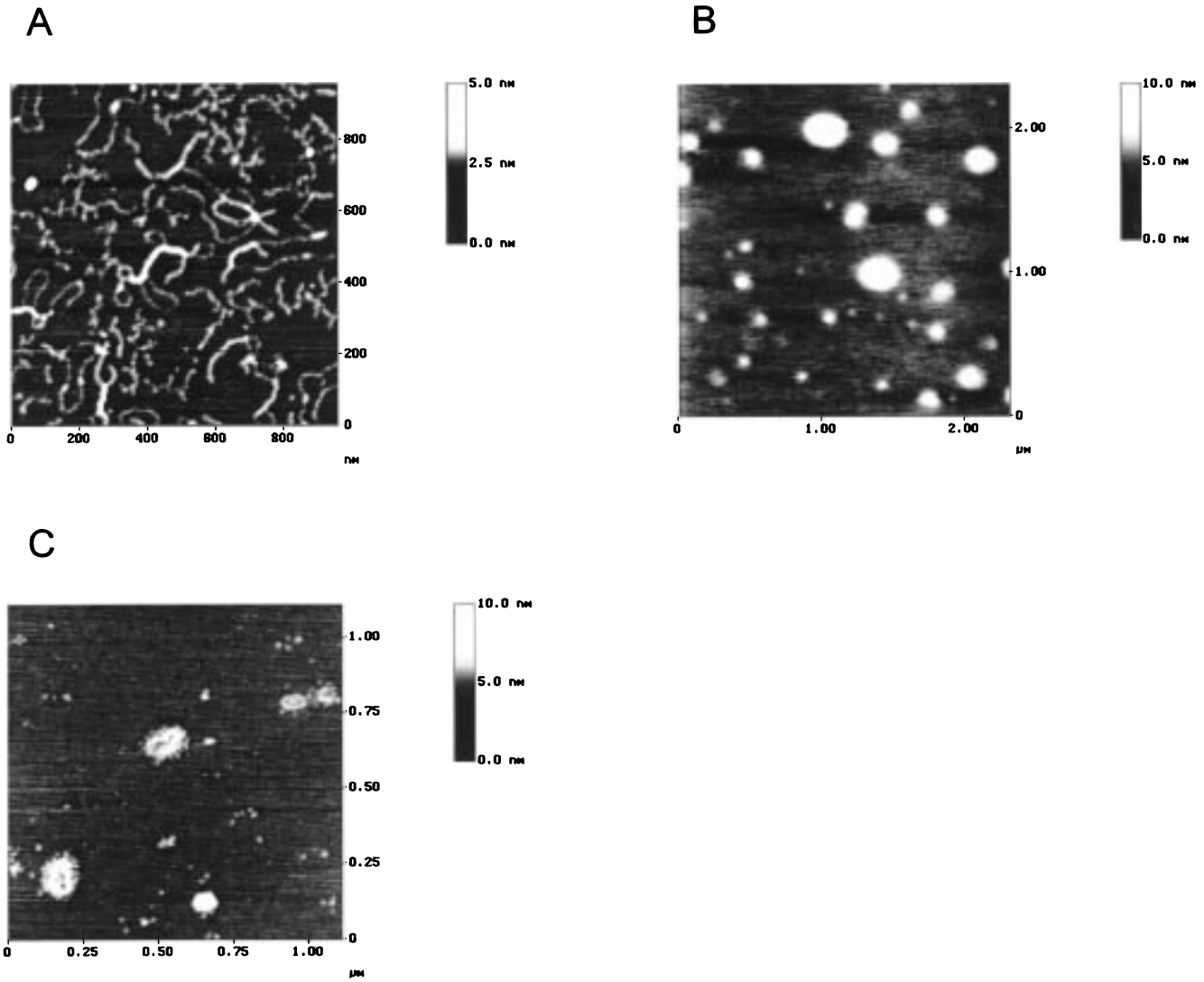


Figure 3. The atomic force microscopy images of the mPEG-*b*-PLL dendrimer/pSV-*β*-gal complex. Charge ratios of copolymer/DNA = 1, 2, and 4 (A, B, and C). The image mode was set to tapping mode. The white color indicates a height more than the designated nm above the mica surface. The *x* and *y* dimensions are scaled as shown.

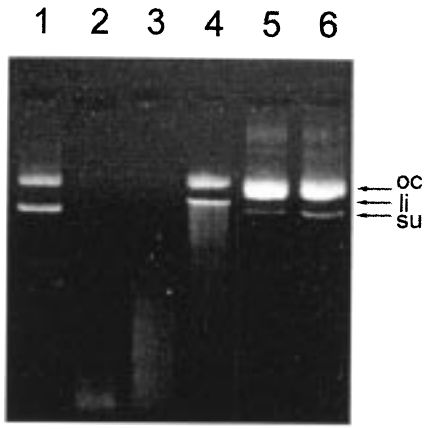


Figure 4. Stability of mPEG-*b*-PLL/plasmid DNA complexes to DNase I at various charge ratios. Undigested plasmid DNA (lane 1), Charge ratio of copolymer/DNA = 0, 0.5, 1, 2, and 4 (lanes 2, 3, 4, 5, and 6, respectively). The positions of the open circular (*oc*), linear (*li*), and supercoiled (*su*) forms are indicated on the right.

Moreover, the amount of supercoiled DNA increased as the charge ratio increased. Even though the complex could not completely protect the plasmid DNA, it is thought to be valuable in considering the recent report that the open circular form of plasmid DNA gave almost the same gene expression efficiency relative to supercoiled DNA (12).

In conclusion, it was proved that this novel linear/dendrimer block copolymer could self-assemble with plasmid DNA at physiological condition, forming a compact and water-soluble polyionic complex. The formed complex was found to take a globular shape with a relatively narrow size distribution. Nuclease resistance of the complex proved that the copolymer increased much the stability of the complexed plasmid DNA. In viewing the results obtained, this copolymer could be valuable in in vitro and/or in vivo delivery of genetic materials, such as antisense or plasmid DNA. Such a study is now in progress in our laboratory.

ACKNOWLEDGMENT

This work was supported by grants from the Korea Research Foundation, the Center for Molecular Catalysis at Seoul National University, the Inter-University Center of Natural Science Research Facilities, the Ministry of Education in Korea, and the Seoul National University Fund.

LITERATURE CITED

(1) Kataoka, K., Kwon, G. S., Yokoyama, M., Okano, T., and Sakurai, Y. (1993) Block copolymer micelles as vehicles for drug delivery. *J. Controlled Release 24*, 119−132.

(2) Gref, R., Minamitake, Y., Peracchia, M. T., Trubetskoy, V., Torchilin, V., and Langer, R. (1994) Biodegradable Long-Circulating Polymeric Nanospheres. *Science 263*, 1600−1603.

(3) Wolfert, M. A., Schacht, E. H., Toncheva, V., Ulbrich, K., Nazarova, O., and Seymour, L. W. (1996) Characterization of Vectors for Gene Therapy Formed by Self-Assembly of DNA with Synthetic Block Co-polymers. *Hum. Gene Ther. 7*, 2123-2133.

(4) Kabanov, A. V., Vinogradov, S. V., Suzdaltseva, Y. G., and Alakhov, V. Y. (1995) Water-Soluble Block Polycations as Carriers for Oligonucleotide Delivery. *Bioconjugate Chem. 6*, 639−643.

(5) Choi, Y. H., Liu, F., Kim, J. S., Choi, Y. K., Park, J. S., and Kim, S. W. (1998) Poly(ethylene glycol)-grafted poly-L-lysine as polymeric gene carrier. *J. Controlled Release 54*, 39−48.

(6) Katayose, S., and Kataoka, K. (1997) Water-Soluble Polyion Complex Associates of DNA and Poly(ethylene glycol)-Poly(L-lysine) Block Copolymer. *Bioconjugate Chem. 8*, 702−707.

(7) Kataoka, K., Togawa, H., Harada, A., Yasugi, K., Matsumoto, T., and Katayose, S. (1996) Spontaneous Formation of Polyion Complex Micelles with Narrow Distribution from Antisense Oligonucleotide and Cationic Block Copolymer in Physiological Saline. *Macromolecules 29*, 8556−8557.

(8) Bielinska, A., Kukowska-Latallo, J. F., Johnson, J., Tomalia, D. A., and Baker, J. R. (1996) Regulation of in vitro gene expression using antisense oligonucleotides or antisense expression plasmids transfected using starburst PAMAM dendrimers. *Nucleic Acids Res. 24*, 2176−2182.

(9) Tang, M. X., Redemann, C. T., and Szoka, F. C. (1996) In Vitro Gene Delivery by Degraded Polyamidoamine Dendrimers. *Bioconjugate Chem. 7*, 703−714.

(10) Bayer, E., and Mutter, M. (1979) The Liquid-Phase Method for Peptide Synthesis. in *The Peptides* (Gross, E., and Meienhofer, J., Eds.) Vol. 2, pp 285−332, Academic Press, New York.

(11) Aharoni, S. M., Crosby, C. R., III, and Walsh, E. K. (1982) Size and Solution Properties of Globular *tert*-Butyloxycarbonyl-poly(α,ϵ-L-lysine). *Macromolecules 15*, 1093−1098.

(12) Adami, R. C., Collard, W. T., Gupta, S. A., Kwok, K. Y., Bonadio, J., and Rice, K. G. (1998) Stability of Peptide-Condensed Plasmid DNA Formulations. *J. Pharm. Sci. 87*, 678−683.

BC9800668

Bis-Intercalation of Homodimeric Thiazole Orange Dye Derivatives in DNA

Michael Petersen, Atef A. Hamed, Erik B. Pedersen, and Jens Peter Jacobsen*

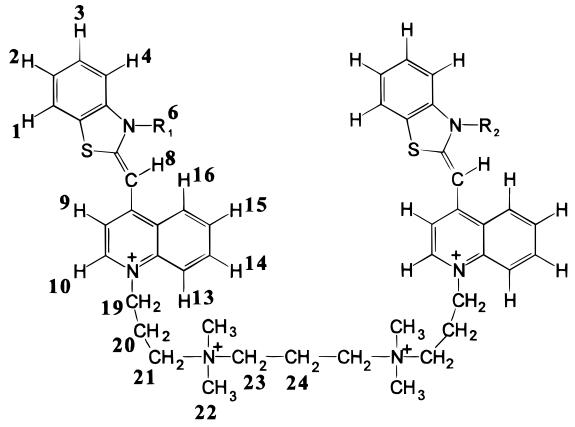
Department of Chemistry, Odense University, Odense M, DK-5230 Denmark. Received June 20, 1998; Revised Manuscript Received November 17, 1998

The thiazole orange dye 1,1′-(4,4,8,8-tetramethyl-4,8-diazaundecamethylene)-bis-4-[(3-methyl-2,3-dihydro-2(3H)-benzo-1,3-thiazolylidene)methyl]quinolinium tetraiodide (TOTO) binds to double-stranded DNA (dsDNA) in a sequence selective bis-intercalation. We have examined the binding of derivatives of TOTO with different substituents on the benzothiazole ring. The analogues are the following: 1,1′-(4,4,8,8-tetramethyl-4,8-diazaundecamethylene)-[4-[3-(benzyl-2,3-dihydro-2-(3H)-benzothiazolylidene)methyl]quinolinium]-[4-[3-(methyl-2,3-dihydro-2-(3H)-benzothiazolylidene)methyl]-quinolinium]tetraiodide (TOTOBzl) and 1,1′-(4,4,8,8-tetramethyl-4,8-diazaundecamethylene)-bis-4-[(3-ethyl-2,3-dihydro-2(3H)-benzo-1,3-thiazole)methyl]quinolinium tetraiodide (TOTOEt). In this paper, we report the synthesis of TOTOBzl and TOTOEt together with the one- and two-dimensional ^{1}H NMR investigations of complexes between these TOTO analogues and the dsDNA oligonucleotide d(CGCTAGCG)$_2$. Both analogues yield extremely stable complexes in which each chromophore is sandwiched between two base pairs in a (5′-CpT-3′):(5′-ApG-3′) site. The linker spans over two base pairs in the minor groove. The benzyl group in TOTOBzl and the ethyl groups in TOTOEt is pointing outward in the major groove.

INTRODUCTION

Interest in nonradioactive detection of nucleic acids has led to the search for DNA[1] stains that are stable under gel electrophoretic conditions. Recently, this has led to the synthesis and characterization of a family of homo- and heterodimeric DNA-binding dyes (Benson et al., 1993a,b; Rye et al., 1992). These dyes form highly fluorescent and stable noncovalent complexes with double-stranded DNA (dsDNA). Prominent among these are 1,1′-(4,4,8,8-tetramethyl-4,8-diazaundecamethylene)-bis-4-[(3-methyl-2,3-dihydro-2(3H)-benzo-1,3-thiazolyl idene)methyl]quinolinium tetraiodide (TOTO, Scheme 1). The enhancement of the fluorescence quantum yield of TOTO upon complex formation with dsDNA is greater than 1000 (Rye et al., 1992), and $t_{1/2}$ for the dissociation of the dsDNA-TOTO complex under gel electrophoretic conditions is approximately 11 h (Benson et al., 1993a). This makes TOTO an excellent choice as a marker with a detection limit of ∼4 pg of DNA (Benson et al., 1993b).

Scheme 1. Numbering Scheme for TOTO, TOTOEt, and TOTOBzl



TOTO: $R_1 = CH_3$ $R_2 = CH_3$

TOTOBzl: $R_1 = CH_2Ph$ $R_2 = CH_3$

TOTOEt: $R_1 = CH_2CH_3$ $R_2 = CH_2CH_3$

We have used ^{1}H NMR spectroscopy to study the binding mode and sequence selectivity of TOTO with various dsDNA oligonucleotides and shown that TOTO binds via bis-intercalation preferentially to oligonucleotides containing the (5′-CTAG-3′)$_2$ binding site (Faridi et al., 1997; Hansen et al., 1996; Jacobsen et al., 1995; Spielmann et al., 1995; Stærk et al., 1997).

The solution structure of the complex of TOTO bis-intercalated in the (5′-CTAG-3′)$_2$ binding site of the d(5′-CGCTAGCG-3′)$_2$ oligonucleotide shows that the strong binding of TOTO is caused by the ability of the TOTO

* To whom correspondence should be addressed. E-mail: jpj@chem.ou.dk.

[1] Abbreviations: AMBER, assisted model building with energy refinement; DNA, deoxyribose nucleic acid; DMSO, dimethyl sulfoxide; dsDNA, double-stranded DNA; DSS, 2,2-dimethyl-2-silapentane-5-sulfonate; EDTA, ethylenediaminetetraacetic acid; HSQC, heteronuclear single quantum coherence; MARDIGRAS, matrix analysis of relaxation for discerning the geometry of an aqueous structure; NMR, nuclear magnetic resonance; NOESY, nuclear Overhauser effect spectroscopy; RANDMARDI, randomized MARDIGRAS; RMD, restrained molecular dynamics; TOCSY, total correlation spectroscopy; TOTO, 1, 1′-(4,4,8,8-tetramethyl-4,8-diazaundecamethylene)-bis-4-[(3-methyl-2,3-dihydro-2(3H)-benzo-1,3-thiazolylidene)methyl]-quinolinium tetraiodide; TOTOBzl,1, 1′-(4,4,8,8-tetramethyl-4,8-diazaundecamethylene)-[4-[3-(benzyl-2,3-dihydro-2-(3H)-benzothiazolylidene)-methyl]quinolinium]-[4-[3-(methyl-2,3-dihydro-2-(3H)-benzothiazolylidene)methyl]quinolinium] tetraiodide; TOTOEt, 1, 1′-(4,4,8,8-tetramethyl-4,8-diazaundecamethylene)-bis-4-[(3-ethyl-2,3-dihydro-2(3H)-benzo-1,3-thiazole)-methyl]quinolinium tetraiodide; TPPI, time proportional phase incrementation.

10.1021/bc980073w CCC: $18.00 © 1999 American Chemical Society
Published on Web 12/31/1998

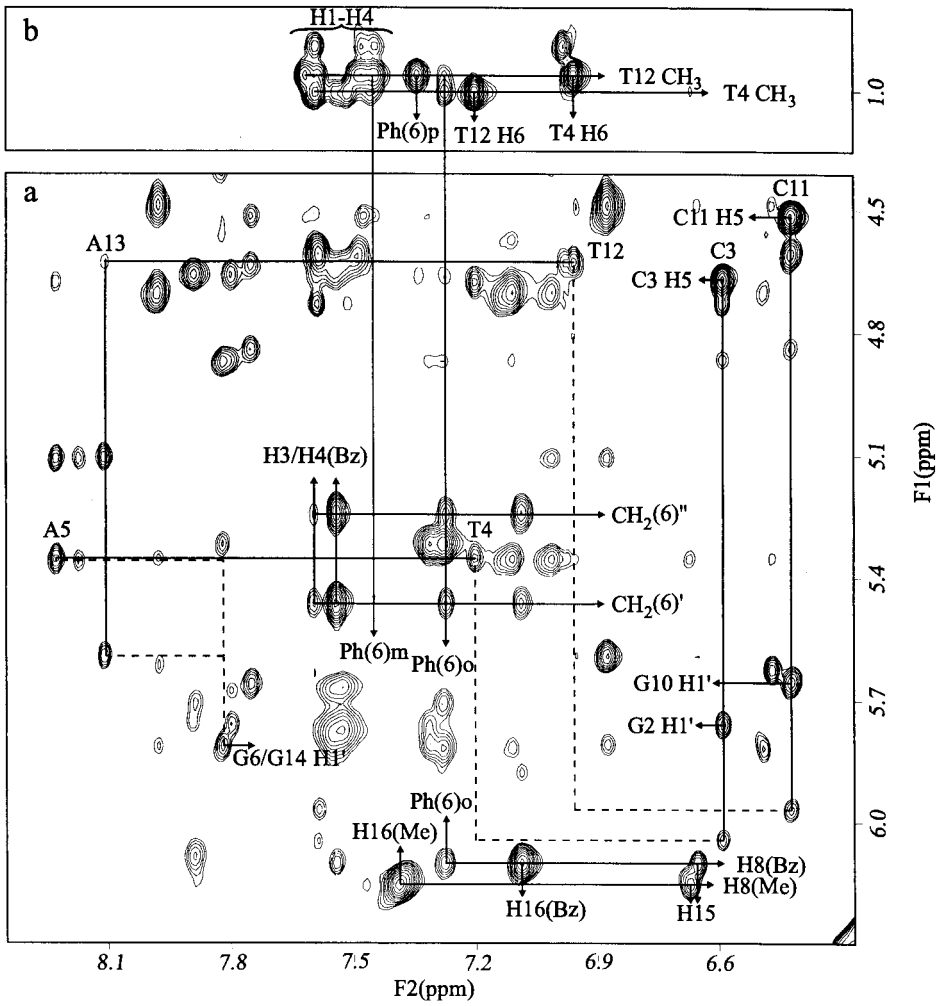


Figure 1. Parts of the 200 ms NOESY spectrum of the TOTOBzl complex recorded in D_2O. Note that the sample contains ca. 20% d(CGCTAGCG)$_2$−TOTO complex. (a) The aromatic to H1′ region. The sequential H1′(n − 1) − H6/H8(n) − H1′(n) connectivity pattern is shown for the 5′−G2-G6−3′ and 5′−G10-G14−3′ dsDNA segments with solid lines. Interruption due to bis-intercalation is shown with broken lines. Some TOTOBzl resonances are marked with solid arrows. (b) The aromatic to methyl region.

chromophores to adapt to the propeller twist of the nucleobases (Spielmann et al., 1995). This is possible since the benzothiazole ring can twist relative to the quinolinium ring due to the flexible cyanine methine bond between. The benzothiazole is intercalated between two pyrimidine bases and the quinolinium ring between the two purine bases. In contrast to other intercalators, the sequence selectivity of TOTO arises directly from the interaction of the intercalated chromophores with the nucleobases. Although the linker of TOTO adds significantly to the binding strength, it is only a spectator with respect to the sequence selectivity. The charged amino groups most probably contribute to the binding free energy by a nonspecific polyelectrolytic contribution.

In this paper, we present the results of one- and two-dimensional ^{1}H NMR studies of complexes between dsDNA and TOTO derivatives. We have synthesized 1,1′-(4,4,8,8-tetramethyl-4,8-diazaundecamethylene)-[4-[3-(benzyl-2,3-dihydro-2-(3H)-benzothiazolylidene)methyl]-quinolinium]-[4-[3-(methyl-2,3-dihydro-2-(3H)-benzothiazolylidene)methyl]quinolinium] tetraiodide (TOTOBzl, Scheme 1) and 1,1′-(4,4,8,8-tetramethyl-4,8-diazaundecamethylene)-bis-4-[(3-ethyl-2,3-dihydro-2(3H)-benzo-1,3-thiazole)methyl]quinolinium tetraiodide (TOTOEt, Scheme 1) and investigated their complexes with the oligonucleotide d(CGCTAGCG)$_2$. This oligonucleotide contains the (5′-CpT-3′):(5′-ApG-3′) and the (5′-ApG-3′):(5′-CpT-3′) sequences.

SYNTHESIS

The major problem in the synthesis of TOTOEt and TOTOBzl was to achieve proper 2-(methylthio)benzothiazolium salts to be used as starting materials for the synthesis of the intermediate monomeric cyanine dyes **6a** and **6b**. According to the procedure of Brooker et al. (1941, 1942), these 2-(methylthio)benzothiazolium salts should be condensed with the quinolinium salt **5** in the presence of triethylamine in methanol. For the synthesis of **6a**, it was decided to use *N*-ethyl-2-(methylthio)-benzothiazolium tetrafluoroborate (**3**) which could be easily obtained in a high yield from commercially available 2-(methylthio)benzothiazole (**1**) by alkylation with triethyloxonium tetrafluoroborate. When it was attempted to N-benzylate compound **1** by treatment with neat benzyl bromide at 100 °C for 12 h in order to obtain a proper benzothiazolium salt for the synthesis of **6b**, a demethylation reaction occurred and compound **2** was isolated in 51% yield. However, S-ethylation with triethyloxonium tetrafluoroborate afforded the adequate starting material **4**. In the final step, TOTOEt was obtained in 85% yield by condensing 2 equiv of the monomeric cyanine dye **6a** with 1 equiv of *N*,*N*,*N*′,*N*′-tetramethyl-1,3-propanediamine in dry methanol according to the procedure of Glazer and co-workers (Rye et al., 1992). Compound **7b**, believed to be formed in situ in this reaction, was also synthesized in a preparative

scale by reacting **6a** with an excess of *N*,*N*,*N*′,*N*′-tetramethyl-1,3-propanediamine. The so formed **7b** could then be used for an alternative synthesis of TOTOEt by condensation with **6a**. TOTOBzl was obtained in a similar way by condensing the compounds **6b** and **7a**.

RESULTS

The d(CGCTAGCG)$_2$−TOTOBzl Complex. *Spectral Data*. The line width observed in the 1D ^{1}H spectrum of the d(CGCTAGCG)$_2$−TOTOBzl complex is approximately 6−7 Hz indicating essentially no dynamic exchange between two or more complexes. The d(CGCTAGCG)$_2$−TOTOBzl complex arises from bis-intercalation in the (5′-CTAG-3′)$_2$ binding site. The amount of this complex is at least 100 times higher than the complex of TOTOBzl in any other site as seen from inspection of the spectra.

The dyad symmetry of the d(CGCTAGCG)$_2$ oligonucleotide is broken upon binding of TOTOBzl resulting in 16 spectroscopically distinct dsDNA residues and two distinct TOTOBzl chromophores henceforth designated as the Me-chromophore and the Bzl-chromophore. The protons of the dsDNA were assigned by conventional methods (Wüthrich, 1986; Feigon et al., 1983; Hare et al., 1983; Scheek et al., 1983, 1984; Boelens et al., 1985) while the TOTOBzl protons were assigned by the strategy usually employed for TOTO analogues (Spielmann et al., 1995).

Figure 1 shows the aromatic to H1′ part of a NOESY spectrum. The sequential connectivity pathway of the H1′(*n* − 1)-H6/H8(*n*)-H1′(*n*) resonances in the intercalation sites is shown with solid lines in Figure 1. Interruption due to intercalation in the 5′−C3pT4−3′ and the 5′−A5pG6−3′ (numbering of the dsDNA in Scheme 3) intercalation sites and similarly at the 5′−C11pT12−3′ and the 5′−A13pG14−3 intercalation sites is indicated with broken lines. The assignment of a few TOTOBzl protons is also indicated.

The interruption of the connectivity pathway combined with a multitude of intermolecular dsDNA-TOTOBzl cross-peaks unambiguously identifies binding in the (5′-CTAG-3′)$_2$ site. H13, H14, and H15 on TOTOBzl yield cross-peaks to A5 H2′/H2″ while H1 and H3 on TOTOBzl have cross-peaks to C3 H2′/H2″. These, and other, NOEs position the benzothiazole rings between C3/C11 and T4/T12 while the quinolinium rings are sandwiched between A5/A13 and G6/G14. The methyl group protons of T4/T12 have an upfield shift of 0.7 ppm and yield NOEs to H1−H4 on TOTOBzl implying that the methyl groups are positioned right above the benzothiazole rings.

The CH$_2$(6) protons on TOTOBzl give rise to two sharp resonances. It is only possible to identify three resonances from the phenyl ring of TOTOBzl; these resonances are identifiable as the ortho, meta, and para protons, respectively, by the magnitude of their NOESY cross-peaks to the methylene protons. The relative conformation of TOTOBzl in the complex is as shown in Scheme 1 as confirmed by prominent H8−H16 cross-peaks.

The NOESY spectra of the complex recorded in H$_2$O contain the normal Watson−Crick NOE connectivity pattern. Chemical shift values of labile protons are included in Table 1.

Intermolecular contacts between the *N*-methyl groups and A5/G6 confirm that the linker crosses the minor groove. The cross-peak pattern observed for the d(CGCTAGCG)$_2$−TOTBzl complex is very similar to that observed for the d(CGCTAGCG)$_2$−TOTO complex (Spielmann et al., 1995).

A ^{1}H,^{13}C-HSQC spectrum gave unambiguous assignment of the H3′ and H4′ protons of the dsDNA. However, not all H5′ and H5″ resonances could be assigned due to spectral overlap. Chemical shift values of all protons are shown in Table 1.

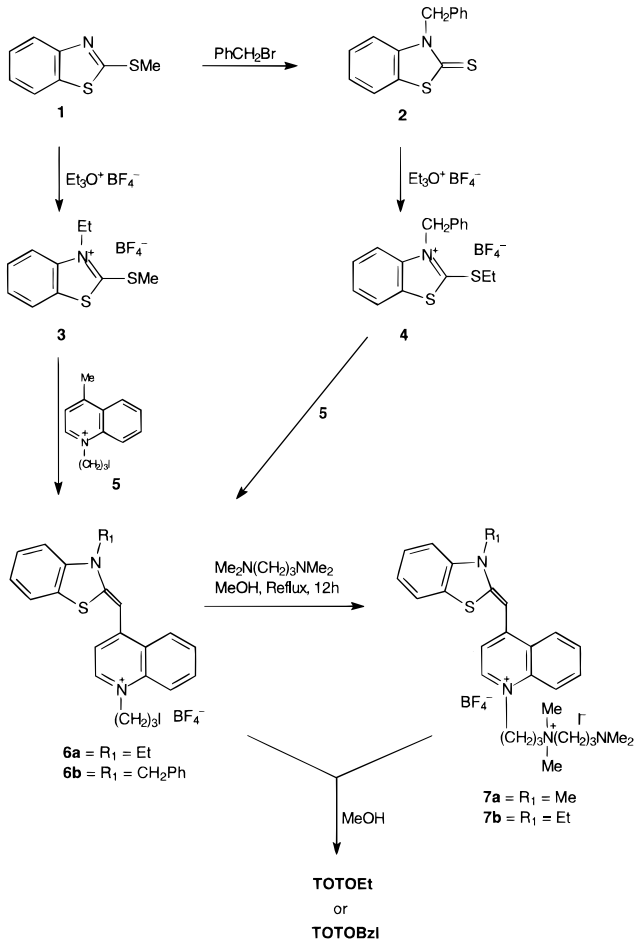
As we observe no exchange cross-peaks between the two strands of the dsDNA in the NOESY spectrum with a mixing time of 200 ms, we conclude that the d(CGCTAGCG)$_2$−TOTOBzl complex has a lifetime on the order of, or above, 200 ms.

Ligand−dsDNA NOE contacts. Interruption of the sequential connectivities in the C3pT4, A5pG6, C11pT12, and A13pG14 base pair steps are a clear indication that TOTOBzl bis-intercalates in the (5′−C3T4A5G6−3′):(5′−C11T12A13G14−3′) site. Intermolecular NOEs between T4 CH$_3$ and H1−H4(Me), T12 CH$_3$ and H1−H4(Bzl), A5 H1′, H3′ and H13−H15(Me), G6 H1′ and H13(Me) A13 H1′, H3′ and H13−H15(Bzl), and G14 H1′ and H13(Bzl) places the two benzothiazoles in the C3pT4 and C11pT12 pyrimidine base pair steps while the quinolinium rings are placed in the A5pG6 and A13pG14 purine base pair steps.

NOEs between a number of minor groove markers (H1′ and H2 of the adenosines in the intercalation site) and the polyamin(propylene)linker positions the linker of TOTOBzl in the minor groove of the dsDNA.

Observation of NOE contacts between protons on the phenyl ring and the methyl groups of T4 and T12 unequivocally places the phenyl ring in the major groove of the dsDNA. NOESY cross-peaks between the amino

Scheme 2. Synthetic Path for the TOTO Analogues



Scheme 3

5' -	**C**1	**G**2	**C**3	**T**4	**A**5	**G**6	**C**7	**G**8	- 3'
3' -	**G**16	**C**15	**G**14	**A**13	**T**12	**C**11	**G**10	**C**9	- 5'

Table 1. ^{1}H Chemical Shift Values (ppm) for the d(CGCTAGCG)$_2$−TOTOBzl Complex Compared with Those of the Free Oligonucleotide in Parentheses[a]

	H6/H8	H1′	H2′	H2″	H3′	H4′	H5/H2/CH$_3$	H1/H3	H4/H6	*H4/H6*
C1	7.53(7.65)	5.68(5.81)	1.92(2.00)	2.33(2.45)	4.67(4.76)	4.02(4.09)	5.78(5.92)			
G2	7.80(1.99)	5.76(5.97)	2.45(2.71)	2.45(2.77)	4.86(5.00)	4.27(4.38)		12.78(13.02)		
C3	6.59(7.44)	6.04(5.98)	1.83(2.07)	2.44(2.51)	4.72(4.78)	4.17(4.24)	4.69(5.39)		6.27(6.58)	8.06(8.27)
T4	7.20(7.41)	5.35(5.60)	1.85(2.14)	2.05(2.44)	4.67(4.88)	4.16(4.14)	1.00(1.70)	13.10(13.76)		
A5	8.23(8.23)	5.35(6.02)	2.81(2.74)	2.72(2.88)	5.11(5.05)	4.29(4.40)	6.97(7.37)		6.68(6.54)	7.31(7.81)
G6	7.82(7.79)	5.82(5.71)	2.64(2.50)	2.70(2.60)	4.87(4.95)	4.57(4.37)		12.02(12.76)		
C7	7.28(7.30)	5.71(5.76)	1.86(1.87)	2.29(2.33)	4.78(4.79)	4.17(4.14)	5.32(5.34)		6.84(6.47)	8.18(8.34)
G8	7.89(7.93)	6.09(6.16)	2.60(2.60)	2.32(2.37)	4.66(4.66)	4.06(4.16)				
C9	7.53(7.65)	5.68(5.81)	1.86(2.00)	2.30(2.45)	4.67(4.76)	4.02(4.09)	5.78(5.92)			
G10	7.75(7.99)	5.65(5.97)	2.54(2.71)	2.44(2.77)	4.84(5.00)	4.24(4.38)		12.75(13.02)		
C11	6.42(7.44)	5.97(5.98)	1.92(2.07)	2.54(2.51)	4.61(4.78)	4.19(4.24)	4.52(5.39)		6.57(6.58)	7.94(8.27)
T12	6.96(7.41)	4.62(5.60)	1.91(2.14)	1.97(2.44)	4.62(4.88)	4.18(4.14)	0.96(1.70)	13.49(13.76)		
A13	8.11(8.23)	5.59(6.02)	2.83(2.74)	2.72(2.88)	5.11(5.05)	4.32(4.40)	6.95(7.37)			
G14	7.82(7.70)	5.82(5.71)	2.64(2.50)	2.67(2.60)	4.87(4.95)	4.53(4.37)		12.01(12.76)		
C15	7.31(7.30)	5.76(5.76)	1.88(1.87)	2.31(2.33)	4.78(4.79)	4.17(4.14)	5.32(5.34)		6.84(6.47)	8.18(8.34)
G16	7.89(7.93)	6.09(6.16)	2.60(2.60)	2.32(2.37)	4.66(4.66)	4.06(4.16)				

TOTOBzl	Me[b]	Bzl[c]	TOTOBzl	Me[b]	Bzl[c]	TOTOBzl	Me[b]	Bzl[c]
H1	7.62	7.59	H15	6.67	6.65	H23″	3.51	3.43
H2	7.45	7.51	H16	7.39	7.09	H24	∼2.5[d]	∼2.5[b]
H3	7.59	7.59	H19′	4.13	4.11	CH$_3$(6)	3.63	
H4	7.48	7.54	H19″	4.70	4.48	CH$_2$′(6)		5.24
H8	6.15	6.10	H20	∼2.5[d]	∼2.5[d]	CH$_2$″(6)		5.45
H9	6.49	6.47	H21′	3.66	3.6	Ph(6), ortho		7.27
H10	7.98	7.98	H21″	3.66	3.71	Ph(6), meta		7.44
H13	7.11	6.87	CH$_3$(22)	3.28	3.29	Ph(6), para		7.34
H14	7.01	6.87	H23′	3.42	3.43			

[a] The values are relative to DSS at 25 °C. [b] Values of the chromophore containg a methyl group on the benzothiazole ring. [c] Values of the chromophore containg a benzyl group on the benzothiazole ring. [d] Overlapping resonances at 2.5 ppm.

Table 2. Observed NOE Contacts between the Phenyl Ring and dsDNA and TOTOBzl Protons

phenyl atom	DNA atom	TOTOBzl atom
ortho	T4 CH$_3$, T12 CH$_3$	CH$_2$′(6), CH$_2$″(6), H8(Bzl), H4(Bzl), H2(Bzl)
meta	T12 CH$_3$, T4 CH$_3$*a*	CH$_2$′(6), CH$_2$″(6)
para	T12 CH$_3$	

[a] Weak NOESY cross-peak.

protons of C3 and CH$_2$(6) and between the para proton of the phenyl ring and the methyl group of T12 show that the phenyl ring points toward the center of the oligonucleotide. The observed NOE contacts between the dsDNA and the phenyl ring of TOTOBzl are shown in Table 2.

Molecular Modeling. A total of 146 distance restraints were incorporated into RMD calculations; 87 of these restraints were found by the RANDMARDI procedure based on 97 NOESY cross-peak volumes; 33 restraints were qualitative restraints found by inspection of the NOESY spectrum with a mixing time of 200 ms and were conservatively chosen as strong (1.8−5.0 Å), medium (1.8−5.5 Å) or weak (1.8−6.0 Å). Four restraints were included to keep the ends of the dsDNA duplex in a B-DNA-like conformation. The remaining 22 of these restraints served to mimic Watson−Crick hydrogen bonding between the two DNA strands as justified by the NOESY spectrum recorded in H$_2$O. As an evaluation of the precision of the distances returned by RANDMARDI, the covalently fixed distances in TOTOBzl were left out of the distance reference file for MARDIGRAS. Consequently, the magnetization transfer for these protons are calculated and the distances returned can be used to evaluate the precision of the RANDMARDI procedure. Four of the 97 intensities used in the calculations stemmed from covalently fixed proton pairs in TOTOBzl and the distances returned for these proton pairs by RANDMARDI were in all cases in error of less than 0.3 Å relative to the covalently known "real" distances. This

Table 3. Distance Restraints Incorporated in the RMD Calculations of the d(CGCTAGCG)$_2$−TOTOBzl Complex[a]

DNA−DNA		DNA−TOTOBzl		TOTOBzl-TOTOBzl	
interresidue	16	C3-TOTOBzl	2 (0)		20
intraresidue	25	T4-TOTOBzl	6 (0)		
		A5-TOTOBzl	5 (13)		
		G6-TOTOBzl	0 (5)		
		C11-TOTOBzl	0 (0)		
		T12-TOTOBzl	5 (0)		
		A13-TOTOBzl	8 (11)		
		G14-TOTOBzl	0 (4)		
total	41	total	26 (33)	total	20

[a] Found by RANDMARDI calculations. Qualitative distance restraints found by inspection of the NOESY spectrum with a mixing time of 200 ms are tabulated in parentheses.

lends credibility to the distances returned by RANDMARDI despite the sparse experimental data and justifies the inclusion of the 87 proton−proton distances in the RMD calculations. A detailed survey of the distance restraints is shown in Table 3.

Convergence. Twenty structures were generated for the dsDNA−TOTOBzl complex with B-DNA conformation as starting structure by RMD calculations. The 20 structures all converged to just one family of structures, and the pairwise root-mean-square (rms) deviation was 0.99 Å. We observed only two violations in excess of 0.2 Å but none in excess of 0.3 Å.

A model structure as the one here presented should not be mistaken for a high-resolution structure which requires a much larger set of experimental data. Due to the rather large number of restraints incorporated in the RMD calculations, the consideration of spin-diffusion effects in the RANDMARDI procedure, and the convergence after the RMD calculations, we have confidence in the model structure obtained and believe it to show a fairly precise "picture" of the structure of the TOTOBzl complex. Hence, we believe that the model structure enables us to determine various aspects of the local

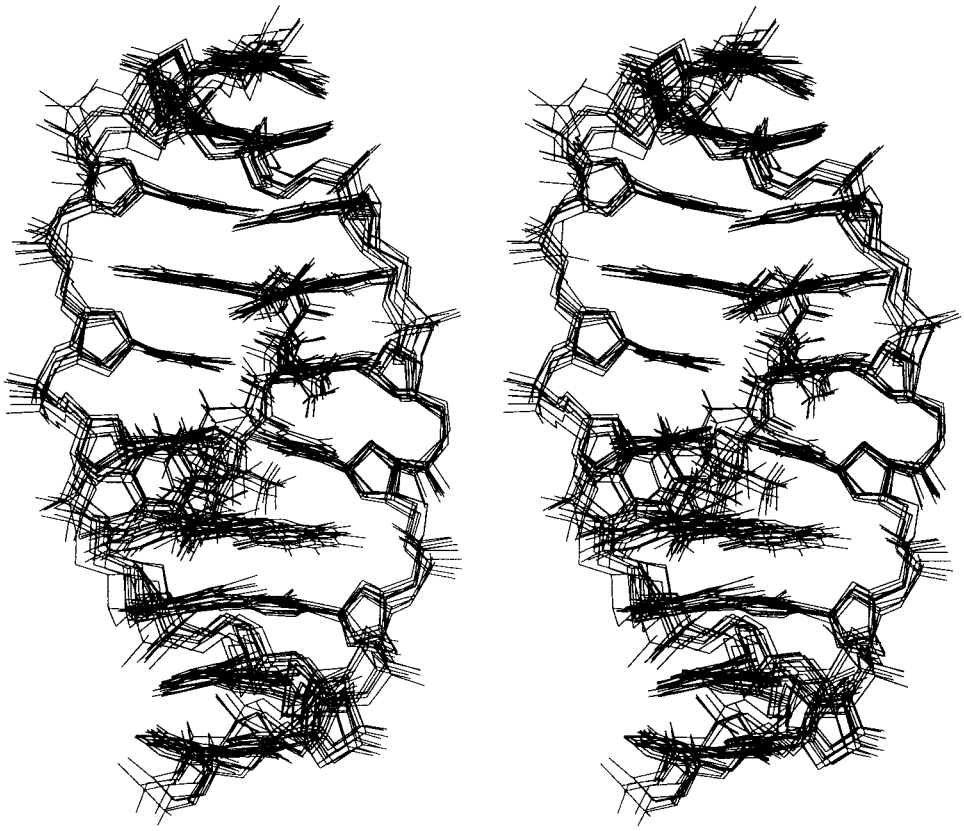


Figure 2. Stereoview of a superposition of 10 structures of the d(CGCTAGCG)$_2$−TOTOBzl complex looking into the major groove. Deoxyribose protons have been omitted for clarity.

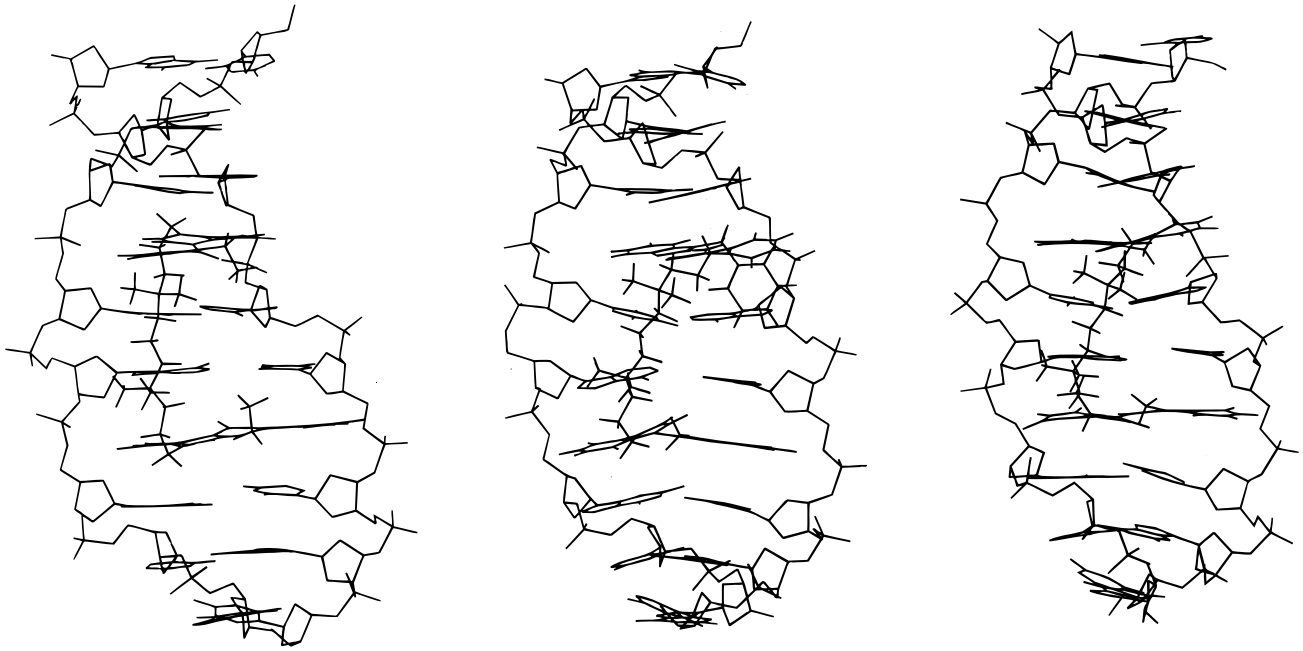


Figure 3. The complexes between d(CGCTAGCG)$_2$ and TOTO (left), TOTOEt (center) and TOTOBzl (right). The d(CGCTAGCG)$_2$-TOTO complex is reproduced from Spielmann et al. (1995). The d(CGCTAGCG)$_2$−TOTOEt complex is reproduced from Petersen and Jacobsen (1998).

structure of the complex. Views of the model structure are shown in Figures 2 and 3.

The d(CGCTAGCG)$_2$−TOTOEt Complex. The line width observed in the 1D ^{1}H NMR spectrum of the d(CGCTAGCG)$_2$−TOTOEt complex is just as narrow as for the TOTOBzl complex, indicating essentially no dynamic exchange between two or more complexes. Furthermore, only one resonance frequency is observed for the protons on each strand of the dsDNA and for each chromophore. This shows that the TOTOEt forms a single complex with d(CGCTAGCG)$_2$ with dyad symmetry. The d(CGCTAGCG)$_2$−TOTOEt complex arises from bis-intercalation in the (5′−CTAG−3′)$_2$ binding site. The amount of this complex is at least 100 times higher than any other complex as seen from inspection of the spectra. A full relaxation matrix analysis employing RAND-

MARDI (Liu et al.,1995) followed by restrained molecular dynamics calculations using cross-peak intensities in NOESY build-up experiments yielded a high-resolution structure of the d(CGCTAGCG)$_2$−TOTOEt complex. This work is reported elsewhere (Petersen and Jacobsen, 1998).

DISCUSSION

The sequence selectivity and the binding mode of the TOTO analogues to the dsDNA oligonucleotide examined in this work are very similar to those of TOTO. In the d(CGCTAGCG)$_2$ oligonucleotide, both TOTOEt and TOTOBzl bind exclusively to the (5′−CTAG−3′)$_2$ site.

Though the mode of binding and selectivity of TOTOEt, TOTOBzl, and TOTO is similar, there are interesting differences in the local structure of the dsDNA and the ligands. These differences are discussed below.

Description of the d(CGCTAGCG)$_2$−TOTOBzl Model Structure. The structure of the d(CGCTAGCG)$_2$−TOTOBzl complex shows that TOTOBzl bis-intercalates in the (5′−CTAG−3′)$_2$ site with the benzothiazole ring systems sandwiched in the CpT base pair steps and the quinolinium ring systems sandwiched in the ApG base pair steps. The N-benzyl group on the benzothiazole is placed in the major groove orientated toward the center of the oligonucleotide, and the polyamin(propylene)linker is in the minor groove. The dsDNA is in an overall B-DNA like conformation.

As can be gleaned from Figure 2 the nucleobases and the intercalating chromophores are fairly well-defined in the model structure while the N-benzyl group and the polyamin(propylene)linker cannot be accurately determined from the spectral data. The positions in the two grooves of the dsDNA are, however, beyond any doubt.

In the complex, the intercalating chromophores stretch across the dsDNA helix; T4 and T12 unstack from A5 and A13 to maximize van der Waals contacts with the intercalating chromophores. The methyl groups of the thymines are placed right on top of the benzothiazoles of TOTOBzl.

Cross-strand NOEs between T12 H3 and A5's amino protons and between the adenosine H2s and the thymidine H1s reveal that normal Watson−Crick base pairing is present in the intercalation site even though the adenosines and thymidines are unstacked.

For the uncomplexed d(CGCTAGCG)$_2$, no cross-peaks are observed between the thymine imino proton and the base-paired adenine amino protons due to exchange with the solvent. In the complex, cross-peaks are observed between T12 H3 and A5's amino protons. This is a testimony of the increased stability of the T12−A5 base pair due to intercalation of the Me-chromophore of TOTOBzl. Intriguingly, no cross-peaks are observed between T4 H3 and A13's amino protons. This can be explained by analysis of the model structure: A5 and T12 stack well with the ring systems of the intercalating Me-chromophore while T4 and A13 do not seem to make any appreciable stacking with the intercalating ring systems of the Bzl-chromophore. Therefore, the stability of the A5−T12 Watson−Crick base pair is enhanced relative to the stability of an A−T base pair in the uncomplexed dsDNA duplex.

Comparison of the Complexes of d(CGCTAGCG)$_2$ with TOTO, TOTOEt, and TOTOBzl. Bearing in mind that the model structure of the TOTOBzl complex is not a high-resolution structure, as are the structures determined of the TOTO and TOTOEt complexes, we refrain from discussing more detailed parameters such as helix parameters. Instead, we are making a qualitative comparison of the three complexes.

Table 4. Observed Twist between the Ring Systems of the Aromatic Chromophores in the TOTO, TOTOBzl, and TOTOEt Complexes and the Chemical Shift Values of the Protons Discussed in the Text

	twist angle[a] (deg)	thymidine H1′ [b]	$\Delta\delta$[c]	thymidine H6[b]	$\Delta\delta$[c]
TOTO	22	4.62	0.98	6.97	0.44
TOTOEt	6	4.96	0.64	7.08	0.33
TOTOBzl	1	5.35	0.25	7.20	0.21
TOTOBzl	25	4.62	0.98	6.96	0.45

[a] Twist angle between the two ring systems of the intercalating chromophore. [b] Chemical shift value of the specified proton on the thymidine adjacent to the intercalating chromophore, values are given (ppm). [c] Change in chemical shift relative to the free dsDNA.

In the three complexes, the dsDNA adopts an overall B-DNA-like geometry. A striking feature of the three complexes is the change in the angle around the cyanine methine bond of the intercalators (Figure 2). This angle defines the angle of the benzothiazole relative to the quinolinium ring. It appears that the substitution of ethyl and benzyl at the benzothiazole N-atom lowers this angle in the complexes relative to the complexes where a N-methyl is present at the benzothiazole (see Table 4).

As for chemical shifts, pronounced changes from free dsDNA are observed for the thymidine H6, H1′, H2′, H2″, and the adenosine H2 protons for the three complexes discussed. These protons are placed in the minor groove of dsDNA, and with the charged polyamin(propylene)-linker of the bis-intercalators "intruding" in this groove, it is to be expected that the electrostatic potential of the minor groove is profoundly altered in the complexes, resulting in changes of chemical shift values of protons positioned herein. The thymidine H6 and H1′ protons, however, seem to occupy exceptional positions as shown by the much different chemical shifts values for the three complexes (see Table 4).

The relationship between the value of the above-mentioned twist angle and the thymidine H6 and H1′ chemical shifts is evident as seen from Table 4. Although it appears that no simple relationship can account for the observations, the qualitative trend is clear that a large twist angle between the chromophores of the bis-intercalator leads to a large change in chemical shift for the thymidine H6 and H1′ protons relative to free dsDNA. Most striking are the results obtained for the TOTOBzl complex where each of the two intercalating chromophores display profoundly different behavior.

As the twist angle between the ring systems of the chromophores is enlarged, the overlap of the π-orbitals of the two ring systems diminishes, resulting in a quenching of the flow of π-electrons between the two ring systems, thus changing the ring current of the intercalating chromophore.

As neither the H2′ nor H2″ protons of the thymidine experience these different changes in chemical shifts it would seem that the change in "environment" for the H6 and H1′ protons is a local feature. This can be rationalized by the intercalating aromatic chromophore inducing a change in the ring current of the thymine ring and should be expected only to affect the protons in close proximity to this ring (Davies, 1978).

CONCLUSION

We have examined the complexes between d(CGCTAGCG)$_2$ and the bis-intercalators TOTOEt and TOTOBzl

resulting in a high-resolution structure of the d(CGCTAGCG)$_2$−TOTOEt complex and a model structure of the d(CGCTAGCG)$_2$−TOTOBzl complex. We have compared these complexes with the previously published high-resolution structure of the d(CGCTAGCG)$_2$−TOTO complex (Spielmann et al., 1995). Though the overall binding of the bis-intercalators are alike with nearest neighbor bis-intercalation in the (5′−CTAG−3′)$_2$ site, we are able to point out pronounced changes in the structure of the dsDNA upon binding of the different bis-intercalators.

There are no indications whatsoever that TOTOBzl or TOTOEt make less stable complexes than TOTO when bound to dsDNA. Our long-term objective of this work is to move the linker of the bis-intercalator from the minor groove to the major groove while retaining TOTO's sequence selectivity. The structure of the TOTOEt complex reveals that the benzothiazole N-ethyl group adopts a geometry near to perfect for the linking of the two chromophores in the major groove while the TOTOBzl complex shows that there is ample room to accommodate a benzyl group. This, thus, renders our goal a distinct future possibility.

EXPERIMENTAL PROCEDURES

Synthesis. *3-Ethyl-2-(methylthio)benzothiazolium Tetrafluoroborate (**3**).* Triethyloxonium tetrafluoroborate (1.90 g, 0.01 mol) in $CHCl_3$ (10 mL) is added with stirring to 2-(methylthio)benzothiazole (1.81 g, 0.01 mol) in $CHCl_3$ (50 mL) at −10 °C. The temperature was allowed to increase to 20 °C, and stirring was continued for 5 h. The precipitate was collected by filtration; yield 2.26 g (75%); mp 172−175 °C.

*3-Benzyl-2-(ethylthio)benzothiazolium Tetrafluoroborate (**4**).* A mixture of 2-(methylthio)benzothiazole (18.1 g, 0.1 mol) and benzyl bromide (51.1 g, 0.3 mol) was heated at 100 °C for 12 h. After cooling to room-temperature, ether (200 mL) was added under stirring and the precipitate of **2** was collected by filtration; yield 13.2 g (51%); mp 150−152 °C; lit. mp 149 °C (Reed et al., 1939). Et_3OBF_4 (1.90 g, 0.01 mol) in 50 mL CH_2Cl_2 was added dropwise to **2** (2.6 g, 0.01 mol) in 50 mL of CH_2Cl_2 at −10 °C with stirring. The temperature was allowed to increase to room temperature during 1 h and the mixture was stirred for 5 h. Compound **4** precipitated as pale yellow crystals on addition of ether; yield 3.3 g (88%); mp 165−168 °C. ^{1}H NMR (DMSO-d_6): δ 1.56 (t, 3H, J = 7.3 Hz, CH_3), 3.68 (q, 2H, J = 7.3 Hz, CH_2), 5.95 (s, 2H, CH_2), 7.31−8.45 (m, 9H, Ar). FAB MS: m/z 286 (M − BF_4). Anal. Calcd for $C_{16}H_{16}NS_2 \cdot BF_4$: C, 51.49; H, 4.32; N, 3.75. Found: C, 51.65; H, 4.09; N, 3.81.

*4-[(3-Ethyl-2(3H)-benzothiazolylidene)methyl]-1-(3-iodopropyl)quinolinium Tetrafluoroborate (**6a**).* Equimolar amounts of **3** and **5** were dissolved in absolute ethanol by heating. One equivalent of triethylamine was added, and the mixture was stirred at room temperature for 30 min. The title compound precipitated on addition of ether; yield 70%; recrystallization from acetone/ether; mp 250−252 °C. ^{1}H NMR (DMSO-d_6): δ 1.40 (t, 3H, J = 7.0 Hz, CH_3), 2.39 (quint, 2H, J = 7.0 Hz, CH_2), 3.35 (t, 2H, J = 7.0 Hz, CH_2), 4.65 (m, 4H, 2 × CH_2), 6.94 (s, 1H, =CH), 7.37−8.80 (m, 10H, Ar). FAB MS m/z 473 (M − BF_4). Anal. Calcd for $C_{22}H_{22}IN_2S \cdot BF_4 \cdot 0.5H_2O$: C, 46.42; H, 4.07; N, 4.92. Found: C, 46.65; H, 3.91; N, 4.89.

*4-[(3-Benzyl-2(3H)-benzothiazolylidene)methyl]-1-(3-iodopropyl)quinolinium Tetrafluoroborate (**6b**).* The title compound was synthesized from equimolar amounts of **4** and **5** in a similar way as **6a**; yield 65%; mp 237−247 °C (dec). ^{1}H NMR (DMSO-d_6): δ 2.38 (quint, 2H, J = 7.0 Hz, CH_2), 3.33 (t, 2H, J = 7.0 Hz, CH_2), 4.64 (t, 2H, J = 7.0 Hz, CH_2), 5.96 (s, 2H, CH_2), 6.99 (s, 1H, =CH), 7.29−8.64 (m, 15H, Ar). FAB MS: m/z 535 (M − BF_4). Anal. Calcd for $C_{27}H_{24}IN_2S \cdot BF_4 \cdot 0.5H_2O$: C, 51.37; H, 3.99; N, 4.44. Found: C, 51.56; H, 3.91; N, 4.44.

1,1′-[1,3-Propanediylbis[(dimethylimino)-3,1-propanediyl]]bis[4-[(3-ethyl-2(3H)-benzothiazolylidene)methyl]quinolinium Tetraiodide, TOTOEt. A suspension of **6a** and 0.5 equiv of *N*,*N*,*N*′,*N*′-tetramethyl-1,3-propanediamine in anhydrous methanol was heated at reflux for 24 h. Recrystallization from DMF/MeOH afforded the title compound as an orange-red solid: yield 85%; mp 248−251 °C (dec). ^{1}H NMR (DMSO-d_6): δ 1.42 (t, 6H, J = 6.8 Hz, 2 × CH_3), 2. 38 (m, 6H, 3 × CH_2), 3.19 (s, 12H, 4 × CH_3), 3.36 (m, 4H, 2 × CH_2), 3.71 (m, 4H, 2 × CH_2), 4.68 (m, 8H, 4 × CH_2), 6.93 (s, 2H, 2 × =CH), 7.35−8.82 (m, 20H, Ar). FAB MS: m/z 1203 (M − I). Anal. Calcd for $C_{51}H_{62}I_4N_6S_2$: C, 46.03; H, 4.70; N, 6.31. Found: C, 46.28; H, 4.85; N, 6.10.

1-[3-[[3-[Dimethyl[3-[4-[(3-methyl-2(3H)-benzothiazolylidene)methyl]quinolinio]-propyl]ammonio]propyl]dimethylammonio]propyl]-4-[(3-benzyl-2(3H)-benzothiazolylidene) − methyl]quinolinium Tetraiodide, TOTOBzl. Equivalent amounts of **6b** and **7a** in anhydrous methanol were refluxed for 12 h. TOTOBzl was precipitated by addition of ether and recrystallized from acetone/ether: yield 90%; mp 228−230 °C (dec). ^{1}H NMR (DMSO-d_6): δ 2.38 (m, 6H, 3 × CH_2), 3.19 (s, 12H, 4 × CH_3), 3.40 (m, 4H, 2 × CH_2), 3.72 (m, 4H, 2 × CH_2), 4.01 (s, 3H, CH_3), 4.70 (m, 4H, 2 × CH_2), 5.97 (s, 2H, CH_2), 6.90 (s, 1H, =CH), 6.97 (s, 1H, =CH), 7.30−8.90 (m, 25H, Ar). FAB MS: m/z 1251 (M − I). Anal. Calcd for $C_{55}H_{62}I_4N_6S_2 \cdot 4H_2O$: C, 45.53; H, 4.86; N, 5.79. Found: C, 45.49; H, 4.89; N, 5.81.

Sample Preparation. The purified oligonucleotide d(CGCTAGCG)$_2$ was purchased from DNA technology, Århus, Denmark, and used without further purification. TOTOEt and TOTOBzl are almost insoluble in water and the complexes with dsDNA was therefore made by the procedure described earlier (Jacobsen et al., 1995). The NMR samples were prepared by dissolving the complexes in 0.5 mL of 10 mM sodium phosphate buffer (pH 7.0), 0.05 mM NaEDTA, 0.01 mM NaN_3, and 0.1 mM DSS. For experiments carried out in D_2O the solid complexes, lyophilized three times from D_2O, were redissolved in 99.96% D_2O (Cambridge Isotope Laboratories). A mixture of 90% H_2O and 10% D_2O (0.5 mL) was used for experiments examining exchangeable protons. The samples were kept in NMR tubes under nitrogen. The final concentration of the complexes were ca. 2 mM.

NMR Experiments. NMR experiments were performed on a Varian Unity 500 spectrometer at 25 °C for the TOTOBzl complex and at 27 °C for the TOTOEt complex. NOESY spectra of the complexes were acquired in D_2O using 1024 complex points in t_2 and a spectral width of 5000 Hz. A total of 512 t_1 experiments were recorded using the States phase cycling scheme. The residual signal from HOD was removed by presaturation. For the TOTOEt complex, spectra with mixing times of 50, 100, 150, and 200 ms were recorded sequentially without removing the sample from the magnet. NOESY spectra of the TOTOBzl complex with mixing times of 100 and 200 ms were acquired at 750 MHz using 2048 complex points in t_2 and a spectral width of 7500 Hz on a Varian INOVA 750 spectrometer. NOESY spectra of the complexes in H_2O were obtained by using a NOESY pulse sequence where the last 90° pulse is replaced by a 1−1 jump-return pulse to suppress the solvent signal (Guéron and Plateau, 1982). The mixing times were 160 ms. In addition, a Watergate NOESY spectrum in H_2O

with a mixing time of 50 ms was recorded of the TOTOEt complex on a Varian Unity+ 500 spectrometer. The NOESY spectra in H_2O were acquired with a spectral width of 10 000 Hz in 2048 complex points using 512 t_1 experiments with 64 scans acquired in each t_1 experiment. NOESY spectra with mixing times of 500 ms were recorded of the free TOTOBzl and TOTOEt in DMSO-d_6.

TOCSY spectra of the complexes with mixing times of 30 and 90 ms were obtained in the TPPI mode using 1024 complex points in t_2 and 512 t_1 experiments with 64 scans each.

DQF−COSY spectra of the complexes were recorded using the States phase cycling scheme with 4096 complex points in t_2 and 1024 t_1 experiments with 64 scans each. Removal of the residual HOD signal was done by presaturation in all spectra.

^1H,^{13}C HSQC spectra in D_2O were recorded for both the complexes: the spectrum of the TOTOEt complex on a Varian Unity+ 500 spectrometer and the spectrum of the TOTOBzl complex on a Varian INOVA 750 spectrometer.

The acquired data were processed using FELIX (version 2.35, Biosym/MSI, San Diego, CA). The spectra were assigned by conventional methods (Wüthrich, 1986; Feigon et al., 1983; Hare et al., 1983; Scheek et al., 1983, 1984; Boelens et al., 1985).

Restrained Molecular Dynamics. The d(CGCTAGCG)$_2$ oligonucleotide and the TOTOBzl molecule were built in INSIGHTII (version 95.0, Biosym/MSI, San Diego, CA). TOTOBzl was manually docked into the model of B-form DNA to obtain the starting model for the structure refinement. The potentials for both DNA and TOTOBzl were assigned by the AMBER force field, modified to accommodate the benzothiazole sulfur atom of TOTOBzl.

The distance restraints obtained from RANDMARDI were incorporated into an energy minimization and a RMD procedure using DISCOVER (version 95.0, Biosym/MSI, San Diego, CA). An initial energy minimization was followed by 28 ps of restrained molecular dynamics: dynamics at 600 K for 4 ps, followed by cooling to 200 K in 50 K steps of 3 ps each. The final structure was then energy minimized to a maximum derivative of 0.01 Å.

The pseudo energy terms used to enforce the restraints were

$$E_{\mathrm{NOE}} = \begin{cases} k_1(r - r_1)^2 & \text{when } r < r_1 \\ 0 & \text{when } r_1 \le r \le r_2 \\ k_2(r - r_2)^2 & \text{when } r > r_2 \end{cases}$$

where r_1 and r_2 are the lower and upper distance bounds determined from the cross-peak volumes; k_1 and k_2 are the force constants. A lower force constant of $k_1 = 50$ kcal/(mol Å^2) and upper force constant of $k_2 = 25$ kcal/(mol Å^2) were employed. The width of the flat region of the potential well reflects the accuracy of a given constraint. A distance dependent dielectric, $\epsilon = r$, was employed to account for solvent effects.

Distance Restraints. *The Initial Model*. An initial model of the d(CGCTAGCG)$_2$−TOTOBzl complex was made with restraints found from the NOESY spectrum with a mixing time of 100 ms. Cross-peak volumes were converted to proton−proton distances by the isolated spin pair approximation (ISPA) using the volumes of covalently fixed dsDNA protons as references (cytosine H5−H6, 2.45 Å; deoxyribose H2′−H2″, 1.78 Å). All lower bounds were set to 1.8, and 1 Å was added to the distances determined to obtain the upper bounds. Distance restraints involving methyl and methylene protons were further loosened. In this manner, a total of 81 distance restraints were obtained (25 of these were intermolecular restraints). A further 22 distance restraints were included to mimic Watson−Crick base pairing. Three hydrogen bonds were included for each of the six C/G base pairs and two for both of the T/A base pairs. Lower and upper bounds were 1.7 and 2.1 Å, respectively. Thus, a total of 103 distance restraints were included in the RMD calculations.

A total of 20 structures were generated by the RMD protocol described above, all structures converged to just one family of structures. A representive structure of this family was chosen for further refinement by including restraints obtained by including a relaxation matrix analysis.

Relaxation Matrix Analysis. A total of 97 cross-peaks on the upper diagonal of the NOESY spectrum with a mixing time of 200 ms were integrated. The RANDMARDI variation of MARDIGRAS was employed to transfer the cross-peak volumes to proton−proton distance restraints taking spin diffusion into account (Borgias and James, 1990; Borgias et al., 1990; Liu et al., 1995). The RANDMARDI procedure generated 50 peak intensity sets and MARDIGRAS calculations were performed on each of those. A "noise level" of five times the measured volume of the weakest cross-peak was used in the RANDMARDI calculaions. Upper and lower bounds were calculated as the average interproton distance ± one standard deviation as found from the MARDIGRAS calculations.

A total of 97 cross-peak volumes were measured in FELIX; of those, 88 cross-peak volumes stemmed from interproton distances not detemined by the covalent geometry of neither the dsDNA nor the TOTOBzl. RANDMARDI returned 87 interproton distances for use in the RMD calculations, and 0.6 Å was added to all upper bounds for these distances before implementation as restraints. The average flat well potential width was 1.34 Å.

ACKNOWLEDGMENT

We thank The Instrumentcenter for NMR spectroscopy of Biological Macromolecules at The Carlsberg Laboratory, Copenhagen, granted by The Danish Natural Science Research Council for providing spectrometer time at the 750 MHz spectrometer.

LITERATURE CITED

Benson, S. C., Singh, P., and Glazer, A. N. (1993a) Heterodimeric DNA-binding dyes designed for energy transfer: synthesis and spectroscopic proporties. *Nucleic Acids Res. 21*, 5727−5735.

Benson, S. C., Mathies, R. A., and Glazer, A. N. (1993b) Heterodimeric DNA-binding dyes designed for energy transfer: stability and applications of DNA complexes. *Nucleic Acids Res. 21*, 5720−5726.

Boelens, R., Scheek, R. M., Dijkstra, K., and Kaptein, R. (1985) Sequential Assigment of Imino- and Amino-Proton Resonances in 1H NMR Spectra of Oligonucleotides by Two-Dimensional NMR Spectroscopy. Application to lac Operator Fragment. *J. Magn. Reson. 62*, 378−386.

Brooker, L. G. S., White, F. L., Keyes, G. H., Smyth, C. P., and Oesper, P. E. (1941) Color and constitution. II. Absorptions of some related vinylene-homologous series. *J. Am. Chem. Soc. 62*, 3192−3203.

Brooker, L. G. S., Keyes, G. H., and Williams, W. W. (1942) Color and constitution. V. The absorption of unsymmetrical cya-

nines. Resonance as a basis for a classification of dyes. *J. Am. Chem. Soc. 63*, 199−210.

Davies, D. B. (1978) Conformations of Nucleosides and Nucleotides. *Prog. NMR Spectrosc. 12*, 135−225.

Faridi, J., Nielsen, K. E., Stein, P. C., and Jacobsen, J. P. (1997) Bis-Intercalation of a Homodimeric Thiazole Orange Dye in DNA: Dynamic Exchange between Two Sites. *J. Biomol. Struct. Dyn. 15*, 321−331.

Feigon, J., Leupin, W., Denny, W. A., and Kearns, D. R. (1983) Two-Dimensional Proton Nuclear Magnetic Resonance Investigation of the Synthetic Deoxyribonucleic Acid Decamer d(ATATCGATAT)$_2$. *Biochemistry 22*, 5943−5951.

Guéron, M., and Plateau, P. (1982) Exchangeable Proton NMR without Base-Line Distortion, Using New Strong-Pulse Sequences. *J. Am. Chem. Soc. 104*, 7310−7311.

Hansen, L. F., Jensen, L. K., and Jacobsen, J. P. (1996) Bis-intercalation of a homodimeric thiazole orange dye in DNA in symmetrical pyrimidine-pyrimidine-purine-purine oligonucleotides. *Nucleic Acids Res. 24*, 859−867.

Hare, D. R., Wemmer, D. E., Chou, S.-H., Drobny, G., and Reid, B. R. (1983) Assignment of the nonexchangeable proton resonances of d(C-G-C-G-A-A-T-T-C-G-C-G) using two-dimensional nuclear magnetic resonance methods. *J. Mol. Biol. 171*, 319−336.

Jacobsen, J. P., Pedersen, J. B., Hansen, L. F., and Wemmer, D. E. (1995) Site selective bis-intercalation of a homodimeric thiazole orange dye in DNA oligonucleotides. *Nucleic Acids Res. 23*, 753−760.

Petersen, M., and Jacobsen, J. P. (1998) Solution Structure of a DNA Complex with the Fluorescent Bis-Intercalator TOTO Modified on the Benzothiazole Ring. *Bioconjugate Chem. 9*, 331−340.

Reed, F. P., Robertson, A., and Sexton, W. A. (1939) Reaction of benzthiazole derivatives. Part II. The Conversion of 1-Alkylthiobenzthiazoles into 1-Thio-2-alkyl-1: 2-dihydrobenzthiazoles. *J. Chem. Soc.* 473−476.

Rye, H. S., Yue, S., Wemmer, D. E., Quesada, M. A., Haugland, R. P., Mathies, R. A., and Glazer, A. N. (1992) Stable fluorescent complexes of double-stranded DNA with bis-intervalating asymmetric cyanine dyes: proporties and applications. *Nucleic Acids Res. 20*, 2803−2812.

Scheek, R. M., Russo, N., Boelens, R., and Kaptein, R. (1983) Sequential Resonance Assigments in DNA 1H NMR Spectra by Two-Dimensional NOE Spectroscopy. *J. Am. Chem. Soc. 105*, 2914−2916.

Scheek, R. M., Boelens, R., Russo, N., Van Boom, J. H., and Kaptein, R. (1984) Sequential Resonance Assigments in 1H NMR Spectra of Oligonucleotides by Two-Dimensional NMR Spectroscopy. *Biochemistry 23*, 1371−1376.

Spielmann, H. P., Wemmer, D. E., and Jacobsen, J. P. (1995) Solution Structure of a DNA Complex with the Fluorescent Bis-Intercalator TOTO Determined by NMR Spectroscopy. *Biochemistry 34*, 8542−8553.

Stærk, D., Hamed, A. A., Pedersen, E. B., and Jacobsen, J. P. (1997) Bis-Intercalation of Homodimeric Thiazole Orange Dyes in DNA: The Effect of Modifying the Linker. *Bioconjugate Chem. 8*, 869−877.

Wüthrich, K. (1986) *NMR of Proteins and Nucleic Acids*, John Wiley & Sons, New York.

BC980073W

Cross-Linking Exogenous Bifunctional Peptides into Fibrin Gels with Factor XIIIa

Jason C. Schense[†,‡] and Jeffrey A. Hubbell*[,‡]

Division of Chemistry and Chemical Engineering, California Institute of Technology, Pasadena, California 91125, and Department of Materials and Institute for Biomedical Engineering, ETH-Zürich and the University of Zürich, Moussonstrasse 18, CH-8044, Zürich, Switzerland. Received June 26, 1998; Revised Manuscript Received October 13, 1998

Bi-domain peptides with a factor XIIIa substrate in one domain and a bioactive peptide in another domain were covalently incorporated into fibrin gels during coagulation through the action of the transglutaminase factor XIIIa. The cross-linking characteristics were determined for two bi-domain peptides with factor XIIIa substrates based on fibrinogen, dYRGD*TIGEGQQHHLGG*-NH_2, and dLRGD*GAKDV*-NH_2, as well as one bi-domain peptide with a substrate sequence based on α_2-plasmin inhibitor, dL*NQEQVSPL*RGD-NH_2, and another with a nonbiological, oligolysine substrate, dLRGD-*KKKK*G-NH_2 (substrate domains in italic). Each of these peptides was able to cross-link into the fibrin gels during coagulation, with the peptide containing the factor XIIIa substrate based on α_2-plasmin inhibitor being incorporated at levels in excess of 8 mol/mol fibrinogen. The structural characteristics of these peptide-modified gels proved to be the same as those for a native fibrin gel. The bioactivity of the incorporated active factors was tested in a neuronal culture model with day 8 chicken dorsal root ganglia using two bioactive sequences, RGD and DGEA, and one inactive control sequence, RDG. Each of these peptides influenced the extension of neurites from the ganglia as expected, indicating that the incorporated factors retained their activity. With the use of soluble competitive inhibitors, it was shown that this effect was due to the covalently incorporated peptides. Through exploiting the role of factor XIIIa in coagulation, we have developed a method by which to impart the character of nonfibrin proteins, such as extracellular matrix proteins, to fibrin, a biological material with many potential therapeutic and academic applications.

INTRODUCTION

Fibrin is a biopolymeric gel that plays an important role in natural wound healing and medicine. Fibrin is formed by the enzymatic polymerization of fibrinogen at most sites of injury, and fibrin can be formed for therapeutic purposes either from purified fibrinogen or from processed blood plasma. Such therapeutic applications include use as an adhesive and sealant and as a vehicle for the local delivery of drugs (*1, 2*). A special feature of fibrin, both formed naturally and therapeutically, is that it is degraded and remodeled by cell-associated enzymatic activity during cell migration and wound healing (*3, 4*). As such, the material differs qualitatively from most synthetic biomaterials employed in medicine, in that there exists an active feedback from the cells in the healing response to the material (leading to degradation of the material) as well as from the material to the cells (providing a mechanical scaffold with biospecific adhesion sites for cell infiltration) (*5*). Our interest in fibrin relates to its use as a therapeutic material, and this report addresses methods by which to harness the enzymatic processes of coagulation to incorporate exogenous bioactive signals into the fibrin network. The processes by which fibrinogen is polymerized into fibrin and by which this fibrin is subsequently degraded have been well characterized. Initially, the protease thrombin cleaves the dimeric fibrinogen molecule at two symmetric sites. Once the fibrinogen is cleaved, a self-assembly step occurs in which the fibrinogen monomers come together and form a noncovalently cross-linked polymer gel via the proteolytic exposure of binding sites (*1*). Factor XIIIa, proteolytically activated from factor XIII by thrombin, may then covalently cross-link this polymer network (see below). Once a cross-linked fibrin gel is formed, the subsequent degradation of the fibrin network is tightly controlled. One of the key molecules in controlling the degradation of fibrin is α_2-plasmin inhibitor (*6*). This molecule is cross-linked to the α chain of fibrin through the action of factor XIIIa (*7*). By attaching to the gel, a high concentration of inhibitor can be localized to the gel. The inhibitor then acts by preventing the binding of plasminogen to fibrin (*8*) and by inactivating plasmin (*6*).

The enzyme factor XIIIa plays an important role in the formation and degradation of fibrin gels (*9*). Factor XIIIa is a transglutaminase, and the specific cross-linking mechanism has been elucidated (*10, 11*). Initially, the zymogen factor XIII is activated by thrombin cleavage to form the active transglutaminase factor XIIIa. This enzyme then proceeds to create primarily intermolecular cross-links between the γ chains in the fibrin network (*12, 13*). These covalent cross-links provide the fibrin gel with significantly greater stability and resistance to protease degradation. Furthermore, factor XIIIa has been shown to cross-link other proteins, including fibronectin to both fibrin (*14*) and collagen (*15*). For several proteins,

* To whom correspondence should be addressed. Tel: +41 1 632 45 75. Fax: +41 1 632 12 14. E-mail: hubbell@biomed.mat.ethz.ch.

† California Institute of Technology.

‡ ETH-Zurich and the University of Zurich.

10.1021/bc9800769 CCC: $18.00 © 1999 American Chemical Society
Published on Web 12/08/1998

the exact amino acid sequence of the factor XIIIa substrate domain has been elucidated, including for fibrin (*12*), fibronectin (*16*), and α_2-plasmin inhibitor (*17*).

Fibrin is a very useful material in several biomedical applications. Its usefulness could be extended further, however, if one could alter the biological character of the fibrin by incorporating within it the biological activity of other proteins, such as those from extracellular matrix proteins including fibronectin, vitronectin, laminin, and collagen (*18*−*20*). In many cases, the bioactive domains, i.e., the regions of the proteins that bind to cell-surface receptors, are known, and these domains can be mimicked with synthetic linear and cyclic peptides (*21*, *22*). Two such sequences that were employed in this study were the tripeptide RGD, derived from many extracellular matrix proteins (*23*), which binds to a variety of integrin receptors (*24*), and the tetrapeptide DGEA, derived from collagen, which binds to the $\alpha_2\beta_1$ integrin (*25*).

Bi-domain peptides were designed and evaluated, with a factor XIIIa substrate in one domain and a bioactive region from fibronectin or collagen in another domain. The extent of incorporation of the exogenous peptide was determined, and the biological activity of such exogenous peptides was examined in the context of nerve regeneration. This technique has provided the ability to transfer biological activity from sources that are usually exogenous to fibrin gels, such as from extracellular matrix proteins, to create three-dimensional matrixes with numerous medical and biological applications.

EXPERIMENTAL PROCEDURES

Peptides and Proteins. Peptides were synthesized on solid resin using an automated peptide synthesizer (9050 Pep Plus Synthesizer, Millipore, Framingham) with standard 9-fluorenylmethyloxycarbonyl chemistry (*26*). All peptides were labeled with a fluorescent probe by including an α-dansylated leucine (Sigma, St. Louis) at the amino terminus of the peptide, except for dYRGD-*TIGEGQQHHLGG*-NH_2, which was dansylated off-line using dansyl chloride (*27*). All other reagents employed in peptide synthesis were purchased from Novabiochem (San Diego). A series of bifunctional peptides was synthesized that contained an RGD sequence coupled to a factor XIIIa substrate sequence (for clarity, the factor XIIIa substrate domains are always shown in italics). These peptides included dYRGD*TIGEGQQHHLGG*-NH_2 (d = dansylated amino acid; sequence from fibrinogen), dLRGD*GAKDV*-NH_2 (sequence from fibrinogen), dL*NQEQVSPL*RGD-NH_2 (sequence from α_2-plasmin inhibitor), and dLRGD*KKKK*G-NH_2 (nonbiological sequence including an oligomer of lysine). Two additional peptides were synthesized with the cross-linking domain from α_2-plasmin inhibitor, one containing a bioactive domain from collagen, dL*NQEQVSPL*DGEA-NH_2, and the other containing a biologically inactive control sequence, dL*NQEQVSPL*RDG-NH_2. Hydrophobic scavengers and cleaved protecting groups were removed by precipitation of the peptide in cold diethyl ether and dissolution in deionized water. After lyophilization, peptides were redissolved in 0.03 M Tris-buffered saline (TBS, pH 7.0) and analyzed using HPLC (Waters; Milford) on a size-exclusion column with TBS.

Fibrinogen solutions were prepared by dissolving fibrinogen (Fluka; Ronkonkoma) in deionized water at 8 mg/mL for 4 h. Dialysis (Spectrum, 6000−8000 MWCO; Laguna Hills) vs 400 vol of TBS, pH 7.4, for 24 h was used to exchange salts present in the protein solution. The resulting solution was then sterilized by filtering through a 0.22 μm syringe filter. The final fibrinogen concentration was determined by measuring the absorbance of the protein solution at 280 nm (*28*). TBS solutions at pH 7.0 that were made with either 50 mM Ca^{2+} or without any Ca^{2+} were sterilized by filtration though a 0.22 μm filter. Fresh thrombin solutions were made by dissolving thrombin (Sigma; St. Louis) in TBS at pH 7.0 at a concentration of 20 units/mL.

Fibrin Formation and Peptide Incorporation. Fibrin gels (200 μL) were made by mixing the four components such that final concentrations of 3.6 mg/mL fibrinogen, 2.5 mM Ca^{2+}, and 2 NIH units/mL of thrombin were obtained with various amounts of peptide added. This solution was allowed to gel for 60 min at 37 °C and 100% relative humidity. The gels were soaked in 0.3 M phosphate-buffered saline (PBS, pH 7.0) so that free peptide was allowed to diffuse out of the fibrin. In some experiments, the buffer was changed after the diffusion of free peptide reached equilibrium as indicated by spectrofluorimetric measurement of the dansyl signal.

To determine the amount of peptide incorporation, fibrin gels were degraded with 0.05 NIH units of plasmin (Sigma, St. Louis), and the resulting solution was analyzed using high-performance liquid chromatography (Waters; Milford). A size-exclusion column (Shodex, polyhydroxymethyl methacrylate packing; New York) was used that had a molecular mass range of 1−100 kDa. Samples were applied to the column and eluted in PBS. The resulting eluent was measured with both an inline ultraviolet and fluorescence detector to measure the presence of degraded fibrinogen and exogenous peptide (via the dansyl label), respectively.

Swelling. Fibrin gels were synthesized as described above with varying amounts of peptide. The gels were soaked in deionized water for 24 h and then weighed. Each gel was added to a preweighed culture dish and placed in a vacuum oven to dry. After all the water had been removed, the weight of the remaining gel was determined and the ratio of wet weight to dry weight was calculated.

Neurite Outgrowth. Dorsal root ganglia were dissected from 8 day old white leghorn chicken embryos (*29*). Ganglia were temporarily stored in modified neurobasal medium, consisting of insulin (5 μg/mL), transferrin (100 μg/mL), progesterone (6.3 ng/mL), putrascine (16.11 μg/mL), selenite (5.2 ng/mL), fibronectin (5 μg/mL), L-glutamine (0.5 mM), L-glutamate (25 μM), murine mouse nerve growth factor (20 ng/mL), 0.2% bovine serum albumin, and 1% antibiotic-antimycotic added to neurobasal medium (Gibco; Grand Island). Fibrin gels (400 μL) were polymerized as described above in the bottom of flat 24-well culture plates, except that the fibrin was polymerized around a dorsal root ganglion, such that one dorsal root ganglion was embedded three-dimensionally inside each gel. The dorsal root ganglia were cultured in 1 mL of modified neurobasal medium and the medium was changed at 3, 6, 9, and 24 h post seeding to wash out non-cross-linked peptide. Dorsal root ganglia were cultured in fibrin gels without added exogneous peptides (all values were normalized to this level of neurite extension in native fibrin), or with added dL*NQEQVSPL*DGEA-NH_2 or dL*NQEQVSPL*RGD-NH_2. As a control, dorsal root ganglia were cultured in fibrin gels with added dL*NQEQVSPL*RDG-NH_2 peptide, which is not biologically active. In each case, peptide was incorporated at 8 mol/mol fibrinogen. As additional controls, dorsal root ganglia were cultured in the three peptide-modified fibrin gels with the corresponding exogenous peptide

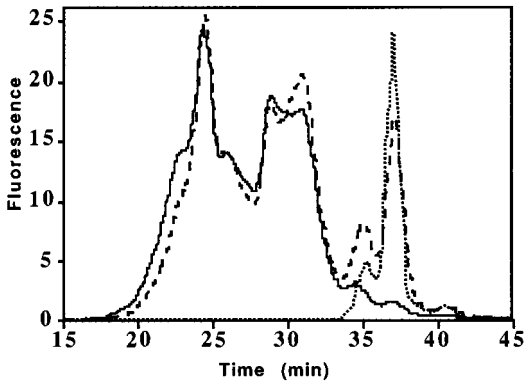


Figure 1. Fluorescence detection of chromatograms of plasmin-degraded gels. Size exclusion chromatography of a degraded gel with the peptide dL*NQEQVSPL*RGD (—) incorporated is shown. The second chromatogram shown (- - -) is identical to the first, except for the addition of free peptide after degradation of the gel with plasmin and the third chromatogram shown (···) represents free peptide eluted alone. The free peptide was observed to elute at longer times, corresponding to a lower molecular weight than the peptide incorporated during coagulation, demonstrating that peptide incorporated via the factor XIIIa substrate was covalently bound to the fibrin network.

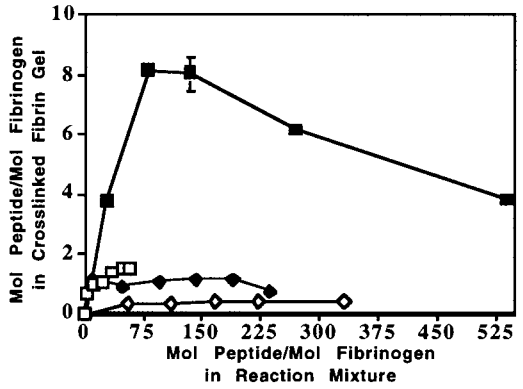


Figure 2. Incorporation of four bi-domain peptides with different factor XIIIa peptide substrates (italics). (■) dL*NQEQVSPL*RGD, from α_2-plasmin inhibitor, (◇) dLRGDAKDV, from fibrinogen, (□) dYRGD*TIGEGQQHHLGG*, from fibrinogen, and (◆) dLRGD*KKKK*G a nonbiological substrate, were each cross-linked into fibrin at a series of initial peptide concentrations, and the extent of incorporation is shown. Mean values and standard error of the mean are shown. The peptide dL*NQEQVSPL*RGD cross-linked more efficiently into the fibrin gel than the other three peptides, and achieved concentrations of up to 8.18 ± 0.09 mol of peptide/mol of fibrinogen.

added after gelation and throughout the culture duration (at 0.67 mg/mL) to serve as a soluble competitive inhibitor.

Images were collected at 24 and 48 h using light microscopy and digital image processing. At each time point, the average neurite length extending from each ganglion was measured as described elsewhere (*30*).

Statistics. Statistical analyses were performed using Statview 4.5. Comparative analyses were completed using analysis of variance (ANOVA) and Fisher's protective *t*-test at a 95% confidence level. Mean values and standard error of the mean are shown.

RESULTS

Calibration. Linear calibration curves were observed for both the incorporated peptides and the major components of the fibrin gels. Peptides were labeled with an α-dansylated amino acid, and this label was detected using an in-line fluorescence detector. Fibrinogen was degraded with plasmin and the correlation between the UV_{280} absorbance signal and protein concentration was determined. It was found the UV_{280} signal was linearly proportional to fibrinogen concentration for both degraded and nondegraded fibrinogen.

Measurement of Peptide Incorporation. To determine the extent of incorporation of the various bi-domain peptides into the fibrin network during coagulation, gels were formed, free peptide was permitted to diffuse out of the network, the fibrin was degraded with plasmin, and the degradation products were analyzed by HPLC to determine the amount of peptide (by fluorescence from the dansyl label) relative to fibrin (by UV absorbance) (Figure 1). Fibrin gels were synthesized and degraded, and the degradation products were analyzed by chromatography. The chromatogram obtained from a degraded, native fibrin gel with UV detection contained a single broad peak that eluted at 24 min (data not shown). The fluorescence signal was collected as well; however, the magnitude of the signal (from gels lacking exogenous peptide) was negligible (data not shown). Fibrin gels modified with different factor XIIIa substrate peptides were formed. The UV signals collected from these gels were consistently identical to that produced by native fibrin lacking exogenous peptides. However, for the peptide-modified gels, a large fluorescence signal appeared at an elution time later than the UV signal, appearing between 24 and 34 min (Figure 1, solid trace). When soluble peptide was added to the degraded peptide-modified fibrin gel, the fluorescence signal seen between 18 and 34 min was essentially identical to that seen in the degraded gel alone. However, the fluorescence signal seen between 34 and 39 min was increased (Figure 1, dashed trace), indicating that the added free peptide was eluting at a later time than peptide which had been incorporated during coagulation. These extra peaks, between 34 and 39 min, correlated directly with those observed for free peptide analyzed alone, in the absence of fibrinogen or fibrin degradation products (Figure 1, dotted trace).

The incorporation of four different bi-domain peptides, each with a different factor XIIIa substrate domain but the same bioactive domain, was determined as a function of exogenous peptide concentration during coagulation (Figure 2). The amount of peptide that was cross-linked into each gel was measured as described above. The bi-domain peptide with the cross-linking domain from α_2-plasmin inhibitor reached a maximum incorporated concentration of 8.18 ± 0.09 mol of peptide/mol of fibrinogen. It was possible to control the amount of peptide that was incorporated within the fibrin gel via the amount of peptide initially incorporated into the fibrinogen solution before coagulation. At initial peptide concentrations in excess of 135 mol of peptide/mol of fibrinogen, the ability of the peptide to cross-link into the gels decreased ($p < 0.05$). The cross-linking of dLRGD*KADV* and dYRGD*TIGEGQQHHLGG*, the two peptides with the fibrinogen factor XIIIa substrate domains, proved to be independent of initial peptide concentration, reaching levels of incorporation of 0.44 ± 0.03 and 1.53 ± 0.04 mol of peptide/mol of fibrinogen, respectively. The lysine oligomer substrate, dLRGD*KKKK*G, displayed a similar cross-linking profile and reached a maximum cross-linking density of 1.18 ± 0.05 mol of peptide/mol oof fibrinogen. When the average efficiency of incorporation (the fraction of exogenous peptide present in the coagulation mixture that was incorporated into the fibrin gel) was measured for each peptide, it was found that the factor XIIIa substrates with a glutamine at the active

Table 1. Extent of Incorporation and Efficiency of Bi-Domain Peptides Containing Different Factor XIIIa Substrates

peptide sequence (factor XIIIa substrate sequence in italics)	maximum cross-linking density (mol of peptide/ mol of fibrinogen)	maximum cross-linking efficiency (%)
dL*NQEQVSPL*RGD	8.18 ± 0.09	14 ± 0.6
dLRGD*AKDV*	0.44 ± 0.03	0.6 ± 0.1
dLRGD*KKKK*G	1.18 ± 0.05	12 ± 5
dYRGD*TIGEGQQHHLGG*	1.53 ± 0.04	29 ± 0.6

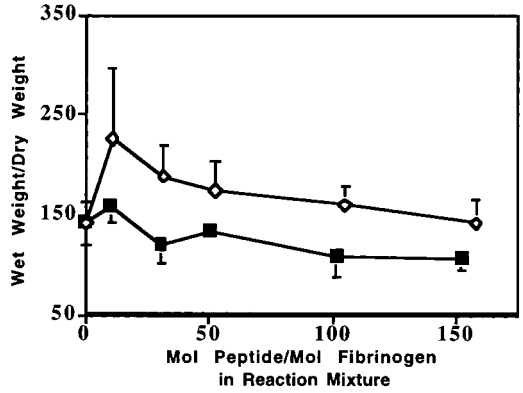


Figure 3. Swelling of the peptide cross-linked gels. Two different peptides, (■) dL*NQEQVSPL*RGD and (◇) dLRGDAKDV, were cross-linked into fibrin gels at a series of concentrations and the amount of swelling, determined by comparing the dry weight to the wet weight, is shown. Upon the basis of the initial volume and amount of material used, the swelling ratio at the time of synthesis before any contraction was 190. Mean values and standard error of the mean are shown. The change in swelling induced by incorporation of these two peptides was statistically insignificant ($p > 0.10$).

site were 3−30 times more efficiently incorporated than the lysine substrates (Table 1).

Swelling. As a measure of disruption of the fibrin network that might potentially occur as a result of the incorporation of exogenous peptide, the swelling of the fibrin gel was measured (Figure 3). Fibrin gels were polymerized as described above and modified separately with two factor XIIIa substrate peptides. The two substrates chosen were dLRGDG*KADV*, based on a fibrinogen substrate site, and dL*NQEQVSPL*RGD, based on the α_2-plasmin inhibitor substrate site. The influence of the incorporation of these peptides on the swelling of the resulting fibrin matrix was determined by comparing swelling to that of unmodified gels as well as to the initial ratio of water-to-protein, 190. When an unmodified fibrin gel was created, the ratio of wet weight to dry weight, 141.8 ± 20.7, was lower than the initial value in the fibrinogen solution before coagulation ($p < 0.05$). The swelling of peptide-modified gels proved to be similar to the swelling of unmodified fibrin gels and was independent of cross-linked peptide density for both peptides tested; no value for either peptide tested was statistically different than that for the unmodified gel ($p > 0.1$).

Neurite Extension. As a measure of the bioactivity of the exogenous peptide, incorporated via the factor XIIIa substrate domain of the bi-domain peptide, a neuronal cell culture model was employed in which neurites extend from dorsal root ganglia taken from day 8 chick embryos cultured within a three-dimensional fibrin network (Figure 4). Three peptides were individually cross-linked into fibrin and tested for their ability to interact with growing neurites in vitro. Each was a bi-domain peptide that contained the α_2-plasmin inhibitor

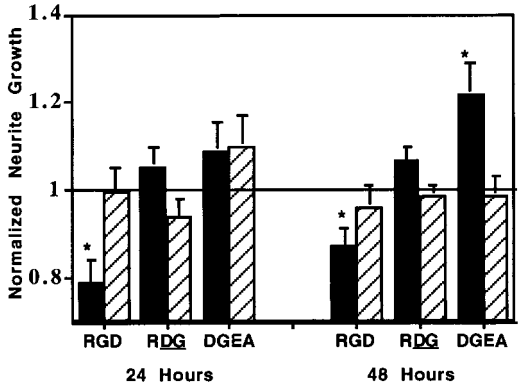


Figure 4. The effect of incorporated peptide at 8 mol of peptide/ mol of fibrinogen on neurite length within three-dimensional fibrin matrixes without (solid bars) and with (hatched bars), the indicated peptide added in soluble form to the culture medium. Neurite growth from day 8 dorsal root ganglia was normalized to growth in unmodified fibrin at 24 and 48 h culture time. All cross-linked peptides contained the substrate sequence dL*NQEQVSPL* and the active sequence as shown. Experiments were performed in triplicate with six dorsal root ganglia and mean values and standard error of the mean are shown; (*) $p < 0.05$ compared to unmodified fibrin. Cross-linking of RGD statistically lowered neurite extension, DGEA increased neurite extension and the inactive control peptide RDG had no effect on neurite extension. In each case, the effect of the cross-linked peptide was neutralized by the addition of the same peptide in soluble form as a competitive inhibitor.

sequence *NQEQVSPL* as the cross-linking substrate. Two active sequences, RGD and DGEA, and one control sequence, RDG, were attached to this factor XIIIa substrate. By incorporating 8 mol of peptide/mol of fibrinogen, statistically different neurite growth was obtained for both of the active sequences. At 24 and 48 h of culture, the incorporation of RGD into the fibrin reduced outgrowth ($p < 0.05$) relative to native fibrin by 21 ± 5.2% at 24 h and 13 ± 4.3% at 48 h. DGEA-modified gels proved to enhance neurite growth, increasing neurite length at 48 h of culture by 22 ± 7.0% ($p < 0.05$) relative to that in native fibrin. The cross-linking of the control peptide, RDG, into the fibrin did not affect the extent of neurite extension ($p = 0.22$). As a final control, peptides were added in the soluble phase in the culture medium as well as cross-linked into the gel to serve as competitive inhibitors. The resulting level of neurite growth returned to the level attained in native fibrin alone in all cases ($p > 0.21$).

DISCUSSION

Fibrin gels provide a unique platform as a biomaterial. In addition to being nontoxic as monomer, polymerized gel, or degraded gel, these materials are also able to interact biologically with cells, inducing proliferation or migration. However, many other proteins contain useful domains that fibrin lacks which would enhance the usefulness of fibrin as a biomaterial, e.g., in wound healing. Through the action of the transglutaminase, factor XIIIa, we sought to augment the native biological characteristics of fibrin to allow it to incorporate the characteristics of other useful proteins such as fibronectin, collagen, or laminin. Fibrinogen was obtained as a protein that was isolated from blood plasma. The transglutaminase zymogen factor XIII was present, as it usually is, as a copurified component in this fibrinogen preparation. Exogenous peptides were readily incorporated through the concerted action of thrombin and factor XIIIa during coagulation to covalently graft these bi-

domain peptides into the fibrin network. A sequence from α_2-plasmin inhibitor served as a particularly effective factor XIIIa substrate to accomplish this end.

Chromatographic analysis of the degradation products of peptide-modified fibrin gels provided information about the peptide incorporation process, allowing the determination of the amount of peptide incorporated as well as proof of the covalent nature of the incorporation. When peptide-modified and native fibrin gels were degraded by the fibrinolytic enzyme plasmin, multiple fragments of differing molecular weights were created. UV absorption was employed as the primary indicator of the presence of fibrin degradation products, and fluorescence measurement was utilized for detection of the exogenous peptide. These two measurements allowed unequivocal determination of the ratio of incorporated exogenous peptide to fibrin. Moreover, they provided strong evidence of covalent incorporation: when free peptide was added to degraded fibrin, it eluted at a low molecular weight, at a position identical to that of the free peptide in a single-component solution, whereas the peptide incorporated during fibrin polymerization eluted at a much higher molecular weight, indicating that it was covalently bound to the fibrin degradation fragments. This was true for all the exogenous peptides examined.

The various factor XIIIa substrates demonstrated different activities for incorporation into the fibrin network during gelation. Two substrate sequences were selected based on cross-linking domains on the γ chain of fibrinogen, one that contains a lysine substrate and one that contains a glutamine substrate. The lysine-based fibrinogen substrate displayed a relatively low maximum cross-linking density of 0.44 mol/mol fibrinogen and the density of incorporation saturated at this level at high concentrations in the fibrin precursor. The glutamine-based sequence could cross-link into the fibrin at a rather high density, 1.53 mol/mol fibrinogen, and the incorporation of this peptide also saturated at high reactant concentrations. The final cross-linking density may have been limited by the mechanism through which both of these peptides were incorporated into the fibrin. Namely, the sites at which these peptides cross-linked into the fibrin gel were the same as those used for intermolecular fibrin cross-linking, and thus the peptides had to compete directly with the polymerizing fibrin gel for the cross-linking sites. During the formation of a fibrin gel, precursor fibrils become ordered, placing the two fibrinogen cross-linking substrates into close proximity (*31*). This alignment enhances cross-linking of the fibrils and may have prevented these two peptides from efficiently competing for cross-linking sites. Interestingly, the fibrinogen-based substrate with a glutamine at the reaction site was incorporated at a more than 3-fold density ($p < 0.01$) and at a more than 48-fold efficiency ($p < 0.01$) than the fibrinogen-based substrate with a lysine at the reactive site.

A nonbiological substrate comprising a tetramer of lysine was also examined. The incorporation of this peptide reached a useful density of 1.18 mol/mol fibrinogen, with a maximum efficiency of 12%. Despite lacking a native substrate sequence, this oligomer was efficiently incorporated into the fibrin gel. This is consistent with studies that have demonstrated that the reactivity of the receptor amine for transglutaminase enzymes is more promiscuous than the glutamine. While small variations in amino acids flanking the glutamine residue in a native substrate can lead to significant changes in cross-linking specificity (*32*), the lysine residue is cross-linked sufficiently well that even nonbiological lysine substrates can be employed with high enzymatic activity (*33*, *34*).

Perhaps the most useful of the factor XIIIa substrates examined for the incorporation of exogenous peptides was a sequence based on the α_2-plasmin inhibitor cross-linking domain. A very high density of incorporation, more than 8 mol/mol fibrinogen in the fibrin gel was achieved. The nature of the cross-linking of the protein α_2-plasmin inhibitor appears to have features that make its factor XIIIa substrate very useful in incorporation of exogenous peptides into fibrin during gelation. The native protein is cross-linked into fibrin gels at a very high density, attaching at up to 17 separate sites on the α chain (*17*). By comparison with the maximum density of incorporation observed in this study of 8 mol of peptide/mol of fibrinogen, it may be that the truncated sequence dL*NQEQVSPL* with the fluorescent marker near the active amino acid does not serve as a substrate for all of these sites, or it may be that competition with contaminant α_2-plasmin inhibitor in the fibrinogen used (not assayed) limited incorporation. Another beneficial property of the factor XIIIa substrate from α_2-plasmin inhibitor is that these sites on the α fibrin chain are not used for intermolecular fibrinogen cross-links. Therefore, a peptide with this substrate would not need to compete with the fibrin itself for cross-linking sites. Interestingly, the chromatographic results obtained with the bi-domain peptide dL*NQEQVSPL*RGD are consistent with its incorporation into the α chain of fibrinogen. The peptide-containing peak (by fluorescence) obtained with this substrate eluted at consistently longer times (lower molecular weight) than those observed with the other three substrates. These smaller fibrin degradation fragments have been reported to be primarily degradation products of the α chain of fibrinogen (*35*, *36*). Previous work has shown that α_2-plasmin inhibitor cross-links only to one of the three chains in fibrinogen, the α chain (*37*, *38*), and the chromatographic result obtained in this study with the bi-domain peptide is consistent with this behavior. As a final feature of the nature of the cross-linking of the factor XIIIa substrate in α_2-plasmin inhibitor, α_2-plasmin inhibitor is known to continue to cross-link onto the fibrin matrix after the formation of the gel, allowing the fibrin gel to form unimpeded. Because of these natural traits, it would seem that the peptide was able to cross-link into the gel at a much higher density than the other substrates tested.

The swelling characteristics of the fibrin gel, specifically the water content, were used as an indication of the disruption of fibrin gel structure by the incorporation of exogenous peptides. The natural intermolecular cross-linking of fibrin limits the swelling of these gels in addition to providing stability. If the incorporation of exogenous peptide interferes with the formation of intermolecular fibrinogen cross-links, the water content in the gel should increase. As an example, two representative peptides were tested; namely a bi-domain peptide with the factor XIIIa substrate from fibrinogen, dLRGD-*GAKDV*, and a bi-domain peptide with the factor XIIIa substrate from the α_2-plasmin inhibitor sequence, dL*N-QEQVSPL*RGD. The amount of water absorbed by the gels comprising either of these peptides was not significantly higher than for a native fibrin gel, suggestive of little disruption of fibrin structure due to peptide incorporation. The peptide with the substrate from fibrinogen demonstrated relatively low incorporation levels, perhaps due to its inability to compete with the fibrin gel itself for enzymatic activity. It is thus likely that this rather subtle change in composition resulted in minimal alter-

ation in fibrin structure. The peptide containing the factor XIIIa substrate from α_2-plasmin inhibitor was incorporated at high levels, up to 8 mol/mol fibrinogen, however, the swelling of these gels remained unchanged as well. The natural role of α_2-plasmin inhibitor is to prevent proteolytic degradation of fibrin after it is cross-linked into the fibrin by factor XIIIa. Therefore, the cross-linking of this protein onto the fibrin is critical for gel stability and apparently is optimally arranged to minimize disruption of the gel structure. This property would appear to have been transferred to the peptide substrate as well, allowing it to cross-link at high densities without affecting the physical character of the fibrin.

A cell culture assay, in which neurites extend from the dorsal root ganglia of embryonic chicks through the fibrin matrix, was employed to assess the bioactivity of the incorporated peptides. All fibrin gels were modified with bi-domain peptides containing the factor XIIIa substrate sequence from α_2-plasmin inhibitor since this peptide had the greatest biological potential due to its high incorporation density. The fibrin gels modified with the exogenous peptides tested demonstrated significantly different neurite extension relative to native fibrin, with the associated active sequences providing the expected activity. Fibrin modified with the inactive control sequence, RDG, resulted in statistically identical neurite extension to that observed in native fibrin. Since the RDG sequence does not have any associated bioactivity, the only possible effect associated with peptide incorporation would be derived from physical changes to the fibrin gel. Incorporation of the this peptide did not affect neurite extension, indicating that any physical changes to the gel must have had a negligible effect in this cell culture model. The incorporation of RGD at 8 mol/mol fibrinogen into fibrin gels resulted in significantly shorter neurites at both 24 and 48 h. RGD modifies cell migration by acting as an adhesion site (*39*). Native fibrin contains two RGD domains per mole of fibrinogen, so this modification led to the formation of gels with 10 mol of RGD/mol of fibrinogen. By creating a material with so much adhesive character, it apparently became more difficult for the advancing neurite to migrate through the gel, leading to slower extension. This observed phenomenon is consistent with the observations of Palecek et al., who demonstrated that, in two dimensions, incorporation of high densities of adhesion ligand resulted in slower cell migration (*40*). This effect depended on the affinity of the ligand for its corresponding adhesion receptor and on cytoskeletal interactions. A sequence derived from collagen, DGEA, was also examined for bioactivity in this neurite extension model. This domain had been previously observed to enhance neurite extension (*41*); a similar observation in this present study suggests that this covalently incorporated exogenous peptide was indeed presented in a manner such that it was both available for receptor binding and biologically active. The control experiments with the peptides included in the culture medium as a soluble competitive inhibitor in which neurite extension was not significantly different than fibrin demonstrated that the observed biological activity was due exclusively to the covalently incorporated adhesion peptide.

Through the use of factor XIIIa, we have developed a consistent method through which the biological character of fibrin can be augmented with active factors, creating a material that can be optimized for various applications in medicine or cell biology. The specificity of the cross-linking enzyme allows us to have good control over the final incorporation density, allowing this material to be used for both therapeutic and academic applications.

ACKNOWLEDGMENT

This work was funded by NIH Predoctoral Training in Biotechnology, Grant GM08346, and by Grant 31-52261 NFP 38 of the Swiss National Science Foundation.

LITERATURE CITED

(1) Sierra, D. H. (1993) Fibrin Sealant Adhesive Systems, A Review of Their Chemistry, Material Properties and Clinical Applications. *J Biomater. Appl. 7,* 309−352.

(2) Zarge, J. I., Husak, V., Huang, P., and Greisler, H. P. (1997) Fibrin Glue Containing Fibroblast Growth Factor Type 1 and Heparin Decreases Platelet Deposition. *Am. J. Surg. 174,* 188−192.

(3) Seeds, N. W., Haffke, S. P., Hawkins, R. L., Krystosek, A., McGuire, P. G., and Verrall, S. (1992) Neuronal Growth Cones: Battering Rams or Lasers? *The Nerve Growth Cone* (P. C. Letourneau, S. B. Kater, and E. R.Macagno, Eds.) pp 219−229, Raven Press, New York.

(4) Krystosek, A., and Seeds, N. W. (1984) Peripheral Neurons and Schwann Cells Secrete Plasminogen Activator. *J. Cell. Biol. 98,* 773−776.

(5) Francis, C. W., Bunce, L. A., and Sporn, L. A. (1993) Endothelial Cell Responses to Fibrin Mediated by FPB Cleavage and the Amino Terminus of the β Chain. *Blood Cells 19,* 291−307.

(6) Aoki, N. (1979) Natural Inhibitors of Fibrinolysis. *Prog. Cardiovasc. Dis. 21,* 267−286.

(7) Sakata, Y., and Aoki, N. (1980) Cross-Linking of α2-Plasmin Inhibitor to Fibrin by Fibrin-stabilizing Factor. *J. Clin. Invest. 65,* 290−297.

(8) Aoki, N., Moroi, M., and Tachiya, K. (1978) Effects of α2-plasmin Inhibitor on Fibrin Clot Lysis. It's Comparison With α2-macroglobulin. *Thromb. Haemost. 39,* 22−31.

(9) Francis, C. W., and Marder, V. J. (1988) Increased Resistance to Plasmic Degradation of Fibrin With Highly Cross-linked α-polymer Chains Formed at High Factor XIII Concentrations. *Blood 71,* 1361−1365.

(10) Pisano, J. J., Finlayson, J. S., and Peyton, M. P. (1968) Cross-link in Fibrin Polymerized by Factor XIII: ϵ-(γ-Glutamyl)lysine. *Science 160,* 892−893.

(11) Folk, J. E. (1969) Mechanism of Action of Guinea Pig Liver Transglutaminase. *J. Biol. Chem. 244,* 3707−3713.

(12) Doolittle, R. F., Chen, R., and Lau, F. (1971) Hybrid Fibrin: Proof of the Intermolecular Nature of $\gamma-\gamma$ Cross-linking Units. *Biochem. Biophys. Res. Commun. 44,* 94−100.

(13) Shainoff, J. R., Urbanic, D. A., and DiBello, P. M. (1991) Immunoelectrophoretic Characterizations of the Cross-linking of Fibrinogen and Fibrin by Factor XIIIa and Tissue Transglutaminase. *J. Biol. Chem. 266,* 6429−6437.

(14) Potts, J. R., Phan, I., Williams, M. J., and Campbell, I. D. (1995) High-resolution Structural Studies of the Factor XIIIa Cross-linking Site and the First Type 1 Module of Fibronectin. *Nat. Struct. Biol. 2,* 946−950.

(15) Mosher, D. F., Schad, P. E., and Kleinman, H. K. (1979) Cross-Linking of Fibronectin to Collagen by Blood Coagulation Factor XIIIa. *J. Clin. Invest. 64,* 781−787.

(16) McDonagh, R. P., McDonagh, J., Petersen, T. E., Thogersen, H. C., Skorstengaard, K., Sottrup-Jensen, L., Magnusson, S., Dell, A., and Morris, H. R. (1981) Amino Acid Sequence of the Factor XIIIa Acceptor Site in Bovine Plasma Fibronectin. *FEBS Lett. 127,* 174−178.

(17) Ichinose, A., Tamaki, T., and Aoki, N. (1983) Factor XIII-mediated Cross-linking of NH2-terminal Peptide of α2-plasmin Inhibitor to Fibrin. *FEBS Lett. 153,* 369−371.

(18) Yamada, Y., and Kleinman, H. K. (1992) Functional Domains of Cell Adhesion Molecules. *Curr. Opin. Cell. Biol. 4,* 819−823.

(19) Engvall, E., and Wewer, U. M. (1996) Domains of Laminin. *J. Cell. Biochem. 61,* 493−501.

(20) Malinda, K. M., and Kleinman, H. K. (1996) The Laminins. *Int. J. Biochem. Cell. Biol. 28,* 957−959.

(21) Yamada, K. M. (1991) Adhesive Recognition Sequences. *J. Biol. Chem. 266,* 12809−12812.
(22) Massia, S. P., and Hubbell, J. A. (1991) An RGD Spacing of 440 nm is Sufficient for Integrin $\alpha_v\beta_3$ Mediated Fibroblast Spreading and 140 nm for Focal Contact Stress Fiber Formation. *J. Cell. Biol. 114,* 1089−1100.
(23) Ignatius, M. J., Large, T. H., Houde, M., Tawil, J. W., Burton, A., Esch, F., Carbonetto, S., and Reichardt, L. F. (1990) Lipoprotein Uptake by Neuronal Growth Cones in Vitro. *J. Cell. Biol. 111,* 709−720.
(24) Hynes, R. O. (1992) Integrins: Versatility, Modulation, and Signaling in Cell Adhesion. *Cell 69,* 11−25.
(25) Zutter, M. M., and Santaro, S. A. (1990) Widespread Histologic Distribution of the $\alpha_2\beta_1$ Integrin Cell-surface Receptor. *Am. J. Path. 137,* 113−120.
(26) Fields, G., and Noble, R. (1990) Solid-Phase Peptide Synthesis Utilizing 9-fluorenylmethoxycarbonyl Amino Acids. *Int. J. Peptide Protein Res. 35,* 161−214.
(27) Varadarajan, A., and Hawthorne, M. F. (1991) Novel Caraboranyl Amino Acids and Peptides: Reagents for Antibody Modification and Subsequent Neutron-Capture Studies. *Bioconjate Chem. 2,* 242−253.
(28) Dellenback, R. J., and Chien, S. (1970) The Extinction Coefficient of Fibrinogen from Man, Dog, Elephant, Sheep, and Goat at 280mμ. *Proc. Soc. Exp. Biol. Med. 134,* 353−355.
(29) Varon, S. J., Nomura, J., Perez-Polo, J. R., and Shooter, E. M. (1972) The Isolation and Assay of the Nerve Growth Factor Proteins. *Methods of Neurochemistry* (R. Fried, Eds.) pp 203−229, New York.
(30) Herbert, C. B., Bittner, G. D., and Hubbell, J. A. (1996) Effects of Fibrinolysis on Neurite Growth From Dorsal Root Ganglia Cultured in Two- and Three-Dimensional Fibrin Gels. *J. Comp. Neurol. 365,* 380−391.
(31) Doolittle, R. F. (1973) Structural Aspects of the Fibrinogen to Fibrin Conversion. *Adv. Protein Chem. 27,* 1−109.
(32) Gorman, J. J., and Folk, J. E. (1981) Structural Features of Glutamine Substrates for Transglutaminases. Specificities of Human Plasma Factor XIIIa and the Guinea Pig Liver Enzyme Toward Synthetic Peptides. *J. Biol. Chem. 256,* 2712−2715.
(33) Fink, M. L., Shao, Y. Y., and Kersh, G. J. (1992) A Fluorometric High-perfomance Liquid Chromatographic Assay for Transglutaminase Activity. *Anal. Biochem. 201,* 270−276.
(34) Parameswaran, K. N., Velasco, P. T., Wilson, J., and Lorand, L. (1990) Labeling of ϵ-lysine Cross-linking Sites in Proteins With Peptide Substrates of Factor XIIIa and Transglutaminase. *Proc. Natl. Acad. Sci. U.S.A. 87,* 8472−8475.
(35) Pizzo, S. V., Schwartz, M. L., Hill, R. L., and McKee, P. A. (1973) The Effect of Plasmin on the Subunit Structure of Human Fibrin. *J. Biol. Chem. 248,* 4574−4583.
(36) Ständler, L., Sillard, R., Bensch, K. W., Ruf, A., Raida, M., Schulz-Knappe, P., Schepky, A. G., Patscheke, H., and Forssmann, W.-G. (1995) In Vivo Degradation of Human Fibrinogen Aα: Detection of Cleavage Sites and Release of Antithrombotic Peptides. *Biochem. Biophys. Res. Commun. 215,* 896−902.
(37) Tamaki, T., and Aoki, N. (1981) Cross-linking of α2-plasmin Inhibitor and Fibronectin to Fibrin by Fibrin-stablizing Factor. *Biochim. Biophys. Acta 661,* 280−286.
(38) Sobel, J. H., and Gawinowicz, M. A. (1996) Identification of the α Chain Lysine Donor Sites Involved in Factor XIIIa Fibrin Cross-linking. *J. Biol. Chem. 271,* 19288−19297.
(39) DiMilla, P. A., Barbee, K., and Lauffenburger, D. A. (1991) Mathematical Model for the Effects of Adhesion and Mechanics on Cell Migration Speed. *Biophys. J. 60,* 15−37.
(40) Palecek, S. P., Loftus, J. C., Ginsberg, M. H., Lauffenburger, D. A., and Horwitz, A. F. (1997) Integrin-ligand Binding Properties Govern Cell Migration Speed Through Cell-substratum Adhesiveness. *Nature 385,* 537−540.
(41) Lander, A. (1989) Understanding the Molecules of Cell Contacts. *J. Trends Neurol. Sci. 12,* 189−195.

BC9800769

Physicochemical Properties and O_2-Coordination Structure of Human Serum Albumin Incorporating Tetrakis(*o*-pivalamido)phenylporphyrinatoiron(II) Derivatives

Teruyuki Komatsu, Kazuyoshi Hamamatsu, Jian Wu, and Eishun Tsuchida*,†

Department of Polymer Chemistry, Advanced Research Institute for Science & Engineering, Waseda University, Tokyo 169-8555, Japan. Received July 16, 1998; Revised Manuscript Received October 12, 1998

Incorporation of tetrakis(*o*-pivalamido)phenylporphyrinatoiron(II) derivatives with a covalently linked axial imidazole (FeP) into human serum albumin (HSA) provides a new type of artificial hemoprotein (HSA-FeP) that binds and releases dioxygen reversibly under physiological conditions (in aqueous media, pH 7.4, 37 °C) and in a fashion similar to hemoglobin and myoglobin. The HSA host adsorbs a maximal eight FeP molecules, and their stepwise equilibrium constants (K_1-K_8) range from 1.2×10^6 to 1.3×10^4 M^{-1}. The major binding sites of the synthetic hemes are identical to those of hemin, bilirubin, and long-chain fatty acids. The red-colored solution of HSA-FeP was stored for three months at 4 °C and could be kept as a freeze-dried powder for more than six months. The solution properties [[HSA]: 5 wt %, FeP/HSA = 1−8 (mol/mol)] satisfy the physiological requirements for dioxygen infusion for potential clinical use; the specific gravity is 1.013, and the viscosity is 1.1 cP. Mixing the solution with human blood does not induce any coagulation and precipitation. On the basis of the gel permeation chromatography, CD spectroscopy, and IEF measurements, the molecular size, second-order structure, and surface charge distribution of the HSA-FeP conjugate are constant and independent of the binding numbers of heme molecules. Furthermore, the O_2-coordination structure of FeP embedded into certain hydrophobic domains of the albumin was confirmed by resonance Raman spectroscopy.

INTRODUCTION

In the bloodstream, serum albumin serves as a *shuttle* that transports an incredible variety of endogenous and exogenous compounds. Interest in this molecular binding led to research involving association studies of HSA with various ligands (Brown, 1976; Kragh-Hansen, 1981; Peters, 1975, 1985). Human serum albumin (HSA) was among the very first proteins crystallized in the microgravity environment of space (Carter et al., 1989, 1994; He et al., 1992). In contrast to the early conception of an oblate ellipsoid shape (140 × 40 Å), HSA is a unique heart-shaped molecule that can be approximated to be an equilateral triangle with sides of 8 nm and a depth of 3 nm. HSA has three homologue domains (I, II, and III) with nine loops formed by 17 disulfide linkages, and each domain is constructed of two subdomains (IA, IB, etc.). The majority of the compounds are bound at one or both sites within specialized cavities of the subdomains IIA and IIIA with typical equilibrium constants (K) ranging 10^6-10^4 M^{-1} (Kragh-Hansen, 1981a). For instance, bilirubin is primarily bound to a site within IIA. The binding behavior of several porphyrin derivatives to HSA has also been studied over the last two decades (Little et al., 1960; Beaven et al., 1974; Muller-Eberhand et al., 1975; Adams et al., 1980), because hemin released from hemoglobin is transported to the liver by albumin for metabolic processing. The primary binding site of hemin is located in the sequence 124−298 of HSA, corresponding to subdomains Ib−IIa (Hrkal et al., 1984), and the immobilization presumably involves coordination of a histidine residue to the central iron (Casella et al., 1993). The hemopexin in plasma definitely attaches to a free heme in both iron(II) and iron(III) states by an axial imidazole coordination (Muller-Eberhand and Morgan, 1975; Morgan et al., 1980; Lamola et al., 1981). One may expect some new functions of these albumin-heme conjugates, but little attention has been generated so far (Marden et al., 1989; Bonaventura et al., 1994).

We have recently found that a tetraphenylporphyrinatoiron(II) derivative with a covalently linked axial base, 2-[8-{*N*-(2-methylimidazolyl)}octanoyloxymethyl]-5,10,15,20-tetrakis(α,α,α,α-*o*-pivalamido)phenylporphyrinatoiron(II) (FeP, Figure 1) (Tsuchida et al., 1994), is efficiently incorporated into the HSA molecule, providing an artificial hemoprotein which is able to bind and release dioxygen reversibly under physiological conditions (in aqueous media, pH 7.4, 37 °C) as hemoglobin (Komatsu et al., 1995; Tsuchida et al., 1997). The imidazole intramolecularly coordinated to the central iron plays a crucial role in the formation of a stable $Fe-O_2$ complex. We report herein the stepwise equilibrium constants for FeP association and the physicochemical properties of the obtained hybrid HSA-FeP. Furthermore, the axial base imidazole and the O_2-coordination structures of FeP embedded into certain domains of the albumin have been clarified by resonance Raman spectroscopy.

EXPERIMENTAL PROCEDURES

Materials and Methods. HSA-FeP with different FeP concentration was prepared according to our previously reported procedure (Tsuchida et al., 1997). An HSA was purchased from Bayer Co., Ltd. (Albumin Cutter, 5 wt %). Protoporphyrin IX disodium salts (PPIX) was gifted from Sato Pharmacy Co., Ltd. Phenol red and palmitic

* To whom the correspondence should be addressed. Phone: +81 3-5286-3120; Fax: +81 3-3205-4740. E-mail: eishun@mn.waseda.ac.jp.

† CREST investigator, JST.

10.1021/bc980084p CCC: $18.00 © 1999 American Chemical Society
Published on Web 12/31/1998

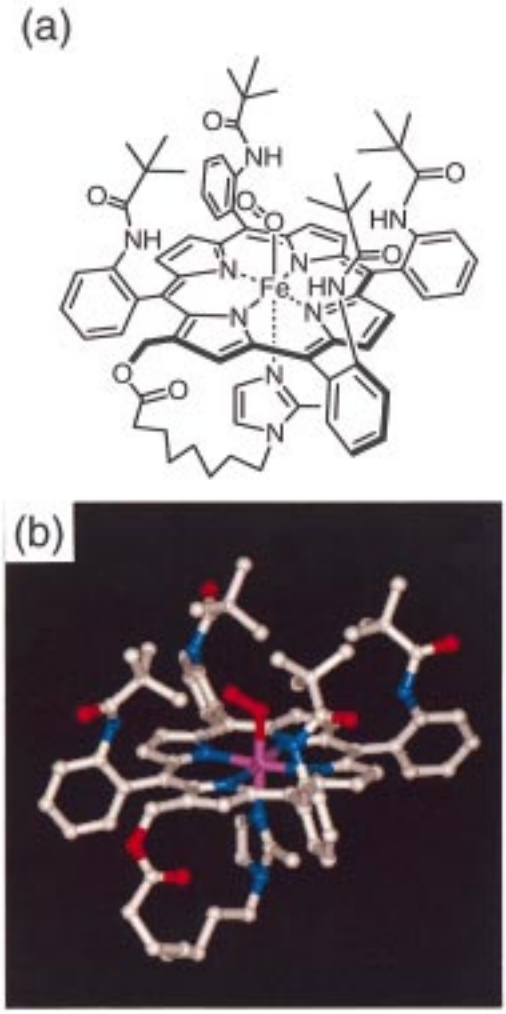


Figure 1. (a) Formula of FeP and (b) computer-simulated structure of dioxygenated FeP. Molecular dynamics and minimization (force field: esff) were performed using an Insight II system (Molecular Simulations Inc.). The structure was generated by alternative minimizations and annealing dynamic calculations from 1000 to 100 K.

acid were purchased from Kanto Chemical Co., Ltd. Pure water (Otsuka Pharmaceutical Co., Ltd.) was used for dilution for HSA and ethanol (>99.5%, Kanto Chemical Co., Ltd.) was for the solvent of FeP. UV−vis absorption spectra were obtained on a Shimadzu V-570 spectrometer.

Equilibrium Constants for FeP Binding to HSA. In the course of preparation of the HSA-FeP solution, the precipitated carbonyl FeP [FeP(CO)] was extracted with $CHCl_3$ and its concentration was determined by the absorption spectra (ϵ_{max} at 420 nm: 2×10^5 $M^{-1}cm^{-1}$). On the basis of the quantitative analysis of this free FeP-(CO) molecule in the solution prepared with different FeP/HSA mixing ratios (1−14 mol/mol), the equilibrium constants were determined using stepwise equilibrium models (Fletcher et al., 1970; Ashbrook et al., 1975).

Binding Sites of FeP in HSA. The association sites of FeP were determined from the competitive binding with other ligands which are well-known to bind the major sites of HSA. Palmitic acid, PPIX, instead of hemin, and phenol red, instead of bilirubin, were used as the inhibitors. The quantitative analysis of FeP was carried out with the hybrid HSA incorporating each inhibitor (molar ratio 1/1). The maximal binding numbers of FeP were decreased to less than the mixing ratio, if the FeP molecule could not displace the inhibitor in competitive binding.

Rheological Properties. The viscosity and density of the solution at 37 °C were measured with an Anton Parr OCR-D oscillatory capillary rheometer and density meter, where the sample in the measuring capillary was set into sinusoidal oscillations at a given frequency of 2 Hz. The shear rate ranged 0.58−358 s^{-1}. The HSA-FeP solution [[HSA]: 5 wt %, FeP/HSA = 4,8 (mol/mol)] was applied to all measurements. The human venous blood were drawn into EDTA containing tube just before use.

Physicochemical Properties. Circular dichroism (CD) spectra were obtained by a JASCO J-725 spectropolarimeter. The HSA concentration was 1.12 μM [FeP/HSA = 1, 4, 8 (mol/mol)], and quartz cuvettes with 1 mm and 10 mm thickness were used for measurements in the ranges 190−250 nm and 250−700 nm, respectively. Isoelectric points and molecular weights were measured by a Pharmacia Phastsystem using isoelectric focusing (IEF) in pH 3−9 Phast Gel IEF 3−9 and native PAGE in Phast Gel Gradient 8−25, respectively. The temperature during the electrophoresis was maintained at 15 °C and the sample concentrations were [HSA] = 3.75 μM. The used markers are Isoelectric Focusing Calibration Kit and LMW Electrophoresis Calibration Kit, respectively. Gel permeation chromatography was performed on a Shimadzu LC-8A chromatograph equipped with a SPD-10A UV−vis detector by using a Shodex GS-620HQ column at room temperature. The HSA-FeP solutions [FeP/HSA = 1, 4, 8 (mol/mol)] were applied to the measurements with phosphate-buffered saline (10 mM, pH 7.3) as the eluent.

Resonance Raman (RR) Spectroscopy. RR spectra were obtained with excitation of the 457.9 nm line of an NEC GLG2162 Ar^+ ion laser in a back-scattering geometry at 25 °C. All the spectra were recorded using a JASCO NRS-2000 laser Raman spectrometer equipped with a CCD multichannel detector. The preparation procedures of the deoxy and dioxygenated HSA-FeP [[HSA]: 5 wt %, FeP/HSA = 4 (mol/mol)] were reported elsewhere (Tsuchida et al., 1997). Calibration of the spectrometer was performed with indene.

RESULTS AND DISCUSSION

Binding Aspects of FeP to HSA. The maximal binding numbers of FeP to one HSA molecule were determined to be eight (Tsuchida et al., 1997). Our second interest in this albumin−heme complex was its nano structure. How strong and at which place are FePs bound in HSA? The binding constants are typically analyzed according to the Scatchard model (Beaven et al., 1974, Halfman and Nishida, 1992), we used, however, another means of analysis with a stepwise equilibrium model (Fletcher et al., 1970; Ashbrook et al., 1975). This model can incorporate many of the concepts in protein−ligand interaction, including cooperativity, the creation of new sites in the binding process, etc.; it is therefore the most satisfactory for protein-heme binding analysis. The magnitude of the binding constants for the FeP association with HSA (K_1−K_8) ranged 1.2×10^6 to 1.3×10^4 M^{-1} (Table 1) in which no cooperative relation was observed. These values are relatively low with respect to those of palmitic acid [K_1−K_8 = (6.2×10^7)−(3.8×10^5) M^{-1}] (Ashbrook et al., 1975) and hemin ($K_1 = 5.0 \times 10^7$ M^{-1}) (Beaven et al., 1974), which have Coulombic interactions with the albumin host through their carboxylic groups. The FeP molecules are probably incorporated into HSA

Table 1. Stepwise Equilibrium Constants of FeP Binding to HSA (M^{-1}) at 25 °C

K_1	K_2	K_3	K_4	K_5	K_6	K_7	K_8
1.2×10^6	7.8×10^4	6.6×10^4	5.3×10^4	2.3×10^4	1.8×10^4	1.7×10^4	1.3×10^4

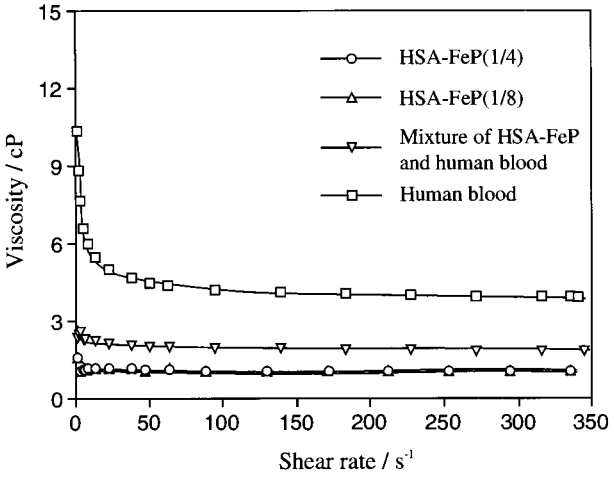


Figure 2. Shear rate dependence of the viscosity of HSA-FeP at 37 °C.

only by hydrophobic interactions, leading to a rather weak nonspecific binding.

The association sites of FeP were estimated from the competitive binding inhibition behavior by other well-known ligands which can bind the typical areas of HSA [palmitic acid (IIIB), PPIX instead of hemin (IB, IIA), and phenol red instead of bilirubin (IIA)]. At an FeP/HSA mixing ratio of 8, the binding numbers were significantly decreased to 7 in all cases; one of the binding regions of the synthetic heme is obviously occupied by the inhibitor ligands. Consequently, the primary binding sites of these ligands are identical to one of the FeP's sites. It is remarkable that the FeP binding was inhibited even by phenol red with a low K_1 of 3.9×10^4 M^{-1} (Kragh-Hansen, 1981b). One of the minor binding sites, at least a fifth one, was definitely blocked by a phenol red molecule.

Structure and Physicochemical Properties. The red-colored solution could be stored for three months at 4 °C; the turbidity at 700 nm was not changed (±4%), and no aggregation was observed for all samples prepared. Furthermore, the solution could be kept as a freeze-dried powder for more than 6 months. The long stability and no blood type, of course, become great advantages of this solution as a dioxygen infusion for potential clinical use.

The solution properties of HSA-FeP sufficiently satisfy the physiological needs. Specific gravities were all 1.013 [FeP/HSA = 1−8 (mol/mol)]. The viscosity behavior showed typical Newtonian type, and a value of 1.1 cP observed at a high shear rate of 230 s^{-1} was much lower than that of human blood (4.0 cP) (Figure 2). Furthermore, the HSA-FeP solution was mixed with fresh drawn human whole blood. The obtained suspension did not show any coagulation or precipitation, and its viscosity behavior was again Newtonian type (1.8 cP at 230 s^{-1}), displaying a good compatibility of HSA-FeP with human blood. The O_2-carrying solution with low viscosity may facilitate circulation and would permit a better exploition of collateral microcirculation.

The physicochemical properties of this artificial hemoprotein were studied. The isoelectric points (pI) of the HSA-FeP [FeP/HSA = 1∼8 (mol/mol)] were all found to be 4.8 from the IEF measurements, values that were exactly the same as that of HSA itself (Figure 3a). In the case of fatty acid binding, the pI value significantly decreased due to partial neutralization of the surface charge. Thus, it can be considered that FeP molecules interact nonspecifically with a part (most probably the hydrophobic region) of albumin, and its surface charge distributions are not influenced.

The native PAGE showed the same molecular sizes for all samples with different FeP binding numbers (Figure 3b). This was rather unexpected, because the molecular volume of FeP (1.3^3 nm^3 estimated by simulation, Figure 1b) is relatively bulky as a ligand for the host albumin. The morphology of HSA should be expanded after the FeP incorporation. GPC measurements also displayed very close peaks for HSA and HSA-FeP that could not be clearly distinguished. Carter (1994) reported some preliminary results on cocrystal structures of HSA with long chain fatty acids of laurate or palmitate in which three or more fatty acids bind to produce significant conformational changes in the albumin. The invariable molecular size of HSA-FeP obviously indicates the weak binding of FePs and conformational flexibility of the HSA molecule, somewhat like a sponge.

Circular dichroism (CD) spectroscopy provides information on the secondary and tertiary structures of HSA and conformation changes that ensue when FeP is bound. The spectral pattern showed typical double-minimum negative peaks in the ultraviolet region independent of

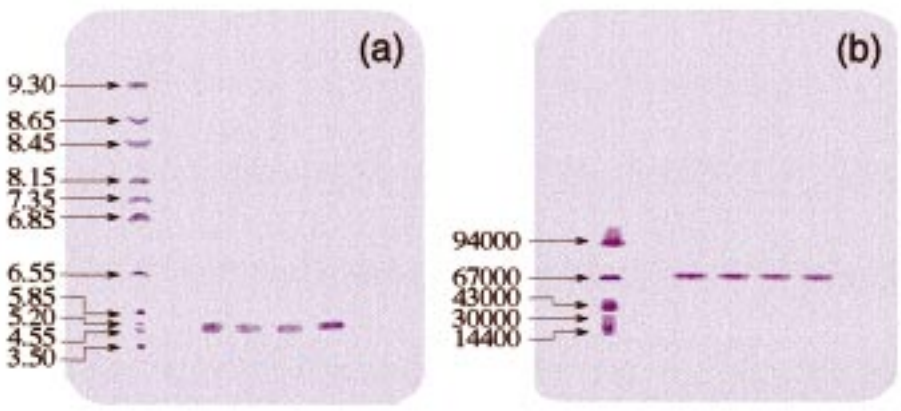


Figure 3. (a) IEF and (b) native-PAGE electrophoretic patterns of HSA and HSA-FeP solution. Lane 1, markers; lane 2, HSA; lane 3, HSA-FeP (1/1); lane 4, HSA-FeP (1/4); lane 5, HSA-FeP (1/8) from the left.

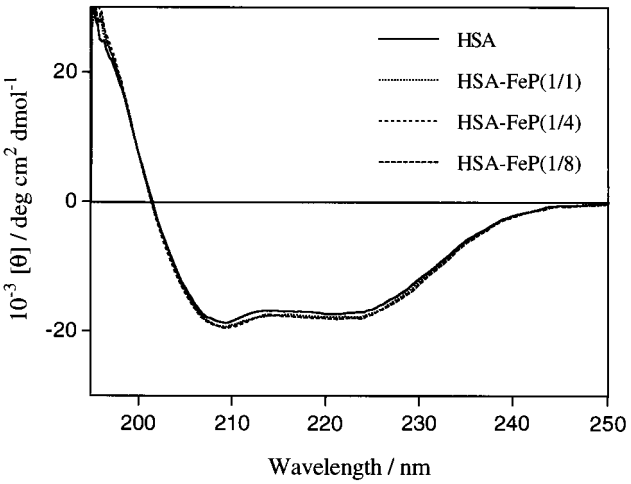


Figure 4. Circular dichroism spectra of the HSA-FeP solution at 25 °C.

the binding numbers of the FeP molecules from one to eight. There are no differences between the HSA-FeP series and HSA itself (Figure 4). The calculated α-helix content was approximately 52%, suggesting that the FeP association did not cause any second- and third-ordered structural changes in HSA. In general, the binding of the heme derivative to the albumin molecule is accompanied by a rise to an extrinsic negative Cotton effect in the Soret band region, because it binds to an albumin through a coordination between the imidazole of histidine and the central iron, allowing a high degree of immobilization (Beaven et al., 1974; Casella et al., 1993). HSA-FeP did not, however, show any CD bands in the Soret region. This observation again indicates a weak interaction between FeP and HSA as an apoprotein.

Attempts to measure the exact molecular mass of HSA-FeP from 67.8 kDa [FeP/HSA = 1 (mol/mol)] to 76.9 kDa [FeP/HSA = 8 (mol/mol)] by a time-of-flight mass spectroscopy with matrix-assisted laser desorption ionization system (Shimadzu Kompact MALDI-4) unfortunately failed. We detected only the 66.5 kDa peak of HSA itself. During the laser ionization, the weakly bound FePs were presumably dissociated from the HSA host. The nonspecific interaction between FeP and HSA was further studied using ultracentrifugation. In all cases, FeP sedimented together with albumin but redispersed again completely on shaking, giving a reddish homogeneous solution which showed the same absorbance at the 420 nm Soret band. We thus concluded that hydrophobic interactions are the major driving force of the FeP binding to HSA and that FeP incorporation does not induce any changes in the highly ordered structure and surface charge distribution of the albumin molecule.

Resonance Raman Studies of Axial Ligand Coordination to FeP Incorporated into HSA. The obtained HSA-FeP has the ability to bind dioxygen reversibly at 37 °C with a constant O_2-binding affinity [$P_{1/2}(O_2)$: 30 Torr], independent of the numbers of associated FePs (Tsuchida et al., 1997). The auto-oxidation reaction of the oxy state (λ_{max}: 548 nm) took place slowly, and the absorption band of 548 nm almost disappeared after 24 h, leading to formation of inactive hemin. The half-life ($\tau_{1/2}$) of the dioxygenated species was 8 h at 25 °C. We employed resonance Raman (RR) spectroscopy to characterize the O_2-coordination structure of the dioxygenated FeP in HSA. Soret band excitation of natural hemoproteins or synthetic porphyrinatoiron(II)s resulted in rich RR spectra consisting of totally symmetric vibrations of

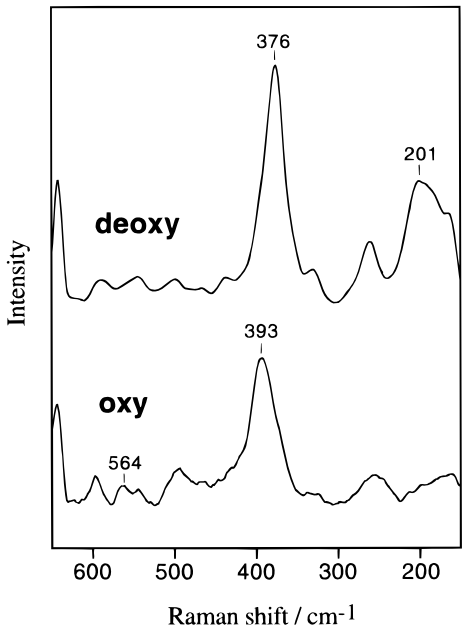


Figure 5. Resonance Raman spectra of the HSA-FeP solution at 25 °C.

the porphyrin macrocycle (Spiro et al., 1975). In the low-frequency RR spectra (<650 cm^{-1}) of the HSA-FeP under argon (i.e., the deoxy form), there is a medium band at 201 cm^{-1} (Figure 5). The five-coordinated species of FeP in CH_2Cl_2 also displayed a similar band at 205 cm^{-1} that has been assigned to the intramolecular coordinated iron−imidazole stretching mode, ν(Fe−N$_\epsilon$) (Wu et al., 1998). The covalently attached imidazole allowed the intramolecular iron−imidazole coordination of FeP even when embedded into a hydrophobic binding domain of the protein, where other peptide residues possibly coordinated to the central iron(II) may exist.

In addition, several porphyrin skeletal modes, that are sensitive to the spin state, have been identified (Burke et al., 1978). For instance, a relatively strong band around 360−395 cm^{-1} for tetraphenylporphyrinatoiron(II) derivatives has been assigned to a deformation mode of the porphyrin ring (ν_8) (Stein et al., 1984). The appearance of a ν_8 band at 376 cm^{-1} for HSA-FeP under argon represented the formation of the high-spin five-coordination state (Figure 5). Other strong bands at 1340−1390 cm^{-1} are generally assigned to a ν_4 frequency, a deformed pyrrole-ring breath-like mode (Oshio et al., 1984; Proniewicz et al., 1986), that depends on the electron density at the π^* antibonding orbital of the porphyrin (Abe et al., 1978). Hence, it is sensitive to the axial coordination state of the central iron. The ν_4 band of the deoxy HSA-FeP at 1356 cm^{-1} corresponding to the five-coordinated high-spin species immediately shifted to 1371 cm^{-1} after exposure to dioxygen. This observation indicated the formation of a six-coordinated low-spin dioxygenated species. At the same time, in the low-frequency region, the ν(Fe−O_2) vibration appeared at 564 cm^{-1}. This frequency mode represented the formation of dioxygenated heme with an end-on type coordinated dioxygen, similar to hemoglobin and myoglobin. All these peak changes have been observed to be reversibly dependent on the O_2 concentration. We concluded that the FePs having an intramolecular coordinated imidazole group obviously bind and release dioxygen in the HSA molecule.

In conclusion, human serum albumin incorporating synthetic hemes as O_2-binding sites provides an O_2-

carrying artificial hemoprotein as a hemoglobin analogue and shows unique physicochemical properties. The heme binding through hydrophobic interaction is relatively weak and does not lead to a change in the morphology and highly ordered structure, as well as the solution properties of HSA, independent of the binding numbers of FeP. The imidazole moiety coordinates to the central iron producing a five-coordinated high-spin species, and the complex forms a reversible and stable dioxygen adduct in HSA. Evaluation of the O_2-delivering efficacy in vivo is now underway using hemorrhagic shocked rats. HSA-FeP acts as a new O_2-carrying hemoprotein molecule capable of replacing hemoglobin in the bloodstream.

There is also current interest in recombinant HSA (rHSA), which has been recently manufactured by gene cloning and expression in *Pichia pastoris* (Sumi et al., 1993). A study on an rHSA−FeP conjugate as a totally synthetic O_2-carrier is also in progress.

ACKNOWLEDGMENT

This work was partially supported by the Health Science Research Grants (Artificial Blood Project), the Ministry of Health and Welfare, Japan.

LITERATURE CITED

Abe, M., Kitagawa, T., and Kyogoku, Y. (1978) Resonance Raman Spectra of Octaethylporphyrinato-Ni(II) and Meso-Deuterated and ^{15}N Substituted Derivatives. II. A Nomal Coordinate Analysis. *J. Chem. Phys. 69,* 4526−4534.

Adams, P. A., and Berman, M. C. (1980) Kinetics and Mechanism of the Interaction Between Human Serum Albumin and Monomeric Haemin, *Biochem. J. 191,* 95−102 (1980).

Ashbrook, J. D., Sector, A. A., Santos, E. C., and Fletcher, E. (1975) Long Chain Fatty Acid Binding to Human Plasma Albumin. *J. Biol. Chem. 250,* 2333−2338.

Beaven, G. H., Chen, S.-H., D'Albis, A., and Gratzer, W. B. A Spectroscopic Study of the Haemin-Human-Serum-Albumin System. (1974) *Eur. J. Biochem. 41,* 539−546.

Bonaventura, J., Brouwer, M., Brouwer, T., Cashon, B., and Cameron, S. (July 1994) Presented in part at the 11th Congress ISABI, Boston.

Brown, J. R. (1976) Serum Albumin: Amino Acid Sequence. in *Albumin Structure, Function and Uses* (V. M. Rosenoer, M. Oratz, and M. A. Rothschild, Eds.) pp 27−51 Pergamon Press, New York.

Burke, J. M., Kincaid, J. R., Peters, S., Gagne, R. R., Collman, J. P., and Spiro, T. G. (1978) Structure-Sensitive Resonance Raman Bands of Tetraphenyl and "Picket Fence" Porphyrin-Iron Complexes, Including an Oxyhemoglobin Analogue. *J. Am. Chem. Soc. 100,* 6083−6088.

Carter, D. C., and Ho, J. X. (1994) Structure of Serum Albumin. *Adv. Protein Chem. 45,* 153−203.

Carter, D. C., He, X.-M., Munson, S. H., Twigg, P. D., Gernert, K. M., Broom, M. B., and Miller, T. Y. (1989) Three-Dimensional Structure of Human Serum Albumin. *Science 244,* 1195−1198.

Casella, L., Gullotti, M., Poli, S., and De Gioia, L. (1993) Haem-Protein Interactions. The Binding of Haem Complexes to Serum Albumin. *Gazz. Chim. Ital. 123,* 149−154.

Fletcher, J. E., Sector, A. A., and Ashbrook, J. D. (1970) Analysis of Macromolecule-Ligand Binding by Determination of Stepwise Equilibrium Constants. *Biochemistry 9,* 4580−4587.

Halfman, C. J., and Nishida, T. (1972) Method for Measuring the Binding of Small Molecules to Proteins from Binding-Induced Alterations of Physical Chemical Properties. *Biochemistry 11,* 3493−3498.

He, X. M., and Carter, D. C. (1992) Atomic Structure and Chemistry of Human Serum Albumin. *Nature 356,* 209−215.

Hrkal, Z., and Klementova, S. (1984) Bilirubin and Haem Binding to Human Serum Albumin Studied by Spectroscopy Methods. *J. Biochem. 16,* 799−804.

Komatsu, T., Ando, K., Kawai, N., Nishide, H., and Tsuchida, E. (1995) O_2-Transport Albumin: A New Hybrid-Haemoprotein Incorporating Tetraphenylporphyrinato-iron(II) Derivative. *Chem. Lett. 1995,* 813−814.

Kragh-Hansen, U. (1981a) Molecular Aspects of Ligand Binding to Serum Albumin. *Pharmacol. Rev. 33,* 17−53.

Kragh-Hansen, U. (1981b) Effect of Aliphatic fatty Acids on the Binding of Phenol Red to Human Serum Albumin. *Biochem. J. 195,* 603−613.

Lamola, A. A., Asher, I., Muller-Eberhard, U., and Poh-Fitzpatrick, M. (1981) Fluorimetric Study of Binding of Protoporphyrin to Haemopexin and Albumin. *Biochem. J. 196,* 693−698.

Little, H. N., and Nelands, J. B. (1960) Binding of Hematin by Human Serum Albumin. *Nature 170,* 913−915.

Marden, M. C., Hazard, E. S., Leclerc, L., and Gibson, Q. H. (1989) Flash Photolysis of the Serum Albumin−Heme-CO Complex. *Biochemistry 28,* 4422−4426.

Morgan, W. T., Smith, A., and Koskelo, P. (1980) The Interaction of Human Serum Albumin and Hemopexin with Porphyrins. *Biochim. Biophys. Acta 624,* 271−285.

Muller-Eberhand, U. and Morgan, W. T. (1975) Porphyrin-Binding Proteins in Plasma. *Ann. N.Y. Acad. Sci. 244,* 625−650.

Oshio, H., Ama, T., Watanabe, T., Kincaid, J., and Nakamoto, K. (1984) Structure Sensitive Bands in the Vibrational Spectra of Metal Complexes of Tetraphenyl-porphine. *Spectrochim. Acta 40A,* 863−870.

Peters, T., Jr. (1975) Serum Albumin. *The Plasma Proteins. Structure, Function and Genetic Control* (F. W. Putnum, Ed.) 2nd ed., pp 133−181, Academic Press, New York.

Peters, T., Jr. (1985) Serum Albumin. *Adv. Protein Chem. 37,* 161−245.

Proniewicz, L. M., Bajdor, K., and Nakamoto, K. (1986) Resonance Raman Spectra of Ferrylporphyrins and Related Compounds in Dioxygen Matrixes. *J. Phys. Chem. 90,* 1760−1766.

Spiro, T. G. (1975) Resonance Raman Spectroscopic Studies of Heme Proteins. *Biochim. Biophys. Acta 416,* 169−187.

Stein, P., Ulman, A., and Spiro, T. G. (1984) Resonance Raman Spectra of S_2TPP, SSeTPP, Se_2TPP and H_2TPP: Extended Tetraphenylporphine Vibrational Assignments and Bonding Effects. *J. Phys. Chem. 88,* 369−374.

Sumi A, Ohtani, W., Kobayashi, K., Ohmura, T., Yokoyama, K., Nishida, M., and Suyama, T. (1993) Purification and Physicochemical Properties of Recombinant Human Serum Albumin. in *Biotechnology of Blood Proteins* (J. Rivat, and J. F. Stolts, Eds.) Vol. 227, pp 293−298, John Libbey Eurotext.

Tsuchida, E., Komatsu, T., Kumamoto, S., Ando, K., and Nishide, H. (1994) Synthesis and O_2−Binding Properties of Tetraphenylporphyrinatoiron(II) Derivatives Bearing a Proximal Imidazole Covalently Bound at the β-pyrrolic Position. *J. Chem. Soc., Perkin Trans. 2 1995,* 747−753.

Tsuchida, E., Ando, K., Maejima, H., Kawai, N., Komatsu, T., Tekeoka, S., and Nishide, H. (1997) Properties of and Oxygen Binding by Albumin-Tetraphenyl-porphinatoiron(II) Derivative Complexes. *Bioconjugate Chem. 8,* 534−538.

Wu, J., Komatsu, T., Tsuchida, E. (1998) Resonance Raman Studies of O_2−Binding to *ortho*-Substituted Tetraphenyl- and Tetranaphthyl-Porphyrinatoiron(II) Derivatives with a Covalently Linked Axial Imidazole. *J. Chem. Soc., Dalton Trans. 1998,* 2503−2506.

BC980084P

Efficient Gene Delivery by a Peptide Derived from a Monoclonal anti-DNA Antibody

Alexandre Avrameas,*,† Thérèse Ternynck,‡ Leila Gasmi,† and Gérard Buttin†

Unité de Génétique Somatique (URA CNRS 1960) and Unité d'Immunocytochimie, Département d'Immunologie, Institut Pasteur, 28 rue du Dr Roux, 75724 Paris Cedex 15, France. Received July 9, 1998; Revised Manuscript Received October 12, 1998

We recently reported that translocating murine polyreactive anti-DNA antibodies can be used as vectors for the transfer of macromolecules into cells growing in culture. We show here that two such monoclonal antibodies (J20.8 and F4.1) conjugated to polylysine with a high (93) but not a low (19) number of lysine residues can transfer genes in the presence of serum. A 30 amino acid long peptide, VAYISRGGVSTYYSDTVKGRFTRQKYNKRA (peptide P3), corresponding to joined heavy-chain complementary-determining regions 2 and 3 of F4.1 antibody and carrying 19 lysine residues at its N-terminal, was found to be an efficient vector for the transfection of the luciferase gene into 3T3 and CCL39 cells in the presence of serum. Addition of 0.23 M glycerol during transfection considerably enhanced gene delivery. These results show that conjugation of a short polylysine tail converted a spontaneously internalizing peptide into a potent nontoxic plasmid vector.

INTRODUCTION

Nonviral gene delivery systems have been developed with the purpose to transfer foreign genes into cells (*1*−*3*). Cationic lipids, like dioctacethylaminodoglycylspermine (*4*) and *N*-(1-(2,3-dioeyloxy)propyl)-*N*,*N*,*N*-trimethylammonium chloride (*5*), and cationic polymers, such as poly(L-lysine) (pLK)[1] conjugates (*6*−*9*) or polyethylenimine (PEI) (*10*), were used as vectors in these experiments. pLK and PEI have also been linked through their amino groups to asialoglycoprotein, transferrin, insulin, immunoglobulin, folate, and lectins in order to achieve greater specificity in cell recognition, without interferring with DNA binding (*11*−*20*). Sometimes helper molecules, like chloroquine, glycerol, or fusogenic peptides, were used to facilitate the delivery of the complex into the cytosol (*17*, *21*−*25*). Chloroquine, a weak base which limits the degradation of DNA by lysozome enzymes, was found to enhance the polyfection (*26*) of cells mediated by pLK conjugates (*21*, *22*). Amphiphilic peptides exhibiting fusogenic properties in acidic medium were used to develop synthetic virus-like gene-transfer vectors (*24*, *25*). Although these helper molecules were inefficient when the transfection step was conducted in medium-containing serum, a peptide containing several histidines was recently reported to improve transfection efficiency without being impaired by the presence of serum (*27*).

Several studies have shown that anti-DNA autoantibodies obtained from humans and mice with lupus are able to penetrate into living cells (*28*−*30*). In a previous study, we showed (*31*) that monoclonal anti-DNA antibodies (mAbs) derived from a nonimmunized (NZB x NZW)F1 mouse accumulated in the nuclei of a variety of cells cultured in serum-containing medium and could be used as vectors for the intracellular transfer of haptens and proteins. Furthermore, we found that the polypeptide, VAYISRGGVSTYYSDTVKGRFTRQKYNKRA (P3), containing heavy-chain complementary-determining regions 2 and 3 (CDR2 and CDR3) from one of these mAbs (F4.1) translocated haptens and proteins across cell membranes but was not effective for gene transfer (*31*). Because these mAbs intensively complexed DNA and thereby altered the electrophoretic migration in agarose, their effectiveness in the transfer and expression of plasmids was also examined. As the DNA binding and translocation capacities of these mAbs are likely to be interdependent, specific conditions had to be defined for each mAb to avoid DNA immunoprecipitation while allowing plasmid transfer, and this idiosyncrasy gave rise to highly variable results from one experiment to another. In the present study, we tried to overcome this lack of reproducibility by using conjugates of these anti-DNA mAbs and pLK (*32*). Moreover, we explored the conditions necessary to obtain optimal polyfections with P3 carrying 19 lysines residues at its N-terminal position (K_{19}−P3). Indeed, because conjugation of low-molecular-weight pLK to a peptide or a polysaccharide (*33*, *34*) has been reported to generate useful carriers for nonviral gene delivery, we examined the possibility that addition of a short lysine tail could be sufficient to make P3 a plasmid vector. We compared the performances of this peptide with those of a peptide IGRIDPANGKTKYAPKFQDKATRSNYYGNSPS (P9.3), derived from an anti-DNA antibody H 9.3 which does not penetrate into cells (31), carrying also 19 lysine residues at its N-terminal position (K_{19}−P9.3). We also compared these peptides with another vector peptide bearing a tryptophan and a cysteine at its amino terminal

* To whom correspondence should be addressed. Fax: 33/1/40613171. Phone: 33/1/45688655. E-mail: alexanav@pasteur.fr.

† Unité de Génétique Somatique.

‡ Unité d'Immunocytochimie.

[1] Abbreviations: CDR, complementary-determining region; CW−K_{18}, cysteine-tryptophan-poly(L-lysine)$_{18}$; DMEM, Dulbecco's modified Eagle's medium; FCS, fetal calf serum; mAbs, monoclonal anti-DNA antibodies; pLK, poly(L-lysine); pLK_{19}, poly(L-lysine)$_{19}$; pLK_{93}, poly(L-lysine)$_{93}$; P3, VAYISRGGVSTYYSDTVKGRFTRQKYNKRA; K_{19}−P3, K_{19}−VAYISRGGVSTYYSDTVKGRFTRQKYNKRA; P9.3, IGRIDPANGKTKYAPKFQDKATRSNYYGNSPS; K_{19}−P9.3 K_{19}−IGRIDPANGKTKYAPKFQDKATRSNYYGNSPS; RLU, relative light units; PEI, polyethylenimine; VH, immunoglobulin heavy-chain variable region; PBS, phosphate-buffered saline.

10.1021/bc980081c CCC: $18.00 © 1999 American Chemical Society
Published on Web 12/15/1998

and 18 lysine residues coupled at its carboxyterminal ($CW-K_{18}$) (*33*). During polyfections in serum-containing medium, we tried to enhance gene delivery by $K_{19}-P3$ and $CW-K_{18}$ peptides by adding chloroquine or glycerol, and found that glycerol considerably improved delivery while chloroquine had only a very limited effect.

MATERIALS AND METHODS

Chemicals. Chloroquine, 1-ethyl-3(3-dimethylaminopropyl)carbodiimide, pLK hydrobromide 1000−4000 (average degree of polymerization 19) (pLK_{19}), and 15000−30000 (average degree of polymerization 93) (pLK_{93}) were purchased from Sigma (St. Louis, MO). PEI 25 (kDa) was from Aldrich (St Louis, MO) and glycerol from Prolabo (Paris, France). Luciferin (luciferase assay substrate), luciferase assay buffer, cell culture lysis buffer, and the complete luciferase assay system were from Promega (Madison, WI).

Preparation of mAb-Polylysine Conjugates. IgG2a F4.1 and J20.8 anti-DNA mAbs derived from the spleen of an (NZB × NZW)F1 lupus mouse and an IgG2a B7.14 not reacting with DNA mAb (negative control) were purified on a protein A-Sepharose column as previously described (*31*). pLK_{19} and pLK_{93} were coupled to mAbs with 1-ethyl-3(3-dimethylaminopropyl)carbodiimide as previously reported (*32*). Conjugates were passed through a protein A-Sepharose column and washed extensively with 1.5 M NaCl to eliminate free pLK. The column-bound conjugates were eluted with citric acid buffer, pH 2.9, and dialyzed against phosphate-buffered saline (PBS).

DNA Purification and Peptide Synthesis. pCMV-LUC plasmid (6.4 kb) carrying the firefly luciferase gene under the control of the human cytomegalovirus promoter was kindly provided by Dr. U. Hazan (Institut Cochin de Génétique Moléculaire, Paris, France). Plasmid DNA was prepared with the Qiagen plasmid Maxi Kit (Courtaboeuf, France) according to the manufacturer's protocols. Peptides $CW-K_{18}$, $K_{19}-P3$, and $K_{19}-P9.3$ were synthesized by Altergen (Strasbourg, France). Briefly, peptides were prepared by solid-phase peptide synthesis on Fmoc amino acid-*p*-alkoxy-benzyl-alcohol-resin (Wang resin). Cleavage was performed with trifluoroacetic acid (TFA); and peptides were purified on a semipreparative Eurosil Bioselect 5 μ 300A (1.6 × 25 cm) C_5 RP-HPLC column eluted at 1.1 mL/min with 0.1% TFA and a 10 to 70% acetonitrile gradient. Peptides were characterized by electrospray mass spectrometry using a VG BioQ triple quadrupole mass spectrometer [mass to charge (*m*/*z*) range 4000] upgraded by the manufacturer so that it gained Quattro II performance (Micromass Ltd, U.K., Altrincham). Scanning was performed in the range 400−1400 in 10 s. The extracting cone voltage was 50 V. The mass spectrometer was calibrated externally by using the horse heart myoglobine multiply charged ions. The mass spectra obtained for each peptide was for $K_{19}-P3$ (calcd 5908.2 Da, found 5908.3 Da), for $K_{19}-P9.3$ (calcd 61767.4 Da, found 61767.5 Da) and for $CW-K_{18}$ (calcd 2642.5 Da, found 2642.6 Da). Lyophilized peptides were dissolved in 0.15 mM NaCl and sterilized by passage through a 0.22 μm filter. To determine precisely the concentrations of the dissolved peptides, aliquots were hydrolyzed with 6 N HCl−0.2% phenol at 110 °C for 20 h in sealed tubes. Norleucine was added as the internal standard. Aliquots of the hydrolysates were analyzed on a Beckman 6300 amino acid analyzer.

Cells and Cell Culture. NIH 3T3 and CCL39 cells (respectively mouse embryo and hamster lung fibroblasts) were cultured in Dulbecco's modified Eagle's medium (DMEM) (Axcell) (St-Genis l'Argentière, France) containing 4 mM L-glutamine, 100 units/mL penicillin, and 0.1 mg/mL streptomycin (Gibco BRL) (Cergy Pontoise, France) (culture medium) and supplemented with 10% fetal calf serum (FCS) (complete medium). Cells were cultured at 37 °C in a humidified atmosphere (92% air and 8% CO_2).

Gel Retardation Assay. The preparation of pCMV-LUC/$K_{19}-P3$ complexes was carried out as follows. Plasmid/$K_{19}-P3$ complexes were prepared by adding 0, 0.005, 0.01, 0.02, 0.03, 0.04, and 0.06 nmol of $K_{19}-P3$ to 0.1 μg of pCMVLUC in 5 μL of 0.15 M NaCl. After 20 min of incubation at 20 °C, each sample was analyzed by electrophoresis for 1 h under 50 V/cm through a 0.8% agarose gel containing ethidium bromide (1 μg/mL of gel) to visualize DNA in a Tris-borate-EDTA buffer (45 mM Tris, 45 mM boric acid, and 1.2 mM EDTA), pH 8.6.

In Vitro Transfections with $pLK_{19}-mAb$ and $pLK_{93}-mAb$ Conjugates. 3T3 cells (8×10^4) were deposited into 24-well tissue culture plates the day before transfection. pCMVLUC-pLK_{19}-mAb or pLK_{93}-mAb conjugate polyplexes were made at the lowest plasmid/conjugate ratio (usually 1/6, w/w) able to completely block all DNA electrophoretic migration. pCMVLUC (2 μg) in 50 μL of 0.15 M NaCl was mixed with 12 μg of K_{19}-mAbs or K_{93}-mAbs (triplicate wells), and kept for 20 min at 20 °C. Just before transfection, cells were washed and incubated with 0.5 mL of complete medium or culture medium containing 2% FCS and 100 μM chloroquine. Polyplexes were added to the cells for 4 h at 37 °C in a humidified atmosphere (92% air and 8% CO_2). The medium was removed and cells were further incubated for 24 h at 37 °C in 1 mL of fresh complete medium.

In Vitro Transfections with $K_{19}-P3$, $K_{19}-P9.3$, or $CW-K_{18}$ Peptides. 3T3 or CCL39 cells (8×10^4) were deposited into 24-well tissue culture plates the day before transfection. Polyplexes were formed between pCMVLUC (3 μg) and different amounts of $CW-K_{18}$, $K_{19}-P3$, $K_{19}-P3$, or free pLK_{19} in 50 μL of 0.15 M NaCl and kept for 20 min at 20 °C. Just before transfection, cells were washed and incubated for various times with 0.5 mL of complete medium containing 0.23 M glycerol or not or culture medium containing 100 μM chloroquine and 2% FCS. Polyplexes were added to the cells for 1.25, 2.5, 5.5, and 24 h at 37 °C in a humidified atmosphere (92% air and 8% CO_2), the medium was removed, and cells were incubated for an additional 24 h at 37 °C in 1 mL of fresh complete medium. PEI (25 kDa) was used as previously described (*35*) at charge ratios (*26*) of 5 or 2.2 in the presence of glycerol. All experiments were run at least three times.

Luciferase Assay. Cells were washed twice with cold PBS. Lysis buffer (100 μL) (Promega) containing 1% Triton X-100 and 2 mM DTT were added to each well of a 24-well tissue culture plate. After 15 min, cell lysates were transferred into a microcentrifuge tube and briefly centrifuged at 13000 *g* to pellet large debris. The luciferase assay reagent (100 μL) containing luciferin was automatically injected into the cell lysate sample (15 μL). Luciferase relative light units (RLU) were recorded on a Lumat LB 9501 luminometer (Berthold Systems, Wildbach, Germany) with 10 s integration. The RLUs were normalized to milligrams of protein. Protein concentrations were determined using the Bradford assay (*36*) with bovine γ globulin as the standard with the Bio-Rad Protein Assay Kit (Ivry sur Seine, France). The number of RLU obtained with 15 μL of a 1 pg/mL luciferase solution was 4000.

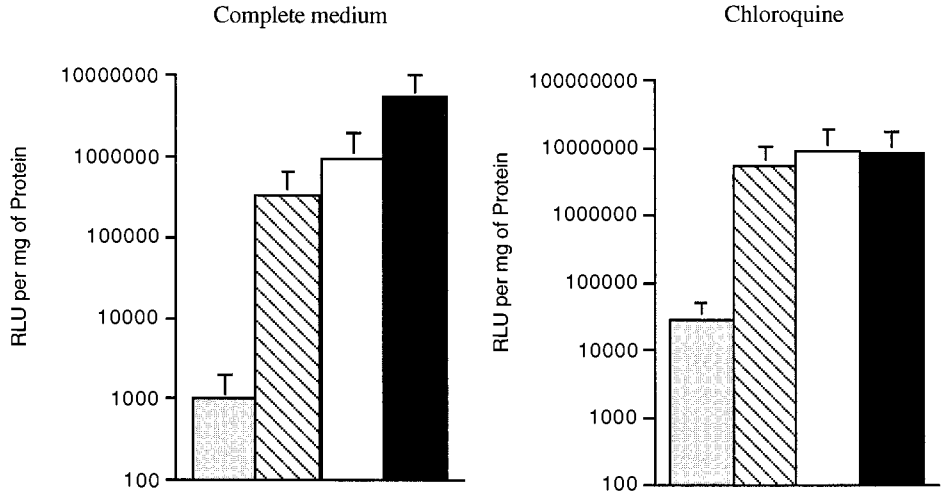


Figure 1. Polyfections of 3T3 cells with pLK_{93} (grey bar) and its conjugates with mAb J20.8 (J20.8-pLK_{93}) (white bar), (B7.14-pLK_{93}) (crosshatched bar), or F4.1 (F4.1-pLK_{93}) (black bar). pCMVLUC (2 μg) and 12 μg of either free pLK_{93}, J20.8-pLK_{93}, B7.14-pLK_{93}, or F4.1-pLK_{93} were combined in 50 μl of 0.15 M NaCl, and the reaction mixtures were incubated for 20 min at 20 °C. Each polyplex was tested in triplicate. Just before transfection, cells were washed and incubated with 0.5 mL of DMEM containing 10% FCS or 2% FCS and 100 μM chloroquine. Polyplexes were added to the cells for 4 h at 37 °C in a humidified atmosphere (92% air and 8% CO_2). The medium was removed and cells were further incubated for 24 h at 37 °C in 1 mL of fresh complete medium. After washing cells were lysed and the luciferase activity was determined. All experiments were carried out at least three times.

RESULTS

Polyfections with pLK_{19}−mAbs and pLK_{93}−mAbs. Transfection of 3T3 cells with pCMVLUC-pLK_{19}−F4.1 or pCMVLUC-pLK_{19}-J20.8 polyplexes at various plasmid/mAbs ratios failed to produce any major luciferase expression. The transfection potential of pCMVLUC-pLK_{93}-mAbs polyplexes was then tested. pLK_{93}-mAbs F4.1 J20.8 both showed high gene-transfer efficiency in complete medium in the absence of chloroquine (Figure 1). pLK_{93}-mAb F4.1 was 5 times more efficient than pLK_{93}-mAb J20.8 and at least 15 times more efficient than pLK_{93}-mAb IgG2a B7.14 used as negative control. Polyplexes formed with mAb had gene-transfer efficiencies 3−4 orders of magnitude higher than those formed with pLK_{93} alone. When the pLK_{93}-mAbs were tested for their gene-transfer efficiencies in medium containing 2% FCS and 100 μM chloroquine, 2- and 10-fold enhancements were noted, respectively, for pLK_{93}−F4.1 and pLK_{93}-J20.8. In contrast, a 16-fold and a 30-fold increase was, respectively, observed with pLK_{93}−B7.14 conjugate and free pLK_{93}.

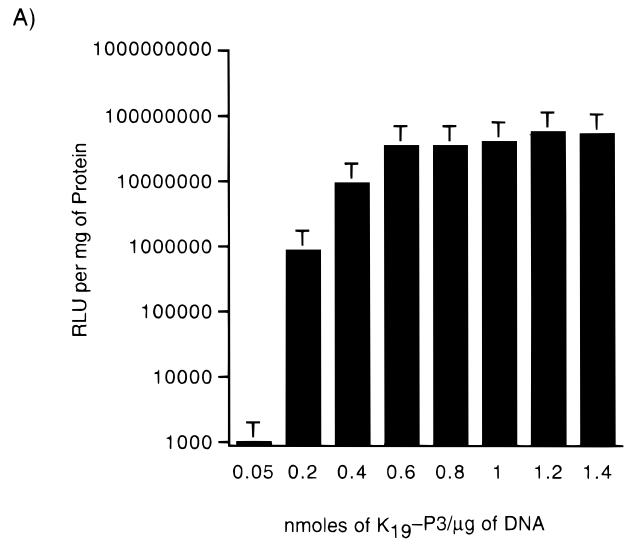
Polyfection of 3T3 Cells with K_{19}−P3, K_{19}−P9.3, and CW−K_{18} Peptides. Luciferase reporter-gene expression was analyzed following transfection of 3T3 cells with the K_{19}−P3 peptide prepared at stoichiometric concentrations ranging from 0.05 to 1.4 nmol of peptides/μg of DNA. Gene expression increased with increasing peptide concentrations reaching a maximum at 0.6 nmol of peptide/μg of DNA that is a charge ratio of 4.4 (Figure 2A). This stoichiometry also corresponds to the optimum gene expression reported for CW−K_{18} (*33*), but does not coincide to the first complete retardation of all DNA in electrophoresis by the K_{19}−P3 peptide; this was obtained at a concentration of 0.2 nmol/μg of DNA (Figure 2B). Remarkably, 0.2 nmol/μg of DNA of CW−K_{18} peptide was also enough to obtain the full condensation of DNA observed with light scattering profile (*33*). At higher proportions, gene expression remained constant.

Kinetics of polyfections in complete medium without helper molecules at a 4.4 charge ratio showed no toxicity during 24 h of incubation with either K_{19}−P3, K_{19}−P9.3, or CW−K_{18} peptides. After 5.5 h of incubation, the luciferase reporter-gene expression was (2−3) × 10^7 RLU/mg of protein for K_{19}−P3 and (1−2) × 10^6 RLU/mg of protein for K_{19}−P9.3 or CW−K_{18} (Figure 3). After 24 h of incubation, transfection was, respectively, enhanced 4-, 10-, and 1.3-fold for CW−K_{18}, K_{19}−P9.3, and K_{19}−P3 peptides as compared to 5.5 h (Figure 3).

Polyfection in complete medium with K_{19}−P3 was 6 times lower than that obtained with PEI (Figure 4A). When the gene-transfer efficiencies of K_{19}−P3 and CW−K_{18} were tested in culture medium containing 2% FCS and 100 μM chloroquine, moderate 2-fold increase, comparable to that observed with pLK_{93}-mAb, was noted. Free pLK_{19} efficiency with or without chloroquine was, respectively, 5 and 100 times weaker than those of CW−K_{18} and K_{19}−P3 peptides.

Polyfection of CCL39 Cells with K_{19}−P3 and CW−K_{18} Peptides. 3T3 cells are a convenient classical model for transfection assays using nonviral vectors. However, because some cell lines are more refractory to transfection, we conducted comparative polyfections with 3T3 and CCL39 cell lines. Polyfection with K_{19}−P3 in complete medium resulted in the expression of 4 × 10^5 RLU/mg of protein in CCL39 cells (Figure 4B), a value that is 2 orders of magnitude lower than that detected with 3T3 cells (compare with Figure 4A). Indeed, absolute values of gene expression obtained with K_{19}−P3 or CW−K_{18} vectors were much lower in CCL39 cells than in 3T3. Their relative rates of gene-expression efficiency remained, however, constant, that is approximately 20 times higher for K_{19}−P3 in both 3T3 and CCL39 cells (compare panels A and B of Figure 4). Polyfections of CCL39 cells with PEI at a charge ratio of 5 also resulted in luciferase gene expression corresponding to no more than 10% of that obtained in 3T3 cells. Polyfections in culture medium containing 2% FCS and 100 μM chloroquine enhanced the expression of the luciferase gene by 3 and 10 times, respectively, with K_{19}−P3 and CW−K_{18} peptides. Free pLK_{19} with or without the addition of helper molecules failed to produce any major reporter gene expression.

Polyfection with K_{19}−P3 and CW−K_{18} Peptides in the Presence of 0.23 M Glycerol. Recent studies have demonstrated that the addition of 1.15 M glycerol during polyfection with DNA−transferrin−polylysine and DNA−



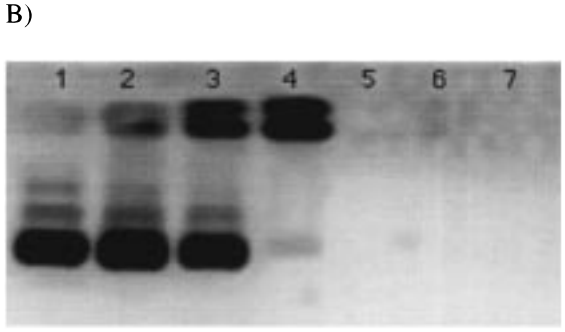


Figure 2. (A) Polyfection of 3T3 cells at various K_{19}−P3/plasmid ratios. Polyplexes between pCMVLUC (3 μg) and various amounts of K_{19}−P3 were made in 50 μL of 0.15 M NaCl (triplicate wells), and the solution was kept for 20 min at 20 °C. Just before transfection, cells were washed and incubated with 0.5 mL of complete medium. Polyplexes were added to the cells for 5.5 h at 37 °C. The subsequent steps were as those described in the legend to Figure 1. (B) Electrophoretic migration of pCMVLUC related to the plasmid/K_{19}−P3 molar ratio. Plasmid/K_{19}−P3 complexes were prepared by adding 0(1), 0.005 (2), 0.01 (3), 0.02 (4), 0.03 (5), 0.04 (6), and 0.06 (7) nmol of K_{19}−P3 for 0.1 μg of pCMVLUC in 5 μL of 0.15 M NaCl. After 20 min of incubation at 20 °C, each sample was analyzed by electrophoresis for 1 h under 50 V/cm through a 0.8% agarose gel containing ethidium bromide (1 μg/mL of gel) to visualize DNA in a Tris-borate-EDTA buffer (45 mM Tris, 45 mM boric acid, and 1.2 mM EDTA) pH 8.6.

polylysine complexes dramatically increases transgene expression (*23*, *37*). Using 3T3 cells, we found that 0.23 M glycerol was sufficient to maximize gene expression without the toxicity that we observed at 1.15 M when either K_{19}−P3 or CW−K_{18} peptides were used at a charge ratio of 2.2. When polyfections were carried out in 3T3 cells in the presence of 0.23 M glycerol, K_{19}−P3 was as efficient as PEI in the absence of glycerol (Figure 4A). In contrast, at a charge ratio of 2.2, PEI effectiveness decreased by almost 2 orders of magnitude while K_{19}−P3 remained at least equally effective (Figure 4A). Luciferase gene expression in CCL39 cells was increased by at least 1.5 orders of magnitude when polyfections mediated by K_{19}−P3 or CW−K_{18} peptides, but not by PEI, were performed in complete medium containing 0.23 M glycerol (Figure 4B). PEI effectiveness in the presence of glycerol was similar in both cell lines (Figure 4). In general, polyfections in the presence of 0.23 M glycerol except for PEI were much more effective (2−10 times)

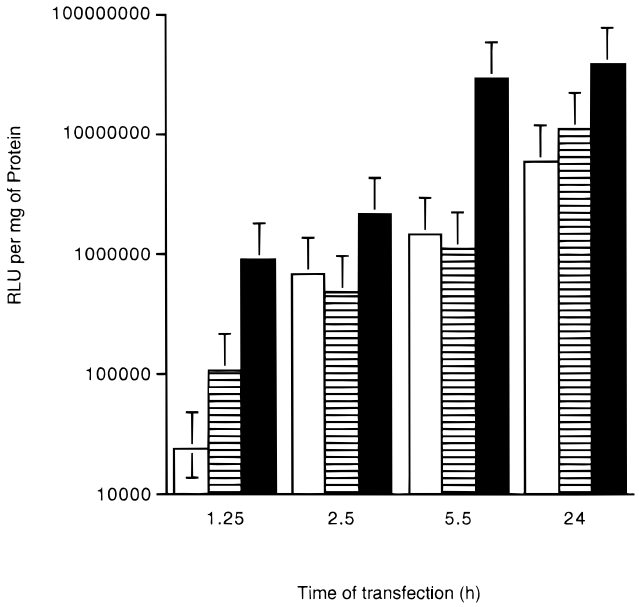


Figure 3. Polyfection of 3T3 cells incubated for various times with plasmid-peptide complexes. Polyplexes between 3 μg of pCMVLUC and 1.8 nmol of CW−K_{18} (white bar), K_{19}−H9.3 (crosshatched bar), or K_{19}−P3 (black bar) were made in 50 μL of 0.15 M NaCl (in triplicate wells), and the solution was kept for 20 min at 20 °C. Just before transfection, cells were washed and incubated with 0.5 mL of complete medium. Polyplexes were added to the cells for various times at 37 °C. The subsequent steps were as those described in the legend to Figure 1.

than those obtained in the presence of chloroquine (Figure 4A and B).

DISCUSSION

The naturally occurring polyreactive anti-DNA mAbs J20.8 and F4.1, recovered as hybridoma secretion products derived from the spleen cells of a nonimmunized mouse, penetrate and accumulate in the nuclei of a variety of cultured cells (*31*). In the present study, these antibodies conjugated to polylysine were tested as transfection vectors. mAbs-pLK_{19} conjugates were inefficient, probably because the proportion of lysine residues added was low by comparison to the long polypeptide chain of the mAbs. In contrast, conjugates of anti-DNA mAbs with pLK_{93} proved to be potential nonviral vectors for in vitro polyfections in the presence of serum. The observation that polyfection with J20.8 was 5 times lower than with F4.1 may be a reflection of each mAb's distinct kinetics of intracellular transit and/or its capacity to bind to distinct epitopes differently expressed at the cell surface (*38*). The experiments conducted with pLK_{93}-mAbs or free pLK_{93} showed toxicity for 3T3 cells (about 10−30%) which has not been analyzed but is presumably explained by the use of high molecular weight polydisperse poly-L-lysine (*39*).

Taken together, the above observations prompted us to substitute F4.1 mAb with the P3 peptide containing the heavy-chain CDR2 and CDR3 sequences of this antibody. P3 was previously shown to penetrate into various cell lines and to translocate proteins, but it failed to serve as a vector for delivery and expression of plasmid genes. The addition of 19 lysine residues to P3 generated an effective vector for gene transfer. In agreement with the reported properties of low-molecular-weight polylysine conjugates (*33*, *34*, *39*), K_{19}−P3 was not toxic. K_{19}−P3 turned out to be 10−20 times more efficient than CW−K_{18} peptide or than K_{19}−P9.3 peptide which was

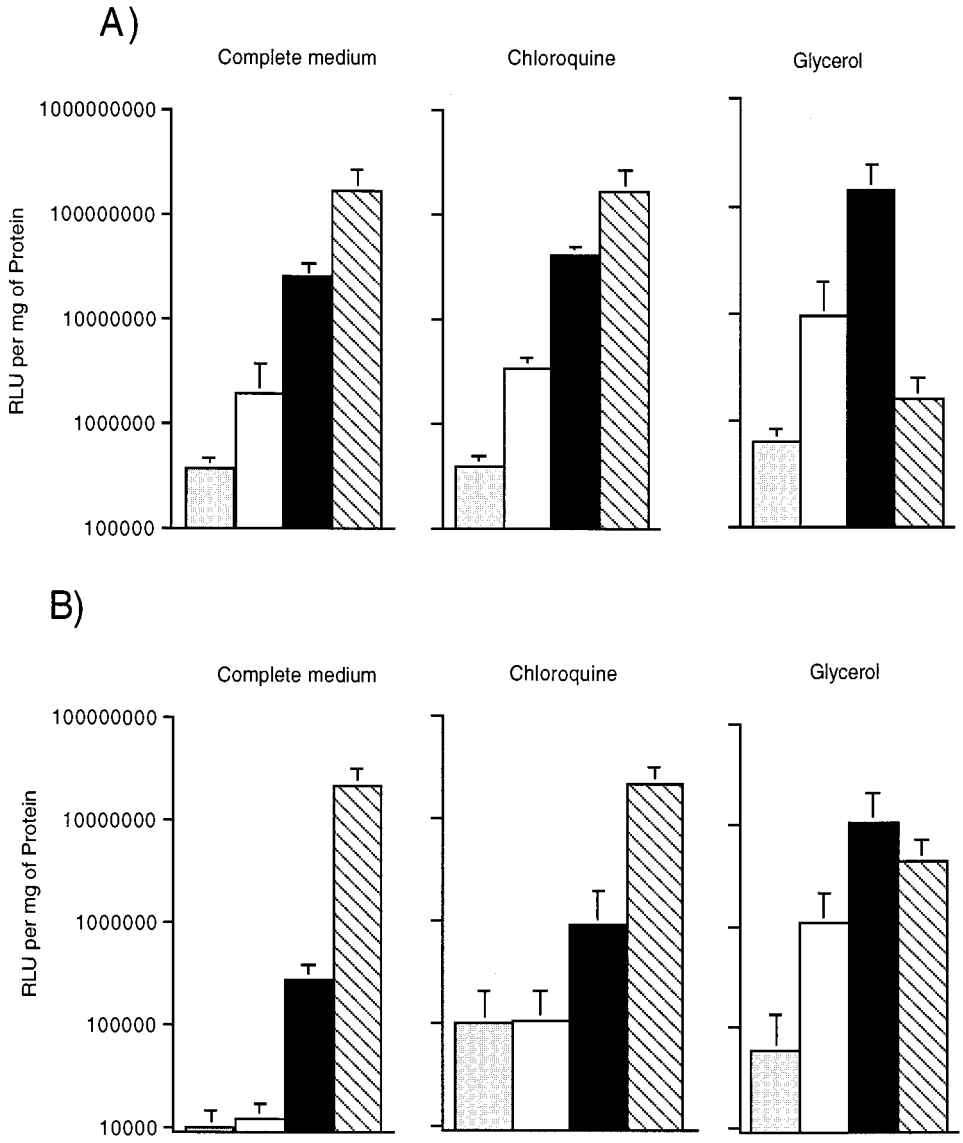


Figure 4. Polyfection of 3T3 (A) or of CCL39 (B) cells in the presence of helper molecules. Polyplexes formed between pCMVLUC (3μg) and 1.8 nmol and 0.9 nmol (in the presence of 0.23 M of glycerol) of either pLK_{19} (grey bar), $CW-K_{18}$ (white bar), or $K_{19}-P3$ (black bar) peptides, or 45 and 20 nmol (in the presence of 0.23 M of glycerol) of PEI (crosshatched bar). Polyplexes were made in 50 μL of 0.15 M NaCl, and the solution was kept for 20 min at 20 °C. Just before transfection, cells were washed and incubated with 0.5 mL of complete medium containing 0.23 M glycerol or not or culture medium containing 100 μM chloroquine and 2% FCS. Polyplexes were added to the cells for 5.5 h at 37 °C. The subsequent steps were as those described in the legend to Figure 1.

derived from a nonpenetrating anti-DNA antibody (H9.3) for gene transfer into 3T3 cells. Indeed, the values we observed in the present experiments for the expression of the luciferase gene driven by the $CW-K_{18}$ peptide in 3T3 cells (10^6 RLU/mg of protein) were comparable to those previously reported by Wadhwa et al. (*33*) for HepG2 cells. These results indicate that linking the mAb-derived P3 peptide to K_{19} makes a gene-delivery vector considerably more efficient than free K_{19}. Transfection of 3T3 cells gave 2−6% green cells when they were transfected with pCMV carrying the gene of the green fluorescent protein (data not shown).

In CCL39 cells, all attempted polyfections, even with PEI polyplexes, were less efficient although anti-DNA mAbs or P3 peptide penetrated into this cell line equally well as into 3T3 cells (*31*). This finding suggests that polyfection efficiency is not governed only by the ability of anti-DNA mAb conjugates or $K_{19}-P3$ to enter cells but also by the capacity of each cell line to transfer the DNA to the nucleus.

To enhance gene delivery by $K_{19}-P3$, we examined the possibility of adding chloroquine or glycerol helper molecules. Chloroquine did not markedly enhance polyfection. It is interesting to note that the recovery of luciferase activity after polyfections in the presence of glycerol at a 1.1 charge ratio was 2−3 orders of magnitude greater than without glycerol (data not shown), thereby confirming that the glycerol effect increased when the charge ratio of polylysine conjugates decreased (*37*). Glycerol stimulation of the activity of the cytomegalovirus promoter governing luciferase gene expression has been clearly ruled out (*37*). Evidence has been obtained to support the hypothesis that polylysine conjugates and glycerol may synergize their abilities to rupture membranes of internal vesicles, such as early endosomes (*37*). Our data do not evoke a likely mechanism of glycerol action, but the observation that chloroquine, unlike glycerol, did not greatly enhance polyfection by $K_{19}-P3$ remains consistent with the interpretation that glycerol enhances cellular uptake of the compact

polyplex particles (*23*). In our experiments, glycerol was used at 0.23 M, rather than 1.15 M as in previous studies (*23*), because at that relatively high concentration, significant toxicity was noted under our culture conditions.

Glycerol markedly improved gene delivery with peptides-K_{19}, but not with free pLK_{19}. This result is in contrast to those reported with free high-molecular-weight polydisperse polylysine (pLK_{250}), whose efficiency as a vector was enhanced by glycerol as was that of the transferrin-pLK_{250} conjugate (*24*). The difference may be attributable to the properties of the polyelectrolyte complexes arising from the complexation of DNA with polylysines of different molecular weights. The low-molecular-weight polylysines form condensates 20−30 nm in diameter, while pLK_{250} conjugates form condensates 100−200 nm in diameter (*39*), and thus they may need less glycerol to improve gene delivery than larger polyplexes. The addition of glycerol to the medium for K_{19}−P3 polyfection, as compared to complete medium, enhanced the efficiency of gene delivery 38 times in CCL39 but only 5 times in 3T3 cells. This finding suggests that glycerol is an efficient helper molecule, especially in cells that are poorly transfected, like CCL39 cells. Our data also demonstrated that a long peptide (30 amino acids) bound to K_{19} residues is a very efficient nontoxic gene vector able to preserve the property of low-molecular-weight polylysine to condense actively DNA into small particles. The rationale for constructing P3 peptide was to identify the specific sequences governing the internalization potential of a polyreactive mAb. Different CDR combinations from F4.1 and many other cell-penetrating anti-DNA mAbs can now be tested; some of them might possess selective capacities of internalization depending on the cell lines used. Indeed, preliminary experiments performed with several peptides derived from other translocating anti-DNA mAbs have shown different efficiencies and cell specificities for gene delivery. These observations prompt us to think that K_{19} conjugated to peptides naturally preselected in anti-DNA mAbs may represent an unlimited source of building blocks for gene-delivery vectors with different specificities.

ACKNOWLEDGMENT

We are grateful to Dr. U. Hazan, Institut Cochin de Génétique Moléculaire, for kindly providing the pCMV-LUC plasmid. A.A. received fellowships from Institut Pasteur-Weizmann Institut and Institut Pasteur-Canam. This work was supported in part by the Université Pierre et Marie Curie.

LITERATURE CITED

(1) Behr, J. P. (1994) Gene transfer with synthetic cationic amphiphiles: prospects for gene therapy. *Bioconjugate Chem. 5*, 382−389.

(2) Ledley, F. D. (1995) Nonviral gene therapy: the promise of genes as pharmaceutical products. *Hum. Gene Ther. 6*, 1129−1144.

(3) Christiano, R. J., and Roth, J. A. (1995) Molecular conjugates: a targeted gene delivery vector for molecular medicine. *J. Mol. Med. 73*, 479−486.

(4) Behr, J. P., Demeneix, B., Loeffer, J. P., and Perez-Mutul, J. (1989) Efficient gene transfer into mammalian primary endocrine cells with lipopolyamine-coated DNA. *Proc. Natl. Acad. Sci. U.S.A. 86*, 6982−6986.

(5) Felgner, P. L., Gadek, T. R., Holm, M., Roman, R., Chan, H. W., Wenz, M., Northrop, J. P., Ringold, G. M., and Danielsen, M. (1987) Lipofection: a highly efficient, lipid-mediated DNA transfection procedure. *Proc. Natl. Acad. Sci. U.S.A. 84*, 7413−7417.

(6) Monsigny, M., Roche, A. C., Midoux, P., and Mayer, R. (1994) Glycoconjugates as carriers for specific delivery of therapeutic drugs and genes. *Adv. Drug Delivery Rev. 14*, 1−24.

(7) Wagner, E., Curiel, D. T., and Cotten, M. (1994) Delivery of drugs, proteins and genes into cells using transferrin as ligand for receptor-mediated endocytosis. *Adv. Drug Delivery Rev. 14*, 113−136.

(8) Frese, J. J., Wu, C. H., and Wu, G. Y. (1994) Targeting of genes to the liver with glycoprotein carriers. *Adv. Drug Delivery Rev. 14*, 137−153.

(9) Cristiano, R. J., and Curiel, D. T. (1996) Strategies to accomplish gene delivery via the receptor-mediated endocytosis pathway. *Cancer Gene Ther. 3*, 49−57.

(10) Boussif, O., Lezoualc'h, F., Zanta, M. A., Mergny, M. D., Scherman, D., Demeneix, B., and Behr, J. P. (1995) A versatile vector for gene and oligonucleotide transfer into cells in culture and in vivo: polyethylenimine. *Proc. Natl. Acad. Sci. U.S.A. 92*, 7297−7301.

(11) Wu, G. Y., and Wu, C. H. (1988) Evidence for targeted gene delivery to HepG2 hepatoma cells in vitro. *Biochemistry* 27, 887−892.

(12) Wu, G. Y., and Wu, C. H. (1988) Receptor-mediated gene delivery and expression in vivo. *J. Biol. Chem. 263*, 14621−14624.

(13) Merwin, J. R., Noell, G. S., Thomas, W. L., Chiou, H. C., DeRome, M. E., McKee, T. D., Spitalny, G. L., and Findeis, M. A. (1994) Targeted delivery of DNA using YEE $(galNAcAH)_3$, a synthetic glycopeptide ligand for the asialoglycoprotein receptor. *Bioconjugate Chem. 5*, 306−311.

(14) Huckett, B., Ariatti, M., and Hawtrey, A. O. (1990) Evidence for targeted gene transfer by receptor-mediated endocytosis. Stable expression following insulin-directed entry of NEO into HepG2 cells. *Biochem. Pharmacol. 40*, 253−263.

(15) Thurnher, M., Wagner, E., Clausen, H., Mechtler, K., Rusconi, S., Dinter, A., Birnstiel, M. L., Berger, E. G., and Cotten, M. (1994) Carbohydrate receptor-mediated gene transfer to human T-leukaemic cells. *Glycobiology 4*, 429−435.

(16) Rojanasakul, Y., Wang, L. Y., Malanga, C. J., Ma, J. K. H., and Liaw, J. (1994) Targeted gene delivery to alveolar macrophages via Fc receptor-mediated endocytosis. *Pharm. Res. 11*, 1731−1736.

(17) Midoux, P., Mendes, C., Legrand, A., Raimond, J., Mayer, R., Monsigny, M., and Roche, A. C. (1993) Specific gene transfer mediated by lactosylated poly(L-lysine) into hepatoma cells. *Nucleic Acid Res. 21*, 871−878.

(18) Wagner, E., Zenke, M., Cotten, M., Beug, H., and Birnstiel, M. L. (1990) Transferrin-polycation conjugates as carriers for DNA uptake into cells. *Proc. Natl. Acad. Sci. U.S.A. 87*, 3410−3414.

(19) Yin, W., and Cheng, P. W. (1994) Lectin conjugate-directed gene transfer to airway epithelial cells. *Biochem. Biophys. Res. Commun. 205*, 826−833.

(20) Gottschalk, S., Cristiano, R. J., Smith, L. C., and Woo, S. L. (1994) Folate receptor mediated DNA delivery into tumor cells: protosomal disruption results in enhanced gene expression. *Gene Ther. 1*, 185−191.

(21) Erbacher, P., Roche, A. C., Monsigny, M., and Midoux, P. (1995) Glycosylated polylysine/DNA complexes: gene transfer efficiency in relation with the size and the sugar substitution level of glycosylated polylysines and with the plasmid size. *Bioconjugate Chem. 6*, 401−410.

(22) Erbacher, P., Roche, A. C., Monsigny, M., and Midoux, P. (1996) Putative role of chloroquine in gene transfer into a human hepatoma cell line by DNA/lactosylated polylysine complexes. *Exp. Cell Res. 225*, 186−194.

(23) Zauner, W., Kichler, A., Schmidt, W., Sinski, A., and Wagner, E. (1996) Glycerol enhancement of ligand-polylysine/DNA transfection. *Biotechniques 20*, 905−913.

(24) Planck, C., Oberhauser, B., Mechtler, K., Koch, C., and Wagner, E. (1994) The influence of endosome-disruptive peptides on gene transfer using synthetic virus-like gene transfer systems. *J. Biol. Chem. 269*, 12918−12924.

(25) Murata, M., Kagiwada, S., Takahashi, S., and Ohnishi, S. (1991) Membrane fusion induced by mutual interaction of the

two charge-reversed amphiphilic peptides at neutral pH. *J. Biol. Chem. 266*, 14353−14358.
(26) Felgner, P. L., Barenholz, Y., Behr, J. P., Cheng, S. H., Cullis, P., Huang, L., Jessee, J. A., Seymour, L., Szoka, F., Thierry, A. R., Wagner, E., and Wu, G. (1997) Nomenclature for synthetic gene delivery systems. *Hum. Gene Ther. 8*, 511−512.
(27) Midoux, P., Kichler, A., Boutin, V., Maurizot, J. C., and Monsigny, M. (1998) Membrane permeabilization and efficient gene transfer by a peptide containing several histidines. *Bioconjugate Chem. 9*, 260−267.
(28) Alarcon-Segovia, D., Ruiz-Arguelles, A., and Fishbein, E. (1978) Antibody to nuclear ribonucleoprotein penetrates live human mononuclear cells through Fc receptors. *Nature* (*London*) *271*, 67−69.
(29) Yanase, K., Smith, R. M., Cizman, B., Foster, M. H., Peachey, L. D., Jarett, L., and Madaio, M. P. (1994) A subgroup of murine monoclonal anti-deoxyribonucleic acid antibodies traverse the cytoplasm and enter the nucleus in a time- and temperature-dependent manner. *Lab. Invest. 71*, 52−60.
(30) Zack, D., Stempniak, M., Wong, A. L., Taylor, C., and Weisbart, R. H. (1996) Mechanisms of cellular penetration and nuclear localization of an anti-double strand DNA autoantibody. *J. Immunol. 157*, 2082−2088.
(31) Avrameas, A., Ternynck, T., Nato, F., Buttin, G., and Avrameas, S. (1998) Polyreactive monoclonal anti-DNA antibodies and a derived peptide as vectors for the intracytoplasmic and intranuclear translocation of macromolecules. *Proc. Natl. Acad. Sci. U.S.A. 95*, 5601−5606.
(32) Merwin, J. R., Carmichael, E. P., Noell, G. S., DeRome, M. E., Thomas, W. L., Robert, N., Spitalny, G., and Chiou, H. C. (1995) CD5-mediated specific delivery of DNA to T lymphocytes: compartmentalization augmented by adenovirus. *J. Immunol. Methods 186*, 257−266.
(33) Wadhwa, M. S., Collard, W. T., Adami, R. C., McKenzie, D. L., and Rice, K. G. (1997). Peptide-mediated gene delivery: influence of peptide structure on gene expression. *Bioconjugate Chem. 8*, 81−88.
(34) Wadhwa, M. S., Knoell, D. L., Young, A. P., and Rice, K. G. (1995) Targeted gene delivery with a low molecular weight glycopeptide carrier. *Bioconjugate Chem. 6*, 283−291.
(35) Abdallah, B., Hassan, A., Benoist, C., Goula, D., Behr, J. P., and Demeneix, B. A. (1996) A powerful nonviral vector for in vivo gene transfer into the adult mammalian brain: polyethylenimine. *Hum. Gene Ther. 7*, 1947−1954.
(36) Bradford, M. M. (1976) A rapid and sensitive method for the quantification of microgram quantities of protein utilizing the principle of protein-dye binding. *Anal. Biochem. 72*, 248−254.
(37) Zauner, W., Kichler, A., Schmidt, W., Mechtler, K., and Wagner, E. (1997) Glycerol and polylysine synergize in their ability to rupture vesicular membranes: a mechanism for increased transferrin-polylysine-mediated gene transfer. *Exp. Cell Res. 232*, 137−145.
(38) Sibille, P., Ternynck, T., Nato, F., Buttin, G., Strosberg, A. D., and Avrameas, A. (1997) Mimotopes of polyreactive anti-DNA antibodies identified using phage-display peptide librairies. *Eur. J. Immunol. 27*, 1221−1228.
(39) Wolfert, M. A., and Seymour, L. W. (1996) Atomic force microscopic analysis of the influence of the molecular weight of poly(L)lysine on the size of polyelectrolyte complexes formed with DNA. *Gene Ther. 3*, 269−273.

BC980081C

DNA Interaction and Photocleavage Properties of Porphyrins Containing Cationic Substituents at the Peripheral Position

Sashikumar Mettath,[†] Benjamin R. Munson,[†] and Ravindra K. Pandey*[,†,‡]

Photodynamic Therapy Center, Department of Radiation Biology and Department of Nuclear Medicene, Roswell Park Cancer Institute, Buffalo, New York 14263. Received July 29, 1998; Revised Manuscript Received September 23, 1998

A series of mono- and disubstituted cationic porphyrins (**1**−**8**) were synthesized and investigated for their ability to bind and cleave DNA in the presence of light. In these porphyrins, the cationic substitutuents were introduced at various peripheral positions, i.e., the non-meso positions of the porphyrin system. The modes of binding of these porphyrins to DNA were investigated by UV−vis spectroscopy, circular dichroism, and an unwinding assay. The intrinsic binding constants K_b of these porphyrins to calf thymus DNA was found to be in the range 10^4-10^5 M^{-1}. Two of the zinc(II) complexes of non-meso-substituted cationic porphyrins (**5** and **8**) were found to bind to DNA via intercalation, which is in contrast to the previously reported outside-binding mode for the Zn(II) complexes of meso-substituted cationic porphyrins. Except for monocationic porphyrin **1** and Ni(II) dicationic porphyrin **6**, all the other porphyrins were found to be efficient photocleavers of DNA. The DNA photocleavage characteristics of this series of cationic prophyrins were found to depend on the structural characteristics of the poprhyrins such as (a) length of the side chain of the cationic substituents (**2** vs **4**), (b) the position of the side chain on the porphyrin ring (**4** vs **7**), and (c) the presence of the chelating metal in **3**, **5**, and **8** as compared to the nonmetallo porphyrins **2**, **4**, and **7**, respectively.

INTRODUCTION

Chemical agents which bind and cleave nucleic acids are potentially useful as reagents for accessing structural and genetic information, as well as for development of efficient chemical nucleases (*1*). Such compounds may also be useful as drugs for treatment of cancer, genetic diseases, and viral infections. Among such agents, cationic porphyrins such as meso-tetra-(4-*N*-methylpyridyl)porphyrin [T4MPyP] and its related analogues are known to bind as well as cleave DNA (*2*). Binding studies by others have shown that, in general, the free bases and Cu^{2+} and Ni^{2+} complexes of meso-substituted cationic porphyrins intercalate between the base pairs of the DNA as well as bind in the minor groove by an outside binding mode (*3*, *4*), whereas for Mn^{3+}, Fe^{3+}, Zn^{2+}, and Co^{2+} complexes of these porphyrins, due to the presence of axially bound ligands, intercalation is blocked and only outside binding occurs (*5*, *6*). DNA footprinting studies have shown that Mn^{3+}, Fe^{3+}, Zn^{2+}, and Co^{2} metallocomplexes of T4MPyP bind to the AT rich regions of DNA in the minor groove. The Ni and Cu complexes of T4MPyP were found to intercalate in GC rich regions and bind in the AT rich regions by outside binding mode (*7*−*10*). The affinity of binding to these two regions were different.

Fiel and co-workers found that Fe complexes of T4MPyP can be chemically activated to produce strand breaks in DNA (*11*). Studies by various groups have established that Fe^{3+}, Mn^{3+}, and Co^{2+} complexes of T4MPyP can be activated using a variety of oxidizing agents to produce strand breaks in the DNA (*12*−*14*). Conjugates of cationic manganese porphyrins with ellipticine (*15*, *16*), spermine (*17*), bis(benzimidazole) dye (*18*), peptide nucleic acid (*19*), and oligonucleotides (*20*, *21*) when activated by oxidizing agents have also been found to cleave DNA.

Porphyrins can also be activated by light to produce an effect on biological molecules, and such a methodology has been used in photodynamic therapy for treatment of cancer (*22*, *23*). Fiel and co-workers examined the light activated DNA cleavage property of meso-tetra(*p*-carboxyphenyl)porphine (T4MPyP) and found it to be an efficient cleaver (*24*). The DNA photocleavage properties of a series of cationic porphyrins including the zinc complexes, and porphyrin dimers were studied by Praseuth and co-workers (*25*). They found that the zinc complexes and the dimers were more efficient in cleaving DNA than the corresponding free bases and the monomers. Similarly, Munson et al. have demonstrated that cis and trans isomers of bis(*N*-methyl-4-pyridiumyl)-diphenyl porphyrin intercalates into DNA and also cleaves DNA in the presence of light (*26*).

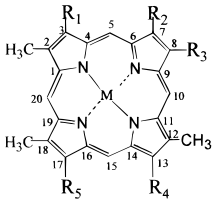
A review of the literature showed that most of the cationic porphyrins studied for their DNA cleavage activity are metalloderivatives of porphyrins possessing cationic substituents at the meso positions and belong to the class of cleavers which needs an activating agent. The few exceptions in which the non-meso-substituted compounds have been studied for their DNA-cleaving abilities are the noncationic chlorins (*27*) and lutetium-(III) texaphrin (*28*). The aim of this work was to investigate the photocleavage and DNA-binding properties of a series of non-meso-substituted cationic porphyrins to further understand the characteristics needed for efficient cleavage of DNA in the presence of light. The structural characteristics of this series of porphyrins that

* Author to whom correspondence should be addressed, Photodynamic Therapy Center. Phone: (716) 845-3203. Fax: (716) 845-8920. E-mail: pdt.ctr@3101med.edu.

[†] Photodynamic Therapy Center.

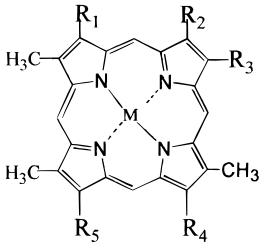
[‡] Department of Nuclear Medicine.

10.1021/bc9800872 CCC: $18.00 © 1999 American Chemical Society
Published on Web 11/07/1998



1. R_1 = H, R_2 = CH_3, R_3= CH=CH-CH_2-$N^+(CH_3)_3I^-$, R_4 = R_5 = $(CH_2)_2CO_2CH_3$, M = 2H
2. R_1 = R_3 = CH_2-$N^+(CH_3)_3I^-$, R_2 = CH_3, R_4 = R_5 =$(CH_2)_2CO_2CH_3$, M = 2H
3. R_1 = R_3 = CH_2-$N^+(CH_3)_3I^-$, R_2 = CH_3, R_4 = R_5 =$(CH_2)_2CO_2CH_3$, M = Zn
4. R_1 = R_3 = -CH=CH-CH_2-$N^+(CH_3)_3I^-$, R_2 = CH_3, R_4 = R_5 = $(CH_2)_2CO_2CH_3$, M= 2H
5. R_1 = R_3 = -CH=CH-CH_2-$N^+(CH_3)_3I^-$, R_2 = CH_3, R_4 = R_5 = $(CH_2)_2CO_2CH_3$, M= Zn
6. R_1 = R_3 = -CH=CH-CH_2-$N^+(CH_3)_3I^-$, R_2 = CH_3, R_4 = R_5 = $(CH_2)_2CO_2CH_3$, M=Ni
7. R_1 = R_4 = -CH = CH-CH_2-$N^+(CH_3)_3I^-$, R_3 = CH_3, R_2 = R_5 = $(CH_2)_2CO_2CH_3$, M = 2H
8. R_1 = R_4 = -CH = CH-CH_2-$N^+(CH_3)_3I^-$, R_3 = CH_3, R_2 = R_5 = $(CH_2)_2CO_2CH_3$, M = Zn

Figure 1. Structure of non-meso-substituted cationic porphyrins that were used in the study.



9. R_1 = H, R_2 = CH_3, R_3= CH=CH_2, R_4 = R_5 = $(CH_2)_2CO_2CH_3$
10. R_1 = R_3 = H, R_2 = CH_3, R_4 = R_5 = $(CH_2)_2CO_2CH_3$, M = 2H
11. R_1 = R_3 = H, R_2 = CH_3, R_4 = R_5 = $(CH_2)_2CO_2CH_3$, M = Zn
12. R_1 = R_3 = -CH=CH_2, R_2 = CH_3, R_4 = R_5 = $(CH_2)_2CO_2CH_3$, M = 2H
13. R_1 = R_3 = -CH=CH_2, R_2 = CH_3, R_4 = R_5 = $(CH_2)_2CO_2CH_3$, M = Zn
14. R_1 = R_3 = -CH=CH_2, R_2 = CH_3, R_4 = R_5 = $(CH_2)_2CO_2CH_3$, M = Ni
15. R_1 = R_4 = -CH = CH_2, R_3 = CH_3, R_2 = R_5 = $(CH_2)_2CO_2CH_3$, M = 2H
16. R_1 = R_4 = -CH = CH_2, R_3 = CH_3, R_2 = R_5 = $(CH_2)_2CO_2CH_3$, M = Zn

Figure 2. Structure of porphyrins that were used as starting materials for synthesis of non-meso-substituted cationic porphyrins.

were varied to understand their effect on the DNA cleavage activity were (i) number of cationic substituents, (ii) the length of the carbon chain between the cationic group(s) and the porphyrin, (iii) the position of the cationic substituents on the porphyrin ring, and (iv) the effect of the coordinated metal.

MATERIAL AND METHODS

Synthesis of Porphyrins. The cationic porphyrins **1**−**8** (shown in Figure 1) were prepared from their respective porphyrins **9**−**16** (shown in Figure 2) by following the general scheme shown in Figure 3 (*29*). For the preparation of the moncationic porphyrin **1**, 8-vinyl porphyrin **9** obtained from dueteroporphyrin via a series of reactions, was used as the starting material. Reaction of **9** with Eschenmoser's salt [CH_2=$N^+(Me)_2I^-$] led to the formation of the dimethyl amino derivative, which on treatment with methyl iodide gave the desired cationic porphyrin **1**. Cationic porphyrins **2**−**8** were similarly prepared from porphryins **10**−**16**, respectively.

Porphyrin **15** in which the cationic substituents were introduced at the vinyl groups in diagonal position (ring A and ring C) to form porphyrin **7** was prepared by following the scheme shown in Figure 4 (*30*). In brief, the acetoxy methyl pyrrole **17** was condensed with the α-free pyrrole **18** in the presence of Montmorillonite K 10 and pyrromethane **19** was obtained in 85% yield (*31*). Reaction of **19** with TFA/triethyl orthoformate gave the

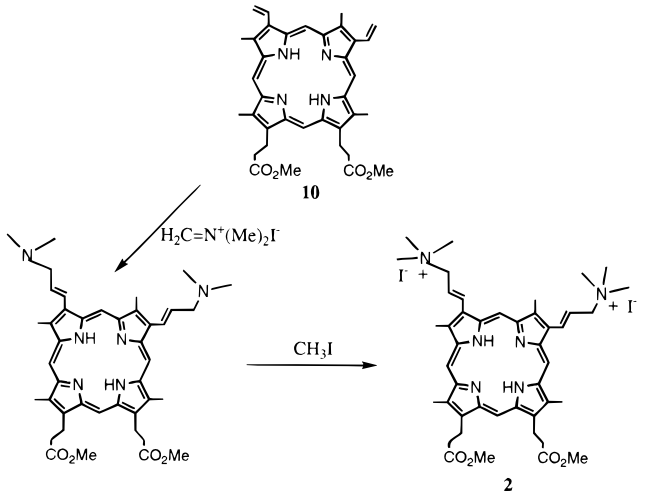


Figure 3. General scheme for the synthesis of non-meso-substituted cationic porphyrins.

monoformyl pyrromethane **20** in 70% yield. Hydrogenation of the benzyl ester functionality gave pyrromethane **21** as monocarboxylic acid, which on self-condensation under McDonald's reaction conditions produced bis(2-chloroethyl) porphyrin **22**. The chloroethyl functionalities were then converted to vinyl substituents by refluxing in NaOH/pyridine solution to obtain **16**. The divinyl free porphyin **15**, obtained upon removal of the zinc metal from porphyrin **16** was converted to the cationic porphyrin **7** by reaction with Eschenmoser's salt, followed by treatment with methyl iodide. All the new compounds were characterized by NMR and mass spectrometry analysis.

DNAs. Calf thymus DNA was purchased from Sigma Chemical and dissolved in BPES buffer (without NaCl) for the binding studies. Plasmid DNA used was the 4752 bp circular pCAT-control from Promega, amplified in *Escherichia coli* strain DH5α. The DNA was isolated and purified using cesium chloride and dissolved in TE buffer. Polydeoxyguanylic deoxycytidylic acid (poly[d(G.C)].poly[d(G.C)]) and polydeoxyadenylic thymidylic acid (poly[d(A.T)].poly[d(A.T)]) were purchased from ICN and were dissolved in BPES buffer (without NaCl) (*3*).

Hypochromicity Studies. All UV−vis spectrophotometric measurements were done on Genesys 5 spectrophotometer (5 nm spectral bandwidth). The hypochromicity in the Soret band of the cationic porphyrins caused by their interaction with calf thymus DNA and the polynucleotides poly[d(G.C)].poly[d(G.C)] and poly[d(A.T)].poly[d(A.T)] was determined as follows. Initially, visible absorption spectra of these porphyrins was determined at a concentration of $\sim 10^{-6}$ M. Calf thymus DNA, poly[d(A.T)].poly[d(A.T)] or poly[d(G.C)].poly[d(G.C)] was added in increments of 1−2 μL until no further decrease in the Soret band was observed. Buffer blanks were used to compensate for the dilution effect. The percentage hypochromicity was determined from the equation $(OD_f - OD_b/OD_f) \times 100$, where OD_f and OD_b represent the optical density of the free porphyrin and the mixture of free porphyrin and porphyrin bound to DNA, respectively.

Intrinsic Binding Constant K_b. The intrinsic binding constant K_b was determined by using the formula

$$[DNA]/(\epsilon_A - \epsilon_F) = [DNA]/(\epsilon_B - \epsilon_F) + 1/K_b(\epsilon_B - \epsilon_F)$$

where ϵ_A, ϵ_F, and ϵ_B correspond to A_{obsd}/[porphyrin], the extinction coefficient for the free porphyrin and the

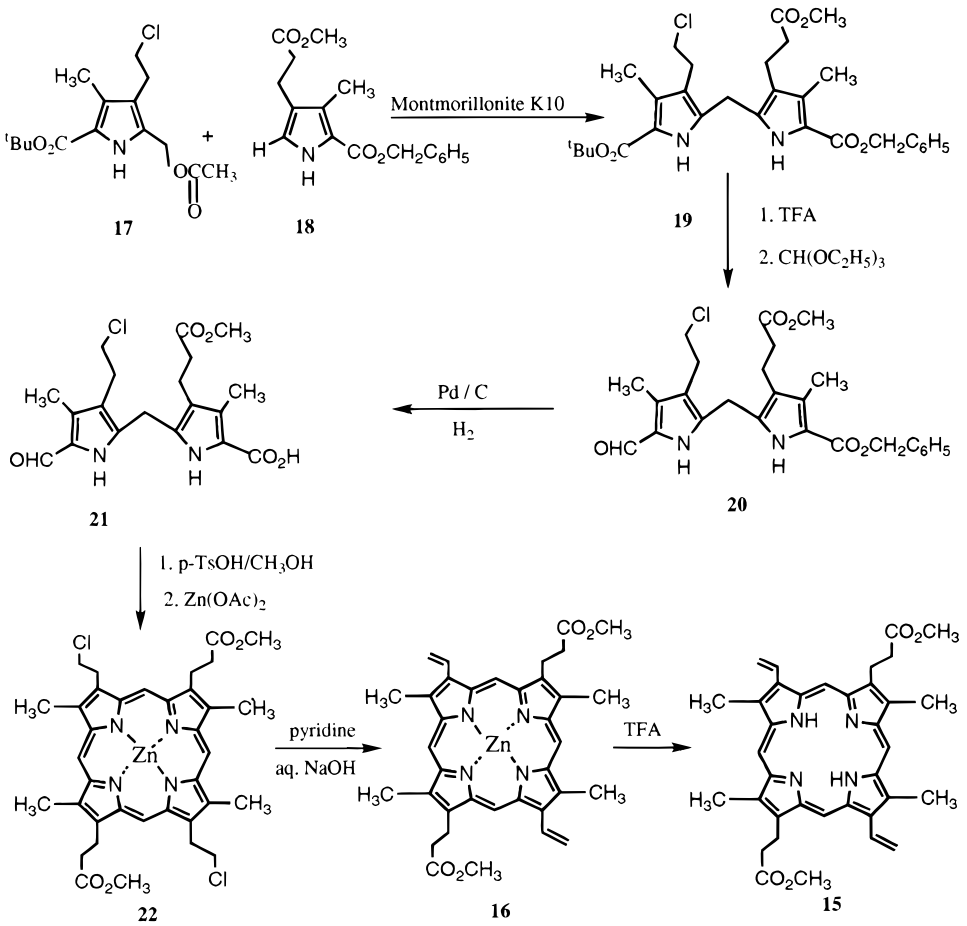


Figure 4. Synthetic strategy for the preparation of symmetrical porphyrins **15** and **16**.

extinction coefficient for the porphyrin complex in fully bound form, respectively. A plot of [DNA]/($\epsilon_A - \epsilon_F$) vs [DNA] will have a slope of 1/($\epsilon_B - \epsilon_F$) and a *y*-axis intercept equal to 1/K_b ($\epsilon_B - \epsilon_F$). The binding constant K_b was calculated from the ratio of the slope to the *y*-axis intercept.

Circular Dichroism (CD) Studies. CD spectra were recorded on a Jasco J-600 spectropolarimeter with a spectral bandwidth of 2 nm. The path length was 1 mm. The DNA (calf thymus DNA, poly[d(A.T)].poly[d(A.T)] or poly[d(G.C)].poly[d(G.C)]) was added to the porphyrins, and after an incubation period of 15 min, the samples were scanned in the visible region (320−480 nm). The *r* value, the ratio of the concentration of the porphyrins to the concentration of DNA, was less than 0.5. The baseline correction was applied using the buffer before scanning the samples.

DNA Unwinding Experiments. DNA unwinding assays were performed in two steps. First, closed supercoiled DNA (form I) pCAT (0.5 μg) was relaxed with wheat germ topoisomerase I (Promega Corp., Madison, WI). This was followed by a second topoisomerase-mediated relaxation in the presence of porphyrin. Specifically, topoisomerase I (2 units) was incubated at 37 °C for 30 min with 0.5 μg of form I pGS81 DNA first in the absence and then for 30 min in the presence of porphyrin in 25 μL of buffer containing 25 mM Tris-HCl, pH 7.9, 25 mM NaCl, 1 mM EDTA, 1 mM DTT, and 10% glycerol. The assay was stopped with 3 μL of 10% SDS and subjected to 1% agarose gel electrophoresis at 15 V for 20 h. After addition of the cationic porphyrin to DNA, care was taken to prevent exposure of the mixture to light.

Exposure of DNA/Porphyrin to Light. The solution of cationic porphyrins was added to the plasmid DNA in a 1.5 mL eppendorf microtube such that the *r* value was 0.5 or less. The tubes were placed 4 cm from a 15 W fluorescent daylight lamp and exposed to light for times ranging 0−90 min. The photoexposure ranged from 4.0 × (10^{-5} to 10^{-4}) J/cm^2 among various experiments. After exposure of the DNA to light, 1/10 volume of a solution of 50% glycerol containing 0.25% bromophenol blue was added to the DNA sample and loaded on to a 1% agarose gel and run in a TAE buffer system at 80 V for approximately 1.5 h. The agarose gel was then stained in ethidium bromide (0.25 μg/mL) and photographed. The photographs were analyzed using Image Quant software to quantify the amount of plasmid DNA (form I) remaining after treatment with light.

The singlet oxygen and hydroxyl radical quenching experiments were carried out in a manner similar to the cleavage reactions, with the addition of sodium azide (0.1 M) and mannitol (0.1 M), respectively. Sodium azide or mannitol was added at a final concentration of 0.1 M and exposed to light for varying amounts of time.

RESULTS AND DISCUSSION

Binding Studies. UV−vis absorption spectroscopy, CD spectroscopy, and DNA unwinding assays were used to evaluate the binding of non-meso-substituted cationic porphyrins **1**−**8** to DNA. In general, the hypochromic shift in the Soret band of the porphyrins upon interaction with the DNA indicate binding of the porphyrin to DNA; the sign of the ellipticity obtained in the visible range of the CD scan can point to the nature of the binding.

Table 1

porphyrin	Soret band (nm)	% hypochromicity with CT.DNA	K_b
2	385	29.8	2.32×10^5
3	410	25.4	2.52×10^4
4	385	28.6	3.10×10^5
5	409	49.0	1.12×10^5
6	388	42.7	0.88×10^5
7	382	33.5	0.81×10^5
8	406	41.0	1.34×10^5

Table 2

porphyrin	Soret band (nm)	% hypochromicity with poly dA.dT	% hypochromicity with poly dG.dC
2	385	15.0	28.7
3	410	9.7	5.5
4	385	21.5	35.9
5	409	14.0	25.0
6	388	12.9	22.6
7	382	32.2	41.4
8	406	29.6	46.4

Similarly, the unwinding assay has been used to examine the nature of binding of porphyrins to DNA as described below (*26*, *32*).

(a) UV−Vis Absorption Spectroscopy. A summary of changes in the Soret band of the porphyrins upon interaction with calf thymus DNA is shown in Table 1. These studies were done at an ionic strength (μ) of 0.17. Sodium chloride was excluded in these solutions. Addition of NaCl to these solutions was seen to decrease the hypochromic effects. Porphyrin **1** did not show any hypochromic shift. Porphyrins **5**, **6**, and **8** exhibited hypochromic shifts greater than 35%. All the other porphyrins showed hypochromic shifts in the absorption band in the range 25−33% (Table 1). However, no change in the absorption wavelength of the Soret band has been observed. The intrinsic binding constant, K_b for the binding of these porphyrins to calf thymus DNA was determined by the method reported in the literature (*33*−*35*). The binding constant for all the compounds **2**−**8** except **4** were found to be in the range of $\sim 10^5$; for **4** it was in the range of 10^4. However, because of the limitations imposed due to the aggregation of the cationic porphyrins, some variation in the value of the intrinsic binding constant, K_b cannot be ruled out. Attempts to find the number of binding sites by Scatchard plot proved to be difficult due to aggregation. Similarly, Sehlstedt et al. have also reported difficulty in finding the DNA binding constants of cobalt porphyrins due to aggregation effects (*36*). The hypochromic shift in the Soret band of the porphyrins upon interaction with copolymers poly-[d(A.T)].poly[d(A.T)] and poly[d(G.C)].poly[d(G.C)] was also determined and are shown in Table 2. The hypochromic shifts in the Soret band in the range 9.7−29.6% were observed upon binding of these porphyrins to poly-[d(A.T)].poly[d(A.T)] and in the range 5.5−46.4% upon unbinding to poly[d(G.C)].poly[d(G.C)].

(b) CD Studies. CD studies have been extensively used to study the binding of small molecules including porphyrins to DNA (*3*, *5*, *35*−*37*). In the visible range (320−480 nm), the porphyrins alone as well as the DNA by themselves do not show any ellipticity. However, an induced CD spectrum is obtained if there is a binding between the porphyrin and the DNA. The shapes of the curves obtained gave information about the nature of the binding. The mode of binding of the porphyrins **2**−**8** to calf thymus DNA, the copolymers poly[d(G.C)].poly-[d(G.C)] and poly[d(A.T)].poly[d(A.T)] were hence investigated by CD. None of these porphyrins showed any

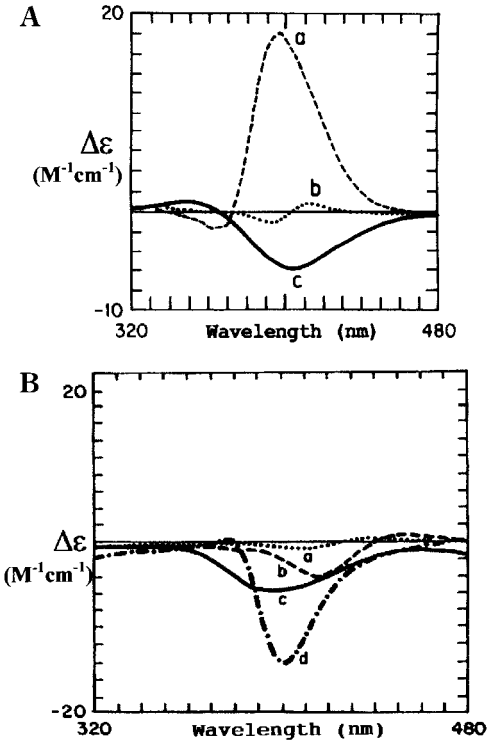


Figure 5. Visible CD spectra of CT. DNA in BPES/no salt buffer with porphyrins **2**−**8**. (A) **2** (line a), **3** (line b), **4** (line c). (B) **5** (line b), **6** (line d), **7** (line c), **8** (line a). $R < 0.5$, $\mu = 0.017$.

ellipticity in the visible range (320−480 nm) or in the UV range (220−300 nm). Interaction of the porphyrins **2**−**8** with calf thymus DNA and copolymers poly-[d(A.T)].poly[d(A.T)] and poly[d(G.C)].poly[d(G.C)] resulted in the formation of induced CD spectrums in the visible range (320−400 nm). The results of these interactions are shown in Figures 5 (interaction with calf thymus DNA), 6 (interaction with poly[d(A.T)].poly-[d(A.T)]), and 7 (interaction with poly[d(G.C)].poly-[d(G.C)]).

Porphyrin **2** (line a, Figure 5A) upon binding to calf thymus, DNA showed a strong positive peak centered at 396 nm, whereas compound **3** (line b, Figure 5A), the zinc complex, showed a weak positive peak and a weak negative peaks centered at 413 and 394 nm, respectively. Porphyrin **4** (line c, Figure 5A) and its metallocomplexes **5** (line b, Figure 5B) and **6** (line d, Figure 5B) all showed negative ellipticity; however, the intensity of the peaks as well as the wavelength at maximum peak height differed. Similarly, compound **7** (line c, Figure 5B) showed a strong negative peak upon interaction with calf thymus DNA. For the zinc complex **8**, a very weak ellipticity pattern was obtained, and changes in the *r* value did not cause any change in the shape of the spectra.

The visible CD spectrums obtained upon binding of porphyrins **2**−**8** with poly[d(A.T)].poly[d(A.T)] are shown in Figure 6. Porphyrin **2** upon interaction with poly-[d(A.T)].poly[d(A.T)] (line a, Figure 6a) showed a strong positive peak centered at 393.0 nm, whereas for porphyrins **3** and **4**, very weak and broad negative peaks (lines b and c in Figure 6A, respectively) were obtained. Compound **6** showed strong negative peaks centered at 402 nm (line b, Figure 6B), whereas compounds **5** and **8** exhibited broad peaks centered at 396 and 412 nm, respectively (lines a and d, Figure 6B). The interaction of compound **7** with poly[d(A.T)].poly[d(A.T)] did not result in any ellipticity.

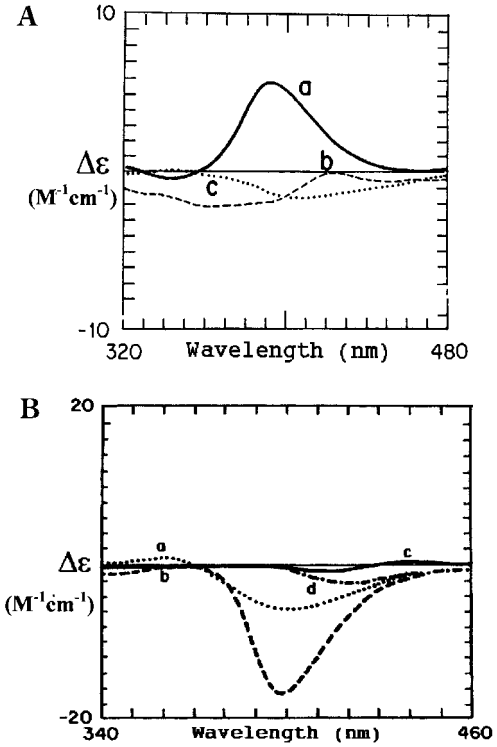


Figure 6. Visible CD spectra of poly[d(A−T)].poly[d(A−T)] in BPES/no salt buffer with porphyrins **2**−**8**. **(**A) **2** (line a), **3** (line b), **4** (line c). (B) **5** (line d), **6** (line b), **7** (line c), **8** (line a). R < 0.5, $\mu = 0.017$.

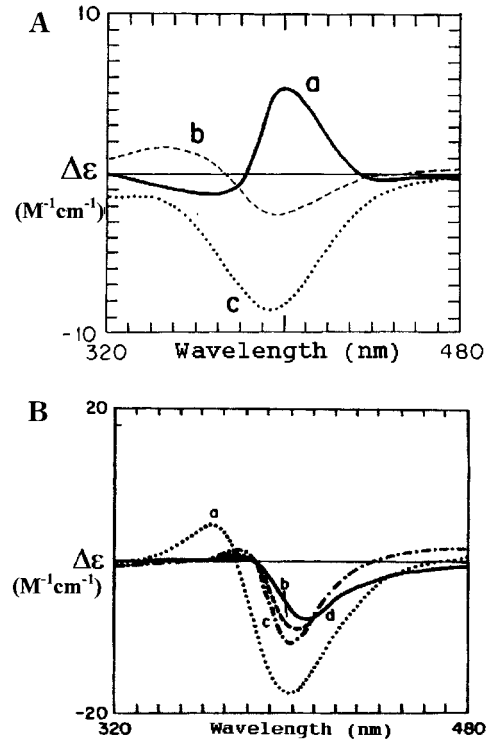


Figure 7. Visible CD spectra of poly[d(G−C)].poly[d(G−C)] in BPES/no salt buffer with porphyrins **2**−**8**. (A) **2** (line b), **3** (line a), **4** (line c). (B) **5** (line d), **6** (line b), **7** (line a), **8** (line c). R < 0.5, $\mu = 0.017$.

The interaction of porphyrins **2**−**8** with poly[d(G.C)]. poly[d(G.C)] is shown in the Figure 7. A strong positive peak was obtained in the visible CD spectra for compound **3** (line a, Figure 7A), upon binding to poly[d(G.C)].poly-[d(G.C)]. In the visible range, the binding of all the other porphyrins to poly[d(G.C)].poly[d(G.C)] resulted in negative ellipticity. These interactions are represented by lines b and c in Figure 7A, for **2** and **4**, respectively, and lines a−d in Figure 7B for the compounds **7**, **6**, **8**, and **5**, respectively.

(c) Unwinding Assay. The ability of compounds to intercalate to DNA can be checked by the unwinding assay using topoisomerase I (*26*, *32*). The DNA that is used in this assay is negatively supercoiled DNA. The supercoiled DNA is first converted to relaxed supercoiled DNA using topoisomerse I. The compounds were then added to interact with the DNA, and the assay was continued for 30 min in the presence of topoisomerase I. Compounds that intercalate into DNA induce supercoiling of DNA and, beyond a certain r value, complete supercoiling to negatively supercoiled DNA is obtained. The binding of porphyrins **2**−**8** were studied using unwinding assay and are shown in Figure 8 a−d. Porphyrins **2**, **3**, **4**, **6**, and **7** [porphyrins 2, 3, 4 (Figure 8, panels a−c), 6 (Figure 8D, lanes 11−13), and 7 (Figure 8D, lanes 2−4)], exhibit only a very weak unwinding of DNA, whereas porphyrins **5** (lanes 8−10, Figure 8D) and **8** (lanes 5−7, Figure 8D) caused complete unwinding to form supercoiled DNA. These unwinding assays indicate that compounds **5** and **8** are able to intercalate into DNA.

Photosensitized Cleavage of DNA. A convenient way to assess the ability of a cationic porphyrin to photocleave DNA is to measure the conversion of supercoiled DNA (form I) to form II (*26*). In the presence of light, all the cationic porphyrins, except **6** and **1**, were able to nick closed circular DNA (form I) to convert it into relaxed closed circular DNA (form II) in varying amounts. The amount of form II created depended upon the amount of exposure to visible light, the porphyrin that was used, and ratio of the concentration of the porphyin to that of the DNA. DNA (form I) was quantified by densitometry studies using Image Quanta software. Upon exposure to light for 90 min, all the porphyrins (r = 0.5), except **1** and **6**, were able to convert over 80% of DNA (form I) to DNA (form II) and not much difference in cleavage efficiency was observed. However, upon exposure to light for shorter time periods up to 60 min, differences in the efficiency of DNA cleavage by various porphyrins were observed. In the case of compound **5** (Figure 9b, lanes 13−16), within 15 min of exposure to light (lane 13), over 95% of the DNA (form I) was converted to form II, and 100% conversion was seen upon exposure to light for 60 min (lane 15). For compounds **2**, **3**, and **4**, the amount of DNA converted to form II in 15 min was 38.33, 49.81, and 50.93%, respectively, as shown in lanes 2, 7, and 12 of Figure 9a, respectively. Compounds **7** and **8** caused the conversion of 33.44 and 39.20% of the DNA form I to form II in 15 min (lanes 3 and 8 of Figure 9b, respectively). Compound **6 (**lanes 18−20**)**, the nickel complex, did not cause any cleavage of DNA (form I) even after exposure to light for an extended period of time (90 min). Similarly, the monocationic compound **1** also did not cause any cleavage of DNA (results not shown). The comparison of the DNA cleaving efficiencies of these porphyrins is shown in Table 3 (*37*).

The species responsible for causing the DNA cleavage is believed to be singlet oxygen. Singlet oxygen is generated upon transfer of energy from an excited porphyrin in the triplet state to oxygen in ground state (triplet state). The transfer of energy causes the conversion of oxygen to excited singlet state. The Ni complex **6** does not generate singlet oxygen, and this could explain the noncleavage of the DNA by this compound. For the other porphyrins, if singlet oxygen is the primary agent responsible for the cleavage of DNA, irradiation of the

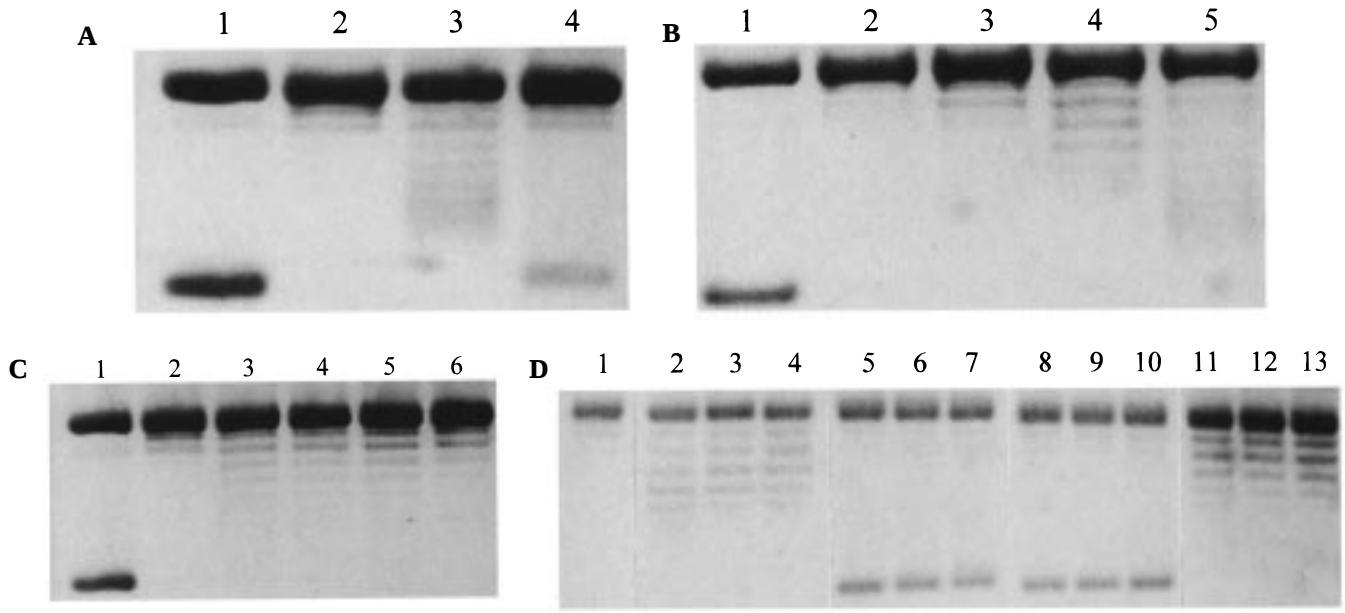


Figure 8. Agarose gel electrophoresis of supercoiled DNA relaxed by topoisomerase I in the presence of cationic non-meso-substituted porphyrins **2**−**8**. (A) Lane 1 is DNA form I and relaxed DNA. Lane 2 is control, DNA relaxed in the presence of topoisomerase I. Lanes 3 and 4, DNA relaxed in the presence of 19 and 38 μM of porphyrin **2**, respectively. (B) Lane 1 is DNA form I and relaxed DNA; lane 2 is control, i.e., DNA relaxed in the presence of topoisomerase I. Lanes 3−5 contain DNA relaxed in the presence of 14, 28, and 56 μM of porphyrin **3**, respectively. (C) Lane 1 is DNA form I. Lanes 2 and 6 are control, DNA relaxed in the presence of topoisomerase I. Lanes 3−5 DNA relaxed in the presence of 28, 42, and 60 μM of porphyrin **4**, respectively. (D) Lane 1 is control, DNA form I treated with topoisomerase I, lanes 2−4, DNA relaxed in the presence of 14, 10, and 7 μM of porphyrin **7**, respectively. Lanes 5−7, DNA relaxed in the presence of 14, 10, and 7 μM of porphyrin **8**, respectively. Lanes 8−10, DNA relaxed in the presence of 14, 10, and 7 μM of porphyrin **5**, respectively. Lanes 11−13 DNA relaxed in the presence of 14, 10, and 7 μM of porphyrin **6**, respectively.

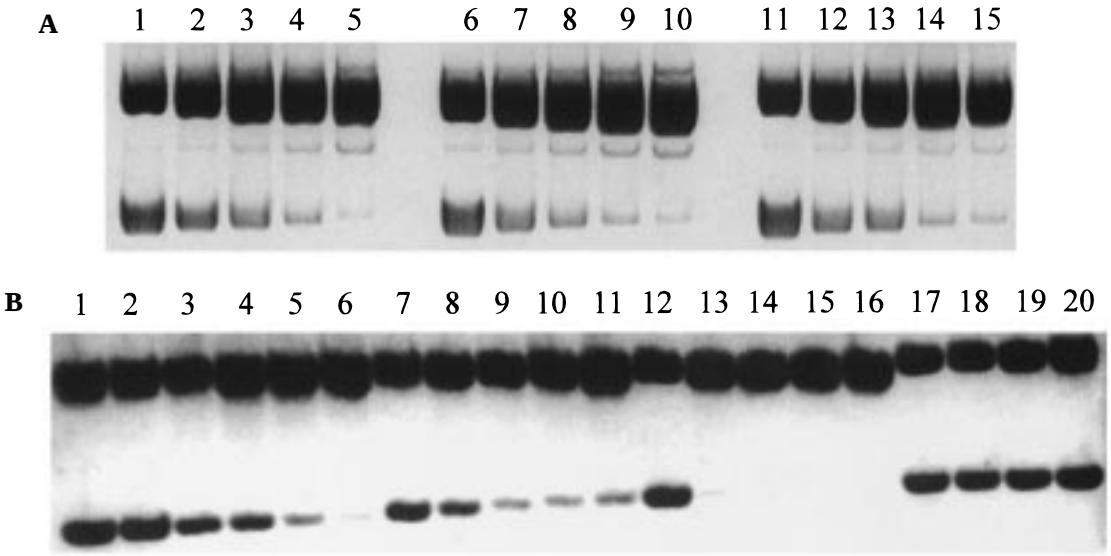


Figure 9. Agarose gel electrophoresis of plasmid DNA (form I) photosensitized with porphyrins **2**-**8**. Plasmid DNA (10 μL, 1 μg/10 μL) was added to eppendorf microtubes containing the porphyrins (10 μL, 75 μmol) and exposed to light for durations ranging 15−90 min and subsequently separated on 1% agarose gel. (A) Photocleavage of plasmid DNA (form I) by porphyrins **2**, **3**, and **4**. Lanes 1, 6, and 11 are controls and contain no porphyrins. Lanes 2−5: DNA + porphyrin **2**, treated with light for 15, 30, 60, and 90 min, respectively. Lanes 7−10: DNA + porphyrin **3**, treated with light for 15, 30, 60, and 90 min, respectively. Lanes 12−15: DNA + porphyrin **4**, treated with light for 15, 30, 60, and 90 min, respectively. (B) Photocleavage of plasmid DNA (form I) by porphyrins **5**, **6**, **7**, and **8**. Lanes 1, 7, 12, and 17 are controls and contains no porphyrins. Lanes 2−6: DNA + porphyrin **7** treated with light for 0, 15, 30, 60, and 90 min, respectively. Lanes 8−11: DNA + porphyrin **8** treated with light for 15, 30, 60, and 90 min, respectively. Lanes 13−16: DNA + porphyrin **5** treated with light for 15, 30, 60, and 90 min, respectively. Lanes 18−20: DNA + porphyrin **6** treated with light for 15, 60, and 90 min, respectively.

porphyrin−DNA complex in the presence of a singlet oxygen quencher should result in the decrease of the amount of DNA cleavage (*16*, *24*). As expected, a decrease in the cleavage of DNA was observed upon irradiation in the presence of sodium azide (100 mM), a well-known $^1O_2$ quencher (see Figure 10). No decrease in the cleavage was observed when the studies were done in the presence of equivalent concentration of NaCl (100 mM). DNA cleavage was also studied in the presence of hydroxyl radical scavenger mannitol (100 mM), and no discernible decrease in the cleavage of the DNA was observed (results not shown). These results indicate that singlet oxygen is the major species responsible for the cleavage of DNA.

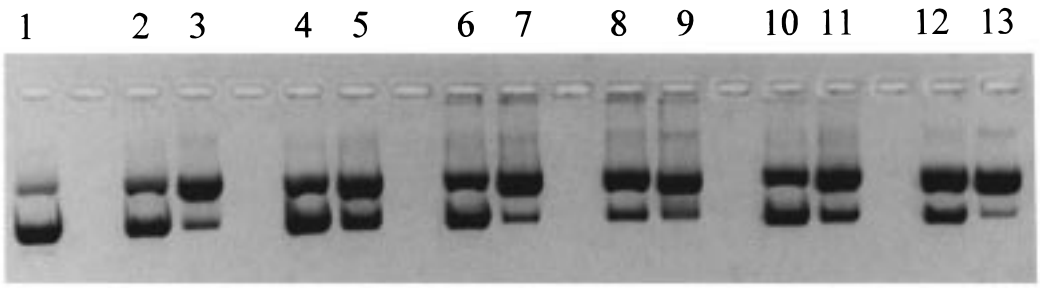


Figure 10. Agarose gel electrophoresis of plasmid DNA (form I) photosensitized with porphyrins **2**−**8** in the presence of 0.1 M sodium azide for 45 min. Lane 1 contains only DNA. Lanes 2 and 3: DNA photostosenstized with porphyrin **2** in the presence and absence of 0.1 M sodium azide, respectively. Lanes 4 and 5: DNA photostosensitized with porphyrin **3** in the presence and absence of 0.1 M sodium azide, respectively. Lanes 6 and 7: DNA photostosenstized with porphyrin **4** is the presence and absence of 0.1 M sodium azide, respectively. Lanes 8 and 9: DNA photostosensitized with porphyrin **5** is the presence and absence of 0.1 M sodium azide, respectively. Lanes 10 and 11: DNA photostosensitized with porphyrin **7** is the presence and absence of 0.1 M sodium azide, respectively. Lanes 12 and 13: DNA photostosensitized with porphyrin **8** in the presence and absence of 0.1 M sodium azide, respectively.

Table 3

porphyrin	% of DNA form I cleaved at 15 min	% of DNA form I cleaved at 60 min
1		
2	38.33	88.31
3	49.81	93.67
4	50.73	91.22
5	95.86	100
6		
7	33.44	80.44
8	39.20	80.27

Binding Characteristics. The hypochromicity values obtained for the interaction of compounds **5**, **6**, and **8**, with calf thymus DNA are 49.0, 42.7, and 41.0%. The hypochromicity values obtained for the other porphyrins are in the range 25.4−33.5%. In the literature, hypochromicity values greater than 35% have been considered as one of the characteristics of intercalators (*1*, *3*, *5*). Interaction of all the porphyrins, with poly[d(A.T)].poly[d(A.T)] and poly[d(G.C)].poly[d(G.C)], also resulted in hypochromic shifts in the absorbance of the Soret band. However, for all the porphyrins except **3**, higher hypochromicity value was obtained upon interaction with poly[d(G.C)].poly[d(G.C)] than poly[d(A.T)].poly[d(A.T)], probably indicating a slight preference for GC rich sites.

The nature of the binding of the porphyrins to the DNA has been generally interpreted from the shape of the induced CD bands obtained upon the interaction of the porphyrins with calf thymus DNA, poly[d(G.C)].poly[d(G.C)] and poly[d(A.T)].poly[d(A.T)]. In general, intercalation of the porphyrins is usually seen at GC-rich sites and is denoted by negative peaks in the CD spectrums with calf thymus DNA and poly[d(G.C)].poly[d(G.C)] (*3*, *5*, *38*−*40*), whereas outside binding has usually been observed at AT-rich sites and is denoted by positive peaks in the CD spectrums with calf thymus DNA and poly[d(A.T)].poly[d(A.T)] (*5*, *38*, *39*). The interpretations of the CD spectrums obtained for all porphyrins upon interaction with calf thymus DNA, poly[d(A.T)].poly[d(A.T)] and poly[d(G.C)].poly[d(G.C)] as well as the results from the unwinding assay can be interpreted as follows. (a) Porphyrin **2** shows a positive peak with calf thymus DNA (Figure 5a) and poly[d(A.T)].poly[d(A.T)] (Figure 6a) and weak positive and negative peaks with poly[d(G.C)].poly[d(G.C)] (Figure 7a), indicating an outside binding mode with preference to AT. The negative peak with poly dG.dC does point toward a small amount of binding at GC sites. The unwinding assay also indicates that this compound does not intercalate (Figure 8a). (b) Porphyrin **3** shows a weak positive peak and a weak negative peak with calf thymus DNA (Figure 5a), a weak negative peak with poly[d(A.T)].poly[d(A.T)] (Figure 6a), and a strong positive peak with poly[d(G.C)].poly[d(G.C)] (Figure 7a). Binding at GC-rich sites is generally by intercalation and indicated by a negative peak upon binding to poly[d(G.C)].poly[d(G.C)], hence the positive peak upon interaction with GC-rich sites could indicate an outside binding mode.

(c) Porphyrins **4**, **6**, and **7**; all three porphyrins show a strong negative peak in the visible CD with CT.DNA (Figure 5), a weak negative peak with poly[d(A.T)].poly[d(A.T)] (Figure 6), and a strong negative peak with poly[d(G.C)].poly[d(G.C)] (Figure 7). The nature of the peaks obtained indicate an intercalative mode of binding with preferential binding to GC-rich sites, with some binding to AT sites. However, the unwinding assays (Figure 8, panels c and d) indicate that these compounds are able to unwind the DNA to only a smaller extent. The combined results from these two assays point toward an outside binding mode with at GC-rich sites. (d) Porphyrin **5** shows a broad negative peak with calf thymus DNA and poly[d(A.T)].poly[d(A.T)] and a strong negative peak with poly[d(G.C)].poly[d(G.C)]. The CD spectrums indicate an intercalative mode of binding at GC-rich sites and also a weak binding at AT sites. However, the negative CD pattern upon interaction with poly[d(A.T)].poly[d(A.T)] is unusual as compared to meso-substituted porphyrins, wherein a positive ellipticity is obtained for binding at AT sites. The unwinding assay also indicates that this porphyrin does intercalate into DNA. (e) Porphyrin **8** shows very weak negative peak in the visible range spectrums with calf thymus DNA (Figure 5b) and poly[d(A.T)].poly[d(A.T)] (Figure 6b). A strong negative peak as well as a small positive peak is obtained in visible range with poly[d(G.C)].poly[d(G.C)] (Figure 7b). The negative peak obtained upon binding of **8** to poly[d(G.C)].poly[d(G.C)] indicates intercalation at GC sites. The small positive peak does point toward a small amount of outside binding at GC-rich sites. The unwinding assay also indicates an intercalative mode of binding.

DNA Cleavage Characteristics. The amount of DNA cleaved by the various porphyrins upon exposure to light for 15 and 60 min is shown in Table 3. The factors affecting the efficiency of DNA cleavage seem to be complex (*37*), however, certain porphyrins, structural characteristics needed for efficient cleavage of DNA can be elicited from these data. Among the factors that affect the cleavage efficiency are (a) the number of charges, (b) length and position of the side chain connecting the cationic substituent to the porphyrin macrocycle, and (c) the presence of chelated metal at the core of the porphyrin ring.

(a) Number of Charges. Our studies with various cationic porphyrins show that a minimum of two charges is needed for the binding and cleavage of DNA by cationic porphyins. For example, montocationic porphyrin **1** did not show any cleavage of DNA even after incubation with light 90 min under the condition used for all the other porphyrins.

(b) Length of the Side Chain of the Cationic Substituents. Dicationic porphyrins **2** and **4** are both linked to the porphyrin macrocycle by side chains at positions 3 and 8. However, in porphyrin **4**, the length of the side chain is extended by two more carbon atoms. This increase in the length of the side chain is seen to increase the efficiency of cleavage. Porphyrin **2** is able to convert 38.33% of DNA form I to form II and form III in the presence of light for 15 min; however, under the same conditions, porphyrin **4** is able to cleave 50.73% of DNA form I to DNA form II.

(c) Position of the Cationic Substituent on the Porphyrin System. In our attempts to understand the effect of the position of the cationic charges, porphyrins **4** and **7** were used as sensitizers. In porphyrin **4**, the charged group is substituted at positions 3 and 8, whereas in compound **7**, the charged groups are present at positions 3 and 13 of the porphyrin ring system. Porphyrin **4** converted 50.73% of the DNA form I to form II and form III in 15 min (Figure 9a, lane 12), and under the same conditions, porphyrin **7** was able to convert 33.44% of the DNA form I to form II (Figure 9b, lane 3).

(d) Effect of Chelated Metal. Compared to the nonmetalated analogues **2**, **4**, and **7**, the zinc analogues **3**, **5**, and **8** were found to have a higher efficiency of photocleavage of DNA.

CONCLUSION

The absorption, circular dichroism, unwinding assays, and the DNA photocleavage evidence from the present study shows that non-meso-substituted cationic porphyrins bind, as well as photocleave, DNA efficiently. On the basis of the DNA-binding studies and unwinding assays, it is suggested that the nature of binding of non-meso-substituted cationic porphyrins is different from that of the cationic meso-substituted pyridyl porphyrins. The results from the absorption spectroscopy, CD, and unwinding studies point toward intercalation as a mode of binding for the Zn(II) porphyrins **5** and **8**. The nature of the binding obtained for zinc porphyrins **5** and **8** is surprising, due to the presence of the nonplanar substituents as well as the presence of metal zinc, both of these characteristics are thought to block intercalation (*5*, *41*, *42*). Furthermore, the negative ellipticity obtained in the visible CD spectrums with calf thymus DNA and poly-[d(G.C)].poly[d(G.C)] for porphyrins **4**, **6**, and **7** indicate an intercalative mode of binding; however, this binding mode is not supported by unwinding assay. Again, the positive peak with poly[d(G.C)].poly[d(G.C)] and negative peak with poly[d(A.T)].poly[d(A.T)] for porphyrin **3** completely differ from the ellipticity obtained under similar conditions for meso-substituted cationic porphyrins. These studies show that the binding of porphyrins is complex, and from the presently existing model with meso-substituted cationic porphyrins, it is difficult to come to any precise conclusion regarding the binding mode obtained for non-meso-substituted cationic porphyrins. Clearly, further research in this area is needed to understand the binding characteristics of these types of porphyrins to DNA. To shed more light on the exact nature of the binding of these porphyrins to DNA, molecular modeling and DNA footprinting studies are underway.

ACKNOWLEDGMENT

We thank Drs. R. J. Fiel, T. J. Dougherty, and R. Shibata for their suggestions during this project. We also thank Drs. M. J. Levine and N. Ramasubbu (Research Center in Oral Biology, SUNY, Buffalo) for allowing us the use of Jasco J-600 spectropolarimeter (supported by Grant DE 08240).

LITERATURE CITED

(1) Sigman, D. S. (1990) Chemical Nucleases. *Biochemistry 29*, 9097−9105.

(2) Fiel, R., Jenkins, B., and Alderfer, J. (1990) Cationic Porphyrins − DNA Complexes. in *23rd Jerusalem Symposium in Quantum Chemistry and Biochemistry* (B. Pullman and J. Jortner, Eds.) Kluwer Academic Press, Netherlands.

(3) Fiel, R. J., Howard, J. C., Mark, E. H., and Datta-Gupta, N. (1979) Interaction of DNA with porphyrin ligand: evidence for intercalation. *Nucleic Acids Res. 6*, 3093−3118.

(4) Banville, D. S., Marzill, L. G., and Wilson, W. D. (1983) ^{31}P NMR and viscometric studies of the interaction of meso-tetra-(4-*N*-methylpyridyl) porphine and its Ni(II) and Zn(II) derivatives to DNA′. *Biochem. Biophys. Res. Commun. 113*, 148−154.

(5) Pasternack, R. F, Gibbs, E. J., and Villafranca, J. J. (1983) Interaction of porphyrins with Nucleic Acids. *Biochemistry 22*, 2406−2414.

(6) Fiel, R. J. (1989) Porphyrin Nucleic Acid Interactions: A review. *J. Biomol. Struct Dyn. 6*, 1259−1274.

(7) Ward, B., Skorobogaty, A and Dabrowiak, J. C. (1986) DNA cleavage specificity of a group of cationic metalloporphyrins. *Biochemistry 25*, 6875−6883.

(8) Ford, K. G., and Neidle, S. (1995) Perturbations in DNA structure upon interaction with porphyrins revealed by chemical probes, DNA footprinting and molecular modelling. *Biorg. Med. Chem. 3*, 671−677.

(9) Bromley, S. D., Ward, B. W., and Dabrowiak, J. C. (1986) Cationic porphyrins as probes of DNA structure. *Nucleic Acids Res. 14*, 9133−9147.

(10) Ward, B., Skorobogaty, A., and Dabrowiak, J. C. (1986) DNA binding specificity of a series of cationic metalloporphyrin complex. *Biochemistry 25*, 7827−7833.

(11) Fiel R. J, Beerman, T. A, Mark, E. H, and Datta-Gupta, N. (1982) DNA strand scission activity of metalloporphyrins. *Biochem. Biophys. Res. Commun. 107*, 1067−1074.

(12) Byrnes, R. W., Fiel, R. J., and Datta-Gupta, N. (1988) DNA strand scission by iron comples of meso−Tetra(N−Pyridyl)-Porphines *Chem.-Biol Interact. 67*, 225−241.

(13) Fouquet, E., Pratviel, G., Bernadou, J., and Meunier, B. (1987) Nuclease activity of a water soluble manganese porphyrin associated with potassium hydrogen persulphate: oxidative cleavage of DNA. *J. Chem. Soc., Chem. Commun.* 1169−1170.

(14) Pratviel, G., Bernadou, J., Ricci, M., and Meunier, B. (1989) Magnesium monoperoxophthalate: An efficient single oxygen atom donor in DNA cleavage catalysed by mettaloporphyrins. *Biochem. Biophys. Res. Commun. 160*, 1212−1218.

(15) Ding, L., Etemad-Moghadam, G., Cros, S., Auclair, C., and Bernard, M. (1989) Cytotoxic hybrid molecules Metalloporphyrin − Ellipticine having a high affinity for DNA. *J. Chem. Soc., Chem. Commun.* 1711−1713.

(16) Sentagne, C., Meunier, B., and Paillous, N. (1992) DNA cleavage photoinduced by new water − soluble zinc porphyrins linked to 9-methoxyellipticine. *J. Photochem. Photobiol. B 16*, 47−59.

(17) Jakobs, A., Bernadou, J., and Meunier, B. (1997) Preparation of teracationic metalloporpyrin-spermine conjugates. *J. Org. Chem. 62*, 3505−3510.

(18) Frau, S., Bernadou, J., and Meunier, B. (1997) Nuclease activity and binding characteristics of a cationic "Manganese

Porphyrin−Bis(benzimidazole) Dye (Hoechst 33259)". *Bioconjugate Chem. 8*, 222−231.
(19) Bigey, P., Sonnichsen, S. H., Meunier, B., and Nielsen, P. (1997) DNA binding and cleavage by a cationic manganese porphyrin−peptide nucleic acid conjugate. *Bioconjugate Chem. 8*, 267−270.
(20) Mestre, B., Jakobs, A., Pratviel, G, and Meunier, B. (1996) Structure/nuclease activity relationships of DNA cleavers based on cationic metalloporphyrin-oligonucleotide conjugates. *Biochemistry 35*, 9140−9149.
(21) Bigey, P., Pratviel, G., and Meunier, B. (1995) Cleavage of double stranded DNA by metalloporphyrin − linker − oligonucleotide, molecules: influence of the linker. *Nucleic Acid Res. 23*, 3894−3900.
(22) Dougherty, T. J., Gomer, C. J., Henderson, B. W., Jori, G., Kessel, D., Korbelik, M., Maon, J., Peng, Q. (1998) Photodynamic Therapy. *J. Natl. Cancer Inst. 90*, 889−905.
(23) Henerson, B. W., and Dougherty, T. J., Eds. (1992) Photodynamic Therapy: Basic principles and clinical applications, New York, Marcel Dekker.
(24) Fiel, R. J., Datta-Gupta, N., Mark, E. H., and Howard, J. C. (1981) Induction of DNA damage by porphyrin photosensitizers. *Cancer Res. 41*, 3543−3545.
(25) Prasueth, D., Gaudemer, A., Verlhac, J., Kraljic, I., Sissoeff, I., and Guille, E. (1986) Photocleavage of DNA in the presence of synthetic water soluble porphyrins. *Photochem. and Photobiol. 44*, 717−724.
(26) Munson, B. R. and Fiel, R. J. (1992) DNA intercalation and photosensitization of cationicmeso-substituted porphyrin. *Nucleic Acid Res. 20*, 1315−1319.
(27) Boutorine, A. S., Brault, D., Takasugi, M., Delgado, O., and Helene, C., (1996) Chlorin-oligonucleotide conjugates: synthesis, properties and red light-induced photochemical sequence-specific DNA cleavage in duplexes and triplexes. *J. Am. Chem. Soc. 118*, 9469−9476.
(28) Magda, D., Wright, M., Miller, R. A., Sessler, J. L., and Sansom, P. I. (1995) Sequence specific photocleavage of DNA by an expanded porphyrin with irradiation above 700 nm. *J. Am. Chem. Soc. 117*, 3629−3630.
(29) Pandey, R. K., Shiau, F., Smith, N. W., Dougherty, T. J., and Smith, K. M. (1992) Syntheses of water soluble cationic porphyrins and chlorins. *Tetrahedron 48*, 7591−7600.
(30) Pandey, R. K., Shiau, F. Y., Ramachandran, K., Dougherty, T. J., and Smith, K. M. (1992) Long wavelength photosensitizers related to chlorins and bacteriochlorins for use in photodynamic therapy. *J. Chem. Soc., Perkin Trans. 1* 1377−1385.
(31) Jackson, A. H., Pandey, R. K., Roberts, E., and Rao, K. R. N. (1985) Reaction on solid supports Part II: A conveninet method for synthesis of pyrromethanes using a Montmorillonite clay as catalyst. *Tetrahedron Lett. 26*, 793−796.
(32) Keller, W., (1975) Determination of the number of spherical turns in simian virus 40 DNA by gel electrophoresis. *Proc. Natl. Acad. Sci. U.S.A. 72*, 4876−4880.
(33) Wolfe, A., Shimer, G. H., and Meehan, T., (1987) Polycyclic aromatic hydrocarbon physically intercalate into duplex region of denatured DNA. *Biochemistry 26*, 6392−6396.
(34) Pyle, A. M., Rehmann, J. P., Mesoyrer, R., Kumar, C. V., Turro, N. J., and Barton, J. K. (1989) Mixed-ligand complexes of ruthenium(II): factors governing binding to DNA. *J. Am. Chem. Soc. 111*, 3051−3058.
(35) Bhattacharya, S., and Mandal, S. S. (1996) DNA cleavage by intercalatable cobalt-bispicoylamine complexes activated by visible light. *Chem. Commun.* 1515−1516.
(36) Sehlstedt, U., Kim, S. K., Carter, P., Goodisman, J., Vollano, J. F., Norden, B., and Dabrowiak, J. C. (1994) Interaction of cationic porphyrins with DNA. *Biochemistry 33*, 417−426.
(37) The factors influencing the relative photocleavage efficiencies of the different chromophores, other than their structural differences, are complex and could reflect affects such as binding affinities and singlet oxygen quantum yield. As suggested by one of the reviewers, another important factor that can effect the DNA cleaving efficiency is the exact number of porphyrin molecules bound to double stranded DNA, which is difficult to establish, due to aggregation effects.
(38) Carvlin, M. J., Datta-Gupt, N., and Fiel, R. J. (1982) Circular dichroism spectroscopy of a cationic porphyrin bound to DNA. *Biochem. Biophys. Res. Commun. 108*, 66−73.
(39) Carvlin, M. J., and Fiel, R. J. (1983) Intercalative and nonintercalative binding of a large cationic porphyrin ligand to calf thymus. *Nucleic Acid Res. 11*, 6121−6140.
(40) Carvlin, M. J., Mark, E., and Fiel, R., Intercalative and nonintercalative binding of a large cationic porphyrin ligands to polynucleotides. *Nucleic Acids Res. 11*, 6141−6154.
(41) Sari, M. A., Battioni, J. P., Dupre, D., Mansuy, D., and Lepecq, J. B. (1996) Mode of interaction and apparent binding constants of meso-tetraaryl porphyrins bearing between one and four positive charges with DNA. *Biochem. Biophys. Res. Commun. 141*, 643−649.
(42) Sari, M. A., Battioni, J. P., Dupre, D., Mansuy, D., and Lepecq, J. B. (1990) Interaction of cationic porphyrins with DNA: Importance of the number and position of the charges and minimum structural requirements for intercalation. *Biochemistry 29*, 4205−4215.

BC9800872

Evaluation of the in Vivo Biodistribution of Indium-111 and Yttrium-88 Labeled Dendrimer-1B4M-DTPA and Its Conjugation with Anti-Tac Monoclonal Antibody†

Hisataka Kobayashi,‡ Chuanchu Wu,§ Meyoung-Kon Kim,‡ Chang H. Paik,‡ Jorge A. Carrasquillo,*,§ and Martin W. Brechbiel§

National Institutes of Health, Bethesda, Maryland 20892. Received August 4, 1998; Revised Manuscript Received September 29, 1998

We evaluated the in vivo biodistribution of indium- and yttrium-labeled second-generation polyamidoamine dendrimer (PAMAM) conjugated with 2-(*p*-isothiocyanatobenzyl)-6-methyl-diethylenetriaminepentaacetic acid (1B4M), a derivative of DTPA. In addition, we conjugated PAMAM-1B4M to humanized anti-Tac IgG (HuTac) and evaluated its in vitro and in vivo properties. PAMAM-1B4M was labeled with ^{111}In at 37−48 MBq/mg (1.0−1.3 mCi/mg) or with ^{88}Y at 3.7−4.8 MBq/mg (0.1−0.13 mCi/mg), and an aliquot of radiolabeled conjugate was saturated with the corresponding stable yttrium or indium. Nontumor-bearing nude mice were injected intravenously with 55.5−66.6 kBq (1.5−1.8 μCi) of ^{88}Y-labeled PAMAM-1B4M or with 185 kBq (5 μCi) of ^{111}In-labeled PAMAM-1B4M. The mice were then sacrificed at 15 min, 90 min, 1 day, and 4 days postinjection. Then the PAMAM-1B4M was conjugated with HuTac and labeled with ^{111}In at 111−259 MBq/mg (3−7 mCi/mg). Another preparation of ^{111}In-labeled HuTac-PAMAM-1B4M was saturated with stable indium. Immunoreactivity of both preparations and biodistribution in normal mice 1 h after injection and in ATAC4 and A431 tumor-bearing mice 18 h after injection were evaluated and compared with those of ^{111}In-labeled 1B4M-HuTac. We noted significantly higher accumulations ($p < 0.05$) of ^{111}In-labeled and ^{88}Y-labeled unsaturated PAMAM-1B4M than saturated preparations in the liver, kidney, spleen, and bone at most time points. The whole-body clearance times of unsaturated preparations were significantly slower than those of saturated preparations at all time points, with the exception of 168 h for ^{111}In-labeled PAMAM-1B4M. The saturated preparation of ^{111}In-labeled HuTac-PAMAM-1B4M showed lower hepatic uptake (27 ± 2%ID/g) than the unsaturated (32 ± 2%ID/g), but greater than the HuTac-1B4M control (10 ± 0%ID/g). The splenic uptake showed 15 ± 1, 38 ± 5, and 8 ± 1%ID/g for the saturated, unsaturated, and control, respectively. The biodistribution of the dendrimer conjugated HuTac in normal organs of tumor-bearing mice was similar to nontumor-bearing mice. Specific tumor (ATAC4) uptake was higher than that in nonspecific tumor (A431). In conclusion, we evaluated the biodistribution of radiolabeled PAMAM-1B4M. We noted high accumulation in the liver, kidney, and spleen, which significantly decreased when the chelates were saturated with the stable element. A similar phenomenon was observed between unsaturated and saturated ^{111}In-labeled HuTac-PAMAM-1B4M, indicating that the PAMAM dendrimer had a detrimental effect on biodistribution.

INTRODUCTION

Starburst polyamidoamine (PAMAM)[1] dendrimers are a new class of highly branched spherical polymers that are highly soluble in aqueous solution and have a unique surface of primary amino groups (*1*, *2*). Compared with many other types of dendritic macromolecules that recently have been synthesized, PAMAM dendrimers are the only class of macromolecules that are unidispersed and show high charge densities restricted to the surface of the molecule (*3*). The defined structure and large number of surface amino groups of PAMAM dendrimers have led to their use as substrates for the attachment of chelating agents to antibodies (*2*, *4*, *5*) and in the preparation of novel magnetic resonance imaging (MRI) contrast agents (*6*). In addition, they have been used successfully to transfer nucleic acids into mammalian cells (*7*, *8*).

Radiolabeled antibodies have been extensively evaluated for radioimmunodetection and radioimmunotherapy of cancer (*9*−*11*). In addition to ^{131}I, ^{90}Y has been used for radioimmunotherapy (*12*−*14*). Initially, cyclic or mixed anhydride of diethylenetriaminepentaacetic acid (DTPA) was used for ^{90}Y labeling. Unfortunately, this chelate was not optimal since it prematurely released the ^{90}Y, which increased bone uptake (*15*, *16*). More stable chelates have since been generated (*17*, *18*) to address this problem. While 1,4,7,10-tetraazacyclododecane tetraacetic acid (DOTA), a macrocyclic chelating agent, has

† Presented at the 45th annual meeting of Society of Nuclear Medicine in Toronto, ON, Canada on June 6−11, 1998.

* To whom correspondence should be addressed. Department of Nuclear Medicine, National Institutes of Health, Bldg. 10, Room 1C-401, 10 Center Drive, MSC 1180, Bethesda, MD 20892-1180. Tel: 301-496-5675. Fax: 301-496-0114; E-mail: jorge@nmdpet.cc.nih.gov.

‡ Nuclear Medicine Department, Warren G. Magnuson Clinical Center.

§ Chemistry Section, Radiation Oncology Branch, National Cancer Institute.

[1] Abbreviations: polyamidoamine dendrimer, PAMAM; 2-(*p*-isothiocyanatobenzyl)-6-methyl-diethylenetriaminepentaacetic acid, 1B4M; 2-(p-SCN-Bz)-cyclohexyl-diethylenetriaminepentaacetic acid, CHX; humanized anti-Tac IgG, HuTac; %ID/g, percent injected dose per gram.

10.1021/bc980091d CCC: $18.00 © 1999 American Chemical Society
Published on Web 12/10/1998

excellent stability in vivo and in vitro for ^{90}Y, the metal−DOTA complex is slow to form (*16*, *19*). Approaches that may overcome this problem include prolonged incubation with the ^{90}Y or high doses of ^{90}Y, which may damage the antibody's immunoreactivity if radioprotectants are not used (*20*). Another approach is that of using higher temperature incubations (*21*), although in our experience, we have not been greatly successful with this approach (*2*), perhaps because of the DOTA variant that we utilized. Although large numbers of chelating groups can be conjugated to the antibody in an attempt to improve the kinetics, this often results in a drop in immunoreactivity (*22*). Problems similar to those encountered with ^{90}Y are likely to be encountered with α emitters, such as ^{212}Bi or ^{213}Bi that are being investigated for radioimmunotherapy. Previous work has attempted to take advantage of PAMAM dendrimers by conjugating multiple chelates to the dendrimer and attaching this dendrimer-chelate construct to the antibody through a single attachment site (*2*). Wu et al., using a second-generation ($G = 2$) PAMAM dendrimer, were able to attach either 2-(*p*-isothiocyanatobenzyl) (p-SCN-Bz)-DOTA or 2- (p-SCN-Bz)-cyclohexyl-diethylenetriaminepentaacetic acid (CHX) chelates to the dendrimer, and their preliminary in vitro results indicated a potential for greatly improving the radiolabeling kinetics and the specific activity of the ^{90}Y- or ^{212}Bi-labeled monoclonal antibody, a noted hindrance for the routine use of DOTA conjugated to antibodies in the conventional way (*2*). In addition, antibodies have been considered as targeting agents to be used with MRI. In this case, high molar concentrations are required with atom such as gadolinium (*6*). This study is an in vivo extension of our previous work (*2*).

We evaluated the biodistribution of a monoclonal antibody labeled with ^{111}In via a PAMAM dendrimer conjugated to 1B4M chelate (*16*). Because preliminary in vivo studies with this reagent showed large uptakes in liver and spleen, we evaluated the biodistribution of the PAMAM-1B4M labeled with ^{111}In and ^{88}Y, which was not conjugated to an antibody. In addition, we determined whether saturating the PAMAM-1B4M conjugate with stable indium or yttrium would alter its biodistribution. We chose to work with 1B4M rather than DOTA because of its greater availability and in order to provide proof-of-principal.

MATERIALS AND METHODS

Monoclonal Antibody. The anti-Tac IgG2a was produced and characterized as previously described (*23*). The humanized anti-Tac antibody (HuTac) was genetically constructed, as previously described, by combining the complementarity-determining regions of the murine anti-Tac antibody with the human IgG1κ framework and constant regions (*24*).

Conjugation of Chelates to Dendrimer. We used second-generation PAMAM dendrimer with an ethylenediamine core that possesses 16 amino groups and has a molecular mass of 3256 Da (Aldrich Chemical Co., Milwaukee, WI) (*1*). This dendrimer (10 μM in 10 mL of H_2O) was reacted with 240 μmol of 2-(*p*-isothiocyanatobenzyl)-6-methyl-diethylenetriaminepentaacetic acid (1B4M) at 40 °C, adjusted to pH 9 with 1 M NaOH, for 24 h. One-half of the 1B4M was added at the beginning, and the remainder was added after 8 h as a solid form. The resulting preparations were purified by diafiltration using a stirred cell (Amicon Co., Beverly, MA) with a 3 kDa membrane (Omega 3K; Filtron Technology Co., Northborough, MA). This resulted in an average of 14.3 1B4M ligands on a dendrimer, as determined by a colorimetric assay (*25*). An average of one free amine was available for further chemical reaction and conjugation to the monoclonal antibody, as described below.

Conjugation of Dendrimer-Chelates with Antibody. The method of conjugation of PAMAM-1B4M with antibody was performed as previously described (*2*). Briefly, to provide a free thiol group, the remaining primary amine on the PAMAM-1B4M constructs was reacted with a 5-fold molar excess of sulfosuccinimidyl 6-[3′-(2-pyridyldithio)propionamido]hexanoate (sulfo-LC-SPDP, Pierce Chemical Co., Rockford, IL), in 0.1 M HEPES buffer, at pH 8.5 for 1 h at room temperature. A free sulfhydryl group was generated by reacting the above product with solid dithiothreitol for 15 min at a final concentration of 25 mM. The product was purified by diafiltration using a stirred cell (Amicon Co.) with a 3 kDa membrane (Omega 3K; Filtron Technology Co.).

The HuTac (5 mg/mL) was first reacted with sulfosuccinimidyl 4-(*N*-maleimidomethyl)cyclohexane-1-carboxylate (sulfo-SMCC; Pierce Chemical Co.) in bicarbonate buffer, pH 8.5, at room temperature for 20 min, at an initial sulfo-SMCC-to-HuTac ratio of 4:1. The unreacted reagent was removed by Sephadex G50 size-exclusion chromatography with aqueous 0.02M Bis-Tris/HCl and 0.1 M NaCl, pH 7.0, as eluant.

The thiol-containing PAMAM-1B4M construct was then conjugated with HuTac-SMCC at pH 7.0, at room temperature for 30 min, at a 1.5:1 molar ratio, respectively. HuTac-PAMAM-1B4M conjugates were separated from unmodified antibody, unreacted PAMAM-1B4M, and higher-molecular-weight species, which arose from multiple sulfhydryl groups attached to the dendrimer, by HPLC using a MONO Q anion-exchange column (5 × 600 mm, Pharmacia, Uppsala, Sweden) coupled in tandem with a TSK 3000SW preparative size-exclusion column (21 × 600 mm, Toso Haas, Tokyo, Japan) by a Pharmacia V7 valve eluted with 0.05 M PBS, pH 7.2, at a flow rate of 1.0 mL/min. The mean ratio of dendrimer to antibody was 0.8−1:1 (*2*). Isoelectric focusing experiments on a PhastGel IEF 3-9 (Pharmacia Biotech AB, Uppsala, Sweden) with the Phast System (Pharmacia Biotech AB) to determine the pI of PAMAM-1B4M were not successful because PAMAM-1B4M stayed at the site of application.

Radiolabeling of PAMAM-1B4M or HuTac-PAMAM-1B4M. Carrier-free $^{111}InCl_3$ was purchased from NEN DuPont (Boston, MA). Carrier-free ^{88}Y (Los Alamos National Laboratory, Los Alamos, NM) was further purified from metal contaminants by column extraction chromatography (*26*). The PAMAM-1B4M or HuTac-PAMAM-1B4M conjugates were reacted with ^{111}In or ^{88}Y at pH 5.5−6.5 for 30 min at room temperature as previously described (*2*, *16*, *18*, *26*). To remove any nonincorporated free radiometal, 10 μL of 0.1 M EDTA was added and purified by HPLC using a TSK 3000 SW size-exclusion column (Toso Haas) eluted with PBS, pH 7.2, at a flow rate of 1.0 mL/min. The resulting purified materials were referred to as "unsaturated" because on the average they had <1 radiometal (^{111}In or ^{88}Y) per molecule.

To evaluate the effect on biodistribution of saturating the 1B4M chelates, the PAMAM-1B4M or HuTac-PAMAM-1B4M was saturated with either nonradioactive indium or yttrium. Preparation method was the same as described above, except that excess cold indium or yttrium chloride was added to the reaction mixture and incubated for 5 min before the addition of EDTA and column purification. Radiolabeling yields were >85% for

all the conjugates, and their specific activities ranged from 3.7 to 4.8 MBq/mg (0.1−0.13 mCi/mg) for ^{88}Y-labeled PAMAM-1B4M; 37−48 MBq/mg (1.0−1.3 mCi/mg) for ^{111}In-labeled PAMAM-1B4M; and 111−259 MBq/mg (3−7 mCi/mg) for ^{111}In-labeled HuTac-PAMAM-1B4M.

All radiolabeled PAMAM-1B4M preparations, including the HuTac conjugates, were analyzed by HPLC using TSK 2000SW (Toso Haas) size-exclusion columns connected to an on-line γ detector (γRAM, IN/US Systems, Inc., Fairfield, NJ). The columns were eluted with 0.067 M PBS, 0.1 M KCl buffer (pH 6.8), with a flow rate of 0.5 mL/min. The same HPLC system was used to analyze collected urine.

Immunoreactivity. The immunoreactivity of the radiolabeled monoclonal antibody was determined by use of a modification of the cell-binding assay of Lindmo et al. (*27*) as we previously described (*28*). Aliquots of the ^{111}In-labeled HuTac-PAMAM-1B4M (3 ng/100 μL) were incubated for 2 h at 4 °C with 1×10^6 to 4×10^7 SP2/Tac cells. The cell-bound radioactivity was separated by centrifugation and counted in a γ counter. Nonspecific binding to the cells was examined under conditions of antibody excess (25 μg of nonradiolabeled anti-Tac antibody). As a control, we determined the immunoreactivity of ^{111}In-labeled 1B4M-HuTac.

Tumor-Bearing Animal Models. Tumor xenografts were generated with the ATAC4 cell line, which expresses the IL-2Rα receptor but does not secrete it into the circulation. This cell line was generated by genetically transfecting the plasmid encoding the IL-2Rα and a neomycin-resistant gene into receptor-negative A431 cells (*29*). The A431 cells, which were obtained originally from G. Todaro (National Institutes of Health, Bethesda, MD), are a human epidermoid carcinoma line that does not express IL-2Rα. Both cell lines were grown in RPMI 1640 medium (GIBCO Laboratories, Grand Island, NY) containing 10% fetal calf serum (GIBCO Laboratories, Grand Island, NY) and 0.03% L-glutamine, at 37 °C, in 5% CO_2, which was occasionally supplemented with 750 mg/mL sulfate Geneticin (GIBCO Laboratories) to avoid the growth of transformed ATAC4 cells. Tumor xenografts were established by s.c. inoculation of 4×10^6 ATAC4 and 5×10^6 A431 cells. The ATAC4 tumors in this study were 0.68 ± 0.31 g and the A431 were 0.55 ± 0.10 g in the HuTac-PAMAM-1B4M group and 0.76 ± 0.12 g for ATAC4 and 0.49 ± 0.14 g for the A431 tumor in the HuTac-1B4M control group.

Biodistribution Study. Biodistribution studies were performed in 5−6-week-old female athymic nude mice weighing 16−21 g (Harlan Sprague Dawley, National Cancer Institute, Frederick, MD). All studies were approved by the Clinical Centers' Animal Care and Use Committee. Mice were euthanized with CO_2 inhalation and exsanguinated by cardiac puncture prior to dissection. Aliquots of blood and all major organs were removed, weighed on an analytical balance, and the radioactivity was counted in a well-type γ counter (Autogamma, Packard Instrument Company, Downers Grove, IL). All data were decay corrected. When dual isotope studies were performed, the counts were corrected for decay and spillover. Under our counting conditions, ^{111}In (100−500 keV) had a 0.02% spillover and ^{88}Y (600−2000 keV) a 42% spillover into each other's window. The whole-body clearance was determined by summing the radioactivity measured in blood, individual organs, and in the remaining carcass. Random urine samples were taken shortly before sacrifice and analyzed with a size-exclusion HPLC system.

The biodistribution of ^{111}In-labeled unsaturated or saturated HuTac-PAMAM-1B4M was evaluated in two groups of three mice each. In addition, as a control, ^{111}In-labeled 1B4M-HuTac was injected into six mice. These groups of nontumor-bearing nude mice were sacrificed at 1 h after injection, and biodistribution studies were performed. In addition, two groups of three tumor-bearing mice each underwent a biodistribution study 18 h after injection of ^{111}In-labeled unsaturated HuTac-PAMAM-1B4M or ^{111}In-labeled 1B4M-HuTac.

Two groups of four mice each were injected i.v. with ^{111}In-labeled unsaturated [185 kBq (5 μCi)] or saturated [185 kBq (5 μCi)] PAMAM-1B4M and sacrificed at 15 min, 45 min, 90 min, 360 min, 24 h, 48 h, and 96 h after injection. Another two groups of four mice each received ^{88}Y-labeled unsaturated [62.9 kBq (1.7 μCi)] or saturated [55.5 kBq (1.5 μCi)] PAMAM-1B4M, and were then sacrificed at 15 min, 90 min, 24 h, and 96 h after injection. Biodistribution studies and whole-body clearance were performed as described above. In addition, urine was collected and analyzed at 15, 45, and 90 min to evaluate the urinary excretion of the radiolabeled PAMAM-1B4M.

To validate the reproducibility from one labeling to another, on the biodistribution of unsaturated and saturated PAMAM-1B4M, we co-injected ^{111}In-labeled and ^{88}Y-labeled unsaturated PAMAM-1B4M in one group of four mice and ^{111}In-labeled and ^{88}Y-labeled saturated PAMAM-1B4M in another group of four mice. The biodistribution was then evaluated at 15 min, 90 min, 24 h, and 96 h after injection.

To determine if the metal ion used to saturate the PAMAM-1B4M affected its biodistribution, cross-saturation studies were performed. PAMAM-1B4M trace-labeled with ^{111}In [185 kBq(5 μCi)] was saturated with cold yttrium, or ^{88}Y trace-labeled PAMAM-1B4M [55.5 kBq (1.5 μCi)] was saturated with cold indium. Mice were injected i.v. with these reagents and sacrificed at 15 min, 90 min, 24 h, and 96 h after injection. The biodistribution study was done as described above.

Statistical Analysis. We performed the statistical analysis using the one-way analysis of variance (ANOVA), with pairwise comparison using the Bonferroni method (Sigmastat, Jandel Scientific, San Rafael, CA).

RESULTS

Quality Control and Immunoreactivity. Radiochemical purity of all the ^{111}In-labeled HuTac-PAMAM-1B4M and ^{111}In-labeled or ^{88}Y-labeled PAMAM-1B4M preparations were >99% as determined by size-exclusion HPLC. Although the total binding was similar for both preparations, the nonspecific binding for the HuTac-PAMAM conjugates was higher and therefore had slightly lower immunoreactivity than that of the ^{111}In-labeled 1B4M-HuTac (Table 1) these immunoreactivity levels are similar to those we have observed for ^{125}I-labeled HuTac.

Biodistribution Studies. The ^{111}In-labeled unsaturated HuTac-PAMAM-1B4M showed higher hepatic and splenic accumulation than the ^{111}In-labeled saturated HuTac-PAMAM-1B4M (Table 2). However, the hepatic and splenic accumulation of ^{111}In-labeled saturated HuTac-PAMAM-1B4M was still significantly higher than that of ^{111}In-labeled 1B4M-HuTac ($p < 0.001$, Anova). The blood clearance of both unsaturated and saturated ^{111}In-labeled HuTac-PAMAM-1B4M were much faster than that of ^{111}In-labeled 1B4M-HuTac. Additional biodistribution studies were performed at 18 h to evaluate delayed kinetics and tumor uptake. As noted in the 1 h

Table 1. Immunoreactivity Test for ^{111}In-Labeled HuTac-PAMAM-1B4M and ^{111}In-Labeled 1B4M-HuTac

	^{111}In-labeled HuTac-PAMAM-1B4M (unsaturated)	^{111}In-labeled HuTac-PAMAM-1B4M (saturated)	^{111}In-labeled 1B4M-HuTac
total binding[a]	81.4−83.2[d]	79.5[e]	84.3−85.6[d]
nonspecific binding [b]	7.1−8.5[d]	6.4[e]	1.7−2.1[d]
estimated immunoreactivity (specific binding)[c]	72.7−74.3[d]	73.1[e]	82.4−83.5[d]

[a] Data are expressed as a range of percentage of total radioactivity added per well. [b] Percentages of total activity added that bound to antigen-positive cells under conditions of antibody excess (25 μg). [c] Total radiolabeled antibody bound minus nonspecific binding. [d] Range from the results of preparations at three different times. [e] Value from the result of preparation at a single time.

Table 2. Biodistribution of ^{111}In-Labeled HuTac-PAMAM-1B4M and ^{111}In-Labeled 1B4M-HuTac 1 h after Injection[a]

organs /preparation	blood	liver	kidney	intestine	stomach	spleen	lung	whole body[b]
unsaturated HuTac-PAMAM-1B4M[b]	23.1 ± 0.4	32.0 ± 1.8	8.5 ± 0.3	1.8 ± 0.1	0.9 ± 0.1	37.5 ± 5.3	8.7 ± 1.7	99.9 ± 0.1
saturated HuTac-PAMAM-1B4M[b]	24.2 ± 0.4	26.5 ± 1.8	6.8 ± 1.0	1.9 ± 0.1	1.0 ± 0.1	14.9 ± 0.8	10.1 ± 1.5	100.4 ± 1.2
1B4M-HuTac[c]	36.8 ± 3.8	10.2 ± 0.2	8.0 ± 0.8	2.6 ± 0.1	1.2 ± 0.4	7.7 ± 1.1	15.2 ± 2.2	101.9 ± 1.5

[a] Data were expressed as %ID/g ± SD, except whole body, which is expressed as the percentage of the ID ± SD. [b] $n = 3$ mice. [c] $n = 6$ mice.

Table 3. Biodistribution of ^{111}In-Labeled HuTac-PAMAM-1B4M and ^{111}In-Labeled 1B4M-HuTac 18 h after Injection in Tumor-Bearing Mice[a]

organs/preparation	blood	liver	kidney	intestine	stomach	spleen	lung	A431 (Tac−)	ATAC4 (Tac+)	whole body[b]
unsaturated HuTac-PAMAM-1B4M[b]	5.5 ± 1.0	30.8 ± 2.6	5.2 ± 0.2	1.6 ± 0.5	0.8 ± 0.2	14.8 ± 2.8	3.4 ± 0.1	3.0 ± 0.2	8.2 ± 1.0	98.6 ± 0.0
1B4M-HuTac[b]	15.5 ± 0.2	5.1 ± 1.3	5.1 ± 0.1	1.3 ± 0.3	0.7 ± 0.2	3.3 ± 0.7	7.6 ± 1.7	3.4 ± 0.2	14.3 ± 1.6	100.9 ± 1.0

[a] Data were expressed as %ID/g ± SD, except whole body, which is expressed as the percentage of the ID ± SD. [b] $n = 3$ mice.

Table 4. Comparative Biodistribution of ^{111}In-Labeled or ^{88}Y-Labeled PAMAM-1B4M Unsaturated or Saturated with Stable 1n(III) or Y(III) in the Liver, Kidney, Spleen, and Bone Various Times after Injection[a]

radioisotope		^{111}In			^{88}Y		
saturation/organ	time	no	cold In	cold Y	no	cold In	cold Y
liver	15 min	24.4 ± 1.3	18.1 ± 2.7	11.8 ± 1.5	22.4 ± 0.8	15.8 ± 1.0	9.4 ± 0.4
	90 min	23.7 ± 0.7	19.2 ± 2.1	10.6 ± 1.1	21.7 ± 1.6	16.6 ± 2.0	10.8 ± 0.3
	1 day	22.3 ± 0.9	17.8 ± 1.7	10.3 ± 1.1	18.0 ± 0.8	15.3 ± 2.0	8.2 ± 0.6
	4 day	19.9 ± 2.1	16.5 ± 1.3	9.6 ± 1.0	11.9 ± 0.8	10.4 ± 1.1	6.7 ± 0.7
kidney	15 min	73.6 ± 4.7	42.5 ± 3.5	27.9 ± 1.7	88.9 ± 2.9	64.5 ± 4.5	31.9 ± 4.0
	90 min	90.3 ± 7.8	40.7 ± 5.6	16.7 ± 1.6	82.4 ± 2.7	50.0 ± 9.7	41.6 ± 2.1
	1 day	60.6 ± 3.5	33.7 ± 5.4	13.6 ± 1.2	68.1 ± 4.0	44.8 ± 1.4	18.6 ± 2.3
	4 day	22.9 ± 2.1	16.6 ± 1.9	8.4 ± 0.4	36.8 ± 4.6	12.5 ± 1.3	6.4 ± 0.7
spleen	15 min	10.6 ± 0.5	6.1 ± 0.6	6.0 ± 0.9	10.0 ± 1.4	8.3 ± 1.4	4.7 ± 0.7
	90 min	7.8 ± 0.4	5.5 ± 0.6	3.1 ± 0.5	6.2 ± 0.9	5.4 ± 0.3	2.6 ± 0.2
	1 day	6.8 ± 0.9	4.4 ± 0.2	2.9 ± 0.2	5.0 ± 0.3	4.8 ± 0.7	1.7 ± 0.1
	4 day	6.0 ± 0.3	4.2 ± 0.4	2.6 ± 0.3	3.1 ± 0.3	3.1 ± 0.5	1.7 ± 0.1
bone	15 min	6.9 ± 0.2	5.5 ± 0.7	5.3 ± 1.2	9.8 ± 0.1	6.4 ± 1.0	4.7 ± 0.2
	90 min	6.2 ± 0.8	4.9 ± 0.6	4.1 ± 1.0	9.3 ± 0.1	6.0 ± 0.5	5.6 ± 0.5
	1 day	6.1 ± 0.6	4.5 ± 0.4	3.6 ± 0.3	7.4 ± 0.4	5.4 ± 0.7	4.7 ± 0.4
	4 day	5.6 ± 0.2	4.6 ± 0.2	3.5 ± 0.6	6.2 ± 0.5	5.3 ± 0.7	4.3 ± 0.3

[a] Data are expressed %ID/g ± SD.

biodistribution results in nontumor-bearing nude mice, the blood clearance of the ^{111}In-labeled HuTac-PAMAM-1B4M was faster than that of ^{111}In-labeled HuTac-1B4M. Although specific tumor uptake was seen at 18 h, the tumor uptake for the HuTac-PAMAM-1B4M was lower than that for HuTac-1B4M (Table 3).

The blood clearance of both ^{111}In- and ^{88}Y-labeled PAMAM-1B4M was rapid. The greatest concentrations of ^{111}In- and ^{88}Y-labeled PAMAM-1B4M were in the kidney, liver, spleen, and bone. There were very few differences in organ accumulation amounts of either the unsaturated ^{111}In- or the unsaturated ^{88}Y-labeled PAMAM-1B4M (Table 4). Significant differences between unsaturated and saturated preparations were seen in the biodistribution of both ^{111}In-labeled (Figure 1) and ^{88}Y-labeled PAMAM-1B4M (Figure 2). For both ^{111}In-labeled and ^{88}Y-labeled PAMAM-1B4M, saturation with their respective nonradioactive metals resulted in decreased activity of ^{111}In or ^{88}Y in the liver, kidney, spleen, and bone ($p < 0.05$).

The whole-body clearances were also significantly faster for saturated than unsaturated preparations radiolabeled with ^{111}In or ^{88}Y at all time ($p < 0.01$), except 168 h for ^{111}In-labeled PAMAM-1B4M (Figure 3). Both ^{111}In-labeled and ^{88}Y-labeled PAMAM-1B4M, unsaturated and saturated, were excreted into the urine, and HPLC analysis showed that the excreted products had the same retention time as the intact dendrimer (data not shown).

The co-injection studies with ^{111}In- and ^{88}Y-labeled unsaturated PAMAM-1B4M or ^{111}In- and ^{88}Y-labeled saturated PAMAM-1B4M showed similar biodistribution for these as for single isotopes (data not shown).

The ^{111}In-labeled PAMAM-1B4M saturated with cold yttrium showed significantly lower hepatic, renal, and splenic accumulations than either the ^{111}In-labeled unsaturated PAMAM-1B4M or the ^{111}In-labeled PAMAM-1B4M saturated with cold indium ($p < 0.05$; except in the spleen at 15 min). Although ^{88}Y-labeled PAMAM-1B4M saturated with cold indium showed lower hepatic

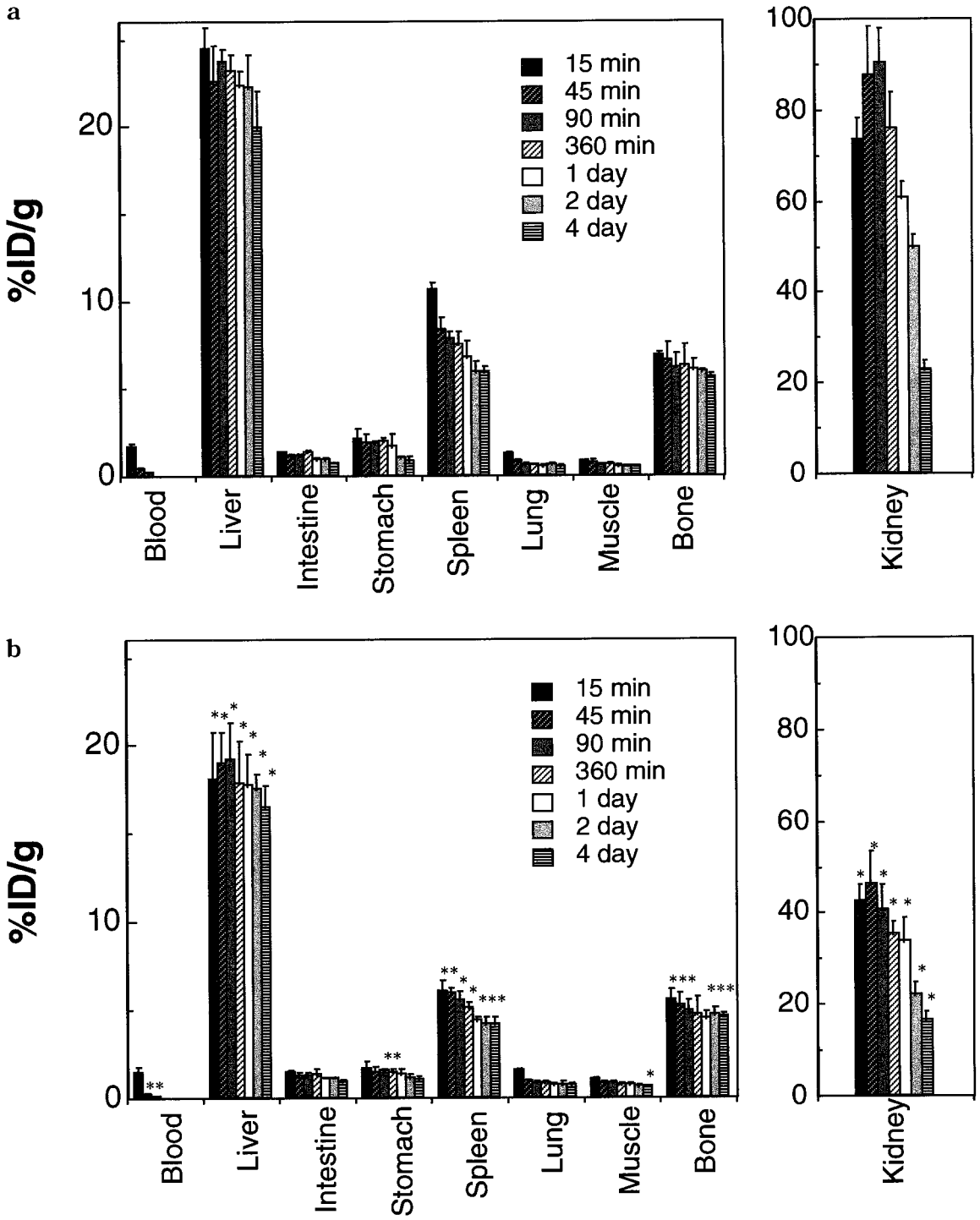


Figure 1. Plots of the biodistribution of ^{111}In-labeled PAMAM-1B4M (a) and ^{111}In-labeled PAMAM-1B4M saturated with cold indium (b). Nontumor-bearing nude mice were sacrificed in groups of four at 15 min, 45 min, 90 min, 360 min, 24 h, 48 h, and 96 h postinjection. The percentages of the injected dose per gram of tissue (%ID/g) in all major organs and in blood are shown. Data are expressed as means ±SD. The asterisks in panel b indicate significant differences ($p < 0.05$) compared with ^{111}In-labeled unsaturated PAMAM-1B4M.

and renal accumulations than ^{88}Y-labeled unsaturated PAMAM-1B4M ($p < 0.05$; except in the liver at 4 day), ^{88}Y-labeled PAMAM-1B4M saturated with cold indium showed higher hepatic and splenic accumulation than that saturated with cold yttrium ($p < 0.01$; except in the kidney at 90 min) (Table 4). The whole-body clearance showed that the saturated PAMAM-1B4M cleared more rapidly than the nonsaturated ($p < 0.01$; except for ^{111}In saturated with cold indium at 4 days) and that the PAMAM-1B4M saturated with yttrium cleared the fastest ($p < 0.01$) (Figure 3).

DISCUSSION

As far as we know, this is the first study to evaluate the biologic properties of an antibody that has been radiolabeled via a dendrimer-chelate combination. A few studies have investigated the use of antibody-dendrimer conjugates for tumor targeting (*2*, *4*, *30*). As expected from such work, attaching a dendrimer to the antibody had little effect on its immunoreactivity (*2*, *4*, *5*). Although retention of immunoreactivity is a prerequisite

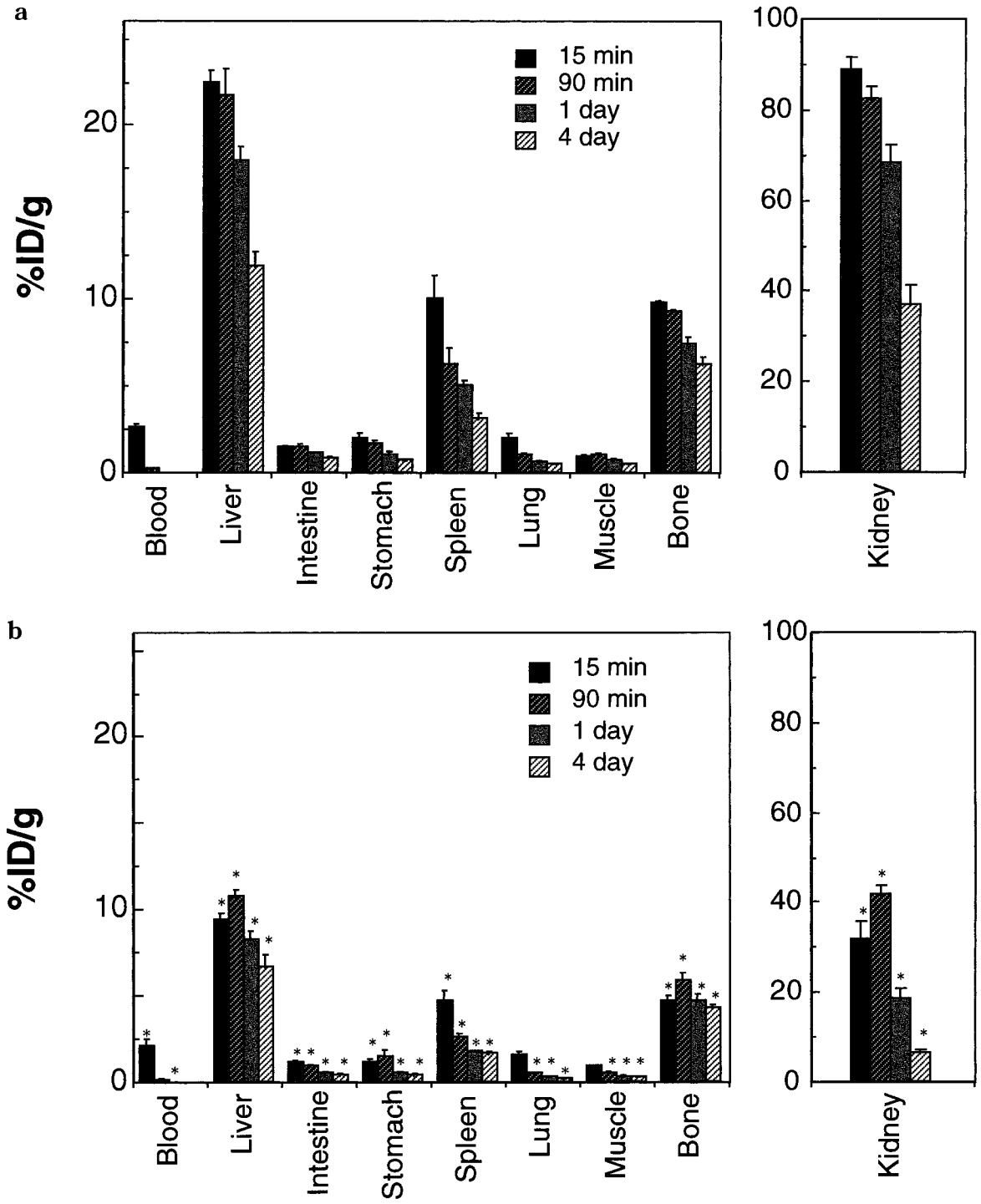


Figure 2. Plots of the biodistribution of ^{88}Y-labeled PAMAM-1B4M (a) and ^{88}Y-labeled PAMAM-1B4M saturated with cold yttrium (b) in nontumor-bearing mice. Animals were sacrificed in groups of four at 15 min, 90 min, 24 h, and 96 h postinjection. The percentages of the injected dose per gram of tissue (%ID/g) in all major organs and in blood are shown. Data are means ±SD. The asterisks in panel b indicate significant differences ($p < 0.05$) compared with ^{88}Y-labeled unsaturated PAMAM-1B4M.

when labeling an antibody, it is also important that the radiolabeling process not adversely affect the biodistribution.

Unfortunately, our results show that the ^{111}In-labeled HuTac-PAMAM-1B4M has altered clearance when compared to the HuTac conventionally labeled with ^{111}In. These altered kinetics were unfavorable because there was fast clearance from the blood and higher clearance into the liver and spleen. This was similar to what was reported by Barth et al., when they used a dendrimer labeled directly with Bolton−Hunter reagent (*4*). While this suggested that the faster clearance was related to the dendrimer itself, the alteration in clearance between saturated and unsaturated antibody conjugates suggested that additional factors related to the 1B4M metal complex itself were important. Roberts et al. evaluated the biodistribution in mice of [^{14}C]methylated dendrimers ranging from third to seventh generation (*31*). Their study of the methylated third generation dendrimer ($G = 3$), which is one generation larger than the one we studied, showed accumulation in liver, spleen, kidney, and pancreas. Methylated $G = 3$ has a molecular mass of 5.2 kDa, which is smaller than that of PAMAM-1B4M, ranging 7.6−9.3 kD. The surface charge on the methy-

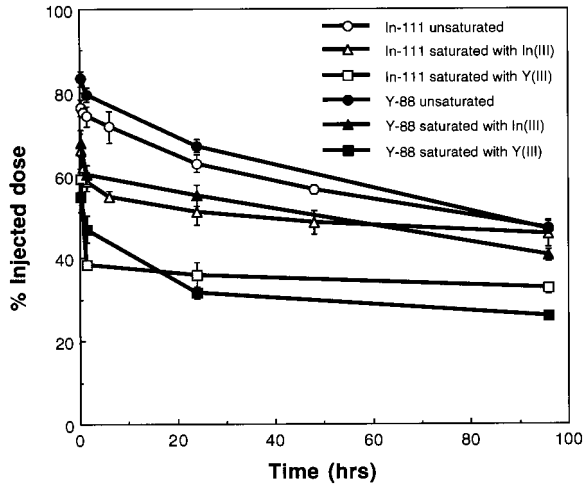


Figure 3. The whole-body retention of six preparations: ^{111}In-labeled (open symbols) or ^{88}Y-labeled (solid symbols); unsaturated (circles), saturated with stable indium (triangles) or saturated with stable yttrium (squares). Data are expressed as %ID retained in the whole body (means ± SD).

lated $G = 3$ is strongly positive. In contrast, unsaturated PAMAM-1B4M is strongly negative, although, after saturation with cold +3 metal ions, the overall charge is more positive. These differences in charge may be responsible for the higher accumulation of PAMAM-1B4M in the kidney and liver that we saw.

Other studies have evaluated the effect of alterations in pI on antibody biodistribution. ten Kate et al. (*32*) reported that changes in pI had a significant effect on antibody biodistribution. The pI change of an IgG resulted in faster blood clearance and less organ uptake. In addition, decreasing pI of small antibody fragments resulted in much lower renal accumulation than the unmodified dsFv fragment (*33*).

The altered kinetics of the ^{111}In-labeled HuTac-PAMAM-1B4M conjugate and the changes observed by saturating the 1B4M with cold radiometals directed us to evaluate the biodistribution of the PAMAM-1B4M with no antibody attached. Although the dendrimer itself is a polycation, in our studies, a mean of 14.3 1B4M groups were substituted, and therefore, this charge may be responsible for the fast clearance into liver and spleen. Saturation with cold metals caused a significant decrease in liver and spleen uptake and more rapid renal clearance. Among the most interesting aspects of this work is the greater effect of saturating the conjugate with yttrium rather than with indium in affecting the whole-body clearance of the PAMAM-1B4M. Our studies suggest that charge and molecular weight are not the only factors affecting biodistribution when cold radiometals were used for saturation, since the final charge and molecular weight should be similar whether indium or yttrium is used for saturation. Other studies show that, in the case of other branch polylysine structures, factors such as size or molecular configuration may affect biodistribution (*34*).

The exact changes in charge as a result of our modifications are complex. If one conjugates the 1B4M-DTPA to protein, the resulting change in charge is a sum of the −2 charge of the DTPA at physiological pH and the depletion of the +1 charge associated with the ϵ-amine of the lysine to which the ligand is now covalently linked via the newly formed thiourea structure. Radiolabeling with a +3 metal ion then returns the charge to the initial overall conditions. This of course neglects any charge balancing contributions of counterions such as H^+, Na^+, K^+, Ca^{2+}, etc. To assess the effect on charge due to the dendrimer, one must first assume that the 14 interior structural tertiary amines contribute to charge and that the 16 exterior primary amines are eliminated by use of one for linkage to protein with the remainder being used for 15 1B4M-DTPA molecules. The potential charge of this structure would be as high as −17, dropping to −14 after radiolabeling assuming just one ^{111}In atom per structure, and then finally after saturation with +3 metal ion becoming as high as +28. Again, these numbers neglect the presence of counterions. The effects of these changes in charge to the protein is strictly speculative and one must consider that while these may seem to be large swings in charge, the overall change to the entire protein charge, i.e., pI, may in fact be negligible, or at least be a local effect. While clearly there is a relationship between charge and organ deposition/clearance, the fact that the overall change in charge from negative to positive, i.e., unsaturated vs saturated, effected better results but not "normal" results would then imply that charge alone is not the determining factor and that other physical characteristics are involved. The lower generation level of PAMAM dendrimers may exhibit substantial back-folding of terminal groups into the dendrimer interior (*35, 36*). It is possible that the act of saturating the chelating surface with metals may inhibit the back-folding and keep the surface charge negative. Therefore, this saturation could decrease the interaction between cell membrane and the PAMAM-1B4M and possibly result in decreased hepatic and splenic uptake. In addition, this hypothesis could explain the difference of hepatic and renal uptake between yttrium and indium saturation if their atomic size differences affected the amount of back-folding. Whether this would happen in higher generation PAMAM dendrimers is not to be determined.

We used the 1B4M to chelate the indium and yttrium because these radiometals require a chelate that will hold the isotope tightly, since, if released from the chelate, these metals would have undesirable targeting and adverse dosimetry (*37*−*39*). In the case of ^{90}Y, the initial chelates used had been developed for ^{111}In, and their stability for ^{90}Y was suboptimal (*15*). As a result of advances in bifunctional chelate technology for ^{90}Y (*40*), several preclinical studies with new chelates indicate that isothiocyanatobenzyl derivatives of DTPA (SCN-Bz-DTPA) have greater stability for ^{90}Y than cyclic anhydride of DTPA, resulting in less bone uptake of ^{90}Y (*15, 41*−*43*). Although our studies were performed with 1B4M because of it greater availability, we believe that similar findings would be observed with DOTA or CHX chelates and therefore 1B4M use was adequate for proof-of-principal.

In conclusion, radiolabeled HuTac-PAMAM-1B4M has a different biodistribution than native HuTac. The faster blood clearance and greater liver and spleen accumulation are likely to be detrimental from an imaging and dosimetry point of view. While saturation of the conjugate with either indium or yttrium partially reversed the differences in biodistribution, its liver and spleen accumulation is still higher than that of native HuTac. Evaluation of the radiolabeled PAMAM-1B4M suggested that some of the uptake in liver and spleen depended on the conjugate itself. In the future we will evaluate other dendrimers which differ in their composition and that may have different physical characteristics.

ACKNOWLEDGMENT

We thank Dr. T. A. Waldmann of the Metabolism Branch, Division of Clinical Sciences, National Cancer

Institute, National Institutes Health, for kindly providing the HuTac.

LITERATURE CITED

(1) Tomalia, D. A., Naylor, A. M., and Goddard, W. A. III (1990) Starburst dendrimers: Molecular-level control of size, shape, surface chemistry, topology, and flexibility from atoms to macroscopic matter. *Angew. Chem., Int. Ed. Engl. 29*, 138−175.

(2) Wu, C., Brechbiel, M. W., Kozak, R. W., and Gansow, O. A. (1994) Metal-chelate-dendrimer-antibody constructs for use in radioimmunotherapy and imaging. *Bioorg. Med. Chem. Lett. 4*, 449−454.

(3) Frechet, J. M. (1994) Functional polymers and dendrimers: reactivity, molecular architecture, and interfacial energy. *Science 263*, 1710−1715.

(4) Barth, R. F., Adams, D. M., Soloway, A. H., Alam, F., and Darby, M. V. (1994) Boronated starburst dendrimer-monoclonal antibody immunoconjugates: evaluation as a potential delivery system for neutron capture therapy. *Bioconjugate Chem. 5*, 58−66.

(5) Singh, P., Moll, F., III, Lin, S. H., Ferzli, C., Yu, K. S., Koski, R. K., Saul, R. G., and Cronin, P. (1994) Starburst dendrimers: enhanced performance and flexibility for immunoassays. *Clin. Chem. 40*, 1845−1849.

(6) Wiener, E. C., Brechbiel, M. W., Brothers, H., Magin, R. L., Gansow, O. A., Tomalia, D. A., and Lauterbur, P. C. (1994) Dendrimer-based metal chelates: a new class of magnetic resonance imaging contrast agents. *Magn. Reson. Med. 31*, 1−8.

(7) Behr, J. P. (1993) Synthetic gene-transfer vectors. *Acc. Chem. Res. 26*, 274−278.

(8) Kukowska-Latallo, J. F., Bielinska, A. U., Johnson, J., Spindler, R., Tomalia, D. A., and Baker, J. R., Jr. (1996) Efficient transfer of genetic material into mammalian cells using Starburst polyamidoamine dendrimers. *Proc. Natl. Acad. Sci. U.S.A. 93*, 4897−4902.

(9) Larson, S. M. (1990) Clinical radioimmunodetection, 1978−1988: overview and suggestions for standardization of clinical trials. *Cancer Res. 50*, 892s−898s.

(10) Goldenberg, D. M., and Larson, S. M. (1992) Radioimmunodetection in cancer identification. *J. Nucl. Med. 33*, 803−814.

(11) Carrasquillo, J. A. (1996) Radioimmunotherapy of leukemia and lymphoma. In *Principles of Nuclear Medicine* (H. Wagner, Ed.) pp 1117−1132, W. B. Saunders and Co., Philadelphia.

(12) Waldmann, T. A., White, J. D., Carrasquillo, J. A., Reynolds, J. C., Paik, C. H., Gansow, O. A., Brechbiel, M. W., Jaffe, E. S., Fleisher, T. A., Goldman, C. K., Top, L. E., Bamford, R., Zaknoen, S., Roessler, E., Kasten-Sportes, C., England, R., Litou, H., Johnson, J. A., Jackson-White, T., Manns, A., Hanchard, B., Junghans, R. P., and Nelson, D. L. (1995) Radioimmunotherapy of interleukin-2R alpha-expressing adult T-cell leukemia with yttrium-90-labeled anti-Tac. *Blood 86*, 4063−4075.

(13) Knox, S. J., Goris, M. L., Trisler, K., Negrin, R., Davis, T., Liles, T.-M., Grillo-Lopes, A., Chinn, P., Varns, C., Ning, S.-C., Fowler, S., Deb, N., Becker, M., Marquez, C., and Levy, R. (1996) Yttrium-90-labeled anti-CD20 monoclonal antibody therapy of recurrent B-cell lymphoma. *Clin. Cancer Res. 2*, 457−470.

(14) Denardo, S. J., Richman, C. M., Goldstein, D. S., Shen, S., Salako, Q., Kukis, D. L., Meares, C. F., Yuan, A., Welborn, J. L., and Denardo, G. L. (1997) Yttrium-90/indium-111-DOTA-peptide-chimeric L6: Pharmacokinetics, dosimetry and initial results in patients with incurable breast cancer. *Anticancer Res. 17*, 1735−1744.

(15) Roselli, M., Schlom, J., Gansow, O. A., Raubitschek, A., Mirzadeh, S., Brechbiel, M. W., and Colcher, D. (1989) Comparative biodistributions of yttrium- and indium-labeled monoclonal antibody B72.3 in athymic mice bearing human colon carcinoma xenografts. *J. Nucl. Med. 30*, 672−682.

(16) Camera, L., Kinuya, S., Garmestani, K., Brechbiel, M. W., Wu, C., Pai, L. H., McMurry, T. J., Gansow, O. A., Pastan, I., Paik, C. H., and Carrasquillo, J. A. (1994) Comparative biodistribution of indium- and yttrium-labeled B3 monoclonal antibody conjugated to either 2-(p-SCN-Bz)-6-methyl-DTPA (1B4M-DTPA) or 2-(p-SCN-Bz)-1, 4, 7, 10-tetraazacyclododecane tetraacetic acid (2B-DOTA). *Eur. J. Nucl. Med. 21*, 640−646.

(17) Roselli, M., Schlom, J., Gansow, O. A., Brechbiel, M. W., Mirzadeh, S., Pippin, C. G., Milenic, D. E., and Colcher, D. (1991) Comparative biodistribution studies of DTPA-derivative bifunctional chelates for radiometal labeled monoclonal antibodies. *Int. J. Rad. Appl. Instrum. B 18*, 389−394.

(18) Camera, L., Kinuya, S., Garmestani, K., Wu, C., Brechbiel, M. W., Pai, L. H., McMurry, T. J., Gansow, O. A., Pastan, I., Paik, C. H., and Carrasquillo, J. A. (1994) Evaluation of the serum stability and in vivo biodistribution of CHX-DTPA and other ligands for yttrium labeling of monoclonal antibodies. *J. Nucl. Med. 35*, 882−889.

(19) Li, M., Meares, C. F., Zhong, G. R., Miers, L., Xiong, C. Y., and DeNardo, S. J. (1994) Labeling monoclonal antibodies with ^{90}yttrium- and ^{111}indium-DOTA chelates: a simple and efficient method. *Bioconjugate Chem. 5*, 101−104.

(20) Chakrabarti, M. C., Le, N., Paik, C. H., De Graff, W. G., and Carrasquillo, J. A. (1996) Prevention of radiolysis of monoclonal antibody during labeling. *J. Nucl. Med. 37*, 1384−1388.

(21) Lewis, M. R., Raubitschek, A., and Shively, J. E. (1994) A facile, water-soluble method for modification of proteins with DOTA. *Bioconjugate Chem. 5*, 565−576.

(22) Sakahara, H., Endo, K., Nakashima, T., Koizumi, M., Ohta, H., Torizuka, K., Furukawa, T., Ohmomo, Y., Yokoyama, A., Okada, K., Yoshida, O., and Nishi, S. (1985) Effect of DTPA conjugation on the antigen binding activity and biodistribution of monoclonal antibodies against alpha-fetoprotein. *J. Nucl. Med. 26*, 750−755.

(23) Uchiyama, T., Nelson, D. L., Fleisher, T. A., and Waldmann, T. A. (1981) A monoclonal antibody (anti-Tac) reactive with activated and functionally mature human T cells. II. Expression of Tac antigen on activated cytotoxic killer T cells, suppressor cells, and on one of two types of helper T cells. *J. Immunol. 126*, 1398−1403.

(24) Queen, C., Schneider, W. P., Selick, H. E., Payne, P. W., Landolfi, N. F., Duncan, J. F., Avdalovic, N. M., Levitt, M., Junghans, R. P., and Waldmann, T. A. (1989) A humanized antibody that binds to the interleukin 2 receptor. *Proc. Natl. Acad. Sci. U.S.A. 86*, 10029−10033.

(25) Pippin, C. G., Parker, T. A., McMurry, T. J., and Brechbiel, M. W. (1992) Spectrophotometric method for the determination of a bifunctional DTPA ligand in DTPA-monoclonal antibody conjugates. *Bioconjugate Chem. 3*, 342−345.

(26) Wu, C., Kobayashi, H., Sun, B., Yoo, T. M., Paik, C. H., Gansow, O. A., Carrasquillo, J. A., Pastan, I., and Brechbiel, M. W. (1997) Stereochemical influence on the stability of radio-metal complexes in vivo. Synthesis and evaluation of the four stereoisomers of 2-(*p*-nitrobenzyl)-trans-CyDTPA. *Bioorg. Med. Chem. 5*, 1925−1934.

(27) Lindmo, T., Boven, E., Cuttitta, F., Fedorko, J., and Bunn, P. A., Jr. (1984) Determination of the immunoreactive fraction of radiolabeled monoclonal antibodies by linear extrapolation to binding at infinite antigen excess. *J. Immunol. Methods 72*, 77−89.

(28) Kobayashi, H., Yoo, T. M., Kim, I. S., Kim, M.-K., Le, N., Webber, K. O., Pastan, I., Paik, C. H., Eckelman, W. C., and Carrasquillo, J. A. (1996) L-lysine effectively blocks renal uptake of ^{125}I- or ^{99m}Tc-labeled anti-Tac dsFv. *Cancer Res. 56*, 3788−3795.

(29) Kreitman, R. J., and Pastan, I. (1994) Recombinant single-chain immunotoxins against T and B cell leukemias. *Leuk. Lymphoma 13*, 1−10.

(30) Roberts, J. C., Adams, Y. E., Tomalia, D., Mercer-Smith, J. A., and Lavallee, D. K. (1990) Using starburst dendrimers as linker molecules to radiolabel antibodies. *Bioconjugate Chem. 1*, 305−308.

(31) Roberts, J. C., Bhalgat, M. K., and Zera, R. T. (1996) Preliminary biological evaluation of polyamidoamine (PAM-AM) Starburst dendrimers. *J. Biomed. Mater. Res. 30*, 53−65.

(32) ten Kate, C. I., Fischman, A. J., Rubin, R. H., Fucello, A. J., Riexinger, D., Wilkinson, R. A., Du, L., Khaw, B. A., and Strauss, H. W. (1990) Effect of isoelectric point on biodistribution and inflammation: imaging with indium-111-labeled IgG. *Eur. J. Nucl. Med. 17*, 305−309.

(33) Kim, I. S., Yoo, T. M., Kobayashi, H., Kim, M.-K., Le, N., Han, E. S., C., W. Q., Pastan, I., Carrasquillo, J. A., and Paik, C. H. (1997) Acylation with glycolate lowers pI of dsFv and reduces renal uptake of its Tc-99m label (abstract). *J. Labeled Compd. Rad. XL*, 422−424.

(34) Clegg, J. A., Hudecz, F., Mezo, G., Pimm, M. V., Szekerke, M., and Baldwin, R. W. (1990) Carrier design: Biodistribution of branched polypeptides with a poly(L-lysine) backbone. *Bioconjugate Chem. 1*, 425−430.

(35) Lescanec, R. L., and Muthukumar, M. (1990) Configurational characteristics and scaling behavior of starburst molecules—A conputational study. *Macromolecules 23*, 2280−2288.

(36) Mansfield, M. L., and Klushin, L. I. (1993) Monte Carlo studies of dendrimer macromolecules. *Macromolecules 26*, 4262−4268.

(37) Hnatowich, D. J., Virzi, F., and Doherty, P. W. (1985) DTPA-coupled antibodies labeled with yttrium-90. *J. Nucl. Med. 26*, 503−509.

(38) Stewart, J. S., Hird, V., Snook, D., Sullivan, M., Hooker, G., Courtenay-Luck, N., Sivolapenko, G., Griffiths, M., Myers, M. J., Lambert, H. E., Mason, W. P., Soutter, W. P., and Epenetos, A. A. (1989) Intraperitoneal radioimmunotherapy for ovarian cancer: pharmacokinetics, toxicity, and efficacy of I-131 labeled monoclonal antibodies. *Int. J. Radiat. Oncol. Biol. Phys. 16*, 405−413.

(39) Stewart, J. S., Hird, V., Snook, D., Dhokia, B., Sivolapenko, G., Hooker, G., Papadimitriou, J. T., Rowlinson, G., Sullivan, M., Lambert, H. E., Coulter, W. P., Mason, W. P., Soutter, W. P., and Epenetos, A. A. (1990) Intraperitoneal yttrium-90-labeled monoclonal antibody in ovarian cancer. *J. Clin. Oncol. 8*, 1941−1950.

(40) Brechbiel, M. W., Gansow, O. A., Atcher, R. W., Schlom, J., Esteban, J., Simpson, D., and Colcher, D. (1986) Synthesis of 1-(p-isothiocyanatobenzyl) derivatives of DTPA and EDTA. Antibody labeling and tumor-imaging studies. *Inorg. Chem. 25*, 2772−2781.

(41) Kozak, R. W., Raubitschek, A., Mirzadeh, S., Brechbiel, M. W., Junghaus, R., Gansow, O. A., and Waldmann, T. A. (1989) Nature of the bifunctional chelating agent used for radioimmunotherapy with yttrium-90 monoclonal antibodies: critical factors in determining in vivo survival and organ toxicity. *Cancer Res. 49*, 2639−2644.

(42) Sharkey, R. M., Motta-Hennessy, C., Gansow, O. A., Brechbiel, M. W., Fand, I., Griffiths, G. L., Jones, A. L., and Goldenberg, D. M. (1990) Selection of a DTPA chelate conjugate for monoclonal antibody targeting to a human colonic tumor in nude mice. *Int. J. Cancer 46*, 79−85.

(43) Washburn, L. C., Sun, T. T., Lee, Y. C., Byrd, B. L., Holloway, E. C., Crook, J. E., Stubbs, J. B., Stabin, M. G., Brechbiel, M. W., Gansow, O. A., and Steplewski, Z. (1991) Comparison of five bifunctional chelate techniques for ^{90}Y-labeled monoclonal antibody CO17-1A. *Int. J. Rad. Appl. Instrum. B 18*, 313−321.

BC980091D

Universal Isolation of Cross-Linked Peptides: Application to Neurofibrillary Tangles

Xiaohui Chen,[†,‡] Devayani Eswaran,[†,‡,||] Mark A. Smith,[§] George Perry,[§] and Vernon E. Anderson*[,‡]

Department of Biochemistry, Case Western Reserve University, 10900 Euclid Avenue, Cleveland, Ohio 44106-4935. Received August 11, 1998; Revised Manuscript Received October 19, 1998

A universal procedure to isolate cross-linked peptides has been demonstrated. The procedure relies on initially converting the ϵ-amino groups of lysine to dimethyl lysine by reductive methylation with sodium cyanoborohydride and formaldehyde. The lysine-modified protein is proteolytically cleaved and the resulting α-amino groups derivatized with methoxypoly(ethylene glycol)$_{5000}$ succinyl hydroxysuccinimide. Any unintentional derivatization of tyrosine side chains can be reversed by incubation under mildly alkaline conditions. The cross-linked polypeptides contain two poly(ethylene glycol)$_{5000}$ chains while non-cross-linked peptides contain a single poly(ethylene glycol)$_{5000}$ chain. The two populations of peptides can be separated by gel filtration chromatography. This procedure has been shown capable of isolating cross-linked peptides using glutathione, lysozyme, chemically cross-linked hemoglobin, and neurofibrillary tangles isolated from the brain of a case of Alzheimer's disease.

The determination of the sites of cross-links of proteins has been a central feature of protein structure determination from the initial work on insulin (Ryle et al., 1955). The location of disulfide cross-links has played a central role in the study of protein folding (Darby and Creighton, 1995, 1997). The use of cross-linking reagents, both specific (Wells and Yount, 1979) and nonspecific, e.g., Cervoni et al. (1994), has provided valuable information on the tertiary and quaternary structure of proteins. A wide variety of pathological processes including atherosclerosis and Alzheimer's disease have been characterized by the occurrence of proteinaceous deposits. It has been suggested that one cause of deposit formation and/or existence may be the generation of cross-linked proteins resulting in a decreased solubility and resistance to proteolytic removal of the aggregate (Munch et al., 1997).

Previous methods for isolating cross-links have relied on two separate approaches. The first is a prior knowledge of the chemical structure or property of the cross-link. Thus, fluorescent cross-linkers have been utilized (Mornet et al., 1985) to assist in the recovery of cross-linked peptides. Alternatively, careful characterization of a proteolytic peptide map can be used to identify new peptides following treatment with a cross-linker (Giorgianni et al., 1997).

Both of the classical approaches of isolating cross-links will fail when both the chemical mechanism of cross-linking is uncertain and the identity of the cross-linked proteins uncertain or derived from impure biological matrixes rendering the peptide maps inherently irreproducible. In this contribution, we describe a method and demonstrate its implementation at isolating an ensemble of cross-linked peptides to permit their further characterization by other analytical methods. This procedure, shown in concept in Scheme 1, relies on the obvious premise that cross-linked peptides will contain two α-amino groups while all other peptides will contain at most one α-amino group. To prevent the ϵ-amino groups of lysine from confounding the analysis, these amino groups must be derivatized prior to the proteolytic generation of the cross-linked peptides. A conceptually similar approach was taken by Jue and Doolittle (1985) to label the N-terminus of peptides.

The N-terminal derivatization suggested in Scheme 1 has three essential requirements: (1) the derivatization must be close to quantitative; (2) the product must permit the separation of peptides that contain one derivative from the cross-linked peptides which contain two of the derivatives, independent of what amino acid side chains are present in the peptide; and (3) the chemistry must result in the derivatization of only the α-amino group. In this contribution, we demonstrate that the *N*-hydroxysuccinimidyl ester of poly(ethylene glycol) succinate fulfills these three requirements and permits the universal isolation of cross-linked peptides.

MATERIALS AND METHODS

Chemicals. The methoxypoly(ethylene glycol)$_{5000}$ succinyl hydroxysuccinimide (PEG-*O-succinyl-O*−*Su*)[1] was purchased from Shearwater Polymers Inc. Sodium cyanoborohydride, succinic anhydride, chymotrypsin, Pronase, fluorescamine, sodium sulfite, bismuth nitrate, 5,5′-dithio bis(2-nitrobenzoic acid) (DTNB), trinitrobenzenesulfonate (TNBS), dithiothreitol (DTT), bovine insulin, and all amino acids, peptides, and buffers were purchased from Sigma Chemical Co. Potassium iodide

* To whom correspondence should be addressed. E-mail: anderson@biochemistry.cwru.edu. Phone: 216-368-2599. Fax: 216-368-3419.

† These two authors contributed equally to the experimental work and primary authorship of this paper.

‡ Department of Biochemistry, Case Western Reserve University School of Medicine.

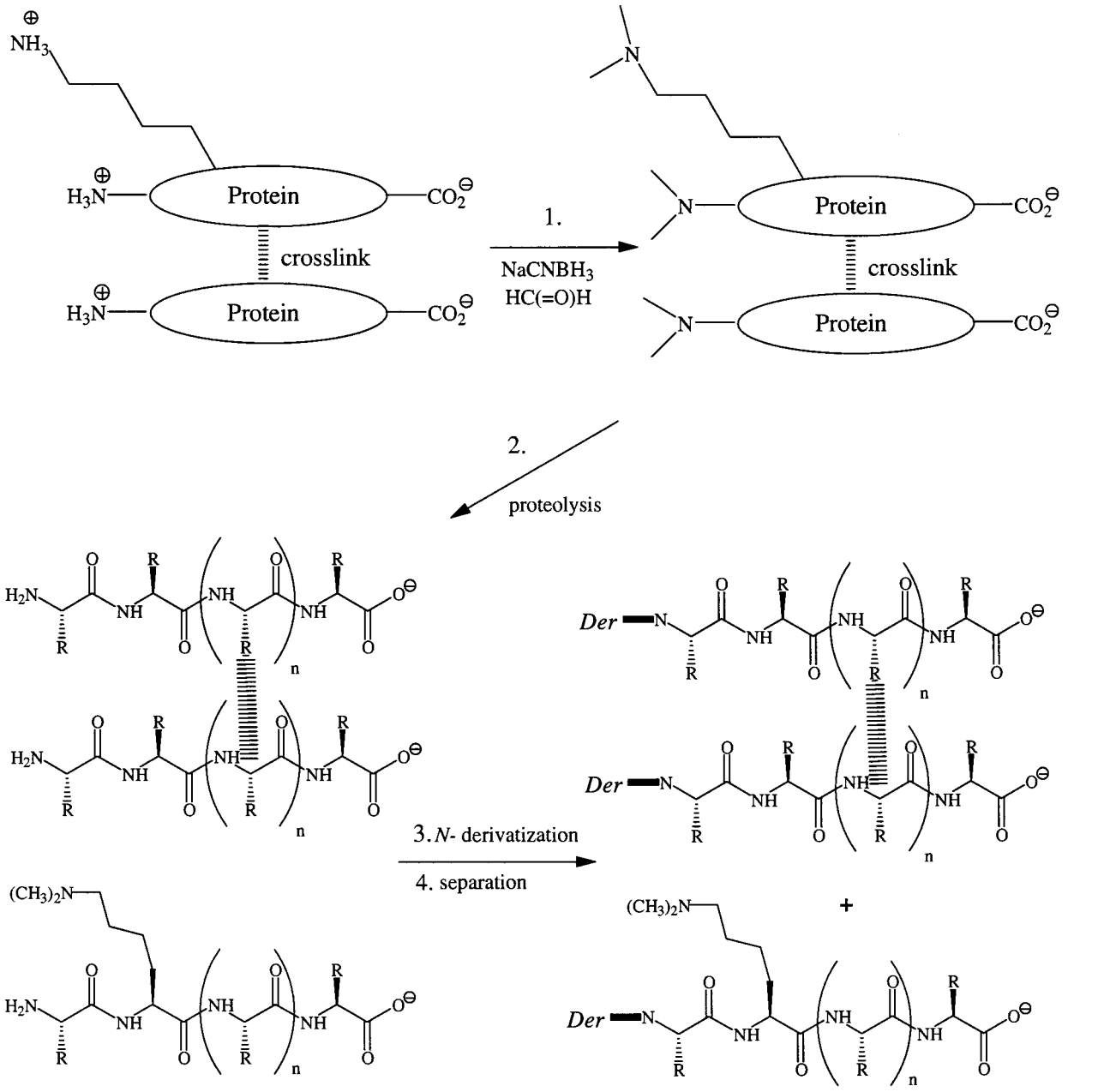
|| Current address: 182 St. Mary's Rd., Apt 1A, R.A. Puram, Chennai 600028, India.

§ Department of Pathology, Case Western Reserve University School of Medicine.

[1] Abbreviations: DTNB, 5,5-dithio bis(2-nitrobenzoic acid); DTT, dithiothreitol; MDC−Hb2, β1-Lys82-N_ϵ trimesyl β2-Lys82-N_ϵ 5-(*N*′-dansyl cadaverine) cross-linked hemoglobin; NTB, 2-nitro-5-thiobenzoate; NTSB, 2-nitro-5-thiosulfobenzoate; PEG-*O-succinyl-O*−*Su*, methoxypoly(ethylene glycol)succinyl hydroxysuccinimide; SDS, sodium dodecyl sulfate.

10.1021/bc980098v CCC: $18.00 © 1999 American Chemical Society
Published on Web 12/18/1998

Scheme 1

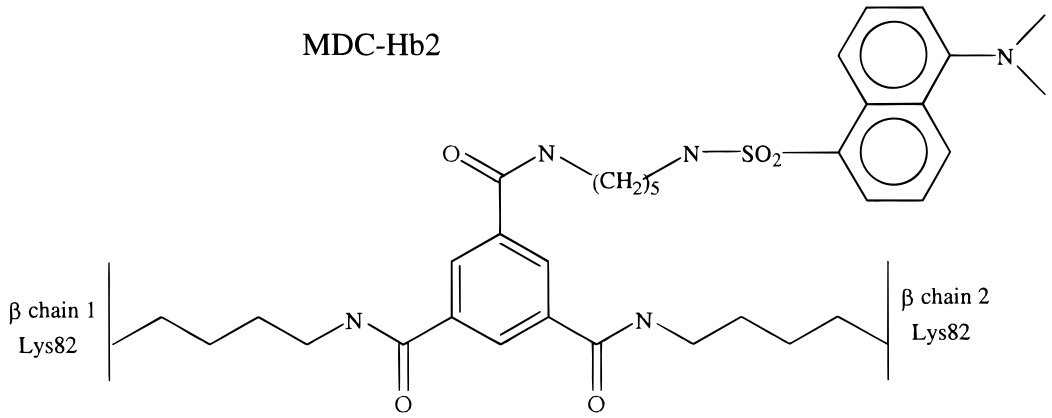


was purchased from Aldrich Chemical Co. Hydroxylamine hydrochloride, acetic anhydride, ammonium acetate, sodium phosphate, sodium sulfate, sodium sulfite, sodium borate, sodium hydroxide, concentrated HCl, formaldehyde, acetone, and acetonitrile were purchased from Fisher Scientific. 2-Nitro-5-thiosulfobenzoate (NTSB) was synthesized as previously decribed (Thannhauser et al., 1987). Superdex 200 PG gel and PD-10 desalting columns were purchased from Pharmacia Biotech. Brain samples of cases of Alzheimer's disease case were from the CWRU brain bank. Hemoglobin was obtained from Dr. K. Magnus (Department of Biochemistry, CWRU). Hemoglobin cross-linked with a fluorescent cross-linker, MDC−Hb2 shown in Scheme 2, was a generous gift from Hemosol Inc. (Etobicoke, Canada) (Jones et al., 1993; Kluger et al., 1992; Schumacher et al., 1995).

Insoluble Paired Helical Filaments and Control Fractions. Hippocampus and temporal cortex with meninges and white matter removed from a case of Alzheimer's disease (77 year old) was homogenized in 5 vol of 50 mM Tris-HCl, pH 7.6 (buffer A), with 0.1 g of sodium dodecyl sulfate (SDS)/g of wet tissue. After centrifugation at 10000*g* for 4 h at 22 °C, the supernatant was removed, and the pellet was rehomogenized in buffer A with 1% SDS. After centrifugation at 25000*g* for 1 h, the pellet was again homogenized in buffer A with 1% SDS and 10% sucrose, layered over a gradient of 1.0, 1.2, and 2.0 M sucrose/buffer A, and centrifuged for 1 h at 72000*g*. The insoluble paired helical filament fraction at the 1.2−2.0 M interface was used in further experiments.

Gel Filtration Chromatography. A 420 mL Superdex 200 PG gel in a Pharmacia XK 26/100 column was used for most separations. In some early experiments, a 320 mL Pharmacia 26/60 HiLoad Superdex 200 PG gel filtration column was used. Constant flow was maintained with a Pharmacia P-500 FPLC system and the column effluent monitored with a 20 μL flow cell in an HP 8452A diode array spectrophotometer and constant volume fractions collected in an Isco Retriever II fraction collector.

Scheme 2



Modification of the Amino Group of the Cross-Linked Protein. Initial protection of protein lysine ϵ-amino groups as shown in Scheme 1 was accomplished by acetylation, succinylation, or reductive methylation, which proved to be most useful. Acetylation was accomplished by infusion of acetic anhydride at a flow rate of 0.9 μL/min using a syringe pump, into 1 mL of solution containing 1−3 mg of protein in 0.1 M phosphate buffer at pH 8.0 until a final concentration of 150 mM was achieved. The infusion procedure permitted the pH to be held constant at 8.0 by the manual dropwise addition of 1 M NaOH. Succinylation, after the method of Kooistra et al. (Kooistra et al., 1979), was achieved by addition of 1 mg of solid succinic anhydride to a 1 mL of solution containing 1−2 mg of protein in 0.1 M phosphate buffer at pH 8.0 with constant stirring. The pH of the solution dropped to 5.5, after 12 min, it was increased to 8.0 by titration with 1 M NaOH. Then, another addition of succinic anhydride was performed. This process was repeated for a total of five additions. The pH was increased to 8.0 at the end of each 12 min interval. Reductive methylation followed the procedure of Jentoft and Dearborn (1983). Formaldehyde and sodium cyanoborohydride were both added to a 1 mg/mL protein solution in 50 mM sodium phosphate buffer, pH 7.0, to final concentrations of 10 mM, and the was reaction allowed to proceed at ambient temperature for 24 h. The mixture was then dialyzed extensively against 0.2 M sodium phosphate buffer, pH 8.0, or alternatively desalted by elution with water through a PD-10 desalting column, preequilibrated with water.

The extent of the amino group modification was determined by detection of residual primary amines using a TNBS assay (Snyder and Sobocinski, 1975) or in later experiments with the more sensitive fluorescamine assay (Udenfriend et al., 1972).

Protease Digestion. The N-modified and desalted protein was then cleaved with the proteases chymotrypsin and Pronase to generate free amino termini. Except where noted, chymotrypsin was added first in a 1:50 (w:w) protease-to-protein ratio. The cleavage reaction was incubated for 5 h at 37 °C. Pronase was then added to the protein solution in a 1:50 (w:w) protease-to-protein ratio and incubated for 24 h at 37 °C. For the brain sample solution, only Pronase was added in a 1:25 (w:w) protease-to-protein ratio and incubated for 30 h at 37 °C.

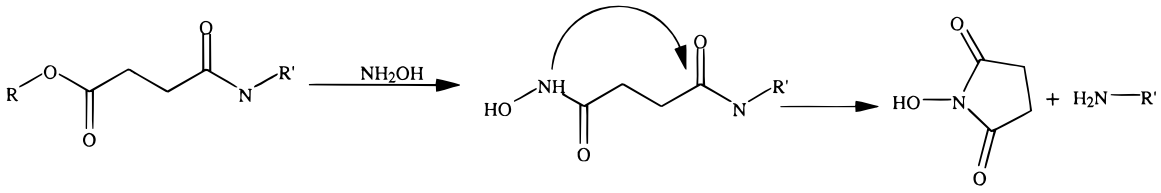
Derivatization of the Proteolytically Liberated Peptide N-Termini with PEG-O-succinyl-O−Su. Following proteolysis, solid PEG-*O-succinyl-O−Su* was added into the above peptide solution with constant stirring to produce a concentration of 10 mg/mL. After 15 min, approximately 4 μL of 1 M NaOH was added to raise the pH back to 8.0. Then, an additional 10 mg/mL of PEG-*O-succinyl-O−Su* was added. This process was repeated to a total of seven PEG-*O-succinyl-O−Su* additions (final concentration of 70 mg/mL). The pH of the solution was increased to 8.0 by titration with 1 M NaOH at the end of each 15 min reaction.

Selective Hydrolysis of PEG-O-succinyl-O-Tyr. The modification of tyrosine with PEG-*O-succinyl-O−Su* revealed that the phenoxyl group of the side chain is derivatized to a small extent, forming the PEG-*O-succinyl-O*-Tyr phenyl ester. To unambiguously identify the doubly labeled peptides as cross-linked peptides, it is imperative to remove the PEG-*O-succinyl* tag from the side chain of tyrosine residues. After derivatizing the peptides with PEG-*O-succinyl-O−Su*, as described above, the phenyl ester linkage in PEG-*O-succinyl-O-Tyr* moiety was selectively hydrolyzed by titration to pH 11 with saturated trisodium phosphate. The reaction mixture was maintained at pH 11 for 30 min at ambient temperature and the reaction stopped by reducing the pH to 8.0 with acetic acid. This mild alkaline hydrolysis additionally hydrolyzes PEG-*O-succinyl-S−Cys* thiolesters but unfortunately will also cleave disulfide bonds. However, it does not hydrolyze the PEG-*O-succinyl* oxygen ester.

Separation of Peptides Containing either One or Two PEG_{5000} Chains. The PEG-*O-succinyl-O−Su* derivatized peptides were separated on a Pharmacia XK26/100 Superdex 200 PG gel filtration column, preequilibrated with 50 mM ammonium acetate, pH 5.0, and eluted with the same buffer. The PEG-*O-succinyl-O−Su* derivatized peptides (1 mL) were injected, and eluted at 1 mL/min, collecting 4 mL fractions. The gel filtration column was calibrated with PEG-*O-succinyl-O−Su* derivatized tryptophan and lysine nitroanilide which served as models for peptides containing either one or two PEG_{5000} chains, respectively. The tryptophan and lysine nitroanilide derivatives could be identified by their UV absorbance at 280 and 318 nm, respectively.

Quantitation of Disulfide Bonds. Fractions from the Superdex gel chromatography could be analyzed for disulfide bonds employing a 2-nitro-5-thiosulfobenzoate (NTSB) assay (Thannhauser et al., 1987). From each fraction, 1 mL was taken to dryness in a centrifugal vacuum concentrator, redissolved in 20 μL of water, and added into a 300 μL of NTSB assay solution, consisting of 250 μM NTSB, 50 mM glycine, 100 mM sodium sulfite, and 3 mM EDTA. The concentration of disulfide bonds

Scheme 3



was calculated from the increase in the 2-nitro-5-thiobenzoate (NTB) absorbance at 412 nm, $\epsilon_{412} = 13\ 600\ M^{-1}\ cm^{-1}$.

Hydroxaminolysis of PEG-O-succinyl-N-peptide. To permit further analysis of the fractions containing peptides with two PEG_{5000} chains, it is useful to be able to remove the N-terminal PEG-*O-succinyl* label. The treatment of the PEG-*O-succinyl*-labeled peptides with hydroxylamine, cleaves the PEG-*O-succinyl* ester, and the HONH-*succinyl-N*-peptide subsequently cyclizes releasing *N*-hydroxysuccinimide and the peptide with an unblocked amino terminus as shown in Scheme 3.

This cyclization of succinyl hydroxamate with cleavage of an amide is a known facile reaction (Notari, 1969). The reaction was monitored by following the release of ionized *N*-hydroxysuccinimide, $\lambda_{max} = 260$ nm. To effect this cleavage, *N*,*N*′-(PEG-*O-succinyl*)$_2$glutathione was isolated by chromatography and solid hydroxylamine was added to a final concentration of 0.8 M. The pH was adjusted to 9.5 with 1 M NaOH, and the reaction mixture held at 40 °C for 2 h (Notari, 1969). To analyze the time course of reaction, aliquots of the reaction at 30 min intervals up to 2 h were analyzed by gel filtration HPLC using a 30 cm Phenomenex Biosep SEC S2000 column eluted with 100 mM ammonium acetate buffer, pH 5, at a flow rate of 1 mL/min. The eluate was monitored at 280 nm and each 1 mL fraction analyzed for the presence of PEG by the addition of an equal volume of Dragendorff's reagent (0.11 M potassium iodide and 0.6 mM bismuth nitrate in 3.5 M acetic acid) (Rubia and Gomez, 1977) which generates an orange solution ($\lambda_{max} = 524$ nm) or precipitate in the presence of PEG.

Desalting Cross-Linked Peptides. Following hydroxaminolysis, the reaction mixture contained newly regenerated peptides, ammonium acetate, PEG_{5000}, hydroxylamine, and N-hydroxysuccinimide. To remove the PEG_{5000} and the excess hydroxylamine prior to further analysis, the solution was fractionated using a 1 g C_{18} solid-phase extraction column washed with 10 mL of 1 M sodium sulfate and 2 mL of water and eluted with 50% acetonitrile. Solid sodium sulfate was added to the peptide solution to a final concentration of 1 M prior to being loaded onto the solid-phase extraction column. Hydroxylamine and PEG_{5000} were removed by the wash, and the peptides were eluted in an elution volume of 1.5−2 mL of 50% acetonitrile.

RESULTS

Protection of ϵ-Amino Groups. Quantitative derivatization of lysine ϵ-amino groups has been accomplished by many procedures. In our hands, the best procedure was reductive methylation. This procedure had the benefits of retaining the positive charge for solubility while only chemically altering the protein amines, leaving Cys, His, and Tyr residues unmodified. To demonstrate that the conditions chosen successfully derivatized all of the ϵ-amino groups, lysozyme was chosen as a test protein. Following reductive methylation, less than 1% of the initially present amino groups was detected by fluorescamine assay. In all protein methylations monitored, the reaction with fluorescamine decreased by at least 99%. In the presence of aggregates, the potential exists that ϵ-amino groups could be inaccessible to both methylation and fluorescamine. However, extensive reaction times and elevated temperatures should prevent this from being a difficulty.

Derivatization of Amino Termini with PEG-O-succinyl-O−Su. The derivatization of the proteolytically generated α-amino groups was moderately successful. The aqueous derivatization with a hydroxysuccinimide ester represents a competition between hydrolysis and aminolysis. The pH of this reaction is the crucial parameter, lowering the pH makes the reaction more specific for amines and decreases the rate constant for hydrolysis at the price of increasing the required reaction time. We adopted a repetitive addition, titration scheme to neutralize the acid generated during hydrolysis of the excess reagent. In favorable cases, this repetitive procedure derivatized over 90% and, in the worst case, 70% of the amino groups, corresponding to a predicted complete derivatization of at least half of all cross-linked peptides.

Hydrolysis of PEG-O−Suc-O-Tyr. Control reactions with tyrosine indicated that some O-esterification of tyrosine with PEG-*O−succinyl-O−Su* occurred at pH 8.0. To define conditions required to hydrolyze PEG-*O−succinyl-O-Tyr*, the peptide YGGFL was intentionally N- and O-derivatized by raising the pH of the derivatization reaction. The O-Tyr ester hydrolysis can be monitored by following the appearance of tyrosine phenoxide at 292 nm (Edelhoch, 1967) and was shown to be complete in 30 min at pH 11. This mild alkaline hydrolysis effectively cleaves both phenyl and thiolesters while leaving the PEG-*O−Suc-N-peptide* ester and amide linkages uncleaved. Any histidine derivatization would generate an unstable acyl-imidazole that hydrolyzes at neutral pH.

Protein Hydrolysis. Proteolytic treatment with Pronase generates very small cross-linked peptides as it has endopeptidase activity as well as exopeptidase peptidase activities (Narahashi and Yanagita, 1967) which permits small modified peptides to be isolated (Catley et al., 1969). The use of more specific proteases such as trypsin will generate larger peptides that retain more sequence information. In our standard procedure the initial cleavage with chymotrypsin was introduced to enhance the efficacy of the Pronase cleavage.

Separation of Doubly and Singly Derivatized Peptides. The gel filtration separation of lysine nitroanilide and tryptophan derivatized with PEG-*O-succinyl-O−Su* on this column is shown in Figure 1. Lysine nitroanilide derivatized with two PEG_{5000} chains eluted between 239 and 277 mL and the tryptophan derivative containing a single PEG_{5000} chain eluted between 277 and 332 mL on the Superdex XK26/100 column. The elution volumes for peptides containing either one or two PEG_{5000} chains were relatively consistent and had a resolution of 1.2−1.3. These elution volumes compare to that of a globular protein with an M_r of 5−10 times the nominal molecular weight of the polymer. Insulin with three amino groups,

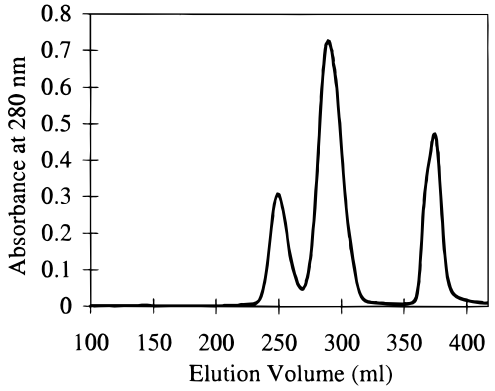


Figure 1. Gel filtration chromatogram of PEG-*O-succinyl-N*-Trp and N_α,N_ϵ-bis(PEG-*O*-succinyl-)lysine nitroanilide as singly and doubly labeled calibrators on an XK 26/100 Superdex 200PG column. The elution volumes of the tryptophan and lysine derivatives define the volumes for the elution of peptides containing either one or two PEG_{5000} chains, respectively. UV analysis of the fractions indicated that the first peak contained only the lysine derivative, the second peak contained the tryptophan derivative and the third peak was largely hydroxysuccinimide.

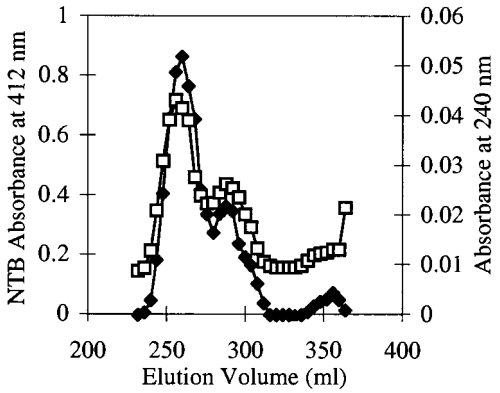


Figure 2. Gel filtration chromatogram of N_α,N_a'-bis(PEG-*O-succinyl*)glutathione by an XK 26/100 Superdex 200 PG column with the fractions monitored either by UV absorbance at 240 nm (□) or by using the NTSB assay for disulfide bonds (◆).

was derivatized with PEG-*O-succinyl-O−Su*. The triply derivatized insulin eluted well before the lysine nitroanilide standard. This early eluting triply labeled species was pooled, reduced with DTT, and then rechromatographed on the same gel filtration column. Two peaks were observed, one from the doubly labeled β-chain (the amino terminus and carboxy terminal lysine would both be derivatized) eluted and the other from the singly labeled α-chain. The coelution of the PEG-*O-succinyl*-derivative of the 21 amino acid insulin α-chain with the singly labeled standards suggests that the size of the derivatized oligopeptide will not significantly alter the chromatographic behavior of the PEG-*O-succinyl*-peptides.

Glutathione was used for the studies of both column recovery and derivatization efficiency. Glutathione was derivatized with PEG-*O-succinyl-O−Su* as described in the Materials and Methods. Derivatized glutathione was then chromatographed on the Superdex XK26/100 column. Using the NTSB assay for disulfide bonds, the recovery of cross-linked peptides was determined to be greater than 80%. The result with NTSB also showed that doubly labeled glutathione eluted between 236 and 276 mL and singly labeled glutathione eluted between 276 and 316 mL (Figure 2). The ratio of doubly labeled: singly labeled glutathione was 2.3:1. Thus, the efficiency

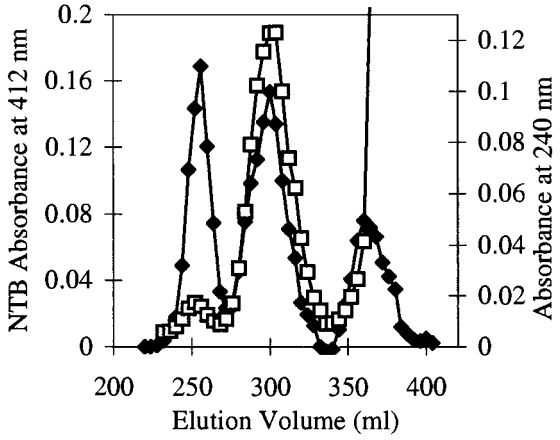


Figure 3. Gel filtration chromatogram of reductively methylated lysozyme, proteolytically digested, and derivatized with PEG-*O-succinyl-O−Su* monitored at 240 nm (□) or by NTSB assay for disulfide bonds (◆).

of derivatization of the glutathione amines was 85%. The pK_a of the α-amino group of glutathione of 8.5 is higher than expected for the α-amino peptides, so that the efficiency of derivatization of the α-amino groups of peptides at pH 8.0 might be anticipated to be better. The incomplete derivatization results from the competitive hydrolysis of PEG-*O-succinyl-O−Su* by water. While more complete derivatization might be anticipated with additional PEG-*O-succinyl-O−Su*, higher concentrations of PEG_{5000} become counterproductive in the subsequent chromatographic separation. The requirement for excess derivatizing reagent made it difficult to use an affinity matrix with their attendant low capacities for the chromatographic resolution singly and doubly labeled peptides.

Hydroxaminolytic Liberation of Cross-Linked Peptides from PEG-O-succinyl-N-peptide. Removal of PEG-*O-succinyl* moiety is desirable for planned sequencing studies of cross-linked peptides by Edman degradation or by mass spectrometry. Hydroxaminolysis was shown to remove the PEG-*O-succinyl* label from the derivatized peptides, as depicted in Scheme 3. The peptide MeOSuc-Ala-Ala-Pro-Val was used as a standard to determine the required reaction conditions. With peptides, the cleavage was additionally demonstrated by separating the liberated peptide from the polymeric PEG. Doubly labeled *N*,*N*′-(PEG-*O-succinyl*)$_2$-glutathione was subjected to hydroxaminolysis, and the products separated by HPLC gel filtration. Following hydroxaminolysis, the PEG elution volume increased from 11 to 13 min, consistent with the release from the doubly labeled peptide with a nominal M_r in excess of 10 000 to the elution volume of a standard monomeric PEG_{5000} while the glutathione eluted in the included volume. Analyses at varying times were consistent with the spectrophotometric studies, indicating that the hydroxaminolysis was complete in under 1 h.

Lysozyme. Lysozyme is cross-linked by four disulfide bonds. To demonstrate the method, peptides cross-linked by disulfides were isolated by the protocol outlined in Scheme 1. Lysozyme was methylated and desalted as described, digested with chymotrypsin and Pronase, and derivatized with PEG-*O-succinyl-O−Su*. The gel filtration chromatogram of the lysozyme derived peptides is shown in Figure 3. Each fraction was concentrated and then tested for disulfide bonds by using the NTSB assay. The ratio of underivatized: singly labeled: doubly labeled peptides was 2:2.1:1.5 based on the NTSB assay. The

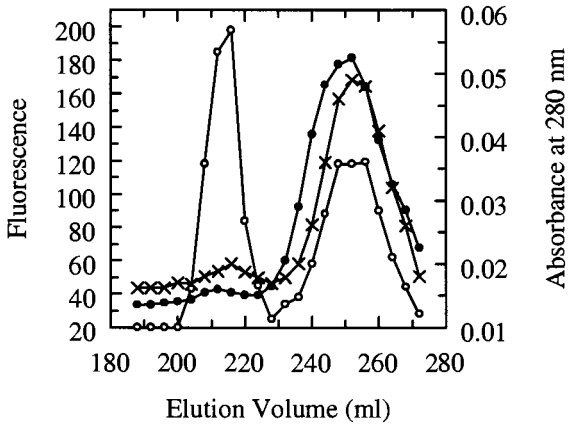


Figure 4. Gel filtration chromatograms of cross-linked and un-cross-linked hemoglobin by 26/60 Hiload Superdex 200 PG column, following reductive methylation, digestion with chymotrypsin and Pronase, and derivatization with PEG-*O-succinyl-O−Su*, followed by mild alkaline hydrolysis. The column fractions of the derivatized un-cross-linked hemoglobin peptides were monitored at 280 nm (×). The fractions of the derivatized cross-linked hemoglobin peptides were monitored by both UV at 280 nm (●) and the dansyl fluorescence at 550 nm (○) with excitation at 340 nm. The major fluorescent peak eluting around 215 mL elutes corresponds to the elution volume of peptides containing two PEG_{5000} chains by this column.

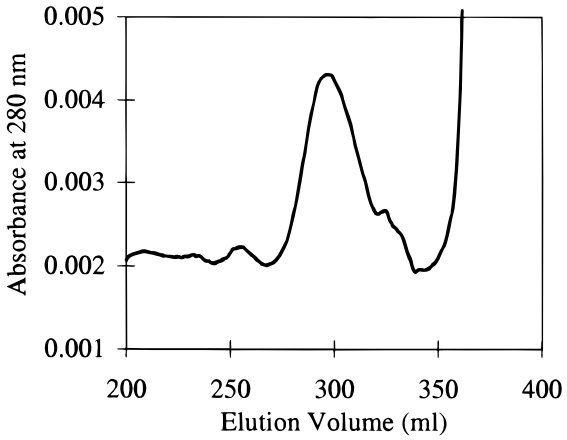


Figure 5. Gel filtration chromatogram of protein isolated from neurofibrillary tangles from Alzheimer disease that was reductively methylated, Pronase digested, PEG-*O-succinyl-O−Su* derivatized, and finally subjected to mild alkaline hydrolysis. The peptides eluted are monitored by absorbance at 280 nm. The peak eluting at 250 mL, elutes at the position expected for cross-linked peptides but not linear peptides. Unlike the previous examples this peak is small when compared to the monomeric fraction eluting at 300 mL because the cross-link is unknown and cannot be specifically detected.

apparent lower yield based on disulfide bonds, when compared with that of glutathione, may result from (1) free thiols generation from the cleavage of disulfide bonds since NTSB assay detects both free thiol and disulfide and (2) incomplete proteolysis. An inherent requirement of the protocol is that the proteolysis generates a new α-amino group in the sequence prior to the amino acid whose side chain participates in the cross-link. In lysozyme, Cys-6 forms a disulfide bond with Cys-127. To isolate a peptide with this cross-link, the proteolysis must cleave the peptide backbone before Cys-6 and between Cys-115 and Cys-127. Failure to proteolytically cleave before Cys-6 would result in cross-linked peptide with only one α-amino group because the N-terminal of lysozyme has been blocked by dimethylation. Thus, the apparent low efficiency may be a function both of disulfide cleavage and incomplete proteolysis. Even with this difficulty, this chromatogram clearly demonstrates the potential separation of a pool of cross-linked peptides obtained from a protein with intramolecular cross-links.

Hemoglobin. MDC−Hb2 (shown in Scheme 2) and control human hemoglobin were both treated according to Scheme 1 as follows: reductive methylation, desalting of protein, proteolytic digestion with chymotrypsin and Pronase, PEG-*O-succinyl-O−Su* derivatization, mild alkaline hydrolysis of labile PEG_{5000} esters, gel filtration chromatography, and fluorescent measurement of the collected fractions. The chromatograms of the cross-linked hemoglobin (3 mg) and un-cross-linked hemoglobin (3 mg) produced by monitoring the fluorescence at 550 nm with excitation at 340 nm and by monitoring the absorbance at 280 nm are shown in Figure 4. The peptides generated from proteolytic digestion of the cross-linked hemoglobin were separated by gel filtration column into three peaks, doubly labeled, singly labeled and underivatized peptides in the order of increased retention time. From the fluorescence assay of the fractions, it is obvious that the cross-linked peptide containing the dansyl group was concentrated in the first peak. This particular cross-linked protein was selected because (1) there is a single cross-link per 68 kDa hemoglobin tetramer and (2) the dansyl moiety on the cross-link can be identified by monitoring fluorescence, permitting the spectral identification of cross-linked peptides and their separation to be monitored.

In the control experiment, un-cross-linked hemoglobin was treated according to the same procedure. The chromatogram monitored by UV absorbance at 280 nm showed only one peak at the same retention time of the peptides containing a single PEG_{5000} chain, indicating that the protocol does not produce false positive signals by incorporation of two PEG_{5000} chains by unanticipated derivatization of amino acid side chains.

Insoluble Paired Helical Filaments of Alzheimer's Disease. An enriched fraction of paired helical filaments, the component structures of neurofibrillary tangles, from a case of Alzheimer's disease containing 0.4 mg of protein was treated by using the same procedure as for hemoglobin, except the fluorescence analysis of the chromatographic fractions was not required. The chromatogram obtained monitoring absorbance at 280 nm to detect peptides containing aromatic residues is shown in Figure 5. The peak with elution volume of 240−268 mL was that of the peptides containing two PEG_{5000} chains and are presumptively cross-linked peptides derived from neurofibrillary tangles. There were no disulfide bonds or free thiols detected in these fractions using the NTSB and DTNB assays, respectively. Therefore, the identification of peptides derivatized with two PEG_{5000} chains is suggestive of the existence of cross-link(s) in the neurofibrillary tangles. Further characterization of these putative cross-link(s) is being undertaken by mass spectrometry. Hydroxaminolysis will liberate the parent peptides and permit the reversed-phase HPLC-mass spectrometric characterization of this pool of peptides in our laboratory.

DISCUSSION

Cross-linking has proven to be a powerful method of studying protein structure, by demonstrating that the two cross-linked groups must, for the chemical reaction to have occurred, have been in close proximity. While cross-linked peptides can be identified when a control peptide map exists or when the cross-linker contains a detectable marker, neither of these restrictions applies when cross-linked peptides are sought from a biological

sample cross-linked by unknown processes. Scheme 1 presented a conceptual approach to isolating cross-linked peptides independent of the chemical nature or origin of the cross-link. All of the chemistry proposed is precedented and was substantiated in the studies reported.

The main issue presented in Scheme 1 is the selection of an amine-derivatizing reagent that will quantitatively react with the α-amino groups, including the secondary amine of proline, liberated by the partial hydrolysis of the protein backbone. Our initial concept was to use myristoyl isothiocyanate, as the development of Edman degradation has substantiated that derivatization of the amino terminal group with isothiocyanates can be quantitative and yet easily removed by acid-catalyzed cyclization. We envisioned a separation based on reversed-phase HPLC. The difficulties of peptide solubility both before and after derivatization prevented the realization of this approach. The choice of PEG-*O-succinyl-O−Su* as the derivatizing reagent was in response to difficulties in maintaining peptide and reagent solubility. The PEG_{5000} chain is miscible with water and imparts enhanced aqueous solubility to derivatized peptides and minimizes interactions with the gel filtration matrix. Alternative derivatization conditions or reactive PEG_{5000} substituent may permit an increase in the efficiency of the derivatization conditions. Incorporation of a radioactive label into the PEG, e.g., using [^{14}C]succinic anhydride to form the succinate ester, would permit the described assay to become a method of quantifying the isolated cross-links.

The second major consideration in Scheme 1 is the choice of proteolytic conditions. As noted, one of the virtues of reductive methylation of the ϵ-amino groups is that this derivatization is stable to acid hydrolysis. Thus, quantitative hydrolysis with 6 N HCl or weak acid hydrolysis would be possible, allowing the described method to isolate all acid-stable cross-links. This is potentially an important virtue for handling insoluble protein aggregates. A similar method exists based on α-amino acids ability to chelate diphenylborinic acid (Graham and Gallop, 1994). However, this approach has the absolute requirement that the protein be hydrolyzed completely to its constituent amino acids, preventing any sequence information from being retained in the cross-linked peptides.

Conclusion. A protocol has been proposed that permits the isolation of cross-linked peptides independent of the chemical nature of the cross-link. The validity of the key premise of this scheme, that the two amino termini of cross-linked peptides can be derivatized to permit separation from linear peptides, has been clearly demonstrated. Separation of PEG-*O-succinyl-O−Su*-derivatized peptides by gel filtration chromatography has been shown capable of isolating disulfide-bond cross-links from proteins of known sequence, a single fluorescent cross-linked peptide from the large number of proteolytic peptides of hemoglobin, and most provocatively, a potential pool of cross-linked peptides isolated from neurofibrillary tangles obtained from an Alzheimer's disease brain.

ACKNOWLEDGMENT

This publication was supported in part by NIH Grant AG-14249.

LITERATURE CITED

Catley, B. J., Moore, S., and Stein, W. H. (1969) *J. Biol. Chem. 244*, 933−936.
Cervoni, L., Ferraro, A., Giartosio, A., Wang, C., and Turano, C. (1994) *Arch. Biochem. Biophys. 311*, 35−41.
Darby, N., and Creighton, T. E. (1995) *Methods Mol. Biol. 40*, 219−252.
Darby, N., and Creighton, T. E. (1997) *Mol. Biotech. 7*, 57−77.
Edelhoch, H. (1967) *Biochemistry 6*, 1948−1954.
Giorgianni, F., Beranova, S., Wesdemiotis, C., and Viola, R. E. (1997) *Arch. Biochem. Biophys. 341*, 329−336.
Graham, L., and Gallop, P. M. (1994) *Anal. Biochem. 217*, 298−305.
Jentoft, N., and Dearborn, D. G. (1983) *Methods Enzymol. 91*, 570−579.
Jones, R. T., Head, C. G., Fujita, T. S., Shih, D. T., Wodzinska, J., and Kluger, R. (1993) *Biochemistry 32*, 215−223.
Jue, R. A., and Doolittle, R. F. (1985) *Biochemistry 24*, 162−170.
Kluger, R., Wodzinska, J., Jones, R. T., Head, C., Fujita, T. S., and Shih, D. T. (1992) *Biochemistry 31*, 7551−7559.
Kooistra, T., Duursma, A. M., Bijsterbosch, M. K., Bouma, J. M., and Gruber, M. (1979) *Biochim. Biophys. Acta 587*, 299−311.
Mornet, D., Ue, K., and Morales, M. F. (1985) *Proc. Natl. Acad. Sci. U.S.A. 82*, 1658−62.
Munch, G., Mayer, S., Michaelis, J., Hipkiss, A. R., Riederer, P., Muller, R., Neumann, A., Schinzel, R., and Cunningham, A. M. (1997) *Biochim. Biophys. Acta 1360*, 17−29.
Narahashi, Y., and Yanagita, M. (1967) *J. Biochem. (Tokyo) 62*, 633−641.
Notari, R. E. (1969) *J. Pharm. Sci. 58*, 1069−73.
Rubia, L. B., and Gomez, R. (1977) *J. Pharm. Sci. 66*, 1656−1657.
Ryle, A. P., Sanger, F., Smith, L. F., and Kitai, R. (1955) *Biochem. J. 60*, 541.
Schumacher, M. A., Dixon, M. M., Kluger, R., Jones, R. T., and Brennan, R. G. (1995) *Nature 375*, 84−87.
Smith, C. D., Carney, J. M., Starke-Reed, P. E., Oliver, C. N., Stadtman, E. R., Floyd, R. A., and Markesbery, W. R. (1991) *Proc. Natl. Acad. Sci. U.S.A. 88*, 10540−10543.
Snyder, S. L., and Sobocinski, P. Z. (1975) *Anal. Biochem. 64*, 284−288.
Thannhauser, T. W., Konishi, Y., and Scheraga, H. A. (1987) *Methods Enzymol. 143*, 115−119.
Udenfriend, S., Stein, S., Bohlen, P., Dairman, W., Leimgruber, W., and Weigele, M. (1972) *Science 178*, 871−872.
Wells, J. A., and Yount, R. G. (1979) *Proc. Natl. Acad. Sci. U.S.A. 76*, 4966−7490.

BC980098V

Integrated "3+1" Oxorhenium(V) Complexes as Estrogen Mimics

Marc B. Skaddan, and John A. Katzenellenbogen*

Department of Chemistry, University of Illinois, 600 S. Mathews Avenue, Urbana, Illinois 61801.
Received August 19, 1998; Revised Manuscript Received October 7, 1998

The diagnosis and staging of breast cancer could be improved by the development of imaging radiopharmaceuticals that provide a noninvasive determination of the estrogen receptor (ER) status of tumor cells. Toward this goal, we have synthesized a number of integrated "3+1" oxorhenium(V) complexes designed to mimic estradiol and a class of nonsteroidal estrogens, the tetrahydrochrysenes (THC). The monodentate component of the estradiol mimic is a *p*-hydroxyphenethyl thiol ligand with ethyl substituents at the benzylic and homobenzylic positions. Model complexes of this ligand were easily made, but steric hindrance of the secondary thiol prevented the formation of the complex with the disubstituted ligand. The three "3+1" oxorhenium(V) complexes prepared to mimic the THC class mimics represent the first pyridinedithiol rhenium complexes of their kind to be made. These complexes are quite stable to air and moisture. The target tridentate ligand was prepared from chelidamic acid, and the VT NMR of the rhenium complex displays interesting fluxional behavior. The binding affinities of these complexes for the estrogen receptor are low, and their lipophilicities are rather high. Nevertheless, our findings provide a further refinement of our understanding of ligand structure-binding affinity correlations for the estrogen receptor.

INTRODUCTION

Metastatic breast cancer is the most prevalent form of cancer of women in the United States and is the number one killer of women ages 40−55 (*1*). Recent figures show that a woman's lifetime risk of developing breast cancer is 1 in 8 (*2*). Early detection is imperative for breast cancer survival, as the 5 year survival rate for localized breast cancer is 96% (*3*). However, if the cancer has spread regionally, the survival rate drops to 75%, and distant metastases further reduce the survival rate to 20% (*3*). Clearly, better diagnostic techniques for early detection would increase survival.

Breast cancers that retain estrogen receptor (ER)[1] can usually be treated effectively by endocrine therapy, such as the use of the antiestrogen tamoxifen. In fact, about 60% of ER+ patients respond to endocrine therapy, whereas the response of ER− patients is much lower (*4*). However, only 70% of breast cancers are ER+; so, it is important to be able to determine the ER status of each tumor.

Current methods used to determine the ER status of breast tumor cells are invasive and do not fully account for cell heterogeneity. One way to eliminate the invasiveness and minimize the heterogeneity problems of current tumor ER assays would be to image breast tumors based on their content of ER, using positron-emission tomography (PET) or single photon emission computed tomography (SPECT). These techniques utilize the emission characteristics of certain radionuclides attached to radiopharmaceuticals that have appropriate distribution properties to image tissues. Considerable advances have been made in the development of steroids labeled with either fluorine-18 for PET imaging (*5*−*16*) or iodine-123 for SPECT imaging (*5*, *17*−*21*) of ER+ breast tumors. However, the radionuclide of choice for breast tumor imaging would be Tc-99m, due to its convenient 6 h half-life and its wide availability.

We have been interested in the development of Tc-99m-containing steroid mimics for use as imaging agents for receptor-positive breast tumors. In the "conjugated" or "pendant" design, a Tc-99m containing moiety is tethered to an existing steroid, such as progesterone or estradiol (**1**) (*22*−*29*). Such complexes are generally stable, but their large overall size can greatly affect their physical properties and their affinity for steroid receptors (*22*, *29*). Smaller complexes are produced by the alternative "integrated" approach, in which part of the steroid backbone itself is replaced by the requisite Tc-99m chelate (*30*−*32*). One way to incorporate Tc-99m into such integrated complexes is via the "3+1" design, in which a tridentate and monodentate ligand surround an oxometal core (*33*). The advantage of such a design is the well-established stability of many "3+1" complexes themselves (*27*−*29*, *33*−*35*), compared with that of the related 2+2 complexes. In addition, appropriately designed "3+1" complexes lack syn and anti stereoisomers that are often produced in the tetradentate oxorhenium and technetium complexes.

We report here the synthesis of several "3+1" oxorhenium complexes that are in the series of the estradiol mimic **2** and the tetrahydrochrysene (THC) mimic **4** (Figure 1). The syntheses involve rhenium as the surrogate metal for Tc-99m (*36*). As is illustrated in Figure 1, estradiol mimic **2** would contain a tridentate aliphatic ligand (where the heteroatom X could be a sulfur, oxygen, or alkyl nitrogen), intended to mimic the D-ring of estradiol. The monodentate ligand is aromatic, with a 2 carbon "spacer" separating the phenyl ring from the thiol, and is intended to mimic the A, B, and C rings of estradiol. The THC mimic **4** involves thiophenol as the

* To whom correspondence should be addressed. Phone: (217) 333-6310. Fax: (217) 333-7325. E-mail: jkatzene@uiuc.edu.

[1] Abbreviations: ER, estrogen receptor; DHP, dihydropyran; MEM, methoxyethoxymethyl; MOPS, 3-morpholinopropanesulfonic acid; PET, positron emission tomography; RBA, receptor-binding affinity; SPECT, single photon emission computerized tomography; THC, tetrahydrochrysene.

10.1021/bc980094q CCC: $18.00 © 1999 American Chemical Society
Published on Web 12/11/1998

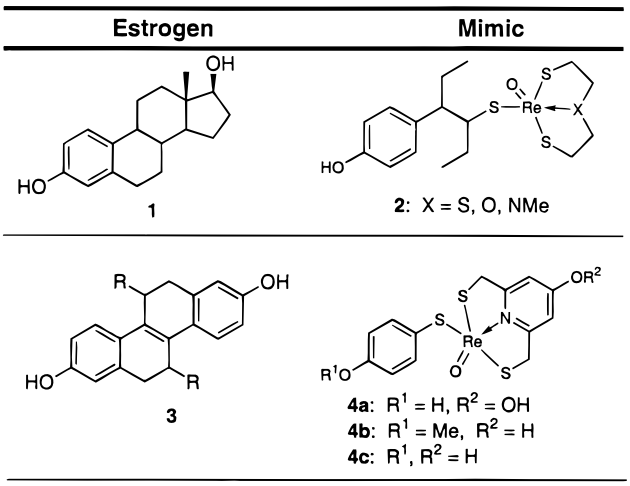


Figure 1. Estrogens and their mimics.

monodentate ligand and a unique pyridinedithiol as the tridentate ligand. In this case, both ligands are equally involved in mimicking the rings of THC.

EXPERIMENTAL SECTION

General. All reagents and solvents were obtained from Aldrich, Acros, Alfa Aesar, or Fisher. All reactions were performed under a nitrogen atmosphere unless otherwise indicated. THF was distilled from sodium/benzophenone immediately prior to use. Methylene chloride was distilled from CaH_2 prior to use. Triethylamine was dried by distillation from CaH_2 and stored over KOH. Dimethylformamide was distilled from and stored over 4 Å molecular sieves. MeOH was distilled from Mg/I_2 and stored over 3 Å molecular sieves. Hexanes were distilled from calcium sulfate (Drierite) before use in flash chromatography.

Reaction progress and flash chromatography was monitored by analytical thin-layer chromatography. Silica gel used in flash chromatography was 32−63 μm. Radial chromatography (Chromatotron, Harrison Research, model 7924T) was performed using a circular glass plate with a 2 mm depth of silica gel 60 PF_{254} (with gypsum). TLC plates were visualized using short-wave UV light (254 nm), potassium permanganate, or phosphomolybdic acid.

^1H and ^{13}C NMR were obtained at 400 or 500 MHz and are reported in parts per million relative to incomplete deuteration signals of $CDCl_3$, CD_3OD (CD_3 signal used), DMSO-d_6 or acetone-d_6. Mass spectra were obtained with a VG Instruments 70-VSE (EI, CI) or a VG Instruments ZAB−SE (FAB) mass spectrometer. Melting points are uncorrected. Elemental analyses were performed by the Microanalytical Service Laboratory of the University of Illinois.

4-Methoxyphenethyl Thioacetate (8a). MsCl (770 μL, 9.94 mmol) was added dropwise to a solution of 4-methoxyphenethyl alcohol (1.01 g, 6.63 mmol) and Et_3N (1.40 mL, 9.94 mmol) in THF (40 mL) at 0 °C. A white ppt of Et_3N hydrochloride formed immediately. The reaction was stirred for 1 h, at which time potassium thioacetate (2.27 g, 19.9 mmol) in DMF (10 mL) was added, resulting in an orange solution which turned red after several h. After 6 h, the reaction was stopped and concentrated, then dissolved in CH_2Cl_2 (60 mL). This was washed with saturated LiCl twice, followed by a wash with brine and then water (30 mL). The brine and water washes were separately back-extracted with CH_2Cl_2 (30 mL). The organics were then combined, dried over Na_2SO_4, filtered, and concentrated to a dark oil. Flash chromatography (60% CH_2Cl_2/PhH) and radial chromatography (30% EtOAc/Hex), followed by Kugelrohr distillation (125 °C, 0.9 mmHg) provided **8a** as a yellow oil (1.06 g, 76%). ^1H NMR ($CDCl_3$, 400 MHz): δ 2.33 (s, 3H, $-SCOCH_3$), 2.95 [ABq, J_{AB} = 7.3 Hz, $\Delta\upsilon$ = 119 Hz, 2H, $Ar(CH_2)_2SCOCH_3$], 2.95 [ABq, J_{AB} = 6.3 Hz, $\Delta\upsilon$ = 102 Hz, 2H, $Ar(CH_2)_2SCOCH_3$], 3.79 (s, 3H, $ArOCH_3$), 6.84 (d, J = 8.8 Hz, 2, ArH), 7.14 (d, J = 8.9 Hz, 2H, ArH). ^{13}C NMR ($CDCl_3$, 100 MHz): δ 30.6, 30.7, 34.8, 55.2, 113.8, 129.5, 132.0, 158.2, 195.7. MS (EI, 70 eV): m/z 210 (M^+, 5), 134 (100), 121 (64). HRMS calcd for $C_{11}H_{14}O_2S$: 210.0715. Found: 210.0715.

4-Methoxyphenethyl Thiol (9a). A solution of 1 M HCl in MeOH/dioxane was prepared by diluting commercially available 4 M HCl/dioxane with freshly distilled, degassed MeOH. Following Okuno's procedure (*37*), 4 mL of this solution was added to **8a** (200 mg, 0.951 mmol) and the reaction was refluxed at 80 °C under Ar for 3 h. The reaction was then concentrated under high vacuum overnight, providing an orange oil which was Kugelrohr distilled (65 °C, 0.2 mmHg) to provide **9a** as a pungent-smelling yellow oil (70.1 mg, 44%). ^1H NMR ($CDCl_3$, 400 MHz): δ 1.37 (t, J = 7.8 Hz, 1H, −SH), 2.75 (m, 2H, $ArCH_2CH_2SH$), 2.87 (t, J = 7.3 Hz, 2H, $ArCH_2CH_2SH$), 3.80 (s, 3H, $ArOCH_3$), 6.85 (d, J = 8.7 Hz, 2H, ArH), 7.11 (d, J = 8.7 Hz, 2H, ArH). MS (CI, CH_4): m/z 168 (M^+, 22), 135 (100), 61 (23). HRMS calcd for $C_9H_{13}OS$: 169.0686. Found: 169.0687.

(4-Methoxyphenethylthiolato)(3-thiapentane-1,5-dithiolato)oxorhenium(V) (5a). A solution of bis(2-mercaptoethyl)sulfide (35.5 μL, 0.272 mmol) and **9a** (45.8 mg, 0.272 mmol) in CH_3CN (1 mL) was added dropwise to a solution of $[BnEt_3N]ReOCl_4$ (*38*) (146 mg, 0.272 mmol) in MeOH (1 mL) at 0 °C, followed by Et_3N (114 μL, 0.816 mmol). A brown solution immediately formed. After stirring for 1 h, the crude mixture was concentrated and purified by flash chromatography (CH_2Cl_2) to produce **5a** as a foamy red solid (78.7 mg, 55%). IR (NaCl): 959 cm^{-1} (Re═O); mp 51−53 °C (dec). ^1H NMR ($CDCl_3$, 400 MHz): δ 1.95 [ddd, J = 14.6, 10.1, 4.7 Hz, 2H, $-S(CH_2)_2S-$], 3.07−3.17 [m, 4H, $-S(CH_2)_2Ar-$], 3.80 (s, 3H, $ArOCH_3$), 3.91 [ddd, J = 10.2, 4.1, 1.5 Hz, 2H, $-S(CH_2)_2S-$], 4.00−4.06 [m, 2H, $-S(CH_2)_2S-$], 4.29 [ddt, J = 13.4, 4.9, 1.3 Hz, 2H, $-S(CH_2)_2S-$], 6.85 (d, J = 8.6 Hz, 2H, ArH), 7.24 (d, J = 8.6 Hz, 2H, ArH). MS (CI, CH_4): m/z 523 (M + H^+ for ^{187}Re, 3), 521 (M + H^+ for ^{185}Re, 2), 227 (19), 195 (51), 135 (100), 121 (20). HRMS calcd for $C_{13}H_{20}O_2S_4{}^{187}Re$: 520.9876. Found: 520.9893.

4-Hydroxyphenethyl Thioacetate (8b). Diisopropyl azodicarboxylate (4.27 mL, 21.7 mmol) was added dropwise to a solution of PPh_3 (5.70 g, 21.7 mmol) in THF (75 mL) at 0 °C. A white precipitate of the ylide formed, and the heterogeneous solution was stirred in an ice bath for 30 min. A solution of the 4-hydroxyphenethyl alcohol (1.00 g, 7.24 mmol) in THF was added slowly to the ylide, followed by thiolacetic acid (1.55 mL, 21.7 mmol). The reaction was stirred for 1 h at 0 °C, then room-temperature overnight, changing from a white to green to a golden yellow color during this time. The reaction was then concentrated and purified by flash chromatography twice (2.5% MeOH/CH_2Cl_2 and 2.5% acetone/CH_2Cl_2), yielding **8b** as a yellow oil (756 mg, 53%). ^1H NMR ($CDCl_3$, 400 MHz): δ 2.34 (s, 3H, $-SCOCH_3$), 2.95 [ABq, J_{AB} = 7.2 Hz, $\Delta\upsilon$ = 127 Hz, 2H, $Ar(CH_2)_2SCOCH_3$], 2.95 (ABq, J_{AB} = 6.1 Hz, $\Delta\upsilon$ = 110 Hz, 2H, $Ar(CH_2)_2SCOCH_3$), 6.07 (s, 1, ArOH), 6.80 (d, J = 8.3 Hz, 2H, ArH), 7.07 (d, J = 8.1 Hz, 2H, ArH). ^{13}C NMR ($CDCl_3$, 100 MHz): δ 30.6, 30.8, 34.7, 115.3, 129.6, 131.8, 154.3, 197.3. MS (EI,

70 eV): *m*/*z* 197 (M + H, 44), 120 (100), 107 (66). HRMS calcd for $C_{10}H_{12}O_2S$: 196.0558. Found: 196.0558.

4-Hydroxyphenethyl Thiol (9b). Ten milliliters of 1 M HCl in MeOH/dioxane (vide supra) was added to **8b** (466 mg, 2.37 mmol), and the reaction was refluxed at 80 °C under Ar for 3 h. Following evaporation of the solution under high vacuum, Kugelrohr distillation (75 °C, 0.1 mmHg) provided **9b** as a near-colorless oil (338 mg, 92%). ^{1}H NMR ($CDCl_3$, 400 MHz): δ 1.37 (t, J = 7.7 Hz, 1H, S*H*), 2.75 [m, 2H, Ar(CH_2)$_2$SH], 2.85 [m, 2H, Ar(CH_2)$_2$SH], 4.70 (s, 1H, ArO*H*), 6.78 (d, J = 8.4 Hz, 2H, Ar*H*), 7.07 (d, J = 8.1 Hz, 2H, ArH). ^{13}C NMR ($CDCl_3$, 100 MHz) δ 26.3, 39.2, 115.3, 129.8, 132.0, 153.9. MS (EI, 70 eV): *m*/*z* 154 (M^+, 27), 120 (81), 107 (100). Anal. Calcd for $C_8H_{10}OS$: C, 62.30; H, 6.54. Found: C, 62.28; H, 6.59.

(4-Hydroxyphenethylthiolato)(3-thiapentane-1,5-dithiolato)oxorhenium(V) (5b). A solution of bis(2-mercaptoethyl)sulfide (39.3 μL, 0.301 mmol) and **9b** (46.4 mg, 0.301 mmol) in CH_3CN (0.8 mL) was added dropwise to a solution of [BnEt_3N]ReOCl_4 (161 mg, 0.301 mmol) in MeOH (1 mL) at 0 °C under Ar, followed by Et_3N (1 drop). A red precipitate immediately formed. After stirring for 2 h at 0 °C, the crude mixture was concentrated and purified by radial chromatography (1% acetone/CH_2Cl_2) to produce a red residue. This was dissolved in CH_2Cl_2, and ether was slowly added over the top of the CH_2Cl_2 layer. Crystals immediately formed. After 24 h, the mixture was filtered to give **5b** as red crystals (37.4 mg, 24%). IR (KBr): 955 cm^{-1} (Re═O); mp 153−155 °C (dec). ^{1}H NMR (CD_2Cl_2, 400 MHz): δ 1.97 [ddd, J = 14.5, 10.4, 5.0 Hz, 2H, −S(CH_2)$_2$S−], 3.02 [m, 2H, Ar(CH_2)$_2$S−], 3.10 [ddd, J = 14.4, 13.2, 4.1 Hz, 2, −S(CH_2)$_2$S−], 3.95 [m, 2H, Ar(CH_2)$_2$S−], 4.29 [ddt, J = 13.4, 4.8, 1.2 Hz, 2H, −S(CH_2)$_2$S−], 5.19 (s, 1H, ArO*H*), 6.77 (d, J = 8.5 Hz, 2H, Ar*H*), 7.17 (d, J = 8.3 Hz, 2H, Ar*H*). ^{13}C NMR (CD_2Cl_2, 100 MHz): δ 38.8, 39.1, 44.1, 47.0, 115.3, 129.9, 132.9, 155.4. MS (FAB): *m*/*z* 509 (M^+ for ^{187}Re, 16), 507 (M^+ for ^{185}Re, 10), 307 (74), 289 (48), 154(100), 136 (94). HRMS Calcd for $C_{12}H_{18}O_2S_4{}^{187}$Re: 508.9747. Found: 508.9741.

2-(4-Hydroxyphenyl)butanoic Acid (12). Following the procedure by Aaron (*39*), sodium (1.58 g, 69.2 mmol) was added to a solution of naphthalene (8.87 g, 69.2 mmol) in THF (60 mL) and was stirred for 4 h with occasional sonication, during which time it turned the characteristic deep blue color. This was added to a solution of 4-methoxyphenylacetic acid (5.00 g, 30.1 mmol) in THF (70 mL) dropwise, which was then stirred for several h. The reaction was then cooled in an ice bath, and to it, EtBr (2.56 mL, 34.3 mmol) was added dropwise. The ice bath was removed, and the reaction was stirred overnight. It was then quenched with water (20 mL), concentrated, dissolved in ether, and extracted with 1 M Na_2CO_3 (3 × 25 mL). The extracts were washed with ether, then acidified and extracted with ether. The ether extracts were dried with Na_2SO_4, concentrated, and distilled (131 °C, 0.5 mmHg) to provide **11** as a yellow oil (5.28 g), which was used in the next step without further purification.

The yellow oil was refluxed with HBr (15 mL) and acetic acid (15 mL) for 16 h. It was neutralized with saturated Na_2CO_3, extracted into CH_2Cl_2, washed with saturated Na_2CO_3, and acidified with HCl. The aqueous washes were back-extracted with CH_2Cl_2. The organics were combined, dried with Na_2SO_4, and purified by flash chromatography (5% MeOH/CH_2Cl_2 to 10% MeOH/CH_2Cl_2) to give **12** as a slightly yellow solid (715 mg, 13% two-step yield): mp 125.5−129 °C. ^{1}H NMR (CD_2Cl_2/CD_3OD, 500 MHz): δ 0.87 (t, J = 7.4 Hz, 3H, −CH_3), 1.71 (dquin, J = 13.7, 7.4 Hz, 1H, −CH_2Me), 2.02 (dquin, J = 13.4, 7.5 Hz, 1H, −CH_2Me), 3.36 (t, J = 7.6 Hz, 1H, C*H*), 6.75 (d, J = 8.7 Hz, 2H, Ar*H*), 7.13 (d, J = 8.4 Hz, 2H, Ar*H*). ^{13}C NMR (CD_3OD, 100 MHz): δ 12.5, 27.8, 54.0, 116.2, 129.9, 131.7, 157.5, 178.5. MS (CI, CH_4): *m*/*z* 181 (M + H^+, 49), 163 (15), 149 (11), 135 (100), 121 (8), 107 (14). HRMS Calcd for $C_{10}H_{13}O_3$: 181.0865. Found: 181.0870.

2-(4-Hydroxyphenyl)butanol (13). A solution of **12** (180 mg, 0.924 mmol) in THF (10 mL) was added to a solution of LAH (4.33 mg, 4.7 mmol) in THF (1 mL), and the reaction was stirred overnight. The reaction was quenched with saturated potassium sodium tartrate, and the gummy aluminum salts from the reaction were filtered through Celite. Concentration, followed by radial chromatography (2.5−10% MeOH/CH_2Cl_2) provided **13** as an off-white solid (34.9 mg, 23%). ^{1}H NMR ($CDCl_3$/CD_3OD, 500 MHz): δ 0.80 (t, J = 7.4 Hz, 3H, −CH_3), 1.49 [ddq, J = 13.6, 9.5, 7.4 Hz, 1H, −CH(CH_2OH)CH_2-CH_3], 1.68 [dqd, J = 13.5, 7.4, 5.4 Hz, 1H, −CH(CH_2OH)-CH_2CH_3], 2.61 [ddt, J = 9.5, 8.4, 5.4 Hz, 1H, −C*H*(CH_2-OH)Et], 3.66 [dd, J = 10.8, 8.4 Hz, 1H, −CH(CH_2OH)Et], 3.75 [dd, J = 10.8, 5.5 hz, 1H, −CH(CH_2OH)Et], 6.75 (d, J = 8.7 Hz, 2H, Ar*H*), 7.02 (d, J = 8.6 hz, 2H, Ar*H*). ^{13}C NMR (CD_2Cl_2, CD_3OD, 100 MHz): δ 12.0, 25.4, 49.9, 67.5, 115.6, 129.4, 133.9, 155.5. MS (CI, CH_4): *m*/*z* 167 (M + H^+, 27), 149 (33), 135 (100), 107 (97). HRMS Calcd for $C_{10}H_{15}O_2$: 167.1072. Found: 167.1078.

2-(4-Hydroxyphenyl)butyl Thioacetate (14). DIAD (83.0 μL, 0.420 mmol) was added dropwise to a solution of PPh_3 (110 mg, 0.420 mmol) in THF (5 mL) at 0 °C. Following formation of the white ylide precipitate, the solution was stirred for 30 min, at which time a solution of **13** (34.9 mg, 0.210 mmol) in THF was added dropwise, followed by thiolacetic acid (1.54 mL, 21.6 mmol). The reaction was stirred for 1 h at 0 °C, then overnight at room temperature. The reaction was then concentrated, and purification by radial chromatography (1% acetone/CH_2Cl_2) provided **14** as a slightly yellow oil (33.3 mg, 71%). ^{1}H NMR ($CDCl_3$, 400 MHz): δ 0.78 (t, J = 7.4 Hz, 3H, −CH(CH_2SCOCH_3)CH_2CH_3], 1.56 (ddq, J = 13.5, 9.6, 7.4 Hz, 1H, −CH(CH_2SCOCH_3)CH_2CH$_3$], 1.78 (dqd, J = 13.5, 7.4, 5.0 Hz, 1H, −CH(CH_2SCOCH_3)CH_2CH$_3$], 2.29 (s, 3H, −SCOCH_3), 2.58 [dddd, J = 9.6, 8.4, 6.6, 5.0 Hz, 1H, −C*H*(CH_2SCOCH_3)Et], 3.04 (dd, J = 13.3, 8.5 Hz, 1H, −CH(CH_2SCOCH_3)Et], 3.21 [dd, J = 13.3, 6.6 Hz, 1H, −CH(CH_2SCOCH_3)Et], 5.56 (s, 1H, −O*H*), 6.79 (d, J = 8.5 Hz, 2H, Ar*H*), 7.01 (d, J = 8.5 Hz, 2H, ArH). ^{13}C NMR ($CDCl_3$, 100 MHz): δ 12.0, 28.5, 30.6, 35.7, 46.4, 115.2, 128.7, 135.2, 154.3, 196.8. MS (CI, CH_4): *m*/*z* 225 (M + H^+, 7), 149 (100), 135 (23), 131 (36), 107 (48). HRMS calcd for $C_{12}H_{17}O_2S$: 225.0949. Found: 225.0950.

2-(4-Hydroxyphenyl)butanethiol (15). Five milliliters of 1 M HCl in MeOH/dioxane (vide supra) was added to **14** (18.5 mg, 0.0825 mmol), and the reaction was refluxed at 80 °C under Ar for 3 h. Following evaporation of the solution under high vacuum, Kugelrohr distillation (65 °C, 0.1 mmHg) provided **15** as a near-colorless oil which crystallized in the collection flask to a white solid (17.2 mg, 100%). mp 64−65.5 °C. ^{1}H NMR ($CDCl_3$, 400 MHz): δ 0.81 (t, J = 7.3 Hz, 3, −CH_3), 1.19 (ddd, J = 8.6, 7.5, 0.6 Hz, 1H, −S*H*), 1.57 (m, 1H −CH_2CH$_3$), 1.82 (m, 1H, −CH_2CH$_3$), 2.56 (m, 1H, C*H*), 2.74 (m, 2H, −CH_2SH), 4.73 (s, 1H, O*H*), 6.80 (d, J = 8.3 Hz, 2H, Ar-3H), 7.04 (d, J = 8.5 Hz, 2, Ar-2H). ^{13}C NMR ($CDCl_3$, 100 MHz): δ 12.1, 28.3, 31.0, 50.3, 115.3, 129.0, 135.3, 154.1. MS (CI, CH_4): *m*/*z* 183 (M + H^+, 36), 149 (56), 135 (52), 107 (100), 89 (18). Anal. Calcd for $C_{10}H_{14}OS$: C, 66.65; H, 7.83. Found: C, 66.69; H, 8.08.

[2-(4-Hydroxyphenyl)butanethiolato](3-thiapentane-1,5-dithialato)oxorhenium(V) (6). A solution of **15** (19.3 mg, 0.106 mmol) and bis(2-mercaptoethyl)sulfide (13.0 μL, 0.106 mmol) in CH_3CN (0.6 mL) was added dropwise to a solution of $[BnEt_3N]ReOCl_4$ (56.8 mg, 0.106 mmol) in MeOH (1 mL). A reddish solid immediately precipitated from solution. To this was added Et_3N (1 drop), and the reaction was stirred at 0 °C for 1 h. The reaction was concentrated, then purified by radial chromatography (1% acetone/CH_2Cl_2) to give **6** as a red powder (17 mg, 31%). IR (KBr): 932 cm^{-1} (Re═O); mp 188−189 °C, dec. ^{1}H NMR (DMSO-d_6, 500 MHz): δ 0.71 (t, J = 7.4 Hz, 3H, −C*H*3), 1.54 (m, 1H, −CH_2CH$_3$), 2.21 [m, 2H, −S(CH_2)$_2$S−], 2.76 (m, 1H, CH), 3.01 [m, 2H, −S(CH_2)$_2$S−], 3.76 (dd, J = 12.8, 7.1 Hz, 1H, −CHCH_2S−), 3.86 (dd, J = 13.0, 7.5 Hz, 1H, −CHCH_2S−), 4.03 [m, 2H, −S(CH_2)$_2$S−], 4.27 [dt, J = 12.5, 6.1 Hz, 2H, −S(CH_2)$_2$S−], 6.67 (d, J = 8.4 Hz, 2H, Ar-3H), 7.00 (d, J = 8.4 Hz, 2H, Ar-2H), 9.11 (s, 1H, O*H*). ^{13}C NMR (d_6-DMSO, 125 MHz): δ 12.1, 27.8, 43.0, 43.1, 45.5, 49.2, 115.0, 128.4, 134.7, 155.6. MS (FAB): *m*/*z* 537 (M, ^{187}Re isotope, 3). HRMS calcd for $C_{14}H_{22}O_2S_4{}^{187}Re$: 537.0060. Found: 537.0054.

1-(*p*-Anisyl)-butan-2-one (17). Following the synthesis according to Myers (*40*), NaOMe (13.7 g, 253 mmol) was added in portions over a period of 3 h to a solution of distilled *p*-anisaldehyde (31.0 g, 228 mmol) and ethyl α-bromobutyrate (44.5 g, 228 mmol) with cooling in an ice bath. After stirring for 2 days, the crude reaction was diluted with water, acidified with acetic acid, and extracted with ether. The organics were dried over Na_2SO_4, filtered, and concentrated to a yellow oil. The oil was Kugelrohr distilled, and after a forerun of anisaldehyde was collected (∼10 g, 90 °C, 0.1 mmHg), the epoxides were collected (110−115 °C, 0.1 mmHg) to give **16** as a slightly yellow oil (39.4 g, 69%, 100% corrected). A smaller portion was further purified by radial chromatography (20% EtOAc/Hex) and redistilled to give analytically pure material. MS (CI, CH_4): *m*/*z* 251 ($M + H^+$, 12), 237 (16), 177 (100), 149 (16), 121 (10). Anal. Calcd for $C_{14}H_{18}O_4$: C, 67.18; H, 7.25. Found: C, 67.10; H, 7.04.

A solution of NaOH (6.92 g, 173 mmol) in EtOH (110 mL) was added to the epoxide and refluxed 3 h, at which time it was cooled and concentrated. It was then diluted with water (35 mL) and washed with ether (75 mL). This was followed by acidification with 6 M HCl and extraction with ether. The ether was then washed with water (2 × 50 mL) and water (50 mL) with a trace amount of $NaHCO_3$. The organics were dried over Na_2SO_4, filtered, and concentrated. The concentrate was then heated on an oil bath at 90−100 °C for 4 h, then 130 °C for 1 h. After cooling, the red oil was dissolved in ether (100 mL) and washed sequentially with 1 M NaOH (50 mL), water (2 × 40 mL), and brine (40 mL). The organics were dried over Na_2SO_4, and concentrated to an orange oil. Kugelrohr distillation (90 °C, 0.1 mmHg) provided **17** as a slightly yellow oil (21.2 g, 76%). ^{1}H NMR ($CDCl_3$, 400 MHz): δ 1.01 (t, J = 7.3 Hz, 3H, −CH_2CH_3), 2.45 (q, J = 7.3 Hz, 2H, −CH_2CH$_3$), 3.61 (s, 2H, ArCH_2COEt), 3.78 (s, 3H, −OCH_3), 6.85 (d, J = 8.8 Hz, Ar*H*), 7.11 (d, J = 8.8 Hz, 2H, Ar*H*). ^{13}C NMR ($CDCl_3$, 100 MHz) δ 7.7, 34.9, 48.7, 55.1, 114.0, 126.4, 130.2, 158.5, 209.2. MS (EI, 70 eV): *m*/*z* 178 (M^+, 23), 121 (100), 91 (10), 78 (23), 57 (12). Anal. Calcd for $C_{11}H_{14}O_2$: C, 74.13; H, 7.92. Found: C, 74.20; H, 7.99.

4-(4-Methoxyphenyl)-3-hexanone (18). Following the procedure by Myers (*40*), EtI (28.1 mL, 351 mmol) was added dropwise to a slurry of **17** (20.9 g, 117 mmol) and NaOMe (12.6 g, 234 mmol) in an ice bath. The solution was then refluxed, adding excess EtI when needed to keep the reaction stirring. After 1 h, the reaction was cooled, concentrated, and diluted with 10 mL of water. This was then extracted with ether (30 mL). The ether layer was washed with 10% NaS_2O_3 (10 mL), water (10 mL), and brine (10 mL). The ether layer was then dried with Na_2SO_4, filtered, and concentrated to a yellow oil. Kugelrohr distillation (81 °C, 0.1 mmHg) provided **18** as a slightly yellow oil (21.4 g, 89%). A small portion was purified by radial chromatography (20% EtOAc/hexane) and redistilled to give analytically pure product. ^{1}H NMR ($CDCl_3$, 400 MHz): δ 0.80 (t, J = 7.4 Hz, 3H, −CHCH$_2$CH_3), 0.94 (t, J = 7.3 Hz, 3H, −COCH$_2$CH_3), 1.66 (dquin, J = 13.8, 7.5 Hz, 1H, −CHCH_2CH$_3$), 2.01 (dquin, J = 13.7, 7.3 Hz, 1H, −CHCH_2CH$_3$), 3.46 [t, J = 7.5 Hz, 1H, Ar−C*H*(Et)COEt], 2.37 (ABqq, J_{AB} = 7.3 Hz, $\Delta\nu$ = 16.7 Hz, J = 7.3 Hz, 2H, −COCH_2CH$_3$), 3.77 (s, 3H, ArOCH_3), 6.84 (d, J = 8.8 Hz, 2H, Ar*H*), 7.11 (d, J = 8.7 Hz, 2H, Ar*H*). ^{13}C NMR δ 7.8, 12.0, 25.2, 34.8, 55.1, 59.5, 114.0, 129.1, 131.1, 158.6, 211.4. MS (EI, 70 eV): *m*/*z* 206 (M^+, 14), 149 (100), 121 (44), 91 (13). Anal. Calcd for $C_{13}H_{18}O_2$: C, 75.69; H, 8.79. Found: C, 75.88; H, 8.94.

4-(4-Hydroxyphenyl)-3-hexanone (19). HBr (15 mL) and acetic acid (15 mL) were added to **18**, and the mixture was refluxed for 5 h and then cooled. The reaction was diluted with water (40 mL) and extracted with ether (3 × 40 mL). The ether layer was washed with saturated $NaHCO_3$ until neutral to pH paper. The ether was then washed with 10% $Na_2S_2O_3$ (30 mL) and water (40 mL). The phenol was extracted with 1 M NaOH (2 × 40 mL), acidified with HCl, and extracted with ether (3 × 35 mL). The ether layer was washed with water (30 mL), brine (40 mL), then dried with Na_2SO_4, filtered, and concentrated to provide **19** as a brown solid (5.73 g, 88%): mp 64−65.5 °C. ^{1}H NMR ($CDCl_3$, 400 MHz): δ 0.80 (t, J = 7.3 Hz, 3H, −CHCH$_2$CH_3), 0.96 (t, J = 7.3 Hz, 3H, −COCH$_2$CH_3), 1.69 (dquin, J = 13.7, 7.6 Hz, 1H, −CHCH_2CH$_3$), 2.01 (dquin, J = 13.7, 7.3 Hz, 1H, −CHCH_2-CH$_3$), 2.42 (ABqq, J_{AB} = 7.4 Hz, $\Delta\nu$ = 18.4 Hz, J = 7.3 Hz, 2H, −COCH_2CH$_3$), 3.50 [t, J = 7.5 Hz, 1H, ArC*H*(Et)-COEt], 6.89 (d, J = 8.7 Hz, 2H, Ar*H*), 6.96 (s, 1H, ArO*H*), 7.05 (d, J = 8.5 Hz, 2H, Ar*H*). ^{13}C NMR ($CDCl_3$, 100 MHz): δ 7.9, 12.0, 25.1, 35.0, 59.6, 115.7, 129.3, 130.4, 155.2, 213.7. MS (EI, 70 eV): *m*/*z* 192 (M^+, 16), 135 (100), 107 (55). Anal. Calcd for $C_{12}H_{16}O_2$: C, 74.97; H, 8.39. Found: C, 75.12; H, 8.40.

4-[4-(2-Methoxyethoxymethoxy)phenyl]-3-hexanone (20). To a solution of NaH (1.25 g, 31.2 mmol) and THF (20 mL), cooled to 0 °C, was added **19** (4.00 g, 20.8 mmol) slowly. After stirring for 30 min, MEMCl (7.25 mL, 41.6 mmol) was added slowly. This was stirred for 6 h at room temperature, then quenched with MeOH with cooling and concentrated. The residue was dissolved in 110 mL of ether, then washed with 15% NaOH (2 × 40 mL), water (40 mL), and brine (45 mL). The ether layer was dried over Na_2SO_4 and concentrated to a yellow oil. Flash chromatography (10% acetone/CH_2Cl_2) and radial chromatography (2.5% acetone/CH_2Cl_2) provided **20** as a slightly yellow oil (4.91 g, 84%). ^{1}H NMR ($CDCl_3$, 400 MHz): δ 0.79 (t, J = 7.4 Hz, 3H, −CHCH$_2$CH_3), 0.93 (t, J = 7.3 Hz, 3H, −COCH$_2$CH_3), 1.65 (dquin, J = 13.8, 7.5 Hz, 1H, −CHCH_2CH$_3$), 2.00 (dquin, J = 13.8, 7.3 Hz, 1H, −CHCH_2CH$_3$), 2.36 (ABqq, JAB = 7.3 Hz, $\Delta\nu$ = 16.1 Hz, J = 7.3 Hz, 2H, −COCH_2CH$_3$), 3.35 [s, 3H, CH_3O(CH$_2$)$_2$-OCH$_2$OAr], 3.46 [t, J = 7.4 Hz, 1H, ArC*H*(Et)COEt], 3.54 [m, 2H, CH$_3$O(CH_2)$_2$OCH$_2$OAr], 3.80 [m, 2H, CH$_3$O(CH_2)$_2$-OCH$_2$OAr], 5.23 [s, 2H, CH$_3$O(CH$_2$)$_2$OCH_2OAr], 6.97 (d, J = 8.9 Hz, 2H, Ar*H*), 7.10 (d, J = 8.5 Hz, 2H, Ar*H*). ^{13}C NMR ($CDCl_3$, 100 MHz): δ 7.8, 12.0, 25.3, 34.9, 58.9,

59.5, 67.5, 71.5, 93.4, 116.4, 129.1, 132.5, 156.3, 211.4. MS (EI, 70 eV): *m/z* 280 (M^+, 8), 223 (38), 149 (4), 135 (9), 107 (10), 89 (100), 59 (88), 43 (33). Anal. Calcd for $C_{16}H_{24}O_4$: C, 68.54; H, 8.63. Found: C, 68.30; H, 8.90.

4-[4-(2-Methoxyethoxymethoxy)phenyl]-3-hexanol (21). A solution of **20** (2.48 g, 8.85 mmol) in THF (10 mL) was added to a slurry of LAH (839 mg, 22.1 mmol) in THF (15 mL) at 0 °C. The reaction was warmed to room temperature and stirred for 1.5 h. It was quenched sequentially with 840 μL of water, 840 μL of 15% NaOH, and 2.5 mL of water. The white slurry was then passed through Celite and concentrated. Flash chromatography (10% acetone/CH_2Cl_2) provided **21** as a colorless oil (2.24 g, 90%). ^{1}H NMR ($CDCl_3$, 400 MHz, major diastereomer): δ 0.75 (t, J = 7.4 Hz, 3H, $-CH_3$), 0.95 (t, J = 7.4 Hz, 3H, $-CH_3$), 1.27 (d, J = 5.0 Hz, 1H, OH), 1.29 [ddq, J = 13.9, 8.2, 7.3 Hz, 1H, $-$CH(OH)CH_2-CH$_3$], 1.55 [dqd, J = 13.9, 7.5, 3.9 Hz, 1H, $-$CH(OH)-CH_2CH$_3$], 1.63 [ddq, J = 13.6, 10.3, 7.3 Hz, 1H, $-$CH-(CH_2CH$_3$)Ar], 1.75 [dqd, J = 13.6, 7.4, 4.9 Hz, 1H, $-$CH(CH_2CH$_3$)Ar], 2.43 [dt, J = 10.4, 5.2 Hz, 1H, $-$CH(Et)Ar], 3.36 [s, 3H, CH_3O(CH$_2$)$_2$CH$_2$OAr], 3.56 [m, 2H, CH$_3$O(CH_2)$_2$CH$_2$OAr], 3.61 [m, 1H, $-$CH(OH)Et], 3.82 [m, 2H, CH$_3$O(CH_2)$_2$CH$_2$OAr], 5.25 [s, 2H, CH$_3$O-(CH$_2$)$_2$CH_2OAr], 7.00 (d, J = 8.8 Hz, 2H, ArH), 7.11 (d, J = 8.6 Hz, 2H, ArH). ^{13}C NMR ($CDCl_3$, 100 MHz, major diastereomer): δ 10.1, 12.2, 25.0, 27.8, 52.6, 58.9, 67.5, 71.6, 76.0, 93.5, 116.1, 129.8, 134.4, 155.9. MS (EI, 70 eV): *m/z* 282 (M^+, 1), 223 (30), 148 (56), 136 (36), 107 (19), 89 (100), 59 (92). HRMS Calcd for $C_{16}H_{26}O_4$: 282.1831. Found: 282.1841.

4-[4-(2-Methoxyethoxymethoxy)phenyl]-3-thioacetyl-hexane (22). Triethylamine (1.66 mL, 11.9 mmol) and MsCl (0.921 mL, 11.9 mmol) were added to a solution of **21** (2.24 g, 7.93 mmol) in THF (15 mL) and cooled to 0 °C in an ice bath. The reaction was stirred for 30 min at 0 °C, then for 1 h at room-temperature. Reaction was stopped and diluted with 20 mL of water. Following concentration, the aqueous layer was extracted with ether (1 × 40 mL, 1 × 15 mL). The organics were combined and washed with water (15 mL), dried with Na_2SO_4, and concentrated to a yellow oil (2.72 g, 91%). This was used in the next step without further purification.

The mesylate (361 mg, 0.960 mmol) was combined with tetrabutylammonium thioacetate [760 mg, 2.39 mmol, prepared according to Logusch (*41*)] in DMF (2 mL). This was heated at 50 °C overnight. The crude mixture was diluted with ether, washed with saturated LiCl, water, and brine, then dried over Na_2SO_4, filtered, and concentrated to a dark oil. This was purified by radial chromatography (0.5% acetone/CH_2Cl_2) to provide the thioacetate **22** as a yellow-orange oil (121 mg, 37%). ^{1}H NMR ($CDCl_3$, 400 MHz, major diastereomer): δ 0.68 (t, J = 7.4 Hz, 3H, CH_3), 0.84 (t, J = 7.3 Hz, 3H, CH_3), 1.24 [m, 1H, $-$CH(SCOCH$_3$)CH_2CH$_3$], 1.56 [m, 2H, $-$CH(SCOCH$_3$)CH_2-CH$_3$], 1.93 [dqd, J = 13.6, 7.4, 3.8 Hz, 1H, $-$CH(CH_2CH$_3$)-Ar], 2.34, (s, 3H, $-$SCOCH_3), 2.52 [ddd, J = 11.1, 8.6, 3.8 Hz, 1H, $-$CH(CH_2CH$_3$)Ar], 3.37 [s, 3H, CH_3O(CH$_2$)$_2$-CH$_2$OAr], 3.56 [m, 2H, CH$_3$O(CH_2)$_2$CH$_2$OAr], 3.68 [td, J = 8.9, 3.5 Hz, 1H, $-$CH(Et)Ar], 5.25 [s, 2H, CH$_3$O-(CH$_2$)$_2$CH_2OAr], 6.97 (d, J = 8.6 Hz, 2H, ArH), 7.08 (d, J = 8.6 Hz, 2H, ArH). ^{13}C NMR ($CDCl_3$, 100 MHz, major diastereomer): δ 11.0, 12.2, 25.4, 26.4, 30.8, 50.8, 51.6, 59.0, 57.6, 71.6, 93.6, 115.9, 129.4, 135.6, 155.8, 195.9. MS (EI, 70 eV): *m/z* 340 (M^+, 1), 264 (40), 223 (51), 135 (21), 107 (15), 89 (100), 59 (75). HRMS calcd for $C_{18}H_{28}O_4S$: 340.1708. Found: 340.1709.

3-Mercapto-4-(4-hydroxyphenyl)hexane (23). Ten milliliters of 1 M HCl in MeOH/dioxane was added to **22** (121 mg, 0.350 mmol) and the reaction was refluxed at 80 °C under Ar for 3 h. Evaporation of the solvent under high vacuum provided a dark oil. Purification by radial chromatography (0.5% acetone/CH_2Cl_2) gave the thiol **23** as a yellow-orange oil (34.1 mg, 46%). ^{1}H NMR ($CDCl_3$, 400 MHz, major diastereomer): δ 0.73 (t, J = 7.3 Hz, 3H, CH_3), 0.95 (t, J = 7.3 Hz, 3H, CH_3), 1.26 [m, 1H, $-$CH(SH)CH_2CH$_3$], 1.31 (d, J = 7.2 Hz, 1H, $-$SH), 1.63 [m, 2H, ArCH(CH_2CH$_3$)CH(SH)CH_2CH$_3$], 2.03 [dqd, J = 13.5, 7.4, 3.8 Hz, 1H, $-$CH(CH_2CH$_3$)Ar], 2.50 [ddd, J = 11.0, 7.4, 3.5 Hz, 1H, $-$CH(Et)Ar], 2.87 [dtd, J = 9.2, 7.3, 3.5 Hz, 1H, $-$CH(SH)Et], 5.09 (s, 1H, Ar$-$OH), 6.78 (d, J = 8.3 Hz, 2H, ArH), 7.02 (d, J = 8.5 Hz, 2H, ArH). MS (CI, CH_4): *m/z* 211 ($M + H^+$, 40), 177 (100), 135 (72), 121 (14), 107 (80). HRMS Calcd for $C_{12}H_{19}OS$: 211.1157. Found: 211.1161.

2,6-Bis(thiacetomethyl)pyridine (25). DIAD (4.25 mL, 21.6 mmol) was added dropwise to a solution of PPh_3 (5.67 g, 21.6 mmol) in THF (100 mL) at 0 °C. Following formation of the white ylide precipitate, the solution was stirred for 30 min, at which time a solution of 2,6-pyridinedimethanol (1.00 g, 7.19 mmol) in THF/DMF was added dropwise, followed by thiolacetic acid (1.54 mL, 21.6 mmol). The reaction was stirred for 1 h at 0 °C, then overnight at room temperature. A green slurry developed immediately upon addition of the thiolacetic acid, which eventually changed to a yellow color. The reaction was then concentrated and purified by flash chromatography (5% MeOH/CH_2Cl_2) and radial chromatography (CH_2Cl_2 to 5% MeOH/CH_2Cl_2). Recrystallization from EtOAc/hexanes 3 times provided **25** as yellow crystals (980 mg, 53%): mp 46.5−47.5 °C. ^{1}H NMR ($CDCl_3$, 400 MHz): δ 2.36 (s, 6H, $-$SCOCH_3), 4.22 (s, 4H, ArCH_2SCOCH$_3$), 7.21 (d, J = 7.7 Hz, 2H, ArH), 7.56 (t, J = 7.7 Hz, 1H, ArH). ^{13}C NMR ($CDCl_3$, 100 MHz): δ 30.2, 35.0, 121.6, 137.4, 157.0, 194.9. MS (CI, CH_4): *m/z* 256 ($M + H^+$, 100), 214 (55). Anal. Calcd for $C_{11}H_{13}NO_2S_2$: C, 51.74; H, 5.13; N, 5.49; S, 25.11. Found: C, 51.64; H, 5.19; N, 5.42; S, 25.07.

2,6-Dithiomethylpyridine Hydrochloride (26). Four milliliters of 1 M HCl in MeOH/dioxane (vide supra) was added to **25** (200 mg, 0.783 mmol) and the reaction was refluxed at 80 °C under Ar for 3 h. Evaporation under high vacuum provided **26** as a slightly yellow solid (144 mg, 89%). This solid was used in the next reaction without further purification. ^{1}H NMR (CD_3OD, 400 MHz) δ 4.09 (s, 4H, ArCH_2SH), 7.93 (d, J = 8.0 Hz, 2H, ArH), 8.48 (t, J = 8.0 Hz, 1H, ArH). MS (CI, CH_4): *m/z* 172 (M + H^+, 100), 138 (39).

(4-Hydroxythiophenolato)(2,6-dithiomethylpyridinato)oxorhenium(V) (4b). A solution of **26** (28.0 mg, 0.172 mmol) and 4-hydroxythiophenol (24.1 mg, 0.172 mmol) in CH_3CN (0.6 mL) and MeOH (0.4 mL) was added to a solution of [BnEt$_3$N]ReOCl$_4$ in MeOH (1 mL) under an Ar atmosphere. A brownish solution formed immediately, which intensified when Et_3N (95.9 μL, 0.688 mmol) was added. The reaction was stirred for 1 h, concentrated, and purified by radial chromatography (1% acetone/CH_2Cl_2) to give **4b** as a red solid (47.2 mg, 55%). IR (KBr): 962 cm^{-1} (Re═O); mp 108−112 °C (dec). Normal-phase HPLC [t_R = 8.6 min, 50% hexane/50% (5% IPA/CH_2Cl_2), UV detection] showed only one visible peak. ^{1}H NMR (acetone-d_6, 400 MHz): δ 4.8−5.6 (bm, 5H, $-$SCH_2pyr, ArOH), 6.89 (d, J = 8.7 Hz, 2H, $-$SArH), 7.53 (d, J = 8.7 Hz, 2H, $-$SArH), 7.70−7.88 (bd, 2H, pyrH), 7.97 (t, J = 7.7 Hz, 1H, pyr-4H). MS (EI, 70 eV): *m/z* 497 (M^+, 100), 372 (80). HRMS Calcd for $C_{13}H_{12}NO_2S_3{}^{187}$-Re: 496.9588. Found: 496.9581.

(4-Methoxythiophenolato)(2,6-dithiomethylpyridinato)oxorhenium(V) (4c). A solution of **26** (20 mg, 0.0927 mmol) and 4-methoxythiophenol (13.0 mg, 0.0927 mmol) in a 1:1 mixture of MeOH/CH_3CN (1 mL) was added dropwise to a solution of $[BnEt_3N]ReOCl_4$ in MeOH (1.5 mL). This was followed by the dropwise addition of Et_3N (52 μL, 0.371 mmol), and the reaction was stirred for 1 h, then warmed to 40 °C for 15 min. Concentration, followed by radial chromatography (CH_2Cl_2) provided **4c** as a dark red solid (18.5 mg, 39%). IR (KBr): 964 cm^{-1} (Re═O); mp 103 °C (dec). ^1H NMR (CD_2Cl_2, 500 MHz): δ 3.85 (s, 3H, Ar−OCH_3), 4.8−5.6 (m, 4H, pyr-CH_2S−), 6.96 (d, J = 8.8 Hz, −SAr*H*), 7.59 (d, J = 8.9 Hz, 2H, −SAr*H*), 7.78 (bd, 2H, pyr*H*), 7.97 (t, J = 7.7 Hz, 1H, pyr*H*). MS (FAB): m/z 511 (M + H^+ for ^{187}Re, 8), 509 (M + H^+ for ^{185}Re, 4), 141 (100). HRMS Calcd for $C_{14}H_{14}NO_2S_3{}^{187}Re$: 510.9744. Found: 510.9741.

Dimethyl Chelidamate (28). Using the procedure by Bradshaw (*42*), chelidamic acid (6.00 g, 32.8 mmol), MeOH (80 mL), and concentrated H_2SO_4 (1.2 mL) were combined and refluxed for 21 h. The reaction was cooled, neutralized with saturated Na_2CO_3, and reacidified with concentrated HCl. This was diluted with water (80 mL) and extracted with CH_2Cl_2 (1 × 100 mL, 2 × 50 mL). The organics were combined, dried with Na_2SO_4, filtered, and concentrated to a yellow solid. Two recrystallizations from MeOH gave **28** as a light yellow solid (3.51 g, 51%): mp 168.5−169.5 °C [lit. (*42*) 169−169.5 °C]. ^1H NMR ($CDCl_3$, 400 MHz): δ 3.96 (s, 6H, ArCO_2CH_3), 7.80 (bs, 2H, pyr*H*), 9.8−10.2 (bs, 0.4H, pyrO*H*), 11.4−11.9 (bs, 0.4H, pyrO*H*). MS (EI, 70 eV): m/z 211 (M^+, 100), 183 (71), 167 (15), 153 (96), 121 (52), 92 (64), 79 (8), 68 (14), 59 (31). Anal. Calcd for $C_9H_9NO_5$: C, 51.19; H, 4.30; N, 6.63. Found: C, 51.16; H, 4.24; N, 6.63.

Dimethyl 4-[(Tetrahydro-2-pyranyl)oxy]-2,6-pyridinedicarboxylate (29). To a solution of **28** (3.11 g, 14.7 mmol) in CH_2Cl_2 (44 mL) was added 3,4-dihydro-2*H*-pyran (6.72 mL, 73.6 mmol) and pyridinium *p*-toluenesulfonate (377 mg, 1.50 mmol). The reaction was stirred overnight at room temperature. The crude reaction mixture was washed with brine (2 × 15 mL) and water (20 mL), dried over Na_2SO_4, filtered, concentrated, and recrystallized from EtOAc/hexane to give **29** as white crystals (2.97 g, 68%): mp 119.5−121.5 °C [lit. (*42*) 120−121.5 °C]. ^1H NMR ($CDCl_3$, 400 MHz): δ 1.5−1.78 (m, 3H, THP), 1.82−2.04 (m, 3, THP), 3.61−3.80 (m, 2H, THP), 3.98 (s, 6H, pyrCO_2CH_3), 5.66 (t, J = 2.75 Hz, 1H, THP), 7.92 (s, 2H, pyr*H*). ^{13}C NMR ($CDCl_3$, 100 MHz): δ 17.9, 24.7, 29.5, 53.1, 62.0, 96.3, 116.0, 149.6, 165.06, 165.12. MS (CI, CH_4): m/z 296 (M + H^+, 5), 240 (13), 212 (100), 85 (26), 57 (11). Anal. Calcd for $C_{14}H_{17}NO_6$: C, 56.94; H, 5.80; N, 4.74. Found: C, 56.80; H, 6.99; N, 4.73.

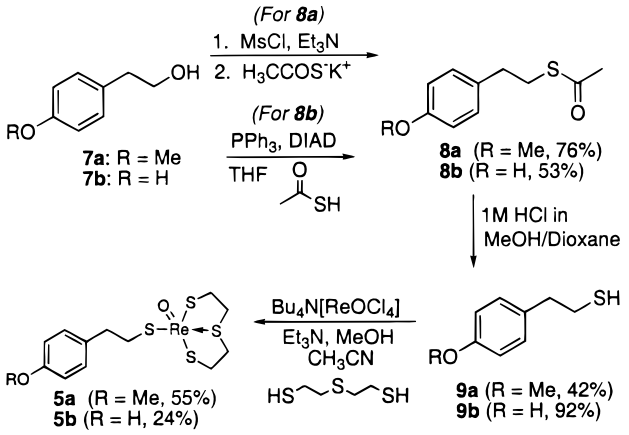
4-(Tetrahydro-2H-2-pyranyloxy)-2,6-bis(hydroxymethyl)pyridine (30). Following the procedure used by Scrimin (*43*), $NaBH_4$ (1.06 g, 28.1 mmol) was added to a solution of **29** in EtOH (90 mL). Crushed $CaCl_2$ (3.11 g, 28.1 mmol) was then added slowly to the reaction, producing a heterogeneous pink color. After stirring overnight, the reaction was diluted with water (100 mL), and the EtOH was removed by evaporation in vacuo. The residue was added to brine (100 mL), and extracted with $CHCl_3$ (4 × 200 mL). This was evaporated to a light green oil, which solidified upon standing under vacuum for several days, giving a crude mass of 1.53 g (69%). Recrystallization from EtOAc provides **30** as off-white crystals (1.14 g, 51%): mp 115−116 °C. ^1H NMR (CD_3OD, 500 MHz): δ 1.5−1.75 (m, 2H, THP), 1.8−2.0 (m, 3H, THP), 2.70 (bs, 2H, pyrCH_2O*H*), 3.58 (dtd, J = 11.3, 4.1, 1.5 Hz, 1H, THP), 3.77 (ddd, J = 11.4, 10.1, 3.2 Hz, 1H, THP), 4.61 (s, 4H, pyrCH_2OH), 5.55 (t, J = 3.2 Hz, 1H, THP), 6.89 (s, 2H, pyr*H*). MS (CI, CH_4): m/z 240 (M + H^+, 13), 222 (10), 184 (25), 156 (100), 85 (35). Anal. Calcd for $C_{12}H_{17}NO_4$: C, 60.24; H, 7.16; N, 5.85. Found: C, 59.93; H, 7.13; N, 5.85.

4-(Tetrahydro-2H-2-pyranyloxy)-2,6-bis(thioacetylmethyl)pyridine (31). Diisopropyl azodicarboxylate (2.30 mL, 11.5 mmol) was added slowly to a solution of PPh_3 (3.01 g, 11.5 mmol) in THF (75 mL) at 0 °C. Upon formation of the white ylide precipitate., the reaction was stirred for 30 min at 0 °C. A solution of **30** (1.08 g, 4.50 mmol) in THF/DMF was added to the reaction, followed by thiolacetic acid (820 μL, 11.5 mmol). The reaction was stirred for 1 h at 0 °C, then overnight at room temperature. The reaction was concentrated, redissolved in CH_2Cl_2 (60 mL), and washed with saturated LiCl (2 × 30 mL) and brine (1 × 30 mL). The organic layer was dried over Na_2SO_4, filtered, and concentrated. After three flash chromatography purifications (5% MeOH/CH_2Cl_2), the thioacetate **31** was isolated as a yellow oil (1.15 g, 72%). ^1H NMR ($CDCl_3$, 400 MHz): δ 1.24 (m, 2H, THP), 1.52−2.0 (m, 6H, THP), 2.34 (s, 6H, −SCOCH_3), 3.60 (dtd, J = 11.1, 4.0, 1.5 Hz, 1H, THP), 3.76 (m, 1H, THP), 4.14 (ABq, J_{AB} = 13.8 Hz, $\Delta\upsilon$ = 13.8 Hz, 4H, ArCH_2SCOMe), 6.86 (s, 2H, pyrH). ^{13}C NMR ($CDCl_3$, 100 MHz): δ 18.2, 24.8, 29.7, 30.2, 35.4, 61.9, 95.7, 109.6, 158.4, 164.4, 194.9. MS (CI, CH_4): m/z 356 (M + H^+, 5), 300 (15), 272 (81), 247 (26), 205 (55), 161 (100), 147 (32), 119 (89), 85 (34), 57 (16). HRMS Calcd for $C_{16}H_{22}NO_4S_2$: 356.0997. Found: 356.0997.

[4-Hydroxy-2,6-bis(thiomethyl)pyridinato][4-hydroxythiophenolato]oxorhenium(V) (4a). A solution of 1 M HCl in MeOH/dioxane (1 mL) was added to **31** (50 mg, 0.141 mmol) and refluxed at 80 °C for 3 h under Ar. Concentration under high vacuum provided the dithiol HCl salt **32** as an extremely hygroscopic off-white solid, which darkened with time at room temperature. A solution of the thiol (25.2 mg, 0.113 mmol) and *p*-hydroxythiophenol (15.8 mg, 0.113 mmol) in 1:1 MeOH/CH_3CN (1 mL) was added to a solution of $[BnEt_3N]ReOCl_4$ in MeOH (1 mL) at 0 °C under Ar. This was followed by the dropwise addition of Et_3N (16 μL, 0.113 mmol), resulting in a dark solution. The reaction was warmed to room temperature for 45 min. Concentration, followed by radial chromatography (5−10% MeOH/CH_2Cl_2), provided a red, sticky oil, which when slowly evaporated from CH_2Cl_2 provided **4a** as red solid (22.5 mg, 39%). IR (NaCl): 965 cm^{-1} (Re═O); mp ∼100 °C (dec). ^1H NMR (DMSO-d_6, 400 MHz, 95 °C): δ 4.98 (ABq, J_{AB} = 17.6 Hz, $\Delta\upsilon$ = 195 Hz, 4H, pyrCH_2S−), 6.76 (d, J = 8.5 Hz, 2H, −SAr*H*), 7.25 (s, 2H, pyr*H*), 7.28 (d, J = 8.5 Hz, 2H, −SAr*H*). ^{13}C NMR ($CD_3OD/CDCl_3$, 100 MHz): δ 51.2, 106.7, 134.8, 138.0, 155.8, 168.8. MS (FAB): m/z 514 (M^+ for ^{187}Re, 3), 512 (M^+ for ^{185}Re, 2), 461 (100). HRMS calcd for $C_{13}H_{13}NO_3S_3{}^{187}Re$: 513.9615. Found: 513.9613.

Measurement of the Octanol/Water Partition Coefficient. The log $P_{o/w}$ values were estimated from log k'_w values determined by reversed-phase HPLC following the method outlined by Minick (*44*). A Chromegabond C8 (5 mm, 60 Å, ES Industries) 15 cm × 4.6 mm column served as the stationary phase. The organic mobile phase was methanol containing 0.25% (v/v) 1-octanol, and the aqueous phase consisted of octanol-saturated water containing 0.25% (v/v) M MOPS (3-morpholinopropanesulfonic acid, Sigma) buffer and 0.15% (v/v) *n*-decylamine, adjusted to pH 7.4. The flow rate was 1 mL/min.

Scheme 1



Estrogen Receptor Binding Affinity. Receptor-binding affinity (RBA) values were determined by a competitive radiometric binding assay, using tritiated estradiol as the tracer and lamb uterus cytosol as the source of receptor, according to a previously established method (*45*).

RESULTS AND DISCUSSION

Syntheses. *Synthesis of Complexes That Mimic Estradiol (**5ab**, **6**, and **2**).* Before the preparation of the precursor monodentate ligand for **2**, we first synthesized some model compounds which were intended to not only help us determine the route by which to introduce the thiol to monodentate ligands but also serve as a "reference" to compare relative-binding affinities to **2**. These complexes included one with a simple phenethyl thiol monodentate ligand (**5a,b**) and one with an ethyl group at the benzylic position of the monodentate ligand (**6**).

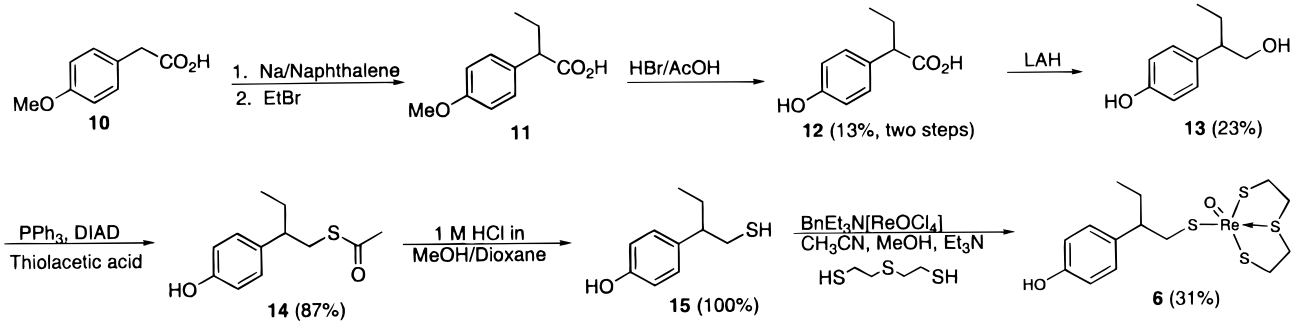
The synthesis of the first model systems **5a** and **5b** follows the straightforward route outlined in Scheme 1. Starting with the parent phenethyl alcohol (**7a**, **7b**), either Mitsunobu or mesylation-displacement with potassium thioacetate work well in generating the thioacetates **8a** and **8b**, respectively. Treatment of the thioacetate with anhydrous HCl in methanol/dioxane generates the free thiols **9a** and **9b** cleanly. Attempts to free the thiol under alkaline conditions (e.g., K_2CO_3 in MeOH/H_2O and LAH) only resulted in formation of the disulfide, even when strictly anaerobic conditions were observed. Complexation of these thiols with the commercially available bis(2-mercaptoethyl) sulfide and a readily available rhenium source, $Bu_4N[ReOCl_4]$ (*38*), furnished the desired complexes **5a** and **5b** in modest yields.

The synthesis of the monoethyl model system **6** is outlined in Scheme 2 and is analogous to the syntheses of **5a** and **5b**. Carboxylic acid **11** is prepared from *p*-methoxyphenylacetic acid (**11**), using a known literature procedure (*39*), and is used without purification in the deprotection step to afford phenol **12** in low yield. Reduction with LAH generates alcohol **13** in low yield because of difficulties in the workup. A Mitsunobu reaction on the alcohol provides the thioacetate **14** in good yield. The thiol **15** is then released in a manner analogous to **9a** and **9b**, and the complex is obtained without complication.

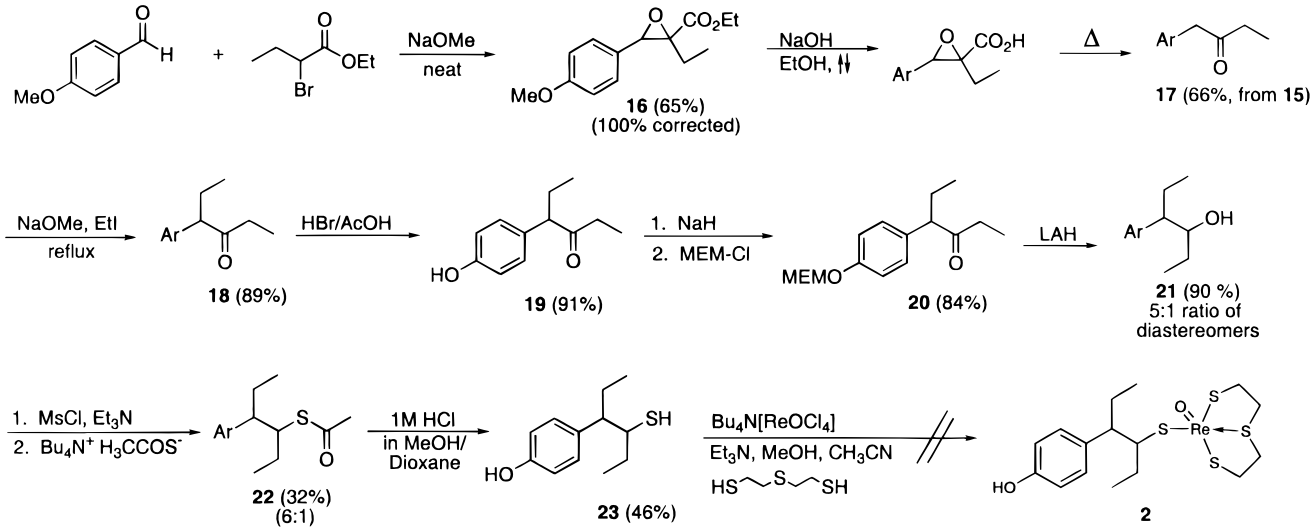
The attempted synthesis of desired complex **2** is described in Scheme 3. The skeleton for the monodentate ligand was generated by first reacting *p*-anisaldehyde and ethyl *a*-bromobutyrate in a Darzens reaction to afford the glycidic ester **16** in good yield (*40*). Saponification, followed by thermal decarboxylation produced ketone **17** in good yield (*40*). Ethylation of the more stable benzylic enolate with EtI as the solvent afforded the branched ketone **18** in excellent yield. Deprotection with HBr and AcOH produced the free phenol **19**, again in excellent yield (*40*). After reprotection with the MEM group, the protected ketone **20** was reduced by LAH reduction to generate the alcohol **21** as a 5:1 mixture of diastereomers by NMR (presumably 3R*,4S*:3R*,4R* according to Felkin-Ahn rules). We did not separate the diastereomers at this point because we chose to determine the relative-binding affinities of the diastereomeric mixture of rhenium complexes, not knowing which would be of higher affinity. If appreciable binding were observed, we then would have made efforts to separate the two diastereomers.

Mesylation of alcohol **21**, followed by displacement with thioacetate, generated the thioacetate **22** in low yield. A competing elimination reaction to produce the trisubstituted olefin and the difficulty of an S_N2 attack of the thioacetate on the highly hindered secondary carbon are thought to be responsible for the low yield. Typical Mitsunobu conditions to generate the thioacetate failed for this reaction. In addition, attempts to form the thiol via BuLi-assisted reductive fragmentation of a thioketal (derived from ketone **20**) failed (*46*), and reduction of the Lawesson's Reagent-produced thioketone (also derived from ketone **20**) was also unsuccessful. The thioacetate **22** was subjected to the same acidic conditions as in Schemes 1 and 2 to generate the thiol **23** in modest yield; the yield was again limited by acid-catalyzed formation of the olefin. However, in contrast to thiols **9ab** or **15**, when the thiol was subjected to the standard complexation conditions, complex **2** failed to form. Efforts to generate the complex by changing the temperature, order of reagent addition, and rhenium source also failed. It is believed that the difficulty in producing this complex is again due to the highly hindered nature of the secondary thiol used in the reaction, especially considering the fact that complexation of thiol **15**, which lacks just one of the

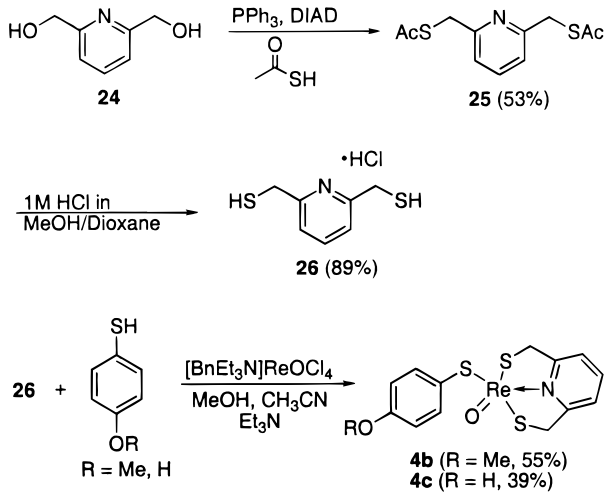
Scheme 2



Scheme 3



Scheme 4



ethyl groups, results in clean formation of complex **6** (Scheme 2).

*Synthesis of Complexes That Mimic a Tetrahydrochrysene Estrogen (**4a**−**c**).* Complexes **4a**−**c** were designed to mimic a tetrahydrochrysene (THC) estrogen (cf. Figure 1). The reasoning behind including complexes with and without the *p*-hydroxy functionality on the tridentate ligand was to compare the effect this would have on the relative-binding affinity. One would expect the binding to be appreciably higher in **4a** where both hydroxyls are present, as this best represents the THC that the complex is trying to mimic. Alternatively, when one removes the *p*-hydroxy group from the tridentate ligand (as in **4b** and **4c**) or protects the hydroxy on the monodentate ligand (**4b**), one should see a dramatic drop in binding affinity compared to **4a**.

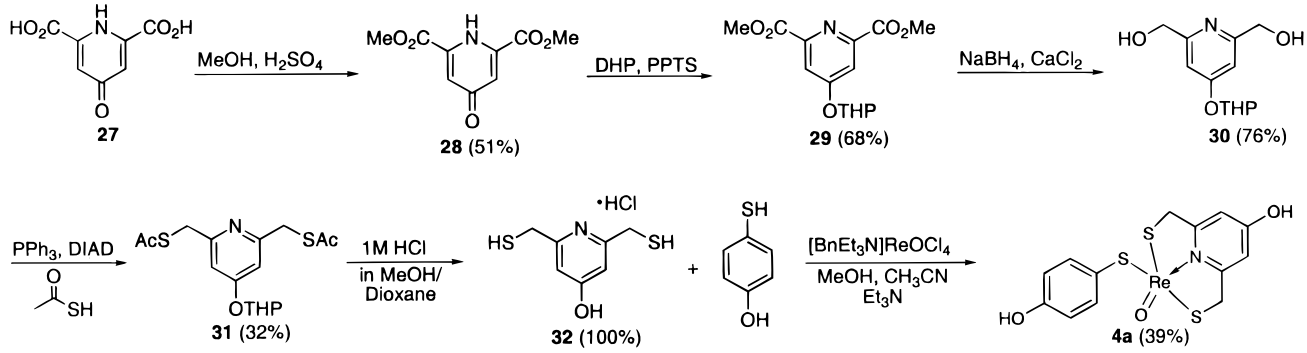
We synthesized the tridentate pyridine dithiol ligand for **4b** and **4c**, which does not contain the *p*-hydroxy group, by starting with commercially available 2,6-pyridinedimethanol (**24**, Scheme 4). The Mitsunobu reaction was then used to transform the diol **24** into the dithioacetate **25** after recrystallization. Thioacetate **25** was then treated with anhydrous hydrochloric acid under argon to afford the dithiol **26** as the HCl salt in good yield. Subjecting the crude dithiol **26** to standard complexation conditions with either *p*-methoxythiophenol or *p*-hydroxythiophenol afforded the red complexes **4b** and **4c**, respectively.

A concern that we had prior to the successful formation of these complexes was that the planar aromatic pyridine would inhibit bonding of the tridentate ring to the oxorhenium core, because of the rigidity it enforces on the framework of the tridentate ligand. However, all complexation reactions involving this type of tridentate ligand went smoothly, and all of the complexes produced were stable to air and moisture for extended periods of time. To our knowledge, this is the first example of a benzylic dithiopyridine complexed to an oxorhenium center.

The synthesis of complex **4a** requires the use of a starting material which will eventually give a tridentate ligand having a *p*-hydroxy functionality. To this end, we started with commercially available chelidamic acid (**27**, Scheme 5). Esterification provides the diester **28**, which, upon protection of the phenol with DHP, gives the fully protected diester **29** (*42*). Although LAH was not effective in reducing the diesters, a mixture of $NaBH_4$ and $CaCl_2$ produced diol **30** in good yield (*43*). The thioacetates were then introduced by using the standard Mitsunobu conditions to give the dithioacetate **31**. Removal of the thioacetates under acidic conditions also conveniently removed the THP group, giving the desired tridentate dithiol **32** as the very hygroscopic HCl salt, in quantitative yield. The crude **32** was then subjected to the standard complexation conditions to give the novel rhenium complex **4a** in modest yield.

*Variable Temperature NMR Studies on the Fluxional 3+1 Complex **4a**.* An X-ray crystal structure of a complex similar to **4b** (where there is no *para* hydroxyl on the pyridine ring) shows that the arenethiolate ligand is bent toward one side of the molecule (*47*). Therefore, **4a** is asymmetric, and VT NMR studies on **4a** seem to confirm this observation (Figure 2). At −60 °C, the rotation of the arenethiolate ligand is slow on the NMR time scale, and the magnetically inequivalent benzylic and meta protons of the tridentate ligand appear as two sharp sets of AB quartets and two singlets, respectively. As the temperature is elevated, these peaks start to coalesce as the arenethiolate ligand flips back and forth more rapidly. This is evident at 16 °C where these signals are significantly broadened. At 95 °C, the rotation of the arenethiolate ligand is fast on the NMR time scale, and one observes a symmetric time-averaged structure. This is evident by the fact that the two singlets at −60 °C have now nicely coalesced into one singlet at 95 °C. Similarly,

Scheme 5



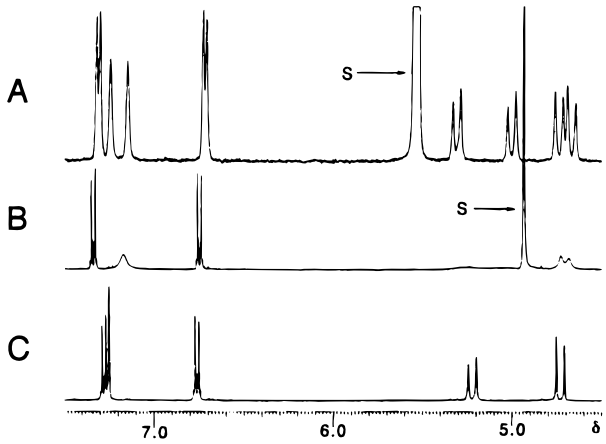


Figure 2. VT NMR of **4a** [A (CD_3OD, −60 °C); B (CD_3OD, 16 °C); C (DMSO-d_6, 95 °C)].

Table 1. Relative-Binding Affinity (RBA) and Log $P_{o/w}$ Values of Rhenium Complexes

complex	RBA (0 °C)	log $P_{o/w}$
1	100	3.98
5a	<0.006	
5b	0.018	
6	0.005	
4a	0.035	5.35
4b	<0.01	4.14
4c	0.01	3.46

the two sets of AB quartets at −60 °C have coalesced into one AB quartet at 95 °C.

Estrogen Receptor Binding Affinities and Lipophilicities. The ER binding affinities and lipophilicities of the rhenium complexes **5a**−**b**, **6**, and **4a**−**c** are shown in Table 1. The affinities were expressed as relative-binding affinities (RBA), where estradiol has a value of 100. RBA values were determined by a competitive radiometric binding assay at 0 °C, using lamb cytosol as the source for ER and [^{3}H]estradiol as the tracer. Unfortunately, all complexes showed only micromolar affinities for the ER. Considering the low RBA values of the estradiol mimic series, **5ab** and **6**, it is unlikely that the introduction of the second ethyl group would have changed the binding affinities dramatically had we been successful in preparing complex **2**. The THC mimic series (**4a**−**c**) also showed very low-binding affinities. There is a reasonable trend in the values, in that the complexes with one or more phenols show better RBA values than those without (**4a** > **4c** > **4b**). However, the significance of this trend at very low affinities is uncertain.

The lipophilicities of the THC mimics were determined by measuring their log $P_{o/w}$ values according to the method of Minick (*44*). The values of **4b** and **4c** (4.14 and 3.46, respectively) are rather similar to that of estradiol, while **4a**, which one would expect to be even more polar than **4c** because of the addition of a hydroxyl group, has a remarkably high log $P_{o/w}$ value of 5.35 by this method, even though normal-phase TLC and solubility in polar organic solvents show the opposite trend. The unique and not well-understood properties of this novel rhenium complex structure, especially its interactions with the reversed-phase HPLC column used to determine the log $P_{o/w}$ in this experiment, might contribute to this unexpected result. It is interesting to note, however, that Kung and co-workers reported a similar finding in comparing the log $P_{o/w}$ values of N_2S_2 oxotechnetium complexes of the diamine vs amine-amide type (*48*). The replacement of two hydrogens with an oxo substituent in this case resulted in an 8-fold increase in the log $P_{o/w}$ value.

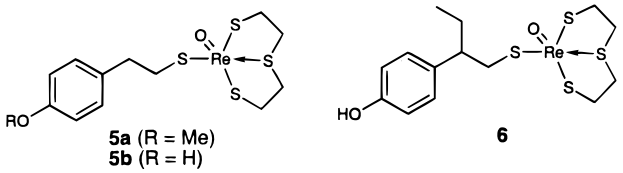
CONCLUSIONS

We have described the synthesis of a number of novel "3+1" oxorhenium(V) complexes (**4a**−**c**, **5ab**, and **6**) for use as estrogen mimics and have determined their binding affinites for the estrogen receptor (ER). We were also able to synthesize the monodentate ligand **23** needed to prepare complex **2** (the best mimic of estradiol); however, the hindered nature of the thiol in **23** prevented this ligand from complexing with rhenium to form the desired complex. The relative-binding affinity (RBA) values of the estradiol model complexes (**5a**, **5b**, and **6**) are low (the highest value is 0.018% vs 100% for estradiol) and indicate that these complexes are not, in fact, good mimics of estradiol.

The series of pyridinedithiol complexes **4a**−**c** as mimics for THC have also been synthesized. These pyridinedithiol oxorhenium complexes are the first of their kind. The complexes are quite stable to air and moisture, and VT NMR studies reveal the fluxional nature of the arenethiolate ligand in these complexes. These complexes also have poor binding affinity to the ER. The lipophilicity of complexes **4b** and **4c** is fairly close to that of estradiol, while complex **4a** shows a log $P_{o/w}$ value much higher than expected. Even though molecular modeling suggests that the distance between the phenolic hydroxyl groups in complex **4a** is actually comparable to that of diethylstilbestrol compounds (*49*), the location of the polar and bulky square pyramidal oxorhenium core toward the center of a normally lipophilic region of steroidal and nonsteroidal estrogens might account for the low binding affinity observed for the THC class mimics (*30*).

The low binding affinity of all complexes described here is probably due to the poor geometric and electronic match between the complexes and the native ligands. Future work on these integrated complexes will involve

Chart 1



5a (R = Me)
5b (R = H)

6

the use of a chelate system whose geometry (e.g., square planar) and arrangement of polar moieties is more akin to that of the native ligands.

ACKNOWLEDGMENT

We are grateful for the support of this research through grants from the Department of Energy (DE FG02 86ER60401) and the National Institutes of Health (PHS 5 R01 CA25836). The assistance of Ms. Kathy E. Carlson in the receptor-binding experiments is appreciated. Helpful discussions regarding molecular modeling, log $P_{o/w}$ measurements, and X-ray crystal structures from Frank Wüst are also deeply appreciated. NMR experiments were performed in the Varian Oxford Instrument Center for Excellence NMR Laboratory (VOICE NMR Lab), in part funded by grants from the National Institutes of Health (PHS 1 S10 RR1044-01), the National Science Foundation (NSF CHE 96-0152), and the Keck Foundation. Mass spectral data were acquired on spectrometers purchased with funds in part from the Division of Research Resources, National Institutes of Health (RR 01575 and RR 04648), the National Science Foundation (PCM 8121494), and the National Institute of General Medical Sciences (GM27029).

LITERATURE CITED

(1) Harris, J. R., Lipman, M. E., Veronesi, U., and Willett, W. (1992) Breast cancer. *N. Engl. J. Med. 327*, 319.

(2) Feuer, E. J., Wun, L. M., Boring, C. C., Flanders, W. D., Timmel, M. J., and Tong, T. (1993) The lifetime risk of developing breast cancer. *J. Natl. Cancer Inst. 85*, 892.

(3) American Cancer Society (1996) *Cancer Facts and Figures*.

(4) McGuire, W. L. (1975) *Estrogen Receptors in Human Breast Cancer*. Raven Press, New York.

(5) Cummins, C. H. (1993) Radiolabeled steroidal estrogens in cancer research. *Steroids 58*, 245.

(6) VanBrocklin, H. F., Pomper, M. G., Carlson, K. E., Welch, M. J., and Katzenellenbogen, J. A. (1992) Preparation and evaluation of 17-ethynyl-substituted 16α-[^{18}F]fluoroestradiols: Selective receptor-based PET imaging agents. *Int. J. Rad. Appl. Instrum. B 19*, 363−374.

(7) VanBrocklin, H. F., Carlson, K. E., Katzenellenbogen, J. A., and Welch, M. J. (1993) 16*β*-([^{18}F]Fluoro)estrogens: Systematic investigation of a new series of fluorine-18-labeled estrogens as potential imaging agents for estrogen-receptor-positive breast tumors. *J. Med. Chem. 36*, 1619−1629.

(8) VanBrocklin, H. F., Rocque, P. A., Lee, H. V., Carlson, K. E., Katzenellenbogen, J. A., and Welch, M. J. (1993) 16*β*-[^{18}F]Fluoromoxestrol: a potent, metabolically stable positron emission tomography imaging agent for estrogen receptor positive human breast tumors. *Life Sci. 53*, 811−819.

(9) VanBrocklin, H. F., Liu, A., Welch, M. J., O'Neil, J. P., and Katzenellenbogen, J. A. (1994) The synthesis of 7α-methyl-substituted estrogens labeled with fluorine-18: Potential breast tumor imaging agents. *Steroids 59*, 34−45.

(10) Kochanny, M. J., VanBrocklin, H. F., Kym, P. R., Carlson, K. E., O'Neil, J. P., Bonasera, T. A., Welch, M. J., and Katzenellenbogen, J. A. (1993) Fluorine-18-labeled progestin ketals: Synthesis and target tissue uptake selectivity of potential imaging agents for receptor-positive breast tumors. *J. Med. Chem. 36*, 1120−1127.

(11) Brandes, S. J., and Katzenellenbogen, J. A. (1987) Fluorinated androgens and progestins: molecular probes for androgen and progesterone receptors with potential use in positron emission tomography. *Mol. Pharmacol. 32*, 391−403.

(12) Buckman, B. O., Bonasera, T. A., Kirschbaum, K. S., Welch, M. J., and Katzenellenbogen, J. A. (1995) Fluorine-18-labeled progestin 16α,17α-dioxolanes: Development of high-affinity ligands for the progesterone receptor with high in vivo target site selectivity. *J. Med. Chem. 38*, 328−337.

(13) Pomper, M. G., Katzenellenbogen, J. A., Welch, M. J., Brodack, J. W., and Mathias, C. J. (1988) 21-[^{18}F]Fluoro-16α-ethyl-19-norprogesterone: Synthesis and target tissue selective uptake of a progestin receptor based radiotracer for positron emission tomography. *J. Med. Chem. 31*, 1360−1363.

(14) Pomper, M. G., Pinney, K. G., Carlson, K. E., van Brocklin, H., Mathias, C. J., Welch, M. J., and Katzenellenbogen, J. A. (1990) Target tissue uptake selectivity of three fluorine-substituted progestins: Potential imaging agents for receptor-positive breast tumors. *Int. J. Rad. Appl. Instrum. B 17*, 309−319.

(15) Verhagen, A., Luurtsema, G., Pesser, J. W., de Groot, T. J., Wouda, S., Oosterhuis, J. W., and Vaalburg, W. (1991) Preclinical evaluation of a positron emitting progestin ([^{18}F]-fluoro-16α-methyl-19-norprogsterone) for imaging progesterone receptor positive tumours with positron emission tomography. *Cancer Lett. 59*, 125−132.

(16) Verhagen, A., Elsinga, P. H., de Groot, T. J., Paans, A. M. J., deGoeij, C. C. J., Sluyser, M., and Vaalburg, W. (1991) A fluorine-18 labeled progestin as an imaging agent for prostestin receptor positive tumors with positron emission tomography. *Cancer Res. 51*, 1930−1933.

(17) Hochberg, R. B., Hoyte, R. M., and Rosner, W. (1985) E−17α-(2-[^{125}I]iodovinyl)-19-nortestosterone: The synthesis of a gamma emitting ligand for the progesterone receptor. *Endocrinology 117*, 2550−2552.

(18) Hochberg, R. B., MacLusky, N. J., Chambers, J., Eisenfeld, A. J., Naftolin, F., and Schwartz, P. E. (1985) Concentration of [16α-^{125}I]iodoestradiol in human ovarian tumors in vivo and correlation with estrogen receptor content. *Steroids 46*, 775−778.

(19) Hoyte, R. M., Rosner, W., Johnson, I. S., Zielinski, J., and Hochberg, R. B. (1985) Synthesis and evaluation of potential radioligands for the progesterone receptor. *J. Med. Chem. 28*, 1695−1699.

(20) Lamb, D. J., Bullock, D. W., Hoyte, R. M., and Hochberg, R. B. (1988) D9-[16α-^{125}I]iodo-19-nortestosterone: a gamma-emitting photoaffinity label for the progesterone receptor. *Endocrinology 122*, 1923−1932.

(21) Salman, M., Stotter, P. L., and Chamness, G. C. (1989) ^{125}I−Ligand for progesterone receptor: 17α-(6′-iodohex-1′-ynyl)-19-nortestosterone. *J. Steroid Biochem. 33*, 25−31.

(22) DiZio, J. P., Fiaschi, R., Davison, A., Jones, A. G., and Katzenellenbogen, J. A. (1991) Progestin−rhenium complexes: Metal-labeled steroids with high receptor binding affinity, potential receptor-directed agents for diagnostic imaging or therapy. *Bioconjugate Chem. 2*, 353.

(23) DiZio, J. P., Anderson, C. J., Davison, A., Ehrhardt, G. J., Carlson, K. E., and Welch, M. J. (1992) Technetium- and rhenium-labeled progestins: Synthesis, receptor binding and in vivo distribution of an 11*β*-substituted progestin labeled with technetium-99 and rhenium-186. *J. Nucl. Med. 33*, 558.

(24) O'Neil, J. P., Carlson, K. E., Anderson, C. J., Welch, M. J., and Katzenellenbogen, J. A. (1994) Progestin radiopharmaceuticals labeled with technetium and rhenium: Synthesis, binding affinity, and in vivo distribution of a new progestin N_2S_2-metal conjugate. *Bioconjugate Chem. 5*, 182.

(25) Top, S., Vessieres, A., and Jaouen, G. (1994) Synthetic strategy for organometallic complexes of rhenium with exceptionally high affinity for the oestradiol receptor; their potential use as imaging and therapeutic agents. *J. Chem. Soc., Chem. Commun.* 453.

(26) Top, S., El Hafa, H., Vessieres, A., Quivy, J., Vaissermann, J., Hughes, D. W., McGlinchey, M. J., Mornon, J. P., Thoreau, E., and Jaouen, G. (1995) Rhenium carbonyl complexes of *β*-estradiol derivatives with high affinity for the estradiol receptor: An approach to selective organometallic radiopharmaceuticals. *J. Am. Chem. Soc. 117*, 8372.

(27) Wüst, F., Spies, H., and Johannsen, B. (1996) Synthesis of "3+1" mixed-ligand oxorhenium(V) complexes containing modified 3,17β-estradiol. *Bioorg. Med. Chem. Lett. 6*, 2729.

(28) Wüst, F., Spies, H., and Johannsen, B. (1997) Synthesis of 17α-substituted mercaptoalkynyl derivatives of 3,17β-estradiol. *Tetrahedron Lett. 38*, 2931.

(29) Wüst, F. R., Carlson, K. E., Katzenellenbogen, J. A., Spies, H., and Johannsen, B. (1999) Synthesis and binding affinities of new 17α-substituted estradiol-rhenium mixed-ligand and thioether-carbonyl complexes. *Steroids* (in press).

(30) Hom, R. K., and Katzenellenbogen, J. A. (1997) Synthesis of a tetradentate oxorhenium(V) complex mimic of a steroidal estrogen. *J. Org. Chem. 62*, 6290.

(31) Sugano, Y., and Katzenellenbogen, J. A. (1996) Synthesis of tetradentate bisamino-bisthiol complexes of oxorhenium(V) as structural mimics of steroids. *Bioorg. Med. Chem. Lett. 6*, 361.

(32) Chi, D. Y., O'Neil, J. P., Anderson, C. J., Welch, M. J., and Katzenellenbogen, J. A. (1994) Homodimeric and heterodimeric bis(aminothiol) oxometal complexes with rhenium(V) and technetium(V). Control of heterodimeric complex formation and an approach to metal complexes that mimic steroid hormones. *J. Med. Chem. 37*, 928.

(33) Spies, H., Fietz, T., Glaser, M., Pietzsch, H. J., and Johannsen, B. (1995) *The "n+1" concept in the synthesis strategy of novel rhenium and technetium tracers* (M. Nicolini, G. Bandoli, and U. Mazzi, Eds.)Vol. 4, pp 243−246, SGEditoriali, Padova, Italy.

(34) Mastrostamatis, S. G., Papadopoulas, M. S., Pirmettis, I. C., Paschali, E., Varvarigou, A. D., Stassinopolou, C. I., Raptapoulou, C. P., Terzis, A., and Chiotellis, E. (1994) Tridentate ligands containing the SNS donor atom set as a novel backbone for the development of technetium brain-imaging agents. *J. Med. Chem. 37*, 3212.

(35) Pirmettis, J. C., Papadopoulas, M. S., Mastrostamatis, S. G., Raptopoulou, C. P., Terzis, A., and Chiotellis, E. (1996) Synthesis and characterization of oxotechnetium(V) mixed-ligand complexes containing a tridentate N-substituted bis-(2-mercaptoethyl)amine and a monodentate thiol. *Inorg. Chem. 35*, 1685.

(36) Niccolini, M., Bandoli, G., and Mazzi, U. (1995) *Technetium and Rhenium in Chemistry and Nuclear Medicine 4*, SGEditoriali, Padova, Italy.

(37) Okuno, H., Uoto, K., Tomohiro, T., and Youinou, M. T. (1990) Synthesis of tetranuclear iron-sulphur protein analogues with tetrathiol ligands attached to macrocycles which provide intramolecular hydrophobic domains. *J. Chem. Soc., Dalton Trans.* 3375.

(38) Spies, H., Fietz, T., Pietzsch, H. J., Johannsen, B., Leibnitz, P., Reck, G., Scheller, D., and Klosterman, K. (1995) Neutral oxorhenium(V) complexes with tridentate dithiolates and monodentate alkane- or arene-thiolate coligands. *J. Chem. Soc., Dalton Trans.* 2277.

(39) Aaron, C., Dull, D., Schmiegel, J. L., Jaeger, D., Ohashi, Y., and Mosher, H. S. (1967) The resolution and configuration of α-substituted phenylacetic acids. *J. Org. Chem. 32*, 2797.

(40) Myers, T. C., Pratt, R. J., Morgan, R. L., O'Donnell, J., and Jensen, E. V. (1955) Hormone analogues. I. Preparation of intermediate ketones for the synthesis of stilbestrol analogues. *J. Am. Chem. Soc. 77*, 5655.

(41) Logusch, E. W. (1988) A simple preparation of *S*-alkyl homocysteine derivatives: *S*-phosphonomethyl homocysteines as inhibitors of glutamine synthetase. *Tetrahedron Lett. 29*, 6055.

(42) Bradshaw, J. S., Colter, M. L., Nakatsuji, Y., Spencer, N. O., Brown, M. F., Izatt, R. M., Arena, G., Tse, P.-K., Wilson, B. E., Lamb, J. D., and Dalley, N. K. (1985) Proton-ionizable crown compounds. 2. Synthesis, complexation properties, and structural studies of macrocyclic polyether-diester ligands containing a 4-hydroxypyridine subcyclic unit. *J. Org. Chem. 50*, 4865.

(43) Scrimin, P., Tecilla, P., Tonellato, U., and Vendrame, T. (1989) Aggregate structure and ligand location strongly influence Cu^{2+} binding ability of cationic metallosurfactants. *J. Org. Chem. 54*, 5988.

(44) Minick, D. J., Frenz, J. H., Patrick, M. A., and Brent, D. A. (1988) A comprehensive method for determining hydrophobicity constants by reverse-phase high-performance liquid chromatography. *J. Med. Chem. 31*, 1923.

(45) Katzenellenbogen, J. A., Johnson, H. J., Jr., and Myers, H. N. (1973) Photoaffinity labels for estrogen binding proteins of rat uterus. *Biochemistry. 12*, 4085.

(46) Wilson, S. R., Caldera, P., and Jester, M. A. (1982) Synthesis of sulfides and mercaptans from thioketals. *J. Org. Chem. 47*, 3319.

(47) The crystal structure of this complex was kindly provided by Frank Wüst at the Forschungszentrum Rossendorf e.V., Dresden, Germany.

(48) Meegalla, S. K., Plossl, K., Kung, M. P., Chumpradit, S., Stevenson, D. A., Kushner, S. A., McElgin, W. T., Mozley, P. D., and Kung, H. F. (1997) Synthesis and characterization of Tc-99m labeled tropanes as dopamine transporter imaging agents. *J. Med. Chem. 40*, 9−17.

(49) Wüst, F. R. (1998) Forschungszentrum Rossendorf e.V., Dresden, Germany (personal communication).

BC980094Q

TECHNICAL NOTES

Comparison of the Stability of Technetium-Labeled Peptides to Challenge with Cysteine

M. A. Stalteri,[†] S. Bansal,[‡] R. Hider,[‡] and S. J. Mather*[,†,‡]

Imperial Cancer Research Fund, Department of Nuclear Medicine, St. Bartholomew's Hospital, West Smithfield, London EC1A 7BE, U.K., and Department of Pharmacy, King's College, London, U.K. Received April 30, 1998; Revised Manuscript Received September 29, 1998

We have labeled a series of short peptides with technetium-99m either by direct labeling at pH 11 or by exchange from [^{99m}Tc]technetium glucoheptonate. Typical labeling yields obtained were as follows: *N*-acetyl-Gly-Cys(*S*-Acm)-Gly-Cys(*S*-Acm)-Gly-NH_2 (Acm = acetamidomethyl) 99%, *S*-benzoyl-mercaptoacetyltriglycine (*S*-Benzoyl-MAG3) 95%, mercaptoacetyldiglycine-NH_2 (MAG2-NH_2) 94%, MAG3 92%, *N*-acetyl-Aib-Aib-Cys-NH_2 (Aib = aminoisobutyric acid) 91%, Gly-Gly-Gly-Gly 90%, *N*-acetyl-Gly-Gly-Cys-Gly 87%, cyclo-1,4-(Gly-Gly-Gly-Gln) 40%, *S*-methyl-MAG2-NH_2 0%. In the absence of cysteine, all of the labeled peptides were quite stable in solution, with at least 80−90% of the labeled peptide remaining at 24 h. The order of stability of the labeled peptides to challenge with cysteine was found to be MAG3 > *S*-benzoyl-MAG3 > *N*-acetyl-Gly-Cys(*S*-Acm)-Gly-Cys(*S*-Acm)-Gly-NH_2 > *N*-acetyl-Aib-Aib-Cys-NH_2 > MAG2-NH_2 > *N*-acetyl-Gly-Gly-Cys-Gly > cyclo-1,4-(Gly-Gly-Gly-Gln) > Gly-Gly-Gly-Gly. The peptides without a sulfur donor were least stable to challenge with cysteine.

INTRODUCTION

Radiolabeled peptides have great potential as radiopharmaceuticals (Fischman, 1993; Thakur, 1995; Hom and Katzenellenbogen, 1997; Liu et al., 1997). Naturally occurring peptides are involved in many biological processes, where they may function as hormones, neurotransmitters, cytokines or growth factors. The low molecular weights of peptides, compared to other biomolecules such as antibodies and antibody fragments, result in faster localization and blood clearance. The rapid pharmacokinetics are ideal for labeling peptides with a radioisotope that has a short half-life, such as technetium-99m (Lister-James et al., 1997).

In previous work (Mather et al., 1995), we described the use of hybrid peptides which contain both receptor-binding and technetium-chelating amino acid sequences. Such peptides can easily be prepared by solid-phase synthesis techniques, and amino acid sequences designed to chelate technetium can be incorporated at sites where the biological activity will not be affected. This approach has also been used by Lister-James et al. (Lister-James et al., 1995, 1996; Pearson et al., 1996a,b) in the development of technetium-labeled somatostatin receptor-binding peptides and thrombus imaging peptides.

The renal function agent MAG3 was the first peptide-derived technetium chelator to be developed. Deprotonation of three of the amide nitrogens and deprotection/deprotonation of the sulfur during the labeling process gives an N3S triamide thiol ligand which forms a stable complex with a technetium(V) oxo core. MAG2 forms a similar type of complex with technetium-99m, acting as a tetradentate S,N,N,O donor ligand, with the terminal carboxyl group acting as an O donor (Johannsen et al., 1993). N4 donor tetrapeptides, such as tetraglycine, also form stable complexes with technetium-99m, with three deprotonated amide nitrogens and one amine nitrogen coordinated to technetium (Vanbilloen et al., 1995).

In previous work (Mather et al., 1995), we investigated the use of the peptide sequence Gly-Gly-Cys as a technetium chelator. Like MAG3, the Gly-Gly-Cys sequence can act as a triamide thiol ligand. Lister-James and coworkers have developed peptides with the technetium-chelating sequences Gly-Gly-Cys, Cys-Gly-Cys and Lys-Gly-Cys, which provide triamide thiol, diamide dithiol, and diamide amine thiol chelating ligands, respectively (Lister-James et al., 1996). Peers et al. are developing peptides for imaging inflammation using the *N*-dimethyl-Gly-Ser-Cys sequence as a technetium chelator (Peers et al., 1997). Peptide sequences therefore show great promise as chelators for technetium-99m. Factors such as the overall charge around the metal center or the side chains on the chelating amino acids may affect the biodistribution and receptor-binding affinity of technetium-labeled peptides, but the performance of a particular chelator will also depend on its ability to retain the technetium in vivo. Trans-chelation to other sulfur-containing ligands has been shown to be an important route of radiopharmaceutical instability (Pearson et al., 1996a). Thus, it would be useful to explore the technetium chelating abilities of different peptide sequences and the stability of their complexes.

In the present work, we have investigated the labeling,

* To whom correspondence should be addressed. Phone: 44-171-601-7153. Fax: 44-171-796-3907. E-mail: mather@icrf.icnet.uk.
[†] St. Bartholomew's Hospital.
[‡] King's College.

10.1021/bc9800466 CCC: $18.00 © 1999 American Chemical Society
Published on Web 12/16/1998

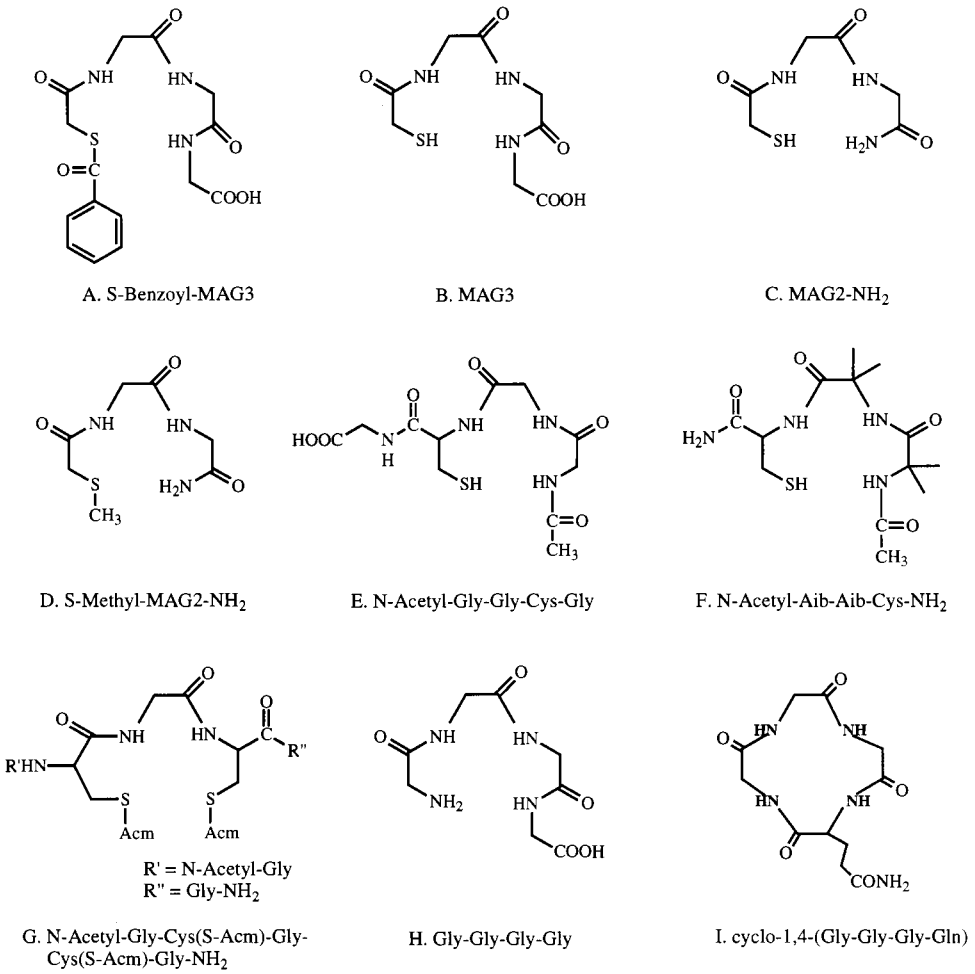


Figure 1. Structures of the peptide derivatives (a) *S*-benzoyl-MAG3, (b) MAG3, (c) MAG2-NH_2, (d) S-methyl-MAG2-NH_2, (e) *N*-acetyl-Gly-Gly-Cys-Gly, (f) *N*-acetyl-Aib-Aib-Cys-NH_2, (g) *N*-acetyl-Gly-Cys(*S*-Acm)-Gly-Cys(*S*-Acm)-Gly-NH_2, (h) Gly-Gly-Gly-Gly, and (i) cyclo-1,4-(Gly-Gly-Gly-Gln).

solution stability, and stability to cysteine challenge of a series of peptides (Figure 1), including the sequences -Gly-Gly-Cys-, -Cys-Gly-Cys-, MAG3, and tetraglycine in order to compare their suitability as technetium chelators.

MATERIALS AND METHODS

Radioisotope. Sodium [^{99m}Tc]pertechnetate was obtained from an Amertec II technetium-99m generator (Amersham, UK).

Reagents for Peptide Synthesis. Tetraglycine was obtained from Sigma (Poole, U.K.). *S*-Benzoyl-MAG3 was obtained as a commercial kit (TechneScan MAG3, Mallinckrodt Medical, Petten, Holland). *p*-(9-Fluorenylmethoxycarbonyl-amino)-2,4-dimethoxybenzyl)phenoxyacetic acid (Rink amide linker), Tentagel resin, suitably protected Nα-9-fluorenylmethyloxycarbonyl (Fmoc) amino acids, and [2-(1*H*-benzotriazole-1-yl]-1,1,3,3-tetramethyluronium tetrafluoroborate (TBTU) were obtained from NovaBiochem (U.K.). Dimethylformamide (DMF) was freshly distilled by fractional distillation at reduced pressure. All organic solvents were of analytical reagent grade quality or better. 2-[(Triphenylmethyl)thio]acetic acid was prepared by reaction of mercaptoacetic acid with triphenylmethanol and boron trifluoride etherate in acetic acid according to published methods (Brenner et al., 1984).

Peptide Synthesis. Peptides were synthesized by solid-phase methods using a Milligen Biosearch 9050 Pepsynthesizer. Concentrations were performed under reduced pressure at temperatures of <30 °C. Positive FAB-MS were recorded on a double focused VG-Analytical 70-250S mass spectrometer. The FAB ions were produced by a beam of xenon atoms, 6 keV, from a matrix of 3-nitrobenzyl alcohol. HPLC was performed on a Waters Powerline System with a 990 photodiode array detector. The system was fitted with a Vydac reversed-phase C-18 column (218TP54) and a semipreparative column. Solvent system A was 0.1% trifluoroacetic acid (TFA) and B was 0.1% TFA in 90% acetonitrile; 10% water was employed for both analytical (1 mL/min) and preparative (5 or 7 mL/min) separations and detection was at 230 nm.

Synthesis of *N*-Acetyl-Aib-Aib-Cys-NH_2. Solid-phase synthesis was performed on Tentagel resin (1 g, 0.41 mequiv/g, 0.41 mmol). Nα-Fmoc deprotection was performed with a flow of 20% piperidine in DMF for 12 min. Fmoc-Cys(Trt)OPfp (Trt = trityl, Pfp = pentafluorophenyl) was coupled for 1 h in the presence of 1-hydroxybenzotriazole (HOBt), Fmoc-Aib-OH (4 equiv) was coupled for 2 h by recirculation after in situ preactivation with TBTU (3.9 equiv) and *N*-ethylmorpholine (NEM) (6 equiv), and N-terminal acetylation was performed with acetic anhydride (10% in DMF for 20 min). Each deprotection and acylation was followed by a DMF wash cycle for 15 min. After completion of the synthesis, the resin was washed with methanol (30 mL) then ether (30 mL) and dried in vacuo for 3 h. The peptide was cleaved from

the linker by treatment with TFA, water, phenol, triisopropylsilane (95:3:1:1, 15 mL, v/v) for 1 h followed by filtration, and the resin was washed with TFA (2 × 10 mL). The combined TFA solution was concentrated to dryness and the remaining material was precipitated by trituration with diethyl ether and then extracted with water. The crude product was obtained by lyophilization of the aqueous phase. The peptides MAG2-NH_2, *S*-methyl-MAG2-NH_2, *N*-acetyl-Gly-Gly-Cys-Gly, and *N*-acetyl-Gly-Cys(*S*-Acm)-Gly-Cys(*S*-Acm)-Gly-NH_2 were prepared in a manner similar to that described above.

MAG2-NH_2, FAB-MS $(M + Na)^+$: 228 calcd, 228 found. MAG3, FAB-MS $(M + Na)^+$: 286 calcd, 286 found.

N-Acetyl-Gly-Cys(Acm)-Gly-Cys(Acm)-Gly-NH_2, FAB-MS $(M+H)^+$: 579 calcd, 579 found.

Synthesis of cyclo-1,4-(Gly-Gly-Gly-Gln). Fmoc-Glu(OH)-OAll (All = allyl) was prepared by reaction of Fmoc-Glu(OtBu)-OH with allyl alcohol and diisopropylethylamine (DIPEA) followed by treatment with TFA according to published procedures (Kates et al., 1993). The Nα-Fmoc-Glu(OH)OAll was coupled to the Rink amide linker-Tentagel resin (0.27 mequiv/g, 1 g, 0.27 mmol) in DMF using TBTU (0.337 g, 1 mmol) and NEM (1.5 mmol), and the assembly of the peptide was completed as described above to afford Fmoc-Gly-Gly-Gly-Glu(Rink amide linker-Tentagel resin)-OAll. The allyl group from the α-carboxy group of the glutamate was removed by treatment with $Pd(PPh3)_4$ (2.7 mmol, 0.5 g) and HOBt (1.35 mmol, 40 mg), in a mixture of DMSO/DMF (1:1, 10 mL) under an argon atmosphere and in the dark for 18 h. On completion, the peptide-resin was filtered and washed with 0.5% DIPEA and 0.5% sodium diethyldithiocarbamate in DMF until the yellow coloration of the $Pd(PPh3)_4$ had been removed. The Nα-Fmoc group was removed with piperidine and the resin was washed with DMF. Cyclization of the peptide was performed with diisopropylcarbodiimide and HOBt, and the peptide was cleaved from the linker as described above and purified by HPLC.

FAB-MS$(M + Na)^+$: 320 calcd, 320 found.

High-Pressure Liquid Chromatography. Reversed-phase HPLC was performed using a Beckman System Gold dual pump system with a Beckman 166 UV detector at 220 nm, a 50 μL injection loop, and a Beckman Ultrasphere 5 μ ODS 4.6 mm × 25 cm column. Technetium-99m-labeled peptides were eluted at a flow rate of 1.0 mL/min using a 0.01 M sodium phosphate pH 6.0 (buffer A) to methanol (buffer B) gradient as follows: at $t = 0$ min, 5% B; $t = 3$ min, 5% B to 95% B over 10 min, linear gradient; $t = 13$ min, 95% B for 10 min; $t = 23$ min, 95% B to 5% B over 5 min, linear gradient; $t = 28$ min, 5% B for 2 min. Radioactivity was measured using a NaI(Tl) flow-through detector connected to a multichannel analyzer. The recovery was determined by collecting the eluate from the HPLC column for 30 min from the time of injection, and counting 1 mL aliquots in an LKB Wallac CompuGamma CS gamma counter, together with 1 mL aliquots of an appropriate dilution of the injectate.

Labeling with Technetium-99m. *Exchange Labeling.* A commercial glucoheptonate kit (Glucoheptoscint, Medgenix diagnostics, Fleurus, Belgium) containing 150 mg of sodium glucoheptonate, 50 mg of calcium glucoheptonate, 1.0 mg of stannous chloride dihydrate, and 0.3 mg of sodium sulfite was reconstituted with 2 mL of nitrogen-purged saline, divided into 200 μL aliquots and stored at −20 °C. A small amount of peptide was weighed accurately, and the appropriate amount of nitrogen-purged 0.5 M sodium phosphate buffer, pH 11, was added to give a 1 mg/mL peptide solution. The peptide solution was divided into 100 μL aliquots and stored at −20 °C. One hundred microliters of the reconstituted glucoheptonate kit was added to 100 μL of peptide solution. The mixture was vortexed, 100 μL of sodium [^{99m}Tc]pertechnetate (5−8 mCi) in saline was added, and the solution was either incubated at room temperature for 30 min or heated at 90 °C for 10 min in a shielded water bath, cooled to room temperature, and analyzed by reversed-phase HPLC.

Direct Labeling. Two microliters of a freshly prepared 113 mg/mL (0.5 M) solution of stannous chloride dihydrate in 1 M HCl was added to 100 μL of a 1 mg/mL peptide solution in 0.5 M sodium phosphate pH 11. One hundred microliters of sodium [^{99m}Tc]pertechnetate (5−8 mCi) in saline was then added, followed by 50 μL of 0.5 M sodium triphosphate. The solution was incubated at room temperature for 1 h, or heated at 90 °C in a water bath for 10 min, then analyzed by reversed-phase HPLC.

Labeling of *S*-Benzoyl-MAG3. *S*-Benzoyl-MAG3 was labeled essentially according to the manufacturer's instructions with 30 mCi of sodium [^{99m}Tc]pertechnetate in 4 mL of saline. The kit was then heated for 10 min in a boiling water bath, cooled to room temperature, and analyzed by reversed-phase HPLC.

Stability of Technetium-99m-Labeled Peptides. Peptides were labeled with technetium-99m as described above and analyzed by RP-HPLC. Eleven microliters of 0.5 M sodium phosphate buffer, pH 3, was added to 200 μL of technetium-99m-labeled peptide solution in order to adjust the pH to 7. The peptide solutions were then incubated at room temperature for 24 h. At various time points, aliquots of the solutions were removed and analyzed by RP-HPLC.

Cysteine Challenge. The pH of the technetium-99m-labeled peptide solutions was adjusted to pH 7 with 0.5 M phosphate buffer, and the solutions were diluted to a peptide concentration of 0.25 mg/mL. L-Cysteine hydrochloride monohydrate was dissolved in 0.5 M phosphate buffer to give 25 and 5 mg/mL solutions of cysteine with a pH of 7. Thirty microliters of each cysteine solution was added to 270 μL of labeled peptide solution, and the resulting solutions were incubated at 37 °C. The ^{99m}Tc-labeled peptides were not purified after labeling, and therefore tin and unlabeled peptides remained present in the solutions. The progress of the reactions was followed by RP-HPLC with radiometric detection.

RESULTS

Radiolabeling. The peptides shown in Figure 1 were labeled with technetium-99m either by direct labeling using stannous chloride dihydrate as the reducing agent or by exchange from [^{99m}Tc]technetium glucoheptonate using a commercial glucoheptonate kit. The reaction mixtures were either incubated at room temperature or heated to 90 °C for 10 min and then cooled to room temperature. *S*-Benzoyl-MAG3 was obtained as a commercial kit and was labeled by exchange from [^{99m}Tc]-tartrate with heating at 100 °C for 10 min. The labeling efficiencies were measured by reversed-phase HPLC with radiometric detection using a C18 column and a 0.01 M sodium phosphate pH 6.0 to methanol gradient. Typical labeling efficiencies for the peptides are given in Table 1, and HPLC radiochromatograms of the labeled peptides are shown in Figure 2. Peptides containing sulfur donors were labeled by transchelation from glucoheptonate or tartrate, whereas peptides without a sulfur donor were labeled by direct labeling. The peptides *N*-Acetyl-Aib-Aib-

Table 1. Labeling Yield and HPLC Data for ^{99m}Tc-Labeled Peptides

complex[a]	ligand type	retention time (min)	labeling yield (%)[b]	labeling method[c]	tin/peptide molar ratio
$[^{99m}TcO(MAG3)]^{2-}$ [d]	triamide thiol	9.0	95	1	0.08
$[^{99m}TcO(MAG3)]^{2-}$ [e]	triamide thiol	8.9	92	2	0.6
$[^{99m}TcO(MAG2\text{-}NH_2)]^{-}$	triamide thiol	13.5	94	2	0.5
$[^{99m}TcO(S\text{-methyl-MAG2-}NH_2)]$	triamide thioether		0	2	0.5
$[^{99m}TcO(N\text{-acetyl-Gly-Gly-Cys-Gly})]^{2-}$	triamide thiol	12.2	87	2	0.7
$[^{99m}TcO(N\text{-acetyl-Aib-Aib-Cys-}NH_2)]^{-}$	triamide thiol	13.2, 14.5	91	2	0.7
$[^{99m}TcO(N\text{-acetyl-Gly-Cys-Gly-Cys-Gly-}NH_2)]^{-}$	diamide dithiol	11.0	99	2	1.3
$[^{99m}TcO(Gly\text{-Gly-Gly-Gly})]^{-}$	triamide amine	10.5	90	3	2.5
$[^{99m}TcO(\text{cyclo-1,4-(Gly-Gly-Gly-Gln)})]^{-}$	tetraamide	12.0, 12.8	40	3	3.0
$[^{99m}TcO(\text{glucoheptonate})_2]^{-}$		2.3			
$^{99m}TcO_4^-$		3.1			

[a] Carboxylic acid groups are deprotonated under the conditions used for labeling and HPLC. [b] Average of several labelings. [c] 1 = exchange from 99mTc-tartrate, 2 = exchange from 99mTc-glucoheptonate, 3 = direct labeling. [d] Commercial kit containing *S*-benzoyl-MAG3. [e] Unprotected MAG3.

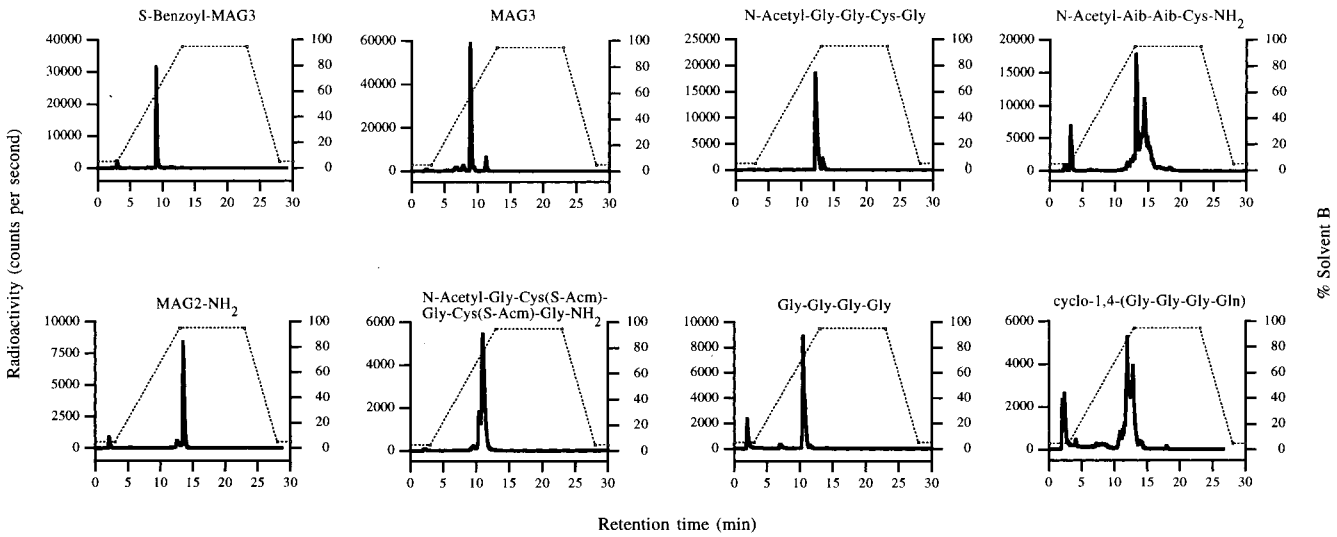


Figure 2. Reversed-phase HPLC radiochromatograms of the ^{99m}Tc-labeled peptides. Beckman Ultrasphere 5 μ ODS column; mobile phase 0.01 M sodium phosphate, pH 6.0 (A), methanol (B) gradient; flow rate 1.0 mL/min. (a) *S*-benzoyl-MAG3; (b) MAG3; (c) *N*-acetyl-Gly-Gly-Cys-Gly; (d) MAG2-NH_2; (e) *N*-acetyl-Aib-Aib-Cys-NH_2; (f) *N*-acetyl-Gly-Cys(*S*-Acm)-Gly-Cys(*S*-Acm)-Gly-NH_2; (g) Gly-Gly-Gly-Gly; (h) cyclo-1,4-(Gly-Gly-Gly-Gln).

Cys-NH_2, *N*-Acetyl-Gly-Cys(*S*-Acm)-Gly-Cys(*S*-Acm)-Gly-NH_2, and cyclo-1,4-(Gly-Gly-Gly-Gln) show more than one major peak in the HPLC radiochromatograms.

Typical labeling yields obtained were as follows: *N*-acetyl-Gly-Cys(*S*-Acm)-Gly-Cys(*S*-Acm)-Gly-NH_2 99%, *S*-benzoyl-MAG3 95%, MAG2-NH_2 94%, MAG3 92%, *N*-acetyl-Aib-Aib-Cys-NH_2 91%, Gly-Gly-Gly-Gly 90%, *N*-acetyl-Gly-Gly-Cys-Gly 87%, cyclo-1,4-(Gly-Gly-Gly-Gln) 40%, S-methyl-MAG2-NH_2 0%.

Stability of Technetium-99m-Labeled Peptides at pH 7. The pH of the labeled peptide solutions was adjusted to pH 7, and the solutions were incubated at room temperature for 24 h. The stability of the labeled peptides was monitored by RP-HPLC with radiometric detection. In the absence of cysteine, all of the labeled peptides were quite stable, with at least 80−90% of the labeled peptide remaining at 24 h.

Stability to Challenge with Cysteine. The stability of solutions of the labeled peptides at pH 7 and 37 °C to a challenge with cysteine at cysteine/peptide ratios of 2/1 and 10/1(w/w), corresponding to cysteine/peptide molar ratios in the ranges 3.4−6.0/1 and 17−30/1, was compared. The progress of the reactions was followed by HPLC. Figure 3 shows HPLC radiochromatograms of the reaction of technetium-99m-labeled *N*-acetyl-Gly-Gly-Cys-Gly with cysteine. The results of the cysteine challenge experiments are shown in Figure 4. The order of stability of the labeled peptides to challenge with cysteine was found to be MAG3 > *S*-benzoyl-MAG3 > *N*-acetyl-Gly-Cys(*S*-Acm)-Gly-Cys(*S*-Acm)-Gly-NH_2 > *N*-acetyl-Aib-Aib-Cys-NH_2 > MAG2-NH_2 > *N*-acetyl-Gly-Gly-Cys-Gly > cyclo-1,4-(Gly-Gly-Gly-Gln) > Gly-Gly-Gly-Gly. The peptides without a sulfur ligand were least stable to challenge with cysteine.

DISCUSSION

Five of the peptides we chose to study were triamide thiol ligands (Table 1). The other four peptides we studied included a triamide thioether, a diamide dithiol, a triamide amine and a tetraamide ligand, respectively. The peptides with a sulfur donor were labeled by transchelation from ^{99m}Tc-glucoheptonate or from ^{99m}Tc-tartrate in the case of *S*-benzoyl-MAG3. The peptides cyclo-1,4-(Gly-Gly-Gly-Gln) and Gly-Gly-Gly-Gly, which have a tetraamide and a triamide amine set of donors, respectively, were labeled by direct labeling at pH 11. High labeling yields were obtained for all the peptides except cyclo-1,4-(Gly-Gly-Gly-Gln) and *S*-methyl-MAG2-NH_2. All of the labeled peptides were stable in solution at pH 7.

In the case of the peptides *N*-acetyl-Aib-Aib-Cys-NH_2, *N*-acetyl-Gly-Cys(*S*-Acm)-Gly-Cys(*S*-Acm)-Gly-NH_2, and cyclo-1,4-(Gly-Gly-Gly-Gln), multiple unresolved peaks were present in the HPLC radiochromatograms. Square

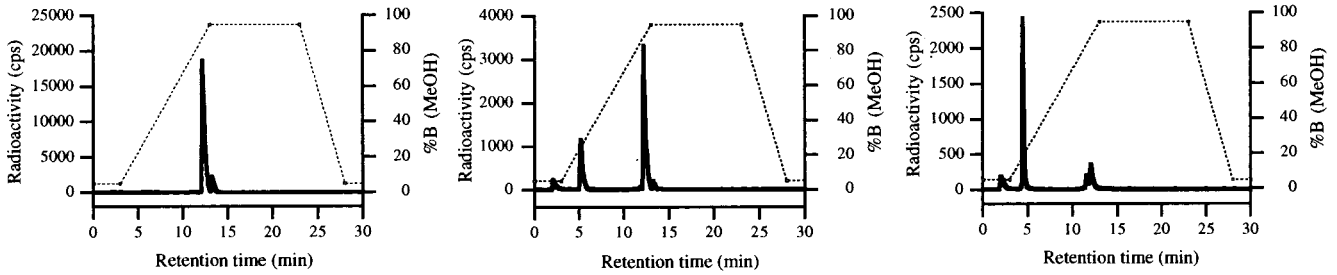


Figure 3. Reversed-phase HPLC radiochromatograms showing the time course of the reaction of ^{99m}Tc-labeled *N*-acetyl-Gly-Gly-Cys-Gly with cysteine. Beckman Ultrasphere 5 μ ODS column; mobile phase 0.01 M sodium phosphate pH 6.0 (A), methanol (B) gradient; flow rate 1.0 mL/min. (a) $t = 0$, (b) 10/1 cysteine/peptide, $t = 0.5$ h; retention times ^{99m}Tc-cysteine 5.2 min; [^{99m}TcO(*N*-acetyl-Gly-Gly-Cys-Gly)]$^{2-}$ 12.2 min, (c) 10/1 cysteine/peptide, $t = 2$ h; retention times ^{99m}Tc-cysteine 4.4 min; [^{99m}TcO(*N*-acetyl-Gly-Gly-Cys-Gly)]$^{2-}$ 11.6 min.

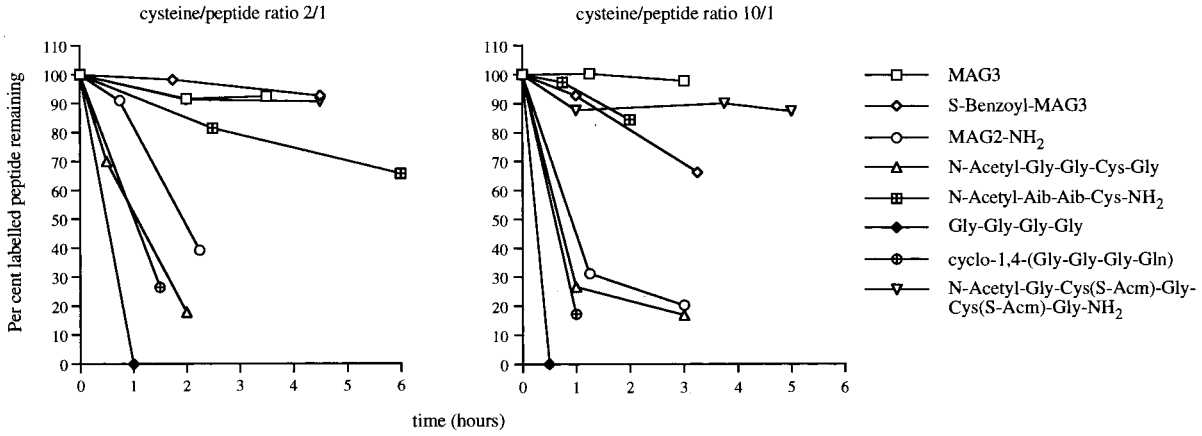


Figure 4. Percent of ^{99m}Tc remaining bound to peptide versus time after incubation with cysteine at 37 °C for cysteine-to-peptide ratios of 2/1 (left panel) and 10/1 (right panel).

pyramidal oxo-technetium complexes containing chiral centers on the ligand backbone may form diastereomers. (Liu et al., 1997). In the peptide cyclo-1,4-(Gly-Gly-Gly-Gln), the α carbon of the Gln residue is chiral. The Gln side chain can be either syn or anti with respect to the technetium-oxo core, thus diastereomers can be formed. *N*-Acetyl-Gly-Cys(*S*-Acm)-Gly-Cys(*S*-Acm)-Gly-NH_2 is a pentapeptide, and so more than one mode of coordination is possible. Diastereomers can be separated by HPLC, but the gradient we used was possibly too steep to resolve the various components.

Syn and anti isomers of square pyramidal complexes with a Tc-oxo core may show differences in stability and biodistribution (Vanbilloen et al., 1991), and it is therefore also possible that different isomers will show different stabilities to challenge with cysteine (Sharma, 1998). However, in the case of the peptides *N*-acetyl-Aib-Aib-Cys-NH_2, *N*-acetyl-Gly-Cys(*S*-Acm)-Gly-Cys(*S*-Acm)-Gly-NH_2, and cyclo-1,4-(Gly-Gly-Gly-Gln), which showed multiple unresolved components on HPLC analysis, we found no evidence that one of the components was more or less stable to cysteine than the others.

The low labeling efficiency obtained for cyclo-1,4-(Gly-Gly-Gly-Gln) may be due to the slow kinetics of labeling observed with macrocyclic ligands (Simon et al., 1981), or it may be due to the relative sizes of the technetium oxo core and the macrocyclic ring formed by the cyclic peptide. The 14 membered ring formed by the peptide may be either too small or too large for the technetium to be bound strongly in the plane of the four amide nitrogens. When the reaction mixture was monitored for several hours at room temperature after the initial heating step, the percent of labeled peptide was found to increase with time, from 40% at 30 min to 77% at 3 h. It is also possible that heating for 10 min is not enough to deprotonate the amide nitrogens. We obtained somewhat higher labeling yields at pH 12, but cleavage of peptide bonds is also more likely to occur at a pH greater than 11 (Bormans et al., 1995).

We chose to study the peptide *S*-methyl-MAG2-NH_2 in order to determine what effect, if any, the *S*-Me group would have on labeling and stability by comparison with MAG2-NH_2. Unprotected thiol groups are generally not stable and may oxidize to form disulfides, so it is more convenient to block the thiol with a protecting group (Bodanszky, 1988). Protecting groups such as *S*-benzoyl and *S*-acetamidomethyl are easily removed on heating to 100 °C for a short time (Liu and Edwards, 1995). However, some protecting groups, such as *S*-benzyl and *S*-benzamidomethyl, are more difficult to remove under the conditions used for radiolabeling (Bormans et al., 1995). We did not expect the *S*-methyl group of *S*-methyl-MAG2-NH_2 to be cleaved during the labeling, however the total failure of *S*-methyl-MAG2-NH_2 to label was somewhat unexpected. The N2S2 ligand *N*,2-methylthiobenzyl-*N*′-(1-oxo-2-mercapto-2-methyl)propyl ethylenediamine, which has one thiol sulfur donor, and one thioether sulfur donor forms a neutral complex with technetium (Oya et al., 1995). Thioether ligands coordinated to technetium are also found in technetium complexes of sulfur macrocycles (White et al., 1992).

Instability of radiolabeled peptides in vivo can occur through two principal routes; through proteolytic degradation of the peptide backbone by serum proteases or by transchelation of the technetium to other high-affinity binding sites. The first route of breakdown can be minimized by the use of unnatural amino acids such as D-optical isomers and through cyclization of the peptide.

The second route can be overcome by the use of suitable high-affinity chelators which prevent transfer of the radiolabel to other competing ligands in vivo. Since technetium shows a high affinity for sulfur-containing molecules, its tendency to transchelate in vivo can be modeled in vitro by challenge with the sulfur containing amino acid cysteine.

The peptides examined in this study fall into two clear categories as far as their stability to cysteine challenge is concerned. The thiol-containing ligands show much greater stability that those relying entirely on coordination by amide nitrogens. This suggests that sulfur-containing sequences would provide the chelators of choice for use in receptor-binding peptides. However, in addition to this requirement, this study points to a number of other desirable properties in a peptide technetium chelator which would help in the design of the optimal peptide sequence.

MAG3 shows greater stability than MAG2-NH2. Since the only difference between the two molecules is the terminal carboxylate, this group must assist the stability of the complex, either by unexpected involvement in coordination of the technetium or by steric hindrance of competing ligands attacking from the base of the pyramidal complex. This effect is also observed if the terminal amide nitrogen is acetylated as in the *N*-acetyl-gly-gly cys-gly sequence.

However, the presence of bulky substituents on the peptide backbone produces a marked increase in stability as can be observed in a comparison of *N*-acetyl-gly-gly cys-gly and *N*-acetyl-aib-aib-cys-gly. Such substituents will tend to promote the folding of the peptide in a manner which tends to favor coordination of the technetium with consequent increase in the stability of the complex.

The presence of two thiols in the sequence does not necessarily produce an advantage over one, since both the MAG3 complexes and *N*-acetyl-gly-cys-gly-cys-gly-NH2 show little or no instability in this assay. However, the dithiol sequence achieves this without the presence of the protective terminal carboxyl group. It seems likely therefore that in the absence of the carboxylate, two sulfurs are better than one.

The sequence showing the poorest stability to cysteine challenge was the open-chain tetraglycine sequence; however, cyclization of the peptide showed little if any increase in stability, perhaps, as suggested above, because the technetium is not fully located within the cage of the macrocycle.

The ultimate performance of a radiolabeled receptor-binding sequence will depend on a number of factors, in particular its affinity for the receptor, its pattern of biodistribution, and its in vivo stability. An advantage of the hybrid peptide approach is that the chelation sequence and the sequence responsible for receptor binding can be optimized independently. However, changes in both of these regions of the peptide are likely to result in an alteration in biodistribution since they will alter the hydrophilicity and possibly the resulting charge of the molecule. The rules which govern the influence of peptide structure on its biodistribution are not yet clearly understood and further studies on the factors which control this relationship are required before an optimal design for these radiopharmaceuticals can be realized.

CONCLUSION

Short peptide sequences can be incorporated into receptor-binding peptides to provide a radiolabeling site for technetium-99m. These peptides can be radiolabeled with high efficiency and high solution stability. Increased protection against possible loss of the radiolabel in vivo can be provided by the presence in the chelation sequence of either two sulfur atoms or one sulfur atom and a pendant carboxyl group on the terminal nitrogen. A further increase in stability is provided by the presence of bulky peptide side chains. This information will be of value in the design of optimized peptide chelators for technetium-99m.

ACKNOWLEDGMENT

We gratefully acknowledge the financial support of the Imperial Cancer Research Fund and the use the facilities of the Dominion House Centre for Clinical Research. We thank Angela Glenn for technical assistance with the peptide synthesis.

LITERATURE CITED

(1) Bodanszky, M. (1988) *Peptide Chemistry*, Springer-Verlag, Berlin.

(2) Bormans, G., Cleynhens, B., Adriaens, P., Vanbilloen, H., De Roo, M., and Verbruggen, A. (1995) Investigation of the labeling characteristics of Tc-99m-mercaptoacetyltriglycine. *Nucl. Med. Biol. 22*, 339−349.

(3) Brenner, D., Davison, A., Lister-James, J., and Jones, A. G. (1984) *Inorg. Chem. 23*, 3793−3797.

(4) Fischman, A. J., Babich, J. W., and Strauss, H. W. (1993) A ticket to ride: peptide radiopharmaceuticals. *J. Nucl. Med. 34*, 2253−2263.

(5) Hom, R. K., and Katzenellenbogen, J. A. (1997). Technetium-99m-labeled receptor-specific small-molecule radiopharmaceuticals: recent developments and encouraging results. *Nucl. Med. Biol. 24*, 485−498.

(6) Johannsen, B., Noll, B., Leibnitz, P., Reck, G., Noll, S., and Spies, H. (1993) Technetium and rhenium complexes of mercapto-containing peptides. 1. Tc(V) and Re(V) complexes with mercaptoacetyl diglycine (MAG_2) and X-ray structure of $AsPh_4[TcO(MAG_2)]\cdot C_2H_5OH$. *Inorg. Chim. Acta 210*, 209−214.

(7) Kates, S. A., Solé, N. A., Johnson, C. R., Hudson, D., Barany G., and Albericio, F. (1993) *Tetrahedron Lett. 34*, 1549.

(8) Lister-James, J., McBride, W. J., Buttram, S., Civitello, E., Martel, L. J., Pearson, D. A., Wilson, D. M., and Dean, R. T. (1995) Technetium-99m chelate-containing receptor-binding peptides. In *Technetium and rhenium in chemistry and nuclear medicine.* (M. Nicolini, G. Bandoli, and U. Mazzi, Eds.), Vol. 4, pp 269−274, SG Editoriali, Padova, Italy.

(9) Lister-James, J., Moyer, B. R., and Dean, T. (1996) Small peptides radiolabeled with ^{99m}Tc. *Q. J. Nucl. Med. 40*, 221−233.

(10) Lister-James, J., Moyer, B. R., and Dean, R. T. (1997) Pharmacokinetic considerations in the development of peptide-based imaging agents. *Q. J. Nucl. Med. 41*, 111−118.

(11) Liu, S., and Edwards, D. S. (1995) New N2S2 diamidedithiol and N3S triamidethiols as bifunctional chelating agents for labeling small peptides with technetium-99m. In *Technetium and rhenium in chemistry and nuclear medicine.* (M. Nicolini, G. Bandoli, U. Mazzi, Eds.) Vol. 4, pp 383−393, SG Editoriali, Padova, Italy.

(12) Liu, S., Edwards, D. S., and Barrett, J. A. (1997) 99mTc labeling of highly potent small peptides. *Bioconjugate Chem. 8*, 621−636.

(13) Mather, S. J., Ellison, D., and Bard, D. S. (1995) Technetium-99m labeled hybrid receptor-binding peptides. In Technetium and rhenium in chemistry and nuclear medicine. (M. Nicolini, G. Bandoli, U. Mazzi, Eds.) Vol. 4, pp 491−497, SG Editoriali, Padova, Italy.

(14) Oya, S., Kung, M. P., Frederick, D., and Kung, H. F. (1995) New bisaminoethanethiol (BAT) ligands which form two interconvertible Tc-99m complexes. *Nucl. Med. Biol. 22*, 749−757.

(15) Pearson, D. A., Lister-James, J., McBride, W. J., Wilson, D. M., Martel, L. J., Civitello, E. R., Taylor, J. E., Moyer, B. R., and Dean, R. T. (1996a) Somatostatin receptor-binding peptides labeled with technetium-99m: Chemistry and initial biological studies. *J. Med. Chem. 39*, 1361−1371.

(16) Pearson, D. A., Lister-James, J., McBride, W. J., Wilson, D. M., Martel, L. J., Civitello, E. R., and Dean, R. T. (1996b) Thrombus imaging using technetium-99m-labeled high-potency GPIIb/IIIa receptor antagonists.Chemistry and initial biological studies. *J. Med. Chem. 39*, 1372−1382.

(17) Peers, S. H., Paul, C., Woodruff, L., Thornback, J. R., Goodbody, A. E., and Bolton, C. (1997) The study of Tc-99m RP128 in experimental allergic encephalomyelitis (EAE), an animal model of multiple sclerosis. *J. Nucl. Med. 38*, 187P−188P (abstract).

(18) Sharma, S. (1998) Differential stability of syn and anti isomers in Tc-99m complexes-evidence from cysteine challenge studies. *Q. J. Nucl. Med. 42* (3) (Suppl. 1), 39.

(19) Simon, J., Troutner, D. E., and Volkert, W. A. (1981) Radiochemical characterisation of Tc-cyclam. *J. Radiochem. Radioanal. Lett. 47*, 111.

(20) Thakur, M. L. (1995) Radiolabeled peptides: Now and the future. *Nucl. Med. Commun. 16*, 724−732.

(21) VanBilloen, H., Bormans, G., Heylen, J., Hoogmartens, M., DeRoo, M., and Verbruggen, A. (1991), Complexes of technetium-99m with tetraglycine and tetra-L-alanine and their biodistribution in mice. *J. Labeled Compd. Radiopharm. 30*, 42−44.

(22) Vanbilloen, H. P., Bormans, G. M., De Roo, M. J., and Verbruggen, A. M. (1995) Complexes of technetium-99m with tetrapeptides, a new class of ^{99m}Tc-labeled agents. *Nucl. Med. Biol. 22*, 325−338.

(23) White, D. J., Kuppers, H. J., Edwards, A. J., Watkin, D. J., and Cooper, R. S. (1992). Crown thioether chemistry. The first homoleptic thioether complex of technetium, and its potential application in tumor imaging. *Inorg. Chem. 31*, 5351−5352.

BC9800466

L-Glutamic Acid and L-Lysine as Useful Building Blocks for the Preparation of Bifunctional DTPA-like Ligands†

Pier Lucio Anelli,* Franco Fedeli, Ornella Gazzotti, Luciano Lattuada, Giovanna Lux, and Fabrizio Rebasti

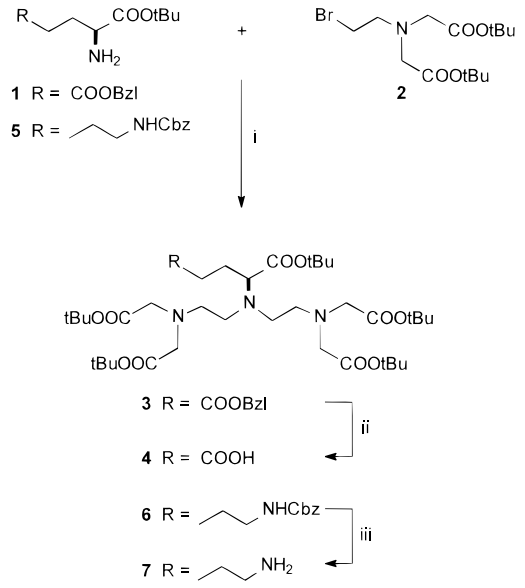
Bracco spa, Milano Research Centre, via E. Folli 50, 20134 Milano, Italy. Received December 26, 1997; Revised Manuscript Received November 19, 1998

Bisalkylation of suitably protected L-glutamic acid and L-lysine derivatives with *tert*-butyl *N*-(2-bromoethyl)iminodiacetate **2**, followed by deprotection of the *ω* functional group affords *N*,*N*-bis[2-[bis[2-(1,1-dimethylethoxy)-2-oxoethyl]amino]ethyl]-L-glutamic acid 1-(1,1-dimethylethyl) ester **4** and N^2,N^2-bis[2-[bis[2-(1,1-dimethylethoxy)-2-oxoethyl]amino]ethyl]-L-lysine 1,1-dimethylethyl ester **7**. Such compounds feature a carboxylic or an amino group, respectively, which are available for conjugation with a suitable partner via formation of an amide bond. The conjugates, which can be prepared in this way, contain a chelating subunit in which all five acetic residues of DTPA are available for the complexation of metal ions. Direct bisalkylation of glycine with **2** promptly gives *N*,*N*-bis[2-[bis[2-(1,1-dimethylethoxy)-2-oxoethyl]amino]ethyl]glycine **11**. The latter allows to achieve conjugates in which the central acetic group of DTPA is selectively converted into an acetamide.

Diethylenetriaminepentaacetic acid (DTPA) is a very efficient chelating agent for the complexation of the gadolinium ion. The corresponding complex, due to its high in vivo stability, has been safely used as contrast agent in MRI over the past decade (*2*). Conjugation of DTPA-like ligands to macromolecules (*3*), iodinated synthons (*4*) or bile acids (*5*) has been recently pursued to achieve MRI contrast agents featuring improved organ specificity. The most popular way to conjugate DTPA to other molecules involves the conversion of one of the four equivalent carboxylic groups into a carboxamide via DTPA bisanhydride (*6*). Besides being not selective, due to the concomitant formation of some diamide (*7*), this methodology has the disadvantage of yielding conjugates containing a ligand weaker than DTPA. Indeed, such decrease in chelating ability of DTPA-like ligands in which one of the carboxylic group has been converted into a carboxamide is well-known (*8*).

Nevertheless, due to its chemical stability, amide bond is one of the preferred choices for the preparation of conjugates containing metal complexes which have to be administered in vivo. Therefore, we became interested in the preparation of DTPA ligands bearing either a carboxylic group or an amino group available for conjugation. Williams and Rapoport recently introduced a simple methodology which is a breakthrough in the synthesis of DTPA-like ligands (*9*). We have now found that L-glutamic acid and L-lysine, after suitable protections and using such methodology, conveniently yield functionalized DTPA pentaesters which are versatile intermediates for the preparation of conjugates of metal complexes. Since DTPA-like ligands have been proposed for the chelation of radionuclides [e.g., ^{111}In(III), ^{212}Bi(III), and ^{90}Y(III)] (*10*, *11*) we believe that the above intermediates could also be of some importance for the preparation of new radiopharmaceuticals.

Scheme 1[a]



[a] (i) **1** EtOH/H_2O, pH 8; for **5** MeCN/pH 8 phosphate buffer; (ii) H_2, 5% Pd/C, EtOH; (iii) H_2, 5% Pd/C, MeOH.

L-Glutamic acid 5-benzyl ester (*12*) was converted, with isobutene in dioxane in the presence of H_2SO_4, into the 1-*tert*-butyl 5-benzyl diester **1** (*13*), which was directly reacted with bromide **2** in EtOH/H_2O at pH 8 to afford hexaester **3** in only 31% yield (Scheme 1). The isolation of **3** in fair yields is related to the easy lactamization of both **1** and the monoalkylated intermediate. However, in our hands the dialkylation of **1** in homogeneous phase proved to be the best procedure, even better then the reaction under Rapoport's two-phase conditions (i.e., MeCN/pH 8 phosphate buffer). Cleavage of the benzyl ester protection of **3** by hydrogenolysis yielded the monoacid pentaester **4**.

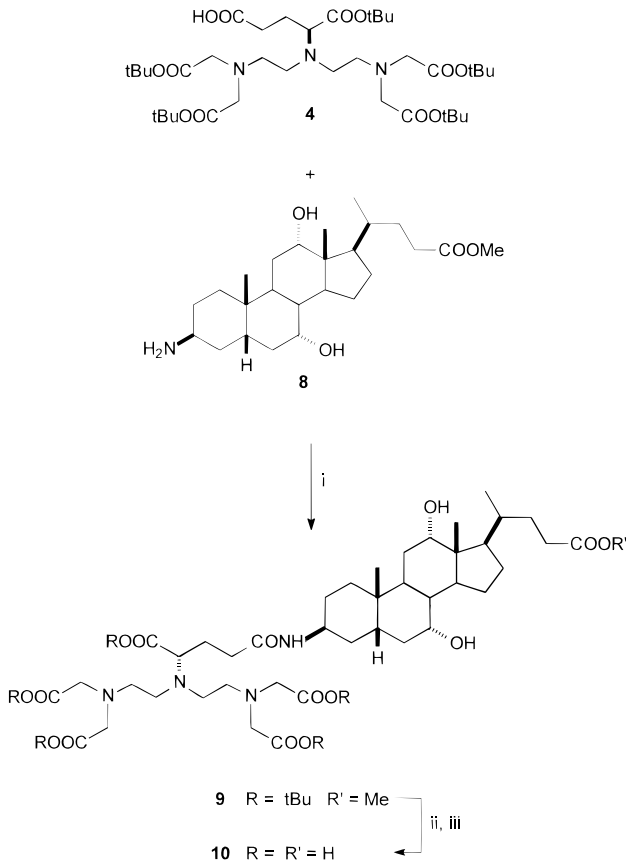
On the other hand, to obtain a DTPA pentaester with a free amino group, commercially available N^6-Cbz L-

† Presented in part at the 35th National Organic Chemistry Symposium, San Antonio, TX, June 1997.

* To whom correspondence should be addressed. Phone: +39 02 21772353. Fax: +39 02 26410678.

10.1021/bc970212u CCC: $18.00 © 1999 American Chemical Society
Published on Web 12/31/1998

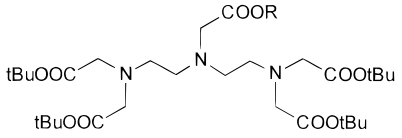
Scheme 2[b]



[b] (i) DEPC, Et_3N, DMF; (ii) CF_3COOH, CH_2Cl_2; (iii) NaOH, pH 13.

lysine was esterified in *tert*-butyl acetate in the presence of $HClO_4$ to afford **5**. Subsequent dialkylation with bromide **2** in MeCN/pH 8 phosphate buffer afforded protected pentaester **6**. Classical removal of the Cbz moiety by hydrogenolysis yielded the amino pentaester **7** (Scheme 1).[1] It must be stressed that Rapoport demonstrated that, under the reaction conditions that they developed for the dialkylation of amino esters, no racemization is observed. Pentaesters **4** and **7** can be easily reacted with substrates containing amino or carboxylic functionalities, respectively, and subsequently, the *tert*-butyl ester groups can be removed using routine methodologies. According to this strategy, conjugates containing DTPA subunits, in which all five acetic groups are available for complexation, are promptly achieved. Indeed, we synthesized ligand **10** by coupling of **4** to aminocholic methyl ester **8** (*14*) (Scheme 2). On complexation with Gd(III) ligand **10** gives rise to a complex which will be studied as MRI contrast agent in comparison with other bile acid conjugates (*5*). We also investigated the preparation of a synthon in which the acetic residue on the central nitrogen atom of DTPA can be selectively activated. Compound **11** has been recently prepared by hydrogenolysis of the corresponding mixed monobenzyl tetra-*tert*-butyl ester of DTPA **12** in its turn obtained through a synthetic route involving time consuming protection-deprotection of diethylenetriamine (*15*).

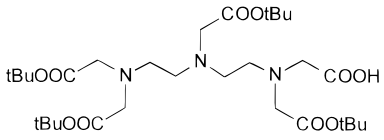
[1]Similarly, reaction of *O*-benzyl-L-serine *tert*-butyl ester with bromide **2** under Rapoport's conditions, followed by hydrogenolysis of the benzyl group, yielded a DTPA pentaester bearing an hydroxymethyl moiety on the central acetic residue. Such derivative can also be used for the preparation of conjugates.



11 R = H

12 R = Bzl

We found that dialkylation of glycine benzyl ester (*16*) with **2** directly affords pentaester **12** of DTPA which can be hydrogenated in MeOH in the presence of 10% Pd/C to give **11**. More surprisingly, we realized that dialkylation of glycine with **2** in $EtOH/H_2O$ at pH 10 straightforwardly leads to **11** in 70% yield after flash chromatography. Tetraester **11** is a very convenient intermediate for the synthesis of conjugates containing DTPA monoamide subunits. In this respect, the preparation of **11** appears less troublesome and quicker than that of the unsymmetrical tetraester **13**, which has been recently prepared with a six step synthesis (*17*).



13

It is noteworthy that DTPA polyesters **4**, **7**, and **11** are all prepared using bromide **2**, which indeed proved to be a very versatile intermediate.

A limit to the direct application of compounds **4**, **7**, and **11** for the preparation of conjugates is represented by the absence, in the substrate to which they have to be coupled, of chemical bonds labile under conditions of cleavage of the *tert*-butyl ester groups. This drawback can be circumvented, reacting **4** and **11** with either *N*-(2-aminoethyl)maleimide (*17*) or *S*-(2-pyridylthio)cysteamine (*18*) to give, after deprotection of the *tert*-butyl ester functions, bifunctional ligands which can be coupled to SH containing substrates (e.g., proteins). A similar strategy could be exploited for the use of **7**.

EXPERIMENTAL PROCEDURES

General Comments. All reagents were purchased from Fluka Chemie AG (Buchs, Switzerland), Aldrich (Milwakee, WI) and Merck KGaA (Darmstadt, Germany). ^1H and ^{13}C NMR spectra were recorded at 200 and 50 MHz, respectively, on a Bruker AC 200 spectrometer. Electrospray ionization was performed on a Finnigan TSQ 700 triple quadrupole mass spectrometer fitted with a Finnigan ESI interface, dissolving the samples in MeOH, H_2O/MeOH, or H_2O/MeCN. Optical rotations (10^{-1} deg cm^2 g^{-1}) were measured with a Perkin-Elmer 341 polarimeter. Melting points were determined with a Büchi 510 apparatus and are uncorrected. Preparative HPLC was performed on a Merck KGaA Prepbar 100 apparatus.

***N,N*-Bis[2-[bis[2-(1,1-dimethylethoxy)-2-oxoethyl]-amino]ethyl]-L-glutamic acid 1-(1,1-dimethylethyl) 5-(Phenylmethyl) Diester (3).** L-Glutamic acid 5-benzyl ester (*12*) (171 g, 0.72 mol) was added to a mixture of 98% H_2SO_4 (50.5 mL, 0.93 mol) in dioxane (500 mL) at 20 °C and the solution was stirred over 6 days under an isobutylene atmosphere (132 kPa). Crushed ice (720 g) was added to the reaction mixture, and then a solution of K_2CO_3 (128.5 g, 0.93 mol) in water (350 mL) was added dropwise over 1 h. The precipitate, containing the start-

ing monoester (60 g, 0.25 mol) and salts, was filtered and the solution freeze-dried. L-Glutamic acid 1-*tert*-butyl 5-benzyl diester **1** thus obtained (137.8 g; 0.47 mol; 65%) was dissolved in EtOH (780 mL) and water (170 mL) and bromoderivative **2** (*9*) (247 g; 0.7 mol) was added at 5 °C. The mixture was maintained at pH 8 by means of a pH-stat apparatus with 10 N NaOH. After 48 h at 5 °C and 98 h at 25 °C further, bromoderivative **2** was added (106 g, 0.3 mol). After 120 h at 25 °C and 22 h at 50 °C, the mixture was neutralized with 36% HCl and filtered. After evaporation of EtOH, the solution was diluted with water (300 mL) and extracted with *n*-hexane (1 × 1100 mL, 1 × 300 mL). The combined organic phase was washed with water (250 mL), dried, and evaporated. The residue (322 g) was purified by a first flash chromatography with 1:4 EtOAc/*n*-hexane followed by a second flash chromatography using CH_2Cl_2 → 1:12 Et_2O/CH_2Cl_2 as the eluent. Evaporation gave **3** (122.8 g, 0.147 mol, 31%) as a yellow oil. $[\alpha]_D^{20}$: −30.43 (*c* 5.5, $CHCl_3$). ^{1}H NMR ($CDCl_3$): δ 1.40 (s, 45H), 1.92 (m, 2H), 2.45 (m, 2H), 2.70 (m, 8H), 3.40 (m, 9H), 5.05 (s, 2H), 7.29 (m, 5H). ^{13}C NMR ($CDCl_3$): δ 24.7 (CH_2), 28.0 (CH_3), 28.1 (CH_3), 30.7 (CH_2), 50.0 (CH_2), 53.7 (CH_2), 55.8 (CH_2), 63.2 (CH), 65.9 (CH_2), 80.6 (C), 80.7 (C), 127.9 (CH), 128 (CH), 128.3 (CH), 136.0 (C), 170.3 (CO), 171.9 (CO), 173.1 (CO). Anal. ($C_{44}H_{73}N_3O_{12}$) C, H, N. MS: *m*/*z* 836 $[M + H]^+$, 858 $[M + Na]^+$.

***N*,*N*-Bis[2-[bis[2-(1,1-dimethylethoxy)-2-oxoethyl]-amino]ethyl]-L-glutamic acid 1-(1,1-Dimethylethyl) Ester (4).** Pd (5%) on carbon (16 g) was added to a solution of **3** (121 g, 142 mmol) in EtOH (800 mL), and the suspension was stirred over 2 h under a hydrogen atmosphere (111 kPa) at 20 °C. The mixture was filtered over Millipore FH 0.45 μm, the solution evaporated and the residue purified by flash chromatography eluting with 1:2 EtOAc/*n*-hexane → EtOAc. Evaporation gave **4** (59.3 g, 56%) as a very viscous yellow oil. $[\alpha]_D^{20}$: −13.49 (*c* 2.3, $CHCl_3$). ^{1}H NMR ($CDCl_3$): δ 1.36 (s, 45H), 1.95 (m, 2H), 2.65 (m, 2H), 2.85 (m, 8H), 3.42 (s, 8H), 3.85 (dd, 1H). ^{13}C NMR ($CDCl_3$): δ 24.3 (CH_2), 27.9 (CH_3), 28.0 (CH_3), 31.6 (CH_2), 40.6 (CH_2), 53.0 (CH_2), 55.5 (CH_2), 63.6 (CH), 80.8 (C), 81.1 (C), 170.3 (CO), 171.1 (CO), 176.9 (CO). Anal. ($C_{37}H_{67}N_3O_{12}$) C, H, N. MS: *m*/*z* 746 $[M + H]^+$, 768 $[M + Na]^+$.

***N*^{6}-[(Phenylmethoxy)carbonyl]-L-lysine 1,1-Dimethylethyl Ester (5).** $HClO_4$ (70%, 19.5 mL) was added dropwise to a suspension of *N*^{6}-[(phenylmethoxy)-carbonyl]-L-lysine (56 g, 0.2 mol) in *tert*-butyl acetate (700 mL) to afford a clear solution. After 20 h, 10% Na_2CO_3-(aq) (600 mL) was dripped into the solution obtaining precipitation of the unreacted starting material which was filtered. NaOH (10 N) was added to adjust to pH 10 the aqueous phase then the organic phase was separated, washed with water (5 × 50 mL) and dried (Na_2SO_4). Evaporation gave **5** (53.5 g, 79%) as a colorless oil. $[\alpha]_D^{20}$: +8.88 (*c* 4.9, $CHCl_3$). ^{1}H NMR ($CDCl_3$): δ 1.30−1.80 (m, 15H), 3.10−3.35 (m, 3H), 4.90 (br s, 1H), 5.05 (s, 2H), 7.03 (m, 5H). ^{13}C NMR ($CDCl_3$): δ 22.6 (CH_2), 27.9 (CH_3), 29.5 (CH_2), 34.4 (CH_2), 40.7 (CH_2), 54.7 (CH), 66.3 (CH_2), 80.7 (C), 127.9 (CH), 128.3 (CH), 136.5 (C), 158.3 (CO), 175.2 (CO). Anal. ($C_{18}H_{28}N_2O_4$) C, H, N; H, calcd: 8.33. Found: 8.80. MS: *m*/*z* 337 $[M + H]^+$, 359 $[M + Na]^+$.

***N*^{6}-[(Phenylmethoxy)carbonyl]-*N*^{2},*N*^{2}-bis[2-[bis[2-(1,1-dimethylethoxy)-2-oxoethyl]amino]ethyl]-L-lysine 1,1-Dimethylethyl Ester (6).** Phosphate buffer (1 L; 2 M, pH 8) was added to a solution of compound **5** (81 g, 0.24 mol) and bromoderivative **2** (209 g, 0.59 mol) in CH_3CN (900 mL), and the mixture was vigorously stirred for 2 h. The two phases were separated and the aqueous phase replaced with fresh phosphate buffer (800 mL, 2 M, pH 8). After 48 h, the mixture was separated and the organic layer concentrated to dryness. The residue was dissolved in CH_2Cl_2 (1 L), washed with water (2 × 50 mL), dried (Na_2SO_4), and evaporated. The residue was purified by flash chromatography with 1:2 EtOAc/*n*-hexane to give **6** (190 g, 90%) as a very viscous yellow oil. $[\alpha]_D^{20}$: −26.40 (*c* 4.98, $CHCl_3$). ^{1}H NMR ($CDCl_3$): δ 1.20−1.80 (m, 51H), 2.75 (m, 8H), 3.20 (m, 3H), 3.40 (s, 8H), 5.10 (s + br s, 3H), 7.23 (m, 5H). ^{13}C NMR ($CDCl_3$): δ 23.1 (CH_2), 27.9 (CH_3), 28.1 (CH_3), 29.3 (CH_2), 40.6 (CH_2), 50.0 (CH_2), 53.4 (CH_2), 55.8 (CH_2), 63.7 (CH), 66.1 (CH_2), 80.4 (C), 80.5 (C), 127.7 (CH), 127.8 (CH), 128.2 (CH), 136.6 (C), 156.2 (CO), 170.4 CO), 172.5 (CO). Anal. ($C_{46}H_{78}N_4O_{12}$) C, H, N. MS: *m*/*z* 337 $[M + H]^+$, 359 $[M + Na]^+$.

***N*^{2},*N*^{2}-Bis[2-[bis[2-(1,1-dimethylethoxy)-2-oxoethyl]-amino]ethyl]-L-lysine 1,1-Dimethylethyl Ester (7).** Pd (5%) on carbon (9 g) was added to a solution of **6** (180 g, 0.2 mol) in MeOH (1 L) and the suspension was stirred over 2 h under a hydrogen atmosphere at 20 °C. The mixture was filtered over Millipore HA 0.45 μm and evaporated. The residue was dissolved in 0.5 N HCl and the solution maintained under vacuum for 10 min, then 1 N NaOH was added and the product extracted with Et_2O. The solution was evaporated and the residue was purified by flash chromatography with MeOH to give **7** (90 g, 60%) as a very viscous yellow oil. $[\alpha]_D^{20}$: −27.97 (*c* 5.7, $CHCl_3$). ^{1}H NMR ($CDCl_3$): δ 1.20−1.90 (m, 51H), 2.60−2.85 (m, 10H), 3.12 (m, 1H), 3.40 (s, 8H). ^{13}C NMR ($CDCl_3$): δ 23.3 (CH_2), 28.0 (CH_3), 29.6 (CH_2), 33.4 (CH_2), 41.6 (CH_2), 50.2 (CH_2), 53.5 (CH_2), 55.7 (CH_2), 64.2 (CH), 80.2 (C), 170.3 (CO), 172.4 (CO). Anal. ($C_{38}H_{72}N_4O_{10}$) C, H, N; H, calcd: 9.74. found: 10.25. MS: *m*/*z* 745 $[M + H]^+$, 767 $[M + Na]^+$.

[3β(S),5β,7α,12α]-3-[[5-(1,1-Dimethylethoxy)-4-[bis-[2-[bis[2-(1,1-dimethylethoxy)-2-oxoethyl]amino]eth-yl]amino]-1,5-dioxopentyl]amino]-7,12-dihydroxycholan-24-oic Acid Methyl Ester (9). Monoacid pentaester **4** (18.6 g, 25 mmol), (3β,5β,7α,12α)-3-amino-7,12-dihydroxycholan-24-oic acid methyl ester (*14*) (11.6 g, 27.5 mmol) and diethyl cyanophosphonate (DEPC) (4.8 g, 29.6 mmol) were dissolved in DMF (500 mL). The resulting solution was cooled to 0 °C and Et_3N (2.7 g, 26.2 mmol) was added dropwise. After 30 min at 0 °C and 1 h at room temperature, the solution was evaporated and the residue dissolved in EtOAc (200 mL). The organic phase was washed with 5% $NaHCO_3$ (aq) (2 × 100 mL) then with brine (2 × 100 mL), dried, and evaporated. The crude product was purified by flash chromatography with EtOAc to give **9** (21 g, 73%) as a yellowish solid: mp 54−57 °C. ^{13}C NMR ($CDCl_3$): δ 12.3 (CH_3), 17.1 (CH_3), 22.8 (CH_3) 23.1 (CH_2), 24.5 (CH_2), 25.4 (CH_2), 25.9 (CH), 27.3 (CH_2), 28.0 (CH_3), 28.3 (CH_2), 30.7 (CH_2), 30.9 (CH_2), 31.0 (CH_2), 32.8 (CH_2), 33.5 (CH_2), 34.5 (CH_2), 35.1 (CH), 35.2 (C), 37.0 (CH), 39.2 (CH), 41.6 (CH), 45.1 (CH), 46.4 (C), 47.0 (CH), 49.4 (CH_2), 51.3 (CH_3), 53.1 (CH_2), 55.7 (CH_2), 63.2 (CH), 68.2 (CH), 72.9 (CH), 80.6 (C), 80.7 (C), 170.5 (CO), 172.2 (CO), 172.4 (CO), 174.6 (CO). Anal. ($C_{62}H_{108}N_4O_{15}$) C, H, N. MS: *m*/*z* 1150 $[M + H]^+$, 1172 $[M + Na]^+$.

[3β(S),5β,7α,12α]-3-[4-Carboxy-4-[bis[2-[bis(car-boxymethyl)amino]ethyl]amino]-1-oxobutyl]amino]-7,12-dihydroxycholan-24-oic Acid (10). CF_3COOH (399 g, 3.5 mol) was added dropwise in 30 min to a solution of hexaester **9** (96.5 g, 0.084 mol) in CH_2Cl_2 (360 mL) at 0 °C. The reaction mixture was stirred at room temperature for 18 h and then evaporated, and the

residue was taken up with fresh CF_3COOH (114 g, 1 mol). After an additional 24 h, the reaction mixture was diluted with Et_2O (700 mL) to afford a precipitate that was filtered and suspended in H_2O. The mixture was basified to pH 13 with 10 N NaOH to give a clear solution. After 1 h, MeCN (300 mL) was added then the solution was acidified to pH 2 with 37% HCl. Slow evaporation under vacuum of the organic solvent gave precipitation of a white solid that was filtered off. The crude product was purified by preparative reversed-phase HPLC [Lichroprep RP-18 column, 50 × 250 mm, 25−40 μm, Merck KGaA; with 80% 0.01 M KH_2PO_4/20% MeCN for 105 min then 50% 0.01 M KH_2PO_4/50% MeCN for 20 min; flow rate 90 mL/min, monitored on-line by UV at 200 nm]. Fractions containing the product were combined, neutralized to pH 7 with 10 N NaOH, and evaporated under reduced pressure to give a solid (product mixed with inorganic salts) that was dissolved in H_2O (790 mL). The solution was heated at 50 °C and, while maintained under vigorous stirring, slowly acidified to pH 2.1 with 37% HCl (48 mL) to yield a white precipitate. The suspension was allowed to cool spontaneously to room temperature, and the precipitate was filtered, washed with H_2O (2 × 25 mL), and dried to give **10** (33.1 g, 46%) as a white solid. mp 193−195 °C. ^{13}C NMR (D_2O + KOD): δ 15.0 (CH_3), 19.6 (CH_3), 25.2 (CH_3), 25.8 (CH_2), 26.6 (CH_2), 28.4 (CH_2), 28.7 (CH), 30.1 (CH_2), 30.7 (CH_2), 33.2 (CH_2), 35.0 (CH_2), 35.6 (CH_2), 36.2 (CH_2), 37.0 (CH_2), 37.3 (C), 38.3 (CH), 39.1 (CH), 41.9 (CH), 44.3 (CH), 48.6 (CH), 49.0 (C), 50.4 (CH_2), 54.9 (CH_2), 60.5 (CH_2), 68.7 (CH), 71.0 (CH), 75.7 (CH), 177.5 (CO), 177.7 (CO), 177.8 (CO), 180.4 (CO), 186.8 (CO). Anal. ($C_{41}H_{66}N_4O_{15}$) C, H, N. MS: *m*/*z* 853 $[M - H]^-$.

***N,N*-Bis[2-[bis[2-(1,1-dimethylethoxy)-2-oxoethyl]-amino]ethyl]glycine (11).**

Method a. Phosphate buffer (50 mL, 2 M, pH 8) was added to a solution of glycine benzyl ester (*16*) (2.44 g, 14.8 mmol) and bromoderivative **2** (11.5 g, 32.6 mmol) in CH_3CN (100 mL), and the mixture was vigorously stirred for 24 h. The mixture was separated, the organic phase evaporated, and the residue flash chromatographed with $CHCl_3$. The yellow oil obtained (6.5 g) was dissolved in MeOH (50 mL), and 10% Pd on carbon (0.7 g) was added. The suspension was stirred over 24 h under a hydrogen atmosphere at 20 °C. The mixture was filtered over Millipore FH 0.45 μm and evaporated to give **11** (4.87 g, 53%) as a yellow oil.

Method b. NaOH (10 M) (10 mL) was added to a solution of glycine (12 g, 0.160 mol) in water (100 mL) and 95% EtOH (100 mL) until pH 10 was reached. A solution of bromoderivative **2** (120 g, 0.341 mol) in 95% EtOH (100 mL) was added dropwise, maintaining at pH 10 by means of a pH-stat apparatus. After 18 h, EtOH was removed under reduced pressure, and the solution was acidified to pH 3.5 with 12 N HCl and extracted with CH_2Cl_2 (2 × 300 mL). The combined organic phases were washed with water (2 × 100 mL), dried (Na_2SO_4), and evaporated. The residue was purified by flash chromatography using CH_2Cl_2 → CH_2Cl_2/MeOH/25% NH_4OH-(ag) 150:13:1 as the eluent. Evaporation of the solvent gave a pale yellow oil which was treated with petroleum benzine (boiling range 60−80 °C; 3 × 400 mL) until **11** (69 g, 70%) was obtained as a white crystalline solid. mp 93 °C. ^1H NMR ($CDCl_3$): δ, 1.46 (s, 36H), 2.99 (t, 4H), 3.10 (br t, 4H), 3.45(s, 8H), 3.56 (s, 2H). ^{13}C NMR ($CDCl_3$): δ, 28.5 (CH_3), 51.2 (CH_2), 53.9 (CH_2), 56.4, (CH_2), 57.0 (CH_2), 82.0 (C), 170.8 (CO). Anal. ($C_{30}H_{55}N_3O_{10}$) C, H, N. MS: *m*/*z* 618 $[M + H]^+$, 640 $[M + Na]^+$.

LITERATURE CITED

(1) Anelli, P. L., Fedeli, F., Gazzotti, O., Lattuada, L., and Rebasti, F. Presented in part at 35th National Organic Chemistry Symposium, San Antonio, TX, June 1997, paper T166.

(2) Weinmann, H. J. (1994) Characteristics of Gd-DTPA dimeglumine in *Magnevist monograph* (R. Felix, A. Heshiki, N. Hosten, and H. Hricak, Eds.) pp 5−14, Blackwell Scientific Publications, Oxford.

(3) Weiner, E. C., Brechbiel, M. W., Brothers, H., Magin, R. L., Gansow, O. A., Tomalia, D. A., and Lauterbur, P. C. (1994) Dendrimer-based metal chelates: a new class of magnetic resonance imaging contrast agents. *Magn. Reson. Med. 31*, 1−8.

(4) Anelli, P. L., Calabi, L., de Haën, C., Fedeli, F., Losi, P., Murru, M., and Uggeri, F. (1995) A new approach to hepatospecific MRI contrast agents: gadolinium complexes conjugated to iodinated synthons. *Gazz. Chim. Ital. 126*, 89−97.

(5) Anelli, P. L., Calabi, L., de Haën, C., Lattuada, L., Lorusso, V., Maiocchi, A., Morosini, P., and Uggeri, F. (1997) Hepatocyte-directed MR contrast agents. Can we take advantage of bile acids? *Acta Radiol. 38* (*Suppl. 412*), 125−133.

(6) Hnatowich, D. J., Layne, W. W., and Childs, R. L. (1982) The preparation and labeling of DTPA-coupled albumin. *Int. J. Appl. Radiat. Isot. 33*, 327−332.

(7) Maisano, F., Gozzini, L., and de Haën, C. (1992) Coupling of DTPA to proteins: a critical analysis of the cyclic dianhydride method in the case of insulin modification. *Bioconjugate Chem. 3*, 212−217.

(8) Sherry, A. D., Cacheris, W. P., and Kuan, K.-T. (1988) Stability constants for Gd^{3+} binding to model DTPA-conjugates and DTPA-proteins: implications for their use as magnetic resonance contrast agents. *Magn. Reson. Med. 8*, 180−190.

(9) Williams, M. A., and Rapoport, H. (1993) Synthesis of enantiomerically pure diethylenetriaminepentaacetic acid analogues. L-Phenylalanine as the educt for substitution at the central acetic acid. *J. Org. Chem. 58*, 1151−1158.

(10) Gansow, O. A., Brechbiel, M. W., Mirzadeh, S., Colcher, D., and Roselli, M. (1990) Chelates and antibodies: current methods and new directions. in *Cancer imaging and radiolabeled antibodies* (D. M. Goldenberg, Ed.) pp 153−171, Kluwer Academic Publishers, Dordrecht, The Netherlands.

(11) Cummins, C. H., Rutter, E. W., Jr., and Fordyce, W. A. (1991) A convenient synthesis of bifunctional chelating agents based on diethylenetriaminepentaacetic acid and their coordination chemistry with yttrium(III). *Bioconjugate Chem. 2*, 180−186.

(12) Guttmann, St., and Boissonnas, R. A. (1958) Synthèse du *N*-acétyl-L−séryl-L-tyrosyl-L−séryl-L−méthionyl-γ-L-glutamate de benzyle et de peptides apparentés. *Helv. Chim. Acta 41*, 1852−1867.

(13) Roeske, R. (1963) Preparation of *tert*-butyl esters of free amino acids. *J. Org. Chem. 28*, 1251−1253.

(14) Anelli, P. L., Lattuada, L., and Uggeri, F. (1998) One-pot Mitsunobu-Staudinger preparation of 3-aminocholan-24-oic acid esters from 3-hydroxycholan-24-oic acid esters. *Synth. Commun. 28*, 109−117.

(15) Platzek, J., Niedballa, U., and Raduchel, B. (1996) U.S. Patent 5,514,810, *Chem. Abstr. 125*, 87212.

(16) Miller, H. K., and Warlsch, H. (1952) Benzyl esters of amino acids. *J. Am. Chem. Soc. 74*, 1092−1093.

(17) Arano, Y., Uezono, T., Akizawa, H., Ono, M., Wakisaka, K., Nakayama, M., Sakahara, H., Konishi, J., and Yokoyama A. (1996) Reassessment of diethylenetriaminepentaacetic acid (DTPA) as a chelating agent for indium-III labeling of polypeptides using a newly synthesized monoreactive DTPA derivative. *J. Med. Chem. 39*, 3451−3460.

(18) Hayward, M. M., Adrian, J. C. and Schepartz, A. (1995) Convenient synthesis of bifunctional metal chelates. *J. Org. Chem. 60*, 3924−3927.

BC970212U

Analysis of Nonlinear Quenching of Terbium(III):Dipicolinic Acid Complex Fluorescence by Chelators and Chelate-Conjugated Macromolecules

Charles G. Sanny* and Joseph A. Price

Department of Biochemistry/Microbiology, Oklahoma State University College of Osteopathic Medicine, 1111 West 17th Street, Tulsa, Oklahoma 74107. Received February 16, 1998; Revised Manuscript Received October 20, 1998

The terbium-dipicolinic acid complex (Tb(III):DPA) fluorescence quenching method of Ma, Hwang, and Lee [*Pharm. Res.* (1993) *10*, 204−207] was used at a lower initial concentration of Tb(III):DPA (0.2 μM compared to 1.0 μM) to minimize the concentration of chelate-conjugated macromolecules required for estimating concentrations of metal-binding sites. Fluorescence quenching by either EDTA, diethylenetriaminepentaacetic acid (DTPA), poly (L-lysine)-DTPA, or poly (L-lysine)-DTPA linked to mouse IgG (IgG-PL-DTPA) was nonlinear, suggesting initial binding of chelator results in minimal change in Tb(III):DPA complex fluorescence. On the basis of the law of mass action and nonlinear curve fitting, the data suggests a three-site binding model for Tb(III):DPA complex formation in which the binding of the first and second DPA produce the majority of complex fluorescence. Initial binding of chelators to the complex results in only slight decreases in fluorescence with the majority of fluorescence quenching resulting from dissociation of more than one DPA from the complex. Although fluorescence quenching was nonlinear, binding capacity of each chelator relative to either EDTA or DTPA (as suggested by Ma et al.) could be used to estimate the concentration of metal-binding sites consistent with concentrations reported in the literature using either radionuclides or nuclear magnetic resonance. Estimation of chelating groups on chelate-conjugated macromolecules at lower concentrations would minimize the amount of sample required for analysis during synthesis and isolation of chelate-conjugated macromolecules. The suggested model for the stoichiometry of Tb(III):DPA complex fluorescence may be useful in further refinement of methods for estimating chelator concentrations and for design of fluorescent probes for chelate-conjugated macromolecules.

INTRODUCTION

Chelate-conjugated macromolecules such as monoclonal antibodies linked to chelating polymers have become important tools for a wide variety of studies including radioimmunoimaging, radioimmunotherapy, NMR-tomography, and in vitro immunoassays (*1, 2*). Ma, Hwang, and Lee (*3*) have described a terbium−dipicolinic acid complex fluorescence quenching method for estimating chelating groups in chelate-conjugate macromolecules which is simple, rapid, and does not require radionuclides. This method was based on the assumptions that (1) the displacement of dipicolinic acid from the complex by stronger chelators is quantitative, (2) the resulting terbium−chelator complex is nonfluorescent, and (3) the reduction in fluorescence is linear with chelator or other chelate-coupled macromolecule concentration. To minimize the concentration of chelate-conjugated macromolecules required for analysis, the procedure of Ma et al. (*3*) was used at a lower concentration of terbium-dipicolinic acid complex (0.2 μM compared to 1.0 μM). Quenching by chelators and chelate-conjugated macromolecules at the lower initial concentration of the fluorescent complex was nonlinear. This communication describes the use of nonlinear analysis to estimate chelator concentrations at lower concentations than previously reported (*3*). Also, revised models are presented for turbium−dipicolinic acid complex fluorescence and for fluorescence quenching by chelators and chelate-conjugated macromolecules.

* To whom correspondence should be addressed. E-mail: sanny@okway.okstate.edu. Phone: (918) 561-8245. Fax: (918) 561-8414.

MATERIALS AND METHODS

Materials. Terbium(III) chloride hexahydrate and ethylenediaminetetraacetic acid (EDTA) were purchased form Aldrich Chemical Co. (Milwaukee, WI). Dipicolinic acid (pyridine-2,6-dicarboxylic acid) (DPA), diethylenetriaminepentaacetic acid (DTPA), poly L-lysine (PL25, 25 000 kDa), and *N*-(2-hydroxyethyl)piperazine-*N*′-(2-ethanesulfonic acid) (HEPES) and mouse IgG were purchased from Sigma (St. Louis, MO). Poly (L-lysine)-diethylenetriaminepentaacetic acid (PL25-DTPA) and PL25-DTPA linked to mouse IgG (IgG-PL25-DTPA) were prepared according to Manabe et al. (*4*) and Torchilin et al. (*5*), respectively.

Fluorescence Measurements. Fluorescence measurements were obtained using an RFM-2001 spectrofluorometer and standard cuvette holder from Photon Technologies International (Monmouth Jct., NJ) with excitation at 276 nm and emission from 470 to 510 nm. Fluorescence was determined from either the emission at 491 nm or the baseline corrected area of the emission peak from 477 to 507 nm.

Fluorescence measurements were normalized to percent fluorescence by the following equation:

$$\%F = F_{\text{sample}}/F_{\text{std}} \times 100 \quad (1)$$

10.1021/bc980018n CCC: $18.00 © 1999 American Chemical Society
Published on Web 12/03/1998

where %F is the normalized fluorescence, and F_{sample} and F_{std} are fluorescence of sample and of 0.2 μM Tb(III) in 1 μM DPA, respectively.

Standard curves of Tb(III):DPA complex fluorescence were obtained using Tb(III) concentrations ranging from 0 to 0.4 μM in 2 mM HEPES (pH 7.0, 0.9% NaCl) with either a DPA/Tb(III) ratio of 5 as recommended by Ma et al. (*3*), or at a constant concentration (2 μM) of DPA.

Fluorescence Quenching Measurements. Quenching of Tb(III):DPA complex fluorescence was measured using 0.2 μM Tb(III) in 2 mM HEPES (pH 7.0, 0.9% NaCl) containing DPA at a DPA/Tb(III) ratio of 5 as recommended by Ma et al. (*3*). Fluorescence measurements were obtained at increasing concentrations of either DTPA or EDTA from 0 to 1 μM or either PL25-DTPA (0−52 nM) or IgG-PL25-DTPA (0−44 nM).

Apparent Chelator-Binding Parameters and Stoichiometry of Fluorescence Quenching. Apparent binding constants and stoichiometry of fluorescence quenching by chelator were evaluated using the law of mass action for the reactions

$$(1)\ F_{cplx} + aS \leftrightarrow FS_a \text{ and } (2)\ F_{cplx} + bS \leftrightarrow NS_b:$$

$$K_{xa} = [FS_a]/([F_{cplx}][S]^a) \quad (2A)$$

$$K_{xb} = [NS_b]/([F_{cplx}][S]^b) \quad (2B)$$

where K_{xa} and K_{xb} are apparent association constants, $[F_{cplx}]$, $[S]$, $[FS_a]$, and $[NS_b]$ are the concentrations of the fluorescent complex, free terbium binding sites on chelator, fluorescent complex bound to chelator, and non-fluorescent turbium:chelator complex in the mixture, respectively, and a and b are reaction coefficients. The total number of chelator-binding sites in the reaction mixture can be defined as $cX_o = S + aFS_a + bNS_b$ where X_o is the initial molar concentration of chelator and c is the number of binding sites per chelator. By substitution, eqs 2A and 2B can be written as

$$K_{xa} = [FS_a]/([F_{cplx}][cX_o - aFS_a - bNS_b]^a) \quad (2C)$$

$$K_{xb} = [NS_b]/([F_{cplx}][cX_o - aFS_a - bNS_b]^b) \quad (2D)$$

Also,

$$\%F = p([F_{cplx}]_o - [NS_b]) \quad (3)$$

where $[F_{cplx}]_o$ is the initial concentration of the fluorescent complex and p is a fluorescence proportionality constant.

The amount of chelator required to produce a 50% decrease in fluorescence was estimated using a simple logistic dose−response function (LDR) of the form

$$\%F = \%F_{max}/[1 + ([X]_o/D_{50})^m] \quad (4)$$

where $\%F_{max}$ is the maximum percent fluorescence, $[X_o]$ is the initial concentration of chelator, D_{50} is the initial concentration of chelator resulting in 50% reduction of %F, and m is a slope factor (*6*).

Apparent DPA-Binding Parameters and Stoichiometry of Complex Fluorescence. A fluorescence titration curve was obtained using 0.2 μM $TbCl_3$ and increasing concentrations of DPA from 0 to 1 μM. Apparent binding constants and stoichiometry of DPA binding to Tb(III) to form a fluorescent complex were evaluated using the law of mass action for the reaction Tb(III) + nDPA⇔ $Tb(DPA)_n$:

$$K_n = [Tb(DPA)_n]/([Tb(III)][DPA]^n) \quad (5A)$$

$$K_n = [Tb(DPA)_n]/[([Tb(III)]_o - [Tb(DPA)_n])([DPA]_o - n[Tb(DPA)_n])^n] \quad (5B)$$

where K_n is an apparent association constant, $[Tb(DPA)_n]$, $[Tb(III)]$, $[DPA]$, $[Tb(III)]_o$, and $[DPA]_o$ are the concentrations of the fluorescent complex, free Tb(III), free DPA, initial Tb(III), and initial DPA in the mixture, respectively, and n is the reaction coefficient. Also, if %F is proportional to the concentration of $Tb(DPA)_n$, then

$$\%F = p[Tb(DPA)_n] \quad (6)$$

where p is a fluorescence proportionality constant.

Standard error of the curve fit. The standard error for each nonlinear regression curve fit [SE (fit)] was calculated as SE (fit) = square-root(sum of squares of the residuals/regression degrees of freedom). The residuals are the difference between the observed fluorescence and the calculated fluorescence. The regression degrees of freedom are the number of observations minus 1 minus the number of parameters in the curve-fit equation.

RESULTS

Standard curves of Tb(III):DPA complex fluorescence are shown in Figure 1. At a constant concentration of DPA (2 μM), the curve was linear throughout a Tb(III) concentration range 0−0.4 μM [$r^2 > 0.999$, SE (fit) = 4.1]. Within the same Tb(III) concentration range with a DPA/Tb(III) ratio of 5, complex fluorescence was approximately linear [$r^2 = 0.995$, SE (fit) = 11.9]; however, the curve deviated from linearity, suggesting complex dissociation.

Fluorescence quenching of the Tb(III):DPA complex by EDTA, DTPA, PL25-DTPA, and IgG-PL25-DTPA, respectively, are shown in Figures 2−5. EDTA, DTPA, and PL25-DTPA produced pronounced sigmoid-shaped quenching curves, suggesting initial binding of chelator results in minimal change in Tb(III):DPA complex fluorescence. The fluorescence quenching curves were modeled to law of mass action eqs 2A−D and 3 and to the logistic dose response eq 4. Curve-fit parameters are listed in Tables 1 and 2. Quenching equivalents defined as DTPA/X = $D_{50,DTPA}/D_{50,X}$ and EDTA/X = $D_{50,EDTA}/D_{50,X}$, where $D_{50,DTPA}$, $D_{50,EDTA}$, and $D_{50,X}$ are the D_{50} of DTPA, EDTA, and chelator X, respectively, are also listed in Table 2.

To determine Tb(III):DPA complex saturation conditions, 0.2 μM $TbCl_3$ was titrated with DPA up to a DPA/Tb(III) ratio of 5 as shown in Figure 6. The resulting saturation curve was modeled to the law of mass action (eqs 5A,B and 6). Curve-fit parameters were $n = 1.63$, $K_n = 29.0\ \mu M^{-n}$, and $p = 526\%F/\mu M$ [SE (fit) = 1.7]. At a DPA/Tb(III) ratio of 5, the observed %F(100) was approximately 95.1% of the maximum %F(105) predicted by eqs 5A,B and 6 for 0.2 μM Tb(III):DPA complex fluorescence.

DISCUSSION

Ma, Hwang, and Lee have described a fluorescence-quenching method using Tb(III) (1 μM) and dipicholinic acid (5 μM) for estimating chelating groups in chelate-conjugate macromolecules (*3*). This method of analysis was based on a fluorescence quenching model where Tb-(III) alone has low fluorescence, $Tb(DPA)_3^{3-}$ has strong fluorescence, and Tb(III) bound to chelator has no fluorescence. Fluorescence-quenching curves were fit to linear regression equations of fluorescence intensity and

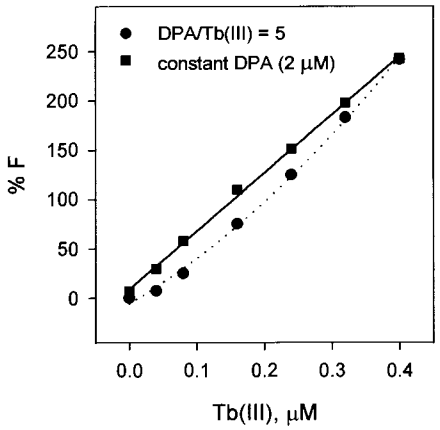


Figure 1. Fluorescence of Tb(III):DPA complex at various concentrations of Tb(III).

Table 1. LMA Curve-Fit Paramaters

	parameter					
chelator	K_{xa} (μM^{-a})	K_{xb} (μM^{-b})	*a*	*b*	*c*	SE (fit)
DTPA	1.7×10^2	7.6×10^5	0.47	1.5	1.0	1.9
EDTA	4.0×10^2	6.6×10^4	0.60	1.4	0.57	1.3
PL25-DTPA	1.5×10^3	5.6×10^5	0.62	1.5	15	2.0
IgG-PL25-DTPA	7.0×10^1	2.5×10^3	0.30	1.3	25	1.5

Table 2. LDR Curve-Fit Paramaters

	parameter				
chelator (X)	D_{50} (μM)	*m*	DTPA/X	EDTA/X	SE (fit)
DTPA	1.8×10^{-1}	3.9	1.0	1.9	5.0
EDTA	3.4×10^{-1}	4.6	0.54	1.0	1.7
PL25-DTPA	1.4×10^{-2}	6.2	14	25	0.9
IgG-PL25-DTPA	6.4×10^{-3}	2.0	29	54	0.1

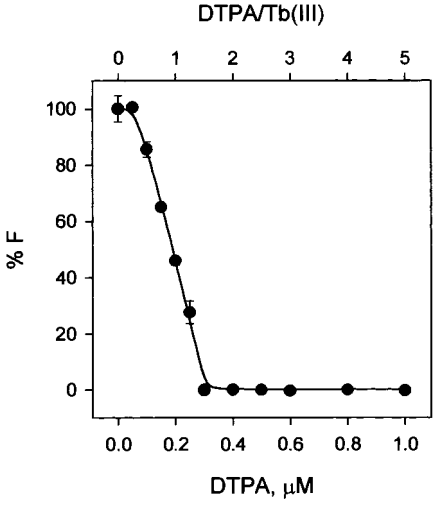


Figure 2. Fluroescence of Tb(III):DPA complex at various concentrations of DTPA. Solid line, law of mass action curve fit.

initial chelator concentrations, with characteristic intercepts and slopes for each chelator. The relative number of molecules of different quenching reagents equivlent to one molecule of DTPA was calculated from the slopes of the quenching curves relative to the slope of the DTPA quenching curve.

In the current study, using higher sensitivity fluorometry and lower concentrations of Tb(III) (0.2 μM) and DPA (1 μM), fluorescence quenching by chelators was not linear (Figures 2−5) but rather sigmoidal suggesting

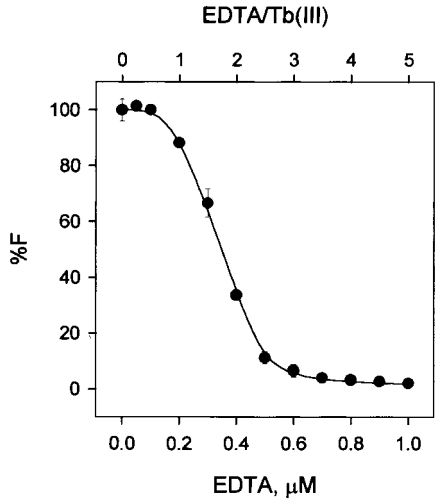


Figure 3. Fluorescence of Tb(III):DPA complex at various concentrations of EDTA. Solid line, law of mass action curve fit.

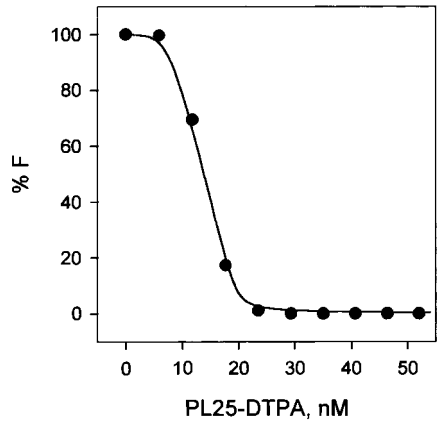


Figure 4. Fluorescence of Tb(III):DPA complex at various concentrations of PL25-DTPA. Solid line, law of mass action curve fit.

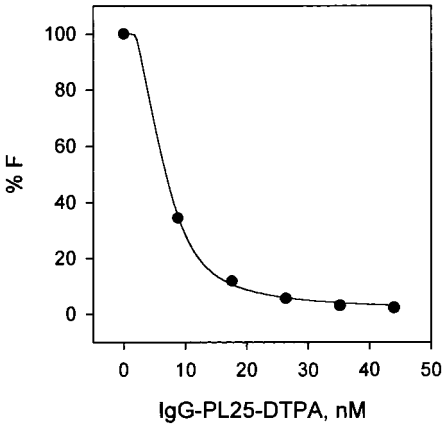


Figure 5. Fluorescence of Tb(III):DPA complex at various concentrations of IgG-PL25-DTPA. Solid line, law of mass action curve fit.

initial binding of chelator to the Tb(III):DPA complex may produce only small changes in fluorescence. The formation of a fluorescent Tb:DPA:chelator complex would be possible if there were coordination bonds not involved with chelator binding that could be filled by DPA. EDTA, for example, could occupy up to six out of eight coordination bonds leaving at least two available for DPA binding. At higher chelator concentations, the DPA would be

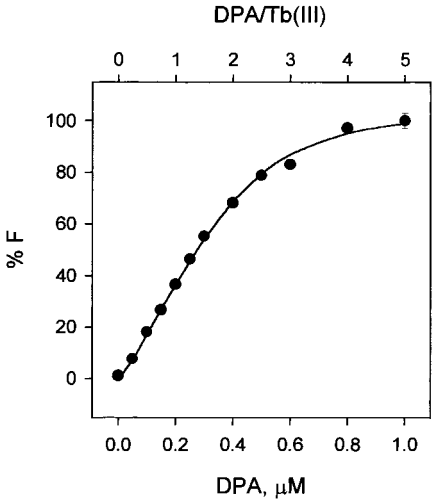


Figure 6. Fluorescence of $TbCl_3$ (0.2 μM) at increasing concentrations of DPA. Solid line, law of mass action curve-fit for Tb(III) + nDPA ↔ $Tb(DPA)_n$, % F = p*[$Tb(DPA)_n$]; $n = 1.63$, $K_n = 29.0\ \mu M^{-n}$, $p = 526\%$ F/μM.

displaced, resulting in complete quenching of fluorescence. Curves representing a nonlinear fluorescence quenching model (eqs 2A−D and 3; Table 1) are included in Figures 2−5. The stoichiometry of chelator binding as reflected by the reaction coefficients *a* and *b* listed in Table 1 suggests that approximately 1/3 of total chelator bound does not significantly change fluorescence of the Tb(III):DPA complex.

The potential formation of fluorescent Tb(III):DPA:chelator complexes is also supported by the fluorescence titration of Tb(III) with DPA (Figure 6). Stoichiometry of DPA binding to Tb(III) as evaluated using the law of mass action (eqs 5A,B and 6) suggests that maximum fluorescence may be achieved when less than 3 DPAs are bound per Tb(III) (i.e., $n = 1.6$). On the basis of a three-site binding model for Tb(III):DPA complex formation (Scheme 1), total fluorescence would depend on the concentration of each of three Tb(III):DPA complexes [i.e., Tb(III):(DPA), Tb(III):$(DPA)_2$, or Tb(III):$(DPA)_3$] and on the fluorescence proportionality constant for each complex. If fluorescence intensity depends primarily on one or two DPAs bound per Tb(III), then initial binding of chelator may significantly decrease the concentration of the Tb(III):DPA_3 complex by forming fluorescent Tb(III):DPA_2:chelator or Tb(III):DPA:chelator complexes, thus a change in fluorescence would be minimal. Subsequent changes in fluorescence at higher chelator concentrations could result when the Tb(III):$(DPA)_2$:chelator or Tb(III):(DPA):chelator complex concentrations decrease. The slightly sigmoidal shape of the fluorescence titration curve (Figure 6) would suggest that fluorescence of the Tb(III):DPA:chelator complex would be less than the Tb(III):$(DPA)_2$:chelator complex.

The values of the apparent association constants (K_{xa}, K_{xb}) listed in Table 1 for the binding of DTPA or EDTA to the fluorescent Tb(III):DPA complex are less than the reported values of the formation constants for the Tb(III):DTPA ($K_f = 5 \times 10^{13}\ \mu M^{-1}$) or Tb(III):EDTA ($K_f = 9 \times 10^{8}\ \mu M^{-1}$) complexes (*7*). Differences in values would be expected in this study where the binding of chelator to Tb(III) is in the presence of excess DPA which also binds to Tb(III), thus the apparent association constant for chelator binding to the fluorescent Tb(III):DPA complex would be less than the association constants for chelators binding to Tb(III) alone. The parameters in Table 1 are minimum values required to fit a model curve (eqs 2A−D and 3) to the observed data based on nonlinear least-squares analysis. Greater values for association constants are possible, although higher values would not necessarily improve the curve fit. The curve fit parameters are valid for the proposed reaction model (eqs 2A−D and 3), thus comparisons of reaction paramaters with others in the literature also requires a comparison of the reaction models used in calculating the association constants. The relative magnitudes of the binding constants determined in this study are consistent with published data (i.e. DTPA > EDTA ≫ DPA) (*7*).

The inclusion of the coefficient c (number of binding sites per chelator, Table 1) or the DTPA/X ratio (Table 2) provided means of evaluating the binding capacity of each chelator relative to DTPA. The relative binding capacity of each chelator was EDTA < DTPA < PL25-DTPA < IgG-PL25-DTPA. The weaker chelating ability of EDTA ($c = 0.57$; DTPA/X = 0.54) is to be expected from the fewer carboxyl groups available for chelation for EDTA (four) compared to DTPA (five) as suggested by Ma et al. (*3*). Also, the larger size of DTPA compared to EDTA may result in greater chelating ability of DTPA for lanthanide series ions.

Scheme 1. Three Site Binding Model for Tb(III):DPA Fluorescent Complex Formation[a]

A. Binding

1	Tb(III) + DPA <=> Tb(III):DPA	K_1 = [Tb(III):DPA] /{[Tb(III)]*[DPA]}
2	Tb(III):DPA + DPA <=> Tb(III):$(DPA)_2$	K_2 = [Tb(III):$(DPA)_2$] /{[Tb(III):DPA]*[DPA]}
3	Tb(III):$(DPA)_2$ + DPA <=> Tb(III):$(DPA)_3$	K_3 = [Tb(III):$(DPA)_3$] /{[Tb(III):$(DPA)_2$]*[DPA]}

B Fluorescence

1 $\%F_1 = p_1*[Tb(III):DPA] = p_1*K_1*[Tb(III)]*[DPA]$

2 $\%F_2 = p_2*[Tb(III):(DPA)_2] = p_2*K_1*K_2*[Tb(III)]*[DPA]^2$

3 $\%F_3 = p_3*[Tb(III):(DPA)_3] = p_3*K_1*K_2*K_3*[Tb(III)]*[DPA]^3$

[a] K_1−K_3, association constants; $\%F_1$ − $\%F_3$, complex fluorescence; p_1−p_3, fluorescence proportionality constants.

Fluorescence quenching by the chelate-conjugated macromolecules PL25-DTPA and IgG-PL25-DTPA reflects the expected higher binding capacity for these molecules. On the basis of the curve fit parameters *c* in Tables 1 and DTPA/X and EDTA/X in Table 2, PL25-DTPA and IgG-PL25-DTPA have approximately 14−15 and 18−29 times the binding capacity of DTPA and 25−26 and 33−54 times the binding capacity of EDTA, respectively. The data also suggests (based on DTPA/X and EDTA/X, Table 2) that up to two PL25-DTPAs may be bound per IgG. Fluorescence quenching by IgG-PL25-DTPA may also include Tb(III) and DPA binding to other sites on IgG, thus analysis of fluoresence quenching by IgG alone would be necessary to assess relative chelator concentration of chelate-conjugated IgG.

Estimates of chelating capacity by fluorescence quenching may underestimate the number of chelating groups in chelate-conjugated macromolecules. Tb(III) binding to PL25-DTPA as determined by fluorescence quenching suggests approximately 0.4−0.6 DTPA and approximately 1.0−1.1 EDTA equivalent Tb(III)-binding sites/kDa of PL25. Using ^{153}Gd(III) binding to PL14-DTPA (PL14 = 14 kDa), Manabe, Longley, and Furmanski (*4*) detected approximately 3 DTPA/kDa PL14. Torchilin et al. (*5*), using radiometric determination of ^{111}In(III) binding and nuclear resonance determination of Gd(III) binding to PLn-DTPA (PLn = 4, 14, or 55 kDa), conjugated monoclonal antimyosin antibody estimated from 1.6 to 5.4 cations bound/kDa PLn. As suggested by the data shown in Figures 2 and 3, approximately 1.5−2.0 DTPA/Tb(III) and >2.5 EDTA/Tb(III) are required to quench fluorescence, thus the actual number of chelating groups on PL25-DTPA or IgG-PL25-DTPA per kilodalton PL25 would be comparable to that reported by others.

In conclusion, as proposed by Ma et al. (*3*), the method of fluorescence quenching of the Tb(III):DPA complex by chelators is rapid, simple, and has merit in estimating low concentrations of chelating groups in chelate-conjugated macromolecules. Using high sensitivity fluorometry and lower initial concentrations of the Tb(III):DPA fluorescent complex, nonlinear curve fitting of fluorescence quenching facilitated the estimation of chelating groups at lower concentration limits. The estimation of chelating groups on chelate-conjugated macromolecules at lower concentrations would minimize the amount of sample required for analysis during synthesis and isolation of chelate-conjugated macromolecules for various procedures including radioimmunoimaging, radioimmunotherapy, NMR-tomography, and in vitro immunoassays. The data also suggested a model for the stoichiometry of Tb(III):DPA complex fluorescence consistent with the observed fluorescence quenching by chelators. An understanding of the mechanism of Tb:DPA complex fluorescence and fluorescence quenching would be useful in further refinement of methods for estimating chelator concentrations and for design of fluorescent probes.

ACKNOWLEDGMENT

The authors wish to thank the Office of Research and the Department of Biochemistry/Microbiology of the Oklahoma State University College of Osteopathic Medicine and the Department of Surgery (Research Section) of the University of Oklahoma Health Sciences Center (Tulsa Campus) for their financial support.

LITERATURE CITED

(1) Torchlin, V. P., and Klibanov, L. (1991) The antibody-linked chelating polymers for nuclear therapy and diagnostics. *Crit. Rev. Ther. Drug Carrier Sys. 7*, 275−308.

(2) Kassis, A. I. (1991) Optimizing antibodies for use in nuclear medicine. *J. Nucl. Med. 32*, 1751−1753.

(3) Ma, W., Hwang, K. J., and Lee, V. H. L. (1993) A fluorescence quenching method for estimating chelating groups in chelate-conjugate macromolecules. *Pharm. Res. 10*, 204−207.

(4) Manabe, Y., Longley, C., and Furmanski, P. (1986) High-level conjugation of chelating agents onto immunoglobulins: Use of an intermediary poly (L-lysine)-diethylenetriaminepentaacetic acid carrier. *Biochim. Biophys. Acta 883*, 460−467.

(5) Torchilin, W. P., Klibanov, A. L., Nossiff, N. D., Slinkin, M. A., Strauss, H. W., Haber, E., Smirnov, V. N., and Knaw, B. A. (1987) Monoclonal antibody modification with chelate-linked high-molecular-weight polymers: Major increases in polyvalent cation binding without loss of antigen binding. *Hybridoma 6*, 229−240.

(6) Rodbard, D., and Hutt, D. M. (1974) Statistical analysis of radioimmunoassays and immunoradiometric (labeled antibody) assays. A generalized weighted, iterative, least-squares method for logistic curve fitting. *Radioimmunoassay and Related Procedures in Medicine,* Vol. I, pp 165−192, International Atomic Energy Agency, Vienna.

(7) Moeller, T. (1973) *Comprehensive Inorganic Chemistry* (J. C. Bailar, H. J. Emeleus, R. Nyholm, and A. F. Trotman-Dickenson, Eds.) Vol. 4, p 29, Pergamon, Oxford.

BC980018N

Biotin-Conjugated Polychelating Agent

Vladimir P. Torchilin*

Center for Imaging and Pharmaceutical Research, Department of Radiology, Massachusetts General Hospital and Harvard Medical School, 149 13th Street, Charlestown, Massachusetts 02129. Received May 27, 1998

A procedure is described for preparing a polychelating agent−biotin conjugate through the interaction of biotin-maleimide with poly-L-lysine modified with multiple residues of diethylenetriaminepentaacetic acid and containing amino-terminal pyridylthio-propionate group. The conjugate can be easily loaded with multiple metal atoms, such as ^{111}In, and preserves its ability to specifically interact with avidin (as avidin-agarose). Polychelate-biotin conjugate may be used for signal amplification in visualization and analytical protocols involving the application of the avidin-biotin system.

The avidin-biotin system is well studied and used for different biochemical and biomedical applications including analytical ones, for review see ref *1*. Its application is based on the ability of avidin macromolecule to bind four biotin molecules with extremely high affinity ($K_d \approx 10^{-15}$ M). In particular, the authors of ref *1* mention the application of avidin-biotin complex in affinity chromatography, affinity cytochemistry, cell cytometry, blotting technology, immunoassay, histopathology staining, gene probes, and bioaffinity sensors. Avidin-biotin complex is also being used for targeted delivery of diagnostic and therapeutic agents. For the latter purpose, a ligand is modified either with avidin or with biotin and is then allowed to accumulate in a target area. Then, the pharmaceutical agent is administered as a conjugate with biotin (if avidin is accumulated in the target) or with avidin (if the target contains biotin) and concentrates locally in the desired area due to the fast formation of avidin-biotin complex. Since the in vivo stability of biotin association with various biological (macro) molecules was repeatedly confirmed (see, for example, refs *2* and *3* and references therein), the approach is currently finding growing application.

Recently, the (strept) avidin-biotin system was also used for the visualization of various pathological conditions including tumors (*4*, *5*). The approach is based on the observation that infected, inflamed, necrotic, and malignant areas are able to nonspecifically accumulate large protein molecules, such as immunoglobulins or albumin (*6*, *7*) or even nanoparticulates (*8*) via the mechanism of impaired filtration. It was suggested to use (strept) avidin itself or (strept) avidin-antibody conjugate as a tumor-accumulating substance, and after its preliminary injection and accumulation, to target (i.e., to visualize) the tumor with a biotin-associated label (*9*−*11*). Different heavy metal ions serve usually as those labels, such as ^{111}In and ^{99m}Tc (for γ-immunoscintigraphic visualization); Gd and Mn (for magnetic resonance imaging), or ^{186,188}Re and ^{90}Y (for tumor radiotherapy) (*10*).

Whenever biotin has to be modified with a reporter metal for in vitro or in vivo application, to couple metals with biotin, the latter is first chemically modified with a metal-chelating moiety (*11*). However, the insufficient ability to load biotin with a metal might be considered as one of the potential limitations of the proposed scheme. All techniques described so far involved the use of biotin carrying just a single chelating group, i.e. capable of binding just one metal atom, which results in the insufficient signal multiplication from biotin in both, in vitro and in vivo analytical (imaging) procedures. Thus, in vivo it should result in relatively low label accumulation in the target (tumor), especially when the size of the target is small and/or the quantity of avidin in the target is low. This makes γ- and MR-imaging as well as radiotherapy difficult enough, since the efficacy of all in vivo protocols depend on the quantity of a label delivered to the target. The sensitivity of various analytical in vitro protocols involving avidin-biotin application also might suffer because of insufficient biotin load with tracers.

This report describes an attempt to increase biotin load with a marker metal. With this in mind, the scheme was developed of biotin modification with single-terminus reactive chelating polymers containing multiple chelating groups and able to chelate firmly multiple metal atoms (their exact number in each particulate case can be controlled by the length of a chelating polymer). Such polymers were developed by us earlier for the modification of monoclonal antibodies used for γ-immunodiagnostics (*12*−*14*), see also ref *15* for review.

Materials. Biotin-maleimide [*N*-biotinoyl-*N*′-(6-maleimidohexanoyl)hydrazide, BMA], *N*-(carbobenzyloxy)-poly-DL-lysine (CBZ-PLL; MW 4000), diethylenetriaminepentaacetic acid cyclic anhydride (caDTPA), dithiothreitol (DTT), N-succinimidyl 3-(pyridyldithio) propionate (SPDP), guanidine chloride, and all solvents and buffer components were obtained from Sigma Chemical Co., St. Louis, Mo.[1] Prepacked 1 mL avidin-agarose columns (Immuno-Pure AffinityPak) were acquired from Pierce (Rockford, IL).

* To whom correspondence should be addressed. Current address: Department of Pharmaceutical Sciences, Northeastern University, Mugar Building 312, 360 Huntington Avenue, Boston, MA 02115.

[1]Abbreviations: BMA, *N*-biotinoyl-*N*′-(6-maleimidohexanoyl)-hydrazide; PLL, poly-DL-lysine; CBZ-PLL, *N*-(carbobenzyloxy)-poly-DL-lysine; caDTPA, diethylenetriamine pentaacetic acid cyclic anhydride; DTT, dithiothreitol; SPDP, *N*-succinimidyl 3-(pyridyldithio)propionate; DTPA-PLL-PDP, *N*-terminal-activated chelating polymer; DTPA-PLL-SH, chelating polymer with free terminal SH-group; DTPA-PLL-biotin, conjugate of chelating polymer with biotin; DTPA-biotin, conjugate of monomeric DTPA with biotin; HBS, HEPES-buffered saline.

10.1021/bc9800567 CCC: $18.00 © 1999 American Chemical Society
Published on Web 12/24/1998

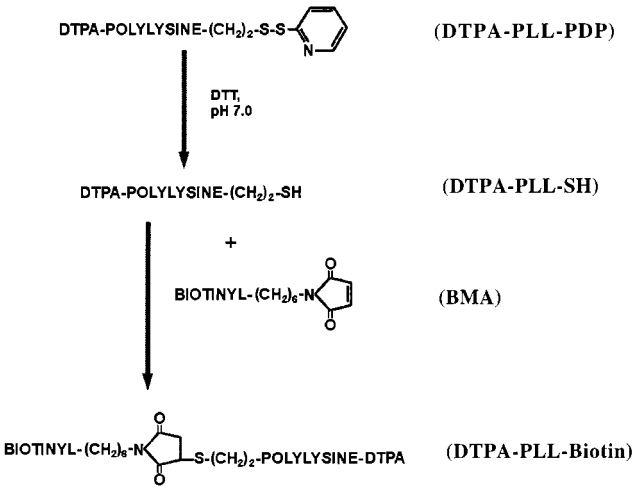


Figure 1. The scheme of DTPA-PLL-biotin synthesis. Starting DTPA-PLL-PDP was prepared as in ref 13.

Synthesis. N-Terminal-activated chelating polymer DTPA-PLL-PDP was prepared as in ref *14* by modification of the unprotected terminal amino group in CBZ-PLL with SPDP, subsequent deprotection of CBZ-PLL-PDP with HBr/CH_3COOH, and interacting free amino groups of PLL-PDP with caDTPA. For this purpose, 3.5 μmol of SPDP was reacted with 0.8 μmol of CBZ-PLL (MW 4000) in 350 μL of DMFA in the presence of 0.14 μL of triethylamine at 4 °C overnight. The product was precipitated with water and CBZ deprotected with 250 μL of 36% HBr in acetic acid. The resulting PLL-PDP was precipitated with diethyl ether and freeze-dried. DTPA residues were incorporated into PLL-PDP by reacting the latter with 50-fold molar excess of caDTPA at pH 8.2. In order to diminish possible cross-linking of PLL chains by bifunctional caDTPA, mixed DTPA anhydride can be used instead of caDTPA (*16*). However, HPLC analysis of DTPA-PLL-PDP obtained by both protocols provides similar patterns demonstrating the absence of olygomeric structures. As was demonstrated in our previous reports using the titration of remaining free amino groups with trinitrobenzene sulfonic acid of direct binding of ^{111}In (*12*−*14*, *17*), in such conditions 15−20 DTPA residues can be reproducibly incorporated into a single chain of DTPA-PLL(4000)-PDP.

To derivatize biotin with DTPA-PLL, DTPA-PLL-PDP (10 mg/mL in HEPES buffered saline, HBS, pH 7.0) was first reduced with 5 mM DTT in HBS for 2 h at room temperature. The product was purified from low-molecular-weight reactants by centrifugation on Sephadex G-10 minicolumn (Pharmacia). The resulting chelating polymer with free terminal SH-group was conjugated with BMA. For this purpose, 100 μg of DTPA-PLL-SH was incubated with 6 μg of BMA (added as 10% solution in DMSO), which corresponds to molar ratio DTPA-PLL-SH:BMA ca. 2:1, in 0.5 mL of HBS, pH 7.4, for 1 h at room temperature. The resulting DTPA-PLL-biotin (mixed with nonreacted DTPA-PLL-SH and BMA) was separated from low-molecular-weight reactants, including BMA, by centrifugation on Sephadex G-10 minicolumn. The synthesis scheme is presented in Figure 1.

DTPA-PLL-biotin (as a mixture with nonreacted DTPA-PLL-SH) and control DTPA-PLL-SH (same molar quantities as DTPA-PLL) were labeled with ^{111}In via the transchelation mechanism. For this purpose, 150 μL of 0.1 M citrate, pH 5.3, was added to 100 μg of each polymer in 0.5 mL of HBS, then polymer solutions were supplemented with ca. 300 μCi of ^{111}In (as $^{111}InCl_3$ in HCl and NEN) and incubated for 1 h at room temperature. Free ^{111}In was separated from ^{111}In-labeled polymers by centrifugation on Sephadex G-10 mincolumn.

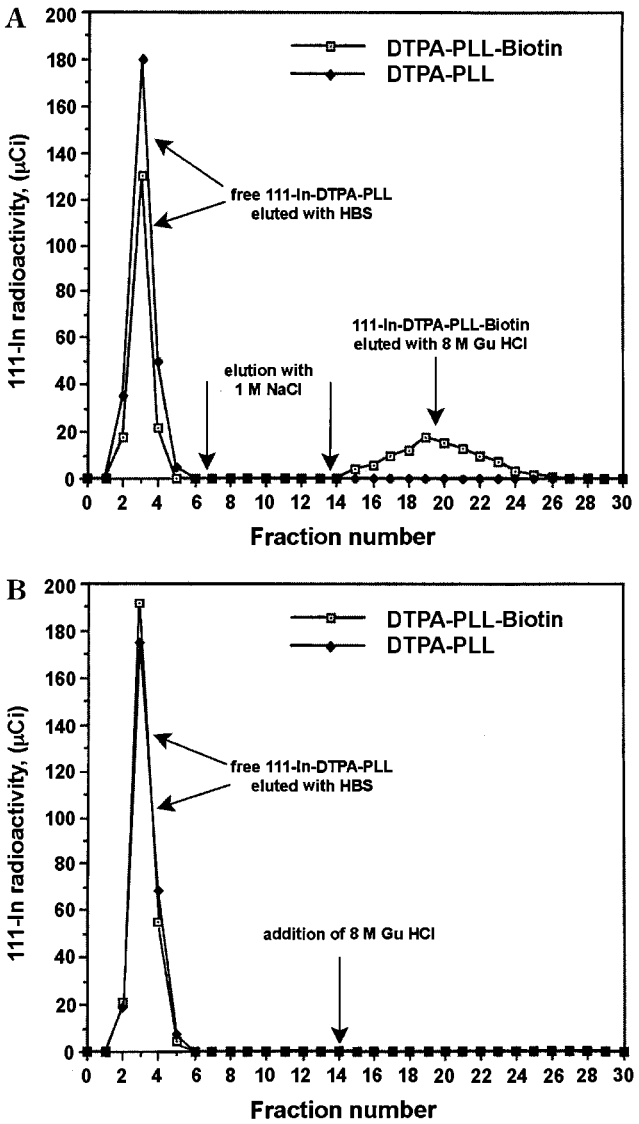


Figure 2. Chromatography of ^{111}In-labeled DTPA-PLL-biotin and control DTPA-PLL on avidin-agarose without (A) and with (B) column presaturation with free biotin. Column volume, 5 mL; samples were applied in 0.5 mL of HBS, pH 7.4 (other details in the text).

RESULTS AND DISCUSSION

Sephadex G-10 chromatography of ^{111}In-labeled samples demonstrated that both the eluate with DTPA-PLL-Biotin and eluate with DTPA-PLL-SH contained ca. 250 μCi of ^{111}In radioactivity (of ca. 300 μCi added to each sample). It proves efficient and similar labeling of chelates in both polymers.

To check the efficacy of biotin derivatization with DTPA-PLL, a gel-chromatography of both ^{111}In-labeled DTPA-PLL-Biotin and control DTPA-PLL-SH on avidine-agarose column equilibrated with HBS was performed. The results of this experiment are presented in Figure 2A. Upon washing column with HBS, all applied polymer-bound radioactivity was eluted in case of control chelating polymer, DTPA-PLL-SH. However, only 60% of applied radioactivity was eluted in case of labeled DTPA-PLL-Biotin. Forty percent of applied radioactivity remained on the column. This avidin-agarose-bound radioactivity

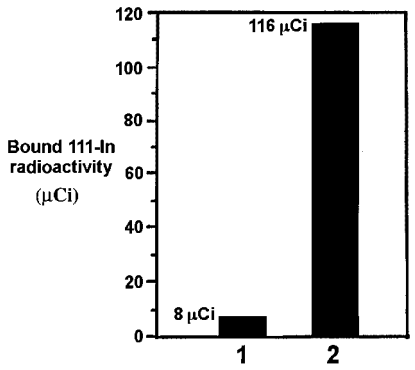


Figure 3. Radioactivity (^{111}In) binding with avidin-agarose via DTPA-biotin (1) and DTPA-PLL-Biotin (2). For conditions, see Figure 2.

cannot be eluted by washing the column with 1 M NaCI (which excludes any nonspecific interactions, such as electrostatic ones), but was eluted as a broad peak with 8 M guanidine chloride, which is known to slowly dissociate avidin-biotin complex (*18*). However, presaturation of the avidine-agarose column with pure nonlabeled biotin results in identical elution pattern for both polymers: HBS is able to elute all applied radioactivity for both, DTPA-PLL-biotin and control DTPA-PLL-SH (Figure 2B). It clearly proves that the reaction mixture after DTPA-PLL-biotin synthesis, together with nonbiotinylated DTPA-PLL, contains also polychelate-conjugated biotin which preserves its ability to specifically interact with avidin with very high affinity since, like in case of the native biotin-to-avidin interaction, only 8 M guanidine chloride is able to slowly dissociate the complex formed. Probably, negatively charged polychelator forms rigid rod-like "tail" attached to biotin "head" and does not create any steric hindrances for the biotin-to-avidin interaction. Since in the reaction mixture, DTPA-PLL-SH:BMA molar ratio was 2:1 and avidine-agarose adsorbs ca. 40% of applied reaction mixture (following the radioactivity data), we can easily calculate that the coupling yield of BMA and DTPA-PLL-SH is ca. 80% relative to BMA. Thus, even in the case of relatively low-molecular-weight PLL, it is possible to couple a PLL tail containing 15−20 DTPA residues (it means the same number of diagnostic or therapeutic metal atoms) to a single biotin molecule.

To prove the practical significance of polychelate-biotin and its superiority over traditional single chelate-modified biotin, we compared the quantity of radioactivity which can be delivered to the avidin-agarose column by ^{111}In-loaded DTPA-biotin (was purchased from Sigma as DTPA-α,ω-bis-biocytinamide) and DTPA-PLL-Biotin under similar conditions. Both reagents, taken in similar quantities as biotin, were incubated with the same quantity of ^{111}In in the same conditions, and reaction mixtures were directly applied onto identical avidin-agarose minicolumns. After washing columns with HBS (to remove all components containing no biotin moiety), the radioactivity remaining on both columns (i.e., attached to avidin via biotin residues) was measured. The results presented in Figure 3 clearly shows that DTPA-PLL-biotin is able to deliver to avidin-containing matrix almost 15 times more radioactivity than DTPA-biotin (which corresponds well with the presence of ca. 15 DTPA groups in DTPA-PLL-biotin compared with a single DTPA group in routine DTPA-biotin).

Thus, the possibility of increasing loading of biotin with metal (radio)isotopes via chelating polymers is demonstrated. Chelate-PLL-biotinyl conjugates (with various chelates) can be used to amplify the signal from avidin-bound biotin in various analytical systems in vitro and to enhance a diagnostic and/or therapeutic metal targeting to a preaccumulated avidin or avidinylated molecules in vivo. The medical application of this approach might be especially attractive, and one can speculate that the local metal concentration can be achieved suitable for γ-imaging, radiotherapy, and MR diagnostics of avidin-containing targets (tumors, infarcts, necrotic tissues etc.). Sure, additional in vivo studies have to be performed to investigate the pharmacokinetics of biotin-polychelate compared to biotin-monochelate (in particular liver uptake which might be higher for biotin-polychelate if the presence of DTPA residues will not compensate sufficiently positive charge of PLL) before making a more definite conclusion concerning the clinical (diagnostic) applicability of a new conjugate. However, the benefit of using biotin-polychelate conjugates is evident for in vitro analytical biochemistry, where it might be successfully applied as an amplification system in analytical procedures involving the use of the avidin-biotin system.

LITERATURE CITED

(1) Wilchek, M., and Bayer, E. A. (1988) The avidin-biotin comples in bioanalytical applications. *Anal. Biochem. 171,* 1−32.

(2) Paganelli, G., Samuel, A., Magnani, P., Siccardi, A., and Fazio, F. (1995) Potential of the avidin-biotin system for diagnostic application. in *Handbook on Targeted Delivery of Imaging Agents* (V. Torchilin, Ed.) pp 289−303, CRC Press, Boca Raton, FL.

(3) Jeong, J. M., Saga, T., Lee, J., and Koh, C.-S. (1995) Avidin-biotin system for targeting metastases: basic aspects. in *Handbook on Targeted Delivery of Imaging Agents* (V. Torchilin, Ed.) pp 305−319, CRC Press, Boca Raton, FL.

(4) Hnatowich, D. J., Virzi, F., and Rusckowski, M. (19897) Investigation of avidin and biotin for imaging applications. *J. Nucl. Med. 28,* 1294−1302.

(5) Rusckowski, M., Fritz, B., and Hnatowich, D. J. (1992) Localization of infection using streptavidin and biotin: an alternative to nonspecific polyclonal immunoglobulin. *J. Nucl. Med. 33,* 1810−1815.

(6) Rubin, R. H., Fischman, A. J., Needleman, M., Wilkinson, R., Callahan, R. J., Khaw, B.A., Hansen, W. P., Kramer, R. B., and Strauss, H. W. (1989) Radiolabeled, nonspecific polyclonal human immunoglobulin in the detection of focal inflammation by scintigraphy: comparison with gallium-67-citrate and technitium-99m-labeled albumin. *J. Nucl. Med. 30,* 385−389.

(7) Goh, A. S. W., Aw, S. E., Sundram, F. X., Ang, E. S., Goh, S. K., and Leong, K. H. (1990) Imaging of focal inflammation with 99m-Tc-labeled human polyclonal immunoglobulin G. *Nucl. Med. Commun. 11,* 843−856.

(8) Palmer, T. N., Caride, V. J., Caldecourt, M. A., Twicjler, J., and Abdullah, V. (1984) The mechanism of liposome accumulation in infarction. *Biochim. Biophys. Acta 797,* 363−368.

(9) Kalofonos, H. P., Rusckowski, M., Siebecker, D. A., Sivolapenko, G. B., Snook, D., Lavender, J. P., Epenetos, A. A., and Hnatowich, D. J. (1990) Imaging of tumor in patients with indium-111-labeled biotin and streptavidin-conjugated antibodies: preliminary communication. *J Nucl. Med. 31,* 1791−1796.

(10) *Antibodies in Radiodiagnosis and Therapy* (1989) (Zalutsky, M. R., Ed.) CRC Press, Boca Raton, FL.

(11) Virzi, F., Fritz, B., Rusckowski, M., Gionet, M., Misra, H., and Hnatowich, D. J. (1991) New In-111-labeled biotin derivatives for improved immunotargeting. *Nucl. Med. Biol. 18,* 719−726.

(12) Torchilin, V. P., Klibanov, A. L., Nossiff, N. D., Slinkin, M. A., Strauss, H. W., Haber, E., Smirnov, V. N., and Khaw, B. A. (1987) Monoclonal antibody modification with chelate-linded high-molecular-weight polymers: major increase in

polyvalent cation binding without loss of antigen binding. *Hybridoma 6*, 229−240.
(13) Slinkin, M. A., Klibanov, A. L., and Torchilin, V. P. (1991) Terminal-modified polylysine-based chelating polymers: highly efficient coupling to antibody with minimal loss in immunoreactivity. *Bioconjugate Chem. 2*, 342−348.
(14) Torchilin, V. P., Trubetskoy, V. S., Narula, J., Khaw, B. A., Klibanov, A. L., and Slinkin, M.A. (1993) Chelating polymer modified monoclonal antibodies for radioimmunodiagnostics and radioimmunotherapy. *J. Controlled Release 24*, 111−118.
(15) Torchilin, V. P., and Klibanov, A. L. (1991) The antibody-linked chelating polymers for nuclear therapy and diagnostics. *CRC Crit. Rev. Ther. Drug Carrier Syst. 7*, 275−308.
(16) Krejcarek, G.E., and Tucker, K.L. (1977) Covalent attachment of chelating groups to macromolecules. *Biochem. Biophys. Res. Commun. 77*, 581−584.
(17) Trubetskoy, V. S., Narula, J., Khaw, B. A., and Torchilin, V. P. (1993) Chemicallly optimized antimyosin Fab conjugates with chelating polymers: importance of the nature of the protein-polymer single site covalent bond for biodistribution and infarct localization. *Bioconjugate Chem. 4*, 251−255.
(18) Green, N. M., and Toms, E. J. (1972) The dissociation of avidin-biotin complexes by guanidinium chloride. *Biochem. J. 130*, 707−711.

BC9800567

Enzyme-Assisted Synthesis and Structural Characterization of Nitrocatechol Glucuronides

Leena Luukkanen,[†] Ilkka Kilpeläinen,[‡] Heli Kangas,[†] Pekka Ottoila,[§] Eivor Elovaara,[||] and Jyrki Taskinen*,[†]

Department of Pharmacy, Division of Pharmaceutical Chemistry, POB 56, FIN-00014, University of Helsinki, Finland, Institute of Biotechnology, NMR Laboratory, FIN-00014, University of Helsinki, Finland, Orion Corporation, Orion Pharma, POB 65, FIN-02101 Espoo, Finland, and Finnish Institute of Occupational Health, FIN-00250 Helsinki, Finland. Received June 8, 1998; Revised Manuscript Received November 7, 1998

Enzyme-assisted synthesis and characterization are described for 3-O-β-D-glucuronides **1b**−**4b** of the aglycons *E*- and *Z*-2-cyano-*N*,*N*-diethyl-3-(3,4-dihydroxy-5-nitrophenyl)propenamide (entacapone), **1a** and **2a**, respectively, 3-(3,4-dihydroxy-5-nitrobenzylidene)-2,4-pentanedione (nitecapone) **3a** and 4′-methyl-3,4-dihydroxy-5-nitrobenzophenone (tolcapone) **4a**, and 1-*o*- and 2-*o*-glucuronides **5b** and **6b** of the aglycon 1,2-dihydroxy-4-nitrobenzene **5a**. Liver microsomes from rats pretreated with Aroclor 1254 were used as catalyst in the synthesis. Glucuronidation was regio- and stereoselective in the case of **1a**−**4a**; only one product was observed by HPLC, HPTLC, and NMR. The glucuronidation of 1,2-dihydroxy-4-nitrobenzene **5a** resulted in equal amounts of 1-O-β-D- and 2-O-β-D-glucuronides. Purification of the crude products by C_{18} solid-phase extraction and/or flash chromatography gave compounds **1b**−**6b** in 38−98% yields (50−84 mg). The structures of the glucuronides were characterized on the basis of UV and IR spectra and confirmed with FAB-MS and NMR spectroscopy.

INTRODUCTION

Nitrocatechol derivatives entacapone (E-isomer) **1a**, its Z-isomer (*Z*-entacapone) **2a**, nitecapone **3a**, and tolcapone **4a** (Figure 1) are potent inhibitors of catechol-*O*-methyltransferase (EC 2.1.1.6, COMT), with K_i values in the nanomolar range (*1*). Entacapone and tolcapone are used clinically as adjuncts in the L-DOPA therapy of Parkinson's disease (*2*). The main biotransformation reaction for these compounds is glucuronidation (*3*−*5*), catalyzed by UDP-glucuronosyltransferase, UGT, enzyme family (EC 2.4.1.17). Products of the enzymatic reactions represent the β-anomer. Futile cycling, including the glucuronidation and subsequent hydrolysis of the conjugates by β-glucuronidase, may affect the net glucuronidation in vivo (*6*, *7*) since microsomal β-glucuronidase (EC 3.2.1.31) egasyn complex is located within the lumen of the endoplasmic reticulum (*8*), as is the active site of UGTs (*9*). The hydrolysis of nitrocatechol glucuronides by β-glucuronidase from *Escherichia coli* in the intestine may also be of importance in vivo as suggested by the biliary excretion of nitrocatechol glucuronides (*10*).

Well-characterized reference glucuronides are needed for pharmacokinetic and toxicokinetic studies as well as for enzyme kinetic studies of both glucuronidation by UGTs and glucuronide hydrolysis by β-glucuronidase.

A variety of methods are available for the synthesis of β-glucuronide conjugates (*11*). Most synthetic methods yield mixtures of α- and β-anomers and side-products such as ortho ester.

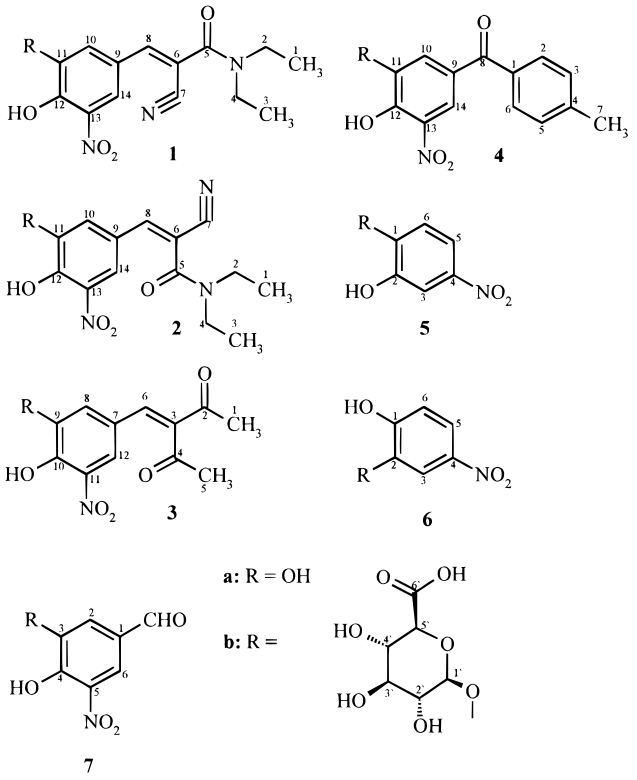


Figure 1. Structures of the nitrocatechol derivatives and their glucuronides.

Enzyme-assisted synthesis offers an alternative way of producing glucuronides. The advantage of biocatalyzed reactions is that the formation of solely the biologically relevant stereo- and regioisomeric products can be expected. Glucuronides have been prepared in laboratory scale by batch synthesis with microsomal enzyme sus-

* To whom correspondence should be addressed. Phone: 358 9 70859191. Fax: 358 9 70859556. E-mail: Jyrki.Taskinen@helsinki.fi.
[†] Department of Pharmacy.
[‡] Institute of Biotechnology.
[§] Orion Corporation.
[||] Finnish Institute of Occupational Health.

10.1021/bc980064n CCC: $18.00 © 1999 American Chemical Society
Published on Web 12/31/1998

Table 1. Yields and Purities of the Glucuronides 1b−6b

	yield		impurities, %	
product	%	mg	Aglycon	UDP, UDPGA, SL
1b	76	73	0.5	<0.1
2b	94	84	0.1	<0.5
3b	46	51	0.8	<0.5
4b	75	60	0.5	<0.1
5b	38[a]	29	nd	<0.5
6b	38[a]	21	nd	<0.5

[a] The yield includes both isomers; nd, not detected.

pensions (*12, 13*), microsomal enzymes immobilized to alginate (*14*), agarose (*15, 16*), and IAM HPLC (*17*) column and by microsomal enzymes trapped to hollow fiber systems (*18*).

This paper describes the synthesis and characterization of glucuronides of COMT inhibitors and some other nitrocatechols using rat liver microsomes as biocatalyst. Pure stereo- and regioisomeric glucuronides **1b−6b** were readily prepared in 50 mg scale, a quantity large enough for enzyme kinetic studies in vitro and for the reference standards required in pharmacokinetic and metabolism studies in vivo.

RESULTS AND DISCUSSION

Glucuronides of five nitrocatechol derivatives were prepared using liver microsomes from rats pretreated with Aroclor 1254 as biocatalyst. The purification by solid-phase extraction or flash chromatoraphy gave compounds **1b−6b** in 38−94% (50−84 mg) yields (Table 1).

The UGT activity in rat liver was increased by animal pretreatment with Aroclor 1254, which is a mixture of polychlorinated biphenyls. The specific UGT activities toward tolcapone and entacapone in liver microsomes from Aroclor 1254 (Aro) treated rats were 2- and 5-fold, respectively, relative to untreated or phenobarbital (PB)-treated rats. Glucuronidation may occur species dependently. Two glucuronides of nitecapone (*4*) and *Z*-entacapone (*3*) have been found in rat urine but only one glucuronide in human urine (*3, 4*). Surprisingly, only one glucuronide was formed for each aglycon **1a−4a** by liver microsomes from Aroclor 1254-treated rats. The observed regioselectivity of the reaction in vitro was not due to enzyme induction since only one glucuronide was produced with liver microsomes from untreated rats, too.

The glucuronidation of each nitrocatechol derivative was characterized by following the formation of the glucuronides **1b−6b** against time, protein concentration, and substrate concentration by HPLC. The reaction conditions were chosen by minimizing the amount of protein, maximizing the substrate concentration and optimizing against time.

An attempt was made to prepare nitecapone glucuronide **3b** by using rat liver microsomes immobilized to alginate beads (*14*). The reaction was incomplete resulting in low yield (38%). Further, the tight binding of the aglycon substrate and its degradation products to the matrix prevented repeated use of the beads.

The solubility of the aglycon substrates was in most cases (*Z*-entacapone, tolcapone, and 4-nitrocatechol) the rate-limiting factor of the glucuronidation, but entacapone inhibited its own glucuronidation at concentrations above 2 mM. This problem could be circumvented by adding the aglycon substrate to the reaction mixture in two portions after which the yield was increased from 50 to 76%.

During long incubations at pH 7.4, the side chain of entacapone **1a**, its Z-isomer **2a**, and nitecapone **3a** underwent nonenzymatic cleavage through *retro* aldol condensation. The product of the cleavage, 3,4-dihydroxybenzaldehyde **7a**, was also glucuronidated by rat liver microsomes. The identity of 3,4-dihydroxy-5-nitrobenzaldehyde glucuronide **7b** was determined by negative ion FAB mass spectrometry, $(M - H)^- = 358$. In the purification of **3b** by flash chromatography, the degradation product of the cleavage **7a** could not be fully separated from the glucuronide **3b**. Excess concentration of the aglycon substrate rather than the cosubstrate could not therefore be used in the synthesis of **3b**. The cleavage occurs in neutral conditions (*4*) and might have been prevented by lowering the pH of the reaction mixture.

D-Saccharic acid 1,4-lactone (SL) was included in the incubation medium to prevent cleavage of the generated glucuronides by endogenous β-glucuronidase. In the absence of SL, the cleavage of the glucuronides **1b−6b** was significant only after several hours of incubation.

The negative ion FAB spectra of the glucuronides **1b−6b** typically showed the loss of glucuronic acid. The deprotonated molecular ions $(M - H)^-$ and deprotonated aglycon fragments $(M - H - 176)^-$ were detected as diagnostic peaks. The exact masses obtained by high-resolution FAB mass spectrometry corresponded well with the calculated ones.

^1H and ^{13}C NMR spectra in D_2O were fully assigned on the basis of double quantum filtered correlation spectroscopy (DQF COSY), heteronuclear multiple quantum correlation (HMQC), and heteronuclear multiple bond connectivity (HMBC) spectra. For the sugar moiety, the DQF COSY spectra revealed the expected coupling network. The anomeric proton $H_{1'}$ was identified by the characteristic chemical shift near 5.2 ppm. The coupling constants between $H_{1'}$ and $H_{2'}$ (7 Hz) were in good agreement with the expected β-configuration. The site of glucuronidation was determined from the coupling between the anomeric proton $H_{1'}$ and the aromatic carbon of the glycosidic bond and from the absence or presence of long-range coupling between the aromatic carbon of the glycosidic bond and aromatic protons H_{10} and H_{14} in **1b−4b** (H_3, H_5, and H_6 in **5b** and **6b**). The NMR spectra confirmed the structures of the glucuronides **1b−6b** as stated in Figure 1.

For glucuronides **1b−4b**, the reaction was highly regioselective, producing 3-O-β-D-glucuronides in high yield. The glucuronidation of 4-nitrocatechol resulted in equal amounts of 1-O- and 2-O-glucuronides **5b** and **6b**. The products **1b−6b** were pure β-anomers and contained only minor amounts of the known impurities, indicating the superiority of the biocatalyzed reaction over chemical synthesis. In our laboratory this method has been successfully applied to the synthesis of glucuronides of other compounds, such as steroids and hydroxylated metabolites of polycyclic aromatic hydrocarbons, as well. The results will be reported elsewhere.

EXPERIMENTAL PROCEDURES

Chemicals. Entacapone, its Z-isomer, nitecapone, and tolcapone were from Orion Pharma (Espoo, Finland). All other reagents were of analytical grade. UDPGA, UDP, and SL were from Sigma Chemical Co. (St. Louis, MO).

Animal Treatment and Preparation of Microsomes. Eight adult male Wistar rats were obtained from the Helsinki University Breeding Center (Finland) and treated with as described previously (*19*). The treatment of the animals was approved by the local Ethical Committee for Animal Studies. Liver microsomes were prepared as described previously (*19*).

Table 2. Incubation Conditions for Glucuronides 1b−6b

compd	substrate (mM)	protein (mg/mL)	UDPGA (mM)	DMSO (%)	time (h)
1b	5.0[a]	0.8	10		19
2b	5.0	1.4	9.0		5
3b	10	0.9	5.0		20
4b	3.5	1.4	8.5	10	6
5b	8.0	1.2	13		2
6b	8.0	1.2	13		2

[a] **1a** was added in two portions, 30.5 mg in the beginning and 30.5 mg after 6 h.

Table 3. Purification of Glucuronides 1b−6b

compd	method[a]	wash	elution
1b	SPE[b]	15% MeOH[d]	40% MeOH
2b	SPE	15% MeOH	40% MeOH
3b	flash[c]	1 N HCl	10% ACN[e]/1 N HCl
	SPE	H_2O	MeOH
4b	SPE	H_2O	15% ACN
5b	flash	1 N HCl	5% MeOH/1 N HCl
	flash	H_2O	5% MeOH
6b	flash	1 N HCl	5% MeOH/1 N HCl
	flash	H_2O	5% MeOH

[a] If two methods were applied consecutively, both are listed. [b] Solid-phase extraction (Bakerbond C_{18} Polar Plus, 3 g). [c] Flash-chromatography (Baker octadecyl 40 μm, 60 Å, 2.5 × 25 cm). [d] Methanol. [e] Acetonitrile.

Enzyme Reactions. All enzyme reactions were carried out in a water bath (37 °C) in 50 mM phosphate buffer (pH 7.4, 5 mM $MgCl_2$, 5 mM D-saccharic, acid 1,4-lactone) with continuous stirring and the reactions were stopped with 10% of ice-cold perchloric acid. The precipitated proteins were removed by centrifugation (3500 rpm, 10 min) and filtration (Schleicher & Schuell ME 25/21, 0.45 μm, Dassel, Germany) of the supernatants. The detailed reaction conditions are given in Table 2.

Purification of Glucuronides 1b−6b. Glucuronides **1b−6b** were purified by solid-phase extraction cartridges (Bakerbond C-18 Polar Plus 3 g) or by flash chromatography (Baker octadecyl 40 μm, 60 Å) in a 2 × 25 cm column (Table 3). After elution, organic solvents were evaporated by rotary evaporator and the aqueous residues were frozen and dried under vacuum with phosphorus pentoxide.

HPLC. (System 1) The formation of the glucuronides was followed by liquid chromatography (HP 1090 Liquid Chromatograph, Pye Unicam PU4020 UV detector and HP 35900 Interface) with a 3.9 × 150 mm Waters NovaPak C_{18} or Waters Symmetry C_{18} column and a Merck 4 × 30 mm precolumn packed with 5 μm LiChrospher RP-18. The detector was set to the UV absorption maximum of each aglycon substrate and glucuronide conjugate at pH 2.0. The flow rate was 1 mL/min. The mobile phase consisted of 5−30% acetonitrile in 0.5% acetic acid.

(System 2) The impurities in the glucuronides **1b−6b** were quantified with (Waters 510 HPLC Pump, Waters 717 plus Autosampler) Micra NPS, 3 μm, 4.6 × 33 mm C_{18} column and electrochemical detection (ESA Coulochem II, 5010 Analytical Cell) with electrode 1 set to 0 mV and electrode 2 set to 250 mV. The flow rate (5% ACN/ 20 mM phosphate buffer, 10 mM citric acid, pH 2.2, 0.15 mM Na_2-edetate) was 0.8 mL/ min.

(System 3) Entacapone glucuronide **1b**, its Z-isomer **2b**, and 4-nitrocatechol 1-O- and 2-O-glucuronides **5b** and **6b** contained small amounts of the other isomer as impurity and they were quantified by liquid chromatography (HP 1090 Liquid Chromatograph, Pye Unicam PU4020 UV detector and HP 35900 Interface) with a 3.9 × 150 mm Waters NovaPak C_{18} column and a Merck 4 × 30 mm precolumn packed with 5 μm LiChrospher RP-18. The mobile phase consisted of 20 mM ammonium acetate in 5−10% acetonitrile/water, and the flow rate was 1 mL/ min.

HPTLC. UDP, UDPGA, and SL contents of the products were determined by thin-layer chromatography by the method of Bansal and Gessner (*20*) but without radioactive label. Compounds **1b−6b** (50 μg) and 0.25−2.5 μg of UDP, UDPGA, and D-saccharic acid 1,4-lactone were applied on a Merck Silica gel 60 F_{254} HPTLC plate using the Linomat IV spray-on technique (Camag). After ascending chromatography in a Camag twin-trough chamber, the plates were scanned with a Camag TLC Scanner II controlled by a computer running Camag CATS software version 3.14.

UV−Vis, IR, and Mass Spectra. UV−vis spectra were recorded with a Philips PU8700 UV−vis spectrophotometer at pH 7.4 (50 mM phosphate buffer) and pH 2.0 (0.5% acetic acid). Molar absorptivities (ϵ) were calculated from 0.06 mM solutions. Infrared spectra were recorded with a Pye Unicam SP3-200 infrared spectrophotometer from KBr tablets. The fluorescence spectrum of nitecapone was also recorded at pH 7.4 and pH 2.0. FAB mass spectra were recorded on a JEOL JMS-HX100 instrument. Low-resolution spectra were obtained in negative ion mode using a 50/50 mixture of glycerol and DMSO as the matrix. Accurate mass measurements at a resolution of 5000 were made in positive or negative ion mode with use of glycerol as the matrix and reference compound.

NMR Spectra. For NMR spectroscopy the samples were deuterium exchanged twice by lyophilizing with excess D_2O. The final samples were prepared by dissolving the compounds (5−15 mg) in 0.7 mL of D_2O (Sigma 99.9% ^2H) in a 5 mm NMR tube. A small amount of acetone was added to the solution as an internal standard (^1H δ 2.225 ppm, ^{13}C δ 30.55 ppm). All spectra were recorded at 300 K (27 °C) on a Varian Unity 500 spectrometer. The HMQC spectra were recorded using the pulse sequence of Summers et al. (*21*). The delay for polarization transfer was set for an assumed ^1J(C, H) of 140 Hz and the delay after the BIRD portion of the pulse sequence was set to 200 ms. GARP-1 decoupling was used in the carbon channel during acquisition (*21*). The relaxation delay between scans was 1 s. The ^1H and ^{13}C spectra of glucuronides **1b−6b** were assigned based on DQF COSY, HMQC, and HMBC. HMQC and HMBC were used in concert to accomplish full ^1H and ^{13}C assignment.

Enzyme-Assisted Synthesis of Nitrocatechol Glucuronides and Physicochemical Characterization Data. *E-5-(2-Cyano-2-(N,N-diethylcarbamoyl)vinyl)-2-hydroxy-3-nitrophenyl-β-D-glucopyranosiduronic Acid,* ***1b***. The yield was 73 mg (76%). The product contained 0.4% entacapone, 0.04% *Z*-entacapone, 0.43% 3,4-dihydroxy-5-nitrobenzaldehyde, 0.73% *Z*-entacapone glucuronide, and less than 0.1% SL, UDP, and UDPGA.

Mp: declines above 120 °C. IR ν_{max} (KBr): 3420s, 3000m, 2205w, 1735s, 1615s, 1540s, 1265s, 1070s cm^{-1}. λ_{max} (ϵ_{max}): 223 and 308 (24426) nm (pH 2), 240, 286, and 369 (32 319) nm (pH 7.4). $[M + H]^+$: 482.1409. NMR: δ_H (500 MHz, D_2O): 1.25 (3H, m, $^3J_{HH} = 7$ Hz, CH_3), 1.33 (3H, t, $^3J_{HH} = 7$ Hz, CH_3), 3.52 (2H, q, $^3J_{HH} = 7$ Hz, CH_2), 3.62 (2H, q, $^3J_{HH} = 7$ Hz, CH_2), 3.76 (1H, m, $H_{3'}$), 3.77 (1H, m, $H_{4'}$), 3.79 (1H, m, $H_{2'}$), 4.24 (1H, d, $^3J_{HH} = 9$ Hz, $H_{5'}$), 5.22 (1H, d, $^3J_{HH} = 7$ Hz, arom. $H_{1'}$), 7.58 (1H, s, aliph. H_8), 8.07 (1H, d, $^4J_{HH} = 2$ Hz, arom. H_{14}), 8.12 (1H, s, arom. H_{10}). δ_C (500 MHz, D_2O): 13.0 (C_1), 14.1 (C_3),

42.4 (C_2), 45.7 (C_4), 72.5 (C_{17}), 73.6 ($C_{2'}$), 76.1 ($C_{4'}$), 76.2 ($C_{5'}$), 102.0 ($C_{1'}$), 106.3 (C_6), 117.4 (C_7), 120.8 (C_{10}), 124.3 (C_{14}), 124.4 (C_9), 136.4 (C_{13}), 148.1(C_{11}), 148.5 (C_{12}), 149.6 (C_8), 165.7 (C_5), 173.3 ($C_{6'}$).

Z-5-(2-Cyano-2-(N,N-diethylcarbamoyl)vinyl)-2-hydroxy-3-nitrophenyl-β-D-glucopyranosiduronic Acid, ***2b***. The yield was 63 mg (70%). The product contained 0.15% *Z*-entacapone, 0.05% entacapone, 3.61% entacapone glucuronide, and less than 0.1% D-saccharic acid 1,4-lactone, UDP, and UDPGA.

Mp: declines above 120 °C. IR ν_{max} (KBr): 3420s, 3000m, 2205w, 1735s, 1620s, 1540s, 1275s, 1080s, 1055s cm^{-1}. λ_{max} (ϵ_{max}): 223 and 308 (21157) nm (pH 2), 240, 286, and 369 (27 020) nm (pH 7.4). $[M + H]^+$: 482.1383. NMR δ_H (500 MHz, D_2O): 1.00 (3H, t, $^3J_{HH} = 7$ Hz, C*H*$_3$), 1.16 (3H, t, $^3J_{HH} = 7$ Hz, C*H*$_3$), 3.45 (2H, m, C*H*$_2$), 3.48 (2H, m, C*H*$_2$), 3.69 (1H, m, $H_{4'}$), 3.70 (1H, m, $H_{3'}$), 3.73 (1H, m, $H_{2'}$), 4.14 (1H, d, $^3J_{HH} = 9$ Hz, $H_{5'}$), 5.13 (1H, d, $^3J_{HH} = 8$ Hz, arom. $H_{3'}$), 7.48 (1H, d, $^4J_{HH} = 2$ Hz, arom. H_{10}), 7.60 (1H, s, aliph. H_8), 7.91 (1H, d, $^4J_{HH} = 2$ Hz, arom. H_{14}). δ_C (500 MHz, D_2O): 12.7 (C_1), 14.1 (C_3), 41.4 (C_2), 45.4 (C_4), 72.5 ($C_{3'}$), 73.7 ($C_{2'}$), 76.2 ($C_{4'}$), 76.4 ($C_{5'}$), 102.5 ($C_{1'}$), 108.5 (C_9), 117.9 (C_7), 122.3 (C_{14}), 123.7 (C_{10}), 124.5 (C_6), 136.7 (C_{13}), 147.7 (C_8), 148.3 (C_{12}), 148.6 (C_{11}), 164.3 (C_5), 173.6 ($C_{6'}$).

5-(2-Acetyl-3-oxobut-1-enyl)-2-hydroxy-3-nitrophenyl-β-D-glucopyranosiduronic Acid, ***3b***. The yield was 75% (60 mg). The product contained 0.70% 3,4-dihydroxy-5-nitrobenzaldehyde (NMR), 0.79% nitecapone, and less than 0.5% SL, UDP, and UDPGA.

Mp: declines above 120 °C. IR ν_{max} (KBr): 3400s, 3300s, 2920m, 1700s, 1655s, 1615s, 1535s, 1350s, 1080s cm^{-1}. λ_{max} (ϵ_{max}): 223 and 298 (20 589) nm (pH 2), 237, 288, and 372 (25446) nm (pH 7.4). $[M + H]^+$: 442.1013. NMR δ_H (500 MHz, D_2O): 2.22 (3H, s, C*H*$_3$), 2.40 (3H, s, C*H*$_3$), 3.60 (1H, m, $H_{3'}$), 3.62 (1H, m, $H_{4'}$), 3.64 (1H, m, $H_{2'}$), 4.11 (1H, d, $^3J_{HH} = 10$ Hz, $H_{5'}$), 4.99 (1H, d, $^3J_{HH} = 7$ Hz, arom. $H_{1'}$), 7.24 (1H, d, $^4J_{HH} = 2$ Hz, arom. H_8), 7.54 (1H, s, arom. H_6), 7.84 (1H, d, $^4J_{HH} = 2$ Hz, arom. H_{12}). δ_C (500 MHz, D_2O): 25.5 (C_5), 31.1 (C_1), 71.2 ($C_{3'}$), 72.2 ($C_{2'}$), 74.8 ($C_{5'}$), 74.8 ($C_{4'}$), 100.8 ($C_{1'}$), 120.7 (C_{12}), 122.4 (C_8), 123.6 (C_7), 135.3 (C_{11}), 139.9 (C_6), 141.4 (C_3), 146.3 (C_{10}), 146.7 (C_9), 172.0 ($C_{6'}$), 201.0 (C_4), 215.4 (C_2), 165.7 (C_5).

2-Hydroxy-5-(4-methylphenyl)carbonyl-3-nitrophenyl-β-D-glucopyranosiduronic Acid, ***4b***. The yield was 75% (60 mg). The product contained 1.00% tolcapone and less than 0.1% saccharic acid 1,4-lactone, UDP, and UDPGA.

Mp: declines above 116 °C. IR ν_{max} (KBr): 3400s, 2925m, 1740s, 1650s, 1610s, 1540s, 1300s, 1070s cm^{-1}. λ_{max} (ϵ_{max}): 220 and 276 (28681) nm (pH 2), 236, 270, and 340 (22 340) nm (pH 7.4). $[M + H]^+$: 482.1409. NMR δ_H (500 MHz, D_2O): 2.37 (3H, s, C*H*$_3$), 3.58 (1H, m, $H_{4'}$), 3.59 (1H, m, $H_{3'}$), 3.67 (1H, m, $H_{2'}$), 3.94 (1H, dd, $^3J_{HH} = 7$ Hz, $^4J_{HH} = 2$ Hz, $H_{5'}$), 5.10 (1H, d, $^3J_{HH} = 8$ Hz, arom. $H_{1'}$), 7.28 (2H, d, $^3J_{HH} = 8$ Hz, arom. $H_{3,5}$), 7.52 (2H, d, $^3J_{HH} = 8$ Hz, arom. $H_{2,6}$), 7.67 (1H, d, $^4J_{HH} = 2$ Hz, arom. H_{10}), 8.14 (1H, d, $^4J_{HH} = 2$ Hz, arom. H_{14}). δ_C (500 MHz, D_2O): 20.6 (C_7), 71.0 ($C_{3'}$), 72.1 ($C_{2'}$), 74.6 ($C_{5'}$), 74.7 ($C_{4'}$), 100.2 ($C_{1'}$), 122.0 (C_{14}), 122.6 (C_{10}), 126.9 (C_{13}), 129.0 (C_5), 129.8 (C_6), 132.9 (C_1), 134.8 (C_9), 144.9 (C_4), 145.9 (C_{11}), 148.5 (C_{12}), 172.3 ($C_{6'}$), 196.1 (C_8).

2-Hydroxy-4-nitrophenyl-β-D-glucopyranosiduronic Acid, ***5b***. The combined yield for glucuronides **5b** and **6b** was 38% (29 mg 5b). The product contained less than 0.5% D-saccharic acid 1,4-lactone, UDP, and UDPGA.

Mp: declines above 119 °C. IR ν_{max} (KBr): 3400s, 2920m, 1735s, 1600m, 1515s, 1350s, 1280s, 1220s, 1075s cm^{-1}. λ_{max} (ϵ_{max}): 215, 236, and 299 (5736) nm (pH 2), 306 (5623) nm (pH 7.4). $[M - H]^-$: 330.0513. NMR δ_H (500 MHz, D_2O): 3.55 (3H, m, $H_{2'}$, $H_{3'}$, and $H_{4'}$), 4.05 (1H, m, $H_{6'}$), 5.10 (1H, m, arom. $H_{1'}$), 7.02 (1H, d, $^3J_{HH} = 9$ Hz, arom. H_6), 7.52 (1H, d, $^4J_{HH} = 3$ Hz, arom. H_3), 7.56 (1H, dd, $^3J_{HH}$=9 Hz, $^4J_{HH}$=3 Hz, arom. H_5). δ_C (500 MHz, D_2O): 71.4 ($C_{3'}$), 72.6 ($C_{2'}$), 75.0 ($C_{4'}$), 75.2 ($C_{5'}$),100.2 ($C_{1'}$), 111.9 (C_3), 115.2 (C_6), 117.4 (C_5), 143.0 (C_2), 145.9 (C_4), 150.4 (C_1), 172.2 ($C_{6'}$).

2-Hydroxy-5-nitrophenyl-β-D-glucopyranosiduronic Acid, ***6b***. The yield was 21 mg **6b**. The product contained less than 0.5% D-saccharic acid 1,4-lactone, UDP, and UDPGA.

Mp: declines above 126 °C. IR ν_{max} (KBr): 3360s, 2920m, 1730m, 1590s, 1510s, 1340s, 1290s, 1075s cm^{-1}. λ_{max} (ϵ_{max}): 215, 231, and 329 (5782) nm (pH 2), 263 and 413 (11091) nm (pH 7.4). $[M - H]^-$: 330.0502. NMR δ_H (500 MHz, D_2O): 3.69 (1H, m, $H_{3'}$), 3.70 (1H, m, $H_{4'}$), 3.72 (1H, m, $H_{2'}$), 4.19 (1H, m, $H_{5'}$), 5.26 (1H, d, $^3J_{HH} = 7$ Hz, arom. $H_{1'}$), 7.01 (1H, d, $^3J_{HH} = 9$ Hz, arom. H_6), 7.90 (1H, dd, $^3J_{HH} = 9$ Hz, $^4J_{HH} = 3$ Hz, arom. H_5), 7.94 (1H, d, $^4J_{HH} = 3$ Hz, arom. H_3). δ_C (500 MHz, D_2O): 72.6 ($C_{3'}$), 73.8 ($C_{2'}$), 76.3 ($C_{4'}$), 76.5 ($C_{5'}$), 101.9 ($C_{1'}$), 113.6 (C_3), 117.4 (C_6), 122.1 (C_5), 141.6 (C_1), 145.2 (C_2), 154.2 (C_4), 174.4 ($C_{6'}$).

ACKNOWLEDGMENT

We wish to thank the Technology Development Center in Finland (TEKES) for financial support and Orion Pharma for generously providing entacapone and its Z-isomer, nitecapone, tolcapone, and 3,4-dihydroxybenzaldehyde. We also wish to thank Professor Gösta Brunow for his helpful advice. The present work is associated with study project no. BMH4-97-2621 financed by the EU Biomed 2 program.

LITERATURE CITED

(1) Lotta, T., Vidgren, J., Tilgmann, C., Ulmanen, I., Melén, K., Julkunen, I., and Taskinen, J. (1995) Kinetics of human soluble and membrane-bound catechol O-methyltransferase: A revised mechanism and description of the thermolabile variant of the enzyme. *Biochemistry 34*, 4202−4210.

(2) Kaakkola, S., Gordin, A., and Männistö, P. T. (1994) General properties and clinical possibilities of new selective inhibitors of catechol O-methyltransferase. *Gen. Pharmac. 25* (5), 813−824.

(3) Wikberg, T., Vuorela, A., Ottoila, P., and Taskinen, J. (1993) Identification of major metabolites of the catechol-*O*-methyltransferase inhibitor entacapone in rats and humans. *Drug Metab. Dispos. 21* (1), 81−92.

(4) Taskinen, J., Wikberg, T., Ottoila, P., Kanner, L., Lotta, T., Pippuri, A., and Bäckström, R. (1991) Identification of major metabolites of the catechol-*O*-methyltransferase-inhibitor nitecapone in human urine. *Drug Metab. Dispos. 19*, 178−183.

(5) Da Prada, M., Borgulya, J., Napolitano, A., and Zürcher, G. (1994) Improved therapy of Parkinson's disease with tolcapone, a central and peripheral COMT inhibitor with an S-adenosyl-L-methionin-sparing effect. *Clin. Neuropharm. 17* (Suppl. 3), S26−S37.

(6) Whiting, J. F., Narciso, J. P., Chapman, V., Ransil, B. J., Swank, R. T., and Collan, J. L. (1993) Deconjugation of bilirubin-IX alpha glucuronides: a physiologic role of hepatic microsomal beta-glucuronidase. *J. Biol. Chem. 268*, 23197−23201.

(7) Dwivedi, C., Downie, A. A., and Webb, T. E. (1987) Net glucuronidation in different rat strains: importance of microsomal β-glucuronidase. *FASEB J. 1* (4), 303−307.

(8) Brown, J., Novak, E. K., Takeuchi, K., Medda, S., Moore, K., and Swank, R. T. (1987) Lumenal localization of the microsomal β-glucuronidase-egasyn complex. *J. Cell Biol. 105*, 1571−1578.

(9) Kinosaki, M., Masuko, T., Sogawa, K., Iyanagi, T., Yamamoto, T., Hashimoto, Y., and Fujii-Kuriyama, Y. (1993) Intracellular localization of UDP-glucuronosyltransferase expressed from the transfected cDNA in cultured cells. *Cell Struct. Funct. 18*, 41−51.

(10) Wikberg, T., and Vuorela, A. (1994) Metabolite profiles of two ^{14}C-labeled catechol-*O*-methyltransferase inhibitors, nitecapone and entacapone, in rat and mouse urine and rat bile. *Eur. J. Drug Metab. Phamacokinet. 19* (2), 125−135.

(11) Kaspersen, F. M., and van Boeckel, C. A. A. (1987) A review of the methods of chemical synthesis of sulphate and glucuronide conjugates. *Xenobiotica 17* (12), 1451−1471.

(12) Andersen, J. V., Dalgaard, L., and Hansen, S. (1989) Enzymic synthesis of two glucuronides of the hydroxyisoxazole GABA-agonist, THIP, and the in vivo glucuronidation of THIP in rat. *Xenobiotica 19* (12), 1399−1406.

(13) Johnson, D. B., Swanson, M. J., Barker, C. W., Fanska, C. B., Murrill, E. E. (1979) Preparation of 3-benzo[*a*]pyrenyl-*β*-D-glucopyranosiduronic acid in multimilligram quantities by microsomal UDP-glucuronosyltransferase. *Prep. Biochem. 9* (4), 391−406.

(14) Haumont, M., Magdalou, J., Ziegler, J.-C., Bidault, R., Siest, J.-P., and Siest, G. (1991) Immobilization of microsomes into alginate beads is a convenient method for producing glucuronides from drugs. *Appl. Microbiol. Biotechnol. 35*, 440−446.

(15) Gilissen, R. A. H. J., Meerman, J. H. N., and Mulder, G. J. (1992) Immobilization of solubilized UDP-glucuronosyltransferase from rat liver microsomes to Sepharose 4B. *Biochem. Pharmacol. 43* (12), 2661−2663.

(16) Studenberg, S. D., Price-Raybuck, D. L., Unger, S. E., Shockcor J., and Brouwer, K. L. (1995) Characterization of p-hydroxyphenobarbital glucuronide generated from immobilized rat hepatic UDP-glucuronosyltransferase. *J. Pharm. Sci. 84* (9), 1134−1136.

(17) Alebic-Kolbah, T., and Wainer, I. W. (1993) Microsomal immobilized-enzyme-reactor for on-line production of glucuronides in a HPLC column. *Chromatographia 37* (11−12), 608−612.

(18) Tegtmeier, F., Belsner, K., and Brunner, G. (1988) Enzymatic synthesis of glucuronides using lipophilic hollow fiber membranes. *Bioproc. Eng. 3*, 43−47.

(19) Luukkanen, L., Elovaara, E., Lautala, P., Taskinen, J., and Vainio, H. (1997) Characterization of 1-hydroxypyrene as a novel marker substrate of 3-methyl-cholanthrene inducible phenol UDP-glucuronosyltransferase(s). *Pharm. Toxicol. 80*, 152−158.

(20) Bansal, K., and Gessner T. (1980) A unified method for the assay of uridinediphosphoglucuronyltransferase activities toward various aglycons using uridine diphospho(U-^{14}C)-glucuronic acid. *Anal. Biochem. 109* (2), 321−328.

(21) Summers, M. F., Marzilli, L. G., and Bax, A. (1986) Complete proton and ^{13}carbon assignments of coenzyme B_{12} through the use of new two-dimensional NMR experiments. *J. Am. Chem. Soc. 108* (15), 4285.

BC980064N

MARCH/APRIL 1999
Volume 10, Number 2

© Copyright 1999 by the American Chemical Society

Bioconjugate Chemistry

COMMUNICATIONS

Paramagnetic Oligonucleotides: Contrast Agents for Magnetic Resonance Imaging with Proton Relaxation Enhancement Effects

Jennifer V. Hines,*,† Ghada M. Ammar,† Jill Buss,† and Petra Schmalbrock‡

Division of Medicinal Chemistry & Pharmacognosy, College of Pharmacy, and Department of Radiology, College of Medicine, The Ohio State University, Columbus, Ohio 43210. Received September 2, 1998

An antisense paramagnetic oligonucleotide analogue targeted to a model macromolecular receptor (5S rRNA) was prepared. The paramagnetic agent's relaxivity (dependence of the relaxation rate on paramagnetic agent concentration) in the presence and absence of the macromolecular receptor was measured at 1.5 and 6.3 T. The relaxivity of the targeted agent increased specifically in the presence of the macromolecular receptor (16% at 6.3 T and 15% at 1.5 T). This effect was specific for a paramagnetic oligonucleotide targeted to the receptor and was larger than the relaxivity enhancement due simply to receptor-induced viscosity differences. Maximizing this relaxivity enhancement of tumor targeted paramagnetic oligonucleotides will aid in contrast agent development for magnetic resonance imaging.

In addition to clinical assessment, cross-sectional diagnostic imaging procedures such as computed tomography (CT) and magnetic resonance imaging (MRI) are currently used to increase the accuracy of cancer diagnosis and staging. Currently approved MRI contrast agents either are tissue-nonspecific (Gd-DTPA, Figure 1) or target normal tissue providing only "cold" spot imaging (superparamagnetic iron oxide) which reduces their value in accurately detecting primary neoplasia or metastases (*1*−*3*). Development of cancer-targeted contrast imaging agents for providing "hot" spot MR imaging would improve the sensitivity of MRI for tumor detection over current methods. Biostable oligonucleotide analogues targeted to diseased tissue, either as an antisense agent to overexpressed mRNA (*4*) or as a ligand (aptamer) to a disease-specific receptor (*5*), have been investigated for other imaging methods but have not been thoroughly investigated as paramagnetic contrast agents for MRI. To optimize contrast agents for MRI, it is useful to maximize not only target localization but also the proton relaxation enhancement (PRE) (*6*) effect upon target binding. Maximizing the PRE effect increases the signal difference between targeted and nontargeted tissues, thus reducing toxicity by reducing the dose necessary for adequate contrast enhancement. We report the preparation of an antisense paramagnetic oligonucleotide targeted to a model macromolecular receptor and the demonstration of a specific PRE effect upon target binding. This information will aid in the development of paramagnetic oligonucleotide contrast agents for MRI.

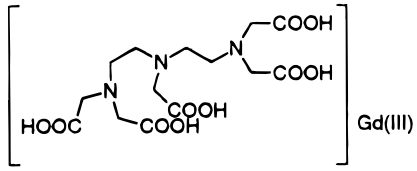


Figure 1. Gd-DTPA−diethylenetriaminepentaacetic acid.

MR contrast imaging relies on the effect a paramagnetic species has on the observed longitudinal and transverse relaxation rates ($1/T_1$ and $1/T_2$, respectively) of solvent (water) nuclei (*6*). Differential relaxation rates due to paramagnetic contrast agents can enhance the MR

* To whom correspondence should be addressed. Phone: (614) 688-4008. Fax: (614) 292-2435. E-mail: hines.89@osu.edu.
† College of Pharmacy.
‡ College of Medicine.

10.1021/bc980103v CCC: $18.00 © 1999 American Chemical Society
Published on Web 02/03/1999

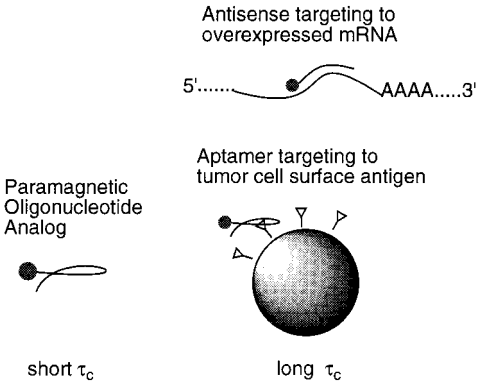


Figure 2. Antisense and aptamer-based targeting strategies.

image obtained and thus lead to better diagnosis. The relaxation rates are linearly dependent on the concentration of the paramagnetic species M where relaxivity (R_1) is defined as

$$(1/T_1)_{obs} = (1/T_1)_d + R_1[M] \quad (1)$$

where $(1/T_1)_d$ is the diamagnetic contribution to the observed relaxation rate $(1/T_1)_{obs}$.[1] A similar relationship applies to T_2 for R_2 relaxivity. The most widely investigated paramagnetic ions for T_1 contrast work are chelated Gd(III), Mn(II), and Fe(III).

The relaxivity is dependent on many factors, including magnetic field strength, correlation time (τ_c, tumbling rate in solution), and inner-sphere and outer-sphere water around the paramagnetic ion (*6*). Of particular importance is the fact that an increase in the correlation time of the paramagnetic species results in increased relaxivity. When the paramagnetic species is targeted to a macromolecular receptor and has a significant change in correlation time upon receptor binding, this leads to a proton relaxation enhancement (PRE) effect or increased relaxivity in the presence of the macromolecular receptor (*6*). Maximizing the PRE effect enhances the image contrast that can be achieved with a targeted contrast agent beyond that which can be achieved with currently available nonspecific agents.

Biopolymers such as paramagnetic antibodies targeted to tumor-specific antigens have been investigated for use as MRI contrast agents. The paramagnetic metal enhances the relaxivity (R_1) of bulk water, while the antibody provides tumor localization. Antibodies with only paramagnetic chelates attached, however, are not very effective contrast agents due to their large size, the lack of access of bulk water to the paramagnetic center, and very small correlation time change (and hence small relaxivity change) upon target binding (*6*). Only the superparamagnetic particle−antibody complexes are useful candidates. Porphyrins (*8*), liposomes (*9*), and polysaccharides (*10*, *11*) have also been investigated for tissue-specific delivery of relaxation agents. An alternative to these agents which has not been thoroughly investigated is the use of targeted paramagnetic oligonucleotide analogues.

Biostable oligonucleotide analogues can provide tumor-specific delivery of contrast agents (Figure 2) either as an antisense agent to mRNA overexpressed in a cancer cell (*4*) or as an aptamer to a cell surface (*12*). The main advantage of an oligonucleotide-based delivery agent over an antibody is size. Many oligonucleotide antisense agents and aptamers to complex targets have tight binding specificity contained within a relatively small piece of oligonucleotide (20−40 nucleotides ≅ 7−14 kDa) (*13*). Consequently, the correlation time of the free oligonucleotide analogue versus the oligonucleotide when bound to the target is different. This difference is sufficient to induce a PRE effect. The extent and lifetime of bound water in nucleic acids (*14*) can also be exploited to further enhance the PRE effect.

[1] Often, the terms $1/T_1$ and R_1 are used interchangeably; however, the explicit definition of relaxivity (R_1) is that shown in eq 1 (*6*) and is used accordingly throughout this paper.

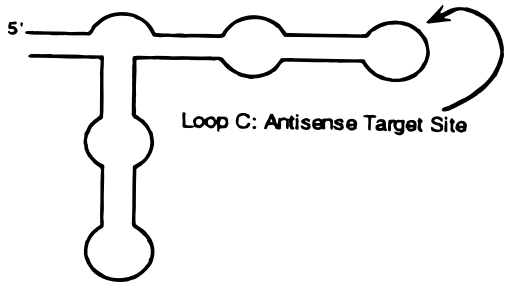


Figure 3. Secondary structure of 5S rRNA and antisense target site.

Our model system for investigating and ultimately optimizing the PRE effect for an antisense paramagnetic oligonucleotide uses 5S rRNA as the macromolecular target and a complementary 6mer sequence as the antisense agent. The *Escherichia coli* 5S rRNA was purchased and renatured (*15*). We chose the sequence 5′-CGGCAT-3′ (**ON-1**) which is complementary to nucleotides 39−44 in 5S rRNA (Figure 3) (*15*). We chose the sequence 5′-AAAAAA-3′ ($\mathbf{A_6}$) as a control to monitor relaxivity changes due to viscosity differences. Since there is no complementary binding site for $\mathbf{A_6}$ on 5S rRNA, relaxivity changes in the presence of 5S rRNA will depend only on viscosity changes due to the macromolecule. **ON-1** and $\mathbf{A_6}$ were purchased with a 5′-amino linker and reacted with DTPA dianhydride (**2**, Scheme 1). The resulting chelate conjugates were treated with $GdCl_3$ followed by size-exclusion chromatography and dialysis to prepare the paramagnetic−oligonucleotide chelate complexes. HPLC and MALDI-TOF analyses indicated there was pure product with no degradation or dimer formation. DTPA content was verified by spectrophotometric analysis (*16*).

On the basis of the correlation time of 5S rRNA (10 ns) (*17*) and of a 6mer oligonucleotide (1 ns) (*18*), there should be a significant change in the correlation time of the 6mer oligonucleotide chelate upon binding to the 5S rRNA target. Such a change in the correlation time should result in a PRE effect as discussed earlier. An electron spin resonance study with a TEMPO-modified single-stranded oligonucleotide showed that there was a change in the correlation time upon binding a complementary region of 5S rRNA (*19*).

The buffered renatured 5S rRNA (*15*) was used to prepare sample paramagnetic agent:5S rRNA ratios of 0:1, 0.25:1, 0.5:1, 0.75:1, and 1:1. Equivalent samples containing just buffered paramagnetic agent were also prepared. Inversion−recovery studies for measuring the T_1 values of the bulk water were carried out at 6.3 and 1.5 T. At 6.3 T, all buffered samples were in 95% D_2O/5% H_2O. Due to the sequential nature of the experiments, a full inversion−recovery experiment for determining each individual T_1 was prohibitively long. Consequently, the T_1s were estimated from the null spectrum of a 180−D_2−90−acquire pulse sequence where $T_1 = D_2/\ln 2$ (*20*). At 1.5 T, buffered samples in H_2O were placed in a 96-

Scheme 1. Synthesis of Paramagnetic Oligonucleotides

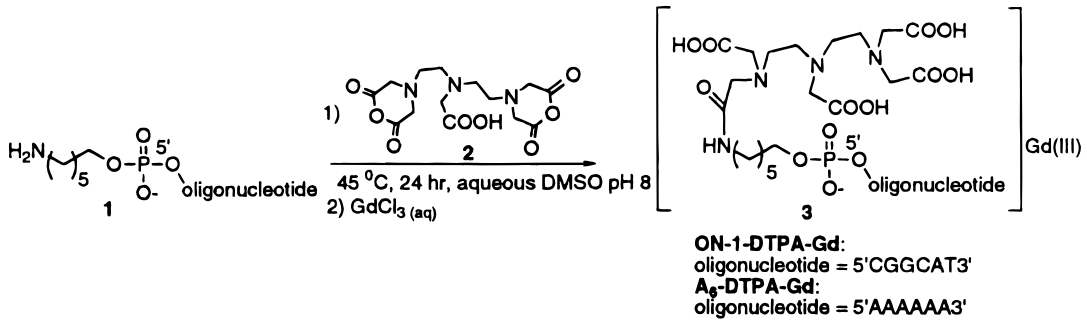


Table 1. R_1 Relaxivity of Paramagnetic Oligonucleotides at 6.3 T[a]

	R_1[b] (mM^{-1} s^{-1})	% PRE[c]
ON-1−DTPA-Gd	8.84	−
ON-1−DTPA-Gd and 5S rRNA[d]	10.24	16
A_6−DTPA-Gd	13.49	−
A_6−DTPA-Gd and 5S rRNA[d]	13.90	3
ON-1−DTPA-Gd and dextran[e]	9.13	3

[a] In 10 mM Tris-HCl (pH 6.9), 10 mM $MgCl_2$, 20 mM $Na_2B_4O_7$ buffer. Relaxation studies were performed at 300 K on a Bruker 6.3 T 270 MHz NMR spectrometer. [b] See the text for R_1 determination. Error estimated to be less than 5% based on replicate T_1 determinations.

Table 2. R_1 Relaxivity of Paramagnetic Oligonucleotides at 1.5 T[a]

	R_1[b] (mM^{-1} s^{-1})	% PRE[c]
ON-1−DTPA-Gd	85	−
ON-1−DTPA-Gd and 5S rRNA[d]	98	15
A_6−DTPA-Gd	156	−
A_6−DTPA-Gd and 5S rRNA[d]	168	7.7

[a] In 10 mM Tri- HCl (pH 6.9), 10 mM $MgCl_2$, 20 mM $Na_2B_4O_7$ buffer. Relaxation studies were performed at room temperature on a GE/Signa 1.5 T MR imager with the wrist coil as the receiver coil and the large volume body coil as the radio frequency transmitter. A single slice that was 4 mm thick was acquired corresponding to 40% of the sample height. The field of view was 12 cm × 9 cm and the matrix size 256 × 256 points. An inversion recovery fast spin-echo (IR-FSE) program was used with TIs (delay time for monitoring inversion recovery) of 50, 200, 300, 500, 700, 900, 1100, 1500, 1800, 2100, 2500, 3200, and 4000 ms with a constant TE (echo time) and TR (repetition time) of 16 and 8000 ms, respectively. [b] See the text for R_1 determination. Error estimated to be 5% based on replicate R_1 determinations. [c] Proton relaxation enhancement (% R_1 enhancement in the presence of a macromolecule); see the text. [d] At 0.006 mM in 5S rRNA.

well polypropylene tube array and surrounded by buffer to minimize magnetic susceptibility problems. To investigate the possibility of the nucleic acid binding to the well walls, which could potentially affect the relaxation measurements, duplicates of the samples were placed in wells previously treated with a siliconizing agent and then rinsed with 95% ethanol and air-dried.

To avoid difficulties with phase variation across the image, MR systems typically generate magnitude images. Thus, only the absolute value of the MR signal was measured. Images were analyzed using IDL (Research Systems Inc.), and the image intensities of each sample well (7 mm × 7 mm, 14 pixel × 14 pixel image) were measured over an area of 121 pixels. The intensities at different TIs were analyzed using SigmaPlot (Jandell Scientific). A nonlinear curve fit of the form

$$I_\tau = |I_\infty(1 - Ce^{-\tau/T_1})| \qquad (2)$$

was applied where τ is the delay time TI, T_1 is the spin−lattice relaxation time, I_τ is the image intensity at delay time τ (=TI), I_∞ is the image intensity when $\tau = \infty$, and $C \approx 2$. I_∞, C, and T_1 were treated as adjustable parameters. The resulting $1/T_1$ values were then plotted versus the paramagnetic agent concentrations. The relaxivity (R_1) was calculated for each experiment using a linear regression fit to the equation $(1/T_1)_{obs} = R_1x + b$, where $(1/T_1)_{obs}$ is measured in s^{-1} and x (the paramagnetic agent concentration) in millimolar. Using our experimental conditions for sample preparation, data acquisition, and analysis, the relaxivity measured for Gd-DTPA ($R_1 = 4.43$ mM^{-1} s^{-1} at 1.5 T) compares favorably with the literature value (*21*, *22*).

The antisense paramagnetic oligonucleotide targeted to 5S rRNA produced a 16% PRE effect at 6.3 T (Table 1) and a 15% PRE effect at 1.5 T (clinical MR field strength, Table 2). The nonspecific effect that viscosity changes would have on the observed relaxivity of the paramagnetic oligonucleotides due to the presence of a macromolecule was estimated two different ways. The R_1 of **ON-1−DTPA-Gd** in the presence of dextran (MW = 40 kDa ≅ 5S rRNA) was measured. The other viscosity control involved measuring the R_1 of **A_6−DTPA-Gd** in the presence of 5S rRNA. Both methods for estimating viscosity effects indicated the same enhancement of R_1 (3%, Table 1) in the presence of a macromolecule. On the basis of these controls, the enhancements simply due to viscosity were smaller than the PRE effects due to the targeted paramagnetic oligonucleotide binding to the 5S rRNA target. This indicates that a PRE effect can be observed when paramagnetic oligonucleotide analogues bind specifically to a macromolecular receptor. Maximizing this PRE effect will be useful in adding hot spot contrast to MR imaging with diseased tissue-targeted paramagnetic oligonucleotide analogues.

As mentioned above, in the 96-well array used for the MRI experiment we were concerned there might be some nonspecific attachment to the well sides. However, no significant difference in R_1 values was seen between the treated and the nontreated wells. An additional control was run to determine if there was any nonspecific attraction between Gd-DTPA and 5S rRNA. No significant difference in the R_1 values for Gd-DTPA in the presence (5.22 mM^{-1} s^{-1} at 6.3 T) or absence (5.20 mM^{-1} s^{-1} at 6.3 T) of 5S rRNA was detected. While the PRE for **A_6−DTPA-Gd** at 1.5 T was significantly smaller than that for **ON-1−DTPA-Gd**, we were somewhat surprised that it was larger than that at 6.3 T. It is possible that **A_6−DTPA-Gd** hydration differences for samples with and without 5S rRNA are affecting the PRE at 1.5 T more than at 6.3 T.

Since unchelated lanthanide ions and certain lanthanide complexes can lead to RNA degradation (*23*), we investigated whether any 5S rRNA degradation was occurring due to the paramagnetic oligonucleotides. UV

melting (*24*) of 1:1 **ON-1**−**DTPA-Gd**:5S rRNA and 1:1 **A_6**−**DTPA-Gd**:5S rRNA each showed a slight decrease in T_m ($\Delta T_m = 5$ °C) compared to that of 5S rRNA alone (approximate $T_m = 75$ °C). The predicted T_m for the **ON-1**−**DTPA-Gd**:5S rRNA duplex is 20 °C; however, the expected hyperchromicity upon melting would be very small relative to the 5S rRNA hyperchromicity and, thus, was not detected. Denaturing polyacrylimide gel studies for detecting full-length 5S rRNA and any degradation products were also carried out. Under the ratio and incubation time conditions used in the NMR and MRI studies, no degradation was observed. However, some degradation was observed at a ratio of 2:1.

While 5S rRNA degradation effects could affect the observed R_1 values, there was no difference in the degradation effects of **ON-1**−**DTPA-Gd** versus **A_6**−**DTPA-Gd** on 5S rRNA. Consequently, degradation does not appear to contribute to the observed difference in PRE between the targeted **ON-1**−**DTPA-Gd** and the viscosity control **A_6**−**DTPA-Gd**. The degradation is most likely due to gadolinium having one less ligand in the oligonucleotide−DTPA-Gd complexes than in Gd-DTPA, leading to an increased likelihood of free Gd^{3+} and nonspecific degradation. Since Gd-DTPA alone does not degrade 5S rRNA under the conditions used in the NMR and MRI studies or at a 2:1 ratio of paramagnetic agent: 5S rRNA as determined by UV melting and gel studies, we believe that utilizing a more stable chelate (DTPA isothiocyanate) (*25*) will reduce the degradation effects we are observing. This analogue allows full chelation of Gd^{3+} (stability constant equivalent to that of Gd-DTPA) with an added tether for conjugation to a macromolecule.

In summary, these studies indicate that paramagnetic oligonucleotides targeted to a macromolecule produce a PRE effect which is specific and greater than simple viscosity differences in the presence of the macromolecular receptor. Maximizing this PRE effect will lead to enhanced MR image contrast with paramagnetic oligonucleotides targeted to tumors since it enhances relaxivity without increasing the paramagnetic agent concentration. We are currently investigating the optimal biophysical features necessary to maximize the PRE effect of tumor-targeted biostable paramagnetic oligonucleotide analogues. Results from these experiments will be presented in due course.

ACKNOWLEDGMENT

This work was supported by The American Cancer Society of Ohio. We thank Profs. E. Wisner and I. Tinoco, Jr., for helpful discussions.

LITERATURE CITED

(1) Sabel, M., and Aichinger, H. (1996) Recent Developments in Breast Imaging. *Phys. Med. Biol. 41*, 315−368.

(2) Greenfield, G. B., Arrington, J. A., and Kudryk, B. T. (1993) MRI of Soft Tissue Tumors. *Skeletal Radiol. 22*, 77−84.

(3) Tanimoto, A., Satoh, Y., Uasa, Y., Jinzaki, M., and Hiramatsu, K. (1997) Performance of Gd-EOB-DTPA and Superparamagnetic Iron Oxide Particles in the Detection of Primary Liver Cancer: A Comparative Study by Alternative Free-Response Receiver Operating Characteristic Analysis. *J. Magn. Reson. Imaging 7*, 120−124.

(4) Dewanjee, M. K., Ghafouripur, A. K., Kapadvanjwala, M., Dwanjee, S., Serafini, A. N., Lopez, D. M., and Sfakianakis, G. N. (1994) Noninvasive Imaging of C-myc Oncogene Messenger RNA with Indium-111-antisense Probes in a Mammary Tumor-Bearing Mouse Model. *J. Nucl. Med. 35*, 1054−1063.

(5) Charlton, J., Sennello, J., and Smith, D. (1997) In Vivo Imaging of Inflammation using an Aptamer Inhibitor of Human Neutrophil Elastase. *Chem. Biol. 4*, 809−816.

(6) Lauffer, R. B. (1987) Paramagnetic Metal Complexes as Water Proton Relaxation Agents for NMR Imaging: Theory and Design. *Chem. Rev. 87*, 901−927.

(7) Teifenauer, L. X., Kuhne, G., and Andres, R. Y. (1993) Antibody-Magnetite Nanoparticles: In Vitro Characterization of a Potential Tumor-Specific Contrast Agent for Magnetic Resonance Imaging. *Bioconjugate Chem. 4*, 347−352.

(8) van Zijl, P. C., Place, D. A., Cohen, J. S., Faustino, P. J., Lyon, R. C., and Patronas, N. J. (1990) Metalloporphyrin Magnetic Resonance Contrast Agents. Feasibility of Tumor-Specific Magnetic Resonance Imaging. *Acta Radiol. Suppl. 374*, 75−79.

(9) Storrs, R. W., Tropper, F. D., Li, H. Y., Song, C. K., Kuniyoshi, J. K., Sipkins, D. A., Li, K. C. P., and Bednarski, M. D. (1995) Paramagnetic Polymerized Liposomes: Synthesis, Characterization, and Applications for Magnetic Resonance Imaging. *J. Am. Chem. Soc. 117*, 7301−7306.

(10) Rongved, P., and Laveness, J. (1991) Water-Soluble Polysaccharides as Carriers of Paramagnetic Contrast Agents for Magnetic Resonance Imaging: Synthesis and Relaxation Properties. *Carbohydrate Res. 214*, 315−323.

(11) Rebizak, R., Schaefer, M., and Dellacherie, E. (1997) Polymeric Conjugates of Gd^{3+}-Deithylenetriaminepentaacetic Acid and Dextran. 1. Synthesis, Characterization, and Paramagnetic Properties. *Bioconjugate Chem. 8*, 605−611.

(12) Schering, A.-G. (1996) Ger. Offen. DE 4424923; *Chem. Abstr. 124*, 283703.

(13) Wang, Y., and Rando, R. R. (1995) Specific Binding of Aminoglycoside Antibiotics to RNA. *Chem. Biol. 2*, 281−290.

(14) Johannesson, H., and Halle, B. (1998) Minor Groove Hydration of DNA in Solution: Dependence on Base Composition and Sequence. *J. Am. Chem. Soc. 120*, 6859−6870.

(15) Goringer, H. U., and Wagner, R. (1988) 5S RNA Structure and Function. *Methods Enzymol. 164*, 721−737.

(16) Pippin, C. G., Parker, T. A., McMurry, T. J., and Brechbiel, M. W. (1992) Spectrophotometric Method for the Determination of a Bifunctional DTPA Ligand in DTPA-Monoclonal Antibody Conjugates. *Bioconjugate Chem. 3*, 342−345.

(17) Marshall, G., and Smith, J. L. (1980) Raman and $^{19}F(^1H)$ Nuclear Overhauser Evidence for a Rigid Solution Conformation of *Escherichia coli* 5-Fluorouracil 5S Ribonucleic Acid. *Biochemistry 19*, 5955−5959.

(18) Cantor, C. R., and Schimmel, P. R. (1980) *Biophysical Chemistry II: Techniques for the Study of Biological Structure and Function*, p 461, Freeman & Co., San Francisco.

(19) Murakami, A., Nagahara, S., Nakaura, M., Uematsu, H., Mukae, M., and Makino, K. (1990) Structural Analysis of Nucleic Acids by Labeled Oligonucleotides. *Nucleic Acids Res. Symp. Ser. 22*, 27−28.

(20) Derome, A. E. (1987) *Modern NMR Techniques for Chemistry Research*, pp 86−89, Pergamon, Oxford, U.K.

(21) Steen, R. G., Gronemeyer, S. A., Kingsley, P. B., Reddick, W. E., Langston, J. S., and Taylor, J. S. (1994) Precise and Accurate Measurement of Proton T1 in Human Brain in vivo: Validation and Preliminary Clinical Application. *J. Magn. Reson. Imaging 4*, 681−691.

(22) Donahue, K. M., Weisskoff, R. M., and Burstein, D. (1997) Water Diffusion and Exchange as They Influence Contrast Enhancement. *J. Magn. Reson. Imaging 7*, 102−110.

(23) Kazunari, M., and Komiyama, M. (1997) Enormously fast RNA hydrolysis by Lanthanide(III) Ions Under Physiological Conditions: Eminent Candidates for Novel Tools of Biotechnology. *Jpn. J. Biochem. 122*, 387−394.

(24) Puglisi, J. D., and Tinoco, I., Jr. (1989) Absorbance Melting Curves of RNA. *Methods Enzymol. 180*, 304−325.

(25) Brechbiel, M. W., Gansow, O. A., Atcher, R. W., Schlom, J., Esteban, J., Simpson, D. E., and Colcher, D. (1986) Synthesis of 1-(*p*-Isothiocyanatobenzyl) Derivatives of DTPA and EDTA. Antibody Labeling and Tumor-Imaging Studies. *Inorg. Chem. 25*, 2772−2781.

BC980103V

ARTICLES

^{99m}Tc-Labeled MIBG Derivatives: Novel ^{99m}Tc Complexes as Myocardial Imaging Agents for Sympathetic Neurons

Zhi-Ping Zhuang,[†] Mei-Ping Kung,[†] Mu Mu,[†] Catherine Hou,[†] and Hank F. Kung*[,†,‡]

Departments of Radiology and Pharmacology, University of Pennsylvania, Philadelphia, Pennsylvania 19104.
Received November 29, 1997; Revised Manuscript Received October 1, 1998

Radioactive-iodine-labeled meta-iodobenzylguanidine (MIBG) is currently being used as an in vivo imaging agent to evaluate neuroendocrine tumors as well as the myocardial sympathetic nervous system in patients with myocardial infarct and cardiomyopathy. It is generally accepted that MIBG is an analogue of norepinephrine and its uptake in the heart corresponds to the distribution of norepinephrine and the density of sympathetic neurons. A series of MIBG derivatives containing suitable chelating functional groups N_2S_2 for the formation of $[Tc^{v}O]^{3+}N_2S_2$ complex was successfully synthesized, and the ^{99m}Tc-labeled complexes were prepared and tested in rats. One of the compounds, [^{99m}Tc]**2**, tested showed significant, albeit lower, heart uptakes post iv injection in rats (0.21% dose/g at 4 h) as compared to [^{125}I]MIBG (1.7% dose/g at 4 h). The heart uptake of the ^{99m}Tc-labeled complex appears to be specific and can be reduced by co-injection with nonradioactive MIBG or by pretreatment with desipramine, a selective norepinephrine transporter inhibitor. Further evaluation of the in vitro uptake of [^{99m}Tc]**2** in cultured neuroblastoma cells displayed consistently lower, but measurable uptake (approximately 10% of that for [^{125}I]MIBG). These preliminary results suggested that the mechanisms of heart uptake of [^{99m}Tc]**2** may be related to those for [^{125}I]MIBG uptake. If suitable ^{99m}Tc-labeled MIBG derivatives can be further developed, the prevalent availability of ^{99m}Tc in nuclear medicine clinics will allow them to be readily available for widespread application.

INTRODUCTION

In the past 15 years meta-iodobenzylguanidine (MIBG,[1] Figure 1) has attracted widespread acceptance as an imaging agent for studying norepinephrine neuronal function. Initially, radioiodine-labeled MIBG was developed as a norepinephrine analogue which localized in the adrenal medulla (*1*). The molecule was designed as a congener of an antihypertensive drug, guanethidine, whose pharmacological action is directly related to inhibition of the release of norepinephrine from adrenergic nerve endings. Using cloned cell lines (CV-1, green monkey kidney cells, and HeLa cells) expressing specific dopamine, norepinephrine, and serotonin transporters, MIBG uptake was reported to be mediated specifically by the norepinephrine transporter with a K_m value of 264 nM. The specific uptake was blocked by desipramine (DMI), a specific norepinephrine transporter inhibitor, and unaffected by dopamine and serotonin transporter inhibitors (*2*). As an analogue of norepinephrine, [^{131}I]-MIBG localizes in the tumors and provides a useful diagnostic tool of neuronal storage of norepinephrine (*1*, *3*). It was later discovered that [^{131}I]MIBG is useful as an agent for neuroendocrine tumor (neuroblastomas and pheochromocytomas) imaging and therapy (*4*).

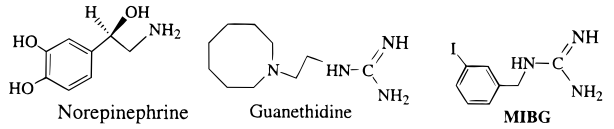


Figure 1. Chemical structures of norepinephrine, guanethidine, and meta-iodobenzylguanidine (MIBG).

One other important observation of using MIBG was that it also localized in myocardium (*5*). It was systematically established by the research group at the University of Michigan and others that the pharmacokinetics of MIBG are indeed related to norepinephrine uptake and release (*6*−*9*). Recent studies in denervated dog heart strongly suggested that the localization of MIBG reflected the integrity of adrenergic neurons. The cardiac scan at time points later than 1 h after injection of [^{123}I]MIBG provides a closed resemblance of the distribution of the sympathetic nerve endings (*9*−*11*). It was suggested that

* Address correspondence to this author at the Department of Radiology, University of Pennsylvania, 3700 Market St., Room 305, Philadelphia, PA 19104. Telephone: (215) 662-3096. Fax: (215) 349-5035. E-mail: kunghf@sunmac.spect.upenn.edu.

[†] Department of Radiology.

[‡] Department of Pharmacology.

[1] Abbreviations: MIBG, meta-iodobenzylguanidine; DMI, desipramine; ECD, ethylene cysteine dimer; TRODAT-1, [2-[[2-[[[3-(4-chlorophenyl)-8-methyl-8-azabicyclo[3.2.1]oct-2-yl]methyl]-(2-mercaptoethyl)amino]ethyl]amino]ethanethiolato(3−)-*N2,N2′,S2,S2′*]oxo-[1*R*-(*exo-exo*)]; LAH, lithium aluminum hydride; THF, tetrahydrofuran; Boc, *tert*-butoxycarbonyl; TLC, thin-layer chromatography; HPLC, high-performance liquid chromatography; NET, norepinephrine transporter; DAT, dopamine transporter; TMS, tetramethylsilane; DCC, 1,3-dicyclohexylcarbodiimide; DMF, *N*,*N*-dimethylformamide; PTLC, preparative thin-layer chromatography; MPLC, medium-performance liquid chromatography; EDTA, ethylenediaminetetraacetic acid disodium salt; PC, partition coefficient.

10.1021/bc970207q CCC: $18.00 © 1999 American Chemical Society
Published on Web 01/22/1999

assessment of the sympathetic nervous system by MIBG imaging may be important for patients with ventricular tachycardia, cardiomyopathy, and arrhythmia (*12*). Thus, MIBG scan may have predictable value for patients at risk of sudden death (*12*−*15*) and patients with diabetes (*16*, *17*). However, due to the limited supply of [^{123}I]MIBG, large-scale clinical studies are not readily achievable (*12*).

Due to the popularity of ^{99m}Tc routinely used in the clinical community, there is a strong need to develop ^{99m}Tc-based compounds, which can be used on a routine basis. Our successful development of [^{99m}Tc]TRODAT-1, a SPECT imaging agent targeting dopamine transporters (DAT) in humans (*18*), opened up a new avenue. The similar strategy aimed at developing ^{99m}Tc-labeled agents for other specific binding sites can be applied, by which they may provide important clinical applications. The $[Tc^{v}O]^{3+}N_2S_2$ complex was chosen for the initial attempt to prepare ^{99m}Tc-labeled MIBG derivatives because this complex has been successfully applied in the development of a brain perfusion imaging agent, [^{99m}Tc]ECD (ethylene cysteine dimer) (*19*−*21*), as well as for the DAT imaging agent, [^{99m}Tc]TRODAT-1 (*22*). Other ^{99m}Tc complexes may be possible, but in this initial report we are going to concentrate on the $[Tc^{v}O]^{3+}N_2S_2$ complexes.

If ^{99m}Tc-labeled MIBG derivatives can be successfully developed based on the same $[Tc^{v}O]^{3+}N_2S_2$ complex, the prevalent availability of ^{99m}Tc in nuclear medicine clinics will permit a widespread clinical application on patients with myocardial disease or various endocrine tumors. We report herein the initial effort in preparing novel ^{99m}Tc-labeled MIBG derivatives, which may potentially be valuable for routine clinical imaging study of the sympathetic nervous system of the heart.

EXPERIMENTAL PROCEDURES

General. Reagents used in the syntheses were purchased from Aldrich (Milwaukee, WI) or Fluka (Ronkonkoma, NY), and were used without further purification unless otherwise indicated. Anhydrous Na_2SO_4 was used as a drying agent. Reaction yields are reported without attempts at optimization. ^{1}H NMR spectra were obtained on a Bruker spectrometer (Bruker AC 200; 200 MHz). Chemical shifts are reported as δ values with chloroform or TMS as the internal reference. Coupling constants are reported in hertz. The multiplicity is defined by s (singlet), d (doublet), t (triplet), br (broad), and m (multiplet). Elemental analyses were performed by Elemental Analysis Laboratory, University of Pennsylvania. Mass spectrometry was performed by the Mass Spectrometry Center, University of Pennsylvania.

***N*-3-Cyanophenyl-2-(4′-methoxybenzyl)mercaptoacetamide (5).** A mixture of 3-aminobenzonitrile (1.18 g, 10 mmol), 2-(4-methoxybenzyl)mercaptoacetic acid (**4**, 2.12 g, 1 equiv), and DCC (2.18 g, 1 equiv) in CH_2Cl_2 (30 mL) was stirred under reflux overnight. After the mixture was cooled to room temperature, water was added and extracted with CH_2Cl_2. The organic extracts was dried and concentrated to give the crude product, which was purified by medium-pressure liquid chromatography (MPLC) (Hex:EtOAc = 5:1) to give 2.17 g of product (70%).

^{1}H NMR: 3.31 (2H, s, Ar-C$\underline{H}_2$-S-), 3.70 (3H, s, OC$\underline{H}_3$), 3.74 (2H, CO-C$\underline{H}_2$-S-), 6.78 (2H, dot, J = 8.6, 2.5 Hz, Ar$\underline{H}$), 7.18 (2H, d,t, J = 8.6, 2.5 Hz, Ar$\underline{H}$), 7.35−7.40 (2H, m, Ar$\underline{H}$), 7.54−7.63 (1H, m, Ar$\underline{H}$), 7.78 (1H, m, Ar$\underline{H}$), 8.4 (1H, br, CON$\underline{H}$).

Anal. ($C_{17}H_{16}N_2O_2S$): Calcd: C, 65.36; H, 5.16; N, 8.97. Found: C, 65.02; H, 5.08; N, 8.94.

3-Aminomethylphenyl-2-(4′-methoxybenzyl)mercaptoethylamine (6). To a suspension of LAH (0.72 g, 18.9 mmol) in THF (15 mL) was added dropwise a solution of **5** (1.19 g, 3.8 mmol) in THF (15 mL) at room temperature. The mixture was stirred under reflux for 1 h and stirred at room temperature overnight. Water (0.9 mL), NaOH (1 M, 0.9 mL), and additional water (2.7 mL) were added successively with caution to decompose excess LAH. The resulting mixture was stirred at room temperature for another 10 min, and the mixture was filtered through Celite. The filtrate was concentrated and purified by preparative thin-layer chromatography (PTLC) (CH_2Cl_2:MeOH:NH_4OH = 9:1:0.1) to give 633 mg of oil (55%).

^{1}H NMR: 2.68 (2H, t, J = 6.4 Hz, NHC$\underline{H}_2$), 3.27 (2H, t, J = 6.4 Hz, S-C$\underline{H}_2$), 3.68 (2H, s, Ar-C$\underline{H}_2$-S), 3.77 (2H, s, Ar-C$\underline{H}_2$-NH$_2$), 3.79 (3H, s, OCH_3), 6.47 (1H, d,d, J = 7.8, 2.0 Hz, Ar$\underline{H}$), 6.54 (1H, s, Ar$\underline{H}$), 6.65 (1H, d, J = 7.5 Hz, Ar$\underline{H}$), 6.84 (2H, d,t, J = 8.6, 2.8 Hz, Ar$\underline{H}$), 7.12 (1H, t, J = 7.7 Hz, Ar$\underline{H}$), 7.22 (2H, d,t, J = 8.6, 2.1 Hz, Ar$\underline{H}$).

Anal. ($C_{17}H_{22}N_2OS\cdot0.25H_2O$): Calcd: C, 66.52; H, 7.39; N, 9.13. Found: C, 66.70; H, 7.38; N, 8.98.

3-(*N*′-*tert*-Butoxycarbonyl)aminomethylphenyl-2-(4′-methoxybenzyl)mercaptoethylamine (7). To a solution of **6** (100 mg, 0.33 mmol) and Et_3N (0.1 mL) in CH_2Cl_2 (5 mL) was added dropwise a solution of $(Boc)_2O$ (72 mg, 1 equiv) in CH_2Cl_2 (2 mL) at 0 °C. The mixture was stirred at 0 °C for 1 h. Water was added, and the reaction mixture was extracted with CH_2Cl_2. The combined organic extract was dried, concentrated, and purified by PTLC (Hex:EtOAc = 3:2) to give 107 mg of product (80%).

^{1}H NMR: 1.47 (9H, s, Boc-H), 2.67 (2H, t, J = 6.4 Hz, NHC$\underline{H}_2$), 3.21 (2H, t, J = 6.4 Hz, S-C$\underline{H}_2$), 3.68 (2H, s, Ar-C$\underline{H}_2$-S), 3.79 (3H, s, OC$\underline{H}_3$), 4.22 (2H, d, J = 5.8 Hz, Ar-C$\underline{H}_2$-NH$_2$), 6.47 (1H, d, J = 6.7 Hz, Ar$\underline{H}$), 6.49 (1H, s, Ar$\underline{H}$), 6.62 (1H, d, J = 7.5 Hz, Ar$\underline{H}$), 6.85 (2H, d,t, J = 8.6, 2.8 Hz, S-Ar$\underline{H}$), 7.08 (1H, t, J = 7.6 Hz, Ar$\underline{H}$), 7.22 (2H, d,t, J = 8.6, 2.0 Hz, Ar$\underline{H}$).

Anal. ($C_{22}H_{30}N_2O_3S$): Calcd: C, 65.64; H, 7.50; N, 6.96. Found: C, 65.46; H, 7.57; N, 6.74.

***N*-3-(*N*′-*tert*-Butoxycarbonyl)aminomethylphenyl-*N*-2-(4′-methoxybenzyl)mercaptoethyl-2-chloroacetamide (8).** To a solution of **7** (100 mg, 0.25 mmol) and Et_3N (0.1 mL) in CH_2Cl_2 (5 mL) was added a solution of chloroacetyl chloride (34 mg, 1.2 equiv) in CH_2Cl_2 (1 mL) at 0 °C in an ice bath. The mixture was stirred at room temperature for 1 h. Water was added, and the reaction mixture was extracted with CH_2Cl_2. The combined extracts were dried, concentrated, and purified by PTLC (Hex:EtOAc = 1:1) to give 116 mg of product (97%).

^{1}H NMR: 1.45 (9H, s, Boc-H), 2.53 (2H, t, J = 7.6 Hz, NHC$\underline{H}_2$), 3.69 (2H, s, Ar-C$\underline{H}_2$-S), 3.81 (3H, s, OC$\underline{H}_3$), 3.78−3.85 (4H, m, S-C$\underline{H}_2$, COCH_2Cl), 4.32 (2H, d, J = 6.2 Hz, Ar-C$\underline{H}_2$-NH$_2$), 6.78 (2H, d,t, J = 8.6, 2.8 Hz, Ar$\underline{H}$), 7.07−7.72 (6H, m, Ar$\underline{H}$).

Anal. ($C_{24}H_{31}ClN_2O_4S\cdot0.5H_2O$): Calcd: C, 59.07; H, 6.61; N, 7.26. Found: C, 59.33; H, 6.54; N, 7.13.

***N*-3-(*N*′-*tert*-Butoxycarbonyl)aminomethylphenyl-*N*-2-(4′-methoxybenzyl)mercaptoethylaminoacetamide (10).** A mixture of **8** (390 mg, 0.81 mmol), 2-(4-methoxybenzyl)-mercaptoethylamine **9** (320 mg, 2 equiv), KI (50 mg, 0.3 mmol), and K_2CO_3 (500 mg, 4.5 equiv) in DMF (10 mL) was stirred at room temperature overnight. Water was added and the reaction mixture was extracted with a mixed solvent (CH_2Cl_2:MeOH = 9:1). The combined extract was dried, condensed, and purified by PTLC (CH_2Cl_2:MeOH = 95:5) to give 387 mg of product (74%)

^{1}H NMR: 1.45 (9H, s, Boc-H), 2.44−2.67 (6H, m, NHCH$_2$-, SCH$_2$-), 3.02 (2H, s, CO-CH$_2$-NH), 3.64 (2H, s, Ar-CH$_2$-S), 3.65 (2H, s, Ar-CH$_2$-S), 3.77 (6H, s, OCH$_3$), 3.70−3.83 (2H, m, CONCH$_2$-), 4.30 (2H, d, J = 5.9 Hz, ArCH$_2$NHBoc), 6.74−6.86 (4H, m,ArH), 6.98−7.39 (8H, m, ArH).

Anal. ($C_{34}H_{45}N_3O_5S_2\cdot 2H_2O$): Calcd: C, 60.42; H, 7.30; N, 6.21. Found: C, 60.89; H, 7.02; N, 5.72.

***N*-3-Aminomethylphenyl-*N*-2-(4′-methoxybenzyl)-mercaptoethyl-2-(4-methoxybenzyl)mercapto-ethylaminoacetamide (11).** Compound **10** (387 mg, 0.6 mmol) was dissolved in HCl−EtOAc (10 mL, 3 M), and the mixture was stirred at room temperature for 1 h. The solvent was removed, and the residue was dissolved in MeOH (1 mL). Water (5 mL) was added, and the solution was adjusted to pH 10 with concentrated NH_4OH. The resulting mixture was extracted with a mixed solvent (CH_2Cl_2:MeOH = 9:1). The combined extracts were dried, evaporated, and purified by PTLC (CH_2Cl_2:MeOH:NH_4OH = 9:1:0.2) to give 288 mg of product (88%).

^{1}H NMR: 2.42−2.67 (6H, m, NHCH$_2$-, SCH$_2$-), 3.03 (2H, s, Ar-CH$_2$-NH$_2$), 3.63 (2H, s, Ar-CH$_2$-S), 3.65 (2H, s, Ar-CH$_2$-S), 3.75 (6H, s, OCH$_3$), 3.79−3.83 (2H, m, CONCH$_2$-), 3.86 (2H, s, COCH$_2$N-), 6.76 (2H, d,t, J = 8.6, 2.9 Hz, ArH), 6.80 (2H, d,t, J = 8.6, 2.9 Hz, ArH-), 6.95−7.38 (8H, m, ArH).

Anal. ($C_{29}H_{37}N_3O_3S_2\cdot 1.5H_2O$): Calcd: C, 61.40; H, 7.11; N, 7.41. Found: C, 61.59; H, 6.96; N, 7.17.

***N*^{2}-3-{*N*-2-(4-Methoxy)benzylmercaptoethyl-*N*-2-[*N*′-2-(4-methoxy)benzylmercaptoethyl]aminoethyl}-aminobenzyl-*N*^{1},*N*^{3}-di-*tert*-butoxycarbonylguanidine (12).** To a suspension of LAH (28 mg, 0.73 mmol) in THF (3 mL) was added a solution of **11** (100 mg, 0.19 mmol) in THF (3 mL) dropwise at room temperature. The reaction mixture was stirred under reflux for 1 h after which one 1 drop of H_2O, 1 drop of NaOH (1 M), and 3 drops of H_2O were added successively to decompose the excess LAH. The resulting mixture was filtered, and the filtrate was concentrated to give 100 mg of crude product, 3-{*N*-2-(4-methoxy)benzylmercaptoethyl-*N*-2-[*N*′-2-(4-methoxy)benzylmercaptoethyl]aminoethyl}amino-benzylamine, which is pure enough for the next reaction without further purification.

^{1}H NMR: 2.53−2.76 (8H, m, S-CH$_2$-, NCH$_2$-), 3.65 (2H, s, Ar CH$_2$-S-), 3.68 (2H, m, Ar-CH$_2$-NH$_2$), 3.71 (2H, s, Ar-CH$_2$-S-), 3.78 (3H, s, OCH$_3$), 3.79 (3H, s, OCH$_3$), 6.49 (1H, d,d, J = 8.2, 2.3 Hz, ArH), 6.62 (2H, m, ArH), 6.80−6.87 (4H, m, ArH), 7.11−7.30 (5H, m, ArH).

A mixture of the amine obtained above (260 mg, 0.50 mmol) and 1,3-bis(*tert*-butoxycarbonyl)-2-methyl-2-thio-pseudourea (156 mg, 1 equiv) in THF (10 mL containing 0.2 mL of water) was stirred at 65 °C for 3 h. The solvent was removed, and the residue was purified by PTLC (CH_2Cl_2:CH_3OH = 93:7) to give 124 mg of product, **12** (33%).

^{1}H NMR: 1.46 (9H, s, Boc-H), 1.51 (9H, s, Boc-H), 2.52−2.80 (8H, m, -CH$_2$-), 3.32−3.46 (4H, m, -CH$_2$-), 3.60 (2H, s, Ar-CH$_2$-S-), 3.67 (2H, s, Ar-CH$_2$-S-), 3.77 (3H, s, OCH$_3$), 3.78 (3H, s, OCH$_3$), 4.52 (2H, d, J = 4.9 Hz, Ar-CH$_2$-NH-), 6.50 (1H, d,d, J = 8.1, 2.3 Hz, ArH), 6.58−6.65 (2H, m, ArH), 6.79−6.96 (4H, m, ArH), 7.04−7.32 (5H, m, ArH), 8.55 (1H, t, J = 4.5 Hz, Ar-CH$_2$-NH-), 11.52 (1H, s, NHBoc).

Anal. ($C_{40}H_{57}N_5O_6S_2$): Calcd: C, 62.55; H, 7.48; N, 9.32. Found: C, 62.54; H, 6.96; N, 9.12.

***N*^{2}-3-[*N*-2-Mercaptoethyl-*N*-2-(*N*′-2-mercaptoeth-yl)aminoethyl]aminobenzylguanidine (13).** Compound **12** (124 mg, 0.16 mmol) in TFA (5 mL) was stirred at room temperature for 30 min, and the mixture was cooled to 0 °C in an ice bath. Anisole (2 drops) was added followed by $Hg(OAc)_2$ (123 mg, 1.2 equiv). The mixture was stirred at 0 °C for 1 h. Solvent was removed by vacuum, and ether was added. The solid, which was produced after adding the ether, was collected by filtration and washed with ether to give 180 mg of white solid which was dissolved in a mixed solvent (20 mL, EtOAc:EtOH = 1:1) to which H_2S gas was bubbled through for 10 min. The mixture was filtered through Celite and washed with MeOH. The filtrate was condensed to give an oil, which was washed with $CHCl_3$ 3 times to give 66 mg of **13** (73%).

^{1}H NMR: 2.68 (2H, t, J = 6.9 Hz, -CH$_2$-), 2.82 (2H, t, J = 6.1 Hz, -CH$_2$-), 3.24 (4H, t, J = 6.9 Hz, -CH$_2$-), 3.57 (2H, t, J = 7.0 Hz, -CH$_2$-), 3.74 (2H, t, J = 7.0 Hz, -CH$_2$-), 4.35 (2H, s, -Ar-CH$_2$-N-), 6.71−6.81 (3H, ArH), 7.21−7.30 (1H, m, ArH).

HRMS calcd($C_{14}H_{25}N_5S_2$): m/z 328.1629 (M^++1); Found: m/z 328.1613 (M^++1).

Anal. ($C_{14}H_{25}N_5S_2\cdot 5CF_3COOH$): Calcd: C, 32.11; H, 3.37; N, 7.82. Found: C, 32.59; H, 3.53; N, 8.12.

***N*-3-Chloromethylbenzylphthalimide (14).** To a solution of α,α′-*m*-dichloroxylene (1.3 g, 7.4 mmol) in DMF (4 mL) was added potassium phthalimide (925 mg, 5 mmol) in solid form. The reaction mixture was heated to 70 °C under stirring for 2 h. The reaction mixture was cooled to room temperature, and DMF was removed under vacuum. The residue was purified by MPLC (hexane:EtOAc = 2:1) to give 1.01 g of white solid (70%).

^{1}H NMR: 4.55 (2H, s, ClCH$_2$-Ar), 4.84 (2H, s, Ar-CH$_2$-N-), 7.26−7.44 (4H, m, ArH), 7.67−7.75 (2H, m, ArH), 7.83−7.89 (2H, m, ArH).

Anal. ($C_{16}H_{12}ClNO_2$): Calcd: C, 67.26; H, 4.23; N, 4.90. Found: C, 67.47; H, 4.09; N, 4.91.

***N*-3-{*N*′-2-(4-Methoxy)benzylmercaptoethyl-*N*′-2-[*N*″-2-(4-methoxy)benzylmercaptoethyl]aminoethyl}-aminomethylbenzylphthalimide (17a).** The mixture of **14** (286 mg, 1 mmol), amine **16a** (420 mg, 1 equiv), K_2CO_3 (552 mg, 4 equiv), and KI (50 mg, 0.3 mmol) in DMF (5 mL) was stirred at room temperature overnight. Water was added, and the mixture was extracted with a mixed solvent (CH_2Cl_2:MeOH = 9:1). The combined organic extract was dried over Na_2SO_4 and filtered. The filtrate was evaporated under vacuum to give the crude product, which was purified by PTLC (EtOAc) to give 330 mg of product, **17a** (49.5%).

^{1}H NMR: 2.33−2.74 (12H, m, -CH$_2$-), 3.52 (2H, s, Ar-CH$_2$-S), 3.53 (2H, s, Ar-CH$_2$-S), 3.64 (2H, s, Ar-CH$_2$-N-), 3.76 (6H, s, OCH$_3$), 4.81 (2H, s, Ar-CH$_2$-NCO-), 6.76−6.83 (4H, m, ArH), 6.99−7.32 (8H, m, ArH), 7.56−7.71 (2H, m, ArH), 7.77−7.86 (2H, m, ArH).

MS: m/z 670 (M^++1).

Anal. ($C_{38}H_{43}N_3O_4S_2\cdot 2H_2O$): Calcd: C, 64.65; H, 6.71; N, 5.95. Found: C, 64.90; H, 6.37; N, 5.96.

***N*-3-{*N*′-2,2-Dimethyl-2-(4-methoxy)benzyl-mercaptoethyl-*N*′-2-[*N*″-2,2-dimethyl-2-(4-methoxy)-benzylmercaptoethyl]aminoethyl}aminomethyl-benzylphthalimide (17b).** The same procedure for preparation of **17a** was employed using **14** (286 mg, 1 mmol), **16b** (476 mg, 1 equiv), K_2CO_3 (552 mg, 4 equiv), and KI (100 mg, 0.6 mmol) in DMF (5 mL) to give 476 mg of product, **17b** (66%).

^{1}H NMR: 1.29 (12H, s, -CH$_3$), 2.50 (2H, s, -CH$_2$-), 2.61 (4H, s, -CH$_2$-), 2.66 (2H, s, -CH$_2$-), 3.63 (2H, s, Ar-CH$_2$S-), 3.67 (2H, s, Ar-CH$_2$S-), 3.71 (2H, s, Ar-CH$_2$-N-), 3.75 (3H, s, OCH$_3$), 3.76 (3H, s, OCH$_3$), 4.81 (2H, s, Ar-CH$_2$−NCO), 6.79 (4H, d,d, J = 8.6, 0.8 Hz, ArH), 7.19 (4H, d,d, J = 8.6, 1.7 Hz, ArH), 7.27−7.34 (3H, m, ArH),

7.40 (1H, br, ArH), 7.68 (2H, d,d, J = 5.4, 3.1 Hz, ArH), 7.81 (2H, d,d, J = 5.6, 3.1 Hz, ArH).

Anal. ($C_{42}H_{51}N_3O_4S_2 \cdot 0.5H_2O$): Calcd: C, 68.63; H, 7.13; N, 5.80. Found: C, 68.49; H, 6.93; N, 5.45.

3-{*N*-2-(4-Methoxy)benzylmercaptoethyl-*N*-2-[*N*′-2-(4-methoxy)benzylmercaptoethyl]aminoethyl}-aminomethylbenzylamine (18a). To a solution of **17a** (510 mg, 0.76 mmol) in MeOH (10 mL) was added hydrazine anhydrate (0.3 mL) at room temperature. The mixture was stirred at room temperature overnight. The precipitate was removed by filtration, and the filtrate was concentrated to give 325 mg of white solid (79%), which was pure enough for the next reaction without further purification.

^{1}H NMR: 2.40−2.64 (12H, m, -CH$_2$-), 3.52 (2H, Ar-CH$_2$-), 3.55 (2H, Ar-CH$_2$-), 3.62 (2H, Ar-CH$_2$-), 3.73 (6H, s, OCH$_3$-), 3.79 (2H, Ar-CH$_2$-), 6.79 (4H, d,d, J = 8.6, 3.0 Hz, ArH), 7.10−7.27 (8H, m, ArH).

MS: m/z 540 (M^++1).

Anal. ($C_{30}H_{41}N_3O_2S_2 \cdot 0.5H_2O$): Calcd: C, 65.66; H, 7.71; N, 7.66. Found: C, 65.53; H, 7.61; N, 7.51.

3-{*N*-2,2-Dimethyl-2-(4-methoxy)benzylmercaptoethyl-*N*-2-[*N*′-2,2-dimethyl-2-(4-methoxy)-benzylmercaptoethyl]aminoethyl}aminomethylbenzylamine (18b). The same procedure for preparation of **18a** was employed with **17b** (476 mg, 0.66 mmol) and hydrazine (0.2 mL) in MeOH (15 mL) to give 335 mg of product, **18b** (86%).

^{1}H NMR: 1.23 (6H, s, -CH$_3$), 1.32 (6H, s, -CH$_3$), 2.42 (2H, s, -CH$_2$-), 2.51−2.59 (4H, m, -CH$_2$-), 2.64 (2H, s, -CH$_2$-), 3.59 (2H, Ar-CH$_2$-), 3.68 (2H, Ar-CH$_2$-), 3.70, 3.71 (10H, s, OCH$_3$-, Ar-CH$_2$-), 6.78 (4H, d,d, J = 8.7, 2.2 Hz, ArH), 7.14−7.32 (8H, m, ArH).

Anal. ($C_{34}H_{49}N_3O_2S_2 \cdot 0.5H_2O$): Calcd: C, 67.51; H, 8.33; N, 6.61. Found: C, 67.28; H, 8.22; N, 6.76.

***N*^{2}-3-{*N*-2-(4-Methoxy)benzylmercaptoethyl-*N*-2-[*N*′-2-(4-methoxy)benzylmercaptoethyl]aminoethyl}-aminomethylbenzyl-*N*^{1},*N*^{3}-di-*tert*-butoxycarbonylguanidine (19a).** To a mixture of **18a** (100 mg, 0.19 mmol) and 1,3-bis(*tert*-butoxycarbonyl)-2-methyl-2-thiopseudourea (54 mg, 1 equiv) in THF (3 mL) was added 6 drops of water, and the mixture was stirred at 65 °C for 3 h. The solvent was removed, and the residue was purified by PTLC (CH_2Cl_2:CH_3OH = 9:1) to give 94 mg of product, **19a** (65%).

^{1}H NMR: 1.46 (9H, s, tert-CH$_3$), 1.51 (9H, s, tert-CH$_3$), 2.44−2.72 (12H, m, CH$_2$), 3.56 (2H, s, Ar-CH$_2$-N-), 3.60 (2H, s, Ar-CH$_2$-S-), 3.64 (2H, s, Ar-CH$_2$-S-), 3.77 (6H, s, OCH$_3$), 4.60 (2H, d, J = 5.1 Hz, Ar-CH$_2$-NH-), 6.81 (4H, d,d, J = 8.6, 3.2 Hz, CH$_3$O-ArH), 7.13−7.32 (8H, m, ArH), 8.54 (1H, t, J = 4.7 Hz, Ar-CH$_2$-NH-), 11.53 (1H, s, NHBoc).

HRMS calcd($C_{41}H_{59}N_5O_6S_2$): m/z 782.3915 (M^++1); found: m/z 782.3937 (M^+ + 1).

Anal. ($C_{41}H_{59}N_5O_6S_2 \cdot 1.5H_2O$): Calcd: C, 60.86; H, 7.72; N, 8.66. Found: C, 60.56; H, 6.53; N, 9.08.

***N*^{2}-3-{*N*-2,2-Dimethyl-2-(4-methoxy)benzylmercaptoethyl-*N*-2-[*N*′-2,2-dimethyl-2-(4-methoxy)-benzylmercaptoethyl]aminoethyl}aminomethylbenzyl-*N*^{1},*N*^{3}-di-*tert*-butoxycarbonylguanidine (19b).** The same procedure for preparation of **19a** was employed using **18b** (138 mg, 0.23 mmol) and 1,3-bis(*tert*-butoxycarbonyl)-2-methyl-2-thiopseudourea (80 mg, 1 equiv) to give 96 mg of product, **19b** (49%).

^{1}H NMR: 1.29 (6H, s, -CH$_3$-), 1.32 (6H, s, -CH$_3$-), 1.47 (9H, s, tert-CH$_3$), 1.52 (9H, s, tert-CH$_3$), 2.50 (2H, s, -CH$_2$-), 2.64 (4H, s, -CH$_2$-), 2.67 (2H, s, -CH$_2$-), 3.63 (2H, s, Ar-CH$_2$-), 3.70 (2H, s, Ar-CH$_2$-), 3.73 (2H, s, Ar-CH$_2$-), 3.76 (6H, s, OCH$_3$-), 4.60 (2H, d, J = 4.9 Hz, Ar-CH$_2$NH-), 6.80 (4H, d,d, J = 8.5, 1.7 Hz, ArH), 7.19−7.29 (8H, m, ArH).

Anal. ($C_{45}H_{67}N_5O_6S_2 \cdot 1.5H_2O$): Calcd: C, 62.47; H, 8.15; N, 8.10. Found: C, 62.29; H, 7.11; N, 8.43.

***N*^{2}-3-[*N*-2-Mercaptoethyl-*N*-2-(*N*′-2-mercaptoethyl)aminoethyl]aminomethylbenzylguanidine (20a).** The same procedure for preparation of **13** was employed by using **19a** (350 mg, 0.45 mmol) in TFA (10 mL), Hg(OAc)$_2$, (341 mg), and anisole (4 drops) to give 150 mg of product, **20a** (37%).

^{1}H NMR: 2.85 (4H, m, -CH$_2$-), 3.04−3.45 (8H, m, -CH$_2$-), 4.27 (2H, s, Ar-CH$_2$-N-), 4.45 (2H, s, Ar-CH$_2$-NH-), 7.46 (4H, m, ArH).

HRMS calcd($C_{15}H_{27}N_5S_2$): m/z 342.1786 (M^++1); found: m/z 342.1778 (M^+ + 1).

Anal. ($C_{15}H_{27}N_5S_2 \cdot 5CF_3COOH$): Calcd: C, 32.94; H, 3.54; N, 7.68. Found: C, 32.52; H, 3.66; N, 7.66.

***N*^{2}-3-[*N*-2,2-Dimethyl-2-mercaptoethyl-*N*-2-(*N*′-2,2-dimethyl-2-mercaptoethyl)aminoethyl]aminomethylbenzylguanidine (20b).** The same procedure for preparation of **13** was employed by using **19b** (84 mg, 0.1 mmol), TFA (4 mL), Hg(OAc)$_2$ (77 mg), and anisole (2 drops) to give 50 mg of product, **20b** (68%).

^{1}H NMR: 1.37 (6H, s, CH$_3$-), 1.41 (6H, s, CH$_3$-), 2.80 (2H, s, N-CH$_2$-), 3.03 (2H, t, J = 6.5 Hz, N-CH$_2$-CH$_2$-NH-), 3.07 (2H, s, N-CH$_2$-), 3.29 (2H, t, J = 6.8 Hz, N-CH$_2$-CH$_2$-NH-), 3.92 (2H, s, Ar-CH$_2$-), 4.43 (2H, s, Ar-CH$_2$-NH-), 7.40 (4H, m, ArH).

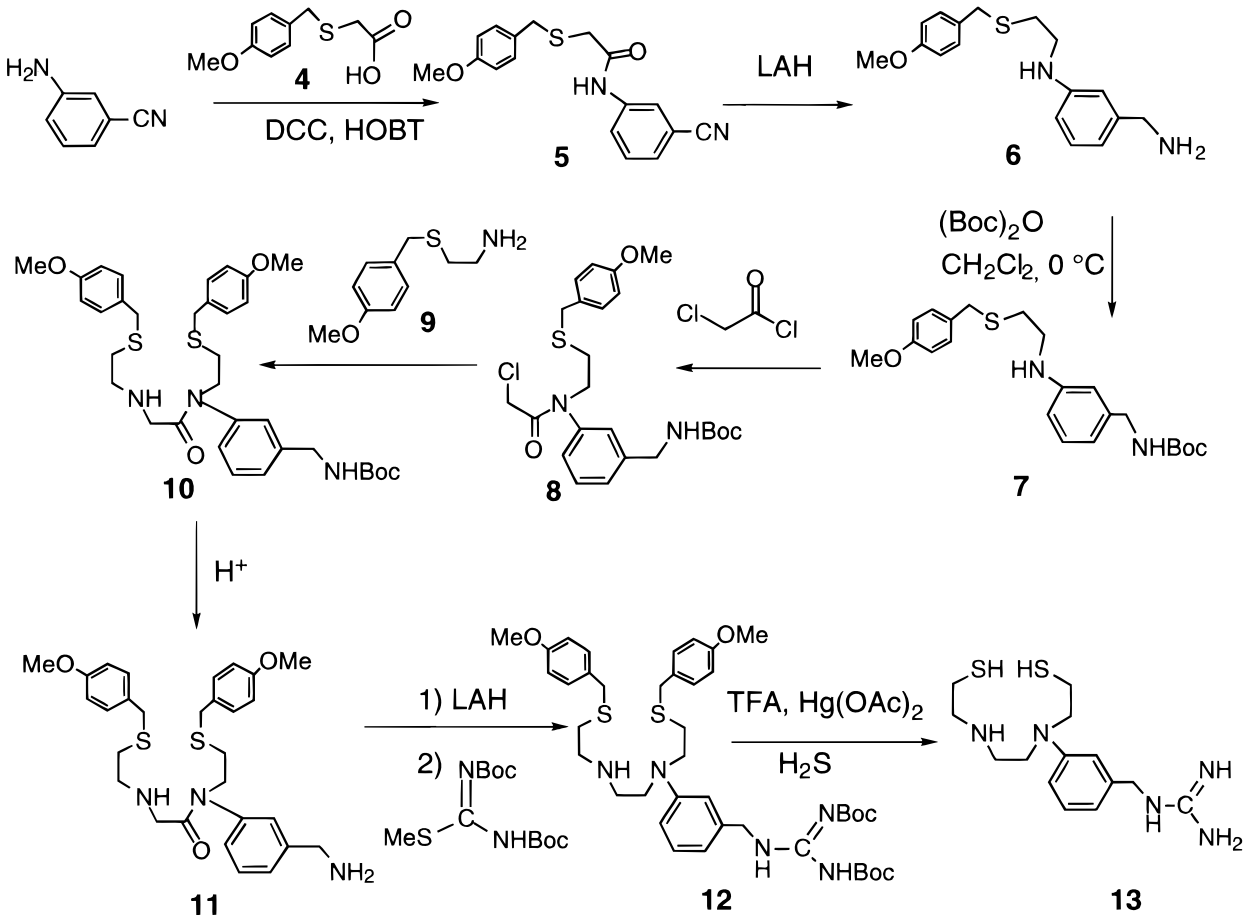
Anal. ($C_{19}H_{35}N_5S_2 \cdot 5CF_3COOH$): Calcd: C, 35.99; H, 4.16; N, 7.24. Found: C, 36.27; H, 4.15; N, 8.03.

Radiolabeling Procedure. Unlabeled MIBG was prepared by the same two-step method employed for the synthesis of **13** and **20** from **11** and **18**. Labeling of MIBG with ^{125}I was performed by the ammonium sulfate, heat-mediated exchange procedure according to a published method (*1*). A generic description for preparation of all the ^{99m}Tc-labeled complexes is described as the following: A small amount of N_2S_2 ligand (1−2 mg) dissolved in 100 μL of EtOH was mixed with 200 μL of HCl (1 N) and 1 mL of Sn-glucoheptonate solution (containing 12 μg of $SnCl_2$ and 120 μg of Na-glucoheptonate, pH 6.67) and 50 μL of EDTA solution (0.1 N). [^{99m}Tc]Pertechnetate solution (100−200 μL; ranging from 1 to 3 mCi) was then added. The reaction was heated for 30 min at 100 °C, and cooled to room temperature. The reaction mixture was directly analyzed on either TLC (EtOH:concentrated NH_3 = 9:1) or ITLC SG (100% MeOH) to determine the purity of the product. For the animal study, the mixture was neutralized with phosphate buffer to pH 5.0. The ratio of the amount of ligand (a possible pseudo-carrier) to [^{99m}Tc]pertechnetate used for labeling was carefully monitored to result in a final dosing solution with less than 10 μg/Kg body weight/dose (*23*).

Partition Coefficients. Partition coefficients were measured by mixing ^{99m}Tc-labeled complexes or [^{125}I]MIBG with 3 g each of 1-octanol and buffer (pH 7.0 or 7.4, 0.1 M phosphate) in a test tube. The test tube was vortexed for 3 min at room temperature, and then centrifuged for 5 min. Two weighed samples (0.5 g each) from the 1-octanol and buffer layers were counted in a well counter. The partition coefficient was determined by calculating the ratio of cpm/g of octanol to that of buffer. Samples from the octanol layer were repartitioned until consistent partition coefficient values were obtained. The measurement was repeated 3 times.

Biodistribution in Rats. Male Sprague-Dawley rats (225−300 g) allowed free access to food and water were used for in vivo biodistribution studies (*24*, *25*). While

Scheme 1



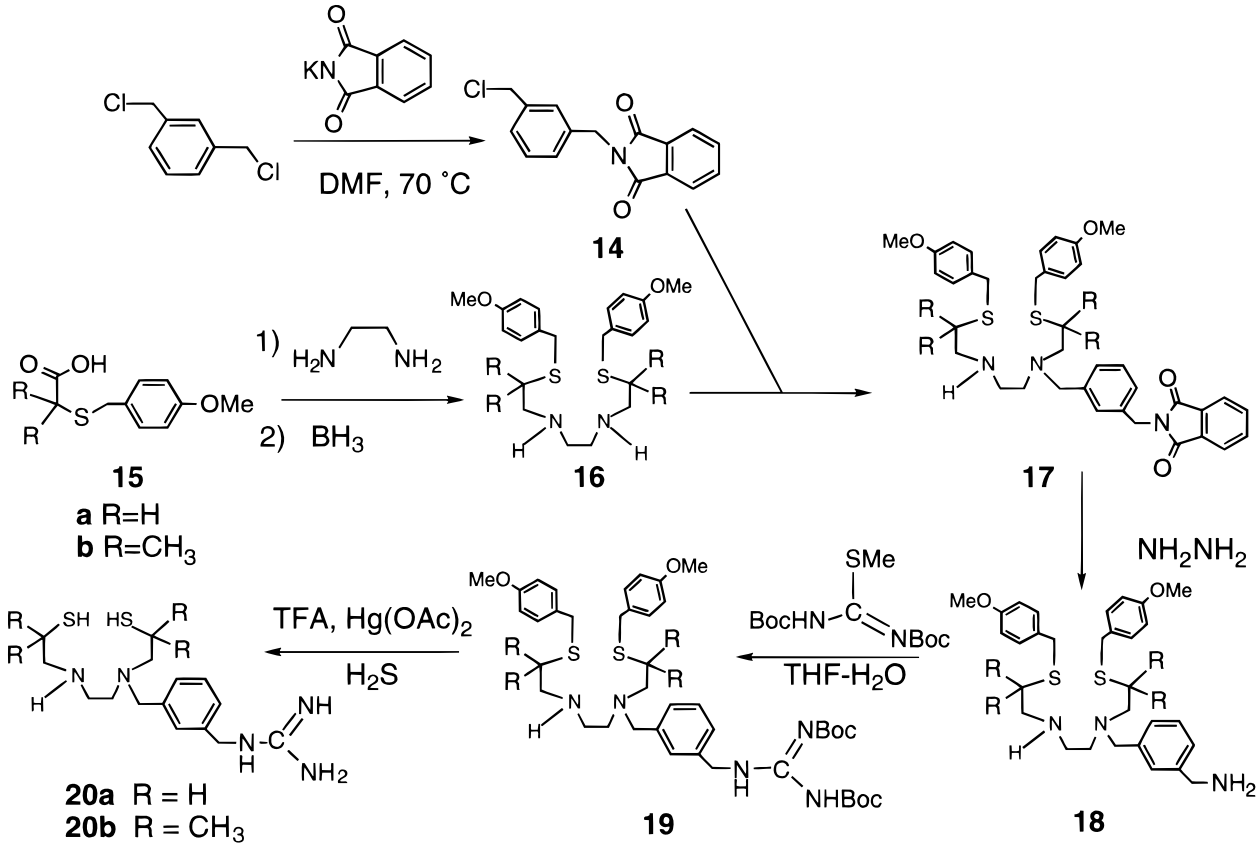
under ether anesthesia, 0.2 mL of a saline solution containing ^{99m}Tc-labeled agents (5−10 μCi) was injected directly into the femoral vein of rats, and the rats were sacrificed by cardiac excision at various time points postinjection. The organs of interest were removed and weighed, and the radioactivity was counted with an automatic gamma counter (Packard 5000). The percentage dose per gram of organ was calculated by a comparison of the tissue counts to suitably diluted aliquots of the injected material. For the dual-tracer experiment, [^{99m}Tc]**2** (5−10 μCi) and [^{125}I]MIBG (1−5 μCi) were coinjected together to the rats, and the biodistribution was performed as described. The samples were counted for ^{99m}Tc activity at the day of the experiment using the energy window of ^{99m}Tc (80−200 keV), and after a 3-day decay period, ^{125}I activity in the samples was determined and used without further decay correction. Blocking studies were carried out either by pretreating rats with desipramine (10 mg/kg, ip) 30 min prior to tracer injection or by coinjecting nonradioactive MIBG (1 mg/kg) together with the tracers.

Uptake Studies in Cultured Cells. The human neuroblastoma cell lines SK-N-SH (uptake-1 positive) and SK-N-MC (uptake-1 negative) (*26*) were purchased from the American Type Culture Collection (Rockville, MD). Cell uptake study was performed similar to that reported previously for MIBG and its related derivatives (*27*). Briefly, bulk quantities of cells were grown in Falcon tissue culture flasks (75 cm^2) at 37 °C in a 5% CO_2 humidified atmosphere. The culture medium was minimal essential medium (MEM) supplemented with glutamine, Earl's salts, sodium pyruvate, and 10% fetal bovine serum. The cells were seeded into 24-well plates [(2−4) × 10^5 cells/per well in 500 μL of medium] and incubated at 24 h at 37 °C. The transporters for dopamine (DAT) or norepinephrine (NET) expressed in the pig kidney cell line (LLC-PK1) were kindly provided by Dr. Rudnick (Yale University, New Haven, CT). These cells, grown as a monolayer culture as described (*28*), were seeded and incubated similarly to SK-N-SH cells. On the day of the experiment, [^{125}I]MIBG and [^{99m}Tc]**2** in the medium were incubated with cells in phosphate-buffered saline (PBS) for 60 min. The cells were solubilized with 500 μL of 0.5 N NaOH and then counted for the associated activity in a gamma counter (Packard 5000). Nonspecific activity was determined either by preincubating cells with DMI (50 μM) or by measuring tracer binding to SK-N-MC cells. Both methods gave similar results.

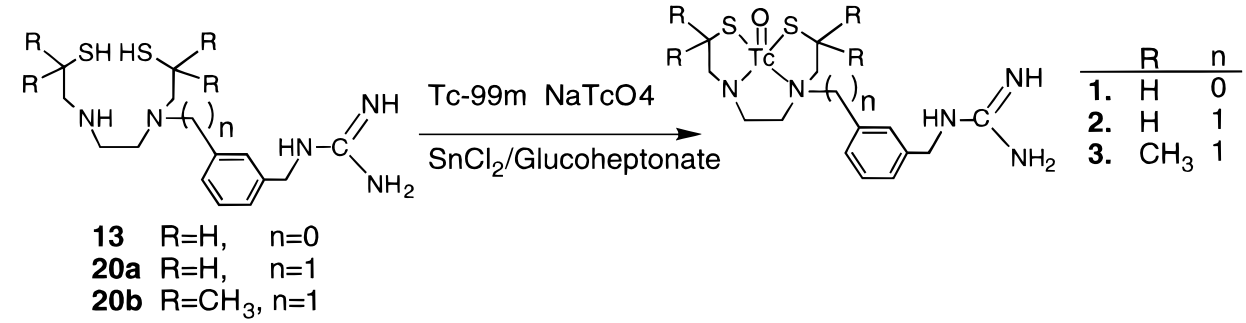
RESULTS

Synthesis of Ligands. Ligands **13**, **20a**, and **20b**, were prepared by reactions described in Schemes 1 and 2. For the synthesis of ligand **13**, a stepwise approach was used to build the N_2S_2 ligand system. The starting material, 3-aminobenzonitrile, was reacted with 2-(4-methoxybenzyl)mercaptoacetic acid, **4**, in the presence of DCC to produce the amide **5** in 70% yield. Reduction of the amide and the nitrile groups by LAH produced the desired amine **6** (55% yield). Selective protection of **6** with $(Boc)_2O$ resulted in **7** (80% yield). The protected amine, **7**, was acylated with chloroacetyl chloride by which the desired amide, **8**, was produced in 97% yield. Substitution of chlorine in **8** with 2-(4-methoxybenzyl)mercaptoethylamine, **9**, afforded **10** (yield 74%). Deprotection of the Boc group on **10** by acid gave amine **11** (yield 88%).

Scheme 2



Scheme 3



Reduction of the amide moiety of **11** followed by a selective alkylation of the primary amine of the reductive product with 1,3-bis(*tert*-butoxycarbonyl)-2-methyl-2-thiopseudourea in THF (*29*) introduced the guanidine moiety. This two-step reaction produced **12** in 33% yield. A one-pot reaction was used to remove both Boc and methoxybenzyl protection groups simultaneously. This was accomplished by treating **12** with TFA and $Hg(OAc)_2$ followed by treatment with H_2S to give the final product **13** (73%). The other two ligands, **20a** and **20b**, were prepared by reactions described in Scheme 2. To synthesize **20a** and **20b**, 2 equiv of α,α′-*m*-dichloroxylene was reacted with potassium phthalimide to give monophthalimide **14** in 70% yield. Monoalkylation of **16a** (*30*) or **16b** (*31*) by **14** produced the desired N_2S_2 derivatives **17a**,**b** directly. In this selective monoalkylation reaction, when 1 equiv of **16a** was used, the ratio of monoalkylation vs dialkylation was 2:1; when 2 equiv of **16a** was used in the same reaction, the ratio was increased to 4:1. In the case of preparation of **17b**, the reaction was much slower compared to that of **17a**, and no dialkylation product was detected even when 1 equiv of **16b** was used, which is likely due to the steric hindrance of tetramethyl substitution on **16b**. The yield of **17b** was improved from 33% to 66% by adding KI to the same reaction mixture. Hydrolysis of phthalimide of **17a** and **17b** with hydrazine afforded amines **18a** and **18b** in 79% and 86% yield, respectively. The same procedure for introducing the guanidine moiety as that reported for **13** was used to produce **20a** and **20b** in 37% and 68% yield, respectively.

Preparation of ^{99m}Tc-Labeled MIBG Derivatives. Preparation of ^{99m}Tc-labeled compounds from the free thiols, **13**, **20a**, and **20b**, was achieved by using stannous(II) glucoheptonate as the reducing agent for [^{99m}Tc]pertechnetate (Scheme 3). Formations of ^{99m}Tc-labeled complexes resulted in similar R_f values (0.1−0.2) as that of [^{125}I]-MIBG by a similar TLC method [Whatman silica gel plates (PESIL G/UV) under various solvent systems (data not shown)]. Using a solvent system of ethanol/concentrated NH_3 (9:1), the blank labeling reaction (without adding the ligand) showed one peak, most likely the ^{99m}Tc glucoheptonate peak with a R_f value of 0.8−0.9. The radiochemical purity of the final complexes evaluated on TLC (EtOH:concentrated NH_3 = 9:1) showed greater

Table 1. Biodistribution in Rats after iv Injections of ^{99m}Tc-Labeled Complexes 1, 2, and 3 (% Dose/g, Average of 3 Rats ± SD)

	[^{99m}Tc]**1**		[^{99m}Tc]**2**		[^{99m}Tc]**3**	
organ	2 min	30 min	2 min	30 min	2 min	30 min
blood	1.01 ± 0.15	0.37 ± 0.07	0.30 ± 0.03	0.07 ± 0.006	1.04 ± 0.09	0.03 ± 0.003
heart	**0.52 ± 0.05**	**0.24 ± 0.04**	**0.67 ± 0.07**	**0.41 ± 0.01**	**0.18 ± 0.009**	**0.034 ± 0.002**
muscle	0.18 ± 0.01	0.07 ± 0.001	0.04 ± 0.01	0.04 ± 0.004	0.04 ±0.006	0.015 ± 0.0003
lung	2.92 ± 0.35	1.65 ± 0.14	1.42 ± 0.12	0.75 ± 0.03	0.26 ± 0.05	0.064 ± 0.008
kidney	2.48 ± 0.39	1.46 ± 0.40	8.63 ± 0.71	5.70 ± 0.78	4.78 ± 0.05	4.68 ± 0.64
spleen	0.94 ± 0.34	1.13 ± 0.05	0.51 ± 0.08	0.31 ± 0.03	0.40 ± 0.09	0.08 ± 0.01
liver	4.17 ± 0.24	4.08 ± 0.73	3.68 ± 0.49	2.09 ± 0.77	3.96 ± 0.50	1.41 ± 0.20
skin	0.13 ± 0.02	0.13 ± 0.003	0.17 ± 0.02	0.11 ± 0.002	0.06 ± 0.01	0.04 ± 0.003
brain	0.02 ± 0.008	0.01 ± 0.003	0.01 ± 0.00	0.006 ± 0.001	0.01 ± 0.002	0.002 ± 0.000
heart:BL ratios	**0.51**	**0.65**	**2.23**	**5.85**	**0.17**	**1.13**

Table 2. Dual-Tracer Biodistribution of [^{99m}Tc]2 and [^{125}I]MIBG in Sprague-Dawley Rats (iv Injection, % Dose/g, Average of 3 Rats ± SD)

organ	2 min	1 h	2 h	4 h
		[^{99m}Tc]2		
blood	0.25 ± 0.04	0.056 ± 0.01	0.033± 0.004	0.026 ± 0.004
heart	**0.45 ± 0.03**	**0.26 ± 0.03**	**0.22 ± 0.01**	**0.21 ± 0.01**
heart:BL ratios	**1.86**	**4.69**	**6.66**	**8.11**
		[^{125}I]MIBG		
blood	0.50 ± 0.08	0.17 ± 0.02	0.14 ± 0.01	0.13 ± 0.02
heart	**3.35 ± 0.24**	**2.68 ± 0.16**	**2.11 ± 0.09**	**1.70 ± 0.20**
heart:BL ratios	**6.68**	**15.76**	**15.07**	**13.0**

than 95% purity (R_f = 0.15). Alternately, the formed complexes were evaluated on ITLC SG (Gelman Sciences) with 100% MeOH as the solvent. Without any chelating agent present, the reduced pertechnetate (most likely chemical form is TcO_2) moved slightly from the origin (R_f = 0.15). Formation of the ^{99m}Tc-labeled MIBG derivatives gave R_f values around 0.4, in contrast to the R_f value of 1.0 in the absence of the new ligands (data not shown). These results lend support to the formation of the proposed ^{99m}Tc-labeled complexes ([^{99m}Tc]**1**, [^{99m}Tc]**2**, and [^{99m}Tc]**3**). These complexes were stable up to 6 h in phosphate buffer (pH 5.0) when evaluated in the same TLC system at room temperature. It is important to note that the labeling reaction may produce isomers. Attempts were made to separate the ^{99m}Tc-labeled complexes on either TLC or HPLC (normal phase or reversed phase columns) with various solvent combinations but without any success. A more systematic effort is currently being made to identify possible isomers, which may not be detected by the TLC system described above.

Biodistribution Study of ^{99m}Tc-Labeled MIBG Derivatives in Rats. Lipophilicities, as measured by the partition coefficient (PC) between 1-octanol and pH 7.0 phosphate buffer, of these ^{99m}Tc-labeled complexes were comparable to that of [^{125}I]MIBG (PC = 1.1 for [^{125}I]MIBG and 1.99, 6.74, and 4.54 for [^{99m}Tc]**1**, [^{99m}Tc]**2**, and [^{99m}Tc]**3**, respectively). Preliminary biodistribution studies of these ^{99m}Tc-labeled MIBG derivatives showed reasonably good heart uptakes in rats (Table 1). The initial heart uptake of [^{99m}Tc]**3** (heart uptake 0.18 and 0.034% dose/g, at 2 and 30 min, respectively) clearly indicated that this compound is the least favorable one among all three ^{99m}Tc complexes in terms of penetrating the cell membrane to localize in heart tissues. It is likely that, despite the advantage of adding a tetramethyl group on the molecule, which increases the lipophilicity (may facilitate diffusion process), the bulk hindrance may play an even more important role in obstructing the ability of this molecule to cross the membrane. We therefore concentrated on studying compounds [^{99m}Tc]**1** and [^{99m}Tc]**2**, without the tetramethyl substitution groups. It appears that compounds [^{99m}Tc]**1** and [^{99m}Tc]**2** are both interesting, with similar heart uptakes at 2 and 30 min (0.52 and 0.24% dose/g for [^{99m}Tc]**1** and 0.67 and 0.41% dose/g for [^{99m}Tc]**2**, respectively). However, [^{99m}Tc]**2** displayed a higher heart-to-blood ratio (5.85) at 30 min as compared to that of [^{99m}Tc]**1** (0.65). Therefore, compound [^{99m}Tc]**2** was chosen for further studies in rats. It is interesting to note that these three ^{99m}Tc-labeled complexes displayed different uptakes in other organs such as lung and liver. [^{99m}Tc]**1** appeared to be more concentrated in these two organs and was slowly washed out as compared to [^{99m}Tc]**2** and [^{99m}Tc]**3**. In contrast, [^{99m}Tc]**1** displayed lower accumulation in kidney as compared to [^{99m}Tc]**2** and [^{99m}Tc]**3**.

The dual-tracer biodistribution study provides a direct comparison of heart uptake and washout between the ^{99m}Tc-labeled agent and [^{125}I]MIBG. Therefore, a dual-tracer experiment, the biodistribution of [^{99m}Tc]**2** and [^{125}I]MIBG, in Sprague-Dawley rats was carried out (Table 2). In these preliminary experiments using tracer doses, the loading doses for nonradioactive MIBG and also the ligands for making technetium complexes were kept below 10 μg/kg per rat per dose, so the concentrations of carrier or pseudo-carrier will not be sufficient to compete for the norepinephrine uptake sites (*23*). [^{99m}Tc]**2** displayed the desired heart uptake and slow washout (0.45% dose/g at 2 min and 0.21% dose/g at 4 h, respectively; see Table 2). However, in a direct comparison with [^{125}I]MIBG, the heart uptake of the ^{99m}Tc-labeled complex was approximately one-eighth of that for [^{125}I]MIBG (3.35 and 1.71% dose/g at 2 and 4 h, respectively). Unlike [^{125}I]MIBG, the contrast between heart vs blood at 4 h for [^{99m}Tc]**2** appeared to be lower (8.11 and 13.00 for [^{99m}Tc]**2** and [^{125}I]MIBG, respectively). The preliminary data are encouraging in that it is the first time a ^{99m}Tc-labeled MIBG derivative displays a measurable heart uptake. To specifically examine whether the heart uptake is related to norepinephrine distribution, we have performed the dual-tracer experiment in rats either by coinjecting nonradioactive MIBG (1.0 mg/kg) or by pretreating rats with desipramine (DMI, specific norepinephrine transporter blocker) prior to tracer injection. In rats with a coinjected loading dose of MIBG (1.0 mg/kg), the heart uptake of [^{125}I]MIBG was blocked by 47.5% at 2 h, while there was about 32.0% blockade of

Table 3. Biodistribution of [^{99m}Tc]2 and [^{125}I]MIBG (Dual-Isotope Experiment) in Rats with or without Coinjection of Nonradioactive MIBG (% Dose/g, Average of 3 Rats ± SD)[a]

	control		treated (nonradioactive MIBG)			
organ	2 min	2 h	2 min	% of blocking	2 h	% of blocking
			[^{99m}Tc]2			
blood	0.28 ± 0.05	0.046 ± 0.01	0.40 ± 0.05		0.043 ± 0.01	
heart	**0.53 ± 0.06**	**0.22 ± 0.01**	**0.36 ± 0.04**	**32.1**[b]	**0.15 ± 0.01**	**32.0**[b]
heart:BL ratios	**1.89**	**4.78**	**0.90**		**3.58**	
			[^{125}I]MIBG			
blood	0.47 ± 0.09	0.11 ± 0.01	0.79 ± 0.05		0.13 ± 0.02	
heart	**3.14 ± 0.20**	**2.17 ± 0.07**	**1.99 ± 0.03**	**36.7**[b]	**1.14 ± 0.12**	**47.5**[b]
heart:BL ratios	**6.59**	**19.37**	**2.51**		**8.61**	

[a] In treated rats: MIBG (1.0 mg/kg) was coinjected together with the tracers, [^{99m}Tc]**2** and [^{125}I]MIBG. [b] $p < 0.05$, Student's *t*-test.

Table 4. Blocking Studies with Desipramine on Dual-Tracer Uptakes in Rats (% Dose/g, Average of 3 Rats ± SD)[a]

	control		treated (desipramine; DMI)			
organ	2 min	2 h	2 min	% of blocking	2 h	% of blocking
			[^{99m}Tc]2			
blood	0.49 ± 0.03	0.064 ± 0.004	0.35 ± 0.05		0.054 ± 0.011	
heart	0.46 ± 0.06	0.23 ± 0.03	0.37 ± 0.09	20[b]	0.20 ± 0.02	12[b]
adrenal gland	0.61 ± 0.11	0.23 ± 0.01	0.52 ± 0.09		0.21 ± 0.04	
heart:BL ratios	0.94	3.62	1.05		3.81	
			[^{125}I]MIBG			
blood	0.64 ± 0.06	0.14 ± 0.01	0.65 ± 0.06		0.091 ± 0.01	
heart	3.04 ± 0.15	2.29 ± 0.25	2.23 ± 0.72	27[b]	1.58 ± 0.22	32[b]
adrenal gland	2.47 ± 0.30	1.50 ± 0.19	0.52 ± 0.09		1.73 ± 0.88	
heart:BL ratios	4.75	16.20	3.41		17.36	

[a] Control rats and rats pretreated with desipramine (DMI); 10 mg/kg, ip 30 min prior to tracer injection was used for this study. [b] $p < 0.05$, Student's *t*-test.

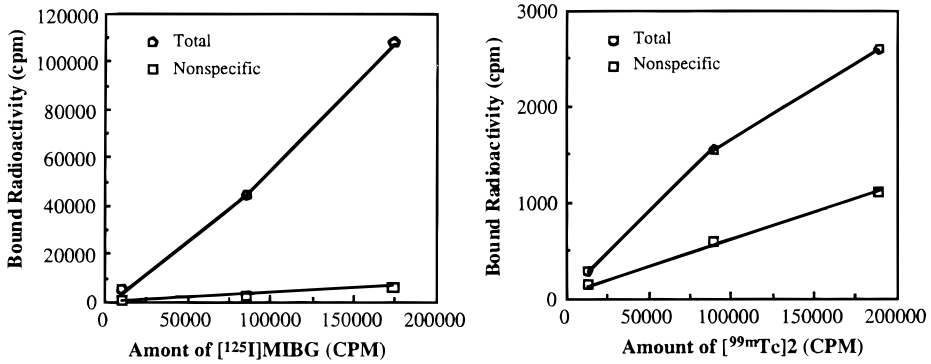


Figure 2. Uptake of [^{99m}Tc]**2** and [^{125}I]MIBG in SK-N-SH human neuroblastoma cells in vitro as a function of tracer concentration (in cpm). The data shown above were from a set of representative experiments.

heart uptake for [^{99m}Tc]**2** at the same time point (Table 3). This result suggests that the heart uptake of [^{99m}Tc]**2** may be related to the MIBG uptake.

To test the hypothesis that the binding of [^{99m}Tc]**2** is specific for norepinephrine transporters, rats were pretreated with desipramine (DMI; 10 mg/kg) ip for 30 min prior to tracer injection, and the same biodistribution was carried out (see Table 4). Even though the specific blockade for [^{99m}Tc]**2** is smaller than that of [^{125}I]MIBG (12% vs 32% reduction, respectively), the result is consistent with the notion that the new ^{99m}Tc-labeled complex, [^{99m}Tc]**2**, displayed specific binding to norepinephrine transporters.

Uptake Studies in Cells Expressing Monoamine Transporters. Cell uptakes of [^{99m}Tc]**2** were evaluated together with [^{125}I]MIBG in either SK-N-SH neuroblastoma cells or LLC-NET and LLC-DAT cells. [^{99m}Tc]**2** uptake by SK-N-SH cells, like [^{125}I]MIBG, increased as a function of input activity (Figure 2). The specific uptake of [^{99m}Tc]**2** was found, however, to be much lower than that of [^{125}I]-MIBG (about one-tenth). A higher nonspecific uptake of [^{99m}Tc]**2** (approximately 40% of total uptake) was observed in contrast to low nonspecific uptake for [^{125}I]-MIBG (10%). Interestingly, a similar specific uptake of [^{99m}Tc]**2** was also observed in LLC-NET cells but not in LLC-DAT cells (data not shown). The data are consistent with the results for [^{125}I]MIBG and related derivatives in the same SK-N-SH cells reported previously (*27*).

DISCUSSION

In the last 10 years, the localization of myocardial adrenergic nerve endings in normal subjects and patients with various cardiac diseases has been reported (*9*, *10*, *12*). MIBG in its ^{123}I-labeled form is the imaging agent of choice, and it is now commercially available in Japan and in Europe, which attests to its importance as a clinical diagnostic tool. MIBG initially was designed as an attempt to attach a more stable iodine at the meta position of benzenylguanidine as an adrenal medulla imaging agent (*1*, *3*). It is generally accepted that the iodine substitution at the paraposition is subjected to rapid in vivo deiodination. However, at the practical level, a comparable ^{99m}Tc-labeled MIBG derivative will provide a much wider clinical acceptance. In developing ^{99m}Tc-

labeled MIBG derivatives, in vivo deiodination is not a subject of concern; therefore, it is likely that the $[Tc^{v}O]^{3+}N_2S_2$ complex can be attached to benzylguanidine and both meta- and para-substituted ^{99m}Tc derivatives may be potentially useful.

We made the initial attempt to replace the iodo group at the meta position of MIBG with $[Tc^{v}O]^{3+}N_2S_2$ complex. Three complexes, [^{99m}Tc]**1**, -**2**, and -**3**, were prepared and tested. By substituting the iodo group with $[Tc^{v}O]^{3+}N_2S_2$ complex, the resulting ^{99m}Tc complexes displayed comparable lipophilicities as the parent MIBG molecule (reflected by comparable partition coefficients). However, the ^{99m}Tc complexes displayed a lower heart uptake in rats. It is possible that these complexes with enlarged molecular size due to $[Tc^{v}O]^{3+}N_2S_2$ complex prohibit their easy passage through the cell membranes.

Dual-tracer distribution studies clearly delineated that the ^{99m}Tc-labeled complex [^{99m}Tc]**2**, similar to [^{125}I]MIBG, was concentrated in the heart. It remained trapped in the heart for up to 4 h postinjection. Despite the lower amount of heart uptake, [^{99m}Tc]**2** closely resembled [^{125}I]-MIBG, i.e., displayed significantly reduced heart uptake when coinjected with nonradioactive MIBG or pretreated with desipramine, a norepinephrine transporter inhibitor. Two components of MIBG uptake have been identified: (a) the specific neuronal uptake-1 pathway mediated by NE transporters, which is blocked by desipramine (*6*); and (b) the nonspecific uptake-2 pathway (possibly by a simple diffusion mechanism). Both pathways are considered to be involved when [^{123}I]MIBG was used for myocardial imaging. It is likely that the heart uptake of ^{99m}Tc-labeled compound, [^{99m}Tc]**2**, derived from [^{125}I]-MIBG, also contained specific and nonspecific pathways and only the specific pathway can be blocked by pretreatment with desipramine (less than 20% for [^{99m}Tc]-**2**). The smaller percentage of the specific uptake-1 pathway observed with [^{99m}Tc]**2** could be likely due to the presence of the mixtures of diastereomers. It is also possible that only a certain structure conformation or configuration of the ^{99m}Tc complex can be preferably recognized by the specific uptake-1 pathway but not the other diastereomers. We attempted to separate different diastereomers using various HPLC columns and solvent combinations but without any success. Future efforts will be directed to the separation of individual isomers of the ^{99m}Tc complexes and the evaluation of the isolated isomer for their in vivo distribution.

The specific activity of radiolabeled MIBG appears to be important for the in vivo localization (*23*). An initial report by Wieland et al. used an exchange reaction for preparation of radiolabeled MIBG (*1*). The exchange reaction requires the use of a higher quantity of nonradioactive MIBG, which leads to a lower specific activity. Biodistribution studies in rats, as predicted, showed a substantially decreased heart uptake when nonradioactive carrier was added. The saturable uptake in the heart is consistent with the proposed mechanism of uptake and retention. Consistent heart uptake was observed in rats only when the loading nonradioactive dose was below 12 μg/kg (*23*). Recent studies showed that the no-carrier-added preparation, using the corresponding 3-trimethylsilylbenzylguanidine as the starting material, clearly suggested that the uptake in the heart of mice is carrier-dependent (*32*, *33*). It was also reported that in humans the heart uptake appeared to be higher when the no-carrier-added preparation of MIBG was used (the carrier-added preparation specific activity was 2 mCi/μmol for 5.4 mCi dose/70 kg man = 10.6 μg/kg). However, the image quality was not significantly improved in subjects receiving the no-carrier-added preparation of MIBG. It was suggested that the in vivo de-iodination might be more significant at a lower "carrier" dose (higher specific activity); therefore, the background level was higher. To avoid carrier effect, the loading dose for nonradioactive MIBG or unchelated technetium ligand used for the study was kept below 10 μg/kg per rat.

The uptake of MIBG into SK-N-SH cells by an active uptake-1 mechanism was reported previously (*2*). The substantially lower accumulation (one-tenth) of the ^{99m}Tc-labeled compound, [^{99m}Tc]**2**, as compared to that of MIBG in SK-N-SH cells, was observed (Figure 2). This lower cellular uptake is consistent with the finding of lower heart uptake in rat biodistribution (the heart uptake was one-eighth of that for MIBG). Further studies will endeavor to determine the specificity of the cellular uptake of these ^{99m}Tc-labeled complexes. It is suggested that an ideal Tc-99m-labeled agent should have the following properties: (i) A heart uptake of at least 0.75% dose/organ at 2 h post iv injection into rats (this is about 50% of that reported for [^{125}I]MIBG) and a heart vs blood ratio (percentage dose:gram ratio) $\geq$10 at 2 h postinjection. (ii) A specific heart uptake selective to norepinephrine storage sites (i.e., the uptake can be significantly reduced after pretreatment of "cold" MIBG or desipramine, DMI). The ^{99m}Tc-labeled analogue of MIBG should have a selective uptake similar to that of [^{125}I]-MIBG (at least 50% of the binding is related to selective norepinephrine distribution).

In conclusion, initial results of a series of novel ^{99m}Tc-labeled MIBG derivatives showed mixed results. At least in principle, it appears feasible to replace the iodine of MIBG with a $[Tc^{v}O]^{3+}N_2S_2$ complex. The heart uptake in rats for this series of compounds is relatively low (about one-eighth of that of MIBG). The other challenge is that the ligand may form several isomers of ^{99m}Tc complexes, resulting in differential biodistribution in vivo We are currently preparing additional compounds to ameliorate the deficiencies mentioned above, and we remain optimistic that agents with desirable properties could be developed in the future for imaging myocardial sympathetic neuronal functions

ACKNOWLEDGMENT

We thank Susan West and Laura Danich for their assistance in preparing the manuscript. This work was supported by the U.S. grants awarded by the U.S. Department of Energy (DOE-ER61657) and the National Institutes of Health (NS 18509).

LITERATURE CITED

(1) Wieland, D. M., Wu, J.-l., Brown, L. E., Mangner, T. J., Swanson, D. P., and Beierwaltes, W. H. (1980) Radiolabeled adrenergic neuron-blocking agents: adrenomedullary imaging with [^{131}I]iodobenzylguanidine. *J. Nucl. Med. 21*, 349−353.

(2) Glowniak, J. V., Kilty, J. E., Amara, S. G., Hoffman, B. J., and Turner, F. E. (1993) Evaluation of metaiodobenzylguanidine uptake by the norepinephrine, dopamine and serotonin transporters. *J. Nucl. Med. 34*, 1140−1146.

(3) Wieland, D. M., Mangner, T. J., Inbasekaran, M. N., Brown, L. E., and Wu, J.-l. (1984) Adrenal medulla imaging agents: a structure-distribution relationship study of radiolabeled aralkylguanidines. *J. Med. Chem. 27*, 149−155.

(4) Shapiro, B., Sisson, J. C., Shulkin, B. L., Gross, M. D., and Zempel, S. (1995) The current status of meta-iodobenzylguanidine and related agents for the diagnosis of neuro-endocrine tumors [review; 60 refs]. *Q. J. Nucl. Med. 39*, 3−8.

(5) Wieland, D. M., Brown, L. E., Rogers, W. L., Worthington, K. C., Wu, J.-L., Clinthorne, N. H., Otto, C. A., Swanson, D.

P., and Beierwaltes, W. H. (1981) Myocardial imaging with a radioiodinated norepinephrine storage analogue. *J. Nucl. Med. 22*, 22−31.

(6) Sisson, J. C., Wieland, D. M., Sherman, P., Mangner, T. J., Tobes, M. C., and Jacques, J., S. (1987) Metaiodobenzylguanidine as an index of the adrenergic nervous system integrity and function. *J. Nucl. Med. 28*, 1620−1624.

(7) McGhie, A. I., Corbett, J. R., Akers, M. S., Kulkarni, P., Sills, M. N., Kremers, M., Buja, M. L., Durant-Reville, M., Parkey, R. W., and Willerson, J. T. (1991) Regional cardiac adrenergic function using I-123 *meta*-iodobenzylguanidine tomographic imaging after acute myocardial infarction. *Am. J. Cardiol. 67*, 236−242.

(8) Kline, R. C., Swanson, D. P., Wieland, D. M., Thrall, J. H., Gross, M. D., Pitt, B., and Beierwaltes, W. H. (1981) Myocardial imaging in man with I-123 metaiodobenzylguanidine. *J. Nucl. Med. 22*, 129−132.

(9) Dae, M. W., O′Connell, J. W., Botvinick, E. H., and Michael, C. (1995) Acute and chronic effects of transient myocardial-ischemia on sympathetic-nerve activity, density, and norepinephrine content. *Cardiovasc. Res. 30*, 270−280.

(10) Demarco, T., Dae, M., Yuengreen, M. S. F., Kumar, S., Sudhir, K., Keith, F., Amidon, T. M., Rifkin, C., Lau, D., Botvinick, E. H., and Chatterjee, K. (1995) I-123 metaiodobenzylguanidine scintigraphic assessment of the transplanted human heart: evidence for late reinnervation. *J. Am. Coll. Cardiol. 25*, 927−931.

(11) Merlet, P., Caussin, C., Poiseau, E., Piot, O., Mazière, B., and Syrota, A. (1996) In vivo assessment of neurotransmitter system in cardiovascular diseases. Clinical issues [review]. *Q. J. Nucl. Med. 40*, 108−120.

(12) Dae, M. W. (1995) Scintigraphy of myocardial innervation with metaiodobenzylguanidine (MIBG): is there a clinical application? [editorial]. *J. Nucl. Cardiol. 2*, 151−154.

(13) Fagret, D., Wolf, J.-E., and Cornet, M. (1989) Myocardial uptake of *meta*-[^{123}I]-iodobenzylguanidine ([^{123}I]-MIBG) in patients with myocardial infarct. *Eur. J. Nucl. Med. 15*, 624−628.

(14) Fagret, D., Wolf, J.-E., Vanzetto, G., and Borrel, E. (1993) Myocardial uptake of metaiodobenzylguanidine in patients with left ventricular hypertrophy secondary to valvular aortic stenosis. *J. Nucl. Med. 34*, 57−60.

(15) Merlet, P., Valette, H., Dubois-Randé, J. L., Moyse, D., Duboc, D., Dove, P., Bourguignon, M., Benvenuti, C., Duval, A.-M., Agostini, D., Loisance, D., Castaigne, A., and Syrota, A. (1992) Prognostic value of cardiac metaiodobenzylguanidine imaging in patients with heart failure. *J. Nucl. Med. 33*, 471−477.

(16) Schnell, O., Muhr, D., Dresel, S., Weiss, M., Haslbeck, M., and Standl, E. (1997) Partial restoration of scintigraphically assessed cardiac sympathetic denervation in newly diagnosed patients with insulin-dependent (type 1) diabetes mellitus at one-year follow-up. *Diabetic Med. 14*, 57−62.

(17) Schnell, O., Muhr, D., Weiss, M., Dresel, S., Haslbeck, M., and Standl, E. (1996) Reduced myocardial ^{123}I-metaiodobenzylguanidine uptake in newly diagnosed IDDM patients. *Diabetes 45*, 801−805.

(18) Kung, H. F., Kim, H.-J., Kung, M.-P., Meegalla, S. K., Plössl, K., and Lee, H.-K. (1996) Imaging of dopamine transporters in humans with technetium-99m TRODAT-1. *Eur. J. Nucl. Med. 23*, 1527−1530.

(19) Walovitch, R. C., Hill, T. C., Garrity, S. T., Cheesman, E. H., Burgess, B. A., O'Leary, D. H., Watson, A. D., Ganey, M. V., Morgan, R. A., and Williams, S. J. (1989) Characterization of technetium-99m-L,L-ECD for brain perfusion imaging, Part 1: Pharmacology of technetium-99m ECD in nonhuman primates. *J. Nucl. Med. 30*, 1892−1901.

(20) Léveillé, J., Demonceau, G., DeRoo, M., Rigo, P., Taillefer, R., Morgan, R. A., Kupranick, D., and Walovitch, R. C. (1989) Characterization of technetium-99m-L,L-ECD for brain perfusion imaging, Part 2: biodistribution and brain imaging in humans. *J. Nucl. Med. 30*, 1902−1910.

(21) Walovitch, R. C., Franceschi, M., Picard, M., Cheesman, E. H., Hall, K. M., Makuch, J., Watson, M. W., Zimmerman, R. E., Watson, A. D., and Ganey, M. V. (1991) Metabolism of [^{99m}Tc]-L,L-ethyl cysteinate dimer in healthy volunteers. *Neuropharmacology 30*, 283−292.

(22) Meegalla, S. K., Plössl, K., Kung, M.-P., Chumpradit, S., Stevenson, D. A., Kushner, S. A., McElgin, W. T., Mozley, P. D., and Kung, H. F. (1997) Synthesis and characterization of Tc-99m labeled tropanes as dopamine transporter imaging agents. *J. Med. Chem. 40*, 9−17.

(23) Mock, B. H., and Tuli, M. M. (1987) Influence of specific activity on myocardial uptake of ^{123}I-mIBG in rats. *Nucl. Med. Commun. 9*, 663−667.

(24) Kung, H. F., Molnar, M., Billings, J. J., Wicks, R., and Blau, M. (1984) Synthesis and biodistribution of neutral lipid-soluble Tc-99m complexes that cross the blood-brain barrier. *J. Nucl. Med. 25*, 326−332.

(25) Kung, H. F., Yu, C. C., Billings, J. J., Molnar, M., and Blau, M. (1985) Synthesis of new bis-aminoethanethiol (BAT) derivatives: possible ligands for Tc-99m brain imaging agents. *J. Med. Chem. 28*, 1280−1284.

(26) Biedler, J. L., Helson, L., and Sprengler, B. A. (1973) Morphology and growth, tumorigenicity and cytogenetics of human neuroblastoma cells in continuous culture. *Cancer Res. 33*, 2643−2652.

(27) Vaidyanathan, G., Zhao, X.-G., Strickland, D. K., and Zalutsky, M. R. (1997) No-carrier-added iodine-131-FIBG: evaluation of an MIBG analogue. *J. Nucl. Med. 38*, 330−334.

(28) Gu, H., Wall, S. C., and Rudnick, G. (1994) Stable expression of biogenic amine transporters reveals differences in inhibitor sensitivity, kinetics, and ion dependence. *J. Biol. Chem. 269*, 7124−7130.

(29) Monache, G. D., Botta, B., Delle Monache, F., Espinal, R., De Bonnevaux, S. C., De Luca, C., Botta, M., Corelli, F., and Carmignan, M. (1993) Novel hypotensive agents from Verbesina caracasana. 2. Synthesis and pharmacology of caracasanamide. *J. Med. Chem. 36*, 2956−2963.

(30) Oya, S., Plössl, K., Kung, M.-P., Stevenson, D. A. and Kung, H. F. (1998) Small and neutral TcO(V) BAT, bisaminoethanethiol (N_2S_2) complexes for developing new brain imaging agents. *Nucl. Med. Biol. 25*, 135−140.

(31) Ohmomo, Y., Francesconi, L. C., Kung, M.-P., and Kung, H. F. (1992) New conformationally restricted [^{99m}Tc]N_2S_2 complexes as myocardial perfusion imaging agents. *J. Med. Chem. 35*, 157−162.

(32) Vaidyanathan, G., and Zalutsky, M. R. (1993) No-carrier-added synthesis of *meta*-[^{131}I]iodobenzylguanidine. *Int. J. Radiat. Appl. Instrum., Part A, Appl. Radiat. Isot. 44*, 621−628.

(33) Vaidyanathan, G., and Zalutsky, M. R. (1995) No-carrier-added *meta*-[^{123}I]iodobenzylguanidine: synthesis and preliminary evaluation. *Nucl. Med. Biol. 22*, 61−64.

BC970207Q

Synthesis and Characterization of a Photoactivatable Glycoaryldiazirine for Surface Glycoengineering

Yann Chevolot,*,† Odile Bucher,‡ Didier Léonard,† Hans Jörg Mathieu,† and Hans Sigrist‡

Département des Matériaux, LMCH, Ecole Polytechnique Fédérale de Lausanne (EPFL), CH-1015 Lausanne, Switzerland, and CSEM (Centre Suisse d'Electronique et de Microtechnique SA), Jaquet-Droz 1, CH-2007 Neuchâtel, Switzerland . Received May 12, 1998; Revised Manuscript Received October 15, 1998

Biological systems make considerable use of specific molecular interactions. Many biomolecules involved in biorecognition are glycosylated, the carbohydrate moiety playing an essential role. Controlled surface glycoengineering is thus of crucial importance in biosensing, cell guidance, and biomedical applications. This study describes the synthesis of an aryldiazirine-derivatized galactose and the functionalization of surfaces by carbohydrates using photochemical immobilization techniques. A photoactivatable glycosylated reagent was synthesized by addition of thiogalactopyranose to the maleimide group of *N*-[*m*-[3-(trifluoromethyl)diazirin-3-yl]phenyl]-4-maleimidobutyramide (MAD) to give *N*-[*m*-[3-(trifluoromethyl)diazirin-3-yl]phenyl]-4-[3-thio (1-D-galactopyranosyl)succinimidyl]butyramide (MAD-Gal). The structure of the newly synthesized molecule was confirmed by UV spectroscopy, photoactivation, ^{1}H NMR, and ^{13}C NMR. MAD-Gal was immobilized on thin diamond films by photoactivation of the diazirine function (350 nm). Surface modification was investigated by XPS (X-ray photoelectron spectroscopy) and ToF-SIMS (time-of-flight secondary ion mass spectrometry). Imaging ToF-SIMS was applied to detect glycopatterns generated by mask-assisted lithography.

INTRODUCTION

Biological systems make considerable use of surface glycosylation. Indeed glycosylated molecules are involved in, for example, cell recognition (including species discrimination), blood group typing, blood coagulation cascade, and asialoglycoprotein recognition (*1*−*3*). Tissue engineering requires control of specific cell receptor interactions at material surfaces through oriented immobilization of biologically active molecules such as carbohydrates.

Carbohydrate immobilization is reported in the literature for galactose (*4*), melibiose (*5*), mannose (*5, 6*), lactose (*7*), starch (*8*), lactosaminide (*9*), and heparin (*5, 10*−*15*). This has been achieved mainly by thin-film adsorption (weak interactions) or by covalent binding. Adsorption of molecules through weak interactions (ionic in the case of heparin (*13*)) may reverse with time. Covalent immobilization was reported for polymer substrates by divinyl sulfone activation for mannose (*5*), reductive amination for melibiose on polyacrylamide (*5*), the bisorane method for lactose and *N*-acetylglucosamine (*5*), CNBr activation for heparin (*5*), reductive amination of nitrous acid treated heparin (*13*), and copolymerization for galactose (*4)* and lactosaminide (*9*). Galactose-derivatized polymers were used for the study of hepatocyte adhesion (e.g. PVLA,[1] poly(vinylbenzyl-β-D-lactonamide) (*7, 16*)). However, this kind of immobilization is not surface specific, unless coated. Furthermore, it is performed on polymeric materials and is not addressable. Photochemical procedures were applied for heparin (*10*−*12, 14, 15*) and dermatan (*14*) immobilization. Photoactivatable reagents generate very reactive intermediates that allow immobilization of the molecules onto various substrates, as well as addressable immobilization. Erdtmann et al. (*14*) used a nitrene generating reagent to achieve immobilization of heparin and dermatan on cellulose membranes. The membranes were first modified with 4-azido-1-fluoro-2-nitrobenzene. Guire (*10, 11*) immobilized heparin on polyurethane: albumin was first photoimmobilized on polyurethane, and heparin was then linked to albumin using 1-ethyl-3-[3-(dimethylamino)-propyl]carbodiimide chemistry. These strategies combine thermochemistry and photochemistry for surface immobilization. The development of a single step photochemical process would provide a more convenient tool for light addressable surface patterning.

Utilizing diazirine as a photoactivatable function, a reactive carbene is generated by thermochemical or light activation. The carbene may insert into C−H, C−C, C═C, N−H, O−H, and S−H bonds (*17*). Carbene-mediated target molecule binding has been reported for TiO_2/SiO_2 (*18*), silicon (*19, 20*), silicon nitride (*19*−*21*), diamond (*19, 20, 22*) and FEP-OH (hydroxylated fluorinated ethyleneepropylene) (*23*). Shergold et al. (*22*) used diazomethane, and Gao et al. (*18*) used an aryldiazirine-derivatized bovine serum albumin (T-BSA), while other investigations were carried out with the photoreagent MAD (*19*−*21, 23, 24*) (Figure 1). The energy used for photolabel

* To whom correspondence should be addressed. Phone: ++41 21 693 4124. Fax: ++41 21 693 3946. E-mail: chevolot@lmch.dmx.epfl.ch.

† Ecole Polytechnique Fédérale de Lausanne.

‡ Centre Suisse d'Electronique et de Microtechnique SA.

[1] Abbreviations: MAD, *N*-[*m*-[3-(trifluoromethyl)diazirin-3-yl]phenyl]-4-maleimidobutyramide; MAD-Gal, *N*-[*m*-[3-(trifluoromethyl)diazirin-3-yl]phenyl]-4-[3-thio(1-D-galactopyranosyl)-succinimidyl]butyramide; BSA, bovine serum albumin; FEP-OH (hydroxylated fluorinated ethyleneepropylene); EDTA, ethylenediaminetetraacetic acid; TFA, trifluoroacetic acid; PVLA, poly(vinylbenzyl-β-D-lactonamide); XPS, X-ray photoelectron spectroscopy; ToF-SIMS, time-of-flight secondary ion mass spectrometry; UHV, ultrahigh vacuum; CVD, chemical vapor deposition; fwhm, full width half maximum; ROI, region of interest.

10.1021/bc980050h CCC: $18.00 © 1999 American Chemical Society
Published on Web 02/04/1999

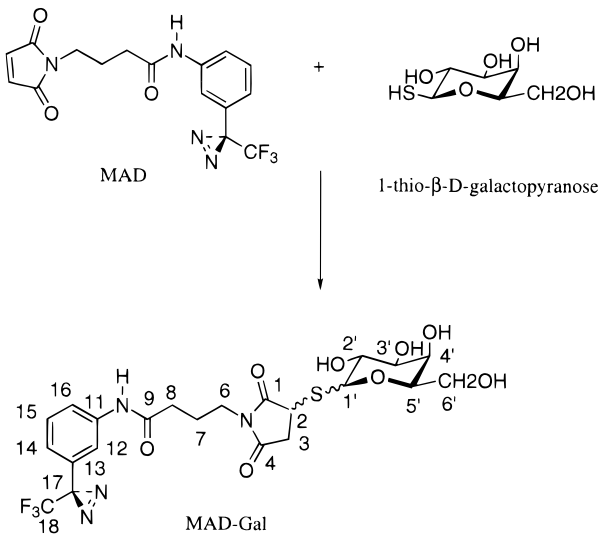


Figure 1. Reaction of 1-thio-β-D-galactopyranose with MAD, yielding *N*-[*m*-[3-(trifluoromethyl)diazirin-3-yl]phenyl]-4-(3-thio-(1-D-galactopyranosyl)succinimidyl)butyramide (MAD-Gal).

activation does not impair biological functions ((*24*) and unpublished results).

This work presents the derivatization of MAD with 1-thio-β-D-galactopyranose to give *N*-[*m*-[3-(trifluoromethyl)diazirin-3-yl]phenyl]-4-[3-thio(1-D-galactopyranosyl)-succinimidyl]butyramide (Figure 1). The parent molecule MAD provides a maleimide function, allowing the reaction with thiogalactopyranose. Both MAD and its derivative MAD-Gal contain the diazirine function that yields carbenes upon light activation at 350 nm. The synthesis, purification, and bulk analysis of MAD-Gal are described.

MAD-Gal was then immobilized on diamond. Due to its physical properties and biocompatibility (*25*−*27*), diamond and diamond-like carbon are widely used in biomedical applications. For example, thin film coatings are applied to stents and carbon is identified as a good substrate for biosensor applications (*28*). Therefore, surface modification of diamond functionalized by biological molecules to obtain specific interaction with analytes or cells is of great interest. Structured surfaces (photopatterning) can be used for probing or controlling interactions of cells or macromolecules at the surfaces of materials (i.e. implants and biosensing). The immobilization of MAD-Gal on diamond is confirmed by surface analysis techniques such as XPS (X-ray photoelectron spectroscopy) and ToF-SIMS (time-of-flight secondary ion mass spectrometry). Imaging ToF−SIMS is applied to detect glycopatterns generated by mask-assisted lithography.

EXPERIMENTAL SECTION

Materials. *Synthesis and Characterization.* MAD was synthesized according to Collioud et al. (*24*). 1-Thio-β-D-galactopyranose was purchased from Aldrich. Uvasol quality solvents (Merck) were used for chemical reactions. The HPLC grade solvents were purchased from Romil (Switzerland). Trifluoroacetic acid (TFA) was purchased from Sigma. MAD-Gal was purified by HPLC using a wide-pore butyl (C4) Bakerbond standard column (dimensions 4.6 × 250 mm; particle size 5 mm; Baker Inc., Phillipsburg, NJ) on a Bio-Cad system. The 1D ^{1}H NMR, 2D ^{1}H/^{1}H COSY NMR, ^{13}C NMR, and DEPT ^{13}C NMR spectra were collected at the University of Bern on a Bruker 500 MHz NMR using D_2O as solvent.

Surface Analysis. XPS analysis was performed under UHV conditions (~10^{-9} Torr) using a PHI 5500 (Perkin-Elmer, USA) system equipped with a hemispherical analyzer and a nonmonochromatized Mg Kα radiation source. The analyzed area was 0.12 mm^2, and spectra were recorded with a takeoff angle of 45° (with respect to the surface). Pass energies used for survey scans and high-resolution elemental scans were 93.5 and 23.5 eV, respectively. No sample charge-up was observed. For each sample, three areas were analyzed. For evaluation of the XPS spectra, the absolute peak areas were calculated using a parabolic interpolation routine, and background subtraction was applied. Resulting values were normalized to the step size to give the intensity in electronvolts per second. Sensitivity factors (S_i) were 0.296, 0.711, 0.477, 1.000, and 0.570 (*29*) for C 1s, O 1s, N 1s, F 1s, and S 2p, respectively. Atomic percentages of selected elements (x) were calculated using the above sensitivity factors and the equation: $X\% = (I_x/S_x)/(\sum I_i/S_i)$. Diamond chemical shift was chosen as the reference at 284.2 eV (*30*). It was confirmed with gold as internal standard.

ToF-SIMS was performed on commercial equipment from PHI-EVANS & Associates (described in (*31, 32*)) equipped with a pulsed FEI Ga^+ ion gun operated at 15 kV for high mass resolution. The sample surface was biased ±3 kV with respect to the grounded extraction electrode for positive/negative mode SIMS, respectively. The 800−850 pA dc ion beam current was pulsed at a 5 kHz repetition rate (pulse width of about 8 ns, as measured with the unbunched beam). The analyzed area was estimated to be a square of 84 μm × 84 μm. Spectra were acquired in the high mass resolution mode (bunched beam). The total ion dose for a typical spectrum was on the order of 9 × 10^{11} ions/cm^2, which is within the so-called "static" conditions (*33*). The mass resolution obtained for $Si^{+/-}$ on a Si wafer was $m/\Delta m$ > 3600 in the positive mode and >3000 in the negative mode. Normalized values were calculated by dividing the absolute intensity of secondary ions by the corrected total intensity (=total intensity from which intensities of H^{+-} of all inorganic peaks and of the main peaks of ubiquitous contaminants were subtracted). Images were also collected in the high mass resolution mode. The high mass resolution conditions were similar to those described above except for analyzed area (180 μm × 180 μm) and analysis time (20 min), but the ion dose was similar (8 × 10^{11} ions/cm^2).

Methods. *Synthesis of N-[m-[3-(Trifluoromethyl)diazirin-3-yl]phenyl]-4-[3-thio(1-D-galactopyranosyl)succinimidyl]butyramide.* 1-Thio-β-D-galactopyranose (1.5 mg) was dissolved in 150 μL of buffer A (20 mM citric acid, 35 mM Na_2HPO_4, 108 mM NaCl, 1 mM ethylenediaminetetraacetic acid (EDTA)) and 150 μL of ethanol. MAD (3.3 mg) was dissolved in 150 μL of ethanol and an additional 150 μL of buffer A. Both solutions were mixed. The mixture was stirred and allowed to react at room temperature for 90 min, to give MAD-Gal. The product was purified by HPLC. The HPLC flow rate was 2 mL/min. For gradient elution (0 min, 100% A; 5 min, 100% A; 20 min, 70% A; 30 min, 0% A; 40 min, 0% A), solvent B was added to solvent A (solvent A, 0.1% TFA in water; solvent B, 0.1% TFA in acetonitrile/water (4:1 by volume)). Detection was performed at 254 nm and fractions of the eluant were collected. ^{13}C NMR (D_2O chemical shift (δ) in parts per million): 179.14, 178.40, 177.99, 177.86, 173.30, 137.79, 129.53, 129.38, 122.46, 121.84, 118.32, 84.42, 84.27, 78.99, 78.91, 73.84, 73.66, 69.73, 69.68, 68.58, 68.49, 60.80, 60.69, 39.61, 38.66, 38.46, 37.71, 35.83, 33.57, 22.68, 22.57.

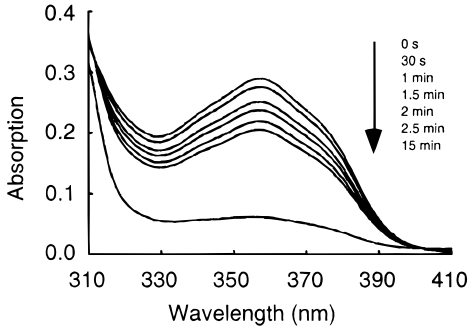


Figure 2. UV absorption spectra of MAD-Gal before and after irradiation for differing lengths of irradiation time.

Immobilization of MAD-Gal on Diamond. Hot filament CVD deposited thin-film diamond (*34*) was used as the substrate to exploit MAD-Gal immobilization. Pristine samples (5×5 mm^2) were washed (5 min ultrasonic bath in hexane and in ethanol) and dried for 2 h at room temperature under vacuum (~6 mbar). Then, MAD-Gal (10 μL, 0.25 mM in ethanol) was deposited as a droplet released from a syringe. The samples were dried for 2 h at room temperature under vacuum (30−40 mbar). They were irradiated for 20 min with the Stratalinker light source (0.95 mW/cm^2) and washed by ultrasound treatment twice in ethanol (5 min) and twice in hexane (5 min). The investigated samples are referenced as follows: **A** (washed surface), **B** (MAD-Gal deposited, no illumination performed before final washing), and **C** (MAD-Gal deposited, illumination and final washing). Patterning was performed with a mask consisting of 40 μm × 40 μm square windows separated by 40 μm bridges. MAD-Gal was deposited on the diamond surface before mask-assisted illumination and final washing.

RESULTS AND DISCUSSION

Chemical Characterization of MAD-Gal. The reaction between 1-thio-β-D-galactopyranose and MAD, yielding MAD-Gal, is displayed in Figure 1. HPLC analysis of the educts revealed a retention time of 37.41 min for MAD and approximately 15 min for 1-thio-β-D-galactopyranose, which was detected with 5,5′-dithiobis(2-nitrobenzoïc acid) (*35*). HPLC separation of the reaction mixture revealed a major peak with a retention time of 33.68 ± 0.07 min (88.2% of the total area). Minor byproducts with retention times of 33.06 ± 0.02 and 35.61 ± 0.02 min (0.6% and 11.2% of the total area, respectively), were observed. We suggest that they are products of the reaction of molecular oxygen with the thiols. During concentration of the eluant, thermal degradation may occur. Indeed, a peak with retention time of 35.99 min (10% area) was observed upon rechromatography of concentrated MAD-Gal. To avoid any thermal or light degradation of MAD-Gal, it was stored at −20 °C in the dark. MAD has shown to be stable over a period of at least 8 months under such conditions (*24*). In the immobilization experiments, MAD-Gal was dissolved in ethanol. Exposure to artificial light, unfiltered sunlight, or heat (over 30 °C) was avoided. These solutions were also stored at −20 °C.

The UV absorption spectrum of the product corresponding to the peak with the retention time of 33.68 min (major peak) shows an absorption band at 357 nm, characteristic of the diazirine function (*23*). Figure 2 indicates that the absorbance diminished with increasing light exposure at 357 nm, demonstrating exposure time dependent photoactivation and, thus, conversion of the diazirines into carbenes.

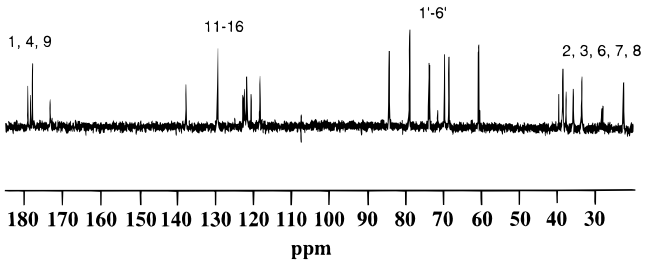


Figure 3. ^{13}C NMR overview spectrum of MAD-Gal.

In Figure 1, carbon and hydrogen atoms are numbered to facilitate the discussion of the NMR spectra. The ^{13}C NMR spectrum showed four separated areas corresponding to the ^{13}C nuclei of the amide function, the aromatic ring, the carbohydrate moiety, and the alkyl chain, respectively (Figure 3). The split signals of carbons 1, 2, 3, 4, 6, and 7 and of the carbohydrate moiety indicate the occurrence of two stereoisomers detected in similar proportions. Indeed, the sulfhydryl groups can attack the maleimide group above or below the plane of the ring, leading to two configurations of carbon 2. Consequently, the nuclei of both compounds in the vicinity of carbon 2 can appear at different chemical shifts. The DEPT (distortionless enhancement through polarization transfer) sequence analysis demonstrated that the peaks of the alkyl chain (22.57, 22.68, and 33.57 ppm) and C6′ (60.69 and 60.37 ppm, corresponding to the two isomers) correspond to secondary carbons. Other peaks appearing at 28.32, 27.99, 60.37, 71.52, 120.68, and 122.86 ppm were attributed to undefined contaminations.

The ^{1}H NMR spectrum of the purified product confirmed the presence of aromatic (6.5−7.5 ppm), alkyl (3.2−1.6 ppm), and carbohydrate protons (4.8−3.4 ppm) (Figure 4a). The ^{1}H/^{1}H COSY-NMR spectrum of MAD-Gal is displayed in Figure 4b. The two-proton signal at 1.8 ppm was connected with the peaks at 2.3 and 3.4 ppm. It was attributed to proton 7. The peak at 2.3 ppm was also a two-proton signal. Peaks at 2.3 and 3.4 ppm were attributed to proton 8 and proton 6, respectively. The two peaks at 4.1 and 4.2 ppm corresponded to $^1/_2$ of a proton signal each. The former was connected to the signal at 2.7 and 3.14 ppm, whereas the latter was connected to the peaks appearing at 2.8 and 3.14 ppm. According to the integration, peaks at 2.7 and 2.8 ppm represented the signal of a $^1/_2$ proton each. The wide peak at 3.14 ppm was a one-proton signal. Thus, the peaks at 4.1 and 4.2 ppm corresponded to H-2 in two configurations. The peaks at 2.7 and 2.8 ppm corresponded to H-3a (one for each stereoisomer), and the peak at 3.14 ppm consisted of two peaks (shown by COSY) and corresponded to H-3b. According to the integration, the peak at 4.4 ppm was also $^1/_2$ of a proton signal. The chemical shift corresponded to H-1′ of β-thiogalactopyranose. H-1′ for the second stereoisomer (also β) was at 4.7 ppm, within the water signal. Peaks between 3.9 and 3.4 ppm corresponded to protons 2′, 3′, 4′, and 5′.

In summary, the results confirmed the structure of MAD-Gal. NMR analyses sustain that the final product is a mixture of two stereoisomers detected approximately in the same quantities.

Surface Photobonding and Surface Analysis. MAD-Gal was deposited on washed diamond surfaces. The solvent was removed under vacuum to avoid the reaction of carbenes with solvent molecules. Next, the diazirines were activated by light (350 nm) and modified surfaces were extensively washed. It was expected that

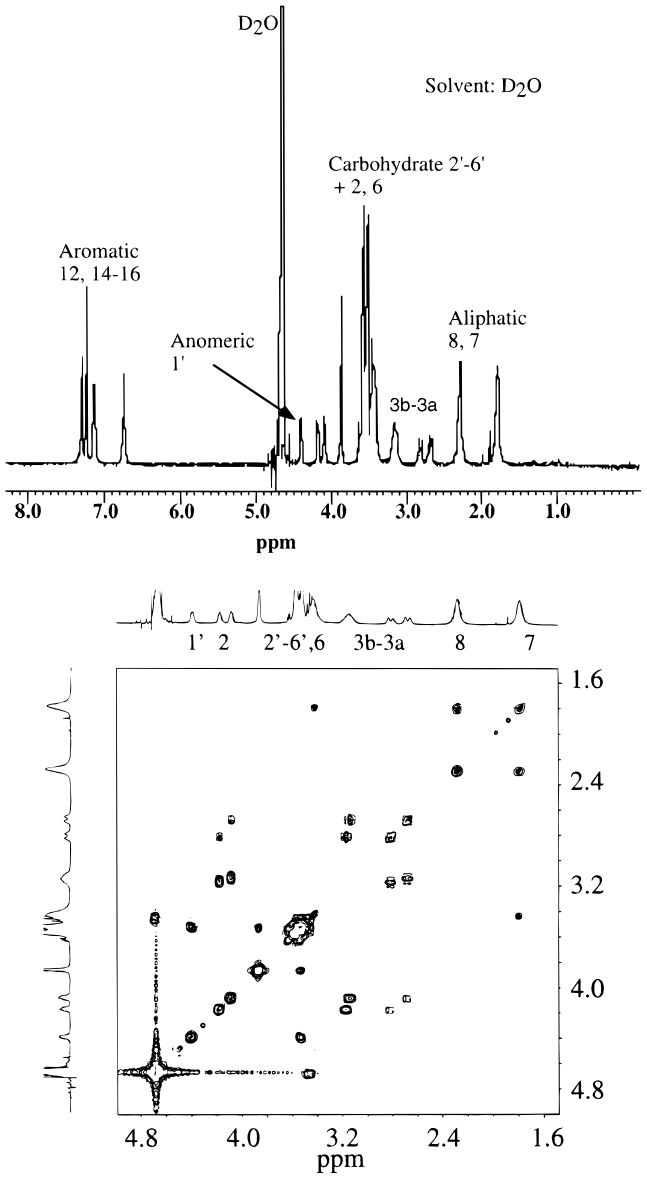


Figure 4. (a, top) ^{1}H NMR spectrum of MAD-Gal. (b, bottom) ^{1}H/^{1}H NMR COSY NMR spectrum of MAD-Gal.

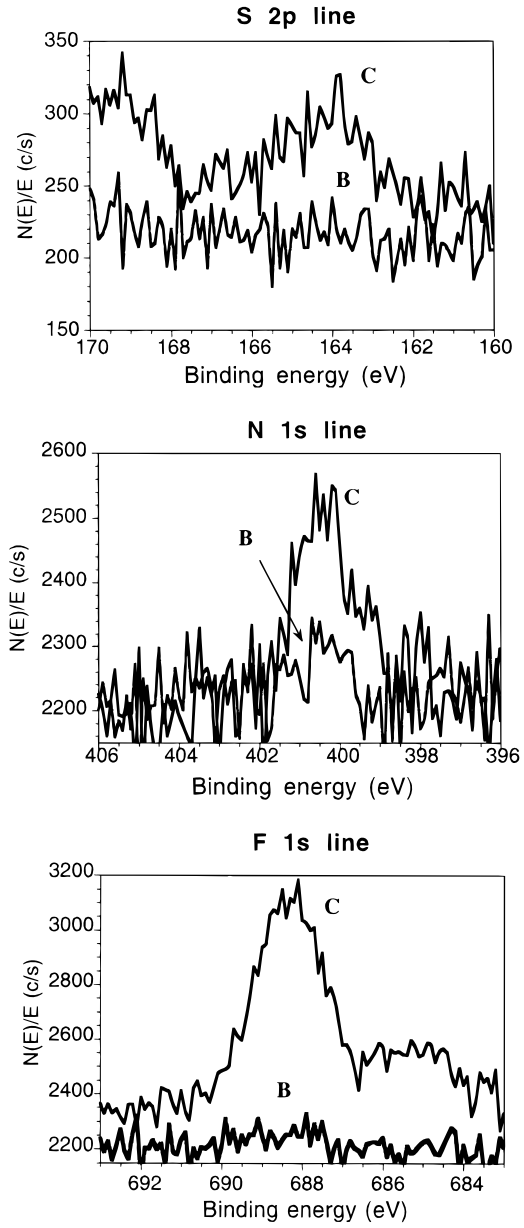


Figure 5. (a, top) S 2p XPS spectra of samples **B** and **C** (**B**, MAD-Gal on diamond, not irradiated, washed; **C**, MAD-Gal on diamond, irradiated and washed). The chemical shift corresponds to a C−S bond. S is only detected on sample **C**. (b, middle) N 1s XPS spectra of samples **B** and **C**. Nitrogen is only present on sample **C** (**B**, MAD-Gal on diamond, not irradiated, washed; **C**, MAD-Gal on diamond, irradiated and washed). The chemical shift corresponds to an amide. (c, bottom) F 1s XPS spectra of samples **B** and **C** (**B**, MAD-Gal on diamond, not irradiated, washed; **C**, MAD-Gal on diamond, irradiated and washed). Fluorine is only present on sample **C**. The chemical shift corresponds to a C−F bond. F is only detected on sample **C**.

this final washing step removed most of the physically adsorbed but not the covalently bound MAD-Gal molecules.

XPS wide scans of samples **A** and **B** exhibited intense photoelectron peaks at about 285 and 532 eV corresponding to the C 1s and O 1s lines. For sample **B**, on one area only, very low intensity peaks were observed around 400 and 688 eV corresponding to the N 1s and F 1s lines, respectively. According to the structure of the molecule (Figure 1), oxygen, fluorine, nitrogen, and sulfur were expected to be detected on diamond surfaces with grafted MAD-Gal. For sample **C**, XPS wide scans exhibited intense peaks corresponding to C 1s (285 eV), O 1s (532 eV), and F 1s (688 eV). Lower intensity peaks were observed at 165 and 400 eV corresponding to S 2p and N 1s, respectively. The binding energy of the S 2p line confirmed a C−S bond (Figure 5a) (*36*, *37*), and that of the N1s line corresponded to the chemical shift of an amide function (Figure 5b) (*38*). The F 1s chemical shift confirmed the presence of C−F (Figure 5c) (*36*, *38*). Results shown in parts a and b of Figure 5 indicated that XPS analysis of N and S on sample **C** was close to the instrumental detection limit (10^{12}−10^{13} molecules/cm^2).

The elemental compositions of samples **A**, **B**, and **C** are displayed in Table 1. For sample **A**, oxygen has an atomic percentage of 6%. Its presence at diamond surfaces can be explained by the fact that, during the hot filament CVD process, oxygen was incorporated to give a very complex surface with various functionalities (*39*, *40*): lactone, ether, carboxylic acid, and alcohol. The presence of oxygen on diamond surfaces was consistent with the various contributions in the C 1s envelope (data not shown) and the full width half maximum (fwhm) of diamond contribution to C 1s (*39*). Except on one area, the sample **B** spectrum did not exhibit fluorine or

Table 1. XPS C, O, N, F, and S Atomic Percentages for Samples A, B, and C[a]

	A	B	C
C	93.9 ± 0.6	92.3 ± 1.39	88.7 ± 1.7
O	6.0 ± 0.6	7.5 ± 1.05	9.8 ± 1.61
N	0 ± 0	0.42*	0.6 ± 0.07
F	0 ± 0	0.16*	0.8 ± 0.19
S	0 ± 0	0 ± 0	0.08 ± 0.07

[a] Mean values for three areas except for values marked with an asterisk, for which only one area is displayed (see text). The investigated samples are denoted as follows: **A**, washed surface; **B**, MAD-Gal deposited, no illumination performed before final washing; **C**, MAD-Gal deposited, illumination and final washing.

Table 2. Negative Mode ToF-SIMS Corrected Total Intensity and Normalized ToF-SIMS Intensities (‰) for Samples A, B and C (Average of Three Spectra)[a]

	A	B	C
cor tot.[b]	313 ± 12.9	409 ± 11.9	408 ± 20.24
C^-	74 ± 2.5	108 ± 1.6	62.9 ± 1.2
O^-	200 ± 7.2	162 ± 2.1	184.9 ± 0.7
F^-	29 ± 2.53	6 ± 0.33	197 ± 3.1
CF_3^-	7 ± 0.75	0.7 ± 0.02	8.59 ± 0.29
S^-	1.87 ± 0.18	0.9 ± 0.05	10.3 ± 0.05
SO_4^-	0.78 ± 0.20	1.34 ± 0.07	1.47 ± 0.02
$C_4H_4NO_2^-$	0.07 ± 0.01	0.08 ± 0.01	1.05 ± 0.06
$C_5H_5O_2S^-$	0.11 ± 0.01	0.03 ± 0.00	0.15 ± 0.02

[a] The investigated samples are denoted as follows: **A**, washed surface; **B**, MAD-Gal deposited, no illumination performed before final washing; **C**, MAD-Gal deposited, Illumination and final washing. [b] Negative mode ToF-SIMS corrected total intensity ($\times 10^4$).

nitrogen, illustrating the efficiency of the washing step to remove physisorbed molecules. O and C atomic percentages were intermediate between those of samples **C** and **A**. The elemental composition of sample **C** was characterized by significant amounts of fluorine and nitrogen at the surface. Sulfur was also detected, but at a very low intensity, and the oxygen content was higher for sample **C** than for sample **B**. XPS data revealed an F/N ratio of 1.3, which was close to the theoretical value (1.5). However, the F/S ratio was higher than 3, indicating a possible partial loss of sulfur during XPS analysis.

Table 2 displays the corrected total intensity ($\times 10^4$, denoted "cor tot.") of negative mode ToF-SIMS spectra and normalized ToF-SIMS intensities (‰) of selected peaks for samples **A**, **B**, and **C**. F^-, CNO^- (an amide related ion), and CF_3^- fragments were related to the MAD moiety of the molecule (*20*). $C_4H_4O_2N^-$ (*20*) was identified as part of the succinimidyl group. S^- (not correlated to SO_4^-) and $C_5H_5O_2S^-$ were specifically related to the carbohydrate moiety (*41*, *42*). It should be noted that the mass resolution allowed the separation between S^- and O_2^- and between the peak at 129.01 amu ($C_5H_5O_2S^-$) and those appearing at 129.06 and 129.13 amu (not illustrated). Due to its high sensitivity, ToF-SIMS analysis revealed F where XPS analysis failed (samples **A** and **B**). Moreover, S was easily detected compared to XPS for sample **C**. All the characteristic ions of MAD-Gal showed lower intensities on sample **B** than on sample **C**. The results further confirmed that the washing procedure removed most of the physisorbed molecules.

The oxygen XPS signal and oxygen-containing ToF-SIMS ions were expected characteristic fragments of MAD-Gal. The data presented here (Tables 1 and 2) are of low information value, due to signals contributed by the substrate.

MAD-Gal surface patterning was performed using contact mode, mask-assisted lithography. Figure 6 presents the image of F^- ions and documents addressable immobilization of the photoreagent MAD-Gal. The figure shows three regions-of-interest (ROI) areas from which spectra were collected. Table 3 displays the normalized ToF-SIMS intensities (‰) of MAD-Gal characteristic ions for the three ROIs. ROIs 1 and 3 were light-exposed, whereas ROI 2 was a masked region. Areas where characteristic signatures of MAD-Gal were observed corresponded to the light-exposed domains. However, it was noted that the nonexposed ROI 2 exhibited detectable amounts of MAD-Gal fragments (higher than those observed on sample **B**), indicating the limitations of contact mode, mask-assisted patterning.

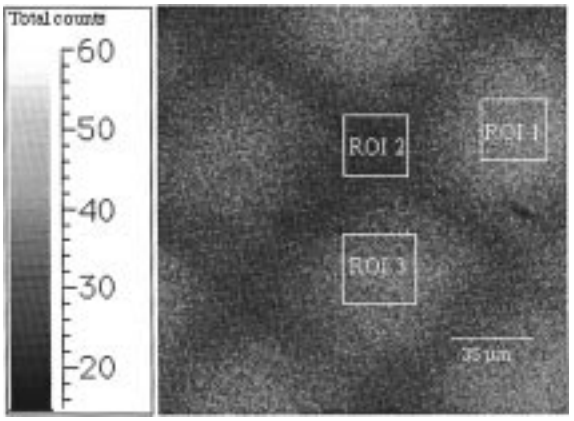


Figure 6. Negative mode ToF-SIMS image of F^- after mask-assisted patterning of MAD-Gal on thin film diamond. The pattern was generated with a mask consisting of 40 μm × 40 μm square windows separated by 40 μm bridges. The mask was placed on a MAD-Gal-coated diamond surface before irradiation. Negative ToF-SIMS images were recorded after irradiation and final washing of the surfaces.

Table 3. Negative Mode Normalized ToF-SIMS Intensities (‰) for the Spectra Corresponding to the Three Regions of Interest (ROIs) Displayed in Figure 6[a]

	ROI 1	ROI 2	ROI 3
F^-	141.3	97.7	145.3
CF_3^-	6.6	4.3	5.7
S^-	7.4	3.6	6.2
SO_4^-	1.0	1.1	0.8
CNO^-	12.7	8.8	12.0
$C_4H_4O_2N^-$	0.3	0.2	0.3
$C_5H_5O_2S^-$	0.1	0.01	0.1

[a] ROIs 1 and 3 were light-exposed, whereas ROI 2 was a masked region.

DISCUSSION

Great efforts are made in biomaterial science to generate bioactive surfaces with grafted oriented biomolecules. Molecular orientation is needed for biological interactions with modified surfaces. Carbohydrates are known to be involved in many biological phenomena. Linear and complex carbohydrate structures are present at biosurfaces in specific orientations and in defined structural (3-D) arrangements. In this study, oriented surface immobilization is implicated in the asymmetric molecular structure of MAD-Gal.

Maleimido groups are known to react readily with accessible sulfhydryl groups (*24*). Chemical and structural analyses have demonstrated that the addition of 1-thio-β-D-galactopyranose to MAD occurred at the maleimido group. The reaction produced two stereoisomeric glycosylated photoreagents. No attempts have been made to separate the isomers.

Diamond surfaces possess various types of surface functions (*39*) which figure as candidates for carbene

insertion. Surface analysis techniques provided strong evidence that MAD-Gal was successfully grafted to the diamond surface. The surface analyses and related phenomena are described in detail in (*42*). They also indicated that the applied wash procedure removed most but not all of the physically adsorbed molecules. A total of 10^{-8} mol/cm^2 (6.02×10^{15} molecules/cm^2) of MAD-Gal was deposited at the sample surfaces. The XPS signal of the molecule after photoimmobilization and washing was close to the detection limit of this technique. Therefore, the surface density of the molecule was estimated to be $10^{12}-10^{13}$ molecules/cm^2 (*20*). The efficiency of the grafting is estimated to be between 1% and 1‰. Optimization of the grafting will be considered. However, for future purposes (i.e. biological applications), such densities should not be a problem. Biomolecules can exhibit biological activity at very low concentration, as demonstrated by Massia et al. (*43*) in the case of surface-grafted peptides.

ToF-SIMS imaging allowed visualization of topically addressed MAD-Gal. However, the patterns obtained were not as distinct as expected. A possible explanation is the position of the mask during the illumination, which was positioned above but not close enough to the surface, and the diffraction of light under the mask.

In summary, the new photoreagent MAD-Gal was successfully synthesized as demonstrated by ^{13}C NMR, ^{1}H NMR, and UV absorption spectroscopy. Photoimmobilization of MAD-Gal on diamond surfaces via diazirine insertion was illustrated by XPS and ToF-SIMS surface analyses. The feasibility of surface patterning was demonstrated, although the lateral resolution was limited.

Biological tests are in progress to identify the remaining biological activity of photoimmobilized MAD-Gal molecules. Primary results with rat hepatocyte cultures are encouraging. However, the implicated surface orientation of MAD-Gal awaits further experimental documentation with biological systems.

ACKNOWLEDGMENT

Financial support from the Swiss Priority Program on Material Research is gratefully acknowledged.

LITERATURE CITED

(1) Lee, Y. C., and Lee, R. T. (1995) Carbohydrate-Protein Interaction: Basis of Glycobiology. *Acc. Chem. Res. 28*, 321−327.

(2) Monsigny, M. (1995) Glycotechnologies: les Biotechnologies Douces. *Biofutur 142*, 27−32.

(3) Petrak, K. (1994) Introduction: Physical Basis of Specific Interactions Involving Carbohydrates. *Adv. Drug Deliv. Rev. 13*, 211−213.

(4) Hatanaka, K., Takeshige, H., and Akaike, T. (1994) Synthesis of New Polymer Containing Uridine and Galactose as Pendent Groups. *Carbohydr. Chem. 13*, 603−610.

(5) Hermanson, G. T., Mallia, A. K., and Smith, P. K. (1992) *Immobilized Affinity Ligand Techniques* (G. T. Hermanson, A. K. Mallia, and P. K. Smith, Eds.), pp 158−167, Academic Press, London.

(6) Largent, B. L., Walton, K. M., Hoppe, C. A., Lee, Y. C., and Schnaar, R. L. (1984) Carbohydrate-Specific Adhesion of Alveolar Macrophages to Mannose-Derivatized Surfaces. *Biol. Chem. 259*, 1764−1769.

(7) Kobayashi, K., Kobayashi, A., and Akaike, T. (1994) Culturing Hepatocytes on Lactose Carrying Polystyrene Layer via Asialoglycoprotein Receptor-Mediated Interactions. *Methods Enzymol. 247*, 409−419.

(8) Onyiriuka, E. C. (1996) Modification of Polystyrene Cell Culture Surfaces by Grafting a Thin Film of Starch. *J. Adhes. Sci. Technol. 10*, 617−633.

(9) Kobayashi, K., Akaike, T., and Usui, T. (1994) Synthesis of Poly(N-Acetyl-*β*-Lactosaminide-Carrying Acrylamide): Chemical-Enzymatic Process. *Methods Enzymol. 242*, 226−235.

(10) Guire, P. E. (1990) Method of Improving the Biocompatibility of Solid Surfaces (Bio-Metric Systems, Inc.). U.S. Patent 4,973,493.

(11) Guire, P. E. (1990) Biocompatible Coating for Solid Surfaces (Bio-Metric Systems, Inc.). U.S. Patent 4,979,959.

(12) Anderson, A. B., Enrico, L. S., Melchior, M. J., Pietig, J. A., Tran, L. V., Tran, T. H., and Duquette, P. H. (1994) Photochemical Immobilization of Heparin to Reduce Thrombogenesis. Proceedings of 20th Annual Meeting in conjunction with the 26th International Biomaterials Symposium, Boston (Society of Biomaterials, Ed.), p 75.

(13) Courtney, J. M., Yu, J., and Sundaram, S. (1993) Immobilization of Macromolecules for Obtaining Biocompatible Surfaces. *Immobilised Macromolecules: Application Potentials* (U. B. Sleytr, Ed.), pp 175−193, Springer, London.

(14) Erdtmann, M., Keller, R., and Baumann, H. (1994) Photochemical Immobilization of Heparin, Dermatan Sulphate, Dextran Sulphate and Endothelial Cell Surface Heparan Sulphate onto Cellulose Membrane for the Preparation of Athrombogenic and Antithrombogenic Polymers. *Biomaterials 15*, 1043−1049.

(15) Anderson, A. B., Tran, T. H., Hamilton, M. J., Chudzik, S. J., Hasting, B. P., Melchior, M. J., and Hergenrother, R. W. (1996) Platelet Deposition and Fibrinogen Binding on Surfaces Coated with Heparin or Friction-Reducing Polymers. *Am. J. Neuroradiol. 17*, 859−863.

(16) Adachi, N., Maruyama, A., Ishihara, T., and Akaike, T. (1994) Cellular Distribution of Polymer Particles Bearing Various Densities of Carbohydrate Ligands. *J. Biomater. Sci. Polymer Edn. 6*, 463−479.

(17) Sigrist, H., Collioud, A., Clémence, J. F., Gao, H., Luginbuhl, R., Sanger, M., and Sundarababu, G. (1995) Surface Immobilization of Biomolecules by Light. *Opt. Eng. 34*, 2339−2348.

(18) Gao, H., Sanger, M., Luginbuhl, R., and Sigrist, H. (1995) Immunosensing with Photoimmobilized Immunoreagents on Planar Optical Wave Guides. *Biosensors and Bioelectronics 10*, 317−328.

(19) Léonard, D., Chevolot, Y., Bucher, O., Tang, X. M., Mathieu, H. J., and Sigrist, H. (1997) Aryldiazirine photoimmobilisation on silicon, silicon nitride and diamond substrates studied by XPS and ToF−SIMS. Proceedings of ECASIA, Göteborg (I. Olefjord, L. Nyborg, and D. Briggs, Eds.), pp 135−138, Wiley, Chichester, U.K.

(20) Léonard, D., Chevolot, Y., Bucher, O., Sigrist, H., and Mathieu, H. J. (1998) ToF-SIMS and XPS Study of Photoactivatable Reagents designed for Surface Glycoengineering: Part 1: N-(m-(3-(trifluoromethyl) diazirine-3-yl) phenyl)-4-maleimido-butyramide (MAD) on silicon, silicon nitride and diamond. *Surf. Interface Anal. 26*, 783−792.

(21) Gao, H., Luginbuhl, R., and Sigrist, H. (1997) Bioengineering of Silicon Nitride. *Sens. Actuators, B 38−39*, 38−41.

(22) Shergold, H. L., and Hartley, C. J. (1982) The Surface Chemistry of Diamond. *Int. J. Miner. Process. 9*, 219−233.

(23) Clémence, J. F., Ranieri, J. P., Aebischer, P., and Sigrist, H. (1995) Photoimmobilization of a Bioactive Laminin Fragment and Pattern-Guided Selective Neuronal Cell Attachment. *Bioconjugate Chem. 6*, 411−417.

(24) Collioud, A., Clémence, J. F., Sanger, M., and Sigrist, H. (1993) Oriented and Covalent Immobilization of Target Molecules to Solid Supports: Synthesis and Application of a Light-Activable and Thiols Cross-Linking Reagent. *Bioconjugate Chem. 4*, 528−536.

(25) Dion, I., Baquey, C., and Monties, J. R. (1993) Diamond: the Biomaterial of the 21st Century? *Int J. Artif. Organs 16*, 623−627.

(26) Butter, R. S., and Lettington, A. H. (1995) Diamond-Like Carbon for Biomedical Applications (review). *J. Chem. Vapor Deposition 3*, 182−192.

(27) Tang, L., Tsai, C., Gerberich, W. W., Kruckeberg, L., and Kania, D. R. (1995) Biocompatibility of Chemical-Vapor-Deposited Diamond. *Biomaterials 16*, 483−488.

(28) Göpel, W., and Heiduschka, P. (1995) Interface Analysis in Biosensor Design. *Biosens. Bioelectron. 10*, 853−883.
(29) Perkin-Elmer (1992) *Multi-Technique ESCA Operator's Reference Manual (625612: C)*, Perkin-Elmer, Eden Prairie, USA.
(30) Benndorf, C., Hadenfeldt, S., Luithardt, W., and Zhukov, A. (1996) Photoelectron Spectroscopic Investigations and Exoelectron Emission of CVD Diamond Surfaces Modified with Oxygen and Potassium. *Diamond Relat. Mater. 5*, 784−789.
(31) Franzreb, K., Mathieu, H. J., and Landolt, D. (1995) Reactive Ion Sputter Depth Profiling of Tantalum Oxides: a Comparative Study Using ToF-SIMS and Laser-SNMS. *Surf. Interface Anal. 23*, 641−651.
(32) Schueler, B. W. (1992) Microprobe Imaging by Time-of-Flight Secondary Ion Mass Spectrometry. *Microsc. Microanal. Microstruct. 3*, 119−139.
(33) Briggs, D. (1992) Static SIMS-Surface Analysis of Organic Materials. *Practical Surface Analysis* (D. Briggs and M. P. Seah, Eds.) pp 367−423, Wiley, Chichester, U.K.
(34) Mueller, C., Haenni, W., Binggeli, M., and Hintermann, H. E. (1993) Uniform Diamond Coatings on 4 in Si Wafers. *Diamond Relat. Mater. 2*, 1211.
(35) Habeeb, A. F. S. A. (1972) Reaction of Protein Sulfhydryl Groups with Ellman's Reagent. *Methods Enzymol. 25*, 457−464.
(36) Moulder, J. F., Stickle, W. F., Sobol, P. E., and Bomben, K. D. (1992) *Handbook of X-ray Photoelectron Spectroscopy* (J. Chastain, Ed), Perkin-Elmer, Eden Prairie, MN.
(37) Davies, M. C., Lynn, R. A. P., Davis, S. S., Hearn, J., Watts, J. F., Vickerman, J. C., and Paul, A. J. (1993) Preparation of Polymer Latex Particles with Immobilized Sugar Residues and their Surface Characterisation by X-ray Photoelectron Spectroscopy and Time-of-Flight Secondary Ion Mass Spectroscopy. *Langmuir 9*, 1637−1645.
(38) Beamson, G., and Briggs, D. (1992) *High-Resolution XPS of Organic Polymers*, Wiley, Chichester, U.K.
(39) Evans, S. (1992) Surface Properties of Diamond. *The Properties of Natural and Synthetic Diamond* (J. E. Field, Ed.), pp 181−214, Academic Press, London.
(40) MacNamara, K. M., Williams, B. E., Gleason, K. K., and Scruggs, B. E. (1994) Identification of Defects and Impurities in Chemical-Vapor-Deposited Diamond through Infrared Spectroscopy. *J. Appl. Phys. 76*, 2466−2472.
(41) Léonard, D., Chevolot, Y., Bucher, O., Tang, X. M., Mathieu, H. J., and Sigrist, H. (1998) ToF-SIMS Study of Photoactivatable Reagents Designed for Surface Glycoengineering. *Proceedings of SIMS XI*, Orlando (G. Gillen, J. B. R. Lareau, and F. Stevie, Eds.), pp 529−532, Wiley, Chichester, U.K.
(42) Léonard, D., Chevolot, Y., Bucher, O., Sigrist, H., and Mathieu, H. J. (1998) TOF-SIMS and XPS Study of Photoactivatable Reagents designed for Surface Glycoengineering: Part 2: N−(m-(3-(trifluoromethyl) diazirine-3-yl) phenyl)-4-(−3-thio (1-D-galactopyranosyl)-succinimidyl) -butyramide (MAD-Gal) on diamond. *Surf. Interface Anal. 26*, 793−799.
(43) Massia, S. P., and Hubbell, J. A. (1991) An RDG Spacing of 440 nm is Sufficient for Integrin, $\alpha_v\beta_3$-mediated Fibroblast Spreading and 140 nm for Focal Contact and Stress Fiber Formation. *J. Cell Biol. 114*, 1089−1100.

BC980050H

Structure-Binding Relationships for the Interaction between a Vancomycin Monoclonal Antibody Fab Fragment and a Library of Vancomycin Analogues and Tracers

Maciej Adamczyk,* Jonathan Grote, Jeffrey A. Moore, Sushil D. Rege, and Zhiguang Yu

Diagnostics Division Organic Chemistry (9-NM), Abbott Laboratories, Building AP 20, 100 Abbott Park Road, Abbott Park, Illinois, 60064. Received November 6, 1998; Revised Manuscript Received December 23, 1998

A series of vancomycin analogues and tracers were synthesized, and their binding interactions with an anti-vancomycin Fab fragment were evaluated under mass transport limiting conditions using surface plasmon resonance detection. Differences observed in binding interactions were utilized to define the vancomycin structural elements critical for antibody recognition. Major structural regions of vancomycin shown to play an important role in anti-vancomycin Fab fragment recognition include two sugar moieties and one chlorinated phenyl ring. The *N*-methylleucyl residue, the carboxy terminal residue, and residues in the peptide-binding region of vancomycin have minimal impact on the anti-vancomycin Fab fragment/vancomycin binding interaction. The selection of an antibody with such binding properties plays a critical role in the development of a vancomycin immunoassay that employs stable calibrators and controls.

INTRODUCTION

The definition of a well-characterized immunoreagent has been expanded in recent years (*1, 2*). Haptens and tracers have been characterized traditionally for their identity and purity. Advances in electrophoresis, HPLC, and ESI and MALDI MS methods have permitted similar characterization of antibodies and immunoconjugates (*1, 3, 4*). Although important, such characterization is less critical to assay development than the structure−function relationships of the immunoreagents. This includes a more complete understanding of the molecular features critical for specific recognition between ligands (haptens and tracers) and antibodies. These molecular features can be identified through a rigorous evaluation of the binding interactions between antibodies and structurally modified haptens and tracers.

A method utilizing automated surface plasmon resonance technology has recently been demonstrated to be useful for studying the binding interactions between a monoclonal antibody Fab fragment and structurally modified ligands (*5, 6*). This method involves an immobilized ligand and a soluble ligand free in solution competing for binding sites on a single antibody Fab fragment. If high-density immobilized ligand surfaces are employed and the association rate between the antibody Fab fragment and the immobilized ligand is $\geq 1 \times 10^5$ M^{-1} s^{-1}, the observed binding will be limited by mass transfer (*7, 8*). Under such conditions, initial binding rates are directly proportional to the amount of free antibody Fab fragment (not bound to soluble ligand) in solution and independent of the interaction kinetics or analyte-ligand affinity. Measuring concentrations of free antibody Fab fragment in equilibrium solutions with different concentrations of structurally modified ligand allows one to determine binding affinities and relate these results to structural features critical for recognition.

* To whom correspondence should be addressed. Phone: (847) 937-0225. Fax: (847)938-8927. E-mail: maciej.adamczyk@abbott.com.

Vancomycin (**1**, Figure 1) is the antibiotic drug of choice for the treatment of Gram-positive infections caused by methicillin resistant *Staphylococcus aureus* (*9*). It is also the treatment of choice in bacterial infections in patients allergic to β-lactam antibiotics (*10*). For the safe and effective use of this drug, quantitation of its levels in patient blood is required to maintain therapeutic levels (*11, 12*). Immunoassay techniques requiring structurally modified vancomycin tracers are frequently employed for this purpose. However, the antibiotic is rich in functionality from which to covalently attach signal-generating moieties. Here, we describe the preparation of several vancomycin analogues and tracers and the binding studies carried out on an automated BIAcore 2000 designed to evaluate the structural regions of vancomycin critical to recognition by an anti-vancomycin Fab fragment and those vancomycin regions which can be structurally modified with minimal impact to the binding interaction.

MATERIALS AND METHODS

Protein A Affinity-Pak columns and ImmunoPure Fab preparation kits, BupH phosphate-buffered saline packs, Slide-A-Lyzer 10K MWCO dialysis cassettes, the Micro BCA protein assay kit, and the Immunopure Mouse IgG $F(ab')_2$ fragment were obtained from Pierce (Rockford, IL). Microconcentrators were obtained from Millipore Corp. (Bedford, MA). Vancomycin (**1**) was obtained from the Chemical and Agricultural Products Division, Abbott Laboratories (Abbott Park, IL). Anti-vancomycin mAb was obtained from the Abbott cell culture facility (Abbott Park, IL) (*13*). (N^{α},N^{ϵ}-diacetyl)KdAdA tripeptide was obtained from Peninsula Laboratories (Belmont, CA). Aminocaproate-derivatized (N^{ϵ}-acetyl)KdAdA tripeptide was obtained from Research Genetics (Huntsville, Al). Biotin active ester (**2**) was prepared by the method of Wilchek (*14*). 6-Carboxyfluorescein active ester (**3**) was prepared by the method of Adamczyk et al. (*15*). Acridinium chemiluminescent label (**4**) was prepared following the general procedure of Mattingly et al. (*16, 17*).

10.1021/bc980135i CCC: $18.00 © 1999 American Chemical Society
Published on Web 02/25/1999

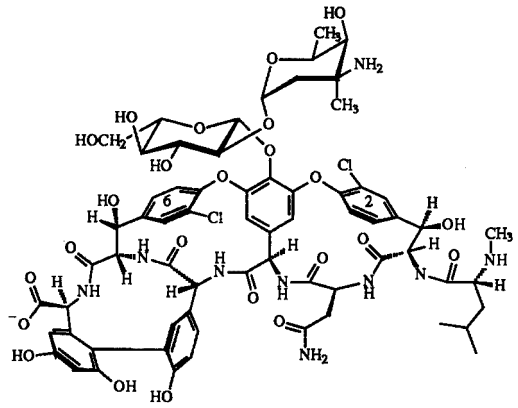


Figure 1. Structure of vancomycin.

Desvancosaminylvancomycin (**5**), aglucovancomycin (**6**), and *N*-acetylvancosaminylvancomycin (**7**) were prepared by the method of Kannan et al. (*18*). Ring-2 dechlorovancomycin (**8**) was prepared by the method of Harris et al. (*19*). Crystalline degradation product (CDP, **10**) was prepared by the method of Marshall (*20*). Ring-2 dechloroCDP (**12**) was prepared by the method of Harris et al. (*19*). All other reagents used in synthesis were obtained from Aldrich Chemical Co. (Milwaukee, WI) and utilized without further purification. Synthesized compounds were purified by HPLC [Waters (Millford, MA) Delta Prep 3000 Preparative Chromatography system equipped with a Lambda-Max 481 UV detector, a model 740 data module, and a 40 × 100 mm μBondapak C18 column]. Analytical HPLC was performed with the same system using an 8 × 100 mm μBondapak C18 column. HPLC columns were eluted with a linear gradient of 5 to 50% CH_3CN in 50 mM ammonium formate (solvent A) or isocratically in aqueous CH_3CN containing trifluoroacetic acid (v:v:v, CH_3CN/H_2O/TFA; solvent B) as noted. Elution profiles were recorded at 254 nm. Electrospray ionization mass spectrometry (ESI/MS) was carried out on a Perkin-Elmer (Norwalk, CT) Sciex API 100 Benchtop system employing the Turbo IonSpray ion source. Protein was analyzed by SDS−PAGE on a Bio-Rad Minigel system (Hercules, CA) utilizing 12.5% polyacrylamide gels (7 cm × 10 cm × 1 mm), followed by staining with Coomassie Blue. Surface plasmon resonance measurements were carried out on a BIAcore 2000 (BIAcore, Inc., Piscataway, NJ) automated system using CM-5 four-channel sensor chips. Reagents for the BIAcore instrument consisted of HBS buffer [10 mM Hepes (pH 7.4), 150 mM NaCl, 3.4 mM EDTA, and 0.05% surfactant P-20], a coupling kit containing *N*-hydroxysuccinimide (NHS), *N*-ethyl-*N*-(3-diethylaminopropyl)carbodiimide (EDAC), and 1 M ethanolamine hydrochloride (pH 8.5), all from BIAcore, Inc.

Preparation of AglucoCDP (11). Crystalline degradation product (CDP, **10**) (*20*) (100 mg, 0.069 mmol) in 1 N HCl (3 mL) was heated on a water bath for 1 h. The mixture was cooled to ambient temperature, and the solid was filtered off. The crude product was dissolved in saturated $NaHCO_3$, purified by preparative HPLC (solvent A over 20 min; flow rate, 45 mL/min), and lyophilized (45 mg, 57%). Analytical HPLC (solvent A over 20 min; flow rate, 2 mL/min): retention time, 9.4 min, 99%. ESI MS *m/z*: 1145 (MH^+).

General Procedure for Preparation of *N*-Vancosaminyl-Derived Vancomycin Tracers. To a solution of vancomycin (**1**) (482 mg, 0.33 mmol) in dry DMF (6 mL) were added active ester **2**, **3**, or **4** (0.36 mmol) and triethylamine (0.91 mL, 6.6 mmol). After stirring for 24 h at ambient temperature under N_2, the crude reaction mixtures were purified by preparative HPLC and lyophilized.

Compound **13** was obtained from **1** and biotin-active ester (450 mg, 81%). Preparative HPLC: solvent A over 20 min; flow rate, 45 mL/min. Analytical HPLC (solvent A over 15 min; flow rate, 2 mL/min): retention time, 9.4 min, 99%. ESI/MS *m/z*: 1674 (MH^+), 1305 (MH^+ − vancosaminylbiotin), 1143 (MH^+ − disaccharide − biotin), 554 (disaccharide + biotin + Na^+).

Compound **14** was obtained from **1** and 6-carboxyfluorescein-active ester (20 mg, 11%). Preparative HPLC: solvent B, 30:70:0.1; flow rate, 45 mL/min. Analytical HPLC (solvent B, 30:70:0.1; flow rate, 2 mL/min): retention time, 4.0 min, 99%. ESI/MS *m/z*: 1809 (MH^+), 904 (MH_2^{2+}), 1305 (MH^+ − vancosaminylfluorescein), 1143 (MH^+ − disaccharide − fluorescein), 665 (disaccharide + fluorescein).

Compound **15** was obtained from **1** and acridinium-active ester (409 mg, 70%). Preparative HPLC: solvent A over 20 min; flow rate, 45 mL/min. Analytical HPLC (solvent A over 20 min; flow rate, 2 mL/min): retention time, 10.4 min, 99%. ESI/MS *m/z*: 2016 (MH^+), 1305 (MH^+ − vancosaminylacridinium), 1143 (MH^+ − disaccharide − acridinium), 710 (disaccharide + acridinium).

General Procedure for Preparation of *N*-Methylleucyl-Derived Vancomycin Tracers. To a solution of vancomycin (**1**) (296 mg, 0.20 mmol) in DMSO (10 mL) were added biotin or 10-(3-sulfopropyl)-*N*-tosyl-*N*-(3-carboxypropyl)acridinium-9-carboxamide (0.20 mmol) and *N*-hydroxybenztriazole (33 mg, 0.24 mmol). Dicyclohexylcarbodiimide (206 mg, 1.0 mmol) was added, and the mixtures were stirred for 72 h at ambient temperature under N_2. The crude reaction mixtures were purified by preparative HPLC and lyophilized.

Compound **16** was obtained from **1** and biotin (136 mg, 40%). Preparative HPLC: solvent A over 20 min; flow rate, 45 mL/min. Analytical HPLC (solvent A over 20 min; flow rate, 2 mL/min): retention time, 9.4 min, 99%. ESI/MS *m/z*: 1675 (MH^+), 1531 (MH^+ − vancosamine), 1372 (MH^+ − disaccharide), 838 (MH_2^{2+}).

Compound **17** was obtained from **1** and 10-(3-sulfopropyl)-*N*-tosyl-*N*-(3-carboxypropyl)acridinium-9-carboxamide (190 mg, 35%). Preparative HPLC: solvent A over 20 min; flow rate, 45 mL/min. Analytical HPLC (solvent A over 15 min; flow rate, 2 mL/min): retention time, 12.1 min, 99%. ESI/MS *m/z*: 2016 (MH^+), 1874 (MH^+ − vancosamine), 1711 (MH^+ − disaccharide), 694 (*N*-methylleucylacridinium).

General Procedure for Preparation of Carboxyl-Derived Vancomycin Tracers. (A) Compound **9** was prepared according to the method of Sundram and Griffin (*21*). Briefly, to a solution of vancomycin (**1**) (500 mg, 0.35 mmol) and hexanediamine hydrochloride (196 mg, 1.04 mmol) in anhydrous DMSO/DMF (v:v, 1:1, 8 mL) at 0 °C were added HBTU (262 mg, 0.69 mmol) and diisopropylethylamine (480 μL, 2.76 mmol). After stirring for 72 h at ambient temperature, the crude reaction mixture was purified by preparative HPLC (solvent B, 17:83:0.0; flow rate, 40 mL/min) and lyophilized (228 mg, 43%). Analytical HPLC (solvent B, 17:83:0.0; flow rate, 2 mL/min): retention time, 7.9 min, 99%. ESI/MS *m/z*: 1548 (MH^+). (B) To a solution of compound **9** (19 mg, 12 μmol) in dry DMF (0.5 mL) were added active ester **2**, **3**, or **4** (12 μmol) and triethylamine (2 μL, 12 μmol). After stirring for 24 h at ambient temperature under N_2, the crude reaction mixtures were purified by preparative HPLC and lyophilized.

Compound **18** was obtained from **9** and biotin-active ester (9 mg, 31% based on recovered starting material). Preparative HPLC: solvent B, 20:80:0.05; flow rate, 40 mL/min). Analytical HPLC (solvent B, 20:80:0.05; flow rate, 2 mL/min): retention time, 6.1 min, 99%. ESI/MS *m/z*: 1797 ($M + Na^+$), 1775 (MH^+), 1632 (MH^+ − vancosamine), 1469 (MH^+ − disaccharide).

Compound **19** was obtained from **9** and 6-carboxyfluorescein-active ester (4 mg, 26% based on recovered starting material). Preparative HPLC: solvent B, 27:73:0.05; flow rate, 40 mL/min. Analytical HPLC (solvent B, 27:73:0.05; flow rate, 2 mL/min): retention time, 7.5 min, 99%. ESI/MS *m/z*: 1929 ($M + Na^+$), 1907 (MH^+), 1764 (MH^+ − vancosamine), 1600 (MH^+ − disaccharide).

Compound **20** was obtained from **9** and acridinium-active ester (3 mg, 35% based on recovered starting material). Preparative HPLC: solvent B, 27:73:0.05; flow rate, 40 mL/min. Analytical HPLC (solvent B, 27:73:0.05; flow rate, 2 mL/min): retention time, 5.8 min, 99%. ESI/MS *m/z*: 2137 ($M + Na^+$), 2115 (MH^+), 1972 (MH^+ − vancosamine), 1810 (MH^+ − disaccharide).

Anti-Vancomycin Monoclonal Antibody Preparation. Anti-vancomycin mAb, which was raised against vancomycin coupled through the carboxylate to thyroglobulin via a 4-aminobutyrate linker (*13*), was purified on an Affinity-Pak Protein A column according to the manufacturer's protocol. Briefly, the cell culture medium containing mAb (25.4 mg) was clarified by centrifugation (3500*g*, 30 min) and filtered through a 0.2 μm filter, and the supernatant was applied to the Affinity-Pak Protein A column which had been equilibrated with 12 mL of IgG binding buffer. After washing with IgG binding buffer, the antibody was eluted with 6 mL of IgG elution buffer to a vial containing 1.0 mL of 1.5 M Tris buffer, pH 9.0. The purified IgG was dialyzed against PBS buffer (20 mM phosphate and 30 mM NaCl, pH 7.2) for 12 h at 4 °C and then concentrated to approximately 10 mg/mL in an Amicon Microcon-50 microconcentration device. The mAb concentration was 12.4 mg/mL as determined by the micro-BCA protein assay (*22*). The total recovery of the purified mAb was 18.6 mg.

Anti-Vancomycin Fab Fragment Preparation. The digestion of anti-vancomycin mAb was carried out with the ImmunoPure Fab preparation kit following the manufacturer's protocol. Briefly, purified anti-vancomycin mAb (∼12 mg) in digestion buffer (0.5 mL; 20 mM sodium phosphate, 10 mM EDTA, and 30 mM cysteine, pH 7.0) was incubated for 5 h in a 37 °C incubator shaker with immobilized papain in digestion buffer (0.5 mL). Papain-digested anti-vancomycin mAb was then passed through a preequilibrated immobilized protein-A column (2 mL) supplied with the kit to remove undigested mAb and the Fc fragment. The protein-A column was washed with an additional 13 mL of ImmunoPure binding buffer. The column flow-through and column washes containing the Fab fragment were pooled and dialyzed against PBS buffer for 12 h at 4 °C and concentrated in a Centriprep-10 concentration device. The concentration of the anti-vancomycin Fab fragment was 2.0 mg/mL as determined by the micro-BCA method using mouse IgG $(F_{ab}')_2$ as the standard. Purified anti-vancomycin Fab fragment was characterized by SDS−PAGE and LC/ESI mass spectrometry. The molecular masses of the heavy and light chains of the Fab fragment were 23 986 and 24 033 Da, respectively. All studies described were conducted with the Fab fragment of anti-vancomycin mAb to eliminate the complexity associated with the bivalency of the monoclonal antibody.

Preparation of Biosensor Surfaces. Immobilization of vancomycin analogue **9** or the aminocaproate-derivatized (N^{ϵ}-acetyl)KdAdA tripeptide via amine coupling to the CM-5 sensor chip was performed by a previously described method (*6*). Briefly, a continuous flow of HBS buffer at 10 μL/min was initiated over the biosensor surface. The carboxymethylated dextran matrix on the sensor surface was activated by a 3.5 min injection of a solution of 0.05 M NHS and 0.2 M EDAC. A solution of **9** or the aminocaproate-derivatized (N^{ϵ}-acetyl)KdAdA tripeptide (10 μM) and ethanolamine (990 μM; 1 mM total amine in HBS buffer) was then injected (7 min), followed by a 7 min injection of 1.0 M ethanolamine hydrochloride to block remaining unreacted active ester groups. Blank surfaces were generated under identical conditions omitting the ligand immobilization step.

Solution Competition Analysis of the Vancomycin Analogue/Anti-Vancomycin Fab Fragment Binding Interaction. Solution competition studies were carried out on a BIAcore 2000 following the general procedure previously described (*6*). Biosensor surfaces were regenerated after each injection with successive 1 min pulses of 6, 6, and 1.5 M guanidine hydrochloride. Initial rates of binding of anti-vancomycin Fab fragment to the biosensor surface were measured over a 15 s window beginning 20 s postinjection. Data were evaluated by nonlinear regression analysis using the solution affinity model built into BIAevaluation 3.0 software (BIAcore, Inc).

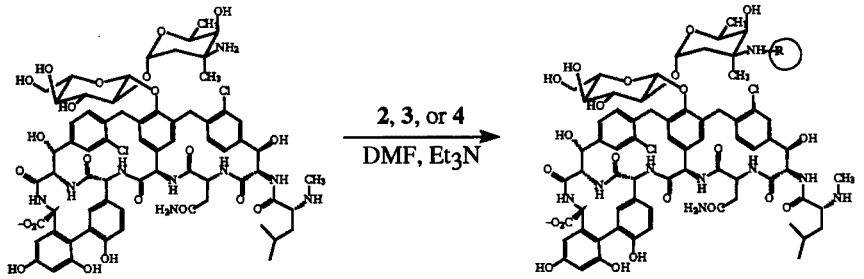
RESULTS

Preparation of Vancomycin Analogues and Tracers. Vancomycin analogues lacking the sugars or the ring-2 chlorine were prepared as previously described (*18*, *19*). Tracers **13**−**15**, containing a derivatized *N*-vancosaminyl carbohydrate moiety, were prepared in 11−81% yield by coupling vancomycin with the NHS active esters of biotin (**2**), 6-carboxyfluorescein (**3**), or 10-(3-sulfopropyl)-*N*-tosyl-*N*-(3-carboxypropyl)acridinium-9-carboxamide (**4**) and purification by preparative HPLC (Scheme 1). Vancomycin tracers **16** and **17**, bearing a derivatized *N*-methylleucyl moiety, were prepared in 40 and 35% yield, respectively, by coupling vancomycin with free biotin or acridinium acid in the presence of *N*,*N*′-dicyclohexylcarbodiimide and *N*-hydroxybenztriazole (Scheme 1). Analogue **9**, containing an aminoalkyl linker on the free carboxyl functionality of vancomycin, was prepared by the method of Sundram and Griffin (*21*). Coupling of **9** with the NHS active esters of biotin (**2**), 6-carboxyfluorescein (**3**), or 10-(3-sulfopropyl)-*N*-tosyl-*N*-(3-carboxypropyl)acridinium-9-carboxamide (**4**), as above, provided mixtures of the carboxyl and *N*-vancosaminyl carbohydrate derivatized vancomycin tracers. Repeated purifications by preparative HPLC provided pure carboxyl-modified tracers **18**−**20** in 26−35% yield (Scheme 1). Crystalline degradation product analogues were prepared following literature procedures or the general methodology described for preparation of vancomycin analogues. The structures of all vancomycin analogues and tracers and the CDP analogues utilized in this study are summarized in Table 1.

Preparation of an Immobilized Vancomycin Biosensor Surface. Initial attempts to generate a biosensor surface involved immobilization of vancomycin through the primary amine of the vancosamine sugar moiety via amine coupling to the activated carboxymethyl dextran surface of a CM-5 sensor chip. Subsequent binding studies with saturating amounts of anti-vancomycin Fab

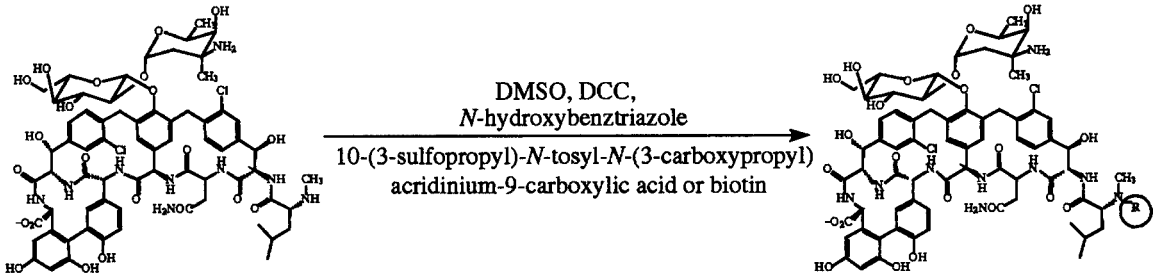
Scheme 1

N-Vancosaminyl Derived Tracers



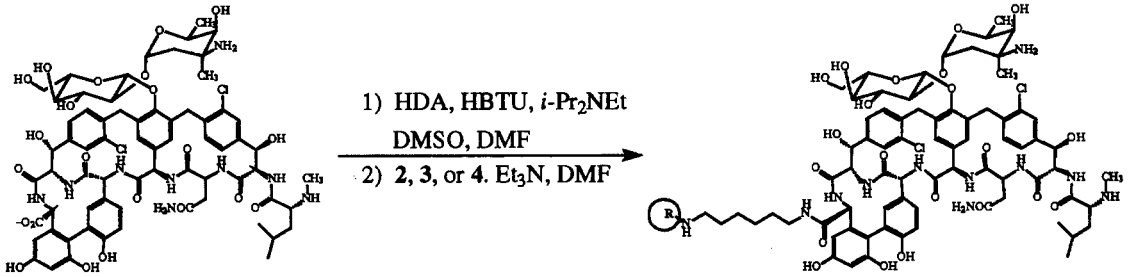
(1) (13-15)

N-Methylleucyl Derived Tracers

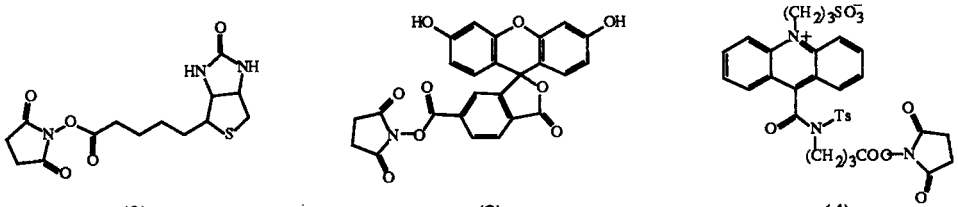


(1) (16 & 17)

Carboxyl-HDA Derived Tracers



(1) (18-20)

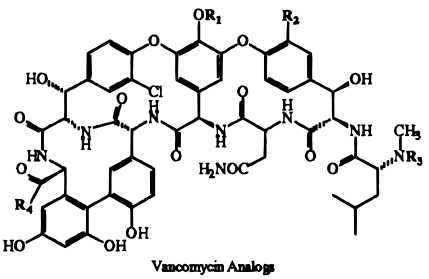


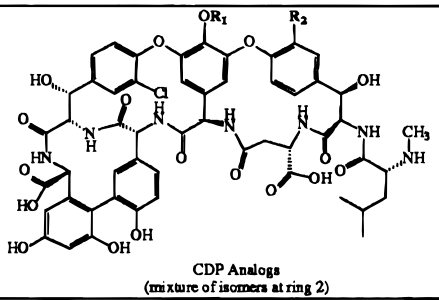
(2) (3) (4)

fragment showed that these surfaces had minimal binding capacity and a relatively low affinity for the antibody fragment. In contrast, immobilization of vancomycin derivative **9**, containing the aminoalkyl linker from the free carboxyl functionality, under identical conditions to the activated carboxymethyl dextran surface provided biosensors with relatively high binding capacity ($RU_{max} \approx 4000$) and high affinity for anti-vancomycin Fab fragment. Additional binding studies of the anti-vancomycin Fab fragment to the immobilized aminoalkyl-modified vancomycin surface demonstrated the binding to be limited by mass transfer and suitable for use in the solution binding studies described below.

Determination of Binding Affinities of Vancomycin Analogues and Tracers for Anti-Vancomycin Fab Fragment. The binding affinity of anti-vancomycin Fab fragment for several vancomycin analogues and tracers was determined from solution competition experiments. Initially, known concentrations of anti-vancomycin Fab fragment (0−22 nM) were injected over the aminoalkyl vancomycin biosensor surface, and the initial rate of binding for each anti-vancomycin Fab fragment

Table 1. Structures of Vancomycin Analogues and Tracers





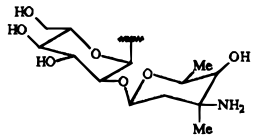
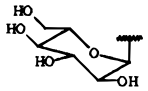
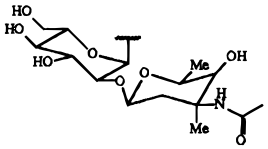
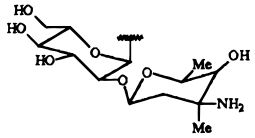
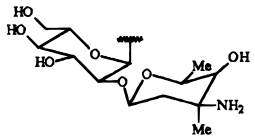
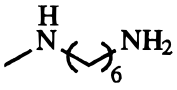
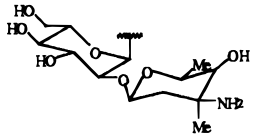
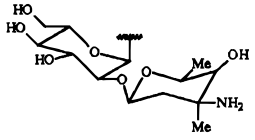
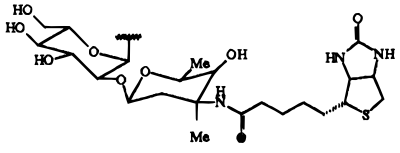
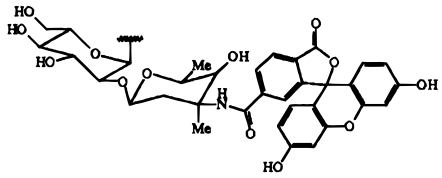
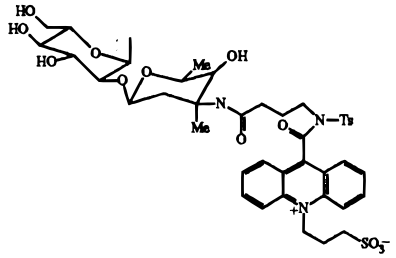
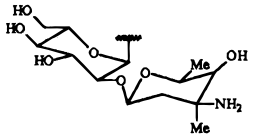
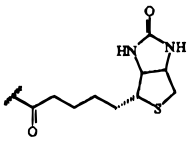
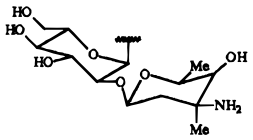
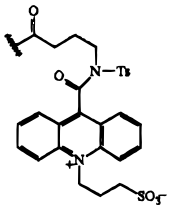
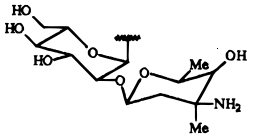
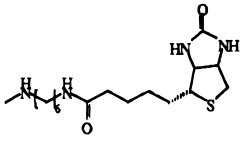
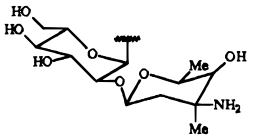
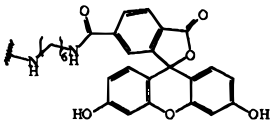
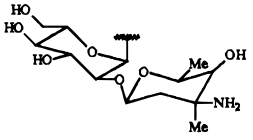
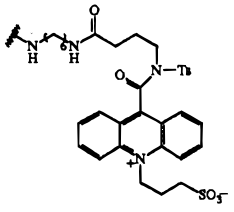
Compound	R_1	R_2	R_3	R_4
Vancomycin Analogs				
(1)		Cl	H	OH
(5)		Cl	H	OH
(6)	H	Cl	H	OH
(7)		Cl	H	OH
(8)		H	H	OH
(9)		Cl	H	
CDP Analogs				
(10)		Cl	(-)	(-)
(11)	H	Cl	(-)	(-)
(12)		H	(-)	(-)
N-Vancosaminyl Derived Tracers				
(13)		Cl	H	OH

Table 1 (Continued)

Compound	R_1	R_2	R_3	R_4
(14)		Cl	H	OH
(15)		Cl	H	OH
N-Methylleucyl Derived Tracers				
(16)		Cl		OH
(17)		Cl		OH
Carboxyl Derived Tracers				
(18)		Cl	H	
(19)		Cl	H	
(20)		Cl	H	

concentration was determined. A plot of initial binding rate versus concentration of anti-vancomycin Fab fragment was fit using a 4-parameter logistic (general model in BIAevaluation 3.0) providing a standard curve. Several standard curves were generated during the course of these studies and all were identical within experimental error. A fixed concentration of anti-vancomycin Fab fragment (20 nM) was then mixed with 12 concentrations of each vancomycin analogue or tracer and allowed to reach equilibrium. The equilibrium mixtures were individually injected over the aminoalkyl vancomycin biosensor surface, and the concentration of free anti-vancomycin Fab fragment remaining was quantitated by determination of the initial rate of binding to the biosensor surface as described above. A plot of free anti-vancomycin Fab fragment versus total concentration of added analogue or tracer provides a competition curve. Figure 2 shows typical competition curves for studies conducted here. The data points represent the experimentally determined concentrations of free anti-vancomycin Fab fragment in equilibrium solutions at a given concentration of soluble analogue or tracer. The curves represent the best nonlinear fit of the data using eq 1 (solution affinity model in BIAevaluation 3.0 software)

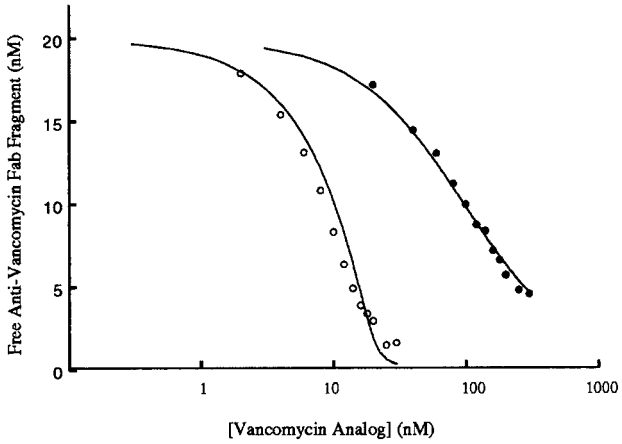


Figure 2. Solution competition curves for determination of equilibrium dissociation constants. Ring-2 dechlorovancomycin (**8**, ●); Biotinylated carboxyl-HDAvancomycin tracer (**18**, ○). The fixed concentration of anti-vancomycin Fab fragment was 20 nM.

$$\mathrm{Fab_f} = \frac{\mathrm{Fab_T} - A - K_D}{2} + \sqrt{\frac{(\mathrm{Fab_T} - A - K_D)^2}{4} - A \times \mathrm{Fab_T}} \quad (1)$$

where $\mathrm{Fab_f}$ is the concentration of free anti-vancomycin Fab fragment in equilibrium solutions, $\mathrm{Fab_T}$ is the total concentration of anti-vancomycin Fab fragment in solution (20 nM), A is the total concentration of added vancomycin analogue or tracer, and K_D is the equilibrium dissociation constant for the binding of the vancomycin analogue or tracer to anti-vancomycin Fab fragment in solution.

The structure-binding relationships for the interaction between vancomycin analogues and the anti-vancomycin Fab fragment, as measured by changes in the equilibrium dissociation constants (K_D), are summarized in Table 2. Vancomycin and the *N*-acetylvancosaminyl-derivatized vancomycin analogue (**7**) bind exceedingly tight with K_D values being outside the range for which the BIAcore instrument can accurately provide values from solution competition studies. Incorporation of the aminoalkyl linker on the free carboxyl functionality of vancomycin, providing **9**, which was used for preparation of the immobilized vancomycin biosensor surface, has minimal effect on the anti-vancomycin Fab fragment recognition in solution. Removal of the ring-2 chlorine atom from vancomycin results in a significant loss in binding recognition by the antibody fragment (cf. **8**). Cleavage of one or both of the carbohydrate rings from vancomycin by acid hydrolysis providing **5** and **6**, respectively, results in a further sequential loss in binding recognition by the antibody fragment with the loss of each monosaccharide. Anti-vancomycin Fab fragment binding interactions with vancomycin degradation products were extremely weak relative to the native antibiotic binding interaction. Crystalline degradation product (**10**) binds with a K_D of 488 ± 34 nM. Removal of the chlorine atom from the 2-position again results in a significant loss in binding recognition by the anti-vancomycin Fab fragment and, complete hydrolysis of the carbohydrate rings, providing **11**, results in a binding interaction with the anti-vancomycin Fab fragment too weak to be determined by the solution competition studies.

The structure-binding relationships for the binding interaction between vancomycin tracers and the anti-vancomycin Fab fragment, as measured by changes in the equilibrium dissociation constants (K_D), are summarized in Table 3. The binding interactions vary depending on the label contained on the tracer. However, *N*-methylleucyl- (**16** and **17)** and carboxyl-HDA-derived tracers (**18**−**20**) containing the same label bind the antibody fragment with similar affinities. In contrast, *N*-vancosaminyl-derived tracers (**13**−**15**) containing the equivalent label bind the antibody fragment substantially weaker.

Table 2. Structure-Binding Relationships for the Interaction between Vancomycin Analogues and the Anti-Vancomycin Fab Fragment[a]

analogue	equilibrium dissociation constant (K_D) (nM)
vancomycin (**1**)	≤0.2[b]
desvancosaminylvancomycin (**5**)	587 ± 27
aglucovancomycin (**6**)	42 000 ± 1000
N-acetylvancosaminylvancomycin (**7**)	≤0.2[b]
ring-2 dechlorovancomycin (**8**)	87 ± 4
carboxyl-HDAvancomycin (**9**)	0.32 ± 0.04
CDP (**10**)	488 ± 34
AglucoCDP (**11**)	≥50 000[c]
ring-2 dechloroCDP (**12**)	6000 ± 100

[a] Values are average equilibrium dissociation constants obtained from triplicate measurements. [b] K_D was too small to be reliably measured by solution affinity experiments. [c] K_D was too large to be reliably measured by solution affinity experiments.

Table 3. Structure-Binding Relationships for the Interaction between Vancomycin Tracers and the Anti-Vancomycin Fab Fragment[a]

	derivatization site (nM)		
derivative	*N*-vancosaminyl	*N*-methylleucyl	carboxyl-HDA
biotin	584 ± 19	≤0.2[b]	≤0.2[b]
fluorescein	76 ± 3	*c*	204 ± 6
acridinium	1200 ± 100	25 ± 0.7	26 ± 0.9

[a] Values are average equilibrium dissociation constants obtained from triplicate measurements. [b] K_D was too small to be reliably measured by solution affinity experiments. [c] Not determined.

Evaluation of a Vancomycin/KdAdA Tripeptide Binding Interaction on Anti-Vancomycin Fab Fragment Recognition. To further evaluate the topology of vancomycin critical for anti-vancomycin Fab fragment recognition, the role of residues located in the peptide-binding pocket of the antibiotic was investigated (Figure 3). For these studies an (N^{ϵ}-acetyl)KdAdA tripeptide containing an aminocaproate linker from the amino terminus was immobilized via amine coupling to an activated carboxymethyl dextran surface of a CM-5 sensor chip. Vancomycin (0.5 μM) binds to this surface (Figure 4). However, since the mass of the antibiotic is small, the instrumental response is relatively small (~50 RU at equilibrium). In contrast, injection of a vancomycin (0.5 μM)/anti-vancomycin Fab fragment (1 μM) complex, in which ≥99% of the vancomycin is bound by the antibody fragment, results in an approximately 10-fold increase in response due the increased mass of the complex (Figure 4). Anti-vancomycin Fab fragment alone has no affinity for the immobilized tripeptide surface (Figure 4). To further verify that the peptide and antibody-binding pockets of vancomycin were mutually exclusive, the vancomycin/anti-vancomycin Fab fragment solution binding interaction was reinvestigated under the conditions described above in the presence of (N^{a},N^{ϵ}-diacetyl)-KdAdA tripeptide (500 μM). The K_D value obtained for the vancomycin/anti-vancomycin Fab fragment binding interaction in solution in the presence of (N^{a},N^{ϵ}-diacetyl)-

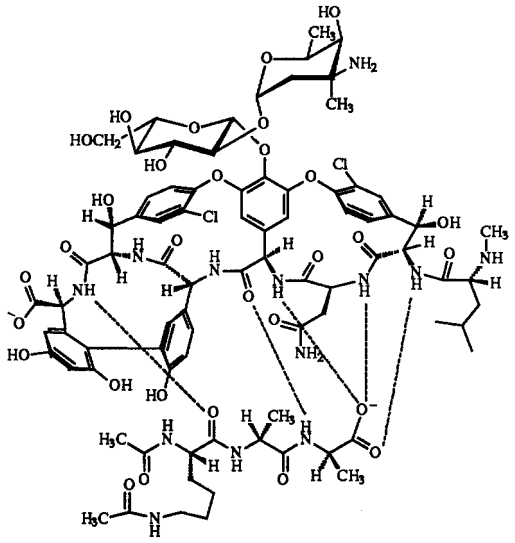


Figure 3. Proposed model for the binding interaction between vancomycin (**1**) and a cell wall peptide analogue (N^{α},N^{ϵ}-diacetyl)-KdAdA (*28*). Dashed lines indicate hydrogen bonds.

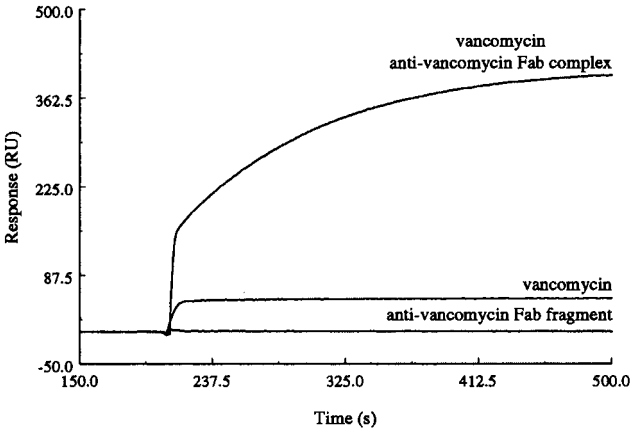


Figure 4. Binding of vancomycin, anti-vancomycin Fab fragment, and vancomycin/anti-vancomycin Fab fragment complex to aminocaproate-derivatized (N^{ϵ}-acetyl)KdAdA tripeptide biosensor surface.

KdAdA tripeptide was identical to the value obtained in the absence of the tripeptide (≤0.2 nM).

DISCUSSION

Reagent design plays an important role in rational immunoassay development. Specifically, the molecular architecture of an immunogen used for triggering an antigenic response is critical to the production of antibodies exhibiting the desired ligand binding characteristics. Important features of immunogen design can include the attachment site of a spacer arm to the ligand, the structure of the spacer arm, and the method employed for coupling the hapten to a carrier molecule. Likewise, some molecular features of the complementary ligand and labeled tracers will be important for recognition by the elicited antibody. The goal of tracer design is to produce ligands containing a signal-generating moiety, which exhibit diagnostically useful binding characteristics. Two approaches to immunoreagent design have been investigated. The design of homologous immunoreagents involves preparation of an immunogen and a tracer from the same hapten. Alternatively, in design of heterologous immunoreagents the immunogen and tracer are prepared from haptens with distinct points of attachment. In the present study, several vancomycin tracers (homologous and heterologous) were prepared, and their binding interactions with an anti-vancomycin Fab fragment were investigated. Several vancomycin analogues were also prepared and tested to further evaluate the structural regions of the antibiotic critical for recognition by the antibody fragment.

The inherent reactivity of vancomycin allows for the preparation of several analogues. Removal of the sugars from vancomycin occurs by mild acid hydrolysis (*18*, *20*). Crystalline degradation product (CDP, **10**) is formed in solution at ambient temperature by rearrangement of vancomycin with concomitant hydrolytic loss of ammonia (*23*). The antibiotic further contains several phenols that are susceptible to oxidative conditions and eight racemizable asymmetric centers. In contrast, the reactivity and complexity of vancomycin makes the preparation of tracers a challenge. As a result, literature reports of vancomycin tracers are limited, and no structural assignments have been provided (*24*−*26*). Tracers designed and synthesized here were derivatized on the vancosaminyl, *N*-methylleucyl, and carboxy terminal residues of vancomycin. The vancosaminyl and *N*-methylleucyl derivatized tracers (heterologous) were synthesized in good to moderate yield. The carboxyl derivatized tracers (homologous) were obtained in lower yields due to competing derivatization reactions yielding products, which were difficult to separate from the desired material. All tracers were isolated in >99% purity as determined by analytical HPLC. The structural assignments for all tracers were confirmed by mass spectral fragmentation patterns.

Aminoalkyl modified vancomycin (**9**) was immobilized on biosensor surfaces and utilized for all solution competition experiments. Analogue **9** contains two primary amines that can potentially react with the activated carboxymethyl dextran of a CM-5 sensor chip to produce a heterogeneous surface. Results obtained using underivatized vancomycin immobilized surfaces indicate that if coupling does occur via the primary amine of the vancosamine sugar moiety it is minor. Coupling of **9** results in a vancomycin-immobilized surface with high affinity and high-binding capacity for anti-vancomycin Fab fragment. This suggests the majority of coupling occurs via the primary amine of the aminoalkyl linker conjugated to the carboxy terminus of vancomycin. The possible generation of heterogeneous vancomycin biosensor surfaces in this manner does not effect the solution competition experiments, since all studies were conducted under mass transport limiting conditions with concentrations of free antibody fragment in equilibrium solutions being determined from a standard curve.

Solution competition studies show the antibody fragment binds vancomycin and the aminoalkyl modified vancomycin (**9**) with high affinity. However, hydrolysis of the two sugar moieties or removal of the ring-2 chlorine atom from vancomycin results in significant losses in binding affinity. The anti-vancomycin Fab fragment also exhibits minimal binding interactions with CDP analogues. In fact, binding interactions observed with CDP analogues and vancomycin analogues lacking the sugar moieties were outside the diagnostically relevant range for the vancomycin immunoassay (*13*). This is critical as assay specificity relies on the ability of the mAb to distinguish between vancomycin and its metabolites (i.e., CDP and other structurally similar compounds). The decreased binding recognition of the anti-vancomycin Fab fragment for CDP is attributed to a conformational change which occurs in the vancomycin to CDP transformation due to a ring expansion relieving the strain in

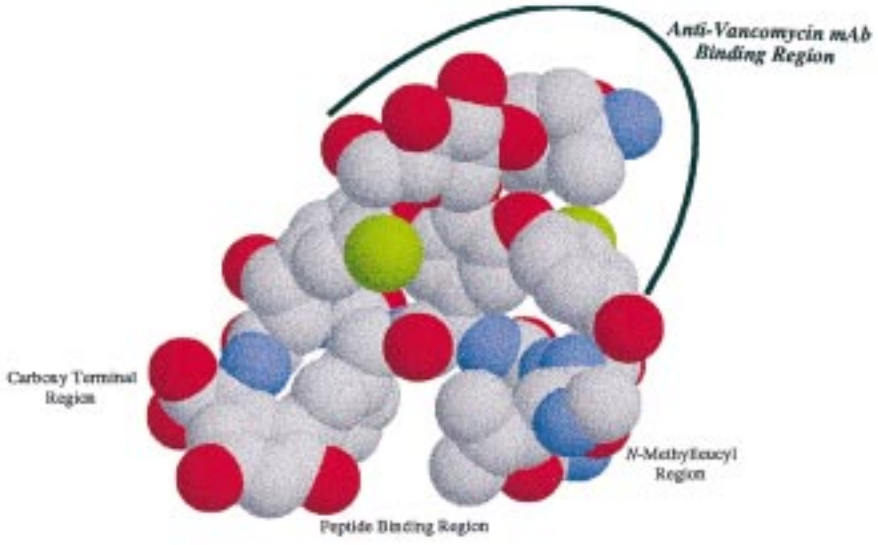


Figure 5. Space filling model of vancomycin showing a proposed anti-vancomycin mAb binding region. Color scheme: carbons (grey), chlorines (green), oxygens (red), and nitrogens (blue). Structure adapted from PDB file 1AA5 using SymApps 5.1 (Bio-Rad Laboratories).

the peptide backbone of the macrocycle (*23*). Crystalline degradation product (CDP, **10**) actually exists as an equilibrium mixture (2:3) of atropisomers differing in the orientation of the chlorine containing ring-2 residue (*23*). The orientation of the chlorine containing ring-2 residue in the major isomer differs from that in vancomycin by 180°. The minor isomer corresponds to the orientation found in vancomycin. The ring-2 orientation conversion is restricted in vancomycin. This reorientation of the chlorine atom in CDP can partially account for the decreased binding interaction observed with anti-vancomycin Fab fragment.

Results obtained for the binding interactions between vancomycin tracers and the anti-vancomycin Fab fragment are consistent with the vancomycin analogue binding studies. The *N*-methylleucyl and carboxy terminal residues of vancomycin can be structurally modified with minimal impact to the anti-vancomycin Fab fragment binding interaction. In contrast, derivatization of the vancosaminyl sugar residue of vancomycin with biotin, fluorescein, or acridinium labels results in a substantial loss in binding recognition by the antibody fragment. Interestingly, acetylation of the same vancosaminylamine does not affect the binding interaction. This suggests that the antibody-binding pocket may accommodate small structural modifications at the amino functionality and that the amine is not directly involved in the binding interaction.

Vancomycin manifests its antibiotic action by binding the carboxy terminal d-Ala-d-Ala peptides of the lipid-PP-disaccharide-pentapeptide intermediates involved in the biosynthesis of the bacterial cell wall peptidoglycan (*27*). This inhibits cross-linking of the chains in the growing cell wall peptidoglycan making the cell susceptible to lysis through osmotic shock. Binding of the carboxy terminal d-Ala-d-Ala peptides to vancomycin has been shown to occur in the concave pocket of vancomycin through five hydrogen bonds between the peptide and the amide backbone of the antibiotic (Figure 3) (*28*). To investigate the role this region played, if any, in anti-vancomycin Fab fragment binding recognition, we evaluated the vancomycin/anti-vancomycin Fab fragment binding interaction in the presence of KdAdA model peptides. Direct binding studies of a vancomycin/anti-vancomycin Fab fragment complex to an aminocaproate-derivatized (N^{ϵ}-acetyl)KdAdA tripeptide biosensor surface demonstrated the peptide and antibody fragment could bind vancomycin simultaneously. This observation was further confirmed by determination of the vancomycin/anti-vancomycin Fab fragment solution binding affinity in the presence of (N^{α},N^{ϵ}-diacetyl)KdAdA tripeptide. The results obtained were essentially identical to the value obtained in the absence of the tripeptide.

The selection of an anti-vancomycin mAb that binds vancomycin at a site independent from that of the peptide-binding site is notable. The degradation of vancomycin to CDP is relatively facile and can lead to problems associated with stability of immunoassay components (i.e., calibrators, controls, and tracers) and cross reactivity with degradation products. Certain peptidoglycan analogues have been shown to inhibit the degradation of vancomycin to CDP resulting in reagent stabilization (*29*). The mAb selected and utilized here not only is highly specific for vancomycin but can also be used in the presence of peptides that stabilize the assay components without interfering with the immunoassay (*13*).

A proposed antibody binding region consistent with all observations is shown in Figure 5. Major structural regions of vancomycin shown to be critical for recognition by the anti-vancomycin Fab fragment include the disaccharide moiety and the ring-2 chlorine atom. Additional structural features of vancomycin critical to recognition by the anti-vancomycin Fab fragment may exist but cannot be evaluated from the results obtained here.

CONCLUSION

A series of vancomycin analogues and tracers were synthesized, and their binding interactions with an anti-vancomycin Fab fragment were evaluated under mass transport limiting conditions using surface plasmon resonance. The results show that two sugar moieties and one chlorinated phenyl ring play important roles in the antibody binding interaction. The *N*-methylleucyl and carboxy terminal residues have minimal contact with the antibody binding pocket and can be structurally modified to generate tracers with little impact on the binding interaction. Additionally, KdAdA model peptides were

shown to bind to vancomycin at a site independent from that of the mAb-binding site and as a result can be used to stabilize immunoassay components.

LITERATURE CITED

(1) Henry, C. (1996) FDA, reform, and the well-characterized biologic. *Anal. Chem. 68*, 674A−677A.

(2) Adamczyk, M., Gebler, J. C., Gunasekera, A. H., Mattingly, P. G., and Pan, Y. (1997) Immunoassay reagents for thyroid testing. 2. Binding properties and energetic parameters of a T_4 monoclonal antibody and its Fab fragment with a library of thyroxine analog biosensors using surface plasmon resonance. *Bioconjugate Chem. 8*, 133−145.

(3) Adamczyk, M., Buko, A., Chen, Y. Y., Fishpaugh, J. A., Gebler, J. C., and Johnson, D. D. (1994) Characterization of protein-hapten conjugates. 1. Matrix-assisted laser desorption ionization mass spectrometry of immuno BSA-hapten conjugates and comparison with other characterization methods. *Bioconjugate Chem. 5*, 631−635.

(4) Adamczyk, M., Gebler, J. G., and Mattingly, P. G. (1996) Characterization of protein-hapten conjugates. 2. Electrospray mass spectrometry of bovine serum albumin-hapten conjugates. *Bioconjugate Chem. 7*, 475−481.

(5) Rauffer, N., Zeder-Lutz, G., Wenger, R., Van Regenmortel, M. H. V., and Altschuh, D. (1994) Structure-activity relationships for the interaction between cyclosporin A derivatives and the Fab fragment of a monoclonal antibody. *Mol. Immunol. 31*, 913−922.

(6) Adamczyk, M., Johnson, D. D., Mattingly, P. G., Moore, J. A., and Pan, Y. (1998) Immunoassay reagents for thyroid testing. 3. Determination of the solution binding affinities of a T_4 monoclonal antibody Fab fragment for a library of thyroxine analogs using surface plasmon resonance. *Bioconjugate Chem. 9*, 23−32.

(7) Karlsson, R., Fagerstam, L., Nilshans, H., and Persson, B. (1993) Analysis of active antibody concentration. Separation of affinity and concentration parameters. *J. Immunol. Methods 166*, 75−84.

(8) Karlsson, R. (1994) Real-time competitive kinetic analysis of interactions between low-molecular-weight ligands in solution and surface-immobilized receptors. *Anal. Biochem. 221*, 142−151.

(9) Kirby, W. M. M. (1981) Vancomycin therapy in severe staphylococcal infections. *Rev. Infect. Dis. 3*, 5236−5239.

(10) Ingerman, M. J., and Santoro, J. (1989) Vancomycin a new old agent. *Infect. Dis. Clin. North Am. 3*, 641−651.

(11) Pryka, R. D., Rodvold, K. A., and Erdman, S. M. (1991) An updated comparison of drug dosing methods. IV. Vancomycin. *Clin. Pharmacokinet. 20*, 463−476.

(12) Ryback, M. J., and Boike, S. C. (1986) Monitoring vancomycin therapy. *Drug Intell. Clin. Pharm. 20*, 757−761.

(13) Adamczyk, M., Brate, E. M., Chiappetta, E. G., Ginsburg, S., Hoffman, E., Klein, C., Perkowitz, M. M., Rege, S. D., Chou, P. P., and Constantino, A. G. (1998) Development of a quantitative vancomycin immunoassay for the Abbott AxSYM Analyzer. *Ther. Drug Monit. 20*, 191−201.

(14) Wilchek, M., and Bayer, E. A. (1990) Biotin-containing reagents. In *Avidin-Biotin Technology* (M. Wilchek, Ed.) pp 123−138, Academic Press, New York.

(15) Adamczyk, M., Fishpaugh, J., and Heuser, K. (1997) Preparation of succinimidyl and pentafluorophenyl active esters of 5- and 6-carboxyfluorescein. *Bioconjugate Chem. 8*, 253−255.

(16) Mattingly, P. G. (1991) Chemiluminescent 10-methylacridinum-9-(N-sulfonylcarboxamide) salts. Synthesis and kinetics of light emission. *J. Biolumin. Chemilumin. 6*, 107−114.

(17) Mattingly, P. G., and Bennett, L. (1995) Chemiluminescent acridinium salts, U.S. patent 5,468,646.

(18) Kannan, R., Harris, C. M., Harris, T. M., Waltho, J. P., Skelton, N. J., and Williams, D. H. (1988) Function of amino sugar and N-terminal amino acid of the antibiotic vancomycin in its complexation with cell wall peptides. *J. Am. Chem. Soc. 110*, 2946−2953.

(19) Harris, C. M., Kannan, R., Kopecka, H., and Harris, T. M. (1985) The role of chlorine substituents in the antibiotic vancomycin: Preparation and characterization of mono- and didechlorovancomycin. *J. Am. Chem. Soc. 107*, 6652−6658.

(20) Marshall, F. J. (1965) Structure studies on vancomycin. *J. Org. Chem. 8*, 18−22.

(21) Sundram, U. N., and Griffin, J. H. (1995) General and efficient method for the solution- and solid-phase synthesis of vancomycin carboxamide derivatives. *J. Org. Chem. 60*, 1102−1103.

(22) Smith, P. K., Krohn, R. I., Hermanson, G. T., Mallia, A. K., Gartner, F. H., Provenzano, M. D., Fujimoto, E. K., Goeke, N. M., Olson, B. J., and Klenk, D. C. (1985) Measurement of protein using bicinchoninic acid. *Anal. Biochem. 150*, 76−85.

(23) Harris, C. M., Kopecka, H., and Harris, T. M. (1983) Vancomycin: Structure and transformation to CDP-I. *J. Am. Chem. Soc. 105*, 6915−6922.

(24) Colbert, D. L., Smith, D. S., and Landon, J. (1993) Dissociation of fluorescein-labelled haptens from polyclonal antibodies. The influence of hapten molecular weight. *J. Immunol. Methods 161*, 269−272.

(25) Schwenzer, K. S., Wang, C.-H. J., and Anhalt, J. P. (1983) Automated fluorescence polarization immunoassay for monitoring vancomycin. *Ther. Drug Monit. 5*, 341−345.

(26) Fong, K.-L. L., Ho, D.-H. W., Bogerd, L., Pan, T., Brown, N. S., Gentry, L., and Bodey, G. P. (1981) Sensitive radioimmunoassay for vancomycin. *Antimicrob. Agents Chemother. 19*, 139−143.

(27) Walsh, C. T., Fisher, S. L., Park, I.-S., Prahalad, M., and Wu, Z. (1996) Bacterial resistance to vancomycin: five genes and one missing hydrogen bond tell the story. *Chem. Biol. 3*, 21−28.

(28) Barna, J. C. J., and Williams, D. H. (1984) Structure and mode of action of glycopeptide antibiotics of the vancomycin group. *Annu. Rev. Microbiol. 38*, 339−357.

(29) Harris, C. M., Kopecka, H., and Harris, T. M. (1985) The stabilization of vancomycin with peptidoglycan analogs. *J. Antibiot. 38*, 51−57.

BC980135I

High-Efficiency Intracellular Magnetic Labeling with Novel Superparamagnetic-Tat Peptide Conjugates

Lee Josephson, Ching-Hsuan Tung, Anna Moore, and Ralph Weissleder*

Center for Molecular Imaging Research, Massachusetts General Hospital, Boston, Massachusetts 02129.
Received October 19, 1998; Revised Manuscript Received January 4, 1999

A biocompatible, dextran coated superparamagnetic iron oxide particle was derivatized with a peptide sequence from the HIV-tat protein to improve intracellular magnetic labeling of different target cells. The conjugate had a mean particle size of 41 nm and contained an average of 6.7 tat peptides. Derivatized particles were internalized into lymphocytes over 100-fold more efficiently than nonmodified particles, resulting in up to 12.7×10^6 particles/cell. Internalized particles localized in cytoplasm and nuclear compartments as demonstrated by fluorescence microscopy and immunohistochemistry. Labeled cells were highly magnetic, were detectable by NMR imaging, and could be retained on magnetic separation columns. The described method has potential applications for in vivo tracking of magnetically labeled cells by MR imaging and for recovering intracellularly labeled cells from organs.

INTRODUCTION

Cell labeling with ferro/supermagnetic substances is an increasingly common method for in vitro cell separation (*1*). Magnetically labeled cells can also be detected by magnetic resonance imaging (*2*−*5*). Most current labeling techniques utilize one of two approaches: (i) attaching magnetic particles to the cell surface (*6*) or (ii) internalizing biocompatible magnetic particles by fluid phase endocytosis (*3, 5*), receptor mediated endocytosis (*7*) or phagocytosis (*2*). The first approach is limited to ex vivo use (*8*). The second approach is limited by the fact that many cells, such as lymphocytes, do not possess high-efficiency internalizing receptors and that the fluid phase pathway is relatively inefficient (*5*). It would therefore be highly desirable to develop a technique of high efficiency intracellular magnetic labeling for in vivo magnetic separation and/or imaging of a wide variety of cells. Such techniques are expected to be of particular importance as cell-based genetic therapies are being developed.

We hypothesized that a superparamagnetic iron oxide with a membrane translocating signal (MTS) peptide attached might be capable of producing high levels of cell internalization. Several MTSs have been described including the third helix of the homeodomain of Antennapedia (*9*), peptide derived from anti-DNA monoclonal antibody (*10*), VP22 herpes virus protein (*11, 12*), and HIV-1 tat peptide (*13*). HIV-1 tat protein is an 86 amino acid polypeptide and is essential for viral replication. It has been shown to freely travel through cellular and nucleic membranes (*14, 15*). Its membrane translocational property is dominated by a short signal, GRKKRRQRRR (amino acid residues 48−57). More recently, it has been demonstrated that the core peptide itself rather than the entire protein is capable of translocating a variety of molecules, including fluorescent probes (*16*), peptides (*17*), pathogenic epitopes (*18*), and proteins (*13, 19*−*21*). Here we report that tat peptide (residues 48−57) derivatized superparamagnetic iron oxide nanoparticles (41 nm) are internalized into cells over 100-fold more efficiently than has been reported to date. The novel compound may thus serve as a reagent for magnetic resonance imaging of cell trafficking and/or magnetic separation of in vivo homed cells.

* To whom correspondence should be addressed. Tel: (617) 726-8226. Fax: (617) 726-5708. E-mail: weissleder@helix.mgh.harvard.edu.

EXPERIMENTAL PROCEDURES

Peptide Synthesis. A peptide containing the translocation sequence of the tat peptide was synthesized on an automatic synthesizer (PS3, Rainin, Woburn, MA) by Fmoc chemistry using 2-(1H-benzotriazole-1-yl)-1,1,3,3-tetramethyluronium hexafluorophosphate (HBTU)/*N*-hydroxybenzotriazole (HOBt) as activating agent. The peptide is referred to as tat(FITC). The sequence is Gly-Gly-Cys-*Gly-Arg-Lys-Lys-Arg-Arg-Gln-Arg-Arg-Arg*- Lys-(FITC)-NH_2 (the italicized amino acids correspond to residues 48−57 of the tat protein). Fmoc-Lys(Dde) was anchored to 0.1 mmol of Rink amide MBHA resin (NovaBiochem, San Diego, CA) and followed with other amino acids, e.g., Fmoc-Arg(Pbf), Fmoc-Gln(Trt), Fmoc-Lys(Boc), Fmoc-Gly, and Fmoc-Cys(Trt). The N-terminal was finally capped with t-Boc-Gly. Thereafter, the Dde group on the C-terminal lysine residue was selectively removed with 10 mL of 2% hydrazine in DMF (2×3 min) and the deprotected amino group was reacted with 0.4 mmol of fluorescein isothiocyanate (FITC) (Aldrich, Milwaukee, WI) in 5 mL of DMSO/diisopropylethylamine (20% v/v) overnight. The peptide was cleaved by 5 mL of TFA/thioanisole/ethandithiol/anisole (90/5/3/2) and purified by C18 reversed-phase HPLC. MALDI-MS ($M + H)^+$: 2130.4 (calc.), 2130.3 (found).

Synthesis of Amine Terminated Cross-Linked Superparamagnetic Iron Oxide (CLIO−NH2) (II). A monodispersed superparamagnetic iron oxide colloid (MION) **I** was synthesized and cross-linked with epichlohydrin (Aldrich) to prepare **II** as described (*22*). Briefly, amination was achieved by the addition of 50 mL of concentrated ammonia/200 mL of the MION colloid, followed by heating at 37 °C overnight. The mixture was incompatible with ultrafiltration equipment, so low molecular weight materials were removed by dialysis against

10.1021/bc980125h CCC: $18.00 © 1999 American Chemical Society
Published on Web 02/26/1999

water using dialysis tubing (12−14K cutoff) (Spectra/Por, Laguna Hills, CA). Air was then bubbled through the colloid for 24 h at 37 °C. The colloid was subjected to pressure dialysis with the addition of 10 vol of 5 mM sodium citrate, pH 8. These steps fully oxidize any ferrous iron and remove traces of low molecular weight materials. Final concentration was 26 mg Fe/mL.

Synthesis of 2-Pyridyl Disulfide Derivatized Superparamagnetic Iron Oxide (III). To 1.2 mL of **II** (31.2 mg Fe, 557 μmol) was added 1.2 mL of 0.1 M phosphate buffer, pH 7.4, and 2 mL of *N*-succinimidyl 3-(2-pyridyldithio)propionate (SPDP) (Molecular Biosciences, Boulder, CO) in DMSO (25 mM, 50 μmol). The mixture was allowed to stand for 60 min at room temperature. Low molecular impurities were removed by PD-10 columns (Sigma Chemical, St. Louis, MO) equilibrated with 0.01 M Tris and 0.02 M citrate, pH 7.4 buffer. The pooled void volume of 4.4 mL was recovered, containing **III** at a concentration of 7 mg Fe/mL.

To measure the number of 2-pyridyl disulfide groups attached, 0.2 mL of the solution above was added to 0.2 mL of 0.05 M DTT in 0.1 M phosphate, pH 7.4. The mixture was allowed to stand for 30 min at room temperature. A microconcentrator, 30 kDa cutoff (Amicon, Beverly, MA) was used to separate the product of the reduction, pyridine-2-thione (P2T), from iron. The concentration of P2T was determined using an extinction coefficient at 343 nm of 8100 M^{-1} cm^{-1}. Results are expressed as the number of SPDP groups per particle, i.e., per crystal, assuming 2064 Fe atoms/crystal (*23*).

Synthesis of Superparamagnetic Iron Oxide-Tat-(FITC) (CLIO−Tat) (IV). To 2.3 mL of **III** (16.1 mg/Fe, 288 μmol) was added 1.9 mL of tat(FITC), (803 μM, 1.52 μmol, as determined by FITC absorbance, extinction coefficient of 73 000 M^{-1} cm^{-1} at 494 nm in 0.1 M phosphate buffer). The mixture was allowed to react overnight at room temperature. The solution was applied to PD-10 columns equilibrated as above and the excluded volume containing **IV** saved. To measure the number of tat(FITC) groups attached, the colloid was reacted with DTT and applied to a microconcentrator as above. Released peptide in the filtrate was quantitated using FITC fluorescence read against a standards of FITC.

^{111}In Labeling of IV. To permit **IV** to chelate indium, it was reacted with DTPA dianhydride (Aldrich). **IV** was exhaustively dialyzed against 2.5 mM citrate, pH 6.5 (Spectra/Por membrane, 12−14 kDa cutoff). To 0.6 mL of iron oxide (17.1 μmol of Fe, 8.28 nmol of crystal with 56 nmol of tat-peptide attached) were added 0.1 mL of 0.1 M tetraborate buffer, pH 8.5, and 0.2 mL of 0.14 mM DTPA dianhydride in DMSO (0.028 μmol). The reaction was allowed to proceed at room temperature for 60 min. Unreacted DTPA was removed by using a PD-10 column, equilibrated with 0.02 M sodium citrate, pH 6.5. The samples were applied to the columns which was spin for 5 min at 800*g*. To the filtrate was added 0.72 mCi of ^{111}In (NEN Life Sciences, Boston, MA), which was allowed to react for 3 h at room temperature. The separation procedure was repeated with 45−50% of the radioactivity passing through the column.

Cellular Uptake Assays. Lymphocytes were prepared from mouse spleen as previously described (*5*). Briefly, mice (n = 2) were sacrificed under general anesthesia by lethal intravenous injection of sodium pentobarbital (220 mg/kg, Anpro, Arcadia, CA) and their spleens removed using aseptic procedures. Lymphocytes were obtained by disrupting the spleen between sterile frosted histology slides and dispersed in RPMI 1640 medium (Cellgro, Mediatech, Washington, DC) supplemented with 10% fetal bovine serum. After an initial centrifugation, erythrocytes were lysed by resuspending the cell pellet in 0.83% ammonium chloride in distilled water. To remove the majority of the monocyte/macrophage population, the nonadherent cells were transferred into a new flask after 1 h and counted. This method yielded a cell population containing about 95% lymphocytes, as determined by morphology. Cells were counted and their viability was determined with the Trypan Blue exclusion assay.

The uptake of ^{111}In-labeled **IV** in mouse lymphocytes was measured as previously described (*5*). To determine the amount of superparamagnetic particle associated with cells, we used a simple cell binding assay. Cell suspensions (10^6 cells) were placed into plastic tubes containing 1 mL of the media with different concentrations of ^{111}In-**IV**. Cells were incubated at 37° C for 1 h and then washed three times by centrifugation through a step gradient of 40% Histopaque-1077 (Sigma) in Hanks' balanced salt solution (Mediatech). After the last centrifugation and aspiration of the supernatant, cell pellets were counted in a gamma counter (1289 Compugamma LS; Wallac, Turku, Finland).

Fluorescence Microscopy. Lymphocytes, natural killer (NK) cells, and HeLa cells were further used for fluorescent microscopy. HeLa cells were grown to confluence on glass cover slips in 12 well plates (Becton Dickinson, Bedford, MA). The culture MEM (Minimum essential medium) was replaced with 500 μL of **IV** in MEM media, 0.2 mg Fe/mL. Same amount of **IV** was added to cell suspensions of NK cells and mouse lymphocytes. After 30 min at 37 °C the cells were washed 3 times with HBSS and analyzed by fluorescence microscopy. All images were obtained using a cooled charge coupled device (Photometrics, Tucson, AZ), operated via a linked Power Macintosh 7600/120 computer.

Immunohistochemical Stain for Dextran. To evaluate cellular localization of **IV**, HeLa cells were plated on glass cover slips in a 12 well plate at 60% confluency 24 h before the experiment. Cells were incubated with **IV** for 1 h at 20 μg of Fe, washed extensively with HBSS and fixed with MeOH:acetone (1:1) mixture for 10 min at −80° C. After fixation cells were incubated with anti-dextran IgA antibody W1329 (generous gift from Dr. Glaudemans) (*24*), followed by incubation with secondary biotinylated goat anti-mouse IgA antibody (Sigma). Biotin was probed for with avidin peroxidase (Bio-Rad, Hercules, CA). The color reaction was revealed with DAB Fast substrate tablets (Sigma).

Physical Properties of the Superparamagnetic Iron Oxide Particles. Relaxivity, iron concentration, and size by light scattering were measured as described (*23*). Special phantoms were constructed for NMR imaging that consisted of 10^7 cells embedded in agar to prevent drying and susceptibility artifacts. Freshly isolated lymphocytes were labeled with **IV** or **I**, and sedimented cell pellets were resuspended in 30 μL of warm agarose and placed into holes previously stenciled into the agarose. Each well was then sealed with an additional 0.5 mL of agarose. NMR imaging was performed with a 1.5 T superconducting magnet (Signa 5.0; GE Medical Systems, Milwaukee, WI) using a 5 in. surface coil. The imaging protocol consisted of coronal T1 weighted spin−echo (SE 300/11 where the first number represents the repetition time, TR, and the second number the echo time, TE), T2 weighted SE (SE 2000/102) or T2* gradient echo sequence (Steady-State Free Precession pulse sequence with TR/TE 50/60 and a flip angle of 20°) representative of commonly used pulse sequences in

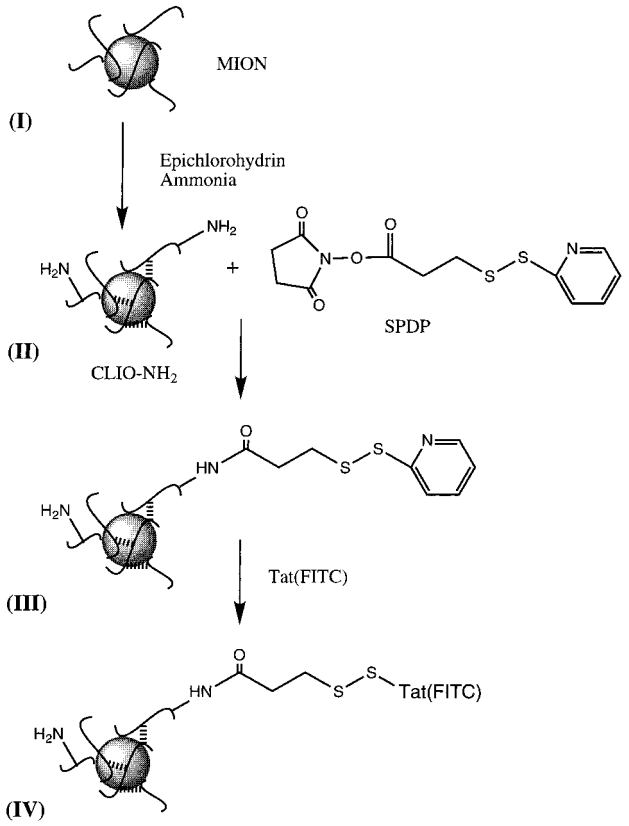


Figure 1. Synthetic scheme of superparamagnetic iron oxide-Tat peptide conjugate

clinical imaging. Slice thickness was 3 mm. The field of view (FOV) was 10 or 12 cm^2, using an 256 × 192 imaging matrix and 2−4 acquisition averages.

RESULTS AND DISCUSSION

A variety of MTS peptides have been used as vectors to carry various payloads into cells (*10, 25*−*27*). These reports inspired us to test whether MTS conjugated to nanometer sized superparamagnetic iron oxide particles could be used for intracellular magnetic cell labeling. Among the reported MTS peptides, HIV-1 tat is unique in that it is one of the shortest MTS signals. Tat peptides have been used to internalize different compounds into cells, such as peptides (*17*) and proteins (*13, 19*−*21*). Although it has been reported that tat peptide with extensions on both ends has a higher efficiency (*13*), we chose to use the shortest tat peptide (residues 48−57) (*17*) for our conjugate. The tat peptide was modified to carry a fluorescein isothiocyanate (FITC) tag, to follow the peptide during conjugation and as a marker for fluorescence microscopy. A Gly-Gly-Cys peptide was incorporated to the N-terminus to introduce a mono reactive sulfhydryl group.

The fluorescent peptide was attached to the amino group of a cross-linked dextran iron oxide (**1**) using SPDP (Figure 1). Reacting **II** with SPDP, the amino groups on **II** were converted to sulfhydryl groups, which were initially protected with 2-pyridyl disulfide. The degree of substitution was determined by reduction with DTT followed by ultrafiltration to free solutions of iron. Measuring the specific absorption of the released pyridine-2-thione at 343 nm, an average of 14 sulfhydryl groups was determined per particle.

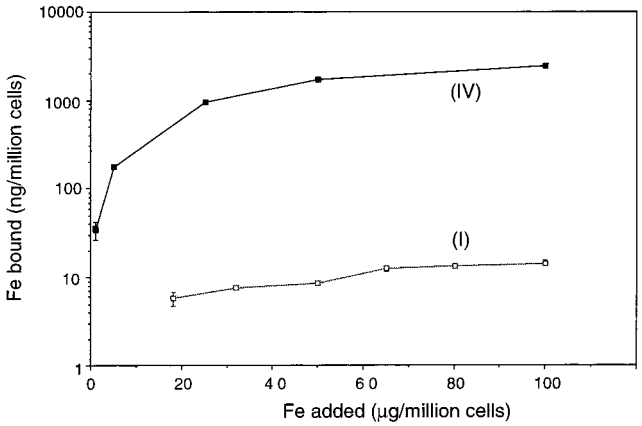


Figure 2. Uptake of **IV** and **I** by mouse lymphocytes at 37 °C for 1 h. **I** was prepared as described in ref *5*. Note the logarithmic *Y* axis. Cellular uptake of control peptide-particles were similar to **I** (data not shown).

Tat(FITC) was attached to activated **III** at pH 7.4 through a disulfide exchange reaction. After separating the free peptide from the conjugate **IV** by a size-exclusion column, a small portion of **IV** was used to determine the number of tat(FITC) per particle using the DTT reduction reaction and ultrafiltration. Released peptide was quantitated by determining FITC fluorescence against a FITC standard at 494 nm. An average of 6.7 peptides were thus attached per particle.

The physical properties of the superparamagnetic iron oxide colloids involved in this study are summarized in Table 1. No significant difference in the particle size was observed after peptide attachment. In addition, the similar relaxivity (values) of **II**, **III**, and **IV** indicate that the magnetic property of the colloid is unaffected by the reactions performed to attach tat(FITC).

A high cellular uptake of **IV** could be demonstrated in all three cell types tested in this study: murine lymphocytes, human natural killer cells and HeLa cells. With murine lymphocytes, the uptake of radioactive **IV** was quantified and compared to **I** (*5*) (Figure 2). Over a wide concentration range, the uptake of **IV** was about 100-fold higher than that of a conventional nonmodified magnetic particle. At the highest concentration of **IV** employed, 100 μg of Fe/million cells, there was an uptake of 2535 ng of iron/million cells corresponding to 12.7 × 10^6 particles/cells. Under similar conditions but using **I**, mouse peritoneal macrophages internalized 970 ng (*2*), while splenic lymphocytes, human and rat lymphocytes took up only 18.7, 27.9, and 11.5 ng, respectively (*5*). The concentration dependence of the uptake of **IV** was such that even at 20 μg of Fe/million cells, mouse lymphocytes internalized 981 ng/million cells (Figure 2), an amount equivalent to that obtained with macrophages at 100 μg of Fe/million cells.

Table 1: Physical Properties of Superparamagnetic Iron Oxide Colloids

compd	surface	size (nm)	2-pyridyl per particle	tat(FITC) per particle	R1[a]	R2[a]
II	cross-linked aminated dextran	37.1	ND	ND	22.4	76.7
III	cross-linked dextran-S-S-2Py	ND	14.3	ND	22.4	74.2
IV	cross-linked dextran-tat(FITC)	41.3	ND	6.7	22.3	71.9

[a] mM^{-1} s^{-1}.

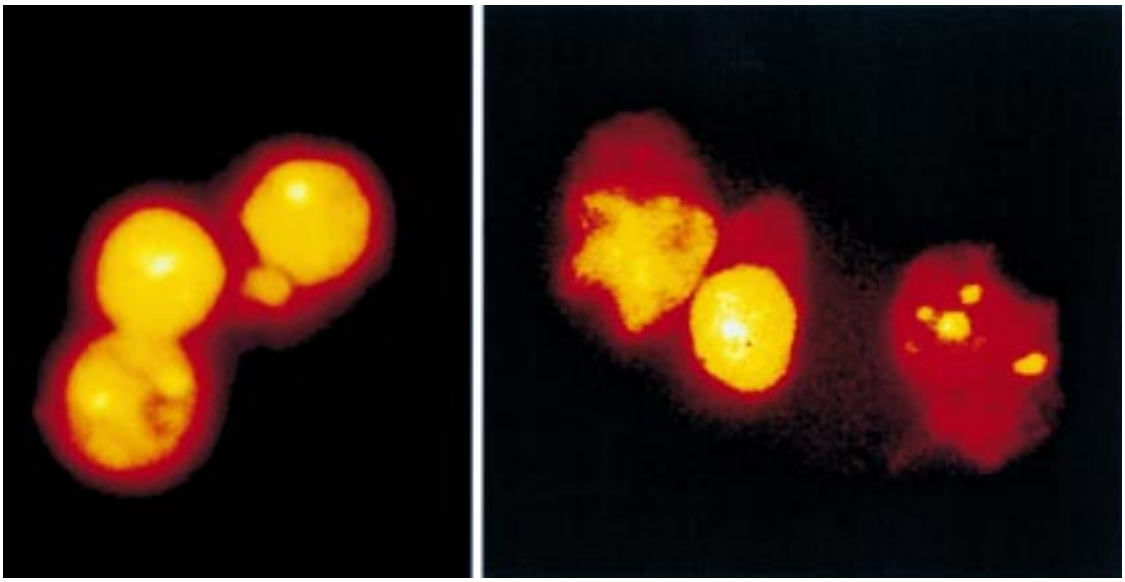


Figure 3. Fluorescence microscopy of murine lymphocytes (left) or activated human NK cells (right) 30 min after incubation with **IV**. The label is clearly contained within lymphocytes, particularly the nucleus and nucleoli. The shape of activated NK is slightly irregular representing terminal tufts. No significant intracellular fluorescence was observed when cells were labeled with FITC-**II** under identical conditions (not shown).

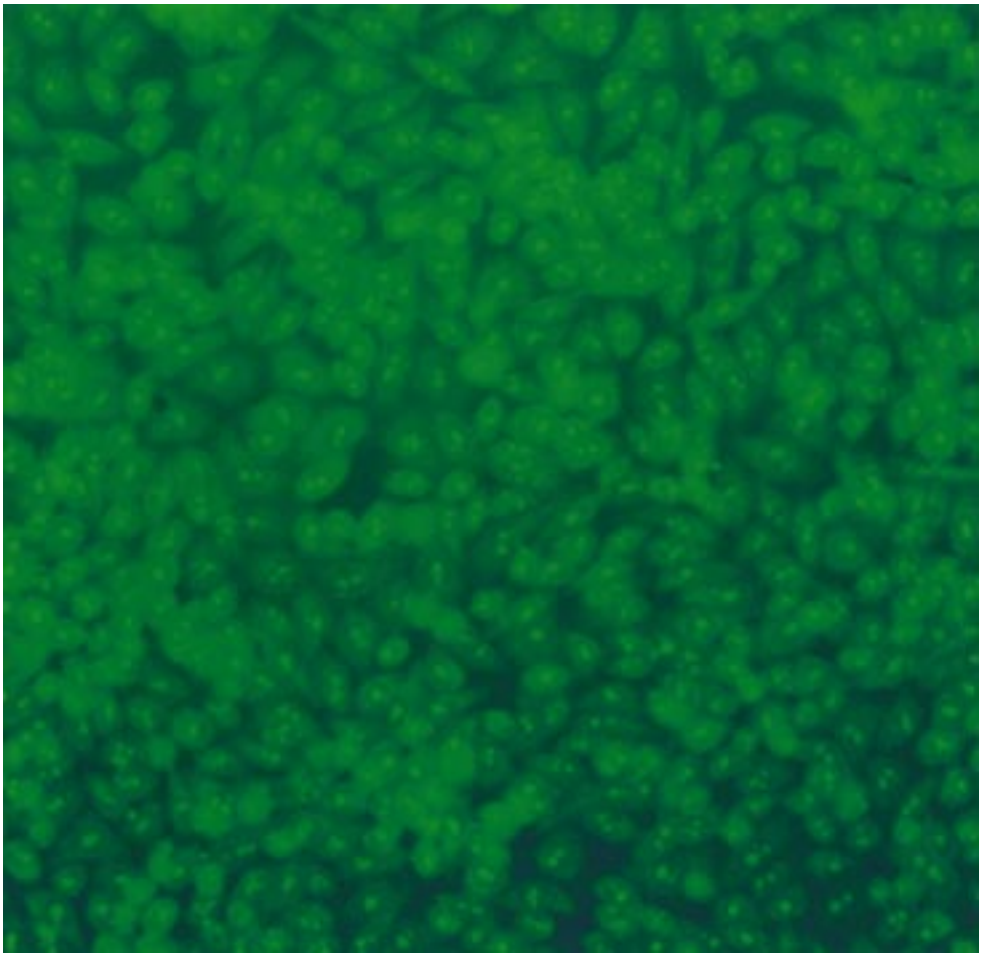


Figure 4. Fluorescence microscopy of HeLa cells incubated with **IV**.

Figure 3 shows the intracellular distribution of **IV** by fluorescence microscopy in murine lymphocytes and activated human NK cells. Fluorescence signal was distributed in the cytoplasm with particularly high concentrations in the nucleus and nucleolus. There was a notable lack of punctate staining as is observed with lysosomal accumulation where receptor-mediated or fluid phase endocytosis pathways are used for magnetic cell labeling (*5*). Intracellular location of **IV** was also examined in HeLa cells, which are commonly used in studies of MTS biology. Figure 4 shows HeLa cells after an incubation of 30 min with a concentration of 0.2 mM of Fe **IV**. A pronounced nuclear accumulation was observed in virtually all cells examined. Cells were not fixed to

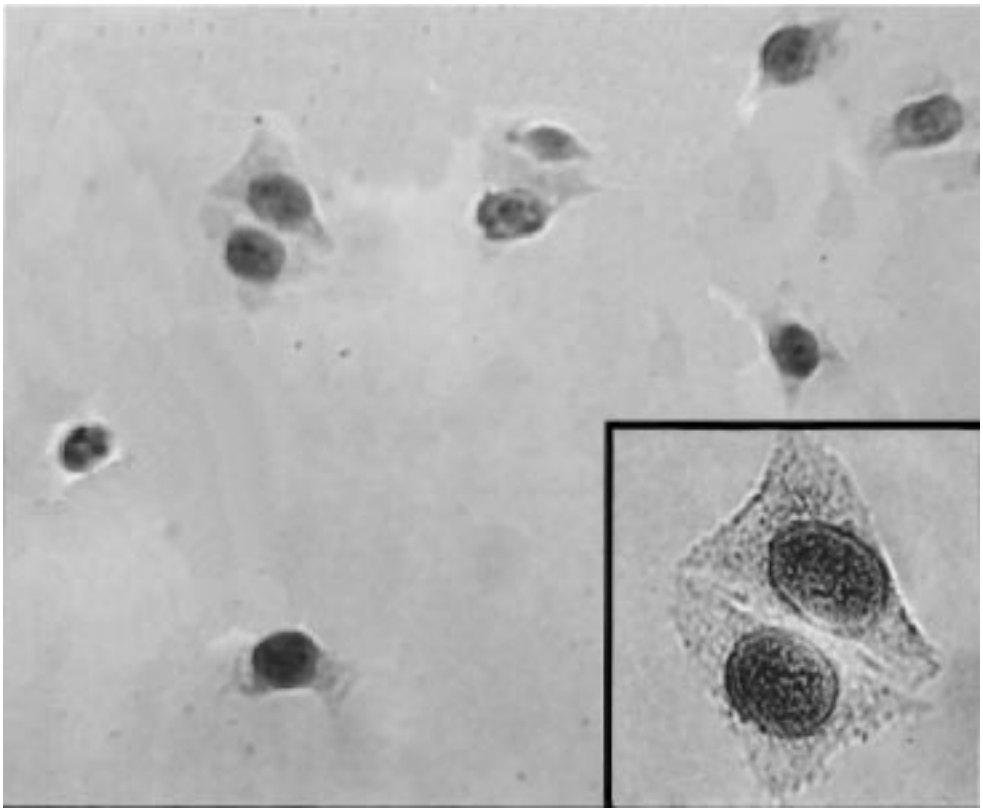


Figure 5. Anti-dextran staining of HeLa cells incubated with **IV**. (Inset) Magnification at 600×. The brown reaction product represents dextran within cell and the nucleus.

avoid possible alterations due to the fixing procedure. No significant cellular internalization was observed for the control compounds consisting of GRGDSPGGCK(FITC)-NH_2-**II** conjugate or FITC-**II**.

The linkage between the superparamagnetic iron and tat (FITC) peptide of conjugate **IV** is a reversible disulfide bond. Under physiological conditions, it is possible that the peptide is released from the particle. Although the fluorescence signal was clearly intracellular, we performed additional experiments to exclude the possibility of peptide dissociation. Briefly, cells were stained for dextran using a monoclonal antibody (*24*). As shown in Figure 5, dextran was concentrated in and distributed through the nucleus thus confirming internalization of the entire construct **IV**. This suggests that the uptake and nuclear localization of **IV** seen by fluorescence microscopy corresponds to the intact particle and not the dissociated peptide-tat (FITC).

Finally, we compared the magnetic effects of cellular internalization of **IV** and **I**. These studies were performed with lymphocytes incubated with either compound and then subjected to MR imaging using different pulse sequences. Figure 6 summarizes these results. Signal intensity differences were most marked with the T2 and T2* weighted sequences as predicted by theory. For example, **IV**-labeled cells produced a much lower signal intensity than did **I**-labeled cells (Figure 6). These results are entirely consistent with quantitative cell uptake studies (Figure 2) and attest to the feasibility of MR imaging of labeled cells. Furthermore, 95% of lymphocytes labeled with **IV** were retained on magnetic separation columns whereas cells labeled with **I** were not (data not shown).

We describe the synthesis and properties of a functionalized, biocompatible iron oxide particle containing multiple copies of a membrane translocating tat peptide.

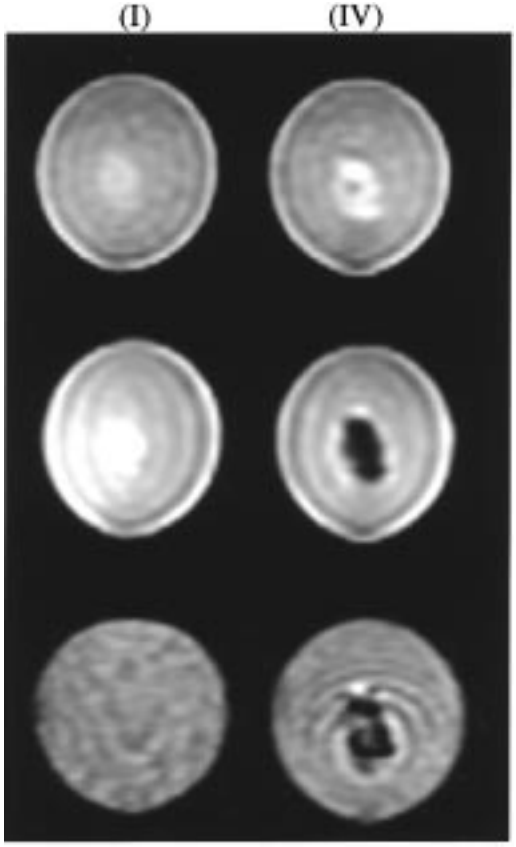


Figure 6. Comparative NMR imaging of **I** or **IV** labeled lymphocytes. (Top) T1 weighted spin−echo sequence (SE 300/11); middle T2 weighted sequences (FSE 2000/102); (bottom) T2* weighted sequence (SSFP 50/60/20°). Each well measures 2 cm in diameter and each agar plug contains a 20 μL insert with 10^7 labeled cells. Cell concentration and incubation conditions among the two samples are identical.

To the best of our knowledge, our study is the first to show that relatively short MTS signals can internalize entire nanometer sized magnetic particles into cells. A second type of tat (FITC) conjugate was synthesized devoid of the C-terminal GGC sequence. Both conjugates were internalized in a similar manner (data not shown). Utilizing the above-described approach, a variety of studies are currently being conducted to further explore the exact mechanism of cellular internalization of **IV** conjugates. Preliminary trypan blue exclusion toxicity studies showed no cellular toxicity at incubation concentrations used for MR imaging (up to 30 μg of Fe). Apart from more elaborate toxicity studies, additional MR imaging studies are underway to determine the threshold of cell detection by NMR imaging. Initial feasibility studies have also shown that magnetically labeled cells are indeed recoverable by magnetic cell separation technique after intravenous administration.

LITERATURE CITED

(1) Olsvik, O., Popovic, T., Skjerve, E., Cudjoe, K. S., Hornes, E., Ugelstad, J., and Uhlen, M. (1994) Magnetic separation techniques in diagnostic microbiology. *Clin. Microbiol. Rev. 7*, 43−54.

(2) Weissleder, R., Cheng, H. C., Bogdanova, A., and Bogdanov, A. (1997) Magnetically labeled cells can be detected by MR imaging. *J. Magn. Reson. Imaging 7*, 258−63.

(3) Yeh, T. C., Zhang, W., Ildstad, S. T., and Ho, C. (1993) Intracellular Labeling of T-Cells with Superparamagnetic Contrast Agents. *Magn. Reson. Med. 30*, 617−25.

(4) Yeh, T. C., Zhang, W., Ildstad, S. T., and Ho, C. (1995) In Vivo Dynamic MRI Tracking of Rat T-Cells Labeled with Superparamagnetic Iron-Oxide Particles. *Magn. Reson. Med. 33*, 200−208.

(5) Schoepf, U., Marecos, E., Melder, R., Jain, R., and Weissleder, R. (1998) Intracellular magnetic labeling of lymphocytes for in vivo trafficking studies. *BioTechniques 24*, 642−51.

(6) Handgretinger, R., Lang, P., Schumm, M., Taylor, G., Neu, S., Koscielnak, E., Niethammer, D., and Klingebiel, T. (1998) Isolation and transplantation of autologous peripheral CD34+ progenitor cells highly purified by magnetic-activated cell sorting. *Bone Marrow Transpl. 21*, 987−93.

(7) Moore, A., Basilion, J. P., Chiocca, E. A., and Weissleder, R. (1998) Measuring transferrin receptor gene expression by NMR imaging. *Biochim. Biophys. Acta 1402*, 239−49.

(8) Tsai, E., Bogdanov, A., Papisov, M., Brady, T. J., and Weissleder, R. (1992) Lymphocytes as drug carriers for MR contrast agents. Society of Magnetic Resonance in Medicine, 11th Annual Meeting, August 8−14, Berlin.

(9) Derossi, D., Calvet, S., Trembleau, A., Brunissen, A., Chassaing, G., and Prochiantz, A. (1996) Cell internalization of the third helix of the Antennapedia homeodomain is receptor-independent. *J. Biol. Chem. 271*, 18188−93.

(10) Avrameas, A., Ternynck, T., Nato, F., Buttin, G., and Avrameas, S. (1998) Polyreactive anti-DNA monoclonal antibodies and a derived peptide as vectors for the intracytoplasmic and intranuclear translocation of macromolecules. *Proc. Natl. Acad. Sci. U.S.A. 95*, 5601−6.

(11) Phelan, A., Elliott, G., and O'Hare, P. (1998) Intercellular delivery of functional p53 by the herpesvirus protein VP22. *Nat. Biotechnol. 16*, 440−3.

(12) Elliott, G., and O'Hare, P. (1997) Intercellular trafficking and protein delivery by a herpesvirus structural protein. *Cell 88*, 223−33.

(13) Fawell, S., Seery, J., Daikh, Y., Moore, C., Chen, L. L., Pepinsky, B., and Barsoum, J. (1994) Tat-mediated delivery of heterologous proteins into cells. *Proc. Natl. Acad. Sci. U.S.A. 91*, 664−8.

(14) Frankel, A. D., and Pabo, C. O. (1988) Cellular uptake of the tat protein from human immunodeficiency virus. *Cell 55*, 1189−93.

(15) Mann, D. A., and Frankel, A. D. (1991) Endocytosis and targeting of exogenous HIV-1 Tat protein. *EMBO J. 10*, 1733−9.

(16) Vives, E., Brodin, P., and Lebleu, B. (1997) A truncated HIV-1 Tat protein basic domain rapidly translocates through the plasma membrane and accumulates in the cell nucleus. *J. Biol Chem. 272*, 16010−7.

(17) Vives, E., Granier, C., Prevot, P., and Lebleu, B. (1997) Structure−activity relationship study of the plasma membrane translocating protential of a short peptide from HIV-1 Tat protein. *Lett. Pept. Sci. 4*, 1−8.

(18) Schluesener, H. J. (1996) Protection against experimental nervous system autoimmune diseases by a human immunodeficiency virus-1 Tat peptide-based polyvalent vaccine. *J. Neurosci. Res. 46*, 258−62.

(19) Efthymiadis, A., Briggs, L. J., and Jans, D. A. (1998) The HIV-1 Tat nuclear localization sequence confers novel nuclear import properties. *J. Biol. Chem. 273*, 1623−8.

(20) Pepinsky, R. B., Androphy, E. J., Corina, K., Brown, R., and Barsoum, J. (1994) Specific inhibition of a human papillomavirus E2 trans-activator by intracellular delivery of its repressor. *DNA Cell Biol. 13*, 1011−9.

(21) Anderson, D. C., Nichols, E., Manger, R., Woodle, D., Barry, M., and Fritzberg, A. R. (1993) Tumor cell retention of antibody Fab fragments is enhanced by an attached HIV TAT protein-derived peptide. *Biochem. Biophys. Res. Commun. 194*, 876−84.

(22) Palmacci, S., and Josephson, L. (1993) *Synthesis of polysaccharide covered superparamagnetic oxide colloids*, U.S. Patent 5,262,176.

(23) Shen, T., Weissleder, R., Papisov, M., Bogdanov, A., and Brady, T. J. (1993) Monocrystalline iron oxide nanocompounds (MION): physiocochemical properties. *Magn. Reson. Med. 29*, 599−604.

(24) Nashed, E. M., and Glaudemans, C. P. (1996) Observations on the binding of four anti-carbohydrate monoclonal antibodies to their homologous ligands. *J. Biol. Chem. 271*, 8209−14.

(25) Pooga, M., Soomets, U., Hallbrink, M., Valkna, A., Saar, K., Rezaei, K., Kahl, U., Hao, J. X., Xu, X. J., Wiesenfeld-Hallin, Z., Hokfelt, T., Bartfai, T., and Langel, U. (1998) Cell penetrating PNA constructs regulate galanin receptor levels and modify pain transmission in vivo. *Nat. Biotechnol. 16*, 857−61.

(26) Rojas, M., Donahue, J. P., Tan, Z., and Lin, Y. Z. (1998) Genetic engineering of proteins with cell membrane permeability. *Nat. Biotechnol. 16*, 370−5.

(27) Chaloin, L., Vidal, P., Lory, P., Mery, J., Lautredou, N., Divita, G., and Heitz, F. (1998) Design of carrier peptide−oligonucleotide conjugates with rapid membrane translocation and nuclear localization properties. *Biochem. Biophys. Res. Commun. 243*, 601−8.

BC980125H

Novel Paramagnetic Macromolecular Complexes Derived from the Linkage of a Macrocyclic Gd(III) Complex to Polyamino Acids through a Squaric Acid Moiety

Silvio Aime,*,† Mauro Botta,† Simonetta Geninatti Crich,† Giovanni Giovenzana,‡ Giovanni Palmisano,§ and Massimo Sisti‡

Dipartimento di Chimica IFM, Università di Torino, via P. Giuria 7, I-10125 Torino, Italy, Dipartimento di Chimica Organica ed Industriale, Università di Milano, Viale Venezian 21, I-20133 Milano, Italy, and Dipartimento di Scienza e Tecnologia del Farmaco, Università di Torino, via P. Giuria 9, I-10125 Torino, Italy.
Received March 16, 1998; Revised Manuscript Received October 15, 1998

Macromolecular Gd(III) complexes may find useful application as contrast agents for magnetic resonance angiography (MRA). Herein two novel systems are reported, namely $Gd(DO3ASQ)_3-lys_{16}$ and $Gd(DO3ASQ)_{30}-orn_{114}$. Their syntheses are based on the ability of the squaric acid moiety to act as a linker between the DO3A (1,4,7,10-tetraazacyclododecane-1,4,7-triacetic acid) chelate moiety and the polyamino acidic chain. Moreover, the squaric acid participates in the coordination cage of the Gd(III) ion. The investigation of ^1H and ^{17}O NMR relaxation processes of solvent water nuclei allowed a detailed characterization of the systems under study. $Gd(DO3ASQ)_{30}-orn_{114}$ displays a remarkable ability to enhance the water proton relaxation rate of its solutions, and it may be considered as potential contrast agent for MRA applications.

INTRODUCTION

The search for macromolecular Gd(III) complexes (*1*, *2*) has been an important issue in the past decade of development of contrast agents (CA) for magnetic resonance imaging (MRI) (*3*−*5*). This interest is even stronger now that magnetic resonance angiography (MRA) is becoming a procedure of widespread use. These macromolecular systems provide both an enhanced ability to catalyze solvent proton relaxation rates [through the occurrence of a long molecular reorientational time τ_R (*6*, *7*)] and an increased lifetime of the CA in the circulating blood by avoiding the extravasation typical of the small-sized Gd(III) complexes commonly employed in MRI investigations. It was earlier reported that an easy way to attach a chelating moiety to a macromolecule consists of forming an amide linkage with the reaction of an amino group on the macromolecule and the bis(anhydride) derivative of DTPA. This procedure has been used to prepare systems such as $(GdDTPA)_n$−albumin and $(GdDTPA)_n$−polylysine (*8*, *9*).

The main drawback in the use of the bifunctional dianhydride DTPA stems from the occurrence of undesiderable intra- and intermolecular cross-linking reactions. Intermolecular cross-linking may be reduced by the use of low protein concentrations, but this has no effect on intramolecular cross-linking, which represents a major risk in the case of highly flexible macromolecules such as polylysine (*10*). The diconjugation of DTPA is expected to cause a large reduction of the thermodynamic stability of the metal complexes as proved in a detailed study on model systems (*11*). The search has then been addressed to methods that preclude diconjugation of the chelate, for instance, through the use of the monoanhydride derivative of DTPA (*12*). However, as outlined also by other authors (*10*), the synthesis of the latter ligand appears to be difficult to reproduce and the yields are invarianty low. For the same purpose other authors have dealt with functionalized DOTA chelates (*13*). Again, the employed procedures are rather laborious and troublesome. On this basis, the need for a monoreactive chelate derivative that would enable extensive and specific activation of amino groups in macromolecules is still vivid.

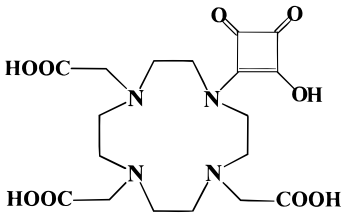
The effectiness of paramagnetic CAs is represented by their relaxivity (r_{1p}); that is, the water proton relaxation rate of a 1 mM solution of the Gd(III) chelate, that, at the magnetic fields usually employed in MRI (0.5−1.5 T), is roughly proportional to the molecular reorientation time (τ_R) of the complex. Unfortunately, the relaxivity of such systems is not as high as one would expect on the basis of their molecular weights. Possible causes for such behavior may be either the occurrence of internal motions that reduce the effective molecular reorientation time or the presence of a relatively long exchange lifetime (τ_M) of the coordinated water molecule or both. As far as the exchange of the water molecule coordinated to the Gd(III) ion is concerned, the enhancement of the solvent relaxation rate (R_{1p}^{is}) is "quenched" when τ_M is longer than the relaxation time of these protons (T_{1M}) (*14*).

Indeed, a number of bis(amide) DTPA Gd(III) complexes have been reported to have τ_M values of ∼1 μs at room temperature (*15*), whereas other DTPA- and DOTA-like (1,4,7,10-tetraazacyclododecane-*N*,*N*′,*N*″,*N*‴-tetraacetic acid) Gd(III) complexes display shorter τ_M values (*14*). On this basis, it was deemed of interest to explore alternative routes to obtain conjugates between macromolecular substrates and Gd(III) chelate moieties different from DTPA-amide. Since it has been recently reported that squaric esters readily react with amino groups (*16*), under mild conditions, we decided to explore

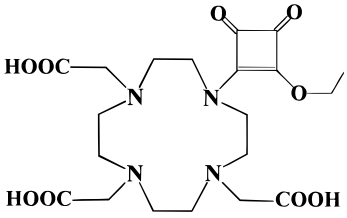
* Author to whom correspondence should be addressed [fax (+39)-11-670-7524; e-mail aime@silver.ch.unito.it].
† Dipartimento di Chimica IFM.
‡ Dipartimento di Chimica Organica ed Industriale.
§ Dipartimento di Scienza e Tecnologia del Farmaco.

10.1021/bc980030f CCC: $18.00 © 1999 American Chemical Society
Published on Web 02/05/1999

Scheme 1



DO3ASQ



DO3ASQ-est

their use in the formation of stable linkages between Gd(III) complexes and NH_2 moieties on macromolecular substrates. Furthermore, once the squaric ester derivatives are bonded to an amino nitrogen of a tetraazacyclododecane macrocycle as in DO3ASQ and DO3ASQ-est ligands (Scheme 1), they may show coordination properties analogous to those displayed by an acetate arm in the parent DOTA ligand.

EXPERIMENTAL PROCEDURES

Syntheses. *Synthesis of 10-(2-Ethoxy-3,4-dioxo-1-cyclobutenyl)-1,4,7,10-tetraazacyclododecane-1,4,7-triacetic Acid, (Tri)-tert-Butyl Ester (**3**).* To a stirred solution of the triester (**1**) [1,4,7,10-tetraazacyclododecane-1,4,7-triacetic acid, (tri)-*tert*-butyl ester] (*17*), kindly provided by Bracco (Bracco S.p.A., Milano, Italy) (3.3 g, 6.1 mmol) in ethanol (50 mL) is added a solution of diethyl squarate (1.24 g, 7.73 mmol) in one portion. The resulting mixture is stirred overnight at room temperature and then evaporated in vacuo. The product is purified by column chromatography (SiO_2, $CHCl_3$/acetone 50:50 → 10:90), yielding 3.60 g (92.7%) of **3** as a light yellow viscous oil: ^{1}H NMR (300 MHz, $CDCl_3$) δ 4.72 q[2H] (J = 7.1 Hz), 3.93 t[2H] (J = 6.0 Hz), 3.78 t[2H] (J = 6.0 Hz), 3.26 s[2H], 3.25 s[4H], 2.98 m[4H], 2.72 m[8H], 1.42 s[27H], 1.30 t[3H] (J = 7.1 Hz); ^{13}C NMR (75.5 MHz, $CDCl_3$) δ 189.0, 182.1, 176.1, 172.0, 170.6, 81.0, 69.2, 58.0, 57.6, 56.7, 55.6, 54.8, 54.6, 53.2, 53.0, 52.1, 52.0, 49.6, 48.7, 28.1, 15.8; IR (neat) 2979, 2932, 2848, 1797, 1731, 1714, 1613 cm^{-1}; MS(CI), m/z 640 (MH^+), 611 (−CO); R_f (TLC) = 0.78 (SiO_2, acetone).

Synthesis of 10-(2-Hydroxy-3,4-dioxo-1-cyclobutenyl)-1,4,7,10-tetraazacyclododecane-1,4,7-triacetic Acid (Trifluoroacetate) (DO3ASQ). To a stirred solution of the tetraester **3** (3.27 g) in THF (20 mL) is added concentrated HCl (37%, 2.5 mL), and the mixture is stirred for 24 h at room temperature. Diethyl ether (20 mL) is slowly added to form a two-phase system, which is allowed to stand at room temperature overnight. The crystalline product DO3ASQ is isolated by filtration, washed with diethyl ether, and dried in vacuo. The product is recrystallized from water, obtaining 2.88 g: mp 223−225 °C (dec); ^{1}H NMR (D_2O, 200 MHz) δ 4.25 m[4H], 3.60 m[4H], 3.48 m[4H], 3.46 s[6H], 3.08 m[4H]; ^{13}C NMR (D_2O, 50.3 MHz) δ 198.6, 190.0, 184.2, 179.4, 170.5, 56.4, 55.6, 55.2, 54.1, 52.2, 49.3; IR (Nujol mull) 3500−2500 (bb), 1813, 1751, 1694, 1665 cm^{-1}.

Synthesis of 10-(2-Ethoxy-3,4-dioxo-1-cyclobutenyl)-1,4,7,10-tetraazacyclododecane-1,4,7-triacetic Acid (Trifluoroacetate) (DO3ASQ-est). A solution of compound **3** (204.0 mg, 0.3194 mmol) in trifluoroacetic acid (1 mL) was stirred overnight at room temperature. After evaporation to dryness, the residue was dissolved in methanol (1 mL); slow addition of diethyl ether (10 mL) caused the precipitation of DO3ASQ-est as a white powder, which was collected by centrifugation, washed with diethyl ether, and dried in vacuo (140.7 mg): mp 170−175 °C (dec); ^{1}H NMR (D_2O, 200 MHz) δ 4.65 q[2H] (J = 7.0 Hz), 3.82−3.51 m[10H], 3.16−3.00 m[12H], 1.36 t[3H] (J = 7.1 Hz).

Syntheis of Polylysine Conjugate. Polylysine hydrobromide (**5**, 49.1 mg; Sigma, St. Louis, MO) is dissolved in 250 μL of H_2O; triethylamine (500 μL) is added to the clear solution and, after 5 min, a solution of the tetraester **4** (33.6 mg) in 750 μL of ethanol is added in one portion. The mixture is stirred at room temperature for 72 h, with the disappearance of **4** (SiO_2, $CHCl_3$/MeOH 9:1) monitored by TLC. The mixture is evaporated in vacuo and the residue dissolved in neat trifluoroacetic acid (3 mL) and stirred overnight at room temperature; the solution is evaporated, and the residue is dissolved in 1 mL of methanol. By slow addition of a 4-fold volume of diethyl ether, the conjugate (**7**) precipitated as a white amorphous powder, which was collected by centrifugation, repeatedly washed with diethyl ether, and dried in vacuo (yield = 69.7 mg).

The presence of unconjugated DO3ASQ monomer has been ruled out on the basis of HPLC analysis. The experimental setup of HPLC analysis is as follows: Hamilton PRP-1 column (5 μm, 250 × 4 mm), UV detector at 260 nm, isocratic elution with a 10:90 mixture of acetonitrile/TBOH, 0.02 M, pH 6.5 by H_2SO_4; elution flux = 1 mL/min. The samples were derivatized by treatment with a 0.01 M $CuSO_4$ solution.

Synthesis of Polyornithine Conjugate. Polyornithine hydrochloride (**5**, 51.6 mg; Sigma) is dissolved in 500 μL of H_2O; triethylamine (500 μL) is added to the clear solution and, after 5 min, a solution of the tetraester **4** (60.9 mg) in 500 μL of ethanol is added in one portion. The mixture is stirred at room temperature for 72 h, with the disappearance of **4** (SiO_2, $CHCl_3$/MeOH 9:1) monitored by TLC. The mixture is evaporated in vacuo and the residue dissolved in neat trifluoroacetic acid (3 mL) and stirred overnight at room temperature; the solution is evaporated, and the residue is dissolved in 1 mL of methanol. By slow addition of a 4-fold volume of diethyl ether, the conjugate (**7**) precipitated as a white amorphous powder, which was collected by centrifugation, repeatedly washed with diethyl ether, and dried in vacuo (yield = 72.7 mg).

The absence of unconjugated DO3ASQ monomer has been checked by HPLC as described above for the polylysine conjugate.

Preparation of the Gd(III) Complexes. The complexation has been carried out by adding stoichiometric amounts of $GdCl_3$ to the aqueous solutions of the ligands at neutral pH and at room temperature. The formation of the complex has been followed by measuring the solvent proton relaxation rate ($1/T_1$). The presence of an excess of free Gd(III) ions, which yields a noticeable increase of the observed relaxation rate, may be quickly removed by centrifugation of the solution brought to basic pH.

NMR Measurements. The longitudinal water proton relaxation rate was measured by using a Stelar Spin-

master spectrometer [Stelar, Mede (PV) Italy] operating at 20 MHz, by means of the standard inversion−recovery technique (16 experiments, 2 scans). A typical 90° pulse width was 3.5 μs, and the reproducibility of the T_1 data was ±0.5%. The temperature was controlled with a Stelar VTC-91 air-flow heater equipped with a copper−constantan thermocouple (uncertainty of ±0.1 °C).

The proton $1/T_1$ NMRD profiles were measured over a continuum of magnetic field strength from 0.00024 to 1.2 T (corresponding to 0.01−50 MHz proton Larmor frequency) on the Koenig−Brown field-cycling relaxometer installed at the NMR relaxometry laboratory of the University of Torino (Italy). The relaxometer works under complete computer control with an absolute uncertainty in $1/T_1$ of ±1%. Details of the instrument and of the data acquisition procedure may be found elsewhere (*18*).

Variable-temperature ^{17}O NMR measurements were recorded on a JEOL EX-90 (2.1 T) spectrometer, equipped with a 5 mm probe, by using a D_2O external lock. Experimental settings were as follows: spectral width = 10000 Hz, pulse width = 7 μs, acquisition time = 10 ms, 1000 scans, and no sample spinning. Solutions containing 2.6% of ^{17}O isotope (Yeda, Israel) were used. The observed transverse relaxation rates (R^{O}_{2obs}) were calculated from the signal width at half-height. The ^{1}H and ^{13}C NMR spectra of the ligands were performed on a Bruker AC-200 spectrometer (7.1 T). *tert*-Butyl alcohol (1%) was used as internal reference ($\delta^{1H} = 1.29$ ppm, $\delta^{13C} = 31.3$ ppm, and $\delta^{31P} = 0$ ppm) for ^{1}H/^{13}C NMR spectra recorded using as solvent D_2O (99.8%, Merck, Darmstadt, Germany).

THEORY

^{1}H Water Relaxation Rate. The longitudinal water proton relaxivity r^{H}_{1p} is defined as the paramagnetic contribution to the observed water proton relaxation rate (R^{H}_{1obs}) of a 1 mM solution of the paramagnetic metal complex:

$$r^{H}_{1p} = R^{H}_{1obs} - R^{H}_{1d} \quad (1)$$

In eq 1 R^{H}_{1d} is the water proton relaxation rate in the presence of an equimolar amount of a diamagnetic analogue of the paramagnetic compound which, for diluted solutions, may be made equal to the value of 0.38 s^{-1}, that is, the relaxation rate of pure water at 298 K. The observed relaxivity results from contributions arising from water molecules in the inner- and outer-coordination spheres of the metal ion:

$$r^{H}_{1p} = r^{His}_{1p} + R^{Hos}_{1p} \quad (2)$$

r^{His}_{1p} deals with the contribution arising from the exchange of the water directly coordinated to the paramagnetic metal ion and is given by

$$R^{His}_{1p} = (Cq/55.6)(T^{H}_{1M} + \tau^{H}_{M}) \quad (3)$$

where C is the molar concentration of the complex, q the hydration number, T^{H}_{1M} the longitudinal relaxation time of the inner-sphere water protons, and τ^{H}_{M} their residence lifetime. The Solomon−Bloembergen theory (*19*) describes the magnetic field dependence of T^{H}_{1M}, which, for a Gd(III) chelate, is given by

$$\frac{1}{T^{H}_{1M}} = \frac{2}{15}\frac{2\gamma_H^2 g_e^2 \mu_B^2 S(S+1)}{r_H^6}\left[\frac{3\tau_{c1}}{1+\omega_H^2\tau_{c1}^2} + \frac{7\tau_{c2}}{1+\omega_S^2\tau_{c2}^2}\right] \quad (4)$$

where S is the electron spin quantum number [$^7/_2$ for Gd(III)], γ_H is the proton nuclear magnetogyric ratio, μ_B is the Bohr magneton, g_e is the Landè factor for the free electron, r_H is the distance between the metal ion and the inner-sphere water protons, ω_H and ω_S are the proton and electron Larmor frequencies ($\omega_S = 658\omega_H$), respectively, and τ_{ci} ($i = 1, 2$) are the correlation times related to the modulation of the electron−proton dipolar coupling. Such an interaction may be modulated by the reorientation of the paramagnetic species, τ_R, by the residence lifetime of the inner-sphere water molecule (τ_M) and by the electronic relaxation times, T_{iE}.

$$\tau_{ci}^{-1} = \tau_R^{-1} + \tau_M^{-1} + T_{iE}^{-1} \quad (5)$$

In analogy with the nuclear relaxation time also the electronic relaxation processes depend on the magnetic field strength. For Gd(III) complexes T_{iE} are related to the modulation of the zero field splitting (ZFS) of the electronic spin states due to the dynamic distortions of the ligand field interaction and, according to the Blombergen−Morgan theory (*20*), their magnetic field dependence is given by the following equations:

$$T_{1E}^{-1} = \frac{1}{25}\Delta^2\tau_v[4S(S+1) - 3]\left(\frac{1}{1+\omega_S^2\tau_v^2} + \frac{4}{1+4\omega_S^2\tau_v^2}\right) \quad (6)$$

$$T_{2E}^{-1} = \frac{1}{50}\Delta^2\tau_v[4S(S+1) - 3] \times \left(3 + \frac{5}{1+\omega_S^2\tau_v^2} + \frac{2}{1+4\omega_S^2\tau_v^2}\right) \quad (7)$$

where Δ^2 is the trace of the square of the transient ZFS tensor and τ_v is the correlation time related to its modulation. The outer-sphere term, R^{Hos}_{1p}, describes the contribution arising from the water molecules diffusing near the paramagnetic chelate and, according to the model of Hwang and Freed (*21*), may be related to the minimum distance between the metal and the diffusing water molecules, a, the relative solute−solvent diffusion coefficient, D, and the electronic relaxation times, T_{iE}

$$R^{Hos}_{1p} = C^{os}\left(\frac{1}{aD}\right)[7J(\omega_S) + 3J(\omega_H)] \quad (8)$$

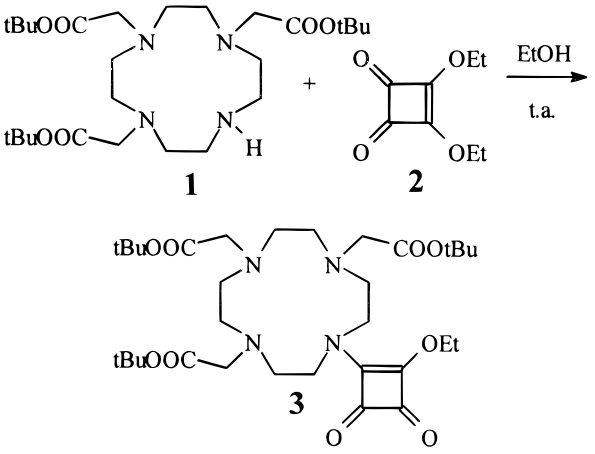
where C^{os} is a constant (5.8×10^{-13} s^{-2} M^{-1}) and the dependence on the electronic relaxation times is expressed in the non-Lorentzian spectral density functions $J(\omega_i)$.

^{17}O Water Relaxation Rate. The residence lifetime of a water molecule directly coordinated to a paramagnetic metal ion (τ^{O}_{M}) may be evaluated by measuring the temperature dependence of the paramagnetic contribution (R^{O}_{2p}) to the observed ^{17}O water solvent transverse relaxation rate

$$R^{O}_{2p} = R^{O}_{2obs} - R^{O}_{2d} \quad (9)$$

where, in analogy with ^{1}H measurements, the diamagnetic term R^{O}_{2d} is measured on a solution containing a diamagnetic analogue of the chelate of interest. (We used ^{17}O NMR data of LaDOTA.) R^{O}_{2p} is related to τ^{O}_{M} through

Scheme 2



the values of $\Delta\omega_M^O$ (which is the ^{17}O chemical shift difference between coordinated and bulk water molecule) and R_{2M}^O (which is the transverse relaxation rate of the coordinated water oxygen) (*22*):

$$R_{2p}^O = \frac{qC}{55.6}\tau_M^{O-1}\frac{R_{2M}^{O\,2} + \tau_M^{O-1}R_{2M}^O + \Delta\omega_M^{O\,2}}{(R_{2M}^O + \tau_M^{O-1})^2 + \Delta\omega_M^{O\,2}} \quad (10)$$

The temperature dependence of $\Delta\omega_M^O$ is described by the equation

$$\Delta\omega_M^O = \frac{g_e\mu_B S(S+1)B_0}{3k_B T}\frac{A}{\hbar} \quad (11)$$

where B_0 is the magnetic field strength (2.11 T in this work) and $A/\hbar$ is the Gd-^{17}O scalar coupling constant [the value of which for polyaminocarboxylate Gd(III) complexes may be reasonably fixed to -3.8×10^6 rad s^{-1}].

For relatively small-sized Gd(III) chelate and at the field of 2.11 T used in this work, R_{2M}^O is dominated by the electron−nucleus scalar interaction:

$$R_{2M}^O = \frac{1}{3}\left(\frac{A}{\hbar}\right)^2 S(S+1)\left(\tau_{E1} + \frac{\tau_{E2}}{1+\omega_S^2\tau_{E2}^2}\right) \quad (12)$$

$$\tau_{E2}^{-1} = T_{iE}^{-1} + (\tau_M^O)^{-1} \quad (13)$$

Finally, the temperature dependence of R_{2P}^O is expressed in terms of the Eyring relationship for τ_M^O and τ_v

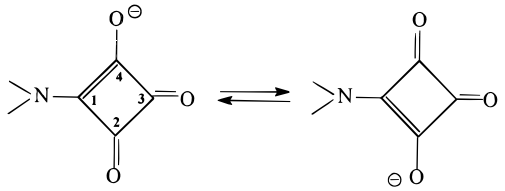
$$(\tau_j)_T^{-1} = \frac{(\tau_j^{-1})^{298.15}T}{298.15}\exp\left[\frac{\Delta H_j}{R}\left(\frac{1}{298.15} - \frac{1}{T}\right)\right] \quad (14)$$

where j refers to the two different dynamic processes involved (j = v, M) and ΔH_j is the corresponding activation enthalpy.

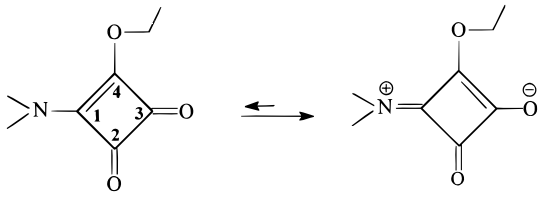
RESULTS AND DISCUSSION

Synthesis of the Ligands DO3ASQ and DO3ASQ-est. The ligands reported herein were prepared starting from diethyl squarate **2** (Scheme 2). The reactivity of this compound toward amines has been already investigated (*23*−*25*). Diethyl squarate may be selectively converted into the corresponding mono- or bis(amide)s (*26*, *27*) simply by varying the experimental conditions. Reaction of a slight excess of diethyl squarate **2** with DO3A−*tert*-butyl ester (**1**) in ethanol at room temperature gave, after silica gel chromatography, nearly quantitative yields of tetraester **3**.

Scheme 3



Scheme 4



The ligand **4** was obtained in good yield by reacting **3** with concentrated HCl/THF at room temperature, which promotes the simultaneous hydrolysis of the *tert*-butyl and ethyl ester groups.

^{13}C NMR Characterization of DO3ASQ and DO3ASQ-est Ligands. The ^{13}C NMR spectra of DO3ASQ and DO3ASQ-est provide useful insights to predict the coordination properties of these ligands. In fact, whereas the chemical shifts of the ^{13}C resonances of the macrocyclic ring and of the acetate arms (see Experimental Procedures) are very similar in the two ligands, a noticeable difference exists as far as the cyclobutenedione (squaric) group resonances are concerned. In DO3ASQ the squaric acid moiety gives raise to three resonances with the relative intensity ratio of 1:2:1 at 197.1 (C-3), 189.7 (C-2 and C-4), and 183.2 (C-1) ppm, respectively, owing to the delocalization of the negative charge (Scheme 3) as outlined by the remarkable downfield shift of C-3 with respect to C-2/C-4. On the other hand, in the case of DO3ASQ-est, there are four, equally intense, squaric ester derivative resonances at 190.3 (C-2), 184.8 (C-1), 175.4 (C-4), and 174.5 (C-3) ppm, respectively. Because it is well established that a heteroatom substituent (alkoxy or amino) deactivates the nonadjacent carbonyl group through resonance delocalization (*28*, *29*), the contribution of this resonance form A-2, reported in Scheme 4, is also evident from the large upfield shift of C-3. Thus, the strong upfield shift of C-3 suggests a large decrease of its carbonylic character, which is consistent with a shift in the equilibrium represented in Scheme 4. Besides the squaric acid resonances, the overall ^{13}C NMR spectrum of the DO3ASQ-est, recorded at 25 °C, supports this hypothesis as it shows 18 different signals resulting from the hindered rotation around the bond between carbon (C-1) of the squaric ester moiety and the macrocyclic nitrogen (i.e., vinylogous amide functionality).

Thus, we expect that in DO3ASQ the squaric moiety may participate in the chelation of a Ln^{3+} ion through the negatively charged oxygen at one of the equivalent C-2 or C-4 sites, whereas in DO3ASQ-est the coordination might involve either the oxygen of the carbonyl C-2 functionality or the estereal oxygen.

Chelation of the Gd(III) ions from both DO3ASQ and DO3ASQ-est occurs instantaneously, at room temperature, by mixing equimolar solutions of the reagents.

^{1}H and ^{17}O Relaxometric Investigations of DO3ASQ and DO3ASQ-est Gd(III) Complexes. The

Table 1. Best Fitting Parameters Obtained from the Analysis of the NMRD Profiles (298 K, pH 7.0, 1 mM) and of the Temperature Dependence of $^{17}O-R_{2p}$ (2.1 T, pH 7.0, 50 mM) for Aqueous Solutions of DO3ASQ and DO3ASQ-est-Gd(III) Chelates

	q	Δ^2 (s^{-2})/10^{19}	τ_v (ps)	τ_R (ps)	τ_M (ns)	r (Å)	ΔH_v (kJ mol^{-1})	ΔH_M (kJ mol^{-1})
Gd-DO3ASQ	1	6.3 ± 0.4	19 ± 3	78 ± 2	134	2.98	1.3	41
Gd-DO3ASQ-est	1	5.5 ± 0.4	18 ± 3	83 ± 2	200	2.98	2.0	42

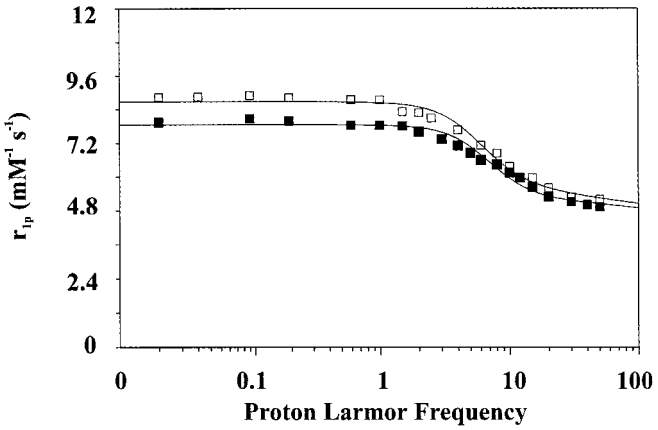


Figure 1. $1/T_1$ NMRD profile of a 1 mM aqueous solution of GdDO3ASQ (■) and GdDO3ASQ-est (□) at 25 °C and pH 7. The solid curves through the data points were calculated with the parameters of Table 1. The lower curves represent the outer sphere contributions to the overall relaxivity.

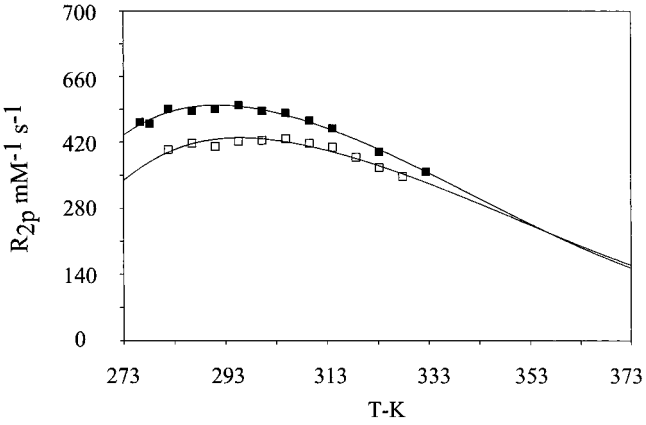
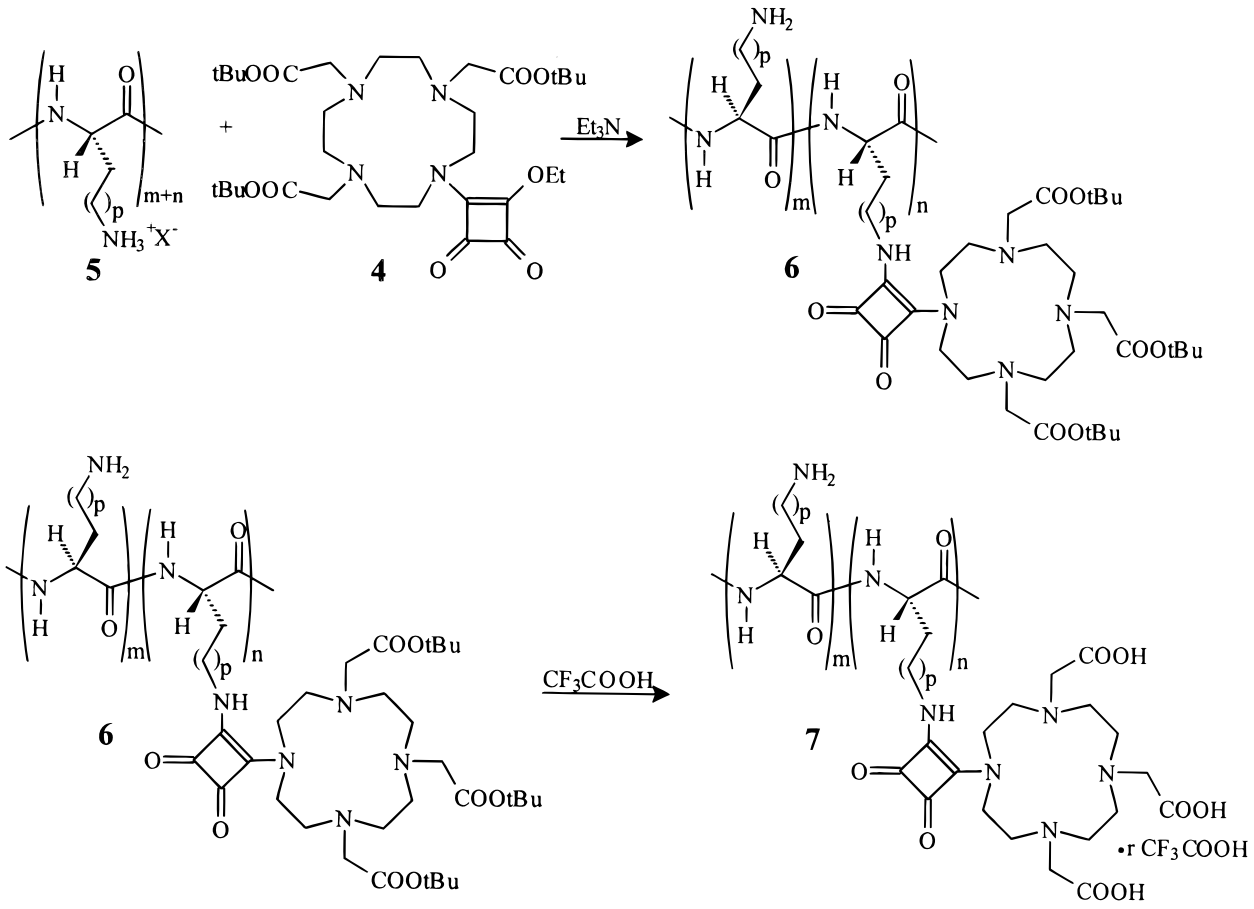


Figure 2. Temperature dependence of the transverse water ^{17}O relaxation rate at 2.1 T and pH 7 for 50 mM solution of GdDO3ASQ (■) and GdDO3ASQ-est (□). The solid curves through the data points were calculated with the parameters of Table 1.

relaxivities at 20 MHz and 25 °C of GdDO3ASQ and GdDO3ASQ-est are 5.3 and 5.6 mM^{-1} s^{-1}, respectively, that is, in the upper range of values for related polyamino polycarboxylate Gd(III) complexes containing one coordinated water molecule (q = 1) (*5*, *14*). The NMRD profiles of GdDO3ASQ and GdDO3ASQ-est (Figure 1) closely resemble those obtained for a number of DOTA-like Gd(III) complexes, and Table 1 shows the parameters obtained by fitting the experimental data to the Solomon−Bloembergen−Morgan and Freed equations. Thus,

Scheme 5



the occurrence of $q = 1$ implies that the squaric acid moiety is involved in the coordination scheme of these complexes.

A parameter particularly important for the forthcoming application of these complexes is represented by the residence lifetime of the coordinated water molecule at the metal site (τ_M). As has been demonstrated in several recent publications (*15*, *30*, *31*), the exchange rate of the coordinated water molecule (τ_M^{O-1}) may be accurately determined by the measurement of the solvent water $^{17}O-T_2$ at variable temperature. In fact, the temperature dependence of R_{2M}^O may be fitted in terms of the temperature dependence of τ_M^O, τ_v, and $\Delta\omega_M^O$. In Figure 2 the R_{2p}^O data for GdDO3ASQ and GdDO3ASQ-est measured over an extended temperature range are reported, and the calculated values of the relevant parameters obtained from the fitting procedure to the above-reported theory are shown in Table 1.

From this procedure we obtained, at 298 K, τ_M values of 134 ns for GdDO3ASQ and 200 ns for GdDO3ASQ-est. These values are similar to those reported for other DTPA- and DOTA-like Gd(III) complexes and are almost 1 order of magnitude shorter than those obtained at the same temperature for the corresponding complexes with bis(amide)−DTPA ligands. Thus, although still far from optimum τ_M values of 10−20 ns, which ensure maximum relaxation enhancement (*14*) for systems with long τ_R and T_{1E}, the exchange lifetime of the coordinated water in these Gd(III) chelates of squaric acid containing ligands should not represent a limiting factor in attaining a relaxation enhancement for conjugates in which the paramagnetic moiety is attached to macromolecular substrates of molecular mass up to 30−40 kDa.

Synthesis of the Conjugates with Polylysine and Polyornithine. The tetraester **3** (Scheme 5) was employed for the synthesis of polylysine−DO3ASQ and polyornithine−DO3ASQ conjugates. For this purpose we chose two polyamino acids endowed with a large difference in the number of monomeric units in their chain, that is, polylysine ($n = 16$) and polyornithine ($n = 114$). The "second amidation step" implied the reaction with an amino group in the presence of a base (generally a tertiary amine). Due to the low solubility of polylysine and polyornithine in solvents other than water, the coupling reaction was run in a water/ethanol mixture, in the presence of triethylamine. The reaction of the two polymers with **3** required 72 h to reach completion; the two conjugates were isolated by adding diethyl ether to a methanolic solution of the crude hydrolysis product. All of the added chelate bound almost quantitatively to yield $(DO3ASQ)_n-lys_{16}$ and $(DO3ASQ)_m-orn_{114}$ respectively. n and m numbers were estimated to be ∼3 and ∼30 on the basis of the observation that all of the added compound **3** was consumed. These numbers have been confirmed by the results of the titration with Gd^{3+} ions (vide infra). The number of chelate moieties on each polyamino acidic chain is an average value as we have not attempted any separation of the reaction products. The conjugates so obtained were directly used for the complexation of the paramagnetic ion.

Synthesis and Relaxometric Characterization of DO3ASQ−lys$_{16}$ and DO3ASQ−orn$_{114}$ Gd(III) Complexes. The dropwise addition of a $GdCl_3$ solution to 1 mM aqueous solutions of $(DO3ASQ)_n-lys_{16}$ and $(DO3ASQ)_m-orn_{114}$ at room temperature led to the prompt chelation of the metallic ions by the chelate moieties on the polyamino acidic substrate. The formation of the macromolecular complex has been monitored

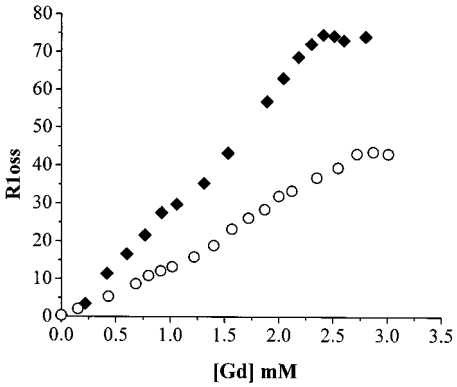


Figure 3. Longitudinal water proton relaxation rate of 0.078 mM $(DO3ASQ)_{30}-orn_{114}$ (◆) and 1 mM $(DO3ASQ)_3-lys_{16}$ (○) ligand solutions as a function of the Gd(III) ion concentration added to solutions.

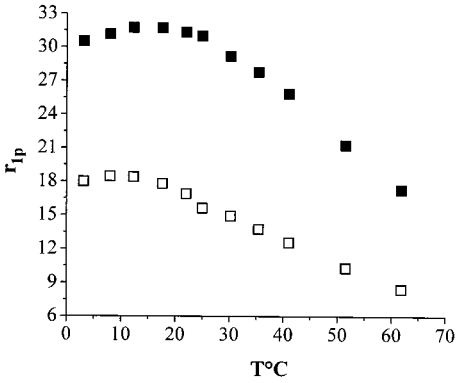


Figure 4. Temperature dependence of the longitudinal proton relaxivity at 20 MHz and pH 7 of $Gd(DO3ASQ)_{30}-orn_{114}$ (■) and $Gd(DO3ASQ)_3-lys_{16}$(□) water solutions.

by measuring the relaxation time of the water protons. Each addition of Gd(III) ions corresponds to an increase of the observed relaxation rate (not a linear increase as the successive coordination of metal ions causes a progressive increase of the molecular weight and an eventual change in the overall polymer structure). The titration end point (Figure 3) is clearly detected and allows us to establish the relative metal chelate/polyamino acid ratio, thus yielding the following stoichiometries: $Gd(DO3ASQ)_3-lys_{16}$ (MW ≅ 5000) and $Gd(DO3ASQ)_{30}-orn_{114}$ (MW ≅ 35000); their relaxivities are 15.6 and 31.0 mM^{-1} s^{-1}, respectively. To get more insight into the understanding of the various parameters determining the observed relaxivities of these paramagnetic macromolecular complexes, we measured both the temperature dependence of proton r_{1p} at 0.47 T and the temperature dependence of $^{17}O-R_2$ at 2.1 T. From the data reported in Figure 4, it is clearly shown that from room to high temperature, the relaxivities of $Gd(DO3A)_3-lys_{16}$ and $Gd(DO3A)_{30}-orn_{114}$ are not limited by τ_M; that is, the condition $T_{1M} > \tau_M$ holds (eq 1). At lower temperatures the decreased exchange rate and the concomitant shortening of T_{1M} (as a consequence of the elongation of τ_R) yield the typical flattening of the profile of r_{1p} versus T, expected for systems whose $\tau_M > T_{1M}$. This is confirmed by analyzing the water $^{17}O-R_{2p}$ variable temperature profiles (Figure 5) from which the τ_M values obtained for both macromolecular complexes are relatively short and similar to those determined for the free Gd complexes. Table 2 shows that the other parameters and the reorientational correlation time (τ_R) display values comparable to those of the free complexes. This finding supports the view that each Gd ion owns one water molecule, pointing

Table 2. ^{17}O NMR Best Fitting Parameters Obtained from the Analysis of the Temperature Dependence of R^{O}_{2p} for 11 mM Aqueous Solution of the Gd(III) Complexes

	q	Δ^2 (s^{-2})/10^{19}	τ_v (ps)	τ_M (ns)	ΔH_v (kJ mol^{-1})	ΔH_M (kJ mol^{-1})
$Gd(DO3ASQ)_{30}$−orn_{114}	1	4.4	11	153	4.3	31
$Gd(DO3ASQ)_3$−lys_{16}	1	4.5	29	197	1.5	45

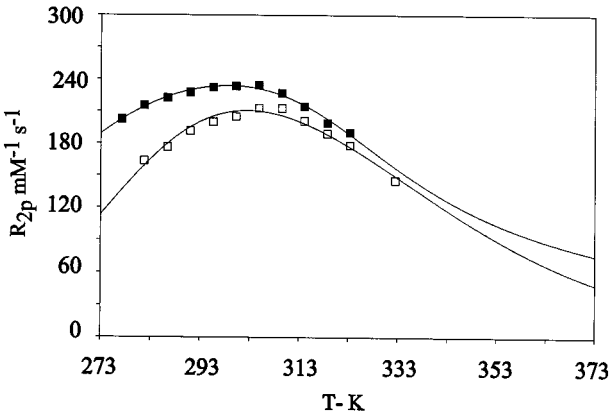


Figure 5. Temperature dependence of the transverse water ^{17}O relaxation rate at 2.1 T and pH 7 for 11.0 mM solutions of $Gd(DO3ASQ)_{30}$−orn_{114} (■) and $Gd(DO3ASQ)_3$−lys_{16} (□). The solid curves through the data points were calculated with the parameters of Table 2.

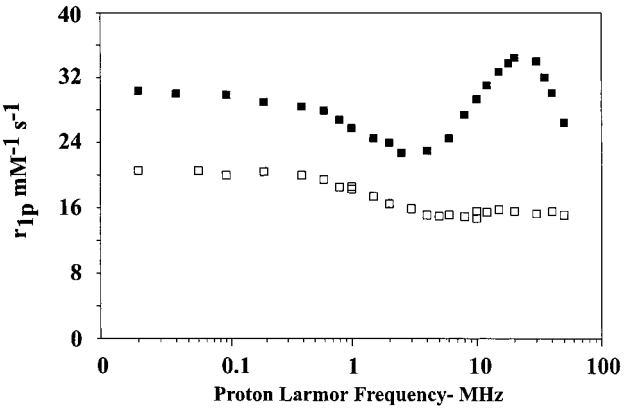


Figure 6. $1/T_1$ NMRD profile of a 1 mM aqueous solution of $Gd(DO3ASQ)_{30}$−orn_{114} (■) or $Gd(DO3ASQ)_3$−lys_{16} (□) at 25 °C and pH 7.

out that the squaric group maintains its ability to coordinate the metal ion. The linkage to the polyamino acidic residue yields to the transformation of one of the $C_{(2/4)}$−O bonds of the squaric acid moiety into a C−N bond; thus, it seems likely that the coordination to the Gd(III) center occurs through the carbonyl (C-2) functionality. On this basis it seems likely that an analogous binding scheme may occur also in the case of the monomeric GdDO3ASQ-est.

The NMRD profiles of $Gd(DO3A)_3$−lys_{16} and $Gd(DO3A)_{30}$−orn_{114} (Figure 6) show a relaxivity increase at ∼20−30 MHz typical of slowly tumbling paramagnetic systems. Only in the case of $Gd(DO3A)_{30}$−orn_{114} does the NMRD profile display the shape of the relaxivity peaks commonly found for paramagnetic protein conjugates. Furthermore, the extent of the observed relaxivity enhancements is not proportional to the molecular weights of the two systems to suggest that large internal motions overlap the reorientational processes of the whole molecules. As in the case of the noncovalent paramagnetic adducts with albumin, the data in the low-field region of the NMRD profile cannot be fitted with the r_{1p} values calculated on the basis of the Solomon−Bloenbergen−Morgan theory. Likely, the high relaxivities observed in the 0.01−3 MHz region are indicative of additional contributions arising mainly from water molecules bound to the surface of the macromolecular substrate in the proximity of the paramagnetic center (*32*, *33*).

CONCLUDING REMARKS

In summary, the results herein reported show that, for the formation of conjugates with macromolecular substrates, an easy alternative to the use of DTPA anhydride is now available leading to Gd(III) chelates that display quite good relaxivities and do not suffer the limitation of the long exchange lifetime. Particularly interesting is the $(GdDO3ASQ)_{30}$−orn_{114} conjugate, which has an r_{1p} value, at 39 °C, of 26.5 mM^{-1} s^{-1}, significantly higher than the r_{1p} values reported by Brasch et al. for other macromolecular CAs such as $(GdDTPA)_n$−polylysine (r_{1p} = 13.1 mM^{-1} s^{-1}) and $(GdDTPA)_n$−albumin (r_{1p} = 14.4 mM^{-1} s^{-1}), respectively (*1*).

Furthermore, with respect to the use of DTPA−bis(anhydride), there is the advantage that, by applying the method herein described, no cross-linking between the macromolecular chain occurs. The easiness found in the anchoring procedure of the chelate moiety to the macromolecular substrates suggests that this route based on squaric acid conjugates may find a wide generalization. As far as the specific substrates considered in this work are concerned, polyamino acidic chains containing a high number of Gd(III) chelates may be used as high relaxivity markers for systems able to target selected tissues or organs.

ACKNOWLEDGMENT

Financial support from Bracco S.p.A. (Milano, Italy), CNR, and MURST is gratefully acknowledged. This work was carried out under the scheme of the EU-COST-D8 Program and the EU-BIOMED II-MACE Project. We gratefully acknowledge the stimulating discussion with Prof. I. Bertini, C. Luchinat, L. Casella, and their collegues.

LITERATURE CITED

(1) Brasch, R. C. (1991) Rationale and Applications for Macromolecular Gd-Based Contrast Agents. *Magn. Reson. Med. 22*, 282−287.

(2) Schuhmann-Giampieri, G., Schmitt-Willich, H., Frenzel, T., Press, W., and Weinmann, H. (1991) In vivo and in vitro evaluation of Gd-DTPA-polylysine as a macromolecular contrast agent for resonance magnetic imaging. *Invest. Radiol. 269*, 69−78.

(3) Kumar, K., and Tweedle, M. F. (1993) Macrocyclic polyaminocarboxylate complexes of lanthanides as magnetic resonance imaging contrast agents. *Pure Appl. Chem. 65*, 515−520.

(4) Rinck, P. A. (1993) *Magnetic Resonance in Medicine*, pp 155−174, Blackwell Scientific Publications, Oxford, U.K.

(5) Peters, J. A., Huskens, J., and Raber, D. J. (1996) Lanthanide induced shifts and relaxation rate enhancements. *Prog. NMR Spectrosc. 28*, 283−350.

(6) Lauffer, R. B. (1987) Paramagnetic Metal Complexes as Water Proton Relaxation Agents for NMR Imaging: Theory and Design. *Chem. Rev. 87*, 901−927.

(7) Lauffer, R. B., Brady, T. J., Brown, R. D., III, Baglin, C., and Koenig, S. H. (1986) $1/T_1$ NMRD Profiles of solutions of

Mn(II) and Gd(III) Protein-Chelate Conjugates. *Magn. Reson. Med. 3*, 541−548.
(8) Sieving, P. F., Watson, A. D., and Rocklage, M. R. (1990) Preparation and characterization of paramagnetic polychelates and their protein conjugates. *Bioconjugate Chem. 1*, 65−71.
(9) Spanoghe, M., Lanens, D., Dommisse, R., Van Der Linden, A., and Alderweireldt, F. (1992) Proton relaxation enhancement by means of serum albumin and poly-L-lysine labeled with DTPA-Gd3+: relaxivities as a function of molecular weight and conjugation efficiency. *Magn. Reson. Imaging 109*, 13−21.
(10) Maisano, F., Gozzini, L., and de Haen, C. (1992) Coupling of DTPA to proteins: A critical analysis of the cyclic dianhydride method in the case of insulin modification. *Bioconjugate Chem. 3*, 212−217.
(11) Sherry, A. D., Cacheris, W. P., and Kuan, K. T. (1988) Stability constants for Gd^{3+} binding to model DTPA-conjugates and DTPA-proteins: implications for their use as magnetic resonance contrast agents. *Magn. Reson. Med. 8*, 180−190.
(12) Halpern, S., Stern, P., Hagan, P., Chen, A., Frincke, J., Bartholomew, R., David, G., and Adams, T. (1983) Labeling of monoclonal antibodies with indium(III): technique and advantages compared to radioiodine labeling. In *Radioimmunoimaging and Radioimmunotherapy* (S. W. Burchiel and B. A. Rhodes, Eds.), pp 197−205, Elsevier Science Publishing, New York.
(13) Parker, D. (1990) Tumor targeting with radiolabeled macrocycle-antiboby congjugates. *Chem. Soc. Rev. 19*, 271−291.
(14) Aime, S., Botta, M., Fasano, M., and Terreno, E. (1998) Lanthanide(III) chelates for NMR biomedical applications. *Chem. Soc. Rev. 27*, 19−29.
(15) Powell, D. H., Ni, Dhubhghaill, O. M., Pubanz, D., et al. (1996) Structural and Dynamic Parameters Obtained from ^{17}O NMR, EPR, and NMRD Studies of Monomeric and Dimeric Gd^{3+} Complexes of Interest in Magnetic Resonance Imaging: An Integrated and Theoretically Self-Consistent Approach. *J. Am. Chem. Soc. 118*, 9333−9346.
(16) Tietze, L. F., Schroter, C., Gabius, S., Brinck, U., Goerlach-Graw, A., and Gabius, H. J. (1991) Conjugation of p-Aminophenyl Glycosides with Squaric Acid Diester to a Carrier Protein and the Use of the Neoglycoprotein in the Histochemical Detection of Lectins. *Bioconjugate Chem. 2*, 48−53.
(17) Chang, C. A., Francesconi, L. C., Malley, M. F., et al. (1993) Synthesis, Characterization, and Crystal Structure of MDO3A (M = Fe, Gd) and Na[M(DOTA)] (M = Fe, Y, Gd). *Inorg. Chem. 32*, 3501−3508.
(18) Koenig, S. H., Brown, R. D., III, and Gupta, R. K., Eds. (1987) *NMR Spectroscopy of Cells and Organism*, CRC Press, Boca Raton, FL.
(19) Banci, L., Bertini, I., and Luchinat, C. (1991) *Nuclear and Electron Relaxation*, VCH, Weinheim, Germany.
(20) Bloembergen, N., and Morgan, L. O. (1961) Proton Relaxation Times in Paramagnetic Solutions. Effects of Electron Spin Relaxation. *J. Chem. Phys. 34*, 842−850.
(21) Hwang, L. P., and Freed, J. H. (1975) Generalized Einstein Relations for Rotational and Translational Diffusion of Molecules Including Spin. *J. Chem. Phys. 63*, 118−130.
(22) Swift, T. J., and Connick, R. E. J. (1962) NMR Relaxation Mechanisms of O^{17} in Aqueous Solutions of Paramagnetic Cations and the Lifetime of Water Molecules in the First Coordination Sphere. *J. Chem. Phys. 37*, 307.
(23) Schmidt, A. H., and Ried, W. (1978) Die Praparative Chemie der Cyclobutenedione; Synthese von Cyclobutendion und dressen Alkyl-, Alkenyl- und aryl- Derivaten. *Synthesis*, 1−22.
(24) Knorr, H., and Ried, W. (1978) Die Praparative Chemie der Cyclobutenedione; Reaktionen von Alkyl-, Alkenyl- and Arylcyclobutendionen. *Synthesis*, 649−666.
(25) Schmidt, A. H., and Ried, W. (1978) Die Praparative Chemie der Cyclobutenedione: Synthese von Quadratsaure, Benzocyclobutendion und deren Derivaten. *Synthesis 8*, 68−80.
(26) Tietze, L. F., Arlt, M., Beller, M., Glusenkamp, K. H., Jahde, E., and Rajewsky, M. F. (1991) Bioisosteric Replacement of the a-Aminocarboxylic Functionality in 2-Amino-5-phosphonopentanoic Acid Yield Unique 3,4-Diamino-3-cyclobutene-1,2-dione Containing NMDA Antagonists. *Chem. Ber. 124*, 1215−1221.
(27) Kinney, W. A., Lee, N. E., Garrison, D. T., Podlesny, E. J., Jr., Simmonds, J. T., Bradlett, D., Notvest, R. R., Kowal, D. M., and Tasse, R. P. (1992) Squaric Acid Diethyl Ester: A New Coupling Reagent for the Formation of Drug Biopolymer Conjugates. Synthesis of Squaric Acid Ester Amides and Diamides. *J. Med. Chem. 35*, 4720−4738.
(28) Liebeskind, L. S., Granberg, K. L., and Zhang, J. (1992) A Strategy for Generalization of the Regiospecific Synthesis of Substituted Quinones from Cyclobutenediones. *J. Org. Chem. 57*, 4345−4352.
(29) Liebeskind, L. S., and Sun, L. J. (1995) Construction of Highly-substituted Aromatics Bearing Acyl Substituents Using Cyclobutenedione Technology: Vinylketene-Based Benzannulations using 3-Acyl-4-(substituted amino) cyclobutenediones. *J. Org. Chem. 60*, 8194−9201.
(30) Micksei, K., Powell, D. H., Helm, L., Brucher, E., and Merbach, A. E. (1993) Water Exchange on $[Gd(H_2O)_8]^{3+}$ and $[Gd(PDTA)(H_2O)_2]^-$ in Aqueous Solution: a Variable-Pressure, -Temperature and -Magnetic Field ^{17}O NMR Study. *Magn. Reson. Chem. 31*, 1011−1020.
(31) Micksei, K., Helm, L., Brucher, E., and Merbach, A. E. (1993) ^{17}O NMR Study of Water Exchange on $[Gd(DTPA)(H_2O)]^{2-}$ and $[Gd(DOTA)(H_2O)]^-$ Related to NMR Imaging. *Inorg. Chem. 32*, 3844−3850.
(32) Aime, S., Botta, M., Fasano, M., Geninatti Crich, S., and Terreno, E. (1996) Gd(III) Complexes as Contrast Agents for Magnetic Resonance Imaging: a Proton Relaxation Enhancement Study of the Interaction with Human Serum Albumin. *J. Biol. Inorg. Chem. 1*, 312−319.
(33) Aime, S., Botta, M., Geninatti Crich, S., et al. (1997) Towards MRI contrast agents of improved efficacy. NMR relaxometric investigations of the binding interaction to HSA of a novel heptadentate macrocyclic triphosphonate Gd(III)-complex. *J. Biol. Inorg. Chem. 2*, 470−479.

BC980030F

CORRECTIONS

Volume 10, Number 2, March/April 1999.

Silvio Aime,* Mauro Botta, Simonetta Geninatti Crich, Giovanni Giovenzana, Giovanni Palmisano, and Massimo Sisti

NOVEL PARAMAGNETIC MACROMOLECULAR COMPLEXES DERIVED FROM THE LINKAGE OF A MACROCYCLIC GD(III) COMPLEX TO POLYAMINO ACIDS THROUGH A SQUARIC ACID MOIETY

On page 195, the reaction arrows in Schemes 3 and 4 should be replaced with ↔. In addition, on page 195, right column, in the sixth sentence of the second full paragraph, the following change should be made. "Thus, the strong upfield shift of C-3 suggests a large decrease of its carbonylic character, which is consistent with a shift in the equilibrium represented in Scheme 4." should be changed to "Thus, the strong upfield shift of C-3 suggests a large decrease of its carbonylic character, which is indicative that A-2 contributes more to the resonance hybrid than A-1."

BC990056M

10.1021/bc990056m
Published on Web 06/25/1999

Synthesis and Characterization of Photoreactive Insulin-like Growth Factor 1 Derivatives for Receptor Analysis

Marlies Fabry*

Deutsches Wollforschungsinstitut an der RWTH Aachen e.V., 52062 Aachen, Germany. Received May 19, 1998; Revised Manuscript Received September 23, 1998

Recombinant human insulin-like growth factor 1 (hIGF-1) was reacted with 4-azidosalicylic acid (Asa) to synthesize photoreactive IGF-1 derivatives. Depending on the time of reaction and the Asa/IGF-1 ratio, a mixture of mono-, bis-, and trisacylated derivatives and one tetraacylated derivative was produced, which was separated by reversed-phase HPLC. HPLC, PAGE, and MALDI mass spectrometry were used to determine the degree of the acylation and location of the photolabel insertion. After iodination of the three monoacylated photoreactive IGF-1 derivatives, the specific labeling of the receptor could be proved. Together with a comparative investigation in which B29-Asa−insulin was used, the results suggest corresponding contact areas for IGF-1 and insulin with the insulin receptor ectodomain.

INTRODUCTION

Insulin-like growth factor 1 (IGF-1)[1] is a growth factor that exhibits structural and functional homology to insulin. The single-chain protein consists of 70 amino acids forming four peptide domains: the B (1−29), C (30−41), A (42−62), and D domains (63−70). The A and B domains are structurally homologous to the insulin A and B chains; the C domain corresponds to the C peptide of proinsulin, while the D domain does not have an equivalent in proinsulin or insulin. As in insulin, six cysteine residues form three disulfide links (Rinderknecht and Humbel, 1978; Blundell et al., 1983). Whereas IGF-1 has a key function in the regulation of cellular proliferation and differentiation, insulin regulates a broad spectrum of metabolic processes. The action of both polypeptide hormones is mediated by the interaction with their specific membrane receptors.

Like their ligands, the insulin and IGF-1 receptor exhibit a remarkable homology with regard to their amino acid sequence and molecular structure. Both receptors have the same heterotetrameric $\alpha_2\beta_2$ structure. The ligand-binding α-domains are completely extracellular and have a cysteine-rich domain. The β-subunits cross the plasma membrane and contain the cytoplasmatic phosphotyrosine kinase domain. Ligand binding induces autophosphorylation of the receptors and subsequently phosphorylation of cytoplasmatic proteins (Ullrich et al., 1985, 1986; Ebina et al., 1985).

Despite the high degree of homology of the ligands as well as the receptors, insulin and IGF-1 exhibit only weak cross reactivity. The affinity of binding of each ligand to the receptor of the other ligand is about 1% (Kjeldsen et al., 1991; Schumacher et al., 1991). Nevertheless, cross reactivity and homology between ligands and receptors suggest an analogous mechanism of ligand−receptor interaction for IGF-1 and insulin.

Photoaffinity labeling is a powerful chemical approach in structural biology (Kojro et al., 1993; Zhou et al., 1997) and has already proven to be very useful in the identification of the area of binding of insulin to its receptor (Wedekind et al., 1989; Yip, 1992; Fabry et al., 1992; Whaugh et al., 1989; Kurose et al., 1994). Analogous studies with the IGF-1 receptor should now provide additional information about the ligand specificity. In this paper, the preparation and characterization of photoreactive IGF-1 derivatives are reported. These derivatives were used to label IGF-1 receptors and to further investigate the IGF-1 and insulin receptor systems.

MATERIALS AND METHODS

Chemicals. Recombinant human insulin-like growth factor 1 (hIGF-1) was a donation from Lilly Research Laboratories (Indianapolis, IN). HPLC-grade acetonitrile, TFA, and TPCK−trypsin were from Merck. Carrier-free ^{125}I was purchased from Amersham. 4-(Azidosalicyloyl)-*N*-hydroxysuccinimide ester was synthesized as described elsewhere (Fabry and Brandenburg, 1992). Human IGF-1 receptor was isolated from transfected NIH-3T3 fibroblasts (Lammers et al., 1989). Clones of transfected CHO-K1 cells that overexpress the IR921 protein were selected. This is the soluble ectodomain of the human insulin receptor in which the heterotetrameric $(\alpha\beta_0)_2$ receptor was truncated following residue 921 (Schaefer et al., 1992).

Preparation of Asa−IGF-I Derivatives. Asa-OSu was dissolved in DMF (90 μg/10 μL) and added in 4 portions to a 70 μL solution containing 500 μg of IGF-1 dissolved in 0.1 M sodium phoshate buffer (pH 7.4) which was being stirred at room temperature protected from light. After 5−10 min, the reaction was quenched with 10 μL of ethanolamine. The mixture was separated on a Sephasil C-18 SC 2.1/10 column using the SMART system (Pharmacia) and a gradient from 20 to 48%

* To whom correspondence should be addressed: Deutsches Wollforschungsinstitut, Veltmanplatz 8, D-52062 Aachen, Germany. E-mail: fabry@dwi.rwth-aachen.de. Fax: ++49 (0)241 44 69 100. Phone: ++49 (0)241 44 69 146.

[1] Abbreviations: Asa, 4-azidosalicylic acid; DMF, dimethylformamide; IGF-1, insulin-like growth factor 1; IR921, insulin receptor ectodomain; MALDI mass spectrometry, matrix-assisted laser desorption/ionization mass spectrometry; OSu, *N*-hydroxysuccinimidyl; PAGE, polyacrylamide gel electrophoresis; TFA, trifluoroacetic acid; TPCK, tosylphenylchloromethyl ketone.

10.1021/bc980051+ CCC: $18.00 © 1999 American Chemical Society
Published on Web 02/17/1999

acetonitrile in 0.1% TFA over the course of 90 min. The proteins were detected by measuring the absorbance at 214, 256, and 280 nm. Fractions were collected automatically into 0.5 mL Eppendorf tubes and lyophilized by SpeedVac vacuum centrifugation.

Degree of Acylation and Location of the Photolabel. The different Asa−IGF-1 derivatives separated by reversed-phase HPLC were analyzed by acid−urea PAGE with 8 M urea and 0.9 M acetic acid at pH 4 using a 15% polyacrylamide gel (Poole et al., 1974) and MALDI mass spectrometry to determine the degree of acylation. The mass spectra were obtained on a Bruker Biflex III TOF instrument (Bruker-Franzen Analytik, Bremen, Germany) equipped with a 337 nm nitrogen laser using sinapinic acid as the matrix, acetonitrile/TFA as the solvent, and standard experimental parameters (3 ns pulse duration, linear mode, 100−150 laser spots). To locate the position of the photolabel, IGF-1 and the monoacylated products were digested with trypsin after reduction and carboxymethylation (Honegger and Humbel, 1986). The digests were subjected to MALDI mass spectrometry to evaluate the change of the fragmentation pattern compared to that of unlabeled IGF-1. For reduction and carboxymethylation of disulfide bonds, the lyophilized proteins (10 μg) were dissolved in 20 μL of 6 M guanidinium hydrochloride, 0.5 M Tris, and 5 mM EDTA (pH 8.5) containing 40 nmol of dithiothreitol, flushed with nitrogen, and kept at room temperature in darkness for 3 h. Then, 400 nmol of iodoacetic acid was added, and the solution was further incubated under nitrogen for 2 h. The reaction was stopped by addition of 2 μL of mercaptoethanol. The proteins were desalted by reversed-phase HPLC with the same column using a 90 min gradient from 16 to 48% acetonitrile in 0.1% TFA at a flow rate of 100 μL/min and dried. The reduced products were identified by acid−urea PAGE. The enzymatic cleavage was performed by addition of 0.5 μg of TPCK−trypsin to the proteins dissolved in 30 μL of 0.1 M ammonium bicarbonate (pH 8), followed by incubation at room temperature for 18 h. To stop the reaction, 0.1% TFA was added and proteins were dried by SpeedVac vacuum centrifugation and washed with water twice. The digestion products were then studied with MALDI mass spectrometry.

Radioiodination/Iodine Analysis. IGF-1 and the Asa−IGF-1 derivatives were iodinated according to the chloramine T method (Yip et al., 1993) with the following modification of reaction conditions; 4 μg of IGF-1 or the derivative was dissolved in 20 μL of 0.4 M sodium phosphate buffer (pH 7.5), and then 100 μCi of carrier-free ^{125}I (IMS 30, Amersham) was added. Iodination was started by addition of 5 μL of chloramine T (100 ng/1 μL of 0.04 M sodium phoshate buffer) and continued for 3 min at room temperature. The reaction was stopped by adding 10 μL of tyrosine (0.2 mg/mL) and KI (1 mg/mL). The reaction mixture was applied to a SepPak C-18 cartridge (Waters Corp.) that had been equilibrated with 0.1% TFA/acetronitrile (90/10 v/v). After washing, the iodinated derivatives were eluted with 60% acetronitrile in 0.1% TFA into 50 mM ammonium bicarbonate, lyophilized, and stored at −20 °C. To define the ^{125}I position, approximately 50 000 cpm carboxymethylated protein was digested with TPCK−trypsin as described above, and the digest was separated by reversed-phase HPLC with a gradient of 15 to 40% acetonitrile in 0.1% TFA over the course of 100 min at a flow rate of 100 μL/min.

Assay of IGF-1 Receptor Binding. Binding of [^{125}I]-IGF-1 to plasma membranes of NIH-3T3 cells (50 μg of protein/sample) and competition with IGF-1 and the Asa−IGF-1 derivatives were assessed as described previously (Schumacher et al., 1991). Plasma membranes were prepared according to a previously published procedure (Breiner et al., 1993).

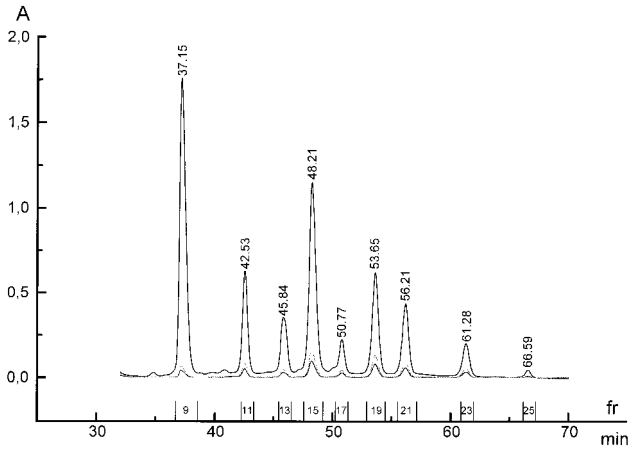


Figure 1. Reversed-phase HPLC separation of the reaction mixture of 4-(azidosalicyloyl)-*N*-hydroxysuccinimide (Asa-OSu) with IGF-1. Fifty micrograms of the reaction mixture was loaded onto a C-18 column and separated with a flow rate of 100 μL/min using a 20 to 48% acetonitrile gradient over the course of 90 min. Proteins were monitored at 215, 256, and 280 nm. IGF-1 and the Asa derivatives were identified by acid−urea PAGE (Figure 2) and MALDI mass spectrometry (Table 1).

Photoaffinity Labeling. Plasma membranes (protein content of at least 30 μg) prepared from NIH-3T3 fibroblasts or IR921 were incubated with the photoreactive IGF-1 derivatives (approximately 500 000 cpm, 2.95 nM) in 50 μL of KRH buffer [50 mM Hepes, 13 mM NaCl, 5.1 mM KCl, and 1.3 mM Mg_2SO_4 (pH 7.8)] at 15 °C for 90 min. Membrane pellets were washed once with KRH buffer and photolyzed by irradiation with three flashes (each 1000 Ws) of an UV flash apparatus ("Lizzy", Raytest) in 20 μL of KRH buffer. When the soluble IR921 was labeled, noncovalently bound ligand was removed by precipitation with polyethylene glycol and γ-globulin after photolysis (Fabry et al., 1992). The membrane pellets were solubilized in SDS sample buffer in the presence of dithiothreitol and analyzed by SDS−PAGE (7.5%). Gels were dried prior to autoradiography.

Time Course of the Tryptic Digestion of the Photoaffinity-Labeled Ectodomain. IR921 was labeled with B29-Asa−insulin and B27-Asa−IGF-1. Digestion was carried out with 30 μg/mL TPCK−trypsin at room temperature (reaction times indicated). Aliquots were taken, and the reaction was stopped by addition of Laemmli sample buffer and heating for 5 min at 95 °C and analyzed by SDS−PAGE (12.5%).

RESULTS AND DISCUSSION

Preparation of Asa−IGF-1 Derivatives. By reaction of the photoreagent, the *N*-hydroxysuccinimide ester of 4-azidosalicylic acid, with unprotected IGF-1, four free amino groups, the α-amino group in B1 and the three ϵ-amino groups of B27-, D65-, and D68-lysine, can be substituted. The resulting mixture of reaction products, varying in degree and site of acylation, can be separated by reversed-phase HPLC due to differences in charge and hydrophobicity (Figure 1).

Proteins were detected at the leading wavelength of 214 nm. Two secondary wavelengths at 256 and 280 nm were of interest for the detection of aromatic or modified amino acids. Since the photolabel also absorbs at 256 and 280 nm, the absorbance ratios A_{214nm}/A_{256nm} and $A_{214nm}/$

Table 1. Absorbance Ratios of the HPLC Fractions for Reaction of Asa-OSu with IGF-1 (Figure 1)[a]

HPLC fraction	A_{214nm}/A_{256nm}	A_{214nm}/A_{280nm}	A_{256nm}/A_{280nm}	assumed number of photogroups
9	45.0	28.0	0.63	0
11	12.9	8.1	0.7	1
13	16.2	10.4	0.64	1
15	13.3	8.0	0.6	1
17	8.5	6.5	0.62	2
19	8.2	5.0	0.63	2
21	7.8	5.0	0.63	2
23	5.2	3.1	0.63	3
25	5.6	3.5	0.62	3

[a] Absorptions were simultaneously monitored at 214, 256, and 280 nm.

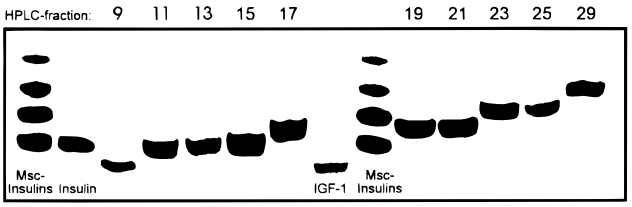


Figure 2. Acid−urea PAGE of the HPLC fractions, and reaction of Asa-OSu with IGF-1 (Figure 1). Msc-insulins are a standard mixture of differently charged insulins. Fraction 9 contains unmodified IGF-1 with the same mobility as the standard IGF-1. Fractions 11, 13, and 15 correspond to monoacylated, fractions 17, 19, and 21 to bisacylated, and fractions 23 and 25 to trisacylated Asa−IGF-1, and fraction 29 corresponds to tetraacylated Asa−IGF-1.

A_{280nm} change characteristically with the degree of acylation (Table 1). Thus, a first classification of the products according to their degree of acylation was possible. Fraction 9 exhibits the typical absorption characteristics of native IGF-1 ($45A_{214nm}/A_{256nm}$ and $28A_{214nm}/A_{280nm}$).

The acid−urea PAGE (Figure 2) confirmed that fraction 9 contained IGF-1 and fractions 11, 13, and 15 the monoacylated products, followed by three bisacylated IGF-1 derivatives (fractions 17, 19, and 21), and two trisacylated products (fractions 23 and 25). When the reaction was carried out with a 5-fold excess of active ester and a reaction time of 5 min, 29% of the IGF-1 was not modified, 41% monoacylated, 23% bisacylated, and 4% trisacylated. With the same Asa-OSu/IGF-1 ratio and a longer reaction time, there was actually less educt, but the amount of more highly acylated products increased considerably: 4% nonacylated IGF-1 and 11% monoacylated, 33% bisacylated, 46% trisacylated, and 7.5% tetraacylated IGF-1 derivatives (see Figure 2, fraction 29).

For native IGF-1, the mass determined by MALDI mass spectrometry corresponds to the calculated mass. For the Asa−IGF-1 derivatives, mass shifts of 1−3-fold minus 28 Da were found in addition to the expected data.[2] The mass spectrum for B27-Asa−IGF-1 is given in Figure 3. This mass shift can be explained by a partial photoactivation of the aryl azides effected by the laser energy of the spectrometer during measurement leading to the formation of nitrene with elimination of nitrogen and possibly an addition of two atoms of hydrogen. Normally, this reaction leads to a covalent binding to the receptor.

Location of the Photolabel. Tryptic digestion of reduced IGF-1 leads to the formation of six fragments, T1−T6 (Rinderknecht and Humbel, 1978; Honegger and Humbel, 1986). The substitution sites of the photolabel at B1-glycine, B27-lysine, or D65/D68-lysine are within

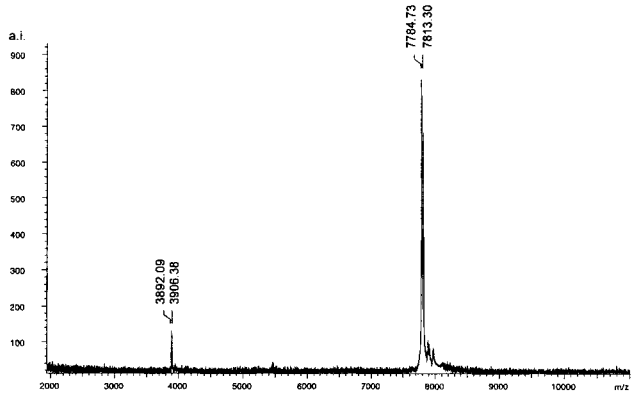


Figure 3. MALDI mass spectrum of B27-Asa−IGF-1 (calculated mass of 7810.3 Da; fraction 11 of the reversed-phase HPLC separation, Figure 1). In addition to the observed mass of 7813.3 Da, a second peak with a mass 28.6 Da lower and the corresponding doubly protonated proteins were detected. The spectrum was recorded using sinapinic acid as the matrix.

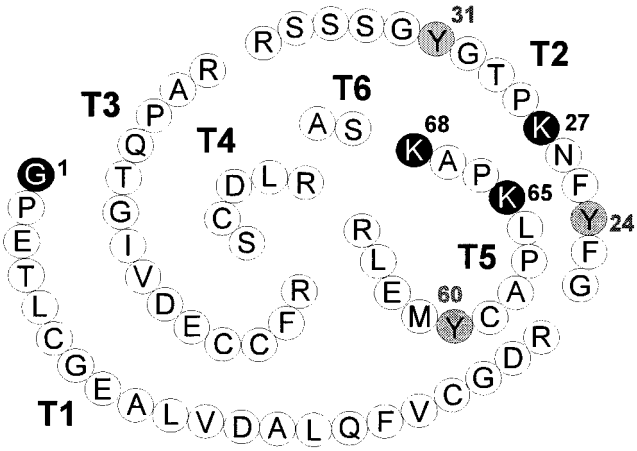


Figure 4. Amino acid sequence of IGF-1 showing tryptic peptides T1−T6, the acylation sites of the photolabel Asa (black), and the positions of iodination (gray).

tryptic fragments T1, T2, or T5, respectively (Figure 4). The mass values of the fragments are changed characteristically due to substitution.

IGF-1 and the three monoacylated IGF-1 derivatives were reduced, carboxymethylated, and treated with trypsin after reversed-phase HPLC purification. The peptides were analyzed by MALDI mass spectrometry.

Under the conditions used, trypsin cleaved IGF-1 and its derivatives completely and as expected.[3] Additionally, at the sequence position S^{C35}-R^{C36}-R^{C37}-A^{C38}, a shifting of the cleavage occurred. As a result, tryptic fragment T2 with two C-terminal arginines and tryptic fragment T3 without the N-terminal arginine were found. At the second position with two arginine residues in sequence, L^{A54}-R^{A55}-R^{A56}-L^{A57}, cleavage occurred only between the two arginines.

The mass analyses of the tryptic fragments of the three monoacylated IGF derivatives confirmed the complete elimination of nitrogen from the photofragments. In fraction 11, a mass shift of the tryptic fragment T2 from 1668.78 to 1803.76 Da was observed, corresponding to the activated photogroup (Figure 5). In fraction 15, this caused a shift of the mass of fragment T1 from 2310.28 to 2445.07 Da. Due to the acylation at D68-lysine, no tryptic cleavage of the peptide of fraction 13 was possible.

[2] Interested investigators can request molecular mass data from Fabry@dwi.rwth-aachen.de.

[3] Molecular mass data also available via e-mail from Fabry@dwi.rwth-aachen.de.

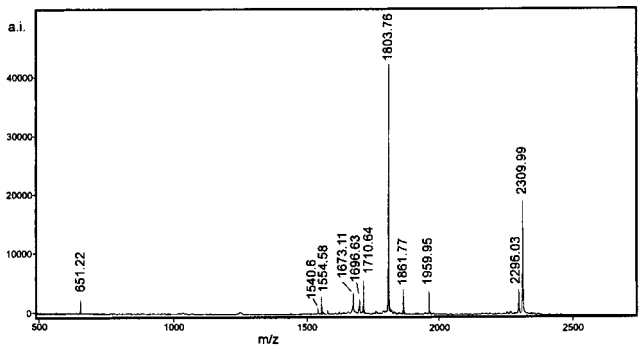


Figure 5. MALDI mass spectrum of the tryptic peptide map of B27-Asa−IGF-1. In addition to the native tryptic peptides, a peak at *m*/*z* 1803.76 corresponding to the photofragment T2 with Asa in position B27 was observed. The spectrum was recorded using α-cyano-4-hydroxycinnamic acid as the matrix.

Therefore, this photofragment was enlarged not only by the mass of the activated photogroup but also by the two C-terminal amino acids serine and alanine. As a result, it could be confirmed that fraction 11 contained B27-Asa−IGF-1 (t_R = 42.53 min, Figure 1), fraction 13 D68-Asa−IGF-1 (t_R = 45.84 min), and fraction 15 B1-Asa−IGF-1 (t_R = 48.21 min). The derivative acylated in position B27 was of special interest, because here the photogroup is directly located within the postulated binding area (Blundell et al., 1983).

Radioiodination and Analysis of the Position of ^{125}I. To verify that after tryptic digestion of radioactive IGF−receptor conjugates the resulting binding fragments are still detectable, the insertion of iodine was investigated. Iodine can be inserted onto three tyrosine residues in positions 24, 31, and 60 (Figure 4), as well as into the photolabel itself. Under the conditions used, radioiodination of IGF-1 results in the formation of three monoiodo isomers and radioiodination of the mono-Asa−IGF-1 derivatives forms four isomers.

To clarify the site of iodination, radiolabeled IGF-1 and the three mono-Asa−IGF-1 derivatives were reduced, carboxymethylated, and digested with trypsin. Since fragments T1 and T3 only contain phenylalanine, fragment T5 only contains tyrosine, and fragment T2 contains phenylalanine as well as tyrosine, typical absorbance ratios were obtained. The elution profile given in Figure 6 and the assignment were identical to the tryptic peptide map of Honegger and Humbel (1986), who determined the primary structure of the hormone isolated from bovine serum. The tryptic mapping of [^{125}I]IGF-1 revealed the presence of three radioactive peaks. They correspond to tryptic fragment T5 with iodine in position tyrosine 60 and to fragment T2, one with iodine in position tyrosine 24 and one in position tyrosine 31 (Figure 4). When the photolabel is inserted into position B1, tryptic fragment T1 that is not radioactive without the photolabel now is radioactive. Therefore, the reversed-phase HPLC separation of the tryptic map of B1-Asa−IGF-1 shows a fourth radioactive peak neighboring fragment T1 (Figure 6, t_R = 74.4 min); here, 30% of the iodine was inserted into the N-terminal photolabel (Figure 6, histogram). Fragments T2 and T5 are radioactive without photolabel, but the elution time of the photofragments is much longer compared to those of the radioactive fragments without photolabel. Iodine is inserted into position tyrosine 60 of B27-Asa−IGF-1 to a small extent; iodination of tryptic fragment T2 (with two tyrosine residues and one photogroup) is strongly preferred. For fragment T5, insertion of the photolabel in D65/D68 increases the iodine uptake from 11 to 21%.

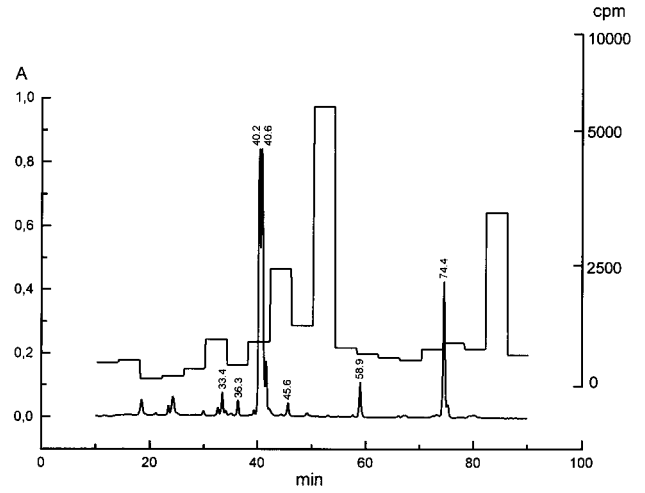


Figure 6. Reversed-phase HPLC separation of the tryptic peptide map of carboxymethylated IGF-1 (lower UV curve) with the corresponding radioactivity profile of B1-Asa−IGF-1 (upper histogram). The digest was fractionated on a C-18 column at a flow rate of 100 μL/min using a 10 to 40% acetonitrile gradient over the course of 100 min. Fractions (400 μL) were collected, and the amount of radioactivity was counted.

Table 2. Receptor Binding of Native IGF-1 and Asa−IGF-1 Derivatives

HPLC fraction	derivative	$K_D \pm$ SD (nM)	relative biological binding affinity (%)
9	IGF-1	0.72 ± 0.36	100
11	B27-Asa−IGF-1	6.3 ± 0.44	11.5
13	D65/D68-Asa−IGF-1	1.2 ± 0.14	59
15	B1-Asa−IGF-1	0.61 ± 0.04	120
17	bis-Asa−IGF-1	4 ± 0.36	18.5
19	bis-Asa−IGF-1	15 ± 1.80	4.8
21	bis-Asa−IGF-1	7 ± 0.98	10.4
23	tris-Asa−IGF-1	12 ± 1.68	6.3
25	tris-Asa−IGF-1	9.2 ± 1.47	7.9
27	tris-Asa−IGF-1	18 ± 1.62	4.1
29	tetra-Asa−IGF-1	15 ± 1.05	4.8

As a conclusion, it can be expected that after tryptic digestion of the covalent hormone−receptor conjugate binding fragments are still detectable because the point of receptor labeling and ^{125}I would not be separated.

Receptor Binding Studies. To determine the binding characteristics of the photo-IGF-1 derivatives, saturation binding experiments were carried out with [^{125}I]IGF-1 on plasma membranes of NIH-3T3 cells that overexpress wild-type IGF-1 receptors (Table 2). The binding affinities of the three monoacylated photo-IGF-1 derivatives differed considerably, indicating the importance of the substituted positions for receptor binding. The severest impairment of receptor binding was caused by a modification of position B27, which is within the postulated binding area. The derivative acylated in position B1 showed an even slightly higher binding affinity than native IGF-1, indicating that this position is not significantly involved in receptor binding. The binding affinity of the derivative with modification of the C-terminal D domain was intermediate. As expected, the binding affinity decreased with a further increase in the degree of acylation, with the exception of a bisacylated derivative that showed a rather low binding affinity of 4.8% compared with that of IGF-1.

Photoaffinity Labeling. Figure 7A shows the results of the photoaffinity labeling of plasma membranes of NIH-3T3 cells overexpressing the human IGF-1 receptor with the three mono-Asa−IGF-1 derivatives analyzed by SDS−PAGE. Specifically labeled bands with M_rs of

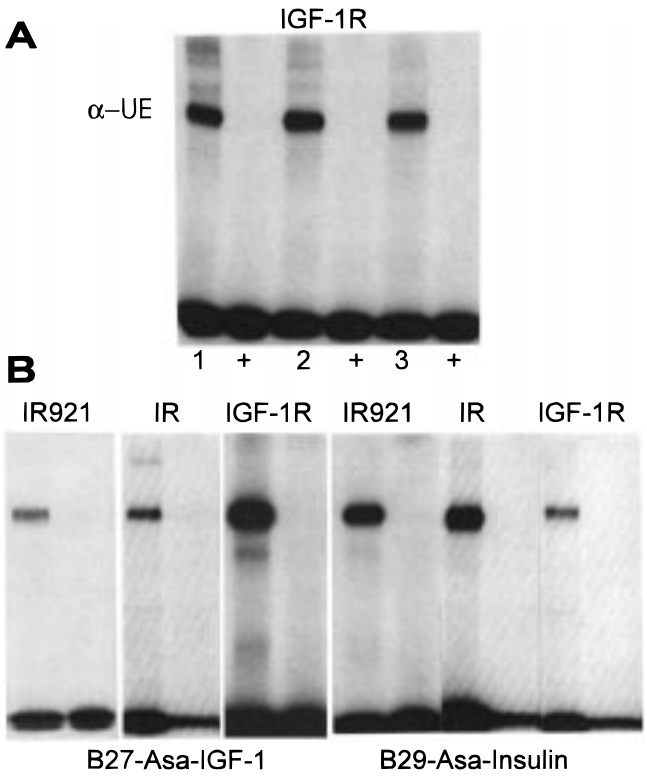


Figure 7. (A) Photoaffinity labeling of the IGF-1 receptor with B27-Asa−IGF-1 (1), D65/D68-Asa−IGF-1 (2), and B1-Asa−IGF-1 (3). Lanes marked with + are protein labeling (control) with an excess of IGF-1 (10^{-5} M). (B) Photoaffinity labeling of the IGF-1 receptor (IGF-1R), insulin receptor (IR), and insulin receptor ectodomain (IR921) with B27-Asa−IGF-1 and B29-Asa−insulin, as analyzed by SDS−PAGE under reducing conditions and autoradiography.

120 000 Da correspond to the hormon binding α-subunit. The B1-, B27-, and D65/D68-Asa−IGF-1 derivatives revealed no detectable difference in the degree of labeling of the receptor. The efficiency of photolabeling was approximately 10% (calculated as the extent of incorporation of radioactivity into the IGF-1 receptor α-subunit vs the total amount of radioactivity applied onto SDS−PAGE). In Figure 7B, the photoaffinity labeling of insulin receptor ectodomain (IR921), native insulin (IR), and IGF-1 receptors (IGF-1R) of NIH-3T3 cells with B27-Asa−IGF-1 and B29-Asa−insulin is compared. Photo-IGF-1 labels the insulin receptor and vice versa; photoinsulin also labels the IGF-1 receptor. The soluble ectodomain is strongly labeled by insulin (maximum of 40%) but only weakly by IGF-1 (approximately 5%).

The tryptic peptide maps of the photoinsulin and IGF-1 IR921 conjugates are very similar (Figure 8). SDS−PAGE of the cleavage products under reducing conditions indicated for labeling with photoinsulin major fragments of 97, 72, 59, 31, 28, and 22 kDa and for labeling with photo-IGF-1 of 94, 68, 58, 32, 29, 24, and 23 kDa. For both labels, weak bands at 43 and 13 kDa were also observed. The high correspondence of the digestion pattern indicates identical fragments and thus identical binding areas.

The synthesis of a series of photoreactive hormone derivatives for cross-linking described here will facilitate the construction of a detailed interaction map of the insulin and IGF-1 receptors and their ligands. Synthesis and radioiodination of the ligands as well as photoaffinity labeling of the receptors are possible within a short period of time. The method presented is a powerful tool for detecting and comparing specific binding areas of ligands and their receptors.

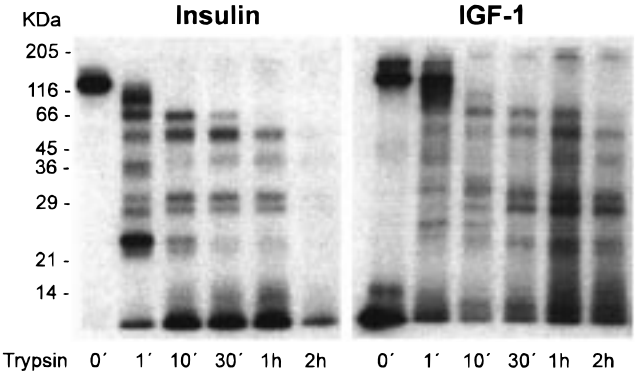


Figure 8. Time course of the tryptic digestion of the insulin receptor ectodomain labeled with B29-Asa−insulin and B27-Asa−IGF-1. Receptors were photoaffinity labeled as described in Materials and Methods. At the indicated time points, aliquots were withdrawn and analyzed by SDS−PAGE (12.5%) and autoradiography.

ACKNOWLEDGMENT

We thank Lilly Research Laboratories (Indianapolis, IN) for providing recombinant human insulin-like growth factor 1 (hIGF-1) and Dr. E. Schaefer (Quality Controlled Biochemicals, Hopkinton, MA) for the insulin receptor ectodomain IR921. The NIH-3T3 cell lines overexpressing the human IGF-1 and insulin receptor were kindly provided by Prof. A. Ullrich (MPI für Biochemie, Martinsried, Germany). I thank Dr. D. Waidelich (PerSeptive Biosystems, Wiesbaden, Germany) for the mass spectra of the tryptic digests and Mr. S. Rütten for his technical assistance. This work was supported by a Lise Meitner Grant from the Ministry of Higher Education and Research of the State of North Rhine-Westphalia.

LITERATURE CITED

(1) Blundell, T. L., Bedarkar, S., and Humbel, R. E. (1983) Tertiary structures, receptor binding, and antigenicity of insulinlike growth factors. *Fed. Proc. 42*, 2592−2597.
(2) Breiner, M., Weiland, M., Müller-Wieland, D., Streicher, R., Fabry, M., and Joost, H. G. (1993) Heterogeneity of insulin receptors in rat tissues as detected with the partial agonist B29,B29′-suberoyl-insulin. *Mol. Pharmacol. 44*, 271−276.
(3) Ebina, Y., Ellis, L., Jarnagin, K., Edery, M., Graf, L., Clauser, E., Ou, J., Masiarz, F., Kan, Y. W., Goldfine, I. D., Roth, R. A., and Rutter, W. J. (1985) The human insulin receptor cDNA: the structural basis for hormone-activated transmembrane signalling. *Cell 40*, 747−758.
(4) Fabry, M., and Brandenburg, D. (1992) Design and synthesis of a novel biotinylated photoreactive insulin for receptor analysis. *Biol. Chem. Hoppe-Seyler 373*, 143−150.
(5) Fabry, M., Schaefer, E., Ellis, L., Kojro, E., Fahrenholz, F., and Brandenburg, D. (1992) Detection of a new hormone contact site within the insulin receptor ectodomain using a novel photoreactive insulin. *J. Biol. Chem. 267*, 8950−8956.
(6) Honegger, A., and Humbel, R. E. (1986) Insulin-like growth factors I and II in fetal and adult bovine serum. *J. Biol. Chem. 261*, 569−575.
(7) Kjeldsen, T., Andersen, A. S., Wiberg, F. C., Rasmussen, J. S., Schäfer, L., Balschmidt, P., Moller, K. B., and Moller, N. P. H. (1991) The ligand specificities of the insulin receptor and the insulin-like growth factor I receptor reside in different regions of a common binding site. *Proc. Natl. Acad. Sci. U.S.A. 88*, 4404−4408.
(8) Kojro, E., Eich, P., Gimpl, G., and Fahrenholz, F. (1993) Direct identification of an extracellular agonist binding site in the renal V_2 vasopressin receptor. *Biochemistry 32*, 13537−13544.

(9) Kurose, T., Pashmforoush, M., Yoshimasa, Y., Carroll, R., Schwartz, G. P., Burke, G. T., Katsoyannis, P. G., and Steiner, D. F. (1994) Cross-linking of a B25 azidophenylalanine insulin derivative to the carboxyl-terminal region of the α-subunit of the insulin receptor. *J. Biol. Chem*. *269*, 29190−29197.

(10) Lammers, R., Gray, A., Schlessinger, J., and Ullrich, A. (1989) Differential signalling potential of insulin- and IGF-1 receptor cytoplasmic domains. *EMBO J. 8*, 1369−1375.

(11) Poole, T., Leach, B. S., and Fish, W. W. (1974) Analysis of polypeptide molecular weights by electrophoresis in urea. *Anal. Biochem*. *60*, 595−607.

(12) Rinderknecht, E., and Humbel, R. E. (1978) The amino acid sequence of human insulin-like growth factor I and its structural homology with proinsulin. *J. Biol. Chem*. *253*, 2769−2776.

(13) Schaefer, E., Erickson, H. P., Ferderwisch, M., Wollmer, A., and Ellis, L. (1992) Structural organisation of the human insulin receptor ectodomain. *J. Biol. Chem*. *267*, 23393−23402.

(14) Schumacher, R., Mosthaf, L., Schlessinger, J., Brandenburg, D., and Ullrich, A. (1991) Insulin and insulin-like growth factor I binding specificity is determined by distinct regions of their cognate receptors. *J. Biol. Chem*. *266*, 19288−19295.

(15) Ullrich, A., Bell, J. R., Chen, E. Y., Herrera, R., Petruzzelli, L. M., Dull, T. J., Gray, A., Coussens, L., Liao, Y.-C., Tsubokawa, M., Mason, A., Seeburg, P. H., Grunfeld, C., Rosen, O. M., and Ramachandran, J. (1985) Human insulin receptor and its relationship to the tyrosine kinase family of oncogenes. *Nature 313*, 756−760.

(16) Ullrich, A., Gray, A., Tam, A. W., Yang-Feng, T., Tsubokawa, M., Collins, C., Henzel, W., Le Bon, T., Kathuria, S., Chen, E., Jacobs, S., Francke, U., Ramachandran, J., and Fujita-Yamaguchi, Y. (1986) Insulin-like growth factor I receptor primary structure: comparison with insulin receptor suggests structural determinants that define functional specificity. *EMBO J. 5*, 2503−2512.

(17) Waugh, S. M., DiBella, E. E., and Pilch, P. F. (1989) Isolation of a proteolytically derived domain of the insulin receptor containing the major site of cross-linking/binding. *Biochemistry 28*, 3448−3455.

(18) Wedekind, F., Baer-Pontzen, K., Bala-Mohan, S., Choli, D., Zahn, H., and Brandenburg, D. (1989) Hormone binding site of the insulin receptor. *Biol. Chem*. *Hopppe-Seyler 370*, 251−258.

(19) Yip, C. C. (1992) The insulin-binding domain of insulin receptor is encoded by exon 2 and exon 3. *J. Cell Biochem*. *48*, 19−25.

(20) Yip, C. C., Hsu, H., Olefsky, J. M., and Seely, L. (1993) Preparation of $N^{\epsilon B28}$-monoazidobenzoyl insulin-like growth factor I and photoaffinity labeling of insulin-like growth factor I receptor. *Peptides 14*, 325−330.

(21) Zhou, A. T., Bessalle, R., Bisello, A., Nakamoto, C., Rosenblatt, M., Suva, L. J., and Chorev, M. (1997) Direct mapping of an agonist-binding domain within the parathyroid hormone/parathyroid hormone-related protein receptor by photoaffinity crosslinking. *Proc. Natl. Acad. Sci. U.S.A. 94*, 3644−3649.

BC980051+

Optimized Conditions to Couple Two Water-Soluble Biomolecules through Alkylamine Thiolation and Thioetherification

Laurent Meunier, Sylvain Bourgerie, Roger Mayer, Annie-Claude Roche, and Michel Monsigny*

Glycobiologie, Centre de Biophysique Moléculaire, CNRS, Rue Charles Sadron, 45071 Orléans Cedex 02, France. Received June 16, 1998; Revised Manuscript Received October 5, 1998

A simple method for introducing, in buffered saline, a reactive sulfhydryl group on water-soluble molecules bearing an alkyl-amino group is described. This method is based on the use of two water-soluble reagents: 2-iminothiolane and 6,6′-dithiodinicotinic acid. The first one is open upon reaction with an amino group, and the generated thiol group is immediately protected by action of the second reagent. The optimal conditions were determined by taking into account the stability and the reactivity of both reagents with regards to pH and temperature. This method was validated through two applications, the substitution of bovine serum albumin with a bromoacetyl peptide and the substitution of an amino link at the 5′ end of an oligonucleotide by reaction with either a fluorescent tag, iodoacetamidofluorescein, or a bromoacetyl peptide, upon reduction of the protected disulfide bridge with a third water-soluble reagent, namely tris(2-carboxyethyl)phosphine.

INTRODUCTION

A number of molecules, including antibodies (Carlsson et al., 1978; Duncan et al., 1983; Karacay et al., 1997), enzymes (Yoshitake et al., 1979), liposomes (Lasch et al., 1987), or toxins (Lambert et al., 1985) have been thiolated and then substituted with other molecules.

One of the procedures used for the preparation of protein conjugates is to link the two partners through either a disulfide bridge or a thioether bond. Heterobifunctional reagents such as *N*-succinimidyl 3-(2-pyridyldithio)propionate (SPDP) (Carlsson et al., 1978), *S*-acetyl thioacetic acid (Duncan et al., 1983), or homocysteine thiolactone (Leanza et al., 1992) are commonly used to add a thiol group to a protein.

Alternatively, 2-iminothiolane, which reacts with an amino group and generates a free thiol group (Traut et al., 1973; Jue et al., 1978; Singh et al., 1996) can be used. King et al. (1978) used a mixture of 2-iminothiolane and dithiodipyridine to prepare protein conjugates via an intermolecular disulfide bond, dithiopyridine being used to protect the generated thiol groups. The advantage of 2-iminothiolane over SPDP is that it is more hydrophilic and preserves a positive charge on lysine side chains. Indeed, with 2-iminothiolane, the surface charge distribution of the protein is unperturbed (Jue et al., 1978), whereas with SPDP the positive charge of the free lysine residue is lost upon substitution; this induces a decrease in the solubility of the substituted protein. However, as shown earlier and especially by Singh et al. (1996), the adduct obtained upon reaction of 2-iminothiolane on an amino group is labile as long as the thiol group is free. It is therefore very useful to immediately substitute the thiol group by adding a protective reagent such as dithiodipyridine (King et al., 1978). However, dithiodipyridine, which must be used in large excess, is unfortunately slightly water soluble; in contrast, 6,6′-dithiodinicotinic acid is highly water soluble, and therefore, it may be used in a high concentration without requiring the presence of any organic solvent. Upon reaction of 6,6′-dithiodinicotinic acid with a thiol group, the carboxylated pyridinethione released is easily titrated thanks to its high absorbance at 344 nm (Grassetti et al., 1969), as in the case of pyridinethione.

We describe a simple, optimized method for the derivatization of a protein and of an oligonucleotide in buffered saline by introducing a thiol-reactive group on these molecules. This method is based on the use of three water-soluble reagents, namely 2-iminothiolane, 6,6′-dithiodinicotinic acid, and tris(2-carboxyethyl)phosphine (TCEP). The two first reagents used in conjunction led to a protected thiol derivative. Then, the use of TCEP together with halogeno-acetyl derivatives led to the substitution of molecules of interest with either a fluorescent tag or a peptide.

EXPERIMENTAL PROCEDURES

Materials. 2-Iminothiolane, tris(2-carboxyethyl)phosphine, iodoacetamidofluorescein, or lissamine rhodamine sulfonyl chloride were purchased from Molecular Probes (Leiden, The Netherlands); 6,6′-dithiodinicotinic acid, dithiodipyridine, triisopropylsilane, iodoacetamide, ϵ-amino caproic acid, DABCO and 5,5′-dithiobis(2-nitrobenzoic acid or Ellman's reagent) were from Aldrich (Saint Quentin Fallavier, France).

An 5′-alkylamine pentacosanucleotide $^{+}NH_3$-$(CH_2)_6$-O-PO_2-$^{5'}$CTC TCG CAC CCA TCT CTC TCC TTC T$^{3'}$-PO_2-O-$(CH_2)_{12}$OH phosphodiester (specific for a sequence encompassing the gag AUG of HIV) was kindly provided by Drs. U. Asseline and N. T. Thuong (CBM-CNRS, Orléans, France).

* To whom correspondence should be addressed. Tel: +33 (0)2 38 25 55 57. Fax: +33 (0)2 38 69 00 94. E-mail: monsigny@cnrs-orleans.fr.

[1] Abbreviations: DABCO = 1,4-diazabicyclo(2.2.2)octane; DMEM = Dulbecco's modified Eagle's medium; DMF = dimethylformamide; FBS = fetal bovine serum; F-BSA = fluoresceinylated-bovine serum albumin; HIV = human immunodeficiency virus; NLS = nuclear localization signal; PBS = phosphate buffered saline; R-BSA = rhodaminylated-bovine serum albumin; SDS = sodium dodecyl sulfate; SPDP = *N*-succinimidyl 3-(2-pyridyldithio)propionate; TCEP = tris(2-carboxyethyl)phosphine; TEAA = triethylammonium acetate.

10.1021/bc980069k CCC: $18.00 © 1999 American Chemical Society
Published on Web 01/22/1999

Fluorescein-labeled serum albumin (F-BSA) and rhodamine-labeled serum albumin (R-BSA) were prepared by allowing fluorescein isothiocyanate (isomer-I) or lissamine rhodamine sulfonyl chloride to react with bovine serum albumin as previously described (Roche et al., 1983; Monsigny et al., 1984).

Peptide Synthesis. The SV40 karyophilic peptide YPKKKRKVEDPR (M_r 1665), an NLS peptide (Yoneda et al., 1987), and the KDEL peptide YGEEDTSEKDEL (M_r 1533), a reticulum endoplasmic retention signal (Munro and Pelham, 1987), were prepared by solid-phase synthesis on an Applied 433 A synthesizer (Foster city, CA) using an Fmoc strategy starting from a 4-(hydroxymethyl)phenoxymethyl resin and monitoring the coupling efficiency by conductimetry. At the last step, bromoacetic anhydride reacted with the N_α-amino terminal group to form the N_α-(bromoacetyl)-protected peptide-resin (Arar et al., 1995). The peptides were further deprotected and released from the resin by incubation in a trifluoroacetic acid/water/phenol/triisopropylsilane mixture (88:5:5:2) for 3 h. After precipitation and washing with *tertio*-butylmethyl ether, the peptides were dried under reduced pressure. The bromoacetyl peptides were characterized by matrix-assisted laser desorption ionization time-of-flight mass spectrometry using a Finnigan MAT Lasermat 2000 instrument (San Jose, CA) and an α-cyano-4-hydroxycinnamic acid matrix (Aldrich). Their purity was checked by capillary electrophoresis on a P/ACE 5500 instrument (Beckman, Fullerton, CA) equipped with a P/ACE diode array detector and a fused-silica capillary equilibrated in sodium borate buffer, pH 8.6 (Kit Beckman).

pH and Temperature Influence on the Stability and on the Reactivity of 2-Iminothiolane. The 6,6′-dithiodinicotinic acid (5 mM) was dissolved in 1 mL of 50 mM sodium borate buffer containing 2 M sodium acetate, in the presence or in the absence of ϵ-amino caproic acid (20 mM). The pH was adjusted between 8.0 and 9.2 by adding 0.5 N NaOH. One micromole of 2-iminothiolane (from a freshly prepared 73 mM stock solution) was added, and the reaction was performed either at 25 °C or on ice.

After different incubation times, the amount of released sulfhydryl groups was determined by measuring the absorbance of carboxylated pyridinethione [ϵ_{344nm} = 10 000 according to Grassetti et al. (1969)].

Synthesis of F-BSA-NLS Using 2-Iminothiolane and 6,6′-Dithiodinicotinic Acid. F-BSA (0.3 μmol) was dissolved in 4 mL of 50 mM sodium borate buffer, pH 9.0, containing 2 M sodium acetate. A solution of 6,6′-dithiodinicotinic acid (45 μmol) in 1 mL of the buffer was adjusted at pH 9.0 by addition of 0.5 N NaOH. Then, 2-iminothiolane (30 μmol) was added. The mixture was incubated for 12 h on ice. F-BSA-(dithionicotinic acid)$_n$ was purified by gel filtration on an Ultrogel GF 05 column (50 × 2 cm) (Sepracor, Villeneuve-la-Garenne, France) eluted with a *n*-butanol/water (5:95) mixture at 4 °C. The fluorescent fractions were collected.

After freeze-drying, F-BSA-(dithionicotinic acid)$_n$ (0.28 μmol, 93% yield) was dissolved in 4 mL of 50 mM sodium phosphate buffer, pH 8.0, containing 2 M sodium acetate. The mixture was degassed by freezing at −20 °C and then thawing under reduced pressure. The solution was maintained under argon throughout the reaction to prevent air oxidation of sulfhydryl groups. The disulfide bridges were reduced with TCEP (4.5 μmol) at 25 °C then bromoacetyl-peptide NLS (8 μmol) was added in 2 M sodium acetate and 50 mM sodium phosphate buffer, pH 8.0. The mixture was stirred for 4 h. Remaining thiol groups were substituted by adding an excess of iodoacetamide (30 μmol) in 200 μL DMF (5% of the buffer volume), and the solution was stirred further for 2 h. The F-BSA-NLS was purified at 4 °C by gel filtration on Ultrogel GF 05 equilibrated with water containing 5% *n*-butanol. The number of peptides linked to F-BSA was estimated by electrophoresis in an 8% polyacrylamide gel (Laemmli, 1970) in the presence of 0.1% SDS. After freeze-drying, 0.255 μmol of F-BSA-NLS was collected which represented a yield of 85%.

Synthesis of F-Oligonucleotide Using 2-Iminothiolane and 6,6′-Dithiodinicotinic Acid. A 5′-hexylamine phosphodiester oligonucleotide (0.125 μmol) was dissolved in 0.5 mL of 2 M sodium acetate and 50 mM sodium borate buffer pH 9.0. 2-Iminothiolane (12.5 μmol) and 6,6′-dithiodinicotinic acid (19 μmol) were added in 0.5 mL of the same buffer adjusted at pH 9.0. The mixture was incubated on ice, and the oligonucleotide thiolation was monitored by HPLC.

Analyses were carried out using a Waters system (Saint-Quentin-en-Yvelines, France) with a Millennium software, on a Nova-Pack C18 (Waters) column (0.4 × 15 cm; particle size, 10 μm), with a linear gradient from 5 to 30% solvent B in solvent A over 30 min (flow rate 1 mL/min; solvent A: 95% 0.1 M triethylammonium acetate (TEAA), pH 7.0/5% acetonitrile; solvent B, 5% 0.1 M TEAA, pH 7.0/95% acetonitrile). The elution was monitored by UV absorbance at 260 nm using a Waters photodiode array detector.

The thiolated oligonucleotide was precipitated by adding 2.5 vol of ethanol. The precipitate was then dissolved in distilled water and loaded onto a Biogel P2 column (20 × 1 cm) (Bio-Rad, Oxfordshire, England) eluted with 5% *n*-butanol. Fractions containing the oligonucleotide were pooled and, upon freeze-drying, stored at −20 °C.

The thiolated oligonucleotide, dissolved in 0.5 mL of 2 M sodium acetate, 50 mM phosphate buffer, pH 8.0, was reduced with 2 equiv of TCEP (0.25 μmol). Iodoacetamidofluorescein (20 equiv) was dissolved in the same buffer and slowly added to the oligonucleotide solution under stirring. The reaction was performed under argon at 25 °C for 3 h. To remove the fluorescein excess, the oligonucleotide was precipitated by adding 2.5 vol of ethanol. The fluoresceinylated oligonucleotide was purified by chromatography on Biogel P2 or by HPLC before its characterization by mass spectrometry. The negative ion electrospray mass spectra were obtained using a Platform quadrupole mass spectrometer (VG Biotech, Fisons Instruments, Altrincham, U.K.) equipped with an electrospray atmospheric pressure ionization source.

Synthesis of Oligonucleotide-KDEL Peptide Conjugate Using 2-Iminothiolane and 6,6′-Dithiodinicotinic Acid. The 5′-hexylamine phosphodiester oligonucleotide was thiolated as described above. All the solutions used were degassed under reduced pressure and then gassed with argon. The reduction of the dithionicotinic acid-oligonucleotide and the coupling reaction with the KDEL peptide bearing a N_α-bromoacetyl reactive group were simultaneously conducted. The thiolated oligonucleotide (0.125 μmol dissolved in 0.5 mL of 2 M sodium acetate, 50 mM phosphate buffer pH 8.0) was mixed with the N_α-bromoacetyl-KDEL peptide (1.25 μmol dissolved in 0.25 mL of the same buffer) and with TCEP (0.25 μmol in 7 μL of the same buffer). The reaction was stirred under argon for 3 h. The oligonucleo-peptide-KDEL was purified by HPLC on a LiChrospher 100 RP-18 E (Merck) column (10 × 250 mm; particule size, 10 μm) with a linear gradient from 10 to 30% solvent B in solvent A over 30 min (flow rate 3 mL/min; solvent A,

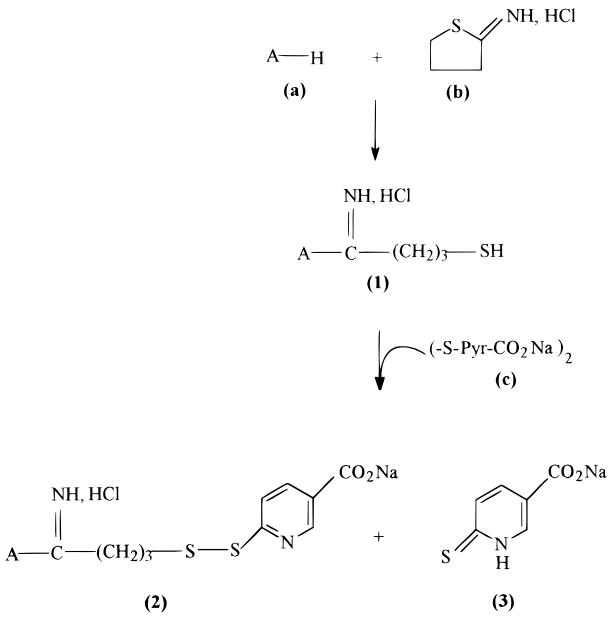


Figure 1. Scheme of the reaction of 2-iminothiolane (b) with an amine bearing molecule (a) (A = R-NH) or water (A = OH) followed by substitution with 6,6′-dithiodinicotinic acid (c). **1**, a thiolated compound; **2**, a dithionicotinic acid-substituted compound; and **3**, the carboxylated pyridinethione released. It should be noted that there is a large excess of 2-iminothiolane and 6,6′-dithiodinicotinic acid over the concentration of the amine and therefore the amount of carboxypyridinethione obtained is much larger than that expected from the reaction with the thiolgroup linked to the aminogroup.

95% 0.1 M triethylammonium acetate (TEAA), pH 7.0/5% acetonitrile; solvent B, 5% 0.1 M TEAA, pH 7.0/95% acetonitrile). The elution was monitored by UV absorbance at 260 nm using a Waters photodiode array detector. The oligonucleo-peptide was then characterized by a polyacrylamide (15%) gel electrophoresis, using a 10 cm long slab for 3 h under 70 V, in a tris-borate-EDTA buffer (TBE), pH 8.0. The oligonucleotides were then stained with methylene blue.

Microinjection into Somatic Cells and Confocal Microscopy Analysis. HeLa cells (10^5 cells/well) were grown for 24 h on CELLocate microgrid coverslips (Eppendorf, Hamburg, Germany). Both R-BSA and F-BSA-NLS were co-injected at 5 mg/mL into the cytosol of cells by using a microinjector 5242 and a micromanipulator 5170 (Eppendorf, Hamburg, Germany). Cells were incubated for 30 min at 37 °C in complete medium (DMEM supplemented with 10% FBS) in a 5% CO_2 air atmosphere. Cells were then fixed with 2% *p*-formaldehyde in PBS for 30 min and were mounted in PBS/glycerol (1:1, v/v) containing 1% DABCO as an antifading agent (Johnson et al., 1982). Cells were observed with a MRC 1024 confocal microscope (BioRad, Oxfordshire, U.K.) equipped with a Nikon Optiphot epifluorescence microscope (Nikon, Tokyo, Japan) and a 60× Planapo objective (numerical aperture 1.4).

RESULTS

Stability and Reactivity of 2-Iminothiolane Related to pH and Temperature. The thiolation scheme of an amino group with 2-iminothiolane and 6,6′-dithiodinicotinic acid is presented in Figure 1. Each molecule of dithiodinicotinic acid which reacts with a molecule containing a sulfhydryl group releases one molecule of carboxylated pyridinethione.

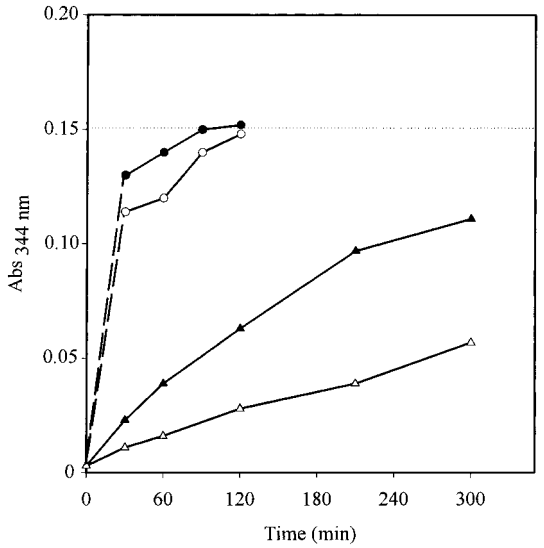


Figure 2. Hydrolysis and aminolysis of 2-iminothiolane at pH 8.6 and 25 °C in the presence (●) or in the absence (○) of ϵ-amino caproic acid, and at pH 8.6 on ice in the presence (▲) or in the absence (△) of ϵ-amino caproic acid. The absorbance of carboxylated pyridinethione released was measured at 344 nm.

The optimal conditions leading to the substitution of an ϵ-amino group were determined by using ϵ-amino caproic acid as a model compound. The stability and the reactivity of 2-iminothiolane were checked in the absence or in the presence of ϵ-amino caproic acid.

The coupling reaction was conducted in the presence of a high ionic strength buffer, 2 M sodium acetate; indeed, 2-iminothiolane was found to be less susceptible to degradation when it was kept in such a high ionic strength buffer. The extent of the reaction was monitored by measuring the absorbance increase at 344 nm. The rapid increase of the absorbance at 344 nm of a solution of 2-iminothiolane and 6,6′-dithiodinicotinic acid at pH 8.6 and 25 °C (Figure 2), in the absence of ϵ-amino caproic acid, indicated a spontaneous hydrolysis of 2-iminothiolane. However, in the presence of ϵ-amino caproic acid, the increase in absorbance was slightly faster showing that 2-iminothiolane was both aminolyzed and hydrolyzed (Figure 2). The spontaneous hydrolysis at pH 8.6, in the absence of ϵ-amino caproic acid was slower at low temperature (on ice) allowing a more efficient aminolysis (Figure 2).

To determine the optimal coupling conditions, the reaction was performed on ice at pH between 8.0 and 9.2 (Figure 3). The 6,6′-dithiodinicotinic acid was found to be quite stable on ice and at pH around 9.2. Concerning 2-iminothiolane, its rates of both hydrolysis and aminolysis increased with pH but the aminolysis reaction appeared to be optimal when the reaction was conducted at pH 9.0. At higher pH, the rate of hydrolysis increased faster than that of aminolysis. On these bases, the optimized conditions are those conducted on ice at pH 9.0 in a high salt buffered solution.

Preparation of F-BSA-NLS. 2-Iminothiolane and 6,6′-dithiodinicotinic acid were used to add thiol reactive groups to a protein (F-BSA). After 12 h of incubation under optimized conditions (pH 9.0, on ice) and purification by gel filtration, the number of sulfhydryl groups added to F-BSA, determined on an aliquot of F-BSA-(dithionicotinic acid)$_n$ by measuring the amount of carboxylated pyridinethione released upon reduction with TCEP, was found to be about 15. When the reaction was conducted at pH 8.0, the substitution was less efficient

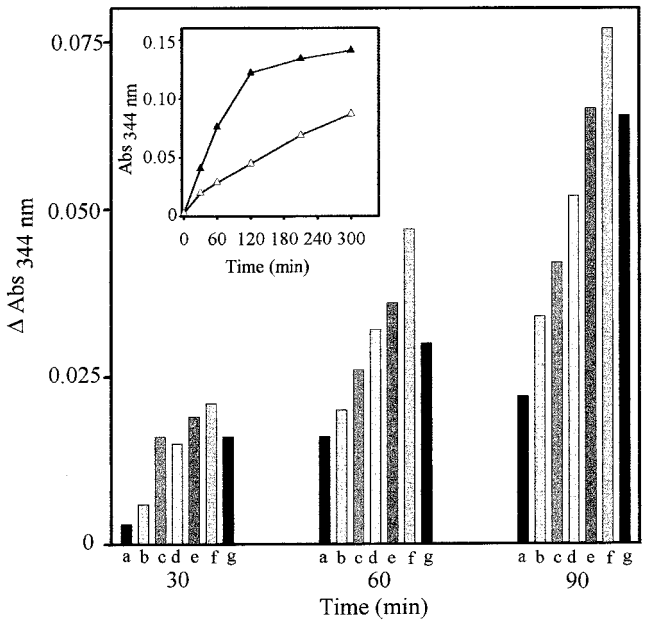


Figure 3. Time-course studies of the reaction of 2-iminothiolane with ϵ-amino caproic acid on ice at pH 8.0 (a); pH 8.2 (b); pH 8.4 (c); pH 8.6 (d); pH 8.8 (e); pH 9.0 (f); pH 9.2 (g). ΔAbs is the difference between the absorbances of the released carboxylated pyridinethione at 344 nm in the presence and in the absence of ϵ-amino caproic acid. Inset: monitored time-course studies of the release of carboxylated pyridinethione at pH 9.0 on ice. The absorbance of released carboxylated pyridinethione was measured at 344 nm in the presence (▲) or in the absence (△) of ϵ-amino caproic acid.

by a factor of 0.7. The number of NLS peptide linked to F-BSA through a thioether bond was determined by electrophoresis in SDS−polyacrylamide gel. Under reducing and denaturing conditions, the electrophoretic mobility of F-BSA-NLS decreased with the number of peptides bound. An average of 10 NLS peptides was found to be bound on one F-BSA molecule. A control study using the bromoacetyl-peptide-NLS with native nonthiolated BSA to estimate the extent of the reaction of bromoacetyl-peptide on lysine and histidine residues was performed at pH 8.0 and 9.5: no substitution could be evidenced upon monitoring the migration of the protein in SDS−PAGE.

To assess the intracellular fate of the F-BSA-NLS conjugate, F-BSA-NLS and R-BSA were co-injected into the cytosol of HeLa cells. The F-BSA-NLS, as expected, was localized in the nucleus within 30 min incubation at 37 °C, whereas R-BSA stayed in the cytosol (Figure 4) showing that the F-BSA-NLS conjugate, prepared as described above, was selectively and efficiently transported through the nuclear pore to the nucleus.

Derivatization of an Oligonucleotide on its 5′ End. The same method was used to introduce a thiol group on a phosphodiester oligonucleotide substituted with an amino group on its 5′-end. The reaction was monitored by HPLC (Figure 5). The thiolated oligonucleotide (peak 2) was eluted 2 min after the oligonucleotide (peak 1). After 7 h, about 60% of the oligonucleotide was thiolated and the reaction was almost completed after 12 h (Figure 5B). By comparison, the reaction with dithiodipyridine instead of 6,6′-dithiodinicotinic acid appeared less efficient: only 60% of oligonucleotide was thiolated after 12 h. It is important to notice that due to the low solubility of dithiodipyridine in aqueous solvent, dithiodipyridine had to be previously dissolved in dimethylformamide and added to the oligonucleotide which was in aqueous solution. The final concentration in dimethylformamide was 30%. Conversely, using 6,6′-dithiodinicotinic acid, there was no need of any organic solvent.

The sulfhydryl group may be used to couple an oligonucleotide to another molecule with a reactive group such as a sulfhydryl or a bromoacetyl group leading to either a disulfide bridge or a thioether linkage, respectively. To test the reactivity of the thiolated oligonucleotide, 20 equiv of iodoacetamidofluorescein in 2 M sodium acetate and 50 mM sodium phosphate buffer at pH 8.0 was added to a solution of dithionicotinic acid-oligonucleotide conjugate reduced with 2 equiv of TCEP. Under these conditions, the reaction was complete within 3 h. The fluorescent oligonucleotide was purified by HPLC (Figure 6) before characterization by mass spectrometry. The experimental mass of the fluorescent oligonucleotide (8195 ± 2 Da) was in agreement with the calculated mass (8196.6 Da).

In the same manner, a N_α-bromoacetyl-peptide containing a KDEL motif was coupled to the thiolated oligonucleotide reduced with 2 equiv of TCEP. The reaction was stopped after 3 h and the oligonucleopeptide was characterized by polyacrylamide (15%) gel electrophoresis. The purified oligonucleo-peptide (Figure 7, lane 3) had a migration slower than that of the oligonucleotide protected with dithionicotinic acid derivative (Figure 7, lane 1). After 3 h, the major compound was the expected oligonucleo-peptide; a small amount of the monomeric-reduced oligonucleotide, which had not reacted with the peptide, was however still present (Figure 7, lane 2). It should be emphasized that, under these conditions, the dithionicotinic acid-oligonucleotide derivative did not lead to any significant amount of a dimeric oligonucleotide (Figure 7, lane 1).

DISCUSSION

The present report describes an optimized and simple technique for obtaining water-soluble conjugates based on the use of two selected water-soluble reagents: 2-iminothiolane to add a reactive thiol group on a compound bearing an aminoalkyl residue and 6,6′-dithiodinicotinic acid to immediately protect the newly generated thiol.

Dealing with highly hydrophilic components such as proteins or oligonucleotides, it is worthwhile to define efficient conditions which avoid any organic solvent. 2-Iminothiolane is very soluble in aqueous solution and, therefore, can be easily used in a large excess without adding any organic solvent.

Dithiodipyridine has been used in conjunction with 2-iminothiolane to introduce dithiopyridyl groups into proteins (King et al., 1978). Unfortunately, dithiodipyridine has a limited water solubility; it is therefore usually dissolved in an organic solvent such as dimethylformamide or methanol. Conversely, sodium 6,6′-dithiodinicotinate is highly soluble in aqueous solution. Furthermore, 6,6′-dithiodinicotinic acid was preferred to another thiol reagent such as the Ellman's reagent [5,5′-dithiobis(2-nitrobenzoic acid)] because, in preliminary experiments the substitution of thiolated BSA led to precipitation of the adduct. In addition, the dithiopyridine derivative upon reduction led to a single thiol, the released protecting group becoming a nonreactive pyridinethione derivative. Conversely, upon reduction, dithionitrobenzoic acid derivative led to two thiols: one born by the molecule of interest, and the other by the released protective group.

TCEP was used to reduce quantitatively disulfide bridges of small molecules (Burns et al., 1991) leading

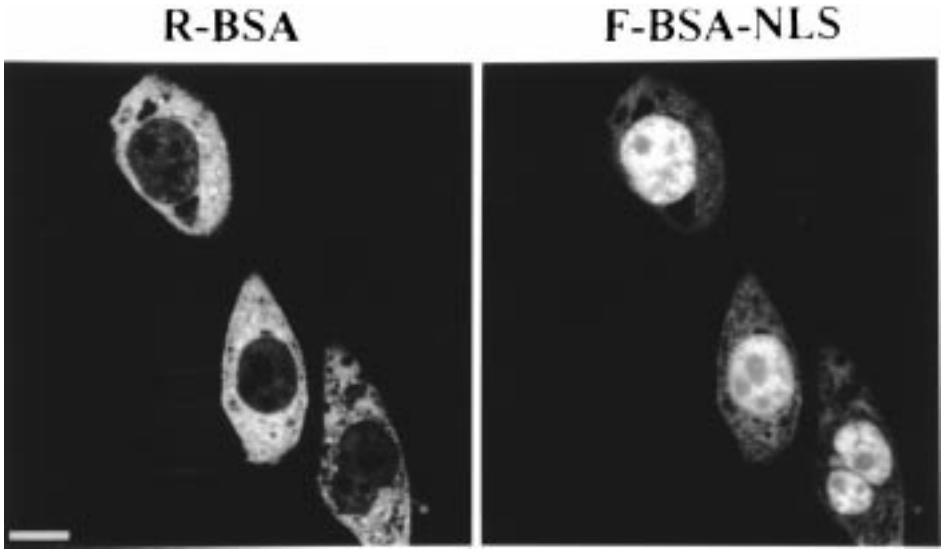


Figure 4. HeLa cells, co-injected with both F-BSA-NLS and R-BSA, in their cytoplasm were then incubated for 30 min at 37 °C in DMEM containing 10% FBS and then observed in a confocal microscope after fixation as described in the Experimental Procedures. Scale bar, 10 μm.

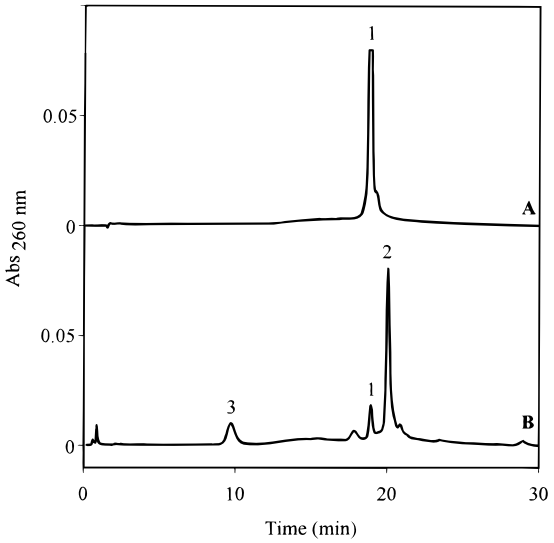


Figure 5. HPLC analysis of thiolated oligonucleotide formation using the conditions described in the Experimental Procedures. (A) unmodified oligonucleotide; (B) reaction after 12 h. Peak 1, the unmodified oligonucleotide, and peak 2, the thiolated oligonucleotide. Peak 3 corresponds to 6,6′-dithiodinicotinic acid.

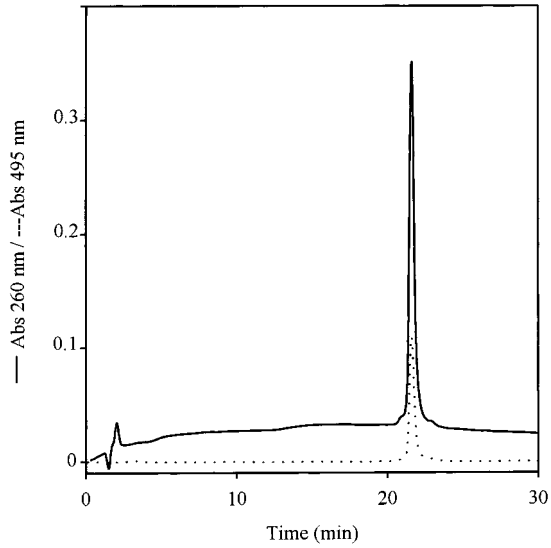


Figure 6. HPLC analysis of fluorescein-substituted oligonucleotide as described in the Experimental Procedures. Solid line, monitoring at 260 nm; broken line, monitoring at 495 nm.

to two thiols; acting on an alkyldithionicotinic acid, TCEP leads to a free alkylthiol and to carboxypyridinethione. Initially, the reduction was performed for 30 min at pH 7.0 before adding the thiol reagent (Arar et al., 1995). Under those conditions, optimized for the use of TCEP, we were unable to form a fluorescent oligonucleotide (results not shown). The thiol adduct formed by the reaction of an amine with iminothiolane is rapidly converted to nonthiol products with a loss of ammonia as shown by Singh et al. (1996), except when it is substituted; therefore, it is important to increase the rate of the reaction. For this reason, the reaction was performed at pH 8.0, and both the reduction and the substitution of the newly formed thiol were simultaneously conducted. Therefore, the optimal conditions are a compromise to take into account the relative instability of both the iminothiolane adducts and TCEP. Indeed, TCEP is stable at or below pH 7.0; it is slowly oxidized in water at higher pH. However, by adding both a slight excess of TCEP and a larger excess of a thiol reagent (iodoacetamidofluorescein) at the same time, at pH 8.0, the reduction was complete and the formation of a stable thioether was fast enough to efficiently avoid any substantial rearrangement of the primary iminothiolane adduct. Under similar conditions, TCEP was found to reduce the dithionicotinic acid linked to a protein such as thiolated BSA or thiolated immunoglobulin. The reduction of the intramolecular disulfide bridges under nondenaturing conditions is unlikely. In control experiments, thiolated human IgG treated with TCEP was not dissociated in subunits upon subsequent denaturation in the presence of SDS (results not shown). In addition, TCEP was selected among a series of reducing agents such as mercaptoethanol, thioglycolic acid, and dithiothreitol for three main reasons: the first one is because TCEP is hydrophilic and highly water soluble, the second one is that the reduction is roughly stoichiometric with regards to the concentration of dithiodinicotinic acid, and the third one because TCEP is oxidized into a nonreactive TCEPoxide making the reaction strictly irreversible. The two last characteristics are specific to such a compound

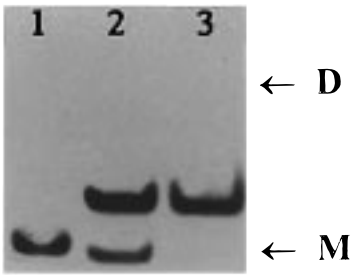


Figure 7. Polyacrylamide gel electrophoresis of oligonucleotide and derivatives conducted for 3 h on a 15% polyacrylamide gel, 10 cm long at 7 V/cm. Lane 1 is the dithionicotinic acid-oligonucleotide derivative, alone. Lane 2 is the mixture after 3 h reaction containing the dithionicotinic acid-oligonucleotide and the oligonucleo-peptide. Lane 3 is the HPLC purified oligonucleotide-KDEL peptide conjugate. Oligonucleotides were stained with methylene blue, the peptide not being stained under these conditions. The M arrow shows the migration of the reduced monomeric oligonucleotide and the D arrow shows the position of the dimeric oligonucleotide.

and are not shared with the reducing agents containing free thiol groups.

Several previous papers described different methodologies to incorporate thiol groups into proteins by using 2-iminothiolane. Jue et al. (1978) showed that 2-iminothiolane was quite stable at pH 8.0 at 7 °C; they also showed that sulfhydryl groups were slowly exposed in the absence of any primary amine at 25 °C at the same pH. Lasch et al. (1987) used 2-iminothiolane at pH 8.5 and 23 °C to thiolate liposomes, and Singh et al. (1996) used it at pH 8.0 on ice to thiolate BSA. Tarentino et al. (1993) used 2-iminothiolane for the introduction of a sulfhydryl group into oligosaccharyl-glycosylamines deriving from asparagine-linked glycans at pH 8.8 at 25 °C. Under their conditions, we were unable to introduce more than a few sulfhydryl groups onto F-BSA (results not shown).

The optimal conditions in using 2-iminothiolane were determined. At 25 °C, 2-iminothiolane was found to be almost totally degraded within 1 h. Conversely, when the reaction was performed at low temperature, about 17 protein amino groups were substituted. The optimal pH was found to be around 9.0. This optimal pH allowed the addition of 15 thiol groups on F-BSA by using a 100-fold excess in thiolation reagent; this excess corresponds to 1.8-fold excess based on the number of lysyl residues in BSA. In their study on the decay of thiol groups in a sample of BSA modified with 2-iminothiolane, Singh et al. (1996) introduced two thiol groups per BSA at pH 8.0 on ice using a 42-fold molar excess of 2-iminothiolane per molecule of BSA.

In addition to the thiolation of a protein, the thiolation of a 5′-ω-hexylamine oligonucleotide derivative was investigated. For the ϵ-amino groups of a protein or for the single ω-alkylamino group of an oligonucleotide, the reactivity even at pH 9.0 requires a large excess of 2-iminothiolane and therefore an excess of a thiol-specific reagent to protect the newly added thiol. Because of the high pK of an ϵ-amino group (around 10.5), the pH must be as high as possible. But because spontaneous hydrolysis of 2-iminothiolane when the solution is strongly basic, the optimal pH is lower than the pK of the acceptor amino group. Furthermore, the rate of the spontaneous hydrolysis of 2-iminothiolane increased more rapidly with an increase in temperature than that of aminolysis; therefore, by working at low temperature (close to 0 °C), the spontaneous hydrolysis is slow enough to allow an efficient aminolysis in the presence of ϵ-amino groups. Finally, because the rate of the spontaneous hydrolysis of 2-iminothiolane at pH 9.0 is not negligible even at low temperature, an excess of 2-iminothiolane is required to ensure a high yield of substitution of the ϵ-amino groups or ω-amino groups. The optimal conditions described here allow the substitution of about one-fourth of the ϵ-amino groups of a protein such as BSA, and almost quantitatively (about 95%), the amino group of the hexylamine linked to an oligonucleotide.

Alternatively, Gaur et al. (1989) shows in a short note that it is possible to introduce a protected thiol group on an alkylamine at the 5′ end of an oligonucleotide in hydroorganic solvent (a mixture of water and acetonitrile) by using a very large excess of 500-fold SPDP and an acylating catalyst.

The method described in the present paper was mainly developed with the aim to substitute water-soluble biomolecules such as proteins or oligonucleotides with ligands or recognition signals in a high yield by avoiding the use of any organic solvent. The yield of the substitution of oligonucleotides and BSA was not dependent on the oligonucleotides used nor on the BSA batches used. Concerning the substitution of proteins, the use of three water-soluble reagents, namely 2-iminothiolane, 6,6′-dithiodinicotinic acid, and tris(carboxyethyl)phosphine, allows a very efficient thiolation of the amino groups and finally a high substitution of the protein with molecules of interest such as a peptide. Because the primary thiolation reaction does not require any organic solvent and does not neutralize the positive charge of the protein amino groups, the highly thiolated protein obtained remains very water-soluble. Concerning the oligonucleotides, the thiol derivatives are much more easily substituted than the alkylamine derivatives. Therefore, when an oligonucleotide has to be substituted twice, the best way is to use commercially available oligonucleotide derivatives with an alkylamine at one end and a protected alkylthiol at the other end. The first step is the linkage of a substituant on the thiol group, the second step is the addition of a new thiol group by reaction of 2-iminothiolane on the available alkylamine and its temporary protection with the water-soluble dithiodinicotinic acid, and finally, the third step is the addition of the second substituant on the newly added thiol derivative. This bisubstituted oligonucleotide can bear two substituants linked by two thioether bonds or two substituants linked by both a thioether bond and a disulfide bond.

ACKNOWLEDGMENT

We thank Drs. Ulysse Asseline and N. T. Thuong and Yves Aubert, Centre de Biophysique Moléculaire, CNRS, Orléans, France, for the preparation of oligonucleotides and Alain Deroussent, Institut Gustave Roussy, Villejuif, France, for running the electrospray mass spectrometer. This work was supported by grants from the Agence Nationale de Recherches sur le SIDA (ANRS), from the Association de Recherche sur le Cancer (ARC 6132), and from the Ligue Nationale contre le Cancer. L.M. received a fellowship from the MENESR. S.B. is the recipient of a postdoctoral fellowship from the ANRS, R.M. is Research Director CNRS, A.C.R. is Research Director INSERM, and M.M. is a professor at the University of Orléans.

LITERATURE CITED

Arar, K., Aubertin, A. M., Roche, A. C., Monsigny, M., and Mayer, R. (1995) Synthesis and antiviral activity of peptide−

oligonucleotide conjugates prepared by using N_α-bromoacetyl peptides. *Bioconjugate Chem. 6*, 573−577.

Burns, J. A., Bulter, J. C., Moran, J., and Whitesides, G. M. (1991) Selective reduction of disulfides by tris(2-carboxyethyl)-phosphine. *J. Org. Chem. 56*, 2648−2650.

Carlsson, J., Drevin, H., and Axén, R. (1978) Protein thiolation and reversible protein−protein conjugaison. *Biochem. J. 173*, 723−737.

Duncan, R. J., Weston, P. D., and Wrigglesworth, R. (1983) A new reagent which may be used to introduce sulfhydryl groups into proteins, and its use in the preparation of conjugates for immunoassay. *Anal. Biochem. 132*, 68−73.

Gaur, R. K., Sharma, P., and Gupta, K. C. (1989) A simple method for the introduction of thiol group at 5′-termini of oligodeoxynucleotides. *Nucleic Acids Res. 17*, 4404.

Grassetti, D. R., Murray, J. F., and Ruan, H. T. (1969) The interaction of 6,6′-dithiodinicotinic acid with thiols and with Ehrlich ascites tumor cells. *Biochem. Pharmacol. 18*, 603−611.

Johnson, G. D., Davidson, R. S., McNamee, K. C., Russel, G., Goodwin, D., and Holborow, E. J. (1982) Fading of immunofluorescence during microscopy: a study of the phenomenon and its remedy. *J. Immunol. Methods 55*, 231−242.

Jue, R., Lambert, J. M., Pierce, L. R., and Traut, R. R. (1978) Addition of sulfhydryl groups to *Escherichia coli* ribosomes by protein modification with 2-iminothiolane (methyl 4-mercaptobutyrimidate). *Biochemistry 17*, 5399−5405.

Karacay, H., Sharkey, R. M., Govindan, S. V., McBride, W. J., Goldenberg, D. M., Hansen, H. J., and Griffiths, G. L. (1997) Development of a streptavidin-anti-carcinoembryonic antigen antibody, radiolabeled biotin pretargeting method for radioimmunotherapy of colorectal cancer. Reagent development. *Bioconjugate Chem. 8*, 585−594.

King, T. P., Li, Y., and Kochoumian, L. (1978) Preparation of protein conjugates via intermolecular disulfide bond formation. *Biochemistry 17*, 1499−1506.

Laemmli U, K. (1970) Cleavage of structural proteins during the assembly of the head of bacteriophage T4. *Nature 227*, 680−685.

Lambert, J. M., Senter, P. D., Yau-Young, A., Blattler, W. A., and Goldmacher, V. S. (1985) Purified immunotoxins that are reactive with human lymphoid cells. Monoclonal antibodies conjugated to the ribosome-inactivating proteins gelonin and the pokeweed antiviral proteins. *J. Biol. Chem. 260*, 12035−12041.

Lasch, J., Niedermann, G., Bogdanov, A. A., and Torchilin, V. P. (1987) Thiolation of preformed liposomes with iminothiolane. *FEBS. Lett. 214*, 13−16.

Leanza, W. J., Chupak, L. S., Tolman, R. L., and Marburg, S. (1992) Acidic derivatives of homocysteine thiolactone: utility as anionic linkers. *Bioconjugate Chem. 3*, 514−518.

Monsigny, M., Roche, A. C., and Midoux, P. (1984) Uptake of neoglycoproteins via membrane lectin(s) of L 1210 cells evidenced by quantitative flow cytofluorometry and drug targeting. *Biol. Cell. 51*, 187−196.

Munro, S., and Pelham, H. R. B. (1987) A C-terminal signal prevents secretion of luminal ER proteins. *Cell 48*, 899−907.

Roche, A. C., Barzilay, M., Midoux, P., Junqua, S., Sharon, N., and Monsigny, M. (1983) Endocytosis of glycoconjugates by Lewis lung carcinoma cells. *J. Cell Biochem. 22*, 131−140.

Singh, R., Kats, L., Blättler, W. A., and Lambert, J. M. (1996) Formation of N-substituted 2-iminothiolane when amino groups in proteins and peptides are modified by 2-iminothiolane. *Anal. Biochem. 236*, 114−125.

Tarentino, A. L., Phelan, A. W., and Plummer, T. H. (1993) 2-iminothiolane: a reagent for the introduction of sulphydryl groups into oligosaccharide derived from asparagine-linked glycans. *Biochemistry 30*, 279−285.

Traut, R. R., Bollen, A., Sun, T.-.T., Hershey, J. W. B., Sundberg, J., and Pierce, L. R. (1973) Methyl 4-mercaptobutyrimidate as a cleavable cross-linking reagent and its application to the *Escherichia coli* 30s ribosome. *Biochemistry 12*, 3266−3273.

Yoneda, Y., Arioka, T., Imamoto-Sonobe, N., Sugawa, H., Shimonishi, Y., and Uchida, T. (1987) Synthetic peptides containing a region of SV 40 large T-antigen involved in nuclear localization direct the transport of proteins into the nucleus. *Exp. Cell Res. 170*, 439−452.

Yoshitake, S., Yamada, Y., Ishikawa, E., and Masseyeff, R. (1979) Conjugation of glucose oxidase from *Aspergillus niger* and rabbit antibodies using N-hydroxysuccinimide ester of N-(4-carboxycyclohexylmethyl)maleimide. *Eur. J. Biochem. 101*, 395−399

BC980069K

Tresyl-Mediated Synthesis: Kinetics of Competing Coupling and Hydrolysis Reactions as a Function of pH, Temperature, and Steric Factors

Jeffrey J. Sperinde, Benjamin D. Martens, and Linda G. Griffith*

Massachusetts Institute of Technology, Department of Chemical Engineering and Division of Bioengineering and Environmental Health, MIT 66-466, 25 Ames Street, Cambridge, Massachusetts 02139. Received June 19, 1998

Kinetic parameters have been measured for coupled nucleophilic and solvolytic reactions of 2,2,2-trifluoroethanesulfonyl (tresyl)-modified poly(ethylene glycol) based on a system of coupled differential equations implied by recently proposed elementary reaction mechanisms. Fitted kinetic parameters were found to be strong functions of pH, temperature, and steric factors. To maximize the total yield of coupled amine as well as the fraction of secondary amine linkages, our model predicts that it is desirable to run tresyl coupling reactions at low temperatures at pH ~8.0, depending on the amine pK_a for primary, unhindered amines. For branched primary amines, our data favor room temperature at a slightly higher pH.

INTRODUCTION

Nearly two decades ago, 2,2,2-trifluoroethanesulfonyl chloride (tresyl chloride) was introduced as a more reactive alternative to *p*-toluenesulfonyl chloride (tosyl chloride) in activating hydroxyl groups to covalent modification for the preparation of affinity chromatography supports (Nilsson and Mosbach, 1981). Tresyl chloride has found wide use in solid support activation as well as extensive use in poly(ethylene glycol) (PEG) activation for PEG modification of small drugs and proteins for biological stabilization and immuno-modulation (Harris, 1992).

It had long been assumed that the reaction mechanism for tresyl-mediated coupling was identical to that of tosyl chloride and other sulfonyl chlorides where the substituted sulfonyl acts as a leaving group. Recently, it has been suggested that alternative mechanisms may prevail. Demiroglou et al. (1994) proposed a mechanism in which the sulfonyl sulfur is retained throughout the entire coupling reaction. On the basis of experimental evidence, Gais and Ruppert (1995) as well as King and Gill (1995, 1996) corrected this postulated mechanism to include nucleophile addition by an β-elimination/Michael-type addition reaction. The present understanding of tresyl reactions in aqueous media includes three pathways (Scheme 1): hydrolysis, nucleophilic displacement, and β-elimination/addition.

Experimental work regarding tresyl-chloride-mediated coupling has been focused on determining the molecular structure of reaction products, yet for practical application of tresyl-mediated coupling, it is necessary to know how reaction conditions may affect the coupling yield. Here, we report effective rate constants for the recently elucidated reaction network for tresyl-mediated coupling, using PEG-Tr as a model. We further examine the effects of temperature, pH, and steric factors that affect yields of the reaction products.

The central goal of this research was to define rate constants useful in predicting coupling rates, product distributions, and product yields for tresyl-mediated coupling based on fundamental parameters such as pH, temperature, steric effects, and nucleophilic amine pK_a. It has recently been shown that pH can play a large role in hydrolysis rates and coupling products (King and Gill, 1996). Here, we sought to define the role of pH, temperature, and steric effects through the measurement of apparent rate constants that might be representative of the elementary reaction mechanisms involved in tresyl-mediated coupling of amine nucleophiles to tresylated PEG.

* To whom correspondence should be addressed. Phone: (617) 253-0013. Fax: (617) 258-5042. E-mail: griff@mit.edu.

MATERIALS AND METHODS

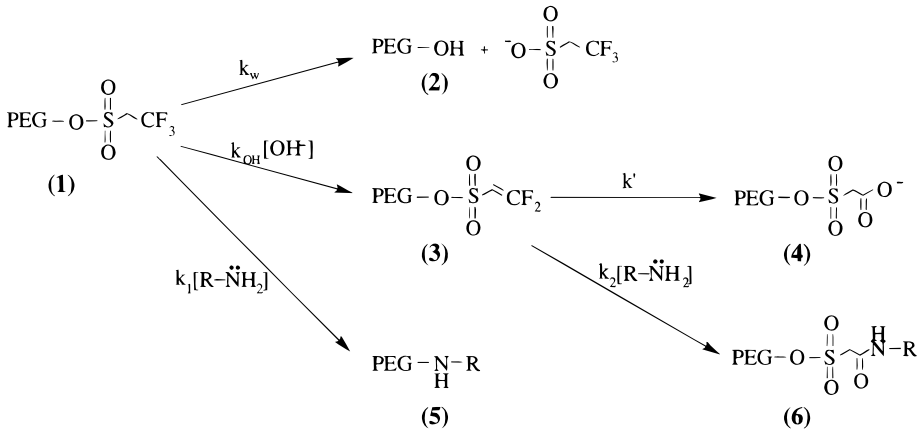
Poly(ethylene glycol) (MW = 6000) was purchased from Fluka. Tresyl chloride (2,2,2-trifluoroethanesulfonyl chloride), L-phenylalanine (Phe), and N^2-(carbobenzyloxy)-L-lysine (αCBZ-Lys) was from Aldrich. Glycyl-DL-phenylalanine (Gly-Phe) was from Sigma.

Synthesis of Tresylated PEG (1). The general synthesis procedure for PEG tresylation is detailed elsewhere (Sperinde and Griffith, 1997), employing a method similar to that of Nilsson and Mosbach (1984). In the present study, dihydroxyl PEG (6000 MW) was used as the starting material. Briefly, the tresylation was performed in a dried solution (over molecular sieves previous to tresylation) of PEG$-OH_2$ in methylene chloride (10 mL/g PEG) under argon with triethylamine as an acid acceptor. Purified PEG-Tr_2 was obtained by successive reprecipitations from acidified methanol, using decreasing concentrations of acid. Residual triethylamine was found to be 0.02 wt % by ^{1}H NMR. On the basis of sulfur elemental analysis, tresylation was approximately 100%, with 3.08 g/mmolTr [52.2% C, 8.54% H, 1.04% S]. Each tresyl group (=[1], see Scheme 1) of PEG-Tr_2 is assumed to react independently; therefore, designations "PEG-Tr" and "PEG-Tr_2" are used interchangeably.

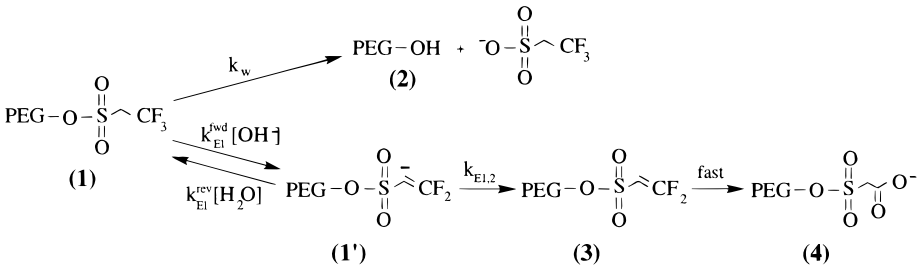
Isolated Hydrolysis Reaction. Progress of the hydrolysis reaction was monitored by continuous titration. A weighed amount of PEG-Tr_2 (about 50 mg) was added to a measured volume (about 100 mL) of Milli-Q water. The solution was stirred continuously. Dilute potassium

10.1021/bc980070j CCC: $18.00 © 1999 American Chemical Society
Published on Web 02/24/1999

Scheme 1



Scheme 2



hydroxide (20 mM) was added as needed to maintain the pH within 0.05 units of desired pH as measured by a standard calomel electrode. The amount and time of addition of each acid aliquot was recorded. Continuous titration experiments were run at 22 ± 1 °C with pH 6.0, 7.0, 7.5, 8.0, 8.5, and 9.0 and at 4 ± 0.2 °C with pH 8.0, 8.5, and 9.0. Each continuous titration reaction was monitored for 80 min. For slower reactions at 4 ± 0.2 °C with pH 5.0, 6.0, and 7.0, base was required much less often to maintain the desired pH. In these three conditions, the rate of acid evolution was measured by the rate of pH change, where the pH was always maintained within ±0.1 pH units of the desired level. These three slower reactions were run at higher PEG-Tr_2 concentrations (about 2 mg/mL) and were maintained over a number of days, with frequent recalibration of the pH meter.

The measurement of moles of base added to maintain constant pH was used to calculate moles of tresyl groups consumed. By reaction stoichiometry, 4 mol of base is required to neutralize the acid evolved by the conversion of R-Tr to R-$OSO_2CH_2COO^-$, and 1 mol of base is required to neutralize the hydrolysis of R-Tr to R-OH and $^-OSO_2CH_2CF_3$. The fractional conversion of tresyl groups (X_{Tr}) was calculated on the basis of the weight of PEG-Tr_2 used in each experiment (measured to ±0.1%), using the value of 3.08 g of PEG/mmol of Tr noted above, confirmed by total hydrolysis of PEG-Tr_2.

Simultaneous Coupling/Hydrolysis Reaction. A measured amount of PEG-Tr to make a final concentration of 40 mM in tresyl was added to a solution 100 mM in primary amine and 400 mM in potassium phosphate at the desired pH. The extent of the coupling reaction was measured as a function of time by periodic sampling of the reaction solution by a HPLC Hitachi L-7200 autosampler. The aliquot was immediately injected onto one TSK G4000PW and one TSK G2000PW column in series. The mobile phase was 0.50 M sodium chloride with 10 mM potassium phosphate and 4% acetonitrile at pH 4 delivered by a Hitachi L-7100 pump. Detection was by a Hitachi L-7420 UV−vis detector at 260 nm where PEG-Tr has an insignificant absorbance. For each measurement, the fraction of amine bound to PEG was calculated as the integral of absorbance at 260 nm for the PEG peak (first to elute) divided by the total integral (PEG peak + free amine peak). Amines examined include glycyl-phenylalanine, phenylalanine, and α-CBZ-lysine. All amines were examined at 4 and 22 °C.

Algorithm for Rate Constant Fitting. Whereas analytical solutions to rate equations were unavailable, rate constants were fit using standard Fortran models extracted from Numerical Recipes (Press et al., 1986). The rate constants were fit by an iterative process. A fourth-order Runge−Kutta routine was used to generate data for conversion as a function of time from a set of guessed rate constants. This generated data was then compared with measured data to calculate a new set of more accurate rate constants. A Levenberg−Marquardt (LM) χ-squared minimization routine generated this new guess. The same Runge−Kutta routine was used within the LM routine as well to calculate the necessary partial derivatives ($\partial\chi/\partial k_i$) for each rate constant, k_i. This process was repeated iteratively until χ was approximately minimized ($\chi_{n+1}/\chi_n < 0.0001\%$).

The data were separated for rate constant analysis by nucleophile ($n = 3$) and by temperature ($n = 2$). For each of these six data groups, rate constants were optimized by the LM method for all pHs simultaneously.

RESULTS AND DISCUSSION

A number of reaction pathways for tresylated species have recently been elucidated, yet kinetic data which could be used to maximize desired products is somewhat limited. The goal of this work is to measure apparent rate constants for a reaction network that describes the set of possible reactions for the displacement of tresyl groups by primary amines in an aqueous environment as a

function of pH temperature and steric factors. This has been undertaken in two steps. First, in the absence of an amine nucleophile, rate constants for hydrolysis and hydroxyl-mediated tresylate conversion were measured. Second, with knowledge of the solvent-mediated reactions, rate constants for coupling of various primary amine species were measured by fitting to a kinetic model consistent with known reaction mechanisms.

Rate Constants for Hydrolytic Processes. King and Gill have shown that the ethyl trifluoroethanesulfonate in the absence of a nucleophile will hydrolyze to different species depending on the solution pH (King and Gill, 1996) as can be inferred from Scheme 2. They reported data at 25 °C supporting a traditional sulfonate ester hydrolysis pathway (first-order rate constant = k_w) at low pH and reversible E1cB reaction at high pH (pseudo-first-order rate constant = $k_{OH}[OH^-]$) in which the first step is rate limiting. Given the set of reactions in Scheme 2, the disappearance of PEG-Tr (1) can be written as

$$-\frac{d[PEG-Tr]}{dt} = (k_w + k_{OH}[OH^-])[PEG-Tr]$$

where

$$k_{OH} = \frac{k_{E1}^{fwd} k_{E1,2}}{k_{E1}^{rev}[H_2O] + k_{E1,2}}$$

The integrated form of this equation in terms of conversion ($\equiv X_{Tr}$) is

$$-\ln(1 - X_{Tr}) = (k_w + k_{OH}[OH])t = k_{h,app}t$$

where

$$X_{Tr} = 1 - \frac{[PEG-Tr]}{[PEG-Tr]_0}$$

This equation implies that a plot of $-\ln(1 - X_{Tr})$ versus time would be linear, with the slope equal to (k_w + $k_{OH}[OH^-]$). By varying the pH, unique values for k_w and k_{OH} can be computed. Data for hydrolysis reactions are plotted in Figure 1 at 4 °C for pH 8−9 and 22 °C for pH 6−9.

Our data for the hydrolysis of tresylated PEG at 4 and 22 °C supports the model given in Scheme 2. Linearity of the $\ln(1 - X_{Tr})$ plot (Figure 1) confirms that the first hydrolysis step is rate limiting under almost all conditions studied. The pH 9.0, 22 °C reaction deviates somewhat from linearity, indicating that one or more of the multiple steps between 3 and 4 of Scheme 1 may be limiting in the high pH regime.

To derive rate constants k_w and k_{OH}, the apparent hydrolysis rate $k_{h,app}$ was fit by a least-squares method to $k_{h,app} = k_w + k_{OH}[OH^-]$ separately for 4 and 22 °C as shown in Figure 2. Table 1 shows the rate constants fit to the data in Figure 2.

The hydrolysis rate constant k_w was found to be a stronger function of temperature than k_{OH}, the apparent rate constant for the addition−elimination pathway. The low-temperature dependence of k_{OH} may point to a significant influence of k_{E1}^{rev}, consistent with a reversible E1cB mechanism. Because k_w is of a similar order of magnitude as $k_{OH}[OH^-]$ around room temperature and slightly basic pHs, this difference in temperature dependence might allow for the control of the distribution of products by manipulating pH and temperature. This will depend on the kinetics of S_N2 nucleophilic displacement discussed below.

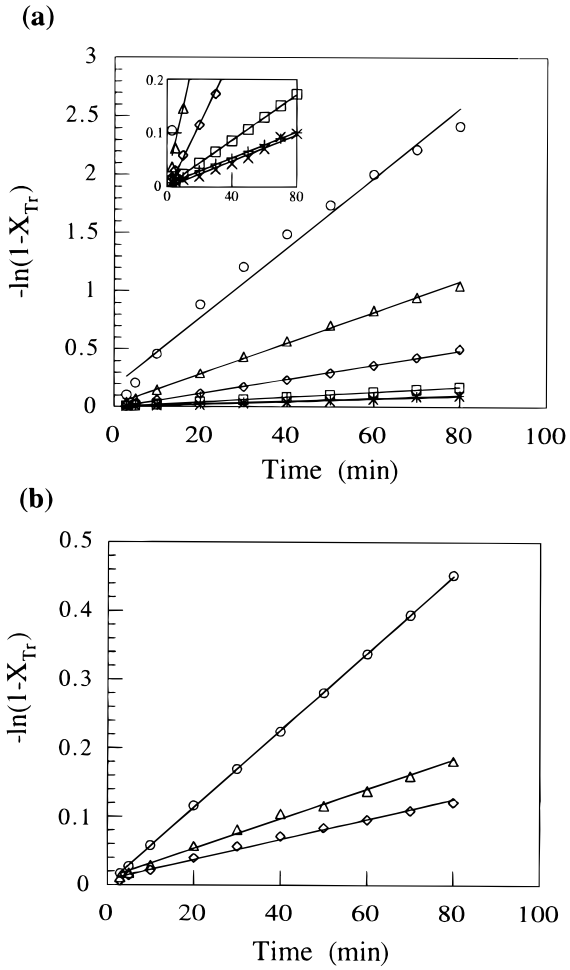


Figure 1. Hydrolysis reaction at 22 °C (1a) at pH 6.0 (×), pH 7.0 (+), pH 7.5 (□), pH 8.0 (◇), pH 8.5 (△), pH 9.0 (○), and 4 °C (1b) at pH 8.0 (◇), pH 8.5 (△), and pH 9.0 (○). All reactions were followed by titration as detailed in the Materials and Methods. Conversion of tresyl groups ($X_{Tr} = 1 - [1]/[1]_0$) was calculated on the basis of the initial concentration of tresyl groups for each experiment.

Development of a Tresyl-Mediated Coupling Model. It has been suggested that there are at least two pathways by which nucleophilic amines can couple to tresylated species (Scheme 1) [Gais and Ruppert, 1995; King and Gill, 1995; ref 6 in King (1996)]. The first pathway involves an S_N2 nucleophilic displacement, similar to that which is observed for other sulfonate leaving groups. This S_N2 pathway is thought to be minor or undetectable at very high pH (King and Gill, 1996). At high pH, the second pathway has been observed that is thought to go through an addition−elimination intermediate (3) (King and Gill, 1995). This intermediate can undergo further modifications to an inactive product (4), or it can react with an amine to give a coupled product (6).

The apparent first-order rate dependence of the addition−elimination pathway for hydrolysis suggests that $k' \gg k_{OH}[OH^-]$. This implies that as 3 is formed it is rapidly converted to a mixture of 4 and 6, such that [3] ≪ [1]. We can describe the fraction of 3 that becomes 6 as α, given by the following approximation:

$$\frac{d[6]}{dt} \approx \alpha(k_1[OH^-][1])$$

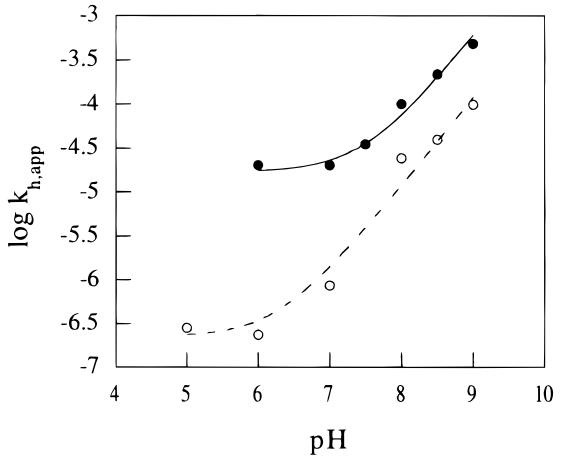


Figure 2. Least-squares fit for hydrolysis reaction ($k_{h,app} = k_w + k_{OH}[OH^-]$) for 22 °C (●) and 4 °C (○). Values of $k_{h,app}$ are taken from the slopes of curves in Figure 1 for faster reactions (points where log $k_{h,app} > -5$) and from the rate of pH change (see Materials and Methods) for slower reactions (points where log $k_{h,app} < -5$).

where

$$\alpha = \frac{k_2[\mathrm{N:}]}{k_2[\mathrm{N:}] + k'}; \; [\mathrm{N:}] \equiv \text{unprotonated amine}$$

As suggested by the hydrolysis experiments, the above assumption should hold at least for pH ≲9.0. Because reactions governed by k_2 and k' are downstream of the rate-limiting step, (1 → 3), the absolute magnitudes of k_2 and k' cannot be measured independently. Only the ratio k_2/k' can be calculated.

The rate constants k_w and k_{OH} are known from the previous section (Table 1). Here we will fit k_1 and k_2/k' for each amine species at each temperature, based on measured coupling data for a set of model amines. On the basis of Scheme 1 and the above approximation, we can write the following differential equations that describe the concentrations of the reaction components as a function of time:

$$\frac{\mathrm{d}[1]}{\mathrm{d}t} = (k_w + k_{OH}[OH^-] + k_1[\mathrm{N:}])[1]$$

$$\frac{\mathrm{d}[2]}{\mathrm{d}t} = k_w[1]$$

$$\frac{\mathrm{d}[4]}{\mathrm{d}t} = (1 - \alpha)k_{OH}[OH^-][1]$$

$$\frac{\mathrm{d}[5]}{\mathrm{d}t} = k_1[\mathrm{N:}][1]$$

$$\frac{\mathrm{d}[6]}{\mathrm{d}t} = \alpha k_{OH}[OH^-][1]$$

$$\frac{\mathrm{d}[\mathrm{N}]_{total}}{\mathrm{d}t} = -(k_1[\mathrm{N:}] + \alpha k_{OH}[OH^-])[1]$$

The $[OH^-]$ concentration was calculated using the measured pH and the ion product of water, K_w, at the appropriate temperature (see Table 2):

$$[OH^-] = K_W(T) \times 10^{pH}$$

Table 1. Hydrolysis Rate Constants

temp (°C)	k_w (10^{-6} s^{-1})	k_{OH} (10^3 s^{-1} M^{-1})
4	0.22	68
22	17.0	78.3

Table 2. Ionization Constants

temp (°C)	pK_w[a]	pK_a Gly-Phe	pK_a Phe	pK_a αCBZ-Lys
4	14.78	8.6	9.6	11.3
22	14.08	8.1	9.1	10.7

[a] pK_w from Marshall and Franck (1981). The amine pK_as at 4 and 22 °C were calculated as explained in the text from literature values at 25 °C for glycylphenylalanine (Biester and Ruoff, 1959) and phenylalanine (Nevenzel et al., 1949). The pK_a of the αCBZ-Lys was assumed to be similar to lysine (Ellenbogen, 1952) and 6-aminohexanoic acid (Smith and Smith, 1942), which have similar pK_as.

The concentration of unprotonated amine was calculated from an algebraic variant of the Henderson–Hasselbach equation as

$$[\mathrm{N:}] = [\mathrm{N}]_{total}\frac{10^{\{pH - pK_a(T)\}}}{1 + 10^{\{pH - pK_a(T)\}}}$$

Both K_w and the pK_a for each amine species vary with temperature (Table 2). The pK_as for the various amine species were adjusted for temperature based on the van't Hoff equation by

$$pK_a(T_2) = pK_a(T_1) - \log\left\{\exp\left[-\frac{\Delta H°}{R}\left(\frac{1}{T_1} - \frac{1}{T_2}\right)\right]\right\}$$

The temperature adjustments to the pK_a are significant, yet small enough to allow for use of approximate values for $\Delta H°$. For example, variations in $\Delta H°$ on the order of 10 kJ/mol imply differences in pK_a of only 0.1 pH unit at 4 °C. The heat of ionization for the α-amine of phenylalanine was taken as 44 kJ/mol (Izatt et al., 1961). The heat of ionization for the α-amine of glycylphenylalanine was also approximated as 44 kJ/mol based on the observation that chemical substituents removed from the α-amine have little effect on the $\Delta H°$. For example, enthalpy literature values for similar molecules such as glycine (King, 1951), glycylglyine (Smith and Smith, 1942), and phenylalanine (above) were all given as 44 kJ/mol. The heat of ionization for the α-amine of α-CBZ-lysine was assumed to be similar to α-dimethyllysine (Marini et al., 1971) at 52 kJ/mol. Heat capacities, defined as the change in $\Delta H°$ with temperature, were assumed to be insignificant based on typical literature values. For example, the heat capacity for a prototypical α-amine of glycine (King, 1951) predicts only a 0.2 kJ/mol difference in $\Delta H°$ between 4 and 22 °C.

To test the robustness of this tresyl reaction network model, we chose to experimentally study three model amine compounds (Figure 3)—a high pK_a species, αCBZ-lysine; a low pK_a species, glycyl-phenylalanine; and a more sterically hindered amine of intermediate pK_a, phenylalanine—to probe for possible steric inhibition. On the basis of the results from the hydrolysis experiments, a pH range of 7.5–8.5 was chosen for study so that $k_{OH}[OH^-]$ is of the same order as k_w for maximum resolution of the various pathways. Experiments at room temperature (22 °C) and in a 4 °C cold room were conducted to measure the effects of temperature.

Figure 4 shows measured reaction time courses and curves predicted by the model for the three model amines at three pHs and two temperatures. The best-fit rate

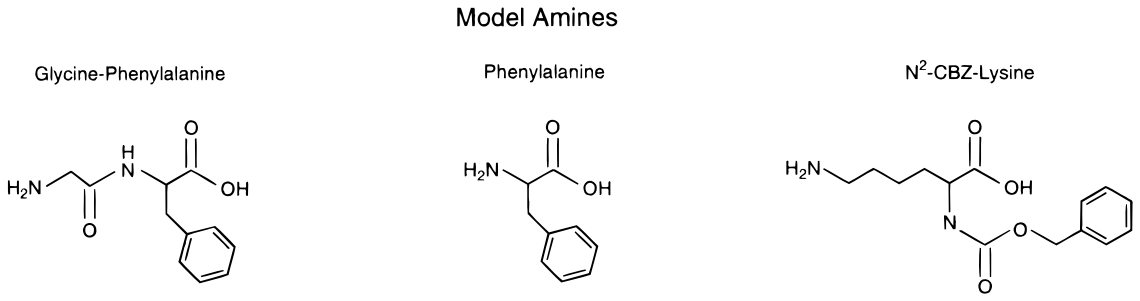


Figure 3. Model primary amines used in coupling studies. Compounds were chosen to span a range of pK_as (see Table 2). Glycine-phenylalanine, phenylalanine, and αCBZ-lysine were chosen as models for peptidyl N-termini, branched amines, and protein surface-presented lysines, respectively.

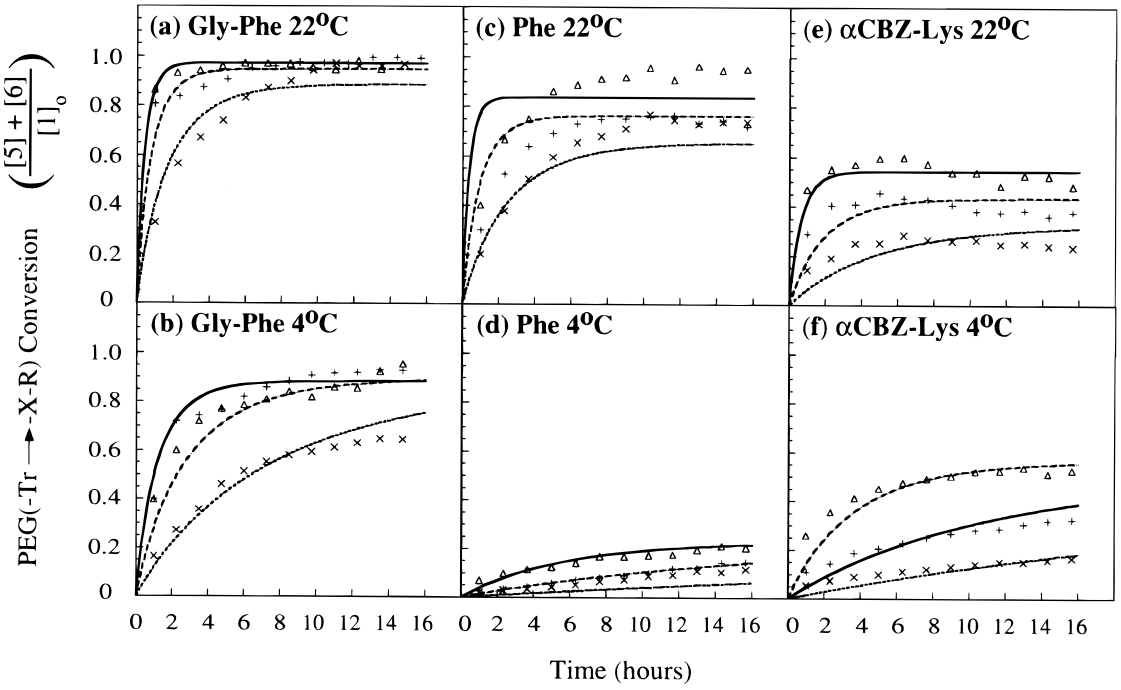


Figure 4. PEG(−Tr → −X−R) conversion data and model fit for the reaction PEG-Tr + H_2N−R → PEG−X−R where X = (NH) or [$OSO_2CH_2C(O)NH$]. Each panel (a−f) is fit by a single set of rate constants to the mechanism prescribed in Scheme 1. Data [symbols, (×) pH 7.5; (+) pH 8.0; (△) pH 8.5] and model predictions [lines, pH 7.5 (- - -); pH 8.0 (— —); pH 8.5 (—)] are given for Gly-Phe at 22 °C (1a), Gly-Phe at 4 °C (1b), Phe at 22 °C (1c), Phe at 4 °C (1d), αCBZ-Lys at 22 °C (1e) and αCBZ-Lys at 4 °C (1f). Conversion data [=([5] + [6])/$[1]_o$] was measured as the fraction of tresyl groups converted to PEG−N−R.

Table 3: Tresyl-Mediated Coupling Effective Rate Constants

	Gly-Phe		Phe		αCBZ-Lys	
rate constant[a]	4 °C	22 °C	4 °C	22 °C	4 °C	22 °C
k_1 (10^{-2} s^{-1} M^{-1})	0.48(0.02)	0.69(0.05)	0.16(0.01)	3.1(0.2)	25(2)	29(2)
k_2/k' (10^2 M^{-1})	13(6)	*b*	*c*	0.63(0.16)	12(6)	5.4(1.3)

[a] Rate constants are given as value (standard deviation). The large standard deviation in the case of k_2/k' for αCBZ-Lys at 4 °C reflects a relative insensitivity of the fit to this parameter.

constants from the χ-squared minimization fitting routine are given in Table 3. The model reaction network (Scheme 1) was able to fit the observed data quite well considering that a single set of rate constants were fit to all pH values simultaneously. In all cases, the model was able to capture the long time behavior trend as a function of reaction pH, as well as the final conversion. The transient behavior was also fit acceptably well in all cases, with the exception of phenylalanine at 22 °C (Figure 4c). The transient portion of Figure 4c suggests a weaker dependence on pH than predicted with [N:] as the driving force, possibly due to an effect of the proximity of the carboxylate group to the nucleophilic amine.

Temperature Effects. The reaction temperature can have a profound influence on the kinetics and product distribution in tresyl-mediated reactions as illustrated in Figure 4. In general it can be said that room-temperature reactions lead to higher total coupling yields. Yet, our data suggest that the distribution of the coupled products, 5 and 6, can also be affected by temperature.

Our data suggest that at lower temperatures, a higher proportion of 5 is formed relative to 6. This is evident from the temperature influence on the initial step of the reaction. Whereas k_w and k_{OH} appear to have significant temperature dependencies, k_1 appears to be only slightly affected by temperature. This suggests that lowering the temperature serves to increase the relative yield of 5. The ratio of k_2/k' is also a function of temperature. The apparent activation energy of k_2 is higher than that of the hydrolysis rate constant, k', as suggested by our data

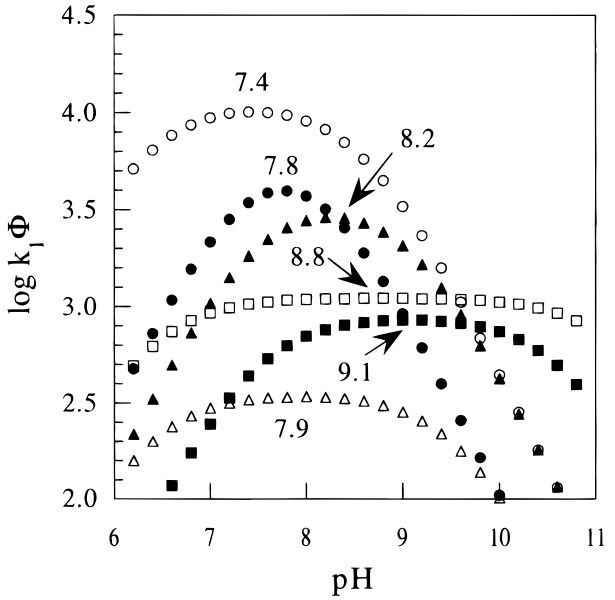


Figure 5. Plot of relative rates of reactions with PEG-Tr in terms of $k_1\Phi$ (see text). Curves at given at 4 °C (open symbols) and 4 °C (filled symbols) for Gly-Phe (○/●), Phe (Δ/s) and αCBZ-Lys (□/■) The pH where $k_1\Phi$ is a maximum is indicated (numeral) for each curve. Maximal $k_1\Phi$ predicts an optimal pH for (1 → 5)-type coupling.

(Table 3). Thus, our data indicate that higher temperatures yield more 6 relative to 4. It should be noted that higher temperatures also contribute to increased hydrolysis through the (1 → 2) pathway.

Temperature also has a small, but significant effect on pK_w and the pK_as of the amines as shown in Table 2.

pH Effects. Increasing the pH of the reaction solution increases the rate of conversion of tresyl species, through the addition−elimination pathway as well as the amine-nucleophilic displacement pathway shown in Scheme 1. Increasing the hydroxyl concentration increases the flux through the addition−elimination pathway (1→ 3). Increasing the pH also has the effect of creating a larger concentration of unprotonated amines, increasing the amine-nucleophilic displacement as well as the conversion of 3 to 6.

The reaction pH has an especially strong influence on the initial fate of 1. A detailed analysis and discussion of similarly competing pH-dependent reactions can be found in the literature (King et al., 1992, 1994). In the present case, the relative values of k_w, $k_{OH}[OH^-]$, and k_1-[N:] must be considered to optimize the amount of 5 formed relative to 2 and 3. This can be quantified as

$$\frac{\text{rate}_{1\to5}}{\text{rate}_{1\to2} + \text{rate}_{1\to3}} = \frac{k_1[\text{N:}]}{k_w + k_{OH}[OH^-]} = k_1[\text{N}]_{total}\Phi$$

where

$$\Phi = \frac{\dfrac{[\text{N:}]}{[\text{N}]_{total}}}{k_w + k_{OH}[OH^-]}$$

The parameter Φ then expresses the relative rates as a function of pH, regardless of the absolute concentration of amine and the particular value of k_1 and $[N]_{total}$. In Figure 5 we show a plot of $\log(k_1\Phi)$ versus pH for the three model amines at 4 and 22 °C. By solving for $\partial\Phi/\partial pH = 0$, the pH that maximizes Φ is found to be

$$pH|_{max\Phi} = \frac{pK_w + pK_a + \log\left(\dfrac{k_w}{k_{OH}}\right)}{2}$$

This defines the optimal pH for (1 → 5)-type coupling. It can be seen from Figure 5 that $\Phi(pH|_{max\Phi})$ increases with decreasing pK_a, predicting a lower required amine concentration, but longer reaction times. Decreasing temperature has the effect of somewhat increasing $\Phi(pH|_{max\Phi})$ as well as $pH|_{max\Phi}$.

On the basis of Scheme 1, the interplay of the pH effect on hydroxyl and unprotonated amine concentration can be separated into three regimes: $[OH^-] \ll k_w/k_{OH}$, $[OH^-] \approx k_w/k_{OH}$, and $[OH^-] \gg k_w/k_{OH}$. At low pHs, only hydrolysis (1 → 2) and nucleophilic substitution (1 → 5) are significant, yet a large concentration of the amine species will be needed to favor addition over hydrolysis due to the low fraction of unprotonated amines at low pH. In the intermediate regime, all three pathways can be significant; however, the (1 → 5) pathway can be made dominant with a lower amine concentration than is needed for the later low pH regime. In the high pH regime, hydrolysis is insignificant relative to the first step in the addition−elimination pathway (1 → 3). This regime can prove to be impractical because $[OH^-]$ increases faster than [N:] with increasing pH, requiring a large excess of amines.

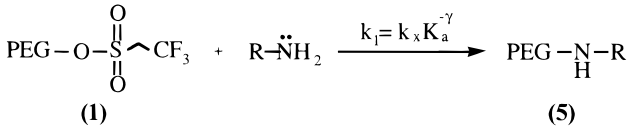
In our model, we have attempted to represent all reactions in terms of possible elementary reactions. However, in the case of k_1, in particular, our data suggests that there might be a dependence on the amine pK_a that would not be consistent with the assertion that k_1 is an elementary reaction. It can be seen from Table 3 that k_1 increases with pK_a. This trend acts in the opposite direction but with a smaller magnitude than the pK_a dependence imposed by using [N:] as the effective amine dependence. Attempts to fit the data with $k_1[N]_{total}$ as the driving force failed to yield a fit comparable to that of k_1[N:] as the driving force.

In an attempt to fit all the data for k_1 to a single rate relation, an empirical model was developed for the S_N2 reaction as shown in Scheme 3. This empirical rate equation fits the data of all temperatures, reaction pHs, and amines except for the phenylalanine 4 °C reaction, possibly for steric reasons. The correlation of the empirical rate equation with the measured values for k_1 is illustrated in Figure 6. It is interesting to note that the k_1 dependence on $K_a^{-0.63}$ is invariant with temperature, although only limited data is available at 4 °C. The consistency of this empirical relation across the variety of amines may indicate a slightly different dependence than the concentration of unprotonated amine, [N:].

Steric Effects. Phenylalanine was expected to be the most sterically inhibited. The effect was most noticeable at 4 °C (Figure 4d). This is best illustrated in Figure 6, where the phenylalanine 4 °C reaction is well removed from the trends established by all other rate constants. It is also possible that steric factors rather than the pK_a dependence supported above may account for the higher values of k_1 for αCBZ-Lys as compared to glycyl-phenylalanine 4 °C.

Control of Product Distribution. It could be argued that the relative amount of 5-type, 2° amine linkages and 6-type, sulfonyl linkages may be more important than total yields, especially since 6-type linkages may be subject to slow hydrolytic cleavage. In general, it would be desirable to maximize the number of 5-type, secondary amine linkages. Our model predicts that reactions run

Scheme 3



[b] k' was found to be negligible as compared to k_2 under the conditions examined. [c] k_2 was found to be negligible as compared to k' under the conditions examined.

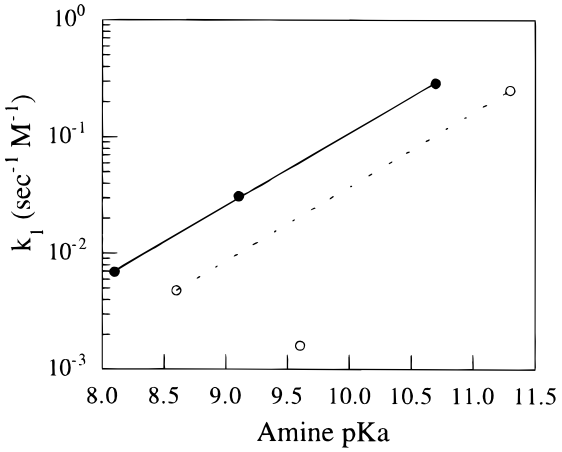


Figure 6. Empirical correlation (see Scheme 3) for rate constant k_1 at 22 °C (●) and 4 °C (○) with the amine pK_a (see Table 2) fit to $k_1 = k_x K_a^{-\gamma}$ where k_x(22 °C) = 6.4 × 10^{-8} M^{-1} s^{-1}, k_x(4 °C) = 1.6 × 10^{-8} M^{-1} s^{-1}, γ(22 °C) = 0.62, and γ(4 °C) = 0.63. Fit at 4 °C (- - -) is included to illustrate the similarity in γ to the fit at 22 °C (—) even though the data point at pK_a = 9.6 is omitted due to suspicion of steric influences.

at 4 °C would have more secondary amine bonds than at 22 °C for a given amine concentration. In general, the fraction of secondary amine linkages increases with increasing amine concentration by increasing the rate of 1 → 5 relative to 1 → 2 + 3.

The distribution of 4 and 6 from 3 is best described by α. At any given time, α is the instantaneous fraction of 3 that will become 6:

$$\alpha = \frac{k_2[\mathrm{N:}]}{k_2[\mathrm{N:}] + k'} = \frac{\dfrac{\mathrm{d}[6]}{\mathrm{d}t}}{\dfrac{\mathrm{d}[4]}{\mathrm{d}t} + \dfrac{\mathrm{d}[6]}{\mathrm{d}t}}$$

Because α is a function of [N:], its value changes as the reaction progresses. To compare values of k_2 for the three model amines at both temperatures, it is instructive to compare the initial value of α. α will tend to decrease somewhat from its initial value as free amines are consumed. Figure 7 shows α(t = 0) for the 18 curves examined. The value of α was found to be consistently larger at 22 °C than at 4 °C. For any given amine, the initial value of α is a increasing function of reaction pH through the dependence of [N:] on the solution pH. α was found to be a decreasing function of pK_a, with a value approaching unity for 100 mM glycyl-phenylalanine at 22 °C, suggesting that the driving force for this coupling pathway has a stronger dependence on solution pH than is exerted through [N:].

CONCLUSIONS

With the judicious choice of reaction temperature and pH, tresyl-mediated couplings can be achieved with high yields. To maximize the total yield and the fraction of secondary amine linkages, our model predicts that it is

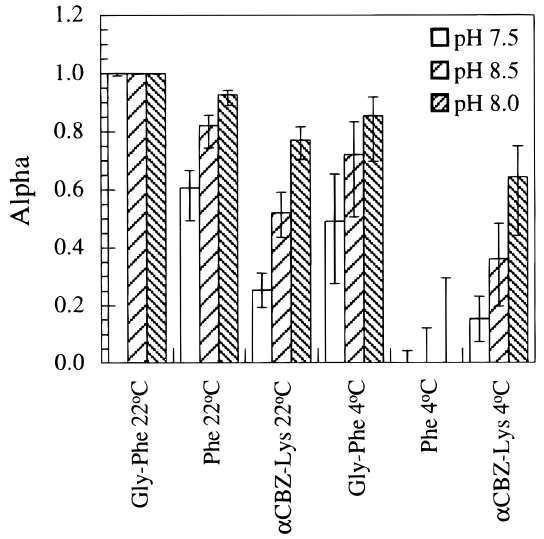


Figure 7. Plot of the initial distribution of products from ref *3*, given as α (= $\mathrm{rate}_{3\to6}/\mathrm{rate}_{3\to4+6}$), based in Scheme 1 and measured rate constants, k_2/k'. Because α is a function of the concentration of the nucleophilic species [N:], α is expected to be a function [N:], and will decrease with time proportional to the depletion of [N:]. Error bars are 95% confidence intervals.

desirable to run tresyl coupling reactions at lower temperatures around pH 8, depending on the amine pK_a as specified by the above equation for $\mathrm{pH}|_{\max\Phi}$ and illustrated in Figure 5. Although total yields ([5] + [6]) may be higher at elevated pH levels (Figure 4), 6-type amide linkages may be unstable over prolonged periods in aqueous environments. Where reactions must be run at higher temperatures due to solubility limitations, maximal secondary amine linkages are predicted at slightly higher pH levels to overcome the higher rate of hydrolysis (k_w).

Where the choice of nucleophilic amine is possible, it is advantageous to use an amine of low pK_a to maximize the concentration of the unprotonated species. This points to an advantage of coupling peptides via an N-terminal glycine rather than through an ϵ-amine group of a lysine residue.

When coupling to tresylated species via a lysyl ϵ-amine is necessary, as may be the case with certain proteins, low temperature at pH ∼8.8 is indicated (Figure 5). In this case high concentrations of amine are necessary, even beyond the 100 mM amine used here, to achieve high yields of secondary amine linkages. Beyond pH ∼8.8, additional tresyl conversion (Figure 4) is predicted to be largely through 6-type amide linkages.

In some applications, it may be the nucleophilic amine that is limiting, rather than the tresyl-activated species. Such a case is encountered in attaching pendant PEG chains to proteins or small molecules. When the tresylated species is used in large excess, it can be seen from Scheme 1 that the 1 → 3 pathway (∼[Tr]) can quickly become dominant over the 1 → 5 pathway (∼[N:][Tr]). This raises the concern that the limited number of amines might be consumed in a 3 → 6 reaction, disfavoring 1 → 5. To maximize secondary amine linkages in this case, it is advantageous to run under conditions where α is small (Figure 7), i.e., at a somewhat lower pH than prescribed by Figure 5.

ACKNOWLEDGMENT

The financial support of NSF BES9632714, the MIT NIH Biotechnology Training Grant, NIH GM50047, and the MIT Center for Biomedical Engineering Seed Grant

are gratefully acknowledged. The authors are also indebted to Gizette V. Sperinde for assembling and optimizing the Fortran code used herein.

LITERATURE CITED

Biester, J. L., and Ruoff, P. M. (1959) Structural influences on the stability of dipeptide-metal ion complexes. *J. Am. Chem. Soc. 81*, 6517−6521.

Demiroglou, A., Bandel-Schlesselmann, and C., Jennissen, H. P. (1994) A novel reaction sequence for the coupling of nucleophiles to agarose with 2,2,2-trifluoroethanesulfonyl chloride. *Angew. Chem., Int. Ed. Engl. 33*, 120−123.

Ellenbogen, E. (1952) Dissociation constants of peptides. I. A survey of the effect of optical configuration. *J. Am. Chem. Soc. 74*, 5198−5201.

Gais, H.-J., and Ruppert, S. (1995) Modification and immobilization of proteins with polyethylene glycol tresylates and polysaccharide tresylates: evidence suggesting a revision of the coupling mechanism and the structure of the polymer−polymer linkage. *Tetrahedron Lett. 36*, 3837−3838.

Harris, J. M. (1992) Introduction to biotechnical and biomedical applications of ploy(ethylene glycol). In *Poly(Ethylene Glycol) Chemistry* (J. M. Harris, Ed.) pp 1−12, Plenum Press, New York.

Izatt, R. M., Wrathall, J. W., and Anderson, K. P. (1961) Studies of the copper(II)-alanine and phenylalanine systems in aqueous solution. Dissociation and formation constants as a function of temperature. *J. Phys. Chem. 65*, 1914−1915.

King, E. J. (1951) The ionization constants of glycine and the effect of sodium chloride upon its second ionization. *J. Am. Chem. Soc. 73*, 155−159.

King, J. F., and Gill, M. S. (1995) Reactions of Neopentyl 2,2,2-trifluoroethanesulfonate (tresylate) with nucleophiles: a model study for the coupling of nucleophiles with tresyl agarose. *Angew. Chem., Int. Ed. Engl. 34*, 1612−1613.

King, J. F., and Gill, M. S. (1996) Alkyl 2,2,2-trifluoroethanesulfonates (tresylates): elimination-addition vs bimolecular nucleophilic substitution in reactions with nucleophiles in aqueous media. *J. Org. Chem. 61*, 7250−7255.

King, J. F., Guo, Z. R., and Klassen, D. F. (1994) Nucleophilic Attack vs General Base Assisted Hydrolysis in the Reactions of Acetic Anhydride with Primary and Secondary Amines. pH-Yield Studies in the Recognition and Assessment of the Nucleophilic and General Base Reactions. *J. Org. Chem. 59*, 1095−1101.

King, J. F., Rathore, R., Lam, J. Y. L., Guo, Z. R., and Klassen, D. F. (1992) pH Optimization of Nucleophilic Reactions in Water. *J. Am. Chem. Soc. 114*, 3028−3033.

Marini, M. A., Berger, R. L., Lam, D. P., and Martin, C. J. (1971) Thermal titrimetric evaluation of the heats of ionization of the commonly occurring amino acids and their derivatives. *Anal. Biochem. 43*, 188−198.

Marshall, W. L., and Franck, E. U. (1981) Ion product of water substance, 0−1000C, 1−10,000 bars, new international formulation and its background. *J. Phys. Chem. Ref. Data 10*, 295−304.

Nevenzel, J. C., Shelberg, W. E., and Niemann, C. (1949) The apparent ionization constants and ultraviolet spectra of o-, m- and p-chloro and p-sulfamyl-DL-phenylalanine. *J. Am. Chem. Soc. 71*, 3024−3026.

Nilsson, K., and Mosbach, K. (1981) Immobilization of enzymes and affinity ligands to various hydroxyl group carrying supports using highly reactive sulfonyl chlorides. *Biochem. Biophys. Res. Commun. 102*, 449−457.

Nilsson, K., and Mosbach, K. (1984) Immobilization of ligands with organic sulfonyl chlorides. In *Methods in Enzymology* (W. B. Jakoby, Ed.) Vol. 104, pp 56−69, Academic Press, New York.

Press, W. H., Flannery, B. P., Teukolsky, S. A., and Vetterling, W. T. (1986) *Numerical Recipies*, Cambridge University Press, Cambridge.

Smith, E. R. B., and Smith, P. K. (1942) Thermodynamic properties of solutions of amino acids and related substances. *J. Biol. Chem. 146*, 187−195.

Sperinde, J. J., and Griffith, L. G. (1997) Synthesis and characterization of enzymatically-cross-linked poly(ethylene glycol) hydrogels. *Macromolecules 30*, 5255−5264.

BC980070J

Methods for Dual, Site-Specific Derivatization of Bovine Pancreatic Trypsin Inhibitor: Trypsin Protection of Lysine-15 and Attachment of Fatty Acids or Hydrophobic Peptides at the N-Terminus

Chadler T. Pool[†] and Thomas E. Thompson,*[,‡]

Department of Biochemistry and Molecular Genetics, University of Virginia, Charlottesville, Virginia 22908.
Received June 25, 1998; Revised Manuscript Received December 21, 1998

To produce a series of model membrane proteins, bovine pancreatic trypsin inhibitor (BPTI) has been modified by specifically attaching reporter groups to Lys-15 and fatty acids or hydrophobic peptides at the N-terminus. Lys-15 of BPTI was protected by trypsin bound to BPTI, then *O*-methylisourea (OMIU) was used to guanidinate all unprotected lysines. The N-terminal amine was then reacted with several saturated fatty acid anhydrides from 8 to 18 carbons in length, or with an SMCC cross-linker. Cysteine-containing hydrophobic peptides, cleaved from resin in the presence of sodium dodecyl sulfate (SDS), were then attached to the protein via the N-terminal cross-linker. The methods described yield a unique, chemically modified protein which can carry site-specific modifications at two distinct residues. The resulting proteins are ideal for diffusional or partitioning studies on model and biological membranes.

INTRODUCTION

We are interested in generating a series of unobtrusive, fluorescently labeled, model transbilayer proteins and fatty-acylated proteins capable of spontaneously inserting into the hydrophobic core of membranes in order to measure accurately the insertion and diffusion of membrane proteins and assess the factors influencing these processes. To accomplish this goal, we have devised methods for site-specifially attaching fatty acids or hydrophobic peptides, along with reporter groups to bovine pancreatic trypsin inhibitor (BPTI).[1] The choice of BPTI as the carrier protein was based on the stability of the protein, its compact structure, and its high aqueous solubility.

To attach peptides specifically to the N-terminus of BPTI, Ebina et al. (1989) and Moll and Thompson (1994) have both utilized *O*-methylisourea (OMIU) to derivatize the four lysine residues of BPTI. OMIU has been used extensively and has been shown to be very specific in its reactivity toward only the ϵ-amino groups of lysine and not N-terminal α-amines (Hughes et al., 1949; Chervenka and Wilcox, 1956). Derivatization of BPTI with OMIU thus yields a protein with all four lysine residues guanidinated (G-BPTI) and the N-terminal amine available for the attachment of peptides, fatty acids, or other groups. To create a second specific labeling site, we protected lysine-15 of BPTI with trypsin. Following guanidination of the BPTI/trypsin complex with OMIU, a fatty acid or cross-linker was attached specifically to the N-terminus of BPTI. Upon dissociation of the trypsin, lysine-15 of BPTI was labeled with an amine-reactive reporter group. Other, less specific strategies for dual protein modifications have been reported previously (Babbitt et al., 1984; Amir and Haas, 1987); however, such strategies generally are specific for only certain modifications or subsequent chromatographic separation of multiple products is required.

The cleavage and handling of hydrophobic peptides is difficult due to their insolubility and propensity to irreversibly aggregate. Moll and Thompson (1994) attached polyalanine peptides to G-BPTI by employing detergents during both the cleavage from the resin and attachment to G-BPTI. We have employed a similar strategy here to attach other, more hydrophobic peptides to guanidinated, trypsin-protected BPTI (K15-G-BPTI).

The N-hydroxysuccinimide ester of palmitic acid has usually been used in the presence of detergents to chemically attach fatty acids to proteins (Lee and Kim, 1995; Huang et al., 1980; Babbitt and Huang, 1985). Detergents, however, can pose difficult purification problems. As an alternative, we have developed a novel tetrahydrofuran (THF) based solvent system which eliminates the need for detergents. As acylating reagents we employed fatty acid anhydrides which are commercially available in a variety of chain lengths.

We describe here, methods for the synthesis and cleavage of hydrophobic peptides, and novel strategies for the site-specific attachment of these hydrophobic peptides or fatty acids to the N-terminus of trypsin-protected, guanidinated BPTI (K15-G-BPTI). We show that trypsin can effectively protect lysine-15 of BPTI from guanidination by OMIU and thereby provide a second specific site for the attachment of a reporter group. Figure

* To whom correspondence should be addressed.

[†]Central Research Division, Pfizer Inc., Box 0067, Eastern Point Rd., Groton, CT 06340. E-mail: chadler_t_pool@groton.pfizer.com. Phone: 860-715-5407.

[‡]Permanent address: University of Virginia, Department of Biochemistry and Molecular Genetics, Charlottesville, VA 22908.

[1] Abbreviations: BPTI, bovine pancreatic trypsin inhibitor; OMIU, *O*-methylisourea; G-BPTI, BPTI with all four lysine residues guanidinated; K15-G-BPTI, BPTI with all lysines except lysine-15 guanidinated; NSP, *N*-succinimidylpropionate; SDS, sodium dodecyl sulfate; THF, tetrahydrofuran; TBMether, *tert*-butyl methyl ether; TFA, trifluoroacetic acid; CF, 5-(and 6-)-carboxyfluoroscein; PFH, propionic acid:formic acid:water (2:1:2); MALDI−TOF, matrix-assisted laser-desorption ionization−time-of-flight; CAD, collision-activated dissociation; ESI, electrospray ionization; FRAP, fluorescence recovery after photobleaching; dH_2O, deionized water.

10.1021/bc9800771 CCC: $18.00 © 1999 American Chemical Society
Published on Web 02/24/1999

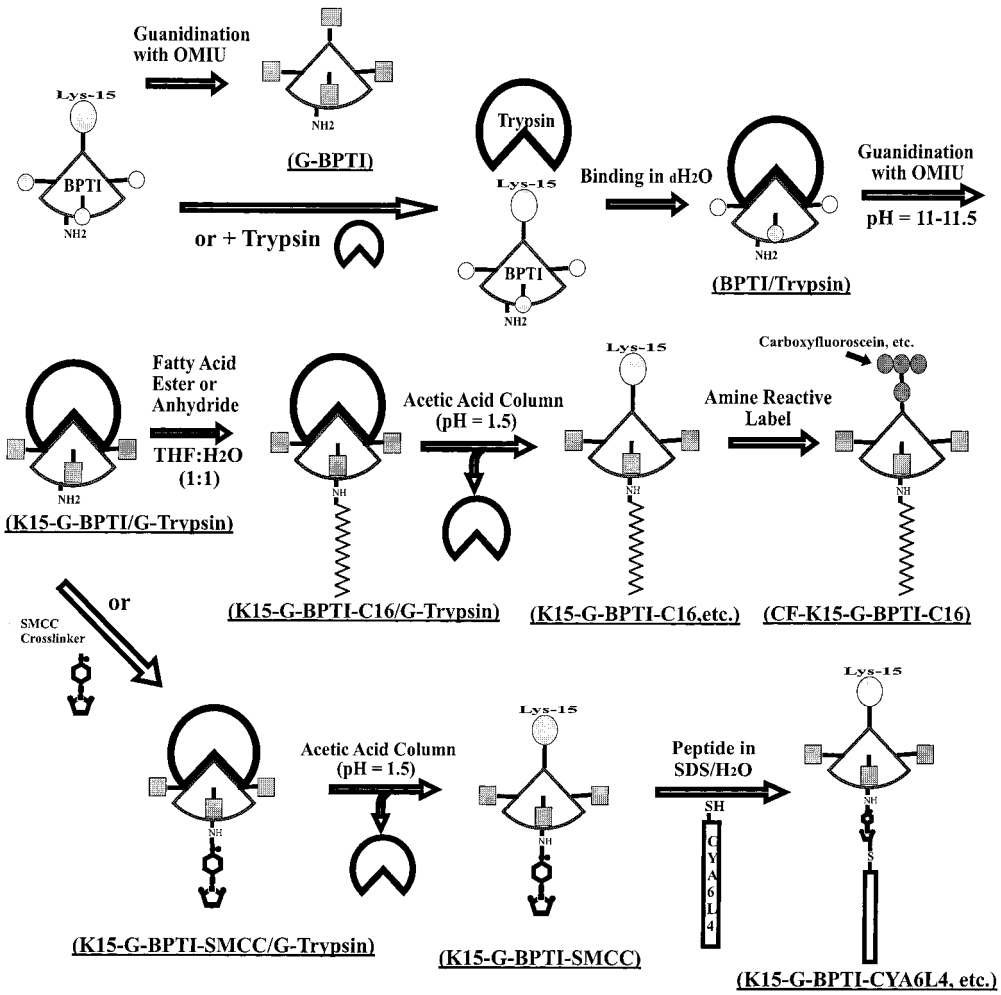


Figure 1. A diagram depicting the steps involved in site-specifically attaching fatty acids, hydrophobic peptides, and reporter groups to BPTI. Lysine residues are depicted as circles, and homoarginine residues as squares. Each step in the synthesis was characterized using reversed-phase HPLC and/or MALDI and ESI mass spectrometry. The names used in reference to each structure are indicated below the corresponding structures.

1 outlines the strategy of the chemical modifications described in this paper. The resulting proteins are ideal for experiments such as membrane diffusion studies or partitioning studies due to their small size, stability, and well-defined structure and composition. In a more general sense, these methods yield a unique carrier protein site-specifically modified at two separate sites.

MATERIALS AND METHODS

Materials. Bovine pancreatic trypsin inhibitor (BPTI) was purchased from Bayer Corporation (Kankakee, IL). Fisher Scientific (Pittsburgh, PA) supplied the barium hydroxide, glycine, sodium chloride, and calcium chloride. Sephadex CM-25 ion-exchange resin and Sephadex G-50 super fine gel filtration resins were obtained from Pharmacia (Uppsala, Sweden), and Spectra/Por 3 regenerated cellulose dialysis membranes (3500 MWCO) were obtained from Spectrum (Houston, TX). *N*-α-Benzoyl-L-arginine-*p*-nitroanilide (L-BAPA), *N*-Hydroxybenzotriazole (HOBt) and all Fmoc amino acids were obtained through Bachem (King of Prussia, PA). Arg-C and Lys-C endoproteinases were obtained from Boehringer Mannheim Corp. (Indianapolis, IN). OMIU, trypsin (type III, bovine pancreas), Trizma-HCl and the N-hydroxysuccinimide ester of palmitic acid (NHS-palmitate), all amino acids, sodium bicarbonate, bromocresol green, ammonium bicarbonate, boric acid, ferric chloride, ninhydrin, TRIZMA base, and all fatty acid anhydrides were purchased from Sigma Chemical Co. (St. Louis, MO). 5-(and 6-)-Carboxyfluorescein was purchased from Molecular Probes (Eugene, OR). TLC plates were from Analtech (Newark, DE). Sulfo-SMCC heterobifunctional crosslinker was purchased from Pierce (Rockford, IL). Tritiated acetic anhydride was purchased from Amersham (Arlington Heights, IL). 2-(1H-Benzotriazole-1-yl)-1,1,3,3-tetramethyluronium hexafluorophosphate (HBTU), and Nα-Fmoc-Nϵ-tBoc-lysine Wang resin were purchased from Nova Biochem (San Diego, CA). Peptide amide resin (PAL) was purchased from Perseptive Biosystems (Framingham, MA). All other reagents were obtained from Aldrich (Milwaukee, WI).

Guanidination of BPTI/Trypsin Complex with OMIU. The method used to guanidinate the lysine residues of the BPTI/trypsin complex was similar to that of Chervenka and Wilcox (1956) with some modifications. One hundred milligrams of BPTI was dissolved in 10 mL of water and combined with 368.5 mg of trypsin yielding a BPTI to trypsin ratio of 1:1. Twenty grams of OMIU was dissolved in 40 mL of deionized water with stirring at room temperature. This solution was then put on ice, and 40 g of barium hydroxide (anhydrous) was added while stirring. The solution was diluted with water to a final volume of 200 mL. This solution was then centrifuged twice at 10 000 rpm for 20 min, and the supernatants were saved. The pH of the supernatant was then decreased to 11.4 by addition of concentrated hydrochloric

acid. The BPTI/trypsin solution was then added to the OMIU solution on ice and allowed to react for 7 days with stirring at 4 °C. Following the 7 day period, the reaction mixture was dialyzed and purified on a CM-25 ion-exchange column using a 0.02 M glycine buffer (pH 10.5) and eluted with a 0 to 1 M NaCl gradient. The lyophilized complex was then chromatographed on a Sephadex G-50 super fine gel filtration column (1.5 × 45 cm) using an ammonium bicarbonate buffer at pH 7.8. Yields for the K15-G-BPTI/G-trypsin complex were greater than 70%. To dissociate K15-G-BPTI from G-trypsin, the complex was chromatographed on a Sephadex G-50 super fine column (1.5 × 45 cm) equilibrated with a 100 mM acetic acid buffer at pH 1.5 (Ebina et al., 1989). Protein absorbance was monitored at 280 nm. Yields of K15-G-BPTI from this column were always greater than 95%. The purified K15-G-BPTI was characterized by MALDI−TOF and ESI mass spectrometry and amino acid analysis.

Digestion and Sequencing of K15-G-BPTI. K15-G-BPTI was reduced and carboxymethylated as described by Crestfield et al. (1963). Lys-C digestion of the protein was performed by dissolving 0.15 μmol of K15-G-BPTI (reduced and carboxymethylated) and 0.1 mg of Lys-C endoproteinase in 1 mL of buffer containing 5 mM tris and 2 mM EDTA at pH 8.5. The digestion was carried out for 16 h at 37 °C and monitored by MALDI−TOF mass spectrometry. Collision activated dissociation electrospray ionization mass spectrometry (CAD ESI-MS) was used to sequence peptides of interest.

Acylation of G-BPTI and K15-G-BPTI/G-Trypsin with Fatty Acid Anhydrides. A total of 1.5 μmol of G-BPTI or 0.5 μmol of K15-G-BPTI/G-trypsin was dissolved in 1 mL of 100 mM phosphate buffer (pH 7.8). A total of 100 μmol of acid anhydride was then dissolved in 1 mL of THF and added to the protein solution while stirring. For the anhydrides of caprylic acid and capric acid (which are liquids at room temperature), the reagents were added to protein solutions to which 1 mL of THF had already been added. After a reaction time of 1 h, the protein was precipitated by addition of excess THF. Those reactions involving myristic-, palmitic-, and stearic acid anhydrides were performed in a 50 °C water bath to increase the reactivity and solubility of the anhydrides. Yields for the palmitoylated and myristoylated proteins were between 10 and 20%, approximately 30% for C12-G-BPTI, and over 70% for C8-G-BPTI and C10-G-BPTI.

Gel Filtration Chromatography of Acylated G-BPTI and K15-G-BPTI/G-Trypsin. Following reaction with fatty acid anhydrides, G-BPTI samples were dissolved in 1−2 mL of 5% acetic acid and chromatographed on a Sephadex G-25 column (1.5 × 25 cm) equilibrated with the same. The protein eluted in the void volume and was collected and lyophilized. Following the acylation reaction, K15-G-BPTI/G-trypsin samples were dissolved in 2−3 mL of 50 mM ammonium bicarbonate (pH 7.9) and were chromatographed on a Sephadex G-50 column (1.5 × 45 cm) equilibrated with the same buffer. The intact complexes were lyophilyzed then dissolved in 1−2 mL of 100 mM acetic acid (pH 1.5), allowed to equilibrate for 20 min, and chromatographed on a Sephadex G-50 super fine column (1.5 × 45 cm) equilibrated with the same buffer (Ebina et al., 1989). Protein absorbance was monitored at 280 nm during all runs.

Fatty-Acylated G-BPTI and K15-G-BPTI Analysis and Purification by Reversed-Phase HPLC. All solvents were vacuum filtered using an Amicon 0.25 micron filter and degassed under reduced pressure. Solvent A consisted of 0.1% trifluoroacetic acid (TFA) in glass-distilled water. Solvent B consisted of acetonitrile: 1-propanol:iso-butyl alcohol in a ratio of 2:5.5:2.5 plus 0.1% TFA. Samples were dissolved in deionized water and diluted in half with 0.2% TFA. A Zorbax 300SB-C3 semipreparative reversed-phase column (9.4 mm × 25 cm) (MAC-MOD Analytical Inc., Chadds Ford, PA) was used for all purifications. The HPLC system consisted of a Beckman System Gold programmable solvent module 126 and detector module 166, interfaced with an NEC PC-8300 computer. The linear gradient used for purifying the acylated proteins started at 30% B and increased to 90% B over 10 min. Peaks of interest were *immediately* diluted with water and frozen in liquid nitrogen for lyophilization.

Attachment of sulfo-SMCC Cross-Linker to G-BPTI and K15-G-BPTI/G-Trypsin Complex. A total of 1.5 μmol of G-BPTI or 0.5 μmol of K15-G-BPTI/G-trypsin was dissolved in 1 mL of 100 mM phosphate buffer at pH 7.8. To this was added 4 mg of sulfo-SMCC cross-linker, and the reaction was stirred for 10−15 min. The reaction mixture was then chromatographed on a Sephadex G-50 column (1.5 × 45 cm) equilibrated with 100 mM acetic acid at pH 1.5. In initial experiments, the K15-G-BPTI/G-trypsin complex was first chromatographed on a Sephadex G-50 column (1.5 × 45 cm) equilibrated with 50 mM ammonium bicarbonate (pH 7.8) to determine if the complex remained intact following the attachment of the cross-linker.

Synthesis of Hydrophobic Peptides. Fmoc-based automated synthesis was performed on a Symphony peptide synthesizer (Protein Technologies Inc., Tucson, AZ) on low substitution Wang or Pal resins (0.15−0.20 mmol/g). Capping was performed with acetic anhydride following each coupling cycle. Following automated synthesis, the final residues were attached manually. The peptides were radiolabeled by either capping with tritiated acetic anhydride following the final coupling reaction or by using tritiated Fmoc-leucine amino acids which were synthesized using established protocols involving a trimethylsilyl intermediate (Chang et al., 1980; Bolin et al., 1989). Peptides containing N-terminal cysteines were synthesized using a PAL resin affording an amide group at the C-terminus.

Cleavage of Peptides Using Sodium Dodecyl Sulfate (SDS). The solution used to cleave the peptides from the resin was a modified form of that used by Moll and Thompson (1994) and consisted of 950 μL of trifluoroacetic acid (TFA), 25 μL of water, 25 μL of triethylsilane or triisopropyl silane, and 2−5 mg of SDS. The supernatant containing the cleaved peptide was then separated from the resin, and the TFA was reduced to a volume of 100 μL under a stream of dry nitrogen. A total of 1.5 mL of *cold* TBMether was then added, and the solution was stored at −20 °C for 30 min. (To reduce any peroxides present, the TBMether was distilled over $LiAlH_4$ and cooled to −20 °C immediately before use.) The peptide/SDS precipitate was pelleted in a microfuge. The ether was then removed and the pellet dried under nitrogen. The pellet was placed under high vacuum for 30 min to remove any residual ether.

Coupling of Peptides to (K15)-G-BPTI-SMCC. The peptide/SDS complex was immediately dissolved in 1 mL of 100 mM phosphate buffer at pH 6.6. A total of 1.5 μmol of G-BPTI-SMCC or 0.5 μmol of K15-G-BPTI-SMCC was then added to the peptide solution and incubated at room temperature for 1 h. The reaction was stopped by flash freezing the solution in liquid nitrogen followed by lyophilization.

Gel Filtration of (K15)-G-BPTI-Peptide/SDS Complex. To separate the (K15)-G-BPTI-Peptide conjugate from the SDS, gel filtration was performed using a Sephadex G-25 column and PFH buffer. The (K15)-G-BPTI-Peptide/SDS complex was dissolved in 1−3 mL of PFH buffer (depending on the solubility of the sample), loaded on the column and chromatographed at a flow rate of 0.1 mL/min. Protein absorbance was monitored at 280 nm and radioactivity was measured using liquid scintillation. The protein peak was then diluted with water and lyophilized. The method of Sokoloff and Frigon (1981) was used to assay for the presence of SDS.

Gel Filtration and Refolding of the (K15)-G-BPTI-Peptide Conjugate. Initial separation of G-BPTI-Peptide from G-BPTI was achieved using a Sephadex G-50 column (1.5 × 120 cm) equilibrated with 50 mM ammonium bicarbonate (pH 7.8). Following the elution of the proteins, the fractions were kept as dilute solutions overnight. Peaks of interest were then lyophilized.

HPLC Purification of G-BPTI-Peptide Conjugates. The HPLC system used to separate the unmodified protein from that with attached peptide was the same as described above. However, the gradient was more shallow consisting of a change in organic phase from 10 to 30% over 30 min. It was found to be crucial to freeze the purified proteins in liquid nitrogen immediately following elution from the column. If fractions were allowed to stand for more than 30 min before freezing, the resulting lyophylized proteins were mostly insoluble.

Labeling of G-BPTI and K15-G-BPTI-C16,14,12 with ^{3}H-NSP. K15-G-BPTI-C16,14,12 samples were dissolved in 0.5 mL of 100 mM borate buffer (pH 9.5). G-BPTI-C16,14,12 proteins were then added to these samples until the absorbance at 280 nm was greater than 0.5 absorbance units (∼0.6 mM). ^{3}H-NSP (150 μCi) was then dissolved in 150 μL of THF and added to the proteins while stirring. An additional 75 μCi of NSP was added to the reaction after 20 min. After 1 h, the reaction was quenched by addition of 1.5 mL of 1 M hydroxylamine (pH 9) and equilibrated for 1 h. G-BPTI samples were prepared in the same manner, except that a phosphate buffer at pH 7.8 was used in place of the borate buffer. Following treatment with hydroxylamine, the samples were purified on a Sephadex G-25 column (1.5 × 25 cm) equilibrated with 5% acetic acid. The purified samples were then characterized by MALDI−TOF mass spectrometry and liquid scintillation.

Fluorescent Labeling of K15-G-BPTI-C16 at Lys-15. A total of 30 μmol of K15-G-BPTI-C16 was dissolved in 250 μL of phosphate buffer (100 mM, pH 7.9), while 2 mg of 5-(and 6-)-carboxyfluoroscein, succinimidyl ester (CF) was dissolved in 200 μL of dry DMF. Twenty-five microliters of the CF was added dropwise, very slowly, to the protein solution stirring in a minireaction vessel. The reaction vessel was covered in foil and the reaction was allowed to proceed for 1 h at which time 25 μL of 3 M hydroxylamine (pH 8.5) was added to quench the reaction and cleave any esters which may have formed with tyrosine side chains. The entire sample was then diluted with phosphate buffer to 2 mL and desalted on a Millipore spin concentrator (5000 MWCO). The product was characterized by UV spectroscopy and MALDI−TOF mass spectrometry.

RESULTS

Guanidination of BPTI/Trypsin Complex. Figure 2A shows that on a cation-exchange column, the fully guanidinated BPTI (M_r = 6684) elutes at a higher NaCl concentration than K15-G-BPTI (M_r = 6641). Gel filtration was also performed to show that the peak corresponding to fully guanidinated BPTI (NaCl concentration of 0.45−0.55 M) consisted of unassociated G-BPTI and G-trypsin, while the larger peak (NaCl concentration of 0.3−0.4 M) contained protein present as intact complex. These results demonstrate that ion exchange chromatography provides an effective means for separating the dissociated proteins from intact complex and thereby a means for purifying the fully guanidinated G-BPTI from the trypsin-protected K15-G-BPTI.

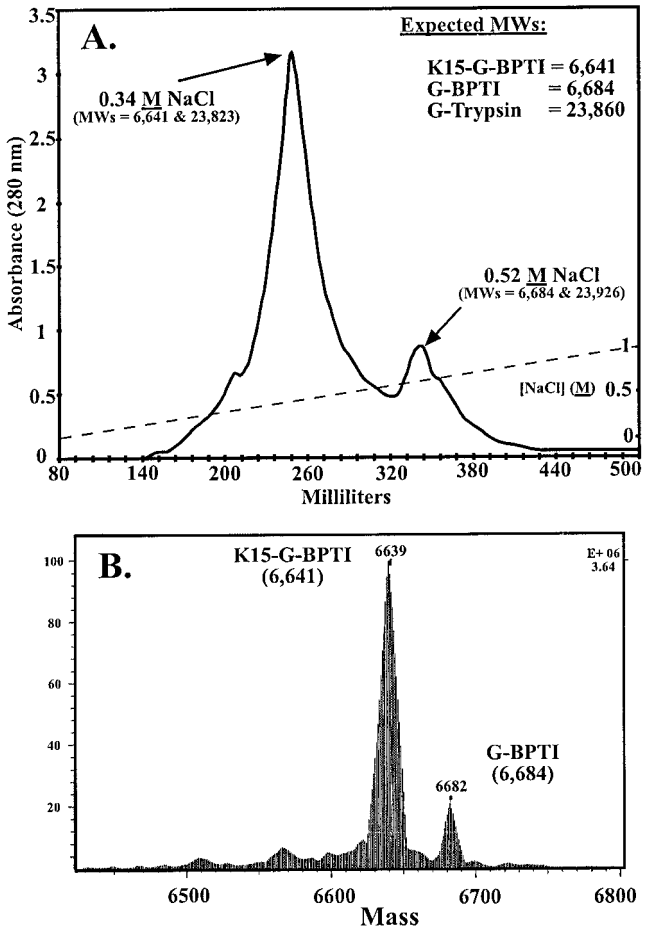


Figure 2. (A) Elution profile obtained for the K15-G-BPTI/G-trypsin complex on a Sephadex CM-25 cation exchange column (0.02 M glycine, pH 10.5) with a gradient of 0 to 1 M NaCl. For each peak, the NaCl concentration is given, as well as the relative molecular mass (MW in figure) of each molecular species eluting in that peak. The relative molecular masses calculated for the three expected derivatives are also given. (B) ESI mass spectrum obtained for the lower relative molecular mass species from the 0.34 M NaCl peak in panel A. The relative molecular masses expected for each peak are given below the names of the two protein derivatives.

Figure 2B shows the ESI mass spectrum obtained for K15-G-BPTI. The major peak at 6639 corresponds to the relative molecular mass of 6641 expected for BPTI with one unguanidinated lysine residue. The peak at 6682 indicates that a small fraction of fully guanidinated BPTI had reassociated with trypsin during the derivatization reaction. This was not surprising since the pK_a of homoarginine is well above 11.5 and under the reaction conditions used, the guanidinium group on a derivatized lysine-15 would therefore possess a positive charge facilitating the formation of a salt bridge with aspartic acid 189 in the active-site pocket of trypsin.

Protease Digestion and CAD Sequencing of K15-G-BPTI. To verify that lysine-15 was the sole, underiva-

tized lysine residue on K15-G-BPTI, an Arg-C endoproteinase digestion was performed. While analyzing the mass spectrum from the digest, we discovered that Arg-C endoproteinase had not only cleaved at arginine residues, but had also cleaved after the guanidinated lysine residues. Since the digestion at these homoarginine residues was incomplete, as well as unexpected, the resulting mass spectrum of the digest was difficult to interpret.

We therefore decided to use Lys-C endoproteinase to digest K15-G-BPTI. Since Lys-C cleaves C-terminal to lysine residues, only one cleavage site at lysine-15 was expected. Figure 3A shows the primary structure of BPTI with the expected Lys-C cleavage site indicated at lysine-15. Figure 3B shows the MALDI−TOF mass spectrum of the Lys-C digest of K15-G-BPTI. The peaks at 1844 and 5178 correspond, respectively, to peptides consisting of residues 1−15 and 16−58 of BPTI. The presence of these peptides indicates that K15-G-BPTI was cleaved at lysine-15. The peaks at 2205 and 2910 were not assigned and are not consistent with cleavage at any of the lysine residues. Thus, it was concluded that the only remaining lysine residue on K15-G-BPTI had to be lysine-15. Control digests of native BPTI showed products consistent with cleavage at all four lysine residues.

Since unassigned peaks were observed during the Lys-C digest, we decided to use collision activated dissociation (CAD) sequencing of the 1844 peptide from the Lys-C digest to confirm that it did indeed consist of residues 1−15 of BPTI (Figure 3C). Since fragmentation of peptides occurs preferentially at amide bonds in CAD experiments, the peaks resulting from the fragmentation were analyzed for relative molecular masses corresponding to cleavages at those bonds. The insert of Figure 3C shows the sequence of BPTI from residues 1−15. The relative molecular masses above the sequence correspond to those expected for peptides resulting from single cleavages of the peptide at each residue starting from arginine-1. The relative molecular masses below the sequence correspond to those expected for peptides resulting from single cleavages of the peptide at each residue starting at lysine-15. Unfortunately, when using this method, preferential cleavage tends to occur on the N-terminal side of proline residues resulting in a significant fraction of peptides corresponding to double cleavages. The second row of relative molecular masses above the sequence correspond to those expected for peptides initially cleaved at proline residues.

The CAD sequencing data showed that large peaks occurred at 920 and 921 as a result of the preferential cleavage of the BPTI peptide between glutamate-7 and proline-8. The appearance of these and other peaks corresponding to fragmentation products expected from the given sequence, indicates that the Lys-C endoproteinase cleavage product weighing 1844 did correspond to residues 1−15 of BPTI. The results from the Lys-C cleavage and sequencing, coupled with the ESI mass spectra, conclusively show that trypsin effectively protects lysine-15 of BPTI from guanidination and that all other lysines on BPTI, as well as on trypsin, became fully guanidinated during the derivatization with OMIU.

Fatty Acylation of K15-G-BPTI/G-Trypsin Complex. The (50% THF)/(50% aqueous phosphate buffer, pH 7.8) utilized here for attaching the fatty acid anhydrides proved essential in maintaining the solubility of both the anhydrides and proteins without the need for detergents. BPTI has been shown to be stable in 70% methanol, 70% ethanol, and 50% acetone (Kassel, 1970). We have demonstrated here that both the inhibitor and the

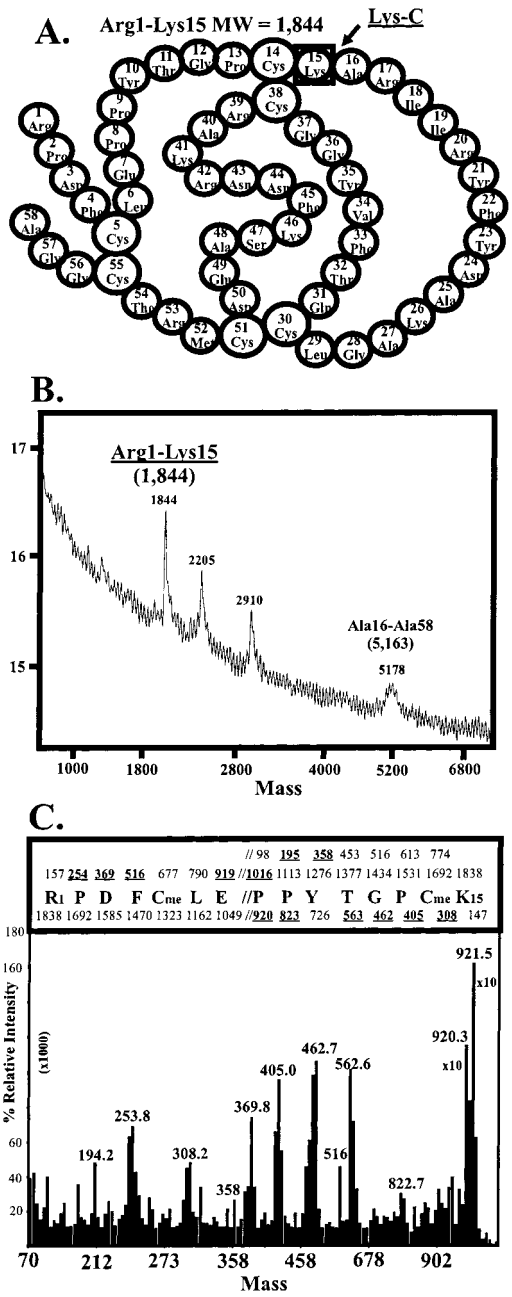


Figure 3. (A) Primary structure of BPTI, the expected site of cleavage of K15-G-BPTI by Lys-C endoproteinase and the calculated relative molecular mass for the peptide resulting from such a cleavage. (B) MALDI−TOF mass spectrum obtain from the Lys-C cleavage of K15-G-BPTI. (C) Graphical display of the data obtained from the CAD sequencing of the 1844 relative molecular mass peptide from panel B. Each labeled peak corresponds to a cleavage product consistent with values calculated from the first 15 residues of BPTI. The insert displays the sequence of the first 15 residues of BPTI with the relative molecular mass calculated for fragmentation of the peptide at each respective peptide bond. Since fragmentation occurred preferentially at proline-8, the relative molecular masses calculated for double fragmentations at this site are given on a second line above the sequence. The peptide fragments observed in the spectrum are in bold and underlined.

inhibitor/trypsin complex are stable in 50% THF. The use of THF aided in the purification of the derivatized proteins as well, since addition of excess THF precipitates the proteins which can then be simply collected as a pellet.

By performing the reaction at pH 7.8, we were able to eliminate nearly all acylation of tyrosine residues (pK_a

≈ 10). Other studies have also shown that at pH values below 8, α-amino groups are much more reactive than ϵ-amino groups (Rana and Meares, 1990; Wetzel et al., 1990). Thus, a pH of 7.8 significantly enhanced the selectivity of the acylation reactions described here. The yields, however, ranged from over 70% for G-BPTI-C8 and -C10 to only about 10% for G-BPTI-C14 and -C16. In preliminary experiments using a borate buffered system (pH 8.5 or 9.5), we have obtained yields of nearly 100% (data not shown). Although multiple tyrosine residues were found to be acylated, such side reactions were reversible with hydroxylamine. Thus, once these reaction conditions have been refined, much higher yields should be realized in future experiments.

Following acylation of the K15-G-BPTI/G-trypsin complex, gel filtration revealed that a small fraction (always less than 5%) of the complex does dissociate during the course of the reaction. However, these proteins were easily purified from the intact complex. Figure 4A displays the elution profile obtained for a palmitoylated K15-G-BPTI/G-trypsin complex on a pH 1.5 acetic acid column used to dissociate the complex. Under these conditions, almost all of the complex dissociated and the K15-G-BPTI-C16 was well resolved from the dissociated trypsin. The disparity in peak size is due to the much larger absorbance of trypsin at 280 nm. Unlike previous studies (Ebina et al., 1989), these conditions provide a complete dissociation of the complex in one chromatographic run. Figure 4B shows an HPLC elution profile obtained for K15-G-BPTI-C16 following dissociation of the complex on the acetic acid column, while Figure 4C shows the MALDI-MS obtained for K15-G-BPTI-C16 following HPLC purification. Both indicate that the product is clean and is modified as expected.

Reversed-Phase HPLC of Acylated Proteins. The solvent system employed was based on that used by Moll and Thompson (1994) to purify polyalanines attached to G-BPTI. The final mobile phase (or solvent B) used in our experiments consisted of 20% acetonitrile, 55% 1-propanol, and 25% iso-butanol. Isobutanol is quite nonpolar with a relative polarity of 3.0 (water = 10.2), however, at this concentration was miscible with water and was found to improve resolution and shorten the retention time of the proteins. A very steep gradient of 6% B/min was also found to enhance resolution. Figure 5 displays the elution profile of each of the acylated-G-BPTIs examined and shows that all of the acylated proteins are well resolved from the unmodified G-BPTI (see also Figure 4B).

Site-Specific Attachment of Reporter Groups. To show that these acylated proteins can be used in a fluorescence recovery after photobleaching (FRAP) experiment or other experiments requiring a fluorescent label, it was necessary to show that lysine-15 could be labeled with an amine-specific fluorophore. The NHS-ester of 5-(and 6-)carboxyfluoroscein (CF) was chosen due to its high quantum yield, low cost, wide use as a general fluorophore, and its susceptibility to bleaching, which is important for FRAP experiments. Both mass and absorbance spectra indicated that the ratio of attachment of the fluorophore to K15-G-BPTI-C16 was 1:1.

Initial attempts at labeling K15-G-BPTI-C16 with tritiated *N*-succinimidyl propionate (^{3}H-NSP) were unsuccessful. The pK_a of the ϵ-amino group on lysine-15 is between 9.8 and 10.4 (Mathews and van Holde, 1990), and thus, the phosphate buffer initially used at pH 7.8 could not deprotonate the ϵ-amine which is necessary for its reaction with ^{3}H-NSP. Morrison et al. (1986) have shown that there is a very significant difference in the

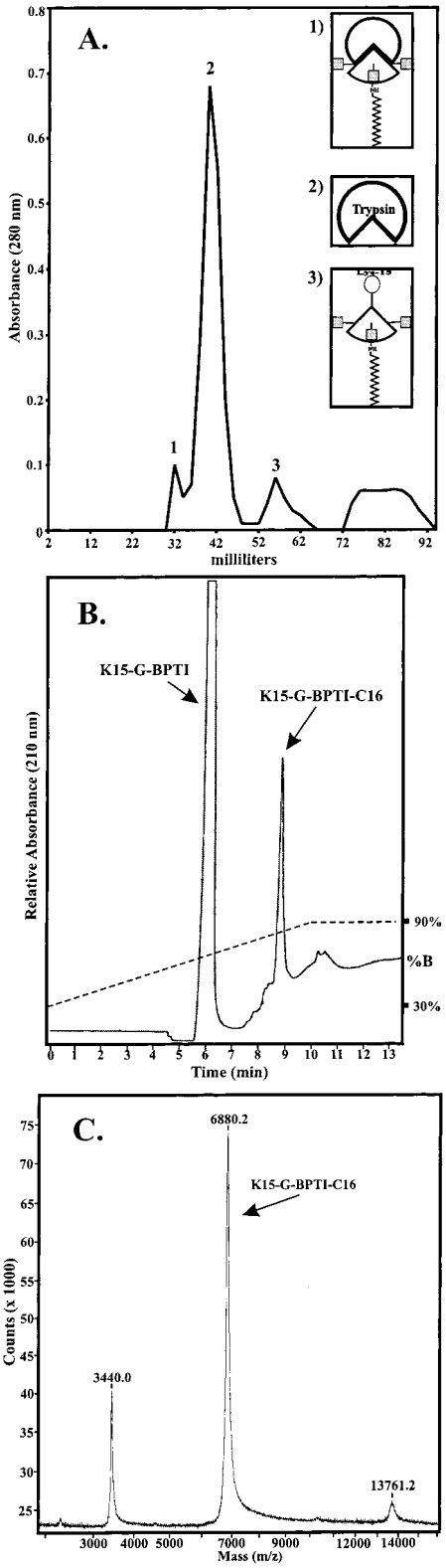


Figure 4. (A) Elution profile obtained for a palmitoylated K15-G-BPTI/G-trypsin complex on a Sephadex G-50 superfine column (1.5 × 45 cm; 100 mM acetic acid, pH 1.5). Protein absorbance was monitored at 280 nm. The peaks are numbered and the structures (from Figure 1) corresponding with the relative molecular masses measured in each peak are indicated. (B) C-3, reversed-phase HPLC elution profile obtained for K15-G-BPTI-C16 from acetic acid column in Figure 4A. The organic phase (B) consisted of acetonitrile:1-propanol:isobutanol (2:5.5:2.5). (C) MALDI-MS of K15-G-BPTI-C16 HPLC peak. Relative molecular mass calculated for [M + H$^+$] (6880.0). The peak at 3440 corresponds to [M + 2H$^+$], and the peak at 13 761.2 corresponds to a gas-phase dimer.

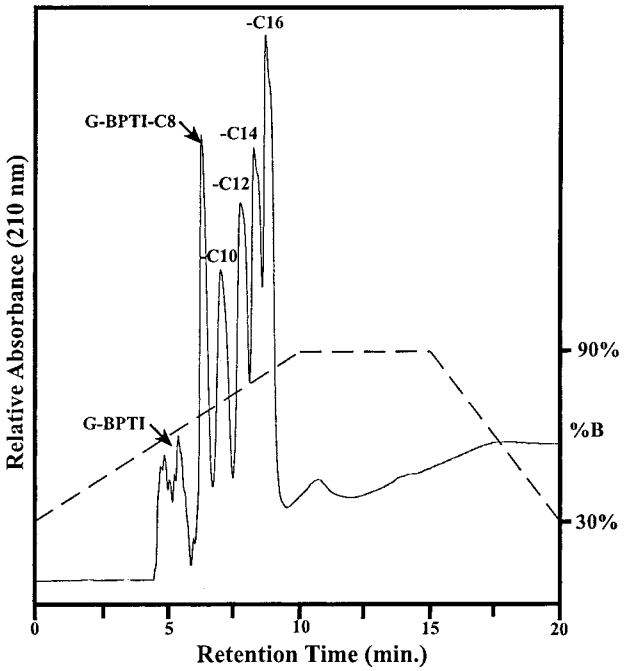


Figure 5. Elution profile obtained on a C-3 reversed-phase HPLC column (9.4 × 250 mm) for a series of G-BPTI proteins N-terminally acylated with fatty acids ranging in length from 8 to 16 carbons. The organic phase (B) consisted of acetonitrile: 1-propanol:isobutanol (2:5.5:2.5). The retention times for each of the proteins are as follows: G-BPTI, 5.3 min; G-BPTI-C8, 6.4 min; G-BPTI-C10, 7.1 min; G-BPTI-C12, 7.8 min; G-BPTI-C14, 8.4 min; G-BPTI-C16, 8.8 min; and G-BPTI-C18, 9.5 min (G-BPTI-C18 not shown in Figure 5). The peaks around 5 min correspond to G-BPTI and to excess TFA introduced during dilution of the samples.

reactivity of NSP with coagulation factor X between pH 7.5 and 9.0. Thus, a borate buffer at pH 9.5 was employed. The reaction proceeded well at this pH; however, in addition to the amide bond at lysine-15, esters were formed with tyrosine residues. These esters were easily cleaved with hydroxylamine yielding a molecule radiolabeled specifically at lysine-15.

Labeling of the α-amine of G-BPTI proved much less problematic due to its lower pK_a. This lower pK_a allowed the reaction to be performed in phosphate buffer at pH 7.8 with no labeling observed at tyrosine residues. The difference in labeling between G-BPTI and K15-G-BPTI-C16 at pH 7.8 indicates that the labeling indeed occurred at the N-terminus of G-BPTI and Lysine-15 of K15-G-BPTI-C16, respectively.

Attachment of sulfo-SMCC to G-BPTI and K15-G-BPTI/G-Trypsin. During the initial course of these reactions, mass spectra indicated the addition of a second linker to some proteins after 10 min. Since the half-life of the NHS-ester was determined to be around 4 min, the species appearing after 10 min was assumed to be due to the reaction of the maleimide group on SMCC with a cysteine residue on G-BPTI. The lag time before the attachment of the second cross-linker supports this assumption, since it is also reasonable that under these conditions, the attachment of a cross-linker to a cysteine residue involved in a disulfide bridge would take longer than the reaction of an NHS-ester with a free amino group.

Therefore, to reduce the fraction of proteins with a second cross-linker attached, the time of the reaction was limited to 10−15 min. It was found that, in this time frame, approximately 30−50% of the total protein received one cross-linker and approximately 10% received two. No proteins with three cross-linkers were observed. Gel filtration showed that the complex remained intact, indicating that lysine-15 remained protected during the reaction. Experiments monitoring the stoichiometry of attachment of free cysteine with the proteins indicated only one reactive maleimide group per protein.

Due to the significant hydrolysis of maleimide groups above pH 8 (Ishikawa et al., 1983), acidic conditions were used during purification of G-BPTI-SMCC and K15-G-BPTI-SMCC. The stability of the maleimide at acidic pH was particularly convenient since it was necessary to dissociate the K15-G-BPTI/G-trypsin complex on a gel filtration column at pH 1.5 (see Figure 4).

Peptide Cleavage Procedures. The method used to cleave the hydrophobic peptides from resin was a modified version of that described by Moll and Thompson (1994) to cleave polyalanine peptides. The goal of our study was to develop a cleavage procedure that could be performed on small amounts of resin, allowing the peptides to be coupled to proteins within a few hours following cleavage. Such a method would eliminate the need for further reduction of cysteine residues on the peptides and allow for cleavage of only necessary amounts of peptide such that unneeded peptide could be kept protected and attached to resin.

Performing cleavages on small resin samples of 20−30 mg (3−4.5 μmol of crude peptide) and using dry nitrogen to remove most of the cleavage solution made it possible to couple peptides to G-BPTI within 2 h of cleavage. Triethylsilane and water were used as scavengers because their volatility allowed them to be easily removed following cleavage. By performing all steps in 1.5 mL eppendorf tubes, microfuges could be used for pelletting the peptides making the procedure quicker and more convenient than methods used in the past. An important step in the procedure proved to be the distillation of TBMether immediately before precipitation of the peptide/SDS complex. Prior to distillation, TBMether can contain peroxides which will oxidize cysteine residues.

Synthesis/Characterization of K15-G-BPTI-Peptide Conjugates. To separate the peptide−protein conjugate from the SDS following the coupling reaction, a propionic acid, formic acid, and water (PFH) buffer was used. Figure 6A shows the elution profile obtained for K15-G-BPTI-CYA_6L_4 using this column. The majority of the radioactivity elutes with the protein, indicating that a significant amount of peptide was attached to the protein. The peak corresponding to the acridine orange assay for SDS indicates that the protein is well resolved from the detergent-containing fractions. All syntheses yielded elution profiles very similar to Figure 6A, indicating that this method completely dissociates SDS from the proteins.

Figure 6B shows the elution profile for the same K15-G-BPTI-CYA_6L_4 protein on a Sephadex G-50 gel filtration column. The protein−peptide conjugate elutes slightly ahead of the unmodified protein as indicated by both the protein absorbance and tritium profiles. This column also serves to separate the protein from any unattached peptides as evidenced by the small radiolabeled peak around 145 mL corresponding to residual peptide. Dilution of the proteins on this column facilitated the refolding of denatured forms of the protein that were observed during HPLC purification.

Many different peptides were attached to G-BPTI and K15-G-BPTI using these methods. Peptides attached included CYA_6, CYA_6L_2, $CYA_6L_2A_2$, CYA_6L_4, and $CYA_{14}L_2A_6$. Yields varied from around 80% for attachment of

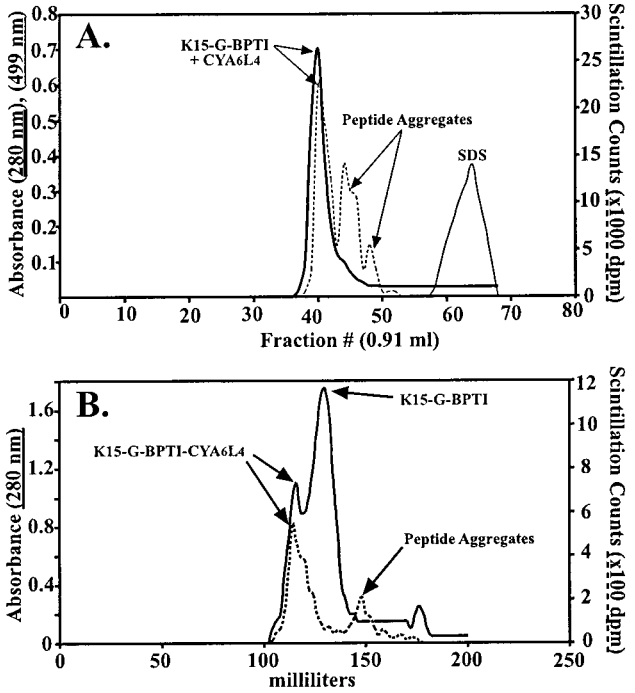


Figure 6. (A) Elution profile obtained on a Sephadex G-25 superfine column (1.5 × 25 cm; propionic acid:formic acid:water, 2:1:2) of the reaction mixture used to couple CYA_6L_4 to K15-G-BPTI-SMCC. Protein and peptide absorbance was measured at 280 nm (solid, bold line), and radiolabeled peptide was assayed using liquid scintillation (dotted line). SDS was assayed by partitioning of SDS/acridine orange complexes into toluene and subsequent absorbance of the complexes at 499 nm (solid, line). (B) Elution profile for the main 280 nm peak from panel A on a Sephadex G-50 superfine (1.5 × 120 cm; 50 mM ammonium bicarbonate, pH 7.8) gel filtration column. Protein and peptide absorbance was measured at 280 nm (solid line), and radiolabeled peptide was assayed by liquid scintillation (dotted line).

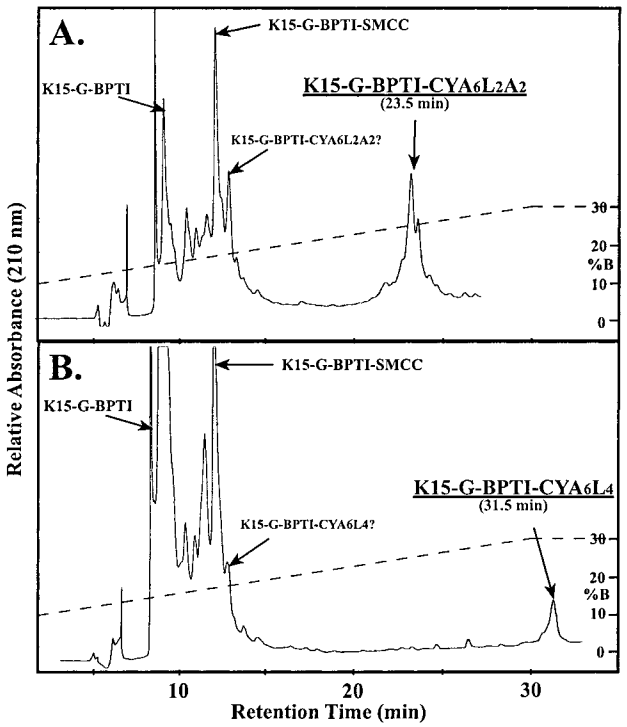


Figure 7. HPLC elution profiles obtained for (A) K15-G-BPTI-$CYA_6L_2A_2$ and (B) K15-G-BPTI-A_6L_4 on a C-3 reversed-phase column (9.4 × 250 mm). The organic phase consisted of acetonitrile:1-propanol:isobutanol (2:5.5:2.5).

CYA_6 and 60% for $CYA_6L_2A_2$ to less than 1% for the attachment of $CYA_{14}L_2A_6$. The predominant factor limiting coupling of the peptides to K15-G-BPTI was the concentration of peptides' free sulfhydryl groups. Thus, yields could be improved dramatically if the yields of full-length peptide were increased.

HPLC Purification of K15-G-BPTI-Peptide Conjugates. Figure 7 shows the HPLC elution profile for K15-G-BPTI-$CYA_6L_2A_2$, and K15-G-BPTI-CYA_6L_4. Using G-BPTI as an internal standard, it was observed that the yield for K15-G-BPTI-CYA_6L_4 was much lower than that for K15-G-BPTI-$CYA_6L_2A_2$. Since the peptides were capped following each coupling cycle, only full-length peptides should have possessed an N-terminal cysteine residue. Thus, the lower yield was primarily due to a lower yield of full-length peptide, which reduced the concentration of peptide containing free sulfhydryls.

The appearance of two peaks for K15-G-BPTI-$CYA_6L_2A_2$ was a concern; however, ESI mass spectrometry verified that the protein in each peak has the expected relative molecular mass of 8024. Also, since the K15-G-BPTI-$CYA_6L_2A_2$ from these peaks was shown to be a good inhibitor of trypsin (data not shown), it was assumed that the two peaks must simply corresponded to two slight structural isoforms of the same protein.

DISCUSSION

The goal of these studies was to create a series of unobtrusive, fluorescently labeled, model transbilayer proteins and fatty-acylated proteins capable of spontaneously inserting into the hydrophobic core of membranes. To create such a protein, we have developed methods for chemically modifying BPTI to contain two specific, reactive sites. To either site, an amine-reactive reporter group may be attached. We have developed methods for coupling fatty acids specifically to the N-terminus without the need for detergents. As an alternate procedure, we have also developed methods for handling and specifically linking hydrophobic peptides to the N-terminus.

To create two specific sites on BPTI for attachment of different groups, we protected Lys-15 of BPTI from modification with OMIU by binding trypsin to the inhibitor. The coupling of a trypsin protection strategy with derivatization by OMIU was unique and significant in two respects. First, these studies are the first time that a derivatization has been performed on a BPTI/trypsin complex above pH 10.0. Second, OMIU does not derivatize the α-amino group of the N-terminus, which results in a BPTI molecule (K15-G-BPTI) with two sites available for the attachment of labels, peptides, fatty acids, or other moieties. Past studies using trypsin to protect lysine-15 employed reagents that modified all unprotected amino groups, thus eliminating the possibility for a second site-specific modification (Ebina et al., 1989; Elkana, 1974). Also, since trypsin survives the modification and stays complexed with K15-G-BPTI, trypsin can be used to further protect lysine-15 during the attachment of other groups to the N-terminal α-amino group. These studies show that trypsin does effectively protect Lys-15 from derivatization and extend to a higher pH, data from past studies showing the extreme stability of the complex formed between BPTI and trypsin (Lazdunski et al., 1974; Levilliers et al., 1970; Delaage and Lazdunski, 1968).

The reaction conditions and reagents used here to fatty acylate the N-terminus of G-BPTI and K15-G-BPTI/G-trypsin are unique in several respects. The use of THF to maintain the solubility of the reagents provides a means for reacting hydrophilic proteins with hydrophobic

fatty acid esters and anhydrides without detergents. This solvent system eliminates the need for dialysis or excessive washing of the protein as described in other methods (Robert et al., 1993; Lee and Kim, 1995; Huang et al., 1980; Babbitt and Huang, 1985) and simplifies purification by allowing the modified protein to be precipitated with excess THF. The use of fatty acid anhydrides for the acylation of G-BPTI is also unique and establishes a simple method for attaching various lengths of fatty acids to proteins and peptides, since the anhydrides of fatty acids of up to 22 carbons in length are commercially available. At pH values below 8, these methods could provide a general means for specific N-terminal fatty acylation of proteins.

To attach hydrophobic peptides to BPTI, we have developed methods for the cleavage and handling of hydrophobic peptides and the attachment of these types of peptides to K15-G-BPTI via an SMCC cross-linker attached at the N-terminus (K15-G-BPTI-SMCC). The entire cleavage process takes only 2 h which allows the peptides to be conjugated to the K15-G-BPTI-SMCC before significant oxidation of cysteine residues can occur. These procedures eliminate the need for further reduction of cysteine-containing peptides prior to conjugation with K15-G-BPTI-SMCC. Unlike past methods (Moll and Thompson, 1994), our methods make small-scale cleavages practical allowing unused peptide to remain resin bound. Although further studies, including peptide mapping, should be performed to ensure the absolute specificity of cross-linker and peptide attachment, our results indicate that these methods can be used to attach very hydrophobic peptides to the N-terminus of K15-G-BPTI and that the stoichiometry of attachment is 1:1.

The methods described here provide a realistic means for producing model membrane proteins containing N-terminal fatty acyl groups or hydrophobic peptides. Because BPTI is a small, stable, highly soluble protein, it is expected to have minimal interactions with any other membrane proteins. Since the site of attachment of fluorescent labels and other reporter groups at lysine-15 is on the opposite pole of K15-G-BPTI, these groups should not effect membrane binding or diffusion. Moll and Thompson (1994) studied the partitioning of peptide−G-BPTI conjugates prepared in a manner very similar to those described here and found them satisfactory as biophysical probes. We have also examined the membrane binding and self-association properties of the fatty-acylated proteins described here (Pool and Thompson, 1998). Both studies attest to the utility of these proteins as model systems for studying protein−membrane and protein−protein interactions.

ACKNOWLEDGMENT

The authors would like to thank Dr. Mike Kinter and Dr. Nicholas Sherman for their assistance in obtaining and interpreting the mass spectral data, Linda Beggerly for her assistance in synthesizing the hydrophobic peptides, and David Singleton for critical reading of the manuscript. This work was supported by NIH Grants GM-14628 and GM-23573.

LITERATURE CITED

Amir, D., and Haas, E. (1987) Estimation of intramolecular distance distributions in bovine pancreatic trypsin inhibitor by site-specific labeling and nonradiative excitation energy-transfer measurements. *Biochemistry 26*, 2162−2175.

Babbitt, B., and Huang, L. (1985) α-Bungarotoxin immobilized and oriented on a lipid bilayer vesicle surface. *Biochemistry 24*, 15−21.

Babbitt, B., Huang, L., and Freire, E. (1984) Thermotropic and dynamic characterization of interactions of acylated α-bungarotoxin with phospholipid bilayer membranes. *Biochemistry 23*, 3920−3926.

Bolin, D., Sytwu, I, Humiec, F., and Meienhofer, J. (1989) Preparation of oligomer-free Nα-Fmoc and Na-urethane amino acids. *Int. J. Pept. Protein Res. 33*, 353−359.

Chang, C., Waki, M., Ahmad, M., Meienhofer, J., Lundell, E., and Haug, J. (1980) Preparation and Properties of Na-9-Fluorenylmethyloxycarbonylamino Acids Bearing *tert*-Butyl Side Chain Protection. *Int. J. Pept. Protein Res. 15*, 59−66.

Chervenka, C., and Wilcox, P. (1956) Chemical Derivatives of Chymotrypsin: II. Reaction with ortho-methylisourea. *J. Biol. Chem. 222*, 635−647.

Crestfield, A., Moore, S., and Stein, W. (1963) The Preparation and Enzymatic Hydrolysis of Reduced and S-Carboxymethylated Proteins. *J. Biol. Chem. 238*, 622−627.

Delaage, M., and Lazdunski, M. (1968) Trypsinogen, trypsin, trypsin-substrate and trypsin-inhibitor complexes in urea solutions. *Eur. J. Biochem. 4*, 378−384.

Ebina, S., Lerner, R. A., and Wright, P. E. (1989) Chemical modification of bovine pancreatic trypsin inhibitor for single site coupling of immunogenic peptides for NMR conformational analysis. *J. Biol. Chem. 264*, 7882−7888.

Elkana, Y. (1974) The Use of Fluorescence Techniques in the Study of the Interaction of the Basic Trypsin Inhibitor of Bovine Pancreas, Selectively Labeled at Lysine 15, with Chymotrypsin and Trypsin. In *Bayer-Symposium V "Proteinase Inhibitors"* (H. Fritz, H. Tschesche, L. Greene, and E. Truscheit, Eds.) pp 445−453, Springer-Verlag, Berlin.

Huang, A., Huang, L., and Kennel, S. J. (1980) Monoclonal antibody covalently coupled with fatty acid. A reagent for in vitro liposome targeting. *J. Biol. Chem. 255*, 8015−8018.

Hughes, W., Saroff, H., and Carney, A. (1949) Preparation and Properties of Serum and Plasma Proteins. XXII. A Crystallizable Guanidinated Derivative of Human Serum Albumin. *J. Am. Chem. Soc. 71*, 2476−2480.

Ishikawa, E., Imagawa, M., Hashida, S., Yoshitake, S., Hamaguchi, Y., and Ueno, T. (1983) Enzyme-labeling of antibodies and their fragments for enzyme immunoassay and immunohistochemical staining. *J. Immunoassay 4*, 209−327.

Kassel, B. (1970) Bovine Trypsin-Kallikrein Inhibitor (Kunitz Inhibitor, BPTI, Polyvalent Inhibitor of Bovine Organs). In *Proteolytic Enzymes (*G. Perlman and L. Laszlo, Eds.) pp 844−852, Academic Press, New York.

Lazdunski, M., Vincent, J., Schweitz, H., Peron-Renner, M., and Pudles, J. (1974) The Mechanism of Association of Trypsin (or Chymotrypsin) with the Pancreatic Trypsin Inhibitors (Kunitz and Kazal) Kinetics and Thermodynamics of the Interaction. In *Bayer-Symposium V "Proteinase Inhibitors"* (H. Fritz, H. Tschesche, L. Greene, and E. Truscheit, Eds.) pp 420−431, Springer-Verlag, Berlin.

Lee, E. O., and Kim, J. D. (1995) Palmitoyl lysozyme-induced stabilization of PE (phosphatidylethanolamine) liposomes and their interaction with *Candida albicans*. *J. Biochem. 117*, 54−58.

Levilliers, N., Peron, M., Arrio, B., and Pudles, J. (1970) On the mechanism of action of proteolytic inhibitors. IV. Effect of 8 M urea on the stability of trypsin in trypsin-inhibitor complexes. *Arch. Biochem. Biophys. 40*, 474−483.

Mathews, C., and van Holde, K. (1990) In *Biochemistry* (D. Bowen, Ed.) The Benjamin/Cummings Publishing Co, Red Wood.

Moll, T. S., and Thompson, T. E. (1994) Semisynthetic proteins: model systems for the study of the insertion of hydrophobic peptides into preformed lipid bilayers. *Biochemistry 33*, 15469−15482.

Morrison, S. A., Lidonnici, K., and Jesty, J. (1986) Effect of limited modification of amino groups on the reactivity of human factor Xa. *Biochim. Biophys. Acta 884*, 409−418.

Pool, C. T., and Thompson, T. E. (1998) Chain Length and Temperature Dependence of the Reversible Association of

Model-Acylated Proteins with Lipid Bilayers. *Biochemistry 37* (28), 10246−10255.

Rana, T. M., and Meares, C. F. (1990) N-Terminal modification of immunoglobulin polypeptide chains tagged with isothiocyanato chelates. *Bioconjugate Chem. 1*, 357−362.

Robert, S., Domurado, D., Thomas, D., and Chopineau, J. (1993) Fatty acid acylation of RNase A using reversed micelles as microreactors [published erratum appears in *Biochem. Biophys. Res. Commun.* (1994) *198* (1), 410]. *Biochem. Biophys. Res. Commun. 196*, 447−454.

Sokoloff, R. L., and Frigon, R. P. (1981) Rapid spectrophotometric assay of dodecyl sulfate using acridine orange. *Anal. Biochem. 118*, 138−141.

Wetzel, R., Halualani, R., Stults, J. T., and Quan, C. (1990) A general method for highly selective cross-linking of unprotected polypeptides via pH-controlled modification of N-terminal α-amino groups. *Bioconjugate Chem. 1*, 114−122.

BC9800771

Labeling of Monoclonal Antibodies with Diethylenetriaminepentaacetic Acid-Appended Radioiodinated Peptides Containing D-Amino Acids†

Serengulam V. Govindan,*,‡ M. Jules Mattes,§ Rhona Stein,§ Bill J. McBride,‡ Habibe Karacay,‡ David M. Goldenberg,§ Hans J. Hansen,‡ and Gary L. Griffiths‡

Immunomedics, Inc., 300 American Road, Morris Plains, New Jersey 07950, and Garden State Cancer Center, 520 Belleville Avenue, Belleville, New Jersey 07109. Received June 26, 1998; Revised Manuscript Received November 18, 1998

The optimal use of radioiodinated internalizing monoclonal antibodies (mAbs) for radioimmunotherapy necessitates the development of practical methods for increasing the level of retention of ^{131}I in the tumor. Lysosomally trapped ("residualizing") iodine radiolabels that have been previously designed are based mostly on carbohydrate−tyramine adducts, but these methods have drawbacks of low overall yields and/or high levels of mAb aggregation. We have developed a method using thiol-reactive diethylenetriaminepentaacetic acid (DTPA)−peptide adducts wherein the peptides are assembled with one or more D-amino acids, including D-tyrosine. Two such substrates, R-Gly-D-Tyr-D-Lys[1-(*p*-thiocarbonylaminobenzyl)DTPA], referred to as IMP-R1, and [R-D-Ala-D-Tyr-D-Tyr-D-Lys]$_2$(CA-DTPA), referred to as IMP-R2, wherein R is 4-(*N*-maleimidomethyl)cyclohexane-1-carbonyl, were synthesized by preparing functional group-protected peptides on a solid phase, selectively derivatizing the lysine side chain with 1-(*p*-isothiocyanatobenzyl)DTPA or DTPA dianhydride (CA-DTPA), deprotecting other functional groups, and finally derivatizing the peptide's N-terminus so it contained a maleimide group. Radioiodinations of the peptides followed by conjugations to disulfide-reduced mAbs, carried out as a one-vial procedure, resulted in 32−89% overall yields, at specific activities of 1.8−11.1 mCi/mg, with less than 2% aggregation. Two internalizing mAbs, LL2 (anti-CD 22 B-cell lymphoma mAb) and RS7 (an anti-adenocarcinoma mAb which targets EGP-1 antigen), labeled with this procedure exhibited a 2−3-fold better cellular retention in Ramos and Calu-3 tumor cell lines, in vitro, respectively, compared to the same mAbs radioiodinated with the chloramine-T method. The rationale for the new approach, syntheses, radiochemistry and in vitro data are presented.

INTRODUCTION

The current status of radiolabeled mAbs[1] in cancer diagnosis and therapy, and possible approaches for improved methods, have been discussed in recent reviews (*1*−*3*). Among the significant issues to consider are the role of mAb metabolism after internalization in tumor cells and the subsequent fate of the attached radionuclide, because this process affects tumor dosimetry (*4*). Radioiodine is released from the cell as iodotyrosine after lysosomal processing of radioiodinated mAbs, while a radiometal label on mAbs is trapped in lysosomes after such processing (*4*, *5*). With radioiodinated mAbs, the residence times of the nuclide in tumor and tumor-to-nontumor discrimination are reduced, and in the case of ^{131}I, the dosimetric advantage of the isotope's 8 day half-life is diminished. This scenario potentially applies to most mAbs which bind to the tumor cell surface, since it has been shown in in vitro studies that most bound mAbs are catabolized with a half-life of 1−2 days (*4*, *6*). The need to develop practical methods to enhance the residence time of radioiodine in tumors is therefore compelling.

To increase the residence time of radioiodine inside cells, mAbs have been labeled with radioiodinated nonmetabolizable carbohydrate−tyramine adducts. Dilactitoltyramine (DLT; *7*−*9*) and tyraminecellobiose (TCB; *10*) are two substrates of this class which have been frequently utilized for this purpose. After mAb processing,

† Presented in part at the 215th American Chemical Society National Meeting, Dallas, TX, March 1998, 45th annual meeting of the Society of Nuclear Medicine, Toronto, ON, June 1998, and Seventh Conference on Radioimmunodetection and Radioimmunotherapy of Cancer, Princeton, NJ, October 1998.

* To whom correspondence should be addressed. Phone: (973) 605-8200. Fax: (973) 605-1103.

‡ Immunomedics, Inc.

§ Garden State Cancer Center.

[1] Abbreviations: Aloc, allyloxycarbonyl; BOC, *tert*-butyloxycarbonyl; tBu, *tert*-butyl; Bz-DTPA, benzyl-DTPA; CA-DTPA, cyclic DTPA dianhydride; CEA, carcinoembryonic antigen; cpm, counts per minute; CT, chloramine-T; DIC, diisopropylcarbodiimide; DIEA, diisopropylethylamine; DLT, dilactitoltyramine; DMF, dimethylformamide; DTPA, diethylenetriaminepentaacetic acid; DTT, dithiothreitol; EDTA, ethylenediaminetetraacetic acid; EGP-1, epithelial glycoprotein-1; Et_3N, triethylamine; Fmoc, fluorenylmethoxycarbonyl; HOAc, acetic acid; HOBt, 1-hydroxybenzotriazole; HPLC, high-performance liquid chromatography; IMP-R1, Immunomedics peptide-residualizing 1; IMP-R2, Immunomedics peptide-residualizing 2; IMR, immunoreactivity; ITC-Bz-DTPA, 1-(*p*-isothiocyanatobenzyl)DTPA; mAb, monoclonal antibody; MCC, 4-(*N*-maleimidomethyl)cyclohexane-1-carbonyl; MW, molecular mass; PBS, phosphate-buffered saline; RAIT, radioimmunotherapy; SDS−PAGE, sodium dodecyl sulfate−polyacrylamide gel electrophoresis; SE-HPLC, size-exclusion HPLC; SIPC, succinimidyl 5-iodo-3-pyridinecarboxylate; sulfo-SMCC, sulfosuccinimidyl 4-(*N*-maleimidomethyl)cyclohexane-1-carboxylate; TCA, trichloroacetic acid; TCB, tyraminecellobiose; TFA, trifluoroacetic acid.

10.1021/bc980075g CCC: $18.00 © 1999 American Chemical Society
Published on Web 02/11/1999

the radioiodinated carbohydrate metabolite is trapped ("residualized") in lysosomes. Stein et al. (*9*) have observed a >3-fold advantage in the level of tumor cell retention of [^{125}I]DLT-labeled mAbs RS7 and RS11 in vitro over a 69 h period, and a pronounced dosimetric (*9*) and therapeutic (*11*) advantage in animal experiments in which the Calu-3 lung carcinoma cell line was used, compared to data obtained using the same antibodies radioiodinated with the chloramine-T method. Similar advantages were reported by Mattes et al. (*12*) in the [$^{125/131}$I]DLT labeling of anti-lymphoma antibody LL2. Ali et al. (*10*) have reported improved tumor retention of radio-
iodine when mAbs were labeled with radioiodinated TCB.

However, these carbohydrate-based iodine radiolabels have certain practical drawbacks. In the case of DLT, the level of overall radioiodine incorporation into mAbs is only 3−6% (*9*, *12*) which results in very low specific activities. With TCB, the conjugation to mAbs makes use of cyanuric chloride as the cross-linker, which produces 10−25% mAb aggregation (*10*). In both cases, the mAb labeling is a multistep procedure. These limitations may impede further development of these agents for clinical use.

Another reported method involves using *N*-succinimidyl 5-iodo-3-pyridinecarboxylate (SIPC), as exemplified in the labeling of the anti-epidermal growth factor variant III mAb L8A4 (*13*). The major intracellularly trapped low-molecular mass catabolite, after internalization and processing of the radiolabeled mAb−antigen complex, was found to be a 5-iodonicotinic acid−lysine conjugate. The level of intracellular retention, in the HC2 20 d2 cell line, of L8A4 mAb radioiodinated by the SIPC method was 68% higher at 2 h than that of the same mAb radioiodinated with the iodogen method, although this difference was reduced at the 20 h time point. In vivo, the amounts of tumor-associated radioactivities in athymic mice bearing HC2 20 d2 xenografts were 25% higher for the mAb labeled with SIPC than for the iodogen mode of radioiodination at time points up to 48 h, but the levels were equalized for both the labels at the 72 h time point. However, the former label also cleared faster from normal organs and thus gave rise to better tumor-to-organ ratios (*13*).

Radiometalated mAbs constitute another class of residualizing labels. The radionuclides from indium- and yttrium-labeled mAbs, for instance, are residualized in the lysosomes in the form of the lysine adducts of the respective metal chelates (*14*). The metal chelators in these cases are usually aminopolycarboxylates, such as EDTA or DTPA.

The goal of this study was to devise a practical method for the production of residualizing radioiodine, based on what was known about the residualization of metal chelates. We hypothesized that if an aminopolycarboxylate, such as DTPA, were attached to the ϵ-amine of D-lysine, and the latter was further elaborated by sequential couplings to one or more D-amino acids, including D-tyrosine, the result would be a DTPA-attached peptide wherein the peptide bonds would be relatively resistant to the action of proteases in the lysosomes. The N-terminus of the peptide could be coupled to a cross-linker, such as sulfo-SMCC, carrying a thiol-reactive group. Radioiodination of such an entity, followed by conjugation to a thiol-containing mAb, could generate a residualizing iodine label, while concurrently enabling the desired yield and specific activity enhancements in radiolabeling.

This work was carried out mainly using internalizing mAbs LL2 and RS7. LL2 is a pan-B-cell mAb, whose binding is restricted to B cells, and is one of a number of mAbs that belong to the CD22 cluster (*15*, *16*). Its internalization has been studied (*12*, *17*). RS7, an internalizing mAb, targets epithelial glycoprotein EGP-1, which is expressed in a number of carcinoma cell lines (*18, 19*). LL2 belongs to the IgG_{2a} isotype, while RS7 belongs to the IgG_1 class. In this report, we describe the syntheses of two bifunctional substrates,[2] IMP-R1 and IMP-R2, the radiochemistry of mAb labelings, and a proof of concept that radiolabeling internalizing mAbs using these radioiodinated peptides leads to enhanced retention of radioiodine in tumor cells.

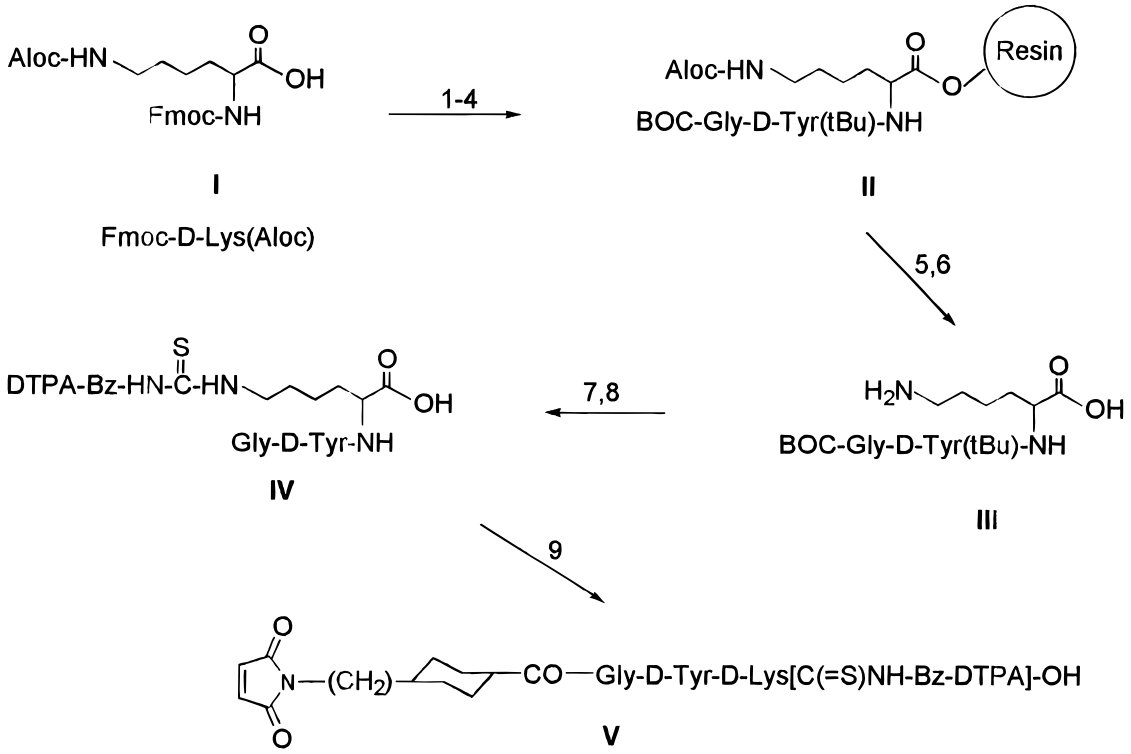
EXPERIMENTAL PROCEDURES

General Procedures. Monoclonal antibodies were obtained from Immunomedics' and the Garden State Cancer Center's antibody production laboratories. 2-Chlorotrityl chloride resin and protected D-amino acids were obtained from Advanced ChemTech (Louisville, KY) and used as received. Sulfo-SMCC was purchased from Pierce (Rockford, IL) and Molecular Biosciences, Inc. (Boulder, CO). All other chemicals and solvents (high-purity grade) were obtained from Advanced ChemTech, Aldrich Chemical Co. (Milwaukee, WI), Fisher Scientific (Pittsburgh, PA), and J. T. Baker (Phillipsburg, NJ). Na^{125}I, Na^{131}I, and $^{111}InCl_3$ were purchased from NEN Life Science Products (Boston, MA). All nonaqueous reactions were carried out under argon or nitrogen. Electrospray mass spectral (ESMS) data were obtained from Mass Consortium (San Diego, CA) and were recorded using either a Hewlett-Packard 1100 MSD or an API 1 Perkin-Elmer SCIEX electrospray mass spectrometer. Exact mass determinations by high-resolution mass spectra were obtained using FAB on a VG ZAB-VSE mass spectrometer. Amino acid analyses were carried out at the Scripps Research Institute Core facility (La Jolla, CA). Analytical HPLC analyses of peptides were carried out using a Waters PrepLC 4000 system using a Nova Pak C-18 (4 μm, 8 mm × 100 mm) Radial Pak cartridge, equipped with a UV detector (220 nm), and using a gradient elution consisting of buffers A (0.1% aqueous TFA) and B (9:1 acetonitrile/water in 0.1% TFA). [The gradient was as follows: 100% A changing to 100% B over the course of 10 min (linear gradient) at a flow rate of 3 mL/min, changing to a flow rate of 5 mL/min at 10.1 min, and remaining isocratic at 100% B at this flow rate for the next 5 min.] Unless otherwise stated, purified peptides were found to be eluted essentially as single peaks under these HPLC analytical conditions. Preparative HPLC was performed on a Waters PrepLC 4000 system using a Delta Pak C-18 (15 μm, 100 Å, 4 cm × 31 cm) or Nova Pak C-18 (6 μm, 60 Å, 2.5 cm × 20 cm) preparative HPLC column. HPLC analyses of radiolabeled mAbs were carried out on an analytical Bio-Sil 250 size-exclusion column, in series with a guard column (both from Bio-Rad Laboratories, Hercules, CA), using 0.2 M sodium phosphate buffer (pH 6.8) as the mobile phase at a flow rate of 1 mL/min, with in-line UV (280 nm) and radioactivity detection. Cell lines were obtained from American Type Culture Collection (Rockville, MD), cultured as previously described (*9*, *12*), and were routinely tested for mycoplasma by the Mycotect assay (Life Technologies, Gaithersburg, MD).

Synthesis of IMP-R1 (Scheme 1). Fmoc-D-lysine-(Aloc) (0.325 g) was dissolved in anhydrous dichlo-

[2] IMP-R1 and IMP-R2 were previously referred to as "DPep" and "DDipep", respectively.

Scheme 1[a]

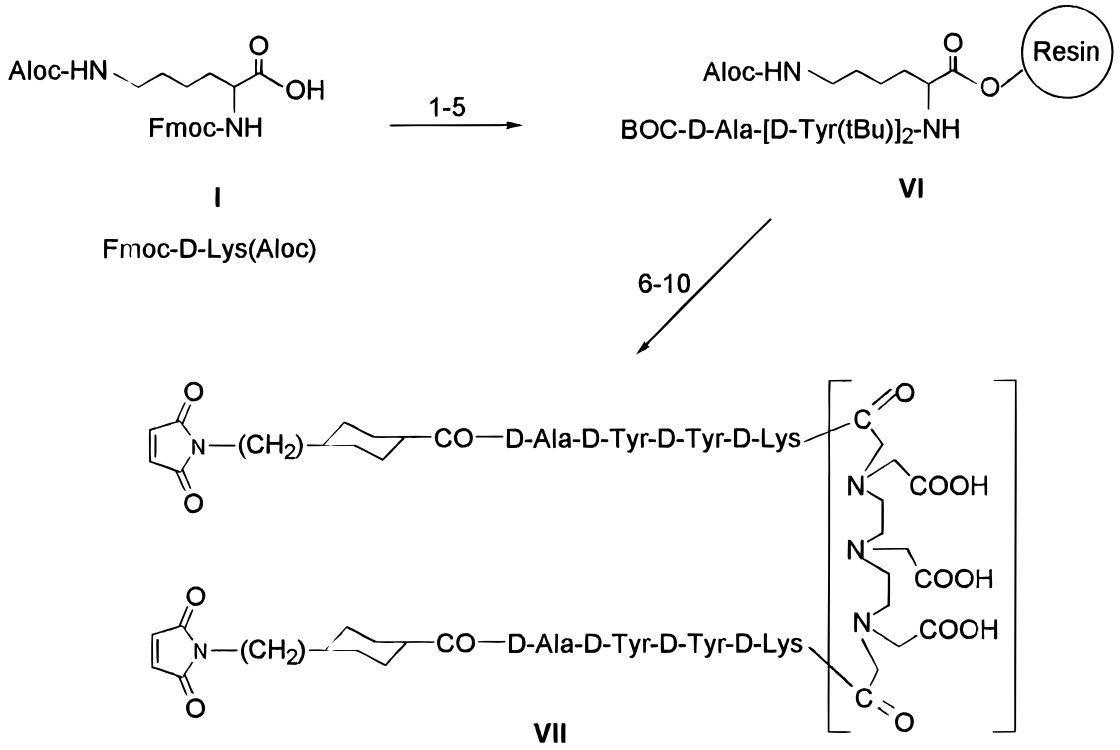


[a] (1) 2-Chlorotrityl chloride resin, DIEA, CH_2Cl_2, 18 h; (2) 20% piperidine/DMF; (3) Fmoc-D-Tyr(tBu), activated with HOBt and DIC, DIEA, step 2; (4) BOC-Gly, activated with HOBt and DIC, DIEA; (5) $[(C_6H_5)_3P]_4Pd$, Bu_3SnH; (6) 1:1:8 HOAc/CF_3CH_2OH/CH_2Cl_2, 3% TFA; (7) ITC-Bz-DTPA, pH 8.5; (8) TFA; (9) sulfo-SMCC, pH 7.0−7.2, 1 h.

romethane (5 mL) and mixed with DIEA (0.55 mL). The solution was mixed with 0.5 g of 2-chlorotrityl chloride resin at room temperature for 18 h. The resin was filtered, washed with solvents, and dried in a stream of nitrogen. The rest of the steps for the synthesis of resin-bound BOC-Gly-D-Tyr(tBu)-D-Lys(Aloc) followed standard Fmoc protocol (*20*, *21*) utilizing, sequentially, Fmoc-D-tyrosine(tBu) and BOC-glycine. The Aloc protecting group was removed by adding a solution of 0.1547 g of tetrakis-(triphenylphosphine)palladium(0) in a mixture consisting of dichloromethane (40 mL), acetic acid (2 mL), and DIEA (5 mL), followed by the addition of tributyltin hydride (5 mL). After 1 h, the filtered resin was washed with solvents, dried, and treated with 10 mL of 1:1:8 acetic acid/trifluoroethanol/dichloromethane, containing 3% TFA, for 1 h. The peptide, cleaved from the resin, was collected by filtration of the reaction mixture. Solvent removal furnished the protected peptide **III** as a gummy material which was essentially pure as determined by HPLC (>95%), and was used as such. It had a retention time (HPLC) of 7.10 min. The electrospray mass spectrum exhibited an M + H peak at *m/e* 523 (positive ion mode) and an M − H peak at *m/e* 521 (negative ion mode). This product (53 mg, 0.1 mmol) was derivatized with ITC-Bz-DTPA (0.2 mmol) in water (pH 8.5) at 37 °C for 4 h. HPLC analysis indicated ~65% conversion. Preparative purification via reverse-phase HPLC furnished 30 mg of the precursor of **IV** as a colorless solid. It had a retention time (HPLC) of 7.54 min. The mass spectrum exhibited an M + H peak at *m/e* 1063 (positive ion mode) and an M − H peak at *m/e* 1061 (negative ion mode). This material was then treated with 0.8 mL of a mixture consisting of TFA (2 mL), dichloromethane (0.5 mL), 0.12 mL of 1:3 (v/v) ethanedithiol/anisole, and 0.06 mL of water and the mixture stirred for 1 h at room temperature, and the product (**IV**, >98% pure as determined by HPLC) was precipitated with diethyl ether. It had a retention time (HPLC) of 5.31 min. Mass spectrum: M + H at *m/e* 907, M − H at *m/e* 905. Exact mass: calcd for M + Na 929.3327, found 929.3370 (mass spectrum). Amino acid analysis, found (expected): Gly, 1.05 (1); Tyr, 0.92 (1); Lys, 0.95 (1). The intermediate **IV** (25 mg) was reacted with a 5-fold molar excess of sulfo-SMCC in 0.1 M sodium phosphate (pH periodically adjusted to be in the range of 7.0−7.2) for 1 h. The reaction proceeded with ~50% efficiency (HPLC). Preparative reverse-phase HPLC yielded IMP-R1 (**V**). It had a retention time (HPLC) of 6.36 min. Electrospray mass spectrum: M+H at *m/e* 1126 (positive ion mode) and M−H at *m/e* 1124 (negative ion mode). Additionally, the mass spectra exhibited peaks at *m/e* 1186 and 1184 in the two ion modes, respectively, which were about 30% of the intensity of the main mass peak (see Results and Discussion). Exact mass: calcd for M + H 1126.4423, found 1126.4381 (mass spectrum). A repetition of the last step using >95% pure sulfo-SMCC gave IMP-R1 whose mass spectrum showed a negligible peak at *m/e* M + H + 60.

Synthesis of IMP-R2 (Scheme 2). The resin-bound Fmoc-D-Lys(Aloc) was elaborated to **VI** via treatment with two successive D-tyrosine(tBu) units followed by BOC-D-alanine. After the Aloc group removal, the ϵ-amine at the C-terminus of the resin-bound peptide was reacted with a 6-fold molar excess of CA-DTPA in DMF, added in portions over the course of 1 h. After workup involving filtering and washing the resin with solvents, the final peptide was cleaved from the resin under mild acidic conditions. The product was purified by preparative reverse-phase HPLC. Cleavage of BOC and tBu protecting groups using TFA/dichloromethane/anisole produced the precursor to the title compound. It had a retention time (HPLC) of 5.44 min. Electrospray mass spectrum: *m/e* 1445 (M + H). Exact mass: calcd for M + Na

Scheme 2[a]



[a] (1−3) Steps 1−3 of Scheme 1; (4) step 3 of Scheme 1; (5) BOC-D-Ala, activated with HOBt and DIC, DIEA; (6 and 7) steps 5 and 6 of Scheme 1; (8) DTPA dianhydride, DMF, Et_3N; (9 and 10) steps 8 and 9 of Scheme 1.

1466.6456, found 1466.6489 (mass spectrum). Amino acid analysis, found (expected): Ala, 2.10 (2); Tyr, 3.69 (4); Lys, 2.22 (2). This intermediate was further derivatized with a 10-fold excess of sulfo-SMCC as described previously. Purification by preparative reverse-phase HPLC yielded IMP-R2 (**VII**). It had a retention time (HPLC) of 6.99 min. Electrospray mass spectrum: *m/e* 1883 (M + H). In addition, a peak at *m/e* 1943 (M + H + 60) was observed (see Results and Discussion). Reaction yields were estimated by HPLC analyses of reaction mixtures. The precursor to the DTPA-coupled peptide was obtained in >95% yield, and the coupling to CA-DTPA gave ~80% yield; the TFA deprotection proceeded in >95% yield, and the final derivatization with sulfo-SMCC resulted in ~40% conversion.

Stock aqueous solutions (0.75−1.24 mM, pH 5.6) of the peptides were aliquoted in several vials and stored frozen (−80 °C). For radioiodinations, 5−7 μL (~6 nmol) of the peptide solution was used.

Radioiodination and Conjugation to mAb-SH. *DTT Reduction of mAbs.* Intact IgG of LL2 (0.55 mL, 13 mg/mL) or RS7 (0.55 mL, 9 mg/mL) was mixed with 0.55 mL of 0.1 M sodium phosphate (pH 7.0), 0.11 mL of 0.5 M sodium borate buffer (pH 8.5), and 6 μL of a freshly prepared DTT solution (2.6 M). The solution was purged with argon to exclude the presence of air, incubated at room temperature for 30 min, and purified with centrifugation SEC (*22*) on two successive 3 mL columns of Sephadex G50/80 in 0.1 M sodium phosphate (pH 6.6). Another method involved mixing 0.1 mL of IgG (8−10 mg/mL) with 6 μL of 0.1 M aqueous EDTA (pH 7) and 6 μL of 40 mM DTT, purging with an inert gas such as argon, incubating at 37 °C in a water bath for 40−50 min, and purifying as described above.

Iodogen Method. Twenty microliters of a diluted solution of PBS [0.8 mL of water and 0.02 mL of 0.5 M PBS (pH 7.5)] was added to 3−5 μL of $Na^{125}I$ (2 mCi) in the activity vial. Buffered $Na^{125}I$ was transferred into a septum-sealed 1 mL vial containing the peptide solution (5−7 μL, 6 nmol) and a coating of iodogen (60 μg). The vial was shaken every 5 min for 20−30 min, and the solution was syringed out into a second septum-sealed vial containing a (4-hydroxyphenyl)acetic acid solution (40 mM, 1.5 μL). After 2−5 min, DTT-reduced antibody (0.5 mg) was added and the vial contents were incubated for a further 40 min. [Although DTT reduction was carried out on ~1−7 mg scale for convenience, only a small portion was used for conjugating to radioiodinated IMP-R1 or -R2.] The rest of the processing and purification were as described below for the chloramine-T method.

Chloramine-T (CT) Method. To $Na^{125}I$ (2 mCi) in the activity vial were added PBS (0.5 M, pH 7.5, 20 μL), a peptide solution (5−7 μL, 6 nmol), and aqueous chloramine-T (4.4 mM, 20 μL). After 1−2 min, piperidine (14 mM, 20 μL), (4-hydroxyphenyl)acetic acid (5 mM, 20 μL), and potassium iodide (5 mM, 20 μL), each in water or 50 mM sodium phosphate (pH 7.5), were added sequentially, and the mixture was incubated for 1 min. Reduced IgG (0.2−0.5 mg) was then added, and the mixture was incubated for 20−30 min. Finally, aqueous sodium tetrathionate (50 mM, 20 μL) was added and the mixture incubated for 5 min. The iodination mixture was diluted with 0.25 mL of a solution of 40 mM PBS/10 mM sodium iodide, containing 0.02% sodium azide and 0.1% gelatin (pH 7.0), and transferred onto a 3 mL size-exclusion column of Sephadex G50/80 equilibrated in 50 mM PBS (pH 7.0). The vial was further rinsed, and the rinse was also transferred. Purification was carried out via centrifugation SEC.

Radiolabelings of mAbs with ^{111}In, [^{125}I]DLT, and $^{125/131}I$ (CT Method). These labelings were carried out as reported (*9*, and references therein). For ^{111}In labelings, conjugates of RS7 and LL2 intact mAbs with ITC-Bz-DTPA were used, unless otherwise stated.

Immunoreactivity (IMR). Comparisons of IMRs of the various RS7 preparations were carried out via a direct cell binding assay as described previously (*18*). Antigen-expressing cells (typically ME180 cells) were washed with PBS (Dulbecco's PBS without calcium and magnesium), and the cell suspension (100 μL) was mixed with labeled mAb (~50000 cpm) and 25 μL of either an unlabeled irrelevant mAb or an unlabeled specific mAb (RS7). A minimum of a 100-fold excess of unlabeled mAb was used. After incubation for 1 h at 4 °C with shaking, the mixture was diluted with PBS containing 1% horse serum, cells were pelleted for 5 min at 400*g*, and the amount of radioactivity associated with the pellet was counted. Data from triplicate experiments were computed as average percentages of specific bindings. Results obtained at two or three cell concentrations were compared to determine if a plateau of mAb excess had been reached.

In Vitro Antibody Retention Experiments. These studies were carried out as described in detail in published work (*6, 9*). Raji, Calu-3, and ME180 cell lines were grown in RPMI 1640 medium (Gibco, Grand Island, NY) supplemented with 5% fetal bovine serum, 5% horse serum, penicillin, streptomycin, glutamine, and sodium pyruvate (Gibco). All incubations were carried out in tissue culture medium at 37 °C. Confluent cells in 96-well plates were incubated with 5×10^5 cpm of labeled antibody for 2 h and then washed four times with media by centrifugation. Tissue culture medium (0.2 mL) was added, and incubation was continued for specified times as indicated in the Results. Cells remained viable for at least 3 days. At indicated times, 0.1 mL of the medium was removed, and after washing via centrifugation, the cells were solubilized with 2.0 M NaOH to determine the amounts of cell-bound radioactivity. After the total counts per minute were determined in the culture medium, iodinated mAbs were precipitated with 5 mL of cold 10% trichloroacetic acid, the indium samples were precipitated with 10 mL of methanol with the use of 1.0 mg of bovine IgG as a carrier protein, and the precipitates were collected by centrifugation. The amounts of precipitable radioactivity and soluble radioactivity in the supernatant were thus determined. The extents of antigen-specific bindings, determined by adding a large excess of unlabeled specific mAbs (50 μg/mL) in control wells, were >90%. Each mAb processing experiment was carried out in triplicate unless otherwise stated.

RESULTS

Solid-phase peptide syntheses were carried out utilizing a standard Fmoc strategy (*20, 21*). The functional group-protected peptide was assembled on the 2-chlorotrityl chloride resin; the Aloc group was selectively deprotected by a Pd(0)-mediated reaction (*23*), and the peptide was cleaved from the resin under mild acidic condition. This was followed by the derivatization of the lysine side chain, the cleavage of BOC and tBu groups, and finally the reaction of the amine terminus with sulfo-SMCC. Differential protections of the ϵ-amine of D-lysine and the peptide's N-terminus, with Aloc and BOC protecting groups, respectively, which were cleaved under different conditions, enabled differential derivatizations of the amines. The methods used for peptide bond formation are known to cause negligible racemization (*21*).

The intermediates prior to SMCC derivatization, in both IMP-R1 and IMP-R2, were characterized by electrospray mass spectra, by exact mass analyses, by high-resolution mass spectrometry, and by amino acid analyses. After derivatization with the cross-linker, both the bifunctional substrates exhibited M + H + 60 peaks (estimated to be 30%) in the electrospray mass spectra in addition to the expected mass peaks, as a result of an impurity (M + 60) present at the same level in the particular lot of sulfo-SMCC used.[3] This suggested that in the particular lot of the cross-linker used, perhaps the maleimide group's functional purity was compromised by a 1,4-addition of acetic acid, or some other entity with a molecular mass of 60 Da, to the same.[3] The consequence of the presence of a M + 60 side product is in the lowering of the observed overall radioiodination−conjugation yield, but does not otherwise affect the utility aspect of the radiolabeled conjugates. The preparation of IMP-R1 was repeated when >95% pure sulfo-SMCC (including maleimide purity) was made available from a different commercial source. As expected, the mass spectrum of this preparation of IMP-R1 exhibited only a negligible level of the previously seen impurity.

Disulfide reduction was carried out using DTT. Reduced IgGs (3.8−5.6 mg/mL) were estimated to contain 8.84 thiols (for LL2) and 8.95 thiols (for RS7) per IgG molecule by Ellman's assay (*24*), corresponding to the breakage of four disulfide bonds. Under a variety of conditions, using up to 250 molar equiv of DTT, 8−9 thiols per IgG were produced (not shown). Using 2-mercaptoethanol, the number of thiol groups produced per IgG was 4−5, but the final radioiodinated mAbs derived thereof were not different from those derived from the DTT-reduced IgGs in terms of in vitro and in vivo characteristics (not shown).

Radiolabeling consisted of peptide radioiodination and subsequent conjugation to reduced IgG. Only the combined yield of the radioiodination and the conjugation steps (overall yield) was determined routinely. Overall yields were based on the amount of radioactivity recovered after purification by centrifugation SEC. The radioactive material obtained after purification was determined to be the relevant mAb, based on the retention time on analytical SE-HPLC. In a few cases where the HPLC analyses showed the presence of a slower-eluting component (low-molecular mass entity, such as a labeled peptide not completely removed by the purification method, usually <5%), overall yields were appropriately corrected. Specific activities were calculated from the amount of radioactivity in the purified final material and the antibody content in the same. The latter was derived from the amount of mAb used, and correcting for the customary loss of ~5% of the protein on the size-exclusion column. On a few occasions, we also determined the peptide radioiodination yields by analytical size-exclusion HPLC. The HPLC sample consisted of an aliquot of radiolabeling mixture prior to quenching with (4-hydroxyphenyl)acetic acid, which was treated with sodium metabisulfite to reduce reactive iodine to sodium iodide. Panels A and B of Figure 1 show the results from size-exclusion radio-HPLC analyses of $Na^{125}I$ and the reaction mixture of [125I]IMP-R1 radioiodination, respectively. Areas under the broad peptide peak and the sodium iodide peak in the HPLC chromatogram of IMP-R1 radioiodination (Figure 1B) are seen integrated in a 7:3 ratio, indicating a 70% incorporation of radioiodine in the peptide. The mAb conjugation yield was not determined separately, but was computed from the overall and radioiodination yields. For instance, a high overall yield

[3] The supplier concurred with our finding about the specific product lot (communication of April 14, 1998). A conversation with the supplier indicated that that lot of the material contained acetate.

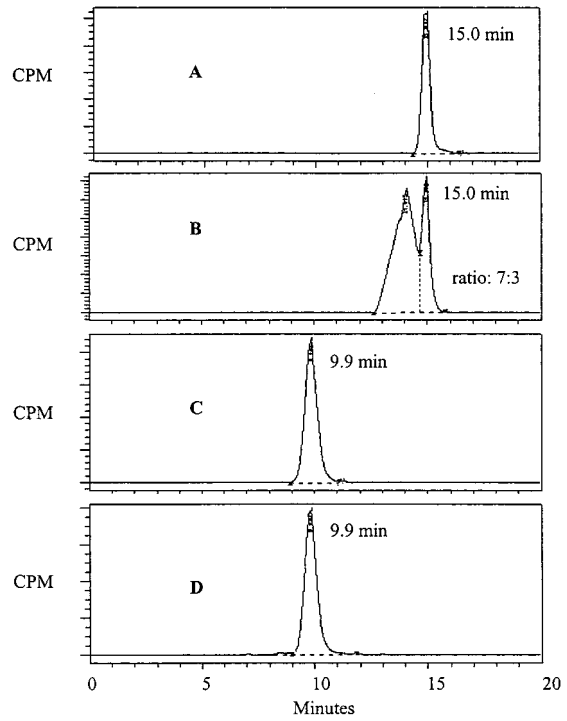


Figure 1. Analytical size-exclusion HPLC analyses, with radiomatic detection, of representative radioiodinations. (A) $Na^{125}I$. (B) [^{125}I]IMP-R1 radioiodination mixture (chloramine-T method), treated with sodium metabisulfite. Although a baseline separation is not achieved, the sodium iodide peak can be distinguished from the broad peptide peak. (C) Purified [^{125}I]-IMP-R1−RS7. (D) Purified [^{125}I]IMP-R2−RS7.

(74−89%), when IMP-R2 was used, implied a minimum average of 85% yield for each of the two steps. Panels C and D of Figure 1 display radio-HPLC traces of purified [^{125}I]IMP-R1−RS7 and [^{125}I]IMP-R2−RS7, respectively. The recoveries from the HPLC columns were judged to be good, based on empirical correlations of the amounts of radioactivity injected onto the HPLC column with the millivolt outputs, and comparing the same with historical data. In one instance, the actual recovery, as determined for purified [^{125}I]IMP-R1−RS7, was quantitative.

Table 1 contains incorporations, specific activities, and levels of aggregation (determined from HPLC) for representative labelings of LL2 and RS7 mAbs which are the internalizing mAbs of focus in this study. Table 1 also gives two entries (14 and 15) of data obtained with a CEA mAb, MN-14 (*25*), and LL1 which is another internalizing anti-lymphoma mAb (*26*), to demonstrate the generality of the labeling method. The control experiment (entry 16) served to ensure that, when the described procedures were used, nonspecific labeling of mAb was negligible (less than 0.5%) when the peptide was not present. The data in Table 1 fall into three distinct patterns. (i) When iodogen was used for the radioiodination of IMP-R1, the overall yield was 21−30% (entries 1−4). (ii) The CT-mediated labeling of IMP-R1 offered better overall labeling yields (32−44%) at specific activities of 1.7−2.0 mCi/mg (entries 5−9). (iii) The CT-mediated iodination of IMP-R2 gave much enhanced yields and specific activities (>74% yield, 5−11 mCi/mg; entries 10−15). The level of aggregation was usually less than 2%. A level of aggregation of about 5% was seen in some initial LL2 labelings with [^{125}I]IMP-R1 using the iodogen method, but this was not observed subsequently (not shown).

In a single radiolabeling of RS7 carried out with a newer preparation of IMP-R1 (the latter prepared using >95% pure sulfo-SMCC), an overall yield of ∼42% was achieved with a doubling of the specific activity from 2 to 4 mCi/mg.

Table 1. Overall Incorporations, Specific Activities, and Aggregate Content of Purified [^{125}I]IMP-R1/R2−mAb-SH Conjugates for Representative Labelings[a]

	substrate	mAb-SH	mCi used	% yield[b]	mCi/mg[c]	% aggregation[d]
1[e]	IMP-R1	LL2	1.97	21.2	0.83	0.9
2[e]	IMP-R1	RS7	1.78	24.1	0.85	0.0
3[e]	IMP-R1	RS7	1.32	30.4	0.81	0.0
4[e]	IMP-R1	RS7	1.46	26.6	0.94	0.9
5	IMP-R1	LL2	2.24	43.9	1.98	<2.0
6	IMP-R1	LL2	2.29	32.0	1.77	<2.0
7	IMP-R1	LL2	2.36	37.2	1.85	0.9
8	IMP-R1	LL2	2.24	43.8	2.07	0.0
9	IMP-R1	RS7	2.18	37.6	1.73	0.0
10	IMP-R2	LL2	1.80	74.0	5.10	1.1
11	IMP-R2	LL2	2.58	86.3	5.32	1.8
12	IMP-R2	RS7	1.72	75.0	5.51	1.3
13	IMP-R2	RS7	2.12	80.0	7.25	1.6
14	IMP-R2	MN-14	2.41	85.7	7.25	0.2
15	IMP-R2	LL1	2.00	89.4	11.1	0.6
16	control[f]	LL2	2.09	<0.5	N/A[g]	N/A

[a] Chloramine-T as the oxidant in peptide iodination unless otherwise stated. [b] Overall isolated yield. [c] Specific activity of the purified product. [d] Determined by HPLC analysis. [e] Iodogen as the oxidant in peptide labeling. [f] No peptide was used in this control. [g] N/A, not applicable.

Immunoreactivities (IMRs) of labeled RS7 preparations were determined with a direct cell binding assay (*18*). Representative data of percent average bindings (with <5% variations from the mean, in each case, of triplicate data) were 69.3 and 65.7% for [^{131}I]RS7(conventional label), 78.4 and 72.6% for [^{125}I]IMP-R1−RS7, 72.3 and 58.2% for [^{125}I]DLT−RS7, and 52.1 and 43.9% for [^{111}In]-RS7, with numbers in each set corresponding to binding at 2×10^7 and 1×10^7 cells/mL, respectively. In a separate experiment (with no blocking performed), the percent average bindings from duplicate data were 73.1, 69.4, and 66.3% for the [^{125}I]IMP-R2 label and 75.3, 70.7, and 56.2% for the conventional ^{131}I label, with numbers in each set corresponding to binding at 2×10^6, 1×10^6, and 5×10^5 cells/mL, respectively.

Results from in vitro antibody retention experiments are shown in Figures 2−4. In Figure 2A, we compare the processing of [^{125}I]IMP-R1−LL2 with that of [^{125}I]LL2 (CT) by Raji cells. At 45 h, the amount of cell-bound radioactivity for IMP-R1 label was 37.9% of the initially bound value, which was 2 times that for the conventional (CT) label. Panels B and C of Figure 2 pertain to intact and degraded mAbs in the supernatant, respectively, for the two labels compared. In a different experiment (not shown in the figure), the amounts of Raji cell-retained radioactivity, up to 5 days, were compared for three groups of radiolabeled LL2: (i) [^{125}I]IMP-R1−LL2, (ii) [^{111}In]LL2, prepared by labeling IMP-R1 with ^{111}In acetate, followed by coupling to DTT-reduced LL2, and (iii) [^{125}I/In]IMP-R1−LL2 which was prepared by first labeling LL2 with [^{125}I]IMP-R1, followed by labeling with excess indium acetate (cold). Retentions, expressed as the average of three measurements (with the spread within 5% of the mean), were as follows: for [^{125}I]IMP-R1−LL2, 94.7 (2 h), 66.8 (18.5 h), 63.8 (26 h), 51.1 (48 h), and 35.4% (115 h); for [^{111}In]IMP-R1−LL2, 89.2 (2 h), 69.4 (18.5 h), 68.1 (26 h), 49.8 (48 h), and 34.1% (115 h); and for [^{125}I/In]IMP-R1−LL2, 95.2 (2 h), 66.5 (18.5 h), 59.6 (26 h), 49.0 (48 h), and 33.5% (115 h).

Panels A−C of Figure 3 show the Calu-3 cell binding data for RS7 preparations containing [^{125}I]IMP-R1, [^{125}I]-

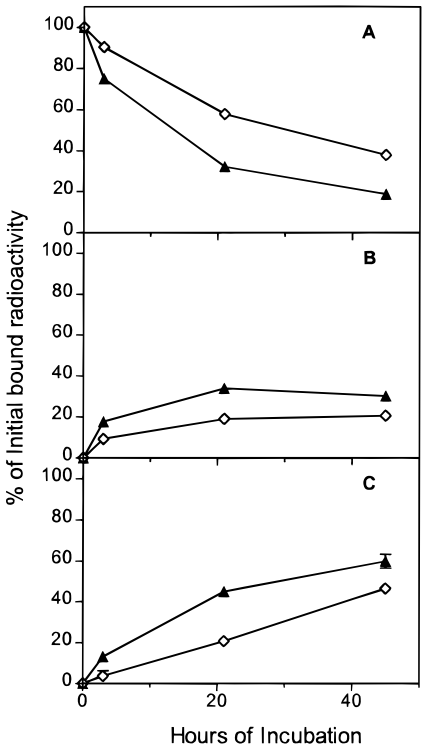


Figure 2. Processing of radiolabeled LL2 bound to Raji cells in vitro. LL2 was labeled with either [125I]IMP-R1 (◇) or 125I by the chloramine-T method (▲). (A) Amount of cell-bound radioactivity in counts per minute. (B) Counts per minute released intact into the supernatant. (C) Counts per minute released degraded into the supernatant. Results shown are average of triplicate data; standard deviations for most data are low and are not readily seen.

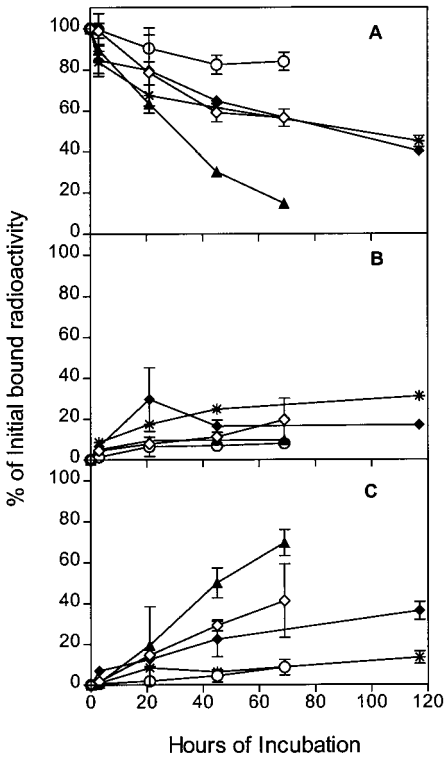


Figure 3. Processing of radiolabeled RS7 bound to Calu-3 cells in vitro. RS7 was labeled with [125I]IMP-R1 (◇), [125I]IMP-R2 (*), [125I]DLT (◆), [111In]benzyl-DTPA (○), or 125I by the chloramine-T method (▲). (A) Amount of cell-bound radioactivity in counts per minute. (B) Counts per minute released intact into the supernatant. (C) Counts per minute released degraded into the supernatant. Results shown are means ± standard deviations of triplicate data.

IMP-R2, [125I]DLT, conventional 125I and 111In labels. Figure 3A shows that at 69 h, the amount of cell-bound radioactivity of the IMP-R1 label is 46% of the amount of the initially bound radioactivity, which is 3 times that of the 14.7% observed for the conventional (CT) label. The tumor cell retentions of the residualizing radioiodine labels derived from IMP-R1, IMP-R2, and DLT are similar and are markedly better than that of the conventional label. The 111In label is seen to be somewhat better than the residualizing iodine labels in this set of experiments.

Panels A−C of Figure 4 show the comparisons of [125I]-IMP-R1, [125I]IMP-R2, [125I]DLT, 125I (CT), and [111In]-benzyl-DTPA labels in the ME180 cell line. As can be seen, the processing patterns of the 111In label and the IMP-R2- and DLT-based radioiodine labels of RS7 are quite similar, and distinctly different from that of the CT-based iodine label of RS7. The [125I]IMP-R1 label is somewhat less well retained than the other three residualizing labels, although it is still retained twice as well as a conventional iodine label as judged from the 69 h cell-bound counts per minute levels. Both Calu-3 (lung adenocarcinoma) and ME180 (cervical carcinoma) cell lines express RS7 antigens, but the antigen density on ME180 is 3 times that on Calu-3. For in vitro analyses, either cell line is conveniently used (*9*, *18*, *19*).

The stabilities of mAbs, labeled with radioiodinated IMP-R1 and IMP-R2 substrates, in cell culture media were determined by TCA precipitation. This revealed an average loss of label of 3%/day and 1%/day, when IMP-R1 and IMP-R2 methods are used, respectively, in various culture media (data not shown).

DISCUSSION

The lysosomal processing of mAbs to the level of amino acids results in the escape of the conventional iodine label of mAbs in the form of iodotyrosine (*5*, *27*). Since the particular label would not be expected to alter the metabolic pathway of mAb itself, it can be concluded that mAbs carrying residualizing labels are likewise processed to the level of amino acids and that the lysosomal retention of residualizing labels must be in the form of low-molecular mass catabolites. It has been suggested (*8*) that carbohydrate-based residualizing labels, such as iodo-TCB or iodo-DLT, are lysosomally trapped because these (i) cannot be digested by lysosomal hydrolases, (ii) are relatively large in size, with molecular masses of >500 Da, and (iii) are hydrophilic. All these factors collectively render the label membrane-impermeable. In the case of metal−DTPA conjugates of mAbs, the final catabolite, metal−DTPA−lysine (*14*), is also a residualizing label for the same reasons. Designing a residualizing radioiodine label modeled on metal−DTPA, as described herein, is attractive in that the DTPA molecule provides polar groups, hydrophilicity, and a size contribution.

It is evident that many other types of residualizing radioiodine labels could be created, which may be functionally similar to those described in this report. The key requirement is that the putative metabolite containing the residualizing label meets the requisite criteria (*8*) for membrane impermeability. We have not yet determined which features of our labels are essential for residualization. More specifically, we do not know if DTPA is a requirement, since certain peptides composed of D-amino acids would probably be effective residualizing labels

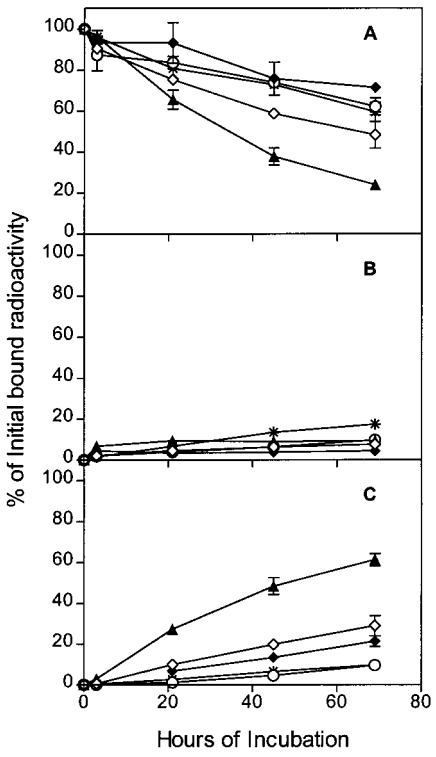


Figure 4. Processing of radiolabeled RS7 bound to ME180 cells in vitro. RS7 was labeled with [^{125}I]IMP-R1 (◇), [^{125}I]IMP-R2 (*), [^{125}I]DLT (◆), [^{111}In]benzyl-DTPA (○), or ^{125}I by the chloramine-T method (▲). (A) Amount of cell-bound radioactivity in counts per minute. (B) Counts per minute released intact into the supernatant. (C) Counts per minute released degraded into the supernatant. Results shown are means ± standard deviations of triplicate data.

themselves. Likewise, we do not know how many amino acids, conjugated to DTPA, are required to achieve good retention; it is possible that tyrosine alone would be sufficient. Considering that many of the residualizing labels are retained intracellularly to similar extents, we did not find a need to further optimize the label design. Rather, our primary goal was to solve the problems that have inhibited the use of the previous residualizing iodine labels for RAIT, namely, low iodination efficiency and low specific activity, and this was achieved. One question is whether iodo-D-tyrosine, coupled to mAbs, can itself be a residualizing label. It is known that iodo-D-tyrosine and iodotyramine are less efficient substrates than iodo-L-tyrosine for the enzyme deiodinase (*28*). However, many studies have clearly demonstrated that the metabolism of mAbs to the level of amino acids is the major factor contributing to reduced retention of internalized radioiodinated mAbs in the tumor, with deiodination playing a minor role, if any (*5*, *27*−*29*). Therefore, if iodinated D-tyrosine is used as a label for mAbs, protein catabolism in lysosomes may also lead to the escape of iodo-D-tyrosine through the lysosomal membrane.

Once the enhanced retention of the [^{125}I]IMP-R1 label was established, we attempted to further improve the mAb radioiodination yields by increasing the tyrosine and the maleimide contents in the peptide. In this respect, the DTPA dianhydride (CA-DTPA) reagent presented an opportunity to readily introduce multiple tyrosines and maleimides on the peptide template. All that was needed was synthesis of a tetrapeptide containing two tyrosines and linking the same to both ends of CA-DTPA, and this was the basis for the preparation of IMP-R2. In fact, the use of IMP-R2, which is also a residualizing label, resulted in substantially higher yields and specific activities of radioiodinated mAbs (Table 1). The type of attachment of DTPA to lysine was not expected to influence residualization, since previouly published work had shown that metalated DTPA−mAb conjugates with either thiourea (*27*) or amide (*14*) bonding of DTPA to mAb lysines generated effective residualizing labels.

Disulfide-reduced mAbs are frequently used for site-specific conjugations since this method offers several advantages, including a minimal impact on immunoreactivity (*30*). IgG_1 and IgG_{2a} classes are known to possess four interchain disulfide bonds and numerous intrachain disulfide bonds, and the interchain bonds are held together by noncovalent forces in addition to the four disulfide bonds (*31*). The intrachain disulfides are inaccessible to reduction by thiol-containing agents even when a high molar excess of the reductant is used. With an up to 250-fold excess of DTT, the cleavage of only four disulfide bonds, corresponding most likely to the four interchain disulfides, is found to occur with the Ellman's assay in this study. This is similar to the results reported for mAb BR96 (*30*). The mAb is found to retain its molecular structure even after the reduction of the four interchain disulfide bonds, as evidenced by SE-HPLC analyses in this study and by SE-HPLC and nondenaturing SDS−PAGE analyses in the work of Willner et al. (*30*).

In initial experiments, the peptide was radioiodinated using iodogen as the oxidant, but this procedure was subsequently replaced by the use of chloramine-T (CT) radioiodination. This resulted in a simpler one-vial method, reduced the process time, and increased the overall yield. To minimize potential damage to the antibody due to CT, piperidine (a secondary amine) was added prior to the conjugation step so that the amine, not the reactive groups in the antigen binding region of the mAb, was chlorinated (*32*). Peptide radioiodination by either iodogen or CT methods led to mAb products which behaved similarly in vitro and in vivo (not shown), but the shorter duration of the CT method improved the conjugation yield, possibly by limiting the degradation of the maleimide group at the labeling pH of 7.5.

The lack of significant aggregation in these radiolabelings, particularly when substrate IMP-R2 was used, is interesting. Substrate IMP-R2 offers the opportunity to cross-link thiol groups from two mAb molecules. Intermolecular cross-linking is possibly inhibited by unfavorable stereoelectronic factors. Also, SDS−PAGE analyses indicated the absence of mAb interchain cross-linking by the two maleimide groups of IMP-R2 (not shown).

Antibody immunoreactivity (IMR) is known to be only minimally affected by the method of conjugation to hinge-region cysteines (*30*). Indeed, IMRs of all radiolabeled RS7 preparations were very similar. Although IMR determinations were not carried out with LL2 preparations, the strong binding seen in the in vitro cell binding experiments as well as in in vivo targeting experiments (not shown) was indicative of the preservation of IMR of LL2 labeled by radioiodinated IMP-R1 or IMP-R2.

The better cellular retention of indium versus residualizing radioiodine labels ([^{125}I]DLT, [^{125}I]IMP-R1, and [^{125}I]IMP-R2) on RS7 in the Calu-3 cell bindings (Figure 3) appears to be contrary to our earlier findings of the similarity of [^{125}I]DLT and [^{111}In]Bz-DTPA labels in vitro and in vivo (*9*). The explanation of this discrepancy must await further experimentation. In the ME-180 cell bindings, however, [^{125}I]IMP-R2, [^{125}I]DLT, and [^{111}In]Bz-DTPA labels on RS7 were seen to be processed similarly,

with the [125I]IMP-R1 label being released somewhat faster. The residualizing iodine labels were retained significantly better than a conventional iodine label in both cell lines. In this study, we have not directly determined either the form in which radiolabels were retained by cells or the subcellular site at which they were retained. However, it can be logically expected that the low-MW lysosomal catabolites in this work would be similar to those in other documented studies (*14*, *27*), and are very likely to contain the iodo-D-Tyr-D-Lys(DTPA) residue.

It must be pointed out that TCA precipitation of supernatants in cell binding studies effectively distinguishes between intact and degraded mAb, with a radioiodine label produced by the chloramine-T method, but with the [I]IMP-R2 label, some of the degradation products are also likely to be precipitated, as indicated by partial precipitation (~25%) of the cysteine adduct of IMP-R2, prepared as a control. In this case, TCA precipitation provides a minimum estimate of the extent of degradation, and an overestimate of the amount of mAb released intact; therefore, the amount of cell-bound radioactivity, as well as the amount of total radioactivity released into the supernatant, provides the most reliable indication of retention. Whether this is also the case with the IMP-R1 label remains to be determined, although the profiles of the intact and the degraded forms of radioactivity released into the supernatant when IMP-R1 is used suggest that the degraded form of the radioactivity is probably not precipitable.

The question of whether a metal (such as indium)−DTPA, rather than unchelated DTPA, should be part of the DTPA−peptide structure was addressed in one of our early experiments. We examined IMP-R1 labeled with 125I alone, with 125I and cold indium acetate, and with 111In acetate. Each of these IMP-R1 radiolabels was conjugated to disulfide-reduced LL2, and the processing by Raji tumor cells in vitro was studied. The tumor cell retentions were almost identical in all three cases. This implied that incorporation of indium in the label design was not a prerequisite for residualization to occur, perhaps because the metal ions present inside the cells or in the medium were themselves available for chelation by the DTPA substructure of the peptides.

In the in vitro studies, we did not examine directly the internalization of the mAb, but rather the retention of the radiolabel which is a function of both internalization and catabolism. Clearly, it is the accumulation of radiolabel in the target cell that is the major consideration for RAIT. Moreover, methods commonly used to assay mAb internalization appear to be unreliable when some residualizing radiolabels are used, as the following example suggests. Lymphoma tumor cells, bound by the labeled mAb [125I]DLT−LL1, were extracted at low pH (under conditions used for extraction of surface-bound mAb) 21 h after mAb binding to the cell surface, a time when virtually all of the mAb had been catabolized (*26*) and the retained radiolabel colocalized with lysosomes (*33*). We found that the majority of the label, shown to be low-MW degradation products by TCA precipitation, was extracted from the cells by treatment with pH 2.0 or 2.5 buffers.[4] Some of the low-pH buffers also caused death of more than half the cells, as determined by exclusion of trypan blue. While cell death could of course allow the release of an intracellular label, we noted that one of the buffers that did not cause substantial cell death still extracted the majority of the [125I]DLT from its intracellular site. We conclude that low-pH treatment may extract intracellular material from cells, possibly by cell toxicity.[4]

In summary, the yield and the specific activity levels obtained in mAb radioiodinations using IMP-R1 and IMP-R2, as well as the enhanced tumor cell retentions observed in in vitro experiments, bode well for the DTPA−peptide approach in the design of residualizing radioiodine. However, the particular choice of the radioiodinating agent for RAIT is not necessarily restricted to these substrates. This flexible peptide approach can be adapted to the synthesis of a number of bifunctional substrates differing in the tyrosine content, the maleimide content, the number of amino acids, and the mode of attachment to DTPA, to maximize mAb radioiodination yields as well as therapeutic indices in in vivo applications. Progress along these lines, together with the details of a series of paired-label in vivo experiments involving RS7 and LL2 mAbs labeled with IMP-R1, IMP-R2, DLT and conventionally (CT method) based radioiodine labels, will be described elsewhere.

[4] M. J. Mattes, unpublished data.

ACKNOWLEDGMENT

We are grateful to Mr. Joseph Donnelly, Ms. Gaik L. Ong, Ms. Susan Chen, and Ms. Hong Xuan for assistance with in vitro cell binding experiments. This work was supported in part by U.S. Public Health Service Outstanding Investigator Grant CA 39841 (D.M.G.), U.S. Public Health Service Grant CA 60039 (R.S.), and SBIR Grant CA 72324 (S.V.G.) from the National Institutes of Health.

LITERATURE CITED

(1) Goldenberg, D. M. (1993) Monoclonal antibodies for cancer detection and therapy. *Am. J. Med. 94*, 297−312.
(2) Knox, S. J. (1995) Overview of studies on experimental radioimmunotherapy.*Cancer Res. 55*, 5832s−5836s.
(3) Buchsbaum, D. J. (1995) Experimental approaches to increase radiolabeled antibody localization in tumors. *Cancer Res. 55*, 5729s−5732s.
(4) Mattes, M. J., Griffiths, G. L., Diril, H., Goldenberg, D. M., Ong, G. L., and Shih, L. B. (1994) Processing of antibody-radioisotope conjugates after binding to the surface of tumor cells. *Cancer 73*, 787−793.
(5) Geissler, F., Anderson, S. K., Venkatesan, P., and Press, O. (1992) Intracellular catabolism of radiolabeled anti-μ antibodies by malignant B-cells. *Cancer Res. 52*, 2907−2915.
(6) Kyriakos, R. J., Shih, L. B., Ong, G. L., Patel, K., Goldenberg, D. M., and Mattes, M. J. (1992) The fate of antibodies bound to the surface of tumor cells *in vitro*. *Cancer Res. 52*, 835−842.
(7) Strobel, J. L., Baynes, J. W., and Thorpe, S. R. (1985) 125-I-Glycoconjugate labels for identifying sites of protein catabolism in vivo: Effect of structure and chemistry of coupling to protein on label entrapment in cells after protein degradation. *Arch. Biochem. Biophys. 240*, 635−645.
(8) Thorpe, S. R., Baynes, J. W., and Chroneos, Z. C. (1993) The design and application of residualizing labels for studies of protein catabolism. *FASEB J. 7*, 399−405.
(9) Stein, R., Goldenberg, D. M., Thorpe, S. R., Basu, A., and Mattes, M. J. (1995) Effects of radiolabeling monoclonal antibodies with a residualizing iodine radiolabel on the accretion of radioisotope in tumors. *Cancer Res. 55*, 3132−3139.
(10) Ali, S. A., Warren, S. D., Richter, K. Y., Badger, C. C., Eary, J. F., Press, O. W., Krohn, K. A., Bernstein, I. D., and Nelp, W. B. (1990) Improving the tumor retention of radioiodinated antibody: Arylcarbohydrate adducts. *Cancer Res. 50*, 783s−788s.
(11) Stein, R., Goldenberg, D. M., Thorpe, S. R., and Mattes, M. J. (1997) Advantage of a residualizing iodine radiolabel for radioimmunotherapy of xenografts of human non-small-cell carcinoma of the lung. *J. Nucl. Med. 38*, 391−395.

(12) Mattes, M. J., Shih, L. B., Govindan, S. V., Sharkey, R. M., Ong, G. L., Xuan, H., and Goldenberg, D. M. (1997) The advantage of residualizing radiolabels for targeting B-cell lymphomas with a radiolabeled anti-CD22 monoclonal antibody. *Int. J. Cancer 71*, 429−435.
(13) Reist, C. J., Garg, P. K., Alston, K. L., Bigner, D. D., and Zalutsky, M. R. (1996) Radioiodination of internalizing monoclonal antibodies using N-succinimidyl 5-iodo-3-pyridinecarboxylate. *Cancer Res. 56*, 4970−4977.
(14) Franano, F. N., Edwards, W. B., Welch, M. J., and Duncan, J. R. (1994) Metabolism of receptor targeted ^{111}In-DTPA-glycoproteins: Identification of ^{111}In-DTPA-ϵ-lysine as the primary metabolic and excretory product. *Nucl. Med. Biol. 8*, 1023−1034.
(15) Stein, R., Belisle, E., Hansen, H. J., and Goldenberg, D. M. (1993) Epitope specificity of the anti-B-cell lymphoma monoclonal antibody, LL2. *Cancer Immunol. Immunother. 37*, 293−298.
(16) Pawlak-Byczkowska, E. J., Hansen, H. J., Dion, A. S., and Goldenberg, D. M. (1989) Two new monoclonal antibodies, EPB-1 and EPB-2, reactive with human lymphoma. *Cancer Res. 49*, 4568−4577.
(17) Shih, L. B., Lu, H.-Z., Xuan, H., and Goldenberg, D. M. (1994) Internalization and intracellular processing of an anti-B-cell lymphoma monoclonal antibody, LL2. *Int. J. Cancer 56*, 538−545.
(18) Stein, R., Chen, S., Sharkey, R. M., and Goldenberg, D. M. (1990) Murine monoclonal antibodies raised against human non-small cell carcinoma of the lung: specificity and tumor targeting. *Cancer Res. 50*, 1330−1336.
(19) Stein, R., Basu, A., Goldenberg, D. M., Lloyd, K. O., and Mattes, M. J. (1994) Characterization of cluster 13: The epithelial/carcinoma antigen recognized by MAb RS7. *Int. J. Cancer 8* (Suppl.), 98−102.
(20) *Novabiochem Catalog and Peptide Synthesis Handbook* (1997/98) Calbiochem-Novabiochem, Nottingham.
(21) Fields, G. B., and Noble, R. L. (1990) Solid phase peptide synthesis utilizing 9- fluorenylmethoxycarbonyl amino acids. *Int. J. Pept. Protein Res. 35*, 161−214.
(22) Penefsky, H. S. (1979) A centrifuged-column procedure for the measurement of ligand binding by beef heart F1. *Methods Enzymol. 56*, 527−530.
(23) Dangles, O., Guibe, F., Balavoine, G., Lavielle, S., and Marquet, A. (1987) Selective cleavage of the allyl and allyloxycarbonyl groups through palladium-catalyzed hydrostannolysis with tributyltin hydride. Application to the selective protection-deprotection of amino acid derivatives and in peptide synthesis. *J. Org. Chem. 52*, 4984−4993.
(24) Ellman, G. L. (1959) Tissue sulfhydryl groups. *Arch. Biochem. Biophys. 82*, 70−77.
(25) Hansen, H. J., Goldenberg, D. M., Newman, E. S., Grebenau, R., and Sharkey, R. M. (1993) Characterization of second-generation monoclonal antibodies against carcinoembryonic antigen. *Cancer 71*, 3478−3485.
(26) Hansen, H. J., Ong, G. L., Diril, H., Valdez, A., Roche, P. A., Griffiths, G. L., Goldenberg, D. M., and Mattes, M. J. (1996) Internalization and catabolism of radiolabeled antibodies to the MHC class-II invariant chain by B-cell lymphomas. *Biochem. J. 320*, 293−300.
(27) Shih, L. B., Thorpe, S. R., Griffiths, G. L., Diril, H., Ong, G. L., Hansen, H. J., Goldenberg, D. M., and Mattes, M. J. (1994) The processing and fate of antibodies and their radiolabels bound to the surface of tumor cells *in vitro*: A comparison of nine radiolabels. *J. Nucl. Med. 35*, 899−908.
(28) Dumas, P., Maziere, B., Autissier, N., and Michel, R. (1973) Specificite de L'iodotyrosine desiodase des microsomes thyroidiens et hepatiques (Specificities of iodo-L-tyrosine desiodase from thyroid and hepatic microsomes). *Biochim. Biophys. Acta 293*, 36−47.
(29) Waldmann, T. A., and Strober, W. (1969) Metabolism of immunoglobulins. *Prog. Allergy 13*, 1−110.
(30) Willner, D., Trail, P. A., Hofstead, H., King, D., Lasch, S. J., Braslawsky, G. R., Greenfield, R. S., Kaneko, T., and Firestone, R. A. (1993) (6-Maleimidocaproyl)hydrazone of doxorubicin: A new derivative for the preparation of immunoconjugates of doxorubicin. *Bioconjugate Chem. 4*, 521−527.
(31) Stevenson, G. T. (1997) Chemical engineering at the antibody hinge. *Chem. Immunol. 65*, 57−72.
(32) Chen, P., Hussain, A., and Tai, H.-H. (1994) An improved method of radioiodination with chloramine T. *Anal. Biochem. 219*, 159−161.
(33) Karacay, H., Ong, G. L., Hansen, H. J., Griffiths, G. L., Goldenberg, D. M., and Mattes, M. J. (1998) Intracellular processing of ^{99m}Tc-antibody conjugates. *Nucl. Med. Commun. 19*, 971−979.

BC980075G

Design, Synthesis, and Spectroscopic Properties of Peptide-Bridged Fluorescence Energy-Transfer Cassettes

Yanlong Li† and Alexander N. Glazer*

Departments of Chemistry and Molecular and Cell Biology, University of California, Berkeley, California 94720.
Received July 6, 1998; Revised Manuscript Received December 1, 1998

A general partial solid-phase synthetic scheme was developed for the synthesis of energy-transfer cassettes with the donor and acceptor dyes bridged by a peptide. In these cassettes, 6-carboxyfluorescein (Fam) served as a donor. For the second dye, 6-carboxy-X-rhodamine (Rox) was used as a fluorescent acceptor or erythrosin B as a quencher. Different peptides bearing Rox at the amino terminus and Fam linked through different diamines to the carboxyl terminus were synthesized to examine the effects of the chain length and rigidity on energy-transfer efficiency. The ratio of emission intensities at 605 nm of the acceptor dye (ROX) in the cassette Rox-GPPPEPPP-*p*-xylylenediamine-Fam versus free ROX with 488 nm excitation was ~14 and is similar to that obtained for optimized oligonucleotide primers bearing the same dyes [Ju, J., Ruan, C., Fuller, C. W., Glazer, A. N., and Mathies, R. A. (1995) *Proc. Natl. Acad. Sci. U.S.A. 92*, 4347−4351].

INTRODUCTION

In recent years, we have developed sets of fluorescence energy-transfer (ET)[1] primers for DNA sequencing and mapping (reviewed in refs *1* and *2*). In these primers, a donor dye is attached to the oligonucleotide at the 5′ end, and the acceptor is attached to a modified thymidine internal in the primer sequence. ET cassettes are superior to single dye-labeled probes because the large acceptor-dependent Stokes shifts allow excellent rejection of adventitious autofluorescence, Raleigh and Raman scattering at the emission wavelength of the acceptor, and because multiplex assays can be carried out by using sets of labels with a common dye as a donor and different dyes as acceptors. In addition, we have developed a general method to tag primers of any sequence with ET-coupled fluorophores using a universal ET cassette which contains a polydideoxyribose phosphate spacer and can be incorporated at the 5′ end of an oligonucleotide primer by conventional automated synthesis (*3*).

Other universal ET cassettes would be useful; ones that could be coupled to any molecule of interest. Such general ET cassettes would need to embody the following components: (i) a donor dye; (ii) an acceptor dye; (iii) a conformationally constrained bridge of readily varied length connecting the donor and acceptor dyes; and (iv) a functional group for attachment of the cassette to target molecules.

We describe here a preliminary examination of alternative ET cassettes which employ 9-phenylxanthene dyes as donor and acceptors (or quenchers) and conformationally constrained peptide derivatives as the bridging moieties. Peptides are particularly attractive bridge candidates because of the convenience of solid-phase synthesis and the availability of a wide range of building blocks. Indeed, peptides bearing donor dyes and quenchers are widely used for proteinase assay (e.g., refs *4*−*13*).

EXPERIMENTAL PROCEDURES

All chemicals were purchased from Aldrich (Milwaukee, WI) except where otherwise indicated. Erythrosin B-5-isothiocyanate and the NHS esters of the 5-carboxy isomers of Fam and Rox were purchased from Molecular Probes (Eugene, OR). Peptides on Merrifield resin were obtained through custom synthesis performed by SynPep (Dublin, CA). Chymotrypsin was purchased from Sigma (St. Louis, MO).

Synthesis of Erythrosin B-Ala-Phe-Ala-Gly-NH-C2-NH-Fam. Erythrosin B isothiocyanate (~4 mg) was dissolved in DMSO (0.2 mL) and added to the peptide AFAG-Merrifield resin (~2 mg of peptide) in an Eppendorf tube. DIPEA (5 μL) was added to this mixture. After vortexing for 2 h, a few resin beads were removed and checked by the Kaiser test for the completeness of dye coupling (*14*). When the reaction was complete, the supernatant was removed by centrifugation. After three sets of alternating washes with DMSO (1.0 mL) and methanol (1.0 mL), the resin beads were added to 30% (v/v) ethylenediamine in methanol (0.2 mL). After vortexing for 2 h, the supernatant was transferred to a fresh Eppendorf tube. Ether (2 mL) was added to precipitate the labeled peptide, erythrosin B-AFAG-NH-C2-NH_2. The precipitate was redissolved in DMSO (0.2 mL) and the

* To whom correspondence should be addressed, Department of Molecular and Cell Biology. Phone: (510) 642-3126. Fax (510) 643-9290. E-mail: glazer@uclink4.berkeley.edu.

† Department of Chemistry. Present address: Gull Laboratories, 1001 East 4800 South, Salt Lake City, UT 84117.

[1] Abbreviations: Fam, 5-carboxyfluorescein; Rox, 5-carboxy-X-rhodamine; DIPEA, *N*,*N*-diisopropylethylamine; DMSO, dimethyl sulfoxide; DMF, *N*,*N*-dimethylformamide; ET, energy transfer; NHS, *N*-hydroxysuccinimide; TEAA, triethylamine acetate; tBoc, *tert*-butyloxycarbonyl; tBu, *tert*-butyl; TFA, trifluoroacetic acid; MMT, monomethoxytrityl. 1× TBE buffer, 89 mM Tris/89 mM boric acid/2 mM EDTA, pH 8.0. The standard one-letter amino acid abbreviations used are E, L-Glu; F, L-Phe; G, Gly; P, L-Pro. Dye-labeled peptides are named systematically by the abbreviation of the first dye (at the N terminus) followed by one letter abbreviations for the amino acid residues, the abbreviation for the diamine and the abbreviation for the second dye (at the C terminus). The ethylenediamine linker was abbreviated as HN-C2-NH.

10.1021/bc980080k CCC: $18.00 © 1999 American Chemical Society
Published on Web 02/26/1999

peptide derivative reprecipitated to remove residual ethylenediamine. The NHS ester of Fam (~2 mg) was dissolved in DMSO (0.2 mL) and added to erythrosin B-AFAG-NH-C2-NH_2 followed by DIPEA (5 μL). After vortexing for 2 h, ethyl acetate (2 mL) was added to precipitate the doubly labeled peptide, erythrosin B-AFAG-NH-C2-NH-Fam. The precipitate was dissolved in methanol, and the doubly labeled peptide purified by reversed-phase HPLC. In the HPLC solvent, the erythrosin B-AFAG-NH-C2-NH-Fam peak showed two visible absorbances at 529 and 495 nm with a A_{529nm}:A_{495nm} ratio of 0.755. In 1× TBE, the erythrosin B absorbance was negligible relative to that of Fam.

Rox-Gly-Pro-Pro-Glu-Pro-Pro-NH-C2-NH-Fam. Ethylenediamine in methanol (30% v/v; 0.2 mL) was added to tBoc-GPPE(-tBu)PP-Merrifield resin (~5 mg of peptide) to give tBoc-GPPE(-tBu)PP-NH-C2-NH_2. This product was then labeled with NHS ester of FAM (~8 mg) to give tBoc-GPPE(-tBu)PP-NH-C2-NH-Fam. After precipitation with ethyl acetate, tBoc-GPPE(-tBu)PP-NH-C2-NH-Fam was added to 75% (v/v) TFA in dichloromethane (0.3 mL) and allowed to deprotect for 1 h. The product, GPPEPP-NH-C2-NH-Fam, was precipitated with ether (2 mL). Addition of the NHS ester of Rox (~5 mg) in DMF (0.1 mL) and DIPEA (5 μL) to GPPEPP-NH-C2-NH-Fam produced Rox-GPPEPP-NH-C2-NH-Fam.

Alternatively, 4-methoxytrityl chloride (~0.5 g) was dissolved in dichloromethane (0.5 mL) and added to GPPEGG-Merrifield resin (~5 mg of peptide). Pyridine (0.5 mL) was added to the above mixture. While stirring, the mixture was heated at 45 °C for 48 h. After completion of the reaction, the peptide was treated as described above to give MMT-GPPEPP-NH-C2-NH_2. The rest of the synthesis was performed as described above except that deprotection was performed with 3% (v/v) TFA in dichloromethane for 5 min.

Mass spectrometry of Rox-GPPEPP-NH-C2-NH-Fam gave $(M + 1)^+$ of 1510 (corresponding to the calculated mass of 1509) and a ratio of A_{495nm} (FAM):A_{585nm} (Rox) of 0.816.

Rox-Gly-Pro-Pro-Glu-Pro-Pro-*p*-xylylenediamine-Fam. This compound was synthesized following the scheme for Rox-GPPEPPNH-C2-NH-Fam except that *p*-xylylenediamine, $C_6H_4(CH_2NH_2)_2$, was used for cleavage. Rox-GPPEPP-*p*-xylylenediamine-Fam purified by HPLC had a ratio of A_{495nm} (FAM):A_{585nm} (Rox) of 0.873.

Rox-Gly-Pro-Pro-Pro-Glu-Pro-Pro-Pro-*p*-xylylenediamine-Fam. This compound synthesized as described for Rox-GPPEPP-*p*-xylylenediamine-Fam except that GPPPEPPP-Merrifield resin was used as the starting material. Rox-GPPPEPPP-*p*-xylylenediamine-Fam purified by HPLC had a ratio of A_{495nm} (FAM):A_{585nm} (Rox) of 0.896.

Hydrolysis of Erythrosin B-AFAG-NH-C2-NH-Fam by Chymotrypsin. Chymotrypsin (0.25 mg) was added to a solution of erythrosin B-AFAG-NH-C2-NH-Fam (1.0 mL, A_{498} = 0.12/cm) in 0.1 mM $CaCl_2$, 50 mM Tris-HCl, pH 8. A control solution was prepared leaving out chymotrypsin. The fluorescence emission spectra of both the sample and the control solutions were measured after 24 h incubation at 37 °C.

Chromatography. HPLC was performed on a Waters 991 system with a photodiode array detector. All runs were carried on a Bio-Rad C18 column (4.6 × 250 mm) with a flow rate of 1.0 mL/min. Purification was performed with a linear gradient from 50% methanol and 50% 0.05 M TEAA to 100% methanol in 10 min. Peaks were collected manually and the solvent removed by vacuum-drying.

Mass Spectrometry. Low-resolution fast-atom bombardment mass spectrometry was performed by Mass Spectrometry Center of University of California, Berkeley.

Absorbance and Fluorescence Spectroscopy. All absorbance spectra were measured in 1× TBE buffer (unless otherwise specified) with a Perkin-Elmer Lambda 6 UV−vis spectrophotometer. The ratio of the extinction coefficients of free Fam at 495 nm to that of free Rox at 585 nm is 1.01. The absorbance of Rox at 495 nm is 7.5% of its absorbance at 585 nm, whereas Fam contributes no absorbance at 585 nm. The ratios of Fam-to-Rox absorbance given for the ET cassettes are corrected for the Rox contribution at 495 nm. Fluorescence emission spectra were collected on a Perkin-Elmer MPF-44B spectrofluorimeter with excitation at 488 nm. The sample absorbance at A_{max} in 1× TBE ranged between 0.010 and 0.012/cm. The bandwidth of the excitation and emission slits was set to 3.0 nm.

RESULTS

In their classic test of the Förster prediction (*15*) that the rate constant for energy transfer is proportional to the inverse sixth power of the distance between the donor and acceptor, Stryer and Haugland (*16*) synthesized oligomers of L-proline as spacers of defined length carrying an α-naphthyl group at the carboxyl end as a donor and a dimethylaminonaphthalenesulfonyl group at the imino end as an acceptor. The synthesis was carried out by the Merrifield solid-phase method, and the acceptor was attached to the imino end of the peptide before release from the resin. Treatment with hydrazine was then used to release the peptide derivative and to provide a reactive group at the carboxyl terminus for the attachment of the donor. However, we found that 9-phenylxanthene dyes subjected to this synthetic procedure were unstable under the conditions of hydrazinolysis.

To address this problem, we examined the use of diamines in place of hydrazine to introduce the attachment site for a dye. Since, in principle, different diamines could be used to effect the release of the peptide, this allowed examination of the effect of the portion of the bridge immediately proximal to one of the dyes on the efficiency of the energy-transfer process. Preliminary experiments showed that primary amines that are liquids or are readily soluble in organic solvents, such as ethylenediamine, 1,3-diaminopropane, and *p*-xylylenediamine, all cleaved 9-phenylxanthene dye-peptide conjugates efficiently from the resin without adverse effect on the dye.

In an initial test of the procedure, we synthesized erythrosin B-AFAG-NH-C2-NH-Fam (Figure 1). This compound was designed with a donor (Fam) and a quencher (erythrosin B) and a chymotrypsin-sensitive Phe−Ala bond to show that this synthetic procedure would be readily applicable to the synthesis of energy-transfer peptides of the type widely used for proteinase assays. The fluorescence emission of Fam at 525 nm was quenched >95% in erythrosin B-AFAG-NH-C2-NH-Fam. A 24 h incubation with chymotrypsin restored the fluorescence emission to 90% that of free 6-carboxyfluorescein (Figure 2).

Figure 3 presents the synthetic scheme for the preparation of peptides which carry Fam as a donor and Rox as acceptor and in which the γ-carboxyl group on a glutamyl residue is available for the conjugation of the ET cassette to a target molecule. With tBoc-GPPE(-tBu)-PP-Merrifield resin as starting material, ethylenediamine

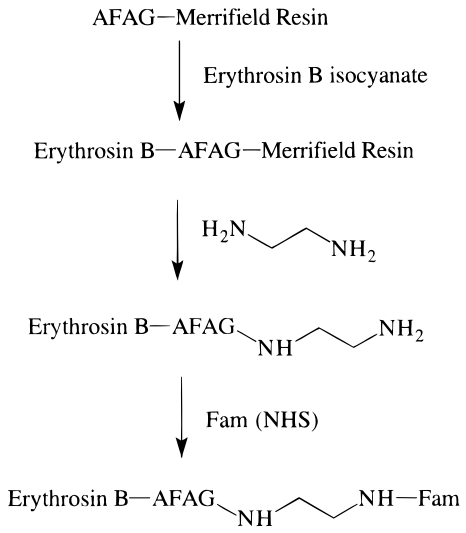


Figure 1. Synthetic scheme for erythrosin B-AFAG-NH-C2-NH-Fam.

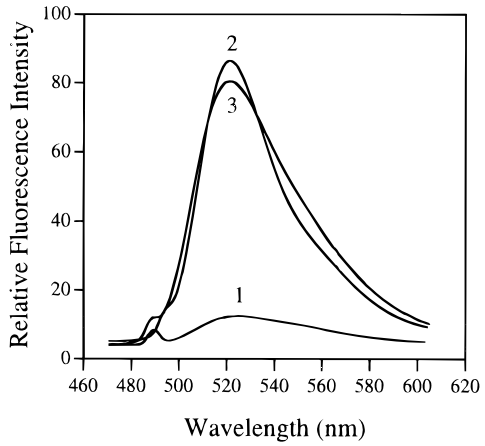


Figure 2. Fluorescence emission with 488 nm excitation of Erythrosin—AFAG-NH-C2-NH-Fam before (curve 1) and after (curve 3) hydrolysis by chymotrypsin. Curve 2 shows the fluorescence emission of an equimolar solution of free Fam. See the Experimental Procedures for details.

cleavage introduced a free amino group at the C-terminus. After conjugation to Fam, the peptide was deprotected with 75% TFA for 1 h to remove the tBoc from the N-terminus. The free N-terminal amine then readily reacted with Rox NHS ester. When a monomethoxytrityl (MMT) group was used to protect the N-terminal amine, deprotection was achieved with 3% TFA in 5 min. The latter procedure is more compatible with syntheses that may involve dyes unstable under strongly acidic conditions. The product Rox-GPPEPP-NH-C2-NH-Fam was obtained with both synthetic schemes (Figure 3). The mass of Rox-GPPEPP-NH-C_2-NH-Fam matched the proposed structure. Rox-GPPEPP-*p*-xylylenediamine-Fam and GPPPEPPP-*p*-xylylenediamine-Fam were synthesized following the same procedure with *p*-xylylenediamine for cleavage from the resin and GPPEPP or GPPPEPPP as the peptide sequences.

When excited at 488 nm, the compound Rox-GPPEPP-NH-C_2-NH-Fam showed strong emission from Rox at 605 nm, but also significant residual fluorescence emission from the donor Fam at 525 nm (Figure 4a). In contrast, Rox-GPPEPP-*p*-xylylenediamine-Fam offered a negligible donor residue emission (Figure 4b). Increase in donor—acceptor separation by two additional prolyl residues in Rox-GPPPEPPP-*p*-xylylenediamine-Fam gave the

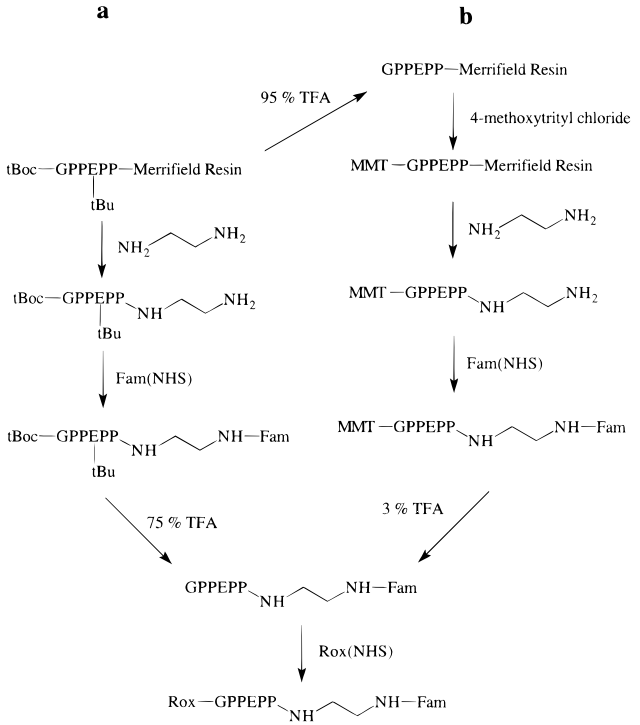


Figure 3. Synthetic schemes for Rox—GPPEPP-NH-C2-NH-Fam.

most pronounced increase of Rox emission on 488 nm excitation, over 13 times that of equimolar free Rox (Figure 4c).

DISCUSSION

We present here a straightforward general procedure which depends largely on solid-phase synthesis for the production of ET peptide cassettes. The novel feature of this procedure is the use of diamines both to release the peptide from the resin and to provide a primary amino group at the C-terminus of the peptide for facile addition of a dye.

This procedure allows the synthesis of ET peptide cassettes varying only in the nature of the diamine at the C-terminus. Surprisingly, different diamines have a substantial impact on the fluorescence emission properties of the ET cassette. With 488 nm excitation, Rox-GPPEPP-NH-C2-NH-Fam and Rox-GPPEPP-*p*-xylylenediamine-Fam (Figure 4, panels a and b) show similar enhancement of Rox fluorescence emission at 605 nm (relative to equimolar free Rox). However, Rox-GPPEPP-NH-C2-NH-Fam shows significant emission from the Fam donor, whereas the donor emission in Rox-GPPEPP-*p*-xylylenediamine-Fam is virtually completely quenched. Thus, the structure (and possibly the rigidity) of the portion of the ET cassette proximal to a dye has a disproportionately large effect on the spectroscopic properties of the cassette. It is customary to link dyes to oligonucleotides (*1, 2*) and the like through long aliphatic tethers. The result reported here suggests that systematic studies of the influence of the structure of these tethers on the fluorescence properties of the ET cassettes would be worthwhile.

Studies of ET cassettes with oligonucleotide and oligodideoxyribose phosphate spacers (*3, 17—20*) have yielded the unexpected result that both the efficiency of energy transfer, as measured by quenching of donor emission, and the intensity of fluorescence emission from the acceptor increase with longer donor—acceptor spacing,

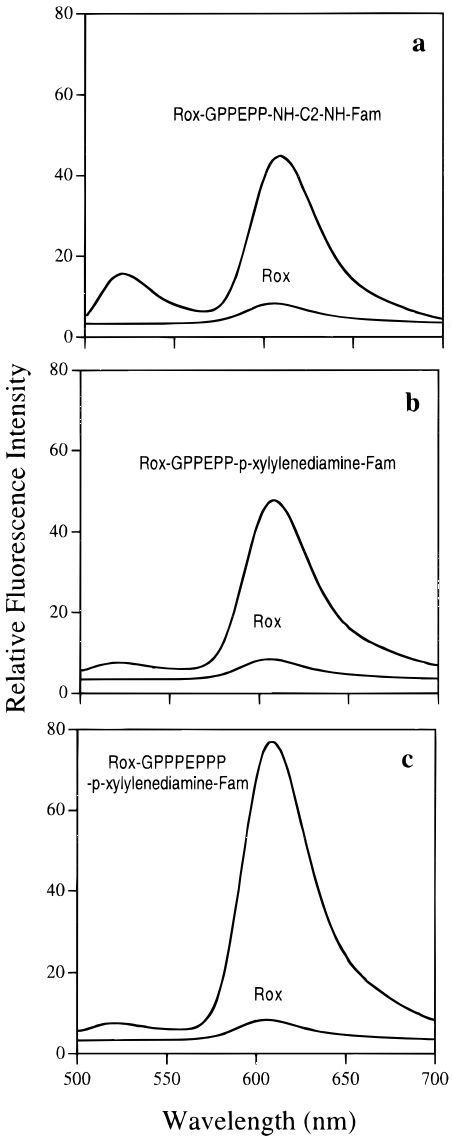


Figure 4. Comparison the fluorescence emission on 488 nm excitation of peptide ET-cassettes with that of an equimolar solution of free Rox. (a) Rox−GPPEPP-NH-C2-NH-Fam versus Rox. (b) Rox−GPPEPP−*p*-xylylenediamine-Fam versus Rox. (c) Rox−GPPPEPPP−*p*-xylylenediamine-Fam versus Rox.

reaching a maximum at a chain length of 8−10 monomer units (*17*−*19*). The inverse result is predicted by the Förster equation (*15*), and such expectation is validated by studies of donor−acceptor pairs bridged by a rigid backbone (*16*). The anomalous behavior of cassettes with oligonucleotide and polydideoxyribose phosphate spacers is attributable to their conformational flexibility which may allow for close contact of donor and acceptor in some conformers with consequent quenching of the emission.

In this report, we examine the dependence of energy transfer in Fam/Rox oligopeptide cassettes on the structure of the spacer separating the dyes. Here, as in oligonucleotide and polydideoxyribose phosphate spacers studied earlier, peptide length-dependent variation in the orientation factor (κ^2) is not likely to be significant because the 9-phenylxanthenes are attached to the oligopeptides through bonds that do not hinder their mobility. Experimental support for this assertion is provided by Stryer and Haugland (*16*), who concluded that a dansyl group attached to the imino end of proline oligopeptides had a fast rotational mobility independent of that of the oligopeptide moiety. They therefore used the average value of κ^2, i.e., 2/3, in the energy-transfer calculations for oligoproline peptides varying in length (*16*). Eisinger and co-workers (*21*, *22*) reached the same conclusion for chromophores attached to polypeptide chains that have little or no secondary or tertiary structure.

The two peptides Rox-GPPEPP-*p*-xylylenediamine-Fam and Rox-GPPPEPPP-*p*-xylylenediamine-Fam differ only in the length of the Pro-containing segments. Both of these ET peptides show near-complete quenching of donor emission. However, the longer peptide, Rox-GPPPEPPP-*p*-xylylenediamine-Fam, gave significantly greater enhancement of Rox fluorescence emission (Figure 4c). The ratio of emissions for 488 nm excitation for this ET cassette versus free ROX approaches 14 and is similar to the ratio of 14 obtained for optimized oligonucleotide primers bearing the same dyes (*2*). The difference in the absorbance spectra of Rox-GPPEPP-*p*-xylylenediamine-Fam (A_{495nm}:A_{585nm} = 0.873) and Rox-GPPPEPPP-*p*-xylylenediamine-Fam (A_{495nm}:A_{585nm} = 0.896) is consistent with lesser dye-dye interaction in the longer ET cassette.

The conformational aspects of the Pro-Pro or Pro-Pro-Pro segments of the oligopeptides deserve a brief comment. Pro is unique among amino acids in that the side chain is bonded covalently to the nitrogen atom of the peptide group. Therefore, the backbone at a Pro residue within an oligopeptide chain has no amide hydrogen for participation in hydrogen bonding or in resonance stabilization of the peptide bond of which it is a part. The cyclic five-membered ring also imposes rigid constraints on rotation about the N−C^{α} bond of the backbone. Pro residues, therefore, do place major constraints on the conformation of the oligopeptide backbone. However, even the Pro-Pro and Pro-Pro-Pro segments of these oligopeptides most likely exist in alternative conformations since the trans form of imide bond involving Pro is only slightly favored (4:1) over the cis form (*23*). These segments are too short to assume a helical conformation. The oligopeptide portion of each of the two ET cassettes thus exists as a population of conformers each varying in the separation between the donor and acceptor dyes.

In conclusion, as for ET primers with oligonucleotide spacers, for ET peptide-based cassettes with partially flexible regions, the optimum donor−acceptor separation will need to be established empirically.

ACKNOWLEDGMENT

We thank Richard A. Mathies for many valuable discussions. This research was supported by Amersham Life Science Inc. and by the Director, Office of Energy Research, Office of Health and Environmental Research of the U.S. Department of Energy under Contract DE-FG-91ER61125. Financial support from the W. M. Keck Foundation is also gratefully acknowledged.

LITERATURE CITED

(1) Glazer, A. N., and Mathies, R. A. (1997) Energy transfer fluorescent reagents for DNA analyses. *Curr. Opin. Biotechnol. 8*, 94−102.

(2) Ju, J., Glazer, A. N., and Mathies, R. A. (1996) *Nat. Med. 2*, 246−249.

(3) Ju, J., Glazer, A. N., and Mathies, R. A. (1996) Cassette labeling for facile construction of energy transfer fluorescent primers. *Nucleic Acids Res. 24*, 1144−1148.

(4) Gershkovich, A., and Kholodovych, V. V. (1996) Fluorogenic substrates for proteases based on intramolecular fluorescence energy transfer (IFETS) *J. Biochem. Biophys. Methods 33*, 135−162.

(5) Matayoshi, E., Wang, G. T., Krafft, G. A., and Erickson, J. (1990) Novel fluorogenic substrates for assaying retroviral proteases by resonance energy transfer. *Science 247*, 954−958.

(6) Wang, G. T., Matayoshi, E., Huffaker, H. J., and Krafft, G. A. (1990) Design and synthesis of new fluorogenic HIV protease substrates based on resonance energy transfer. *Tetrahedron Lett. 31*, 6493−6496.

(7) Garcia-Echeveria, C., and Rich, D. H. (1992) New intramolecularly quenched fluorogenic peptide substrates for the study of the kinetic specificity of papain. *FEBS Lett. 297*, 100−102.

(8) Pennington, M. W. and Thornberry, N. A. (1994) Synthesis of a fluorogenic interleukin-1β converting enzyme substrate based on resonance energy transfer. *Pept. Res. 7,* 72−76.

(9) Geoghegan, K. F. (1996) Improved method for converting an unmodified peptide to an energy-transfer substrate for a proteinase. *Bioconjugate Chem. 7*, 385−391.

(10) Maggiora, L. L., Smith, C. W., and Zhang, Z. Y. (1992) A general method for the preparation of internally quenched fluorogenic protease substrates using solid-phase peptide synthesis. *J. Med. Chem. 35,* 3727−3730.

(11) Contillo, L. G., Singleton, D. H., Andrews, G. C., Spencer, R. W., Faraci, W. S., Martin, W. H., and Stock, I. A. (1994) A general strategy for the synthesis of eosin- fluorescein energy transfer substrates for high sensitivity screening of protease inhibitors. *Techniques in Protein Chemistry* V, pp 493−500, Academic Press, San Diego.

(12) Handa, B. K., Keech, E., Conway, E. A., Broadhurst, A., and Ritchie, A. (1995) Design and synthesis of a quenched fluorogenic peptide substrate for human cytomegalovirus proteinase. *Antiviral Chem. Chemother. 6,* 255−261.

(13) Kornelyuk, A. I., Terentiev, A. G., Fisher, S., and Porter, T. (1995) Synthesis and characterization of fluorogenic peptide substrate of HIV-1 protease based on fluorescence resonance energy transfer. *Biopol. Kletka 11,* 57−61.

(14) Kaiser, E., Colescott, R. L., Bossinger, C. D., and Cook, P. I. (1970) Color test for detection of free terminal amino groups in the solid-phase synthesis of peptides. *Anal. Biochem. 34*, 595−598.

(15) Förster, T. (1948) Zwischenmolekulare energiewanderung und fluoreszenz. *Ann. Physik. 2*, 55−75.

(16) Stryer, L. and Haugland, R. P. (1967) Energy transfer: A spectroscopic ruler. *Proc. Natl. Acad. Sci. U.S.A. 58*, 719−726.

(17) Ju, J., Ruan, C., Fuller, C. W., Glazer, A. N., and Mathies, R. A. (1995) Fluorescence energy transfer dye-labeled primers for DNA sequencing and analysis. *Proc. Natl. Acad. Sci. U.S.A. 92*, 4347−4351.

(18) Ju, J., Kheterpal, I., Scherer, J. R., Ruan, C., Fuller, C. W., Glazer, A. N., and Mathies, R. A. (1995) Design and synthesis of fluorescence energy transfer dye-labeled primers and their application for DNA sequencing and analysis. *Anal. Biochem. 231,* 131−140.

(19) Hung, S.-C., Mathies, R. A., and Glazer, A. N. (1997) Optimization of spectroscopic and electrophoretic properties of energy transfer primers. *Anal. Biochem. 252,* 78−88.

(20) Hung, S.-C., Mathies, R. A., and Glazer, A. N. (1998) Comparison of fluorescence energy transfer primers with different donor−acceptor dye combinations. *Anal. Biochem. 255,* 32−38.

(21) Eisinger, J. (1969) Intramolecular energy transfer in adrenocorticotropin. *Biochemistry 8,* 3902−3908.

(22) Eisinger, J., Feuer, B., and Lamola, A. A. (1969) Intramolecular singlet excitation transfer. Application to polypeptides. *Biochemistry 8,* 3908−3915.

(23) Creighton, T. E. (1984) *Proteins. Structures and Molecular Principles,* pp 163−164, W. H. Freeman & Co., New York.

BC980080K

Comb-Type Prepolymers Consisting of a Polyacrylamide Backbone and Poly(L-lysine) Graft Chains for Multivalent Ligands

Shoichiro Asayama, Atsushi Maruyama,* and Toshihiro Akaike

Department of Biomolecular Engineering, Tokyo Institute of Technology, 4259 Nagatsuta, Midori, Yokohama 226-8501, Japan. Received August 17, 1998

The comb-type copolymers consisting of a polyacrylamide (PAAm) backbone and poly(L-lysine) (PLL) graft chains have been prepared as the "prepolymer" for designing multivalent ligands. To regulate the length and density of the clusters of primary amino groups, the N^{α}-carboxyanhydride of N^{ϵ}-carbobenzoxy (CBZ)-L-lysine was first polymerized using *p*-vinylbenzylamine as an initiator. The resulting poly(CBZ-L-lysine) macromonomer was then radically copolymerized with AAm, followed by the deprotection of amino groups. For the model study, the reactive clusters of primary amino groups were completely converted into anion clusters by the reaction with succinic anhydride. The model multivalent ligands having the biotin label on the PAAm backbone were prepared by the terpolymerization of the macromonomer, AAm, and the biotin derivative having a vinyl group. The enzyme-linked immunosorbent assay showed that the biotin with no spacer on the PAAm backbone was recognized by the avidin−peroxidase conjugate specifically. Therefore, the highly sensitive detection of the interaction between cells and various model multivalent ligands was possible. The selective labeling onto the PAAm backbone revealed that the converted anion clusters of graft chains interacted exclusively with the cell and that the backbone was inert to the interaction with the cell. These results indicate that the various PAAm-*graft*-PLL comb-type copolymers with the defined length and density of the PLL-*grafts* are the potential prepolymers to investigate and to optimize the affinity of the multivalent ligands for receptors.

INTRODUCTION

Cell-surface receptors interact with their specific ligands such as growth factors, hormones, neurotransmitters, cell adhesion molecules, and extracellular matrices (*1*). These receptor−ligand interactions are mainly driven through the combination of electrostatic attraction, hydrogen bonds, and van der Waals attractive force (*2*). Interestingly, in the case of an asialoglycoprotein receptor (ASGP-R[1]), the affinity of the galactosylated protein for the ASGP-R on hepatocytes is enhanced by increasing the number of the galactose residues on the protein (*3*−*6*). Furthermore, the particular geometry of a few galactose residues considerably increases the affinity of the galactosylated ligand for the ASGP-R on the hepatocytes (*7*, *8*).

We reported previously that the multivalent β-galactose ligands of a polystyrene derivative, poly[*N*-(*p*-vinylbenzyl)-4-*O*-β-D-galactopyranosyl-D-gluconamide] [PVLA, poly(vinylbenzyl-β-D-lactonamide)], are recognized by the ASGP-R on the surface of the hepatocytes; namely, the PVLA is found to be an artificial cellular matrix as the useful substratum for hepatocyte culture (*9*−*12*). When a culture dish is coated with a high density of PVLA, the hepatocytes attached on the dish remain spherical and show low DNA synthesis activity. In contrast, the hepatocytes on the coated dish with a low density of PVLA show spread morphology but high DNA synthesis activity (*13*). The particles covered with the PVLA are also recognized by the hepatocytes (*14*, *15*). The particle covered with the high density of β-galactose residues is promptly internalized by ASGP-R-mediated endocytosis, whereas the low density of β-galactose residues on the particle permits the binding to the hepatocyte without internalization (*16*). In these cases, the surface density of β-galactose residues is shown to be influential in the cellular responses and ligand binding. However, the influence of the size and distribution of the galactose cluster is not precisely estimated. The multivalent effect may occur in a variety of receptor−ligand interactions of cell adhesion molecules (*17*−*20*) such as P-selectin recognizing anionic glycoproteins (*21*−*24*).

In this study, we have designed the "prepolymer" for the multivalent ligands which have the well-controlled clusters of ligand molecules. The prepolymer consists of a polyacrylamide (PAAm) (*25*) backbone and poly(L-lysine) (PLL) graft chains. The clusters of primary amino groups on the PLL-*grafts* offer chemical modification sites, so that the amino groups can be converted into galactose clusters by the reaction with lactonolactone (*12*). The length and density of these clusters are properly characterized and controlled by varying the length of the PLL macromonomer or by varying the feed ratio for the

* Author to whom correspondence should be addressed (telephone +81-45-924-5122; fax +81-45-924-5815; e-mail amaruyam@bio.titech.ac.jp).

[1] Abbreviations: ASGP-R, asialoglycoprotein receptor; PVLA, poly[*N*-(*p*-vinylbenzyl)-4-*O*-β-D-galactopyranosyl-D-gluconamide] or poly(vinylbenzyl-β-D-lactonamide); PAAm, polyacrylamide; PLL, poly(L-lysine); THF, tetrahydrofuran; DMF, *N*,*N*-dimethylformamide; OPD, *o*-phenylenediamine dihydrochloride; CBZ, carbobenzoxy group; NCA, N^{α}-carboxyanhydride; NHS, *N*-hydroxysuccinimide; DCC, dicyclohexylcarbodiimide; VBA, *p*-vinylbenzylamine; V-65, 2,2′-azobis(2,4-dimethylvaleronitrile); TFA, trifluoroacetic acid; TEA, triethylamine; TNBS, trinitrobenzenesulfonic acid; GPC, gel permeation chromatography; RI, refractive index; ELISA, enzyme-linked immunosorbent assay; PLLS, succinylated poly(L-lysine); P_n, number-average degree of polymerization; A_{274}, absorbance at 274 nm.

10.1021/bc980093y CCC: $18.00 © 1999 American Chemical Society
Published on Web 02/12/1999

copolymerization with AAm. The various PAAm-*graft*-PLL comb-type copolymers are, therefore, expected to be useful in investigating and optimizing the affinity of the multivalent ligands for receptors.

EXPERIMENTAL PROCEDURES

Materials. Acrylamide (AAm) was purchased from Wako Pure Chemical Industries, Ltd. (Osaka, Japan) and was crystallized from benzene. Hexane was from Kanto Chemical Co., Inc. (Tokyo, Japan) and was washed with concentrated sulfuric acid to remove olefin, followed by water, drying, and distilling over sodium under nitrogen. Ethyl acetate (from Kanto) was dried with K_2CO_3, followed by distilling and redistilling over acetic anhydride to convert ethanol into ethyl acetate under nitrogen. Tetrahydrofuran (THF) was from Kanto and was dried with KOH, followed by distilling over *n*-butyllithium under nitrogen. *N*,*N*-Dimethylformamide (DMF) was from Kanto and was distilled under reduced pressure over $MgSO_4$. (+)-Biotin was purchased from Wako. Streptavidin−horseradish peroxidase conjugate and *o*-phenylenediamine dihydrochloride (OPD) were purchased from Gibco Bethesda Research Laboratories (Grand Island, NY). All other chemicals of a special grade were used without further purification.

Synthesis of Poly[N^{ϵ}-carbobenzoxy (CBZ)-L-lysine] Macromonomers. The N^{α}-carboxyanhydride (NCA) of CBZ-L-lysine (**2**) was prepared in THF, followed by crystallization from THF/hexane and recrystallization from ethyl acetate/hexane according to the method proposed by Daly and Poché (*26*). The NCA (**2**) was dissolved in dehydrated DMF. *p*-Vinylbenzylamine (**1**; VBA) (*27*) was dissolved in dehydrated DMF and added to the solution of **2**. The polymerization reaction was performed with 2.5 g of CBZ-L-lysine NCA (**2**) in 25 mL of DMF at the monomer (**2**)/initiator (**1**) molar ratios of 3, 5, 10, or 20 (for 36 h at 48 °C). The reaction mixture was then poured into a 20-fold volume of diethyl ether. Precipitate was collected by centrifugation and washed with diethyl ether, followed by drying in vacuo.

Synthesis of the Biotin Derivative Having a Polymerizable Group. First, biotinyl-*N*-hydroxysuccinimide ester was prepared from biotin (**7**) and *N*-hydroxysuccinimide (NHS) by coupling with dicyclohexylcarbodiimide (DCC) (*28*). Each reactant was dissolved at 0.07 M concentration in DMF and incubated for 16 h at 50 °C. The mixture was cooled to room temperature, the dicyclohexylurea was filtered off, and the filtrate was dried on a rotary evaporator. The residue was crystallized from 2-propanol. The resulting active ester of biotin and VBA (**1**) were dissolved at 0.06 M concentration in DMF and incubated for 22 h at 25 °C. The mixture was diluted with a 19-fold volume of H_2O, and the precipitate was collected by filtration, followed by washing with H_2O (to remove resulting NHS and unreacted **7**) and diethyl ether (to remove unreacted **1**). The residue was crystallized from DMF/H_2O mixture.

Synthesis of PAAm-*graft*-PLL Comb-Type Copolymers. The resulting macromonomer (**3**) and AAm (**4**) were dissolved in 2.5 mL of DMF at the total monomer concentration of 100 mg/mL. In the case of biotinylation, 5 mg of the resulting biotin monomer (**8**) was added to the above mixture. The radical copolymerization reaction was carried out for 2−4 h at 47 °C in a sealed glass ampule using 10 mM 2,2′-azobis(2,4-dimethylvaleronitrile) (V-65) as an initiator. After the reaction, the content was poured into a large excess of ethanol, and precipitate was dried in vacuo. The crude polymers were dissolved in trifluoroacetic acid (TFA), followed by the addition of thioanisole to deprotect CBZ-amino groups. The final concentrations of thioanisole and the polymer were 0.3−1 M and 20−100 mM (based on the CBZ groups), respectively. The deprotection reaction was carried out for 2.5−3.0 h at 25 °C. The reaction mixture was poured again into a large excess of ethanol. Precipitate was redissolved in TFA and poured into ethanol repeatedly. The precipitate was dried in vacuo, dissolved in water, and obtained by freeze-drying.

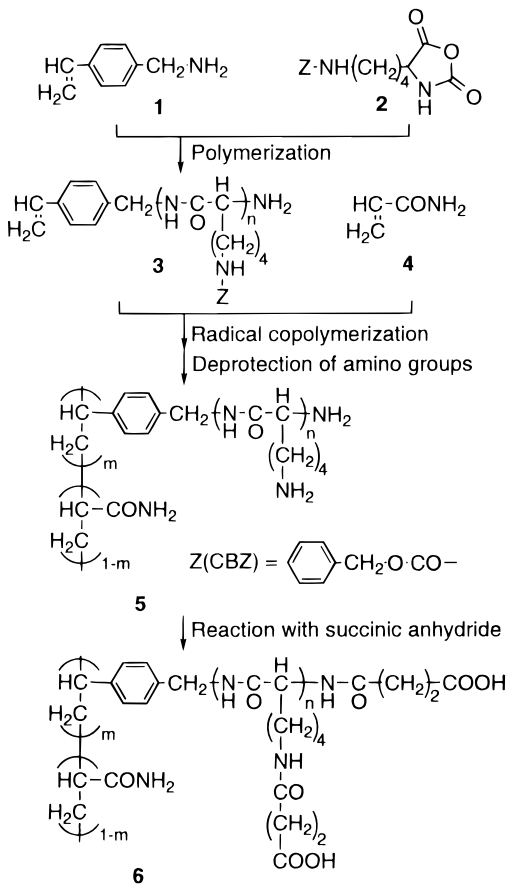
Succinylation of PAAm-*graft*-PLL Comb-Type Copolymers. The resulting copolymer (**5**) or biotinylated **5** was dissolved in 1 mL of H_2O at the concentration of 50 mg/mL, the pH of which was increased to 10 by the addition of triethylamine (TEA). The DMF solution (150 μL) of succinic anhydride (60 mg) was subsequently added to the copolymer aqueous solution. The mixture was incubated for 3 h at 25 °C. The above DMF solution of succinic anhydride was added again to the mixture, the pH of which was adjusted to 10 with TEA. The resulting mixture was further incubated for 1 day at 25 °C. The degree of amino group modification was examined by the spectrophotometric amino group determination with trinitrobenzenesulfonic acid (TNBS) (*29*). The reaction mixture was dialyzed against distilled water using a Spectra/Por 7 membrane (molecular weight cutoff = 10^3), followed by freeze-drying.

Gel Permeation Chromatography (GPC). GPC was carried out using a JASCO 880-PU pumping system (Tokyo, Japan) at a flow rate of 1.0 mL/min at 25 °C with Ultrahydrogel 500 and Ultrahydrogel 250 columns (Japan Waters Ltd., Tokyo, Japan). The aqueous solution containing 0.5 M CH_3COOH and 0.3 M Na_2SO_4 was used as a mobile phase. Three hundred microliters of 1 mg/mL samples was injected into the columns. Eluate was detected by a UV (wavelength = 274 nm) detector (875-UV, JASCO), a refractive index (RI) detector (830-RI, JASCO), and a multiangle light scattering detector (Dawn-DSP, Wyatt Technology Co., Santa Barbara, CA).

^{1}H NMR Spectroscopy. Each polymer was dissolved in $(CD_3)_2SO$ (DMSO-d_6) or D_2O (99.8 atom % D; Merck, Darmstadt, Germany). ^{1}H NMR spectra (400 MHz) were obtained by a Varian Unity 400plus spectrometer (Palo Alto, CA) at a probe temperature of 298 K. The chemical shifts are expressed as parts per million using internal DMSO (δ = 2.5 ppm in DMSO-d_6) or HDO (δ = 4.7 ppm in D_2O) molecules as a reference.

Enzyme-Linked Immunosorbent Assay (ELISA) Measuring Polymer−Cell Interaction. Endothelial cells (ECV304, ATCC CRL1998) were seeded in tissue culture wells and allowed to grow to confluence in M199 medium (Gibco) supplemented with 10% heat-inactivated fetal bovine serum. The binding assays between the polymers and the cells were performed in a Sumilon multiwell plate (No. MS-8096F, Sumitomo Bakelite Co., Ltd., Tokyo, Japan) as below. First, the cells were washed once with an isotonic and low-ionic incubation buffer (285 mM sucrose, 10 mM Hepes, 0.9 mM $CaCl_2$, 0.5 mM $MgCl_2$). The confluent cells were incubated with 100 μL/well of the buffer containing each polymer (1 mg/mL) for 2 h at 4 °C. The wells were then washed once with the buffer, followed by the addition of 100 μL of the peroxidase-conjugated streptavidin in the buffer (1 μg/mL). After 1 h of incubation at 4 °C, the wells were washed three times with the buffer. Finally, 100 μL of 1 mg/mL OPD solution (in 50 mM citric acid, 100 mM Na_2HPO_4 buffer, pH 5.0) containing 0.02% H_2O_2 was added to the well as a substrate. Fifty microliters per well of 1.5 M

Scheme 1. Synthesis of PAAm-*graft*-PLL Comb-Type Copolymers



H_2SO_4 was added to stop the enzyme reaction after the incubation at room temperature. The absorbance at 492 nm was measured with an MTP-120 microplate reader (Corona Electric Co., Ltd., Ibaragi, Japan).

Estimation of the Dependence of the Succinylated PAAm-*graft*-PLL (PAAm-*graft*-PLLS) Cell Binding on the Ionic Strength of the Medium. As stated above, the endothelial cells were seeded and washed once with the isotonic and low-ionic incubation buffer. The PAAm-*graft*-PLLS was dissolved in the isotonic buffer containing 10 mM Hepes, 0.9 mM $CaCl_2$, 0.5 mM $MgCl_2$, and various sucrose/NaCl mixtures (285 mM/0 mM, 230 mM/27.5 mM, 155 mM/65 mM, 80 mM/102.5 mM, or 5 mM/140 mM) being added to the cells. These cells were incubated with 100 μL/well of each buffer containing PAAm-*graft*-PLLS (10 μg/mL) for 2 h at 4 °C. The wells were washed once with the isotonic and low-ionic incubation buffer. One hundred microliters of the peroxidase-conjugated streptavidin in the low-ionic buffer (1 μg/mL) containing 1 mg/mL bovine serum albumin was added to the wells. After the incubation for 1 h at 4 °C, the wells were washed three times with the low-ionic buffer. One hundred microliters of a 1 mg/mL OPD solution containing 0.012% H_2O_2 was then added to the well, followed by the measurement of the absorbance at 492 nm.

RESULTS AND DISCUSSION

Synthesis of Poly(CBZ-L-lysine) Macromonomers. To synthesize the graft copolymers (Scheme 1), we chose the macromonomer method (*30*) because it has several advantages over other methods. The length (molecular weight) of the polyamino acid macromonomer is easy to control by varying the feed ratio of monomers to the initiator having a polymerizable functional group. The density of graft chains is also controllable by varying the feed ratio of the macromonomer to comonomers. Therefore, the structure of graft chains would be well-defined and characterized. Furthermore, we are able to vary the properties of backbone polymers by replacing comonomers (*31*).

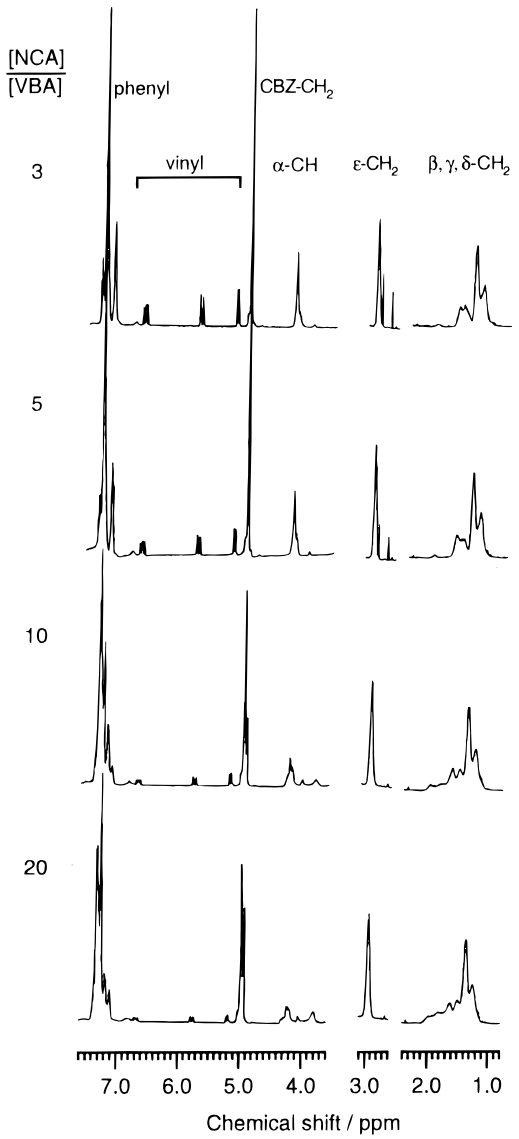


Figure 1. ^{1}H NMR spectra of poly(CBZ-L-lysine) macromonomers in DMSO-d_6. The feed ratio of monomer (NCA) to initiator (VBA) is represented.

Poly(CBZ-L-lysine) macromonomers (**3**) were prepared by the polymerization of CBZ-L-lysine NCA (**2**) using VBA (**1**) as an initiator. The polymerization progressed homogeneously in the solvent of dehydrated DMF. The polymers were purified by precipitating into diethyl ether. The vinyl groups were preserved in the resulting polymer (**3**), which was confirmed by ^{1}H NMR spectroscopy (Figure 1) in DMSO-d_6: δ 5.2 (doublet), 5.8 (doublet), and 6.7 (quartet). The signals of CBZ-L-lysine were also identified: δ 1.2−1.8 (β-, γ-, and δ-methylene protons), 3.0 (ϵ-methylene protons), 4.3 (α-methine protons), 5.0 (CBZ-methylene protons), and 7.2−7.4 (phenyl protons). From the signal ratio of vinyl protons and lysine protons, the number-average degree of polymerization (P_n) of **3** was determined. The result is shown in Table 1. The P_n of **3** almost corresponded with the feed ratio of monomer (**2**) to initiator (**1**). Therefore, it is possible to vary the

Table 1. Polymerization of CBZ-L-lysine NCA Using VBA as an Initiator[a]

sample	in feed: NCA (mmol)	in feed: VBA (mmol)	in feed: [NCA]/[VBA]	polymer P_n[b]
1	8.2	2.7	3	2.6
2	8.2	1.6	5	4.7
3	8.2	0.82	10	8.4
4	8.2	0.41	20	16

[a] Reaction temperature, 48 °C; reaction time, 36 h; solvent, DMF. [b] Determined by ^{1}H NMR.

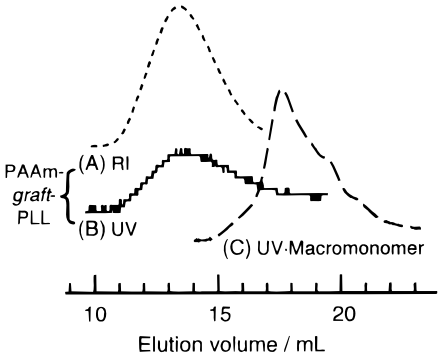


Figure 2. GPC chromatograms of the PAAm-*graft*-PLL comb-type copolymer (sample 4 in Table 2) detected by (A) RI and (B) A_{274}, and (C) the deprotected CBZ-L-lysine macromonomer (sample 3 in Table 1) detected by A_{274}: column, Ultrahydrogel 500 + 250; eluent, 0.5 M CH_3COOH + 0.3 M Na_2SO_4; flow rate, 1.0 mL/min; temperature, 25 °C.

average length of the poly(CBZ-L-lysine) macromonomer (**3**) as the graft chain of PAAm-*graft*-PLL comb-type copolymer (**5**).

Synthesis of PAAm-*graft*-PLL Comb-Type Copolymers. At first, we attempted to deprotect CBZ-amino groups of the macromonomer (**3**) before the copolymerization reaction. However, the undesirable side reaction of vinyl groups occurred when the deprotection was carried out in the TFA/thioanisole mixture. Accordingly, we deprotected CBZ-amino groups after the copolymerization. The radical copolymerization of **3** with AAm (**4**) using the initiator of an azo compound, V-65, was carried out in DMF at 46 °C. During the reaction, a precipitate gradually appeared. After the copolymerization, the mixture was poured into a large excess of ethanol to precipitate the resulting polymer (**5**), together with unreacted **3**, and to remove unreacted **4**. The removal of the unreacted macromonomers (**3**) from the copolymers (**5**) in this step was difficult because the solubility of **3** was similar to that of **5**. Eventually, we were unable to find any selective solvents for the purification. Therefore, we isolated the copolymers after the deprotection of CBZ-amino groups. Because deprotected **3** was soluble in ethanol, the copolymers were isolated by the precipitation into ethanol after the deprotection. Figure 2 shows the representative GPC profiles of the resulting copolymer (**5**) detected by either absorbance at 274 nm (A_{274}) or RI. The A_{274} was mainly attributed to the terminal phenyl groups of the graft chains. The GPC profiles therefore validated the incorporation of the macromonomer (**3**) in the copolymer (**5**) and the removal of unreacted **3**. The number-average molecular weight of the each copolymer determined by GPC was $\sim 3 \times 10^4$. The ^{1}H NMR spectra (Figure 3) of the copolymer showed the characteristic signals of both PLL-*graft* and PAAm backbone: δ 1.4−1.8 (methylene protons of PAAm), 2.1−2.4 (methine protons of PAAm), 3.0 (ϵ-methylene protons of PLL), and 4.3 (α-methine protons of PLL). No residual

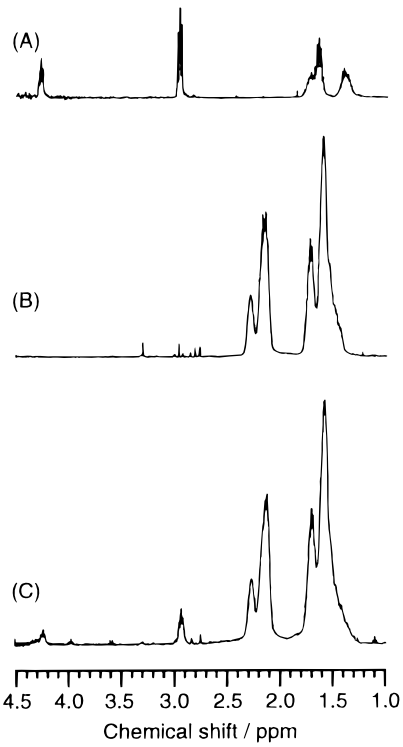


Figure 3. ^{1}H NMR spectra of (A) PLL, (B) PAAm, and (C) PAAm-*graft*-PLL in D_2O.

Table 2. Synthesis of PAAm-*graft*-PLL Comb-Type Copolymers[a]

	monomers: **4**		monomers: **3**		copolymer[b]: **3** (deprotected)	
sample	mg	mg	P_n	10^3 mol fraction	10^3 mol fraction	yield (%)
1	242.5	7.5	4.7	1.6	3.6	45
2	232.5	17.5	4.7	3.8	5.7	40
3	212.5	37.5	4.7	8.9	11	39
4	242.5	7.5	8.4	0.95	0.9	56
5	232.5	17.5	8.4	2.3	2.5	68
6	212.5	37.5	8.4	5.4	3.9	70
7	242.5	7.5	16	0.51	0.5	50
8	232.5	17.5	16	1.2	1.3	60
9	212.5	37.5	16	2.9	2.6	57

[a] Initiator, 10 mM V-65; reaction temperature, 46 °C; solvent, 2.5 mL of DMF; reaction time, 2 h (samples 1, 4, and 7), 3 h (samples 2, 5, and 8), 4 h (sample 3), and 4.5 h (samples 6 and 9). [b] The deprotection reaction of CBZ-amino groups was carried out in TFA/thioanisole mixture at 25 °C: 0.27 M thioanisole/19 mM CBZ, 2.5 h reaction (samples 1, 4, and 7); 0.54 M thioanisole/45 mM CBZ, 2.75 h reaction (samples 2, 5, and 8); and 1.1 M thioanisole/95 mM CBZ, 3.0 h reaction (samples 3, 6, and 9).

CBZ groups were detected in the final polymer samples, indicating the successful deprotection of amino groups. From the signal ratio of the PLL-*grafts* and the PAAm backbone, the content (mole fraction) of **3** in the copolymer was determined. As the mole fraction of **3** in feed increased, the mole fraction in the copolymer increased (Table 2). Furthermore, various macromonomers (**3**) with different P_n were copolymerized. Thus, it is possible to obtain the various PAAm-*graft*-PLL comb-type copolymers (**5**) with the well-controlled length and density of graft chains by using the macromonomer method.

Modification of the Amino Groups of the PAAm-*graft*-PLL Comb-Type Copolymers. We examined the reactivity of the amino groups of the graft chains. Here the acylation of the graft chains by succinic anhydride

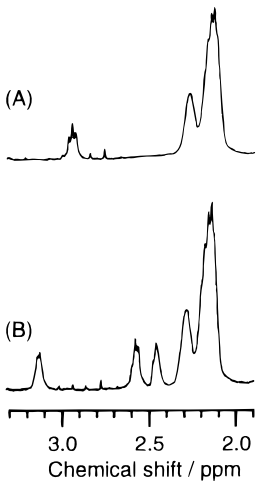


Figure 4. Change in the ^{1}H NMR spectra of the PAAm-*graft*-PLL comb-type copolymer (sample 6 in Table 2) by the reaction with succinic anhydride: (A) before and (B) after the reaction.

was examined. The PAAm-*graft*-PLL (**5**) was dissolved in water, and the pH of the solution was increased to 10 by TEA. The succinic anhydride dissolved in DMF was added to the aqueous solution of the PAAm-*graft*-PLL, which was insoluble in DMF. Thus, the succinylation reaction was carried out in the mixture of water and DMF. The complete succinylation of the amino groups of the graft chains was confirmed by the spectrophotometric amino group titration with TNBS (*29*). Figure 4 shows the ^{1}H NMR spectra of the resulting polymer (**6**) purified by dialysis. After the succinylation (Figure 4B), the signal of ϵ-methylene protons of the PLL-*grafts* shifted downfield (from δ 3.0 to 3.2), and the signals of the methylene protons of succinic acid appeared (δ 2.4−2.6). These results proved the complete succinylation of the amino groups again. The amino groups of the graft chains retained high reactivity, so that the graft chains are expected to be modified with ligand molecules such as β-galactose (unpublished results).

PAAm-*graft*-PLL Comb-Type Copolymers Having the Biotin Label on the Backbone. To analyze the interaction between cells and the comb-type copolymers, we intended to label the PAAm-*graft*-PLL with biotin, which is detected by ELISA using avidin (biotin-binding protein) (*32*). The comb-type copolymer PAAm-*graft*-PLL has two segments, that is, the nonionic backbone of PAAm and the PLL-*graft*. We prefer to incorporate biotin molecules into the PAAm backbone rather than into the PLL-*graft* to minimize the influence on the avidin−biotin binding and the interaction between the PLL-*graft* and the receptor. For the biotin-labeling, the biotin derivative (**8**) having a polymerizable group was prepared and terpolymerized with the poly(CBZ-L-lysine) macromonomer (**3**) and AAm (**4**) (Scheme 2).

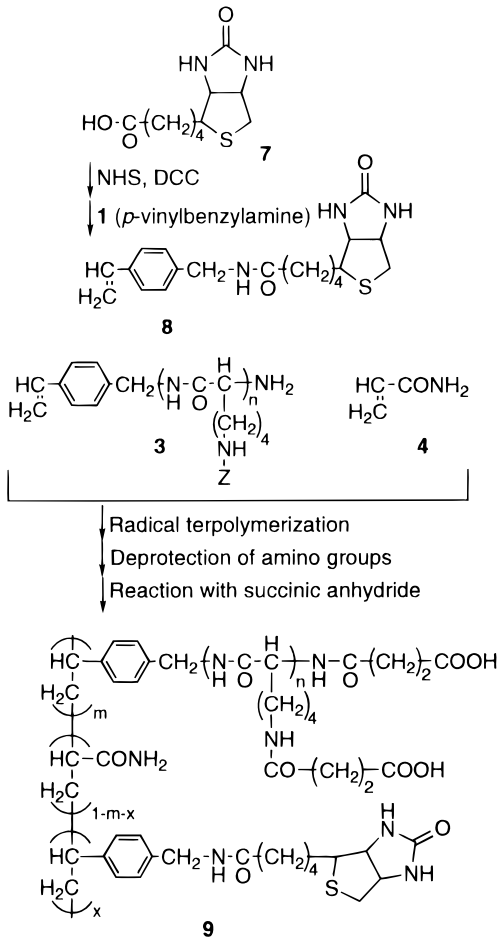
First, the carboxyl group of biotin (**7**) was activated in DMF using NHS and DCC. The active ester of biotin was then reacted with VBA (**1**), resulting in the monomer (**8**) having a vinyl group. The biotin monomer (**8**) was terpolymerized with the macromonomer (**3**) and AAm (**4**). After the deprotection of amino groups, the ^{1}H NMR spectra of the resulting terpolymer were obtained (results not shown). From the signal ratio of methine protons (2.1−2.4 ppm) of the PAAm backbone and ϵ-methylene protons (3.0 ppm) of the PLL-*grafts*, the content (mole fraction) of **3** in the terpolymer was determined (Table 3). However, the ^{1}H NMR signal of **8** in the terpolymer was not detected, presumably because of considerably low feed and thereby low content in the terpolymer. The

Table 3. Biotinylation of PAAm-*graft*-PLL Comb-Type Copolymers[a]

	monomers						copolymer[b]	
	4		**3**		**8**		**3** (deprotected)	
sample	mg	mg	P_n	10^3 mol fraction	mg	10^3 mol fraction	10^3 mol fraction	yield (%)
1	242.5	7.5	8.4	0.95	5	4.1	2.2	26
2	232.5	17.5	8.4	2.3	5	4.2	2.6	39
3	212.5	37.5	8.4	5.4	5	4.6	4.4	45
4	242.5	7.5	16	0.51	5	4.1	1.4	24
5	232.5	17.5	16	1.2	5	4.2	1.7	36
6	212.5	37.5	16	2.9	5	4.6	2.2	46
7	250	0			5	3.9		16

[a] Initiator, 10 mM V-65; reaction temperature, 46 °C; solvent, 2.5 mL of DMF; reaction time, 2 h (samples 1 and 4), 3 h (samples 2 and 5), 4 h (samples 3 and 6), and 1 h (sample 7). [b] The deprotection reaction of CBZ-amino groups was carried out in TFA/thioanisole mixture at 25 °C for 3 h: 0.91 M thioanisole/58 mM CBZ (sample 1); 1.1 M/67 mM, 1.0 M/95 mM, 0.27 M/19 mM, 0.54 M/45 mM, and 1.1 M/95 mM (samples 2−6, respectively).

Scheme 2. Biotinylation of PAAm-*graft*-PLL Comb-Type Copolymers



complete succinylation of the biotinylated PAAm-*graft*-PLL was also carried out in the same way as succinylating the unlabeled PAAm-*graft*-PLL.

Detection of the Interaction between Cells and the Biotinylated PAAm-*graft*-PLLS Comb-Type Copolymers by ELISA. We examined whether the interaction between cells and the PAAm-*graft*-PLLS comb-type copolymers was detected by ELISA. Figure 5 shows the detection of the biotinylated PAAm-*graft*-PLLS (**9**) bound to adherent cells by ELISA using peroxidase-conjugated streptavidin (*33*). The biotinylated PAAm-

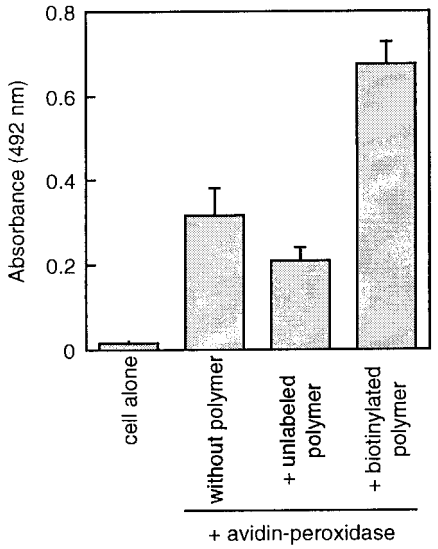


Figure 5. Detection of the interaction between adherent cells and the biotinylated PAAm-*graft*-PLLS comb-type copolymers by ELISA using the peroxidase-conjugated streptavidin. The biotin-labeled (sample 3 in Table 3) or unlabeled (sample 6 in Table 2) PAAm-*graft*-PLLS was added to confluent endothelial cells at 4 °C, as described under Experimental Procedures, followed by the addition of the peroxidase-conjugated streptavidin. After washing, the substrate (OPD + H_2O_2) was added and the color development was read as the absorbance at 492 nm. Symbols and error bars represent the mean and standard deviation of the measurements made in quadruplicate wells.

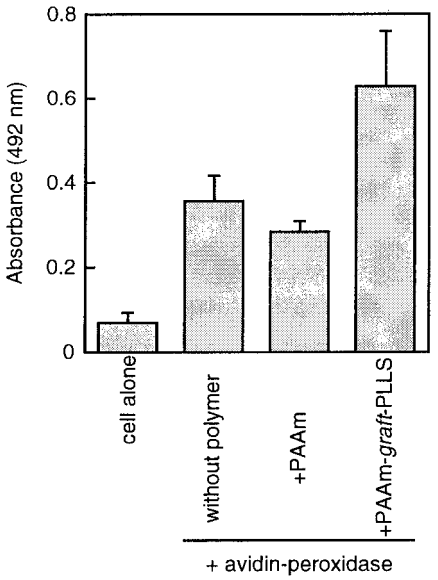


Figure 6. Binding assay between endothelial cells and polymers by ELISA. The binding of the PAAm-*graft*-PLLS (sample 1 in Table 3) or PAAm (sample 7 in Table 3) was determined by the color development of the substrate as described in Figure 5. Symbols and error bars represent the mean and standard deviation of the measurements made in quadruplicate wells.

graft-PLLS (**9**) and not unlabeled copolymer (**6**) showed significant absorbance over the background level. The PAAm-*graft*-PLLS bound to the cells was, therefore, detectable by ELISA using the peroxidase-conjugated streptavidin.

To evaluate the role of graft chains in the binding to the cell, we carried out a set of the ELISA experiments with the PAAm-*graft*-PLLS comb-type copolymer and PAAm homopolymer. As shown in Figure 6, the biotinylated PAAm was not detected. Therefore, the graft chains played a major role in the binding to the cell,

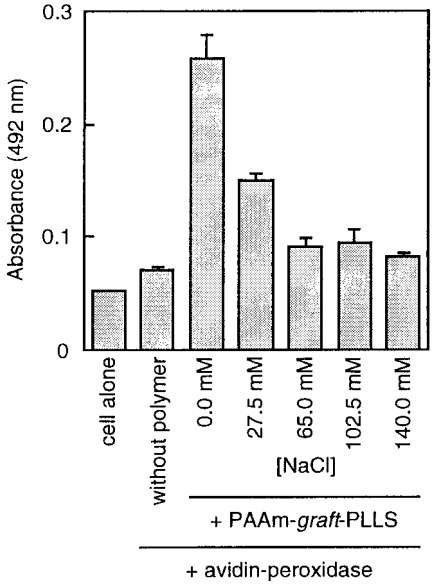


Figure 7. Effect of the ionic strength of the medium on the interaction between endothelial cells and the PAAm-*graft*-PLLS comb-type copolymers. The PAAm-*graft*-PLLS (sample 3 in Table 3) was added to confluent endothelial cells at 4 °C in the isotonic solution containing the indicated concentration of NaCl, as described under Experimental Procedures. The binding of the PAAm-*graft*-PLLS was determined by the color development of the substrate (the absorbance at 492 nm). Symbols and error bars represent the mean and standard deviation of the measurements made in quadruplicate wells.

whereas the PAAm backbone presumably had no interaction with the cell surface.

The ionic interaction between the graft chains and the cell surface was considered the major driving force for the binding to the cell, so that we estimated the effect of the ionic strength of the medium on the interaction of the PAAm-*graft*-PLLS with the cell (Figure 7). The PAAm-*graft*-PLLS was highly bound to the cell under low ionic strength conditions (0 mM NaCl and 285 mM sucrose). However, the increase in the ionic strength of the medium drastically reduced the binding of the PAAm-*graft*-PLLS, leading to almost no binding at physiological ionic strength (140 mM NaCl and 5 mM sucrose). These results proved that the electrostatic attraction between PLLS-*grafts* and the cell surface mainly mediated the binding of the PLLS-*graft* to the cell. In other words, the nonspecific interaction of the PAAm-*graft*-PLLS with the cell was negligible under physiological salt conditions.

Conclusion. We have synthesized the various PAAm-*graft*-PLL comb-type copolymers with the defined length and density of graft chains by using the macromonomer method. The PAAm-*graft*-PLL was synthesized as the "prepolymer" for multivalent ligands. We can introduce the various types of ligand molecules into the graft chains, via the primary amino groups, with certain chemicals such as lactonolactone (*12*) to form ligand clusters. In this paper, the complete modification of the graft chains with succinic anhydride was achieved for the model study to explore the interaction between a cell surface and the resulting polymer having anion clusters (PAAm-*graft*-PLLS). To detect the interaction between the cell surface and the model multivalent ligands having the anion clusters, we prepared the biotin monomer, labeling the prepolymer on the PAAm backbone. By ELISA, we confirmed that the anion clusters of the graft chains worked exclusively for the interaction with the cell and that the PAAm backbone was inert to the interaction with the cell. The anion clusters of the model

multivalent ligand may interact with cation cluster sites [e.g., P-selectin (*21*−*24*, *34*)] or anionic sites [via Ca^{2+} bridges (*35*)] on the cell surface under low ionic strength conditions. From a practical point of view, the nonspecific interaction of the model multivalent ligand PAAm-*graft*-PLLS with the cell was negligible under physiological salt conditions, so that we expect the multivalent effect of ligands to be properly extracted by incorporating ligands of interest into the PLL-*grafts*.

The multivalent effect has been studied by conjugating ligand molecules to soluble polymers or insoluble polymer matrices. In these cases, however, it is difficult to control the density and distribution of ligands. Indeed, the increase of ligand density must result in the formation of the clustered domain of ligands, so that we are unable to distinguish between cluster effect and density effect. The various PAAm-*graft*-PLL comb-type copolymers with the defined length and density of the PLL-*grafts* are the potential prepolymers to investigate and to optimize the affinity of the multivalent ligands for receptors.

ACKNOWLEDGMENT

This work was partially supported by a Grant-Aid (No. 09558115) from the Ministry of Education, Science, Sports and Culture of Japan. We are grateful to Dr. Yoshifumi Watanabe, Dr. Anwarul Ferdous, Dr. Noriyuki Adachi, Dr. Masahiko Morita, and Dr. Tsutomu Ishihara of the Tokyo Institute of Technology for their helpful discussions, technical assistance, and critical reading of the manuscript.

LITERATURE CITED

(1) Goldstein, J. L., Brown, M. S., Anderson, R. G. W., Russell, D. W., and Schneider, W. J. (1985) Receptor-mediated endocytosis: Concepts emerging from the LDL receptor system. *Annu. Rev. Cell Biol. 1*, 1−39.

(2) Hulme, E. C., Ed. (1992) Receptor−Ligand Interactions. *The Practical Approach Series*, IRL Press, Oxford, U.K.

(3) Lee, R. T., and Lee, Y. C. (1980) Preparation and some biochemical properties of neoglycoproteins produced by reductive amination of thioglycosides containing an *ω*-aldehydoaglycon. *Biochemistry 19*, 156−163.

(4) Stowell, C. P., Lee, R. T., and Lee, Y. C. (1980) Studies on the specificity of rabbit hepatic carbohydrate-binding protein using neoglycoproteins. *Biochemistry 19*, 4904−4908.

(5) Kawaguchi, K., Kuhlenschmidt, M., Roseman, S., and Lee, Y. C. (1981) Differential uptake of D-galactosyl- and D-glucosyl-neoglycoproteins by isolated rat hepatocytes. *J. Biol. Chem. 256*, 2230−2234.

(6) Lee, R. T., Myers, R. W., and Lee, Y. C. (1982) Further studies on the binding characteristics of rabbit liver galactose/*N*-acetylgalactosamine-specific lectin. *Biochemistry 21*, 6292−6298.

(7) Rice, K. G., Weisz, O. A., Barthel, T., Lee, R. T., and Lee, Y. C. (1990) Defined geometry of binding between triantennary glycopeptide and the asialoglycoprotein receptor of rat hepatocytes. *J. Biol. Chem. 265*, 18429−18434.

(8) Wu, P., Rice, K. G., Brand, L., and Lee, Y. C. (1991) Differential flexibilities in three branches of an *N*-linked triantennary glycopeptide. *Proc. Natl. Acad. Sci. U.S.A. 88*, 9355−9359.

(9) Kugumiya, T., Yagawa, A., Maeda, A., Nomoto, H., Tobe, S., Kobayashi, K., Matsuda, T., Onishi, T., and Akaike, T. (1992) Investigation of dynamic behaviors of asialoglycoprotein receptors of hepatocytes using a latex probe whose surface was coated with lactose-carrying polystyrene. *J. Bioactive Compatible Polym. 7*, 337−345.

(10) Kobayashi, A., Kobayashi, K., and Akaike, T. (1992) Control of adhesion and detachment of parenchymal liver cells using lactose-carrying polystyrene as substratum. *J. Biomater. Sci. Polym. Ed. 3*, 499−508.

(11) Kobayashi, A., Goto, M., Sekine, T., Masumoto, A., Yamamoto, N., Kobayashi, K., and Akaike, T. (1992) Regulation of differentiation and proliferation of rat hepatocytes by lactose-carrying polystyrene. *Artificial Organs 16*, 564−567.

(12) Kobayashi, K., Sumitomo, H., and Ina, Y. (1985) Synthesis and functions of polystyrene derivatives having pendant oligosaccharides. *Polym. J. 17*, 567−575.

(13) Kobayashi, A., Goto, M., Kobayashi, K., and Akaike, T. (1994) Receptor-mediated regulation of differentiation and proliferation of hepatocytes by synthetic polymer model of asialoglycoprotein. *J. Biomater. Sci. Polym. Ed. 6*, 325−342.

(14) Maruyama, A., Ishihara, T., Adachi, N., and Akaike, T. (1994) Preparation of nanoparticles bearing high-density carbohydrate chains using carbohydrate-carrying polymers as emulsifier. *Biomaterials 15*, 1035−1042.

(15) Cho, C. S., Jeong, Y. I., Ishihara, T., Takei, R., Park, J. U., Park, K. H., Maruyama, A., and Akaike, T. (1997) Simple preparation of nanoparticles coated with carbohydrate-carrying polymers. *Biomaterials 18*, 323−326.

(16) Adachi, N., Maruyama, A., Ishihara, T., and Akaike, T. (1994) Cellular distribution of polymer particles bearing various densities of carbohydrate ligands. *J. Biomater. Sci. Polym. Ed. 6*, 463−479.

(17) Welder, C. A., Lee, D. H. S., and Takei, F. (1993) Inhibition of cell adhesion by microspheres coated with recombinant soluble intercellular adhesion molecule-1. *J. Immunol. 150*, 2203−2210.

(18) Sayre, P. H., Hussey, R. E., Chang, H. C., Ciardelli, T. L., and Reinherz, E. L. (1989) Structural and binding analysis of a two domain extracellular CD2 molecule. *J. Exp. Med. 169*, 995−1009.

(19) Selvaraj, P., Plunkett, M. L., Dustin, M., Sanders, M. E., Shaw, S., and Springer, T. A. (1987) The T lymphocyte glycoprotein CD2 binds the cell surface ligand LFA-3. *Nature 326*, 400−403.

(20) Sayre, P. H., Chang, H. C., Hussey, R. E., Brown, N. R., Richardson, N. E., Spagnoli, G., Clayton, L. K., and Reinherz, E. L. (1987) Molecular cloning and expression of T11 cDNAs reveal a receptor-like structure on human T lymphocytes. *Proc. Natl. Acad. Sci. U.S.A. 84*, 2941−2945.

(21) Varki, A. (1994) Selectin ligands. *Proc. Natl. Acad. Sci. U.S.A. 91*, 7390−7397.

(22) Cecconi, O., Nelson, R. M., Roberts, W. G., Hanasaki, K., Mannori, G., Schultz, C., Ulich, T. R., Aruffo, A., and Bevilacqua, M. P. (1994) Inositol polyanions: Noncarbohydrate inhibitors of L- and P-selectin that block inflammation. *J. Biol. Chem. 269*, 15060−15066.

(23) Mulligan, M. S., Paulson, J. C., Frees, S. D., Zheng, Z. L., Lowe, J. B., and Ward, P. A. (1993) Protective effects of oligosaccharides in P-selectin-dependent lung injury. *Nature 364*, 149−151.

(24) Needham, L. K., and Schnaar, R. L. (1993) The HNK-1 reactive sulfoglucuronyl glycolipids are ligands for L-selectin and P-selectin but not E-selectin. *Proc. Natl. Acad. Sci. U.S.A. 90*, 1359−1363.

(25) Raja, R. H., Herzig, M., Grissom, M., and Weigel, P. H. (1986) Preparation and use of synthetic cell culture surfaces: A new reagent for the covalent immobilization of proteins and glycoproteins on a nonionic inert matrix. *J. Biol. Chem. 261*, 8505−8513.

(26) Daly, W. H., and Poché, D. (1988) The preparation of N-carboxyanhydrides of α-amino acids using bis(trichloromethyl)carbonate. *Tetrahedron Lett. 29*, 5859−5862.

(27) Kobayashi, K., Sumitomo, H., and Ina, Y. (1983) A carbohydrate-containing synthetic polymer obtained from *N*-*p*-vinylbenzyl-D-gluconamide. *Polym. J. 15*, 667−671.

(28) Heitzmann, H., and Richards, F. M. (1974) Use of the avidin−biotin complex for specific staining of biological membranes in electron microscopy. *Proc. Natl. Acad. Sci. U.S.A. 71*, 3537−3541.

(29) Spadaro, A. C. C., Draghetta, W., Lama, S. N. D., Camargo, A. C. M., and Greene, L. J. (1979) A convenient manual trinitrobenzenesulfonic acid method for monitoring amino acids and peptides in chromatographic column effluents. *Anal. Biochem. 96*, 317−321.

(30) Rempp, P. F., and Franta, E. (1984) Macromonomers: Synthesis, characterization and applications. *Adv. Polym. Sci. 58*, 1−53.
(31) Asayama, S., Maruyama, A., Cho, C. S., and Akaike, T. (1997) Design of comb-type polyamine copolymers for a novel pH-sensitive DNA carrier. *Bioconjugate Chem. 8*, 833−838.
(32) Green, N. M. (1975) Avidin. *Adv. Protein Chem. 29*, 85−133.
(33) Green, N. M. (1990) Avidin and streptavidin. *Methods Enzymol. 184*, 51−67.
(34) Takahasi, K., and Sawasaki, Y. (1992) Rare spontaneously transformed human endothelial cell line provides useful research tool. *In Vitro Cell Dev. Biol. 28A*, 380−382.
(35) Maurer, P., Hohenester, E., and Engel, J. (1996) Extracellular calcium-binding proteins. *Curr. Opin. Cell Biol. 8*, 609−617.

BC980093Y

^{99m}Tc-Labeling and in Vivo Studies of a Bombesin Analogue with a Novel Water-Soluble Dithiadiphosphine-Based Bifunctional Chelating Agent

Srinivasa R. Karra,[†] Roger Schibli,[†,‡] Hariprasad Gali,[†,‡] Kattesh V. Katti,[†] Timothy J. Hoffman,[†,§,∥] Chris Higginbotham,[∥] Gary L. Sieckman,[∥] and Wynn A. Volkert*[,†,∥]

Department of Radiology, Department of Chemistry, and Department of Medicine, University of Missouri—Columbia, Columbia, Missouri 65211, and H. S. Truman Memorial Veterans Hospital, Columbia, Missouri 65212. Received August 19, 1998; Revised Manuscript Received December 2, 1998

Recent progress in the synthesis of water-soluble phosphine ligand systems and their corresponding ^{99m}Tc complexes prompted the development of a new bifunctional chelating agent (BFCA) based on a tetradentate dithiadiphosphine framework (P_2S_2-COOH). The detailed synthesis of this new BFCA is described here. The corresponding ^{99m}Tc complex, ^{99m}Tc−P_2S_2-COOH, can be formed in >95% yield. To demonstrate the potential of this chelate to efficiently label peptides, ^{99m}Tc−P_2S_2-COOH was coupled to the N-terminal region of the truncated nine-amino acid bombesin analogue, 5-Ava-Gln-Trp-Ala-Val-Gly-His-Leu-Met-NH_2 [BBN$^{(7-14)}$], to form ^{99m}Tc−P_2S_2−BBN$^{(7-14)}$. Conjugation to the peptide was performed in borate buffer (pH 8.5) by applying the prelabeling approach in yields of >60%. In competitive binding assays, using Swiss 3T3 mouse fibroblast cells against [^{125}I-Tyr^4]bombesin, Re−P_2S_2−BBN$^{(7-14)}$ exhibited an IC_{50} value of 0.8 ± 0.4 nM. The pharmacokinetic studies of ^{99m}Tc−P_2S_2−BBN$^{(7-14)}$ and its ability to target tissue expressing gastrin-releasing peptide (GRP) receptors were performed in normal mice. The ^{99m}Tc−P_2S_2−BBN$^{(7-14)}$ exhibited fast and efficient clearance from the blood pool (0.6 ± 0.1% ID, 4 h postinjection) and excretion through the renal and hepatobiliary pathways (56.4 ± 8.2 and 28.1 ± 7.9% ID, 4 h postinjection, respectively). Significant uptake in the pancreas was observed (pancreatic acini cells express bombesin/GRP receptors), producing pancreas:blood and pancreas:muscle ratios of ca. 22 and 80, respectively, at 4 h postinjection.

INTRODUCTION

Small receptor-avid peptides have attracted considerable interest for use in thrombus, inflammation, and tumor imaging and tumor treatment (*1*, *2*, and references cited therein). A number of malignant tumors overexpress certain types of receptors on their surface which make them potential targets for imaging and therapy with radiolabeled synthetic antagonists and agonists. The 14-amino acid peptide bombesin (BBN) isolated from the skin of the amphibian Bombina and related gastrin-releasing peptides (GRP) exhibit an enhanced response in a variety of tumor tissues, e.g., in small cell lung, prostate, breast, and colon cancer (*3*−*6*). Analogues of bombesin with modified structures exhibited a similar or even higher affinity for these receptors (*7*−*9*). Today, corresponding synthetic peptides can be readily generated through automated solid phase techniques. For our studies, we produced and used the nine-amino acid bombesin analogue BBN$^{(7-14)}$ as a vehicle to target GRP receptors (Figure 1). The peptide BBN$^{(7-14)}$ has proved in the literature to be a potent GRP agonist. It can be radiolabeled with $^{123/131}$I or ^{105}Rh for potential nuclear medical applications by virtue of its retention of a high binding affinity for GRP receptors (*10*, *11*). We introduced an additional spacer function in the form of 5-aminopentanoic acid to the N-terminal region of the peptide to avoid interference of the chelating moiety with the receptor binding C-terminus of the peptide.

Most of the bifunctional chelating agents reported in the literature for labeling biomolecules with ^{99m}Tc and $^{186/188}$Re are based on N_2S_2 or N_3S frameworks. Sometimes, harsh reaction conditions (e.g., high temperatures and extended reaction times) are required to form the corresponding complexes with high specific activity or the labeling efficiency is low. Furthermore, these chelate moieties can exhibit often unfavorable physicochemical characteristics (e.g., high lipophilicity), which can play a critical role in maintaining high receptor binding affinity and in tumor uptake and also in the rate and route of clearance of a biomolecule from target and nontargeted tissues. The hydrazinonicotinamide (HYNIC) ligand system in combination with coligands offers today the only important alternative to the NS systems (*12*, *13*).

Our group is focused on the development of hydrophilic chelating moieties to achieve efficient clearance of the ^{99m}Tc or ^{188}Re conjugate from the blood pool through the kidneys into the urine with low retention of the radioactivity in the liver and the kidney. Initial in vitro and in vivo studies with water-soluble dithiadiphosphine ligand systems (Figure 2, I) and their corresponding technetium and rhenium complexes, synthesized in our laboratory, showed that they are highly soluble and

* To whom correspondence should be addressed: Department of Radiology, 409 Lewis Hall, University of Missouri, Columbia, MO 65211. E-mail: wynn_volkert@muccmail.missouri.edu. Phone: (573) 882-7695. Fax: (573) 882-6129.

[†] Department of Radiology, University of Missouri—Columbia.

[‡] Department of Chemistry, University of Missouri—Columbia.

[§] Department of Medicine, University of Missouri—Columbia.

[∥] H. S. Truman Memorial Veterans Hospital.

10.1021/bc980096a CCC: $18.00 © 1999 American Chemical Society
Published on Web 02/09/1999

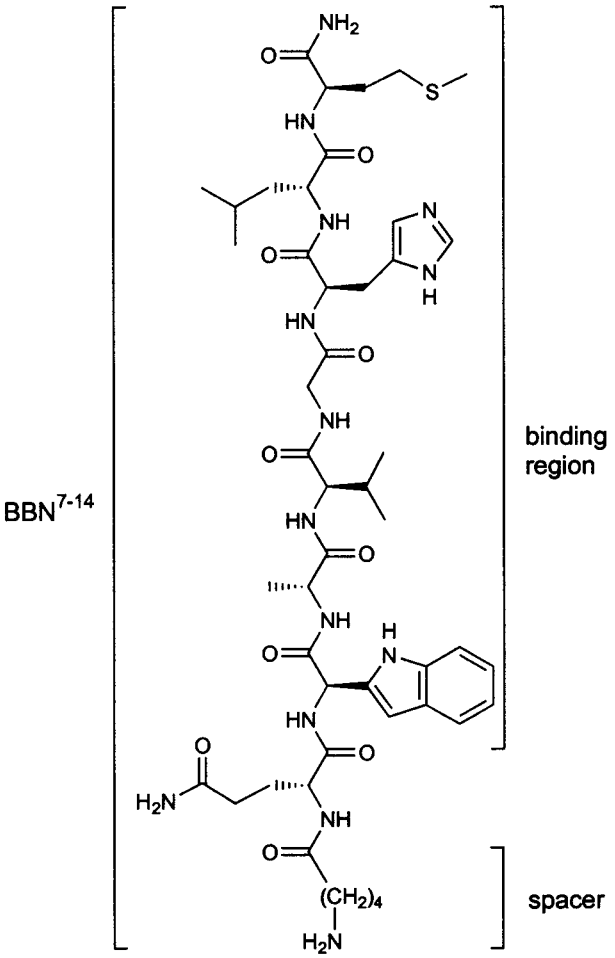
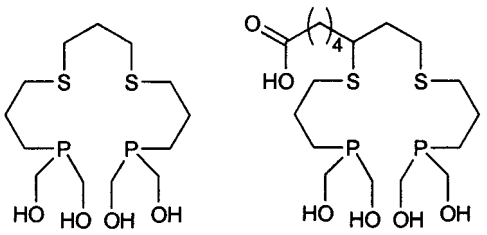


Figure 1. Bombesin analogue BBN$^{(7-14)}$.



I **II**

Figure 2. Structure of the model, dithiadiphosphine ligand P_2S_2 (I) and structure of the bifunctional dithiadiphosphine ligand P_2S_2-COOH (**4a**) (II) used for the studies.

stable in aqueous solutions (*14*−*16*). The excellent water solubility is facilitated by the positive overall charge of the chelate and by the four hydroxymethyl groups on the phosphine functionalities. The combination of sulfur and phosphorus exhibits enhanced σ-donor and good π-accepting properties for stabilizing the metal center. We recently developed the P_2S_2-COOH (**4b**) BFCA based on the dithiadihydroxymethylphosphine framework shown in Figure 2 (II). The complex with ^{99m}Tc demonstrated excellent in vitro and in vivo stability and the desirable clearance and excretion properties (*17*).

This study describes the synthesis and the radiolabeling of the new BFCA **4b** and demonstrates the utility of **4b** in labeling small bioactive peptides. The procedure of labeling BBN$^{(7-14)}$ with ^{99m}Tc−P_2S_2-COOH and the in vitro and in vivo behavior of the conjugate M−P_2S_2−BBN$^{(7-14)}$ (M = ^{99m}Tc or Re) are also presented.

EXPERIMENTAL PROCEDURES

Materials. All chemicals were obtained from either Aldrich Chemical Co. or Fisher Scientific. Diethyl (3-bromopropyl)phosphonate was synthesized utilizing Arbuzov Reaction and refluxing triethyl phosphite in a 10-fold excess of 1,3-dibromopropane for 1 h and then purified by vacuum distillation. DL-6,8-Dihydrothioctic acid and $ReO_2(py)_4Cl$ were synthesized according to the literature procedures (*18*, *19*). The Fmoc-protected amino acids were purchased from Nova Biochem. The chemicals and solvents were of reagent grade and were used without further purification. Na[$^{99m}TcO_4$] was eluted from a ^{99}Mo/^{99m}Tc generator (Mallinckrodt Medical, Inc.) using 0.9% saline. CF-1 normal mice were purchased from Taconic Labs. Swiss 3T3 mouse fibroblast cell lines were obtained from American Type Culture Collection (ATCC) and maintained and grown in the University of Missouri Cell and Immunology Care facilities. The [^{125}I-Tyr^4]-bombesin was purchased from DuPont Merck Pharmaceuticals. The peptide was synthesized on a Synergy 432A personal peptide synthesizer from Applied Biosystems.

Nuclear magnetic resonance spectra were recorded on a Bruker ARX-300 spectrometer. The ^{1}H and ^{13}C chemical shifts are reported relative to residual solvent protons as a reference, while the ^{31}P shifts are reported relative to an external reference of 85% H_3PO_4. IR spectra were recorded on a Mattson Galaxy Series FTIR 3000 spectrometer. FAB-mass spectral analyses were performed by the mass spectrometry laboratories at Washington University (St. Louis, MO). HPLC analyses were performed on a Waters 600E system equipped with a Waters 486 tunable absorption detector, a radiometric detector system, and a Waters 746 Data Module integrating recorder. HPLC solvents consisted of H_2O containing 0.1% trifluoroacetic acid (solvent A) and acetonitrile containing 0.1% trifluoroacetic acid (solvent B). For the radiochemical experiments (analysis and purification), a C-18 Hamilton PRP-1 column (10 μm, 150 mm × 4.1 mm) was used. The HPLC gradient system started with 95% A/5% B from 0 to 2 min followed by a linear gradient from 95% A/5% B to 50% A/50% B from 2 to 17 min. The gradient remained at 50% A/50% B for 9 min before ramping back to 95% A/5% B at 26 min. The flow rate was 1.5 mL/min. For the purification and quality control of the peptide, a C-18 Phenomenex Jupiter column (250 mm, 10 μm) was used. The gradient started with a linear gradient from 95% A/5% B to 30% A/70% B over the course of 25 min.

Preparation of Compound 1. A suspension of 60% NaH in mineral oil (6.5 g, 0.16 mol) was placed in a 1 L two-necked flask fitted with a septum and a N_2 inlet. The mineral oil was extracted with dry hexane (3 × 25 mL). The remaining NaH was suspended in dry THF (100 mL). Dihydrolipoic acid (10.5 g, 0.05 mol) in THF (15 mL) was added dropwise under N_2 via a syringe at 0 °C. The suspension was stirred for 30 min. Diethyl (3-bromopropyl)phosphonate (27.2 g, 0.10 mol) in THF (200 mL) was added slowly while the mixture was constantly being stirred. After 1 h, the excess NaH was quenched with 5 N HCl (50 mL). THF was removed under reduced pressure, and 500 mL of dichloromethane was added to the residue. The organic layer was washed with water (3 × 25 mL) and brine (100 mL) and dried over anhydrous Na_2SO_4. After removal of the solvent, the crude product was purified on a silica gel column (98:2 dichloromethane/methanol). The yield was 25.6 g (90%): LR-FAB-MS *m*/*z* 565.4 [M + 1]$^+$; IR (NaCl cell) 1724 cm^{-1} (s, $\nu_{C=O}$); ^{1}H NMR ($CDCl_3$) δ 4.17−4.13 (m, 8H), 2.79−2.66 (m, 8H),

2.36 (t, 2H), 2.15−1.99 (m, 4H), 1.90−1.3 (m, 8H), 1.36 (t, 12H); ^{13}C NMR ($CDCl_3$) δ 180.4, 61.4 (d, J = 6.4 Hz), 61.3 (d, J = 6.4 Hz), 44.5, 36.8, 34.5 (d, J = 13.8 Hz), 32.3 (d, J = 18.2 Hz), 30.5 (d, J = 18.2 Hz), 28.8, 26.4, 25.57, 24.23 (d, J = 141.4 Hz), 24.18 (d, J = 141.4 Hz), 22.6 (d, J = 4.4 Hz), 22.2 (d, J = 4.4 Hz), 16.2 (d, J = 6.0 Hz); ^{31}P NMR ($CDCl_3$) δ 31.8 (s), 31.6 (s).

Preparation of Compound 2. *N*-Methylmorpholine (2.3 g, 0.022 mol) and isobutyl chloroformate (3.1 g, 0.022 mol) were added to a solution of **1** (11.3 g, 0.02 mol) in dry THF (100 mL) at −15 °C under N_2. After 10 min, a solution of aniline (2.0 g, 0.022 mol) in THF (25 mL) and triethylamine (2.2 g, 0.22 mol) in THF (25 mL) were added at −15 °C. The mixture was allowed to warm to room temperature and stirred for 2 h. The precipitate of *N*-methylmorpholine hydrochloride was filtered, and the solvent was removed. The crude product was purified on a neutral alumina column (70:30 chloroform/hexane). The yield was 10.9 g (85%): LR-FAB-MS m/z 640.3 $[M + 1]^+$; IR (NaCl cell) 1657 cm^{-1} (s, $\nu_{C=O}$);^{1}H NMR ($CDCl_3$) δ 8.85 (br s, 1H), 7.62 (d, 2H, J = 7.6 Hz), 7.28 (dd, 2H, J_1 = 12.0 Hz, J_2 = 7.6 Hz), 7.05 (t, 1H, $J_1 = J_2$ = 7.4 Hz), 4.09 (m, 8H), 2.75−2.52 (m, 8H), 2.4−2.35 (2H), 2.0−1.5 (m, 15H), 1.33 (t, 6H, $J_1 = J_2$ = 7.1 Hz), 1.32 (t, 6H, $J_1 = J_2$ = 7.1 Hz); ^{13}C NMR ($CDCl_3$) δ 171.7, 138.7, 128.4, 123.3, 119.5, 61.4 (d, J = 5.9 Hz), 44.4, 36.9, 34.5, 34.3, 32.2 (d, J = 17.7 Hz), 30.8 (d, J = 17.7 Hz), 28.7, 26.0, 24.2 (d, J = 140.5 Hz), 24.1 (d, J = 142.6 Hz), 22.7 (d, J = 4.2 Hz), 22.2 (d, J = 4.3 Hz), 16.2 (d, J = 5.9 Hz); ^{31}P NMR ($CDCl_3$) δ 31.5 (s), 31.4 (s).

Preparation of Compound 3. Compound **2** (6.4 g, 0.01 mol) was dissolved in dry diethyl ether (100 mL) and the mixture placed in a 500 mL flask fitted with a reflux condenser. The solution was cooled to 0 °C, and 1 M $LiAlH_4$ in ether (15 mL, 0.15 mol) was added dropwise via a syringe under N_2. After the mixture was stirred at room temperature for 30 min, the reaction mixture was diluted with diethyl ether (200 mL). Then, a saturated solution of Na_2SO_4 (25 mL) was added at 0 °C to quench the excess $LiAlH_4$. The organic layer was cannulated and the ether removed under reduced pressure at room temperature to give the crude diphosphine **3**, which was used without further purification: ^{31}P NMR ($CDCl_3$) δ −137.5 (s).

Preparation of Compound 4a. The crude diphosphine **3** was dissolved in degassed ethanol (15 mL). A solution of 37% formaldehyde (9 g, 0.1 mol) in ethanol (5 mL) and 5 mL of 30% HCl was added, and the mixture was stirred for 10 min under N_2 at room temperature and then refluxed for 5 h. The solvents were removed under reduced pressure to give the crude (hydroxymethyl)phosphonium chloride **4a**. The crude product was purified with a reverse phase Sep-Pak C-18 column using a water/methanol gradient. The yield was 3.0 g (45%): LR-FAB-MS m/z 573.6 $[M - Cl]^+$; ^{1}H NMR (D_2O) δ 4.49 (m, 12H), 2.75−2.5 (m, 7H), 2.45−2.20 (m, 6H), 2.0−1.20 (m, 12H); ^{13}C NMR (D_2O) δ 180.0, 51.1 (d, J = 54.5 Hz), 45.1, 34.8, 34.7, 32.7 (d, J = 15.9 Hz), 31.2 (d, J = 15.8 Hz), 29.3, 26.6, 25.2, 22.4 (d, J = 4.1 Hz), 21.9 (d, J = 4.1 Hz), 13.7 (d, J = 41.2 Hz), 13.6 (d, J = 41.1 Hz); ^{31}P NMR (D_2O) δ 28.6 (s).

Preparation of Compound 4c. A solution of compound **4a** (901 mg, 1.48 mmol) in water (100 mL) was added to a solution of $[ReO_2(py)_4]Cl$ (py = pyridine) (200 mg, 0.37 mmol) in water (25 mL), and the reaction mixture was refluxed for 5 h. The reaction solution was concentrated and purified on a reverse phase Sep-Pak C-18 column (35 cm^3, 10 g) using a water/methanol gradient to obtain pure compound **4c** as a purple viscous oily liquid. The yield was 148 mg (55% based on Re): LR-FAB-MS m/z 694.9 $[M - Cl]^+$; IR (NaCl cell) 3333 (bs, ν_{O-H}), 1724 (s, $\nu_{C=O}$), 912 (s, ν_sO═Re═O), 795 cm^{-1} (s, ν_{as}O═Re═O); ^{1}H NMR (D_2O) δ 4.30 (m, 8H), 3.43 (br s, 4H), 3.20 (br s, 1H), 2.90 (br t, 2H), 2.45 (br m, 5H), 2.19 (br t, 6H), 1.66 (br m, 2H), 1.31 (br m, 4H); ^{13}C NMR (D_2O) δ 179.1 (s), 59.4 (s), 58.9 (s), 58.5 (d), 58.0 (d), 49.9 (s), 38.4 (s), 37.2 (s), 34.0 (s), 33.3 (s), 33.1 (s), 30.1 (s), 24.5 (s), 24.2 (s), 20.9 (s), 17.8 (d), 17.5 (d); ^{31}P NMR (D_2O) δ −7.9 (d, J_{PP} = 12 Hz), −8.8 (d, J_{pp} = 12 Hz).

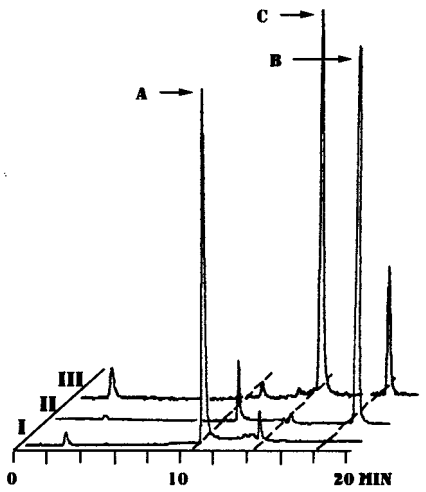


Figure 3. ^{99m}Tc HPLC traces of the products formed during the labeling procedure: (A) ^{99m}Tc−P_2S_2-COOH, (B) ^{99m}Tc−P_2S_2−PFP, and (C) ^{99m}Tc−P_2S_2−BBN$^{(7-14)}$. A reverse phase C-18 column was used for the characterization and purification of the compounds.

^{99m}Tc-Labeling of 4b. For the preparation of the ligand, 5 mg (8.2 μmol) of **4a** was dissolved in 1 mL of H_2O. One hundred microliters of a 1 M $NaHCO_3$ buffer solution (pH 9) was added to produce **4b**. Thirty microliters of the stock solution of **4b** was added to 500 μL of Na[$^{99m}TcO_4$] in saline and the mixture vortexed. The technetium was reduced by addition of 10 μL of a degassed, presaturated stannous tartrate solution to form ^{99m}Tc−P_2S_2-COOH within 10 min at room temperature. The formation of the product was confirmed by reverse phase HPLC (>95% yield). The retention time of Na[$^{99m}TcO_4$] was 1.2 min, whereas ^{99m}Tc−P_2S_2-COOH had a retention time of 10.9 min (Figure 3, I).

Activation of the Acid Functionality of ^{99m}Tc−P_2S_2-COOH. The carboxylic acid group of ^{99m}Tc−P_2S_2-COOH was activated with pentafluorophenol (PFP) using 1-ethyl-3-[3-(dimethylamino)propyl]carbodiimide methiodide (EDC) to form ^{99m}Tc−P_2S_2−PFP ester. Ten milligrams of EDC (0.3 mmol) and 6 mg of PFP (0.3 mmol in 100 μL of acetonitrile) were added to 500 μL of a freshly prepared ^{99m}Tc−P_2S_2-COOH solution in a 10 mL test tube. The reaction mixture was vortexed for 1 min and kept at room temperature for 20 min. The solution was centrifuged for 2 min, and the aqueous layer was separated from the oily drops of PFP containing >80% of the initial activity in the form of ^{99m}Tc−P_2S_2−PFP. The product was separated from the excess PFP by HPLC after dissolving the oily drops in 200 μL of acetonitrile. The activated ester had a retention time of 18.1 min (Figure 3, II), whereas PFP had a retention of 20.4 min (monitored at 254 nm) on the reverse phase HPLC system. The aqueous layer contained 20% of the initial radioactivity in form of ^{99m}Tc−P_2S_2−PFP (ca. 60%) and some unreacted ^{99m}Tc−P_2S_2-COOH (ca. 40%).

Coupling of ^{99m}Tc−P_2S_2−PFP Ester to BBN$^{(7-14)}$. The pH of a previously HPLC-purified solution of ^{99m}Tc−

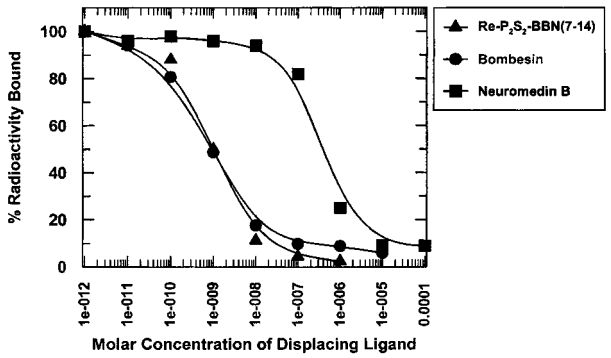


Figure 4. Competitive binding of peptide Re−P_2S_2−BBN$^{(7-14)}$ vs [^{125}I-Tyr^4]bombesin using Swiss 3T3 mouse fibroblast cells. Competitive binding of bombesin and Neuromedin B vs [^{125}I-Tyr^4]bombesin in the same cell line performed as controls which have IC_{50} values of 4 and 1000 nM, respectively (*22*).

P_2S_2−PFP was adjusted to 8.5 using borate buffer (0.1 M). Approximately 1 mg of BBN$^{(7-14)}$ (0.9 μmol) was added to a 500 μL aliquot of a ^{99m}Tc−P_2S_2−PFP solution and the reaction mixture vortexed for 1 min and incubated for 30 min at room temperature. The reaction was monitored by reverse phase HPLC. The final product [^{99m}Tc−P_2S_2−BBN$^{(7-14)}$] was separated from excess BBN$^{(7-14)}$ using the standard HPLC gradient. The conjugate exhibited a retention time of 14.6 min (Figure 3, III), whereas the free BBN$^{(7-14)}$ exhibited a retention time of 12.3 min. The coupling yields were usually between 70 and 80% as determined radiometrically.

Preparation of the Re Analogue of the Conjugate. The Re−P_2S_2−BBN$^{(7-14)}$ was synthesized by solid phase peptide synthesis. ReO_2−P_2S_2-COOH was introduced in the last step of the peptide synthesis. After the peptide was cleaved from the resin, the product was purified by reverse phase HPLC. The molecular constitution of Re−P_2S_2−BBN$^{(7-14)}$ was confirmed by FAB mass spectroscopy. The FAB mass spectral analysis confirmed the presence of a $[O{=}Re{=}O]^+$ core. This is in agreement with the observation made by Smith et al. for similar Re(V) complexes with P_2S_2 ligands (*15*). The conjugate exhibited a retention time of 15.2 min (monitored at 350 nm): FAB-MS *m/e* (M + 1) calcd 1616.89, found 1616.4.

In Vitro Binding Assay of Re−P_2S_2−BBN$^{(7-14)}$. In vitro BBN−receptor binding capabilities of the labeled peptide were assessed utilizing displacement binding assays conducted at 37 °C in Swiss 3T3 fibroblast cells with a method similar to that designed by Mahmoud et al. (*20*). The IC_{50} value was determined for the non-radiolabeled Re−P_2S_2−BBN$^{(7-14)}$ analogue by analyzing displacement of bound [^{125}I-Tyr^4]bombesin (Figure 4). In vitro binding assays were performed under identical conditions using active BBN and Neuromedin B as positive and negative controls, respectively (Figure 4).

Biodistribution of ^{99m}Tc−P_2S_2−BBN$^{(7-14)}$ in Normal Mice. Normal CF-1 mice (average weight, 25 g) were used for the biodistribution studies (Tables 1 and 2). The pH of the HPLC-purified ^{99m}Tc−P_2S_2−BBN$^{(7-14)}$ solution was adjusted to physiological conditions using a 0.01 M phosphate buffer (pH 7.4). Aliquots (80−100 μL) of the labeled peptide solution (55−75 kBq) were injected into each animal via the tail vein. Tissues and organs were excised from the sacrificed animals 30 min, 1 h, and 4 h postinjection. The organs and tissue were weighed; the activity was counted in a NaI counter, and the percent injected dose per organ and the percent injected dose per gram were calculated. The % ID in whole blood was estimated assuming a blood volume of 6.5% of the total body weight. Receptor blocking studies were also carried out where excess BBN$^{(7-14)}$ was administered to animals for in vivo saturation of GRP receptors prior to injection of ^{99m}Tc−P_2S_2−BBN$^{(7-14)}$ (Tables 3 and 4). In these studies, each animal received a subcutaneous injection of 1 mg of BBN$^{(7-14)}$ dissolved in 100 μL of a mixture of saline/acetonitrile/DMF (90:5:5) 35 min prior to the injection of ^{99m}Tc−P_2S_2−BBN$^{(7-14)}$. Control (unblocked) animals received an injection of 100 μL of the solvent mixture without BBN$^{(7-14)}$ 35 min prior to the injection of ^{99m}Tc−P_2S_2−BBN$^{(7-14)}$. The animals were sacrificed 30 min postinjection and the tissues removed, weighed, and counted as previously described.

Table 1. Biodistribution (% ID per Organ)[a] of ^{99m}Tc−P_2S_2−BBN$^{(7-14)}$ in Normal Mice as a Function of Time after Intravenous Administration

organ	0.5 h[b]	1 h	4 h
brain	0.04 ± 0.02	0.01 ± 0.01	0.03 ± 0.3
blood[c]	1.7 ± 0.03	0.9 ± 0.50	0.6 ± 0.07
heart	0.1 ± 0.01	0.1 ± 0.02	0.1 ± 0.02
lung	0.2 ± 0.03	0.1 ± 0.02	0.1 ± 0.03
liver	10.0 ± 1.50	7.4 ± 1.10	5.3 ± 0.80
intestines	30.8 ± 1.82	33.1 ± 3.95	28.1 ± 7.94
stomach	0.7 ± 0.33	0.7 ± 0.11	0.4 ± 0.10
kidneys	2.1 ± 0.10	1.7 ± 0.10	1.3 ± 0.15
pancreas	6.8 ± 0.90	4.7 ± 0.53	2.4 ± 0.25
urine	36.3 ± 2.80	43.8 ± 2.90	56.5 ± 8.20

[a] Values represent the mean ± SD ($n = 5$) of the percent injected dose per organ. [b] $n = 4$. [c] The total blood volume is estimated to be 6.5% of the body weight.

Table 2. Biodistribution (% ID per Gram)[a] of ^{99m}Tc−P_2S_2−BBN$^{(7-14)}$ in Normal Mice as a Function of Time after Intravenous Administration

organ	0.5 h[b]	1 h	4 h
brain	0.04 ± 0.01	0.1 ± 0.1	0.11 ± 0.07
blood[c]	1.0 ± 0.20	0.5 ± 0.28	0.4 ± 0.06
heart	0.4 ± 0.03	0.4 ± 0.20	0.1 ± 0.02
lung	1.1 ± 0.16	0.8 ± 0.23	0.4 ± 0.20
liver	6.9 ± 1.11	5.1 ± 0.45	4.0 ± 0.86
kidneys	6.3 ± 0.17	4.8 ± 0.48	3.7 ± 0.44
pancreas	21.3 ± 2.10	17.4 ± 3.40	8.5 ± 1.25
muscle	0.3 ± 0.10	0.1 ± 0.05	0.1 ± 0.02

[a] Values represent the mean ± SD ($n = 5$) of the percent injected dose per gram unless otherwise indicated. [b] $n = 4$. [c] The total blood volume is estimated to be 6.5% of the body weight.

Table 3. BBN Receptor Blocking Studies in Normal Mice (% ID per Organ)[a]

organ	unblocked	blocked[b]	organ	unblocked	blocked[b]
stomach	0.6 ± 0.10	0.3 ± 0.10	liver	9.1 ± 2.40	8.7 ± 1.67
blood[c]	1.3 ± 0.60	1.4 ± 0.34	kidneys	2.0 ± 0.20	1.7 ± 0.10
urine	44.4 ± 7.30	55.1 ± 2.60	pancreas	6.5 ± 0.25	0.6 ± 0.33
intestines	27.0 ± 6.90	23.6 ± 4.43			

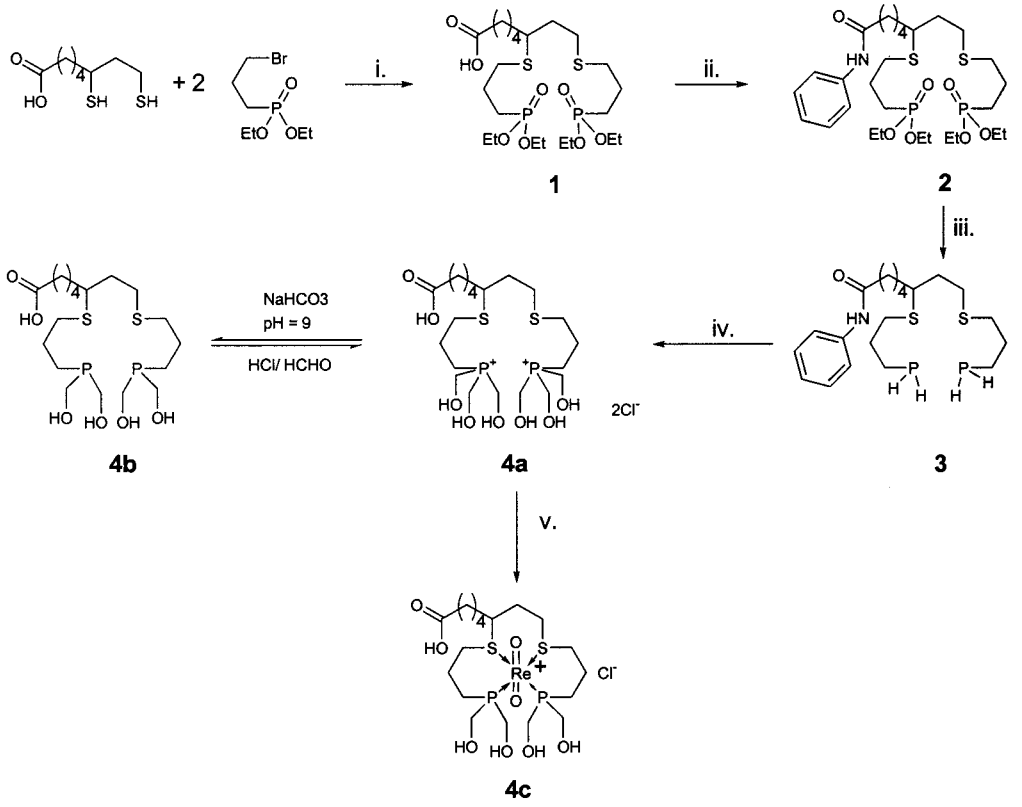
[a] $n = 5$. [b] One milligram of BBN$^{(7-14)}$ was subcutaneously administered 35 min prior to the injection of ^{99m}Tc−P_2S_2−BBN$^{(7-14)}$. [c] The total blood volume is estimated to be 6.5% of the body weight.

Table 4. BBN Receptor Blocking Studies in Normal Mice (% ID per Gram)[a]

organ	unblocked	blocked[b]	organ	unblocked	blocked[b]
blood[c]	0.7 ± 0.36	0.8 ± 0.20	kidneys	5.1 ± 0.50	4.5 ± 0.40
muscle	0.2 ± 0.10	0.1 ± 0.10	pancreas	20.2 ± 1.70	1.7 ± 1.20
liver	6.0 ± 1.10	5.9 ± 1.10			

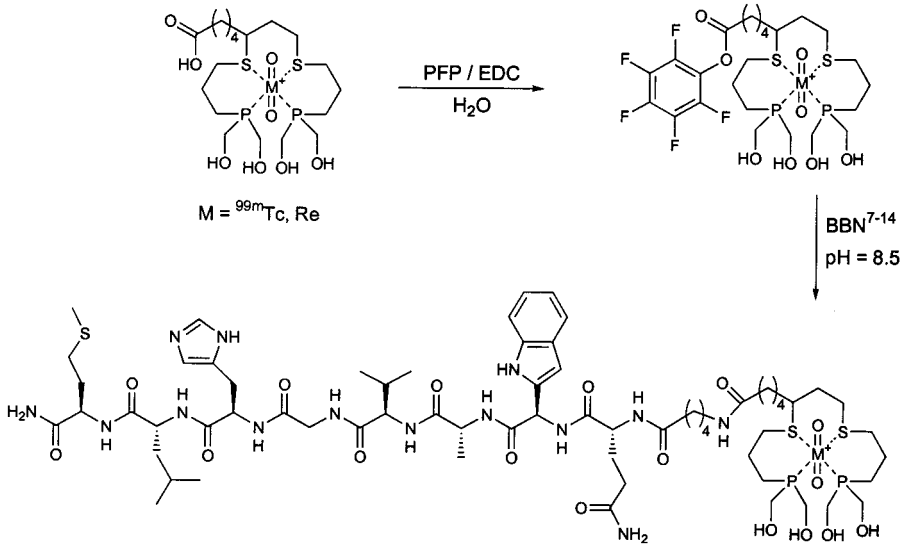
[a] $n = 5$. [b] One milligram of BBN$^{(7-14)}$ was subcutaneously administered 35 min prior to the injection of ^{99m}Tc−P_2S_2−BBN$^{(7-14)}$. [c] The total blood volume is estimated to be 6.5% of the body weight.

Scheme 1. Synthesis of the P_2S_2-COOH Ligand and Its Complexation with Re(V)



i. NaH, THF; ii. N-methylmorpholine, isobutyl chloroformate, aniline, THF; iii. $LiAlH_4$, Et_2O; iv. HCHO, 5 N HCl, ethanol; v. $ReO_2(py)_4Cl$, H_2O Reflux, 5h

Scheme 2. Procedure for Labeling BBN$^{(7-14)}$ with ^{99m}Tc−P_2S_2-COOH



RESULTS AND DISCUSSION

The crucial molecular building block for the bifunctionalization of the P_2S_2 ligand system is the commercially available DL-α-lipoic acid. The bifunctional ligand **4a** was produced in four steps outlined in Scheme 1. The synthetic procedure for forming the P_2S_2 backbone is identical with that applied for the underivatized P_2S_2 ligand (Figure 2, I) described by Smith et al. (*15*). The carboxylic acid was protected with aniline for the reduction step of the phosphonate groups using a procedure described by Barton et al. (*21*). The (hydroxymethyl)-phosphonium chloride **4a** was prepared by formylation of the P−H bonds of **3** in oxygen-free ethanol in the presence of excess aqueous formaldehyde and hydrochloric acid. In the same step, the carboxylic acid function was deprotected.

The new compounds, **1**, **2**, and **4b**, were characterized by ^{1}H, ^{13}C, and ^{31}P NMR and IR spectroscopy and mass spectrometry. Compound **3**, which is an intermediate, was characterized by ^{31}P NMR spectroscopy only. Ligands **4a,b** are highly soluble in water. The formation of the phosphonium salt of the ligand **4** has two advantages.

(1) Purification of the phosphonium salt **4a** is more convenient than that of **4b**. (2) Due to the formation of the phosphonium salt, the P^{III} centers are protected against oxidation, and the ligand can be stored under aerobic conditions for a long period of time. This is an important advantage for a kit formulation in which ligand systems with (hydroxymethyl)phosphine groups are used. **4a** can be readily converted into **4b** by adding small amounts of a base before complexation with a metal center. It is noteworthy that **4b** is oxidatively stable even under high levels of dilution in aqueous media for several hours, which was confirmed in the ^{31}P NMR experiments.

The prelabeling approach was selected to radioactively conjugate the peptide, as difficulties were encountered in activating the carboxylic acid in **4a,b**. ^{99m}Tc−P_2S_2-COOH can be produced either by direct reduction of Na[$^{99m}TcO_4$] with stannous tartrate in the presence of **4b** (total ligand concentration in the samples is on the order of 10^{-5} M) or by the ligand exchange reaction starting with [^{99m}Tc]gluconate and **4b** at room temperature (*17*). In both cases, the complex was efficiently produced (>95%) as a single species which was confirmed by HPLC (Figure 3, I). However, we were only able to form the active ester complex ^{99m}Tc−P_2S_2−PFP in good yields in the absence of the trans-chelating gluconate ligand. Therefore, only direct reduction of the ^{99m}Tc center in the presence of **4b** was employed for these studies. ^{99m}Tc−P_2S_2−PFP was produced in good yields (>90%) in a 0.9% saline solution using an excess of EDC and PFP at room temperature. The HPLC profile again showed the formation of a single species (Figure 3, II). ^{99m}Tc−P_2S_2−PFP is remarkably stable under acidic conditions and could be purified and collected by HPLC where only minor reformation of ^{99m}Tc−P_2S_2-COOH was observed 2 h after collection of ^{99m}Tc−P_2S_2−PFP. For the final labeling step of BBN$^{(7-14)}$, the pH of the purified ^{99m}Tc−P_2S_2−PFP solution was adjusted to 8.5 using a 0.1 M borate buffer. An aliquot of 500 μL of the ^{99m}Tc−P_2S_2−PFP solution was added to 1 mg of the peptide and the mixture incubated at room temperature. HPLC profile III, shown in Figure 3, revealed that after 30 min ^{99m}Tc−P_2S_2−BBN$^{(7-14)}$ was formed as a single species in approximately 80% yield. Extension of the incubation time did not lead to the complete formation of the conjugate due to the decomposition of the remaining ^{99m}Tc−P_2S_2−PFP back to ^{99m}Tc−P_2S_2-COOH. The labeled peptide was separated from unlabeled BBN$^{(7-14)}$ by HPLC and collected into 0.1 M phosphate buffer to achieve physiological pH conditions for use in animal studies.

To evaluate the biological activity of the labeled peptide in vitro, the ability of the nonradioactive conjugate Re−P_2S_2−BBN$^{(7-14)}$ to bind to the GRP receptors on Swiss 3T3 mouse fibroblast cells was examined. The cell binding studies were carried out using [^{125}I-Tyr^4]bombesin as the competitive BBN analogue. The results of the experiments shown in Figure 4 demonstrated the high binding affinity of Re−P_2S_2−BBN$^{(7-14)}$. The IC_{50} value was determined to be 0.8 ± 0.4 nM and is comparable with those of bombesin and its analogues that are considered to have sufficiently high binding affinity for potential use as targeting vectors for GRP receptor-expressing cancers in vivo.

Results of the in vivo biodistribution experiments with ^{99m}Tc−P_2S_2−BBN$^{(7-14)}$ in normal mice are summarized in Tables 1 and 2. The conjugate ^{99m}Tc−P_2S_2−BBN$^{(7-14)}$ exhibited rapid clearance from the blood pool (0.6 ± 0.07% ID at 4 h postinjection) and nontargeted tissues. The excretion of the radioactivity from the body occurs in both the renal (56.5 ± 8.20% ID, 4 h postinjection) and the hepatobiliary (liver and intestines, ca. 35% ID, 4 h postinjection) pathways. Only small amounts of activity were retained in the kidneys 4 h postinjection (1.3 ± 0.15% ID). There was some retention of the conjugate in the liver (5.3 ± 0.80% ID, 4 h postinjection). The amount of radioactivity found in the stomach, an indication of an in vivo decomposition of a ^{99m}Tc conjugate and the reformation of [$^{99m}TcO_4$]$^-$, was negligible (0.4 ± 0.10% ID, 4 h postinjection). This provides important evidence that the P_2S_2 ligand system is capable of stabilizing ^{99m}Tc even under in vivo conditions. A significant uptake of radioactivity was observed in the pancreas (4.7 ± 0.53 or 17.4 ± 3.40% ID/g, 1 h postinjection), demonstrating the ability of ^{99m}Tc−P_2S_2−BBN$^{(7-14)}$ to target in vivo GRP-expressing cells (acini cells in the pancreas express GRP receptors that are accessible to the blood stream). The pancreas:muscle and pancreas:blood ratios (based on % ID per gram) reached a maximum of 80 and 22, respectively, at 4 h postinjection. Furthermore, receptor blocking studies with BBN$^{(7-14)}$ confirmed the specificity of BBN$^{(7-14)}$ or ^{99m}Tc−P_2S_2−BBN$^{(7-14)}$ toward the GRP receptors. The difference in the uptake of ^{99m}Tc−P_2S_2−BBN$^{(7-14)}$ in the pancreas with and without subcutaneous injection of 1 mg of BBN$^{(7-14)}$ is significant (0.6 ± 0.33 and 6.5 ± 0.25% ID, respectively). The uptake of the ^{99m}Tc-labeled peptide in all other organs and tissue was not affected by the blocking experiment (Tables 3 and 4).

CONCLUSION

The detailed synthesis and characterization of the first water-soluble, bifunctional chelator **4a,b** based on a P_2S_2 framework is presented. Furthermore, the ability of the novel BFCA to form an in vitro and in vivo stable complex with ^{99m}Tc and its utility for the radiolabeling of receptor-avid peptides are demonstrated. Although the prelabeling procedure with ^{99m}Tc−P_2S_2-COOH is time-consuming, a P_2S_2 chelating system might, in the future, serve as a potential alternative to the known tetradentate N_2S_2, N_3S, and HYNIC ligand systems. In fact, recent experiments showed that the synthetic precursor **3** (after deprotection of the acid function) can be efficiently attached to the N-terminal function of peptides. The hydroxymethyl functions are subsequently introduced to the $[H_2P]_2S_2$ peptide conjugate to achieve the favorable in vivo characteristics of the chelating moiety. This enables in the future a more convenient postlabeling approach of a P_2S_2-functionalized peptide.

ACKNOWLEDGMENT

This work was supported by NIH Grant R01-CA72421, DuPont-Merck Pharmaceuticals, and the Departments of Chemistry and Radiology of the University of Missouri—Columbia.

LITERATURE CITED

(1) Liu, S., Edwards, D. S., and Barrett, J. A. (1997) ^{99m}Tc Labeling of High Potent Small Peptides. *Bioconjugate Chem. 8*, 621−636.

(2) Lister-James, J., Moyen, B. R., and Dean, T. (1996) Small peptides radiolabeled with ^{99m}Tc. *Q. J. Nucl. Med. 40*, 221−233.

(3) Moody, T. W., Carney, D. N., Cuttita, F., Quattrocchi, K., and Minna, J. D. (1985) High affinity of receptors for bombesin/GRP-like peptides on human small cell cancer. *Life Sci. 37*, 105−113.

(4) Qin, Y., Ertl, T., Cai, R. Z., Halmos, G., and Schally, A. V. (1994) Inhibitory effect of bombesin receptor antagonist RC-

3095 on the growth of human pancreatic cancer cells *in vivo* and *in vitro*. *Cancer Res. 54*, 1035−1041.
(5) Pinski, J., Schally, A. V., Halmos, G., Yano, T., Szepeshazi, K., and Groot, K. (1994) Somatostatin analogues and bombesin/gastrin releasing peptide antagonist RC-3095 inhibit the growth of glioblastomas *in vitro* and *in vivo*. *Cancer Res. 54*, 5895−5901.
(6) Radulovic, S., Miller, G., and Schally, A. V. (1991) Inhibition of growth of HT-29 human colon cancer xenografs in nude mice by treatment with bombesin/gastrin releasing peptide antagonist (RC-3095). *Cancer Res. 51*, 6006−6009.
(7) Jensen, R. T., Jones, S. W., Folkers, K., and Gardner, J. D. (1984) A synthetic peptide that is a bombesin receptor antagonist. *Nature 309*, 61−63.
(8) Safavy, A., Khazaeli, M. B., Qin, H., and Buchsbaum, D. J. (1997) Synthesis of Bombesin Analogues for Radiolabeling with Rhenium-188. *Cancer Suppl. 80*, 2354−2359.
(9) Baidoo, K. E., Lin, K.-S., Zhan, Y., Finley, P., Scheffel, U., and Wagner, H. N., Jr. (1998) Design, Synthesis, and Initial Evaluation of High-Affinity Technetium Bombesin Analogues. *Bioconjugate Chem. 9*, 218−225.
(10) Hoffman, T. J., Sieckman, G. L., and Volkert, W. A. (1995) Targeting Small Cell Lung Cancer Using Iodinated Peptide Analogs. *J. Labelled Comp. Radiopharm. 37*, 321−323.
(11) Li, N., Hoffman, T. J., Sieckman, G. L., Ochrymowycz, L. A., Higginbotham, C., Strutman, M., Volkert, W. A., and Ketring, A. R. (1996) *In vitro* and *in vivo* characterization of Rh-105-Tetrathiamacrocycle conjugate of a bombesin analogue. *J. Nucl. Med. 37* (Suppl.), 61P.
(12) Barrett, J. A., Crocker, A. C., Damphousse, D. J., Heminway, S. J., Liu, S., Edwards, S. D., Lazewatsky, J. L., Kagan, M., Mazaika, T. J., and Carroll, T. R. (1997) Biological Evaluation of Thrombus Imaging Agents Utilizing Water-Soluble Phosphines and Tricine as Coligands When Used to Label a Hydrazinonicotinamide-Modified Cyclic Glycoprotein IIb/IIa Receptor Antagonist with ^{99m}Tc. *Bioconjugate Chem. 8*, 155−160.
(13) Edwards, S. D., Liu, S., Barrett, J. A., Harris, A. R., Looby, R. J., Ziegler, M. C., Heminway, S. J., and Carroll, T. R. (1997) New and Versatile Ternary Ligand Systems for Technetium Radiopharmaceuticals: Water-Soluble Phosphines and Tricine as Coligands in Labeling a Hydrazinonicotinamide-Modified Cyclic Glycoprotein IIb/IIa Receptor Antagonist with ^{99m}Tc. *Bioconjugate Chem. 8*, 146−154.
(14) Smith, C. J., Reddy, V. S., Karra, S. R., Katti, K. V., and Barbour, L. J. (1997) Synthesis and Coordination Chemistry of the First Water-Soluble Dithio-Bis(phosphine) Ligands $[(HOH_2C)_2P(CH_2)_2S\text{-}X\text{-}S(CH_2)P(CH_2OH)_2]$ (X = $(CH_2)_3$ or C_6H_4). X-ray Crystal Structure of $[Pd[(HOH_2C)_2P(CH_2)_2S\text{-}(CH_2)_3S(CH_2)P(CH_2OH)_2](Cl)_2$. *Inorg. Chem. 36*, 1786−1791.
(15) Smith, C. J., Katti, K. V., Volkert, W. A., and Barbour, L. J. (1997) Synthesis and Characterization of Chemically Flexible, Water-Soluble Dithio-Bis(phosphine) Compounds: $(HOH_2C)_2P(CH_2)_2S(CH_2)_3S(CH_2)_2P(CH_2OH)_2$, $(HOH_2C)_2P\text{-}(CH_2)_2S(CH_2)_4S(CH_2)_2P(CH_2OH)_2$, and $(HOH_2C)_2P(CH_2)_3S\text{-}(CH_2)_3S(CH_2)_3P(CH_2OH)_2$. Systematic Investigation of the Effect of Chain Length on the Coordination Chemistry of Rhenium(V). X-ray Crystal Structure of $[ReO_2(HOH_2C)_2P\text{-}(CH_2)_2S(CH_2)_3S(CH_2)_2P(CH_2OH)_2]_2(Cl)_2$, $[ReO_2(HOH_2C)_2P\text{-}(CH_2)_2S(CH_2)_4S(CH_2)_2P(CH_2OH)_2]_2(ReO_4)_2$, and $[ReO_2(HOH_2C)_2P\text{-}(CH_2)_2S(CH_2)_3S(CH_2)_2P(CH_2OH)_2](Cl)$. *Inorg. Chem. 36*, 3928−3935.
(16) Smith, C. J., Li, N., Katti, K. V., Higginbotham, C., and Volkert, W. A. (1997) *In vitro* and *in vivo* Characterization of Novel Water-Soluble Dithio-Bisphosphine ^{99m}Tc Complexes. *J. Nucl. Med. Biol. 24*, 685−691.
(17) Schibli, R., Karra, S. R., Gali, H., Katti, K. V., Higginbotham, C., and Volkert, W. A. (1998) *In vitro* and *in vivo* Characterization of a Novel Bifunctionalized Water-Soluble Dithia-Bisphosphine ^{99m}Tc Complex. *Radiochim. Acta* (In press).
(18) Wagner, A. F., Walton, E., Boxer, G. E., Pruss, M. P., Holly, F. W., and Folkers, K. (1956) Properties and derivatives of α-lipoic acid. *J. Am. Chem. Soc. 78*, 5079−5081.
(19) Beard, J. H., Casey, J., and Murmann, R. K. (1965) The preparation and properties of $[Re(amine)_4O_2]^+$ type ions. *Inorg. Chem. 4*, 797−803.
(20) Mahmoud, S., Stanley, J., Taylor, J., Bogden, A., Moreau, J. P., Coy, D., Avis, I., Cuttitta, F., Mulshine, J. L., and Moody, T. W. (1991) [Psi 13, 14] bombesin analogues inhibit growth of small cell lung cancer *in vitro* and *in vivo*. *Cancer Res. 51*, 1798−1802.
(21) Barton, F. H. R., Herve, Y., Potier, P., and Thierry, J. (1988) Manipulation of the carboxylic groups of α-amino acids and peptides using radical chemistry based on esters of N-hydroxy-2-thiopyridone. *Tetrahedron 44*, 5479−5486.
(22) Moody, T. W., Venugopal, R., Hu, V., Gozes, Y., McDermed, J., and Leban, J. J. (1996) BW 1023490: A new GRP receptor antagonist for small-cell lung cancer cells. *Peptides 17*, 1337−1343.

BC980096A

Synthesis and Electrochemistry of Anthraquinone−Oligodeoxynucleotide Conjugates

Neil A. Whittemore,[†] Adam N. Mullenix,[†] Gopal B. Inamati,[‡] Muthiah Manoharan,[‡] P. Dan Cook,[‡] Albert A. Tuinman,[†] David C. Baker,[†] and James Q. Chambers*[,†]

Department of Chemistry, University of Tennessee, Knoxville, Tennessee 37996-1600, and Chemistry Division, Isis Pharmaceuticals, Carlsbad Research Center, 2292 Faraday Avenue, Carlsbad, California 92008. Received August 19, 1998; Revised Manuscript Received December 10, 1998

Electroactive oligodeoxynucleotides (ODNs) with specific base sequences have a potential application as electrical sensors for DNA molecules. To this end, a phosphoramidite that bears a 9,10-anthraquinone (AQ) group tethered to the 2′-O of the uridine via a hexylamino linker, 2′-*O*-[6-[2-oxo(9,10-anthraquinon-2-yl)amino]hexyl]-5′-*O*-(4,4′-dimethoxytrityl)uridine 3′-[2-(cyanoethyl)bis(1-methylethyl)-phosphoramidite] (**3**), has been synthesized and used to prepare three ODNs with tethered AQs using standard phosphoramidite chemistry. The synthetic methodology thus allows the synthesis of ODNs with electroactive tags attached to given locations in the base sequence. Cyclic voltammetric behavior of these AQ−ODN conjugates was examined in aqueous buffer solutions at a hanging mercury drop electrode. At slow sweep rates, nearly reversible two-electron waves characteristic of an adsorbed anthraquinone/hydroquinone redox couple was observed for all of the AQ−ODN conjugates. Approximate Langmuirian isotherms were found for the AQ−ODNs with molecular footprints, calculated from the saturation coverages, that scaled with molecular size. The cyclic voltammetric response of the duplexes formed from the AQ−ODNs and their complementary ODN was complicated by the competitive adsorption of the individual ODNs and possibly the duplex species as well.

INTRODUCTION

The exquisite selectivity provided by Nature in the formation of DNA double helices via Watson−Crick hydrogen-bonded base pairs is arguably unmatched among molecular recognition strategies. Hybridization of complementary oligonucleotides, if confined to a small volume element or interface, is the basis of a selective nucleic acid sensor using conventional (e.g., radiochemical) means of distinguishing double-helix from single-strand (ss) structures (*1*). Much of this research is highly interdisciplinary, involving both the synthesis of modified oligonucleotides and their study by different physicochemical techniques (*2*). The use of fluorescent oligonucleotide probes is well established and the basis of commercial DNA analyzers. Reviews of the older literature on this topic are available (*3*, *4*), and a summary of recent attempts to improve detection of the hybridization event was given by Thiel et al. (*5*), who used surface plasmon resonance imaging to differentiate between ss- and ds-DNA.

A modified electrode surface in which an electroactive probe has been incorporated would have many attractive features common to modern electroanalytical techniques. These include in situ analysis of small volumes and possibly no requirement for washing of excess reactants from the surface reaction layer. Ideally, a surface-attached oligodeoxynucleotide (ODN) with an attached electroactive group would mimic natural DNA, which gives well-defined faradaic signals for ss-DNA and not ds-DNA (*6*−*8*). An ideal tag for this purpose would give a persistent signal, preferably electrochemically reversible, in a potential region well removed from where natural DNA and RNA are electroactive, such that the signal could be easily interrogated in a sensor configuration. ODNs with attached electroactive groups or tags have been described by several groups (*9*−*13*). These applications have involved chromatographic separation of the ss- and ds-DNAs with electrochemical detection of the tag, although Xu and Bard used electrochemical luminescence to detect ds-DNA with an end-tethered Ru(bpy)$_3^{2+}$ group (*14*).

The above strategy can be contrasted to other electrochemical means of detecting ds-DNA that have appeared in recent years, many of which involve the use of electroactive intercalators that selectively bind to double-helix structures. Most of these methods require the addition of a solution species, the intercalator, to perform the analysis. Thus, hybridization can be detected by the preconcentration or binding of the intercalator to a surface-confined DNA molecule, which leads to an increase in the signal. Transition metal complexes, which bind to DNA to give electroactive complexes (*15*−*17*), have been used in this manner (*16*, *18*−*21*), as have a variety of other species, including a Hoechst dye (*22*), ethidium (*23*), methylene blue (*24*), daunomycin (*25*), and aromatic amines (*26*). Other electrochemical approaches involve the enhancement of the electrocatalytic current for oxidation of ds-DNA by intercalating redox couples (*27*−*30*), use of the Fe(CN)$_6^{3-/4-}$ couple as a permeability marker (*31*), and an attenuation of the poly(pyrrole) doping process by a tethered oligonucleotide in the double-helix form (*32*).

Described below are the synthesis and electrochemical behavior of ODNs with 9,10-anthraquinone (AQ) groups

* To whom correspondence should be addressed. Telephone: (423) 974-3437. Fax: (423) 974-3454. E-mail: jqchambers@utk.edu.

[†] University of Tennessee.

[‡] Isis Pharmaceuticals.

10.1021/bc980095i CCC: $18.00 © 1999 American Chemical Society
Published on Web 02/05/1999

Scheme 1

5'-d(AU*G CAT TCT GCC CCC AAG AG)-3'

1a

5'-d(ATG CAT TCU* GCC CCC AAG AG)-3'

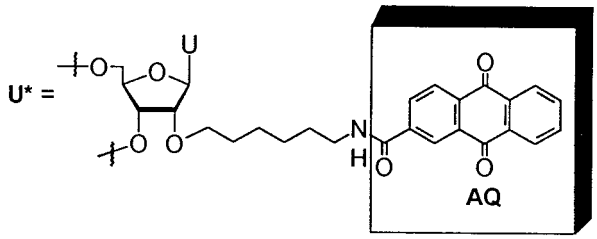
1b

5'-d(AU*G CAT TCU* GCC CCC AAG AG)-3'

1c

5'-d(GAU*CT)-3'

2



tethered to the 2′-O of a uridine unit (see Scheme 1). While this work focuses on the electrode reactions, others have prepared ODNs with tethered quinone groups for different applications. An increase in stability has been noted for nucleic acid duplexes modified at the sugar 2′-position (*33*), including several studies in which pendant AQ groups were used (*34*−*36*). Rokita and co-workers have used tethered quinones for photochemical methylation of DNA with known sequences at specific sites (*37*, *38*), and Gasper and Schuster found photooxidation of GG sites in a DNA double helix possessing an end-tethered anthraquinone group (*39*). Cohen and co-workers utilized 5′-linked AQ−ODNs to demonstrate that AQ derivatives can be delivered to target nucleic acids (mRNA or DNA) (*40*). AQ tags were chosen for the present study since they can withstand the conditions required for the solid-phase synthesis of ODNs (*33*, *39*), while also exhibiting a two-electron electrode reaction characteristic of the quinone/hydroquinone couple. The formal potential of this couple is well separated from potentials of redox reactions associated with the ODNs. In addition, the electrochemical signal provides a means of studying interfacial electron and proton transfer reactions of immobilized oligonucleotide probes on electrode surfaces.

EXPERIMENTAL PROCEDURES

All reactions were monitored by thin-layer chromatography (TLC). Adsorption chromatography was carried out using E. Merck silica gel products: (a) TLC on 0.2 mm aluminum-backed plates or (b) column chromatography using 230−400 mesh silica gel. Visualization of the TLC plates was achieved with 254 nm UV light and by spray-heat development using a *p*-anisaldehydesulfuric acid reagent (*41*). The solvent systems for adsorption chromatography were (A) 1:1 ethyl acetate/hexanes, (B) 95:5 dichloromethane/methanol, (C) 3:1 ethyl acetate/hexanes, (D) 9:1 dicholoromethane/methanol, (E) 99:1 dichloromethane/methanol, and (F) 65:35:trace ethyl acetate/hexanes/triethylamine. All reactions were carried out under a nitrogen atmosphere unless otherwise indicated. Solvents were evaporated under an aspirator vacuum at about 25 °C unless otherwise indicated. Elemental analyses were furnished by Atlantic Microlab, Inc. (Atlanta, GA). ^{1}H and ^{13}C NMR spectra were recorded at 400.13 and 100.61 MHz, respectively, unless stated otherwise. ^{19}F NMR spectra were recorded on a JEOL FX90Q spectrometer at 84.24 MHz using an external standard of trifluoroacetic acid-*d*. ^{31}P NMR spectra were recorded at 161.9 MHz using an external standard of phosphoric acid (85%) at 37 °C.

Positive ion electrospray mass spectra of the modified nucleosides were acquired on a Quattro-II quadrupole instrument (Micromass Inc., Manchester, U.K.) by infusion (5 μL/min) of a ca. 1 μM solution of the analyte in methanol. Data were averaged in the "multichannel acquisition" mode over a 2 min acquisition period. Conversely, negative ion electrospray mass spectra of the unmodified ODNs were obtained on the same instrument by infusion (5 μL/min) of a ca. 1 μM solution of the analyte in 1:1 methanol/water that contains 0.15% triethylamine. The averaging of the data was performed as described above.

The AQ−ODNs were synthesized using a Perspective Biosystems Expedite 8901 Nucleic Acid Synthesis System (PE Applied Biosystems, Foster City, CA)

Preparative reversed-phase HPLC on the monotritylated AQ−ODNs was performed on a Waters 600E instrument (260 nm) equipped with a Waters Delta Pak C4 column (7.8 mm × 300 mm) and a Waters 991 integrator (Waters Corp., Milford, MA). The solvent systems used for reversed-phase HPLC were (G) 50 mM triethylammonium acetate at pH 7.0 and (H) acetonitrile. The gradient system employed was 95:5 G:H for 5 min with a linear increase to 4:6 G:H over the course of 50 min (method A) using a flow rate of 2.5 mL/min. The purity of the AQ−ODNs was determined utilizing a Waters Delta Pak C4 column (3.9 mm × 300 mm) and the same gradient system as described above at a flow rate of 1.5 mL/min (method B).

Additional analysis of the AQ−ODNs was conducted with capillary gel electrophoresis (CGE). A 100 μL aliquot of the ODN (0.2 OD) was injected into a Beckman P/ACE System 5000 Capillary Gel Electrophoresis unit, coupled to a UV−vis detector (Beckman and Coulter, Inc., Fullerton, CA) that was equipped with a column (27 cm in total length with an effective length of 20 cm) of 12% linear polyacrylamide in a buffer of 7 M urea and 0.2 M bis tris borate. A voltage of 500 V/cm was supplied to the column at ca. 40 °C. A typical analysis was completed in 12 min (method A).

Prior to acquisition of the negative ion electrospray mass spectra of the AQ−ODNs on a HP 59987A series II API 5989A mass spectrometer (Hewlett-Packard Co., Palo Alto, CA), ca. 0.5 OD was desalted by osmosis from water that contained ammonium hydroxide using a Millipore VS 0.025 μm filter (Millipore Corp.). After 1 h, the purified sample was then dissolved in 1:1 2-propanol/water (100 μL). Before the sample was infused into the spectrometer, a 2.5 μL aliquot of piperidine (100 mM) was added.

A Shimadzu UV-2101PC UV−vis scanning spectrophotometer was used to determine the ϵ_{max} of the novel AQ−ODNs (Shimadzu Corp., Kyoto, Japan). Melting points of the ODNs were determined using an HP model 8452A diode array spectrophotometer equipped with an HP model 89090A Peltier temperature controller (Hewlett-Packard Co.).

The electrochemical studies were performed using a hanging mercury drop electrode (HMDE) purchased from EG&G (Oak Ridge, TN). The electrode area was 0.0225 cm^2 for most of the voltammetric experiments; details are given elsewhere (*42*). The reference electrode was a Ag/

AgCl wire immersed directly in the test solution. A Cypress model CS-2Ra (Cypress Systems, Inc., Lawrence, KS) potentiostat was used. Calculation of the cyclic voltammograms was carried out using software supplied by CH Instruments, Inc. (Cordova, TN).

Materials and Solvents. Solutions of nonmodified phosphoramidites (0.1 M) were used as purchased from PE Applied Biosystems. 5′-d(ATG CAT TCT GCC CCC AAG AG)-3′ (**7**) was supplied by Operon Technologies, Inc. (Alameda, CA). The other unmodified ODN 5′-d(CTC TTG GGG GCA GAA TGC AT)-3′ (**6**) was furnished by Isis Pharmaceuticals (Carlsbad, CA). The entire amount of the ODNs was diluted to 10 mL with sterile deionized water. Anhydrous solvents were prepared as follows. Dichloromethane and pyridine were distilled from calcium hydride at atmospheric pressure, and 1,4-dioxane was distilled from lithium aluminum hydride.

9,10-Anthraquinone-2-carboxylic Acid 2,3,4,5,6-Pentafluoro Phenyl Ester (9). To a solution of **8** (2.1 g, 7.9 mmol) in dichloromethane (50 mL) at 0 °C were added DCC (0.67 g, 4.3 mmol) and 2,3,4,5,6-pentafluorophenol (0.90 g, 4.3 mmol). The suspension was allowed to warm to room temperature overnight. The crude reaction mixture was adsorbed onto silica gel and submitted to column chromatography (hexanes), affording **9** as a pale yellow solid (1.25 g, 45%): mp 197−205 °C; R_f = 0.91 (solvent A); ^{1}H NMR ($CDCl_3$) δ 7.88 (m, 2H), 8.37 (m, 2H), 8.50 (d, 1H, J = 8.15 Hz), 8.58 (dd, 1H, J = 1.52 Hz, J = 8.09 Hz), 9.13 (d, 1H, J = 1.33 Hz); ^{19}F NMR ($CDCl_3$) δ −152.35 (d, 2F, J = 18.31 Hz), −157.23 (t, 1F, J = 21.98 Hz), −161.98 (dd, 2F, J = 18.31 Hz, J = 21.98 Hz); ^{13}C NMR ($CDCl_3$ and 2 drops of DMSO-d_6) δ 127.19, 127.69, 129.34, 131.59, 133.13, 133.72, 134.34, 134.84, 137.01, 160.92, 181.35, 181.68. Higher-order resonances associated with the pentafluoro moiety are between δ 120 and 150. Anal. Calcd for $C_{21}H_7F_5O_4$: C, 60.30; H, 1.69. Found: C, 60.23; H, 1.71.

2′-*O*-[6-[2-Oxo(9,10-anthraquinon-2-yl)amino]hexyl]-5′-*O*-(4,4′-dimethoxytrityl)uridine (10). To a solution of **9** (1.0 g, 2.4 mmol) in dichloromethane (40 mL) at 0 °C was added pyridine (0.19 mL, 2.4 mmol). Compound **4** (*43*) (1.4 g, 2.2 mmol) was then added. After 50 min, the reaction mixture was allowed to warm to room temperature for a further 3 h. The crude reaction mixture was then adsorbed onto silica gel and subjected to flash chromatography (solvent C), which afforded a pale yellow, glassy material **10** (1.6 g, 83%): R_f = 0.44 (solvent B); ^{1}H NMR (DMSO-d_6) δ 1.34 (bm, 4H), 1.54 (bm, 4H), 3.07−3.50 (bm, 3H, obscured by the H_2O signal), 3.50−3.67 (overlapping resonances, 3H), 3.71 (s, 6H), 3.98 (bs, 1H), 3.91 (bs, 1H), 4.18 (t, 1H, J = 5.23 Hz), 5.11 (bs, 1H, exchanges with D_2O), 5.28 (d, 1H, J = 8.04 Hz), 5.81 (d, 1H, J = 3.15 Hz), 6.88 (d, 4H, J = 8.65 Hz), 7.11−7.50 (overlapping resonances, 9H), 7.73 (d, 1H, J = 8.04 Hz), 7.91 (dd, 2H, J = 3.36 Hz, J = 5.21 Hz), 8.04−8.41 (overlapping resonances, 4H), 8.61 (s, 1H), 8.88 (t, 1H, J = 4.80 Hz), 11.35 (bs, 1H, exchanges with D_2O); ^{13}C NMR (DMSO-d_6) δ 26.28, 28.89, 29.04, 54.99, 62.58, 68.47, 69.82, 79.12, 80.91, 82.60, 85.87, 87.14, 101.43, 113.20, 125.42, 126.75, 126.96, 127.68, 127.84, 129.73, 132.73, 132.99, 134.39, 134.56, 135.05, 135.32, 139.50, 140.14, 144.60, 150.25, 158.10, 162.95, 164.44, 182.06; ESIMS calcd for $C_{51}H_{48}N_3O_{11}$ 878.3, found $[M + Na]^+$ 902.1 and $[M + K]^+$ 918.0. Anal. Calcd for $C_{51}H_{48}N_3O_{11}\cdot 2H_2O$: C, 66.95; H, 5.73; N, 4.59. Found: C, 66.96; H, 5.57; N, 4.44.

2′-*O*-[6-[2-Oxo(9,10-anthraquinon-2-yl)amino]hexyl]-uridine (5). Compound **10** (0.33 g, 0.38 mmol) was stirred with a 3% (v/v) dichloroacetic acid/dichloromethane solution (7 mL) for 10 min. The crude reaction mixture was subjected to flash chromatography (solvent A → ethyl acetate, followed by dichloromethane → E) to afford a pale yellow amorphous powder **5** (0.13 g, 60%). Lyophilization with 1,4-dioxane afforded an off-white, fluffy solid: R_f = 0.39 (solvent D); ^{1}H NMR (DMSO-d_6) δ 1.31 (bm, 4H), 1.53 (bm, 4H), 3.40−3.63 (overlapping resonances, 6H), 3.86 (dd, 2H, J = 2.28 Hz, J = 4.56 Hz), 4.06 (dd, 2H, J = 5.28 Hz, J = 5.9 Hz, signal collapses to a triplet upon the addition of D_2O), 5.02 (d, 1H, J = 5.9 Hz, exchanges with D_2O), 5.10 (t, 1H, J = 5.14 Hz, exchanges with D_2O), 5.63 (dd, 1H, J = 2.06 Hz, J = 7.87 Hz), 7.76−8.10 (overlapping resonances, 3H), 8.13−8.43 (overlapping resonances, 4H), 8.64 (bd, 1H, J = 2.54 Hz), 8.90 (t, 1H, J = 5.08 Hz), 11.31 (s, 1H); ^{13}C NMR (DMSO-d_6) δ 25.32, 26.45, 29.07, 29.23, 60.74, 68.59, 69.92, 81.34, 85.31, 86.39, 101.98, 102.05, 125.80, 125.90, 127.02, 127.37, 133.24, 133.30, 139.79, 140.65, 140.77, 163.49, 165.04, 182.46. Anal. Calcd for $C_{30}H_{31}N_3O_9\cdot 0.5C_4H_8O_2$ (1,4-dioxane): C, 61.83; H, 5.67; N, 6.76. Found: C, 61.87; H, 5.78; N, 6.60.

2′-*O*-[6-[2-Oxo(9,10-anthraquinon-2-yl)amino]hexyl]-5′-*O*-(4,4′-dimethoxytrityl)uridine 3′-[2-(Cyanoethyl)bis(1-methylethyl)phosphoramidite] (3). Compound **10** (1.12 mmol, 0.98 g, dried in vacuo for 12 h) was dissolved in dichloromethane (ca. 1 mL) that was added under a blanket of argon. To the solution were added diisopropylammonium tetrazolide (1.13 mmol, 2.0 g) and 2-(cyanoethyl)-*N*,*N*,*N*′,*N*′-tetraisopropyl phosphorodiamidite (2.25 mmol, 0.14 g). After being stirred overnight, the crude reaction mixture was purified by column chromatography (solvent F), which afforded the phosphoramidite **3** (0.750 g, 64%): R_f = 0.36 (solvent F); ^{31}P NMR ($CDCl_3$) δ 150.89; FABMS calcd for $C_{60}H_{66}N_5O_{12}P$ 1079.45, found $[M + H]^+$ 1080.11 and $[M + Na]^+$ 1102.23.

General Procedure for the Synthesis of 2′-O-Modified AQ−ODNs 1a−c and 2. All of the AQ−ODNs were synthesized (2 μmol scale)—at least two batches were prepared of each modified ODN—using standard instrument chemistry with the exception of the step of incorporating the modified uridine moiety. This was accomplished by coupling the growing oligomer twice per cycle (5 min for each cycle) utilizing an acetonitrile solution of phosphoramidite **3** (0.08−0.1 M). At the end of the synthetic sequence, the final DMT group was left intact. After treatment with ammonium hydroxide (28−30%) for ca. 16 h at 55 °C, the CPG was removed by filtration through a Gelman 0.45 μm nylon acrodisc syringe filter (Pall Gelman Sciences, Ann Arbor, MI). The crude ODNs were purified employing reversed-phase HPLC (method A). Final detritylation was accomplished with acetic acid (80%) for ca. 30 min. The trityl residues and excess salt were removed by passing the AQ−ODNs through a column of Sephadex G-25 (Sigma, St. Louis, MO). Analytical details of AQ−ODNs were as follows.

5′-d(AU*G CAT TCT GCC CCC AAG AG)-3′ (1a): t_R = 21.77 min (HPLC using method B); t_R = 4.12 min (CGE using method A); ESIMS calcd for $C_{213}H_{262}N_{75}O_{121}P_{19}$ m/z 6397.4, found m/z 6398.8.

5′-d(ATG CAT TCU* GCC CCC AAG AG)-3′ (1b): t_R = 19.97 min (HPLC using method B); t_R = 5.89 min (CGE using method A); ESIMS calcd for $C_{213}H_{262}N_{75}O_{121}P_{19}$ m/z 6397.4, found m/z 6398.6.

5′-d(AU*G CAT TCU* GCC CCC AAG AG)-3′ (1c): t_R = 22.84 min (HPLC using method B); t_R = 8.16 min (CGE using method A); ESIMS calcd for $C_{233}H_{279}N_{76}O_{125}P_{19}$ m/z 6732.7, found m/z 6732.9.

5′-d(GAU*CT)-3′ (2): t_R = 34.72 min (HPLC using method B); t_R = 7.98 min (CGE using method A); ^{1}H NMR (D_2O) δ 5.84−5.88 (overlapping resonances, 3H), 5.98 (d,

1H, $J = 7.55$ Hz), 6.13 (d, 1H, $J = 6.45$ Hz), 6.10−6.30 (overlapping resonances, 3H), 7.53 (d, 1H, $J = 6.59$ Hz), 7.74 (s, 1H), 7.80−7.90 (overlapping resonances, 4H), 8.07−8.15 (overlapping resonances, 3H), 8.20 (s, 1H), 8.24 (s, 1H), 8.34 (d, 1H, $J = 1.78$ Hz); ^{31}P NMR (D_2O) δ −0.32, −0.28, −0.11, 0.11; ESIMS calcd for $C_{69}H_{80}N_{18}O_{33}P_4$ m/z 1813.4, found m/z 1813.2.

Determination of the Concentration of the Novel ODNs 1a−c. To accurately determine the concentration of AQ−ODNs **1a**−**c**, a stock solution of 20−60 ODs of each of the modified oligomers (dependent on the amount available) was prepared in sterile, deionized water (10 mL). The contribution of AQ to the ϵ_{260} for modified AQ−ODN **1a** was added to the ϵ_{260} for 5′-AUG CAT TCT GCC CCC AAG AG-3′, which was calculated from the nearest-neighbor effect (*44*). The ϵ_{260} of AQ was determined to be 26 400 M^{-1} cm^{-1} by subtracting the ϵ_{260} of uridine from the ϵ_{260} of monomer **5**. Thus, the ϵ_{260} of **1a** was determined to be 214 000 M^{-1} cm^{-1} (260 nm). By measuring the absorbance at 260 nm, we found the concentration of the stock solution of **1a** to be 2.09×10^{-5} M. Similarly, the concentrations of the stock solutions of **6** ($\epsilon_{260} = 194\,000$ M^{-1} cm^{-1}) and **7** ($\epsilon_{260} = 188\,000$ M^{-1} cm^{-1}) were determined to be 2.04×10^{-5} and 2.83×10^{-5} M, respectively.

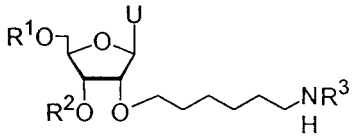
Electrochemical Studies. Cyclic voltammetry (CV) was carried out using aqueous buffers containing NaCl at various concentrations. For the pH studies on compounds **2** and **5** (see below), 0.125 M phosphate and acetate buffers were used for pH <7 and Britton−Robinson (BR) (*45*) buffers were used for pH >7. The latter buffer system was also used for the determination of the adsorption isotherms at pH 7.15. Before measurements were taken, solutions were purged with purified nitrogen that had been passed through a column containing Mn(II) oxide dispersed on a vermiculite support to remove oxygen.

Hybridization Conditions. Hybridization solutions were prepared by mixing equimolar aliquots (ca. 50 μL) of the stock solutions with 2−3 mL of buffer solution. Temperature profiles were obtained by heating the cell to 90 °C for 10 min, followed by slow cooling in 1 °C increments while measuring the absorbance at 260 nm. Once confirmation of duplex formation was achieved, CV was performed on the solution as described above. Initial experiments used either the pH 7.15 BR buffer solution containing 0.25 M NaCl and 3.6 mM EDTA or a 0.01 M ammonium acetate/0.001 M ammonium chloride buffer. The ammonium acetate buffers were chosen to mimic the conditions of Bayer et al. (*46*), who detected duplexes in solution using electrospray mass spectroscopy (albeit at higher concentrations). The latter experiments were performed in 0.1 M phosphate buffer (pH ∼7) containing 0.05 M NaCl and 5 mM EDTA. In the latter procedure, melting curves were obtained for solutions before exposure to the HMDE conditions, and the voltammetric behavior was compared to that of an identical solution that was not thermally cycled. Spurious voltammetric waves were obtained for solutions of **1a** and **6** that had been exposed to the HMDE conditions before thermal cycling.

RESULTS AND DISCUSSION

Synthesis of 2′-O-Modified ODNs. Entry into the novel oligomers **1a**−**c** and **2** was crucial for this study (refer to Scheme 1). The key intermediate in the synthetic sequence was the electroactive phosphoramidite **3** (Scheme 2). Additionally, the strategy provided access to the free nucleoside **5** that was required to establish the experimental conditions required to observe the distinctive electrochemical signature of the quinone moiety. Initially, the 3-(3-methyl-1,4-naphthoquinon-2-ylsulfanyl)propionyl reporter group of Chatterjee and Rokita (*38*) was employed. However, when the precursor to the conjugates was subjected to concentrated ammonia, to mimic the final deblocking step in the synthesis of ODNs (*47*), deleterious side reactions took place. Accordingly, an AQ tag was employed in this work since these conjugates are known to survive the conditions of the oligonucleotide synthesis (*34*, *40*).

Scheme 2



3: R^1 = DMT; R^2 = $(i\text{-Pr})_2$N–P(O)(O)CN; R^3 = AQ

4: R^1 = DMT; R^2 = H; R^3 = H

5: R^1 = H; R^2 = H; R^3 = AQ

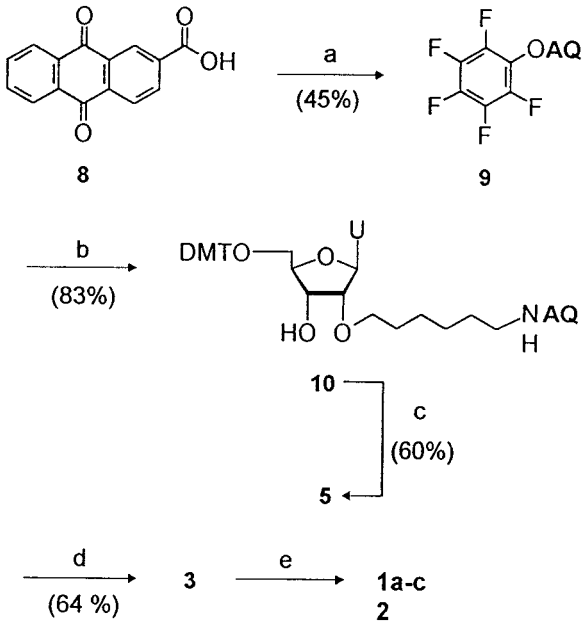
3′-d(TAC GTA AGA CGG GGG TTC TC)-5′

6

3′-d(GAG AAC CCC CGT CTT ACG TA)-5′

7

Scheme 3[a]



[a] (a) DCC, 2,3,4,5,6-pentafluorophenol, CH_2Cl_2, 0 °C → room temperature over the course of 12 h; (b) **4**, pyr, CH_2Cl_2, 0 °C for 50 min, room temperature for 3 h; (c) 3% (v/v) $Cl_2CHCOOH$ in CH_2Cl_2, 10 min; (d) diisopropylammonium tetrazolide, 2-(cyanoethyl)-*N*,*N*′,*N*′,*N*-tetraisopropyl phosphoramidite, CH_2Cl_2, room temperature for 12 h; (e) automated ODN synthesizer.

Compound **9** was synthesized utilizing DCC to condense **8** with 2,3,4,5,6-pentafluorophenol (Scheme 3). Addition of **9** to **4** (*43*) in the presence of pyridine secured the modified nucleoside **10**. With this essential intermediate in hand, (a) phosphoramidite **3** was prepared using

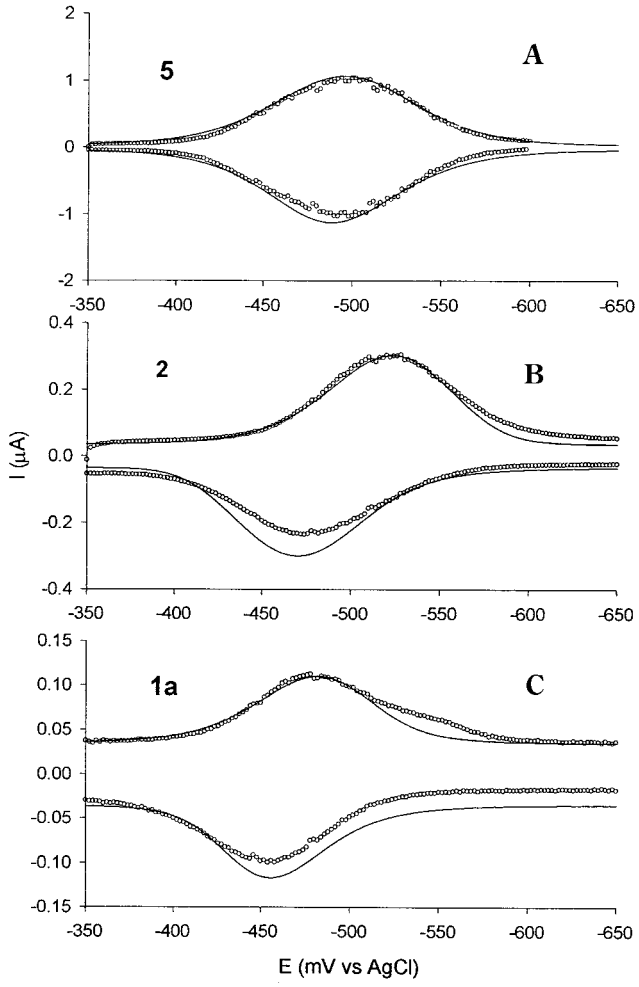


Figure 1. Typical cyclic voltammograms (○) of compounds (A) **5** (pH 7.15), (B) **2** (pH 7.77), and (C) **1a** (pH 7.15) at 100 mV/s with accompanying EE mechanism simulations (solid lines). Simulation parameters were as follows: (A) $k_{s1} = 100\ s^{-1}$, $k_{s2} = 20\ s^{-1}$, $E°_1 = -0.475$ V, and $E°_2 = -0.510$ V; (B) $k_{s1} = 100\ s^{-1}$, $k_{s2} = 2\ s^{-1}$, $E°_1 = -0.510$ V, and $E°_2 = -0.490$ V; and (C) $k_{s1} = 100\ s^{-1}$, $k_{s2} = 5\ s^{-1}$, $E°_1 = -0.470$ V, and $E°_2 = -0.470$ V.

standard methodology (*43*) and (b) removal of the 4,4′-dimethoxyltrityl (DMT) group was readily achieved with a 3% (v/v) dichloroacetic acid in CH_2Cl_2 (*47*) solution to afford free ribonucleoside **5**. A standard protocol was performed to obtain AQ–ODNs **1a**–**c** and **2** from **3** on an automated oligonucleotide synthesizer (*48*). Prior to removal of the final DMT group, the resulting oligomers were purified using reversed-phase HPLC.

Cyclic Voltammetry. Before studies were carried out on oligomers **1a**–**c**, cyclic voltammetry was performed on aqueous buffer solutions of **2** and **5**. Immediately upon extrusion of a HMDE into a dilute aqueous solution of these AQ–ODNs, the presence of an adsorbed layer of electroactive AQ was indicated by the appearance of a voltammetric wave with a wave shape indicative of a redox process for a surface-confined species. Typical voltammograms are shown in Figure 1. These voltammograms are similar to those reported by Forster, in both position and shape, for related simple AQs on HMDEs (*49*). Thus, it appears that the AQ groups readily adsorb on and remain in close electrical contact with the mercury surface despite the presence of the oligonucleotide substitutent.

The cyclic voltammograms of 20-mers **1a**–**c** were similar to those of **2** and **5**, except that the magnitudes of the current and the corresponding surface charge were smaller. Figure 1C shows a typical cyclic voltammogram for **1a**, which has an AQ group tethered to the second nucleotide from the 5′-phosphate end of the base sequence. The shapes of the voltammetric waves for all the compounds studied at sweep rates of less than ca. 1 V/s were symmetrical, or nearly so, with peak separations ($E_p^{anod} - E_p^{cath}$) of a few millivolts and minimal faradaic current at potentials on the wings of the voltammogram. These observations are consistent with formation of a self-assembled layer on the electrode surface. It will be argued below that these films must possess a fair degree of order as well.

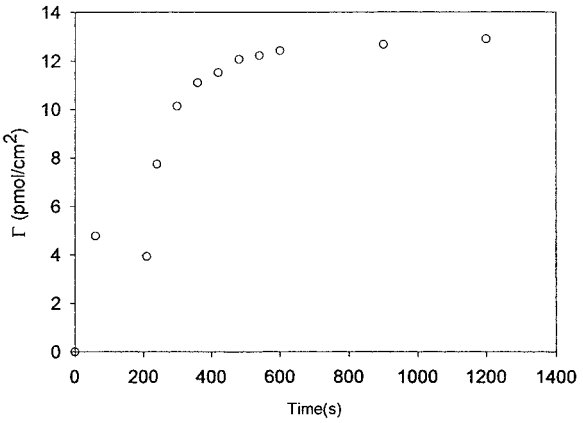


Figure 2. Surface coverage vs exposure time of the HMDE drop to 0.4 μM **1a** BR buffer (pH 7.15).

The voltammograms in Figure 1, which do not have ideal Nernstian shapes for an *n*-electron process, have been fit to a simple global EE mechanism (i.e., two successive electron additions) (*50*). This approach gave good fits to the slow sweep rate voltammograms of all the conjugates, including the splitting that was evident in the cyclic voltammograms at pH values of less than ca. 6 and the narrowing of the voltammograms at pH >7. In this simple analysis, it is assumed that the electron additions would be accompanied by protonation steps. It is realized that the formal potentials and rate constants used in these calculations are necessarily not unique. A more detailed analysis of the electrode kinetics for these surface layers will be published elsewhere.

With time after the extrusion of a new mercury surface, the magnitude of the waves for all the AQ species increased, and then leveled off, reaching a plateau after 5–10 min, while maintaining an approximately constant shape. This behavior is shown in Figure 2, where the surface coverage was calculated using the charge necessary to reduce the adsorbed species from Faraday's law in the usual fashion. At the sweep rates of these experiments, an *n* value of 2 was assumed for the reduction of the AQ moiety.

$$AQ + 2H^+ + 2e^- \rightleftarrows AQH_2 \qquad (1)$$

The solutions used to obtain the data of Figure 2 contained an excess of EDTA to scavenge metal ions, in particular adventitious Hg(II) species which are difficult to eliminate in HMDE voltammetry. The cathodic current evident as a shoulder on the negative side of the peak voltammogram of **1c** in Figure 1 is likely due to the reduction of accumulated Hg(II). In the absence of EDTA, the cathodic charge continued to increase with time, and the wave shape changed, indicative of overlapping redox processes. This behavior is attributed to the reduction of the Hg(II) species accumulated by the oligonucleotide

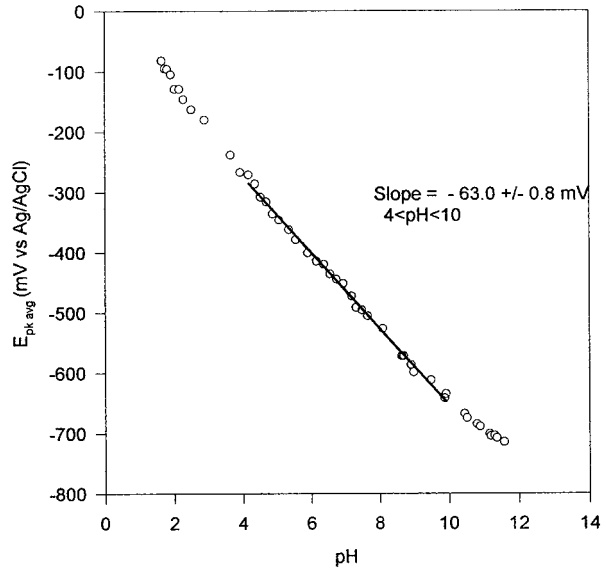


Figure 3. Average peak potential [$(E_{pk}^{a} + E_{pk}^{c})/2$] pH study for compound **5**.

surface layer. The ability of nucleic acids to coordinate mercury species is well documented (*51*).

The pH dependence of the $E^{o\prime}$ [$=(E_{pk}^{a} + E_{pk}^{c})/2$] for the AQ/$AQH_2$ couple of compound **5** is shown in Figure 3. The response is close to 60 mV/pH unit over a wide pH range. This is consistent with the two-electron, two-proton stoichiometry of eq 1 and with the Pourbaix diagrams of simple anthraquinones (*52*). A similar behavior was obtained for pentamer **2**. Due to the limited amounts of the 20-mers that are available, full pH studies were not carried out for these compounds, but the peak potential data were consistent with Figure 3 and eq 1. The fact that the apparent $E^{o\prime}$ values exhibited a lack of gross dispersion indicates that the surface layers possess a fair degree of order with respect to the location of the AQ/AQH_2 couple.

Adsorption Isotherms. The concentration dependence of the voltammograms for all of the AQ−ODN conjugates was examined in neutral pH phosphate buffer solutions. Limiting saturation surface coverages were seen at concentrations in the micromolar range, indicating a high affinity of all of the compounds for the mercury electrode surface. This is not surprising in view of the known affinity of the purine and pyrimidine bases, native DNA and RNA (*7*), and the AQ unit itself for mercury electrode surfaces. Figures 4 and 5 show the Γ versus concentration behavior for compounds **5** and **1a**, respectively, along with fits to the simple Langmuir adsorption isotherm model.

Although the agreement with the Langmuir model is not perfect, the fits are good enough to provide a means of comparing the AQ−ODN conjugate voltammetry as a function of chain length and degree of substitution. First, the molecular footprints calculated from the limiting Γ_{max} values

$$\text{footprint} = (\Gamma_{max} N_{av} \times 10^{-14})^{-1}\ \text{nm}^2/\text{molecule} \quad (2)$$

scale with the size of the *n*-mers and the degree of substitution; see Table 1. The sizes of the footprints per substituted uridine ring indicate a closely packed surface layer.

The footprint calculation of eq 2 assumes that the *n* value of the electrode reaction is two for compounds **1a**, **1b**, **2**, and **5**, and four for compound **1c**, which possesses

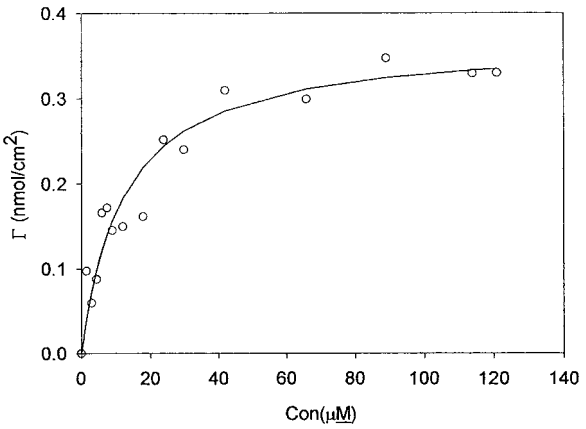


Figure 4. Adsorption isotherm of compound **5** in pH 7.15 BR buffer with 0.25 M NaCl (○). The line is a calculated Langmuir isotherm where $\Gamma_{max} = 0.369$ nmol cm^{-2} and $\beta = 1.01 \times 10^5$ M^{-1}.

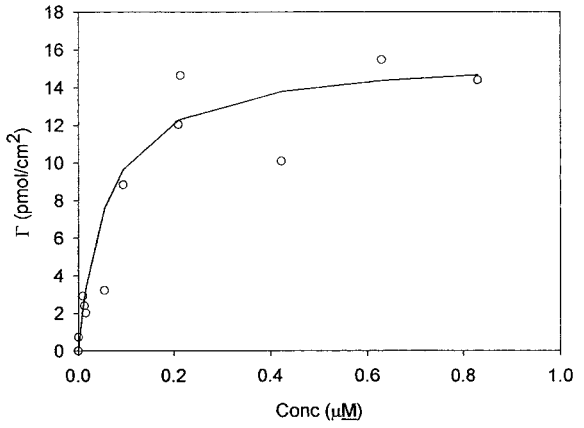


Figure 5. Adsorption isotherm of compound **1a** in pH 7.15 BR buffer with 0.25 M NaCl (○). The line is a calculated Langmuir isotherm where $\Gamma_{max} = 15.7$ pmol cm^{-2} and $\beta = 1.7 \times 10^7$ M^{-1}.

Table 1. Langmuir Adsorption Isotherm Parameters for AQ Conjugates at Hg in pH 7.1 Buffer Solution

	footprint (nm²/molecule)	β (M^{-1})	ΔG_{ads} (kJ/mol)
2	0.48	1.01×10^5	−28
5	1.99	7.9×10^7	−45
1a	11.0	8.50×10^6	−40
1b	10.5	2.69×10^7	−42
1c	11.1	3.2×10^7	−43

two pendant AQ groups. Significantly, the footprint for the latter was in agreement with those of the other 20-mers, indicating that both AQ groups were involved in the electrochemical reactions. At faster sweep rates, a splitting of the cathodic wave was seen in the voltammograms of the disubstituted 20-mer.

The packing density of **5**, ca. 0.5 nm²/molecule, is on the order of magnitude expected for a much smaller benzohydroquinone based on van der Waals radii (*53*). This indicates that the AQ group in the adsorbate is oriented in an edge-pendant configuration with respect to the electrode surface. The observed reversibility of the electrode reaction also suggests that the AQ groups are close to the mercury surface. It should be noted that the charge under the voltammetric waves decreased significantly at faster sweep rates (up to 30−50% of the charge for the voltammograms of Figure 1). This is indicative of kinetic limitations on the electrode reaction which are beyond the scope of this report. However, possible kinetic limitations would decrease the surface charge and in-

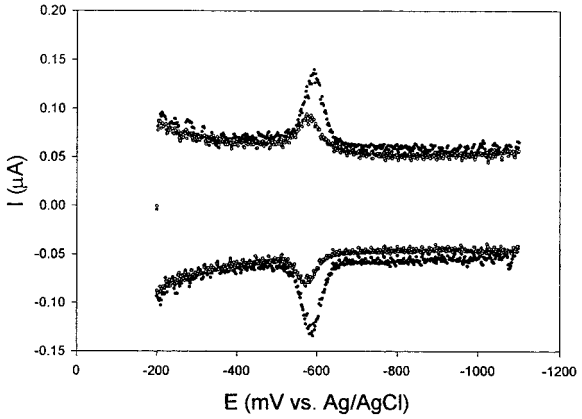


Figure 6. Cyclic voltammogram of (●) **1a** and (○) **1a** and complementary strand **6** in 0.01 M NH_4Ac and 0.001 M NH_4Cl, with a sweep rate of 0.1 V s^{-1}, a 0.0225 cm^2 HMDE, and an accumulation time of 5 min.

crease the calculated values of the footprints, which assume a two-electron *n* value.

The Langmuirian behavior of the Γ data also affords a quantitative measure of the affinity of the molecules for the electrode surface via the following relationship between the free energy of adsorption (ΔG_{ads}) and the Langmuir energy coefficient (β):

$$\Delta G_{ads} = -RT \ln(\beta) \tag{3}$$

The large absolute values of the negative free energy of adsorption for the AQ bioconjugates indicate a strong affinity of the mercury surface for these single-strand DNA molecules.

Competitive Adsorption of ODNs. Several experiments were performed to examine the effect of hybridization of the DNA chain on the voltammetric response. The results from one such experiment are shown in Figure 6, which shows the voltammogram of **1a** in the absence and presence of an equimolar concentration of its complementary strand, compound **6**, in an ammonium acetate buffer solution. In the presence of the complementary strand, the electrochemical signal was attenuated significantly, while the wave shape remained approximately constant. However, this result is complicated by the competitive adsorption displacement of the tagged 20-mer from the electrode surface by the untagged chain. In the buffer solution of Figure 6, essentially identical behavior was observed when a noncomplementary sequence, compound **7**, was added to the solution.

The facile competitive nature of the adsorption process is demonstrated by the experiment whose results are depicted in Figure 7. Here the voltammetric charge for **1a** was measured as a function of the amount of added untagged 20-mer in phosphate buffer solution. Within a few seconds, apparent equilibrium surface coverage by both compounds is observed. The data are in agreement with the following equation for competitive Langmuirian adsorption of two species with identical saturation surface coverages (*54*).

$$\Gamma_1 = \frac{\Gamma_s \beta_1 C_1}{1 + \beta_1 C_1 + \beta_2 C_2} \tag{4}$$

This equation can be rearranged into the following linear form

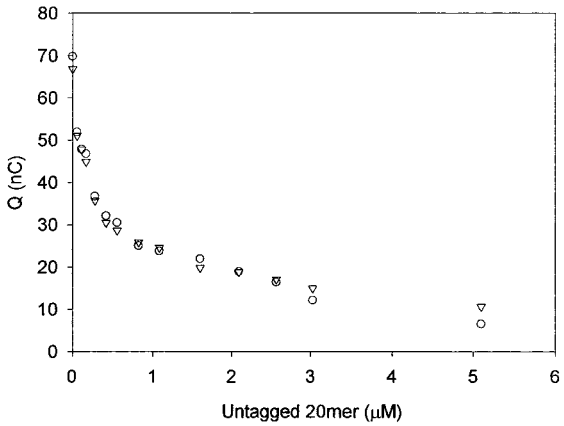


Figure 7. Competitive adsorption study of compounds **1a** and **7** at a HMDE. Conditions were 0.216 μM **1a** in pH 7.15 BR buffer, with 0.25 M NaCl and 3.6 mM EDTA: (○) cathodic charge or (▽) anodic charge.

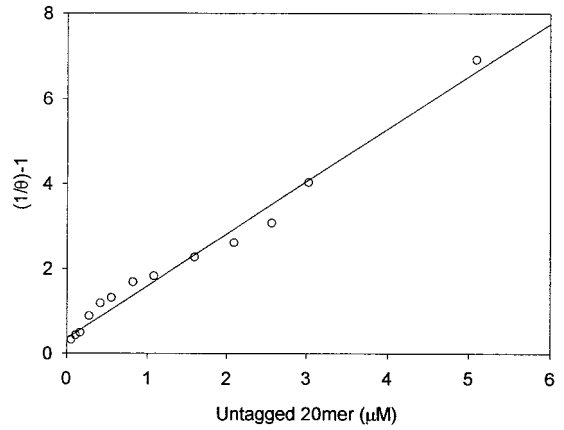


Figure 8. Linear competitive adsorption model.

$$\frac{1}{\theta_1} - 1 = \frac{1}{\beta_1 C_1} + \frac{\beta_2 C_2}{\beta_1 C_1} \tag{5}$$

where C_1 is the concentration of the tagged 20-mer **1a**, C_2 is the concentration of the added untagged 20-mers (**6** or **7**), and θ_1 is the fractional surface coverage of the tagged compound. The corresponding plot is shown in Figure 8. Calculation of the relative β values from the slope of the line in Figure 8 reveals that the untagged 20-mer is adsorbed less strongly than the tagged 20-mer by 4 kJ/mol.

Effect of Duplex Formation. The surface state of these AQ−ODNs in the presence of its complementary strand, i.e., adsorbed ss-DNA versus adsorbed ds-DNA, is difficult to establish in the absence of additional information. The possibility exists that a duplex structure of these ODNs would unzip and adsorb on the mercury electrode in the single-strand form. There is ample precedent for this in the classical work of Palecek on native DNA electrochemistry (*7*), and the large negative free energy of adsorption could provide the driving force for this process. In addition, the crowded packing of these molecules on the electrode surface may not allow enough space for surface hybridization (*55*).

To confirm that a duplex was present in the solutions containing both a tagged 20-mer and its complementary strand, the melting/annealing process was followed by monitoring the UV absorption spectrum as a function of temperature. Figure 9 shows a cooling absorbance trace for a solution of **1a** and its complementary strand, which exhibits a melting point at 66 °C. Interestingly, the

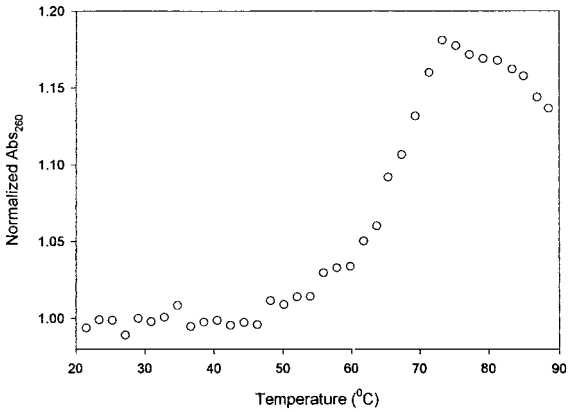


Figure 9. Typical melting curve for 0.35 μM **1a** and **6** in pH 6.83 0.1 M phosphate buffer, with 0.1 M NaCl.

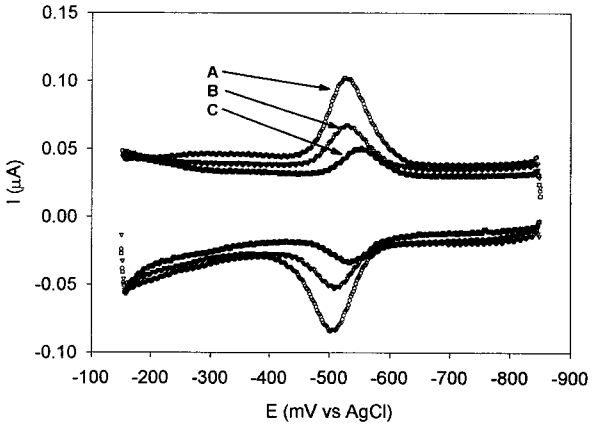


Figure 10. Cyclic voltammogram of **1a** with complementary 20-mer **6**: (A) 0.695 μM **1a** in pH 7.4 phosphate buffer (0.1 M), with 0.05 M NaCl and 5 mM EDTA; (B) addition of an equal amount of compound **6** at room temperature; and (C) after heating to 90 °C and cooling to room temperature. The sweep rate was 0.1 V s^{-1}.

melting temperatures of the untagged duplex, i.e., **6·7**, and the duplexes of the AQ−ODNs were approximately the same, indicating that the tethered AQ group is not intercalated in the duplex structure. In pH 7.4, 0.1 M phosphate buffer containing 0.05 M NaCl and 5 mM EDTA, the T_m (ΔT_m) values were 66.4, 68.3 (1.9), 68.4 (2.0), and 69.1 (2.7) °C for the duplexes of **6** with **7**, **1a**, **1b**, and **1c**, respectively. Somewhat larger ΔT_m values were seen for 2′-O-modified ribonucleotides with an intercalating substituent, 2-aminoanthraquinone, tethered on shorter linker arms (*35*).

Cyclic voltammetry experiments carried out in parallel with the melting curves gave further support to the competitive nature of the adsorption equilibria that are at play at the electrode surface. In these experiments, solutions containing equimolar amounts of a tagged AQ−ODN and either its complementary (**6**) or a noncomplementary (**7**) ODN species were split into two parts and subjected to both CV and UV−vis analysis. The resulting voltammograms for compound **1a** are shown in Figures 10 and 11 for a pH 7.4 phosphate buffer. The cyclic voltammograms marked A in these figures were obtained with solutions containing **1a** at a concentration sufficient to give a limiting surface coverage of the AQ−ODN. Addition of the complementary strand to the solution resulted in an attenuation of the signal; refer to the cyclic voltammogram marked B in Figure 10. However, this result cannot be distinguished from simple competitive adsorption of an untagged ODN since essentially identical behavior was seen when the experiment was repeated with a noncomplementary sequence; see the cyclic voltammogram marked B in Figure 11.

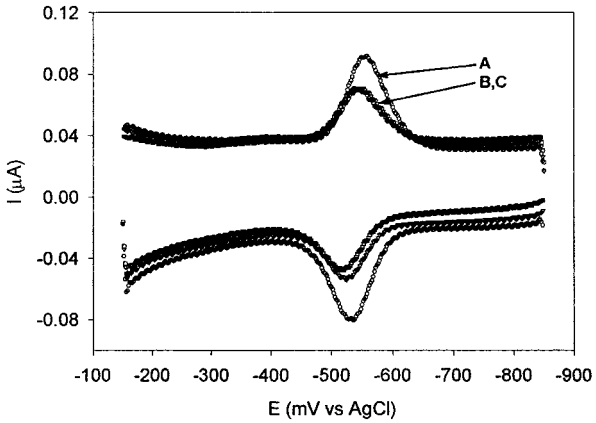


Figure 11. Cyclic voltammogram of **1a** with noncomplementary 20-mer **7**. Conditions were the same as those described in the legend of Figure 10.

Significantly, however, when the solution containing **1a** and its complement was annealed at 90 °C, followed by slow cooling to room temperature, the resulting cyclic voltammogram obtained on the solution was further attenuated and shifted to slightly more negative potential; see the cyclic voltammogram marked C in Figure 10. The corresponding cyclic voltammogram obtained for the control solution with the noncomplementary species **7** (cyclic voltammogram marked C in Figure 11) was not attenuated. These results are best understood if the hybridization is slow in these dilute solutions at room temperature. In this case, the attenuation seen in the cyclic voltammograms marked B in Figures 10 and 11 could be due to competitive adsorption as described above.

While the further attenuation seen in the cyclic voltammogram marked C in Figure 10 appears to be related to formation of the duplex species in solution, the physical phenomenon responsible for this effect is not clear. One possibility is that the duplex **1a·6** species is electroinactive or not adsorbed on the electrode surface and that the signal obtained after solution hybridization is due to adsorbed **1a** in equilibrium with a decreased concentration of **1a** in the bulk of the solution. Alternatively, the duplex **1a·6** might adsorb on the electrode with a footprint that is larger than the combined footprints of the tagged and untagged 20-mers. More likely, the duplex **1a·6** is electroactive, but has a smaller adsorption coefficient (β) than the single-strand ODNs since the DNA bases are not free to interact with the surface, so that when the duplex is formed in solution, the surface layer is no longer at saturation coverage. In any case, the possibility of a simple in situ electrochemical detection of the hybridization event based on these results is problematic without a different strategy and further modification of the electrode surface.

CONCLUSIONS

(1) We have demonstrated that AQ−ODNs, which bear one or more reporter groups, can be prepared with a modified uridine moiety in any location in a specific sequence utilizing standard phosphoramidite methodology.

(2) The AQ conjugates form compact surface layers on Hg electrodes with molecular footprints, calculated from the saturation coverages, that scale with molecular size.

The cyclic voltammetry is consistent with rapid electron transfer and little dispersion of $E^{\circ\prime}$ values. This indicates that the AQ groups are located in a uniform position in a compact surface layer and are not insulated from the electrode surface since facile transfer of electrons through the adsorbed ss-DNA layer is unlikely.

(3) The cyclic voltammetric response of the ds-AQ−20-mers is complicated by the competitive adsorption of the individual ss-20-mers and possibly the ds-20-mers as well. At room temperature in aqueous buffer solutions, equilibrium surface coverages are established more rapidly than the hybridization kinetics, which are much slower than the CV time scale.

(4) Accumulation of adventitious Hg(II) ions is a problem, which has not been fully realized in previous work, when HMDEs are used for voltammetric sensing of DNA.

ACKNOWLEDGMENT

This research was supported by the National Science Foundation (NSF Grant CHE-9616994) and The University of Tennessee (Knoxville, TN).

LITERATURE CITED

(1) Chee, M., Yang, R., Hubbell, E., Berno, A., Huang, X. C., Stern, D., Winkler, J., Lockhart, D. G., Morris, M. S., and Fodor, S. P. A. (1996) Accessing genetic information with high-density DNA arrays. *Science 274*, 610−614.

(2) Kessler, C. (1992) *Nonradioactive Labeling and Detection of Biomolecules*, Springer-Verlag, Berlin.

(3) Englisch, U., and Gauss, D. H. (1991) Chemically Modified Oligonucleotides. *Angew. Chem., Int. Ed. 30*, 613−629.

(4) Asseline, U., Thoung, N. T., and Helene, C. (1997) Synthesis and properties of oligonucleotides covalently linked to intercalating agents. *New J. Chem. 21*, 5−17.

(5) Thiel, A. J., Frutos, A. G., Jordan, C. E., Corn, R. M., and Smith, L. M. (1997) In Situ Surface Plasmon Resonance Imaging Detection of DNA Hybridization to Oligonucleotide Arrays on Gold Surfaces. *Anal. Chem. 69*, 4948−4956.

(6) Palecek, E. (1983) Modern Polarographic (Voltammetric) Techniques in Biochemistry and Molecular Biology. In *Topics in Bioelectrochemistry and Bioenergetics* (G. Milazzo, Ed.) Vol. 5, pp 65−155, Wiley, New York.

(7) Palecek, E. (1988) New Trends in Electrochemical Analysis of Nucleic Acids. *Bioelectrochem. Bioenerg. 20*, 179−194.

(8) Hall, J. M., Moore-Smith, J., Bannister, J. V., and Higgins, I. J. (1994) An Electrochemical Method for Detection of Nucleic Acid Hybridisation. *Biochem. Mol. Biol. Internat. 32*, 21−28.

(9) Jacobson, K. B., Arlinghus, H. F., Schmitt, H. W., Sachleben, R. A., Brown, G. M., Thonnard, N., Sloop, F. V., Foote, R. S., Larimer, F. W., et al. (1991) An Approach to the Use of Stable Isotopes for DNA Sequencing. *Genomics 9*, 51−59.

(10) Sloop, F. V., Brown, G. M., Sachleben, R. A., Garrity, M. L., Elbert, J. E., and Jacobson, K. B. (1994) Metalloorganic Labels for DNA Sequencing and Mapping. *New J. Chem. 18*, 317−326.

(11) Takenaka, S., Uto, Y., Kondo, H., Ihara, T., and Takagi, M. (1994) Electrochemically Active DNA Probes: Detection of Target DNA Sequences at Femtomole Level by HPLC with Electrochemical Detection. *Anal. Biochem. 218*, 436−443.

(12) Ihara, T., Maruo, Y., Takenaka, S., and Takagi, M. (1996) Ferrocene-oligonucleotide conjugates for electrochemical probing of DNA. *Nucleic Acids Res. 24*, 4273−4281.

(13) Uto, Y., Kondo, H., Abe, M., Suzuki, T., and Takenaka, S. (1997) Electrochemical analysis of DNA amplified by the polymerase chain reaction with a ferrocenylated oligonucleotide. *Anal. Biochem. 250*, 122−124.

(14) Xu, X.-H., and Bard, A. J. (1995) Immobilization and Hybridization of DNA on an Aluminum(III) Alkanebisphosphonate Thin Film with Electrogenerated Chemiluminescent Detection. *J. Am. Chem. Soc. 117*, 2627.

(15) Carter, M. T., Rodriquez, M., and Bard, A. J. (1989) Voltammetric Studies of the Interaction of Metal Chelates with DNA. 2. Tris-Chelated Complexes of Cobalt(III) and Iron(II) with 1,10-Phenanthroline and 2,2-Bipyridine. *J. Am. Chem. Soc 111*, 8901.

(16) Rodriguez, M., and Bard, A. J. (1990) Electrochemical Studies of the Interaction of Metal Chelates with DNA. 4. Voltammetric and Electrogenerated Chemiluminescent Studies of the Interaction of Tris(2,2-bipyridine)osmium(II) with DNA. *Anal. Chem. 62*, 2658.

(17) Welch, T. W., Corbett, A. H., and Thorp, H. H. (1995) Electrochemical Determination of Nucleic Acid Diffusion Coefficients through Noncovalent Association of Redox-Active Probes. *J. Phys. Chem. 99*, 11757−11763.

(18) Millan, K. M., Saraullo, A., and Mikkelsen, S. R. (1994) Voltammetric DNA Biosensor for Cystic Fibrosis Based on a Modified Carbon Paste Electrode. *Anal. Chem. 66*, 2943−2948.

(19) Wang, J., Rivas, G., Parrado, C., Cai, X., and Flair, M. N. (1997) Electrochemical biosensor for detecting DNA sequences from the pathogenic protozoan *Cryptosporidium parvum*. *Talanta 44*, 2003−2010.

(20) Wang, J., Rivas, G., Cai, X. H., Dontha, N., Shiraishi, H., Luo, D. B., and Valera, F. S. (1997) Sequence-specific electrochemical biosensing of *M. tuberculosis* DNA. *Anal. Chim. Acta 337*, 41−48.

(21) Zhao, Y.-D., Pang, D.-W., Wang, Z.-L., Cheng, J.-K., and Qi, Y.-P. (1997) DNA-modified electrodes. Part 2. Electrochemical characterization of gold electrodes modified with DNA. *J. Electroanal. Chem.*, 203−209.

(22) Hasshimoto, K., Ito, K., and Ishimori, Y. (1994) Sequence-specific gene detection with a gold electrode modified with DNA probes and an electrochemically active dye. *Anal. Chem. 66*, 3830.

(23) Liu, S., Ye, J., He, P., and Fang, Y. (1996) Voltammetric determination of sequence-specific DNA by electroactive intercalator on graphite electrode. *Anal. Chim. Acta 335*, 239.

(24) Kelley, S. O., Barton, J. K., Jackson, N. M., and Hill, M. G. (1997) Electrochemistry of Methylene Blue Bound to a DNA-Modified Electrode. *Bioconjugate Chem. 8*, 31−37.

(25) Palanti, S., Marrazza, G., and Mascini, M. (1996) Electrochemical DNA probes. *Anal. Lett. 29*, 2309−2331.

(26) Wang, J., Rivas, G., Luo, D., Cai, X., Valera, F. S., and Dontha, N. (1996) DNA-Modified Electrode for the Detection of Aromatic Amines. *Anal. Chem. 68*, 4365.

(27) Johnston, D. H., Glasgow, K. C., and Thorp, H. H. (1995) Electrochemical Measurement of the Solvent Accessibility of Nucleobases Using Electron Transfer between DNA and Metal Complexes. *J. Am. Chem. Soc. 117*, 8933−8938.

(28) Johnston, D. H., and Thorp, H. H. (1996) Cyclic Voltammetry Studies of Polynucleotide Binding and Oxidation by Metal Complexes: Homogeneous Electron-Transfer Kinetics. *J. Phys. Chem. 100*, 13837−13843.

(29) Napier, M. E., and Thorp, H. H. (1997) Modification of Electrodes with Dicarboxylate Self-Assembled Monolayers for Attachment and Detection of Nucleic Acids. *Langmuir 13*, 6342.

(30) Napier, M. E., Loomis, C. R., Sistare, M. F., Kim, J., Eckhardt, A. E., and Thorp, H. H. (1997) Probing Biomolecule Recognition with Electron Transfer: Electrochemical Sensors for DNA Hybridization. *Bioconjugate Chem. 8*, 906−913.

(31) Tohda, K., Ameniya, S., and Umezawa, Y. (1997) Channel Mimetic Sensing Membranes for Nucleotides Based on Multitopic Hydrogen Bonding. *Isr. J. Chem. 37*, 267−275.

(32) Korri-Youssoufi, H., Garnier, F., Srivastava, P., Dodillot, P., and Yassar, A. (1997) Toward Bioelectronics: Specific DNA Recognition Based on an Oligonucleotide-Functionalized Polypyrrole. *J. Am. Chem. Soc. 119*, 7388−7389.

(33) Freier, S. M., and Altmann, K.-H. (1997) The ups and downs of nucleic acid duplex stability: structure−stability studies on chemically-modified DNA:RNA duplexes. *Nucleic Acids Res. 25*, 4429.

(34) Yamana, K., Nishijima, Y., Ikeda, T., Gokota, T., Ozaki, H., Nakano, H., Sangen, O., and Shimidzu, T. (1990) Synthesis and Interactive Propeties of an Oligonucleotide with

Anthraquinone at the Sugar Fragment. *Bioconjugate Chem. 1*, 319−324.
(35) Keller, T. H., and Häner, R. (1993) Synthesis and hybridization properties of oligonucleotides containing 2′-O-modified ribonucleotides. *Nucleic Acids Res. 21*, 4499−4505.
(36) Deshmukh, H. M., Joglekar, S. P., and Broom, A. D. (1995) Self-Complementary Oligodeoxyribonucleotides Containing 2′-*O*-(Anthraquinone-2-methyl)adenosine. *Bioconjugate Chem. 6*, 578−586.
(37) Kang, H., and Rokita, S. E. (1996) Site-specific and photoinduced alkylation of DNA by a dimethylanthraquinone-oligodeoxynucleotide conjugate. *Nucleic Acids Res. 24*, 3896−3902.
(38) Chatterjee and Rokita, S. E. (1994) The Role of a Quinone Methide in the Sequence Specific Alkylation of DNA. *J. Am. Chem. Soc. 116*, 1690−1697.
(39) Gasper, S. M., and Schuster, G. G. (1997) Intramolecular Photoinduced Electron Transfer to Anthraquinone Linked to Duplex DNA: The Effect of Gaps and Traps on Long-Range radical Cation Migration. *J. Am. Chem. Soc. 119*, 12762−12771.
(40) Mori, K., Subasinghe, C., and Cohen, J. S. (1989) Oligodeoxynucleotide analogs with 5-linked anthraquinone. *FEBS Lett. 249*, 213−218.
(41) Schaumberg, J. P., Hokanson, G. C., French, J. C., Smal, E., and Baker, D. C. (1985) 2′-Chloropentostatin, a new inhibitor of adenosine deaminase. *J. Org. Chem 50*, 1651.
(42) Wagner, G. J., and Chambers, J. Q. (1997) Electrochemistry of Covalently Mercurated Uridine Nucleotides. *Langmuir 13*, 3529−3541.
(43) Manoharan, M., Tivel, K. L., Andrade, L. K., and Cook, P. D. (1995) 2-*O*- and 3-*O*-Pyrimidine Aminotether-Containing Oligonucleotides: Synthesis and Conjugation Chemistry. *Tetrahedron Lett. 36*, 3647−3650.
(44) Fasman, G. D. (1985) *Handbook of Biochemistry and Molecular Biology: Nucleic Acids*, 2nd ed., Vol. 1, p 589, CRC Press, Cleveland, OH.
(45) Dean, J. A. (1985) *Lange's Handbook of Chemistry*, 13th ed., McGraw-Hill, New York.
(46) Bayer, E., Bauer, T., Schmeer, K., Bleicher, K., Maier, M., and Gaus, H.-J. (1994) Analysis of Double-Stranded Oligonucleotides by Electrospray Mass Spectrometry. *Anal. Chem. 66*, 3858−3863.
(47) Atkinson, T., and Smith, M. (1984) Solid-Phase Synthesis of Oligodeoxynucleotides by the Phosphite-triester Method. In *Oligonucleotide Synthesis: A Practical Approach* (M. J. Gait, Ed.) pp 35−81, IRL Press, Washington, DC.
(48) Manoharan, M., Tivel, K. L., and Cook, P. D. (1995) Lipidic Nucleic Acids. *Tetrahedron Lett. 36*, 3651−3654.
(49) Forster, R. J. (1996) Reversibly Adsorbed Monolayers on Microelectrodes: Effect of Potential on the Adsorption Thermodynamics. *Anal. Chem. 68*, 3143.
(50) Meunier-Prest, R., and Laviron, E. (1992) Electrochemical Reactions with Protonations at Equilibrium. Part XV. The 2-electron, 2-proton Bi-cubic Scheme. *J. Electroanal. Chem. 328*, 33−46.
(51) Sletten, E., and Nerdal, W. (1997) Interaction of Mercury with Nucleic Acids and Their Components. In *Metals in Biology* (A. Sigel and H. Sigel, Eds.) Vol. 34, pp 479−501, Marcel Dekker, New York.
(52) Ksenzhek, O. S., Petrova, S. A., Oleinik, S. V., Kolokyazhnyi, M. V., and Moskovskii, V. Z. (1977) Investigation of the redox properties of quinoid compounds. II. Anthraquinone and its derivatives. *Soviet Electrochemistry 13*, 151−158.
(53) Salaita, G. N., and Hubbard, A. T. (1992) Adsorbed Organic Molecules at Well-Defined Electrode Surfaces. In *Molecular Design of Electrode Surfaces, Techniques of Chemistry* (R. W. Murray, Ed.) Vol. XXII, John Wiley & Sons, New York.
(54) Bard, A. J., and Faulkner, L. R. (1980) In *Electrochemical Methods: Fundamentals and Applications*, John Wiley & Sons, New York.
(55) Herne, T. M., and Tarlov, M. J. (1997) Characterization of DNA Probes Immobilized on Gold Surfaces. *J. Am. Chem. Soc. 119*, 8916−8920.

BC980095I

Inhibition of Viral Adhesion and Infection by Sialic-Acid-Conjugated Dendritic Polymers

Jon D. Reuter,[†,‡] Andrzej Myc,[†] Michael M. Hayes,[†] Zhonghong Gan,[§] Rene Roy,[§] Dujie Qin,[∥] Rui Yin,[∥] Lars T. Piehler,[∥] Roseita Esfand,[∥] Donald A. Tomalia,[∥] and James R. Baker, Jr.*[,†]

Center for Biologic Nanotechnology, Department of Internal Medicine, Division of Allergy, 1150 West Medical Center Drive, Room 9220 MSRB III, University of Michigan, Unit for Laboratory Animal Medicine, University of Michigan, Ann Arbor, Michigan 48109, Department of Chemistry, University of Ottawa, Canada, and Michigan Molecular Institute, Midland, Michigan 48640. Received August 19, 1998;
Revised Manuscript Received December 21, 1998

Multiple sialic acid (SA) residues conjugated to a linear polyacrylamide backbone are more effective than monomeric SA at inhibiting influenza-induced agglutination of red blood cells. However, "polymeric inhibitors" based on polyacrylamide backbones are cytotoxic. Dendritic polymers offer a nontoxic alternative to polyacrylamide and may provide a variety of potential synthetic inhibitors of influenza virus adhesion due to the wide range of available polymer structures. We evaluated several dendritic polymeric inhibitors, including spheroidal, linear, linear-dendron copolymers, comb-branched, and dendrigraft polymers, for the ability to inhibit virus hemagglutination (HA) and to block infection of mammalian cells in vitro. Four viruses were tested: influenza A H2N2 (selectively propagated two ways), X-31 influenza A H3N2, and sendai. The most potent of the linear and spheroidal inhibitors were 32−256-fold more effective than monomeric SA at inhibiting HA by the H2N2 influenza virus. Linear-dendron copolymers were 1025−8200-fold more effective against H2N2 influenza, X-31 influenza, and sendai viruses. The most effective were the comb-branched and dendrigraft inhibitors, which showed up to 50000-fold increased activity against these viruses. We were able to demonstrate significant ($p < 0.001$) dose-dependent reduction of influenza infection in mammalian cells by polymeric inhibitors, the first such demonstration for multivalent SA inhibitors. Effective dendrimer polymers were not cytotoxic to mammalian cells at therapeutic levels. Of additional interest, variation in the inhibitory effect was observed with different viruses, suggesting possible differences due to specific growth conditions of virus. SA-conjugated dendritic polymers may provide a new therapeutic modality for viruses that employ SA as their target receptor.

INTRODUCTION

Influenza virus is a highly contagious, enveloped RNA virus which is responsible for several severe pandemics (Mulder and Hers, 1972). Two envelope glycoproteins, hemagglutinin (HA) and neuraminidase (NA), determine the antigenic specificity of viral subtypes (Lamb and Krug, 1996). The virus is highly mutagenic, and frequent alterations in HA glycosylation leading to altered antigenicity are considered to be responsible for the episodic resurgence of influenza. The capacity to modify viral antigenic sites enables influenza virus to overcome inhibitory effects of neutralizing antibodies and elude many anti-viral compounds including neuraminidase inhibitors (Lamb and Krug, 1996; Schulze, 1997).

The first step of infection by influenza virus is the binding of the viral HA to sialic acid receptors on the host cell, followed by receptor-mediated endocytosis of the virus into the cell (Wiley and Skehel, 1987). One potential approach to anti-viral therapy involves the inhibition of virus/host cell binding via blocking of the viral receptor (Kiefel et al., 1996; Weis et al., 1988). Ideal preventative agents must be nontoxic to mammalian cells, broadly specific across viral subtypes and cost effective. Previous reports have demonstrated that millimolar concentrations of solubilized monomeric sialic acid (SA) prevent influenza A agglutination of chicken erythrocytes (cRBC), presumably by binding to the HA molecule on the virus (Pritchett and Paulson, 1987; Weis et al., 1988). However, host cell viral receptor sialyl moieties have great lateral mobility on the cellular surface, allowing each influenza virion to use the estimated 300−600 envelope hemagglutinin spikes to develop strong polyvalent binding to host cell receptors (Choi et al., 1997; Weis et al., 1988). Thus, while the binding of soluble α-sialoside monomeric derivatives to hemagglutinin is very weak ($K_D \approx 2$ mM), cooperative interaction allows influenza virus attachment to the surface of an erythrocyte with K_D (HA) over $<10^{-12}$ M (Pritchett and Paulson, 1987; Sauter et al., 1989). Nonphysiological and potentially toxic concentrations of soluble monomeric SA are required to competitively disrupt this polyvalent interaction and prevent viral internalization into the cells. Moreover, soluble monomeric SA is vulnerable to enzymatic breakdown when exposed to biological fluids. Soluble monomeric SA also must compete with host sialosides attached to glycoproteins and glycolipids, and its use is therefore unlikely to be an effective strategy to prevent viral infection (Pritchett and Paulson, 1987).

To circumvent these problems, multiple sialyl moieties were conjugated to a synthetic polymer backbone to provide a polyvalent inhibitor. With this strategy, the

* To whom correspondence should be addressed. Phone: (734) 647-2777. Fax: (734) 936-2990. E-mail: jbakerjr@umich.edu.
[†] Center for Biologic Nanotechnology.
[‡] Unit for Laboratory Animal Medicine.
[§] Department of Chemistry.
Michigan Molecular Institute.

10.1021/bc980099n CCC: $18.00 © 1999 American Chemical Society
Published on Web 02/24/1999

polymeric inhibitor molecule can potentially interact with many HA moieties on a single virus, leading to increased binding affinity. In addition, the sialyl moiety is more stable when conjugated to polymer in a manner similar to the higher stability of immobilized enzymes (Trevan, 1980). Whitesides and co-workers have successfully conjugated SA residues to a polyacrylamide backbone, and this material demonstrates enhanced inhibition of viral agglutination of cRBC at concentrations between $10^{-4}-10^{-7}$ M SA in solution (Choi et al., 1997; Mammen et al., 1995; Spaltenstein and Whitesides, 1991). This demonstrated that coupling SA to a synthetic polymer backbone can enhance the inhibition of viral adhesion of SA 25-fold greater than the best naturally occurring inhibitor (Mammen et al., 1995). However, we have found linear polyacrylamide to be toxic to mammalian cells and the acrylamide monomer is a potent neurotoxin in animals (Mangan and Snyder, 1978; Schaumburg et al., 1989; Spencer and Schaumburg, 1975), and this limits its utility in vivo.

Roy and co-workers tried an alternative multivalent approach to influenza virus inhibition, attaching sialic acid groups to the periphery of several generations of small polylysine dendrimers (Roy et al., 1993). It was found that as the number of surface sialic acid moieties was increased from 2 to 16 (along with the dendrimer size), the potency of the inhibitors increased to approximately that of Whitesides' much larger polysialoside inhibitors. It seemed that the branching architecture could hold advantages over the more conventional linear inhibitors such as increased polyvalent binding with reduced toxicity. Further explorations of this concept with other relatively small, dendritic carbohydrate inhibitors have allowed improvements in lectin binding (Roy, 1996). Recent results from the same group suggest that PAMAM dendrimers above G1 have superior lectin binding properties (Zanini et al., 1998).

The objective of this study was to assess the efficacy of novel polymer-based decoys to prevent viral adhesion and infection. In analyzing these agents, we hope to identify structure−function relationships in these inhibitors. The present approach uses inert, nontoxic and structurally well-defined dendritic polymers conjugated with sialic acid as polyvalent inhibitors of viral adhesion. We screened a variety of these polymer conjugates for the ability to prevent adhesion of several strains of virus. We also confirmed for the first time that these polymer conjugates could prevent viral infection in mammalian cells.

MATERIALS AND METHODS

Virus and Antisera. Influenza virus A/AA/6/60 (H2N2) strain passaged in mice and another passaged in chickens (Herlocher et al., 1996) were graciously donated by Dr. Hunein Maassab (Department of Public Health, University of Michigan, Ann Arbor, MI). X-31 (A/Aichi/2/68 × A/PR/8/34) influenza A H3N2 virus was kindly provided by Mr. Alan R. Douglas, NIMR, London, United Kingdom. Sendai/52 virus was obtained from ATCC (Rockville, MD). Viruses were propagated in embryonated chicken eggs using standard methods described elsewhere (Barrett and Inglis, 1985). Infectious allantoic fluid was collected and centrifuged at 2000−3000 rpm for 10 min. The supernatant was cultured on blood agar to screen for potential bacterial contamination. As an extra precaution, the supernatant was passed through a 0.2 mm filter and stored in aliquots of 10^8 pfu/mL at −80 °C.

Ferret anti-influenza A H2N2 polyclonal antibody was donated by Dr. Hunein Maassab (Department of Public Health, University of Michigan, Ann Arbor, MI). Rabbit anti-X31 polyclonal antisera was graciously provided by Alan R. Douglas (NIMR, London, United Kingdom).

Dendritic Polymers. Linear polyacrylamide polymers were synthesized similar to previous reports using a modified form with the same SA group (Choi et al., 1997; Roy et al., 1992). Synthesis of comb-branched (Figure 1, structure II) and dendrigrafts (Figure 1, structure III) polymers (Tomalia et al., 1991), spheroidal dendrimer (Figure 1, structure IV) (Kim et al., 1996; Roy, 1996; Roy et al., 1993, 1994; Tomalia et al., 1985), and linear-dendron architectural copolymers (Figure 1, structure V) (Yin et al., 1998) were accomplished as reported elsewhere.

Briefly, linear polyethyleneimine (PEI) required for the construction of the comb-branched, dendrigraft (Tomalia et al., 1991), and linear-dendron architectural copolymers (Yin et al., 1998) was obtained by either partial (30%, for the first two architectures) or full (for the latter) acid hydrolysis of polyethyloxazoline (PEOx). The PEOx was in turn prepared by the living cationic polymerization of ethyl oxazoline, initiated by methyl *p*-toluenesulfonate.

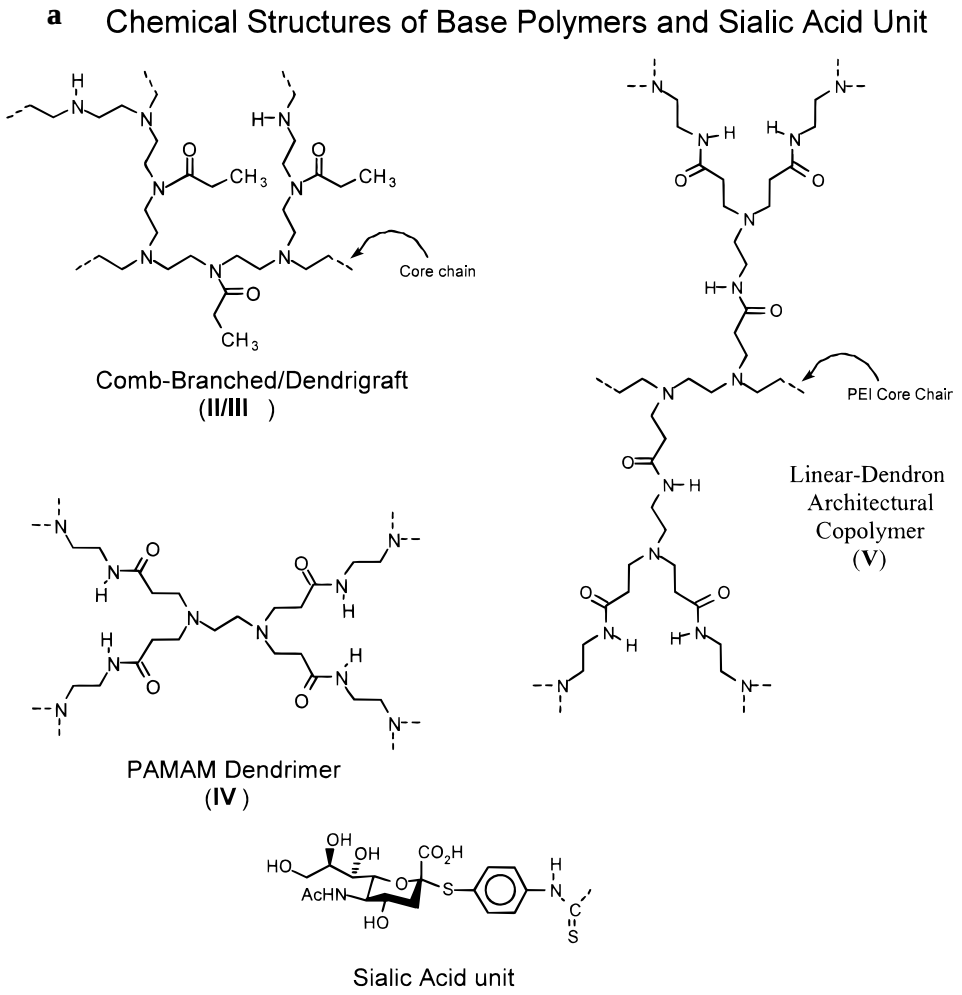
Comb-branched (G0) polymers were prepared by grafting living cationic PEOx chains (initiated as above) onto linear PEI. Reiteration of the hydrolysis and grafting steps led to dendrigraft polymers of increasing generation (Figure 1, structure II). Linear-dendron architectural copolymers were prepared by employing the methyl acrylate Michael addition/EDA amidation sequence used for the PAMAM synthesis (see above) with linear PEI as the core instead of EDA. This led to a polymer consisting of a PEI core functionalized with PAMAM dendrons along its length (Figure 1, structure V).

PAMAM dendrimers (Tomalia et al., 1985) were prepared by Michael addition of methyl acrylate to ethylenediamine (EDA), followed by amidation of the tetraester product with an excess of EDA to produce the G0 product. Continued similar alternating Michael addition/amidation reactions with the G0 product (and succeeding generations) led to PAMAM dendrimers of the desired generation, with primary amine end groups (Figure 1, structure IV). Those PAMAM dendrimers listed in Table 1b with variable degrees of conjugation contain a mixed hydroxyl/amine surface.

The conjugation of sialic acid to the backbone dendritic polymers was carried out by reacting primary or secondary amine groups of the polymers with a protected, isothiocyanate-derivatized sialate. Deprotection of the blocking groups led to polymers conjugated to sialic acid groups via an aromatic thiourea linker (Zanini et al., 1998).

Backbone polymers were characterized by ^{1}H and ^{13}C NMR spectroscopy, SEC-RI, MALDI MS, and MALLS. The conjugates were characterized by UV−vis and ^{1}H and ^{13}C NMR spectroscopy. Molecular weights of dendrigraft conjugates were calculated from amide hydrolysis and grafting efficiencies, as determined by ^{1}H NMR. Ultraviolet spectroscopy was utilized for quantitative measurement of the chromophore-linked sialic acid molarity at a wavelength of 248−250 nm. Decoy polymers were reconstituted with sterile Dulbecco's PBS (D-PBS) (Life Technologies, GibcoBRL, Gaithersburg, MD), mixed overnight on a tube rotator at room temperature, and stored at 4 °C.

Hemagglutination Inhibition Assay (HAI). Assays were performed with 0.5% chicken red blood cells (cRBC) as previously described (Kendal and Dowdle, 1986) with minor modifications. *N*-Acetylneuraminic acid type IV (Sigma Chemical Co.) was employed as internal monomer



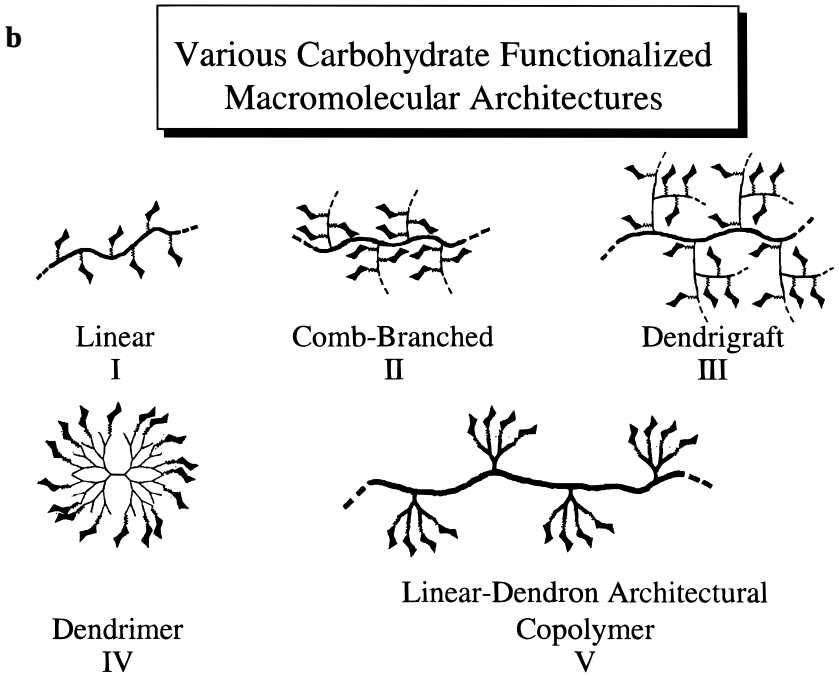


Figure 1. (a) Chemical structures of base polymers and sialic acid unit. (b) Model representations of sialic-acid-conjugated polymeric inhibitor subunits used to inhibit viral infection. (I) Linear polymer, (II) comb-branched polymer, (III) dendrigraft polymer, (IV) spheroidal dendrimer, (V) linear-dendron architectural copolymers. Structures are not drawn to scale.

SA standard. Potential inhibitor and virus (25 μL each) were incubated together for 30 min at 37 °C. After incubation, 50 μL of cRBC was added to each well and incubated for one additional hour. PBS was prepared

Table 1. Hemagglutination Inhibition Activity of Polymeric Inhibitors with Various Strains of Influenza A and Sendai Virus[a]

description	architectural type	molecular weight	influenza A H2N2 chicken	influenza A H2N2 mouse	X-31	sendai
(a) Linear Polyacrylamide Inhibitors						
N-acetylneuraminic acid	monomer	309.3	4000	4000	4000	4000
NeuAc-polysuccinimidyl acrylate NeuAc/ester 1/2[c]	I	68 000	*b*	ND	ND	*b*
NeuAc-polysuccinimidyl acrylate NeuAc/ester 1/5	I	38 000	65	ND	ND	*b*
NeuAc-polysuccinimidyl acrylate NeuAc/ester 1/10	I	28 000	47	ND	ND	*b*
GM3 polymer GM3/polymer 1/10	I	36 000	56	ND	ND	35
(b) Polyamidoamine (PAMAM) Spheroidal Dendrimers						
N-acetylneuraminic acid	monomer	309.3	4000	4000	4000	4000
PAMAM G0 (100%)	IV	2351	*b*	ND	ND	ND
PAMAM G1 (100%)	IV	5098	*b*	ND	ND	ND
PAMAM G2 (100%)	IV	10 592	*b*	ND	ND	ND
PAMAM G3 (100%)	IV	21 581	*b*	ND	ND	ND
PAMAM G2 OH/NeuAc 25/75	IV	8762	*b*	ND	ND	*b*
PAMAM G5 OH/NeuAc 50/50	IV	58 233	*b*	ND	ND	*b*
PAMAM G5 OH/NeuAc 75/25	IV	43 592	*b*	ND	ND	*b*
PAMAM G5 OH/NeuAc 67/33	IV	48 168	*b*	ND	ND	*b*
(c) Linear-Dendron Architectural Copolymers						
N-acetylneuraminic acid	monomer	309.3	4000	4000	4000	4000
PEI/PAMAM G0 (0%)	I	15 700	*b*	*b*	*b*	*b*
PEI/PAMAM G0 (100%)	I	63 760	*b*	48.8	78.8	4.8
PEI/PAMAM G0 (28%)	I	29 060	*b*	*b*	*b*	*b*
PEI/PAMAM G0 (9%)	I	20 120	*b*	*b*	*b*	*b*
PEI/PAMAM G0 (5%)	I	18 250	*b*	*b*	*b*	*b*
PEI/PAMAM G1 (100%)	V	110 590	*b*	290	*b*	3.7
PEI/PAMAM G1 (20%)	V	57 340	*b*	*b*	*b*	*b*
PEI/PAMAM G1 (9%)	V	46 860	*b*	*b*	*b*	*b*
PEI/PAMAM G1 (5%)	V	43 310	*b*	*b*	*b*	*b*
PEI/PAMAM G2 (100%)	V	213 960	*b*	520	6.5	6.6
PEI/PAMAM G2 (23%)	V	127 890	*b*	*b*	*b*	*b*
PEI/PAMAM G2 (11%)	V	105 780	*b*	*b*	*b*	*b*
PEI/PAMAM G2 (5%)	V	93 910	*b*	*b*	*b*	*b*
(d) Comb-Branched and Dendrigraft Polymers						
N-acetylneuraminic acid	monomer	309.3	4000	4000	4000	4000
comb-branched polymer G0 (0%)	II	1.66×10^5	*b*	*b*	*b*	*b*
comb-branched polymer G0 (43%)	II	2.54×10^5	*b*	*b*	1.5	0.2
comb-branched polymer G0 (17%)	II	2.00×10^5	*b*	*b*	*b*	10
comb-branched polymer G0 (10%)	II	1.86×10^5	*b*	*b*	*b*	*b*
comb-branched polymer G0 (5%)	II	1.76×10^5	*b*	*b*	*b*	*b*
dendrigraft polymer G1 (51%)	III	1.56×10^6	*b*	2260	1.0	0.1
dendrigraft polymer G1 (15%)	III	1.16×10^6	*b*	*b*	*b*	112
dendrigraft polymer G1 (8%)	III	1.09×10^6	*b*	*b*	*b*	*b*
dendrigraft polymer G1 (5%)	III	1.05×10^6	*b*	*b*	*b*	*b*
dendrigraft polymer G2 (41%)	III	8.57×10^6	*b*	1725	0.7	0.1
dendrigraft polymer G2 (13%)	III	6.82×10^6	*b*	*b*	*b*	66.5
dendrigraft polymer G2 (7%)	III	6.41×10^6	*b*	*b*	*b*	*b*
dendrigraft polymer G2 (5%)	III	6.29×10^6	*b*	*b*	*b*	*b*
dendrigraft polymer G3 (56%)	III	5.82×10^7	*b*	2475	0.2	0.1
dendrigraft polymer G3 (15%)	III	4.19×10^7	*b*	*b*	*b*	66.5
dendrigraft polymer G3 (10%)	III	4.00×10^7	*b*	*b*	*b*	*b*
dendrigraft polymer G3 (5%)	III	3.79×10^7	*b*	*b*	*b*	*b*

[a] Values in parts a and b are reported in terms of the lowest effective polymer concentration (μM) in solution; values in parts c and d are reported in terms of the lowest effective micromolarity SA in solution. [b] No ability to prevent agglutination of *N*-acetylneuraminic acid type IV at the concentration of 1×10^{-3} M SA in solution. [c] Numbers in parentheses represent percent SA conjugation to free amine groups on the polymer.

with 0.1 M sodium phosphate and 0.13 M sodium chloride in double distilled water with the final pH adjusted to 7.4.

MDCK Cellular Toxicity Assay. Madin Darby Canine Kidney (MDCK) cells (American Type Culture Collection [ATCC], Rockville, MD) were grown to a monolayer in 96-well microtiter plates in Minimal Essential Medium (MEM) Eagle (Mediatech, Inc., Herndon, VA), 10% fetal bovine serum (Hyclone, Logan, UT), 0.1 mM MEM Nonessential Amino Acids Solution, 2 mM L-Glutamine, 1.0 mM MEM sodium pyruvate, 100 units/mL Penicillin 100 μg/mL Streptomycin (Life Technologies, GibcoBRL, Gaithersburg, MA). MDCK cells were washed with Dulbecco's PBS (D-PBS) and incubated with 100 μL of the virus/potential inhibitor mixture diluted in serum free medium for 1 h. Cells were visually inspected for cytopathic effect using an inverted microscope and quantification of cell viability was performed using the MTT (3-(4,5-dimethylthiazol-2-yl)-2,5-diphenyltetrazolium bromide) spectrophotometric assay (Watanabe et al., 1994; Schulze, 1997) read at 595 nm with an ELISA reader.

Enzyme-Linked Immunosorbant Assay (ELISA) Infection Assays. All polymeric inhibitors were standardized to 5×10^{-3} M SA and incubated with an equal volume of influenza virus at a final concentration of 5.0

$\times 10^7$ pfu/mL for 30 min at 37 °C. The monomeric SA was diluted in serum free MEM and 1 M HEPES solution to a neutral pH. Polymeric inhibitors were diluted in serum free MEM to the desired concentration and incubated with MDCK cells as described below.

An ELISA was used to detect and quantitate soluble viral proteins in the supernatant from the infected cells. MDCK cells were prepared as described in the MDCK cellular toxicity assay above. Culture media were removed and cells were washed with sterile D-PBS. A total of 100 μL of the inoculum was added to each well and incubated for one hr at 37 °C with 5% CO_2. One hour later, the inoculum was replaced with fresh serum-free culture medium and incubated for 24 h at 37 °C in 5% CO_2.

Culture media from virus-infected MDCK cells were transferred to another 96-well microtiter plate pretreated with 0.5% glutaraldehyde for 1 h at 56 °C. Plates were then washed with PBS and blocked with 1% dry milk in PBS for 30 min at 37 °C. A total of 100 μL of ferret anti-influenza A antibody (1:1000 dilution) was added to the wells for 1 h at 37 °C. The wells were washed four times with washing buffer (PBS and 0.05% Tween-20) and incubated with goat anti-ferret biotinylated antibody (Kirkegaard and Perry Laboratories, Gaithersburg, MA) for 30 min at 37 °C, then washed four times again and incubated with streptavidin-peroxidase (Sigma), washed again, and then incubated with 1-Step turbo TMB-ELISA substrate (Pierce, Rockford, IL). The reaction was stopped with 1 N sulfuric acid and plates were read at a wavelength of 450 nm in an ELISA reader.

Data Analysis. All experiments were done in triplicate. Significance testing using the Student's *t*-test and regression analysis was done using Microsoft Excel SR-1, 1997, software. Significance was defined with $\alpha = 0.05$. Significance in the hemagglutination inhibition assay was defined as at least a 4-fold change in titer.

RESULTS

The concentration of monomeric SA that effectively inhibited viral agglutination of cRBC was determined. Free SA at a concentration of 4×10^{-3} M was shown to inhibit agglutination of cRBC caused by three different influenza viral strains and sendai virus. In subsequent hemagglutination inhibition assays, a concentration of 4×10^{-3} M SA was used as a standard concentration of free sialic acid for comparison with the polymeric agents.

Linear Polyacrylamide Polymers. Preliminary studies showed that three of four linear polyacrylamide polymers (Figure 1, structure I) were 64−128-fold more effective (concentrations $\sim 10^{-4}$ M) at inhibiting influenza A H2N2 (chicken passaged) virus agglutination of cRBC than the monomeric SA on a molar basis as measured in the HAI assay (Table 1a). The strongest inhibitor of these four was the compound with 20% of available binding sites conjugated to SA. Those with either higher or lower levels were less effective. However, these polymeric inhibitors were extremely toxic to MDCK cells at 10^{-6} M concentration (1000-fold lower than the effective HAI concentration; data not shown) and therefore could not be evaluated in the infectivity study.

Spheroidal Dendrimers. Of the spheroidal polyamidoamine (PAMAM) dendrimers (Figure 1, structure IV) tested, only one compound was more effective on a molar basis of polymer (32-fold) than monomeric SA at inhibiting cRBC agglutination of influenza A H2N2 (chicken passaged; see Table 1b). None of the spheroidal dendrimers were found to be effective at blocking sendai virus adhesion. Unconjugated generation five spheroidal dendrimers tested as a control also showed no ability to block viral adhesion.

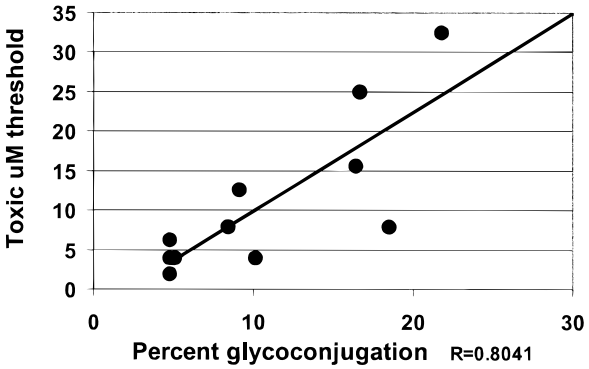


Figure 2. Inverse relationship between toxicity to MDCK cells and percentage SA conjugation of protonated primary and/or secondary amine binding termini observed for linear-dendron architectural copolymers (Figure 1, structure V). Those with all of the available primary amine sites conjugated to SA were nontoxic to mammalian cells.

Linear-Dendron Architectural Copolymers. On the basis of this information, we sought to determine if a nontoxic, linear backbone structurally similar to polyacrylamide could be equally effective in preventing viral cRBC agglutination. To test this hypothesis, we constructed 12 branched polyethylenimine-PAMAM linear-dendron architectural copolymers (Figure 1, structure V) with varying amounts of sialic acid moieties conjugated to the primary amine termini and screened them for efficacy in the HAI assay. These polymers, intended to be rod-shaped, at higher generations have the tree-like branching structure of PAMAM dendrons attached to the linear backbone (Figure 1, structure V). When these polymeric inhibitors had all of the primary amine groups conjugated to sialic acid, they were up to 1000-fold more effective at preventing cRBC agglutination caused by influenza A H2N2 (mouse passaged), H3N2 (X-31), and sendai viruses when compared to monomeric SA at the same molarity of sialic acid in solution (M SA, Table 1c). Hemagglutination by X-31 influenza and sendai viruses in particular was highly susceptible to the inhibitory effects of these conjugates. In contrast, these polymers failed to prevent agglutination of cRBC caused by the influenza A H2N2 (chicken passed) virus. Conjugates with 30% or less sialyl conjugation were ineffective with all tested viruses. We observed a negative correlation between the percentage of sialyl conjugation and cytotoxicity with these polymers (Figure 2). The unconjugated polyethylenimine backbone was cytotoxic to mammalian cells in vitro, while structures with 100% sialic acid conjugation at the same concentrations were not.

Comb-Branched and Dendrigraft Polyethylenimine Polymers. In the next set of experiments, we tested the efficacy of sialic-acid-conjugated comb-branched and dendrigraft (Figure 1, structures II and III) polymers to inhibit HA mediated by influenza and sendai viruses. These polymeric inhibitors are constructed of many chains of polyethylenimine in a "branch upon branch" comblike structure and have sialyl moieties conjugated to secondary amines. Those polymers with approximately 50% of secondary amines conjugated to sialic acid demonstrated a significant inhibition of cRBC agglutination caused by X-31 and sendai viruses at molar concentrations up to 50000-fold lower SA molarity than monomeric SA (Table 1d). These conjugates showed only moderate inhibition of cRBC agglutination caused by influenza A

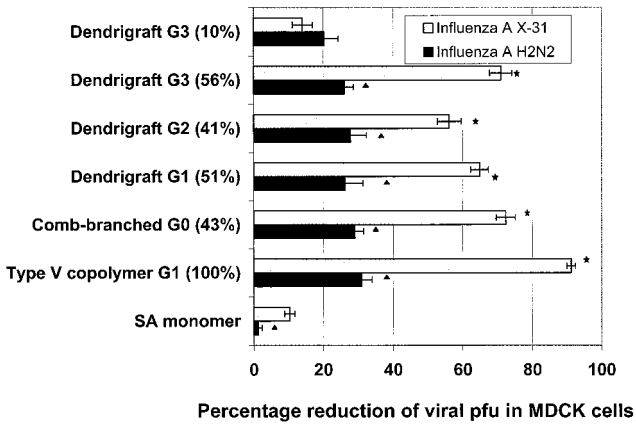


Figure 3. Percentage reduction of influenza A H2N2 (mouse passaged) and influenza A H3N2 (X-31) virus (pfu/well) treated with linear-dendron architectural copolymers (structure V), comb-branched (structure II), and dendrigraft (structure III) polymers on MDCK cells using ELISA. Numbers in parentheses represent percent SA conjugation to free amine binding sites on the polymer backbone. Note the viral strain variation in susceptibility to the inhibitors. All samples were standardized to 5×10^{-3} M SA. (★) Significantly less virus isolated from cells treated with decoy polymers than from virus treated with the unconjugated polymer backbone or monomeric SA ($p < 0.001$). (▲) Significantly different amounts of virus isolated from cells infected with either influenza A H2N2 or X-31 virus treated with the same inhibitor ($p < 0.05$).

H2N2 (mouse passaged) virus and were not effective in preventing cRBC agglutination of the influenza A H2N2 (chicken passaged) virus. Those with less than 13% of amines conjugated to sialyl groups were ineffective with all tested viruses. None of the tested comb-branched or dendrigraft polymeric inhibitors, regardless of the percentage of sialyl conjugation, were toxic to MDCK cells, even at concentrations as high as 1 mM SA (data not shown).

Prevention of Influenza Infection. On the basis of the HAI screening data, we attempted to determine if the most effective inhibitors (Figure 1, structures II, III, and IV) would be able to prevent viral infection of MDCK cells cultured in vitro. Using ELISA to measure the infection levels, buffered monomeric 2.5 mM SA showed a significant difference in inhibitory effect on X-31 virus infection compared to influenza A H2N2 (mouse passaged) virus (10 and 2%, respectively, $p < 0.05$). Several sialic-acid-conjugated comb-branched, dendrigraft, and linear-dendron architectural copolymers significantly ($p < 0.001$) inhibited influenza H2N2 (mouse passaged) and X-31 virus infection at 2.5 mM SA concentration (Figure 3). Inhibition data obtained from ELISA correlated well with those obtained from the HAI assay. Polymeric architectures that did not inhibit hemagglutination (e.g., dendrigraft G3 [10%]) consistently failed to show inhibitory effect on either X-31 or influenza A H2N2 (mouse passaged) viral infection of MDCK cells as tested in the ELISA. X-31 virus was significantly more susceptible to the dendrimer inhibitors than the influenza A H2N2 (mouse passaged) virus ($p < 0.01$). The reduction of X-31 virus ranged from 55% to over 90%, while for influenza A H2N2 the range was 23−35%. This significant viral variation to dendritic polymer inhibition observed during the in vitro infection assay was comparable to that which was observed in the HAI assay.

Unexpectedly, the unconjugated PEI polymer backbone (0.17 mM) showed some ability to inhibit (<20%) influenza A H2N2 (mouse passaged) virus infection in the MDCK cellular infection assay as determined by ELISA. However, this effect was not seen with the X-31 virus (<6%).

DISCUSSION

It is theorized that a significant proportion of the estimated 300−600 hemagglutinin glycoprotein spikes on an influenza virion must be blocked to effectively prevent viral adhesion to target cells (Mammen et al., 1995). Due to the low-affinity interaction between monomeric SA and viral HA, high concentrations of monomeric SA would be required to inhibit influenza virus. However, these concentrations are not biologically or medically feasible due to rapid enzymatic breakdown of the SA monomer (Kelm and Schauer, 1997) and the potential tissue toxicity of the high concentrations of SA. Spherical dendrimers are capable of inhibiting influenza viral agglutination of cRBC, as are linear polyacrylamide polymers. Due to their cellular toxicity, however, linear polyacrylamide polymers could not be evaluated in the infection assay. Linear-dendron architectural copolymers and dendrigraft polymers (Figure 1, structures V and III, respectively) were approximately 50 000 times stronger inhibitors of influenza viral agglutination of cRBC than monomeric SA and approximately 500 times stronger than other types of polymeric inhibitors. For the first time, it has been shown that sialic-acid-conjugated dendritic polymers are capable of inhibiting viral infection of mammalian cells in vitro and do not exhibit cytotoxicity at potentially therapeutic concentrations.

The action of SA-conjugated polymers is not fully understood (Mammen et al., 1995). These structures may act as decoy molecules with a high polyvalent binding to the hemagglutinin glycoprotein spikes and therefore compete with the host cell receptor binding by blocking virus adhesion. Some reports suggest that the cooperative interaction of SA moieties dramatically increases binding affinity to the virus (Choi et al., 1997; Mammen et al., 1995, 1998). In addition to this effect, we believe another factor also may contribute to inhibit viral adhesion to the host cell: the backbone of the virus-bound polymeric inhibitor provides a mass effect that may interfere with interactions between the virus and cell. It is also thought that these hydrophilic polymers have a large hydration effect, increasing nonspecific steric inhibition. Together, the specific affinity of HA for SA receptors and backbone hindrance may be inhibiting virus absorption in a synergistic manner.

Specific variations in dendritic polymer architecture selectively enhance the ability to inhibit virus. Spheroidal dendrimer architecture (Figure 1, structure IV) has a fixed, rigid size and shape, which may limit its ability to interact with the virus. These dendrimers are relatively small (1−10 nm) when compared to influenza virus (∼120 nm). Thus, it may take many more dendrimer inhibitors per virion in solution to block virus adhesion to the target cell. Linear-dendron architectural copolymers (Figure 1, structure V) are larger and more flexible than the spherical polymers and, therefore, potentially interact with the virus more efficiently. It is also possible that the unbound backbone and polymer groups block additional binding sites between virus and target by preventing the interaction. Comb-branched polymers and dendrigrafts (Figure 1, structures II and III) have a scaffolding-type of structure that combines the exponential surface binding capacity of the spherical dendrimers and the plasticity of the linear-dendron architectural copolymers (Figure 1, structure V). These dendritic

polymers theoretically have the ability to conform and wrap around receptor sites maximizing steric hindrance. However, the addition of excess branches may lead to entanglement of the SA-bound branches and actually limit virus/receptor interaction. The early generation (G0, G1) linear-dendron architectural copolymers and dendrigrafts (Figure 1, structures V and III, respectively) show the same ability to inhibit virus as hyperbranched, later generation (G2, G3) inhibitors (when standardized to the same SA molarity concentration). Thus, the advantage offered by the additional branching rapidly diminishes.

Only those dendrimers with all of the exterior primary and/or secondary amine binding sites conjugated to sialyl groups were effective at inhibiting viral adhesion and infection. One explanation is that the dendrimer polyvalent attraction to viral HA is only strong enough to effectively compete with the host cell receptors when maximally conjugated. An alternative hypothesis is that the protonated primary amines create charge repulsion between the decoy inhibitor and the virus (or create internal ionic binding between carboxylates and amines within decoy conjugates). With spheroidal dendrimers or linear-dendron architectural copolymers (Figure 1, structures IV and V), all of the amine sites within the polymer are exposed and able to be conjugated. However, with comb-branched and dendrigraft polymers (Figure 1, structures II and III), only approximately 50% of the amine sites are available to undergo conjugation, with the remaining sites buried within the polymer. The minor inhibition of influenza H2N2 viral infection in tissue culture by the unconjugated PEI backbone may be attributable to a type of nonspecific binding.

Initial PAMAM structures contained varying ratios of hydroxyl/SA moieties based on previous reports of ideal mole fractions of SA/acrylamide ranging from 0.05 to 0.6 (Choi et al., 1997; Spaltenstein and Whitesides, 1991). However, we found no correlation between the partial degree of sialyl moiety conjugation of the PAMAMs and the ability to prevent viral adsorption to cRBC. Due to their lack of activity in our HAI screening assay, these structures were not included in further studies. Also, given our finding that maximal conjugation of the larger polymers was required for any anti-viral activity, we hypothesize that 100% conjugation of the PAMAMs would be required for them to become effective. However, at this time, we do not have the capability to consistently synthesize higher generation PAMAM dendrimers with 100% conjugation. Both the degree of sialic acid conjugation and the polymer size appear to influence the ability of the polymer to inhibit influenza via polyvalent binding forces and steric hindrance. Investigation into these concepts is ongoing.

Creating polymeric inhibitors that are not toxic or irritating to tissues can be problematic. The polyacrylamide backbone causes significant cytotoxic effect to tissue culture cells, and the monomer is a known neurotoxin to humans. Conjugating all of the primary amine termini with SA mitigated the toxicity of a polyamine backbone and this suggests that the amino groups are responsible for the observed cellular damage. The potential inhibitor diversity with this polymer backbone is therefore somewhat limited due to this factor. However, when the PEI backbone is used to create a scaffold type of structure, as with dendrigraft polymers, the toxicity is markedly reduced. This may be because of internalization (i.e., sheltering) of the unreacted, protonated amines and the presence of secondary amine sites instead of primary.

Strain variation may be as important as the differences between polymeric inhibitors. Strain-specific viral variation to anti-viral therapy has been observed many times in the literature (Hartley et al., 1997; Kiefel et al., 1996; Schulze, 1997). Alternations or mutations in glycosylation of the HA glycoprotein of influenza virus are responsible for changes in virulence and, ultimately, resistance to previously protective antibodies (Lamb and Krug, 1996). Because influenza A virus must adhere to the target cell through the HA−SA interaction to cause infection, it was theorized that these polymeric inhibitors could be used to block this interaction, regardless of the specific viral antigenicity. However, significant variation was seen in influenza H2N2 strains when a given parent virus was passaged in a different host. These viruses have distinct phenotypic and genotypic characteristics, and specific point mutations have been identified which are common to all virulent viruses but absent from attenuated viruses (Herlocher et al., 1996). The virus-specific hemagglutinins in these two strains have not yet been sequenced, but may help explain the differences in susceptibility to dendritic polymers. Sendai virus in the closely related *Paramyxoviridae* family shares affinity for sialyl receptors on host cells. This virus allows further evaluation of polymeric sialyl receptor and viral hemagglutinin interaction. Sendai virus is the most susceptible to the effects of the dendritic polymer inhibition, suggesting that differences in the hemagglutinin are responsible for altered affinity to sialyl moieties and possible conformational changes in the structure of the glycoprotein. There are many SA structures found in nature (Kelm and Schauer, 1997). Influenza A typically binds to α-2,3-linked or α-2,6-linked SA, while sendai virus uses α-2,3-linked and α-2,8-linked SA as receptors. The significant viral variation in susceptibility to polymeric inhibitor inhibition seen in this study was not expected and must be further evaluated. On the basis of our findings, it is clear that one needs to evaluate several strains of influenza virus when assessing the efficacy of potential influenza inhibitors.

In conclusion, this study has shown that variations in dendritic architecture have a profound effect on the potency of sialate-based polymeric viral inhibitors. In addition, the effectiveness of the inhibitors increases with the degree of sialic acid substitution on the "surface" of these polymers. For a given inhibitor, we saw significant variation in the degree of inhibition for each virus, effects that will require further study for a more complete understanding. Finally, a significant reduction in cell toxicity was observed for those inhibitors based on dendritic architecture (when compared to those based on linear polymers) and with increasing SA surface substitution.

ACKNOWLEDGMENT

This work was supported by DARPA (Defense Advanced Research Project Agency) Contract MDA 972-1-007 of the Unconventional Pathogen Countermeasures Program and National Institutes of Health (NIH) Training Grant RR0 7008-21. The authors wish to thank Dr. H. Maassab for his generous donation of influenza virus, antisera and chicken erythrocytes, Mr. A. R. Douglas for his kind donation of X-31 virus and antisera, Y. Zhu for her preparation of type (V) copolymer backbones, Dr. M. Anderson for her work with viral propagation, and P. and L. Balogh for their help with polymer illustrations.

LITERATURE CITED

(1) Barrett, T., and Inglis, S. C. (1985) Growth purification and titration of influenza viruses. in *Virology: a Practical Approach* (W. J. Mahy, Ed.) pp 119−151, IRL Press, Washington, DC.

(2) Choi, S.-K., Mammen, M., and Whitesides, G. M. (1997) Generation and in situ evaluation of libraries of poly(acrylic acid) presenting sialosides as side chains as polyvalent inhibitors of influenza-mediated hemagglutination. *J. Am. Chem. Soc. 119*, 4103−4111.

(3) Hartley, C. A., Reading, P. C., Ward, A. C., and Anders, E. M. (1997) Changes in the hemagglutinin molecule of influenza type A (H3N2) virus associated with increased virulance for mice. *Arch. Virol. 142*, 75−88.

(4) Herlocher, M. L., Clavo, A. C., and Maassab, H. F. (1996) Sequence comparison of A/AA/6/60 influenza viruses: mutations which may contribute to attenuation. *Virus Res. 42*, 11−25.

(5) Kelm, S., and Schauer, R. (1997) Sialic Acids in Molecular and Cellular Interactions. *Int. Rev. Cytol. 175*, 137−240.

(6) Kendal, A. P., and Dowdle, W. R. (1986) Influenza Virus. in *Manual of Clinical Laboratory Immunology*, 3rd ed. (N. R. Rose, H. Friedman, J. L. Flatly, Eds.) pp 515−520, American Society for Microbiology, Washington, DC.

(7) Kiefel, M. J., Beisner, B., Bennett, S., Holmes, I. D., and Itzstein, M. (1996) Synthesis and biological evaluation of N-acetylneuraminic acid-based rotavirus inhibitors. *J. Med. Chem. 39*, 1314−1320.

(8) Kim, R. M., Manna, M., Hutchins, S. T., Griffin, P. R., and Yates, N. A. (1996) Dendrimer-supported combinatorial chemistry. *Proc. Natl. Acad. Sci. 93*, 10012−10017.

(9) Lamb, R. A., and Krug, R. M. (1996) Orthomyxoviridae: The Viruses and Their Replication. in *Fields Virology*, 3rd ed. (B. N. Fields, D. M. Knipe, P. M. Howley, Eds.) pp 1353−1395, Lippincott-Raven Publishers, Philadelphia.

(10) Longo, M. L., Waring, A. J., and Hammer, D. A. (1997) Interaction of the influenza hemagglutinin fusion peptide with lipid bilayers: Area expansion and permeation. *Biophys. J. 73*, 1430−1439.

(11) Mammen, M., Dahmann, G., and Whitesides, G. M. (1995) Effective inhibitors of hemagglutination by influenza virus synthesized from polymers having active ester groups. Insight into mechanism of inhibition. *J. Med. Chem. 38*, 4179−4190.

(12) Mammen, M., Choi, S.-K., and Whitesides, G. M. (1998) Polyvalent interactions in biological systems: implications for design and use of multivalent ligands and inhibitors. *Angew. Chem., Int. Ed. Engl. 37*, 2754−2794.

(13) Mangan, D., and Snyder, I. S. (1978) The effect of acrylamide on human polymorphonuclear neutrophils in vitro. *Br. J. Ind. Med. 35*, 305−311.

(14) Mulder, J., and Hers, J. F. Ph. (1972) *Influenza*, Wolter-Noordhoff Publishing, Groningen, The Netherlands.

(15) Pritchett, T. J., and Paulson, J. C. (1989) Basis for the potent inhibition of influenza virus infection by equine and guinea pig α-2macroglobin. *J. Biol. Chem. 256*, 9850−9858.

(16) Roy, R. (1996) Glycopolymers: A new class of biopolymers. *Polymer News 21*, 226−232.

(17) Roy, R., Tropper, F. D., and Romanowska, A. (1992) New strategy in glycopolymer synthesis. Preparation of antigenic water-soluble poly(acrylamide-*co*-p-acrylamidophenyl *β*-lactoside). *Bioconjugate Chem. 3*, 256−261.

(18) Roy, R., Zanini, D., Meunier, S. J., and Romanowska, A. (1993) Solid-phase synthesis of dendritic sialoside inhibitors of influenza A virus Haemagglutinin. *J. Chem. Soc., Chem. Commun.* 1869−1872.

(19) Roy, R., Zanini, D., Meunier, S. J., and Romanowska, A. (1994) *ACS Symp. Ser. 560*, 104−119.

(20) Sauter, N. K., Bednarski, M. D., Wurzburg, B. A., Hanson, J. E., Whitesides, G. M., Skehel, J. J., and Wiley, D. C. (1989) Hemagglutinins from two influenza virus variants bind to sialic acid derivatives with millimolar dissociation constants: a 500-MHz proton nuclear magnetic resonance study. *Biochemistry 28*, 8388−8396.

(21) Schaumburg, H. H., Arezzo, J. C., and Spencer P. S. (1989) Delayed onset of axonal neuropathy in primates after prolonged low-level administration of a neurotoxin. *Ann. Neur. 26*, 576−579.

(22) Schulze, I. T. (1997) Effects of glycosylation on the properites and functions on influenza virus hemaggluntinin. *J. Infect. Dis. 176* (Suppl 1), S24−28.

(23) Skehel, J. J., Bayley, P. M., Brown, E. B., Martin, S. R., Waterfield, M. D., White, J. M., Wilson, I. A., and Wiley, D. C. (1982) Changes in the conformation of influenza virus hemagglutinin at the pH optimum of virus-mediated membrane fusion. *Proc. Natl. Acad. Sci. U.S.A. 79*, 968−972.

(24) Spaltenstein, A., and Whitesides, G.M. (1991) Polyacrylamides bearing pendant α-sialoside groups strongly inhibit agglutination of erythrocytes by influenza virus. *J. Am. Chem. Soc. 113*, 686−687.

(25) Spencer, P. S., and Schaumburg, H. H. (1975) Nervous system degeneration produced by acrylamide monomer. *Environ. Health Perspect. 11*, 129−133.

(26) Tomalia, D. A., Baker, H., Dewald, J. R., Hall, M., Kallos, G., Martin, S., Roeck, J., Ryder, J., and Smith, P. (1985) A New Class of Polymers: Starburst-Dendritic Macromolecules. *Polymer J.* (Tokyo) *17*, 117−132.

(27) Tomalia, D. A., Hedstrand, D. M., and Ferritto, M. S. (1991) Combburst(TM) Dendrimer Topology. *Macromolecules 24*, 1435−1438.

(28) Trevan, M. D. (1980) *Immobilized Enzymes: an introduction and applications in biotechnology*, Wiley, New York.

(29) Watanabe, W., Konno, K., Ijichi, K., Inoue, T., Yokota, T., and Shigeta, S. (1994) MTT colorimetric assay system for the screening of anti-orthomyxo- and anit-paramyxoviral agents. *J. Virol. Methods 48*, 257−265.

(30) Weis, W., Cusack, S., Paulson, J. C., Skehel, J. J., and Wiley, D. C. (1988) Structure of the influenza virus haemagglutinin complexed with its receptor, sialic acid. *Nature 333*, 426−431.

(31) Wiley, D. C., and Skehel, J. J. (1987) The structure and function of the hemagglutinin membrane glycoprotein of influenza virus. *Annu. Rev. Biochem. 56*, 365−394.

(32) Yin, R., Zhu, Y., Tomalia, D. A., and Ibuki, H. (1998) Architechtural Copolymers: Rod-Shaped, Cylindrical Dendrimers. *J. Am Chem. Soc. 120*, 2678−2679.

(33) Zanini, D., and Roy, R. (1998) Practical Synthesis of Starburst PAMAM α-Thiosialodendrimers for Probing Multivalent Carbohydrate-Lectin Binding Properties. *J. Org. Chem. 63*, 3486−3491.

BC980099N

Monoclonal Antibody Conjugates of Doxorubicin Prepared with Branched Linkers: A Novel Method for Increasing the Potency of Doxorubicin Immunoconjugates

H. Dalton King,*[,†] Derek Yurgaitis,[†] David Willner,[†] Raymond A. Firestone,[†,‡] Michael B. Yang,[§] Shirley J. Lasch,[§] Karl Erik Hellström,[∥] and Pamela A. Trail[§]

Bristol Myers Squibb Pharmaceutical Research Institute, 5 Research Parkway, Wallingford, Connecticut 06492, and Princeton, New Jersey, 08543. Received August 28, 1998; Revised Manuscript Received December 28, 1998

Immunoconjugates of monoclonal antibody BR96 and Doxorubicin have been prepared using a novel series of branched hydrazone linkers. Since each linker bound to the mAb carries two DOX molecules, the DOX/mAb molar ratios of these conjugates were approximately 16, twice that of those previously prepared with single-chain hydrazone linkers. The conjugates were stable at a physiological pH of 7, but released DOX rapidly at lysosomal pH 5. The branched series of BR96 conjugates demonstrated antigen-specific cytotoxicity, and were more potent in vitro than the single-chain conjugate on both a DOX (4−14-fold) and mAb (7−23-fold) basis. The results suggest that, by using the branched linker methodology, it is possible to significantly reduce the amount of mAb required to achieve antigen-specific cytotoxic activity. In this paper, the synthesis and in vitro biology of branched chain immunoconjugates are described.

Monoclonal antibody conjugates have been shown to be effective targeting vehicles for cytotoxic drugs such as doxorubicin (*1*). We have previously demonstrated the antitumor activity of BR96-DOX conjugates in the treatment of human tumor xenografts in mice and rats (*2*, *3*). The BR96 mAb identifies a Lewis y (Le^y)-related tumor-associated antigen expressed at high density on the majority of human carcinomas (*4*). BR96 is rapidly internalized following antigen-specific binding (*4*, *5*). The BR96-DOX conjugates employed a hydrazone linkage to C-13 of DOX (*6*−*8*) and a thioether linkage to the mAb (*2*, *9*). Hydrazones of this nature are stable at normal physiological pH 7, but once internalized into the acidic compartment of endosomes/lysosomes, hydrolysis occurs liberating free DOX (*6*, *7*). The thioether linkage is formed by the reaction of BR96 thiol groups, generated by mild DTT reduction of four interchain disulfides, with the linker **1**. Therefore, the observed molar ratio (DOX/mAb) of these first generation BR96 conjugates was typically 8 (*2*, *9*). BR96-DOX conjugates produced antigen-specific antitumor activity and were more potent, were more active, and produced less systemic toxicity than unconjugated DOX in vivo (*2*, *3*, *9*).

We have previously demonstrated that it is possible to increase the potency of lysine-linked SPDP-hydrazone conjugates by increasing the DOX/mAb molar ratio from 1 to 8 (*10*). When the molar ratio was increased beyond 8, significant losses in antigen-specific binding were observed. A similar loss in both binding avidity and antigen-specific potency was observed by other investigators as molar ratios of directly linked DOX conjugates exceeded 10 (*11*).

In the studies described here we evaluated the potential to increase the potency of BR96-DOX conjugates by attaching more than one drug per thiol group generated on the mAb. This approach employs a *branched* linker (Scheme 1), carrying two hydrazide functional groups for the attachment of DOX. With the single branch point, MR's are expected to approach 16, twice that of the prototype conjugate BR96-DOX. For these conjugates to be effective, they must maintain binding avidity and be capable of undergoing acid-catalyzed hydrolysis at rates similar to that of BR96-DOX (*9*).

For the branched linkers **2** and **3**, we used L-glutamic acid as the synthetic template to attach the required functionality. The two carboxyl groups were converted to hydrazides for DOX attachment, and the amino group was extended to a maleimide for mAb thiol group attachment. The length of the maleimide tether was varied (n = 2, 3, and 5) to evaluate solubility and other subtle aspects of conjugate synthesis. To avoid potential crowding of the DOX moieties, we also synthesized an extended series **3** in which a β-alanyl unit was inserted at each glutamic acid carboxyl group. Finally, to evaluate the susceptibility of a typical branched linker to enzymatic degradation, we synthesized a D-glutamic acid analogue of **2b** (Schemes 2 and 3).

EXPERIMENTAL PROCEDURES

General. All reactions utilizing nonprotic solvents were carried out under inert N_2 atmosphere. Reaction solvents were freshly opened Aldrich "Sure-Seal" quality. All other solvents and reagents were reagent grade and used without further purification. Bio-Beads SM-2 chromatographic support was supplied by Bio-Rad Laboratories. ^{1}H NMR and ^{13}C NMR spectra were obtained at

* To whom correspondence should be addressed. E-mail: kingd@bms.com.

† Bristol Myers Squibb Pharmaceutical Research Institute, Wallingford, CT.

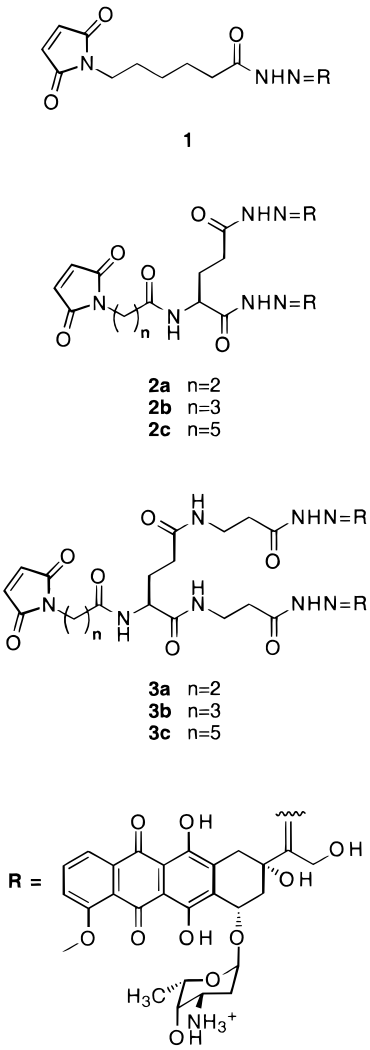
‡ Current address: Boehringer Ingelheim Pharmaceuticals, Ridgefield, CT.

§ Bristol Myers Squibb Pharmaceutical Research Institute, Princeton, NJ.

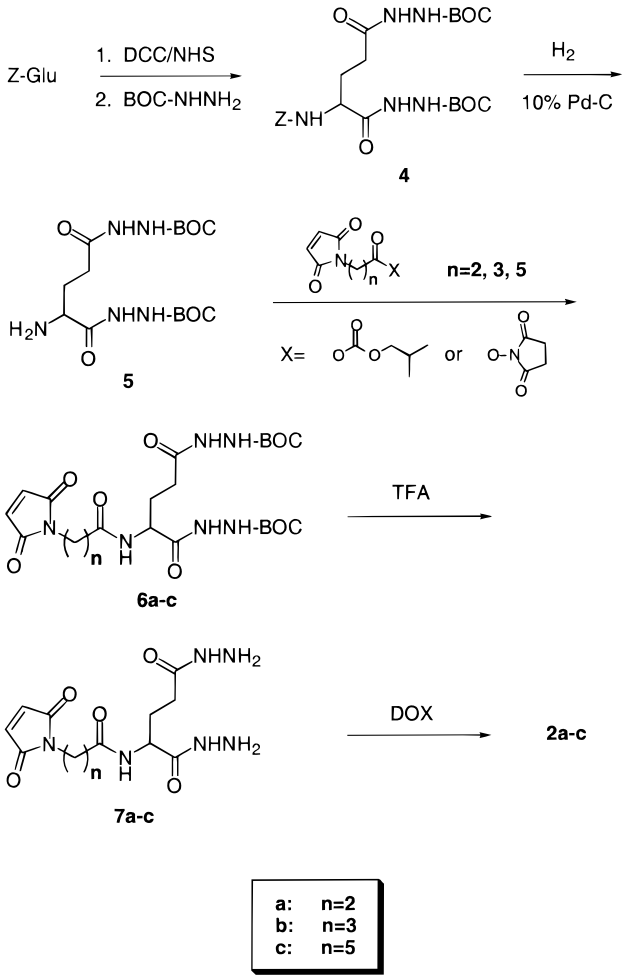
∥ Original address: Bristol Myers Squibb Pharmaceutical Research Institute, Seattle, WA. Current address: Pacific Northwest Research Foundation, Seattle, WA.

10.1021/bc980100i CCC: $18.00 © 1999 American Chemical Society
Published on Web 02/24/1999

Scheme 1. Branched DOX Hydrazone Linkers



Scheme 2. Synthesis of Series 2



300 and 75 MHz, respectively, in the indicated solvents. Internal referencing was used and chemical shifts are reported in ppm. FTIR's were obtained as KBr pellets. Melting points are uncorrected. Elemental analyses were provided by Oneida Research Services.

TLC was carried out on Analtech silica gel GHLF plates, generally with 10−20% MeOH in methylene chloride as the eluting solvent, and visualized with UV light and chemical staining. Flash chromatography was carried out on Merck silica gel 60 (230−400 mesh). Routine HPLC of synthetic compounds was performed on a Perkin-Elmer 410 Pump and LC-235 Detector. HPLC columns were supplied by Phenomenex (IB-Sil 5 C-18). All compounds were homogeneous by TLC and/or HPLC.

HPLC Analysis of Conjugates. SEC−HPLC analysis of conjugates was carried out on a Toyo Soda 5u TSK column (3000SW XL, 300 mm × 7.5 mm) equipped with a 5u TSK (3000SW XL, 40 mm × 6.0 mm) guard column. Samples were eluted at a flow rate of 1.0 mL/min with isocratic 0.2 M KH_2PO_4, 0.9% NaCl, pH 6.8, and monitored at 280 and 495 nm.

HIC−HPLC analysis was carried out on a Biorad Biogel TSK-phenyl-5-PW column (75 mm × 7.5 mm). Samples were eluted under a 35 min gradient of 100% buffer A to 100% buffer B at 1.0 mL/min. Buffer A was 2 M NaCl, 25 mm NaH_2PO_4 (pH 7.0). Buffer B was 80% 50 mM NaH_2PO_4 (pH 7.0), 10% 2-propanol, and 10% acetonitrile. Eluant was monitored at 280 and 495 nm.

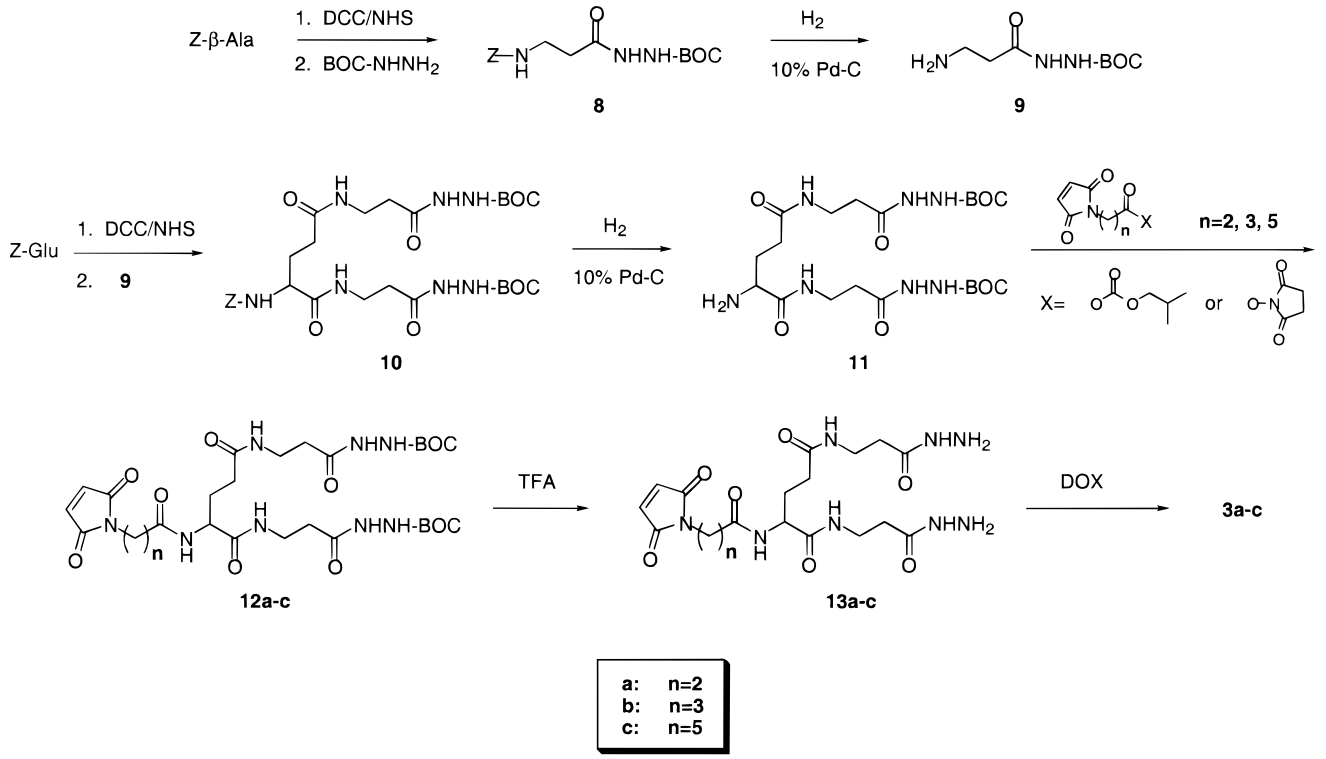
SYNTHESIS

***Z*-Glutamyldi(Boc)hydrazide 4.** *Z*-Glutamic acid (42.20 g, 150 mmol) and *N*-hydroxysuccinimide (34.53 g, 300 mmol) were dissolved in 150 mL of DMF at 0 °C under dry N_2. A 0.5 M solution of dicyclohexylcarbodiimide in methylene chloride (600 mL, 300 mmol) was added dropwise over a 1 h period with stirring. The reaction was stored at 4 °C in the refrigerator for 18 h. Dicyclohexylurea precipitate (65.48 g, 98%) was filtered, and the filtrate was added directly to solid *tert*-butylcarbazate (39.65 g, 300 mmol). After being stirred at room temperature for 48 h, the reaction was rotary evaporated to an oil, which was redissolved in 300 mL of ethyl acetate/200 mL of ether. The organic layer was extracted three times with 200 mL of 10% citric acid, 3 times with 200 mL of saturated aqueous sodium bicarbonate, and once with 100 mL of brine. The organic layer was dried over sodium sulfate and rotary evaporated to a foam. Flash chromatography was carried out on silica gel (4 in. × 19 in.) with ethyl acetate−hexane 2:1, 12 L. Pure fractions containing product **4** were pooled and concentrated to a foam by rotary evaporation to yield, after drying under high vacuum, 55.24 g (72%).

^{1}H NMR ($CDCl_3$): δ 1.44 and 1.47 (2s, 18H), 1.9−2.4 (bm, 4H), 4.32 (bm, 1H), 5.06 (dd, J = 12, 16 Hz, 2H), 5.55 (d, J = 6 Hz, 1H), 6.5 (bd, 2H), 7.31 (bm, 5H), 9.6 (s, 1H), and 9.9 (s, 1H). Mass Spec.: FAB 510 ($M + H^+$), 532 ($M + Na^+$), 548.1 ($M + K^+$). Anal.: $C_{23}H_{35}N_5O_8$ C, H, N.

***Z*-(D)-Glutamyldi(Boc)hydrazide D-4.** This compound was prepared on an identical scale by a method

Scheme 3. Synthesis of Series 3



similar to that used for **4**. Flash chromatography was carried out on silica gel (4 in. × 18 in.) with the following gradient: (1) CH_2Cl_2, 2 L, (2) CH_2Cl_2-methanol 25:1, 4 L, and (3) CH_2Cl_2−methanol 9:1, 6 L. Yield of D-**4** was 59.11 g (77%).

^{1}H NMR ($CDCl_3$): δ 1.44 and 1.47 (2s, 18H), 1.9−2.4 (bm, 4H), 4.32 (bm, 1H), 5.06 (dd, J = 12, 16 Hz, 2H), 5.57 (d, J = 7 Hz, 1H), 6.6 (m, 2H), 7.31 (bm, 5H), 9.60 (s, 1H), and 9.87 (s, 1H). Mass Spec.: FAB 532 $(M + Na^+)$, 549 $(M + K^+)$. Anal.: $C_{23}H_{35}N_5O_8$ C, H, N.

Glutamyldi(Boc)hydrazide 5. *Z*-Glutamyldi(Boc)-hydrazide **4** (19.59 g, 38.44 mmol) was hydrogenated along with 2 g of 10% Pd−C in 200 mL of MeOH at 50 psi for 3 h. The reaction was filtered through Celite and rotary evaporated. The resulting foam was dried under high vacuum to yield **5** (14.40 g, 100%).

^{1}H NMR (d_4-methanol): δ 1.42 and 1.45 (2s, 18H), 1.9 (bm, 2H), 2.35 (t, J = 7 Hz, 2H), 3.34 (t, 7 Hz, 1H). Mass Spec.: DCI 376 $(M + H)^+$. Anal.: $C_{15}H_{29}N_5O_6 \cdot 0.5H_2O$ C, H, N.

(D)-Glutamyldi(Boc)hydrazide D-5. This compound was prepared from D-**4** (23.05 g, 45.2 mmol) by an similar procedure to that used for **5**. Crude product was purified by flash chromatography on silica gel (2 in. × 20 in.) with the following gradient: (1) CH_2Cl_2−methanol 25:1, 600 mL, (2) CH_2Cl_2−methanol 9:1, 6 L, and (3) CH_2Cl_2−methanol 8:2, 4 L. Pure fractions were pooled and rotary evaporated. Drying under high vacuum yielded pure D-**5** (13.51 g, 80%).

^{1}H NMR (d_4-methanol): δ 1.46 and 1.47 (2s, 18H), 1.94 (bm, 2H), 2.33 (t, J = 7 Hz, 2H), 3.34 (t, J = 7 Hz, 1H). Mass Spec.: FAB 376 $(M + H)^+$, 398 $(M + Na)^+$, 414 $(M + K)^+$. Anal.: $C_{15}H_{29}N_5O_6 \cdot 0.5H_2O$ C, H, N.

Maleimidopropionylglutamyldi(Boc)hydrazide 6a. Maleimidopropionic acid (636 mg, 3.76 mmol) and *N*-hydroxysuccinimide (476 mg, 4.14 mmol) were dissolved in 10 mL of DMF at 0 °C. A 0.5 M solution of DCC in CH_2Cl_2 (7.6 mL, 3.8 mmol) was added and the reaction allowed to stand for 20 h at 4 °C. After filtration of the DCU precipitate, the filtrate was added to **5** (1.27 g, 3.38 mmol) and the mixture was stirred at room temperature for 2.5 days. Solvents were partially removed by rotary evaporation. The oil was dissolved in 100 mL of ethyl acetate, then extracted three times with 100 mL of 10% citric acid, three times with 100 mL of saturated aqueous sodium bicarbonate, and three times with 100 mL of H_2O. The organic layer was dried over sodium sulfate and rotary evaporated to a foam. This was purified by flash chromatography on silica gel (2 in. × 11 in.) with CH_2Cl_2−acetic acid−methanol 93:2:5. Pure fractions were pooled, rotary evaporated, and dried under high vacuum to yield **6a** as a foam (1.22 g, 69%).

^{1}H NMR (d_4-methanol): δ 1.46 (s, 18H), 2.01 (m, 2H), 2.33 (t, 7 Hz, 2H), 2.51 (t, J = 7 Hz, 2H), 3.76 (t, J = 7 Hz, 2H), 4.34 (t, J = 7 Hz, 1H), 6.80 (s, 2H). Mass Spec.: FAB 549.4 $(M + Na)^+$, 565.3 $(M + K)^+$. Anal.: $C_{22}H_{34}N_6O_9 \cdot 2HOAc$ C, H, N.

Maleimidobutyrylglutamyldi(Boc)hydrazide 6b. This compound was prepared by a method analagous to that used for **6a** from maleimidobutyric acid (1.9 g, 10.3 mmol). Crude product was purified through a plug of silica gel with CH_2Cl_2−acetic acid−methanol 93:2:5, rotary evaporated, and dried under high vacuum to yield **6b** as a foam (3.50 g, 63%).

^{1}H NMR (d_4-methanol): δ 1.36 and 1.37 (2s, 18H), 1.77 (p, J = 7 Hz, 2H), 2.00 (bm, 2H), 2.14 (t, J = 7 Hz, 2H), 2.26 (t, J = 7 Hz, 2H), 3.43 (t, J = 7 Hz, 2H), 4.26 (t, J = 7 Hz, 1H), 6.71 (s, 2H). Mass Spec.: 541 $(M + H)^+$, 563 $(M + Na)^+$, 579 $(M + K)^+$. Anal.: $C_{23}H_{36}N_6O_9 \cdot 0.75H_2O$ C, H, N.

Maleimidobutyryl-(D)-glutamyldi(Boc)hydrazide D-6b. Maleimidobutyric acid (1.832 g, 10.0 mmol) was dissolved with *N*-methylmorpholine (1.21 mL, 11.0 mmol) in 60 mL of dry THF under N_2 at 0 °C. Isobutylchloroformate (1.30 mL, 10.0 mmol) was added dropwise, followed 10 min later by the addition of (D)-Glutamyldi-(Boc)hydrazide (D-**5**) (3.754 g, 10.0 mmol). Stirring was continued for 1 h at 0 °C. The reaction was rotary

evaporated to a foam, which was then dissolved in 150 mL of EtOAc. The organic layer was washed two times with 100 mL of 10% citric acid and two times with 100 mL of saturated $NaHCO_3$. The organic layer was concentrated to a foam, which was purified by flash chromatography on silica gel (2 in. × 11 in.) with CH_2Cl_2−acetic acid−methanol 95:2:3, 2 L, followed by CH_2Cl_2−acetic acid−methanol 93:2:5, 1 L. Pure fractions were pooled and rotary evaporated to a foam. Drying under high vacuum yielded **6b** (3.25 g, 60%).

^{1}H NMR (d_4-methanol): δ 1.45 and 1.46 (2s, 18H), 1.86 (p, J = 7 Hz, 2H), 2.09 (bm, 2H), 2.24 (t, J = 7 Hz, 2H), 2.35 (t, J = 7 Hz, 2H), 3.52 (t, J = 7 Hz, 2H), 4.35 (t, J = 7 Hz, 1H), 6.81 (s, 2H). Mass Spec.: 563 $(M + Na)^+$, 579 $(M + K)^+$. Anal.: $C_{23}H_{36}N_6O_9 \cdot 0.75H_2O$ C, H, N.

Maleimidocaproylglutamyldi(Boc)hydrazide 6c. This compound was prepared by a method analagous to that used for **6a** from maleimidocaproic acid (4.22 g, 20 mmol). Crude product was purified by flash chromatography on silica gel (2 in. × 10 in.) with 4 L of CH_2Cl_2−acetic acid−methanol 97:1:2. Pure fractions were pooled, rotary evaporated, and dried under high vacuum to yield **6c** as a foam (6.40 g, 56%).

^{1}H NMR (d_4-methanol): δ 1.2 (p, J = 7 Hz, 2H), 1.40 (s, 18H), 1.5 (m, 4H), 2.0 (bm, 2H), 2.14 (t, J = 7 Hz, 2H), 2.28 (t, J = 7 Hz, 2H), 3.41 (t, J = 7 Hz, 2H), 4.29 (t, J = 7 Hz, 1H), 6.72 (s, 2H). Mass Spec.: FAB 569 $(M + H)^+$, 591 $(M + Na)^+$, 607 $(M + K)^+$. Anal.: $C_{25}H_{40}N_6O_9 \cdot 0.5H_2O$ C, H, N.

Maleimidopropionylglutamyldihydrazide Ditrifluoroacetate 7a. Maleimidopropionylglutamyldi(Boc)-hydrazide **6a** (1.50 g, 2.85 mmol) was stirred in 15 mL of CH_2Cl_2/trifluoroacetic acid (1:1) under N_2 for 1.5 h. Solvents were removed by rotary evaporation. Ether was added and coevaporated three times, and then the resulting solid was triturated with ether. The solid was filtered and dried under high vacuum to yield **7a** (1.6 g, 100%).

^{1}H NMR (d_4-methanol): δ 1.99 and 2.16 (2m, 2H), 2.41 (t, J = 7 Hz, 2H), 2.53 (t, J = 7 Hz, 2H), 3.80 (dt, J = 2, 7 Hz, 2H), 4.38 (dd, J = 5, 4 Hz, 1H), 6.81 (s, 2H). Mass Spec.: FAB 349.2 $(M + Na)^+$, 365.1 $(M + K)^+$. Anal.: $C_{12}H_{18}N_6O_5 \cdot 2.8$TFA C, H, N.

Maleimidobutyrylglutamyldihydrazide Ditrifluoroacetate 7b. This compound was prepared by a similar procedure from **6b** (3.50 g, 6.47 mmol). Yield of **7b** was 3.8 g (100%).

^{1}H NMR (d_4-methanol): δ 1.87 (p, J = 7 Hz, 2H), 2.0 and 2.2 (2m, 2H), 2.27 (t, J = 7 Hz, 2H), 2.44 (m, 2H), 3.53 (t, J = 7 Hz, 2H), 4.42 (dd, J = 5, 4 Hz, 1H), 6.82 (s, 2H). Mass Spec.: FAB 341 $(M + H)^+$, 363 $(M + Na)^+$, 379 $(M + K)^+$. Anal.: $C_{13}H_{20}N_6O_5 \cdot 3.15$TFA C, H, N.

Maleimidobutyryl-(D)-glutamyldihydrazide Ditrifluoroacetate D-7b. This compound was prepared by a similar procedure from D-**6b** (2.06 g, 3.81 mmol). Yield of D-**7b** was 2.2 g (100%).

^{1}H NMR (d_4-methanol): δ 1.79 (p, J = 7 Hz, 2H), 1.9 and 2.1 (2m, 2H), 2.18 (t, J = 7 Hz, 2H), 2.37 (m, 2H), 3.45 (t, J = 7 Hz, 2H), 4.35 (dd, J = 5, 4 Hz, 1H), 6.73 (s, 2H). Mass Spec.: FAB 341 $(M + H)^+$, 363 $(M + Na)^+$, 379 $(M + K)^+$. Anal.: $C_{13}H_{20}N_6O_5 \cdot 2.5$TFA C, H, N.

Maleimidocaproylglutamyldihydrazide Ditrifluoroacetate 7c. This compound was prepared by a similar procedure from **6c** (5.96 g, 10.5 mmol). Yield of **7c** was 6.3 g (100%).

^{1}H NMR (d_4-methanol): δ 1.22 (p, J = 7 Hz, 2H), 1.52 (m, 4H), 1.92 and 2.09 (2m, 2H), 2.18 (t, J = 7 Hz, 2H), 2.35 (m, 2H), 3.41 (t, J = 7 Hz, 2H), 4.35 (dd, J = 5,4 Hz, 1H), 6.72 (s, 2H). Mass Spec.: FAB 369 $(M + H)^+$, 391 $(M + Na)^+$, 407 $(M + K)^+$. Anal.: $C_{15}H_{24}N_6O_5 \cdot 2.5$TFA C, H, N.

Maleimidopropionylglutamyldihydrazone of Doxorubicin 2a. Maleimidopropionylglutamyldihydrazide ditrifluoroacetate **7a** (600 mg, 1.07 mmol) and DOX·HCl (1.24 g, 2.14 mmol) were dissolved in 600 mL of methanol over a period of 3 h. The reaction was concentrated to 100 mL by rotary evaporation, then stirred for 3 days. The reaction was further concentrated to 12 mL and eluted on an LH-20 column (2 in. × 10 in.) with methanol. Chromatography was repeated in the same system on mixed fractions. The purified product was rotary evaporated to a red film and dried under high vacuum to yield **2a** (776 mg, 50%).

^{1}H NMR (d_4-methanol): (selected peaks) δ 1.34 (2d, J = 7 Hz, 6H), 4.07 (2s, 6H), 6.79 (s, 2H), 7.5−8.0 (m, 6H). Mass Spec.: FAB 1375.4 $(M - H)^-$. Ionspray: 1377.2 (MH^+). HRMS: calculated $(M + Na)^+$ 1399.4506; observed 1399.4455. Anal.: $C_{66}H_{72}N_8O_{25} \cdot 2HCl \cdot 3.0H_2O$ C, H, N.

Maleimidobutyrylglutamyldihydrazone of Doxorubicin 2b. This compound was prepared by a similar procedure from **7b** (1.00 g, 1.76 mmol) and DOX·HCl (2.05 g, 3.53 mmol). Yield of **2b** was 1.32 g (51%).

^{1}H NMR (d_4-methanol): (selected peaks) δ 1.33 (2d, J = 7 Hz, 6H), 4.06 (2s, 6H), 6.80 (s, 2H), 7.5−8.0 (m, 6H). Mass Spec.: FAB 1392 (MH^+), 1413.4 $(M + Na)^+$, 1429 $(M + K)^+$. Ionspray: 1392.5 $(M + H)^+$, 1414.4 $(M + Na)^+$. HRMS: calculated $(M + Na)^+$ 1413.4663; observed 1413.4609. Anal.: $C_{67}H_{74}N_8O_{25} \cdot 2HCl \cdot 4.0H_2O$ C, H, N.

Maleimidobutyryl-(D)-glutamyldihydrazone of Doxorubicin D-2b. This compound was prepared by a similar procedure from D-**7b** (570 mg, 1.00 mmol) and DOX·HCl (1.34 g, 2.30 mmol). Yield of D-**2b** was 420 mg (30%).

^{1}H NMR (d_4-methanol): (selected peaks) δ 1.30 (2s, 6H), 4.07 (2s, 6H), 6.80 (s, 2H), 7.5−8.0 (m, 6H). Mass Spec.: FAB 1392.0 (MH^+), 1414.9 $(M + Na)^+$, 1429.7 $(M + K)^+$. HRMS: calculated $(M + Na)^+$ 1413.4663; observed 1413.4603. Anal.: $C_{67}H_{74}N_8O_{25} \cdot 2HCl \cdot 3.5H_2O$ C, H, N.

Maleimidocaproylglutamyldihydrazone of Doxorubicin 2c. This compound was prepared by a similar procedure from **7c** (298 mg, 0.50 mmol) and DOX·HCl (580 mg, 1.00 mmol). Yield of **2c** was 510 mg (68%).

^{1}H NMR (d_4-methanol): (selected peaks) δ 1.34 (2s, 6H), 4.08 (2s, 6H), 6.76 (s, 2H), 7.5−8.0 (m, 6H). Mass Spec.: FAB 1420 (MH^+), 1442.3 $(M + Na)^+$. Ionspray: 1419.6 $(M + H)^+$. HRMS: calculated $(M + Na)^+$ 1441.4976; observed 1441.4924. Anal.: $C_{69}H_{78}N_8O_{25} \cdot 2HCl \cdot 4H_2O$ C, H, N.

***Z*-β-Alanyl(BOC)hydrazide 8.** *Z*-β-Alanine (8.93 g, 40 mmol), *tert*-butylcarbazate (5.29 g, 40 mmol), and EDCI (8.00 g, 42 mmol) were stirred in 200 mL of CH_2Cl_2 for 1.5 h at room temperature. The reaction was extracted three times with 200 mL of 0.1 M acetic acid, twice with 200 mL of saturated aqueous sodium bicarbonate, and once with 200 mL of water. The organic layer was dried over sodium sulfate, rotary evaporated, and dried under high vacuum to yield **8** as a foam, 12.42 g (92%).

^{1}H NMR (d_6-DMSO): δ 1.38 (s, 9H), 2.25 (t, J = 7 Hz, 2H), 3.19 (q, J = 7 Hz, 2H), 4.99 (s, 2H), 7.3 (m, 6H), 8.21 (s, 1H), 9.56 (s, 1H). Mass Spec.: FAB 338 $(M + H)^+$. Anal.: $C_{16}H_{23}N_3O_5$ C, H, N.

β-Alanyl(BOC)hydrazide 9. 8 (15.25 g, 45.2 mmol) was hydrogenated at 50 psi in 200 mL of methanol with 3 g of 10% Pd−C for 4 h. The reaction was filtered

through Celite, rotary evaporated, and dried under high vacuum to yield **9** as a hygroscopic foam, 9.2 g (100%).

^{1}H NMR (d_4-methanol): δ 1.40 (s, 9H), 2.32 (t, J = 7 Hz, 2H), 2.88 (t, J = 7 Hz, 2H). Mass Spec.: FAB 204.2 $(M + H)^+$. Anal.: $C_8H_{17}N_3O_3 \cdot 0.5H_2O$ C, H, N.

***Z*-Glutamyldi[*β*-alanyl(Boc)hydrazide] 10.** *Z*-Glutamic acid (3.86 g, 13.7 mmol) and *N*-hydroxy succinimide (3.17 g, 27.5 mmol) were dissolved in 80 mL of DMF at 0 °C under dry N_2. A 0.5 M solution of dicyclohexylcarbodiimide in methylene chloride (55 mL, 27.5 mmol) was added, and the reaction was stored at 4 °C for 24 h. Dicyclohexylurea precipitate was filtered, and the filtrate was added to **9** (6.00 g, 29.5 mmol). After the mixture was stirred at room temperature for 15 h, the reaction was rotary evaporated to an oil, which was redissolved in 150 mL of ethyl acetate. The organic layer was extracted three times with 100 mL of 10% citric acid, 3 times with 100 mL of saturated aqueous sodium bicarbonate, and three times with 100 mL of brine. The organic layer was dried over sodium sulfate and rotary evaporated to a foam. Flash chromatography was carried out on silica gel (2 in. × 11 in.) with 1 L of CH_2Cl_2/methanol 25:1 followed by 3 L of CH_2Cl_2/methanol 9:1. Pure fractions containing product **10** were pooled and concentrated to a foam by rotary evaporation to yield, after drying under high vacuum, 6.70 g (75%).

^{1}H NMR ($CDCl_3$): δ 1.42 (s, 18H), 2.03 and 2.32 (2m, 8H), 3.5 (m, 4H), 4.35 (t, J = 7 Hz, 1H), 5.05 (dd, J = 18 Hz, 2H), 6.22 (d, J = 7 Hz, 1H), 6.49 (d, J = 18 Hz, 2H), 7.30 (s, 5H), 7.42 (m, 1H), 7.58 (m, 1H). Mass Spec.: DCI 652 $(M + H)^+$, 674 $(M + Na)^+$, 690 $(M + K)^+$. Anal.: $C_{29}H_{45}N_7O_{10}$ C, H, N.

Glutamyldi[*β*-alanyl(Boc)hydrazide] 11. *Z*-Glutamyldi[*β*-alanyl(Boc)hydrazide] **10** (3.52 g, 5.40 mmol) was hydrogenated along with 1 g of 10% Pd−C in 75 mL of MeOH at 50 psi for 2 h. The reaction was filtered through Celite and rotary evaporated. The resulting foam was dried under high vacuum to yield **11** (2.77 g, 99%).

^{1}H NMR (d_4-methanol): δ 1.46 (s, 18H), 1.91 (m, 2H), 2.25 (t, J = 7 Hz, 2H), 2.42 (q, J = 8 Hz, 4H), 3.35 (t, J = 8 Hz, 1H), 3.44 (m, 4H). Mass Spec.: FAB 518 $(M + H)^+$, 540 $(M + Na)^+$, 556 $(M + K)^+$. Anal.: $C_{21}H_{39}N_7O_8 \cdot 1.5H_2O$ C, H, N.

Maleimidopropionylglutamyldi[*β*-alanyl(Boc)hydrazide] 12a. Maleimidopropionic acid (399 mg, 2.36 mmol) and *N*-hydroxy succinimide (272 mg, 2.36 mmol) were dissolved in 30 mL of CH_2Cl_2/3 mL of DMF at 0 °C. A 0.5 M solution of DCC in CH_2Cl_2 (4.7 mL, 2.36 mmol) was added and the reaction mixture stirred for 3 h at room temperature. After filtration of the DCU precipitate, the filtrate was added to **11** (1.10 g, 2.13 mmol) and the reaction mixture stirred at room temperature for 1 day. Solvents were removed by rotary evaporation. The oil was purified by flash chromatography on silica gel (2 in. × 10 in.) with 500 mL of CH_2Cl_2, 2 L of CH_2Cl_2/methanol 95:5, and 2 L of CH_2Cl_2/methanol 9:1. Pure fractions were pooled, rotary evaporated, and dried under high vacuum to yield **12a** as a foam (850 mg, 60%).

^{1}H NMR (d_4-methanol): δ 1.46 (s, 18H), 1.82 and 2.04 (2m, 2H), 2.23 (t, J = 8 Hz, 2H), 2.40 (m, 4H), 2.52 (t, J = 7 Hz, 2H), 3.45 (m, 4H), 3.78 (t, J = 7 Hz, 2H), 4.20 (dd, J = 8 Hz, 1H), 6.81 (s, 2H). Mass Spec.: FAB 669 $(M + H)^+$, 691 $(M + Na)^+$, 707 $(M + K)^+$. Anal.: $C_{28}H_{44}N_8O_{11} \cdot 2H_2O$ C, H, N.

Maleimidobutyrylglutamyldi[*β*-alanyl(Boc)hydrazide] 12b. This compound was prepared by a similar procedure from maleimidobutyric acid (432 mg, 2.36 mmol). Yield of **12b** was 800 mg (55%).

^{1}H NMR (d_4-methanol): δ 1.46 (s, 18H), 1.87 (m, 3H), 2.08 (m, 1H), 2.24 (m, 4H), 2.41 (m, 4H), 3.45 (m, 6H), 4.23 (dd, J = 8 Hz, 1H), 6.82 (s, 2H). Mass Spec.: FAB 683 $(M + H)^+$, 705 $(M + Na)^+$, 721 $(M + K)^+$. Anal.: $C_{29}H_{46}N_8O_{11} \cdot 1.5H_2O$ C, H, N.

Maleimidocaproylglutamyldi[*β*-alanyl(Boc)hydrazide] 12c. Maleimidocaproic acid (453 mg, 2.14 mmol) and *N*-methylmorpholine (239 mg, 2.36 mmol) were dissolved in 25 mL of dry THF under Ar at −5 °C. Isobutylchloroformate (263 mg, 1.93 mmol) was added. After 5 min, **11** (1.0 g, 1.93 mmol) was added as a THF solution and the reaction mixture stirred for 3 h with warming to room temperature. Ethyl acetate (150 mL) was added, and then the solution was extracted three times with 75 mL of 10% citric acid, three times with 75 mL of saturated aqueous sodium bicarbonate, and three times with 75 mL of water. The organic layer was dried over sodium sulfate, then passed through a plug of silica gel with CH_2Cl_2/methanol 9:1. The purified product was rotary evaporated and dried under high vacuum to give **12c**, 800 mg (58%).

^{1}H NMR (d_4-methanol): δ 1.30 (m, 2H), 1.46 (s, 18H), 1.60 (m, 4H), 1.88 and 2.06 (2m, 2H), 2.22 (t, J = 7 Hz, 4H), 2.41 (t, J = 7 Hz, 4H), 3.44 (m, 6H), 4.24 (dd, J = 9 Hz, 1H), 6.80 (s, 2H). Mass Spec.: FAB 711.4 $(M + H)^+$, 733.2 $(M + Na)^+$, 749.3 $(M + K)^+$. Anal.: $C_{31}H_{50}N_8O_{11} \cdot 1.0H_2O$ C, H, N.

Maleimidopropionylglutamyldi[*β*-alanylhydrazide] 13a. Maleimidopropionylglutamyldi[*β*-alanyl(Boc)-hydrazide] **12a** (850 mg, 1.27 mmol) was stirred in 15 mL of CH_2Cl_2/trifluoroacetic acid (1:1) under N_2 for 1.5 h. Solvents were removed by rotary evaporation. Ether was added and coevaporated three times, and then the resulting solid was triturated with ether. The solid was filtered and dried under high vacuum to yield **13a** (890 mg, 100%).

^{1}H NMR (d_4-methanol): δ 1.83 and 2.02 (2m, 2H), 2.23 (t, J = 7 Hz, 2H), 2.52 (q, J = 7 Hz, 6H), 3.47 (m, 4H), 3.78 (dt, J = 7, 3 Hz, 2H), 4.13 (dd, J = 5, 4 Hz, 1H), 6.82 (s, 2H). Mass Spec.: FAB 469.0 $(M + H)^+$, 491.1 $(M + Na)^+$, 507.1 $(M + K)^+$. Anal.: $C_{18}H_{28}N_8O_7 \cdot 3.75TFA \cdot 0.25Et_2O$ C, H, N.

Maleimidobutyrylglutamyldi[*β*-alanylhydrazide] 13b. This compound was prepared by a similar procedure from **12b** (800 mg, 1.17 mmol). Yield of **13b** was 840 mg (100%).

^{1}H NMR (d_4-methanol): δ 1.88 (m, 3H), 2.06 (m, 1H), 2.26 (t, J = 7 Hz, 4H), 2.51 (t, J = 7 Hz, 4H), 3.50 (m, 6H), 4.18 (dd, J = 5, 4 Hz, 1H), 6.82 (s, 2H). Mass Spec.: FAB 483.2 $(M + H)^+$, 505.1 $(M + Na)^+$, 521.1 $(M + K)^+$. Anal.: $C_{19}H_{30}N_8O_7 \cdot 3.5TFA \cdot 0.25Et_2O$ C, H, N.

Maleimidocaproylglutamyldi[*β*-alanylhydrazide] 13c. This compound was prepared by a similar procedure from **12c** (800 mg, 1.13 mmol). Yield of **13c** was 870 mg (100%).

^{1}H NMR (d_4-methanol): δ 1.31 (p, J = 7 Hz, 2H), 1.61 (m, 4H), 1.85 and 2.03 (2m, 2H), 2.24 (t, J = 7 Hz, 4H), 2.50 (t, J = 7 Hz, 4H), 3.47 (m, 6H), 4.19 (dd, J = 5, 4 Hz, 1H), 6.80 (s, 2H). Mass Spec.: Ionspray 511.1 $(M + H)^+$, 533.0 $(M + Na)^+$. Anal.: $C_{21}H_{34}N_8O_7 \cdot 2.75TFA \cdot 0.25Et_2O$ C, H, N.

Maleimidopropionylglutamyldi[*β*-alanylhydrazone] of Doxorubicin 3a. Maleimidopropionylglutamyldi[*β*-alanylhydrazide] ditrifluoroacetate **13a** (1.0 g, 1.44 mmol) and DOX·HCl (1.68 g, 2.88 mmol) were dissolved in 600 mL of methanol over a period of 3 h. The reaction was concentrated to 100 mL by rotary evaporation, then stirred for 1 day. After further concentration to 10 mL, elution on an LH-20 column (2 in. × 10 in.) with

methanol/DMF (1:1) was carried out. The purified product was concentrated by rotary evaporation and precipitated by the addition of acetonitrile. The red solid was isolated by centrifugation and dried under high vacuum to yield **3a** (450 mg, 20%).

^{1}H NMR (d_4-methanol): δ 1.29 (2bd, 6H), 4.04 (s, 6H), 6.80 (s, 2H), 7.5−8.0 (m, 6H). Mass Spec.: Ionspray 1519.6 $(M + H)^+$, 1541.2 $(M + Na)^+$. HRMS: calculated $(M + Na)^+$ 1541.5249; observed 1541.5187. Anal.: $C_{72}H_{82}N_{10}O_{27}$·2HCl·7H_2O C, H, N.

Maleimidobutyrylglutamyldi[β-alanylhydrazone] of Doxorubicin 3b. This compound was prepared by a similar procedure from **13b** (280 mg, 0.395 mmol). Chromatography was carried out on an LH-20 column (1 in. × 15 in.) with methanol/DMF (1:1). The purified product was concentrated by rotary evaporation and precipitated by the addition of acetonitrile. The red solid was isolated by centrifugation and dried under high vacuum to yield **3b** (325 mg, 51%).

^{1}H NMR (d_4-methanol): δ 1.30 (m, 6H), 4.04 (s, 6H), 6.78 (s, 2H), 7.4−8.0 (m, 6H). Mass Spec.: FAB 1533.7 $(M + H)^+$, 1555.5 $(M + Na)^+$, 1572.4 $(M + K)^+$. Anal.: $C_{73}H_{84}N_{10}O_{27}$·2HCl·7H_2O C, H; N; calcd, 8.08; found, 7.41.

Maleimidocaproylglutamyldi[β-alanylhydrazone] of Doxorubicin 3c. By using the procedure of **3b**, we prepared this compound from **13c** (148 mg, 0.20 mmol). Yield of **3c** was 162 mg (50%).

^{1}H NMR (d6-DMSO): δ 1.20 (m, 6H), 4.0 (s, 6H), 6.95 (s, 2H), 7.5−8.1 (m, 6H). Mass Spec.: FAB 1561 $(M + H)^+$, 1583.4 $(M + Na)^+$, 1599.9 $(M + K)^+$. Anal.: $C_{75}H_{88}N_{10}O_7$·2HCl·7H_2O C, H, N.

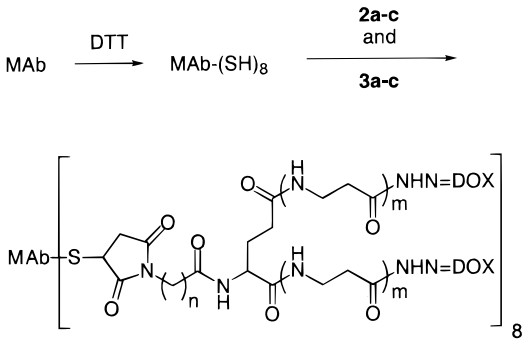
CONJUGATE SYNTHESIS

Monoclonal Antibodies. BR96 is a chimeric (mouse/human IgG1) mAb which identifies a Le^y-related tumor-associated antigen expressed on carcinomas of the lung, colon, breast, and ovary. The mAb is rapidly internalized following antigen-specific binding (*2*, *4*, *9*). Doxorubicin immunoconjugates of various DOX/mAb molar ratios were prepared with both chimeric BR96 and control human IgG.

Thiolation. *Method A*. On a scale ≤3 g, BR96 and IgG were reduced by a previously reported method (*9*). In a typical example, 1.54 g of BR96 (180 mL at 53.4 μM, 9.6 μmol) was deoxygenated by cycling several times between vacuum and Ar atmosphere. This was then treated with 34 mM DTT (2.0 mL, 68.0 umol in Ar-bubbled PBS, pH 7.0) and stirred at 37 °C under Ar for 3 h. Removal of low molecular weight compounds was accomplished by ultrafiltration against PBS, pH 7.0, in an Amicon stirred cell at 4 °C. A 400 mL Amicon cell was fitted with an Amicon YM30 filter (molecular weight cutoff 30000) and charged to 40 psi with Ar. Cell eluant was monitored for thiol content with Ellman's reagent (*12*) until a baseline reading at 412 nm was obtained. Concentrations of protein and thiol groups were determined according to the previously reported method (*9*). In this example, 1.47 g of reduced BR96 (190 mL at 48.57 μM mAb, 412.7 μM thiol) was obtained, for a yield of 95% and a thiol titer of 8.5 mol of thiol groups/mol of BR96.

Method B. On a scale >3 g, the same procedure was utilized for the DTT reaction, with the exception that the mAb solutions were deoxygenated by bubbling with Ar. Purification after DTT reduction was accomplished by ultrafiltration in a Filtron Minisette unit. The Minisette was fitted with two Filtron 30K cassettes and was connected to a Watson Marlow 604S pump with Bioprene tubing. The mAb solution was ultrafiltered at 0 °C under Ar against Ar-bubbled PBS, pH 7.0 (eluant flow rate 100−150 mL/min, 25 psi backpressure), while continually monitoring eluant for thiol content as above. In a typical example, a 6.6 g batch of BR96 (550 mL at 75.3 μM) yielded 6.1 g of reduced BR96 (800 mL at 47.6 μM mAb, 398 μM thiol) for a yield of 92% and thiol titer of 8.4 mol of thiol groups/mol of BR96.

Scheme 4. Conjugation of Branched Linkers to mAb's BR96 and IgG



	n	m
MAb-2a	**2**	**0**
MAb-2b	**3**	**0**
MAb-2c	**5**	**0**
MAb-3a	**2**	**1**
MAb-3b	**3**	**1**
MAb-3c	**5**	**1**

Table 1. Representative Immunoconjugates

conjugate[a]	SH titer	MR	yield (%)	aggregate (%)	unconjugated DOX (%)[b]	unreacted mAb (%)
BR96-**2a**	7.9	15.6	94	4.5	bld[c]	nd[d]
IgG-**2a**	10.0	15.9	87	3.1	bld	
BR96-**2b**	8.5	15.1	100	0.5	0.04	nd
IgG-**2b**	8.6	14.5	100	<3	0.20	
BR96-D-**2b**	8.4	15.3	41[e]	4.7	0.10	nd
IgG-D-**2b**	8.6	15.4	57	<3	0.18	
BR96-**2c**	7.2	14.6	96	7.0	0.04	nd
IgG-**2c**	9.9	16.2	86	12.7	0.21	
BR96-**3a**	7.9	11.7	100	2.4	1.81	nd
IgG-**3a**	9.4	14.7	71	<3	1.40	
BR96-**3b**	7.9	11.9	100	3.2	2.36	nd
IgG-**3b**	9.9	16.2	75	<3	bld	
BR96-**3c**	6.8	13.9	50[e]	4.1	bld	nd

[a] MAb-**linker**; Linkers and conjugates defined in Schemes 1 and 4. [b] Sum of unconjugated linker and free DOX. [c] Below limits of detection. [d] None detected. [e] Unoptimized.

Conjugation. The following procedure, for the conjugation of BR96 and **2b**, is typical of that used for all linkers cited herein. To reduced BR96 from Method A (125 mL, 6.07 μmol mAb, 51.5 μmol thiol) was added dropwise at 0 °C under Ar a solution of **2b** (93 mg, 67.2 umol) in 5 mL of Ar-bubbled H_2O. After being stirred for 30 min, the reaction mixture was filtered through a 0.22μ sterile filter. Conjugate was purified at 4 °C by percolation (approximately 2 mL/min) through a 1 in. × 36 in. Bio-Beads column (initially prepared by swelling and packing in methanol, then equilibrated in H_2O, and finally PBS, pH 7.0). The purified conjugate was filtered again through a 0.22μ sterile filter to yield 155 mL of BR96-**2b** (BR96, 39.13 μM; DOX, 589.0 μM; MR, 15.1 mol of DOX/mol of BR96; yield, 100%). Conjugate was frozen in liquid N_2 and stored at −80 °C. Conjugation results for all linkers **2** and **3** are shown in Scheme 4 and Table 1.

Synthesis of Thioethers 14−16 (Scheme 5). Compounds **1**−**3** (3−5 mg) were dissolved in MeOH (**1**) or H_2O

Table 2. Hydrolysis of Representative Thioether-Modified Linkers and Immunoconjugates at pH 5 and 7

	$T_{1/2}$ (h)			$T_{1/2}$ (h)	
linker	pH 5[a]	pH 7[b]	conjugate[c]	pH 5[a]	pH 7[b]
14	3.5	>120	BR96-**1**	3.2	>158
			BR96-**2a**	6.5	>300
			IgG-**2a**	5.4	>300
15b	19	>400	BR96-**2b**	6.1	>160
			IgG-**2b**	5.3	>235
			BR96-D-**2b**	5.5	>300
			IgG-D-**2b**	5.5	>300
15c	14	>420	BR96-**2c**	6.1	450
			IgG-**2c**	7.0	>415
			BR96-**3a**	2.5	>300
			IgG−**3a**	2.4	>300
16b	1.5	120	BR96-**3b**	3.5	>85
			IgG-**3b**	2.7	>300
16c	2.5	60	BR96-**3c**	3.2	>117

[a] 100 mM NaOAc. [b] 100 mM Na_2HPO_4. [c] MAb-**linker**; Linkers and conjugates defined in Schemes 1 and 4.

(**2**-**3**) and treated for 10 min with 100 mL of 2-mercaptoethanol. Solvent was removed under vacuum and the residue washed with Et_2O. Complete conversion to the thioether was verified by ^1H NMR and a shift in HPLC retention time.

Determination of Hydrolysis Kinetics of 14−16. Stock solutions (10 mM) of **14**−**16** were freshly prepared in H_2O. Aliquots were diluted to a final concentration of 30 mM in either 100 mM NaOAc, pH 5.0, or 100 mM Na_2HPO_4, pH 7.0, then incubated (stoppered test tube) at 37 °C in a thermostat-regulated H_2O bath. RP−HPLC was used to monitor the formation of DOX in solution and the disappearance of starting materials until equilibrium was reached. Conditions for the analyses were 50 mL injection; Phenomenex IB−Sil 5 C-18 column; mobile phase 44:56 H_2O−MeOH with 6% NH4OAc; flow rate 1.5 mL/min; UV detection 235 nm. Free DOX was quantitated by integrating the 7.5 min peak (positively identified by comparison to a DOX standard) and represented as the percent of total DOX in solution vs time. Half-lives for the appearance of DOX were calculated from these curves and are listed in Table 2.

Determination of Conjugate Hydrolysis Kinetics. Conjugates at approximately 10 mg/mL were diluted 1:3 into either 100 mM NaOAc, pH 5.0, or 100 mM Na_2HPO_4, pH 7.0. The solutions were placed into a temperature-controlled (37 °C) autosampler for RP−HPLC. Samples were taken and analyzed automatically at timed intervals by the autosampler. Conditions for the analyses were Jones Chromatography Apex C-18 5μ column; mobile phase 70:30 MeOH−30mM ammonium phosphate, pH 4.5; flow rate 1.5 mL/min; fluorescence exitation 233 nm, emission 570 nm; UV detection 235 nm. DOX·HCl standards were analyzed before and after the experiment. The results are expressed as percents of total DOX released. Half-lives for the appearance of DOX were calculated from these curves and are listed in Table 2.

In Vitro Cytotoxicity Assays. In vitro cytotoxicity assays were performed as described previously (*10*) using the BR96 expressing human lung carcinoma line L2987 (*2*). Briefly, monolayer cultures of L2987 cells were harvested and resuspended to 1×10^5/mL in RPMI-1640 containing 10% heat inactivated fetal calf serum (RPMI-10%FCS). Cells (0.1 mL/well) were added to each well of 96 well microtiter plates and incubated overnight at 37 °C in a humidified atmosphere containing 5% CO_2. Medium was removed from the plates and serial dilutions of DOX or mAb-DOX conjugates added to the wells. All dilutions were performed in quadruplicate. Cells were exposed to DOX or mAb-DOX conjugates for 2 h at 37 °C in a humidified atmosphere of 5% CO_2. Plates were centrifuged (200*g*, 5 min), the drug or conjugate removed, and the cells washed 3× with RPMI−10% FCS. The cells were cultured in RPMI−10% FCS (37 °C, 5% CO_2) for an additional 48 h. At this time the cells were pulsed for 2 h with 1.0 μCi/well of [^{3}H]thymidine (New England Nuclear, Boston, MA). Cells were harvested onto glass fiber mats (Skatron Instruments, Inc.,Sterling, VA), dried, and filter bound [^{3}H]thymidine radioactivity determined (β-Plate scintillation counter, Pharmacia LKB Biotechnology, Piscataway, NJ). Inhibition of [^{3}H]thymidine uptake was determined by comparing the mean CPM for treated samples with that of the mean CPM of the untreated control.

RESULTS AND DISCUSSION

Linker Synthesis. The branched linkers were synthesized using L- or D-glutamic acid as a convenient template. The two carboxyl groups of glutamic acid were converted to hydrazides, either directly as in **2** (Scheme 2), or via an extended β-alanine spacer as in **3** (Scheme 3). The amino group of glutamic acid was extended using an amide linkage with maleimidoalkanoic acids of varying length to introduce a terminal maleimide group.

The two series of linkers **2** and **3** were synthesized by parallel procedures. For the **2** series, *Z*-Glu was doubly activated with DCC/NHS to give the bis-succinimdyl carbonate which was directly coupled with *tert*-butyl carbazate to give **4**. Catalytic hydrogenation gave the free amine **5**. The maleimidoalkanoyl tether was attached to **5** by either of two amide coupling methods, yielding **6a**−**6c**. The unprotected bis-hydrazides **7a**−**7c** were generated by treatment with 50% TFA in CH_2Cl_2. Condensation of **7a**−**7c** with DOX in MeOH in the presence of catalytic TFA[1] was monitored by RP−HPLC, which showed that the reaction progressed through a monohydrazone species to give bis-hydrazones **2a**−**2c**. The final products were generally isolated in good yield and purity after chromatography on Sephadex LH-20 in methanol (*13*). Included in this series is one D-analogue, D-**2b**, which was synthesized by an identical procedure from *Z*-D-Glu.

In the **3** series, the hydrazide linkage was initially installed on the β-alanine unit before attachment to *Z*-Glu. Thus, *Z*-β-Ala was activated with DCC/NHS and coupled to *tert*-butyl carbazate to give **8**. Catalytic hydrogenation generated **9**, which was coupled to *Z*-Glu in a manner similar to that used for **4** to generate the extended bis-hydrazide **10**. Continuing the parallel sequence, **10** was elaborated to the extended bis-hydrazones **3a**−**3c**.

Our earliest attempt at the synthesis of glutamyldihydrazides made use of the attachment of a maleimidoglycine unit to **5** to give **6** ($n = 1$), with the ultimate goal of extension to **2** ($n = 1$). In a similar manner, **12** ($n = 1$) was synthesized.[2] It was felt that linkers with short tethers would be the most H_2O soluble. We unexpectedly found that **6** ($n = 1$) was unstable in methanol. NMR studies showed that it decomposed with a $T_{1/2}$ of about 24 h at room temperature to yield a maleamate. By contrast, **12** ($n = 1$) was completely stable, as were all

[1] Prior experience with the synthesis of unbranched DOX hydrazones has shown TFA to be an effective catalyst in this reaction (*8*). Advantageously bound TFA, from the previous synthetic step, acted as catalyst in the preparation of **2a**-**2c**.

[2] Data not shown.

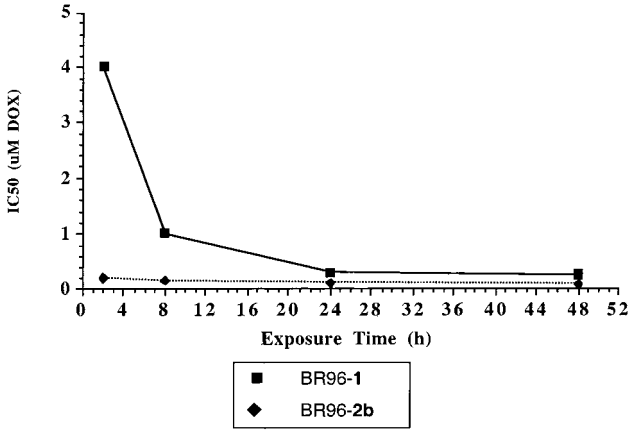


Figure 1. Relative in vitro potencies of branched and linear conjugates evaluated as a function of in vitro exposure time.

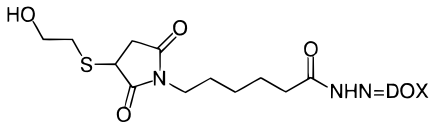
compounds with $n \geq 2$. Appparently **6** ($n = 1$) is a uniquely activated electrophile toward protic solvolysis by virtue of the hydrazide groups at close proximity. Because methanol was a crucial solvent during later stages of the syntheses, we decided to abandon maleimidoglycine linkers in general. Ultimately, this proved to be inconsequential in regard to solubility, since all members of the **2** and **3** series which were synthesized were fully soluble in H_2O as HCl salts.

Conjugation of Linkers to Monoclonal Antibodies. We have previously shown that mild treatment of BR96 with DTT reduces a maximum of 4 interchain disulfide bonds to yield 8 thiol groups, which, upon reaction with the single-chain maleimide **1** gave immunoconjugates with MR's equal to 8 (*9*). The reduction procedure is generally applicable and was used with minor modifications in this work to generate immunoconjugates of branched linkers. Thus, mAb (either BR96 or control IgG) was treated with a 7-fold excess of DTT with exclusion of O_2 at 37 °C for 3 h. For syntheses ≤3 g, reduced mAb was purified by diafiltration in an Amicon stirred cell device. For larger scale syntheses (3−9 g), a Filtron minisette was used. In either case removal of small molecules was rapid (about 3 h for the Amicon device and 30 min for the Filtron minisette) and efficient, generating SH titers of about 8 for BR96 and 10 for IgG. Conjugation of a 1.3 molar excess of branched linkers (based on SH titer) for 30 min at 0 °C was followed by chromatography on Bio-Beads to remove unreacted linker. MR values of 14−16 DOX/mAb were obtained for the **2** series, consistent with the SH titer generated. Protein recoveries were generally good with yields in the range of 85−100%. For reasons not readily apparent, lower MR values were obtained for the **3** series than for the **2** series. Results for some representative immunoconjugates are summarized in Table 1.

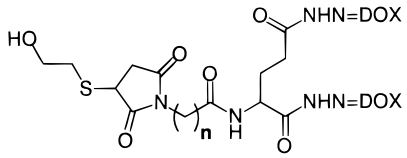
In our earlier work, we reported that BR96-DOX, prepared from the single-chain linker **1**, was a single molecular entity with molecular weight 160000 (*9*). Conjugates prepared from **2** and **3** also were shown by SEC−HPLC to be monomeric, usually containing <5% aggregate. In this study we also used HIC chromatography to verify the absence of unreacted Ab. Finally, these immunoconjugates were shown by RP−HPLC to contain <2−3% unconjugated DOX or DOX linker (Table 1).

Hydrolysis Kinetics. We have previously shown that **1** and its mAb conjugates are stable at pH 7, yet hydrolyze rapidly at pH 5 to release free DOX (*9*). In this study, it was also necessary to examine the hydrolytic

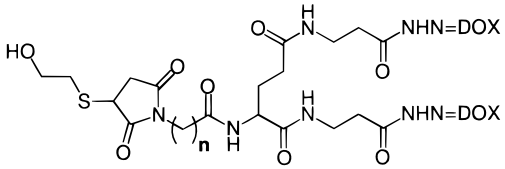
Scheme 5. 2-Mercaptoethanol Adducts of 1−3



14



15b n=3
15c n=5



16b n=3
16c n=5

stability of branched linkers **2** and **3**. For this purpose we decided to convert our linkers **1**−**3** to thioether derivatives **14**−**16** (Scheme 5) by reaction with 2-mercaptoethanol. The thioethers were more soluble in aqueous buffers than their parent maleimides and more closely mimicked the mAb conjugate, which itself is a thioether. The conversion of thioethers **14**−**16** to DOX was followed at pH 5 and 7 by RP−HPLC, and $T_{1/2}$ values calculated for disappearance of starting material. Results are summarized in Table 2.

Within each series of linkers, $T_{1/2}$ values are equivalent and show that there is no effect due to the length of the tether. It is interesting to note that **15** (derived from the compact series **2**) is considerably more stable at pH 5 and 7 than **16** (derived from the extended series **3**). It is possible that stacking interactions are greater for **15** and that attack by water on the hydrazone bond is hindered due to steric constraints. Furthermore, it is seen that **16** hydrolyzes at a rate equal to that of the single-chain linker **14** (derived from **1**) at both pH values. This observation is consistent with **16** adopting a more extended conformation, similar to **14**, where the hydrazone bond is less hindered to attack by water.

We also examined the hydrolysis rates of the actual conjugates derived from **2** and **3** as a function of pH. In this case, RP−HPLC was used to monitor the levels of free DOX in solution generated over time from the immunoconjugate. Results from Table 2 show that the same trends are maintained as for the thioether derivatives, albeit at rates 2−10× faster at pH 5. General acid catalysis provided by acidic residues on the protein may account for the increase in hydrolysis rates. Stereochemistry of the Glu residue has no effect on conjugate hydrolysis rates. Immunoconjugates derived from **2** are about twice as stable as those of **3** or **1** (our prototype

Table 3. Cytotoxicity of Linear and Branched DOX Hydrazone Conjugates

linker	type	molar ratio (mean ± SD)	IC_{50} (mean ± SD) DOX (μM)	IC_{50} (mean ± SD) mAb (μM)	specificity ratio[a]
1	linear	7.8 ± 0.3	2.8 ± 0.8	0.30 ± 0.09	8
2a	branched	15.3 ± 0.5	0.2 ± 0.08	0.013 ± 0.006	>25
2b	branched	13.3 ± 1.7	0.58 ± 0.29	0.045 ± 0.01	>25
D-**2b**	branched	13.3 ± 0.7	0.2 ± 0.03	0.015 ± 0.003	>25
2c	branched	14.3 ± 1.7	0.34 ± 0.26	0.026 ± 0.021	>25
3a	branched	11.7 ± 0.8	0.5 ± 0.08	0.04 ± 0.02	>25
3b	branched	11.9 ± 0.25	0.4 ± 0.1	0.033 ± 0.009	>25
	free DOX		0.26 ± 0.09		

[a] Specificity Ratio defined as the following: IC_{50} IgG-DOX/IC_{50} BR96-DOX.

single-chain linker) at pH 5, a factor which is probably not significant in vivo. We believe that a $T_{1/2}$ of 5−7 h is sufficient for efficient release of DOX within the tumor lysosome.

In Vitro Potency of Linear and Branched DOX Hydrazone Conjugates. The in vitro potency of immunoconjugates prepared with different branched linkers is shown in Table 3. The conjugates evaluated in this study had molar ratios which ranged from 7.0 to 15.3, contained <5% aggregate, and retained ≥95% binding activity relative to mAb BR96. When the concentration of DOX required to produce 50% cytotoxicity was evaluated, the branched BR96-DOX conjugates were 4−14-fold (IC_{50} values of 0.2−0.58 μM equivalent DOX) more potent than the linear BR96-**1** conjugate (2.8 μM DOX equivalent DOX) on an equivalent DOX basis. The branched BR96-DOX conjugates were as potent as unconjugated DOX, whereas the linear BR96-**1** conjugate was approximately 20-fold less potent. As shown in Table 3, the increased potency of the branched chain conjugates on a DOX basis coupled with the increased DOX/mAb molar ratios of these conjugates translates into a 7−23-fold increase in potency on a mAb basis. For example, the IC_{50} of the branched D-**2b** conjugate (0.015 μM mAb) was 20-fold lower than that of the linear **1** conjugate (0.3 μM mAb). We conclude, therefore, that branched BR96-DOX conjugates deliver an increased concentration of DOX per molecule of BR96, resulting in a significant increase in the in vitro potency of the conjugate on both a DOX and mAb basis.

The mechanism responsible for the >2-fold increase in in vitro potency corresponding to the doubling of the DOX/mAb molar ratio is not clear at this time. However, in additional in vitro experiments (Figure 1), the relative potencies of the branched and linear conjugates were evaluated as a function of the in vitro exposure time. These studies demonstrated that the enhancement in potency of branched conjugates was seen only following exposure times of ≤2h (the standard exposure time for these assays). With longer exposure times, 8−24 h, the branched conjugates were approximately twice as potent as the linear **1** conjugate. These data suggest either that the branched conjugates are internalized more rapidly than the linear conjugates or that DOX is more rapidly released from the branched conjugates in lysosomes following internalization.

The branched and linear chain BR96-DOX conjugates demonstrated antigen-specific cytotoxicity; however the specificity ratios of the branched conjugates were much higher than the linear conjugates. BR96-DOX conjugates were significantly more potent than IgG-DOX conjugates prepared at a similar molar ratio using the same linker.

CONCLUSION

In this work, we have introduced the novel concept of branched DOX hydrazone linkers for mAb conjugates. With a single branch point, these linkers have enabled us to successfully synthesize conjugates with mole ratios twice that of conjugates derived from similar single-chain DOX linkers. The new conjugates were generally obtained in good yield and were found to contain little or no aggregates, unreacted mAb, unreacted DOX hydrazone linkers, or free DOX. They demonstrate appropriate hydrolysis kinetics, releasing DOX rapidly at pH 5 while stable at pH 7. Conjugates derived from series **3** hydrolyze at the same rate at pH 5 as BR96-DOX, which is about twice as fast as those derived from series **2**. Neither this factor nor others such as the length of the maleimide tether or the configuration of the Glu residue are reflected, though, in in vitro cytotoxicity. The BR96 branched hydrazone conjugates were more potent than the linear DOXHZN conjugate on both a DOX (4−14-fold) and a mAb (7−23-fold) basis. These data suggest that utilizing the branched hydrazone methodology offers a potential advantage in conjugate potency and provides a means to significantly reduce the amount of mAb required to achieve activity. The in vivo biology of the branched chain conjugates is the subject of a later manuscript.

ACKNOWLEDGMENT

We acknowledge Michael Walker (BMS-Wallingford) and Y. Pendri (BMS-New Brunswick) for their assistance in various aspects of this work, and the BMS Analytical Chemistry Group (Ed Pack, Sadia Abid, and Tony Spears) for chromatographic assistance. Finally, we thank Drs. Dinesh Vyas and Terry Doyle for their support.

Supporting Information Available: Analytical data for the compounds described in the Synthesis section. This material is available free of charge via the Internet at http://pubs.acs.org.

LITERATURE CITED

(1) Trail, P. A., Willner, D., and Hellstrom, K. E. (1995) Site-directed delivery of anthracyclines for cancer therapy. *Drug Dev. Res. 34*, 196−209.

(2) Trail, P. A., Willner, D., Lasch, S. J., Henderson, A. J., Hofstead, S. J., Casazza, A. M., Firestone, R. A., Hellström, I., and Hellström, K. E. (1993) Cure of xenografted human carcinomas by BR96-Doxorubicin immunoconjugates. *Science 261*, 212−215.

(3) Sjogren, H. O., Isaksson, M., Willner, D., Hellstrom, I., Hellstrom, K. E., and Trail, P. A. (1997) Antitumor activity of carcinoma-reactive BR96-doxorubicin conjugate against human carcinomas in athymic mice and rats and syngeneic rat carcinomas in immunocompetent rats. *Cancer Res. 57*, 4530−4536.

(4) Hellström, I., Garrigues, H. J., Garrigues, U., and Hellström, K. E. (1990) Highly tumor-reactive, internalizing, mouse monoclonal antibodies to Le^y-related cell surface antigen. *Cancer Res. 50*, 2183−2190.

(5) Garrigues, J., Garrigues, U., Hellström, I., and Hellström, K. E. (1993) Le^y specific antibody with potent anti-tumor activity is internalized and degraded in lysosomes. *Am. J. Pathol. 142*, 607−622.

(6) Kaneko, T., Willner, D., Monkovic, I., Knipe, J. O., Braslawsky, G. R., Greenfield, R. S., and Vyas, D. M. (1991) New hydrazone derivatives of adriamycin and their immunoconjugates − a correlation between acid stability and cytotoxicity. *Bioconjugate Chem. 2*, 133−141.

(7) Braslawsky, G. R., Kadow, K. F., Knipe, J., McGoff, K., Edson, M., Kaneko, T., and Greenfield, R. S. (1991) Adriamycin(hydrazone)-antibody conjugates require internalization and intracellular acid hydrolysis for antitumor activity. *Cancer Immunol. Immunother. 33*, 367.

(8) Greenfield, R. S., Kaneko, T., Daues, A., Edson, M. A., Fitzgerald, K. A., Olech, L., Grattan, J. A., and Braslawsky, G. R. (1990) Evaluation in vitro of adriamycin − immunoconjugates synthesized using an acid sensitive hydrazone linker. *Cancer Res. 50*, 6600−6607.

(9) Willner, D., Trail, P. A., Hofstead, S. J., King, H. D., Lasch, S. J., Braslawsky, G. R., Greenfield, R. S., Kaneko, T., and Firestone, R. A. (1993) (6-Maleimidocaproyl)hydrazone of doxorubicin − a new derivative for the preparation of immunoconjugates of doxorubicin. *Bioconjugate Chem. 4*, 521−527.

(10) Trail, P. A., Willner, D., Lasch, S. J., Henderson, A. J., Greenfield, R. S., King, D., Zoeckler, M. E., and Braslawsky, G. R. (1992) Antigen specific activity of carcinoma reactive BR64-adriamycin conjugates evaluated in vitro and in human tumor xenograft models. *Cancer Res. 52*, 5693−5700.

(11) Shih, L. B., Goldenberg, D. M., Xuan, H., Lu, H., Sharkey, R. M., and Hall, T. C. (1991) Anthracycline immunoconjugates prepared by a site specific linkage via an amino-dextran intermediate carrier. *Cancer Res. 51*, 4192−4198.

(12) Riddles, P. W., Blakeley, R. L., and Zerner, B. (1979) Ellman's reagent: 5,5′-Dithiobis(2-nitrobenzoic acid)-A reexamination. *Anal. Biochem. 94*, 75.

(13) Henry, D. W., and Tong, G. L. (1978) Bis-hydrazones of daunomycin and adriamycin. U.S. Patent 4112217.

BC980100I

© 1999 American Chemical Society, Bioconjugate Chem., King bc980100i Supporting Info Page 1

ANALYTICAL DATA

Z-Glutamyldi(Boc)hydrazide **4**

Anal. $C_{23}H_{35}N_5O_8$

Calculated C, 54.21; H, 6.92; N, 13.74. Found C, 53.96;H, 6.91; N, 13.41.

Z-(D)-Glutamyldi(Boc)hydrazide **D-4**

Anal. $C_{23}H_{35}N_5O_8$

Calculated C, 54.21; H, 6.92; N, 13.74. Found C, 53.99;H, 6.92; N, 13.50.

Glutamyldi(Boc)hydrazide **5**

Anal. $C_{15}H_{29}N_5O_6 \cdot 0.5\ H_2O$

Calculated C, 46.87; H, 7.87; N, 18.22. Found C, 46.96; H, 7.74; N, 18.02.

(D)-Glutamyldi(Boc)hydrazide **D-5**

Anal. $C_{15}H_{29}N_5O_6 \cdot 0.5\ H_2O$

Calculated C, 46.87; H, 7.87; N, 18.22. Found C, 46.85; H, 7.63; N, 17.98.

Maleimidopropionylglutamyldi(Boc)hydrazide **6a**

Anal. $C_{22}H_{34}N_6O_9 \cdot 2HOAc$

Calculated C, 48.29; H, 6.55; N, 13.00. Found C, 48.15; H, 6.48; N, 13.28.

Maleimidobutyrylglutamyldi(Boc)hydrazide **6b**

Anal. $C_{23}H_{36}N_6O_9 \cdot 0.75\ H_2O$

Calculated C, 49.86; H, 6.82; N, 15.17. Found C, 50.21; H, 6.72; N, 14.79.

Maleimidobutyryl-(D)-glutamyldi(Boc)hydrazide **D-6b**

Anal. $C_{23}H_{36}N_6O_9 \cdot 0.75\ H_2O$

Calculated C, 49.86; H, 6.82; N, 15.17. Found C, 50.25; H, 6.65; N, 14.80.

© 1999 American Chemical Society, Bioconjugate Chem., King bc980100i Supporting Info Page 2

Maleimidocaproylglutamyldi(Boc)hydrazide **6c**

Anal. $C_{25}H_{40}N_6O_9 \cdot 0.5\ H_2O$

Calculated C, 51.98; H, 7.15; N, 14.55. Found C, 51.79; H, 6.96; N, 14.39.

Maleimidopropionylglutamyldihydrazide ditrifluoroacetate **7a**

Anal. $C_{12}H_{18}N_6O_5 \cdot 2.8$ TFA

Calculated C, 32.75; H, 3.25; N, 13.02. Found C, 33.04; H, 3.37; N, 12.72.

Maleimidobutyrylglutamyldihydrazide ditrifluoroacetate **7b**

Anal. $C_{13}H_{20}N_6O_5 \cdot 3.15$ TFA

Calculated C, 33.14; H, 3.34; N, 12.01. Found C, 33.49; H, 3.52; N, 11.64.

Maleimidobutyryl-(D)-glutamyldihydrazide ditrifluoroacetate **D-7b**

Anal. $C_{13}H_{20}N_6O_5 \cdot 2.5$ TFA

Calculated C, 34.57; H, 3.63; N, 13.44. Found C, 34.75; H, 3.50; N, 13.11.

Maleimidocaproylglutamyldihydrazide ditrifluoroacetate **7c**

Anal. $C_{15}H_{24}N_6O_5 \cdot 2.5$TFA

Calculated C, 36.76; H, 4.09; N, 12.86. Found C, 36.66; H, 4.22; N, 12.72.

Maleimidopropionylglutamyldihydrazone of Doxorubicin **2a**

Anal. $C_{66}H_{72}N_8O_{25} \cdot 2HCl \cdot 3.0H_2O$

Calculated C, 52.70; H, 5.36; N, 7.45. Found C, 52.57; H, 5.25; N, 7.33.

Maleimidobutyrylglutamyldihydrazone of Doxorubicin **2b**

Anal. $C_{67}H_{74}N_8O_{25} \cdot 2HCl \cdot 4.0H_2O$

Calculated C, 52.38; H, 5.51; N, 7.29. Found C, 52.38; H, 5.58; N, 7.50.

Maleimidobutyryl-(D)-glutamyldihydrazone of Doxorubicin **D-2b**

Anal. $C_{67}H_{74}N_8O_{25} \cdot 2HCl \cdot 3.5H_2O$

Calculated C, 52.69; H, 5.48; N, 7.34. Found C, 52.74; H, 5.57; N, 7.47.

Maleimidocaproylglutamyldihydrazone of Doxorubicin **2c**

Anal. $C_{69}H_{78}N_8O_{25} \cdot 2HCl \cdot 4H_2O$

Calculated C, 52.98; H, 5.67; N, 7.16. Found C, 52.96; H, 5.39; N, 7.45.

Z- β -Alanyl(BOC)hydrazide **8**

Anal. $C_{16}H_{23}N_3O_5$

Calculated C, 56.96; H, 6.87; N, 12.45. Found C, 57.19; H, 7.05; N, 12.57.

β -Alanyl(BOC)hydrazide **9**

Anal. $C_8H_{17}N_3O_3 \cdot 0.5H_2O$

Calculated C, 45.27; H, 8.55; N, 19.80. Found C, 45.51; H, 8.17; N, 19.49.

Z-Glutamyldi[β -Alanyl(Boc)hydrazide] **10**

Anal. $C_{29}H_{45}N_7O_{10}$

Calculated C, 53.45; H, 6.96; N, 15.04. Found C, 53.10; H, 6.90; N, 14.91.

Glutamyldi[β -Alanyl(Boc)hydrazide] **11**

Anal. $C_{21}H_{39}N_7O_8 \cdot 1.5H_2O$

Calculated C, 46.31; H, 7.77; N, 18.00. Found C, 46.34; H, 7.42; N, 17.90.

Maleimidopropionylglutamyldi[β -Alanyl(Boc)hydrazide] **12a**

Anal. $C_{28}H_{44}N_8O_{11} \cdot 2H_2O$

Calculated C, 47.72; H, 6.87; N, 15.90. Found C, 47.70; H, 6.57; N, 15.83.

Maleimidobutyrylglutamyldi[β -Alanyl(Boc)hydrazide] **12b**

Anal. $C_{29}H_{46}N_8O_{11} \cdot 1.5H_2O$

Calculated C, 49.08; H, 6.96; N, 15.79. Found C, 48.85; H, 6.65; N, 15.73.

Maleimidocaproylglutamyldi[β -Alanyl(Boc)hydrazide] **12c**

Anal. $C_{31}H_{50}N_8O_{11} \cdot 1.0H_2O$

Calculated C, 51.09; H, 7.19; N, 15.38. Found C, 51.43; H, 7.00; N, 15.08.

Maleimidopropionylglutamyldi[β -Alanylhydrazide] **13a**

Anal. $C_{18}H_{28}N_8O_7 \cdot 3.75TFA \cdot 0.25Et_2O$

Calculated C, 34.80; H, 3.77; N, 12.25. Found C, 34.63; H, 4.04; N, 12.20.

Maleimidobutyrylglutamyldi[β -Alanylhydrazide] **13b**

Anal. $C_{19}H_{30}N_8O_7 \cdot 3.5TFA \cdot 0.25Et_2O$

Calculated C, 36.03; H, 4.03; N, 12.45. Found C, 36.00; H, 4.29; N, 12.26.

Maleimidocaproylglutamyldi[β -Alanylhydrazide] **13c**

Anal. $C_{21}H_{34}N_8O_7 \cdot 2.75TFA \cdot 0.25Et_2O$

Calculated C, 39.20; H, 4.70; N, 13.30. Found C, 39.32; H, 4.58; N, 13.06.

Maleimidopropionylglutamyldi[β -Alanylhydrazone] of Doxorubicin **3a**

Anal. $C_{72}H_{82}N_{10}O_{27} \cdot 2HCl \cdot 7H_2O$

Calculated C, 50.32; H, 5.75; N, 8.15. Found C, 50.20; H, 5.49; N, 8.44.

Maleimidobutyrylglutamyldi[β -Alanylhydrazone] of Doxorubicin **3b**

Anal. $C_{73}H_{84}N_{10}O_{27} \cdot 2HCl \cdot 7H_2O$

Calculated C, 50.61; H, 5.82; N, 8.08. Found C, 50.83; H, 5.60; N, 7.41.

© 1999 American Chemical Society, Bioconjugate Chem., King bc980100i Supporting Info Page 5

Maleimidocaproylglutamyldi[β-Alanylhydrazone] of Doxorubicin **3c**

Anal. $C_{75}H_{88}N_{10}O_7 \cdot 2HCl \cdot 7H_2O$

Calculated C, 51.17; H, 5.95; N, 7.96. Found C, 51.04; H, 5.61; N, 8.29.

Targeting Folate Receptor with Folate Linked to Extremities of Poly(ethylene glycol)-Grafted Liposomes: In Vitro Studies

Alberto Gabizon,[†] Aviva T. Horowitz,[†] Dorit Goren,[†] Dinah Tzemach,[†] Frederika Mandelbaum-Shavit,[‡] Masoud M. Qazen,[§] and Samuel Zalipsky*[,§]

Sharet Institute of Oncology and Department of Bacteriology, Hadassah-Hebrew University Medical Center and Medical School, Jerusalem, Israel, and SEQUUS Pharmaceuticals, Inc., 960 Hamilton Court, Menlo Park, California 94025 . Received September 11, 1998; Revised Manuscript Received November 30, 1998

Conjugates of three components, folic acid−poly(ethylene glycol)−distearoylphosphatidylethanolamine (FA−PEG−DSPE), derived from PEG with molecular masses of 2000 and 3350 Da were synthesized by a carbodiimide-mediated coupling of FA to H_2N-PEG−DSPE. The conjugates were characterized by ^1H NMR, MALDI-TOF, and HPLC analysis of enzymatic cleavage with carboxypeptidase G. As a prototype of a folate receptor (FR)-targeted system, the conjugates were formulated at 0.5 mol % phospholipid in hydrogenated phosphatidylcholine/cholesterol liposomes with or without additional methoxyPEG2000−DSPE. In vitro binding studies were performed with sublines of M109 (murine lung carcinoma) and KB (human epidermal carcinoma) cells each containing high and low densities of FR. FA−PEG−DSPE significantly enhanced liposome binding to tumor cells. The best binding was observed when FA−PEG liposomes contained no additional mPEG−lipid. In fact, our experiments showed that the presence of mPEG on liposomal surfaces significantly inhibited FA−PEG−liposome binding to FR. Increasing the molecular mass of the PEG tether from 2000 to 3350 Da improved the FR binding, particularly in the case of mPEG-coated liposomes. The FA−PEG liposomes bound to M109-HiFR cells very avidly as demonstrated by the inability of free FA (used in a 700-fold excess either at the beginning or at the end of the incubation) to prevent the cell binding. This is in contrast to the 5−10-fold lower cell binding activity of mPEG−FA compared to that of free FA, and likely to be related to the multivalent nature of the liposome-bound FA. Only 22% of FA−PEG3350 and 32% of FA−PEG3350/mPEG cell-associated liposomes could be removed by exposure to pH 3, conditions that dissociate FA−FR, suggesting that more than two-thirds of the bound liposomes were internalized during incubation for 24 h at 37 °C. FA-targeted liposomes also show enhanced nonspecific binding to extracellular tissue culture components, a phenomenon especially relevant in short incubation time experiments.

INTRODUCTION

Recent advances in the design of liposomes based on surface modification with poly(ethylene glycol) (PEG)[1] have resulted in new formulations of small (<100 nm), long-circulating vesicles (*1*). The brush-like coat of PEG molecules attached to liposomal bilayer builds up a sterically repulsive shield that protects the liposome surface from nonspecific opsonization by plasma proteins, thus interfering with liposome recognition and clearance from circulation by the macrophages of the reticuloendothelial system (*2*, *3*). The improved pharmacokinetic properties of these PEG-grafted liposomes (*4*), and specifically their long circulation time, result in increased levels of localization into tumor tissues with high microvascular permeability (*5*). However, these liposomes remain mostly in the extracellular fluid and are not taken up by tumor cells (*6*).

For efficient drug delivery, a carrier system should facilitate not only tumor localization but also intracellular access. Therefore, significant effort has been focused on exploiting natural endocytosis pathways for targeting macromolecules or particulate carriers into living cells. The methodology has generally involved the chemical coupling of a normally endocytosed ligand to the carrier, followed by exposure of the resulting conjugate to receptor-bearing cells. Using this strategy, a variety of ligands such as antibodies, growth factors, or cytokines have served as vehicles for introducing drugs, proteins, and nucleic acids into target cells (*7*). In the case of ligand-mediated targeting of PEG-grafted liposomes, it is advantageous to link the ligand moieties to distal end groups of the PEG chains (*8*−*11*). It has been demonstrated recently using a surface forces apparatus that linking via a long PEG spacer expands the receptor-accessible range by almost the entire length of the fully stretched PEG tether (*12*). This may offer a major targeting advantage compared to ligand attachment

* To whom correspondence should be addressed. Telephone: (650) 323-9011. Fax: (650) 617-3080. E-mail: SamuelZ@SEQUUS.com.

[†] Sharet Institute of Oncology, Hadassah-Hebrew University Medical Center and Medical School.

[‡] Department of Bacteriology, Hadassah-Hebrew University Medical Center and Medical School.

[§] SEQUUS Pharmaceuticals, Inc.

[1] Abbreviations: PEG, poly(ethylene glycol); mPEG, methoxy-PEG; FA, folic acid; FR, folate receptor; PBS, phosphate-buffered saline; PL, phospholipid; EDTA, ethylenediaminetetraacetic acid; DSPE, distearoylphosphatidylethanolamine; HSPC, hydrogenated soy phosphatidylcholine; Chol, cholesterol; MALDI-TOFMS, matrix-assisted laser desorption ionization time-of-flight mass spectrometry; CPG, carboxypeptidase G; PI-PLC, phosphatidylinositol-phospholipase C; RPMI medium (also known as RPMI 1640), cell culture medium developed at Roswell Park Memorial Institute.

10.1021/bc9801124 CCC: $18.00 © 1999 American Chemical Society
Published on Web 02/04/1999

directly to phospholipid (PL) membrane. In another example, it was shown that incorporation of sialyl Lewis X−PEG2000−DSPE into unilamellar liposomes resulted in a striking enhancement in the level of binding to E-selectin, 3 orders of magnitude higher than that of the free oligosaccharide ligand (*13*).

Antibody targeting to erbB2-overexpressing human carcinomas, using anti-erbB2 monoclonal antibody-bearing hydrazide−PEG liposomes (immunoliposomes), was examined by our group (*14*). We obtained specific and pronounced binding of immunoliposomes to erbB2-overexpressing cells in vitro. However, failure of the antibody-targeted liposomes to induce internalization by target cells was probably a major factor preventing the translation of specific binding into improved antitumor efficacy of doxorubicin-loaded immunoliposomes (*15*). Confirming the importance of internalization, Park et al. (*16*) have observed enhanced therapeutic efficacy with doxorubicin encapsulated in liposomes targeted with an anti-erbB2 antibody Fab fragment that causes liposome internalization into several breast cancer cell lines.

In recent years, it has been demonstrated that receptor-mediated uptake of the vitamin folic acid (FA) could also be exploited to facilitate entry of an attached molecule, macromolecule, or liposome into cells (*10*, *17*−*19*). Notably, it has been reported that the covalent conjugation of FA to liposomes through a PEG spacer permitted avid uptake of liposomes by KB cells (human nasopharyngeal cancer cell line) (*10*, *20*−*22*). The binding of these FA-targeted liposomes to KB cells could be competitively inhibited by excess free FA or by an antiserum against the FA receptor, demonstrating that the interaction is mediated by the cell surface FA-binding protein. The folate receptor (FR) is a glycosylphosphatidylinositol-linked membrane glycoprotein of 38 kDa located in caveolae that participates in the cellular accumulation of folates in a number of epithelial cells through the process of potocytosis (*23*−*25*). In this process, ligand-bound receptor is sequestered in caveolae, followed by internalization into postcaveolar plasma vesicles, released from the receptor via an intravesicular reduction in pH, and subsequently transported into the cytoplasm for polyglutamation. Ligand-free receptor is then recycled to the cell surface by reopening of the caveolae (*25*, *26*). A soluble form of the receptor, the folate-binding protein, was first described 30 years ago (*27*).

Cell surface receptors for folic acid are generally overexpressed in human cancer cells. The human FR happens to be largely overexpressed in ovarian cancer (80−90% of the cases), where it constitutes a useful marker (*28*−*30*). Enhanced expression of human FR has also been reported in malignant cell lines (>20-fold) (*31*), in human brain tumors (*31*), and in lung tumors (*32*). In addition, the receptor has been mapped to 11q13 (*31*), a region amplified in more than 20% of the samples from head and neck and breast tumors. In normal human tissues, detectable FR has a limited distribution, mainly in kidneys, lungs, choroid plexus, and placenta. The receptors in each of these tissues, except placenta, are localized in the apical membrane surface, i.e., facing away from the blood (toward urine, airway, and CSF) and hence inaccessible to FA conjugates administered intravenously (*19*). These observations suggest that the receptor may be a useful target for the development of selective cancer therapy.

Here we describe the synthesis and characterization of a folate−PEG−distearoylphosphatidylethanolamine (FA−PEG−DSPE) conjugate and summarize our in vitro findings with methoxy-PEG (mPEG)-grafted liposomes bearing the above conjugate specifically designed for targeting to the FR. Our results are in agreement with previous reports pointing at the feasibility of targeting liposomes using a FA ligand (*19*). However, we also find that the liposome mPEG coating interferes significantly with liposome binding and uptake by cells expressing FR at a high level. Optimal liposome−cell association was obtained when liposomes were prepared with a small fraction of the FA−PEG conjugate and no additional mPEG coating. When FA was conjugated using a longer polymer chain, PEG3350, liposome interaction with target cells was enhanced compared to that with the shorter PEG2000 tether commonly used for liposome coating.

MATERIALS AND METHODS

Synthesis and Characterization of FA−PEG−DSPE and mPEG−FA. Folic acid (Fluka, 100 mg, 0.244 mmol) was dissolved in DMSO (4 mL). Amino-PEG2000−DSPE (*33*) (400 mg, 0.14 mmol) and pyridine (2 mL) were added to the FA−DMSO solution followed by dicyclohexylcarbodiimide (130 mg, 0.63 mmol). The reaction was continued at room temperature for 4 h. TLC on silica gel GF (75:36:6 chloroform/methanol/water) showed a new spot ($R_f = 0.57$) due to the formation of the product. The disappearance of amino-PEG−DSPE ($R_f = 0.76$) from the reaction mixture was confirmed by ninhydrin spray. Pyridine was removed by rotary evaporation. Water (50 mL) was added to the reaction mixture. The solution was centrifuged to remove trace insolubles. The supernatant was dialyzed in Spectra/Por CE (Spectrum, Houston, TX) tubing (MW cutoff of 300 000) against saline (50 mM, 2 × 2000 mL) and water (3 × 2000 mL). The dyalizate, containing only the product (single spot by TLC), was lyophilized and the residue dried in vacuo over P_2O_5. The yield was 400 mg (90%). Exactly the same protocol was used to prepare FA−PEG−DSPE from H_2N-PEG3350−DSPE. In a similar procedure, FA was attached to mPEG2000-NH_2 (*34*). The product, mPEG−FA, was purified on a silica gel (70−200 mesh, 60 Å) column using a stepwise gradient of methanol (10 to 80%) in chloroform and then chloroform/methanol/water (65:30:5) for the elution of the pure product.

UV Analysis. Folate content values determined by quantitative UV spectrophotometry of the conjugates in methanol (0.05 mg/mL) using FA the extinction coefficient ϵ value of 27 500 M^{-1} cm^{-1} at a λ_{max} of 285 nm. The following FA content values were calculated: 0.29 mmol/g (94% of the theoretical value, 0.31 mmol/g) for FA−PEG2000−DSPE, 0.21 mmol/g (97% of the theoretical value, 0.22 mmol/g) for FA−PEG3350−DSPE, and 0.40 mmol/g (98% of the theoretical value, 0.41 mmol/g) for mPEG2000−FA.

^{1}H NMR (360 MHz, DMSO-d_6/CF_3CO_2D, ~10:1 v/v) for FA−PEG−DSPE: δ 0.84 (t, CH_3, 6H), 1.22 (s, CH_2, 56H), 1.49 (m, CH_2CH_2CO, 4H), 2.1−2.3 (overlapping 2 × t, CH_2CH_2CO and m, CH_2 of Glu, 8H), 3.2 (m, CH_2CH_2N, 4H), 3.50 (s, PEG, ~180H and ~300H for derivatives of PEG2000 and -3350, respectively), 4.02 (t, CH_2OCONH, 2H), 4.1 (dd, *trans*-PO_4CH_2CH, 1H), 4.3 (dd, *cis*-PO_4CH_2CH, 1H), 4.37 (m, α-CH, 1H), 4.60 (d, 9-CH_2N, 2H), 5.15 (m, PO_4CH_2CH, 1H), 6.65 (d, 3′,5′-H, 2H), 7.65 (d, 2′,6′-H, 2H), 8.77 (s, C7-H, 1H).

^{1}H NMR (360 MHz, DMSO-d_6/CF_3CO_2D, ~10:1 v/v) for mPEG−FA: δ 1.85−2.1 (m, β-CH_2 of Glu, 2H), 2.3 (m, γ-CH_2 of Glu, 2H), 3.11 (m, CH_2CH_2N, 4H), 3.50 (s, PEG, ~180H), 4.3 and 4.37 (minor and major α-CH_2 of Glu,

1H), 4.60 (9-CH_2N, 2H), 6.65 (d, 3′,5′-H, 2H), 7.66 (d, 2′,6′-H, 2H), 8.77 (s, C7-H, 1H).

Mass Spectra (MALDI-TOFMS). The spectra were obtained by Charles Evans & Associates (Redwood City, CA) with a PHI-EVANS MALDI triple electrostatic analyzer time-of-flight mass spectrometer (desorption laser operating at 337 nm, with a 600 ps pulse width), utilizing gentrinsic acid as a matrix material. The spectra exhibited a bell-shaped distribution of 44 Da-spaced lines centered at 3284 Da for FA−PEG2000−DSPE (calculated molecular mass of 3200 Da), 4501 Da for FA−PEG3350−DSPE (calculated molecular mass of 4540 Da), and 2400 Da for mPEG−FA (calculated molecular mass of 2423 Da).

HPLC Monitoring of CPG-Mediated Cleavage. An HPLC system, Shimadzu 10 A, equipped with a Phenomenex Prodigy C8 (4.6 mm × 50 mm) column was used at a flow rate of 1 mL/min, while monitoring at a λ of 285 nm. For analysis of FA−PEG−DSPE, the system was used in isocratic mode, with methanol/10 mM sodium phosphate at pH 7.0 (92:8 v/v). The conjugate eluted as a single peak with a retention time of 5.7 min. Analysis of mPEG−FA was performed in a gradient mode, using 10 mM sodium phosphate (pH 7.0) with methanol (0 to 35% over the course of 25 min). The conjugate eluted as a single peak with a retention time of 19.6 min. In both cases, it was possible to follow the enzymatic cleavage of pteroate from the FA moiety of the conjugates by the decrease in the total conjugate peak area. A solution of FA−PEG−DSPE (0.1 mg/mL) was prepared in 150 mM Tris buffer (pH 7.3). An aliquot (10 μL) of this solution was injected into the HPLC system to obtain the time zero peak integration. Enzyme carboxypeptidase G (CPG, Sigma, 1 unit) was added to the FA−PEG−DSPE solution. The resulting solution was incubated at 30 °C, and aliquots (10 μL) were injected into the HPLC system at different time intervals. The rate of enzymatic hydrolysis is rather fast initially, but it slows after incubation for 4 h. Additional 1 unit aliquots of CPG were added to the reaction mixture at 4 and 20 h time points. Data were collected for up to 27 h. Despite the prolonged incubation times and multiple additions of the enzyme, the size of the conjugate peak did not diminish beyond 20% of the initial integration value, indicating that 80% of the FA−PEG−DSPE was γ-carboxyl-linked. The experiment performed with mPEG−FA as a substrate showed that ~90% of the FA residues in this conjugate were γ-carboxyl-linked.

Liposome Preparation. Hydrogenated soybean phosphatidylcholine (HSPC) was from Avanti Polar Lipids (Birmingham, AL), and cholesterol (Chol) was from Sigma (St. Louis, MO); methoxyPEG2000−DSPE (mPEG−DSPE) was prepared as described previously (*35*). Liposomes with six different compositions (molar ratios in parentheses) were tested here: HSPC/Chol/FA−PEG-2000−DSPE (99.5:70:0.5), HSPC/Chol/FA−PEG3350−DSPE (99.5:70:0.5), HSPC/Chol/mPEG−DSPE (99.5:70:0.5), HSPC/Chol/FA−PEG2000−DSPE/mPEG−DSPE (92.5:70:0.5:7), HSPC/Chol/FA−PEG3350−DSPE/mPEG−DSPE (92.5:70:0.5:7), and HSPC/Chol/mPEG−DSPE (92.5:70:7.5). Since all preparations contained HSPC, Chol, and DSPE, we will refer to them by their type of FA−PEG/mPEG content (for a schematic diagram, see Figure 1). All liposome preparations were spiked with a trace amount of [^{3}H]Chol-hexadecyl ether (NEN, Boston, MA). Liposomes were made by hydration at 55−60 °C of either a thin dry lipid film obtained by rotary evaporation of a chloroform/methanol (1:1) lipid solution or a freeze-dried lipid "cake" obtained by lyophilization of a *tert*-butyl alcohol lipid solution. The buffer was 5% dextrose/15 mM Hepes (pH 7.4) at a concentration of 50−100 μmol of PL/mL. The course of hydration was followed by high-pressure extrusion through double-stacked polycarbonate membranes with pore sizes from 1.0 to 0.05 μm using a stainless steel device from Lipex Biomembranes (Vancouver, BC). Liposomes were sterilized by filtration through 0.22 μm cellulose membranes. Liposome characterization included the PL concentration based on phophorus content, the FA concentration based on the UV absorbance of folic acid at 285 nm after liposome disruption in sodium dodecyl sulfate solution (10%), the vesicle size as determined by dynamic laser scattering, and, in some preparations, free fatty acid content to check for PL hydrolysis. All liposome preparations had a mean vesicle size between 70 and 90 nm with a standard deviation of <25% and a unimodal size distribution. PL hydrolysis was not detected in the preparations tested here.

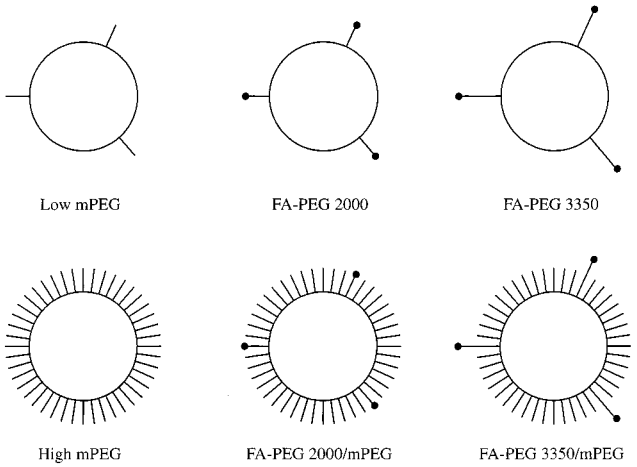


Figure 1. Schematic diagram of the liposome formulations tested in this study emphasizing the presence or absence of FA−PEG−DSPE with a short (PEG2000) or long (PEG3350) spacer arm and the presence or absence of mPEG.

Cell Culture and Binding Studies. *Medium.* Cells were cultured in normal or FA-free RPMI medium (RPMI-1640, Biological Industries, Beyt Haemek, Israel), with 10% fetal bovine serum (GIBCO, Grand Island, NY), 2 mM glutamine, 50 units/mL penicillin, and 50 μg/mL streptomycin. The concentration of FA in the serum-containing FA-free medium is only 3 nM, as opposed to 2.26 μM (1 mg/L) under normal culture conditions. Cells were routinely passed by treatment with a trypsin (0.05%)/EDTA (0.02%) solution in calcium- and magnesium-free phosphate-buffered saline (PBS).

Cell Lines. M109, a murine lung carcinoma line of BALB/c mice (*36*), and a subline of these cells, M109R, displaying multidrug resistance (an approximately 100-fold increased resistance to doxorubicin) were used in most of the experiments. Both cell lines express in vitro low amounts of FA receptors and are therefore referred to as M109-LoFR and M109R-LoFR, respectively. By culturing these cells in FA-free medium for several passages, we obtained two sublines expressing a high amount of FA receptors and adapted to grow under low-FA conditions with generation doubling times similar to the lines of origin. They are referred to as M109-HiFR and M109R-HiFR, respectively, to emphasize the overexpression of folic acid receptors.

KB cells, a human nasopharyngeal epidermal carcinoma (*37*), were also grown in low-FA medium to obtain cells overexpressing folic acid receptors, KB-HiFR cells.

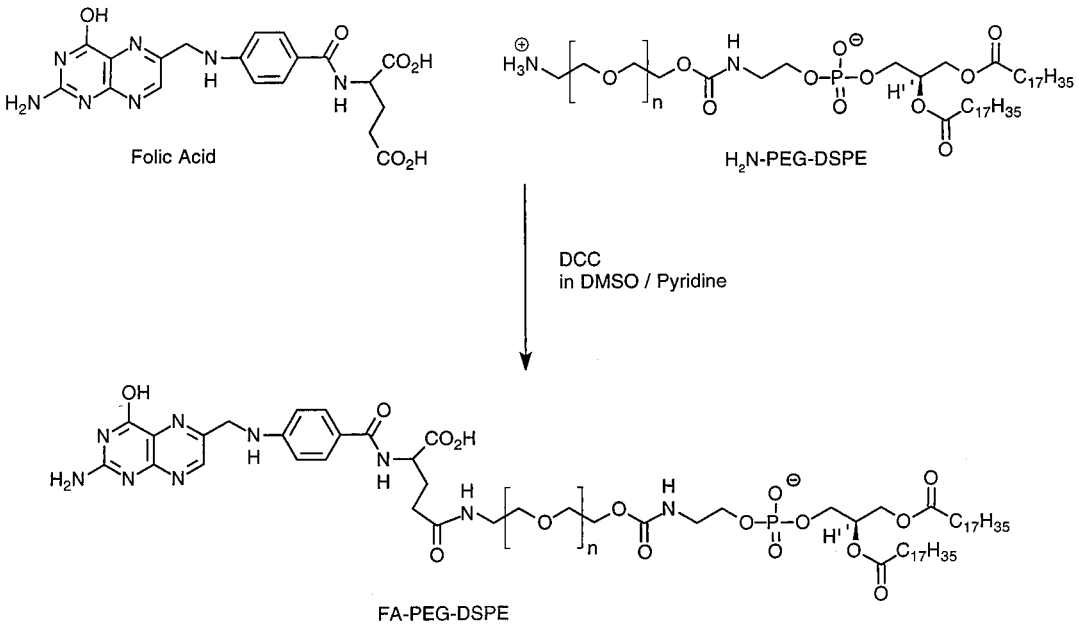


Figure 2. Synthesis of the FA−PEG−DSPE conjugate. Only the structure of the main product, the active γ-carboxyl-linked conjugate, is shown ($n \approx 45$ for PEG2000, $n \approx 76$ for PEG3350).

Other cell lines used in this study are A375, a human melanoma line, and normal human fibroblasts which were kindly provided by the Genetics Department of Hadassah Hebrew University Hospital.

Cell Binding of Free Folate or Liposomes. Binding was assayed through measurement of the level of cell-associated liposomal [^{3}H]Chol or [^{3}H]FA (Amersham, U.K.). Forty-eight hours prior to an assay, 5×10^5 cells were seeded per 35 mm dish, to obtain a concentration of about 10^6 cells/plate. Plates preincubated with medium and serum for 2 days, without cells, were used as controls. For the assays, plates were washed twice with FA-free RPMI medium, and incubated at 37 °C with 1 mL of FA-free RPMI medium containing 0.1 μM radiolabeled FA or liposomes in amounts of 30−300 nmol of PL. After incubation, the plates were rinsed three times with 2 mL of ice-cold PBS, and the radiolabels were extracted with 1 mL of 0.5 N NaOH overnight, followed by neutralization with 1 mL of 0.5 N HCL. To analyze exclusively radioactivity associated with cells, cells were released from plates with the trypsin/EDTA treatment, washed three times with PBS, and then extracted following the same procedure. The amount of radioactivity was determined by liquid scintillation counting. On the basis of the specific ratio of counts per minute per PL for each liposome formulation, the results were translated into picomoles of PL per 1 million cells.

For acid wash treatment following binding, each dish was washed twice with acidified saline (pH 3), followed by washing with PBS, and then the compound extracted as described above.

For treatment of cells with phosphatidylinositol-phospholipase C (PI-PLC), 2-day-old cell monolayers were rinsed twice with FA-free RPMI medium and incubated for 60 min at 37 °C with 0.1 unit/mL PI-PLC (Boehringer, Mannheim, Germany) in 1 mL of FA-free RPMI medium. Each dish was rinsed twice with FA-free RPMI medium and assayed for FA or liposome binding as described above.

In experiments performed with cells in suspension, cells from monolayers were released with the trypsin/EDTA treatment, followed by three washes (7 min, 500*g* centrifugation) in FA-free RPMI medium. The suspended cells ($1-10 \times 10^6$ cells/mL) were incubated with radiolabeled free FA or liposomes (concentration as indicated for each experiment) for 30 min to 24 h in 5 mL plastic tubes. Unbound material was removed by four washes with PBS.

RESULTS

Preparation and Characterization of FA Conjugates. Folate−PEG−DSPE conjugates were prepared, as shown in Figure 2, via a dicyclohexylcarbodiimide-mediated coupling of FA to H_2N-PEG−DSPE. The starting amino-PEG lipids were synthesized from PEG with molecular masses of 2000 and 3350 Da according to the previously described method (*33*). Using the same coupling method, we also prepared the mPEG−FA conjugate. This material represents FA conjugated to PEG with a molecular mass of 2000 Da without the PL moiety. The structures of the purified conjugates were corroborated by ^{1}H NMR, MALDI-TOFMS, and UV analysis. Since carbodiimide-activated FA can couple with H_2N-PEG−DSPE via either α- or γ-carboxyl groups of its glutamate residue, and it is known that only the γ-conjugate is capable of binding to the FR, it was important to determine the relative amounts of each α- and γ-carboxyl-linked conjugate. Our HPLC assay did not separate the two isomeric conjugates. It was previously shown that the α-conjugates of FA are inert with respect to carboxypeptidase G (CPG), while the γ-conjugates are subject to pteroate-glutamate cleavage at an appreciable rate (*18*, *38*, *39*). The enzymatic cleavage was followed by disappearance of the conjugate peak by HPLC. This reaction proceeded up to 80% conversion despite prolonged incubation times and multiple additions of the enzyme, indicating that FA−PEG−DSPE contained 80% γ-linked and the remaining 20% α-linked conjugates. Using the same approach (HPLC followup of CPG cleavage), we determined that ~90% of the mPEG−FA was linked through the γ-carboxyl group. These proportions of α- and γ-products are consistent with the previously reported results obtained with the FA−desferal conjugate synthesized under similar conditions (*18*).

Binding and Uptake of Free FA by M109 and Other Cell Lines. As indicated in Materials and Meth-

Table 1. Binding of Folic Acid to Various Cell Lines in Culture Plates[a]

cell line	folic acid (fmol/10^6 cells)
M109-LoFR	20 ± 6
M109-LoFR[b]	25 ± 13
M109R-LoFR	27 ± 10
M109-HiFR	678 ± 255
M109R-HiFR	2179 ± 430
KB-LoFR	456 ± 79
KB-LoFR[b]	6725 ± 323
KB-HiFR	9730 ± 79
A375	168 ± 33
NHF	45 ± 3

[a] Incubation time of 30 min at 37 °C. [b] After incubation in FA-depleted medium for 24 h.

ods, three of the cell lines tested here (M109, M109R, and KB cells) were induced to upregulate their FA receptors by consecutive passages in FA-depleted medium (3 nM FA). This resulted in three cell sublines referred to as HiFR with a 20−80-fold increase in FA binding capacity compared to those of the parental cell lines, which are known as LoFR (Table 1). We also used normal human fibroblasts in early passage, and a human melanoma line A375, to obtain a spectrum of different cell lines with a broad range of receptor expression levels (Table 1). When the lines with the lowest (M109-LoFR) and highest (KB-HiFR) amount of receptors are compared, differences in FA binding capacity up to 485-fold were observed.

All of the above experiments were carried out with a 30 min incubation with FA at 37 °C in FA-depleted medium. M109-LoFR and KB-LoFR cells were also assayed for FA binding following 24 h of incubation in FA-depleted medium (Table 1). Under these conditions, M109-LoFR did not upregulate the amount of FA binding. In contrast, KB-LoFR showed a 15-fold increase in the level of FA binding, indicating rapid upregulation of receptor expression.

In further experiments used to characterize the binding of FA with the FR-overexpressing M109-HiFR cell line, we made the following observations (data not shown).

(i) The extent of binding is directly proportional to the number of cells in the range of 10^5 to 1.5×10^6 cells/plate.

(ii) Monolayer cultures of M109R-HiFR cells pretreated with PI-PLC lose 99% of their FA receptors, as shown by the binding assay with FA, indicating that the overexpressed FR is bound to the cell membrane by a glycophospholipid anchor. In contrast, trypsin treatment does not damage the FR, as indicated by the fact that (a) radiolabeled FA binds to a similar extent to plated cells and to suspension cells after trypsinization and (b) cell-bound radiolabeled FA is almost fully recovered (91 ± 11%) after trypsinization.

(iii) Only 2 ± 1% of the FA remains bound to M109R-HiFR cell monolayers following acid wash (pH 3), indicating that the binding of FA to the overexpressed receptors is pH-sensitive. To prevent internalization, the FA binding assay took place at ∼1 °C for 30 min. When M109R-HiFR cells were incubated for 4 h at 37 °C with radiolabeled FA, and then submitted to acid wash, 30−40% of the ligand is retained by cells. This is most likely the fraction of FA ligand that is internalized by cells, thus avoiding the pH-induced dissociation from the receptor.

Competition Binding Study with FA, mPEG−FA, and Free PEG. In this experiment, M109R-HiFR cells were exposed to a constant amount of radiolabeled FA at a concentration of 0.1 μM and increasing concentrations of "cold" FA, mPEG−FA, and free PEG (from 0.1 to 100 μM). Both the PEG2000 and mPEG2000−FA used here were freely water-soluble, not lipid-linked, compounds. The latter derivative can be viewed as a monovalent version of FA−PEG2000−liposome as depicted in Figure 1. As seen in Figure 3, mPEG−FA was less effective than free FA in competing with radiolabeled FA, suggesting that the attachment of PEG to the vitamin molecule diminishes by 5−10-fold the extent of binding of FA to the receptor, whereas free PEG did not inhibit binding at all.

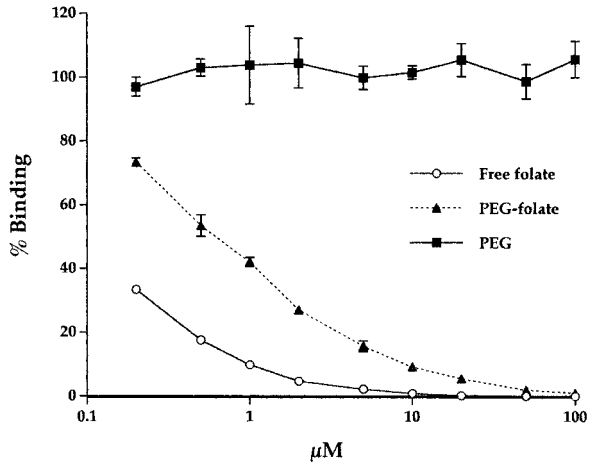


Figure 3. Competition study of binding to cellular folate receptor with free folic acid, free PEG2000, and the mPEG2000−FA conjugate. Radiolabeled FA was added at a concentration of 0.1 μM to M109R-HiFR cell monolayers which were incubated at 37 °C for 30 min with or without the competitors at the concentrations shown.

Enhanced in Vitro Cell Binding of FA-Targeted Liposomes. The liposome formulations tested were as described in Materials and Methods and as schematically depicted in Figure 1. Since the plain (nontargeted) high-mPEG and low-mPEG formulations behaved similarly in vitro, data are presented only for the high-mPEG liposomes which is the formulation with Stealth properties most commonly used in vivo (*1*). Folate-targeted liposomes contained the FA−PEG−DSPE conjugate derived from PEG with a molecular mass of 2000 or 3350 Da at a molar fraction of ∼0.5% of total liposomal PL.

The binding of radiolabeled FA-targeted liposomes and nontargeted liposomes was assayed on monolayer cultures of M109R-HiFR and M109-LoFR cells at 37 °C for 24 h. Figure 4A shows the amounts of liposomes bound to trypsin-released cells, expressed as the amount of PL per 1 million cells. The level of binding of plain mPEG liposomes was very low and similar for both high- and low-FA receptor cell lines. The targeted formulation with the highest binding efficiency was FA−PEG3350 (26-fold increase over that of nontargeted liposomes). Addition of mPEG (7% of PL) to the formulation or shortening of the PEG tether from 3350 to 2000 reduced the level of binding substantially. The level of binding was always greater for M109-HiFR cells than for M109-LoFR cells, regardless of the type of FA-targeted liposome used, although the differences were much less striking than those seen in Table 1 with free FA binding. The highest-affinity liposomal formulation, FA−PEG3500, showed the lowest relative increase of binding (∼30%) when the LoFR and HiFR cells were compared.

Figure 4B presents the results obtained when similar experiments were performed with KB cells. Once again, the addition of mPEG reduced the efficiency of binding,

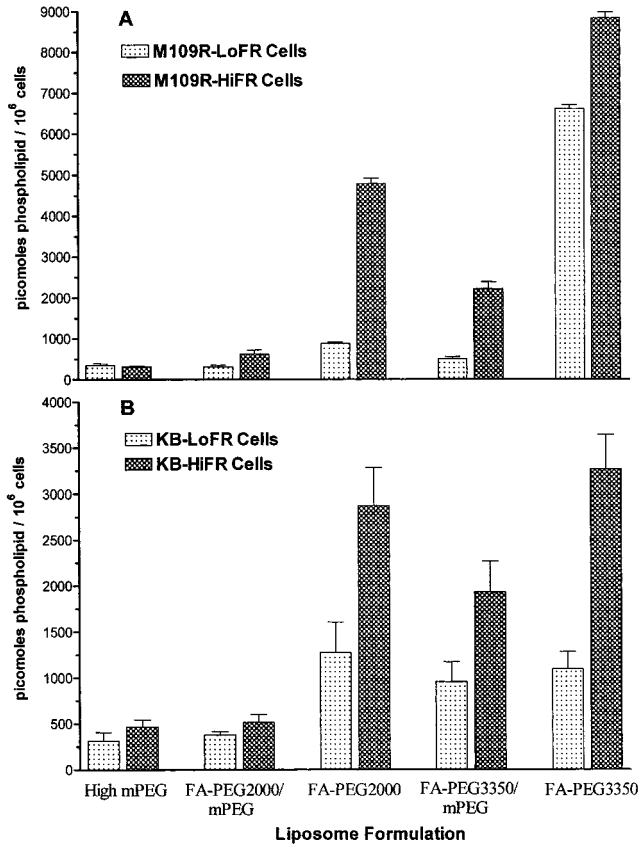


Figure 4. Binding of various FA-bearing and control liposomes to M109-LoFR and M109R-HiFR cells (A) and to KB-LoFR and KB-HiFR cells (B). The results were obtained after incubation for 24 h at 37 °C in the presence of 300 nmol of PL/mL. Cells were seeded 48 h prior to liposome exposure. See Figure 1 for the designation of various liposome formulations.

Table 2. Inhibition of Binding of FA-Bearing Liposomes to M109R-HiFR Cells by Free FA of Acid Wash[a]

	% inhibition	
liposomal formulation	FA−PEG3350	FA−PEG3350/mPEG
1 mM FA at time 0[b]	46 ± 8	86 ± 6
1 mM FA after 24 h[c]	2 ± 3	8 ± 4
acid wash after 24 h[d]	22 ± 2	32 ± 5

[a] M109R-HiFR cells were incubated for 24 h with 300 nmol/mL of FA liposomes. [b] Results obtained after the continuous presence of free folic acid from time 0. [c] Results obtained after folic acid was added for 2 h after incubation for 24 h with liposomes. [d] Results obtained after cells were washed with acid saline (pH 3) after incubation for 24 h with liposomes.

and in the presence of mPEG, FA−PEG3350 was markedly superior to FA−PEG2000. However, when mPEG was absent, the use of the longer PEG spacer did not appreciably increase the level of binding to KB cells. Also, the differences between KB-HiFR and KB-LoFR were in some instances smaller than in the case of M109 cells, a finding related perhaps to the rapid upregulation of FR receptors in KB cells during the 24 h incubation period (Table 1).

Effects of Acid Wash and Competition with FA on Cell Binding and Internalization of FA−PEG Liposomes. To determine if the cell-associated liposomes are cell surface-bound or internalized into cells, an acid wash with saline (pH 3) was performed at the end of the binding assay. The results shown in Table 2 indicate that only 22% of the FA−PEG3350 and 32% of the FA−PEG3350/mPEG liposomes could be removed, which means that more than two-thirds of the cell-associated liposomes have been internalized by M109-HiFR cells. Also shown in Table 2 are results from competition studies with 1 mM folic acid (~700-fold excess compared to the concentration of liposome-bound FA) either at the beginning or at the end of the binding assay. It was found that folic acid only partially inhibits liposome binding, especially when the higher-affinity, mPEG-free liposomes were used. When FA was added at the end of liposome incubation, it was unable to displace any significant amount of FA-bearing liposomes from the cells despite the fact that, according to acid wash experiments, approximately 20−30% of the liposomes were still bound to the cell surface. These experiments demonstrate the greater binding avidity of FA−PEG liposomes over free FA for the cellular FR, which is in contrast to 5−10-fold less efficient binding of the monovalent analogue, mPEG−FA. The stronger binding of FA liposomes is probably related to the multivalent presentation of FA residues on the liposomal platform.

Nonspecific Binding of FA-Targeted Liposomes to Extracellular Components. Unexpectedly, during the course of this study we observed substantial and rapid (within 30 min) binding of FA-presenting liposomes to serum and extracellular components adhered to tissue culture plates. Although most of our investigations on this effect were carried out with the FA−PEG/mPEG liposome formulation (results shown in Table 3), it should be noted that the nonspecific binding to extracellular plate components was observed with FA−PEG liposomes as well.

When binding of free FA to monolayer cultures was assayed by direct extraction from the plates without detaching the cells, the results were similar to those obtained when extraction was performed from trypsin-detached cells; i.e., 92 ± 2% of the total amount of FA bound to the plate was actually cell-associated after incubation for only 30 min. In contrast, after a short incubation time of 30 min, FA-bearing liposomes exhibited a high level of binding to nontrypsinized plates and a minimal level of binding to trypsin-released cells, accounting for only 6 ± 3% of the total counts bound to the nontrypsinized plate. In these experiments, most of the liposomes were released from the plate by trypsin treatment and were found in the cell-free supernatant, indicating that the binding site is extracellular and trypsin-sensitive, in direct contrast to that of cellular FR (data not shown). Moreover, there was no difference in the amounts of binding of FA-targeted liposomes when plates with HiFR and LoFR M109 cells were compared (Table 3). We also observed substantial binding of FA-targeted liposomes to serum-coated, cell-free plates. Plain, nontargeted, liposomes did not adhere to plates or cells under the same conditions (Table 3), indicating that the FA residue of targeted liposomes was responsible for this type of binding.

When the incubation time is prolonged from 30 min to 4 and 24 h, the level of specific cellular binding of FA-targeted liposomes increases gradually while the level of nonspecific extracellular binding remains unchanged or even decreases. At 24 h, FR-mediated cellular binding accounts for 50 to >90% of the total liposome binding to the plate, depending on the type of FA liposome tested.

To determine whether the binding of FA-targeted liposomes to extracellular components of cell culture plates is due to an extracellular FR present in serum and/or shed by cell monolayers, we examined their binding to plates coated with folate binding protein (Sigma), which is the soluble form of the FR. No binding of the FA−PEG/mPEG liposomes was observed, despite the fact

Table 3. Binding of FA-Bearing Liposomes, Control Nontargeted Liposomes, and Free FA to Plates with Serum Components or Monolayer Cell Cultures[a]

plates	liposomes (pmol of PL/plate)		free FA (fmol/plate)
	plain high mPEG	FA−PEG2000/ mPEG	
uncoated, cell-free	7 ± 4	31 ± 4	not detectable
serum-coated, cell-free	8 ± 3	809 ± 72	4 ± 3
laminin-coated, cell-free	3 ± 4	6 ± 8	1 ± 1
folate binding protein-coated, cell-free	6 ± 8	26 ± 12	1034 ± 56
M109-LoFR cells,[b] serum coated	25 ± 13	2564 ± 677	20 ± 6
M109R-HiFR cells,[b] serum coated	22 ± 12	2496 ± 868	2179 ± 430
M109R-HiFR laminin-coated[c]	18 ± 3	25 ± 6	1817 ± 252

[a] In a 35 mm empty plastic dish with incubation for 30 min at 37 °C. Liposome concentration of 30 nmol of PL/mL. [b] Two day monolayer confluent cultures (about 10^6 cells/plate) grown in medium with 10% fetal bovine serum. [c] About 10^6 cells attached to laminin-coated plates for 4 h in serum-free medium.

that free FA binds avidly in the same assay (Table 3). To investigate further the involvement of serum or cell-secreted proteins (unrelated to FR), we used laminin-coated plates. Within 4 h of incubation on laminin-coated plates and serum-free medium, M109-HiFR cells are firmly attached and spread. This enabled us to carry out liposome binding experiments before secreted or shed cellular components accumulate in the extracellular medium, and without the confounding factor of serum proteins. The level of binding of FA-targeted liposomes to laminin-coated plates was extremely low, and equivalent to only about 1% of the amount of binding to the same cell monolayers grown for 48 h with serum (Table 3).

These results support the contention that the extracellular binding component is present in serum and its level increases significantly in the presence of products shed from cell monolayers. The extracellular binding is likely to be related to a nonspecific binding of FA liposomes to proteins of the plate extracellular matrix, perhaps an opsonizing effect due to the recognition of an acidic carboxyl group on the surface of FA-targeted liposomes. This notion is further supported by the observation that free glutamic acid (1 mM) competes effectively with the binding of FA liposomes to the extracellular plasma component, but not with the cellular FR binding (data not shown).

DISCUSSION

The need to develop targeted liposomes with PEG coating is derived from our strategy for liposome targeting to tumors which consists of two steps: an initial step of extravasation into the tumor interstitial fluid based on the "Enhanced Permeability and Retention" effect (*40*) followed by a second step of direct interaction with a receptor on the membrane of tumor cells leading to internalization of liposome contents (*41*). The first step of tumor localization requires liposomes to be long-circulating, stable, and small, probably <100 nm in diameter (*5*), such as a class of PEG-coated liposomes referred to as Stealth (*1*). Extravasation is the rate-limiting step for tumor localization and should not be affected by a small-sized targeting ligand directed to the tumor cell (*14*, *15*). However, once liposomes reach the tumor cell microenvironment, the targeting effect may play an important role in facilitating the intracellular delivery of liposome contents.

The FA receptor has been proposed as a target for cancer drug delivery and immunotherapy (*17*, *31*, *42*, *43*). For liposome-mediated delivery in particular, Lee and Low have pioneered this approach using FA as a ligand attached to the PL bilayer of liposomes through a PEG spacer. Their work with KB cells overexpressing FA receptors has demonstrated the feasibility and efficiency of this targeting system (*10*, *20*, *44*). The advantages of FA-mediated targeting include the small size of the ligand, as opposed to the bulkiness, and potential immunogenicity of proteins (*45*), and the internalization of the ligand−receptor complex which should facilitate intracellular delivery of the therapeutic agent. In addition, FR overexpression is common as the α-isoform in malignant tumors of epithelial origin, and as the *β*-isoform in malignant tumors of nonepithelial origin (*46*), suggesting that this approach can be applied to a wide spectrum of neoplastic diseases. The main concern of FA targeting is the potential damage to normal tissues which generally express low to moderate amounts of the *β*-isoform of FR (*46*, *47*), an issue which needs to be evaluated.

Our approach to the synthesis of PEG−FA conjugates, in particular FA−PEG−DSPE, involved carbodiimide-mediated coupling of FA to readily attainable H_2N-PEG derivatives. This constitutes a cleaner and more straightforward approach to the target conjugates in comparison to the previously published examples (*10*, *20*). We also provide here, for the first time, a complete chemical characterization of these conjugates, including NMR, MALDI-MS, UV, and HPLC-mediated followup analysis of the CPD cleavage. According to these criteria, the conjugate preparations were highly pure (>94%) and contained predominantly (≥80%) the biologically active, *γ*-carboxyl-linked, form of FA. Folate−PEG−DSPE conjugates were incorporated into liposomes with or without additional mPEG−DSPE. As discussed in detail elsewhere (*48*), this method is preferable to conjugation of the ligand to preformed liposome (*10*).

In the experiments reported here, we examined the FA-mediated targeting of liposomes using a similar PEG spacer approach of Lee and Low (*10*, *20*, *44*), although the liposome tracer was different, a radiolabeled nondegradable cholesterol ether molecule which is a component of the liposome bilayer in this study, as opposed to encapsulated calcein or doxorubicin used by Lee and Low. This study demonstrates clearly that coupling of FA to the extremities of PEG chains grafted on liposomes is an effective way of targeting liposomes to tumor cells, especially when these cells overexpress FR, increasing the level of liposome cell binding by 26-fold. This is achieved with only about 100−250 FA−PEG residues per vesicle exterior. The estimated number of vesicles internalized by each tumor cell is very large, in the range of 50000−100000, stressing the potential of this approach for intracellular delivery of large payloads. Of note, the increase in the level of liposome binding and/or targeting is also important in the case of tumor cells not submitted to repeated passages in FA-depleted medium for further overexpressing FR. As a result, HiFR and LoFR M109

cells, which show enormous differences (80-fold, Table 1) with regard to the level of uptake of free FA, differ only by a relatively small factor (1.3−5.4 depending on the PEG tether with or without additional mPEG, Figure 4) when the uptake of FA-bearing liposomes is examined. This cannot be related to a difference in affinity of the respective ligands since mPEG−FA actually shows a lower affinity for the FR than for free FA (Figure 3). One likely explanation of these results is that a large part of the overexpressed receptors plays no essential role in liposome binding (estimated number of receptors per M109-HiFR cell is approximately 1 million). The number of liposomes which can interact with FR-enriched membrane areas in the vicinity of caveolae is physically limited. Once bound, a liposome may encompass an area of the cell membrane in which the number of FR exceeds the number of the liposomal FA residues, therefore rendering a fraction of the FR superfluous. Therefore, under in vitro conditions of liposome excess, an equivalent number of liposomes may bind to cells having a large difference in the number of FR.

Our experiments point at a clear interference of mPEG coating, which is mainly needed to combine extended systemic circulation in vivo with the targeting effect of FA. This interference of mPEG coating was more pronounced with FA−PEG2000−DSPE than with FA−PEG3350−DSPE. The longer arm of the latter ligand probably enables a better interaction with the FR away from the shielding effect of the mPEG2000 coating. The interference of the grafted mPEG with FA−PEG recognition by its receptor was much more marked for M109-HiFR cells than for KB-HiFR cells (4.0- vs 1.7-fold binding inhibition, respectively, using FA−PEG3350−DSPE, Figure 4), suggesting that the cell type is an important factor. This is worth noting in light of the results of Lee and Low (*20*, *44*), who reported equally effective cell binding regardless of the additional mPEG coating, using high-FR-expressing KB cells. In any case, the mPEG−lipid content might be an important variable in determining the liposome cell binding properties.

Recently, Kirpotin et al. (*49*) found that the binding activity of immunoliposomes was negatively affected in a dose-dependent fashion by the actual amount of mPEG present on the liposome surface, but only when the Fab′ ligand was linked to the lipid anchor directly. When the antigen was bound through a PEG spacer, mPEG−lipid content had no effect on the antigen binding activity. Inhibition of receptor binding by mPEG grafted to the same liposome surface as the ligand has been previously reported for cases involving both large, protein-based ligands (*8*, *11*, *49*, *50*) and also small molecules (*51*, *52*). In the current study, for the first time, we observed the negative effect of grafted mPEG on the binding of a PEG-tethered ligand, FA−PEG, even though the length of the PEG tether was equal or even greater than that of the mPEG. This is a somewhat surprising finding, in light of our previous experience with sialyl Lewis X−PEG2000 liposomes (SLX content of 0.5−5 mol %), which exhibited markedly enhanced E-selectin binding with minimal influence of the mPEG2000−DSPE content in the 4.5−0 mol % range (*13*). Furthermore, the FA−PEG binding inhibition caused by grafted mPEG is difficult to rationalize in light of previous measurements of the thickness of the mPEG2000 steric barrier (≤50 Å) (*53*−*55*) and the PEG2000-tethered ligand−receptor interaction range (≈150 Å) (*12*), although the latter measurement was taken in the absence of additional mPEG. Perhaps the explanation lies in the nature of the ligand itself, for example, in its potential to form hydrogen bonds with PEG, thus contributing to the PEG-tethered FA being shielded in the PEG layer surrounding the liposome.

Finally, our observations on the nonspecific binding of FA-targeted liposomes to extracellular components underscore the need for a cautious evaluation of the in vitro binding assays. The in vivo relevance of this nonspecific binding as a factor interfering with specific targeting is still uncertain and needs to be clarified in biodistribution studies of FA-targeted liposomes in tumor-bearing animals.

ACKNOWLEDGMENT

This project was supported by a grant to A. Gabizon, A. T. Horowitz and D. Goren from the Israel Science Foundation and by SEQUUS Pharmaceuticals Inc.

LITERATURE CITED

(1) D. Lasic and F. Martin, Eds. (1995) *Stealth Liposomes*, CRC Press, Boca Raton, FL.

(2) Torchilin, V. P., Omelyanenko, V. G., Papisov, M. I., Bogdanov, A. A., Trubetskoy, V. S., Herron, J. N., and Gentry, C. A. (1994) Polyethylene glycol on the liposome surface: On the mechanism of polymer-coated liposome longevity. *Biochim. Biophys. Acta 1195*, 11−20.

(3) Zalipsky, S. (1995) Chemistry of polyethylene glycol conjugates with biologically active molecules. *Adv. Drug Delivery Rev. 16*, 157−182.

(4) Papahadjopoulos, D., Allen, T. M., Gabizon, A., Mayhew, E., Matthay, K., Huang, S. K., Lee, K. D., Woodle, M. C., Lasic, D. D., Redeman, C., and Martin, F. J. (1991) Sterically stabilized liposomes: Improvements in pharmacokinetics and tumor therapeutic efficacy. *Proc. Natl. Acad. Sci. U.S.A. 88*, 11460−11464.

(5) Gabizon, A. (1995) Liposome circulation time and tumor targeting: Implications for cancer chemotherapy. *Adv. Drug Delivery Rev. 16*, 285−294.

(6) Huang, S. K., Lee, K.-D., Hong, K., Field, D. S., and Papahadjopoulos, D. (1992) Microscopic localization of sterically stabilized liposomes in colon carcinoma-bearing mice. *Cancer Res. 52*, 5135−5143.

(7) R. Duncan and T. Connors, Eds. (1996) Drug targeting in cancer therapy. *Journal of Drug Targeting*, Vol. 3 (special issue 5), pp 317−410.

(8) Blume, G., Cevc, G., Crommelin, M. D. J. A., Bakker-Woudenberg, I. A. J. M., Kluft, C., and Storm, G. (1993) Specific targeting with poly(ethylene glycol)-modified liposomes: coupling of homing devices to the ends of the polymeric chains combines effective target binding with long circulation times. *Biochim. Biophys. Acta 1149*, 180−184.

(9) Zalipsky, S., Puntambekar, B., Bolikas, P., Engbers, C. M., and Woodle, M. C. (1995) Peptide attachment to extremities of liposomal surface grafted PEG chains: Preparation of the long-circulating form of laminin pentapeptide, YIGSR. *Bioconjugate Chem. 6*, 705−708.

(10) Lee, R. J., and Low, P. S. (1994) Delivery of liposomes into cultured KB cells via folate receptor-mediated endocytosis. *J. Biol. Chem. 269*, 3198−3204.

(11) Zalipsky, S., Hansen, C. B., Lopes de Menezes, D. E., and Allen, T. M. (1996) Long-circulating, polyethylene glycol-grafted immunoliposomes. *J. Controlled Release 39*, 153−161.

(12) Wong, J., Kuhl, T. L., Israelashvili, J. N., Mullah, N., and Zalipsky, S. (1997) Direct measurement of tethered ligand−receptor interaction potential. *Science 275*, 820−822.

(13) DeFrees, S. A., Phillips, L., Guo, L., and Zalipsky, S. (1996) Sialyl Lewis^x liposomes as a multivalent ligand and inhibitor of E-Selectin mediated cellular adhesion. *J. Am. Chem. Soc. 118*, 6101−6104.

(14) Goren, D., Horowitz, A. T., Zalipsky, S., Woodle, M. C., Yarden, Y., and Gabizon, A. (1996) Targeting of Stealth liposomes to erbB2 (Her/2) receptor: In vitro and in vivo studies. *Br. J. Cancer 74*, 1749−1756.

(15) Goren, D., and Gabizon, A. (1998) Pharmacologic advantages of antracyclines encapsulated in polyethylene glycol coated Stealth liposomes: Potential for tumor targeting. In *Medical applications of liposomes* (D. Lasic and D. Papahadjopoulos, Eds.) pp 259−274, Elsevier Science B. V., Amsterdam.

(16) Park, J. W., Hong, K., Carter, P., Asgari, H., Guo, L. Y., With, C., Shalabi, R., Kotts, C., Keller, G. A., Wood, W. I., Papahadjopoulos, D., and Benz, C. C. (1995) Development of anti-p185HER2 immunoliposomes for cancer therapy. *Proc. Natl. Acad. Sci. U.S.A. 92*, 1327−1331.

(17) Leamon, C. P., and Low, P. P. (1991) Delivery of macromolecules into living cells: A method that exploits folate receptor endocytosis. *Proc. Natl. Acad. Sci. U.S.A. 88*, 5572−5576.

(18) Wang, S., Lee, R. J., Mathias, C. J., Green, M. A., and Low, P. S. (1996) Synthesis, purification, and tumor cell uptake of ^{67}Ga-desferoxamine-folate, a potential radiopharmaceutical for tumor imaging. *Bioconjugate Chem. 7*, 56−62.

(19) Wang, S., and Low, P. S. (1998) Folate-mediated targeting of antineoplastic drugs, imaging agents, and nucleic acids to cancer cells. *J. Controlled Release 53*, 39−48.

(20) Lee, R. J., and Low, P. S. (1995) Folate-mediated tumor cell targeting of liposome-entrapped doxorubicin in vitro. *Biochim. Biophys. Acta 1233*, 134−144.

(21) Wang, S., Lee, R. J., Cauchon, G., Gorenstein, D. G., and Low, P. S. (1995) Delivery of antisense oligonucleotides against the human epidermal growth factor into cultured KB cells with liposomes conjugated to folate via polyethylene glycol. *Proc. Natl. Acad. Sci. U.S.A. 92*, 3318−3322.

(22) Vogel, K., Wang, S., Lee, R. J., Chmielewski, J., and Low, P. S. (1996) Peptide-mediated release of folate-targeted liposome contents from endosomal compartments. *J. Am. Chem. Soc. 118*, 1581−1586.

(23) Kamen, B. A., and Capdevila, A. (1986) Receptor-mediated folate accumulation is regulated by the cellular folate content. *Proc. Natl. Acad. Sci. U.S.A. 83*, 5983−5987.

(24) Kamen, B. A., Wang, M. T., Streckfuss, A. J., Peryea, X., and Anderson, R. G. W. (1988) Delivery of folates to the cytoplasm of MA104 cells is mediated by surface membrane receptor that recycles. *J. Biol. Chem. 263*, 13602−13609.

(25) Anderson, R. G. W., Kamen, B. A., and Rothberg, K. G. (1992) Potocytosis sequestration and transport of small molecules. *Science 255*, 410−411.

(26) Rothberg, K. G., Ying, Y., Kohlhouse, J. F., Kamen, B. A., and Anderson, R. G. W. (1990) The glycophospholipid-linked folate receptor internalizes folate without entering the clathrin-coated pit endocytic pathway. *J. Cell Biol. 110*, 637−649.

(27) Ghitis, J., and Lora, C. (1967) The folate receptor in milk. *Am. J. Clin. Nutr. 20*, 1−4.

(28) Coney, L. R., Tomassetti, A., Carayannopoulos, L., Frasca, V., Kamen, B. A., Colnaghi, M. I., and Zurawski, V. R. J. (1991) Cloning of a tumor-associated antigen: MOv18 and MOv19 antibodies recognize a folate binding protein. *Cancer Res. 51*, 6125−6132.

(29) Campbell, I. G., Jones, T., and Trowsdale, J. (1991) High-affinity folate-binding protein is a marker for ovarian cancer. *Cancer Res. 51*, 5329−5338.

(30) Mantovani, L. T., Miotti, S., and Menard, S. (1994) Folate binding protein distribution in normal tissues and biological fluids from ovarian carcinoma patients as detected by the monoclonal antibodies Mov18 and Mov19. *Eur. J. Cancer 30A*, 363−369.

(31) Weitman, S. D., Lark, R. H., Coney, L. R., Fort, D. W., Frasca, V., Zurawski, V. R., and Kamen, B. A. (1992) Distribution of the folate receptor GP38 in normal and malignant cell lines and tissues. *Cancer Res. 52*, 3396−3401.

(32) Franklin, W. A., Waintrub, M., Edwards, D., Christensen, K., Prendegrast, P., Woods, J., Bunn, P. A., and Kolhouse, J. F. (1994) New anti-lung cancer antibody cluster 12 reacts with human folate receptors present on adenocarcenoma. *Int. J. Cancer, Suppl. 8*, 89−95.

(33) Zalipsky, S., Brandeis, E., Newman, M. S., and Woodle, M. C. (1994) Long-circulating, cationic liposomes containing amino-PEG-phosphatidylethanolamine. *FEBS Lett. 353*, 71−74.

(34) Zalipsky, S., Gilon, C., and Zilkha, A. (1983) Attachment of drugs to polyethylene glycols. *Eur. Polym. J. 19*, 1177−1183.

(35) Zalipsky, S. (1993) Synthesis of an end-group functionalized polyethylene glycol-lipid conjugate for preparation of polymer-grafted liposomes. *Bioconjugate Chem. 4*, 296−299.

(36) Marks, T. A., Woodman, R. J., Geran, R. I., Billups, L. H., and Madison, R. M. (1977) Characterization and responsiveness of the Madison 109 lung carcinoma to various antitumor agents. *Cancer Treat. Rep. 61*, 1459−1470.

(37) Saikawa, Y., Price, K., Hance, K. W., Chen, T. Y., and Elwood, P. C. (1995) Structural and functional analysis of the human KB cells folate receptor gene P4 promoter: cooperation of three clustered Sp1-binding sites with initiator region for basal promoter activity. *Biochemistry 34*, 9951−9961.

(38) Fan, J., Pope, L. E., Vitols, K. S., and Huennekens, F. M. (1991) Affinity labeling of folate proteins with the *N*-hydroxysuccinimide ester of the γ-isomer of fluorescein-methotrexate. *Biochemistry 30*, 4573−4580.

(39) Levy, C. C., and Goldman, P. (1967) The enzymatic hydrolysis of methotrexate and folic acid. *J. Biol. Chem. 242*, 2933−2938.

(40) Maeda, H., Seymour, L. W., and Miyamoto, Y. (1992) Conjugates of anticancer agents and polymers: Advantages of macromolecular therapeutics in vivo. *Bioconjugate Chem. 3*, 351−362.

(41) Gabizon, A. (1995) Stealth liposomes and cancer targeting: A realistic compromise in drug delivery. *J. Liposome Res. 5*, 705−710.

(42) Kranz, D. M., Patrick, T. A., Brigle, K. E., Sprinella, M. J., and Roy, E. J. (1995) Conjugates of folate and anti-T-cell-receptor antibodies specifically target folate-receptor-positive tumor cells for lysis. *Proc. Natl. Acad. Sci. U.S.A. 92*, 9057−9061.

(43) Kranz, D. M., Manning, T. C., Rund, L. A., Cho, B. K., Gruber, M. M., and Roy, E. J. (1998) Targeting tumor cells with bispecific antibodies and T cells. *J. Controlled Release 53*, 77−84.

(44) Lee, R. J., and Low, P. S. (1997) Folate-targeted liposomes for drug delivery. *J. Liposome Res. 7*, 455−466.

(45) Harding, J. A., Engbers, C. M., Newman, M. S., Goldstein, N. I., and Zalipsky, S. (1997) Immunogenicity and pharmacokinetic attributes of poly(ethylene glycol)-grafted immunoliposomes. *Biochim. Biophys. Acta 1327*, 181−192.

(46) Ross, J. F., Chaudhuri, P. K., and Ratnam, M. (1994) Differential regulation of folate receptor isoforms in normal and malignant tissues in vivo and in established cell lines. *Cancer 73*, 2432−2443.

(47) Gates, S. B., Mendelsohn, L. G., and Shackelford, K. A. (1996) Characterization of folate receptor from normal and neoplastic murine tissue: influence of dietary folate on folate receptor expression. *Clin. Cancer Res. 2*, 1135−1141.

(48) Zalipsky, S., Mullah, N., Harding, J. A., Gittelman, J., Guo, L., and DeFrees, S. A. (1997) Poly(ethylene glycol)-grafted liposomes with oligosaccharide or oligopeptide ligands appended to the termini of the polymer chains. *Bioconjugate Chem. 8*, 111−118.

(49) Kirpotin, D., Park, J. W., Hong, K., Zalipsky, S., Li, W.-L., Carter, P., Benz, C. C., and Papahadjopoulos, D. (1997) Sterically stabilized anti-HER2 immunoliposomes: design and targeting to human breast cancer cells in vitro. *Biochemistry 36*, 66−75.

(50) Klibanov, A., Maruyama, K., Beckerleg, A. M., Torchilin, V. P., and Huang, L. (1991) Activity of amphipatic poly(ethylene glycol) 5000 to prolong the circulation time of liposomes depends on the liposome size and is unfavorable for immunoliposome binding to target. *Biochim. Biophys. Acta 1062*, 142−148.

(51) Mori, A., Klibanov, A. L., Torchilin, V. P., and Huang, L. (1991) Influence of the steric barrier activity of amphipatic poly(ethylene glycol) and ganglioside GM1 on the circulation time of liposomes and on the target binding of immunoliposomes in vivo. *FEBS Lett. 284*, 263−266.

(52) Noppl-Simson, D. A., and Needham, D. (1996) Avidin−biotin interactions at vesicle surfaces: Adsorption and binding, cross-bridge formation, and lateral interactions. *Biophys. J. 70*, 1391−1401.
(53) Needham, D., McIntosh, T. J., and Lasic, D. D. (1992) Repulsive interactions and mechanical stability of polymer-grafted lipid membranes. *Biochim. Biophys. Acta 1108*, 40−48.
(54) Woodle, M. C., Collins, L. R., Sponsler, E., Kossovsky, N., Papahadjopoulos, D., and Martin, F. J. (1992) Sterically stabilized liposomes: Reduction in electrophoretic mobility but not electrostatic surface potential. *Biophys. J. 61*, 902−910.
(55) Kuhl, T. L., Leckband, D. e., Lasic, D. D., and Israelachvili, J. N. (1994) Modulation of interaction forces between bilayers exposing short-chained ethylene oxide headgroups. *Biophys. J. 66*, 1479−1488.

BC9801124

Duplex Recognition by Oligonucleotides Containing 2′-Deoxy-2′-fluoro-D-arabinose and 2′-Deoxy-2′-fluoro-D-ribose. Intermolecular 2′-OH−Phosphate Contacts versus Sugar Puckering in the Stabilization of Triple-Helical Complexes

Christopher James Wilds and Masad José Damha*

Department of Chemistry, Otto Maass Chemistry Building, McGill University, 801 Sherbrooke Street West, Montreal, Quebec, Canada H3A 2K6. Received September 24, 1998;
Revised Manuscript Received December 1, 1998

To gain insight into the origins of the large binding affinity of RNA toward target duplexes, 2′-deoxy-2′-fluororibonucleic acid (2′F-RNA) and 2′-deoxy-2′-fluoroarabinonucleic acid (2′F-ANA) were tested for their ability to recognize duplex DNA, duplex RNA, and RNA−DNA hybrids. 2′F-RNA, 2′F-ANA, and the corresponding control single-stranded (ss) DNA strands were shown to form triple-helical complexes only with duplex DNA and hybrid DNA (Pu)−RNA (Py), but not with duplex RNA and hybrid RNA (Pu)−DNA (Py). In contrast, an RNA third strand recognized all four possible duplexes (DD, DR, RD, and RR) as previously demonstrated by Roberts and Crothers [(1992) *Science 258*, 1463−1466]. The 2′F-RNA (C3′-endo) strand exhibited significantly reduced affinity for duplexes compared to an unmodified RNA (C3′-endo) strand. These findings are consistent with the intermolecular 2′-OH−phosphate contact mechanism proposed by Escudé et al. [(1993) *Nucleic Acids Res. 24*, 5547−5553], as a ribo 2′-F atom should not interact with a negatively charged phosphate. In addition, they emphasize the role of the 2′-OH ribose as a general recognition and binding determinant of RNA. The 2′-F arabino modification (2′F-ANA, C2′-endo) led to a considerable increase in the binding affinity for duplex DNA, as compared to those of DNA and 2′F-RNA third strands. This is likely to be the result of a greater population of C2′-endo pucker of the 2′F-ANA compared to DNA. The enhancement observed for 2′F-ANA strands toward duplex DNA is comparable to that observed with 2′-OMe RNA. Since 2′F-ANA has been shown to be more resistant to nuclease degradation than DNA, these results are likely to stimulate experimental work on arabinose derivatives in laboratories concerned with targeting DNA sequences in vivo ("antigene" strategy).

INTRODUCTION

The ability of single-stranded (ss) DNA or RNA to hybridize complementary nucleic acids, in a sequence-specific manner, is a fundamental characteristic of these molecules (*1*). The familiar double-helical structure of DNA is a consequence of this type of association (*2*). Of special interest are the hybridization properties of modified nucleic acids because of their potential use as molecular biology probes (*3*), and as chemotherapeutic agents that form double-stranded complexes with target mRNA ("antisense" approach; *4*). Interest in modified oligonucleotides has recently intensified due to the realization that they can be used as "antigene agents" forming intermolecular triplexes with DNA sequence (*5*−*7*). Several nucleic acid triple helices have been characterized, which fall into two distinct classes depending on the orientation of the third strand. In the more common triplex pattern known as the "pyrimidine" (or "parallel") motif, pyrimidine-rich oligonucleotides bind parallel to the purine strand of the target duplex, forming *T*·AT and C^+·GC triplets (*5*−*7*), while in the alternative "purine" (or "antiparallel") triplex motif, purine-rich third strands bind in an antiparallel orientation, generating *G*·GC, *A*·AT, and *T*·AT triads (*8*, *9*).

Investigations from several laboratories have established that the chemical nature of the sugar rings has a dramatic influence on the stability of triplexes (*10*−*13*). For example, in pyrimidine motif triplexes, a more stable triplex is formed when the third strand is RNA rather than DNA. In addition, a third RNA strand forms a stable triplex with all duplex combinations (i.e., DD, DR, RD, and RR, where the first letter represents the purine strand and the second the pyrimidine strand), whereas a third DNA strand forms a stable triplex only with DD and DR duplexes. The structural basis for these effects is unknown. Possible explanations include (a) a specific intermolecular contact of the 2′-OH group of the RNA third strand with proximal phosphate groups of the underlying Watson−Crick duplex (*12*) and (b) different sugar puckering forms of RNA and DNA (*5*, *14*). Thus, with some exceptions, the DNA sugars generally assume a C2′-endo conformation, while RNA sugars generally assume a C3′-endo conformation (*1*). Interestingly, these puckering modes seem to prevail in triple-helical complexes. For example, C2′-endo sugars are mainly observed in triple helices formed with a DNA strand, while C3′-endo sugars are mainly found in triple helices containing an RNA third strand (*15*−*17*).

Cuenoud and co-workers examined recently the properties of 2′-*O*-alkylamino RNA with regard to binding to duplex DNA, and found that this modification led to a considerable increase in the binding affinity compared

* To whom correspondence should be addressed. E-mail: damha@omc.lan.mcgill.ca. Phone: (514) 398-7552. Fax: (514) 398-3797.

10.1021/bc9801171 CCC: $18.00 © 1999 American Chemical Society
Published on Web 02/11/1999

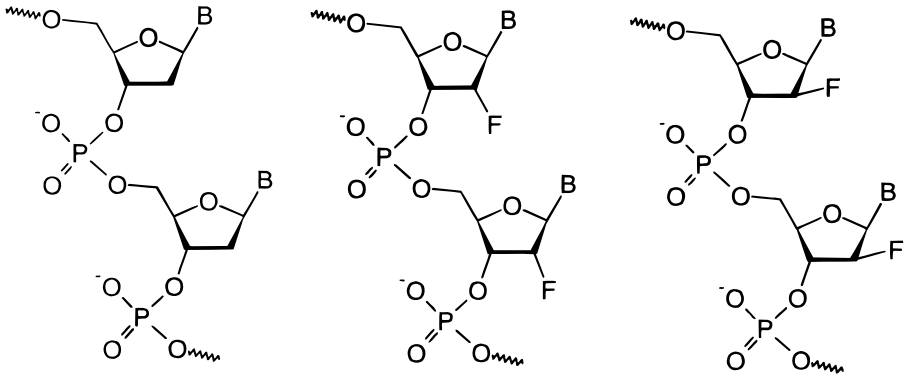


Figure 1. Structures of DNA, 2′-deoxy-2′-fluororibonucleic acid (*R*′, **1**), and 2′-deoxy-2′-fluoroarabinonucleic acid (*A*′, **2**) strands.

to that of an unmodified DNA third strand (*18*). While these findings are consistent with the proposed intermolecular OH−phosphate contact (i.e., a 2′-*O*-alkyl-NH_3^+−phosphate interaction should be stronger than a 2′-OH−phosphate interaction), they do not rule out mechanism b. The sugar conformation of 2′-*O*-alkylamino RNA is unknown, as is its ability to associate with duplex DR, RD, and RR. Our laboratory has recently reported on arabinonucleic acids (ANA), the 2′-epimer of RNA, with regard to triplex formation (*14*). The inversion of configuration at the 2′-stereocenter led to a significant decrease in the binding affinity compared to that of the RNA third strand. Moreover, the ANA strand was able to hybridize only to DD and DR duplexes, and not to RD and RR duplexes. Thus, in terms of binding properties, ANA mimics DNA, not RNA. Since the loss of stability may be due to the disruption of the 2′-OH−phosphate contact, and/or a change in the sugar conformation to C2′-endo (observed often in arabinonucleotide residues; *14*, and references therein), it is difficult to ascertain the nature of the observed effects. It is important to understand the role that sugar conformation has on triplex stability so that puckering and intermolecular contact effects can be distinguished from one another. A thorough understanding of these factors is crucial for the design of future generation oligonucleotide analogues.

To help identify the role played by sugar conformation, we have examined the properties of 2′-deoxy-2′-fluororibonucleic acids (2′F-RNA, **1**) and 2′-deoxy-2′-fluoroarabinonucleic acid (2′F-ANA, **2**) with regard to triplex formation (Figure 1). Since 2′F-RNA lacks the protic 2′-OH group and its puckering is C3′-endo, like that of natural RNA, it provides a unique opportunity to clarify the stabilizing influence of RNA strands on triple-helical complexes. The 2′F-arabino modification should stabilize the C2′-endo form (*14*, *19*) and thus serves as a reference point for evaluating the importance of sugar puckering (C3′-endo vs C2′-endo) in the stabilization of triple helices (Figure 2). Our results are described below.

EXPERIMENTAL PROCEDURES

General Methods. Molar extinction coefficients for oligonucleotides were calculated from those of the mononucleotides and dinucleotides according to nearest-neighboring approximations (*20*). The values for the hybrid hairpins were assumed to be the sum of their D and R components: DD, 26.5; DR, 27.1; RD, 26.7; RR, 27.7; *D*, 9.1; and *R*, 9.6 ($\times 10^4$ M^{-1} cm^{-1}). Molar extinction coefficients for 2′F-ANA and 2′F-RNA strands (*A*′ and *R*′) were assumed to be the same as that of the corresponding DNA strand (9.1 $\times$ 10^4 M^{-1} cm^{-1}). Complexes were prepared by mixing equimolar amounts of interacting strands, e.g., *R*′ and hairpin DD, and lyophilizing the resulting mixture to dryness. The resulting pellet was then redissolved in the buffer. The solutions were at a concentration of 2 μM in each strand, with 100 mM NaOAc and 1 mM EDTA (pH 5.5). The solutions were then heated to 80 °C for 15 min, cooled slowly to room temperature, and stored at 4 °C overnight before measurements were taken. Melting curves were determined using a Varian Cary model 1 UV spectrophotometer equipped with a Peltier temperature programmer for automatically increasing the temperature at a rate of 0.5 °C/min. Melting temperatures (T_m) were calculated from the first derivative of the melting curves. Gel electrophoresis (mobility shift assays) and CD measurements were carried out as described previously (*14*).

Oligonucleotide Synthesis. 1′-(2-Deoxy-2-fluoro-β-D-arabinofuranosyl)thymine (2′F-aT) and 1′-(2-deoxy-2-fluoro-β-D-arabinofuranosyl)cytosine (2′F-aC) were synthesized according to published procedures (*21*, *22*). They were elaborated to the 5′-*O*-(4-monomethoxytrityl)-3′-*O*-(2-cyanoethyl-*N*,*N*-diisopropyl)phosphoramidite derivatives of 2′F-aT and 2′F-aC(N^4-Bz) according to literature procedures (*23*). 1′-(2′-Deoxy-2′-fluoro-β-D-ribofuranosyl)-thymine (2′F-rT) and its 5′-*O*-(4,4′-dimethoxytrityl)-3′-*O*-(2-cyanoethyl-*N*,*N*-diisopropyl)phosphoramidite derivative were a gift from Y. Sanghvi (Isis Pharmaceuticals) (*24*). The β-anomeric configuration of these nucleoside derivatives was established with two-dimensional nuclear Overhauser effect (nOe) experiments (NOESY). For example, the NOESY spectrum of 2′F-rT displayed both H2′/H6 (moderate) and H3′/H6 (strong) correlations, as expected, whereas only the H3′/H6 correlation was observed with 2′F-aT. Also consistent with the β-configuration at the glycosidic bond is the observation of nOes between H4′ and H1′ for both 2′F-rT and 2′F-aT (data not shown). 5′-*O*-(4,4′-Dimethoxytrityl)-2′F-rC(N^4-Bz) 3′-*O*-(2-cyanoethyl-*N*,*N*-diisopropyl)phosphoramidite was purchased from Glen Research (Sterling, VA).

Oligonucleotides 2′F-RNA (*R*′) and 2′F-ANA (*A*′) were synthesized on an Applied Biosystems 381A synthesizer using slight modifications of our published protocols (*14*). Couplings proceeded in good yields (>90%) as judged by the trityl assay. The oligomers were isolated by polyacrylamide gel electrophoresis (PAGE) followed by gel filtration (desalting) on a Sephadex G-25 column (*23*).

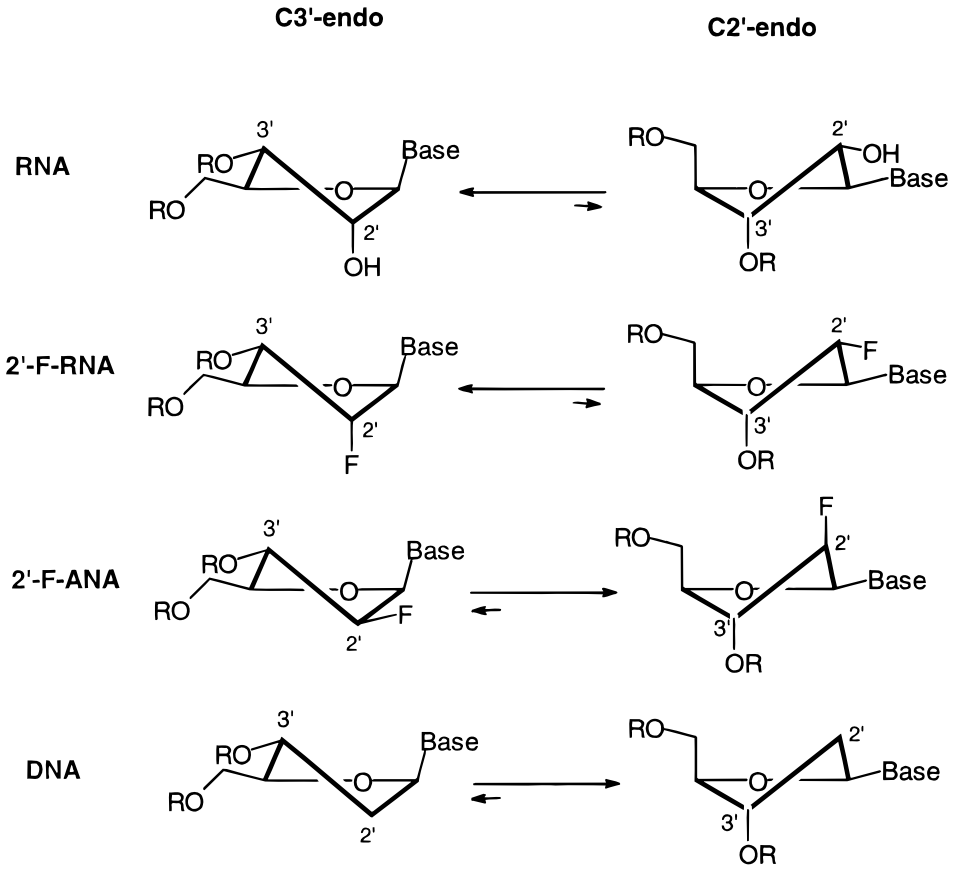


Figure 2. Sugar puckering conformational equilibrium for RNA, 2′F-RNA, 2′F-ANA, and DNA. In the most stable conformations of 2′F-RNA (C3′-endo) and 2′F-ANA (C2′-endo), the 2′-F atom is pseudoaxial and gauche with respect to ring oxygen O4′ ("gauche effect").

Isolated yields were 10−20 A_{260} units (ca. 1 mg). The isolated product gave satisfactory MALDI-TOF mass spectra (*A′*, calcd M^+ 3682.5, found M^+ 3681.7; *R′*, calcd M^+ 3682.5, found M^+ 3681.3). The hairpin duplexes DR, RD, and RR and the control strand *R* were synthesized according to the method of Damha and Ogilvie (*23*). The DD hairpin and *D* sequence were obtained commercially.

RESULTS AND DISCUSSION

Experimental Design. Experiments were carried out with polypyrimidines *R′* and *A′* and hairpin target duplexes having all four possible duplex combinations with each of the two duplex strands composed of either DNA or RNA (i.e., DD, DR, RD, and RR; Figure 3). The known DNA (*D*) and RNA (*R*) third strands served as controls. This experimental design was selected since Roberts and Crothers had used it successfully in analyzing the effects of the DNA and RNA composition of pyrimidine motif triple helices (*10*). Triple helix formation was monitored via native gel electrophoresis (*25*; Figure 4A,B) and CD (*10*; Figure 5A,B), whereas the melting behavior of complexes was assessed by obtaining UV melt curves (Figure 6A,B and Table 1).

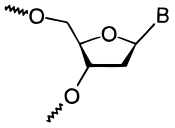
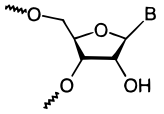
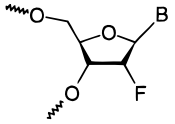
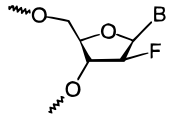
As previously demonstrated (*10*), the RNA (*R*) third strand formed a triple-helical complex with all four duplexes, whereas the DNA (*D*) strand formed a triplex only with duplex DD and DR. This was indicated by the presence of two transitions in the absorbance versus temperature profile of single stands and duplex mixtures (e.g., *D* + DD and *R* + DD; see Figure 6). The low-temperature transition corresponds to dissociation of the third strand from the target duplexes, whereas the high-temperature transition corresponds to the melting of the



Figure 3. Base sequence of hairpin duplexes (DD, DR, RD, and RR) and third strands (D, R, *A′*, and *R′*) selected for study. DNA sequences are shown in bold.

hairpin duplexes (*10*). These assignments are based upon the observations that the low-temperature transition disappears at neutral pH (due to destabilization of C^+·GC triads), and the fact that only the high-temperature transition is observed when a solution of duplex alone was heated under identical conditions. These results were confirmed by native polyacrylamide gel electrophoresis and CD (data not shown).

Table 1

third strand		Δ T_m / triad	
type	structure	DD target	DR target
DNA		0	0
RNA		+ 1.8	+ 2.8
2'F-RNA		- 0.3	+0.4
2'F-ANA		+ 0.8	+ 0.7

2′F-RNA (*R*′) versus RNA (*R*) as a Third Strand. The CD spectra of a 1:1 mixture (5 °C) of *R*′ and DD and of *R* and DD are quite similar in the region of 240−320 nm, suggesting that *R*′ and DD and *R* and DD triplexes have similar helical conformations (Figure 6A). This was also true for the CD spectra of *R*′ and DR and of *R* and DR (Figure 6B). The differences are mainly located in the region around 280 nm, where the (+) band of the *R*′ triplexes is blue shifted and greater in magnitude than that observed for the *R* triplexes.

If the 2′-OH groups of RNA (*R*) third strands were indeed positioned to interact specifically with nearby phosphate groups, one might expect that replacing the 2′-OH group with a 2′-F group would destabilize the triplex. If puckering was the most important effect, however, one may actually observe stabilization of the complex since the C3′-endo sugar population of 2′F-RNA (*R*′) is larger than that of RNA (*26*). Thermal dissociation data for the triplex formed from *R*′ and DD and *R*′ and DR in fact support the proposed intermolecular contact, since the ribo 2′-F modification significantly reduced the affinity of *R*′ for the duplexes to a level similar to that of the DNA third strand (Table 1). For example, the temperature at which *R*′ dissociates from duplex DD is only 36 °C, a value significantly lower than that observed for the *R* strand (62 °C). Also significant is the finding that *R*′, like *D* strands (and unlike *R* strands), is unable to form a stable triplex with RD and RR (Figure 4A). We conclude that the 2′-OH ribose group, not the C3′-endo pucker of third strands, is essential for the formation of *R* and RD and *R* and RR triple helices.

2′F-ANA (*A*′) versus DNA (D) as a Third Strand. As shown in Table 1, the 2′-F arabino sugar modification (C2′-endo) led to an increase in the binding affinity compared to that of the unmodified DNA (C2′-endo), although the magnitude of the effect was smaller than that observed for RNA (*R*). It is also worth noting that *A*′ strands and 2′-O-methylated RNA display comparable triplex binding enhancement with respect to *D* third strands (*15*, *18*, *27*). The higher affinity of 2′F-ANA (*A*′) compared to *D* for DD and DR duplexes is consistent with expectations of a more preorganized state (higher percentage of C2′-endo population) of the *A*′ strand relative

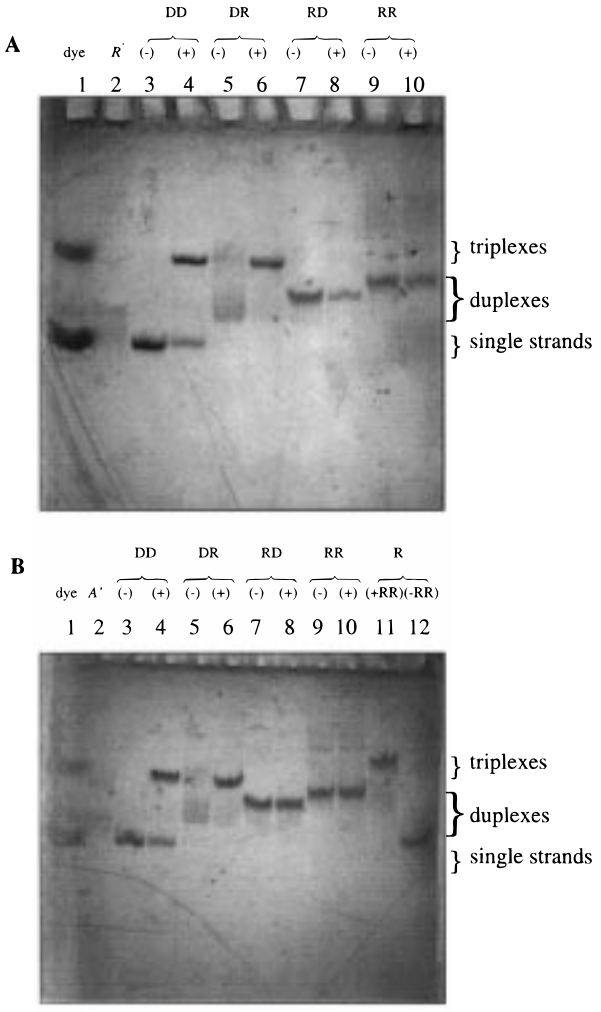


Figure 4. Gel shift mobility assay under nondenaturing conditions, with 20% polyacrylamide at 4 °C and pH 5.0. The marker dyes are xylene cyanol (XC) and bromophenol blue (BPB). Hairpins either alone (−) or in the presence (+) of 2′F-RNA (A) or 2′F-ANA (B) are indicated. Evidence of the formation of the control triplex R·RR is seen in lane 11 of Figure 4B.

to the *D* strand (*14*, *19*), whereas the stabilizing effect seen for 2′-OMe RNA is most likely hydrophobic in nature (*15*, *27*).

Also shown in Figure 5 (panels C and D) are the CD spectra of 1:1 mixtures of *A*′ and DD and of *A*′ and DR at 5 °C, along with the spectra of the control *D* and DD and *D* and DR mixtures. The spectra of the triplexes containing *A*′ strands are characterized by (+) bands that are blue-shifted relative to the *D* triplexes. In the case of *A*′ and DR, the CD spectrum is dominated by a very large molar ellipticity of the (+) band (e.g., compared to the CD spectra of *A*′ and DR and *D* and DR; Figure 5D) which may be attributed to a more effective $\pi-\pi$ overlap of the base triplets.

As in the case for *D* strands, only triplexes derived from *A*′ and DD and from *A*′ and DR, but not from *A*′ and RR and *A*′ and RD, were observed (Figure 4B). Thus, the entropic advantage exhibited by *A*′ strands over *D* strands is not sufficient to effect binding to RR or RD under the conditions used. In the case for the two triplexes that do not form (*A*′ and RD and *A*′ and RR), only the transition corresponding to the self-association of the *A*′ strand ($T_m \simeq 44$ °C) is seen at low temperatures (data not shown). This self-associating structure of *A*′ is evident because of the presence of numerous bands in a

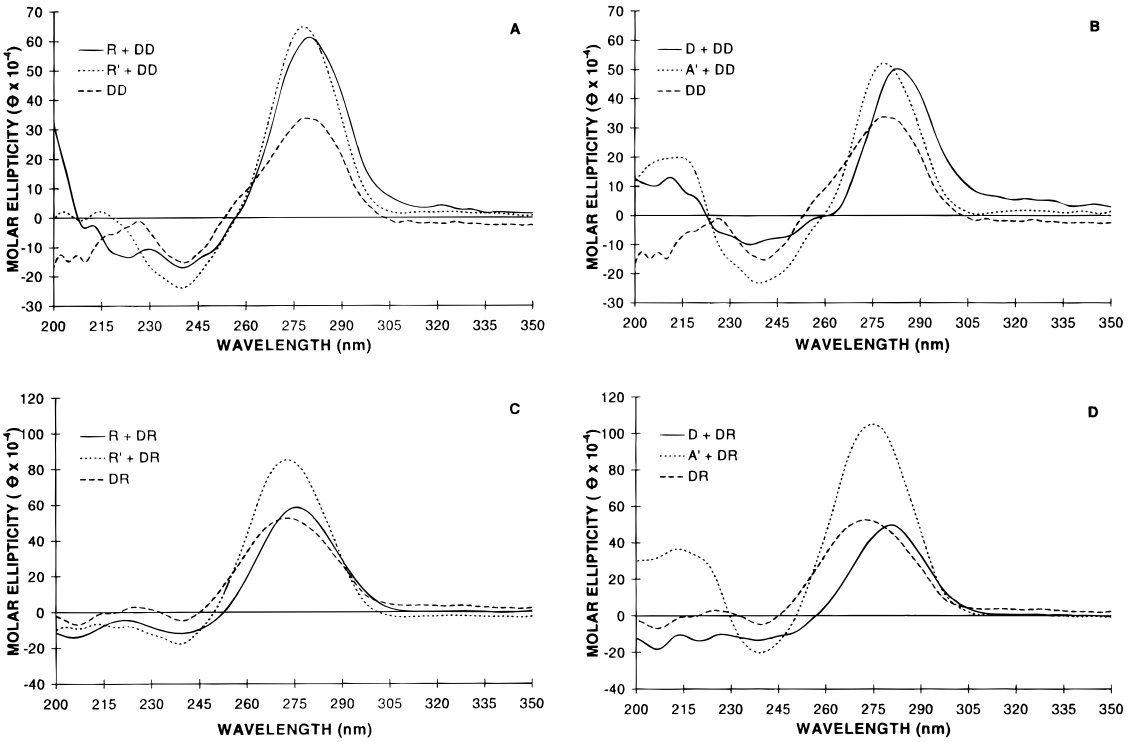


Figure 5. (A−D) Circular dichroism (CD) of hairpin duplexes and triple-helical complexes. The concentration is 2 μM in each strand, and the buffer is 100 mM sodium acetate and 1 mM EDTA (pH 5.5).

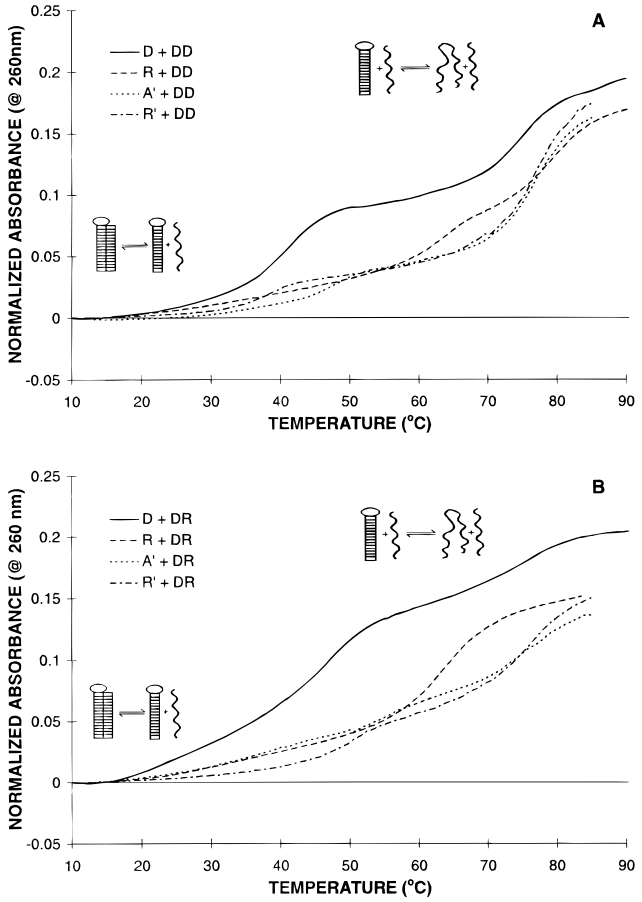


Figure 6. (A and B) Ultraviolet (UV) melting curves of complexes (2 μM) in 100 mM sodium acetate and 1 mM EDTA (pH 5.5). The cartoons indicate the transition from triplex to duplex plus third strand, and from the latter to completely dissociated complexes.

gel run under nondenaturing conditions (e.g., Figures 4B and 7B). This property is shared with the corresponding *D* (*10*), ANA (*16*), and 2′F-RNA strands, but not with RNA or 2′,5′-linked RNA (*28*) strands which appear as a single, well-defined band under the same conditions. The self-associating structures of *D* and other deoxycytidine-rich sequences have been described in detail (*10*, *29*), and are believed to be complexes in which the cytosines are base paired ($C{\cdot}C^+$).

SUMMARY

Our findings are consistent with the work of Escudé and co-workers, who proposed that interactions between the 2′-hydroxyl group of an RNA third strand and the phosphates of the polypurine strand play an important role in determining the relative stabilities of pyrimidine motif triple-helical complexes (*12*). In addition, they emphasize the role of the 2′-OH ribose as a general recognition and binding determinant of ribonucleic acids. An important observation made from this study was that 2′F-ANA shows considerable binding affinity for duplex DNA, relative to DNA and 2′F-RNA third strands. Since 2′F-ANA (*30*) and ANA (*31*) elicit RNaseH activity when bound to single-stranded RNA (*32*) and bind to duplex DNA (this work and ref *14*), our results are likely to stimulate experimental work on arabinose derivatives in laboratories concerned with targeting DNA and RNA sequences in vivo (antigene and antisense strategies).

ACKNOWLEDGMENT

This research was supported by a grant from the National Science and Engineering Council of Canada (NSERC-Strategic Program). We also gratefully acknowledge postgraduate scholarships from NSERC and FCAR to C.J.W. We also thank the referees for thoughtful criticism and suggestions, and A. Noronha for assistance in experiments and in preparing the manuscript. The

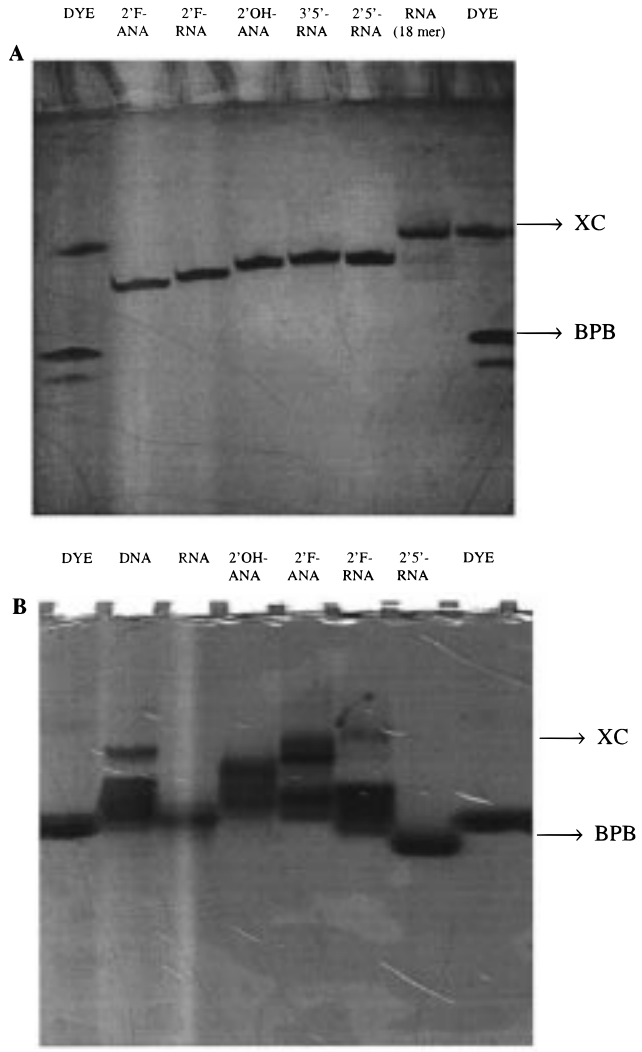


Figure 7. Polyacrylamide (20%) gel electrophoresis of single strands under (A) denaturing (7 M urea) and (B) nondenaturing conditions at 5 °C and pH 5.0. The dye lanes contain xylene cyanol (XC) and bromophenol blue (BPB). Bands are visualized using UV shadowing under nondenaturing conditions and stained with the reagent Stains-All (Sigma) for native conditions.

2′F-rT monomer was generously provided by Dr. Y. Sanghvi (Isis Pharmaceuticals).

LITERATURE CITED

(1) Saënger, W. (1984) *Principles of Nucleic Acids Structure*, Springer-Verlag, New York.

(2) Watson, J. D., and Crick, F. H. C. (1953) A structure for deoxyribose nucleic acid. *Nature 171*, 737−738.

(3) Urdea, M., Horn, T., Fultz, T., Anderson, M., Runnings, J., Hamren, S., Ahle, D., and Chang, C.-A. (1991) Branched DNA amplification multimers for the sensitive, direct detection of human hepatitis viruses. *Nucleic Acids Res. Symp. Ser. 24*, 197−200.

(4) Uhlmann, E., and Peyman, A. (1990) Antisense oligonucleotides: a new therapeutic principle. *Chem. Rev. 90*, 543−584.

(5) Moser, H. E., and Dervan, P. B. (1987) Sequence-specific cleavage of double helical DNA by triple helix formation. *Science 238*, 645−650.

(6) Le Doan, T., Perrouault, L., Praseuth, D., Habhoub, N., Decout, J.-L., Thuong, N. T., Lhomme, J., and Hélène C. (1987) Sequence-specific recognition, photocrosslinking and cleavage of the DNA double helix by an oligo-[α]-thymidylate covalently linked to an azidoproflavine derivative. *Nucleic Acids Res. 15*, 7749−7760.

(7) Thuong, N. T., and Hélène, C. (1993) Sequence-specific recognition and modification of double-helical DNA by oligonucleotides. *Angew. Chem. 32*, 666−690.

(8) Cooney, M., Czernuszewicz, G., Postel, E. H., Flint, S. J., and Hogan, M. E. (1988) Site-specific oligonucleotide binding represses transcription of the human c-myc gene in vitro. *Science 241*, 456−459.

(9) Beal, P. A., and Dervan, P. B. (1991) Second structural motif for recognition of DNA by oligonucleotide-directed triple-helix formation. *Science 251*, 1360−1363.

(10) Roberts, R. W., and Crothers, D. M. (1992) Stability and properties of double and triple helices: dramatic effects of RNA or DNA backbone composition. *Science 258*, 1463−1466.

(11) Han, H., and Dervan, P. B. (1993) Sequence-specific recognition of double-helical RNA and RNA·DNA by triple helix formation. *Proc. Natl. Acad. Sci. U.S.A. 90*, 3806−3810.

(12) Escudé, C., Francois, J.-C., Sun, J., Gunther, O., Sprinzl, M., Garestier, T., and Hélène, C. (1993) Stability of triple helices containing RNA and DNA strands: experimental and molecular modeling studies. *Nucleic Acids Res. 21*, 5547−5553.

(13) Semerad, C. L., and Maher, L. J. (1994) Exclusion of RNA strands from a purine motif triple helix. *Nucleic Acids Res. 22*, 5321−5325.

(14) Noronha, A., and Damha, M. J. (1998) Triple helicies containing arabinonucleotides in the third (Hoogsteen) strand: effects of inverted stereochemistry at the 2′ position of the sugar moiety. *Nucleic Acids Res. 26*, 2665−2671.

(15) Dagneaux, C., Liquier, J., and Taillandier, E. (1995) FTIR study of a nonclassical dT10*dA10-dT10 intramolecular triple helix. *Biochemistry 34*, 14815−14818.

(16) Taillandier, E., and Liquier, J. (1992) Infrared spectroscopy of DNA. In *Methods in Enzymology* (J. E. Dahlberg and D. M. J. Lilley, Eds.) Vol. 211, pp 307−335, Academic Press, Orlando, FL.

(17) Srinivasan, A. R., and Olson, W. K. (1998) Molecular models of nucleic acid triple helices I: DNA and RNA backbone complexes. *J. Am. Chem. Soc. 120*, 484−491.

(18) Cuenoud, B., Casset, F., Hüsken, D., Natt, F., Wolf, R. M., Altmann, K.-H., Martin, P., and Moser, H. E. (1998) Dual recognition of double-stranded DNA by 2′-aminoethoxy-modified oligonucleotides. *Angew. Chem., Int. Ed. 37*, 1288−1291.

(19) Ikeda, H., Fernandez, R., Wilk, A., Barchi, J. J., Huang, X. L., and Marquez, V. E. (1998) The effect of two antipodal fluorine induced sugar puckers on the conformation and stability of the Dickerson-Drew dodecamer duplex d[CGC-GAATTCGCG]$_2$. *Nucleic Acids Res. 26*, 2237−2244.

(20) Puglisi, J. D., and Tinoco, I., Jr. (1989) Absorbance melting curves of RNA. In *Methods in Enzymology* (J. E. Dahlberg and J. N. Abelson, Eds.) Vol. 180, pp 304−325, Academic Press, Orlando, FL.

(21) Tann, C. H., Brodfuehrer, P. R., Brundidge, S. P., Sapino, C., Jr., and Howell., H. G. (1985) Fluorocarbohydrates in synthesis. An efficient synthesis of 1-(2-deoxy-2-fluoro-β-D-arabinofuranosyl)-5-iodouracil (β-FIAU) and 1-(2-deoxy-2-fluoro-β-D-arabinofuranosyl) thymine (β-FMAU). *J. Org. Chem. 50*, 3644−3647.

(22) Howell, H. G., Brodfuehrer, P. R., Brundidge, S. P., Benigni, D. A., and Sapino, C., Jr. (1988) Antiviral nucleosides. A stereospecific, total synthesis of 2′-fluoro-2′-deoxy-β-D-arabinofuranosyl nucleosides. *J. Org. Chem. 53*, 85−88.

(23) Damha, M. J., and Ogilvie, K. K. (1993) Oligoribonucleotide Synthesis. In *Protocols for Oligonucleotides and Analogues: Synthesis and Properties, Methods in Molecular Biology* (S. Agrawal, Ed.) pp 84−114, Humana Press, Totowa, NJ.

(24) Kawasaki, A. M., Casper, M. D., Freier, S. M., Lesnik, E. A., Zounes, M. C., Cummins, L. L., Gonzalez, C., and Cook, P. D. (1993) Uniformly modified 2′-deoxy-2′-fluoro phosphoramidite oligonucleotides as nuclease-resistant antisense compounds with high affinity and specificity for RNA targets. *J. Med. Chem. 36*, 831−841.

(25) Kibler-Herzog, L., Kell, B., Zon, G., Shinozuka, K., Mizan, S., and Wilson, W. D. (1990) Sequence dependent effects in methylphosphonate deoxyribonucleotide double and triple helical complexes. *Nucleic Acids Res. 18*, 3545−3555.

(26) Sanghvi, Y. S., and Cook, D. P. (1994) Carbohydrates: synthetic methods and applications in antisense therapeutics an overview. In *Carbohydrate Modifications in Antisense Research* (Y. S. Sanghvi and D. P. Cook, Eds.) ACS Symposium Series 580, pp 1−22, American Chemical Society, Washington, DC.

(27) Escudé, C., Sun, J. S., Garestier, T., Rougée, M., and Hélène, C. (1992) Stable triple helices are formed upon binding of RNA oligonucleotides and their 2′-O-methyl derivatives to double helical DNA. *C. R. Acad. Sci., Ser. III 315*, 521−525.

(28) Damha, M. J., and Noronha, A. (1998) Recognition of nucleic acid double helices by homopyrimidine 2′,5′-linked RNA. *Nucleic Acids Res. 26*, 5152−5156.

(29) Singh, S., Patel, P. K., and Hosur, R. V. (1997) Structural polymorphism and dynamism in the DNA segment GATCTTCCCCCCGGAA: NMR investigations of hairpin, dumbbell, nicked duplex, parallel strands, and i-motif. *Biochemistry 36*, 13214−13222.

(30) Kois, P., Tocik, Z., Spassova, M., Ren, W.-Y., Rosenberg, I., Soler, J. F., and Watanabe, K. A. (1993) Synthesis and some properties of modified oligonucleotides. 2. Oligonucleotides containing 2′-deoxy-2′-fluoro-β-D-arabinofuranosyl pyrimidine nucleosides. *Nucleosides Nucleotides 12*, 1093−1109.

(31) Giannaris, P. A., and Damha, M. J. (1994) Hybridization properties of oligoarabinonucleotides. *Can. J. Chem. 72*, 909−918.

(32) Damha, M. J., Wilds, C. J., Noronha, A., Brukner, I., Borkow, G., Arion, D., and Parniak, M. A. (1998) Hybrids of RNA and arabinonucleic acids (ANA and 2′F-ANA) are substrates of ribonuclease H. *J. Am. Chem. Soc. 120*, 12976−12977.

BC9801171

TECHNICAL NOTES

Quantitative Analysis of Derivatized Proteins Prepared with Pyridyl Disulfide-Containing Cross-Linkers by High-Performance Liquid Chromatography

Dong Hee Na, Byung Ho Woo, and Kang Choon Lee*

Drug Targeting Laboratory, College of Pharmacy, SungKyunKwan University, 300 Chonchon-dong, Jangan-ku, Suwon City 440-746, Korea. Received March 11, 1998; Revised Manuscript Received November 30, 1998

Determination of the introduced moieties into derivatized proteins is an essential step in the preparation and quality control of chemically defined immunoconjugates. For the derivatized proteins using pyridyl disulfide-containing cross-linkers such as *N*-succinimidyl 3-(2-pyridyldithio)propionate (SPDP) and 4-succinimidyloxycarbonyl-α-methyl-α-(2-pyridyldithio)toluene (SMPT), the derivatization degree (ratio of pyridyl disulfide moieties to protein) has been traditionally determined by measuring the absorbance of both the derivatized protein and 2-thiopyridone (2-TP) released from the dithiothreitol (DTT) treatment (spectrophotometric method). This method, however, causes several problems including false high and low determinations of the protein and 2-TP, respectively, low selectivity, poor reproducibility, and relatively large amounts of sample consumption. A quantitative determination method of the derivatization ratios using bovine serum albumin derivatized with SPDP and SMPT as the model system has been developed. The concentration of protein and 2-TP released from the DTT treatment of derivatized proteins was determined directly without consideration of different reagents used and their concentrations. The present HPLC method was proved to be better in terms of accuracy, selectivity, and reproducibility with micro sample consumption. Moreover, this HPLC method can be directly applied to all derivatized proteins prepared with pyridyl disulfide-containing cross-linkers.

INTRODUCTION

The majority of immunoconjugates including immunotoxins consisting of monoclonal antibody and toxin have been synthesized according to chemical methods with cleavable heterobifunctional cross-linkers (*1*−*4*). A major concern in immunoconjugate research is the synthesis and testing of the heterogeneous mixture without proper separation and characterization of the chemically defined immunoconjugates. Recently, there is increasing interest among pharmaceutical scientists in developing specific and reproducible chemical methods in the preparation of immunotoxins and appropriate controls and validatable assays (*5*). Determination of the introduced moieties into the protein derivatized with cross-linkers is therefore an essential step in the preparation and quality control of chemically defined immunoconjugates (*6*−*7*).

The derivatization degree (ratio of pyridyl disulfide moieties to protein) of the derivatized proteins prepared with pyridyl disulfide-containing cross-linkers (*8*−*20*) has been traditionally determined by using the spectrophotometric method (SP method), which measures the absorbances of both protein derivatized and 2-thiopyridone (2-TP) released from the derivatized protein by reaction with dithiothreitol (DTT) at 280 and 343 nm, respectively (*8*). This method, although simple, raises several concerns including false high or low determination of the protein and 2-TP concentration, respectively, low selectivity, and poor reproducibility due to the spectral interference of the introduced moieties (*9*, *10*). In addition, it requires a large amount of sample consumption. Furthermore, this method has not been modified appropriately for all of the derivatized proteins prepared from different cross-linkers. Pyridyl disulfide moieties of the derivatized protein from different cross-linkers, for example, (2-pyridyldithio)-propionate (PP) from *N*-succinimidyl 3-(2-pyridyldithio)-propionate (SPDP) and α-methyl-α-(2-pyridyldithio)-toluene (MPT) from 4-succinimidyloxycarbonyl-α-methyl-α-(2-pyridyldithio)toluene (SMPT), have their own absorbance at 280 nm (A_{280}) in addition to protein. Therefore, these moieties may exert different effects on the A_{280} in protein assay (*8*, *9*).

In this study, we developed a quantitative determination method of the derivatization ratios of protein modified with pyridyl disulfide-containing heterobifunctional cross-linkers by measuring the protein and 2-TP using size exclusion and C-18 reversed phase HPLC, respectively. This new HPLC method was compared with the SP method using bovine serum albumin (BSA) derivatized with SPDP and SMPT as the model system.

MATERIALS AND METHODS

Materials. BSA (fraction V) and DTT were obtained from Sigma (St. Louis, MO). BSA was further purified by using a Sephadex G-100 column, and the purified fraction (MW 66000) was used. SPDP and SMPT were purchased from Pierce (Rockford, IL). 2-Thiopyridone (2-

* Author to whom correspondence should be addressed (fax 82-331-290-7724; e-mail kclee@yurim.skku.ac.kr).

10.1021/bc980029g CCC: $18.00 © 1999 American Chemical Society
Published on Web 02/17/1999

mercaptopyridine) was obtained from Aldrich (Milwaukee, WI), and HPLC grade methanol was purchased from J. T. Baker (Phillipsburg, NJ). All other materials were of reagent grade.

BSA Conjugation with SPDP and SMPT. Each of 0−16 molar excess of SPDP or SMPT solutions (20 mM in dimethyl sulfoxide) was added to 1 mL of BSA (5×10^{-2} mM) in 10 mM phosphate buffer containing 0.15 M NaCl (PBS, pH 7.4). The reaction mixtures were incubated for 30 min at room temperature, and the excess of reagent was then removed by gel filtration on a Sephadex G-25 column (Sigma) equilibrated with PBS. Fractions with an absorbance >1.0 at 280 nm (~8 mL) were collected and used in the assay. The derivatization ratio was determined by measuring the concentration of both BSA and 2-TP released by DTT treatment of the derivatized BSA using both the SP and HPLC methods described below.

SP Method. This method was performed as described previously (*8*). In brief, BSA concentration was determined by measuring the A_{280} using a Spectronic 1201 UV−vis spectrophotometer (Milton Roy, Rochester, NY). The amount of pyridyl disulfide moiety (PP or MPT) in the derivatized BSA was determined by measuring the absorbance of 2-TP at 343 nm (A_{343}), which was released by adding 20 μL of 1 M DTT in deionized water to the derivatized BSA solution (980 μL) after 1 h of incubation at room temperature. The molar concentration of 2-TP was calculated using its molar extinction coeffcient $E_{343} = 8.08 \times 10^3\ M^{-1}\ cm^{-1}$ (*21*). In the determination of the molar concentration of BSA, an erroneously high BSA concentration due to pyridyl disulfide moieties was corrected by subtracting the A_{280} contribution of the pyridyl disulfide moieties (2-pyridyl disulfide structure) in the derivatized BSA from the total A_{280} using the equation

$$\text{pyridyl disulfide moieties/1 molecule of BSA} = A_{343} \times 40.3/(A_{280} \times 8.08 - A_{343} \times 5.10) \quad \text{(a)}$$

The molar extinction coefficient of BSA at 280 nm was measured as $E_{280} = 4.03 \times 10^4\ M^{-1}\ cm^{-1}$ using purified BSA described under Materials. E_{280} of pyridyl disulfide moiety (PP or MPT) in the derivatized BSA was adopted as used previously without correction as $E_{280} = 5.10 \times 10^3\ M^{-1}\ cm^{-1}$ (*8*, *9*, *11*, *19*, *21*).

HPLC Method. The concentration of BSA of the derivatized BSA was determined by a size exclusion HPLC using a BIOSEP SEC-S2000 column (300 × 7.8 mm, Phenomenex). PBS (pH 7.4) was used as a mobile phase, and the flow rate was 1 mL/min. Each 20 μL of standard and sample solutions was injected onto the HPLC, and the effluent was detected at 215 nm. The concentration of 2-TP released from the derivatized BSA solution by DTT treatment was determined by a reversed phase HPLC using a LiChrospher 100 RP-18 column (125 × 4.0 mm, 5 μm, Merck, Darmstadt, Germany) at 343 nm. The mobile phase was composed of distilled water with a linear gradient of 0−30% (v/v) methanol for 10 min. The flow rate of the mobile phase and the injection volume were 1 mL/min and 20 μL, respectively. A Gynkotek HPLC system with model 480 pumps, a model GINA50 autosampler, a model UVD340S photodiode array detector and Gynkosoft (Gynkotek, Munich, Germany) was adopted.

RESULTS AND DISCUSSION

The important point of the required and ideal characteristics of immunotoxin conjugates is that the cross-linking process must minimize the deactivation and polymerization of both the antibody and toxin. In general, the chemistry of bioconjugation gives rise to various structures, resulting in a heterogeneous population of products that are difficult to separate from each other (*5*, *22*, *23*). These products usually consist of a major component containing equimolar amounts of antibody and toxin and several other conjugates with two or more toxin molecules per molecule of antibody. This heterogeneity results from the introduction of varying numbers of derivatized moieties per molecule of antibody (*24*). Due to the nature of the chemical reaction between the *N*-succinimidyl or hydrazide groups of the cross-linkers and the primary amino or carbohydrate groups of the antibody, the populations of antibody molecules substituted with none, one, two, three, and more than three pyridyl disulfide groups are obtained and the microenvironment of the protein attached linker will most likely affect the conjugation of antibody with toxin. Thus, it is very important to reproducibly determine the extent of derivatization exactly.

To determine the derivatization degrees of modified proteins by cross-linkers, both protein and pyridyl disulfide moieties of derivatized proteins must be assayed precisely. Determination of protein by measuring A_{280} adopted in the SP method is not strictly quantitative and is fairly adequate for crude protein mixtures, because this assay is based on the strong absorbance of tyrosine, phenylalanine, and tryptophan residues. Different proteins may therefore have widely varying molar extinction coefficients, and the absorbance must be partially corrected for interfering substances in the range of 0.2−2 mg/mL (*25*). Because all of the pyridyl disulfide moieties of derivatized proteins have their own A_{280} values, an erroneously high protein concentration is obtained when calculation is done on the basis of absorbance at 280 nm.

For the SPDP-derivatized BSA, the additional A_{280} by the pyridyl disulfide moieties has been calculated using the molar extinction coefficients of the PP moiety in derivatized BSA at 280 nm ($E_{280} = 5.10 \times 10^3\ M^{-1}\ cm^{-1}$). This E_{280} value of the PP moiety in the derivatized protein is not a measured value but a calculated value from the absorbance of SPDP or 2,2′-dipyridyl disulfide (2-Py-S−S-Py) (*8*, *21*). This means that the SP method must be validated and confirmed by the experimental method. Also, the SP method has not been modified adequately for different derivatized proteins prepared from different cross-linkers. Different pyridyl disulfide moieties of the derivatized proteins are obtained depending upon the cross-linkers used, for example, (2-pyridyldithio)propionate (PP) from SPDP and α-methyl-α-(2-pyridyldithio)-toluene (MPT) from SMPT. Therefore, if the concentration of BSA of the SMPT-derivatized BSA is determined in the same manner as in SPDP derivatization, false high protein concentrations may result due to differences in the contribution of A_{280} between PP from SPDP and MPT from SMPT (*9*, *11*, *19*).

To assess the effect of the introduced moiety on the A_{280} value of derivatized BSA, the absorbance of each derivatized BSA prepared from different ratios of cross-linkers to BSA and fractionated by size exclusion HPLC was measured using the SP method. Higher ratios of the cross-linker to BSA resulted in higher A_{280} (data not shown). In the case of SMPT derivatization, the additional absorbance from pyridyl disulfide moieties introduced was higher than that of SPDP derivatization, resulting from the methyl toluene moiety in addition to the PP moiety. Therefore, specific equations for different

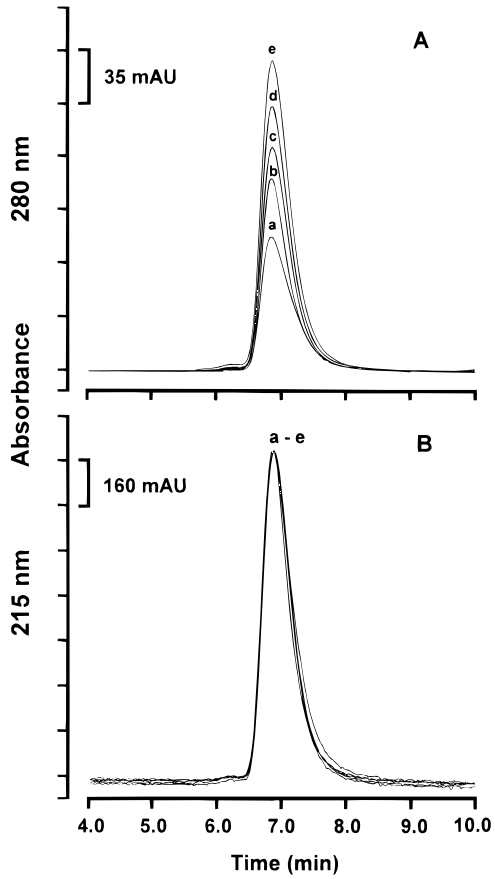


Figure 1. Size exclusion HPLC chromatograms of SPDP-derivatized BSA prepared from 0 to 8.7 molar excess of SPDP: (A) 280 nm detection; (B) 215 nm detection; (a) underivatized BSA; (b−e) SPDP-derivatized BSA (SPDP/BSA molar ratio: b, 1:1; c, 2.6:1; d, 5.0:1; e, 8.7:1).

derivatized proteins must be confirmed to determine the accurate derivatization ratios.

In the HPLC method, the detection wavelength was set at 215 nm, which was sensitive to the peptide bonds. To determine the effect of the pyridyl disulfide moiety on the detection wavelengths, the HPLC chromatograms obtained at both wavelengths of 215 and 280 nm were compared (Figure 1). In contrast to the increased absorbance as a result of increased concentration of cross-linkers at 280 nm, no additional absorbance of the introduced moieties into the derivatized protein was observed at 215 nm. This means that no correction is needed to measure the protein concentration regardless of the cross-linkers and reaction conditions used. Therefore, this HPLC method may be applied to all of the derivatized proteins prepared with pyridyl disulfide-containing cross-linkers. In addition, the detection sensitivity of protein at 215 nm was 13 times higher than that at 280 nm. From the HPLC method, the correlation coefficient of the detector linearity was found to be >0.999 over the concentration range 1.5−15.2 μM in 10 mM PBS (pH 7.4)

The introduced moieties, PP from SPDP and MPT from SMPT, have been routinely quantitated by measuring the difference in the absorbance before and after DTT treatment of derivatized proteins at 343 nm using the molar extinction coefficient $E_{343} = 8.08 \times 10^3\ M^{-1}\ cm^{-1}$ without separation of 2-TP from the reaction solution. However, it is laborious to obtain reproducible data because the value of A_{343} of 2-TP is variable depending upon the reaction conditions, for example, pH, reagents used and

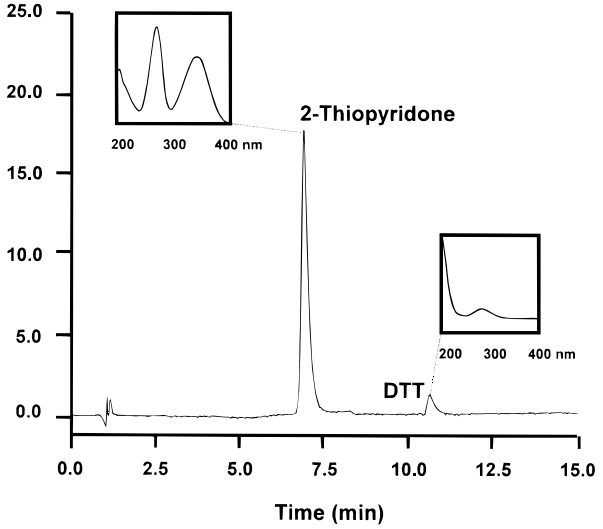


Figure 2. Reversed phase HPLC chromatogram of SPDP-derivatized BSA treated with DTT at 343 nm and the identification of the peak by photodiode array detection: (Insets) absorbance curves of 2-thiopyridone and DTT.

their concentrations, and proteins derivatized (*7*, *8*, *21*, *26*). Moreover, this method was found to be unreliable because the DTT treatment changes the absorbance at 280 nm, resulting in small baseline changes at 343 nm that are of an order of magnitude similar to those expected for the released 2-TP (*10*). In fact, the HPLC chromatogram of the reaction mixture shows the presence of the DTT peak detected at 343 nm (Figure 2), indicating that DTT used as a reducing agent might cause falsely high concentrations of 2-TP, especially for proteins with a low degree of derivatization and high concentrations of DTT under the SP method. As an alternative method, the measurement of sulfhydryl groups in the DTT-treated derivatized protein using Ellman's reagent has its own limitation, due to possible damage of endogenous disulfide bonds and unfavorable effects of the reaction conditions (*8*, *10*).

In the present HPLC method, the concentration of 2-TP released from the DTT treatment of SPDP- or SMPT-derivatized BSA was determined with photodiode array detection at 343 nm. 2-TP was well resolved as shown in Figure 2. The linearity was observed over the range of 2−80 μM in 10 mM PBS (pH 7.4), with the correlation coefficient being >0.999. Using this HPLC method, 2-TP released from other proteins prepared with various pyridyl disulfide-containing cross-linkers may be determined quantitatively without any interference from the reagents or reaction conditions used.

The derivatization ratios determined according to the SP and HPLC methods were compared (Table 1). The ratios of the SPDP-derivatized BSA were comparable between these two methods. However, there was a significant difference in the derivatization ratios for the SMPT-derivatized BSA. At low derivatization ratios <1, these differences were relatively small. However, the differences became significant at higher derivatization ratios. The derivatization ratios from the SP method were determined to be lower than those from the HPLC method. The reason for this might be due to the falsely high BSA concentration caused by a partial correction for the contribution of MPT moiety on the A_{280} by using the correction factor of PP instead of MPT. For both derivatized BSAs, the HPLC method showed better reproducibility than the SP method. In the HPLC method, intraday ($n = 5$) and interday ($n = 6$, data not shown)

Table 1. Comparison of the Derivatization Ratios of SPDP- and SMPT-Derivatized BSA Determined by Spectrophotometric and HPLC Methods (Intraday, $n = 5$)

	spectrophotometric method					
	conventional[a]		corrected[b]		HPLC method	
reaction ratio[c] (M/M)	deriv ratio obtained (M/M)	CV (%)	deriv ratio obtained (M/M)	CV (%)	deriv ratio obtained (M/M)	CV (%)
SPDP-Derivatized BSA						
1	0.48 ± 0.06	12.25			0.53 ± 0.02	4.38
2	1.08 ± 0.05	5.00			1.08 ± 0.03	3.04
4	2.62 ± 0.07	2.81			2.59 ± 0.03	1.04
8	5.09 ± 0.10	1.89			5.03 ± 0.06	1.25
16	9.14 ± 0.24	2.64			8.68 ± 0.08	1.01
SMPT-Derivatized BSA						
1	0.62 ± 0.03	4.82	0.66 ± 0.03	5.10	0.68 ± 0.01	1.75
2	1.13 ± 0.03	3.05	1.26 ± 0.04	3.39	1.42 ± 0.01	1.02
4	2.15 ± 0.05	2.27	2.65 ± 0.07	2.80	2.74 ± 0.01	0.46
8	3.31 ± 0.05	1.65	4.64 ± 0.11	2.32	4.45 ± 0.06	1.30
16	4.72 ± 0.09	1.90	7.98 ± 0.26	3.24	6.78 ± 0.12	1.77

[a] Ratio from the conventional E_{280} value of introduced moiety; $E_{280} = 5.1 \times 10^3$ M^{-1} cm^{-1}. [b] Ratio from the new E_{280} value of introduced moiety; $E_{280} = 8.6 \times 10^3$ M^{-1} cm^{-1}. [c] Reaction ratio = cross-linker/BSA.

coefficients of variation (CV) ranged from 1.01 to 4.38% in SPDP-derivatized BSA and from 0.46 to 1.77% in SMPT-derivatized BSA, respectively. In the SP method, intraday ($n = 5$) and interday ($n = 6$, data not shown) CVs ranged from 1.89 to 12.25% in SPDP-derivatized BSA and from 1.65 to 4.82% in SMPT-derivatized BSA, respectively.

These results indicate that the SP method, although simple, is not quantitative and may be suitable for the SPDP-derivatized protein. To apply the SP method to SMPT-derivatized protein, a new molar absorption coefficient of MPT moiety at 280 nm was calculated as $E_{280} = 8.6 \times 10^3$ M^{-1} cm^{-1} on the basis of the data obtained by using the HPLC method. Consequently, in SMPT-derivatized BSA, the derivatization ratio can be calculated by using the equation (Table 1):

$$\text{MPT moieties/1 molecule of BSA} = A_{343} \times 40.3/(A_{280} \times 8.08 - A_{343} \times 8.60) \quad \text{(b)}$$

Likewise, a specific equation may be constructed for any derivatized protein prepared by an individual pyridyl disulfide-containing heterobifunctional cross-linker.

In conclusion, we have developed a quantitative HPLC method to determine the derivatization ratios of the modified protein prepared by pyridyl disulfide-containing heterobifunctional cross-linkers. In contrast to the SP method, the concentration of the protein and 2-TP released from the DTT treatment of derivatized proteins can be assayed directly without interference from different reagents (proteins, cross-linkers, and DTT) and their concentrations. This HPLC method was proved to be better in terms of accuracy, selectivity, and reproducibility, requiring micro sample consumption. Therefore, this HPLC method may be directly applied to other derivatized proteins prepared with pyridyl disulfide-containing cross-linkers.

ACKNOWLEDGMENT

This work was supported by Korean Science and Engineering Foundation Grant 97-04-03-12-01-3.

LITERATURE CITED

(1) Jansen, F. K., Bourrie, B., Dussossoy, D., Gros, O., Vic, P., Vidal, H., and Gros, P. (1988) Toxin selection and modification: Utilization of the A chain of ricin. In *Immunotoxins* (A. E. Frankel, Ed.), pp 97−111, Kluwer Academic Publishers, Boston, MA.

(2) Wong, S. S. (1993) *Chemistry of Protein Conjugation and Cross-linking*, CRC Press, Boca Raton, FL.

(3) Hermanson, G. T. (1996) Immunotoxin conjugation techniques. *Bioconjugate Tech.*, pp 494−527, Academic Press, San Diego, CA.

(4) Thrush, G. R., Lark, L. R., Clinchy, B. C., and Vitetta, E. S. (1996) Immunotoxins: An update. *Annu. Rev. Immunol. 14*, 49−71.

(5) Byrn, S. R., and Stowell, J. G. (1995) Drug targeting using conjugates: The importance of pharmaceutical chemistry. *J. Drug Target. 3*, 239−421.

(6) Vogel, C.-W. (1988) Synthesis of antibody conjugates with cobra venom factor using heterobifunctional crosslinking reagents. In *Antibody-Mediated Delivery Systems* (J. D. Rodwell, Ed.), pp 191−224, Dekker, New York.

(7) Singh, V., and Curtiss, R., 3rd. (1994) Effect of amino group modification of ovine luteinizing hormone (oLH) by N-succinimidyl 6-[3-(2-pyridyldithio)propionate] hexanoate, a long chain N-succinimidyl-3-(2-pyridyldithio) propionate (SPDP) on immunological and biological properties: a comparative study with SPDP modified oLH. *Mol. Cell. Biochem. 130*, 83−90.

(8) Carlsson, J., Drevin, H., and Axen, R. (1978) Protein thiolation and reversible protein−protein conjugation. N-Succinimidyl 3-(2-pyridyldithio) propionate, a new heterobifunctional reagent. *Biochem. J. 173*, 723−737.

(9) Ghetie, V., Till, M. A., Ghetie, M.-A., Uhr, J. W., and Vitetta, E. S. (1990) Large scale preparation of an immunoconjugate constructed with human recombinant CD4 and deglycosylated ricin A chain. *J. Immunol. Methods 126*, 135−141.

(10) Ansell, S. M., Tardi, P. G., and Buchkowsky, S. S. (1996) 3-(2-Pyridyldithio)propionic acid hydrazide as a cross-linker in the formation of liposome-antibody conjugates. *Bioconjugate Chem. 7*, 490−496.

(11) Vallera, D. A., Burns, L. J., Frankel, A. E., Sicheneder, A. R., Gunther, R., Fajl-Peczalska, K., Pennell, C. A., and Kersey, J. H. (1996) Laboratory preparation of a deglycosylated ricin toxin A chain containing immunotoxin directed against a CD7 T lineage differentiation antigen for phase I human clinical studies involving T cell malignancies. *J. Immunol. Methods 197*, 69−83.

(12) Singh, V., Mavila, A. K., and Kar, S. K. (1993) Comparison of the cytotoxic effect of hormonotoxins prepared with the use of heterobifunctional cross-linking agents N-succinimidyl 3-(2-pyridyldithio) propionate and N-succinimidyl 6-[3-(2-pyridyldithio) propionamido]hexanoate. *Bioconjugate Chem. 4*, 473−482.

(13) Uckun, F. M., Myers, D. E., Irvin, J. D., Kuebelbeck, V. M., Finnegan, D., Chelstrom, L. M., and Houston, L. L. (1993) Effects of intermolecular toxin-monoclonal antibody linkage on the in vivo stability, immunogenicity and anti-leukemic activity of B43 (Anti-CD19) pokeweed antiviral protein immunotoxin. *Leukemia Lymphoma 9*, 459−476.

(14) Woo, B. H., Lee, J. T., and Lee, K. C. (1996) Effects of intermolecular linkage on stability and cytotoxicity of Fab-Ricin A immunotoxins. *Proc. Int. Symp. Controlled Release Bioact. Mater. 23*, 629−630.

(15) Matsunaga, T., Kawasaki, M., Yu, X., Tsujimura, N., and Nakamura, N. (1996) Chemiluminescence enzyme immunoassay using bacterial magnetic particles. *Anal. Chem. 68*, 3551−3554.

(16) Wawrzynczak, E. J., Zangemeister-Wittke, U., Waibel, R., Henry, R. V., Parnell, G. D., Cumber, A. J., Jones, M., and Stahel, R. A. (1992) Molecular and biological properties of an abrin A chain immunotoxin designed for therapy of human small cell lung cancer. *Br. J. Cancer 66*, 361−366.

(17) Thorpe, P. E., Wallace, P. M., Knowles, P. P., Relf, M. G., Brown, N. F., Watson, G. J., Knyba, R. E., Wawrzynczak, E. J., and Blakey, D. C. (1987) New coupling agents for the synthesis of immunotoxins containing a hindered disulfide bond with improved stability in vivo. *Cancer Res. 47*, 5924−5931.

(18) Engert, A., Diel, V., Schnel, R., Radszuhn, A., Hatwig, M. T., Drillich, S., Schon, G., Bohlen, H., Tesch, H., Hansmann, M. L., Barth, S., Schindler, J., Ghetie, V., Uhr, J., and Vitetta, E. (1997) A phase-I study of an anti-CD25 ricin A-chain immunotoxin (RFT5-SMPT-dgA) in patients with refractory Hodgkin's lymphoma. *Blood 89*, 403−410.

(19) Sanchez, E. F., Buah, L. R., Swenson, S., and Markland, F. S. (1997) Chimeric fibrolase: covalent attachment of an RGD-like peptide to create a potentially more effective thrombolytic agent. *Thromb. Res. 87*, 289−302.

(20) Zara, J., Pomato, N., McCabe, R. P., Bredehorst, R., and Vogel, C.-W. (1995) Cobra Venom Factor Immunoconjugates: Effect of carbohydrate-directed versus amino group-directed conjugation. *Bioconjugate Chem. 6*, 367−372.

(21) Stuchbury, T., Shipton, M., Norris, R., Malthouse, J. P. G., Brocklehurst, K., Herbert, J. A. L., and Suschitzky, H. (1975) A reporter group system with both absolute and selective specificity for thiol groups and an improved fluorescent probe containing the 7-nitrobenzo-2 oxa-1,3-diazole moiety. *Biochem. J. 151*, 417−432.

(22) Lappi, D. A., Matsunami, R., Martineau, D., and Baird, A. (1993) Reducing the heterogeneity of chemically conjugated targeted toxins: homogeneous basic FGF-saporin. *Anal. Biochem. 212*, 446−451.

(23) Woo, B. H., Lee, J. T., and Lee, K. C. (1994) Ricin A immunotoxins of IgG and Fab of anti-CALLA monoclonal antibody: Effect of water soluble long-chain SPDP on conjugate yield, immunoselectivity and cytotoxicity. *Arch. Pharm. Res. 17*, 452−457.

(24) Ghetie, V., Swindell, E., Uhr, J. W., and Vitetta, E. S. (1993) Purification and properties of immunotoxins containing one vs. two deglycosylated ricin A chains. *J. Immunol. Methods 166*, 117−122.

(25) Bollag, D. M., Rozycki, M. D., and Edelstein, S. J. (1996) *Protein Methods*, pp 57−81, Wiley-Liss, New York.

(26) Grassetti, D. R., and Murray, Jr., J. F. (1967) Determination of sulfhydryl groups with 2,2′- or 4,4′-dithiodipyridine. *Arch. Biochem. Biophys. 119*, 41−49.

BC980029G

Thiol-Reactive Luminescent Chelates of Terbium and Europium

Jiyan Chen and Paul R. Selvin*

Physics Department and Center for Biophysics, University of Illinois, Urbana, Illinois 61801.
Received September 17, 1998; Revised Manuscript Received November 18, 1998

Thiol-reactive lanthanide complexes have been synthesized that are luminescent when bound to terbium and/or europium. The complexes consist of a diethylenetriaminepentaacetate (DTPA) chelate covalently joined through one amide bond to a chromophore, carbostyril 124, and via a second amide bond to a maleimide, bromoacetamide, or pyridyldithio moiety. Site-specific attachment and characterization of the complexes attached to DNA-activating protein NtrC, to various sites on myosin, or to DNA are presented. The compounds coordinate a surprisingly large number of ligation sites of terbium when a hydrazide spacer is used between the chelate and thiol-reactive moiety, although this extra ligation can cause quenching when europium is used. Synthesis is a simple two- or three-step reaction, and purification is straightforward. The compounds should be useful as nonisotopic replacements, as long-lifetime probes in imaging, and as donors in luminescence resonance energy transfer. They are examples of a wide class of chelates that can be made conjugatable via readily available hetero- or homo-bifunctional linkers.

INTRODUCTION

Luminescent lanthanide chelates are of interest in time-resolved fluorescence assays (reviewed in refs *1* and *2*) as long-lifetime (millisecond) probes to increase contrast in fluorescence imaging when autofluorescence is a problem (*3*, *4*) and as donors in resonance energy transfer experiments (*5*−*12*). The chelate of diethylenetriaminepentaacetic acid covalently joined to a chromophore, 7-amino-4-methyl-2(1*H*)-quinolinone (also named carbostyril 124 or cs124), makes an excellent donor in energy transfer experiments (*7*, *8*, *10*) and can be conjugated to amine-containing macromolecules via either the anhydride or isothiocyanate forms (*13*). The conversion of one or even two DTPA[1] carboxyl groups to amides does not affect the coordination (*14*), and a sufficiently high binding constant is maintained for most purposes. Pyridyldithio forms of DTPA and triethylenetetraaminehexanoic acid, which are luminescent with europium, have been made previously by placing the reactive moiety on the chromophore (*15*). Other thiol-reactive chelates have also been developed (*16*).

Here we present the synthesis of maleimide, bromoacetamide, and pyridyldithio forms of DTPA−cs124 for reaction with thiols. We have recently used the maleimide form in energy transfer experiments on the muscle protein myosin (*17*). The synthesis is a simple two- or three-step reaction in which the dianhydride of DTPA is first reacted with the 7-amino of cs124 and then with a hetero-bifunctional compound containing an amino on one end and a thiol-reactive moiety on the other end. Alternatively, the second anhydride can be reacted with a diamino compound, which is then further reacted with an NHS−thiol reactive cross-linker. When the linker contains a hydrazide, under favorable conditions we find the carbonyl can ligate the lanthanide, resulting in a higher terbium quantum yield.

EXPERIMENTAL METHODS

Chemicals and Materials. The following were purchased from Aldrich: diethylenetriaminepentaacetic acid dianhydride (caDPTA); 7-amino-4-methyl-2(1*H*)-quinolinone (also named carbostyril 124 or cs124); anhydrous dimethyl sulfoxide, dimethylformamide, and hydrazine (Sure/Seal bottles); triethylamine (dried by activated molecular sieves before use); ethylenediamine (redistilled); C18-silica on glass-backed TLC plates (150 μm layer thickness); 3-maleimidopropionic acid *N*-hydroxylsuccinimide ester; acetonitrile (99.93%, HPLC grade). Glacial acetic acid and ammonium hydroxide were purchased from Fisher Scientific. *N*-Hyroxysuccinimidyl bromoacetate was purchased from Molecular Biosciences (Boulder, CO). Glutathione (reduced form) was purchased from Sigma. 3-(2-Pyridyldithiol)propionyl hydrazide (PDPH) was purchased from Pierce. ϵ-Maleimidocaproic acid hydrazide−HCl (EMCH) was from Bioaffinity Systems (Roscoe, IL). cDNA for the cys73 mutant of myosin regulatory light chain (RLC) was the generous gift of Dr. Susan Lowey. NtrC (mutant D54C) was the generous gift of Dr. Michael Nohaile. Distilled and deionized water (18 MΩ cm^{-1}) was used throughout. All glassware was washed with a mixed acid solution and thoroughly rinsed with deionized, distilled water (*18*). All plastic labware was purchased from Bio-Rad (metal-free). All chemicals were of the purest grade available.

Purification. Reverse-phase high-performance liquid chromatography was performed at room temperature on a Waters model 600 system with a Dynamax 60 Å C_{18} column (10 or 25 mm i.d. × 250 mm, Rainin, at 3 or 8

* Address correspondence to this author at the Loomis Laboratory of Physics, 1110 W. Green St., University of Illinois, Urbana, IL 61801 [e-mail selvin@uiuc.edu; telephone (217) 244-3371; fax (217) 244-7187].

[1]Abbreviations: DTPA, diethylenetriaminepentaacetic acid; caDTPA, dianhydride of DTPA; cs124 or carbostyril 124, 7-amino-4-methyl-2(1*H*)-quinolinone; DMSO, dimethyl sulfoxide; DMF, dimethylformamide; EDA, ethylenediamine; EMCH, ϵ-maleimidocaproic hydrazide; EMPH, ϵ-maleimidoproprionic hydrazide; PDPH, 3-(2-pyridyldithiol)propionic hydrazide; HMM, heavy meromyosin; RLC, regulatory light chain of myosin; NtrC, nitrogen regulatory protein C; RP-TLC, reverse-phase thin-layer chromatography.

10.1021/bc980113w CCC: $18.00 © 1999 American Chemical Society
Published on Web 02/05/1999

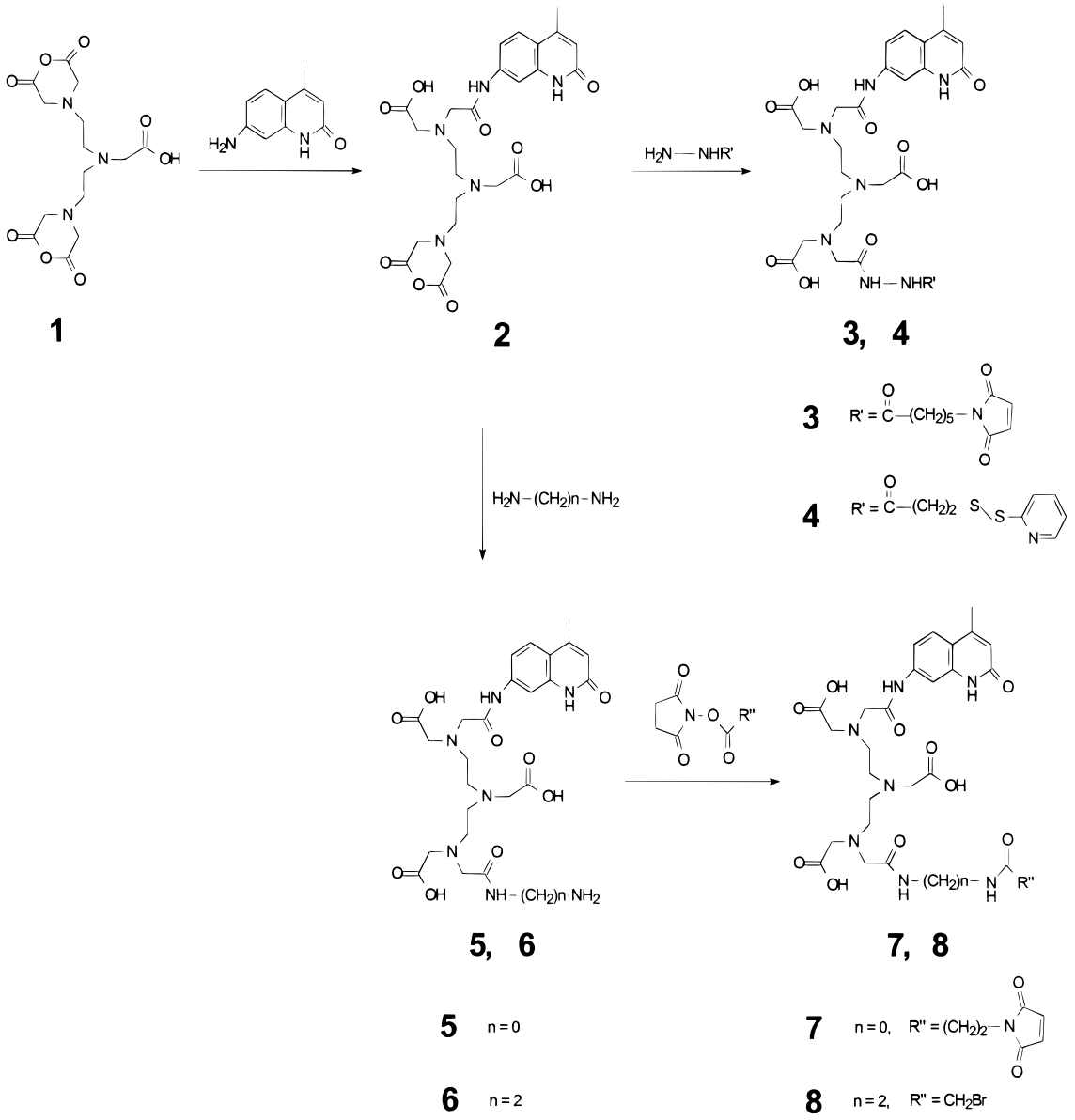


Figure 1. Synthetic reaction scheme for thiol-reactive DTPA−cs124 chelates.

mL/min, respectively) using a linear gradient (solvent A = 0.1 M triethylammonium acetate, pH 6.5; solvent B = acetonitrile). Fractions were vacuum-dried at room temperature, and the powder was stored at −80 °C.

Spectroscopy. Time-resolved and gated luminescence measurements were made on a laboratory-built spectrometer described previously (*8*, *10*), employing a 5 ns excitation pulse at 337 nm followed by time-resolved detection of lanthanide emission (*8*, *10*).

Synthesis (Figure 1). *DTPA−cs124−EMPH (**7**).* caDTPA (**1**) (50 mg, 141 μmol) was dissolved in 0.5 mL of anhydrous DMSO. Triethylamine (20 μL, 141 μmol) dried over molecular sieves was added to the caDTPA−DMSO solution. A solution of cs124 (19 mg, 109 μmol, 0.77 equiv in 0.5 mL of anhydrous DMSO) was added dropwise. The reaction was carried out at room temperature for 30 min, and then 10.7 μL of anhydrous hydrazine (282 μmol, 2 equiv) was added to above the reaction mixture. Fifteen minutes later, one-third of the solution was added to solid 3-maleimidopropionic acid *N*-hydroxysuccinimide ester (25 mg, 2 equiv) at room temperature and the reaction quenched after 30 min by adding 7 mL of aqueous triethylammonium acetate (TEAA) (0.1 M, pH 6.5). The remaining two-thirds of the solution was stored at −80 °C for future reaction. Alternatively, the intermediate product DTPA−cs124−hydrazide (**5**) was first purified by HPLC, redissolved in DMSO, and reacted with *N*-hydroxysuccinimide ester as above. This eliminated contaminating DTPA−$(cs124)_2$ in the final product (see directly below).

The reactions were monitored by C18 RP-TLC. When acetonitrile/TEAA (2:8, v/v) was used as RP-TLC developing system, the R_f values of DTPA−cs124, DTPA−cs124−hydrazine, and DTPA−cs124−hydrazine−maleimide were 0.67, 0.60, and 0.40, respectively. The final product was purified by HPLC using a 40-min linear gradient, from 10 to 20% solvent B. Three major peaks with 12.2, 17.6, and 20.2 min retention times were collected and characterized as DTPA−cs124, DTPA−$(cs124)_2$, and DTPA−cs124−hydrazine−maleimide (DTPA−cs124−EMPH), respectively. [HPLC purification of the intermediate product, DTPA−cs124−hydrazine, when done, eliminated the $(DTPA-cs124)_2$ peak from the final reaction.] FAB-MS (glycerol matrix) of the 20.2 min retention time peak shows mass (MH^+) of 715.2686 (found); 715.2687 (calculated). The product was dried on

a Speed-vac and stored either at −80 °C in solid form or in TEAA buffer at ∼30 mM DTPA−cs124−EMPH.

The thiol reactivity of the DTPA−cs124−EMPH was tested by adding an excess of solid glutathione (reduced form) with a solution of DTPA−cs124−EMPH in 0.1 M TEAA (pH 6.5) at room temperature for 1 h and then checked on RP-TLC and MS. The RP-TLC showed the DTPA−cs124−EMPH peak disappeared and a more rapidly moving peak appeared; high-resolution FAB-MS (glycerol as matrix) of the reaction mixture showed 1022.35; 1022.35 (calcd). These results indicate complete reaction of starting material into product.

*DTPA−cs124−EMCH (**3**).* To a solution of caDTPA (27.6 mg, 77 μmol) in 1 mL of DMSO was added dropwise cs124 (13.5 mg, 77 μmol) in 200 μL of DMSO, and the mixture was vortexed immediately. Two or four hours later, solid EMCH (27.6 mg,105 μmol) was added, and the mixture was vortexed until the EMCH had dissolved. The reaction proceeded overnight and was then frozen at −70 °C until purification. Immediately before HPLC purification, 9× volume of 0.5 M triethylammonium acetate, pH 6.5, was added to quench the reaction. The product was purified by reverse-phase HPLC using a 30 min linear gradient from 10 to 45% solvent B at 3 mL/min. The product was collected as a well-resolved peak at 22 min and immediately frozen and lyophilized to dryness. Yield was ∼25%, estimated by HPLC profile. FAB-MS: *m/e* 757 (glycerol matrix).

*DTPA−cs124−EDA−Bromoacetamide (**8**).* DTPA−cs124−ethylenediamine (**6**) (DTPA−cs124−EDA) was synthesized as reported previously (*13*). To a solution of DTPA−cs124−EDA (5.9 mg, 10 μmol, containing about an equal amount of DTPA−cs124) in 1 mL of TEAA (0.1 M, pH 8.5) was added *N*-hydroxysuccinimidyl bromoacetate (NHS-Br, 10 mg, 3 equiv). With vigorous stirring, the white solid of NHS-Br was dissolved gradually in the reaction solution over a few minutes at room temperature. The reaction was complete in 30 min. The R_f value of DTPA−cs124−EDA−bromoacetyl (DTPA−cs124−EDA−Br) was 0.45 [C18 RP-TLC in acetonitrile/TEAA (2:8, v/v)]. The newly formed compound showed full reactivity with glutathione (reduced form), monitored by RP-TLC. The final product was purified by HPLC (45-min linear gradient, from 10 to 25% solvent B at 8 mL/min), and the peaks at 18.8 and 25.2 min retention times were collected and characterized as DTPA−cs124 and DTPA−cs124−EDA−Br. High-resolution FAB-MS (glycerol as matrix) of the 25.2 min retention time peak shows 712.1942 (found); 712.1942 (calcd)

*PDPH−DTPA−cs124 (**4**).* Cs124 (10.5 mg, 60 μmol) was dissolved in 0.3 mL of dry DMSO and added dropwise to a 0.9 mL solution of caDTPA (21 mg, 61 μmol) in dry DMSO and allowed to react at room temperature for 45 min. Solid PDPH (10.7 mg, 47 μmol) was added to 1 mL of the above solution and allowed to react for >2.5 h at room temperature. Solid caDTPA (1.1 mg, 3 μmol) was occasionally added in an attempt to bind any residual free cs124 or PDPH. The reaction was quenched by addition of an equal volume of 400 mM sodium bicarbonate, pH 7.0. Purification was by HPLC (gradient: 0−14% solvent B from 4 to 14 min, 14−20% solvent B from 14 to 84 min, at 8 mL/min). The product at 51 min was dried on a Speed-vac, redissolved in water, passed through a C18 Sep-Pak (Waters), eluting with 50:50 acetonitrile/water and dried to give a white powder. The product was identified by FAB mass spectrometry, UV−vis, and lanthanide luminescence. Reaction with 2.4× glutathione (20 mM sodium bicarbonate, pH 7.0) resulted in increased absorbance in the 310−380 nm range due to release of the absorbing pyridyl group [$\epsilon_{343} = 8.1 \times 10^3\ M^{-1}\ cm^{-1}$ (*19*)], indicating nearly quantitative reaction with the PDPH moiety. FAB-MS, *m/e* 758.

Addition of Metal. $TbCl_3$ or $EuCl_3$ was added to the chelate in a 0.9:1 mole ratio at >0.1 mM concentration at pH 6−7, usually in 0.1 M TEAA, pH 6.5, buffer and allowed to bind on ice for ∼15 min. The complex was either stored at −80 °C or used immediately for reaction with biomolecules.

Coupling to Biomolecules. Coupling of Tb−DTPA−cs124−EMPH with the regulatory light chain of myosin, a 20 kDa calmodulin-like protein has been described (*17*), although we now routinely omit the reductant TCEP. We have also coupled it to a cysteine mutant of RLC (cys73) (*20*) at 25 μM protein with a 5-fold excess of chelate and to a single-cysteine mutant (D54C) of NtrC protein, a 20 kDa protein for which the atomic structure has been solved by NMR (*21*). Tb−(Eu−)DTPA−cs124−EDA−Br was coupled to heavy meromyosin (HMM), a 400 kDa fragment of myosin (∼14 μM protein), at a ratio varying from 2:1 to 10:1, and the reaction was carried out on ice overnight in 20 mM Mops, pH 7.0/5 mM $MgCl_2$. The excess lanthanide chelates were removed by passing the reaction mixture through a Sephadex G-25 size exclusion column. Tb−EMCH−DTPA−cs124 was reacted with a DNA (5′-$HSCH_2CH_2NHPO_3$−CCT-AGC-CAG-TGG), containing a free thiol at the 5′ end [introduced by coupling of cystamine via a slight modification of the method of Chu and Orgel (*22*)], and HPLC purified.

RESULTS AND DISCUSSION

Figure 1 shows the synthetic pathway for the various thiol-reactive chelates. HPLC, mass spectra, reaction with small or large thiol-containing molecules, and lanthanide luminescence all prove the chelates' structures and reactivities. The products were generated either in a two-step (one-pot) reaction, where DTPA dianhydride was first reacted with cs124 and then to an amine-thiol cross-linker (such as EMCH or PDPH), or via a three-step (one- or two-pot) procedure where a DTPA−cs124−diamine compound was generated and the free amine converted into a thiol-reactive entity via reaction with an NHS-thiol cross-linker. The former has greater simplicity but was not always possible. In particular, we made DTPA−cs124−EMPH both ways, but with the two-step reaction, HPLC retention of the DTPA−cs124−EMPH was similar to that of the byproduct DTPA−$(cs124)_2$, and more significantly, dramatically different yields were found, possibly due to variability in the purity of the starting EMPH material.

General Overview. The excited-state lifetime and emission spectra of Tb^{3+} and Eu^{3+} in the thiol-reactive chelates are shown in Table 1 and Figures 2 and 3. Figure 3 shows that both lanthanides have the usual sharply spiked emission spectrum. Table 1 and Figure 2 show that the lifetimes of both lanthanides are, as expected, in the millisecond range. The exact lifetimes depends on the lanthanide, chelate, and linker between maleimide and chelate and what they are attached to. For lanthanides, one of the main determinants of lifetime is the number of waters bound to the lanthanide (*23*). DTPA or DTPA−cs124 coordinates eight of nine possible sites, and the remaining site is filled by a water molecule, which reduces the excited-state lifetime through vibrational quenching. Surprisingly, for the chelate derivatives reported here, this last site can be filled by the carbonyl oxygen of the hydrazide (but not ethylenediamine) linker (see also Coordination Sites). For terbium, this is advan-

Table 1. Lifetimes of Thiol-Reactive Europium and Terbium Complexes in H_2O and D_2O, Their Ratio, and the Number of Coordinated Waters in the Lanthanide Primary Sphere[a]

lanthanide complexes[a]	τ_{H_2O} (ms)	τ_{D_2O} (ms)	τ_{H_2O}/τ_{D_2O}	no. of waters
Tb−(Eu−)DTPA−cs124[b]	1.55 (0.62)	2.63 (2.42)	0.59 (0.26)	1.1 (1.26)
Tb−(Eu−)DTPA−cs124−AH[c]	1.91 (Q)	2.31 (Q)	0.83	0.37
Tb−(Eu−)DTPA−cs124−EDA−bromoacetyl[d]	1.51 (0.60)	2.70 (2.37)	0.56 (0.28)	1.22 (1.32)
Tb−(Eu−)DTPA−cs124−EMPH[e]	1.51 (0.55)	2.53 (2.05)	0.60 (0.27)	1.13 (1.40)
Tb−DTPA−cs124−EMPH−R[f]	18% 0.46 82% 1.80			
Eu−DTPA−cs124−EMPH−R'[g]	0.62			
Tb−DTPA−cs124−EMCH−R[h]	1.60	2.1	0.76	0.6
Tb−(Eu−)DTPA−cs124−PDPH[i]	1.82 (1.32)	2.22 (2.32)		0.41 (0.34)

[a] The measurements for the free reactive chelates were taken in 20 mM MOPS/5 mM $MgCl_2$, pH 7.0, at room temperature. Numbers in parentheses are for Eu^{3+}; those not in parentheses are for Tb^{3+}. [b] Data from ref *24*. [c] DTPA−cs124−AH = DTPA−cs124−acetic hydrazide = $CH_3CONHNH_2$−DTPA−cs124. Synthesis followed the general protocol outlined in Figure 1: reaction of caDTPA with cs124 followed by addition of an excess of $CH_3CONHNH_2$ and HPLC purification. [d] Tb^{3+} lifetime decreases *slightly* when conjugated to proteins (see Figure 1). [e] Free chelate. Tb lifetimes are major component. There was a minor short-lifetime (<0.5 ms) component as well. [f] Conjugated to NtrC in buffer defined above (footnote *a*) such that there is <1 Tb chelate per protein. [g] Conjugated to glutothione. Lifetime indicates ligation of carbonyl hydrazide from linker is not occurring. Conjugated to DNA it is highly quenched due to extra ligation (data not shown). [h] Conjugated to single-stranded 12-mer DNA in 20 mM $MgCl_2$/50 mM NaCl/10 mM Tris, pH 8.0. [i] Unconjugated compound showed very large concentration-dependent quenching. To achieve the reported Tb lifetimes required titrations down to 5 nM. Tb lifetime was biexponential, with 75% of population corresponding to long-lifetime reported; shorter lifetime was ≈0.5 ms. Eu lifetimes could not be accurately determined at these concentrations. The results for Eu are reported in the presence of glutothione, which displaced the pyridyl group of PDPH, produced a large (>200-fold) increase in signal, and largely eliminated the concentration quenching.

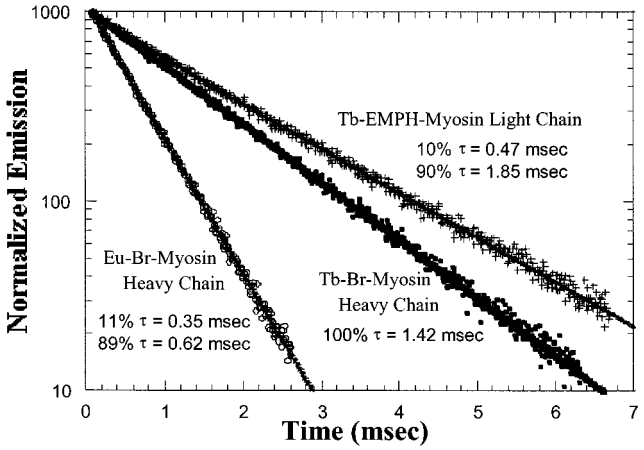


Figure 2. Lifetime of Tb^{3+} and Eu^{3+} bound to seven or eight attached to myosin fragments.

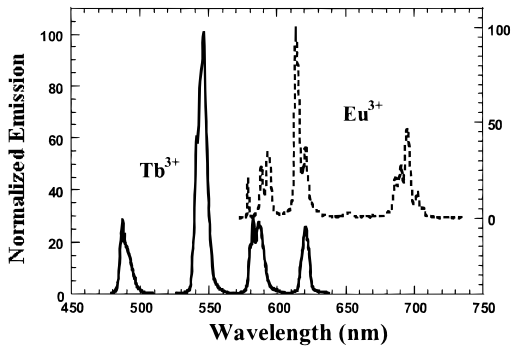


Figure 3. Normalized Tb and Eu emission spectra in DTPA−cs124−EDA−Br. Tb^{3+} and Eu^{3+} display their characteristic sharply spiked spectra. Free chelate dissolved in 20 mM Mops, pH 7.0/5 mM $MgCl_2$ at a concentration of 0.5 μM. Resolution is 0.3 nm, excitation was at 40 Hz of 3.4 μJ/pulse at 337 nm for Eu, 2.0 μJ/pulse for Tb; integration time is 1 s for Tb and 10 s for Eu. Note that signal is normalized. Tb emission is considerably brighter (roughly 20×) than Eu emission. Eu spectrum is displaced for clarity of presentation.

tageous. However, for europium, with one exception (PDPH bound to glutathione), this ligation causes very large quenching, presumably through vibrational deactivation. Single-exponential lifetimes (as opposed to biexponential) are also advantageous, and the bromoacetamide chelate produces this, whereas the maleimide can be either single exponential or biexponential, depending on the biomolecule attachment site and solvent conditions. In all cases, coupling to thiol-containing biomolecules could be monitored by comparing the absorbance of the cs124 when coupled to DTPA (12000 M^{-1} cm^{-1}) at 337 nm to that of the biomolecule (typically 260 nm for DNA, 280 nm for proteins). [The absorption spectra has been reported (*24*).] For DTPA−cs124−PDPH, coupling could also be monitored by the release of the pyridylthio group. Reaction with the RLC was also monitored by MALDI mass spectroscopy.

Specific Thiol-Reactive Forms. *Maleimide.* The maleimide form has the advantage of quick and efficient reaction with thiols. Tb−DTPA−cs124−EMPH was previously attached to the regulatory light chain of myosin and used successfully as a donor in resonance energy transfer experiments in myosin (*17*) (see Figure 2). To further characterize this reaction, we have now performed mass spectrometry (MALDI) on the chelate bound to a single-cysteine (cys73) mutant of RLC. Two peaks of molecular weight of 20002.9 and 19285.2 in approximately 4:1 ratio were found (data not shown). The former is labeled RLC, and the latter is unlabeled RLC. Note that the difference in mass is 717.7, in excellent agreement with the mass of EMPH−DTPA−cs124. The mass spectrometery data also show that labeling is efficient (∼80% yield based on relative peak heights) and, as expected for a maleimide, is likely highly specific for thiols as only one chelate per protein is bound. Previous energy transfer measurements using this chelate-labeled protein further indicate that the label is bound specifically to cysteine-108 (*17*). The excited-state lifetime of Tb in this reaction was biexponential, with a minor, short-lifetime component and with a major long-lifetime component of ∼1.8 ms at room temperature (2.0 ms at 4 °C) (Table 1 and Figure 2). The brightness of the terbium−maleimide when bound to RLC was equivalent to or slightly brighter than that of free Tb−DTPA−cs124 (the unreactive, no linker parent compound), which we have previously shown to have a 2 pM detection limit.

In addition, the EMPH or EMCH chelate was reacted with thiolated DNA, with NtrC, and with the heavy chain of myosin at cysteine-707. When attached to the 5′ end of thiolated DNA, Tb−DTPA−cs124−EMPH went from biexponential to single exponential at higher salt. With

NtrC it was also biexponential, although in both cases the short-lifetime component was a minority (10−20%). Finally, because the maleimide forms were made using a hydrazide linker, the number of waters bound to the terbium was decreased in most cases (discussed further below), which results in longer lifetime (>1.8 versus 1.5 ms without hydrazide; Table 1), higher quantum yield, and brighter emission compared to those without the extra ligation. Europium in the EMPH linker was highly quenched under conditions where extra ligation was present, such as bound to the 5′ end of thiolated DNA, but displayed its usual 0.6 ms unquenched lifetime in H_2O-based buffer when extra ligation did not occur (see Table 1, footnote *g*).

Bromoacetamide. The bromoacetamide form has the distinct advantage of being single exponential with terbium and either single exponential with europium or at worst having a minor (10%) quenched component (Figure 2). The terbium brightness in the unconjugated bromoacetamide chelate (**8**) was equivalent to the unreactive form (Tb−DTPA−cs124 with no linkers). We found, however, the reactivity of bromoacetamide chelates to be significantly less than that of maleimides. It was sufficiently reactive with cysteine-707 on myosin, a site that is known to be highly reactive, but was not sufficiently reactive for labeling the regulatory light chain of myosin.

PDPH. The PDHP−DTPA−cs124 reacts rapidly with thiols to form a reducible disulfide bridge, with the release of pyridylthio. Because the PDPH chelate contains a hydrazide linker, it displays the long lifetime with terbium. Interestingly, this probe appears to be a useful reagent for the detection of glutathione or possibly other small thiol peptides, as it is highly quenched in the absence of glutathione and has a 200-fold intensity increase in its presence.

Coordination State. The number of waters bound to the primary ligation sphere can be calculated by comparing the lifetimes in H_2O and D_2O and using the equation of Horrocks and Sudnik (*23*). The results are shown in Table 1. Recently, Parker et al. have shown that ligated amide N−H bonds can deactivate the excited state of Eu^{3+} with an efficiency equivalent to approximately one-sixth that of a ligated OH bond, so the number of water molecules reported in Table 1 is likely overstated by about this amount (*25*). By comparing the free DTPA−cs124 to DTPA−cs124−acetic hydrazide it can be seen that the number of water molecules decreases for terbium, which we interpret as being due to the ligation of the amide−carbonyl in the hydrazide linkage. This ligation is advantageous, as mentioned above, in that it increases the terbium quantum yield and also results in 1.8-fold higher intensity. The ligation is fairly weak (order of kT) as it is temperature dependent, with lifetime increasing from 1.85 ms at room temperature to ∼2.0 ms at 4 °C for the EMPH derivative. For the DTPA−cs124−EMCH chelate this ligation is even weaker. This weak ligation is not surprising given that it arises from a seven-membered ring formation. Slight changes, such as using an ethylenediamine instead of hydrazine or using DTPA−cs124−triglyceride (*24*) eliminates this extra ligation. Similar subtle changes exist depending on what is bound to at the end of the hydrazine linkage. For example, unconjugated DTPA−cs124 hydrazine−maleimide compounds do not display this extra ligation, whereas we have found that when conjugated to certain proteins, the extra ligation occurs. Surprisingly, this hydrazide ligation tends to efficiently quench the europium excited state, with the exception of Eu bound to DTPA−cs124−PDPH coupled to glutathione (Table 1).

In summary, we have made a number of different thiol-reactive forms of the luminescent lanthanide chelate DTPA−cs124. The maleimide form (**7**) appears to be the most versatile with terbium as it is highly reactive, specific, and bright. A drawback is its biexponential excited-state lifetime when conjugated to some biomolecules. The bromoacetamide derivative overcomes this drawback when it is sufficiently reactive. Overall, the synthetic route is simple and amenable to modification such that a wide variety of different linker lengths can be readily made. These have already been shown to be useful donors in resonance energy transfer experiments in which specific reaction with protein thiols is required.

ACKNOWLEDGMENT

This work was supported initially by NIH Grant AR44420 and later by Amersham Inc. We thank Dr. Michael Nohaile for the gift of NtrC protein and Dr. Susan Lowey for the gift of cDNA for mutant RLCs. We also thank Dr. Ming Xiao for assistance in RLC labeling and Dr. Handong Li for assistance with mass spectroscopy.

LITERATURE CITED

(1) Soini, E., and Lovgren, T. (1987) *CRC Crit. Rev. Anal. Chem. 18*, 104−154.
(2) Sammes, P. G., and Yahioglu, G. (1996) *Nat. Prod. Rep. 13*, 1−28.
(3) Seveus, L., et al. (1994) *Microsc. Res. Tech. 28*, 149−154.
(4) Marriott, G., Heidecker, M., Diamandis, E. P., and Yan-Marriott, Y. (1994) *Biophys. J. 67*, 957−965.
(5) Stryer, L., Thomas, D. D., and Meares, C. F. (1982) in *Annual Review of Biophysical Bioengineering* (L. J. Mullins, Ed.), pp 203−222, Annual Reviews, Inc.: Palo Alto, CA.
(6) Mathis, G. (1993) *Clin. Chem. 39*, 1953−1959.
(7) Selvin, P. R., Rana, T. M., and Hearst, J. E. (1994) *J. Am. Chem. Soc. 116*, 6029−6030.
(8) Selvin, P. R., and Hearst, J. E. (1994) *Proc. Natl. Acad. Sci. U.S.A. 91*, 10024−10028.
(9) Mathis, G. (1995) *Clin. Chem. 41*, 1391−1397.
(10) Selvin, P. R. (1996) *IEEE J. Sel. Top. Quantum Electron.: Lasers Biol. 2*, 1077−1087.
(11) Root, D. D. (1997) *Proc. Natl. Acad. Sci. U.S.A. 94*, 5685−5690.
(12) Heyduk, E., Heyduk, T., Claus, P., and Wisniewski, J. R. (1997) *J. Biol. Chem. 272*, 19763−19770.
(13) Li, M., and Selvin, P. R. (1997) *Bioconjugate Chem. 8*, 127−132.
(14) Selvin, P. R., Jancarik, J., Li, M., and Hung, L.-W. (1996) *Inorg. Chem. 35*, 700−705.
(15) Heyduk, E., and Heyduk, T. (1997) *Anal. Biochem. 248*, 216−227.
(16) Takalo, H., Mukkala, V.-M., Mikola, H., Liitti, P., and Hemmila, I. (1994) *Bioconjugate Chem. 5*, 278−282.
(17) Burmeister-Getz, E., Cooke, R., and Selvin, P. R. (1998) *Biophys. J. 75*, 2451−2458.
(18) Thiers, R. C. (1957) *Methods Biochem. Anal. 5*, 273−335.
(19) Pierce Catalog (1994).
(20) Wolff-Long, V., Tao, T., and Lowey, S. (1995) *J. Biol. Chem. 270*, 31111−31118.
(21) Nohaile, M., Kern, D., Wemmer, D., Stedman, K., and Kustu, S. (1997) *J. Mol. Biol. 273*, 299−316.
(22) Chu, B. C., and Orgel, L. E. (1988) *Nucleic Acids Res. 16*, 3671−3691.
(23) Horrocks, W. D., Jr., and Sudnick, D. R. (1979) *J. Am. Chem. Soc. 101*, 334−350.
(24) Li, M., and Selvin, P. R. (1995) *J. Am. Chem. Soc. 117*, 8132−8138.
(25) Dickins, R. S., Parker, D., Desousa, A. S., and Williams, J. A. G. (1996) *Chem. Commun. 6*, 697−698.

BC980113W

Total Solid-Phase Synthesis of 1,4,7,10-Tetraazacyclododecane-*N*,*N*′,*N*″,*N*‴-tetraacetic Acid-Functionalized Peptides for Radioimmunotherapy

James J. Peterson, Roger H. Pak, and Claude F. Meares*

Department of Chemistry, University of California, One Shields Avenue, Davis, California 95616-5295.
Received September 25, 1998; Revised Manuscript Received December 12, 1998

A convenient approach to the functionalization of peptides with the macrocyclic 1,4,7,10-tetraazacyclododecane-*N*,*N*′,*N*″,*N*‴-tetraacetic acid (DOTA) moiety has been developed. Protected components (using *tert*-butyl or *tert*-butyloxycarbonyl groups) of both the peptide and the chelate were assembled on the same solid resin support. Deprotection and cleavage of the resin-bound DOTA−peptides were performed in one step using a trifluoroacetic acid cleavage mixture to yield free DOTA−peptide amides.

INTRODUCTION

Bifunctional chelating agents derived from the macrocyclic 1,4,7,10-tetraazacyclododecane-*N*,*N*′,*N*″,*N*‴-tetraacetic acid (DOTA)[1] have been used for studies in vivo due to the extraordinary stability of its complexes with many useful metals under physiologic conditions (*1*−*4*). Introduction of peptide/protein conjugation functionality to DOTA can originate either from the ring methylene carbons (*4*−*6*) or, more simply, through one of the four carboxylates of the macrocycle (*3*, *6*, *10*).[2] For the latter strategy, activation of a carboxylate group with isobutyl chloroformate (*7*−*9*) allows conjugation to a peptide (*10*). The DOTA should be monofunctionalized to prevent cross-linking of peptides. One disadvantage of this method is the low solubility of DOTA (<20 mM) (*8*, *10*) in anhydrous organic solvents.[3] We were able to circumvent this difficulty by synthesizing DOTA stepwise on the peptide N-terminus, using solid-phase synthesis methodology (Scheme 1). The selectivity in the *alkylation* of polyazamacrocycles (*12*) and the high solubility (>4 M) of the macrocycle cyclen in an appropriate organic solvent were also important.

EXPERIMENTAL PROCEDURES

Reagents. Fmoc-protected amino acids and BOP reagent for manual synthesis were purchased from BACHEM California, Inc. Fmoc-protected amino acids in 1 mmol cartridges, HMP resin, and reagents for automated synthesis (using "FastMoc" chemistry) were purchased from ABI. Cyclen sulfate, anhydrous NMP, anhydrous DMF, bromoacetyl bromide, chloroacetyl chloride, *tert*-butyl-2-bromoacetate, redistilled DIEA, piperidine, acetic anhydride, NBP, and HOBt were purchased from Aldrich Chemical Co. PEGA Rink amide resin was purchased from Nova-Biochem. Polypropylene chromatography columns (fritted) used for solid-phase peptide synthesis were purchased from Bio-Rad (parts 731-0003 and 732-1010). TFA and TIPS were purchased from Acros Organics or Fisher Scientific. Ammonia gas was purchased from Matheson. All buffers and cleavage cocktails were made using pure water (18 MΩ cm^{-1} resistivity). The ninhydrin test kit was purchased from ABI.

High-Performance Liquid Chromatography. For analytical HPLC, a Dynamax 60 Å (8 μm, 4.6 mm × 250 mm) C_{18} reversed-phase column was used at a flow rate of 1 mL/min. For semipreparative HPLC, a Phenomenex Magellan 100 Å (5 μm, 10 mm × 250 mm) C_{18} reversed-phase column was used at a flow rate of 3 mL/min. HPLC buffers are as follows: buffer system A, 0.068 M NH_4OAc (pH 4.8) versus CH_3CN; and buffer system B, 0.1% TFA/H_2O versus 0.1% TFA/CH_3CN. Eluting samples were detected at 280 nm unless otherwise indicated. For gradient 1, hold at 0% CH_3CN for 5 min and proceed to 50% by 35 min. For gradient 2, hold at 20% CH_3CN for 5 min and proceed to 50% by 23 min. For gradient 3, hold at 25% CH_3CN for 5 min and proceed to 50% by 25 min. For gradient 4, hold at 0% CH_3CN for 5 min, proceed to 50% in 10 min, and proceed to 70% in 15 min. Samples collected during HPLC were lyophilized at least twice on a Savant model SVC-100H Speed-Vac lyophilizer before analysis.

NMR Spectroscopy. ^1H NMR spectra were recorded on a General Electric QE 300 spectrometer at 300 MHz. Chemical shifts are reported relative to HDO (4.80 ppm) or $CHCl_3$ (7.26 ppm).

* To whom correspondence should be addressed: Department of Chemistry, University of California, One Shields Avenue, Davis, CA 95616-5295. Telephone: (530) 752-0936. Fax: (530) 752-8938. E-mail: cfmeares@ucdavis.edu.

[1]Abbreviations: ABI, Applied Biosystems, Inc.; BOP, (benzotriazolyloxy)tris(dimethylamino)phosphonium hexafluorophosphate; cyclen, 1,4,7,10-tetraazacyclododecane; DCM, dichloromethane; DIEA, diisopropylethylamine; DOTA, 1,4,7,10-tetraazacyclododecane-*N*,*N*′,*N*″,*N*‴-tetraacetic acid; ESI-MS, electrospray ionization mass spectrometry; Et_2O, diethyl ether; F*, (*S*)-*p*-nitrophenylalanine; Fmoc, fluoren-9-ylmethyloxycarbonyl; HMP, hydroxymethylphenoxy resin; HOBt, 1-hydroxybenzotriazole; NMP, 1-methyl-2-pyrrolidone; NBP, (nitrobenzyl)pyridine; NO_2Phe, (*S*)-*p*-nitrophenylalanine; PEG, polyethylene glycol; PEGA, bis(2-acrylamidoprop-1-yl) polyethylene glycol cross-linked dimethylacrylamide and mono(2-acrylamidoprop-1-yl)-(2-aminoprop-1-yl) polyethylene glycol (800); SPPS, solid-phase peptide synthesis; TIPS, triisopropylsilane.

[2]This is a very practical alternative, since the resulting loss of metal−chelate stability (*8*) has been found to be insignificant in serum (with ^{111}In or ^{90}Y), or when subjected to DTPA challenge (*3*).

[3]The purity and counterion form of DOTA must be carefully defined and reliable. For example, we purchased DOTA that was only 25% pure as determined with a ^{57}Co metal binding assay (*11*).

10.1021/bc980118t CCC: $18.00 © 1999 American Chemical Society
Published on Web 02/11/1999

Scheme 1. Solid-Phase Synthesis of DOTA−Peptides

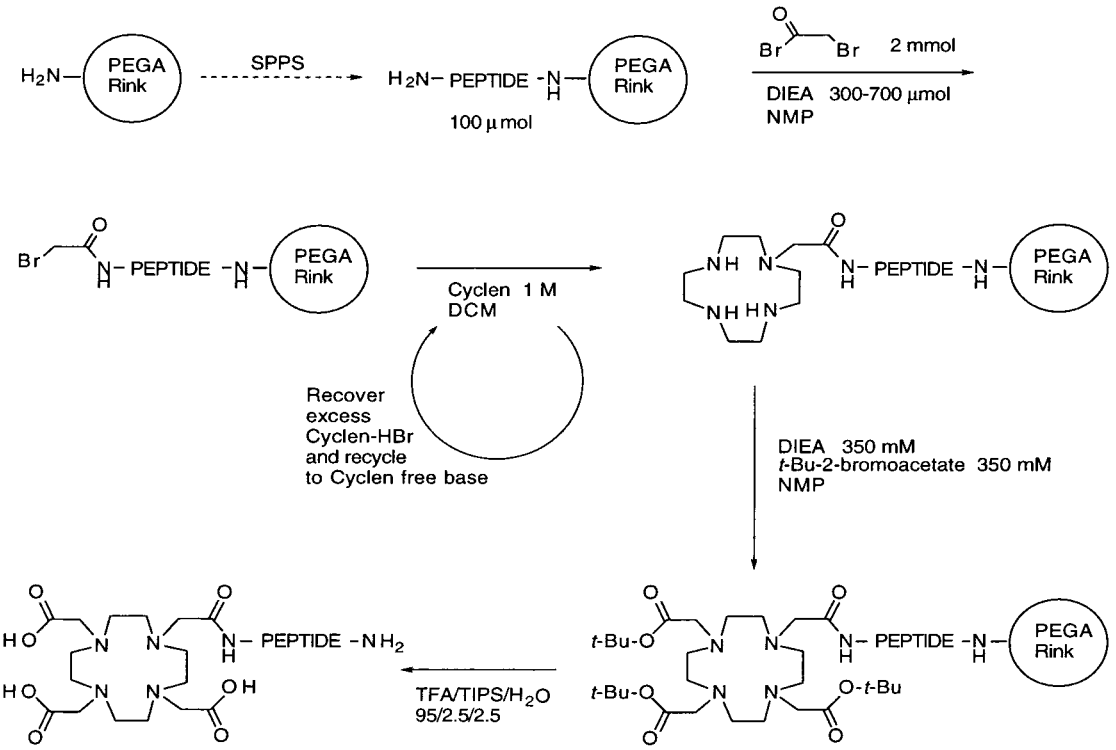


Table 1. Sequence, HPLC, and ESI-MS Data of DOTA−Peptide Amides

compd/sequence	purity of crude product by HPLC (%)[a]	HPLC retention time (min)[b]	purified yield (%)[c]	ESI-MS $[M + H]^+$ *m/z* (calcd/found)
1/DOTA−GGGF*-NH_2	65−84	14.8	32	767.3/768.0
2/DOTA−GFQGVQFAGF*-NH_2	40−60	27.4	20	1486.7/1486.0
3/DOTA−GFGSVQFAGF*-NH_2	40−75	26.8	12	1446.7/1445.0
4/DOTA−GFGSTFFAGF*-NH_2	58−87	28.3	20	1467.7/1468.0
5/DOTA−GLVGGAGAGF*-NH_2	62−63	23.0	31	1235.6/1236.0
6[d]/DOTA−GGVLRAGFK-NH_2	48	23.7	37	667.8/667.6[e]
7/DOTA−GGFLGLGAGF*-NH_2	52−84	29.0	23	1325.7/1325.7
8/DOTA−KLLKLLLKLYKKLLKLLK-NH_2	28	20.1	12	2594.6/2594.4[f]
9[d]/DOTA−GKLLKLLLKL*p*YKKLLKLLK-NH_2	47	19.3	18	2729.8/2730.0[f]

[a] Range of purities found by integration of the peak area of an HPLC trace (detection at 280 nm) for different batches (at least two) of each DOTA−peptide. [b] For peptides **1**−**7**, we used gradient 1 and buffer system A, while for peptides **8** and **9**, we used gradient 4 and buffer system B. [c] The purified yield is based on the substitution level of completed peptide resins. [d] Milder conditions used for synthesis (chloroacetyl chloride). [e] Mass calculations are for the $[M + 2H]^{2+}$ species. [f] Due to a distribution of charged states for this species, the spectrum was deconvoluted using MaxEnt software to determine the mass on the true mass scale.

Mass Spectrometry. ESI-MS was performed on a Fisons Instruments VG Quattro triple-quadrupole spectrometer using an eluent of 0.1% HCOOH/49.95% H_2O/49.95% CH_3CN at a flow rate of 5 μL/min. The cone voltage was set to 50 V. The source temperature was set to 80 °C. Calibration of the mass scale was performed using a solution of PEG 300, PEG 600, and PEG 1000 as a calibration standard. Molecular weights of multiply charged peptides were determined by mathematical transformation (deconvolution) of the electrospray spectra to a true mass scale spectrum using the maximum entropy transformation algorithm MaxEnt.

Peptide Synthesis. Peptides were synthesized using either a multiple parallel manual synthesis apparatus (peptides **1**−**7**, see Table 1) or an ABI model 430A automated peptide synthesizer (peptides **8** and **9**). All parent peptides were fully characterized by amino acid analysis and mass spectrometry before the parent peptide−resin was subjected to DOTA functionalization.

Parallel Manual Synthesis of Peptide−Resins 1−7. Using the multiple synthesis apparatus described previously (*13*), 17 peptides were manually synthesized in parallel within 10 days. Standard Fmoc SPPS was carried out according to the preactivation method of Hudson et al. (*14*). A simple method of assaying the activity of the HOBt esters used for SPPS was also employed (*13*).

PEGA Rink resin (10 g, 2 mmol, stored in CH_3OH) was delivered to a 250 mL polypropylene-fritted reaction vessel fashioned from a Bio-Rad Polyprep Column. Dry argon was introduced to the reaction column from below the frit to bubble-stir the slurry using the frit as a bubbler. The resin was washed with 4 × 60 mL of DCM (5 min/wash) and then with 5 × 60 mL of DMF (5 min/wash). Solvent was drained through the frit into a vacuum filter flask using positive argon pressure from above the swollen resin. Fmoc-L-NO_2Phe-OH (4.51 g, 10.4 mmol) and HOBt (1.41 g, 10.4 mmol) were placed in a dry pear-shaped flask and dissolved in 25 mL of dry DMF. To this solution was added 2.61 mL of redistilled DIEA (15 mmol). BOP reagent (5 g, 11.3 mmol) was dissolved in a separate dry pear-shaped flask with 5 mL

of dry DMF and syringed into the Fmoc-L-NO_2Phe-OH solution. After preactivation for 10 min, a 20 μL aliquot containing the active ester was checked for acylating activity and the Fmoc-L-NO_2Phe active ester solution was added to the swollen resin in the polypropylene reaction column. After 2.5 h, the peptide−resin tested nearly negative for free amines (<5 μmol/g) as determined by using the ABI ninhydrin test kit. After 3 h, the resin was washed with 5 × 60 mL of dry DMF and residual amines were capped using 2 mL of acetic anhydride (21 mmol) and 1 mL of DIEA (5.7 mmol) in a total slurry volume of 125 mL. After 1.5 h, the resin was washed with 5 × 60 mL of DMF (5 min/wash) and then treated with 20% piperidine in DMF in a total slurry volume of 125 mL for 20 min. The resin was then washed with 5 × 100 mL of DMF (5 min/wash).

Two more cycles of coupling and deprotection as described above were utilized until the common resin L-Ala-Gly-L-NO_2Phe-PEGA Rink was constructed. The resin was then portioned equally into 17 smaller 50 mL reaction vessels fashioned from 50 mL polypropylene conical flasks and Bio-Rad disposable polypropylene columns (part 732-1010). These reaction vessels were fitted to an 18-reaction vessel capacity multiple SPPS apparatus, and the balance of each peptide was synthesized in parallel at a rate of one amino acid per day. Each night, resins were stored in DCM in their amino-terminal form. At the conclusion of the syntheses, resins were stored in their amino-terminal form in ethanol at −20 °C. Resins were not dried, but stored swollen in solvent according to the manufacturer's suggestions. Completed resins were found to swell to 0.16 g/mL in DMF (average of four measurements). To determine the final substitution level for each resin, ninhydrin analyses (average of five measurements) were performed at the conclusion of the syntheses.

Synthesis of Peptide−Resins 8 and 9 by Automated Peptide Synthesis. Two peptide−resins were synthesized on an ABI model 430A automated peptide synthesizer on a 0.1 mmol scale using the manufacturer's "FastMoc" methodology, which involves HBTU activation of amino acids. Solid support was PEGA Rink amide resin (0.05 mmol/g). An automated resin sampler was programmed to aliquot samples of resin after coupling steps were completed. These resin samples were typically in the range of 3−5 mg and were tested by ninhydrin analysis (ABI test kit) to determine the completeness of coupling which was determined to be >98% for all steps. Peptide−resin **9**, Fmoc-GKLLKLLLKL*p*YKKLLKLLK−PEGA Rink, was initially synthesized with a free hydroxyl on the Tyr residue, which was subsequently protected as the *tert*-butyl phosphotriester upon global phosphorylation using the method of Perich (*15*). All other Fmoc-amino acids were incorporated with side chain protecting groups. After synthesis was complete, Fmoc-peptide−resins were stored at −20 °C in anhydrous NMP until further use. Immediately prior to subsequent alkylation steps, the Fmoc-peptide−resins were amino-terminus deprotected by treatment with 5 mL of 20% piperidine/DMF for 5 min followed by another treatment for 10 min. The peptide−resin was then washed with 5 × 5 mL of DMF (5 min/wash) and 5 × 5 mL of NMP (5 min/wash).

Preparation of Cyclen Free Base. Cyclen sulfate (5.12 g, 13.9 mmol) was stirred vigorously in DCM (125 mL) in a 250 mL round-bottom flask fitted to a reflux condenser and septum for the gas inlet tube and vent needle. Ammonia gas was filtered and dried through a 300 mm × 50 mm column of KOH pellets and bubbled into the suspension (being stirred) for 9 h. The precipitated $(NH_4)_2SO_4$ was filtered off, and the supernatant was again treated with ammonia gas for an additional 2 h. The flask was sealed and the mixture allowed to stir overnight. A second batch of $(NH_4)_2SO_4$ precipitate was filtered off, and the supernatant was rotary evaporated to give white cyclen free base in quantitative yield. ^{1}H NMR ($CDCl_3$): δ 2.61 (s). ESI-MS: *m*/*z* calcd $(M + H)^+$ 173.2, found 173.5.

Cyclen Recovery Procedure. Excess cyclen in DCM, which had been recovered after reaction with alkylating peptide resin (see below), was concentrated by rotary evaporation and recycled to the free base. As an example, 1.6 g of recovered cyclen oil was taken up in 80 mL of CH_3OH, and 15 mL of concentrated HCl was added dropwise. The mixture was then stirred for 6 h, and the CH_3OH was rotary evaporated. Cyclen hydrochloride was then converted to the free base in the same manner as cyclen sulfate (see above). Peptide **2** DOTA−GFQGVQ-FAGF*-NH_2 was synthesized using recycled cyclen.

General Synthesis of DOTA−Peptides. A general method for the synthesis of DOTA−peptides is shown by example using the synthesis of DOTA−GGFLGLGAGF*-NH_2. All other DOTA−peptides followed a similar synthetic procedure.

Step 1. Acylation with Bromoacetyl Bromide. NH_2-GGFLGLGAGF*−PEGA Rink resin (0.59 g, 92 μmol) was washed with 5 × 5 mL of dry NMP. The resin slurry volume was adjusted to 5.8 mL with NMP and vortex mixed. To the vortexing slurry were added 80 μL (460 μmol) of DIEA, and then 180 μL (2 mmol) of bromoacetyl bromide. The resin was vortex mixed for 1 h, and washed with 5 × 5 mL of dry NMP and 10 × 5 mL of dry DCM. A 5 mg sample of resin was assayed by ninhydrin for free amines and found to be negative for free amines (<5 μmol/g). A 1 mg sample was removed and treated with NBP (3 g in 60 mL of acetone). The yellow resin turned royal blue upon treatment with NH_3(g), indicating the presence of alkylating species (the reactive bromoacetyl moiety).

Alternate Step 1. Acylation with Chloroacetyl Chloride. NH_2-GGVLRAGFK−PEGA Rink resin (0.1 g, 16 μmol) was washed with 5 × 2 mL of dry NMP. The resin slurry volume was adjusted to 1.1 mL and the slurry vortex mixed. To the vortexing slurry were added 80 μL (115 μmol) of DIEA, and then 29 μL (364 μmol) of chloroacetyl chloride. The resin was vortex mixed for 72 min, and then washed with 5 × 2 mL of dry NMP and 10 × 2 mL of dry DMSO. A 5 mg sample of resin was assayed by ninhydrin for free amines and found to be negative for free amines (<10 μmol/g). A 1 mg sample was removed and soaked with NBP (3 g in 60 mL of acetone) for 30 min at 35 °C. The yellow resin turned violet upon treatment with NH_3(g), indicating the presence of alkylating species (the reactive chloroacetyl moiety).

Step 2. Immobilization of Cyclen by the Haloacetyl-Peptide−Resin. The bromoacetyl-GGFLGLGAGF*−PEGA Rink resin was gravity drained and vortex mixed. Over a period of less than 10 s, 1.4 mL of 4.3 M cyclen free base in dry DCM was added to the resin that was being vortexed. This gave a total volume of 5.4 mL for a final cyclen concentration of 1.1 M. The slurry was vortex mixed for 2.5 h, checked for alkylating species via NBP test (negative), and washed with 6 × 5 mL of dry DCM (the washes pooled for the recycling procedure), 5 × 5 mL of dry DMSO (to remove any insoluble cyclen mixed salts), and 5 × 5 mL of dry NMP. A 43 mg sample of the cyclen−peptide−resin was removed, washed with 8 × 5 mL of DCM, and dried with flowing argon gas. Standard

peptide cleavage (see below) resulted in a product that was purified on HPLC (gradient 1, buffer system A). The major peak was collected and determined to be cyclen−GGFLGLGAGF*-NH_2. HPLC purity: 69%. ESI-MS: *m/z* calcd for $C_{53}H_{82}N_{16}O_{13}$ $(M + H)^+$ 1151.7, found 1151.0; calcd for $(M + 2H)^{2+}$ 576.4, found 576.2.

Step 3. Alkylation of Immobilized Cyclen−Peptide with tert-Butyl 2-Bromoacetate. The slurry volume of cyclen−GGFLGLGAGF*−PEGA Rink resin was adjusted to 5.3 mL with dry NMP. DIEA (366 μL, 2.1 mmol) and then *tert*-butyl 2-bromoacetate (310 μL, 2.1 mmol) were added to give final concentrations of 0.35 M. The resin was vortex mixed for 13.5 h, and then washed with 5 × 5 mL of DMF and 6 × 5 mL of DCM. An analytical sample of resin was removed and the product cleaved from the resin (see below). After collection of product fractions from C_{18} HPLC (gradient 1, buffer system A), ESI-MS of the cleaved DOTA−peptide amide indicated completion of the reaction and the absence of significant impurity corresponding to incomplete alkylation. The remaining resin was then dried by flowing argon over the drained bed for several hours.

Step 4. Cleavage of the DOTA−Peptide Amide from Solid Support and HPLC Purification. The dried DOTA−peptide−resin was weighed (0.576 g, 82 μmol), and a cleavage cocktail of TFA, TIPS, and H_2O (95:2.5:2.5, v/v) was added (10 mL). After vortex mixing for 2.5 h, the eluent was collected and the resin was washed with 5 × 4 mL of cocktail. The combined eluents were rotary evaporated to approximately 500 μL. Cold Et_2O (10 mL) was added and the solution cooled for 30 min at −20 °C. The precipitate was centrifuged at 800*g* at 4 °C for 5 min. The Et_2O was decanted and the pellet resuspended in another 10 mL of cold Et_2O. This centrifuge/wash procedure was repeated for a total of five washes. The precipitate was dried under vacuum and weighed (70 mg). The precipitate was taken up in 5 mL of 20% DMSO/water, filtered through a 0.45 μm membrane, and HPLC analyzed using gradient 1 with buffer system A on a Dynamax analytical C_{18} column. The major peak (retention time of 29 min) comprised 54% of the integrated chromatogram. The crude material was HPLC purified using gradient 2 with buffer system A on a Magellan C_{18} semipreparative column (retention time of 13 min). The product was lyophilized twice. The yield was 25 mg, or 19 μmol (23% based on ninhydrin-quantitated substitution of 156 μmol/g × 0.91 for *t*-Bu-DOTA−GGFLGL-GAGF*−resin).[4] ESI-MS: *m/z* calcd for $C_{59}H_{88}N_{16}O_{19}$ $(M + H)^+$ 1325.6, found 1325.7; calcd for $(M + 2H)^{2+}$ 663.3, found 663.7. Amino acid analysis confirmed the correct composition of amino acids. A stock solution of DOTA−GGFLGLGAGF*-NH_2 was prepared in 1:1 DMSO/0.1 M triethylammonium acetate, and the concentration was determined with a ^{57}Co metal binding assay (11.7 mM). This value compared well with the spectrophotometrically determined value (13.4 mM) obtained from absorbance at 280 nm when 2.5 μL of this stock was diluted in 500 μL of 0.1 M sodium phosphate (pH 7.0) using an ϵ of 9050 M^{-1} cm^{-1} (280 nm) for *p*-nitrophenylalanine at pH 7.

RESULTS

A variety of peptide−resins were synthesized, by manual and automated methods, for use as scaffolds for the construction of the DOTA moiety on their amino termini. The crude unmodified peptides, when cleaved from the resin, were typically >90% pure as determined by HPLC.

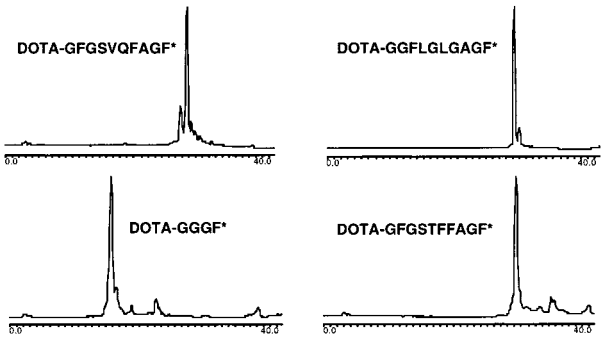


Figure 1. HPLC chromatograms of the crude cleavage products for several DOTA−peptide amides on an analytical C_{18} column. All DOTA−peptide amides were deprotected and cleaved from PEGA Rink amide resin using a cleavage cocktail of 95% TFA/2.5% TIPS/2.5% H_2O. After precipitation from cold Et_2O, DOTA−peptides were dissolved in 20% DMSO/H_2O and filtered before HPLC analysis. The major peak in each chromatogram was determined to be the desired product.

Functionalization of the amino terminus of the peptide−resin was provided through the use of the bifunctional bromoacetyl bromide or chloroacetyl chloride. Since the acyl halide functionality is much more reactive than the alkyl halide with respect to amine nucleophilic attack, acylation was the preferred reaction pathway. Initial acylation experiments using peptide−HMP resins (polystyrene-based) followed by cyclen alkylation resulted in a complex mixture of byproducts. Analysis of the bromoacetyl-peptide−HMP resins using 1.1 M NH_3 as the nucleophile showed that simple polystyrene-based peptide−resins treated with bromoacetyl bromide were poor alkylating agents in DCM when compared to peptide−poly(ethylene glycol) acrylamide resins. We therefore used the PEGA−Rink resins as the solid phase for our peptide syntheses.

Milder reaction conditions in which chloroacetyl chloride was used were also successful, despite the less reactive chloroacetyl electrophile. Preliminary tests of the alkylation step in which NH_3 was used as the nucleophile showed that the chloroacetyl group is significantly less reactive toward NH_3 than the bromoacetyl group in DCM. Nevertheless, alkylation of cyclen by the chloroacetyl group was accomplished in both DMSO and DCM. Recovery of unreacted cyclen was further simplified by the fact that the resulting cyclen mixed salt was in the hydrochloride form and required one less step for recycling to the free base form.

During the cyclen alkylation step, it was feared that a considerable amount of cross-linked peptide−cyclen−peptide products might have resulted since cyclen has four nucleophilic sites. However, products such as peptide−DOTA−peptide were not detected by mass spectrometry (sub-picomole limits of detection). Rather, the most significant impurity for the multistep DOTA functionalization of peptide−resin was typically one with a mass corresponding to underalkylation of immobilized cyclen−peptide by *tert*-butyl 2-bromoacetate (i.e., two groups instead of three). The purity of the cleaved DOTA−peptides as measured by integration of their HPLC chromatograms was high enough to yield useful amounts of pure material. Table 1 displays the sequences, HPLC purities, yields, and ESI-MS data of the DOTA−peptide amides. Figure 1 displays the HPLC

[4]The factor of 0.91 is derived from the fact that *t*-Bu-DOTA adds to the weight of the peptide resin, and the substitution level of 156.1 μmol/g must be adjusted accordingly to 142 μmol/g.

chromatograms of several of these DOTA−peptide amides.

DISCUSSION

Peptide linkers can potentially improve the efficacy of targeting radionuclides to tumors (*10*, *13*); practical synthesis of peptides bearing strong metal-binding groups makes it possible to test various strategies efficiently. A combined procedure where both the DOTA and the DOTA-linked peptide amide are synthesized on a single support offers many advantages. The peptidyl solid support can be thought of as a purification column, eliminating the costly and laborious HPLC steps utilized to purify the chelate, the peptide, and the chelate-modified peptide. The time to synthesize one DOTA−peptide amide is significantly reduced, since byproducts and unreacted starting materials are simply eluted during the wash steps. The procedure can take as little as 4 days from bare PEGA Rink resin to HPLC-purified DOTA−peptide.

The gravimetric yields of DOTA−peptide realized with this method are not yet characteristic of what can be expected of SPPS. For example, solid-phase synthesis yields of the peptides alone are typically >90%. However, the DOTA−peptide yields are comparable to those realized with other methods where only one of multiple sites on a macrocycle is modified. Using a solid-phase chemistry solvent such as DCM provides practical advantages for the use of cyclen in our synthetic route. Not only does the resin swell effectively in DCM, but also cyclen is highly soluble in this solvent, allowing us to use the principle of excess and avoid cross-linking. The recovery of unreacted cyclen is also easily and rapidly accomplished in DCM. The use of *tert*-butyl 2-bromoacetate (*16*) affords a carboxyl-protected DOTA moiety which, when utilized in an orthogonal protection scheme, allows further manipulation of the resin-bound peptide. This may prove useful in the synthesis of peptides with multiple functionalities.

The variety of peptides that have been DOTA-functionalized on the solid phase testifies to the general utility of this synthetic route. Milligram quantities of DOTA peptides have been rapidly and efficiently made and purified. These DOTA−peptides can be further investigated for use in radioimmunoconjugates or targeted delivery vehicles for radioisotopes.

ACKNOWLEDGMENT

This work was supported by NIH Research Grants CA16861 (C.F.M.) and CA47829 (G. L. DeNardo, principal investigator). R.H.P. was supported by NIH Postdoctoral Fellowship CA71177. We thank Dr. Vincent Jacques for helpful discussions.

LITERATURE CITED

(1) Desreux, J. F. (1980) Nuclear magnetic resonance spectroscopy of lanthanide complexes with a tetraacetic tetraaza macrocycle. Unusual conformation properties. *Inorg. Chem. 19*, 1319−1324.

(2) Loncin, M. F., Desreux, J. F., and Merciny, E. (1986) Coordination of lanthanides by two polyamino polycarboxylic macrocycles: Formation of highly stable lanthanide complexes. *Inorg. Chem. 25*, 2646−2648.

(3) Lewis, M. R., Raubitschek, A., and Shively, J. E. (1994) A facile, water soluble method for modification of proteins with DOTA. Use of elevated temperature and optimized pH to achieve high specific activity and high chelate stability in radiolabeled immunoconjugates. *Bioconjugate Chem. 5*, 565−576.

(4) Moi, M. K., Meares, C. F., and DeNardo, S. J. (1988) The peptide way to macrocyclic bifunctional chelating agents: Synthesis of 2-(*p*-nitrobenzyl)-1,4,7,10-tetraazacyclododecane-*N*,*N*′,*N*″,*N*‴-tetraacetic acid and study of its yttrium(III) complex. *J. Am. Chem. Soc. 110*, 6266−6267.

(5) Renn, O., and Meares, C. F. (1992) Large scale synthesis of the bifunctional chelating agent 2-(*p*-nitrobenzyl)-1,4,7,10-tetraazacyclododecane-*N*,*N*′,*N*″,*N*‴-tetraacetic acid, and the determination of its enantiomeric purity by chiral chromatography. *Bioconjugate Chem. 3*, 563−569.

(6) Cox, J. P. L., Craig, A. S., Helps, I. M., Jankowski, K. J., Parker, D., Eaton, M. A. W., Millican, A. T., Millar, K., Beeley, N. R. A., and Boyce, B. A. (1990) Synthesis of C- and N-functionalized derivatives of 1,4,7-triazacyclononane-1,4,7-triyltriacetic acid (NOTA), 1,4,7,10-tetraazacyclododecane-1,4,7,10-tetrayltetraacetic acid (DOTA), and diethylenetriaminepentaacetic acid (DTPA): Bifunctional complexing agents for the derivatization of antibodies. *J. Chem. Soc., Perkin Trans. 1*, 2567−2576.

(7) Sieving, P. F., Watson, A. D., and Rocklage, S. M. (1990) Preparation and characterization of paramagnetic polychelates and their protein conjugates. *Bioconjugate Chem. 1*, 65−71.

(8) Sherry, A. D., Brown, R. D., III, Geraldes, C. F. G. C., Koenig, S. H., Kuan, K.-T., and Spiller, M. (1989) Synthesis and characterization of the gadolinium(3+) complex of DOTA-propylamide: A model DOTA-protein conjugate. *Inorg. Chem. 28*, 620−622.

(9) Wu, C., Verzi, F., and Hnatowich, D. J. (1992) Investigations of N-linked macrocycles for ^{111}In and ^{90}Y labeling of proteins. *Nucl. Med. Biol. 19*, 239−244.

(10) Li, M., and Meares, C. F. (1993) Synthesis, metal chelate stability studies, and enzyme digestion of a peptide-linked DOTA derivative and its corresponding radiolabeled immunoconjugates. *Bioconjugate Chem. 4*, 275−283.

(11) Meares, C. F., McCall, M. J., Reardan, D. T., Goodwin, D. A., Diamante, C. I., and McTigue, M. (1984) Conjugation of antibodies with bifunctional chelating agents: Isothiocyantate and bromoacetamide reagents, methods of analysis, and subsequent addition of metal ions. *Anal. Biochem. 142*, 68−78.

(12) Kruper, W. J., Rudolf, P. R., and Langhoff, C. A. (1993) Unexpected selectivity in the alkylation of polyazamacrocycles. *J. Org. Chem. 58*, 3869−3876.

(13) Peterson, J. J., and Meares, C. F. (1998) Cathepsin substrates as cleavable peptide linkers in bioconjugates, selected from a fluorescence quench combinatorial library. *Bioconjugate Chem. 9*, 618−626.

(14) Hudson, D. (1988) Methodological implications of simultaneous solid-phase peptide synthesis. 1. Comparison of different coupling procedures. *J. Org. Chem. 53*, 617−624.

(15) Perich, J. (1992) Efficient solid-phase synthesis of mixed Thr(*P*)-, Ser(*P*)- and Tyr(*P*)-containing phosphopeptides by "global" "phosphite-triester" phosphorylation. *Int. J. Pept. Protein Res. 40*, 134−140.

(16) Liberatore, F. A., Comeau, R. D., McKearin, J. M., Pearson, D. A., Belonga, B. Q., III, Brocchini, S. J., Kath, J., Phillips, T., Oswell, K., and Lawton, R. G. (1990) Site-directed chemical modification and cross-linking of a monoclonal antibody using equilibrium transfer alkylating cross-link reagents. *Bioconjugate Chem. 1*, 36−50.

BC980118T

MAY/JUNE 1999
Volume 10, Number 3

© *Copyright 1999 by the American Chemical Society*

Bioconjugate Chemistry

COMMUNICATIONS

Molecular Chaperone-Like Activity of Hydrogel Nanoparticles of Hydrophobized Pullulan: Thermal Stabilization with Refolding of Carbonic Anhydrase B

Kazunari Akiyoshi,* Yoshihiro Sasaki, and Junzo Sunamoto*

Department of Synthetic Chemistry and Biological Chemistry, Graduate School of Engineering, Kyoto University, Yoshida-Hommachi, Sakyo-ku, Kyoto 606-8501, Japan. Received October 26, 1998

We have been studying the formation of hydrogel nanoparticles by the self-aggregation of hydrophobized polysaccharide and the effective complexation between these nanoparticles as a host and various globular soluble proteins as a guest. This paper describes a new finding that refolding of the heat-denatured enzyme effectively occurs with the nanoparticles and β-cyclodextrin according to a mechanism similar to that of a molecular chaperone. In particular, the irreversible aggregation of carbonic anhydrase B (CAB) upon heating was completely prevented by complexation between the heat-denatured enzyme and hydrogel nanoparticles formed by the self-aggregation of cholesteryl group-bearing pullulan (CHP). The complexed CAB was released by dissociation of the self-aggregate upon the addition of β-cyclodextrin. The released CAB refolded to the native form, and almost 100% recovery of the activity was achieved. The thermal stability of CAB was drastically improved by capture of the unfolded form which was then released to undergo refolding.

Most proteins irreversibly aggregate upon heating. Molecular chaperones selectively trap heat-denatured proteins (*1*−*3*) or their intermediates in refolding (*4*, *5*) to prevent their irreversible aggregation. The host chaperone releases the protein in a refolded form through a change in the conformation of the complex with the aid of ATP and another co-chaperone. Chaperonins, which have multiple subunits and a cage-like structure, are a well-investigated family of molecular chaperones (*6*). For example, GroEL acts as a host in macromolecular self-assembly by enclosing a folding intermediate protein as a guest in its central hydrophobic cavity (*6*). This is an interesting example of host−guest chemistry in a macromolecular system.

Surfactants (*7*, *8*) and cyclodextrins (*9*) are known to prevent the aggregation of the partly intermediate protein that is formed in the refolding process and in heat denaturation. Gellman et al. demonstrated an interesting system for protein refolding via the sequential use of low molecular weight surfactants and cyclodextrins as a stripping agent (*10*). In their system, however, it is sometimes difficult to completely remove the surfactant after treatment. Water-soluble polymers such as poly(ethylene oxide) (*11*) and polyamino acids (*12*) also prevent protein aggregation, although their efficiency is low.

The amphiphilic nature of proteins, especially their

* To whom correspondence should be addressed.

10.1021/bc9801272 CCC: $18.00 © 1999 American Chemical Society
Published on Web 03/10/1999

hydrophobicity, is important in the complexation between a chaperone and denatured protein. To mimic or simulate the function of molecular chaperones, we newly designed an amphiphilic hydrogel nanoparticle that behaves as a host for a guest protein. Hydrophobized polysaccharides such as cholesteryl group-bearing pullulan (CHP) spontaneously form hydrogel nanoparticles in water by intra- and/or intermolecular self-aggregation (*13, 14*). Furthermore, these hydrogel nanoparticles spontaneously complex with various soluble proteins or enzymes in water (*15*−*17*). In these cases, we have observed several different types of complexation, as follows. Type I: Enzymes such as α-chymotrypsin or horseradish peroxidase are complexed by polysaccharide nanoparticles at room temperature or physiological temperature and lose their enzyme activity in the complex (*15*). Type II: Enzymes are complexed in the native form and retain their activity even in the complex, for example, lipase (unpublished result). In both cases, the complexed proteins gain substantial thermal stabilization due to fixation of the proteins or enzymes in the hydrogel matrix of the nanoparticles.

In this work, we newly report another interesting type of complexation: Type III. In this case, carbonic anhydrase B (CAB) was complexed quantitatively by the nanoparticles in a heat-denatured form above its denaturation temperature (55 °C). Another interesting and important finding is that complexed CAB was effectively (almost quantitatively) released in its refolded native form in the presence of β-cyclodextrin. This is similar to the two-step mechanism of a molecular chaperone, that is, capture of a heat-denatured protein and release of the refolded protein. In addition, this system provided effective thermal stabilization of CAB. In this paper, we describe this unique behavior of hydrogel nanoparticles of CHP self-aggregate, which is different from those previously reported for the immobilization and stabilization of enzymes or proteins in an ordinary polymer matrix.

The preparation and characterization of CHP nanoparticles have been reported elsewhere (*13, 14*). Cholesteryl group-bearing pullulan (CHP-108−0.9, where the molecular weight of the parent pullulan was 108 000 and the degree of substitution of the cholesteryl moiety per 100 glucose units was 0.9) was used in this study. The average hydrodynamic radius (R_H) of the nanoparticles was approximately 18 nm by dynamic light scattering. The apparent molecular weight (8.2×10^5) and the aggregation number of the self-aggregate (approximately 7) were determined by the static light-scattering method. The root-mean-square radius of gyration (R_G) was 15.1 nm. The association of cholesteryl moieties provides noncovalently cross-linked points in hydrogel nanoparticles (*14*).

The heat-induced aggregation of CAB (molecular weight 30 000, 0.06 mg/mL, 2 μM) was investigated by the light-scattering method at 400 nm in the absence and presence of CHP. When CAB was heated above its denaturation temperature (55 °C) to 63 °C, aggregation started within 5 min (Figure 1). The hydrophobic portions of globular protein are exposed upon partial unfolding of the protein under heating. This results in aggregation of the protein. This aggregation of CAB was significantly prevented in the presence of CHP nanoparticles. When the molar ratio of CHP nanoparticles to CAB was above 0.2, the solution was optically clear even after heating at 63 °C for 40 min. In contrast, the parent pullulan did not show the same behavior even at a rather high concentration of pullulan. Thus, CHP nanoparticles effectively prevented the aggregation and sedimentation of heat-denatured CAB. This effect is similar to the behavior of a molecular chaperone in nature.

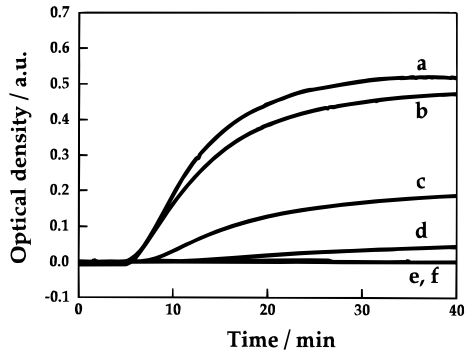


Figure 1. Self-aggregation of CAB in the presence of CHP nanoparticles and pullulan at 63 °C: (a) free CAB (0.06 mg/mL, 2 μM). (b) Pullulan (molecular weight 108 000), 0.15 mg/mL. (c) CHP nanoparticles (0.082 mg/mL, 0.1 μM as CHP nanoparticles concentration): CAB (0.06 mg/mL, 2 μM) = 0.05:1 (as a molar ratio). (d) CHP nanoparticles: CAB = 0.1:1. (e) CHP nanoparticles: CAB = 0.2:1; and (f) CHP nanoparticles, CAB = 1:1.

A mixture of the CHP nanoparticles (2 μM, as a molar per nanoparticle) and CAB (2 μM) was incubated at 70 °C for 10 min and then cooled to 25 °C. Quantitative complexation between CAB and the CHP nanoparticles was confirmed by high-performance size-exclusion chromatography (HPSEC, Superdex 200HR column, Pharmacia, UV detection at 280 nm) (data not shown). No spontaneous dissociation of CAB was observed even after storage for a week at room temperature. The CHP nanoparticles did not complex with native CAB at 25 °C even after incubation for 32 h. The secondary structure of native CAB consists of 6.6% α-helical and 30.9% β-forms (*17*). With the CHP−CAB complex, the proportions of the helical and β-forms were computationally estimated to be 24.6% and 12.0%, respectively, on the basis of the CD spectrum. The heat denaturation and subsequent complexation of CAB with CHP nanoparticles induced a large conformational change in its secondary structure. Goto and co-workers previously pointed out the possibility that the α-helical intermediate of denatured protein is a nonhierarchical intermediate of β-sheet proteins such as CAB (*18*). CHP nanoparticles may capture the heat-denatured intermediate of CAB.

The change in the mean residual ellipticity of CAB was investigated in the presence of CHP as a function of temperature at 222 nm. The mixture of CAB and CHP nanoparticles was gradually heated from 25 to 70 °C at 0.17 °C/min and then cooled to 25 °C at the same rate (Figure 2). No significant change was observed in the secondary structure of CAB upon heating to 40 °C. At around 50 °C, however, the ellipticity showed a large sigmoidal decrease. This temperature coincides with the denaturation temperature of CAB. CHP nanoparticles themselves do not show any structural change even after heating to 70 °C. The nanoparticles selectively and effectively complex only with heat-denatured CAB. The increased hydrophobicity of the denatured unfolded protein may prefer complexation with amphiphilic hydrogel nanoparticles compared to the completely folded native protein.

The dynamics of a chaperone function are controlled by suitable effectors (*6*). ATP interacts with the chaperone−protein complex and induces a conformational change in the chaperone to release the bound protein, accompanied by complete refolding, and the original protein

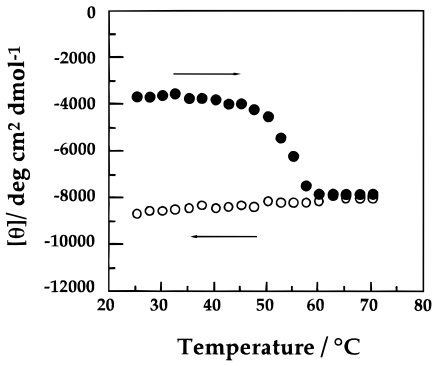


Figure 2. Mean residual ellipticity (θ) at 222 nm as a function of temperature in 50 mM Tris-sulfate (pH 7.5). A solution mixture of CAB and CHP nanoparticles was heated from 25 to 70 °C at 10 °C/h and then cooled to 25 °C: [CHP nanoparticles] = [CAB] = 15 μM.

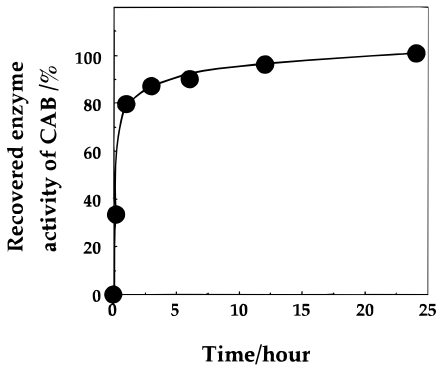


Figure 3. Recovery of enzyme activity of complexed CAB in the prescence of β-cyclodextrin (3 mM) at 25 °C in 50 mM Tris-sulfate buffer (pH 7.5).

activity is fully recovered. CHP self-aggregates undergo dissociation with the addition of β-cyclodextrin (*19*). The cross-linking domains provided by the hydrophobic cholesteryl groups are destructed upon encapsulation of the cholesteryl moiety by the β-cyclodextrin cavity. Destruction of the nanoparticles subsequently induces the release of complexed CAB. To the CHP−CAB complex, which was prepared by mixing the CHP nanoparticles (2 μM) and CAB (2 μM) at 70 °C for 10 min, was added β-cyclodextrin (3 mM), and the mixture was kept for 24 h at 25 °C. HPSEC analysis of the reaction mixture showed a complete release of free CAB (data not shown) from the complex under these conditions. Figure 3 shows the recovery of the enzyme activity of CAB with the addition of β-cyclodextrin as a function of incubation time.[1] Complexed CAB (2 μM) did not show any enzyme activity in the absence of β-cyclodextrin. However, with the addition of β-cyclodextrin (3 mM) to the complex (CHP, 2 μM), 90% of the enzyme activity recovered after 6 h, and recovery was almost 100% after 24 h. The mixture of CAB and CHP nanoparticles was heated for 10 min at various temperatures and then cooled to 25 °C. The enzyme activity that remained after the addition

[1] An aliquot containing CAB was heated at 70 °C for 10 min in 50 mM Tris, pH 7.5, and then chilled to room temperature for 10 min. A dry acetonitrile solution (0.2 mL) of 10 mM *p*-nitrophenylacetate (pNPA) was added to 1.8 mL of the sample solution (CAB, 1.8 μM in 50 mM Tris-sulfate, pH 7.5). After 20 s of mixing, an increase in the *p*-nitrophenolate concentration was monitored by the absorbance at 400 nm as a function of time. The percent recovery of enzyme activity was calculated on the basis of the initial velocity of the activity of native CAB (*20*).

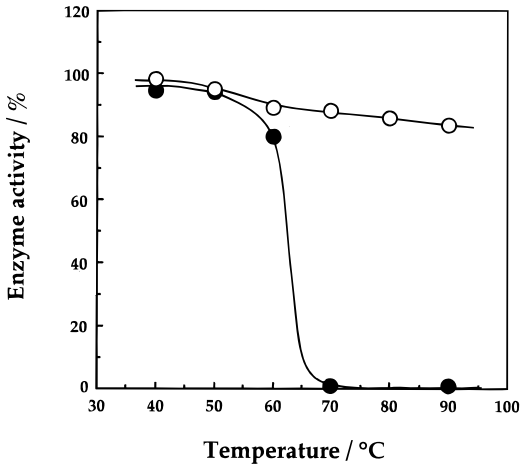


Figure 4. Stability of CAB in the presence of CHP nanoparticles at various temperatures. The mixture of CAB (2 μM) and CHP nanoparticles (2 μM) was treated for 10 min at various temperatures. The *p*-nitrophenyl acetate hydrolysis by CAB was monitored at 25 °C in 50 mM Tris-sulfate buffer, pH 7.5, after the addition of β-cyclodextrin.

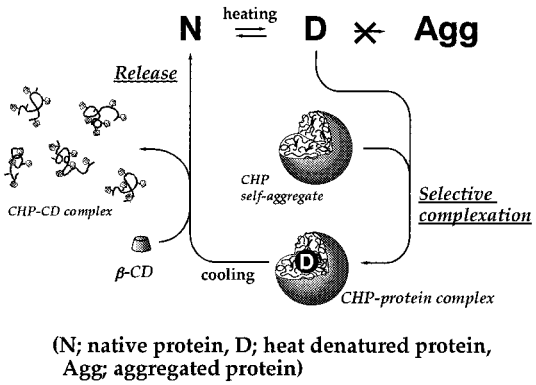


Figure 5. Schematic representation of controlled association between CHP nanoparticles and CAB.

of β-cyclodextrin was investigated (Figure 4). The irreversible heat denaturation of CAB was effectively prevented by complexation with CHP nanoparticles even at higher temperatures. As a result, the thermal stability of CAB was drastically enhanced in this system.

In conclusion, in this study, we mimicked the complex function of a molecular chaperone using a relatively simple system consisting of CHP self-aggregate nanoparticles and β-cyclodextrin. Figure 5 shows a schematic two-step mechanism, that is, the capture of heat-denatured unfolded protein and the release of the refolded form. Through this processes, the enzyme gains significant thermal stabilization. This is a novel method for the thermal stabilization of enzymes using the well-controlled association with a simple macromolecule. Protein refolding in urea or GuHCl-induced denaturation system is under investigation using a similar hydrophobized polysaccharide system.

ACKNOWLEDGMENT

This research was supported by a Grant-in-Aid for Scientific Research from the Ministry of Education, Science, Sports and Culture, Japan. Y.S. gratefully acknowledges a predoctoral fellowship from the Japan Society for the Promotion of Science.

LITERATURE CITED

(1) Höll Neugebauer, B., Rudolph, R., Schmidt, M., and Buchner, J. (1991) Reconstitution of a heat shock effect in vitro:

influence of GroE on the thermal aggregation of α-glucosidase from yeast. *Biochemistry 30*, 11609−11614.
(2) Taguchi, H., and Yoshida, M. (1993) Chaperonin from Thermus thermophilus can protect several enzymes from irreversible heat denaturation by capturing denaturation intermediate. *J. Biol. Chem. 268*, 5371−5375.
(3) Kawata, Y., Nosaka, K., Hongo, K., Mizobata, T., and Nagai, J. (1994) Chaperonin GroE and ADP facilitate the folding of various proteins and protect against heat inactivation. *FEBS Lett. 345*, 229−232.
(4) Weissman, J. S., Hohl, C. M., Kovalenko, O., Kashi, Y., Chen, S., Braig, K., Saibil, H. R., Fenton, W. A., and Horwich, A. L. (1995) Mechanism of GroEL action: productive release of polypeptide from a sequestered position under GroES. *Cell 83*, 577−587.
(5) Mayhew, M., da Silva, A. C., Martin, J., Erdjument Bromage, H., Tempst, P., and Hartl, F. U. (1996) Protein folding in the central cavity of the GroEL-GroES chaperonin complex. *Nature 379*, 420−426.
(6) Braig, K., Otwinowski, Z., Hegde, R., Boisvert, D. C., Joachimiak, A., Horwich, A. L., and Sigler, P. B. (1994) The crystal structure of the bacterial chaperonin GroEL at 2.8 A [see comments]. *Nature 371*, 578−586.
(7) Tandon, S., and Horowitz, P. M. (1986) Detergent-assisted refolding of guanidinium chloride-denatured rhodanese. The effects of lauryl maltoside. *J. Biol. Chem. 261*, 15615−15681.
(8) Tandon, S., and Horowitz, P. M. (1987) Detergent-assisted refolding of guanidinium chloride-denatured rhodanese. The effects of the concentration and type of detergent. *J. Biol. Chem. 262*, 4486-4491.
(9) Karuppiah, N., and Sharma, A. (1995) Cyclodextrins as protein folding aids. *Biochem. Biophys. Res. Commun. 211*, 60−66.
(10) Rozema, D., and Gellman, S. H. (1995) Artificial chaperones: Protein refolding via sequential use of detergent and cyclodextrin. *J. Am. Chem. Soc. 117*, 2373−2374; (1996) Artificial chaperone-assisted refolding of carbonic anhydrase B. *J. Biol. Chem. 271*, 3478−3487.
(11) Cleland, J. L., Hedgepeth, C., and Wang, D. I. (1992) Polyethylene glycol enhanced refolding of bovine carbonic anhydrase B. Reaction stoichiometry and refolding model. *J. Biol. Chem. 267*, 13327−13334.
(12) *Cosolvent effects on refolding and aggregation.* Cleland, J. L., and Wang, D. I. (1993) in Biocatalist design for stability and specificity, ACS Symposium Series, pp 151−166.
(13) Akiyoshi, K., and Sunamoto, J. (1996) Supramolecular assemblies of hydrophobized polysaccharide. *Supramol. Sci. 3*, 157−163.
(14) Akiyoshi, K., Deguchi, S., Tajima, H., NIshikawa, T., and Sunamoto, J. (1997) Microscopic structure and thermoresponsiveness of a hydrogel nanoparticle by self-assembly of a hydrophobized polysaccharide. *Macromolecules 30*, 857−861.
(15) Nishikawa, T., Akiyoshi, K., and Sunamoto, J. (1994) Supramolecular assembly between nanoparticles of hydrophobized polysaccharide and soluble protein complexation between the self-aggregate of cholesterol-bearing pullulan and alpha-chymotrypsin. *Macromolecules 27*, 7654−7659.
(16) Nishikawa, T., Akiyoshi, K., and Sunamoto, J. (1996) Macromolecular complexation between bovine serum albumin and the self-assembled hydrogel nanoparticle of hydrophobized polysaccharides. *J. Am. Chem. Soc. 118*, 6110−6115.
(17) Akiyoshi, K., Nishikawa, T., Shichibe, S., and Sunamoto, J. (1995) Stablization of insulin upon supramolecular complexation with hydrophobized polysaccharide nanoparticle. *Chem. Lett.*, 707−708.
(18) Shiraki, K., Nishikawa, K., and Goto, Y. (1995) Trifluoroethanol-induced stabilization of the alpha-helical structure of beta-lactoglobulin: implication for non-hierarchical protein folding. *J. Mol. Biol 245*, 180−194.
(19) Akiyoshi, K., Sasaki, Y., Kuroda, K., and Sunamoto, J. (1998) Controlled association of hydrophobized polysaccharide by cyclodextrin. *Chem. Lett.*, 93−94.
(20) Pocker, Y., and Guilbert, L. J. (1972) Catalytic versatility of erythrocyte carbonic anhydrase. Kinetic studies of the enzyme-catalyzed hydrolysis of methylpyridyl carbonates. *Biochemistry 11*, 180−190.

BC9801272

ARTICLES

Synthesis of Novel Europium-Labeled Estradiol Derivatives for Time-Resolved Fluoroimmunoassays

Niko Meltola,*,† Piitu Jauria,†,‡ Petri Saviranta,† and Heikki Mikola§

University of Turku, Medical Physics and Chemistry and Department of Biotechnology, P.O. Box 123, FIN-20521 Turku, Finland, and Wallac Oy, P.O. Box 10, FIN-20101 Turku, Finland . Received January 26, 1998; Revised Manuscript Received November 30, 1998

The *O*-(5-carboxypentyl)-, *O*-(4-aminobutyl)-, *O*-(6-aminohexyl)oximes of 2- and 4-formylestradiol as well as the 4-carboxyethylthioether derivative of estradiol were synthesized. These estradiol derivatives were characterized using IR-, ^{1}H-, and ^{13}C NMR spectroscopy. All synthesized estradiol derivatives were labeled with europium chelates. These "tracers" were purified and tested in a competitive time-resolved fluoroimmunoassay with monoclonal antibody (SSI 57-2) raised against the 6-*O*-(carboxymethyl)oxime-bovine serum albumin derivative of estradiol. All the tested europium-labeled estradiol-4-derivatives were bound by the antibody, whereas tracers linked via position 2 were not recognized by this antibody. It was observed that tracers conjugated via C-4 gave more sensitive standard curves than tracers conjugated via C-6. Especially, the estradiol-4-thioether derivative was found to be highly useful in time-resolved fluoroimmunoassays of estradiol while using this antibody.

INTRODUCTION

In many biochemical applications, haptens coupled covalently to other molecules are needed (*1*). For example, in affinity chromatography and in immunoassays, haptens coupled covalently onto either a solid matrix, a carrier molecule, or a label molecule are used. The coupling site, the chemical structure of the linkage, and the length of the spacer arm between the hapten and the label or the carrier molecule play important roles in the biochemical recognition reactions (*1*−*3*). Usually before coupling, a spacer arm and/or a suitable reactive group has to be introduced to the hapten molecule. In steroid immunoassay procedures and in antibody rising *O*-(carboxyalkyl)oximes, hemisuccinates, carboxyalkyl ethers, and thioethers are frequently used to couple the steroids to proteins or to the label molecule (*1, 4*).

For the raising of anti-steroid antibodies, steroids conjugated to macromolecular carriers have to be used as immunogens. The specificities of the antibodies obtained partly depend on the nature of the linkage and the coupling site of the steroid on the carrier. We have studied the binding properties of a monoclonal anti-estradiol antibody (SSI 57-2) using time-resolved fluoroimmunoassay. In these assays, we used estradiol derivatives labeled with europium chelates, which give a strong, long decay-time fluorescence, creating high specific activity in the labeled immunoreagents (*5*−*7*). The monoclonal antibody used here has been raised against 6-oxoestradiol 6-(*O*-carboxymethyl)oxime-bovine serum albumin immunogen. This immunogen has a distorted steroid core compared to free estradiol because of the double bonding of the nitrogen to position C-6 (*8*). The used anti-estradiol antibody has a much higher affinity to derivatives linked via C-6 than to free estradiol (*9*) mainly due to the bridge effect also described elsewhere (*8, 10*). It was our aim to design new estradiol derivatives that behave as similarly to free estradiol as possible while using this antibody. Because of the aromatic A ring of estradiol, conjugations to the A ring do not cause any distortions in the core structure. In addition, our previous studies (*9*) show that this anti-estradiol antibody has 90% cross-reactivity to estradiol-4-derivative, which means that the antibody binds estradiol and estradiol-4-derivatives by almost the same selectivity. On the basis of the reasons above, we describe here the synthesis of some estradiol 4-alkyloxime and 4-thioether derivatives and their labeling with a europium chelate. These europium-labeled estradiol derivatives, called tracers, were briefly tested in a competitive time-resolved fluoroimmunoassay with the monoclonal anti-estradiol antibody in order to study their binding to the antibody and, thus, to find a useful estradiol derivative to be used as a panning antigen.

EXPERIMENTAL PROCEDURES

Materials. The reagents for syntheses were purchased from either Aldrich-Chemie, Fluka, Sigma, or E. Merck and used without further purification. Europium-labeled 6-oxoestradiol 6-(*O*-carboxymethyl)oxime (abbreviated as E2-6-CMO-Eu), the europium chelates used for labeling (*11*), and aminooxyalkylamines (*12*) and aminooxyalkanoic acids (*13*) were obtained from Wallac. The solvents

* To whom correspondence should be addressed, Medical Physics and Chemistry. E-mail: niko.meltola@utu.fi. Phone: +358 2 333 7057. Fax: +358 2 333 7060.

† Department of Biotechnology.

‡ Present address: InnoTrac Diagnostics Oy, Tykistökatu 6 A7, FIN-20520 Turku, Finland.

§ Wallac Oy.

10.1021/bc980013q CCC: $18.00 © 1999 American Chemical Society
Published on Web 03/13/1999

were p.a. grade from either E. Merck, Aldrich-Chemie, or Lab-Scan and were used as received unless otherwise stated. NMR spectra were recorded on either JEOL JNM-LA400 or JEOL JNM-A500 spectrometers using deuterated chloroform as a solvent and tetramethylsilane as internal standard. Mass spectra (MS) were recorded on a VG7070E spectrometer and IR spectra on a Perkin-Elmer 1600 FTIR spectrophotometer. The UV spectrum was recorded on a Shimadzu UV-2100 spectrophotometer. Thin-layer chromatography (TLC) plates and silica gel for short-column chromatography were obtained from E. Merck. Purification of the europium-labeled estradiol derivatives was performed using a Superdex Peptide column (Pharmacia) with UV detection at 276 nm (Uvicord UV Monitor from Pharmacia). The murine anti-estradiol antibody; SSI 57-2 (IgG_1, κ) was obtained from Statens Seruminstitut (Denmark). Rabbit anti-mouse IgG microtitration plates, 1234 DELFIA fluorometer, DELFIA assay buffer, DELFIA wash solution, and DELFIA enhancement solution were from Wallac.

4- and 2-Formylestra-1,3,5(10)-trien-3,17β-diol (2 and 3). A solution of ethylmagnesium bromide was prepared from magnesium turnings (410 mg, 16.9 mmol) and ethyl bromide (1.27 mL, 16.9 mmol) in sodium-dried diethyl ether (115 mL). 17β-Estradiol (**1**) (1.00 g, 3.67 mmol) in anhydrous toluene (270 mL) was added dropwise to this solution. Paraformaldehyde (0.88 g, 29.4 mmol) and triethyl phosphate were then added to the mixture. The mixture was heated at 80 °C for 20 h. Hydrochloric acid (5%) was added, and layers were separated. The aqueous layer was extracted with toluene/diethyl ether (1/1 v/v). Combined organic extracts were washed with water, dried over magnesium sulfate, filtered, and evaporated to dryness. The residue was chromatographed on a short silica gel column. Elution with chloroform (technical grade) gave a mixture of 4- and 2-formyl-17β-estradiol (**2** and **3**) 688 mg (62%).

*4-Formyl-17β-estradiol (**2**).* ^{1}H NMR (δ ppm): 12.00 (1H, s, ArOH), 10.38 (1H, s, CHO), 7.49 (1H, d, J = 8.9 Hz, H-1), 6.79 (1H, d, J = 8.9 Hz H-2), 3.74 (1H, m, H-17), 0.79 (3H, s, CH_3-18).

*2-Formyl-17β-estradiol (**3**).* ^{1}H NMR (δ ppm): 10.79 (1H, s, ArOH), 9.81 (1H, s, CHO), 7.43 (1H, s, H-1), 6.70 (1H, s, H-4), 3.74 (1H, m, H-17), 0.80 (3H, s, CH_3-18). IR (film): 3413, 2931, 2869, 1653, 1571, 1488, 1239 cm^{-1}.

4-Formylestra-1,3,5(10)-trien-3,17β-diol 4-[*O*-(5-carboxypentyl)]oxime (4) and 2-formylestra-1,3,5-(10)-trien-3,17β-diol 2-[*O*-(5-carboxypentyl)]oxime (5). A mixture of 4- and 2-formyl-17β-estradiol (**2** and **3**) (52.8 mg, 0.176 mmol) was dissolved in pyridine (0.5 mL), and 6-(aminooxy)hexanoic acid hydrobromide (40.0 mg, 0.176 mmol) was added. According to TLC (dichloromethane/methanol 10/1, v/v) the reaction occurred immediately. The reaction mixture was stirred overnight at room temperature and hydrochloric acid was added. The solution was extracted with ethyl acetate. The organic layer was washed with water and dried over sodium sulfate. After filtration, the solution was evaporated to dryness and purified by preparative TLC (2 mm silica gel plate) using dichloromethane and methanol (10/1, v/v) as an eluent. Extraction with dichloromethane/methanol (5/1, v/v) gave a mixture of desired 4- and 2-carboxypentyloxime derivatives (**4** and **5**) 48.8 mg (64%).

*4-Carboxypentyloxime Derivative (**4**).* ^{1}H NMR (δ ppm): 10.34 (1H, s, ArOH), 8.54 (1H, s, $-$CH$=$N$-$), 7.25 (1H, d, J = 8.8 Hz, H-1), 6.80 (1H, d, J = 8.8 Hz, H-2), 4.16 (2H, m, $=$N$-$O$-$CH$_2-$), 3.74 (1H, t, H-17), 0.78 (3H, s, CH_3-18).

*2-Carboxypentyloxime Derivative (**5**).* ^{1}H NMR (δ ppm): 9.66 (1H, s, ArOH), 8.11 (1H, s, $-$CH$=$N$-$), 7.02 (1H, s, H-1), 6.69 (1H, s, H-4), 4.16 (2H, m, $=$N$-$O$-$CH$_2-$), 3.74 (1H, t, H-17), 0.77 (3H, s, CH_3-18). IR (film): 3430, 2933, 2870, 1728, 1393, 1260 cm^{-1}.

4-Formylestra-1,3,5(10)-trien-3,17β-diol 4-[*O*-(6-Aminohexyl)]oxime (8) and 2-formylestra-1,3,5(10)-trien-3,17β-diol 2-[*O*-(6-aminohexyl)]oxime (9). A mixture of 4- and 2-formyl-17β-estradiol (**2** and **3**) (100 mg, 0.33 mmol) was dissolved in pyridine (1.5 mL), and 6-(aminooxy)hexylamine hydrochloride (379 mg, 1.66 mmol) was added. The reaction was complete in 1 h. Pyridine was evaporated and the residue was purified by preparative TLC using chloroform/methanol (10/3, v/v) as eluent. Extraction with the same solvent gave a mixture of 4- and 2-aminohexyloxime derivatives (**8** and **9**) 75 mg (54%).

*4-Aminohexyloxime Derivative (**8**).* ^{1}H NMR (δ ppm): 8.55 (1H, s, $-$CH$=$N$-$), 7.25 (1H, d, J = 8.8 Hz, H-1), 6.80 (1H, d, J = 8.8 Hz, H-2), 4.15 (2H, m, $=$N$-$O$-$CH$_2-$), 3.70 (1H, t, H-17), 0.77 (3H, s, CH_3-18).

*2-Aminohexyloxime Derivative (**9**).* ^{1}H NMR (δ ppm): 8.12 (1H, s, $-$CH$=$N$-$), 7.04 (1H, s, H-1), 6.69 (1H, s, H-4), 4.15 (2H, m, $=$N$-$O$-$CH$_2-$), 3.70 (1H, t, H-17), 0.77 (3H, s, CH_3-18). IR (film): 3376, 2928, 2863, 1628, 1385, 1265 cm^{-1}.

4-Formylestra-1,3,5(10)-trien-3,17β-diol 4-[*O*-(4-aminobutyl)]oxime (10) and 2-formylestra-1,3,5(10)-trien-3,17β-diol 2-[*O*-(4-aminobutyl)]oxime (11). A mixture of 4- and 2-formyl-17β-estradiol (**2** and **3**) (30 mg, 0.1 mmol) was dissolved in pyridine (1.0 mL), and 4-(aminooxy)butylamine hydrochloride (28 mg, 0.2 mmol) was added. The reaction mixture was stirred overnight at room temperature. Pyridine was evaporated and the residue was purified by preparative TLC using chloroform/methanol (10/3, v/v) as eluent. Extraction with the same solvent gave a mixture of 4- and 2-aminobutyloxime derivatives (**10** and **11**) 18 mg (47%).

*4-Aminobutyloxime Derivative (**10**).* ^{1}H NMR (δ ppm): 8.55 (1H, s, $-$CH$=$N$-$), 7.25 (1H, d, J = 8.8 Hz, H-1), 6.81 (1H, d, J = 8.8 Hz, H-2), 4.17 (2H, m, $=$N$-$O$-$CH$_2-$), 3.73 (1H, t, H-17), 0.78 (3H, s, CH_3-18).

*2-Aminobutyloxime Derivative (**11**).* ^{1}H NMR (δ ppm): 8.12 (1H, s, $-$CH$=$N$-$), 7.03 (1H, s, H-1), 6.70 (1H, s, H-4), 4.17 (2H, m, $=$N$-$O$-$CH$_2-$), 3.73 (1H, t, H-17), 0.78 (3H, s, CH_3-18). IR (film): 3332, 2923, 2871, 1627, 1385, 1265 cm^{-1}.

4,5-Epoxy-17β-hydroxyestran-3-one (17). 19-Nortestosterone (**16**) (980 mg, 3.57 mmol) was dissolved in methanol (100 mL) and the solution was cooled to 5 °C. Aqueous NaOH (5.4 mL, 4 M) and H_2O_2 (0.54 mL, 30%) were added, and the mixture was allowed to stand at 5 °C for 3.5 h. The solution was acidified with glacial acetic acid (2 mL), concentrated to 30 mL, diluted with water, and extracted with ethyl acetate. The organic layer was washed with $NaHCO_3$ (5% aq) and water, dried over sodium sulfate, and evaporated to dryness. The crude product (970 mg, 93%) was used for the next synthesis step without further purification.

^{1}H NMR (δ ppm): 3.66 (1H, t, J = 8.5 Hz, H-17), 3.04 (1H, s, H-4), 0.78 (3H, s, CH_3-18). ^{13}C NMR (δ ppm): 206.82 (C-3), 81.56 (C-17), 67.50 (C-5), 61.75 (C-4). IR (film): 1705 cm^{-1}.

4,5-Epoxy-17β-hydroxyestr-1-en-3-one (18). The crude 4,5-epoxy-17β-hydroxyestran-3-one (**17**) (900 mg, 3.10 mmol) was dissolved in 2-methyl-2-propanol (200 mL). Acetic acid (3 mL, glacial) and selenium dioxide (688 mg, 6.20 mmol) were added to the solution. The mixture was refluxed under nitrogen atmosphere for 42 h, filtered

through a Celite layer, and the filtrate was evaporated to dryness. The residue was dissolved in ethyl acetate, washed 3 times with $NaHCO_3$ (5% aq), washed once with water, and dried over sodium sulfate. After removal of the solvent, the product was purified by short-column chromatography on silica gel (petroleum ether/ethyl acetate, 5/2, v/v). Yield: 382 mg (43%).

^{1}H NMR (δ ppm): 6.77 (1H, dd, J = 10.5 and 5.4 Hz, H-1), 5.95 (1H, dd, J = 10.5 and 1.2 Hz, H-2), 3.65 (1H, t, J = 8.5 Hz, H-17), 3.24 (1H, s, H-4), 2.61 (1H, dd, J = 10.7 and 5.4 Hz, H-10), 0.82 (3H, s, CH_3-18). ^{13}C NMR (δ ppm): 196.03 (C-3); 148.32 (C-1); 124.95 (C-2); 81.52 (C-17); 63.86 (C-5); 61.91 (C-4). IR (film): 1682 cm^{-1}.

3,17β-Dihydroxyestra-1,3,5(10)-trien-4-(2-carboxyethyl)thioether (19). 4,5-Epoxy-17β-hydroxyestr-1-en-3-one (**18**) (415 mg, 1.44 mmol) was dissolved in methanol (4 mL), and Tris-HCl-buffer (4 mL, 0.2 M, pH 7.5) and mercaptopropionic acid (250 μL, 3.5 mmol) were added. The pH of the reaction mixture was adjusted to 9.0 with sodium hydroxide, and the mixture was stirred at 62 °C for 20 h. The mixture was washed with ethyl acetate, and the product was precipitated from aqueous layer by adjusting pH to 2.5 with hydrochloric acid. The product was filtered off, washed with water and dried in a vacuum desiccator. Yield: 411 mg (76%).

^{1}H NMR (δ ppm): 7.42 (1H, d, J = 8.5 Hz, H-1), 6.81 (1H, d, J = 8.5 Hz, H-2), 3.70 (1H, t, J = 8.5 Hz, H-17), 2.88 (2H, t, J = 7.1 Hz, Ar−S−CH_2−), 2.54 (2H, t, J = 7.1 Hz, −CH_2COOH), 0.77 (3H, s, CH_3-18). ^{13}C NMR (δ ppm): 174.19 (−COOH); 155.31 (C-3); 141.45 (C-5); 132.95 (C-10); 127.80 (C-1); 116.93 (C-4); 111.82 (C-2); 81.22 (C-17). IR (film): 1700 cm^{-1}. MS: 376 (M^+); 304 (M − CH_2CH_2COOH); 272 (M − SCH_2CH_2COOH). UV (EtOH): λ_{max} = 293 nm.

Labeling of Carboxy and Amino Derivatives of Estradiol with Europium Chelate. The carboxy derivatives of estradiol were labeled with 4-aminobenzyldiethylenetriaminetetraacetic acid europium chelate in a mixture of dioxane and 4-morpholineethanesulfonic acid buffer (0.5 M, pH 5.5) using 1-(3-dimethylaminopropyl)-3-ethylcarbodiimide as an activator. The reaction mixture was stirred for 2 h at room temperature, evaporated to dryness and the product was purified by preparative TLC using acetonitrile/water (2/1, v/v) as an eluent (*3*).

The amino derivatives of estradiol were labeled with 4-isothiocyanatobenzyldiethylenetriaminetetraacetic acid europium chelate in pyridine/water/triethylamine (90/15/1, v/v/v). After reaction (2 h), the solution was evaporated to dryness and the product was purified by preparative TLC using acetonitrile/water (2/1, v/v) as an eluent (*4*).

All the labeled estradiol derivatives were further purified on a Superdex Peptide column using 0.05 M Tris-HCl buffer [pH 7.5, containing 0.05 M NaCl and 20% (v/v) acetonitrile] as eluent. The fractions were detected by UV absorption at 276 nm and checked for europium content by DELFIA enhancement solution and time-resolved fluorometer as described later. The chromatogram of europium-labeled estradiol 4- and 2-carboxypentyloxime derivatives is shown by way of an example in Figure 1. The retention times of all europium-labeled estradiol derivatives obtained using a flow rate of 1 mL/min are given in Table 1.

Time-Resolved Fluoroimmunoassays. The synthesized and purified europium-labeled estradiol derivatives were tested in a time-resolved fluoroimmunoassay (*4*). Assays were carried out by adding 200 μL of anti-estradiol antibody (5 ng/mL) to prewashed rabbit anti-mouse IgG microtitration wells and, after a 2 h incubation, washing the wells four times with wash solution (DELFIA Platewash). The tracer solution (200 μL) was added, and after 2 h incubation, the unbound tracer was washed away. Enhancement solution (200 μL) was dispensed into the wells and incubated for 30 min in order to release the europium ion from the chelate into the solution and enhance the fluorescence. The enhanced fluorescence signal was then measured with the 1234 DELFIA research fluorometer. All the dilutions of antibody, estradiol and tracers were made in assay buffer and all the measurements were made in duplicate.

The affinity constants were determined by Scatchard analysis (*14*) of binding data obtained from the immunoassays described above. The amount of binding sites was titrated with increasing concentrations (0.05−20 nM) of labeled estradiol derivatives.

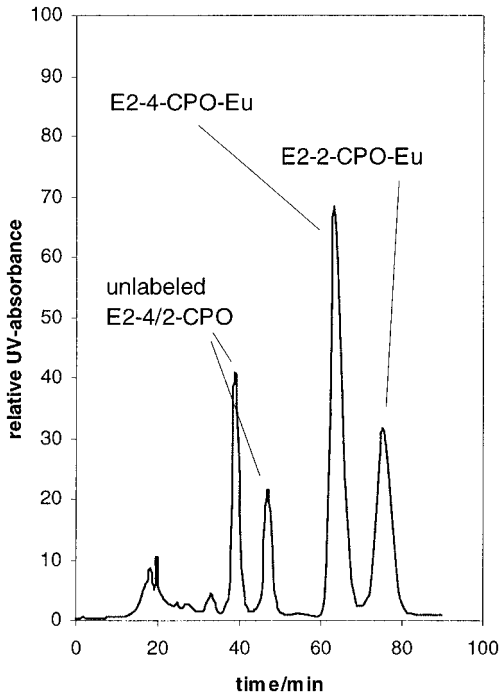
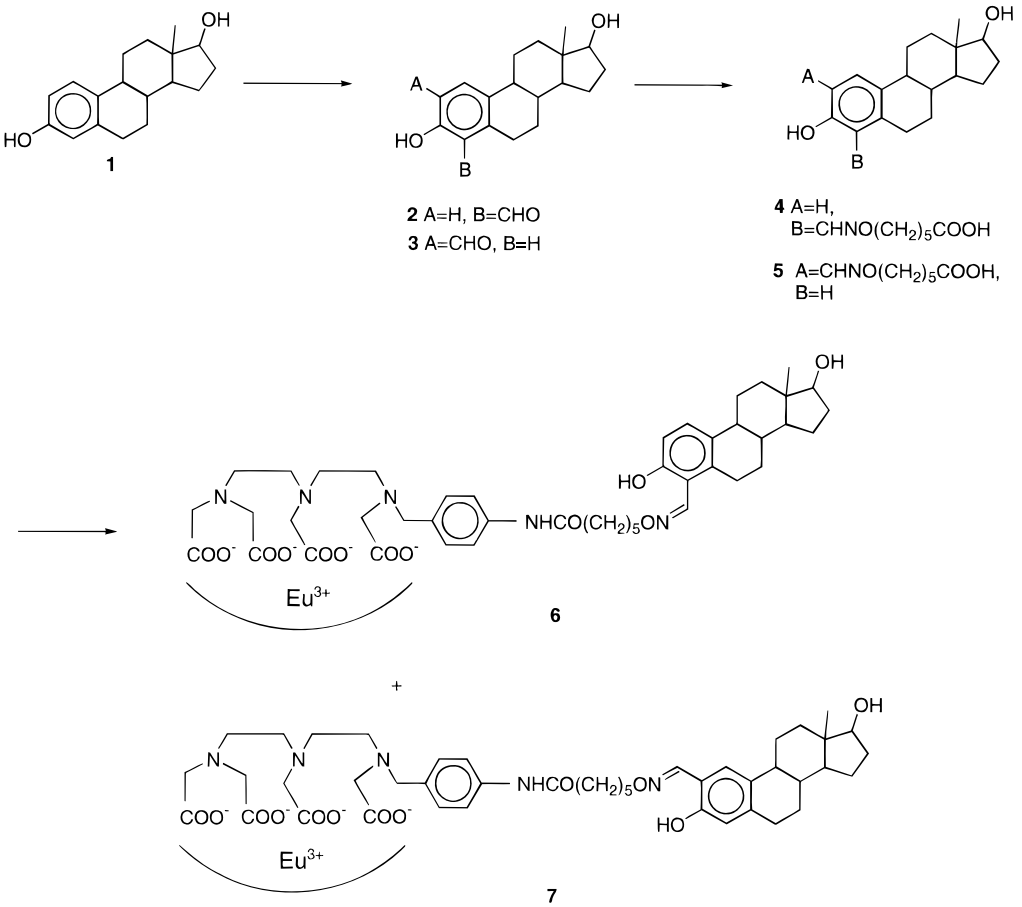


Figure 1. Purification of europium-labeled estradiol-4- and 2-carboxypentyloximes (E2-4-CPO-Eu and E2-2-CPO-Eu) (**6**, **7**).

Table 1. Retention Times of Europium-Labeled Estradiol Derivatives at Purification with Superdex Peptide Column

name	abbreviation	retention time (min)
4-formylestra-1,3,5(10)-trien-3,17β-diol 4-[*O*-(5-carboxypentyl)] oxime europium chelate	E2-4-CPO-Eu	63
2-formylestra-1,3,5(10)-trien-3,17β-diol 2-[*O*-(5-carboxypentyl)] oxime europium chelate	E2-2-CPO-Eu	75
4-formylestra-1,3,5(10)-trien-3,17β-diol 4-[*O*-(6-aminohexyl)] oxime europium chelate	E2-4-AHO-Eu	91
2-formylestra-1,3,5(10)-trien-3,17β-diol 2-[*O*-(6-aminohexyl)] oxime europium chelate	E2-2-AHO-Eu	106
4-formylestra-1,3,5(10)-trien-3,17β-diol 4-[*O*-(4-aminobutyl)] oxime europium chelate	E2-4-ABO-Eu	55
2-formylestra-1,3,5(10)-trien-3,17β-diol 2-[*O*-(4-aminobutyl)] oxime europium chelate	E2-2-ABO-Eu	61
estra-1,3,5(10)-trien-3,17β-diol 4-(2-carboxyethyl)thioether europium chelate	E2-4-CET-Eu	30

Scheme 1. Synthesis of Europium-Labeled Estradiol-4- and 2-Carboxypentyloximes (6, 7)



The standard curves for estradiol were obtained with competitive fluoroimmunoassay using double antibody technique (*4*), in which the anti-estradiol antibody was captured on to the solid phase by secondary antibody (anti-mouse IgG), whereafter estradiol standards were added together with the tracer to the wells. Estradiol inhibits the binding of the labeled derivative, resulting in a descending standard curve.

RESULTS AND DISCUSSION

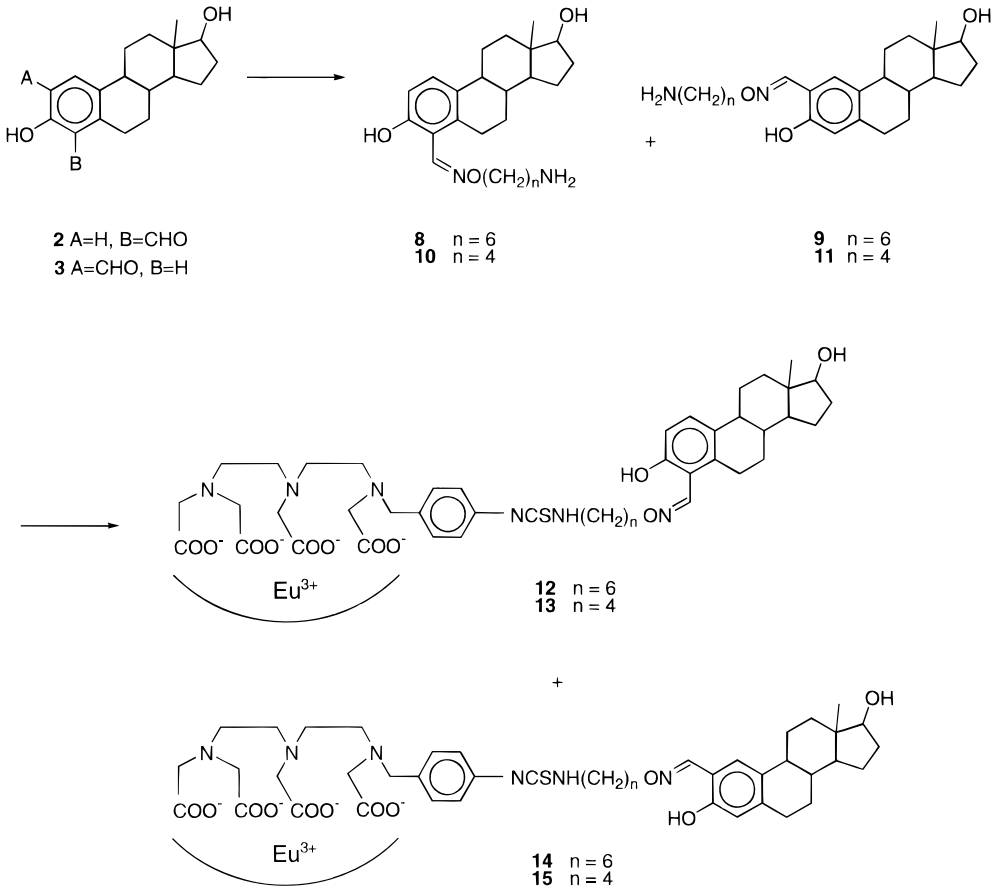
Syntheses. On the basis of our previous good experiences with oxime-type spacers (*4*, *12*, *15*), we synthesized estradiol-4 derivatives starting with the introduction of a formyl moiety into position 4. Selective formylation of estradiol into position 2 has been published by Brueggemeier et al. (*16*); however the regioisomeric 4-formylestradiol could not be obtained by this route. Pert et al. (*17*) have published the synthetic route for 2- and also for 4-formylestradiol. The synthesis of 4-formylestradiol seemed laborious, and the overall yield was quite low. The procedure that Xie et al. (*18*) have used for the formylation of 17α-ethynylestradiol seemed attractive, because in this procedure there is no need of protective groups, and both 2- and 4-formyl-17α-ethynylestradiol were obtained in a single step in relative good yield. We used the same procedure for the synthesis of 2- and 4-formylestradiol (Scheme 1). The reaction occurred smoothly and the product obtained was as expected, a mixture of 4-formylestradiol (**2**) and 2-formylestradiol (**3**) with a total yield of 62%. Total separation of these two isomers was laborious and unnecessary at this stage. For partial purification, we used a short silica gel column where the faster moving 4-formylestradiol (**2**) could be enriched from 1/5 to 3/2 for further reactions.

Introduction of the oxime linkers (Schemes 1 and 2) was performed by dissolving a mixture of formylestradiol into pyridine and adding aminooxy compounds into the solution (*12*). The reaction was complete in a few minutes due to the relatively high reactivity of the salicylaldehyde-type formylestradiol. The reaction mixture was stirred at room temperature for longer period to make sure there was no starting material left. The reaction conditions were not optimized and better results may be obtained by using another solvent or temperature. All estradiol-oxime derivatives, except for europium-labeled ones, were characterized as a mixture of two isomers using ^{1}H NMR and IR spectroscopy.

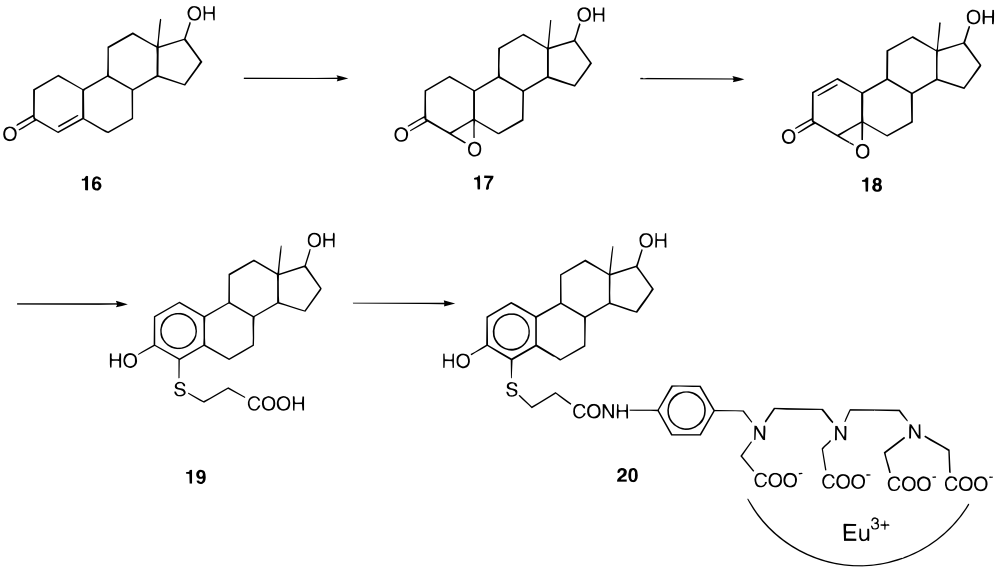
The thioether derivative (**19**) was synthesized (Scheme 3) starting from 19-nortestosterone (**16**) using previously published methods (*19*, *20*). The 19-nortestosterone (**16**) was converted to its epoxy derivative (**17**) by oxidation with alkalic hydrogen peroxide. The 4,5-epoxy-17β-hydroxyestran-3-one was obtained in 93% yield and was used for the next synthesis step without further purification. Oxidation with selenium oxide gave the desired 4,5-epoxy-17β-hydroxyestr-1-en-3-one (**18**) with 43% yield after purification by short-column chromatography. The previous two reactions were scaled up and compounds **17** and **18** were obtained in approximately the same yields (90 and 40%) as before. The mercaptopropionic acid was introduced into the 4,5-epoxy-17β-hydroxyestr-1-en-3-one (**18**) by modifying the method of Ghaffari et al. (*21*). The product (**19**) was obtained in 76% yield. The estra-1,3,5(10)-trien-3,17β-diol 4-(2-carboxyethyl)thioether (**19**) was characterized using ^{1}H NMR, ^{13}C NMR, IR, and UV spectroscopy. Mass spectrometry was also used to confirm the desired structure.

All the synthesized estradiol amino and carboxy de-

Scheme 2. Synthesis of Europium-Labeled Estradiol-4- and 2-aminoalkyloximes (12-15)



Scheme 3. Synthesis of Europium-Labeled Estradiol-4-(2-carboxyethyl)thioether (20)



rivatives were labeled with europium chelate and purified using first preparative TLC and then HPLC on a Superdex Peptide column (Table 1 and Figure 1).

Tracer Testing. For testing of the tracers, we used a buffer-based model system. The results from the affinity measurements, analyzed according to the Scatchard equation (*14*), are shown in Figure 2. As expected, the affinity of the anti-estradiol antibody to europium-labeled 6-oxoestradiol-6-CMO used as an internal standard was the highest because it was the immunogen used to raise the antibody. Estradiol-4-derivatives have considerably lower affinity as shown in Figure 2 and Table 2. In general, antibodies are expected to have lower affinity to steroids, which differ from the immunogen with regard to positions where direct contact is made with antibody side chains (*22*). The chemical structure of the linkage between the label and steroid also affects the process of the antibody recognition (*2*). This has also been observed in our studies. The antibody had a higher affinity to the thioether derivative than to the oxime derivatives when coupled to position C-4 of estradiol (Figure 2). This can be explained by hydrogen bond between oxime-nitrogen

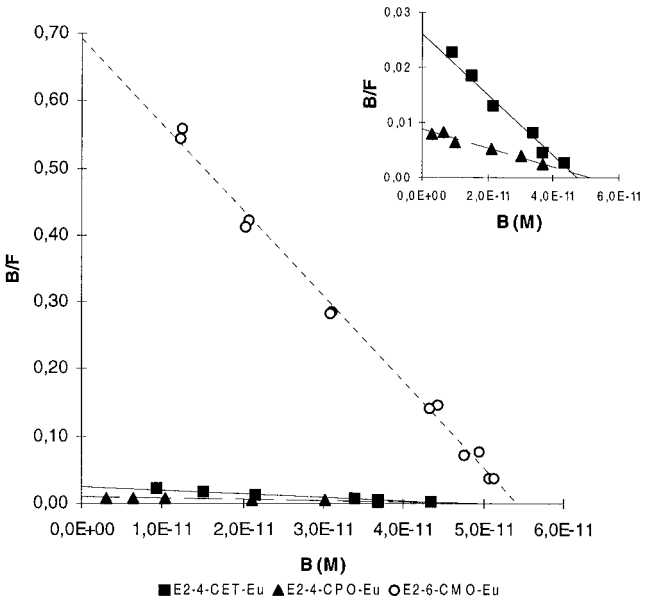


Figure 2. Scatchard analysis of equilibrium binding data for an anti-estradiol antibody. The plot includes only one oxime-derivative by the way of an example. Each point is the mean of two determinations.

Table 2. IC_{50} Values, Signal Levels, and Affinities of the Tested Estradiol Tracers

tracer	IC_{50}[a] (nM)	corr B_o[b] (cps)	bg[c] (cps)	K_a (M^{-1})
E2-6-CMO-Eu	8.1	37 068	477	1.3×10^{10}
E2-4-CPO-Eu	4.0	36 182	5148	1.7×10^{8}
E2-4-AHO-Eu	4.9	43 288	12 222	1.9×10^{8}
E2-4-CET-Eu	6.1	35 773	729	5.5×10^{8}
E2-4-ABO-Eu	7.8	34 366	10 978	1.6×10^{8}

[a] IC_{50} values are determined as estradiol concentration for 50% displacement of maximum binding in the absence of unlabeled estradiol. [b] Signal in the absence of unlabeled estradiol. [c] Instrumental background and nonspecific binding.

and 3-hydroxyl group, which obviously has a negative effect on antibody recognition.

In summary, all the tested europium-labeled estradiol-4-derivatives were bound by the antibody (SSI 57-2), whereas tracers linked via position 2 were not recognized by this antibody. This was anticipated because in the previous studies (*9*), the same antibody had only slight cross-reactivity with estradiol-2-derivatives. Figure 3 shows estradiol standard curves with three different tracers. The curves show a trend in sensitivity depending on the position of the linkage. Tracers conjugated via C-4 give more sensitive standard curves than tracers conjugated via C-6. This can also be seen in Table 2, where IC_{50} values are lower when using tracers conjugated via C-4. The reason for higher background signal with oxime derivatives is unspecific binding, resulting partly from the higher tracer concentration needed because of the lower affinity of these derivatives.

Our results demonstrate that the new estradiol derivatives synthesized here, especially the thioether derivative, are useful tracers in the immunochemical characterization of the anti-estradiol Mab SSI 57-2. Because this antibody is a representative of a large group of monoclonal antibodies raised with estradiol-6-CMO conjugates, we foresee that our tracers will be potentially suitable for the other Mabs, too. Furthermore, as these new conjugates do not exhibit considerable bridge effect (unlike the 6-CMO derivatives), they could be used as panning antigens in the search of improved anti-E2-6-CMO antibody variants from large mutant libraries using

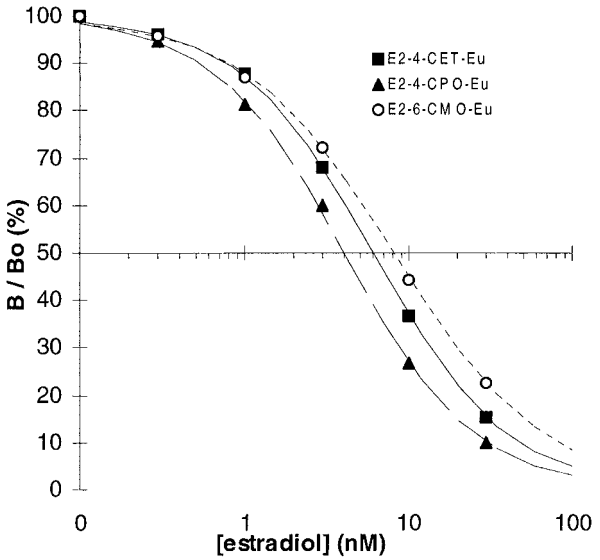


Figure 3. Estradiol displacement curves with different europium-labeled estradiol derivatives in the time-resolved fluoroimmunoassay. *B* is binding at the estradiol concentration indicated, B_o is maximum binding without unlabeled estradiol.

the phage display technology (*23*). When used as a panning antigen, these estradiol derivatives can be conjugated with biotin instead of a europium chelate. We are currently using such biotinylated estradiol-4-thioether derivative for the panning of a mutant phage library derived from Mab SSI 57-2 (to be published elsewhere).

ACKNOWLEDGMENT

We are grateful to Dr. V.-M. Mukkala for his valuable advise in the field of synthetic chemistry. This work was supported by Academy of Finland and Technology Development Centre Finland.

LITERATURE CITED

(1) Pratt, J. J. (1978) Steroid immunoassay in clinical chemistry. *Clin. Chem. 24*, 1869−1890.

(2) Tiefenauer, L. X., and Andres, R. Y. (1990) Biotinyl-estradiol derivatives in enzyme immunoassays: Structural requirements for optimal antibody binding. *J. Steroid Biochem. 35*, 633−639.

(3) Mikola, H., and Miettinen, P. (1991) Preparation of europium labeled derivatives of cortisol for time-resolved fluoroimmunoassays. *Steroids 56*, 17−21.

(4) Mikola H., Sundell, A.-C., and Hänninen, E. (1993) Labeling of estradiol and testosterone alkyloxime derivatives with a europium chelate for time-resolved fluoroimmunoassays. *Steroids 58*, 330−334.

(5) Soini, E., and Lövgren, T. (1987) Time-resolved fluorescence of lanthanide probes and applications in biotechnology. *CRC Crit. Rev. Anal. Chem. 18*, 105−154.

(6) Lövgren, T., Hemmilä, I., Pettersson, K., and Halonen, P. (1985) Time-resolved fluorometry in immunoassays. In *Alternative immunoassays* (W. P. Collins, Ed.) Wiley, Chichester, NY.

(7) Lövgren, T. (1987) Time-resolved fluoroimmunoassays of steroid hormones. *J. Steroid Biochem. 27*, 47−51.

(8) Tiefenauer, L. X., Bodmer, D. M., Frei, W., and Andres, R. Y. (1989) Prevention of bridge binding in immunoassays: a general estradiol tracer structure. *J. Steroid Biochem. 32*, 251−257.

(9) Lamminmäki, U., Villoutreix, B. O., Jauria, P., Vihinen, M., Nilsson, L., Teleman, O., Saviranta, P., and Lövgren, T. (1997) Structural analysis of an anti-estradiol antibody. *Mol. Immunol. 34*, 1215−1226.

(10) Allen, R. M., and Redshaw, M. R. (1978) The use of homologous and heterologous ^{125}I-radioligands in the radioimmunoassay of progesterone. *Steroids 32*, 467−486.
(11) Mukkala, V.-M., Mikola, H., and Hemmilä, I. (1989) The synthesis and use of activated N-benzyl derivatives of diethylenetriaminetetraacetic acids: Alternative reagents for labeling of antibodies with metal ions. *Anal. Biochem. 176*, 319−325.
(12) Mikola, H., and Hänninen, E. (1992) Introduction of aliphatic amino and hydroxy groups to ketosteroids using O-substituted hydroxylamines. *Bioconjugate Chem. 3*, 182−186.
(13) Mikola, H. (Unpublished results).
(14) Scatchard, G. (1949) The attractions of proteins for small molecules and ions. *Annals. N. Y. Acad. Sci. 51*, 660−672.
(15) Meltola, N., and Mikola, H. (unpublished results).
(16) Lovely, C. J., and Brueggemeier, R. W. (1994) Synthesis of 2-substituted hydroxyalkyl and aminoalkyl estradiols. *Tetrahedron Lett. 35*, 8735−8738.
(17) Pert, D. J., and Ridley, D. D. (1989) Formylation of oestrogens. *Aust. J. Chem. 42*, 405−419.
(18) Xie, R., Chen, Q., Xie, J., and Zhao, H. (1990) A new efficient synthetic method for 2- and 4-hydroxy-17α-ethynylestradiol. *Steroids 55*, 488−490.
(19) Mihailovic, M. Lj., Forsek, J., and Lorenc, Lj. (1977) A novel procedure for the aromatization of ring A in 19-nortestosterone. *Tetrahedron 33*, 235−237.
(20) Le Quesne, P. W., Abdel-Baky, S., Durga, A. V., and Purdy, R. H. (1986) Active nonaromatic intermediates in conversion of the steroidal estrogens into catechol estrogens. *Biochemistry 25*, 2065−2072.
(21) Ghaffari, M. A., and Abul-Hajj, Y. J. (1990) Reaction of thiol nucleophiles with 1,2-epoxy-and 4,5-epoxy-estrene-3-one-17β-ols. *J. Steroid Biochem. Mol. Biol. 37*, 237−244.
(22) Gani, M., Coley, J., Piron, J., Humphrey, A. S., Arevalo, J., Wilson, I. A., and Taussig, M. J. (1994) Monoclonal antibodies against progesterone: effect of steroid-carrier coupling position on antibody specificity. *J. Steroid Biochem. Mol. Biol. 48*, 277−282.
(23) Hoogenboom, H. R., Griffiths, A. D., Johnson, K. S., Chiswell, D. J., Hudson, P., and Winter, G. (1991) Multi-subunit proteins on the surface of filamentous phage: Methodologies for displaying antibody (Fab) heavy and light chains. *Nucleic Acids Res. 19*, 4133−4137.

BC980013Q

Toward an in Vitro Test for the Diagnosis of Allergy to Penicillins. Synthesis, Characterization, and Use of β-Lactam and β-Lactam Metabolite Poly-L-lysines Which Recognize Human IgE Antibodies

Ezio Bolzacchini, Viviana Consonni, Paola Gramatica, Simone Meinardi, Marco Orlandi, Bruno Rindone,* and Roberto Todeschini

Dipartimento di Scienze dell'Ambiente e del Territorio, Universita' di Milano, Via Emanueli 15, I-20126 Milano, Italy

Miguel Blanca and Cristobalina Mayorga

Carlos Haya Hospital, Malaga, Spain. Received February 3, 1998; Revised Manuscript Received December 18, 1998

Conjugates of poly-L-lysine (PLL) containing a penicillin or a penicilloyl residue were prepared and characterized by ^{1}H NMR and by size-exclusion (SE) HPLC. These conjugates were used in a radio allergo sorbent tests (RAST) test for the determination of allergy toward β-lactams. The chemiometric evaluation of the data indicates that allergy to amoxycillin is different from allergy to the other β-lactams tested. Furthermore, careful chemical characterization of the conjugates appears to be crucial to obtain meaningful information from the RAST data.

INTRODUCTION

Despite a recent claim suggesting the overestimation of allergy to penicillin (*1*), most research groups agree with the importance of this pathology (*2*), which may cause severe health problems (*3*).

Hypersensitivity reactions to β-lactams are the most frequent type of adverse drug reaction mediated by an immunological mechanism (*4*, *5*). Penicillin allergy has been deeply studied and considered to be the model for drug allergy (*6*−*8*).

Penicillins are low molecular weight substances which are not themselves antigenic but give rise to a number of different antigenic determinants either by metabolism in vivo or by breakdown in vitro before administration (*9*).

In early studies with benzylpenicillin in man and animals (*10*, *11*), it was demonstrated that penicillin interacts covalently with serum proteins (*12*) forming immunogenic conjugates (*13*) which can produce severe anaphylactic reactions.

The major antigenic determinant is the penicilloyl group derived from the cleavage of the β-lactam ring of penicillin (*12*), and many allergic reactions to penicillin are due to antibodies specific to this group (*14*). Other β-lactam cleavage products may also act as haptens and are known as "minor determinants" (*15*). These are associated with the majority of the severe immediate reactions to penicillin G (*16*). Human IgE to penicillin itself has been clearly documented in a previous paper (*17*).

Skin tests are often used for the diagnosis of penicillin allergy (*18*−*21*). These appear to be positive in approximately 60% of predictive cases in allergic reaction to penicillin or its derivatives (*22*). The materials used for "in vivo" tests are essentially penicillin−poly-L-lysine conjugates (*23*). Several "in vitro" tests for the determination of allergy to penicillin derivatives are also based on penicillin−protein conjugates (*24*). Penicillin-related RAST requires a carrier-drug structure to present the drug molecule to the specific antibody (*25*). These conjugates are not generally chemically well characterized, and this has a consequence in the uncertainty about the structure of the determinant(s).

A chemical characterization of these compounds is also necessary since penicillin conjugates with tissue macromolecules (proteins, carbohydrates, and lipids) are the compounds which elicit antibody formation (*26*, *27*). Moreover, knowledge of the structure of the antigenic determinants of penicillin conjugates may allow the preparation of monovalent derivatives which could be used to desensitize patients prior to administration of the drug (*28*).

EXPERIMENTAL PROCEDURES

Instrumentation. NMR spectra were measured in D_2O at 25 °C using a Bruker AC300 instrument. HPLC analyses were performed with a Waters 600E HPLC. The detector was a Hewlett-Packard 1040 Diode Array Detector. The γ-counter was a Packard Cobra instrument.

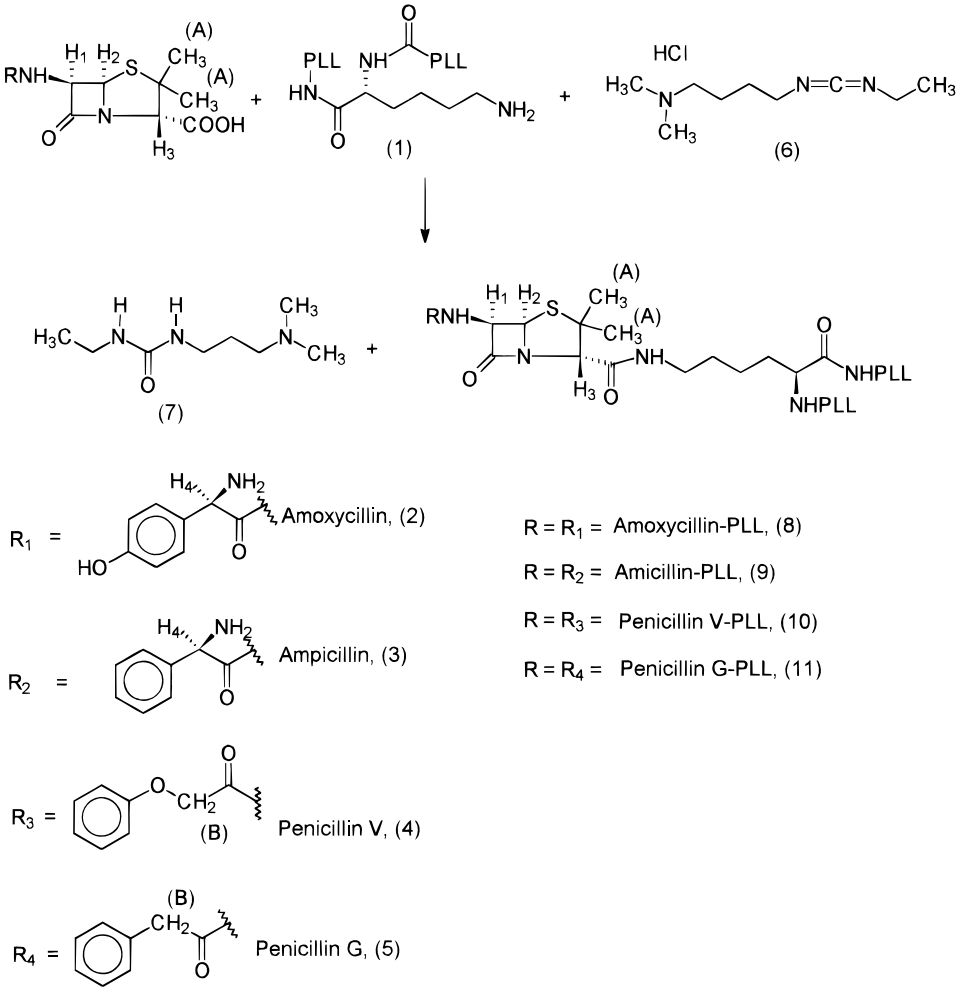
Reagents. Poly-L-lysine (L-PLL) hydrobromide ($n \approx 145$) was purchased from Sigma Chemicals, *N*-(3-dimethylaminopropyl)-*N*′-ethylcarbodiimide (ECDI) was an Aldrich product; all the β-lactam antibiotics were Farmitalia Carlo Erba products. Membranes for dialysis were Spectra/Por products. Paper disks were activated with cyanogen bromide. Labeled, affinity purified, anti-human IgE from goat was a Pharmacia product.

Preparation of the Conjugates. A total of 0.09 mmol of β-lactam was added to a solution of L-PLL (*1*) (13 mg, 0.0007 mmol) in 5 mL of 0.2 M aqueous buffer, pH 7.2 (K_2HPO_4/KH_2PO_4) (or 0.2 M aqueous buffer, pH 8.5 for K_2HPO_4/KH_2PO_4), and the resulting solution was stirred

* To whom correspondence should be addressed. Phone: ++39 02 64474302. Fax: ++39 02 64474300. E-mail: Bruno.Rindone@unimi.it.

10.1021/bc980023r CCC: $18.00 © 1999 American Chemical Society
Published on Web 04/08/1999

Scheme 1



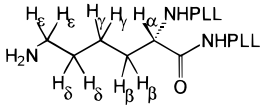
at 4 °C. After 5 min, 17 mg (0.09 mmol) of *N*-(3-dimethylaminopropyl)-*N′*-ethylcarbodiimide (*10*) was added, and this solution was stirred at 4 °C for 12 h. Low molecular weight reagents and byproducts were removed by dialysis for 120 h at 4 °C with a 3500 Da cutoff membrane. The product was then obtained by lyophilization.

Radio Allergo Sorbent Test (RAST). RAST assays were carried out as previously described (*25*, *29*, *30*). Cyanogen bromide activated cellulose disks were used as the solid phase. The disks were bound to different conjugates. This was made in duplicate using 30 μL of serum and 30 μL of radiolabeled anti-IgE antibody (Pharmacia, Uppsala, Sweden). Results obtained were expressed as percentage of label uptake respect to the maximum counts after subtracting the uptake of the respective carrier single disk. Optimal cutoff points between positive and negative were determined by receiver operator control curves (ROC) using a negative control group of subjects with no history of allergy to penicillin and a negative skin test to all the penicillin determinants (*31*).

RESULTS AND DISCUSSION

The reaction of poly-L-lysine (L-PLL-NH_2), **1**, average MW, 20 kDa (*32*) with excess penicillins [amoxycillin (**2**, AXO), ampicillin (**3**, AMP); penicillin V (**4**, PV); penicillin G (**5**, PG)] (Scheme 1) was performed at pH 7.2, in the presence of the water-soluble carbodiimide **6** (ECDI) (*33*), and gave, after extensive dialysis at 0 °C, the conjugates **8**−**11**. These were constituted of a family of poly-L-lysines derivatized at the primary amino group at C_ϵ with a β-lactam fragment. The lysine residue resonated as shown in Table 1. This resulted from the ^{1}H NMR spectrum in D_2O.

Table 1



PLL	H_α	H_β	H_γ	H_δ	H_ϵ
Amoxycillin-PLL, **8**	4.25 (t)	1.75 (m)	1.40 (t)	1.75 (m)	3.00 (t)
Ampicillin-PLL, **9**	4.25 (t)	1.75 (m)	1.40 (t)	1.75 (m)	3.00 (t)
Penicillin V-PLL, **10**	4.30 (t)	1.75 (m)	1.45 (m)	1.75 (m)	3.00 (s)
Penicillin G-PLL, **11**	4.30 (m)	1.70 (m)	1.40 (m)	1.70 (m)	3.00 (s)

The NMR signals of the β-lactam-derived part of the molecule are shown in Table 2, together with the signals of the parent β-lactam. In the preparations performed at pH 7.2 and 4 °C, H_1 and H_2 appeared in the region δ 5.20−5.60, respectively, with a $J = 5-7$ Hz. Hence, they were in the same position and had the same multiplicity as the corresponding protons in the starting materials. In particular, the coupling constants showed also that the chirality at C_6 and C_7 had been retained. The aromatic hydrogens of the penicillin residue appeared at δ 7.30−7.50 as multiplets. These attributions were confirmed by ^{1}H-COSY experiments.

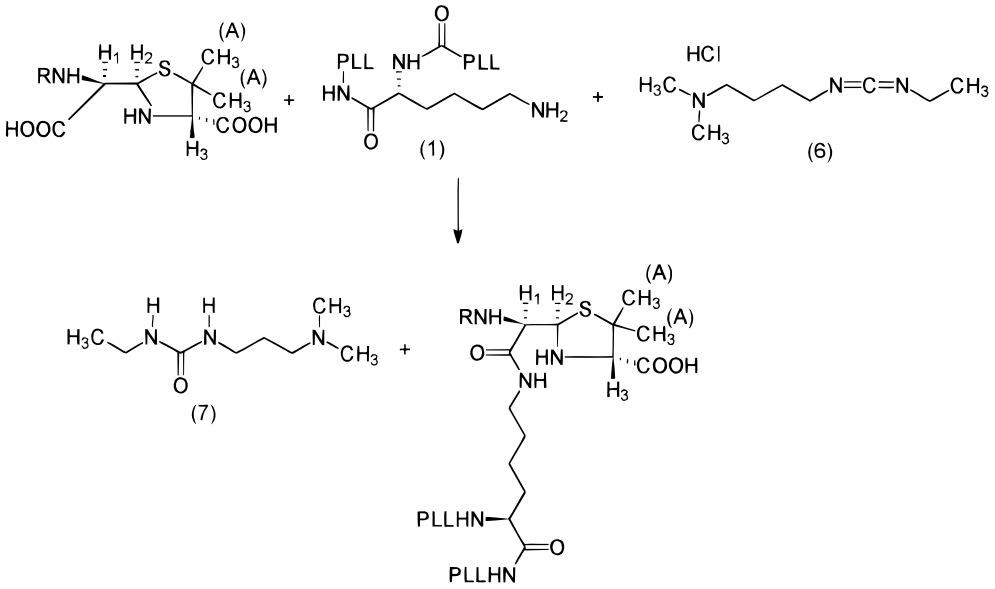
The integration of the aromatic protons and H_α suggested that the family of derivatized poly-L-lysine mol-

Table 2. ^{1}H NMR Spectra of β-Lactams and β-Lactam−poly-L-lysine Conjugates in D_2O at Different pHs (δ = ppm; J = Hz)

	amoxycillin, **2**	amoxycillin-PLL, **8**	amoxycilloyl-PLL, **12**		amoxycillin, **2**	amoxycillin-PLL, **8**	amoxycilloyl-PLL, **12**
H_1	5.60 (d) $J = 4.7$	5.60 (d) $J = 6.0$	*a*	CH_3 (A)	1.50 (s)	1.50 (s)	*a*
H_2	5.70 (d) $J = 4.7$	5.70 (d) $J = 6.0$	*a*	CH_3 (B)	1.45 (s)	1.50 (s)	*a*
H_3	4.20 (s)	4.80 (s)	*a*	H Ar	6.80 (d) $J = 8.8$	6.80 (m)	6.90 (m)
H_4	4.96 (s)	4.80 (s)	*a*		7.50 (t) $J = 8.8$	7.50 (m)	7.35 (m)
	ampicillin, **3**	ampicillin-PLL, **9**	ampicilloyl-PLL, **13**		ampicillin, **3**	ampicillin-PLL, **9**	ampicilloyl-PLL, **13**
H_1	5.50 (d) $J = 5.8$	5.60 (m)	4.20 (d) $J = 7.1$	H_4	5.20 (s)	5.60 (s)	4.60 (s)
H_2	5.50 (d) $J = 5.8$	5.60 (m)	5.10 (d) $J = 7.1$	CH_3 (A)	1.40 (s)	1.35(s)	1.15 (s)
H_3	4.10 (s)	4.35 (s)	3.25 (s)	H Ar	7.50 (m)	7.50 (m)	1.30 (s)
	penicillin V, **4**	penicillin V-PLL, **10**	penicilloyl V-PLL, **14**		penicillin V, **4**	penicillin V-PLL, **10**	penicilloyl V-PLL, **14**
H_1	5.60 (d) $J = 4.2$	5.45 (d) $J = 5.0$	4.30 (d) $J = 5.0$	CH_2 (B)	4.75 (m)	4.70 (m)	4.70 (m)
H_2	5.60 (d) $J = 4.2$	5.55 (d) $J = 5.0$	5.00 (d) $J = 5.0$	H Ar	7.10 (m)	7.00 (m)	7.10 (m)
H_3	4.20 (m)	4.20 (m)	3.50 (s)		7.50 (m)	7.40 (m)	7.40 (m)
CH_3 (A)	1.50 (s)	1.50 (s)	1.20 (s) 1.50 (s)				
	penicillin G, **5**	penicillin G-PLL, **11**	penicilloyl G-PLL, **15**		penicillin G, **5**	penicillin G-PLL, **11**	penicilloyl G-PLL, **15**
H_1	5.40 (d) $J = 7.2$	5.40 (d) $J = 10.0$	4.80 (d) $J = 8.0$		1.55 (s)	3.65 (m)	1.60 (s)
H_2	5.50 (d) $J = 7.2$	5.50 (d) $J = 10.0$	5.10 (d) $J = 8.0$	CH_2 (B)	3.65 (t)	3.65 (m)	3.70 (m)
H_3	4.20 (s)	4.10 (s)	3.40 (s)	H Ar	7.35 (m)	7.40 (m)	
CH_3 (A)	1.45 (s)	1.60 (s)	1.30 (s)				

[a] Complex mixture of ring fission products.[a]

Scheme 2



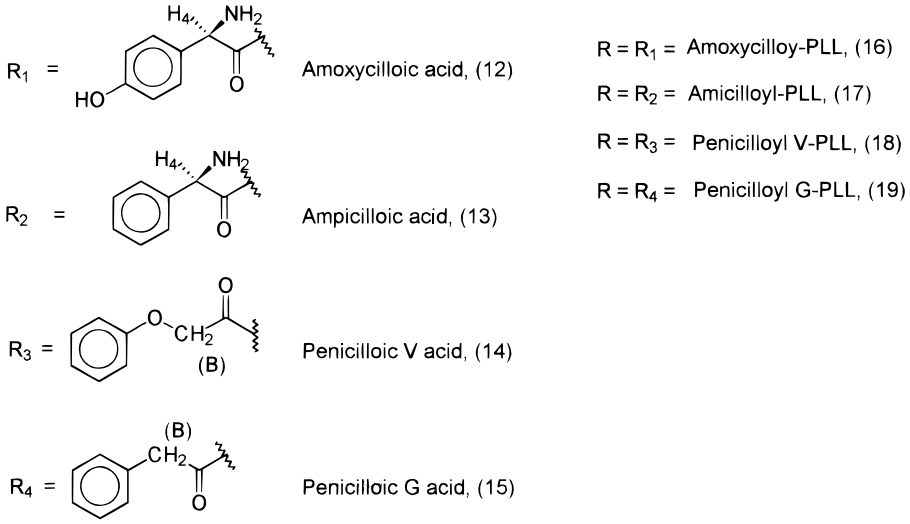


Table 3. Hapten Density for the Different Hapten−Poly-L-lysine Conjugates

	% hapten/PLL	hapten/Lys
amoxycillin-PLL, **8**	9.00	10.8
ampicillin-PLL, **9**	9.50	10.5
penicillin V-PLL, **10**	8.60	11.6
penicillin G-PLL, **11**	10.1	9.91
amoxycilloyl-PLL, **12**	12.0	8.30
ampicillyl-PLL, **13**	7.00	14.1
penicilloyl V-PLL, **14**	8.60	11.6
penicilloyl G-PLL, **15**	16.0	6.24

ecules constituting the conjugate contained the hapten density shown in Table 3. This evaluation of hapten density of a polypeptide or a protein turned out to be by far more precise that the spectrophotometric determination.

It has been pointed out that a too low percent haptenization of the protein carrier lowers the effectiveness of the conjugate in eliciting Wheal-and-Flare in penicillin-sensitized human subjects (*34*). Using penicilloylated bovine serum albumin (BSA) as the immunizing antigen in mice, it was found that an epitope number higher than 11 penicilloyl residues/protein molecule induces significant antibody formation after a single injection, whereas 0.6 penicilloyl residues/BSA molecule do not induce penicilloyl-specific antibodies (*35*).

When the reaction of the β-lactam was performed at alkaline pH (8.5), this resulted in the formation of a different type of conjugate **12**−**15**. In fact, Table 1 shows the opening of the β-lactam ring, thus allowing the conjugation with L-PLL via the carboxylic acid resulting from the cleavage of the β-lactam ring (Scheme 2). In the reaction of amoxycillin **2** at pH 8.5, the resulting mixture was constituted of amoxycilloyl-PLL **12,** 60%, and a complex mixture of other ring fission products (Scheme 2).

Other authors have prepared penicillin−L-polylysine conjugates. The alkaline pH was generally used. In particular, a recent synthetic method (*36*) forms a benzylpenicilloyl−L-polylysine (BPO-L-PLL), and this conjugate has been used in the determination of IgE antibodies to the BPO determinant (*30*).

All the conjugates previously described were then used in a RAST (*37*). The conjugates were immobilized in paper disks and used to test the presence of human IgE antibodies in the sera of some 30 patients known to be allergic to penicillins. Ten sera had been shown by conventional clinical tests to be only specific to amoxycillin (group A), 10 other sera were shown by conventional clinical tests to be specific only to penicillin G (group B), and further 10 sera where shown by conventional clinical tests to be positive to both amoxycillin and penicillin G (group C). The results are shown in Table 4.

The principal component analysis (PCA) (*38*) was used to evaluate the information contained in the experimental data (distribution, clusters, outliers, etc.) and the relationships among the variables. PCA was performed on the experimental data (30 patient sera × 8 β-lactams, Table 4); the first three principal components explain 95% of the total data variability.

The meaning of the PCs and the relationships among the variables were evaluated from the two biplots PC1 vs PC2 and PC1 vs PC3 (i.e., the contemporary scatter plot of both loadings and scores). The first component is the allergenic power of all the combined considered drugs (81% of explained variance); the second component is the

Table 4. RAST Analysis of the Sera[a]

serum no.	PG-PLL 7.2	PG-PLL 8.5	PV-PLL 7.2	PV-PLL 8.5	AX-PLL 7.2	AX-PLL 8.5	AMP-PLL 7.2	AMP-PLL 8.5
				Sera Specific to Amoxycillin				
1	6.31	3.85	1.42	2	9.13	8.7	4.77	13.7
2	0.64	2.9	1.05	1.9	1.62	2.2	0.59	7.3
3	2.14		2.07		2.99		2.03	
4	5.41	0.1	0.92	1.24	34.21	31.71	0.07	9.51
5	0.79	0.32	1.44	0.67	0.99	5.39	0.55	2.95
6	0.26	0.15	0	0.65	1.09	26.88	0	7.77
7	0.21	0	0.25	0.48	0.19	0.30	0.25	0.09
8	0	0	0.18	0.17	0	0	0.04	0.01
9	0.28	0.16	0.36	0.25	0.30	0.43	0.11	3.19
10	0.18	0	0.18	0.13	0.28	0	0.23	0
				Sera Specific to Penicillin G				
11	8.07	6.24	10.74	4.44	2.63	0.34	1.88	3.94
12	27.13	30.5	23.07		12.04		10.64	
13	11.15	17.6	13.41	12.1	3.06	1	3.06	15.7
14	0.68	0.76	9.71	0.60	0.85	0.10	0.72	0.18
15	1.07	0.75	2.48	0.75	0.89	0	0.62	0.13
16	4.78	6.5	5.58		0.57	0.42	0.86	5.27
17	0.18	3.7	0.06	2.89	0	0	0.02	13.44
18	0	0.47	0.02		0	0.26	0	1.68
19	0	3.82	0	1.32	0	0	0	0.18
20	2.15	4.66	0.92	1.47	1.72	0.01	0.03	2.65
				Sera Specific to Amoxycillin and Penicillin G				
21	0.72	0.3	1.96	2.7	0.06	0.5	0.79	9.3
22	0.72	0.4	0.06	0.8	0.59	0.5	0.77	0.7
23	53.21	76.4	48.35	43.1	28.06	46.1	26.16	85.1
24	22.05	16.19	21.13	2.62	1.77	2.61	3.72	20.65
25	5.02	1.95	6.33	2.3	4.11	1.72	2.91	3.59
26	0.19	0.18	0.03	0.39	0.15	1.46	0.06	13.57
27	1.74	2.70	1.08	2.09	0.43	0.81	0.48	2.36
28	0	1	0	0.27	0	0	0	11.87
29	8.81	12.2	6.32	8.57	0.12	5.89	0.54	15.54
30	9.37	8.22	0.33	6.65	8.03	14.11	6.53	15.66

[a] Results were expressed as percentage of label uptake respect to the maximum counts of radiolabeled anti IgE added.

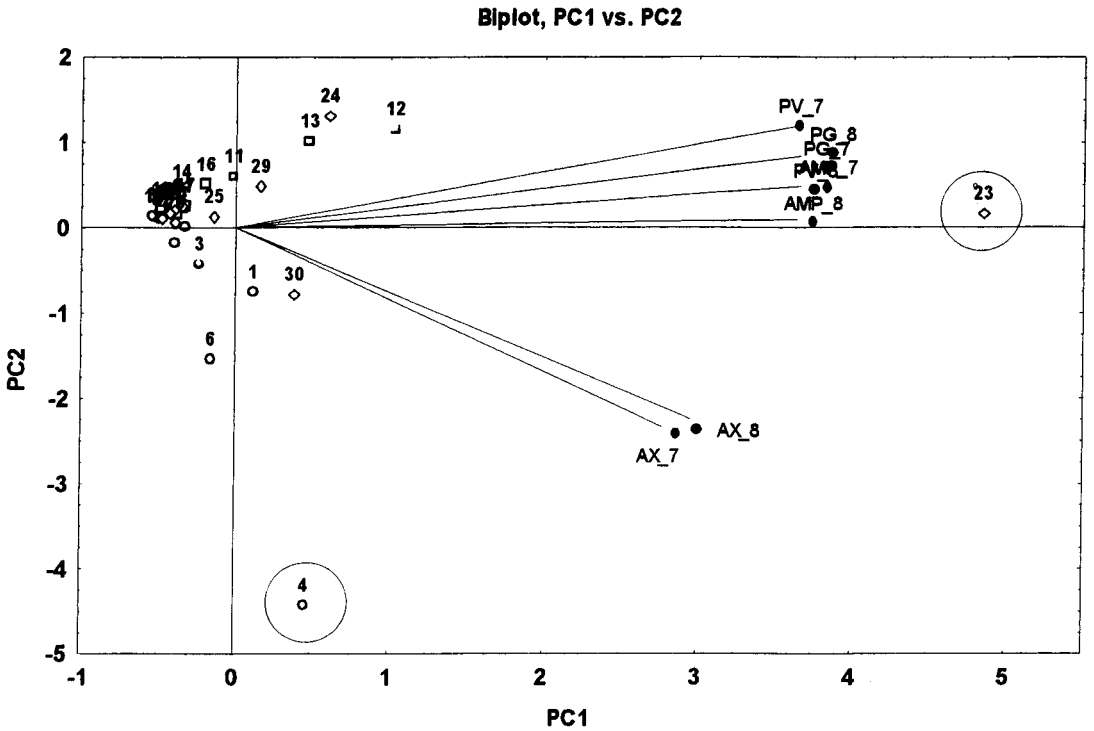


Figure 1. Biplot PC1 vs PC2. Variables in black (loadings); samples (patient sera) are divided in allergic to amoxycillin (circles), allergic to penicillin G (squares), and allergic to both drugs (rhombs). Patients 4 and 23 are highlighted with a big circle.

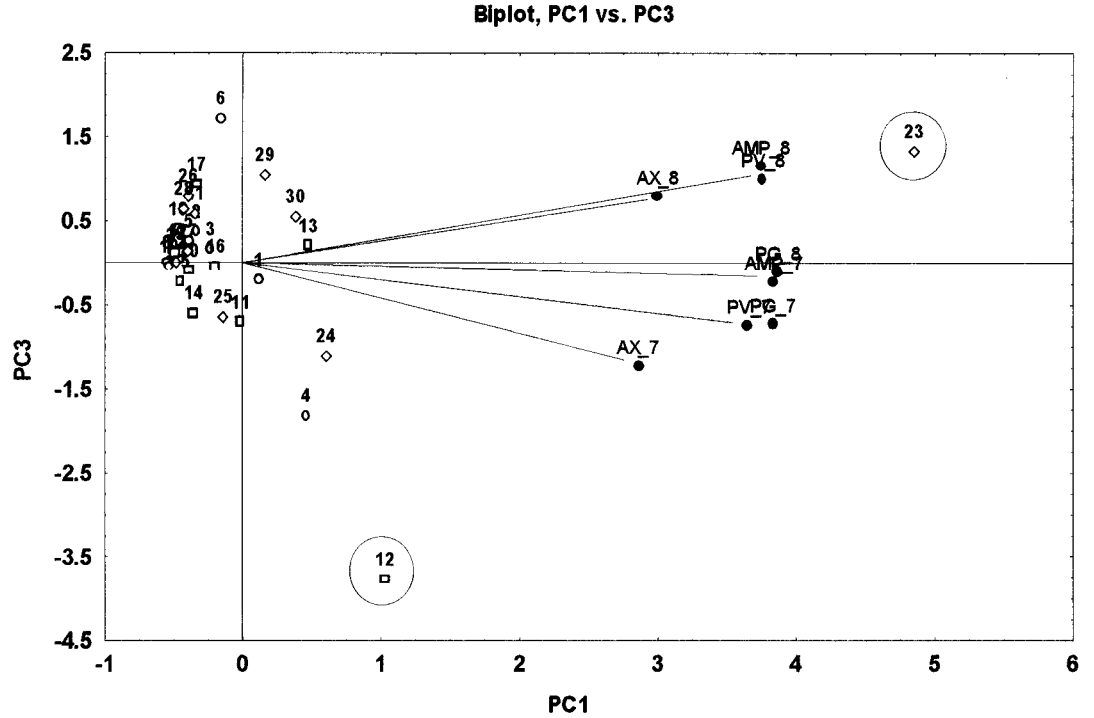


Figure 2. Biplot PC1 vs PC3. Variables in black (loadings); samples (patient sera) are divided in allergic to amoxycillin (circles), allergic to penicillin G (squares), and allergic to both drugs (rhombs). Patients 12 and 23 are highlighted with a big circle.

different action of amoxycillin with respect to the remaining β-lactams (11% of explained variance, Figure 1).

Concerning the patients, the analysis highlights patient 23 as the most allergic to all the β-lactams. Furthermore, patient 4 is characterized by a strong reactivity to amoxycillin (Figure 1).

The third component (4% of explained variance) shows the different behavior exhibited by the conjugates prepared at pH 7.2 in comparison with those prepared at pH 8.5, in particular related to amoxycillin (Figure 2). This component shows the high sensitivity to conjugates prepared at pH 7.5 for patient 12.

In conclusion, the in vitro determination of human IgE antibodies to β-lactams shows that patients may have both anti-penicillyl and anti-penicilloyl IgE antibodies. The chemometric evaluation of the data indicates that allergy to amoxycillin is different from allergy to the other β-lactams tested. Furthermore, careful chemical characterization of the conjugates appears to be crucial to obtain meaningful information from the RAST data.

ACKNOWLEDGMENT

This work was supported by NATO Contract CRG-971196 and by a CNR grant. We thank our students Aldo Comi, Luciana Monti, and Barbara Avogadro for their collaboration in the experimental work.

LITERATURE CITED

(1) Surtees, S. J., Stockton, M. G., and Gietzen, T. W. (1991) Allergy to penicillin, fable or fact? *Br. Med. J. 302*, 105−106.
(2) Pearson, C. R. (1991) Allergy to penicillin. *Br. Med. J. 302*, 1462; Walley, T., and Coleman, J. (1991) *Br. Med. J. 302*, 1462−1463; McSharry, C., Lewis, C., and Kirkwood, E. (1991) *Br. Med. J. 302*, 1463; Surtees, S. J., Stockton, M. G., and Gietzen, T. W. (1991) *Br. Med. J. 302*, 1463.
(3) Sogon, D. D. (1984) Penicillin Allergy. *J. Allergy Clin. Immunol. 74*, 589−593.
(4) de Weck A. L. (1983) Penicillins and cephalosporins. In *Allergic reactions to drugs* (A. L. de Weck, and H. Bundgaard, Eds.) pp 423−464, Springer-Verlag, Berlin.
(5) Blanca, M., Vega, J. M., Garcia, J., Miranda, A., Carmona, M. J., and Juarez, C. (1994) New aspects of allergic reactions to betalactams: Cross-reactions and unique specificities. *Clin. Exp. Allergy 24*, 407−415.
(6) Adkinson, N. F., Jr., Thompson, W. L., Maddrey, W. C., and Lichtenstein, L. M. (1971) Routine use of penicillin skin testing in an inpatient service. *N. Eng. J. Med. 285*, 22−24.
(7) Levine, B. B., and Zolov, D. M. (1969) Prediction of penicillin allergy by immunological tests. *J. Allergy Clin. Immunol. 43*, 231−244.
(8) Audicana, M., Bernaola, G., Urrutia, Y., Echechipia, S., Gastaminza, G., Muñoz, D., Fernandez, E., and Fernandez de Corres, L. (1994) Allergic reactions to betalactams: studies in a group of patients allergic to penicillin and evaluation of cross-reactivity with cephalosporin. *Allergy 49*, 108−113.
(9) De Weck, A. L. (1974) Low Molecular Weight Antigens. *Sela The Antigens*, Vol. 2, pp 141−248, Academic Press, New York.
(10) Parker, C. W., de Weck, A. L., Kewrn, M., and Eisen, H. N. (1962) The preparation and some properties of penicillenic acid derivatives relevant to penicillin hypersensitivity. *J. Exp. Med. 115*, 803.
(11) Levine, B. B., and Ovary, Z. (1961) Studies of the mechanism of the formation of the penicillin antigen III: The N(D(Benzyl penicilloyl) group as an antigenic determinant responsible for hypersensitivity to penicillin G. *J. Exp. Med. 114*, 875−881.
(12) Beeley, L. (1984) Allergy to penicillin. *Br. Med. J. 288*, 511−512.
(13) Atsumi, T., Nishida, K., and Horiuchi, Y. (1967) The heterogeneity of combining sites of benzylpenicillin antibodies obtained from a single rabbit: Fractionation of antibodies with a specific immunoadsorbent. *J. Immunol. 99*, 1286−1293.
(14) Erffmeyer, J. E. (1981) Adverse reactions to penicillin. *Ann. Allergy 47*, 288−300.
(15) Levine, B. B., and Redmond, A. P. (1969) Minor Haptenic determinant-specific Reagents of Penicillin Hypersensitivity in Man. *Int. Arch. Allergy Appl. Immunol. 35*, 445−455.
(16) Levine, B. B., Redmond, A. P., and Fellner, A. J. (1966) Penicillin Allergy and the Heterogeneous Immune Response of Man to Benzylpenicillin. *J. Clin. Invest. 45*, 1895−1906.
(17) Caneva, E., Di Gennaro, P., Farina, F., Orlandi, M., Rindone, B., and Falagiani, P. (1983) Synthesis and characterisation of a penicillinpolylysine (PG-PLL) which recognizes human IgE anti-penicillin antibodies and preparation of an antibody directed to PG-PLL. *Bioconjugate Chem. 4*, 309−313.
(18) Ressler, C., and Mendelson, L. M. (1987) Skin Test for Diagnosis of Penicillin Allergy. Current Status. *Ann. Allergy 59*, 167−170.
(19) Van Dellen, R. D. (1981) Skin Testing for Penicillin Allergy. *J. Allergy Clin. Immunol. 68*, 169−180.
(20) Van Arsdel, P. P., Jr. (1978) Adverse Drug Reactions. In *Allergy, Principles and Practice* (E. Middleton, Jr., C. E. Reed, and F. F. Ellis, Eds.) pp 1153−1154.
(21) Sullivan, T. J., Wedner, H. J., Shatz, G. S., Yecies, L. D., and Parker, C. W. (1981) Skin testing to detect penicillin allergy. *J. Allergy Clin. Immunol. 68*, 171−180.
(22) Silviu-Dan, F., Shawn, R. N., and Warrington, R. J. (1993) The frequency of skin test reactions to side-chain penicillin determinants. *J. Allergy Clin. Immunol. 91*, 694−701.
(23) Parker, C. W. (1967) Conjugation of penicillin and its derivatives. In *Methods in Immunology and Immunochemistry* (C. A. Williams, and M. W. Chase, Eds.) Vol. 1, pp 133−143.
(24) Wide, L., Bennich, H., and Johansson, S. G. O. (1967) Diagnosis of allergy by an in vitro test for allergen antibodies. *Lancet 2*, 1105−1107.
(25) Blanca, M., Moreno, F., Mayorga, C., Garcia, J., Fernandez, M., Perez, E., Juarez, C., and Suau, R. (1994) The nature of the carrier in the RAST assay influences the capacity for detecting IgE antibodies to penicillins. *J. Clin. Immunoassay 17*, 166−170.
(26) Kristoffersson, A., Ahlstedt, S., Petterson, E., and Svard, P. O. (1977) A radioimmunoassay for Detection of Penicilloylated Protein Contaminants in Penicillin Preparations. *Int. Arch. Allergy Appl. Immunol. 55*, 13−22.
(27) Landsteiner, K. (1962) *The Specificity of Serological Reactions*, Dover, New York; Eisen. H, N. (1959) In *Cellular and Humoral Aspects of the Hypersensitive State* (H. S. Lawrence, and Haeber, Eds.) New York.
(28) Schwartz, M. A. (1969) Chemical Aspects of Penicillin Allergy. *J. Pharm. Sci. 58*, 643−661.
(29) Edwards, R. G., Spackman, D. A., and Dewdney, J. M. (1982) Development and use of three new radioallergosorbent tests in the diagnosis of penicillin allergy. *Int. Arch. Allergy Appl. Immunol. 68*, 352−357.
(30) Blanca, M., Mayorga, C., Perez, M., Suau, R., Juarez, C., Vega, J. M., Carmona, M. J., Perez Estrada, M., and Garcia, J. (1992) Determination of IgE antibodies to the benzyl penicilloyl determinant. A comparison between poly-L-lysine and human serum albumin as carriers. *J. Immunol. Methods 153*, 99−105.
(31) García, J. J., Blanca, M., Moreno, F., Vega, J. M., Mayorga, C., Fernández, J., Juárez, C., Romano, A., and de Ramón, E. (1997) Determination of IgE antibodies to the benzylpenicilloyl determinant: A comparison of the sensitivity and specificity of three radio allergo sorbent test methods. *J. Clin. Lab. Anal. 11*, 251−257.
(32) Wakana, H., Shigaki, T., and Saito, N. (1982) Intramolecular alpha helix-beta structure-random coil Transitions in Polypeptides. *Biochem. Chem. 16*, 275−285.
(33) Khorana, H. G. (1953) The Chemistry of Carbodiimides. *Chem. Rev. 53*, 145−166.
(34) Levine, B., and Redmond, A. P. (1968) The Nature of the Antigen−Antibody Complexes Initiating the Specific Wheal-and-Flare Reaction in Sensitized Man. *J. Clin. Invest. 47*, 556−567.
(35) Kristofferson, A., Ahlsted, S., and Svard, P. O. (1977) Antigens in Penicillin Allergy. *Int. Arch. Allergy Appl. Immunol. 55*, 23−28.
(36) Edwards, R. G., Speckman, D. A., and Dewdney, J. M. (1982) Development and use of three radioallergosorbent tests in the diagnosis of penicillin allergy. *Int. Arch. Allergy Appl. Immunol. 68*, 352−357.
(37) Ceska, M., Eriksson, R., and Varga, J. M. (1972) Radioimmunosorbent assay of allergens. *J. Allergy Clin. Immunol. 49*, 1−9.
(38) Jackson, J. E. (1991) *A User's Guide to Principal Components*, Wiley, New York; Frank, I. E., and Todeschini, R. (1994) *The Data Analysis Handbook*, Elsevier, Amsterdam.

BC980023R

Closo-Dodecaborate(2-) as a Linker for Iodination of Macromolecules. Aspects on Conjugation Chemistry and Biodistribution

Vladimir Tolmachev,*[,†,‡] Jacek Koziorowski,[§,∥] Igor Sivaev,[⊥] Hans Lundqvist,[†] Jörgen Carlsson,[†] Anna Orlova,[§] Lars Gedda,[†] Pär Olsson,[†] Stefan Sjöberg,[§] and Anders Sundin[#]

Division of Biomedical Radiation Sciences, Box 535, S-751 21, Uppsala University, Uppsala, Sweden, Uppsala University PET-Centre, Uppsala University, Uppsala, Sweden, Department of Organic Chemistry, Uppsala University, Uppsala, Sweden, Nesmeyanov Institute of Organo-Element Compounds, Moscow, Russia, RRC "Kurchatov Institute", Moscow, Russia, and Institute for Medical Radiobiology, Paul Scherrer Institut, Villigen, Switzerland. Received March 18, 1998; Revised Manuscript Received January 29, 1999

Boron-containing compounds like *closo*-dodecaborate(2-) are in theory suitable for radioactive labeling with halogens. The boron−halogen bond is stronger than carbon−halogen bond and is not likely to be recognized by deiodinating enzymes in vivo. Peptides and proteins may be conjugated with various *closo*-dodecaborate(2-)-containing ligands, and thereafter, the conjugate can be iodinated. Since *closo*-dodecaborate(2-) is more avidly iodinated than tyrosine in moderately acidic media, such conjugates may be directly labeled on the boron part with radioisotopes of iodine using the standard Chloramine-T procedure. Mercapto-undecahydro-*closo*-dodecaborate(2-) (BSH) was reacted with the double bond of allyldextran to form a boronated dextran compound of the molecular size of about 70 kDa. This compound, in the text denoted as Dx-BS, and cesium dodecahydro-*closo*-dodecaborate(2-) were labeled using iodine-125. The two compounds were administered to rats in order to study their in vivo stability. The results indicate that iodinated Dx-BS is stable for about 20 h in vivo. The degradation rate, as indicated by thyroid uptake, was found low. [^{125}I]Iodo-*closo*-dodecaborate(2-), which is a possible degradation product of [^{125}I]Dx-BS-I, was rapidly excreted in urine without significant accumulation in any organ.

INTRODUCTION

Iodine isotopes play a fundamental role both in biomedical research and in clinical practice (Dewanjee, 1992), and a variety of decay schemes for these different iodine isotopes allow for a wide range of applications in the field of nuclear medicine. A convenient radionuclide for laboratory studies and for radioimmunoassay is ^{125}I [$T_{1/2}$= 60 days,100% electron capture (EC)] (Cleeland et al., 1976), while ^{131}I ($T_{1/2}$= 8 days, β^-) is the most frequently used isotope for systemic radionuclide therapy (Wilbur et al., 1989; O'Doherty et al., 1993; Press et al., 1996; Troncone and Rufini, 1997). ^{123}I ($T_{1/2}$=13.3 h, 100% EC) is widely used for diagnostic purposes in γ-scintigraphy and SPECT [see, e.g. Killen et al. (1989), Kulkarni and Corbett (1990), and Kusic et al. (1990)]. In the past few years, there has been a growing interest in the long-lived positron emitter ^{124}I ($T_{1/2}$= 4.2 days, 23% β^+) for labeling of macromolecules as positron emission tomography (PET) tracers (Arbit et al., 1995; Carnochan et al., 1994; Young et al., 1995).

It has been advocated that the use of radioiodine is advantageous compared with radiometals for labeling of antibodies intended for in vivo applications (Larson and Carrasquillo, 1988). During the past decade, radioiodinated antibodies have been used both for radioimmunodetection (Delaloye et al., 1986; Bischof-Delaloye et al., 1989; Gasparini et al., 1994) and for radioimmunotherapy (RIT) (Knox, 1995; Lashford et al., 1988).

A problem associated with in vivo applications of radioiodinated radioimmunoconjugates is the loss of the iodine label from the targeting compound in a tumor (Zalutsky and Narula, 1988; Zalutsky et al., 1989; Wilbur et al., 1989). This process is probably the reason for the lower tumor accumulation of radioiodine than radiometals as shown in a number of dual-labeling studies (Khaw et al., 1986; Bischof Delaloye et al., 1997; Meijs et al., 1997). It was believed for a long time that the structural similarity between iodotyrosines and the thyroid hormones, which are substrates for deiodinases, was the major cause for the loss of radioiodine from monoclonal antibodies (mAbs) in vivo (Zalutsky, 1988; Khaw et al., 1986). For this reason, alternative strategies for protein radioiodination were sought to provide iodination sites on the mAbs, with a high C−I bond strength, which are dissimilar in structure to iodotyrosines and thyroxine (Garg et al., 1991). This search resulted in the development of various radioiodinating reagents which contained radioiodine attached to a nonphenolic benzene ring (Zalutsky and Narula, 1987; Zalutsky and Narula, 1988; Wilbur et al., 1989), 4-methyl-benzoate (Garg et al., 1993), pyridinecarboxylate (Garg et al., 1991), or vinyl moiety (Hadley and Wilbur, 1990) instead of a tyrosine-like moiety.

* To whom correspondence should be addressed. Phone: (46) 18-4713840. Fax: (46) 18-4713432. E-mail: Vladimir.Tolmachev@bms.uu.se.
† Division of Biomedical Radiation Sciences.
‡ RRC "Kurchatov Institute".
§ Department of Organic Chemistry.
∥ Institute for Medical Radiobiology.
⊥ Nesmeyanov Institute of Organo-Element Compounds.
Uppsala University PET-Centre.

10.1021/bc980033s CCC: $18.00 © 1999 American Chemical Society
Published on Web 04/08/1999

The same concept was initially the basis of this study where derivatives of *closo*-dodecaborate dianion were chosen as linkers for attachment of iodine to targeted conjugates. The rationale for this approach was (1) *closo*-dodecaborate(2-) may be easily iodinated (Knoth et al., 1964; Srebny and Preetz, 1984; Haeckel and Preetz, 1995; Wilbur et al., 1995); (2) the B−I bond is stronger than the C−I bond (220 kJ/mol versus 209 kJ/mol) (Kerr, 1992); (3) Derivatives of *closo*-dodecaborate(2-) can be conjugated to biomolecules (Holmberg and Meurling, 1993; Gedda et al., 1996); and (4) the assumption that no enzymatic system exists in laboratory animals or in human for detachment of iodine from boron.

One strategy in our laboratory in the development of compounds for tumor targeting is the use of dextran conjugated to a target-seeking moiety to create a spacer to attach therapeutic radionuclides or other cytotoxic substances at a suitable distance from the antigen- or receptor-binding site. Receptor-specific proteins and shorter peptides, like mAbs or their fragments, epidermal growth factor (EGF), and somatostatin may be conjugated to dextran without destroying the receptor specificity (Holmberg et al., 1994a,b; Andersson et al., 1991; Lövqvist et al., 1993; Olsson et al., 1994; Zhao et al., 1998). Dextran may also protect peptides from fast biodegradation (Andersson et al., 1991, 1992; Carlsson et al., 1994; Lindström and Carlsson, 1993).

To evaluate the stability of the iodine−boron bond in vivo, we used compound 4 (Dx-BS) in this study. This compound was radioiodinated and injected intravenously in rats. It has been shown previously that Dx-BS may be conjugated with EGF, and that such a conjugate, without iodine label on boron, binds to cultured glioma cells (Gedda et al., 1996). The biodistribution in rats of iodinated *closo*-dodecaborate(2-), an expected catabolite of Dx-BS, was also investigated.

A general problem in the design of radioimmunoconjugates is the choice of labeling strategy. In the present experiment, there were two possible approaches: (1) to label *closo*-dodecaborate(2-) with iodine first and then attach it to the dextran-containing targeted conjugate and (2) to bind *closo*-dodecaborate(2-) to the conjugate and then iodinate.

In the first case, the position of the label is more predictable, but the conjugation-labeling yield is generally lower than that of direct halogenation. The second approach probably leads to a higher yield, but suffers from the risk of iodinating the tyrosine residues of the peptide part, which is often vulnerable to biodegradation. This drawback may, however, be overcome if *closo*-dodecaborate(2-) is iodinated at a lower pH, i.e., under conditions when the tyrosine ring is not so easily iodinated (Knight and Welch, 1978). To study the feasibility of such an approach, a competitive iodination of *closo*-dodecaborate(2-) and tyrosine was performed at different pH-values of the reaction mixture.

The aims of the study were (1) to develop a convenient method for no-carrier added labeling of *closo*-dodecaborate(2-) and its derivatives with iodine, (2) to evaluate the possibility to direct the iodine label to boron but not to tyrosine, via pH variation during labeling, (3) to evaluate the in vivo stability of the iodine label on *closo*-dodecaborate(2-), and (3) to study the pharmacokinetics of [^{125}I]Dx-BS-I and of [^{125}I]iodo-*closo*-dodecaborate(2-).

MATERIALS AND METHODS

Materials. ^{125}I (3.7 GBq/mL) for labeling was from Amersham Int. plc., Little Chalfont, Buckinghamshire, U.K. Cesium carbonate was heated at 300 °C during 60 min and dissolved in methanol to a concentration of 5 mg/mL before use. Water solutions of Chloramine-T (4 mg/mL) and sodium metabisulfite (4 mg/mL) (Sigma Chemical Co., St. Louis, MO) were prepared immediately before iodination. IodoGen (Pierce, supplied by Soccochim SA, Lausanne, Switzerland) was dissolved in methylene chloride (1 mg/mL), 100 μL of the solution was added into 300 μL ReactiVials (Pierce, supplied by Soccochim SA, Lausanne, Switzerland), and the solvent was evaporated under a gentle stream of nitrogen, leaving a thin film of IodoGen.

NAP-5 columns (Sephadex G-25 gel, Pharmacia, Sweden) were used for separation of labeled dextran from low-molecular-weight components.

Radioactivity measurements were done with an automatic γ counter (LKB Wallac Oy, Turku, Finland).

The radio-TLC identity of the compounds was assessed by coelution with corresponding cold standards.

Preparation of Dx-BS. The Dx-BS compound (76 kDa dextran, 40−50 boron cages/dextran molecule) was produced as described by Gedda et al. (1996). Briefly, 2 g of 70 kDa dextran, 0.5 g NaOH, and 20 mg $NaBH_4$ were mixed in 15 mL of distilled water at 40 °C. Allyl bromide (3.5 g, 2.5 mL) was added and the reaction allowed to proceed at 60 °C for about 3 h. After neutralization, the allyldextran was purified by precipitation with ethanol three times, then lyophilized and stored at −70 °C. The degree of allyl substitution was calculated by elemental analysis of carbon and hydrogen in the allylated and native dextran (Gedda et al., 1996).

For attachment of boron cages, 20 mg of BSH and 20 mg of $(NH_4)_2S_2O_8$ were mixed with 20 mg of allyldextran dissolved in 200 μL of distilled water. The reaction continued for 2 h at 50 °C with stirring. Then, dextran-BSH was purified from uncoupled BSH and other low-molecular-weight compounds on a NAP-5 column (equilibrated with distilled water). The high-molecular-weight fraction (first 900 μL) was eluted instead of the recommended 1.0 mL, to avoid any contaminants of low-molecular-weight compounds. The amount of boron added to the dextran was determined with ICP-AES, and substitution rates were calculated (Gedda et al., 1996). Dx-BS was dissolved in 0.25 M phosphate buffered saline (PBS), pH 7.5, to a concentration of 20 mg/mL and stored frozen before use.

Iodination of Dx-BS Conjugate. [^{125}I]Iodide solution (5 μL) was mixed with 20 μL of Dx-BS solution and 20 μL of PBS and 10 μL of Chloramine-T solution in water were added. After vortexing, the mixture was incubated at room temperature for 5 min and then quenched by adding 20 μL of sodium metabisulfite solution.

Alternatively, 10 μL of Dx-BS was mixed with 80 μL of citrate buffer (pH 4.0) in the IodoGen coated vessel, and 5 μL of [^{125}I]iodide was added. After vortexing, the mixture was incubated at room temperature during 5 min, and the high-molecular-weight fraction was separated from unreacted iodine without quenching using gel-filtration.

Separation of iodinated Dx-BS from low-molecular-weight components was performed on a NAP-5 column equilibrated with PBS. After passing of the void volume (500 μL), fractions of 200 μL were collected. The radioactivity in each fraction, as well as reaction vial and the column, was measured to determine the labeling yield. The high-molecular- weight fractions were pooled and diluted in PBS for use in the biodistribution experiments.

One problem was found in the purification step of [^{125}I]-Dx-BS-I after the labeling since 30% of the added

radioactivity was retained in the NAP-5 column. Washing the column with more buffer did not elute more radioactivity. Free iodine is easily eluted, and the remaining radioactivity was most likely attached to Dx-BS nonspecifically interacting with the column matrix. Pretreating the column with nonlabeled *closo*-dodecaborate(2-) did not help. Work is in progress to develop another size-exclusion chromatographic method that will avoid this problem and that will increase the total labeling yield.

Iodination of Cesium *Closo*-Dodecaborate(2-). Solution of potassium dodecahydro-*closo*-dodecaborate(2-) in water (10 μL, 10 mg/mL) was mixed with 30 μL of PBS and 5 μL of [^{125}I]iodide. After addition of 10 μL of Chloramine-T solution and vortexing, the mixture was incubated during 5 min at room temperature. The reaction was quenched with 20 μL of sodium metabisulfite solution.

The iodinated *closo*-dodecaborate(2-) was purified as follows: 150 μL of water was added to the reaction mixture, and *closo*-dodecaborate(2-) was precipitated with 20 μL of tetraphenylphosphonium chloride. The mixture was passed through a 0.45 μm filter, and the residue was washed with 500 μL of water. More than 90% of the initial iodine radioactivity was associated with the residue. After drying over phosphorus pentoxide, the residue was redissolved in 600 μL of acetonitrile. A total of 400 μL of water was added, and acetonitrile was evaporated under a gentle flow of argon. The newly formed residue was filtered out, washed with water (400 μL), and dried during 4 h over phosphorus pentoxide. After redissolving in 600 μL of methanol, *closo*-dodecaborate(2-) (both labeled and unreacted) was precipitated with the solution of cesium carbonate in methanol. After additional washing with methanol, the residue was redissolved in water and used for injection in experimental animals. Quality control was performed on Silica gel coated TLC aluminum plates (Merck) using methylene chloride:acetone (1:4) as an eluent. R_f values were found: 0.71 for iodinated dodecaborate, and 0.41 for iodide.

Competitive Iodination of *Closo*-Dodecaborate-(2-) and Tyrosine. Tyrosine and sodium *closo*-dodecaborate(2-) (100 μL of each) were added from 5 mg/10 mL of stock solutions into a ReactiVial coated with 10 μg of IodoGen. The molar amount of tyrosine was 0.276 μmol and that of sodium *closo*-dodecaborate(2-) 0.266 μmol. Tyrosine and *closo*-dodecarborate(2-) was dissolved in one of the following: (a) 0.1 M phosphate buffer, pH 7; (b) 0.1 M borate buffer, pH 9; (c) 0.1 M citrate buffer, pH 4; (d) 0.1 M phosphate buffer, pH 6; (e) 0.1 M acetate buffer, pH 5; or (f) 0.1 M borate buffer, pH 8. After careful mixing, 10 μL of [^{125}I]iodide in 0.1 M phosphate buffer, pH 7, was added to the vial, and the reaction mixture was incubated at room temperature. After 1 and 5 min of incubation, aliquots were taken for radio-TLC analysis. TLC analysis was performed on silica-coated glass plates (Merck, Silica gel 60 F254) using methylene chloride:acetone (1:3) as eluent. Radiochromatograms were quantitatively evaluated using Berthold tracemaster 20 (Berthold AG, Regensdorf, Switzerland) radio-TLC scanner. In these conditions R_f values were [^{125}I]-monoiodotyrosine, about 0; [^{125}I]iodide, 0.6; *closo*-dodecaborate(2-) and [^{125}I]iodo-*closo*-dodecaborate(2-), 0.81.

Animal Experiments. Twenty-three male Sprague−Dawley rats (BK Universal AB, Stockholm, Sweden) weighing 240−300 g were used. The animals were housed in an isolated room at 25 °C, constant air humidity, and a 12 h light/12 h dark cycle. They were fed ad libitum with sterilized water and standard pellet diet. For anesthesia, Inactin (5 mg/mL, 0.25 mL/100 g of body weight) was administered intraperitoneally. Under anesthesia, an incision was made in the right groin and the femoral vein was isolated and cannulated with a plastic catheter. About 0.25 MBq (0.25−0.30 mL) of [^{125}I]Dx-BS-I (n = 11) or [^{125}I]iodo-*closo*-dodecaborate(2-) (n=12) was administered intravenously to each rat using 1 mL syringes. After injection, the catheter was rinsed with saline. The radioactivity of each syringe was measured before and after injection. Samples of each labeled compounds were taken as standards for the distribution study.

The animals were sacrificed under anesthesia by desanguination and dissected in groups of three rats and with occasional groups of two rats at 0.5, 1, 3, and 6 h after injection and in the [^{125}I]Dx-BS-I experiment also at 20 h. At each time-point, blood and urine were drawn, and various organs and tissues were collected. The samples were weighed and measured for radioactivity corrected for background. Accumulation of the radioactivity in each organ was calculated as the percent injected dose per gram.

Table 1. Iodination of Sodium *Closo*-Dodecaborate(2-) Using IodoGen at Different pH

pH	buffer	iodination yield (%)[a]
4	citrate-phosphate	88−95
5	acetate	87−88
6	phosphate	90−97
7	phosphate	85−87
7.4	phosphate buffered saline	96−97
8.1	phosphate	44−45
9.1	borate	27−28

[a] The iodination yields were determined using radio-TLC, as described in the text.

Table 2. Competitive Iodination of Tyrosine and *Closo*-Dodecaborate(2-)[a]

pH	percent of iodine incorporated into tyrosine	percent of iodine incorporated into *closo*-dodecaborate(2-)	ratio of iodinated tyrosine to iodinated *closo*-dodecaborate(2-)
4	13	87	0.15
5	12	89	0.13
6	42	58	0.72
7	70	30	2.33
8	93	7	13.3
9	94	6	15.6

[a] A mixture of tyrosine and cesium *closo*-dodecaborate(2-) was iodinated using IodoGen at different pH. The iodination yields were determined using radio-TLC, as described in the text.

RESULTS

Labeling Chemistry. The labeling yield of *closo*-dodecaborate dianion, assessed by radio-TLC, was 85−97% in the pH range 4−7.4, but decreased at higher pH (Table 1). The yield was similar using Chloramine-T and IodoGen, giving the same yield at 1 and 5 min of incubation. The unreacted iodine was identified through TLC-analysis as free iodide. The labeling yield was found to be independent of pH within the range 4−7.4. The main factor influencing the labeling yield was the quality of [^{125}I]iodide. "Old" iodide samples, which had been stored for 2 months or more, gave lower iodination yield. Radio-TLC analysis of such samples showed that appreciable amounts of radioactivity had R_f values different from the R_f of iodide.

The results of the competitive iodination of tyrosine and dodecaborate are given in Table 2. Note the different pH dependencies between labeling of tyrosine and *closo*-

Table 3. Tissue Distribution of Radioiodine after i.v. Administration of [^{125}I]iodo-*Closo*-Iodododecaborate(2-) in Rats

	% ID/g tissue[a]			
tissue	0.5 h	1 h	3 h	6 h
blood	1.063 ± 0.162	0.774 ± 0.089	0.471 ± 0.148	0.180 ± 0.031
urinary bladder	1.155 ± 0.403	1.204 ± 0.356	1.096 ± 0.482	0.822 ± 0.065
kidney	1.198 ± 0.469	1.238 ± 0.315	1.023 ± 0.175	0.433 ± 0.047
spleen	0.208 ± 0.019	0.137 ± 0.092	0.136 ± 0.045	0.050 ± 0.012
pancreas	0.254 ± 0.028	0.206 ± 0.045	0.154 ± 0.051	0.062 ± 0.017
liver	0.544 ± 0.052	0.531 ± 0.120	0.309 ± 0.066	0.126 ± 0.025
stomach	0.180 ± 0.027	0.130 ± 0.019	0.081 ± 0.020	0.035 ± 0.009
small intestine	0.168 ± 0.018	0.148 ± 0.029	0.097 ± 0.013	0.054 ± 0.011
colon	0.200 ± 0.020	0.213 ± 0.045	0.172 ± 0.036	0.048 ± 0.013
heart	0.457 ± 0.120	0.317 ± 0.063	0.181 ± 0.058	0.067 ± 0.010
lungs	0.812 ± 0.310	0.494 ± 0.106	0.478 ± 0.261	0.166 ± 0.028
muscle	0.201 ± 0.047	0.128 ± 0.016	0.090 ± 0.027	0.027 ± 0.003
bone	0.191 ± 0.043	0.145 ± 0.022	0.101 ± 0.034	0.034 ± 0.008
skin	0.430 ± 0.083	0.332 ± 0.054	0.181 ± 0.120	0.072 ± 0.013
testicle	0.067 ± 0.004	0.110 ± 0.016	0.099 ± 0.010	0.071 ± 0.008
brain	0.036 ± 0.005	0.023 ± 0.006	0.016 ± 0.004	0.006 ± 0.001
thyroid	0.445 ± 0.070	0.311 ± 0.039	0.227 ± 0.064	0.132 ± 0.017
salivary gland	0.410 ± 0.079	0.252 ± 0.042	0.196 ± 0.067	0.058 ± 0.008

[a] Mean ± SD (n = 3).

dodecaborate(2-), and that even in a moderately acidic water solution, the radioiodine label was preferentially bound to *closo*-dodecaborate(2-) rather than to the tyrosine residues.

The labeling of Dx-BS conjugate was equally efficient at pH 7 and 4. Typically, about 60% of the eluted radioiodine was associated with the high-molecular-weight fraction.

Distribution of [^{125}I]Iodo-*Closo*-Dodecaborate-(2-). The tissue distribution of [^{125}I]iodo-closo-dodecaborate(2-) is presented in Table 3. [^{125}I]Iodo-*closo*-dodecaborate(2-) was not accumulated in any organ, and the uptakes in most tissues were very low. The high ^{125}I content in the kidneys and urine indicated a rapid elimination of [^{125}I]iodo-*closo*-dodecaborate(2-) by urinary excretion. The radioactivity concentration in blood decreased quite rapidly after the injection to an "intermediate" level. The fact that the uptake in heart and lungs was somewhat higher than in the other normal tissues merely reflects the high blood volume of these organs. Note that there was no accumulation of radioiodine in the stomach and in the thyroid. Hence, throughout the observation time, the iodine content of the thyroid was lower than that in blood, and tended to decrease over time (Figure 2). The radioactivity uptake in the stomach, generally considered to represent free iodide, was 0.28 ± 0.057% ID at 30 min and 0.23 ± 0.02% ID at 1 h after injection.

Distribution of [^{125}I]-Dx-BS-I. The distribution of [^{125}I]-Dx-BS-I in various organs and tissues is given in Table 4. The radioactivity was accumulated to a high degree in kidney, liver and spleen. The uptakes in these organs reached maximum values between 3 and 6 h after injection and then slowly decreased. The radioactivity was mainly excreted through the kidneys but radioactivity was detected in the feces 20 h after injection. No appreciable accumulation of radioactivity was observed in the other organs. The thyroid uptake increased over the observation time. However, the value of the thyroid uptake was only 0.073 ± 0.003% ID at 20 h after injection.

DISCUSSION

During the past few years, knowledge regarding dehalogenation mechanisms of iodinated compounds in vivo has increased considerably. Directly radioiodinated proteins, after cellular uptake, undergo catabolism accompanied by a rapid loss of cell-bound radioactivity. This is mainly due to a fast membrane transport of iodotyrosine, whereas free iodide accounts for a minor part of the cellular radioactivity losses (Geissler et al., 1992; Press et al., 1996; Stein et al., 1997). Procedures have been suggested to overcome this problem, e.g., by the use of so-called residualizing labels based on aryl carbohydrate adducts (Ali et al., 1990). A small molecule, stable to metabolic degradation, is labeled with radioiodine after which it is attached to the main molecule, e.g., a targeting peptide or protein. After internalization, the protein may still undergo degradation, but the labeled products are not easily excreted from the cell. Radioiodinated dilac-

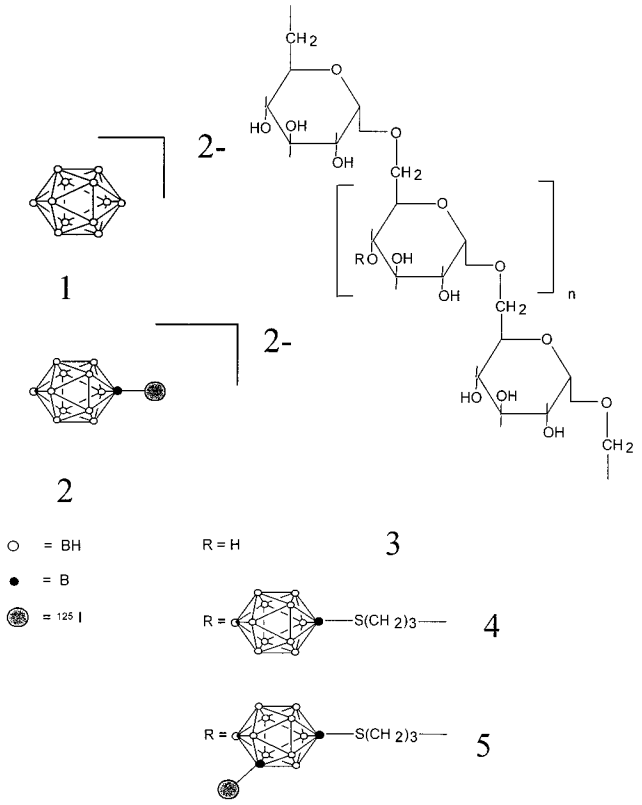


Figure 1. Structures of dodecahydro-*closo*-dodecaborate(2-) (1), iodo-undecahydro-*closo*-dodecaborate(2-) (2), dextran (3), product of the radical addition of mercapto-undecahydro-*closo*-dodecaborate(2-) (BSH) to the double bond of allyldextran (Dx-BS) (4), and radioiodinated Dx-BS (5).

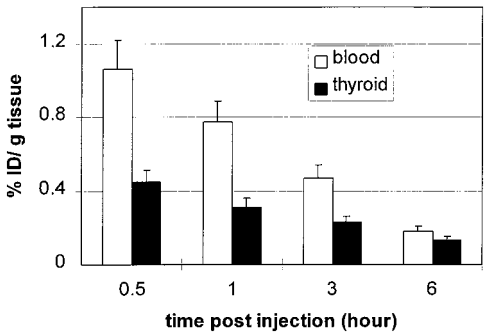


Figure 2. Accumulation of radioactivity in blood and thyroid after injection of radioiodinated *closo*-dodecaborate(2-).

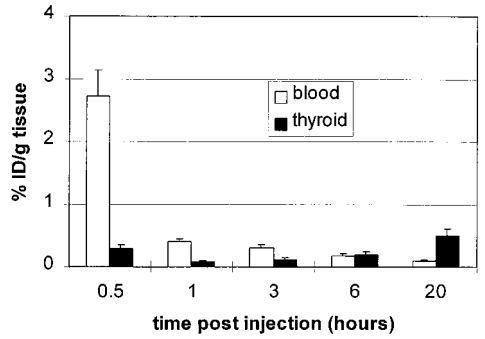


Figure 3. Accumulation of radioactivity in blood and thyroid after injection of radioiodinated [^{125}I]Dx-BS-I.

titol-tyramine or tyramine-cellobiose seem in this aspect more promising than nonphenolic linkers in order to enhance cellular retention of radioiodine (Stein et al., 1997; Reist et al., 1995).

So far, indirect labeling methods have been used, i.e., the residualizing linkers are first radiolabeled and then conjugated, often with a low efficiency, which is the main disadvantage. Thus, Stein et al. (1997) stated that the delivery of absorbed dose using [^{131}I]dilactitol-tyramine was limited by the low conjugation efficiency of prelabeled linker. Low conjugation yields, 30−40%, and a possible aggregation of antibodies when using tyramine-cellobiose were observed by Reist et al. (1995).

Thus, it would be of advantage to do the conjugation step first, i.e., targeting molecule to residualizing linker. After a purification step that hopefully can separate the conjugate from starting material, the conjugate could then be directly labeled. The advantages should be that the starting material is well characterized, the labeling is fast and gives high labeling yields, and also the final purification step is simple. However, the labeling conditions must preferably direct the label to the linker molecule and not to the rest of the conjugate. Furthermore, the biological function of the conjugate must not be severely affected.

An example of such a direct labeling procedure was recently suggested at our laboratory. A conjugate of mouse epidermal growth factor and dextran modified with tyrosine, (mEGF)-dextran-tyrosine, was iodinated using the Chloramine-T method (Zhao et al., 1998). Since the dextran contained more tyrosine (5−15) than the mEGF (5), the radioactive label was concentrated to the dextran-tyrosine part (65−75%). The intracellular retention of radioiodine delivered by such a conjugate was improved in comparison with a homologous mEGF-dextran labeled only in the peptide part thus proving that dextran-tyrosine has a residualizing function. However, this method can be applied only if the targeting molecule contains no or a few tyrosine residues.

In this study, we suggest a new type of residualizing linker, dextran conjugated with *closo*-dodecaborate(2-), which permits direct labeling. Nonradioactive iodo-derivatives of *closo*-dodecaborate were studied and characterized earlier (Knoth et al., 1964; Srebny and Preetz, 1984; Haeckel and Preetz, 1995; Wilbur et al., 1995). Boron-containing compounds are interesting since the boron−iodine bond is stronger than the carbon−iodine bond and no enzymatic system in vivo is known to cleave this bond. *Closo*-Dodecaborate(2-) can, as shown here, easily be labeled with iodine at various pH using standard methods such as Chloramine-T or IodoGen. A new labeling strategy may then be applied where the conjugation step [*closo*-dodecaborate(2-)-sugar to protein] is the first step. At pH 5, a rather mild labeling condition for most proteins, a high labeling yield is obtained for the *closo*-dodecaborate(2-) residues, whereas the protein tyrosine is poorly labeled (Table 1). Since the radioiodination yield of *closo*-dodecaborate does not depend on pH, the difference in the yields in competitive experiments, which were performed for nearly equimolar amounts of tyrosine and *closo*-dodecaborate, should be due to different impact of pH variation on the iodination kinetics of these two compounds.

The stability test, using [^{125}I]Dx-BS-I as a model compound, was designed to prove the stability of the radioactive label bound to the *closo*-dodecaborate(2-) in vivo. Dextran per se is known to be resistant to metabolic degradation (Mowry and Millican, 1953). Previous studies of our group have shown that both tritium and radioiodine labels attached to the dextran part of targeting conjugates possess an enhanced stability after intracellular uptake (Andersson et al., 1991; Zhao et al., 1998). In vivo, dextran is accumulated in lysosomes after kidney uptake (Christenses and Maunsbach, 1981). Dextran might also undergo liver uptake mediated by receptors for asialoglycoproteins (Nishikawa et al., 1992) when injected in rats at doses below 1 mg/kg of body weight. The interaction with these receptors leads to internalization and quick degradation of glycoproteins in lysosomes (Duncan and Welch, 1993). Thus, [^{125}I]Dx-BS-I administered at low amounts in vivo could be exposed to lysosomal digestion, but the carbohydrate backbone is assumed to be stable to degradation and will not readily be excreted from the cells. Loss of the radioactivity from liver and kidney may then be ascribed mainly to cleavage of boron−iodine bond or to detachment of [^{125}I]iodo-*closo*-dodecaborate(2-) from dextran.

The expected in vivo distribution of [^{125}I]Dx-BS-I was verified in the animal studies. High radioactivity uptake was found in liver and kidneys reaching a maximum at 3−6 h after injection. At this time the blood pool was cleared of [^{125}I]Dx-BS-I. Thereafter, a small decrease in kidney and liver radioactivity was observed that probably corresponded to exocytosis or a degradation and slow release of radioactivity. The thyroid uptake of radioactivity increased over time but was only 0.072 ± 0.003% ID at 20 h. This is low in comparison with previous results on thyroid accumulation of iodine in mice after injection of various mAbs and fragments iodinated by other techniques. Zalutsky and Narula (1987) reported radioactivity uptake of 1.39 and 2.37% ID in mouse thyroid at 24 h when injecting iodinated IgG labeled by the use of ATE and IodoGen, respectively. Although the comparison is made between different rodent species, the difference is considerable and supports the assumption that the iodine is firmly attached to the boron compound.

Liver and kidney are organs where the highest rate of radioiodine loss is expected (Khaw et al., 1986). Our data

Table 4. Tissue Distribution of Radioiodine after Administration of [^{125}I]Dx-BS-I in Rats

	% ID/g tissue[a]				
tissue	0.5 h	1 h	3 h	6 h	20 h
blood	2.724 ± 0.402	0.394 ± 0.026	0.307 ± 0.083	0.182 ± 0.039	0.098 ± 0.005
urinary bladder	0.050 ± 0.018	0.067 ± 0.009	0.070 ± 0.011	0.093 ± 0.008	0.093 ± 0.005
kidney	0.710 ± 0.043	4.007 ± 0.195	4.459 ± 0.089	4.203 ± 0.537	3.834 ± 0.286
spleen	0.077 ± 0.001	1.096 ± 0.047	1.523 ± 0.160	1.238 ± 0.006	0.946 ± 0.011
pancreas	0.029 ± 0.003	0.063 ± 0.001	0.061 ± 0.005	0.056 ± 0.005	0.066 ± 0.004
liver	0.363 ± 0.027	2.804 ± 0.072	3.760 ± 0.066	3.636 ± 0.046	3.334 ± 0.179
stomach	0.014 ± 0.002	0.043 ± 0.006	0.043 ± 0.000	0.023 ± 0.006	0.027 ± 0.001
small intestine	0.022 ± 0.004	0.121 ± 0.020	0.110 ± 0.026	0.128 ± 0.079	0.060 ± 0.009
colon	0.022 ± 0.007	0.047 ± 0.011	0.076 ± 0.026	0.058 ± 0.022	0.087 ± 0.032
heart	0.050 ± 0.007	0.095 ± 0.005	0.075 ± 0.013	0.056 ± 0.012	0.038 ± 0.001
lungs	0.064 ± 0.011	0.124 ± 0.007	0.126 ± 0.026	0.034 ± 0.034	0.085 ± 0.009
muscle	0.006 ± 0.001	0.018 ± 0.003	0.011 ± 0.001	0.010 ± 0.001	0.016 ± 0.002
bone	0.020 ± 0.002	0.039 ± 0.001	0.040 ± 0.006	0.041 ± 0.000	0.040 ± 0.010
skin	0.011 ± 0.001	0.033 ± 0.001	0.031 ± 0.004	0.024 ± 0.001	0.026 ± 0.000
testicle	0.007 ± 0.001	0.024 ± 0.003	0.041 ± 0.003	0.043 ± 0.006	0.039 ± 0.001
brain	0.004 ± 0.001	0.010 ± 0.000	0.007 ± 0.002	0.007 ± 0.003	0.005 ± 0.001
thyroid	0.291 ± 0.077	0.078 ± 0.000	0.114 ± 0.006	0.195 ± 0.028	0.490 ± 0.052
salivary gland	0.019 ± 0.003	0.047 ± 0.001	0.044 ± 0.010	0.031 ± 0.002	0.035 ± 0.006

[a] Mean ± SD ($n = 3$ or $n = 2$).

indicate that the dextran-associated label was stable after internalization. A comparison was made to a directly labeled peptide, [^{125}I]mEGF, which was tested in the same Sprague−Dawley rats using a similar experimental protocol (Scott-Robson et al., 1991) as for the [^{125}I]Dx-BS-I. After receptor-mediated uptake, iodinated mEGF is efficiently transported into the intracellular compartment (Todderud and Carpenter, 1989). We assume that [^{125}I]Dx-BS-I is transported to the same compartments, the lysosomes, and is exposed to similar degradation conditions. The rapid blood clearance of [^{125}I]mEGF is an advantage since the organ loss of radioactivity directly reflects the degradation rate and is not obscured by blood radioactivity. The comparison of data shows a fast degradation of [^{125}I]mEGF, e.g., more than a 3-fold decrease of the liver radioactivity during 2 h, whereas the radioactivity loss of [^{125}I]Dx-BS-I was minor.

[^{125}I]Iodo-*closo*-dodecaborate(2-), a probable degradation product of the conjugate, was found to be rapidly eliminated from the circulation and excreted in urine without accumulation in any organ. The radioactivity uptake in the stomach, generally considered to represent free iodide, was 0.23 ± 0.02% ID at 1 h after injection. In distribution studies performed in mice (Zalutsky and Narula, 1988; Garg et al. 1991), the uptake of free radioiodine in the stomach was in the range 14−25% at 1 h after injection. Although the comparison is made between two species, the difference between the previous studies in mice and the present experiment, i.e., 2 orders of magnitude, is persuasive. This indicates that in the clinical situation the degradation products will probably not contribute to the background, which might improve the tumor to normal tissue ratio.

Systemic injection of dextran leads to an elevated uptake in liver, spleen, and kidney. It is possible that this will also be true for, e.g., a tumor-seeking peptide and that a part of the conjugate will be directed to these organs, thus competing with the desired tumor uptake. However, Nishikawa et al. (1992) have shown in rats that the hepatic uptake of dextran may be receptor mediated, and the co-injection of nonlabeled dextran could therefore decrease the liver uptake considerably if such receptors are present in humans. Since dextran is nontoxic (Molteni, 1979), an injection of a large amount of dextran before injection of dextranated targeting conjugates is possible.

Generally, increased and prolonged uptake in excretory organs is typical for residualizing labels. A similar effect of prolonged retention of the residualizing label in liver, spleen, and kidney was reported by Reist et al. (1995) when they compared a distribution of mAb H10 labeled by IodoGen and by tyramine-cellobiose. Longer hepatic and renal retention of metal chelates, which are residualizing labels, in comparison with iodine have been observed in numerous dual label studies (Khaw et al., 1986; Meijs et al., 1997; Schott et al., 1992; Ryser et al., 1992). Prolonged retention of ^{111}In in liver and kidney was the reason for Larson and Carrasquillo (1988) to state that conventional iodine label is better for certain applications than metal label, despite better accumulation of radioindium in tumor sites. Several studies (Press et al., 1996; Duncan and Welch, 1993; Behr et al., 1998) suggest that protracted renal and hepatic retention is provided by the same mechanism, which provides prolonged retention of residualizing label inside tumor cells. For this reason, this problem can be alleviated only by modification of the pharmacokinetics of the whole targeted radioconjugate to prevent capture in liver and kidney. Thus, promising results were obtained in decrease of kidney accumulation of radiometal labeled peptides using lysine or poly-lysine (Behr et al., 1998; De Jong et al., 1995; Bernard et al., 1997; De Jong et al., 1998). However, the problem is far from solved at the moment. It is possible that in the future the kind of label will be chosen for a given patient on a basis of individual optimization.

The present study indicates that radioiodinated [^{125}I]Dx-BS-I conjugated to a tumor-seeking molecule can provide a stable residualizing iodine label which, if applied to a relevant targeting agent, will be of interest for imaging and therapy.

ACKNOWLEDGMENT

This research has been supported by the Swedish Cancer Society and the Royal Swedish Academy of Sciences. Jacek Koziorowski thanks the Swiss National Fund (3100-045665.95/1) for financial support.

LITERATURE CITED

Ali, S. A., Warren, S. D., Richter, K. Y., Badger, C. C., Eary, J. F., Press, O. W., Krohn, K. A., Bernstein, I. D., and Nelp, W.

B. (1990) Improving of the retention of radioiodinated antibody: aryl carbohydrate adducts. *Cancer Res. 50*, 783−788.

Andersson, A., Holmberg, A., Carlsson, J., Carlsson, J., Ponten, J., and Westermark, B. (1991) Binding of epidermal growth factor-dextran conjugates to cultured glioma cells. *Int. J. Cancer 47*, 439−444.

Andersson, A., Capala, J., and Carlsson, J. (1992) Effects of EGF-dextran-tyrosine-^{131}I conjugates on the clonogenic survival of cultured glioma cells. *J. Neuro-Oncology 14*, 213−223.

Arbit, E., Cheung, N. K., Yeh, S. D., Daghighian, F., Zhang, J. J., Cordon-Cardo, C., Pentlow, K., Canete, A, Finn, R., and Larson, S. M. (1995) Quantitative studies of monoclonal antibody targeting to disialoganglioside GD2 in human brain tumours. *Eur. J. Nucl. Med. 22*, 419.

Behr, T. M., Goldenberg, D. M., and Becker, W. (1998) Reducing the renal uptake of radiolabeled antibody fragments and peptides for diagnostics and therapy: present status, future prospects and limitations. *Eur. J. Nucl. Med. 25*, 201−212.

Bernard, B. F., Krenning, E. P., Breeman, W. A., Rolleman, E. J., Bakker, W. H., Visser, T. J., Macke, H., and de Jong, M. (1997) D-lysine reduction of indium-111 octreotide and yttrium-90 octreotide renal uptake. *J. Nucl. Med. 38*, 1929−1933.

Bischof-Delaloye, A., Delaloye, B., Buchegger, F., von Fieldner, V., Gilgien, W., Studer, A., Curchod, S., Moisman, F., Pettavel, J., and Mach, J.-P. (1989) Clinical value of immunoscintigraphy in colorectal carcinoma patients: a prospective study. *J. Nucl. Med. 30*, 1646−1656.

Bischof-Delaloye, A., Delaloye, B., Buchegger, F., Vogel, C.-A., Gillet, M., Mach, J.-P., Smith, A., and Schubiger, P. A. (1997) Comparison of copper-67 and iodine-125-labeled anti-CEA monoclonal antibody biodistribution in patients with colorectal tumors. *J. Nucl. Med. 38*, 847−853.

Carlsson, J., Gedda, L., Grönvik, C., Hartman, T., Lindstrom, A., Lindstrom, P., Lundqvist, H., Lovqvist, A., Malmqvist, J., and Olsson, P. (1994) Strategy for boron neutron capture therapy against tumor cells with overexpression of the epidermal growth factor receptor. *Int. J. Radiat. Oncol. Biol. Phys. 30*, 105−115.

Carnochan, P., Trivedi, M., Young, H., Eccles, S., Potter, G., Haynes, B., and Ott, R. (1994) Biodistribution and kinetics of radiolabeled pyrrolidino-4-iodo-tamoxifen: prospects for pharmacokinetic studies using PET. *J. Nucl. Biol. Med. 38*, 96.

Christensen, E. I., and Maunsbach, A. B. (1981) Dextran is resistant to lysosomal digestion in kidney tubules. *Virchows Arch. (Cell Pathol.) 37*, 49−59.

Cleeland, R., Christenson, J, Usategui-Gomez, M., Heveran, J., Davis, R., and Grunberg, E. (1976) Detection of drugs of abuse by radioimmunoassay: a summary of published data and some new information. *Clin. Chem. 22*, 712−725.

De Jong, M., Breeman, W. A., Bernard, B. F., Rolleman, E. J., Hofland, L. J., Visser, T. J., Setyono-Han, B., Bakker, W. H., van der Pluijm, M. E., and Krenning, E. P. (1995) Evaluation in vitro and in rats of ^{161}Tb-DTPA-octreotide, a somatostatin analogue with potential for intraoperative scanning and radiotherapy. *Eur. J. Nucl. Med. 22*, 608−616.

De Jong, M., Bakker, W. H., Breeman, W. A., Bernard, B. F., Hofland, L. J., Visser, T. J., Srinivasan, A., Schmidt, M., Behr, M, Mäcke, H. R., and Krenning, E. (1998) Pre-clinical comparison of [DTPA^0] octreotide, [DTPA^0, Tyr^3] octreotide and [DOTA^0, Tyr^3] octreotide as carriers for somatostatin receptor-targeted scintigraphy and radionuclide therapy. *Int. J. Cancer. 75*, 406−411.

Delaloye, B., Bischof-Delaloye, A., Buchegger, F., von Fieldner, V., Grob, J.-P., Volant, J.-C., Pettavel, J., and Mach, J.-P. (1986) Detection of colorectal carcinoma by emission computerized tomography after injection of ^{123}I-labeled Fab or F(ab')2 fragments from monoclonal anti-carcinoembryonic antigen antibodies. *J. Clin. Invest. 77*, 301−311.

Dewanjee, M. K. (1992) *Radioiodination: theory, practice, and biomedical applications*; Kluwer academic publishers: Boston, MA.

Duncan, J. R., and Welch, M. J. (1993) Intracellular metabolism of indium-111-DTPA labeled receptor targeted proteins. *J. Nucl. Med. 34*, 1728−1738.

Garg, S., Garg, P. K., and Zalutsky, M. H. (1991) N-succinimidyl-5-(trialkylstannyl)-3-pyridinecarboxylates: a new class of reagents for protein radioiodination. *Bioconjugate Chem. 2*, 50−56.

Garg, S., Garg, P. K., and Zalutsky, M. H. (1993) N-succinimidyl-4-methyl-3-(tri-*n*-butylstannyl)benzoate: synthesis and potential utility for the radioiodination of monoclonal antibodies. *Nucl. Med. Biol. 20*, 379−387.

Gasparini, M., Buraggi, G. L., Regalia, E., Maffioli, L., Balzarini, L., and Gennari L. (1994) Comparison of radioimmunodetection with other imaging methods in evaluating local relapses of colorectal carcinoma. *Cancer 73*, 864−849.

Gedda, L., Olsson, P., Ponten, J., and Carlsson, J. (1996) Development and in vitro studies of epidermal growth factor-dextran conjugates for boron-neutron capture therapy. *Bioconjugate Chem. 7*, 584−591.

Geissler, F., Anderson, S. K., Venkatesan, P., and Press, O. (1992) Intracellular catabolism of radiolabeled anti-μ antibodies by malignant B-cells. *Cancer Res. 52*, 2907−2915.

Haeckel, O., and Preetz, W. (1995) Darstellung und Kristallstrukturen von Dipyridiniomethan-Monohalogenohydro-closo-Dodecaboraten(2-), $[(C_5H_5N)_2CH_2][B_{12}H_{11}X]$; X = Cl, Br, I. Z. *Anorg. Allg. Chem. 621*, 1454−1458.

Holmberg, A., and Meurling, L. (1993) Preparation of sulfhydrylborane-dextran conjugates for boron neutron capture therapy. *Bioconjugate Chem. 4*, 570−573.

Holmberg, A., Silen, Å., Marquez, M., Bergwall, R., Westlin, J.-E., and Nilsson, S. (1994a). An alternative method of labeling antibodies with ^{99m}Tc. *Antibody Immunoconj. Radiopharm. 7*, 149−154.

Holmberg, A., Marquez, M., Westlin, J.-E., and Nilsson, S. (1994b). Preparation, in vitro binding and technetium-99m labeling of somatostatin-dextran conjugates. *Antibody Immunoconj. Radiopharm. 7*, 253−259.

Kerr, J. A. (1992) Strengths of chemical bonds. in *Handbook of chemistry and physics*, 72nd ed. (D. R. Lide, Ed.) pp 9-105 to 9-113, CRC press, Boca Raton, FL.

Khaw, B. A., Cooney, J., Edingtom, T., and Strauss, H. W. (1986) Differences in experimental tumor localisation of dual-labeled monoclonal antibody. *J. Nucl. Med. 27*, 1293−1299.

Killen, A. R., Oster, G., and Colditz, G. A. (1989) An assessment of the role of ^{123}I−N-isopropyl-*p*-iodoamphetamine with single-photon emission computed tomography in the diagnosis of stroke and Alzheimer's disease. *Nucl. Med. Commun. 10*, 271−284.

Knight, L. C., and Welch, M. J. (1978) Sites of direct and indirect halogenation of albumin. *Biochim. Biophys. Acta 534*, 185−195.

Knoth, W. H., Miller, H. C., Sauer, J. C., Balthis, J. H., Chia, Y. T., and Muetterties, E. L. (1964) Chemistry of Boranes. IX. Halogenation of $B_{10}H_{10}2$- and $B_{12}H_{12}2$-. *Inorg. Chem. 3*, 159−167.

Knox, S. J. (1995) Overview of studies on experimental radioimmunotherapy. *Cancer Res. (Suppl.) 55*, 5832s−5836s.

Kulkarni, P. V., and Corbett, J. R. (1990) Radioiodinated tracers for myocardial imaging. *Semin. Nucl. Med. 20*, 119−129.

Kusic, Z., Becker, D. V., Saenger, E. L., Paras, P., Gartside, P., Wessler, T., and Spaventi, S.(1990) Comparison of technetium-99m and iodine-123 imaging of thyroid nodules: correlation with pathologic findings. *J. Nucl. Med. 31*, 393−399.

Larson, S. M., and Carrasquillo, J. A. (1988) Advantages of radioiodine over radioindium labeled monoclonal antibodies for imaging solid tumors. *Nucl. Med. Biol. 15*, 231−233.

Lashford, L. S., Davies, A. G., Richardson, R. B., Broune, S. P., Bullimore, J. A., Eckhert, H., Kemshead, J. T., and Coakham, H. B. (1988) A pilot study of ^{131}I monoclonal antibodies in the therapy of leptomengial tumors. *Cancer 61*, 857−868.

Lindström, A., and Carlsson, J. (1993) Penetration and binding of epidermal growth factor-dextran conjugates in spheroids of human glioma origin. *Cancer Biother. 8*, 145−158.

Lövqvist, A., Lindström, A., and Carlsson, J. (1993) Binding, internalisation and excretion of TGF-alfa-dextran associated

radioactivity in cultured human glioma cells. *Cancer Biother. 8*, 345−356.

Meijs, W. E., Haisma, H. J., Klok, R. P., van Gog, F. B., Kievit, E., Pinedo, H. M., and Herscheid, J. D. M. (1997) Zirconium-labeled monoclonal antibodies and their distribution in tumor-bearing nude mice. *J. Nucl. Med. 38*, 112−118.

Molteni, L. (1979) Dextrans as drug carriers. in *Drug carriers in biology and medicine* (G. Gregoriadis, Ed.) pp 107−125, Academic Press, London.

Mowry, R. W., and Nillican, R. C. (1953) A histological study of the distribution and fate of dextran in tissue of the mouse. *Am. J. Pathol. 29*, 523−545.

Nishikawa, M., Yamashita, F., Takakura, Y., Hashida, M., and Sezaki, H. (1992) Demonstration of the receptor-mediated hepatic uptake of dextran in mice. *J. Pharm. Pharmocol. 44*, 396−401.

O'Doherty, M. J., Nunan, T. O., and Croft, D. N. (1993) Radionuclides and therapy of thyroid cancer. *Nucl. Med. Commun. 14*, 736−755.

Olsson, P., Lindström, A., and Carlsson, J. (1994) Internalization and excretion of epidermal growth factor-dextran associated radioactivity in cultured human squamous-carcinoma cells. *Int. J. Cancer 56*, 529−537.

Press, O. W., Shan, D., Howell-Clark, J., Eary, J., Appelbaum, F. R., Metthews, D., King, D. J., Haines, M. R., Hamann, P., Hinman, L., Shochat, D., and Bernstein, I. D. (1996) Comparative metabolism and retention of iodine-125, yttrium-90, and indium-111 radioimmunoconjugates by cancer cells. *Cancer Res. 56*, 2123-2129.

Reist, G. J., Archer, G. E., Kurpad, S. N., Wikstrand, C. J., Vaidyanathan, G., Willingham, M. C., Moscatello, D. K., Wong, A. J., Bigner, D. D., and Zalutsky, M. R. (1995) Tumor-specific anti-epidermal growth factor receptor variant III monoclonal antibodies: use of the tyramine-cellobiose radioiodination method enhances cellular retention and uptake in tumor xenografts. *Cancer Res. 55*, 4375−4382.

Ryser, J. E., Jones, R. M., Egeli, R., Pelegrin, A., Rose, K., Kurt, A. M., Perin, M., Broquet, P. E., Ambrosetti, P., Fisch, I., Pochon, S., Donath, A., Mach, J. P., and Offord, R. E. (1992) Colon carcinoma immunoscintigraphy by monoclonal anti-CEA antibody labeled with gallium-67-aminooxyacetyldeferroxamine. *J. Nucl. Med. 33*, 1766−1773

Schott, M. E., Milenic, D. E., Yokota, T., Whitlow, M., Wood, J. F., Fordyce, W. A., Cheng, R. C.; Schlom, J. (1992) Differential metabolic patterns of iodinated versus radiometal chelated anticarcinoma single-chain Fv molecules. *Cancer Res. 52*, 6413−6417.

Scott-Robson, S., Capala, J., Carlsson, J., Malmborg, P., and Lundqvist, H. (1991) Distribution and stability in the rat of a ^{76}Br/^{125}I-labeled polypeptide, Epidermal growth factor. *Nucl. Med. Biol. 18*, 241−246.

Srebny, H.-G., and Preetz, W. (1984) Darstellung, 11B−NMR− und Schwingugsspektren isomerenreiner Halogenohydrododecaborate $X_nB_{12}H_{12-n}^{2-}$; X = Cl, n = 1−3; X = Br, n = 1, 2; X = I, n = 1. Z. Naturforsch., Teil B. *Chem. Sci. 39*, 189−196.

Stein, R., Goldenberg, D. M., Thorpe, S. R., and Mattes, M. J. (1997) Advantage of a residualizing iodine radiolabel for radioimmunotherapy of xenografts of human nonsmall-cell carcinoma of the lung. *J. Nucl. Med. 38*, 391−395.

Todderud, G., and Carpenter, G. (1989) Epidermal growth factor: the receptor and its function. *BioFactors 2*, 11−15.

Troncone, L., and Rufini V. (1997) ^{131}I-MIBG therapy of neural crest tumours (review). *Anticancer Res. 17*, 1823−1831.

Wilbur, D. S. (1992) Radiohalogenation of proteins: an overview of radionuclides, labeling methods, and reagents for conjugate labeling. *Bioconjugate Chem. 3*, 433−470.

Wilbur, D. S., Hadley, S. W., Hylarides, M. D., Abrams, P. G., Beaumier, P. A., Morgan, A. C., Reno, J. M., and Fritzberg, A. R. (1989) Development of a stable radioiodinating reagent to label monoclonal antibodies for radiotherapy of cancer. *J. Nucl. Med. 39*, 216−226.

Wilbur, D. S., Hamlin, D. K., Buhler, K. R., Srivastava, R. R., Stray, J. E., Daniel, J., and Vessela, R. J. (1995) Comparison of in vivo distributions of simple radioiodinated borane and carborane cage molecules. *Q. J. Nucl. Med. 39*, 51−52.

Young, H., Carnochan, P., Trivedi, M., Potter, G. A., Eccles, S. A., Haynes, B. P., Jarman, M., and Ott, R. J. (1995) Pharmacokinetics and biodistribution of radiolabeled idoxifene: prospects for the use of PET in the evaluation of a novel antioestrogen for cancer therapy. *Nucl. Med. Biol. 22*, 405−411.

Zalutsky, M. R (1988). Radiohalogenation of antibodies: chemical aspects. in *Radiolabeled monoclonal antibodies for imaging and therapy* (S. C. Srivastava, Ed.) pp 195−214, Plenum Press, New York.

Zalutsky, M. R., and Narula, A. S. (1987) A method for the radiohalogenation of proteins resulting in decreased thyroid uptake of radioiodine. *Appl. Radiat. Isot. 38*, 1051−1055.

Zalutsky, M. R., and Narula, A. S. (1988) Radiohalogenation of a monoclonal antibody using an N-succinimidyl-3-(tri-*n*-butylstannyl)benzoate intermediate. *Cancer Res. 48*, 1446−1450.

Zalutsky, M. R., Noska, M. A., Colapinto, E. V., Garg, P. K., and Bigner, D. D. (1989) Enhanced tumor localization and in vivo stability of a monoclonal antibody radioiodinated using N-succinimidyl-3-(tri-*n*-butylstannyl)benzoate. *Cancer Res. 49*, 5543−5549.

Zhao, Q., Blomquist, E., Bolander, H., Gedda, L., Hartvig, P., Jahnson, J.-K., Lundquist, H., Mellstedt, H., Nilsson, S., Nister, M., Sundin, A., Tolmachev, V., Westlin, J.-E., and Carlsson, J. (1998) Conjugate chemistry, iodination and cellular binding of mEGF-dextran-tyrosine. Preclinical tests in preparation for clinical trials. *Int. J. Mol. Med. 1*, 693−702.

BC980033S

New Use of Cyanosilane Coupling Agent for Direct Binding of Antibodies to Silica Supports. Physicochemical Characterization of Molecularly Bioengineered Layers

Sandrine Falipou, Jean-Marc Chovelon,*,† Claude Martelet,† Jacqueline Margonari,‡ and Dominique Cathignol‡

Laboratoire d'Ingénierie et Fonctionnalisation des Surfaces, CNRS/UMR 5621, Ecole Centrale de Lyon, BP163 69131 Ecully Cedex, France, and INSERM, Unité 281: Recherches sur la Détection et le Traitement de la Prolifération Tissulaire par Agents Physiques. 151, Cours Albert Thomas 69424 Lyon Cedex 03, France.
Received April 10, 1998; Revised Manuscript Received February 4, 1999

A simple protocol to fix biological species to silica-based surfaces (silica microbeads and glass slides), using a bifunctional silane reagent (3-cyanopropyl dimethyl chlorosilane), is presented. This silane reagent was used without further derivatization. This system led to strong, but not covalent, linkage of antibodies through their glycosylated regions (OH groups) to solid supports. The use of a microsized sample revealed that the coupling process depends not only on physicochemical interactions but also on steric phenomena, and in this case, it was shown that a molecule acting as a spacer was required for more efficient cell fixation. Here, monoclonal mouse antibodies against the CD45 molecule expressed on rat lymphocytes (MAR anti CD45 Ab) were linked to lymphocytes, and as spacers, sheep anti-mouse antibodies (SAM Ab) were immobilized on silica surfaces, allowing the cells to stick to the floating hollow silica microbeads by simple incubation. Under such conditions, a single microbead can fix several cells. The potential of this hollow, low-density support is in ultrasound applications, for the destruction by cavitation phenomena of cells selectively fixed onto such a support. Such a study can serve as a basic model for various microbiosystems involving cell manipulation.

INTRODUCTION

Since the first work of Nelson and Griffin (*1*), fixing biologicals onto a variety of solid inorganic supports has become a widely used technique.

A great number of biomedical applications, especially diagnostic, involve binding biospecies (antigen, antibody, and enzyme) to various solid matrixes. For example, biosensing applications require the biospecies involved to be grafted onto silicon, polymers, or metallic-based materials (*2*, *3*). For immunoaffinity chromatography, functionalized beads are required. The various functionalization methods are often tedious, rather expensive, and can denature the biological species (*4*). Moreover, the efficiency of the grafting processes must often be characterized through topographical studies (atomic force microscopy) or analytical investigations. For this purpose, substrates such as mica or glass slides with similar reactivity and with a well-controlled surface state (low roughness) are used (*5*, *6*).

Various chemical reagents can be used to modify surfaces in order to immobilize proteins (*7*). For example, surfaces can be activated with reagents such as BrCN or derivatized with linkers such as triazines, epoxy, aryl azides, isothiocyanates, *N*-hydroxysuccinimides, silanes, etc. Bifunctional silanes with a $(MeO)_3Si(CH_2)_nX$ structure, where X represents a reactive moieties such as an amine or a glycidoxy group, were used extensively in the 1970s as coupling agents to link proteins to various inorganic solid supports (*8*). Very often, after silanization, the reactive moieties must be derivatized prior to protein immobilization. This additional step is not always easy to realize and a direct coupling procedure without the use of an intermediary step would be of interest.

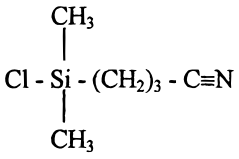


Figure 1. Bifunctional silane reagent: 3-cyanopropyl dimethyl chlorosilane.

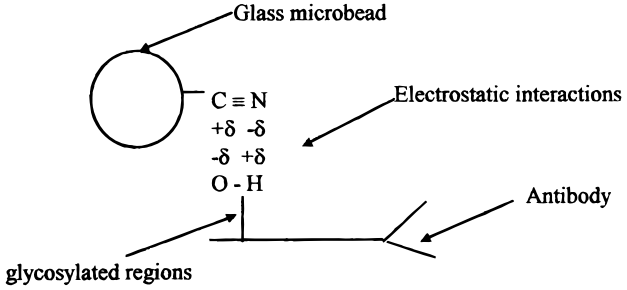


Figure 2. Antibody coupling to silica or glass surfaces.

In this paper, a simple protocol to fix biological species to silica-based surfaces by using a bifunctional silane reagent (3-cyanopropyl dimethyl chlorosilane, cf. Figure 1) is presented. This silane reagent was used without further derivatization. Such a system has already been shown to induce a strong, but not covalent linkage, of antibodies to solid supports, through their glycosylated regions (OH groups) (cf. Figure 2) (*9*). Moreover, antibodies fixed onto a cyanosilanized silica substrate have been

* To whom correspondence should be addressed. Phone: 33 (0) 4 72 18 62 52. Fax: 33 (0) 4 78 33 15 77. E-mail: chovelon@ec-lyon.fr.
† Laboratoire d'Ingénierie et Fonctionnalisation des Surfaces.
‡ INSERM.

10.1021/bc9800421 CCC: $18.00 © 1999 American Chemical Society
Published on Web 04/09/1999

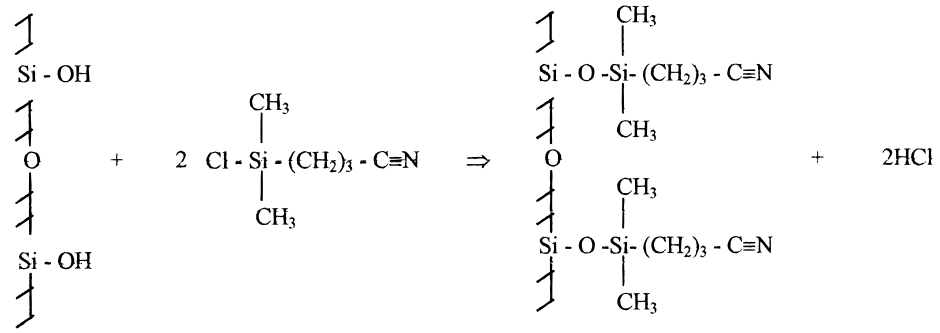


Figure 3. Activation of glass surface by silane reagent.

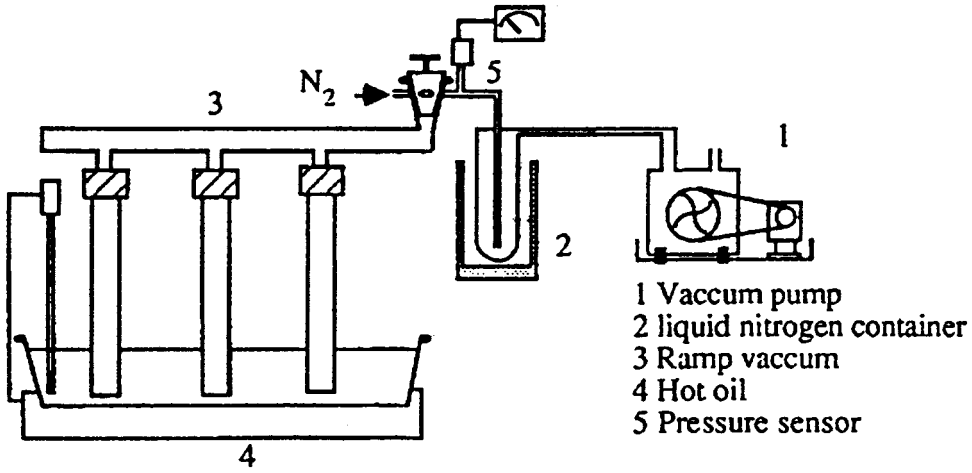


Figure 4. Vapor phase deposition device.

Table 1. Contact Angle Measurements on Glass Slides

substrate	liquid	treatment	angle (deg)	standard deviation	number of measures
glass slides	pure water	none	34.2	7.0	27
		sulfochromic at 70−80 °C	<15		
		blank	40.6	1.7	16
		silanization	71.5	1.8	27

Table 2. Surface Roughness Parameter Evolution

substrate	roughness (rms) (nm)
nontreated glass slide	0.3
silanized glass slide	0.7
silanized glass slide + antibodies	>5

found to resist acid washing. During such treatments, a partial reorganization of the antibody layer was observed, inducing an increase in antibody activity (*10*).

The efficiency of such a silanization process resulting in a high rate of immobilized antibodies on the silica surfaces has been demonstrated by using glass slides which allow various methods of physicochemical characterization.

Subsequently, antibodies anchored on floating silica hollow microbeads were proved to be able to recognize CD45 rat cells.

The originality of this study is that such hollow, low-density silica microbeads have never been used before. This solid support was chosen because it is inexpensive and could also be used in ultrasound applications. Cavitation could be used for the destruction of cells in vitro (*11*): gas bubbles in the suspension could collapse and damage cell membranes causing their death. Thus, acoustic cavitation could be used as an alternative medical therapy for cancer treatment. F. Prat et al. (*12*) obtained subsequent hepatic lesions in vivo in the rabbit by acoustic cavitation, coupling the injection of artificial bubbles in the liver with ultrasonic treatment. It is worth noting that pressures generated during the collapse could attain tens of thousands of bars (*13*).

EXPERIMENTAL SECTION

Reagents. 3-Cyanopropyl dimethyl chlorosilane was purchased from Aldrich and was used as received. According to the suppliers, its purity was 95%, the remaining 5% being mainly composed of disilane form, which resulted from the condensation of the molecule, and was nonreactive toward the surface. The following commercial analytical grade reagents were used: sulfuric acid and potassium dichromate from Merck, tetrahydrofuran from Sigma, xylene from Carlo Erba, and 2-methylbutane from Aldrich.

Low-density hollow silica microbeads (SDT-60:0.6 g cm^{-3}) were obtained from NewMet.

The sulfochromic solution was prepared by mixing 15 g of potassium dichromate, 5 mL of deionized water, and 80 mL of 96% concentrated sulfuric acid.

Purified sheep anti-mouse monoclonal antibody, purified mouse anti-rat CD45RC (clone OX22) monoclonal antibody, and biotin-conjugated mouse anti-rat CD45RC (clone OX22) monoclonal antibody were obtained from Pharmingen. A FITC-conjugated $F(ab')_2$ fragment of goat anti-mouse antibody was purchased from Dako. Ficolite was obtained from Dutscher.

Phosphate-buffered saline (PBS), bovine serum albumin (BSA), and Tween 20 were from Sigma, carbonate/bicarbonate buffer was prepared by mixing Na_2CO_3 0.1 M and $NaHCO_3$ 0.1 M and adjusting the pH to 9.4. Barbital (Veronal) buffer was prepared by dissolving 4.12 g of sodic veronal and 0.8 g of veronal in 1 L of distilled

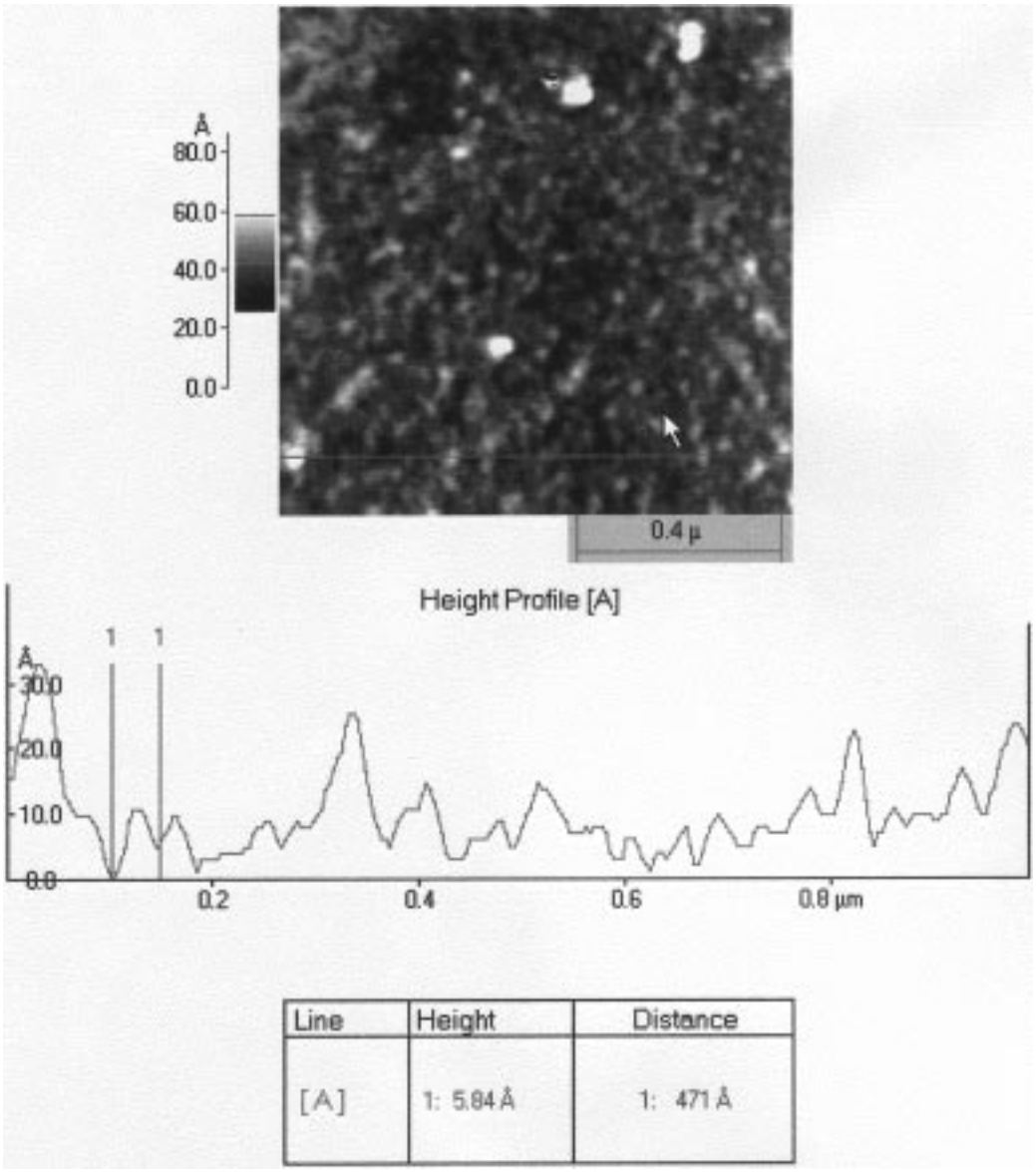


Figure 5. AFM image of silanized surface and profile corresponding to the line shown in the image. The height and the distance are measured between lines 1.

water and adjusting the pH to 8.6. Citrate buffer was prepared by mixing 1.78 g of Na_2HPO_4, 0.7 g of citric acid, and 134 mL of distilled water.

Sample Surface Preparation. Silica surface cleaning and hydroxylation are important in the grafting process. Glass slides were first degreased under ultrasonic stirring with acetone. Due to the difficulties of handling them, silica microbeads were not degreased before the hydroxylation treatment. This first step is not critical, as grease residues should be completely eliminated in the following which involves strong oxidizing reagents.

Glass slides and floating silica microbeads were treated with sulfochromic solution for 30 min at 70−80 °C to remove any coatings or contaminates and to create hydroxyl reactive functions at the surface. Glass slides were washed with deionized water and dried by a pure nitrogen stream. The washing procedure used for microbeads is more critical since they are far more difficult to handle than glass slides. After the sulfochromic treatment, the microbeads were allowed to float to the top of the suspension while the underlying fluid was drawn off. Then deionized water was added to the microbeads which were once again allowed to float. This process was repeated until the sulfochromic solution was completely eliminated. Then, the microbeads were partially dried at 100 °C in air.

Silane Activation (Figure 3). After the cleaning process, the glass slides and microbeads were dried at 140 °C under vacuum (0.1 Pa) for 2 h in order to remove the physisorbed water (Figure 4).

For the glass slides, pure silane was introduced under nitrogen atmosphere whereas the microbeads were first placed in a solution of 5×10^{-2} mol of silane in 2-methyl butane, to ensure that they would be well wetted. For the latter, the solvent was removed in the following step under vacuum.

The condensation reaction on the silica sample was performed in sealed vessels under vacuum for 48 h at 70 °C.

The excess silane was eliminated by washing with THF, xylene, and deionized water. The glass slides were blown dry with dry nitrogen, whereas the microbeads, were allowed to dry in air at ambient temperature. Although the cleaning and the treating processes are slightly different for each substrate, the surface reactivities to silane reagents are assumed to be quite similar.

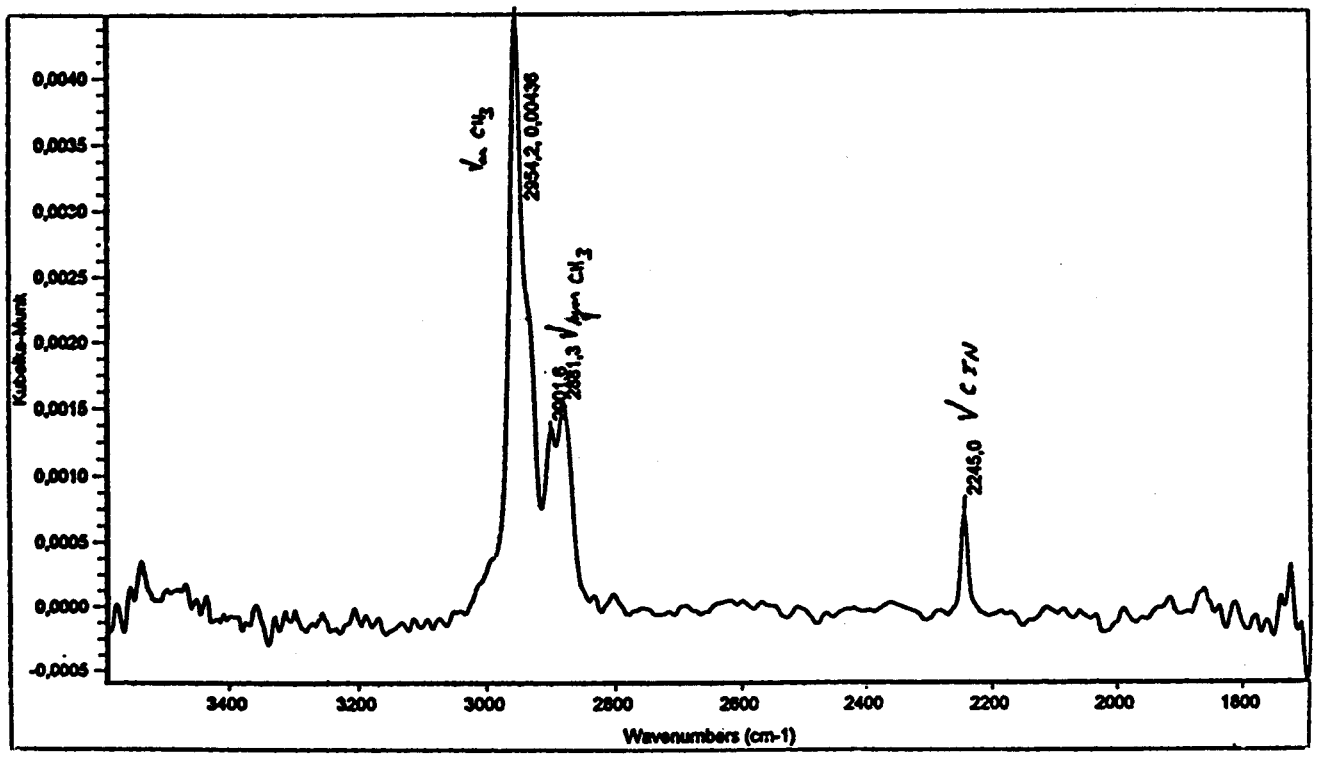
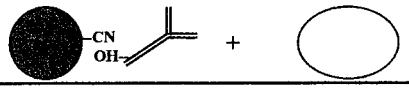
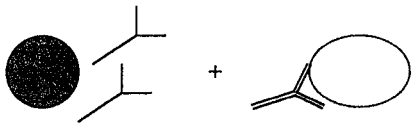
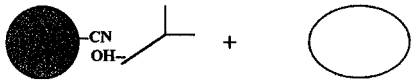
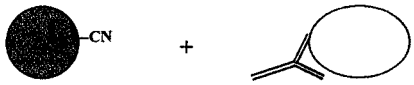
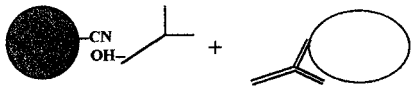
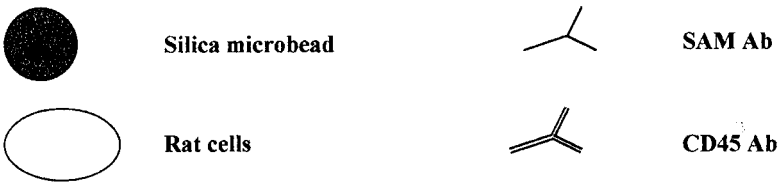


Figure 6. Infrared spectrum of cyanosilane deposited on microbeads.

Table 3. Results of the Cell Binding Assays

Substrate and fixation mode	Results	Schematic representation of molecular assemblies
(1) silane-activated microbeads with CD45 Ab	+/-	
(2) non-silanized microbeads sensitized cells	-	
(3) silane-activated microbeads with SAM Ab non sensitized cells	-	
(4) silane-activated microbeads without SAM Ab sensitized cells	+/-	
(5) silane-activated microbeads with SAM Ab sensitized cells	+	



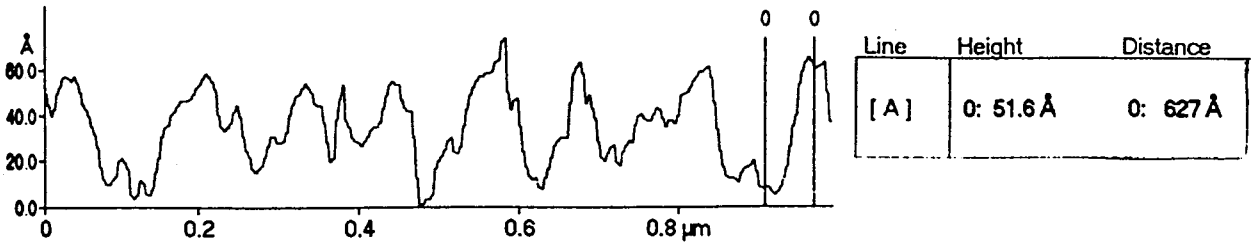


Figure 7. AFM profile of the surface after antibody grafting. The height and the distance are measured between lines 0.

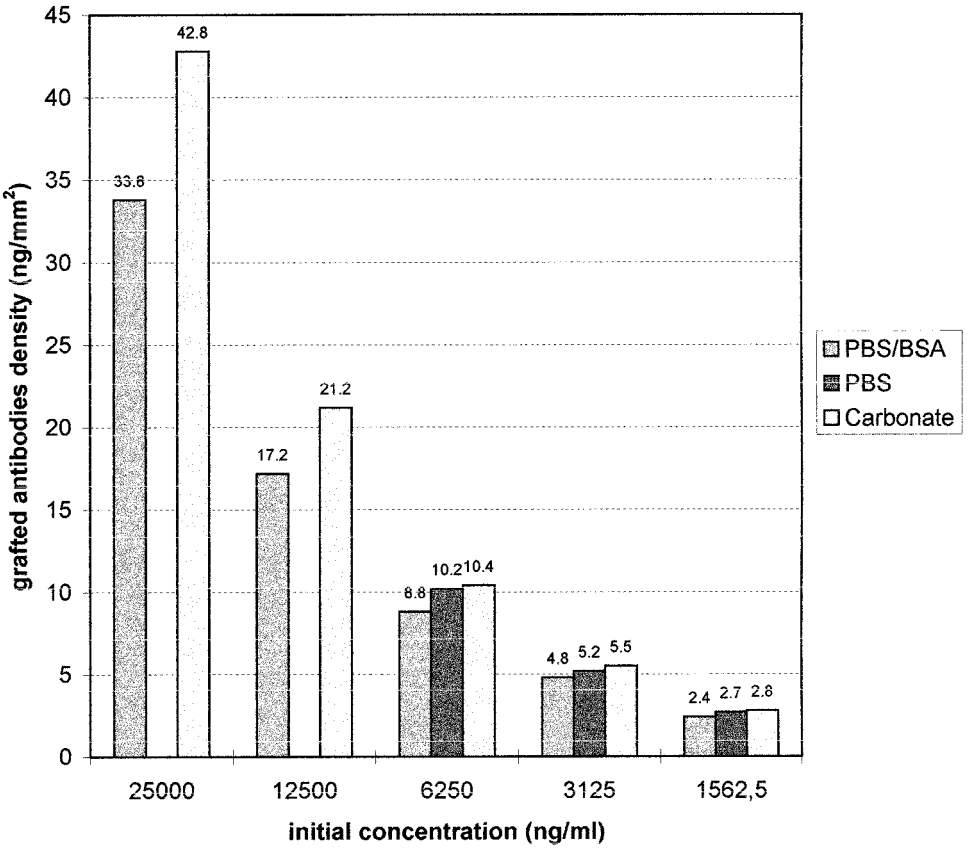


Figure 8. Antibody density per surface unit on glass slide versus the initial concentration for different buffers.

Of course, the possibility that solvent may penetrate the cyanosilane molecules of the microbeads is not excluded.

Contact Angle Measurements on Planar Substrates. As the silanized surfaces are more hydrophobic compared to the hydroxylated ones, the efficiency of the silanization process can be controlled by measuring the contact angles.

Contact angles were measured by the sessile drop method on a Digidrop instrument. (GBX Scientific Instruments).

Measurements were made on drops of pure water deposited at 22 °C under an atmosphere saturated with humidity to obtain reproducible conditions.

A video camera equipped with an image analyzer visualized the shape of the drop and gave the contact angle between water drop and silica surface.

The reported contact angles are the average of at least 15 drops for each surface treatment. The macroscopic homogeneity of the surface structure can be estimated by its standard deviation. These measurements are used to control each sample at each step of the silanization process by reference to the values obtained for at least 3 samples and 15 drops of distilled water.

Atomic Force Microscopy. Atomic force microscopy (AFM) images were obtained in air using a Park Scientific Instrument (Autoprobe). V-shaped cantilevers (PSI) with a normal spring constant of 0.05 N m^{-1} and a pyramidal Si_3N_4 tip were used in this study. Either 100 $\times$ 100 μm^2 or 5 $\times$ 5 μm^2 scanners were used. Images were flattened with only a second order correction. Images were taken in the contact or tapping modes.

Surface evolution was tracked using root-mean-squared surface roughness (rms), measured for each step of the silanization and antibody fixation processes.

Infrared Spectroscopy on Microbeads. Methods previously described do not allow the characterization of microspherical substrates. Infrared measurements were made by the Service Central d'Analyses of the CNRS on a Nicolet 20SXC instrument (diffuse reflection mode). Results were given after accumulations of 2048 scans.

Immobilization of Immunological Species on Silanized Substrates and Analysis of Ab Content by Competitive ELISA Assay: Use of Glass Slides for Technical Purposes. Mouse anti-rat CD45RC antibody was placed on silanized slides of defined surfaces at concentrations ranging from a few nanograms per milliliter to several micrograms per milliliter. Antibodies were allowed to adsorb for 1 h at 37 °C and 1 night at 4 °C in a wet atmosphere. Various buffers for dilution and washing were studied: phosphate-buffered solution, pH 7.4 (PBS),

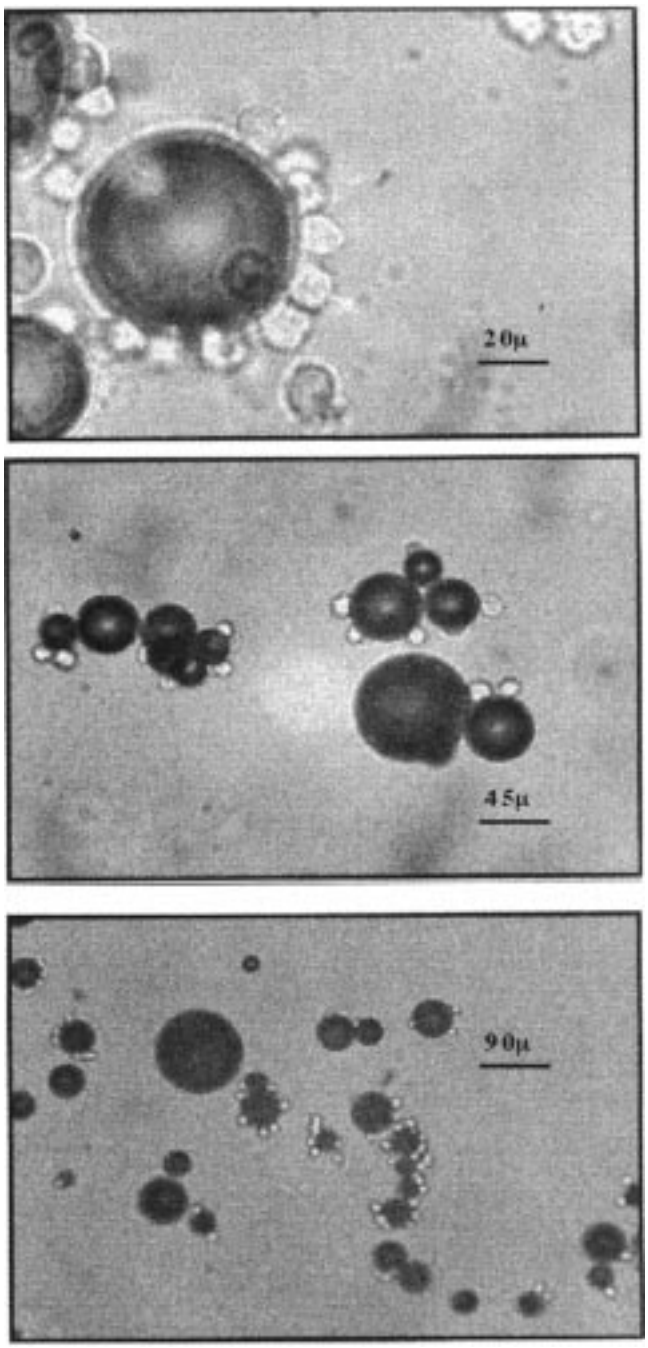


Figure 9. Photographs of cells around silica microbeads.

phosphate-buffered solution/bovine serum albumine at pH 7.4 (PBS/BSA) and carbonate/bicarbonate at pH 9.4.

Concentrations of less than 5 μg/mL could not be obtained by direct enzymatic methods of quantification (for example with a goat anti-mouse horseradish peroxidase monoclonal). Thus, a competitive technique was used in association with the amplified visualization of antibody fixation (an enzymatic reaction with biotinylated mouse antibody and a streptavidin/enzyme complex for binding).

First the optimum optical density curve for biotinylated anti CD45 dilutions was defined. The dilution which gave 50% of the maximal OD was retained.

Second, optical density was tested when nonbiotinylated anti-CD45 antibody dilutions were added to the previously defined biotinylated anti-CD45 dilution.

Finally, the same competition analysis was carried out for the glass slides: the glass slides and 400 μL Mouse anti-CD45 in concentrations ranging from a few nanograms per milliliter to several micrograms per milliliter were incubated with constant agitation for 1 h at 37 °C and 1 night at 4 °C. The quantity of nonbound antibodies remaining in the liquid was measured by competing with biotin-conjugated antibody at the previously determined concentration, and the results obtained by comparison with the curve defined at the second step were read at 492 and 620 nm. The difference between the total amount used for incubation and the residual one after incubation represented the amount of absorbed antibodies per surface unit.

Preparation of Rat Lymphocytes for Cell-Immobilization Experiments. Fresh rat blood (approximately 15 mL) was collected and heparinized. The blood was diluted by half, and 15 mL of diluted blood was added to 50 mL centrifuge tubes containing 15 mL of Ficolite. The tubes were then centrifuged at 1000*g* for 13 min at ambient temperature to obtain a cell density gradient. The resulting layer of peripheral blood lymphocytes, which possess CD45 antigen on their surface, was delicately removed from each tube and pooled.

Cells were washed in PBS containing albumin (PBS/BSA 1%) and spun down 3 times for 13 min at 500*g* and low temperature. A batch of four tubes, each containing 1×10^7 cells in 50 μL of PBS/BSA, was prepared, and 100 μL of a 5 μg/mL dilution of anti-CD45 antibody was added to each tube before incubation for 30−60 min at 4 °C.

After washing in PBS/BSA, cells were counted with a hemocytometer for viability.

Immobilization of Cells onto Silica Microbeads. The experiments and control were carried out using silanized or nonsilanized substrates and different fixation modes were tested using monoclonal mouse anti rat antibodies, which recognize CD45 molecules expressed on rat lymphocytes. Another biochemical link was tested with the insertion of an antibody between the complex cells/CD45 and the substrate SAM Ab.

In all cases, cells were added to the microbeads in a ratio higher than 5×10^5 cells/mg of microbeads.

The volume was 500 μL to 1 mL, and the microbeads and cells were incubated for 2 h at 4 °C with agitation. After incubation, centrifuging at 450−500*g* allowed microbeads to float to the top of the suspension whereas nonfixed cells fell to the bottom. Then, the effluent was drawn off. Floating microbeads were observed under the microscope and photographs of the cell were taken.

RESULTS AND DISCUSSION

Silanization Process. Considering the geometry of the silica beads, classical methods of characterization of the silanization cannot be applied. Of these methods, the contact angle measurements offer the most significant wettability test when pure fluids and smooth surface are used. So, to evaluate the wettability after silanization on flat sample, glass slides were used.

Such silica-based samples should behave similarly to microbead ones.

For silane-treated and untreated glass slides, Table 1 summarizes contact angle results at equilibrium.

When no treatment was applied, the value obtained showed great standard deviation ($\theta = 34.2 \pm 7°$), reflecting the heterogeneity of the surface.

The surface of glass slides, when treated by hot sulfochromic solution, is almost totally wetted by water ($\theta < 15°$) demonstrating the efficiency of such a cleaning procedure. Surface hydrophilicity is due to the presence

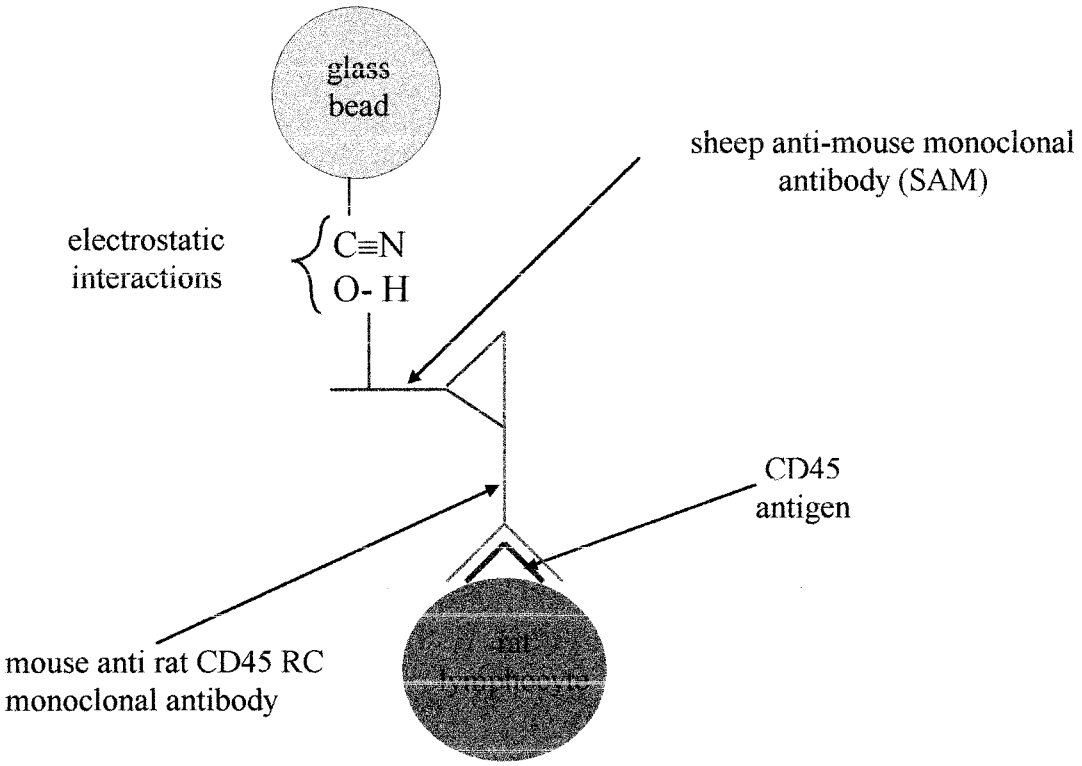


Figure 10. Rat cell immobilization by silane-activated glass beads with SAM Ab.

of a great number of hydroxyl groups on the surface which are required for the silanization process (Figure 4). Great care must be taken with cleaned samples, as organic molecules can readily be adsorbed on these reactive surfaces, inducing an increase of the contact angle within a few minutes. Because of this, as soon as the treatment is finished, the samples are placed under vacuum.

After silanization, contact angles increase up to around 71.5 ± 1.8° proving the presence of silane. This surface treatment induces a more homogeneous surface (low standard deviation).

To be sure that no contamination takes place, a sample treated by this process but without the silanization step was tested. In this condition, the value of the contact angle increased up to 40.6°: lower than the value obtained with the silane, but higher than that obtained after sulfochromic treatment.

AFM technique was used to characterize the molecular organization of silane on glass slides. Substrate modifications after reaction were checked by measuring surface roughness variations.

Table 2 shows the evolution of this surface roughness parameter (rms).

The roughness of the silanized surface was found to be higher than the untreated one (rms = 0.7 nm compared to 0.3 nm), values which could be compared to those obtained by Perrin et al. (*14*) who used the same chain length for the silane reagent.

Figure 5 obtained in tapping mode (1 μm × 1 μm) shows that the silane layer was dense and relatively homogeneous, except for a small number of pinhole defects. Thanks to these defects, the thickness of one layer was evaluated at 0.58 nm, as shown in Figure 5. This figure also shows a thicker area, proving that in some cases aggregates can be formed. It is noteworthy that by using silane molecules with long alkyl chains [Si−$(CH_2)_{17}CH_3$, for example], a monolayer with almost no defects was observed (*15*). Such aggregates are known (*16*) to be induced by nonuniform reactions on the surface which lead to the formation of at least two different distributions of attached ligands: the expected siloxane bonds and hydrogen bonds between cyano groups and free surface silanols. Although nonuniform reactions take place, the architecture of the film obtained thus appears quite similar for various tested samples. In addition, these interactions are strong enough to resist several washing processes.

The presence of silane on treated microbeads was confirmed by the diffuse reflection infrared spectroscopy method.

Figure 6 shows the presence of nitrile and alkyl functions at the surface of the microbeads, whereas no peaks were obtained with untreated microbeads.

According to the infrared analysis conditions used and taking into account the sensitivity of the apparatus, if only one monolayer was present on the surface, no peak would be visible. In our case, the presence of nitrile and alkyl peaks confirmed that the silanization process had occurred, forming a few aggregates.

In this context, silanization effects would appear to similar for both substrates.

Immobilization of Immunological Species. Figure 7 shows an AFM profile taken in tapping mode in air from antibodies deposited onto cyanosilane. The profile showed aggregates which were about 5 nm high. These aggregates suggest that lateral interactions occur between the adjacent IgG molecules. It was not surprising to find such lateral interactions, as this protein has some self-aggregating properties.

The height of these molecules roughly matched the known size of one IgG molecule (5 × 15 nm) (*4*) set horizontally confirming the orientation of the antibodies and thus the nature of the link (electrostatic interactions between OH groups of the glycosylated regions on the Fc fragment of antibodies and CN functions of the silane).

Optimization of Antibody Fixation: ELISA Assay. The ELISA assay was done with mouse anti-rat CD45RC

in concentrations ranging from a few nanograms per milliliters to several micrograms per milliliter in different buffers: PBS, PBS/BSA (1%), and carbonate/bicarbonate. This assay was used to determine the optimum mouse anti-rat CD45RC level coupled to well-defined surfaces of glass slides activated with the cyanosilane by varying the antibody concentration and the incubation buffer.

The antibody surface density was given as a function of initial antibody concentration in solution for three buffers.

Results are shown in Figure 8. Concerning the nonspecific binding, measurements carried out on unsilanized slides lead to an adsorption rate which never exceeds 3%.

These results showed the validity of the cyanosilane coupling agent for the immobilization of antibodies onto glass or silica surfaces.

The most suitable buffer was found to be the carbonate buffer with a pH of 9.4.

Cell Binding. Table 3 compares cell immobilization behavior in various fixation modes. The fixation control was carried out by a camera coupled to an optical microscope, and results were expressed as + for subsequent immobilization (a mean number of at least one cell fixed to bead after centrifuging at 450−500*g*), ± for weak immobilization (some beads fix no cells), and − for no immobilization of cells on the substrate.

This table shows that only activated microbeads with SAM Ab incubated with sensitized cells subsequently immobilize cells (in the table, the fifth substrate and fixation mode). In this case, microbeads grafted with SAM Ab, which acts as a spacer, allow cells sensitized with CD45 Ab to approach the microbeads better, which is in good agreement with the literature (*17*). Figure 9 shows photographs of cell aggregation around microbeads. The architecture of the biochemical link between cells and microbeads is given in Figure 10. Moreover, by fixing SAM Ab, which is able to recognize mouse species on lymphocytes, to substrates, unexpected antibody fixation to or removal from substrates could be minimized.

The experimental procedure was validated by producing blanks to confirm that no fixation occurs when microbeads were not silanized and also that SAM Ab does not recognize CD45 molecules expressed on lymphocytes.

CONCLUSION

By applying a specific functionalization process, activated hollow silica microbeads were shown to be able to fix rat cells strongly and selectively. Efficient fixation of antibodies was obtained with a reproducible silane layer, through electrostatic interactions between the OH groups of the glycosylated regions on the Fc fragments and CN groups of the silane. The recognizing capabilities of the Fab groups are preserved when this type of fixation method is used. A further step could be the destruction of the cells as the microbeads could be destroyed under ultrasonic power. Such a process could be used successfully to separate different strains of cells.

LITERATURE CITED

(1) Nelson, J. M., and Griffin, E. G. (1916) *J. Am. Chem. Soc. 38*, 1109.

(2) Maupas, H. (1995) Thesis of Ecole Centrale Lyon.

(3) Maupas, H., Saby, C., Martelet, C., Jaffrezic-Renault, N., Soldatkin, A. P., Charles M−H., Delair, T., and Mandrand, B. (1996) *J. Electroanal. Chem. 406*, 53.

(4) Harlow, E., and Lane D. (1991) *Anticorps: un manuel de laboratoire*, Editions Pradel, Paris.

(5) Karraasch, S., Dolder, M., Schabert, F., Ramsden, J., and Engel A. (1993) *Biophys. J. 65*, 2437.

(6) Browning-Kelley, M. E., Wadu-Mesthrige, K., Hari, V., and Liu, G. Y. (1997) *Langmuir 13*, 343.

(7) Taylor, R. F. (1991) Fundamentals and Applications. *Protein immobilization*, Marcel Dekker Inc.

(8) Plueddemann, E. P. (1982) *Silane Coupling Agents*, Plenum Press, New York.

(9) Saby, C., Jaffrezic-Renault, N., Martelet, C., Colin, B., Charles, M.-H, Delair, T., and Mandrand D. (1993) *Sensors Actuators B, 15−16*, 458.

(10) Billard, V., Martelet, C., Binder, P., and Therasse, J. (1991) *Anal. Chim. Acta 249*, 367.

(11) Prat, F., Chapelon, J. Y., Chauffert, B., Ponchon, T., and Cathignol, D. (1991) *Cancer Res. 51* (11), 3024.

(12) Prat, F., Ponchon, T., Berger, J. Y., Chapelon, J. Y., Gagnon, P., and Cathignol, D. (1991) *Gastroenterology 100* (5), 1345.

(13) Church, C. (1989) *J. Acoust. Soc. Am. 86* (1), 215.

(14) Perrin, A., Lanet, V., and Theretz, A. (1997) *Langmuir 13*, 2557.

(15) Duchet, J. *Système modèle Polyéthylène/verre: rôle de chaînes connectrices greffées sur l'adhésion*, Thesis, Université Claude Bernard Lyon 1.

(16) Suffilk, B. R., and Gilpin, R. K. (1986) *Anal. Chim. Acta 181*, 259.

(17) *DYNAL*, Technical Handbook, second ed.

BC9800421

Recognition of Novel Amphiphiles with Many Pendent Mannose Residues by Con A†

Koji Tagawa, Naoko Sendai, Kohji Ohno, Tomoaki Kawaguchi, and Hiromi Kitano*

Department of Chemical and Biochemical Engineering, Toyama University, Toyama 930-8555, Japan

Takayuki Matsunaga

Toyama Prefectural Institute of Pharmaceutical Science, Kosugi, Toyama 939-0363, Japan. Received July 15, 1998; Revised Manuscript Received November 19, 1998

Novel amphiphiles which carry many mannose residues as side chains were prepared by telomerization of *N*-methacryloylaminopropyl D-mannopyranoside (α:*β* = 20:1), *N*-methacryloylaminohexyl D-mannopyranoside (α:*β* = 20:1), or 3-(2-methacryloylaminoethylthio)propyl D-mannopyranoside (α:*β* = 4:1) using a lipophilic radical initiator. The mannose-carrying amphiphiles incorporated in liposomes were recognized by a lectin from *Canavalia ensiformis* (Con A), which was proven by the increase in turbidity of the liposome suspension after mixing with Con A. The interaction between sugar residues on the liposome surface and the lectin was largely affected by the degree of polymerization (DP) and the surface density of the amphiphile in the liposomes. The distance between the sugar residues and the polymer main chain did not affect the specific recognition by the lectin significantly in the liposome system, whereas it appreciably affected the recognition in the water-soluble polymer system. The association constants (K_a) of the amphiphiles (DP ≃ 18) with Con A ($0.3-2.2 \times 10^6$ M^{-1} at 25 °C) were much larger than that of α-methyl D-mannopyranoside (8.2×10^3 M^{-1}) due to the "*cluster effect* ". The positive entropy change (20−52 J/mol K) for the binding of Con A to mannose residues on the liposome surface showed that the recognition in the liposome system was largely promoted by the release of water molecules from both the sugar residues on the liposome surface and the binding site of Con A.

INTRODUCTION

Sugar chains in glycolipids and glycoproteins on cell membranes are, in general, made of limited kinds of monosaccharides such as glucose, galactose, mannose, fucose, *N*-acetylgalactosamine, and sialic acids (*N*-acetyl neuraminic acid) (*1*). However, oligosaccharides are able to have a larger number of structures compared with oligopeptides and oligonucleotides that are composed of an equivalent number of residues. Because of this diversity of sugar derivatives, sugar chains are essential moieties to take charge of various information in living bodies. For example, sugar chains are closely related to recognition phenomena *in vivo* (e.g., cell−cell recognition and adhesion, bacteria or viruses' infection, and immunological protection system). Since the specific receptors for sugars have been found to locate on various cell surfaces, targeting devices utilizing the recognition of sugar chains have been frequently investigated in recent years. For example, there are many studies on drug targeting using the galactose-receptor on the surface of parenchymal hepatocytes (*2*), the mannose-receptor on Kupffer cells (*3*) or various macrophages (*4*). Furthermore, some sugars above cell walls or around biopolymers can be used even for evasion from the uptake by the cells in reticuloendothelial systems (RES)[1] (*5*).

Meanwhile, we previously prepared liposome-forming amphiphiles having pH or temperature responsiveness by polymerization of acrylic acid or *N*-isopropylacrylamide, respectively, with a lipophilic radical initiator (*6*) or lipophilic chain-transfer reagent (*7*). Sugar-carrying amphiphiles were also prepared using a lipophilic radical initiator and sugar-carrying vinyl monomers (*8*−*11*). These hybrid amphiphiles with many monomer residues in their head region would be strong candidates as a component in drug delivery systems (DDS).

In this report, we prepared novel amphiphilic compounds with many pendent mannose residues in their hydrophilic headgroup by telomerization of mannose-carrying vinyl monomers using a lipophilic radical initiator. Recognition of the mannose-carrying amphiphilic compounds by a lectin from *Canavalia ensiformis* (Concanavalin A, Con A) was investigated in the liposome

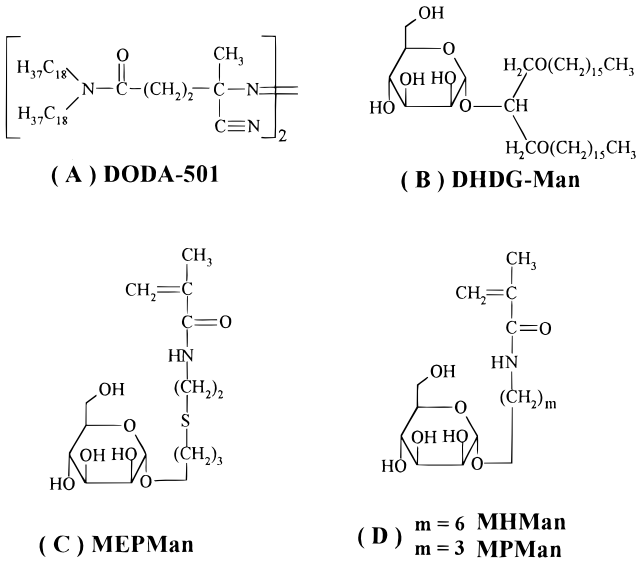
† Presented at the 45th Annual Meeting of the Society of Polymer Science, Japan, in Nagoya in May 1996.

* To whom correspondence should be addressed.

[1] Abbreviations: Con A, Concanavalin A; DDS, drug delivery systems; DLS, dynamic light scattering; DODA, dioctadecylamine; DODA-PMHMan, dioctadecylamine−poly(*N*-methacryloylaminohexyl D-mannopyranoside) conjugate; DODA-PMPMan, dioctadecylamine−poly(*N*-methacryloylaminopropyl D-mannopyranoside) conjugate; DODA-PMEPMan, dioctadecylamine−poly(3-(2-methacryloylaminoethylthio)propyl D-mannopyranoside) conjugate; DHDG-Man, 1,3-di-*O*-hexadecyl-2-*O*-(α-mannosyl)glycerol; DODA-501, azo radical initiator with dioctadecyl groups; DP, degree of polymerization; DDPC, bis(*trans*,*trans*-2,4-dioctadecadienoyl)phosphatidylcholine; MHMan, N-methacryloylaminohexyl D-mannopyranoside; MPMan, N-methacryloylaminopropyl D-mannopyranoside; MEPMan, 3-(2-methacryloylaminoethylthio)propyl D-mannopyranoside; RES, reticuloendothelial systems; THF, tetrahydrofuran; DMF, *N*,*N*-dimethyl formamide; V-50, 2,2′-azobis(2-amidinopropane) dihydrochloride; V-501, 4,4′-azobis(cyanovaleric acid).

10.1021/bc980083x CCC: $18.00 © 1999 American Chemical Society
Published on Web 04/22/1999

Scheme 1. Chemical Structure of Lipophilic Radical Initiator, Mannose-Carrying Lipid, and Mannose-Carrying Monomers



system. The association constants for Con A to mannose-carrying amphiphiles incorporated in liposomes were also estimated.

EXPERIMENTAL PROCEDURES

Materials. A lipophilic radical initiator (DODA-501, Scheme 1A) was prepared from dioctadecylamine (DODA, Fluka, Switzerland) and 4,4′-azobis(cyanovaleric acid) (V-501, Wako Pure Chemicals, Osaka, Japan) as previously reported (*6*). Succinimidyl methacrylate was prepared as described before (*11*). 1,3-Di-*O*-hexadecylglycerol was synthesized by the reaction of epichlorohydrin and 1-hexadecanol in the presence of sodium hydride at 80 °C overnight (*13*). A lectin, concanavalin A (Con A) from *Canavalia ensiformis*, was purchased from Sigma. Bis(*trans*,*trans*-2,4-dioctadecadienoyl)phosphatidylcholine (DDPC) was kindly donated from the Japan Fat & Oil Co, Tokyo, Japan. 2,2′-Azobis(2-amidinopropane)dihydrochloride (V-50) was kindly donated from Wako Pure Chemicals. Other reagents were commercially available. A Milli-Q grade water was used for preparation of sample solutions.

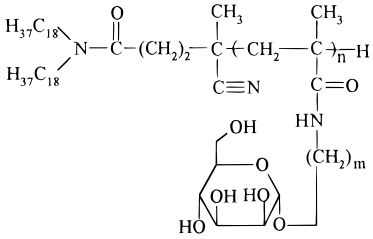
Preparation of 3-(2-Methacryloylaminoethylthio)-propyl D-Mannopyranoside (MEPMan, Scheme 1C). 3-(2-Aminoethylthio)propyl D-mannopyranoside (2.40 g, 8.1 mmol), which was prepared by the method reported by Lee and Lee (*14*), was coupled with an equivalent amount of succinimidyl methacrylate (1.48 g, 8.1 mmol) and dry triethylamine (0.80 g, 7.9 mmol) in the presence of (dimethylamino)pyridine (100 mg) and hydroquinone (30 mg) in dry DMF (20 mL) for 24 h. The solution mixture was condensed by evaporation and purified by a silica gel column chromatography two times [eluting solutions; methanol (first purification) and ethyl acetate: *n*-hexane: methanol = 1:1:6) (second)] (MEPMan, 1.87 g, 63% yield). ^{1}H NMR (400 MHz, D_2O): δ 5.56 (s, 1H, CH_2=C<, Z-form H), 5.32 (s, 1H, CH_2=C<, E-form H), 4.71 (d, 1H, J = 1.6 Hz, H_1), 4.51 (d, 1H, H_1), 3.44 (t, 2H, −SCH_2CH_2N−), 3.33 (t, 2H, −CH_2CH_2CH_2S−), 2.52 (m, 2H, >CH_2) and 1.79 (s, 3H, −CH_3). The anomeric ratio of MEPMan was estimated as α:β = 4:1 by ^{1}H NMR [δ 4.71 (α) and 4.51 (β)]. IR (KBr): O−H stretching of mannose 3316 cm^{-1}, C=O stretching of secondary amide 1616 cm^{-1}, N−H deformation of secondary amide 1541 cm^{-1}, CH_2 ν_{as} 2924 cm^{-1}, CH_2 ν_s 2853 cm^{-1}, C=C stretching 1654 cm^{-1}. Anal. calcd for $C_{15}H_{26}O_7NS\cdot 2H_2O$: C, 47.88; H, 8.05; N, 3.72. Found: C, 47.04; H, 7.37; N, 3.56.

Preparation of *N*-Methacryloylaminopropyl D-Mannopyranoside (MPMan, Scheme 1D). *N*-Methacryloylaminopropyl alcohol was prepared by the coupling of 3-amino-1-propanol (6.15 g, 82 mmol) with succinimidyl methacrylate (10 g, 55 mmol) and 4-(dimethylamino)pyridine (100 mg) in dry chloroform (100 mL). The solution mixture was condensed by evaporation and purified by a silica gel column chromatography (ethyl acetate: *n*-hexane: methanol = 6:3:1). Tetra-*O*-acetyl D-mannopyranoside (1.5 g, 4.3 mmol), which was prepared by the method described before (*15*), was reacted with trichloroacetonitrile (1.6 g, 11 mmol) in the presence of anhydrous cesium carbonate (0.50 g, 1.5 mmol), and afterward, with *N*-methacryloylaminopropanol (0.68 g, 4.7 mmol) in the presence of trimethylsilyl trifluoromethanesulfonate (0.85 g, 3.8 mmol). The oily product was deacetylated with a 28% methanol solution of sodium methoxide (200 μL) as a catalyst and purified by a silica gel chromatography (methanol:chloroform = 1:2). (MPMan, 0.48 g, 50% yield). ^{1}H NMR (400 MHz, D_2O): δ 5.61 (s, 1H, CH_2=C<, Z-form H), 5.37 (s, 1H, CH_2=C<, E-form H), 4.77 (d, 1H, J = 1.6 Hz, H_1), 4.58 (d, 1H, H_1), 3.87−3.28 (11H, others), 1.86 (s, 3H, −CH_3), and 1.17 (m, 6H, >CH_2). The anomeric ratio of MPMan was estimated as α:β = 20:1 by ^{1}H NMR [δ 4.77 (α) and 4.58 (β)]. IR (KBr) O−H stretching of mannose 3435 cm^{-1}, C=O stretching of secondary amide 1620 cm^{-1}, N−H deformation of secondary amide 1561 cm^{-1}, CH_2 ν_{as} 2930 cm^{-1}, CH_2 ν_s 2877 cm^{-1}, C=C stretching 1655 cm^{-1}. Anal. calcd for $C_{13}H_{23}O_7N\cdot 1.5H_2O$: C, 46.98; H, 7.88; N, 4.21. Found: C, 46.30; H, 7.17; N, 3.89. By the similar procedure, *N*-methacryloylaminohexyl D-mannopyranoside was prepared (MHMan, α:β = 20:1, Scheme 1D).

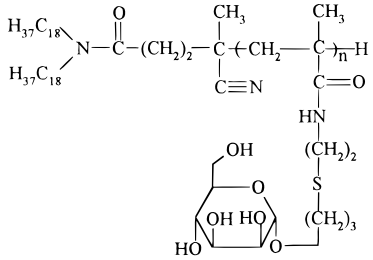
Preparation of Mannose Lipid (DHDG-Man, Scheme 1B). Following the method of Minamikawa et al. (*15*), 1,3-di-*O*-hexadecyl-2-*O*-(2,3,4,6-tetra-*O*-acetyl α-mannosyl)glycerol was prepared by the coupling of 1,3-di-*O*-hexadecylglycerol (820 mg, 1.5 mmol) and 2,3,4,6-tetra-*O*-acetylmannosyl 1-α-trichloroacetimidate (500 mg, 1.0 mmol) in the presence of trimethylsilyl trifluoromethanesulfonate (270 mg, 1.2 mmol) in dry chloroform [20 mL, molecular sieves 4A (1 g) were added] for 6 h at 0 °C. After purification, the residual oil was mixed with a 28% methanol solution of sodium methoxide (100 μL) for deacetylation. The solution mixture was condensed by evaporation and purified by a silica gel column chromatography (methanol:chloroform = 1:7). (DHDG-Man, 290 mg, 46% yield). ^{1}H NMR (400 MHz, $CDCl_3$): δ 5.09 (d, 1H, J = 2.0 Hz, H_1), 3.96−3.14 (m, 19H, others), 1.4−1.1 (m, 52H, CH_2 of hexadecyl chains) and 0.88 (t, 6H, CH_3 of hexadecyl chains). IR (KBr): O−H stretching of mannose 3449−3294 cm^{-1}, CH_2 ν_{as} 2918 cm^{-1}, CH_2 ν_s 2850 cm^{-1}, C−O−C stretching of glycerol moiety 1140−1061 cm^{-1}. Anal. calcd for $C_{43}H_{86}O_9$: C, 70.02; H, 11.78. Found: C, 69.96; H, 11.92.

Preparation of Mannose-Carrying Homopolymer. MPMan (180 mg, 570 mmol), V-50 (1.6 mg, 5.7 mmol) as initiator, and cystamine hydrochloride (3.3 mg, 29 mmol) as chain-transfer reagent were dissolved in water (10 mL). After a N_2 gas was passed through the solution for 5 min, the mixture was tightly sealed and incubated for 24 h at 70 °C. The solution mixture was repeatedly ultrafiltrated with water (Amicon Model 8010; membrane, YM-1; exclusion limit, 1000) to remove small impurities. The viscous solution retained above the

Scheme 2. Chemical Structure of Mannose-Carrying Amphiphiles



(A) m = 6 **DODA-PMHMan**
m = 3 **DODA-PMPMan**



(B) DODA-PMEPMan

membrane was lyophilized (91 mg, PMPMan, 59% yield). The degree of polymerization (DP) of the homopolymer was determined as 17 by the conductometric titration of amino group at the end of the polymer. IR (KBr) O−H stretching of mannose 3394 cm^{-1}, CH_2 ν_{as} 2939 cm^{-1}, CH_2 ν_s 2863 cm^{-1}, C═O stretching of secondary amide 1641 cm^{-1}, N−H deformation of secondary amide 1532 cm^{-1}, C−O−C stretching of glycerol moiety 1132−1045 cm^{-1}. Anal. calcd for C_2H_8NSCl $(C_{13}H_{23}O_7N)_{17}$·$18H_2O$: C, 46.92; H, 7.00; N, 4.48. Found: C, 46.90; H, 7.53; N, 4.34. By the similar procedure, PMHMan (DP = 16) was prepared (120 mg, 35% yield).

Preparation of Mannose-Carrying Amphiphiles by Polymerization. DODA-501 (31 mg, 23 μmol) in THF (5 mL) and MPMan (290 mg, 940 μmol) in methanol (5 mL) were mixed in a small round-bottomed flask. After passing a N_2 gas through the solution for 5 min, the reaction mixture was tightly sealed and incubated for 24 h at 70 °C. After evaporation of the solvent, the mannose-carrying amphiphile was purified by washing with *n*-hexane (to remove unreacted initiator) and subsequently with cold water (to remove polymers without lipophilic end group). The amphiphile, which had been dispersed in water by a vortex mixer and subsequently by an ultrasonifier (Astrason W-385, Heat Systems-Ultrasonics, Inc., NY) at 50 °C for 3 min, was further purified by passing through a GPC column (2 × 20 cm, Sephacryl S-200; mobile phase, water) and lyophilized (126 mg, DODA-PMPMan, 42% yield, Scheme 2A). IR (KBr) O−H stretching of mannose 3370 cm^{-1}, C≡N stretching 2245 cm^{-1}, C═O stretching of secondary amide 1616 cm^{-1}, C═O stretching of tertiary amide 1654 cm^{-1}, N−H deformation of secondary amide 1529 cm^{-1}, CH_2 ν_{as} 2923 cm^{-1}, CH_2 ν_s 2853 cm^{-1}. The DP value of the amphiphiles was determined as 18 by elemental analyses and NMR. Anal. calcd for $C_{42}H_{82}ON_2$ $(C_{13}H_{23}O_7N)_{18}$·$36H_2O$: C, 48.92; H, 8.44; N, 4.13. Found: C, 48.49; H, 7.66; N, 4.06.

Using the similar method, dioctadecylamine−poly(*N*-methacryloylaminohexyl D-mannopyranoside) conjugate (DODA-PMHMan, DP = 9, 18, 23 and 25, Scheme 2A) and dioctadecylamine−poly[3-(2-methacryloylaminoethylthio)propyl D-mannopyranoside] conjugate (DODA-PMEPMan, DP = 17, Scheme 2B) were prepared (Table 1). Because of the difficulty to purify amphiphilic compounds, the yields of mannose-carrying amphiphiles were in general very low (Table 1).

Table 1. Preparation of Mannose-Carrying Amphiphiles

amphiphile	DODA-501 (mg)	mannose-carrying vinyl monomer (mg)	solvent (mL)	product (mg) (yield in %)	DP[a]
DODA-PMHMan	18	200	30[b]	62 (27)	25
DODA-PMHMan	47	250	40[c]	82 (13)	23
DODA-PMHMan	49	260	40[d]	46 (12)	18
DODA-PMHMan	160	440	40[c]	94 (10)	9
DODA-PMPMan	31	290	10[c]	126 (42)	18
DODA-PMEPMan	110	610	50[e]	116 (10)	17

[a] Degree of polymerization. [b] THF:MeOH:H_2O = 1:1:1. [c] THF:MeOH = 1:1. [d] THF:MeOH:H_2O = 3:3:2. [e] THF:MeOH = 2:1.

Preparation of Liposome. DDPC was dissolved in chloroform (1 mL) in a small round-bottomed flask, and the solvent was evaporated. The thin lipid membrane formed was dispersed in a Hepes buffer (pH 8.2, 10 mM) in which the mannose-carrying amphiphile had been dispersed beforehand using a vortex mixer at 50 °C. The dispersion was further sonicated by the ultrasonifier for 3 min while a N_2 gas was passed through the dispersion. The liposome (small uni-lamellar vesicle, SUV) dispersion was passed through a syringe filter (Millipore Millex-GV; pore size, 0.22 μm) and finally irradiated in a quartz cell by a UV lamp (UI-5010, Ushio, Tokyo, Japan) at room temperature for 4 h to polymerize the dienoyl groups of DDPC. The progress of polymerization was followed by the decrease in absorbance at 258 nm by using a UV−vis spectrometer (Ubest-35, Japan Spectroscopic Co., Tokyo, Japan).

Dynamic Light Scattering Method. Hydrodynamic diameter of SUV liposomes composed of mannose-carrying amphiphile, and DDPC was determined by the dynamic light scattering (DLS) method (DLS-7000, Otsuka Electronics, Hirakata, Japan. light source, He−Ne laser 632.8 nm).

Turbidity Measurements. The lectin-induced agglutination of liposomes was followed by the increase in decadic absorbance at 350 nm by using a stopped flow spectrophotometer (RA-401, Otsuka Electronics, Hirakata, Japan). The observation cell was thermostated by a water bath (Neslab RTE−8, Neslab Instruments, Inc., Portsmouth, NH). To get reliable data, the measurements were carried out 5 or 6 times at various lectin concentrations. The uncertainties of the rate of turbidity change were within 10%.

Association Constants for Con A to Mannose-Carrying Liposomes. The association constant, K_a, between Con A, L, and the mannose-carrying amphiphile, S, (eq 1) was determined by the Scatchard plot.

$$L + S \overset{K_a}{\rightleftharpoons} L{\cdot}S \qquad (1)$$

The ratio of the concentration of free Con A to that of the complex with Con A is given by the eq 2.

$$[L{\cdot}S]/[L] = K_a(n[S]_o - [L{\cdot}S]) \qquad (2)$$

where [L·S] and [L] refer to the concentration of bound Con A and that of free Con A, respectively, and $[S]_o$ refers to the total concentration of mannose-carrying am-

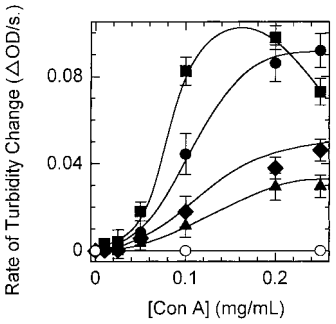


Figure 1. Effect of concentration of Con A on the turbidity change after the addition of Con A to the liposome suspension at 25 °C. Wavelength = 350 nm. Content of mannose-carrying lipid = 20 wt %. [Liposome] = 50 μg of lipid/mL. 10 mM HEPES buffer (pH 8.2) containing 0.1 mM $CaCl_2$ and 0.1 mM $MnCl_2$. (○) DHDG-Man; (▲) DODA-PMHMan DP = 9, (◆) DP = 18, (●) DP = 23, and (■) DP = 25.

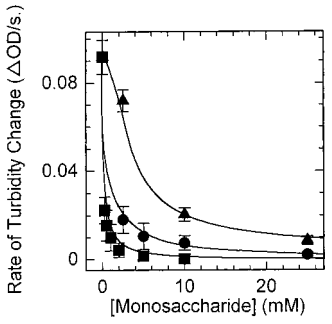


Figure 2. Inhibitory effects of monosaccharides on the rate of turbidity change in the aggregation of mannose-carrying liposomes by Con A at 25 °C. Wavelength = 350 nm. Content of DODA-PMHMan (DP = 23) = 20 wt %. [Liposome] = 50 μg of lipid/mL. [Con A] = 0.25 mg/mL. (▲) Glucose; (●) mannose; (■) α-methyl D-mannopyranoside.

phiphiles. A plot of [L·S]/[L] versus [L·S] should ideally give a straight line with a slope $-K_a$. The association constant obtained from the plot was expressed in inverse molarity, assuming a molecular weight of 26 500 for four subunits in Con A (*16*).

The mannose-carrying liposome suspension in a test tube (1 mL) was incubated with various concentrations of Con A (1 mL) at 25 °C for 1.5 h. The Con A bound to the liposome (actually the aggregates of liposomes cross-linked by Con A molecules) was removed with a syringe filter (Millipore Millex-GV; pore size, 0.22 μm), and the absorbance of the filtrate at 280 nm was measured. Although the filter of low protein binding was used to remove the liposome−Con A aggregates, free Con A was observed to adsorb to the filter a little. Therefore, we at first estimated the relationship between the absorption of filtrate (2 mL) at 280 nm vs the concentration of free Con A before the filtration, and the amount of Con A bound to the liposome was calculated with the help of this calibration curve.

Estimation of Contents of Phospholipids and Sugar Residues in Liposomes. The contents of phospholipids and sugar residue in the liposomes were estimated by the Bartlett method (*17*) and phenol-sulfuric acid method (*18*), respectively.

RESULTS AND DISCUSSION

A. Recognition of Pendent Mannose Residues on Liposomes by Con A. The physically stabilized liposomes could be easily prepared by the photoirradiation of liposomes composed of glycolipids and the polymerizable phospholipid (DDPC) (*19*). The liposomes prepared here probably bring about the phase separation of the mannose-carrying amphiphiles in the liposomes by two-dimensional photopolymerization of DDPC molecules (*20*). Using the DLS method, diameters of the liposomes (SUV) composed of polymerized DDPC and DODA-PMPMan, DODA-PMHMan, or DODA-PMEPMan were estimated to be 1300−1400 Å on average, respectively, and the diameters of the liposomes did not change for at least 1 month (data were not shown).

Turbidity of mannose-carrying liposome suspension at 350 nm was rapidly increased by the addition of Con A (Figure 1). The initial slope of the turbidity change increased both with the concentration of Con A and the degree of polymerization of mannose-carrying amphiphiles incorporated in the liposome. The latter is because a steric hindrance for the lectin to approach mannose residues on the liposome surface decreased with the DP value. When the mannose-carrying liposome consisted of 1,3-di-*O*-hexadecyl-2-*O*-(α-mannosyl)glycerol (DHDG-Man), and polymerized DDPC was incubated with the Con A solution, the turbidity did not increase at all, because the mannose residues were too close to the liposome surface.

Next, the effects of various monosaccharides on the Con A-induced turbidity change of mannose-carrying liposome dispersions were examined (Figure 2). It was previously reported that the inhibition activity of α-methyl D-mannopyranoside (α-MeMan) was much higher than any other monosaccharide (*21*). The tendency observed in Figure 2 is consistent with the data reported previously. Furthermore, the subsequent addition of monosaccharides to the dispersion of mannose-carrying liposome−Con A aggregates induced the prompt reduction of turbidity (data not shown). These results strongly support that the turbidity change is due to the specific recognition of mannose residues on the liposomes by Con A, and subsequent aggregation of liposomes mediated by the tetrameric lectin molecules.

It should be mentioned here that the sugar-carrying amphiphiles prepared here were stably incorporated in the liposome membrane. For example, after passing a gel permeation chromatography (GPC) column (Sephacryl S-200, 2 × 20 cm), the contents of phospholipid and manno-lipid in the DODA-PMPMan (DP = 18) − polymerized DDPC liposome estimated by the Bartlett method and phenol-sulfuric acid method, respectively, were the same as those without the GPC treatment (91% of the manno-lipid was retained in the liposome after the GPC). Furthermore, after the GPC, the DODA-PMPMan-polymerized DDPC liposome mixed with the Con A solution showed a quite similar turbidity change to the liposome of the same concentration without the GPC treatment.

B. Effect of the Distance between the Polymer Chain and Mannose Residues on the Recognition by Con A. Figure 3a shows that the rate of turbidity change was not dependent on the distance between the polymer main chain and mannose residues as for the amphiphiles with the same DP value [DODA-PMPMan (DP = 18) and DODA-PMHMan (DP = 18)]. We had expected that the rate of turbidity change of DODA-PMHMan (the distance between the polymer main chain and mannose residue, about 14 Å) would be larger than that of DODA-PMPMan (about 9 Å).

The results obtained here suggest the following situation: In the liposome system, the steric hindrance of the gigantic carrier liposome for Con A molecule to approach the mannose residues was dominant, and Con A could limitedly bind the end mannose residues in the

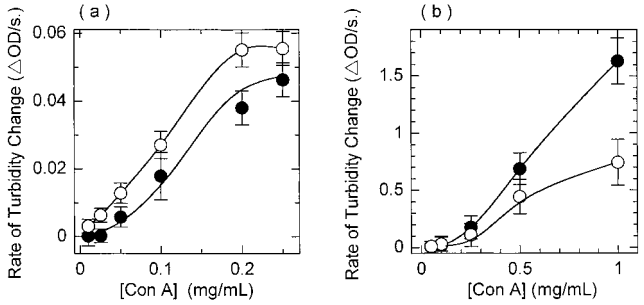


Figure 3. Effect of concentration of Con A on the rate of turbidity change after the addition of Con A at 25 °C. Wavelength = 350 nm. (a) Liposome suspension. Content of mannose-carrying amphiphile = 20 wt %. [Liposome] = 50 μg of lipid/mL. (○) DODA-PMPMan (DP = 18); (●) DODA-PMHMan (DP = 18). (b) Solution of mannose-carrying polymer. [Polymer] = 50 μg/mL. (○) PMPMan (DP = 17); (●) PMHMan (DP = 16).

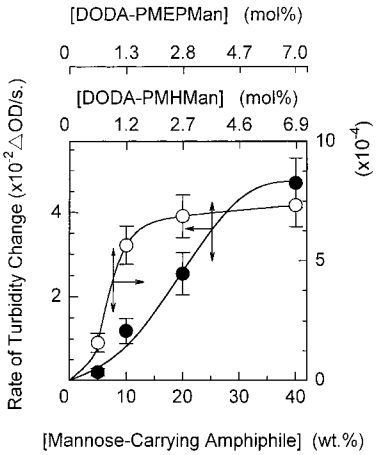


Figure 4. Effect of mannose-carrying amphiphile content in the liposome on the rate of turbidity change after the addition of Con A into the liposome suspension at 25 °C. Wavelength = 350 nm. [Liposome] = 50 μg of lipid/mL. [Con A] = 0.1 mg/mL. (○) DODA-PMEPMan (DP = 17) (α:β = 4:1); (●) DODA-PMHMan (DP = 18) (α:β = 20:1).

polymer chain. Consequently, the effect of spacer length in the liposome systems on the recognition did not clearly appear.

In the water-soluble polymer system, on the contrary, the length of spacer (Figure 3b) appreciably affected the turbidity change. In the absence of the gigantic carrier liposome, Con A can make a multidirectional approach to the mannose residues in the polymer. The difference in the distances between the mannose residue and polymer main chain, therefore, became effective in the recognition of the mannose residue by Con A molecule.

C. Effect of the Content of Mannose-Carrying Amphiphile on the Recognition by Con A. Figure 4 shows the effect of mol percent of mannose-carrying amphiphile (DODA-PMEPMan and DODA-PMHMan) on the turbidity change. The distances between mannose residues and polymer chain in these amphiphiles were comparable (about 14 Å). It is very clear that there was a steep increase in the rate of turbidity change at a low content of mannose-carrying amphiphile in both systems. The presence of threshold value in 5 mol % of lactosylceramide in liposomes at the lectin-induced aggregation was previously reported (*22*). In the present liposome systems, however, the turbidity increased with time at the very small mole percent of mannose-carrying amphiphile, probably because many mannose residues are present in a polar head region of one lipid molecule, which makes it unnecessary for the lectin to bind to

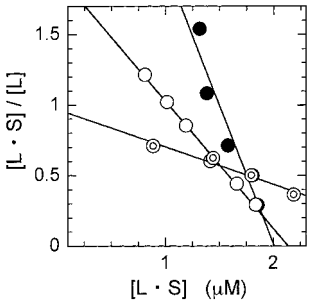


Figure 5. Scatchard plots for the binding of mannose-carrying liposomes to Con A at 25 °C. (○) DODA-PMPMan (DP = 18); (●) DODA-PMHMan (DP = 18); (◎) DODA-PMEPMan (DP = 17).

Table 2. Association Constants (K_a) for the Complexation of Con A with Mannose-Carrying Amphiphiles and Sugar Derivatives at 25 °C

amphiphiles	K_a ($\times 10^6$ M^{-1})[a]
DODA-PMHMan (DP = 18)	2.2 ± 0.1
DODA-PMPMan (DP = 18)	0.9 ± 0.1
DODA-PMEPMan (DP = 17)	0.3 ± 0.03
sugar derivatives	**K_a (M^{-1})[b]**
α-methyl D-glucopyranoside	2.0×10^3
α-methyl D-mannopyranoside	8.2×10^3
oligosaccharide[c]	1.4×10^6

[a] In the 10 mM Hepes buffer (pH 8.2) containing 0.1 mM $CaCl_2$ and 0.1 mM $MnCl_2$. [b] Ref *23*. [c] (GlcNAc(β1,2)−Man)$_2$−(α1,6, α1,3)Man−OH.

plural number of mannose-carrying amphiphiles on each liposome to bring about the significant aggregation, and consequently, the agglutinability of the lectin at the very small mol percent of mannose-carrying amphiphile was observed. A similar tendency was observed in the lectin-induced aggregation of liposomes that contained glucose- or galactose-carrying amphiphiles prepared with the lipophilic radical initiator (*8*, *9*).

It should be noted here that the scales of ordinate in the figure are different for two kinds of mannose-carrying amphiphiles. Con A possesses about 30 times the binding ability to α-derivatives compared with that to β-derivatives (*21*). Therefore, it is understandable that DODA-PMHMan (α:β = 20:1) which contained many α-form mannose residues in one lipid molecule was much more easily recognized than DODA-PMEPMan (α:β = 4:1).

D. Association Constants for Con A to Mannose-Carrying Amphiphiles. The association constants for Con A to various mannose-carrying liposomes obtained by the Scatchard plot (exemplified in Figure 5) are shown in Table 2. The K_a values were much lager than those of α-MeMan and α-MeGlc (*23*) and similar to the value of a branched penta-saccharide shown in the footnote c of the table. These results show that sugar residues incorporated in polymer chain as pendent groups enhance appreciably the affinity for Con A compared with monosaccharides. This is called the "*cluster effect* " which enhances the apparent affinity of cluster glycosides toward lectins without significantly changing the sugar concentration (*2a*, *24*). Previously we examined catalytic behavior of galactose oxidase at lipid bilayer−liquid interfaces (*10*, *11*), and observed that the affinity of galactose oxidase for the amphiphiles that carried many pendent galactose residues was much higher (10^4 times at the most) than those for various galactose derivatives with low molecular weight.

E. Thermodynamic Parameters for Mannose-Carrying Amphiphile-Con A System. Thermodynamic

Table 3. Thermodynamic Parameters for the Complexation of Con A with Mannose-Carrying Amphiphiles[a] and Sugar Derivatives[b]

	$\Delta G°$ [c] (kJ/mol)	$\Delta H°$ (kJ/mol)	$\Delta S°$ (J/mol K)
amphiphiles			
DODA-PMHMan (DP = 18)	−36.0	−30.1	20
DODA-PMPMan (DP = 18)	−33.8	−22.8	37
DODA-PMEPMan (DP = 17)	−30.6	−15.1	52
sugar derivatives			
α-methyl D-glucopyranoside	−18.8	−27.6	−29
α-methyl D-mannopyranoside	−22.3	−34.3	−41
oligosaccharide[d]	−35.1	−44.3	−31

[a] In the 10 mM HEPES buffer (pH 8.2) containing 0.1 mM $CaCl_2$ and 0.1 mM $MnCl_2$. [b] Calculated from the data by Mandal et al. (*23*). [c] Temp at 25 °C. [d] (GlcNAc(β1,2)−Man)$_2$−(α1,6 α1,3)Man−OH.

parameters for the K_a values of Con A−mannose-carrying amphiphiles were estimated by the van't Hoff plot (Table 3). The enthalpy change has been interpreted in terms of differences in the interactions between the solvent and lectin and between the ligand and lectin (*25*). These interactions involve hydrogen bonding and electrostatic and van der Waals interactions (*26*). On the other hand, the increase in entropy change is associated with the release of water from the binding site of the lectin and the sugar residue into bulk solvent (*25*).

The absolute value of enthalpy change for the DODA-PMHMan system was larger than that for the DODA-PMPMan system. This difference might be due to the strength of hydrophobic interaction between the spacer part and the binding site of the lectin, because the DODA-PMHMan has three more methylene groups in its spacer part than the DODA-PMPMan. It was reported that the binding of 4-methylumbelliferyl α-D-galactopyranoside with L-14 lectin was about 50-fold larger than that of D-galactose due to the presence of large nonpolar aglycon (*27*). In the DODA-PMEPMan system, on the contrary, the presence of thioether group in the spacer part might reduce the hydrophobic interaction with the lectin, resulting in the smallest absolute value of enthalpy change.

The entropy change for the binding of Con A to mannose residues on the liposome surface was positive in all the mannose-carrying amphiphiles examined here, which is in contrast with the negative value for various sugar derivatives with low molecular weight (*23*). Therefore, the binding process between the pendent mannose-carrying liposomes and Con A were entropically driven by the dehydration effect rather than enthalpically driven.

It is indispensable for the safe usage and effective action of medicine to selectively deliver the medicine to the target parts. This is a final goal of pharmacology. For the achievement of the goal, a lot of attempts to modify medicine itself or to incorporate the medicine in the microparticles have been carried out. Liposomes, unnecessary to say, are quite attractive material as drug carrier to achieve the targeting. Meanwhile, the activated macrophages play an important role in the host defense against neoplasias (*28*). In this case, after being activated by the uptake of the liposomes which incorporate biological response modifiers, the macrophages arrive at the tumoricidal state and destroy the tumorigenic cells. Taking account of the previous reports that mannosylated liposomes were easily taken up by Kupffer cells (*3*) or macrophages (*4*) in greater amounts than the nontargeted liposomes, the mannose-carrying amphiphilic compounds prepared here have a possibility to be used as a tool not only for the DDS to target cells with sugar receptors, such as Kupffer cells or other macrophages, but also for the activation of these cells to join the self-defense system against neoplasias.

ACKNOWLEDGMENT

We are grateful to Wako Pure Chemicals for their kind donation of V-501 and V-50. This work was supported by the Grant-in-Aid for Scientific Research on Priority Areas (08246222, 09232223, 09240213, and 10126221) from the Ministry of Education, Science, Sports and Culture.

LITERATURE CITED

(1) Jones, M. N. (1994) Carbohydrate-Mediated Liposomal Targeting and Drug Delivery. *Adv. Drug Delivery Rev. 13*, 215−250.

(2) (a) Connolly, D. T., Townsend, R. R., Kwaduchi, K., Bell, W. R., and Lee, Y. C. (1982) Binding and Endocytosis of Cluster Glycosides by Rabbit Hepatocytes. *J. Biol. Chem. 257*, 939−945. (b) Spanjer, H. H., Van Berkel, T. J., Scherphof, G. L., and Kempen, H. J. M. (1985) The Effect of a Water-Soluble Tris-Galactose Terminated Cholesterol Derivative on the in Vivo Fate of Small Unilamellar Vesicles in Rats. *Biochim. Biophys. Acta 816*, 396−402.

(3) (a) Muller, C. D., and Schubor, F. (1989) Neo-Mannosylated Liposomes: Synthesis and Interaction with Mouse Kupffer Cells and Resident Peritoneal Macrophages. *Biochim. Biophys. Acta 986*, 97−105. (b) Ghosh, P., Das, P. K., and Bachhawant, B. K. (1982) Targeting of Liposomes towards Different Cell Types of Rat Liver through the Involvement of Liposomal Surface Glycolipids. *Arch. Biochem. Biophys. 213*, 266−270.

(4) (a) Hoppe, C. A., and Lee, Y. C. (1983) The Binding and Processing of Mannose-Bovine Serum Albumin Derivatives by Rabbit Alveolar Macrophages. *J. Biol. Chem. 258*, 14193−14199. (b) Stahl, P. D., Rodman, J. S., Miller, M. J., and Schlesinger, P. H. (1978) Evidence for Receptor-Mediated Binding of Glycoproteins, Glycoconjugates, and Lysosomal Glycosidase by Alveolar Macrophages. *Proc. Natl. Acad. Sci. U.S.A.* 75, 1399−1403. (c) Barratt, G., Tenu, J. P., Yapo, A., and Petit, J. F. (1986) Preparation and Characterization of Liposomes Containing Mannosylated Phospholipids Capable of Targeting Drugs to Macrophages. *Biochim. Biophys. Acta 862*, 153−164.

(5) Allen, T. M. (1989) Stealth Liposomes: Avoiding Reticuloendothelial Uptake. in *Liposomes in the Therapy of Infection Diseases and Cancer* (G. Lopez Berestain, and I. J. Fidler, Eds.) pp 405−415, Alan R. Liss, New York.

(6) Kitano, H., Akatsuka, Y., and Ise, N. (1991) pH-Responsive Liposomes Which Contain Amphiphiles Prepared by Using Lipophilic Radical Initiator. *Macromolecules 24*, 42−46.

(7) Kitano, H., Maeda, Y., Takeuchi, S., Ieda, K., and Aizu, Y. (1994) Liposomes Containing Amphiphiles Prepared by Using a Lipophilic Chain Transfer Reagent: Responsiveness to External Stimuli. *Langmuir 10*, 403−406.

(8) Kitano, H., and Ohno, K. (1994) Sugar-Containing Lipids Prepared by Using a Lipophilic Radical Initiator: Interfacial Recognition by Lectin as Studied by Using the Multiple Internal Reflection Fluorescence Method. *Langmuir 10*, 4131−4135.

(9) Kitano, H., Sohda, K., and Kosaka, A. (1995) Galactose-Containing Amphiphiles Prepared with a Lipophilic Radical Initiator. *Bioconjugate Chem. 6*, 131−134.

(10) Ohno, K., Sohda, K., Kosaka, A., and Kitano, H. (1995) Galactose-Containing Amphiphiles Prepared with a Lipophilic Radical Initiator: Association Processes between Liposomes Triggered by Enzymatic Reaction. *Bioconjugate Chem. 6*, 361−366.

(11) (a) Ohno, K., and Kitano, H. (1998) Catalytic Properties of Galactose Oxidase to Liposome-Forming Amphiphiles Which Have Many Pendent Galactose Residues. *Bioconjugate Chem. 9*, 548−554. (b) Kawaguchi, T., Tagawa, K., Senda, F., Matsunaga, T., and Kitano, H. (1999) Recognition of

Amphiphiles with Many Pendent Galactose Residues by *Ricinus communis* Agglutinin. *J. Colloid Interface Sci. 210*, 290−295.
(12) Kitano, H., Wolf, H., and Ise, N. (1990) pH-Responsive Release of Fluorophore from Homocysteine-Carrying Polymerized Liposomes. *Macromolecules 23*, 1958−1961.
(13) Kuwamura, T. (1961) Long Chain Aliphatic Derivatives of Glyceryl α,α′-Diethers. *Kogyo Kagaku Zasshi 64*, 1958−1964.
(14) Lee, R. T., and Lee, Y. C. (1974) Synthesis of 3-(2-Aminoethylthio)propyl Glycosides. *Carbohydr. Res. 37*, 193−201.
(15) Minamikawa, H., Murakami, T., and Hato, M. (1994) Synthesis of 1,3-Di-*O*-alkyl-2-*O*-(β-glycosyl)glycerols Bearing Oligosaccharides as Hydrophilic Groups. *Chem. Phys. Lipids 72*, 111−118.
(16) Kalb, A. J., and Lusting, A. (1968) The Molecular Weight of Concanavalin A. *Biochim. Biophys. Acta 168*, 366−367.
(17) Bartlett, G. R. (1959) Phosphorus Assay in Column Chromatography. *J. Biol. Chem. 234*, 466−468.
(18) Dubois, M., Gilles, K., Hamilton, J. K., Rebers, P. A., and Smith, F. (1956) Colorimetric Method for Determination of Sugars and Related Substances. *Anal. Chem. 28*, 350−356.
(19) (a) Ringsdorf, H., Schlarb, B., and Venzmer, J. (1988) Molecular Architecture and Function of Polymeric Oriented Systems: Models for the Study of Organization, Surface Recognition, and Dynamics of Biomembranes. *Angew. Chem., Int. Ed. Eng. 27*, 113−158. (b) Kitano, H., Kato, N., Tanaka, N., and Ise, N. (1988) Mutual Recognition between Polymerized Liposomes: Enzyme and Enzyme Inhibitor System. *Biochim. Biophys. Acta 942*, 131−138. (c) Kitano, H., Kato, N., and Ise, N. (1988) Mutual Recognition between Polymerized Liposomes: Macrophage Model System by Polymerized Liposomes. *J. Am. Chem. Soc. 111*, 6809−6813.
(20) Wagner, N., Does, K., Koch, H., and Ringsdorf, H. (1981) Incorporation of ATP Synthetase into Long-Term Stable Lipsomes of a Polymerizable Synthetic Sulfolipid. *FEBS Lett. 132*, 313−318.
(21) Goldstein, I. J., Hollerman, C. E., and Smith, E. E. (1965) Protein-Carbohydrate Interaction. II. Inhibition Studies on the Interaction of Concanavalin A with Polysaccharides. *Biochemistry 4*, 876−883.
(22) Curatolo, W., Yau, A. O., Small, D. M., and Sears, B. (1978) Lectin-Induced Agglutination of Phospholipid/Glycolipid Vesicles. *Biochemistry 17*, 5740−5744.
(23) Mandal, D. K., N. Kishore, N., and Brewer, C. F. (1994) Thermodynamics of Lectin-Carbohydrate Interactions. Titration Microcalorimetry Measurements of Binding of N-Linked Carbohydrates and Ovalbumin to Concanavalin A. *Biochemistry 33*, 1149−1156.
(24) Lee, R. T., and Lee, Y. C. (1994) in *Neoglycoconjugates: Preparation and Application* (Y. C. Lee, and R. T. Lee, Eds.) pp 23−50, Academic Press, San Diego.
(25) Schwarz, F. P., Puri, K. B., Bhat, R. G., and Surolia, A. (1993) Thermodynamics of Monosaccharide Binding to Concanavalin A, Pea (*Pisum sativum*) Lectin, and Lentil (*Lens culinaris*) Lectin. *J. Biol. Chem. 268*, 7668−7677.
(26) (a) Bessler, W., Shafer, J. A., and Goldstein, I. J. (1974) A Spectrophotometric Study of the Carbohydrate Binding Site of Concanavalin A. *J. Biol. Chem. 249*, 2819−2822. (b) Schwarz, F. P., Puri, K. B., and Surolia, A. (1991) Thermodynamics of the Binding of Galactopyranoside Derivatives to the Basic Lectin from Winged Bean (*Psophocarpus tetrogonolobus*). *J. Biol. Chem. 266*, 24344−24350.
(27) Ramkumar, R., Surolia, A., and Podder, S. K. (1995) Energetics of Carbohydrate Binding by a 14 kDa S-Type Mammalian Lectin. *Biochem. J. 308*, 237−241.
(28) (a) Fidler, I. J. (1985) Macrophages and Metastasis Biological Approach to Cancer Therapy. Presidential Address. *Cancer Res. 45*, 4714−4726. (b) Sone, S. (1986) Role of Alveolar Macrophages in Pulmonary Neoplasias. *Biochim. Biophys. Acta 823*, 227−245.

BC980083X

Polymeric Gadolinium Chelate Magnetic Resonance Imaging Contrast Agents: Design, Synthesis, and Properties

David L. Ladd,*,† Robert Hollister,† Xin Peng,‡ Donna Wei, Gang Wu,§ Daniel Delecki,† Robert A. Snow,† John L. Toner,|| Kenneth Kellar,† Jennifer Eck,⊥ Vinay C. Desai,† Gemma Raymond,† Lewis B. Kinter,# Terry S. Desser M. D.,▽ and Daniel L. Rubin M. D.▽

Torsten Almén Research Center, Nycomed Amersham Imaging, 466 Devon Park Drive, Wayne, Pennsylvania 19087 . Received July 23, 1998; Revised Manuscript Received February 8, 1999

We have synthesized and evaluated five series of polymeric gadolinium chelates which are of interest as potential MRI blood pool contrast agents. The polymers were designed so that important physical properties including molecular weight, relaxivity, metal content, viscosity, and chelate stability could be varied. We have shown that, by selecting polymers of the appropriate MW, extended blood pool retention can be achieved. In addition, relaxivity can be manipulated by changing the polymer rigidity, metal content affected by monomer selection, viscosity by polymer shape, and chelate stability by chelator selection.

INTRODUCTION

The use of paramagnetic gadolinium chelates to enchance magnetic resonance imaging (MRI) examinations has become increasingly important (Hohenschuh and Watson, 1997). The gadolinium-containing contrast agents that are currently approved for human use (Omniscan, Magnevist, Prohance, and Dotarem) are all low molecular weight chelates. When administered parenterally, these agents rapidly extravasate out of the circulation into the interstitial space. For some imaging applications (Brasch, 1992), it would be desirable to have an agent that was largely retained within the intravascular space during the time frame of an MRI examination, a so-called "blood pool" agent. Several approaches have been explored in the quest for MR blood pool agents including: (1) low MW Gd-chelates that bind to serum proteins (Lauffer et al., 1996; Wallace et al., 1998), (2) iron oxide particles (Engelbrecht et al., 1998), (3) Gd-liposomes (Unger et al., 1990), and (4) polymeric Gd-chelates. While others have prepared polymeric Gd-chelates by grafting chelators onto preformed polymers such as albumin (Schmiedl et al., 1987), polylysine (Schuhmann-Giampieri et al., 1991), dextran (Rebizak et al., 1998; Casali et al., 1998), and dendrimers (Schwickert et al., 1995), we have focused our efforts to obtain MR blood pool agents primarily on wholly synthetic polymers.

As contrast agents for MRI, the potential advantages of macromolecular complexes in comparison to the currently available monomeric low molecular weight complexes are well recognized (Brasch, 1991). An increased lifetime of the contrast agent in the blood pool has been identified as an important feature in both blood pool and dynamical tumor imaging (Brasch, 1991; Desser et al., 1994a). However, increasing the lifetime in the blood pool is a necessary, but not sufficient, criteria for attaining a useful contrast agent. The agent must also fulfill additional safety related criteria. The ideal Gd-based MR blood pool contrast agent will reside in the blood pool long enough to allow for convenient MR imaging, then clear from the blood pool rapidly after completion of the MR imaging procedure. For dynamical tumor imaging, the situation is even more complicated (Desser et al., 1994a; Roberts et al., 1997). The uptake and clearance from tumors depends on many factors, including the size and structure of the contrast agent (Roberts et al., 1997). Whatever the application, the agent should be a benign, low-volume parenteral that is completely eliminated from the body within a reasonable time. However, except for possibly the dendrimer-based gadolinium chelates, little attention has been given to the design of macromolecular complexes which have a basic structure that can easily be altered to control the resulting physical properties and size. Such a structure that can easily be altered is important, because it allows optimization of the contrast agent with respect to blood pool lifetime or tumor uptake and clearance. Within the basic structure of these complexes, the molecular weight, as well as other important physical properties including relaxivity, metal content, viscosity, and chelate stability, can be optimized. This report describes the design rationale that we employed and the results that were obtained with five series of polymeric gadolinium chelates. Since the polymers described herein are prototypical, not all of the above parameters were optimized, or even measured, for each polymer. Indeed, optimization of all of the parameters for a given agent is probably not feasible due to the interrelationship of the parameters studied, which necesitates the need to make compromises when designing a new agent. Thus, for each series, one or more features were chosen to be modified to illustrate the effect on a given parameter and to demonstrate the feasibility of modifying the key attributes of an MR blood pool polymer.

* To whom correspondence should be addressed. Phone: 610-225-4349. Fax: 610-225-4413. E-mail: david.ladd@US.Nycomed-Amersham.com.

† Nycomed Amersham Imaging.

‡ SmithKline Beecham.

§ Bristol Myers Squibb.

|| Abbott Laboratories.

⊥ Sanofi Research Division.

Astra Pharmaceuticals.

▽ Department of Radiology, Stanford University School of Medicine and VA Palo Alto Health Care System.

10.1021/bc980086+ CCC: $18.00 © 1999 American Chemical Society
Published on Web 03/19/1999

EXPERIMENTAL PROCEDURES

General Procedures. The identity of all intermediates was confirmed by ^{1}H NMR spectroscopy; purity was assessed by silica gel TLC. Molecular weight, polydispersity, and purity of polymers were determined by size-exclusion-HPLC.

Molecular Weight Determinations. Molecular weights and molecular weight distributions were obtained by size exclusion-HPLC comparing the polymers to a set of PEG standards obtained from American Polymer Standards Corp. A Perkin-Elmer series 200 analytical HPLC fitted with a series of three Supelco 30 cm × 7.8 mm size-exclusion columns comprised of a Progel-TSK G2000 SWXL, a Progel-TSK G3000 SWXL, and a Progel-TSK G4000 SWXL were employed. Detection was with a refractive index detector. The method involved 20 μL injections of 1 mg/mL solutions of the polymer samples, a mobile phase comprised of 30% acetonitrile:70% pH 6.8 phosphate buffer, a flow rate of 0.6 mL/min, and a 60 min isocratic program. Turbochrome software was used to control the program and Turbogel software to do the MW analysis.

Rabbit Blood Pool Retention Measurements. Formulations of polymers in isotonic saline were injected into the lateral ear vein of New Zealand white rabbits via a 21-gauge Butterfly needle at doses of 0.06 or 0.10 mmol of Gd/Kg. Arterial blood samples for relaxivity measurement were obtained via a catheter placed percutaneously into the lateral ear artery. Blood samples were withdrawn and collected into heparin tubes at 0, 5, 15, 30, 60, 120, 360, 600, and 1440 min following the injection (note: in some experiments every time point was not collected). T_1 measurements were made on the blood samples using a Bruker Mini-Spec operating at 20 MHz and 40 °C.

^{153}Gd Labeling of Polymers. Unmetalated polymers were dissolved in 0.1 M, pH 5.0, sodium acetate buffer and treated with ^{153}Gd by addition of $^{157}GdCl_3$ containing approximately 0.1% (w/w) $^{153}GdCl_3$ (Amersham, Arlington Heights, IL). The DTPA polymers were reacted for 15 min at room temperature, and the DOTA polymers were reacted for 2 h at 50 °C. The radiolabeling efficiencies as determined by instant thin-layer chromatography (ITLC) and HPLC were found to be >99%. The labeled polymers were purified by preparative SEC-HPLC, and the test article was diluted in 0.9% sterile saline, pH 6.5, to a final concentration of approximately 30 mM Gd.

Rat Blood Pool Retention Measurements. Six rats (0.35−0.45 Kg) previously prepared with polyurethane catheters were injected intravenously with 0.08 mmol of Gd/Kg (approximately 0.5 mL containing 1 mCi) of test article. Blood samples (100 mL) were withdrawn at 0.042, 0.08, 0.17, 0.33, 0.5, 0.75, 1, 1.25, 1.5, 2, 4, 6, 24, 48, and 168 h and the radioactivity quantitated using a γ counter.

Viscosity Measurements. The viscosities were measured in water with a Brookfield viscometer (model LVCP DVII-plus) equipped with a cone and plate spindle and a jacketed sample cell for temperature control. The temperature was controlled with a LAUDA RM6 circulating water bath. The viscometer was calibrated using Brookfield viscosity standards that ranged from 5 to 100 cP.

Relaxation Rate Measurements. The proton longitudinal relaxation rate ($1/T_1$) for aqueous solutions of the polymers was measured by the inversion−recovery method using a Bruker Minispec PC 120/125/10 Vts NMR Process Analyzer operating at 0.47 T and 40 °C. The relaxivity of a given polymer was calculated by subtracting the $1/T_1$ of pure water from the $1/T_1$ measured for the polymer-containing solution and dividing this quantity by the concentration of gadolinium as determined by ICP. The relaxivities were found to be independent of gadolinium concentration.

Polyoxyethylene Bis(chloride) (3). To a solution of poly(ethylene glycol) [**2**, average MW, 1.45K] (1000 g, 0.69 mol) in 1.5 L of toluene (60−80 °C) were added $SOCl_2$ (200 mL, 2.76 mol) and DMF (10 mL) dropwise over 10 min. The reaction mixture was heated on a steam bath for 1 h. An analysis by TLC (CH_2Cl_2:MeOH; 6:1) indicated that a very small amount of starting material still remained. An additional 20 mL of $SOCl_2$ was added to the reaction, and it was heated on the steam bath for another 20 min to drive the reaction to completion. After cooling the reaction to 0 °C with an ice bath, 1 N NaOH (2.5 L) was carefully introduced to neutralize the solution and the layers were separated. The aqueous layer was washed with CH_2Cl_2 (3 × 1 L), and the combined CH_2Cl_2 layers were washed with water (2 × 1 L) and dried with $MgSO_4$. It was filtered and concentrated under reduced pressure to give a light yellow oil. The product was precipitated by adding TBME (2 L) to the residue with cooling and stirring. The filtered product was dried in the oven under vacuum overnight to yield 941 g (94%) of the titled compound as a white solid. An analysis by HPLC indicated that the purity of the product was 99.86% with no oligomer present. Anal. calcd for $C_{64}H_{128}O_{31}Cl_2$: C, 52.49; H, 8.81; Cl, 4.84. Found: C, 51.94; H, 8.43; Cl, 5.00.

Polyoxyethylene Bis(azide) (4). To a suspension of polyoxyethylene bis(chloride) (**3**, 500 g, 0.336 mol) and KI (139 g, 0.841 mol) in 1500 mL of DMF was added NaN_3 (109 g, 1.68 mol). The suspension was heated on a steam bath at 70 °C for 12 h to give a yellow solution. After cooling the reaction to room temperature, 2.5 L of water was added and the solution was extracted with CH_2Cl_2 (3 × 1 L). The combined CH_2Cl_2 layers were washed with water (3 × 1 L), dried over $MgSO_4$, filtered, and concentrated under reduced pressure to give a light yellow oil. The product was precipitated out by adding TBME (1 L) to the residue with cooling and stirring. The filtered product was dried in the oven under vacuum overnight at room temperature to yield 452 g (90%) of the PEG diazide as a white solid. An analysis by HPLC indicated that the purity of the product was 99.2% with no oligomers present. Anal. calcd for $C_{64}H_{128}O_{31}N_6$: C, 52.09; H, 8.73; N, 5.69. Found: C, 52.50; H, 8.58; N, 5.11.

Polyoxyethylene Bis(amine) (5). To a solution of polyoxyethylene bis(azide) (**4**, 176 g, 0.117 mol) in 1 L of 1 N HCl was added Pd/C (17.6 g). The suspension was hydrogenated at 45 psi for 15 h. An aliquot withdrawn from the reaction indicated no more starting material by TLC (CH_2Cl_2:MeOH; 4:1), and the catalyst was removed by carefully filtering through a short plug of Celite. The filtrate was neutralized with 10% NaOH to pH 5−6 and extracted with CH_2Cl_2 (3 × 600 mL) to remove the impurities. The aqueous solution was neutralized with 35% NaOH to pH >10 and extracted with CH_2Cl_2 (2 × 500 mL). The CH_2Cl_2 layer was washed with water (500 mL), brine (500 mL), and dried over $MgSO_4$. The filtrate was concentrated under reduced pressure to give a light yellow oil. The product was precipitated by adding TBME (1 L) to the residue with cooling and stirring. The filtered product was dried in the oven under vacuum at room-temperature overnight to give 138 g (81% yield) of the titled compound as a white solid. Analysis by HPLC indicated that the purity of the product was 96.9% with no oligomer detected by gel chromatography. Anal. calcd

for $C_{64}H_{132}O_{31}N_2$: C, 53.92; H, 9.33; N, 1.96. Found: C, 53.24; H, 9.35; N, 1.66.

Preparation of Polymer NC 66368 (1a). [Note: WFI (water for injection) is used for this entire process.] To a solution of polyoxyethylene bis(amine) (**5**, 550 g, 0.380 mol) in 5500 mL of water was added triethylamine (159 mL, 1.14 mol) and DTPA-dianhydride (**6**, 149 g, 0.418 mol). The suspension was stirred at room temperature and gave a clear solution after 10 min. The reaction was stirred for an additional 50 min, and a solution of $GdCl_3 \cdot 6H_2O$ (156 g, 0.418 mol) in 2000 mL of water was added. The reaction mixture was checked with PAR reagent to be sure only a slightly excess of $GdCl_3 \cdot 6H_2O$ was added. The complexed solution (pH 2) was neutralized to pH ~5 with 10% NaOH and then diafiltered using a Pellicon diafiltration unit with a 10K cutoff filter for 10 turnovers: A 10% NaCl (USP grade) solution (filtered through a 0.22 μ filter) was used for the first four turnovers and water was used for the remaining six turnovers. At the end of the diafiltration, the solution was concentrated to half of its original volume (pH 7), filtered through a 0.22 μ filter and then lyophilized for 3 days leaving (532 g, 80%) a sponge-like product. MW = 20 200; $p = 1.63$. Total Gd = 7.09% w/w. KF moisture = 2.55%. Elemental analysis; anal. calcd for $[C_{80}H_{152}GdN_5O_{40}]_x$: C, 48.50; H, 7.73; N, 3.53. Found (corrected for H_2O): C, 48.14; H, 7.91; N, 3.29.

Preparation of Polymer NC 22181 (10a). (Note: WFI is used for this entire process). To a solution of hexamethylenediamine (**8**, 200 g, 1.72 mol) in 4 L of DMSO was added triethylamine (810 mL, 5.52 mol) and DTPA-dianhydride (**6**, 664 g, 1.84 mol). The suspension was stirred at room temperature for 45 h, and a light yellow solution was obtained. Four liters of EtOAc was added to the solution, and product (**9**) was precipitated as an oil. Solvent was decanted, and the oil product was further washed with EtOAc (2 × 2 L). After the oil product was dried under vacuum for 1 h, it was dissolved in 4 L of water and $GdCl_3 \cdot 6H_2O$ (312 g) was added (PAR reagent was used to ensure that no excess Gd^{3+} was added). The solution was neutralized to pH ~5 with NaOH and filtered through a 0.45 μ filter. The filtered solution was diafiltered using a Pellicon diafiltration unit with a 10K cutoff filter for 10 turnovers: A 10% NaCl (USP grade) solution (filtered through a 0.22 μ filter) was used for the first five turnovers and water was used for the remaining five turnovers. At the end of the diafiltration, the solution was concentrated to half of its original volume (pH 7), filtered through a 0.22 μ filter and then lyophilized for 3 days leaving (203 g) a sponge-like product (**10a**). MW = 18 900; $p = 1.51$. Total Gd = 22.00% w/w. KF moisture = 10.68%. Elemental analysis; anal. calcd for $[C_{20}H_{32}GdN_5O_8]_x$ (corrected for H_2O and NaCl): C, 33.54; H, 5.70; N, 9.78. Found: C, 33.44; H, 5.77; N, 9.63; Na, 0.69; Cl, 0.98.

In a similar manner polymers **10a** of different MWs were prepared using the following conditions:

expt	mmol of **8**	mmol of **6**	base/mmol	DMSO (mL)	reaction time (h)	molecular mass (kDa)/ polydispersity
1	5.1	5.5	NaOH/16.5	18	50	8.8/1.50
2	51.0	55.0	Et_3N/159.	206	18	14.2/1.54
3	645.	678.	Et_3N/2030.	2500	168	18.1/1.34
4	129.1	135.5	Et_3N/406.6	250	24	21.0/1.39

In experiment 3, intermediate **9** was precipitated with ether prior to complexation with $GdCl_3 \cdot 6H_2O$; in experiments 1, 2, and 4, the reaction mixtures were diluted with water and then complexed with $GdCl_3 \cdot 6H_2O$.

Preparation of Polymer NC 22177 (16a). A solution of methoxy-PEG of average MW 550 (**11**, 66.67 g, 0.1212 mol; Sigma Chemical Co.) in 1000 mL of toluene was refluxed with azeotropic removal of water for several hours. The cooled toluene solution was treated with triethylamine (55.75 mL, 0.4 mol), 4-(dimethylamino)-pyridine (2.96 g, 0.0242 mol) and tosyl chloride (69.33 g, 0.3636 mol) and heated in an oil bath at 60 °C for 48 h. The reaction mixture was then cooled and filtered. The filtrate was extracted three times with water. The combined aqueous extracts were washed three times with ether, then extracted three times with chloroform. The chloroform extracts were dried over anhydrous $MgSO_4$ and concentrated to yield 47.58 g (56%) of product **12**. A solution of 14.96 g (21.25 mmol) of **12** in 150 mL of absolute EtOH was treated with 31.8 mL (213 mmol) of tris(2-aminoethyl)amine (**13**). The reaction mixture was heated in a stainless steel bomb at 160 °C for 16 h. The solvent was removed by evaporation and the residue dissolved in 257 mL of water and made basic with 42.5 mL of 1 N NaOH. The basic solution was washed twice with ether, then extracted twice with chloroform. The chloroform extracts were dried over anhydrous $MgSO_4$; solvent evaporation followed by heating at 90 °C under vacuum (1 mm) to remove residual tris(2-aminoethyl)-amine (**13**) yielded 12.14 g (84%) of **14** as a viscous tan oil. A solution of 4.23 g (6.24 mmol) of **14** in 42 mL of acetonitrile was treated with triethylamine (2.61 mL, 18.7 mmol) and diethylenetriaminepentaacetic acid dianhydride (**6**) (3.34 g, 9.36 mmol). After 1.0 h at room temperature, 168 mL of water was added and the solution was stirred for 30 min. The solution of crude polymer **15** was treated with gadolinium(III) chloride hexahydrate (3.65 g, 9.83 mmol) then diafiltered against water in a diafiltration cell equipped with a 10 000 MW cutoff membrane. The pH of the solution was adjusted to 7 with NaOH, then the solution was filtered through a 0.2 mm nylon filter. Lyophilization yielded 4.15 g of product (**16a**) of average molecular mass 13 600 Da ($p = 1.36$) as determined by SEC-HPLC using PEG molecular mass standards; 15.6% gadolinium by weight.

Preparation of Polymer NC 100203 (24a). A solution of 5.00 g of **19** (hydrobromide salt; WO 93/02045), methyl bromoacetate (0.795 mL), tetramethylguanidine (14.0 mL), and 100 mL of acetonitrile was refluxed for 3 h. The reaction mixture was then concentrated and the residual oil taken up in toluene and washed three times with water. The toluene solution was dried over anhydrous magnesium sulfate and concentrated to 4.46 g of product **20**. A solution of 4.10 g of **20** in 82 mL of methanol was treated with 41 mL of tris(2-aminoethyl)amine and stirred for 3 days at room temperature under N_2. The solution was concentrated under reduced pressure (1 mm) at 60 °C then taken up in $CHCl_3$ and washed four times with water, dried over anhydrous $MgSO_4$, and concentrated to 4.56 g of **21**.

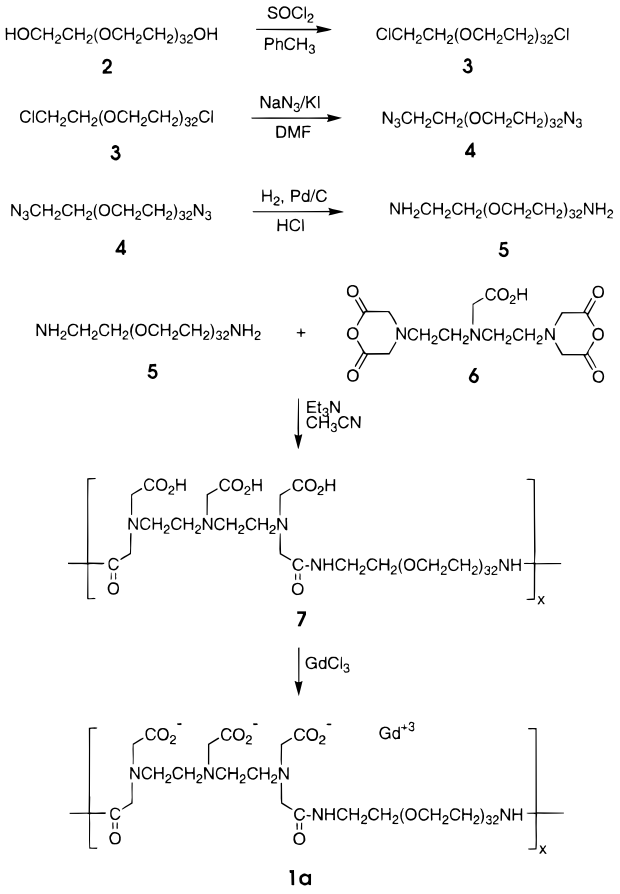
A solution of 3.989 g of **17** (Shearwater Polymers, Inc.) in 26.8 mL of CH_2Cl_2 was treated with 270.5 mg of *N*-hydroxysuccinimide and 2.579 mL of a 1 M solution of dicyclohexylcarbodiimide in CH_2Cl_2 for 2 h.

The above reaction mixture of **18** was treated with a solution of 0.776 g of **21** in 23 mL of CH_2Cl_2 for 1 h, filtered, and concentrated to give 3.81 g of **22**. The tri-*tert*-butyl ester **22** (4.78 g) was treated with 48 mL of CH_2Cl_2 and 5 mL of TFA for 16 h, a second 5 mL portion of TFA was added, and the reaction continued for 16 h; a third 5 mL portion of TFA was added, and the reaction

continued for another 16 h, after which NMR indicated incomplete reaction. A fourth 5 mL portion of TFA was added, and after 4 days, the reaction was concentrated to dryness; NMR still indicated incomplete reaction. The crude product was treated with 25 mL of neat TFA for 16 h, after which NMR indicated complete reaction. The reaction mixture was then concentrated and taken up in 100 mL of water, and the pH was raised to 7.0 with 2 N KOH. The solution was then diafiltered vs water in a stirred cell with a YM-3 membrane (Amicon, Inc., Beverly, MA) and lyophilized to give 3.56 g of **23**. A 1.55 g sample of **23** in 31 mL of water was treated with 0.185 g of $GdCl_3 \cdot 6H_2O$; the pH was maintained at 4.5 with 1 N NaOH for 16 h. The pH was lowered to 3.0 with 1 N HCl, and then the solution was diafiltered vs water in a stirred cell with a YM-3 membrane (Amicon, Inc., Beverly, MA). The pH was adjusted to 7.0, and the solution lyophilized to give to give 1.41 g of **24a** of average molecular mass 16 200 Da ($p = 1.36$) as determined by SEC-HPLC using PEG molecular mass standards; 2.51% Gd by weight determined by ICP. The R_1 relaxivity was determined to be 6.6 mM^{-1} s^{-1} using a Bruker Mini-Spec operating at 20 MHz and 40 °C.

Preparation of Polymer NC 100372 (34). To a solution of 24.6 g (0.062 mol) of 6-aminocaproic acid benzylester *p*-toluenesulfonic acid salt and 20 g (0.19 mol) of sodium carbonate in 460 mL of 50% water in methylene chloride was added dropwise over 45 min a solution of 10 mL (0.13 mol) of chloroacetyl chloride in 230 mL of methylene chloride. Stirring was continued at room temperature under a nitrogen atmosphere for 2 h. The organic phase was separated and dried over anhydrous magnesium sulfate. Evaporation of the solvent left 18.4 g of crude product **28** which was further purified by flash chromatography on silica gel eluting with CH_2Cl_2. A solution of 0.676 g (1.14 mmol) of **19**, 0.338 g (1.14 mmol) of **28,** and 0.43 mL (3.4 mmol) of 1,1,3,3-tetramethylguanidine in 14 mL of acetonitrile was stirred at room temperature under a nitrogen atmosphere for 18 h. Volatiles were removed under reduced pressure, and the residue was partitioned with a mixture of toluene and water.The toluene phase was separated and washed with water, then dried over anhydrous magnesium sulfate, filtered from the drying agent, and concentrated to yield 0.79 g of product **29**. A solution of 5.0 g (6.4 mmol) **29** in 200 mL of methanol was treated with 0.5 g of 10% palladium on carbon and hydrogenated on a PARR shaker for 17 h. After the uptake of hydrogen had ceased, the catalyst was removed by careful filtration through a bed of Celite. The volatiles were removed from the filtrate using reduced pressure, and the residue obtained was triturated well with dry ethyl ether. The ether phase was decanted and concentrated under reduced pressure to yield 2.3 g of the product **30** as a white glass. Another 1.4 g of less pure product remained after the ether trituration. To a stirring solution of 2.25 g (3.30 mmol) of **30** (previously dried via azeotropic distillation from methylene chloride) and 0.43 g (3.6 mmol) of dry *N*-hydroxysuccinimide in 45 mL of methylene chloride at room temperature and under a nitrogen atmosphere was added dropwise, in 5 min, a solution of 7.4 mL (3.7 mmol) of 0.5 M *N*,*N*-dicyclohexylcarbodiimide in methylene chloride. After the addition was complete, stirring was continued at room temperature under nitrogen for about 17 h. The reaction slurry was filtered, and the volatiles were removed from the filtrate under reduced pressure to yield 2.7 g of the product **31** as a white glass. A solution of 0.437 g (0.076 mmol) of third generation PAMAM dendrimer (Meltzer et al., 1992) and 2.6 g (2.7 mmol) of **31** in 20 mL of

Scheme 1



anhydrous dimethyl sulfoxide was stirred at room temperature under a nitrogen atmosphere for 3 days. Most of the solvent was removed under reduced pressure at 60 °C, and the viscous residue was triturated with absolute ethyl ether three times, decanting each time, leaving a residue which was dried under high vacuum yielding 1.6 g of product **32**. The average number of unreacted amines on the PAMAM dendrimer moiety of compound **32** was determined to be approximately four by a ninhydrin assay (Curotto and Aros, 1993).

Elemental analysis calcd for $C_{905}H_{1,573}N_{191}O_{225}$, corrected for water of hydration: C, 51.14%; H, 7.46%; N, 12.6%. Found: C, 51.44%; H, 7.66%; N, 12.18%.

Treatment of 1 g (0.5 mmol) of **32** with 50 mL of a 25% trifluoroacetic acid solution in methylene chloride at 0 °C under a nitrogen atmosphere was followed by allowing the stirring reaction mixture to warm to ambient temperature during 1 h after which the volatiles were removed under reduced pressure. The residue was triturated with absolute ethyl ether, the ether decanted, and the residue dried under vacuum. The reaction was repeated with 50% trifluoroacetic acid for overnight reaction time. The volatiles were removed under reduced pressure, and the resulting residue stirred with absolute ethyl ether for 2 h, then filtered, washed with ether, and dried in a vacuum oven at 50 °C to give 0.9 g. The 0.9 g was dissolved in 10 mL of deionized water and filtered, and the pH of the filtrate was raised to 8 with 2 N potassium hydroxide solution. This solution was then diafiltered in an Amicon stirred cell against water using a 5000 Da cutoff membrane for 30 turnovers totaling 300 mL. The purified solution was filtered through a 0.2 μ filter and lyophilized yielding a tan foam which was dried under high vacuum and 40 °C to afford 0.4 g of **33**

Table 1. Physicochemical and Biological Data for Polymeric Gadolinium Chelates

compound	molecular mass (kDa)	$T_{1/2}$ [n] rabbit	$T_{1/2}$ [n] rat	%Gd (w/w)	R_1 (mM^{-1} s^{-1})[d]	viscosity (cP)[a] (100 mM Gd)	rat 7 day bone retention[m]
magnevist	0.9	0.77 ± 0.05	0.33[g]	16.8	3.8 ± 0.15	2.9[f]	0.21 ± 0.05[g,h]
1a (NC 66368)	20.2	6.22 ± 0.13[i,j]		7.1 ± 0.28	6.0 ± 0.24	56.1[b]	3.50 ± 0.68
10a (NC 22181)	18.9	1.64 ± 0.20[k]		22.0 ± 0.88	9.5 ± 0.39		4.91 ± 0.83
16a (NC 22177)	13.6	9.38 ± 0.68[i]		15.6 ± 0.62	10.1 ± 0.41	2.2[c]	
24a (NC 100203)	16.2		2.96 ± 0.13[l]	2.5 ± 0.10	6.6 ± 0.31		0.76 ± 0.30
34 (NC 100372)	18.2[e]		0.53 ± 0.06	17.3[e]			0.62 ± 0.08

[a] **1a**, 45.3 cP at 20 °C for 210 mg of polymer/mL; **16a**, 5.1 cP at 25 °C for 199 mg of polymer/mL. [b] 20 °C. [c] 25 °C. [d] 20 MHz, 40 °C. [e] Calculated value; Gd chelate was prepared in situ from $^{153}GdCl_3/^{157}GdCl_3$. [f] 500 mM Gd, 37 °C. [g] Weinmann et al. (1984). [h] Whole body minus liver, spleen and kidney. [i] Significantly different from Magnevist, $p < 0.01$. [j] Significantly different from **10a**, $p < 0.01$. [k] Significantly different from **16a**, $p < 0.01$. [l] Significantly different from **34**, $p < 0.05$. [m] Percent injected dose. [n] Mean ± standard deviation.

(polydispersity of 1.06). Elemental analysis calcd for $C_{665}H_{1193}N_{191}O_{205}$ (corrected for water and potassium): C, 48.07; H, 7.96; N, 16.10; K, 2.35. Found: C, 48.17, 48.32; H, 7.70, 7.52; N, 15,48, 15.99; K, 2.88, 3.17.

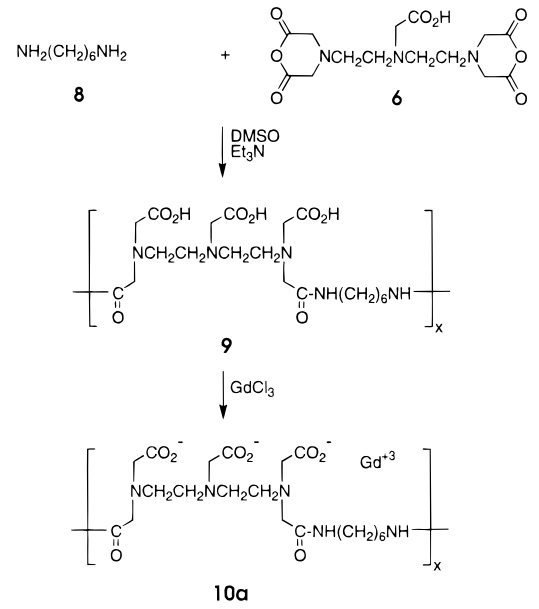
RESULTS AND DISCUSSION

Initially, we prepared (Desser et al., 1994a) a series of copolymers of diethylenetriaminepentaacetic acid (DTPA) and poly(ethylene glycol) (PEG) diamines chelated to gadolinium (**1**, Gd-DTPA-PEGs) ranging in MW from 10.8 to 83.4 kDa as shown in Scheme 1. PEG-diamine (**5**) was prepared in two steps from poly(ethylene glycol) (**2**) and polymerized with the dianhydride of DTPA (**6**) and the resultant polymer (**7**) chelated with gadolinium to produce the Gd-DTPA-PEG polymer (**1a**). DTPA was selected as the chelator based upon its successful use in the marketed agents Omniscan and Magnevist; poly(ethylene glycol) diamines were chosen based upon the well-established biocompatability, hydrophilicity, and synthetic accessibility of PEG derivatives (Zalipsky, 1995). The Gd-DTPA-PEG polymers were evaluated (Desser et al., 1994a) in a rabbit model to (1) identify the molecular weight above which Gd-DTPA-PEG polymers behave as blood pool agents and (2) to analyze the tumor enhancement dynamics as a function of polymer molecular weight in a rabbit tumor model. This study showed that linear Gd-DTPA-PEG polymers with a molecular mass of 20 kDa and higher exhibited significant blood pool retention over a 60 min time frame. Therefore, we focused upon a Gd-DTPA-PEG polymer (**1a**, NC 66368) with a molecular mass of ~20 kDa prepared from polyethene glycol of MW 1450 (Scheme 1) as our initial lead structure.

While NC 66368 proved to be efficacious in the rabbit tumor model (Desser et al., 1994a) and a model demonstrating time-of-flight magnetic resonance angiography (TOF-MRA) (Desser et al., 1994b), it possessed some shortcomings. The low R_1 relaxivity (6.0) combined with the low gadolinium content (7.1%) made it necessary to administer large amounts of polymer in order to achieve adequate doses of gadolinium to produce the required t_1 shortening. In addition, as the formulation concentration of NC 66368 was increased to minimize the injection volume, the solution viscosity became unacceptably high (56.1 cP for a 100 mM Gd formulation, see Table 1).

One approach to addressing the shortcoming of NC 66368 was to design an analogous series of copolymers (**10**) of diethylenetriaminepentaacetic acid with short-chain alkyldiamines in place of the longer chain poly(ethylene glycol) diamines (Scheme 2). While these polymers had the expected increase in gadolinium content, from 7.1% for **1a** to 22.0% for **10a**, they also exhibited (Kellar et al., 1997) unexpected increases in R_1 relaxivity, from 6.0 for **1a** to 9.5 for **10a**. A subset of this series, analogues of **10** in which the spacer length (n) was

Scheme 2



varied, was found to have relaxivities up to 20.7 (Kellar et al., 1997). This combination of increased gadolinium content and increased relaxivity resulted in significant decreases in the amount of polymer required for imaging studies. From this series of polymers, NC 22181 (**10a**) was identified as a significantly improved lead. Like NC 66368, NC 22181 has been shown to be an effective contrast agent for MRA imaging in rabbits (T. Desser and D. L. Rubin, unpublished data) and an effective agent for MR urography in pigs (Nolte-Ernsting et al., 1997). While blood pool retention is known to be affected by polymer MW, size, shape, and charge (Petrak and Goddard, 1989), within a given series in which MW and consequently size is the only variable, it would be expected that blood pool retention would be determined by MW. However, this relationship would not necessarily hold up comparing polymers across series as more than one variable could be changing. Therefore, the results from the Gd-DTPA-PEG polymer series could not be used to confidently predict the minimal MW required for NC 22181 to act as a blood pool agent, and thus polymers ranging in molecular mass from 9 to 21 kDa were prepared and evaluated in the rabbit model. The results of this study are summarized in Figures 2 and 3. The data shows that NC 22181 of molecular mass 14 kDa and above has a prolonged blood pool phase reflected in significantly increased blood half-lives and decreased volumes of distribution and thus would qualify as a candidate MR blood pool imaging agent.

A third approach to designing blood pool agents was aimed primarily at addressing the relaxivity and viscosity

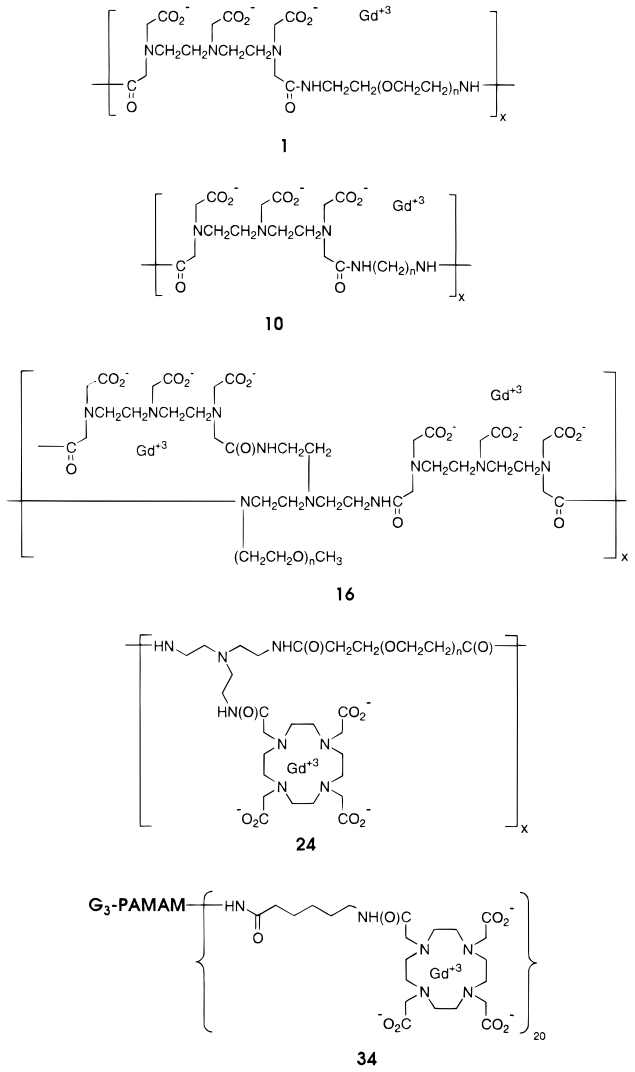


Figure 1. Polymeric gadolinium chelates.

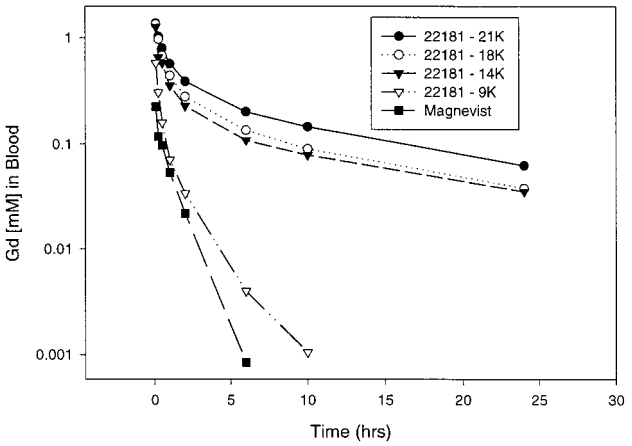


Figure 2. Blood retention vs time for NC 22181 of four different molecular weights and Magnevist.

issues. A series was designed (Ladd, 1996) to produce polymers with a more globular shape than the above two linear polymers. The nonlinear shape was achieved by appending poly(ethylene glycol) chains to the polymer backbone [vs incorporation of poly(ethylene glycol) chains into the polymer backbones of **1** and **10**] and incorporating interchain cross-links through the DTPA moieties (Scheme 3). Methoxy-PEG-triamine (**14**) was prepared from the methoxy-PEG-tosylate (**12**), polymerized with

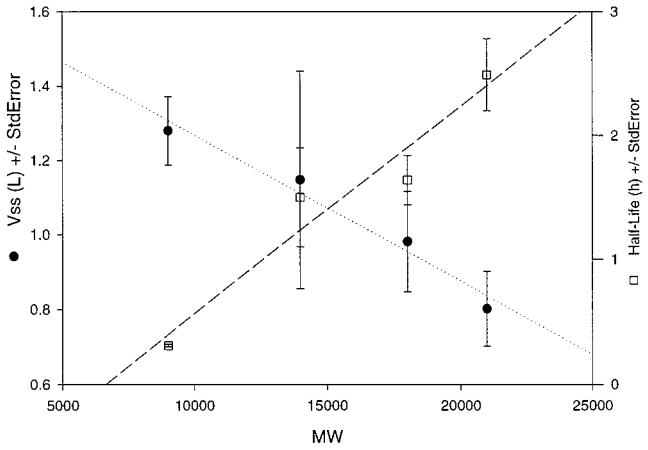
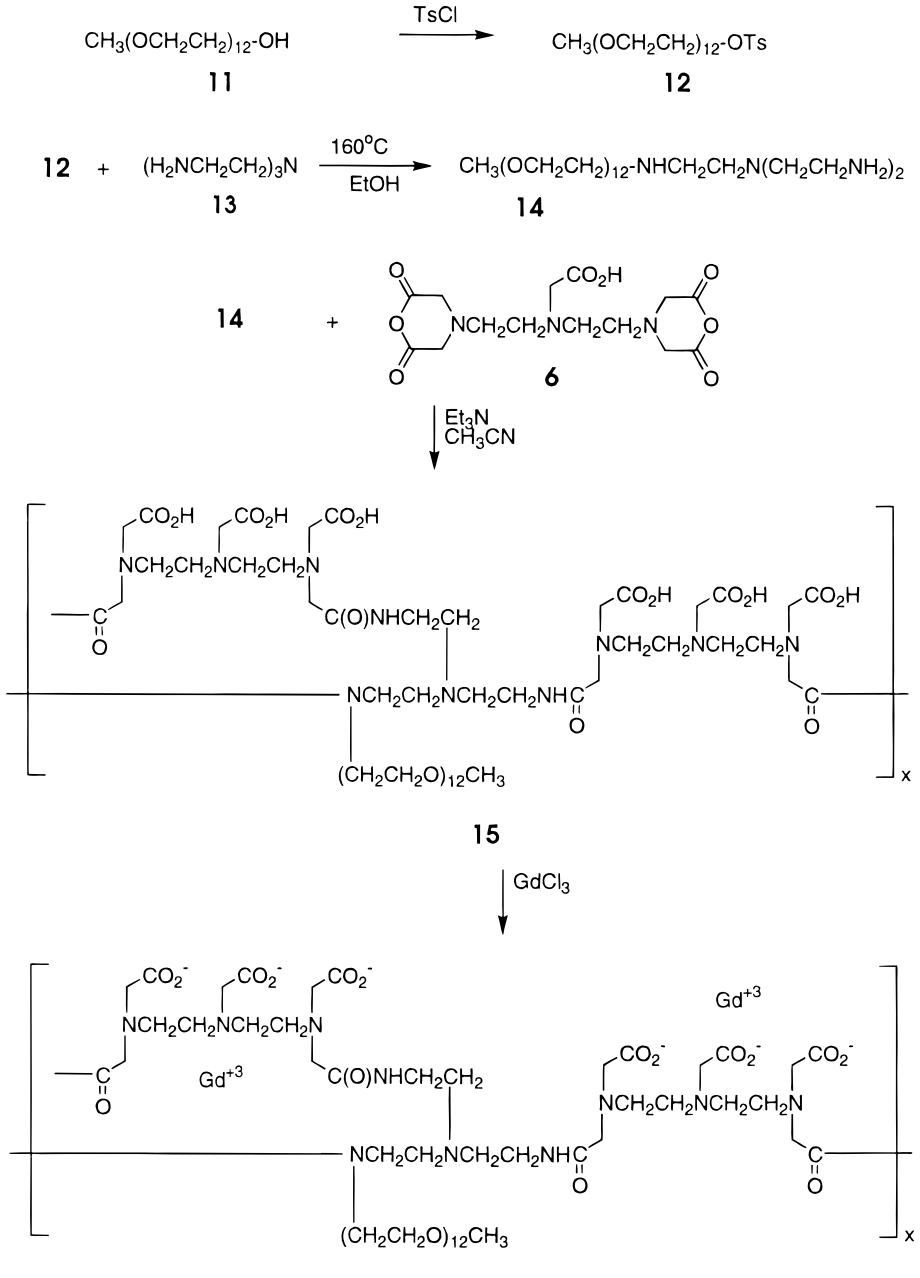


Figure 3. Volume of distribution and overall blood clearance half-life vs molecular weight for NC 22181 of four different molecular weights.

1.5 equiv of DTPA dianhydride and chelated with gadolinium to give **16a**. It was expected that the more globular shape of **16a** would result in lower viscosity solutions and that the increased rigidity resulting from cross-linking would result in higher relaxivities. This was indeed found to be the case. Solutions of **16a** had considerably lower viscosities than solutions of **1a** when compared on the basis of similar gadolinium concentration or polymer concentration (see Table 1). The relaxivity of **16a** (10.1) was found to be 68% higher than for the linear, non-cross-linked polymer **1a**.

Since blood pool gadolinium polymers, by design, reside in the body for extended periods of time, there is an increased opportunity for in vivo metal dissociation (Cacheris et al., 1990; Wedeking et al., 1992; Duncan et al., 1994; Deal et al., 1996; Corot et al., 1998). This is illustrated by the percentage of the injected dose recovered in the bone at 7 days (Table 1). For example, Magnevist with a short half-life has bone gadolinium retention of 0.21% of the injected dose (% ID), while the two DTPA based polymers (**1a** and **10a**) showed higher levels of retention at 7 days, 3.50 and 4.91%ID, respectively. Only bone data at 7 days is reported in Table 1 as no other major organs retained significant amounts of metal and bone retention is generally considered to be a good measure of long term gadolinium retention. Traditionally, reduction of metal retention has been addressed by the choice of chelator. Therefore, in response to the concern of long term metal retention, a series of polymers was designed which employ the macrocyclic chelator DOTA in place of the linear chelator DTPA. Macrocyclic Gd-DOTA chelates which are found in the marketed agents Prohance and Dotarem are known (Wedeking et al., 1992) to be more thermodynamically and kinetically stable than linear Gd-DTPA chelates. Scheme 4 shows the synthesis of a DOTA polymer (**24a**). The PEG-bis-NHS ester (**18**) was polymerized with the tri-*tert*-butyl ester-DOTA-diamine (**21**), and the resultant polymer (**22**) deprotected with TFA and chelated with gadolinium. The requirement that the DOTA nucleus maintains at least three carboxylates to maintain the desired tight metal binding necessitated trade offs that resulted in a polymer with less than optimal properties. Appending the chelator to the polymer backbone through a single amide bond resulted in a nonrigid structure and consequently a relatively low R_1 relaxivity of 6.6. Because the polymerization of **21** with PEG-bis-NHS esters was not a very efficient process, a high molecular mass PEG monomer

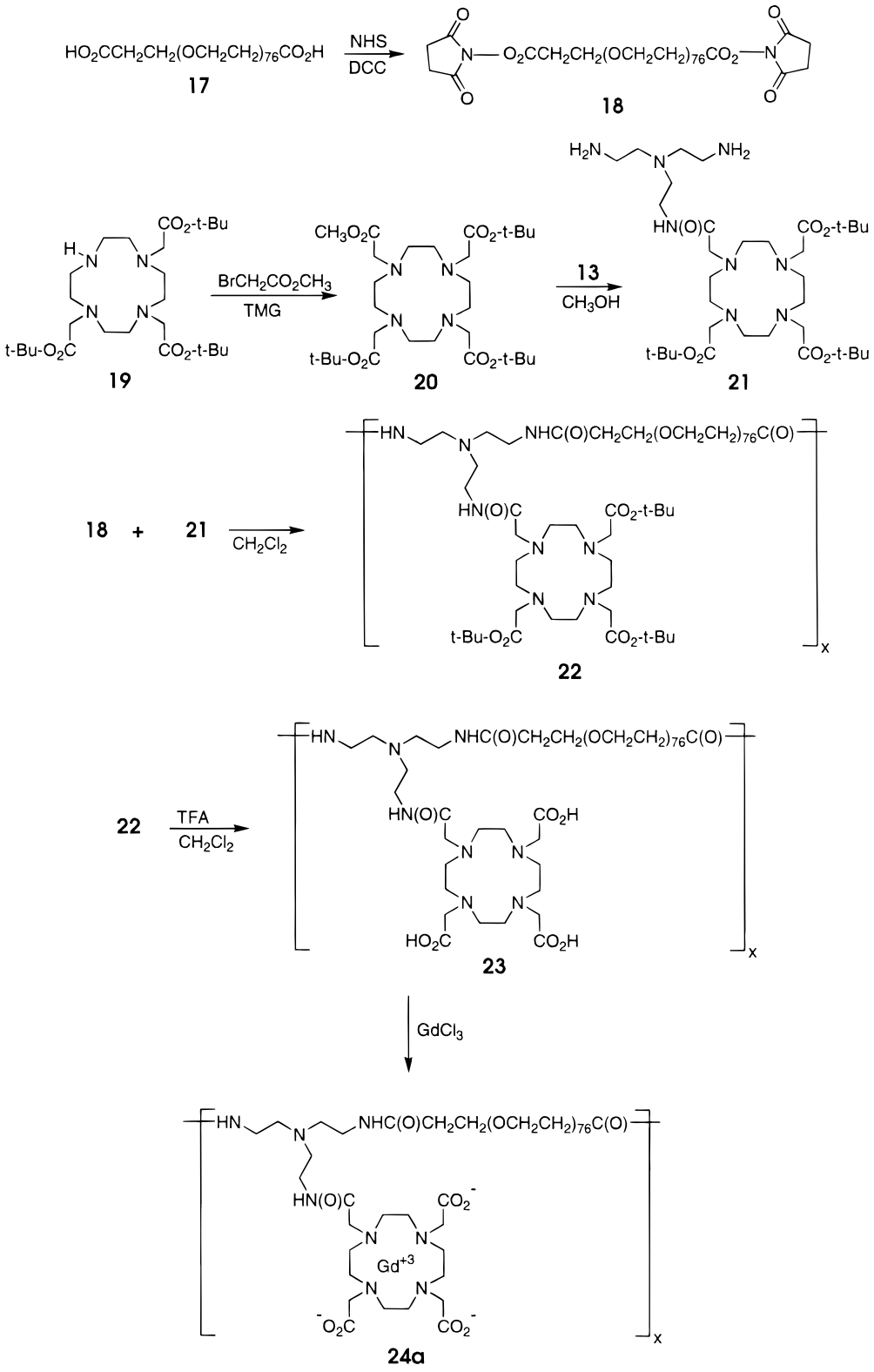
Scheme 3



(**18**, molecular mass = 3.4 kDa) was needed to form a polymer with the requisite MW for blood pool retention resulting in a low metal content for the polymer (2.5%). As anticipated, the 7 day bone retention for **24a** (0.76% ID) was significantly lower than for the two DTPA based polymers (**1a** and **10a**). While it is recognized that **24a** is structurally dissimilar to **1a** and **10a**, its significant blood half-life in rats qualifies it as a blood pool agent and therefore the reduced bone retention is meaningful.

An additional example of a polymeric Gd-DOTA (**34**) was prepared (Scheme 5) by grafting DOTAs onto the surface of a dendrimer. While various linkers and chemistries have been employed (Lewis et al., 1994; Li et al., 1994; McCall et al., 1990; Kline et al., 1991; Brasch et al., 1994; Kubomura et al., 1993; Schmitt-Willich et al., 1992) to graft DOTA macrocycles onto a variety of macromolecules, we chose to use the novel intermediate **31**. DOTA-tris(*tert*-butyl ester) activated ester (**31**) was designed to couple DOTA to the dendrimer via conversion of one of the four DOTA carboxylates to an amide of aminocaproic acid, thus placing the chelators at a reasonable distance from the surface of the dendrimer. Intermediate **28** was prepared from amino-ester **27** (Goodacre et al., 1977), which was prepared (Callahan et al., 1988) from **25** (Sigma). When activated ester **31** was reacted with a third generation PAMAM dendrimer, approximately 20 of the 24 surface amino groups on the dendrimer were derivatized to form the DOTA grafted dendrimer **32**. Deprotection of **32** with TFA followed by metalation with gadolinium chloride produced the chelated polymer **34**. Like **24a**, **34** was found to have less 7 day bone retention (0.62% ID) than the DTPA-based polymers **1a** and **10a**. While the blood half-life of globular polymer **34** was determined to be longer than Magnevist, it was considerably shorter than the linear DOTA polymer **24a** which likely is a reflection of the influence of shape on polymer retention.

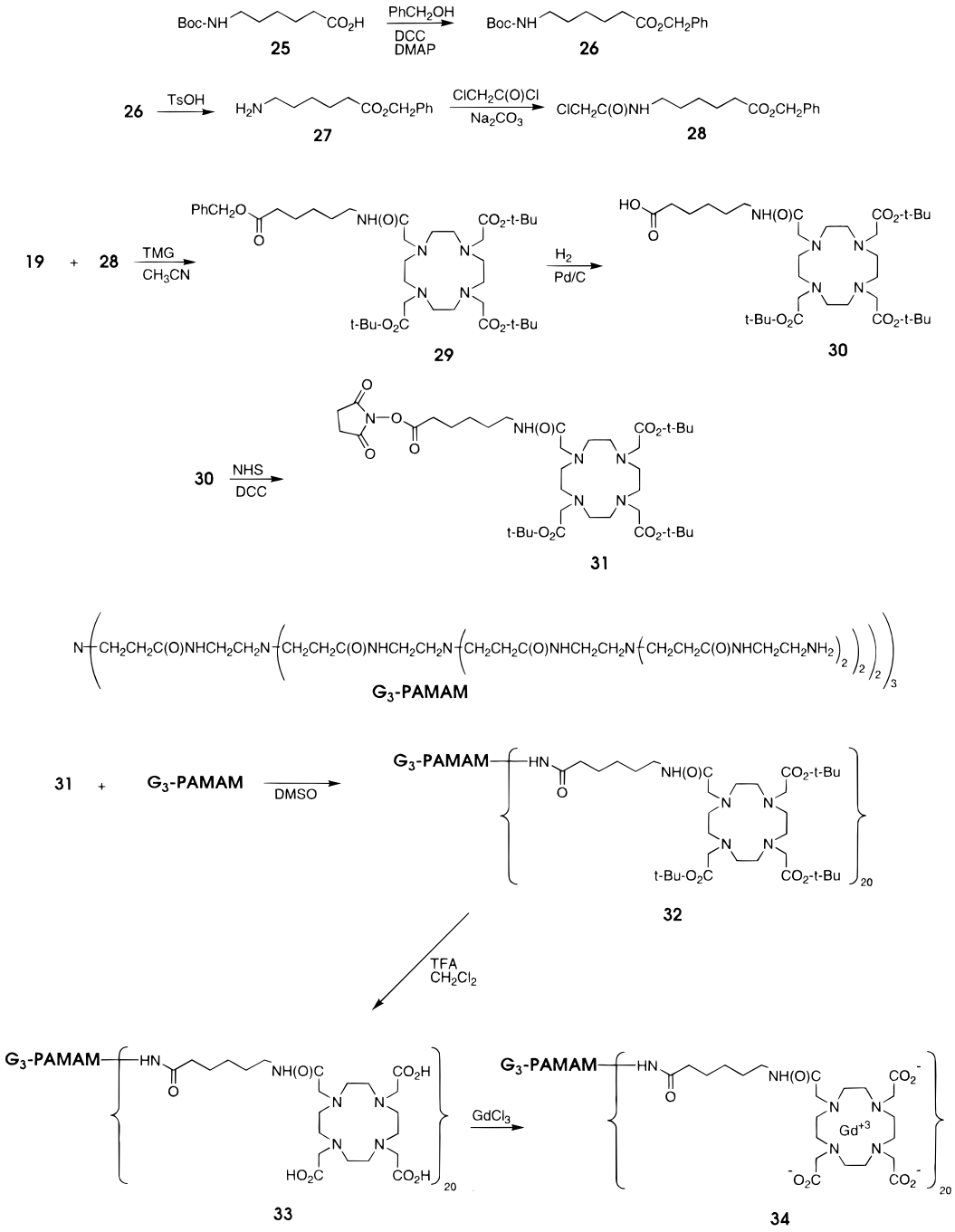
Scheme 4



CONCLUSION

We have shown that polymeric gadolinium chelates with extended blood pool retention can be obtained by selecting polymers of the appropriate MW. For example, with linear copolymers of DTPA and PEG-diamines (**1**), it was found that polymers of 20 kDa and higher are blood pool agents as are linear copolymers of DTPA and alkyldiamines (**10**) of 14 kDa and higher. For polymer **10a** (NC 22181), linear relationships were found for both overall blood clearance half-lives and volumes of distribution vs MW within the range of MWs studied (Figure 3). In addition, with copolymers **10** a significant decrease in dose was realized as a consequence of these polymer's increased metal contents and higher relaxivities. It has also been shown that additional features which are important to achieve a pharmaceutically acceptable contrast agent can be controlled by the design of the polymer. Changing the shape of the polymer from linear as are

Scheme 5



series **1** and **10** to the more globular series **16** resulted in decreased viscosity as well as increased relaxivity. Potential in vivo metal dissociation was addressed by designing a polymer series (**24**) which employs the DOTA chelator which is known to form gadolinium chelates that are both kinetically and thermodynamically more stable than DTPA gadolinium chelates. Finally, we designed a polymer (**34**) that conceptually incorporates most of the above desirable features. The DOTA-dendrimer construct is globular with tight binding gadolinium chelators capable of incorporating a high percentage of metal. In summary, we have demonstrated that the principal characteristics of polymeric gadolinium chelates including blood retention, metal content, viscosity, chelate stability, and relaxivity can be manipulated by the choice of features incorporated into the polymer.

To the best of our knowledge, this report is the first study that addresses the rational design of polymeric MR blood pool contrast agents. The purpose of this study was not to evaluate every parameter for each class of polymer, but to emphasize the relative importance of each parameter. We hope that this paper serves as the basis for further work to develop agents to satisfy an important unmet medical need.

LITERATURE CITED

Brasch, R. C. (1991) Rational and applications for macromolecular Gd-based contrast agents. *Magn. Reson. Med. 22*, 282−287.

Brasch, R. C. (1992) New Directions in the Development of MR Imaging Contrast Media. *Radiology 183*, 1−11.

Brasch, R. C., Mann, J. S., and Nitecki, D. E. (1994) Macromolecular Contrast Media for MR Imaging. WO 9427498, Dec. 8, 1994.

Cacheris, W., Quay, S. C., and Rocklage, S. M. (1990) The Relationship Between Thermodynamics and the Toxicity of Gadolinium Complexes. *Magn. Reson. Imaging 8*, 467−481.

Callahan, J. F., Newlander, K. A., Bryan, H. G., Huffman, W. F., Moore, M. L., and Yim, N. C. F. (1988) Synthesis of 6,6-Pentamethylene-2-aminosuberic Acid. A Key Intermediate in the Synthesis of Dicarba Analogues of Vasopressin Antagonists. *J. Org. Chem. 53*, 1527−1530.

Casali, C., Janier, M., Canet, E., Obadia, J. F., Benderbous, S., Corot, C., and Revel, D. (1998) Evaluation of Gd-DOTA-Labeled Dextran Polymer as an Intravascular MR Contrast Agent for Myocardial Perfusion. *Acad. Radiol. 5* (Suppl. 1), S214−S218.

Corot, C., Idee, J.-M., Hentsch, A.-M., Santus, R., Mallet, C., Goulas, V., Bonnemain, B., and Meyer, D. (1998) Structure−Activity Relationship of Macrocyclic and Linear Gadolinium Chelates: Investigation of Transmetalation Effect on the Zinc-Dependent Metallopeptidase Angiotensin-Converting Enzyme. *J. Magn. Reson. Imaging 8*, 695−702.

Curotto, E., and Aros, F. (1993) Quantitative Determination of Chitosan and the Percentage of Free Amino Groups. *Anal. Biochem. 211*, 240−241.

Deal, K. A., Motekaitis, R. J., Martell, A. E., and Welch, M. J. (1996) Evaluation of the Stability and Animal Biodistribution of Gadolinium(III) Benzylamine-Derivatized Diethylenetriaminepentaacetic Acid. *J. Med. Chem. 39*, 3096−3106.

Desser, T. S., Rubin, D. L., Muller, H. H., Fan, Q., Khodor, S., Zanazzi, G., Young, S. W., Ladd, D. L., Wellons, J. A., Kellar, K. E., Toner, J. L., and Snow, R. A. (1994a) Dynamics of Tumor Imaging with Gd-DTPA-Polyethylene Glycol Polymers: Dependence on Molecular Weight. *J. Magn. Reson. Imaging 4*, 467−472.

Desser, T. S., Rubin, D. L., Fan, Q., Muller, H. H., Young, S. W., Kellar, K. E., Wellons, J. A., Ladd, D. L., Toner, J. T., and Snow, R. A. (1994b) Quantitation of Saturation Effects versus Dose in Three-Dimensional Time-of Flight Magnetic Resonance Angiography with Blood-Pool Contrast Agents. *Invest. Radiol. 29*, S65−S68.

Duncan, J. R., Franano, F. N., Edwards, W. B., and Welch, M. J. (1994) Evidence of Gadolinium Dissociation from Protein-DTPA-Gadolinium Complexes. *Invest. Radiol. 29*, S58−S61.

Engelbrecht, M. R., Saeed, M., Wendland, M. F., Canet, E., Øksendal, A. N., and Higgins, C. B. (1998) Contrast-Enhanced 3D-TOF MRA of Peripheral Vessels: Intravascular Versus Extracellular MR Contrast Media. *J. Magn. Reson. Imaging 8*, 616−621.

Goodacre, J., Jeffries, L., Nayler, J. H. C., Ponsford, R. J., and Stirling, I. (1977) Antibacterial Halogenoacetyl Derivatives of Amino Acids and Simple Peptides. *J. Med. Chem. 20*, 1445−1448.

Hohenschuh, E., and Watson, A. D. (1997) Contrast Media: Theory and Mechanisms of Contrast-Enhancing Agents. in *Magnetic Resonance Imaging of the Body, Third Edition* (C. B. Higgins, H. Hricak, and C. A. Helms, Eds.) pp 1439−1464, Lippincott-Raven Press, New York.

Kellar, K. E., Henrichs, P. M., Hollister, R., Koenig, S. H., Eck, J., and Wei, D. (1997) High Relaxivity Linear Gd(DTPA)-Polymer Conjugates: The Role of Hydrophobic Interactions. *Magn. Reson. Med. 38*, 712−716.

Kline, S. J., Betebenner, D. A., and Johnson, D. K. (1991) Carboxymethyl-Substituted Bifunctional Chelators: Preparation of Aryl Isothiocyanate Derivatives of 3-(Carboxymethyl)-3-azapentanedioic Acid, 3,12-Bis(carboxymethyl)-6,9-dioxa-3,12-diazatetradecanedioic Acid, and 1,4,7,10-Tetraazacyclododecane-N,N′,N″,N‴-tetraacetic Acid for Use as Protein Labels. *Bioconjugate Chem. 2*, 26−31.

Kubomura, K., Seri, S., Iwai, K., and Azuma, M. (1993) Tetraazacyclododecane tetraacetic acid derivatives and the use thereof as diagnositic agents. European Patent Application 565930A1.

Ladd, D. L. (1996) Low Viscosity Chelating Polymers. WO 9600588, Jan. 11, 1996.

Lauffer, R. B., Parmelee, D. J., Ouellet, H. S., Dolan, R. P., Sajiki, H., Scott, D. M., Bernard, P. J., Buchanan, E. M., Ong, K. Y., Tyeklá, Z., Midelfort, K. S., McMurry, T. J., and Walovitch, R. C. (1996) MS-325: A Small-Molecule Vascular Imaging Agent for Magnetic Resonance Imaging. *Acad. Radiol. 3*, S356−S358.

Lewis, M. R., Raubitschek, A., and Shively, J. E. (1994) A Facile Water-Soluble Method for Modification of Proteins with DOTA. Use of Elevated Temperature and Optimized pH To Achieve High Specific Activity and High Chelate Stability in Radiolabeled Immunoconjugates. *Bioconjugate Chem. 5*, 565−576.

Li, M., Meares, C. F., Zhong, G.-R., Miers, L., Xiong, C.-Y., and DeNardo, S. J. (1994) Labeling Monoclonal Antibodies with ^{90}Yttrium- and ^{111}Indium-DOTA Chelates: A Simple and Efficient Methodol. *Bioconjugate Chem. 5*, 101−104.

McCall, M. J., Diril, H., and Meares, C. F. (1990) Simplified Method for Conjugating Macrocyclic Bifunctional Chelating Agents to Antibodies via 2-Iminothiolane. *Bioconjugate Chem. 1*, 222−226.

Meltzer, A. D., Tirrell, D. A., Jones, A. A., Inglefield, P. T., Hedstrand, D. M., and Tomalia, D. A. (1992) Chain Dynamics in Poly(amido amine) Dendrimers. A Study of ^{13}C NMR Relaxation Parameters. *Macromolecules 25*, 4541−4548.

Nolte-Ernsting, C., Adam, G., Bucker, A., Berges, S., Bjornerud, A., and Gunther, R. W. (1997) Contrast-Enhanced Magnetic Resonance Urography. First Experimental Results with a Polymeric Gadolinium Bloodpool Agent. *Invest. Radiol. 32*, 418−423.

Petrak, K., and Goddard, P. (1989) Transport of macromolecules across the capillary walls. *Adv. Drug Delivery Rev. 3*, 191−214.

Rebizak, R., Schaefer, M., and Dellacherie, E. (1998) Polymeric Conjugates of Gd^{3+}-Diethylenetriaminepentaacetic Acid and Dextran. 2. Influence of Spacer Arm Length and Conjugate Molecular Mass on the Paramagnetic Properties and Some Biological Parameters. *Bioconjugate Chem. 9*, 94−99.

Roberts, H. C., Saeed, M., Roberts, T. P. L., Muhler, A., Shames, D. M., Mann, J. S., Stiskal, M., Demsar, F., and Brasch, R. C. (1997) Comparison of Albumin-$(Gd\text{-}DTPA)_{30}$ and Gd-DTPA-24-Cascade-Polymer for Measurements of Normal and Abnormal Microvascular Permeability. *J. Magn. Reson. Imaging 7*, 331−338.

Schmiedl, U., Ogan, M., Paajanen, H., Marotti, M., Crooks, L. E., Brito, A. C., and Brasch, R. C. (1987) Albumin Labeled with Gd-DTPA as an Intravascular, Blood Pool-Enhancing Agent for MR Imaging: Biodistribution and Imaging Studies. *Radiology 162*, 205−210.

Schmitt-Willich, H., Platzek, J., Gries, H., Schuhmann-Giampieri, G., and Frenzel, T. (1992) New macrocyclic polymer complexes useful as X-ray and NMR contrast agents, and in radio-diagnosis and therapy of tumours. European Patent Application 512661A1.

Schuhmann-Giampieri, G., Schmitt-Willich, H., Frenzel, T., Press, W.-R., and Weinmann, H.-J. (1991) In Vivo and In Vitro Evaluation of Gd-DTPA-Polylysine as a Macromolecular Contrast Agent for Magnetic Resonance Imaging. *Invest. Radiol. 26*, 969−974.

Schwickert, H. C., Roberts, T. P. L., Mühler, A., Stiskal, M., Demsar, F., and Brasch, R. C. (1995) Angiographic properties of Gd-DTPA-24-cascade-polymer- a new macromolecular MR contrast agent. *Eur. J. Radiol. 20*, 144−150.

Unger, E., Cardenas, D., Zerella, A., Fajardo, L. L., and Tilcock, C. (1990) Biodistribution and clearance of liposomal gadolinium-DTPA. *Invest. Radiol. 25*, 638−644.

Wallace, R. A., Haar, J. P., Miller, D. B., Woulfe, S. R., Polta, J. A., Galen, K. P., Hynes, M. R., and Adzamli, K. (1998) Synthesis and Preliminary Evaluation of MP-2269: A Novel, Nonaromatic Small-Molecule Blood-Pool MR Contrast Agent. *Magn. Reson. Med. 40*, 733−739.

Wedeking, P., Kumar, K., and Tweedle, M. F. (1992) Dissociation of Gadolinium Chelates in Mice: Relationship to Chemical Characteristics. *Magn. Reson. Imaging 10*, 641−648.

Weinmann, H.-J., Brasch, R. C., Press, W.-R., and Wesbey, G. E. (1984) Characteristics of Gadolinium-DTPA Complex: A Potential NMR Contrast Agent. *Am. J. Roentgenol. 142*, 619−624.

Zalipsky, S. (1995) Functionalized Poly(ethylene glycol) for Preparation of Biologically Relevant Conjugates. *Bioconjugate Chem. 6*, 150−165.

BC980086+

Ternary Conjugates of Guanosine Monophosphate as Initiator Nucleotides for the Enzymatic Synthesis of 5′-Modified RNAs

Burckhard Seelig and Andres Jäschke*

Institut für Biochemie, Freie Universität Berlin, Thielallee 63, D-14195 Berlin. Received July 23, 1998; Revised Manuscript Received October 26, 1998

We give a detailed account on the enzymatic synthesis of RNA conjugates by T7 RNA polymerase using modified initiator nucleotides during transcription. Following two different routes, ternary conjugates of guanosine-5′-monophosphate, poly(ethylene glycol), and anthracene were synthesized via phosphoramidite intermediates and characterized by a variety of spectroscopic techniques. Up to a degree of polymerization n_{PEG} of about 17, these conjugates were efficiently incorporated into RNA by T7 RNA polymerase at the 5′-termini, thereby giving access to RNA conjugates required for biochemical studies as well as for the exploration of the catalytic potential of ribonucleic acids. The resulting conjugates are intact and functional.

INTRODUCTION

Oligonucleotide conjugates have found many uses in biochemical research and medical diagnostics, and a large number of conjugate groups have been used (Agrawal, 1994; Beaucage and Iyer, 1993; Goodchild, 1990). The most common strategies for site-specific conjugation of oligonucleotides are (i) transformation of the conjugate group into a phosphoramidite and direct incorporation during automated solid-phase synthesis of oligonucleotides and (ii) incorporation of a reactive linker during oligonucleotide synthesis and postsynthetic attachment of the conjugate group to this linker.

While these conjugation strategies work well with short oligonucleotides accessible by chemical synthesis, the possibilities to conjugate enzymatically synthesized long nucleic acid sequences are very limited [e.g., Oh and Pace (1994) and Tong et al. (1993)]. This is especially problematic with ribonucleic acids, where chemical synthesis is normally limited to a chain lengths of about 50 nucleotides. Most RNAs of biological interest are much longer, and for biochemical studies they are either isolated from biological sources or prepared by enzymatic transcription from DNA templates using viral RNA polymerases (Milligan et al., 1987). To study RNA processing, translocation, or ribozyme reaction mechanisms, it is highly desirable to have simple and reliable methods available that allow the site-specific incorporation of conjugate groups (Bevilacqua et al., 1994; Igloi, 1996; Moore and Sharp, 1992).

Recently, ternary RNA conjugates have successfully been used for the in vitro selection of new catalytic RNA species (Tarasow et al., 1997; Wiegand et al., 1997; Seelig and Jäschke, 1999). A key feature of these strategies is the use of synthetic RNA conjugate libraries in which a small organic residue as a potential reactant is attached to each individual sequence of a combinatorial RNA pool via a flexible polymeric tether. These RNA conjugates are then incubated with a second reactant carrying a biotin tag. If an RNA molecule catalyzes the reaction of the attached reactant with the biotinylated free reactant, the reaction product would also carry the biotin tag and could be isolated by affinity chromatography. The RNA part of the isolated conjugate is then enzymatically amplified. The cycle of conjugation, reaction, selection, and amplification is repeated until the active species are sufficiently enriched from the ancestral RNA pool. This approach was successfully applied to the selection of RNA Diels–Alderases and RNA amide synthases (Tarasow et al., 1997; Wiegand et al., 1997; Seelig and Jäschke, 1999).

Toward the same end, we have described the synthesis of multifunctional RNA conjugates in which a small organic molecule is site-specifically attached to the 3′-terminal hydroxyl group of the RNA via a long flexible poly(ethylene glycol) tether harboring a photocleavage site (Hausch and Jäschke, 1997). In that case, we made use of an enzymatic two-step procedure involving preparation of the unmodified RNA molecule by enzymatic transcription and subsequent addition of a conjugated dinucleotide by T4 RNA ligase.

In a recent short communication, we have described an enzymatic one-step procedure which permits an easy access to RNA 5′-conjugates (Seelig and Jäschke, 1997). This procedure is based on the known tolerance of T7 RNA polymerase toward certain chemical modifications in the initiation step (Pitulle et al., 1992). The conjugate group is added at the 5′-end during transcription by T7 RNA polymerase, which utilizes ternary conjugates of guanosine monophosphate, poly(ethylene glycol), and anthracene (as a potential organic reactant) exclusively during the initiation, but not during the elongation steps. While a number of reports have been published on the use of different initiator nucleotides, a systematic investigation of this method has not been carried out so far. Here, we give a detailed account on the chemical synthesis of ternary initiator nucleotides with varying lengths of the poly(ethylene glycol) linker, an investiga-

* To whom correspondence should be addressed. Phone: (49) 30 838 6023. Fax: (49) 30 838 6413. E-mail jaschke@chemie.fu-berlin.de.

[1] Abbreviations: DMF, *N*,*N*-dimethylformamide; DNA, deoxyribonucleic acid; dsDNA, double-stranded DNA; HEPES, *N*-(2-hydroxyethyl)piperazine-*N*′-(2-ethanesulfonic acid); MALDI-TOF, matrix-assisted laser desorption/ionization time-of-flight (mass spectrometry); NTPs, (ribo)nucleoside 5′-triphosphates; PCR, polymerase chain reaction; PEG, poly(ethylene glycol); RNA, ribonucleic acid.

10.1021/bc980085h CCC: $18.00 © 1999 American Chemical Society
Published on Web 04/06/1999

tion of their enzymatic incorporation, and a detailed characterization of the enzymatically synthesized conjugates.

MATERIALS AND METHODS

General. Poly(ethylene glycol) was purchased from Fluka; all other chemicals, buffers, solvents and reagents were obtained as the highest commercial grade available and used without further purification. Reactions were carried out at room temperature unless stated otherwise. Silica gel (0.063−0.200 mm) for column chromatography was obtained from J. T. Baker. HPLC purification was performed on a Beckman System Gold chromatograph using an Ultrasphere ODS reversed-phase column (4.6 × 250 mm, flow 1 mL/min). NMR spectra were recorded using a Bruker A250 (^{13}C) and a Bruker AMX500 (^{1}H, ^{31}P). ESI mass spectra were recorded on a Finnigan MAT 7M spectrometer, and MALDI TOF mass spectra were obtained using a Bruker Reflex spectrometer. UV spectra were recorded with a Shimadzu UV-160A.

Mono-[9-(methyl)anthracene]-PEG 600 Conjugate and Mono-[9-(methyl)anthracene]-PEG 1500 Conjugate 1. PEG 600 (3.6 g, 6 mmol) or PEG 1500 (9 g, 6 mmol) was dried in vacuo (P_4O_{10}) and dissolved in dry benzene (30 mL). *n*-Butyllithium (2.5 mL, 6.2 mmol, 2.5 M solution in hexane) was added dropwise under vigorous stirring. After further stirring for 2 h, benzene was removed by rotary evaporation, and the product was redissolved in dry *N*,*N*-dimethylformamide (45 mL). 9-(Chloromethyl)anthracene (1.36 g, 6 mmol) was added, and the mixture was stirred for 2 h at room temperature. The solvent was removed under reduced pressure, and the resulting oil subjected to silica gel chromatography (CH_2Cl_2/MeOH 96:4 v/v for PEG 600 conjugate and CH_2Cl_2/MeOH 9:1 v/v for PEG 1500 conjugate). Concentration in vacuo afforded mono-[9-(methyl)anthracene]-PEG 600 **1** with a yield of 39% [mono-[9-(methyl)anthracene]-PEG 1500 with a yield of 48%], referred to PEG. ^{1}H NMR (250 MHz, [D$_1$]CHCl$_3$, 25 °C): δ = 3.5−3.8 (m, 56 H; CH_2−O for n = 14), 5.6 (s, 2H; CH_2−Ar), 7.48 (m, 4H; H-2/H-3/H-6/H-7), 8.0 (d, 2H; H-1/H-8), 8.4 (d, 2H; H-4/H-5), 8.42-(s, 1H; H-10). ^{13}C NMR (63 MHz, [D$_1$]CHCl$_3$, 25 °C): δ = 131.2, 130.8, 128.8, 128.6, 128.1, 125.9, 124.7, 124.3. ESI$^+$-MS: calculated for $C_{43}H_{68}O_{15}$ (n = 14) [MH$^+$] = 825.0, found 825.

Mono-[9-(methyl)anthracene]-PEG 600-(2-cyanoethyl-*N*,*N*-diisopropyl)-phosphoramidite 2. Mono-[9-(methyl)anthracene]-PEG 600 **1** (260 mg, 325 μmol) was coevaporated twice from CH_2Cl_2/pyridine (9:1 v/v) and dried in vacuo overnight (P_4O_{10}). *N*,*N*-Diisopropylethylamine (585 μL, 3.25 mmol) and dichloromethane (1 mL, refluxed with CaH_2 and distilled in the dark immediately before use) were added under argon. (2-Cyanoethyl-*N*,*N*-diisopropyl)chlorophosphoramidite (73 μL, 325 μmol) was added dropwise, and the mixture was stirred for 30 min in the dark. A total of 50 μL of anhydrous methanol was added, and the reaction mixture was diluted with CH_2Cl_2 to 30 mL. After extraction with saturated $NaHCO_3$ solution and with water, the organic phase was dried over Na_2SO_4 and solvent was removed under reduced pressure to yield 190 mg (58%) of phosphoramidite **2**, which was used for coupling without further purification.

^{31}P NMR (202 MHz, [D$_1$]CHCl$_3$, 20 °C): δ = 146.05 ppm.

2′-O,3′-O,*N*^{2}-Triisobutyrylguanosine 3. N^2-Isobutyryl-5′-*O*-(4,4′-dimethoxytrityl)guanosine (3.28 g, 5 mmol) was added to a solution of isobutyric anhydride (8.33 mL, 50 mmol) in pyridine (50 mL) and stirred for 20 h. Pyridine was distilled off, and the residue was dissolved in water (50 mL) and extracted with dichloromethane (200 mL). After extraction with saturated $NaHCO_3$ solution, saturated NaCl solution and water, the organic phase was dried over Na_2SO_4 and solvent was removed under reduced pressure. The residue was subjected to silica gel chromatography (CH_2Cl_2/MeOH/triethylamine 96:4:0.25 v/v). The pooled fractions were evaporated to dryness and detritylated with trichloroacetic acid (3%) in dichloromethane for 2 min. The solution was extracted with saturated $NaHCO_3$ solution, saturated NaCl solution, and water. After evaporation, the final purification by silica gel chromatography (CH_2Cl_2/MeOH 98:2 v/v) gave 775 mg (31%) of 2′-O,3′-O,N^2-triisobutyrylguanosine **3**. ^{1}H NMR (500 MHz, [D$_1$]CHCl$_3$, 20 °C): δ 1.0−1.23 (m, 18 H; 6 × CH_3-Ibu), 2.4, 2.6 (2 × septet, 2 × 1H; CH-2′,3′-Ibu), 2.78 (septet, 1H; CH-N^2-Ibu), 3.74 (dd, 1H; H-5′), 3.92 (dd, 1H; H-5′), 4.2 (q, 1H; H-4′), 5.63 (dd, 1H; H-3′), 5.86 (d, 1H; H-1′), 5.91 (t, 1H; H-2′), 7.8 (s, 1H; H-8). ^{13}C NMR (63 MHz, [D$_1$]CHCl$_3$, 25 °C): δ = 18.5-18.8 (9 × CH_3), 33.5, 33.7 (CH-2′,3′-Ibu), 36.1 (CH-N^2-Ibu), 61.7 (C-5′),71.1 (C-4′), 72.3 (C-2′), 84.4 (C-1′), 87.4 (C-3′), 122.1 (C-5), 138.9 (C-8), 147.6 (C-4), 148 (C-6), 155.3 (C-2), 175.3 (C=O, 2′-Ibu), 175.8 (C=O, 3′-Ibu), 179.4 (C=O, N^2-Ibu). ESI$^+$-MS calculated for $C_{22}H_{31}O_8N_5$ [M$^+$]: 493. Found: 493.

2′-O,3′-O,*N*^{2}-Triisobutyrylguanosine-(2-cyanoethyl-*N*,*N*-diisopropyl)phosphoramidite 4. 2′-O, 3′-O, N^2-Triisobutyrylguanosine **3** (493 mg, 1 mmol) was dried in vacuo overnight (P_4O_{10}) and dissolved in dichloromethane (4 mL, refluxed with CaH_2 and distilled in the dark immediately before use) under argon. *N*,*N*-Diisopropylethylamine (1.22 mL, 7 mmol) was added, and (2-cyanoethyl-*N*,*N*-diisopropyl)chlorophosphoramidite (340 μL, 1.5 mmol) was added dropwise and the mixture was stirred for 30 min in the dark. A total of 100 μL of anhydrous methanol was added, and the reaction mixture was diluted with CH_2Cl_2 to 30 mL. After extraction with saturated $NaHCO_3$ solution and with water, the organic phase was dried over Na_2SO_4 and solvent was removed under reduced pressure. The yielded phosphoramidite **4** was used for coupling without further purification. TLC in $CHCl_2$/MeOH/triethylamine (90:10:0.25 v/v) showed the product spot (R_f = 0.68) and the pale spot of the starting material (R_f = 0.48), indicating almost complete conversion.

Initiator Nucleotide 6. Route 1: 2′-O,3′-O,N^2-Triisobutyrylguanosine **3** (30 mg, 60 μmol) and 1.5 equiv of mono-[9-(methyl)anthracene]-PEG 600-(2-cyanoethyl-*N*,*N*-diisopropyl)phosphoramidite **2** (90 mg, 90 μmol) was coevaporated twice from pyridine and dried in vacuo overnight (P_4O_{10}). The two components were dissolved in anhydrous acetonitrile (5 mL), and a solution of tetrazole in acetonitrile (510 μL/0.47 M, 240 μmol) was added under argon. The mixture was stirred for 15 min, and iodine (450 μL/0.1 M in tetrahydrofurane/collidine/water 2:2:1 v/v, 45 μmol) was added. After 5 min, the mixture was diluted with an aqueous solution of sodium thiosulfate (5 mL/1 M, 5 mmol), and the product was extracted with dichloromethane (50 mL). The organic phase was extracted with saturated $NaHCO_3$ solution and water and dried over Na_2SO_4. The solvent was removed under reduced pressure, and the residue was subjected to silica gel chromatography (CH_2Cl_2/MeOH 85/15). The fractions **5** with the typical additive anthracene/guanosine UV spectrum were pooled and deprotected with aqueous ammonia (4 mL, 33%) at 55 °C overnight. After evaporation to dryness, product **6** was finally purified and fractionated according to the degree of polymerization of PEG by isocratic HPLC using 38% acetonitrile in 100 mM

triethylammonium acetate (TEAA), pH 7.0. The fractions were lyophilized.

Route 2: Mono-[9-(methyl)anthracene]-PEG 600 **1** (1.2 g, 1.5 mmol) or mono-[9-(methyl)anthracene]-PEG 1500 (2.25 g, 1.5 mmol) and 0.67 equiv of 2′-O,3′-O,N^2-triisobutyrylguanosine-(2-cyanoethyl-*N*,*N*-diisopropyl)phosphoramidite **4** (1 mmol) and were coevaporated twice from pyridine and dried in vacuo overnight (P_4O_{10}). The two components were dissolved in anhydrous acetonitrile (10 mL) and a solution of tetrazole in acetonitrile (8.5 mL/0.47 M, 4 mmol) was added under argon. The mixture was stirred for 15 min and iodine (12 mL/0.1 M in tetrahydrofurane/collidine/water 2:2:1 v/v, 1.2 mmol) was added. After 5 min, the mixture was diluted with an aqueous solution of sodium thiosulfate (1 M) until the brown color of iodine disappeared. The product was extracted with dichloromethane (70 mL). The organic phase was extracted with saturated $NaHCO_3$ solution and with water and dried over Na_2SO_4. The solvent was removed under reduced pressure and the product **5** was chromatographically purified, deprotected, and finally HPLC-purified exactly as described for route 1.

MALDI$^+$-MS calcd for $C_{45}H_{65}O_{18}N_5P$ ($n = 10$) [MH^+]: 994.4. Found: 994. Calcd for $C_{93}H_{159}O_{42}N_5P$ ($n = 34$) [MH^+]: 2050.27. Found: 2049.6. UV (H_2O): λ_{max}= 254.5, 348, 365, 385, 277 nm (shoulder). Fluorescence spectrophotometry (H_2O): emission at $\lambda = 419$ nm upon exitation at $\lambda = 254$ nm (Figure 1).

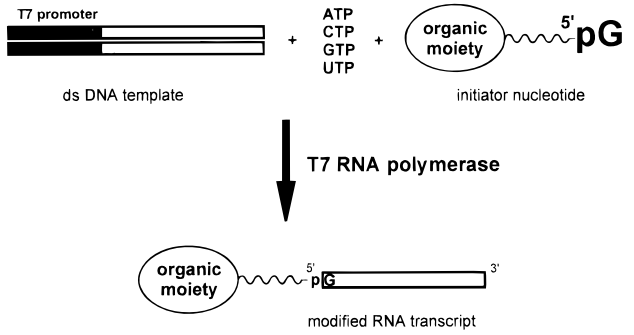
T7 Transcriptions. T7 transcriptions were performed essentially as described (Milligan et al., 1987). DNA templates for T7 transcription were synthesized by standard phosphoramidite chemistry and purified by reversed-phase HPLC (C18) using a gradient from 8 to 32% acetonitrile in 100 mM triethylammonium acetate, pH 7.0, in 30 min. The DNA template for the 25 nt transcript was a duplex of a 44-mer (3′-AG ATT ATG CTG AGT GAT ATC CTC GAG TCG GAA GTG ACG AGG TGG-5′) and a 38-mer (5′-TC TAA TAC GAC TCA CTA TAG GAG CTC AGC CTT CAC TGC-3′), prepared by heating a mixture of the two DNA strands to 95 °C for 3 min and then cooling to room temperature in 1 h. The DNA templates for the randomized 113 and 159 nt transcripts were prepared essentially as described (Hausch and Jäschke, 1997) with completely randomized regions of 74 and 120 nt, respectively, flanked by constant sequences at the termini.

The transcription reactions were run in 80 mM HEPES (pH 7.5), 1 mM spermidine, 22 mM $MgCl_2$, 10 mM dithiothreitol, 120 μg/mL bovine serum albumin, 4 mM NTPs (except GTP), 3 μM [α-^{32}P]CTP (0.2 μCi/μL from Amersham Buchler), 1 μM dsDNA template, 0.5 units/μL ribonuclease inhibitor (MBI Fermentas), and 1 unit/μL T7 RNA polymerase (Stratagene). The concentrations of GTP and initiator nucleotide **6** were varied as indicated in each experiment. The reaction mixtures were incubated at 37 °C for 3 h. After transcription, the RNA was heated in loading buffer containing 50% formamide at 95 °C for 2 min immediately prior to loading on an analytical 15% (25 nt transcript) or 10% (113/159 nt transcript) denaturing polyacrylamide gel. Products were separated on a 24 cm vertical gel apparatus, and the band was located by autoradiography, cut out, and Cerenkov counted in a Beckman LS 6000 SC liquid scintillation counter to determine yields.

RESULTS AND DISCUSSION

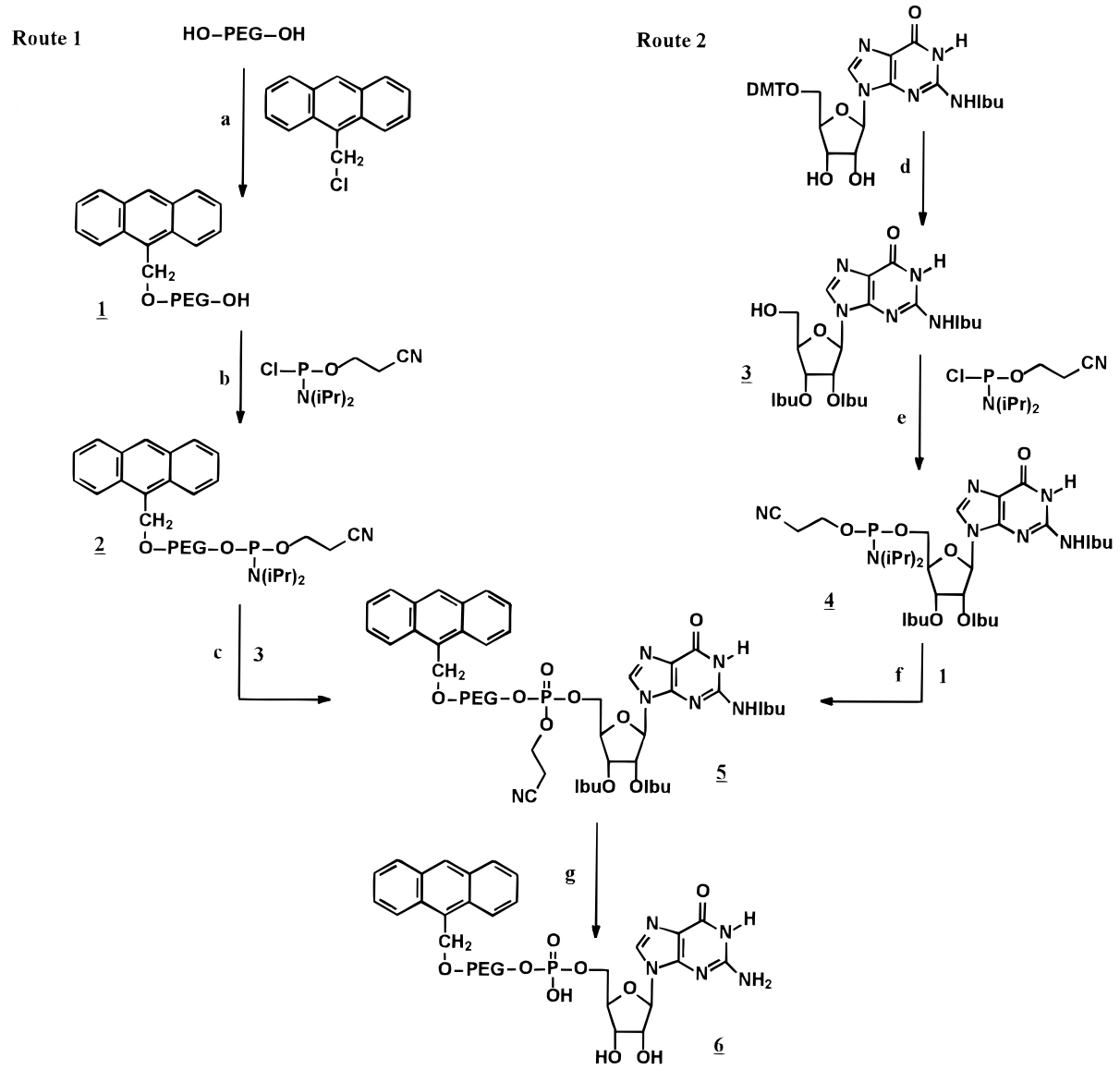
Design, Synthesis, and Characterization of the Initiator Nucleotides. The most common method to synthesize RNA in the laboratory is in vitro transcription. The DNA-dependent RNA polymerase of bacteriophage T7 recognizes and binds to specific double-stranded DNA promotor sequences and starts transcription right behind the promotor by using ribonucleotide-5′-triphosphates according to the sense strand of the DNA duplex. Synthesis stops at the end of the DNA template (runoff transcription). The first incorporated nucleotide is always GTP. The polymerase has been shown to be rather tolerant toward certain modifications at the 5′-position of this first guanosine in the initiation step (Martin and Coleman, 1989). Therefore, the use of 5′-modified guanosines as "initiator nucleotides" has been described for the incorporation of cap-analogues, nucleoside monophosphates, or thiophosphates as well as short oligonucleotides and fluorescence-labeled nucleotides at 5′-terminal positions of RNA transcripts (Burgin and Pace, 1990; Darzynkiewicz et al., 1988; Logsdon et al., 1992; Pitulle et al., 1992). These initiator nucleotides cannot be incorporated during elongation, since they are lacking the essential 5′-triphosphate.

Scheme 1. General Scheme for 5′-Conjugation by Runoff Transcription Using Ternary Initiator Nucleotides



To develop a generally applicable method to attach labels, fluorophores, cross-linkers or reactive groups to long RNA molecules without interfering with the overall RNA structure, we chose to investigate ternary conjugates in which the organic moiety is attached to the 5′-position of guanosine via a polymeric tether (Scheme 1). As the organic moiety, we chose anthracene primarily for use of the resulting conjugates in selection experiments similar to those described by Tarasow et al. (1997), i.e., for the selection of RNA molecules catalyzing Diels−Alder reactions from combinatorial libraries (Seelig and Jäschke, 1999). Additionally, anthracene turned out to be a convenient molecule to study because (i) it is a highly sensitive fluorophore and can thus be easily detected, (ii) attachment of anthracene to an RNA molecule causes significant shifts in reversed-phase HPLC, and (iii) the specific reactivity of anthracene provides an additional means to study the properties of the conjugates. We used poly(ethylene glycol) as a tether because it is highly flexible, water soluble, and its chemical properties are known to be compatible with RNA chemistry (Jäschke, 1997; Jäschke et al., 1996). To select catalysts from libraries without prior structural knowledge, the use of polydisperse PEG was thought to be beneficial because a range of different tether lengths would allow the system to find the optimum tether length itself. We designed initiator nucleotide **6**, consisting of guanosine monophosphate, esterified with the terminal PEG hydroxyl group, while the other end of the PEG chain was connected to the anthracene ring system via an ether linkage (Scheme 2).

Scheme 2. Synthesis of Initiator Nucleotides[a]



[a] (a) benzene, *n*-butyllithium; DMF; (b) CH_2Cl_2, *N*,*N*-diisopropylethylamine; (c) acetonitrile, tetrazole; iodine; (d) pyridine, isobutyric acid; CH_2Cl_2, trichloroacetic acid (e) CH_2Cl_2, *N*,*N*-diisopropylethylamine; (f) acetonitrile, tetrazole; iodine; (g) 33% aqueous ammonia.

Initiator nucleotides **6** were synthesized by two different ways (Scheme 2). In the first route, PEG 600 was converted into the alcoholate and reacted with 9-chloromethylanthracene. The resulting mixture was chromatographically fractionated, and monoanthracene-PEG **1** was reacted with (2-cyanoethyl-*N*,*N*-diisopropyl)chlorophosphoramidite to give phosphoramidite **2**. 2′-O,3′-O,N^2-Triisobutyrylguanosine **3** was prepared from 5′-*O*-dimethoxytrityl-N^2-isobutyrylguanosine and reacted with **2** in the presence of tetrazole. After coupling, the reaction mixture was oxidized and purified by column chromatography on silica gel. **5** was deprotected using aqueous ammonia giving initiator nucleotide **6**, which was fractionated by reversed-phase HPLC according to the number of ethylene glycol units into 12 product peaks.

Alternatively, 2′-O,3′-O,N^2-triisobutyrylguanosine **3** was reacted with (2-cyanoethyl-*N*,*N*-diisopropyl)chlorophosphoramidite to give a protected guanosine-5′-phosphoramidite **4** which allowed an easier chromatographic purification, compared to polydisperse **2**. After reaction with **1** and tetrazole, oxidation, deprotection, and purification, **6** was obtained. Total yields were generally higher with route 2, which was also used for the synthesis of derivatives with higher n_{PEG}, starting from PEG 1500.

As observed with oligonucleotide−PEG conjugates (Jäschke et al., 1993, 1994, 1996), the degree of polymerization (number of CH_2CH_2O units) of the coupled PEG influences the molecular properties of the conjugates. For initiator nucleotides **6**, single degrees of polymerization were eluted sequentially in reversed-phase HPLC, giving a characteristic elution pattern. Figure 1a shows the chromatogram of initiator nucleotides derived from PEG 1500. For PEG 600, similar chromatograms were observed at lower acetonitrile concentrations (Seelig and Jäschke, 1997). The UV spectra of the conjugates show the typical features of both anthracene (absorbance maximum at 254.5 nm, "fingers" at 348, 365, and 385 nm) and guanosine (shoulder at 277 nm, see Figure 1b), and no influence of n_{PEG} on the spectroscopic properties was observed. Upon UV excitation at 254 nm, the initiator nucleotides show a typical blue anthracene fluorescence with an emission maximum at 419 nm (Figure 1c). The correct composition was corroborated by MALDI mass spectrometry (Figure 1d), and the mea-

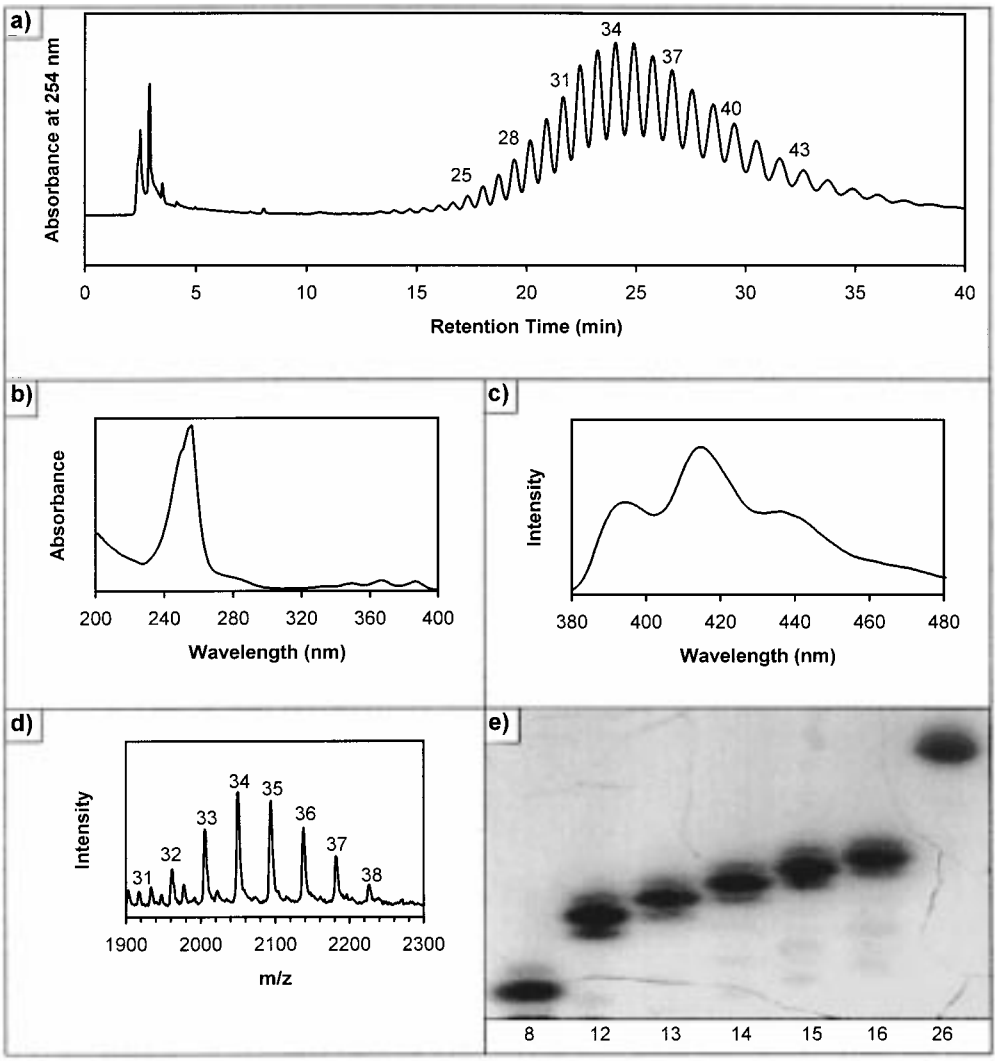


Figure 1. (a) Reversed-phase HPLC of initiator nucleotides **6** (PEG 1500). Eluent: 38% acetonitrile in 100 mM triethylammonium acetate, pH 7.0. The figures at the peaks indicate the respective degree of polymerization. (b) UV spectrum of the peak eluted at 13.2 min. (c) Fluorescence spectrum measured on excitation at 254 nm at a concentration of 1 μM. (d) MALDI mass spectrum of polydisperse **6** (PEG 1500). (e) Electrophoretic analysis of **6** with varying n_{PEG}. Two A_{260} units each of HPLC-purified **6** (n_{PEG} = 8−35) were loaded in 50% formamide and ran on a 15% denaturing polyacrylamide gel. Bands were visualized by epiillumination at 254 nm and photographed.

sured *m*/*z* values were in good agreement with the calculations (typically ±0.5 Da). The molecular masses of neighboring peaks differ by 44 Da, i.e., by the size of one CH_2CH_2O unit. Electrophoretic mobility decreases with increasing size of the PEG chain (Figure 1e). Generally, the electrophoretic mobility is rather low, due to the low charge-to-mass ratio. On a 15% denaturing polyacrylamide gel, **6** with n_{PEG} = 8 has about the mobility of an 32-mer oligonucleotide.

Enzymatic Synthesis and Characterization of Ternary RNA Conjugates. To investigate whether T7 RNA polymerase incorporates the synthesized initiator nucleotides, HPLC-purified monodisperse **6** with n_{PEG} = 10 was added to standard transcription reactions from a short synthetic DNA template, while the concentration of GTP was reduced accordingly (Figure 2). Since T7 RNA polymerase always generates a mixture of correct transcripts and molecules with an additional nucleotide appended to the 3′-end, RNA transcripts of 25 (*n*-mer, band 5) and 26 nucleotides (*n*+1-mer, band 4), respectively, were generated. With increasing concentration of **6,** two new bands with lower electrophoretic mobility (1 and 2) appeared in the autoradiogram (Figure 2a). Upon excitation with 254 nm UV light, these bands showed the typical blue anthracene fluorescence. (Figure 2b). The third fluorescent band found on the photograph (band 3) does not contain RNA and is a decomposition product arising from **6** during incubation. Transcription reactions using polydisperse initiator nucleotides give complex mixtures of varying electrophoretic mobility with the longer oligomers moving slower than the shorter ones. The percentage of RNA molecules being coupled to anthracene is a function of the ratio of **6** to GTP, while the overall transcription yield drops with decreasing GTP concentration (Figure 2c). Bands were excised from the gel, eluted, and analyzed by MALDI mass spectrometry. The *n*-mer conjugate band 2 was found to have a molecular weight of 8623.3 (calculated 8623.7 for $[MH^+]$), indicating that no other modifications had taken place. A typical mass spectrum for a mixture of *n*+1-mers is shown in Figure 2d (n_{PEG} = 15), and three signals were found at *m*/*z* =9104.6, 9126.9, and 9145.3, while the calculated values with the arbitrarily appended "*n*+1"-nucleotide were 9106 (for N=C), 9107 (U), 9130 (A), and 9146 (G).

To investigate whether T7 RNA polymerase could also be used to fuse even larger molecules to RNA, we then systematically studied the dependence of the enzymatic

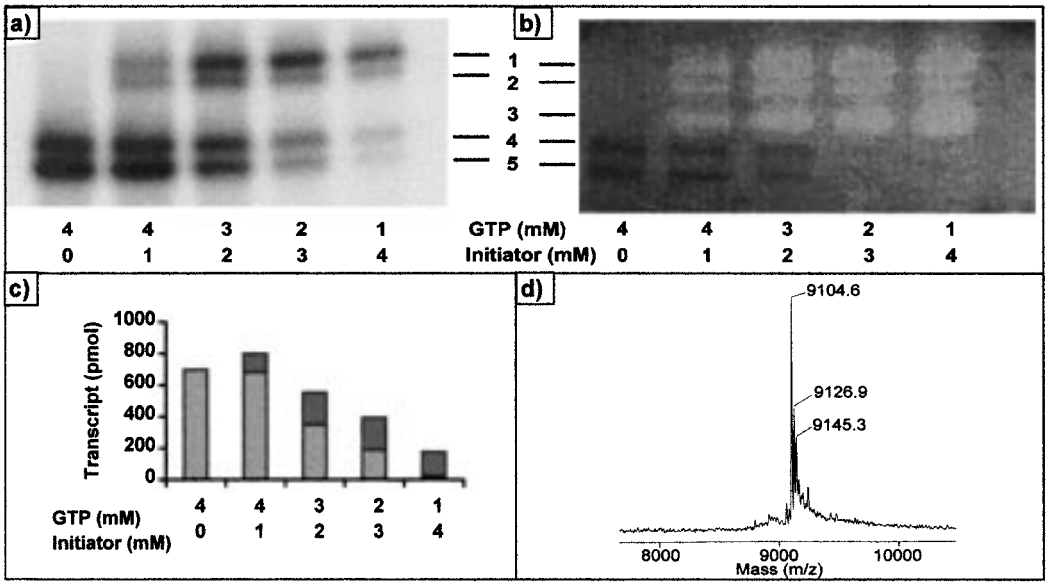


Figure 2. T7 transcriptions using initiator nucleotides **6** (n_{PEG} = 10). (a) Transcription by T7 RNA polymerase of a short DNA oligonucleotide duplex (see Materials and Methods). Autoradiogram of a 15% denaturing polyacrylamide gel. Nucleotide sequence of transcripts (bands 1,2,4,5), 5′(anthracene-PEG-)G GAG CUC AGC CUU CAC UGC UCC ACC (N)3′ (N = A, C, G or U); band 5, unmodified *n*-mer transcript; band 4, *n*+1-mer; band 2, anthracene-PEG-conjugate, *n*-mer; band 1, anthracene-PEG-conjugate; *n*+1-mer. (b) Fluorescence photograph of the same gel upon epiillumination at 254 nm. (c) Dependence of transcription yields on the composition of the transcription mixture. Light gray, unmodified RNA; dark filling, RNA conjugates. (d) MALDI mass spectrum of *n*+1-mer conjugates (equivalent to band 1 in Figure 2a) with n_{PEG} = 15. Bands were excised from the gel and eluted.

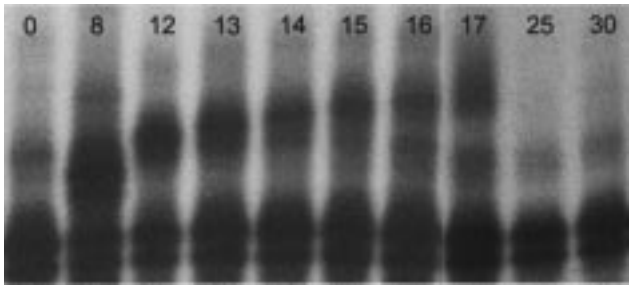


Figure 3. Electrophoretic analysis of transcripts prepared using **6** with varying n_{PEG}. Templates and conditions were identical to Figure 2. c_{GTP} was 4 mM, and $c_{Initiator}$ was 1 mM. HPLC-purified initiator nucleotide fractions were used. Bands were visualized by autoradiography.

incorporation on the length of the PEG tether. Transcription mixtures were prepared from individual HPLC fractions of initiator nucleotides derived from PEG 600 and PEG 1500, respectively. These fractions contained each at least 80% of one single degree of polymerization. To ensure sufficient yield of total transcript, GTP was kept at 4 mM, while initiators **6** were used at 1 mM. Figure 3 shows the autoradiograms of 15% denaturing polyacrylamide gels with n_{PEG} varying from 8 to 30. Up to n = 13, the initiators **6** are efficiently incorporated giving transcripts with the electrophoretic mobility decreasing with increasing n_{PEG}. From n = 14, a decline in the yield of conjugate occurs, while no significant effect on the yield of unmodified transcript is observed. From n = 25, no incorporation at all can be detected. These results demonstrate that initiator nucleotides **6** of this type can be used to introduce a poly(ethylene glycol) spacer of up to 50 atoms, while longer spacers are not incorporated.

Longer RNA transcripts up to 159 base pairs containing regions of randomized sequence for in vitro selection experiments were efficiently transcribed and conjugated

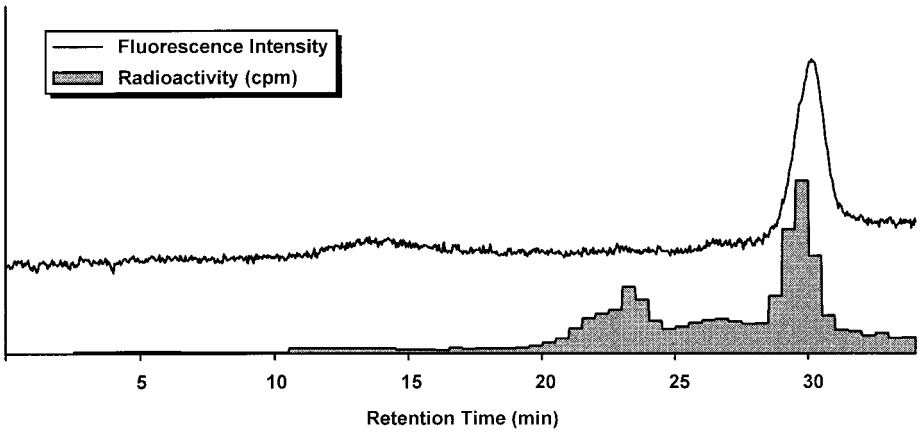


Figure 4. Reversed-phase HPLC analysis of a transcription reaction from a randomized ds DNA pool in the presence of polydisperse **6**. Nominal length of transcripts: 159 nucleotides. Separation was carried out on a C_4 column using a linear gradient of 1 to 32% acetonitrile in 40 min at a flow rate of 1 mL/min. Fluorescence detection was carried out with a Shimadzu RF 535 HPLC fluorescence detector using an excitation wavelength of 254 nm and an emission wavelength of 419 nm. Fractions of 500 μL were collected and analyzed by Cerenkov counting.

in the presence of initiator nucleotides **6** and using appropriate double-stranded DNA template molecules. A ratio of 3 mM GTP/2 mM **6** gave an average of 57% of the transcripts conjugated at their 5′-ends with only marginally lower total yield, compared with transcription in the absence of **6**. Quantitative separation, however, was not achieved under standard electrophoresis conditions due to the fact that the mass difference caused by coupling of anthracene−PEG is smaller than the mass dispersion caused by randomization of large parts of the molecules. Reversed-phase HPLC of transcript mixtures using a C4 column with fluorescence detection and Cerenkov counting of collected fractions turned out to be suitable for purification and quantification of incorporation (Figure 4). As expected, anthracene caused a significantly increased retention, and two peaks were detected containing radioactivity, with only the second showing anthracene fluorescence.

RNA-linker−anthracene conjugate libraries prepared by this method have successfully been used in selection experiments toward RNA Diels−Alderases. In short, these experiments involve incubation of the conjugate library with biotin maleimide, and biotinylated RNA species are isolated by affinity chromatography on immobilized streptavidin. These RNAs are then efficiently reverse transcribed and PCR amplified, demonstrating that conjugation does not interfere with recognition of RNA by polymerases. Repetitive rounds of conjugation, selection, and amplification were carried out, leading to the enrichment of highly active Diels−Alder catalysts (Seelig and Jäschke, 1999).

CONCLUSION

Methods for the site-specific incorporation of nonnucleotide moieties into RNA are valuable tools in RNA biochemistry and for the expansion of RNA catalysis beyond self-modification. The approach described here for coupling of anthracene−PEG derivatives allows the incorporation of a single conjugate group at the 5′-position of a transcript with high efficiency in a single step. The guanosine part of the initiator nucleotides represents the minimum substrate for T7 RNA polymerase (Martin and Coleman, 1989), and up to about $n_{PEG} = 13$, the poly(ethylene glycol) linker does not interfere with the transcription reaction. Combined with data from other publications (Martin and Coleman, 1989; Pitulle et al., 1992), the results indicate that a poly(ethylene glycol) linker attached to the 5′-phosphate of GMP could be used to incorporate various other molecules into RNA, too. The chemical synthesis of the described initiator nucleotides **6** is straightforward and can be easily carried out on a multigramm scale, thereby allowing the production of quantities sufficient for numerous preparative transcription reactions.

Using polydisperse poly(ethylene glycols), libraries of initiator nucleotides were synthesized differing only in the number of ethylene glycol units, thereby spanning a distance from about 20 to 60 Å from the 5′-end of the RNA to the attached moiety. This could be useful for finding the optimum length of the linker for applications were distances are critical (Cload et al., 1993) or as a mobility modifier for coding purposes (Baron et al., 1996; Grossman et al., 1994).

Finally, terminal coupling of PEG has been reported to increase the resistance of oligonucleotides to degradation in biological media and also to alter the pharmacokinetic properties, so enzymatic PEGylation strategies might provide an elegant alternative to the chemical methods described (Jäschke et al., 1994; Kawaguchi et al., 1995; Manoharan et al., 1995).

ACKNOWLEDGMENT

This work was supported by the Deutsche Forschungsgemeinschaft (Grants Ja 794/1 and SFB 344, TP B10 to A.J.). We acknowledge additional support by Prof. V. A. Erdmann, and spectrometric measurements performed by Drs. P. Franke, A. Schäfer and E. Nordhoff.

LITERATURE CITED

Agrawal, S., Ed. (1994) *Protocols for oligonucleotide conjugates*, Humana Press, Totowa, NJ.

Baron, H., Fung, S., Aydin, A., Bähring, S., Luft, F. C., and Schuster, H. (1996) Oligonucleotide ligation assay (OLA) for the diagnosis of familial hypercholesterolemia. *Nat. Biotechnol. 14*, 1279−82.

Beaucage, S. L., and Iyer, R. P. (1993) The functionalization of oligonucleotides via phosphoramidite derivatives. *Tetrahedron 49*, 1925−1963.

Bevilacqua, P. C., Li, Y., and Turner, D. H. (1994) Fluorescence-detected stopped flow with a pyrene labeled substrate reveals that guanosine facilitates docking of the 5′ cleavage site into a high free energy binding mode in the Tetrahymena ribozyme. *Biochemistry 33*, 11340−11348.

Burgin, A. B., and Pace, N. R. (1990) Mapping the active site of ribonuclease P RNA using a substrate containing a photoaffinity agent. *EMBO J. 9*, 4111−4118.

Cload, S. T., Richardson, P. L., Huang, Y. H., and Schepartz, A. (1993) Kinetic and thermodynamic analysis of RNA binding by tethered oligonucleotide probes: alternative structures and conformational changes. *J. Am. Chem. Soc. 115*, 5005−5014.

Darzynkiewicz, E., Stepinsky, J., Ekiel, I., Jin, Y., Haber, D., Sijuwade, T., and Tahara, S. M. (1988) b-globin mRNAs capped with m7G, m2,2,7G or m2,3,2,7G differ in intrinsic translation efficiency. *Nucleic Acids Res. 16*, 8953−8962.

Goodchild, J. (1990) Conjugates of oligonucleotides and modified oligonucleotides: a review of their synthesis and properties. *Bioconjugate Chem. 1*, 165−187.

Grossman, P. D., Bloch, W., Brinson, E., Chang, C. C., Eggerding, F. A., Fung, S., Iovannisci, D. A., Woo, S., and Winn-Deen, E. S. (1994) High-density multiplex detection of nucleic acid sequences: oligonucleotide ligation assay and sequence-coded separation. *Nucleic Acids Res. 22*, 4527−4534.

Hausch, F., and Jäschke, A. (1997) Libraries of multifunctional RNA conjugates for the selection of new RNA catalysts. *Bioconjugate Chem. 8*, 885−890.

Igloi, G. (1996) Nonradioactive Labeling of RNA. *Anal. Biochem. 233*, 124−129.

Jäschke, A. (1997) Oligonucleotide-poly(ethylene glycol) conjugates−synthesis, properties and applications. In *Chemistry and Biological Applications of PEG* (J. M. Harris, and S. Zalipsky, Eds.) Vol. 680, pp 265−283, ACS Symp. Ser. Washington DC.

Jäschke, A., Bald, R., Nordhoff, E., Hillenkamp, F., Cech, D., Erdmann, V. A., and Fürste, J. P. (1996) Synthesis and analytical characterization of RNA-poly(ethylene glycol) conjugates. *Nucleosides Nucleotides 15*, 1519−1529.

Jäschke, A., Fürste, J. P., Cech, D., and Erdmann, V. A. (1993) Automated incorporation of poly(ethylene glycol) into synthetic oligonucleotides. *Tetrahedron Lett. 34*, 301−304.

Jäschke, A., Fürste, J. P., Nordhoff, E., Hillenkamp, F., Cech, D., and Erdmann, V. A. (1994) Synthesis and properties of oligodeoxyribonucleotide- poly(ethylene glycol) conjugates. *Nucleic Acids Res. 22*, 4810−4817.

Kawaguchi, T., Asakawa, H., Tashiro, Y., Juni, K., and Sueishi, T. (1995) Stability, specific binding activity, and plasma concentration in mice of an oligodeoxynucleotide modified at 5′-terminal with poly(ethylene glycol). *Biol. Pharm. Bull. 18*, 474−476.

Logsdon, N., Lee, C. G., and Harper, J. W. (1992) Selective 5′ modification of T7 RNA polymerase transcripts. *Anal. Biochem. 205*, 36−41.

Manoharan, M., Tivel, K. L., Andrade, L. K., Mohan, V., Condon, T. P., Bennet, C. F., and Cook, P. D. (1995) Oligonucleotide conjugates—alteration of the pharmacokinetic properties of antisense agents. *Nucleosides Nucleotides 14*, 969−973.

Martin, C. T., and Coleman, J. E. (1989) T7 RNA polymerase does not interact with the 5′-phosphate of the initiating nucleotide. *Biochemistry 28*, 2760−2762.

Milligan, J. F., Groebe, D. R., Witherell, G. W., and Uhlenbeck, O. C. (1987) Oligoribonucleotide synthesis using T7 RNA polymerase and synthetic DNA templates. *Nucleic Acids Res. 15*, 8783−8798.

Moore, M. J., and Sharp, P. A. (1992) Site-specific modification of pre-mRNA: the 2′-hydroxyl groups at the splice sites. *Science 256*, 992−997.

Oh, B. K., and Pace, N. R. (1994) Interaction of the 3′-end of tRNA with ribonuclease P RNA. *Nucleic Acids Res. 22*, 4087−4094.

Pitulle, C., Kleineidam, R. G., Sproat, B., and Krupp, G. (1992) Initiator oligonucleotides for the combination of chemical and enzymatic RNA synthesis. *Gene 112*, 101−105.

Seelig, B., and Jäschke, A. (1997) Site-specific modification of enzymatically synthesized RNA: transcription initiation and Diels−Alder reaction. *Tetrahedron Lett. 38*, 7729−7732.

Seelig, B., and Jäschke, A. (1999) A small catalytic RNA motif with Diels−Alderase activity. *Chem. Biol. 6*, 167−176.

Tarasow, T. M., Tarasow, S. L., and Eaton, B. E. (1997) RNA-catalysed carbon−carbon bond formation. *Nature 389*, 54−57.

Tong, G., Lawlor, J. M., Tregear, G. W., and Haralambidis, J. (1993) The synthesis of oligonucleotide−polyamide conjugate molecules suitable as PCR primers. *J. Org. Chem. 58*, 2223−2231.

Wiegand, T. W., Janssen, R. C., and Eaton, B. E. (1997) Selection of RNA amide synthases. *Chem. Biol. 4*, 675−683.

BC980085H

Synthesis of CpFe(CO)(L) Complexes of Hydantoin Anions (Cp = η^5-C_5H_5, L = CO, PPh_3), and the Use of the 5,5-Diphenylhydantoin Anion Complexes as Tracers in the Nonisotopic Immunoassay CMIA of This Antiepileptic Drug

Anne Vessières,*,† Konrad Kowalski,‡ Janusz Zakrzewski,*,‡ Andrzej Stepien,§ Mieczyslaw Grabowski,§ and Gérard Jaouen†

Ecole Nationale Supérieure de Chimie de Paris, Laboratoire de Chimie Organométallique, UMR CNRS 7576, 11, rue Pierre et Marie Curie, 75231 Paris Cedex 05, France, and Department of Organic Chemistry, Department of Crystallography, University of Łodz, Narutowicza 68, 90-136 Łodz, Poland. Received July 29, 1998; Revised Manuscript Received December 3, 1998

As part of our ongoing development of the CMIA nonisotopic immunoassay method, in which the tracers are metal carbonyl complexes and detection is by Fourier transform infrared spectroscopy, we examined the potential use as tracers of the complexes $CpFe(CO)_2$(5,5-diphenylhydantoin) **2d** and CpFe(CO)(PPh_3)(5,5-diphenylhydantoin) **3**. The present study involved the synthesis of a series of hydantoin complexes (**2a**−**2d**), in particular that of the derivative of 5,5-diphenylhydantoin **2d**. The structure of **2d** was confirmed by X-ray crystallography. The infrared analysis, establishing the position and intensity of the characteristic metal−carbonyl peaks of complexes **2d** and **3** in the 1850−2200 cm^{-1} region, shows that measurement of the absorbance values of these characteristic peaks will permit quantitative analysis in the picomole range, the norm for routine use in immunoassay and thus suitable for use as CMIA tracers. Cross-reaction rates of these tracers with anti-DPH specific antibodies show that **2d** and **3** are both recognized by anti-DPH antibodies (cross-reaction rates 43 and 20%, respectively). In developing a CMIA of DPH with these tracers, it was found that **3**, with a single, intense band at 1977 cm^{-1}, had very promising IR characteristics for use in multiassay CMIA, but probably owing to its relatively weak affinity for the antibodies, it was not possible to develop a CMIA for DPH using this tracer. Complex **2d**, however, showed better recognition by the antibodies, and using this complex as a tracer, it was possible to develop a particularly sensitive monoassay of DPH by the CMIA method.

INTRODUCTION

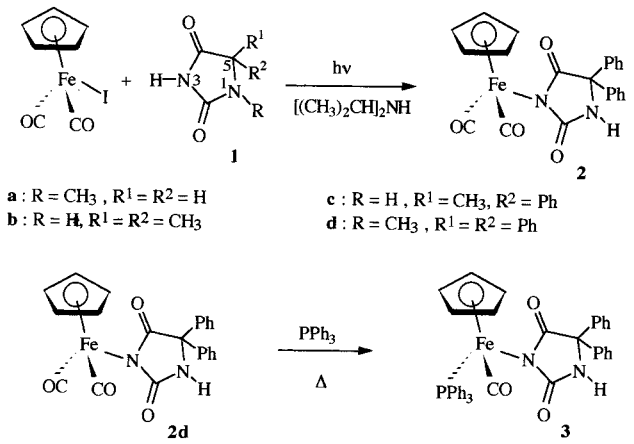
We recently developed a new type of nonisotopic immunoassay termed carbonyl metallo immuno assay (CMIA)[1], using metal carbonyl complexes as tracers and Fourier transform infrared spectroscopy (FT-IR) as the detection method. The feasibility of the method was first shown in the case of the monoimmunoassay of three antiepileptic drugs, phenobarbital (*1*), diphenylhydantoin (DPH) (*2*), carbamazepine (*3*) and of a circulating hormone, cortisol (*4*). These experiments allowed us to establish the strengths of this new assay method, which include the absence of nonspecific signals (due to the entirely exogenous nature of the metal carbonyl tracers), and the fact that a metal carbonyl tracer can be synthesized for any given hapten. Clearly the greatest strength of the CMIA method, however, is the potential it affords to perform multiimmunoassays of two (*5*) or three (*6*) analytes simultaneously. Although the development of nonisotopic immunoassays has received considerable attention over the past few years, there have been few breakthroughs in the area of the simultaneous multiassay, owing to the difficulty of finding tracers that give simultaneously analyzable signals. Such analyses would however meet a number of clearly defined needs (thyroid checks, allergen studies, testing of patients on multiple medications, emergency toxicology), and some authors have suggested that this is one of the major challenges in the area of immunoassay development today (*7*, *8*). It is interesting to note, for example, that the radioactive tracers that led to the first immunoassays and the enzymatic tracers that are in most frequent use today cannot be used for more than a double immunoassay. The only promising routes at present appear to be those offered by fluorescent lanthanides (*9*) and metal carbonyl tracers. In simultaneous analysis by CMIA, the starting point is the search for new metal carbonyl complexes possessing $\nu_{(CO)}$ vibration peaks that can be individualized and simultaneously analyzed by infrared in a mixture containing the other tracers that have already been developed. The characteristics of a good tracer are the following: it must be stable in biological media (pH buffer 7.4) and possess intense $\nu_{(CO)}$ vibration peaks in the 1850−2200 cm^{-1} region, thus permitting quantitative analysis in the picomole range. We have previously tested the following complexes: (η^6-C_6H_5-R)$Cr(CO)_3$, (R-C≡C-R′)$Co_2(CO)_6$, (η^5-C_5H_4-R)$Mn(CO)_3$. To extend the range of available tracers, we felt it would be of interest to examine the potential for use in CMIA of $CpFe(CO)_2$ and

* To whom correspondence should be addressed.
† Ecole Nationale Supérieure de Chimie de Paris.
‡ Department of Organic Chemistry.
§ Department of Crystallography.

[1] CMIA, carbonyl metallo immuno assay; DPH, 5,5-diphenylhydantoin; FT-IR, Fourier transform infrared spectroscopy; BSA, bovine serum albumin.

10.1021/bc980089m CCC: $18.00 © 1999 American Chemical Society
Published on Web 05/17/1999

Scheme 1



$CpFe(CO)(PPh_3)$ moieties, which permit the formation of novel complexes of DPH in which the drug is directly bonded to the metal atom. The full development of the CMIA of DPH, a drug widely used in the treatment of epilepsy, using **2d** and **3** as tracers, will permit a clearer assessment of the individual potential of these complexes for the purpose.

RESULTS AND DISCUSSION

(I) Synthesis of the Tracers. Synthesis of $CpFe(CO)_2^-$ Complexes of Hydantoin Anions. We recently studied the photochemical substitution reaction of the iodide ligand in cyclopentadienyl iron dicarbonyl iodide [$CpFe(CO)_2I$] by an anion derived from an acidic NH group. Our study included pyrroles, indoles, imides, and uracils (*10*), and we attempted to extend this study to the hydantoins, in particular 5,5-diphenylhydantoin (DPH), with the aim of using the resulting complex as a tracer in the CMIA of DPH.

We have found that illumination with visible light of $CpFe(CO)_2I$ in the presence of hydantoins **1a**, **1b**, and **1d** in benzene leads to the formation in high yield of a single, yellow product **2a**, **2b**, and **2d**, respectively (Scheme 1).

The structures of these products were confirmed by elemental analyses and by IR and NMR data. The IR spectra of the hydantoin starting material in chloroform solutions display two bands in the region of carbonyl stretching vibrations: a weak band at ~1750−1770 cm^{-1} and a strong band at ~1720−1730 cm^{-1}. In the spectra of their $CpFe(CO)_2$ complexes, **2**, these two bands are shifted toward lower wavenumbers: 1715−1730 (weak) and 1650−1660 (strong). The same phenomenon was observed on going from phthalimide to $CpFe(CO)_2$-(η^1-*N*-phthalimidato) (*10c*). The ^{13}C NMR spectrum of hydantoin **1a** in $CDCl_3$ solution shows two carbonyl resonances at 170.2 and 156.6 ppm. The corresponding $CpFe(CO)_2$ complex **2a** displays two carbonyl resonances of the hydantoin ligand at 182.8 and 168.0 ppm, i.e., shifted downfield 11.4−12.6 ppm. These downfield shifts are very close to those observed on going from phthalimide to $CpFe(CO)_2$(η^1-*N*-phthalimidato), (13.5 ppm) (*10c*), which is in keeping with the coordination of the $CpFe(CO)_2$ moiety to the nitrogen bound to two carbonyls, i.e., to N(3). Conclusive evidence for this type of coordination is provided by the X-ray structure of **2d** (see below).

In the case of hydantoin **1c**, the same treatment gave a mixture of yellow and orange products. We were able to obtain the yellow product in a pure form by column chromatography. Its IR spectrum was very similar to those of **2a**, **2b**, and **2d**, which together with the NMR data, suggested the structure **2c**. Our attempts to isolate the orange product in the pure form by column chromatography met with failure. It was always contaminated with variable amounts of **2c**. The IR spectra of this material showed three distinct bands in the region of 1800−1600 cm^{-1}, namely at 1735, 1660, and 1615 cm^{-1} (all bands with comparable intensity). We have suggested that this material could be the isomeric complex **2c′** having the $CpFe(CO)_2$ moiety bound to deprotonated N(1) contaminated with **2c**, as indicated by the presence of the characteristic IR band at 1660 cm^{-1} and by TLC. It is likely that this product is kinetically labile and undergoes isomerization to **2c** during the separation procedure.

Synthesis of $CpFe(CO)(PPh_3)$(5,5-diphenylhydantoin) 3. **3** was prepared by the standard method (*10b*), by refluxing **2d** in benzene in the presence of triphenylphosphine (Scheme 1).

(II) X-ray Crystal Structure of 2d. The crystal structure of **2d** provides unambiguous evidence that the $CpFe(CO)_2$ moiety binds to deprotonated N(3) of the DPH molecule. A perspective view of **2d** is presented in Figure 1, and this also includes the atomic numbering scheme. Crystal data and structure refinement details are listed in Table 1, final atomic coordinates in Table 2, and selected bond lengths and angles in Table 3.

In the crystals of **2d**, the monomers are held together by two intermolecular (symmetry dependent) hydrogen bonds N(2)−H(2)···O(1) to effectively become dimeric molecules. The N(2)−O(1) distance of 2.84 Å is typical for strong hydrogen bonds. As found in similar structures, the coordination around the iron atom is pseudo-octahedral (three-legged piano-stool geometry). The two CO ligands and N(1) atom occupy three *fac* positions, and the cyclopentadienyl ring acting in a tridentate mode occupies the three remaining positions. In accord with this description, the angles C(31)FeN(1) and C(31)FeC(41) are close to 90° [93.3(2)−94.3(2)°]. The cyclopentadienyl ring is planar [maximum deviation from the best plane being 0.004(9) Å]. All the carbon atoms of this ring have high displacement parameters (>0.1 $Å^2$). The Fe−N(1) distance of 1.949(3) Å is similar to that found in $CpFe(CO)_2$(*N*-phthalimidato), 1.956(3) Å, and substantially shorter than that observed in the analogous florafur [5-fluoro-2(2-tetrahydrofuryl)uracil] complex, 1.991(4) Å.

(III) FT-IR Spectroscopy Study of the Organometallic Complexes 2d and 3. **2d** and **3** constitute potential tracers for an immunoassay of DPH by CMIA. The preliminary step in this assay is FT-IR quantification of the metal carbonyl entities by measurement of the absorbance values of the characteristic $\nu_{(CO)}$ vibration bands that appear in the 1800−2200 cm^{-1} region. These bands offer the dual advantage of possessing intensities 7−10 times higher than all the other bands of the spectrum and of occurring in a region which is normally devoid of other bands. The 1800−2200 cm^{-1} sections of the IR spectra of these complexes are shown in Figure 2. In this region, **2d** shows two narrow and intense peaks at 2010 and 2054 cm^{-1}, and **3** a single peak at 1977 cm^{-1}.

For the CMIA of DPH, we chose to work in the presence of 50 pmol of one of the tracers **2d** and **3**. The quantitative analysis of these tracers was performed using a light-pipe cell with an optical path length of 2 cm for an internal volume of only 30 μL (*12*). We have shown that this cell permits quantitative analysis of organometallic complexes in the picomole or even femtomole range (*13*). In the case of **2d** and **3** the absorbance values of the peaks at 2054 and 2010 cm^{-1} (**2d**) and 1977

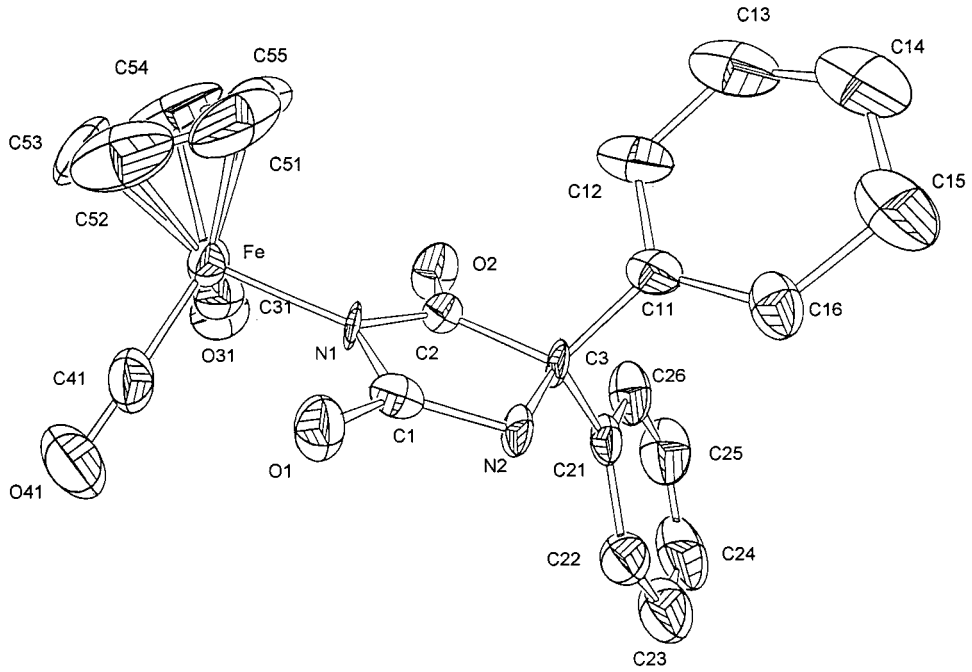


Figure 1. A perspective view of the **2d** molecule with the numbering scheme.

Table 1. Crystal Data and Structure Refinement[a]

(a) Crystal Parameters	
empirical formula	$C_{22}H_{16}FeN_2O_4$
formula weight	428.23
crystal system	triclinic
crystal color	orange
crystal size (mm)	0.2 × 0.1 × 0.1
space group	*P*1
a (Å)	10.7226(8)
b (Å)	12.0069(8)
c (Å)	8.4584(5)
α (deg)	94.408(5)
β (deg)	105.546(5)
γ (deg)	108.001(5)
Z	2
d_x (Mg m^{-3})	1.447
d_o (Mg m^{-3})	1.446
V (Å^3)	982.5(1)
F(000)	440
μ(Cu/Kα) (mm^{-1})	6.432
T (K)	293
(b) Data Collection and Refinement	
θ range for data collection	$3.93 < \theta < 60.05$
data collected (*h*, *k*, *l*)	$-11 \le h \le 10$, $-13 \le k \le 13$, $0 \le l \le 9$
reflection collected	2331
independent observed reflections	1440
refinement method	full-matrix least-squares on F^2
final R^b	0.0313
$\Delta\rho_{min}$ (e Å^{-3})	−0.180
$\Delta\rho_{max}$ (e Å^{-3})	0.201
goodness-of-fit[c]	1.045

[a] Rigaku diffractometer; graphite monochromated CuKα radiation (λ = 1.541 78 Å). [b] $R = \sum|F_o - F_c|/\sum F_o$. [c] Goodness of fit = $[\sum w|F_o^2 - F_c^2|^2/(N_o - N_v)]^{1/2}$ where N_o is the number of observation and N_v the number of variables.

Table 2. Final Atomic Coordinates for Non-Hydrogen Atoms in 2d

label	*x*/*a*	*y*/*b*	*z*/*c*	U_{eq}
FE	0.026 58 (7)	0.725 09 (5)	0.265 94 (7)	0.0458 (4)
C51	−0.056 (1)	0.8526 (6)	0.1952 (8)	0.103 (4)
C52	−0.1569 (6)	0.7485 (8)	0.1660 (9)	0.101 (4)
C53	−0.136 (1)	0.6782 (6)	0.054 (1)	0.148 (5)
C54	−0.025 (1)	0.739 (1)	0.0194 (9)	0.19 (1)
C55	0.0220 (8)	0.8442 (9)	0.106 (1)	0.157 (7)
C31	−0.0073 (4)	0.5734 (4)	0.2848 (5)	0.058 (2)
O31	−0.0371 (3)	0.4749 (2)	0.2948 (3)	0.086 (2)
C41	0.0514 (4)	0.7331 (4)	0.4787 (5)	0.066 (3)
O41	0.0614 (3)	0.8057 (3)	0.6140 (4)	0.105 (2)
N1	0.2218 (3)	0.7558 (2)	0.2978 (3)	0.035 (2)
C1	0.3282 (5)	0.8597 (3)	0.3894 (4)	0.035 (2)
O1	0.3099 (2)	0.9418 (2)	0.4672 (3)	0.047 (1)
N2	0.4504 (5)	0.8560 (3)	0.3815 (3)	0.036 (2)
C3	0.4342 (4)	0.7550 (3)	0.2600 (4)	0.031 (2)
C2	0.2793 (4)	0.6884 (3)	0.2236 (4)	0.038 (2)
O2	0.2147 (3)	0.5894 (2)	0.1366 (3)	0.059 (1)
C11	0.5201 (4)	0.6808 (3)	0.3300 (4)	0.038 (2)
C12	0.6137 (5)	0.7134 (5)	0.4866 (5)	0.062 (3)
C13	0.6920 (7)	0.6430 (7)	0.5446 (8)	0.088 (4)
C14	0.6754 (7)	0.5415 (6)	0.4486 (9)	0.088 (4)
C15	0.5827 (6)	0.5065 (4)	0.2918 (8)	0.079 (3)
C16	0.5066 (5)	0.5768 (4)	0.2331 (6)	0.057 (3)
C21	0.4685 (4)	0.7994 (3)	0.1066 (4)	0.035 (2)
C22	0.5928 (5)	0.8855 (4)	0.1301 (5)	0.050 (2)
C23	0.6312 (6)	0.9296 (4)	−0.0035 (7)	0.065 (3)
C24	0.5428 (7)	0.8859 (5)	−0.1623 (6)	0.077 (3)
C25	0.4198 (7)	0.8003 (4)	−0.1878 (5)	0.075 (3)
C26	0.3816 (5)	0.7574 94)	−0.0546 (5)	0.057 (3)

cm^{-1} (**3**) are closely proportional to the quantity of tracer, in the range of 0−50 pmol (Table 4) which is an appropriate range for immunoassay. For quantification of **2d** later in this study, the peak at 2054 cm^{-1} (analytical peak) will be used.

With a view to the possible utilization of these complexes as tracers in a simultaneous multiimmunoassay by CMIA, the number, position, and intensities of the $\nu_{(CO)}$ bands of **2d** and **3** were compared with those of the tracers already available. These values are shown in Table 4. It should be noted first that the peaks of **2d** do not overlap at all with those of the chromium carbonyl tracer, which would permit the simultaneous quantification of the two markers $Cr(CO)_3$ and $CpFe(CO)_2$ and consequently a double immunoassay. Also, the ϵ values of the analytical peaks of these moieties are closely comparable (1096−1542), which would allow the same analytical sensitivity for the two tracers. Complex **3** in particular possesses only a single CO ligand and thus only one $\nu_{(CO)}$ vibrational peak at 1977 cm^{-1}, which has no overlap with the characteristic peaks of the tracers

Table 3. Selected Bond Lengths (Å) and Angles (deg)

	(a) Fe Coordination Sphere		
Fe−N1	1.949 (3)	Fe−C53	2.037 (8)
Fe−C31	1.773 (4)	Fe−C54	2.043 (8)
Fe−C41	1.770 (4)	Fe−C55	2.04 (1)
Fe−C51	2.042 (8)		
Fe−C52	2.038 (7)	C31−Fe−C41	94.3 (2)
	(b) Heterocyclic Ligand		
N1−C2	1.366 (6)		
C2−O2	1.232 (3)		
N1−C1	1.399 (4)		
C1−O1	1.239 (5)		
C2−C3	1.536 (5)		
C3−N2	1.463 (4)		
N2−C1	1.343 (8)		
C3−C11	1.513 (5)		
C3−C21	1.531 (5)		
Fe−N1−C1	124.8 (3)	N2−C3−C11	113.3 (3)
Fe−N1−C2	127.5 (2)	N2−C3−C21	109.6 (3)
C1−N1−C2	107.4 (3)	C2−C3−C11	112.1 (3)
N1−C1−O1	123.7 (4)	C2−C3−C21	112.2 (3)
N1−C1−N2	110.4 (3)	C11−C3−C21	110.4 (3)
O1−C1−N2	125.8 (3)	N2−C3−C2	98.8 (3)
N1−C2−O2	124.4 (4)	C1−N2−C3	111.9 (4)
N1−C2−C3	110.5 (3)		
O2−C2−C3	125.1 (4)		
	(c) CO Ligands		
C41−O41	1.146 (5)	Fe−C41−O41	176.4 (4)
C31−O31	1.141 (5)	Fe−C31−O31	176.0 (4)
	(d) Hydrogen Bonds		
D−H···A	D−A	H···A	D−H···A
N2−H2···O1	2.835 (4)	1.99 (2)	1.66 (2)

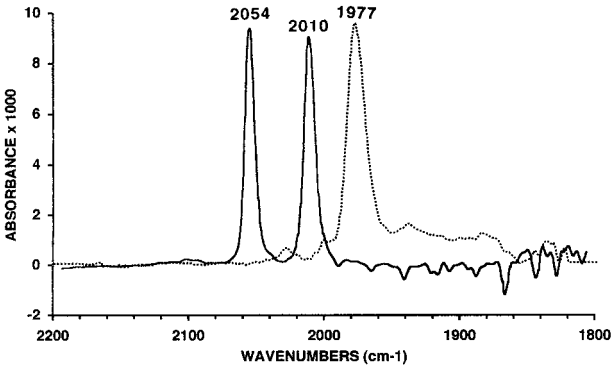


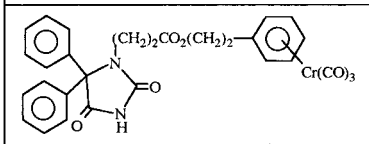
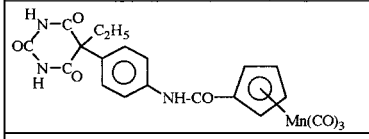
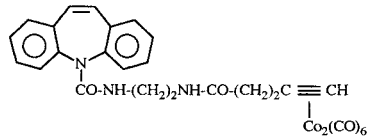
Figure 2. FT-IR spectra (80 pmol in CCl_4) of **2d** (—) and **3** (- - -). Expansion of the ν(CO) region between 2200 and 1900 cm^{-1}.

for dicobalt hexacarbonyl, **6**, and manganese tricarbonyl, **5**, which we already have available. In addition, this peak has a high ϵ value (1238). The characteristics of this tracer in infrared spectroscopy thus appear highly favorable for a multiimmunoassay by CMIA.

(IV) Biochemical Study. The components for an immunoassay by CMIA are three in number: the analyte (i.e., the substance to be assayed, here DPH), the tracer, which is a derivative of the analyte onto which a marker has been attached to permit quantification at low quantities, here $CpFe(CO)_2$ or $CpFe(CO)(PPh_3)$, and the specific antibodies of the substance to be assayed (Scheme 2).

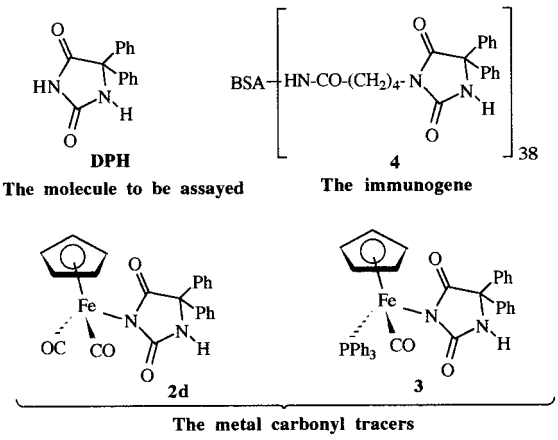
Preparation and Specificity of anti-DPH Antibodies. DPH is a hapten, i.e., a molecule of low molecular weight with no antigenic properties. For this reason, anti-DPH antibodies can only be obtained after coupling this molecule to a vector protein such as bovine serum albumin (BSA). In the case of DPH, we chose to synthesize the immunogen DPH-3-valerate-BSA, **4** (Scheme 2). It is obtained by coupling DPH-valeric acid to BSA, using 1-ethyl-3-(3-dimethylaminopropyl)carbodiimide (EDAC).

Table 4. Infrared Characteristics of the Metal Carbonyl Complexes in the ν(CO) Region

Metal carbonyl complexes	ν(CO), cm^{-1}	$\epsilon^{a)}$
2d	2054[c] 2010	1096 1157
3	1977	1238
 **4**[b]	1971[c] 1898	1542[d]
 **5**[e]	2032[c] 1955	1212[d]
 **6**[f]	2094 2056[c] 2027	3355[d]

[a] Molar extinction coefficient (cm^{-1} M^{-1}) measured in a light-pipe cell, 20 mm path length, filled volume, 30 μL as described in ref *13* with a Bomen MB100 equipped with a InSb detector. Measurements are done in CCl_4 except for **5** where it is done in $CHCl_3$. [b] Prepared as described in ref *2*. [c] Analytical band of the complex, i.e., the band used to performed quantitative analysis. [d] ϵ value for the analytical band of the complex. [e] Prepared as described in ref *5*. [f] Prepared as described in ref *3*.

Scheme 2. Molecules Involved in the Carbonyl Metallo Immunoassay (CMIA) of DPH



Injection of rabbits with this immunogen gives anti-DPH specific antibodies (*2*).

Measurement by Radioimmunoassay (RIA) of the Cross-Reaction Rates of Tracers 2d and 3 to anti-DPH Specific Antibodies. In order for the organometallic complexes **2d** and **3** to be useful as tracers in a CMIA assay, they must be recognized by the available anti-DPH specific antibodies. To ascertain this, an RIA test was performed to determine cross-reaction rate (CR%) of the complexes relative to the anti-DPH specific antibodies. **2d** and **3** showed a CR% of 43 and 20%, respectively, showing that the two complexes are recognized by anti-DPH antibodies and are thus candidates for use as tracers in CMIA. However, **2d** has much better

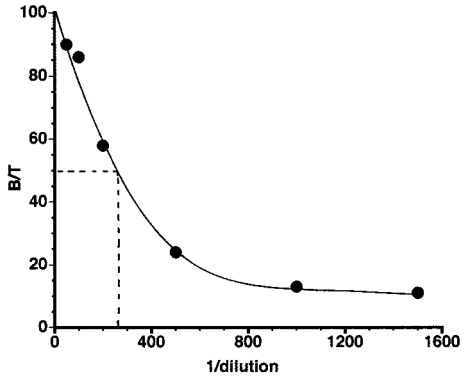


Figure 3. Antiserum dilution curve of anti-DPH antibodies by CMIA (50 pmol of **2d**, quantification of the free fraction of the tracer by FT-IR spectroscopy).

recognition than **3**, probably owing to the high level of steric crowding of the PPh_3 ligand.

CMIA Determination of the Titer Value of anti-DPH Antibodies Using 2d or 3 as Tracer. Once tracers and specific antibodies for the substance to be assayed have been obtained, the immunoassay itself can be started, beginning with a titration curve. These curves are obtained by incubating a fixed quantity of tracer (50 pmol) in the presence of increasing dilutions of anti-DPH antibodies. At the end of the incubation period (2 h at room temperature), the free and bound fractions of the tracer are separated by extraction using isopropyl ether. The organic fraction containing the free fraction is recovered and evaporated on a Speed-Vac. The FT-IR spectrum of each fraction is obtained after redissolving the residue in CCl_4 and quantification of the tracer is performed by measuring the absorbance of the analytical peak of each tracer (2054 cm^{-1} for **2d** and 1977 cm^{-1} for **3**). The starting point for a titration curve by CMIA is thus a series of IR spectra corresponding to the quantity of free tracer (**2d** or **3**) present in each fraction. When **2d** is used as the tracer, the curve shown in Figure 3 is obtained. The titer value of the antibody tested, which by definition is the inverse value of the dilution corresponding to $B/T = 50\%$, is 250 in this case. This value is entirely satisfactory and permits the further development of the immunoassay of DPH by CMIA.

In the case of **3**, the binding rate of the tracer to the anti-DPH antibody is low, in fact with 50 pmol of tracer, only 35% is bound for the first point of the curve (antibody dilution 1/50; data not shown). By extrapolation, a titer value of 25 is obtained, which is insufficient to permit further development of the immunoassay with the combination anti-DPH antibody/tracer **3**.

Acquisition of a Standard Assay Curve of DPH by CMIA Using 2d as Tracer. The titer value is an indication of the quantity of antibodies present in the antisera under study and of their affinity for the tracer. However, it does not give any indication of the feasibility of the assay itself, in particular regarding the capacity of the antibody−tracer complex to displace the analyte. This must be established by acquisition of a standard curve to allow quantitative assay of the analyte. This curve is obtained by incubating a fixed quantity of tracer (50 pmol of **2d**) in the presence of a fixed dilution of antibody (equal to the titer value, i.e., 1/250) and increasing quantities of DPH, between 10 and 200 pmol. After incubation, separation of the free and bound fractions and quantification of the tracer by FT-IR, a curve is obtained as shown in Figure 4. This curve has the classic appearance of the curves obtained by other types of immunoassay, such as radioimmunoassay, and is an indication of the feasibility of performing a monoimmunoassay of DPH by CMIA using **2d** as tracer. Several comments are suggested by this particular curve. First, it is noteworthy that the B/B_0 value goes as low as approximately 9%, indicating a low nonspecific binding rate of the tracer with the antibody. This can be explained by the fact that the chemical structure of the tracer, with a direct bond between the drug and the organometallic moiety, is completely different from the structure of the immunogen, where a spacer connects DPH to BSA. This eliminates the possibility of binding of **2d** to anti-spacer antibodies and a concomitant rise in the nonspecific binding rate.

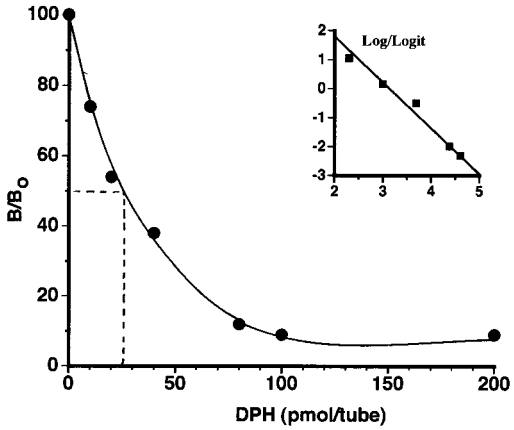


Figure 4. Standard cure of DPH by CMIA (50 pmol of **2d**, quantification of the free fraction of the tracer by FT-IR spectroscopy). (Inset) Log/Logit transformation of the curve.

Another interesting result is the quantity of DPH needed to reach a B/B_0 value of 50%. This value is calculated by linearization of the standard curve shown in Figure 4 by the log/logit function (Figure 4, inset). The value found is 23 pmol, signifying that the highest sensitivity of the assay will be obtained around this value, i.e., for quantities of DPH between 10 and 50 pmol. This is of particularly high sensitivity. This result may be explained by the cross-reaction rate of 43% obtained for **2d**. This rate is high enough to permit binding of the tracer and antibody, but not too high to allow its later displacement by small quantities of DPH. The compromise between these parameters is particularly advantageous in this case. Taking into account the range of measurement for serum concentrations, which is between 2.5 and 40 μg/mL, the assay can be performed with less than a microliter of serum.

Conclusion and Future Perspectives. We have synthesized a series of novel metal carbonyl complexes of phenytoins, in particular the complexes $CpFe(CO)_2$-DPH, **2d**, and $CpFe(CO)(PPh_3)$-DPH, **3**. The study described here demonstrates the feasibility of a monoassay of DPH by CMIA, using the metal carbonyl tracer **2d**, thus adding a new type of metal carbonyl moiety to the list of those suitable for use with this assay method. On the other hand, the affinity of **3** for the anti-DPH antibodies we obtained is too low to permit immunoassay using the antibody/tracer combination we currently have. The interest of **3** for multiimmunoassay is clear, however, because the metal carbonyl entity $CpFe(CO)(PPh_3)^-$ shows in IR a single, high-intensity $\nu_{(CO)}$ peak at 1977 cm^{-1}, which is a region where the dicobalt hexacarbonyl and manganese tricarbonyl tracers do not absorb. The very high steric crowding of the PPh_3 ligand is no doubt the reason for the greatly reduced affinity of the tracer **3** for the antibodies. Replacement of the triphenylphos-

phine by less bulky P-ligands is expected to produce a tracer with better antibody affinity.

EXPERIMENTAL PROCEDURES

Materials. All syntheses were carried out under argon. Solvents were dried using standard procedures. Chromatographic separations were carried out on silica gel 60 (Merck, 230−400 mesh ASTM). $CpFe(CO)_2I$ was prepared according to King (*11*). 5,5-Diphenylhydantoin (DPH), bovine serum albumine (BSA), 1-ethyl-3-[3-(dimethylaminopropyl)]carbodiimide (EDAC), Freund's complete and incomplete adjuvant, charcoal (Norit A) and dextran T70, were purchased from Sigma. [4-^{14}C]DPH (specific activity, 107 GBq/mmol) was supplied by DuPont, NEN Products (Boston MA). Other compounds were commercally available (Aldrich, Fluka) and were used as received. NMR spectra were run on a Varian Gemini 200 BB spectrometer (200 MHz for ^{1}H) in $CDCl_3$ solutions and referenced toward internal Me_4Si. Mass spectra were determined on an LKB 2001 spectrometer. Elemental analyses were done by the Analytical Services of the CBMiM PAN (Łodz).

X-ray Structure Determination for 2d. Crystals of **2d** were grown from layered dichloromethane-hexane for 2 days. Crystal data and details of the data collection and refinement are listed in Table 1. The intensities were corrected for Lorenz and polarization effects. No absorption correction was applied. The structure was solved by Patterson method and refined by the full-matrix least-squares method using the SHELXS programs (*14*). All non-hydrogen atoms were refined anisotropically. H atoms for the Cp ring were refined isotropically by the "riding mode". The remaining H atoms were located in the difference map and refined isotropically.

General Procedure for the Synthesis of the $CpFe(CO)_2$-Hydantoins (2a−2d). $CpFe(CO)_2I$ (455 mg, 1.5 mmol), hydantoin (1.0 mmol), benzene (15 mL), and diisopropylamine (1 mL) were introduced to a glass tube, saturated with argon, and photolyzed with visible light (4 × 150 W domestic tungsten lamps). The photolyzed mixture was magnetically stirred and externally cooled by immersion in a water−ice bath. During the photolysis, the initial black coloration of the photolyte turned yellow. After 3 h of photolysis, the solid, diisopropylamine hydroiodide, formed and was filtered off and washed with a small volume of benzene. The filtrate was evaporated to dryness, and the residue dissolved in chloroform and chromatographed on Kieselgel 60 (6 g) using chloroform as eluent. The yellow band which followed the black band of the unreacted $CpFe(CO)_2I$ was collected and evaporated to dryness. The products were crystallized from dichloromethane-hexane. In the case of **1c,** the chromatography yields two overlapping bands (yellow and orange). These bands can be separated on a longer column to give pure yellow **2c** and orange **2c′**, presumably the N1 addition product contaminated with **2c**.

Yields (%): **2a**, 96; **2b**, 85; **2c**, 76; **2d**, 94. (**2a**) ^{1}H NMR ($CDCl_3$): 5.09 (s, 5H, Cp), 3.74 (s 2H, CH_2), 2.93 (s 3H, Me). ^{13}C NMR: 212.36 (Fe−CO); 182.75 and 167.86 (C-2 and C-4), 84.97 (Cp); 55.00 (N-Me), 30.30 (C-5). IR ($CHCl_3$, cm^{-1}): 2060, 2000, ($\nu_{C\equiv O}$), 1710 (w), 1650 (s) ($\nu_{C=O}$). (**2b**) ^{1}H NMR ($CDCl_3$): 5.60 (s, 1H, N−H), 5.08 (s, 5H, Cp) 1,28 (s 6H, Me). ^{13}C NMR: 212.27 (Fe−CO); 190.69 and 167.41 (C-2 and C-4); 84.95 (Cp); 61.28 (C-5), 25.65 (Me). IR ($CHCl_3$, cm^{-1}): 2060, 2000, ($\nu_{C\equiv O}$), 1715 (w), 1650 (s) ($\nu_{C=O}$). (**2c**)^{1}H NMR ($CDCl_3$): 7.5−7.3 (m, 5H, Ph), 6.01(s, 1H, NH) 5.02 (s, 5H, Cp), 1.67 (s, 3H, Me).^{13}C NMR: 212.19 and 212.11 (Fe−CO), 188.14 and 167.79 (C-2 and C-4); 141.12 (ipso Ph); 128.50, 127.51 and 125.12 (other Ph); 84.97 (Cp), 66.34 (C-5); 20.07 (Me). IR ($CHCl_3$): 2060, 2000, ($\nu_{C\equiv O}$), 1730 (w), 1660 (s) ($\nu_{C=O}$). (**2d**) ^{1}H NMR ($CDCl_3$): 7.30 (bs,10H, Ph) 6.46 (s, 1H, NH), 5.03 (s, 5H, Cp).^{13}C NMR: 212.12 (Fe−CO), 185.57 and 167.65 (C-2 and C-4); 141.56 (*ipso* Ph), 128.42, 127.65 and 126.84 (other Ph); 85.01 (Cp); 73.13 (C-5). IR ($CHCl_3$) 2040, 1990 ($\nu_{C\equiv O}$); 1720 (w), 1650(s) ($\nu_{C=O}$).

Elemental Analyses (Calcd/Found). (**2a**) $C_{11}H_{10}N_2O_4Fe$ (MW 290.06): C (45.55/45.37); H (3.47/3.48); N (9.66/9.93). (**2b**) $C_{12}H_{12}N_2O_4Fe$ (MW 304.09): C (47.40 /47.52); H (3.98/4.21); N (9.21/9.35). (**2c**) $C_{17}H_{14}N_2O_4Fe$ (MW 366.16): C (55.57/55.88); H (3.85/3.88); N (7.65/7.82). (**2d**) $C_{22}H_{16}N_2O_4Fe$ (MW 428.23): C (61.71/61.54); H (3.77/3.96); N (6.54/6.61)

Mass Spectra (EI, 15 eV, *m/e*, [(intensity)]. (**2a**) 290 (6%) M; 262 (3%) M − CO; 234(100%) M − 2CO; 186 (18%). (**2b**) 304 (5%) M; 276(2%) M − CO; 248 (98%) M − 2CO; 186 (100%). (**2c**) No M peak observed; 310 (13%) M − 2CO; 186 (100%). (**2d**) No M peak observed; 372 (1.6%) M − 2CO; 186 (100%).

Melting Points. (**2a**) 94−96 °C; (**2b**) 159−162 °C (decomp.); (**2c**) decomp. 169 °C; (**2d**) decomp. 182 °C.

Synthesis of $CpFe(CO)(PPh_3)$-5,5-diphenylhydantoin 3. **2d** (221 mg, 0.51 mmol) and triphenylphosphine (186 mg, 0.71 mmol) were refluxed in benzene (8 mL) for 3.5 h. After evaporation to dryness, the residue was dissolved in chloroform and chromatographed. The brown-red band was collected to give **3** as a brown-red solid, crystallized form dichloromethane-hexane. Yield: 58.6%. Melting point.: 130 °C (decomp.). Elemental analysis (calcd/found): $C_{39}H_{31}N_2O_3PFe$ C (70.71/70.83); H (4.72/4.92) N (4.23/4.32). ^{1}H NMR ($CDCl_3$): 7.1−7.25 (m, 25H, Ph), 6.85 (bs 1H, NH), 4.58 (s 5H, Cp). IR ($CHCl_3$): 1980 ($\nu_{C\equiv O}$), 1710 (w), 1625 (s) ($\nu_{C=O}$).

FT-IR Spectroscopy. Infrared spectra for characterization of the products were recorded in $CHCl_3$ on a Specord 75 IR spectrometer. Infrared spectra for quantitative analyses were recorded on a benchtop Bomem, MB-100 FT-spectrometer equipped with a liquid nitrogen-cooled, 1.00 mm^2 InSb (indium antimonide) detector and a microbeam attachment which reduced the 6.00 mm incident IR beam to a 1.00 mm diameter focal beam by means of a 90°, off-axis, 100 mm focal length, gold-coated parabolic mirror. The spectral data were manipulated on an NEC APC IV microcomputer. Routinely, 20 scans were coadded (data collection time: 1.1 min). The absorbance values were baseline corrected and determined using the program "Trend Line Analysis" contained in the Bomem software. With this spectrometer configuration, the samples have to be handled manually. A more detailed description is given in a previous paper (*13*). The IR solution cell used was an ultralow volume, gold light-pipe cell with a fill volume of 30 μL and an optical path length of 20 mm (*12*).

Preparation of Rabbit anti-DPH Antibodies. Polyclonal antisera were produced in "fauves de Bourgogne" rabbits, by subcuteneous administration of [(DPH-VA)-BSA] immunogen prepared as described in ref *2*. Each rabbit received 1 mL of an initial emulsion consisting of 250 μg of the immunogen (lyophilized fraction) in 25% water and 75% Freund's complete adjuvant (*15*). Boosters injections identical in composition and amount to the intitial injection (excepted that Freund's incomplete adjuvant was used) were given monthly 4 weeks after the primary for up to 60 weeks. Blood (5−10 mL) was taken 10−15 days after each booster, kept at room-temperature one night, then centrifuged. Sera were then separated in 150 μL fractions and stored at −20 °C.

Study of Cross-Reactions by RIA. Fractions of 500 μL containing 50 μL of antibody (final dilution 1/250), 50 μL (30 pmol) of [^{14}C]DPH, and increasing amounts of

2d or **3** in 500 μL of RIA buffer (Na_2HPO_4, 30 mM; NaH_2PO_4, 30 mM; NaCl, 160 mM; gelatine, 1 g/L; and sodium azide, 30 mM; pH 7.4) were incubated for 2 h at 0 °C. At the end of the incubation period, the free and bound fractions were separated by DCC treatment (1.25% charcoal, 0.125% dextran; final concentration). The supernatant liquids were transferred into vials, and the radioactivity was counted on an LKB Rackbeta counter. The cross-reactivity (CR%) is equal to the quantity (pmol) of **2d** or **3** displacing 50% of [^{14}C]DPH/quantity (pmol) of DPH displacing 50% of [^{14}C]DPH.

Titration Curves by CMIA. Fractions of 500 μL containing 50 pmol of **2d** or **3**, 50 μL of anti-DPH antibody (1/30 to 1/3000) in CMIA buffer (Na_2HPO_4, 30 mM; NaCl, 160 mM; sodium azide, 30 mM; and glycerol, 10% v/v) were incubated at 0 °C for 2 h. At the end of the incubation period, the free and bound fractions of the tracer were separated by selective solvent extraction of the free fraction with isopropyl ether in the following manner: 1.0 mL of the organic solvent saturated in buffer was added to each tube, the mixtures were vortexed for 1 min, and then 750 μL of the organic phase which contained the free tracer were withdrawn and transferred immediatly to 1.5 mL Eppendorf tubes. The solutions were quickly evaporated to dryness on a Speed Vac (Savant) concentrator. Samples for IR analysis were obtained by dissolving the dry residues in 30 μL of CCl_4. The FT-IR spectra were immediately recorded on a Bomem Michelson 100 FT spectrometer using the gold light-pipe cell described previously (*12*). The absorbance of the 2054 cm^{-1} (for **2d**) or 1977 cm^{-1} (for **3**) peak was proportional to the free fractions of the tracer (F = free). The absorbance of the total quantity of tracer (T) present in the incubation buffer was obtained following extraction of a 500 μL fraction containing an identical quantity of tracer but no antibodies. The bound fraction (*B*) was calculated from the difference $T - F$. Titration curves were then constructed by plotting the B/T ratio for each sample versus the inverse of the dilution of the antibodies. The linearization of this curve is obtained by plotting ln(amount of DPH in the tube) versus logit Y, with $Y = \ln[B/B_0/100 - (B/B_0)]$.

Standard Curves by CMIA. Fractions of 500 μL containing a dilution of the anti-DPH antibody equal to the titer value, 50 pmol of **2d**, 50 μL of various quantities of DPH, and 350 μL of CMIA buffer were incubated at room temperature for 1 h. Separation of the free and bound fractions was performed by solvent extraction with isopropyl ether, and determination of the bound fractions was performed as described for the titration curves by CMIA. B_o is the B value obtained in the absence of DPH. Standard curves were then obtained by plotting the B/B_o ratios against the amounts of DPH added.

ACKNOWLEDGMENT

We wish to thank Professor Pierre Brossier (Université de Dijon, France) for providing anti-DPH antibodies, Michèle Salmain for helpful discussion, Annie Cordaville for technicial assistance and Barbara McGlinchey for her assistance in translating the manuscript.

LITERATURE CITED

(1) Salmain, M., Vessières, A., Brossier, P., Butler, I. S., and Jaouen, G. (1992) Carbonylmetalloimmunoassay (CMIA), a new type of nonradioisotopic immunoassay. I. Principles and application to phenobarbital assay. *J. Immunol. Methods 148*, 65−75.

(2) Varenne, A., Vessières, A., Brossier, P., and Jaouen, G. (1994) Application of the nonradioisotopic carbonyl metalloimmunoassay (CMIA) to diphenylhydantoin. *Res. Commun. Chem. Pathol. Pharmacol. 84*, 81−92.

(3) Varenne, A., Vessières, A., Salmain, M., Brossier, P., and Jaouen, G. (1995) Production of specific antibodies and development of a nonisotopic immunoassay for carbamazepine by the Carbonyl Metallo Immuno Assay (CMIA) method. *J. Immunol. Methods 186*, 195−204.

(4) Philomin, V., Vessières, A., and Jaouen, G. (1994) New applications of Carbonyl metallo Immunoassay (CMIA): a nonradioisotopic approach to cortisol assay. *J. Immunol. Methods 171*, 201−210.

(5) Varenne, A., Vessières, A., Salmain, M., Brossier, P., and Jaouen, G. (1996) Quantitative analysis of mixtures of metal carbonyl complexes by Fourier transform infrared spectroscopy. Application to the simultaneous double immunoassay of antiepileptic drugs by the non isotopic CMIA method. *Anal. Biochem. 242*, 172−179.

(6) Varenne, A., Ph.D. (1994) Université Paris VI, France.

(7) Kricka, L. J. (1994) Selected strategies for improving sensitivity and reliability of immunoassays. *Clin. Chem. 40*, 347−357.

(8) Ekins, R. (1994) Immunoassay: recent developments and future directions. *Nucl. Med. Biol. 21*, 495−521.

(9) Xu, Y. Y., Pettersson, K., Blomberg, K., Hemmilä, I. A., Likola, H., and Lövgren, T. (1992) Simultaneous quadruple-label fluorometric immunoassay of thyroid-stimulating hormone, 17α-hydroxyprogesterone, immunoreactive trypsin, and creatine kinase MM isoenzyme in dried blood spots. *Clin. Chem. 38*, 2038−2043.

(10) (a) Zakrzewski, J. (1987) The photoreaction of the (η^5-C_5H_5)Fe(CO)$_2$I-diisopropylamine system with pyrrole and indole. *J. Organomet. Chem. 327*, C41−C42. (b) Zakrzewski, J. (1989) The photosubstitution of iodide in (η^5-C_5H_5)Fe(CO)$_2$I, Synthesis of cyclopentadienyl iron dicarbonyl and carbonylphosphine complexes containing η^1-N-imidato(-1)ligands. *J. Organomet. Chem. 359*, 215−219. (c) Bukowska-Strzyzewska, M., Tosik, A., Wodka, D., and Zakrzewski, J. (1994) The X-ray crystal structure, ^{13}C and ^{15}N NMR spectra of (η^5-C_5H_5)Fe(CO)$_2$ (η^1-N-phthalimidato). *Polyhedron 13*, 1689−1694. (d) Rudolf, B., and Zakrzewski, J. (1994) (η^5-C_5H_5)Fe(CO)$_2$-complex of maleimide anion: an organometallic carbonyl probe for biomolecules containing HS groups *Tetrahedron Lett. 35*, 9611−9612. (e) Zakrzewski, J., Tosik, A., and Bukowska-Strzyzewska, M. (1995) Photochemical reaction of (η^5-Cyclopentadienyl)dicarbonyliron iodide-diisopropylamine with 1-substituted uracils. Crystal structure of the (η^5-C_5H_5)Fe(CO)$_2$-complex of deprotonated 5-fluoro-1-(tetrahydro-2-furyl) uracil (Ftorafur). *J. Organomet. Chem. 495*, 83−90. (f) Klys, A., Zakrzewski, J., and Giannotti, C. (1997) (η^5-Cyclopentadienyl) Fe(CO)$_2$-complex of the (L)- and (D)- tryptophan methyl ester N-anion: synthesis and acylation of the amino function, *J. Organomet. Chem. 531*, 91−94. (g) Kazimierczak, A., Zakrzewski, J., Salmain, M., and Jaouen, G. (1997) Cyclopentadienyl iron dicarbonyl (η^1-N-Phthalimidato) complexes containing an isothiocyanate function: synthesis and application to protein side-chain selective labeling, *Bioconjugate Chem. 8*, 489−494.

(11) King, R. B. (1965) Cyclopentadienyl iron dicarbonyl iodide. *Organometallic Syntheses*, Academic Press, New York.

(12) Vessières, A., Jaouen, G., Salmain, M., and Butler, I. S. (1990) An ultralow volume, gold light-pipe cell for the IR analysis of dilute organic solutions. *Appl. Spectrosc. 44*, 1092−1094.

(13) Salmain, M., Vessières, A., Jaouen, G., and Butler, I. S. (1991) Fourier transform infrared spectroscopy method for the quantitative trace analysis of transition metal carbonyl labeled bioligands. *Anal. Chem. 63*, 2323−2329.

(14) (a) Sheldrick, G. M. (1985) SHELX86. Program for the solution of crystal structures. University of Gottingen, Germany. (b) Sheldrick, G. M. (1993) SHELX93. Program for the solution of crystal structures. University of Gottingen, Germany.

(15) Herbert, W. J. (1978) Mineral-oil adjuvants and the immunization of laboratory animals. In *Handbook of Experimental Immunology* (D. M. Weir, Ed.) Appendix 3, Blackwell Scientific Publ., Oxford.

BC980089M

Intracellular Metabolic Fate of Radioactivity after Injection of Technetium-99m-Labeled Hydrazino Nicotinamide Derivatized Proteins

Masahiro Ono,[†] Yasushi Arano,*[,†] Tomoya Uehara,[†] Yasushi Fujioka,[†] Kazuma Ogawa,[†] Shinji Namba,[†] Takahiro Mukai,[‡] Morio Nakayama,[§] and Hideo Saji[†]

Department of Patho-Functional Bioanalysis, Graduate School of Pharmaceutical Sciences, Kyoto University, Yoshida-shimoadachi-cho, Sakyo-ku, Kyoto 606-8501, School of Pharmaceutical Sciences, Nagasaki University, 1-14 Bunkyo-machi, Nagasaki 852-8131, Department of Radiopharmaceutical Chemistry, Faculty of Pharmaceutical Sciences, Kumamoto University, Oe-Honmachi, Kumamoto 862-0973, Japan.
Received September 9, 1998; Revised Manuscript Received February 8, 1999

Hydrazino nicotinate (HYNIC) has been shown to produce technetium-99m (^{99m}Tc)-labeled proteins and peptides of high stability with high specific activities. However, persistent localization of radioactivity was observed in nontarget tissues such as the liver and kidney after administration of [^{99m}Tc]HYNIC-labeled proteins and peptides, which compromises the diagnostic accuracy of the radiopharmaceuticals. Since lysosomes are the principal sites of intracellular catabolism of proteins and peptides, ^{99m}Tc−HYNIC-labeled galactosyl-neoglycoalbumin (NGA) was prepared using tricine as a co-ligand to investigate the fate of the radiolabel after lysosomal proteolysis in hepatocytes. When injected into mice, over 90% of the injected radioactivity was accumulated in the liver after 10 min injection. At 24 h postinjection, ca. 40% of the injected radioactivity still remained in liver lysosomes. Size-exclusion HPLC analyses of liver homogenates at 24 h postinjection showed a broad radioactivity peak ranging from molecular masses of 0.5−50 kDa. RP-HPLC analyses of liver homogenates suggested the presence of multiple radiolabeled species. However, most of the radioactivity migrated to lower molecular weight fractions on size-exclusion HPLC after treatment of the liver homogenates with sodium triphenylphosphine-3-monosulfonate (TPPMS). The TPPMS-treated liver homogenates showed a major peak at a retention time similar to that of [[^{99m}Tc](HYNIC−lysine)(tricine)(TPPMS)] on RP-HPLC. Similar results were obtained with urine and fecal samples. These findings suggested that the chemical bonding between ^{99m}Tc and HYNIC remains stable in the lysosomes and following excretion from the body. The persistent localization of radioactivity in the liver could be attributed to the slow elimination rate of the final radiometabolite, [[^{99m}Tc](HYNIC−lysine)(tricine)$_2$], from lysosomes, and subsequent dissociation of one of the tricine co-ligands in the low pH environment of the lysosomes in the absence of excess co-ligands, followed by binding proteins present in the organelles. The findings in this study also suggested that the development of appropriate co-ligands capable of preserving stable bonding with the Tc center is essential to reduce the residence time of radioactivity in nontarget tissues after administration of [^{99m}Tc]HYNIC-labeled proteins and peptides.

INTRODUCTION

Radiopharmaceuticals derived from low molecular weight peptides and antibody fragments have been used for visualization of the sites of tumors, infections, and thromboses at early postinjection times (*1*−*3*). The pharmacokinetics of these molecules are well matched with the physical half-life of ^{99m}Tc, the most widely used and the least expensive radionuclide for external imaging. Some peptides contain the N_4 tetraamide (Gly-Gly-Gly), N_3S triamidethiol (Gly-Gly-Cys), or N_2S_2 diamidedithiol (Cys-Gly-Cys) tripeptide sequence (*4*−*7*), which form stable ^{99m}Tc complexes with the $[Tc{=}O]^{3+}$ core. However, the radiolabeling of these tripeptide sequences may require harsh conditions such as high pH and high temperatures. In addition, ^{99m}Tc labeling may lead to the loss of receptor-binding affinity if the tripeptide sequence constitutes part of the receptor-binding motif. Furthermore, some peptides and proteins do not possess such endogenous binding sites to form ^{99m}Tc chelate with high stability. Thus, attachment of appropriate chelating agents to proteins or peptides constitutes a major strategy for labeling of these molecules with ^{99m}Tc for in vivo applications.

Hydrazino nicotinate (HYNIC) is one of the most attractive bifunctional coupling agents for labeling of peptides and proteins with ^{99m}Tc. Indeed, HYNIC provides ^{99m}Tc-labeled nonspecific human IgG, human serum albumin, Fab fragment, chemotactic peptides, and RGD peptides with high specific radioactivities and high radiochemical yields (*8*−*13*). Previous studies indicated that HYNIC acts as a monodentate or bidentate ligand to form a mixed ligand ^{99m}Tc complex in the presence of appropriate co-ligands such as glucoheptonate or tricine (*8*, *14*). Both Tc−hydrazido and Tc−diazenido bonds have been reported and characterized by X-ray crystallography (*15*−*19*). A recent study also suggested that HYNIC

* To whom correspondence should be addressed. Phone: 81-75-753-4608. Fax: 81-75-753-4568. E-mail: arano@pharm.kyoto-u.ac.jp.

[†] Graduate School of Pharmaceutical Sciences, Kyoto University.

[‡] School of Pharmaceutical Sciences, Nagasaki University.

[§] Faculty of Pharmaceutical Sciences, Kumamoto University.

10.1021/bc980105f CCC: $18.00 © 1999 American Chemical Society
Published on Web 04/29/1999

requires two tricine ligands to complete the coordination sphere regardless of whichever type of bond ^{99m}Tc and HYNIC may form (*12*).

When administered in vivo, [^{99m}Tc]HYNIC-labeled proteins and peptides show localization of radioactivity in target tissues. However, high and persistent radioactivity levels were also observed in the liver and kidney where catabolism of the parent proteins and peptides occurs, which compromises the diagnostic accuracy of these radiopharmaceuticals (*8*, *20*−*22*). Since indium-111 (^{111}In)-labeled proteins and peptides also show persistent localization of radioactivity in tissues in which they are catabolized due to the slow elimination rates of the final radiometabolites generated after lysosomal proteolysis in these tissues (*23*−*27*), similar mechanisms may be responsible for the long residence times of the radioactivity derived from [^{99m}Tc]HYNIC-labeled proteins and peptides in these tissues. Decomposition or exchange reactions of the [^{99m}Tc]HYNIC−tricine mixed ligand complex may also account for the long residence times of the radioactivity in the lysosomal compartment where the complexes are present at very low ligand concentrations in the low pH environment. Indeed, decomposition of a [^{99m}Tc]HYNIC-conjugated peptide was indicated in a dilute solution (*12*). However, little is known regarding the retention of radioactivity at the sites of catabolism after administration of [^{99m}Tc]HYNIC-labeled proteins and peptides (*22*). Since HYNIC allows preparation of a variety of ^{99m}Tc-labeled proteins and peptides, the chemical design of HYNIC-based chelating agents that circumvent such undesirable localization of radioactivity is required. Thus, understanding of the fate of ^{99m}Tc after metabolism of [^{99m}Tc]HYNIC-labeled proteins and peptides is essential.

Since lysosomes are the principal sites of intracellular catabolism of proteins and peptides (*28*), metabolic analysis of [^{99m}Tc]HYNIC-labeled proteins in the lysosomal compartment of the liver or kidney would provide insight into the mechanisms responsible for the prolonged radioactivity levels in these organs. Galactosyl-neoglycoalbumin (NGA) is incorporated by hepatic parenchymal cells via receptor-mediated endocytosis immediately after administration (*29*). Use of NGA as a carrier protein provides explicit information regarding the fate of radioactivity after lysosomal proteolysis in hepatocytes without being affected by transchelation of radiolabels in plasma or redistribution of radiometabolites generated elsewhere in the body to the liver (*24*, *30*). In addition, a recent study indicated that an [^{111}In]DTPA-adduct of lysine was generated as the final radiometabolite in the liver and kidney when ^{111}In-labeled NGA and antibodies using cyclic DTPA dianhydride (cDTPA) as the bifunctional chelating agent (BCA) were administered into animals (*31*).

In the present study, NGA was used as a model protein, and biodistribution and subcellular localization of the radioactivity in the murine liver was investigated after administration of [^{99m}Tc]HYNIC-labeled NGA using tricine as the co-ligand. Radiometabolites retained in the liver and excreted from the body were analyzed to determine the fate of the radiolabel, ^{99m}Tc, after lysosomal proteolysis in hepatocytes. Factors affecting the long residence time of radioactivity in nontarget tissues after administration of [^{99m}Tc]HYNIC-labeled proteins and peptides will be discussed. Since HYNIC generates ^{99m}Tc-labeled proteins and peptides in the presence of two tricine co-ligands (*12*, *14*, *32*), ^{99m}Tc-labeled HYNIC−NGA and HYNIC−lysine are abbreviated as [[^{99m}Tc](HYNIC−NGA)(tricine)$_2$] and [[^{99m}Tc](HYNIC−lysine)(tricine)$_2$], respectively.

MATERIALS AND METHODS

Reagents and Chemicals. [^{99m}Tc]Pertechnetate ($^{99m}TcO_4^-$) was eluted in saline solution on a daily basis from Daiichi Radioisotope Laboratory generators (Chiba, Japan). Reversed-phase high-performance liquid chromatography (RP-HPLC) was performed with a Cosmosil 5 C_{18}-MS column (4.6 × 150 mm, Nacalai Tesque, Kyoto) at a flow rate of 1 mL/min with a gradient mobile phase starting from 100% A (0.1% aqueous trifluoroacetic acid) to 100% B (acetonitrile with 0.1% trifluoroacetic acid) in 30 min (solvent system 1). RP-HPLC was also performed with a gradient mobile phase starting from 10% acetonitrile in 0.05 M phosphate buffer (pH 7.0) to 90% acetonitrile in the same buffer in 20 min and the final solvent composition was maintained for a further 10 min (solvent system 2). Size-exclusion HPLC was performed using a 5 Diol-300 column (7.5 × 600 mm, Nacalai Tesque) connected to a 5 Diol-300 guard column (7.5 × 50 mm, Nacalai Tesque), eluted with 0.1 M phosphate buffer (pH 6.8) at a flow rate of 1 mL/min. The eluent was collected with a fraction collector (RediFrac; Pharmacia Biotech, Tokyo) at 30 s intervals, and the radioactivity levels in each fraction (500 μL) were determined with an auto well counter (ARC-2000; Aloka, Tokyo). TLC analyses were performed with silica plates (Merck Art 5553) with a mixture of 10% aqueous ammonium chloride-methanol (1:1) or saline as developing solvents. Proton nuclear magnetic resonance (^{1}H NMR) spectra were recorded on a Bruker AC-200 spectrometer, and the chemical shifts are reported in parts per million downfield from an internal tetramethylsilane standard. Fast atom bombardment mass spectra (FAB-MS) were obtained with a JMS-HX/HX 110 A model (JEOL Ltd., Tokyo). Sodium triphenylphosphine-3-monosulfonate (TPPMS) was purchased from Tokyo Kasei Kogyo Co. Ltd. (Tokyo), and other reagents were of reagent grade and used as received. To facilitate collection of urine and feces after administration of radiolabeled NGA, mice were housed in metabolic cages (Metabolica, MM type; Sugiyama-Gen Iriki Co. Ltd., Tokyo). Succinimidyl 6-hydrazinopyridine-3-carboxylate hydrochloride (SHNH) was synthesized according to the procedure of Abrams et al. (*8*).

Synthesis of Galactosyl-Neoglycoalbumin (NGA). Cyanomethyl-2,3,4,6-tetra-*O*-acetyl-1-β-galactopyranoside, synthesized according to the procedure of Lee et al. (*33*), was conjugated with human serum albumin (HSA, A-3782; Sigma Co., St. Louis, MO), according to the procedure of Stowell et al. (*34*). The phenol-sulfuric acid reaction (*35*) indicated that 43 galactose units were attached to each HSA molecule.

Synthesis of HYNIC−Lysine. Boc-protected SHNH (500 mg, 1.43 mmol), prepared by the method of Abrams et al. (*8*), in 15 mL of dry acetonitrile was added to a solution of α-Boc-L-lysine (352 mg, 1.43 mmol) in saturated $NaHCO_3$ (5 mL) at 0 °C. The reaction mixture was stirred at room temperature for 6 h. After filtration to remove white precipitates, the filtrate was cooled to 0 °C, and the solution was acidified to pH 2−3 with concentrated H_2SO_4 before extraction with ethyl acetate (20 mL × 4). The organic layers were combined and dried over anhydrous calcium sulfate. After removing the solvent in vacuo, the oily residue was chromatographed on silica gel using a mixture of chloroform-methanol-acetic acid (10:1:0.1) as the eluent to produce Boc-HYNIC-

α-Boc-L-lysine as white crystals (532 mg, 75.9%). ^{1}H NMR (CD_3OD): δ 1.26−1.81 [6H, m, $(CH_2)_3$], 1.43 (9H, s, Boc), 1.46 (9H, s, Boc), 3.39 (2H, t, NCH_2), 4.23 (1H, q, CH), 6.46 (1H, d, pyridine), 7.82 (1H, dd, pyridine), 8.10 (1H, d, pyridine). Anal. calcd for $C_{22}H_{35}O_7N_5 \cdot CH_3COOH$: C, 53.23; H, 7.21; N, 12.94. Found: C, 53.06; H, 7.04; N, 12.88. FAB-MS calcd for $C_{22}H_{36}O_7N_5$ (MH^+): *m/z* 482. Found: *m/z* 482.

Boc-HYNIC-α-Boc-L-lysine dissolved in 2 mL of dry ethyl acetate was added to a solution of 4 N HCl prepared in 2 mL of dry ethyl acetate. The reaction mixture was stirred at room temperature for 1 h. The HCl salt of HYNIC−lysine precipitated as white crystals (160 mg, 91.4%). ^{1}H NMR (DMSO-d_6): δ 1.36−1.87 [6H, m, $(CH_2)_3$], 3.24 (2H, t, NCH_2), 3.86 (1H, q, CH), 6.93 (1H, d, pyridine), 8.16 (1H, dd, pyridine), 8.67 (1H, d, pyridine). Anal. calcd for $C_{12}H_{21}O_3N_5Cl_2 \cdot 1/3\ C_4H_{10}O \cdot 3H_2O$: C, 37.66; H, 6.60; N, 16.47. Found: C, 37.65; H, 6.88; N, 16.35. FAB-MS calcd for $C_{12}H_{20}O_3N_5$ (MH^+): *m/z* 282. Found: *m/z* 282.

Preparation of HYNIC−NGA Conjugate. The conjugation reaction of HYNIC with NGA was performed according to the procedure of Abrams et al. (*8*) with slight modifications as follows: Briefly, 10 μL of SHNH (8.3 mg/100 μL) in dimethyl sulfoxide (DMSO) was added dropwise to a 1 mL of stirred NGA solution (20 mg/mL) in 0.15 M borate buffer (pH 8.5). The solution was stirred gently for 2 h at room temperature protected from the light. The HYNIC−NGA conjugate was purified by Sephadex G-50 (Pharmacia Biotech Co. Ltd., Tokyo) column chromatography (1.8 × 40 cm) equilibrated and eluted with 10 mM citrate buffer (pH 5.2). The protein fractions were subsequently concentrated to 5 mg/mL by ultrafiltration (8 MC model, Amicon Grace, Tokyo). The number of HYNIC groups attached per molecule of NGA was determined by measuring the hydrazino groups with *p*-nitrobenzaldehyde, according to the method of King et al. (*36*).

^{99m}Tc Labeling of HYNIC−NGA and HYNIC−Lysine. To a solution of HYNIC−NGA (100 μL; 5.0 mg/mL) in 10 mM citrate buffer (pH 5.2) was added an equal volume of [^{99m}Tc]tricine$_2$ prepared by the method of Larsen et al. (*14*), and the mixture was incubated for 1 h at room temperature. [[^{99m}Tc](HYNIC−NGA)(tricine)$_2$] was purified by the centrifuged column procedure using a Sephadex G-50 column equilibrated and eluted with 0.1 M phosphate buffer (pH 7.0) (*37*). Radiochemical yields of [[^{99m}Tc](HYNIC−NGA)(tricine)$_2$] were determined by size-exclusion HPLC and TLC developed with saline. In a control study, unmodified NGA was labeled with [^{99m}Tc]tricine$_2$, according to the procedures described above.

A solution of [^{99m}Tc]tricine$_2$ (100 μL) was added to a 100 μL of HYNIC−lysine solution (2 mg/mL) in 10 mM citrate buffer (pH 5.2), and the reaction mixture was incubated for 1 h at 37 °C. Radiochemical yields were assessed by size-exclusion HPLC, RP-HPLC, and TLC developed with a mixture of 10% aqueous ammonium chloride-methanol (1:1).

[[^{99m}Tc](HYNIC−Lysine)(Tricine)(TPPMS)] Ternary Mixed Ligand Complex. A solution of [[^{99m}Tc]-(HYNIC−lysine)(tricine)$_2$] (100 μL) prepared as described above was mixed with 100 μL of TPPMS solution (5 mg/mL) in 0.1 M acetate buffer (pH 3.0). The solution was acidified to pH 3 with 0.1 N HCl and incubated at 37 °C for 1 h. The reaction mixture was analyzed by RP-HPLC, size-exclusion HPLC and TLC developed with a mixture of 10% aqueous ammonium chloride-methanol (1:1).

Plasma Stability of [[^{99m}Tc](HYNIC−NGA)(Tricine)$_2$]. [[^{99m}Tc](HYNIC−NGA)(tricine)$_2$] was diluted 20-fold with freshly prepared murine plasma, and the solution was incubated at 37 °C for 24 h. After 1 and 24 h of incubation, 50 μL aliquots of the samples were drawn, and the radioactivity was analyzed by size-exclusion HPLC and TLC developed with saline.

In Vivo Studies. The protein concentration of [[^{99m}Tc](HYNIC−NGA)(tricine)$_2$] was adjusted to 90 μg/mL with saline. Biodistribution studies were performed by the intravenous administration of [[^{99m}Tc](HYNIC−NGA)-(tricine)$_2$] to 6-week-old male ddY mice (27−30 g) (*38*). Groups of five mice each were administered 9 μg (37−56 KBq) of [[^{99m}Tc](HYNIC−NGA)(tricine)$_2$] prior to sacrificing the animals at 10 and 30 min and 1, 3, 6, and 24 h postinjection by decapitation. Previous studies indicated that under these conditions radiolabeled NGAs are incorporated by parenchymal cells of murine liver via receptor-mediated endocytosis (*24*, *30*). Tissues of interest were removed, weighed and the radioactivity counts were determined with an auto well γ counter (ARC 2000). To determine the amounts and routes of excretion of radioactivity from the body, mice were housed in metabolic cages for 24 h after administration of [[^{99m}Tc](HYNIC−NGA)(tricine)$_2$], and urine and feces were collected and the radioactivity was determined.

The subcellular distribution of radioactivity in the murine liver was investigated by perfusing the organ in situ with cold 0.25 M sucrose buffered with 10 mM phosphate buffer (pH 7.4) at 1 and 24 h postinjection of [[^{99m}Tc](HYNIC−NGA)(tricine)$_2$]. The liver was treated according to the procedure described previously (*24*, *30*). Briefly, the isolated organ was minced with scissors, suspended in 4 vol of the same buffer prior to homogenization by hand with a Dounce homogenizer (20 strokes). This was followed by two final strokes in an ice-cooled Potter-Elvehjem homogenizer with a Teflon pestle rotated at 800 rpm. The resulting homogenate was centrifuged twice for 5 min at 340 *g* at 4 °C. The isolated supernatant was then layered on top of iso-osmic (0.25 M sucrose) 37.5% Percoll (9 mL, Pharmacia Biotech Co. Ltd.) at a density of 1.08 g/mL. After centrifugation at 20000*g* (RP 30 rotor; Hitachi Co. Ltd., Tokyo) for 90 min at 4 °C, the gradients were collected in 14 fractions. β-Galactosidase was used as a marker enzyme for lysosomes (*39*, *40*) and its activity in each fraction was determined using *p*-nitrophenyl β-galactopyranoside as the substrate (*41*). The density and radioactivity counts of the respective fraction were also determined.

The radiolabeled species remaining in the liver at 1 and 24 h postinjection and excreted in the urine and feces by 24 h postinjection of [[^{99m}Tc](HYNIC−NGA)(tricine)$_2$] (133−266 KBq) were analyzed according to the procedure described previously (*24*, *30*). Briefly, the murine liver was perfused in situ with cold 0.1 M Tris-citrate buffer (pH 6.5) containing 0.15 M NaCl, 0.02% sodium azide, 1 TIU/mL aprotinin, 2 mM benzamidine-HCl, 2 mM iodoacetamide, 1 mM phenylmethanesulfonyl fluoride, and 5 mM diisopropyl fluorophosphate before the hepatic samples (1 g each) were isolated. Each tissue sample was placed in a test tube and subjected to three cycles of freezing (dry ice-acetone bath) and thawing. After addition of 5 vol of the same buffer containing an additional 35 mM β-octyl-glucoside, the samples were homogenized with a Polytron homogenizer (PT 10-35, Kinematica GmbH, Littau, Switzerland) set at full speed with three consecutive 30 s bursts prior to centrifugation at 48000*g* for 20 min at 4 °C (Himac CS-120 Centrifuge; Hitachi

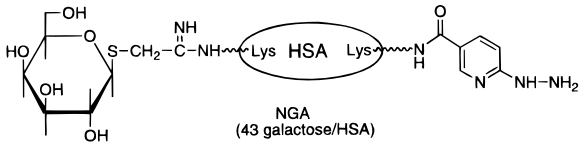


Figure 1. Chemical structure of HYNIC−NGA.

Co. Ltd., Tokyo). The supernatant was separated from the pellet, and the radioactivity was counted. In a procedure similar to that used for liver tissue, fecal samples were homogenized in the presence of 0.1 M phosphate buffer (pH 6.0) before centrifugation at 10000*g* for 20 min at 4 °C. The liver, feces, and urine samples were analyzed immediately by size-exclusion HPLC and TLC after filtration through a polycarbonate membrane with a pore diameter of 0.45 μm (Nacalai Tesque). Each sample was also analyzed immediately by RP-HPLC after ultrafiltration with a 10 kDa cutoff membrane (Microcon-10, Amicon).

Since TPPMS forms a ternary mixed ligand complex with [[^{99m}Tc](HYNIC−peptide)(tricine)$_2$] (*32*), the liver homogenates were reacted with TPPMS and the reaction products were analyzed to further characterize the radiometabolites retained in the liver. The supernatants of the liver homogenates (100 μL) were mixed with a 100 μL solution of TPPMS (5 mg/mL) in 0.1 M acetate buffer (pH 3.0) after filtration through a polycarbonate membrane with a pore diameter of 0.45 μm. After acidification to pH 3 with 0.1 N HCl, the reaction mixture was incubated at 37 °C for 1 h. The reaction mixture was analyzed by size-exclusion HPLC and TLC after filtration through a polycarbonate membrane with a pore diameter of 0.45 μm. Each sample was also analyzed by RP-HPLC after filtration through a 10 kDa cutoff ultrafiltration membrane. The fecal homogenates and urine samples obtained at 24 h postinjection of [[^{99m}Tc](HYNIC−NGA)-(tricine)$_2$] were also reacted with TPPMS by similar procedures, and the radioactivity in the reaction mixture was analyzed.

RESULTS

In Vitro Studies. HYNIC−NGA conjugate (Figure 1) was prepared by reaction of the active esters of SHNH with ϵ-amine residues of the NGA. Three HYNIC groups were attached per molecule of NGA as determined by measuring the hydrazine groups. After purification by the centrifuged column procedure, [[^{99m}Tc](HYNIC−NGA)(tricine)$_2$] was obtained with radiochemical yields over 95% as determined by size-exclusion HPLC and TLC. The reaction of [^{99m}Tc]tricine$_2$ with unmodified NGA resulted in only 5.4% of the radioactivity associated with protein. Figure 2 shows size-exclusion radiochromatograms of [[^{99m}Tc](HYNIC−NGA)(tricine)$_2$] before and after incubation in freshly prepared murine plasma for 24 h. The radioactivity associated with NGA fractions was unchanged before (98.7%) and after 24 h incubation (97.6%). Similar results were obtained by TLC analyses.

In Vivo Studies. The biodistribution of radioactivity after intravenous administration of [[^{99m}Tc](HYNIC−NGA)(tricine)$_2$] is summarized in Table 1. At 10 min postinjection, more than 92% of the injected radioactivity was accumulated in the liver. The radioactivity was gradually eliminated from the liver by hepatobiliary excretion as the major excretion route. At 24 h postinjection, over 38% of the injected radioactivity was still retained in the liver. During the same postinjection period, 38 and 14% of the injected radioactivity was excreted in the feces and urine, respectively.

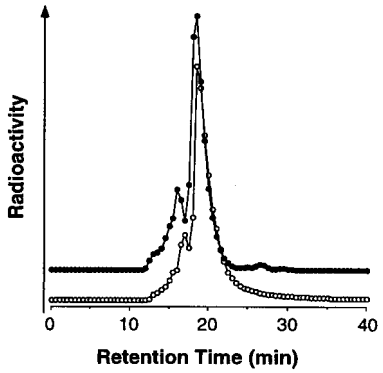


Figure 2. Size-exclusion radiochromatograms of [[^{99m}Tc]-(HYNIC−NGA)(tricine)$_2$] before (○) and after (●) incubation in freshly prepared murine plasma at 37 °C for 24 h.

Table 1. Biodistribution of Radioactivity after Intravenous Administration of [[^{99m}Tc](HYNIC−NGA)(tricine)$_2$] in Mice[a]

tissue	10 min[b]	30 min[b]	1 h[b]	3 h[b]	6 h[b]	24 h[b]
blood[c]	0.27	0.18	0.09	0.13	0.08	0.01
	(0.02)	(0.01)	(0.02)	(0.02)	(0.02)	(0.01)
liver	92.30	88.71	84.56	75.10	63.29	38.77
	(2.65)	(1.44)	(2.48)	(4.07)	(5.26)	(4.10)
intestine	0.36	4.34	7.61	14.54	20.88	2.23
	(0.09)	(0.62)	(0.91)	(0.97)	(2.14)	(0.52)
kidney	0.30	0.33	0.38	0.45	0.53	0.38
	(0.05)	(0.03)	(0.05)	(0.09)	(0.11)	(0.04)
spleen	0.08	0.08	0.08	0.09	0.06	0.04
	(0.04)	(0.01)	(0.01)	(0.03)	(0.01)	(0.03)
stomach	0.31	0.55	0.58	0.70	0.71	0.42
	(0.16)	(0.28)	(0.25)	(0.15)	(0.33)	(0.35)
feces						38.27
						(3.80)
urine						13.67
						(0.59)

[a] Expressed as % injected dose. Each value represents the mean (s.d.) for five animals at each interval. [b] Time after administration. [c] Expressed as percent dose per gram.

The Percoll density gradient centrifugation profiles of radioactivity in the liver at 1 and 24 h postinjection of [[^{99m}Tc](HYNIC−NGA)(tricine)$_2$] are illustrated in Figure 3. Each liver homogenate showed a major radioactivity peak at a density of ca. 1.10 g/mL, which correlated well with the β-galactosidase activity profiles.

The supernatants of the liver homogenates were obtained with radiochemical efficiencies of over 90%. After filtration of the liver supernatant at 1 and 24 h postinjection through the polycarbonate membrane, the radioactivity was recovered in the filtrates with 86.1 and 92.3% efficiencies, respectively. When analyzed by size-exclusion HPLC, while the liver supernatant at 1 h depicted a major radioactivity peak at a retention time close to that of [[^{99m}Tc](HYNIC−lysine)(tricine)$_2$] (Figure 4C), radioactivity was also detected in fractions over 10 kDa (Figure 4A). A significant increase in radioactive fractions over 10 kDa was observed with the liver supernatant at 24 h postinjection (Figure 4B). Under these conditions, the parental [[^{99m}Tc](HYNIC−NGA)-(tricine)$_2$] had a retention time of 18 min (Figure 4, panels A and B). On TLC analyses, the liver homogenates had radioactivity at the origin with a broad peak at R_f values of 0.5−0.65. The liver supernatant at 1 h postinjection was recovered in the filtrate with 76.3% efficiency after filtration through a 10 kDa cutoff ultrafiltration membrane, whereas the radioactivity recovered in the filtrate decreased to 54.3% after filtration of the liver supernatant at 24 h postinjection. RP-HPLC radiochromatograms

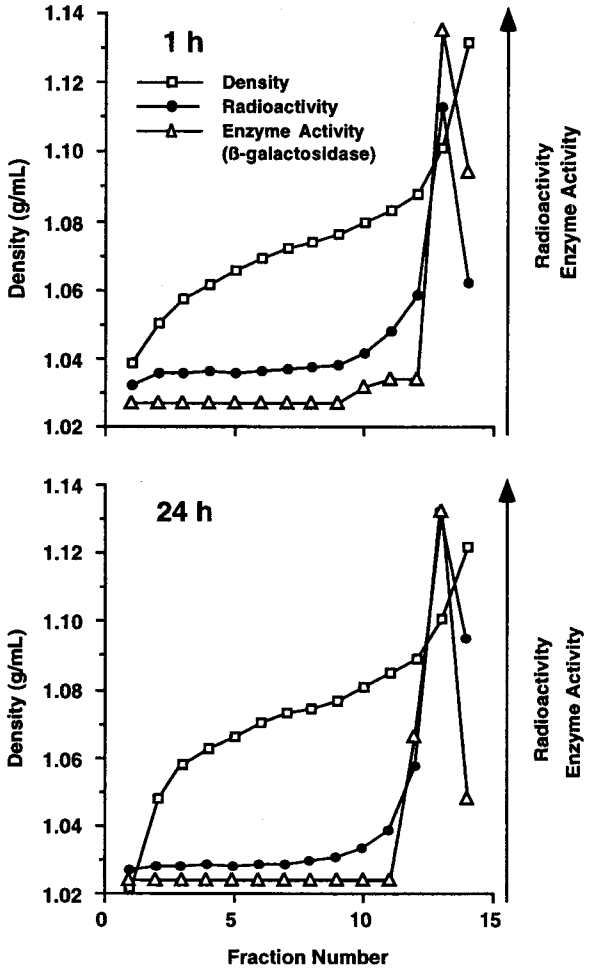


Figure 3. Percoll density gradient centrifugation profiles of liver homogenate at 1 and 24 h postinjection of [[^{99m}Tc](HYNIC−NGA)(tricine)$_2$]. In both preparations, a single radioactivity peak (●) that coincided with β-galactosidase activity (△) was detected at a density (□) of ca. 1.10 g/mL.

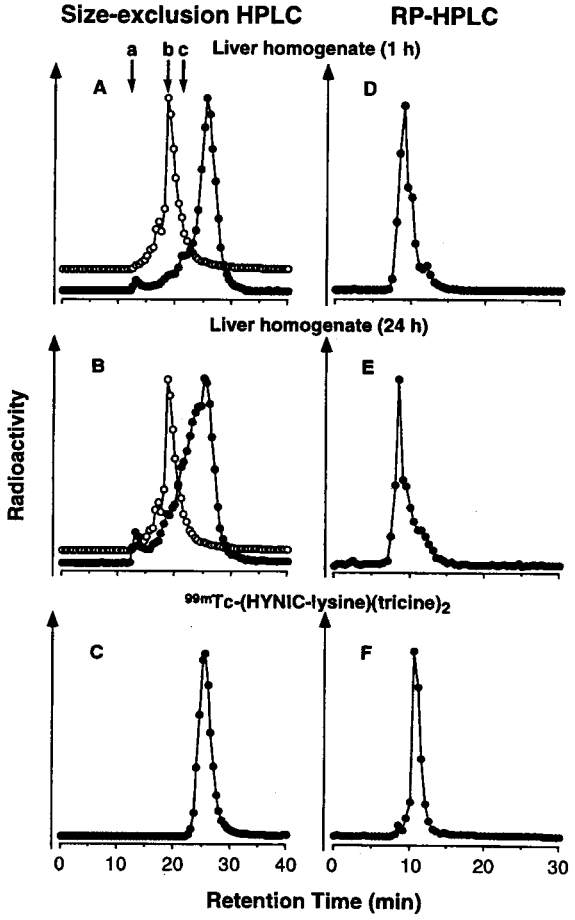


Figure 4. Analyses of liver homogenates (●) at 1 and 24 h postinjection of [[^{99m}Tc](HYNIC−NGA)(tricine)$_2$] (○) by size-exclusion HPLC (A and B) and RP-HPLC using solvent system 1 (D and E). Radiochromatograms of [[^{99m}Tc](HYNIC−lysine)-(tricine)$_2$] when analyzed by size-exclusion HPLC (C) and RP-HPLC (F). Under these conditions, thyroglobulin (a; 670 kDa), bovine serum albumin (b; 68 kDa) and cytochrome C (c; 13 kDa) had retention times of 13, 18, and 21 min, respectively, on size-exclusion HPLC.

of the liver supernatant at 1 and 24 h postinjection using the solvent system 1 are shown in Figure 4, panels D and E. Both supernatants showed similar radiochromatograms with a major radioactivity peak at a retention time of 8−9 min and a shoulder at a retention time of 11 min. Under these conditions, [[^{99m}Tc](HYNIC−lysine)-(tricine)$_2$] showed a radioactivity peak at a retention time of 11 min (Figure 4F). RP-HPLC analyses of the liver homogenates using solvent system 2 showed a radioactivity peak at a retention time of 4 min (Figure 6, panels A and B).

The radiochromatograms of the TPPMS-treated liver homogenates are illustrated in Figures 5 and 6. The radioactivity recovered in the filtrates was 91.1 and 88.6% after filtration of the TPPMS-homogenates obtained at 1 and 24 h postinjection through a polycarbonate membrane, respectively. On size-exclusion HPLC, a significant decrease in the radioactive fractions over 10 kDa was observed with TPPMS-treated liver homogenate at 24 h postinjection. The reaction product of [[^{99m}Tc]-(HYNIC−lysine)(tricine)$_2$] and TPPMS showed a single radioactivity peak at a retention time of 26 min on size-exclusion HPLC (Figure 5C). The radioactivity recovered in the filtrates increased to 89.2 and 91.1% for the TPPMS-treated liver homogenates obtained at 1 and 24 h postinjection after filtration through a 10 kDa cutoff ultrafiltration membrane. On RP-HPLC using solvent system 1, the TPPMS-treated liver homogenates showed a sharp radioactivity peak at a retention time of 17 min for both preparations, which was identical to that of the reaction product of [[^{99m}Tc](HYNIC−lysine)(tricine)$_2$] and TPPMS (Figure 5F). This was confirmed by co-chromatographic analyses (data not shown). Under these conditions, the reaction products of [^{99m}Tc]tricine$_2$ and TPPMS showed a radioactivity peak at a retention time of 13 min on RP-HPLC. Similar results were obtained on RP-HPLC analyses of the liver homogenates using solvent system 2, where both TPPMS-treated liver homogenates and [[^{99m}Tc](HYNIC−lysine)(tricine)$_2$] showed a single radioactivity peak at a retention time of 8.5 min, as shown in Figure 6. On TLC analyses, both TPPMS-treated liver homogenates and the reaction product of [[^{99m}Tc](HYNIC−lysine)(tricine)$_2$] and TPPMS showed a radioactivity peak at an R_f value of 0.7.

Figure 7 shows radiochromatograms of fecal and urine samples analyzed by size-exclusion HPLC and RP-HPLC using solvent system 1. Supernatants of feces were obtained with an efficiency of 54.6%. The recovered radioactivities in the filtrates after filtration though the polycarbonate membrane and the ultrafiltration membrane were 66.7 and 82.5% for feces and 96.9 and 98.3% for urine samples, respectively. Both fecal and urine samples showed a single radioactivity peak on size-exclusion HPLC at a retention time of 26 min (Figure 7, panels A and B). On RP-HPLC, a broad radioactivity

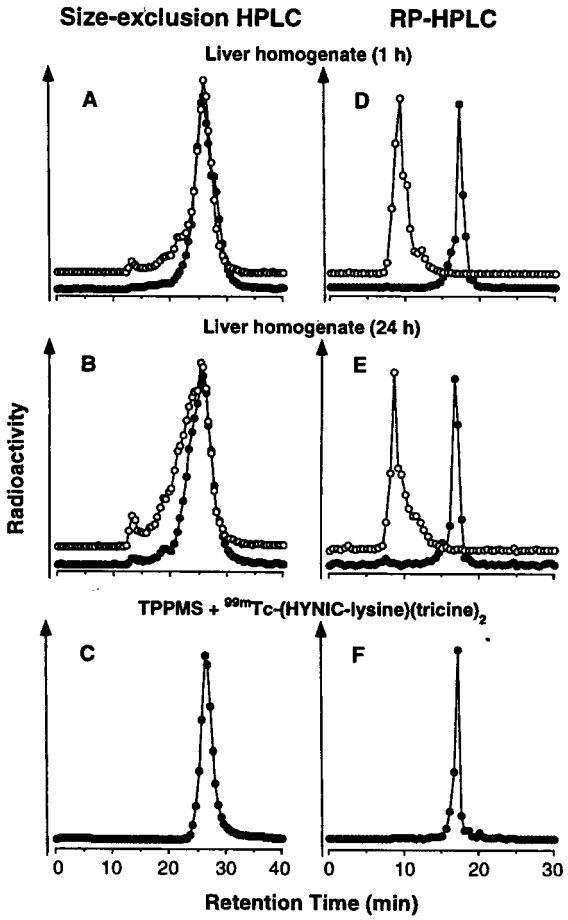


Figure 5. Radiochromatograms of liver homogenates at 1 and 24 h postinjection before (○) and after (●) TPPMS treatment by size-exclusion HPLC (A and B) and RP-HPLC using solvent system 1 (D and E). The reaction product of [[^{99m}Tc](HYNIC−lysine)(tricine)$_2$] with TPPMS was analyzed by size-exclusion HPLC (C) and RP-HPLC (F).

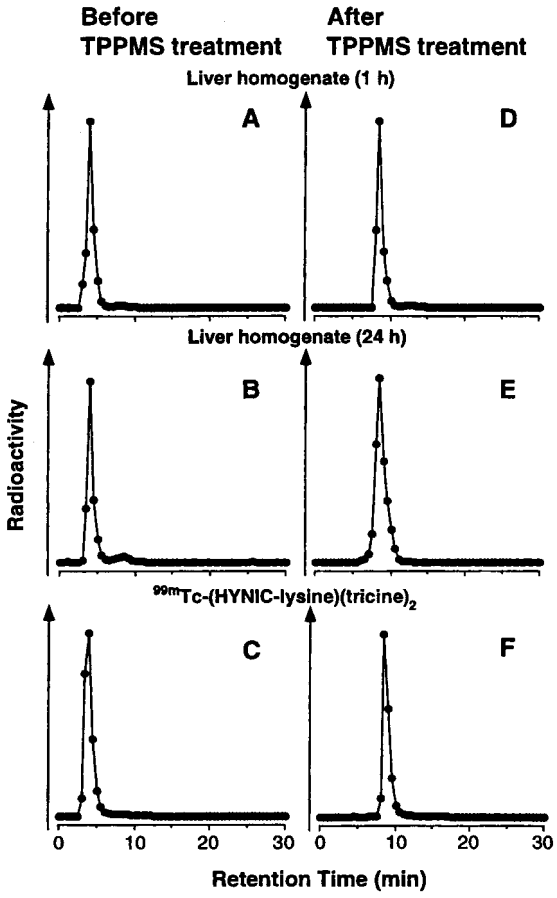


Figure 6. RP-HPLC radiochromatograms of liver homogenates at 1 and 24 h postinjection before and after treatment with TPPMS using solvent system 2. RP-HPLC radiochromatograms of [[^{99m}Tc](HYNIC−lysine)(tricine)$_2$] are also shown before and after treatment with TPPMS under similar conditions (C and F).

profile at a retention time of around 9 min was observed with both preparations using solvent system 1 (Figure 7, panels C and D). After TPPMS treatment, both feces and urine preparations showed migration of the radioactivity peaks to a retention time of 17 min, which was identical to that of the reaction product between [[^{99m}Tc](HYNIC−lysine)(tricine)$_2$] and TPPMS (Figure 7, panels E and F). Similar results were obtained by TLC analyses, where both preparations showed a radioactivity peak at an R_f value of 0.7 after TPPMS treatment.

DISCUSSION

Selective complexation of ^{99m}Tc to the HYNIC moiety was indicated by the exchange reaction of [^{99m}Tc]tricine$_2$ with HYNIC−NGA as shown by the small amounts of ^{99m}Tc attached to unmodified NGA. Unchanged size-exclusion HPLC radiochromatograms before and after incubation for 24 h in murine plasma reinforced the stable chemical bonding between ^{99m}Tc and HYNIC (Figure 2). In biodistribution studies, persistent localization of the radioactivity was observed in the murine liver in which catabolism of NGA occurs following the administration of [[^{99m}Tc](HYNIC−NGA)(tricine)$_2$] (Table 1). These findings using NGA as a model protein were in good agreement with those of previous studies using [^{99m}Tc]HYNIC-labeled proteins in experimental animals (*8*, *42*, *43*).

Radioactivity in the liver homogenates was copurified with lysosomes at 1 and 24 h postinjection of [[^{99m}Tc](HYNIC−NGA)(tricine)$_2$] (Figure 3), as observed in previous studies using ^{111}In-labeled NGAs with cDTPA or 1-(4-isothio,cyanatobenzyl)ethylenediaminetetraacetic acid (SCN−Bz-EDTA) as the BCAs (*24*, *26*, *31*, *44*, *45*). Previous studies also showed that both ^{111}In-labeled NGAs generated lysine-adducts ([^{111}In]DTPA-lysine and [^{111}In]SCN−Bz-EDTA-lysine) as the major final radiometabolites in murine hepatocytes and the slow elimination rates of the radiometabolites from the lysosomal compartment of hepatocytes are responsible for the persistent localization of the radioactivity in the liver. Since HYNIC was also conjugated to the ϵ-amine residues of NGA, lysine-adduct of HYNIC was prepared and radiolabeled with [^{99m}Tc]tricine$_2$ as a standard compound for subsequent analyses of the radioactivity retained in the liver and excreted in the urine and feces.

On size-exclusion HPLC analyses, the liver homogenates registered a radioactivity peak at a retention time representative of low molecular weight compounds such as [[^{99m}Tc](HYNIC−lysine)(tricine)$_2$] (Figure 4), as observed with ^{111}In-labeled NGAs. In contrast to ^{111}In-labeled NGAs, radiolabeled species were also registered in higher molecular weight fractions and the proportion of the fractions increased with postinjection interval. This was reflected in the decreased recovery of radioactivity in the filtrates of liver homogenates at 24 h postinjection using 10 kDa cutoff ultrafiltration membranes. Since generation of the final radiometabolites of ^{111}In-labeled NGAs was complete within 1 h postinjection (*24*, *30*), the time-dependent increase in high molecular weight frac-

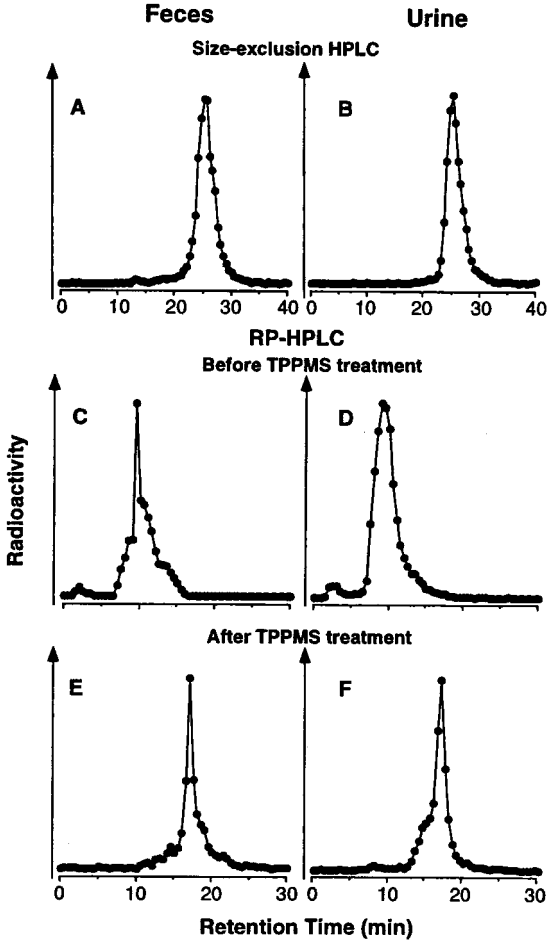


Figure 7. Analyses of feces and urine samples obtained at 24 h postinjection of [[^{99m}Tc](HYNIC−NGA)(tricine)$_2$] by size-exclusion HPLC (A and B) and RP-HPLC (C and D) using solvent system 1. After reacting with TPPMS, both preparations were analyzed by RP-HPLC (E and F).

tions suggested binding of radiometabolites derived from [[^{99m}Tc](HYNIC−NGA)(tricine)$_2$] with proteins present in the lysosomes, which would constitute a major reason for the long residence time of radioactivity in the liver.

To further understand the persistent localization of the radioactivity in the liver after administration of [[^{99m}Tc]-(HYNIC−NGA)(tricine)$_2$], radiolabeled species retained in the liver at the two postinjection intervals were analyzed. Both liver homogenates showed a broad radioactivity peaked at a retention time close to that of [[^{99m}Tc](HYNIC−lysine)(tricine)$_2$] (Figure 4), suggesting that multiple radiolabeled species derived from [[^{99m}Tc]-(HYNIC−lysine)(tricine)$_2$] would be present in the liver homogenates. Since [[^{99m}Tc](HYNIC−lysine)(tricine)$_2$] showed no change in RP-HPLC radiochromatograms after removing excess ligands (data not shown), the broad radioactivity of the liver homogenates suggested the formation of new mixed ligand ^{99m}Tc complexes. On the other hand, the reaction mixture of the liver homogenates with TPPMS showed RP-HPLC radiochromatograms similar to that of the reaction product of [[^{99m}Tc](HYNIC−lysine)(tricine)$_2$] and TPPMS (Figures 5 and 6). A recent study of [^{99m}Tc]HYNIC-labeled peptides showed that [[^{99m}Tc](HYNIC−peptide)(tricine)$_2$] reacts with TPPMS to provide a new ternary mixed ligand complex [[^{99m}Tc]-(HYNIC−peptide)(tricine)(TPPMS)], in which one tricine co-ligand was replaced with one TPPMS molecule (*32*). It has also been reported that [[^{99m}Tc](HYNIC−peptide)-(tricine)$_2$] gradually decomposed to hydrophilic ^{99m}Tc species in a dilute solution (*12*). Furthermore, the binding of [^{99m}Tc]HYNIC-labeled antibodies and DNA with serum proteins was observed (*11*, *46*). Thus, the findings in this study, together with those results of previous studies, suggested that [[^{99m}Tc](HYNIC−lysine)(tricine)$_2$] would be generated as the final radiometabolite after lysosomal proteolysis of [[^{99m}Tc](HYNIC−NGA)(tricine)$_2$] in the murine liver. However, one of the two tricine co-ligands of the metabolite would be replaced with amino acids to generate new mixed ligand ^{99m}Tc complexes of high protein binding ability or with amine residues of proteins present in the organelles, facilitated by a low pH environment in the absence of excess co-ligand.

The radiolabeled species excreted in the urine and feces were present as multiple low molecular weight compounds (Figure 7). However, since the TPPMS-treatment of urine samples and fecal extracts showed migration of the radioactivity with a retention time similar to that of [[^{99m}Tc](HYNIC−lysine)(tricine)(TPPMS)] on RP-HPLC, the radiolabeled species excreted from the body appeared to still retain the [[^{99m}Tc]HYNIC−tricine] bond in the absence of excess co-ligands. The multiple peaks in urine and feces determined by RP-HPLC also suggested the participation of amino acids in the mixed ligand [^{99m}Tc]-HYNIC complexes generated in the lysosomes of the liver.

In conclusion, the findings in this study implied that the bonding between ^{99m}Tc and HYNIC is extremely stable at low pH in the absence of excess co-ligands. The persistent localization of radioactivity in the liver after administration of [[^{99m}Tc](HYNIC−NGA)(tricine)$_2$] was attributed to the slow elimination rate of the final radiometabolite, [[^{99m}Tc](HYNIC−lysine)(tricine)$_2$] from the lysosomes, and subsequent replacement of one of the tricine co-ligands with amino acids to generate new ternary mixed ligand complexes of high protein binding ability or with amine residues of proteins in the lysosomes, presumably due to the low pH environment of the organelles and the absence of excess co-ligands. These findings also suggested that the development of appropriate co-ligands that form stable [^{99m}Tc]HYNIC−[co-ligand] mixed complexes at low pH in the absence of excess co-ligands is essential to reduce localization of radioactivity in nontarget tissues after administration of ^{99m}Tc-labeled proteins using HYNIC.

LITERATURE CITED

(1) Barrett, J. A., Damphousse, D. J., Heminway, S. J., Liu, S., Edwards, D. S., Looby, R. J., and Carroll, T. R. (1996) Biological evaluation of ^{99m}Tc-labeled cyclic glycoprotein IIb/IIIa receptor antagonists in the canine arteriovenous shunt and deep vein thrombosis models: effects of [^{99m}Tc]chelator-peptide conjugates. *Bioconjugate Chem. 7*, 203−208.

(2) Vallabhajosula, S., Moyer, B. R., James, J. L., McBride, B. J., Lipszyc, H., Lee, H., Bastidas, D., and Dean, R. T. (1996) Preclinical evaluation of technetium-99m-labeled somatostatin receptor-binding peptides. *J. Nucl. Med. 37*, 1016−1022.

(3) Verhaar, M. J., Keep, P. A., Hawkins, R. E., Robson, L., Casey, J. L., Pedley, B., Borden, J. A., Begent, R. H. J., and Chester, K. A. (1996) Technetium-99m radiolabeling using a phage-derived single-chain Fv with a C-terminal cysteine. *J. Nucl. Med. 37*, 868−872.

(4) Vanbilloen, H. P., Bormans, G. M., Deroo, M. J., and Verbruggen, A. M. (1995) Complexes of technetium-99m with tetrapeptides, a new class of Tc-99m-labelled agents. *Nucl. Med. Biol. 22*, 325−338.

(5) Pearson, D. A., Lister James, J., McBride, W. J., Wilson, D. M., Martel, L. J., Civitello, E. R., Taylor, J. E., Moyer, B. R., and Dean, R. T. (1996) Somatostatin receptor-binding peptides labeled with technetium-99m: chemistry and initial biological studies. *J. Med. Chem. 39*, 1361−1371.

(6) Bogdanov, A. J., Petherick, P., Marecos, E., and Weissleder, R. (1997) In vivo localization of diglycylcysteine-bearing synthetic peptides by nuclear imaging of oxotechnetate transchelation. *Nucl. Med. Biol. 24*, 739−742.

(7) Chang, F., Rusckowski, M., Qu, T., and Hnatowich, D. J. (1997) Early results in the irrational design of new bifunctional chelators. *Cancer 80*, 2347−2353.

(8) Abrams, M. J., Juweid, M., tenKate, C. I., Schwartz, D. A., Hauser, M. M., Gaul, F. E., Fuccello, A. J., Rubin, R. H., Strauss, H. W., and Fischman, A. J. (1990) Technetium-99m-human polyclonal IgG radiolabeled via the hydrazino nicotinamide derivative for imaging focal sites of infection in rats. *J. Nucl. Med. 31*, 2022−2028.

(9) Babich, J. W., Graham, W., Barrow, S. A., Dragotakes, S. C., Tompkins, R. G., Rubin, R. H., and Fischman, A. J. (1993) Technetium-99m-labeled chemotactic peptides: comparison with indium-111-labeled white blood cells for localizing acute bacterial infection in the rabbit. *J. Nucl. Med. 34*, 2176−2181.

(10) Verbeke, K., Hjelstuen, O., Debrock, E., Cleynhens, B., De Roo, M., and Verbruggen, A. (1995) Comparative evaluation of $^{99}Tc^{m}$-Hynic-HSA and $^{99}Tc^{m}$-MAG_3−HSA as possible blood pool agents. *Nucl. Med. Commun. 16*, 942−957.

(11) Hnatowich, D. J., Winnard, P., Jr., Virzi, F., Fogarasi, M., Sano, T., Smith, C. L., Cantor, C. R., and Rusckowski, M. (1995) Technetium-99m labeling of DNA oligonucleotides. *J. Nucl. Med. 36*, 2306−2314.

(12) Liu, S., Edwards, D. S., Looby, R. J., Harris, A. R., Poirier, M. J., Barrett, J. A., Heminway, S. J., and Carroll, T. R. (1996) Labeling a hydrazino nicotinamide-modified cyclic IIb/IIIa receptor antagonist with ^{99m}Tc using aminocarboxylates as coligands. *Bioconjugate Chem. 7*, 63−71.

(13) Ultee, M. E., Bridger, G. J., Abrams, M. J., Longley, C. B., Burton, C. A., Larsen, S. K., Henson, G. W., Padmanabhan, S., Gaul, F. E., and Schwartz, D. A. (1997) Tumor imaging with technetium-99m-labeled hydrazinonicotinamide-Fab′ conjugates. *J. Nucl. Med. 38*, 133−138.

(14) Larsen, S. K., Solomon, H. F., Caldwell, G., and Abrams, M. J. (1995) [^{99m}Tc]tricine: a useful precursor complex for the radiolabeling of hydrazinonicotinate protein conjugates. *Bioconjugate Chem. 6*, 635−638.

(15) Abrams, M. J., Larsen, S. K., Shaik, S. N., and Zubieta, J. (1991) Investigation of techenetium-organohydrazine coordination chemistry. The crystal and molecular structure of $[TcCl_2(C_8H_5N_4)(PPh_3)_2]\cdot 0.75C_7H_8$ and $[TcNCl_2(PPh_3)_2]\cdot 0.25CH_2Cl_2$. *Inorg. Chim. Acta 185*, 7−15.

(16) Abrams, M. J., Larsen, S. K., and Zubieta, J. (1991) Investigation of the technetium-hydrazido core. Synthesis and structural characterization of $[(n\text{-}C_4H_9)N][Tc_2(NNPh_2)_2(C_6Cl_4O_2)_4]\cdot CH_2Cl_2\cdot 2CH_3OH$, a Tc(V)/Tc(IV) catecholate complex with the hydrazido ligands adopting the unusual n1 bridging model. *Inorg. Chem. 30*, 2031−2035.

(17) Nicholson, T., Cook, J., Davison, A., Rose, D. J., Maresca, K. P., Zubieta, J. A., and Jones, A. J. (1996) The synthesis and characterization of $[MCl_3(N{=}NC_5H_4NH)(HN{=}NC_5H_4N)]$ from $[MO_4]^-$ (where M = Re, Tc) organodiazenido, organodiazene-chelate complexes. The X-ray structure of $[ReCl_3(N{=}NC_5H_4NH)(HN{=}NC_5H_4N)]$. *Inorg. Chim. Acta 252*, 421−426.

(18) Nicholson, T., Cook, J., Davison, A., Rose, D. J., Maresca, K. P., Zubieta, J. A., and Jones, A. J. (1996) The synthesis, characterization and X-ray crystal structure of the rhenium organodiazenido, organodiazene complex of $[ReCl_2(PPh_3)(N{=}NC_5H_4NH)(HN{=}NC_5H_4N)]$. *Inorg. Chim. Acta 252*, 427−430.

(19) Liu, S., Edwards, D. S., and Barrett, J. A. (1997) ^{99m}Tc Labeling of highly potent small peptides. *Bioconjugate Chem. 8*, 621−636.

(20) Callahan, R. J., Barrow, S. A., Abrams, M. J., Rubin, R. H., and Fischman, A. J. (1996) Biodistribution and dosimetry of technetium-99m-hydrazino nicotinamide IgG: comparison with indium-111-DTPA-IgG. *J. Nucl. Med. 37*, 843−846.

(21) Claessens, R. A., Boerman, O. C., Koenders, E. B., Oyen, W. J., van der Meer, J. W., and Corstens, F. H. (1996) Technetium-99m labelled hydrazinonicotinamide human non-specific polyclonal immunoglobulin G for detection of infectious foci: a comparison with two other technetium-labelled immunoglobulin preparations. *Eur. J. Nucl. Med. 23*, 414−421.

(22) Claessens, R. A., Koenders, E. B., Oyen, W. J. G., and Corstens, F. H. (1996) Retention of technetium-99m in infectious foci in rats after release from technetium-99m labelled human non-specific polyclonal immunoglobulin G: a dual-label study with hydrazinonicotinamide and iminothiolano immunoglobulin. *Eur. J. Nucl. Med. 23*, 1536−1539.

(23) Akizawa, H., Arano, Y., Uezono, T., Ono, M., Fujioka, Y., Uehara, T., Yokoyama, A., Akaji, K., Kiso, Y., and Saji, H. (1998) Renal metabolism of ^{111}In-DTPA-D-Phe^1-octreotide in vivo. *Bioconjugate Chem. 9*, 662−670.

(24) Arano, Y., Mukai, T., Uezono, T., Wakisaka, K., Motonari, H., Akizawa, H., Taoka, Y., and Yokoyama, A. (1994) A biological method to evaluate bifunctional chelating agents to label antibodies with metallic radionuclides. *J. Nucl. Med. 35*, 890−898.

(25) Bass, L. A., Lanahan, M. V., Duncan, J. R., Erion, J. L., Srinivasan, A., Schmidt, M. A., and Anderson, C. J. (1998) Identification of the soluble in vivo metabolites of indium-111-diethylenetriaminepentaacetic acid-D-Phe^1-octreotide. *Bioconjugate Chem. 9*, 192−200.

(26) Duncan, J. R., and Welch, M. J. (1993) Intracellular metabolism of indium-111-DTPA-labeled receptor targeted proteins. *J. Nucl. Med. 34*, 1728−1738.

(27) Franano, F. N., Edwards, W. B., Welch, M. J., and Duncan, J. R. (1994) Metabolism of receptor targeted In-111-DTPA-glycoproteins: identification of In-111-DTPA-epsilon-lysine as the primary metabolic and excretory product. *Nucl. Med. Biol. 21*, 1023−1034.

(28) Alberts, B., Bray, D., Lewis, J., Raff, M., Roberts, K., and Watson, J. D. (1983) Membrane transport of macromolecules and particles; exocytosis and endocytosis. *Molecular Biology of The Cell*, pp 302−317, Garland Publishing Inc. New York.

(29) Ashwell, G., and Harford, J. (1982) Carbohydrate-specific receptors of the liver. *Annu. Rev. Biochem. 51*, 531−554.

(30) Arano, Y., Mukai, T., Akizawa, H., Uezono, T., Motonari, H., Wakisaka, K., Kairiyama, C., and Yokoyama, A. (1995) Radiolabeled metabolites of protein play a critical role in radioactivity elimination from the liver. *Nucl. Med. Biol. 22*, 555−564.

(31) Rogers, B. E., Franano, F. N., Duncan, J. R., Edwards, W. B., Anderson, C. J., Connett, J. M., and Welch, M. J. (1995) Identification of metabolites of In-111-diethylenetriaminepentaacetic acid monoclonal antibodies and antibody fragments in vivo. *Cancer Res. 55*, S5714−S5720.

(32) Edwards, D. S., Liu, S., Barrett, J. A., Harris, A. R., Looby, R. J., Ziegler, M. C., Heminway, S. J., and Carroll, T. R. (1997) New and versatile ternary ligand system for technetium radiopharmaceuticals: water soluble phosphines and tricine as coligands in labeling a hydrazinonicotinamide-modified cyclic glycoprotein IIb/IIIa receptor antagonist with ^{99m}Tc. *Bioconjugate Chem. 8*, 146−54.

(33) Lee, Y. C., Stowell, C. P., and Krantz, M. J. (1976) 2-Imino-2-methoxyethyl 1-thioglycosides: new reagents for attaching sugars to proteins. *Biochemistry 15*, 3956−3963.

(34) Stowell, C. P., and Lee, Y. C. (1980) Preparation of some new neoglycoproteins by amidination of bovine serum albumin using 2-imino-2-methoxyethyl 1-thioglycosides. *Biochemistry 19*, 4899−4904.

(35) Dubois, M., Gilles, K. A., Hamilton, J. K., Rebers, P. A., and Smith, F. (1956) Colorimetric method for determination of sugars and related substances. *Anal. Chem. 28*, 350−356.

(36) King, T. P., Zhao, S. W., and Lam, T. (1986) Preparation of protein conjugates via intermolecular hydrazone linkage. *Biochemistry 25*, 5774−5779.

(37) Meares, C. F., McCall, M. J., Reardan, D. T., Goodwin, D. A., Diamanti, C. I., and McTigue, M. (1984) Conjugation of antibodies with bifunctional chelating agents: isothiocyanate and bromoacetamide reagents, methods of analysis, and subsequent addition of metal ions. *Anal. Biochem. 142*, 68−78.

(38) Imai, S., Morimoto, J., Tsubura, T., Esaki, K., Michalides, R., Holms, R. S., Deimling, O., and Higlgers, J. (1986) Genetic

marker patterns and endogenous mammary tumor virus genes in inbred mouse strains in Japan. *Exp. Anim. 35*, 263−276.

(39) Alquier, C., Guenin, P., Munari-Silem, Y., Audebet, C., and Rousset, B. (1985) Isolation of pig thyroid lysosomes. *Biochem. J. 232*, 529−537.

(40) Caimi, L., Marchesini, S., Aleo, M. F., Bresciani, R., Monti, E., Casella, A., Guidici, M. L., and Preti, A. (1989) Rapid preparation of a distinct lysosomal population from myelinating mouse brain using Percoll gradients. *J. Neurochem. 52*, 1722−1728.

(41) Distler, J., and Jourdian, G. W. (1978) B-Galactosidase from bovine testes. *Methods Enzymol. 50* (part C), 514−520.

(42) Fritzberg, A. R., Berninger, R. W., Hardley, S. W., and Wester, D. W. (1988) Approaches to radiolabeling of antibodies for diagnosis and therapy of cancer. *Pharm. Res. 5*, 325−334.

(43) Liu, S., Edwards, D. S., Looby, R. J., Poirier, M. J., Rajopadhye, M., Bourque, J. P., and Carroll, T. R. (1996) Labeling cyclic glycoprotein IIb/IIIa receptor antagonists with Tc-99m by the preformed chelate approach: Effects of chelators on properties of [Tc-99m]chelator-peptide conjugates. *Bioconjugate Chem. 7*, 196−202.

(44) Arano, Y., Mukai, T., Uezono, T., Motonari, H., Wakisaka, K., and Yokoyama, A. (1994) Biological comparison of DTPA and SCN−Bz-EDTA as a chelating agent for indium labeling of antibodies. *J. Laballed Compd. Radiopharm. 35*, 381−383.

(45) Mukai, T., Arano, Y., Nishida, K., Sasaki, H., Saji, H., and Nakamura, J. (1999) Pharmacokinetic estimation of ^{111}In-DTPA-labeling for assessment of sites of protein catabolism in vivo. *J. Pharm. Pharmacol. 51*, 15−20.

(46) Hnatowich, D. J., Mardirossian, G., Rusckowski, M., Fogarasi, M., Virzi, F., and P. Winnard, J. (1993) Directly and indirectly technetium-99m-labeled antibodies-a comparison of in vitro and animal in vivo properties. *J. Nucl. Med. 34*, 109−119.

BC980105F

Temperature Control of Biotin Binding and Release with A Streptavidin-Poly(*N*-isopropylacrylamide) Site-Specific Conjugate

Zhongli Ding, Cynthia J. Long, Yoshiki Hayashi, Esma V. Bulmus, Allan S. Hoffman,*,† and Patrick S. Stayton*,‡

Department of Bioengineering, University of Washington, Seattle, Washington 98195.
Received September 11, 1998; Revised Manuscript Received February 2, 1999

The many laboratory and diagnostic applications utilizing streptavidin as a molecular adaptor rely on its high affinity and essentially irreversible interaction with biotin. However, there are many situations where recovery of the biotinylated molecules is desirable. We have previously shown that poly(*N*-isopropylacrylamide) (PNIPAAm), a temperature-sensitive polymer, can reversibly block biotin association as the polymer's conformation changes at its lower critical solution temperature (LCST). Here, we have constructed a streptavidin−PNIPAAm conjugate which is able to bind biotin at room temperature or lower and release bound biotin at 37 °C. The conjugate can repeatedly bind and release biotin as temperature is cycled through the LCST. A genetically engineered streptavidin mutant, E116C, which has only one cysteine residue, was conjugated site specifically via the sulfhydryl groups with a PNIPAAm that has pendent sulfhydryl-reactive vinyl sulfone groups. The conjugation site is near the tryptophan 120 residue, which forms a van der Waals contact with biotin that is important in generating the large binding free energy. The temperature-induced conformational change of the polymer at position 116 may lead to structural changes in the region of tryptophan 120 that are responsible for the reversible binding between biotin and the conjugated streptavidin.

INTRODUCTION

Diverse and widespread applications utilizing streptavidin as a molecular adaptor have been developed that utilize the tight binding of biotin to the protein (ca. 10^{13-15} M^{-1}) (*1*). Streptavidin can be detected and quantitated with high sensitivity in such complexes by labeling it with enzymes, fluorescent, chemiluminescent, or radioactive agents, and metals. Labeled streptavidin has been used to detect proteins on a cell surface (*2*), to visualize and quantitate blots (*3*−*7*), and to perform an enzyme-linked immunosorbent assay ELISA (*8*−*12*). Streptavidin can also be readily immobilized at surfaces to capture biotinylated molecules or cells. These surfaces are used to detect and separate molecules or cells of interest from complex mixtures (*13*, *14*). Isolation of polymerase chain reaction (PCR) products is simplified by employing streptavidin-immobilized magnetic microbeads (*15*−*17*). Streptavidin has also been investigated for targeted delivery of drugs or immunotoxins (*18*).

These applications rely on the essentially irreversible binding of biotin and streptavidin. However, there are many cases in which dissociation of bound biotin is desired to recover biotinylated molecules or cells, or to release therapeutic reagents at targeted sites. Currently, harsh denaturing conditions are used to dissociate biotin from streptavidin (*19*). These denaturing conditions are undesirable especially to bioseparations. Thus, it is an important goal to effect the capture and release of biotinylated molecules and cells under mild conditions. We have developed a streptavidin−temperature sensitive polymer conjugate in which the polymer is covalently and site specifically linked to the outer edge of the biotin-binding site (*20*). The biotin-binding sites of the conjugate can be blocked by a small change of temperature. The collapse of the polymer did not release bound biotin, however. Morag et al. (*21*) have derivatized the tyrosine residues within the binding sites of avidin or streptavidin with tetranitromethane. The nitro-avidin is able to bind biotin at low pH and release bound biotin at high pH.

Our approach to developing a reversible biotin-binding system is to site specifically conjugate a stimuli-sensitive polymer to streptavidin. Control of biotin-binding is achieved by manipulating the conformation of the polymer, which can be specifically designed to respond sharply to changes in temperature, pH, and even light. For example, we have previously conjugated PNIPAAm to an N49C mutant of streptavidin to reversibly block biotin binding. PNIPAAm is a temperature-sensitive polymer that exhibits lower critical solution temperature (LCST) behavior, in which the polymer changes from a water-soluble coil to a water-insoluble collapsed (dehydrated) globule as temperature increases through the LCST. PNIPAAm and other stimuli-sensitive polymers have been used for enzyme recovery (*22*−*24*), affinity separation (*25*), immunoassay (*26*), and drug delivery (*27*, *28*). In this paper, we present our investigation of a new streptavidin conjugation site, that was designed near an important binding site residue. By changing the location of the mutation site of streptavidin and the structure of the polymer, we are now able both to block biotin binding and to release the bound biotin by changing temperature.

EXPERIMENTAL PROCEDURES

Materials. *N*-Isopropylacrylamide (NIPAAm, Eastman Kodak, Rochester, NY) was purified by recrystalli-

* To whom correspondence should be addressed.
† Box 352255. Phone: 206-543-9423. Fax: 206-543-6124. E-mail: hoffman@bioeng.washington.edu.
‡ Box 352125. Phone: 206-685-8148. Fax: 206-685-8256. E-mail: stayton@bioeng.washington.edu.

10.1021/bc980108s CCC: $18.00 © 1999 American Chemical Society
Published on Web 04/22/1999

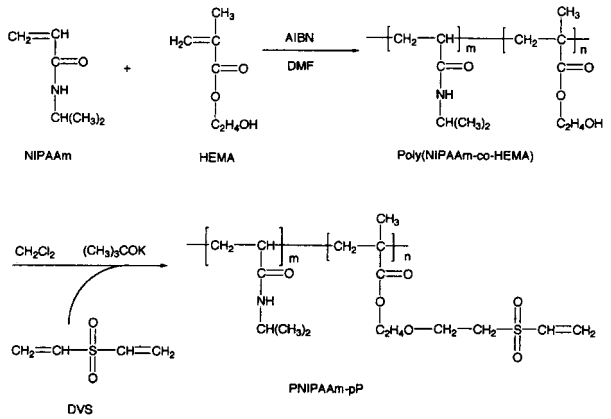


Figure 1. Scheme of synthesis and derivatization of poly(NIPAAm-*co*-HEMA).

zation from *n*-hexane. Methanol was used to recrystallize 2,2′-azoisobutyronitrile (AIBN) (J. T. Baker, Phillipsburg, NJ). To purify 2-hydroxyethyl methylacrylate (Aldrich, Milwaukee, WI), distillation under reduced pressure was employed. Divinyl sulfone (DVS) and d-biotin were purchased from Aldrich (Milwaukee, WI) and used without treatment. d-[8,9-^{3}H]Biotin is a product of Amersham Life Science (Buckinghamshire England). Trypsin, type III from bovine pancreas, was purchased from Sigma (Sigma, St. Louis, MO). Dehydrated dimethylformamide (Sigma, St. Louis, MO) was used without further treatment. Tris-(2-carboxyethyl) phosphine (HCl) (TCEP) (Pierce, Rockford, IL) was used as received. Tosyl-activated magnetic microbeads (DYNABEADS M-280, Dynal, Inc. Lake Success, NY) (TMB) were used. All other reagents were of analytical grade. *Msc*I and *Mlu*I restriction enzymes and T4 DNA Ligase were purchased from New England Biolabs (Beverly, MA). Qiaex II kit for extracting DNA was purchased from Qiagen (Santa Clarita, CA). pET21a vector was obtained from Novagen (Madison, WI).

Preparation and Activation poly(NIPAAm). A copolymer of (NIPAAm-*co*-HEMA) was prepared by free-radical polymerization using AIBN as an initiator, as shown in Figure 1. NIPAAm (11.3 g), HEMA (0.503 mL), and AIBN (0.164 g) were added to 50 mL of dehydrated DMF. The solution was degassed by freezing, evacuating, and thawing three times and then sealed. Polymerization was carried out at 60 °C for 20 min. The conversion of monomers was controlled within 20% in order to obtain relatively homogeneous composition of copolymer. The copolymer was collected by precipitation in diethyl ether and dried in a vacuum oven. For further purification, the dried copolymer was redissolved in 40 mL of dichloromethane and precipitated in diethyl ether. The molecular weight of the copolymer was determined by vapor pressure osmometry (VPO, model OSV111 from Knauer, German). Proton NMR spectroscopy was performed with a Bruker 200 MHz instrument to evaluate the composition of the copolymer. ^{1}H NMR (dimethyl sulfoxide-d_6): 5.05 ppm (1H, −OH) and 7.25 ppm (1H, −NH).

The hydroxyl groups of HEMA in the copolymer were further reacted with DVS in alkaline conditions, as shown in Figure 1. The copolymer and DVS were dissolved in dichloromethane. The solution was purged with nitrogen at room temperature for 30 min before addition of 0.03 g of potassium tert-butoxide. The reaction was carried out at room temperature for 16 h under protection of nitrogen. The derivatized copolymer was isolated by precipitation in diethyl ether. The derivatized copolymer was submitted to NMR analysis and Ellman's reagent analysis (*29*, *30*) for determination of VS content. ^{1}H NMR (dimethyl sulfoxide-d_6): 6.21 ppm (2H, $=CH_2$), 6.97 ppm (1H, $-SO_2CH=$), and 7.20 ppm (1H, −NH). In the Ellman's assay, the polymer was reacted with excess of cystamine followed by titrating the remaining cystamine with Ellman's reagent. Since the copolymer has pendant reactive groups, the VS groups, the copolymer is denoted as PNIPAAm-pP. Thermal responsiveness of PNIPAAm-pP was determined spectroscopically using 0.23 wt % of copolymer solution.

Genetic Engineering of Streptavidin. The streptavidin mutant E116C was constructed by site-directed, cassette mutagenesis, using a synthetic "core" streptavidin gene previously designed and constructed for protein expression in *Escherichia coli* (*31*). Oligonucleotides were designed to substitute glutamic acid at position 116 with cysteine. The following sense and anti-sense oligonucleotides were obtained from Integrated DNA Technologies (Coralville, IA) (the bold-face type indicates amino acid change): 5′CCAGTACGTTGGTGGTGCTGAAGCTCGTATCAACACCCAGTGGTTGTTGACCTCCGGCACCACC**TGC**GCTAA-3′ and 3′GGTCATGCAACCACCACGACTTCGAGCATAGTTGTGGGTCACCAACAACTGGAGGCCGTGGTGG**ACG**CGATTGCGC-5′.

The streptavidin gene in pUC18 was digested with *Msc*I and *Mlu*I restriction enzymes, isolated on a 1.2% agarose gel, extracted, and purified using Qiaex II kit. The synthetic oligonucleotides, designed with *Msc*I and *Mlu*I ends, were annealed then ligated into the pUC18/StAv vector using T4 DNA Ligase. The DNA sequence of the mutant gene was confirmed using automated dyedeoxy sequencing (PE Applied Biosystems, Foster City, CA). The streptavidin mutant (StAv/E116C) gene was subsequently subcloned into pET21a for expression in *E. coli* strain BL21(DE3). The protein was expressed and refolded using established protocols. Analysis of the E116C streptavidin mutant included SDS−PAGE, mass spectrometry, and biotin-binding studies.

Conjugation of Polymer to Protein. Conjugation between E116C and PNIPAAm-pP was carried out in 100 mM sodium tetraborate buffer, pH 8.5, containing 50 mM sodium chloride and 5 mM EDTA at 4 °C for 16 h. Cysteine residues of E116C form disulfide bonds during storage. To reduce disulfide bonds to sulfhydryl groups, TCEP at 50-fold molar excess to E116C was used. PNIPAAm-pP in 50-fold molar excess to E116C was used in order to obtain high conjugation efficiency. The conjugate, denoted as E116C-pP, was separated from unconjugated E116C by thermal-induced precipitation, i.e., centrifuging the mixture at 15 000 rpm (31000*g*) for 15 min at 37 °C. The unconjugated E116C was retained in the supernatant. The thermal-induced precipitation was repeated twice for further purification.

Immobilization of Conjugates. Tosyl-activated magnetic beads were used to immobilize the conjugate, E116C, and trypsin-pP. E116C-pP conjugate dissolved in 100 mM sodium tetraborate buffer, pH 9.5 (concentration = 100 μg/mL) was mixed with TMB in a ratio of E116C-pP:TMB = 100 μg:1 mg. The mixture was rotated head-over-end at 37 °C for 16 h. The E116C-pP immobilized beads (E116C-pP-TMB) were washed with and redispersed in 100 mM sodium phosphate buffer, pH 7.4 (PB). The efficiency of immobilization was determined by mass balance determination of protein loss from solution, which was quantified by the absorbance at λ = 280 nm. A trypsin-pP immobilized magnetic bead surface was used as a control.

Biotin-Binding Assay. [^{3}H]Biotin was employed to quantitate biotin binding. To eliminate unconjugated

biotin-binding sites from interfering with biotin-binding assay, the E116C-pP-TMB was presaturated with cold biotin at 37 °C. To do so, $10^{-9}-10^{-10}$ mol of E116C-pP-TMB was incubated at 37 °C for 1 h followed by mixing with 10-fold excess unlabeled biotin at 37 °C. The mixture was incubated at 37 °C for 1 h to allow complete biotin binding to the unconjugated sites. Unbound biotin was removed by washing the beads with PB at 37 °C five times. [^{3}H]Biotin was then added to the presaturated E116C-pP-TMB at 37 °C. One hour incubation was allowed to reach an equilibrium. An aliquot was taken from the supernatant to determine the [^{3}H]biotin concentration in the supernatant using a β-counter (LS7000 Liquid scintillation system, Beckman Instruments, Inc. Fullerton, CA). The bead suspension was then incubated at 4 °C for 1 h to reach a biotin-binding equilibrium before the biotin concentration of the supernatant was measured. Temperature cycling continued three times. [^{3}H]Biotin concentration of supernatant after incubation at each temperature was determined by a β-counter. Bound biotin was quantitated by the following formula:

$$Q_T = Q_0 - Q_{S/N,T}$$

where Q_T is the bound biotin (mol) at temperature T (°C), Q_0 is the total amount of [^{3}H]biotin (mol) added to the E116C-pP-TMB suspension, and $Q_{S/N,T}$ is the quantity of [^{3}H]biotin (mol) remaining in the supernatant after incubation at temperature T (°C)

The blocking or releasing efficiency was represented by following formula:

$$B\ (\%) = (Q_{4°C} - Q_{37°C}) \times 100/Q_{4°C}$$

Measurement of Cumulative Release of Bound Biotin. Immobilized E116C or E116C-pP-TMB, which was presaturated with cold biotin at 37 °C, was mixed with [^{3}H]biotin at 4 °C for 1 h to allow biotin binding. The mixtures were then incubated at 37 °C for 1 h. To collect the released biotin, the supernatant was removed from the mixture after incubation at 37 °C. The beads were washed with prewarmed (37 °C) PB and then redispersed in the same volume of PB for the next cycle. [^{3}H]Biotin concentration in the supernatant was measured to quantify the cumulative release of [^{3}H]biotin.

RESULTS AND DISCUSSION

P(NIPAAm-*co*-HEMA) and PNIPAAm-pP were characterized by VPO, ^{1}H NMR, and Ellman's reagent. VPO analysis showed that the P(NIPAAm-*co*-HEMA) had a number average molecular weight (Mn) of 7500. ^{1}H NMR analysis demonstrated that all of the hydroxyl groups in the copolymer were converted to vinyl sulfone groups in the derivatization step. Analysis using Ellman's Reagent showed that the vinyl sulfone group content in the copolymer was 4.5 mol %, indicating that every copolymer chain had an average of three vinyl sulfone groups. Figure 2 shows the thermal-responsive properties of P(NIPAAm-*co*-HEMA) and PNIPAAm-pP. It is interesting that the LCST of P(NIPAAm-*co*-HEMA) (32.1 °C) is similar to that of a NIPAAm homopolymer (32−33 °C). Vinyl sulfone derivatization makes polymer more hydrophobic because the LCST of PNIPAAm-pP (27.5 °C) is lower than that of P(NIPAAm-*co*-HEMA). The LCST of PNIPAAm-pP in PB (20.2 °C) is much lower than that in water (27.5 °C). Hence, the salt has a strong effect on the thermal-responsiveness of PNIPAAm-pP.

Studies have shown that the tryptophan-120 plays an important role in generating a large binding free energy

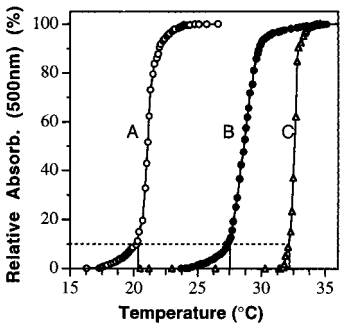


Figure 2. The LCSTs of PNIPAAm-pP in sodium phosphate buffer (A), in deionized and distilled water (B), and that of poly(NIPAAm-*co*-HEMA) in deionized and distilled water (C). Polymer concentration was 0.20 wt %. The LCST is defined as the temperature at which the polymer solution is of 10% of maximum turbidity.

by forming van der Waals contact with biotin (*31*). Conformational change at this site may affect the binding properties significantly. Hence, we desinged a conjugation site near the tryptophan-120. Site-directed mutagenesis techniques were used to replace the native glutamate at position 116 with cysteine. As shown in Figure 3, this cysteine is near tryptophan-120, located on the same loop that contributes to the binding site from an adjacent subunit. Conjugation of the polymer to the E116C mutant was achieved by reacting the vinyl sulfone groups of the PNIPAAm-pP with the genetically engineered sulfhydryl groups (*29*), as shown in Figure 4. Since every monomer of E116C mutant has only one cysteine, the conjugation is site specific. To avoid possible reaction between the vinyl sulfone and primary amines of the protein, which becomes significant only at higher pH (*32*), we used pH 8.5 for the conjugation to minimize this side reaction. The conjugation reaction is quite efficient. A typical conjugate yield is 70%. The conjugate was subsequently immobilized on magnetic microbeads. A commonly used method to immobilize streptavidin on a surface is to use biotinylated solid substrates. However, such biotin-immobilized streptavidin may release from the surface due to the exchange of immobilized biotin with free biotin. Therefore, covalent linkage was used to immobilize streptavidin onto magnetic microbeads, as shown in Figure 4. The efficiency of immobilization, or the percentage of protein which is immobilized, ranged from 30 to 80%.

To maximize the sensitivity of analysis of the temperature responsiveness of the conjugate, the E116C-pP-TMB system was presaturated with biotin at 37 °C. Our studies have indicated that not all of the biotin-binding sites of an E116C molecule are conjugated with copolymer. The biotin-binding properties of the polymer-conjugated sites should show temperature dependence while the unconjugated sites should not show a significant effect of temperature on binding or release of biotin. Presaturating the unconjugated sites with unlabeled biotin reduces the signal from unconjugated binding sites.

Figure 5 shows the changes in the biotin-binding capacity of the E116C-pP-TMB as a function of temperature. The first temperature cycle shows that the polymer at position 116 can block the association of biotin at 37 °C while leaving the binding site open to biotin at 4 °C. In the second cycle, when the temperature was increased from 4 to 37 °C, where the polymer collapsed, a significant fraction of the bound biotin was released. When the temperature was decreased from 37 to 4 °C, the unoccupied polymer-conjugated sites were able to rebind biotin. Therefore, biotin can be bound to and released

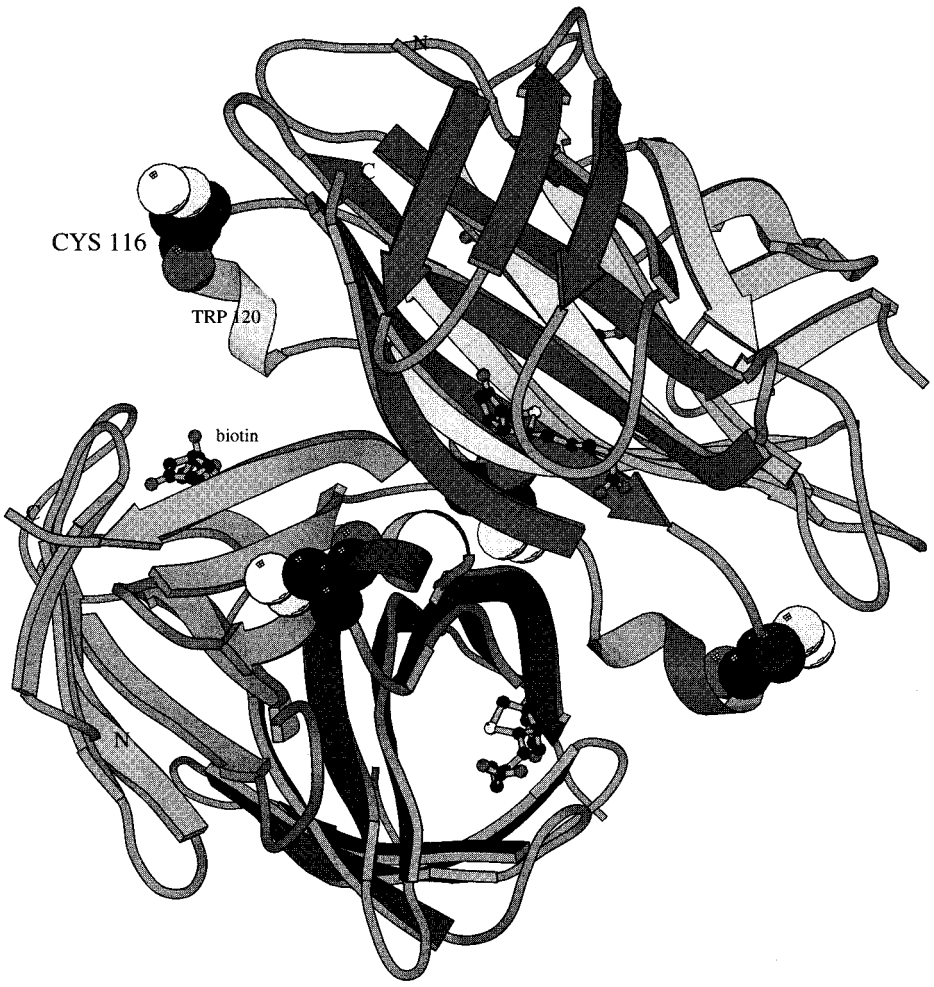


Figure 3. Computer model of the E116C mutant binding site.

from the conjugate by changing the temperature from below to above the polymer's LCST.

The biotin-binding properties of the unconjugated E116C streptavidin are shown in Figure 6 which demonstrates that the immobilized E116C mutant does not display a significant temperature-dependent change of % biotin bound over one cycle. Furthermore, Figure 7 shows that neither a control trypsin-PNIPAAm immobilized conjugate nor the unreacted magnetic bead surface adsorbs or traps biotin at 37 or 4 °C. These controls support the conclusion that the temperature responsiveness of biotin binding shown in Figure 5 is due to the unique site-specific conjugation of E116C with the thermally sensitive PNIPAAm.

To further investigate the release of bound biotin from polymer-conjugated sites, we have conducted cumulative release experiments. Figure 8 shows that all of the bound biotin to the polymer-conjugated sites is released after four washing cycles. It is also shown that repeatedly changing the temperature is necessary to release all of the bound biotin. It should be noted that the complete release of bound biotin is not a consequence of protein denaturation because the conjugate is able to bind biotin after the washes. Figure 8 also shows that about 17% of bound biotin is released from immobilized E116C streptavidin with four washes. Streptavidin has an off-rate of 3.24×10^{-5} (s^{-1}) at 37 °C and 1.03×10^{-7} (s^{-1}) at 4 °C (*33*). It has also been shown that biotin-binding activity decreases when streptavidin is immobilized on a solid surface (*34*). In the cumulative release experiments, the biotin concentration of supernatant was very low because the supernatant was replaced with fresh buffer in every cycles. All these facts may contribute to the release of small amounts of bound biotin from the E116C. However, the biotin release from E116C is significantly less than that from the conjugate.

While the precise mechanism by which polymer collapse causes release of biotin cannot be determined experimentally, it is likely that the polymer conformational change alters the conformation of the tryptophan 120 loop. The radius of the PNIPAAm molecules reduces to half of its original radius upon collapse (*35*, *36*). This conformational change is transmitted to the biotin-binding site, as demonstrated by the change in biotin affinity that leads to biotin release. Because one PNIPAAm-pP chain contains three vinyl sulfone groups on average, it is possible that one copolymer chain is conjugated to more than one site on the protein. We observed such multiple-point conjugation, as indicated by formation of insoluble gel when conjugation was performed at high concentrations of protein and the polymer. The multiple-point conjugation may transmit the conformational change from the polymer to the protein more efficiently.

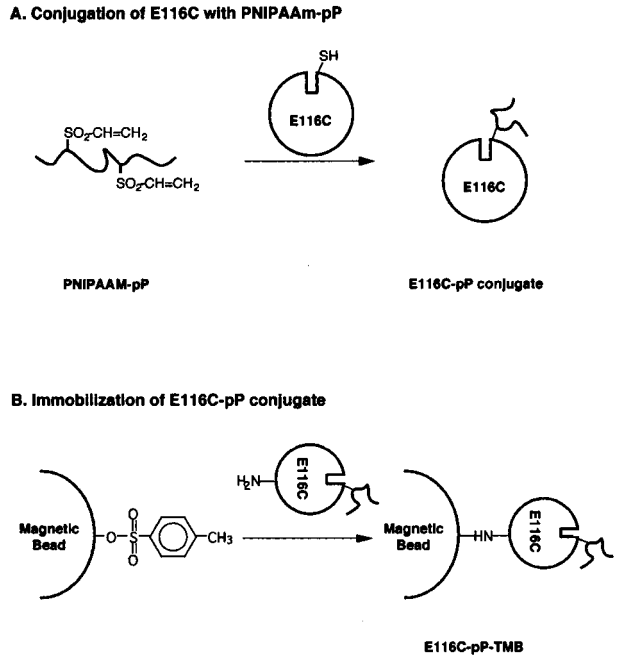


Figure 4. Conjugation of E116C with PNIPAAm-pP and immobilization of E116C-pP conjugate.

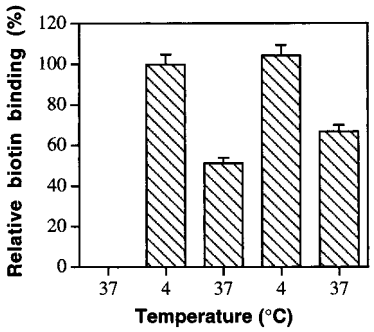


Figure 5. Temperature effect on biotin binding to immobilized E116C-pP conjugate. The data presented are an average of triplicate determinations. The amount of bound biotin at the first 37 °C is zero. Magnetic beads (Dynal M-280) immobilized with 5.4×10^{-10} mol of E116C-pP were used for the assay. Sodium phosphate buffer, pH 7.4, 100 mM was used as the medium.

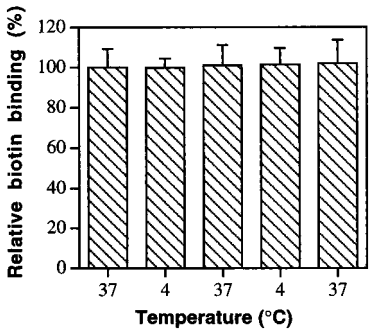


Figure 6. Temperature effect on biotin binding to immobilized E116C. The data presented are an average of triplicate determinations. Magnetic beads (Dynal M-280) immobilized with 5.4×10^{-10} mol of E116C were used for the assay. Sodium phosphate buffer, pH 7.4, 100 mM was used as the medium.

CONCLUSIONS

We have prepared a new site-specific conjugate of streptavidin with a temperature-sensitive polymer. When this conjugate is thermally stimulated, it is able to reversibly bind and release biotin because of the unique combination of specific conjugation sites on a genetically engineered protein and a stimuli-responsive copolymer. The conjugate binds biotin at 4 °C where the polymer is hydrated and releases a significant fraction of bound biotin at 37 °C where the polymer is collapsed. By combining temperature cycling between 4 and 37 °C with washing at 37 °C, all of the bound biotin can be released. The conjugate is immobilized on magnetic microbeads and can be used to capture and to recover biotin. This system is potentially useful for separation and recovery of biotinylated substances without the need for harsh elution conditions.

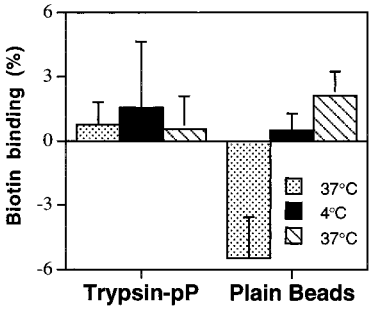


Figure 7. Nonspecific adsorption of biotin to various surfaces. The data presented are an average of triplicate determinations. Magnetic beads (Dynal M-280) immobilized with 1.0×10^{-9} mol of trypsin-pP were used for the assay. Sodium phosphate buffer, pH 7.4, 100 mM was used as the medium.

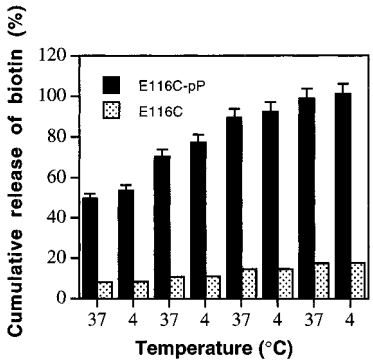


Figure 8. Cumulative release of bound biotin from immobilized E116C and E116C-pP. The data presented are an average of duplicate experiments. Magnetic beads (Dynal M-280) immobilized with 5.4×10^{-10} mol of E116C-pP were used for the assay. Sodium phosphate buffer, pH 7.4, 100 mM was used as the medium.

ACKNOWLEDGMENT

We would like to thank Prof. J. Milton Harris for his advise on derivatization of polymer hydroxyl to vinyl sulfone groups. The NIH (Grant No. R01GM53771), UW Office of Technology Transfer, the Washington Research Foundation and the Washington Technology Center are gratefully acknowledged for their support of this project.

LITERATURE CITED

(1) Weber, P. C., Ohlendore, D. H., Wendoloski, J. J., and Salemme, F. R. (1989) Structural origins of high-affinity biotin binding to streptavidin. *Science 243*, 85−8.

(2) Gallivan, J. P., Lester, H. A., and Dougherty, D. A. (1997) Site-specific incorporation of biotinylated amino acids to identify surface-exposed residues in integral membrane proteins. *Chemistry Biol. 4*, 739−49.

(3) Peranen, J. (1992) Rapid affinity-purification and biotinylation of antibodies. *Biotechniques 13*, 546−9.

(4) King, G., Payne, S., Walker, F., and Murray, G. I. (1997) A highly sensitive detection method for immunohistochemistry using biotinylated tyramine. *J. Pathol. 183*, 237−41.
(5) Narendja, F. M., and Sauermann, G. (1994) The use of biotinylated poly(ADP-ribose) for studies on poly(ADP-ribose)-protein interaction. *Anal. Biochem. 220*, 415−9.
(6) Stevenson, B. R., Richards, C. L., Howarth, A. G., Maraj, V. A., and Hibbard, J. G. (1994) Quantitative immunoblot detection of rare proteins in whole cell extracts using biotin-strepavidin reagents. *J. Exp. Zool. 268*, 224−8.
(7) Hoeltke, H. J., Ettl, I., Strobel, E., Leying, H., Zimmermann, M., and Zimmermann, R. (1995) Biotin in vitro translation, nonradioactive detection of cell-free synthesized proteins. *Biotechniques 18*, 900−4, 906−7.
(8) Stephens, R. W., Pedersen, A. N., Nielsen, H. J., Hamers, M. J. A. G., Hoyer, H. G., Ronne, E., Dybkjaer, E., Dano, K., and Bruenner, N. (1997) ELISA determination of soluble urokinase receptor in blood from healthy donors and cancer patients. *Clin. Chem. 43*, 1868−76.
(9) Gutierrez, R., Garcia, T., Gonzalez, I., Sanz, B., Hernandez, P. E., and Martin, R. (1997) A quantitative PCR-ELISA for the rapid enumeration of bacteria in refrigerated raw milk. *J. Appl. Microbiol. 83*, 518−23.
(10) Muller, R. (1997) Timed ELISA: An alternative approach to quantitative enzyme-linked immunosorbent assay. *Biotechnol. Appl. Biochem. 26*, 73−78.
(11) Schlosser, M., Hahmann, J., Ziegler, B., Augstein, P., and Ziegler, M. (1997) Sensitive monoclonal antibody-based sandwich ELISA for determination of the diabetes-associated autoantigen glutamic acid decarboxylase GAD65. *J. Immunoassay 18*, 289−307.
(12) Shankar, G., and Cohen, D. A. (1997) Enhanced cytokine detection by a novel cell culture-based ELISA. *J. Immunoassay 18*, 371−88.
(13) Kossek, S., Padeste, C., and Tiefenauer, L. (1996) Immobilization of streptavidin for immunosensors on nanostructured surfaces. *J. Mol. Recognit. 9*, 485−7.
(14) Kim, D. R., and McHenry, C. S. (1996) Biotin tagging deletion analysis of domain limits involved in protein-macromolecular interactions. Mapping the tau binding domain of the DNA polymerase III alpha subunit. *J. Biol. Chem. 271*, 20690−8.
(15) Refseth, U. H., Fangan, B. M., and Jakobsen, K. S. (1997) Hybridization capture of microsatellites directly from genomic DNA. *Electrophoresis 18*, 1519−23.
(16) Rolfs, A., and Weber, I. (1994) Fully automated, nonradioactive solid-phase sequencing of genomic DNA obtained from PCR. *Biotechniques 17*, 782−4.
(17) Pettersson, B., Johansson, K. E., and Uhlen, M. (1994) Sequence analysis of 16S rRNA from mycoplasmas by direct solid-phase DNA sequencing. *Appl. Environ. Microbiol. 60*, 2456−61.
(18) Muzykantov, V. R., Gavriluk, V. D., Reinecke, A., Atochina, E. N., Kuo, A., Barnathan, E. S., and Fisher, A. B. (1995) The functional effects of biotinylation of anti-angiotensin-converting enzyme monoclonal antibody in terms of targeting in vivo. *Anal. Biochem. 226*, 279−87.
(19) Weidner, J., Eigel, A., Horst, J., and Koehnlein, W. (1994) Nonisotopic detection of mutations using a modified single-strand conformation polymorphism analysis. *Human Mutat. 4*, 55−6.
(20) Stayton, P. S., Shimoboji, T., Long, C., Chilkoti, A., Chen, G., Harris, J. M., and Hoffman, A. S. (1995) Control of protein−ligand recognition using a stimuli-responsive polymer. *Nature 378*, 472−4.
(21) Morag, E., Bayer, E. A., and Wilchek, M. (1996) Reversibility of biotin-binding by selective modification of tyrosine in avidin. *Biochem. J. 316*, 193−9.
(22) Ding, Z. L., Chen, G. H., and Hoffman, A. S. (1996) Synthesis and purification of thermally sensitive oligomer-enzyme conjugates of poly(N-isopropylacrylamide)-trypsin. *Bioconjugate Chem. 7*, 121−5.
(23) Ding, Z. L., Chen, G., and Hoffman, A. S. (1998) Unusual properties of thermally sensitive oligomer-enzyme conjugates of poly(N-isopropylacrylamide)-trypsin. *J. Biomed. Mater. Res. 39*, 498−505.
(24) Takei, Y. G., Matsukata, M., Aoki, T., Sanui, K., Ogata, N., Kikuchi, A., Sakurai, Y., and Okano, T. (1994) Temperature-responsive bioconjugates. 3. Antibody-poly (N−isopropylacrylamide) conjugates for temperature-modulated precipitations and affinity bioseparations. *Bioconjugate Chem. 5*, 577−82.
(25) Chen, J. P., and Hoffman, A. S. (1990) Polymer-protein conjugates. II. Affinity precipitation of human IgG by poly(N-isopropylacrylamide)-protein A conjugates. *Biomaterials 11*, 631−4.
(26) Monji, N., and Hoffman, A. S. (1987) A novel immunoassay system and bioseparation process based on thermal phase separating polymers. *Appl. Biochem. Biotechnol 14*, 107−20.
(27) Hoffman, A. S., Afrassiabi, A., and Dong, L. C. (1986) Thermally reversible hydrogels: II. Delivery and selective removal of substances in aqueous solutions. *J. Controlled Rel. 4*, 213−22.
(28) Yoshida, R., Kaneko, Y., Sakai, K., Okano, T., Sakurai, Y., Bae, Y. H., and Kim, S. W. (1994) Positive thermosensitive pulsatile drug release using negative thermosensitive hydrogels. *J. Controlled Rel. 32*, 97−102.
(29) Morpurgo, M., Veronese, F. M., Kachensky, D., and Harris, J. M. (1996) Preparation and characterization of poly(ethylene glycol) vinyl sulfone. *Bioconjugate Chem. 7*, 363−8.
(30) Riddles, P. W., Blakeley, R. L., and Zerner, B. (1983) Reassessment of Ellman's reagent. *Methods Enzymol. 91*, 49−60.
(31) Chilkoti, A., Tan, P. H., and Stayton, P. S. (1995) Site-directed mutagenesis studies of the high-affinity streptavidin−biotin complex: contributions of tryptophan residues 79, 108, and 120. *Proc.Natl. Acad. Sci. U.S.A. 92*, 1754−8.
(32) Magnani, M., Chiarantini, L., and Mancini, U. (1994) Preparation and characterization of biotinylated red blood cells. *Biotechnol. Appl. Biochem. 20*, 335−45.
(33) Unpublished data.
(34) Huang, S. C., Stump, M. D., Weiss, R., and Caldwell, K. D. (1996) Binding of biotinylated DNA to streptavidin-coated polystyrene latex: effects of chain length and particle size. *Anal. Biochem. 237*, 115−22.
(35) Wu, C., and Zhou, S. (1995) Thermodynamically stable globule state of a single poly(N-isopropylacrylamide) chain in water. *Macromolecules 28*, 5388−90.
(36) Tiktopulo, E. I., Uversky, V. N., Lushchik, V. B., Klenin, S. I., Bychkova, V. E., and Ptitsyn, O. B. (1995) "Domain" coil-globule transition in homopolymers. *Macromolecules 28*, 7519−24.

BC980108S

Hemolytic Activity of pH-Responsive Polymer-Streptavidin Bioconjugates†

Chantal A. Lackey,‡ Niren Murthy,‡ Oliver W. Press,§ David A. Tirrell,|| Allan S. Hoffman,*,⊥ and Patrick S. Stayton*,#

Department of Bioengineering and Department of Medicine, University of Washington, Seattle, WA 98195, and Department of Chemical Eng'g, Calif. Institute of Technology, Pasadena CA. Received September 11, 1998; Revised Manuscript Received March 11, 1999

Drug delivery systems that increase the rate and/or quantity of drug release to the cytoplasm are needed to enhance cytosolic delivery and to circumvent nonproductive cell trafficking routes. We have previously demonstrated that poly(2-ethylacrylic acid) (PEAAc) has pH-dependent hemolytic properties, and more recently, we have found that poly(2-propylacrylic acid) (PPAAc) displays even greater pH-responsive hemolytic activity than PEAAc at the acidic pHs of the early endosome. Thus, these polymers could potentially serve as endosomal releasing agents in immunotoxin therapies. In this paper, we have investigated whether the pH-dependent membrane disruptive activity of PPAAc is retained after binding to a protein. We did this by measuring the hemolytic activity of PPAAc−streptavidin model complexes with different protein to polymer stoichiometries. Biotin was conjugated to amine-terminated PPAAc, which was subsequently bound to streptavidin by biotin complexation. The ability of these samples to disrupt red blood cell membranes was investigated for a range of polymer concentrations, a range of pH values, and two polymer-to-streptavidin ratios of 3:1 and 1:1. The results demonstrate that (a) the PPAAc−streptavidin complex retains the ability to lyse the RBC lipid bilayers at low pHs, such as those existing in endosomes, and (b) the hemolytic ability of the PPAAc−streptavidin complex is similar to that of the free PPAAc.

INTRODUCTION

There are now many biomolecular drugs in development for the treatment of a wide variety of medical ailments. These therapeutics include DNA for gene therapies, oligonucleotides for antisense therapies, and protein or peptide drugs and toxins for disease (e.g., cancer) therapies. A significant problem with the development of many DNA and protein therapies is the delivery of the biomolecule to the proper intracellular site. The efficacy of DNA and protein therapeutics is often limited by cellular trafficking processes that shunt the agents to undesirable compartments or recycle them out of the cell (*1*). Both DNA and protein therapeutics rely on complicated trafficking routes initiated with receptor-mediated endocytosis followed by transport through endosomal, endoplasmic reticulum, and/or trans-Golgi compartments. The efficiency of delivery across these compartments to the cytosol, a necessary step in gene therapy and many protein therapies, is often the limiting factor in treatment efficacy.

When drugs and their complexes or conjugates with carriers are endocytosed, they are often rapidly trafficked from early endosomes to late endosomes, and eventually to lysosomes where they are degraded (*2*). Internalized drugs are not normally released into the cytoplasm of the cell. An important example is the Immunotoxin family, which exploits the specificity of monoclonal antibodies for delivery of toxins to specific cellular and tissue targets. The most commonly utilized toxins are ricin, a plant toxin from the seeds of *Ricinus communis*, and the bacterial toxins *Diphtheria* toxin and *Pseudomonas* exotoxin A (*3*). The efficacy of immunotoxins has been shown to be dependent on the specific monoclonal antibody used (*3*). Antibodies internalized by endocytosis are often trafficked to lysosomes where they are degraded (*4*), unlike the native toxin which is translocated into the cytosol (*5*). Previous attempts to circumnavigate this trafficking limitation include the modification of ricin A chain by the addition of endoplasmic reticulum and Golgi retention sequences (*6*), the use of endosome-destabilizing peptides (*7*), and pH-triggered bispecific antibodies (*8*, *9*).

We have been investigating pH-sensitive or "intelligent" polymers that are capable of lysing red blood cells at pH values observed in endosomes, while being non-disruptive at a physiologic pH of 7.4. These are based on α-alkyl acrylic acids. One example is poly(2-ethylacrylic acid) (PEAAc),[1] which has been shown to have pH-dependent membrane-disruptive properties in liposomes (*10*). A pH-triggered conformational change occurs at pH

† C.A.L. was awarded the 1998 Controlled Release Society-Cygnus Graduate Student Award for Outstanding Work in Drug Delivery for this work.

* To whom correspondence should be addressed.

‡ Department of Bioengineering.

§ Department of Medicine.

|| Department of Chemical Eng'g.

⊥ Department of Bioengineering, Box 352255. Phone: 206-543-9423. Fax: 206-543-6124. E-mail: hoffman@bioeng.washington.edu.

Department of Bioengineering, Box 352125. Phone: 206-685-8148. Fax: 206-685-8256. E-mail: stayton@bioeng.washington.edu.

[1] PEAAc, poly(2-ethylacrylic acid); PPAAc, poly(2-propylacrylic acid); PPAAc−NH_2, amine-terminated PPAAc; PPAAc-biotin, biotinylated PPAAc; RBC, red blood cell; GPC, gel permeation chromatography; NHS-LC-biotin, Sulfosuccinimidyl-6-(biotinamido)-6-hexanoate; HABA, hydroxyazobenzene-2-carboxylic acid; SDS−PAGE, sodium dodecyl sulfate−polyacrylamide gel electrophoresis.

10.1021/bc980109k CCC: $18.00 © 1999 American Chemical Society
Published on Web 04/24/1999

6.3 and below (*11*, *12*). At these lower pH conditions, PEAAc appears to permeabilize phosphatidylcholine (PC) membranes, disrupt the lamellar structure of lipid bilayers, and form mixed micelles composed of polymer and lipid. This process has a high efficiency, and the disruption of PC membranes in liposomes is general, as PEAAc disrupts distearoyl, dipalmitoyl, dimyristoyl, dilauroyl, and dioleoyl PC at low pH (*10*). These observations suggested that these polymers may be useful as a new class of drug delivery formulation components that enhance delivery of biomolecules to the cytoplasm.

We have recently shown that PEAAc and PPAAc efficiently induce red blood cell (RBC) hemolysis at lower pHs, such as those existing in endosomes (*13*, *14*). To be effective in assisting endosomal release of therapeutics, PEAAc and PPAAc must retain their hemolytic activity when conjugated to a protein. In this paper, we have prepared complexes of PPAAc and streptavidin at stoichiometries of 1:1 and 3:1 polymer to protein. This serves as a model to test the ability of the membrane−disruptive polymer when linked to a protein to disrupt the lipid bilayers of RBC membranes at the pHs existing in endosomes.

EXPERIMENTAL PROCEDURES

Polymer Preparation. Amine-terminated PPAAc (PPAAc−NH_2) was synthesized using established chain-transfer free-radical polymerization techniques. The propyl acrylic acid monomer was mixed with 1 mol % initiator (azobisisobutyronitrile) and 4 mol % chain-transfer agent (cysteamine). The mixture was degassed by first freezing in liquid nitrogen, and subsequently placed under vacuum and thawed. This was repeated three times. Polymerization was carried out at 60 °C. Two different PPAAc preparations were used in subsequent experiments. The product of the first PPAAc polymerization reaction was fractionated by preparative gel permeation chromatography (GPC), while ether precipitation was used to remove small polymer chains from the second PPAAc polymerization products.

Biotinylation of PPAAc. PPAAc−NH_2 was biotinylated using sulfosuccinimidyl-6-(biotinamido)-6-hexanoate (EZ-Link sulfo-NHS-LC−biotin, Pierce). PPAAc−NH_2 was dissolved in 0.1 M sodium phosphate and 0.15 M NaCl, pH 7.4. The NHS-LC-biotin was dissolved in water at a concentration of 20 mg/mL and added to each of the polymers at a 20 times molar excess. This was reacted for 2 h at room temperature. The biotinylation was repeated using a 15 times molar excess of biotin to maximize the yield of biotinylated polymer molecules. The samples were purified using a PD-10 desalting column (Pharmacia) in order to ensure that all the free biotin was removed. Absorbance at 220 nm was used to detect which fractions contained polymer, and these fractions were subsequently pooled.

Determination of Concentration of PPAAc−Biotin. To determine the concentration of the biotinylated PPAAc (PPAAc−biotin), the neutravidin-HABA dye assay was used. A total of 1.5 mg of neutravidin (Molecular Probes) was dissolved in 3 mL of 0.1 M sodium phosphate and 0.15 M NaCl, pH 7.4. 4′-Hydroxyazobenzene-2-carboxylic acid (HABA) (Sigma) was dissolved in 10 mM NaOH at a concentration of 2.42 mg/mL (10 mM), and 75 μL was added to the protein. D-Biotin (Sigma) was dissolved in 0.1 M sodium phosphate and 0.15 M NaCl, pH 7.4, at a concentration of 0.5 mM. This solution was added in 10 μL aliquots to the protein−HABA complex, while the absorbance at 500 nm was measured after each addition. By plotting the absorbance at 500 nm versus the amount of biotin added, the calibration curve was constructed. In parallel, incremental amounts of PPAAc−biotin were added to the neutravidin and HABA solution, and the absorbance at 500 nm was measured. The slope of the curve generated was compared to the calibration curve in order to determine the concentration.

Hemolysis Assay. The pH-dependent membrane-disruptive activity of the PPAAc was measured using a red blood cell (RBC) hemolysis assay. RBCs were harvested by centrifuging whole blood for 4 min. They were washed three times with 100 mM dibasic sodium phosphate at the desired pH, and resuspended in the same buffer to yield the initial volume. They were diluted 10 times in the same buffer, and 200 μL of this suspension was used for each tube. This yields 10^8 RBCs per tube. Each tube contained 800 μL of buffer, 200 μL of the RBC suspension, and the polymer. Each sample was done in triplicate, and was then repeated to verify reproducibility. The tubes were incubated for an hour and a half in a 37 °C incubator. They were spun for 5 min at full speed in the microcentifuge. Lysis was determined by measuring the absorbance of the supernatant at 541 nm, reflecting the amount of hemoglobin which had been released into the supernatant. Percent hemolysis was calculated assuming 100% lysis to be measured by the hemoglobin released by the red blood cells in water; controls of RBCs in buffer with no polymer or in buffer with added streptavidin were also run.

RESULTS

Polymer Preparation and Properties. To investigate the importance of polymer polydispersity, the PPAAc was fractionated by preparative GPC. The resulting polymer mixture displayed an average molecular mass that is equivalent to a PEG standard of 20 kDa. We found that the hemolytic activity of the polymer was not strongly dependent on the degree of polydispersity, as ether-precipitated PPAAc with higher polydispersities demonstrated the same hemolytic activity as fractionated PPAAc.

Biotinylation of PPAAc. The neutravidin-HABA assay was used to determine the fraction of PPAAc that was biotinylated. The results demonstrate that no detectable quantity of the polymer remains unbiotinylated. In addition, if unbiotinylated PPAAc remained in the mixture, we would expect that the concentration dependence of the hemolysis assay (below) would be shifted to reflect the higher concentration added by the nonderivatized polymer. The biotinylation of PPAAc was also verified with an SDS−PAGE gel shift assay (Figure 2). Samples of streptavidin alone, a physical mixture of streptavidin and PPAAc−NH_2, and a complex of streptavidin and PPAAc−biotin were analyzed. The biotin−streptavidin affinity was exploited to create the streptavidin−biotinylated polymer complex as diagrammed in Figure 3. Because the polymer is negatively charged at neutral pH, the streptavidin−biotinylated PPAAc complex migrates further in the gel. The physical mixture of streptavidin and PPAAc−NH_2 does not display a shift in electrophoretic mobility, indicating that the interaction between streptavidin and PPAAc is specifically mediated by biotin.

Hemolysis Assay. The abilities of five different samples to hydrolyze RBCs were compared. Test samples included amine-terminated PPAAc; biotinylated PPAAc; a physical mixture of streptavidin + amine-terminated PPAAc; a streptavidin−biotinylated PPAAc complex; streptavidin alone; and RBCs alone. The abilities of these samples to

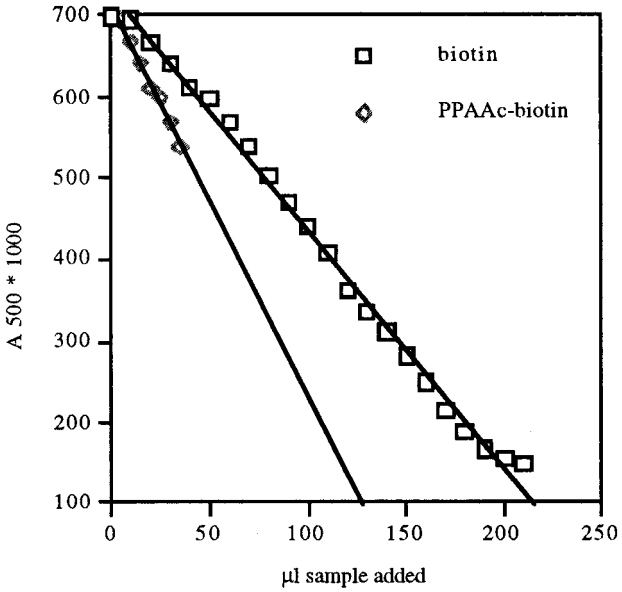


Figure 1. Determination of PPAAc-biotin concentration using the neutravidin/HABA assay.

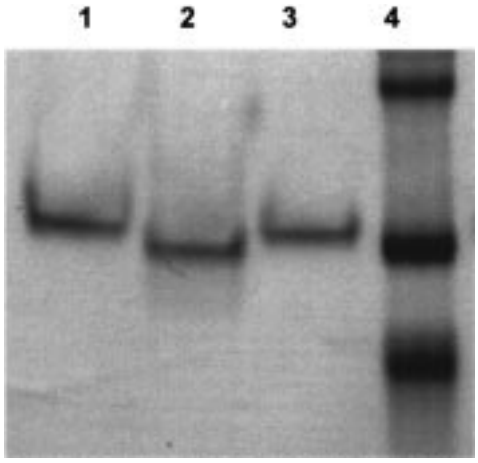


Figure 2. (1) PPAAc−NH_2 + Streptavidin, (2) PPAAc-biotin/Streptavidin, (3) Streptavidin, (4) MW marker.

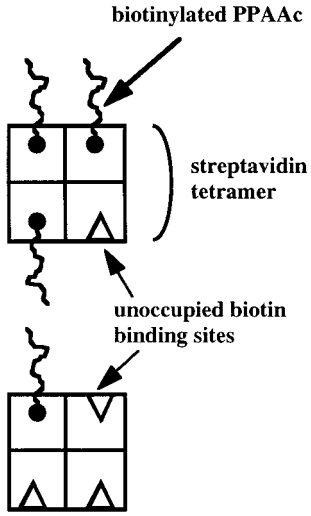


Figure 3. Schematic of the streptavidin−polymer model system with the 3:1 and 1:1 polymer:protein ratios.

disrupt RBC membranes was investigated for a range of polymer concentrations, a range of pH values, and for two polymer-to-streptavidin ratios of 3:1 and 1:1. Figure 4 shows the effect of concentration of PPAAc on hemolysis

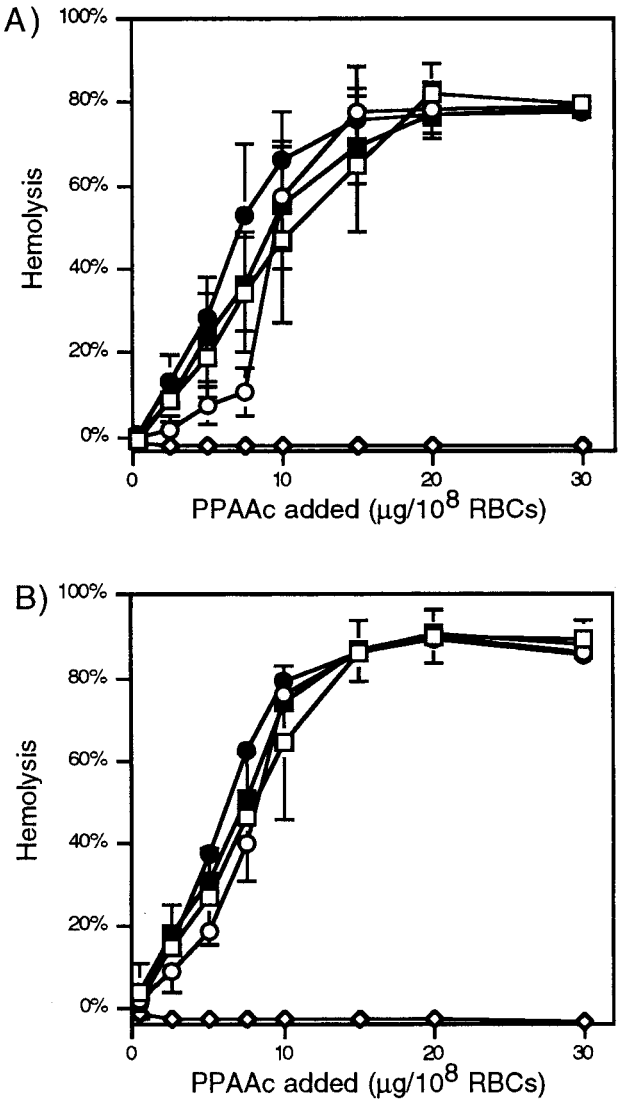


Figure 4. Concentration dependence of hemolytic activity for PPAAc−NH_2 (open squares), PPAAc-biotin (open circles), streptavidin + PPAAc−NH_2 physical mixture (closed squares), streptavidin/PPAAc-biotin complex (closed circles), and streptavidin alone (diamonds), with a polymer:protein stoichiometry of 3:1 (A) and 1:1 (B).

at pH 5 for a polymer-to-protein ratio of 3:1 (Figure 4A) and 1:1 (Figure 4B). All the samples containing PPAAc display equivalent hemolytic activity, as illustrated by the superimposable curves of all derivatives of PPAAc, which are normalized to the weight of PPAAc in each sample. The maximum hemolytic capability is reached at roughly 15 μg of PPAAc per 10^8 RBCs. Figure 5 displays the % hemolysis versus pH for PPAAc at a concentration of 15 μg of polymer per 10^8 RBCs. Results for polymer-to-protein ratios of 3:1 and 1:1 are presented in Figure 5. A sharp dependence on pH is demonstrated, with no significant hemolytic activity at pH 7.4 and a maximum achieved by pH 6.3.

DISCUSSION

The results show that PPAAc hemolyzes red blood cells with the same efficiency whether as a free polymer or complexed via biotin to the protein streptavidin. The hemolysis versus concentration profile is virtually identical for all samples containing PPAAc, indicating that the hemolytic activity of PPAAc is not affected by its linkage to a protein. Hemolysis by PPAAc reaches its maximum

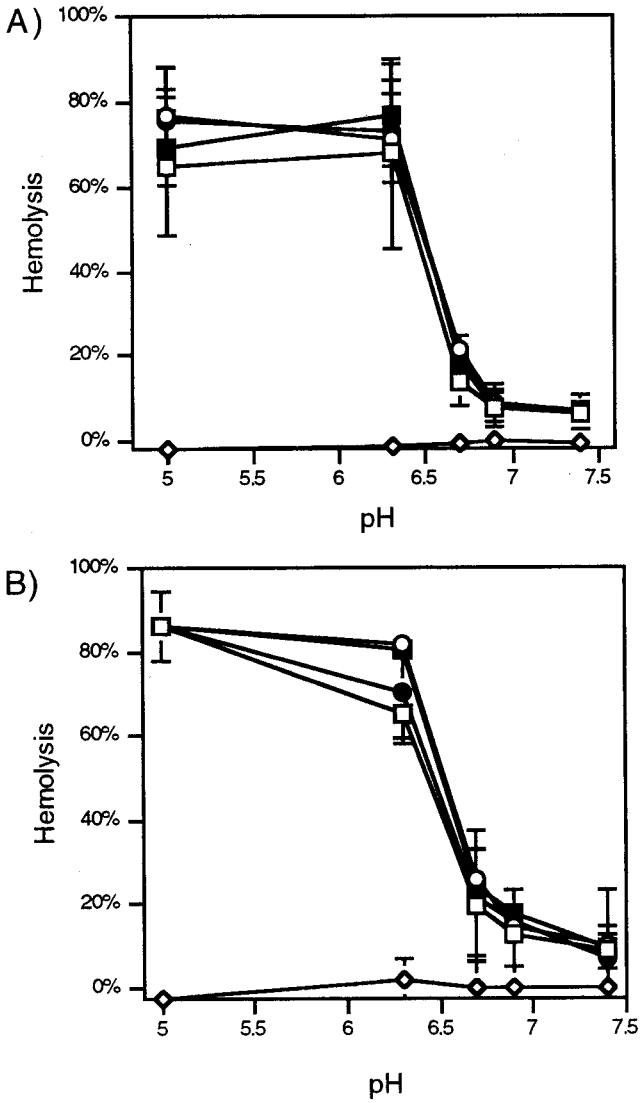


Figure 5. pH dependence of hemolytic activity for PPAAc−NH_2 (open squares), PPAAc-biotin (open circles), streptavidin + PPAAc−NH_2 physical mixture (closed squares), streptavidin/PPAAc-biotin complex (closed circles), and streptavidin alone (diamonds), with a polymer:protein stoichiometry of 3:1 (A) and 1:1 (B). All samples with polymer contained 15 μg of PPAAc.

at ca. 15 μg of polymer/10^8 red blood cells, which corresponds to ca. 4.5×10^6 molecules of PPAAc/red blood cell. Since polymer-to-protein ratios of 3:1 and 1:1 displayed equivalent activity, we can conclude that it is unnecessary to have more than one polymer chain complexed per protein molecule to achieve a highly efficient membrane lytic activity. The hemolysis versus pH curves were also identical for the free PPAAc and for the PPAAc−protein conjugates at both PPAAc:protein ratios. The hemolysis is strongly pH dependent, with the transition from negligible lysis to maximum lysis occurring as the pH decreases over a narrow range from pH 6.9 to 6.3. Thus, linkage of PPAAc to the protein does not affect the pH-dependent conformational and physical change of the polymer and its ability to disrupt the RBC membrane.

We have not investigated the mechanism of this action, but Tirrell and co-workers have studied the disruption of liposomes by PEAAc (*15*). Their surface tensiometry results were consistent with a micellization process driven by hydrophobic interactions of the polymer and the lipid bilayer. Such a mechanism is similar to that seen for amphiphilic, α-helix-based polypeptides, but the polymer is unlikely to adopt a secondary structure, implying that the hydrophobic-to-hydrophilic ratio is the most important factor in liposome micellization (*15*). They also found that the rate of micellization was determined by the rate and extent of PEAAc absorption, which in turn was determined by the lateral compressibility of the membrane (*16*). In comparison, melittin, the most membrane disruptive peptide known, was less effective on a molar basis (*17*).

The ability of the PPAAc−streptavidin complexes to disrupt RBC membranes at lowered pHs, such as those present in endosomes, suggests that these unusual pH-responsive polymers represent a new avenue to facilitate endosomal release and to improve the intracellular delivery of protein or DNA therapeutics.

ACKNOWLEDGMENT

This work was supported by the NIH (NIGMS Grant R01-GM53771-02), the UW Center for Nanotechnology (graduate fellowships to C.A.L. and N.M.), the Office of Technology Transfer at UW, the Washington Technology Center, and the Washington Research Foundation.

LITERATURE CITED

(1) Press, O. W., Martin, P. J., Thorpe, P. E., and Vitetta, E. S. (1988) Ricin A-chain containing immunotoxins directed against different epitopes on the CD2 molecule differ in their ability to kill normal and malignant T cells. *J. Immunol. 141*, 4410−7.

(2) Mukherjee, S., Ghosh, R. N., and Maxfield, F. R. (1997) Endocytosis. *Physiol. Rev. 77*, 759−803.

(3) Blakey, D. C. (1992) Drug targeting with monoclonal antibodies. A review. *Acta Oncol. 31*, 91−7.

(4) Press, O. W., Hansen, J. A., Farr, A., and Martin, P. J. (1988) Endocytosis and degradation of murine anti-human CD3 monoclonal antibodies by normal and malignant T-lymphocytes. *Cancer Res. 48*, 2249−57.

(5) Wawrzynczak, E. J. (1991) Systemic immunotoxin therapy of cancer: advances and prospects. *Br. J. Cancer 64*, 624−30.

(6) Zhan, J., Stayton, P., and Press, O. W. (1998) Modification of ricin A chain, by addition of endoplasmic reticulum (KDEL) or Golgi (YQRL) retention sequences, enhances its cytotoxicity and translocation. *Cancer Immunol., Immunother. 46*, 55−60.

(7) Tolstikov, V. V., Cole, R., Fang, H., and Pincus, S. H. (1997) Influence of endosome-destabilizing peptides on efficacy of anti-HIV immunotoxins. *Bioconjugate Chem. 8*, 38−43.

(8) Raso, V., Brown, M., McGrath, J., Liu, S., and Stafford, W. F. (1997) Antibodies capable of releasing diphtheria toxin in response to the low pH found in endosomes. *J. Biol. Chem. 272*, 27618−22.

(9) Raso, V., Brown, M., and McGrath, J. (1997) Intracellular targeting with low pH-triggered bispecific antibodies. *J. Biol. Chem. 272*, 27623−8.

(10) Thomas, J. L., and Tirrell, D. A. (1992) Polyelectrolyte-sensitized phospholipid vesicles. *Acc. Chem. Res. 25*, 336−42.

(11) Borden, K. A., Eum, K. M., Langley, K. H., and Tirrell, D. A. (1987) On the mechanism of polyelectrolyte-induced structural reorganization in thin molecular films. *Macromolecules 20*, 454−6.

(12) Eum, K. M., Langley, K. H., and Tirrell, D. A. (1989) Quasi-elastic and electrophoretic light scattering studies of the reorganization of dioleoyl phosphatidylcholine vesicle membranes by poly(2-ethylacrylic acid). *Macromolecules 22*, 2755−60.

(13) (a) Murthy, N., Robichaud, J., Stayton, P. S., Press, O. W., Hoffman, A. S., and Tirrell, D. A. (1998) Design of polymers to increase the efficiency of endosomal release of drugs. *Proc. Intl. Symp. Control. Relat. Bioact. Mater. 25*, 224−5. (b) Lackey, C. A., Murthy, N., Stayton, P. S., Press, O. W., Hoffman, A. S., and Tirrell, D. A. (1998) *Proc. Intl. Symp. Control. Relat. Bioact. Mater. 25*, 87−8.

(14) Murthy, N., Robichaud, J. R., Tirrell, D. A., Stayton, P. S., and Hoffman, A. S. (1998) The design and synthesis of polymers for eukaryotic membrane disruption. *J. Controlled Rel.* (Submitted for publication).

(15) Thomas, J. L., Barton, S. W., and Tirrell, D. A. (1994) Membrane solubilization by a hydrophobic polyelectrolyte: surface activity and membrane binding. *Biophysical J. 67*, 1101−6.

(16) Thomas, J. L., Devlin, B. P., and Tirrell, D. A. (1996) Kinetics of membrane micellization by the hydrophobic polyelectrolyte poly(2-ethylacrylic acid). *Biochim. Biophys. Acta 1278*, 73−8.

(17) Dempsey, C. E. (1990) The actions of melittin on membranes. *Biochim. Biophys. Acta 1031*, 143−61.

BC980109K

Efficient Gene Transfer by Histidylated Polylysine/pDNA Complexes

Patrick Midoux* and Michel Monsigny

Centre de Biophysique Moléculaire, Glycobiologie CNRS UPR4301 and University of Orléans, rue Charles-Sadron, F-45071 Orléans Cedex 02, France. Received September 14, 1998; Revised Manuscript Received December 22, 1998

Plasmid/polylysine complexes, which are used to transfect mammalian cells, increase the uptake of DNA, but plasmid molecules are sequestered into vesicles where they cannot escape to reach the nuclear machinery. However, the transfection efficiency increases when membrane-disrupting reagents such as chloroquine or fusogenic peptides, are used to disrupt endosomal membranes and to favor the delivery of plasmid into the cytosol. We designed a cationic polymer that forms complexes with a plasmid DNA (pDNA) and mediates the transfection of various cell lines in the absence of chloroquine or fusogenic peptides. This polymer is a polylysine (average degree of polymerization of 190) partially substituted with histidyl residues which become cationic upon protonation of the imidazole groups at pH below 6.0. The transfection efficiency was optimal with a polylysine having 38 ± 5% of the ϵ-amino groups substituted with histidyl residues; it was not significantly impaired in the presence of serum in the culture medium. The transfection was drastically inhibited in the presence of bafilomycin A_1, indicating that the protonation of the imidazole groups in the endosome lumen might favor the delivery of pDNA into the cytosol.

INTRODUCTION

Poly-L-lysine, which strongly interacts with DNA, may be used to compact plasmid DNA (pDNA) in order to increase the uptake of foreign genes in mammalian cells with the aim to transfect them. The resulting polyplexes—a polyplex is a cationic polymer/DNA complex (*1*)—are taken up by the cells via either a nonspecific endocytosis or a receptor-mediated endocytosis after polylysine substitution with a recognition signal (for reviews, see refs *2*−*5*). However, one of the main limiting factors for the transfection is the inefficacy of the delivery of plasmids into the cytosol from the endocytotic vesicles. Indeed, upon internalization, most of the plasmid molecules are sequestered for several hours into vesicles from where very few plasmid molecules can escape to reach the nuclear machinery. Polyfection—polyfection is a polyplex-mediated transfection—was shown to be much more efficient when cells were incubated in the presence of membrane-disrupting agents such as chloroquine (*6*−*8*), glycerol (*9*), or fusogenic peptides which destabilize the membrane of acidic vesicles containing polyplexes (*7*, *10*−*17*). Therefore, the designing of cationic polymers inducing pDNA compaction and membrane disruption in a slightly acidic medium will be good candidates to help the pDNA to enter the cells and to escape the endocytotic pathway leading to the delivery to lysosomes. Knowing that (i) the imidazole group of histidine has a p*K* around 6.0 and thus becomes cationic in a slightly acidic medium and (ii) poly-L-histidine mediates an acid-dependent fusion and leakage of negative charged liposomes (*18*, *19*), we planned to use a histidylated cationic polymer as a vector for transfecting cells. Because poly-L-histidine is not charged at pH 7.4 and does not form complexes with pDNA at neutral pH, polylysine was partially substituted with histidyl residues.

In the present work, we show that (i) histidylated poly-L-lysine was suitable to make complexes with pDNA and to efficiently transfect various cell lines in the absence of chloroquine or fusogenic peptides; (ii) the highest gene transfer efficiency was obtained with a polylysine (average degree of polymerization of 190) having 38 ± 5% of the ϵ-amino groups substituted with histidyl residues; (iii) the transfection was rather insensitive to the presence of serum in the culture medium; and (iv) the transfection efficiency depended on the protonation of the imidazole groups in the acid lumen of intracellular vesicles.

MATERIALS AND METHODS

Preparation of Partially Histidylated Polylysine (His-pLK). Poly-L-lysine and HBr 30000−50000 (pLK,[1] DP = 190) (Bachem Feinchemikalien, Bubendorf, Switzerland) (1 g in 200 mL H_2O) were passed through an anion-exchange column (Dowex 2 × 8, $^-$OH form, 20−50 mesh) in order to remove bromide ions (*20*). The eluate was neutralized with a 10% *p*-toluenesulfonic acid solution in water and freezed-dried. pLK *p*-toluenesulfonate salt (50 mg; 0.86 μmol) in 3 mL of dimethyl sulfoxide (Aldrich, Strasbourg, France) in the presence of diisopropylethylamine (42 μL; 288 μmol) (Aldrich) was reacted for 24 h at 20 °C with (Boc)His(Boc)-OH (32 mg; 96 μmol) (Novabiochem, Bad Soden, Germany) in the presence of benzotriazol-1-yl-oxy-tris-(dimethylamino) phosphonium hexafluorophosphate (Richelieu Biotechnologies, Saint Hyacinthe, Canada) (43 mg; 97 μmol). The N-protecting Boc groups were removed by acidic treatment by adding 20 mL of H_2O/trifluoroacetic acid mixture (1:1; v/v) for 24 h at 20 °C. Water and trifluoroacetic acid were removed under reduced pressure. The polymer was precipitated by adding 10 vol of 2-propanol and spun down by centrifugation (1800*g* for 15 min). The pellet was washed with 2-propanol, collected by centrifugation (1800*g* for 15 min), solubilized in distilled water, and freeze-dried. The average number of His molecules bound

* To whom correspondence should be addressed. Fax: 33 (0)2 38 69 00 94. Phone: 38 (0)2 38 25 55 95. E-mail: midoux@cnrs-orleans.fr.

[1] Abbreviations: DP, average degree of polymerization; DTT, dithiothreitol; EDTA, ethylenediaminetetraacetate; FBS, fetal bovine serum; His, histidyl residue; PBS, phosphate-buffered saline; pLK, poly-L-lysine.

10.1021/bc9801070 CCC: $18.00 © 1999 American Chemical Society
Published on Web 03/11/1999

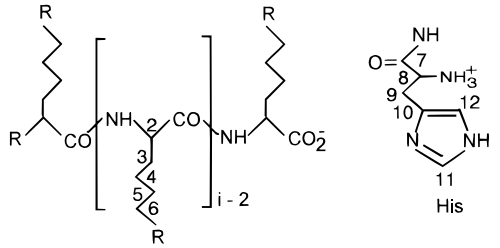


Figure 1. Schematic structure of histidylated polylysine. i = DP; R = NH_3^+ or His.

per pLK molecule was determined by ^{1}H NMR spectroscopy at 300 MHz in D_2O according to $x = 6(h_{8.7}/h_{Lys})$DP, where $h_{8.7}$ was the value of the integration of the signal at 8.7 ppm corresponding to the proton (1H C_{12}) of His (Figure 1), h_{Lys} was in the range 1.3−1.9 ppm corresponding to the 6 methylene protons (C_3, C_4 and C_5) of lysine residues (Figure 1), and DP was the degree of polymerization of pLK. The number of His residues bound per pLK molecule was 70. Histidylated polylysine was fluoresceinylated by using fluoresceinyl isothiocyanate (FITC isomer I, Molecular Probe, La Jolla, CA) as previously described (*7*).

Cells and Cell Culture. COS-7 (SV40 transformed kidney cells of African green monkey, ATCC CRL 1651, ATCC, Rockville, MA), 293-T7 (human embryonic kidney producing T7 RNA polymerase) (*21*), and Rb1 (rabbit smooth muscle cells) (*22*) cells were cultured in DMEM (Gibco, Renfrewshire, U.K.) supplemented with 10% heat inactivated fetal bovine serum (FBS, Gibco); HeLa cells (ATCC CCL 2.1) in DMEM with 5% FBS; B16 cells (murine melanoma cells, ATCC CRL 6322) in DMEM with 10% heat-inactivated new borne calf serum (Gibco); HepG2 (human hepatoma cells, ATCC HB 8065), MCF-7 cells (human breast adenocarcinoma cells, ATCC HTB22), and HOS cells (human osteosarcoma cells, ATCC CRL 1543) in MEM (Gibco) with 10% heat inactivated FBS; 16HBE cells (human airway epithelial cells) in DMEM with 10% heat-inactivated FBS in fibronectin-coated culture plates; A549 cells (human nonsmall cell lung carcinoma cells, ATCC CCL 185) in RPMI with 10% heat-inactivated FBS. All culture media were supplemented with 2 mM L-glutamine (Merck, Darmstadt, Germany) and antibiotics (100 units/mL penicillin and 100 μg/mL streptomycin, Eurobio, France). Cells were grown at 37 °C in a humidified atmosphere containing 5% CO_2 and 95% air. Cells were harvested by treatment with PET [PBS with 0.02% (w/v) EDTA and 2.5 μg/mL trypsin] at 37 °C for 5 min. Cells were mycoplasma free as evidenced by bisbenzimidazole (Hoechst 33258) (*23*).

Plasmids. pSV2*LUC* plasmid (5 kb) was an expression vector encoding the firefly luciferase gene under the control of the SV40 T large antigen promoter (*24*). pUT650 plasmid (5.15 kb) (CAYLA, Toulouse, France) was an expression vector encoding the firefly luciferase gene under the control of the human cytomegalovirus promoter. Supercoiled DNA plasmids were isolated by a standard alkaline lysis method followed by CsCl gradient centrifugation in the presence of ethidium bromide, extensive extraction with *n*-butanol, and precipitation with ethanol.

Polyfection. Polyplexes (histidylated polylysine or polylysine/pDNA complexes) were prepared by adding, under agitation, polymers in 0.3 mL of serum-free DMEM, pH 7.4 to 5 μg (1.5 pmol) of plasmid in 0.7 mL of serum-free DMEM. The mixed solution was kept for 30 min at 20 °C before use. Adherent cell lines [(2−4) × 10^5 cells] were plated (day 0) into 4 cm^2 culture dishes (12-well culture plates). On day 1, the medium was removed and 1 mL of a solution containing a polyplex supplemented with 1% FBS, unless otherwise specified, was added into each well. After 4 h of incubation at 37 °C in a humidified atmosphere (95% air, 5% CO_2), the medium was removed and cells were further incubated at 37 °C in 2 mL of the relevant complete culture medium in a humidified atmosphere (95% air, 5% CO_2). When used, chloroquine (100 μM) was added to the transfection solution, which was immediately supplemented with 1% FBS and put into each well. When used, the fusogenic peptide (E5CA, GLFEAIAEFIGGWEGLIEGCA) (*7*) (10 μM) was added and the transfection solution was immediately supplemented with 1% FBS and put into each well.

Polyethylenimine (PEI 25 kDa from Aldrich) (4.5 mg) was dissolved in 10 mL of H_2O, neutralized with HCl, and sterilized by filtration. Polyplexes were prepared by mixing 10 μL of PEI in 50 μL of 0.15 M NaCl with 5 μg (1.5 pmol) plasmid in 50 μL 0.15 M NaCl. The mixed solution was kept for 30 min at 20 °C. Then, the solution supplemented with 1 mL of DMEM containing 10% FBS was added into each well. After 4 h of incubation at 37 °C in a humidified atmosphere (95% air, 5% CO_2), the medium was removed and cells were further incubated at 37 °C in 2 mL of the relevant complete culture medium in a humidified atmosphere (95% air, 5% CO_2).

Luciferase Assay. Luciferase gene expression was measured by monitoring its luminescence activity according to De Wet et al. (*25*). The medium was discarded, and the cells were washed three times with PBS. The homogenization buffer (200 μL of 8 mM $MgCl_2$, 1 mM DTT, 1 mM EDTA, 1% Triton X100, 15% glycerol, 25 mM Tris-phosphate buffer, pH 7.8) was poured into each well, and the tissue culture plates were kept for 15 min at 20 °C. The solution was recovered and further spun down (5 min at 800*g*). A total of 95 μL of a 2 mM ATP solution in the homogenization buffer without Triton X100 was added to 60 μL of supernatant, and the solution was shaken with a vortex. The luminescence was recorded for 4 s in a Lumat LB 9501 luminometer (Berthold, Wildbach, Germany) upon addition of 150 μL of a 167 mM luciferin solution in water. Measurements were done in duplicate. The data shown correspond to the number of relative light units (RLU) from 10^6 cells. The number of RLU of 1 pg/mL of luciferase was 2000 under these assay conditions.

ζ Potential Measurement. Polyplexes were prepared in 10 mM NaCl, 1 mM MOPS, and 0.1 mM EDTA, at pH 7.2 to a pDNA final concentration of 10 μg/mL. ζ potential was measured by using a ZetaSizer 3000 (Malvern Instruments, Orsay, France) with the following parameters: viscosity, 1.014 cP; dielectric constant, 79; temp, 25 °C; *F*(Ka), 1.50 (Smoluchowsky); current, 10 mA.

RESULTS

Polyfection by Using Histidylated Polylysine. Histidylated polylysine containing 84 histidyl residues (His_{84}-pLK) (Figure 1) was complexed in 1 mL of serum-free DMEM at pH 7.4 with pUT650 plasmid encoding the luciferase gene, and the polyplexes were used to transfect HepG2 cells. The luciferase activity in the cell lysates was compared to that obtained after polyfection with pLK/pUT650 complexes in the absence and in the presence of either chloroquine or E5CA, a fusogenic peptide. Regarding to the luciferase activity, the polyfection was very efficient with His_{84}-pLK/pDNA complexes and very inefficient with pLK/pDNA complexes. The luciferase activity was 4.5 orders of magnitude (10^7

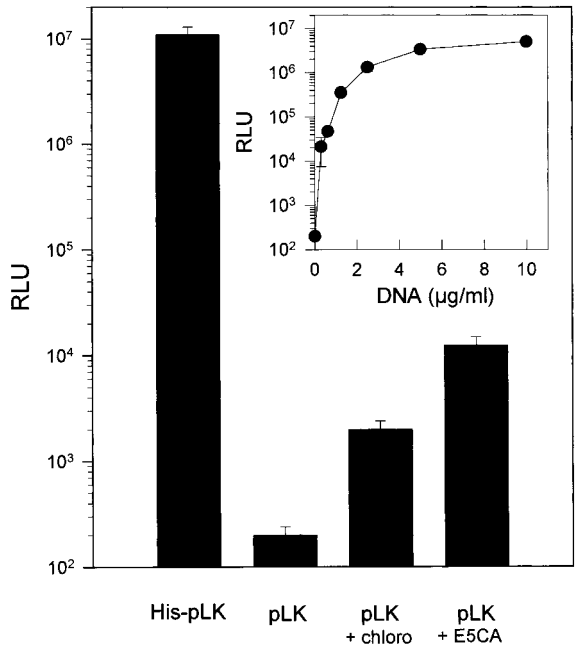


Figure 2. Histidylated polylysine mediated polyfection. Polyplexes were prepared by mixing either His_{84}-pLK (40 μg) or pLK (5 μg) in 0.3 mL of serum-free DMEM with 10 μg (3 pmol) of pUT650 plasmid in 0.7 mL of serum-free DMEM. The solution was kept for 30 min at 20 °C. When it is relevant the solution was made 100 μM in chloroquine or 10 μM in E5CA. HepG2 cells (3×10^5 cells plated in a 4 cm^2 well) were incubated for 4 h at 37 °C with polyplexes in the presence of 5% FBS. Then cells were washed and incubated in complete culture medium containing 10% FBS. The gene expression was determined 48 h later by assaying the luciferase activity in cell lysates. RLU, the number of relative light units, represents the luciferase activity in 10^6 cells. (Inset) Concentration dependence of polyfection with His_{84}-pLK/pDNA complexes.

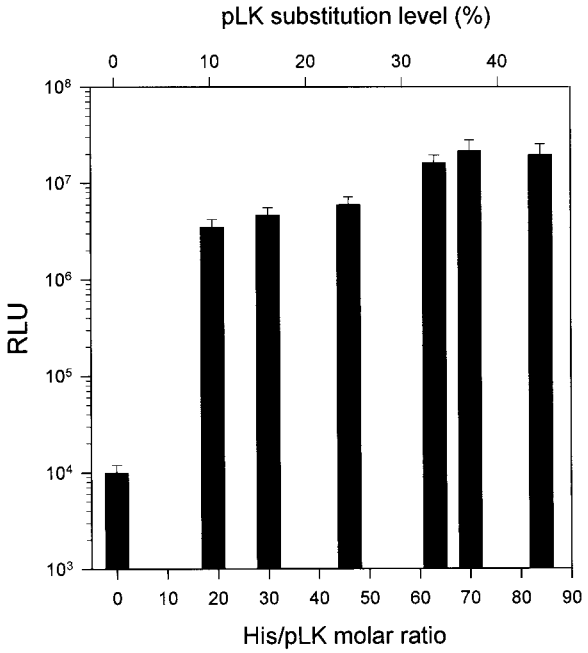


Figure 3. Histidylated polylysine mediated polyfection:influence of the His/pLK ratio. Polyplexes were prepared by mixing pLK substituted with histidyl residues in 0.3 mL of serum-free DMEM with 10 μg (3 pmol) of pUT650 plasmid in 0.7 mL of serum-free DMEM. The solution was kept for 30 min at 20 °C. HepG2 cells (3×10^5 cells plated in a 4 cm^2 well) were incubated for 4 h at 37 °C with polyplexes in the presence of 1% FBS. Then, cells were washed and incubated in complete culture medium containing 10% FBS. The gene expression was determined 48 h later by assaying the luciferase activity in cell lysates. RLU, the number of relative light units, represents the luciferase activity in 10^6 cells.

RLU/10^6 cells) higher than with pLK/pDNA complexes (200 RLU/10^6 cells); it was 3.5 (2×10^7 RLU/10^6 cells) and 3 (10^7 RLU/10^6 cells) orders of magnitude higher than with pLK/pDNA complexes in the presence of chloroquine and the fusogenic peptide, respectively (Figure 2). The luciferase activity was maximal when the cells were incubated for about 3−4 h in the presence of His_{84}-pLK/pDNA complexes (data not shown); increasing the incubation period (up to 24 h) did not increase the luciferase activity. It is noteworthy to emphasize that no cytoxicity was observed whatever the incubation duration (from 4 to 24 h) in the presence of the polyplexes. The amount of plasmid was varied between 0.05 and 10 μg, keeping constant the histidylated polylysine/pDNA ratio equal to 4:1 (weight by weight), the number of cells per well [(2−3) $\times 10^5$ cells in a 4 cm^2 well] and the volume (1 mL) of the solution containing the polyplexes. The polyfection was maximal in the presence of 5 μg of plasmid. Increasing the amount of plasmid did not increase the luciferase activity (Figure 2 inset). Increasing the number of cells per well did not increase the luciferase activity.

Optimal Number of Histidyl Residues on One Polylysine Molecule. HepG2 cells were transfected by using polyplexes made with pUT650 and polylysine substituted with different number of histidyl residues. The luciferase activity in cell lysates was maximal with polylysine substituted with 72 ± 9 histidyl residues/pLK molecule corresponding to 38 ± 5% substitution of the polylysine ϵ-amino groups (Figure 3). When polyfection was performed with pLK containing 20 histidyl residues, the luciferase activity was 10-fold lower than with pLK substituted with 70 histidyl residues.

Influence of the Histidylated Polylysine/pDNA Molar Ratio. The luciferase activity was maximal with polyplexes made by complexing 10 μg of plasmid with 30 (polymer/pDNA molar ratio of 183) to 40 μg (polymer/pDNA molar ratio of 244) of His_{84}-pLK (Figure 4). Increasing the molar ratio did not increase the luciferase activity. The efficiency decreased 10-fold when the molar ratio was down to 122 (20 μg of His_{84}-pLK) and was completely inefficient when the molar ratio was lower than 60 (10 μg of His_{84}-pLK). Under conditions optimal for transfection, polyplexes were positively charged with a ζ potential of +24 mV (Figure 4).

Influence of the Serum Concentration. Polyfection with His_{70}-pLK was not impaired in the presence of serum. The luciferase activity was 2-fold greater in the presence of 5 and 10% FBS than in the presence of 1% FBS, and it was as large in the presence of 20% FBS as in the presence of 1% FBS (Figure 5).

Gene Transfer into Various Cell Lines. The transfection of different mammalian cell lines including human hepatoma cells (HepG2), human breast adenocarcinoma cells (MCF-7), human epidermoid carcinoma cells (HeLa), human osteosarcoma cells (HOS), human airway epithelial cells (16HBE), murine melanoma cells (B16), and simian kidney cells (COS) was assessed by using His_{70}-pLK/pUT650 complexes and rabbit smooth muscle cells (Rb-1) by using His_{70}-pLK/pSV2*LUC* complexes. All the cell lines (except COS cells) were efficiently transfected with luciferase activity ranging from 2×10^6 to 10^7 RLU/10^6 cells (Figure 6). The transfection was compared with that obtained with PEI/pDNA complexes (Table 1). Depending on the cell line, the transfection by His-pLK/pDNA complexes was as effective or less effective (up to 20-fold) than with PEI/pDNA complexes.

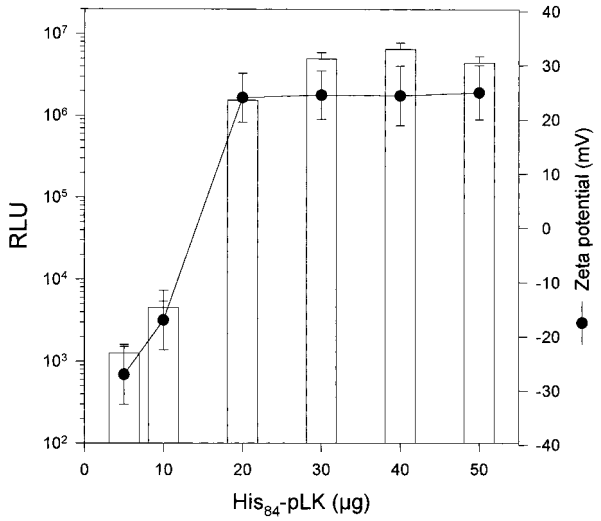


Figure 4. Histidylated polylysine mediated polyfection:influence of the polymer/pDNA ratio and ζ potentials of polyplexes. Polyplexes were prepared by mixing 10 μg (3 pmol) of pUT650 plasmid in 0.7 mL of serum-free DMEM with different amounts of histidylated polylysine (His_{84}-pLK) in 0.3 mL of serum-free DMEM. The solution was kept for 30 min at 20 °C. HOS cells (2×10^5 cells/4 cm^2) were incubated for 4 h at 37 °C with polyplexes in the presence of 5% FBS. Then cells were washed and incubated in complete culture medium containing 10% FBS. The gene expression was determined 48 h later by assaying the luciferase activity in cell lysates. RLU, the number of relative light units, represents the luciferase activity in 10^6 cells.

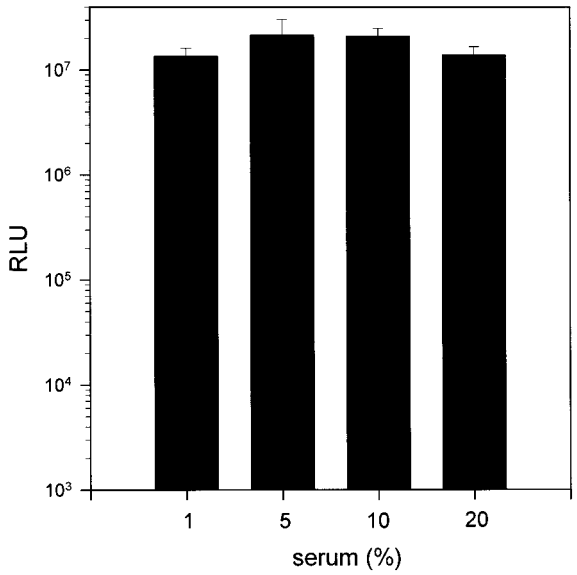


Figure 5. Histidylated polylysine mediated polyfection:influence of the serum. HepG2 cells (3×10^5 cells/4 cm^2 well) were incubated for 4 h at 37 °C with 5 μg/mL of the polyplexes (His_{70}-pLK/pUT650) in the presence of various amount of FBS. Then, cells were washed and incubated in complete culture medium containing 10% FBS. The gene expression was determined 48 h later by assaying the luciferase activity in cell lysates. RLU, the number of relative light units, represents the luciferase activity in 10^6 cells.

Influence of the Endosomal pH. Histidylated polylysine is supposed to increase the delivery of pDNA into the cytosol via membrane destabilization of acidic endocytotic vesicles containing His_{70}-pLK/pDNA complexes following the protonation of the imidazole groups. This was assessed by transfecting cells in the absence or in the presence of bafilomycin A_1, an inhibitor of vacuolar ATPase endosomal proton pump (*26*). When the polyfection of Rb-1 cells by His_{70}-pLK/pSV2*LUC* complexes was performed in the presence of 200 nM bafilomycin A_1, the luciferase activity into cells was about 3 order of magnitude lower than in the absence of bafilomycin A_1 (Figure 7). A flow cytometry analysis showed that, in the absence of bafilomycin A_1 , the polyplexes were in acidic compartment as evidenced by a 1.8-fold increase of the cell fluorescence intensity after a postincubation in the presence of monensin (*27*, *28*); conversely, the fluorescence intensity of cells incubated in the presence of bafilomycin A_1 did not increase upon a postincubation in the presence of monensin (data not shown). Therefore, the decrease of the transfection efficiency of histidylated polylysine/pDNA complexes in the presence of bafilomycin A_1 , indicated that the protonation of the imidazole groups in acidic medium was involved in the polyfection process.

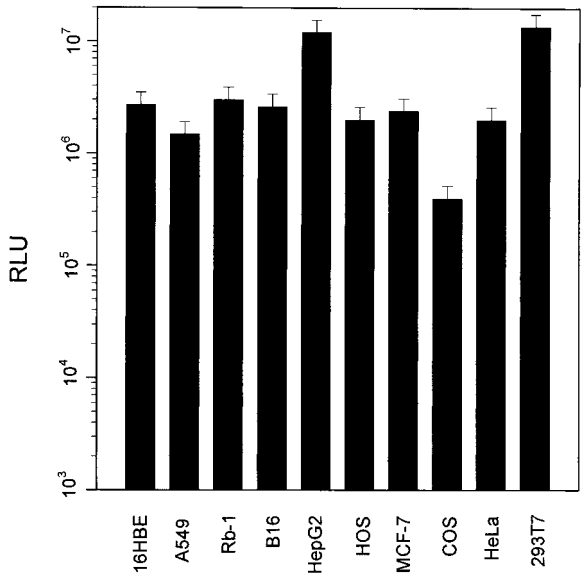


Figure 6. Histidylated polylysine mediated polyfection of various cell lines. Polyplexes were prepared by mixing His_{70}-pLK (30 μg) in 0.3 mL serum-free DMEM with 10 μg (3 pmol) of plasmid (pUT650 or pSV2*LUC* for Rb-1 cells) in 0.7 mL of serum-free DMEM. The mixed solution was kept for 30 min at 20 °C. Cell lines [$(2-3) \times 10^5$ cells/4 cm^2 well] were incubated for 4 h at 37 °C with polyplexes in the presence of 10% FBS. Then, cells were washed and incubated in complete culture medium containing 10% FBS. The gene expression was determined 48 h later by assaying the luciferase activity in cell lysates. RLU, the number of relative light units, represents the luciferase activity in 10^6 cells.

Table 1. Comparison of the Transfection Efficiency by Using Either Histidylated Polylysine or Polyethylenimine as DNA Carriers[a]

cells	PEI/His-pLK	cells	PEI/His-pLK
B16	5.8	A549	21
293	0.6	Rb-1	17

[a] Cells (2×10^5 cells/4 cm^2 well) were transfected for 4 h at 37 °C with 5 μg/mL (pUT650 or pSV2*LUC* for Rb-1 cells) complexed with either His-pLK or PEI in the presence of 10% FBS. Then, cells were washed and incubated in complete culture medium containing 10% FBS. The gene expression was determined 48 h later by assaying the luciferase activity in cell lysates. PEI/His-pLK represents the ratio of the luciferase activity into cells transfected by PEI polyplexes to the luciferase activity into cells transfected by His-pLK polyplexes.

DISCUSSION

The introduction in mammalian cells of a foreign gene as a plasmid DNA by nonviral vectors requires the entry of the plasmid into the cell and then into the nucleus.

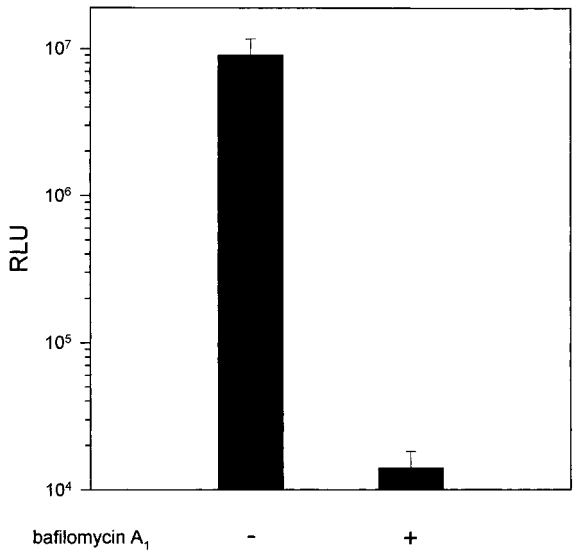


Figure 7. Influence of bafilomycin A1 on the polyfection efficiency. Rb-1 cells (2×10^5 cells/4 cm^2 well) were incubated at 37 °C in the presence of 1 mL His_{70}-pLK/pSV2*LUC* complexes (5 μg of pDNA) and in the absence or in the presence of 200 nM bafilomycin A_1. After 4 h, the cells were washed and incubated in complete culture medium containing 10%. The gene expression was determined 48 h later by assaying the luciferase activity in cell lysates. RLU, the number of relative light units, represents the luciferase activity in 10^6 cells.

The compaction of a pDNA in the presence of polylysine increases its uptake by the cells via making the endocytotic process more easy. Once complexed and taken up by cells, plasmids are sequestered for several hours in vesicular compartments from where they cannot escape to reach the nucleus. The delivery of the pDNA into the cytosol should be obtained from early acidic vesicles formed during polyplex uptake under the condition that the endosomal membrane is disrupted by devices bound to the plasmid-associated carrier working at a weakly acidic medium. In this study, we show that partial substitution of poly-L-lysine with histidyl residues results in a cationic polymer that forms complexes with a plasmid DNA at pH 7.4. These complexes actively transfect cells in culture in the absence of any helper compounds such as chloroquine or a fusogenic peptide. Optimal conditions for transfection were found when polylysine was substituted with 72 ± 9 histidyl residues, corresponding to a polylysine substitution level of $38 \pm 5\%$; the efficiency was 10-fold lower when polylysine substitution was down to 10%. The polyfection was efficient when the global charge of the polyplexes was slightly positive (ζ potential = +24 mV), which likely increased their binding on the cell surface and facilitated their uptake by the cells.

The polyplexes are internalized by the cells in acidic compartments. The mechanism of polyfection mediated by histidylated polyplexes is not yet known, but it is supposed that a subsequent delivery of pDNA into the cytosol occurs by the membrane destabilization of acidic vesicles containing polyplexes, upon the protonation of imidazole groups. Although, there is no evidence that the DNA leaves endocytotic vesicles, this statement is supported by (i) the fact that poly-L-histidine induces fusion of lipid bilayers (*18*, *19*) and (ii) the fact that bafilomycin A_1 which is known to impair the acidification of the lumen of the endosomes, made polyfection inefficient. Poly-L-histidine destabilizes lipid bilayers in a slightly acidic medium and induces fusion upon protonation of the imidazole groups by increasing interactions between this polymeric polycation and the membrane phospholipids (*18*). In acidic medium, poly-L-histidine is more fusogenic than polylysine: efficient fusion of negatively charged liposomes (phosphatidylserine liposomes) occurs at a ratio of the positive charge of poly-L-histidine to the negative charge of the liposomes equal to 0.2 while it occurs at a ratio equal to 1 in the case polylysine. Recently, we have reported that the amphipatic peptide H5WYG (GLFHAIAHFIHGGWHGLIHGWYG) containing five histidyl residues, which does not adopt a helical structure in acidic medium, permeabilizes cell membranes in such an acidic medium (pH 6.4) (*17*). In addition, this peptide increased the expression efficiency when a gene is transferred into cells as glycosylated polylysine/pDNA complexes; the transfection was also inhibited in the presence of bafilomycin A_1 (*17*). These results suggest that the generation of cationic charges via the protonation of several imidazole groups bound to pDNA inside the endosomes consecutively to the acidification of their lumen is a suitable approach to modify the intracellular routing of pDNA, especially its delivery into cytosol. Therefore, the mechanism involved for polyfection with histidylated polylysine could be different from that of polyethylenimine which is supposed to act as a buffer, preventing acidification of the endosomal lumen and inducing the swelling of these vesicles, leading to a membrane destabilization (*29*).

The transfection efficiency by using histidylated polylysine/pDNA complexes was greater than by using polylysine/pDNA complexes in the presence of either chloroquine or the fusogenic peptide E5CA. Chloroquine concentrates in the acidic compartments and prevents the delivery of the endosomal content to lysosomes; it induces the formation of large endosome-derived vacuoles. In addition, it allows the dissociation of pDNA/polylysine conjugate complexes (*8*). Anionic permeabilizing peptides, adopting an α-helical structure at pH <5.5, may destabilize the membrane of weakly acidic vesicles containing the polyplexes leading to the delivery of pDNA into the cytosol. Histidylated polyplexes were efficient for all cell types tested while the efficiency of anionic peptides such as E5CA depends on several parameters in relation with the cell type. These parameters include the number of vesicles containing both polylysine/pDNA complexes and peptides separately taken up, the peptide concentration, and the luminal pH of the vesicles. In addition, histidylated polylysine may destabilize membranes as well as H5WYG peptide at a pH less acidic than E5CA peptide and thus may be effective in early endosomes at pH around 6.4; at this pH, anionic peptides were inefficient.

Chloroquine and fusogenic peptides cannot be used in vivo. Indeed, (i) they are small molecules which are cleared soon after their injection; (ii) chloroquine must concentrate in acidic vesicles and reach a high concentration before being able to induce an efficient transfection (*8*); (iii) polyplex solution to be injected cannot contain a high concentration of chloroquine, because above 1 mM chloroquine, polyplexes start to dissociate (*8*); (iv) the effect of anionic peptides bearing negative charges at neutral pH is inhibited in the presence of serum probably because they bind to serum proteins, and in addition, the effect is diminished when they are chemically linked to polyplexes. With histidylated polylysine, the membrane-disrupting device is bound to the plasmid and the transfection efficiency was not significantly reduced in the presence of serum up to 20%.

In conclusion, histidylated polylysine, a synthetic compound, easy to prepare and to purify, is a good

nonviral vector for gene transfer into mammalian cells. Histidylated polylysine gives polyplex formulation suitable for transferring gene in vivo. In addition, histidylated polylysine may be substituted with recognition signal molecules in order to deliver the gene into cells which specifically express a related receptor; this aspect is currently under development in our laboratory.

ACKNOWLEDGMENT

We express our gratitude to Dr. A. B. Brasier (Massachusetts General Hospital, Boston, MA) for pSV2*LUC* plasmid, Dr. D. C. Gruenert (Gene Therapy Core Center, University of California, San Francisco), Dr. M. Nachtigal (University of South Carolina, Columbia, SC), and Dr. L. Huang (University of Pittsburgh, Pittburgh, PA) for 16HBE, Rb-1, and 293-T7 cells, respectively. We thank Mahajoub Bello-Roufaï for ζ potential measurements and Sophie Fauvin and Suzanne Nuques for their skillful technical helps in cell culture and transfections. We thank Françoise Fargette for the preparation of plasmids and Henri Labbé for his skillfull assistance in NMR spectroscopy. This work was partly supported by grants from ANRS (ANRS No. 97003), Ministère de la Recherche et de la Technologie (ACCSV14 No. 9514104), Ligue Nationale Contre le Cancer, Biotechnocentre and EU (BIO4-CT97-2216). Michel Monsigny is Professor at the University of Orléans. Patrick Midoux is Research Director at INSERM.

LITERATURE CITED

(1) Felgner, P. L., Barenholz, Y., Behr, J. P., Cheng, S. H., Cullis, P., Huang, L., Jessee, J. A., Seymour, L., Szoka, F., Thierry, A. R., Wagner, E., and Wu, G. (1997) Nomenclature for synthetic gene delivery systems. *Hum. Gene Ther. 8*, 511−512.

(2) Monsigny, M., Roche, A. C, Midoux, P., and Mayer R. (1994) Glycoconjugates as carriers for specific delivery of therapeutic drugs and genes. *Adv. Drug Delivery Rev. 14*, 1−24.

(3) Wagner, E., Curiel, D. T., and Cotten, M. (1994) Delivery of drugs, proteins and genes into cells using transferrin as a ligand for receptor-mediated endocytosis. *Adv. Drug Delivery Rev. 14*, 113−136.

(4) Frese, J., Jr., Wu, C. H., and Wu, G. Y. (1994) Targeting of genes to the liver with glycoprotein carriers. *Adv. Drug Delivery Rev. 14*, 137−153.

(5) Cristiano, R. J., and Curiel, D. T. (1996) Strategies to accomplish gene delivery via the receptor-mediated endocytosis pathway. *Cancer Gene Ther. 3*, 49−57.

(6) Zenke, M., Steinlein, P., Wagner, E., Cotten, M., Beug, H., and Birnstiel, M. L. (1990) Receptor-mediated endocytosis of transferrin-polycation conjugates: an efficient way to introduce DNA into hematopoietic cells. *Proc. Natl. Acad. Sci. U.S.A. 87*, 3655−3659.

(7) Midoux, P., Mendes, C., Legrand, A., Raimond, J., Mayer, R., Monsigny, M., and Roche, A. C. (1993) Specific gene transfer mediated by lactosylated poly-L-lysine into hepatoma cells. *Nucleic Acids Res. 21*, 871−878.

(8) Erbacher, P., Roche, A. C., Monsigny, M., and Midoux, P. (1996) Putative role of chloroquine in gene transfer into a human hepatoma cell line by pDNA/lactosylated polylysine complexes. *Exp. Cell Res. 225*, 186−194.

(9) Zauner, W., Kichler, A., Schmidt, W., Sinski, A., and Wagner, E. (1996) Glycerol enhancement of ligand-polylysine/DNA transfection. *BioTechniques 20*, 905−913.

(10) Wagner, E., Plank, C., Zatloukal, K., Cotten, M., and Birnstiel, M. L. (1992) Influenza virus hemagglutinin HA-2 N-terminal fusogenic peptides augment gene transfer by transferrin-polylysine-DNA complexes: toward a synthetic virus-like gene-transfer vehicle. *Proc. Natl. Acad. Sci. U.S.A. 89*, 7934−7938.

(11) Plank, C., Zatloukal, K., Cotten, M., Mechtler, K., and Wagner, E. (1992) Gene transfer into hepatocytes using asialoglycoprotein receptor mediated endocytosis of DNA complexed with an artificial tetra-antennary galactose ligand. *Bioconjugate Chem. 3*, 533−539.

(12) Plank, C., Oberhauser, B., Mechtler, K., Koch, C., and Wagner, E. (1994) The influence of endosome-disruptive peptides on gene transfer using synthetic virus-like gene transfer systems. *J. Biol. Chem. 269*, 12918−12924.

(13) Haensler, J., and Szoka, F. C. (1993) Polyamidoamine cascade polymers mediate efficient transfection of cells in culture. *Bioconjugate Chem. 4*, 372−379.

(14) Gottschalk, S., Sparrow, J. T., Hauer, J., Mims, M. P., Leland, F. E., Woo, S. L. C., and Smith, L. C. (1996) A novel DNA-peptide complex for efficient gene transfer and expression in mammalian cells. *Gene Ther. 3*, 448−457.

(15) Zauner, W., Blaas, D., Kuechler, E., and Wagner, E. (1995) Rhinovirus-mediated endosomal release of transfection complexes. *J. Virol. 69*, 1085−1092.

(16) Wymn, T. B., Nicol, F., Zelphati, O., Scaria, P. V., Plank, C., and Szoka, F. C. (1997) Design, synthesis, and characterization of a cationic peptide that binds to nucleic acids and permeabilizes bilayers. *Biochemistry 36*, 3008−3017.

(17) Midoux, P., Kichler, A., Boutin, V., Maurizot, J. C., and Monsigny, M. (1998) Membrane permeabilization and efficient gene transfer by a peptide containing several histidines. *Bioconjugate Chem. 9*, 260−267.

(18) Wang, C.-Y., and Huang, L. (1984) Polyhistidine mediates an acid-dependent fusion of negatively charged liposomes. *Biochemistry 23*, 4409−4416.

(19) Uster, P. S., and Deamer, W. D. (1985) pH-dependent fusion of liposomes using titratable polycations. *Biochemistry 24*, 1−8.

(20) Derrien, D., Midoux, P., Petit, C., Negre, E., Mayer, R., Monsigny, M., and Roche, A. C. (1989) Muramyl dipeptide bound to poly-L-lysine substituted with mannose and gluconoyl residues as macrophage activators. *Glycoconjugate J. 6*, 241−255.

(21) Li, S., Brisson, M., He, Y., and Huang, L. (1997) Delivery of a PCR amplified DNA fragment into cells: a model for using synthetic genes for gene therapy. *Gene Ther. 4*, 449−454.

(22) Nachtigal, M., Nagpal, M. L., Greenspan, P., Nachtigal, S. A., and Legrand, A. (1989) Characterization of a continuous smooth muscle cell line derived from rabbit aorta. *In Vitro Cell. Dev. Biol. 25*, 892−898.

(23) Chen, T. R. (1977) In situ detection of mycoplasma contamination in cell cultures by fluorescent Hoeschst 33258 stain. *Exp. Cell Res. 104*, 255−262.

(24) Brasier, A. R., Tate, J. E., and Habener, J. F. (1989) Optimized use of the firefly luciferase assay as a reporter gene in mammalian cell lines. *BioTechniques 7*, 1116−1123.

(25) De Wet, J. R., Wood, K. V., De Luca, M., Helinsky, D. R., and Subramani, S. (1987) Firefly luciferase gene: structure and expression in mammalian cells. *Mol. Cell. Biol. 7*, 725−737.

(26) Bowman, E. J., Siebers, A., and Altendorf, K. (1988) Bafilomycins: a class of inhibitors of membrane ATPases from microorganisms, aminal cells, and plant cells. *Proc. Natl. Acad. Sci. U.S.A. 85*, 7972−7976.

(27) Monsigny, M., Roche, A. C., and Midoux, P. (1984) Uptake of neoglycoproteins via membrane lectin(s) of L1210 cells evidenced by quantitative flow cytofluorometry and drug targeting. *Biol. Cell 51*, 187−196.

(28) Midoux, P., Roche, A. C. and Monsigny, M. (1987) Quantitation of the binding, uptake, and degradation of fluoresceinylated neoglycoproteins by flow cytometry. *Cytometry 8*, 327−334.

(29) Boussif, O., Lezoualc′h, F., Zanta, M. A., Mergny, M. D., Scherman, D., Demeinex, B., and Behr, J. P. (1995) A versatile vector for gene and oligonucleotide transfer into cells in culture and in vivo. *Proc. Natl. Acad. Sci. U.S.A. 92*, 7297−72301.

BC9801070

Temperature Sensitization of Liposomes Using Copolymers of *N*-Isopropylacrylamide

Hiroshi Hayashi,[†] Kenji Kono,*[,‡] and Toru Takagishi[‡]

Shiga Central Research Laboratories, Noevir, Co., Ltd., Yokaichi, Shiga 527-8588, Japan, and Department of Applied Materials Science, College of Engineering, and Department of Applied Bioscience, Research Institute for Advanced Science and Technology, Osaka Prefecture University, Sakai, Osaka 599-8531, Japan.
Received September 15, 1998; Revised Manuscript Received December 30, 1998

To obtain liposomes which release the contents in response to ambient temperature, liposomes modified with copolymers of *N*-isopropylacrylamide with varying lower critical solution temperatures have been designed. Poly(*N*-isopropylacrylamide-*co*-acrylamide)s with various compositions were synthesized by free-radical copolymerization. The lower critical solution temperature of the polymer increased with increasing acrylamide content in the polymer. Poly(*N*-isopropylacrylamide-*co*-acrylamide-*co*-*N*,*N*-didodecylacrylamide)s were also prepared via the same method as the thermosensitive polymers having anchor groups to the liposome membrane. Calcein-loaded dioleoylphosphatidylethanolamine/egg yolk phosphatidylcholine (6:4, w/w) liposomes were coated with these polymers by incubating the liposomes with aqueous solutions of the polymers. The liposomes hardly released the contents below the lower critical solution temperature of the polymer, but the release was greatly enhanced above that temperature. The liposomes were also made from a mixture of the same lipids and the polymer. The liposome revealed a more drastic release property than the liposomes prepared by the incubation with the polymer solution, because the polymer chains were bound on both surfaces of the membrane. The close relationship between lower critical solution temperatures of the polymers and temperature regions where enhancement of the release from the polymer-fixed liposomes demonstrates that the release was triggered by alteration of the polymers from a hydrophilic state to a hydrophobic state occurring at their lower critical solution temperatures.

INTRODUCTION

Since liposomes made from naturally occurring lipids are biocompatible, their application to drug delivery systems has been extensively attempted (*1*). To elevate their usefulness, a number of liposomes with various functionalities have been designed. While several approaches to the production of functional liposomes have been employed, one of the most effective methods is modification of liposomes with functional polymers (*2*, *3*). For example, pH sensitization of liposomes using poly(2-ethylacrylic acid) has been reported by Tirrell and coworkers (*4*). They have shown that release of the contents from the polymer-modified liposomes is triggered under weakly acidic conditions. Also, Kitano et al. have prepared pH-responsive liposomes by using amphiphiles having acrylic acid oligomer moieties (*5*).

Recently, temperature sensitization of liposomes has been attempted using poly(*N*-isopropylacrylamide) [poly(NIPAM)][1] (*6*−*9*). It is well-known that poly(NIPAM) shows a lower critical solution temperature (LCST) at 30−35 °C (*10*, *11*). The polymer is hydrophilic and soluble in water below the LCST, but becomes hydrophobic and forms an insoluble aggregate above that temperature due to hydrophobic interactions and hydrogen bondings (*11*, *12*). Therefore, if the polymer chains are fixed on the liposome membrane, release of the contents from the liposomes is expected to be controlled by the interaction between the polymer and liposome membrane in a temperature-dependent fashion. In a previous study, we have demonstrated that liposomes bearing poly(NIPAM) release the contents above its LCST (*7*, *13*). In addition, aggregation and fusion of poly(NIPAM)-coated liposomes were induced above the LCST, indicating that surface property of the liposome is also made temperature sensitive by modification of liposomes with poly(NIPAM) (*14*).

Because temperature sensitivity of the liposome is considered to be given by alteration of the polymer chain from the hydrophilic state to the hydrophobic state in response to the ambient temperature, it is expected that liposomes which reveal the response at a desired temperature are obtained by the modification with polymers having LCST at that temperature. It is known that LCST of poly(NIPAM) can be controlled by copolymerization of NIPAM with comonomers with varying hydrophobicity or hydrophilicity (*15*−*17*).

The object of this study is to examine the possibility of temperature sensitization of liposomes using thermosensitive polymers which exhibit LCST at varying temperatures. We prepared phosphatidylcholine-phosphatidylethanolamine (4:6, w/w) liposomes modified with poly(NIPAM-*co*-acrylamide) with varying NIPAM/acryl-

* To whom correspondence should be addressed. Phone: +81-722-54-9330. Fax: +81-722-54-9913. E-mail: kono@chem.osakafu-u.ac.jp.

[†] Shiga Central Research Laboratories.

[‡] Osaka Prefecture University.

[1] Abbreviations: NIPAM, *N*-isopropylacrylamide; AAM, acrylamide; NDDAM, *N*,*N*-didodecylacrylamide; DOPE, L-α-dioleoylphosphatidylethanolamine; EYPC, egg yolk phosphatidylcholine; AIBN, azobis(isobutyronitrile); Tris, tris(hydroxymethyl)-aminomethane; EDTA, ethylenediaminetetraacetic acid; LCST, lower critical solution temperature; Mw, weight average molecular weight; Mn, number average molecular weight.

10.1021/bc980111b CCC: $18.00 © 1999 American Chemical Society
Published on Web 03/12/1999

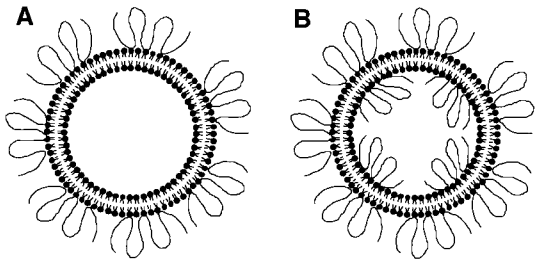


Figure 1. Schematic illustration of two types of polymer-fixed liposomes prepared in this study. (A) Liposomes having polymer chains on outer surface of membrane. (B) Liposomes having polymer chains on both surfaces of membrane.

amide (AAM) ratios and found that release of entrapped calcein from the copolymer-modified liposomes was greatly promoted above the LCST of the polymers. A close relationship between the temperature region where enhancement of the release was observed and the LCST of the polymer is reported.

EXPERIMENTAL SECTION

Materials. L-α-Dioleoylphosphatidylethanolamine (DOPE), egg yolk phosphatidylcholine (EYPC), and calcein were purchased from Sigma (St. Louis, MO). *N*-Isopropylacrylamide (NIPAM) was obtained from Tokyo Kasei (Tokyo, Japan). Azobis(isobutyronitrile) (AIBN), tris(hydroxymethyl)aminomethane (Tris), *N*,*N*-dimethylformamide, and ethylenediaminetetraacetic acid (EDTA) were supplied from Kishida Chemical (Osaka, Japan). *N*,*N*-Didodecylacrylamide (NDDAM) was prepared as described elsewhere (*18*). NIPAM and AIBN were purified by recrystallization from benzene-*n*-hexane and methanol, respectively.

Polymer Synthesis. Poly(NIPAM) and three kinds of poly(NIPAM-*co*-AAM)s were prepared by free-radical polymerization using AIBN as the initiator. NIPAM and AAM in the ratio of 10/0, 9/1, 8/2, or 7/3 (total 10 mmol) and AIBN (0.03 mmol) were dissolved in freshly distilled tetrahydrofuran (10 mL), and then the solution was heated to 60 °C for 6 h in N_2 atmosphere. The polymer was recovered by precipitation with diethyl ether and dried under vacuum. The polymer was dissolved in water, dialyzed against water for 4 days, and then recovered by lyophilization. Four kinds of poly(NIPAM-*co*-AAm-*co*-NDDAM)s were obtained by the same procedure except that NIPAM, AAM, and NDDAM in the ratios of 99/0/1, 89.1/9.9/1, 79.2/19.8/1, and 69.3/29.7/1 (total 10 mmol) were used as the monomers. Composition of polymers was estimated by elemental analysis and ^{1}H NMR.

Cloud Point Determination. Optical density of aqueous copolymer solutions (5 mg/mL) in 140 mM NaCl and 10 mM Tris-HCl-buffered solution (pH 7.4) at 500 nm was monitored using a spectrophotometer (Jasco V-520) with a water-jacketed cell holder coupled with a circulating bath. Temperature was raised at 0.3 °C/min. Cloud points were taken as the initial break points in the resulting transmittance versus temperature curves.

Liposome Preparation. Two types of polymer-fixed liposomes, namely liposomes having polymer chains on the outer surface of the membrane (Figure 1A) and liposomes having polymer chains on both sides of the membrane (Figure 1B), were prepared. Liposomes having polymer chains on the outer surface were obtained as follows. To a dry, thin membrane consisting of a mixture of DOPE (6 mg) and EYPC (4 mg), 1.5 mL of aqueous calcein solution (63 mM, pH 7.4) was added and sonicated for 15 min under an N_2 atmosphere using a probe-type sonicator (Tomy Seiko, UD-201). A given volume of polymer solution (10 mg/mL) containing 63 mM calcein (pH 7.4) was added to liposome suspension and kept at 5 °C for 12 h. Liposomes having polymer chains on both surfaces of the membrane were made by vortexing polymer/lipid mixed membranes in an aqueous 63 mM calcein solution and subsequent extrusion through a polycarbonate membrane filter with a pore size of 100 nm in an ice-cooled water bath. Free calcein and free polymer were removed by gel permeation chromatography on a Sephacryl-400 column at 4 °C using 10 mM Tris-HCl-buffered solution containing 140 mM NaCl and 0.1 mM EDTA at pH 7.4 as an eluent.

Calcein Release from Liposome. The release measurements were performed according to the method previously reported (*7*, *13*). An aliquot of dispersion of liposomes encapsulating 63 mM calcein was added to 2 mL of 10 mM Tris-HCl, 140 mM NaCl, and 0.1 mM EDTA solution (pH 7.4) in a quartz cell (final concentration of the lipids 5.0 μM) at a given temperature and the fluorescence intensity of the solution was monitored using a spectrophotofluorimeter (Hitachi, F-3010). The excitation and monitoring wavelengths were 490 and 520 nm, respectively. The percent release of calcein from liposome was defined as

$$\% \text{ release} = (F^t - F^i)/(F^f - F^i) \times 100$$

where F^i and F^t mean the initial and intermediary fluorescence intensities of the liposome suspension, respectively. F^f is the fluorescence intensity of the liposome suspension after the addition of Triton X-100 (final concentration, 0.15%). Since release of calcein was very fast above LCST of the copolymer, it was impossible to determine F^i. In contrast, release was slow below the LCST, and liposome hardly released calcein at 10 °C. Therefore, we used initial fluorescence intensity of the liposome suspension at 10 °C for F^i. Change in fluorescence intensity depending on temperature was corrected although the change was not significant under the experimental conditions.

Other Methods. The amount of polymer bound onto liposome was estimated by HPLC on an Asahipak GF-310HQ column using methanol as an eluent, according to the method previously reported (*14*). NMR spectra were taken with a JEOL JNM-GX 270 MHz instrument. Differential scanning calorimetry (DSC) was performed with a Seiko Electronics DSC 120 microcalorimeter. Size of liposome was evaluated by dynamic light scattering (Otsuka Electronics, LPA3100S). The weight average molecular weight (Mw) and the number average molecular weight (Mn) of polymers were estimated by GPC on a Shodex KD-803 columns (Showa Denko) using *N*,*N*-dimethylformamide as an eluent and poly(ethylene glycol) as the standard.

RESULTS AND DISCUSSION

Characterization of Thermosensitive Polymers. As thermosensitive polymers with varying LCSTs, we prepared three kinds of poly(NIPAM-*co*-AAM)s with different NIPAM/AAM ratios as well as homopolymer of NIPAM. Also, we synthesized three kinds of poly(NIPAM-*co*-NDDAM-*co*-AAM)s and poly(NIPAM-*co*-NDDAM) which correspond to analogues of these poly(NIPAM-*co*-AAM)s and poly(NIPAM) with anchor groups to the liposome membrane. Already, many studies have shown that poly(NIPAM) having hydrophobic groups can be fixed on liposome membranes through hydrophobic interactions between the hydrophobic groups and lipid membranes

Table 1. Composition and Molecular Weight of Thermosensitive Polymers

polymer	composition: NIPAM/AAM/NDDAM (mol/mol/mol)	Mw	Mw/Mn
poly(NIPAM)	100/0/0	8900	2.2
poly(NIPAM-AAM10)	89.6/10.4/0	8500	2.2
poly(NIPAM-AAM20)	76.8/23.2/0	8200	2.2
poly(NIPAM-AAM30)	65.3/34.7/0	14 000	2.5
poly(NIPAM-NDDAM)	98.9/0/1.1	10 000	2.1
poly(NIPAM-NDDAM-AAM10)	86.7/12.3/1.0	9300	2.2
poly(NIPAM-NDDAM-AAM20)	73.5/25.5/1.0	10 700	2.3
poly(NIPAM-NDDAM-AAM30)	63.0/35.9/1.1	12 000	2.3

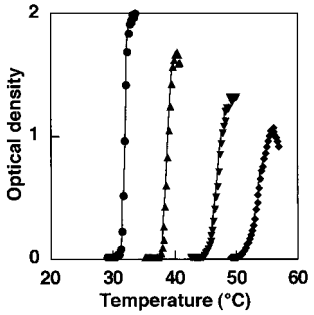


Figure 2. Cloud point curves for solutions of poly(NIPAM) (●), poly(NIPAM-*co*-AAM10) (▲), poly(NIPAM-*co*-AAM20) (▼), and poly(NIPAM-*co*-AAM30) (◆) in 10 mM Tris-HCl buffered solution containing 140 mM NaCl at pH 7.4.

(*7*, *13*, *14*, *19*). Composition, weight average molecular weight, and polydispersity index (Mw/Mn) of these polymers are listed in Table 1.

To determine the LCSTs of these polymers in the Tris-HCl-buffered solution, cloud point and DSC measurements were performed. Figure 2 illustrates typical cloud point curves for solutions of poly(NIPAM) and poly(NIPAM-*co*-AAM)s in the Tris-HCl-buffered solution. The solutions of poly(NIPAM) and poly(NIPAM-*co*-AAM10) exhibited sharp increases in optical density at 32 and 39 °C, respectively. Similarly, aqueous solutions of poly(NIPAM-*co*-AAM20) and poly(NIPAM-*co*-AAM30) displayed increases in optical density around 48 and 54 °C, respectively, although the optical density rose and reached a maximum in relatively broader temperature regions, compared with the cases of poly(NIPAM) and poly(NIPAM-*co*-AAM10). However, the cloud point measurement showed that LCST of poly(NIPAM-*co*-AAM) is elevated with increasing amount of the AAM content. Incorporation of AAM to the polymer chain increases hydrophilicity of the polymer chain, resulting in the increased LCST.

Figure 3 represents typical DSC curves of these polymer solutions. Each polymer solution exhibited an endotherm near the cloud point of the polymer. For example, the solution of poly(NIPAM) revealed an endotherm centered at 32 °C, which is the same to the LCST estimated from the cloud point measurement. However, the endotherm was seen between 27 and 37 °C. Since the endotherm is mainly related to the destruction of water around the hydrophobic N-isopropyl groups by hydrophobic interactions between the hydrophobic groups (*17*), this result suggests that hydrophobicity of the polymer chain was changing in this temperature region. In the case of poly(NIPAM-*co*-AAM), an endotherm appeared at a higher temperature region depending on the AAM content, which is consistent with the result of cloud point measurement. As is apparent in Figure 3, ΔH of the phase separation of the polymer solution decreased with increasing AAM content of the polymer. Feil et al. have reported that ΔH of the phase separation of NIPAM copolymer solutions is directly

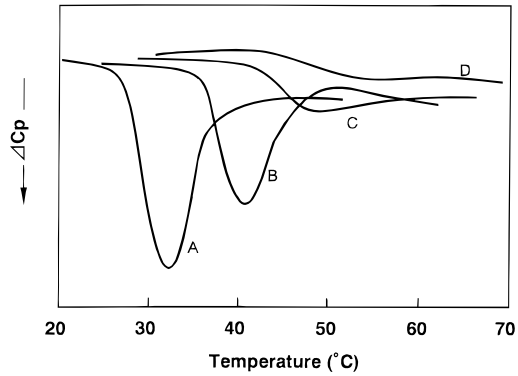


Figure 3. Microcalorimetric endotherms for poly(NIPAM) (A), poly(NIPAM-*co*-AAM10) (B), poly(NIPAM-*co*-AAM20) (C), and poly(NIPAM-*co*-AAM30) (D) in 10 mM Tris-HCl-buffered solution containing 140 mM NaCl at pH 7.4. The samples (100 mg/ml, 50 μL) were heated at 0.5 °C/min.

Table 2. LCST of Polymers

polymer	cloud point (°C)	T_{max}[a] (°C)	ΔH (cal/g of NIPAM unit)
poly(NIPAM)	32.0	32.2	5.6
poly(NIPAM-AAM10)	39.0	40.3	4.6
poly(NIPAM-AAM20)	47.2	48.0	2.0
poly(NIPAM-AAM30)	53.2	55.0	0.8
poly(NIPAM-NDDAM)	28.0	28.1	5.3
poly(NIPAM-NDDAM-AAM10)	33.8	35.5	3.5
poly(NIPAM-NDDAM-AAM20)	39.6	45.0	0.8
poly(NIPAM-NDDAM-AAM30)	46.2	n.d.[b]	

[a] Temperature of peak maximum of calorimetric endotherm. [b] Not detected.

related to its phase separation temperature and a higher LCST leads to a reduced ΔH, because an increase in temperature leads to a reduction in the structuring of water around the N-isopropyl groups (*17*). Since poly(NIPAM-*co*-AAM) with a higher AAM content has a higher LCST, it reveals a smaller ΔH of the phase separation.

Cloud point temperatures, DSC endothermic peaks, and ΔH for solutions of poly(NIPAM), poly(NIPAM-*co*-AAM)s, poly(NIPAM-*co*-NDDAM), and poly(NIPAM-*co*-AAM-*co*-NDDAM)s prepared in this study are summarized in Table 2. LCSTs of poly(NIPAM-*co*-AAM)s and poly(NIPAM-*co*-AAM-*co*-NDDAM)s as a function of AAM content are shown in Figure 4. As is seen in Figure 4, LCSTs of these polymers are linear functions of the AAM content. Also, incorporation of ca. 1 mol % of NDDAM unit caused a decrease in LCST by about 6−7 °C.

Release Property of Thermosensitive Polymer-Fixed Liposomes. As a lipid for liposome preparation, phosphatidylcholines are used most frequently. However, in a previous study, we have shown that interaction of poly(NIPAM) with phosphatidylcholine membranes is not strong enough to destroy the membranes (*7*). Recently, we have found that incorporation of phosphatidyletha-

Table 3. Preparation of Liposomes[a]

liposome	polymer	polymer added (mg/mg lipid)	polymer fixed (mg/mg lipid)	average diameter (nm)
liposome-1	none			119
liposome-2	poly(NIPAM-NDDAM)	0.5	0.09	112
liposome-3	poly(NIPAM-NDDAM-AAM10)	0.1	0.04	110
liposome-4	poly(NIPAM-NDDAM-AAM10)	0.5	0.11	118
liposome-5	poly(NIPAM-NDDAM-AAM10)	1.0	0.12	110
liposome-6	poly(NIPAM-NDDAM-AAM20)	0.5	0.12	117
liposome-7	poly(NIPAM-NDDAM-AAM30)	0.5	0.09	115
liposome-8(E)	poly(NIPAM-NDDAM-AAM10)	0.1	0.08	142
liposome-9(E)	poly(NIPAM-NDDAM-AAM10)	0.5	0.18	132

[a] Liposome-8(E) and liposome-9(E) were prepared by vortexing and subsequent extrusion. Other liposomes were prepared by sonication and subsequent incubation with polymers.

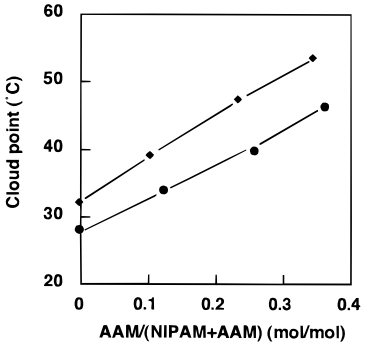


Figure 4. Lower critical solution temperature of poly(NIPAM-*co*-AAM) (◆) and poly(NIPAM-*co*-NDDAM-*co*-AAM) (●) as a function of AAM content.

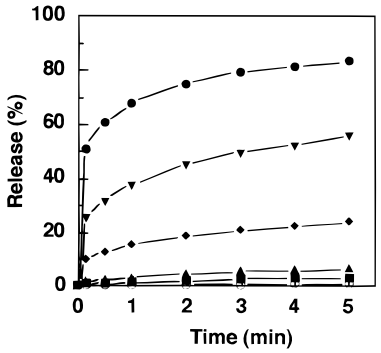


Figure 5. Release profiles of calcein from poly(NIPAM-*co*-NDDAM-*co*-AAM10)-fixed liposome in 10 mM Tris-HCl-buffered solution containing 140 mM NaCl and 0.1 mM EDTA at 20 (○), 30 (■), 35 (▲), 40 (◆), 45 (▼), and 50 °C (●). The liposome-4 was used.

nolamine enhances the polymer−membrane interaction, possibly because phosphatidylethanolamine possesses ability to form hydrogen bondings with the polymer (*18*). Therefore, in this study, we used EYPC/DOPE (4/6, w/w) as liposome lipids. While DOPE liposomes cannot be obtained under neutral conditions due to its strong tendency to take on a hexagonal (H_{II}) phase, liposomes were readily obtained from a mixture of EYPC and DOPE (4/6,w/w) at pH 7.4.

EYPC/DOPE liposomes were prepared by sonication and were coated with poly(NIPAM-*co*-NDDAM) or poly(NIPAM-*co*-AAM-*co*-NDDAM) by incubating the liposome with the polymer. The liposomes obtained by this procedure are considered to have the polymer chains only on the outer surface of the membrane as shown in Figure 1A. The amounts of the polymer added and adsorbed on the liposomes and diameter of the liposome are listed in Table 3. When the EYPC/DOPE liposomes were incubated with poly(NIPAM-*co*-NDDAM-*co*-AAM10) in the ratio of 0.1:1 (polymer/lipid, w/w), 0.04 mg of the polymer was adsorbed onto 1 mg of the liposomal lipid. By increasing the polymer/lipid ratio to 0.5:1 (w/w) during the incubation, amount of the polymer adsorbed onto the liposome increased to 0.11 mg/mg lipid. However, further increase in polymer/lipid ratio to 1:1 (w/w) during the incubation resulted in almost the same amount of the adsorbed polymer. When 0.5 mg of each polymer was added per 1 mg of liposomal lipid, 0.09−0.12 mg of the polymer was adsorbed onto 1 mg of the liposomal lipid. Diameters of the polymer-fixed liposomes were 110−118 nm and approximately the same to the diameter of the bare liposome, indicating that aggregation or fusion of the liposomes did not occur during the incubation of the liposomes with these polymers.

Figure 5 shows typical profiles of calcein release from poly(NIPAM-*co*-NDDAM-*co*-AAM10)-fixed liposome at various temperatures. The liposome hardly released calcein below 35 °C. However, the release was promoted remarkably with rising temperature above 35 °C. Since long alkyl chains on NDDAM units are considered to be inserted into membranes (*19*), these groups might not affect the transition of the polymer chains of NIPAM and AAM units existing in the aqueous environment. Thus, it is likely that the polymer chain of poly(NIPAM-*co*-NDDAM-*co*-AAM10) undergoes the hydrated coil-dehydrated globule transition at the LCST of poly(NIPAM-AAM) with the same AAM/NIPAM ratio, which is estimated to be ca. 40 °C from Figure 4. Therefore, the enhancement of calcein release observed around 40 °C is considered to be triggered by the transition of the polymer chain attached on the liposome surface.

As is seen in Figure 5, calcein release became more significant with raising temperature above 40 °C. While phase separation of the aqueous poly(NIPAM-AAM10) solution occurred in a very narrow temperature region (Figure 2), the DSC measurement indicated that dehydration of the polymer chain still proceeded above the phase transition temperature (Figure 3). In the case of poly(NIPAM-AAM10), an endotherm of the phase separation was seen between 36 and 50 °C. Thus, it is likely that the polymer chains becoming more hydrophobic with rising temperature above 40 °C destabilized the liposome membrane more strongly.

Figure 6 shows an effect of the amount of the polymer fixed on the liposome on its release property. While fixation of the polymer did not affect the release property of the liposome at 35 °C, which is lower than the polymer's LCST, extent of the release increased with increasing amount of the polymer at 45 and 50 °C, which are higher than the LCST. Thus, the liposomes having a larger amount of the polymer revealed a more significant temperature response. While extent of the release was elevated with increasing amount of the polymer above the LCST, further improvement of temperature response

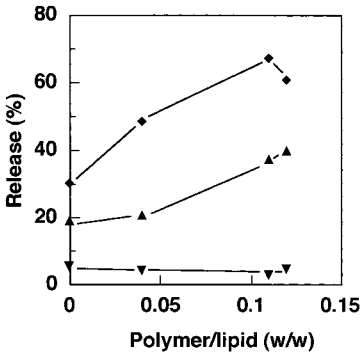


Figure 6. Effect of amount of polymer fixed on liposome on release property at 35 (▼), 45 (▲), and 50 °C (◆). Poly(NIPAM-*co*-NDDAM-*co*-AAM10) was used. Percent release after 1 min incubation is shown.

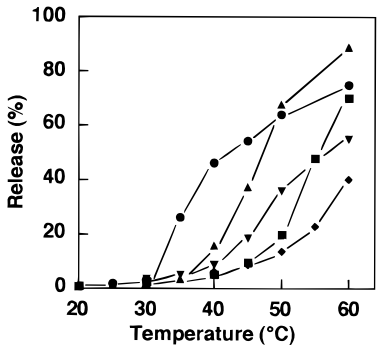


Figure 7. Percent release of calcein from liposomes modified with poly(NIPAM-*co*-NDDAM) (●), poly(NIPAM-*co*-NDDAM-*co*-AAM10) (▲), poly(NIPAM-*co*-NDDAM-*co*-AAM20) (■), and poly-(NIPAM-*co*-NDDAM-*co*-AAM30) (◆) and unmodified liposome (▼) in 10 mM Tris-HCl-buffered solution containing 140 mM NaCl and 0.1 mM EDTA at pH 7.4. Percent release after 1 min incubation is shown. The liposomes-1, 2, 4, 6, and 7 were used.

seems not to be achieved by fixation of more than 0.11 mg of the polymer/1 mg of liposomal lipid.

If release of calcein is triggered by alteration of the polymer chain from a hydrophilic state to hydrophobic state, the critical temperature for the onset of release should be controlled by using polymers with a LCST of a desired temperature. To examine if the calcein release is really triggered by the hydrophilic-to-hydrophobic change of the polymer chains, release properties of various poly(NIPAM-*co*-NDDAM-*co*-AAM)-fixed liposomes were investigated.

Figure 7 depicts percent release of calcein from these liposomes as a function of temperature. These liposomes revealed an enhanced release at different temperatures. For the poly(NIPAM-*co*-NDDAM)-coated liposome, enhancement of the release started between 30 and 35 °C, which corresponds to the LCST of poly(NIPAM). Similarly, poly(NIPAM-*co*-NDDAM-*co*-AAM10)-fixed, poly-(NIPAM-*co*-NDDAM-*co*-AAM20)-fixed, and poly(NIPAM-*co*-NDDAM-*co*-AAM30)-fixed liposomes promoted the contents release from around 40, 50, and 50−55 °C, respectively, which are very close to LCSTs of poly-(NIPAM-*co*-AAM) with same NIPAM/AAM ratios, which are estimated from the result of Figure 4 to be ca. 40, 49, and 55 °C, respectively. This result clearly indicates that the contents release was triggered by the hydrophilic−hydrophobic change of the polymer fixed on the liposome.

A remarkable release was also observed for the unmodified liposome above 45 °C. Because DOPE has a tendency to take on a hexagonal phase and this tendency should increase with temperature, it is possible that DOPE molecules formed the nonbilayer structure in the liposome membrane and caused destabilization of the membrane above that temperature. We examined the occurrence of the bilayer−nonbilayer phase transition in the unmodified liposome membrane by a fluorometric analysis using a fluorescent lipid, dioleoyl-*N*-(7-nitrobenz-2-oxa-1,3-diazol-4-yl)phosphatidylethanolamine (*13*, *22*). The result suggested that the transition takes place between 40 and 45 °C, which is the temperature region where the contents release from the unmodified liposome was promoted (result not shown).

As is seen in Figure 7, calcein release from poly-(NIPAM-*co*-NDDAM-*co*-AAM20)- and poly(NIPAM-*co*-NDDAM-*co*-AAM30)-fixed liposomes was still on a low level around 45−55 °C. This fact suggests that the hydrated polymer chains increased stability of the liposome. It has been reported that, in order for bilayer-to-hexagonal transitions to occur in phosphatidylethanolamine membranes, the membranes have to come into a close contact (*20*, *21*); under nonaggregating conditions such as dilute suspensions of unilamellar liposomes, the phase transition of phosphatidylethanolamine membrane does not take place even above its phase transition temperature (*23*). We have already shown that hydrated poly(NIPAM) chains stabilize DOPE liposomes and suppress occurrence of the bilayer-to-hexagonal transition in the liposome membrane, probably by preventing the bilayer contact between liposomes (*13*). However, under a condition where the polymer chains are dehydrated, the polymer chains interact with the liposome membrane through hydrophobic interactions and hydrogen bondings (*18*). This interaction should promote formation of the nonbilayer structure in the membrane and induce destabilization and/or rupture of the liposome. In fact, it is known that nonpolar molecules such as alkanes promote the formation of the hexagonal phases (*24*). Thus, it may be considered that the primary role of the polymer is the control of the transition to the nonbilayer phase in the liposome membrane. Several stimuli-sensitive liposomes have been prepared using bilayer-to-nonbilayer transitions of phosphatidylethanolamine membranes. Among them are photosensitive liposomes reported by O'Brien and co-workers (*25*, *26*) and target-sensitive liposomes by Huang and his colleagues (*27*).

It is expected that liposomes having the polymer chains on both surfaces of the membrane (Figure 1B) exhibit a more drastic temperature response than liposomes having the polymer chains only on the outer surface (Figure 1A). Thus, two kinds of liposomes of the former type, liposome-8(E) and liposome-9(E), were prepared from the polymer−lipid mixtures. The diameter of the liposome and the amount of the polymer fixed on the liposome are shown in Table 3. Since the liposome-9(E) has 0.18 mg of the polymer/1 mg of the liposomal lipid, density of the polymer chain on the liposome surface may be considered to be roughly the same to that on the outer surface of the liposome-4, which is calculated to have ca. 0.2 mg of the polymer/1 mg of the liposomal lipid. Figure 8 illustrates typical examples of release profiles of calcein from the liposome-9(E). While only a limited extent of release was seen below 35 °C, an intensive and fast release occurred above 45 °C. In comparison with the case of liposome-4 (Figure 5), the release from the liposome-9(E) above the LCST of the polymer is apparently more drastic.

Temperature dependence of the release from these liposomes is shown in Figure 9. Whether the liposome has the polymer chains on the outer surface or on both

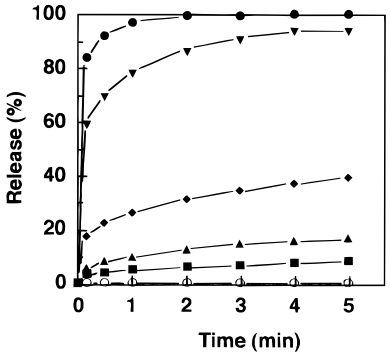


Figure 8. Release profiles of calcein from liposome having polymer on both surfaces of membrane in 10 mM Tris-HCl-buffered solution containing 140 mM NaCl and 0.1 mM EDTA at 20 (○), 30 (■), 35 (▲), 40 (◆), 45 (▼), and 50 °C (●). The liposome-9(E) was used.

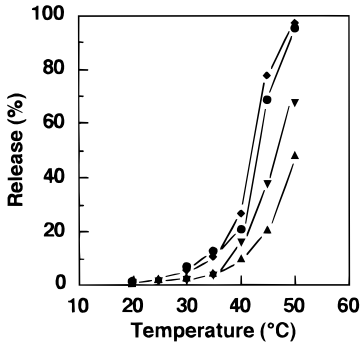


Figure 9. Comparison of release property of liposomes having poly(NIPAM-*co*-NDDAM-*co*-AAM10) on outer surface (▲, ▼) and on both surfaces (●, ◆) of membrane. Percent release of calcein from liposome-3 (▲), liposome-4 (▼), liposome-8(E) (●), and liposome-9(E) (◆) after 1 min incubation is shown as a function of temperature.

surfaces, the release was enhanced remarkably above ca. 40 °C. Although the liposome-8(E) has a lower amount of polymer than the liposome-4, the former revealed a more drastic release. About 70% of the contents was released in 1 min from the liposome-8(E) at 45 °C, whereas only 38% was released from the liposome-4 in the same period. The liposome-9(E) exhibited slightly more drastic release than the liposome-8(E). These results indicate that temperature-sensitive release property of the liposome can be improved by fixing the polymer on both surfaces of the liposome membrane.

Recently, we have found that poly(NIPAM) chain hardly influences fluidity of the hydrophobic region of phospholipid membranes but decreases fluidity of the surface region of membrane above its LCST, suggesting that the hydrophobic polymer chain interacts mainly with the surface region of liposome membrane (*18*). Therefore, in the case of liposome having polymer chains only on the outer surface, the polymer might disturb mainly the outer leaflet of the membrane. Since the inner leaflet of the liposome membrane acts as a barrier to the permeation of calcein, release from the liposome was relatively low. In contrast, for the liposome having the polymer chains on both surfaces of the membrane, the polymer chains destabilize both leaflets of the membrane, and hence, a more intensive release was induced above the LCST. As is seen in Figure 9, the liposome-9(E) might release only less than 15% of the contents at 37 °C, which is the physiological temperature, but about 80% of the contents was released in 1 min at 45 °C. Therefore, this liposome may be useful as a temperature-sensitive drug delivery system.

In conclusion, calcein-loaded EYPC/DOPE liposomes modified with the NIPAM copolymers with varying LCSTs were prepared. It was found that the polymer-fixed liposome hardly released the contents below its LCST, whereas the release was strongly promoted above the LCST. A close relationship between temperature region where the release was enhanced and LCST of the polymer was observed. The results obtained in this study indicate that liposomes which reveal the response at a desired temperature region can be made by modification of liposomes with a NIPAM copolymer, which exhibits a LCST at that temperature. Also, it was shown that temperature response of the liposome can be improved by fixing the polymer on both surfaces of the membrane. Some liposomes prepared in this study exhibited the response around the physiological temperature. Release of the contents from these liposomes might be triggered by the heating of a region of the body. Thus, these liposomes may have potential usefulness as a site-specific drug carrier with temperature sensitivity.

ACKNOWLEDGMENT

The authors thank Mr. Ryoichi Nakai, Osaka Prefecture University, for help concerning GPC measurement.

LITERATURE CITED

(1) Lasic, D. D. (1993) *Liposomes: from physics to applications*, Elsevier, Amsterdam.

(2) Ringsdorf, H., Schlarb, B., and Venzmer, J. (1988) Molecular architecture and function of polymeric oriented systems: models for the study of organization, surface recognition, and dynamics of biomembranes. *Angew. Chem., Int. Ed. Engl. 27*, 113−158.

(3) Thomas, J. L., and Tirrell, D. A. (1992) Polyelectrolyte-sensitized phospholipid vesicles. *Acc. Chem. Res. 25*, 336−342.

(4) Maeda, M., Kumano, A., and Tirrell, D. A. (1988) H^+-induced release of contents of phosphatidylcholine vesicles bearing surface-bound polyelectrolyte chains. *J. Am. Chem. Soc. 110*, 7455−7459.

(5) Kitano, H., Akatsuka, Y., and Ise, N. (1991) pH-Responsive liposomes which contain amphiphiles prepared by using lipophilic radical initiator. *Macromolecules 24*, 42−46.

(6) Wu, X. S., Hoffman, A. S., and Yager, P. (1992) Conjugation of phosphatidylethanolamine to poly(N-isopropylacrylamide) for potential use in liposomal drug delivery systems. *Polymer 33*, 4659−4662.

(7) Kono, K., Hayashi, H., and Takagishi, T. (1994) Temperature-sensitive liposomes: liposomes bearing poly(N-isopropylacrylamide). *J. Controlled Release 30*, 69−75.

(8) Kitano, H., Maeda, Y., Takeuchi, S., Ieda, K., and Aizu, Y. (1994) Liposomes containing amphiphiles prepared by using a lipophilic chain transfer regent: responsiveness to external stimuli. *Langmuir 10*, 403−406.

(9) Winnik, F. M., Adronov, A., and Kitano, H. (1995) Pyrene-labeled amphiphilic poly-(N-isopropylacrylamides) prepared by using a lipophilic radical initiator: synthesis, solution properties in water, and interactions with liposomes. *Can. J. Chem. 73*, 2030−2040.

(10) Heskins, M., and Guillet, J. E., (1968) Solution properties of poly(N-isopropylacrylamide). *J. Macromol. Sci. Chem. A2*, 1441−1455.

(11) Schild, H. G., and Tirrell, D. A. (1990) Microcalorimetric detection of lower critical solution temperatures in aqueous polymer solutions. *J. Phys. Chem. 94*, 4352−4356.

(12) Schild, H. G. (1992) Poly(N-isopropylacrylamide): experiment, theory and application. *Prog. Polym. Sci. 17*, 163−249.

(13) Hayashi, H., Kono, K., and Takagishi, T. (1996) Temperature-controlled release property of phospholipid vesicles bearing a thermo-sensitive polymer. *Biochim. Biophys. Acta 1280*, 127−134.

(14) Hayashi, H., Kono, K., and Takagishi, T. (1998) Temperature-dependent associating property of liposomes modified with a thermosensitive polymer. *Bioconjugate Chem. 9*, 382−389.
(15) Taylor, L. D., and Cerankowski, L. D. (1975) Preparation of films exhibiting a balanced temperature dependence to permeation by aqueous solution: a study of lower consolute behavior. *J. Polym. Sci., Polym. Chem. Ed. 13*, 2551−2570.
(16) Ringsdorf, H., Venzmer, J., and Winnik, F. M. (1991) Fluorescence studies of hydrophobically modified poly(N-isopropylacrylamides). *Macromolecules 24*, 1678-1686.
(17) Feil, H., Bae, Y. H., Feijen, J, and Kim, S. W., Effect of comonomer hydrophilicity and ionization on the lower critical solution temperature of N-isopropylacrylamide copolymers. *Macromolecules 26*, 2496−2500.
(18) Kono, K., Henmi, H., Yamashita, H., Hayashi, H., and Takagishi, T., Improvement of temperature-sensitivity of poly(N-isopropylacrylamide)-modified liposomes. *J. Controlled Release* (In press).
(19) Ringsdorf, H., Venzmer, J., and Winnik, F. M. (1991) Interaction of hydrophobically-modified poly-N-isopropylacrylamides with model membranes- or playing a molecular accordion. *Angew. Chem., Int. Ed. Engl. 30*, 315−318.
(20) Ellen, H., Bentz, J., and Szoka, F. C. (1984) pH-Induced destabilization of phosphatidylethanolamine-containing liposomes: role of bilayer contact. *Biochemistry 23*, 1532−1538.
(21) Siegel, D. (1984) Inverted micellar structures in bilayer membranes: formation rates and half-lives. *Biophys. J. 45*, 399−420.
(22) Hong, K., Baldwin, P. A., Allen, T. M., and Papahadjopoulos, D. (1988) Fluorometric detection of the bilayer-to-hexagonal phase transition in liposomes. *Biochemistry 27*, 3947-3955.
(23) Allen, T. M., Hong, K., and Papahadjopoulos, D. (1990) Membrane contact, fusion, and hexagonal (H_{II}) transitions in phosphatidylethanolamine liposomes. *Biochemistry 29*, 2976−2985.
(24) Seddon, J. M. (1990) Structure of the inverted hexagonal (H_{II}) phase and nonlamellar phase transitions of lipids. *Biochim. Biophys. Acta 1031*, 1−69.
(25) Lamparski, H., Liman, U., Barry, J. A., Frankel, D. A., Ramaswani, V., Brown, M. F., and O'Brien, D. F. (1992) Photoinduced destabilization of liposomes. *Biochemistry 31*, 685-694.
(26) Bennett, D. E., and O'Brien, D. F. (1995) Photoactivated enhancement of liposome fusion. *Biochemistry 34*, 3102−3113.
(27) Ho, R. J. Y., Rouse, B. T., and Huang, L. (1987) Target-sensitive immunoliposomes as an efficient drug carrier for antiviral activity. *J. Biol. Chem. 262*, 13973−13978.

BC980111B

Electrostatic Interactions of Redox Cations with Surface-Immobilized and Solution DNA

Adam B. Steel,*,† Tonya M. Herne, and Michael J. Tarlov*

Process Sensing Group, NIST, Gaithersburg, Maryland 20899. Received September 18, 1998; Revised Manuscript Received January 5, 1999

Association constants for ruthenium(III) hexaamine and cobalt(III) tris(2,2′-bipyridine) with solution and surface-immobilized DNA were determined. The interaction of the cationic redox molecules with calf thymus DNA was monitored via normal pulse voltammetry with analysis of the mass-transfer limited current assuming a discrete binding-site model. Single-stranded DNA was immobilized on gold via self-assembly of a 5′ hexanethiol linker. Double-stranded surface-immobilized DNA was produced by hybridization of a complementary target to surface-immobilized single strands. The interaction between the metal complexes and surface-immobilized DNA was determined using chronocoulometry to construct adsorption isotherms. The measured binding constants for the cationic redox molecules with solution, surface-immobilized single-stranded, and double-stranded DNA are well-correlated, even as a function of ionic strength. The agreement between the determined association constants for the surface-immobilized and solution DNA indicates the potential utility of DNA-derivatized electrodes for examination of small molecule interactions with nucleic acids.

INTRODUCTION

Heterogeneous DNA hybridization, the association of a solution-phase single strand with its immobilized complementary strand at a solid surface, has received considerable attention as an alternative to current DNA diagnostic methods because it is more labor, time, and material efficient (*1*). While biosensors based on heterogeneous hybridization at arrays are now being commercially developed, the physical characteristics of the surface-immobilized DNA are at present poorly understood (*2*). Of particular interest is the influence of surface immobilization on small molecule binding to DNA. In this report, we compare the electrostatic binding of small redox molecules to DNA in solution and immobilized on alkanethiol-modified gold surfaces.

Small molecule binding to DNA has been researched in great detail due to its importance in strand scission mediation, as a structural probe, and as a model for protein−nucleic acid interactions (*3*). Binding modes include covalent attachment, electrostatic attraction, and intercalation into the hydrophobic regions of the DNA. The interaction between a molecule and DNA is often an interplay of the available binding modes. Studies of the binding of electrochemically active small molecules to solution-phase DNA have provided association constants for a wide range of organic and metal chelate compounds (*3*, *4*). The binding constants can be subsequently decomposed into contributions for each type of interaction to provide a more detailed picture of the bound complex.

DNA biosensors have been developed based on an electrochemical signal change for the interaction of small molecules with oligonucleotides immobilized on an electrode surface (*1*, *5*). We recently reported an electrochemical method to determine DNA immobilized on gold based on the electrostatic accumulation of electroactive metal complexes with the nucleotide phosphate backbone (*6*). The quantitative validity of this method rests heavily on using molecules that interact with DNA predominately through electrostatic attraction. As such, small, highly charged redox cations such as ruthenium hexaamine (RuHex) and cobalt trisbipyridyl (CoBPY) were selected as electrochemical markers. In this paper, we report the binding constants for RuHex and CoBPY with solution and surface-immobilized DNA.

EXPERIMENTAL SECTION

Materials. All reagents were obtained from Aldrich Chemical, unless otherwise noted. All solutions were made with deionized water (18 MΩ cm resistivity) from a Barnstead NANOpure system (*7*). Calf thymus DNA was obtained from Sigma Chemical Co. (St. Louis, MO) and was used as received. Concentrated DNA solutions (3−6 mM in nucleotide phosphate) were prepared by dissolving the solid sodium salt of DNA in the measurement electrolyte. Synthetic DNA oligonucleotide probes were purchased from Research Genetics (Huntsville, AL). The probe oligonucleotide contained a 6-mercaptohexyl linker at the 5′ end and 25 bases with the sequence 5′-$HS(CH_2)_6$-CAC GAC GTT GTA AAA CGA CGG CCA G-3′. The complementary single-stranded target was a 25mer with the sequence 5′-CTG GCC GTC GTT TTA CAA CGT CGT G-3′. 6-Mercapto-1-hexanol (MCH) and 2-mercapto-1-ethanol (MCE) were purified using flash chromatography (silica, chloroform). Hexaammineruthenium(III) chloride (99%) (Strem Chemical, Newburyport, MA) was used as received. Tris(2,2′-bipyridyl) cobalt(III) perchlorate was prepared using the procedure of Dollimore and Gillard and recrystallized twice from water prior to use (*8*).

Electrode Preparation. Gold electrodes were prepared by rf sputter deposition of ca. 20 nm of a chromium adhesion layer followed by ca. 200 nm of gold (each 99.99% purity) onto glass microscope slides. Electrodes were cleaned by exposure to warm piranha solution [70% concentrated sulfuric acid, 30% peroxide solution (30%); **WARNING**: piranha reacts violently with organic sol-

* To whom correspondence should be addressed.

† Current address: Gene Logic, Inc. 708 Quince Orchard Rd., Gaithersburg, MD 20878.

10.1021/bc980115g Not subject to U.S. Copyright. Published 1999 by American Chemical Society
Published on Web 03/06/1999

vents] for 12 min. The electrodes were rinsed thoroughly with deionized water and placed in monolayer deposition solutions while wet.

MCE- and MCH-modified surfaces were prepared from 1 mM aqueous solutions. DNA-modified surfaces were prepared using our previously described procedure (*9*). Briefly, mixed monolayer surfaces containing thiolated probe DNA (ss-DNA) and MCH were prepared by immersing the clean gold substrate in a 1.0 μM solution of probe oligonucleotide in 1.0 M potassium phosphate buffer, pH 7, for 15 min, rinsing with 10 mM NaCl, 5 mM Tris buffer, pH 7.4 (R-BFR) for 5 s, immersing in a 1.0 mM MCH solution in deionized water for 1 h, and finally rinsing with R-BFR for 5 s and drying under a stream of nitrogen. Surface-immobilized double-stranded DNA (ds-DNA) was obtained by hybridization of the immobilized ss-DNA to the complementary target at 35 °C for 60 min in 1.0 M NaCl, 10 mM Tris buffer, and 1 mM EDTA, pH 7.4. The concentration of complementary target was 1.0 μM. Upon removal from the hybridization reaction solution, the electrodes were rinsed with R-BFR for 5 s and dried under a stream of nitrogen prior to electrochemical characterization.

Instrumentation. Cyclic voltammetry (CV), normal pulse voltammetry (NPV), and chronocoulometry (CC) were performed with a CH Instruments (Cordova, TN) model 660 electrochemical analyzer (*7*). The following parameters were employed: CV, sweep rate = 100 mV/s; NPV, pulse duration = 100 ms, pulse frequency = 1 s^{-1}, step increment = 4 mV; CC, pulse period = 500 ms, pulse width = 500 mV. Ultraviolet-visible spectra were obtained on a Perkin-Elmer Lambda Bio 20 spectrophotometer (*7*).

Procedures. All electrochemical characterizations were performed in a single-compartment cell with a 10 mL volume. The working electrodes were prepared as described above. A saturated calomel electrode (SCE) and platinum wire gauze served as the reference and counter electrodes, respectively. Supporting electrolyte, 10 mM Tris buffer, pH 7.4 (E-BFR), was deoxygenated via purging with nitrogen gas for 10 min prior to measurements, and the cell was blanketed with nitrogen for the experiment duration. All experiments were carried out at laboratory ambient temperature (21−24 °C).

Binding constants for redox cations with calf thymus DNA in solution were calculated following the DNA titration strategies of the Bard (*3e*) and Thorp (*3h*) groups. Aliquots of solution containing 50 μM redox cation and 3.0 mM nucleotide phosphate were added to a solution containing 50 μM redox cation in 10 mM Tris buffer. For competitive binding studies, NaCl was added to the Tris buffer. Normal pulse voltammograms were collected for each nucleotide phosphate concentration at a MCE-modified electrode. MCE-modified electrodes were used in place of a bare gold electrode because the self-assembled monolayer blocks nonspecific adsorption of the redox molecule and DNA without affecting the reaction kinetics (*10*).

Binding constants for redox cations with surface-immobilized ss- and ds-DNA were calculated from adsorption isotherms. The amount of redox cation accumulated at the electrode surface due to the presence of nucleotide phosphate was determined via chronocoulometry as previously described (*6*). In brief, double layer charge determinations were made in the electrolyte buffer without redox cation. When a redox cation is added to the low ionic strength electrolyte, the redox cation exchanges with the native charge compensation cation, accumulating at that interface. The amount of accumulated redox cation can then be measured using chronocoulometry, a current integration technique, under equilibrium conditions. The number of redox cations at the electrode surface is determined from the difference in chronocoulometric intercepts for the identical potential step experiment in the presence and absence of redox cation. Accumulation of the redox cation at the electrode surface does not significantly alter the double layer charge for the electrode based on experiments using an equivalent potential step magnitude but over a region where the redox cation is not electroactive. Adsorption isotherms were constructed by adding aliquots of a redox cation solution to 10 mL of electrolyte buffer, stirring the solution, and waiting 1 min prior to recording the chronocoulometric trace. Variable waiting periods were used to ensure that the system had reached equilibrium; 30 s of equilibration time was found to be sufficient.

RESULTS AND DISCUSSION

Solution-Phase DNA Interactions. Association constants for electrostatic binding of RuHex and CoBPY to DNA were determined following the method of the Bard and Thorp groups (*3e,h*). High-affinity binding to DNA, as is the case for the redox molecules under consideration here, is best described by a discrete site model. Free small molecule and DNA-binding sites, of a fixed size *s* in base pairs, are in equilibrium with the bound species. An expression for the bound fraction as a function of the association constant, *K*, and the binding site size, *s*, can be derived from the equilibrium constant expression

$$X_b = \frac{b - \left(b^2 - \frac{2K^2[M][NP]}{s}\right)^{1/2}}{2K[M]} \quad (1a)$$

$$b = 1 + K[M] + \frac{K[NP]}{2s} \quad (1b)$$

where X_b is the bound mole fraction, [M] is the total metal ion concentration, and [NP] is the nucleotide phosphate concentration. Equation 1 is valid for noncooperative, nonspecific binding to a unique binding site on DNA. Values for the binding constant, *K*, and the binding site size, *s*, are determined by nonlinear regression analysis of bound fraction versus nucleotide phosphate profiles.

The bound fraction of redox molecule was determined from the plateau current in normal pulse voltammograms obtained during the titration of redox molecule with calf thymus DNA (*3h*). The plateau current diminishes upon the addition of DNA because the effective diffusion coefficient of the redox molecule is lowered by binding to DNA. The bound mole fraction, assuming rapid exchange between free and bound states on the voltammetric time scale, is given by a ratio of squared current differences

$$X_b = \frac{i^2 - i_o^2}{i_{sat}^2 - i_o^2} \quad (2)$$

where i_o is the plateau current in the absence of DNA and i_{sat} is the current at complete saturation.

Because we are interested in promoting electrostatic attraction between the redox cations and nucleotide phosphate backbone, DNA titrations were performed in the absence of excess electrolyte cation. Titration data are given in Figure 1 for both RuHex and CoBPY with the associated nonlinear regression best-fits to eqs 1a and 1b. The regression analysis results are summarized in Table 1. The association constant for the smaller, harder RuHex is an order of magnitude larger than that for

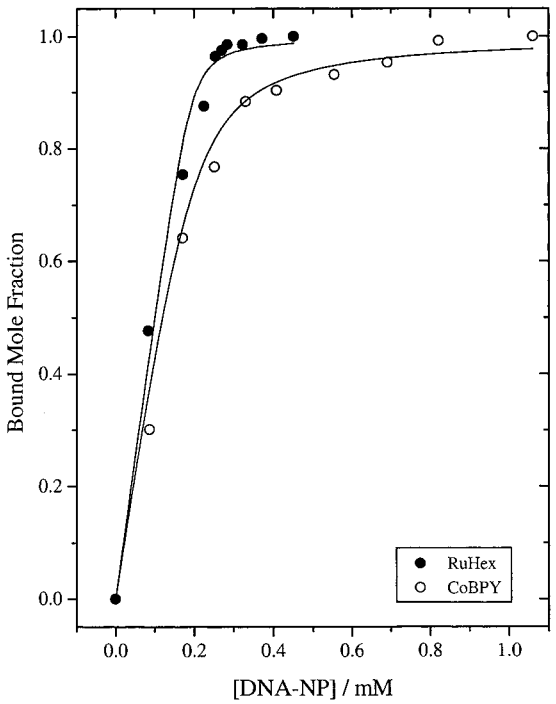


Figure 1. Plot of the bound mole fraction of 50 μM metal complex upon titration with calf thymus DNA in 10 mM Tris buffer, pH 7.4, no excess Na^+, and associated nonlinear least-squares fits to eq 1. Binding titrations are given for ruthenium(III) hexaamine (RuHex, closed circles) and cobalt(III) trisbipyridal (CoBPY, open circles).

Table 1. Binding Constants of RuHex and CoBPY to Calf Thymus DNA in Solution

complex	excess [Na^+] (mM)	K^a (M^{-1})	s^a (bp)
RuHex	0	1.2×10^6	2.0
	10	5.0×10^5	2.5
	100	6.0×10^4	4.0
CoBPY	0	2.0×10^5	2.0
	10	4.5×10^4	3.0
	15[b]	5.8×10^4	3.0

[a] The binding constant, *K*, and binding site size, *s*, were calculated from linear regression analysis of titration data in electrolytes with increasing excess sodium ion concentration. [b] Reference *3h*.

CoBPY. The binding site sizes obtained for RuHex and CoBPY in the absence of excess electrolyte cation are the same, within the experimental uncertainty. Furthermore, the binding site size of 2.0 base pairs approaches the theoretical saturated binding site size of 1.5 base pairs for complete charge compensation of the nucleotide phosphate by trivalent redox cation. We note that the sodium ion concentration in these experiments is equivalent to the nucleotide phosphate concentration, roughly 1 mM, so that a significant amount of sodium cation is available in solution to compete with the redox cation for the anionic phosphate-binding sites. It is not surprising then that the theoretical saturated binding site size of 1.5 base pairs/trivalent redox cation is not achieved.

The influence of a competing cation, e.g., sodium, was studied further by measuring the binding constant, *K*, and site size, *s*, in solutions with increasing ionic strength. Binding isotherms for RuHex are given in Figure 2 with the accompanying nonlinear regression analysis fits. The data are summarized in Table 1. As would be expected, the binding constant decreases and the effective binding site size increases with increasing ionic strength. Our results are in good agreement with those reported by Welch et al. (*3h*).

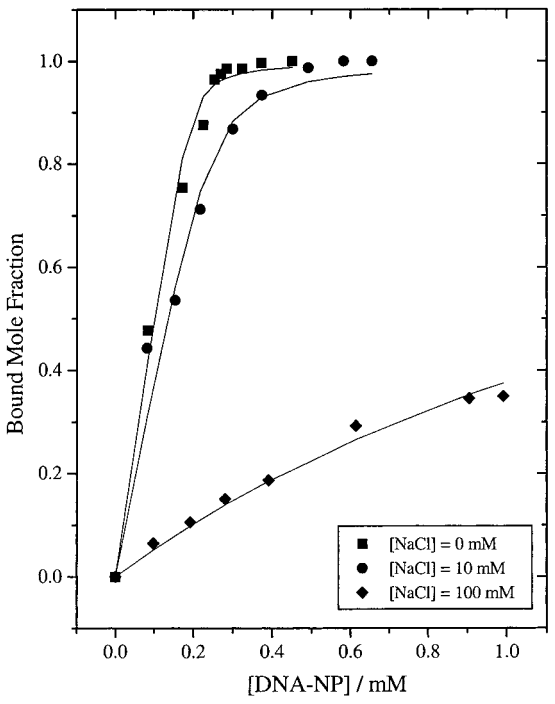


Figure 2. Plot of the bound mole fraction of 50 μM RuHex upon titration with calf thymus DNA in 10 mM Tris buffer, pH 7.4 with increasing excess Na^+ and associated nonlinear least-squares fits to eq 1. Binding titrations were performed with excess sodium concentrations of 0 (squares), 10 (circles), and 100 (diamonds) mM.

Surface-Immobilized DNA. Study of the interactions of small molecules with surface-immobilized oligonucleotides is important for the developing field of DNA diagnostics. Of particular interest here is the interaction of electrostatically bound molecules to DNA immobilized on gold. Attachment of DNA to an electrode surface provides a convenient means to probe the interactions of redox molecules and DNA, as shown by Kelley et al. (*1a*). Surfaces modified with ss-DNA and ds-DNA were prepared to determine if molecule binding affinity is a function of DNA structure (i.e., single-strand vs duplex DNA).

Cationic RuHex interacts strongly with the polyanionic backbone of surface-immobilized DNA. The strong interaction is manifested in cyclic voltammograms as a post-wave shoulder attributable to surface-confined species (*11*). Five consecutive voltammograms for a ss-DNA-modified electrode in 50 μM RuHex are given in Figure 3. The overlap of all of the voltammograms is evidence that equilibrium has been established in the system. Also shown in Figure 3 is a series of voltammograms taken after exposing the electrode to 50 μM RuHex solution, then transferring the electrode to a redox-free buffer for measurement. Removal of the electrode from the redox-containing solution allows us to ascribe the peak at -272 mV to surface-confined redox molecules. Further confirmation that the peak at -272 mV is due to a surface-confined species is determined from scan rate dependence studies. The peak currents at -168 mV (diffusion-limited) and -272 mV (surface-confined) are plotted as a function of scan rate in Figure 4. The peak current at -272 mV is linear with scan rate, indicating a surface-confined reaction, while the peak current data for -168 mV is indicative of the mass-transfer limited reaction.

The voltammetry of CoBPY at DNA-modified electrodes does not exhibit a post-wave, as was observed for RuHex, reflecting the difference in the relative strength

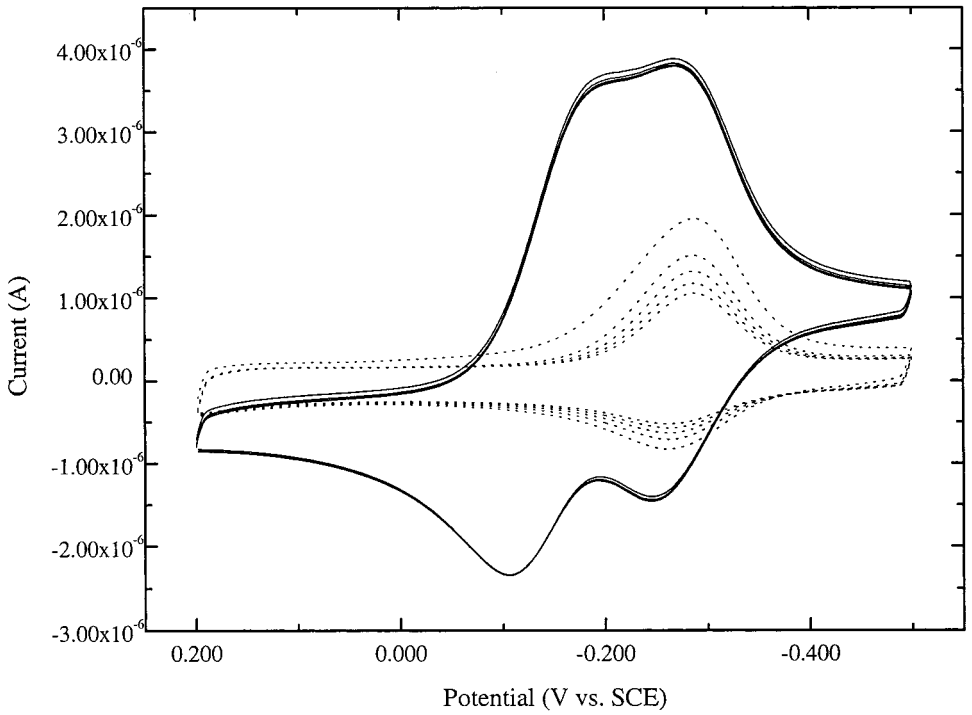


Figure 3. Cyclic voltammetry of RuHex at ss-DNA modified electrode. The first five cycles, $v = 100$ mV/s, for an electrode in 50 μM RuHex, 10 mM Tris, pH 7.4 (solid line), and an electrode that was incubated in same solution for 1 min, washed, and transferred to 10 mM Tris, pH 7.4, for measurement (dotted line).

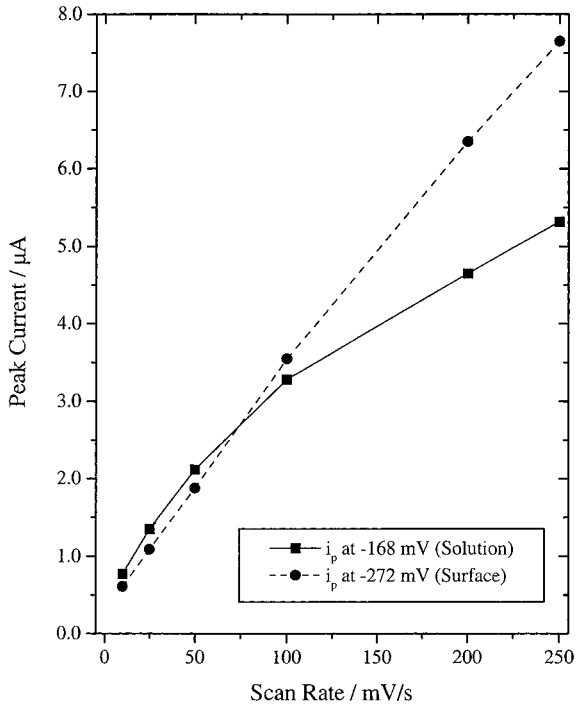


Figure 4. Plot of the peak currents at −168 (squares) and −272 mV (circles) versus scan rate for a ss-DNA modified electrode in 50 μM RuHex, 10 mM Tris, pH 7.4. The lines are given as a guide to the eye only.

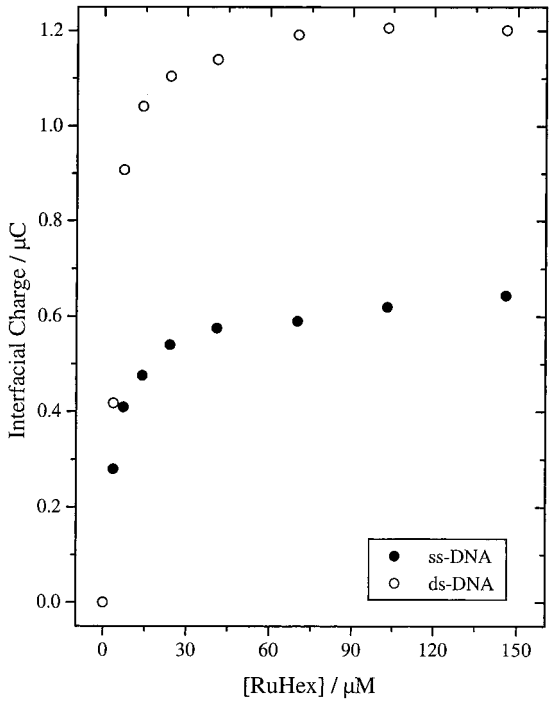


Figure 5. Adsorption isotherms of RuHex at ss-DNA (closed circles) and ds-DNA (open circles) modified electrodes. The interfacial charge due to adsorbed RuHex was determined from the increase in chronocoulometric intercept with increasing metal complex concentration.

of the redox cation/DNA interaction (*11*). Loading experiments, such as those included for RuHex in Figure 3, show that CoBPY does accumulate at the electrode surface.

Determination of Redox Molecule Affinities for Surface-Immobilized DNA. The binding constants of redox molecules with ss- and ds-DNA were determined from adsorption isotherms. The amount of surface-confined redox molecule was measured using chronocoulometry. Binding isotherms for RuHex at ss- and ds-DNA modified electrodes in E-BFR are given in Figure 5. An association constant, K, was calculated from the isotherm data using the Langmuir adsorption isotherm model. The Langmuir model assumes that the every binding site is equivalent and that the ability of a molecule to bind is independent of occupation of nearby sites. A linearized form of the Langmuir isotherm in terms of the solution

Table 2. Binding Constants of RuHex and CoBPY to ss- and ds-DNA Immobilized on an Electrode Surface

complex	excess [Na^+] (mM)	K/ss-DNA[a] (M^{-1})	K/ds-DNA[a] (M^{-1})
RuHex	0	$(2.2 \pm 0.9) \times 10^6$	$(1.3 \pm 0.4) \times 10^6$
	10	$(3.7 \pm 2.2) \times 10^5$	$(3.0 \pm 0.6) \times 10^5$
	100	$(2.7 \pm 1.6) \times 10^4$	$(4.1 \pm 0.8) \times 10^4$
CoBPY	0	$(2.7 \pm 0.5) \times 10^5$	$(1.6 \pm 0.3) \times 10^5$
	10	$(6.9 \pm 0.3) \times 10^4$	$(5.6 \pm 0.4) \times 10^4$

[a] The binding constants, K, were determined from Langmuir analysis of adsorption isotherm data in electrolytes containing the listed excess sodium ion concentrations. The average and standard deviation on at least three measurements per entry are given.

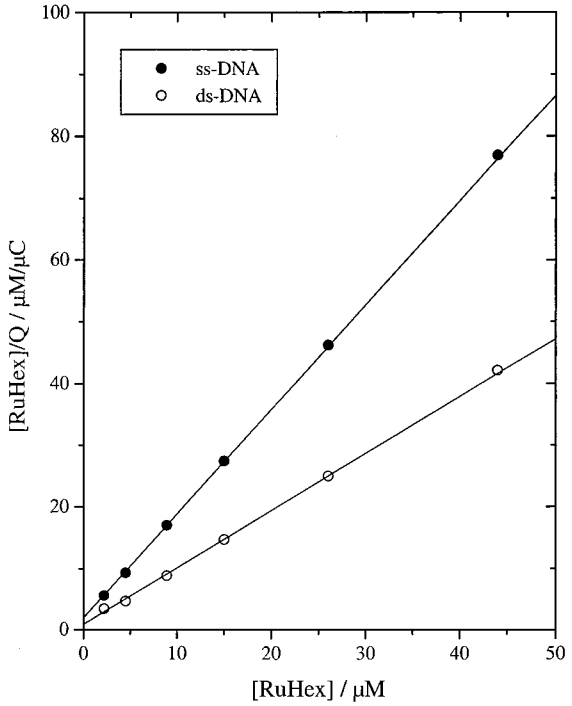


Figure 6. Linearized Langmuir isotherm. The adsorption isotherm data for RuHex at ss-DNA (closed circles) and ds-DNA (open circles) modified electrodes in accordance with eq 3. The lines are the least-squares best-fit to the data used to calculate the binding constants given in Table 2.

redox cation concentration, [M], the accumulated charge at the electrode surface, Q, and the saturated charge, Q_{sat}, is given by eq 3.

$$\frac{[M]}{Q} = \frac{[M]}{Q_{sat}} + \frac{1}{KQ_{sat}} \quad (3)$$

Results of Langmuir analysis of isotherm data are given in Table 2. The binding isotherm data for RuHex at ss- and ds-DNA modified electrodes in E-BFR (no added NaCl) are plotted in the linearized Langmuir plot in Figure 6. The saturation coverages of RuHex are 0.6 and 1.2 μC/cm^2 for ss- and ds-DNA modified surfaces, respectively. Binding constants calculated from the plots in Figure 6 are 2.1×10^6 and 1.1×10^6 M^{-1} for ss- and ds-DNA, respectively.

The doubling of the redox molecule coverage in going from ss- to ds-DNA is particularly satisfying because it indicates that all of the ss-DNA is hybridized when we form our ds-DNA samples. The doubling of saturated redox molecule coverage is a result of our probe and target having the same length so that forming the hybrid doubles the number of binding sites (nucleotide phosphates) at the electrode surface. We have previously shown that the interaction of RuHex with surface-immobilized DNA can be used as a means to quantitate the surface density of DNA when the length of the probe and target are known (*6*). The DNA surface densities calculated from the saturated RuHex coverages in Figure 6 are 3.2×10^{12} probes/cm^2 and hybrids/cm^2.

Comparison of the binding constants in Table 2 shows that these cations interact equivalently with ss- and ds-DNA over the range of ionic strengths studied. The correspondence of these binding constants indicates that electrostatic attraction is the predominant contributor to the overall metal chelate−DNA interaction. Comparison of the association constants in Tables 1 and 2 shows that binding affinity is not affected by end-tethering DNA to a surface.

CONCLUSION

We have shown that electrostatic binding of select cationic molecules to DNA is not affected by immobilization of the nucleic acid to a surface. Thus, DNA-derivatized electrodes provide a convenient and potentially powerful means to study the interactions of small molecules with nucleic acids. We intend to explore the utility of the techniques outlined herein for the investigation of other small molecule−DNA interactions.

LITERATURE CITED

(1) (a) Kelley, S. O., Barton, J. K., Jackson, N. M., and Hill, M. G. (1997) *Bioconjugate Chem. 8*, 31. (b) Chan, V., Graves, D. J., and McKenzie, S. E. (1995) *Biophys. J. 69*, 2243. (c) Wang, J., Cai, X., Rivas, G., Shiraishi, H., Faria, P. A. M., and Donta, N. (1996) *Anal. Chem. 68*, 2629. (d) Hashimoto, K., Ito, K., and Ishimori, Y. (1994) *Anal. Chem. 66*, 3830. (e) Millan, K. M., and Mikkelsen, S. R. (1993) *Anal. Chem. 65*, 2317.

(2) (a) Chan, V., Graves, D. J., Fortina, P., and McKenzie, S. E. (1997) *Langmuir 13*, 320. (b) Chan, V., Graves, D. J., and McKenzie, S. E. (1995) *Biophys. J. 69*, 2243.

(3) (a) Barton, J. K., Danishefsky, A. T., and Goldberg, J. M. (1984) *J. Am. Chem. Soc. 106*, 2172. (b) Kelly, J. M., Tossi, A. B., McConnell, D. J., and OhUigin, C. (1985) *Nucleic Acids Res. 13*, 6017. (c) Barton, J. K. (1986) *Science 233*, 727. (d) Dervan, P. B. (1986) *Science 233*, 464. (e) Carter, M. T., Rodriguez, M., and Bard, A. J. (1989) *J. Am. Chem. Soc. 111*, 8901. (f) Meyer-Almes, F. J., and Porschke, D. (1993) *Biochemistry 32*, 4246. (g) Murphy, C. J., Arkin, M. R., Ghatlia, N. D., Bossmann, S., Turro, N. J., and Barton, J. K. (1994) *Proc. Natl. Acad. Sci. U.S.A. 91*, 5315. (h) Welch, T. W., and Thorp, H. H. (1996) *J. Phys. Chem. 100*, 13829. (i) Wang, J., Rivas, G., Cai, X., Donta, N., Shiraishi, H., Luo, D., and Valera, F. S. (1997) *Anal. Chim. Acta 337*, 41. (j) Pang, D., and Abruna, H. D. (1998) *Anal. Chem. 70*, 3162.

(4) Mahadevan, S., and Palaniandavar, M. (1997) *Inorg. Chim. Acta 254*, 291.

(5) (a) Zhao, Y., Pang, D., Wang, Z., Cheng, J., and Qi, Y. (1997) *J. Electroanl. Chem. 431*, 203. (b) Palanti, S., Marrazza, G., and Mascini, M. (1996) *Anal. Lett. 29*, 2309. (c) Napier, M. E., and Thorp, H. H. (1997) *Langmuir 13*, 6342.

(6) Steel, A. B., Herne, T. M., and Tarlov, M. J. (1998) *Anal. Chem. 70*, 4670.

(7) Certain commercial products and instruments are identified to adequately specify the experimental procedure. In no case does such identification imply endorsement by the authors or NIST.

(8) Dollimore, L. S., and Gillard, R. D. (1973) *J. Chem. Soc., Dalton Trans.* 933.

(9) Herne, T. M., and Tarlov, M. J. (1997) *J. Am. Chem. Soc. 119*, 8916.

(10) Terrattaz, S., Cheng, J., Miller, C. J., and Guiles, R. D. (1996) *J. Am. Chem. Soc. 118*, 7857.

(11) Bard, A. J., and Faulkner, L. R. (1980) *Electrochemical Methods*, p 527, John Wiley & Sons, New York.

BC980115G

Site-Specific Modification of a Single-Chain Antibody Using a Novel Glyoxylyl-Based Labeling Reagent

Zhan G. Zhao,[†,‡] Jin S. Im,[†,§] Kit S. Lam,*[,†,§,||] and Douglas F. Lake*[,†,§]

Arizona Cancer Center, 1515 North Campbell, Tucson, Arizona 85724, and Department of Microbiology and Immunology and Department of Medicine University of Arizona, Tucson, Arizona 85721 .
Received September 29, 1998; Revised Manuscript Received February 25, 1999

A novel, highly specific protein modification approach is described. By using conventional molecular cloning techniques, a protein can be constructed and expressed such that the N-terminal residue is replaced by cysteine. Its 1,2-aminothiol structure reacts very specifically with a glyoxylyl group at pH 7 or below, forming a relatively stable thiazolidine bridge. Therefore, a glyoxylyl-based labeling agent (e.g., radioactive tags, fluorescent probes, biotin) can be used to specifically modify a protein at its N-terminus. To highlight this novel approach, a recombinant anti-insulin single chain antibody (scFv) was specifically biotinylated at its N-terminus even in the presence of other proteins in the total cell lysate. The glyoxylyl-biotinylated scFv retained binding activity similar to unmodified scFv.

INTRODUCTION

One of the major efforts in bioconjugate chemistry research is to develop methods for the derivatization of macromolecules in a site-specific manner (*1*). Commonly, peptides and proteins are modified either on the side chains of lysine residues by using amine-reactive reagents or on the side chains of cysteine residues by using thiol-reactive reagents. Less popular methods include derivatization at the tyrosine residue side chains (*2*) and the enzyme-catalyzed reverse proteolytic reactions at the C-terminal carboxylate group (*3*). Among all these methods, only the enzyme-catalyzed reverse proteolytic reaction is truly site specific. Amine-reactive reagents, which include reagents based on active esters (e.g., N-hydroxysuccinimide ester), isothiocyanides, aldehydes, and sulfonyl halides, etc., react predominately with ϵ-amino functional groups and to a lesser extent α-amino functional groups. Despite the mild conditions under which these reagents are used, heterogeneity of the modified products arises because of the high abundance of lysine residues in proteins and many peptides. Thiol-reactive reagents, such as the maleimide-based reagents and the haloacetic-based reagents, are somewhat more selective because of the lower abundance of cysteine residues in peptides and proteins. In cases where all thiol groups are involved in disulfide bond formation, one can introduce a single surface-accessible thiol into the target protein by site-directed mutagenesis (*4*). Although thiol-reactive reagents are more specific than the amine-reactive reagents, reactions with other nonthiol nucleophiles are possible, especially when the modification is forced by use of excess maleimide-based reagents resulting in modification of the side chains of histidine, lysine, α-amino groups of peptides (*5*).

An interesting approach to label only the N-termini was developed by Geoghegan et al. (*6*) and Gaertuer et al. (*7*). This approach takes advantage of the special reactivity of IO_4^- toward vicinal $-OH$ and $-NH_2$ groups which exist in N-terminal serine or threonine. The 2-amino alcohol group can be easily oxidized by periodate at pH 7, generating a glyoxylyl group which specifically reacts with either a hydrazide group (*6*) or an aminooxy group (*8*). This approach has been used for specific labeling of interleukin-8 at the N-terminus with aminooxy-functionalized fluorescent probes (*9*) and poly(ethylene glycol) polymers (*8*). Later, Zhang and Tam (*10*) extended this approach by using a 1,2-aminothiol-based biotinylation agent which specifically react with the N-terminal glyoxylyl group forming a stable thiazolidine ring.

To avoid potential oxidation of peptides and proteins by periodate, we developed an alternative approach which utilizes a glyoxylyl-based labeling agent to specifically label a synthetic peptide by reacting with either an N-terminal cysteine or a side-chain-attached cysteine resulting in a thiazolidine ring bridge (*11*). We also proposed that this approach could also be used to label a protein at its N-terminus where the original residue can easily be changed to cysteine using site-directed mutagenesis (*11*). In this paper, we report the cloning and expression of a recombinant protein with cysteine added to its N-terminus and the procedure of using a glyoxylyl-based modification reagent to label this protein at the N-terminus either before or after its purification. To highlight this novel approach, we chose to modify a recombinant anti-insulin antibody, designated HB125 scFv[1] (*12*), and a glyoxylyl-functionalized biotin as the modification agent. The conjugate products were then analyzed by Western blot in conjunction with streptavidin-alkaline phosphatase. A flexible and hydrophilic linker molecule was also synthesized and used in the synthesis of labeling agents in order to limit any unwanted structural perturbations of the protein being modified.

MATERIALS AND METHODS

(+)-Biotin, 4,7,10-trioxa-1,13-tridecanedeamine, succinic anhydride, tetrakis(triphenylphosphine) palla-

* To whom correspondence should be addressed.
[†] Arizona Cancer Center.
[‡] Current address: SIDDCO, Inc., 9040 S. Rita Road, Suite 2338, Tucson, AZ 85747.
[§] Department of Microbiology and Immunology.
[||] Department of Medicine.

10.1021/bc980120k CCC: $18.00 © 1999 American Chemical Society
Published on Web 04/24/1999

Scheme 1. Synthesis of Linker Molecule, Fmoc-Ttds-OH

$H_2N(CH_2)_3O(CH_2CH_2O)_2(CH_2)_3NH_2$

↓ Succinic Anhydride

$H_2N(CH_2)_3O(CH_2CH_2O)_2(CH_2)_3NHCOCH_2CH_2COOH$

↓ Fmoc-OSu

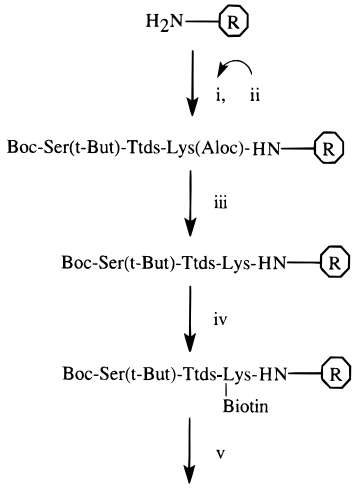
Fmoc-$HN(CH_2)_3O(CH_2CH_2O)_2(CH_2)_3NHCOCH_2CH_2COOH$

(Fmoc-Ttds-OH)

dium(0), and sodium periodate were purchased from Aldrich (Milwaukee, WI); Fmoc-Lys(Aloc)-OH was from SNPE (Princeton, NJ); Boc-Ser(t-but)-OH and Fmoc-Osu were purchased from Advanced ChemTech (Louisville, KY). All other reagents and solvents were purchased from commercial sources and used without purification. ISMS and FABMS were acquired at the Mass Spectoscopy Facility, College of Pharmacy, University of Arizona. HRFABMS was acquired at the Mass Spectroscopy Facility, Department of Chemistry, University of Arizona. HPLC was carried out on an ISCO two-solvent system (Lincoln, NE). For analytical work, a column 250 × 4 mm i.d. (vydac) was used at a flow rate of 10 mL/min. Solvent A was prepared by adding 2 mL of TFA to 4 L of water. Solvent B was prepared by adding 1.7 mL of TFA to 500 mL of water and making up to 4 L with acetonitrile.

Synthesis of Fmoc-Protected 4,7,10-Trioxa-1,13-tridecanediamine Succinimic Acid (Fmoc-Ttds), (Scheme 1). 4,7,10-Trioxa-1,13-tridecanediamine (2.22 g, 10 mmol) was dissolved in 50 mL of CH_3CN and placed in a 250 mL flask with magnetic stirring. Succinic anhydride (1 g, 10 mmol) in 25 mL of CH_3CN was added dropwise over an hour. The reaction was allowed to proceed for an additional 3 h at room temperature. After the waxy product settled, organic solvent was decanted and discarded. The product was rediluted in 100 mL of 50% aqueous CH_3CN and chilled in an ice bath for 30 min before Fmoc-OSu (4.4 g, 13 mmol) in 25 mL of CH_3CN was added. Enough diisopropylethylamine was then added to maintain pH 8−9 throughout the reaction. After stirring for 10 h at room temperature, the solvents were removed in vacuo. The resultant product was dissolved in 100 mL of 5% $NaHCO_3$ and washed with EtOAc. The aqueous phase was then acidified with 1 N HCl to pH 2 and extracted 3 times with 50 mL of EtOAc. The combined organic phase was washed with distilled H_2O and dried over anhydrous Na_2SO_4. The evaporation of organic solvent gave 4 g of product (75% yield). Molecular weight calculated for this compound: 543.5. Found: 543.2 by ion spray mass spectroscopy (ISMS).

Scheme 2. Sythesis of Glyoxylyl-Functionalized Biotin



[a] (i) AA, DIC, HOBt (AA = Fmoc-Lys(Aloc)-OH, Fmoc-Ttds-OH, Boc-Ser(t-But)-OH; (ii) 20% piperidine in DMF; (iii) tetrakis(triphenylphosphine) palladium(0); (iv) biotin, HTBU, HOBt, DIEA; v, 10% TFA in DCM; (vi) $NaIO_4$ (0.02 M NaAc, 0.02 M EDTA, pH 4.2).

Synthesis of Glyoxylyl Functionalized Biotin (Glyoxylyl-Biotin). Synthesis of the glyoxylyl functionalized biotin (glyoxylyl-biotin) is outlined in Scheme 2. Briefly, protected tripeptide, Boc-Ser-Ttds-Lys(aloc)-resin, was synthesized with Fmoc solid-phase chemistry (*13*). Deprotection of lysine side chain, Lys(Aloc), was carried out by Loffexís procedure (*14*) with tetrakis (triphenyl phosphine) palladium(0) as the reducing agent. The on-bead biotinylation was performed by using HBTU and HOBt as the coupling agents. Enough (40−50%) diisopropylethylamine (DIEA) was added to dissolve biotin which is not soluble in pure DMF. The biotinylated tripeptide was then cleaved from the Rink resin with 95% TFA−5% H_2O, and purified on preparative HPLC (ISCO, Lincoln, NE) using a linear gradient of 0 to 50% (by vol) B over 30 min. The product, Ser-Ttds-Lys(biotin)-NH_2, has the expected molecular weight as determined by HRFABMS (M + H calculated for $C_{33}H_{61}O_{10}S$ 761.4231, found 761.4241). The biotinylated tripeptide was quantitatively oxidized following a published procedure (*6*). The resulting glyoxylyl functionalized biotin (glyoxylyl-biotin) was purified by preparative HPLC. After loading the filtered reaction solution onto the column, the inorganic salts were eluted for 10 min with solvent A. The product was then eluted off with a linear gradient of 0 to 100% (by vol) B over 15 min. The molecular weight was determined by FabMS (M + H, 730.3, observed 729.7, and M + H + H_2O, 748.3, observed 747.6). However, the signal was too small for a high-resolution MS analysis, probably because no ionizable group was present in the molecule. A similar result was also observed by Rose et al. (*15*).

Construction of N-Terminal Cysteine Anti-Insulin scFv (NCscFv). Wild-type anti-insulin scFv(WTscFv) constructed from murine anti-insulin IgG1 (HB125) hybridoma, obtained from ATCC, was molecularly cloned into pET21d expression vector as previously reported (*12*). WTscFv was amplified from this vector using a 5′ primer which has a cysteine codon at the 5′ end (5′-

[1] Abbreviations: HBTU, *O*-benzotriazol-*N*,*N*,*N*′*N*′-tetramethyl-uronium-hexafluorophosphate; HOBt, *N*-hydroxybenzotriazol; DIEA, diisopropylethylamine; TFA, trifluoroacetic acid; ISMS, ion spray mass spectroscopy; FABMS, fast-atom bombardment mass spectroscopy; HRFABMS, high-resolutioin fast-atom bombardment spectroscopy; scFv, single-chain Fv; NCscFv, N-terminal cysteine-containing scFv; WTscFv, wild-type scFv; IPTG, isopropylthio-β-galactoside; NHS-LC-biotin, sulfosuccinimidyl-6-(biotinamido) hexanoate; BCIP, 5-bromo-4-chloro-3-indolyl phosphate; NBT, nitroblue tetrazolium; IMAC, immobilized metal affinity chromatography; Ttds, 4,7,10-trioxa-1,13-tridecanediamine succinimic acid.

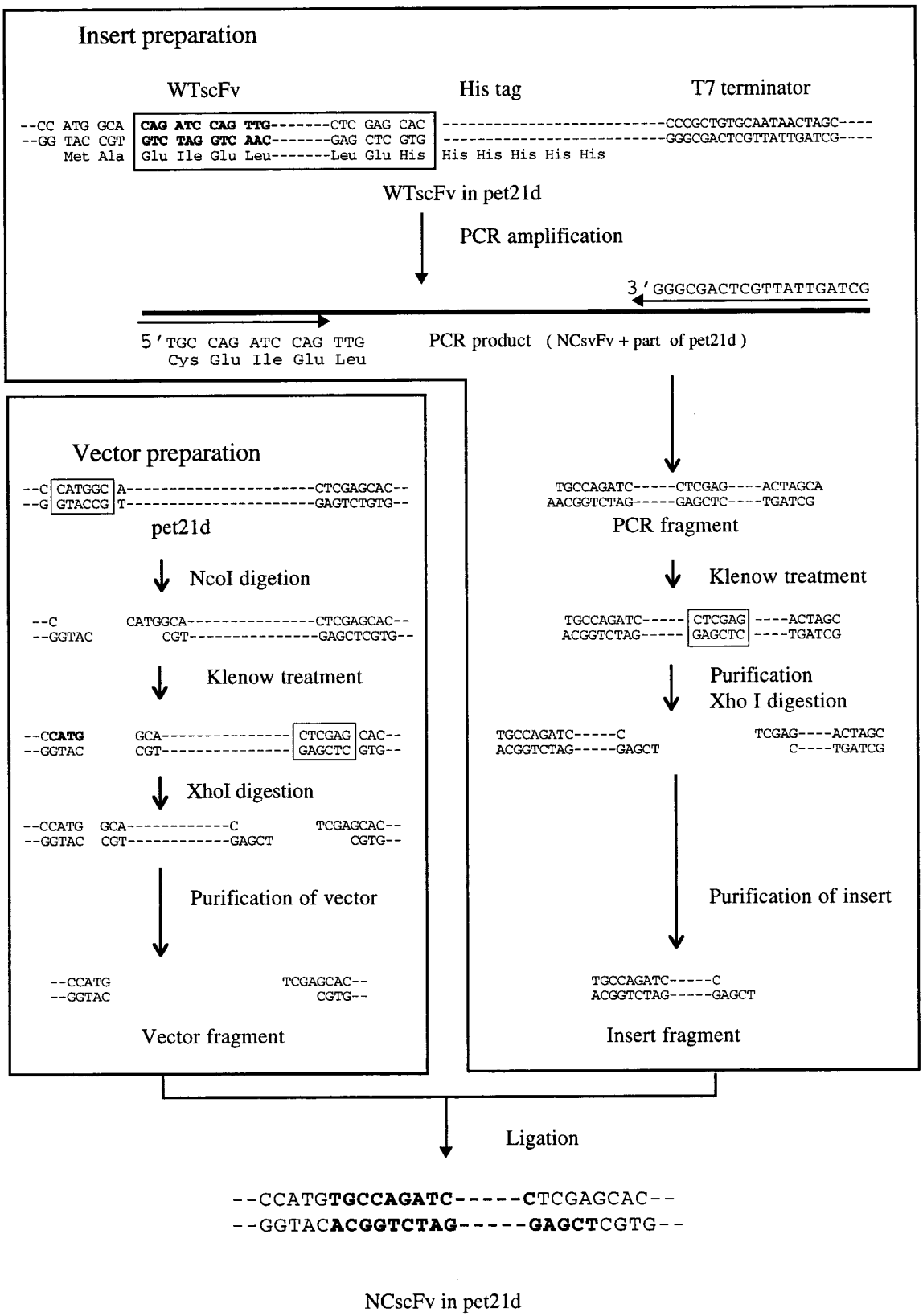


Figure 1. Construction of N-terminal cysteine-containing scFv Vector preparation. Pet21d vector was digested with *Nco*I, followed by Klenow treatment to make blunt ends. After digestion with *Xho*I, the vector was purified. Insert preparation. WTscFv in pet21d was amplified with a 5′ primer hybridizing to the WTscFv with an N-terminal cysteine codon "TGC" and 3′ T7 terminator primer hybridizing to the vector. The resultant NCscFv was blunt ended with Klenow enzyme and purified. The NCscFv insert was digested with *Xho*I and purified. Vector and insert fragments were ligated together. The new NCscFv was then sequenced to ensure correct reading frame. Dotted lines represent nucleotide sequences.

TGCCAGATCCAGTTG) and a 3′ end T7 terminator primer (5′-GCTAGTTATTGCTCAGCGG) as shown in Figure 1. Briefly, the PCR product was blunt-ended with Klenow enzyme for 30 min at 37 °C, electrophoresed on a 1% agarose gel, and purified using a Qiagen Gel Extraction Kit II. The N-terminal cysteine scFv (NCscFv)

insert was then digested with *Xho*I and purified. To prepare the vector for cloning, pET21d was digested with *Nco*I followed by Klenow treatment which resulted in blunt ends. After Klenow enzyme inactivation, pET21d was digested with *Xho*I. Finally, pET21d and the NCscFv insert were ligated overnight by T4 ligase. The ligation mixture was used to transform Novablue cells on an LB plate containing 50 μg/mL ampicillin. All molecular techniques were carried out according to Ausubel et al. (*16*). Fifty colonies were picked and grown in LB overnight after which minipreps were performed using a standard alkaline lysis procedure. Inserts were identified by PCR screening with 5′ T7 promotor and 3′ T7 terminator primers. Dideoxynucleotide DNA sequencing (*17*) was performed on selected clones to ensure correct position of the N-terminal cysteine codon at the 5′ end of the scFv.

Expression and Preparation of Cell Lysates of NCscFv and WTscFv in *Esherichia coli*. BL21 (DE3) bacterial cells were transformed with pET21d containing either NCscFv or WTscFv genes. One colony of each transformed bacterial cells was grown separately in 50 mL of terrific broth (TB) at 37 °C, 200 rpm to OD = 0.8. IPTG was then added to a final concentration of 1 mM, and the cells were grown for two more hours. Cells were harvested by centrifugation for 5 min in JA 17 rotor at 8000 rpm and resuspended in lysis buffer (50 mM Tris-Cl, pH 8, 1 mM EDTA, and 100 mM NaCl) containing 5 mg of lysozyme. After 1 h incubation at room temperature, the cells were sonicated three times for 15 s, then subjected to centrifugation at 8000 rpm for 5 min. The pellets of lysates were resuspended with 50 mM Tris-Cl, pH 8, and centrifugated. After resuspension in 8 M urea, 5 mM Tris-Cl, pH 8, lysates were sonicated again three times for 30 s each and incubated for 1 h on ice. Urea-solubilized cell lysates were collected after centrifugation. The supernatant was filtered through 0.45 μm membrane filter and saved for purification or direct cell lysate assay.

Purification of NCscFv and WTscFv. The recombinant proteins were purified from the cell lysates on a nickel-sepharose column using previously reported methods (*12*). Fractions were collected and analyzed by SDS−PAGE to determine which fraction contained desired proteins. Further purification of NCscFv for the purpose of protein sequencing was carried out by continuous elution SDS−PAGE gel electrophoresis using model 491 Prep Cell (Bio-Rad). Purified NCscFv was dialyzed against 25 mM triethylamine overnight, lyophilized, and resuspended in 100 μL of distilled water. NCscFv was precipitated at −70 °C overnight after the addition of 900 μL of acetone. The protein pellet was obtained by centrifugation at 13 000 rpm for 30 min and air-dried. The N-terminal cysteine residue of the purified NCscFv was derivatized with 4-vinylpyridine according to the protocol in the Applied Biosystems User Bulletin (no. 28, 1987), and the amino acid sequence was determined by an Applied Biosystems model 470A gas-phase sequencer equipped with a model 120 A path analyzer.

Biotinylation of NCscFv and WTscFv in Cell Lysates. The prepared cell lysates were adjusted to pH 6 with 5× phosphate buffer (0.4 M NaOH, 0.2 M H_3PO_4, and 0.2 M boric acid). One microliter of glyoxylyl-biotin (0.4 mg/ml) or 1 μL of sulfo NHS-LC-biotin (0.4 mg/ml, Pierce, Rockford, IL) was added to 10 μL of cell lysates and incubated at room temperature for 30 min. The glyoxylyl-biotinylation reaction was stopped by adding 1 μL of L-cysteine (0.4 mg/mL) while the NHS-LC-biotin reaction was stopped by adding 1 μL of 150 mM Tris-HCl buffer (pH 7.9).

Biotinylation of Purified WTscFv, NCscFv, and Insulin. Purified protein was refolded using the same methods published before (*12*). WTscFv and NCscFv were finally dialyzed against carbonate buffer (15 mM Na_2CO_3 and 35 mM $NaHCO_3$, pH 8). Sulfo NHS-LC biotin or glyoxylyl-biotin was added to WTscFv or NCscFv solution and incubated for 30 min at RT. The reaction was stopped by Tris HCl (1 M, pH 7.9) or free cysteine (1 mg/mL) for 2 h at RT. Further removal of free reagents from scFv solutions was done by dialyzing against carbonate buffer. Porcine insulin (Sigma, MO) was resuspended in PBS (pH 8.0) according to the manufacturer's instruction and labeled with Sulfo NHS-LC biotin as described above. The insulin solution was dialyzed against PBS (pH 7.3) to remove free reagents.

SDS−PAGE and Western Blotting. Biotinylated cell lysates and purified scFvs were mixed with 2× SDS sample buffer and loaded onto a 9% reducing SDS−PAGE gel. After electrophoresis, the gel was cut in half. One-half of the gel was stained with Coomassie Blue while the proteins on the other half of the gel were transferred to nitrocellulose paper in transfer buffer (25 mM Tris-base, 192 mM glycine, 20% methanol, and 1% SDS, pH 8.3). Transblotting was carried out at 30 V, 4 °C overnight using Trans Blot (Bio-Rad). Nonspecific binding to the nitrocellulose membranes was blocked by phosphate-buffered saline containing 0.1% porcine gelatin and 0.05% Tween-20 (blocking buffer) for 2 h at room temperature. Streptavidin-alkaline phosphatase (Pierce, rockford, IL) diluted in blocking buffer (1:5000 dilution) was incubated with the membranes for 1 h at room temperature. After washing with PBS-0.1% Tween, the membranes were developed by incubating with 5-bromo-4-chloro-3-indolyl phosphate (BCIP)/nitroblue tetrazolium (NBT), both obtained from Amresco (Solon, OH) in alkaline phosphatase buffer, pH 9.4 (1.5% diethanolamine, 0.5% NaN_3, and 1 mM $MgCl_2$)

Insulin-Binding ELISA. A 96 well plate was coated with anti-insulin antibody HB125 (1 μg/mL) for 1 h at 37° and blocked with 3% BSA in phosphate-buffered saline (137 mM NaCl, 2.7 mM KCl, 4.3 mM NaH_2PO_4, and 1.4 mM KH_2PO_4, pH 7.3). Biotinylated insulin (10 nM) was preincubated with various concentrations of competitors such as WTscFv, NCscFv, or glyoxylyl-biotinylated NCscFv for 1 h at RT. After HB125 coated plates were washed with washing buffer (0.05% Tween20 in PBS), preincubated biotinylated insulin and scFv mixtures were then added to HB125 IgG coated plate and incubated for another hour at RT. Unbound insulin, scFv and insulin bound scFv were washed out with washing buffer. Streptavidin-horseradish peroxidase (SA-HRP, Pierce,IL) was added and incubated for 1 h at RT to detect biotinylated insulin bound to HB125. 3,3′5,5′-Tetramethylbenzidine base (TMB, Gibco BRL, MD) was added. Color development was stopped with 0.5 N H_2SO_4 and optical densities (OD) were measured at 450 nm.

RESULTS AND DISCUSSION

Synthesis of Glyoxylyl Functionalized Biotin Reagent (Glyoxylyl-Biotin). One major concern for the synthesis of functionalized biotin (glyoxylyl-biotin) was whether the biotin group, which contains a thioether bond, remained unchanged when subjected to periodate oxidation. Fortunately, our results show that this is not a problem under the reaction conditions. Conventional cross-linking reagents contain a lengthy and flexible linker, but many of them are hydrophobic such as the hexanyl linker in NHS-LC-biotin. In this study we

Table 1. Comparison between the Ligation Methods

	this paper	Georghegan et al., Gaertuer et al., and Tam et al. (*6, 7, 10*)
site of derivatization	*N*-terminal cysteine	N-terminal threonine glyoxylyl group
protein oxidation with sodium periodate	no	yes (convert N-terminal threonine or serine to glyoxylyl group)
derivatizing reagent	glyoxylyl compound	hydrazide or aminooxy compound
specific derivatization without protein purification	yes	to be proven

decided to use a lengthy, flexible, and hydrophilic molecule as the linker in order to minimize any unwanted structural perturbation of the target protein. For this purpose a poly(ethylene glycol) (PEG) linker would be ideal, but the commercially available PEGs usually consist of a mixture of PEG molecules with different molecular weights, thus causing problems in purification and characterization. Therefore, we chose a molecule which is similar to triethylene glycol and derivatized it into a special amino acid, so it can be used in standard Fmoc solid-phase peptide synthesis. As a result, the new biotin reagent shows excellent solubility in both aqueous and polar aprotic solvents. Our experiments also show that the glyoxylyl-based biotin reagent is very stable in both acidic and basic conditions (data not shown). This is clearly an advantage over other common NHS-based or maleimide-based biotinylating reagents. We are currently developing a solution-phase synthesis procedure, so that this glyoxylyl-based reagent can be made in bulk quantities.

Site-Directed Mutagenesis and Expression of Anti-Insulin ScFv Containing N-Terminal Cysteine. As described in Materials and Methods, the codon for N-terminal cysteine was added by PCR-based site-directed mutagenesis of WTscFv creating NCscFv. The NCscFv gene was then cloned into pET21d expression vector. Figure 1 shows the initial DNA sequences of the mutated fragments which contain codons corresponding to formyl-Met-Cys. Then pET21d vector containing NCscFv was used to transform BL21 (DE3) *E. coli* host cells for expression. Since the immunoglobulin fragments produced from the pET21d transformed cells contained a carboxyl $(His)_6$, they were purified on a nickel-agarose column using immobilized metal affinity chromatography (IMAC) (*18*). Distinct bands at approximately 31 kDa can be seen in lanes 2 and 4 of Figure 2, corresponding to the wild-type scFv (WTscFv) and the N-terminal cysteine containing scFv (NCscFv), respectively. Purified anti-insulin NCscFv was subjected to protein microsequencing as described in Materials and Methods. Both DNA and protein sequencing analysis showed that a cysteine residue was successfully added to the N-terminus 5′ of glutamine, which was the first residue of WTscFv (data not shown).

In our bacterial protein expression system, a methionine residue is incorporated at the N-termimus as a part of the universal translation-initiation signal used by prokaryotes as well as eukaryotes. In prokaryotes, the methionyl moiety carried by the initiator tRNA is N-formylated prior to its incorporation. For a significant fraction of intracellular proteins, the amino-terminal methionine is also removed enzymatically by a methionine-specific aminopeptidase after the initiation of translation (*19*, *20*). We took advantage of these N-formyl methionine cleavage mechanisms as demonstrated by our ability to selectively label an N-terminal cysteine. Interestingly, methionine aminopeptidase has been reported to be particularly effective when cysteine is at the penultimate position (*21*).

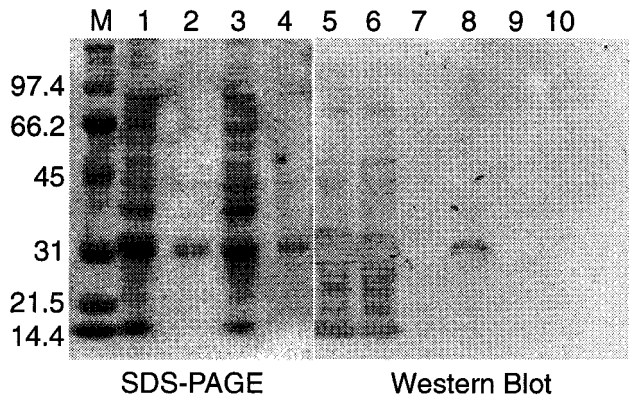


Figure 2. SDS-PAGE and Western blot Analysis of Derivatized proteins. Coomassie Blue stain of SDS/PAGE gel (lane M, 1−4) and Western blot of biotinylated and untreated lysates (lanes 5−10). Bands in lanes 5−10 were detected with streptavidin-alkaline phosphatase using BCIP/NBT as substrates. Lane M, molecular weight marker; lane 1, WTscFv cell lysate; lane 2, purified WTscFv; lane 3, NCscFv cell lysate; lane 4, purified NCscFv; lane 5, sulfo NHS-LC biotin labeled WTscFv cell lysate; lane 6, sulfo NHS-LC biotin labeled NCscFv cell lysate; lane 7, glyoxylyl-biotin labeled WTscFv cell lysate; lane 8, glyoxylyl-biotin labeled NCscFv cell lysate; lane 9, untreated WTscFv cell lysate; lane 10, untreated NCscFv cell lysate.

Biotinylation of Anti-Insulin ScFv in Total Cell Lysates. Total cell lysates that contained either WTscFv or NCscFv were biotinylated with (i) the conventional sulfo NHS-LC-biotin or (ii) our newly developed glyoxylyl-biotin. The streptavidin-alkaline phosphatase system coupled with a colorimetric detection system (BCIP/NBT) was used to detect biotinylated products in the western blot (Figure 2). Biotinylation by sulfo NHS-LC-biotin was essentially identical for both WTscFv lysates (lane 5) and NCscFv lysates (lane 6). This is not suprising since NHS-based reagents label predominantly lysine side chains which are abundant in most proteins. Thus, the western blot pattern of lanes 5 and 6 resembled that of the Coomassie Blue stain as all proteins were labeled (compare lanes 5 and 6 with lanes 1 and 3). When glyoxylyl-biotin was used to biotinylate total lysates, only one predominant band with a molecular mass of approximately 31 kDa in the NCscFv lysate was biotinylated (lane 8). This corresponds to the purified scFv shown in lanes 2 and 4. In contrast, only minor background was detected when the total WTscFv lysate was biotinylated with glyoxylyl-biotin under identical conditions (lane 7). As a negative control, no biotinylation or non-specific binding to streptavidin was detected for the untreated cell lysates (lanes 9 and 10). The above result clearly demonstrates that the glyoxylyl-biotin reagent is highly specific, that it can specifically label the N-terminal cysteine even in the presence of a large number of other proteins, and that glyoxylyl-biotin also works in the presence of 8 M urea under reducing conditions where many other free sulfhydryl groups of other proteins are exposed.

Site-Specific Modification Does Not Significantly Alter the Binding Affinity of Anti-Insulin ScFv.

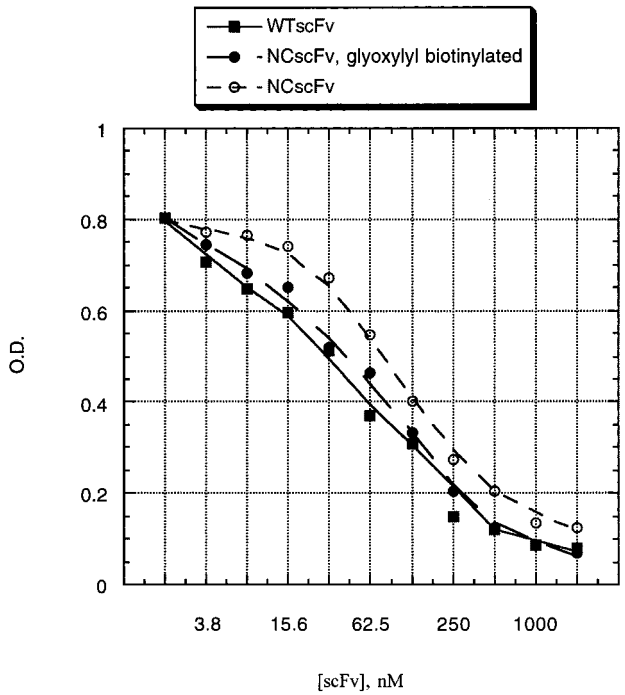


Figure 3. Insulin binding ELISA. A 96 well plate was coated with purified murin anti-insulin antibody (HB125) and blocked. Biotinylated porcine insulin was preincubated with serial dilutions of WTscFv, NCscFv, or glyoxylyl-biotinylated NCscFv, and was then place in HB125 coated 98 well plate. ScFvs and scFv0porcine insulin complex were removed by washing and biotinylated insulin captured by HB125 on plate was detected with SA-HRP and TMB [(■) WTscFv, (○) NCscFv, (●) glyoxylyl-biotinylated NCscFv].

Purified anti-insulin WTscFv and NCscFv were refolded as described (*12*). To investigate the changes in binding affinities of N-terminally mutated anti-insulin scFv to insulin, an insulin binding ELISA was performed with WTscFv, NCscFv, and glyoxylyl-biotinylated NCscFv. First, a 96 well plate was coated with purified parent anti-insulin IgG antibody (HB125). Sulfo NHS-LC biotin-labeled insulin was preincubated with serial dilutions of WTscFv, NCscFv, or glyoxylyl-biotinylated NCscFv prior to adding to HB125-coated plate. During this preincubation step, scFvs bound biotinylated insulin. Since insulin has only one antigenic determinant recognized by parent HB125 anti-insulin antibody, insulin prebound to HB125 scFvs will no longer bind to plate-coated HB125 parent antibody. Thus, only free insulin will be captured by HB125 antibody while scFv−insulin complexes will remain in solution and washed away. Captured insulin was detected with SA-HRP and TMB substrate. The stronger the scFv binds to the insulin, the lesser amount of insulin will be captured by plate bound HB125 antibody, which in turn will lead to a lower OD 450 measurement. Using this assay, the relative reactivities of the three scFvs were assessed (Figure 3). All scFvs, NCscFv, WTscFv, and NCscFv-glyoxyl-biotin, inhibited insulin from binding the parent HB125 IgG in a concentration-dependent manner. WTscFv and glyoxylyl-biotinylated NCscFv similarly inhibit insulin from binding to the parent antibody, whereas the reactivity between insulin and underivatized NCscFv is slightly weaker than the other two in this competition assay. The above study indicates that site-specific modification does not significantly alter the binding affinity of scFv.

Site-Specific Modification. There are several approaches available for site-specific protein modification (*3*, *6*−*8*, *22*, *23*). Among them are the ones developed by Geoghegan (*6*), Gaertuer (*7*), and Tam (*10*). Their approaches are novel and easy to perform compared to other protein-labeling strategies. The strategy we present in this paper is partially inspired by their efforts and, therefore, shares some similarity with their approaches. For example, our method as well as the methods by Geoghegan et al. (*6*), Gaertuer et al. (*7*), or Tam (*10*) use glyoxylyl-based chemistry and both methods result in derivatization at the N-terminus of a protein.

However, there are significant differences between our method and theirs (Table 1). For example, in our method, an N-terminal cysteine is incorporated into the protein using conventional site-directed mutagenesis. Then, the N-terminal cysteine, having a 1,2-aminothiol group, reacts specifically with glyoxylyl reagent forming a thiazolidine ring (*11*). Therefore, the protein itself is not modified after expression in the *E. coli* system. In contrast, the other methods require incorporation of N-terminal threonine or serine into the protein (by site-directed mutagenesis) followed by oxidation with periodate, a condition that potentially can damage the protein. The second difference between the methods is that we introduced a glyoxylyl group into the derivatizing reagent whereas the other methods uses hydrazide, aminooxy, or 1,2-aminothiol groups. Finally, in our approach, the modification reaction can be performed in total cell lysates before proteins fold into their native forms, making this approach attractive for protein purification as well as detection. The reaction between glyoxylyl groups and N-terminal cysteines is extremely selective so that only the target protein is modified at its N-terminal cysteine, even in the presence of many other proteins and biological molecules (Figure 2). It is also important to note that the cell lysates are produced in bacterial cells in reduced form so that in the presence of >6 M urea, the N-terminal cysteine is free from forming disulfide bonds with other cysteine residues. Therefore, the presence of a 1,2-aminothiol structure is assured for the glyoxylyl-based ligation. Under the same conditions, other nonterminal cysteine residues are present in reduced form but are not modified by the glyoxylyl group as observed in our experiments. We believe this approach can be used as a general method to site-specifically label the N-terminus of any recombinant protein. One obvious application is to produce well-defined radioimmunoconjugates for radioimmunotherapy of cancer. Other applications include the selective labeling of sensitive proteins such as enzymes that could be inactivated by oxidation or over modification of free thiol or amino groups.

LITERATURE CITED

(1) Meares, C. F. (1993) Introduction to bioconjugate chemistry. In *Perspectives in Bioconjugate Chemistry* (C. F. Meares, Ed.) pp 1−8, American Chemical Society, Washington, DC.

(2) Brinkley, M. (1993) A brief survey of methods for preparing protein Conjugates with dyes, haptens, and cross-linking reagents. In *Perspectives in Bioconjugate Chemistry* (C. F. Meares, Ed.) pp 59−70, American Chemical Society, Washington, DC.

(3) Rose, K., Vilaseca, L. A., Werlen, R., Meunier, A., Fisch, I., Jones, R. M., and Offord, R. E. (1991) Preparation of well-defined protein conjugates using enzyme-assisted reverse proteolysis. *Bioconjugate Chem. 2*, 154−159.

(4) Wingfield, P., Graber, P., Shaw, A. R., Gronenborn, A. M., Clore, G. M., and MacDonald, H. R. (1989) Preparation, characterization, and application of interleukin-1 mutant protein with surface-accessible cysteine residues. *Eur. J. Biochem. 179*, 565−571.

(5) Smyth, D. G., Blumenfeld, O. O., and Konigsberg, W. (1964) Reaction of *N*-ethylmaleimide with peptides and amino acids. *Biochem. J. 91*, 589−595.
(6) Geoghegan, K. F., and Stroh, J. G. (1992) Site-directed conjugation of nonpeptide groups to peptides and proteins via periodate oxidation of a 2-amino alcohol. Application to modification at N-terminal serine. *Bioconjugate Chem. 3*, 138−146.
(7) Gaertner, H. F., Rose, K., Cotton, R., Timms, D., Camble, R., and Offord, R. E. (1992) Construction of protein analogues by site-specific condensation of unprotected fragments. *Bioconjugate Chem. 3*, 262−268.
(8) Gaertner, H. F., and Offord, R., E. (1996) Site-specific attachment of functionalized poly(ethylene glycol) to the amino terminus of proteins. *Bioconjugate Chem. 7*, 38−44.
(9) Alouni, S., Gaertner, H. F., Mermod, J. J., Power, C. A., Bacon, K. B., Wells, T. N. C., and Proudfoot, A. E. I. (1995) A fluorescent interlukin-8 receptor probe produced by targeted labeling at the amino terminus. *Eur. J. Biochem. 227*, 328−334.
(10) Zhang, L., and Tam, J. P. (1996) Thiazolidine Formation as a General and Site-Specific Conjugation Method for Synthetic Peptides and Proteins. *Anal. Biochem. 233*, 87−93.
(11) Zhao, Z. G., and Lam, K. S. (1995) A novel approach for iodolabeling synthetic peptides. *J. Chem. Soc., Chem. Commun.* 1739−1740.
(12) Lake, D. F., Lam, K. S., Peng, L., and Hersh, E. M. (1994) Molecular cloning, expression and mutagenesis of an anti-insulin single chain Sv (ScFv). *Mol. Immunol. 31*, 845−856.
(13) Atherton, E., and Sheppard, R. C. (1989) *Solid-Phase Peptide Synthesis. A practical Approach*, IRL Press, Oxford.
(14) Loffex, A., and Zhang, H. X. (1992) New side-chain protection of amino acids: Potential use in SPPS. In *Innovative and Perspectives in Solid-Phase Synthesis* (Epton, R., Ed.) pp 77−82, Intercept Limited, Anclover.
(15) Rose, K., Zeng, W., Regamey P.-O., Chernushevich, I. V., Standing, K. G., and Gaertner, H. F. (1996) Natural Peptide as Building Blocks for the Synthesis of Large Protein-like Molecules with Hydrazone and Oxime Linkages, *Bioconjugate Chem. 7*, 552−556.
(16) Ausubel, F. M., Brent, R., Kingston, R. E., Moore, D. D., Seidman, J. G., Smith, J. A., and Sturuhl, K (1989) *Current protocols in Molecular Biology*, Creene Publishing Associates and Wiley-Interscience, New York.
(17) Sanger, F., Nicklen, S., and Coulson A. R. (1977) DNA sequencing with chain-terminating inhibitors. *Proc. Natl. Acad. Sci. U.S.A. 74*, 5463−5467.
(18) Smith, M. C., Furman, T. C., Ingolia, T. D., and Pidgeon, C. (1988) Chelating peptide-immobilized metal ion affinity chromatography. *J. Biol. Chem. 263*, 7211−7215.
(19) Meinnel, T., and Blanquet, S. (1995) Enzymatic properties of *Escherichia coli* peptide deformylase. *J. Bacteriol. 177*, 1883−1887.
(20) Ben-Bassat, A., Bauer, K., Chang, S.-Y., Myambo, K., Boosman, A., and Chang, S. (1987) Processing of the initial methionine from proteins: Properties of the *Escherichia coli* methionine aminopeptidase and its gene structure. *J. Bacteriol. 169*, 751−757.
(21) Hirel, P.-H., Schmitter, J.-M., Dessen, P., Fayat, G., and Blanquet. S. (1989) Extent of N-terminal methionine excision from *Escherichia coli* proteins is governed by the side-chain length of the penultimate amino acid. *Proc. Natl. Acad. Sci. U.S.A. 86*, 8247−8251.
(22) DíSantos, C. S., Nicholson, G. C., Mosely, J. M., Evans, T., Martin, T. J., and Kemp, B. E. (1988) Biologically active derivatizable salmon calcitonin analog: Design, Synthesis and Applications. *Endocrinol. 123*, 1483−1488.
(23) Wetzel, R., Halualani, R., Stults, J. T., and Quan, C. A. (1990) A general method for highly selective cross-linking of unprotected polypeptides via pH-controlled modification of N-terminal alpha-amino groups. *Bioconjugate Chem. 1*, 114−122.

BC980120K

Preparation, ^{99m}Tc-Labeling, and in Vitro Characterization of HYNIC and N_3S Modified RC-160 and [Tyr^3]Octreotide

Clemens Decristoforo and Stephen J. Mather*

Nuclear Medicine Research Laboratory, St. Bartholomews hospital, West Smithfield, London EC1 7BE, U.K.
Received October 5, 1998; Revised Manuscript Received February 1, 1999

The synthesis of conjugates of two somatostatin analogues, RC-160 and [Tyr^3]octreotide with different bifunctional chelators for labeling with Tc-99m, is described. Conjugates with hydrazinonicotinamide (HYNIC) and two N_3S compounds (benzoyl MAG3 and a N_3S adipate derivative) were prepared on a small scale with high purity allowing evaluation of different bifunctional chelators on the same peptide without extensive peptide synthesis. High in vitro stability and retained binding affinity was found for all conjugates except for the N_3S adipate. Peptide conjugates could be labeled at high specific activities (>1 Ci/μmol) with ^{99m}Tc, and different coligands were explored for the HYNIC conjugates. The resulting radiolabeled complexes were highly stable and showed binding affinity to somatostatin receptors in the nanomolar range. Varying labeling yield, stability, lipophilicity, and isomerism were found for different coligands used for labeling HYNIC conjugates, with lower lipophilicity, higher stability, and fewer coordination isomers for EDDA and tricine/nicotinic acid as ternary coligand compared to tricine. In particular, HYNIC complexes showed promising results for further in vivo evaluation.

INTRODUCTION

The radiolabeled somatostatin analogue ^{111}In-DTPA-D-Phe^1-octreotide (Octreoscan) has found a wide clinical application for imaging a range of tumors, including neuroendocrine cancer, carcinoid, and lymphoma (*1*−*4*) but one of the, at least, theoretical disadvantages of this compound is its restricted reactivity to receptor-subtypes SSR2 and SSR5. Recently, it has been demonstrated that another somatostatin analogue (RC-160 or vapreotide) has affinity for a different set of somatostatin receptor subtypes which may increase its usefulness for targeting more common tumors such as those of breast, ovary, exocrine pancreas, prostate, and colon (*5*−*7*). In further contrast to octreotide, RC-160 can also pass the blood-brain barrier and might therefore be used for imaging brain tumors (*8*). RC-160 has previously been radiolabeled with ^{123}I (*9*), ^{111}In (*10*), and recently ^{188}Re (*11*), and high affinity to somatostatin receptors in vivo has been proven.

Although the radiolabel of choice for tumor imaging would be technetium-99m, experience with suitable labeling methods is not yet as great as for other radionuclides [for review, see Liu et al. (*12*)]. The most widely used method for labeling such small highly specific peptides is by conjugation of bifunctional chelators (BFCs) to the peptide. The number of BFCs suitable for labeling with technetium-99m at the high specific activities necessary to permit the use of pharmacologically highly potent peptides in nontoxic doses is limited, but, in recent years, attempts have been made to label various somatostatin analogues with ^{99m}Tc using a number of different BFCs including diamidedithiols, triamidemonothiols and triaminemonothiols (*13*), propyleneamine oxime (*14*), tetramine (*15*), and hydrazinonicotinamide (HYNIC) (*16*). Such methods are generally considered more appropriate than the alternative approach of direct labeling following reduction of the disulfide bridge (*17*, *18*), which forms ^{99m}Tc complexes of uncertain structure and raises concerns with regard to the retention of specific binding to somatostatin receptors.

The aim of this study was to perform a comparison of some of the BFCs previously described, in order that some recommendations can be made on the most suitable system for technetium labeling of these small peptides. This report describes the small-scale preparation of conjugates of RC-160 and [Tyr^3]octreotide (TOC) with different BFCs, based on the triamidemonothiol and HYNIC cores. Results from ^{99m}Tc-labeling experiments using different coligand systems and in vitro evaluations of the resulting ^{99m}Tc complexes are reported and provide data for direct comparison of different BFCs.

EXPERIMENTAL PROCEDURES

Materials. Reagents were purchased from Aldrich-Sigma Chemical Co. except where otherwise stated and used as they were received.

6-BOC-hydrazinopyridine-3-carboxylic acid (BOC-HYNIC) was synthesized and characterized according to Abrams et al. (*19*).

2,3,5,6,-Tetrafluorothiophenyl-*S*-(1-ethoxyethyl)mercaptoacetamidoadipoylglycylglycine [N_3S-adipate (*20*)] was a gift from Alan R. Fritzberg (NeoRx Corporation, Seattle, WA).

N-Hydroxysuccinimide-*S*-acetyl-mercaptoacetyltriglycin [S-acetyl-NHS-MAG3 (*21*)] was a gift from Donald J. Hnatowich (University of Massachusetts, Worcester, MA).

S-Benzoyl-mercaptoacetyltriglycine (S-benzoyl-MAG3) was a gift from Ole K. Hjelstuen (Isopharma Radiopharmaceuticals, Oslo, Norway).

[Lys^5-BOC]RC-160, RC-160, [Tyr^3, Lys^5-BOC]octreotide, and [Tyr^3]octreotide (TOC) were synthesized by Bachem UK Ltd.

* To whom correspondence should be addressed. Phone: 44-171-601-7153. Fax: 44-171-796-3907. E-mail: mather@icrf.icnet.uk.

10.1021/bc980121c CCC: $18.00 © 1999 American Chemical Society
Published on Web 03/31/1999

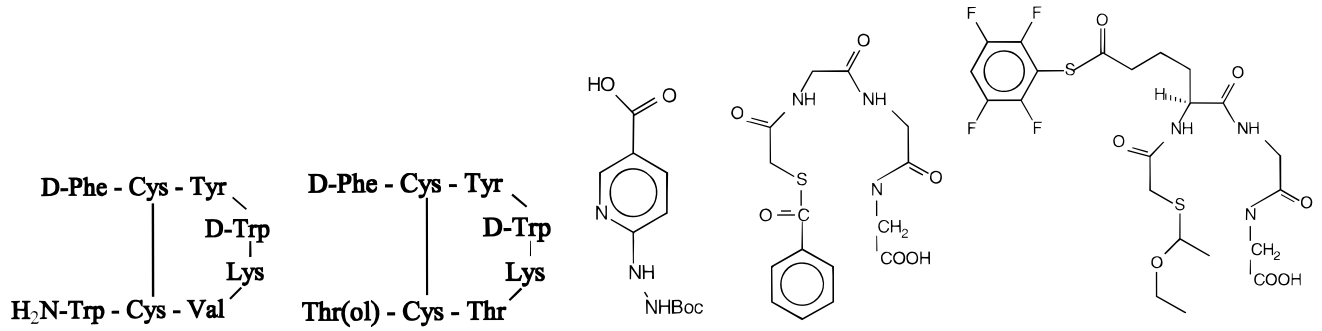


Figure 1. Structures of peptides and BFCs used. From left to right: RC-160, [Tyr^3]octreotide BOC-HYNIC, benzoyl-MAG3, N_3S-adipate.

(3-[^{125}I]iodotyrosyl^{11})Somatostatin-14 ([^{125}I]SST14) was purchased from Amersham Life Science Ltd. (Amersham, U.K.).

$Na^{99m}TcO_4^-$ was obtained from commercial $^{99}Mo/^{99m}Tc$ generator (Nycomed Amersham). Deionized water was obtained from a ELGA Elgastat UHP Water System and was of >18 MΩ quality.

INSTRUMENTS AND METHODS

HPLC. A Beckman solvent module 125 with Beckman UV detector 166NM and radiometric detection was used for reversed-phase HPLC analysis and preparation. A Beckman Ultrasphere ODS 5 μm, 4.6 × 250 mm column, flow rates of 1 mL/min, and UV detection at 220 nm were employed together with the following solvent systems. Method 1: acetonitrile/0.1%TFA/water. Gradient: 0−3 min 0% ACN; 3−13 min 0 to 50% ACN; 13−23 min 50% ACN, 23−26 min 50 to 70% ACN, 26−27 min 70 to 0% ACN. Method 2: acetonitrile/0.01 N phosphate buffer, pH 6.2. Gradient as in method 1. Method 3: acetonitrile/0.1% TFA/water; 0−3 min 0% ACN; 3−10 min 0 to 40% ACN; 10−20 min 40% ACN; 20−23 min 40 to 70% ACN; 26−27 min 70 to 0% ACN. Method 4: acetonitrile/0.01 N phosphate buffer, pH 6.2; 0−3 min 0% ACN; 3−10 min 0 to 25% ACN; 10−20 min 25% ACN; 20−23 min 25 to 70% ACN; 26−27 min 70 to 0% ACN.

Methods 1 and 2 were used for analyses of RC-160 conjugates, methods 3 and 4 for TOC conjugates.

TLC. Instant thin-layer chromatography on silica gel (ITLC-SG, Gelman Sciences) was performed using different mobile phases. 2-Butanone was used to determine the amount of free $^{99m}TcO_4^-$ ($R_f = 1$), and the PBS buffer was used to determine non-peptide-bound ^{99m}Tc coligand and $^{99m}TcO_4^-$ ($R_f = 1$), 50% acetonitrile/water for ^{99m}Tc colloid ($R_f = 0$).

SPE Purification. For purification of the radiolabeled peptide for stability studies, a solid-phase extraction (SPE) method was used. The radiolabeling mixture was passed through a C18-SEPPAK-Mini cartridge (Waters, Milford, MA). The cartridge was washed with 5 mL of water, the radiolabeled peptide eluted with 80% acetonitrile, and the organic solvent evaporated under vacuum. This method efficiently removed all hydrophilic impurities ($^{99m}TcO_4^-$, ^{99m}Tc coligand) and ^{99m}Tc colloid to a concentration of less than 2% when tested by HPLC or TLC.

Synthesis of Peptide Conjugates. Structures of RC-160, [Tyr^3]octreotide (TOC), and the BFC used are shown in Figure 1.

Synthesis of HYNIC-RC-160. A total of 0.3 mg of BOC-HYNIC, 2.0 mg of *O*-(7-azabenzotriazolyl)-1,1,3,3-tetramethyluronium hexafluorophosphate (HATU), and 5 mg of diisopropyethylamine (DEA) in 300 μL of DMF were reacted for 15 min. A total of 60 μL of this solution was added to 1.0 mg of Lys-BOC-RC-160 in 20 μL of DMF/5 μL of water and allowed to react for 1 h. To stop the reaction, 1 mL of water was added, and the resulting solution was passed through a C18 SEPPAK cartridge (Waters, Milford, MA) washed with additional 5 mL of water and finally eluted with 1 mL of 100% acetonitrile. The acetonitrile solution was reduced under vacuum to a volume of 100 μL. A total of 300 μL of TFA and 10 μL of thioanisole were added and reacted for 10 min. The solution was evaporated to dryness, and the residue dissolved in 200 μL of 50% ethanol and purified on HPLC using method 1. The peak of HYNIC-RC-160 was collected and stored in the HPLC eluent at −20 °C under nitrogen. Further characterization was performed by HPLC analysis and matrix assisted laser desorption ionization MS on a Lasermat 2000 (Finnigan Mat).

Synthesis of S-Acetyl-MAG3-RC-160. A total of 0.3 mg of Lys-BOC RC-160, 1.0 mg of S-acetyl-NHS-MAG3, and 1 mg of DEA were reacted for up to 3 h. SEPPAK purification and deprotection was carried out as described for HYNIC-RC-160.

Synthesis of S-Benzoyl-MAG3-RC-160. A total of 2.2 mg of S-benzoyl-MAG3, 1.0 mg of HATU, and 1 mg of DEA in 170 μL of DMF were reacted for 15 min. A total of 40 μL of this solution was added to 0.4 mg of Lys-BOC-RC-160 in 20 μL of DMF/5 μL of water and allowed to react for 1 h. SEPPAK purification and deprotection was carried out as described for HYNIC-RC-160.

Synthesis of N_3S-RC-160. A total of 0.4 mg of N_3S adipate, 0.67 mg of Lys-BOC-RC-160, and 0.3 mg of DEA in 150 μL of DMF were incubated for 80 min. SEPPAK purification and deprotection was carried out as described for HYNIC-RC-160.

Synthesis of S-Benzoyl-MAG3- and HYNIC-TOC. Conjugates were prepared in the same way as the RC-160 conjugates corrected for molecular weight, purified and analyzed by HPLC method 3.

^{99m}Tc Labeling. *[^{99m}Tc]HYNIC conjugate.* Tricine as coligand: in a rubber sealed vial, 10 μg of HYNIC conjugate was incubated with 0.5 mL of tricine solution (100 mg/mL in 25 mM succinate buffer, pH 5.0), 0.5 mL of $^{99m}TcO_4^-$ solution (100−1000 MBq), and 25 μL of tin(II) solution (10 mg of $SnCl_2 \cdot 2H_2O$ in 10 mL of nitrogen purged 0.1 N HCl) for 30 min at room temperature.

Ethylendiaminediacetic acid (EDDA) as coligand: 10 μg of HYNIC-RC-160 was incubated with 0.5 mL of solution of EDDA (10 mg/mL, pH 7.0), 0.5 mL of $^{99m}TcO_4^-$ solution (100−1000 MBq), and 5−10 μL of tin(II) solution (10 mg of $SnCl_2 \cdot 2H_2O$ in 10 mL of nitrogen purged 0.1 N HCl) for 60 min at room temperature.

Nicotinic acid/tricine as coligands: 10 μg of HYNIC-RC-160, 0.4 mL of tricine solution (100 mg/mL in 25 mM

succinate buffer, pH 5.0), 0.1 mL of nicotinic acid (NA) (20 mg/mL in 25 mM succinate buffer pH 5.0), 0.5 mL of $^{99m}TcO_4^-$ solution (100−500 MBq), and 25 μL of tin(II) solution (10 mg of $SnCl_2 \cdot 2H_2O$ in 10 mL of nitrogen purged 0.1 N HCl) were heated at 100 °C for 15 min.

[^{99m}Tc]MAG3 Conjugate. A total of 10 μg of S-benzoyl-MAG3 conjugate was heated with 0.5 mL of sodium tartrate (100 mg/mL in 0.1 M phosphate buffer, pH 7.2), 1.5 mL of $^{99m}TcO_4^-$ solution (100−1000 MBq), and 40 μL of tin(II) solution (10 mg of $SnCl_2 \cdot 2H_2O$ in 10 mL of nitrogen purged 0.1 N HCl) at 100 °C for 15 min.

[^{99m}Tc]N_3S-RC-160. A total of 10 μg of N_3S-RC-160, 1.0 mL of glucoheptonate solution (40 mg/mL pH 2.5), 0.5 mL of $^{99m}TcO_4^-$ solution (100−1000 MBq), and 20 μL of tin(II) solution (10 mg of $SnCl_2 \cdot 2H_2O$ in 10 mL of nitrogen purged 0.1 N HCl) were heated at 80 °C for 20 min.

In Vitro Characterization of Radiolabeled Peptides. *Stability*. The stability of the radiolabeled peptides in aqueous solution was tested by incubation of the SPE purified peptide in 0.1 M phosphate buffer and in a solution containing 1000-fold excess cysteine over the peptide at pH 7.4 at room temperature up to 24 h. Cysteine, naturally occurring and a strong chelating compound for technetium, is thought to be responsible for in vivo degradation of ^{99m}Tc complexes and is frequently used for in vitro stability studies (*22*). As a control, the stability of [^{99m}Tc]tetraglycine, a technetium complex with a low complex stability (*23*), was tested in parallel. Stability in fresh human plasma was also measured at 37 °C for up to 4 h followed by precipitation of plasma protein with acetonitrile. Degradation of the ^{99m}Tc complex was assessed by TLC and HPLC.

Somatostatin Receptor Binding. The binding affinity of peptide conjugates was tested in a competition assay against [^{125}I]SST14 as described elsewhere (*24*). Mouse pituitary [AtT20 cells, expressing SST receptors subtype 2 and 5 (*25*)] and rat pancreatic [AR42J cells, expressing SST receptors subtype2 (*26*)] tumor cell membranes were used as a source for somatostatin receptors and were separated from free radioligand by filtration through glass fiber filters (Whatman GF/C), and IC_{50} values were calculated following nonlinear regression with Origin software (Microcal Origin 5.0, Northampton MA). The specific binding of the ^{99m}Tc-labeled peptides was determined by competition against unmodified RC-160 in a similar assay. K_d values of ^{99m}Tc-labeled peptide conjugates were determined in radioligand saturation assays using AR42J cell membranes as receptor source.

RESULTS

Synthesis of Peptide Conjugates. HPLC analysis of reaction mixtures of different RC-160 conjugates is shown in Figure 2, preparation of TOC conjugates gave similar results. Quantitative peptide coupling of BOC-HYNIC (Figure 2C, peak 3) and S-benzoyl-MAG3, using HATU, as well as of the N_3S adipate active STFP ester was achieved within 1 h. For the *N*-hydroxysuccinimide-activated S-acetyl-MAG3, no quantitative reaction could be achieved in DMF even at high molar excess of the activated ester over the peptide. Deprotection of the peptide conjugates with TFA resulted in one major HPLC-peak for HYNIC-RC-160 (Figure 2D, peak 4) and S-benzoyl-MAG3 (Figure 2F, peak 5). Overall yields were >50% for both these BFCs. In the case of S-acetyl-MAG3, multiple peaks were observed, indicating instability of the conjugate under acidic conditions (Figure 2E) and no pure peptide conjugate could be isolated. The N_3S-RC-160 deprotection solution also showed several byproducts

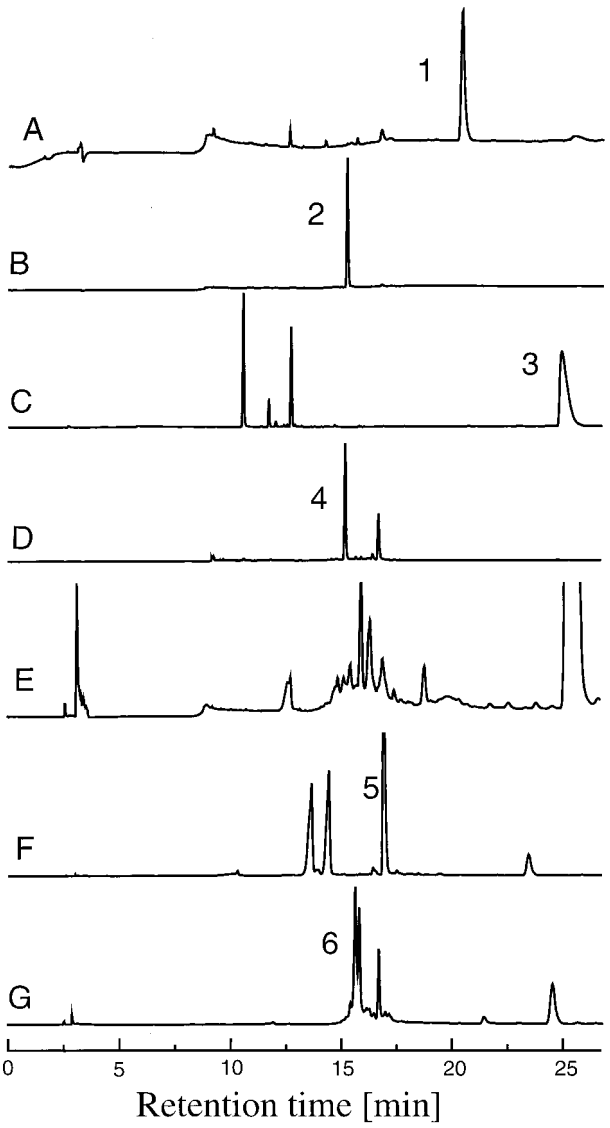


Figure 2. HPLC traces (UV 220 nm, method 1) from the synthesis of RC-160 conjugates. (A) Lys-BOC-RC-160 standard, (B) RC-160 standard, (C) reaction solution of BOC-HYNIC-RC-160 before deprotection, (D) deprotection solution of HYNIC-RC-160, (E) deprotection solution of S-acetyl-MAG3-RC-160, (F) deprotection solution of S-benzoyl-MAG3-RC-160, (G) deprotection solution of N_3S-RC-160. Peaks marked with numbers: 1, Lys-BOC-RC-160; 2, RC-160; 3, BOC-protected-HYNIC-RC-160; 4, HYNIC-RC-160 (deprotected); 5, S-benzoyl-MAG3-RC-160; 6, N_3S-RC-160.

Table 1. Molecular Weight of Peptide Conjugates Determined by Laser Desorption MS Compared with the Theoretical Value

mass	calculated	found
HYNIC-RC-160	1264.5	1265.0
S-benzoyl-MAG3-RC-160	1479.6	1479.4
N_3S-RC-160	1533.6	1462.4
HYNIC-TOC	1170.5	1170.0
S-benzoyl-MAG3-TOC	1383.5	1383.4

(Figure 2G), and the overall yield was <20%. Mass spectrometry data are summarized in Table 1. For HYNIC-RC-160 and S-benzoyl-MAG3, as well as for the TOC conjugates, the calculated MW matched well with the experimental value and the conjugates were stable for several months. N_3S-RC-160 showed a significantly lower MW than calculated, its difference matching the S-ethylethoxy protection group, indicating a cleavage during the deprotection reaction. The stability of this

Table 2. Labeling Yields of Different RC-160 Conjugates (mean of $n = 5$)[a]

peptide	conjugate/coligand	mean (%)	sd (%)
RC-160	N_3S	93.93	4.16
RC-160	MAG3	96.70	1.85
RC-160	HYNIC-tricine	98.86	1.21
RC-160	HYNIC-tricine/NA	97.70	1.8
RC-160	HYNIC-EDDA	69.38	4.58
TOC	MAG3	96.02	4.44
TOC	HYNIC-tricine	98.2	2.64
TOC	HYNIC-tricine/NA	98.7	2.22
TOC	HYNIC-EDDA	63.60	17.90

[a] Conditions: 500 MBq ^{99m}Tc; 10 μg of peptide conjugate

Table 3. Mean K_d Values ($n = 2$) of Different [^{99m}Tc]RC-160 and TOC Conjugates Determined on AR42J Cell Membranes

peptide	conjugate/coligand	K_d (nM)
RC-160	HYNIC-tricine	0.93
RC-160	HYNIC-tricine/NA	1.32
RC-160	HYNIC-EDDA	2.45
RC-160	MAG3	1.46
Tyr octreo	HYNIC-tricine	1.14
Tyr octreo	HYNIC-tricine/NA	2.11
Tyr octreo	HYNIC-EDDA	2.65
Tyr octreo	MAG3	1.11

conjugate was considerably lower, and degradation was seen already after 1 week of storage at −20 °C. Nevertheless the conjugate continued to produce stable and reproducible labeling results and was therefore considered for further evaluation, but no conjugate of TOC was prepared.

^{99m}Tc Labeling. Labeling yields of RC-160 and TOC conjugates at specific activities of approximately 1 Ci/μmol are listed in Table 2, and radiochromatograms for RC-160 conjugates are shown in Figure 3. Almost quantitative labeling (>90%) was achieved for most conjugates and coligand systems. Lipophilic impurities in varying amounts were found in the MAG3 conjugate-labeling mixture (Figure 3D). Labeling HYNIC-RC-160 with EDDA as coligand at room-temperature resulted in an average yield of 69% (Figure 3C), for HYNIC-TOC 63.9%. Labeling yield for the EDDA compounds was independent of pH between 4 and 7.2, and no significant increase was observed by heating the labeling mixture. The optimal EDDA concentration was found to be 5 mg/mL, but the labeling yield was mainly influenced by the concentration of stannous ions in the labeling solution. A rapid decline in labeling yields for HYNIC-RC-160 with increasing amounts of stannous ions was observed (Figure 4) when EDDA was used as coligand. Using pyridine/tricine as ternary ligands, labeling of the peptide conjugate was quantitative, but residues of the binary tricine complex were found when labeling was performed at room temperature. Quantitative labeling to the ternary ligand was only achieved by heating at 100 °C for 15 min.

^{99m}Tc-labeled TOC conjugates showed considerably lower retention times on HPLC compared to their RC-160 counterparts, indicating the considerably lower lipophilicity of this peptide. HPLC profiles were dependent on the pH of the aqueous solvent employed. When water/0.1% TFA HPLC systems were used, retention times were very similar for all ^{99m}Tc-labeled conjugates of the same peptide (see Figure 3, left columns). Using a phosphate buffer at pH 6.2, a better distinction between different labeled peptide conjugates was achieved (see Figure 3, right column). Retention times were in the following order: EDDA-HYNIC < tricine/NA-HYNIC < N_3S < MAG3 < tricine-HYNIC (main peaks) for both RC-160 and TOC conjugates. Multiple peaks were found for tricine as coligands (Figure 3A) and two main peaks for tricine/NA as ternary coligands for HYNIC conjugates (Figure 3B). Except for the N_3S conjugate, this HPLC method allowed efficient separation of the ^{99m}Tc complex from the cold conjugate to yield carrier free Tc complexes that could be used for radioligand binding assays.

Stability of ^{99m}Tc-labeled Peptide Conjugates. ^{99m}Tc-labeled peptide conjugates were stable in aqueous solutions for 24 h, except for tricine-HYNIC conjugates, which, when excess tricine was removed by SEPPAK purification, showed a radiochemical purity of less than 80% after 24 h. Challenge experiments with 1000-fold molar excess of cysteine showed no significant degree of transchelation for N_3S and HYNIC conjugates while, for the MAG3 conjugates, 20% transchelation after 24 h was observed. Results of cysteine challenge experiments are shown for RC-160 in Figure 5, the decrease in the radiochemical purity over time can be related to the transchelation to cysteine. All compounds were stable to 4 h incubation in human plasma, although varying amounts of labeled peptide were protein bound and were precipitated with plasma proteins by acetonitrile, higher amounts for RC-160 compared to TOC.

Receptor Binding. The cold peptide conjugates all showed a high binding affinity on AtT20 and AR42J cell membranes. Competition curves for RC-160 conjugates against [^{125}I]SST14 are shown in Figure 6. For the RC-160 itself, an IC_{50} value of 0.38 nM was calculated while, for S-benzoyl-MAG3-RC-160, binding affinity was almost identical with an IC_{50} of 0.36 nM. HYNIC-RC-160 and N_3S-RC-160 showed a slightly lower binding affinity with IC_{50} values of 1.51 and 1.73 nM, respectively (Figure 6). HYNIC-TOC showed an IC_{50} value of 1.55 nM and S-benzoyl-MAG3-RC-160 of 0.15 nM compared to 0.39 nM for unmodified TOC.

All ^{99m}Tc-labeled conjugates tested showed high specific binding to somatostatin receptors, with calculated K_d values in the nanomolar range, varying from 0.93 to 2.65 nM. Binding affinities were similar for RC-160 and TOC derivatives. K_d values determined on AR42J cell membranes are listed in Table 3. Saturation curves for the ^{99m}Tc-labeled EDDA-HYNIC peptide conjugates are shown as examples in Figure 7.

DISCUSSION

Preparation of Conjugates. RC-160 and [Tyr^3]-octreotide not only have potential clinical utility in their own right but they also represent model compounds which make them ideal for comparison of conjugation and radiolabeling strategies. Both are small octapeptides cyclized through a disulfide bridge and both contain a critical lysine residue, which is essential to preserve in order to retain receptor affinity. The use of a BFC approach for preparation of conjugates for ^{99m}Tc labeling thus requires protection of the lysine-epsilon amino group with a cleavable group like BOC, and conjugation and labeling conditions must be chosen which do not put the disulfide at risk. In addition, many BFCs additionally contain thiols for chelating ^{99m}Tc that also require protection. In this case, the number of protection strategies is very limited. The thiol-protecting group needs to be stable against the slightly alkaline conditions used in the conjugation reaction and also strong acidic conditions during the cleavage of the BOC-amino protection. At the same time, however, the thiol-protecting group must be readily cleaved during the labeling reaction in order to bind ^{99m}Tc. We tested three N_3S-BFCs with different

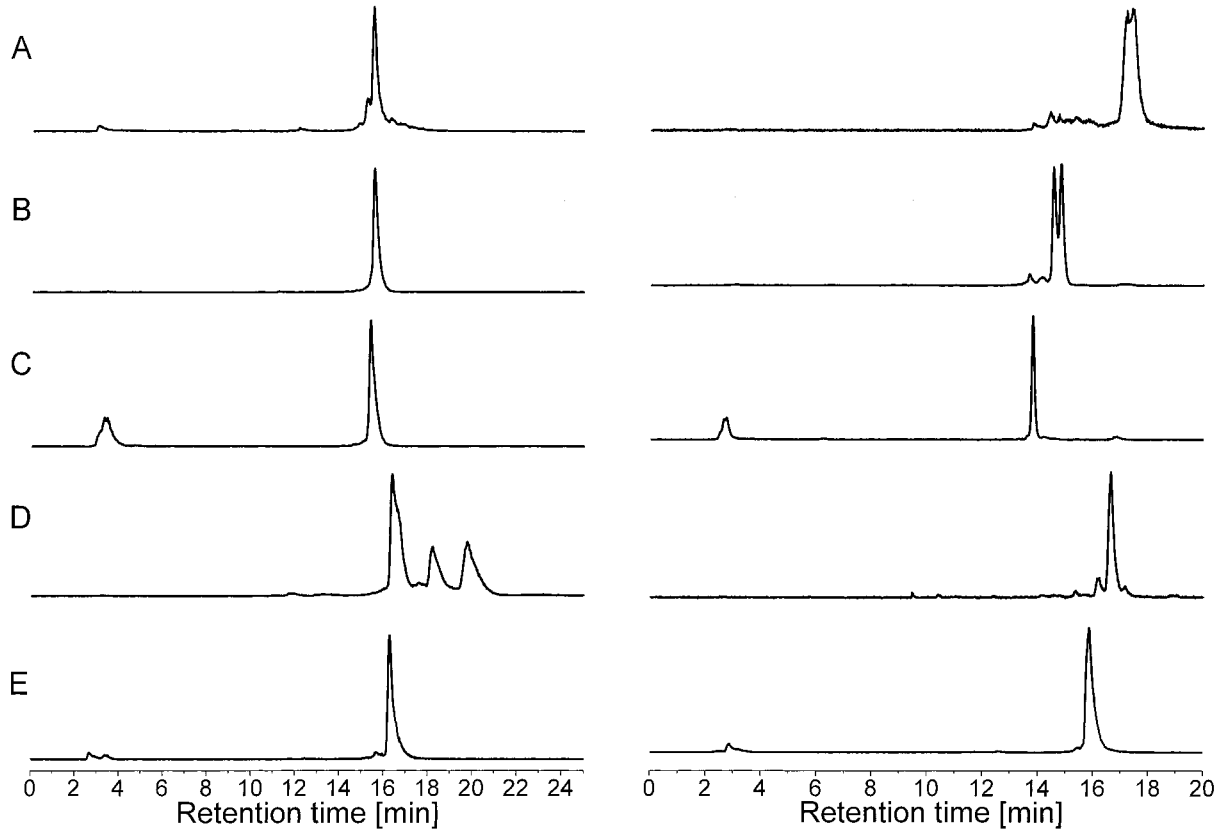


Figure 3. Radiochromatograms of labeling mixtures of different radiolabeled RC-160 conjugates, analyzed by HPLC method 1 (left column) and method 2 (right column). (A) Tricine-HYNIC-RC-160, (B) tricine/NA-HYNIC-RC-160, (C) EDDA-HYNIC-RC-160, (D) MAG3-RC-160, (E) N_3S-RC-160.

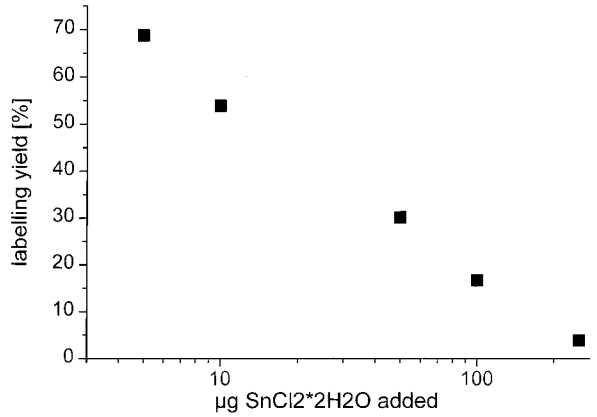


Figure 4. Dependence of labeling yields for EDDA-HYNIC-RC-160 on stannous ion concentration. Conditions for labeling: 10 μg of peptide, 100 MBq ^{99m}Tc.

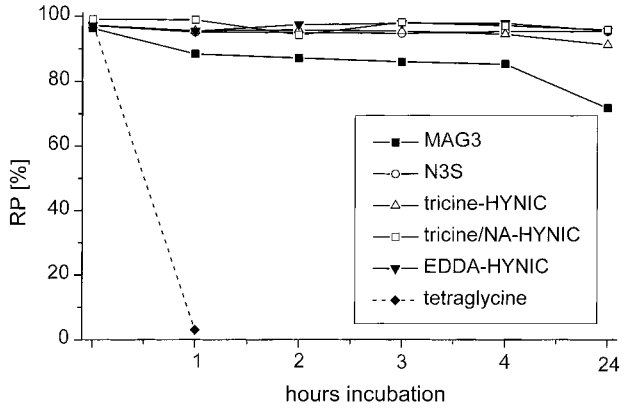


Figure 5. Cysteine challenge of ^{99m}Tc-labeled RC160 conjugates in comparison with [^{99m}Tc]tetraglycine: Radiochemical purity (%) vs time during challenge with 1000-fold excess of cystein over peptide.

protection groups on the thiol (benzoyl-MAG3, acetyl-NHS-MAG3, and ethylethoxy-N_3S adipate). Only the benzoyl group remained stable during the coupling reaction, and both acetyl and ethylethoxy groups were cleaved, mainly during the TFA deprotection reaction.

Using HATU for in situ activation of the free carboxylic acid in the BFC molecule, quantitative coupling yields of the BFC to the peptide and high overall yields on a very small scale (less than 1 mg of peptide) were achieved. Surprisingly, with the N-hydroxysuccinimide-activated ester (NHS-MAG3), which is a widely used system for activating the BFC, even at a high excess of BFC over the peptide, residues of the uncoupled peptide remained which would be likely to cause a problem in the preparation of high-specific activity preparations.

^{99m}Tc Labeling and Stability. Since radiolabeling with technetium requires the use of a reductant, in this case stannous ion, labeling was performed at room temperature, whenever possible, to limit the possibility of a reduction of the disulfide bridge. Although our principle aim was not to achieve the quantitative levels of labeling required for clinical use, sufficiently high labeling efficiencies for in vitro and in vivo evaluations of all the prepared ^{99m}Tc-labeled peptide conjugates were achieved. High specific activity labeling, greater than 1 Ci/mmol could be achieved in all cases. Radiolabeling of HYNIC conjugates requires the use of additional coligands to complete the technetium coordination sphere and our results of labeling using aminocarboxylates as coligands was basically in concordance with the findings

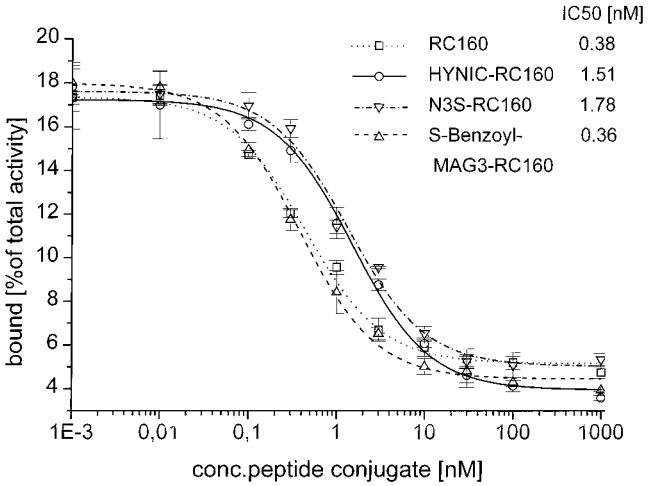


Figure 6. Competition curves of different RC-160 conjugates and calculated IC_{50} values, determined on AtT20-cell membranes, radioligand: [^{125}I]SST14 (data points: bound ± sd).

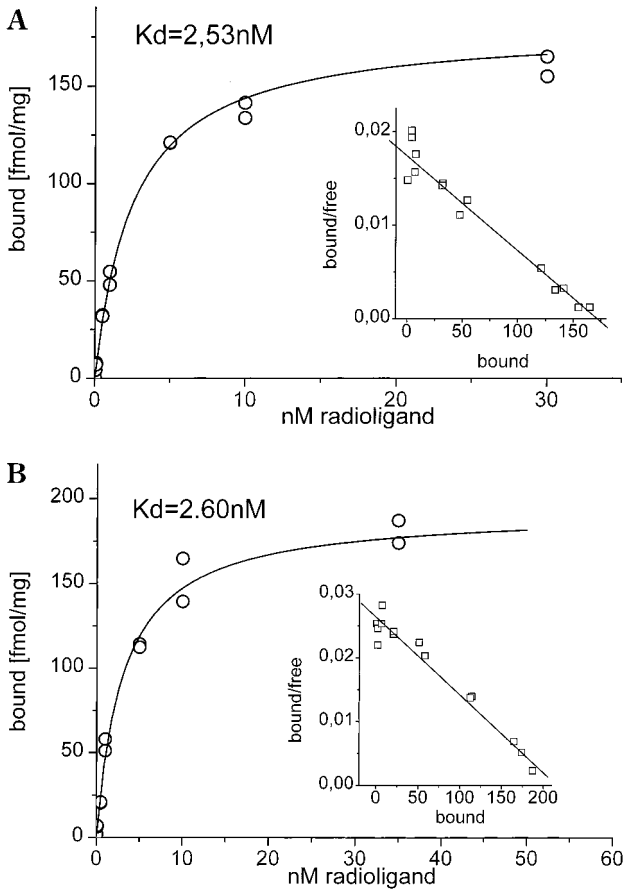


Figure 7. Saturation assays of ^{99m}Tc-labeled EDDA-HYNIC conjugates with respective Scatchard plot, left RC-160 (A), right [Tyr^3]octreotide (B).

of Liu et al. (*27*), who also addressed the problem of specific activity in more detail. Labeled HYNIC conjugates with varying coligands could better be distinguished on HPLC using a phosphate buffer, pH 6.2, gradient than with TFA. For tricine as coligand, a lower in vitro stability (with degradation of the complex especially after removal of excess tricine) and a greater number of isomers were found compared to EDDA. EDDA gave consistently lower labeling yields, but interestingly, we found that the yields were mainly dependent on the amount of stannous ions added and less on the EDDA concentration, pH, or temperature. Although not explored, this presumably relates to differences in the oxidation state of the technetium in the EDDA complex at different stannous ion concentrations.

The high number of isomers and the relatively low stability of ^{99m}Tc-labeled HYNIC modified peptides with tricine as coligand can be overcome by adding a ternary ligand to the labeling solution. We preferred not to use the well characterized triphenylphosphines as described by Edwards et al. (*28*) since their strong reducing properties might affect the disulfide bond. We therefore chose pyridines such as nicotinic acid which were recently described as possible ternary ligands for the tricine-HYNIC system (*29*). Nicotinic acid was compared with other pyridines such as pyridinesulfonic acid or pyridineacetic acid but did not show significantly different properties. To achieve quantitative labeling, heating at 100 °C for 15 min was necessary as ternary ligand complexes were not quantitatively obtained at room temperature. These complexes had a higher stability and lower retention time on HPLC, indicating lower lipophilicity. The number of isomers also was reduced to two compared to more than seven for the tricine binary complex.

^{99m}Tc labeling of the benzoyl-MAG3 conjugates at room temperature failed to achieve complexation, even at high pH [as previously described for MAG3 labeling (*30*)]. Efficient labeling required heating at 100 ˚C to remove the protection group, but even these conditions resulted in the presence of lipophilic impurities possibly due to insufficient deprotection and/or degradation of the peptide conjugate yielding mixed complexes as described for MAG3 itself (*30*−*32*). There was also concern that boiling the peptides in the presence of stannous ion might reduce the disulfide bridge. However, radioligand binding assays showed that the [^{99m}Tc]MAG3 conjugates retain high binding affinity despite this treatment and no difference in retention times or conjugate stability was observed. Studies on tricine/NA ternary ligand systems comparing ternary complexes obtained at room temperature and after heating at 100 °C also showed no difference in the binding affinity of both complexes. These studies prove the stability of the disulfide bridge against reduction by stannous ions even at elevated temperature.

Receptor Binding and Tumor Targeting Properties. In general, all the conjugates prepared and their technetium complexes showed high-affinity specific binding to somatostatin receptors with no relevant differences in binding constants (IC_{50}, K_d values) so far as their likely utility for imaging tumors is concerned. Binding constants of the ^{99m}Tc complexes were in the low nanomolar range, which can be considered sufficiently high for imaging SST-receptors in vivo.

The compounds thus show promise for future tumor-targeting studies initially in animal models and subsequently in patients. Further experiments also have to show the differences of the two investigated peptides described in this study concerning their imaging properties. However, recent publications on ^{111}In-DTPA-RC-160 in comparison with octreotide have shown no advantages of RC-160 in humans (*33*) also no relevant brain uptake was found for the investigated RC-160 derivative (*10*). Whether this holds true for the described ^{99m}Tc-labeled compounds and whether the difference in receptor specificity might offer advantages for RC-160 derivatives remains to be answered.

CONCLUSION

This paper describes the preparation of peptide conjugates using a variety of bifunctional chelate systems suitable for ^{99m}Tc labeling on a small scale using two model peptides. The methods described can be used to evaluate different labeling techniques without extensive and expensive peptide synthesis. Stable HYNIC binary and tertiary complexes in particular could be prepared easily and in high yield. All ^{99m}Tc complexes showed retained binding affinity to somatostatin receptors and further evaluation in vivo will explore their potential for imaging tumors using nuclear medicine techniques.

ACKNOWLEDGMENT

The study described was supported by a EC-"Marie Curie Research Training Grant", proposal E B4001GT9-63891 and the IAEA Coordinated Research Program "^{99m}Tc Labeled Peptides for Imaging of Peripheral Receptors". Special thanks go to H. R. Maecke and M. Behe for their help in the peptide preparation and for sharing their experience in HYNIC labeling. In addition we would like to thank A. R. Fritzberg, D. J. Hnatowich, and O. K. Hjelstuen for the supply of bifunctional chelators.

LITERATURE CITED

Eising, E. G., Bier, D., Knust, E. J., and Reiners, C. (1996) Somatostatin-receptor scintigraphy. Methods, indications, results. *Radiologe 36*, 81−88.

Lamberts, S. W., Chayvialle, J. A., and Krenning, E. P. (1993) The visualization of gastroenteropancreatic endocrine tumors. *Digestion 54* (Suppl. 1), 92−97.

Vekemans, M. C., Urbain, J. L., and Charkes, D. (1995) Advances in radio-imaging of neuroendocrine tumors. *Curr. Opin. Oncol. 7*, 63−67.

Krenning, E. P., Kwekkeboom, D. J., Bakker, W. H., Breeman, W. A., Kooij, P. P., Oei, H. Y., van Hangen, M., Postema, P. T., de Jong M., and Reubi J. C. (1993) Somatostatin receptor scintigraphy with [^{111}In-DTPA-D-Phe] and [^{123}I-Tyr]octreotide: The Rotterdam experience with more than 1000 patients. *Eur. J. Nucl. Med. 20*, 716−731.

Srkalovic, G., Cai, R. Z., and Schally, A. V. (1990) Evaluation of receptors for somatostatin in various tumors using different analogues. *J. Clin. Endocrinol. Metab. 70*, 661−669.

Liebow, C., Reilly, C., Serrano, M., and Schally, A. V. (1989) Somatostain analogues inhibit growth of pancreatic cancer by stimulating tyrosine phosphatase. *Proc. Natl. Acad. Sci. U.S.A.* 86, 2003−2007.

Pinski, J., Milovanovic, T. Y., Yano, T., Hamaoui, A., Radulovic, S., Cai, R. Z., and Schally, A. V. (1992) Biological activity and receptor binding characteristics to various human tumors of acetylated somatostatin receptors. *Proc. Soc. Exp. Biol. Med. 200*, 49−56.

Banks, W. A., Schally, A. V., Barrera, C. M., Fasold, M. B., Durham, D. A., Csernus, V. J., and Kastin, A. J. (1990) Permeability of the murine blood brain barrier to some octapeptide analogues of somatostatin. *Proc. Natl. Acad. Sci. U.S.A. 87*, 6762−6766.

Breeman, W. A. P., Hofland, L. J., Bakker, W. H., van der Pluijm, M., van Koetsveld, P. M., de Jong, M., Setyono-Han, B., Kwekkeboom, D. J., Visser, T. J., Lamberts, S. W. J., and Krenning, E. P. (1993) Radioiodinated somatostatin analogue RC-160: preparation, biological activity, in vivo application in rats and comparison with [^{123}I-Tyr^3]octreotide. *Eur. J. Nucl. Med. 20*, 1089−1094.

Breeman, W. A. P., Hofland, L. J., Pluijm, M.van-der, van Koetsveld, P. M., de Jong, M., Setyono-Han, B., Bakker, W. H., Kweekeboom, D. J., Visser, T. J., Lamberts, S. W. J., and Krenning, E. P. (1994) A new radiolabeled somatostatin analogue [111In-DTPA-D-Phe1]RC-160: preparation, biological activity, receptor scintigraphy in rats and comparison with [111In-DTPA-D-Phe1]octreotide. *Eur. J. Nucl. Med. 21*, 328−335.

Zamora, P. O., Gulhke, S., Bender, H., Diekmann, D., Rhodes, B. A., Biersack, H. J., and Knapp, F. F., Jr. (1996) Experimental radiotherapy of receptor-positive human prostate adenocarcinoma with 188Re-RC-160, a directly radiolabeled somatostatin analogue. *Int. J. Cancer 65*, 214−20.

Liu, S., Edwards, D. S., and Barrett, J. A. (1997) 99mTc labeling of highly potent small peptides. *Bioconjugate Chem. 8*, 621−636.

Valabhajosula, S., Moyer, B. R., Lister-James, J., McBride, B. J., Lipszyk, H., Lee, H., Bastidas, D., and Dean, R. T. (1996) Preclinical evaluation of Technetium-99m-Labeled Somatostatin Receptor-Binding Peptides. *J. Nucl. Med. 37*, 1016−1022.

Maina, T., Stolz, B., Albert, R., Bruns, C., Koch, P., and Mäcke, H. (1994). Synthesis and biological evaluation of a new somatostatin analogue (SDZ 219−387) labeled with technetium-99m. *Eur. J. Nucl. Med. 21*, 437−444.

Maina, T., Stolz, B., Albert, R., Nock, B., Bruns, C., and Mäcke, H. (1995) Synthesis, radiochemistry and biological evaluation of 99mTc[N4-(D)PHE1]-octreotide, a new octreotide derivative with high affinity for somatostatin receptors. in *Technetium and Rhenium in Chemistry and Nuclear Medicine 4* (M. Nicolini, G. Banoli, and U. Mazzi, Eds.) pp 395−400, SG Editorali, Padova.

Mäcke, H. R. and Behe, M. (1996) New octreotide derivatives labeled with technetium-99m. *J. Nucl. Med. 37*, 29P (abstr. 107).

Thakur, M. L., Kolan, H., Wiaderkiewicz, R., Pallela, V. R., Duggaraju, R., and Schally, A. V. (1997) Radiolabeled Somatostatin analogues in Prostate Cancer. *Nucl. Med. Biol. 24*, 105−113.

Kolan, H., Li, J., and Thakur, M. L. (1996) Sandostatin Labeled with 99mTc: In Vitro Stability, In Vivo Validity and Comparison with 111In-DTPA-Octreotide. *Peptide Res. 9*, 144−150.

Abrams, M. J., Juweid, M., tenKate, C. I., Schwartz, D. A., Hauser, M. M., Gaul, F. E., Fuccello, A. J., Rubin, R. H., Strauss, H. W., and Fischman, A. J. (1990) Technetium-99m-human polyclonal IgG radiolabeled via the hydrazino nicotinamide derivative for imaging focal sites of infection in rats. *J. Nucl. Med. 31*, 2022−2028.

Kasina, S., Sanderson, J. A., Fitzner, J. N., Srinivasan, A., Rao, T. N., Hobson, L. J., Reno, J. M., Axworthy, D. B., Beaumier, P. L., and Fritzberg, A. R. (1998) Simplified preformed chelate protein radiolabeling with technetium-99m nercaptoacetamidoadipoylglycylglycine (N3S-Adipate). *Bioconjugate Chem. 9*, 108−117.

Hnatowich, D. J., Qu, T., Chang, F., Ley, A. C., Ladner, R. C., and Rusckowski, M. (1998) Labeling peptides with technetium-99m using a bifunctional chelator of a N-hydroxysuccinimide ester of mercaptoacetyltriglycine. *J. Nucl. Med. 39*, 56−64.

Hnatowich, D. J., Virzi, F., Fogorasi, M., Rusckowski, M., and Winnard, P. (1994) Can a cysteine challenge assay predict the in vivo behavior of 99mTc-labeled antibodies. *Nucl. Med. Biol. 21*, 1035−1044.

Stalteri, M. A., Bansal, S., Hider, R., and Mather, S. J. (1999) Comparison of the stability of technetium labeled peptides to challenge with cysteine. *Bioconjugate Chem. 10*, 130−136.

Hofland, L. J., van Knoetsveld, P. M., Wouters, N., Waaijers, M., Reubi, J. C., and Lamberts, S. W. J. (1992) Dissociation of antiproliferative and antihormoral effects of somatostatin analogue octreotide on 7315b pituitary tumor cells. *Endocrinology 131*, 571−577.

Hofland, L. J., van Knoetsveld, P. M., Waaijers, M., and Lamberts, S. W. (1996) Internalisation of isotope-coupled somatostatin analoges. *Digestion 57* (Suppl. 1), 2−6.

Taylor, J. E., Theveniau, M. A., Bashirzadeh, R., Reisine, T., and Eden, P. A. (1994) Detection of somatostatin receptor subtype 2 (SSTR2) in established tumors and tumor cell lines: evidence for SST2 heterogeneity. *Peptides 15*, 1229−1236.

Liu, S., Edwards, D. S., Looby, R. J., Harris, A. R., Poirier, M. J., Barrett, J. A., Heminway, S. J., and Carroll, T. R. (1996) Labeling a hydrazino nicotinamide-modified cyclic IIb/IIIa

receptor antagonist with 99mTc using aminocarboxylates as coligands. *Bioconjugate Chem. 7,* 63−71.

Edwards, D. S., Liu, S., Barrett, J. A., Harris, A. R., Looby, R. J., Ziegler, M. C., Heminway, S. J., and Carroll, T. R. (1997) New and versatile ternary ligand system for technetium radiopharmaceuticals: water soluble phosphines and tricine as coligands in labeling a hydrazinonicotinamide-modifies cyclic glycoprotein Iib/IIIa receptor antagonist with 99mTc. *Bioconjugate Chem. 8,* 146−154.

Liu, S., Edwards, D. S., and Harris, A. R. (1998) A novel tenary ligand system for ^{99m}Tc-labeling of hydrazio nicotinamide-modified biologically active molecules using imine-N-containing heterocycles as coligands, *Bioconjugate Chem. 9,* 583−595.

Bormans, G., Cleynhens, B., Adriaens, P., Vanbilloen, H., de Roo M., and Verbruggen, A. (1995) Investigation of the labeling characteristics of ^{99m}Tc-Mercaptoacetyltriglycine. *Nucl. Med. Biol. 22,* 339−349.

Millar, A. M. and O'Brien, L. M. (1990) An investigation of fctors that might influence the radiochemical purity and stability of ^{99m}Tc-MAG3. *Eur. J. Nucl. Med. 16,* 615−619.

Noll, B., Johannsen, B., and Spies, H. (1995) Sources of radiochemical impurities in the 99mTc/S-unprotected MAG3 system. *Nucl. Med. Biol. 22,* 1057−1062.

Breeman, W. A. P., Van Hagen, P. M., Kwekkebroom, D. K., Visser, T. J., and Krenning, E. P. (1998) Somatostatin receptor scintigraphy using [^{111}In-DTPA^{0}]RC160 in humans: a comparison with [^{111}In-DTPA^{0}]octreotide. *Eur. J. Nucl. Med. 25,* 182−186.

BC980121C

CORRECTIONS

Volume 10, Number 3, May/June 1999.

Clemens Decristoforo and Stephen J. Mather*

PREPARATION, ^{99m}TC-LABELING, AND IN VITRO CHARACTERIZATION OF HYNIC AND N_3S MODIFIED RC-160 AND [TYR^3]OCTREOTIDE

On pages 437 and 438, the numbers were omitted from the corresponding references. The Literature Cited should appear as follows.

LITERATURE CITED

(1) Eising, E. G., Bier, D., Knust, E. J., and Reiners, C. (1996) Somatostatin-receptor scintigraphy. Methods, indications, results. *Radiologe 36*, 81−88.

(2) Lamberts, S. W., Chayvialle, J. A., and Krenning, E. P. (1993) The visualization of gastroenteropancreatic endocrine tumors. *Digestion 54* (Suppl. 1), 92−97.

(3) Vekemans, M. C., Urbain, J. L., and Charkes, D. (1995) Advances in radio-imaging of neuroendocrine tumors. *Curr. Opin. Oncol. 7,* 63−67.

(4) Krenning, E. P., Kwekkeboom, D. J., Bakker, W. H., Breeman, W. A., Kooij, P. P., Oei, H. Y., van Hangen, M., Postema, P. T., de Jong M., and Reubi J. C. (1993) Somatostatin receptor scintigraphy with [^{111}In-DTPA-D-Phe] and [^{123}I-Tyr]octreotide: The Rotterdam experience with more than 1000 patients. *Eur. J. Nucl. Med. 20,* 716−731.

(5) Srkalovic, G., Cai, R. Z., and Schally, A. V. (1990) Evaluation of receptors for somatostatin in various tumors using different analogues. *J. Clin. Endocrinol. Metab. 70,* 661−669.

(6) Liebow, C., Reilly, C., Serrano, M., and Schally, A. V. (1989) Somatostain analogues inhibit growth of pancreatic cancer by stimulating tyrosine phosphatase. *Proc. Natl. Acad. Sci. U.S.A.* 86, 2003−2007.

(7) Pinski, J., Milovanovic, T. Y., Yano, T., Hamaoui, A., Radulovic, S., Cai, R. Z., and Schally, A. V. (1992) Biological activity and receptor binding characteristics to various human tumors of acetylated somatostatin receptors. *Proc. Soc. Exp. Biol. Med. 200,* 49−56.

(8) Banks, W. A., Schally, A. V., Barrera, C. M., Fasold, M. B., Durham, D. A., Csernus, V. J., and Kastin, A. J. (1990) Permeability of the murine blood brain barrier to some octapeptide analogues of somatostatin. *Proc. Natl. Acad. Sci. U.S.A. 87*, 6762−6766.

(9) Breeman, W. A. P., Hofland, L. J., Bakker, W. H., van der Pluijm, M., van Koetsveld, P. M., de Jong, M., Setyono-Han, B., Kwekkeboom, D. J., Visser, T. J., Lamberts, S. W. J., and Krenning, E. P. (1993) Radioiodinated somatostatin analogue RC-160: preparation, biological activity, in vivo application in rats and comparison with [^{123}I-Tyr^3]octreotide. *Eur. J. Nucl. Med. 20,* 1089−1094.

(10) Breeman, W. A. P., Hofland, L. J., Pluijm, M.van-der, van Koetsveld, P. M., de Jong, M., Setyono-Han, B., Bakker, W. H., Kweekeboom, D. J., Visser, T. J., Lamberts, S. W. J., and Krenning, E. P. (1994) A new radiolabeled somatostatin analogue [^{111}In-DTPA-D-Phe^1]RC-160: preparation, biological activity, receptor scintigraphy in rats and comparison with [^{111}In-DTPA-D-Phe^1]octreotide. *Eur. J. Nucl. Med. 21,* 328−335.

(11) Zamora, P. O., Gulhke, S., Bender, H., Diekmann, D., Rhodes, B. A., Biersack, H. J., and Knapp, F. F., Jr. (1996) Experimental radiotherapy of receptor-positive human prostate adenocarcinoma with ^{188}Re-RC-160, a directly radiolabeled somatostatin analogue. *Int. J. Cancer 65,* 214−20.

(12) Liu, S., Edwards, D. S., and Barrett, J. A. (1997) ^{99m}Tc labeling of highly potent small peptides. *Bioconjugate Chem. 8,* 621−636.

(13) Vallabhajosula, S., Moyer, B. R., Lister-James, J., McBride, B. J., Lipszyk, H., Lee, H., Bastidas, D., and Dean, R. T. (1996) Preclinical evaluation of Technetium-99m-Labeled Somatostatin Receptor-Binding Peptides. *J. Nucl. Med. 37,* 1016−1022.

(14) Maina, T., Stolz, B., Albert, R., Bruns, C., Koch, P., and Mäcke, H. (1994). Synthesis and biological evaluation of a new somatostatin analogue (SDZ 219−387) labeled with technetium-99m. *Eur. J. Nucl. Med. 21,* 437−444.

(15) Maina, T., Stolz, B., Albert, R., Nock, B., Bruns, C., and Mäcke, H. (1995) Synthesis, radiochemistry and biological evaluation of ^{99m}Tc[N_4-(D)PHE$_1$]-octreotide, a new octreotide derivative with high affinity for somatostatin receptors. in *Technetium and Rhenium in Chemistry and Nuclear Medicine 4* (M. Nicolini, G. Banoli, and U. Mazzi, Eds.) pp 395−400, SG Editorali, Padova.

(16) Mäcke, H. R. and Behe, M. (1996) New octreotide derivatives labeled with technetium-99m. *J. Nucl. Med. 37,* 29P (abstr. 107).

(17) Thakur, M. L., Kolan, H., Wiaderkiewicz, R., Pallela, V. R., Duggaraju, R., and Schally, A. V. (1997) Radiolabeled Somatostatin analogues in Prostate Cancer. *Nucl. Med. Biol. 24,* 105−113.

(18) Kolan, H., Li, J., and Thakur, M. L. (1996) Sandostatin Labeled with ^{99m}Tc: In Vitro Stability, In Vivo Validity and Comparison with ^{111}In-DTPA-Octreotide. *Peptide Res. 9,* 144−150.

(19) Abrams, M. J., Juweid, M., tenKate, C. I., Schwartz, D. A., Hauser, M. M., Gaul, F. E., Fuccello, A. J., Rubin, R. H., Strauss, H. W., and Fischman, A. J. (1990) Technetium-99m-human polyclonal IgG radiolabeled via the hydrazino nicotinamide derivative for imaging focal sites of infection in rats. *J. Nucl. Med. 31,* 2022−2028.

(20) Kasina, S., Sanderson, J. A., Fitzner, J. N., Srinivasan, A., Rao, T. N., Hobson, L. J., Reno, J. M., Axworthy, D. B., Beaumier, P. L., and Fritzberg, A. R. (1998) Simplified preformed chelate protein radiolabeling with technetium-99m nercaptoacetamidoadipoylglycylglycine (N_3S-Adipate). *Bioconjugate Chem. 9,* 108−117.

(21) Hnatowich, D. J., Qu, T., Chang, F., Ley, A. C., Ladner, R. C., and Rusckowski, M. (1998) Labeling peptides with technetium-99m using a bifunctional chelator of a N-hydroxysuccinimide ester of mercaptoacetyltriglycine. *J. Nucl. Med. 39,* 56−64.

(22) Hnatowich, D. J., Virzi, F., Fogorasi, M., Rusckowski, M., and Winnard, P. (1994) Can a cysteine challenge assay predict the in vivo behavior of ^{99m}Tc-labeled antibodies. *Nucl. Med. Biol. 21,* 1035−1044.

(23) Stalteri, M. A., Bansal, S., Hider, R., and Mather, S. J. (1999) Comparison of the stability of technetium labeled peptides to challenge with cysteine. *Bioconjugate Chem. 10,* 130−136.

(24) Hofland, L. J., van Knoetsveld, P. M., Wouters, N., Waaijers, M., Reubi, J. C., and Lamberts, S. W. J. (1992) Dissociation of antiproliferative and antihormoral effects of somatostatin analogue octreotide on 7315b pituitary tumor cells. *Endocrinology 131,* 571−577.

(25) Hofland, L. J., van Knoetsveld, P. M., Waaijers, M., and Lamberts, S. W. (1996) Internalisation of isotope-coupled somatostatin analoges. *Digestion 57* (Suppl. 1), 2−6.

(26) Taylor, J. E., Theveniau, M. A., Bashirzadeh, R., Reisine, T., and Eden, P. A. (1994) Detection of somatostatin receptor subtype 2 (SSTR2) in established tumors and tumor cell lines: evidence for SST2 heterogeneity. *Peptides 15,* 1229−1236.

(27) Liu, S., Edwards, D. S., Looby, R. J., Harris, A. R., Poirier, M. J., Barrett, J. A., Heminway, S. J., and Carroll, T. R. (1996) Labeling a hydrazino nicotinamide-modified cyclic IIb/IIIa receptor antagonist with ^{99m}Tc using aminocarboxylates as coligands. *Bioconjugate Chem. 7,* 63−71.

(28) Edwards, D. S., Liu, S., Barrett, J. A., Harris, A. R., Looby, R. J., Ziegler, M. C., Heminway, S. J., and Carroll, T. R. (1997) New and versatile ternary ligand system for technetiumradiopharmaceuticals: water soluble phosphines and tricine as coligands in labeling a hydrazinonicotinamide-modifies cyclic glycoprotein IIb/IIIa receptor antagonist with ^{99m}Tc. *Bioconjugate Chem. 8,* 146−154.

(29) Liu, S., Edwards, D. S., and Harris, A. R. (1998) A novel tenary ligand system for ^{99m}Tc-labeling of hydrazio nicotinamide-modified biologically active molecules using imine-N-containing heterocycles as coligands, *Bioconjugate Chem. 9,* 583−595.

(30) Bormans, G., Cleynhens, B., Adriaens, P., Vanbilloen, H., de Roo M., and Verbruggen, A. (1995) Investigation of the labeling characteristics of ^{99m}Tc-Mercaptoacetyltriglycine. *Nucl. Med. Biol. 22,* 339−349.

(31) Millar, A. M. and O'Brien, L. M. (1990) An investigation of factors that might influence the radiochemical purity and stability of ^{99m}Tc-MAG3. *Eur. J. Nucl. Med. 16,* 615−619.

(32) Noll, B., Johannsen, B., and Spies, H. (1995) Sources of radiochemical impurities in the ^{99m}Tc/S-unprotected MAG3 system. *Nucl. Med. Biol. 22,* 1057−1062.

(33) Breeman, W. A. P., Van Hagen, P. M., Kwekkebroom, D. K., Visser, T. J., and Krenning, E. P. (1998) Somatostatin receptor scintigraphy using [^{111}In-DTPA^0]RC160 in humans: a comparison with [^{111}In-DTPA^0]octreotide. *Eur. J. Nucl. Med. 25,* 182−186.

BC9900688

10.1021/bc9900688
Published on Web 07/19/1999

Recognition of Hairpin-Containing Single-Stranded DNA by Oligonucleotides Containing Internal Acridine Derivatives

Jean-Christophe François* and Claude Hélène

Laboratoire de Biophysique, Muséum National d'Histoire Naturelle, INSERM Unité 201- CNRS UA 481, 43 rue Cuvier, 75231 Paris Cedex 05, France . Received October 7, 1998; Revised Manuscript Received January 27, 1999

Oligodeoxynucleotides with an internal intercalating agent have been targeted to single-stranded sequences containing hairpin structures. The oligonucleotide binds to nonadjacent single-stranded sequences on both sides of the hairpin structure in such a way as to form a three-way junction. The acridine derivative is inserted at a position that allows it to interact with the three-way junction. The melting temperature (T_m) of complexes formed between the hairpin-containing target and oligonucleotides containing one internal acridine derivative was higher than that obtained with the same target and an unmodified oligonucleotide ($\Delta T_m = +13$ °C). The internal acridine provided the oligonucleotide with a higher affinity than covalent attachment to the 5′ end. Oligonucleotides could also be designed to recognize a hairpin-containing single-stranded nucleic acid by formation of Watson−Crick hydrogen bonds with a single-stranded part and Hoogsteen hydrogen bonds with the stem of the hairpin. An internal acridine derivative was introduced at the junction between the two domains, the double helix domain with Watson−Crick base pairs and the triple helix domain involving Hoogsteen base triplets in the major groove of the hairpin stem. Oligonucleotides with an internal acridine or an acridine at their 5′ end have similar binding affinities for the stem-loop-containing target. The bis-modified oligonucleotide containing two acridines, one at the 5′ end and one at an internal site, did not exhibit a higher affinity than the oligonucleotides with only one intercalating agent. The design of oligonucleotides with an internal intercalating agent might be of interest to control gene expression through recognition of secondary structures in single-stranded targets.

INTRODUCTION

Hairpin structures frequently occur in RNA secondary structures and also in DNA sequences that are found near functional loci and therefore seem to play a critical role in gene regulation (*1*). In the antisense strategy where the antisense oligonucleotides are targeted to single-stranded messenger RNAs, it was shown that stem-loop structures can compete with intermolecular hybridization of the oligonucleotides to the complementary sequences (*2*). Nevertheless, hairpin structures could also be exploited in the design of the recognition elements of an oligonucleotide aimed at inhibiting mRNA translation (*3*, *4*) or probing RNA structures (*5*).

We have previously shown that hairpin-containing nucleic acids could bind oligodeoxynucleotides complementary to nonadjacent single-stranded sequences on both sides of the stem-loop sequence (*6*). Oligonucleotides can also bind to hairpin-containing single-stranded nucleic acids (DNA or RNA) by using both triple helix and double helix formation (*3*, *7*−*15*).

In the present paper, we have investigated the effect of introducing an intercalating agent, an acridine derivative, in an oligonucleotide designed to recognize two single-stranded sequences separated by a hairpin structure. We demonstrate that when the acridine is inserted at an internal position close to the bases of the stem loop structure, the resulting complexes are more stable than when it is linked to the 5′ end of the oligonucleotide, suggesting a preferential site of interaction for the acridine ring near the center of the three-way structure.

The formation of triple helices is of interest in both the antisense and the antigene strategies (*16*). Clamp oligonucleotides can bind to an oligopurine sequence in a single-stranded nucleic acid by forming both Watson−Crick and Hoogsteen hydrogen bonds (*17*−*19*). Circular oligonucleotides can also be designed to bind via both double and triple helix formation (*20*, *21*). Recently, it was shown that the incorporation of an acridine derivative at an internal site of an oligonucleotide stabilizes triplexes with an interruption in the oligopurine target sequence and therefore opens new possibilities to extend the range of DNA sequences recognized by triplex-forming oligonucleotides (*22*, *23*). Triplex-specific intercalating agents such as benzopyridoindole and benzopyridoquinoxaline derivative could also be introduced into triplex-forming oligonucleotides to increase binding affinity to the DNA double helices (*24*, *25*).

We have previously demonstrated that antisense oligonucleotides could bind to hairpin-containing single-stranded nucleic acids by using both triple helix and double helix formation (*9*). These oligonucleotides interact with one of the two single-stranded sequences flanking the hairpin via Watson−Crick base pair formation and with the double-stranded stem sequence of the hairpin via Hoogsteen base triplet formation. These newly designed antisense oligonucleotides were called Watson−Crick/Hoogsteen oligonucleotides (abbreviated as WC/H). We have now synthesized WC/H oligonucleotides with an internally incorporated acridine in such a way that the acridine ring is located at the junction between the

* To whom correspondence should be addressed. Phone: 33-1-40-79-37-08. Fax: 33-1-40-79-37-05. E-mail: francois@cimrs1.mnhn.fr.

10.1021/bc9801225 CCC: $18.00 © 1999 American Chemical Society
Published on Web 03/26/1999

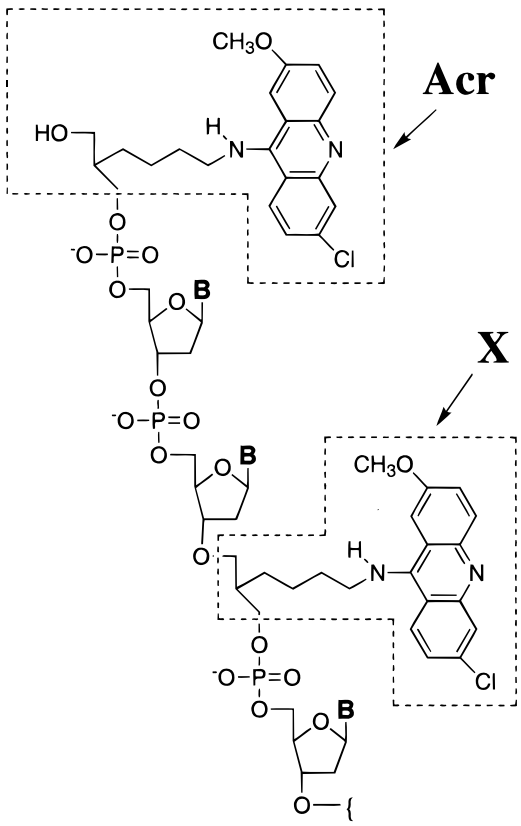


Figure 1. Chemical structures of the internally incorporated acridine within an oligonucleotide and the acridine linked at the 5′ end of an oligonucleotide. Note that the acridine ring covalently linked to the 5′ end was noted in the text as Acr and that the internal acridine derivative was referred to as X. B represents a base.

duplex and triplex portions of the complex. These WC/H oligonucleotides with an internal acridine form more stable complexes with their target than the unmodified oligonucleotides. The binding affinity of the WC/H oligonucleotide with an internal acridine is similar to the binding affinity of the oligonucleotide with an acridine linked to its 5′ end.

MATERIALS AND METHODS

Oligonucleotides. Oligonucleotides and acridine-containing oligonucleotides were synthesized by Eurogentec (Belgium). Acridine phosphoramidite (Glen Research) was either internally incorporated into oligonucleotides in the course of the synthesis or incorporated at the end of synthesis for 5′-linked oligonucleotides. Note that the natural three carbon internucleotidic phosphate distance is maintained in the oligonucleotide containing an internal acridine (Figure 1). The acridine ring was tethered to the backbone via five atoms. The 5′-linked acridine was tethered to the 5′-phosphate group via a seven atom containing linker. A bis-modified oligonucleotide with two acridines, one internal and one linked to the 5′ end, was obtained by the same procedure.

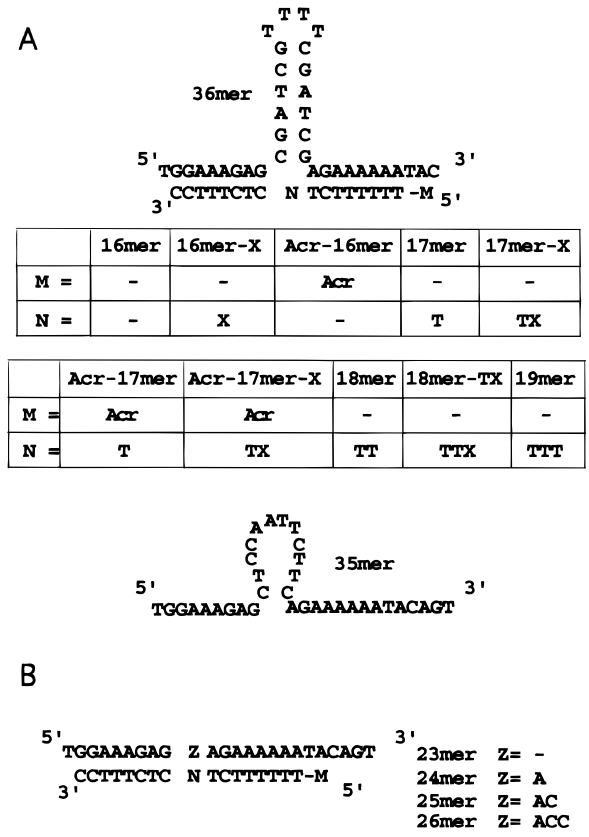
Before utilization, the acridine-oligonucleotide conjugates were purified by gel-filtration on G25 sephadex minicolumns (Boehringer Mannheim) in order to eliminate uncoupled acridine. The quality of acridine-oligonucleotide conjugates was then checked by denaturing gel electrophoresis (20% polyacrylamide/7 M urea). For detection, we used both the UV shadow effect of the oligonucleotide with irradiation at 254 nm on a chromatography paper containing a fluorescent-indicator, (TLC plastic sheets silica gel 60 F254, Merck), and the fluorescence of the incorporated acridine (obtained after excitation at 320 nm). Dark bands at 254 nm (corresponding to absorption of the bases of the oligomers) comigrated with yellow bands at 320 nm (corresponding to the fluorescence of the acridine). With this control assay, all acridine-containing oligonucleotides exhibited only one band that migrated more slowly than the dark band of the unmodified oligonucleotides. The length of 5′ end-labeled unmodified oligonucleotides has also been checked by gel electrophoresis.

The concentration of oligonucleotides and acridine-containing oligonucleotides was determined using the extinction coefficient for acridine at 424 nm, 8500 M^{-1} cm^{-1} or calculated by nearest-neighbor method (*26*) assuming an extinction coefficient for acridine of 85 000 M^{-1} cm^{-1} at 260 nm. The concentration of the oligonucleotide containing two acridine rings was estimated at 260 nm. With this oligonucleotide, calculations using the extinction coefficient at 424 nm gave an underestimated concentration, probably due to the existence of interactions involving the two acridine rings.

Melting Experiments. Absorption spectra were recorded on an UVIKON 940 spectrophotometer with cell holders thermoregulated by a circulating liquid (80% water, 20% ethylene glycol). Sample temperature was decreased from 90 to 5 °C and increased back to 90 °C at a rate of 0.25 °C/min with absorption readings at 260 and 540 nm taken every 5 min. Melting curves were obtained by subtracting the absorbance recorded at 540 nm where none of the constituents absorbed light from that recorded at 260 nm. Under all the experimental conditions described in the figures, all melting profiles were reversible. The melting temperature T_m (±1 °C) was determined as the maximum of the first derivative of melting curves. All the T_m experiments presented in this study were performed with 2 μM hairpin-containing target and 2 μM oligonucleotide ligand, therefore, enabling direct comparison of T_m values. It should be noted that these T_m values depend on the concentration of oligonucleotides. For acridine-containing oligonucleotides, identical melting temperatures were obtained from absorbance measurements at 260 or 425 nm (where acridine absorbs).

RESULTS AND DISCUSSION

Design of Hairpin-Containing Targets and Acridine-Containing Oligonucleotides. In the first DNA model, a single-stranded nucleic acid fragment, 36 nucleotides (nt) in length (36mer) was used as a target for 16mer oligonucleotides linked to an acridine derivative (Figure 2A). The structure of the acridine conjugates is shown in Figure 1. The 36mer can form a hairpin structure with four G·C and two A·T base pairs in the stem and four thymines in the loop. The sequence of the control 35mer was identical to that of the 36mer except that the sequence in the stem-loop $^{5'}$CGATCGTTTTCGATCG$^{3'}$ was changed to $^{5'}$CTCCAATTCTTC$^{3'}$, preventing the formation of a hairpin structure in the 35mer. Three additional nucleotides (AGT) were present at the 3′ end of the 35mer [referred in a previous paper as 35mer-(AAT) (*6*)]. The 16mer oligonucleotides were designed to bind to both sides of the hairpin-containing 36mer forming two mini double helices separated by the stem-loop region (Figure 2A). For comparison with targets containing intervening sequences, oligonucleotides and acridine-oligonucleotide conjugates were targeted to the 23mer, a single-stranded DNA target with no hairpin structure (Figure 2B).



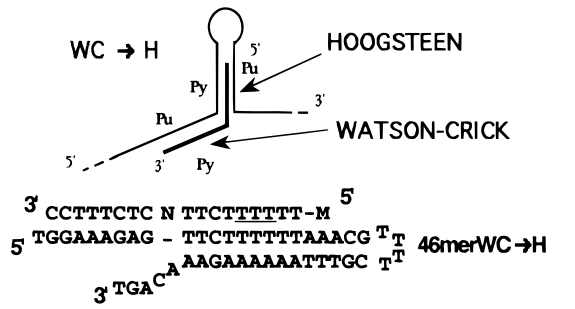
	16mer	16mer-X	Acr-16mer	17mer	17mer-X
M =	-	-	Acr	-	-
N =	-	X	-	T	TX

	Acr-17mer	Acr-17mer-X	18mer	18mer-TX	19mer
M =	Acr	Acr	-	-	-
N =	T	TX	TT	TTX	TTT

Figure 2. (A) Sequences of the hairpin-containing oligonucleotide 36mer and of the 35mer with no hairpin structure. The unmodified ligands, 16mer, 17mer, 18mer, and 19mer together with the sequences of the acridine-modified oligonucleotides are shown. X corresponds to the internal acridine and Acr to the 5′-linked acridine (see Figure 1). (B) Sequences of the 23mer, 24mer, 25mer, and 26mer targets that exhibited no hairpin structure. Sequences of their unmodified or modified oligonucleotide ligands, 16mer, 16mer-X, and Acr-16mer are shown in Figure 2A.

In the second DNA model, the target 46merWC→H has two different domains, a double-stranded stem and a single-stranded sequence, allowing both triple helix and double helix formation with acridine-containing 17mer oligonucleotide ligands (Figure 3). Only one possibility for designing the WC/H targets was studied [see previous paper for details (*9*)]. The single-stranded purine-rich region of the 46mer was chosen to be on the 5′ side of the hairpin and was referred to as the Watson−Crick-toward-Hoogsteen orientation, 46merWC→H in ref *9*. The 17mer oligonucleotides were designed to bind to both single-stranded and double-stranded regions of the hairpin-containing 46merWC→H. The stem sequence in 46merWC→H was chosen to be long enough to give rise to two distinct melting transitions corresponding to oligonucleotide dissociation and stem disruption. It should be noted that the 46merWC→H had a short (5 nt) single-stranded sequence added to the 3′ end of the stem.

Acridine derivatives were either attached to the 5′ end of the oligonucleotides (Acr-16mer and Acr-17mer) or incorporated in the center of the oligonucleotide sequence (for 16mer-X, 17mer-X, and 18mer-X). The acridine of the oligonucleotide ligand was located in the complex formed with the DNA targets, either between the two single-stranded parts of the 36mer (Figure 2) or at the junction between the single-stranded and the double-stranded domains of 46merWC→H (Figure 3). Additional thymines were introduced in replacement of the acridine derivative



	17mer	17mer-X	Acr-17mer	Acr-17mer-X
M =	-	-	Acr	Acr
N =	-	X	-	X

	18mer	18mer-TX	18mer-XT	19mer
M =	-	-	-	-
N =	T	TX	XT	TT

Figure 3. Sequences of the hairpin-containing oligonucleotide 46merWC→H and its ligands: unmodified 17mer, 18mer, 19mer, and 16mer; acridine-containing ligands: 17mer-X, 18mer-TX, 18mer-XT, 16mer-X, and Acr-17mer. Note that single-stranded sequences are present on both the 5′ and 3′ sides of the hairpin of the 46mer WC→H. The mutated oligonucleotide 17mer-Mut $^{5'}$dTTCACTCTTCTCTTTCC$^{3'}$ is identical to the 17mer sequence except for three nucleotides located in the 5′ part of the oligonucleotide (underlined on the ligand sequence). The 16mer and 16mer-X $^{5'}$dTTTTTTCTCTCTTTCC$^{3'}$ lack an internal thymine when compared to the 17mer and 17mer-X, respectively.

or near the acridine derivative to obtain 17mers, 18mers, 19mers, 18mer-TX, and 18mer XT (Figures 2 and 3). A bis-modified oligonucleotide, Acr-17mer-X, with two acridines (one at an internal position and one at the 5′ end of the oligonucleotide) was also targeted to the 36mer (Figure 2A).

Recognition of Two Nonadjacent Sequences by Acridine-Oligonucleotide Conjugates: Model 1. As shown on the melting profile presented in Figure 4A, the melting transitions corresponding to oligonucleotide dissociation and stem fusion of the 36mer were well separated. Melting temperature (T_m) of the stem-loop structure of the 36mer was estimated from the first derivative of melting curves as shown in Figure 4B. The T_m of the $^{5'}$CGATCGTTTTCGATCG$^{3'}$ stem loop in the 36mer was 65 ± 1 °C in the incubation conditions of Figure 4A (0.1 M NaCl). Previous melting experiments have shown that the $^{5'}$CGATCGTTTTCGATCG$^{3'}$ oligonucleotide formed a hairpin structure with a T_m of 70 °C in 0.1 M NaCl (*27*). These results suggested that the addition of flanking sequences to the hairpin-forming sequence $^{5'}$CGATC-GTTTTCGATCG$^{3'}$ decreased by 5 °C the stability of the hairpin in the 36mer.

The unmodified 16mer oligonucleotide binds to the 36mer with a T_m of 25 ± 1 °C at 2 μM concentration in a pH 7.02 buffer containing 50 mM cacodylate and 0.1 M sodium chloride (Figure 4). The addition of an acridine at the 5′ end of the 16mer in Acr-16mer increased the T_m value by 8 °C (Figure 5). This stabilization was already demonstrated for oligonucleotide-acridine conjugates targeted to single-stranded DNA sequences without any secondary structure (*28*, *29*). The 16mer-X with an internal acridine in the center of the 16mer sequence had a higher T_m value (38 ± 1 °C) as compared to the Acr-16mer (T_m = 33 °C) and 16mer (T_m = 25 °C) (Figure

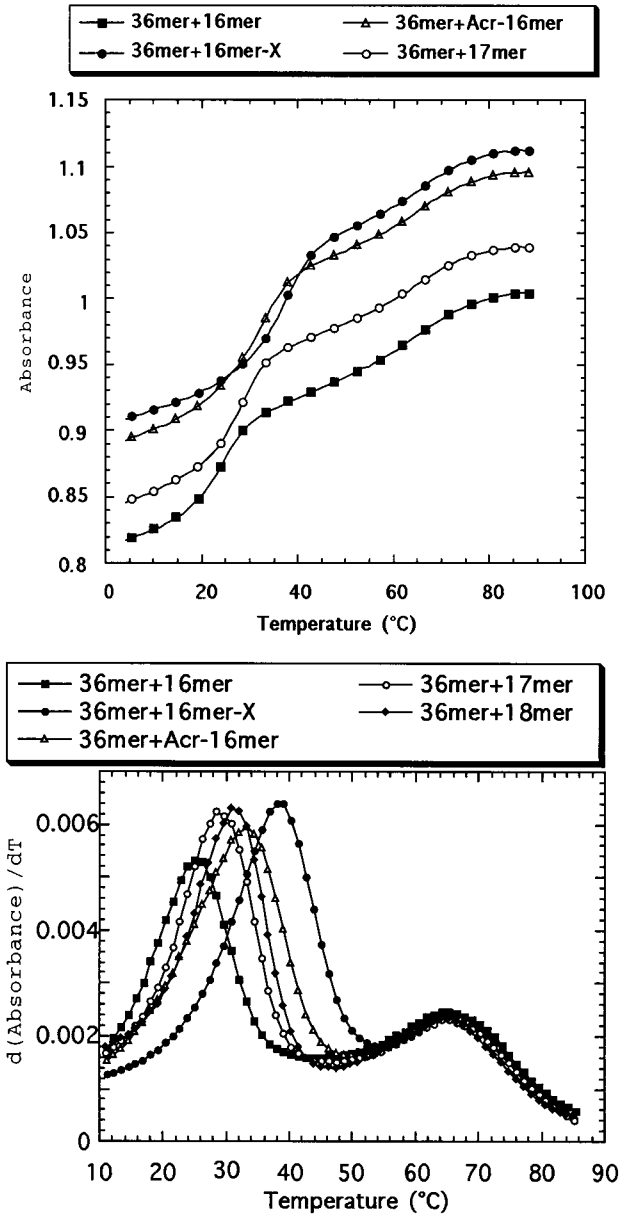


Figure 4. (A) Melting curves measured at 260 nm for 2 μM 36mer bound to 2 μM of 16mer (■), 16mer-X (●), Acr-16mer (△), and 17mer (○) in 50 mM cacodylate buffer, pH 7.02, containing 0.1 M NaCl. The melting temperature corresponding to stem fusion is 65 ± 1 °C. (B) First derivative of the melting curves shown in Figure 4A. Legend symbols are the same as in Figure 4A. In addition the derivative of the melting curve of the 36mer/18mer complex is also shown (◆).

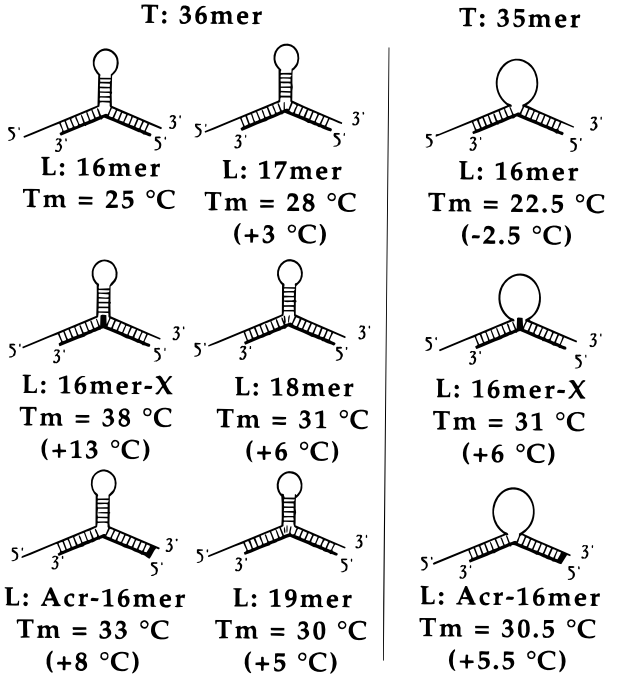


Figure 5. Schematic representations of the complexes formed by acridine-containing and unmodified oligonucleotide ligands (L) with the hairpin-containing 36mer or the 35mer target containing no hairpin structure (T), 36mer and 35mer. Melting temperatures indicated below each complex were obtained with 2 μM/2 μM T/L in the same buffer used in Figure 4. The T_m of the 16mer/36mer (T_m = 25 °C) was taken as reference for the ΔT_m calculations.

5). These results suggested that the location of the acridine in the 16mer-X/36mer complex, near the branch-point of the three-way structure, was likely a preferential site for intercalation of acridine.

The replacement of acridine by one internal thymine (17mer/36mer complex) at the junction between the two single-stranded domains of the 36mer strongly decreased the T_m value from 38 to 28 °C. The 17mer/36mer complex was only slightly stabilized (ΔT_m = +3 °C) as compared to that for the 16mer/36mer complex (Figure 5). The 18mer with two additional thymines had a T_m increased by 6 °C (T_m = 31 °C) (Figure 5), indicating that the introduction of thymines in such structures improved the binding affinity likely via stacking interactions at the branch point as previously described for DNA three-arm junctions (*30*−*33*). No additional increase of stability was observed with the introduction of a third thymine (T_m = 30 °C for the 19mer).

The 17mer-X oligonucleotide with an acridine and a thymine both located at the junction of the three-way structure has a higher melting temperature than the unmodified 17mer [$\Delta T_{m\ (17mer-X/17mer)}$ = +9 °C], but has a melting temperature similar to that of Acr-17mer. The T_m values for complexes with 17mer-X and Acr-17mer are, respectively, 37 and 36.5 °C (data not shown). This result indicated that the addition of acridine either internally or at the 5′ end of the oligonucleotide ligand stabilized to the same extent as the complexes containing one unbound internal thymine (17mer). It should be noted that the replacement of the central thymine in the 17mer by an acridine ring (to obtain the 16mer-X) strongly increased binding affinities as shown by the ΔT_m between the complexes formed by 17mer and 16mer-X [$\Delta T_{m\ (16mer-X/17mer)}$ = +10 °C] (Figure 5). This result indicated that the tricyclic acridine ring interacted as an intercalating agent much better than an additional thymine. The charge of the acridine molecule (assuming that at neutral pH, the ring is still positively charged) may also participate in stabilization of complexes. Nevertheless, this electrostatic stabilization may occur with internal acridine and with acridine linked to the 5′-end of the oligonucleotide ligand. The addition of one thymine in 17mer-X/36mer or two thymines in 18mer-TX/36mer did not give more stable complexes than that formed by 16mer-X/36mer [$T_{m\ (17mer-X/36mer)}$ = 37 °C and $T_{m\ (18mer-TX/36mer)}$ = 38 °C].

In an attempt to increase the binding affinity of 17mer-X ligand to its 36mer target, we have synthesized Acr-17mer-X, an oligonucleotide with two acridine derivatives, one inserted at a internal site and the second one at the 5′ end (Figure 2). Surprisingly, no additional stabilization was observed when compared to the oligo-

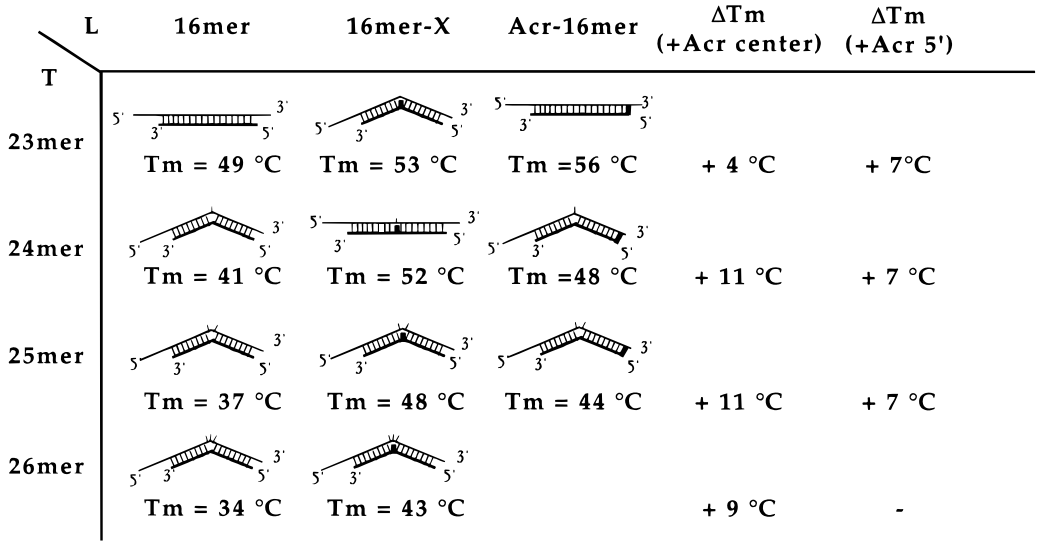


Figure 6. Schematic representations of the complexes formed by acridine-containing and unmodified oligonucleotide ligands (L) with the targets that contains no secondary structures (T), 23mer, 24mer, 25mer and 26mer. Experimental conditions were the same as in Figures 4 and 5. The two columns (to the right of the figure) represent the ΔT_m values with and without acridine attached in the center or at the 5′-end of the ligand for each of the target.

nucleotides with only one acridine, 17mer-X and Acr-17mer [$T_{m\ (Acr-17mer-X/36mer)} = 36$ °C]. The Acr-17mer-X did not give a melting transition when heated alone at 5 μM in the conditions described in Figure 4A (data not shown). However, this does not exclude a stacking interaction between the two acridine rings. 2-Methoxy-6-chloro-9-amino acridine derivatives are known to self-associate in aqueous solutions with a dimerization constant around 10^3 M^{-1} (*34*). In the oligonucleotide, this process becomes intramolecular and can compete with binding of the bis-substituted oligonucleotide to its target sequence.

To determine if the presence of the hairpin structure was necessary for the increase in binding stability of oligonucleotides with an internal acridine, the 35mer which has no hairpin structure but contains the target sequences for each half of the 16mers was synthesized. As shown in Figure 5, the absence of hairpin structure in the 16mer/35mer complexes slightly decreased T_m values, but the addition of acridine either at the 5′ end or internally increased melting temperatures to the same extent [$\Delta T_{m(16mer-X/16mer)} = +8.5$ °C and $\Delta T_{m(Acr-16mer/16mer)} = +8$ °C]. As compared to the hairpin-containing structure [$\Delta T_{m(16mer-X/16mer)} = +13$ °C and $\Delta T_{m(Acr16mer/16mer)} = +8$ °C], there is clearly an increased binding energy of the internal acridine with the hairpin-containing target reflecting the strongest interaction of the acridine with the three-way junction.

Double Helices Formed by Acridine-Oligonucleotide Conjugates and Target Oligonucleotides without Any Secondary Structure. Oligonucleotides and acridine-oligonucleotide conjugates were targeted to the 23mer, a single-stranded DNA target with no secondary structure and no interruption of the complementary sequence of the 16mer and to longer oligomers, 24−26 nt in length, with one, two, or three additional bases at the position where the hairpin sequence of the 36mer was inserted (Figure 2B). All melting temperatures described in Figure 6 were higher than those obtained with targets containing hairpin structures (Figure 5), emphazing the destabilizing role of the hairpin structure in complexes with 36mer. As shown in Figure 6, when the 16mer was targeted successively to the 23mer, 24mer, 25mer, and 26mer, a decrease of T_m values was observed, demonstrating the destabilizing effect of introducing bulges, i.e., nonmatched additional bases (*35*, *36*). Incorporation of an internal acridine in the 16mer sequence (16mer-X) resulted in an increase in binding affinity but to a lesser extent ($\Delta T_{m(16mer-X/23mer)} = +4$ °C, see Figure 6) than that obtained with the 36mer ($\Delta T_{m(16merX/36mer)} = +13$ °C, see Figure 5). Similar results were obtained with oligonucleotides containing an internal acridine ring that were targeted to a target containing an abasic, an apyrimidinic or an apurinic site (*37*, *38*).

In contrast to what was observed with the 16mer/36mer complexes (Figure 5), the Acr-16mer oligonucleotide had a higher T_m value than the 16mer-X when bound to the 23mer ($\Delta T_m = +7$ °C). It should be noted that the stabilization obtained when the acridine was attached to the 5′ end of the 16mer (Acr-16mer) was the same for all targets: 23mer, 24mer, 25mer, and 26mer (Figure 6). For all targets in Figure 6, $\Delta T_{m(Acr-16mer/16mer)}$ was +7 °C. For the 36mer and the 35mer, addition of acridine at the 5′ end resulted in an increase of T_m of +8 °C (Figure 5). These results demonstrated that the intercalating acridine exhibited a similar behavior concerning the stabilization of duplex DNA even if this DNA contained bulged nucleotides or hairpins located 8 nucleotides away from the 5′ end of the oligonucleotide ligand.

The addition of an acridine ring in the center of the 16mer sequence (16mer-X) increased T_m values by +4, +11, and +9 °C for the 16mer-X/23mer, 16mer-X/24 or 25mer, and 16mer-X/26mer, respectively (Figure 6). A stabilization of +8.5 °C was obtained with 16mer-X bound to the 35mer target [($\Delta T_{m(16mer-X/16mer)} = +8.5$ °C, see Figure 5], suggesting that the additional stabilization afforded by an internally attached acridine does not depend on the number of looped-out bases above three bases. The stabilization observed when the 16mer-X binds to the hairpin-containing 36mer ($\Delta T_m = +13$ °C) indicates that the hairpin is formed when the oligonucleotide is bound and that the acridine has a preferential site of interaction at the branch point of the three-way junction.

Recognition of Hairpin-Containing Structures by Acridine-Oligonucleotide Conjugates via Both Watson−Crick and Hoogsteen Hydrogen Bonding: Model 2. We previously demonstrated that the 17mer

Table 1: Melting Temperatures (T_m) for the Dissociation of Oligonucleotide Ligands (L) from a Hairpin-Containing Target (T), 46Mer WC→H[a]

oligonucleotide ligands	T_m (S+) (°C)	ΔT_m (S+)	T_m (°C)	ΔT_m
17mer	34	0	14	0
17mer-X	50	+16	35	+21
Acr-17mer	49	+15	31.5	+17.5
Acr-17mer-X	46	+12	31.5	+17.5
18mer	42	+8	24	+10
18mer-TX	50	+16	34	+20
19mer	39	+5	19	+5
17mer-Mut	26.5	−7.5	12.5	− 1.5

[a] See sequences in Figure 3. Concentration of both the oligonucleotide ligand and the target were 2 μM. Samples were incubated in a 50 mM cacodylate buffer containing 0.1 M NaCl at pH 7.02 in the absence (right columns) or in the presence of 0.2 mM spermine (S+) (left columns). T_m values were determined as described in Materials and Methods and were rounded off to the nearest 0.5 °C and error is estimated at ± 1 °C. Melting temperatures of the stem sequence of the 46mer WC→H are respectively 64 °C and 70 °C in absence and in the presence of 0.2 mM spermine. ΔT_m represents the increase in T_m upon addition of thymines or acridine derivatives for each incubation conditions. The reference is the 17mer complex.

shown in Figure 3 binds to the 46mer WC→H by forming both Watson−Crick and Hoogsteen hydrogen bond interactions (*9*). The difference in stability between the 17mer and the 17mer-Mut complex (ΔT_m = −7.5 °C, Table 1) demonstrated that the 5′ end of the 17mer was bound to the stem sequence of the 46merWC→H via triple helix formation as previously described (*9*).

In the 18mer/46merWC→H complex, the addition of a thymine at the junction of the two domains increased the T_m by +8 °C (Figure 7A and Table 1). As previously reported (*9*), the addition of one nucleotide increases the binding affinity when it is located at the junction of a WC→H complex, but decreased the affinity when it was located at the junction of a H→WC complex (*9*). The addition of two thymines at the junction of 19mer/46merWC→H complex increased T_m by only +5 °C with respect to the 17mer/46merWC→H. The presence of one additional thymine in the 19mer/46merWC→H complex might slightly distort the structure of the 18mer/46merWC→H complex (Table 1).

The introduction of an acridine derivative at the junction between the triple helix and the double helix domains of the 17mer/46merWC→H complex increased the binding affinity by +16 °C (Table 1). The T_m of the 17mer/46merWC→H and 17mer-X/46merWC→H complexes are, respectively, 34 and 50 °C in the presence of 0.2 mM spermine (Figure 7A). It should be noted that the acridine at the junction (in 17mer-X/46merWC→H complex) increases the binding affinity much more than one or two thymines at the junction (in 18mer/46merWC→H and 19mer/46merWC→H complex), demonstrating an important stabilizing role of the intercalating agent at the junction of WC→H structures.

We have also measured the effect of covalent attachment of the acridine derivative to the 5′ end of the 17mer ligand. Acr-17mer binds to the WC→H complex forming a double helix with the 5′ sequence and a triple helix with the stem of the 46merWC→H (Figure 7). The acridine can intercalate in the stem sequence at the junction between the triple helical and the double helical domains as previously demonstrated for triplex-forming acridine-oligopyrimidine conjugates (*39*). The presence of the intercalating agent at the 5′ end of the 17mer (Acr-17mer) increased the T_m by +15 °C (Figure 7 and Table 1), a value close to that obtained with the acridine attached

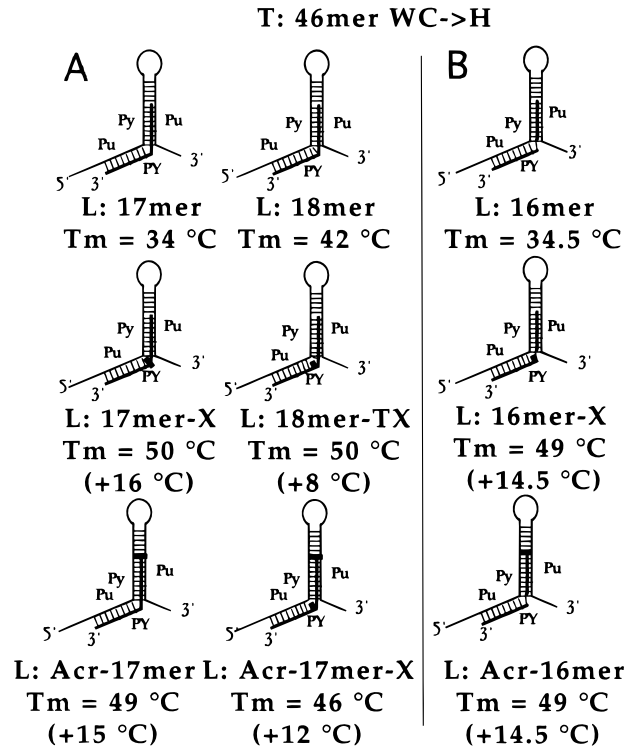


Figure 7. Schematic representations of the complexes formed by the hairpin containing targets (T) 46mer WC→H with the acridine-containing or unmodified oligonucleotide ligands (L). Melting temperatures indicated below each complex were obtained with 2 μM/2 μM T/L in a pH 7.02 cacodylate buffer (50 mM) containing 0.1 M NaCl and either 0.2 mM (A) or 1 mM spermine (B). ΔT_m values are calculated as the difference between the T_m values of the acridine-containing and the corresponding unmodified oligonucleotide.

to the internal site. Surprisingly, the bis-modified oligonucleotide Acr-17mer-X did not exhibit a better affinity for the target 46merWC→H than the acridine-containing oligonucleotides, 17mer-X and Acr-17mer, a similar result to that obtained in the first model of a hairpin target described in this paper (model 1).

To obtain more information on the type of interactions engaged by the internally located acridine, an additional thymine was inserted either between the duplex-forming sequence and the acridine (18mer-XT) or between the acridine and the triplex-forming sequence (18mer-TX). In both cases, the T_m (50 °C) was identical to that of the 17mer-X/46merWC→H complex (only 18mer-TX is shown in Figure 7 and Table 1). As compared to the 18mer, which contains the additional thymine but no acridine, the stabilization afforded by the acridine is only +8 °C as compared to +16 °C for the 17mer. These results demonstrates that two elements contribute to the acridine-induced stabilization: an increased flexibility at the junction between the two domains of the 17mer and a specific interaction of the acridine ring at the junction of the duplex and triplex structures.

Spermine is known to stabilize triple helices (*40*, *39*). When the spermine concentration was raised from 0.2 to 1 mM, the T_m of the 17mer was increased by 3 °C (from 34 to 37 °C). Under these conditions, the lack of a thymine in the triplex-forming sequence of the 16mer decreased the T_m value by 2.5 °C (Figure 7B). Introduction of the intercalating agent in 16mer-X stabilized the interaction with the 46merWC→H target [$\Delta T_{m(16mer-X/16mer)}$ = +14.5 °C] (Figure 7B). A similar stabilization was observed with the 5′-substituted Acr-16mer.

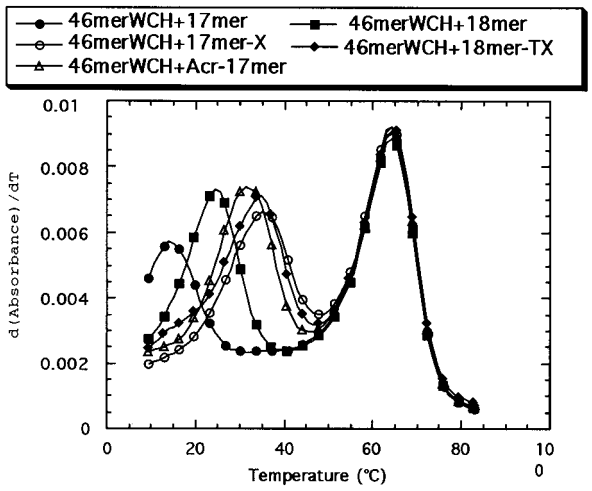


Figure 8. First derivative profiles of the melting curves obtained at 260 nm for 2 μM 46merWC→H bound to 2 μM of 17mer (●), 17mer-X (○), Acr-17mer (△), 18mer (■), and 18mer-TX (◆) in 50 mM cacodylate buffer, pH 7.02, containing 0.1 M NaCl.

Melting experiments with oligonucleotide ligands and the 46merWC→H target were also performed in the absence of spermine. Melting profiles obtained in the absence of spermine with 17mer, 17mer-X, and Acr-17mer bound to the 46merWC→H (Figure 8) demonstrated that the acridine ring better stabilized the complexes when it was located at the internal position than at the 5′ end of the 17mer oligonucleotide [$\Delta T_{m(17mer-X/17mer)} = +21$ °C, $\Delta T_{m(Acr-17mer/17mer)} = +17.5$ °C]. A similar behavior was observed with the 18mer and 18mer-TX (Table 1).

In the 17mer/46merWC→H complex in the absence of spermine, the triplex-forming portion of the 17mer (the 5′ sequence) was not expected to form a stable triple helix with the stem sequence of the 46merWC→H. As a matter of fact, mutations introduced in this part of the 17mer sequence (as in 17mer-Mut) did not markedly change the T_m value of the complex ($\Delta T_m = -1.5$ °C). For the Acr-17mer oligonucleotide, it is likely that a triplex is formed between the 5′ sequence of the 17mer and the stem sequence of the 46mer WC→H with the acridine intercalated at the junction of triplex and duplex domains (*39*). The increase in T_m value obtained when the 17mer is 5′-substituted with acridine (Acr-17mer, $\Delta T_m = +17.5$ °C) and when it is internally substituted (17mer-X, $\Delta T_m = +21$ °C) strongly suggests that 17mer-X also forms a complex involving the triplex portion even in the absence of spermine. The internal acridine could be either intercalated at the junction or located at a preferential binding site within the branch point of the WC→H structure leading to a high stabilization of complexes.

CONCLUSION

In the present study, we demonstrated that an acridine incorporated at an internal site within an oligonucleotide is able to stabilize the binding of this oligonucleotide to a hairpin-containing target sequence when the acridine ring is located at the base of the stem-loop region (model 1). The internal acridine leads to a better stabilization of complexes ($\Delta T_m = +13$ °C) than an acridine covalently linked to the 5′-end of the oligonucleotide ($\Delta T_m = +8$ °C), suggesting the existence of a preferential site of interaction/intercalation for the acridine ring at the three-way junction. The binding of oligonucleotides to hairpin-containing nucleic acids could also be stabilized by insertion of modified bases such as a 5-methyl-N^4-(1-pyrenylmethyl)cytidine or a 2′-deoxy-5-methyl-N^4-(4-phenoxyphenyl)cytidine instead of an acridine ring (*41*−*43*).

Acridine-containing oligonucleotides have also been targeted to hairpin-containing targets in such a way as to form both Watson−Crick base pairs and Hoogsteen base pairs (WC→H recognition, model 2). In the presence of spermine, no differences in stabilization of WC→H complexes were observed between an internal acridine and an acridine linked to the 5′ extremity of the oligonucleotide. Melting temperatures of DNA complexes were increased by +15−16 °C. In the absence of spermine, the oligonucleotide with an internal acridine bound to the hairpin-containing target exhibited a higher stability than the 5′ acridine-oligonucleotide conjugate ($\Delta T_m = +21$ °C compared to +17.5 °C).

What has emerged from our study is that acridine incorporated into an oligonucleotide could be used to recognize hairpin-containing nucleic acids with higher affinity than the unmodified oligonucleotides either by formation of a three-way structure or by a combination of double and triple helix formation. These oligonucleotide-intercalator conjugates are easily synthesized with existing building blocks and provide a new approach to selectively recognize secondary structures in nucleic acids. Their potential applications in the antisense strategy should be evaluated in future investigations.

ACKNOWLEDGMENT

This work was supported in part by the Ligue Nationale contre le Cancer. We thank J. Lacoste, L. Lacroix, J. L. Mergny for helpful discussions, L. N., E. M., and L. L. François for permanent encouragement and D. Perrin for corrections.

LITERATURE CITED

(1) Wells, R. D., Goodman, T. C., Hillen, W., Horn, G. T., Klein, R. D., Larson, J. E., Muller, U. R., Neuendorf, S. K., Panayotatos, N., and Stirdivant, S. M. (1980) DNA structures and Gene regulation. *Prog. Nucleic Acids. Res. Mol. Biol. 24*, 167−267.

(2) Lima, W. F., Monia, B. P., Ecker, D. J., and Freier, S. M. (1992) Implication of RNA structure on Antisense oligonucleotide hybridization kinetics. *Biochemistry 31*, 12055−12061.

(3) Toulmé, J. J., Lettinevez, R., and Brossalina, E. (1996) Targeting RNA structures by antisense oligonucleotides. *Biochimie 78*, 663−673.

(4) Bruice, T. W., and Lima, W. F. (1997) Control of complexity constraints on combinatorial screening for preferred oligonucleotide hybridization sites on structured RNA. *Biochemistry 36*, 5004−5019.

(5) Cload, S. T., Richardson, P. L., Huang, Y. H., and Schepartz, A. (1993) Kinetic and Thermodynamic Analysis of RNA Binding by Tethered Oligonucleotide Probes−Alternative Structures and Conformational Changes. *J. Am. Chem. Soc. 115*, 5005−5014.

(6) François, J. C., Thuong, N. T., and Hélène, C. (1994) Recognition and cleavage of hairpin structures in nucleic acids by oligodeoxynucleotides. *Nucleic Acids Res. 22*, 3943−3950.

(7) Brossalina, E., Pascolo, E., and Toulmé, J.-J. (1993) The binding of an antisense oligonucleotide to a hairpin structure via triplex formation inhibits chemical and biological reactions. *Nucleic Acids Res. 21*, 5616−5622.

(8) Brossalina, E., and Toulmé, J.-J. (1993) A DNA hairpin as target for antisense oligonucleotide. *J. Am. Chem. Soc. 115*, 796−797.

(9) François, J., and Hélène, C. (1995) Recognition and cleavage of single-stranded DNA containing hairpin structures by oligonucleotides forming both Watson−Crick and Hoogsteen Hydrogen Bonds. *Biochemistry 34*, 65−72.

(10) Brossalina, E., Demchenko, Y., Vlassov, V., and Toulmé, J. J. (1996) Triplex-forming oligonucleotides trigger conformation changes of a target hairpin sequence. *Nucleic Acids Res. 24*, 3392−3398.
(11) Mishra, R. K., Le Tinevez, R., and Toulmé, J. J. (1996) Targeting nucleic acid secondary structures by antisense oligonucleotides designed through in vitro selection. *Proc. Natl. Acad. Sci. U.S.A. 93*, 10679−10684.
(12) Moses, A. C., and Schepartz, A. (1996) Triplex tethered oligonucleotide probes. *J. Am. Chem. Soc. 118*, 10896−10897.
(13) Pascolo, E., and Toulmé, J. J. (1996) Double hairpin complexes allow accommodation of all four base pairs in triple helices containing both DNA and RNA strands. *J. Biol. Chem. 271*, 24187−24192.
(14) Moses, A. C., Huang, S. W., and Schepartz, A. (1997) Inhibition of Rev. RRE complexation by triplex tethered oligonucleotide probes. *Bioorg Med. Chem. 5*, 1123−1129.
(15) Moses, A. C., and Schepartz, A. (1997) Kinetics and Mechanism of RNA binding by triplex tethered oligonucleotide probes. *J. Am. Chem. Soc. 119*, 11591−11597.
(16) Thuong, N. T., and Hélène, C. (1993) Sequence-Specific Recognition and Modification of Double-Helical DNA by Oligonucleotides. *Angew. Chem., Int. Ed. 32*, 666−690.
(17) Xodo, L. E., Manzini, G., and Quadrifoglio, F. (1990) Spectroscopic and calorimetric investigation on the DNA triplex formed by d(CTCTTCTTTCTTTTCTTTCTTCTC) and d(GAGAAGAAAGA) at acidic pH. *Nucleic Acids Res. 18*, 3557−3564.
(18) Giovannangéli, C., Montenay-Garestier, T., Rougée, M., Chassignol, M., Thuong, N. T., and Hélène, C. (1991) Single-stranded DNA as a target for triple-helix formation. *J. Am. Chem. Soc. 113*, 7775−7777.
(19) Dsouza, D. J., and Kool, E. T. (1992) Strong Binding of Single-Stranded DNA by Stem-Loop Oligonucleotides. *J. Biomol. Struct. Dyn. 10*, 141−152.
(20) Kool, E. T. (1991) Molecular recognition by circular oligonucleotides: increasing the selectivity of DNA binding. *J. Am. Chem. Soc. 113*, 6265−6266.
(21) Prakash, G., and Kool, E. T. (1992) Structural effects in the recognition of DNA by circular oligonucleotides. *J. Am. Chem. Soc. 114*, 3523−3527.
(22) Zhou, B., Puga, E., Sun, J. S., Garestier, T., and Hélène, C. (1995) Stable triple helices formed by acridine-containing oligonucleotides with oligopurine tracts of DNA interrupted by one or two pyrimidines. *J. Am. Chem. Soc. 117*, 10425−10428.
(23) Kukreti, S., Sun, J. S., Garestier, T., and Hélène, C. (1997) Extension of the range of DNA sequences available for triple helix formation: stabilization of mismatched triplexes by acridine-containing oligonucleotides. *Nucleic Acids. Res. 25*, 4264−4270.
(24) Silver, G. C., Nguyen, C. H., Boutorine, A. S., Bisagni, E., Garestier, T., and Hélène, C. (1997) Conjugates of oligonucleotides with triplex-specific intercalating agents. Stabilization of triple-helical DNA in the promoter region of the gene for the alpha-subunit of interleukin 2 (IL-2R alpha). *Bioconjugate Chem. 8*, 15−22.
(25) Silver, G. C., Sun, J. S., Nguyen, C. H., Boutorine, A. S., Bisagni, E., and Hélène, C. (1997) Stable triple-helical DNA complexes formed by benzopyridoindole- and benzopyridoquinoxaline-oligonucleotide conjugates. *J. Am. Chem. Soc. 119*, 263−268.
(26) Cantor, C. R., Warshaw, M. H., and Shapiro, H. (1970) Oligonucleotide interactions. III. Circular Dichroism studies of the conformation of deoxyoligonucleotides. *Biopolymers 9*, 1059−1077.
(27) Baxter, S. M., Greizerstein, M. B., Kushlan, D. M., and Ashley, G. W. (1993) Conformational properties of DNA hairpins with TTT and TTTT loops. *Biochemistry 32*, 8702−8711.
(28) Asseline, U., Bonfils, E., Dupret, D., and Thuong, N. T. (1996) Synthesis and binding properties of oligonucleotides covalently linked to an acridine derivative: A new study of the influence of the dye attachment site. *Bioconjugate Chem. 7*, 369−379.
(29) Asseline, U., Thuong, N. T., and Hélène, C. (1997) Synthesis and properties of oligonucleotides covalently linked to intercalating agents. *New J. Chem. 21*, 5−17.
(30) Leontis, N. B., Kwok, W., and Newman, J. S. (1991) Stability and structure of three-way DNA junctions containing unpaired nucleotides. *Nucleic Acids Res. 19*, 759−766.
(31) Leontis, N. B., Hills, M. T., Piotto, M., Malhotra, A., Nussbaum, J., and Gorenstein, D. G. (1993) A model for the solution structure of a branched, three-strand DNA complex. *J. Biomol. Struct. Dyn. 11*, 215−223.
(32) Welch, J. B., Duckett, D. R., and Lilley, D. M. J. (1993) Structures of bulged three-way DNA junctions. *Nucleic Acids Res. 21*, 4548−4555.
(33) Zhong, M., Rashes, M. S., Leontis, N. B., and Kallenbach, N. R. (1994) Effects of unpaired bases on the conformation and stability of three-arm DNA junctions. *Biochemistry 33*, 3660−3667.
(34) Young, P. R., and Kallenbach, N. R. (1981) Binding of 9-aminoacridine to deoxydinucleoside phosphates of defined sequence: Preferences and stereochemistry. *J. Mol. Biol. 145*, 785−813.
(35) Lilley, D. M. J. (1995) Kinking of DNA and RNA by base bulges. *Proc. Natl. Acad. Sci. U.S.A. 92*, 7140−7142.
(36) Lilley, D. M. J., Clegg, R. M., Diekmann, S., Seeman, N. C., von Kitzing, E., and Hagerman, P. (1996) A nomenclature of junctions and branch points in nucleic acids. Recommendations 1994. *J. Mol. Biol. 255*, 554−555.
(37) Fukui, K., Morimoto, M., Segawa, H., Tanaka, K., and Shimidzu, T. (1996) Synthesis and properties of an oligonucleotide modified with an acridine derivative at the artificial abasic site. *Bioconjugate Chem. 7*, 349−355.
(38) Fukui, K., and Tanaka, K. (1996) The acridine ring selectively intercalated into a DNA helix at various types of abasic sites: double strand formation and photophysical properties. *Nucleic Acids Res. 24*, 3962−3967.
(39) Sun, J. S., François, J. C., Montenay-Garestier, T., Saison-Behmoaras, T., Roig, V., Thuong, N. T., and Hélène, C. (1989) Sequence-specific intercalating agents. Intercalation at specific sequences on duplex DNA via major groove recognition by oligonucleotide-intercalator conjugates. *Proc. Natl. Acad. Sci. U.S.A. 86*, 9198−9202.
(40) Moser, H. E., and Dervan, P. B. (1987) Sequence specific cleavage of double helical DNA by triple helix formation. *Science 238*, 645−650.
(41) Abdel Aleem, A. A. H., Larsen, E., and Pedersen, E. B. (1995) Synthesis of carboxamide linked dimers, αT*αT and αU^{Cl}*αT. Duplex and triplex stabilities of the corresponding α oligodeoxynucleotides. *Tetrahedron 51*, 7867−7876.
(42) Abdel-Rahman, A. A. H., Ali, O. M., and Pedersen, E. B. (1996) Insertion of 5-Methyl-N^4-(1-Pyrenylmethyl)cytidine into DNA. Duplex, Three-way junction and triplex stabilities. *Tetrahedron 52*, 15311−15324.
(43) Ali, O. M., Franch, T., Gerdes, K., and Pedersen, E. B. (1998) Targeting of nucleic acid junctions: addressing to a branch point an oligodeoxynucleotide conjugated with an intercalator. *Nucleic Acid Res. 26*, 4919−4924.

BC9801225

Chemical Modification to Reduce Renal Uptake of Disulfide-Bonded Variable Region Fragment of Anti-Tac Monoclonal Antibody Labeled with ^{99m}Tc

In S. Kim,[†] Tae M. Yoo,[†] Hisataka Kobayashi,[†] Meyoung-kon Kim,[†] Nhat Le,[†] Q−c. Wang,[‡] Ira Pastan,[‡] Jorge A. Carrasquillo,[†] and Chang H. Paik*,[†]

Nuclear Medicine Department, Warren G. Magnuson Clinical Center, Building 21, Room 136, and Laboratory of Molecular Biology, National Cancer Institute, National Institutes of Health, Bethesda, Maryland 20892.
Received October 26, 1998; Revised Manuscript Received February 4, 1999

The anti-Tac disulfide-bonded variable region fragment (dsFv) is a genetically engineered, 25 kDa, murine monoclonal antibody fragment that recognizes the α subunit of the interleukin-2 receptor (IL-2Rα). The dsFv radiolabeled with the tetrafluorophenyl ester (TFP) of [^{99m}Tc]mercaptoacetyltriglycine ([^{99m}Tc]MAG3-TFP) showed rapid tumor uptake and fast blood clearance in mice, resulting in high tumor-to-nontumor background ratios. However, its high renal uptake was a problem. In this study, we tested the effect of lowering the isoelectric point (pI) of dsFv to <9.3 on renal and tumor uptake. To lower the pI, dsFv was acylated simultaneously with both [^{99m}Tc]MAG3-TFP and TFP-glycolate. The acylation of dsFv decreased its pI and its immunoreactivity inversely proportional to the molar ratio of TFP-glycolate to dsFv, whereas the conjugation of [^{99m}Tc]MAG3-TFP alone did not. When biodistribution studies were performed in nude mice, the effect of the lowered pI was reflected primarily in decreased kidney uptake and whole-body retention, with its highest effect seen at the earliest time point (15 min) after injection. In tumor-bearing nude mice, glycolated [^{99m}Tc]MAG3-dsFv with a pI range of 4.9 to 6.5 accumulated selectively into IL-2 receptor-positive SP2/Tac tumor similar to that of the control [^{125}I]dsFv labeled by the Iodo-Gen method, whereas its renal uptake was 25% of [^{125}I]dsFv at 15 min. At 90 min, the ratios of tumor to receptor-negative SP2/0 tumor, liver, kidney, stomach, and blood had peaked at 10.9, 8.5, 0.3, 5.0, and 6.2, respectively, for the glycolated [^{99m}Tc]MAG3-dsFv. The corresponding ratios for [^{125}I]dsFv were 3.7, 5.0, 0.1, 1.5, and 2.1, respectively.

INTRODUCTION

Anti-Tac monoclonal antibody (anti-Tac MoAb) recognizes the α subunit of IL-2 receptor (IL-2Rα),[1] which is overexpressed on activated T-cells (*1*−*3*), and various malignant lymphomas and leukemias (*4*−*7*). Disulfide-stabilized, variable-region fragments (dsFv) of anti-Tac MoAb were recently produced by recombinant DNA technology (*8*). Amino acid residues in conserved framework regions of both light (V_L) and heavy (V_H) chain variable domains of the anti-Tac antibody were mutated into cysteines at positions compatible with the formation of an interdomain disulfide linkage (i.e., V_H-44gly and V_L-99ser). These mutant V_H and V_L chains were produced in separate *Escherichia coli* cultures from the plasmids pYR43 and pKW50, respectively. The V_H and V_L chains were then combined in equimolar amounts to form an interchain disulfide bridge of the disulfide-bonded Fv molecule. This dsFv bound to IL-2Rα with an affinity identical to that of humanized anti-Tac IgG (K_d = 3 nM) and the corresponding single chain Fv (scFv) (*8*). This dsFv was found to be substantially more stable to denaturation by heat or urea treatment than the scFv.

Anti-Tac dsFv has previously been radiolabeled with ^{125}I (*9*, *10*), ^{18}F (*10*), ^{99m}Tc (*11*), and ^{67}Ga (*12*). Compared to ^{125}I-labeled intact anti-Tac MoAb, these labeled dsFv fragments show improved tumor targeting with faster penetration into tumors due to their small size (25 kDa) (*8*). They also clear faster from blood and most organs, thereby resulting in high tumor-to-nontumor ratios (*9*−*12*). However, these radiolabeled dsFv fragments showed high renal uptake, thus resulting in high renal radiation doses and potentially decreasing imaging sensitivity in the abdomen. High renal accumulation is a common problem for low molecular weight proteins (LMWPs) (*13*). The mechanism of renal uptake and retention of LMWPs is believed to involve glomerular filtration and subsequent reabsorption and catabolism in the proximal tubular cells (*14*). Several investigators have lowered the renal uptake of various LMWPs by infusing basic amino acids such as L-lysine and arginine (*13*, *15*−*19*). These basic amino acids are believed to block the tubular absorption of LMWPs by masking the negatively charged phospholipid bilayers of the tubular cells. We showed previously that the renal uptake of ^{99m}Tc- and ^{125}I-labeled dsFv could be blocked by L-lysine co-injection, in a dose- and time-dependent manner (*20*).

In this study, we lowered the isoelectric point (pI) of dsFv by acylating its amino groups with different concentrations of glycolate molecules. We report the effects of this lowered pI on renal and tumor uptake of ^{99m}Tc-labeled dsFv in nude mice and nude mice xenografted

* To whom correspondence should be addressed. Phone: (301) 496-1426. Fax: (301) 402-4548. E-mail: paik@nmdhst.cc.nih.gov.
[†] Nuclear Medicine Department.
[‡] Laboratory of Molecular Biology.

[1] Abbreviations: dsFv, disulfide-bonded variable region fragment; IL-2Rα, the α subunit of interleukin-2 receptor; pI, isoelectric point; TFP, tetrafluorophenyl; MAG3, mercaptoacetyltriglycine; LMWPs, low-molecular-weight proteins; DMF, dimethylformamide; PBS, sodium phosphate in saline, pH 6.8; Bz, benzoyl.

10.1021/bc980129m Not subject to U.S. Copyright. Published 1999 by American Chemical Society
Published on Web 03/20/1999

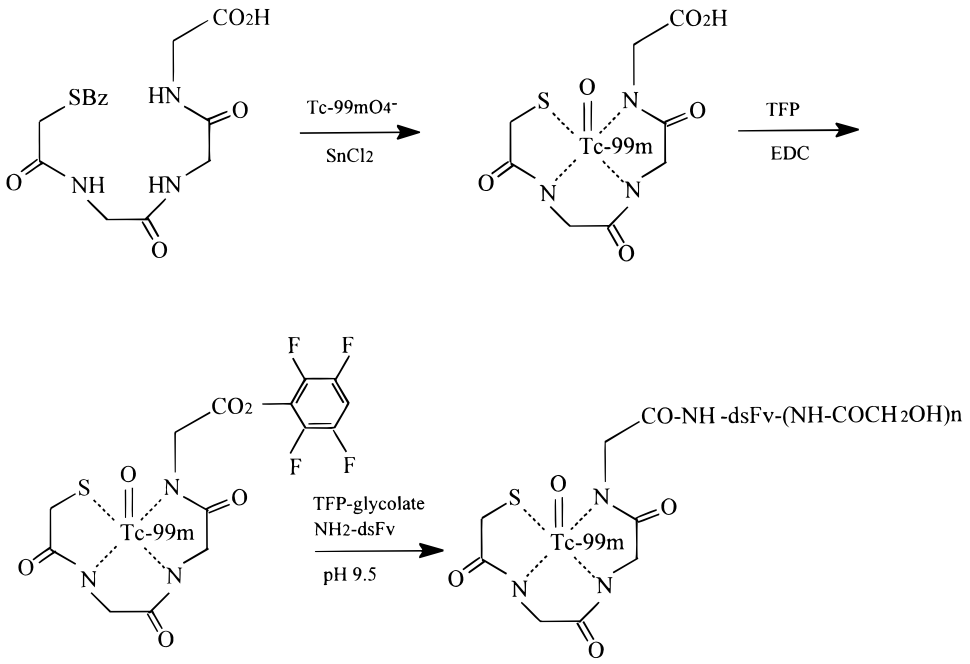


Figure 1. Reaction scheme for the preparation of glycolated [^{99m}Tc]MAG3-dsFv.

with IL-2α-receptor-positive SP2/Tac and receptor-negative SP2/0 cells. The preliminary portion of this work has been previously reported in abstract form (*21*).

MATERIALS AND METHODS

Synthesis. Tetrafluorophenyl (TFP)-glycolate was synthesized as follows. Briefly, 2,3,5,6-tetrafluorophenol (TFP, 100 mmol) and glycolic acid (10 mmol) were reacted in 10 mL of acetonitrile, with dicyclohexylcarbodiimide (12 mmol) used as a coupling agent, for 4 h at room temperature. The ester derivative was purified by normal-phase HPLC equipped with a μPorasil PrepPak cartridge (Waters, Milford, MA, hexane:ethyl acetate:acetic acid = 150:50:1, 5 mL/min). The yield of TFP-glycolate was 56.9%, The melting point of the product was 90.8−91.2 °C, as measured on an electrothermal digital melting point apparatus (Electrothermal, Southend, England), and reported without calibration. ^{1}H NMR ($CDCl_3$): δ 7.12 (m, 1 aromatic *H*), 4.59 (s, 2 CH_2), 3.49 (s, 1 *OH*). Anal. ($C_8H_4O_3F_4$) C, H, F.

Acylation and Radiolabeling with ^{99m}Tc and ^{125}I. Benzoyl (Bz)-MAG3 was synthesized according to the method of Fritzberg et al. (*22*). Bz-MAG3 was radiolabeled with ^{99m}Tc, activated to the TFP ester of ^{99m}Tc MAG3 using the methods of Visser et al. (*23*) and Yoo et al. (*11*), and purified by a Sep-Pak C_{18} column. The purified [^{99m}Tc]MAG3-TFP in acetonitrile was dried with a stream of nitrogen gas and was allowed to react with dsFv (100 μg/100 μL, 4 × 10^{-5} M) in 0.1 M sodium bicarbonate-sodium carbonate buffer (pH 9.5) for 30 min at 4 °C. To acylate the dsFv, we added TFP-glycolate at several different concentrations [TFP-glycolate-to-dsFv molar ratios of 36, 73, and 110 prepared in dimethylformamide (DMF)] to the reaction mixture immediately after we added the dsFv solution to [^{99m}Tc]MAG3-TFP. The amount of DMF added to the reaction mixture was less than 10% of the total volume to prevent the potential deactivation of dsFv by the organic solvent. The conjugation reactions at the molar ratios of 36, 73, and 110 produced glycolated [^{99m}Tc]MAG3-dsFv with pI ranges of 6.6−9.3 (product I), 4.9−6.5 (product II), and 4.4−6.1 (product III). These products were purified on a size-exclusion PD-10 column (Pharmacia Biotech AB, Uppsala, Sweden) with 0.02 M sodium phosphate in saline (PBS). The total reaction scheme is shown in Figure 1. To use as a control for the biodistribution studies, the dsFv was radioiodinated with ^{125}I by the Iodo-Gen method as described previously (*11*). The purity of the radiolabeled dsFv preparations was confirmed with ITLC, paper chromatography and size-exclusion HPLC with a TSK G2000SW column (TosoHass, Philadelphia, PA; 0.067 M sodium PBS−0.1 M KCl, pH 6.8; 1 mL/min).

Isoelectric Focusing and Autoradiography. The radiolabeled dsFv (0.3−1.0 μg) and standard markers with pI values ranging 3.5−9.3 were electrofocused on gels (PhastGel IEF 3-9, Pharmacia Biotech AB, Uppsala, Sweden) using PhastSystem (Pharmacia Biotech AB, Uppsala, Sweden). These gels were then stained with Coomassie Blue R 350 to reveal protein bands and were autoradiographed to reveal radioactive bands using Bioimaging Analyzer BAS-1500 (Fuji Medical Systems, Inc., Stamford, CT). The pI values of the dsFv products were determined by comparing their bands to the standard bands with known pIs.

Immunoreactivity. Immunoreactivity was determined by a modified cell-binding assay of Lindmo et al. (*24*). Aliquots of the radiolabeled dsFvs (0.7−1.0 ng/100 μL) were incubated for 2 h at 4 °C with 1.1 × 10^4 to 4.0 × 10^7 SP2/0 and SP2/Tac cells. Nonspecific binding to the cells was examined under conditions of antibody excess (25 μg of nonradiolabeled anti-Tac IgG antibody). The maximum cell-bound counts, corrected for the nonspecific binding and expressed as a percentage of the total counts, were taken to be the immunoreactivity.

Biodistribution Studies in Nontumor Bearing Mice. Animal studies were performed under an approved Institutional Animal Care and Use Committee protocol. Groups of five female nude mice (NCI, Frederick, MD, 4−7 weeks old, 16−23 g) were used. The mice were injected via the tail vein with either ^{99m}Tc-labeled dsFv or glycolated ^{99m}Tc-labeled dsFv (1.5−6.0 μCi/0.5−1.0 μg), plus [^{125}I]dsFv (0.6−1.6 μCi/0.1−1.0 μg) in 0.2 mL of PBS solution containing 1% BSA. The total dose of dsFv injected was 1.5−2.2 μg. The animals were euthanized

with CO_2 at 15, 45, 90, and 180 min and exsanguinated by cardiac puncture before dissection. Tumors, major organs, blood, and injected-dose standards were weighed, and the radioactivity was counted in a γ counter (Packard Auto-Gamma, Meriden, CT). The percentage of the injected dose per gram (% ID/g) of tissue or blood was calculated and normalized to a 20 g mouse. The whole-body retention was determined by adding the counts in organs, blood and carcasses and dividing by the counts in the injected dose.

Biodistribution Studies in Tumor-Bearing Mice. Tumor xenografts were established by subcutaneous (s.c.) inoculations of 3.5×10^6 SP2/0 cells in the left flanks and same amount SP2/Tac cells in the right flanks of female athymic nude mice ($n = 5$). Biodistribution studies were performed approximately 10 days later, when SP2/Tac tumors weighed a mean of 155 mg (20−477 mg) and SP2/0 tumors a mean of 101 mg (41−172 mg). The mice were injected via the tail vein with a mixture of glycolated ^{99m}Tc-labeled dsFv (product II, 1.7 μCi/1.4 μg) and [^{125}I]-dsFv (1.0 μCi/0.1 μg). Biodistribution was determined as described above for the nontumor-bearing mice.

RESULTS

Radiolabeling and Immunoreactivity. The preformed chelate approach to radiolabel the dsFv involved three steps. Bz-MAG3 was first radiolabeled with ^{99m}Tc producing a quantitative yield of [^{99m}Tc]MAG3 and then activated to TFP ester of [^{99m}Tc]MAG3. The recovery yield of the purified [^{99m}Tc]MAG3-TFP was 70−75%. However, the final conjugation yield of [^{99m}Tc]MAG3-TFP to dsFv was low, 24 ± 8.0% ($n = 8$) because only a low concentration of dsFv (4×10^{-5} M) was used due to a limited amount available and also the very mild reaction conditions (30 min at 4 °C) were selected to minimize potential deactivation of immunoreactivity. The specific activities of the radiolabeled dsFvs ranged from 1.7 to 7.8 μCi/μg. The immunoreactivity of [^{99m}Tc]MAG3-dsFv was similar to that of [^{125}I]dsFv (75%), indicating that the conjugation of a tracer amount of [^{99m}Tc]MAG3 to dsFv did not alter its immunoreactivity. However, the immunoreactivity of glycolated [^{99m}Tc]MAG3-dsFvs was decreased inversely proportional to the TFP-glycolate-to-dsFv molar ratio. The immunoreactivity was decreased by 20% for product II from the TFP-glycolate-to-dsFv molar ratio of 73 and by 35% for product III from the ratio of 110 when compared to [^{125}I]dsFv (75%).

Isoelectric Focusing. The isoelectric focusing experiments showed that the protein bands obtained with Coomassie Blue staining were superimposable on the radioactivity bands, indicating that the ^{99m}Tc labeling reflected the glycolate conjugation (Figure 2). The conjugation of a tracer amount of [^{99m}Tc]MAG3 to dsFv did not change the pI (9.3) of dsFv. However, glycolation decreased the pI of dsFv as the TFP-glycolate to dsFv reaction molar ratio was increased. At molar ratios of 36, 73, and 110, the pI of the glycolated ^{99m}Tc-labeled dsFv decreased to 6.6−9.3 (product I), 4.9−6.5 (product II), and 4.4−6.1 (product III), respectively (Table 1).

Biodistribution Studies. The biodistribution studies of the nonglycolated and the three glycolated products were performed first in nude mice (female, 20 g, $n = 5$) without tumors. For each biodistribution study, [^{125}I]anti-Tac dsFv radiolabeled using the Iodo-Gen method was co-injected as a control to estimate run-to-run variations. Since the run-to-run variations were not significantly large, we used data from all biodistribution experiments to calculate the means and standard deviations for [^{125}I]-anti-Tac dsFv (Table 2). These labeled dsFvs were taken up rapidly by the kidneys such that the amount of radioactivity accumulated in blood and other organs such as liver, spleen, stomach, and intestine was small, generally less than 5% ID/g for a 3 h period. The biodistribution of [^{99m}Tc]MAG3-dsFv differed from that of the glycolated [^{99m}Tc]MAG3-dsFvs; renal uptake, especially at 15 min, was decreased proportionally with the lowering of the pI (Figure 3). Likewise, the whole-body retention of the glycolated products was also much lower, especially at 15 min, proportional to the lowering of the pI (Figure 4). These results appear to indicate that the glycolated [^{99m}Tc]MAG3-dsFv with a lower pI is excreted via the kidneys faster than nonglycolated [^{99m}Tc]MAG3-dsFv. The biodistribution in blood and other organs

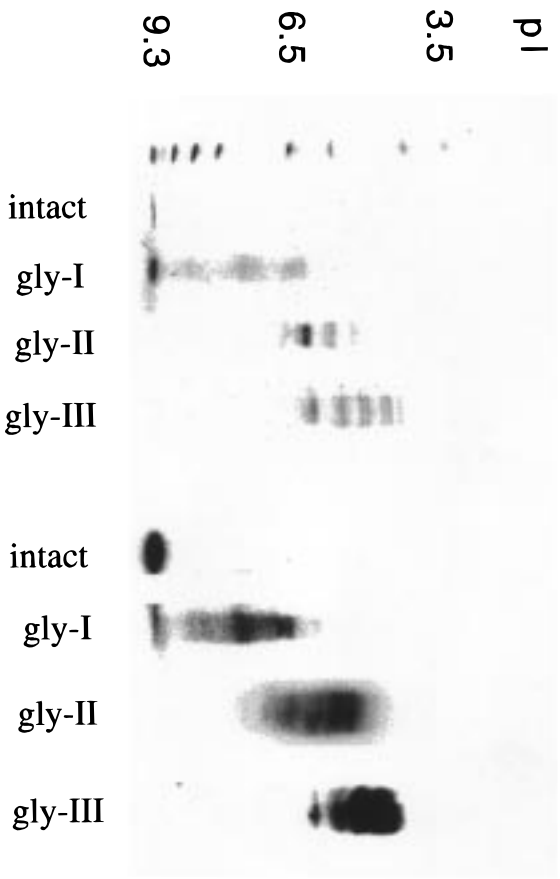


Figure 2. Measurement of isoelectric points on gels from isoelectric focusing experiments. (Left panel) Coomassie blue stain. (Right panel) autoradiography. The lane from the left is for isoelectric point standard molecules. Intact represents [^{99m}Tc]-MAG3-dsFv without glycolate conjugation. Gly-I, II, and III represent glycolated [^{99m}Tc]MAG3-dsFv from the reaction at the TFP-glycolate-to-dsFv molar ratios of 36, 73, and 110, respectively.

Table 1. Effects of TFP-Glycolate Concentration on pI of [^{99m}Tc]MAG3-dsFv

product	[dsFv] (mM)	[TFP-glycolate] (mM)	molar ratio of TFP-glycolate/dsFv	pI[a] range
Tc-99m-MAG3-dsFv	0.04			9.3
product I[b]	0.04	1.44	36:1	6.6−9.3
product II[b]	0.04	2.92	73:1	4.9−6.5
product III[b]	0.04	4.4	110:1	4.4−6.1

[a] pI, isoelectric point. [b] Products I, II, and III represent the products from the reaction of TFP-glycolate to dsFv at a molar ratio of 36, 73, and 110, respectively.

Table 2. Biodistribution of [^{99m}Tc]MAG3-dsFv, Glycolated [^{99m}Tc]MAG3-dsFv (I, II, and III), and [^{125}I]dsFv in Nontumor Nude Mice ($n = 5$)[a]

tissue	[^{99m}Tc]MAG3-dsFv	I	II	III	[^{125}I]dsFv
			15 min		
blood	3.18 ± 0.55[b]	3.36 ± 0.18[b]	2.49 ± 0.34[b]	3.19 ± 0.44[b]	5.07 ± 0.63
liver	2.27 ± 0.20	3.48 ± 0.22[b]	4.70 ± 0.29[b]	2.71 ± 0.25[b]	2.09 ± 0.25
kidney	198.27 ± 17.79	185.25 ± 18.52[b]	64.59 ± 10.24[b]	53.27 ± 5.55[b]	209.47 ± 32.72
intestine	1.38 ± 0.15	1.58 ± 0.13[b]	1.15 ± 0.13[b]	1.63 ± 0.14[c]	1.78 ± 0.23
			45 min		
blood	1.25 ± 0.09[b]	1.51 ± 0.11[b]	1.05 ± 0.10[b]	1.28 ± 0.12[b]	5.86 ± 1.03
liver	1.97 ± 0.22	2.83 ± 0.24[c]	3.28 ± 0.41[b]	1.79 ± 0.24[c]	2.23 ± 0.35
kidney	152.04 ± 6.22[b]	104.60 ± 8.40[b]	41.24 ± 5.08[b]	30.66 ± 3.96[b]	91.36 ± 12.82
intestine	1.97 ± 0.19	2.84 ± 0.29	1.54 ± 0.25[b]	1.78 ± 0.19[b]	2.45 ± 0.47
			90 min		
blood	0.86 ± 0.25[b]	0.75 ± 0.05[b]	0.55 ± 0.08[b]	0.72 ± 0.04[b]	4.64 ± 1.16
liver	1.71 ± 0.54	1.87 ± 0.38	1.82 ± 0.17	1.32 ± 0.25[b]	1.84 ± 0.44
kidney	101.57 ± 27.93[c]	70.72 ± 20.07	18.91 ± 1.50[b]	15.32 ± 1.78[c]	34.75 ± 8.50
intestine	6.11 ± 1.84[b]	2.97 ± 0.62	2.17 ± 0.47	2.58 ± 0.83	2.36 ± 0.51
			180 min		
blood	0.33 ± 0.07[b]	0.48 ± 0.10[b]	0.28 ± 0.03[b]	0.45 ± 0.10[b]	2.81 ± 1.04
liver	1.19 ± 0.38	1.11 ± 0.13	1.09 ± 0.14	0.85 ± 0.10	1.16 ± 0.38
kidney	39.42 ± 15.72[c]	35.63 ± 6.61[b]	8.24 ± 0.81	7.23 ± 0.83[c]	12.06 ± 4.49
intestine	5.00 ± 1.18[b]	3.51 ± 0.86[b]	3.02 ± 0.58[b]	3.05 ± 0.49[c]	1.51 ± 0.51

[a] Data are expressed as the percentage of the injected dose per gram of tissue ± standard deviation. I, II, and III represent the products from the reaction of TFP-glycolate to dsFv at a molar ratio of 36, 73, and 110, respectively. [b] $P < 0.01$ compared with [^{125}I]dsFv. [c] $P < 0.05$ compared with [^{125}I]dsFv.

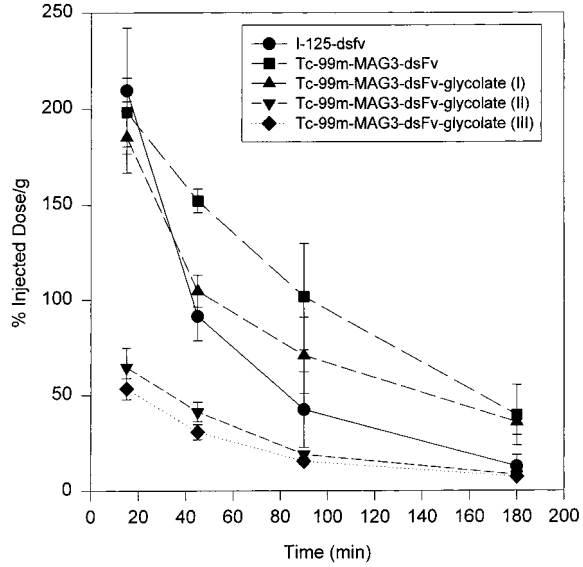


Figure 3. Kidney clearance in nontumor-bearing nude mice ($n = 5$). I, II, and III represent the conjugates from the reaction at the TFP-glycolate-to-dsFv molar ratios of 36, 73, and 110, respectively. The % ID/g of tissue with standard deviation (bar) was plotted against time.

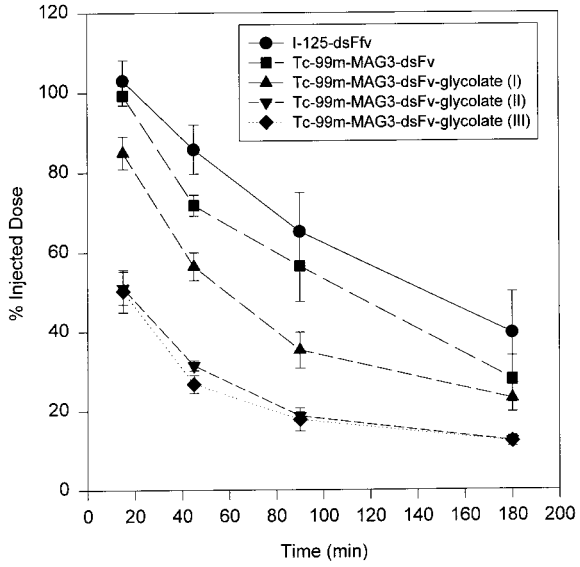


Figure 4. Whole-body clearance in nontumor-bearing nude mice ($n = 5$). I, II, and III represent the conjugates from the reaction at the TFP-glycolate-to-dsFv molar ratios of 36, 73, and 110, respectively. The % ID with standard deviation (bar) was plotted against time.

including liver was very similar between nonglycolated and the three glycolated dsFvs. Compared to [^{99m}Tc]-MAG3-dsFv, [^{125}I]dsFv showed higher blood and stomach accumulation, whereas it cleared faster from kidneys. These results are consistent with our previous findings that showed that [^{125}I]dsFv catabolizes rapidly in kidney and that the radiocatabolite reenters the circulation (*10*, *11*, *20*).

To test the effect of the acylation on tumor targeting, nude mice bearing IL-2 receptor-positive SP2/Tac and receptor-negative SP2/0 tumors were injected intravenously (i.v.) with a total 1.5 μg of product II and [^{125}I]-dsFv. We injected this amount of dsFv because we have previously observed that SP2/Tac tumors shed a small amount of soluble IL-2Rα receptors in the circulation and that the binding of dsFv to the soluble receptors could retain the labeled dsFv longer in the blood when the amount of dsFv was not in a large excess to the soluble receptors (*25*). This biodistribution study in the tumor-bearing mice showed the blood concentrations of the ^{99m}Tc and ^{125}I labels comparable to those in nontumor mice, indicating that a dose of 1.5 μg of dsFv was in gross excess to the soluble receptors. Similar to the biodistribution shown in the nontumor mice, II in the tumor-bearing mice showed a lower uptake in blood and organs including kidney and stomach than the control [^{125}I]dsFv. It is especially interesting to notice that product II showed a drastically reduced renal uptake that was only 25% of that seen in the control [^{125}I]dsFv at 15 min (Figures 5 and 6). However, the renal uptake of product II and [^{125}I]dsFv in the tumor-bearing mice were higher ($p < 0.05$) than those in the nontumor mice at the later time points; at 180 min the renal uptake of product II was 16% ID/g in the tumor-bearing mice vs 8% ID/g in

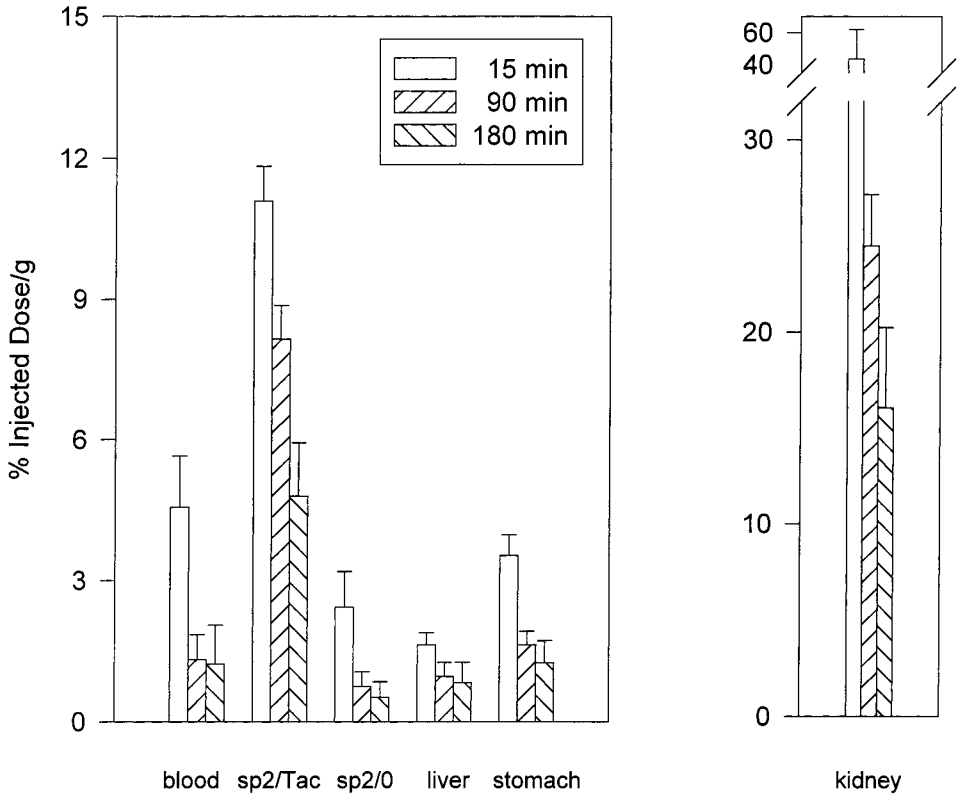


Figure 5. Biodistribution of glycolated [^{99m}Tc]MAG3-dsFv (II) in tumor-bearing nude mice ($n = 5$). The II represents the glycolated [^{99m}Tc]MAG3-dsFv from the reaction at a TFP-glycolate-to-dsFv molar ratio of 73. The % ID/g of tissue with standard deviation (bar) was plotted.

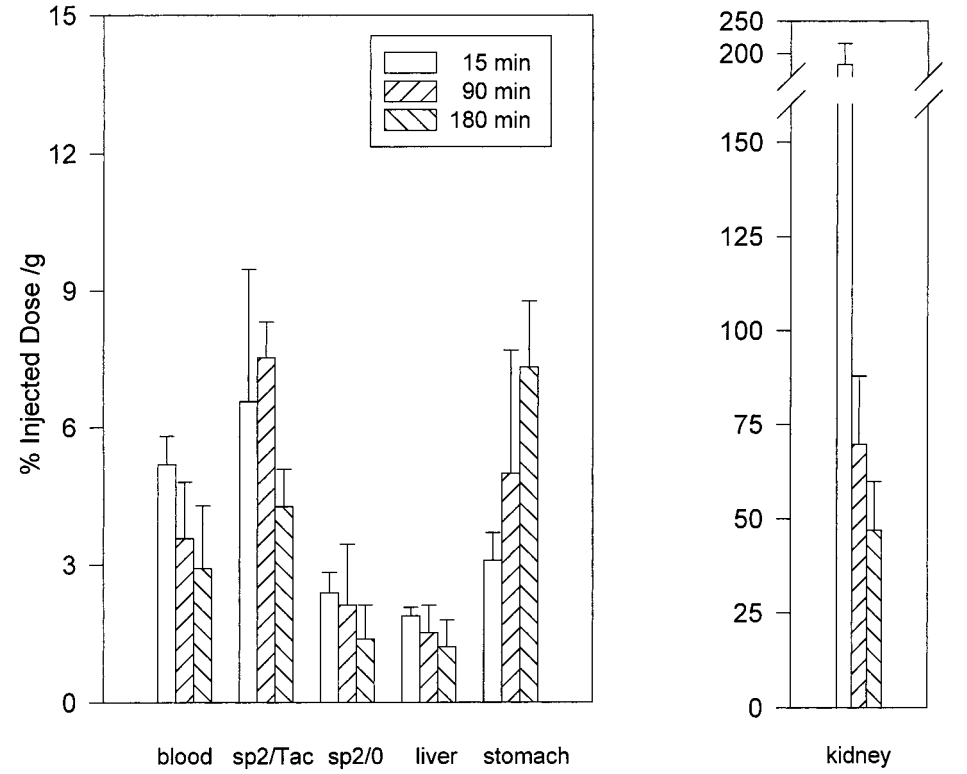


Figure 6. Biodistribution of [^{125}I]dsFv in tumor-bearing nude mice ($n = 5$). The % ID/g of tissue with standard deviation (bar) was plotted.

the nontumor mice. The cause of this higher renal uptake is not known, but it is possible that this higher renal accumulation might be caused by the receptor-bound radioactivity. Product II accumulated selectively into SP2/Tac, similar to that of the control [^{125}I]dsFv at 90 and 180 min (Figures 5 and 6). Since the glycolated [^{99m}Tc]MAG3-dsFv cleared from blood and organs rapidly, whereas it accumulated rapidly in the receptor-positive tumor, high receptor-positive tumor-to-nontumor tissue radioactivity ratios were obtained within 90 min. At 90

min, the ratios of receptor-positive to receptor-negative tumor, liver, kidney, stomach, and blood were 10.9, 8.5, 0.3, 5.0, and 6.2, respectively, for the glycolated [^{99m}Tc]-MAG3-dsFv, whereas the ratios were 3.7, 5.0, 0.1, 1.5, and 2.1, respectively for the control [^{125}I]dsFv. The tumor to nontumor ratios for the glycolated [^{99m}Tc]MAG3-dsFv were higher ($p < 0.05$) than those for the control throughout the 3 h observation.

DISCUSSION

Anti-Tac dsFv is a disulfide-stabilized variable-region fragment with a molecular mass of 25 kDa and a pI of >9.3, thus highly positively charged at physiological pH. The radiolabeled dsFv, due to its small size, is believed to be filtered readily through the glomerulus, but is absorbed by proximal tubular cells via an electrostatic attraction between the positive charge of dsFv and the negative charge of phospholipid bilayers of parenchymal cells of the tubules, resulting in the high renal concentration of radiolabeled dsFv. In this study, we lowered the pI of dsFv by chemical modifications to test whether this lowered pI decreased its renal uptake. The pI of dsFv can be lowered chemically either by the acylation of the ϵ amino group of lysine residues or by the addition of acidic amino acids to the carboxy terminus. We chose the acylation reaction because dsFv has 12 lysine residues whose ϵ amino group is readily acylated.

The acylation of amino groups to the corresponding amides is a common method of neutralizing the positive charges on the proteins (*26*). We used TFP-glycolate as an acylating agent because it is a small molecule with a polar hydroxy group that is expected to cause only a small perturbation to the tertiary structure of dsFv. The conversion of an amino group to an amide by acylation with one glycolate molecule reduces one positive charge from the native dsFv, adds one hydroxyl group, and increases the molecular weight by 58. Thus, the maximum glycolation of all 12 lysine residues would increase the molecular weight of the 25 kDa dsFv by 696, only 2.8% increase in the molecular weight. This study demonstrates that the acylation of the amino groups of dsFv with glycolate molecules lowers its pI inversely proportional to the molar ratio of glycolate-TFP to dsFv (Table 1), and that this lowering of the pI decreases the renal uptake (Figure 3) and the whole-body retention (Figure 4). The effect was especially pronounced at 15 min. At this time, the renal uptake of the labeled, glycolated dsFv with a pI range below 7 was reduced to about 50% ID/g, or 25% of the renal uptake of nonglycolated [^{99m}Tc]MAG3-dsFv, and the whole-body retention of the glycolated dsFv was decreased to 50% ID. These results suggest that one-half of the injected dose was excreted via the kidneys within 15 min for the glycolated dsFv conjugate. These results are consistent with our observation that the [^{99m}Tc]99m activity excreted in urine was all bound to dsFv up to 15 min for the [^{99m}Tc]99m MAG3-dsFv-glycolate prepared at a molar ratio of 73 (data not shown). Since lowering the pI of dsFv reduced renal uptake without altering the blood activity, it is likely that the glomerular filtration was unaffected and that it is the tubular reabsorption that was blocked by the lowering of the pI.

The effect of the lowered pI on the biodistribution of dsFv was somewhat different from that on the biodistribution of ^{111}In-labeled Fab′ (50 kDa), especially in blood concentrations. Tarburton et al. (*27*) reported that the acetylation with acetic anhydride lowered the pI of ^{111}In-labeled Fab′ and that the acetylated [^{111}In]Fab′ showed lower kidney and higher blood concentrations than the nonacetylated [^{111}In]Fab′. A similar result was also reported by Fagnani et al. (*28*) for the [^{111}In]Fab′ that had its pI reduced by conjugation with low-molecular-mass dextran (6000 ± 500 Da). We recently demonstrated that ^{125}I-labeled Fab of anti-Tac monoclonal antibody increased blood concentration, but reduced renal uptake when its pI was lowered by acylation with TFP-glycolate (*29*).

The effect of pI on tumor uptake was investigated with [^{99m}Tc]MAG3-dsFv-glycolate prepared at a TFP-glycolate-to-dsFv reaction molar ratio of 73 because this reaction ratio produced a glycolated dsFv with a pI range below 7 at the expense of only 20% deactivation of immunoreactivity. This glycolated [^{99m}Tc]MAG3-dsFv accumulated selectively into the receptor-positive SP2/Tac tumor with the tumor uptake similar to that of [^{125}I]dsFv at 90 and 180 min. In contrast, the kidney accumulation of the glycolated conjugate was decreased to only 25% of the control [^{125}I]dsFv at 15 min, due to its rapid excretion into urine (Figures 5 and 6), as reflected by a low whole-body retention, with 60% ID remaining at 15 min, compared to 97% ID remaining with [^{125}I]dsFv. In conclusion, this study demonstrated that TFP-glycolate is an efficient acylating agent for lowering the pI of dsFv. This new approach holds promise for enhancing the renal clearance of radiolabeled variable region fragments without altering their tumor uptake.

ACKNOWLEDGMENT

The authors thank Dr. Thomas A. Waldmann for providing SP2/Tac and SP/0 cell lines, David S. Paik for his computational and editorial assistance, and Sue Kendall for her editorial assistance.

LITERATURE CITED

(1) Wolf, R. E., and Brelsford, W. G. (1988) Soluble interleukin-2 receptors in systemic lupus erythematosus. *Arthritis Rheum. 31*, 729−735.

(2) Nakanishi, K., Taniguchi, Y., and Ohta, Y. (1991) Increased soluble interleukin-2 receptor levels in autoimmune thyroid disease. *Acta Endocrinol. 125*, 253−258.

(3) Anasetti, C., Hansen, J. A., Waldmann, T. A., Appelbaum, F. R., Davis, J., Deeg, H. J., Doney, K., Martin, P. J., Nash, R., Storb, R., Sullivan, K. M., Witherspoon, R. P., Binger, M.-H., Chizzonite, R., Hakimi, J., Mould, D., Satoh, H., and Light, S. E. (1994) Treatment of acute graft-versus-host disease with humanized anti-Tac: an antibody that binds to the interleukin-2 receptor. *Blood 84*, 1320−1327.

(4) Kay, N. E., Burton, J., Wagner, D., and Nelson, D. L. (1988) The malignant B cell from B-chronic lymphocytic leukemia patients release Tac-soluble interleukin-2 receptors. *Blood 72*, 447−450.

(5) Richards, J., Mick, R., Latta, J. M., Daly, K., Ratain, M. J., Vardiman, J. W., and Colomb, H. M. (1990) Serum soluble interleukin-2 receptor is associated with clinical and pathologic disease status in hairy cell leukemia. *Blood 76*, 1941−1945.

(6) Motoi, T., Uchiyama, T., Hori, T., Itoh, K., Uchino, H., and Ueda, R. (1989) Elevated serum-soluble interleukin-2 receptor (Tac antigen) levels in chronic myelogenous leukemia patients with blastic crisis. *Blood 74*, 1052−1057.

(7) Ambrosetti, A., Semenzato, G., Prior, M., Chilosi, M., Vinante, F., Vincenzi, C., Zanotti, R., Trentin, L., Portuese, A., Menestrina, F., Perona, G., Agostini, C., and Todeschini, G. (1989) Serum levels of soluble interleukin-2 receptor in hairy cell leukaemia: a reliable marker of neoplastic bulk. *Br. J. Haematol. 73*, 181−186.

(8) Webber, K. O., Reiter, Y., Brinkmann, U., Kreitman, R., and Pastan, I. (1995) Preparation and characterization of a

disulfide-stabilized Fv fragment of the anti-Tac antibody: comparison with its single-chain analogue. *Mol. Immunol. 32*, 249−258.

(9) Webber, K. O., Kreitman, R. J., and Pastan, I. (1995) Rapid and specific uptake of anti-Tac disulfide-stabilized Fv by interleukin-2 receptor-bearing tumors. *Cancer Res. 55*, 318−323.

(10) Choi, C. W., Lang, L., Lee, J. T., Webber, K. O., Yoo, T. M., Chang, H. K., Le, N., Jagoda, E., Paik, C. H., Pastan, I., Eckelman, W. C., and Carrasquillo, J. A. (1995) Biodistribution of ^{18}F- and ^{125}I-labeled anti-Tac disulfide-stabilized Fv fragments in nude mice with interleukin-2 alpha receptor-positive tumor xenografts. *Cancer Res. 55*, 5323−5329.

(11) Yoo, T. M., Chang, H. K., Choi, C. W., Webber, K. O., Le, N., Sood, V. K., Carrasquillo, J. A., Eckelman, W. C., Pastan, I., and Paik, C. H. (1997) Radiolabeling of anti-Tac disulfide-stabilized Fv fragment with Tc-99m and its evaluation in athymic mice with tumor xenografts. *J. Nucl. Med. 38*, 294−300.

(12) Wu, C., Jagoda, E., Brechbiel, M., Webber, K. O., Pastan, I., Gansow, O., and Eckelman, W. C. (1997) Biodistribution and catabolism of ^{67}Ga-labeled anti-Tac dsFv fragment. *Bioconjugate Chem. 8*, 365−369.

(13) Maack, T., Park, C. H., and Camargo, M. J. F. (1992) in Renal filtration, transport, and metabolism of proteins. *The Kidney: Physiology and Pathophysiology* (D. W. Seldin and G. Giebisch, Eds.) 2nd ed., pp 3005−3038, Raven Press, Ltd., New York.

(14) Sumpio, B. E., and Maack, T. (1982) Kinetics, competition, and selectivity of tubular absorption of proteins. *Am. J. Physiol. 243*, F379−F392.

(15) Hammond, P. J., Wade, A. F., Gwilliam, M. E., Peters, A. M., Myers, M. J., Gilbey, S. G., Bloom, S. R., and Calam, J. (1993) Amino acid infusion blocks renal tubular uptake of an indium-labeled somatostatin analogue. *Br. J. Cancer 67*, 1437−1439.

(16) de Jong, M., Breeman. W. A., Bernard, B. F., Rolleman, E. J., Hofland, L. J., Visser, T. J., Setyono-Han, B., Bakker, W. H., van der Pluijm, M. E., and Krenning, E. P. (1995) Evaluation in vitro and in rats of ^{161}Tb-DTPA-octreotide, a somatostatin analogue with potential for intraoperative scanning and radiotherapy. *Eur. J. Nucl. Med. 22*, 608−616.

(17) Morgensen, C. E., and Solling, K. (1977) Studies on renal tubular protein reabsorption: partial and near complete inhibition by certain amino acids. *Scand. J. Clin. Lab. Invest. 37*, 477−486.

(18) Morgensen, C. E., Vittinghus, E., and Solling, K. (1979) Abnormal albumin excretion after two provocative renal tests in diabetes: physical exercise and lysine injection. *Kidney Int. 16*, 385−393.

(19) Rustom, R., Maltby, P., Grime, J. S., Stockdale, H. R., Critchley, M., and Bone, J. M. (1992) Effects of lysine infusion on the renal metabolism of aprotinin (Trasylol) in man. *Clin. Sci. 83*, 295−299.

(20) Kobayashi, H., Yoo, T. M., Kim, I. S., Kim, M.-K., Le, N., Webber, K. O., Pastan, I., Paik, C. H., Eckelman, W. C., and Carrasquillo, J. A. (1996) L-lysine effectively blocks renal uptake of ^{125}I- or ^{99m}Tc-labeled anti-Tac dsFv. *Cancer Res. 56*, 3788−3795.

(21) Kim, I. S., Yoo, T. M., Kobayashi, H., Kim, M.-K, Le, N., Han, E. S., Wang, Q.-C, Pastan, I., Carrasquillo, J. A., and Paik, C. H. (1997) Acylation with glycolate loweres pI of dsFv and reduces renal uptake of its Tc-99m label (Abstract). *J. Labeled Compd. Radiopharm. 15*, 422−424.

(22) Fritzberg, A. R., Kasina, S., Eshima, D., and Johnson, D. L. (1986) Synthesis and biological evaluation of technetium-99m MAG3 as a hippuran replacement. *J. Nucl. Med. 27*, 111−116.

(23) Visser, G. W. M., Gerretsen, M., Herscheid, J. D. M., Snow, G. B., and van Dongen, G. (1993) Labeling of monoclonal antibodies with Rhenium-186 using the MAG3 chelate for radioimmunotherapy of cancer: a technical protocol. *J. Nucl. Med. 34*, 1953−1963.

(24) Lindmo, T., Boven, E., Cuttitta, F., Fedorko, J., and Bunn, P. A., Jr. (1984) Determination of the immunoreactive fraction of radiolabeled monoclonal antibodies by linear extrapolation to binding at infinite antigen excess. *J. Immunol. Methods 72*, 77−89.

(25) Kobayashi, H., Yoo, T. M., Drumm, D., Kim, M.-K., Sun, B.-F., Le. N., Webber, K. O., Pastan, I., Waldmann, T. A., Paik, C. H., and Carrasquillo, J. A. (1997) Improved Biodistribution of ^{125}I-labeled anti-Tac disulfide-stabilized Fv fragment by blocking its binding to the α subunit of the interleukin 2 receptor in the circulation with preinjected humanized anti-Tac IgG. *Cancer Res. 57, 1955−1961.*

(26) Lundblad, R. L. (1991) in The modification of lysine. *Chemical reagents for protein modification* (R. L. Lundblad, Ed.) 2nd ed., pp 129−171, CRC Press, Boca Raton, FL.

(27) Tarburton, J. P., Halpern, S. E., Hagan, P. L., Sudora, E., Chen, A., Fridman, D. M., and Phaff, A. E. (1990) Effect of acetylation on monoclonal antibody ZCE−025 Fab′: distribution in normal and tumor-bearing mice. *J. Biol. Response Mod. 9*, 221−230.

(28) Fagnani, R., Halpern, S., and Hagan, M. (1995) Altered pharmacokinetic and tumor localization properties of Fab′ fragments of a murine monoclonal anti-CEA antibody by covalent modification with low molecular weight dextran. *Nucl. Med. Commun. 16*, 362−369.

(29) Kobayashi, H., Le, N., Kim, I.-S, Kim, M.-K., Pie, J.-E., Drumm, D., Paik, D. S., Waldmann, T. A., Paik, C. H., and Carrasquillo, J. A. (1999) The Pharmacokinetic characteristics of glycolated humanized anti-Tac Fabs are determined by their isoelectric points. *Cancer Res. 59*, 422−430.

BC980129M

NMR Studies of the Metal-Loading Kinetics and Acid−Base Chemistry of DOTA and Butylamide-DOTA

David A. Keire* and Mitsuo Kobayashi

The Beckman Research Institute of the City of Hope, 1450 East Duarte Road, Duarte, California 91010-0269.
Received October 30, 1998; Revised Manuscript Received January 19, 1999

The conjugation of a chelating agent to a protein via a covalent linkage has been previously reported to change the metal-binding characteristics of the chelator. A fundamental understanding of these binding changes would enable design of a new generation of metal-chelating agents for biological applications. To assess the effect of conjugation on the commonly used chelating agent 1 4,7,10-tetraaazacyclododecane-*N*,*N*′,*N*″,*N*‴-tetraaacetic acid (DOTA), we synthesized a model protein conjugate, 1,4,7-tris(carboxymethyl)-10-(butylaminocarboxymethyl)-1,4,7,10-tetraaazacyclododecane (BD) and explored the metal-binding characteristics via NMR. The extent of ionization of the carboxylic acid groups and the two protonated macrocycle nitrogens of DOTA and BD were determined as a function of pH by chemical shift changes in proximal carbon-bonded protons. In addition to the expected sensitivity of the chemical shifts to titration of proximate acidic groups, BD resonances from carbon-bonded protons 10−17 bonds distant from the deprotonation site also shifted significantly, indicating the presence of conformational changes. Furthermore, increased shielding of the amide and alkyl proton signals upon deprotonation of the carboxylic acid groups indicates the presence of pH-dependent hydrogen-bonded BD isoforms. On the basis of these NMR data, we propose new structures for the doubly protonated forms of DOTA and BD. To measure metal loading, the yttrium-loading rates (type I to type II) of DOTA and BD were determined by following the intensity of type I and type II proton signals as a function of time. The yttrium-loading rates of BD are approximately one-half those of DOTA at pHs between 4.6 and 6.5 and 37 °C. The loading rates measured as a function of pH indicate that while both the doubly protonated and singly protonated forms of DOTA are reactive to metal loading, only the singly protonated form of BD is reactive.

INTRODUCTION

The conjugation of metals to proteins via a chelating agent is of fundamental interest in the design of proteins with modified properties. Introduction of a metal center may be used to add radioactive, paramagnetic, or redox character to proteins that lack these properties. For example, radiometals attached to antibodies via a chelating agent have been used for the delivery of therapeutic radiation directly to tumor sites and in the development of new contrast reagents for magnetic resonance imaging [for review, see Alexander (1995)]. However, the conjugation of a chelating agent to protein surface amino groups alters the metal-binding characteristics of the chelating agent, and although a number of applications would benefit from greater understanding of how the metal-binding parameters are modified, very little data exist describing the nature of the changes that occur.

To begin to address this lack of information, we compared the acid−base chemistry and the yttrium metal loading kinetics of 1,4,7,10-tetraazacyclododecane-*N*,*N*′,-*N*″,*N*‴-tetraacetic acid, DOTA,[1] to those of a model protein conjugate, butylamide-DOTA (or BD) by NMR methods. The alkylamide-substituted BD compound is clinically relevant because it mimics the lysine-side-chain protein-conjugate form of the chelating agent. Significant differences in pK_as, kinetics, and structure are observed between the two compounds, and the importance of this to protein conjugate design is discussed.

We chose DOTA for study because it is well-known to form very stable complexes with a wide variety of divalent and trivalent metal ions (Figure 1) (Loncin et al., 1986; Cacheris et al., 1987; Kumar et al., 1989; Broan et al., 1991; Clarke and Martell, 1991a,b). For example, DOTA binds Ca^{2+} and Y^{3+} with stability constants (log K_{LM} = [ML]/[M][L] at 25 °C) of 16.5 and 24.9 M^{-1}, respectively (Alexander, 1995). The tetraaza macrocycle contains a rigid preorganized-binding pocket that allows the formation of highly stable metal chelates. However, at the same time, this rigid pocket leads to a rate of metal incorporation slower than more flexible (and less stable) macrocycles. For example, Gd^{3+} is incorporated into DOTA at a rate 100 times slower than it is into 1,4,7,-10,13,16-hexaazacyclooctadecane-*N*,*N*′,*N*″,*N*‴,*N*⁗,*N*⁗′-hexaacetic acid (Kodama et al., 1991).

The effective ionic radius of the metal is also important to the rate of metal incorporation into DOTA. Larger ionic radii metals such as gadolinium (1.06 Å) and yttrium (1.02 Å) load slowly into DOTA because the binding requires a reorganization of the binding pocket. The metal−DOTA complex formation with these larger radii metals is a two-step process (Kasprzyk and Wilkins, 1982; Wang et al., 1992). Initially, a reversible type I

* To whom correspondence should be addressed. Phone: (626) 357-9711 Ext 3907. Fax: (626) 301-8186. E-mail: dak@ernst.coh.org.

[1] Abbreviations: DOTA, 1,4,7,10-tetraaazacyclododecane-*N*,*N*′,*N*″,*N*‴-tetraaacetic acid; butylamide-DOTA or BD, 1,4,7-tris(carboxymethyl)-10-(butylaminocarboxymethyl)-1,4,7,10-tetraaazacyclododecane; DOTA-OSSu, *N*-hydroxsulfosuccinimide ester of DOTA; sulfo-NHS, *N*-hydroxsulfosuccinimide; EDC, 1-ethyl-3-[3-(dimethylamino)propyl]carbodiimide; MALDI-TOF, matrix-assisted laser-desorption ionization−time-of-flight mass spectrometry.

10.1021/bc980128u CCC: $18.00 © 1999 American Chemical Society
Published on Web 03/19/1999

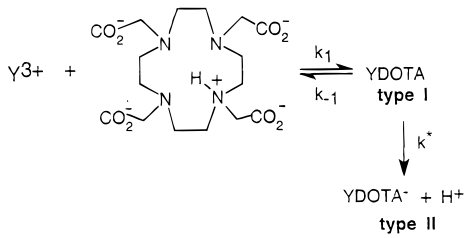


Figure 1. The reaction scheme of the $HDOTA^{3-}$ with Y^{3+}.

adduct forms (ca. $k_1 = 50\ M^{-1}\ s^{-1}$ for Gd^{3+}), followed by a relatively slow forming type II complex (ca. $k^* = 10^{-3}\ s^{-1}$ for Gd^{3+}) that has the metal fully coordinated (Figure 1).

The formation of the fully coordinated metal DOTA complex is highly pH dependent. The singly protonated form of DOTA (LH^{3-}) is the most reactive species, and the doubly protonated LH_2^{2-} form is 4 orders of magnitude less reactive (Wang et al., 1992). Desreux proposed that the slow kinetics of metal−DOTA complex formation is caused, in part, by the dynamics of conversion between isomers of metal−DOTA compounds (Desreux, 1980). Thus, the rate of metal−DOTA complexation is much higher at elevated temperature or with more flexible macrocycles because the rate of conformational change between isomers is more rapid (Desreux, 1980; Kodama et al., 1991).

Despite a relatively slow metal complexation rate, DOTA has been actively studied for use as a metal chelator in biological systems due to its serum stability (Desphande et al., 1990; Li and Meares, 1993; Lewis et al., 1994). The metal-loading yield of free polyaza macrocycles normally exceeds 95% at room temperature in about an hour [e.g., Stimmel et al. (1995)], but it has been observed that upon conjugation to an antibody much lower metal-loading yields are realized. For example, Meares and co-workers incubated $^{88}Y^{3+}$ with an antibody-DOTA conjugate containing a flexible linker for 3 h at room temperature and obtained a 26% radiolabeling yield (Li and Meares, 1993). More recently, two studies have shown that elevated temperature (>40 °C) and optimized pH and the buffer used can greatly improve the yttrium metal incorperation into DOTA-antibody conjugates (Lewis et al., 1994; Govindan et al., 1998). These studies suggest that the chelation properties of free DOTA are altered in protein-chelating agent conjugates and that these changes affect metal-loading efficiency.

Currently, no accepted model explains the observed change in the metal-loading efficiency of DOTA upon conjugation to a protein. A number of possible factors have been proposed to explain the altered metal-loading rates, including the alkyl amide modification of DOTA in the conjugation reaction, competition from other protein metal binding sites, and steric hindrance caused by the conformation of the chelating agent at the protein surface. In this work, a butylamide-DOTA conjugate has been synthesized to explore the effects of an alkyl amide modification on DOTA metal loading kinetics and pK_as.

EXPERIMENTAL PROCEDURES

General. The trisodium salt of DOTA was purchased from Parish Chemical Co. (Orem, UT), and the sulfo-NHS and EDC were purchased from Pierce (Rockford, IL). The butylamine for the conjugation reaction and the yttrium chloride hexahydrate for the metal-loading experiments were procured from Aldrich (Milwaukee, WI). All glassware was acid washed and liberally rinsed with distilled deionized water (Thiers, 1957).

Synthesis and Purification of BD. Synthesis of BD began with the addition of a solution of 60 mg (128 μmol) of DOTA and 56 mg (256 μmol) of sulfo-NHS in 2 mL of H_2O to 0.982 mL (256 μmol) of a freshly prepared solution of EDC (50 mg/mL)[1]. This reaction mixture gave a theoretical concentration of the active ester of 12.7 mM. After 30 min, 25 μL (18.7 mg, 256 μmol) of neat butylamine was added to the reaction mixture, the pH adjusted to 8 with 220 μL of 1 M NaOH, and the solution left overnight. The next morning, the reaction was quenched by lowering the pH of the reaction mixture to 2 with the addition of 670 μL of 1 N HCl. The final mixture contained both doubly and singly modified forms of BD and unmodified DOTA that were separated by reversed-phase HPLC.

The products of the reaction were purified using a Biocad Sprint chromatography system (Perseptive Biosystems, Farmingham, MA), equipped with a 4.6 mm × 10 cm POROS R2 stationary phase column (equivalent to a C18 column) and UV detection at 214 nm. The purification method used a flow rate of 1 mL/min for the wash step and a 4 mL/min flow rate for the linear gradient from 0 to 100% solvent B over 5 min (solvent A, 0.1% TFA; solvent B, 0.1% TFA/90% CH_3CN), beginning 7 min after injection. This method yielded three peaks upon injection of the reaction mixture. The first peak contained unreacted DOTA and other starting material (eluted in the wash step), the second peak contained singly modified BD (also eluted in the wash step, baseline resolved from the first peak), and the third peak contained the doubly conjugated product (eluted in the gradient portion of the method).

The peaks were collected, lyophilized, and identified by their mass-to-charge ratio (vida MALDITOF[1]). The mass-to-charge ratio of the peaks from the HPLC purification were measured on a Kratos Kompact MALDI III spectrometer, using α-cyano-4-hydroxycinnamic acid as the matrix. The spectra were collected in low-mass mode and calibrated with an external standard. A saturated solution of matrix was made in acetone and spotted on the MALDI stage in two 0.5 μL aliquots. The HPLC fraction of each of the peaks was mixed one-to-one with a 70% H_2O/30% CH_3CN/0.1% TFA solution, spotted on the MALDI stage in 1 μL aliquots, and air-dried. Mass-to-charge ratios (MH+) were observed for DOTA, BD, and doubly modified DOTA (2BD) of 406, 460, and 516 amu, respectively.

NMR Measurements. NMR experiments were performed on a Varian Unity Plus 500 MHz spectrometer (Varian Instruments, Palo Alto, CA) with the probe air temperature regulated at 25−37 °C. NMR studies on DOTA and BD in solution were performed at 1−2 mM concentrations in 90% H_2O/10% D_2O solutions with the pH adjusted by addition of HCl or NaOH. All pH measurements were performed with an Orion model 601 pH meter equipped with a combination electrode for 5 mm NMR tubes (Ingold Electrodes, Wilmington, MA). Standard aqueous buffers were used for electrode calibration at pH 4 and 7. All chemical shifts were referenced to the methyl proton signal of sodium-2,2-dimethyl-2-silapentane-5-sulfonate (DSS, at 0 ppm), which was added to the samples.

The assignment of the pH-dependent chemical shifts for BD protons was aided by the observed magnitude of the chemical shift changes during the titration of proximate acidic groups. Those carbon-bonded protons closest to the deprotonation site generally have the largest increase in shielding and, concomitantly, the largest chemical shift changes to lower ppm values. The assign-

ments were confirmed by total correlation spectroscopy [TOCSY (Braunschweiler and Ernst, 1983)] spectra connectivities at selected pHs. Typically, the TOCSYs were performed with 2K points collected in t_2 (32−48 transients/increment), and 256 complex points in t_1 (States et al., 1982). The transmitter channel was used for excitation and observation of the 6000 Hz proton frequency range as well as presaturation of the H_2O signal. Data were processed with zero filling to 2K points in F_1 and shifted sine-bell apodization functions in both F_1 and F_2.

The DOTA and BD type I to type II rate constants (k*) were determined as a function of pH by measuring the intensity of the type I and type II forms as a function of time after the addition of excess yttrium. Typically, 700 μL of a 1 mM BD or DOTA solution was made in 90% H_2O/10% D_2O, the pH adjusted to the desired value with 1 M KOH and 1 N HCl, and a 1D spectrum acquired. Subsequently, 50 μL of a 120 mM yttrium chloride stock solution was added to the NMR tube (ca. 5 mM), and a series of spectra acquired as a function of time over 10 to 14 h. The peak heights of the signals from the acetate methylene group protons in the type I and type II forms were measured from each time-course data set and plotted.

Acid-Dissociation Constants. Acid dissociation constants were determined by fitting NMR chemical shift titration data to monoprotic and diprotic acid models by nonlinear least-squares (Jardetzky and Roberts, 1981; Keire et al., 1992). For a monoprotic acid system, the observed chemical shift is given by the eq 1

$$\delta_{obs} = f_{HA}\delta_{HA} + f_A\delta_A \quad (1)$$

where f_{HA} and f_A represent the mole fractions, and δ_{HA} and δ_A the chemical shifts of the acid in its protonated and deprotonated states. The model equation for a monoprotic acid is obtained by expressing f_{HA} and f_A in terms of the acid dissociation constant, K.

$$\delta_{obs} = \frac{[H^+]\,\delta_{HA} + K\delta_A}{[H^+] + K} \quad (2)$$

The following model equation for the diprotic acid is derived in the same way.

$$\delta_{obs} = \frac{[H^+]^2\delta_{H_2A} + [H^+]K_1\delta_{HA} + K_1K_2\delta_A}{[H^+]^2 + [H^+]K_1 + K_1K_2} \quad (3)$$

The criteria used to select a model were the number of observed inflection points and comparison of the χ^2 values obtained from fitting the data to monoprotic and diprotic models. The DOTA and BD k*s for yttrium were determined by the method of initial rates. Peak intensities were fit to a straight line to determine the initial rate. The fitting of the acid dissociation and rate constants was performed with Mathematica 3.0 (Wolfram Research, Champaign, IL).

RESULTS

Synthesis of BD. The *N*-hydroxysulfo-OSSu active ester of the DOTA carboxylic acids was prepared by a water-soluble method commonly used in peptide synthesis and protein modification (Yamada et al., 1981; Staros et al., 1986; Gilles et al., 1990). A mole ratio of DOTA to sulfo-NHS to EDC of 1:2:2 was used in order to minimize the number of multiply activated DOTA carboxyl groups. The active ester form of DOTA reacts with the primary amine group of the butylamine to form an amide bond in the conjugation reaction. The reaction produced two main products, BD and doubly modified BD (2BD), that were separated by reversed-phase HPLC and identified by their mass-to-charge ratios. The yield of the reaction after purification (based on the DOTA as the limiting reactant) was 38% BD (22.1 mg) and 14% 2BD (9.4 mg).

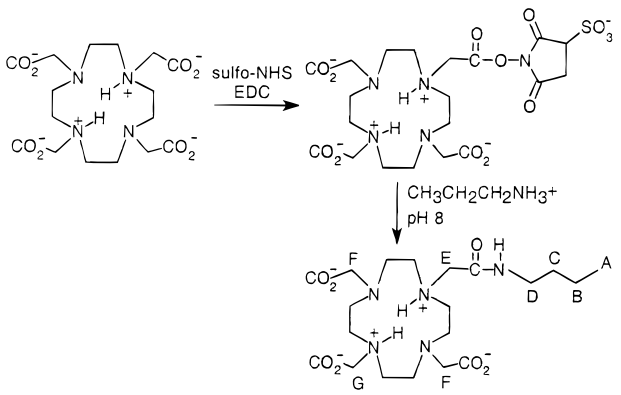


Figure 2. The synthesis of butylamide-DOTA (BD)

NMR pH Titration of DOTA. DOTA and BD have multiple sites with Brønsted acid−base properties in aqueous solution. For DOTA, these are the four carboxylic acid groups and two protonated macrocycle nitrogen protons. Over the range pH 0−13 these groups undergo protonation/deprotonation reactions, and the chemical shifts of the carbon-bonded protons near sites of protonation or deprotonation are expected to change due to through-bond electrostatic effects (Jardetzky and Roberts, 1981). Thus, acid dissociation constants were determined for these groups from the dependence of the chemical shifts of the carbon-bonded protons on pH.

The NMR spectrum of DOTA in aqueous solution consists of two signals, one for the acetate methylene group protons and the other for the macrocycle ethylene protons (Desreux et al., 1981). The signal for the protons on the macrocycle nitrogens are not observable because of exchange broadening (Brucher et al., 1991). Instead, the presence of nitrogen-bound protons in the macrocycle are inferred by the pH dependence of the chemical shifts of other nearby carbon-bonded proton signals at basic pHs. An abrupt change in the chemical shifts is observed at pH 11 is due to K^+ complexation by the fully deprotonated form of DOTA (Clarke and Martell, 1991a).

Macroscopic acid dissociation constants were determined for the various groups by fitting the NMR pH titration data to monoprotic and diprotic models (eqs 1−3). The criteria used to select a model were the number of observed inflection points and the fit of the data based on the χ^2 value. For example, the chemical shifts of the DOTA ethylene proton signal over the range pH 0−7 was fit to a monoprotic model and the acetate chemical shifts were fit to a diprotic model (data not shown). Both the acetate methylene and the macrocycle ethylene signals were fit with a monoprotic model for the amine deprotonation over the range pH 7−11. The chemical shift values of the fully deprotonated and fully protonated forms of DOTA titratable groups (and the intermediate value in the diprotic model) are also obtained from the fits of the NMR pH titration data. The values obtained for the DOTA pK_as and the titration shifts for the acetate and methylene protons are listed in Table 1.

The measured macroscopic pK_as are assigned to protonation of two trans amine nitrogens (designated G amines, 10.26), the two carboxyl groups near the non-

Table 1. Acid Dissociation Constants and Titration Shifts for DOTA in 0.1 M KCl at 25 °C

protons	acetate shift (ppm)	pK_a	ethylene shift (ppm)	pK_a	calculated[a] pK_a	1 M NaCl[b] 25 °C	0.1 M KCl[c] 25 °C	0.1 M KCl[d] 25 °C	0.1 M KNO_3[e] 25 °C
G carboxylates	0.252	1.63	0.103	1.46	1.24	1.71			
					1.84	1.88			
F carboxylates	0.126	4.57			4.27	4.18	3.95	4.41	4.36
					4.87	4.24	4.85	4.54	4.37
G amines	0.368	10.43	0.324	10.08	9.66	9.23	9.69	9.73	9.68
					10.86	11.08	11.14	11.36	11.22

[a] Calculated titration constants from the relationship between macroscopic and microscopic pK_as [see Edsall and Wyman (1958)] and the average of the measured pK_as. [b] Desreux et al. (1981). [c] Clarke and Martell (1991a). [d] Stetter and Frank (1976). [e] Delgado and Fausto Da Silva (1982).

protonated amines (designated F carboxylates, 4.57), and the remaining two carboxylic acid groups near the protonated amines (designated G carboxylates, 1.54). The individual pK_as of the six DOTA protons were calculated using the relationship between macroscopic and microscopic protonation constants (Edsall and Wyman, 1958). The agreement among protonation constants determined for DOTA in Table 1 is reasonably good compared to those measured in other studies by potentiometric and NMR methods (Stetter and Frank, 1976; Desreux et al., 1981; Delgado and Da Silva, 1982; Clarke and Martell, 1991a). The value of the most basic amine pK_a reported in Table 1 is lower than the other measured values presumably because of the effect of the K^+ complexation with the $DOTA^{4-}$ form at pHs above 11.

NMR pH Titration of BD. The conjugation of butylamine with DOTA active ester to form BD greatly increases the number of NMR signals present, whereas only two signals were observed in DOTA spectra (Figure 3). For example, in the conjugate, separate NMR peaks are observed for the acetate and ethylene signals directly adjacent and opposite to the site of the modification because the molecule is no longer symmetric; in symmetrical DOTA, these signals overlap. The separate signals allow the measurement of the microscopic protonation constants of the three carboxylic acid groups and the two macrocyle amines via fits of the pH-dependent chemical shifts of proximal carbon-bonded protons.

These proton signals shift as a function of pH and the protonation state of BD. The 1D 1H NMR spectra of BD as a function of pH for the acetate signals is shown in Figure 3 (similar shifts were observed for the ethylene proton signals). The resonances were individually assigned by comparison with DOTA chemical shifts, their pattern of chemical shift changes with pH, relative intensities, and TOCSY spectra that indicated connectivities between connected ethylene protons or adjacent butylamide proton signals. For example, the methylene protons of the DOTA acetate arm that is involved in the conjugation to butylamine (Figure 4, E protons) exhibits the smallest chemical shift change with titration of the unconjugated carboxylic acids. Similarly, the methylene groups on the carboxylic acids not attached to a protonated nitrogen (Figure 4F) show the smallest perturbation with titration of the two macrocycle nitrogen protons.

In another example, the BD F and G acetate methylene protons give rise to separate signals at low pH (Figure 3). Because the BD G protons are the most DOTA-like acetate methylene protons in BD, they were assigned based on the similarity in chemical shift with the DOTA G proton signal at low pHs (at pH 0.8 BD and DOTA G protons have chemical shifts of 3.935 and 3.992, respectively). In addition, the BD F proton signal can be differentiated from the G signal because it is larger (it arises from four identical protons versus 2 G protons).

To follow the titration shifts of the ethylene signal chemical over the 0−13 pH range, TOCSY spectra were collected at pH 1.24, 2.92, 3.14, 5.70, 7.0, and 9.60. In these experiments, TOCSY connectivities are observed in BD between the G′ and F″ proton signals and the E′ and F′ proton signals. These connectivities, in combination with the pH-dependent shifts were used to assign the macrocycle ethylene proton resonances.

The acetate methylene proton signals (labeled E, F, and G) shift and change shape as a function of the protonation state of BD (Figure 3). For example, the F and G acetate methylene signals at pH 1 are broad and have separate signals. Upon deprotonation of the G carboxylate, these signals move together and overlap, become sharp, and shift to lower chemical shift values. The F and G signals become nonequivalent again upon deprotonation of the F carboxylic acid groups.

The increased shielding (shift to lower chemical shift value) of the methylene signals is expected due to the increased electron density in the adjacent deprotonated carboxylic acid group. Typically, in the absence of structural alterations, the closer that the carbon-bonded proton is to the site of the deprotonation, the greater the magnitude of the chemical shift change. By contrast, deprotonation events that lead to deshielding (movement to higher chemical shift values) for carbon-bonded protons more than 3−5 bonds distant from the site of deprotonation indicate the presence of conformation-dependent through-space interactions.

In particular, the formation of hydrogen bonds between amines and carboxylate groups can be identified from observation of deshielding chemical shift changes as a function of pH (Bundi and Wuthrich, 1979). The chemical shifts change because the N−H bond becomes strongly polarized when the amine or amide proton forms a hydrogen bond, the proton is deshielded and its resonance shifted to higher chemical shift values. Furthermore, the deshielding tends to occur upon titration of carboxylic acid groups because a deprotonated carboxylate forms a stronger hydrogen bond than the protonated form.

Deshielding chemical shift changes attributed to the formation of hydrogen bonds and conformational changes are evident in the NMR pH titration data of BD (Table 2). For example, the E acetate methylene signal is a broad singlet at low pH and upon titration of the G carboxylic acid group shifts to a higher (deshielded) chemical shift value. This signal also sharpens to an AB pattern as the two geminal protons become magnetically nonequivalent (at pH 3.3 $^2J_{AB}$ is −14.2 Hz and $\Delta\nu(\nu_a - \nu_b)$ is 0.033 ppm). With the titration of the F carboxylate groups, the E acetate methylene proton signal is slightly shielded and the AB pattern is altered (at pH 5.5, $\Delta\nu$ is 0.101 ppm).

Simultaneously, the amide, D, and C proton signal chemical shifts decrease upon G deprotonation and increase upon F carboxylate deprotonation (Figure 5). Because the E acetate methylene and butylamide protons (A, B, C, D, and the NH) are 10−17 bonds distant from the site of the G carboxylate deprotonation and 7−12 bonds distant from the site of F carboxylate deprotona-

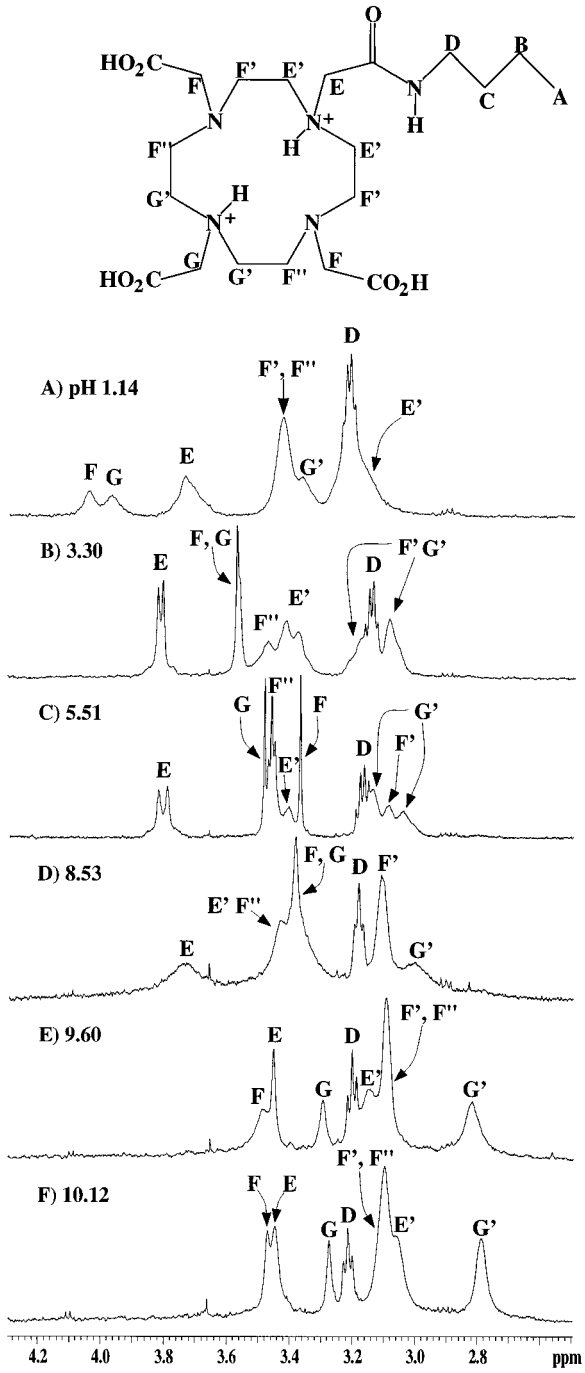


Figure 3. The 2.5−4.3 ppm region of the 500 MHz ^{1}H NMR spectra of 1 mM BD in 90% H_2O/10% D_2O at pH (A) 1.14, (B) 3.30, (C) 5.51, (D) 8.53, (E) 9.60, and (G)10.12. The signals from the various BD protons are labeled in the accompanying structure and the spectra.

tion, these shifts indicate that BD undergoes conformational changes and that these changes are dependent on the protonation state of the molecule. The effects of these structural alterations are evident in the NMR pH titration spectra (the observed chemical shifts, line shapes, and coupling constants are weighted averages of these parameters in the different isomers present at a particular pH).

The BD acetate methylene and macrocycle methylene titration shift data were fit to monoprotic or diprotic models to determine the pK_as of the various functional groups and titration shifts (Table 2). Of note, the fit of pH shifts resulting from titration of the F carboxylate protons revealed two values, 3.52 (±0.12) (three of the

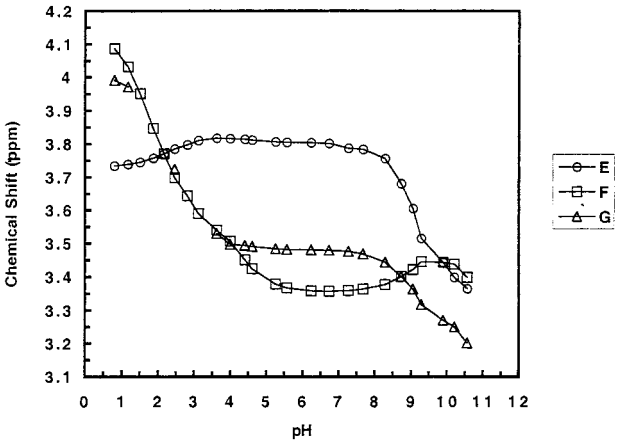


Figure 4. A plot of the chemical shifts of the BD E, F, and G acetate methylene proton signals as a function of pH.

eight values) and 4.53 (±0.24) (five of the eight values). In addition, the formation of a possible hydrogen bond with the pendant arm amide proton is indicated by its deshielding chemical shift change which occurs with the deprotonation of the second F carboxylate group (Table 2).

Yttrium Metal Loading Rates in DOTA. The yttrium metal loading into DOTA over time was monitored by proton NMR (as shown in Figure 6). The rate of the formation of type I complexes is such that by the time the first NMR spectrum is collected after adding excess metal, most of the chelator is in the type I and type II forms. In the presence of the metal, the NMR signals broaden and shift, and, over a period of hours, several of the broad signals disappear. This reflects the transition from the type I to type II complex (Figure 6).

The resonances in the yttrium−DOTA complex previously have been assigned and show that the DOTA protons become magnetically nonequivalent because of the rigid structure induced by metal binding (Broan et al., 1991). The signals labeled F,G in Figure 6A are the methylene protons of the F and G acetate groups of $YDOTA^-$ (an AB pattern with $^2J_{AB}$ of 16 Hz). Three multiplets, J, I, and K, are also observed with a signal intensity ratio of 4:8:4, respectively. Signal *J* is from the ring protons closest to the carboxyl group in the structure induced by metal complexation. The signals in Figure 6A are from the fully metal-loaded form of DOTA (type II complex) and the spectrum in Figure 6B represents a mixture of signals from the type I and type II forms.

With the identity of the type II complex signals established, the broad signals observed in 1H NMR spectra (Figure 6B) of Y−DOTA complexes (that do not correspond to signals in Figure 6A) are assigned to the intermediate type I complex. These type I signals decrease as a function of time after mixing and as the type II signals increase. These data reveal the rate of transition from the type I to type II complex. To determine the initial rates, the intensity of the I and K resonances (at 2.74 and 2.42 ppm, respectively) was plotted as a function of time after adding metal. Table 3 shows the initial rates of yttrium metal loading over the pH range 4.5−6.5 at 37 °C.

Yttrium Metal Loading Rates in BD. The 1H NMR spectrum of the fully metal-loaded (type II) complex of yttrium and BD (Y−BD) has a similar pattern of signals as Y−DOTA (Figure 7A). The resonances of the E, F, and G acetate and the J, I, and K methylene protons of Y−BD appear in the same order as the F, G, J, I, and K signals in Y−DOTA (compare spectra in Figures 6 and 7A).

Table 2. Acid Dissociation Constants[a] and Titration Shifts[b] for BD Protons in 0.1 M KCl at 25 °C

Acid Dissociation Constants

proton(s)	*A*	*B*	*C*	*D*	amide	*E*	*E′*	*F*	*F′*	*G*	*G′*	mean (±std dev)
G carboxylate	2.39	1.98	2.32	2.35	2.46	2.18	2.49	1.90	2.02	2.09	2.57	2.25 (±0.21)
F carboxylates		3.49							3.68	3.40		3.32 (±0.12)
			4.53	4.52	4.40	4.96		4.25				4.53 (±0.24)
E amine	9.07		9.00	9.30		9.04	8.87	9.05		8.92	9.14	9.05 (±0.21)
G amine	10.89	10.56	10.97	10.70		10.77		10.47		10.42	10.85	10.73 (±0.20)

Titration Shifts (ppm)

proton(s)	*A*	*B*	*C*	*D*	amide	*E*	*E′*	*F*	*F′*	*G*	*G′*
G carboxylate	0.009	0.012	0.026	0.085	0.161	−0.088	−0.251	0.539	0.349	0.410	0.340
F carboxylates		0.007	0.010	−0.037	−0.148	0.016		0.221	−0.037	0.128	
E amine	−0.006		−0.011	−0.040		0.402	0.213	−0.137		0.202	0.304
G amine	0.009	−0.006	0.021	0.051		0.111	0.235	0.167		0.117	0.089

[a] The pK_as were calculated from fits to monoprotic and diprotic models of the NMR pH titration data. [b] The titration shifts were calculated from the chemical shift values obtained in the pK_a fits ($\delta_{HA} - \delta_A$).

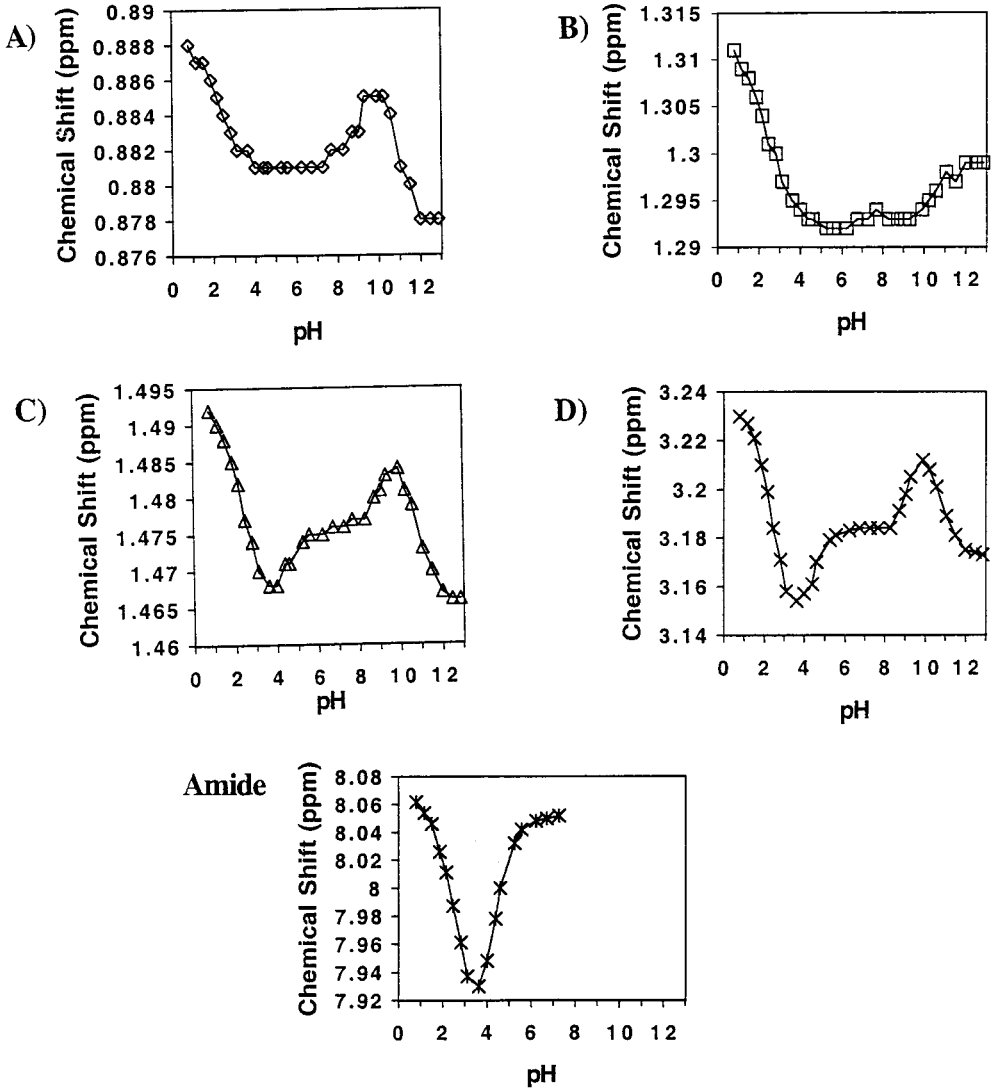


Figure 5. Plots of the chemical shifts of the A, B, C, D, and amide protons of the butylamide portion of BD as a function of pH. The labels are the same as in Figure 1.

However, the E, F, and G acetate methylene protons in Y−BD are split into AB patterns and have different chemical shifts (E being the most deshielded) because of the butylamide substitution. A similar pattern is observed for the macrocycle ring K protons, in which separate signals are observed for the proton next to the E methylene [K(E)], and the F and G methylenes [K(F,G)]. Also, the butylamide D methylene signal is split into a multiplet (vida TOCSY).

The formation of the multiplet patterns in Y−BD for the methylene protons is indicative of the formation of a rigid structure that causes the geminal proton pairs to become magnetically nonequivalent. For example, the splitting of the E and D methylene proton resonances into

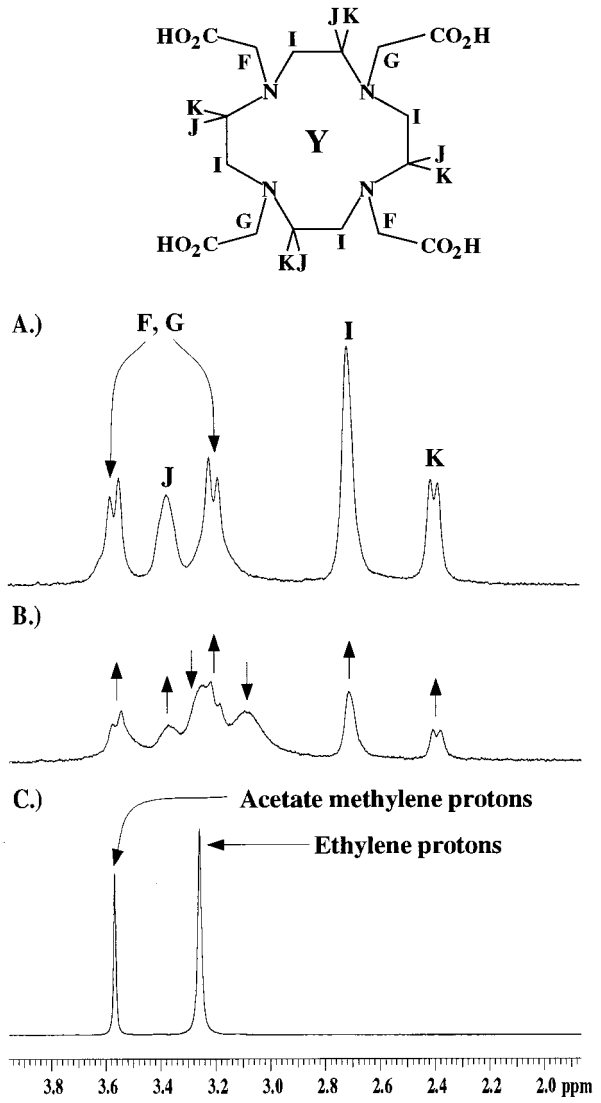


Figure 6. The 1.5−3.9 ppm region of the 500 MHz ^{1}H NMR spectra of (C) a 2 mM solution of DOTA at pH 5, (B) the same solution as in C6 6 min after adding 27 mM Y^{3+}, and (A) the same solution as in panel B acquired 5 h after adding metal. All solutions were 90% H_2O/10% D_2O and the probe air temperature was regulated at 25 °C. Spectra B and C were acquired and displayed with the same parameters and A is labeled as in the accompanying structure. The up and down arrows of spectrum B indicate signals from the type II and type I Y−DOTA complex, respectively, that increase and decrease as a function of time.

Table 3. Rate Constants for Yttrium Metal Loading (Type I to Type II) in DOTA and BD as a Function of pH at 37 °C

pH	*n*	DOTA, k_1 (s^{-1})	BD, k_1 (s^{-1})
4.6	8	0.84 (±0.07) × 10^{-3}	
4.6	4		0.45 (±0.02) × 10^{-3}
5.7	4	1.68 (±0.12) × 10^{-3}	
5.6	4		0.63 (±0.10) × 10^{-3}
6.7	4	2.35 (±0.28) × 10^{-3}	
6.5	3		1.07 (±0.06) × 10^{-3}

AB patterns suggests that metal coordination occurs with the butylamide carbonyl group, fixing the geometry of this portion of BD. At the same time, the A, B, and C proton signals are mostly unchanged, indicating that their environment is not significantly altered by metal binding (although the B proton signal is broadened in the type II complex).

As with Y−DOTA, to determine the BD type I to type II metal loading rate constants, the intensity of three BD proton signals were measured as a function of time after addition of excess yttrium (Table 3). In Figure 7B, the increase in the F,G multiplet pattern at 3.6 ppm and the K(F,G) multiplet at 2.43 ppm and the decrease in the E proton AB pattern doublet at 3.95 ppm peak height as a function of time were plotted and the initial rates determined. The initial rates of yttrium metal loading (type I to type II) into BD as a function of pH at 37 °C are shown in Table 3 and are approximately one-half the rates for DOTA at the same pH.

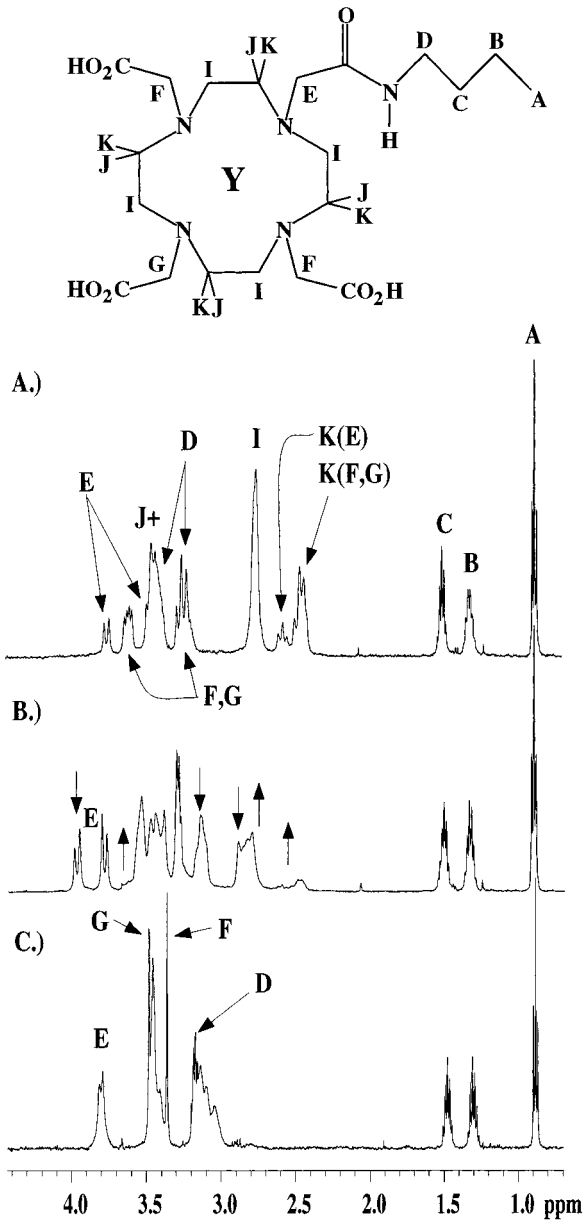


Figure 7. The 0.7−4.4 ppm region of the 500 MHz ^{1}H NMR spectra of (C) a 1 mM solution of BD at pH 7.1, (B) the same solution as in C 6 min after adding 5 mM Y^{3+}, and (A) the same solution as in panel B acquired ca. 24 h after adding metal. All solutions were 90% H_2O/10% D_2O and the probe air temperature was regulated at 37 °C. Spectra B and C were acquired and displayed with the same parameters, and A is labeled as in the accompanying structure. The up and down arrows of spectrum B indicate signals from the type II and type I Y−BD complex, respectively, that increase and decrease as a function of time.

Metal-Loading Forms of DOTA and BD. Examining of the combination of the pK_a and rate data reveals that although both the doubly and singly protonated species of DOTA are reactive to metal loading, only the

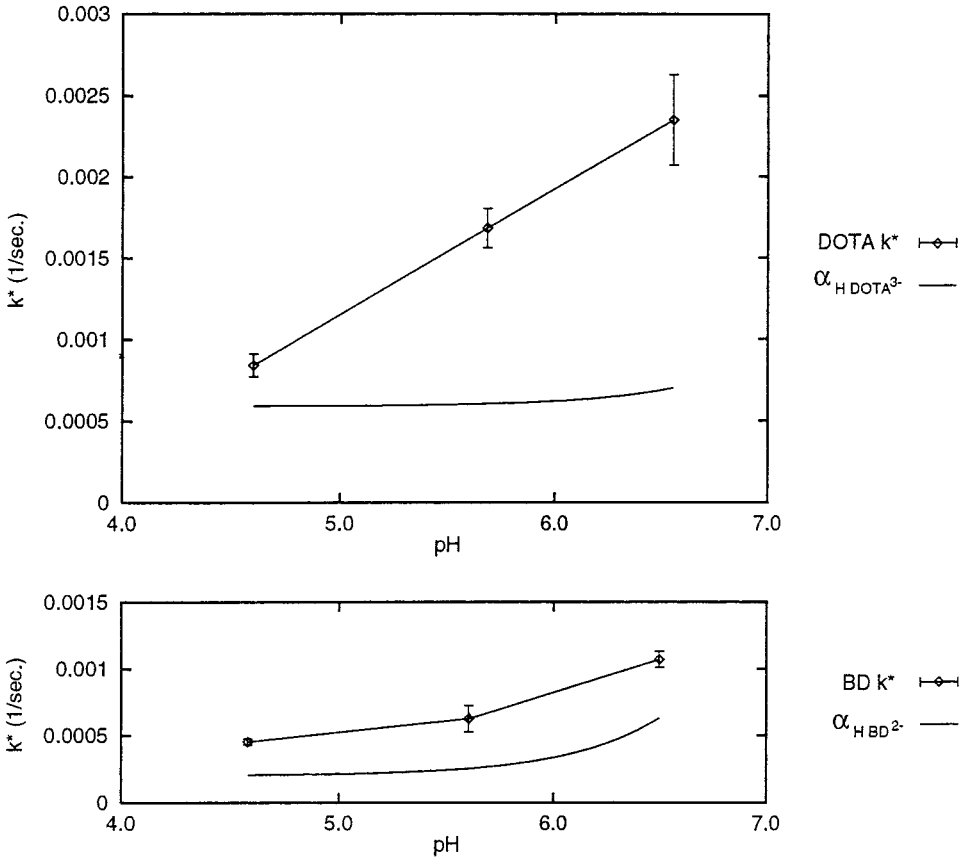


Figure 8. Combined plots of the type I to type II metal loading rate (k*) and the fraction in the singly protonated form of (top) DOTA and (bottom) BD.

singly protonated form of BD is reactive (Figure 8). For DOTA, over the 4.6−6.5 pH range, the change in k* increases more rapidly with pH than the fraction of the chelator in the singly protonated form ($HDOTA^{3-}$) (Figure 8, top). This increase in k* is best explained by metal loading into both the H_2DOTA^{2-} and $HDOTA^{3-}$ forms (the singly protonated form is orders of magnitude more reactive but much less abundant then the doubly protonated form). In contrast, for BD, the change in k* is best fit solely by the increase in the fraction of the singly protonated form (Figure 8 bottom).

DISCUSSION

The modification of a single pendant arm of DOTA to create BD significantly alters the structure and characteristics of the chelator. For example, the NMR pH titration on BD shows a 0.6 pK_a unit decrease in one of the amine nitrogens relative to DOTA. The decrease in the pK_a of the macrocycle amine is important because the singly protonated form is the most reactive to metal loading in both DOTA and BD. The decrease in the pK_a value leads to an increase in the population of the singly protonated form of BD compared to DOTA (at pH 7 the $HDOTA^{3-}$ is 0.002% and HBD^{2-} is 0.009%). Thus, if the macrocycle amine pK_as were the only determinant in the metal-loading rate of BD, BD would metal-load more rapidly than DOTA.

Because the yttrium metal loading rates of BD are approximately one-half the rates measured for DOTA at the same pH and temperature, other factors (e.g., the proton-transfer ability of the pendant arm groups) must be involved in the type I to type II transition. Evidence for the proton-transfer mechanism is observed in ab initio calculations on $Y-H_2DOTA^{2-}$ that show that the pendant carboxylate groups are near enough in space to form hydrogen bonds with the protonated nitrogens of the macrocycle and may act to facilitate the deprotonation of these nitrogens that occurs with metal loading [Jang and Goddard (1999) *J. Am. Chem. Soc.* (Manuscript submitted for publication)].

Consistent with the pendant group proton-transfer mechanism are the observations of Takenouchi et al. (1993a,b) who reported carboxymethyl-substituted derivatives of 6-(4-nitrobenzyl)-1,4,8,11-tetraazacyclotridecane-N,N',N'',N'''-tetraacetic acid (p-NO_2-Bz-TRTA) that showed a distance dependent rate enhancement for Y metal loading. p-NO_2-Bz-TRTA derivatives that contained a (carboxymethyl)amino group appended with a methylene or ethylene spacer increased the Y-metal loading rate by a factor of 2 or had no effect, respectively. Thus, the longer spacer arm may not allow effective proton transfer from the macrocycle nitrogens.

The type I to type II rate constants of DOTA metal loading measured in this work (Table 3) differ from the rate constants measured previously under different conditions. Kodama et al. (1991) reported a $DOTA-Y^{3+}$ metal loading rate of 7.7×10^{-5} s^{-1} (pH 7.8, 25 °C, I = 0.1 from $NaClO_4$ and 25 mM HEPES buffer) compared to value obtained in this work of 2.35×10^{-3} s^{-1} at pH 6.7 and 37 °C (Table 3). Wang et al. (1992) and Wu and Horrocks (1995) measured the pH dependent kinetics of $DOTA-Gd^{3+}$ (pH 3.8−5.8, 25 °C, I = 1 from NaCl and buffer) and $DOTA-Eu^{3+}$ (pH 4.5−5.7, 25 °C, I = 0.1 from KCl and 20 mM buffer) complexation, respectively, and showed rate constants 4−28 times faster (at similar pHs) than the rates measured in this work at 37 °C. These differences are attributed to the sensitivity of DOTA

metal loading rates to pH, ionic strength, temperature, buffer, and the effective ionic radii of the metal used.

DOTA Structure. The structure of DOTA in solution may also influence the kinetics of metal loading. Protonation-state dependent H-bonded forms of DOTA have been proposed to explain the low basicity of two of the macrocycle amine nitrogens (Micheloni et al., 1978; Desreux et al., 1981). Micheloni et al. (1978) first proposed that the two trans protonated macrocycle nitrogens formed intracation H-bonds with the unprotonated macrocycle nitrogens. Later, Desreux (1981) proposed a structure for H_4DOTA that had H-bonds between the two deprotonated G carboxylate groups and the macrocycle G amine protons (a five-membered ring).

For type II complex formation, the possible structures of the H_2DOTA^{2-} and $HDOTA^{3-}$ are the most important because they are reactive to metal loading. Ab initio calculations indicate that in H_2DOTA^{2-} H-bonds between the F carboxylate and G amine groups (an eight-membered ring) are more energetically favorable than H-bonds between the G carboxylate and G amine (Jang and Goddard, unpublished results). The NMR data on DOTA indicates that the H-bonded isoforms must be in fast exchange because only two singlets (from carbon-bonded protons) are observed in the proton NMR spectra. Furthermore, the two macrocycle amine protons may not be observed because of exchange among the possible H-bonded forms between the amines, solvent water, and the macrocycle carboxylates. The exchange mechanism between $-NH$, $-CO^{2-}$, and H_3O^+ or OH^- could also serve as a means to remove protons from the macrocycle ring when metal loading in the type I to type II metal complex forms of DOTA.

Structures of the Various Protonated States of BD. The observed deshielding titration shifts in the BD signals are attributed to the formation of hydrogen-bonded isomers of BD that are protonation-state dependent. The NMR shift data indicates the presence of several pH-dependent hydrogen-bonded structures. The H-bond formation is accompanied by structural changes that affect the chemical shifts of the butylamide portion of BD (Figure 4). Further evidence for the structural alterations is seen in the change in the coupling patterns and line shapes of the E, F, and G protons (Figure 3).

Deriving structure from the titration shift data is complicated by the simultaneous presence of multiple protonated forms of BD. The NMR titration shifts of BD represent a mixture of the effects of the structural changes and the redistribution of electron density caused by titration of proximate groups. These changes can only be interpreted based on a series of structures for each of the protonation states of BD. The BD signals in the NMR spectra represent a population-weighted average of the chemical shifts and line widths of the protonation-state dependent structures present at a particular pH.

The NMR spectra at basic pHs show the macrocycle amine protons exist predominantly in the E−G configuration because of the large titration shift (0.4 ppm, Table 2) of the E acetate methylene proton upon deprotonation of the first macrocycle amine. The BD pK_as have been calculated based on the assumption that the E−G isomer is also favored in the higher protonation states. Thus, the G carboxylate is deprotonated first because it is adjacent to the positively charged protonated macrocycle nitrogen (as in DOTA).

However, the macrocycle amine protons can exist in two different trans isomers (E−G and F−F pairs) that have similar energy in the fully protonated form (Jang and Goddard, unpublished results). If the F−F isomer is present in appreciable amounts (in the fully protonated BD), the assignment of the first deprotonated carboxylate would be one of the two F groups. Further experiments are necessary to clarify the location of the macrocycle amine protons in different protonation states of BD.

For BD, the protonated forms that are most relevant to metal loading are the H_2BD^- and HBD^{2-}. The titration shift data show the amide proton is deshielded (−0.148 ppm, Table 2) upon deprotonation of the second F carboxylate group. This shift indicates the formation of a H-bond involving the amide proton (Bundi and Wuthrich, 1979). For H_2BD^-, we propose that two H-bonds are present, one between the F carboxylate and the butylamide amide (F−HN) and the other between the second F carboxylate and the G amine proton (F−G). The H_2BD^- form may metal-load more slowly than H_2DOTA^{2-} because the BD amide carbonyl is not as facile a proton-transfer mediator as the carboxylate groups of DOTA.

CONCLUSIONS

The ideal chelating agent for biological applications would metal-load rapidly (<1 h) under mild conditions (pH 7 and 25 °C) thereby avoiding protein aggregation and denaturation problems. However, little is known about the effects of conjugation on the metal binding of most chelating agents. This paper provides detailed information regarding the effects of modification of the commonly used chelator DOTA on its pK_as and type I to type II metal loading rates. This information can be used to predict pendant arm modifications that could improve the metal-loading rates of this chelator for biological applications. The DOTA analogue selected for this study mimics the lysine side-chain-conjugated form of DOTA used in radioimmunotherapy of cancer.

The present work shows that the substitution of a single pendant arm of DOTA significantly perturbs the properties of the chelator. The data suggests that DOTA modifications which lower the pK_as of the macrocycle ring amine protons (in the absence of other effects) should increase the rate of type I to type II metal loading reactions at acidic pHs because these DOTA analogues will have a greater population of the reactive singly protonated form. In general, the greater that the electronegativity is of the pendant groups, the greater the acidity of the attached amine. Thus, more electronegative pendant groups than the carboxylates or butylamide could be chosen to decrease the amine pK_as and increase k*. The H-bonding ability of pendant groups may also be important to the deprotonation of the macrocycle for metal loading. Pendant arms that are better proton-transfer mediators may also increase the rate of the metal-loading reaction.

As noted in the Introduction, several possible factors have been proposed to explain the decrease in the metal-loading rates of DOTA when conjugated to a protein. This study shows the modification of the one of the pendant side-chain groups of DOTA to create a model protein conjugated form can be in part responsible for the observed decrease in the rate. In addition, the competition for metal binding by other protein sites and the steric hindrance of the protein to chelate metal loading may further decrease the rate of metal loading. Further studies on the role of these factors on DOTA−protein conjugate metal loading are in progress.

ACKNOWLEDGMENT

This report was supported in part by NIH Grants DK33850 and Cancer Center Core Grant CA33572. Helpful discussion with Dr. M. Lewis (COH), Dr. J.

Shively (COH), Dr. S. Dasgupta (CalTech), Dr. Y. Jang (CalTech), and Dr. W. Goddard (CalTech), and the editing and proofreading of the manuscript by P. C. Haase are gratefully acknowledged.

LITERATURE CITED

(1) Alexander, V. (1995) Design and synthesis of macrocyclic ligands and their complexes of lanthanides and actinides. *Chem. Rev. 95*, 273−342.

(2) Braunschweiler, L., and Ernst, R. R. (1983) Coherence transfer by isotropic mixing: application to proton correlation spectroscopy. *J. Magn. Reson. 53*, 521−528.

(3) Broan, C. J., Cox, J. P. L., Craig, A. S., Kataky, R., Parker, D., Harrison, A., Randall, A. M., and Ferguson, G. (1991) Structure and solution stability of indium and gallium complexes of 1,4,7-triazacyclononanetriacetate and of ytrium complexes of 1, 4, 7, 10-tetraazacyclododecanetetraacetate and related ligands: kinetically stable complexes for use in imaging and radioimmunotherapy. *J. Chem. Soc., Perkins Trans. 2*, 87−99.

(4) Brucher, E., Cortes, S., Chavez, F., and Sherry, A. D. (1991) Synthesis, equilibrium, and kinetic properties of the gadolinium(III) complexes of three triazacyclododecanetriacetate ligands. *Inorg. Chem. 30*, 2092−2097.

(5) Bundi, A., and Wuthrich, K. (1979) Use of amide ^{1}H NMR titration shifts for studies of polypeptide conformation. *Biopolymers 18*, 299−311.

(6) Cacheris, W. P., Nickle, S. K., and Sherry, A. D. (1987) Thermodynamic study of lanthanide complexes of 1,4,7-triazacyclononane-N,N′,N″-triacetic acid and 1,4,7,10-tetraazacyclododecane-N,N′,N″,N‴-tetraacetic acid. *Inorg. Chem. 26*, 958−960.

(7) Clarke, E. T., and Martell, A. E. (1991a) Stabilities of the alkaline earth and divalent transition metal complexes of the tetraazamacrocyclic tetreacetic acid ligands. *Inorg. Chim. Acta 190*, 27−36.

(8) Clarke, E. T., and Martell, A. E. (1991b) Stabilities of the trivalent metal ion complexes of the tetraacetate derivatives of 12-, 13- and 14-membered tetraazomacrocycles. *Inorg. Chim. Acta 190*, 37−46.

(9) Delgado, R., and Da Silva, J. J. R. F. (1982) Metal complexes of cyclic tetra-azatetraacetic acids. *Talanta 29*, 815−822.

(10) Desphande, S. V., DeNardo, S. J., Kukis, D. L., Moi, M. K., McCall, M. J., DeNardo, G. L., and Meares, C. F. (1990) Yttrium-90-Labeled monoclonal antibody for therapy: labeling by a new macrocyclic bifunctional chelating agent. *J. Nucl. Med. 31*, 473−479.

(11) Desreux, J. F. (1980) Nuclear magnetic resonance spectroscopy of lanthanide complexes with tetraacetic tetraaza macrocycle. Unusual conformational properties. *Inorg. Chem. 19*, 1319−1324.

(12) Desreux, J. F., Merciny, E., and Loncin, M. F. (1981) Nuclear magnetic resonance and potentiometric studies of the protonation scheme of two tetraaza macrocycles. *Inorg. Chem. 20*, 987−991.

(13) Edsall, J. T., and Wyman, J. (1958) *Biophysical Chemistry*, Academic Press, New York.

(14) Gilles, M. A., Hudson, A. Q., and Borders, C. L. J. (1990) Stability fo water-soluble carbodiimides in aqueous solution. *Anal. Biochem. 184*, 244−248.

(15) Govindan, S. V., Shih, L. B., Goldenberg, D. M., Sharkey, R. M., Karacay, H., Donnelly, J. E., Losman, M. J., Hansen, H. J., and Griffiths, G. L. (1998) ^{90}Yttrium-labeling complementarity-determining-region-grafted monoclonal antibodies for radioimmunotherapy: Radiolabeling and animal biodistribution studies. *Bioconjugate Chem. 9*, 773−782.

(16) Jardetzky, O., and Roberts, G. C. K. (1981) *NMR in Molecular Biology*, Academic Press, New York

(17) Kasprzyk, S. P., and Wilkins, R. G. (1982) Kinetics of interaction of metal ions with two tetraaza tetraacetate macrocycles. *Inorg. Chem. 21*, 3349−3352.

(18) Keire, D. A., Robert, J. M., and Rabenstein, D. L. (1992) Microscopic protonation equilibria and solution conformations of Coenzyme A and Coenzyme A disulfides. *J. Org. Chem. 57*, 4427−4431.

(19) Kodama, M., Koike, T., Mahatma, A. B., and Kimura, E. (1991) Thermodynamic and kinetic studies of lanthanide complexes of 1,4,7,10,13-pentaazacyclopentadecane-N,N′,-N″,N‴,N⁗-pentaaccetic acid and 1,4,7,10,13, 16-hexaazacyclooctadecane-N,N′,N″,N‴,N⁗,N⁗′-hexaacetic acid. *Inorg. Chem. 30*, 1270−1273.

(20) Kumar, K., Magerstadt, M., and Gansow, O. A. (1989) Lead(II) and bismuth(III) complexes of the polyazacycloalkane-N-acetic acids nota, dota and teta. *J. Chem. Soc., Commun.* 145−146.

(21) Lewis, M. R., Raubitschek, A., and Shively, J. E. (1994) A facile, water-soluble method for modification of proteins with DOTA. Use of elevated temperature and optimized pH to achieve high specific activity and high chelate stability in radiolabeled immunoconjugates. *Bioconjugate Chem. 5*, 565−576.

(22) Li, M., and Meares, C. F. (1993) Synthesis, metal chelate stability studies, and enzyme digestion of a peptide-linked DOTA derivative and its corresponding radiolableled immunoconjugates. *Bioconjugate Chem. 4*, 275−283.

(23) Loncin, M. F., Desreux, J. F., and Merciny, E. (1986) Coordination of lanthanides by two polyamino polycarboxylic macrocycles: formation of highly stable lanthanide complexes. *Inorg. Chem. 25*, 2646−2648.

(24) Micheloni, M., Sabatini, A., Paoletti, P. (1978) Solution chemistry of macrocycles. Part 1. Basicity constants of 1,4,8,-11-tetraazacyclotetradecane, 1,4,8,12-tetraazacyclopentadecane, and 1,4,8,11-tetramethyl-1,4,8,11-tetraazaxyclotetradecane. *J. Chem. Soc., Perkins Trans. 2*, 828−830.

(25) Staros, J. V., Wright, R. W., and Swingle, D. M. (1986) Enhancement by N-hydroxysulfosuccinimide of water-soluble carbodiimide-mediated coupling reactions. *Anal. Biochem. 156*, 220−222.

(26) States, D. J., Haberkorn, R. A., and Ruben, D. J. (1982) A two-dimensional nuclear Overhauser experiment with pure absorption phase in four quadrants. *J. Magn. Reson. 48*, 286.

(27) Stetter, H., and Frank, W. (1976) Complex formation with tetraazacycloalkane-N,N′,N″,N‴-tetraacetic acids as a function of ring size. *Angew. Chem., Int. Ed. Engl. 15*, 686.

(28) Stimmel, J. B., Stockstill, M. E., and Kull, F. C. J. (1995) Yttrium-90 chelation properties of tetraazatetraacetic acid macrocycles, diethylenetriaminepentaacetic acid analogues, and novel terpyridine acyclic chelator. *Bioconjugate Chem. 6*, 219−225.

(29) Takenouchi, K., Tabe, M., Watanabe, K., Hazato, A., Kato, Y., Shionoya, M., Koike, T., and Kimura, E. (1993a) Novel pendant-type macrocyclic bifunctional chelating agents: (carboxymethyl)amino derivatives of 2-(4-nitrobenzyl0−1,4,7,20-tetraazacyclododecane-N,N′,N′,N‴-tetraacetic acid and their complex formation with yttrium(III). *J. Org. Chem. 58*, 6895−6899.

(30) Takenouchi, K., Watanabe, K., Kato, Y., Koike, T., and Kimura, E. (1993b) Novel bifunctional macrocycle chelating agents appended with pendant-type carboxymethylamino ligand and nitrobenzyl group and stability of the $^{88}Y^{III}$ complexes. *J. Org. Chem. 58*, 1955−1958.

(31) Thiers, R. E. (1957) Contamination in trace element analysis and its control. *Methods in Biochemical Analysis*. 273−335,,

(32) Wang, X., Jin, T., Comblin, V., Lopez-Mut, A., Merciny, E., and Desreux, J. F. (1992) A kinetic investigation of the lanthanide DOTA chelates. Stability and rates of formation and of dissociation of a macrocyclic gadolinium(III) polyaza polycarboxylic contrast agent. *Inorg. Chem. 31*, 1095−1099.

(33) Wu, S. L., and Horrocks, W. D. J. (1995) Kinetics of complex formation by macrocyclic polyaza polycarboxylate ligands; detection and characterization of an intermediate in the Eu^{3+}-dota system by laser-excited luminesence. *Inorg. Chem. 34*, 3724−3732.

(34) Yamada, H., Imoto, T., Fujita, K., Okazaki, K., and Motomura, M. (1981) Selective modification of aspartic acid-101 in lysozyme by carbodiimide reaction. *Biochemistry 20*, 4836−4842.

BC980128U

A Synthetic Cysteine Oxidase Based on a Ferrocene-Cyclodextrin Conjugate

Suzanne K. Schreyer and Susan R. Mikkelsen*

Department of Chemistry, University of Waterloo, Waterloo, Ontario, Canada N2L 3G1. Received November 5, 1998; Revised Manuscript Received January 22, 1999

We report a novel synthetic cysteine oxidase consisting of a ferrocene-β-cyclodextrin conjugate in which the ferrocene moiety is bound to the secondary hydroxyl side of the cyclodextrin cavity through an ethylenediamine linker. Cysteine oxidation occurs after the ferrocene group is electrochemically oxidized to the ferricinium form, and this generates a voltammetric electrocatalytic wave, the magnitude of which is related to the rate constant for cysteine oxidation. Comparison of cysteine oxidation rates for the primary and secondary β-cyclodextrin derivatives (105 and 1470 M^{-1} s^{-1}, respectively) shows that the secondary derivatives are more effective synthetic enzymes. Substrate selectivity of the secondary derivative is demonstrated by comparison of oxidation rates for cysteine (1470 M^{-1} s^{-1}) and glutathione (260 M^{-1} s^{-1}) at pH 7.0. The rate constant for cysteine oxidation was 3-fold higher at pH 8.0. With a constant synthetic enzyme concentration, electrocatalytic limiting currents increased linearly with increasing cysteine concentration to a maximum at 6 mM cysteine; above this concentration, the current decreased significantly. These and other results suggest that product inhibition of the catalytic cycle occurs as a result of cystine binding more strongly to the cyclodextrin than cysteine.

INTRODUCTION

Synthetic enzymes have been interesting to chemists and biochemists for several decades. Fundamentally, they are relatively simple models of more complicated biochemical catalysts, possessing both selectivity and enhanced reaction rates in structurally well-defined and relatively small molecules. Their potential applications have encouraged research, since they are expected to be stable under conditions of temperature, pH, and solvent composition that would denature or inactivate natural, protein-based biocatalysts.

In essence, an enzyme may be thought of as a selective substrate-binding site attached rigidly or flexibly to a nearby catalytic site. This simple definition has been realized by various researchers in molecules that selectively catalyze hydrolyses (*1*, *2*), isomerizations (*3*−*5*), addition (*6*), and decarboxylation (*7*). Examples of synthetic oxidoreductases that use cyclodextrins or selective substrate recognition have used attached inorganic catalytic groups [iron−sulfur complexes (*8*), an oxodiperoxomolybdenum complex (*9*), polyamine complexes of various divalent metal ions (*10*), and ferrocene (*11*)] or organic catalysts [porphyrins (*12*, *13*) and flavin analogues (*14*−*18*)] to mimic biological redox processes.

The first synthetic flavoenzyme was reported by Tabushi and Kodera and consisted of riboflavin bound to one of the primary β-cyclodextrin hydroxyl groups (*14*). They reported a 240-fold rate enhancement for the oxidation of *n*-hexyldihydronicotinamide by the primary flavocyclodextrin in comparison with free riboflavin possessing an equivalent but inert substituent.

Ye et al. have reported several studies of β-cyclodextrin derivatized with isoalloxazines (the redox-active part of riboflavin) on either the primary or secondary hydroxyl side of the cavity (*16*, *17*). In this work, the catalysts were compared with free riboflavin for their abilities to oxidize nicotinamides and substituted benzyl acohols (*16*) and to oxidize alcohols or thiols and reduce aldehydes (*17*). Early results showed that *p-tert*-butylbenzyl alcohol was oxidized to its corresponding aldehyde by the secondary flavocyclodextrin 650 times faster than by riboflavin (16a). Subsequent studies with the same flavocyclodextrin revealed that thiol oxidation was effectively catalyzed, and the authors concluded that although the secondary cyclodextrin derivative had a dissociation constant for phenylmethanethiol binding similar to the primary derivative (1.89 mM vs 2.38 mM, respectively), its overall rate (as k_{cat}/K_{diss}) was twice as fast as the primary derivative (0.587 vs 0.246 M s^{-1}) because orientation and alignment of the reacting atoms produced a higher k_{cat} value in the secondary derivative.

Suzuki et al. reported catalytic alcohol oxidation to aldehydes by a primary β-cyclodextrin derivative of ferrocenecarboxylic acid (*11*). In this 1:1 ferrocene:cyclodextrin derivative, all of the remaining hydroxyl groups (14 secondary and six primary hydroxyls) are acetylated, and this results in a lipophilic catalyst. The reactive ferricinium form was generated electrochemically during controlled-potential coulometry experiments using acetonitrile as a solvent. Although kinetic constants are not reported, the authors showed that after 12 h, each catalyst molecule had converted an average of 22 benzyl alcohol molecules and 59 1-naphthalenemethanol molecules to their corresponding aldehyde products; these values are more than 10-fold higher than those obtained after 24 h using methylferrocenecarboxylate, a model catalyst in which substrate binding could not occur. The authors propose a catalytic cycle in which the attached ferrocene, initially bound through the narrower primary opening to the cyclodextrin cavity, is excluded from the

* To whom correspondence should be addressed. Former address: Concordia University, Montreal, Canada. E-mail: mikkels@uwaterloo.ca. Fax (519) 746-0435.

10.1021/bc9801326 CCC: $18.00 © 1999 American Chemical Society
Published on Web 03/24/1999

cavity upon oxidation, allowing substrate binding. Upon substrate oxidation, the attached ferrocene reassociates with the cavity while the oxidation product is excluded.

In this paper, we report the synthesis and preliminary kinetic characterization of two new ferrocene-β-cyclodextrin derivatives. For both, ferrocenemonocarboxaldehyde was reacted with ethylenediamine under reducing conditions prior to reaction with the primary or secondary *p*-toluenesulfonyl derivative of β-cyclodextrin to produce a $-CH_2NHCH_2CH_2NH-$ spacer linking one of the cyclopentadienyl rings of the ferrocene moiety with the cyclodextrin. UV−vis spectrophotometry and electrospray mass spectrometry were used to confirm product structures, and voltammetric experiments were performed to kinetically characterize the two species as synthetic thiol oxidases.

EXPERIMENTAL SECTION

Materials. β-Cyclodextrin hydrate (β-CD), ferrocene carboxaldehyde, dimethylaminomethyl ferrocene, sodium hydride (67% dispersion in mineral oil), *p*-toluenesulfonyl chloride, reduced glutathione, L-cysteine hydrochloride hydrate, sodium formate, *N*,*N*-dimethylformamide, 4A molecular seives, anhydrous pyridine, sodium cyanoborohydride, and 4-(2-hydroxyethyl)-1-piperazineethanesulfonic acid (HEPES) were purchased from Aldrich. Oxidized glutathione, L-cystine dihydrochloride, sodium acetate, dibasic sodium phosphate, and ethylenediamine were purchased from Sigma. Glacial acetic acid, dimethyl sulfoxide, acetone, and HPLC-grade acetonitrile were obtained from Baker. Potassium hexacyanoferrate(II) and monobasic sodium phosphate were obtained from Fisher. Chemicals were of the highest available grade and were used as received. All solutions were made using distilled, deionized water from a Barnstead Nanopure ion-exchange system.

Instrumentation. A Cary 1 double-beam UV-vis spectrophotometer was used to obtain absorbance spectra, with 1 cm quartz cuvettes and blank 0.1 M phosphate buffer, pH 7.0 reference solutions. Purification of β-CD derivatives was done using an HPLC system consisting of a reciprocating pump (Waters model 510), a Rheodyne 2500 injector with a 100 μL sample loop, a 150 × 4.6 mm C18 column (Phenomenex ODP-50 4D) and a refractive index detector (Waters model 410). Electrochemical experiments were performed in nitrogen-deaerated solutions at 25 °C using a BAS 100A potentiostat (Bioanalytical Systems) with glassy carbon or carbon paste working and silver/silver chloride reference electrodes (Bioanalytical Systems) and a coiled NiChrome wire auxiliary electrode. Mass spectra were obtained using an SSQ 700 electrospray mass spectrometer (Finnegan MAT) in the positive ion mode.

Methods. **Preparation of Cyclodextrin Derivatives**. β-CD was initially converted to either the primary or secondary tosylate according to selective literature procedures (*19*, *20*). Briefly, the primary tosylate was formed by combining 2.04 g (1.8 mmol) β-CD with an excess (8.22 g, 43 mmol) of *p*-toluenesulfonyl chloride in 400 mL of pyridine. After 48 h at room temperature, the solution was vacuum distilled to give a viscous yellow liquid. The secondary tosylate was prepared by combining 1.1 g of β-CD with 60 mg of 60% sodium hydride dispersion in 40 mL of DMF (dried over 4A molecular sieves) and stirred at room temperature under dry conditions for 12 h. *p*-Toluenesulfonyl chloride (0.68 g) dissolved in 5 mL of dry DMF was then added, and stirring was continued for 1 h. Water (30 mL) was then added dropwise, and the solution was combined with 500 mL of acetone. The product was collected by filtration as a white precipitate.

Ferrocenecarboxaldehyde (2.14 g, 10.0 mmol) was dissolved in 100 mL of 0.1 M HEPES buffer, 0.60 g (10.0 mmol) of ethylenediamine was added, and the pH was adjusted to 7.5. Sodium cyanoborohydride (6.28 g) was then added, and the solution was stirred at room temperature for 12 h. A 1:1 molar ratio of either the primary or secondary β-CD tosylate was then added to the filtered solution, and the reaction proceeded with stirring at room temperature for 5 days.

Products were purified by reversed-phase HPLC, using a mobile phase consisting of 10% aqueous acetonitrile. Peaks were identified by injecting standard solutions of the starting materials and intermediate product mixtures. The primary ferrocene-β-CD reaction product exhibited a unique redox-active component that eluted at 5.5 min, in comparison with the primary tosylate (13.6 min) and the ferrocenylmethylethylenediamine product mixture (2.3 and 19.5 min). The secondary ferrocene-β-CD product showed two unique components under these conditions (5.9 and 9.8 min), one of which was redox-active with a formal potential of +220 mV vs Ag/AgCl (9.8 min); the component that eluted at 5.9 min is probably a secondary ethylenediamine-β-CD conjugate with no ferrocene attached. The secondary β-CD tosylate eluted at 12.1 min under these conditions. Electrochemical studies by Matsue et al. have shown that noncovalent ferrocene-cyclodextrin association products associate and dissociate so rapidly that the resulting voltammograms display averaged features (*22*); thus, only covalently bound ferrocene-β-CD species would elute under our slower chromatographic conditions.

Purified samples of the primary and secondary β-CD tosylates as well as their ferrocenylmethylethylenediamine-β-CD products (1°-Fc-β-CD and 2°-Fc-β-CD, respectively) were collected for mass spectrometric analysis. Larger quantities of the two ferrocene derivatives were purified and concentrated with a rotary evaporator for electrochemical experiments.

Electrochemical Studies. Glassy carbon working electrodes (0.071 cm^2) were polished prior to each voltammogram using a slurry of 1 μm alumina (Buehler) in water on a polishing cloth (Bioanalytical Systems), and were sonicated in and rinsed with water prior to use. Unless otherwise stated, voltammograms were recorded from 0.0 to 0.7 V (vs Ag/AgCl) at a scan rate of 2 mV/s.

At glassy carbon electrodes, thiol oxidation is kinetically slow, but is facilitated by an EC′ or electrocatalytic reaction mechanism in which an electrocatalyst, such as a ferrocene derivative or hexacyanoferrate (II), is readily oxidized at the electrode and subsequently oxidizes the thiol to the thiyl radical as it is reduced (eqs 1−3):

$$\text{ferrocene} \rightarrow \text{ferricinium} + e^- \quad (1)$$

$$\text{ferricinium} + R{-}SH \xrightarrow{k} \text{ferrocene} + R{-}S\cdot + H^+ \quad (2)$$

$$2R{-}S\cdot \rightarrow R{-}S{-}S{-}R \quad (3)$$

In this scheme, eqs 1 and 3 are expected to proceed rapidly, while the measured *k* values apply to eq 2 as the rate-determining step.

Rate constants for thiol oxidation by electrocatalysts were determined using dilution experiments, with a 10:1 molar ratio of thiol to ferrocene-cyclodextrin conjugate. Under these conditions, the limiting electrocatalytic

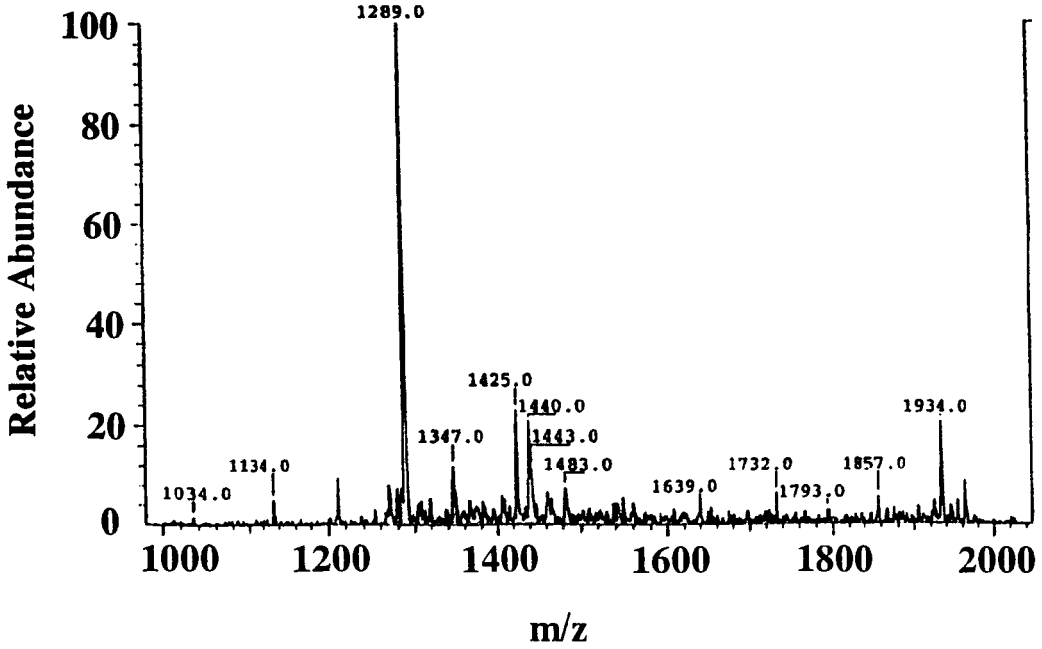


Figure 1. Electrospray mass spectrum of primary tosylate of β-CD dissolved in 10 mM sodium formate. Spectrum has been corrected by subtraction of the atomic weight of sodium.

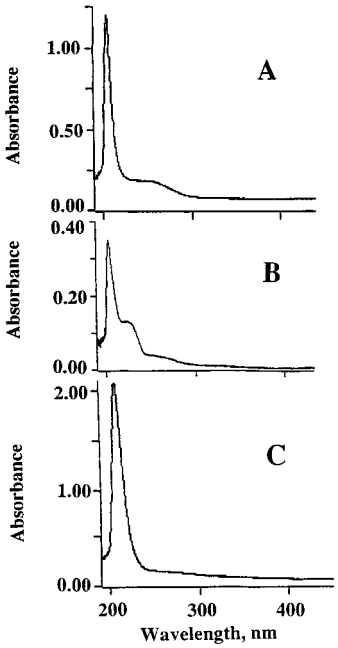


Figure 2. UV−vise spectra of (A) 42 μM dimethylaminomethylferrocene, (B) primary ferrocenylmethylethylenediamine-β-CD, and (C) secondary ferrocenylmethylethylenediamine-β-CD. All species were dissolved in 10 mM phosphate buffer, pH 7.0.

current is described by eq 4, below (*21*):

$$i_{\text{lim}} = nFAC(Dk[\text{thiol}])^{1/2} \quad (4)$$

where i_{lim} is the limiting electrocatalytic oxidation current, n is the number of electrons in the electrochemical reaction, F is Faraday's constant, A is the electrode area, C is the concentration of the electrocatalyst, D is the diffusion coefficient of the electrocatalyst, and k is the rate constant for thiol oxidation, shown in eq 2. Thus, a plot of limiting current against $C[\text{thiol}]^{1/2}$ will have a slope equal to $nFA(Dk)^{1/2}$. Using diffusion coefficients obtained by Matsue et al. of 6.4×10^{-6} and 2.6×10^{-6} cm^2/s for free and CD-bound ferrocenecarboxylic acid at 27 °C (*22*) and 6.50×10^{-6} cm^2/s for hexacyanoferrate(II) (*23*), rate constants are readily calculated.

RESULTS AND DISCUSSION

Structural Characterization of CD Derivatives. Electrospray mass spectrometry was used to characterize the products of the primary and secondary CD tosylation reactions in 0.1 M sodium acetate buffer, pH 4.0, as described by Tinke et al. (*24*) and Lamcharfi et al. (*25*). Under these conditions, a positive ion is generated by the association of sodium ion with the CD. Figure 1 shows the sodium-corrected mass spectrum obtained for the primary tosylation reaction product, where a strong signal can be seen at the expected *m/z* value of 1289, which corresponds to singly tosylated β-CD. Smaller signals at 1134 and 1443 indicate the presence of small quantities of the starting CD and the ditosylated product, respectively. Similar results were observed for the secondary tosylation reaction product: prominent peaks were observed at *m/z* 1134, 1289, and 1443, with the *m/z* 1289 peak being about 5-fold more intense than the *m/z* 1443 peak.

HPLC-purified primary and secondary ferrocenylmethylethylenediamine-β-CD were examined in 0.1 M phosphate buffer, pH 7.0, by UV-vis spectrophotometry and compared with a standard solution of dimethylaminomethylferrocene. The spectra, shown in Figure 2, all possess strong maxima near 205 nm. The molar absorptivity of dimethylaminomethylferrocene at 204 nm (2.71×10^4 M^{-1} cm^{-1}) was used to determine the concentrations of the CD derivatives in subsequent electrochemical experiments.

Electrospray mass spectrometry as described above was used to examine the ferrocene-CD conjugates. Under these conditions, no molecular ion peak was observed at the expected *m/z* value of 1561, but prominent peaks were observed at the much smaller *m/z* values of 403, 457, and 487 for both the primary and secondary conjugates, as shown in Figure 3. Varying the buffer and cone voltage conditions did not result in the expected molecular ion peaks.

The most prominent peaks in the spectra shown in Figure 3, at *m/z* 403.2, can be attributed to the fragmen-

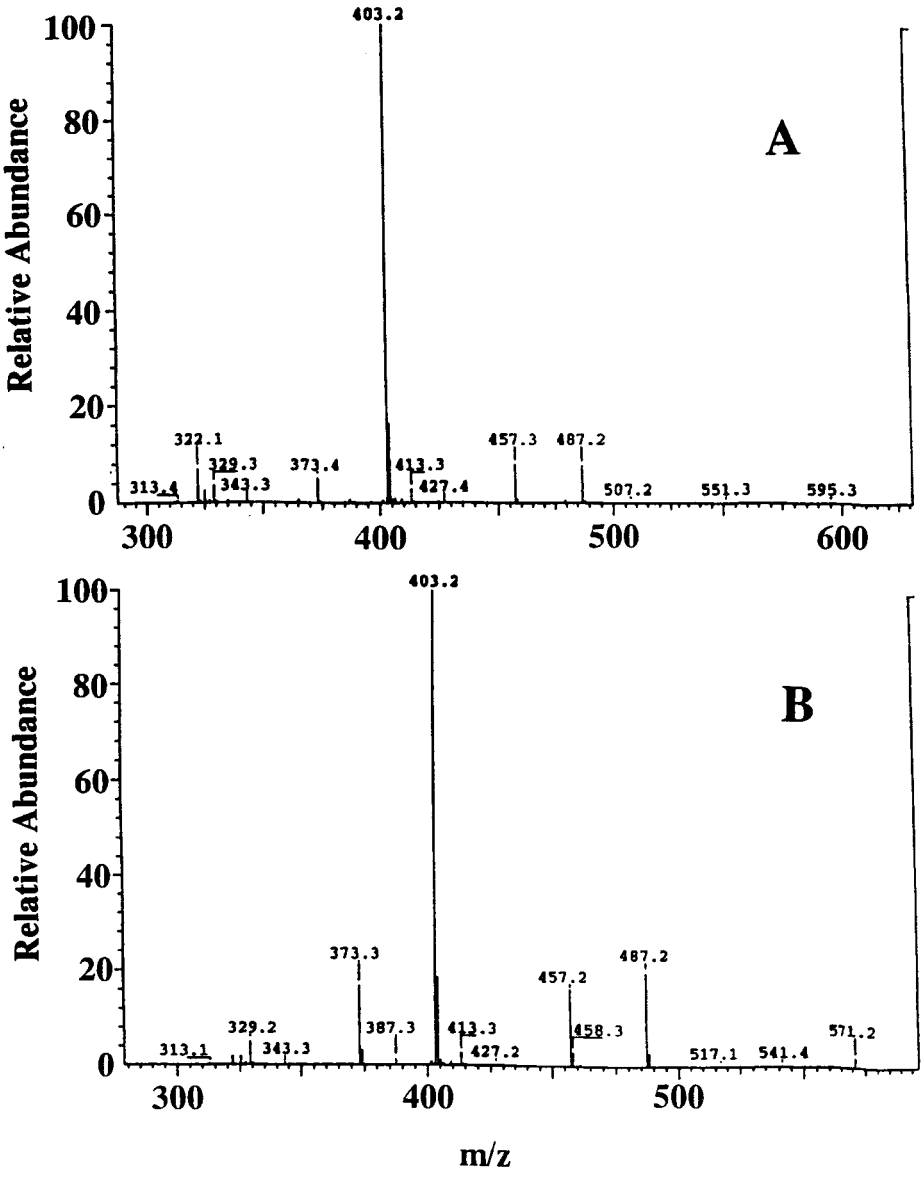


Figure 3. Electrospray mass spectrum of (A) primary ferrocenylmethylethylenediamine-β-CD, and (B) secondary ferrocenylmethylethylenediamine-β-CD, after purification by reversed-phase HPLC. CD derivatives were dissolved in 10 mM aqueous sodium formate. Spectra were not corrected for sodium.

tation products shown in Figure 4, in which the ferrocenylmethylethylenediamine moiety is bound to a single glucose residue through either a primary (Figure 4A) or secondary (Figure 4B) hydroxyl site. This is consistent with recent electrospray ion trap mass spectrometry fragmentation patterns for oligosaccharides observed by Sheeley and Reinhold (*26*).

Electrocatalysis of Thiol Oxidation. Preliminary electrochemical studies were done with simple electrocatalyst species such as ferrocyanide, ferrocenecarboxaldehyde, and dimethylaminomethylferrocene to determine the thiol oxidation rates for their ferricyanide and ferricinium forms by electrocatalytic voltammetry as described in the Experimental Section. Table 1 shows the rates obtained for cysteine and glutathione oxidation in 0.10 M phosphate buffer, pH 7.0, in the presence and absence of free 10 mM β-CD.

Thiol oxidation by ferricyanide has been studied by absorption spectrophotometry, where rate constants of 4.3 and 30 M^{-1} s^{-1} were obtained for the oxidation of mercaptoacetic acid at pH 1.4 and 1.9, respectively (*27*), and a value of 61 M^{-1} s^{-1} was obtained for the oxidation

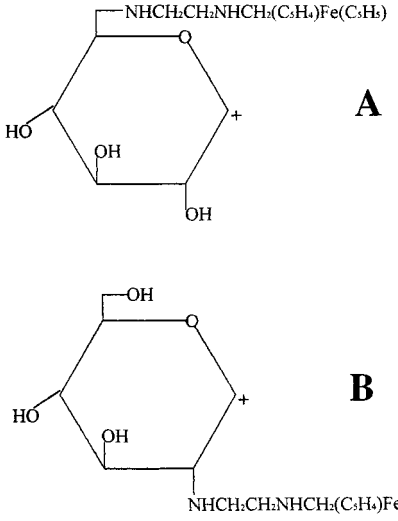


Figure 4. Proposed fragments of (A) primary ferrocenylmethylethylenediamine-β-CD, and (B) secondary ferrocenylmethylethylenediamine-β-CD, each having a mass of 403.2 amu.

Table 1. Rate Constants for the Oxidation of Thiols by Electrocatalysts[a]

electrocatalyst	thiol	[β-CD] (mM)	pH	k (M^{-1} s^{-1})
ferricyanide	GSH	0	7.0	48
		10	7.0	38
	Cys	0	7.0	90
		10	7.0	38
ferriciniumcarbox-aldehyde	GSH	0	7.0	2.1
		10	7.0	21
dimethylaminomethyl-ferricinium	GSH	0	7.0	103
		10	7.0	134
	Cys	0	8.0	30
		10	8.0	23
1°-Fc-β-CD	GSH	0	7.0	143
	Cys	0	7.0	105
2°-Fc-β-CD	GSH	0	7.0	260
	Cys	0	7.0	1470
		0	8.0	4120

[a] Measured by linear-sweep voltammetry (2 mV/s) at glassy carbon electrodes in solutions containing a 10-fold excess of thiol and 10 mM phosphate. Abbreviations: GSH, glutathione; Cys, cysteine; 1°-Fc-β-CD, primary ferrocenylmethylethylenediamine-β-CD; 2°-Fc-β-CD, secondary ferrocenylmethylethylenediamine-β-CD. RSD values were less than 7%.

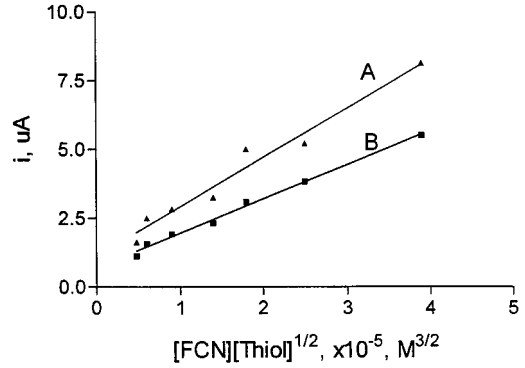


Figure 5. Limiting electrocatalytic current vs [ferricyanide]-[thiol]$^{1/2}$, for (A) cysteine and (B) glutathione oxidation. Data were recorded at 500 mV vs Ag/AgCl following linear-sweep voltammetry at 2 mV/s at a glassy carbon working electrode in 0.10 M phosphate, pH 7.0.

of mercaptopropionic acid at pH 3.8 (*28*). This trend toward increased rates at higher pH values is continued in the values observed in this work. Figure 5 shows plots of limiting electrocatalytic current against [ferricyanide]-[thiol]$^{1/2}$ for the determination of cysteine and glutathione oxidation rate constants. The rate constants compiled in Table 1 indicate not only that the rates of cysteine and glutathione oxidation by ferricyanide (90 and 48 M^{-1} s^{-1}, respectively) are of the same order of magnitude as those reported earlier, but also that the rates are significantly lower when 10 mM β-CD is present. This indicates that both cysteine and glutathione bind β-CD while ferricyanide does not, so that the effective thiol concentration is lower in the presence of the CD.

Results obtained for the two ferrocene derivatives, on the other hand, show increased thiol oxidation rates in the presence of 10 mM β-CD. Dimethylaminomethylferricinium oxidizes glutathione at a 1.3-fold higher rate, while ferriciniumcarboxaldehyde oxidizes glutathione at a 10-fold faster rate in the presence of 10 mM β-CD. These unexpected results are attributed to the simultaneous association of glutathione and ferricinium derivative with free CD. The formation of ternary complexes of CDs with two guest species has been observed previously by stopped-flow kinetic measurements, where association constants for complex formation were determined from CD-catalyzed ester hydrolysis rates that increased in the presence of the second guest species (*29*).

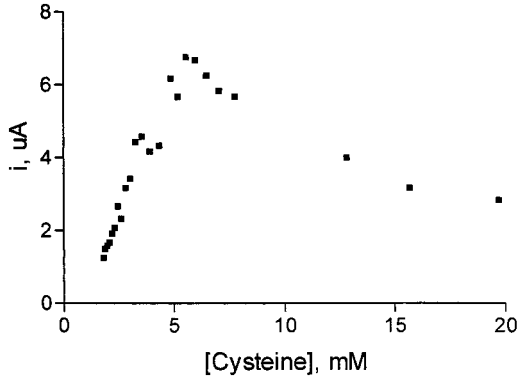


Figure 6. Limiting electrocatalytic current vs cysteine concentration, with [2°-Fc-β-CD] held constant at 0.80 mM. Data were recorded at 500 mV vs Ag/AgCl following linear−sweep voltammetry at 2 mV/s at a glassy carbon working electrode in 0.10 M phosphate, pH 7.0.

Table 1 also shows thiol oxidation rates obtained for the primary and secondary ferrocene derivatives of β-CD. Clearly, the primary derivative does not facilitate thiol oxidation, since rates obtained with this species are not much different than those seen with dimethylaminomethylferrocene; thus, in this derivative, the ferrocene/ferricicinium couple behaves as if it had no CD attached, as long as its lower diffusion coefficient is taken into account. However, the secondary derivative is a much better catalyst of thiol oxidation, especially with cysteine as a substrate: rate constants of 260 and 1470 M^{-1} s^{-1} were observed for glutathione and cysteine oxidation, respectively. Furthermore, if the pH is increased to 8.0 in 0.10 M phosphate, the rate of cysteine oxidation increases to 4120 M^{-1} s^{-1}, while free dimethylaminomethylferrocene shows a rate of 30 M^{-1} s^{-1}. These results suggest that sulfhydryl deprotonation is important during some stage of the reaction, since the pK_a is 8.15 for the cysteine sulfhydryl (*30*). Possibly, the relatively low oxidation rate observed for free dimethylaminomethylferrocene at higher pH is due to the known instability of ferricinium toward nucleophiles (*31*). However, the 140-fold acceleration factor due to covalently bound β-CD is of a similar magnitude to the 650-fold acceleration of *p-tert*-butylbenzyl alcohol oxidation by the secondary flavocyclodextrin derivative reported by Ye et al. (*16a*).

Calibration curves of limiting current against cysteine concentration were obtained while holding the total concentration of secondary ferrocene-β-CD constant. A typical plot, obtained using a glassy carbon working electrode, is shown in Figure 6. A similar curve was observed using a carbon paste working electrode. A linear region can be seen in Figure 6 below 6 mM cysteine, while higher cysteine concentrations yield decreased electrocatalytic wave heights. The shape of this curve suggests product inhibition, in that tighter binding of the disulfide product to the β-CD cavity would effectively reduce the available catalyst concentration; this phenomenon has been documented extensively for enzymatic reactions (*32*). Electrochemical dilution experiments provided confirmation of this type of inhibition. Rate constants observed at pH 7.0 for the oxidation of glutathione by 2°-Fc-β-CD decreased 10-fold when the bulk solution initially contained oxidized glutathione (GS−SG) at half the glutathione concentration. Similarly, when cystine was initially present in the bulk solution at only 4% of the cysteine concentration (this was limited by cystine solubility), the observed rate constant for cysteine oxida-

tion by 2°-Fc-β-CD decreased to less than 10% of the value observed in the absence of cystine. Thus, the disulfide oxidation products appear to associate with the CD cavity more strongly than the sulfhydryl substrates. Despite this, at cysteine concentrations below 6 mM (see Figure 6), 2°-Fc-β-CD appears to be a very effective synthetic cysteine oxidase.

ACKNOWLEDGMENT

The authors are grateful to the Natural Sciences and Engineering Research Council of Canada (NSERC) and Merck Frosst Canada Inc. for financial support.

LITERATURE CITED

(1) Bender, M. L., and Komiyama, M. (1978) *Cyclodextrin Chemistry*, Chapters V, pp 33−50, and VII, pp 61−63, and references therein, Springer-Verlag, New York.
(2) Breslow, R. (1995) Biomimetic Chemistry and Artificial Enzymes: Catalysis by Design *Acc. Chem. Res. 28*, 146−153, and references therein.
(3) Murakami, Y., Hisaeda, Y., Kikuchi, J., Ohno, T., Suzuki, M., Matsuda, Y., and Matsuura, T. (1988) Hydrophobic Vitamin B_{12}. Part 6. Carbon-Skeleton Rearrangement via Formation of Host−Guest Complexes Derived from an "Octopus" Azaparacyclophane and Hydrophobic Vitamin B_{12} Derivatives: A Novel Holoenzyme Model System *J. Chem. Soc., Perkin Trans. 2*, 1237−1246.
(4) Murakami, Y., Hisaeda, Y., and Ohno, T. (1990) Hydrophobic Vitamin B_{12}. VII. Ring-Expansion Reactions Catalyzed by Hydrophobic Vitamin B_{12} in Octopus Azaparacyclophane *J. Coord. Chem. 21*, 13−22.
(5) Murakami, Y., Hisaeda, Y., and Ohno, T. (1991) Hydrophobic Vitamin B_{12}. Part 9. An Artificial Holoenzyme Composed of Hydrophobic Vitamin B_{12} and Synthetic Bilayer Membrane for Carbon-Skeleton Rearrangements *J. Chem. Soc., Perkin Trans. 2*, 405−416.
(6) Nomura, E., Taniguchi, H., and Otsuji, Y. (1994) Calixarene-Catalyzed Generation of Dichlorocarbene and its Application to Organic Reactions: The Catalytic Action of Octopus-Type Calix[6]arene *Bull. Chem. Soc. Jpn. 67*, 792−799.
(7) Ho, M. Y. K., and Rechnitz, G. A. (1987) Highly Stable Biosensor Using an Artificial Enzyme. *Anal. Chem. 59*, 536−537.
(8) Siegel, B. (1979) Preparation and Redox Properties of a Cyclodextrin-Based Ferredoxin Model *J. Inorg. Nucl. Chem. 41*, 609−610.
(9) Bonchio, M., Carofiglio, T., Di Furia, F., and Fornasier, R. (1995) Supramolecular Catalysis: Enantioselective Oxidation of Thioanisole in Water by Hydrogen Peroxide Catalyzed by Mo(VI) in the Presence of β-Cyclodextrin *J. Org. Chem. 60*, 5986−5988.
(10) Tabushi, I., Shimizu, N., Sugimoto, T., Shiozuka, M., and Yamamura, K. (1977) Cyclodextrin Flexibly Capped with Metal Ion. *J. Am. Chem. Soc. 99*, 7100−7103.
(11) Suzuki, I., Chen, Q., Kashiwagi, Y., Osa, T., and Ueno, A. (1993) Electrochemical Conversion of Alcohols into Aldehydes Mediated by Lipophilic β-Cyclodextrin Bearing a Ferrocene Moiety. *Chem. Lett.*, 1719−1722.
(12) Kuroda, Y., Sera, T., and Ogoshi, H. (1991) Regioselectivities and Stereoselectivities of Singlet Oxygen Generated by Cyclodextrin Sandwiched Porphyrin Sensitization. Lipoxygenase-Like Activity *J. Am. Chem. Soc. 113*, 2793−2794.
(13) Kuroda, Y., Ito, M., Sera, T., and Ogoshi, H. (1993) Controlled Electron Transfer between Cyclodextrin-Sandwiched Porphyrin and Quinones. *J. Am. Chem. Soc. 115*, 7003−7004.
(14) Tabushi, I., and Kodera, M. (1987) Flavocyclodextrin as a Promising Flavoprotein Model. Efficient Electron-Transfer Catalysis by Flavocyclodextrin. *J. Am. Chem. Soc. 109*, 4734−4735.
(15) Marzone, M., and Roda, C. (1990) β-Cyclodextrin-(7,8-Dimethylalloxazine) Derivatives as Artificial Oxido-Reductase Agents. *Proc. 5th Int. Symp. Cyclodextrins*, 687−690.
(16) (a) Ye, H., Tong, W., and D'Souza, V. T. (1992) Efficient Catalysis of a Redox Reaction by an Artificial Enzyme. *J. Am. Chem. Soc. 114*, 5470−5472. (b) Ye, H., Rong, D., Tong, W., and D'Souza, V. T. (1992) Artificial Redox Enzymes. Part 4. Structure and Properties. *J. Chem Soc., Perkin Trans. 2*, 2071−2076.
(17) Ye, H., Tong, W., and D'Souza, V. T. (1994) Flavocyclodextrins as Artificial Redox Enzymes. Part 4. Catalytic Reactions of Alcohols, Aldehydes, and Thiols. *J. Chem. Soc., Perkin Trans. 2*, 2431−2437.
(18) Rong, D., Ye, H., Boehlow, T. R., and D'Souza, V. T. (1992) Artificial Redox Enzymes. 1. Synthetic Strategies. *J. Org. Chem. 57*, 163−167.
(19) Melton, L. D., and Slessor, K. N. (1971) Synthesis of Monosubstituted Cyclohexaamyloses. *Carbohyd. Res. 18*, 29−37.
(20) Rong, D., and D'Souza, V. T. (1990) A Convenient Method for Functionalization of the 2-Position of Cyclodextrins. *Tetrahedron Lett. 31*, 4275−4278.
(21) Badia, A., Carlini, R., Fernandez, A., Battaglini, F., Mikkelsen, S. R., and English, A. M. (1993) Intramolecular Electron-Transfer Rates in Ferrocene-Derivatized Glucose Oxidase. *J. Am. Chem. Soc. 115*, 7053−7060.
(22) Matsue, T., Evans, D. H., Osa, T., and Kobayashi, N. (1985) Electron-Transfer Reactions Associated with Host−Guest Complexation. Oxidation of Ferrocenecarboxylic Acid in the Presence of β-Cyclodextrin. *J. Am. Chem. Soc. 107*, 3411−3417.
(23) Adams, R. N. (1969) *Electrochemistry at Solid Electrodes*, p 219, Marcel Dekker, New York.
(24) Tinke, A. P., van der Hoeven, R. A. M., Niessen, W. M. A., van der Greef, J., Vincken, J.-P., and Schols, H. A. (1993) Electrospray Mass Spectrometry of Neutral and Acidic Oligosaccharides: Methylated Cyclodextrins and Identification of Unknowns Derived from Fruit Material *J. Chromatogr. 647*, 279−287.
(25) Lamcharfi, E., Chuilon, S., Kerbal, A., Kunesch, G., Libot, F., and Virelizier, H. (1996) Electrospray Ionization Mass Spectrometry in Supramolecular Chemistry: Characterization of Non-Covalent Cyclodextrin Complexes *J. Mass Spectrom. 31*, 982−986.
(26) Sheeley, D. M., and Reinhold, V. N. (1998) Structural Characterization of Carbohydrate Sequence, Linkage, and Branching in a Quadrupole Ion Trap Mass Spectrometer: Neutral Oligosaccharides and N−Linked Glycans. *Anal. Chem. 70*, 3053−3059.
(27) Kapoor, R. C., Kachhwaha, O. P., and Sinha, B. P. (1969) Oxidation Kinetics of Thioglycolic Acid by Ferricyanide Ion in Acid Medium *J. Phys. Chem. 73*, 1627−1631.
(28) Bohning, J. J., and Weiss, K. (1960) The Kinetics of Oxidation of 3-Mercaptopropionic Acid with Potassium Ferricyanide *J. Am. Chem. Soc. 82*, 4724−4728.
(29) (a) Tee, O. S., Bozzi, M., Clement, N., and Gadosy, T. A. (1995) Catalysis of the Reaction of *p*-Nitrophenyl Alkanoates with Cyclodextrins by Potential Inhibitors: Simple Allosteric Activation. *J. Org. Chem. 60*, 3509−3517. (b) Tee, O. S., and Giorgi, J. B. (1997) The Effect of Alcohols on the Basic Cleavage of *m*-Nitrophenyl Hexanoate by β-Cyclodextrin: Allosteric Reaction Mode Switching. *J. Chem. Soc., Perkin Trans. 2*, 1013−1018.
(30) Martell, A. E., and Smith, R. M. (1974) *Critical Stability Constants*, Vol. I, p 47, Plenum Press, New York.
(31) Prins, R., Korswagen, A. R., and Kortbeek, A. G. T. G. (1972) Decomposition of the Ferricenium Cation by Nucleophilic Reagents. *J. Organomet. Chem. 39*, 335−344.
(32) Rudolph, F. B. (1979) Product Inhibition and Abortive Complex Formation. *Methods Enzymol. 63*, 411−436.

BC9801326

An N_2S_2 Bifunctional Chelator for Technetium-99m and Rhenium: Complexation, Conjugation, and Epimerization to a Single Isomer

Leonard G. Luyt, Hilary A. Jenkins,† and Duncan H. Hunter*

Department of Chemistry, University of Western Ontario, London, Ontario, Canada N6A 5B7. Received November 6, 1998; Revised Manuscript Received January 18, 1999

A bifunctional chelator **6** was prepared bearing an N_2S_2 core for binding rhenium or technetium and a carboxylic acid group for conjugation to amino groups of biomolecules. Complexation of **6** with rhenium(V) resulted in two kinetic isomers, anti-**7** and syn-**7**, being formed in approximately equal amounts. Epimerization with 0.5 M NaOH yields a single isomer anti-**7**, as determined by NMR spectroscopy and single-crystal X-ray analysis. The ^{99m}Tc complex was prepared at the tracer level by reaction of the ligand with $^{99m}TcO_4^-$, tin(II) chloride and sodium gluconate giving a mixture of two isomers, but showing a preference for the anti isomer. Chelation in the presence of 1 M NaOH results in anti-**8** being formed as the sole product. The bifunctional ability of the ligand was explored by amide formation with (*S*)-α-phenethylamine, either by direct DCC coupling or through the N-hydroxy succinimidyl ester **9** intermediate. The deprotected bioconjugate **11** was complexed with rhenium, yielding similar amounts of two isomeric rhenium complexes, anti-**12** and syn-**12**, which were isolated and characterized by NMR spectroscopy. Treatment of the kinetic mixture of anti-**12** and syn-**12** with 1 M NaOH resulted in quantitative conversion to a single rhenium complex anti-**12**. With technetium-99m in 0.1 M sodium acetate, bioconjugate **11** yielded both technetium-99m complexes anti-**13** and syn-**13**, in a 2:1 ratio, respectively. In contrast, complexation in the presence of 1 M NaOH gave only one technetium-99m complex, assigned the structure anti-**13**.

INTRODUCTION

Single photon emission computed tomography (SPECT) imaging with ^{99m}Tc is the most commonly utilized method for routine diagnostic nuclear medicine procedures. ^{99m}Tc is preferred as a radionuclide for its favorable nuclear characteristics, availability, and low cost. A wide variety of ^{99m}Tc-containing radiopharmaceuticals are used (*1*), but only a few receptor-specific small-molecule ^{99m}Tc radiopharmaceuticals have been designed that are directed to bind at specific receptor sites (*2*). Receptor-binding radiotracers allow for the study of changes in receptor concentrations that often accompany disease states or for the imaging of tissues rich in a specific receptor.

One approach to the production of a target-directed ^{99m}Tc radiopharmaceutical is to attach a bifunctional chelator to a biospecific molecule, followed by radiolabeling with ^{99m}Tc. Target-directed radiopharmaceuticals are of importance for diagnostic imaging purposes when ^{99m}Tc is utilized, but also allow for radiotherapy using the chemically analogous ^{186}Re/^{188}Re species (*3*–*5*). For chelating purposes, the amide thiolate ligands (N_2S_2 agents) were attractive since they have been shown to form stable complexes with technetium and rhenium (*6*, *7*). For attachment to a biomolecule, the carboxyl group was selected since many biomolecules contain amino groups available for amide formation.

A number of modifications to the original (*6*, *7*) ethylene/propylene framework of amide thiolate N_2S_2 agents have been made, and analogues bearing carboxyl groups have already been studied as chelating agents (*8*, *9*). However, substituents can introduce stereochemical problems. This is illustrated in Figure 1 for *N*,*N*′-bis(mercaptoacetyl)-2,3-diaminopropanoate (CO_2DADS), where, for R = OH, four stereoisomers are known since each of the anti and syn diastereomers can exist as enantiomers (*10*). All four stereoisomers of these CO_2DADS complexes have been synthesized and differences in biodistribution characteristics were observed (*11*, *12*).

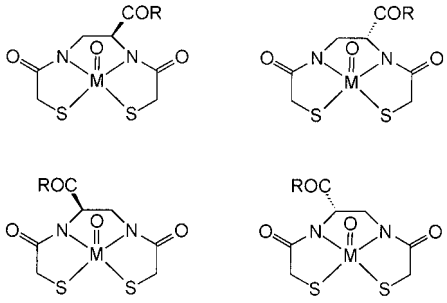


Figure 1. The four anionic stereoisomers formed from chelation of *N*,*N*′-bis(mercaptoacetyl)-2,3-diaminopropanoate (CO_2-DADS) with rhenium or technetium. For R = OH, two sets of enantiomers are formed; for R = chiral biomolecule, four diastereomers are formed.

If the CO_2DADS chelator shown in Figure 1 is attached to a chiral biomolecule (R = chiral molecule), then four different diastereomers will be produced. This could have serious consequences on yields, characterization, and isolation of individual species (*13*), each of which could have differing biological activities. In the case of the dopamine transporter imaging agent [^{99m}Tc]TRODAT-1, the two separated isomers displayed different binding affinities in a SPECT imaging study (*14*).

* To whom correspondence should be addressed. Phone: (519) 679-2111 ext. 6347. Fax: (519) 661-3022. E-mail: dhunter@julian.uwo.ca.

† Presently at Chemistry Department, St. Mary's University, Halifax, Nova Scotia, Canada B3H 3C3.

10.1021/bc980134q CCC: $18.00 © 1999 American Chemical Society
Published on Web 03/05/1999

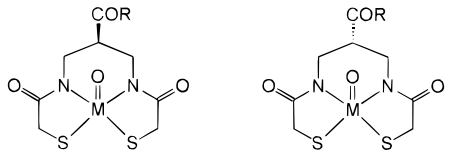


Figure 2. The two anionic isomers formed upon chelation of **6** with rhenium or technetium. For R = OH or R = chiral biomolecule, only two isomers are formed.

In an attempt to minimize the chemical and biological complications of generating multiple stereoisomers, the carboxylic acid linker was placed at the apex of an eventual six membered ring. This is illustrated in Figure 2, which shows that only two stereoisomers (anti and syn) would result with or without attachment to a chiral biomolecule. We have endeavored to keep the chelator as small in size as possible to help minimize disruption on the receptor-binding affinity. The anticipated formal negative charge on the chelate may limit its general applicability as a radiolabel.

EXPERIMENTAL SECTION

Chemicals were purchased from commercial sources as reagent grade and used as received. 2-Triphenylmethylmercaptoacetic acid and dioxobisethylenediaminerhenium(V) chloride were prepared according to literature procedures (*15*, *16)*. ^{1}H NMR spectra were collected on a Varian Gemini-300 or Varian Gemini-200 spectrometer with TMS as an internal reference. ^{13}C NMR and two-dimensional spectra were obtained on a Varian Gemini-300 or Varian 300-XL spectrometer with the ^{13}C acquisition at 75 MHz. ^{1}H spin−spin decoupling NMR spectra were obtained on a Varian Gemini-300 spectrometer. Infrared spectra were recorded in the range 4000−600 cm^{-1} on either a Bruker IFS 5500 FT-IR with a Spectra-Tech diffuse reflectance accessory (DRIFT) or on a Perkin-Elmer 2000 FT-IR utilizing a solution cell or thin film NaCl plate. Routine mass spectra (MS) and negative ion fast-atom bombardment mass spectra (FABMS) were measured on a Finnigan MAT 8200 spectrometer. Melting points were taken on a Gallenkamp or a Fisher−Johns melting point apparatus and are uncorrected. HPLC was performed using either a Varian 5500 or a Dionex DX 300 HPLC under the column and eluent conditions noted in the Experimental Section. Elemental analyses were performed by Guelph Chemical Laboratories Ltd. (Guelph, Ontario). $Na^{99m}TcO_4$ was obtained from a commercial ^{99}Mo/^{99m}Tc generator as supplied by DuPont.

3,3-Dicyano-propionic Acid Ethyl Ester (1). Sodium hydride dispersion (7.89 g of 60% w/w, 0.197 mol) was placed in a three-necked flask with attached dropping funnel, condensor, vacuum inlet, and argon bubbler. The glassware was assembled hot, then twice evacuated and filled with argon. Freshly distilled THF (400 mL distilled from sodium/benzophenone) was added via glass syringe, and the mixture was cooled to 0 °C. Malononitrile (26.1 g, 0.395 mol) was dissolved in 100 mL of distilled THF and added dropwise. After the reaction mixture was warmed to room temperature, ethyl chloroacetate (23.3 g, 0.190 mol) was added, and the mixture was brought to reflux for 2 h. After cooling to room temperature, the THF was removed using a rotary evaporator. The solids were taken up in 250 mL of $CHCl_3$ and washed with two portions of 0.5 M HCl. The organic layer was dried over $MgSO_4$, and the solvent removed by a rotary evaporator. A ^{1}H NMR spectrum of the crude product indicated 63% **1** and 37% 3,3-dicyano-pentanedioic acid diethyl ester byproduct. Using fractional reduced pressure distillation, the desired product was collected over 86−92 °C at 0.2 mmHg, then cooled to allow crystallization. The resulting solid was recrystallized from diethyl ether/petroleum ether to give shiny colorless plates (17.1 g, 59% yield). A sample was further purified by sublimation: mp 70−71 °C. ^{1}H NMR ($CDCl_3$): δ 1.30 (t, 3H, CH_3), 3.04 (d, 2H, CH_2), 4.16 (t, 1H, CH), 4.26 (q, 2H, CH_2O); ^{13}C NMR ($CDCl_3$) δ 13.59 (CH_3), 18.39 (CH), 34.48 (CH_2CO), 62.26 (CH_2O), 111.31 (CN x2), 166.33 (CO). FT-IR (thin film) cm^{-1}: 2263, 1727. HRMS (CI) *m/z*: calcd for $C_7H_8N_2O_2$ $(M + H)^+$ 153.0664. Found: 153.0667. Anal. ($C_7H_8N_2O_2$): C, H, N, O.

4-Amino-3-aminomethyl-butyric Acid Ethyl Ester Dihydrochloride (2). A Parr glass flask was charged with **1** (1.53 g, 10.1 mmol), 50 mL of ethanol (0.2% H_2O as determined by Karl Fischer titration), PtO_2 (148 mg), and 1.73 mL of concentrated HCl (20.8 mmol). The flask was attached to a Parr hydrogenator, twice evacuated and filled with H_2, then filled with H_2 to a pressure of 53 psig. The hydrogenation proceeded at room temperature for 18 h with continuous shaking. The black catalyst was filtered, the solution was transferred to a round-bottom flask, and the ethanol was removed using a rotary evaporator. The product was dried at room temperature under 0.3 mmHg vacuum for 3 h yielding 2.39 g of fluffy white crystals (quantitative yield). This material was used without further purification. ^{1}H NMR (D_2O): δ 1.08 (t, 3H, CH_3), 2.41 (m, 1H, CH), 2.52 (d, 2H, CH_2CO), 2.98 (dd, 4H, NCH_2), 4.01 (q, 2H, CH_2).

***N*-Hydroxysuccinimidyl 2-Triphenylmethylmercaptoacetate (3)**. 2-Triphenylmethylmercaptoacetic acid (4.76 g, 14.2 mmol) and 1.64 g (14.3 mmol) *N*-hydroxysuccinimide (NHS) were added to 25 mL of acetonitrile. The reaction mixture was cooled to 0 °C followed by the addition of 3.01 g (15.7 mmol) 1-(3-dimethylaminopropyl)-3-ethylcarbodiimide hydrochloride (EDC) and 2,4,6-trimethylpyridine (2.1 mL) with subsequent warming to room temperature. The mixture was stirred under argon at room temperature for 3 h and then cooled to 0 °C. The resulting precipitate was removed by filteration and washed with cold acetonitrile to give 5.31 g (yield 86%) of colorless crystals: mp 178.0−179.0 °C. ^{1}H NMR ($CDCl_3$): δ 2.76 (s, 4H, CH_2 succinimidyl), 3.17 (s, 2H, CH_2S), 7.22 to 7.42 (m, 15H, ar). ^{13}C NMR ($CDCl_3$): δ 25.49 (CH_2), 31.38 (CH_2S), 67.98 (CPh_3), 127.09 (ar), 128.19 (ar), 129.43 (ar), 143.48 (ar), 164.99 (CO), 168.54 (CO).

3,3-Bis(triphenylmethylthio-acetidomethyl)propanoic Acid Ethyl Ester (4). A two-necked flask with an attached argon bubbler was charged with 100 mL of CH_2Cl_2, **2** (1.46 g, 6.28 mmol), **3** (5.23 g, 12.1 mmol), and 2.2 mL (12.6 mmol) of *N*,*N*-diisopropylethylamine (DIPEA). The reaction mixture was stirred at room temperature under a flow of argon for 20 h, then transferred to a separatory funnel, washed with saturated $NaHCO_3$ (2 × 75 mL), 0.5 M HCl (2 × 70 mL), and saturated NaCl. The organic layer was dried over $MgSO_4$ and filtered, and the solvent was removed by a rotary evaporator and placed under high vacuum to give 5.05 g of a yellow crystalline solid. Recrystallization from ethyl acetate/hexanes afforded 3.27 g of fine colorless crystals (68% yield): mp 193−194 °C. ^{1}H NMR ($CDCl_3$): δ 1.19 (t, 3H, CH_3), 1.86 (m, 1H, CH), 2.01 (d, 2H, CH_2CO), 2.78 (m, 4H, CH_2N), 3.01 (s, 4H, CH_2−S), 4.06 (q, 2H, CH_2 Et), 6.47 (t, 2H, NH), 7.22 to 7.37 (m, 30H, ar). ^{13}C NMR ($CDCl_3$) δ 14.17 (CH_3), 34.71 (CH_2CO), 35.92 (CH), 36.04 (CH_2S), 39.96 (CH_2N), 60.61 (CH_2O), 67.74 (CPh_3), 126.96 (ar), 128.10 (ar), 129.45 (ar), 143.94 (ar), 168.88 (CO),

172.08 (CO). FT-IR ($CHCl_3$ solution cell): cm^{-1} 3382, 1728, 1664. Anal. ($C_{49}H_{48}N_2O_4S_2$): C, H, N, O, S.

3,3-Bis(triphenylmethylthio-acetamidomethyl)-propanoic Acid (5). To a solution of 25 mL of THF and 25 mL of 1 M NaOH was added **4** (1.00 g, 1.27 mmol). The mixture was stirred at room temperature under argon for 18 h with the reaction progress being monitored by TLC (Silica 60, ethyl acetate). The reaction mixture was acidified by the addition of 25 mL of 1 M HCl. The THF was removed by rotary evaporator and the product extracted with three portions of CH_2Cl_2, which was washed with saturated NaCl and dried over $MgSO_4$. After filtering, the solvent was removed by a rotary evaporator, leaving the crude product as fine colorless crystals (0.93 g). Recrystallization from CH_2Cl_2/hexanes gave the propanoic acid (0.88 g, 0.91 mmol, 91% yield): mp 214−215 °C. ^{1}H NMR ($CDCl_3$): δ 1.72 (m, 1H, CH), 1.93 (d, 2H, CH_2CO), 2.53 (ddd, 2H, CHN x2), 3.00 (ddd, 2H, CHN x2), 3.09 (s, 4H, CH_2S), 6.71 (m, 2H, NH), 7.17 to 7.41 (m, 20H, ar). ^{13}C NMR (d_6-DMSO): δ 33.94 (CH_2CO), 35.21 (CH), 36.02 (CH_2S), 39.96 (CH_2N), 66.10 (CPh_3), 126.81 (ar), 128.08 (ar), 129.10 (ar), 144.06 (ar), 167.65 (CO), 173.38 (CO). FT-IR (thin film) cm^{-1}: 3326, 1718, 1647. Anal. ($C_{47}H_{44}N_2O_4S_2$): C, H, N, O, S.

3,3-Bis(thio-acetamidomethyl)propanoic Acid Oxorhenium(V) (7). A solution of **5** (261 mg, 0.341 mmol) in 14 mL CH_2Cl_2 was cooled to 0 °C with an ice bath. To this were added 8 mL (0.1 mol) of cold trifluoroacetic acid (TFA) and triethylsilane (115 μL, 0.720 mmol). The mixture was stirred at 0 °C for 25 min then warmed to room temperature and transferred to a separatory funnel with additional CH_2Cl_2. Water was added, and the triphenylmethane was extracted with three CH_2Cl_2 extractions.

The aqueous layer containing **6** [3,3-bis(thioacetamidomethylene)propanoic acid] was transferred to a 100 mL flask, and solid sodium acetate was added until the solution tested basic. Dioxobis(ethylenediamine)rhenium-(V) (139 mg, 0.342 mmol) was added and the solution turned a clear yellow color. The mixture was heated to reflux for 45 min with the color turning to red. After cooling to room temperature, tetraphenylarsonium chloride was added (286 mg, 0.682 mmol) with an immediate precipitate formation. The rhenium complex was filtered to give a pale rose powder that was recrystallized from methanol/water, dried under 0.025 mmHg vacuum to give 148 mg of **7** (51% yield) as a mixture of two isomers. ^{1}H NMR (d_6-DMSO): δ 2.17 (m, 1H, CH syn), 2.35 (m, 1H, CH anti), 2.41 (d, 2H, J = 6.5 Hz, CH_2CO_2H anti), 2.44 (d, 2H, J = 6.8 Hz, CH_2CO_2H syn), 2.63 (dd, 2H, J = 13.2, 10.8 Hz, CHN x2 anti), 3.31 (dd, 2H, J = 13.6, 6.6, CHN x2 syn), 3.48/3.79 (AB, 4H, J = 17.2 Hz, CH_2S syn), 3.57/3.64 (AB, 4H, J = 17.1 Hz, CH_2S anti), 3.78 (dd, 2H, J = 13.2, 2.3 Hz, CHN x2 anti), 3.88 (dd, 2H, J = 13.6, 3.1, CHN x2 syn), 7.76−7.90 (40 H, ar). IR (diffuse reflectance): 1712, 1606, 974 (ReO). HRMS, FAB (negative ion) m/z calcd: $C_9H_{12}N_2O_5S_2{}^{187}Re$ 478.9745. Found: 478.9738. HPLC (Dionex IonPac AS9-SC 4.0 × 250 mm; eluent 1.0 mL/min of 20% CH_3CN/80% 0.1 M NaCl, 1.8 mM Na_2CO_3, 1.7 mM $NaHCO_3$ solution; UV detector at 260 nm): product retention times of 10.69 (45%) and 11.65 min (55%).

Epimerization to anti-7. A sample of the epimers **7** (48 mg) was dissolved in 5 mL of methanol with slight warming to assist in the dissolution. To this solution was added 5 mL of 0.5 M sodium hydroxide solution, and the mixture was stirred at room temperature for 30 min. Acidification was carried out by the addition of 1 M HCl until the pH was slightly acidic. The methanol was then removed by a rotary evaporator resulting in a rose-colored powder precipitating from the aqueous solution. The solid was filtered, washed with water, and dried under vacuum, leaving 46 mg (96%) of a single isomer: mp 278−279 °C. ^{1}H NMR (d_6-DMSO): δ 2.35 (m, 1H, CH), 2.41 (d, 2H, J = 6.5 Hz, CH_2CO_2H), 2.63 (dd, 2H, J = 13.2, 10.8 Hz, CHN x2), 3.57/3.64 (AB, 4H, J = 17.1 Hz, CH_2S), 3.78 (dd, 2H, J = 13.2, 2.3 Hz, CHN x2), 7.77−7.90 (20 H, ar). ^{13}C NMR (d_6-DMSO, assignments based on HETCOR): δ 36.86 (CH_2CO_2H), 36.95 (CH_2S), 40.48 (CH), 54.63 (CH_2N), 121.02 (ar), 130.89 (ar), 133.17 (ar), 134.27 (ar), 173.27(CO), 194.25 (CO). HPLC (Dionex IonPac AS9−SC 4.0 × 250 mm; eluent 1.0 mL/min of 20% CH_3CN/80% 0.1 M NaCl, 1.8 mM Na_2CO_3, 1.7 mM $NaHCO_3$ solution; UV detector at 260 nm): product retention time, 11.58 min.

3,3-Bis(thio-acetamidomethyl)propanoic Acid Oxotechnetium(V) (8): **General Method**. A 3 mL vial was charged with 10 μL of aqueous base solution (0.1 M NaOAc or 1.8 mM Na_2CO_3/1.7 mM $NaHCO_3$ or 1 M NaOH), 10 μL of sodium gluconate (10 mM aqueous solution), 50−150 μCi $Na^{99m}TcO_4^-$ in saline, 10 μL of **6** (0.5 mM aqueous solution), and 0.02 mg of $SnCl_2$. The mixture was heated at 70 °C for 40−120 min. The reaction mixture was injected onto a HPLC with an anion-exchange column (Dionex IonPac AS9-SC 4.0 × 250 mm; eluent 1.0 mL/min of 20% CH_3CN/80% 0.1 M NaCl, 1.8 mM Na_2CO_3, 1.7 mM $NaHCO_3$ solution; radiometric γ detector) with resulting product retention times for the two epimers of 11.1 and 12.3 min. The eluent from the HPLC was collected for the period of 11−13 min, thereby allowing for the collection of both isomers of **7**. The collected eluent was counted in a dose calibrator giving a radiochemical yield of 67−88%.

3,3-Bis(triphenylmethylthio-acetamidomethyl)-propanoic Acid *N*-Hydroxysuccinimidyl Ester (9). The acid **5** (407 mg, 0.532 mmol), *N*-hydroxysuccinimide (69 mg, 0.60 mmol) and 1-(3-dimethylaminopropyl)-3-ethylcarbodiimide hydrochloride (118 mg, 0.62 mmol) were placed in a flask with 25 mL of CH_2Cl_2. To this was added 77 μL of 2,4,6-trimethylpyridine (0.58 mmol), and the mixture was stirred at room temperature under argon for 18 h. The reaction mixture was placed in a separatory funnel, washed twice with 0.1 M HCl, water, and saturated NaCl solution. The organic layer was dried over $MgSO_4$ and filtered, and the solvent was removed by a rotary evaporator leaving a clear colorless oil (382 mg, 83%). The product which crystallized when triturated with hexanes was then recrystallized from $CHCl_3$/hexanes and dried under vacuum at room temperature: mp 87 °C (dec). ^{1}H NMR ($CDCl_3$): δ 1.97 (m, 1H, CH), 2.33 (d, 2H, CH_2CO), 2.77 (s, 4H, CH_2 NHS), 2.75−2.99 (m, 4H, CH_2N), 3.05 (d, 4H, CH_2S), 6.61 (t, 2H, NH), 7.17−7.42 (m, 30H, ar). ^{13}C NMR ($CDCl_3$): δ 25.54 (CH_2 NHS), 31.73 (CH_2CO), 35.95 (CH_2S), 36.44 (CH), 39.63 (CH_2N), 67.70 (CPh_3), 126.96 (ar), 128.11 (ar), 129.45 (ar), 143.93 (ar), 167.34 (CO), 168.93 (CO), 169.21 (CO).

***N*-[(*S*)-1-Phenylethyl]-3,3-bis(triphenylmethylthio-acetamidomethyl)propanamide (10)**: **Method A**. The N_2S_2 acid **5** (823 mg, 1.08 mmol), 1-hydroxybenzotriazole (1-HOBT, 184 mg, 1.20 mmol), and dicyclohexylcarbodiimide (DCC, 244 mg, 1.18 mmol) were added to 30 mL of CH_2Cl_2. To this was added (*S*)-1-phenethylamine (137 mg, 1.13 mmol) and 2,4,6-trimethylpyridine (156 μL, 1.18 mmol). The reaction mixture was stirred at room temperature under a constant argon flow for 3 days. The dicyclohexylurea byproduct was removed by filtration. The reaction mixture was placed in a separatory funnel and washed with saturated $NaHCO_3$ (x2), 0.5 N HCl (x2),

and saturated NaCl. The organic layer was then dried over $MgSO_4$, the solvent was removed by a rotary evaporator, followed by drying at room temperature under vacuum to give 1.01 g of a beige solid. This solid was triturated with EtOAc and recrystallized from $CHCl_3$/hexanes to give 821 mg of colorless fine crystals (yield 88%): mp 187−189 °C. ^{1}H NMR ($CDCl_3$): δ 1.43 (d, 3H, CH_3), 1.65 (m, 1H, CH), 1.78 (d, 2H, CH_2), 2.42 (ddd, 1H, CH_2N), 2.54 (ddd, 1H, CH_2N), 2.98 (m, 2H, CH_2NH), 3.03 (s, 4H, CH_2S), 5.02 (quintet, 1H, CHPh), 6.70 (m, 2H, NH x2), 7.16 to 7.42 (m, 35H, ar), 7.81 (d, 1H, NH). ^{13}C NMR ($CDCl_3$): δ 22.42 (CH_3), 36.09 (CH_2S), 36.59 (CH_2), 37.95 (CH), 39.86 (CH_2N), 40.01 (CH_2N), 49.01 (CHPh), 67.75 (CPh_3), 126.17 (Ph), 126.95 (Trt), 128.10 (Trt), 128.45 (Ph), 129.45 (Trt), 143.91 (Trt), 143.95 (Ph), 169.57 (CO), 169.66 (CO). 170.29 (CO). MS (CI, isobutane): *m/z* 867 (M+), 624 (M − trityl), 382 [M − (trityl)$_2$]. HRMS (EI, dprobe): *m/z* calcd: $C_{17}H_{23}N_3O_3S_2$ (detritylated), 381.1181. Found: 381.1169. Anal. ($C_{55}H_{53}N_3O_3S_2$): C, H, N, O, S.

Method B. The succinimidyl ester **9** (155 mg, 0.180 mmol), (*S*)-phenylethylamine (27 mg, 0.220 mmol), and *N,N*-diisopropylethylamine (31 μL, 0.180 mmol) were added to 15 mL of CH_2Cl_2. The reaction contents were stirred at room temperature under argon for 18 h, then transferred to a separatory funnel and washed with 0.1 M HCl, saturated $NaHCO_3$, and saturated NaCl. The organic layer was dried over $MgSO_4$ and filtered, and the solvent was removed by a rotary evaporator and dried under vacuum leaving fine white crystals. Recrystallization from $CHCl_3$/hexanes gave 124 mg of fine white crystals (79%) with characterization consistent to that reported for method A.

***N*-[(*S*)-1-Phenylethyl]-3,3-bis(thio-acetamidomethyl)propanamide (11)**. A two-necked flask containing 10 mL of CH_2Cl_2 was charged with **10** (301 mg, 0.346 mmol). The flask was cooled to 0 °C with an ice bath while under a continuous flow of argon. Trifluoroacetic acid (6 mL, 78 mmol) and triethylsilane (122 μL, 0.762 mmol), both at 0 °C, were added. The reaction mixture was stirred for 30 min with the initially clear and yellow solution turning to clear and colorless. Additional CH_2Cl_2 was added, and the mixture was placed in a separatory funnel then washed twice with water. The organic layer was transferred into a flask, the solvent was removed by a rotary evaporator, and the resulting solid was vacuum-dried at room temperature. The colorless solid was repeatedly triturated with hexane to remove the majority of the triphenylmethane. The crude dithiol product **11** was used without further purification (132 mg). ^{1}H NMR ($CDCl_3$): δ 1.49 (d, 3H, CH_3), 1.98 (t, 2H, SH), 2.08 (m, 3H, CH and CH_2), 2.97 (m, 2H, CH_2N, H_a), 3.22 (d, 4H, CH_2S), 3.40 (m, 2H, CH_2N, H_b), 5.02 (quintet, 1H, NCH), 7.08−7.32 (m, 5H, ar), 7.82 (br.t, 2H, NH), 8.33 (d, 1H, NH).

***N*-[(*S*)-1-Phenylethyl]-3,3-bis(thio-acetamidomethyl)propanamide Oxorhenium(V) (12)**. The crude dithiol **11** (0.346 mmol) was placed in a three-necked flask to which was added trichlorooxobis(triphenylphosphine)-rhenium (288 mg, 0.346 mmol). The flask was evacuated and filled with argon, followed by the addition of 15 mL of 1 M sodium acetate in methanol (degassed for 1 h with bubbling argon). The reaction mixture was brought to reflux, stirred under argon at reflux for 5 h, and then cooled to room temperature. The methanol was removed using a rotary evaporator, and water was added to give a clear solution with a fine brown precipitate. The precipitate was filtered using a sintered glass filter. To the clear brown filtrate was added tetraphenylarsoniumchloride hydrate (162 mg, 0.387 mmol), resulting in the immediate precipitation of pale orange crystals. The crystals were removed by filtration and dried at room temperature under 0.025 mmHg vacuum to give 210 mg (63% for two steps) of a mixture of two isomers. IR (diffuse reflectance): 971 (ReO). HRMS FAB (negative ion) *m/z* calcd: $C_{17}H_{21}N_3O_4S_2187Re$, 582.0531. Found: 582.0567. HPLC using a reversed-phase column indicates that two products are present with retention times of 9.6 (54%) and 11.5 (46%) min under the conditions noted: C_{18} reversed-phase Waters μBondpak 3.9 × 300 mm; eluent 1.0 mL/min of 15% CH_3CN/85% 10 mM KH_2PO_4 solution ramped over 10 min to 30% CH_3CN/70% 10 mM KH_2PO_4 solution, and maintained at that solvent ratio; UV detector at 220 nm.

Epimerization to *anti*-*N*-[(*S*)-1-Phenylethyl)]-3,3-bis(thio-acetamidomethyl)propanamide Oxorhenium(V) (anti-12). The mixture of the two isomers **12** (185.6 mg, 0.192 mmol) was dissolved in 30 mL of methanol followed by the addition of 15 mL of 1 M NaOH. After stirring at room temperature for 30 min, an aliquot was taken and checked by HPLC, indicating 98.8% of a single isomer. Water was added to the flask, and the methanol removed by a rotary evaporator. The rose-colored crystals that formed were filtered and dried under vacuum, yielding 164.4 mg (89%): mp 127−130 °C. ^{1}H NMR ($CDCl_3$): δ 1.48 (d, 3H, CH_3), 2.27 (d, 2H, CH_2CO), 2.56 (m, 1H, CH), 2.87 (m, 2H, CHN x2), 3.59/3.74 or 3.76 (AB, 2H, CHS x2, $|J| = 17.1$ Hz), 3.62/3.74 or 3.76 (AB, 2H, CHS x2, $|J| = 17.1$ Hz), 3.92 (m, 2H, CHN x2), 5.06 (quintet, 1H, CHPh), 5.98 (d, 1H, NH), 7.2−7.8 (ar, 25H). ^{13}C NMR ($CDCl_3$): δ 21.94 (CH_3), 38.61 (CH_2S), 39.99 (CH_2CO), 40.96 (CH), 48.90 (CHPh), 54.90 (CH_2N), 55.04 (CH_2N), 170.4 (NHCO), 195.9 (CO), 196.0 (CO). HPLC of the product was performed under identical conditions as used for compound **12**. The UV chromatogram indicated a single product eluting with a retention time of 9.6 min: C_{18} reversed-phase Waters μBondpak 3.9 × 300 mm; eluent 1.0 mL/min of 15% CH_3CN/85% 10 mM KH_2PO_4 solution ramped over 10 min to 30% CH_3CN/70% 10 mM KH_2PO_4 solution and maintained at that solvent ratio; UV detector at 220 nm.

HPLC Separation of *syn*-*N*-[(*S*)-1-phenylethyl]-3,3-bis(thio-acetamidomethyl)propanamide Oxorhenium(V) (syn-12). A concentrated solution of a mixture of the two isomers (**12**) was prepared in acetonitrile. Semipreparative HPLC was performed on a Varian Vista 5500, with a Varian MicroPak MCH-10 (30 cm × 8 mm) C_{18} reversed-phase column and a UV detector set at 220 nm. The eluent was a gradient from 20% CH_3CN/80% 10 mM KH_2PO_4 solution to 30% CH_3CN/70% 10 mM KH_2PO_4 over 15 min. A flow rate of 2.0 mL/min allowed for the complete separation of the two isomers with retention times of 12.7 and 15.1 min. Two fractions were collected and combined from a total of four HPLC runs. Each was placed in a flask, and the CH_3CN was removed by a rotary evaporator followed by the addition of Ph_4AsCl. The precipitate that formed was collected by filtration and dried under vacuum leaving approximately 2 mg of each isomer. The product eluting at 12.7 min was found to be the anti isomer as shown by ^{1}H NMR spectroscopy. The material eluting at 15.1 min was syn-**12** and was characterized. ^{1}H NMR ($CDCl_3$): δ 1.40 (d, 3H, $J = 6.9$ Hz, CH_3), 2.63 (dd, 2H, CH_2CO), 2.80 (m, 1H, CH), 3.42 (m, 2H, CHN x2), 3.76/3.84 (AB, 2H, CHS x2, $|J| = 17.2$ Hz), 3.86 (m, 2H, CHN x2), 4.04/4.09 (AB, 2H, CHS x2, $|J| = 17.4$ Hz), 5.06 (quintet, 1H, CHPh), 6.13 (d, 1H, NH), 7.2 to 7.9 (ar, 25H). HPLC (conditions

Table 1. Crystal Data and Data Collection Parameters

	anti-**7** Ph_4As
formula	$C_{33}H_{32}AsN_2O_2ReS_2$
FW	861.85
temp (K)	294 (2)
crystal system	orthorhombic
space group	$P2_12_12_1$
Z	4
a (Å)	9.4435 (3)
b (Å)	14.3439 (4)
c (Å)	24.1591 (5)
V (Å^3)	3272.5 (2)
radiation MoKα, λ (Å)	0.710 73
no. of independent reflections	5752
no. of data parameters	405
R_1	0.0246
R_{w2}	0.0558
goodness of fit	0.988

Table 2. Selected Bond Lengths and Bond Angles

Bond Lengths (Å)			
Re−O(1)	1.673 (3)	N(1)−C(3)	1.479 (6)
Re−S(1)	2.2938 (13)	N(2)−C(7)	1.474 (6)
Re−S(2)	2.2954 (13)	C(3)−C(4)	1.498 (6)
Re−N(1)	2.050 (4)	C(4)−C(7)	1.473 (7)
Re−N(2)	2.019 (4)		
Bond Angles (deg)			
O(1)−Re−S(1)	109.03 (13)	Re−N(1)−C(3)	124.0 (3)
O(1)−Re−N(1)	106.8 (2)	Re−N(2)−C(7)	123.7 (3)
O(1)−Re−S(2)	108.47 (13)	N(1)−C(3)−C(4)	113.7 (4)
O(1)−Re−N(2)	110.0 (2)	C(3)−C(4)−C(5)	108.2 (4)
S(1)−Re−S(2)	84.66 (5)	C(3)−C(4)−C(7)	112.5 (5)
S(1)−Re−N(1)	81.97 (11)	C(5)−C(4)−C(7)	111.2 (5)
S(1)−Re−N(2)	141.00 (12)	C(4)−C(7)−N(2)	114.4 (4)
N(1)−Re−N(2)	88.0 (2)		
N(1)−Re−S(2)	144.70 (12)		
S(2)−Re−N(2)	82.19 (11)		

as listed for the semipreparative column): product retention time, 14.9 min.

***N*-[(*S*)-1-Phenylethyl]-3,3-bis(thio-acetamidomethyl)propanamide Oxotechnetium-99m(V) (13)**. A 3 mL vial was charged with 10 μL of 0.1 M sodium acetate, 10 μL of sodium gluconate (10 mM aqueous solution), 100.4 μCi $Na^{99m}TcO_4^-$ in 30 μL of saline, 20 μL of 0.42 mM **11**, and 0.02 mg of $SnCl_2$ in 10 μL of water. The mixture was heated at 60−65 °C for 80 min. From the vial, 47.1 μCi of the reaction mixture was injected onto the HPLC. The eluent at 10−12 min was collected and counted as 34.2 μCi to give a radiochemical yield of 73%. HPLC (C_{18} reversed-phase Waters μBondpak 3.9 × 300 mm; eluent 1.0 mL/min of 15% CH_3CN/85% 10 mM KH_2PO_4 solution ramped over 10 min to 30% CH_3CN/70% 10 mM KH_2PO_4 solution and maintained at that solvent ratio; radiometric γ detector): product retention times, 10.3 and 11.7 min.

Crystal Structure of anti-7. Crystals of anti-**7** were grown from a saturated solution in methanol. A crystal suitable for X-ray analysis was selected and cut to appropriate size and mounted on a glass fiber. Crystal data and refinement parameters for anti-**7** are listed in Table 1, and selected interatomic distances and angles are listed in Table 2. Data were collected on a Nonius Kappa-CCD system at room temperature. Unit cell parameters were calculated from reflections obtained from 10 consecutive data images collected at φ intervals of 1°. One full hemisphere of data was collected by incremental φ scans of 1° followed by 1° ω scans to capture cusp data. Systematic absences and intensity data indicated the space group $P2_12_12_1$. Data were scaled, and empirical absorption corrections were applied using redundant data and XPREP (Shelxtl 5.03). Full-matrix least-squares refinement on F^2 was performed after solving using Patterson methods and the solution package SHELXTL 5.03 (Sheldrick, G. M., Madison, WI). Anisotropic thermal parameters were applied to all nonhydrogen atoms; C6, O4, and O5 were disordered over two positions and refined with site occupancy factors of 0.65 and 0.35. Hydrogen atoms were placed in idealized positions and updated with each least-squares refinement. The absolute structure parameter was −0.017(6). The largest residual peak was found in the lattice and was associated with O4 (0.567 eÅ^{-3}). In the final stages of refinement, $R_1 = 2.46\%$ and $R_{w2} = 5.58\%$.

RESULTS AND DISCUSSION

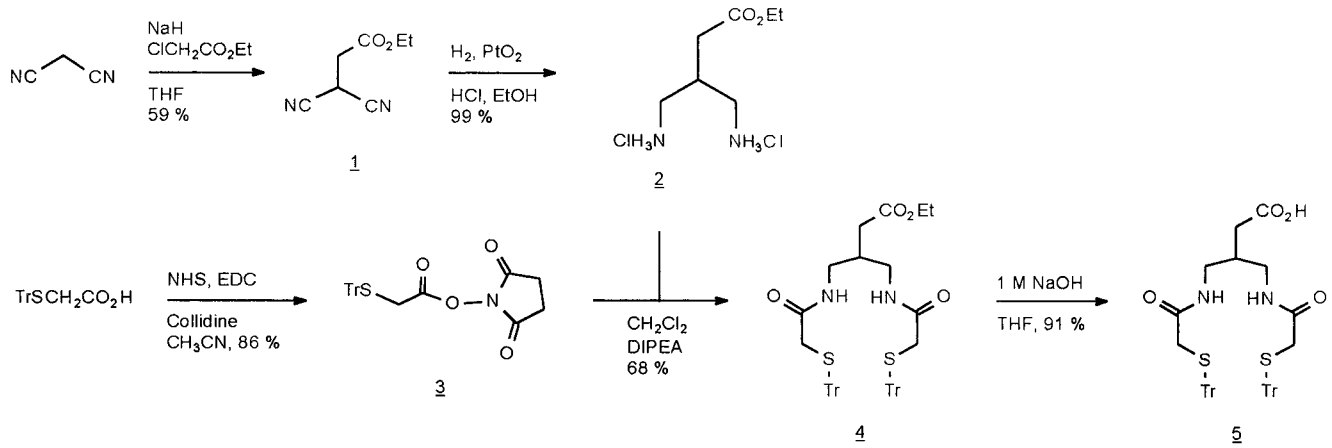
This section presents the synthetic pathway followed for the preparation of the target N_2S_2 chelator bearing a carboxylic acid group. The chelating ability of **6** was demonstrated by complexation of the ligand to both rhenium and technetium-99m. In both cases, the reaction yielded two kinetic isomers, anti and syn, which can be completely converted to the thermodynamically favored anti isomer. Single-crystal X-ray analysis and NMR spectroscopy were used to characterize the rhenium complexes. Finally, the protected chelator **5** was conjugated to (*S*)-α-phenethylamine yielding compound **10**, which after deprotection was also complexed to both rhenium and technetium-99m. Again two kinetic isomers were formed, but only one thermodynamic bioconjugate product resulted. The rhenium isomers were separated and characterized by NMR spectroscopy.

The preparation of the thiol protected N_2S_2 ligand **5** follows a five-step procedure as shown in Scheme 1. The scheme parallels a previously reported pathway for the syntheses of mercaptoamides by using a diamine and two equivalents of a thioglycolate (*17*). The dicyano ester **1** was prepared by alkylation of malononitrile with ethyl chloroacetate. Dialkylation is a significant side reaction in this step as has been noted for various malononitrile alkylations (*18*, *19*). The optimum yield of **1** was obtained with a 2-fold excess of malononitrile over ethyl chloroacetate. The excess malononitrile was removed by extraction followed by fractional vacuum distillation to give **1** in an overall 59% yield. Compound **1** was readily reduced to the 1,3-diamino derivative **2** by catalytic hydrogenation and was isolated as the dihydrochloride in approximately quantitative yield. Attempts to purify this gummy solid by recrystallization or ion-exchange chromatography met with limited success. Instead, **2** was used immediately without further purification.

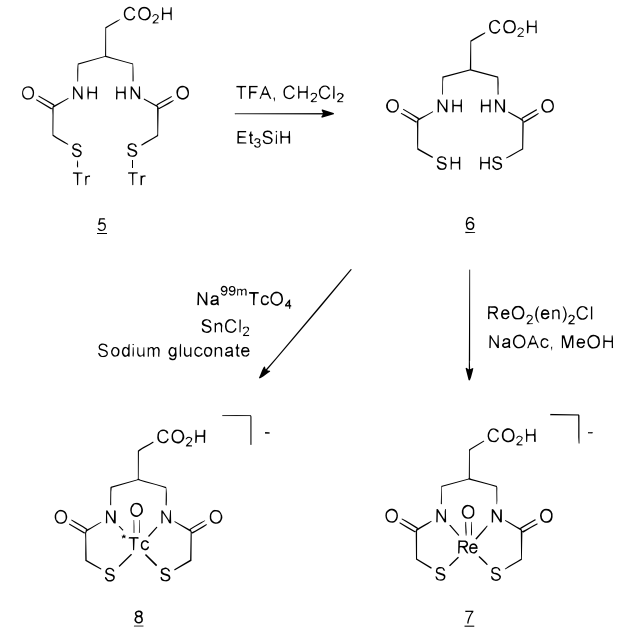
Mercaptoacetic acid was protected using triphenylmethanol (*20*). The procedure for conversion to the N-hydroxy succinimidyl ester **3** was modified from a literature procedure (*21*), using 1-(3-dimethylaminopropyl)-3-ethylcarbodiimide (EDC) as the coupling reagent to give **3** in 86% yield. Compound **4** was synthesized via a conventional amide coupling reaction using the diamine **2** and 2 equiv of the ester **3** in 68% yield. The final step involved the room-temperature saponification to the N_2S_2 carboxylic acid **5**.

As shown in Scheme 2, complex formation with either rhenium or technetium was a two-step process. In the first step, the thiol groups were deprotected using trifluoroacetic acid and triethylsilane or triisopropylsilane as a cation scavenger (*20*). The dithiol intermediate **6** was not purified in order to avoid possible oxidation. Chelation with rhenium was accomplished using a ligand-exchange reaction with $ReO_2(en)_2Cl$ in the presence of sodium acetate. The resultant rhenium complex **7** was precipitated from solution as the tetraphenylarsonium

Scheme 1



Scheme 2



salt. HPLC and ^{1}H NMR spectroscopy ascertained that the reaction product consisted of a mixture of two isomers in an approximate 1:1 ratio. These two epimers were determined to be the anti and syn isomers with respect to the rhenium oxo and carboxylic acid groups. As shown in Figure 3, room-temperature isomerization using a 0.5 M sodium hydroxide solution in water/methanol allowed for the complete conversion of the mixture of epimers to a single isomer. Characterization of this product by ^{1}H NMR spectroscopy and X-ray crystallography indicated that the configuration is anti. In contrast, exposure of the mixture of epimers to 1 M HCl had no effect on the ratio of the two epimers.

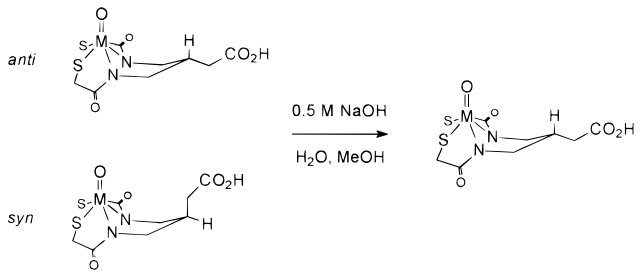


Figure 3. Isomerization at room-temperature results in complete conversion of the mixture of isomers to the anti isomer.

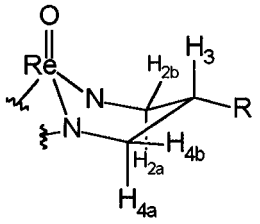
While compounds **7** and **8** are not the first examples of rhenium(V) and technetium(V) N_2S_2 complexes that undergo base-catalyzed isomerization, to our knowledge they are unique in that they form a single stable isomer. It is interesting to note that, in an oxygen-exchange reaction study of N_2S_2 rhenium(V) and technetium(V) DADS complexes (*22*), oxygen exchange was found to be base catalyzed and that no exchange occurred under the acidic conditions employed. In another study, an N_3S peptide chelator for rhenium(V) and technetium(V) was demonstrated to undergo conversion between anti and syn isomers (*23*). This conversion was sufficiently slow that the isomers could be separated by HPLC but sufficiently rapid at room temperature that it prevented isolation of the individual, separated isomers. The structurally related CO_2-DADS rhenium complexes (Figure 1) containing a five-membered ring were not observed to convert from one epimer to another in the pH range of 1−11 (*9*).

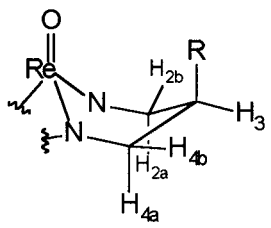
Table 3 shows the ^{1}H NMR analysis which allowed for the determination of the six-membered ring configuration of compounds **7**. Measurement of the coupling constants for the axial (H_{2a}, H_{4a}) and equatorial (H_{2b}, H_{4b}) protons adjacent to the nitrogen atoms allowed for the determination of their spatial relationship to H_3. For anti-**7**, the axial protons next to the nitrogen have two large coupling constants ($|J|$ = 13.2 Hz, $|J|$ = 10.8 Hz) implying a geminal and an axial−axial interaction. Spin−spin decoupling experiments with irradiation at 2.63 ppm converts the doublet of doublets at 3.78 ppm into a broad singlet, and irradiation at 3.78 ppm converts the doublet of doublets at 2.63 ppm into a doublet ($|J|$ = 10.8 Hz). This confirmed that the orientation of H_3 is axial, and therefore, the pendant carboxylic acid group is equatorial.

Since the syn isomer was not isolated, a ^{1}H NMR spectrum could not be acquired. Instead the ^{1}H NMR spectrum was deduced by subtraction of the anti-**7** spectrum from the spectrum of the isomeric mixture of **7**. The doublet of doublets at 3.31 ppm is assigned to the axial protons H_{2a} and H_{4a}, with coupling constants of $|J|$ = 13.6 Hz and $|J|$ = 6.6 Hz, indicating a geminal coupling and an axial−equatorial coupling respectively, consistent with the syn configuration shown in Table 3.

The infrared spectrum (DRIFT) showed a rhenium-oxo stretch at 974 cm^{-1}, in the expected range for a $Re{=}O^{3+}$ core (*9*, *24*). Fast-atom bombardment mass spectroscopy (FABMS) in the negative ion mode confirmed the presence of the rhenium complex with the parent ion peaks at *m*/*z* 479 and 477 with the expected intensity for ^{187}Re/^{185}Re (63:37).

Table 3. Selected ^{1}H NMR Data (300 MHz, d_6-DMSO) for the Anti and Syn[a] Isomers of 7, R = CH_2CO_2H





	anti-7		*syn*-7	
	δ (ppm)	coupling constant (Hz, absolute value)	δ (ppm)	coupling constant (Hz, absolute value)
H(2a) and H(4a)	2.63 (dd, 1H)	$J_{H2a-H2b}$ = 13.2, J_{H2a-H3} = 10.8[b]	3.31 (dd, 1H)	$J_{H2a-H2b}$ = 13.6, J_{H2a-H3} = 6.6[b]
H(2b) and H(4b)	3.78 (dd, 1H)	$J_{H2b-H2a}$ = 13.2, J_{H2b-H3} = 2.3[b]	3.88 (dd, 1H)	$J_{H2b-H2a}$ = 13.6, J_{H2b-H3} = 3.1[b]
H(3)	2.35 (m, 1H)		2.17 (m, 1H)	

[a] Syn-**7** ^{1}H NMR data predicted based on subtraction of the mixture (**7**) and anti-**7** ^{1}H NMR data. [b] Coupling constants for H(2a) are identical for H(4a); likewise, the coupling constants for H(2b) are identical to H(4b).

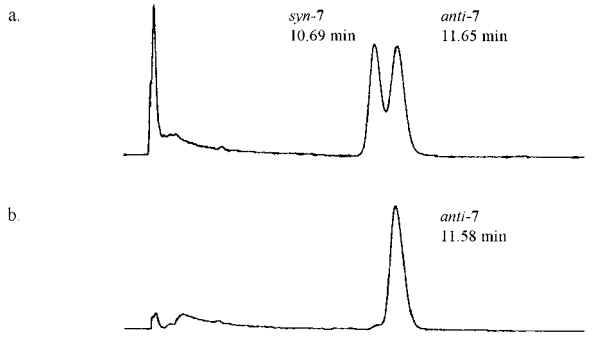


Figure 4. HPLC chromatograms (UV detector) of complex **7** on an anion-exchange column (see Experimental Section for conditions). (a) syn and anti-**7**; (b) anti-**7** after the mixture is exposed to 0.5 M NaOH (water/methanol) at room temperature.

HPLC of Re and ^{99m}Tc Complexes. An anion-exchange column was utilized for the HPLC analysis of the carboxylic acid rhenium complexes **7** and technetium complexes **8**. With rhenium, as can be seen in Figure 4a, the complex formed initially was a 45:55 mixture of two isomers having retention times of 10.7 and 11.7 min (see Experimental Section for conditions). Figure 4b shows the result of an HPLC analysis after treatment of this mixture with 0.5 M NaOH at room temperature for 30 min. Conversion to a single isomer has occurred with the exclusive and later-eluting compound being anti-**7** as established by ^{1}H NMR analysis and X-ray structure determination.

Labeling of the ligand with 99m-pertechnetate was successful using tin(II) chloride, sodium gluconate, and the dithiol ligand **6** in excess. Similar to chelation with rhenium, two isomers of **8** were observed by HPLC. Co-injection of this mixture of technetium-99m isomers along with the mixture of syn and anti isomers of **7** onto an ion-exchange HPLC column allowed for comparison of the retention times of the technetium-99m and rhenium chelates. Elution of the technetium-99m isomers (syn-**8** then anti-**8**) was monitored by a radiometric γ detector (placed in series after the UV detector) with retention times of 11.5 and 12.3 min while the rhenium complexes monitored by a UV detector eluted at 10.7 and 11.7 min. Under the ^{99m}Tc-labeling conditions used, a preference for the later-eluting anti isomer was observed, with radiochemical yields of 67−88%. Labeling of **6** in the presence of 1 M NaOH resulted in only the anti-**8** product being formed. This is consistent with the anti-configuration being thermodynamically preferred for both the rhenium and technetium complexes of **6**. From a practical point of view, this means that labeling of **6** with technetium-99m can result in but one isomer being produced.

Crystal Structure. Crystals of anti-**7** suitable for X-ray diffraction crystallography were grown from a saturated methanol solution. Perspective views of the complex are shown in Figure 5, with crystal data in Table 1 and selected bond lengths and angles in Table 2. The rhenium atom is situated in a square pyramidal geometry with the rhenium atom located 0.6849 Å above the square plane formed by the two nitrogen and two sulfur atoms. The deviation from planarity for the four ligand atoms is 0.0303 Å. The rhenium−oxo bond length is 1.675 Å, within the expected range of 1.66−1.68 Å as noted for similar N_2S_2 chelators (*22*). The molecules pack by intermolecular hydrogen bonding between the carboxylic acid of one molecule and an amide carbonyl of another molecule. HPLC and mixed melting point analysis confirmed that the crystals selected for X-ray analysis consisted solely of the anti isomer. As mentioned earlier, the crystal structure establishes that the later-eluting isomer in Figure 4 is the anti epimer as assigned. It also shows that in the crystalline form the carboxylic acid is situated in an equatorial position. Therefore, the conformation of anti-**7** is the same in both the crystalline form, determined by the crystal structure and, in solution, as determined by ^{1}H NMR spectroscopy.

Bioconjugation. The bifunctional ability of **6** was explored using (*S*)-α-phenethylamine to act as a model of chiral, amine containing pharmaceuticals. As illustrated in Scheme 3, amide formation was accomplished in two ways: by either direct DCC coupling in 88% yield or by first forming a N-hydroxysuccinimidyl (NHS) ester of **6** and subsequent coupling of **9** to the amine in a 66% two-step yield. Direct DCC coupling would be appropriate for compounds bearing available amino groups but not carboxylic acid groups while the NHS ester is appropriate for the technetium-99m labeling of peptides and analogous compounds.

As illustrated in Scheme 4, the complex **11** was chelated with rhenium in a ligand-exchange reaction using either $ReOCl_3(PPh_3)_2$ or $ReO_2(en)_2Cl$ in the presence of sodium acetate. As with **7**, the rhenium chelation product **12** is formed as a mixture of two isomers in a nearly 1:1 ratio. The separation of the two epimers was

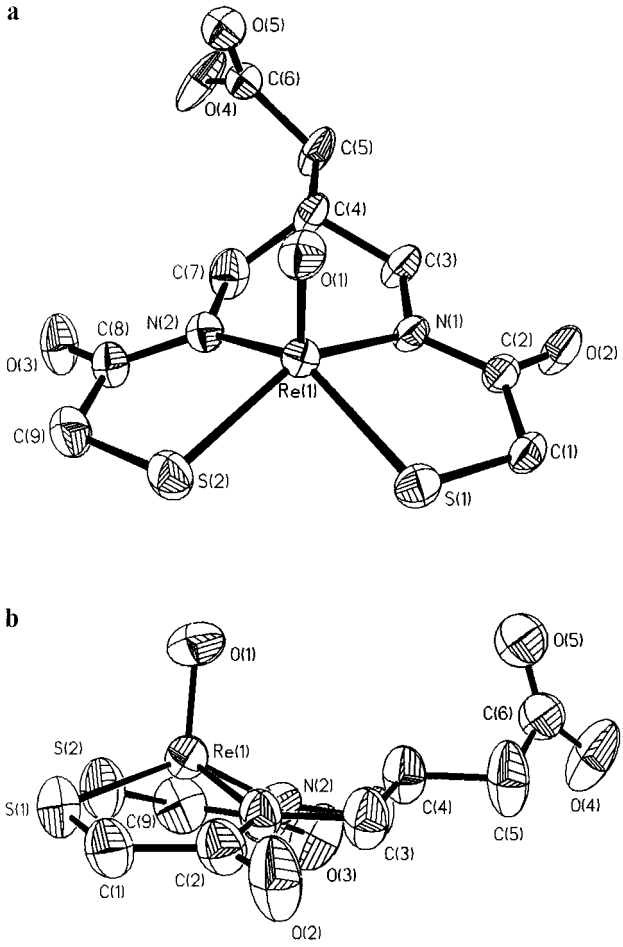
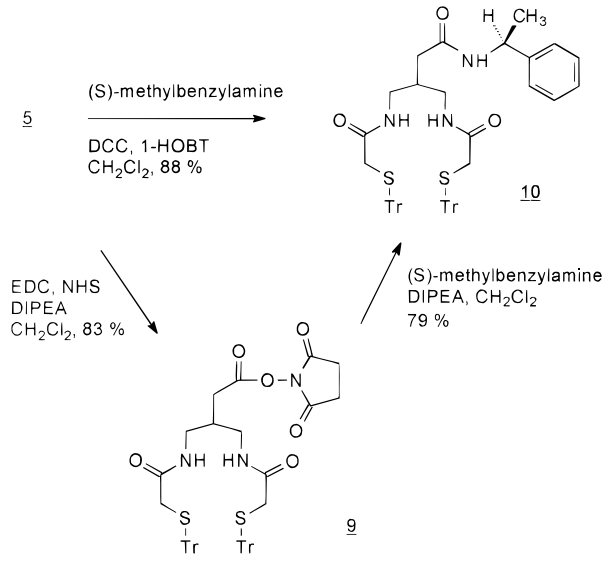


Figure 5. Perspective views of the anion anti-**7**. Thermal ellipsoids are drawn at the 50% probability level. Side view (**b**) indicates the anti arrangement of the rhenium oxo and pendant carboxylic acid functionality.

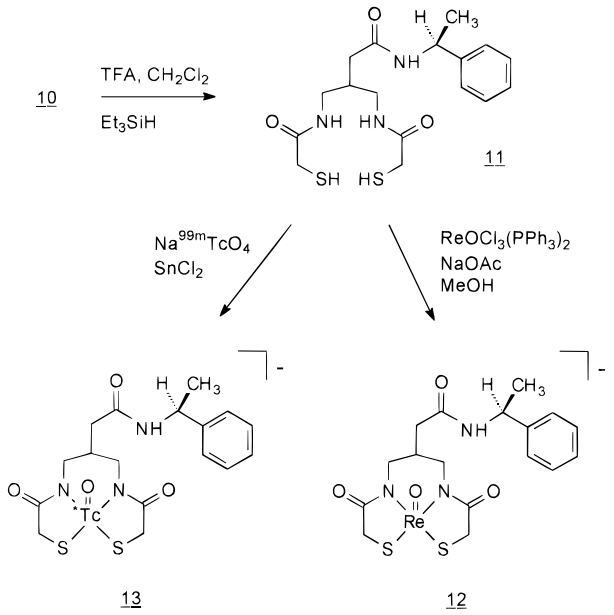
Scheme 3



accomplished using HPLC (C_{18} reversed-phase), with the two isomers having retention times of 9.6 and 11.5 min under the conditions noted in the Experimental Section.

As with **7**, epimerization of this mixture of isomers was accomplished by treating the complexes with 1 M NaOH for 30 min at room temperature. HPLC analysis indicated 98.8% of a single isomer which is the earlier-eluting

Scheme 4



isomer under these HPLC conditions. As described below, identification of the earlier eluting isomer was carried out by ^{1}H NMR spectroscopy resulting in its characterization as anti-**12**. While the anti isomer was readily prepared by epimerization of the mixture of isomers, the syn isomer was isolated by semipreparative HPLC.

The proton NMR spectra for **12** is complicated by the presence of five nonequivalent protons on the six-membered ring ($H_{2a,b}$, H_3, and $H_{4a,b}$). Through COSY and decoupling experiments, the chemical shifts and coupling constants for all five protons were established and are presented in Table 4. The conformation of the six-membered ring was elucidated from the coupling constants of the axial and equatorial protons on H_2 and H_4 as coupled to H_3. For the anti isomer, $|J_{gem}|$ for $H_{2a}-H_{2b}$ and $H_{4a}-H_{4b}$ is 13.1 and 13.6 Hz, respectively. The coupling constant for either axial proton (H_{2a} or H_{4a}) with H_3 is 11.4 Hz, indicating an axial−axial relationship, while the coupling constant for either equatorial proton (H_{2b} or H_{4b}) with H_3 is 2.3 Hz, consistent with a gauche relationship expected for the anti isomer with an equatorial substituent. Spin−spin decoupling ^{1}H NMR experiments verified this assignment and allowed for the chemical shift assignment of the four protons (H_{2a}, H_{2b}, $H_{4a,}$ and H_{4b}).

For the syn isomer, $|J_{gem}|$ for $H_{2a}-H_{2b}$ and $H_{4a}-H_{4b}$ was found to be 14.2 and 14.3 Hz, respectively. The vicinal coupling constants ($J_{2a,3} = J_{4a,3} = 3.5$ Hz and $J_{2b,3} = J_{4b,3} = 3.1$ Hz) were consistent with a gauche relationship as expected for the syn isomer with an axial substituent as illustrated in Table 4.

The infrared spectra (DRIFT) showed the Re=O stretch at 971 cm^{-1}. FABMS in the negative ion mode confirmed the presence of the rhenium complex by exhibiting the characteristic 2:1 rhenium isotopic ratio, with the parent ion peaks at *m*/*z* 582 and 580.

Labeling of **11** with technetium-99m was accomplished with $Na^{99m}TcO_4$ using $SnCl_2$ as the reducing agent and D-gluconate for ligand exchange. Under mild basic conditions (0.1 M NaOAc), the radiochemical yield for **13** was 73%, with a 2:1 ratio between the anti/syn isomers as shown in Figure 6a. When the technetium-99m chelation was carried out in the presence of 1 M NaOH, only the earlier-eluting anti-**13** was formed as indicated by the

Table 4. Selected ^{1}H NMR Data (300 MHz, $CDCl_3$) for the Anti and Syn Isomers of 12, R = $CH_2C(O)NHCH(CH_3)Ph$



	anti-12		*syn*-12	
	δ (ppm)	coupling constant (Hz, absolute value)	δ (ppm)	coupling constant (Hz, absolute value)
H(2a)	2.88 (dd, 1H)	$J_{H2a-H2b}$ = 13.1, J_{H2a-H3} = 11.4	3.43 (dd, 1H)	$J_{H2a-H2b}$ = 14.2, J_{H2a-H3} = 3.5
H(2b)	3.95 (ddd, 1H)	$J_{H2b-H2a}$ = 13.1, $J_{H2b-H3} \approx J_{H2b-H4b} \approx$ 2.3	3.92 (dd, 1H)	$J_{H2b-H2a}$ = 14.3, J_{H2b-H3} = 3.1
H(3)	2.56 (m, 1H)		2.80 (m, 1H)	
H(4a)	2.86 (dd, 1H)	$J_{H4a-H4b}$ = 13.1, J_{H4a-H3} = 11.4	3.40 (dd, 1H)	$J_{H4a-H4b}$ = 14.2, J_{H4a-H3} = 3.5
H(4b)	3.90 (ddd, 1H)	$J_{H4b-H4a}$ = 13.6, $J_{H4b-H3} \approx J_{H4b-H2b} \approx$ 2.3	3.80 (dd, 1H)	$J_{H4b-H4a}$ = 14.3, J_{H4b-H3} = 3.1

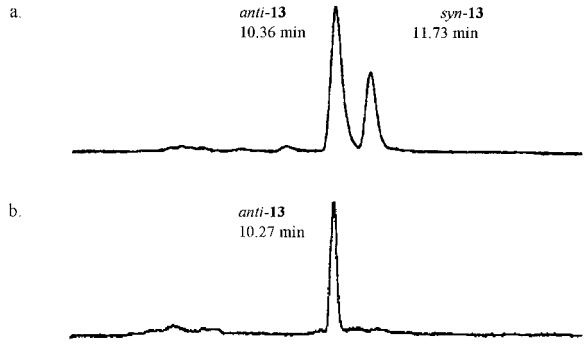


Figure 6. HPLC chromatograms (radiometric γ detector) of complex **13** on a C_{18} reversed-phase column (see Experimental Section for conditions). (a) anti and syn-**13** from chelation in the presence of 0.1 M NaOAc; (b) anti-**13** from chelation in the presence of 1 M NaOH.

HPLC radiometric trace shown in Figure 6b. Co-injection of the rhenium complexes **12** and the technetium-99m complexes **13** was used to compare retention times. Using a C_{18} reversed-phase column, the HPLC eluent was monitored by a UV detector followed in series by a radiometric γ detector. The rhenium epimers **12** had retention times of 9.6 and 11.5 min, while the ^{99m}Tc epimers **13** eluted at 10.3 and 11.7 min. A slight deviation in retention time is expected since the detectors are arranged in series, with the radiometric detector situated after the UV detector.

CONCLUSIONS

An achiral ligand **6** has been prepared in six steps. Chelation of this ligand with rhenium or technetium-99m results in the formation of two isomers as the kinetic products. Equilibration with 0.5 M NaOH yielded a single isomer. This thermodynamically favored epimer is the anti isomer, and this product was fully characterized by NMR spectroscopy and X-ray crystallography.

The bifunctional ability of the ligand was investigated using (*S*)-α-phenethylamine as a model amine, and the resulting complex was chelated with rhenium and technetium-99m. Again, the kinetic products were a mixture of two isomers which was epimerized quantitatively to the anti isomer. This shows that coupling with either NHS or DCC yields amides in good yield and that single isomer bioconjugates can be produced. This will be of value in the preparation and purification of single isomer radiopharmaceuticals and consequently simplify interpretation of potentially complex biodistributions.

ACKNOWLEDGMENT

This work is supported by NSERC (National Science and Engineering Research Council of Canada) and Merck-Frosst. The authors acknowledge the assistance of the Nuclear Medicine Department of the London Health Sciences Centre, University Campus and Surface Science Western. We wish to thank Doug Hairsine for running mass spectra.

Supporting Information Available: Analytical data, supplementary X-ray data. This material is available free of charge via the Internet at http://pubs.acs.org.

LITERATURE CITED

(1) Schwochau, K. (1994) Technetium Radiopharmaceuticals—Fundamentals, Synthesis, Structure, and Development. *Angew. Chem., Int. Ed. Engl. 33*, 2258−2267.

(2) Hom, R. K., and Katzenellenbogen (1997) Technetium-99m-Labeled Receptor-Specific Small-Molecule Radiopharmaceuticals: Recent Developments and Encouraging Results. *Nucl. Med. Biol. 24*, 485−498.

(3) Deutsch, E., Libson, K., Vanderheyden, J., Ketring, A. R., and Maxon, H. R. (1986) The Chemistry of Rhenium and Technetium as Related to the Use of Isotopes of these Elements in Therapeutic and Diagnostic Nuclear Medicine. *Int. J. Radiat. Appl. Instum. Part B: Nucl. Med. Biol. 13* (4), 465−477.

(4) Breitz, H. B., Weiden, P. L., Vanderheyden, J.-L., Appelbaum, J. W., Bjorn, M. J., Fer, M. F., Wolf, S. B., Ratliff, B. A., Seiler, C. A., Foisie, D. C., Fisher, D. R., Schroff, R. W., Fritzberg, A. R., and Abrams, P. G. (1992) Clinical Experience with Rhenium-186-Labeled Monoclonal Antibodies for Radioimmunotherapy: Results of Phase I Trials. *J. Nucl. Med. 33*, 1099−1112.

(5) van Gog, F. B., Visser, G. W. M., Klok, R., van der Schors, R., Snow, G. B., and van Dongen, G. (1996) Monoclonal Antibodies Labelled with Rhenium-186 Using the MAG3 Chelate: Relationship between the Number of Chelated Groups and Biodistribution Characteristics. *J. Nucl. Med. 37-(2)*, 352−362.

(6) Davison, A., Sohn, M., Orvig, C., Jones, A. G., and LeTegola, M. R. (1979) A Tetradentate Ligand Designed Specifically to Coordinate Technetium. *J. Nucl. Med. 20*, 641 (Abstr.).

(7) Davison, A., Jones, A. G., Orvig, C., and Sohn, M. (1981) A New Class of Oxotechnetium(5+) Chelate Complexes Containing a $TcON_2S_2$ Core. *Inorg. Chem. 20* (6), 1629−1631.

(8) Fritzberg, A. R., Kuni, C. C., Klingensmith, W. C., III, Stevens, J., and Whitney, W. P. (1982) Synthesis and Biological Evaluation of Tc-99m N,N′-Bis(mercaptoacetyl)-2,3-diaminopropanoate: A Potential Replacement for ^{131}I *o*-iodohippurate. *J. Nucl. Med. 23*, 592−598.

(9) Rao, T. N., Adhikesavalu, D., Camerman, A., and Fritzberg, A. R. (1990) Technetium(V) and Rhenium(V) Complexes of 2,3-Bis(mercaptoacetamido)propanoate. Chelate Ring Stereochemistry and Influence on Chemical and Biological Properties. *J. Am. Chem. Soc. 112*, 5798−5804.

(10) Costello, C. E., Brodack, J. W., Jones, A. G., Davison, A., Johnson, D. L., Kasina, S., and Fritzberg, A. R. (1983) The Investigation of Radiopharmaceutical Components by Fast Atom Bombardment Mass Spectrometry: The Identification of Tc-HIDA and the Epimers of Tc−CO_2DADS. *J. Nucl. Med. 24*, 353−355.

(11) Bormans, G., Cleynhens, B., José, D., Hoogmartens, M., De Roo, M., and Verbruggen, A. (1990) Synthesis and Biological Characteristics of Four Stereoisomers of ^{99m}Tc-N, N′-bis-(mercaptoacetyl)-2,3-diaminopropionate. *Int. J. Radiat. Appl. Instrum. Part B: Nucl. Med. Biol. 17* (5), 499−506.

(12) Klingensmith, W. C., III, Fritzberg, A. R., Spitzer, V. M., Johnson, D. L., Kuni, C. C., Williamson, M. R., Washer, G., and Weil, R., III (1984) Clinical Evaluation of Tc-99m N,N′-Bis(Mercaptoacetyl)-2,3-Diaminopropanoate as a Replacement for I-131 Hippurate: Concise Communication. *J. Nucl. Med. 25*, 42−48.

(13) Liu, S., Edwards, D. S., and Barrett, J. A. (1997) ^{99m}Tc Labeling of Highly Potent Small Peptides. *Bioconjugate Chem. 8*, 621−636.

(14) Meegalla, S. K., Plössl, K., Kung, M., Stevenson, D. A., Mu, M., Kushner, S., Liable-Sands, L. M., Rheingold, A. L., and Kung, H. F. (1998) Specificity of Diastereomers of [^{99m}Tc]-TRODAT-1 as Dopamine Transporter Imaging Agents. *J. Med. Chem. 41*, 428−436.

(15) Brenner, D., Davison, A., Lister-James, J., and Jones, A. G. (1984) Synthesis and Characterization of a Series of Isomeric Oxotechnetium(V) Diamido Dithiolates. *Inorg. Chem. 23*, 3793−3797.

(16) Johnson, N. P., Lock, C. J. L., and Wolkinson, G. (1964) Amine, Phosphine, and Stibine Complexes of Rhenium-(III), -(IV), and -(V). *J. Chem. Soc.* 1054−1066.

(17) Atkinson, E. R., Handrick, G. R., Bruni, R. J., and Granchelli, F. E. (1965) Potential Antiradiation Drugs. I. Amide, Hydroxamic Acid, and Hydrazine Derivatives of Mercapto Acids. Amino Thioacids. *J. Med. Chem. 8*, 29−33.

(18) Hesse, B. C. (1896) On Malonic Nitrile and Some of Its Derivatives. *Am. Chem. J. 18*, 723−751.

(19) Hessler, J. C. (1899) On Alkyl Malonic Nitriles and Their Derivatives. *Am. Chem. J. 22*, 169−198.

(20) Brenner, D., Davison, A., Lister-James, J., and Jones, A. G. (1984) Synthesis and Characterization of a Series of Isomeric Oxotechnetium(V) Diamido Dithiolates. *Inorg. Chem. 23*, 3793−3797.

(21) Bell, R. A., Hughes, D. W., Lock, C. J. L., and Valliant, J. F. (1996) The synthesis and high-resolution NMR spectroscopy of ethyl N-(2-triphenylmethylthio)ethanoyl-*O*-{4′-[4″-(1″-bis(2‴-chloroethyl)amino)phenyl]butanoyl}-L-seryl-S-benzyl-L-cysteine: a chelate-chlorambucil complex for use as a ligand for ^{99m}Tc radio-imaging. *Can. J. Chem. 74*, 1503−1511.

(22) Chen, B., Heeg, M. J., and Deutsch, E. (1992) Preparation, Characterization, and ^{17}O NMR Kinetic Studies of Analogous Technetium(V) and Rhenium(V) Complexes Which Contain a Seven-Membered Chelate Ring. Single-Crystal Structure Analyses of [Ph_4P][TcO(DBDS)] and [Ph_4P][ReO(DBDS)], Where DBDS is N,N′-Bis(mercaptoacetyl)butane-1,4-diamine. *Inorg. Chem. 31* (22), 4683−4690.

(23) Wong, E., Fauconnier, T., Bennett, S., Valliant, J., Nguyen, T., Lau, F., Lu, L. F. L., Pollak, A., Bell, R. A., and Thornback, J. R. (1997) Rhenium(V) and Technetium(V) Oxo Complexes of an N_2N′S Peptidic Chelator: Evidence of Interconversion between the Syn and Anti Conformations. *Inorg. Chem. 36* (25), 5799−5808.

(24) Davison, A., Orvig, C., Trop, H. S., Sohn, M., Depamphilis, B. V., and Jones, A. G. (1980) Preparation of Oxobis-(dithiolato) Complexes of Technetium(V) and Rhenium(V). *Inorg. Chem. 19*, 1988−1992.

BC980134Q

© 1999 American Chemical Society, Bioconjugate Chem., Luyt bc980134q Supporting Info Page 1

An N_2S_2 Bifunctional Chelator for Technetium-99m and Rhenium: Complexation, Conjugation and Epimerization to a Single Isomer

Leonard G. Luyt, Hilary A. Jenkins[†] and Duncan H. Hunter[*].

Supporting Information

Analytical Data (weight percent composition by element)

3,3-Dicyano-propionic acid ethyl ester (**1**):

	Carbon	Hydrogen	Nitrogen	Oxygen
Calculated	55.26	5.30	18.41	21.03
Observed	55.42	5.14	18.35	21.23

3,3-Bis(triphenylmethylthio-acetidomethyl)propanoic acid ethyl ester (**4**):

	Carbon	Hydrogen	Nitrogen	Oxygen	Sulphur
Calculated	74.21	6.10	3.53	8.07	8.09
Observed	74.23	5.83	3.68	8.15	7.94

3,3-Bis(triphenylmethylthio-acetamidomethyl)propanoic acid (**5**):

	Carbon	Hydrogen	Nitrogen	Oxygen	Sulphur
Calculated	73.79	5.80	3.66	8.37	8.38
Observed	73.44	5.81	3.55	8.33	8.48

N-((S)-1-Phenylethyl)-3,3-bis(triphenylmethylthio-acetamidomethyl)propanamide (**10**):

	Carbon	Hydrogen	Nitrogen	Oxygen	Sulphur
Calculated	76.09	6.15	4.84	5.53	7.39
Observed	76.24	6.11	4.80	5.80	7.36

© 1999 American Chemical Society, Bioconjugate Chem., Luyt bc980134q Supporting Info Page 2

Supplementary X-ray Data

Table 1. Crystal data and structure refinement for *anti*-7.

Identification code	*anti*-7	
Empirical formula	$C_{33}\ H_{33}\ As\ N_2\ O_5\ Re\ S_2$	
Formula weight	862.85	
Temperature	294(2) K	
Wavelength	0.71073 Å	
Crystal system	Orthorhombic	
Space group	P2(1)2(1)2(1)	
Unit cell dimensions	a = 9.4435(3) Å b = 14.3439(4) Å c = 24.1591(5) Å	alpha = 90 deg. beta = 90 deg. gamma = 90 deg.
Volume, Z	3272.5(2) $Å^3$, 4	
Density (calculated)	1.751 Mg/m^3	
Absorption coefficient	4.887 mm^{-1}	
F(000)	1700	
Crystal size	0.30 x 0.20 x 0.20 mm	
Theta range for data collection	1.65 to 25.00 deg.	
Limiting indices	-12<=h<=12, -19<=k<=20, -28<=l<=30	
Reflections collected	22399	
Independent reflections	5752 [R(int) = 0.0452]	
Absorption correction	Semi-empirical	

Max. and min. transmission	0.3158 and 0.2131
Refinement method	Full-matrix least-squares on F^2
Data / restraints / parameters	5749 / 0 / 405
Goodness-of-fit on F^2	0.988
Final R indices [I>2sigma(I)]	R1 = 0.0246, wR2 = 0.0558
R indices (all data)	R1 = 0.0302, wR2 = 0.0693
Absolute structure parameter	-0.017(6)
Extinction coefficient	0.00022(10)
Largest diff. peak and hole	0.567 and -0.649 e.Å^{-3}

Table 2. Atomic coordinates (x 10^4) and equivalent isotropic displacement parameters (Å^2 x 10^3) for *anti*-7. U(eq) is defined as one third of the trace of the orthogonalized Uij tensor.

	x	y	z	U(eq)
Re(1)	9252(1)	9283(1)	3961(1)	44(1)
S(1)	11634(1)	9116(1)	3803(1)	59(1)
S(2)	9016(2)	8841(1)	3053(1)	70(1)
O(1)	8695(4)	8407(2)	4363(2)	61(1)
O(2)	11686(4)	11018(3)	4972(2)	81(1)
O(3)	5775(5)	10518(3)	3184(2)	86(1)
N(1)	9954(4)	10314(3)	4481(2)	45(1)
N(2)	7608(4)	10119(3)	3764(2)	48(1)
C(1)	12396(5)	9875(4)	4321(2)	54(1)
C(2)	11321(5)	10445(4)	4616(2)	51(1)
C(3)	9009(5)	10933(4)	4803(2)	62(1)
C(4)	7467(4)	10729(4)	4722(2)	56(1)

C(5)	6617(5)	11379(5)	5102(3)	76(2)
C(6)	5111(10)	11014(6)	5157(4)	53(2)
O(4)	4190(8)	11644(5)	5049(5)	102(3)
O(5)	4751(6)	10219(5)	5269(2)	70(2)
C(6')	4957(22)	11556(13)	4917(8)	59(4)
O(4')	4401(15)	11946(12)	4561(7)	96(4)
O(5')	4481(19)	10972(12)	5290(6)	92(4)
C(7)	7020(6)	10829(4)	4141(2)	70(2)
C(8)	6833(6)	10048(4)	3285(2)	60(1)
C(9)	7330(6)	9343(5)	2877(2)	75(2)
C(11)	8381(5)	6323(3)	2499(2)	46(1)
C(12)	9667(6)	6675(4)	2334(2)	62(1)
C(13)	9800(7)	7049(4)	1807(2)	74(2)
C(14)	8653(7)	7082(4)	1465(2)	75(2)
C(15)	7359(7)	6736(4)	1641(2)	70(2)
C(16)	7202(6)	6344(4)	2154(2)	59(1)
C(21)	7051(5)	6531(4)	3703(2)	47(1)
C(22)	6158(5)	7199(4)	3488(2)	65(2)
C(23)	5333(6)	7723(4)	3850(3)	75(2)
C(24)	5371(7)	7550(5)	4408(3)	79(2)
C(25)	6262(6)	6897(4)	4615(2)	69(2)
C(26)	7114(6)	6384(4)	4272(2)	56(1)
C(31)	7390(5)	4583(3)	3159(2)	50(1)
C(32)	6741(6)	4180(4)	3622(2)	68(2)
C(33)	6158(7)	3293(4)	3561(3)	81(2)
C(34)	6216(6)	2839(4)	3068(3)	78(2)
C(35)	6836(7)	3236(4)	2620(2)	73(2)
C(36)	7453(6)	4114(4)	2664(2)	60(1)
C(41)	10071(5)	5702(4)	3528(2)	51(1)
C(42)	10854(6)	4914(4)	3427(2)	65(1)
C(43)	12254(7)	4884(5)	3616(3)	85(2)
C(44)	12806(6)	5627(5)	3909(3)	86(2)
C(45)	11987(7)	6387(5)	4016(4)	91(2)
C(46)	10622(6)	6439(4)	3826(2)	66(2)
As(1)	8215(1)	5792(1)	3225(1)	45(1)

Table 3. Bond lengths [Å] and angles [deg] for *anti*-7.

Re(1)-O(1)	1.673(3)
Re(1)-N(2)	2.019(4)
Re(1)-N(1)	2.050(4)
Re(1)-S(1)	2.2938(13)
Re(1)-S(2)	2.2954(13)
S(1)-C(1)	1.808(5)
S(2)-C(9)	1.799(6)
O(2)-C(2)	1.238(6)
O(3)-C(8)	1.230(6)
N(1)-C(2)	1.344(6)
N(1)-C(3)	1.479(6)
N(2)-C(8)	1.373(6)
N(2)-C(7)	1.474(6)
C(1)-C(2)	1.486(7)
C(3)-C(4)	1.498(6)
C(4)-C(7)	1.473(7)
C(4)-C(5)	1.534(7)
C(5)-C(6)	1.521(11)
C(5)-C(6')	1.65(2)
C(6)-O(5)	1.221(11)
C(6)-O(4)	1.280(13)
C(6')-O(4')	1.15(2)
C(6')-O(5')	1.31(3)
C(8)-C(9)	1.488(8)
C(11)-C(12)	1.374(7)
C(11)-C(16)	1.392(7)
C(11)-As(1)	1.918(4)
C(12)-C(13)	1.387(8)
C(13)-C(14)	1.364(8)
C(14)-C(15)	1.386(9)
C(15)-C(16)	1.369(8)
C(21)-C(22)	1.378(7)
C(21)-C(26)	1.392(6)
C(21)-As(1)	1.913(5)
C(22)-C(23)	1.393(8)
C(23)-C(24)	1.371(8)
C(24)-C(25)	1.354(8)
C(25)-C(26)	1.370(7)
C(31)-C(36)	1.371(7)
C(31)-C(32)	1.401(7)

C(31)-As(1)	1.909(5)
C(32)-C(33)	1.394(8)
C(33)-C(34)	1.358(9)
C(34)-C(35)	1.356(8)
C(35)-C(36)	1.392(8)
C(41)-C(42)	1.371(7)
C(41)-C(46)	1.381(7)
C(41)-As(1)	1.904(5)
C(42)-C(43)	1.400(9)
C(43)-C(44)	1.382(9)
C(44)-C(45)	1.361(8)
C(45)-C(46)	1.371(8)

O(1)-Re(1)-N(2)	110.0(2)
O(1)-Re(1)-N(1)	106.8(2)
N(2)-Re(1)-N(1)	88.0(2)
O(1)-Re(1)-S(1)	109.03(13)
N(2)-Re(1)-S(1)	141.00(12)
N(1)-Re(1)-S(1)	81.97(11)
O(1)-Re(1)-S(2)	108.47(13)
N(2)-Re(1)-S(2)	82.19(11)
N(1)-Re(1)-S(2)	144.70(12)
S(1)-Re(1)-S(2)	84.66(5)
C(1)-S(1)-Re(1)	102.3(2)
C(9)-S(2)-Re(1)	101.6(2)
C(2)-N(1)-C(3)	111.6(4)
C(2)-N(1)-Re(1)	124.1(3)
C(3)-N(1)-Re(1)	124.0(3)
C(8)-N(2)-C(7)	111.8(4)
C(8)-N(2)-Re(1)	124.4(3)
C(7)-N(2)-Re(1)	123.7(3)
C(2)-C(1)-S(1)	113.0(3)
O(2)-C(2)-N(1)	121.9(4)
O(2)-C(2)-C(1)	120.5(4)
N(1)-C(2)-C(1)	117.6(4)
N(1)-C(3)-C(4)	113.7(4)
C(7)-C(4)-C(3)	112.5(5)
C(7)-C(4)-C(5)	111.2(5)
C(3)-C(4)-C(5)	108.2(4)
C(6)-C(5)-C(4)	109.4(5)
C(4)-C(5)-C(6')	115.4(8)
O(5)-C(6)-O(4)	121.0(9)
O(5)-C(6)-C(5)	126.9(8)

O(4)-C(6)-C(5)	112.1(9)
O(4')-C(6')-O(5')	132(2)
O(4')-C(6')-C(5)	135(2)
O(5')-C(6')-C(5)	92(2)
N(2)-C(7)-C(4)	114.4(4)
O(3)-C(8)-N(2)	124.0(5)
O(3)-C(8)-C(9)	119.8(5)
N(2)-C(8)-C(9)	116.1(5)
C(8)-C(9)-S(2)	113.3(4)
C(12)-C(11)-C(16)	121.7(5)
C(12)-C(11)-As(1)	118.9(4)
C(16)-C(11)-As(1)	119.4(4)
C(11)-C(12)-C(13)	119.3(5)
C(14)-C(13)-C(12)	119.9(6)
C(13)-C(14)-C(15)	120.1(5)
C(16)-C(15)-C(14)	121.4(5)
C(15)-C(16)-C(11)	117.7(5)
C(22)-C(21)-C(26)	120.2(5)
C(22)-C(21)-As(1)	120.6(4)
C(26)-C(21)-As(1)	119.2(4)
C(21)-C(22)-C(23)	118.7(5)
C(24)-C(23)-C(22)	120.4(6)
C(25)-C(24)-C(23)	120.3(5)
C(24)-C(25)-C(26)	120.8(5)
C(25)-C(26)-C(21)	119.5(6)
C(36)-C(31)-C(32)	120.8(5)
C(36)-C(31)-As(1)	120.1(4)
C(32)-C(31)-As(1)	119.1(4)
C(31)-C(32)-C(33)	117.7(5)
C(34)-C(33)-C(32)	121.0(6)
C(33)-C(34)-C(35)	121.0(6)
C(34)-C(35)-C(36)	119.9(6)
C(31)-C(36)-C(35)	119.5(5)
C(42)-C(41)-C(46)	121.4(5)
C(42)-C(41)-As(1)	118.9(4)
C(46)-C(41)-As(1)	119.7(4)
C(41)-C(42)-C(43)	118.5(6)
C(44)-C(43)-C(42)	120.0(6)
C(45)-C(44)-C(43)	120.0(5)
C(44)-C(45)-C(46)	121.0(6)
C(45)-C(46)-C(41)	119.2(5)
C(41)-As(1)-C(31)	110.3(2)
C(41)-As(1)-C(11)	107.7(2)

C(31)-As(1)-C(11)	108.5(2)
C(41)-As(1)-C(21)	109.6(2)
C(31)-As(1)-C(21)	108.6(2)
C(11)-As(1)-C(21)	112.2(2)

Table 4. Anisotropic displacement parameters ($Å^2$ x 10^3) for *anti*-7.
The anisotropic displacement factor exponent takes the form:
$-2\pi^2$ [$h^2 a^{*2}$ U11 + ... + 2 h k a* b* U12]

	U11	U22	U33	U23	U13	U12
Re(1)	42(1)	41(1)	47(1)	-1(1)	-1(1)	1(1)
S(1)	48(1)	70(1)	60(1)	-9(1)	5(1)	13(1)
S(2)	66(1)	87(1)	56(1)	-22(1)	-2(1)	8(1)
O(1)	64(2)	46(2)	75(2)	10(2)	-6(2)	-10(2)
O(2)	38(2)	105(4)	100(3)	-53(3)	4(2)	-9(2)
O(3)	74(3)	89(3)	95(3)	-16(2)	-42(2)	26(3)
N(1)	33(2)	49(2)	52(2)	-8(2)	4(2)	-1(2)
N(2)	51(2)	42(2)	51(2)	-1(2)	-4(2)	-1(2)
C(1)	33(3)	66(3)	61(3)	-3(3)	0(2)	3(2)
C(2)	41(3)	60(3)	53(3)	-8(2)	2(2)	-4(2)
C(3)	35(3)	66(3)	84(4)	-25(3)	7(2)	-6(2)
C(4)	32(2)	63(3)	71(3)	-25(3)	3(2)	-7(3)
C(5)	30(3)	100(5)	98(5)	-53(4)	5(3)	-2(3)
O(4)	29(3)	63(5)	214(11)	-48(6)	12(5)	2(3)
O(4')	61(8)	121(12)	104(10)	-21(9)	-2(8)	4(8)
C(7)	55(3)	69(4)	86(4)	-17(3)	-12(3)	19(3)
C(8)	57(3)	64(3)	57(3)	-3(3)	-13(3)	2(3)
C(9)	68(3)	98(4)	59(3)	0(4)	-16(2)	4(4)
C(11)	47(3)	47(3)	43(2)	0(2)	3(2)	-2(2)
C(12)	54(3)	67(3)	65(3)	2(3)	5(2)	-7(3)
C(13)	84(4)	85(4)	54(3)	10(3)	18(3)	-11(3)
C(14)	105(5)	68(4)	52(3)	18(3)	6(3)	12(4)
C(15)	81(4)	77(4)	52(3)	0(3)	-16(3)	22(3)
C(16)	55(3)	60(3)	62(3)	3(3)	-10(2)	7(3)
C(21)	40(3)	53(3)	47(3)	0(2)	4(2)	-1(2)

C(22)	56(3)	81(4)	58(3)	0(3)	-1(2)	11(3)
C(23)	59(3)	74(4)	92(5)	-6(3)	5(3)	22(3)
C(24)	69(4)	99(5)	69(4)	-19(4)	22(3)	7(4)
C(25)	70(4)	78(4)	57(3)	4(3)	16(3)	-9(3)
C(26)	57(3)	59(3)	52(3)	-3(2)	4(2)	1(3)
C(31)	50(3)	50(3)	49(3)	3(2)	5(2)	-5(2)
C(32)	77(4)	56(3)	70(3)	0(3)	15(3)	-9(3)
C(33)	103(5)	58(4)	83(5)	10(3)	24(4)	-16(3)
C(34)	73(4)	56(3)	104(5)	3(4)	-5(3)	-14(3)
C(35)	90(5)	68(4)	61(3)	-13(3)	-10(3)	-6(3)
C(36)	62(3)	62(4)	57(3)	0(3)	0(2)	-7(3)
C(41)	52(3)	47(3)	55(3)	1(3)	-5(2)	5(3)
C(42)	70(4)	60(3)	64(3)	-13(3)	-8(3)	16(3)
C(43)	67(4)	97(5)	92(5)	-14(4)	-19(3)	35(4)
C(44)	54(3)	102(5)	101(5)	-16(5)	-20(3)	13(3)
C(45)	71(4)	79(4)	123(6)	-12(4)	-32(4)	-6(3)
C(46)	56(3)	56(3)	87(4)	-11(3)	-15(3)	7(3)
As(1)	43(1)	49(1)	42(1)	1(1)	1(1)	-2(1)

© 1999 American Chemical Society, Bioconjugate Chem., Luyt bc980134q Supporting Info Page 10

Table 5. Hydrogen coordinates (x 10^4) and isotropic displacement parameters ($Å^2$ x 10^3) for *anti*-7.

	x	y	z	U(eq)
H(1A)	9368(4)	8070(2)	4442(2)	92
H(1B)	12907(5)	9500(4)	4589(2)	64
H(1C)	13072(5)	10288(4)	4144(2)	64
H(3A)	9191(5)	11574(4)	4696(2)	74
H(3B)	9236(5)	10872(4)	5192(2)	74
H(4A)	7290(4)	10084(4)	4838(2)	67
H(5A)	7059(5)	11406(5)	5464(3)	91
H(5B)	6604(5)	12003(5)	4948(3)	91
H(4B)	3392(8)	11423(5)	5081(5)	153
H(5'A)	3615(19)	10944(12)	5271(6)	138
H(7A)	5995(6)	10799(4)	4125(2)	84
H(7B)	7303(6)	11440(4)	4010(2)	84
H(9A)	7401(6)	9635(5)	2516(2)	90
H(9B)	6632(6)	8849(5)	2852(2)	90
H(12A)	10439(6)	6663(4)	2573(2)	74
H(13A)	10670(7)	7277(4)	1688(2)	89
H(14A)	8739(7)	7337(4)	1112(2)	90
H(15A)	6581(7)	6771(4)	1406(2)	84
H(16A)	6337(6)	6100(4)	2268(2)	71
H(22A)	6107(5)	7298(4)	3108(2)	78
H(23A)	4752(6)	8193(4)	3713(3)	90
H(24A)	4783(7)	7882(5)	4646(3)	95
H(25A)	6296(6)	6795(4)	4995(2)	82
H(26A)	7730(6)	5942(4)	4418(2)	67
H(32A)	6700(6)	4493(4)	3958(2)	81
H(33A)	5724(7)	3008(4)	3862(3)	98
H(34A)	5824(6)	2247(4)	3037(3)	93
H(35A)	6849(7)	2922(4)	2283(2)	88
H(36A)	7905(6)	4381(4)	2361(2)	73
H(42A)	10463(6)	4412(4)	3237(2)	78
H(43A)	12813(7)	4364(5)	3544(3)	102
H(44A)	13738(6)	5608(5)	4034(3)	103
H(45A)	12359(7)	6879(5)	4221(4)	109
H(46A)	10073(6)	6964(4)	3897(2)	80

Multivalent Thioether−Peptide Conjugates: B Cell Tolerance of an Anti-Peptide Immune Response

David S. Jones,* Stephen M. Coutts, Christina A. Gamino, G. Michael Iverson, Matthew D. Linnik, Martina E. Randow, Huong-Thu Ton-Nu, and Edward J. Victoria

La Jolla Pharmaceutical Company, 6455 Nancy Ridge Drive, San Diego, California 92121.
Received November 17, 1998; Revised Manuscript Received February 19, 1999

Antibodies which bind β_2-glycoprotein I (β_2GPI) are associated with antiphospholipid syndrome. Synthetic peptide mimotopes have been discovered which compete with β_2GPI for binding to selected anti-β_2GPI. A thiol-containing linker was attached to the N-terminus of two cyclic thioether peptide mimotopes, peptides **1a** and **1b**. The resulting peptides, with linker attached, were reacted with two different haloacetylated platforms to prepare four tetravalent peptide-platform conjugates to be tested as B cell toleragens. The linker-containing peptides were reacted with maleimide-derivatized keyhole limpet hemocyanin (KLH) to provide peptide−KLH conjugates. Peptides **1a** and **1b** were also modified by acylation with 3-(4′-hydroxyphenyl)propionic acid *N*-hydroxysuccinimidyl ester. The resulting hydroxyphenyl peptides were radioiodinated and used to measure anti-peptide antibody levels. The KLH conjugates were used to immunize mice to generate an anti-peptide immune response. The immunized mice were treated with the conjugates or saline solution and boosted with the appropriate peptide−KLH conjugate. Three of the four conjugates suppressed the formation of anti-peptide antibody. The stabilities of the conjugates in mouse serum were measured, and the relative stabilities did not correlate with ability to suppress antibody formation.

INTRODUCTION

Multiple copies of a hapten attached covalently to a nonimmunogenic polymeric backbone or platform can tolerize those B lymphocytes producing antibodies that bind the hapten, rendering them nonresponsive to haptenated immunogens (*1*, *2*). The result is a decrease in the amount of antibody produced against the hapten. Molecules such as these, which suppress antibody production by B cells, are called toleragens. For example, 2,4-dinitrophenyl (DNP) groups attached to the D-lysines in polymers consisting of D-amino acids can suppress IgG production in animals which have been immunized with DNP-derivatized proteins. Such findings suggested a therapeutic approach for treatment of autoimmune disorders by specifically tolerizing antigen-specific B cells.

B cell tolerance is the reduction of the ability of a specific B cell to produce antibody. B cell tolerance in vivo can be accomplished by treatment with a toleragen, a molecule bearing multiple copies of hapten. Tolerization of mice, which were immunized with synthetic double stranded oligonucleotides, has been accomplished with a "platform conjugate" consisting of four double-stranded oligonucleotides on a PEG based platform (*3*). This concept was further refined into LJP 394, a molecule designed to treat lupus nephritis (*4*). LJP 394 consists of four double-stranded oligonucleotides connected to a defined platform.

The prospect of developing treatments for other autoimmune diseases has led us to search for peptide mimotopes of naturally occurring antigens. β_2-glycoprotein I (β_2GPI) has been implicated as the natural antigen of what have been historically referred to as anticardiolipin antibodies (ACA), which are associated with arterial and venous thrombosis, recurrent fetal loss, and thrombocytopenia (*5*, *6*). A number of ACA-binding peptides have been discovered by screening random-peptide phage libraries (*7*). Most of these phage-derived ACA-binding peptides are cyclic due to an intramolecular disulfide bond in each. Two analogues of these cyclic peptides have been synthesized as thioether peptide analogues in which the disulfide (S−S) is replaced with a thioether (CH_2−S) (*8*, *9*). Both thioether peptide analogues compete with β_2GPI for ACA which was affinity purified from serum from a single recurrent stroke patient.

The goal of these studies was to develop a method for attaching cyclic thioether peptide analogues to multivalent platforms and test their ability to tolerize an immune response. Thioether peptide analogues were attractive for several reasons. First, a thiol linker can be conveniently used to attach molecules of interest to haloacetylated platforms. A cyclic peptide thioether bond is stable in the presence of a thiol linker, whereas a disulfide bond may be reactive with a thiol linker. Thiol exchange between a thiol and a disulfide can be a rapid reaction leading to mixtures of products (*10*). Second, a thioether bond may be less rapidly metabolized than a disulfide bond (*11*), addressing a major concern with peptide-based drugs.

EXPERIMENTAL PROCEDURES

All chemicals were used as purchased unless otherwise specified. Ethyldiazoacetate, 2-[2-(2-chloroethoxy)ethoxy]-ethanol, BF_3·Et_2O, thiobenzoic acid, 1,8-diazabicyclo-[5.4.0]undec-7-ene (DBU), triphenylmethyl chloride, *p*-nitrophenol, dicyclohexylcarbodiimide (DCC), di-*tert*-butyldicarbonate, 3,5-diaminobenzoic acid, *N*-hydroxysuccinimide (NHS), ethylenediamine, triethyleneglycol bischloroformate, and iodoacetic anhydride were purchased from Aldrich Chemical Co. Maleimidyl-activated KLH

* To whom correspondence should be addressed. Phone: (619) 646-6628. Fax: (619) 626-2845. E-mail: dave.jones@ljpc.com.

10.1021/bc9801373 CCC: $18.00 © 1999 American Chemical Society
Published on Web 04/20/1999

Table 1. Analytical Data

compd	mol. formula	type	calcd	found
4	$C_{17}H_{24}N_2O_6$	EA	C, 57.94; H, 6.86; N, 7.95	C, 58.19; H, 6.67; N, 7.77
5	$C_{21}H_{27}N_3O_8$	EA	C, 56.11; H, 6.05; N, 9.35	C, 55.95; H, 5.91; N, 9.12
7	$C_{22}H_{42}N_4O_{10}$	EA	C, 50.55; H, 8.10; N, 10.72	C, 50.42; H, 7.97; N, 10.45
8	$C_{46}H_{70}N_8O_{16}$	EA	C, 55.74; H, 7.12; N, 11.31	C, 55.37; H, 7.09; N, 11.15
3	$C_{34}H_{42}N_8O_{12}I_4$	EA	C, 32.35; H, 3.35; N, 8.87	C, 31.78; H, 3.05; N, 8.32
10	$C_{17}H_{24}O_6SNa$	MS	(M + Na) 379.1191	(M + Na) 379.1203
11	$C_{29}H_{35}O_5S$	MS	(M + H) 495.2205	(M + H) 495.2216
12	$C_{27}H_{30}O_5S$	EA	C, 69.50; H, 6.48	C, 69.33; H, 6.39
	$C_{27}H_{30}O_5SNa$	MS	(M + Na) 489.1712	(M + Na) 489.1723
13	$C_{33}H_{33}NO_7S$	EA	C, 67.44; H, 5.66; N, 2.38	C, 67.56; H, 5.68; N, 2.68
	$C_{33}H_{33}O_7SNa$	MS	(M + Na) 610.1875	(M + Na) 610.1904
15a	$C_{59}H_{101}N_{15}O_{17}S_2$	MS	(M + H) 1357	(M + H) 1357
15b	$C_{59}H_{104}N_{18}O_{17}S_2$	MS	(M + H) 1402	(M + H) 1402
16a	$C_{270}H_{443}N_{68}O_{80}S_8$	MS	(M + H) 6178	(M + H) 6179
16b	$C_{270}H_{455}N_{80}O_{80}S_8$	MS	(M + H) 6359	(M + H) 6361
17a	$C_{284}H_{485}N_{70}O_{82}S_8$	MS	(M + H) 6449	(M + H) 6449
17b	$C_{284}H_{497}N_{82}O_{82}S_8$	MS	(M + H) 6629	(M + H) 6629
20a	$C_{60}H_{96}N_{15}O_{15}S$		(M + H) 1299	(M + H) 1299
20b	$C_{60}H_{99}N_{18}O_{15}S$	MS	(M + H) 1344	(M + H) 1344

was purchased from Pierce (catalog no. 77105). 3-(4′-Hydroxyphenyl)propionic acid *N*-hydroxysuccinimidyl ester (Taggit) was purchased from Novabiochem. Silica gel chromatography was performed on silica gel (230−400 Mesh ASTM) purchased from Baxter. TLC was performed on silica gel TLC plates (5554) manufactured by EM Separations. Phosphate-buffered saline (PBS) was prepared by dissolving 175 g of NaCl, 6.5 g of $NaH_2PO_4 \cdot H_2O$, and 40.9 g of $Na_2HPO_4 \cdot H_2O$ in H_2O and diluting to a final volume of 20 L. Tris-buffered saline (TBS) was prepared by dissolving 219.9 g of NaCl and 151.4 g of tris(hydroxymethyl)aminomethane in H_2O, adjusting the pH to 8.0, at a final volume of 25 L, with HCl.

Melting points are reported uncorrected. NMR spectra were recorded on a Bruker AC-300 spectrometer with broad band probe. Elemental analyses were performed by Desert Analytics of Tucson, Arizona. Mass spectra were recorded on a Finnigan LC-Q electrospray mass spectrometer or obtained from the Mass Spectroscopy Lab at the Scripps Research Institute, San Diego, CA.

Bis-*N*-(tert-butyloxycarbonyl)diaminobenzoic acid, compound 4. A solution of 7.18 g (32.9 mmol) of di-*tert*-butyldicarbonate in 5.5 mL of MeOH was slowly added to a solution of 2.5 g (16.4 mmol) of 3,5-diaminobenzoic acid and 2.76 g (32.9 mmol) of $NaHCO_3$ in 44.5 mL of H_2O and 22.5 mL of MeOH, and the mixture was stirred at room temperature for 24 h. The mixture was cooled to 0 °C, and 6.53 g of citric acid was added. The mixture was extracted with EtOAc, and the combined EtOAc layers were dried ($MgSO_4$), filtered, and concentrated. The residue was dissolved in 40 mL of Et_2O, and the solution was filtered through Celite. The Et_2O layer was extracted with two 40 mL portions of HCl. The Et_2O layer was dried ($MgSO_4$), filtered, and concentrated to give 3.81 g (66%) of **4** as a foamy pink solid; mp 199 °C. ^{1}H NMR ($CDCl_3$): δ 1.55 (s, 18H), 6.80 (brd, 2H), 7.74 (s, 2H), 7.95 (s, 1H) ^{13}C NMR ($CDCl_3$): δ 28.3, 81.4, 113.1, 115.2, 131.1, 139.6, 153.4, 170.7. MS (ESI): $(M + Na)^+$ 375.2. Anal. ($C_{17}H_{24}N_2O_6$) C, H, N (Table 1).

***N*-Hydroxysuccinimidyl Ester of Compound 4, Compound 5**. Dicyclohexylcarbodiimide (3.34 g, 16.2 mmol) was added to a solution of 3.8 g (10.8 mmol) of compound **4** and 1.24 g (10.8 mmol) of *N*-hydroxysuccinimide in 55 mL of EtOAc which had been cooled to 0 °C, and the resulting mixture was stirred for 18 h allowing to come to room temperature. Acetic acid (0.55 mL) was added to the mixture, and the mixture was stirred for 30 min and placed in the freezer at −20 °C for 2 h. The mixture was filtered to remove solids, and the filtrate was concentrated to give 5.80 g of pink foamy solid. Purification by silica gel chromatography (60/40/1 hexane/EtOAc/HOAc) gave 4.30 g (89%) of compound **5** as a slightly pink solid; mp 133−137 °C. ^{1}H NMR ($CDCl_3$): δ 1.55 (s, 18H), 2.94 (s, 4H), 6.81 (s, 2H), 7.79 (s, 2H), 7.96, (s, 1H). ^{13}C NMR ($CDCl_3$): δ 25.6, 28.2, 81.2, 113.9, 114.3, 126.3, 139.8, 152.3, 161.4, 169.0. MS (ESI): $(M + Na^+)$ 472.2. Anal. ($C_{21}H_{27}N_3O_8$) C, H, N.

Mono-*N*-(tert-butyloxycarbonyl)ethylenediamine, Compound 6. This compound was prepared in a manner similar to that described by Huang (*12*), A solution of 1.5 g (25.0 mmol) of ethylenediamine in 15 mL of CH_2Cl_2 was cooled to 0 °C, and a solution of 1.82 g (8.33 mmol) of di-*tert*-butyldicarbonate was added slowly to the mixture. The mixture was stirred at room temperature for 18 h and filtered, and the filtrate was concentrated. Purification by silica gel chromatography (90/10/1 CH_2Cl_2/MeOH/HOAc) gave 0.98 g (67%) of compound **6** as an oil.

Bis-[N_1-(N_2-(*tert*-butyloxycarbonyl)-2-aminoethyl)-carbamoyl]triethylene Glycol, Compound 7. To a solution of 750 mg (4.25 mmol) of compound **6** and 345 μL (337 mg, 4.25 mmol) of pyridine in 6 mL of CH_2Cl_2 was added 445 μL (559 mg, 2.02 mmol) of triethyleneglycol bis-chloroformate. The mixture was stirred for 3.5 h, and partitioned between 35 mL of CH_2Cl_2 and 35 mL of 1 N HCl. The CH_2Cl_2 layer was washed with H_2O, dried (Na_2SO_4), filtered, and concentrated to give 1.14 g of compound **7** as a white solid; mp 105−110 °C. ^{1}H NMR ($CDCl_3$): δ 1.46 (s, 18H), 3.30 (brd s, 8H), 3.68 (s, 4H), 3.72, (s, 4H), 4.24 (s, 4H), 5.16 (brd s, 2H), 5.56 (brd s, 2H). ^{13}C NMR ($CDCl_3$): δ 28.4, 40.5, 41.2, 64.1, 69.6, 70.6, 79.4, 156.3, 156.9. MS (ESI): $(M + Na^+)$ 545.3. Anal. ($C_{22}H_{42}N_4O_{10}$) C, H, N.

Compound 8. Compound **7** (300 mg, 0.57 mmol) was dissolved in 3.5 mL of CH_2Cl_2, and 3.5 mL of trifluoroacetic acid was added. The mixture was stirred for 3 h at room temperature, and the solution was concentrated to give 398 mg of residue. The residue was dissolved in 1.5 mL of H_2O, and to the resulting solution was added 193 mg (2.30 mmol) of $NaHCO_3$ followed by a solution of 567 mg (1.26 mmol) of compound **5** in 6 mL of dioxane. The mixture was stirred for 3 h, acidified with 1 N HCl, and partitioned between 20 mL of 1 N HCl and 30 mL of EtOAc. The aqueous layer was washed with 2 × 20 mL portions of EtOAc. The combined EtOAc layers were washed with saturated $NaHCO_3$ solution, dried ($MgSO_4$), filtered, and concentrated to give 490 mg (86%) of crude compound **8** as a white foamy solid. Purification by silica

gel chromatography (EtOAc) gave 276 mg (48%) of compound **8** as a white foamy solid; mp 138−140 °C. ^{1}H NMR ($CDCl_3$): δ 1.55 (s, 36H), 3.38 (m, 4H), 3.51 (m, 4H), 3.65 (m, 8H), 4.21 (m, 4H), 5.99 (t, 2H), 7.11 (t, 2H), 7.24 (s, 4H), 7.44 (s, 4H), 7.89 (s, 2H). ^{13}C NMR ($CDCl_3$): δ 28.5, 40.6, 41.0, 64.3, 69.8, 70.8, 80.8, 111.6, 112.0, 135.8, 139.7, 153.1, 157.6, 168.4. Anal. ($C_{46}H_{70}N_8O_{16}$) C, H, N.

Compound 3. Compound **8**, (100 mg, 0.1 mmol) was dissolved in 1 mL of 1/1 TFA/CH_2Cl_2, and the mixture was stirred for 1 h at room temperature. Et_2O was added to the mixture to precipitate the resulting tetraamine salt which was dried under vacuum to give a white crystalline solid. The solid was dissolved in 1 mL of H_2O together with 168 mg (2.0 mmol) of $NaHCO_3$, and the resulting mixture was cooled to 0 °C. To the cooled solution was added a solution of 212 mg (0.6 mmol) of iodoacetic anhydride in 2 mL of dioxane. The mixture was stirred at 0 °C for 15 min, acidified to pH 4 with 1 N H_2SO_4, and partitioned between 10 mL of H_2O and 6 × 10 mL portions of 8/2 CH_2Cl_2/MeOH. The combined organic layers were dried ($MgSO_4$), filtered, and concentrated to give 202 mg of yellow oily solid. Purification by silica gel chromatography (9/1 CH_2Cl_2/MeOH) yielded 57 mg (45%) of compound **3** as a white solid; mp 126−140 °C dec.; ^{1}H NMR (1/1 $CDCl_3$/CD_3OD): δ 3.32 (m, 4H), 3.50 (m, 4H), 3.59 (s, 4H), 3.68 (m, 4H), 3.88 (s, 8H), 4.18 (m, 4H), 7.73 (s, 4H), 7.99 (s, 2H), 8.48 (m, amide protons partially exchanged), 10.41 (s, anilide protons partially exhanged). MS (ESI): *m/z* $(M + H)^+$ 1263, $(M + Na)^+$ 1285. Anal. ($C_{34}H_{42}N_8O_{12}I_4$) C, H, N.

Ethyl-11-chloro-3,6,9-trioxaundecanoate, 9. This compound was prepared as described by Boumrah (*13*). A 0 °C solution of ethyldiazoacetate (11.56 mL; 10.704 g; 110 mmol) in 100 mL of CH_2Cl_2 was added dropwise over 30 min to a solution of 2-[2-(2-chloroethoxy)ethoxy]-ethanol (14.54 mL, 16.86 g, 100 mmol) and BF_3·Et_2O (1.23 mL, 1.066 g, 10 mmol) in 150 mL of CH_2Cl_2, under a nitrogen atmosphere, at 0 °C. The solution was stirred for 30 min at 0 °C, and 100 mL of H_2O was added to the reaction mixture. The mixture was transferred to a separatory funnel and shaken vigorously. The CH_2Cl_2 layer was washed twice with 100 mL of H_2O, dried ($MgSO_4$), filtered, and concentrated. The concentrate was distilled under vacuum to give 14.47 g (57%) of **9** as an oil (bp 94−140 °C, 0.25 mmHg). ^{1}H NMR ($CDCl_3$): δ 1.29 (t, 3H), 3.60−3.81 (m, 12H), 4.16 (s, 2H), 4.22 (q, 2H). ^{13}C NMR ($CDCl_3$): δ 14.1, 42.8, 61.0, 68.9, 70.4, 70.4, 70.5, 70.7, 71.2, 170.6.

Ethyl *S*-Benzoyl-11-mercapto-3,6,9-trioxaundecanoate, 10. A solution of 6.51 g (47.1 mmol) of thiobenzoic acid in 25 mL of dry DMF was added to a 0 °C solution of 10.0 g (39.3 mmol) of **9** in 80 mL of dry DMF. To the mixture was added 10.85 g (78.5 mmol) of DBU in 45 mL of dry DMF. The mixture was stirred at 0 °C for 10 min and heated to 70 °C for 16 h. The mixture was concentrated, and the concentrate was partitioned between 200 mL of CH_2Cl_2 and 2 × 200 mL of 1 N HCl. The CH_2Cl_2 layer was washed with saturated $NaHCO_3$, dried ($MgSO_4$), filtered, and concentrated to give 13.2 g of crude product. Purification by silica gel chromatography (7:3 hexane/ethyl acetate) gave 9.49 g (68%) of **10** as a light yellow oil. ^{1}H NMR ($CDCl_3$): δ 1.30 (t, 3H), 3.31 (t, 2H), 3.69−3.78 (m, 10H), 4.18 (s, 2H), 4.23 (q, 2H), 7.48 (m, 2H), 7.59 (m, 1H), 8.00 (d, 2H). ^{13}C NMR ($CDCl_3$): δ 14.4, 28.7, 60.5, 68.4, 70.1, 70.2, 70.4, 70.6, 127.5, 129.0, 133.5, 137.0, 170.5, 191.5. HRMS (FAB) *m/z* cald for $C_{17}H_{24}O_6SNa$: (M + Na) 379.1191. Found: 379.1203.

Ethyl *S*-Triphenylmethyl-11-mercapto-3,6,9-trioxaundecanoate, 11. A 2.27 M solution of sodium ethoxide in ethanol (10.5 mL, 28.1 mmol) was added under N_2 to a 0 °C solution of 5.0 g (14.0 mmol) of **10** in 15 mL of ethanol, and the mixture was stirred at 0 °C for 30 min. The reaction was acidified to approximately a pH of 2 with 5 N HCl, and the mixture was concentrated. The concentrate was partitioned between 2 × 200 mL of ethyl acetate and 200 mL of 1 N HCl. The combined ethyl acetate layers were dried ($MgSO_4$), filtered, and concentrated. The resulting orange oil was dissolved in 15 mL of CH_2Cl_2, the resulting solution was cooled to 0 °C, and 5.67 mL (5.55 g, 70.15 mmol) of pyridine and 4.30 g (15.43 mmol) of triphenylmethyl chloride was added. The mixture was stirred for 2 h at room temperature and concentrated. The concentrate was partitioned between 3 × 200 mL of ethyl acetate and 200 mL of 1 N HCl. The ethyl acetate layer was dried ($MgSO_4$), filtered, and concentrated. Purification by silica gel chromatography (7:3 hexane/ethyl acetate) gave 4.18 g (60%) of **11** as a viscous oil. ^{1}H NMR ($CDCl_3$): δ 1.28 (t, 3H), 2.46 (t, 2H), 3.32 (t, 2H), 3.47 (m, 2H), 3.60 (m, 2H), 3.69 (m, 2H), 3.73 (m, 2H), 4.14 (s, 2H), 4.21 (q, 2H), 7.20−7.33 (m, 9H), 7.43 (m, 6H). ^{13}C NMR ($CDCl_3$): δ 14.3, 31.9, 61.2, 66.5, 68.7, 69.6, 70.1, 70.3, 70.6, 70.8, 127.1, 128.1, 129.9, 145.0, 170.6. HRMS (FAB) *m/z* calcd for $C_{29}H_{35}O_5S$: (M + H) 495.2205. Found: 495.2216.

***S*-Triphenylmethyl-11-mercapto-3,6,9-trioxaundecanoic acid, 12**. To a solution of 2 g (4.04 mmol) of **11** in 12.2 mL of ethanol was added 1.6 mL (0.648 g; 16.16 mmol) of 10 M NaOH, and the mixture was stirred for 90 min. The mixture was acidified with 1 N HCl to a pH of 2 and partitioned between 200 mL of EtOAc and 200 mL of 1 N HCl. The aqueous layer was washed with two 200 mL portions of EtOAc. The combined EtOAc layers were dried ($MgSO_4$), filtered, and concentrated to give 1.84 g (97%) of **12** as a viscous oil which solidified on standing to give a white solid; mp 59−60 °C. ^{1}H NMR ($CDCl_3$): δ 2.46 (t, 2H), 3.32 (t, 2H), 3.48 (m, 2H), 3.65 (m, 2H), 3.70 (m, 2H), 3.75 (m, 2H), 4.14 (s, 2H), 7.22−7.34 (m, 9H), 7.44 (m, 6H). ^{13}C NMR ($CDCl_3$): δ 31.9, 66.8, 69.6, 69.8, 70.2, 70.4, 71.3, 126.6, 127.8, 129.6, 145.0, 173.2. HRMS (ESI) *m/z* calcd for $C_{27}H_{30}O_5SNa$: (M + Na) 489.1712. Found: 489.1723. Anal. ($C_{27}H_{30}O_5S$) C, H.

4′-Nitrophenyl-*S*-triphenylmethyl-11-mercapto-3,6,9-trioxaundecanoate, 13. To a solution of 1.5 g (3.21 mmol) of **12** in 15 mL of CH_2Cl_2 cooled to 0 °C were added 0.447 g (3.21 mmol) of *p*-nitrophenol and 0.93 g (4.48 mmol) of DCC, and the mixture was stirred at room temperature for 18 h. To the mixture was added 105 μL (0.108 g; 1.79 mmol) of acetic acid, and stirring was continued at room temperature for 1 h. The mixture was placed in the freezer for 30 min and filtered. The filtrate was concentrated, and the residue was purified by silica gel chromatography (70/30/1 hexane/EtOAc/HOAc) to give 1.65 g (87%) of **13** as white crystals; mp 73−74 °C. ^{1}H NMR ($CDCl_3$): δ 2.47 (t, 2H), 3.35 (t, 2H), 3.48 (m, 2H), 3.62 (m, 2H), 3.75 (m, 2H), 3.85 (m, 2H), 4.47 (s, 2H), 7.20−7.35 (m, 11H), 7.42 (m, 6H), 8.29 (d, 2H). ^{13}C NMR ($CDCl_3$): δ 32.0, 66.6, 68.5, 69.6, 70.1, 70.4, 70.8, 71.2, 122.2, 125.2, 126.7, 127.9, 129.6, 145.0, 155.0, 168.5. HRMS (FAB) *m/z* calcd for $C_{33}H_{33}O_7SNa$: (M + Na) 610.1875. Found: 610.1904. Anal. ($C_{33}H_{33}NO_7S$) C, H, N.

Attachment of Linker 13 to 1a, Synthesis of Compound 15a. To 15 mg (0.013 mmol) of compound **1a** were added 160 μL of a solution of 29.5 mg of compound **13** and 17.5 μL of diisopropylethylamine in 0.5 mL of DMF. The mixture was stirred for 2 h and

Table 2. Reduction of Anti-Peptide Antibodies in Mice[a] Treated with Compounds 16a, 16b, 17a, and 17b as Determined by the Farr Assay

	experiment 1 (treatment with **16a**)[b]			experiment 2 (treatment with **16b**)[b]			experiment 3 (treatment with **17a**)[b]			experiment 4 (treatment with **17b**)[b]		
dose (nmol)	mean	SD	reduction	mean	SD	reduction	mean	SD	reduction	mean	SD	reduction
none	203	72		275	188		231	61		275	188	
1.25							298	59	0%			
2.5				59	31	78%	204	94	11%	19	13	93%
5.0	100	71	51%	112	42	41%	192	103	17%	109	62	60%
10.0	82	16	59%	44	16	84%	213	93	8%	52	46	81%
50.0	65	36	68%	73	66	73%	295	127	0%	104	68	62%

[a] Five mice per group were immunized with peptide−KLH conjugate **19a** or **19b**. Three weeks later, the mice were treated with tetravalent peptide conjugate. Five days later, the mice were boosted with peptide−KLH conjugate. Seven days later, the mice were bled. [b] Antigen-binding capacity (ABC) (see refs *15* and *16*). [c] ABC significantly lower than control (experiment 1, $p = 0.0157$; experiment 2, $p = 0.0015$; experiment 4, $p = 0.0015$).

precipitated by addition of Et_2O. The precipitate, compound **14a**, was dried under vacuum and dissolved in 650 μL of a solution of 1/1/0.056/0.040 TFA/CH_2Cl_2/thiophenol/Me_2S, and the solution was allowed to stand for 1 h. Precipitation by addition of Et_2O gave crude compound **15a** which was purified by HPLC (C18, 15−45% CH_3CN/H_2O 0.1% TFA). Fractions containing pure product were lyophilized to give 8.6 mg (48%) of **15a** as a white solid; MS (ESI): *m/z* (M + H) 1357.

Attachment of Linker 13 to 1b, Synthesis of Compound 15b. To 100 mg (0.084 mmol) of compound **1b** was added 1.05 mL of a solution of 88.5 mg of compound **13** and 52.5 μL of diisopropylethylamine in 1.5 mL of DMF. The mixture was stirred for 16 h and precipitated by addition of Et_2O. The precipitate, compound **14b**, was dried under vacuum and dissolved in 3.35 mL of a solution of 1/1/0.056/0.040 TFA/CH_2Cl_2/thiophenol/Me_2S, and the solution was allowed to stand for 2 h. Precipitation by addition of Et_2O gave crude compound **15b** which was purified by HPLC (C18, 15−45% CH_3CN/H_2O 0.1% TFA). Fractions containing pure product were lyophilized to give 60 mg (51%) of **15b** as a white solid; MS (ESI): *m/z* (M + H) 1402.

Conjugate 16a. To a solution of 45 mg (33.2×10^{-6} mol) of **15a** in 3.32 mL of He-sparged pH 8.5, 200 mM borate buffer was added 1.02 mL of a 8.2 mg/mL solution of **3** in MeOH. The mixture was stirred for 16 h and 12 mL of 10% HOAc/H_2O solution was added. The mixture was purified by HPLC (C18, gradient 30−45% CH_3CN/H_2O 0.1% TFA) to give 9.0 mg of **16a**; MS (ESI) *m/z* calcd for $C_{270}H_{443}N_{68}O_{80}S_8$: (M + H) 6178. Found: 6179.

Conjugate 16b. To a solution of 33.1 mg (23.6×10^{-6} mol) of **15b** in 2.8 mL of He-sparged pH 8.5, 100 mM borate buffer was added 707 μL of a 8.4 mg/mL solution of **3** in MeOH. After 2 h, another 6.6 mg of **15b** was added. The mixture was stirred for 3 h and 0.5 mL of 10% HOAc/H_2O solution was added. The mixture was purified by HPLC (C18, gradient 30 to 40% CH_3CN/H_2O 0.1% TFA) to give 23.0 mg of **16b** MS (ESI) *m/z* calcd for $C_{270}H_{455}N_{80}O_{80}S_8$: (M + H) 6359. Found: 6361.

Conjugate 17a. To a solution of 8.6 mg (6.3×10^{-6} mol) of **15a** in 630 μL of He-sparged, pH 8.5, 200 mM borate buffer was added 40 μL of a 40 mg/mL solution of **2** in 9/1 MeOH/H_2O. The mixture was stirred for 24 h, and 1 mL of 10% HOAc/H_2O solution was added. The mixture was purified by HPLC (C18, gradient 25 to 55% CH_3CN/H_2O 0.1% TFA) to give 8.3 mg of **17a**. MS (ESI) *m/z* calcd for $C_{284}H_{485}N_{70}O_{82}S_8$: (M + H) 6449. Found: 6449.

Conjugate 17b. To a solution of 38.0 mg (27.1×10^{-6} mol) of **15b** in 2.7 mL of He-sparged, pH 8.5, 100 mM borate buffer was added 452 μL of a 13.5 mg/mL solution of **2** in MeOH. The mixture was stirred for 2 h and 0.5 mL of 10% HOAc/H_2O solution was added. The mixture was purified by HPLC (C18, gradient 15 to 35% CH_3CN/H_2O 0.1% TFA) to give 20.0 mg of **17b**; MS (ESI) *m/z* calcd for $C_{284}H_{497}N_{82}O_{82}S_8$: (M + H) 6629. Found: 6629.

Preparation of KLH Conjugate, 19a. Compound **15a** (2.5 mg, 1.8 μmol) was dissolved in 0.43 mL of PBS containing 1 mM EDTA, and to the resulting solution was added 0.43 mL of a 10 mg/mL solution of maleimidyl-activated KLH (Pierce Chemical catalog no. 77105) in water. The mixture was tumbled slowly for 2h at room temperature and was exhaustively dialyzed against PBS at 4 °C. The presence of conjugated peptide was demonstrated by the binding of relevant ACA to microplates coated with KLH−peptide conjugate (*14*).

Preparation of KLH Conjugate, 19b. The preparation of **19b** was done essentially similarly to the preparation of **19a** using **15b** instead of **15a**.

Preparation of HOP Peptide, 20a. Compound **20a** was prepared essentially similarly to the preparation of **20b**, using **1a** instead of **1b**, to provide **20a** as a white solid. MS (ESI): *m/z* $(M + H)^+$ 1299.

Preparation of HOP Peptide, 20b. To a solution of 10 mg (8.4 μmol) of peptide **1b** in 840 μL of pH 8.5 200 mM sodium borate buffer was added 110 μL (41.8 μmol) of a solution of a 100 mg/mL solution of 3-(4′-hydroxyphenyl)propionic acid *N*-hydroxysuccinimidyl ester in DMSO. After 2 h, 10 mL of 8/1/1 H_2O/CH_3CN/HOAc was added, and the resulting solution was loaded onto a preparative HPLC column and purified by HPLC (C_{18}, 12 mL/min, gradient 8/2/0.1 H_2O/CH_3CN/TFA to 6/4/0.1 H_2O/CH_3CN/TFA over 40 min, 210 nm, retention time 26−30 min) to provide 6 mg of **20b** as a white solid after lyophilization. MS (ESI): *m/z* $(M + H)^+$ 1343.

In Vivo Biology. Mice (C57Bl/6, five mice per group) were immunized with **19a** or **19b**, a conjugate of the peptide covalently attached to KLH. The immunizations were accomplished by intraperitoneal (IP) injection of 0.5 mL of a solution containing 10 μg of the conjugate (**19a** or **19b**) precipitated on 2 mg of alum and 2×10^9 *Bordetella pertussis* organisms as an adjuvant (*15*). Three weeks after immunization, the mice were injected, IP, with the test toleragens **16a**, **16b**, **17a**, or **17b** at the doses indicated in Table 2. Mice immunized with **19a** were injected with **16a** or **17a**, while mice immunized with **19b** were injected with **16b** or **17b**. A control group was injected with 0.5 mL of saline instead of the toleragen. Five days later, mice in both groups were boosted with the peptide−KLH conjugate in saline solution. Seven days later, all of the mice were bled, and serum was harvested. The anti-peptide antibody levels of the serum, reported as antigen-binding capacity (ABC), was determined by a Farr assay where the radioactive antigen **20a** or **20b** was present at 10^{-8} M (*15*, *16*).

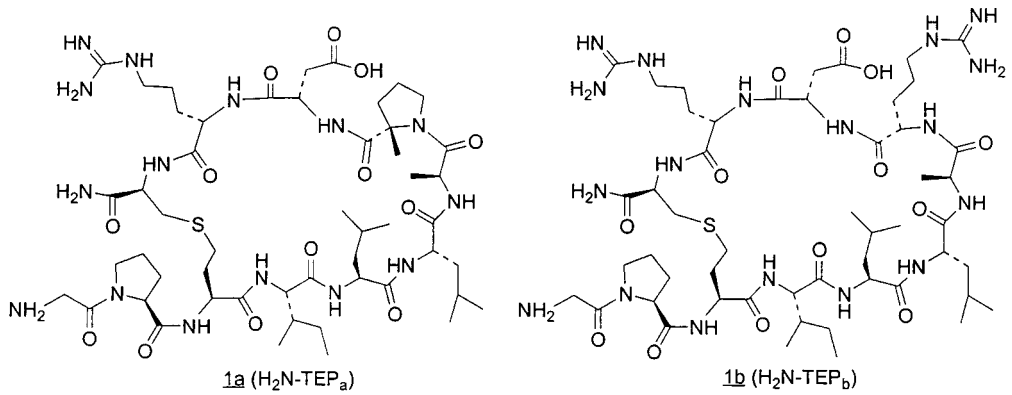


Figure 1.

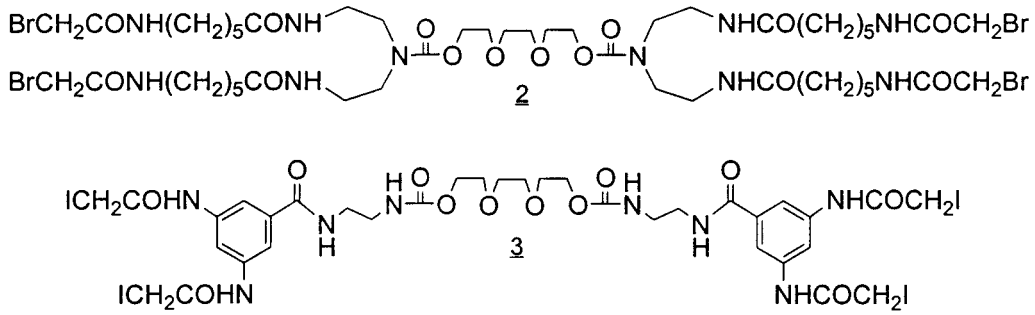


Figure 2.

Determination of Serum Levels of Anti-Peptide Antibodies Using the Farr Assay. Hydroxyphenylated peptide, **20a** or **20b**, was trace radiolabeled as follows. To 50 μg of hydroxyphenylated peptide in 50 μL of, pH 7.5, 100 mM phosphate buffer (PB) was added 1 mCi of ^{125}I (New England Nuclear, NE2−033H) followed by 25 μL of a solution of 2 mg/mL of chloramine T in PB. After 1.5 min, a solution of 25 μL of a solution of 2 mg/mL of sodium metabisulfite in PB was added. The mixture was loaded onto a Sep-pak C_{18} cartridge (Waters part no. 020515), which had been washed with CH_3CN followed of H_2O. The column was eluted with H_2O to wash away salts, then with 50/50 CH_3CN/H_2O to elute peptide. Radiolabeled peptide fractions were pooled and used as radioactive antigen in the Farr assay (*15*). Serum samples from the mice were diluted by factors of 6, 36, and 216 with 10% normal rabbit serum in 0.1 M, pH 8.6, borate buffer, and the radiolabeled peptide was added to the mixture to give a peptide concentration of 10^{-8} M. The IgG was precipitated by addition of an equal volume of saturated ammonium sulfate solution, and the counts in the precipitate were measured to determine the percentage of counts bound to the IgG. The values are reported in Table 2 as antigen-binding capacity (ABC) (*16*).

Serum Stability Studies. To 720 μL of mouse serum (Sigma) was added 80 μL of a 10 mg/mL solution of conjugate (**16a**, **16b**, **17a**, or **17b**) in water, and the mixture was incubated at 37 °C. For each time point, 100 μL of the mixture was added to 900 μL of a cocktail which contained **1b** as an internal standard (80 μL of a 10 mg/mL solution of **1b** in water added to 7.12 mL of a 1 M solution of guanidine HCl in 99/1 water/TFA). The resulting solution was loaded onto a C_{18} Extract Clean column (Alltech Associates Inc., part no. 205 000, 100 mg/1.0 mL) which had been washed with 2 mL of MeOH and 4 mL of water. The peptide conjugate and internal standard were eluted with 1 mL of MeOH, and the eluate was filtered and analyzed by HPLC (C_{18}, gradient 15/85/0.1 CH_3CN/H_2O/TFA to 30/70/0.1 CH_3CN/H_2O/TFA, 0 to 10 min, then 30/70/0.1 CH_3CN/H_2O/TFA to 35/65/0.1 CH_3CN/H_2O/TFA, 10 to 20 min).

DISCUSSION AND RESULTS

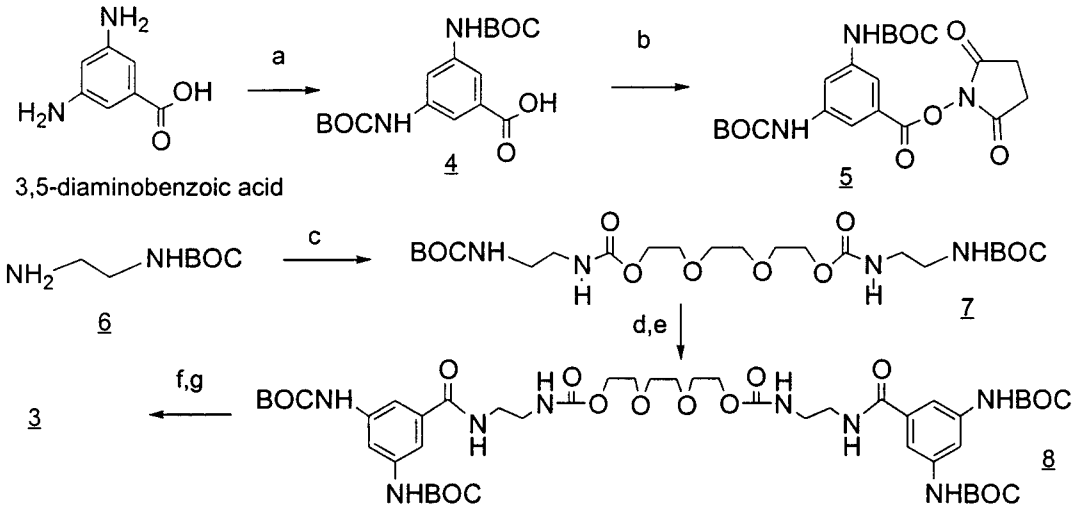
To test the ability of cyclic thioether peptides **1a** and **1b** to effect tolerance when presented on a multivalent platform, chemistry was developed to prepare both tolerageneic and immunogenic conjugates.

Peptides have been conjugated to a variety of substances including other peptides, proteins, and carrier molecules. Some examples of the various methods used are mentioned below. Each method has its own advantages and disadvantages, and the best method for a particular application depends on a number of factors such as what functional groups are present on each partner in the coupling reaction and the solvent compatibility of the partners.

Condensation of protected peptide fragments with amino poly(ethylene glycol) (amino-PEG) has provided PEG−peptide conjugates (*17*). Carboxy-terminal cysteines have been used to link peptides to PEG via disulfide bonds (*18*). Peptide segments have been ligated to provide native proteins by taking advantage of the ability of an N-terminal cysteine on one peptide to react with C-terminal thioesters on another peptide to give a thioester which can rearrange to a natural amide bond (*19*). Ligation via thiazolidine formation between a C-terminal aldehyde and an N-terminal cysteine is another method of connecting two unprotected peptides (*20*). For a review of protein synthesis by chemical ligation see Walker (*21*).

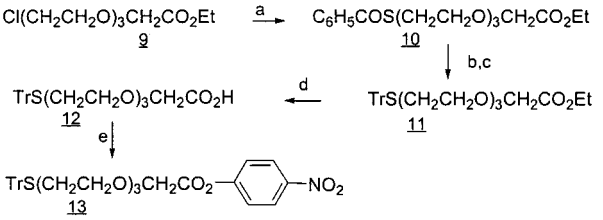
Bromoacetylated peptides have been attached to antibodies (*22*) or ligated to a second cysteine-containing peptide (*23*) via thioether bonds. Peptides with cysteine sulfhydryl groups have been attached to DNA using thioether bonds (*24*). Another method of attaching peptides to other biomolecules is oxime formation between aminooxy peptides and aldehyde or ketone groups (*25*).

Scheme 1[a]



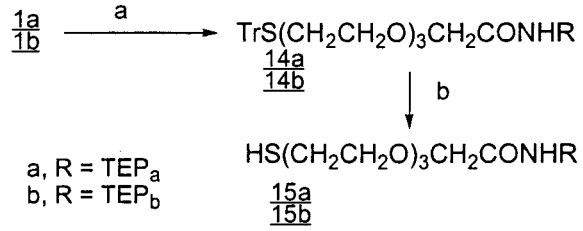
[a] (a) $(BOC)_2O$, MeOH, H_2O, $NaHCO_3$ (66%); (b) NHS, DCC, EtOAc (89%); (c) triethyleneglycol bis-chloroformate, pyridine, CH_2Cl_2 (quantitative); (d) TFA/CH_2Cl_2; (e) compound *5*, $NaHCO_3$, dioxane, H_2O (48%, two steps); (f) TFA/CH_2Cl_2; (g) iodoacetic anhydride, $NaHCO_3$, dioxane, H_2O (45%, two steps).

Scheme 2[a]



[a] (a) Thiobenzoic acid, DBU,DMF (58%); (b) NaOEt, ethanol; (c) trityl chloride, pyridine, CH_2Cl_2 (50%, two steps); (d) NaOH, ethanol (98%); (e) *p*-nitrophenol, DCC, CH_2Cl_2 (87%).

Scheme 3[a]



[a] (a) Compound **13**, DIPEA, DMF; (b) 1/1/0.056/0.04 TFA/CH_2Cl_2/thiophenol/Me_2S (48%, both steps).

Reductive amination of peptide amino groups with oxidized dextran has been used to immobilize peptides on ELISA plates (*26*).

In this report, multivalent thioether peptide conjugates were prepared by first attaching a thiol-containing linker to the thioether peptides, then using the thiol to form a thioether bond with a multivalent haloacetyl platform molecule. This provides a tetravalent conjugate consisting of four identical cyclic thioether peptides attached to a common nonimmunogenic carrier platform. The objective of preparing such conjugates was to test their ability to tolerize an anti-peptide immune response in a model in which mice were immunized with peptide attached to keyhole limpet hemocyanin (KLH).

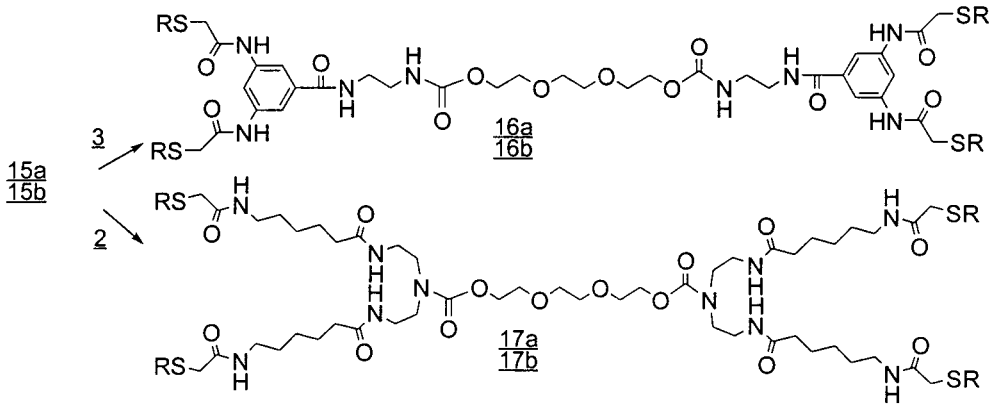
Cyclic thioether peptide analogues **1a** (H_2N-TEP_a) and **1b** (H_2N-TEP_b), which compete with β_2GPI for selected ACA are shown in Figure 1. The sequences of these peptides were derived from phage libraries which contained two fixed cysteines with seven variable amino acids between the cysteines (*27*). Phage which bound ACA were sequenced, and the sequences were used to prepare peptides which bound ACA when oxidized to cyclic disulfides. Peptides **1a** and **1b** are analogues of the primary sequences in which the disulfide bond is replaced with a thioether bridge. In addition peptide **1a** contains an α-methyl proline replacement of a sequence which originally contained a proline at that position. Incorporation of α-methyl proline resulted in tighter binding to ACA and is expected to confer protease resistance.

Peptides **1a** and **1b** were prepared by two different methods for preparing cyclic thioether analogues of cyclic disulfide peptides. Compound **1a** was prepared, as previously described, using a presynthesized thioether intermediate, which was incorporated in solid-phase synthesis (*8*). This method used an amide bond formation to affect cyclization. Compound **1b** was prepared by an alternate method which involved cyclization of a cysteine sulfhydryl with a 4-chloro-2-amino-butyric acid residue which was incorporated in solid-phase synthesis (*9*). The only difference between **1a** and **1b**, is in the fourth amino acid from the C-terminus. Compound **1a** has an (*S*)-α-methylproline at that position, whereas compound **1b** has an arginine at that position. The α-methylproline analogue was included in this study, because it was anticipated that it would have greater metabolic stability. Both analogues have similar ACA binding properties. The relative molar concentrations for 50% inhibition (IC_{50}) of binding of ACA to β_2GPI for **1a** and **1b** are 1.32×10^{-4} M and 2.17×10^{-4} M (*28*).

Tetravalent conjugates of both cyclic thioether peptide analogues, **1a** and **1b**, were prepared using two platforms, compounds **2** and **3**, which are shown in Figure 2. Compound **2** was available from previous studies (*4*). Compound **3** was designed as a hybrid of **2** and a poly(ethylene glycol)-based platform (*3*) which had been previously used successfully in earlier tolerance studies with melittin peptides (*29*).

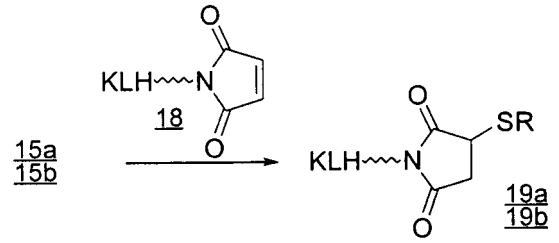
The synthesis of compound **3** is described in Scheme 1. The amino groups of 3,5-diaminobenzoic acid were protected with *tert*-butyloxycarbonyl (BOC) groups to provide compound **4**. Treatment of **4** with *N*-hydroxysuccinimide in the presence of DCC gave the NHS ester, **5**. Mono-BOC-protected ethylenediamine, **6**, (*12*) was condensed with triethylene glycol bis-chloroformate to provide **7**. The BOC groups were removed, and the resulting

Scheme 4[a]



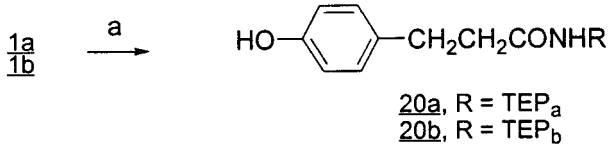
[a] a, R = $(CH_2CH_2O)_3CH_2CONH\text{-}TEP_a$; b, R = $(CH_2CH_2O)_3CH_2CONH\text{-}TEP_b$.

Scheme 5[a]



[a] a, R = $(CH_2CH_2O)_3CH_2CONH\text{-}TEP_a$; b, R = $(CH_2CH_2O)_3CH_2CONH\text{-}TEP_b$.

Scheme 6[a]



[a] (a) 3-(4′-Hydroxyphenyl)propionic acid *N*-hydroxy succinimidyl ester, DMSO, pH 8.5, borate.

diamine was condensed with **5** to provide **8**. Finally, the BOC groups were removed and the resulting amines were acylated with iodoacetic anhydride to provide **3**.

A trityl protected thiol linker, compound **13**, was developed which could be attached to the N-terminus of **1a** or **1b** via acylation. This linker was designed to provide some distance between the platform and the peptide, and to provide water solubility. The synthesis of **13** is diagramed in Scheme 2. Chlorotriethylene glycol was converted to compound **9** by a modification of an existing procedure (*13*). Treatment of **9** with thiobenzoic acid provided the thioester **10**. The thioester was removed by treatment with sodium ethoxide, and the resulting thiol was protected by tritylation to give trityl-thioether **11**. The ester was saponified with sodium hydroxide to provide the acid **12**, which was esterified with DCC and *p*-nitrophenol to provide **13**.

The linker was attached to thioether peptides **1a** ($H_2N\text{-}TEP_a$) and **1b** ($H_2N\text{-}TEP_b$) by acylation at the N-terminus by reaction with **13** as shown in Scheme 3. The resulting peptide products with linker attached, **14a** and **14b**, were treated with trifluoroacetic acid in the presence of scavengers to remove the trityl group and provide **15a** and **15b**, the peptides with the free thiol linker.

Tetravalent conjugates were prepared as described in Scheme 4. Compound **15a** was reacted with platform **3** in pH 8.5 aqueous sodium borate to provide **16a**. Reaction of **15a** with **2** in the same buffer gave conjugate **17a**. Compound **15b** reacted with **3** to give **16b** and with **2** to give **17b**. The reaction mixtures, containing crude conjugates, were loaded directly onto a preparative HPLC column for purification by preparative HPLC.

KLH conjugates **19a** and **19b** were prepared for the purpose of immunizing and boosting mice with peptide. The KLH conjugates were prepared as follows and as described in Scheme 5. A solution of **15a** or **15b** in PBS was added to an aqueous solution of KLH which was modified with maleimide groups on lysine ϵ-amines (compound **18**, Pierce Chemical Co.) resulting in the formation of putative KLH peptide conjugates **19a** and **19b**. These conjugates were not chemically characterized, since KLH itself is an ill-defined multisubunit-containing protein; however, they were characterized by their ability to bind ACA when coated on ELISA plates. The conjugates were also characterized functionally by their ability to elicit an anti-peptide immune response in mice.

Hydroxyphenylated peptides, **21a** and **21b**, were prepared as follows for use in the Farr assay, a solution phase assay for determining antigen binding capacity (ABC) (*15*). Thus, peptides **1a** and **1b** were hydroxyphenylated by adding a solution of 3-(4′-hydroxyphenyl)-propionic acid N-hydroxysuccinimidyl ester (Taggit, Novabiochem) in DMSO to a solution of peptide in pH 8.5 borate buffer to provide **20a** and **20b** as described in Scheme 6.

The Farr assay is a radioimmunoprecipitation assay which measures the amount of radiolabled antigen found in immunoglubulin which has been precipitated in the presence of antigen. The Farr assay is our method of choice for measuring antibody levels when the unbound antigen does not precipitate under the antibody-precipitating conditions. It is our method of choice because it is a relatively simple assay to run, it is reproducible, and it gives a numerical result, the antigen-binding capacity (ABC), which is independent of the dilution at which the assay is run.

An immunization protocol was designed to specifically produce antibodies against the peptide. These anti-peptide antibodies would not exist in the absence of the immunization, because the peptide is totally synthetic. Thus, the ability of compounds **16a**, **16b**, **17a**, and **17b** to tolerate an anti-peptide immune response was tested in mice which were immunized with the relevant peptides conjugated to KLH, conjugates **19a** and **19b**. Three weeks later the mice were treated with one of the tetravalent peptide conjugates, **16a**, **16b**, **17a**, or **17b**. Five days after treatment with the tetravalent peptide conjugates, the mice were boosted with a second administration of the relevant peptide conjugated to KLH (**19a** or **19b**). Seven days after boosting, the ABC of treated and control mice

Table 3. Degradation of Conjugates 16a, 16b, 17a, and 17b in Mouse Serum

compd	time to 50% degradation (h)
16a	10.7
16b	3.6
17a	13.3
17b	3.0

were measured using a Farr assay at dilutions of 1/6, 1/36, and 1/216 (*15*). These data are summarized in Table 2. The specificity of the treatments was demonstrated with measurements of both anti-peptide antibody titers using the Farr assay, and anti-carrier (KLH) antibodies using an ELISA assay (*30*). Three of the conjugates, **16a**, **16b**, and **17b**, resulted in a significant reduction in the anti-peptide antibody levels, whereas, there were no reductions in the anti-KLH antibody levels in any of the experiments (data not shown). Thus, these toleragens were specific for downregulating the anti-peptide response without affecting the response to the protein carrier, KLH. Conjugate **17a** did not reduce the anti-peptide response at the doses used, perhaps due to differences in the distribution, clearance, or metabolic properties of **17a** from the other conjugates. The stabilities of the conjugates in serum were studied to determine if ability to tolerize correlated to metabolic stability. The results, shown in Table 3, indicate that compound **17a** is actually the most stable conjugate of the four conjugates tested in normal mouse serum, so its lack of tolerance activity cannot be explained by the issue of susceptibility to serum proteases.

These studies show that cyclic thioether peptide antigen mimotopes, when presented as a tetravalent conjugate, can cause downregulation of an anti-peptide antibody response. The downregulation is specific to the antibodies against the immunizing peptide as evidenced by no downregulation of antibodies against the carrier protein, KLH, which was used in the immunization. The downregulation is evidence of B cell tolerance, since the tetravalent conjugate is administered 5 days before the boost, at which time little or no toleragen would be present.

LITERATURE CITED

(1) Nossal, G. J. V., Pike, B. L., and Katz, D. H. (1973) Induction of B Cell Tolerance in vitro to 2,4-dinitrophenyl Coupled to a Copolymer of *D*-Glutamic Acid and *D*-Lysine (DNP-*D*-GL). *J. Exp. Med. 138*, 312−317.

(2) Liu, F.-T., Zinnecker, M., Hamaoka, T., and Katz, D. H. (1979) New Procedures for Preparation and Isolation of Conjugates of Proteins and a Synthetic Copolymer of D-Amino Acids and Immunochemical Characterization of Such Conjugates. *Biochemistry 18*, 690−697.

(3) Jones, D. S., Hachmann, J. P., Osgood, S. A., Hayag, M. S., Barstad, P. A., Iverson, G. M., and Coutts, S. M. (1994) Conjugates of Double-Stranded Oligonucleotides with Poly(ethylene glycol) and Keyhole Limpet Hemocyanin: A Model for Treating Systemic Lupus Erythematosus. *Bioconjugate Chem. 5*, 390−399.

(4) Jones, D. S., Barstad, P. A., Field, M. J., Hachmann, J. P., Hayag, M. S., Hill, K. W., Iverson, G. M., Livingston, D. A., Palanki, M. S., Tibbetts, A. R., Yu, L., and Coutts, S. M. (1995) Immunospecific Reduction of Antioligonucleotide Antibody-Forming cells with a Tetrakis-Oligonucleotide Conjugate (LJP 394), a Therapeutic Candidate for the Treatment of Lupus Nephritis. *J. Med. Chem. 38*, 2138−2144.

(5) Kandiah, D. A., Sali, A., Sheng, Y., Victoria, E. J., Marquis, D. M., Coutts, S. M., and Krilis, S. A. (1998) Current Insights into the "Antiphospholipid" Syndrome: Clinical, Immunological, and Molecular Aspects. *Adv. Immunol. 70*, 507−563.

(6) Iverson, G. M., Victoria, E. J., and Marquis, D. M. (1998) Anti-β2 glycoprotein I (β2GPI) autoantibodies recognize an epitope on the first domain of β2GPI. *Proc. Natl. Acad. Sci. 37*, 15542−15546.

(7) Smith, G. N., and Petrenko, V. A. (1997) Phage Display. *Chem. Rev. 97*, 391−410.

(8) Jones, D. S., Gamino, C. A., Randow, M. E., Victoria, E. J., Yu, L., and Coutts, S. M. (1998) Synthesis of a Cyclic-Thioether Peptide Which Binds Anti-Cardiolipin Antibodies. *Tetrahedron Lett. 39*, 6107−6110.

(9) Yu, L., Lai, Y., Wade, J. V., and Coutts, S. M. (1998) A Simple and Efficient Method for the Synthesis of Thioether Cyclic Peptides. *Tetrahedron Lett. 39*, 6633−6636.

(10) Rabenstein, D. L., and Yeo, P. L. (1994) Kinetics and Equilibria of the Formation and Reduction of the Disulfide Bonds in Arginine-Vasopressin and Oxytocin by Thiol/Disulfide Interchange with Glutathione and Cysteine. *J. Org. Chem. 59*, 4223−4229.

(11) Itoh, N., Yoshida, M., Miyamoto, T., Ichinose, H., Wariishi, H., and Tanaka, H. (1997) Fungal Cleavage of Thioether Bond Found in Yperite, *FEBS Lett. 412*, 281−284.

(12) Huang, L., Quada, J. C., and Lown, J. W. (1995) Design, Synthesis, and Sequence Selective DNA Cleavage of Functional Models of Bleomycin. 1. Hybrids Incorporating a Simple Metal-Complexing Moiety of Bleomycin and Lexitropsin Carriers. *Bioconjugate Chem. 6*, 21−33.

(13) Boumrah, D., Campbell, M. M., Fenner, S., and Kinsman, R. G. (1991) Spacer Molecules in Peptide Sequences: Incorporation into Analogues of Atrial Natriuretic Factor. *Tetrahedron Lett. 32*, 7735−7738.

(14) The direct binding ELISA was carried out as follows. Immulon II 96-well microplates (Dynatech laboratories, Inc.) were treated with 100 μL/well of dilutions of KLH−peptide conjugate at concentrations of 0−4 μg/mL in an aqueous solution consisting of 15 mM Na_2CO_3 and 35 mM $NaHCO_3$ for 2 h. The liquid was removed, and each well was treated with 200 μL of 0.5% (w/v) bovine serum albumin (BSA, Sigma Chemical catalog no. A7638) in TBS for 2 h. Each well was washed 5 times with TBS and treated with 100 μL of ACA-6501 serum or normal AB serum diluted in 0.5% BSA/TBS for 1 h with gentle agitation, then washed 5 times with TBS. Each well was treated with goat anti-human IgG alkaline phosphatase conjugate (Zymed, catalog 15, no. 62-8422) diluted 1:1000 in 0.5% BSA-TBS (100 μL) for 1 h, washed 5 times with TBS and developed by adding 100 μL of PPMP solution (7.8 g of phenolphthalein monophosphate and 69.5 g of 2-amino-2-methyl-1-propanol in 100 mL of water and diluted 1:26 with water immediately before use). Color development was stopped by adding 50 μL of 0.2 M Na_2HPO_4 solution to each well. Absorbance at 550 nm was read and plotted vs amount of KLH−peptide added.

(15) Iverson, G. M. (1986) Assay for In Vivo Adoptive Immune Response. in *Handbook of Experimental Immunology, Vol. 2: Cellular Immunology*, 4th ed. (D. M. Weir, and L. A. Herzenberg, Eds.) Chapter 67, pp 67.1−76.8, Blackwell Scientific Publications, Oxford.

(16) The percentage of antigen bound multiplied by the dilution factor is the same as the antigen binding capacity (ABC) up to 35% bound, because the percentage of antigen bound is directly proportional to dilution in that range. For bindings greater than 35%, the log of ABC is proportional to the log of the percentage bound and is calculated by the following formula [ABC = [2 × 1/10 antilog(% bound/35 × log 3.5)] × dilution factor]. Values of ABC reported are the average of ABC values calculated from percentage of antigen bound in the range 10−70% (*15*).

(17) Maeda, M., Izuno, Y., Kawasaki, K., Kanade, Y., Mu, Y., Tsutsumi, Y., Lem, K. W., and Mazumi, T. (1997) Amino Acids and Peptides XXXII: A Bifunctional Poly(Ethylene Glycol) Hybrid of Fibronectin-Related Peptides. *Biochem. Biophys. Res. Commun. 241*, 595−598.

(18) Campbell, R. M., Heimer, E. P., Ahmad, M., Eisenbeis, H. G., Lambros, T. J., Lee, Y., Miller, R. W., Stricker, P. R., and Felix, A. M. (1997) Pegylated Peptides V: Carboxy-Terminal Pegylated Analogues of Growth Hormone Releasing Factor

(GRF) Display Enhanced Duration of Biological Activity In Vitro. *J. Pept. Res. 49*, 527−537.
(19) Dawson, P. E., Muir, T. W., Clark-Lewis, I., and Kent, S. B. H. (1994) Synthesis of Proteins by Native Chemical Ligation. *Science 266*, 776−779.
(20) Botti, P., Pallin, T. D., and Tam, J. P. (1996) Cyclic Peptides from Linear Unprotected Peptide Precursors through Thiazolidine Formation. *J. Am. Chem. Soc. 118*, 10018−10024.
(21) Walker, M. A. (1997) Protein Synthesis by Chemical Ligation of Unprotected Peptides in Aqueous Solution. *Angew. Chem., Int. Ed. Engl. 36*, 1069−1071.
(22) Wilson, K. M., Catimel, B., Mitchelhill, K. I., and Kemp, B. E. (1994) Simplified Conjugation Chemistry for Coupling Peptides to F(ab′) Fragments: Autologous Red Cell Agglutination Assay for HIV-1 Antibodies. *J. Immunol. Methods 175*, 267−273.
(23) Futaki, S., Ishikawa, T., Niwa, M., Kitagawa, K., and Yagami, T. (1997) Embodying a Stable a-Helical Protein Structure through Efficient Chemical Ligation via Thioether Formation. *Bioorg. Med. Chem. 5*, 1883−1891.
(24) Sebestyen, M. G., Ludtke, J. J., Bassik, M. C., Zhang, G., Budker, V., Lukhtanov, E. A., Hagstrom, J. E., and Wolff, J. A. (1998) DNA Vector Chemistry: The Covalent Attachment of Signal Peptides to Plasmid DNA. *Nat. Biotechnol. 16*, 80−85.
(25) Canne, L. E., Ferre-D'Amare, A. R., Burley, S. K., and Kent, S. B. H. (1995) Total Chemical Synthesis of a Unique Transcription Factor-Related Protein cMyc-Max. *J. Am. Chem. Soc. 117*, 2998−3007.
(26) Bocher, M., Boldicke, T., Kiess, M., and Bilitewski, U. (1997) Synthesis of Mono- and Bifunctional Peptide-Dextran Conjugates for the Immobilization of Peptide Antigens on ELISA Plates: Properties and Application. *J. Immun. Methods 208*, 191−202.
(27) Sem, D. S., Baker, B. L., Victoria, E. J., Jones, D. S., Marquis, D., Yu, L., Parks, J., and Coutts, S. M. (1998) Structural Characterization and Optimization of Antibody −Selected Phage Library Mimotopes of an Antigen Associated with Autoimmune Recurrent Thrombosis. *Biochemistry 37*, 16069−16081.
(28) ACA ELISA data were obtained as follows. Polystyrene microtitration plates were coated with cardiolipin (50 μg/well) in ethanol. After evaporation of solvent, wells were blocked (5% fish gelatin/PBS, pH 7.2), washed (TBS, pH 7.4), and coated with β_2GPI (2.3% IgG-depleted normal human serum). Wells were incubated with a mixture of peptide and ACA serum, diluted 1:400 with 3% fish gelatin in 1:1 TBS/PBS, then washed (TBS) and treated with goat anti-human IgG alkaline phosphatase conjugate. After washing with TBS, the wells were treated with colorimetric substrate to determine the amount of ACA bound. The IC_{50} is the concentration of peptide that inhibited ACA binding by 50%.
(29) Unpublished research from this laboratory.
(30) Ferguson, T. A., Beaman, K. D., and Iverson, G. M. (1985) Isolation and Characterization of a T Suppressor Factor by Using a Monoclonal Antibody. *J. Immunol. 134*, 3163−3171.

BC9801373

Technetium-99m-Labeled Medium-Chain Fatty Acid Analogues Metabolized by β-Oxidation: Radiopharmaceutical for Assessing Liver Function

Norio Yamamura,[†] Yasuhiro Magata,[‡] Yasushi Arano,[†] Takayoshi Kawaguchi,[†] Kazuma Ogawa,[†] Junji Konishi,[‡] and Hideo Saji*[,†]

Department of Patho-Functional Bioanalysis, Graduate School of Pharmaceutical Sciences, Department of Nuclear Medicine, Graduate School of Medicine, Kyoto University, Yoshida Shimoadachi-cho, Sakyo-ku, Kyoto, 606-8501, Japan. Received December 28, 1998; Revised Manuscript Received March 8, 1999

External imaging of energy production activity of living cells with ^{99m}Tc-labeled compounds is a challenging task requiring good design of ^{99m}Tc-radiopharmaceuticals. On the basis of our recent findings that ^{11}C- and ^{123}I-labeled medium-chain fatty acids are useful for measuring β-oxidation activity of hepatocytes, we focused on development of ^{99m}Tc-labeled medium-chain fatty acid analogues that reflect β-oxidation activity of the liver. In the present study, monoamine−monoamide dithiol (MAMA) ligand and triamido thiol (MAG) ligand were chosen as chelating groups because of the stability and size of their complexes with ^{99m}Tc and their ease of synthesis. Each ligand was attached to the ω-position of hexanoic acid (MAMA-HA and MAG-HA, respectively). In biodistribution studies, [^{99m}Tc]MAMA-HA showed high initial accumulation in the liver followed by clearance of the radioactivity in the urine. Analysis of the urine revealed [^{99m}Tc]MAMA-BA as the sole radiometabolite. Furthermore, when [^{99m}Tc]MAMA-HA was incubated with living liver slices, generation of [^{99m}Tc]-MAMA-BA was observed. However, [^{99m}Tc]MAMA-HA remained intact when the compound was incubated with liver slices in the presence of 2-bromooctanoate, an inhibitor of β-oxidation. The findings in this study indicated that [^{99m}Tc]MAMA-HA was metabolized by β-oxidation after incorporation into the liver. On the other hand, poor hepatic accumulation was observed after administration of [^{99m}Tc]-MAG-HA.

INTRODUCTION

In the liver, the parenchymal cells are responsible for the metabolism of many substances, and parenchymal cell function is also related to the reserve capacity of the liver (*1*−*3*). Therefore, the development of radiopharmaceuticals which reflect viability of hepatocytes might provide us useful information for predicting prognosis after surgery or determining the efficacy of the treatment.

The β-oxidation of fatty acids is an important pathway for the production of energy for activity of hepatocytes (*4*, *5*). In addition to β-oxidation, however, long-chain fatty acids are esterified and retained in the liver to a fairly large extent. On the other hand, medium-chain fatty acids such as octanoate and hexanoate are recognized only as substrates for β-oxidation and are not esterified in the hepatocytes (*6*−*8*). Indeed, [1-^{11}C]octanoate was metabolized rapidly to $^{11}CO_2$ by β-oxidation and cleared quickly from the liver. In addition, the hepatic elimination rate of the radioactivity was significantly delayed in animal models of hepatitis (*9*). Such characteristics render [1-^{11}C]octanoate useful as a radiopharmaceutical for measuring the viability of hepatocytes by positron emission tomography (PET) imaging.

Medium-chain fatty acid analogues labeled with single photon emitters are more desirable for routine clinical studies to estimate the viability of hepatocytes. We recently found that *p*-[^{123}I]iodophenylenanthic acid ([^{123}I]-IPEA) was taken up by the liver following administration and elimination rate of the final radiometabolite, *p*-iodohippuric acid, from the liver reflected β-oxidation activities of the hepatocytes. A significant delay in elimination of the radioactivity from the liver was observed in hepatitis models (*10*). These findings prompted us to further examine the use of ^{99m}Tc-labeled medium-chain fatty acid analogues for hepatic studies since ^{99m}Tc possesses ideal characteristics for a radiopharmaceutical such as optimal γ-ray energy (141 keV), short half-life (6 h), low-cost, and widespread availability of the ^{99}Mo/^{99m}Tc generator.

Introduction of a chelating group is necessary for labeling of fatty acids with ^{99m}Tc based on the idea of bifunctional chelating agent. A variety of chelating groups have been developed for such purposes. Among these groups, two ^{99m}Tc chelating groups were chosen as candidates in the present study because of the stability and molecular size of their complexes with ^{99m}Tc and ease of synthesis, and each chelating group was attached to the ω-position of hexanoic acid. One was a recently reported monoamine−monoamide dithiol (MAMA) ligand, which forms a stable, neutral, and slightly lipophilic mononuclear ^{99m}Tc complex with pentavalent $^{99m}TcO^{3+}$ (*11*−*13*). The amino nitrogen was the site of attachment to hexanoic acid (MAMA-HA). The other chelating group was a triamide thiol group (N_3S) which has been used clinically as a ^{99m}Tc complex of mercaptoacetylglycylglycylglycine (MAG_3) (*14*−*16*). It forms a negatively charged mononuclear ^{99m}Tc complex with pentavalent $^{99m}TcO^{3+}$. The terminal glycine of MAG_3 was altered to 6-amino-

* To whom correspondence should be addressed. Phone: +81-75-753-4556. Fax: +81-75-753-4568.
[†] Department of Patho-Functional Bioanalysis.
[‡] Department of Nuclear Medicine.

10.1021/bc9801528 CCC: $18.00 © 1999 American Chemical Society
Published on Web 04/16/1999

hexanoic acid (MAG-HA). The biodistribution and metabolism of the two ^{99m}Tc-labeled medium-chain fatty acid analogues were investigated in rats to estimate the molecular design for measuring the viability of hepatocytes.

MATERIALS AND METHODS

Materials. Proton nuclear magnetic resonance (^{1}H NMR) spectra were recorded on a Bruker AC-200 spectrometer, and the chemical shifts are reported in parts per million (ppm) downfield from an internal tetramethylsilane standard. Fast-atom bombardment mass spectra (FABMS) were obtained with a JMS-HX/HX 110 A (JEOL Ltd. Tokyo). Imaging studies were performed using a SPECT2000H-40 (Hitachi Medical Co., Tokyo). [^{99m}Tc]-Pertechnetate ($^{99m}TcO_4^-$) was eluted in saline solution on a daily basis from Daiichi Radioisotopes Labs generator (Chiba, Japan). Reversed-phase high performance liquid chromatography (RP-HPLC) was performed using a Cosmosil 5C_{18}-AR 300 column (150 × 4.6 mm; Nacalai Tesque Co., Ltd., Kyoto). TLC analysis was performed with silica plates (Merck Art 5553). All chemicals were of reagent grade and were used as received.

Synthesis of Tr-MAMA-HA and Its Analogues. *N-[[[2-[(Triphenylmethyl)thio]ethyl]amino]acetyl]-S-(triphenylmethyl)-2-aminoethanethiol (Tr-MAMA) (**3**).* Trityl chloride (27.3 g, 97.9 mmol) and compound **1** (11.1 g, 97.7 mmol) were dissolved in 150 mL of *N*,*N*-dimethylformamide (DMF), and the reaction mixture was stirred for 48 h at room temperature. The solvent was removed in vacuo, and the residue was dissolved in ethyl acetate. After cooling the solution on ice, a saturated solution of $NaHCO_3$ was gradually added. The precipitated white crystals were collected and washed with distilled water to afford compound **2** as the crude product. Crude **2** (9.97 g, 28 mmol) in chloroform (ca. 50 mL) was mixed with triethylamine (14 mL), and the mixture was gradually added to a solution of bromoacetyl bromide (2.84 g, 14 mmol) in 40 mL of chloroform at −78 °C. The reaction mixture was stirred at the same temperature for 30 min and warmed to room temperature over a period of 1 h. After stirring at room temperature for 24 h, the mixture was washed with diluted H_2SO_4 (pH 3), saturated $NaHCO_3$, and brine. The organic layer was dried over anhydrous $CaSO_4$, and the solvent was removed in vacuo. The crude product of compound **3** was obtained after silica gel column chromatography of the oil residue eluted with chloroform. Further purification was performed by silica gel chromatography using ethyl acetate−hexane (60:40) as the eluent to produce 3 (0.95 g, 10.0% from **2**) as a pale yellow oil. ^{1}H NMR ($CDCl_3$): ***δ*** 7.44−7.15 (overlapped m, 30H), 3.07 (td, 2H), 3.02 (s, 2H), 2.45 (t, 2H), 2.38−2.31 (overlapped m, 4H). FABMS calcd for $C_{44}H_{42}N_2OS_2$ ($M + H^+$): m/z 679. Found: 679.

*N-[[[[2-[(Triphenylmethyl)thio]ethyl]amino]carbonyl]-methyl]-N-[2-[(triphenylmethyl)thio]ethyl]-6-aminohexanoic Acid Methyl Ester (**5**).* Methyl 6-bromohexanoate (**4**) (160 mg, 0.77 mmol) in 8 mL of acetonitrile was gradually added to a mixed solution of Tr-MAMA (400 mg, 0.59 mmol) and diisopropylethylamine (120 mg, 1.84 mmol) in 2 mL of acetonitrile. After stirring the reaction mixture at room temperature for 48 h, the solvent was removed in vacuo. The oily residue was purified by silica gel chromatography using ethyl acetate−hexane (95:5) as the eluent to provide compound **5** (117 mg, 24.6%) as a yellow oil. ^{1}H NMR ($CDCl_3$): *δ* 7.43−7.15 (overlapped m, 30H), 3.64 (s, 3H), 3.01 (td, 2H), 2.82 (s, 2H), 2.40−2.33 (overlapped m, 4H), 2.28−2.20 (overlapped m, 6H), 1.59−1.48 (m, 2H), 1.37−1.19 (overlapped m, 4H). FABMS calcd for $C_{51}H_{54}N_2O_3S_2$ ($M + H^+$): *m/z* 807. Found: 807.

*N-[[[[2-[(Triphenylmethyl)thio]ethyl]amino]carbonyl]-methyl]-N-[2-[(triphenylmethyl)thio]ethyl]-6-aminohexanoic Acid (Tr-MAMA-HA) (**6**).* Compound **6** was obtained quantitatively as a viscous yellow oil by hydrolysis of the methyl ester of **5** in 5% NaOH. ^{1}H NMR ($CDCl_3$): *δ* 7.40−7.14 (overlapped m, 30H), 2.99 (td, 2H), 2.87 (s, 2H), 2.40−2.33 (overlapped m, 4H), 2.28−2.20 (overlapped m, 6H), 1.59−1.48 (m, 2H), 1.32−1.21 (overlapped m, 4H). FABMS calcd for $C_{50}H_{52}N_2O_3S_2$ ($M + H^+$): *m/z* 793. Found: 793.

N-[[[[2-[(Triphenylmethyl)thio]ethyl]amino]carbonyl]-methyl]-N-[2-[(triphenylmethyl)thio]ethyl]-4-aminobutyric Acid (Tr-MAMA-BA). *N*-[[[[2-[(Triphenylmethyl)-thio]ethyl]amino]carbonyl]methyl]-*N*-[2-[(triphenylmethyl)thio]ethyl]-4-aminobutyric acid ethyl ester was synthesized by reaction of Tr-MAMA and ethyl bromobutyrate according to the procedure described above with 3.25% yield. ^{1}H NMR ($CDCl_3$): *δ* 7.45−7.15 (overlapped m, 30H), 4.06 (q, 2H), 3.01 (td, 2H), 2.84 (s, 2H), 2.38−2.32 (overlapped m, 4H), 2.29−2.18 (overlapped m, 6H), 1.68−1.26 (m, 2H), 1.20 (t, 3H). After hydrolysis of the ester bond, Tr-MAMA-BA was obtained. ^{1}H NMR ($CDCl_3$): *δ* 7.40−7.17 (overlapped m, 30H), 2.99 (td, 2H), 2.87 (s, 2H), 2.36−2.33 (overlapped m, 4H), 2.30−2.23 (overlapped m, 6H), 1.65−1.62 (m, 2H). FABMS calcd for $C_{48}H_{48}N_2O_3S_2$ ($M + Na^+$): *m/z* 787. Found: 787.

N-[[[[2-[(Triphenylmethyl)thio]ethyl]amino]carbonyl]-methyl]-N-[2-[(triphenylmethyl)thio]ethyl]-2-aminoacetic Acid (Tr-MAMA-AA). This compound was synthesized using Tr-MAMA and methyl bromoacetate according to the procedure described above with 17.5% yield. After hydrolysis, *N*-[[[[2-[(triphenylmethyl)thio]ethyl]amino]-carbonyl]methyl]-*N*-2-[(triphenylmethyl)thio]ethyl]-2-aminoacetic acid (Tr-MAMA-AA) was obtained (72.5%). ^{1}H NMR ($CDCl_3$): *δ* 7.39−7.14 (overlapped m, 30H), 3.10 (s, 2H), 2.99 (s, 2H), 2.98 (td, 2H), 2.50 (t, 2H), 2.34 (t, 2H), 2.24 (t, 2H). FABMS calcd for $C_{46}H_{44}N_2O_3S_2$ ($M + Na^+$): *m/z* 759. Found: 759.

Synthesis of MAG-HA. *S-Acetylthioglycolic Acid N-Hydroxysuccinimide Ester (SATA) (**10**).* *S*-Acetylmercaptoacetic acid (**9**) was synthesized from mercaptoacetic acid (**8**) according to the published procedure (*17*). Compound **9** (5.15 g, 38.5 mmol) and *N*-hydroxysuccinimide (NHS) (4.45 g, 38.5 mmol) were dissolved in 50 mL of anhydrous tetrahydrofurane (THF), and the reaction mixture was stirred at room temperature for 10 min. After cooling on ice, dicyclohexylcarbodiimide (DCC) (7.95 g, 38.5 mmol) in 5 mL of THF was added and the reaction mixture was stirred overnight. The precipitated dicyclohexylurea was removed by filtration, and the solvent was evaporated to dryness in vacuo (*18*). The residue was washed with hexane several times to afford compound **10** as white crystals (7.69 g, 86.3%). ^{1}H NMR ($CDCl_3$): *δ* 3.99 (s, 2H), 2.85 (s, 4H), 2.43 (s, 3H).

*S-Acetylmercaptoglycylglycylaminohexanoic Acid (S-acetyl MAG-HA) (**13**).* *N*-Succinimide ester of Boc-glycylglycine (compound **11**) was prepared by the reaction of Boc-glycylglycine with NHS in the presence of DCC. Compound **11** (2.37 g, 7.2 mmol) in 30 mL of acetonitrile was slowly added to a solution of 6-aminohexanoic acid (0.79 g, 6 mmol) in 0.2 M NaOH at 50−60 °C, and the reaction mixture was refluxed for 2 h. After cooling, the reaction solution on ice, the pH of the solution was brought to ca. 3 with diluted H_2SO_4, followed by extraction with ethyl acetate (20 mL × 3). The organic layers were combined and dried over anhydrous $CaSO_4$. Compound **12** (1.41 g, 56.7% from **11**) was obtained as a

viscous oil after removing the solvent in vacuo. Crude **12** (1.3 g, 3.8 mmol) was then treated with 5% anisol in trifluoroacetic acid (TFA) to deprotect the Boc group. After removing TFA in vacuo, the residue was dissolved in 20 mL of water and the solution was neutralized with 1 M NaOH. This solution was then added dropwise to a solution of SATA (1.04 g, 4.5 mmol) in 20 mL of DMF. After stirring the reaction mixture at room temperature for 2 h, the solvent was removed in vacuo to precipitate compound **13** as white crystals (396 mg, 29.1% from **12**). ^{1}H NMR ($CDCl_3$): δ 8.42 (t, 1H), 8.13 (t, 1H), 7.70 (t, 1H), 3.72 (d, 2H), 3.66 (s, 2H), 3.65 (d, 2H), 3.03 (td, 2H), 2.36 (s, 3H), 2.19 (t, 2H), 1.54−1.21 (overlapped m, 6H). FABMS calcd for $C_{14}H_{23}N_3O_6S$ ($M+H^+$): *m*/*z* 362. Found: 362.

Radiolabeling. ^{99m}Tc complexes of each ligand were prepared by ligand-exchange reaction with $^{99m}TcO_4^-$ reduced with Sn(II) glucoheptonate (GH). A solution of $^{99m}TcO_4^-$ eluted from the generator every morning was added to stock freeze-dried powder of Sn(II) GH (made from 4 g of GH and 1.2 mg of $SnCl_2$ in 50 mL of aqueous solution pH 8.6) to produce a final GH concentration of 3−5 mg/mL. After standing for 10 min, the formation of [^{99m}Tc]GH was ascertained by TLC developed with acetone.

The bistritylated compound **6** (1 mg) was treated with TFA under cation trapping conditions (5% triethylsilane) (*19*). After removing the solvent under a stream of N_2, the residue was neutralized with 1 M NaOH and 0.4 mL of phosphate buffer (0.1 M, pH 8.0). [^{99m}Tc]GH (0.4 mL) was then added to the bisthiol compound, and the reaction mixture was left for 1 h at room temperature. [^{99m}Tc]MAMA-HA was purified by RP-HPLC eluted with a gradient mobile phase starting from 10% acetonitrile in 0.05 M phosphate buffer (pH 7.0) to 100% acetonitrile in 60 min at a flow rate of 1 mL/min at 30 °C (R_t, 14 min for [^{99m}Tc]MAMA-HA, 3 min for [^{99m}Tc]GH). ^{99m}Tc complexes of MAMA-BA and MAMA-AA were prepared by procedures similar to those described above.

^{99m}Tc complex of MAG-HA was also prepared by reaction of [^{99m}Tc]GH with *S*-acetyl MAG-HA as follows. A solution of *S*-acetyl MAG-HA (3 mg) in 1 mL of phosphate buffer (0.1 M, pH 8.0) was mixed with the same volume of [^{99m}Tc]GH, and the reaction mixture was heated at 90−95 °C for 30 min. After cooling, [^{99m}Tc]-MAG-HA was purified by RP-HPLC eluted with a gradient mobile phase starting from 10% methanol in 0.05 M phosphate buffer (pH 7.0) to 50% methanol in 30 min at a flow rate of 1 mL/min at 30 °C (R_t, 20 min for [^{99m}Tc]-MAMA-HA, 3 min for [^{99m}Tc]GH).

The radiochemical yield and purity of ^{99m}Tc-labeled fatty acid analogues were determined by RP-HPLC under the conditions described above and TLC developed with acetone.

Partition Coefficient Determination. The partition coefficients of [^{99m}Tc]MAMA-HA and [^{99m}Tc]MAG-HA were measured by mixing 10 μL of each ^{99m}Tc-labeled compound with 3 g each of 1-octanol and phosphate buffer (0.1 M, pH 7.4) in a test tube. After vortexing for 1 min × 3 times, the solution was left to stand at room temperature for 20 min. Each tube was then centrifuged at 1000 × g for 5 min. Two weighed samples from the 1-octanol and buffer layers were counted in a γ counter. The partition coefficient was determined by calculating the ratio of counts per minute per gram (cpm/g) of octanol to that of buffer.

Cysteine Challenge Assay. To compare the stability of [^{99m}Tc]MAMA-HA and [^{99m}Tc]MAG-HA, a cysteine challenge assay was performed. Both ^{99m}Tc-labeled fatty acid analogues were incubated with 10 μM cysteine, which is the concentration in blood, in phosphate buffer (0.05 M, pH 7.0) at 37 °C. At 5 or 60 min after incubation, the integrity of each was analyzed by RP-HPLC under the conditions used for purification.

Animal Studies. Male Wistar rats (200−250 g) were housed for 1 week under a 12 h light/12 h dark cycle and had free access to food and water for subsequent metabolite analyses in vitro, imaging and biodistribution studies.

Planar imaging studies of ^{99m}Tc-labeled fatty acid analogues were performed as follows. Normal rats were anesthetized with pentobarbital (50 mg/kg i.p.). Dynamic planar scanning (20 s × 30 frames, 1 min × 10 frames, 2 min × 20 frames) was initiated immediately after administration of ^{99m}Tc-labeled compounds (15 MBq/0.5 mL) via the tail vein.

For biodistribution studies, [^{99m}Tc]MAMA-HA (37 kBq in 0.1 mL saline) was administered to normal rats via the tail vein. At appropriate time points after administration, rats were sacrificed by decapitation. Samples of blood and the organs of interest were excised and weighed, and the radioactivity was quantified using a NaI (Tl) γ scintillation counter (Packard Auto-Gamma 500, Packard Inst. Co.). The results are expressed as percent injected dose per gram of blood or organs after decay correction.

Determination of Radiometabolites in Vivo. At 60 min postinjection of [^{99m}Tc]MAMA-HA, urine samples were obtained from the bladder. After filtration of the urine samples through a 10 kDa cutoff ultrafiltration membrane (Molcut II LGC; NIHON MILLIPORE Co, Yonezawa, Japan), the filtrate was analyzed by RP-HPLC eluted with a gradient mobile phase starting from 10% methanol in 0.05 M phosphate buffer (pH 7.0) to 100% methanol in 60 min at a flow rate of 1 mL/min at 30 °C.

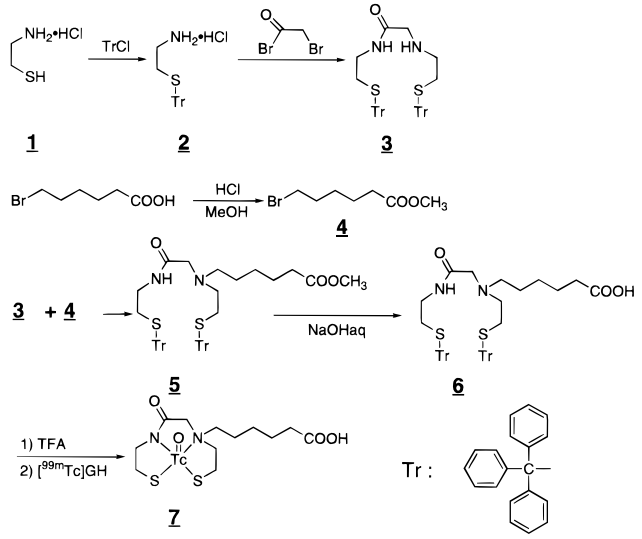
In Vitro Metabolite Studies. Male Wistar rats were anesthetized with pentobarbital (50 mg/kg i.p.), and the rat liver was perfused via the portal vein with O_2/CO_2 (95/5)-saturated cold 20 mM Tris-HCl buffer (pH 7.4) containing 100 mM KCl, 5 mM $MgCl_2$, and 5 mM KH_2PO_4. The rat liver was immediately excised and sliced at a thickness of 300 μm. After weighing, the slices were incubated for 5 min at 37 °C in the presence or absence of 100 μM 2-bromooctanoate which inhibits β-oxidation of long and medium-chain fatty acids (*20*, *21*). Then, [^{99m}Tc]MAMA-HA (3.7 MBq) was added, and the solution was shaken 60 times/min under bubbling O_2/CO_2 (95/5) at 37 °C for 60 min. After addition of 5 mL of acetonitrile, the solution was homogenized and centrifuged at 1000*g* for 20 min to precipitate protein. After removing the organic solvent in vacuo, the residue was filtered through polycarbonate membrane with a pore diameter of 0.22 μm (Hospital/pharmacy Milles GV, Millipore), and the filtrate was analyzed by RP-HPLC as described above. The integrity of the hepatocytes in the slices was determined by measuring lactate dehydrogenase (LDH) activity leaked into the buffer at the end of the incubation. There was no significant difference in LDH activity in the presence or absence of 2-bromooctanoate (3285 ± 367 IU/L vs 3175 ± 478 IU/L, respectively).

Statistical Analyses. Data were analyzed using unpaired two-tailed alternate Welch *t*-tests. A value of $p < 0.05$ was considered significant.

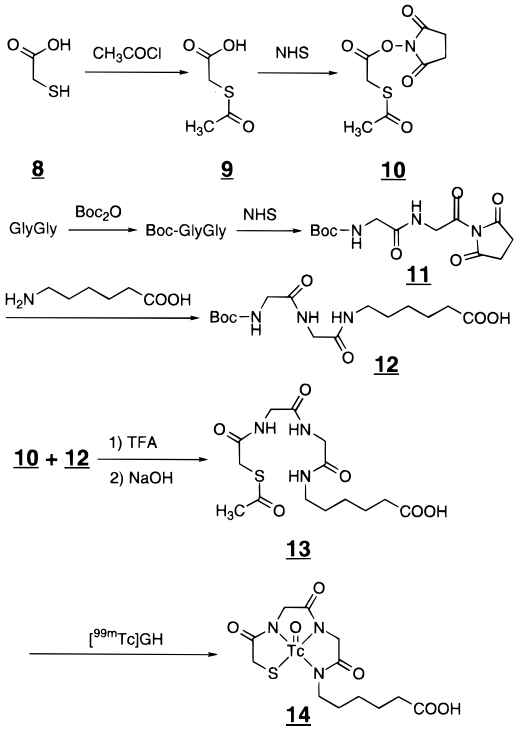
RESULTS

Synthesis of Fatty Acid Analogues. The bistritylated derivative of MAMA-HA (**6**) was synthesized ac-

Scheme 1



Scheme 2



cording to the procedure outlined in Scheme 1. After protecting the thiol group of cysteamine chloride with trityl chloride, the resulting compound **2** was reacted with bromoacetyl bromide to prepare **3**. The amine group of **3** was then alkylated with 6-bromohexanoate to produce **5**. After hydrolysis of the ester group, **6** was obtained as a yellow oil with an overall yield of 2.26%.

The synthetic procedure for *S*-acetyl MAG-HA (**13**) is outlined in Scheme 2. The active ester of **11** was reacted with the amine group of 6-aminohexanoic acid to provide **12**. *S*-Acetyl MAG-HA was obtained as white crystals by the reaction of SATA (**10**) with **12** after deprotecting the Boc group of **12**. The overall yield was 3.70%.

Radiolabeling. [^{99m}Tc]MAMA-HA and [^{99m}Tc]MAG-HA were obtained in radiochemical yields of 77% and 87%, respectively. After RP-HPLC purification, both ^{99m}Tc-labeled fatty acid analogues showed radiochemical purities of over 99% as determined with RP-HPLC and

Table 1. Partition Coefficients of Technecium-99m-Labeled Compounds

	PC[a]
[^{99m}Tc]MAMA-HA	1.06 ± 0.10
[^{99m}Tc]MAG-HA	0.89 ± 0.03[b]

[a] PC, partition coefficient, octanol/phosphate buffer, pH 7.4. [b] $P < 0.05$.

Table 2. Stability of [^{99m}Tc]MAG-HA and [^{99m}Tc]MAMA-HA

	5 min[a]	60 min[a]
[^{99m}Tc]MAG-HA[b]	87.6 (81.2−100)	79.8 (76.9−83.1)
[^{99m}Tc]MAMA-HA[b]	97.2 (96.3−97.9)	87.1 (83.7−93.8)

[a] Values are mean (range) percentages of intact ^{99m}Tc-labeled analogues for three experiments. [b] Each fatty acid analogue labeled with ^{99m}Tc was incubated with 10 μM cysteine in 0.05 M phosphate buffer (pH 7.0) at 37 °C.

Table 3. Biodistribution of [^{99m}Tc]MAMA-HA in Normal Rats[a]

tissue	5 min	20 min	60 min
blood	0.30 (0.28−0.32)	0.21 (0.17−0.26)	0.16 (0.10−0.26)
liver	10.59 (9.78−11.24)	4.30 (3.61−5.60)	2.61 (1.93−3.60)
kidney	8.16 (6.69−9.52)	5.80 (4.87−6.57)	5.25 (3.09−8.13)
spleen	0.06 (0.05−0.06)	0.06 (0.04−0.08)	0.05 (0.01−0.11)
pancreas	0.13 (0.07−0.22)	0.08 (0.06−0.10)	0.09 (0.04−0.18)
lung	0.15 (0.14−0.16)	0.14 (0.08−0.21)	0.12 (0.07−0.19)
heart	0.15 (0.13−0.16)	0.11 (0.08−0.12)	0.07 (0.04−0.12)
intestine	0.17 (0.16−0.18)	0.50 (0.29−0.66)	1.38 (1.37−1.39)

[a] Values are means (range) as % dose/gram tissue for three rats.

TLC. No changes were observed in the radiochemical purities with the two ^{99m}Tc-labeled fatty acids after standing for 24 h at room temperature. On the other hand, the derivatives prepared for metabolite analysis, [^{99m}Tc]MAMA-BA and [^{99m}Tc]MAMA-AA, were obtained in radiochemical yields of 37.4 and 59.7%, respectively; both radiochemical purities were also over 99% after RP-HPLC purification.

Partition Coefficient. Table 1 shows partition coefficients of [^{99m}Tc]MAMA-HA and [^{99m}Tc]MAG-HA at pH 7.4. [^{99m}Tc]MAMA-HA showed a slightly but significantly higher partition coefficient than [^{99m}Tc]MAG-HA.

Cysteine Challenge Assay. Table 2 shows the stability of [^{99m}Tc]MAMA-HA and [^{99m}Tc]MAG-HA. After 60 min of incubation, 88% of [^{99m}Tc]MAMA-HA and 80% of [^{99m}Tc]MAG-HA remained intact, indicating that [^{99m}Tc]-MAMA-HA was more stable than [^{99m}Tc]MAG-HA.

In Vivo Studies. [^{99m}Tc]MAMA-HA showed rapid accumulation of the radioactivity in the liver immediately after administration (Figure 1A). At 60 min postinjection, most of the radioactivity was observed in the kidney and bladder due to its rapid elimination from the liver (Figure 1B). On the other hand, the majority of radioactivity was immediately excreted from the kidney to the bladder after administration of [^{99m}Tc]MAG-HA (Figure 1, panels C and D). Similarly, [^{99m}Tc]MAMA-BA showed rapid excretion of the radioactivity from the kidney into the urine with little radioactivity in the liver (Figure 1E). At 60

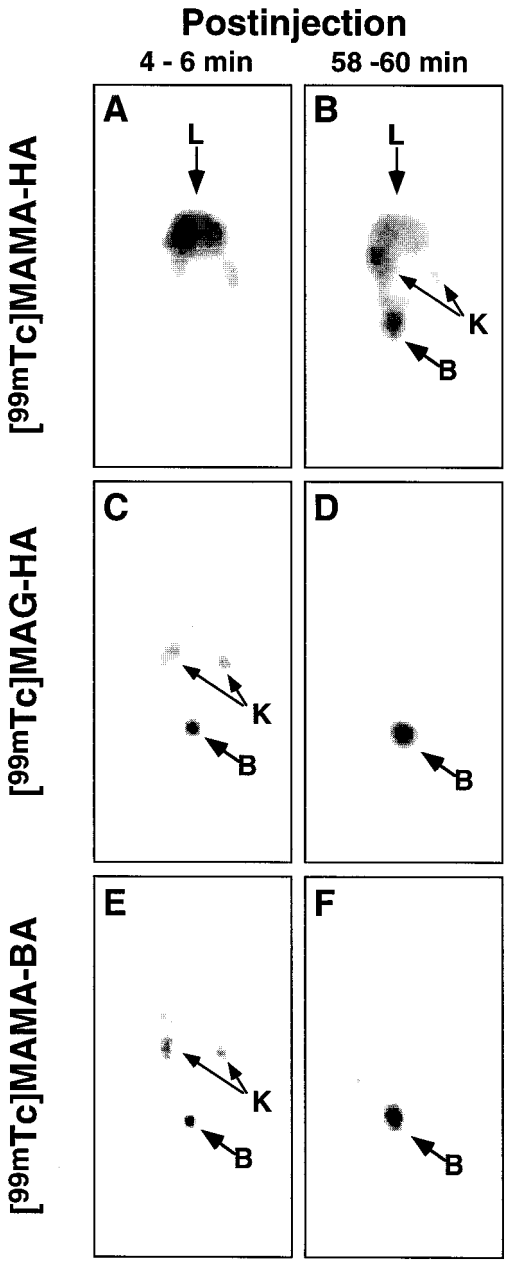


Figure 1. Planar images of ^{99m}Tc-labeled fatty acid analogues. ^{99m}Tc-labeled compounds (15 MBq each) were administered to normal rats via the tail vein. Dynamic scanning was initiated immediately after administration of ^{99m}Tc-labeled compounds. (A) [^{99m}Tc]MAMA-HA, 4−6 min, (B) [^{99m}Tc]MAMA-HA, 58−60 min, (C) [^{99m}Tc]MAG-HA, 4−6 min, (D) [^{99m}Tc]MAG-HA, 58−60 min, (E) [^{99m}Tc]MAMA-BA, 4−6 min, (F) [^{99m}Tc]MAMA-BA, 58−60 min. L, K, and B represent liver, kidney, and bladder, respectively.

min postinjection, radioactivity was observed in the bladder (Figure 1F).

Table 3 summarizes the biodistribution of the radioactivity after administration of [^{99m}Tc]MAMA-HA to normal rats. [^{99m}Tc]MAMA-HA in the liver showed high initial uptake of radioactivity (10.59 % dose/g at 5 min after injection) with low radioactivity levels in the blood for imaging diagnosis. With time, the radioactivity in the liver decreased with only a slight increase in that in the intestine. On the other hand, although the highest radioactivity level was observed in the kidney at 5 min postinjection, high radioactivity levels were still observed at 20 and 60 min postinjection.

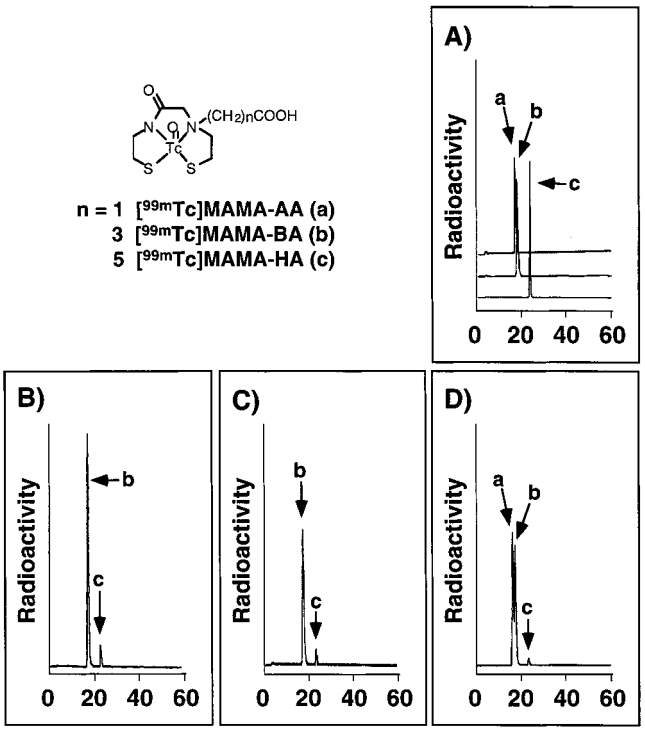


Figure 2. Metabolite analysis of urine samples after administration of [^{99m}Tc]MAMA-HA in rats. Proposed structures of a series of [^{99m}Tc]MAMA derivatives are shown. The parental [^{99m}Tc]MAMA-HA (c) and analytical controls, [^{99m}Tc]MAMA-BA (b) and [^{99m}Tc]MAMA-AA (a), were eluted at retention times of 23, 17, and 16 min, respectively (A). Urine samples showed two radioactivity peaks with a major peak eluted at a retention time of 17 min (B). RP-HPLC analysis of the urine samples coinjected with [^{99m}Tc]MAMA-BA showed a single radioactivity peak at a retention time of 17 min in addition to the peak of [^{99m}Tc]MAMA-HA (C). Cochromatographic analysis of the urine samples with [^{99m}Tc]MAMA-AA showed two peaks well-separated in addition to the peak of [^{99m}Tc]MAMA-HA (D).

The proposed structures of the mother compound [^{99m}Tc]MAMA-HA and its expected radiometabolites, [^{99m}Tc]MAMA-BA and [^{99m}Tc]MAMA-AA, are shown in Figure 2. Figure 2A shows typical radiochromatograms of [^{99m}Tc]MAMA-HA, [^{99m}Tc]MAMA-BA, and [^{99m}Tc]-MAMA-AA. The urine samples showed two well-separated radioactivity peaks at retention times of 17 and 23 min with the former peak representing 82.9 ± 9.0% of the radioactivity in the urine (Figure 2B). Cochromatographic analysis of the urine samples with [^{99m}Tc]MAMA-BA indicated two radioactivity peaks at retention times of 17 and 23 min on RP-HPLC (Figure 2C). However, three radioactivity peaks were detected on RP-HPLC at retention times of 16, 17, and 23 min when the urine sample were cochromatographed with [^{99m}Tc]MAMA-AA (Figure 2D).

In Vitro Metabolite Studies. More than 90% of the radioactivity in the liver homogenate was extracted with acetonitrile. RP-HPLC analysis of the acetonitrile-extracted fraction depicted two radioactivity peaks at retention times of 17 and 23 min when the slices were incubated with [^{99m}Tc]MAMA-HA in the absence of 2-bromooctanoate (Figure 3A) with the former fraction representing 21.2 ± 3.0% of the radioactivity in the supernatant. However, the supernatant showed a single radioactivity peak at a retention time of 23 min (Figure 3B) when incubated with [^{99m}Tc]MAMA-HA in the presence of 2-bromooctanote.

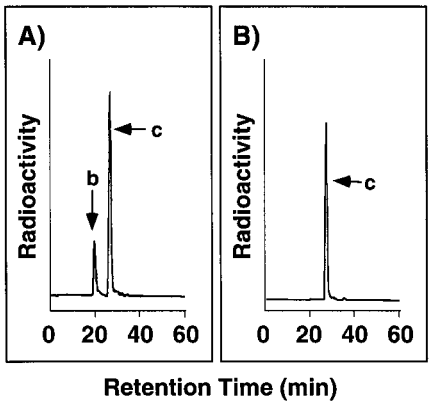


Figure 3. Metabolite analysis of [^{99m}Tc]MAMA-HA in liver slices. The liver slices were incubated with [^{99m}Tc]MAMA-HA for 60 min at 37 °C. Two radioactivity peaks were observed, the former of which had a retention time similar to that of [^{99m}Tc]-MAMA-BA (A). However, RP-HPLC showed a single radioactivity peak with a retention time similar to that of parental [^{99m}Tc]MAMA-HA in the presence of 2-bromooctanoate which inhibits 3-ketothiolase, the last enzyme of the fatty acid oxidation pathway (B).

DISCUSSION

External imaging of energy production levels of living cells with ^{99m}Tc-labeled compounds is a challenging task for the development of ^{99m}Tc-radiopharmaceuticals. Indeed, efforts have been made to develop ^{99m}Tc-labeled long-chain fatty acid analogues for myocardial imaging studies. However, their application has been hampered by poor accumulation in the heart, and it seemed that these ^{99m}Tc-labeled fatty acid analogues were not recognized as substrates for β-oxidation (*22*, *23*).

β-Oxidation is the main pathway providing energy in the liver. On the basis of our recent findings that ^{11}C- and ^{123}I-labeled medium-chain fatty acids were useful for measuring β-oxidation activity of hepatocytes (*9*, *10*), we designed two ^{99m}Tc-labeled medium-chain fatty acid analogues as prototype compounds and evaluated their potential as substrates for β-oxidation in the liver.

In biodistribution studies in rats, [^{99m}Tc]MAMA-HA showed rapid accumulation in the liver following injection. [^{99m}Tc]MAMA-HA also exhibited rapid elimination of the radioactivity from the liver into urine. RP-HPLC analysis of urine samples obtained at 60 min postinjection showed that the major radioactivity peak had a retention time identical to that of [^{99m}Tc]MAMA-BA. This was supported by cochromatographic analyses of the urine samples with [^{99m}Tc]MAMA-BA or [^{99m}Tc]MAMA-AA. In addition, [^{99m}Tc]MAMA-BA showed rapid excretion of the radioactivity into urine via the kidney with little accumulation in the liver, indicating that redistribution of [^{99m}Tc]MAMA-BA generated in the body to the liver was negligible. These findings suggested that [^{99m}Tc]-MAMA-HA would be metabolized to [^{99m}Tc]MAMA-BA in the liver via β-oxidation, and the radiometabolite was excreted from the liver into the urine.

The metabolism of [^{99m}Tc]MAMA-HA to [^{99m}Tc]MAMA-BA by β-oxidation in the liver was also indicated by in vitro studies using living slices of rat liver. [^{99m}Tc]MAMA-BA was observed as the sole radiometabolite after incubation (Figure 3). However, generation of [^{99m}Tc]-MAMA-BA was completely inhibited when [^{99m}Tc]MAMA-HA was incubated with the liver slices in the presence of 2-bromooctanote, an inhibitor of 3-ketothiolase, the last enzyme involved in long- and medium-chain fatty acid oxidation in the mitochondria. These findings implied that after uptake by the liver, [^{99m}Tc]MAMA-HA was recognized as a substrate for β-oxidation and metabolized to [^{99m}Tc]MAMA-BA.

The final radiometabolite of [^{99m}Tc]MAMA-HA was not [^{99m}Tc]MAMA-AA but [^{99m}Tc]MAMA-BA as demonstrated by cochromatographic analyses. Since [^{99m}Tc]MAMA-HA possesses a 6-carbon chain, [^{99m}Tc]MAMA-AA was expected to be the final radiometabolite after β-oxidation. Indeed, our recent study indicated that the radioiodinated medium-chain fatty acid analogue [^{123}I]IPEA was metabolized to iodohippuric acid via iodobenzoate. This suggested that, unlike iodobenzene, the presence of [^{99m}Tc]MAMA chelate might have hindered further recognition of [^{99m}Tc]MAMA-BA by the enzymes that are involved in β-oxidation.

In contrast to [^{99m}Tc]MAMA-HA, [^{99m}Tc]MAG-HA showed little accumulation in the liver after administration. Although [^{99m}Tc]MAG-HA was less stable than [^{99m}Tc]MAMA-HA, about 80% of [^{99m}Tc]MAG-HA was intact even after 60 min of incubation. Since the radioactivity in rats following [^{99m}Tc]MAG-HA injection was rapidly eliminate from blood to urine as shown in Figure 1, panels C and D, the instability of [^{99m}Tc]MAG-HA in the blood was considered not to be a major factor responsible for poor liver uptake. On the other hand, [^{99m}Tc]MAG-HA showed a lower partition coefficient than [^{99m}Tc]MAMA-HA. [^{99m}Tc]MAG-HA had a retention time similar to that of [^{99m}Tc]MAMA-BA, a radiometabolite of [^{99m}Tc]MAMA-HA, on RP-HPLC under the same conditions. Moreover, [^{99m}Tc]MAMA-BA and [^{99m}Tc]MAG-HA showed similar biodistributions. These findings suggested that the low lipophilicity of [^{99m}Tc]MAG-HA was responsible for its poor hepatic accumulation although negatively charged ^{99m}Tc-MAG chelate may also be involved.

In conclusion, [^{99m}Tc]MAMA-HA was metabolized by β-oxidation to [^{99m}Tc]MAMA-BA after uptake into the liver. Thus, [^{99m}Tc]MAMA-HA is the first ^{99m}Tc-labeled compound recognized as a substrate for energy production in living cells. Appropriate lipophilicity of [^{99m}Tc]-MAMA chelate would be useful to facilitate rapid elimination of the final radiometabolite, [^{99m}Tc]MAMA-BA, from the liver into urine without being retained in the hepatocytes. Since the procedure for synthesis of MAMA-HA was applicable to fatty acids with different chain lengths, further derivation of this compound may lead to development of ^{99m}Tc-radiopharmaceuticals more appropriate for visualization of energy production levels in the liver.

LITERATURE CITED

(1) Kudo, M., Todo, A., Ikekubo, K., Hino, M., Ito, H., Yamaguchi, H., Saiki, Y., Yamamoto, K., Yonekura, Y., and Torizuka, K., et al. (1987) Estimation of hepatic functional reserve by asialoglycoprotein receptor-binding, radiolabeled synthetic ligand Tc-99m-galactosyl-neoglycoalbumin—preclinical and clinical studies. *Kaku Igaku (Jpn. J. Nucl. Med.) 24*, 1653−1662.

(2) Kamiike, W., Burdelski, M., Steinhoff, G., Ringe, B., Lauchart, W., and Pichlmayr, R. (1988) Adenine nucleotide metabolism and its relation to organ viability in human liver transplantation. *Transplantation 45*, 138−143.

(3) Lanir, A., Jenkins, R. L., Caldwell, C., Lee, R. G., Khettry, U., and Clouse, M. E. (1988) Hepatic transplantation survival: correlation with adenine nucleotide level in donor liver. *Hepatology 8*, 471−475.

(4) Martin, D. B. (1976) Metabolism and energy mechanisms. Pathophysiology (E. D. Frohlich, Ed.) pp 365−383, Lippincott, Philadelphia.

(5) Zakim, D. (1982) Metabolism of glucose and fatty acids by the liver. *Hepatology* (D. Zakim, and T. D. Boyer, Eds.) pp 76−109, Saunders, Philadelphia.

(6) Fraitz, I. B. (1961) Factors influencing the rates of long-chain fatty acid oxidation and synthesis in mammalian systems. *Physiol. Rev. 41*, 51−129.
(7) Kornberg, A., and Pricer, W. E., Jr. (1953) Enzymatic esterification of α-glycerophosphate by long chain fatty acids. *J. Biol. Chem. 204*, 345−357.
(8) Lossow, W. J., and Chaikoff, I. L. (1955) Carbohydrate sparing of fatty acid oxidation. I. The relation of fatty acid chain length to the degree of sparing. II. The metabolism by which carbohydrate spares the oxidation of palmitic acid. *Arch. Biochem. Biophys. 57*, 23−40.
(9) Yamamura, N., Magata, Y., Kitano, H., Konishi, J., and Saji, H. (1998) Evaluation of [1−^{11}C]octanoate as a new radiopharmaceutical for assessing liver function using positron emission tomography. *Nucl. Med. Biol. 25*, 467−472.
(10) Yamamura, N., Magata, Y., Iida, Y., Kitano, H., Konishi, J., and Saji, H. (1998) Evaluation of radioiodinated medium chain fatty acids as new diagnostic agents for regional liver function. *KAKU IGAKU (Jpn. J. Nucl. Med.) 35*, 595.
(11) Gustavson, L. M., Rao, T. N., Jones, D. S., Fritzberg, A. R., and Srinivasan, A. (1991) Synthesis of a new class of Tc chelating agents: N_2S_2 monoaminemonoamide (MAMA) ligands. *Tetrahedron Lett. 32*, 5485−5488.
(12) O'Neil, J. P., Wilson, S. R., and Katzenellenbogen, J. A. (1994) Preparation and structural characterization of monoamine-monoamide bis(thiol) oxo complex of technetium(V) and rhenium(V). *Inorg. Chem. 33*, 319−323.
(13) Oya, S., Plossl, K., Kung, M. P., Stevenson, D. A., and Kung, H. F. (1998) Small and neutral Tc(V)O BAT, bisaminoethanethiol (N_2S_2) complexes for developing new brain imaging agents. *Nucl. Med. Biol. 25*, 135−140.
(14) Fritzberg, A. R., Kasina, S., Eshima, D., and Johnson, D. L. (1986) Synthesis and biological evaluation of technetium-99m MAG_3 as a hippuran replacement. *J. Nucl. Med. 27*, 111−116.
(15) Taylor, A., Jr., Eshima, D., Fritzberg, A. R., Christian, P. E., and Kasina, S. (1986) Comparison of iodine-131 OIH and technetium-99m MAG_3 renal imaging in volunteers. *J. Nucl. Med. 27*, 795−803.
(16) Taylor, A., Jr., Eshima, D., Christian, P. E., and Milton, W. (1987) Evaluation of Tc-99m mercaptoacetyltriglycine in patients with impaired renal function. *Radiology 162*, 365−370.
(17) Benary, E. (1913) Thiotetronic acid and derivatives. *Ber. 46*, 2103-2107.
(18) Winnard, P., Jr., Chang, F., Rusckowski, M., Mardirossian, G., and Hnatowich, D. J. (1997) Preparation and use of NHS-MAG_3 for technetium-99m labeling of DNA. *Nucl. Med. Biol. 24*, 425−432.
(19) Meltzer, P. C., Blundell, P., Jones, A. G., Mahmood, A., Garada, B., Zimmerman, R. E., Davison, A., Holman, B. L., and Madras, B. K. (1997) A technetium-99m SPECT imaging agent which targets the dopamine transporter in primate brain. *J. Med. Chem. 40*, 1835−1844.
(20) Raaka, B. M., and Lowenstein, J. M. (1979) Inhibition of fatty acid oxidation by 2-bromooctanoate. Including effects of bromooctanoate on ketogenesis and gluconeogenesis. *J. Biol. Chem. 254*, 3303−3310.
(21) Raaka, B. M., and Lowenstein, J. M. (1979) Inhibition of fatty acid oxidation by 2-bromooctanoate. Evidence for the enzymatic formation of 2-bromo-3-ketooctanoyl coenzyme A and the inhibition of 3-ketothiolase. *J. Biol. Chem. 254*, 6755−6762.
(22) Mach, R. H., Kung, H. F., Jungwiwattanaporn, P., and Guo, Y. Z. (1991) Synthesis and biodistribution of a new class of 99mTc-labeled fatty acid analogues for myocardial imaging. *Int. J. Rad. Appl. Instrum. B 18*, 215−226.
(23) Jones, G., Jr., Elmaleh, D. R., Strauss, H. W., and Fischman, A. J. (1994) Synthesis and biodistribution of a new ^{99m}technetium fatty acid. *Nucl. Med. Biol. 21*, 117−123.

BC9801528

Purified Protein Derivative (PPD) as an Immunogen Carrier Elicits High Antigen Specificity to Haptens

Binodh S. De Silva,† Kamal L. Egodage,‡ and George S. Wilson*

Department of Chemistry, Malott Hall, University of Kansas, Lawrence, Kansas 66045. Received June 23, 1998; Revised Manuscript Received February 12, 1999

The effectiveness of the carrier protein in eliciting antigen-specific antibodies was investigated. The effect of the carrier protein was independent of the conjugation chemistry involved. Keyhole limpet hemocyanin (KLH), purified protein derivative (PPD), and ovalbumin (OVA) were used as carrier proteins in the immunization of mice. Three antigens were studied: LY170881 (a small drug molecule), 4-[1′-cyanobenz(*f*)isoindolyl]butyric acid (CBI-butyric acid), and a seven residue peptide GPGRGPG (KLE1). The serum antibody response to the antigen or antigen:BSA conjugate was superior in the case where the PPD:antigen conjugates were used as the immunogen when compared to KLH and OVA. The specificity of the antibodies to the respective antigens vs cross-reactivity with the carrier protein was investigated. PPD-coupled antigen immunized mice generated a higher percentage of antigen-specific hybridomas compared to the other carrier proteins. These findings confirmed PPD as the best carrier molecule for the production of both polyclonal and monoclonal antibodies.

INTRODUCTION

With the advent of monoclonal antibodies (Köhler and Milstein, 1975), many analytical and clinical applications have relied on the highly specific antigen antibody interaction made possible by this methodology. In theory, antibodies could be made to any synthetic molecule, protein, nucleic acid, carbohydrate, or lipoprotein. With the extensive understanding about processes involving the immune system, it has now become possible to characterize the physical requirements of an antigen which result in improved production of antibodies (Eshhar, 1985).

Antigens in general can be classified into two major groups; those that are intrinsically immunogenic and those that have to be conjugated to a carrier to elicit an immune response. There is considerable interest in producing monoclonal antibodies to such small molecules including, for example, drugs, pesticides, and peptides. Typically, an antigen possesses an epitope that can be recognized by surface immunoglobulins on B-cells. However, this is not sufficient to elicit an antibody response. In addition to the B-cell epitope, the antigen has to possess a class II MHC T-cell receptor site that enables the cascade of events resulting in the production of antibodies to a particular antigen of interest. Haptens in classical immunology lack this T-cell epitope. Landsteiner (1936) showed that the T-cell epitope can be introduced by conjugating to a carrier protein, using what he called the "artificial conjugated antigens". Since then, many approaches have attempted to improve the methodology for producing anti-hapten and anti-peptide antibodies. Some of the strategies used are incorporation of T-cell epitopes (Francis et al., 1987; Good et al., 1987), preparation of immunostimulating complexes (Morein et al., 1987), use of a variety of adjuvants and liposomes to enhance the longevity of the antigen of interest in the body (Kawamura and Berzofsky, 1986), and cross-linking of the antigen with antibodies against surface receptors on B-cells, T helper cells or other antigen presenting cells to target the antigen to the cells involved in the immune system (Snider et al., 1987; Hendrickson et al., 1994). Multiple antigen peptide (MAP) where both the B-cell and T-cell epitopes are incorporated into one peptide antigen and synthesized as a single molecule (Tam, 1989) has been successfully used to elicit immune response. This latter approach eliminates the conjugation of peptides to proteins and uses solid-phase peptide synthesis to prepare the immunogen.

Even with the advancement of methodology for the preparation of monoclonal and polyclonal antibodies, the use of the hapten−protein conjugates or peptide−protein conjugates as immunogens still remains the most common method of choice. The simplicity of these techniques, which do not require sophisticated equipment, and the flexibility of choosing a conjugation method applicable to the analyte of interest (use of NH_2, COOH, and SH groups for coupling) favors this mode of immunogen preparation. However, such preparations must strive to preserve the integrity of the antigen structure, since many applications involving these antibodies require the discrimination of analogues with very small conformational differences. There are number of important characteristics to consider when preparing these conjugates. For example, the specificity of the assay, the metabolites of interest, the characteristic site of the antigen that is important for the specificity of the assay, the carrier molecule, epitope density, the method of conjugation, and the chemistry of the linking group between the hapten and the carrier will determine the properties of the resulting antibody.

An important unit of the conjugate is the carrier molecule which provides the T-cell epitope for the production of a successful immune response. Common car-

* To whom correspondence should be addressed. Phone: 785-864-5152. Fax: 785-864-5156. E-mail: wilson@kuhub.cc.ukans.edu.

†Current address: Procter & Gamble Pharmaceuticals, Route 320, Woods Corners, Norwich, NY 13815.

‡ Current address: Monsanto Co., 700 Chesterfield Parkway North, St. Louis, MO 63198.

10.1021/bc9800724 CCC: $18.00 © 1999 American Chemical Society
Published on Web 04/15/1999

rier proteins such as serum albumin (bovine, human) hemocyanin, ovalbumin, g-globulins of various species, thyroglobulin, tetanus toxoid, peptide antigens, and synthetic carriers such as poly-L-lysine have been used extensively (Plaue et al., 1990). The protein carrier chosen must come from a species different from the animal to be immunized (Walker et al., 1973). The proteins to be used as carriers must possess functional groups that can easily be substituted (such as amines or sulfhydryls). The molar ratio of the hapten:protein will greatly influence the immune response and this depends on the coupling method used. Generally a hapten:protein molar ratio of 10:1 is maintained in our laboratory (Tijssen, 1985).

The hapten−protein conjugate once administered to an animal will elicit antibodies that have a specificity to the haptenic group as well as the carrier. While the carrier-specific antibodies could be removed by affinity purification using a column with immobilized carrier protein, antibodies that bind part of the hapten or peptide and the carrier protein will also be removed. More critical, however, is the impact of carrier-specific antibodies on the hybridoma screening process. In the preparation of monoclonal antibodies, the hybridoma supernatants are typically screened first against a hapten−protein conjugate, where the protein is different to that used in the immunization. These supernatants were subsequently screened against the carrier protein used in the immunogen to estimate the number of hybridomas specific to the carrier. If a positive response is obtained, then the well will likely be discarded even if it also may contain antigen-specific antibodies. Since carrier-specific antibodies can correspond to a significant fraction of the antibodies produced, their elimination will greatly simplify identification of the desired antibodies, thus resulting in significantly higher yields of specific antibody hybridoma cell lines.

Keyhole limpet hemocyanin (KLH), ovalbumin (OVA), and bovine serum albumin (BSA) are typical carriers used in the preparation of hapten−protein conjugates. However, purified protein derivative (PPD), currently used in the measurement of T-cell reactivity in persons exposed to tuberculosis or vaccinated with Bacillus Calmette-Guérin (BCG), has been suggested as an ideal carrier candidate (Lachmann et al., 1986).Their studies indicate the advantages of PPD as a carrier molecule and as an adjuvant in vaccine preparations. The present study deals with the properties of PPD as a carrier for the preparation of anti-hapten antibodies. These studies were carried out using two haptens (small organic molecules) and a peptide. The antigens used were LY170881 (a small drug molecule), 4-[1′-cyanobenz(*f*)-isoindolyl]butyric acid (CBI-butyric acid) (Figure 1) and a seven residue peptide, GPGRGPG (KLE1).

EXPERIMENTAL SECTION

Materials and Methods. LY170881 and its conjugates with BSA, PPD, OVA, and KLH were provided by Lilly Laboratories (Indianapolis, IN). The seven residue peptide (GPGRGPG) (KLE1) was synthesized by Coast Scientific Products (La Jolla, CA). 4-[1′-Cyanobenz(*f*)-isoindolyl]butyric acid (CBI-butyric acid) was synthesized at the University of Kansas (Orosz and Carlson, 1990). All buffer components used were of analytical grade and purchased from Fisher Scientific, Fairlawn, NJ. BSA, and KLH were purchased from Sigma Chemical Co. (St. Louis, MO). PPD was provided by Lederle Laboratories, NY.

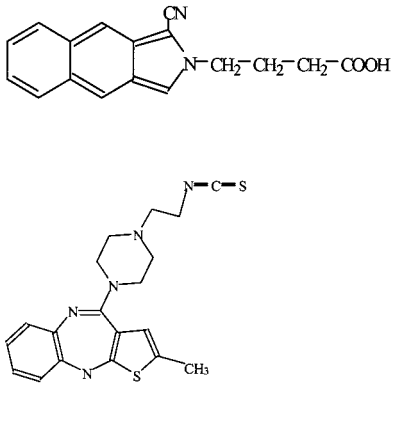


Figure 1. Structures of the antigens used. (A) 4-[1′-Cyanobenz-(*f*)isoindolyl]butyric acid. (B) LY170881.

Table 1. Properties and the Dosage of the Immunogens Used

immunogen	linking group	dose/mouse (μg)
LY170881-PPD	anhydride hemisuccinate	30
LY170881-KLH	anhydride hemisuccinate	30
LY170881-OVA	anhydride hemisuccinate	30
CBI-butyric acid-PPD	carbodiimide	30
CBI-butyric acid-KLH	carbodiimide	10
KLE1-PPD	carbodiimide	25
KLE1-KLH	carbodiimide	25

Preparation of the Immunogens. KLH and PPD were used as the protein carriers in the conjugation of the peptide and CBI-butyric acid used for immunizations.The CBI-butyric acid and the KLE1 peptide were coupled through the −COOH group by first activating it with water-soluble 1-ethyl-3-(3-dimethylaminopropyl)-carbodiimide (EDAC, Pierce, IL) according to the enhanced carbodiimide coupling method of Staros et al. (1986), using sulfo *N*-hydroxysuccinimide (Sulfo-NHS, Pierce, IL) as the enhancer. The molar ratio of KLH: antigen was 1:100. One milligram of antigen was dissolved in 1 mL of 0.01 M phosphate buffer (PB), pH 7.4, containing no azide. EDAC was added to a final concentration of 0.1 M. After stirring for a few minutes, sulfo-NHS was added dropwise (1.25 times antigen concentration). Finally, 1 mg of KLH was added and the solution was made up to 2 mL. The reaction was allowed to proceed for 24 h at room temperature. The order of the addition of the reagents is critical to obtaining a successful conjugate. The PPD-antigen and the BSA−antigen conjugates were prepared in a similar manner using a molar ratio of protein:antigen of 1:10. All conjugates that contained the LY170881 antigen were prepared by the Lilly Laboratories using the mixed anhydride method (Bowsher et al., 1994).

Immunization Schedule. Immunogens were administered to 4−6 week old female BALB/c mice. The immunogens used and their respective dosages are given in Table 1. One week prior to the first immunization with the respective PPD conjugates, the mice were sensitized with 50 μg of Bacillus Calmette-Guérin (BCG; RIBI Immunochemical Research Inc., MT) via the intramuscular (i.m.) route in 50 μL of sterile saline. The rest of the immunization protocol was as follows: the first immunization was intraperitoneal (i.p.) at four sites with 100 μL/site in complete Freund's adjuvant (CFA; Gibco Laboratories, NY) at a 3:1 v/v (adjuvant:conjugate) ratio. The second immunization was intravenous (i.v.) in sterile saline at a ratio of 2:1 v/v (saline:conjugate) after 2 weeks. Biweekly i.p. immunizations (four sites with 100 μL/site)

in incomplete Freund's adjuvant (IFA; Gibco Laboratories, NY) were administered until a desired circulating antibody concentration (1:1000 dilution) specific to each immunogen was attained in the serum. A v/v ratio of 3:1 (IFA:conjugate) was maintained. The conjugates prepared with KLH and OVA as the carriers were employed in mouse immunization in a manner similar to that described above but without the BCG sensitization.

Fusion. Four days after the final immunization, the spleen of the hyperimmunized mouse was fused with the myeloma cell line Sp2/0−Ag-14 (ATCC CRL 1581; American Type Culture Collection, Rockville, MD) according to Galfré and Milstein (1981). A spleen cell: myeloma cell ratio of 10:1 was used and poly(ethylene glycol), molecular weight 3350 (Sigma, St. Louis, MO), was used as the fusogen. Typically, the cell pellet of fused cells is diluted in a large volume (almost 40−50 mL) of growth medium to ensure a reasonable dilution and seeded on 10−12 plates on average, at 50 μL/well. After 2 weeks, the supernatants were screened for specific antibody production using enzyme linked immunosorbent assays (ELISA) as described below.

Screening Procedures. All ELISA procedures were designed to screen for antibodies that reacted with the antigen of interest and the carrier used in the immunizations. Two general ELISA procedures are reported in this manuscript because the antigens used in this work were used for different analytical purposes. The ELISA methods have to be designed in such a way as to get the best antibodies that recognize the antigen of interest and not the carrier protein. Therefore, the following ELISA methods will be described in detail for each antigen.

ELISA Method 1. This ELISA method will allow the selection of antibodies that would recognize the antigen−protein conjugate. The carrier protein used in the ELISA procedure is different from the one that was used in the immunization. This eliminates the selection of antibodies to the carrier protein used in the immunizations. The hybridoma clones that secrete antibodies recognizing the antigen and/or the linking group can be selected using this procedure. This ELISA method was used to screen against BSA−CBI butyric acid and BSA−LY170881 antigen conjugates. The ELISA method used was a modification of Bahr et al. (1980). The ELISA plates (Corning, NY) were coated with 100 μL of antigen−BSA conjugate or the respective carrier proteins (BSA/PPD/KLH/ovalbumin) (10 μg/mL in 0.1 M carbonate buffer, pH 9.35) (plate coating buffer) overnight at 4 °C. The plates were washed four times with 0.01 M PBS containing 0.05% Tween 20 (Sigma, St. Louis, MO) (wash buffer) and patted dry on a stack of paper towels. Wash buffer containing 0.2% BSA (150 μL/well) (ELISA diluent buffer) was added and incubated for 1 h at 37 °C to block the remaining active sites on the plastic surface. The plates were washed four times with wash buffer and patted dry. Serum (1:100 dilution) or culture supernatant (50 μL/well) was added and incubated for 1 h at 37°C. The plates were washed four times with wash buffer and patted dry. Horseradish peroxidase (HRP) labeled goat-anti-mouse (goat anti-Mo−HRP, Organon Teknika Corp., Durham, NC) immunoglobulin (100 μL, 1:10,000 dilution) was added and incubated at 37 °C for an additional hour. The plates were washed four times with Nanopure water (Barnstead, Nanopure II Sybron, Barnstead, MA) and patted dry. A total of 100 μL of HRP substrate (tetramethyl benzidine (TMB) and hydrogen peroxide, KP Laboratories, MD) was added, and after 20 min, the enzyme reaction was quenched with 1 M HCl. The optical density was read at 450 nm using a 96 well plate reader. (V_{max}, Molecular Devices, CA). The screening procedures for LY170881 used the wash buffer and the ELISA diluent buffer recommended by the Lilly Laboratories. In ELISA experiments, using supernatant, serum from an immunized mouse served as the positive control and serum from an unimmunized mouse was used as the negative control.

ELISA Method 2. The primary purpose in preparing antibodies to the peptide, KLE1, was to select antibodies that recognized the native structure of the parent protein. Therefore, during the selection process, it was necessary to identify antibodies that recognized the component peptide only. The following ELISA method was used to fulfill this purpose: 100 μL of the KLE1 peptide antigen (20 μg/mL) was coated on ELISA plates in 0.1 M plate coating buffer and incubated overnight at 4 °C. The plates were washed four times with wash buffer and blocked with 100 μL of 0.2% gelatin in wash buffer to block the remaining active sites on the plates. The plates were incubated at 37 °C for 1 h. The plates were washed four times with wash buffer and patted dry. Serum (1:100 dilution) or culture supernatant (50 μL/well) was added and incubated for 1 h at 37 °C. The plates were washed four times with wash buffer and patted dry. A total of 100 μL of goat anti-Mo−HRP conjugate was added (1:15000 dilution in wash buffer containing 0.2% gelatin) to each well and incubated at 37 °C for an additional hour. The plates were washed four times with Nanopure water and patted dry. A total of 100 μL of HRP substrate was added, and after 20 min, the enzyme reaction was quenched with 1 M HCl. The optical density was read at 450 nm using the 96 well plate reader.

Data Analysis. The statistical analysis of the results was done using the Minitab statistical program (version 8.21, State College, PA).

RESULTS

Serum Response to Antigens. The two ELISA procedures described above were specifically aimed at evaluating the antibody responses to suit the particular analytical method under development. Figures 2 and 3 show the antibody titers in serum for the respective antigens/antigen-BSA and carriers used. At least two mice were immunized with each antigen. The optical density data were statistically analyzed using the Minitab program, and the results for the different animals were pooled where the data showed no significant difference at a 95% confidence level as shown by a one way ANOVA. Figure 2 compares the antibody titers to the peptide, CBI-butyric acid-BSA conjugate, and their respective carrier proteins. When KLH was used as the carrier, the immune response to KLH was far superior to that for the antigen/antigen-BSA of interest. The immune response to PPD on the other hand was significantly lower compared to that for the respective antigens. These results agree with the fact that PPD is a T cell antigen and does not elicit a favorable immune response (Lachman et al., 1986).

Figure 3 shows the serum titers to the LY170881−BSA conjugate and the respective carrier proteins used in the immunization procedures. The antibody responses to the BSA−LY170881 conjugate are comparable to that of the carriers in the case where PPD and OVA were used. The serum titer for PPD is around 51 200 and to OVA is 25 600. The KLH response is far superior to the BSA−LY170881 response.

Fusion. A minimum of two fusions were performed from each category. The hybridoma supernatants were

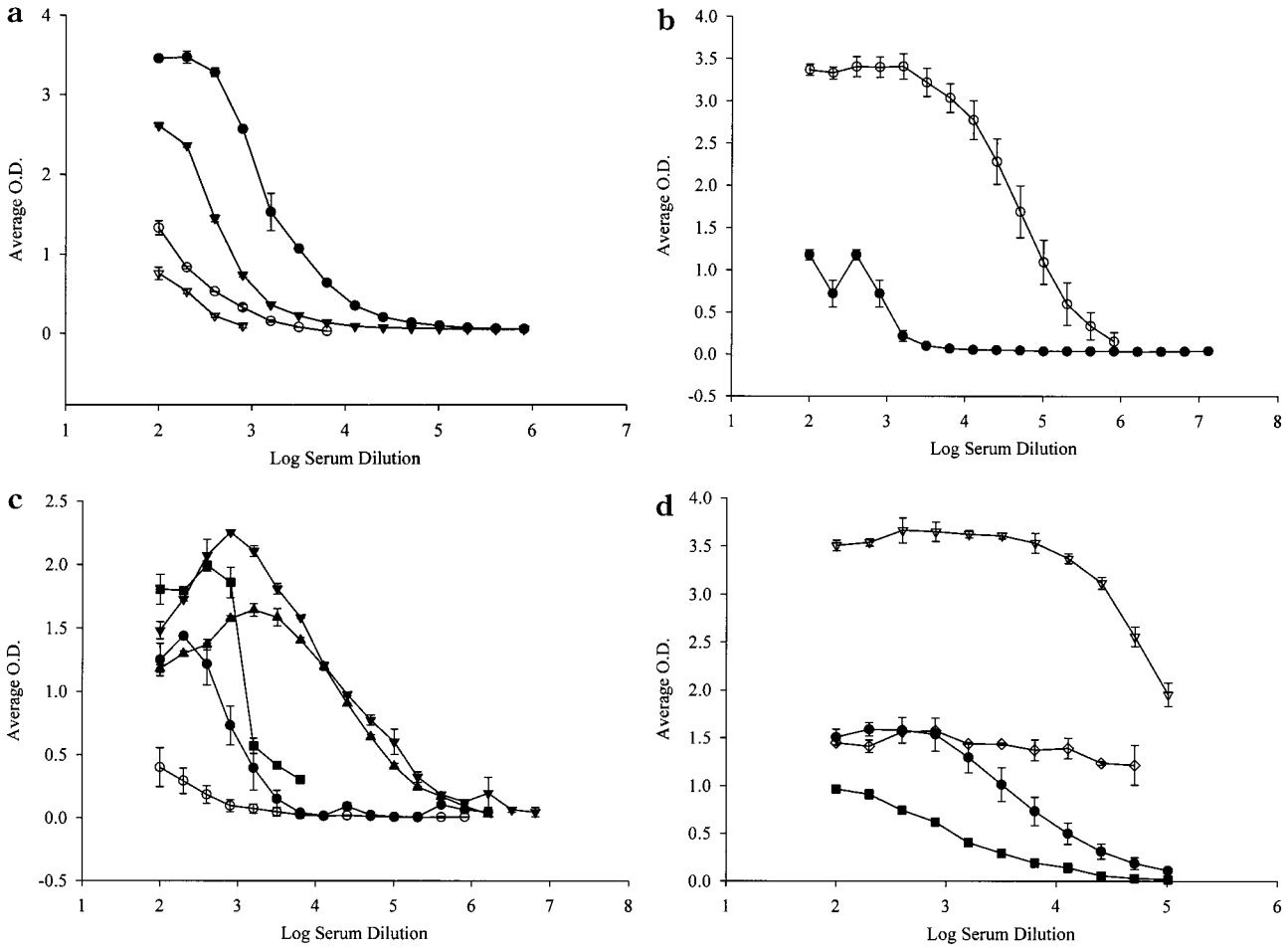


Figure 2. Serum dilution curves for the antigens and their respective carriers used in the immunizations. The solid symbols indicate the response to the antigen or the peptide, and the open symbols indicate the serum response to each carrier molecule. (a) KLE1-PPD [(●, ▼) antigen response for two mice, (○, ▽) carrier for two mice], (b) KLE1-KLH [(●) average antigen response for two mice, (○) average carrier response for two mice], (c) CBI-butyric acid-PPD [(●, ■, ▲, ▼) antigen response for four mice, (○) average carrier response for four mice], (d) CBI-butyric acid-KLH [(●) average antigen response for two mice, (■) antigen response for one mouse, (▽) average carrier response for two mice, (◇) carrier response for one mouse].

tested for the production of antibodies against the BSA-conjugated CBI butyric acid, BSA-conjugated LY170881, KLE1 peptide, and the respective carriers. The results are summarized in Table 2. The percent of specific wells were calculated as follows:

$$\%\ \text{specific wells} = (\text{number of wells positive toward the antigen/carrier})/(\text{total number of growing wells}) \times 100$$

These results clearly indicate that PPD does elicit a superior antigen-specific immune response compared to that of KLH. The percentage of antigen-specific hybridoma wells (Table 2) is about four times higher for PPD than for KLH. The higher percentage of antigen-specific hybridomas makes available a larger number of cell lines from which to choose the appropriate monoclonal antibodies for the specific application. The percentage of specific wells to KLH and OVA was not calculated for the LY170881 antigen, since over 90% of the supernatants screened showed cross reactivity between the carrier and the antigen of interest.

DISCUSSION

This study evaluates the effectiveness of different protein molecules as carriers used in the production of antibodies against haptens and small peptides irrespective of the conjugation process. The primary goal of this project was to enhance the production of anti-hapten/anti-peptide antibodies in systems which are not intrinsically very immunogenic. The ELISA procedures described in the previous section served two purposes: the selection of antigen specific antibodies and the elimination of carrier-specific antibodies. These screening procedures were carefully designed in order to select antigen-specific antibodies which are useful in the analytical procedures that were envisioned for these antibodies. The serum and the fusion results clearly indicate a dramatically reduced carrier response of PPD over KLH and OVA. It has been reported that the efficacy of each carrier protein and the immune response it elicits are difficult to compare since they vary depending on the individual and the species (Pratt, 1978). These variations were taken into consideration during these experiments, and the conditions were kept as comparable as practically possible in designing the immunogens. Furthermore, the animals used were of similar age and belonged to the same species.

The serum titer results we have obtained show great promise when preparing polyclonal antibodies (Figure 2 and Figure 3) and were measured in the serum after the immunization. The low/no titers shown for PPD response is a clear indication of the exceptional effect of PPD in eliciting a specific antibody response to the antigen of

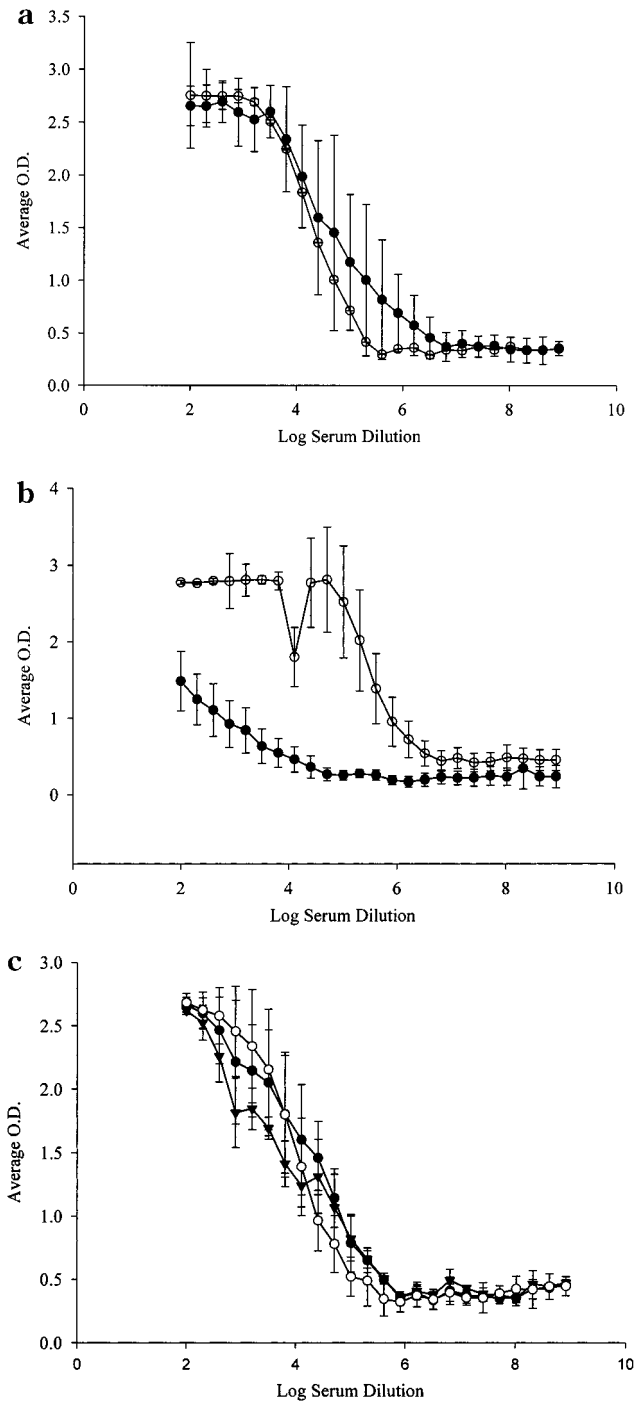


Figure 3. Serum dilution curves for LY170881−BSA conjugate and the carrier proteins used in the immunization. (a) LY170881−PPD [(●) average antigen response for two mice, (○) average carrier response for two mice], (b) LY170881−KLH [(●) average antigen response for two mice, (○) average carrier response for two mice], (c) LY170881−OVA [(●) average antigen response for two mice, (▼) antigen response for one mouse, (○) average carrier response for all three mice].

interest without itself eliciting and immune response. When both KLH and OVA were used, the majority of the time the serum antibody response to the carrier obscured that of the antigen of interest. This poses a great difficulty when purifying the serum to obtain polyclonal antibodies, which are antigen specific, due to the high concentration of antibodies to carrier molecules. The strong carrier response has the effect of reducing the antigen-specific antibody concentration in the IgG fraction.

Table 2. Fusion Results

immunogen	% antigen specificity (a)	% carrier specificity (b)		$[(a)/(a+b)] \times 100$
		PPD	KLH	
KLE-PPD	20	13	na[a]	61
KLE-KLH	7	na	40	15
CBI-butyric acid-PPD	30	7.5	na	80
CBI-butyric acid-KLH	29	na	95	23
LY170881-PPD	4.1	2	na	68

[a] na, not applicable.

The major advantage of producing antigen-specific antibodies lies in the preparation of monoclonal antibodies. When the specificity toward the antigen is greater than that of the carrier, the selection of optimal antibodies for a particular assay becomes trivial. The high percentage of antigen-specific hybridomas (Table 2) in PPD immunized mice confirm the reduction of carrier-specific hybridomas by using PPD as a carrier molecule. In the case of KLE1 peptide, when PPD was used as a carrier molecule 61% of the wells screened for carrier and antigen were antigen specific as opposed to 15% for KLH. The 4-fold increase in the antigen-specific hybridomas will increase the probability of selecting the optimal cell line for the subsequent analytical procedure.

The serum antibody response may or may not be a true predictor of the number of specific hybridoma cells that are produced during a fusion. However, the number of hybridoma wells that cross-reacted with KLH in both the peptide and the CBI-butyric acid was greater than those for PPD (Table 2). The specificity to the antigen is almost 12 times greater when PPD was used as the carrier in CBI-butyric acid. It could be argued that the antigen was not exposed to the surface (epitopic suppression) in KLH due to the large molecular weight of this protein. However, this should be not the case since the molar ratios in each situation were comparable. These results strongly support the fact that PPD is indeed a T-cell antigen.

The KLE1 peptide specificity results are also very encouraging. The fusion results were much superior when the PPD conjugates were used as the immunogen when compared to KLH (Table 2). The results show no advantage to using KLH in obtaining peptide-specific antibodies. Peptides typically have low antigenicity, particularly if they are naturally occurring. To increase the antigenicity, the most common approach has been to use KLH whose immunogenicity KLH masks the production of peptide-specific antibodies, a major disadvantage when preparing peptide-specific antibodies. The role of PPD therefore is to act as a T-cell activation leaving the B-cells to respond to the peptide (Lachmann et al., 1986).

PPD has not been extensively used in the preparation of protein−hapten conjugates. The principal practical use of PPD for the last half century has been as an in vivo diagnostic test for previous encounters with *Mycobacterium tuberculosis* (Lachmann, 1988). However, its potential in the "heterogenization" of tumor cells and the results of these studies in the production of antibodies against tumor antigens has been very encouraging (Lachmann et al., 1981; Sia et al., 1984). PPD has being used by Lachmann et al. (1986) in the preparation of peptide conjugates that were used in the production of anti-peptide antibodies. Antibodies against PPD cannot be precipitated in the Farr assay (Lachmann, 1988), but there has been an ELISA method developed to detect PPD-specific antibodies in the detection of tuberculosis in children (Barrera et al., 1989). Our results do show a

weak antibody response to PPD compared to the other carriers used. On the basis of the Farr assay, Lachmann (1988) defines PPD as a poor B-cell antigen. However, the antibodies that are present in our experiments could be against the impurities present in the protein preparations since it is not clear that the PPD used in most of the clinical testing is of 100% purity (Lachmann et al., 1986). KLH, BSA, and OVA are excellent carrier proteins commonly used in the preparation of hapten−protein conjugates.

We have clearly described the exceptional ability of PPD as a carrier in the production of hapten-specific antibodies. Although this unique characteristic of PPD as a carrier protein is not completely understood, it is assumed that the denatured structure of PPD could be responsible for the activation of T-cell receptors. It is conceivable that as the T-cells recognize processed antigenic epitopes, the heat-denatured PPD could be a potential target for their activation. The activity of PPD is enhanced only in animals previously exposed to *Mycobacterium tuberculosis* or immunized with BCG. These animals show a delayed-type hypersensitivity (DTH) when challenged with PPD. This, on the other hand, may cause a retention of the antigen for a prolonged period of time at the site of the injection, thus giving rise to an adjuvant effect. This has invoked an interest in using PPD in vaccine preparations. Thus PPD has demonstrated its usefulness as a carrier molecule in the preparation of hapten−protein/peptide−protein conjugates and its potential in vaccine preparation as an adjuvant.

ACKNOWLEDGMENT

This work was supported in part by the Center for BioAnalytical Research at University of Kansas, the Procter and Gamble Company, and Eli Lilly Laboratories. We thank Lederle Laboratories for the generous donation of the PPD.

LITERATURE CITED

(1) Bahr, G. M., Rook, G. A. W., Moreno, E., Lydyard, P. M., Modabber, F. Z., and Stanford, J. L. (1980) Use of the ELISA to screen for anti-thymocyte and anti-b_2-microglobulin antibodies in leprosy and SLE. *Immunology 41*, 865−873.

(2) Barrera, L., Miceli, I., Ritacco, V., Torrea, G., Broglia, B., Botta, R., Maldonado, C. P., Ferrero, N., Pinasco, A., Cutillo, I., Cornejo, M., Prokopio, E., and De Kantor, I. (1989) Detection of circulating antibodies to purified protein derivative by enzyme-linked immunosorbent assay: its potential for the rapid diagnosis of tuberculosis. *Pediatr. Infect. Dis. J. 8*, 763−767.

(3) Bowsher, R. R., Compton, J. A., Kirkwood, J. A., Place, G. D., Jones, C. D., Mabry, T. E., Hyslop, D. L., Hatcher, B. L., and De Sante, K. A. (1994) Sensitive and specific radioimmunoassay for Fialuridine: Initial assessment of pharmacokinetics after single oral doses of healthy volunteers. *Antimicrobial Agents Chemother. 38* (9), 2134−2142.

(4) Eshhar, Z. (1985) Monoclonal antibody strategy and techniques. in *Hybridoma technology in the Biosciences and Medicine* (T. A. Springer, Ed.) pp 3−41, Plenum Press, New York.

(5) Francis, M. J., Hastings, G., Syred, A. D., McGinn, B., Brown, F., and Rowlands, D. J. (1987) Nonresponsiveness to a foot and mouth disease virus peptide overcome by of foreign helper T-cell determinants. *Nature 330*, 168−170.

(6) Galfré, G., and Milstein, C. (1981) Preparation of monoclonal antibodies: strategies and procedures. *Methods Enzymol. 73*, 3−46.

(7) Good, M. F., Maloy, W. L., Lunde, M. N., Margalit, H., Cornette, J. L., Smith, G. L., Moss, B., Miller, L. H., and Berzofsky, J. A. (1987) Construction of synthetic immunogen: use of new T-helper epitope on Malaria circumsporozite protein. *Science 235*, 1059−1062.

(8) Hendrickson, T. L., Wilson, G. S., Frazer, J. M., Liu, R.-S., McCormack, R. T., and Wolfert, R. L. (1994) Enhanced immunogenicity of leucine enkephalin following coupling to anti-immunoglobulin and anti-CD3 antibodies. *J. Immunol. Methods 172*, 165−172.

(9) Kawamura, H., and Berzofsky, J. A. (1986) Enhancement of antigenic potency in vitro and immunogenicity in vivo by coupling the antigen to anti-immunoglobulin. *J. Immunol. 136*, 58−65.

(10) Köhler, G., and Milstein, C. (1975) Continuous cultures of fused cells secreting antibody of predefined specificity. *Nature 256*, 495−497.

(11) Lachmann, P. J., Vyakarnam, A., and Sikora, K. (1981) The heterogenization of tumor cells with tuberculin. 1. The coupling of tuberculin to cell surfaces using Con-A as ligand. *Immunology 42*, 329−336.

(12) Lachmann, P. J., Strangeways, L., Vyakarnam, A., and Evan, G. (1986) Raising antibodies by coupling peptides to PPD and immunizing BCG-sensitized animals. *CIBA Foundat. Symp. 119*, 25−57.

(13) Lachmann, P. J. (1988) Purified protein derivative (PPD). *Springer Semin. Immunopathol. 10*, 301−304.

(14) Landsteiner, K. (1936) The serological specificity of proteins. *The Specificity of serological reactions*, pp 9−42, Charles Thomas, Maryland.

(15) Morein, B., Lövgren, K., Höglund, S., and Sundquist, B. (1987) The ISCOM: an immunostimulating complex. *Immunol. Today 8*, 333−338.

(16) Orosz, G., and Carlson, R. G. (1990) (Unpublished data).

(17) Plaue, S., Muller, S., Briand, J. P., and Van-Regenmortel, M. H., (1990) Recent advances in solid-phase peptide synthesis and preparation of antibodies to synthetic peptides. *Biologicals 18* (3), 147−157.

(18) Pratt, J. J. (1978) Steroid Immunoassay in Clinical Chemistry. *Clin. Chem. 24* (11), 1869−1890.

(19) Sia, D. Y., Lachmann, P. J., and Leung, K. N. (1984) Studies in the enhancement of tumor immunity by coupling strong antigens to tumor cells ('heterogenization of tumors'). Helper T cell clones against PPD help other T cells mount antitumor responses to PPD-coupled tumor cells. *Immunology 51*, 755−763.

(20) Snider, D. P., and Segal, D. M. (1987) Targeted antigen presentation using cross-linked antibody heteroaggregates. *J. Immunol. 139*, 1609−1616.

(21) Staros, J. V., Wright, R. W., and Swingle, D. M. (1986) Enhancement by N-hydroxysulfosuccinimide of water-soluble carbodiimide-mediated coupling reactions. *Anal. Biochem. 156*, 220−222.

(22) Tam, J. P. (1989) Immunization with peptide-carrier complexes: traditional and multiple-antigen peptide system. in *Peptide antigens. A practical approach* (G. B. Wisdom, Ed.) pp 83−115, IRL press, New York.

(23) Tijssen, P. (1985) Practice and theory of enzyme immunoassays. in *Laboratory Techniques in biochemistry and molecular biology* (R. H. Burton, and P. H. van Kippenberg, Eds.) pp 279−296, Elsevier, New York.

(24) Walker, C. S., Clark, S. J., and Wotiz, H. H. (1973) Factors involved in the production of specific antibodies to estriol and estradiol. *Steroids 21* (2), 259−283.

BC9800724

Epidermal Growth Factor Radiopharmaceuticals: ^{111}In Chelation, Conjugation to a Blood-Brain Barrier Delivery Vector via a Biotin-Polyethylene Linker, Pharacokinetics, and in Vivo Imaging of Experimental Brain Tumors

Atsushi Kurihara, Yoshiharu Deguchi, and William M. Pardridge*

Department of Medicine, UCLA School of Medicine, Los Angeles, California 90095-1682. Received October 9, 1998; Revised Manuscript Received December 29, 1998

Epidermal growth factor (EGF) is a potential peptide radiopharmaceutical for detection of brain tumors, because many human gliomas overexpress the EGF receptor (EGFR). The transport of EGF to the brain, however, is restricted by the blood-brain barrier (BBB). The purpose of the present study was to develop a vector-mediated brain delivery system for radiolabeled EGF. Human EGF was monobiotinylated with NHS-PEG^{3400}-biotin, where NHS is *N*-hydroxysuccinimide and PEG^{3400} is poly(ethylene glycol) of 3400 Da molecular mass. EGF-PEG^{3400}-biotin was radiolabeled with either ^{125}I or ^{111}In through the metal chelator, diethylenetriaminepentaacetic acid (DTPA). The radiolabeled EGF was then conjugated to a BBB delivery vector comprised of a complex of the OX26 monoclonal antibody (MAb) to the rat transferrin receptor, which was coupled to streptavidin (SA). Following intravenous injection in rats, the ^{125}I conjugate was rapidly degraded in vivo, while the ^{111}In conjugate was metabolically stable. The brain delivery of [^{111}In]DTPA-EGF-PEG^{3400}-biotin was enabled by conjugation with OX26/SA and was optimized by co-injection of unlabeled EGF to saturate EGF receptors in the liver. The specific binding of the [^{111}In]DTPA-EGF-PEG^{3400}-biotin conjugated to OX26/SA to the EGF receptor was confirmed in C6 rat glioma cells, which had been transfected with a gene encoding for the human EGF receptor under the regulation of a dexamethasone-inducible promoter. In vivo studies of C6-EGFR experimental tumors in Fischer 344 rats demonstrated successful brain imaging only when the peptide radiopharmaceutical was conjugated to the BBB delivery system, although the C6-EGFR tumors did not express EGFR in vivo. In conclusion, these studies describe the molecular formulation of a peptide radiopharmaceutical that can be used for imaging brain tumors behind the BBB.

INTRODUCTION

Primary human brain tumors frequently overexpress the receptor for epidermal growth factor (EGF) (*1*−*3*), and EGF peptide radiopharmaceuticals are potential imaging agents for the diagnosis of human brain gliomas (*4*). However, like most other neuropeptides, EGF does not cross the brain capillary endothelial wall (*5*), which makes up the blood-brain barrier (BBB) in vivo. Since the BBB is intact (*6*), until the end stage of most human brain tumors, it may be necessary to conjugate EGF to BBB transport vectors in order to use this peptide as a radiopharmaceutical for imaging human brain tumors. BBB transport vectors include the OX26 monoclonal antibody (MAb), which targets the rat transferrin receptor (*7*), or the anti-human insulin receptor MAb (HIRMAb), which is a BBB delivery vector active in humans or Old World primates such as Rhesus monkeys (*8*). Peptide radiopharmaceuticals may be conjugated to BBB transport vectors using avidin-biotin technology (*7*).

Previous studies describe the biotinylation of human EGF at surface ϵ-amino moieties of lysine residues using a 14 atom bis(aminohexanoyl) spacer arm (-XX-) between the EGF and the biotin (*9*). However, when the EGF-XX-biotin was bound to a conjugate of the OX26 MAb and streptavidin (SA), which is designated OX26/SA, the EGF no longer bound to the EGF receptor on C6 rat glioma cells (*9*). These C6 cells had been transfected with a gene encoding the human EGF receptor under the influence of a dexamethasone-inducible promoter and designated C6EGFRp cells (*10*). Conversely, when the -XX- linker was replaced with a >200 atom linker comprised of poly(ethylene glycol) of 3400 Da molecular mass, designated PEG^{3400}, the binding of the peptide to the EGF receptor was restored despite conjugation to the OX26/SA BBB delivery system (*9*). The radionuclide used in previous studies was ^{125}I, which was added to surface tyrosine residues on EGF.

The present investigations extend these previous studies (*9*) and examine the pharmacokinetics and in vivo metabolic stability of the [^{125}I]EGF-PEG^{3400}-biotin conjugated to OX26/SA. However, the initial studies with the EGF peptide radiopharmaceutical formulated with the ^{125}I radionuclide demonstrated a marked metabolic instability in vivo. Therefore, the present study also describes the preparation of a human EGF peptide radiopharmaceutical that is conjugated with both diethylenetriaminepentaacetic acid (DTPA), to enable chelation with the ^{111}In radionuclide, and monobiotinylation using NHS-PEG^{3400}-biotin, where NHS = *N*-hydroxysuccinimide. The monobiotinylated form of EGF was purified by gel filtration fast-protein liquid chromatography (FPLC) using two columns in series and characterized using

* To whom correspondence should be addressed. Phone: (310) 825-8858. Fax: (310) 206-5163. E-mail: wpardrid@med1.medsch.ucla.edu.

10.1021/bc980123x CCC: $18.00 © 1999 American Chemical Society
Published on Web 03/06/1999

matrix-assisted laser desorption ionization mass spectrometry (MALDI) and sodium dodecyl sulfate−polyacrylamide gel electrophoresis (SDS−PAGE) and Western blotting. The metabolic stability of the EGF conjugate formulated with the ^{111}In radionuclide was demonstrated with FPLC analysis of rat serum taken 60 min after an intravenous (i.v.) injection. The affinity of the EGF peptide radiopharmaceutical conjugated to the BBB delivery system for the human EGF receptor was examined using the C6EGFR cells both in tissue culture and in vivo, wherein experimental brain tumors were formed by implanting the C6EGFR cells into the caudate-putamen nucleus of Fischer 344 rats. Following initial pharmacokinetic analysis, the EGF peptide radiopharmaceutical conjugated to the BBB delivery system and formulated with the ^{111}In radionuclide was used for neuroimaging of experimental brain tumors.

EXPERIMENTAL PROCEDURES

Materials. [^{125}I]Na was supplied by Amersham (Arlington Heights, IL). [^{111}In]Cl_3 was supplied by NEN Life Science Product Inc. (Boston, MA). NHS-PEG^{3400}-biotin was obtained from Shearwater Polymers (Huntsville, AL), where NHS = *N*-hydroxysuccinimide and PEG^{3400} = poly(ethylene glycol) of 3400 Da molecular mass. Diethylenetriaminepentaacetic (DTPA) dianhydride was obtained from Aldrich Chemical Co., Inc. (Milwaukee, WI). Chloramine-T was purchased from MCB Reagents (Cincinnati, OH). Recombinant streptavidin (SA), recombinant human epidermal growth factor (EGF), and all other reagents were obtained from Sigma Chemical Company (St. Louis, MO). Superose 12 HR 10/30 FPLC columns and High-Trap copper affinity columns (1.0 mL) were obtained from Pharmacia Biotech (Piscataway, NJ). C6 rat glioma cells transfected with the gene for the human EGF receptor were kindly provided by Dr. Robert Fenstermaker of the Roswell Park Cancer Institute (Buffalo, NY), and these cells are designated C6EGFRp (*10*). The mouse hybridoma line producing the 528 MAb to human EGFR was obtained from the American Type Culture Collection (Rockville, MD). The anti-human EGFR mouse MAb was purchased from Upstate Biotechnology (Lake Placid, NY), catalog no. 05-101. The ABC-Elite immunocytochemistry kit was obtained from Vector Labs (Burlingame, CA). Mouse IgG1 and IgG2a isotype controls were obtained from Cappel Pharmaceuticals (Aurora, OH).

Preparation of [^{125}I]EGF-PEG^{3400}-biotin. NHS-PEG^{3400}-biotin (65 nmol in 100 μL of 0.05 M $NaHCO_3$) was added in an 8:1 molar ratio to 50 μg of EGF (8.0 nmol in 100 μL of 0.05 M $NaHCO_3$, pH 8.3) followed by incubation at room temperature for 60 min. Of this mixture, 20 μL was added to 20 μL of 0.3 M NaH_2PO_4 (pH 7.0) followed by the addition of 2 mCi of ^{125}I and 10 μL (0.8 μg) of chloramine-T. After a 60 s incubation, an additional 10 μL (0.8 μg) of chloramine-T was added, and 60 s later, the reaction was terminated by the addition of 50 μL (65 nmol) of sodium metabisulfite. Buffer A (0.05 M NaH_2PO_4/0.5 M NaCl/pH 7.0) was added to a volume of 1.0 mL, and the mixture was then applied to a 1.0 mL High-Trap copper affinity column to remove unreacted NHS-PEG^{3400}-biotin, as described previously (*11*). The column was initially washed with 5.0 mL of water and charged with 0.5 mL of 0.1 M $CuSO_4$ followed by washing with 5.0 mL of water, followed by application of the sample. The column was washed with 10 mL of buffer A, and the [^{125}I]EGF-PEG^{3400}-biotin was eluted with 5.0 mL of 50 mM imidazole in buffer A. One milliliter of this eluate (250 μCi) was added to a Centricon-3 microconcentrator (Amicon, Inc., Beverly, MA), and the volume was reduced to 200 μL by centrifugation at 7500 rpm (7500*g*) for 40 min at room temperature. Then [^{125}I]EGF-PEG^{3400}-biotin was purified by size-exclusion chromatography using a TSK-gel G2000$_{SWXL}$ column (TosoHaas, Montgomery, PA) with an elution buffer of 0.01 M NaH_2PO_4/0.15 M NaCl/pH 7.4/0.05% Tween-20 at a flow rate of 0.5 mL/min.

Preparation of [^{111}In]DTPA-EGF-PEG^{3400}-biotin. NHS-PEG^{3400}-biotin (80 nmol in 50 μL of 0.05 M $NaHCO_3$) was added in a 5:1 molar ratio to EGF (16 nmol in 200 μL of 0.05 M $NaHCO_3$) followed by incubation at room temperature for 60 min. To this mixture, 50 μL of 0.43 M $NaHCO_3$ and 850 nmol of DTPA dianhydride (17 μL of a dimethyl sulfoxide solution) were added, followed by incubation at room temperature for 60 min. The entire mixture was then applied to two Superose 12 HR 10/30 FPLC columns in series, followed by the elution in 0.01 M NaH_2PO_4/0.15 M NaCl/pH 7.4 at a flow rate of 0.5 mL/min for 90 min. EGF, containing a single DTPA group and a single PEG^{3400}-biotin moiety and designated DTPA-EGF-PEG^{3400}-biotin, eluted at 52 min from the column, as demonstrated by MALDI (below). Two millicurie of ^{111}In was added to the DTPA-EGF-PEG^{3400}-biotin. After 30 min at room temperature, unreacted free ^{111}In was removed by Sephadex G25 size-exclusion chromatography with an elution buffer of 0.01 M NaH_2PO_4/0.15 M NaCl/pH 7.4 containing 0.05% Tween-20.

Conjugation of [^{125}I]EGF-PEG^{3400}-biotin or [^{111}In]-DTPA-EGF-PEG^{3400}-biotin to OX26/SA. The conjugate of the OX26 MAb and recombinant streptavidin (SA) was prepared with a thiol-ether linkage as described previously (*12*). Briefly, 17 mg of OX26 MAb was thiolated with a 10:1 molar ratio of 2-iminothiolane; 7 mg of recombinant SA was activated with a 20:1 molar ratio of *m*-maleimidobenzoyl *N*-hydroxysuccinimide ester (MBS). The activated SA and the thiolated OX26 were then mixed and incubated at room temperature for 3 h. The OX26/SA conjugate was labeled with 2.5 μCi of [^{3}H]biotin and was purified on a 2.6 × 92 cm column of Sephacryl S300HR (Pharmacia) followed by elution in 0.01 M NaH_2PO_4/0.15 M NaCl/pH 7.4/0.05% Tween-20 at 30 mL/h, and 3 mL fractions were collected. The conjugate peak was separated from either aggregates, unconjugated OX26 MAb, or unconjugated SA. The number of biotin binding sites per OX26/SA conjugate was 3.3 ± 0.3, as determined with the [^{3}H]biotin binding assay (*12*).

The conjugate of [^{125}I]EGF-PEG^{3400}-biotin and OX26/SA was prepared by mixing 1 mL of the imidazole eluate from the High-Trap column containing [^{125}I]EGF-PEG^{3400}-biotin (0.6 nmol) and 400 μg (0.2 nmol) of OX26/SA (*9*). After reduction of the volume to 0.2 mL with a Centricon-30 microconcentrater, [^{125}I]EGF-PEG^{3400}-biotin conjugated to OX26/SA was separated from either [^{125}I]-EGF or unreacted [^{125}I]EGF-PEG^{3400}-biotin by size-exclusion chromatography using a TSK-gel G2000$_{SWXL}$ with an elution buffer of 0.01 M NaH_2PO_4/0.15 M NaCl/pH 7.4/0.05% Tween-20 at a flow rate of 0.5 mL/min.

The conjugate of [^{111}In]DTPA-EGF-PEG^{3400}-biotin and OX26/SA was prepared by mixing [^{111}In]DTPA-EGF-PEG^{3400}-biotin (5 nmol) eluted from Sephadex G25 column with OX26/SA (8 nmol).

Matrix-Assisted Laser Desorption Ionization Mass Spectrometry (MALDI). Mass spectra of DTPA-EGF-PEG^{3400}-biotin eluted from the two Superose 12HR 10/30 FPLC columns in series were recorded with a reflector time-of-flight instrument (PerSeptive Biosystems Voyager RP) used in the linear mode with stainless steel targets. An aliquot of sample solution (0.5 μL) or sample

solution plus internal standard (myoglobin 5 pmol in 0.5 μL of water) was overlaid on top of an aliquot matrix (sinapinic acid), and after drying, the target was inserted into the mass spectrometer, and time/intensity data from 50 to 100 scans was averaged and converted to mass/intensity data using external calibration from myoglobin.

SDS−PAGE and Western Blotting. The change in molecular weight of EGF following conjugation with NHS-PEG^{3400}-biotin was confirmed by SDS−PAGE. The reaction mixture of EGF and varying concentrations of NHS-PEG^{3400}-biotin was applied to a 16.5% SDS−PAGE minigel (Bio-Rad, Rhichmond, CA), and electrophoresis was performed at constant voltage (100 V) for 2 h at room temperature. The gel slab was stained for protein content with Coomassie Blue G250. The incorporation of biotin at the tip of PEG strand was confirmed by Western blotting. Following SDS−PAGE, the gel slab was blotted to a nylon membrane without methanol (100 V, 60 min, 4 °C) and the membrane was subsequently stained for biotin content with the ABC kit (Vector Labs, Burlingame, CA) using avidin and biotinylated peroxidase and diaminobenzidine as chromagen (13). SDS−PAGE molecular weight standards were obtained from Bio-Rad (Richmond, CA).

C6EGFRp Radioreceptor Assay. C6EGFRp cells were grown in Dulbecco's modified Eagle medium (DMEM) with 4.5 g/L D-glucose, 4 mM glutamine, 10% fetal bovine serum, and 250 μg/mL G418, used as a selection agent, in 24-well cluster dishes. For the dexamethasone stimulation condition, the medium was changed to DMEM with 4.5 g/L D-glucose, 4 mM glutamine, 1% fetal bovine serum, and 1 μM dexamethasone 24 h prior to performing radioreceptor assays (*10*). Cells were washed with 0.01 M HEPES/0.15 M NaCl/pH 7.4/0.1% BSA (HBSB buffer), followed by 15 min to 120 min incubation at 37 °C with 200 μL of HBSB buffer containing 1.0 μCi/mL (0.2 nM) of [^{111}In]DTPA-EGF-PEG^{3400}-biotin with and without OX26/SA in the presence and absence of 1 μM unlabeled EGF. After incubation, supernatants were aspirated and the cells were washed two times with cold 0.01 M HEPES/0.15 M NaCl/pH 7.4, and solubilized by the addition of 0.5 mL of 1 N NaOH and incubation at 37 °C for 4 h. ^{111}In radioactivity was counted by γ counter and protein content of the cells was measured with the bicinchoninic acid (BCA) protein assay (Pierce Chemical Co., Rockford, IL). Cell-associated binding (surface-binding and intracellular accumulation) was expressed as percent of medium radioactivity bound per milligram of cell protein.

Pharmacokinetics and Brain Drug Delivery. Male Sprague−Dawley rats weighing 280−350 g were anesthetized with 100 mg/kg ketamine and 2 mg/kg xylazine intraperitoneally (ip). The femoral vein was cannulated with a PE50 cannula and injected with either 5 μCi of [^{125}I]EGF-PEG^{3400}-biotin or 5 uCi of [^{111}In]DTPA-EGF-PEG^{3400}-biotin, with or without conjugation to OX26/SA and either 0 or 16 nmol of unlabeled human EGF. Blood samples (0.25 mL) were collected via a PE50 cannula implanted in the femoral artery at 0.25, 1, 2, 5, 15, 30 and 60 min after the injection of the isotope solution. The blood volume was replaced with an equal volume of saline. After 60 min, the animals were decapitated for removal of the brain, liver, kidney, heart, and lung. The radioactivity in the plasma and organ samples were counted using a γ counter (Beckman Instruments, Inc., Fullerton, CA).

Pharmacokinetic parameters were calculated by fitting the plasma radioactivity data to a biexponential equation (*14*):

$$A(t) = A_1 e^{-k_1 t} + A_2 e^{-k_2 t}$$

where $A(t)$ = % ID/mL plasma and ID = injected dose. For [^{125}I]EGF-PEG^{3400}-biotin, TCA-precipitable radioactivity data was used. The biexponential equation was fit to plasma data by a derivative-free nonlinear regression analysis (PARBMDP, Biomedical Computer P-Series, developed at UCLA Health Science Computing Facilities). The area under the plasma concentration−time curve (AUC), the steady-state volume of distribution (Vss), total plasma clearance (Cl), and the mean residence time (MRT) were calculated from A_1, A_2, k_1, k_2, and the body weight (kg) of the rat as described by Gibaldi and Perrier (*15*). The organ permeability−surface area (PS) product was calculated as

$$\mathrm{PS} = [V_d - V_0]\mathrm{Cp(60min)/AUC(0-60min)}$$

where Cp(60min) is the terminal plasma concentration (dpm/μL) at 60 min after injection, V_d is the tissue volume of distribution determined from the ratio of disintegrations per minute per gram of the tissue to Cp(60min), and V_0 is the organ plasma volume, which has been measured previously (*14*). The organ delivery of the EGF conjugate was determined as

$$\%\ \mathrm{ID/g} = \mathrm{PS} \times \mathrm{AUC(0-60min)}$$

where % ID/g is the percent injected dose taken up per gram of organ.

The metabolic stability in plasma of the [^{125}I]EGF-PEG^{3400}-biotin was determined by trichloroacetic acid (TCA) precipitation of 50 μL aliquots of the plasma sample removed at each time point. The metabolic stability in plasma of the [^{111}In]DTPA-EGF-PEG^{3400}-biotin bound to the OX26/SA conjugate was also examined by elution of plasma through a single Superose 12 HR 10/30 FPLC column. In this study, blood was removed at 60 min following intravenous injection of 60 μCi of [^{111}In]DTPA-EGF-PEG^{3400}-biotin conjugated to OX26/SA and 16 nmol of unlabeled EGF. Fifty microliters of serum sample was applied to the FPLC column, followed by the elution in 0.01 M NaH_2PO_4/0.15 M NaCl/0.05% Tween-20/pH 7.4 at a flow rate of 0.5 mL/min for 50 min. Column fractions (0.5 mL) were assayed for ^{111}In radioactivity.

Intracerebral Tumor Implantation and in Vivo Autoradiography. Male CD Fischer 344 rats weighing 170−180 g were implanted with C6EGFRp cells (*4*, *10*). The rats were anaesthetized with a mixture of ketamine (100 mg/kg) and xylazine (2 mg/kg) ip and fixed in a stereotactic frame. A burr hole was drilled 3 mm to the right of midline, 1 mm posterior to bregma. C6EGFRp cells were suspended in serum-free DMEM containing 1.2% methylcellulose. Five microliters of cell suspension (1×10^5 cells) was injected into the right caudate nucleus at a depth of 4 mm over 10 s, using a 10 μL Hamilton syringe with fixed needle. At the end of the procedure, the viability of the remaining cells was determined by means of the trypan blue exclusion method. To allow for the implanted glioma cells to produce a tumor of a adequate size (~5 mm), in vivo autoradiography studies were carried out 4 weeks following tumor cell implantation (*4*). Tumor-bearing rats were intravenously injected with either [^{111}In]DTPA-EGF-PEG^{3400}-biotin (100 μCi) with OX26/SA and 16 nmol of unlabeled EGF or [^{111}In]-DTPA-EGF-PEG^{3400}-biotin (100 μCi) alone. Sixty minutes after isotope injection, rats were decapitated and the brain was rapidly removed from the cranium and sec-

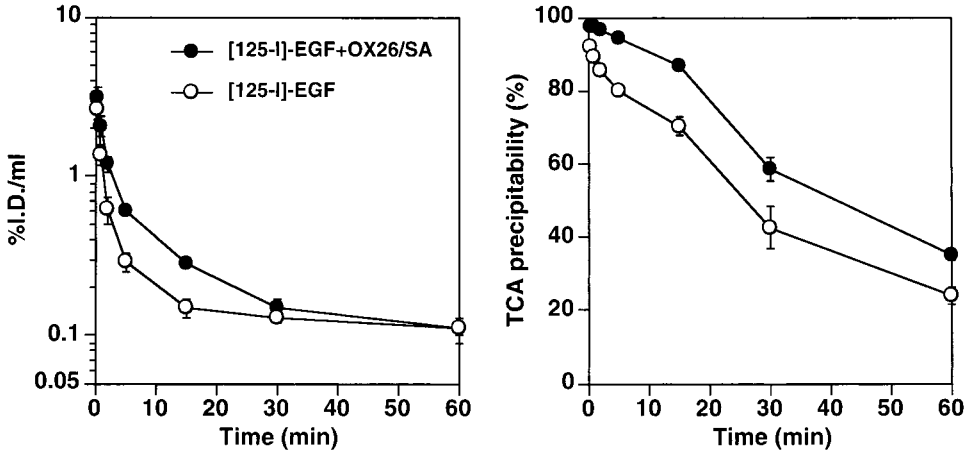


Figure 1. (Right panel) Profile of the TCA-precipitable plasma radioactivity of either unconjugated [^{125}I]EGF-PEG^{3400}-biotin (open circle) or the [^{125}I]EGF-PEG^{3400}-biotin conjugated to the OX26/SA vector (closed circle) after an i.v. injection of 5 μCi/rat. (Left panel) Time course of the percent of plasma radioactivity that is precipitable with TCA after the i.v. injection. Each point represents the mean ±SE of three rats.

tioned into 3 mm slabs. The slabs were plunged into powdered dry ice for rapid freezing over 30 min. Frozen sections of 15 μm were cut and thaw-mounted on glass cover slips. After drying, these cover slips were placed in apposition to Kodak Biomax MS X-ray film and exposed for 4 days at −70 °C with intensifying screen. The film was scanned with a Hewlett-Packard ScanJet IIcx/T flatbed scanner and transferred to Adobe Photoshop on a Power Macintosh 7100/66 microcomputer, followed by colorization with NIH image software, and prints were generated with a Kodak printer.

Immunocytochemistry. The expression of the EGF receptor in the C6EGFRp glioma cells that had been transplanted into the caudate-putamen nucleus of Fischer 344 rats was investigated with immunochemistry at 4 weeks after the implantation of 1×10^5 C6EGFRp cells. Rats were sacrificed and the brain was rapidly removed and frozen in pulverized dry ice. The frozen brain was then embedded in tissue OCT (Tissue Tek II, Miles, Elkhart, IN) and 15 μ frozen sections were obtained with a Bright cryostat. Sections were mounted to glass slides and then fixed in either 100% acetone at −20 °C for 20 min or fixed by drying in an oven at 60 °C for 30 min. Endogenous peroxidase activity was inactivated with 1% H_2O_2 for 5 min at room temperature, and the slides were blocked with 3% horse serum for 30 min at room temperature. Two different primary antibodies were used. The 528 mouse MAb to the human epidermal growth factor receptor was generated from conditioned medium produced from 528 hybridoma cells. The 528 antibody has been demonstrated in previous studies to illuminate the human EGF receptor in experimental brain tumors with immunocytochemistry (*16*). A second primary antibody that was used in these studies was the anti-human EGF receptor mouse monoclonal antibody from Upstate Biotechnology (Lake Placcid, NY). The monoclonal antibodies were used at a concentration of 3 and 10 μg/mL and mouse IgG1 or mouse IgG2$_a$ isotype controls were employed in parallel. Following reaction with a biotinylated horse anti-mouse antibody that had been preabsorbed with rat immunoglobulin (Vector Laboratories, Burlingame, CA, catalog no. BA-2001), the slides were exposed to avidin and biotinylated peroxidase using the vector ABC method (Vector Labs, Burlingame, CA). These slides were lightly counterstained with hematoxylin and mounted. As a control, human glioblastoma multiforme U87 cells, which express the human EGF receptor (*16*), were obtained from the American Type Culture Collection and examined in parallel. These cells formed tumors in the brains of nude rats and the U87 cells, both in cell culture and in vivo as brain tumors, highly expressed immunoreactive human EGF receptor.

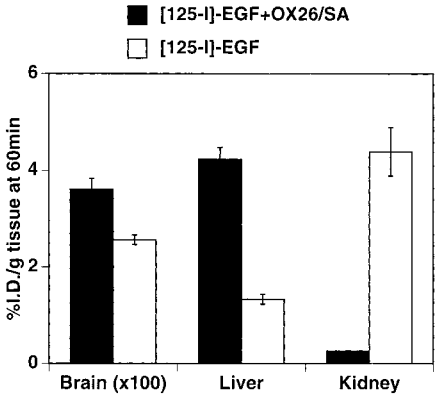


Figure 2. Tissue uptake of unconjugated [^{125}I]EGF-PEG^{3400}-biotin (open column) or the [^{125}I]EGF-PEG^{3400}-biotin conjugated to the OX26/SA vector (closed column) 60 min after the i.v. injection of 5 μCi/rat. Data are mean ±SE (n = 3 rats).

RESULTS

Pharmacokinetics and Brain Uptake of [^{125}I]EGF Conjugate. The [^{125}I]EGF-PEG^{3400}-biotin was prepared and injected intravenously into anesthetized rats with or without conjugation to OX26/SA and the plasma radioactivity profile is shown in Figure 1 (left panel). The EGF radiolabeled with ^{125}I radionuclide was rapidly removed from the plasma compartment despite conjugation to OX26/SA and exhibited reduced metabolic stability based on measurement of plasma radioactivity that was precipitable with trichloroacetic acid (TCA), as demonstrated in Figure 1 (right panel). Analysis of distribution of the EGF conjugate into organs (brain, liver, and kidney) demonstrated the expected redirection of the EGF radiopharmaceutical from kidney to liver following conjugation to the anti-transferrin receptor MAb (Figure 2). However, the brain uptake of the EGF radiopharmaceutical formulated with a ^{125}I radionuclide was low with or without conjugation to OX26/SA (Figure 2). As noted in previous studies (*13*), it is difficult to achieve effective brain uptake of drugs, despite conjugation to BBB delivery systems, when the peptide is inherently metabolically labile. These results indicated

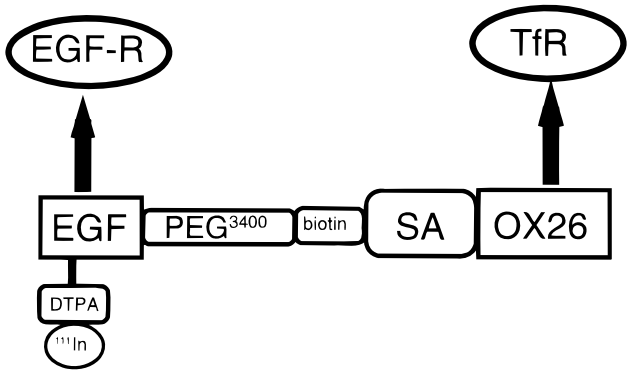


Figure 3. Delivery of radiolabeled EGF through the blood-brain barrier and binding to EGF receptor (EGF-R) overexpressed in glioma cells. The delivery system is comprised of three domains: (i) a glioma binding domain consisting of EGF radiolabeled stably with ^{111}In through the metal chelator, diethylenetriaminepentaacetic acid (DTPA); (ii) a linker domain consisting of *single* strand of PEG^{3400} spacer arm attached to EGF and the biotin moiety, which is in turn bound to streptavidin (SA); (iii) and a BBB transport domain consisting of the OX26 anti-rat transferrin receptor (TfR) monoclonal antibody (MAb), which is conjugated to SA through stable thioether linkage. The OX26 MAb undergoes receptor-mediated transcytosis through the blood-brain barrier via the brain capillary endothelial TfR (*21*). The EGF moiety binds to EGF-R positive glioma cells. The PEG^{3400} linker releases steric hindrance of the OX26 MAb on binding of the EGF to its cognate receptor (*9*). The radioligand ^{111}In is suitable for imaging and confers metabolic stability of the radionuclide moiety compared to ^{125}I.

the necessity of reformulating the EGF peptide radiopharmaceutical with a radionuclide that provided a greater degree of metabolic stability.

Synthesis and Characterization of [^{111}In]EGF Conjugate. The structure of the EGF peptide radiopharmaceutical conjugated to the BBB delivery system and formulated with ^{111}In radionuclide though a DTPA chelator moiety is shown in Figure 3. The placement of a >200 atom linker comprised of PEG^{3400} reduces any steric hindrance between the two components of the conjugate (*9*). The extended linker allows for maintenance of bifunctionality of the conjugate with binding to both the EGF receptor, for imaging brain tumors, and to the transferrin receptor, to enable receptor-mediated transyctosis through the BBB in vivo. Following reaction of DTPA dianhydride with NHS-PEG^{3400}-biotin, the human EGF was eluted through two Superose 12HR gel filtration FPLC columns in series and the elution profile is shown in Figure 4. The identity of the various peaks was determined by either MALDI (Experimental Procedures), or by parallel injection of standards. The EGF peak that contained a single DTPA residue and a single PEG^{3400}-biotin residue was found in peak C, and the measured molecular mass, 10 193 Da, was the expected size, which is approximately 10 200 Da (inset, Figure 4). Following reaction with NHS-PEG^{3400}-biotin, the EGF was also examined with SDS−PAGE, shown in Figure 5. The Coomassie blue stain of the SDS−PAGE gel (Figure 5A) shows the molecular weight of the unconjugated EGF at 6200 Da, and a second band is formed on the gel when NHS-PEG^{3400}-biotin is added, and this band is seen in lanes 1−4 of Figure 5A and migrates at a molecular size of 10 000 Da, which approximates the expected molecular weight, 9900 Da, of EGF with a single PEG^{3400}-biotin residue attached. At the higher molar ratios of NHS-PEG^{3400}-biotin:EGF, an additional band is detected which migrates at 16 000 Da and approximates the expected molecular weight (14 000 Da) of EGF with 2 PEG^{3400}-biotin moieties attached. The attachment of the

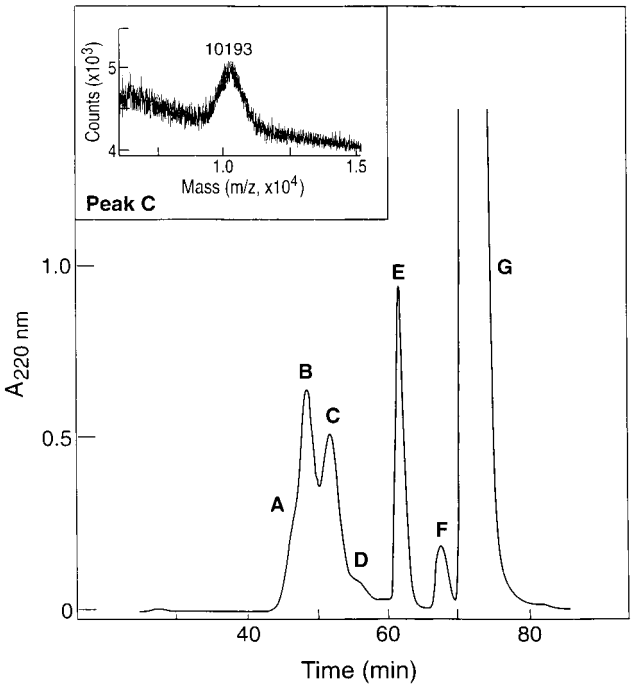


Figure 4. Purification of monobiotinylated DTPA-EGF-PEG^{3400}-biotin by FPLC. Reaction mixture of EGF, NHS-PEG^{3400}-biotin, and DTPA dianhydride was applied to two Superose 12 HR 10/30 FPLC column in series, followed by the elution in 0.01 M NaH_2PO_4/0.15 M NaCl/pH 7.4 at a flow rate of 0.5 mL/min for 90 min. Peak A, EGF-(PEG^{3400}-biotin)$_3$; peak B, DTPA-EGF-(PEG^{3400}-biotin)$_2$; peak C, DTPA-EGF-PEG^{3400}-biotin; peak D, DTPA-EGF; peak E, DTPA; peak F, NHS-PEG^{3400}-biotin; peak G, solvent peak. (Insert) MALDI mass spectra shows mean molecular mass of 10 193 Da for peak C (DTPA-EGF-PEG^{3400}-biotin, theoretical MW, 10 240). Peak A, EGF-(PEG^{3400}-biotin)$_3$ and peak B, DTPA-EGF-(PEG^{3400}-biotin)$_2$ showed molecular masses of 17 500 Da (theoretical 17 542 Da) and 13 801 Da (theoretical 13 891 Da), respectively, with the MALDI analysis. The (PEG^{3400}-biotin)$_n$ nomenclature, where n = 1, 2, or 3, refers to the number of PEG^{3400} strands conjugated to the EGF.

biotin residue was confirmed by Western blotting as shown in Figure 5B. No signal is detected in lanes 5 or 6, which represent reactions that contained either no NHS-PEG^{3400}-biotin or no EGF, respectively. The reaction with a 1:1 molar ratio of NHS-PEG^{3400}-biotin:EGF yields a single prominent band of 9200 Da, and this corresponds to the approximate molecular mass of EGF with a single PEG^{3400}-biotin residue attached. At the higher molar ratios (lanes 1−3) of NHS-PEG^{3400}-biotin:EGF, a second higher molecular weight band is detected of 14 600 Da (Figure 5B), and this approximates the molecular mass of EGF with 2 PEG^{3400}-biotin moieties attached.

Radioreceptor Assays with [^{111}In]EGF Conjugate and C6 Glioma Cells in Tissue Culture. The EGF-PEG^{3400}-biotin formulated with ^{111}In and DTPA radionuclide still actively bound to the EGF receptor on the C6EGFRp cells with or without conjugation to OX26/SA, as shown in Figure 6. Radioreceptor assays performed with the C6EGFRp cells pretreated with 1 μM dexamethasone for 24 h are shown in the right-hand panel of Figure 6, and radioreceptor assays performed with these cells without dexamethasone pretreatment are shown in the left-hand panel of Figure 6. In the absence of dexamethasone pretreatment, there is little induction of the EGF receptor in these cells, which explains the minimal binding of unconjugated [^{111}In]EGF (Figure 6, left-hand panel). However, there was significant binding, even in the C6EGFRp cells that were not pretreated with

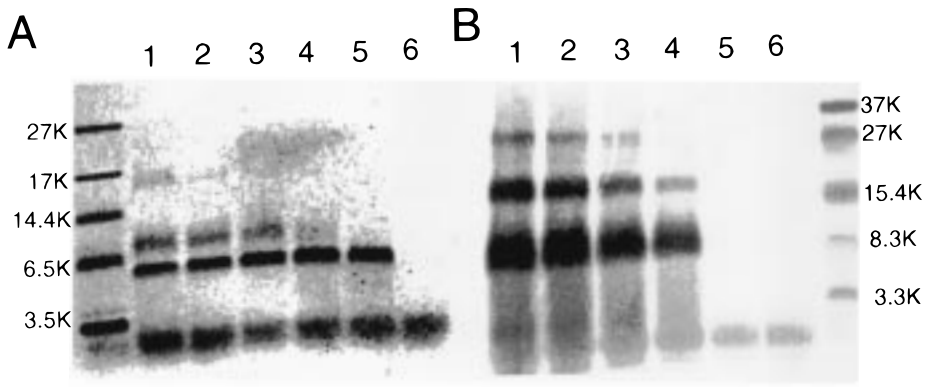


Figure 5. SDS-polyacrylamide gel electrophoresis (A) and Western blotting (B) of EGF-PEG^{3400}-biotin. Reaction mixture of EGF and varying concentration of NHS-PEG^{3400}-biotin was applied to a 16.5% SDS−PAGE minigel. Gel slab was either stained with Coomassie Blue G250 for protein content (panel A), or blotted to a nylon membrane followed by staining with avidin and biotinylated peroxidase to visualize the attachment of PEG^{3400}-biotin to the EGF molecule (panel B). Molar ratio of NHS-PEG^{3400}-biotin: EGF in the reaction mixture was 5:1 (lane 1), 4:1 (lane 2), 2:1 (lane 3), 1:1 (lane 4), 0:1 (lane 5), and 5:0 (lane 6).

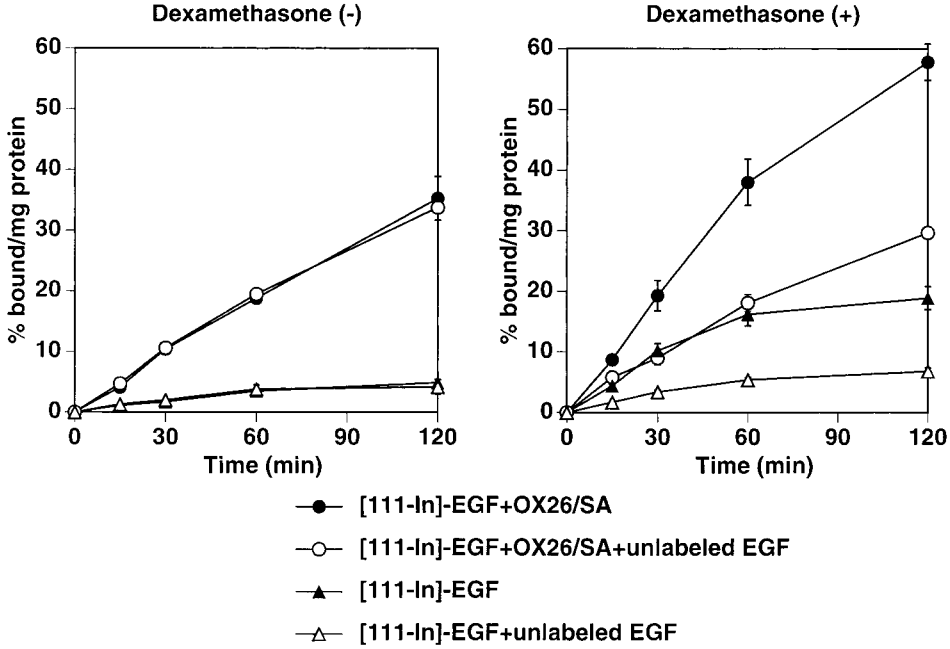


Figure 6. Radioreceptor assay showing time course of binding of either [^{111}In]DTPA-EGF-PEG^{3400}-biotin conjugated to OX26/SA (circles) or binding of [^{111}In]DTPA-EGF-PEG^{3400}-biotin (triangles) to C6 rat glioma cells transfected with the human EGF receptor gene. Assays were performed in the presence (right panel) or absence (left panel) of prior dexamethasone (1 μM) stimulation and in the presence (open symbols) or absence (closed symbols) of 1 μM unlabeled EGF. Each point represents the mean ±SE of three wells.

dexamethasone, of the [^{111}In]EGF-PEG^{3400}-biotin following conjugation to OX26/SA, owing to the expression of transferrin receptor on these cells. The conjugate bound to both transferrin receptor and EGF receptor on the cells, when the EGF receptor was induced by dexamethasone pretreatment (Figure 6, right-hand panel). A saturation analysis demonstrated that the ED_{50} of EGF competition of the binding of [^{111}In]EGF-PEG^{3400}-biotin conjugated to OX26/SA was approximately 1 nM.

Pharmacokinetics and Brain Uptake of [^{111}In]-EGF Conjugate. The pharmacokinetic analysis showed that unconjugated [^{111}In]EGF- PEG^{3400}-biotin was rapidly removed from the bloodstream (Figure 7), similar to the rapid removal of [^{125}I]EGF- PEG^{3400}-biotin from the circulation (Figure 1). For example, the % ID/mL of plasma was approximately 0.1% ID/mL at 10 min for either form of the EGF, indicating that >90% of the peptide had been removed from the circulation within the first 10 min after injection. Following conjugation of [^{111}In]EGF- PEG^{3400}-biotin to OX26/SA, there was some improvement in the plasma AUC (Table 1), but the EGF-PEG^{3400}-biotin conjugated to OX26/SA and formulated with DTPA/^{111}In was still relatively rapidly removed from the bloodstream (Figure 7). Since human EGF is avidly removed from the circulation by the hepatic rat EGF receptor (*17*, *18*), we co-administered a loading dose of unlabeled human recombinant EGF in parallel with the intravenous injection of the EGF-PEG^{3400}-biotin conjugated to OX26/SA and radiolabeled with ^{111}In (Figure 7). The co-injection of the unlabeled EGF resulted in a >4-fold increase in the plasma AUC (Table 1), and the EGF loading also optimized the brain uptake of the conjugate, as shown in Figure 8. In the presence of the unlabeled EGF, the brain uptake of the [^{111}In]EGF-PEG^{3400}-biotin conjugated to OX26/SA was increased more than 10-fold compared to the brain uptake of [^{111}In]EGF-PEG^{3400}-biotin without attachment to the BBB delivery system (Figure 8).

The metabolic stability of the EGF-PEG^{3400}-biotin conjugated to OX26/SA and formulated with DTPA/^{111}In was confirmed by gel filtration FPLC analysis of rat serum taken 60 min after an intravenous injection of the

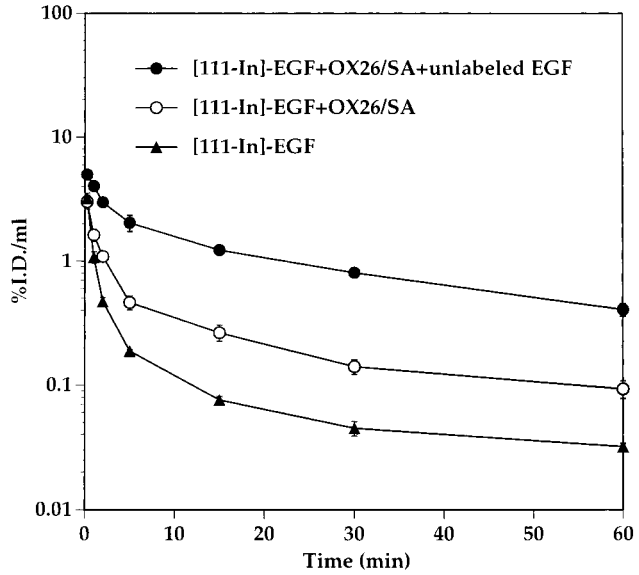


Figure 7. Profile of plasma radioactivity of either unconjugated [^{111}In]DTPA-EGF-PEG^{3400}-biotin (closed triangle), the [^{111}In]-DTPA-EGF-PEG^{3400}-biotin conjugated to the OX26/SA vector (open circle) or [^{111}In]DTPA-EGF-PEG^{3400}-biotin conjugated to the OX26/SA vector and co-injected with 16 nmol of unlabeled EGF (closed circle) after an i.v. injection of 5 μCi/rat. Each point represents the mean ±SE of three rats.

Table 1. Pharmacokinetic Parameters[a]

parameter	[^{111}In]EGF	[^{111}In]EGF + OX26/SA	[^{111}In]EGF + OX26/SA + unlabeled EGF
A_1 (% ID/mL)	3.3 ± 0.7	2.6 ± 0.2	3.5 ± 0.3
A_2 (% ID/mL)	0.11 ± 0.02	0.31 ± 0.03	1.7 ± 0.1
k_1 (min^{-1})	1.1 ± 0.2	0.60 ± 0.11	0.43 ± 0.06
k_2 (min^{-1})	0.044 ± 0.016	0.021 ± 0.001	0.024 ± 0.002
$t_{1/2}^1$ (min)	0.71 ± 0.14	1.2 ± 0.2	1.7 ± 0.2
$t_{1/2}^2$ (min)	33 ± 8	33 ± 2	29 ± 2
AUC(0−60) (% ID min/mL)	6.6 ± 0.6	15 ± 1	63 ± 4
AUC(0−∞) (% ID min/mL)	8.0 ± 0.4	19 ± 1	79 ± 6
Vss (mL/kg)	1297 ± 376	636 ± 7	155 ± 7
Cl (mL/min/kg)	44 ± 3	18 ± 2	4.2 ± 0.3
MRT (min)	30 ± 9	38 ± 5	37 ± 3

[a] Computed from the plasma data in Figure 7. In all cases, the [^{111}In]EGF represents [^{111}In]EGF-PEG^{3400}-biotin.

conjugate (Figure 9). No free EGF was detected, and no significant transfer of the ^{111}In radionuclide to circulating transferrin was detected (peak 4 and 3, respectively, Figure 9). Although there were some transfer of radioactivity to high molecular weight fraction in serum that comigrated with lipoproteins, the principal peak remaining in serum 60 min after intravenous injection was the intact conjugate (peak 2, Figure 9).

In Vivo C6 Glioma Tumor Imaging with [^{111}In]-EGF Conjugate. The quantitative autoradiography (QAR) and tumor imaging using an EGF peptide radiopharmaceutical that is radiolabeled with ^{111}In and administered either with or without the OX26/SA BBB delivery system is shown in Figure 10. The brain images obtained following the intravenous injection of [^{111}In]-EGF-PEG^{3400}-biotin without attachment to the OX26/SA BBB delivery system are shown in the bottom panels (E−H) of Figure 10 and indicate that there is no measurable BBB transport of the peptide radiopharmaceutical into either normal brain or the brain tumor. When the [^{111}In]EGF-PEG^{3400}-biotin is conjugated to OX26/SA and injected intravenously into C6EGFR tumor-bearing rats,

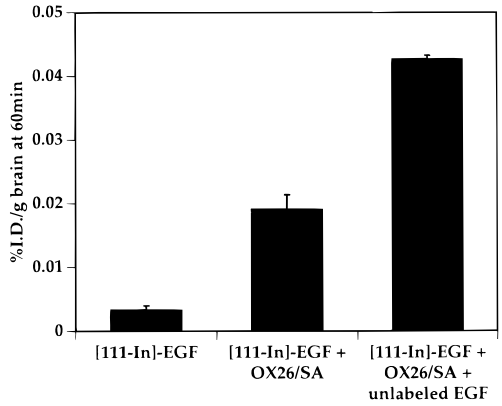


Figure 8. Brain uptake of unconjugated [^{111}In]DTPA-EGF-PEG^{3400}-biotin, [^{111}In]DTPA-EGF-PEG^{3400}-biotin conjugated to the OX26/SA vector, or [^{111}In]DTPA-EGF-PEG^{3400}-biotin conjugated to the OX26/SA vector and co-injected with 16 nmol of unlabeled EGF 60 min after the i.v. injection of 5 μCi/rat. Data are mean ±SE (n = 3 rats).

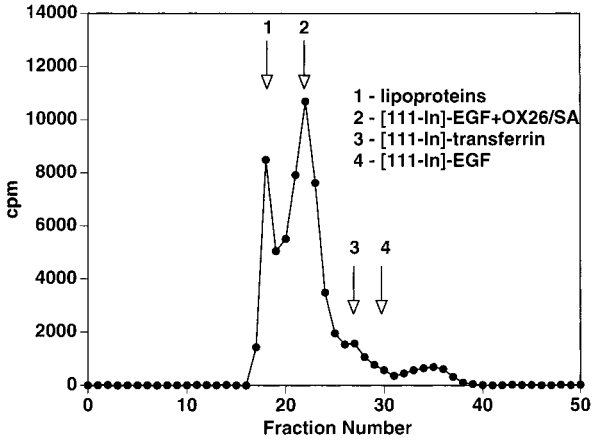


Figure 9. Elution from single Superose 12 HR 10/30 FPLC column of rat serum obtained 60 min after an i.v. injection of 60 μCi of [^{111}In]DTPA-EGF-PEG^{3400}-biotin conjugated to the OX26/SA vector with 16 nmol of unlabeled EGF. Fifty microliters of pooled serum was applied to the FPLC column, followed by the elution in 0.01 M NaH_2PO_4/0.15 M NaCl/0.05% Tween-20/pH 7.4 at a flow rate of 0.5 mL/min for 50 min. Column fractions (0.5 mL) were assayed for [^{111}In]radioactivity. Arrows 1, 2, 3, and 4 indicate elution time of lipoproteins, [^{111}In]DTPA-EGF-PEG^{3400}-biotin conjugated to the OX26/SA, [^{111}In]transferrin, and [^{111}In]DTPA-EGF-PEG^{3400}-biotin, respectively. The result shows that [^{111}In]DTPA-EGF-PEG^{3400}-biotin conjugated to OX26/SA is stable in the circulation at 60 min after i.v. injection in rats.

there is a marked increase in the generalized brain uptake of the peptide radiopharmaceutical owing to transport through the BBB as shown in the top panels (A−D) of Figure 10. The regions of the tumor are clearly demarcated owing to the reduced radionuclide signal emanating from the tumor region. This reduced signal suggested that the C6EGFRp cells, which produce the EGF receptor under the influence of a dexamethasone inducible promoter (*10*), do not express the human EGF receptor in vivo. This was confirmed by immunocytochemistry using two different monoclonal antibodies to the human EGF receptor. Immunocytochemistry of frozen sections of the C6EGFRp tumor showed no visible immunoreactive EGF receptor in the tumor cells in vivo. The positive control cells, U87 human glioma cells, demonstrated high expression of immunoreactive human EGF receptor using either of the monoclonal antibodies (Experimental Procedures).

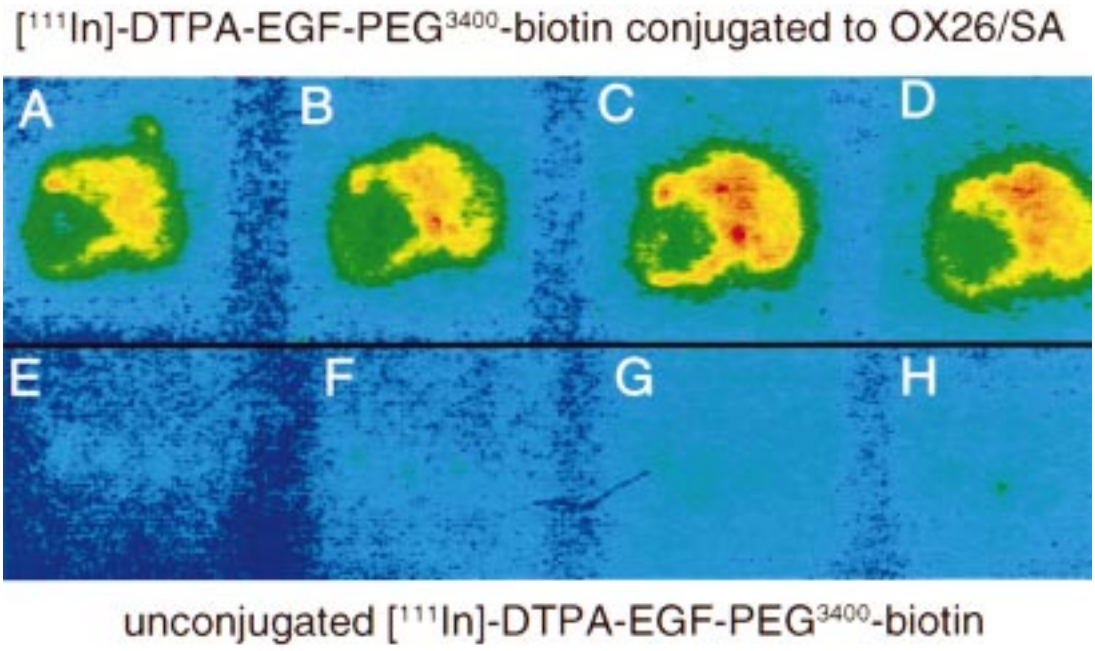


Figure 10. Film autoradiography of brain sections obtained from C6EGFRp tumor-bearing rats injected i.v. with 100 μCi of either [^{111}In]DTPA-EGF-PEG^{3400}-biotin with OX26/SA and 16 nmol of unlabeled EGF (panels A−D) or [^{111}In]DTPA-EGF-PEG^{3400}-biotin alone (panels E−H). The C6EGFRp rat glioma cells (1×10^5 cells/rat) were implanted into the brains of CD Fischer 344 rats and grown for 4 weeks prior to brain distribution experiments. Brains were removed 60 min after the isotope injection. Biomax MS X-ray films were exposed for 4 days at −70 °C with intensifying screen.

DISCUSSION

The results of the present investigation are consistent with the following conclusions. First, formulation of the EGF conjugate with the ^{125}I radionuclide yields a radiopharmaceutical that is metabolically unstable (Figure 1). Second, biotinylation of EGF with NHS-PEG^{3400}-biotin yields a mixture of mono- and dibiotinylated peptide, even at a 1:1 molar ratio of EGF:NHS-PEG^{3400}-biotin, as demonstrated by either SDS−PAGE (Figure 5) or gel filtration FPLC (Figure 4); the EGF construct with a single DTPA residue and a single PEG^{3400}-biotin moiety, such as that depicted in Figure 3, can be purified using two Superose 12HR gel filtration FPLC columns in series (Figure 4). Third, the [^{111}In]EGF-PEG^{3400}-biotin conjugated to OX26/SA binds to both transferrin receptor and EGF receptor in the C6EGFRp cells under the influence of 1 μM dexamethasone, but no specific EGF receptor activity is detected in the cells that are not exposed to dexamethasone (Figure 6). Fourth, the EGF-PEG^{3400}-biotin conjugated to OX26/SA and formulated with the ^{111}In radionuclide shows a high degree of metabolic stability, as low molecular weight ^{111}In-labeled metabolites are not detected in plasma (Figure 9). In contrast, there is a rapid appearance of TCA-soluble low molecular weight ^{125}I metabolites formed in plasma when the ^{125}I radionuclide is used to label the EGF (Figure 1, right panel). Fifth, the [^{111}In]DTPA- EGF-PEG^{3400}-biotin conjugated to OX26/SA is rapidly removed from plasma (Figure 7), and this rapid uptake by peripheral tissues is greatly reduced by co-injection of 16 nmol/rat (100 μg/rat) of unlabeled EGF (Figure 7, Table 1). Sixth, imaging of brain with radiolabeled forms of EGF is not possible when the peptide is not coupled to a BBB drug delivery system (Figure 10, panels E−H), but brain structures and tumors can be imaged with radiolabeled EGF that is conjugated to a BBB drug delivery system using a PEG^{3400} linker (Figure 10, panels A−D).

The plasma AUC and whole body Vss values are comparable for EGF conjugates when either the ^{125}I or the ^{111}In radionuclide is used. For example, the plasma $AUC|_0^\infty$ for [^{125}I]EGF-PEG^{3400}-biotin conjugated to OX26/SA or [^{111}In]DTPA-EGF-PEG^{3400}-biotin conjugated to OX26/SA are 23 ± 2% ID min/mL (data not shown) and 19 ± 1% ID min/mL (Table 1), respectively. When the EGF is conjugated to OX26/SA and co-injected with unlabeled EGF, the plasma $AUC|_0^\infty$ for the ^{125}I and the ^{111}In formulations are 61 ± 8% ID min/mL (data not shown) and 79 ± 6% ID min/mL (Table 1), respectively. However, after uptake by peripheral tissues (e.g., liver and kidney), the ^{125}I radionuclide is rapidly exported to the plasma in the form of low molecular weight TCA soluble metabolites (Figure 1, right panel), but there is no export to plasma of low molecular weight ^{111}In metabolites (Figure 9). These low molecular weight metabolites may include either radiolabeled iodide or amino acids such as iodotyrosine, which are capable of transport through the BBB via carrier-mediated transport and give artifactually high basal uptakes of brain radioactivity (*11*, *19*). Such artifacts are seen in the present study; the basal brain uptake of [^{125}I]EGF-PEG^{3400}-biotin, 0.026 ± 0.001% ID/g (Figure 2), is 10-fold greater than the basal brain uptake of [^{111}In]DTPA-EGF-PEG^{3400}-biotin (Figure 8). The brain uptake of these low molecular weight ^{125}I metabolites would make brain imaging very difficult as it would reduce the signal/noise ratio of the image. Conversely, the brain uptake of radioactivity is negligible when the EGF is administered in the form of the ^{111}In radionuclide, and EGF is not conjugated to a BBB drug delivery system such as OX26/SA (Figure 10, panels E−H). These considerations are further evidence that the measurement of brain uptake of ^{125}I-labeled peptides following peripheral administration is driven principally by the artifactual uptake of low molecular weight metabolites rapidly generated by the degradation of the peptide in noncerebral tissues (*11*).

The synthetic scheme for [^{125}I]EGF-PEG^{3400}-biotin yields a mixture of mono- and dibiotinylated peptide

Table 2. PS Values (μL/min/g)[a]

organ	[^{111}In]EGF	[^{111}In]EGF + OX26/SA	[^{111}In]EGF + OX26/SA + unlabeled EGF
heart	6.3 ± 0.4	2.9 ± 0.7	0.17 ± 0.11
lung	8.9 ± 2.8	11.1 ± 1.9	4.0 ± 0.5
liver	635 ± 33	390 ± 12	74 ± 4
kidney	1006 ± 32	145 ± 13	76 ± 6

[a] Determined at 60 min after intravenous injection. Mean ± S. E. (n = 3 rats). Computed from the plasma data in Figure 7. In all cases, the [^{111}In]EGF represents [^{111}In]EGF-PEG^{3400} biotin.

(Experimental Procedures). Owing to the multivalency of streptavidin binding of biotin, there is a potential for aggregates to form when the ligand is multibiotinylated and bound to OX26/SA. However, in the present studies of the ^{125}I radionuclide formulation, significant aggregates are minimized, as the molar ratio of the [^{125}I]EGF-(PEG^{3400}-biotin)$_2$ and the OX26/SA was approximately 1:1 (Experimental Procedures). Moreover, when the monobiotinylated form of EGF-PEG^{3400}-biotin was purified by two Superose 12HR gel filtration FPLC columns in series (Figure 4) and then radiolabeled with ^{125}I and chloramine T (*9*), there were no significant differences in the plasma radioactivity profiles (unpublished observations).

The conjugation of EGF-PEG^{3400}-biotin to OX26/SA resulted in a redirection of the EGF peptide from kidney to liver (Figure 2, Table 2). The molecular mass of EGF-PEG^{3400}-biotin is approximately 10 000 Da, and the molecular mass of OX26/SA is 200 000 Da. Therefore, following conjugation to OX26/SA, the effective molecular mass of the EGF increases from 10 000 Da to 210 000 Da, and this explains the marked reduction in renal clearance of the EGF conjugate. However, the EGF is still rapidly removed from plasma despite conjugation to OX26/SA (Figure 7). Previous studies have shown that human recombinant EGF is rapidly taken up by the rat EGF receptor in liver in vivo (*17*, *18*). Therefore, we considered that co-injection of unlabeled EGF (100μg/rat) would saturate hepatic uptake of the EGF construct, prolong the circulation time of the imaging agent, and have a beneficial pharmacokinetic effect. This was observed as the plasma AUC$|_0^\infty$ was increased 4-fold from 19 ± 1 to 79 ± 6% ID min/mL following EGF loading (Table 1). The systemic volume of distribution (Vss) was also decreased 4-fold from 637 ± 7 to 157 ± 7 mL/kg following EGF loading (Table 1). The plasma AUC$|_0^\infty$ of [^{111}In]DTPA-EGF-PEG^{3400}-biotin, 8.0 ± 0.4% ID min/mL, is comparable to the plasma AUC for [^{125}I]EGF, 6.8% ID min/mL, which is calculated from the data of Kim et al. (*18*). The principal effect of EGF loading is a 5-fold reduction in the organ clearance by liver, although EGF clearance by heart, lung, and kidney is also decreased by EGF loading (Table 2).

The pharmacokinetic data for [^{111}In]DTPA-EGF-PEG^{3400}-biotin in Tables 1 and 2 allow for comparison with similar data reported previously for [^{125}I]EGF (*17*, *18*). The fact that the plasma clearance for the two formulations of EGF are comparable means that placement of a *single* PEG moiety on a peptide such as EGF does not significantly reduce the rate of plasma clearance of the peptide. Pegylation of proteins is well-known to delay plasma clearance, but this requires the placement of *multiple* PEG moieties on the surface of the protein (*11*).

The EGF peptide radiopharmaceutical depicted in Figure 3 and used for the brain imaging studies shown in Figure 10 embodies three aspects of the formulation that allow for optimization of the brain imaging signal. First, a >200 atom PEG^{3400} linker is placed between the EGF and the biotin to release any steric hindrance caused by binding to streptavidin (*9*). This long flexible arm allows for free binding of the construct to either the EGF receptor or the BBB transferrin receptor. Second, the radionuclide moiety is ^{111}In rather than the ^{125}I used in previous studies (*9*). The use of the ^{111}In radionuclide confers a greater degree of metabolic stability (Figure 9) and a very low basal uptake of the unconjugated peptide (Figure 10). Third, the co-injection of unlabeled EGF inhibits hepatic uptake of the conjugate approximately 5-fold (Table 2), and this optimizes the plasma pharmacokinetics (Table 1, Figure 7) and results in a proportionate increase in brain uptake (Figure 8).

The brain imaging studies in Figure 10 allow for the following conclusions. First, [^{111}In]DTPA-EGF-PEG^{3400}-biotin does not cross either the BBB in normal brain or the blood-tumor barrier (BTB) in the brain tumor (Figure 10, panels E−H). The uptake of the [^{111}In]EGF-PEG^{3400}-biotin in brain is 0.0033 ± 0.0007% ID/g (Figure 8), and this approximates the brain uptake of sucrose (*7*). The failure of EGF to cross the BBB in normal brain is expected based on previous studies (*5*). Although the BTB is more permeable than the normal BBB to small molecules (*20*), the BTB in the C6 glioma is clearly not permeable to the unconjugated EGF peptide radiopharmaceutical, which has a molecular mass of approximately 10 000 Da, as shown in the bottom panels (E−H) of Figure 10. Second, the [^{111}In]DTPA-EGF-PEG^{3400}-biotin does cross the BBB and enter brain following conjugation to OX26/SA. The in vivo QAR studies (Figure 10, panels A− D) show increased brain uptake of the EGF peptide radiopharmaceutical that is attached to the OX26 MAb BBB delivery system. The transcytosis of the OX26 MAb through the BBB has been demonstrated previously at the electron microscopic level with conjugates of OX26 and 5 nm gold (*21*) and at the light microscopic level using autoradiography (*22*). Third, the EGF peptide pharmaceutical conjugated to OX26/SA also crosses the BTB, although the signal in the tumor brain is reduced compared to normal brain (Figure 10, panels A−D). This reduced signal suggested that the human EGF receptor was not expressed by the C6EGFRp cells following implantation in brain and growth as a brain tumor. The absence of EGF receptor in these cells in vivo was confirmed by immunocytochemistry (Results) and is consistent with the tissue culture experiments (Figure 6) showing minimal binding to the EGF receptor in the C6EGFRp cells that were not exposed to 1 μM dexamethasone for 24 h. The expression of the human EGF receptor in the C6EGFRp cells is driven by the dexamethasone-inducible mouse mammary tumor virus long terminal repeat (MMTV-LTR) promoter (*10*). We administered 1 mg/rat of dexamethasone 24 h prior to sacrifice but still could not detect any immunoreactive EGF receptor in these brain tumors in vivo (unpublished observations). Another reason the signal in the brain tumor region is decreased compared to normal brain most likely arises from the decreased vascular density in the brain tumor compared to normal brain. In previous studies with peptide radiopharmaceuticals that were enabled to undergo transport through the BBB by attachment to BBB drug delivery systems, there was a marked increase in the image in gray matter versus white matter in the primate brain in vivo (*8*). This arose from the 3-fold greater vascular density in gray matter versus white matter and, accordingly, the 3-fold greater vascular density of BBB receptor being targeted by the delivery system. The vascular density in the C6 glioma

is probably comparable to the vascular density in white matter, since the rate of cerebral blood flow (CBF) in the C6 glioma approximates white matter CBF, which is only 44% of the CBF in gray matter (*23*).

The present studies show that the C6EGFRp cells express undetectable levels of human EGF receptor when the cells form experimental brain tumors in vivo based on both the in vivo imaging (Figure 10) and the EGFR immunocytochemistry (Results). Experimental tumors such as the U87 human glioblastoma multiforme, which grows as experimental brain tumors in immuno-compromised rodents (*16*), may prove to be a more suitable model for imaging the human EGF receptor in experimental brain tumors in vivo. Factors that will affect the tumor imaging using EGF peptide radiopharmaceuticals that are enabled to cross the BTB include (i) the vascular density and local concentration of transferrin receptor at the BTB and (ii) the local expression of the EGF receptor in the tumor cells and the rate of endocytosis of the EGF into the tumor cells. These receptor systems may be investigated in future imaging of brain tumors using peptide radiopharmaceuticals such as that depicted in Figure 3. The present studies demonstrate that peptide radiopharmaceuticals such as EGF may undergo special molecular formulation to enable both metabolic stability of the radionuclide and transport of the peptide radiopharmaceutical through the BBB in vivo.

ACKNOWLEDGMENT

Margarita Tayag provided expert technical assistance and the manuscript was skillfully prepared by David Kim and Daniel Jeong. This work was supported by a grant from the U.S. Department of Energy. Dr. Kym Faull performed the MALDI analyses. Dr. Dafang Wu asisted with the brain tumor implants.

LITERATURE CITED

(1) Libermann, T. A., Nusbaum, H. R., Razon, N., Kris, R., Lax, I., Soreq, H., Whittle, N., Waterfield, M. D., Ullrich, A., and Schlessinger, J. (1984) Amplification, enhanced expression and possible rearrangement of EGR receptor gene in primary human brain tumours of glial origin. *Nature 313*, 144−147.

(2) Wong, A. J., Bigner, S. H., Bigner, D. D., Kinzler, K. W., Hamilton, S. R., and Vogelstein, B. (1987) Increased expression of the epidermal growth factor receptor gene in malignant gliomas is invariably associated with gene amplification. *Proc. Natl. Acad. Sci. U.S.A. 84*, 6899−6903.

(3) Torp, S. H., Helseth, E., Dalen, A., and Unsgaard, G. (1991) Epidermal growth factor receptor expression in human gliomas. *Cancer Immunol. Immunother. 33*, 61−64.

(4) Capala, J., Barth, R. F., Bailey, M. Q., Fenstermaker, R. A., Marek, M. J., and Rhodes, B. A. (1997) Radiolabeling of epidermal growth factor with 99m-Tc and in vivo localization following intracerebral injection into normal and glioma-bearing rats. *Bioconjugate Chem. 8*, 289−295.

(5) Nave, K. A., Probstmeier, R., and Schachner, M. (1985) Epidermal growth factor does not cross the blood-brain barrier. *Cell Tissue Res. 241*, 453−457.

(6) Blasberg, R. G., and Groothuis, D. R. (1986) Chemotherapy of brain tumors: physiological and pharmacokinetic considerations. *Sem. Oncol. 13*, 70−82.

(7) Pardridge, W. M. (1997) Drug delivery to the brain. *J. Cereb. Blood Flow Metab. 17*, 713−731.

(8) Wu, D., Yang, J., and Pardridge, W. M. (1997) Drug targeting of a peptide radiopharmaceutical through the primate blood-brain barrier in vivo with a monoclonal antibody to the human insulin receptor. *J. Clin. Invest. 100*, 1804−1812.

(9) Deguchi, Y., Kurihara, A., and Pardridge, W. M. (1999) Retention of biologic activity of human epidermal growth factor following conjugation to a blood-brain barrier drug delivery vector via extended poly(ethylene glycol) linker. *Bioconjugate Chem. 10*, 32−37.

(10) Fenstermaker, R. A., Capala, J., Barth, R. F., Hujer, A., Kung, H.-J., and Kaetzel, D. M. (1995) The effect of epidermal growth factor receptor (EGFR) expression on in vivo growth of rat C6 glioma cells. *Leukemia 9*, S106−S112.

(11) Sakane, T., and Pardridge, W. M. (1997) Carboxy-directed pegylation of brain-derived neurotropic factor markedly reduces systemic clearance with minimal loss of biologic activity. *Pharm. Res. 14*, 1085−1091.

(12) Wu, D., and Pardridge, W. M. (1996) Central nervous system pharmacologic effect in conscious rats after intravenous injection of a biotinylated vasoactive intestinal peptide analogue coupled to a blood-brain barrier drug delivery system. *J. Pharmacol. Exp. Ther. 279*, 77−83.

(13) Pardridge, W. M., Wu, D., and Sakane, T. (1998) Combined use of carboxyl-directed protein pegylation and vector-mediated blood-brain barrier drug delivery system optimizes brain uptake of brain-derived neurotrophic factor following intravenous administration. *Pharm. Res. 15*, 576−582.

(14) Kang, Y.-S., and Pardridge, W. M. (1994) Use of neutral avidin improves pharmacokinetics and brain delivery of biotin bound to an avidin-monoclonal antibody conjugate. *J. Pharmacol. Exp. Ther. 269*, 344−350.

(15) Gibaldi, M., and Perrier, D. (1982) *Pharmacokinetics*, Marcel Dekker, Inc., New York.

(16) Huang, H.-J., Nagane, M., Klingbeil, C. K., Lin, H., Nishikawa, R., Ji, X.-D., Huang, C.-M., Gill, G. N., Wiley, H. S., and Cavenee, W. K. (1997) The enhanced tumorigenic activity of a mutant epidermal growth factor receptor common in human cancers is mediated by threshold levels of constitutive tyrosine phosphorylation and unattenuated signaling. *J. Biol. Chem. 272*, 2927−2935.

(17) Kim, D. C., Sugiyama, Y., Fuwa, T., Sakamoto, S., Iga, T., and Hanano, M. (1989) Kinetic analysis of the elimination process of human epidermal growth factor (hEGF) in rats. *Biochem. Pharmacol. 38*, 241−249.

(18) Kim, D. C., Hanano, M., Kanai, Y., Ohnuma, N., and Sugiyama, Y. (1992) Localization of binding sites for epidermal growth factor (EGF) in rat kidney: evidence for the existence of low affinity EGF binding sites on the brush border membrane. *Pharm. Res. 9*, 1394−1401.

(19) Pardridge, W. M. (1981) Enkephalin and blood-brain barrier: studies of binding and degradation in isolated brain microvessels. *Endocrinology 109*, 1138−1143.

(20) Sugita, M., and Black, K. L. (1998) Cyclic GMP-specific Phosphodiesterase Inhibition and Intracarotid Bradykinin Infusion Enhances Permeability into Brain Tumors. *Cancer Res. 58*, 914−920.

(21) Bickel, U., Kang, Y.-S., Yoshikawa, T., and Pardridge, W. M. (1994) In vivo demonstration of subcellular localization of anti-transferrin receptor monoclonal antibody-colloidal gold conjugate within brain capillary endothelium. *J. Histochem. Cytochem. 42*, 1493−1497.

(22) Skarlatos, S., Yoshikawa, T., and Pardridge, W. M. (1995) Transport of [^{125}I]-transferrin through the rat blood-brain barrier in vivo. *Brain Res. 683*, 164−171.

(23) Hiesiger, E. M., Voorhies, R. M., Basler, G. A., Lipschutz, L. E., Posner, J. B., and Shapiro, W. R. (1986) Opening the blood-brain and blood-tumor barriers in experimental rat brain tumors: the effect of intracarotid hyperosmolar mannitol on capillary permeability and blood flow. *Ann. Neurol. 19*, 50−59.

BC980123X

Proximity of a Tat Peptide to the HIV-1 TAR RNA Loop Region Determined by Site-Specific Photo-Cross-Linking

Zhuying Wang, Ikramul Huq, and Tariq M. Rana*

Department of Pharmacology, Robert Wood Johnson Medical School-UMDNJ, and Molecular Biosciences Graduate Program at Rutgers University, 675 Hoes Lane, Piscataway, New Jersey 08854.
Received December 3, 1998; Revised Manuscript Received March 8, 1999

Transcriptional regulation in human immunodeficiency virus type 1 (HIV-1) requires specific interactions of Tat protein with the trans-activation responsive region (TAR) RNA, a 59-base stem-loop structure located at the 5′-ends of all HIV-1 mRNAs. We have used a site-specific cross-linking method based on 4-thio-uracil (4-thioU) photochemistry to determine the interactions of a Tat peptide, Tat(38−72), with the loop region of TAR RNA under physiological conditions. A TAR RNA construct with a single 4-thioU residue at positions U31 in the loop sequence was synthesized by chemical methods. Upon UV irradiation, 4-thioU at U31 formed a covalent cross-link with the Tat peptide. We did not observe any RNA−RNA cross-link formation. Competition experiments revealed that a specific RNA−protein complex formation was necessary for the RNA−protein cross-linking reaction. Our results demonstrate that, during RNA−protein recognition, the Tat peptide is located in close proximity to O^4 of U31 in the TAR RNA loop sequence.

INTRODUCTION

The human immunodeficiency virus type 1 (HIV-1)[1] encodes a transcriptional transactivator protein called Tat, which is expressed early in the viral life cycle and is absolutely required for viral replication and progression of disease (*1*−*3*). In the absence of Tat, most of the viral transcripts terminate prematurely producing short RNA molecules ranging in size from 60 to 80 nucleotides. The Tat protein is a small, cysteine-rich nuclear protein containing 86 amino acids and an arginine-rich RNA-binding region (amino acids 49−57) located in the carboxy-terminal half of the molecule (*1*, *4*). HIV-1 Tat protein acts by binding to the TAR (trans-activation responsive) RNA element, a 59-base stem-loop structure located at the 5′-end of all nascent HIV-1 transcripts (*5*). RNA−protein interaction between TAR and Tat converts RNA polymerase II into its processive form and causes a substantial increase in the production of full-length viral transcripts (*6*−*13*).

TAR RNA was originally localized to nucleotides +1 to +80 within the viral long terminal repeat (LTR) (*14*). Subsequent deletion studies have established that the region from +19 to +42 incorporates the minimal domain which is both necessary and sufficient for Tat responsiveness in vivo (*15*−*17*). TAR RNA contains a six-nucleotide loop and a three-nucleotide pyrimidine bulge which separates two helical stem regions (*5*, *14*, *15*, *18*). The trinucleotide bulge is essential for high affinity and specific binding of the Tat protein (*19*, *20*). Tat protein binds TAR RNA in vitro with high affinity. Due to difficulties in Tat purification, small Tat peptides that specifically bind TAR RNA with high affinity have been used in many Tat−TAR studies (*21*−*27*). In our Tat−TAR photo-cross-linking studies, we used ADP-1, a Tat fragment (37−72), which binds TAR RNA with high specificity and includes the basic and part of the core regions of Tat (*24*). To avoid oxidation problems, we deleted the N-terminal cysteine residue from the ADP-1 sequence (*26*−*28*).

RNA molecules can fold into extensive structures containing regions of double-stranded duplex, hairpins, internal loops, bulged bases and pseudoknotted structures (*29*, *30*). Due to the complexity of RNA structure, the rules governing sequence-specific RNA−protein recognition are not well understood. RNA−protein interactions are vital for many regulatory processes, especially gene regulation where proteins specifically interact with binding sites found within RNA transcripts. Understanding the principles of Tat−TAR interactions is a crucial step for drug design. Although high-resolution NMR information is limited to the TAR RNA component, a structure of the RNA−protein complex is still missing. Therefore, new methods are needed to determine the topology of RNA−protein complexes under physiological conditions. Recently, we have applied photo-cross-linking and affinity cleaving methods to probe RNA folding and RNA−protein interactions under physiological conditions (*26*−*28*, *31*−*34*).

Chemical synthesis of long oligoribonucleotides containing modified nucleosides, such as 29-bases TAR RNA, is still not very efficient. To circumvent this problem, two short oligoribonucleotides were synthesized and annealed together to form a duplex RNA that contained the trinucleotide bulge to create a structure similar to the Tat binding site in TAR RNA (*35*−*37*). Chemically synthesized duplex TAR RNAs without loop residues have been used to study the role of various functional groups in Tat recognition (*35*−*37*). Recently, we and others have performed RNA−protein cross-linking studies on synthetic TAR RNA duplex structures containing Tat-binding bulge sequences (*26*, *38*). Here, we synthe-

* To whom correspondence should be addressed. Phone: (732) 235-4082. Fax: (732) 235-3235. E-mail: rana@umdnj.edu.

[1] HIV-1, Human immunodeficiency virus type 1; TAR, trans-activation response element; EDTA, ethylenediaminetetraacetic acid; 4-thioU, 4-thiouracil; MALDI-TOF MS, matrix-assisted laser desorption ionization/time-of-flight mass spectrometry.

10.1021/bc980145j CCC: $18.00 © 1999 American Chemical Society
Published on Web 05/17/1999

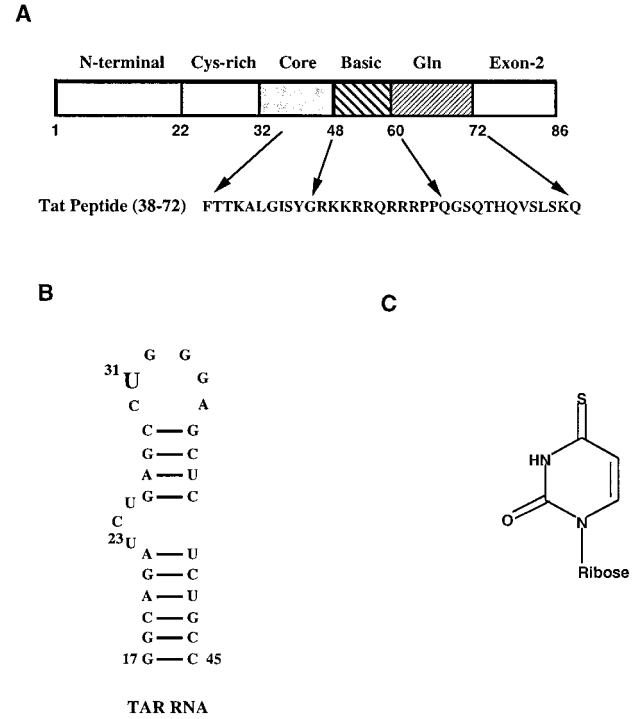


Figure 1. (A) Regions of the HIV-1 Tat protein and sequence of the Tat(38−72) peptide. (B) Secondary structure of TAR RNA used in this study. TAR RNA spans the minimal sequences that are required for Tat responsiveness in vivo (*15*) and for in vitro binding of Tat-derived peptides (*43*). Wild-type TAR contains two non-wild-type base pairs to increase transcription by T7 RNA polymerase. Site of 4-thioU incorporation, U31, is highlighted in the TAR RNA. Numbering of nucleotides in the RNA corrsponds to their positions in wild-type TAR RNA. Incorporation of 4-thioU at position 31 was accomplished by chemical synthesis of RNA (*31, 34*). (C) Structure of 4-thiouridine.

sized a TAR RNA construct (Figure 1) with a single 4-thiouridine (4-thioU) residue at position 31 in the loop sequence. 4-thioU is a very useful photoactivatable probe which has been widely used to study RNA structure (for a review, see ref *39*). This is the first example of chemical synthesis of functional TAR RNA containing loop-residues and a photoactivatible nucleoside. Upon UV irradiation, this 4-thioU labeled RNA formed a covalent cross-link with Tat(38−72) peptide. No RNA−RNA cross-link formation was observed. Competition experiments revealed that a specific RNA−protein complex formation was necessary for the RNA−protein cross-linking reaction. Our results indicate that, during RNA−protein recognition, the Tat peptide is located in close proximity to O^4 of U31 in the TAR RNA loop sequence.

MATERIALS AND METHODS

Buffers. All buffer pH values refer to measurements at room temperature. TK buffer: 50 mM Tris-HCI (pH 7.4), 20 mM KCI, and 0.1% Triton X-100. Transcription buffer: 40 mM Tris-HCI (pH 8.1), 1 mM spermidine, 0.01% Triton X-100, and 5 mM DTT. TBE buffer: 45 mM Tris-borate, pH, 8.0, and 1 mM EDTA. Sample loading buffer: 9 M urea, 1 mM EDTA, and 0.1% bromophenol blue in 1× TBE buffer. Binding buffer: 25 mM Tris-HCI (pH 7.5), 100 mM NaCI, 1 mM $MgCI_2$, and 0.1% Triton X-100. Hydrolysis buffer: 50 mM $Na_2CO_3/NaHCO_3$, pH 9.2. Elution buffer: 1× TBE and 10% sodium acetate (3M), pH 5.5.

RNA Synthesis. RNAs were synthesized by chemical and enzymatic methods. Chemical syntheses were performed on ABI synthesizer model 392 using standard protocols. All the monomers of (2-cyanoethyl)phosphoramidites were obtained from Glen Research (Sterling, VA). Site-specific incorporation of 4-thioU at position 31 in TAR RNA was carried out by chemical synthesis of RNA using triazoloU phosphoramidite as a precursor of 4-thioU (*31*). Synthesis of RNA, deprotection, characterization, and purification were performed as described earlier (*31, 34*). Briefly, incorporation of 4-thioU in the TAR RNA sequence was confirmed by enzymatic digestion. Enzymatic digestion was carried out by incubating 0.2 A_{260} unit of purified oligonucleotide at 37 °C overnight with 6 μL (12 μg) of snake venom phosphodiesterase and 2 μL (2 units) of alkaline phosphatase in a total volume of 78.2 μL of 32 mM Tris, pH 7.5, and 15 mM $MgCl_2$. Nucleosides were recovered by adding 10 μL of 3 M NaOAc, pH 5.2, and 234 μL of 95% ethanol, mixing and chilling to −80 °C for 30 min. After centrifugation at 13 000 rpm for 20 min at 4 °C, the supernatant was taken and dried in Speedvac (Savant) and redissolved in 200 μL of water for HPLC analysis. HPLC analysis of nucleosides was performed as described previously (*31, 33*).

All other RNAs were prepared by in vitro transcription (*40*). The template strand of DNA was annealed to an equimolar amount of top strand DNA, and transcriptions were carried out in transcription buffer and 4.0 mM NTPs at 37 °C for 2−4 h (*41*). For reactions (20 μL) containing 8.0 pmol of template DNA, 40−60 units of T7 polymerase (Promega) was used. Transcription reactions were stopped by adding an equal volume of sample loading buffer. RNA was purified on 20% acrylamide 8 M-urea denaturing gels (*41*). RNAs were stored in DEPC water at −20 °C.

RNAs were 5′-dephosphorylated by incubation with calf intestinal alkaline phophatase (Promega) for 1 h at 37 °C in 50 mM Tris-Cl, pH 9.0, 1 mM $MgCl_2$, 0.1 mM $ZnCl_2$, and 1 mM spermidine. The RNAs were purified by multiple extractions with Tris-saturated phenol and one extraction with 24:1 chloroform:isoamyl alcohol followed by ethanol precipitation. The RNAs were 5′-end-labeled with 0.5 μM [γ-^{32}P]ATP (6000 Ci/mmol) (ICN) per 100 pmol of RNA by incubating with 16 units of T4 polynucleotide kinase (New England Biolabs) in 70 mM Tris-HCl, pH 7.5, 10 mM $MgCl_2$, and 5 mM DTT. RNAs were gel purified on a denaturing gel, visualized by autoradiography, and recovered from gels as described earlier (*41*).

Peptide Synthesis. All Fmoc-amino acids, piperidine, 4-(dimethylamino)pyridine, dichloromethane, *N*,*N*-dimethylforamide, 1-hydroxybenzotriazole (HOBT), 2-(1H-benzotriazo-1-yl)-1,1,3,3-tetramethyluronium hexafluorophosphate (HBTU), diisopropylethylamine, and HMP-linked polystyrene resin were obtained from Applied Biosystems Division, Perkin-Elmer. Trifluoroacetic acid, 1,2-ethanedithiol, phenol, and thioanisol were from Sigma. Tat-derived peptide (from amino acids 38 to 72) was synthesized on an Applied Biosystems 431A peptide synthesizer using standard FastMoc protocols. Cleavage and deprotection of the peptide was carried out in 2 mL of Reagent K for 6 h at room temperature. Reagent K contained 1.75 mL of TFA, 100 μL of thioanisole, 100μL of water, and 50 μL of ethanedithiol (*42*). After cleavage from the resin, peptide was purified by HPLC on a Zorbax 300 SB-C_8 column. The mass of fully deprotected and purified peptides were confirmed by FAB mass spectrometry; calculated mass for Tat(38−72) $C_{175}H_{298}N_{64}O_{43}$ = 4082.7, found = 4083.7 (M + H).

Gel Retardation Assays. RNA−protein binding reactions (20 μL) contained 0.05 μM wild-type, modified TAR, or wild-type TAR RNA and 0−1 μM Tat(38−72) in TK

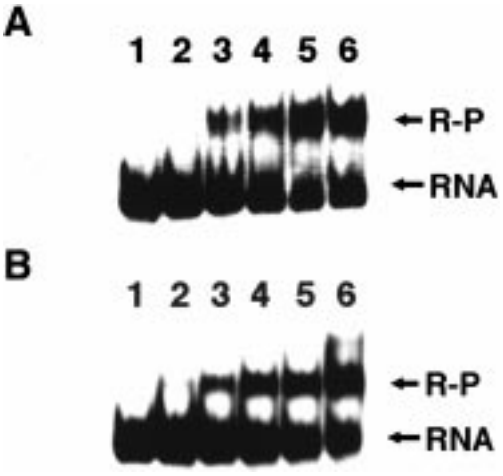


Figure 2. Binding of Tat(38−72) peptide to TAR RNA (A) or 4-thioU-31-modified TAR RNA (B). Binding reactions contained 0.05 μM of 5′-^{32}P-end-labeled RNA and increasing concentration of Tat peptide. Lane 1 was a control lane without the peptide. Complex formation was performed in the TK buffer and incubation at room temperature for 1 h. Complexes were separated from unbound RNA by electrophoresis in nondenaturing 8% polyacrylamide gels containing 0.1% Triton X-100. Gels were run in cold room at 300 V for 2 h. The relative amounts of free and bound RNA were determined by phosphor imaging. RNA−peptide complexes are shown as R-P.

buffer. After 15 min of incubation at room temperature, the complexes were resolved on a nondenaturing 8% acrylamide gels and quantified as described earlier (*26*).

Site-Specific Photo-Cross-Linking Reactions. Typically, 5 pmol of TAR RNA (5′-end labeled with ^{32}P) was mixed with 6 pmol of Tat (38−72) in TK buffer, incubated at room temperature for 10 min, and UV irradiated (360 nm) for 5 min on ice in a Rayonet Photochemical Reactor (RPR-100). After irradiation, 2 μL of Yeast tRNA (20 μg/μL) and 12 μL of sample loading buffer were added to each sample and electrophoresed on 8 M urea-20% acrylamide gels. Efficiencies of cross-linking were determined by a Phosphor Image analysis (Molecular Dynamics).

RNA Sequencing. Alkaline hydrolysis of RNAs was carried out in hydrolysis buffer for 8−12 min at 85 °C. RNAs were incubated with 0.1 units RNAse from *Bacillus cereus* (Pharmacia) per pmol of RNA for 4 min at 55 °C in 16 mM sodium citrate, pH 5.0, 0.8 mM EDTA, 0.5 mg/mL yeast tRNA (Gibco-BRL). This enzyme yields U and C specific cleavage of RNA. Sequencing products were resolved on 20% denaturing gels and visualized by phosphor image analysis.

RESULTS AND DISCUSSION

Tat Binding To Modified TAR RNA. To characterize and evaluate the Tat binding capabilities of 4-thioU containing TAR RNA, we determined the dissociation constants of modified TAR−Tat complexes. Equilibrium dissociation constants of the Tat:TAR complexes were measured using direct electrophoretic mobility assays (*24*, *27*, *33*). A Tat fragment, Tat(38−72), was used in these measurements. A typical gel of these experiments is shown in Figure 2. These results showed that Tat(38−72) binds the 4-thioU-31 modified TAR RNA with a K_D of 0.22 ± 0.05 μM. To compare the Tat-binding affinities of the modified RNA to wild-type RNA, we synthesized an unmodified RNA (Figure 1). Dissociation constants of the unmodified TAR:Tat complexes were determined under the same conditions used for 4-thioU31-TAR:Tat(38−72) complexes. These experiments showed that

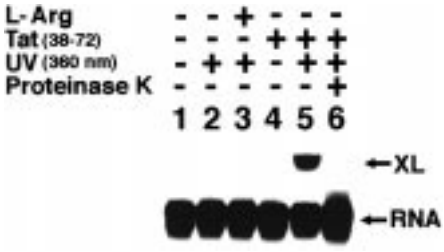


Figure 3. Cross-linking reactions of TAR RNA labeled with 4-thioU at position 31. TAR RNA was labeled with ^{32}P at the 5′-end and UV irradiated at 360 nm. Cross-linked products were resolved on a 20% acrylamide-8 M urea gel and visualized by autoradiography. Lane 1: RNA without irradiation. Lane 2: RNA with irradiation. Lane 3: RNA irradiated with 1 mM L-argininamide. Lane 4: RNA with Tat(38−72) and no irradiation. Lane 5: RNA irradiated in the presence of Tat(38−72). Lane 6: RNA irradiated in the presence of Tat(38−72) and the sample was treated with Proteinase K for 15 min at 55 °C. RNA−protein cross-links are indicated as XL.

the unmodified TAR duplex binds Tat with a K_D of 0.13 ± 0.08 μM (Figure 2). A relative dissociation constant (K_{rel}) can be determined by measuring the ratios of the modified TAR to wild-type TAR dissociation constants (K_D) for Tat(38−72). Our results demonstrate that the calculated value for K_{rel} was 1.7. These results indicate that incorporation of 4-thioU in the TAR loop sequence did not significantly alter the structure of the RNA, thus preserving the Tat-binding affinities of the RNA.

TAR RNA Labeled with 4-thioU at U31 Forms Cross-Link with a Tat Fragment. Specific RNA−protein complexes were formed by adding the approximately equimolar amounts of TAR RNA and the Tat peptide. Under these conditions, electrophoretic mobility-shift assays revealed only one slow-migrating RNA−peptide complex, indicating the absence of other nonspecific RNA−peptide complex formation (*24*, *32*). TAR RNA labeled at its 5′-end with ^{32}P was incubated with the Tat peptide for 10 min in TK buffer and UV irradiated with 360 nm light (see Materials and Methods). Products of the photoreaction were analyzed by denaturing 8 M urea PAGE (Figure 3). Irradiation of the RNA−peptide complex yields band with electrophoretic mobility less than that of RNA (Figure 3, lane 5). Both the peptide and UV irradiation are required for the formation of this cross-linked RNA−protein complex because this cross-linked product is observed only when RNA is irradiated in the presence of Tat peptide (lane 5), and no cross-link is formed with peptide in dark without UV irradiation (lane 4). The formal possibility that the new mobility is due to an alternative RNA−RNA cross-link was ruled out by perfroming proteinase K digestion of the RNA−protein cross-link. RNA−protein cross-link products are degraded by proteinase K enzyme while RNA−RNA cross-link species are stable under these conditions (*26*, *28*). Proteinase K digestion of the RNA−protein cross-link resulted in a loss of RNA−protein cross-link and a gain in free RNA as observed by band intensities on the gel (Figure 3, lane 6). The products of irradiation were also analyzed on a denaturing SDS−15% polyacrylamide gel. Again, a photoproduct with electrophoretic mobility less than that of TAR RNA was observed, which was dependent on the presence of RNA and peptide (data not shown). The photoproduct yields were ∼37% as determined by a Phosphor Image analysis. Since the cross-linked RNA−peptide complex is stable to alkaline pH (9.2), high temperature (85 °C), and denaturing conditions (8 M urea, 2% SDS), we conclude that a covalent bond is

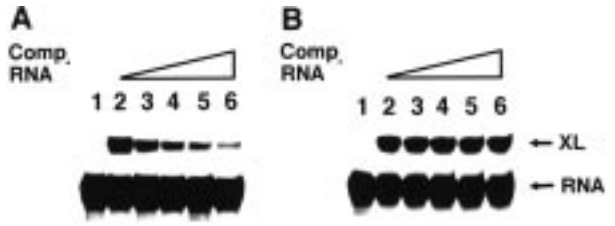


Figure 4. Specificity of the Tat−TAR cross-linking reaction determined by competition assays. RNA−protein complexes were formed between 0.25 μM ^{32}P-5′-end labeled TAR RNA modified with 4-thioU at position 31 and 0.5 μM of Tat(38−72) in the presence of unlabeled wild-type TAR RNA (A) or bulge mutant TAR RNA (B). Concentrations of the competitor RNA in lanes 2, 3, 4, 5, and 6 were 0, 0.5, 0.75, 1.0, and 1.25 μM, respectively. Lane 1 was a control RNA−peptide complex without UV irradiation. RNA−protein cross-link is shown as XL.

formed between TAR RNA and the peptide during the cross-linking reaction.

Specificity of the RNA−Protein Cross-Link Formation. Specificity of the cross-linking reaction was established by competition experiments (*28*). Cross-linking reactions were performed in a 10 μL volume containing 0.25 μM of 5′-^{32}P-labeled 4-thio-U31 modified TAR RNA, 0.5 μM Tat peptide, 25 mM Tris.HCl (pH 7.4), 100 mM NaCl, and up to 1.25 μM unlabeled competitor RNA. Cross-linked products were separated by 8 M urea-20% polyacrylamide gels and visualized by phosphor image analysis. Figure 4 shows that cross-linking was inhibited by the addition of unlabeled wild-type TAR RNA and not by a bulge mutant TAR RNA. Therefore, we conclude that formation of a specific RNA−protein complex between 4-thioU modified TAR RNA and Tat is necessary for photo-cross-linking.

4-Thio-Uridine 31 in TAR RNA Cross-Links to Tat(38−72). Mapping of the cross-link site on TAR RNA to single nucleotide resolution was carried out by partial RNAse digestion and alkaline hydrolysis of the gel-purified RNA−protein cross-link. Fragment sizes are determined by comparison with RNA oligonucleotides of defined sequence and length generated by digesting RNA with RNases T_1 and *B. cereus*. Alkaline hydrolysis of RNA and cross-linked RNA−peptide complex generates a ladder of RNA-degradation products. Bands of cross-linked RNA−peptide complexes migrate slower than corresponding free RNA (lane 3 in Figure 5). Base hydrolysis of the 5′-end-labeled cross-linked complex (lane 3 in Figure 5) results in an RNA ladder in which all fragments up to C30 are resolved. There is an obvious gap in the hydrolysis ladder after C30, indicating that the fragments above C30 from the 5′-end are linked to the Tat peptide (Figure 5, lane 3) that is not seen with the un-cross-linked RNA (lane 2). On the basis of these results, we conclude that 4-thio-U31 of TAR RNA is indeed the site in RNA sequence at which cross-linking occurs.

The basic regions of tat proteins are directly involved in RNA binding. Short basic peptide mimics of this region bind TAR RNA in the bulge region (*21, 23−25, 43*). A number of studies determined the sequence requirements within the basic region of Tat for RNA binding. In vivo experiments using full-length Tat and in vitro studies with synthetic peptides indicate that conservation of overall positive charge including several arginines is essential for TAR RNA recognition. For example, Tat−TAR interactions are not affected by interchanging the basic region sequences of Tat and Rev (*44*). Amino acid substitutions that recreate the consensus sequence of the

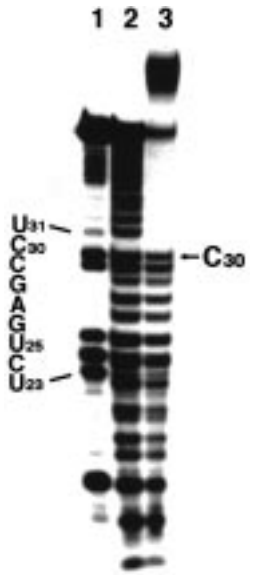


Figure 5. Mapping of cross-linked base in the RNA−protein cross-links by alkaline hydrolysis. Analysis of the RNA−protein cross-link containing 5′-end labeled TAR RNA: *B. cereus* ladder of TAR RNA (lane 1); hydrolysis ladder of TAR RNA (lane 2); hydrolysis ladder of the RNA−peptide cross-link (lane 3). Sequence of the TAR RNA from U23 to U31 is labeled, and a gap in the sequence is obvious after C30 residue indicating that indeed U31 is the cross-linked base.

RNA-binding region (R/KXXRRXRR, where R is arginine, K is lysine, and X is any amino acid) reconstitute a functional Tat protein. These results are in agreement with in vitro peptide studies showing that high-affinity TAR RNA binding requires three of four arginines within the RRXRR stretch, although any one arginine can be substituted, suggesting some redundancy (25). These studies raised the possibility that several amino acids from the RNA-binding region of Tat could be cross-linked to 4-thioU31 in TAR RNA. Although a discrete band for the RNA−protein cross-link was observed in our experiments (Figures 3−5), it is possible that more than one cross-link product is present in the band. To determine the homogeneity of the cross-link products, we analyzed the products by reversed-phase HPLC. Our chromatography data showed that the RNA−protein cross-link products eluted in a single sharp peak from the HPLC column under various solvent systems and gradients (data not shown). These results indicate that homogeneous RNA−protein cross-link products were formed during photo-cross-linking reactions.

Models for Tat−TAR Recognition. Tat protein recognizes the trinucleotide bulge in TAR RNA. Key elements required for TAR recognition by Tat have been defined by extensive mutagenesis, chemical probing, and peptide binding studies (*21−24, 36, 37, 43, 45−48*). Tat interacts with U23, and two other bulge residues, C24 and U25, act as spacers because they can be replaced by other nucleotides or linkers (*24, 35*). Previous studies suggest that Tat protein contacts TAR RNA in a widened major groove (*21, 26, 41*). A rhodium complex, Rh(phen)$_2$phi^{3+}, was used to probe the effect of bulge bases on the major groove width in TAR RNA (*41*). This study showed two important results for Tat−TAR recognition: (i) there is a correlation between major groove opening and Tat binding. At least a two base bulge is required for major groove widening and other conformational changes to facilitate Tat binding. This cannot be accomplished by a single-base bulge. (ii) A Tat peptide occupies the major groove of TAR RNA and abolishes

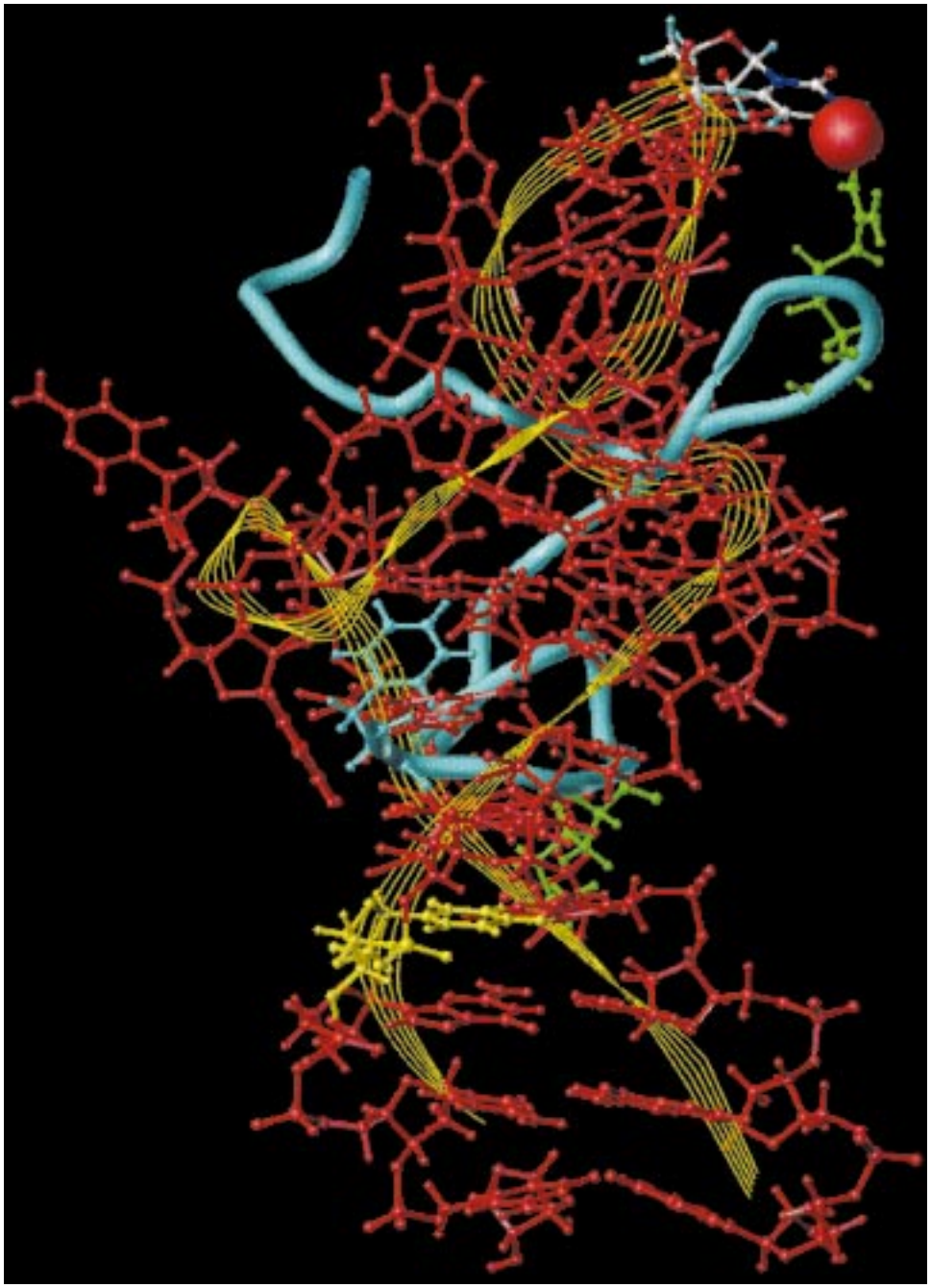


Figure 6. Proposed model for Tat peptide-TAR interactions showing protein orientation and the proximity of U31 to the peptide in the RNA−protein complex. Ribbon structure of TAR RNA is shown in yellow lines and nucleotides in red (*52*). Ribbon structure of the Tat peptide (ribbon/tube) and the amino terminal Phe38 are shown in cyan color. Ribbon structure of the Tat peptide is drawn from Tat protein structure (*53*). Orientation of the Tat peptide is based on previous photo-cross-linking results indicating that Lys41 and Arg57 are close to U42 and U31, respectively (*28, 32*). Lys41 and Arg57 side chains are shown in green. U42 is shown in yellow and U31 in atom-by-type colors. It is evident that O^4 (red spacefill sphere) of U31 is close to Arg57 side chain of the Tat peptide. Structures of RNA and protein were visualized using Insight II software on an IRIS workstation.

access of the rhodium complex (*41*). In addition to the trinucleotide bulge region, two base pairs above and below the bulge also contribute significantly to Tat binding (*21*, *24*). Phosphate contacts below the bulge at positions 22, 23, and 40 are critical for Tat interactions (*23*, *24*, *36*). In a chemical cross-linking study, Gait and co-workers showed that a TAR duplex containing a trisubstituted pyrophosphate replacing the phosphate at 38−39 reacted specifically with Lys51 in the basic region of Tat(37−72) peptide (*38*). We carried out 4-thiouracil-mediated photo-cross-linking studies on Tat−TAR complex and showed that Tat interacts with U23, U38, and U40 in the major groove of TAR RNA (*26*). Our recent cross-linking experiments using 6-thioG-modified TAR RNA demonstrated that Tat interaction with G21 and G26 also takes place in the major groove of RNA (*49*). Taken together, these studies establish that Tat binds TAR RNA at the trinucleotide bulge region and interacts with two base pairs above and below the bulge in the major groove of RNA.

The orientation of a Tat peptide in the Tat−TAR complex was determined by a new method based on psoralen photochemistry (*32*). A psoralen was chemically attached at the amino terminus of a Tat(42−72) peptide. Upon near-ultraviolet irradiation (360 nm), this synthetic psoralen-peptide cross-linked to a single site in TAR RNA

sequence. The RNA−protein complex was purified, and the cross-link site on TAR RNA was determined by chemical and primer extension analyses. These results showed that the amino terminus of Tat(42−72) contacts, or is close to, uridine 42 in the lower stem of TAR RNA (*32*). To define the relative orientation of the C-terminal part of the arginine-rich domain of Tat, we synthesized Tat(38−72) and replaced Arg57 with Cys to introduce a unique thiol group (−SH) in the peptide (*26*). A psoralen derivative which can react with thiol groups was synthesized and used for specific chemical modification of Cys57−Tat(38−72). We used this psoralen−Tat conjugate [psoralen−Cys57−Tat(38−72)] to form a specific complex with TAR RNA. Photo-cross-linking and RNA sequencing results revealed that Cys57 of Tat(38−72) is close to U31 of TAR RNA (*26*).

In a recent report from our laboratory, we applied a site-directed RNA-cleaving strategy to determine the neighborhood of the core domain of a Tat fragment in Tat−TAR complex (*27*). We attached an EDTA analogue to the amino terminus of Tat(38−72) by standard peptide synthesis methods and used this EDTA−Tat conjugate to form a specific complex with TAR RNA. This sequence-specific RNA-binding peptide was converted into a sequence-specific RNA-cleaving peptide by the addition of Fe(II) salt, ascorbate, and H_2O_2. Hydroxyl radicals generated from the tethered Fe(II) cleaved TAR RNA backbone in two localized regions. Site-specific cleavage of TAR RNA was observed at the bulge residues (U23, C24, and U25), in the loop region (G34 and A35), and at the strand opposite the bulge (U40 and C41). These results demonstrate that in the three-dimensional structure of Tat−TAR complex, the Phe38 of Tat(38−72) is located in the proximity of the bulge region and two nucleotides from the loop sequence (*27*).

Here we show that 4-thioU at position 31 cross-links to the Tat peptide. Results from the above studies are summarized in a model for Tat−TAR complex showing the protein orientation, location of N-terminus of the peptide, and U31 functional groups (Figure 6). Our attempts to locate the cross-linked amino acid in the Tat peptide by protein sequencing were not successful. This is not an unexpected result due to the length of the fragment and relatively harsh conditions of peptide sequencing which could result in the destruction of the cross-link between the peptide and RNA (*50*). Previously, we used 4-thioU modified TAR RNA to form Tat−TAR cross-links and we were unable to locate the cross-linked amino acid by Edman protein sequencing (*26*). Recently, Farrow et al. (*51*) applied MALDI-TOF mass spectrometric analysis to locate the cross-link sites in the basic region of a Tat peptide to chemically modified TAR RNA. Farrow et al. (*51*) used a model duplex TAR RNA, and the RNA−protein cross-linked products contained 14−17 nucleotide long RNAs. We followed the methods of Farrow et al. (*51*), and prepared RNA−protein cross-linked products on a large scale and subjected to the MALDI-TOF MS analysis. Due to the larger size of our RNA−protein cross-linked complex, we were unable to analyze it by MALDI-TOF MS. Since our previous findings showed that a psoralen attached to Arg57 formed a cross-link with U31 (*28*), Arg57 is displayed as a potential side chain located in proximity to U31 of TAR RNA. It is important to note that, in previous studies, psoralen was attached to cysteine 57 by a linker of ∼10 Å and psoralen could have preferably photoreacted with uridines in RNA (*28*). Although psoralen photo-cross-linking provides useful information about protein orientation in the Tat−TAR complex, direct interactions and close proximity between the RNA and protein have not been established. Experiments presented in this report show that 4-thioU31 directly contacts Tat peptide. A refined model for Tat−TAR interactions is presented in Figure 6 showing protein orientation and close proximity of U31 to an Arg residue. The RNA structure is derived from ref *52*, and the ribbon structure of Tat(38−72) peptide is based on Tat protein structure (*53*). The Tat peptide is positioned in the major groove of TAR RNA and the RNA is folded to bring O^4 of U31 within 5 Å of Arg57 side chain. All other structural constraints are based on previous photo-cross-linking and affinity cleaving experiments (*26*−*28*, *32*). Due to technical difficulties, we were unable to determine which amino acid formed the cross-link with U31. However, Arg57 is the only amino acid which can be placed in close proximity of U31 in order to generate a structure which is consistent with previous cross-linking and affinity cleaving results.

Mutational analyses have shown that sequences in the loop of TAR RNA are required for trans-activation (*54*, *55*) and not for Tat binding (*35*, *36*, *43*). Tat binds duplex TAR RNA sequences with approximately half the affinity for wild-type TAR RNA (*36*). Duplex TAR RNA sequences have been used previously to study RNA folding and RNA−protein interactions (*26*, *38*, *56*). Recently, Jones and co-workers have identified a novel CDK9-associated C-type cyclin, cyclin T1, which interacts with Tat and increases its affinity and specificity for TAR RNA (*57*). Formation of a specific and high-affinity ternary complexes (Tat:TAR:Cyclin T1) requires sequences in the loop of TAR RNA (*57*). Whether Tat protein or cyclin T1 forms a cross-link with 4-thioU31-modified TAR or not, remains to be determined.

ACKNOWLEDGMENT

We wish to thank Drs. Michael Gait and Thomas Barlow for MALDI-TOF MS analysis and helpful discussions. This work was supported in part by the National Institutes of Health Grants AI 41404 and TW00702 and a Research Career Development Awrad to T.M.R.

LITERATURE CITED

(1) Jones, K. A., and Peterlin, B. M. (1994) Control of RNA Initiation and Elongation at The HIV-1 Promoter. *Annu. Rev. Biochem. 63*, 717−743.
(2) Cullen, B. R. (1998) HIV-1 auxiliary proteins: making connections in a dying cell. *Cell 93*, 685−692.
(3) Emerman, M., and Malim, M. (1998) HIV-1 regulatory/accessory genes: keys to unraveling vial and host cell biology. *Science 280*, 1880−1884.
(4) Cullen, B. R. (1992) Mechanism of action of regulatory proteins encoded by complex retroviruses. *Microbiol. Rev. 56*, 375−394.
(5) Berkhout, B., Silverman, R. H., and Jeang, K. T. (1989) Tat trans-activates the Human Immunodeficiency Virus Through a Nascent RNA Target. *Cell 59*, 273−282.
(6) Kao, S.-Y., Calman, A. F., Luciw, P. A., and Peterlin, B. M. (1987) Antitermination of transcription within the long terminal reppeat of HIV-1 *tat* gene product. *Nature 330*, 489−493.
(7) Laspia, M. F., Rice, A. P., and Mathews, M. B. (1989) HIV-1 tat rotein increases transcriptional initiation and stabilises elongation. *Cell 59*, 283−292.
(8) Feinberg, M. B., Baltimore, D., and Frankel, A. D. (1991) The role of Tat in the human immunodeficiency virus life cycle indicates a primary effect on transcriptional elongation. *Proc. Natl. Acad. Sci. U.S.A. 88*, 4045−4049.
(9) Kato, H., Sumimoto, H., Pognonec, P., Chen, C.-H., Rosen, C. A., and Roeder, R. G. (1992) HIV-1 Tat Acts as a

Processivity Factor in Vitro in Conjuction with Cellular Elongation Factors. *Genes Dev. 6*, 655−666.
(10) Marciniak, R. A., Calnan, B. J., Frankel, D. A., and Sharp, P. A. (1990) HIV-1 Tat Protein Trans-Activates Transcription in Vitro. *Cell 63*, 791−802.
(11) Marciniak, R. A., and Sharp, P. A. (1991) HIV-1 Tat protein promotes formation of more-processive elongation complexes. *EMBO J. 10*, 4189−4196.
(12) Parada, C. A., and Roeder, R. G. (1996) Enhanced processivity of RNA polymerase II triggered by Tat-induced phosphorylation of its carboxy-terminal domain. *Nature 384*, 375−378.
(13) Cujec, T. P., Cho, H., Maldonado, E., Meyer, J., Reinberg, D., and Peterlin, B. M. (1997) The human immunodeficiency virus transactivator Tat interacts with the RNA polymerase II holoenzyme. *Mol. Cell. Biol. 17*, 1817−1823.
(14) Rosen, C. A., Sodroski, J. G., and Haseltine, W. A. (1985) Location of Cis-acting Regulatory Sequences in the Human T cell Lymphotropic Virus type III (HTLV-III/LAV) Long Terminal Repeat. *Cell 41*, 813−823.
(15) Jakobovits, A., Smith, D. H., Jakobovits, E. B., and Capon, D. J. (1988) A Discrete Element 3′ of Human Immunodeficiency Virus 1 (HIV-1) and HIV-2 mRNA Initiation Sites Mediates Transcriptional Activation by an HIV Trans Activator. *Mol. Cell. Biol. 8*, 2555−2561.
(16) Selby, M. J., Bain, E. S., Luciw, P. A., and Peterlin, B. M. (1989) Structure, Sequence, and Position of the Stem-loop in Tar Determine Transcriptional Elongation by Tat through the HIV-1 Long Terminal Repeat. *Genes Dev. 3*, 547−558.
(17) Garcia, J. A., Harrich, D., Soultanakis, E., Wu, F., Zmitsuyasu, R., and Gaynor, R. B. (1989) Human Immunodeficiency Virus Type 1 LTR TATA and TAR Region Sequences Required for Transcriptional Regulation. *EMBO J. 8*, 765−778.
(18) Muesing, M. A., Smith, D. H., and Capon, D. A. (1987) Regulation of mRNA by a Human Immunodeficiency Virus trans-activator protein. *Cell 48*, 691−701.
(19) Dingwall, C., Ernberg, I., Gait, M. J., Green, S. M., Heaphy, S., Karn, J., Lowe, A. D., Singh, M., Skinner, M. A., and Valerio, R. (1989) Human Immunodeficiency Virus Tat protein Binds Trans-activation-responsive Region (TAR) RNA in vitro. *Proc. Natl. Acad. Sci. 86*, 6925−6929.
(20) Dingwall, C., Ernberg, I., Gait, M. J., Green, S. M., Heaphy, S., Karn, J., Lowe, A. D., Singh, M., and Skinner, M. A. (1990) HIV-1 Tat Protein Stimulates Transcription by Binding to the Stem of the TAR RNA Structure. *EMBO J. 9*, 4145−4153.
(21) Weeks, K. M., and Crothers, D. M. (1991) RNA Recognition by Tat-Derived Peptides: Interaction in the Major Groove? *Cell 66*, 577−588.
(22) Calnan, B. J., Tidor, B., Biancalana, S., Hudson, D., and Frankel, A. D. (1991) Arginine-Mediated RNA Recognition: The Arginine Fork. *Science 252*, 1167−1171.
(23) Calnan, B. J., Biancalana, S., Hudson, D., and Frankel, A. D. (1991) Analysis of Arginine-Rich Peptides from the HIV Tat Protein Reveals Unusual Features of RNA Protein Recognition. *Genes Dev. 5*, 201−210.
(24) Churcher, M. J., Lamont, C., Hamy, F., Dingwall, C., Green, S. M., Lowe, A. D., Butler, P. J. C., Gait, M. J., and Karn, J. (1993) High Affinity Binding of TAR RNA by the Human Immunodeficiency Virus Type-1 *tat* Protein Requires Base-pairs in the RNA Stem and Amino Acid Residues Flanking the Base Region. *J. Mol. Biol. 230*, 90−110.
(25) Long, K. S., and Crothers, D. M. (1995) Interaction of human immunodeficiency virus type 1 Tat-derived peptides with TAR RNA. *Biochemistry 34*, 8885−8895.
(26) Wang, Z., and Rana, T. M. (1996) RNA conformation in the Tat-TAR complex determined by site-specific photocross-linking. *Biochemistry 35*, 6491−6499.
(27) Huq, I., and Rana, T. M. (1997) Probing the proximity of the core domain of an HIV-1 Tat fragment in a Tat-TAR complex by affinity cleaving. *Biochemistry 36*, 12592−12599.
(28) Wang, Z., Wang, X., and Rana, T. M. (1996) Protein orientation in the Tat-TAR complex determined by psoralen photocross-linking. *J. Biol. Chem. 271*, 16995−16998.
(29) Tinoco, I., Jr., Puglisi, J. D., and Wyatt, J. R. (1990) RNA folding. *Nucleic Acids Mol. Biol. 4*, 205−226.
(30) Wyatt, J. R., Puglisi, J. D., and Tinoco, I., Jr. (1989) RNA folding: Pseudoknots, loops and bulges. *Bioassays 11*, 100−106.
(31) Shah, K., Wu, H., and Rana, T. M. (1994) Synthesis of uridine phosphoramidite analogues: Reagents for site-specific incorporation of photoreactive sites into RNA sequences. *Bioconjugate Chem. 5*, 508−512.
(32) Wang, Z., and Rana, T. M. (1995) Chemical Conversion of a TAR RNA-Binding Fragment of HIV-1 Tat Protein into a Site-Specific Cross-linking Agent. *J. Am. Chem. Soc. 117*, 5438−5444.
(33) Shah, K., Neenhold, H., Wang, Z., and Rana, T. M. (1996) Incorporation of an artificial protease and nuclease at the HIV-1 tat binding site of trans-activation response RNA. *Bioconjugate Chem. 7*, 283−289.
(34) Ping, Y.-H., Liu, Y., Wang, X., Neenhold, H. R., and Rana, T. M. (1997) Dynamics of RNA-protein interactions in the HIV-1 Rev-RRE complex visualized by 6-thioguanosine-mediated photo-cross-linking. *RNA 3*, 850−860.
(35) Sumner-Smith, M., Roy, S., Barnett, R., Reid, L. S., Kuperman, R., Delling, U., and Sonenberg, N. (1991) Critical chemical features in *trans*-acting-responsive RNA are required for interaction with human immunodeficiency virus tye 1 tat protein. *J. Virol. 65*, 5196−5202.
(36) Hamy, F., Asseline, U., Grasby, J., Iwai, S., Pritchard, C., Slim, G., Butler, P. J. G., Karn, J., and Gait, M. J. (1993) Hydrogen-bonding Contacts in the Major Groove are Required for Human Immunodeficiency Virus Type-1 *tat* Protein Recognition of TAR RNA. *J. Mol. Biol. 230*, 111−123.
(37) Pritchard, C. E., Grasby, J. A., Hamy, F., Zacharek, A. M., Singh, M., Karn, J., and Gait, M. J. (1994) Methylphosphonate mapping of phosphate contacts critical for RNA recognition by the human immunodeficiency virus tat and rev proteins. *Nucleic Acids Res. 22*, 2592−2600.
(38) Naryshkin, N. A., Farrow, M. A., Ivanovskaya, M. G., Oretskaya, T. S., Shabarova, Z. A., and Gait, M. J. (1997) Chemical cross-linking of the human immunodeficiency virus type 1 Tat protein to synthetic models of the RNA recognition sequence TAR containing site-specific trisubstituted pyrophosphate analogues. *Biochemistry 36*, 3496−3505.
(39) Favre, A., and Fourrey, J.-L. (1995) Structural probing of small endonucleolytic ribozymes in solution using thio-substituted nucleobases as intrinsic photolabels. *Acc. Chem. Res. 28*, 375−382.
(40) Milligan, J. F., Groebe, D. R., Witherell, G. W., and Uhlenbeck, O. C. (1987) Oligoribinucleotide synthesis using T7 RNA polymerase and synthetic DNA templates. *Nucleic Acids Res. 15*, 8783−8798.
(41) Neenhold, H. R., and Rana, T. M. (1995) Major Groove Opening at the HIV-1 Tat Binding Site of TAR RNA Evidenced by a Rhodium Probe. *Biochemistry 34*, 6303−6309.
(42) King, D. S., Fields, C. G., and Fields, G. B. (1990) A cleavage method which minimizes side reactions following Fmoc solid-phase peptide synthesis. *Int. J. Pept. Protein Res. 36*, 255−266.
(43) Cordingley, M. G., La Femina, R. L., Callahan, P. L., Condra, J. H., Sardana, V. V., Graham, D. J., Nguyen, T. M., Le Grow, K., Gotlib, L., Schlabach, A. J., and Colonno, R. J. (1990) Sequence-specific Interaction of Tat protein and Tat peptides with the Transactivation-responsive Sequence Element of Human Immunodeficiency Virus Type 1 in vitro. *Proc. Natl. Acad. Sci. U.S.A. 87*, 8985−8989.
(44) Subramanian, T., Govindarajan, R., and Chinnadurai, G. (1991) Heterologous basic domain substitutions in the HIV-1 Tat protein reveal an arginine-rich motif required for trans-activation. *EMBO J. 10*, 2311−2318.
(45) Weeks, K. M., Ampe, C., Schultz, S. C., Steitz, T. A., and Crothers, D. M. (1990) Fragments of the HIV-1 Tat Protein Specifically Bind TAR RNA. *Science 249*, 1281−1285.
(46) Harper, J. W., and Logsdon, N. J. (1991) Refolded HIV-1 Tat Protein Protects Both Bulge and Loop Nucleotides in TAR RNA from Ribonucleolytic Cleavage. *Biochemistry 30*, 8060−8066.
(47) Delling, U., Reid, L. S., Barnett, R. W., Ma, M. Y.-X., Climie, S., Summer-Smith, M., and Sonenberg, N. (1992) Conserved Nucleotides in the TAR RNA stem of Human

Immunodeficiency Virus Type 1 are Critical for Tat Binding and Transactivation: Model for TAR RNA Tertiary Structure. *J. Virology 66*, 3018−3025.

(48) Tao, J., and Frankel, A. D. (1992) Specific binding of arginine to TAR RNA. *Proc. Natl. Acad. Sci. U.S.A. 89*, 2723−2726.

(49) Wang, Z., and Rana, T. M. (1998) RNA-protein interactions in the Tat-*trans*-activation response element complex determined by site-specific photo-cross-linking. *Biochemistry 37*, 4235−4243.

(50) Musier-Forsyth, K., and Schimmel, P. (1994) Acceptor helix interactions in a class II tRNA Synthetase: Photoaffinity cross-linking of an RNA minidulex substrate. *Biochemistry 33*, 773−779.

(51) Farrow, M. A., Aboul-ela, F., Owen, D., Karpeisky, A., Beigelman, L., and Gait, M. J. (1998) Site-specific cross-linking of amino acids in the basic region of human immunodeficiency virus type 1 Tat peptide to chemically modified TAR RNA duplexes. *Biochemistry 37*, 3096−3108.

(52) Aboul-ela, F., Karn, J., and Varani, G. (1995) The structure of the human immunodeficiency virus type-1 TAR RNA reveals principles of RNA recognition by Tat protein. *J. Mol. Biol. 253*, 313−332.

(53) Bayer, P., Kraft, M., Ejchart, A., Westendorp, M., Frank, R., and Rösch, P. (1995) Structural studies of HIV-1 Tat protein. *J. Mol. Biol. 247*, 529−535.

(54) Feng, S., and Holland, E. C. (1988) HIV-1 *tat trans*-activation requires the loop sequence within TAR. *Nature 334*, 165−167.

(55) Berkhout, B., and Jeang, K.-T. (1989) trans activation of human immunodeficiency virus type 1 is sequence specific for both the single-stranded bulge and loop of the trans-acting-responsive hairpin: a quantitative analysis. *J. Virol. 63*, 5501−5504.

(56) Wang, X., Huq, I., and Rana, T. M. (1997) HIV-1 TAR RNA recognition by an unnatural biopolymer. *J. Am. Chem. Soc. 119*, 6444−6445.

(57) Wei, P., Garber, M. E., Fang, S.-M., Fischer, W. H., and Jones, K. A. (1998) A novel CDK9-associated C-type cyclin interacts directly with HIV-1 Tat and mediates its high-affinity, loop specific binding to TAR RNA. *Cell 92*, 451−462.

BC980145J

Accelerated Clearance of Polyethylene Glycol-Modified Proteins by Anti-Polyethylene Glycol IgM

Tian-Lu Cheng,[†,‡] Pin-Yi Wu,[‡] Ming-Fang Wu,[§] Ji-Wang Chern,[∥] and Steve R. Roffler*[,‡]

Institute of Biomedical Sciences, Academia Sinica; Graduate Institute of Life Sciences, National Defense Medical Center; College of Medicine, National Taiwan University; School of Pharmacy, National Taiwan University, Taipei, Taiwan. Received December 2, 1998; Revised Manuscript Received March 3, 1999

Tumor therapy by the preferential activation of a prodrug at tumor cells targeted with an antibody−enzyme conjugate may allow improved treatment efficacy with reduced side effects. We examined antibody-mediated clearance of poly(ethylene glycol)-modified β-glucuronidase (βG−sPEG) as a method to reduce serum concentrations of enzyme and minimize systemic prodrug activation. Enzyme-linked immunosorbent assay and immunoblot analysis of two monoclonal antibodies generated by immunization of BALB/c mice with an antibody−βG−sPEG conjugate showed that mAb 1E8 (IgG1) bound βG and βG−sPEG whereas mAb AGP3 (IgM) bound poly(ethylene glycol). Neither antibody affected the βG activity. mAb 1E8 and AGP3 were modified with 36 and 208 galactose residues (1E8−36G and AGP3−208G) with retention of 72 and 48% antigen-binding activity, respectively, to target immune complexes to the asialoglycoprotein receptor on liver cells. mAb 1E8 and AGP3 cleared βG−PEG from the circulation of mice as effectively as 1E8−36G and AGP3−208G, respectively. mAb AGP3, however, cleared βG−sPEG more completely and rapidly than 1E8, reducing the serum concentration of βG−sPEG by 38-fold in 8 h. AGP3 also reduced the concentration of an antibody−βG−sPEG conjugate in blood by 280-fold in 2 h and 940-fold in 24 h. AGP3-mediated clearance did not produce obvious damage to liver, spleen, or kidney tissues. In addition, AGP3 clearance of βG−sPEG before administration of BHAMG, a glucuronide prodrug of *p*-hydroxyaniline mustard, prevented toxicity associated with systemic activation of the prodrug based on mouse weight and blood cell numbers. AGP3 should be generally useful for accelerating the clearance of PEG-modified proteins as well as for improving the tumor/blood ratios of antibody−βG−PEG conjugates for glucuronide prodrug therapy of cancer.

INTRODUCTION

Drugs, toxins, and isotopes can be selectively delivered to tumors by creating conjugates with monoclonal antibodies (mAb)[1] that preferentially bind tumor-associated antigens. While high serum concentrations of immunoconjugates can increase accumulation and provide more uniform distribution in tumors (Thomas et al., 1989; Fujimori et al., 1990), low serum concentrations of cytotoxic conjugates are preferable to minimize systemic toxicity. High tumor/blood ratios are also desirable for noncytotoxic immunoconjugates such as antibody−enzyme conjugates employed for prodrug activation to minimize systemic prodrug activation.

Tumor/blood ratios of immunoconjugates can be increased by employing an agent that preferentially clears conjugate from the circulation. Avidin has been used to accelerate the clearance of biotinylated antibodies (Klibanov et al., 1988; Stella et al., 1994; Kobayashi et al., 1995) and improve the localization in tumors (Yao et al., 1995; Zhang et al., 1997). Clearance of biotinylated immunoconjugates, however, can be adversely impacted by the high concentrations of endogenous biotin present in serum (Guilarte, 1985) as well as by cleavage of biotin by biotinidase in serum (Wolf et al., 1990). Alternatively, antibodies against primary antibodies (Goldenberg et al. 1987; Sharkey et al., 19984) and antibody−enzyme conjugates (Kerr et al., 1993; Wallace et al., 1994) have also been employed to promote the clearance and tumor localization of immunoconjugates.

In the present study, we were interested in developing a clearance system for PEG-modified conjugates for use in cancer therapy by antibody-directed enzyme activation of glucuronide prodrugs. β-Glucuronidase targeted to tumor cells can activate the glucuronide prodrug (BHAMG) of *p*-hydroxy aniline mustard (pHAM) in vitro (Wang et al., 1992) and cure advanced hepatoma ascites in a rat model (Chen et al., 1997). Antibody−βG conjugates injected intravenously, however, are rapidly cleared from

* To whom correspondence should be addressed. Phone: +886 22 652 3079. Fax: +886 22 782 9142. E-mail: sroff@ibms.sinica.edu.tw.

† Graduate Institute of Life Sciences.

‡ Institute of Biomedical Sciences.

§ College of Medicine.

∥ School of Pharmacy.

[1] Abbreviations: 1E8-*x*G, mAb 1E8 containing *x* galactose moieties per antibody; 5A8-βG−PEG, conjugate formed between mAb 5A8 and βG−sPEG; AGP3-*x*G, mAb AGP3 containing *x* galactose moieties per antibody; βG, *Escherichia coli* β-glucuronidase; βG−sPEG, β-glucuronidase modified with sPEG; βG-tPEG, β-glucuronidase modified with tPEG; BHAMG, glucuronide prodrug of pHAM; BSA, bovine serum albumin; BSA−sPEG, bovine serum albumin modified with sPEG; ELISA, enzyme-linked immunosorbent assay; mAb, monoclonal antibody; PBS, phosphate-buffered saline; PBS-T, PBS containing 0.05% Tween-20; PEG, monomethoxy poly(ethylene glycol); pHAM, *p*-hydroxy aniline mustard; PLT, platelets; RBC, red blood cells; RH1−βG−PEG, conjugate formed between mAb RH1 and βG−sPEG; SDS−PAGE, sodium dodecyl sulfate−polyacrylamide gel electrophoresis; SMCC, succinimidyl-4-(*N*-maleimidomethyl)cyclohexane 1-carboxylate; sPEG, methoxypoly(ethylene glycol) succinimidyl succinate; tPEG, methoxypoly(ethylene glycol) tresylate; WBC, white blood cells.

10.1021/bc980143z CCC: $18.00 © 1999 American Chemical Society
Published on Web 04/17/1999

the circulation before significant tumor accumulation can occur (Cheng et al., 1997). Modification of βG with PEG can extend the half-life of antibody−βG conjugates, decrease normal tissue uptake, and increase the localization of conjugate at solid tumors in nude mice (Cheng et al., 1997). Although the extended half-life of PEG-modified βG conjugates is desirable for improved tumor uptake, at least 5 days were required for the serum concentration of conjugate to reach safe levels before prodrug could be administered (Cheng et al., 1997). Accelerated clearance of conjugates from the circulation may allow earlier prodrug administration when the greatest amount of conjugate is present at tumor cells. In the present study, we generated mAbs against βG and PEG and examined their effect on the clearance of βG−sPEG conjugates. The effect of incorporating galactose residues in the antibodies on the clearance of βG−sPEG conjugates was also examined because galactose can accelerate the removal of proteins from the circulation (Thornburg et al., 1980) by the hepatic asialoglycoprotein receptor (Ong et al., 1991). Rapid clearance of an antibody−carboxypeptidase G2 conjugate by a galactose-modified antibody (Sharma et al., 1990, 1994) allowed earlier administration of a prodrug with reduced toxicity (Rogers et al., 1995). In addition, galactose-modified mAb has also been employed in a clinical trial to remove residual antibody−carboxypeptidase G2 conjugate from the circulation before prodrug administration (Martin et al., 1997). We show that an IgM antibody against PEG can rapidly clear PEG-containing conjugates from the circulation without toxicity and that galactose modification of the IgM is unnecessary.

EXPERIMENTAL PROCEDURES

BSA (Fraction V), sPEG, tPEG, cyanomethyl-2,3,4,6-tetra-*O*-acetyl-1-thio-β-D-galactopyranoside, trinitrobenzenesulfonic acid, fluorescamine, and *p*-nitrophenyl β-D-glucuronide were purchased from Sigma (St. Louis, MO). Sepharose S-200 HR, Sepharose S-300 HR and Sephadex G-25 gels were from Pharmacia Biotech Asia Pacific Ltd. (Taiwan). pHAM and BHAMG were synthesized as described (Roffler et al., 1991). SMCC was from Pierce Chemical Company, Rockford, IL. Second antibodies were purchased from Organon (Durham, NC). FO myeloma cells were purchased from ATCC, Manassas, VA. BALB/c mice were obtained from the animal room of the Institute of Biomedical Sciences, Academia Sinica, Taipei, Taiwan.

PEG-Modification of βG. Recombinant βG was produced and purified as described (Cheng et al., 1997). Twenty milligrams of sPEG per milligram of βG (2 mg/mL) was mixed in coupling buffer (deoxygenated PBS containing 1 mM EDTA, pH 8.0) at room temperature for 2 h before one-tenth the volume of a saturated solution of glycine in coupling buffer was added to stop the reaction. Unreacted PEG was removed by extensive dialysis against PBS or by gel filtration on a 2.5 × 100 cm Sepharose S-200 HR column eluted with PBS at 15 mL/h. Relevant fractions were pooled and concentrated by ultrafiltration to 1.5−2.0 mg/mL for storage at −80 °C. BSA was modified with sPEG in a similar manner. Protein concentrations were determined by the bicinchoninic acid assay (Pierce, Rockford, IL) with BSA employed as the reference protein. The BCA assay was not affected by covalently coupled PEG after removal of free PEG. In some experiments, βG in coupling buffer was modified with 2 mg of sPEG or with 2 or 20 mg of tPEG/mg of βG.

Conjugation of antibodies to βG−sPEG. mAb RH1 (Roffler et al., 1994) and 5A8 (Maloney et al., 1985) were passed through a 2.6 × 30 cm Sephadex G-25 column equilibrated with coupling buffer and concentrated by ultrafiltration to 3 mg/mL. A 4-fold molar excess of SMCC (1 mg/mL in dioxane) was slowly added to the antibodies and allowed to react at room temperature for 50 min. Unreacted SMCC was removed by gel filtration on a 2.6 × 30 cm Sephadex G-25 column equilibrated with coupling buffer. The average number of maleimido groups introduced into antibodies (1−1.5) was assessed as described (Ishikawa et al., 1987). βG−sPEG, prepared as described above, was partially reduced by adding dithiothreitol to a final concentration of 20 mM for 1 h at 37 °C. βG−sPEG was then desalted on a 2.6 × 30 cm Sephadex G-50 column equilibrated with coupling buffer and concentrated to 2 mg/mL. Freshly derivatized antibody and βG−sPEG were immediately mixed at equal molar ratios, concentrated to 2 mg/mL by ultrafiltration and incubated at room temperature for 2 h. Cysteine was added to a final concentration of 2 mM to stop the reaction and the mixture was concentrated by ultrafiltration to about 5 mg/mL. Conjugates were purified by gel filtration on a 2.6 × 100 cm Sepharose S-300 HR column equilibrated with PBS at a flow rate of 15 mL/h. Fractions containing conjugate monomers (antibody/enzyme = 1:1) were pooled and concentrated by ultrafiltration to 1.5−2.0 mg/mL for storage at −80 °C. The yield of conjugates averaged around 35% based on the weight of purified conjugate divided by the total starting weights of antibody and enzyme.

Generation of Monoclonal Antibodies against βG and βG−PEG. Female BALB/c mice were i.v. injected with 200 μg of RH1−βG−PEG in PBS on day 1 and i.p. injected with 100 μg of RH1−βG−PEG on days 7, 14, 21, and 28. Mice received a final i.v. injection of 200 μg of RH1−βG−PEG on day 54. Hybridomas were generated by fusing spleen cells with FO myeloma cells 3 days later (Yeh et al., 1979). Hybridomas were screened by ELISA in 96-well microtiter plates coated with 1 μg/well βG or βG−PEG. Selected hybridomas were cloned 3 times by limiting dilution in 96-well microtiter plates containing thymocyte feeder cells in HT medium supplemented with 15% fetal calf serum. The isotypes and subclasses of mAbs were determined with the Mouse MonoAb-ID kit according to the manufacturer's instructions (Zymed laboratories, South San Francisco, CA). The apparent affinity constants (avidity) of antibodies for βG and βG−sPEG were measured as described (Beatty et al., 1987).

Antibody ELISA. Microtiter plates were coated with 1 μg/well βG, βG−sPEG, BSA, or BSA−sPEG in PBS and blocked with 2% skim milk. Serial dilutions of 1E8 and AGP3 were added to the plates for 1 h at 37 °C. The plates were washed 3 times with PBS-T and 3 times with PBS before horseradish peroxidase conjugated second antibody was added for 1 h at 37 °C. Plates were washed and bound peroxidase activity was measured by adding 100 μL/well ABTS solution [0.4 mg/mL 2,2′-azino-di(3-ethylbenzthiazoline-6-sulfonic acid), 0.003% H_2O_2, 100 mM phosphate-citrate, pH 4.0] for 15 min at room temperature. Absorbance (405 nm) of wells was measured in a microplate reader (Molecular Device, Menlo Park, CA).

Immunoblotting of PEG-Modified Proteins. Samples were electrophoresed in sodium-dodecyl polyacrylamide gels under reducing conditions before overnight transfer to nitrocellulose paper by passive diffusion in blotting buffer (50 mM NaCl, 2 mM EDTA, 0.5 mM 2-mercaptoethanol, and 10 mM Tris-HCl, pH 7.5). Blots were blocked with 5% skim milk and incubated for 1 h at 37 °C with 1E8 or AGP3 ascites diluted 1:2000 in PBS containing

0.05% BSA. Blots were washed 3 times with PBS-T and twice with PBS before incubation with horseradish peroxidase conjugated second antibody for 30 min at 37 °C. Blots were washed and bands were visualized by ECL detection according to the manufacturer's instructions (Pierce, Rockford, IL).

Galactose-modification of antibodies. Cyanomethyl-2,3,4,6-tetra-*O*-acetyl-1-thio-β-D-galactopyranoside was reacted with 0.1 M sodium methoxide in dry methanol for 48 h (Marshall et al., 1995). The methanol was removed by evaporation under vacuum and antibodies (5 mg/mL in pH 8.5 borate buffer) were directly added and allowed to react for 2 h. Different amounts of galactose were incorporated into antibodies by varying the ratio of the reactants. The number of galactose groups introduced into antibodies was estimated by the reduction of trinitrobenzesulfonic acid reactive amine groups after galactose modification (Habeeb, 1966) using a molar extinction coefficient (ϵ^{335}) of 1.31×10^4 for 1E8 and 1.38×10^4 for AGP3. Galactose groups were also estimated by measuring amine groups before and after galactose modification with fluorescamine (Stocks et al., 1986).

Serum Half-Lives of Antibodies. BALB/c mice were i.v. injected with 200 μg of unmodified or galactose-modified antibody. Serum was isolated from blood samples that were periodically removed from the tail vein of mice. The concentrations of 1E8 or AGP3 were determined in duplicate samples by ELISA in microtiter plates coated with βG or βG−sPEG, respectively, by comparison to standard curves generated with known concentrations of the corresponding unmodified or galactose-modified antibody.

Clearance of βG−PEG and 5A8-βG−PEG from Serum. Groups of 3 BALB/c mice were i.v. injected with βG−sPEG or 5A8−βG−PEG at time zero. Blood samples were periodically removed before i.v. injection of unmodified or galactose-modified 1E8 or AGP3 at 24 h. Additional blood samples were taken at subsequent times and the βG activity in duplicate samples was measured using *p*-nitrophenol β-D-glucuronide as substrate (Wang et al., 1992). Sample concentrations were calculated by comparison of absorbance values with a standard curve constructed from known concentrations of βG−sPEG or 5A8−βG−sPEG. For meaningful comparison of clearance results, the measured concentrations of βG−sPEG in mice injected with clearing antibodies were normalized to the mean concentration of βG−sPEG in control (uncleared) mice just before clearance by

$$N_j = (C_{\mathrm{mi}}/C_{\mathrm{i}})C_j$$

where N_j is the normalized serum concentration of βG−sPEG in an experimental mouse at time j, C_{mi} is the mean serum concentration of βG−sPEG in the control group of mice at the last time point before clearance, C_{i} is the serum concentration of βG−sPEG in an experimental mouse at the last time point before clearance, and C_j is the serum concentration of βG−sPEG in an experimental mouse at time j.

Toxicity of Clearance. The number of WBC, RBC, and PLT in groups of 6 BALB/c mice were measured as described (Chen et al., 1997) 1 day before i.v. injection of 50 μg of βG−PEG or PBS. Mice were i.v. injected 24 h later with 300 μg of AGP3 or AGP3−208G or two fractionated 150 μg doses of AGP3−208G separated by 4 h. After allowing 6 h for clearance, mice were i.v. injected with two 7.5 mg/kg doses of BHAMG in PBS. On day 8, the number of WBC, RBC, and PLT in serum samples were determined. On days 3 and 10, the spleen, liver, and kidney were removed from one mouse in each group and fixed in 10% formalin. Ethanol dehydrated samples were embedded in paraffin and cut into 3 μm sections. Sections were then dewaxed with xylene, stained with hematoxylin/eosin, and dehydrated before observation under a light microscope. The weight of mice was followed for 18 days.

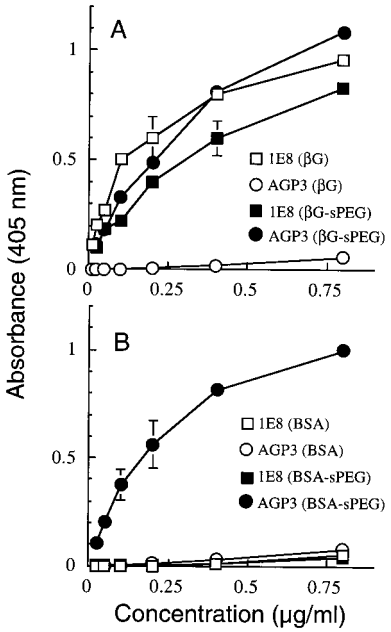


Figure 1. Binding specificity of 1E8 and AGP3. (A) 1E8 or AGP3 antibodies were incubated in microtiter plates coated with βG or βG−sPEG. (B) 1E8 or AGP3 were incubated in microtiter plates coated with BSA or BSA−sPEG. Binding of antibodies was detected by measuring the absorbance of wells at 405 nm as described in the Experimental Procedures. The mean absorbance values of triplicate determinations are shown. Bars, SE.

pH Dependence of βG Activity. Fifteen microliters of βG (4 μg/mL) was mixed in microtiter plates with 200 μl of βG buffer (Wang et al., 1992) with pH values ranging 3−10. Twenty-five microliters of *p*-nitrophenol β-D-glucuronide (32 mM) was added to the wells at 37 °C for 15 min, excess 1 N NaOH was added to adjust the pH to greater than 10, and absorbance was read at 405 nm in a microplate reader. To test the pH stability of βG, enzyme was incubated in βG buffer adjusted to pH values ranging 3−11 for 4 h at 37 °C before neutralization to pH 7.0 and assay of enzymatic activity.

Data Analysis. Statistical significance of differences between mean values was estimated with the shareware program Schoolstat (White Ant Occasional Publishing, West Melbourne, Australia) using the independent *t*-test for unequal variances.

RESULTS

Antibodies against βG−PEG. Monoclonal antibodies against βG−sPEG were generated from spleen cells of mice that had received multiple injections of RH1−βG−PEG. mAb 1E8 (IgG1) and AGP3 (IgM) were selected for further characterization based on preliminary screening by ELISA. 1E8 bound to βG and, to a lesser extent, βG−sPEG (Figure 1A). The apparent affinity constants of 1E8 for βG and βG−sPEG were 0.83 and 1.8 nM, respectively (data not shown). In contrast, AGP3 bound βG−sPEG with an apparent affinity constant of 0.79 nM but did not bind βG (Figure 1A), suggesting that this antibody recognizes PEG chains present on βG−sPEG. AGP3 specificity for PEG was supported by the finding that it

Table 1. Characteristics of Galactose-Modified Monoclonal Antibodies

galactose added[a] (mg/mg)	conjugate	incorporated galactose groups/mAb		activity[d] (% control)	conjugate	incorporated galactose groups/mAb		activity[d] (% control)
		Fluor[b]	TNBS[c]			Fluor[b]	TNBS[c]	
0	1E8	0	0	100	AGP3	0	0	100
0.9	1E8−9G	12 ± 0	7 ± 0.6	100	AGP3−64G	60 ± 18	67 ± 10	72
1.8	1E8−19G	17 ± 2	21 ± 2	82	AGP3−130G	130 ± 4	130 ± 13	64
5.5	1E8−36G	35 ± 0.7	37 ± 2	72	AGP3−208G	210 ± 8	205 ± 21	48
10.9	1E8−46G	48 ± 0.1	44 ± 3	62	AGP3−285G	290 ± 0.1	280 ± 8	43
16.4	1E8−47G	47 ± 0.3	46 ± 2	66	AGP3−295G	310 ± 0.1	280 ± 7	42

[a] The amount of activated galactose added per milligram of antibody. [b] Determined by the fluorescamine method as described by Stocks et al. (1986). [c] Determine by the trinitrobenzesulfonic acid method as described in the Experimental Procedures. [d] Antigen-binding activity determined by ELISA.

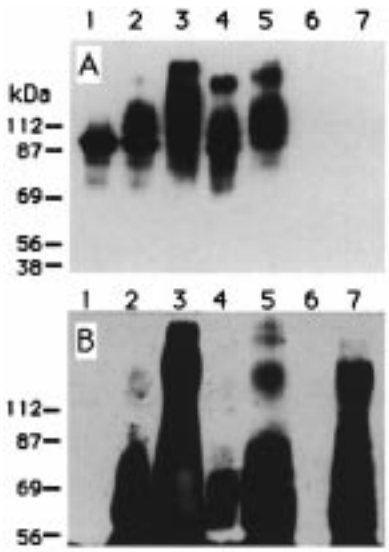


Figure 2. Immunoblot analysis of 1E8 and AGP3 binding. Proteins were electrophoresed in a 3−12.5% gradient reduced SDS−PAGE, transferred to nitrocellulose paper, and probed with 1E8 (A) or AGP3 (B) as described in the Experimental Procedures. Lane 1, βG; lane 2, βG−sPEG (2 mg of sPEG/mg of βG); lane 3, βG−sPEG (20 mg of sPEG/mg of βG); lane 4, βG-tPEG (2 mg of tPEG/mg of βG); lane 5, βG-tPEG (20 mg of tPEG/mg of βG); lane 6, BSA; lane 7, BSA−sPEG (20 mg of sPEG/mg of BSA). kDa, molecular mass in thousands.

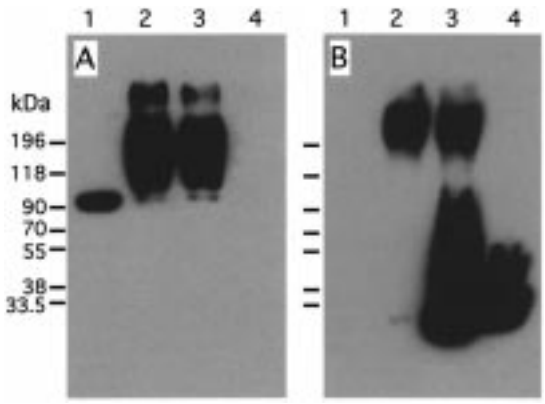


Figure 3. Immunoblot of different βG−PEG preparations. Samples were electrophoresed on a 8% reduced SDS−PAGE, transferred to nitrocellulose paper, and probed with 1E8 (A) or AGP3 (B) as described in the Experimental Procedures. Lane 1, βG; lane 2, βG−sPEG purified by gel filtration; lane 3, βG−sPEG purified by dialysis; lane 4, sPEG neutralized with excess glycine. kDa, molecular mass in thousands.

also bound BSA−sPEG but not BSA (Figure 1B). As expected, 1E8 bound neither BSA nor BSA−sPEG (Figure 1B). Neither mAb affected the activity of βG (results not shown).

The specificity of mAb binding was further examined by immunoblotting. Figure 2A shows that 1E8 detected βG and PEG-modified βG (lanes 1−5), but not BSA or BSA−sPEG (lanes 6 and 7). Figure 2B shows that AGP3, in contrast, did not bind βG (lane 1) or BSA (lane 6) but detected all proteins that incorporated PEG (βG−sPEG, βG−tPEG, and BSA−sPEG). The ability of AGP3 to bind either sPEG or tPEG-modified proteins demonstrates that this antibody binds to poly(ethylene glycol) rather than the linker between PEG and proteins.

Substantial amounts of PEG were present in βG−sPEG preparations purified by dialysis (Figure 3B, lane 3). AGP3 immunoblotting of sPEG after neutralization with glycine (Figure 3B, lane 4) produced a similar smeared band, indicating that the low molecular weight material in βG−sPEG corresponded to free PEG rather than degraded βG−sPEG fragments. Purification of βG−PEG by gel filtration on Sepharose S-200 HR resulted in the removal of free PEG (Figure 3B, lane 2). This βG−sPEG conjugate (Figure 3B, lane 2), containing 9.2 ± 0.3 sPEG groups/βG subunit and possessing 69% of original enzymatic activity, was employed in all subsequent experiments.

Galactose-Modification of Antibodies. 1E8 and AGP3 were modified with galactose to target their uptake by the asialoglycoprotein receptor on hepatocytes. Modification of 1E8 with increasing amounts of activated galactose resulted in the incorporation of up to 47 galactose residues/antibody (Table 1). Introduction of up to 20 galactose residues did not affect the binding of 1E8 to βG whereas greater incorporation of galactose decreased 1E8 activity by about 35%. A maximum of 290 galactose residues could be introduced into AGP3 (Table 1). The greater number of galactose residues incorporated into AGP3 primarily reflects the larger size of the IgM molecule; galactose incorporation for both 1E8 and AGP3 corresponded to 0.3 galactose moieties/kDa of antibody. AGP3 was more sensitive to galactose modification with a 2.4-fold decrease in antigen-binding activity at the highest levels of galactose incorporation.

The half-lives of galactose-modified antibodies were determined in BALB/c mice. Figure 4A shows that 1E8 was eliminated from serum with a half-life of 22 h. Introduction of increasing numbers of galactose residues into 1E8 resulted in progressively faster initial clearance rates. Even at the highest galactose incorporation, however, residual concentrations of 1−4 μg/mL 1E8−46G were present in the serum after 5 h. Unmodified AGP3 cleared from serum with a half-life of 13 h but in contrast to galactose-modified 1E8, almost no residual antibody could be detected in the circulation within 5 h after administration of AGP3 modified with greater than 130 galactose moieties (Figure 4B). On the basis of the elimination kinetics of the antibodies, 1E8−36G and AGP3−208G were selected for further study.

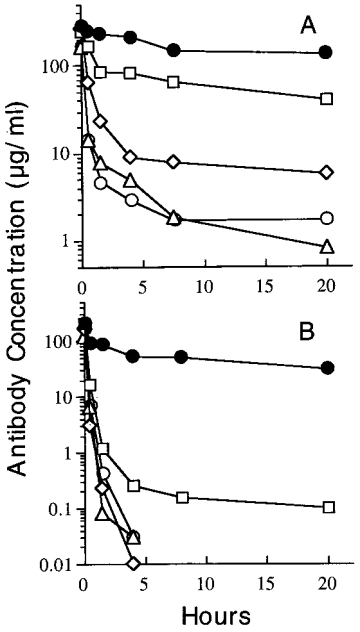


Figure 4. Elimination of galactose-modified antibodies from serum. Single BALB/c mice were i.v. injected with 200 μg of 1E8 (●), 1E8−9G (□), 1E8−19G (◇), 1E8−36G (△), or 1E8−46 (○) (A) or 200 μg of AGP3 (●), AGP3−64G (□), AGP3−130G (◇), AGP3−208G (△), or AGP3−285G (○) (B). The concentrations of antibodies in serum samples taken at the indicated times were measured as described in the Experimental Procedures.

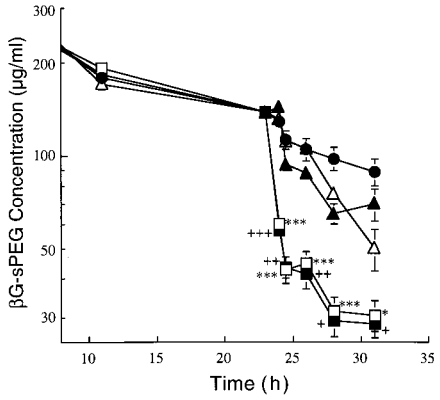


Figure 5. Clearance of βG−PEG by antibodies. Mice injected with 200 μg of βG−sPEG at time 0 were i.v. injected 23 h later with PBS (●) or 250 μg of 1E8 (△), 1E8−36G (▲), AGP3 (□), or AGP3−208G (■). The concentration of βG−sPEG in serum samples was measured and normalized as described in the Experimental Procedures. Mean concentrations from three mice are shown. Significant differences between AGP3 and 1E8 clearance are indicated: (*) $p \leq 0.05$; (**) $p \leq 0.005$; (***) $p \leq 0.0005$. Significant differences between AGP3−208G and 1E8−36G clearance are indicated: (+) $p \leq 0.05$; (++) p ≤ 0.005; (+++) $p \leq 0.0005$. Bars, SE.

In Vivo Clearance of βG−PEG. The ability of antibodies to clear βG−sPEG from the circulation was examined by i.v. injecting mice with 200 μg of βG−sPEG followed 24 h later with 250 μg of unmodified or galactose-modified antibody. Figure 5 shows that both 1E8 and AGP3 accelerated the clearance of βG−sPEG from the circulation. 1E8−36G cleared significantly more βG−sPEG than 1E8 at early times but by 8 h after antibody administration there was no significant difference between these antibodies. AGP3 and AGP3−208G cleared significantly more βG−sPEG than either 1E8 or 1E8−36G at all times examined. βG−sPEG was cleared equally well by AGP3 and AGP3−208G under these experimental conditions.

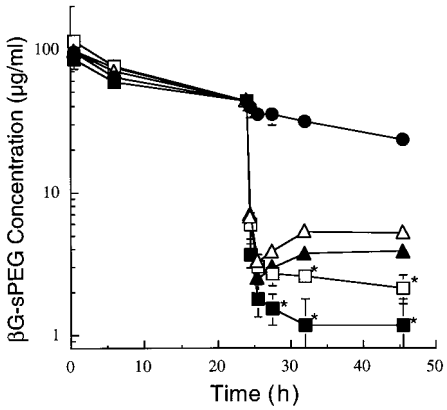


Figure 6. Dose dependence of AGP3 clearance of βG−PEG. Groups of three mice were injected at time 0 with 50 μg of βG−sPEG followed 24 h later by PBS (●), 150 μg of AGP3 (□), 150 μg of AGP3−208G (△), 300 μg of AGP3 (■), or 300 μg of AGP3−208G (▲). The concentration of βG−PEG in serum samples was measured and normalized as described in the Experimental Procedures. Mean concentrations from three mice are shown. Significant differences between AGP3 and AGP3−208G groups are indicated; (*) $p \leq 0.05$. Bars, SE.

Table 2. Clearance of 5A8-βG−PEG by AGP3[a]

		AGP3 clearance	
time (h)	no clearance (μg/mL)	(μg/mL)	reduction[b](fold)
24	24 ± 2.1	37 ± 1.5	1.0
26	18 ± 3.5	0.10 ± 0.001	280
48	6.1 ± 0.7	0.01 ± 0	940

[a] Groups of 3 mice were i.v. injected with 175 μg of 5A8-βG−PEG. At 24 and 25 h, mice were injected with PBS (no clearance) or 300 μg of AGP3. The concentration of 5A8-βG−PEG in serum was determined by measuring βG activity. [b] The ratio of 5A8-βG−PEG concentration in serum without clearance to the concentration with clearance, normalized for the difference in conjugate concentrations at 24 h.

We examined whether increasing the ratio of AGP3 to βG−sPEG would improve clearance. Figure 6 shows that i.v. injection of 150 or 300 μg of AGP3 or AGP3−208G 24 h after i.v. injection of 50 μg of βG−sPEG resulted in rapid removal of 90−95% of the enzyme within 1.5 h. The concentration of βG−sPEG in the circulation, however, rebounded from a minimum of about 2 μg/mL to 4−5 μg/mL 8 h after injection of AGP3−208G. In contrast, the concentration of βG−sPEG decreased to 1.0 μg/mL 8 h after injection of 300 μg of AGP3. Although a dose of 300 μg of AGP3 appeared to more completely clear βG−sPEG compared to 150 μg of AGP3, the difference was only significant ($p \leq 0.05$) 1.5 h after antibody administration. In contrast, clearance of βG−sPEG with both 150 and 300 μg of AGP3 was significantly ($p \leq 0.05$) better than clearance with either dose of AGP3−208G at all times. AGP3 also efficiently cleared 5A8−βG−PEG, reducing the serum concentration of conjugate by 280-fold within 2 h (Table 2).

Prodrug Toxicity After Clearance of βG−sPEG. Clearance of circulating βG−sPEG should reduce systemic activation of the glucuronide prodrug BHAMG, thereby reducing toxicity. Accumulation of cleared immune complexes in organs, however, could result in tissue damage. Organ tissue sections from mice that were injected with PBS or βG−sPEG followed 24 h later by AGP3 and then BHAMG were therefor examined after 3 or 10 days. Figure 7 shows that injection of AGP3 and BHAMG as well as clearance of βG−sPEG with AGP3 before BHAMG administration did not cause obvious

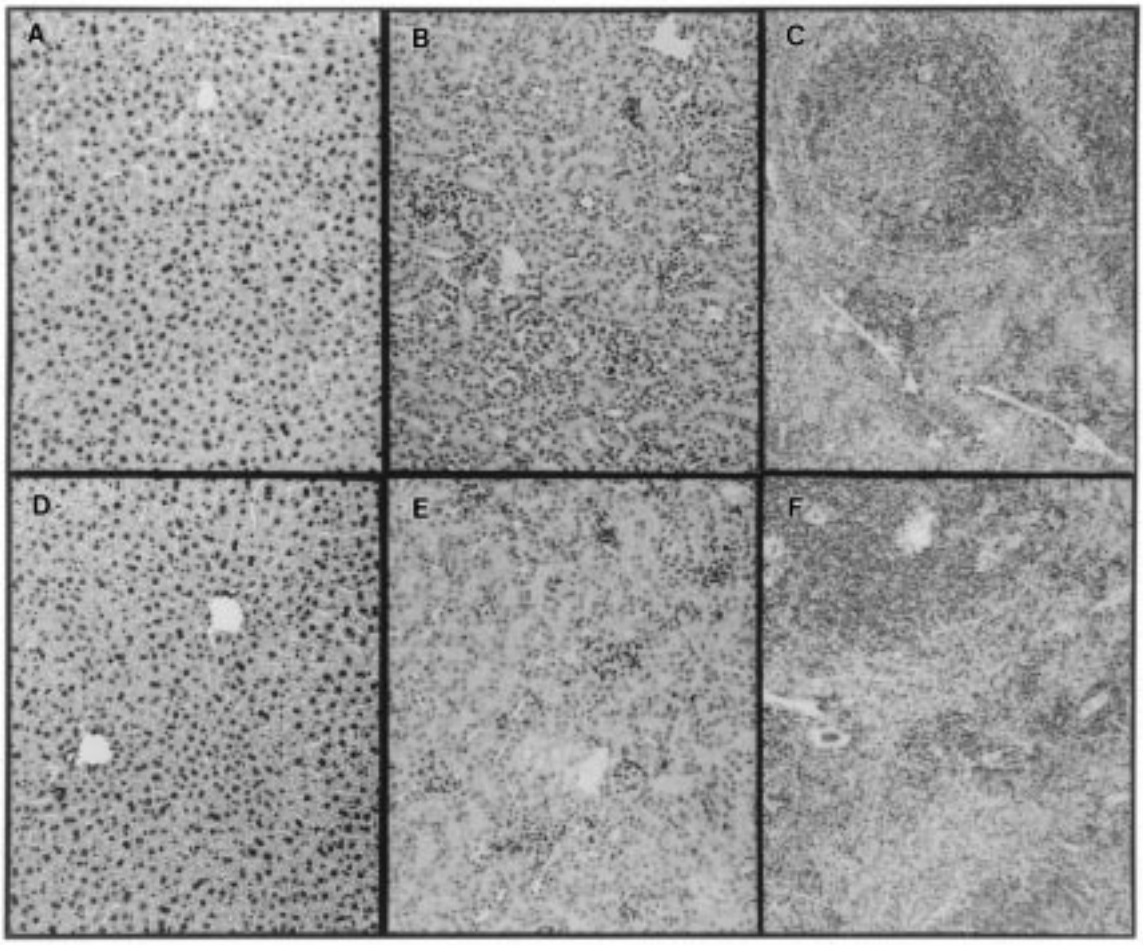


Figure 7. BHAMG-induced organ pathology after βG−PEG clearance. Mice were injected with PBS (A−C) or βG−sPEG (D−F) on day 1. Mice were i.v. injected with AGP3 and BHAMG 24 and 30 h later, respectively. Tissue sections of liver (A, D), kidney (B, E), and spleen (C, F) recovered 10 days later were stained with hematoxylin and eosin.

damage to the liver, spleen, or kidney 10 days after BHAMG administration. Similarly, no tissue damage was observed 3 days after prodrug administration (results not shown).

The toxicity associated with clearance and prodrug administration was also assessed by measuring the weight and blood cells of mice. Administration of AGP3 and 15 mg/kg BHAMG (control group) produced only a small transient decrease in the weight of mice (Figure 8A). In contrast, injection of 50 μg of βG−sPEG 24 h before administration of BHAMG caused significant weight loss and resulted in the death of 1 of 4 mice. Clearance of βG−sPEG with 300 μg of AGP3 or 2 injection of 150 μg of AGP3−208G before prodrug administration prevented significant weight loss compared to the control group. Mice that were cleared with one 300 μg dose of AGP3−208G before injection of BHAMG lost significantly more weight than control mice after day 8, but the loss was much less than in the uncleared mice. Figure 8B shows that the numbers of RBC, PLT, and RBC were significantly reduced in mice injected with βG−sPEG and BHAMG compared to mice injected with AGP3 and BHAMG (control mice). In contrast, the numbers of RBC, WBC, and PLT in mice in which βG−sPEG was cleared with 300 μg of AGP3 before BHAMG administration were not significantly different from control mice. Clearance of βG−sPEG with AGP3−208G before injection of prodrug reduced but did not eliminate hematological toxicity.

AGP3/βG−PEG immune complexes may be routed to the acidic environment of lysosomes after clearance. The effect of pH on βG activity was examined by incubating βG at various pH values for 4 h before neutralization and assay of activity at pH 7.0. βG was irreversibly deactivated at pH values less than 5.0 or greater than 9.0 (Figure 9).

DISCUSSION

We have previously shown that PEG modification of βG increases the tumor localization of antibody−βG conjugates for targeted activation of glucuronide prodrugs (Cheng et al., 1997). PEG-modified βG conjugates, however, are slowly eliminated from the circulation, resulting in low tumor-to-blood ratios. We therefore generated mAbs against βG and PEG and investigated whether these antibodies could accelerate the clearance of βG−sPEG from blood.

mAb 1E8 and AGP3 were modified with galactose to direct uptake of immune complexes by asialoglycoprotein receptors on liver cells (Thornburg et al., 1980; Mattes, 1987). Binding of circulating βG−sPEG by 1E8−36G or AGP3−208G was expected to result in rapid endocytosis, routing to lysosomes and catabolism of enzyme (Ciechanover et al., 1983; Geuze et al., 1983), thereby preventing systemic activation of glucuronide prodrugs. In agreement with previous studies (Mattes, 1987; Sharma et al., 1990), extensive galactose modification of 1E8 and AGP3 (up to 47 and 290 residues, respectively) did not dramati-

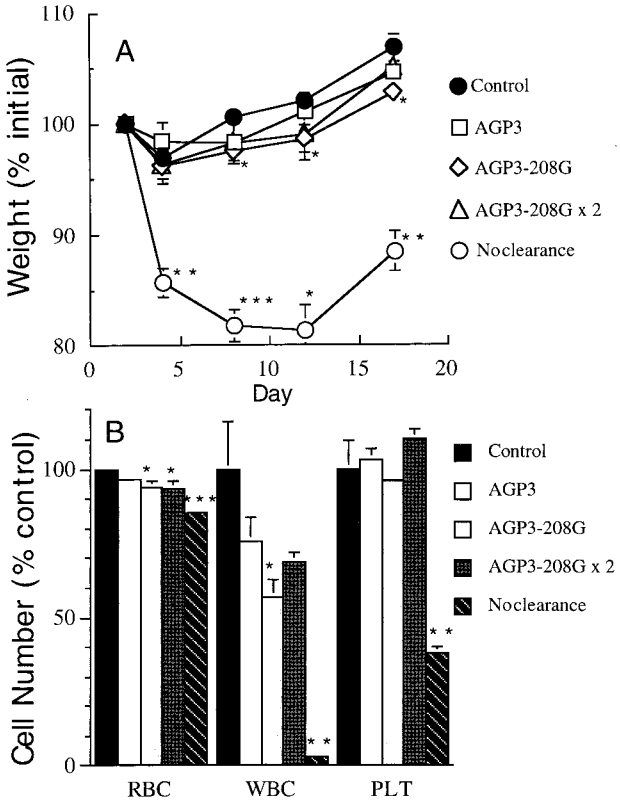


Figure 8. Weight and hematological toxicity of BHAMG after clearance of βG−PEG. Groups of 4 mice were i.v. injected at time zero with PBS (control) or βG−sPEG. Twenty-four hours later, mice received i.v. injections of 300 μg of AGP3 (control and AGP3 groups), 300 μg of AGP3−208G, 150 μg of AGP3−208G (×2, 4 h delay), or PBS (no clearance). Six hours later, all mice were i.v. injected with BHAMG. (A) The time course of mouse weight (% of initial weight) and (B) mean numbers of WBC, RBC, and platelets on day 8 are shown. Significant differences between the control and experimental groups are indicated: (*) $p \leq 0.05$; (**) $p \leq 0.005$; (***) $p \leq 0.0005$. Bars, SE.

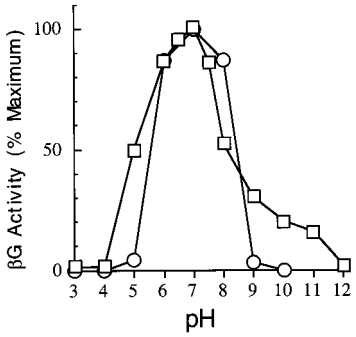


Figure 9. pH sensitivity of βG. βG was assayed for enzymatic activity at various pH values (□) or incubated at the indicated pH for 4 h before neutralization and assay at pH 7.0 (○). Results represent percentage of maximum activity.

cally alter the antigen-binding activity of the antibodies. Increasing the level of galactose residues per antibody did not greatly affect the initial rate of clearance, but did increase the total amount of antibody that was removed from the circulation. For example, the concentrations of 1E8−9G, 1E8−19G, and 1E8−36G in serum were 45, 5.3, and 1.2% of 1E8 levels after 8 h (Figure 4). The galactose-modified antibodies that were not removed from the circulation within the first 5 h exhibited similar elimination kinetics as unmodified 1E8, indicating that a critical number of galactose residues was required for efficient uptake by the asialoglycoprotein receptor, similar to the results found for galactosylated BSA and superoxide dismutase (Nishikawa et al., 1995). The more efficient uptake of galactosylated AGP3 (=99.5% by 4 h for ϵ 130 galactose moieties) compared to galactose-modified 1E8 was unlikely due to differences in the surface density of galactose groups since galactose incorporation was similar based on the molecular weights of 1E8 and AGP3. The asialoglycoprotein receptor is a hetero-oligomer composed of two types of polypeptide chains (Lodish, 1991). High-affinity binding of ligands involves the interaction of three galactose residues in ligands with sites in both polypeptide chains (Rice et al., 1990). Specific orientation of the galactose residues is required for high-affinity receptor binding (Lee et al., 1983; Townsend et al., 1986), suggesting that the orientation of incorporated galactose groups in the pentameric structure of IgM may promote high-affinity binding to the asialoglycoprotein receptor.

AGP3 cleared βG−sPEG more rapidly and completely than 1E8. Hindered binding of 1E8 by PEG chains on βG−sPEG may have contributed to the high residual serum concentrations of βG−sPEG after 1E8 administration. The pentameric structure of AGP3 combined with the presence of multiple PEG chains on each βG tetramer may have promoted the formation of large immune complexes, which are cleared more rapidly than small immune complexes (Roitt et al., 1989). AGP3 appears to produce more rapid and complete clearance than other antibodies previously employed for clearance, which have been limited to IgG fractions of polyclonal antiserum (Bradwell et al., 1983; Sharkey et al., 1984; Pedley et al., 1989; Begent et al., 1989) or monoclonal IgG antibodies (Sharma et al., 1990; Kerr et al., 1993; Haisma et al., 1995; Wallace et al., 1994). Polyclonal IgG antibodies reduced radioimmunoconjugate levels in serum from around 10-fold (Bradwell et al., 1983; Sharkey et al., 1984; Begent et al., 1989) to 130-fold (Pedley et al., 1989) in 24 h whereas monoclonal IgG antibodies reduced the serum levels of antibody−enzyme conjugates from 3−10-fold in a few hours (Sharma et al., 1990; Haisma et al., 1995) to 40−60-fold in 24 h (Kerr et al., 1993; Wallace et al., 1994). In comparison, AGP3 reduced the serum concentration of 5A8−βG−PEG by 280-fold in 2 h and 940-fold in 24 h. Although it is difficult to directly compare clearance results employing different immunoconjugates and experimental conditions, these results suggest that IgM may clear immunoconjugates from blood more rapidly and completely than IgG.

Comparison of AGP3 and AGP3−208G clearance demonstrated that both antibodies initially cleared βG−sPEG with similar rapid kinetics, but that AGP3 removed significantly more βG−sPEG from the circulation than AGP3−208G. The better clearance of unmodified AGP3 can be attributed to the prolonged half-life of AGP3 ($\tau_{1/2}$=13 h) compared to AGP3−208G ($\tau_{1/2}$ < 1 h). βG−sPEG released from normal tissues after rapid removal from blood could be bound and cleared by free AGP3 remaining in the blood pool whereas the rapid endocytosis of both free and complexed AGP3−208G prevented further formation of complexes with βG−sPEG. This behavior is clearly evident in Figure 6 where the concentration of βG−sPEG in the circulation rebounded after an initial period of rapid clearance by AGP3−208G.

One concern of employing IgM to clear proteins is that the immune complexes could be deposited in organs and cause tissue damage. In addition, deposition of βG−PEG on the surface of cells could result in prodrug activation and tissue toxicity. Tissue damage, however, was not

observed after clearance of βG−sPEG with AGP3 and subsequent administration of BHAMG. In addition, clearance of βG−sPEG with AGP3 prevented weight loss and hematological toxicity associated with systemic activation of BHAMG by βG−PEG in the circulation. Soluble IgM immune complexes are primarily removed from the circulation and catabolized by the mononuclear phagocyte system in the liver, spleen, and lungs (Roitt et al., 1989), possibly by receptor-mediated binding of high mannose oligosaccharides exposed upon conformational changes in IgM after binding to antigen (Day et al., 1980). The low toxicity of BHAMG after clearance of βG−sPEG with AGP3 indicates that immune complexes formed between AGP3 and βG−sPEG are rapidly internalized where βG is inactivated, degraded or inaccessible to prodrug. Routing of βG−sPEG to lysosomes is expected to result in loss of enzymatic activity because βG is irreversibly inactivated at pH values lower than 5.0. Deactivation of βG in lysosomes may prevent accumulation of active enzyme and prodrug activation in the liver as observed after antibody-mediated clearance of carboxypeptidase G2 conjugates (Rogers et al., 1995).

PEG modification is a useful technique to improve the stability, prolong serum half-life and decrease the antigenicity and immunogenicity of proteins (Delgado et al., 1992). Because AGP3 binding to PEG is protein independent, this antibody should be generally applicable to the clearance of PEG-modified immunoconjugates. Clearance of immunoconjugates from the circulation can also result in decreased tumor accumulation (Pedley et al., 1989; Sharkey et al., 1992; Kerr et al., 1993), likely due to the generation of a concentration gradient of conjugate from tumor to blood, allowing immunoconjugates that dissociate from tumor antigen to be released into the blood. The large size of IgM may retard passage into the tumor interstitial space, minimizing interactions between localized immunoconjugate and clearing antibody. In addition, the rapid clearance achieved with AGP3 may allow administration of prodrug or other targeting moieties before significant immunoconjugate is released from the tumor. The application of AGP3 for clearing B72.3−βG−PEG conjugates for glucuronide prodrug therapy of colorectal cancer is currently under investigation.

ACKNOWLEDGMENT

Supported by a Grant (NSC88-2314-B001-036) from the National Science Council, Republic of China.

LITERATURE CITED

(1) Beatty, J. D., Beatty, B. G., and Vlahos, W. G. (1987) Measurement of monoclonal antibody affinity by noncompetitive enzyme immunoassay. *J. Immunol. Methods 100*, 173−179.

(2) Begent, R. H. J., Ledermann, J. A., Green, A. J., Bagshawe, K. D., Riggs, S. J., Searle, F., Keep, P. A., Adam, T., Dale, R. G., and Glaser, M. G. (1989) Antibody distribution and dosimetry in patients receiving radiolabeled antibody therapy for colorectal cancer. *Br. J. Cancer 60*, 406−412.

(3) Bradwell, A. R., Vaughan, A., Fairweather, D. S., and Dykes, P. W. (1983) Improved radioimmunodetection of tumours using second antibody. *Lancet i*, 247.

(4) Chen, B. M., Chan, L. Y., Wang, S. M., Wu, M. F., Chern, J. W., and Roffler,S. R. (1997) Cure of malignant ascites and generation of protective immunity by monoclonal antibody-targeted activation of a glucuronide prodrug in rats. *Int. J. Cancer 73*, 392−402.

(5) Cheng, T. L., Chen, B. M., Chan, L. Y., Wu, P. Y., Chern, J. W., and Roffler, S. R. (1997) Poly(ethylene glycol) modification of β-glucuronidase-antibody conjugates for solid-tumor therapy by targeted activation of glucuronide prodrugs. *Cancer Immunol. Immunother. 44*, 305−315.

(6) Ciechanover, A., Schwartz, A. L., and Lodish, H. F. (1983) The asialoglycoprotein receptor internalizes and recycles independently of the transferrin and insulin receptors. *Cell 32*, 267−275.

(7) Day, J. F., Thornburg, R. W., Thorpe, S. R., and Baynes, J. W. (1980) Carbohydrate-mediated clearance of antibody−antigen complexes from the circulation. The role of high mannose oligosaccharides in the hepatic uptake of IgM-antigen complexes. *J. Biol. Chem. 255*, 2360−2365.

(8) Delgado, C., Francis, G. E., and Fisher, D. (1992) The uses and properties of PEG-linked proteins. *Crit. Rev. Therapeut. Drug Carr. Systems 9*, 249−304.

(9) Fujimori, K., Covell, D. G., Fletcher, J. E., and Weinstein, J. N. (1990) A modeling analysis of monoclonal antibody percolation through tumors: a binding-site barrier. *J. Nucl. Med. 31*, 1191−1198.

(10) Geuze, H. J., Slot, J. W., Strous, G. J., Lodish, H. F., and Schwartz, A. L. (1983) Intracellular site of asialoglycoprotein receptor−ligand uncoupling: double-label immunoelectron microscopy during receptor-mediated endocytosis. *Cell 32*, 277−287.

(11) Goldenberg, D. M., Sharkey, R. M., and Ford, E. (1987) Anti-antibody enhancement of iodine-131 anti-CEA radioimmunodetection in experimental and clinical studies. *J. Nucl. Med. 28*, 1604−1610.

(12) Guilarte, T. R. (1985) Radiometric-microbiological assay of biotin in human plasma. *Ann. N. Y. Acad. Sci. 447*, 398−399.

(13) Habeeb, A. (1966) Determination of free amino groups in proteins by trinitrobenzenesulfonic acid. *Anal. Biochem. 14*, 328−336.

(14) Haisma, H. J., Van-Muijen, M., Scheffer, G., Scheper, R. J., Pinedo, H. M., and Boven, E. (1995) A monoclonal antibody against human beta-glucuronidase for application in antibody-directed enzyme prodrug therapy. *Hybridoma 14*, 377−382.

(15) Ishikawa, E., Hashida, S., Kohno, T., and Ohtaki, S. (1987) Modification of monoclonal antibodies with enzymes, biotin, and fluorochromes and their applications. *Monoclonal Antibody Production Techniques and Applications* (L. B. Schook, Ed.) pp 113−139, Marcel Dekker, Inc., New York.

(16) Kerr, D. E., Garrigues, U. S., Wallace, P. M., Hellström, K. E., Hellström, I., and Senter, P. D. (1993) Application of monoclonal antibodies against cytosine deaminase for the in vivo clearance of a cytosine deaminase immunoconjugate. *Bioconjugate Chem. 4*, 353−357.

(17) Klibanov, A. L., Martynov, A. V., Slinkin, M. A., Sakharov, I. Y., Smirnov, M. D., Muzykantov, V. R., Danilov, S. M., and Torchilin, V. P. (1988) Blood clearance of radiolabeled antibody: enhancement by lactosamination and treatment with biotin−avidin or anti-mouse antibodies. *J. Nucl. Med. 29*, 1951−1956.

(18) Kobayashi, H., Sakahara, H., Endo, K., Hosono, M., Yao, Z. S., Toyama, S., and Konishi, J. (1995) Comparison of the chase effects of avidin, streptavidin, neutravidin, and avidin-ferritin on a radiolabeled biotinylated antitumor monoclonal antibody. *Jpn. J. Cancer Res. 86*, 310−314.

(19) Lee, Y. C., Townsend, M. R., Hardy, J., Lönngren, J., Arnarp, M., Haraldsson, M., and Lönn, H. (1983) Binding of synthetic oligosaccharides to the hepatic Gal/GalNAc lectin. Dependence on fine structural features. *J. Biol. Chem. 258*, 199−202.

(20) Lodish, H. F. (1991) Recognition of complex oligosaccharides by the multi-subunit asialoglycoprotein receptor. *Trends Biol. Sci. 16*, 374−377.

(21) Maloney, D. G., Kaminski, M. S., Burowski, D., Haimovich, J., and Levy, R. (1985) Monoclonal anti-idiotype antibodies against the murine B cell lymphoma 38C13: Characterization and use as probes for the biology of the tumor in vivo and in vitro. *Hybridoma 4*, 191−209.

(22) Marshall, D., Pedley, R. B., Melton, R. G., Boden, J. A., and Begent, R. H. J. (1995) Galactosylated streptavidin for improved clearance of biotinylated intact and $F(ab')_2$ fragments of an anti-tumour antibody. *Br. J. Cancer 71*, 18−24.

(23) Martin, J., Stribbling, S. M., Poon, G. K., Begent, R. H., Napier, M., Sharma, S. K., and Springer, C. J. (1997) Antibody-directed enzyme prodrug therapy: pharmacokinetic and plasma levels of prodrug and drug in a phase I clinical trail. *Cancer Chemother. Pharmacol. 40*, 189−201.

(24) Mattes, M. J. (1987) Biodistribution of antibodies after intraperitoneal or intravenous injection and effect of carbohydrate modifications. *J. Natl. Cancer Inst. 79*, 855−863.

(25) Nishikawa, M., Miyazaki, C., Yamashita, F., Takakura, Y., and Hashida, M. (1995) Galactosylated proteins are recognized by the liver according to the surface density of galactose moieties. A*m. J. Physiol. 268*, G849−G856.

(26) Ong, G. L., Ettenson, D., Sharkey, R. M., Marks, A., Baumal, R., Goldenberg, D. M., and Mattes, M. J. (1991) Galactose-conjugated antibodies in cancer therapy: properties and principles of action. *Cancer Res. 51*, 1619−26.

(27) Pedley, R. B., Dale, R., Boden, J. A., Begent, R. H. J., Keep, P. A., and Green, A. J. (1989) The effect of second antibody clearance on the distribution and dosimetry of radiolabeled anti-CEA antibody in a human colonic tumor xenograft model. *Int. J. Cancer 43*, 713−718.

(28) Rice, K. G., Weisz, O. A., Barthel, T., Lee, R. T., and Lee, Y. C. (1990) Defined geometry of binding between triantennary glycopeptides and the asialoglycoprotein receptor of rat hepatocytes. *J. Biol. Chem 265*, 18429−18434.

(29) Roffler, S. R., Wang, S. M., Chern, J. W., Yeh, M. Y., and Tung, E. (1991) Anti-neoplastic glucuronide prodrug treatment of human tumor cells targeted with a monoclonal antibody-enzyme conjugate. *Biochem. Pharmacol. 42*, 2062−2065.

(30) Roffler, S. R., Chan, J., and Yeh, M. Y. (1994) Potentiation of radioimmunotherapy by inhibition of topoisomerase I. *Cancer Res. 54*, 1276−1285.

(31) Rogers, G. T., Burke, P. J., Sharma, S. K., Koodie, R., and Boden, J. A. (1995) Plasma clearance of an antibody-enzyme conjugate in ADEPT by monoclonal anti-enzyme: its effect on prodrug activation in vivo. *Br. J. Cancer 72*, 1357−1363.

(32) Roit, I., Brostoff, J., and Male, D. (1989) Immunology, pp 21.5−21.9, Gower Medical Publishing, London.

(33) Sharkey, R. M., Primus, F. J., and Goldenberg, D. M. (1984) Second antibody clearance of radiolabeled antibody in cancer radioimmunodetection. *Proc. Natl. Acad. Sci. U.S.A. 81*, 2843−2846.

(34) Sharkey, R. M., Boerman, O. C., Natale, A., Pawlyk, D., Monestier, M., Losman, M. J., and Goldenberg, D. M. (1992) Enhanced clearance of radiolabeled murine monoclonal antibody by a synegeic anti-idiotype antibody in tumor-bearing nude mice. *Int. J. Cancer 51*, 266−273.

(35) Sharma, S. K., Bagshawe, K. D., Burke, P. J., Boden, R. W., and Rogers, G. T. (1990) Inactivation and clearance of an anti-CEA carboxypeptidase G2 conjugate in blood after localization in a xenograft model. *Br. J. Cancer 61*, 659−662.

(36) Sharma, S. K., Bagshawe, K. D., Burke, P. J., Boden, J. A., Rogers, G. T., Springer, C. J., Melton, R. G., and Sherwood, R. F. (1994) Galactosylated antibodies and antibody-enzyme conjugates in antibody-directed enzyme prodrug therapy. *Cancer 73*, 1114−20.

(37) Stella, M., DeNardo, P., Paganelli, G., Magnani, P., Mangili, F., Sassi, I., Baratti, D., Gini, P., Zito, F., and Cristallo, M. (1994) Avidin−biotin system in radioimmunoguided surgery for colorectal cancer. Advantages and limits. *Dis. Colon Rectum 37*, 335−343.

(38) Stocks, S. J., Jones, A. J. M., Ramey, C. W., and Brooks, D. E. (1986) A fluorometric assay of the degree of modification of protein primary amines with poly(ethylene glycol). *Anal. Biochem. 154*, 232−234.

(39) Thornburg, R. W., Day, J. F., Baynes, J. W., and Thorpe, S. R. (1980) Carbohydrate-mediated clearance of immune complexes from the circulation. A role for galactose residues in the hepatic uptake of IgG-antigen complexes. *J. Biol. Chem. 255*, 6820−6825.

(40) Thomas, G. D., Chappell, M. J., Dykes, P. W., Ramsden, D. B., Godfrey, K. R., Ellis, J. R. M., and Bradwell, A. R. (1989) Effect of dose, molecular size. affinity, and protein binding on tumor uptake of antibody or ligand: A mathematical model. *Cancer Res. 49*, 3290−3296.

(41) Townsend, R. R., Hardy, M. R., Wong, T. C., and Lee, Y. C. (1986) Binding of N-linked bovine fetuin glycopeptides to isolated rabbit hepatocytes: Gal/GalNAc hepatic lectin discrimination between Galβ(1,4)GalNAc and Galβ(1,3)GalNAc in a triantennary structure. *Biochemistry 25*, 5716−5725.

(42) Wallace, P. M., MacMaster, J. F., Smith, V. F., Kerr, D. E., Senter, P. D., and Cosand, W. L. (1994) Intratumoral generation of 5-fluorouracil mediated by an antibody-cytosine deaminase conjugate in combination with 5-fluorocytosine. *Cancer Res. 54*, 2719−2723.

(43) Wang, S. M., Chern, J. W., Yeh, M. Y., Ng, J. C., Tung, E., and Roffler, S. R. (1992) Specific activation of glucuronide prodrugs by antibody-targeted enzyme conjugates for cancer therapy. *Cancer Res. 52*, 4484−4491.

(44) Wolf, B., Hymes, J., and Heard, G. S. (1990) Biotinidase. *Methods Enzymol. 184*, 103−111.

(45) Yao, Z., Zhang, M., Kobayashi, H., Sakahara, H., Nakada, H., Yamashina, I., and Konishi, J. (1995) Improved targeting of radiolabeled streptavidin in tumors pretargeted with biotinylated monoclonal antibodies through an avidin chase. *J. Nucl. Med. 36*, 837−841.

(46) Yeh, M. Y, Hellström, I., Brown, J. P., Warner, G. A., Hansen, J. A., and Hellström, K. E. (1979) Cell surface antigens of human melanoma identified by monoclonal antibody. *Proc. Natl. Acad. Sci. U.S.A. 76*, 2927−1931.

(47) Yeh, M. Y., Roffler, S. R., and Yu, M. H. (1992) Doxorubicin-monoclonal antibody conjugate for therapy of human cervical carcinoma. *Int. J. Cancer 51*, 274−282.

(48) Zhang, M., Sakahara, H., Yao, Z., Saga, T., Nakamoto, Y., Sato, N., Nakada, H., Yamashina, I., and Konishi, J. (1997) Intravenous avidin chase improved localization of radiolabeled streptavidin in intraperitoneal xenograft pretargeted with biotinylated antibody. *Nucl. Med. Biol. 24*, 61−64.

BC980143Z

5-[3-(*E*)-(4-Azido-2,3,5,6-tetrafluorobenzamido)propenyl-1]-2′-deoxyuridine-5′-triphosphate Substitutes for Thymidine-5′-triphosphate in the Polymerase Chain Reaction

Tatyana S. Godovikova,* Dmitri M. Kolpashchikov,† Tatyana N. Orlova, Vladimir A. Richter, Tamara M. Ivanova, Sergey L. Grochovsky,‡ Tatyana V. Nasedkina,‡ Lubov S. Victorova,‡ and Andrey I. Poletaev‡

Novosibirsk Institute of Bioorganic Chemistry, Siberian Division of the Russian Academy of Sciences, 630090 Novosibirsk, Lavrentiev av. 8, Russia, Novosibirsk State University, Pirogova av. 2, 630090 Novosibirsk, Russia, and Engelhard Institute of Molecular Biology, Russian Academy of Sciences, Vavilova av. 32, 117984 Moscow, Russia. Received December 14, 1998

The DNA targets may be labeled and simultaneously amplified in the polymerase chain reaction (PCR) using a pair of respective primers after elongation with nucleoside-5′-triphosphates carrying photoreactive groups. The amplified DNA may be subsequently photoactivated by irradiation above 300 nm, resulting in photo-cross-linking of the strands. For this goal 5-[3-(*E*)-(4-azido-2,3,5,6-tetrafluorobenzamido)propenyl-1]-, 5-{*N*-[*N*′-(4-azido-2,3,5,6-tetrafluorobenzoyl)-3-aminopropionyl]aminomethyl}-, and 5-{*N*-[*N*′-(2-nitro-5-azidobenzoyl)-3-aminopropionyl]aminomethyl}-2′-deoxyuridine-5′-triphosphate (**VII**, **VIa**, and **VIb**) derivatives have been synthesized. It was found that **VII** is capable of efficiently elongating DNA primers with both Klenow fragment DNA polymerase I and *Thermus aquaticus* DNA polymerase. Thereto, it turned out to provide quantitative incorporation in DNA as revealed by the formation of the full-length amplificate by PCR in the presence of this photoreactive analogue without any dilution with natural dTTP. On the contrary, it was found, that incorporation of **VIa** and **VIb** do not permit further DNA replication.

INTRODUCTION

Nucleoside-5′-triphosphate derivatives carrying a photoreactive aryl azido residue attached to heterocyclic moiety were proposed a few years ago as substrates of the nucleic acid polymerases for the preparation of photoreactive oligonucleotides. UTP and CTP analogues were used for preparation photoreactive transcript, which can be used for affinity labeling of *Escherichia coli* RNA polymerase (*1*, *2*). The dCTP derivative carrying a *p*-perfluoroazido benzoyl residue bound to exocyclic NH_2 group via a $-CH_2CH_2NH-$ spacer was prepared and used for primer extension by a DNA polymerase α-primase complex from human placenta. The duplex obtained was demonstrated to carry out affinity modification of a number of the subunits of the complex (*3*). The same derivative as well as another one, carrying *p*-perfluoroazido benzoyl residue attached to 5-C of dCTP via the spacer $-CH{=}CH-CH_2-NH_2$, was found to be a substrate of the HIV-1 reverse transcriptase, and it was shown that specific modification of DNA template in the complex with the enzyme was carried out (*4*). The primer extension products obtained with 37-meric DNA and M13 DNA templates were found to photo-cross-link with both the enzyme and template DNA (*4*, *5*). Thus, the approach turned out to be promising for the specific labeling of both polymerases and DNA templates. To expand the possibilities of the approach a number of dTTP, dCTP and dATP analogues were prepared as the tools for investigation of nucleic acid—nucleic acid and protein—nucleic acid interactions (*6*).

Recently, we proposed to use this approach to elaborate a new version of the fluorescent DNA probes localization on chromosomes and chromatin (*7*). This version is based upon the elongation of the hybridized probe in the presence of DNA polymerase and a mixture of deoxynucleoside-5′-triphosphate containing a photoreactive analogue of one of the substrates. This procedure permits the subsequent photo-cross-linking of the elongated probe with chromatin, thus making possible the following extensive washing to remove nonspecific signals and, consequently, to achieve higher contrast of the specific one. In our first work, we used a dTTP analogue with 2-nitro-5-azidobenzoyl residue attached to 5-C atom of deoxyuridine-5′-triphosphate via a $-CH_2NHC(O)(CH_2)_2-NH-$ spacer.

Obviously, the efficient incorporation of photoreactive dNTP[1] in the product of DNA replication is one of essential prerequisites for the subsequent efficient cross-linking. The main goal of this work was to prepare the photoreactive nucleoside-5′-triphosphate derivative, which can be efficiently incorporated into DNA primers by DNA polymerases with subsequent cross-linking with the template DNA under irradiation. Since it was shown earlier that, among aryl azides investigated, the *p*-azido perfluorobenzoyl residue is the most reactive toward complementary oligonucleotide chain (*8*, *9*), we have

* To whom correspondence should be addressed. Phone: 007-3832-396274. Fax: (7) (3832) 333677. E-mail: silnik@niboch.nsc.ru.

† Novosibirsk State University.

‡ Engelhard Institute of Molecular Biology.

[1] Abbreviations: (d)NTP, 2′-deoxyribonucleoside-5′-triphosphates; NTP, nucleoside-5′-triphosphates; DMF, dimethylformamide; TEA, triethylamine; TEAB, triethylammonium bicarbonate; DCC, *N*,*N*′-dicyclohexylcarbodiimide; *Taq* DNA polymerase, *Thermus aquaticus* DNA polymerase.

10.1021/bc980144r CCC: $18.00 © 1999 American Chemical Society
Published on Web 04/30/1999

prepared new dNTP analogues, carrying this group connected with pyrimidine heterocycle via two different spacers. One of them, 5-[3-(*E*)-(4-azido-2,3,5,6-tetrafluorobenzamido)propenyl-1]-2′-deoxyuridine-5′-triphosphate, turned out to provide quantitative incorporation in DNA as revealed by the formation of the full-length amplificate in the presence of this dU*TP analogue without any dilution with natural dTTP. The amplified DNA subsequently may be photoactivated by irradiation above 300 nm, leading to the photo-cross-linking of the strands. These results indicate that new photoreactive analogue **VII** can be used for in vitro incorporation into DNA probes to label genetic targets on human metaphase chromosome spreads and interphase nuclei after the formation of covalent links between the photoanchoring probes and template DNA.

EXPERIMENTAL PROCEDURES

Materials. *N*,*N*-Dimethylformamide, acetone, acetonitrile, pyridine, and triethylamine were purified and dried according to standard procedures. Triethyl phosphate, *β*-alanine, DCC, *N*-hydroxysuccinimide, and bis-(tri-*n*-butylammonium)pyrophosphate were purchased from Merck (Germany). Phosphoroxychloride, 2′-deoxyuridine, and 2′-deoxyuridine-5′-triphosphate were purchased from Fluka (Switzerland). Dowex 50W X2 was purchased from Serva (Germany). DEAE-cellulose DE-32 was purchased from Whatman (England). Polynucleotide kinase and dNTP were purchased from NIKTI BAV (Russia). DNA polymerase *Thermus aquaticus* was from Biopol (Russia). [^{32}P]-*o*-phosphate was purchased from "Nuclid Trans" (Moscow, Russia). Other reagents were of analytical grade.

General Methods. ^{1}H NMR spectra were recorded on a Bruker WP-200 SY (200 MHz) and on a Bruker AC-200 (200.132 MHz) spectrometers. All ^{1}H chemical shifts are reported relative to TMS as an internal standard. ^{31}P NMR spectra were recorded on a Bruker AC-200 (81.015 MHz) spectrometer, the ^{31}P chemical shifts are reported using an external standard of 85% H_3PO_4. Infrared spectra were recorded on a Specord M80 (Karl Zeiss, Yena). UV absorption spectra were recorded on a Specord M40 (Karl Zeiss, Yena).

Analytical TLC was carried out on silica gel plates (Merck, DC-Alufolien Kieselgel 60 F_{254}) in ethanol/NH_4-OH, 4:1(v/v), (system A); in dioxane/NH_4OH/water, 6:1:4 (v/v), (system B); and in $CHCl_3$/ethanol, 4:1 (v/v), (system C). The compounds containing amino groups were visualized by the ninhydrin reaction (1% ninhydrin, 2% acetic acid in methanol).

Isolation and purification of the dU*TP derivatives were performed by reversed-phase high-performance liquid chromatography using a LiChrosorb RP-18, 10 μm (Merck, FRG), 4.6 × 250 mm column, a Waters 600E chromatograph, and Waters 484 tunable absorbance detector. A linear gradient (2 mL/min) from 0 to 30% of acetonitrile in 0.05 M TEAB (pH 7.5) was used. Analytical anion-exchange microcolumn chromatography was performed on the Milichrom chromatograph (Russia) using a Polisil-SA, 15 μm (Vector, Russia), 2.5 × 30 mm column. A linear gradient (flow rate 50 μL/min) from 0 to 1 M of NaCl in 7 M urea and 0.01 M Na_2HPO_4 (pH 9) was employed.

The oligodeoxyribonucleotides pd(GACCTGCCACTTTG-GCTGAA) and pd(CACAATGCTGCCTTTTCCAA) were prepared by Dr. Galiya A. Maksakova as described (*10*). The oligonucleotide pd(CACAATGCTGCCTTTTCCAA) was 5′-end labeled using T4-polynucleotide kinase, [γ-^{32}P]-ATP (>3000 Ci/mmol). After purification on 20% polyacrylamide gel under denaturing conditions (8 M urea, 89 mM Tris-H_3BO_3, ~40 °C), oligonucleotide [^{32}P]d-(CACAATGCTGCCTTTTCCAA) was used as a primer in PCR experiments.

The amplification of DNA was performed on a DNA Thermal Cycler Manual (Bis, Russia).

thermal cycling profile	
inital denaturation (25−30 cycles)	95 °C, 3 min
denaturation step	95 °C, 36 s
annealing step	55 °C, 60 s
elongation step	70 °C, 2 min

A 50 μL PCR Mastermix contained 1 μg of each primer, 0.01 μg of DNA template (pTBE−51.1 plasmid), 1.5 mM $MgCl_2$, 67 mM Tris-HCl (pH 8.9), 16 mM $(NH_4)_2SO_4$, 0.05% Tween 20, 0.5 mM solution of dATP, dCTP, dGTP, and either dTTP, the photoreactive 2′-deoxyuridine-5′-triphosphate derivative, or mixture of definite amount of both photoreactive dU*TP and dTTP and 0.5 units of *Taq* DNA-polymerase. The reaction products were separated by agarose gel (2%) electrophoresis. The gels were visualized by ethidium bromide staining or autoradiography.

After synthesis of DNA by PCR in the presence of photoreactive dU*TP analogue **VII**, the PCR products were separated in 10% nondenaturating PAAG in the dark. The amplified DNA was extracted from the gel by electroelution and precipitated by addition of 2% $LiClO_4$ in acetone. The precipitate was carefully washed with acetone (2 × 1.2 mL). UV (H_2O) $\lambda_{max,}$ 268 nm; IR (0.02 mm CaF_2 cuvette) $\nu_{max,}$ 2100 ($-N_3$) cm^{-1}.

The M13mp10 phage DNA was isolated from the culture fluid of a recipient K12 x L1 *E. coli* strain. The primer pd(CCCAGTCACGACGT) was labeled at the 5′-position by [γ-^{32}P]ATP with a specific activity of 1500 Ci/mmol (Radioisotop, Russia) using T4-polynucleotide kinase and annealed with the template at the ratio 1:1 under standard conditions [60 °C, 10 min, in 10 mM Tris-HCl buffer (pH 7.9), 5 mM $MgCl_2$, and 1 mM dithiothreitol]. The primer−template complex was purified by gel filtration on a Bio-Gel A (1.5 mesh) microcolumn, prewashed by 10 mM Tris-HCl (pH 7.6) and 1 mM EDTA.

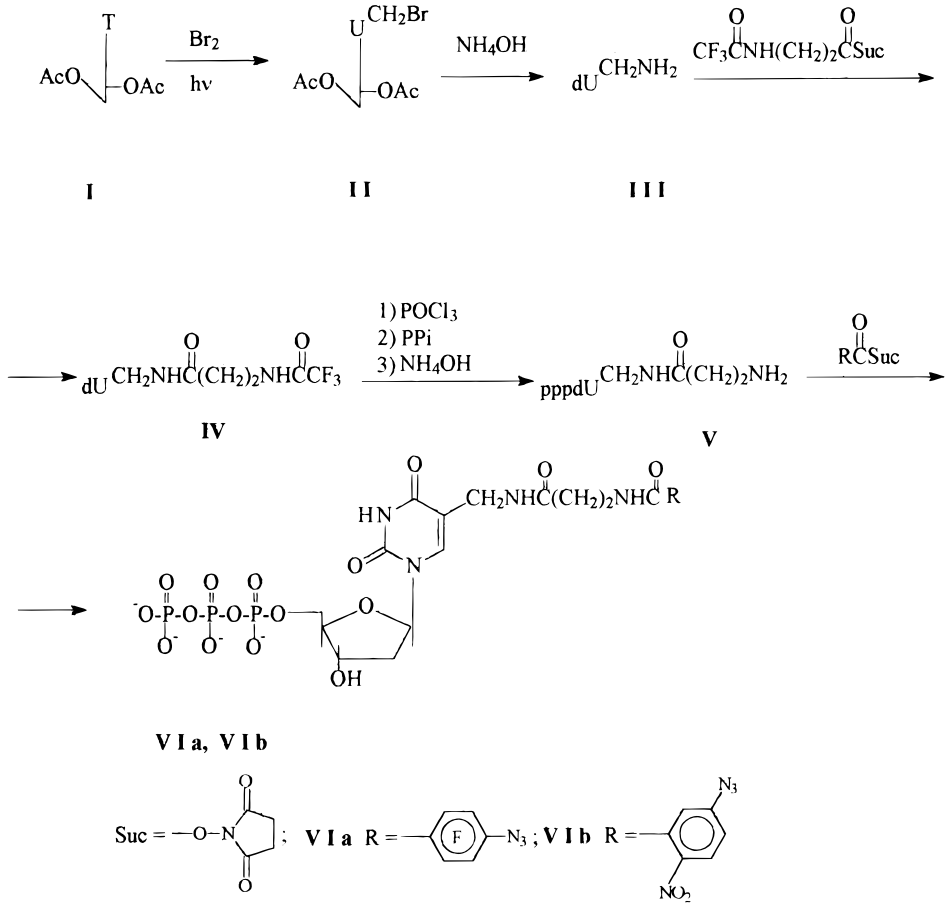
DNA polymerase assays were carried out as described (*11*). The reaction mixture (6 μL) containing 0.2 units of DNA polymerase I Klenow fragment (Promega) or *Taq* DNA polymerase (Biopol, Russia), 10 nM of the primer−template complex, natural substrates (dTTP, dGTP), or the testing compound **VII** was incubated during 15 min at 20 °C for Klenow fragment and 15 min at 72 °C for *Taq* DNA polymerase. The reaction was stopped by addition of 3 μL of formamide containing 0.1% of xylenecyanol, 0.1% of bromophenol blue, and 20 mM EDTA, pH 8.0. The reaction products were separated by electrophoresis in a 20% PAAG under denaturing conditions. The gels were visualized by autoradiography.

N-Hydroxysuccinimide esters of 2-nitro-5-azidobenzoic and 4-azido-2,3,5,6-tetrafluorobenzoic acids were synthesized as described (*12*).

Thymidine monophosphate kinase was isolated from *E. coli* MRE-600 according to the described method (*13*).

Synthesis of 5-{*N*-[3-(trifluoroacetylamino)propionyl]aminomethyl}-2′-deoxyuridine derivative (IV). Compound **IV** was obtained from thymidine in four steps with 68% yield (see Scheme 1) using the method described earlier (*14*): R_f = 0.78 in the system A; UV (H_2O, pH 9) $\lambda_{max,}$ 267 nm (ϵ = 8 800); λ_{min}, 235 nm (ϵ = 3 500). ^{1}H NMR (D_2O): δ 2.35 (m, H2′, 2H), 2.50 (t, J =

Scheme 1



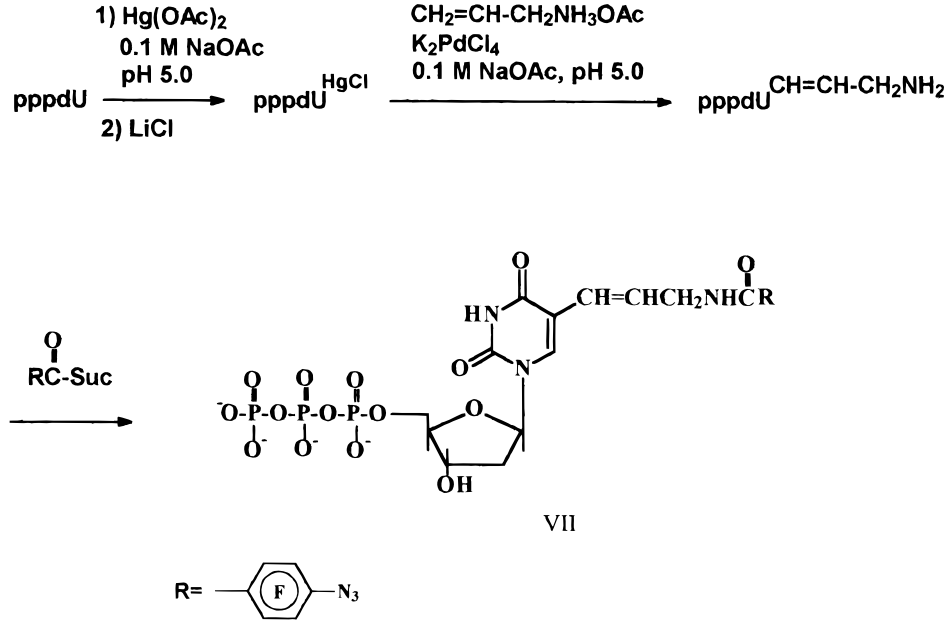
6.0 Hz, H8, 2H), 3.58 (m, H9, 2H), 3.79 (m, H5′, 2H), 4.04 (m, H7, H4′, 3H), 4.45 (m, H3′, 1H), 6.26 (t, J = 6.0 Hz, H1′, 1H), 7.54 (s, H6, 1H).

Synthesis of 5-[*N*-(3-aminopropionyl)aminomethyl]-2′-deoxyuridine-5′-triphosphate derivatives (triethylammonium salt) (V). Compound **V** was obtained from **IV** using the method described earlier for the ATP (*15*). A total of 21 μL (300 μmol) of $POCl_3$ was added to an ice-cooled suspension of **IV** 41.4 mg (100 μmol) in 300 μL of triethyl phosphate. After 16 h at 4 °C, the reaction mixture was treated with a freshly prepared solution of 500 μL of 1 M bis(tri-*n*-butylammonium) pyrophosphate and 100 μL of tri-*n*-butylamine. When the phosphorylation was complete (about 1 min), 10 μL of 1 M triethylammonium bicarbonate was added. After 1 h at room temperature, the reaction mixture was pooled on a rotary evaporator and treated with 10 mL of concentrated aqueous ammonia during 3 h to remove the trifluoroacetic protecting group. The solution was evaporated and diluted with 15 mL of water, and the product was isolated by ion-exchange chromatography on DEAE-cellulose DE-32 (1 × 15 cm) using a gradient of triethylammonium bicarbonate (0.00−0.35 M, pH 7.5). The fraction containing **V** was evaporated and dried in vacuo to give 30 μmol (30%) of **V**: R_f = 0.11 in the system B; UV (H_2O) $\lambda_{max,}$ 268 nm (ϵ = 8800); λ_{min}, 235 nm (ϵ = 3700). ^{31}P NMR (D_2O): δ −21.49 (t, J = 20 Hz, P_β, 1P), −11,16 (d, J = 20 Hz, P_α, 1P), −6.0 (d, J = 20 Hz, P_γ, 1P).

Synthesis of 5-{*N*-[*N*′-(4-azido-2,3,5,6-tetrafluorobenzoyl)-3-aminopropionyl]aminomethyl}-2′-deoxyuridine-5′-triphosphate (lithium salt) (VIa). *N*-Hydroxysuccinimide ester of 4-azido-2,3,5,6-tetrafluorobenzoic acid 4.88 mg (16 μmol) was added to a solution of **V** (4 μmol) in a mixture of DMF (60 μL) and TEA (10 μL). The reaction mixture was kept at room temperature for 4 h and then loaded directly onto a column of DEAE-cellulose DE-32 (1 × 20 cm). A linear gradient (flow rate 0.5 mL/min) from 0.05 to 0.3 M TEAB (pH 7.5) was employed. Fractions containing photoreactive nucleoside-5′-triphosphate were pooled and subjected to reversed-phase HPLC. The product **VIa** was precipitated by addition of 2% $LiClO_4$ in acetone and dried in vacuo. The yield of **VIa** was 87%. The isolated compound was homogeneous as shown by thin-layer and anion-exchange chromatography. R_f = 0.54 in the system B; UV (H_2O) $\lambda_{max,}$ 259 nm (ϵ = 33 900); λ_{min}, 232 nm (ϵ = 10 900). ^{31}P NMR (D_2O): δ −20.9 (t, J = 20 Hz, P_β, 1P), −11.08 (d, J = 20 Hz, P_α, 1P), −5.72 (d, J = 20 Hz, P_γ, 1P). ^{1}H NMR (D_2O): δ 2.43 (dd, J = 6 Hz, J = 2 Hz, H2′, 2H), 2.70 (t, J = 6 Hz, H8, 2H), 3.71 (m, H4′, H9, 3H), 4.30 (m, H3′, H5′, H7, 5H), 6.30 (t, J = 7 Hz, H1′, 1H), 7.90 (s, H6, 1H).

Synthesis of 5-{*N*-[*N*′-(2-nitro-5-azidobenzoyl)-3-aminopropionyl]aminomethyl}-2′-deoxyuridine-5′-triphosphate (lithium salt) (VIb). Compound **VIb** was synthesized from derivative **V** by treatment with *N*-hydroxysuccinimide ester of 2-nitro-5-azidobenzoic acid according to the method described above for the synthesis of **VIa**. The yield of **VIb** was 82%. The isolated compound was homogeneous by thin-layer and anion-exchange chromatography. R_f = 0.55 in the system B; UV (H_2O) λ_{max}, 269 nm (ϵ = 9000), 321 nm (ϵ = 8800); λ_{min}, 245 nm (ϵ = 7900). ^{31}P NMR (D_2O): δ −20.33 (t, J = 20 Hz, P_β, 1P), −10.95 (d, J = 20 Hz, P_α, 1P), −5.10 (d, J = 20 Hz, P_γ, 1P). ^{1}H NMR (D_2O): δ 2.23 (m, H2′, 2H), 2.65 (t, J = 5.2 Hz, H8, 2H), 3.65−3.75 (m, H4′, H9, 3H), 4.16 (m, H3′, H5′, H7, 5H), 6.25 (t, J = 6.5 Hz, H1′, 1H), 7.15 (d, J = 2.3 Hz, H10, 1H), 7.37 (dd, J = 8.9 and 2.3 Hz, H11, 1H), 7.71 (s, H6, 1H), 8.25 (d, H12, 1H).

Scheme 2



Synthesis of 5-[3-(*E*)-(4-Azido-2,3,5,6-tetrafluorobenzamido)-propenyl-1]-2′-deoxyuridine-5′-triphosphate (lithium salt) (VII). Compound **VII** was obtained according to the method of Wlassoff et al. (*6*), described for synthesis of 5-[3-[(*E*)-(2-nitro-5-azidobenzamido)propenyl-1]-2′-deoxyuridine-5′-triphosphate with the use of *N*-hydroxysuccinimide ester of 4-azido-2,3,5,6-tetrafluorobenzoic acid (see Scheme 2). The yield of **VII** (mixture of isomers) was 90%. The separation of isomers was carried out by reversed-phase HPLC. The yield of **VII** (E) was 60%. The isolated compound was homogeneous by thin-layer and anion-exchange chromatography. $R_f = 0.70$ in the system B; UV (H_2O) λ_{max}, 255 nm (ϵ = 32 600); λ_{min}, 218 nm (ϵ = 17 900). IR (KBr) ν_{max}, 2205 ($-N_3$), 1630 ($-C{=}O_{amid}$) cm^{-1}. ^{31}P NMR (D_2O): δ −21.4 (t, J = 20 Hz, P_β, 1P), −10.7 (d, J = 20 Hz, P_α, 1P), −7.8 (d, J = 20 Hz, P_γ, 1P). ^1H NMR (D_2O): δ 2.37 (t, J = 5.5 Hz, H2′, 2H), 4.03 (m, H3′, H4′, H5′, 4H), 4.10 (d, J = 5.0 Hz, H9, 2H), 6.2−6.4 (m, H1′, H7, H8, 3H), 7.9 (s, H6, 1H).

Synthesis of 5-{*N*-[*N*′-(2-nitro-5-azidobenzoyl)-3-aminopropionyl]aminomethyl}-2′-deoxyuridine-[α-^{32}P]-5′-triphosphate (lithium salt) (VI*b). 5-(Trifluoroacetylaminomethyl)-2′-deoxyuridine was synthesized from derivative **III** (0.1 mmol) by treatment with 1 mmol of ethyl trifluoracetate (120 μL) in methanol (1 mL) in the presence of 1.5 mmol of TEA (207 μL). After stirring for 15 h at 20 °C, the solution was evaporated under reduced pressure. The yellow liquid residue was dissolved in 3 mL of water and applied on a Dowex 50W X2 column (1.5 × 20 cm). 5-(Trifluoroacetylaminomethyl)-2′-deoxyuridine was eluted by water, and fractions were evaporated under reduced pressure. The yield was 94%: R_f = 0.73 in system A.

The obtained deoxyuridine analogue was converted to the 5′-*O*-dimethoxytrityl derivative by conventional procedure (*16*) and subjected to phosphorylation with $POCl_3$ using the known method (*15*). Compound **VIII** was obtained by deprotection by incubation in 0.1 N HCl in methanol (0.5 h) followed by treatment with 10 mL of concentrated aqueous ammonia for 3 h. The solution was evaporated, diluted with 15 mL of water and the product was isolated by ion-exchange chromatography on DEAE-cellulose DE-32 (1 × 20 cm) using a gradient of thriethylammonium bicarbonate (0.00−0.2 M, pH 7.5). The fraction containing **VIII** was evaporated and dried in vacuo. The yield of **VIII** was 53%: R_f = 0.76 in system B; UV (H_2O) λ_{max}, 269 nm (ϵ = 8800).

The overall procedure relies on modification of the method of Walseth and Johnson (*17*) for the enzymatic preparation of [α-^{32}P]nucleoside-5′-triphosphates from 5-(aminomethyl)-2′-deoxyuridine-3′-monophosphate and [γ-^{32}P]ATP.

The [α-^{32}P]photoreactive nucleoside-5′-triphosphate derivative **VI*b** was obtained by succesive acylation of NH_2-group of **X** with trifluoroacetyl-β-alanine *N*-hydroxysuccinimide, and benzoylation of deprotected NH_2-group of the β-alanine with 2-nitro-5-azidobenzoic acid *N*-hydroxysuccinimide as described above for compound **VIa**. The yield of **VI*b** was 83%: R_f = 0.30 in system B.

Studies of the Thermolytic Stability of Azido Group of Photoreactive Nucleoside-5′-triphosphate Derivative VII. The thermolytic stability of azido groups of new compouds under the conditions of PCR was studied using the compound **VII**. A 0.5 mM aqueous solution (100 μL) of photoreagent **VII** was subjected to the thermal regime of the amplification procedure. The dU*TP was precipitated by addition of 2% $LiClO_4$ in acetone. The precipitate was carefully washed with acetone (2 × 1.2 mL). IR (KBr) ν_{max}, 2205 ($-N_3$), 1630 ($-C{=}O_{amid}$) cm^{-1}.

Photochemical Behavior of Photoreactive Amplified DNA. A 10^{-7} M solution (20 μL) of photoreactive amplified [^{32}P]DNA in 0.15 M NaCl, 0.1 mM EDTA, and 0.02 M Na_2HPO_4 (pH 9) was pipetted into a 96-well polystyrene plate at 4 °C. Irradiation was carried out by exposing the plate for 18 min to filtered light (300−365 nm) emitted by a high-pressure mercury lamp with an intensity 10^{15} quanta × cm^{-2} × s^{-1}. The irradiated mixture was subjected to electrophoresis in 10% denaturing PAAG and vizualized by radioautography. Quantitative treatment of radioautographs was carried out using Ultrascan laser densitometer (LKB).

RESULTS AND CONCLUSIONS

Synthesis and Characterization of Photoanalogues dU*TP. Synthesis of new dUTP derivatives

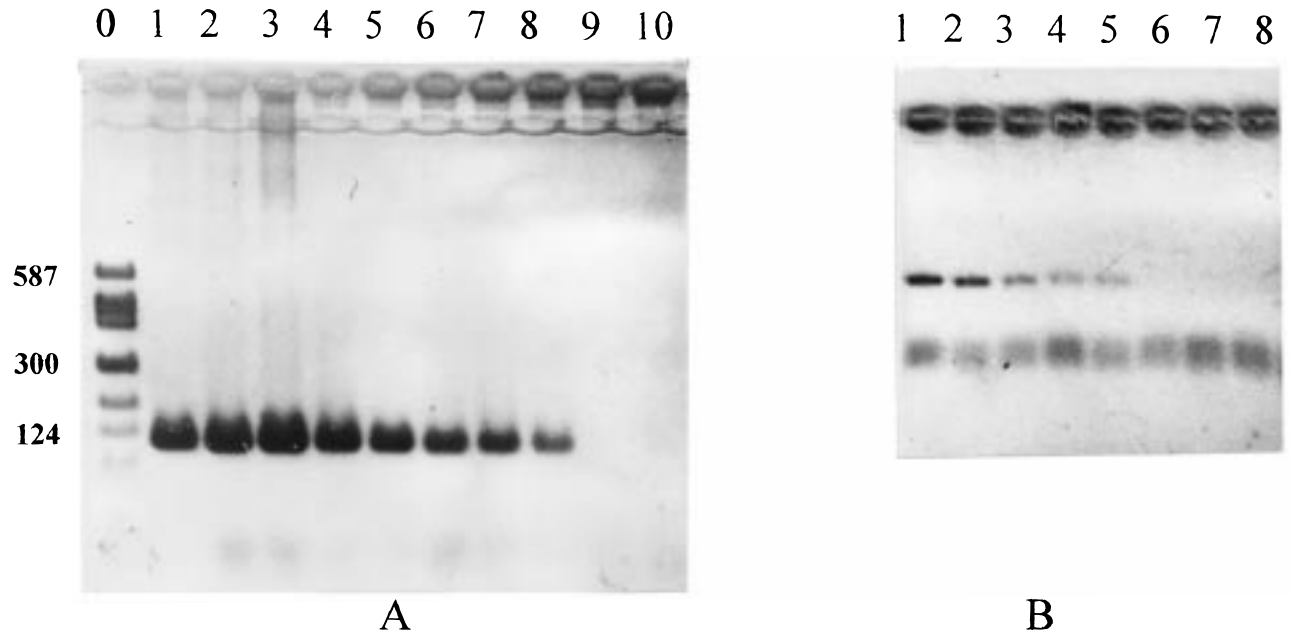


Figure 1. The product of the PCR in the presence of different amount of dU*TP analogue **VIa** (A); analogue **VIb** (B). (A) Lane 1, dTTP only; 2, 10% **VIa**; 3, 20% **VIa**; 4, 50% **VIa**; 5. 60% **VIa**; 6, 70% **VI**a; 7, 80% **VIa**; 8, 85% **VIa**; 9, 90% **VIa**; 10, 100% **VIa**. (B) Lane 1, dTTP only; 2, 10% **VIb**; 3, 20% **VI**; 4, 50% **VIb**; 5, 60% **VIb**; 6, 70% **VIb**; 7, 80% **VIb**; 8, 100% **VIb**; 4 μL from a 50 μL PCR product was analyzed by 2% agarose gel electrophoresis and visualized by ethidium bromide staining. Lane 0 (A), the molecular size marker is pGem-1 (HAE III).

(dU*TP), carrying photoreactive groups, which are highly reactive toward both DNA and proteins were carried out as shown in Schemes 1 and 2.

It is known that the introduction of CH═CH−CH_2−NH_2 spacer to 5-C of 2′-deoxyuridine is accompanied by the formation of isomers with the trans propenyl configuration being the major product (*6*, *18*). We have isolated three isomers of compound **VII** by reversed-phase HPLC. We have proposed that they are E and Z isomers and 5-[3-(4-azido-2,3,5,6-tetrafluorobenzamido)propenyl-2]-2′-deoxyuridine-5′-triphosphate—the product of arylation of allylamine in C2 position, on the basis of ref *18*.

Compounds **I**−**IV** were obtained using the known method (*14*). Reaction of **IV** with $POCl_3$ resulted in the formation of a mixed anhydride, which produced nucleoside-5′-triphosphate **V** under interaction with bis(tri-*n*-butylammonium)pyrophosphate and the following treatment of the reaction mixture with concentrated aqueous ammonia, permitted to remove CF_3CO residue quantitatively off the β-alanyl NH_2-group. Photoreactive derivatives **VIa**,**b** were obtained by benzoylation of aliphatic amino group of **V** with *N*-hydroxysuccinimide esters of 4-azido-2,3,5,6-tetrafluorobenzoic or 2-nitro-5-azidobenzoic acids. The use of the triethylammonium salt of **V** permitted to carry out the reaction in DMF in the presence of triethylamine, thus opening the possibility to achieve higher yields (near 90%) with lower excesses of *N*-hydroxysuccinimide esters.

The structure of photoreactive dU*TP derivatives **VIa**,**b** and **VII** (E) was verified by ^{1}H NMR. The data of anion-exchange chromatography and ^{31}P NMR spectroscopy [the presence of the resonance at δ −21.4 ppm (t, J = 20 Hz, P_β, 1P), −10.7 (d, J = 20 Hz, P_α, 1P), −7.8 (d, J = 20 Hz, P_γ, 1P), for one example, the compound **VII**] proved the presence of the 5′-triphosphate moieties. IR spectra of the compounds obtained revealed the presence of the band at 2205 cm^{-1} (KBr) characteristic of the azido group.

Each photoreactive dU*TP analogue was examined to answer the following questions. Is the dU*TP derivative a substrate for DNA polymerases? Is the newly synthesized DNA containing photoreactive groups a template for the following DNA replication? Is it able to efficiently cross-link with template DNA under irradiation?

Consequently, we have carried out the polymerase chain reaction (PCR) using DNA polymerase *Thermus aquaticus* assays and offering our photoreactive nucleoside-5′-triphosphates as substrates both in the presence and in the absence of dTTP. The amplification of DNA was performed using a pair of oligodeoxyribonucleotide primers which flank a 110 bp region in the gene of the envelope protein E of the tick-borne encephalitis virus. Optimal conditions of PCR for this system with natural nucleoside-5′-triphosphates were elucidated earlier (*19*).

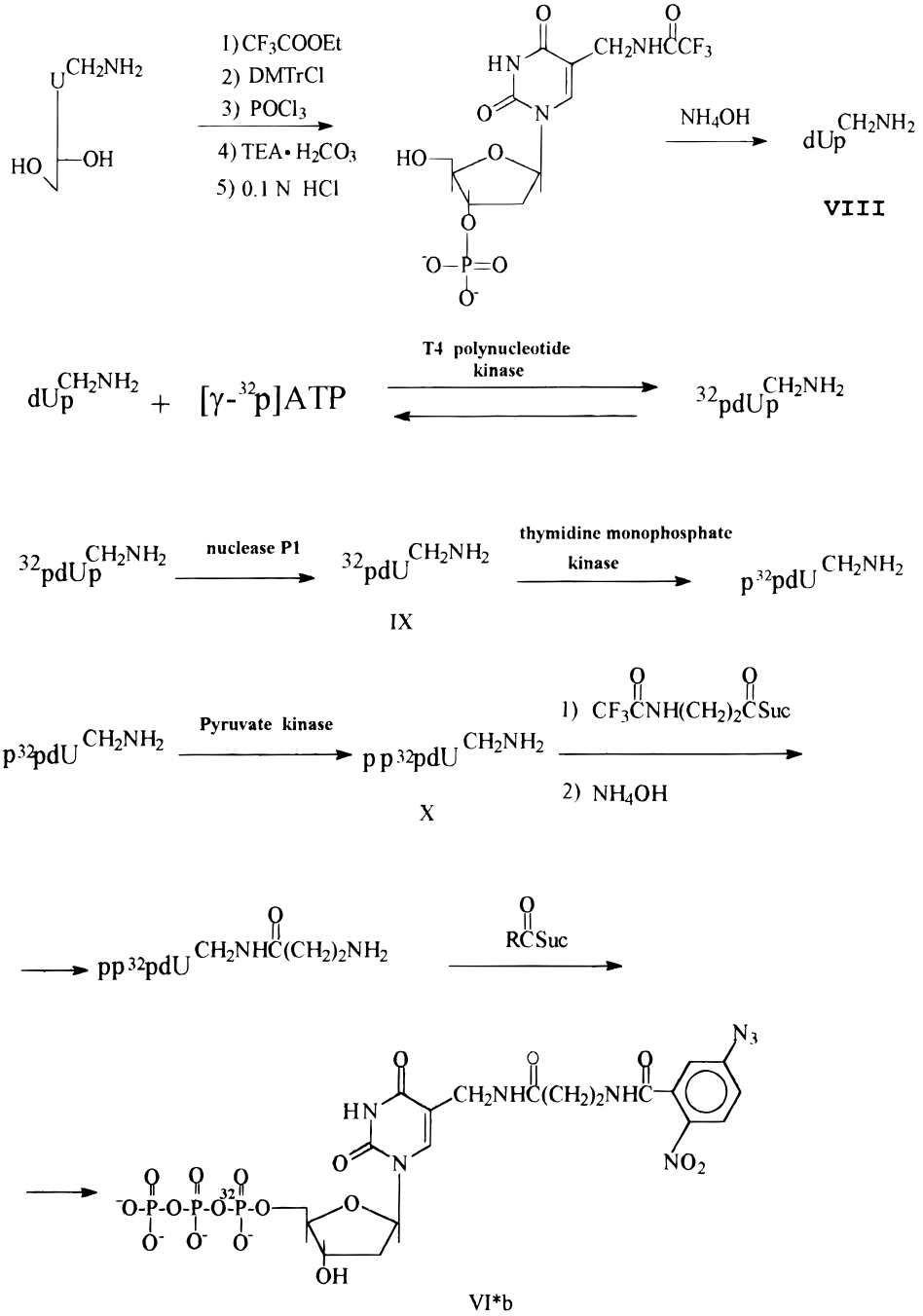
Since azides are known to undergo thermolytic decomposition, the stability of photoreactive nucleoside-5′-triphosphates was preliminary investigated. The thermolytic stability of azido groups of new compounds under the conditions of PCR was studied using the compound **VII**. A 0.5 mM aqueous solution (50 μL) of photoreagent **VII** was subjected to the terminal regime of the amplification procedure. The dU*TP was precipitated by addition of 2% $LiClO_4$ in acetone. The presence of an azido group in the product was proved by IR spectroscopy (the presence of distinct band at 2205 cm^{-1}). The ratio of intensities ν_{2205}/ν_{1630} did not change after treatment in the thermal PCR regime.

When the reaction mixture for PCR with photoanalogues **VIa**,**b** were used in the absence of dTTP, no traces of the full-length primer extension product was observed (Figure 1). The amplified DNA appeared only in the case of simultaneous presence of certain amount of both photoreactive dU*TP and dTTP.

To establish if dU*TP can be used by the DNA polymerase as the substrate, the incorporation of [α-^{32}P]-dU*TP analogue **VIb** in the amplified product was estimated.

Synthesis of the photoreactive [α-^{32}P]dU*TP was fulfilled according to the Scheme 3. Deoxyuridine analogue **III** was converted to 5′-*O*-dimethoxytrityl derivative by

Scheme 3



a conventional procedure and subjected to phosphorylation with $POCl_3$ with subsequent hydrolysis by triethylammonium bicarbonate and deprotection of 5′-OH group by incubation in 0.1 N HCl. The 2′-deoxyuridine-3′-monophosphate analogue **VIII** obtained was enzymatically converted to [5′-^{32}P]2′- deoxyuridine-3′,5′-diphosphate using [γ-^{32}P]ATP and T4 polynucleotide kinase. Then 3′-phosphate was removed by nuclease P1. [5′-^{32}P]-dU*MP (**IX)** was further phosphorylated to dU*DP with nonradioactive ATP using thymidine monophosphate kinase from *E. coli* MRE-600 and to dU*TP (**X**) with phosphoenolpyruvate using pyruvate kinase. Interestingly, despite its high specificity, dTMP kinase turned out to be able to catalyze phosphorylation of **IX**, albeit at lower efficiency as compared with dTMP. The same results were obtained for the analogue with protecting trifluoroacetyl residue on aliphatic amino group.

The [α-^{32}P]photoreactive nucleoside-5′-triphosphate derivative **VI*b** was obtained by succesive acylation of NH_2-group of the compound **X** with trifluoroacetyl-β-alanine *N*-hydroxysuccinimide, removal of trifluoroacetyl residue, and benzoylation of deprotected NH_2-group of the β-alanine with *N*-hydroxysuccinimide ester of 2-nitro-5-azidobenzoic acid as described above for **VIa**.

The product was separated from reaction mixture by ion-exchange and reversed-phase chromatography and analyzed by thin-layer chromatography (TLC). The radiolabeled dU*TP (**VI*b**) had $R_f = 0.3$ on DC-Alufolien Kieselgel TLC plates in the system (B), which is identical with that for nonradioactive photoreactive dU*TP derivative **VIb**.

When the polymerase chain reaction was carried out using the mixture of 50% of photoreactive [α-^{32}P]2′-deoxyuridine-5′-triphosphate derivative **VI*b** and the

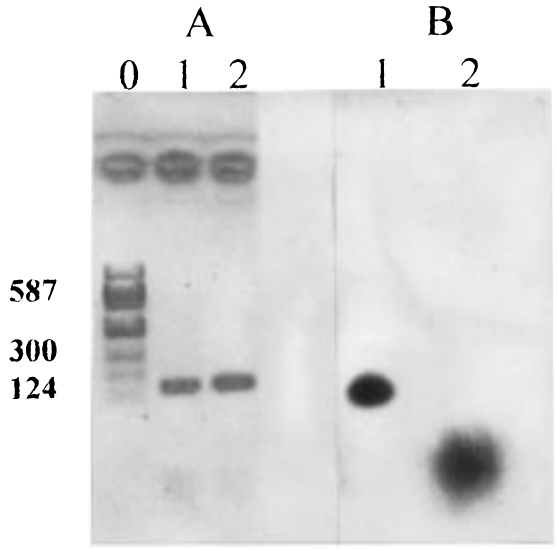


Figure 2. The product of the PCR carried out with 100% dTTP and ^{32}P-foward primer (lane 1); with 50% compound **VI*b** and 50% dTTP (lane 2); lane 0, the molecular size marker as Figure 1. A total of 4 μL from a 50 μL PCR product was analyzed by 2% agarose gel electrophoresis and visualized by ethidium bromide staining (A), autoradiography (B).

dTTP (50%), the formation of full-length amplificate band was observed, as revealed by ethidium bromide staining of the gel (Figure 2A). However, the respective band did not contain any radioactivity (Figure 2B). The radioactive label was observed only in shorter fragments. This indicates that incorporation of the analogue does not permit further elongation. On the contrary, it was found that **VII** (E) replaced dTTP during synthesis of DNA by PCR as revealed by the formation of the full-length amplificate in the presence of this dU*TP analogue without any dilution with natural dTTP (Figure 3). In the same time, we did not obtain full-length amplificate using compounds **VII** (Z) and 5-[3-(4-azido-2,3,5,6-tetrafluorobenzamido)propenyl-2]-2′-deoxyuridine-5′-triphosphate.

The PCR mixture was subjected to electrophoresis in 10% PAAG. The amplified DNA was extracted from the gel by electroelution and inspected by UV and IR spectroscopy. The UV absorption spectra of the product (2×10^{-4} M, H_2O) showed λ_{max} 260 nm characteristic of the oligonucleotide component. IR spectroscopy (2×10^{-4} M, H_2O, 0.02 mm CaF_2 cuvette) proved that analogue **VII** (E) was included into the DNA by PCR (the presence of the characteristic band of the azido group at 2100 cm $^{-1}$).

The photolytic behavior of photoreactive amplified DNA was investigated. The solution of amplified [^{32}P]-DNA (10^{-7} M) in 0.15 M NaCl and 0.02 M Na_2HPO_4 (pH 9) was subjected to photolysis for 18 min and analyzed by denaturing gel electrophoresis. The irradiation time was chosen to be 10-fold greater than the half-life of photolysis. The kinetics of photolysis was studied by recording the IR spectra (2000−3000 cm^{-1}) of the samples irradiated for definite time intervals. As shown in Figure 4, irradiation of the full-length amplificate resulted in the appearance of the cross-linked amplification product (peak 2).

To prove additionally the ability of **VII** (E) to serve a substrate of DNA polymerases, we studied its incorporation into the system: 3′-GGGTCAGTGCTGCAACATTTT-GCTGC... (as a template) and [^{32}P]CCCAGTCACGACGT (as a primer).

It can be seen in Figure 5 that the compond **VII** (E) is incorporated into the DNA chain by the Klenow fragment



Figure 3. The product of the PCR carried out with 100% compound **VII** (E) (lane 1); with 100% dTTP (lane 2). A total of 4 μL from a 50 μL PCR product was analyzed by 2% agarose gel electrophoresis and visualized by ethidium bromide staining.

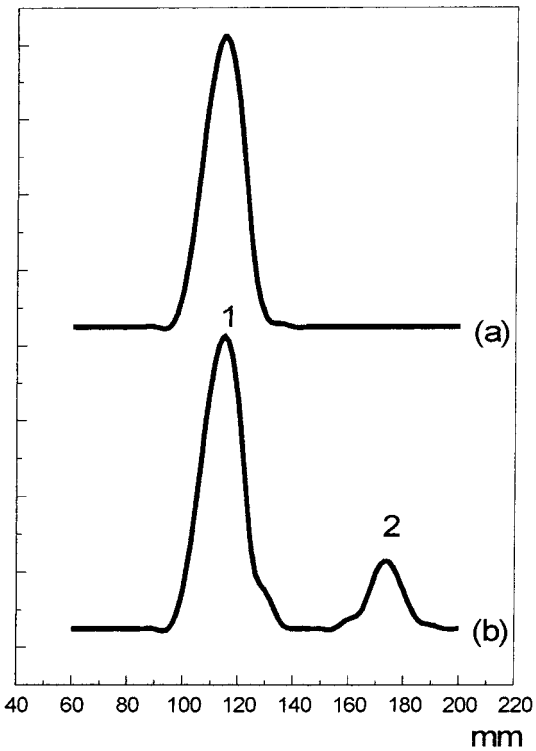


Figure 4. Densitogramms of the gel-radioautographs for the product of the PCR were carried out with 100% compound **VII** and ^{32}P-forward primer. Nonirradiated amplified DNA (a). Irradiated product (b).

of DNA polymerase I (lanes 4−9) and *Taq* DNA polymerase (lanes 13−15). In the control assays, tetradecanucleotide was extended by one residue in the presence of dTTP (lanes 2 and 11) and by three residues in the presence of dTTP and dGTP (lanes 3 and 12) giving

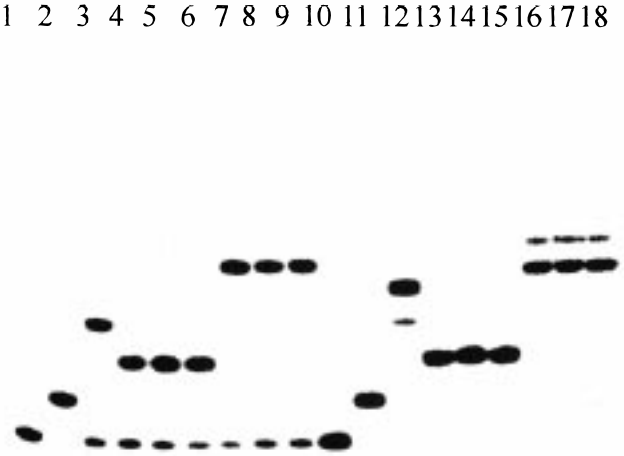


Figure 5. Primer extension catalyzed by Klenow fragment of DNA polymerase I (lanes 1−9) and *Taq* DNA polymerase (lanes 10−18). lanes 1 and 10, enzyme + primer-template 3′GGGTCAGTGCTGCAACATTTTGCTGC (the M13mp10 phage DNA) [^{32}p]CCCAGTCACGACGT (the primer); lanes 2 and 11, as in lanes 1 and 10 + 2 μM dTTP; lanes 3 and 12, as in lanes 2 and 11 + 2 μM dGTP+; lanes 4−6 and 13−15, as in lane 1 + 0.5 μM, 2 μM, and 8 μM compound **VII** (E); lanes 7−9 and 16−18, as in lanes 4−6 and 13−15 + 2 μM dGTP. The reaction products were separated by electrophoresis in the denaturing 20% PAAG.

15-mer and 17-mer, respectivelly. Additionally, there is an 18-mer band most probably due to misincorporation of dGMP residue with formation of mismatched T:G pair, which is most stable among noncanonic pairs (*20*). In the case of the Klenow fragment of *E. coli* DNA polymerase I, displaying 3′-5′ exonuclease activity, which is absent in *Taq* DNA polymerase, low level of a mismatched incomplete nucleotide at the 3′-end was observed. This has been noticed many times before in the systems with a reduced set of substrates (*21*, *22*). Incorporation of one residue of **VII** (E) into a nascent DNA chain would result in formation of a hydrophobic 15-mer of lower electrophoretic mobility (lanes 4−6) as compared with its natural counterpart (lane 2). After addition of dGTP to the assay containing **VII,** one can see the elongation of 15-mer band by two nucleotides (17-mer band) according to the template context (lanes 7−9). The position of 17-mer band corresponds to the mobility of oligonucleotide with two hydrophobic residues. So, we can state that Klenow fragment of *E. coli* DNA polymerase I and *Taq* DNA polymerase are able to incorporate the modified deoxyuridine-5′-phosphate residue with large hydrophobic photoreactive substituents at the 5-position into the 3′-end of the DNA chain keeping the ability of further elongation. Thus, it was shown that the use of modified substrate did not lead to the loss of the specificity of template synthesis.

The unique property of dU*TP analogue **VII** (E) made it possible to use it for direct incorporation in the course of elongation of DNA probes at the template DNA in chromosomes and in interphase chromatin with subsequent cross-linking of the elongated probes with matrixed DNA. This ability might provide a possibility of localization of short probes. We have used this approach for localization of nucleotide sequences on human metaphase chromosomes and interphase nuclei. These results presented in a separate communication (*23*).

ACKNOWLEDGMENT

The authors are grateful E. Yu. Dobrikova for the preparation pTBE-51.1-plasmid DNA, to Dr. V. N. Silnikov for the registration of IR spectra, to V.V. Kandaurova for the registration of NMR spectra, and to Prof. D. G. Knorre for the helpful discussions. This work was supported in part by the grant of the Russian States Program "Human Genome", by the grant of the Russian Fund of Fundamental Investigations, and by the Grant CDA-NIS.

LITERATURE CITED

(1) Hanna, M. M., Dissinger, S., Williams, B. D., and Colston, J. E. (1989) Synthesis and characterization of 5-[(4-Azidophenacyl)thio]uridine 5′-triphosphate, a cleavable photocross-linking nucleotide analogue. *Biochemistry 28*, 5814−5820.

(2) Hanna, M. M., Zhang, Y., Reidling, J. C., Thomas, M. J., and Jou, J. (1993) Synthesis and characterization of a new photo-cross-linking CTP analogue and its use in photoaffinity labeling *E.coli* and T7 RNA polymerases. *Nucleic Acids Res. 21*, 2073−2079.

(3) Doronin, S. V., Dobrikov, M. I., and Lavrik, O. I. (1992) Photoaffinity labeling of DNA polymerase α DNA primase complex based on the catalytic competence of a dNTP reactive analogue. *FEBS Lett. 313*, 31−33.

(4) Doronin, S. V., Dobrikov, M. I., Buckle, M., Roux, P., Buc, H., and Lavrik, O. I. (1994) Affinity modification of human immunodeficiency virus reverse transcriptase and DNA template by photoreactive dCTP analogues. *FEBS Lett. 354*, 200−202.

(5) Dobrikov, M. I., Doronin, S. V., Safronov, I. V., Shishkin, G. I., and Lavrik, O. I. (1994) Affinity modification of M13 DNA by a photoreactive analogue of dNTP promoted by HIV-1 reverse transcriptase. *Chem. Sustainable Devel. 2*, 1−6.

(6) Wlassoff, W. A., Dobrikov, M. I., Safronov, I. V., Dudko, R. Y., Bogachev, V. S., Kandaurova, V. V., Shishkin, G. V., Dymshits, G. M., and Lavrik, O. I. (1995) Synthesis and characterization of (d)NTP derivatives substituted with residues of different photoreagents. *Bioconjugate Chem. 6*, 352−360.

(7) Poletaev, A. I., Nasedkina, T. V., Godovikova, T. S., and Knorre, D. G. (1994) Photoanchoring probes for in situ localization. *Cytometry 7*, 75.

(8) Dobrikov, M. I., Zarytova, V. F., Komarova, N. I., Levina, A. S., Lokhov, S. A., Prikhodjko, T. A., Shishkin, G. V., Tabatadze, D. R., and Zaalishvilli, M. M. (1992) Effective sequence-specific photomodification of nucleic acids by oligonucleotide derivatives bearing aromatic azido groups. *Bioorgan. Khim. 18*, 540−549.

(9) Godovikova, T. S., Berezovskii, M. V., and Knorre, D. G. (1995) Affinity modification of amino acid derivatives of oligonucleotides in complementary complex. *Bioorgan. Khim. 21*, 858−867.

(10) Gryaznov, S. M., Gorn, V. V., Zarytova, V. F., Kumarev, V. P., Levina, A. S., Polistchuk, A. S., Potapov, V. K., Potemkin, G. A., Sredin, Yu. G., and Shabarova, Z. A. (1987) Automatic synthesis of oligodeoxyribonucleotides using phosphitamide method on "Victoria 4M". *Izv. Sib. Otd. Akad. Nauk SSSR 2*, 119−123.

(11) Maniatis, T., Fritsch, E. E., and Sambrook, J. (1984) A laboratory Manual. *Molecular cloning*, pp 241−244, Cold Spring Harbor University Press, Plainview, New York.

(12) Dobrikov, M. I., Prichodjko, T. A., Safronov, I. V., and Shishkin, G. V. (1992) Synthesis of photosensitive kapron membranes. Photoimmobilization of DNA. *Sib. Chim. J. 2*, 18−23.

(13) Richter, V. A., Rabinov, I. V., Kuznetsov, S. A., Pavlii, T. B., and Skoblov, Yu. S. (1988) Purification and same properties of nucleoside monophosphate kinases from *Escherichia coli*. *Prikl. Biokhim. Mikrobiol. 24*, 310−312.

(14) Zarytova, V. F., Komarova, N. I., Levina, A. S., Lokhov, S. A., Tabatadze, D. R., Khalimskaya, L. M., and Alexandrova, L. A. (1993) The synthesis of oligonucleotides carrying deoxyuridine C-5-modified with an aliphatic amino group. *Bioorgan. Khim. 17*, 1059−1065.

(15) Ludwig, J. (1981) A new route to nucleoside-5′-triphosphates. *Acta Biochim. Biophys. Acad. Sci. Hung. 16*, 131−133.

(16) Connolly, B. A. (1991) Oligodeoxynucleotides containing modified bases. In *Oligonucleotided and Analogues. A Practical Approach* (F. Eckstein, Eds.) pp 111−113, Oxford University Press.

(17) Walseth, T. F., and Johnson, R. A. (1979) The enzymatic preparation of [α-^{32}P]nucleoside triphosphates, cyclic [α-^{32}P]-AMP and cyclic [α-^{32}P]GMP. *Acta Biochim. Biophys. Acad. Sci. Hung. 562*, 11−31.

(18) Bergstrom, D. E., and Ogawa, M. K. (1978) C-5 substituted pyrimidine nucleosides. 2. Synthesis via olefin coupling to organopalladium intermediates derived from uridine and 2′-deoxyuridine. *J. Am. Chem. Soc. 100*, 8106−8112.

(19) Godovikova, T. S., Orlova, T. N., Dobrikova, E. Yu., Shamanin, V. A., Zarytova, V. F., Vorobyeva, N. V., Serdyukova, N. A., Shamanina, M. Yu., Petruseva, I. O., and Pitsenko, N. D. (1994) Highly sensitive nonradioactive detection of trick-borne encephalitis virus. *Bioorgan. Khim. 20*, 1196−1205.

(20) Kneal, G., Broun, T., and Kennard, O. (1985). G-T basepare in DNA helix: the crystal structure of d(GGGGTCCC). *J. Mol. Biol. 21*, 805−814.

(21) Hillebrand, G. G., MsGluskey, A. H., Abbott, K. A., Revich, G. G., and Beative, K. L. (1984) Misincorporation during DNA synthesis, analyzed by gel electrophoresis. *Nucleic Acids Res. 12*, 3155−3171.

(22) Huang, P., Farquhar, D., and Plunkett, W. (1990) Selective action of 3′-azido-3′-deoxythymidine 5′-triphosphate on viral reverse transcriptases and human DNA polymerases. *J. Mol. Biol. 265*, 11914−11918.

(23) Nasedkina, T. V., Mal′kov, R. B., Fedorova, L. I., Godovikova, T. S., Kolpashchikov, D. M., and Poletaev, A. I. (1998) Use of photoanchoring DNA probes for FISH. *Cytology 40*, 763−767.

BC980144R

TECHNICAL NOTES

Direct Observation of Fibrinogen−Heparinoid Complexes Formation Using Surface Plasmon Resonance

Nobuyuki Sakamoto, Tomoko Shioya, Takeshi Serizawa, and Mitsuru Akashi*

Department of Applied Chemistry and Chemical Engineering, Faculty of Engineering, Kagoshima University, 1-21-40 Korimoto, Kagoshima 890-0065, Japan. Received December 26, 1997; Revised Manuscript Received December 8, 1998

We analyzed the binding of heparinoid or heparin with fibrinogen by real-time measurement using surface plasmon resonance technology. Poly(glucosyloxyethyl methacrylate) sulfate [poly(GEMA) sulfate] and dextran sulfate were used as heparinoids. The binding ability of each sulfated polymer was estimated by having each polymer-containing buffer interact with the sensor chip surfaces that had immobilized fibrinogen. Dextran sulfate and poly(GEMA) sulfate showed high affinity to the fibrinogen in this experiment, while the heparin did not. All of the dextran sulfates were desorbed from its surface, while about 30% of the poly(GEMA) sulfate remained on the immobilized fibrinogen upon the addition of NaCl to the buffer which was done in order to analyze the desorption of poly(GEMA) sulfate or dextran sulfate from the surface of the fibrinogen. These data show that the type of binding between fibrinogen−poly(GEMA) sulfate was different from that of dextran sulfate, indicating that the interaction between fibrinogen and poly(GEMA) sulfate was caused not only by an electrostatic but also by a hydrophobic force. These results suggest that the interaction mechanism of heparinoids with fibrinogen was different from that of heparin.

INTRODUCTION

Extensive research has been done about the interaction of blood plasma protein with polysaccharide sulfuric acid esters (*1*). Fibrinogen (which is blood clotting factor I), forms a soluble complex with polyanion [sulfate, polyvinyl sulfate, and polyisoprene sulfonate (*2*−*6*)], although fibrinogen contains an overall negative charge in a neutral buffer solution. The distribution of charges on a fibrinogen surface should be heterogeneous. This is a reasonable assumption based on the recently elucidated first-order structure and higher order structures of human fibrinogen (*7*, *8*). In our previous study on glycoside polymer, we found that sulfated poly(glucosyloxyethyl methacrylate) [poly(GEMA) sulfate], which bears sulfated D-(+)-glucose, exhibited anticoagulant activity (*9*), and we studied their anticoagulant mechanism by evaluating various in vitro clotting tests (*10*, *11*). Next, we found that poly(GEMA) sulfate and dextran sulfate formed insoluble complexes with bovine plasma fibrinogen by the turbidity measurement of each complex that contained PBS by using an UV−vis spectroscopy. In our experiment, the amount of poly(GEMA) sulfate−fibrinogen insoluble complex increased with an increase in the amount of poly(GEMA) sulfate. On the other hand, the amount of dextran sulfate−fibrinogen insoluble complex showed a maximum (0.01 mg of dextran sulfate to 4.5 mg of fibrinogen in 1 mL of PBS) when dextran sulfate was added to fibrinogen PBS solution. However, these tendencies were not shown upon the addition of heparin, although heparin has a relatively high charge density (1.5−2.0/pyranose ring). The effects of the inhibition of fibrinogen polymerization by sulfated polymers act on both stages when A and B chains are split by thrombin and on the polymerization of fibrin monomers (*3*). Therefore, we concluded that poly(GEMA) sulfate or dextran sulfate formed insoluble complexes with fibrinogen and then these sulfated polymers appeared to have anticoagulant activity.

Thus far, researchers have clarified the complex formation between fibrinogen and sulfated polymers by precipitation measurements, transmittance measurements using UV−vis spectroscopy, circular dichroism measurements, and electrophoretic mobility measurements with a Tiselius apparatus (*2*, *3*, *5*, *12*). However, there have been few studies about kinetic measurements of these complex formations because it is very difficult to use the radio-labeling and fluorescence-labeling techniques (*13*) for either fibrinogen or sulfated polymers. Moreover, there has been no research about association and dissociation rate constant measurement of interaction between fibrinogen and sulfated polymer in situ. Therefore, a kinetic study on heparinoid−plasma protein interaction would provide significant data in regards to its anticoagulant activity.

In this paper, we analyzed the interactions between plasma fibrinogen and each sulfated polymer at physiological pH values in detail using surface plasmon resonance (SPR) technology (*14*, *15*). The BIAcore system (*16*−*18*) used in this study was produced by Pharmacia Biosensor AB (Uppsala, Sweden). BIAcore is a new type of technology that is designed to analyze label-free

* To whom correspondence should be addressed. Phone: +81-992-85-8320. Fax: +81-992-55-1229. E-mail: akashi@apc.eng.kagoshima-u.ac.jp.

10.1021/bc970218j CCC: $18.00 © 1999 American Chemical Society
Published on Web 03/27/1999

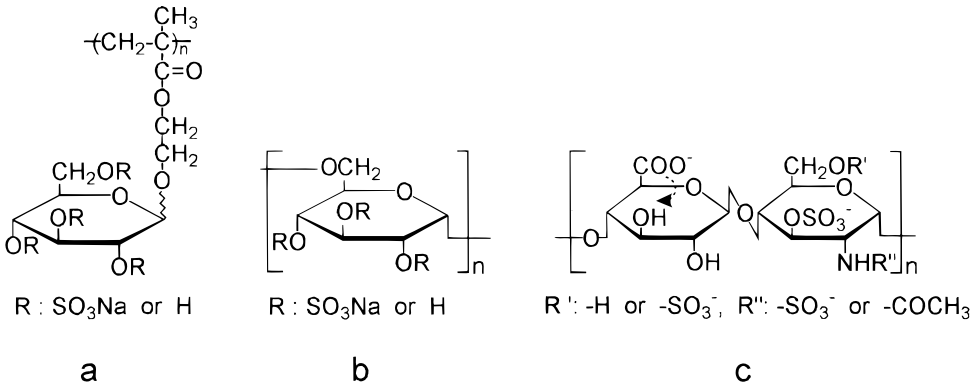


Figure 1. Structure of poly(GEMA) sulfate (a), dextran sulfate (b), and heparin (c).

macromolecular interactions in real-time. The interactions between an immobilized molecule on a sensor chip and ligand is monitored by surface plasmon resonance, which detects changes in mass. We also studied the interactions of fibrinogen or albumin with some sulfated polymers for comparative process. The addition of salt to the buffer for desorption of each sulfated polymer from the immobilized fibrinogen gave insights into the mechanistic aspects of the interactions between each sulfated polymer and fibrinogen.

MATERIALS AND METHODS

Materials. Poly(GEMA) sulfate was obtained by the sulfation of poly(GEMA) (*9*). We estimated the degree of sulfation of the poly(GEMA) sulfate by elemental analysis (which is the number of substituted hydroxyl groups in a glucose unit) to be 3.8. Heparin sodium salt (LotM2E) was purchased from Nacalai Tesque (Kyoto, Japan) and had an anticoagulant activity of 187.5 IU mg^{-1} solid. Dextran sulfate was also purchased from Nacalai Tesque and the degree of sulfation was 2.1. The structures of these sulfated polymers are shown in Figure 1. Bovine plasma fibrinogen and bovine serum albumin were purchased from Sigma (St. Louis, MO). A BIAcore, Sensor Chip CM5 (a carboxymethylated dextran that is coupled to a gold-coated glass surface according to procedures described elsewhere) and an Amine Coupling Kit containing EDC, NHS, and a solution of 1 M ethanol amine hydrochloride that was adjusted to a pH of 8.5 with sodium hydroxide were obtained from Pharmacia Diagnostics AB. All other reagents used were of analytical grade. In addition, MilliQ-grade water was used.

SPR Apparatus. SPR phenomenon was first developed by Otto (*14*) and Kretschmann and Raether (*15*). A laser beam is directed onto the underside of a glass prism, which is an index that is matched to a metal-coated microscope slide and undergoes the total internal reflection at the glass/metal interface. A specific angle of incident beam and surface plasmon at the metal/air interface causes the surface plasmon to be excited and a leads to a subsequent reduction in the intensity of the internally the reflected light. The angle at which this excitation occurs (the SPR angle) is dependent upon the dielectric properties of the layers above the gold surface; therefore, SPR can be used to detect the adsorption of molecules at this interface. In an automatic instrument, BIAcore 2000, the sensor device is composed of three parts: a sensor chip that is a thin film of gold covered with carboxymethylated dextran, a prism which is placed on the opposite glass surface of the chip, and a microfluidices cartridge that can provide proper reaction fluid onto the surface of the sensor chip. As molecules adsorb to the sensor surface, the change in the SPR angle is recorded as a function of time in order to observe the adsorption process onto the sensor surface in real time.

Immobilization of Fibrinogen and Albumin. The immobilization of fibrinogen or albumin on Sensor Chip CM5 in BIAcore was done as follows (*19*, *20*). Separate vials that contained 200 μL of 0.1 M NHS, 0.4 M EDC, and a 1 M ethanolamine hydrochloride solution and a vial for mixing EDC and NHS were placed in an autosampler together with a solution of fibrinogen or albumin that was to be immobilized. A continuous flow pump was filled with PBS buffer (pH 7.4). After Sensor chip CM5 had been conditioned with PBS for a few minutes, an automated immobilization cycle was performed at a flow rate of 5 μL min^{-1}. Eighty microliters of EDC and NHS mix (1/1) was transferred to the mixing vial, and forty microliters of the mixed solution was injected on the surface. Fibrinogen and albumin were dissolved in a 10 mM acetate buffer (pH 5.0) at a concentration of 250 and 400 μg mL^{-1}, respectively. Eighty microliters of each protein solution were then injected, followed by 35 μL of ethanolamine hydrochloride solution. Approximately 1.6×10^4 resonance units (RU) of fibrinogen and 1.2×10^4 RU of albumin were immobilized on the sensor chip. These corresponded to 4.7×10^{-5} nmol mm^{-2} and 17.8×10^{-5} nmol mm^{-2}, respectively, based on the relationship in which 1000 RU equals 1 ng mm^{-2} bound protein (refractive index in protein = 1.6).

Interaction of Sulfated Polymers with Fibrinogen Surface. We estimated the binding of each sulfated polymer to the immobilized fibrinogen as follows: a sensor chip (CM5) with immobilized fibrinogen was brought into contact with the PBS buffer. The flow rate of the buffer solution was kept at a high level (10 μL min^{-1}) in order to prevent mass transport limitation at the sensor surface/solution interface. After reaching a stable baseline (80 s), we injected 40 μL of PBS buffer which contained every sulfated polymer (0.3, 1.5, 3, and 30 μg mL^{-1}), through the fibrinogen surfaces in order to observe the association rate constant (80−320 s). Next, we injected 40 μL of PBS buffer for the purpose of observing the dissociation rate constant (320−560 s). We monitored the changes in the resonance angle consecutively with time intervals of 1 s. This was done for 15−20 min.

Desorptions of Sulfated Polymers from Fibrinogen Surface. We estimated the degree of dissociation of poly(GEMA) sulfates or dextran sulfates from the fibrinogen surface by the addition of NaCl (0.03−3.0 M) in the PBS buffer. After performing the dissociation cycle (560 s, the resonance unit of this point is approximately

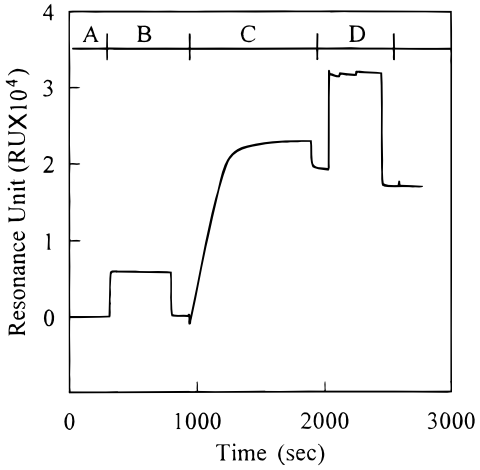


Figure 2. The sensorgram showing the procedure and response of the immobilization of fibrinogen to the sensorchip surface. The letters A, B, C, and D indicate time intervals during which the sensor was in contact with different solutions (A, PBS buffer; B, EDC/NHS; C, acetate buffer with fibrinogen 250 μg mL^{-1}; D, ethanolamine hydrochloride).

constant), we injected NaCl-containing buffer (10 μL) into each of the heparinoid−fibrinogen complex surfaces and the remaining heparinoid on the fibrinogen surface (which was represented by a resonance unit) was estimated as a $\Delta RU_{560s}/\Delta RU_{930s}$ ratio (Figure 6a).

RESULTS AND DISCUSSION

Interactions of Sulfated Polymers with Protein Surface. Figure 2 shows a sensorgram that was recorded during the immobilization of fibrinogen onto the carboxymethylated dextran that covered the sensorchip of a plasmon resonance sensor. The SPR angle is represented as a resonance unit (RU) in BIAcore (0.1° = 1000 RU). During the time interval when the sensor was in contact with the fibrinogen solution, we observed an increase in the resonance unit (RU), which indicates the adsorption of fibrinogen onto the surface. The shape of the response curve (C) indicates that the saturation of the surface with fibrinogen is slow. The RU (after the immobilization of the fibrinogen) was normalized to D as the baseline.

If sulfated polymers are injected, we can monitor the time course of the binding as a change in RU. The sensorgram gives data about the association of the complex that can be followed; the equilibrium or the steady state is readily displaced by the analyte sulfated polymer flow. When the analyte is replaced by a buffer flow, the dissociation of the complex is also monitored. In this study, bovine plasma fibrinogen was covalently coupled to the carboxymethylated dextran surface of the sensorchip as a ligand and sulfated polymer (analyte) buffer solution was flowed. This is because we detect nonspecific adsorbed albumin and fibrinogen on the carboxymethylated dextran surface and we did not detect any adsorbed all sulfated polymers on its surface in the control experiments.

The overlay sensorgrams for the interaction of each sulfated polymer with fibrinogen are shown in Figure 3. We collected binding curves from different batches of proteins because fibrinogen was an unstable protein and tended to denature in the regeneration process. We observed an increase in RU during its contact with a continuous flow (10 μL min^{-1}) of the PBS buffer that contained poly(GEMA) sulfate or dextran sulfate at a concentration of 0.3−30 μg mL^{-1}, indicating a net adsorption of each heparinoid to the immobilized fibrinogen. During subsequent contact with the PBS buffer, the RU decreased slightly, indicating a net desorption of each heparinoid from the fibrinogen (Figure 3, panels a and b). On the other hand, its adsorption of heparin was slightly observed as a refractive index shift (Figure 3c), which indicates its lower affinity for heparin. These results clarified that poly(GEMA) sulfate and dextran sulfate directly formed complexes with fibrinogen; heparin, however, did not. These results are also consistent with our previous research (*10*).

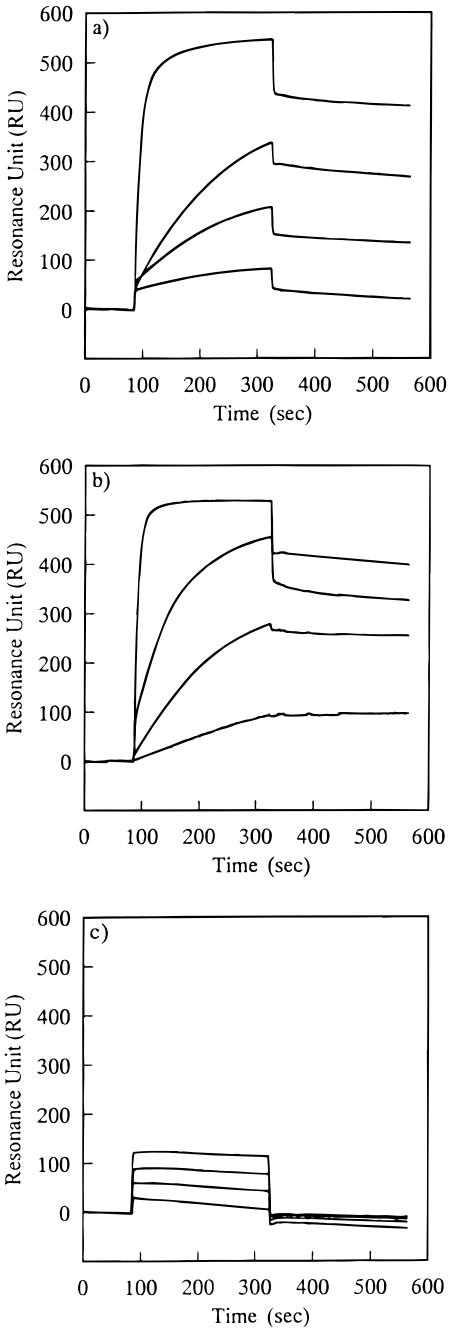


Figure 3. Adsorption of poly(GEMA) sulfate (a), dextran sulfate (b), and heparin (c) to immobilized fibrinogen. Each sulfated polymer concentration is 0.3, 1.5, 3, and 30 μg mL^{-1}. PBS buffer, pH 7.4.

Using the sensorgrams for the binding of poly(GEMA) sulfates and dextran sulfates with fibrinogen (Figure 3, panels a and b) we were able to obtain the maximum binding RU (ΔRU_{max}) of each heparinoid on the fibrinogen surface at a suitable concentration as a function of each

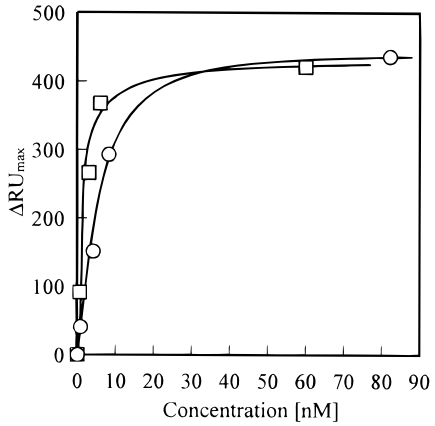


Figure 4. Adsorption isotherms for poly(GEMA) sulfate-binding (○) and dextran sulfate-binding (□) to fibrinogen surfaces. PBS buffer, pH 7.4.

heparinoid concentration (Figure 4). The ΔRU_{max} curves for poly(GEMA) sulfate and dextran sulfate on fibrinogen reached plateaus at a high concentration of heparinoid (30 μg mL^{-1}), indicating that the adsorption behavior of each heparinoid on the fibrinogen was Langmuirian. This suggests that there was neither multilayer aggregation nor heterogeneous adsorption on the fibrinogen surface.

The SPR method can directly evaluate the time-dependent interaction between heparinoid and fibrinogen; the turbidity measurement of the heparinoid−fibrinogen complex, however, cannot. Therefore, association and dissociation processes can be monitored by the SPR method, providing a base for kinetic studies. The time needed to reach an equilibrium state for the binding of each heparinoid (30 μg mL^{-1}) to the fibrinogen surface was about 5 min (Figure 3, panels a and b). In our previous study (*10*), we evaluated the turbidity of the heparinoid−fibrinogen mixture solution in a PBS buffer by allowing a heparinoid−fibrinogen mixture solution to stand for 10 min. The SPR results described above show that the turbidity measurements were done in an equilibrium state. However, another advantage of SPR measurements in regard to analyzing the direct affinity between heparinoid and fibrinogen is because turbidity measurements can only detect large aggregated structures, although the latter is much easier to measure than the former.

We calculated the dissociation constant (K_D) from sensorgrams for the binding of each heparinoid to fibrinogen (Figure 3, panels a and b) by following pseudo-first-order kinetics (BIAcore system manual). We obtained very high correlation coefficients in the determination of K_D for the binding of both heparinoids (~0.99), and a K_D (6.2×10^{-10} M) for the binding of dextran sulfate to fibrinogen was lower than that (3.1×10^{-8} M) for poly(GEMA) sulfate. This might be due to differences in electrostatic force between dextran sulfate and poly(GEMA) sulfate. In this study, we did not confirm the presence of a stoichiometrical complex because the refractive index of poly(GEMA) sulfate and dextran sulfate have not been obtained by anyone yet. If refractive indices of heparinoids are obtained, the interaction mechanism between each heparinoid and fibrinogen can be analyzed in more detail.

The overlay sensorgrams for the interaction of each sulfated polymer with albumin are also shown in Figure 5. We observed lower nonspecific adsorption of all sulfated polymers to the immobilized albumin as a slight refractive index shift. These results indicate the lower

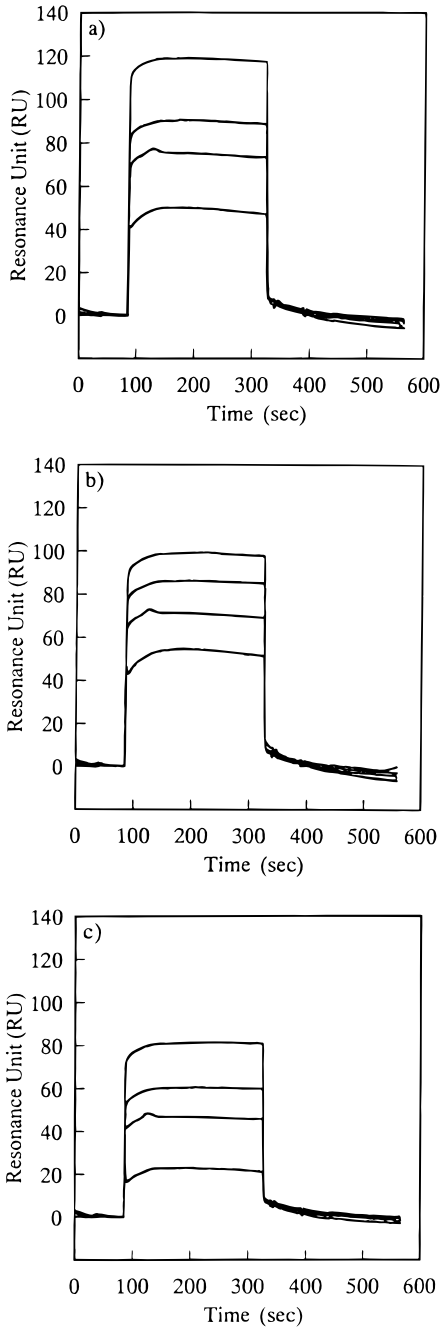


Figure 5. Adsorption of poly(GEMA) sulfate (a), dextran sulfate (b), and heparin (c) to immobilized albumin. PBS buffer, pH 7.4.

affinity of all sulfated polymers for the albumin. However, it seems that the BIAcore system is not able to detect the binding profiles of a lower association constant ($K_D < 10^4$ M). In addition, each sulfated polymer may be prevented from penetrating the albumin-immobilized matrix by steric factors.

Poly(GEMA) sulfate and dextran sulfate showed a high affinity with fibrinogen in this study, while heparin had little or no affinity. The binding amount was dependent on the heparinoid. These results suggest that the interaction mechanism of heparinoid with fibrinogen was different from that of heparin. It is well-known that the aggregation of plasma fibrinogen at physiological pH values is caused by the addition of dextran sulfate, although no aggregations have been observed upon addition of heparin, because of the limited number of

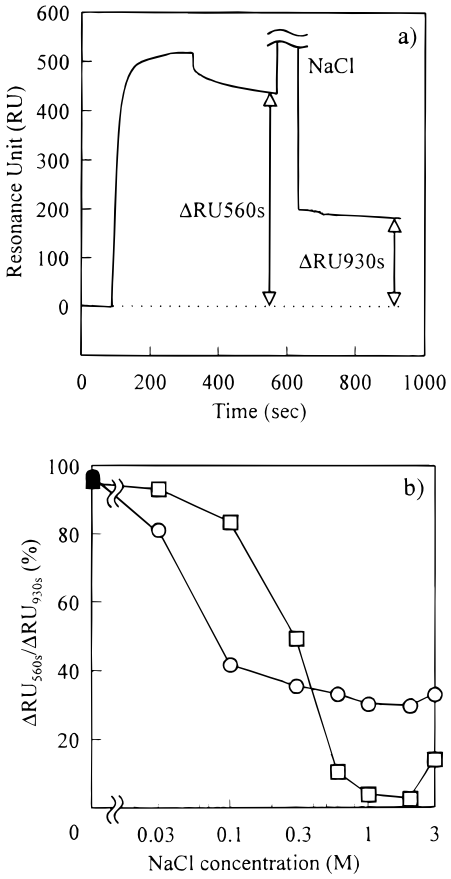


Figure 6. (a) The sensorgram showing the effect of the addition of the 1.0 M NaCl on desorption of poly(GEMA) sulfate from immobilized fibrinogen. (b) Decrease of $\Delta RU_{560s}/\Delta RU_{930s}$ by the desorption of poly(GEMA) sulfate (○) and dextran sulfate (□) from the fibrinogen surface with the addition of NaCl containing PBS buffer.

association constants between heparin and fibrinogen. Therefore, these results are consistent with the above.

Desorption of Sulfated Polymer from Fibrinogen Surface. To obtain data on the binding mechanism of poly(GEMA) sulfate or dextran sulfate to fibrinogen, we examined the degree of dissociation of a sulfated polymer from immobilized fibrinogen in the presence of a NaCl-containing PBS buffer. In general, the interaction of protein with other molecules is believed to be due to (i) ion−ion interaction, (ii) ion−dipole and dipole−dipole interaction, (iii) solvophobic interaction, and (iv) dispersion or van der Waals forces. Our experiment will show if an insoluble complex formation will only lead to an electrostatic interaction between heparinoid and fibrinogen. A sensorgram of the poly(GEMA) sulfate desorption from immobilized fibrinogen with a PBS buffer that contains 1.0 M NaCl is shown in Figure 6a. ΔRU_{560s} indicates the amount of binded heparinoid to the fibrinogen surface after 560 s from the starting point of the experiment. ΔRU_{930s} (RU_{930s} can be seen as a stable baseline because dissociation curve in Figure 6a represents very slow kinetics) indicates the amount of remaining heparinoid on the sensor chips after the injection of NaCl containing buffer (0.03−3.0 M) for 330s to the heparinoid−fibrinogen complexes. We compared the $\Delta RU_{560s}/\Delta RU_{930s}$ values for poly(GEMA) sulfate against NaCl concentration with those for dextran sulfate (Figure 6b). The amount of adsorbed heparinoid to fibrinogen surface decreased with an increase in the ionic strength of the NaCl-containing buffer. Upon the addition of a 1.0 M NaCl containing buffer, all of the dextran sulfates were

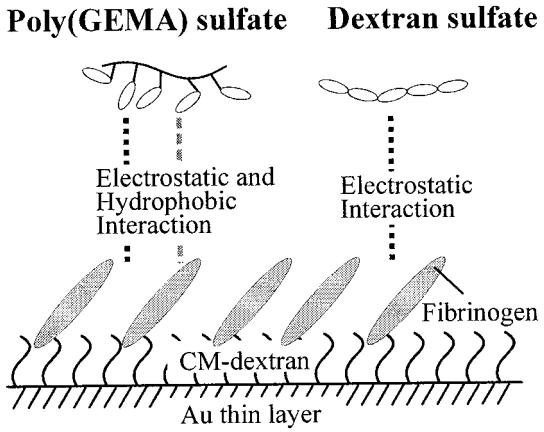


Figure 7. Schematic representation of interaction between each heparinoid and fibrinogen.

desorbed from it, while the poly(GEMA) sulfates were incompletely desorbed, about 30% of poly(GEMA) sulfate remained on the fibrinogen surface despite the presence of a 2.0 M NaCl containing buffer injection. Above concentrations of 2.0 M, we also observed the higher adsorption of both heparinoids to fibrinogen. A consideration of above result can be explained by the denaturing of immobilized fibrinogen. These data show that the binding behavior of poly(GEMA) sulfate with fibrinogen was different from that of dextran sulfate, indicating that the interaction between fibrinogen and poly(GEMA) sulfate was not only caused by electrostatic but also by hydrophobic force (Figure 7). This is because the poly(methacrylate) backbone of poly(GEMA) sulfate is the most hydrophobic part in the polymer. In our previous study, we noted that the interaction mechanism of poly(GEMA) sulfate to fibrinogen was differed from that for dextran sulfate (*10*). This is consistent with our previous research. In further research, we will clarify the formation mechanism of heparinoid−fibrinogen complexes in detail by using different kinds of salt, i.e., by using a lyotropic series that is a defined as the salting-out effects on ions on protein as well as the effects of ions on the surface tension of water (*21*).

The interactions between fibrinogen and sulfated polymers could be observed using the SPR technique in real-time. This is consistent with our turbidity measurement study (*10*). The kinetic constants between heparinoid−fibrinogen can also be obtained. We clarified the differences in the interaction mechanism of poly(GEMA) sulfate to fibrinogen and that of dextran sulfate by using a NaCl-containing buffer. In general, SPR methodology is used for the kinetic determination of the interaction of macromolecules. In this study, we showed that these SPR methods and experimental procedures can be used to obtain data on mechanistic interactions between various sulfated polymers and various plasma proteins by using a salt-containing buffer. This methodology cannot only obtain the kinetic constants between antigen−antibody but also gives us new and valuable insights into physiological mechanistic aspects such as the interactions between body components (proteins, phospholipids, DNAs, and cells) and biomaterials (natural occurring polymers, synthetic polymers, and inorganic materials).

ACKNOWLEDGMENT

This study was financially supported in part by the project entitled “High and Ecological Utilization of Regional Carbohydrates”, through Special Coordination Funds for Promoting Science and Technology (Leading

Research Utilizing Potential of Regional Science and Technology) of the Science and Technology Agency of the Japanese Government, 1997, and this study also was financially supported in part by a Grant-in-Aid for Scientific Research in Priority Areas of "Super-Biosystem Constructed by Cognitive Multidimensional Glyco-molecules" (no. 285/09240105) from the Ministry of Education, Science, Sports and Culture, Japan. The authors thank Dr. Akio Kishida of Kagoshima University for their experimental supports and helpful discussions.

LITERATURE CITED

(1) Gorter, E., and Nanninga, L. (1953) Complexes of heparin and protein. *Discuss. Faraday Soc. 13*, 205−217.
(2) Astrup, T., and Piper, J. (1946) Interaction between fibrinogen and polysaccharide polysulfuric acids. *Acta Physiol. Scand. 11*, 211−220.
(3) Sato, H., Nakanishi, E., and Nakajima, A. (1981) Electrochemical and conformational study of the interactions of fibrinogen with acidic polysaccharides. *Int. J. Biol. Macromol. 3*, 66−70.
(4) Walton, K. M. (1952) The biological behavior of a new synthetic anticoagulant (dextran sulphate) possessing heparin-like properties. *Brit. J. Pharmacol. 7*, 370−391.
(5) Sasaki, S., and Noguchi, H. (1959) Interaction of fibrinogen with dextran sulfate. *J. Gen. Physiol. 43*, 1−12.
(6) Tamada, Y., Makino, K., Yoshida, T., and Taniguchi, Y. (1996) Blood chemical analysis. G. Development of a new blood anticoagulant. *Rinsho-Byori (Japanese) 103*, 192−199.
(7) Doolittle, R. F., Watt, K. W. K., Cottrell, B. A., Strong, D. D., and Riley, M. (1979) The amino acid sequence of the a-chain of human fibringen. *Nature 280*, 464−468.
(8) Doolittle, R. F., Everse, S. J., and Spraggon, G. (1996) Human fibrinogen: anticipationg a 3-dimensional structure. *FASEB J. 10*, 1464−1470.
(9) Akashi, M., Sakamoto, N., Suzuki, K., and Kishida, A. (1996) Synthesis and anticoagulant activity of sulfated glucoside-bearing polymer. *Bioconjugate Chem. 7*, 393−395.
(10) Sakamoto, N., Kishida, A., Maruyama, I., and Akashi, M. (1997) The mechanism of anticoagulant activity of a novel heparinoid sulfated glucoside-bearing polymer. *J. Biomater. Sci. Polym. Ed. 8*, 545−553.
(11) Ohnishi, M., Miyashita, Y., Motomura, T., Sakamoto, N., and Akashi, M. Anticoagulant and antiprotease activities of a heparinoid sulfated glucoside-bearing polymer. *J. Biomater. Sci. Polym. Ed. 9*, 973−984.
(12) Nakajima, E., Sato, H., and Nakajima, A. (1990) Electrophoretic study on a soluble complex of heparin and fibrinogen. *Polym. J. 22*, 510−517.
(13) Hlady, V., Van-Wagenen, R. A., and Andrade, J. D. (1985) Total internal reflection intrinsic fluorescence (TIRIF) spectroscopy applied to protein adsorption. in *Surface and Interfacial Aspects of Biomedical Polymers* (J. D. Andrade, Ed.) Vol. 2, pp 81−119 Plenum Press, New York.
(14) Otto, A. (1968) Excitation of nonradiative surface plasmon waves in silver by the method of frustrated total reflection. *Z. Phys. 216*, 398−410.
(15) Kretschmann, E., and Raether, H. (1968) Radiative decay of nonradiative surface plasmons excited by light. *Z. Naturforsch. 23*, 2135.
(16) Karlsson, R., Michaelsson, A., and Mattsson, L. (1991) Kinetic analysis of monoclonal antibody−antigen interactions with a new biosensor based analytical system. *J. Immunol. Methods 145*, 229−240.
(17) Chaiken, I., Rosé, S., and Karlsson, R. (1992) Analysis of macromolecular interactions using immobilized ligands. *Anal. Biochem. 201*, 197−210.
(18) Altschuh, D., Dubs, M. C., Weiss, E., Zeder-Lutz, G., and Van-Regenmortal, M. H. V. (1992) Determination of kinetic constants for the interaction between a monoclonal antibody and peptides using surface plasmon resonance. *Biochemistry*, *31* 6298−6304.
(19) Johnsson, B, Löfås, S., and Lindqquist, G. (1991) Immobilization of proteins to a carboxymethyldextran-modified gold surface for biospecific interaction analysis in surface plasmon resonance sensors. *Anal. Biochem. 198*, 268−277.
(20) Huber, W., Hurst, J., Schlatter, D., Barner, R., Hübscher, J., Kouns, W. C., and Steiner, B. (1995) Determination of kinetic constants for the interaction between the platelet glycoprotein Iib-IIIa and fibrinogen by means of surface plasmon resonance. *Eur. J. Biochem. 227*, 647−656.
(21) Melander, W., and Horváth, C. (1977) Salt effect on hydrophobic interactions in precipitation and chromatography of proteins: an interpretation of the lyotropic series. *Arch. Biochem. Biophys. 183*, 200−215.

BC970218J

Chemoenzymatic Synthesis of 3′-*O*-(Carboxyalkyl)fluorescein Labels

Maciej Adamczyk,* Jonathan Grote, and Jeffrey A. Moore

Department of Chemistry (D9NM), Abbott Laboratories, Building AP 20, 100 Abbott Park Road, Abbott Park, Illinois, 60064-6016. Received January 23, 1999

A general and versatile method is described for the synthesis of fluorescent labels. Coupling of the 3′-phenol of fluorescein methyl ester with hydroxyalkyl benzyl esters, followed by benzyl ester hydrolysis, provided a series of fluorescein carboxyalkyl ethers. Use of the Mitsunobu reaction allowed for the introduction of linkers of different lengths onto the 3′-phenol of fluorescein. Chemoenzymatic benzyl ester hydrolysis was achieved with LPL-80 lipase, providing pH-independent labels useful for the preparation of fluorescent conjugates.

INTRODUCTION

Fluorescent labels play an important role in a variety of biological and biotechnological applications including fluorescence microscopy, flow cytometry, immunoassay development, and various spectrofluorometic methodologies (*1*−*5*). As the utilization of these fluorescent-dependent applications increases, so does the need for the development of new fluorogenic labels. This need for new fluorogenic labels is particularly true for studying the interactions of fluorescent conjugates with their respective binding proteins or receptors, as the choice of the fluorescent conjugate can be crucial for optimal conjugate performance and cannot usually be made a priori. The factors that affect performance can include the particular fluorescent chromophore utilized in preparation of the conjugate and the location and length of the linker arm employed (*6*−*8*).

The most commonly used fluorescein derivatives include the carboxyfluoresceins, the aminofluoresceins, the fluorescein isothiocyanates, and the aminomethylfluoresceins (*9*). These derivatives allow for conjugation of ligands through the 5- or 6- position of the phenyl ring of fluorescein. Additionally, 4′-(aminomethyl)fluorescein has been utilized for the preparation of tracers used in commercially available immunoassays (*10*, *11*). This fluorescein derivative allows for conjugation through the xanthinyl ring of fluorescein. A series of carboxyalkyl ethers linked through the 3′-phenol of fluorescein would thus represent a significant addition to the repertoire of labels available for conjugation. We describe here the preparation of a series of fluorogenic labels containing linkers of different lengths which permit conjugation through the xanthinyl ring of fluorescein.

EXPERIMENTAL PROCEDURES

All reagents used in syntheses were purchased from Aldrich Chemical Co. (Milwaukee, WI) and utilized without further purification, except lipase LPL-80 (*Pseudomonas sp*.) which was purchased from Amano (Lombard, IL). Solvents (HPLC grade) and silica gel were obtained from E. Merck Science (Gibbstown, NJ) and used without further purification. Hydroxyalkyl benzyl esters were prepared from commercially available hydroxyalkyl acids and benzyl bromide by the method of Ono et al. (*12*). ^{1}H and ^{13}C NMR spectra were recorded at 300 and 75 MHz, respectively, on a Varian Gemini 300 spectrometer (Palo Alto, CA) with TMS as internal standard. Electrospray ionzation mass spectrometry (ESI-MS) was carried out on a Perkin-Elmer (Norwalk, CT) Sciex API 100 benchtop system employing the Turbo IonSpray ion source. Analytical HPLC was performed on a Waters (Millford, MA) RCM C18 (8 × 100 mm) reversed-phase μBondapak column eluting at 2 mL/min with aqueous acetonitrile (v:v, CH_3CN/H_2O) containing 0.05% trifluoroacetic acid as noted. Elution profiles were recorded at 220 nm. Preparative HPLC purification was performed on a Waters RCM C18 (40 × 100 mm) reversed-phase μBondapak column eluting at 40 mL/min with aqueous acetonitrile (v:v, CH_3CN/H_2O) containing 0.05% trifluoroacetic acid as noted, followed by lyophilization. Absorbance spectra were obtained on a Beckman DU 640 spectrophotometer (Fullerton, CA). Fluorescence emission spectra were obtained on an ISS PC1 spectrofluorometer (Champaign, IL).

Fluorescein Methyl Ester (*2*). Fluorescein methyl ester was prepared by an improvement of the method described by Feuerstein (*13*). Briefly, concentrated sulfuric acid (7.5 mL) was added dropwise to a suspension of fluorescein (**1**, 10 g, 30 mmol) in methanol (30 mL). The resulting suspension was refluxed for 14 h with an addition funnel packed with oven dried 3 Å molecular sieves between the pot and condenser to continuously dry the cooled methanol. The mixture was then cooled, and ice (10 g) was added, followed by sodium bicarbonate (30 g). The suspension was filtered and washed with water. The resulting red solid was suspended in 2% aqueous sodium bicarbonate (200 mL), filtered, and washed with water. The washing process was repeated four additional times, the solid was resuspended in 1% HOAc, filtered, and finally washed with water. Drying at 110 °C for 1 h yielded a red solid (10.2 g, 95%). ^{1}H NMR (DMSO-d_6): δ 8.25 (d, 1H, J = 7.4 Hz), 7.90 (td, 1H, J = 7.2, 1.4 Hz), 7.82 (td, 1H, J = 7.4, 1.4 Hz), 7.51 (d, 1H, J = 7.6 Hz), 7.09 (d, 2H, J = 9.2 Hz), 7.00 (d, 2H, J = 1.5 Hz), 6.76 (dd, 2H, J = 9.2, 2.0 Hz), 3.56 (s, 3H). ^{13}C NMR (DMSO-d_6): δ 172.4, 165.1, 158.8, 157.3, 133.5, 133.2, 131.3, 130.8, 130.5, 130.4, 129.3, 121.1, 115.4, 102.8, 52.4. ESI-MS m/z: 347.2 $(M + H)^+$.

General Procedure for Preparation of 3′-*O*-[(Ben-

* To whom correspondence should be addressed. Phone: (847) 937-0225. Fax: (847) 938-8927. E-mail: maciej.adamczyk@abbott.com.

10.1021/bc990009u CCC: $18.00 © 1999 American Chemical Society
Published on Web 04/06/1999

zyl)carboxyalkyl]fluorescein Methyl Esters (*3a*−*e*). To a suspension of fluorescein methyl ester (**2**, 200 mg, 0.58 mmol), triphenylphosphine (227 mg, 0.87 mmol), and a hydroxyalkyl benzyl ester (0.70 mmol) in 50% THF/CH_3CN (4 mL) was added diethyl azodicarboxylate (0.12 mL, 0.64 mmol) (*14*). The mixture was stirred for 1 h, concentrated in vacuo, and filtered through a pad of silica gel. The silica gel was washed with 20% *tert*-BuOMe/CH_2Cl_2, and the filtrate was concentrated in vacuo to a thick oil. Purification by preparative HPLC provided compounds **3a**−**e** as thick red oils.

Compound **3a** was obtained from compound **2** and benzyl glycolate (238 mg, 94%). Preparative HPLC (53:47). Analytical HPLC (60:40): retention time, 5.2 min, >98%. ^{1}H NMR ($CDCl_3$): δ 8.38 (d, 1H, J = 7.2 Hz), 7.84 (m, 2H), 7.37 (m, 12H), 5.29 (s, 2H), 4.95 (s, 2H), 3.65 (s, 3H). ^{13}C NMR ($CDCl_3$): δ 167.3, 166.8, 165.2, 160.3, 157.8, 134.6, 133.3, 133.0, 132.4, 131.6, 129.7, 129.0, 128.8, 123.3, 119.2, 117.4, 117.0, 103.5, 100.9, 67.9, 65.8, 52.7. ESI-MS m/z: 495.5 $(M + H)^+$.

Compound **3b** was obtained from compound **2** and benzyl 4-hydroxybutyrate (212 mg, 72%). Preparative HPLC (56:44). Analytical HPLC (60:40): retention time, 6.0 min, >98%. ^{1}H NMR ($CDCl_3$): δ 8.28 (d, 1H, J = 7.6 Hz), 7.76 (td, 1H, J = 7.3, 1.5 Hz), 7.70 (td, 1H, J = 7.7, 1.5 Hz), 7.35 (m, 6H), 6.96 (m, 3H), 6.76 (m, 3H), 5.14 (s, 2H), 4.15 (t, 2H, J = 6.2 Hz), 3.63 (s, 3H), 2.59 (t, 2H, J = 6.3 Hz), 2.20 (quintet, 2H, J = 6.2 Hz). ^{13}C NMR ($CDCl_3$): δ 172.8, 169.2, 165.2, 160.0, 159.5, 134.4, 132.9, 131.3, 130.8, 130.0, 129.4, 128.7, 128.4, 117.4, 114.9, 105.2, 100.8, 67.8, 66.5, 52.4, 30.4, 24.1. ESI-MS m/z: 523.5 $(M + H)^+$.

Compound **3c** was obtained from compound **2** and benzyl 6-hydroxycaproate (259 mg, 79%). Preparative HPLC (59:41). Analytical HPLC (70:30): retention time, 5.3 min, >98%. ^{1}H NMR ($CDCl_3$): δ 8.34 (d, 1H, J = 7.2 Hz), 7.82 (m, 2H), 7.46 (s, 1H), 7.34 (m, 10H), 7.06 (d, 1H, J = 9.1 Hz), 5.12 (s, 2H), 4.21 (t, 2H, J = 6.1 Hz), 3.63 (s, 3H), 2.39 (d, 2H, J = 7.4 Hz), 1.89 (m, 2H), 1.70 (m, 2H), 1.48 (m, 4H). ^{13}C NMR ($CDCl_3$): δ 173.6, 168.4, 165.3, 160.1, 157.9, 136.1, 133.4, 133.2, 132.0, 131.5, 130.8, 129.9, 129.8, 128.6, 128.2, 123.9, 119.0, 116.8, 116.1, 103.6, 100.3, 70.0, 66.1, 52.6, 34.0, 28.5, 28.3, 25.4, 24.6. ESI-MS m/z: 565.3 $(M + H)^+$.

Compound **3d** was obtained from compound **2** and benzyl 10-hydroxydecanoate (325 mg, 92%). Preparative HPLC (74:26). Analytical HPLC (70:30): retention time, 7.8 min, >99%. ^{1}H NMR ($CDCl_3$): δ 8.36 (d, 1H, J = 7.3 Hz), 7.84 (m, 2H), 7.52 (s, 1H), 7.34 (m, 10H), 7.11 (dd, 1H, J = 9.4, 2.2 Hz), 5.10 (s, 2H), 4.24 (t, 2H, J = 6.4 Hz), 3.64 (s, 3H), 2.36 (t, 2H, J = 7.6 Hz), 1.91 (m, 2H), 1.64 (m, 2H), 1.32 (m, 10H). ^{13}C NMR ($CDCl_3$): δ 173.8, 169.1, 165.2, 160.0, 158.3, 136.1, 133.2, 131.5, 131.1, 129.8, 128.6, 128.2, 123.0, 119.5, 116.4, 103.4, 100.3, 66.2, 52.6, 34.1, 32.2, 29.1, 29.0, 28.9, 28.5, 25.6, 24.7. ESI-MS m/z: 607.4 $(M + H)^+$.

Compound **3e** was obtained from compound **2** and benzyl 12-hydroxydodecanoate (351 mg, 95%). Preparative HPLC (81:19). Analytical HPLC (70:30): retention time, 10.5 min, >99%. ^{1}H NMR ($CDCl_3$): δ 8.37 (d, 1H, J = 7.3 Hz), 7.84 (m, 2H), 7.60 (d, 1H, J = 2.0 Hz), 7.35 (m, 10H), 7.13 (dd, 1H, J = 9.2, 2.3 Hz), 5.11 (s, 2H), 4.27 (t, 2H, J = 6.6 Hz), 3.64 (s, 3H), 2.36 (t, 2H, J = 7.6 Hz), 1.91 (t, 2H, J = 7.6 Hz), 1.64 (t, 2H, J = 6.2 Hz), 1.28 (m, 14 H). ^{13}C NMR ($CDCl_3$): δ 174.2, 169.6, 165.2, 160.0, 158.7, 133.2, 132.1, 131.6, 131.2, 131.0, 129.8, 128.6, 128.2, 122.6, 120.1, 117.0, 116.6, 103.5, 100.3, 66.2, 52.7, 34.3, 29.3, 29.2, 29.1, 29.0, 28.5, 25.7, 24.8. ESI-MS m/z: 635.4 $(M + H)^+$.

General Procedure for Preparation of 3′-*O*-(Carboxyalkyl)fluorescein Methyl Esters (*4a*−*e*). LPL-80 lipase (*Pseudomonas sp*., 100 mg) was added to solutions of 3′-*O*-[(benzyl)carboxyalkyl]fluorescein methyl esters (**3a**−**e**, 0.25 mmol) in CH_3CN/50 mM phosphate buffer (1:1, 10 mL, pH 8), and the reaction mixtures were stirred at ambient temperature for 72−96 h. The reaction mixtures were then transferred to test tubes and additional CH_3CN was added until two distinct layers were present. The resulting clear orange organic phases were separated from the lipase containing aqueous phases and purified directly by preparative HPLC providing acids **4a**−**e** as orange solids.

Compound **4a** was obtained from compound **3a** (92 mg, 91%). Preparative HPLC (40:60). Analytical HPLC (35:65): retention time, 5.5 min, >98%. ^{1}H NMR (CD_3CN): δ 8.27 (dd, 1H, J = 7.8, 1.2 Hz), 7.85 (td, 1H, J = 7.6, 1.6 Hz), 7.79 (td, 1H, J = 7.6, 1.6 Hz), 7.30 (dd, 1H, J = 7.6, 1.2 Hz), 7.17 (d, 1H, J = 2.5 Hz), 7.06 (t, 2H, J = 9.3 Hz), 6.94 (dd, 1H, J = 9.0, 1.6 Hz), 6.59 (dd, 1H, J = 9.6, 2.0 Hz), 6.53 (d, 1H, J = 2.0 Hz), 4.84 (s, 2H), 3.60 (s, 3H). ^{13}C NMR (CD_3CN): δ 174.7, 168.8, 165.4, 156.3, 150.9, 134.2, 133.3, 130.8, 129.7, 125.6, 117.4, 114.8, 103.4, 100.9, 52.3. ESI-MS m/z: 405.2 $(M + H)^+$.

Compound **4b** was obtained from compound **3b** (96 mg, 89%). Preparative HPLC (40:60). Analytical HPLC (50:50): retention time, 3.7 min, >98%. ^{1}H NMR ($CDCl_3$): δ 8.34 (dd, 1H, J = 1.6 Hz), 7.81 (m, 2H), 7.34 (m, 3H), 7.23 (dd, 2H, J = 9.2, 1.4 Hz), 7.13 (dd, 1H, J = 9.3, 2.2 Hz), 7.03 (dd, 1H, J = 9.2, 2.3 Hz), 4.30 (t, 2H, J = 6.3 Hz), 3.64 (s, 3H), 2.59 (t, 2H, J = 6.9 Hz), 2.21 (m, 2H). ^{13}C NMR ($CDCl_3$): δ 179.0, 167.1, 165.1, 159.9, 156.9, 133.4, 132.9, 131.7, 130.6, 130.4, 129.8, 129.7, 124.8, 117.7, 116.7, 116.4, 115.7, 103.6, 100.5, 68.4, 52.4, 29.5, 23.6. ESI-MS m/z: 433.5 $(M + H)^+$.

Compound **4c** was obtained from compound **3c** (99 mg, 83%). Preparative HPLC (48:52). Analytical HPLC (50:50): retention time, 5.5 min, >99%. ^{1}H NMR ($CDCl_3$): δ 8.35 (d, 1H, J = 7.0 Hz), 7.83 (m, 2H), 7.57 (s, 1H), 7.28 (m, 5H), 7.08 (d, 1H, J = 2.0 Hz), 4.25 (t, 2H, J = 6.5 Hz), 3.64 (s, 3H), 2.38 (t, 2H, J = 7.2 Hz), 1.92 (m, 2H), 1.68 (m, 2H), 1.49 (m, 4H). ^{13}C NMR ($CDCl_3$): δ 175.9, 168.9, 165.3, 160.1, 158.3, 133.3, 133.2, 131.5, 131.1, 129.9, 123.4, 119.5, 116.9, 116.3, 103.6, 100.4, 70.1, 52.7, 33.6, 28.3, 28.2, 25.2, 24.3. ESI-MS m/z: 475.3 $(M + H)^+$.

Compound **4d** was obtained from compound **3d** (112 mg, 87%). Preparative HPLC (57:43). Analytical HPLC (60:40): retention time, 5.7 min, >99%. ^{1}H NMR ($CDCl_3$): δ 8.35 (d, 1H, J = 7.8 Hz), 7.82 (m, 2H), 7.53 (d, 1H, J = 2.1 Hz), 7.36−7.20 (m, 5H), 7.10 (dd, 1H, J = 9.2, 2.3 Hz), 4.24 (t, 2H, J = 6.4 Hz), 3.64 (s, 3H), 2.34 (t, 2H, J = 7.6 Hz), 1.90 (t, 2H, J = 6.7 Hz), 1.62 (m, 2H), 1.33 (m, 10H). ^{13}C NMR ($CDCl_3$): δ 176.1, 168.7, 165.2, 160.1, 158.2, 133.2, 132.0, 131.5, 131.1, 130.8, 129.9, 123.6, 119.4, 116.9, 116.3, 103.6, 100.4, 70.3, 52.7, 33.8, 29.0, 28.9, 28.8, 28.4, 25.6, 24.5. ESI-MS m/z: 517.3 $(M + H)^+$.

Compound **4e** was obtained from compound **3e** (107 mg, 80%). Preparative HPLC (68:32). Analytical HPLC (60:40): retention time, 11.0 min, >99%. ^{1}H NMR ($CDCl_3$): δ 8.27 (d, 1H, J = 7.8 Hz), 7.75 (m, 2H), 7.30 (d, 1H, J = 8.6 Hz), 7.08 (d, 1H, J = 2.6 Hz), 7.02 (t, 2H, J = 8.6 Hz), 6.94 (m, 1H), 6.86 (m, 2H), 4.13 (t, 2H, J = 7.6 Hz), 3.64 (s, 3H), 2.35 (t, 2H, J = 7.7 Hz), 1.82 (t, 2H, J = 7.6 Hz), 1.62 (t, 2H, J = 7.6 Hz), 1.25 (m, 14H). ^{13}C NMR ($CDCl_3$): δ 176.4, 168.9, 165.3, 160.2, 158.2, 133.4, 133.3, 132.1, 130.9, 130.0, 123.6, 119.4, 116.8, 103.7, 100.4, 70.3, 52.7, 33.9, 29.1, 29.0, 28.8, 28.5, 25.6, 24.6. ESI-MS m/z: 545.3 $(M + H)^+$.

Scheme 1

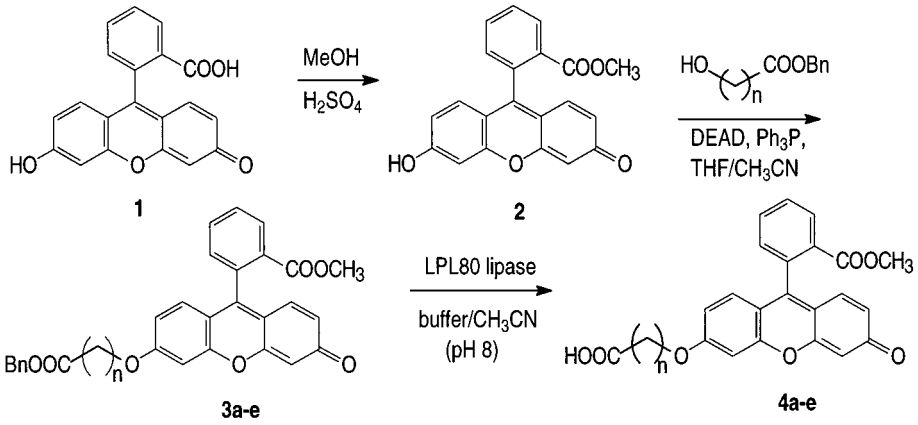
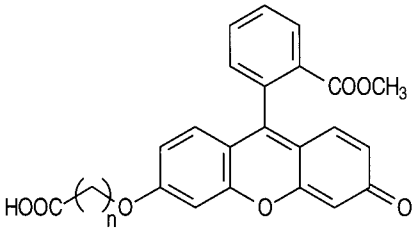


Table 1. Spectral Properties of 3′-*O*-(carboxyalkyl)Fluorescein Methyl Esters



Entry	n	ε ($Abs_{456\ nm}$/M s)[a]	Quantum Yield[b]
4a	1	34,782	0.22 ± 0.03
4b	3	24,086	0.31 ± 0.03
4c	6	25,464	0.21 ± 0.02
4d	9	21,308	0.18 ± 0.03
4e	11	23,417	0.21 ± 0.04
Fluorescein	-	25,427	0.92[c]

[a] Values reported are the average of duplicate determinations. [b] Values reported are the average of triplicate determinations. [c] Obtained from refs *15* and *16*.

Photophysical Studies. All absorbance and fluorescence spectra of 3′-*O*-(carboxyalkyl)fluorescein methyl ester labels (**4a**−**e**) were obtained in 40 mM sodium phosphate, 20% MeOH, pH 7.4. Absorbance and fluorescence spectra of fluorescein were obtained in 10 mM aqueous NaOH. Absorbance spectra were obtained at final concentrations of 2−47 μM (entries 4a and 4e), 2−58 μM (entry 4b), 2−52 μM (entry 4c), 0.3−10 μM (entry 4d), and 1−31 μM (fluorescein). Fluorescence emission spectra were obtained for 50 nM samples with an excitation wavelength of 456 nm and excitation and emission slits of 8 nm. The quantum yield of each label was determined using the expression

$$\frac{Q_{F(sample)}}{Q_{F(fluorescein)}} = \frac{I_{(sample)}}{I_{(fluorescein)}} \frac{\epsilon_{(fluorescein)}}{\epsilon_{(sample)}}$$

where Q_F = quantum yield ($Q_{F(fluorescein)} = 0.92$) (*15*, *16*), I is the total fluorescence emission intensity over all wavelengths, and ϵ is the molar extinction coefficient determined at 456 nm.

RESULTS AND DISCUSSION

The general synthesis of 3′-*O*-(carboxyalkyl)fluorescein methyl esters (**4a**−**e**) is depicted in Scheme 1. Fluorescein (**1**) was esterified in refluxing acidic methanol by the method of Feuerstein (*13*), except that 3 Å molecular sieves were used to absorb water, providing fluorescein methyl ester (**2**) in nearly quantitative yield. Coupling the 3′-phenol of fluorescein methyl ester (**2**) with hydroxyalkyl benzyl esters under Mitsunobu conditions afforded the benzyl protected 3′-*O*-(carboxyalkyl)fluorescein methyl esters (**3a**−**e**) in 72−95% yield (*17*). The syntheses were completed by selective hydrolysis of the benzyl esters of **3a**−**e** by LPL-80 lipase (*Pseudomonas sp*.) providing the desired 3′-*O*-(carboxyalkyl)fluorescein methyl ester labels (**4a**−**e**) in 80−91% yield (*18*, *19*).

Alkylation of the 3′-phenol of fluorescein esters has been reported twice in the literature (*20*, *21*). Lohse et al. synthesized the ethyl ester analogue of **4a** by coupling *tert*-butyl bromoacetate to fluorescein ethyl ester in the presence of diisopropylethylamine (78% yield) (*20*). Likewise, Shubert et al. prepared selected 3′-*O*-(hydroxyalkyl)-fluorescein methyl esters in low to moderate yield (33% for the single yield reported) by coupling dimethoxytrityl protected hydroxyalkyl chlorides to fluorescein methyl ester under basic conditions (*21*). Such O-alkylations are usually efficient using activated alkylhalides, but less effective using long-chain alkylhalides (cf. refs *20*−*22*). On the other hand, an alkylation performed under Mitsunobu conditions is relatively insensitive to alkyl chain length. Such a novel alkylation of the 3′-phenol of fluorescein methyl ester with hydroxyalkyl esters under Mitsunobu conditions is advantageous, since it provides an efficient method for the incorporation of linkers of different lengths.

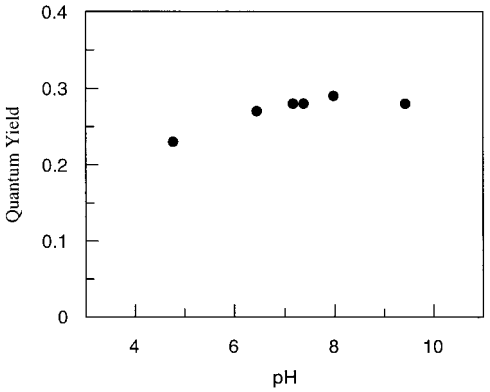


Figure 1. A representative plot of fluorescence quantum yield vs pH (labels **4a**−**e**). Data shown is for compound **4c**.

The choice to use *benzyl* esters in the Mitsunobu coupling was critical. Benzyl esters can be formed selectively in the presence of a terminal hydroxyl functionality (*12*), and are stable to the Mitsunobu coupling conditions. Most importantly, the benzyl ester functionality of the resulting fluorescein intermediates (**3a**−**e**) can be selectively cleaved with LPL-80 lipase without methyl ester cleavage (*18*, *19*).

The spectral properties of labels **4a**−**e** were evaluated and shown to be uniform and comparable to the spectral properties of reported fluorescein mixed ether/esters (*20*, *21*). The UV−visible absorbance spectra of labels **4a**−**e** exhibit absorption maxima at 456 and 481 nm with molar extinction coefficients determined at 456 nm ranging $(2.1-3.5) \times 10^4$ M^{-1} cm^{-1} (Table 1). The fluorescence emission spectra of labels **4a**−**e** are broadened and red-shifted ($\lambda_{max} = 532$ nm) relative to that of fluorescein ($\lambda_{max} = 513$ nm). The fluorescence quantum yields determined for the labels ranged 0.18−0.31 (Table 1). These quantum yield values are consistent with the value reported by Lohse et al. for a pentapeptide conjugate containing the ethyl ester analogue of compound **4a** ($Q_F = 0.18 \pm 0.02$). Furthermore, the quantum yields determined for labels **4a**−**e** are pH independent (pH 4.8−9.4, Figure 1) as the derivatives are locked into a fluorescent quinoid form by virtue of the methyl ester functionality. The pH independence exhibited by labels **4a**−**e** is desirable in situations mandating direct quantification of the fluorophore in different environments (*21*).

In summary, 3′-*O*-(carboxyalkyl)fluorescein methyl esters (**4a**−**e**) were prepared by esterification of fluorescein, Mitsunobu coupling of fluorescein methyl ester with hydroxyalkyl benzyl esters, and selective lipase catalyzed benzyl ester hydrolysis. The Mitsunobu coupling provides an efficient method for incorporation of linkers of different lengths, while utilization of benzyl esters provides a functionality which is both stable to the Mitsunobu reaction and subsequently removable by lipase mediated hydrolysis. This series of pH independent fluorescein labels allows for conjugation through the xanthinyl ring of fluorescein with linkers of different lengths.

LITERATURE CITED

(1) Haugland, R. P., Ed. (1996) *Handbook of Fluorescent Probes and Research Chemicals*, 6th ed., p 679, Molecular Probes, Eugene, OR.

(2) Bright, F. V. (1988) Bioanalytical applications of fluorescence spectroscopy. *Anal. Chem. 60*, 1031A−1039A.

(3) Gordon, G. W., Berry, G., Xiao, H. L., Levine, B., and Herman, B. (1998) Quantitative fluorescence resonance energy transfer measurements using fluorescence microscopy. *Biophys. J. 74*, 2702−2713.

(4) Schwartz, A., Ottinger, J., Wallace, E., Poon, R., and Fernandez-Repollet, E. (1994) Quantitative determination of antibody binding capacity (ABC) by flow cytometry. *Eur. J. Histochem. 38* (*Suppl. 1*), 13−20.

(5) Weber, G. (1997) Fluorescence in biophysics: accomplishments and deficiencies. *Methods Enzymol. 278*, 1−15.

(6) Hosoda, H., Kobayashi, N., Ishii, N., and Nambara, T. (1986) Bridging phenomena in steroid immunoassays. The effect of bridge length on sensitivity in enzyme immunoassay. *Chem. Pharm. Bull. 34*, 2105−2111.

(7) Colbert, D. L., Eremin, S. A., and Landon, J. (1991) The effect of fluorescein labels on the affinity of antisera to small haptens. *J. Immunol. Methods 140*, 227−233.

(8) Buolamwini, J. K., Craik, J. D., Wiley, J. S., Robins, M. J., Gati, W. P., Cass, C. E., and Paterson, A. R. P. (1994) Conjugates of fluorescein and SAENTA (5′-*S*-(2-aminoethyl)-N^6-(4-nitrobenzyl)-5′-thioadenosine): flow cytometry probes for the *es* nucleoside transporter elements of the plasma membrane. *Nucleosides Nucleotides 13*, 737−751.

(9) Mattingly, P. G. (1992) Preparation of 5- and 6-(aminomethyl)fluorescein. *Bioconjugate Chem. 3*, 430−431.

(10) Shipchandler, M. T., Fino, J. R., Klein, L. D., and Kirkemo, C. L. (1987) 4′-[Aminomethyl]fluorescein and its N-alkylated derivatives: useful reagents in immunodiagnostic techniques. *Anal. Biochem. 162*, 89−101.

(11) Adamczyk, M., Grote, J., Douglas, J., Dubler, R., and Harrington, C. (1997) Synthesis of conjugates for a barbiturate screening assay. *Bioconjugate Chem. 8*, 281−288.

(12) Ono, N., Yamada, T., Saito, T., Tanaka, K., and Kaji, A. (1978) A convenient procedure for esterification of carboxylic acids. *Bull. Chem. Soc. Jpn. 51*, 2401−2404.

(13) Feuerstein, W., and Dutoit, M. (1901) Uber Ester des Fluoreszeins. *Ber. Dtsch. Chem. Ges. 34*, 2637−2642.

(14) Additional portions of triphenylphosphine and diethyl azodicarboxylate were added when needed to ensure high yields.

(15) Flemming, G. R., Knight, A. W. E., Morris, J. M., Morrison, R. J. S., and Robinson, G. W. (1977) Picosecond fluorescence studies of xanthene dyes. *J. Am. Chem. Soc. 99*, 4306−4311.

(16) Demas, J. N., and Crosby, G. A. (1971) The measurement of photoluminescence quantum yields. A review. *J. Phys. Chem. 75*, 991−1024.

(17) Mitsunobu, O. (1981) The use of diethyl azodicarboxylate and triphenylphosphine in synthesis and transformation of natural products. *Synthesis*, 1−28.

(18) Adamczyk, M., Gebler, J. C., and Grote, J. (1995) Unexpectedly facile hydrolysis of digoxin esters. The importance of appropriate controls in lipase-mediated hydrolysis. *J. Org. Chem. 60*, 3557−3560.

(19) Adamczyk, M., Grote, J., and Rege, S. (1998) Chemoenzymatic transformations in sensitive systems: lipase mediated hydrolysis of vancomycin esters. *Bioorg. Med. Chem. Lett. 8*, 885−890.

(20) Schubert, F., Cech, D., Reinhardt, R., and Wiesner, P. (1992) Fluorescent labelling of sequencing primers for automated oligonucleotide synthesis. *J. DNA Sequencing Map. 2*, 273−279.

(21) Lohse, J., Nielsen, P. E., Harrit, N., and Dahl, O. (1997) Fluorescein-conjugated lysine monomers for solid-phase synthesis of fluorescent peptides and PNA oligomers. *Bioconjugate Chem. 8*, 503−509.

(22) Carey, F. A., and Sundberg, R. J. (1990) *Advanced Organic Chemistry, Part A: Structure and Mechanism*, Chapter 5, Plenum Press, New York.

BC990009U

Synthesis of Novel Cationic Poly(Ethylene Glycol) Containing Lipids

Uwe Schulze,[†] Hans-Werner Schmidt,*[,‡] and C. R. Safinya*[,†]

Materials Department, Physics Department, and Biochemistry and Molecular Biology Program, University of California, Santa Barbara, California 93106, and Makromolekulare Chemie I und Bayreuther Institut für Makromolekülforschung (BIMF) Universität Bayreuth, 95440 Bayreuth, Germany. Received September 14, 1998; Revised Manuscript Received December 4, 1998

°In this paper, the synthesis of novel divalent cationic lipids with poly(ethylene glycol) segments is described. The lipids consist of an unsaturated double-chain hydrophobic moiety based on 3,4-dihydroxy benzoic acid, attached to a hydrophilic poly(ethylene glycol) spacer which contains a divalent cationic end group. As poly(ethylene glycol) spacers monodisperse triethylene glycol and telechelic poly(ethylene glycol)s with an average degree of polymerization of 9, 23, and 45 were used. The divalent cationic end group was attached by coupling a protected dibasic amino acid to the PEG spacer and following cleavage of the protecting groups. These novel class of cationic lipids is of particular interest for nonviral gene delivery applications.

INTRODUCTION

In the past few years, a very large research effort has been devoted in developing new compounds which are carriers of DNA[1] into human cells. Especially complexes of DNA and cationic liposomes, which are mixtures of neutral and cationic lipids, so-called CL−DNA complexes, seem to be very promising vectors for nonviral gene therapy applications (*1*−*6*). The advantages of these complexes compared to viral methods are lower toxicity, simpler preparation, the lack of immune response from the body and their ability to carry large pieces of DNA.

There are two major arguments for the utilization of lipids with cationic headgroups as DNA carriers. First, the ionic interactions between the positively charged headgroup of the lipid and the negatively charged phosphate groups of the DNA molecule lead to efficient complexation and compaction of DNA mimicking highly compact viral DNA particles. In fact, it has been found that CL−DNA complexes are comprised of highly ordered self-assembled structures, either of the lamellar type (*7*−*10*), or of the inverted hexagonal type (*11*). Second, a positively charged CL−DNA complex is able to interact with the negatively charged cell membrane. This enhances the chances for the complex to enter the cytoplasm of the cell by endocytosis or fusion (*11, 12*). Liposomes for gene therapy applications normally consist of mixtures of neutral lipids and cationic lipids. This enables the independent variation of two important parameters: the charge density of lipid membrane at different neutral lipid/cationic lipid ratios and the overall charge of the CL−DNA complex at different total lipid/DNA ratios (*7, 8, 11*). Commonly used neutral lipids are 1,2-dioleyl-*sn*-glycero-3-phosphocholine (DOPC) and 1,2-dioleyl-*sn*-glycero-3-phosphoethanolamine (DOPE). Scheme 1 shows three of the most commonly used cationic lipids in gene therapy applications (*13*).

In contrast to the cationic lipids shown above, our research goal was to develop a new class of cationic lipids which have a hydrophilic flexible spacer between the hydrophobic alkyl chains and the cationic headgroup. We decided to use poly(ethylene glycol) as spacer unit. PEG is a nonionic water soluble polymer of extremely low immunogenicity which has been studied and applied in a broad range of scientifically and technologically important problems in colloidal science, complex fluids (*14*), drug delivery, and gene therapy (*15*) as well as in biology and biotechnology (*16*−*18*). PEG-containing lipids have also been used in Stealth liposomes (*19*−*22*) as in vivo drug carrier systems. These liposomes consist of closed bilayer shells of phospholipids covered with PEG-based lipids anchored to the membrane. The concept of a poly(ethylene glycol) containing spacer between hydrophobic lipid segments and biologically relevant ligands such as peptides or oligosaccharide-linked glycoproteines is described in studies of Zalipsky et al. (*23, 24*) and Frisch et al. (*25*). Zalipsky reported also on long circulating liposomes containing a monovalent cationic amino-PEG-phosphatidylethanolamine with an average degree of polymerization of the PEG chain of 45 (*26*).

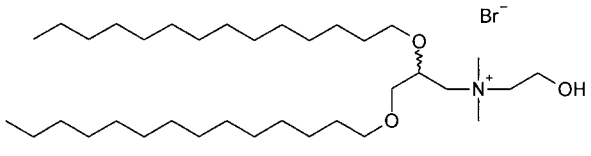
The properties of cationic lipids and their applications in the area of gene therapy may potentially be strongly influenced by the variation of the chain length of the poly(ethylene glycol) spacer and the number of positive charges on the headgroup. To fully explore and elucidate the role of the cationic lipid, we synthesized new types of multivalent cationic lipids. In these lipids, the PEG spacer increases the area per charged lipid. This allows us to directly vary the electrostatic interaction by significantly changing the lipid membrane charge density. In addition, an outer shell of poly(ethylene glycol) seg-

* To whom correspondence should be addressed.
[†] University of California.
[‡] Makromolekulare Chemie I und Bayreuther Institut für Makromolekülforschung (BIMF) Universität Bayreuth.

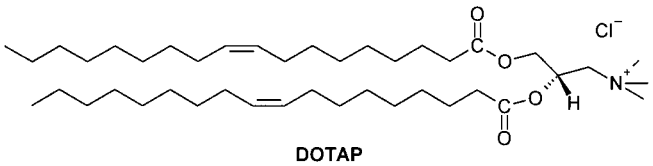
[1]Abbreviations: CL, cationic liposome; COSY, correlation spectroscopy; DCC, *N*,*N*′-dicyclohexyl carbodiimide; DMRIE, 1,2-dimyristoyloxypropyl-3-dimethylhydroxyethylammonium bromide; DMAP, 4-dimethylamino pyridine; DNA, deoxyribonucleic acid; DOPC, 1,2-dioleyl-*sn*-glycero-3-phosphocholine; DOPE, 1,2-dioleyl-*sn*-glycero-3-phosphoethanolamine; DOSPA, 2,3-dioleyloxy-*N*-[2-(sperminecarboxamido)ethyl]-*N*,*N*-dimethyl-1-propanaminium trifluoroacetate; DOTAP, 1,2-dioleyl-3-trimethylammoniumpropane chloride; GPC, gel permeation chromatography; PEG, poly(ethylene glycol); TBAH, tetrabutylammonium hydrogensulfate; tBOC, *tert*-butyloxycarbonyl; TEG, triethylene glycol; THF, tetrahydrofuran; TsCl, *p*-Toluenesulfonyl chloride.

10.1021/bc9801068 CCC: $18.00 © 1999 American Chemical Society
Published on Web 04/21/1999

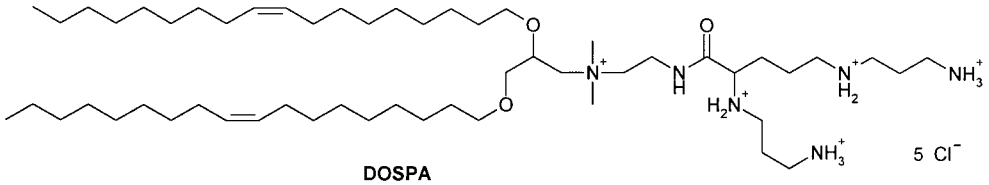
Scheme 1. Cationic Lipids Used in Gene Therapy Applications



DMRIE

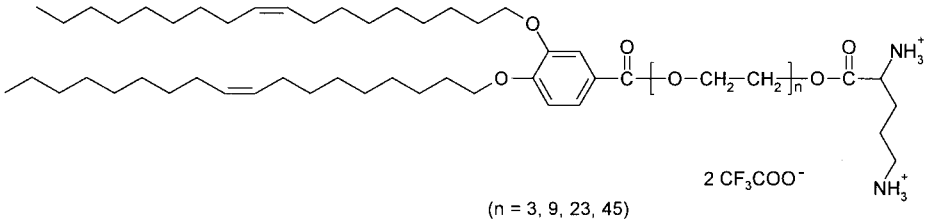


DOTAP



DOSPA

Scheme 2. Cationic Lipids with Poly(ethylene glycol) Spacer Segments



(n = 3, 9, 23, 45)

ments protects the complexes from the immune response of the body (*19*−*22*). This paper describes the synthesis of divalent cationic lipids with poly(ethylene glycol) spacers. The lipids consist of an unsaturated double-chain hydrophobic moiety based on 3,4-dihydroxy benzoic acid, attached to a hydrophilic poly(ethylene glycol) spacer which contains a divalent cationic end group. As poly(ethylene glycol) spacers monodisperse triethylene glycol and telechelic poly(ethylene glycol)s with an average degree of polymerization of 9, 23, and 45 were used. Scheme 2 shows the chemical structure of the cationic lipids presented in this paper.

EXPERIMENTAL PROCEDURES

Materials and Reagents. Oleyl bromide, 3,4-dihydroxy benzoic acid ethyl ester (protocatechuic acid ethyl ester), L-ornithine hydrochloride, di-*tert*-butyl pyrocarbonate, and *N*,*N*′-dicyclohexyl carbodiimide (DCC) were purchased from Sigma. 4-Dimethylamino pyridine (DMAP), *p*-toluenesulfonyl chloride (TsCl), tetrabutylammonium hydrogensulfate (TBAH), acrylonitrile, triethylene glycol (TEG), and poly(ethylene glycol)s (PEG) were obtained from Aldrich. Triethylene glycol and poly(ethylene glycol)s were dried in a vacuum prior to use. All other reagents and solvents were at least analytical grade and used as received.

General Methods. Infrared spectra were recorded on a Perkin-Elmer 1605 FTIR spectrophotometer calibrated using polystyrene film. ^{1}H and ^{13}C NMR spectroscopies were carried out on a Bruker Avance 200 MHz spectrometer. Molecular weight distributions were determined on a gel permeation chromatography system equipped with an Acuflow Series II pump (eluent, THF; flow rate, 1 mL/min), four Phenomenex Phenogel 5 columns (10^5, 10^4, 10^3, and 500 Å pore size), and a VDS Optilab RI-detector. The GPC was calibrated with polystyrene standards. Elemental analysis was carried out on a Control Equipment Corp. organic elemental analyzer model CEC 440HA.

3,4-Di(oleyloxy) Benzoic Acid (1). A total of 5.0 g (15.0 mmol) of oleyl bromide, 1.24 g (6.8 mmol) of protocatechuic acid ethyl ester, 2.8 g (20.4 mmol) of potassium carbonate, and 0.13 g (0.8 mmol) of potassium iodide were suspended in 40 mL of cyclohexanone and stirred at 100 °C for 18 h under nitrogen. Because of the light sensitivity of oleyl bromide, the flask was covered with aluminum foil. The hot reaction mixture was filtered and the solvent was removed in a vacuum. The residue was dissolved in 30 mL of ethanol containing 1.14 g (20 mmol) potassium hydroxide and refluxed for 4 h. The hot reaction mixture was added to 80 mL of water. Acidifying with concentrated hydrochloric acid to pH 1 resulted in the precipitation of a white solid. The solid was filtered off and washed several times with water. The crude acid was recrystallized from 20 mL of ethanol and dried in a vacuum.

Yield: 3.2 g (72%). mp: 60.5 °C. TLC (silica gel) chloroform/methanol (9:1): R_f 0.42. ^{1}H NMR ($CDCl_3$): δ 0.88 (t, 6H), 1.20−1.58 (m, 44H), 1.78−1.96 (m, 4H), 1.96−2.12 (dt, 8H), 4.08 (t, 4H), 5.37 (t, 4H), 6.90 (d, 1H), 7.60 (d, 1H), 7.74 (dd, 1H) ppm.

C18-PEG-OH (2a−d): General Procedure. A total of 1.30 g (2.0 mmol) of 3,4-di(oleyloxy) benzoic acid (**1**), 20 mmol of poly(ethylene glycol), 0.39 g (2.1 mmol) of *p*-toluenesulfonyl chloride, 0.13 g (1.1 mmol) of 4-dimethylamino pyridine, 0.13 g (0.5 mmol) of tetrabutylammonium hydrogensulfate, and 1.9 g (13.6 mmol) of potassium carbonate were suspended in 60 mL of tetrahydrofuran. The reaction mixture was stirred for 24 h

at 45 °C. After cooling to room temperature, the mixture was poured into 700 mL of water and 100 mL of methylene chloride were added. The solution was slowly acidified with dilute hydrochloric acid till pH 1 was reached. The organic layer was separated, washed four times with 400 mL of water and dried over magnesium sulfate. The solvent was removed in a vacuum and the residue dissolved in 40 mL of ethanol. The colorless solution was kept overnight at 4 °C, which resulted in the formation of a white precipitate. After removal of the precipitate by filtration, the solvent was removed in a vacuum. Traces of byproducts could be removed by filtration over an aluminum oxide (basic) containing column (extraction with ethyl acetate and ethanol). The product was dried in a vacuum.

Yield: 60−80%. GPC (THF): M_w/M_n 1.01−1.03. ^{1}H NMR ($CDCl_3$): δ 0.88 (t, 6H), 1.20−1.58 (m, 44H), 1.78−1.96 (m, 4H), 1.96−2.12 (dt, 8H), 3.56−3.90 (m, 4n-2H), 4.08 (t, 4H), 4.45 (t, 2H), 5.37 (t, 4H), 6.90 (d, 1H), 7.60 (d, 1H), 7.74 (dd, 1H) ppm.

Di-*tert*-butyloxycarbonyl-L-ornithine (3). A total of 2.53 g (15 mmol) L-ornithine hydrochloride were dissolved in 12 mL of 2 N sodium hydroxide solution and cooled with an ice−water bath. Within 1 h, 9.8 g (45 mmol) of di-*tert*-butyl pyrocarbonate dissolved in a small amount of tetrahydrofuran and 19 mL of 4 N sodium hydroxide was added in portions to the reaction mixture. The colorless solution was stirred overnight. The solution was acidified with dilute hydrochloric acid and the product extracted twice with 200 mL of ether. The combined ether phases were washed several times with water and dried over magnesium sulfate. The solvent was removed in a vacuum and the product dried in high vacuum at room temperature.

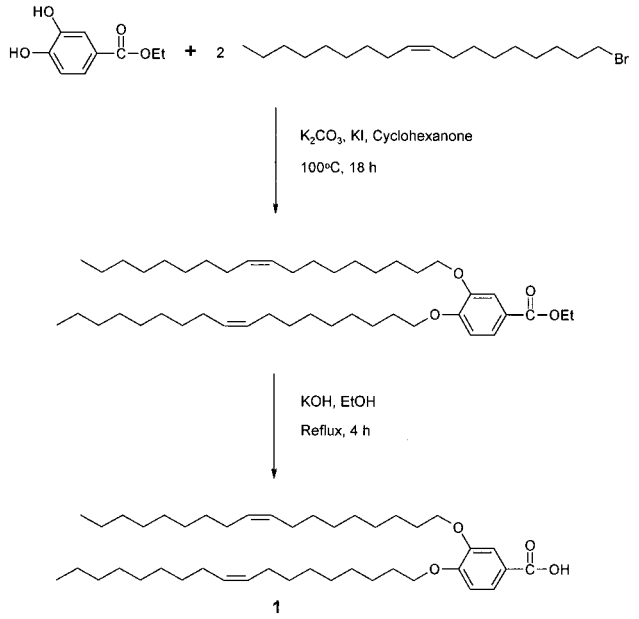
Yield: 4.8 g (97%). ^{1}H NMR ($CDCl_3$): δ 1.45 (s, 18H), 1.65−2.05 (m, 4H), 3.05−3.25 (m, 2H), 4.32 (m, 1H), 4.80 (b, 1H), 5.28 (b, 1H) ppm.

C18-PEG-Orn(BOC) (4a−d): General Procedure. A total of 1.4 mmol of C18-PEG-OH (**2a**−**d**), 0.51 g (1.6 mmol) of di-*tert*-butyloxy-L-ornithine (**3**), and 42 mg (0.35 mmol) of 4-dimethylamino pyridine were dissolved in 40 mL of methylene chloride. A total of 0.35 g (1.7 mmol) of *N,N′*-dicyclohexyl carbodiimide was dissolved in a minimal amount of methylene chloride and added to the reaction mixture. The solution was stirred for 3 h at room temperature. The dicyclohexyl urea was filtered off, and the solvent was removed in a vacuum. The crude product was dissolved in 30 mL of acetone and kept at 4 °C overnight. Dicyclohexyl urea was filtered off again, and the solvent was removed in a vacuum. Traces of unreacted di-*tert*-butyloxy-L-ornithine could be removed by filtration over an aluminum oxide (basic) containing column (elution with acetone). The product was dried in a vacuum.

Yield: 50−95%. GPC (THF): M_w/M_n 1.02−1.05. ^{1}H NMR ($CDCl_3$): δ 0.85 (t, 6H), 1.20−1.58 (m, 44H), 1.40 (s, 18H), 1.65−1.92 (m, 8H), 1.92−2.12 (dt, 8H), 3.02−3.22 (m, 2H), 3.56−3.88 (m, 4n−4H), 4.02 (t, 4H), 4.15 (m, 1H), 4.29 (t, 2H), 4.42 (t, 2H), 5.35 (t, 4H), 6.83 (d, 1H), 7.50 (d, 1H), 7.63 (dd, 1H) ppm.

C18-PEG-Orn (5a−d). General Procedure. A total of 1.0 mmol of C18-PEG-Orn(BOC) (**4a**−**d**) was dissolved in 5 mL of trifluoroacetic acid and cooled with an ice−water bath. After complete dissolution, the solution was stirred for additional 5 min. Longer reaction times may result in an increase of byproducts. The solvent was removed in a vacuum and the residue was dried in high vacuum. The crude product was purified by column chromatography on silica gel and elution with chloroform/methanol (4:1).

Scheme 3. Synthesis of 3,4-Di(oleyloxy) Benzoic Acid (1)



Yield: 30−70%. TLC (silica gel) chloroform/methanol (4:1): R_f 0.20−0.23. ^{1}H NMR ($CDCl_3$): δ 0.84 (t, 6H), 1.20−1.58 (m, 44H), 1.65−1.92 (m, 8H), 1.92−2.09 (dt, 8H), 2.98−3.12 (m, 2H), 3.56−3.90 (m, 4n-4H), 4.04 (t, 4H), 4.12 (m, 1H), 4.24 (t, 2H), 4.45 (t, 2H), 5.34 (t, 4H), 6.84 (d, 1H), 7.51 (d, 1H), 7.61 (dd, 1H), 7.75−8.35 (b, 6H) ppm. ^{13}C NMR ($CDCl_3$): d 14.3, 22.9, 26.3, 27.4, 30.0, 32.1, 69.3, 69.5, 70.0, 111.9, 114.1, 122.2, 130.0, 130.2, 148.1, 153.9, 167.0, 169.2 ppm. Elemental analysis (**5a**) $C_{58}H_{98}N_2O_{12}F_6$: calcd: C, 61.68; H, 8.75; N, 2.48. Found: C, 61.43; H, 9.12; N, 2.41.

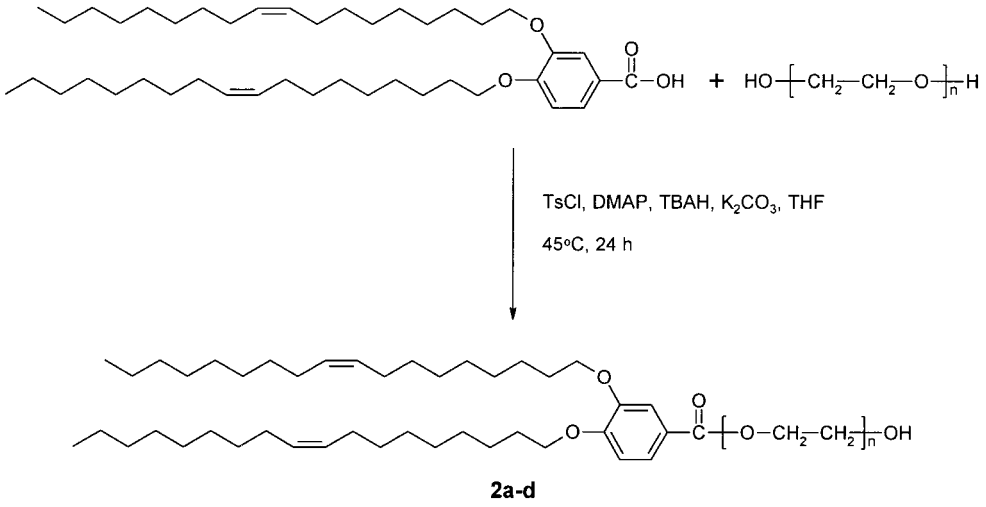
RESULTS AND DISCUSSION

The cationic PEG-containing lipids were synthesized following a route which consists of three main stages: (a) synthesis of the hydrophobic moiety of the lipid; (b) coupling of the hydrophilic PEG spacer segment; (c) attachment of the cationic headgroup to the lipid.

For the synthesis of the hydrophobic moiety of the lipid, we used a dihydroxy- and monocarboxy-substituted benzene ring as a central unit. This substitution pattern enables working with different linkage groups for the aliphatic alkyl chains (ether linkage) and the poly(ethylene glycol) segment (ester linkage). In this paper, we focus on the use of 3,4-dihydroxy benzoic acid which leads to two-chain lipids. Two-chain lipids are also the ones which are commonly found in natural membranes. Altough the benzene ring is an unusual unit in natural lipids there should be pointed out that ether and ester derivatives of the 3,4-dihydroxy benzoic acid (protocatechuic acid) are found in many fruits (*27*). As alkyl chains unsaturated C18 chains were used which will provide strong anchoring of the lipid in the bilayer membrane and chain flexibility due to the cis-double bond. 3,4-Di(oleyloxy) benzoic acid (**1**) was synthesized by etherification of 3,4-dihydroxy benzoic acid ethyl ester with oleyl bromide and following cleavage of the ethyl ester with potassium hydroxide (Scheme 3) (*28*−*30*).

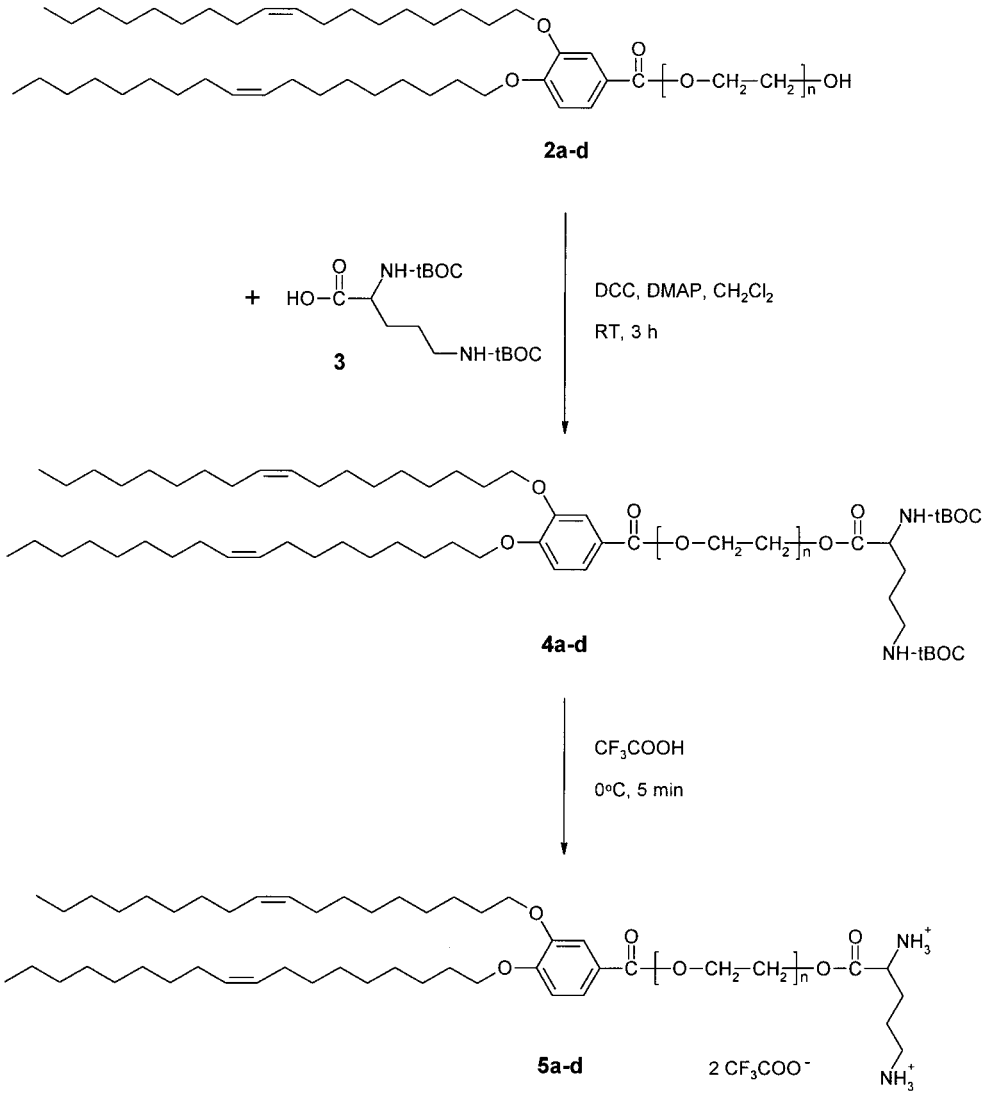
The next synthetic stage is the coupling reaction of 3,4-di(oleyloxy) benzoic acid (**1**) with α,ω-dihydroxy poly(ethylene glycol) (Scheme 4) based on a procedure of

Scheme 4. Synthesis of Hydroxy Functionalized PEG Containing Lipids (2a−d)[a]



[a] a, $n = 3$; b, $n = 9$; c, $n = 23$; d, $n = 45$.

Scheme 5. Synthesis of Cationic PEG Containing Lipids (5a−d)[a]



[a] a, $n = 3$; b, $n = 9$; c, $n = 23$; d, $n = 45$.

Percec et al. (*31*). Poly(ethylene glycol) was used in a 10-fold excess to avoid esterification of both hydroxyl groups. After reaction was completed, the excess PEG was removed by extraction with water followed by filtration of the product over an aluminum oxide (basic) containing column. The absence of traces of excess PEG was checked by gel permeation chromatography. The resulting hydroxy functionalized PEG containing lipids (**2a**−**d**) are useful intermediates for the attachment of a variety of biologically relevant end groups.

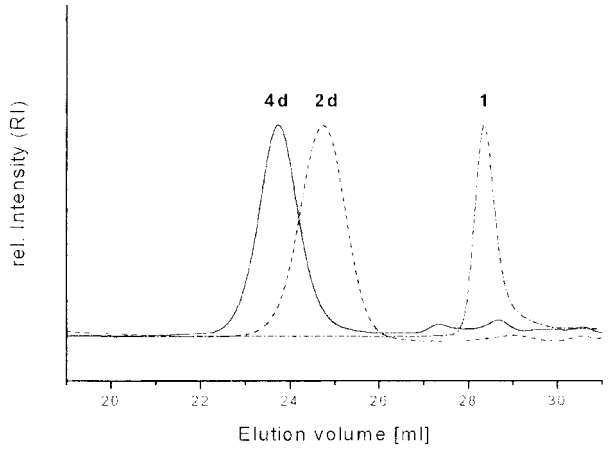


Figure 1. GPC elution diagrams of 3,4-di(oleyloxy) benzoic acid (**1**), the hydroxy functionalized PEG containing lipid (**2d**), and the corresponding PEG containing lipid with the tBOC protected end group (**4d**); eluent, THF; flow rate, 1 mL/min.

The carriers of the positive charge in cationic lipids are amino groups. In this work, we attached a *tert*-butyloxycarbonyl (tBOC) protected dibasic amino acid (L-ornithine) to the free hydroxyl group of the PEG segment (Scheme 5). The use of dicyclohexyl carbodiimide as esterification reagent allows us to run the reaction under mild conditions at room temperature (*32*). The use of a small excess of the protected L-ornithine ensures the complete conversion of the hydroxy functionalized PEG containing lipid. Excess L-ornithine could be removed by filtration over an aluminum oxide (basic) containing column. The purity of the product was checked by GPC and NMR spectroscopy. Figure 1 compares the GPC curves of 3,4-di(oleyloxy) benzoic acid (**1**), the hydroxy functionalized PEG containing lipid (**2d**), and the corresponding PEG containing lipid with the tBOC-protected end group (**4d**). The shift to higher molecular weight (lower elution volume) between the different coupling stages can be clearly observed. In addition, all peaks possess a monomodal distribution.

Cleavage of the *tert*-butyloxycarbonyl protecting groups with trifluoroacetic acid and purification of the crude product by column chromatography on silica gel lead to the cationic polymer lipids (**5a**−**d**) (Scheme 5). The structure was verified by ^{1}H NMR, ^{13}C NMR, COSY-NMR spectroscopy, and elemental analysis.

In conclusion, the successful synthesis of cationic PEG-containing lipids was demonstrated. These lipids have structural advantages compared to other cationic lipids. The divalent cationic headgroup of the lipid may potentially condense neighboring DNA strands, which further compacts DNA inside the complex. These compact structures are thought to enhance the transport of DNA into cells. Of particular interest in this series is the variability of the length of the poly(ethylene glycol) spacer. This spacer is expected to make the DNA strand−strand complexation more efficient and to avoid the immune response from the body by using the Stealth effect.

ACKNOWLEDGMENT

Supported by grants from the UC-Biotechnology Research and Education Program (97-02), NSF (DMR-9624091), and the Petroleum Research Foundation (31352-AC7). The Materials Research Laboratory at Santa Barbara is supported by NSF grant DMR-9632716. U. Schulze gratefully acknowledges a postdoctoral scholarship distributed by the DFG (Schu 1247/1-1).

LITERATURE CITED

(1) Behr, J.-P. (1994) *Bioconjugate Chem. 5*, 382−389.
(2) Felgner, P. L. (1997) *Sci. Am. 276*, 102−106.
(3) Friedmann, T. (1997) *Sci. Am. 276*, 96−101.
(4) Felgner, P. L., and Rhodes, G. (1991) *Nature 349*, 351−352.
(5) Zhu, N., Liggitt, D., Liu, Y., and Debs, R. (1993) *Science 261*, 209−211.
(6) Remy, J.-S., Sirlin, C., Vierling, P., and Behr, J.-P. (1994) *Bioconjugate Chem. 5*, 647−654.
(7) Rädler, J. O., Koltover, I., Salditt, T., and Safinya, C. R. (1997) *Science 275*, 810−814.
(8) Salditt, T., Koltover, I., Rädler, J. O., and Safinya, C. R. (1997) *Phys. Rev. Lett. 79*, 2582−2585.
(9) Lasic, D., Strey, H., Stuart, M., Podgornik, R., and Frederik, P. M. (1997) *J. Am. Chem. Soc. 119*, 832−833.
(10) Pitard, B., Aguerre, O., Airiau, M., Lachagès, A.-M., Boukhnikachvili, T., Byk, G., Dubertret, C., Herviou, C., Scherman, D., Mayaux, J.-F., and Crouzet, J. (1997) *Proc. Natl. Acad. Sci. U.S.A. 94*, 14412−14417.
(11) Koltover, I., Salditt, T., Rädler, J. O., and Safinya, C. R. (1998) *Science 281*, 78−81.
(12) Behr, J.-P. (1994) *Pure Appl. Chem. 66*, 827−835.
(13) Byk, G., Dubertret, C., Escriou, V., Frederic, M., Jaslin, G., Rangara, R., Pitard, B., Crouzet, J., Wils, P., Schwartz, B., and Scherman, D. (1998) *J. Med. Chem. 41*, 224−235.
(14) Lee, V. H. L., Ed. (1991) *Peptide and Protein Drug Delivery*, M. Dekker Inc., New York.
(15) Lasic, D. D., Ed. (1993) *Liposomes: From Physics to Applications*, Elsevier, Amsterdam.
(16) Warriner, H. E., Idziak, S. H. J., Slack, N. L., Davidson, P., and Safinya, C. R. (1996) *Science 271*, 969−973.
(17) Warriner, H. E., Davidson, P., Slack, N. L., Schellhorn, M., Eiselt, P., Idziak, S. H. J., Schmidt, H.-W., and Safinya, C. R. (1997) *J. Chem. Phys. 107*, 3707−3722.
(18) Warriner, H. E., Keller, S. L., Idziak, S. H. J., Slack, N. L., Davidson, P., Zasadzinski, J. P., and Safinya, C. R. (1998) *Biophys. J. 75*, 272−293.
(19) Allen, T. M., and Hansen, C. (1991) *Biochim. Biophys. Acta 1068*, 133−141.
(20) Lasic, D. D., and Needham, D. (1995) *Chem. Rev. 95*, 2601−2628.
(21) Lasic, D. D., and Martin, F. J., Eds. (1995) *Stealth Liposomes*, CRC Press, Boca Raton.
(22) Ceh, B., Winterhalter, M., Frederik, P. M., Vallner, J. J., and Lasic, D. D. (1997) *Adv. Drug Delivery Rev. 24*, 165−177.
(23) Zalipsky, S. (1993) *Bioconjugate Chem. 4*, 296−299.
(24) Zalipsky, S., and Menon-Rudolph, S. (1997) In *Poly(ethylene glycol): Chemistry and Biological Applications* (J. M. Harris, and S. Zalipsky, Eds.) pp 318−341, American Chemical Society, Washington, DC.
(25) Frisch, B., Boeckler, C., and Schuber, F. (1996) *Bioconjugate Chem. 7*, 180−186.
(26) Zalipsky, S., Brandeis, E., Newman, M. S., and Woodle, M. C. (1994) *FEBS Lett. 353*, 71−74.
(27) Billek, G. (1962) *Monatsh. Chem. 93*, 85. Billek, G. (1964) *Monatsh. Chem. 95*, 1044.
(28) Malthête, J., Levelut, A. M., and Nguyen, H. T. J. (1985) *J. Phys. Lett. Paris 46*, L875.
(29) Lattermann, G., and Staufer, G. (1989) *Liq. Cryst. 4*, 347−355.
(30) Staufer, G., and Lattermann, G. (1991) *Macromol. Chem. Phys. 192*, 2421−2431.
(31) Percec, V., Tomazos, D., Heck, J., Blackwell, H., and Ungar, G. (1994) *J. Chem. Soc., Perkin Trans. 2*, 31−44.
(32) Zalipsky, S., Gilon, C., and Zilkha, A. (1984) *J. Macromol. Sci.-Chem. A21*, 839−845.

BC9801068

JULY/AUGUST 1999
Volume 10, Number 4

© *Copyright 1999 by the American Chemical Society*

Bioconjugate Chemistry

COMMUNICATIONS

Enzymatic Cleavage of Peptide-Linked Radiolabels from Immunoconjugates

James J. Peterson and Claude F. Meares*

Department of Chemistry, University of California, One Shields Avenue, Davis, California 95616-5295. Received January 25, 1999

We have incorporated peptides selected by combinatorial library [Peterson, J. J., and Meares, C. F. (1998) *Bioconjugate Chem. 9*, 618−626) into peptide-linked radiolabeled immunoconjugates of the form DOTA-peptide-antibody. Decapeptide linkers -GFQGVQFAGF- and -GFGSVQFAGF-, selected for cleavage by human liver cathepsin B, were rapidly digested in vitro when compared to the simple model tetrapeptide motif of the prototype -GGGF− [Li, M., and Meares, C. F. (1993) *Bioconjugate Chem. 4*, 275−283]. Cleavage properties of these library-selected substrates for cathepsin B compared favorably with decapeptide linkers -GLVGGAGAGF- and -GGFLGLGAGF-, which incorporate two of the most labile extended cathepsin B substrates from the literature. The decapeptide linker -GFGSTFFAGF-, selected from the library for cleavage by human liver cathepsin D, was rapidly digested by cathepsin D while the others were not.

INTRODUCTION

Radioimmunotherapy and imaging use cancer-selective radiolabeled monoclonal antibodies (mAbs) to deliver therapeutic or imaging doses of radiation to the site of disease (*1*−*3*). Undesired accumulation of radioactivity in healthy tissues continues to be an impediment to this approach (*4*−*8*). One possible source of radiation in nontarget organs could be radiometal that has transchelated to proteins such as transferrin (*9*) or albumin (*10*), but this problem has been practically overcome through the use of reagents with high metal-chelate stability (*11*−*14*).

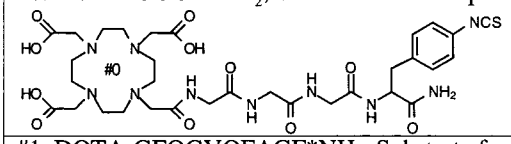
Elimination of radioactivity from the liver, for example, is a complex process involving both enzymatic liberation of low molecular weight radioactive fragments from the targeting molecule (usually an antibody or antibody fragment) and intracellular processing of these fragments (*15*−*18*). One strategy for improved clearance is to insert a metabolizable linker between the tumor-targeting moiety and the radiolabel. Linkers may be designed to mimic natural substrates for enzymes endogenous to the cells of interest, and may include features designed to take advantage of appropriate intracellular pathways of elimination of the resulting low molecular weight fragments (*19*−*21*). The exact conditions in vivo where either cleavage or subsequent metabolite processing will become rate limiting are still unclear, partly because potential linkers are subject to multiple lysosomal enzymes (*22*−*25*) and metabolic pathways (*26, 27*)—all of which are sensitive to variations in linker structure (*8, 16, 17*). Exploration of multiple structures with oligomeric linkers

* To whom correspondence should be addressed. Phone: 530-752-0936. Fax: 530-752-8938. E-mail: cfmeares@ucdavis.edu.

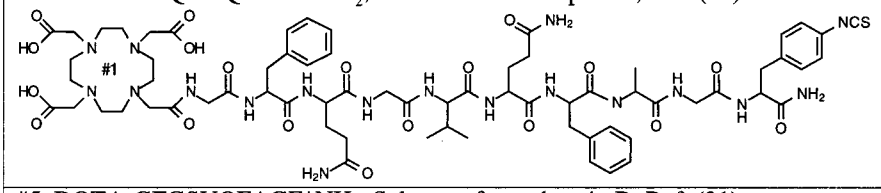
10.1021/bc990010t CCC: $18.00 © 1999 American Chemical Society
Published on Web 05/20/1999

Table 1. DOTA-Peptide Isothiocyanates[a]

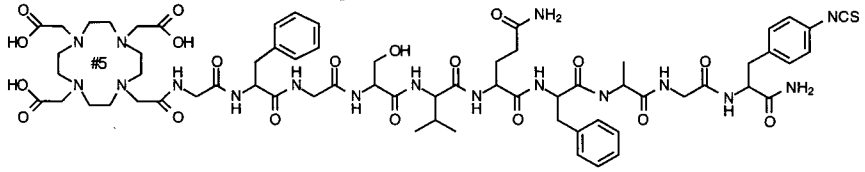
#0. DOTA-GGGF*NH_2; Substrate for cathepsin B; Ref: (30).



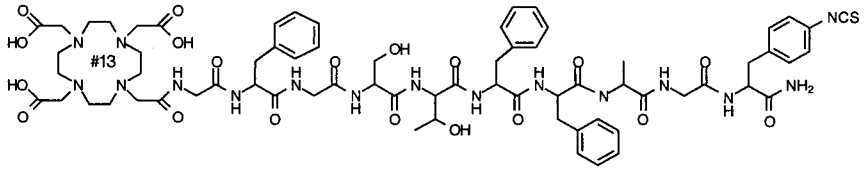
#1. DOTA-GFQGVQFAGF*NH_2; Substrate for cathepsin B; Ref: (31).



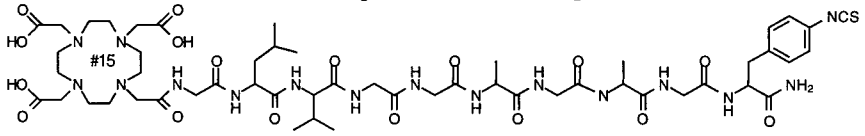
#5. DOTA-GFGSVQFAGF*NH_2; Substrate for cathepsin B; Ref: (31).



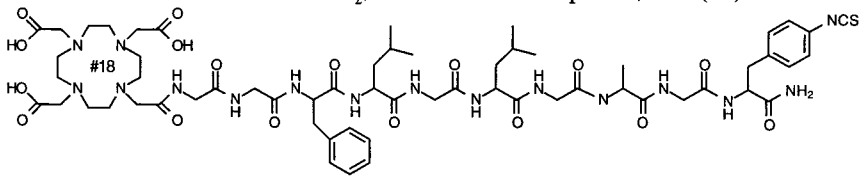
#13. DOTA-GFGSTFFAGF*NH_2; Substrate for cathepsin D; Ref: (31).



#15. DOTA-GLVGGAGAGF*NH_2; Substrate for cathepsin B; Ref: (34).



#18. DOTA-GGFLGLGAGF*NH_2; Substrate for cathepsin B; Ref: (33).



[a] F*, *p*-isothiocyanatophenylalanine.

of readily modified sequence offers a natural approach to further understanding the problem.

Metabolizable linkers explored for reducing radiation in healthy organs during radioimmunotherapy include esters, thioethers, disulfides, amides, and even hydrocarbon chains (*16*, *17*, *20*, *21*, *28*). Although ester linkers exhibit rapid cleavage in the liver, peptide linkers are preferred for their relative stability in circulation (*20*, *21*). It has been demonstrated in vitro that simple tetrapeptides can serve as cleavable linkers for radioimmunotherapy, where cleavage by endoproteases can occur over a period of hours at levels of enzyme expected to be present in vivo (*29*, *30*). The great differences in susceptibility of different peptides to enzymatic cleavage, and the range of possible metabolites resulting from cleavage of polypeptides by different enzymes, afford an opportunity to improve the rate at which radioactive metabolites are eliminated.

Previously, we selected peptide linkers from a combinatorial library using cleavage by specific lysosomal enzymes implicated in hepatic protein turnover: human liver cathepsins B and D (*31*). We have chosen for further study two substrates for cathepsin B and one for cathepsin D, which matched the consensus sequences deduced in that work. Using a convenient solid-phase procedure for the N-terminal functionalization of peptides with the DOTA[1] macrocycle (*32*), we prepared and conjugated peptide-linked chelators to Lym-1, a murine IgG_{2a} mAb used in cancer therapy (*6*). These conjugates were radiolabeled and treated with endoproteases to explore their cleavage properties in vitro compared to the simple prototype DOTA-tetrapeptide-Lym-1 (*30*). In addition, we inserted labile peptide substrates from literature sources (*33*, *34*) into the DOTA-peptide-Lym-1 format for comparison with conjugates derived from our combinatorial selection.

RESULTS AND DISCUSSION

Table 1 gives the formula for each substrate studied. Methods of preparation and comjugation are described in detail in Supporting Information. Thin layer chro-

[1] Abbreviations: DOTA, 1,4,7,10-tetraazacyclododecane-*N*,*N*′,*N*″,*N*‴-tetraacetic acid.

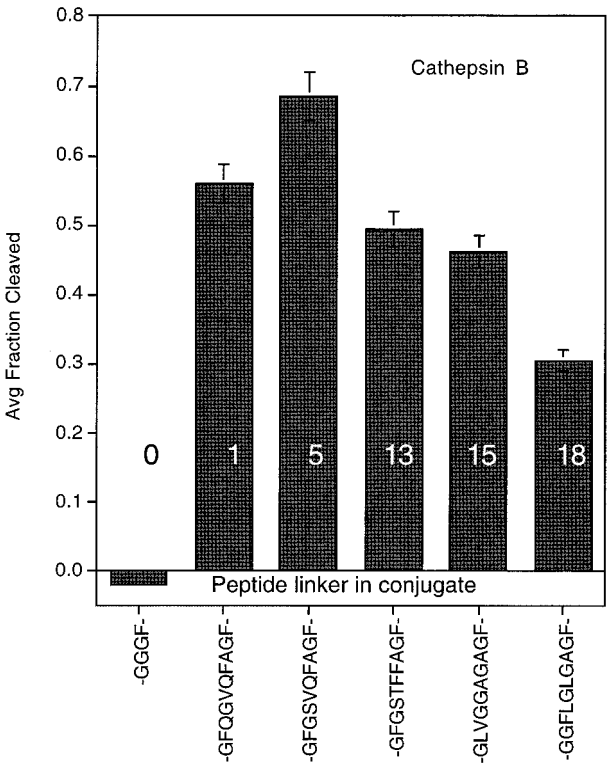


Figure 1. Digestions of ^{90}Y-DOTA-peptide-Lym-1 conjugates with human liver cathepsin B at 37 °C, 0.11 units/mL, 37 min. Experiments were performed in triplicate; error bars represent 1 standard deviation.

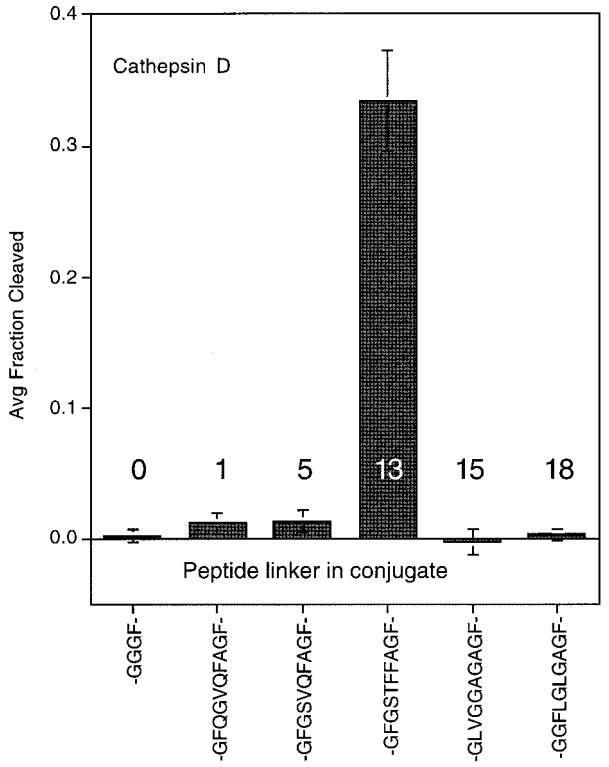


Figure 2. Digestions of ^{90}Y-DOTA-peptide-Lym-1 conjugates with human liver cathepsin D at 37 °C, 0.22 units/mL, 65 min. Experiments were performed in triplicate; error bars represent 1 standard deviation.

matograms showed that the stability of the unconjugated nitro form of each DOTA-peptide-^{90}Y complex was not adversely affected by the enzymatic cleavage buffer. All peptide linkages were stable in cleavage buffer lacking enzyme. Under these conditions [ca. 10-fold lower in enzyme concentration than those previously used (*30*)], no significant cleavage of the prototype DOTA-peptide#0-Lym-1 occurred, while substantial cleavage of all literature and library-based decapeptide conjugates was observed for cathepsin B (Figure 1). The conjugate most labile to cathepsin B (no. 5) was derived from our combinatorial library (*31*). The lability of conjugate 1, also derived from the library for cleavage by cathepsin B, compared favorably with literature-based conjugate 15 (*34*). All decapeptide conjugates were cleaved to a greater extent than conjugate no. 18. Surprisingly, even conjugate 13, selected from the combinatorial library for cleavage by cathepsin *D*, was substantially cleaved during treatment with cathepsin B.

Cathepsin D was able to significantly cleave conjugate 13, while none of the other conjugates were significantly cleaved by this enzyme under these conditions (Figure 2). In our attempts to prepare a literature-based substrate for cathepsin D (*35*), the product was not sufficiently soluble at the DOTA-peptide stage to be readily isolated.

Linkers for radioimmunotherapy that consist of unnatural amide bonds have been referred to as "peptidyl" in the sense that the backbone of the folded antibody flanking each modified lysine may serve as a set of arbitrary peptidyl enzyme substrates (*36*, *37*). It has been found that the potential cleavage sites on Lym-1 provide relatively poor substrates for lysosomal endoproteases when compared to short—or even arbitrary—peptide linkers attached to ϵ-amines on Lym-1 (*29*, *30*). Until very recently (*21*), ester-based linkers (despite their relative lack of stability in plasma) have continued to find favor when compared to simple mono- or diamide linkages, due to their superior elimination properties in healthy tissues (*19*, *20*, *36*−*39*). However, it is unlikely that lysosomal endoproteases are able to participate in catabolic processes involving unnatural amide-based linkers.

Cathepsin D, for example, requires an extended substrate (>5 amino acid residues) for cleavage (*40*, *41*). The cathepsin D results in Figure 2 emphasize the importance of fine structural detail. We and others have found cathepsin D to be a more selective enzyme than cathepsin B (*31*, *42*−*44*).

It is clear from the results in Figure 1 that all conjugates derived from specific substrates for cathepsin B were efficiently cleaved by this enzyme in their bioconjugate form. The effect of linker length on cathepsin B cleavage is still unclear, although the activity of this enzyme may be expected to be hindered by the proximity of the intended substrate to the targeting macromolecule (*31*). Conjugates derived from our combinatorial library were cleaved more quickly than extended cathepsin B substrates from literature that might be considered appropriate candidates for cleavable linkers.

The sensitivity of conjugate 13 (a library substrate selected for cleavage by cathepsin D) to cathepsin B is notable. Our stock of cathepsin B was assayed by the supplier to be over 92% pure by SDS−PAGE, and the method used for its purification was designed to remove cathepsin D (*35*). However, we did not include any specific inhibitors of cathepsin D during cathepsin B cleavage experiments; thus, we cannot rule out the possibility that our stock of cathepsin B was contaminated with traces of cathepsin D.

In conclusion, highly labile cathepsin substrates were derived from a combinatorial library which tapped only

a modest fraction of the potential of this approach (having only four variable positions and nine variable amino acids, or $9^4 = 6561$ unique peptide sequences). It should be possible to make use of a much larger set of amino acid side chains, to incorporate features that may expedite elimination of the fragments as well (*21*, *27*). Subsequent experiments by others have confirmed that the reagents studied here are able to stably link ^{90}Y to Lym-1 for extended periods in human plasma under physiological conditions (David Kukis, personal communication).

ACKNOWLEDGMENT

This work was supported by NIH Research Grants CA16861 (C.F.M.) and CA47829 (G.L. DeNardo P.I.). We thank David Kukis and Drs Gerald and Sally DeNardo for helpful discussions.

Supporting Information Available: Detailed methods of preparation and conjugation, and cathepsin digestion. This material is available free of charge via the Internet at http://pubs.acs.org.

LITERATURE CITED

(1) Sands, H. (1990) Experimental Studies of Radioimmunodetection of Cancer: An Overview. *Cancer Res. 50* (Suppl.), 809s−813s.

(2) Subramanian, R., and Meares, C. F. (1991) Bifunctional Chelating Agents for Radiometal-labeled Monoclonal Antibodies. In *Cancer Imaging with Radiolabeled Antibodies* (D. M. Goldenberg, Ed.) Kluwer Academic Publications, Boston.

(3) Goldenberg, D. M. (1995) Cancer Therapy with Radiolabeled Antibodies. (D. M. Goldenberg, Ed.) CRC Press, Boca Raton.

(4) Hnatowich, D. J. (1990) Antibody Radiolabeling, Problems and Promises. *Nucl. Med. Biol. 17*, 49−55.

(5) Pimm, M. V., Perkins, A. C., and Baldwin, R. W. (1985) Differences in Tumor and Normal Tissue Concentrations of Iodine and Indium Labeled Monoclonal Antibody. II. Biodistribution Studies in Mice with Human Tumor Xenografts. *Eur. J. Nucl. Med. 11*, 300−304.

(6) DeNardo, S. J., DeNardo, G. L., Deshpande, S. V., Adams, G. P., Macey, D. J., Mills, S. L., Epstein, A. L., and Meares, C. F. (1988) The Design of Radiolabeled Monoclonal Antibody for Radioimmunodiagnosis and Radioimmunotherapy. In *Radiolabeled Monoclonal Antibodies for Imaging and Therapy-Potential Problems and Prospects* (S. C. Srivastava, Ed.) Plenum Publishing Corp., New York.

(7) Motta-Hennessy, C., Sharkey, R. M., and Goldenberg, D. M. (1990) Metabolism of Indium-111-Labeled Murine Monoclonal Antibody in Tumor and Normal Tissue of the Athymic Mouse. *J. Nucl. Med. 31*, 1510−1519.

(8) Arano, Y., Mukai, T., Akizawa, H., Uezono, T., Motonari, H., Wakisaka, K., Kairiyama, C., and Yokoyama, A. (1995) Radiolabeled Metabolites of Proteins Play a Critical Role in Radioactivity Elimination from the Liver. *Nucl. Med. Biol. 22*, 555−564.

(9) Hnatowich, D. (1986) Label Stability in Serum of Four Radionuclides on DTPA-coupled Antibodies. An Evaluation. *Int. J. Nucl. Med. Biol. 13*, 353−358.

(10) Cole, W. A., DeNardo, S. J., and Meares, C. F., et al. (1986) Serum Stability of ^{67}Cu Chelates: Comparison with ^{111}In and ^{57}Co. *Int. J. Nucl. Med. Biol. 13*, 363−368.

(11) Deshpande, S. V., Subramanian, R., McCall, M. J., DeNardo, S. J., DeNardo, G. L., and Meares, C. F. (1990) Metabolism of Indium Chelates Attached to Monoclonal Antibody: Minimal Transchelation of Indium from Benzyl-EDTA Chelate in Vivo. *J. Nucl. Med. 31*, 218−224.

(12) Paxton, R. J., Jakowatz, J. G., Beatty, J. D., Beatty, B. G., Vlahos, W. G., Williams, L. E., Clark, B. R., and Shively, J. E. (1985) High Specific-Activity ^{111}In-labeled Anticarcinoembryonic Antigen Monoclonal Antibody: Improved Method for the Synthesis of Diethylenetriaminepentaacetic Acid Conjugates. *Cancer Res. 45*, 5694−5699.

(13) Meares, C. F., Moi, M. K., Diril, H., Kukis, D. L., McCall, M. J., Deshpande, S. V., DeNardo, S. J., Snook, D., and Epenetos, A. A. Macrocyclic Chelates for Diagnosis and Therapy. *Br. J. Cancer 62* (Suppl. X), 21−26.

(14) Lewis, M. R., Raubitschek, A., and Shively, J. E. (1994) A Facile, Water-Soluble Method for Modification of Proteins with DOTA. Use of Elevated Temperature and Optimized pH to Achieve High Specific Activity and High Chelate Stability in Radiolabeled Immunoconjugates. *Bioconjugate Chem. 5*, 565−576.

(15) Duncan, J. R., and Welch, M. J. (1993) Intracellular Metabolism of Indium-111-DTPA-Labeled Receptor Targeted Proteins. *J. Nucl. Med. 34*, 1728−1738.

(16) Faivre-Chauvet, A., Gestin, J. F., Mease, R. C., Sai-Maurel, C., Thedrez, P., Slinkin, M., Meinken, G. E., Srivastava, S. C., and Chatal, J. F. (1993) Introduction of Five Potentially Metabolizable Linking Groups Between ^{111}In−Cyclohexyl EDTA Derivatives and F(ab′)$_2$ Fragments of Anticarcinoembryonic Antigen Antibody-II. Comparative Pharmacokinetics and Biodistribution in Human Colorectal Carcinoma-bearing Nude Mice. *Nucl. Med. Biol. 20*, 763−771.

(17) Quadri, S. M., Vriesendorp, H. M., Leichner, P. K., and Williams, J. R. (1993) Evaluation of In-111- and Yttrium-90-Labeled Linker Immunoconjugates in Nude Mice and Dogs. *J. Nucl. Med. 34*, 938−945.

(18) Gore, S., Morris, A. I., Gilmore, I. T., Maltby, P. J., Thornback, J. R., and Billington, D. (1991) Differences in the Intracellular Processing of the Radiolabel Following Uptake of Iodine-125 and Technetium-99m-Neogalactosyl Albumin by the Isolated Perfused Rat Liver. *J. Nucl. Med. 32*, 506−512.

(19) Arano, Y., Matsushima, H., Tagawa, M., Inoue, T., Koizumi, M., Hosono, M., Sakahara, H., Endo, K., Konishi, J., and Yokoyama, A. (1994) A Newly Designed Radioimmunoconjugate Releasing a Hippurate-like Radiometal Chelate for Enhanced Target/Nontarget Radioactivity. *Nucl. Med. Biol. 21*, 63−69.

(20) Arano, Y., Wakisaka, K., Ohmono, Y., Uezono, T., Akizawa, H., Nakayama, M., Sakahara, H., Tanaka, C., Konishi, J., and Yokoyama, A. (1996) Assessment of Radiochemical Design of Antibodies Using and Ester Bond as the Metabolizable Linkage: Evaluation of Maleimidoethyl 3-(Tri-*n*-butylstannyl)hippurate as a Radioiodination Reagent of Antibodies for Diagnostic and Therapeutic Applications. *Bioconjugate Chem. 7*, 628−637.

(21) Arano, Y., Wakisaka, K., Akizawa, H., Ono, M., Kawai, K., Nakayama, M., Sakahara, H., Konishi, J., and Saji, H. (1998) Assessment of the Radiochemical Design of Antibodies with a Metabolizable Linkage for Target-Selective Radioactivity Delivery. *Bioconjugate Chem. 9*, 497−506.

(22) Huisman, W., Lanting, L., Doddema, H. J., Bouma, J. M. W., and Gruber, M. (1974) Role of Individual Cathepsins in Lysosomal Protein Digestion as Tested by Specific Inhibitors. *Biochim. Biophys. Acta 370*, 297−307.

(23) Blum, J. S., Fiani, M. L., and Stahl, P. D. (1991) Localization of cathepsin D in endosomes: characterization and biological importance. *Adv. Exp. Med. Biol. 306*, 281−287.

(24) Dingle, J. T., Poole, R. A., Lazarus, G. S., and Barrett, A. J. (1973) Immunoinhibition of Intracellular Protein Digestion in Macrophages. *J. Exp. Med. 137*, 1124−1141.

(25) Heymann, E. (1982) Hydrolysis of Carboxylic Ester and Amides. *Metabolic Basis of Detoxification: Metabolism of Functional Group* (W. B. Jakoby, J. R. Bend, and J. Caldwell, Eds.) pp 229−241, Academic Press, New York.

(26) Goldstein, A., Aronow, L., and Kalman, S. M. (1974) Chemical Pathways of Drug Metabolism. *Principals of Drug Action*, pp 242−267. Wiley, New York.

(27) Pisoni, R. L., Thoene, J. L., Lemons, R. M., and Christensen, H. N. (1987) Important Differences in Cationic Amino Acid Transport by Lysosomal System c and System y$^+$ of the Human Fibroblast. *J. Biol. Chem. 262*, 15011−15018.

(28) Haseman, M. K., Goodwin, D. A., Meares, C. F., Kaminski, M. S., Wensel, T. G., McCall, M. J., and Levy, R. (1986) Metabolizable ^{111}In Chelate Conjugated Anti-idiotype Monoclonal Antibody for Radioimmunodetection in Lymphoma Mice. *Eur. J. Nucl. Med. 12*, 455−460.

(29) Studer, M., Kroger, L. A., DeNardo, S. J., Kukis, D. L., and Meares, C. F. (1992) Influence of a Peptide Linker on Biodistribution and Metabolism of Antibody-Conjugated Benzyl-EDTA. Comparison of Enzymatic Digestion in Vitro and in Vivo. *Bioconjugate Chem. 3*, 424−429.
(30) Li, M., and Meares, C. F. (1993) Synthesis, Metal Chelate Stability Studies, and Enzyme Digestion of a Peptide-Linked DOTA derivative and Its Corresponding Radiolabeled Immunoconjugates. *Bioconjugate Chem. 4*, 275−283.
(31) Peterson, J. J., and Meares, C. F. (1998) Cathepsin Substrates as Cleavable Peptide Linkers in Bioconjugates, Selected from a Fluorescence Quench Combinatorial Library. *Bioconjugate Chem. 9*, 618−626.
(32) Peterson, J. J., Pak, R. H., and Meares, C. F. (1999) Total Solid-Phase Synthesis of DOTA-Functionalized Peptides for Radioimmunotherapy. *Bioconjugate Chem. 10*, 316−320.
(33) Putnam, D., Shiah, J.-G., and Kopecek, J. (1996) Intracellularly Biorecognizable Derivatives of 5-Fluoro-uracil. *Biochem. Pharm. 52*, 957−962.
(34) Lalmanach, G., Serveau, C., Brillard-Bourdet, M., Chagas, J. R., Mayer, R., Juliano, L., and Gaurthier, F. (1995) Conserved Cystatin Segments as Models for Designing Specific Substrates and Inhibitors of Cysteine Proteinases. *J. Protein Chem. 14*, 645−653.
(35) Scarborough, P., Topham, C., Richo, G. R., Conner, G. E., Blundell, T. L., and Dunn, B. M. (1993) Exploration of Subsite Binding Specificity of Human Cathepsin D Through Kinetics and Rule-based Molecular Modeling. *Protein Sci. 2*, 264−276.
(36) Paik, C. H., Quadri, S. M., and Reba, R. C. (1989) Interposition of Different Chemical Linkages Between Antibody and ^{111}In-DTPA to Accelerate Clearance from Nontarget Organs and Blood. *Nucl. Med. Biol. 16*, 475−481.
(37) Pak, C. H., Yokoyama, K., Reynolds, J. C., Quadri, S. M., Min, C. Y., Shin, S. Y., Maloney, P. J., Larson, S. M., and Reba, R. C. (1989) Reduction of Background Activities by Introduction of a Diester Linkage Between Antibody and a Chelate in Radioimmunodetection of Tumor. *J. Nucl. Med. 30*, 1693−1701.
(38) Weber, R. W., Boutin, R. H., Nedelman, M. A., Lister-James, J., and Dean, R. T. Enhanced Kidney Clearance with an Ester-Linked 99mTc−Radiolabeled Antibody Fab′-Chelator Conjugate. *Bioconjugate Chem. 1*, 431−437.
(39) Bridger, G. J., Abrams, M. J., Padmanabhan, S., Gaul, F., Larsen, S., Henson, G. W., Schwartz, D. A., Longley, C. F., Burton, C. A., and Ultee, M. E. (1996) A comparison of Cleavable and Noncleavable Hydrazinopyridine Linkers for the ^{99m}Tc Labeling of Fab′ Monoclonal Antibody Fragments. *Bioconjugate Chem. 7*, 255−264.
(40) Barrett, A. J. (1967) Lysosomal Acid Proteinase of Rabbit Liver. *Biochem. J. 104*, 601.
(41) Barrett, A. J. (1970) Purification of Isoenzymes from Human and Chicken Liver. *Biochem. J. 117*, 601−607.
(42) Barrett, A. J. and Kirschke, H. (1981) Cathepsin B, Cathepsin H, and Cathepsin L. *Methods Enzymol. 80*, 535−561.
(43) Barrett, A. J. (1977) In *Proteinases in Mammalian Cells and Tissues* (A. J. Barrett, Ed.) Vol. 2, pp 209−248, Elsevier/North-Holland Biomedical Press, Amsterdam and New York.
(44) Kirschke, H., Langner, J., Riemann, S., Wiederanders, B., Ansorge, S., and Bohley, P. (1980) *Protein Degradation in Health and Disease*, Excerpta Medica, Amsterdam.

BC990010T

© 1999 American Chemical Society, Bioconjugate Chem., Peterson bc990010t Supporting Info Page 1

FOOTNOTES

1. Abbreviations used: BCA, bifunctional chelating agent; DMF, N,N-dimethylformamide; DMSO, methylsulfoxide; DOTA, 1,4,7,10-tetraazacyclododecane-N,N′,N″,N‴-tetraacetic acid; DTPA, diethylenetriamine pentaacetic acid; ESIMS, electrospray ionization mass spectrometry; ITC, isothiocyanate.
2. Radioimmunoconjugates remain fixed at the origin, while low molecular weight impurities such as unreacted radiolabeled BCA or chelate liberated by proteolysis migrate up the plate.
3. The concentration of Lym-1 was determined by measuring its absorbance at 280nm after an appropriate dilution in 0.1M sodium phosphate pH7. ($E^{1\%}_{280}$ = 1.35 (9))

© 1999 American Chemical Society, Bioconjugate Chem., Peterson bc990010t Supporting Info Page 2

EXPERIMENTAL PROCEDURES

Reagents. Fluorescamine, Pd on activated carbon, CCl_4, $CSCl_2$, were purchased from Aldrich Chemical Co. Methanol, NaOH, HCl (aq.), biotechnical grade CF_3COOH, and HPLC grade CH_3CN, and Fuji X-ray film were purchased from Fisher. HPLC grade DMSO was purchased from Fluka. Aqueous 25% tetramethylammonium hydroxide was purchased from Acros Organics. H_2 gas was purchased from Matheson. All buffers were made using 18MΩ•cm water. DOTA-peptides were synthesized as described (2). Human liver cathepsin D was purchased from Calbiochem-Novabiochem Corp. Human liver cathepsin B and Sephadex G-50 was purchased from Sigma. Lym-1 monoclonal antibody was purchased from Techniclone. $^{111}InCl_3$ was kindly provided by the laboratory of Dr David Goodwin. $^{90}YCl_3$ was purchased from Pacific Northwest National Laboratory. Plastic backed thin layer silica gel plates (Kieselgel 60) were purchased from EM Science.

Mass Spectrometry, IR and UV Spectroscopy. Electrospray mass spectrometry was performed on a Fisons Instruments VG Quattro triple quadrupole spectrometer using an eluent of 0.1% HCOOH, 49.95% H_2O, 49.95% CH_3CN at a flow rate of 5μL/min. Cone voltage was set to 50V. Source temperature was set to 80°. Samples collected during HPLC were lyophilized and rewetted at least twice on a Savant model SVC-100H speed-vac lyophilizer before analysis. Calibration of the mass scale was performed using a solution of PEG 300, PEG 600, and PEG 1000 as calibration standard. Infrared spectra were recorded on a Mattson Galaxy Series FTIR 300. UV spectroscopy was performed on a Hewlett-Packard model 8450 UV/vis spectrophotometer.

HPLC. For analytical HPLC a Dynamax microsorb 100 Å 5μm 4.6mm × 250mm C-18 column was used at a flow rate of 1mL/min. For semi-preparative HPLC, a Phenomenex Magellan 100Å 5μm 10 × 250mm C-18 column was used at a flow rate of 3mL/min.

© 1999 American Chemical Society, Bioconjugate Chem., Peterson bc990010t Supporting Info Page 3

HPLC buffers were: Buffer system A=0.068 N NH_4Oac, pH 4.8, vs CH_3CN. Buffer system B=0.1% CF_3COOH in H_2O vs 0.1% CF_3COOH in CH_3CN. Eluting peaks were detected at 280nm unless otherwise indicated.

Gradient 1=Hold 0% CH_3CN for 5 min and linear gradient to 50% by 35min.

Gradient 2=Hold 20% CH_3CN for 5 min and linear gradient to 50% by 23min.

Gradient 3=Hold 25% CH_3CN for 5 min and linear gradient to 50% by 25min.

Thin Layer Chromatography and Imaging. Silica gel thin layer chromatograms were developed on multiple 0.9 × 7.0 cm lanes using a 50:50 mixture of CH_3OH and 10% aqueous NaOAc as the eluent. Chromatograms were first imaged using both X-ray film and an AMBIS radioanalytical imaging system. Fractions of each lane were then cut out using the X-ray image as a template and placed >4 cm apart on AMBIS plates, which were again imaged and quantified using the AMBIS software.

Bifunctional Chelator Synthesis. Several DOTA-peptides containing C–terminal nitrophenylalanine amide were synthesized as described (2). The conversion of DOTA-peptide#18-Lym-1 from the nitro to the isothiocyanato form described below is representative (Scheme S1).

DOTA-peptide #18-L-p-aminophenylalanine amide (2). DOTA-peptide#18-L-p-nitrophenylalanine amide **1** (24mg, 18μmol) was dissolved in 3.0mL water and 1mL CH_3OH in a 25mL pear bottom flask. The pH was adjusted to 10.5 with 0.1N NaOH and 17mg Pd/C was added. The flask was fitted with a vented rubber septum, purged for 5min with argon through a 20-gauge syringe needle, purged 15min with H_2, and charged with H_2 at 5psig. The mixture was vigorously stirred for 15h at room temperature, filtered via 0.45μm syringe filter, and adjusted with 0.1N HCl to pH 5. A small sample was removed for HPLC analysis (gradient #1, buffer system A). A single peak eluting at 27 min was collected and thoroughly lyophilized. The product tested positive for free amine by fluorescamine test (3). Reaction solvent was evaporated to give

© 1999 American Chemical Society, Bioconjugate Chem., Peterson bc990010t Supporting Info Page 4

the sodium salt of **2** (31 mg) in near quantitative yield. ESIMS calc *m/z* $(M+H+Na)^{++}$ for $C_{59}H_{90}N_{16}O_{17}$ = 658.8 *m/z* $(M+H+Na)^{++}$ found = 658.3.

DOTA-peptide#18-p-isothiocyanatophenylalanine amide (3). Compound **2** (30mg) was taken up in 2mL 0.1M HCl, 300mL CCl_4, and 1.7mL $CSCl_2$ and stirred vigorously for 3h. A small aliquot of the aqueous layer was neutralized with NaOH and tested negative for free amines by fluorescamine test. The organic layer was removed, and the aqueous solution was washed 4 × 2mL CH_2Cl_2. After evaporation, crude **3** was dissolved in 2mL HPLC grade DMSO and analyzed by HPLC using gradient 1 buffer system B. The peak eluting at 34min (89% of the total integrated area) using gradient 1 was purified on Magellan C-18 using gradient 3, buffer system B. HPLC solvents were evaporated to yield **3** (20mg, 14.9mmol) after lyophilization. Overall yield of **3** from compound **1**: 83%. IR (KBr) 2102 cm^{-1} (ν N=C=S) ESIMS calc *m/z* $(M+H)^+$ for $C_{59}H_{90}N_{16}O_{17}$ = 1337.7 $(M+H)^+$ found = 1335.3 $(M+2H)^{++}$ found = 668.6. Table S1 shows analytical and yield data for all 5 peptides. All isothiocyanates were stored at 50mM in DMSO at –70°C.

Preparation of DOTA-peptide-Lym-1 conjugates (4). Conjugations were performed in parallel for all bifunctional chelators. Two general procedures were performed. In method 1, isothiocyanate chelators were first labeled with radiometal and then conjugated to Lym-1. In method 2, the isothiocyanates were first conjugated to Lym-1, then radiolabeled.

Method 1. Dilute 5mM solutions of 8μL DOTA-peptide-ITC #0, #1, #5, #13, #15, or #18 (Table S1) in DMSO were buffered with 6μL 0.26M tetramethylammonium acetate pH 5.5, and $^{90}YCl_3$ (2μL; 600μCi) was added to each BCA. For controls, radiometal was incubated with buffer alone and with DTPA alone. The labeling reaction was allowed to proceed for 2h at 40°. An aliquot of each reaction (1μL) was applied to TLC, and 2μL of 0.2M DTPA pH 5.5 was added to the remaining mixture to sequester any unchelated metal. The solution was allowed to react at room temperature for 1.5 h, and

© 1999 American Chemical Society, Bioconjugate Chem., Peterson bc990010t Supporting Info Page 5

another 1μL was removed and analyzed by TLC. Radiolabeled BCA and radiolabeled DTPA migrated at R_f 0.25-0.35 and 0.6, respectively. Lym-1 mAb (9.17mg/mL)[3] was transferred from pH 7 storage buffer to conjugation buffer (0.1M tetramethylammonium phosphate, pH 9) using Sephadex G-50 gel filtration media (4) and 100μL (0.92mg; 5.9nmol) Lym-1 was added to each BCA. Conjugation was allowed to proceed for 3h at 37°C, and the conjugates were purified and buffer exchanged on G-50 gel filtration media into 0.1M tetramethylammonium acetate, pH 4.8. Samples of each conjugate applied to TLC before and after gel filtration confirmed the removal of low molecular weight impurities.[2] Similar labelings were performed with $^{111}InCl_3$.

Method 2. Freshly thawed DOTA-peptide-ITC #0, #1, #5, #13, #15, or #18 (10μL; 50nmol) in DMSO was added to Lym-1 mAb (100μL; 1.67mg; 10.8nmol) in 0.1M tetramethylammonium acetate, pH 8.95. Conjugation was allowed to proceed for 3h at 37°C. Unreacted BCA was removed by gel filtration and the buffer exchanged with 0.4M NH_4OAc, pH 7.0. Conjugate concentration was measured (typically 15mg/mL)[3] and $^{90}YCl_3$ (4μL; 400μCi) was added. The chelation reaction was allowed to proceed for 2.3h at 40°C for every reaction. Reaction mixture aliquots were applied to TLC, and a challenge chelate solution was added (12μL 0.1M DTPA/ 0.5M ammonium citrate, pH 6.5). After 1.5h at 37°C, 1μL aliquots were removed for TLC and the conjugates were purified by gel filtration into 0.1M tetramethylammonium acetate, pH 4.8. Analysis of the TLC plates before and after challenge confirmed removal of unchelated metal by DTPA. TLC analysis before and after final gel filtration confirmed removal of any radiolabeled DTPA or citrate.

***In vitro* Enzymatic Digestions of Protein Conjugates.** Radiolabeled conjugates from method 2 were diluted to 8.5mg/mL in cathepsin cleavage buffer (0.1M tetramethylammonium acetate, pH 4.8) and portioned into 3 × 25μL aliquots for triplicate digestions with cathepsin B, 3 × 25μL aliquots for triplicate digestions with cathepsin D, and 1 × 50μL aliquots for buffer-only controls. Human liver cathepsin B (50μL @ 1.53 units/mL (5)) stored in 50mM NaOAc/ 1mM EDTA, pH 5 was preactivated for 30min with

© 1999 American Chemical Society, Bioconjugate Chem., Peterson bc990010t Supporting Info Page 6

4μL 1M DTT and 2μL of this preactivated enzyme solution was added to three separate 25μL reaction vials for each conjugate at 37°C. Samples were taken at several times during the incubation, and reaction products analyzed by TLC. The object was to find an early time point before all the peptides had been cleaved, at which the differences in substrate properties of the peptides would be readily apparent.

Cathepsin D (2.5μL @ 2.40units/mL (6,7)) was added to another set of three aliquots of each conjugate at 37°C, and reaction aliquots were analyzed as described above for cathepsin B.

Final enzyme concentrations for cathepsin B and D reactions were 0.11units/mL and 0.22 units/mL respectively. For control experiments, each conjugate was exposed to cleavage buffer containing no enzyme, and (separately) the nitro form of DOTA-peptide#0 (2.5mM) was labeled with ^{90}Y and incubated in labeling and cleavage buffers. Proteolytic cleavage was quantified as described above.

RESULTS

Synthesis of Bifunctional Chelating Agents and DOTA-peptide-Lym–1 Conjugates. The preparation of bifunctional chelating agent DOTA-peptide#18-ITC is representative of all five BCAs synthesized (Scheme S1). Conversion of the nitro function to isothiocyanato was modified to accommodate far more hydrophobic peptides and to avoid hydrolysis of the C-terminal amide reported previously (1). For example, during reduction CH_3OH was added to prevent aggregation. To prevent loss of the C-terminal amide, a lower concentration of acid was used in the aqueous phase in the conversion of the aromatic amine to isothiocyanate (8). Despite this precaution, we cannot rule out co-purification of a small amount of C-terminal acid, due to the structural complexity of these high molecular weight BCAs. Hydrolysis of the C-terminal amide would result in a *m/z* one mass unit higher than that calculated for the amide. Although none of the masses in Table S1 are consistent with hydrolysis, our measurements do not

© 1999 American Chemical Society, Bioconjugate Chem., Peterson bc990010t Supporting Info Page 7

have sufficient accuracy to dismiss it. Distinctive IR stretches confirm the presence of the isothiocyanate. Standard size-exclusion and TLC analysis (4) confirmed covalent modification of Lym-1 and stable chelation of either ^{111}In or ^{90}Y in the presence of the challenge chelate, DTPA.

DOTA-peptides #1, #5, #13, and #18 were less soluble in water than DOTA-peptides #0 and #15, whose conjugation consistently resulted in more extensively radiolabeled antibody.

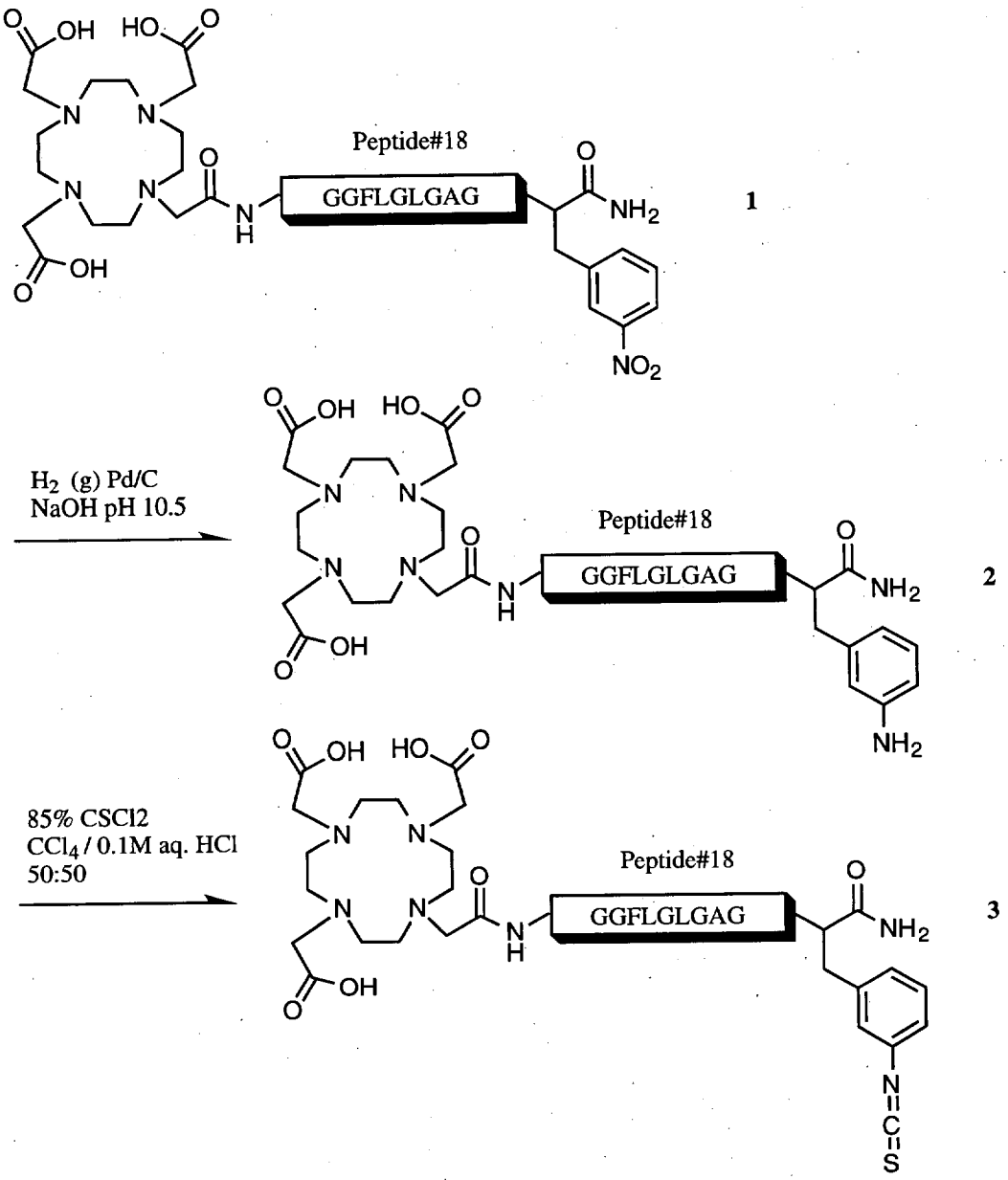
© 1999 American Chemical Society, Bioconjugate Chem., Peterson bc990010t Supporting Info Page 8

REFERENCES

1. Li, M., & Meares, C.F. (1993) Synthesis, Metal Chelate Stability Studies, and Enzyme Digestion of a Peptide-Linked DOTA derivative and Its Corresponding Radiolabeled Immunoconjugates. *Bioconjugate Chem. 4*, 275-283.
2. Peterson, J.J., Pak, R.H., & Meares, C.F. (1999) Total Solid-Phase Synthesis of DOTA-Functionalized Peptides for Radioimmunotherapy. *Bioconjugate Chem. 10*, #2 (bc980118t, published ASAP Feb 11, 1999).
3. Udenfriend, S., Stein, S., Bohlen, P., Dairman, W., Leimgruber, W., Weigele, M. (1972) Fluorescamine: A Reagent for Assay of Amino Acids, Peptides, Proteins, and Primary Amines in the Picomole Range. *Science 178*, 871-872.
4. Meares, C.F., McCall, M.J., Reardan, D.T., Goodwin, D.A., Diamante, C.I. & McTigue, M. (1984) Conjugation of Antibodies with Bifunctional Chelating Agents: Isothiocyanate and Bromoacetamide Reagents, Methods of Analysis, and Subsequent Addition of Metal Ions. *Anal. Biochem. 142*, 68-78.
5. Bajkowski, A. S. & Frankfater, A. (1975) Specific Spectrophotometric Assays for Cathepsin B_1. *Anal. Biochem. 68*, 119-127.
6. Barrett, A. J. (1967) Lysosomal Acid Proteinase of Rabbit Liver. *Biochem. J. 104*, 601.
7. Barrett, A. J. (1970) Purification of Isoenzymes from Human and Chicken Liver. *Biochem. J. 117*, 601-607.
8. Li, M., & Selvin, P.R. (1997) Amine Reactive Forms of a Luminescent Diethylenetriaminepentaacetic Acid Chelate of Terbium and Europium: Attachment to DNA and Energy Transfer Measurements. *Bioconjugate Chem. 8*, 127-132.
9. Haseman, M.K., Goodwin, D.A., Meares, C.F., Kaminski, M.S., Wensel, T.G., McCall, M.J., & Levy, R. (1986) Metabolizable ^{111}In Chelate Conjugated Anti-idiotype Monoclonal Antibody for Radioimmunodetection in Lymphoma Mice. *Eur. J. Nucl. Med.* 12, 455-460.

© 1999 American Chemical Society, Bioconjugate Chem., Peterson bc990010t Supporting Info Page 9

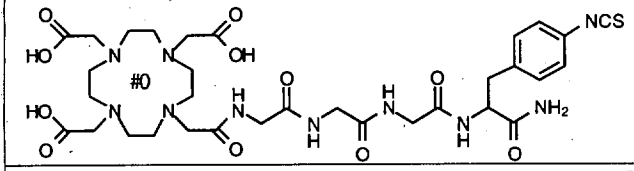
Scheme S1: Conversion of nitro to isothiocyanato



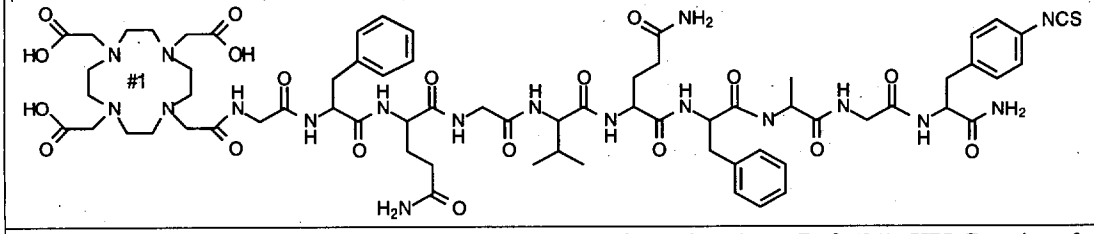
© 1999 American Chemical Society, Bioconjugate Chem., Peterson bc990010t Supporting Info Page 10

Table S1. Data for DOTA-peptide isothiocyanates.[a]

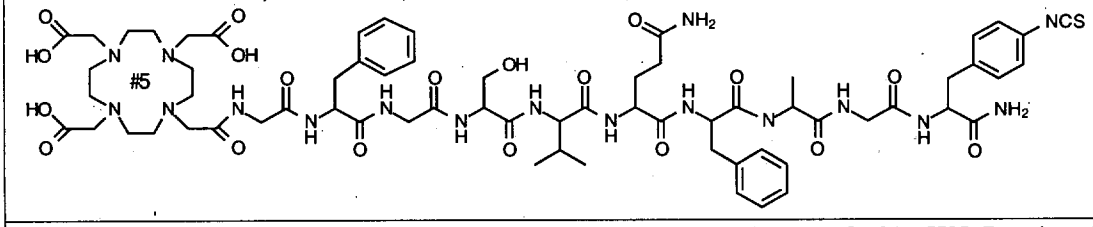
#0. Sequence: DOTA-GGGF*NH_2; Substrate for cathepsin B; Ref: (30); HPLC purity of crude reaction mixture: 80%; Yield: Not determined; Mass: Calc. 780.3; Found: 780.0



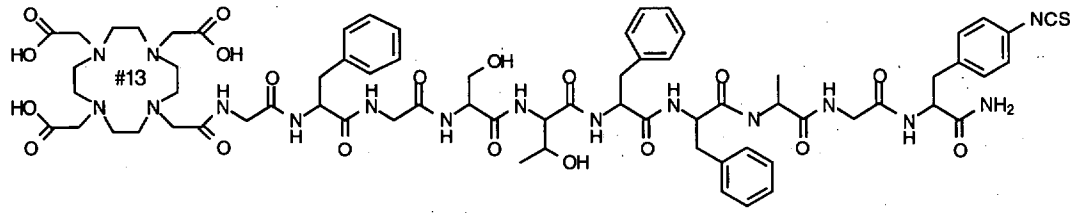
#1. Sequence: DOTA-GFQGVQFAGF*NH_2; Substrate for cathepsin B; Ref: (31); HPLC purity of crude reaction mixture: 95%; Yield: 49%; Mass: Calc. 1499.7; Found 1500.0



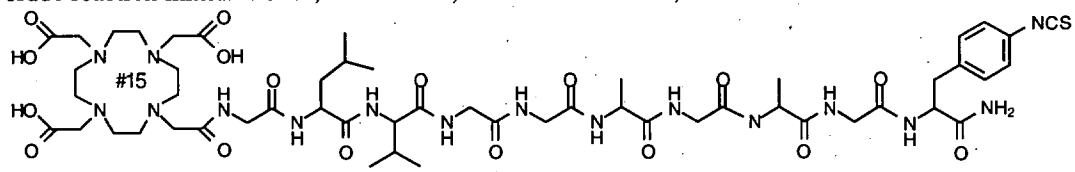
#5. Sequence: DOTA-GFGSVQFAGF*NH_2; Substrate for cathepsin B; Ref: (31); HPLC purity of crude reaction mixture: 76%; Yield: 50%; Mass: Calc. 1458.7; Found 1458.7



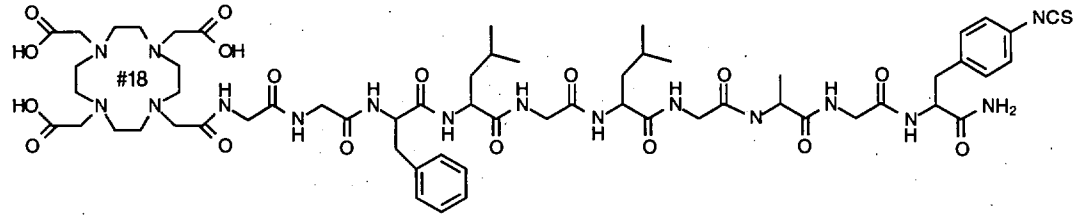
#13. Sequence: DOTA-GFGSTFFAGF*NH_2; Substrate for cathepsin D; Ref: (31); HPLC purity of crude reaction mixture: 67%; Yield: 42%; Mass: Calc. 1479.7; Found 1478.7



#15. Sequence: DOTA-GLVGGAGAGF*NH_2; Substrate for cathepsin B; Ref: (34); HPLC purity of crude reaction mixture: 87%; Yield: 28%; Mass: Calc. 1247.6; Found 1247.5



#18. Sequence: DOTA-GGFLGLGAGF*NH_2; Substrate for cathepsin B; Ref: (33); HPLC purity of crude reaction mixture: 89%; Yield: 83%; Mass: Calc. 1337.7; Found 1335.3



[a] F*, *p*-isothiocyanatophenylalanine

Size Reduction of Galactosylated PEI/DNA Complexes Improves Lectin-Mediated Gene Transfer into Hepatocytes

Thierry Bettinger, Jean-Serge Remy,* and Patrick Erbacher

Laboratoire de Chimie Génétique, Faculté de Pharmacie, CNRS (UMR 7514) et Université Louis Pasteur de Strasbourg, BP 24, F-67401 Illkirch Cedex, France. Received January 13, 1999

Hepatocytes are interesting targets for gene therapy applications. Several hepatocyte-directed gene delivery vectors have been described. For example, simple galactosyl residues coupled to polyethylenimine (PEI) gave an efficient vector which selectively transfected hepatocytes via the asialoglycoprotein receptor-mediated endocytosis [Zanta, M. A., et al. (1997) *Bioconjugate Chem*. *8*, 839−844]. However, the large size of these galactosylated PEI/DNA complexes prevented their use in vivo. We have investigated the role of the saccharide length on the size of glycosylated-PEI/DNA particles. When 5% of the PEI nitrogens were grafted with a linear tetragalactose structure (*l*Gal4), small and stable particles were formed upon complexation with plasmid DNA. These particles were essentially toroids having a size of 50−80 nm and a ζ-potential close to neutrality. Moreover, these slightly charged PEI−*l*Gal4/DNA complexes were as selective as the previously described galactosylated−PEI vector to transfect hepatocytes, but in addition, they were more efficient. It is expected that the properties of the PEI−*l*Gal4/DNA complexes may increase their diffusion into the liver and their efficiency to transfect hepatocytes.

In the nonviral gene delivery field, the cationic polyethylenimine and its derivatives are efficient gene transfer vectors, both in vitro and in vivo (*1*−*5*). Recently, a hepatocyte-directed vector has been developed, consisting of a 5% galactose-bearing polyethylenimine (PEI−Gal)[1] (*6*). The PEI−Gal conjugate was prepared by reductive amination between PEI and lactose in the presence of sodium cyanoborohydride. This vector possesses a DNA-binding domain, an intrinsic endosomal-disrupting activity ("proton sponge" effect), and a galactose specific lectin-binding moiety. The transfection of hepatocytes expressing a galactose-specific membrane lectin was selective and highly efficient. Unfortunately, transmission electron microscopy pictures showed aggregated PEI−Gal/DNA complexes in physiological saline conditions. So, we have investigated the size and the morphology of glycosylated-PEI/DNA complexes (*7*), in relation with the length of the osidyl structure (1−9 units) and the glycosylation extent of the polymer (2.5−25% of grafted nitrogens). Only when 5% of the PEI nitrogens were modified with a linear tetragalactose structure (*l*Gal4), small and stable particles were formed with plasmid DNA.

The 25 kDa PEI (branched polymer, Aldrich) was glycosylated by the reductive amination procedure. Linear tetragalactose (Gal α3 Gal β4 Gal α3 Gal, *l*Gal4, Dextra Laboratories Ltd.) or tetraglucose (Glc α4 Glc α4 Glc α6 Glc, *l*Glc4, Sigma) (5 μmol) and sodium cyanoborohydride (25 μmol, Aldrich) were added to PEI (100 μmol of monomer, 100 μL of a 1 M, pH 7.0, stock solution) in 0.9 mL of borate buffer 0.2 M, pH 8.2, and left for 96 h at rt under continuous stirring. Low molecular weight compounds were removed by gel filtration on a Sephadex G-25 fine column (12.5 × 450 mm, Fluka) in 0.15 M NaCl. The grafting extent of the *l*Gal4 motif per PEI molecule, expressed as a percentage of glycosyl structures per nitrogen, was determined by using the resorcinol/sulfuric acid micromethod (*8*) and was 5%. The polymer amine concentration was determined by the TNBS assay (*9*). PEI−Gal (Figure 1A) and PEI-Glc (data not shown) were prepared as previously described (*6*), except that PEI conjugates were purified by gel filtration (see above). The monosaccharide was unable to prevent particle aggregation in physiological saline conditions (Figure 1A) at PEI nitrogen to DNA phosphate ratios (*N*/*P*) of 3 and 5. Increasing the length of the grafted saccharide to 4 units (*l*Gal4 or *l*Glc4) led to the formation of smaller particles (Figure 1A), which were only slightly charged, as shown by ζ-potential measurements (Figure 1B). In these conditions, the particles were stable, indicating that the linear tetraglycosyl structure (*l*Gal4 or *l*Glc4) was able to prevent aggregation and masked the surface charge (Figure 1, panels A and B). This phenomenon occurred even at high *N*/*P* ratios (≥10). The *N*/*P* ratio slightly influenced the size of tetraglycosyl-PEI/DNA complexes in physiological saline conditions, in contrast to the size of DNA complexed with unmodified PEI, PEI−Gal or other PEI derivatives bearing peptides or proteins (*5*, *10*). The size and morphology of the PEI−*l*Gal4/DNA complexes were determined by negative staining transmission electron microscopy. A homogeneous population of essentially toroidal particles, with a size of 50−80 nm, was observed for *N*/*P* of 5 and 10 (Figure 1C).

We have shown that the terminal galactosyl residues on the PEI−*l*Gal4/DNA complexes were easily accessible and recognized by using a galactose-binding RCA_{120} lectin-mediated agglutination (Figure 2). The recognition

* To whom correspondence should be addressed. Phone: +33-(0)388 676867. Fax: +33(0)388 678891. E-mail: remy@bioorga.u-strasbg.fr.

[1] Abbreviations: PEI, polyethylenimine; Gal, galactose; Glc, glucose; *l*Gal4, linear tetragalactose; *l*Glc4, linear tetraglucose; rt, room temperature.

10.1021/bc990006h CCC: $18.00 © 1999 American Chemical Society
Published on Web 06/05/1999

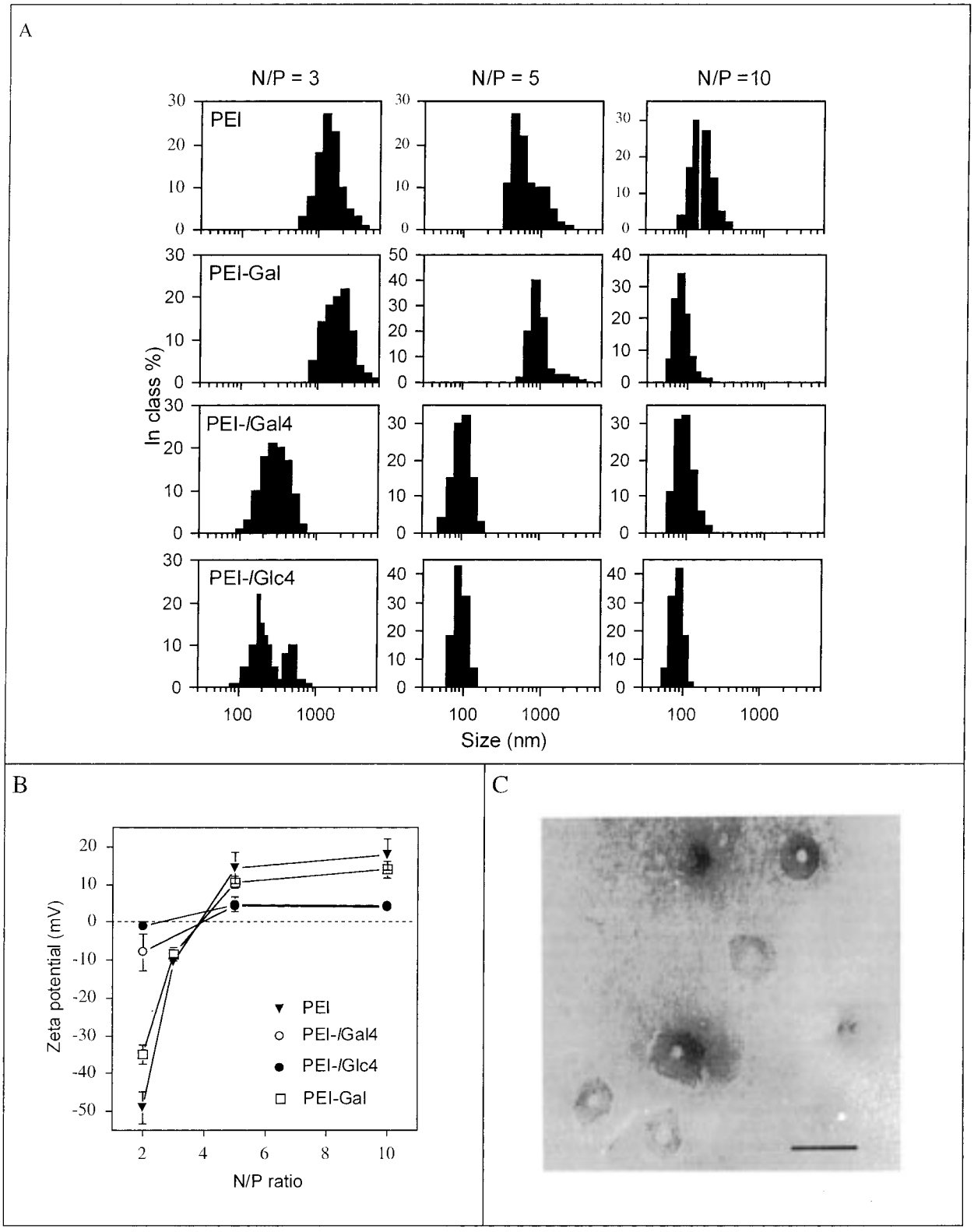


Figure 1. Particle size (A, C) and ζ-potential (B) measurements. DNA (40 μg of pCMVLuc) and the desired amount of glycosylated PEI or unmodified PEI were each diluted separately in 500 μL of a 150 mM NaCl solution. After 10 min, solutions were mixed, homogenized, and left for 10 min. Particle size (A) was determined by dynamic laser light scattering using a Zetamaster 3000 (Malvern Instrument, Orsay, France). ζ-Potential was measured electrophoretically using the same apparatus (B), as previously described (*15*). For transmission electron microscopy (C), a drop (5 μL) of a solution containing the PEI−*l*Gal4/DNA complexes ($N/P = 10$) was added to a carbon-covered grid and left for 1 min. Complexes were negatively stained with 30 μL of an aqueous uranyl acetate solution (1%, w/w), for 20 s. Observations were done at 80 kV on a Philips EM 410 transmission electron microscope, bar is 100 nm.

and agglutination of the PEI−*l*Gal4/DNA complexes by the RCA_{120} lectin were totally reversible after the addition of a 1000-fold molar excess of galactose. Moreover, a nonspecific agglutination mediated by electrostatic interactions was unlikely, as shown by the results obtained with the PEI and PEI−*l*Glc4/DNA complexes, at $N/P = 10$ (Figure 2). These biophysical and recognition properties of PEI−*l*Gal4/DNA complexes confirmed that the

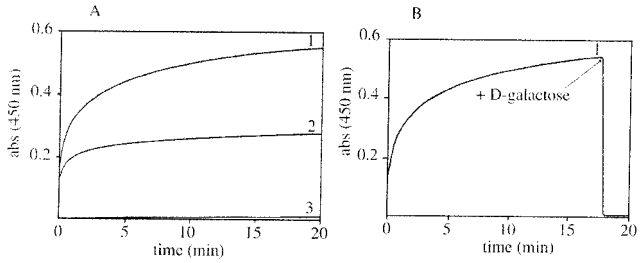


Figure 2. Accessibility of the galactosyl residues at the surface of the complexes. (A) PEI or PEI conjugates/pCMVLuc complexes (20 μg/mL DNA, protocol described in the legend of Figure 1) were incubated in the presence of *Ricinus communis* RCA_{120} lectin (90 μg/mL, Sigma) in 300 μL (total volume) of 10 mM phosphate buffer pH 7, 150 mM NaCl. Agglutination was monitored by following the turbidity at 450 nm, during 20 min. (1) PEI−*l*Gal4/DNA complexes at $N/P = 10$, (2) PEI−*l*Gal4/DNA complexes at $N/P = 5$, and (3) PEI or PEI−*l*Glc4/DNA complexes at $N/P = 10$. (B) The RCA-mediated agglutination of PEI−*l*Gal4/DNA complexes ($N/P = 10$) was reversible when D-galactose was added to a final concentration of 1 M.

glycosyl structures controlled the particle behavior and were exposed at their surface.

Transfections were performed in the presence of 10% serum and without the plate centrifugation step that generally leads to higher efficacies (*6*, *11*). Gene transfer efficiencies were evaluated on the BNL CL.2 murine hepatocyte cell line which expresses a galactose specific membrane lectin (*12*, *13*) and on the HeLa human epitheloid carcinoma cell line which does not express a galactose specific receptor (*14*). In both cases, unmodified PEI-mediated transfection efficiency increased with the *N*/*P* ratio (Figure 3), according to the ionic cell binding mechanism. The PEI−*l*Gal4/DNA complexes showed improved efficiency over PEI−Gal and PEI-mediated gene transfer on BNL CL.2 cells (receptor +), at all *N*/*P* ratios. When *l*Gal4 was replaced by *l*Glc4 motif, transfection efficiencies were comparable to those obtained with the unmodified PEI. On HeLa cells (receptor −), none of the vectors showed any evidence of a selective gene delivery (Figure 3). The differences in expression levels are probably related to differences in the size of particles and to a lesser extent to their surface charge, both important parameters for cellular uptake. At the optimal *N*/*P* ratio, competition experiments with an excess of asialofetuin (20-fold molar excess over galactose), the natural ligand of the asialoglycoprotein receptor, decreased the transfection efficiency of the PEI−*l*Gal4/DNA complexes by 1 order of magnitude on BNL CL.2 cells. In contrast, the transfection of BNL CL.2 cells with PEI or PEI−*l*Glc4/DNA complexes was (only) affected by 2.5 or 5-fold in the presence of asialofetuin or albumin, respectively. The involvement of the asialoglycoprotein receptor was clearly demonstrated by both comparative and competitive experiments showing that transfection of hepatocytes with small and slightly charged PEI−*l*Gal4/DNA complexes was selective and efficient.

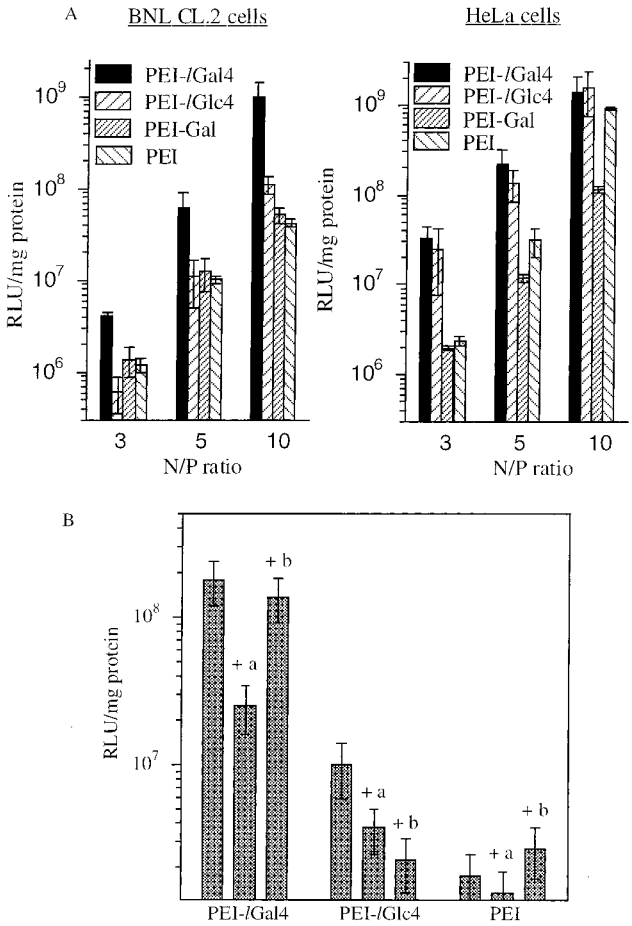


Figure 3. Transfection efficiency of the glycosylated PEI/DNA complexes on the BNL CL.2 murine hepatocyte and HeLa human epitheloid carcinoma cell lines. A day prior to transfection, (5−6) × 10^4 cells/well were seeded in 24 well tissue culture plates and were incubated at 37 °C in a 5% CO_2 humidified atmosphere. Before transfection, cells were supplemented with 1 mL of fresh complete medium containing 10% FCS (DMEM with high glucose (4.5 g/L) for BNL CL.2 and MEM with Earle's salt for HeLa cells). DNA (6 μg of pCMVLuc, for a triplicate experiment) and the desired amount of PEI or PEI conjugates were diluted separately in 150 μL of 0.15 M NaCl. After 10 min, the polycation was added to the DNA, the solution was homogenized and left for 10 min. The polycation/DNA complexes (100 μL/well) were added onto the cells. For the competition experiments, BNL CL.2 cells were transfected with pCMVLuc (1 μg) complexed with PEI−*l*Gal4, PEI−*l*Glc4 or PEI at $N/P = 10$. Before the addition of the polycation/DNA complexes onto the cells, 1 mg of asialofetuin (+a) or bovin serum albumin (+b) was added per well. After 24 h of incubation, cells were lyzed and luciferase gene expression was quantitated using a commercial kit (Promega) and a luminometer (Biolumat LB 9500, Berthold). Results were expressed as light units integrated over 10 s, per mg of cell protein using the BCA assay (Pierce). Values are the mean ± sd of three independent experiments made in triplicate.

ACKNOWLEDGMENT

We thank Jean-Paul Behr for his great interest in this work. T.B. and P.E. are recipient of a doctoral fellowship from the 'Ministère de l'Enseignement Supérieur, de la Recherche et des Technologies' (MESRT) and a postdoctoral fellowship from the 'Association pour la Recherche sur le Cancer' (ARC), respectively.

LITERATURE CITED

(1) Boussif, O., Lezoualch, F., Zanta, M. A., Mergny, M. D., Scherman, D., Demeneix, B., and Behr, J. P. (1995) A versatile vector for gene and oligonucleotide transfer into cells in culture and in vivo: Polyethylenimine. *Proc. Natl. Acad. Sci. U.S.A. 92*, 7297−7301.

(2) Kircheis, R., Kichler, A., Wallner, G., Kursa, M., Ogris, M., Felzmann, T., Buchberger, M., and Wagner, E. (1997) Coupling of cell-binding ligands to polyethylenimine for targeted gene delivery. *Gene Ther. 4*, 409−418.

(3) Goula, D., Remy, J.-S., Erbacher, P., Wasowicz, M., Levi, G., Abdallah, B., and Demeneix, B. (1998) Size, diffusibility and transfection performance of linear PEI-DNA complexes in the mouse central nervous system. *Gene Ther. 5*, 172−177.

(4) Goula, D., Benoist, C., Mantero, S., Merlo, G., Levi, G., and Demeneix, B. (1998) Polyethylenimine-based intravenous delivery of transgenes to mouse lung. *Gene Ther. 5*, 1291−1295.
(5) Erbacher, P., Remy, J.-S., and Behr, J.-P. (1999) Gene transfer with synthetic virus-like particles via the integrin-mediated endocytosis pathway. *Gene Ther. 6*, 138−145.
(6) Zanta, M. A., Boussif, O., Adib, A., and Behr, J.-P. (1997) In vitro gene delivery to hepatocytes with galactosylated polyethylenimine. *Bioconjugate Chem. 8*, 839−844.
(7) Erbacher, P., Bettinger, T., Belguise-Valladier, P., Zou, S., Behr, J.-P., and Remy, J.-S. (1999) Properties of maltose, dextran, poly(ethylene glycol), and antibody derivatives of polyethylenimine. Implications for gene delivery. *J. Gene Med*. (in press).
(8) Monsigny, M., Petit, C., and Roche, A. C. (1988) Colorimetric determination of neutral sugars by a resorcinol sulfuric acid micromethod. *Anal. Biochem. 175*, 525−530.
(9) Snyder, S. L., and Sobocinski, P. Z. (1975) An improved 2,4,6-trinitrobenzenesulfonic acid method for the determination of amines. *Anal. Biochem. 64*, 284−288.
(10) Ogris, M., Steinlein, P., Kursa, M., Mechtler, K., Kircheis, R., and Wagner, E. (1998) The size of DNA/transferrin-PEI complexes is an important factor for gene expression in cultured cells. *Gene Ther. 5*, 1425−1433.
(11) Boussif, O., Zanta, M. A., and Behr, J.-P. (1996) Optimized galenics improve in vitro gene transfer with cationic molecules up to 1000-fold. *Gene Ther. 3*, 1074−1080.
(12) Patek, P., Collins, J., and Cohn, M. (1978) Transformed cell lines susceptible or resistant to in vivo surveillance against tumorigenesis. *Nature 276*, 510−511.
(13) Plank, C., Zatloukal, K., Cotten, M., Mechtler, K., and Wagner, E. (1992) Gene transfer into hepatocytes using asialoglycoprotein receptor mediated endocytosis of DNA complexed with an artificial tetra-antennary galactose ligand. *Bioconjugate Chem. 3*, 533−539.
(14) Midoux, P., Mendes, C., Legrand, A., Raimond, J., Mayer, R., Monsigny, M., and Roche, A. C. (1993) Specific gene transfer mediated by lactosylated poly-L-lysine into hepatoma cells. *Nucleic Acids Res. 21*, 871−878.
(15) Erbacher, P., Zou, S., Bettinger, T., and Remy, J.-S. (1998) Chitosan-based vector/DNA complexes for gene delivery: biophysical characteristics and transfection ability. *Pharm. Res. 15*, 1332−1339.

BC990006H

ARTICLES

Grafting Protein Ligand Monolayers onto the Surface of Microparticles for Probing the Accessibility of Cell Surface Receptors

Andreas Frey,* Barbara Meckelein, and M. Alexander Schmidt

Institut für Infektiologie, Zentrum für Molekularbiologie der Entzündung (ZMBE), Westfälische Wilhelms-Universität Münster, von-Esmarch-Strasse 56, D-48129 Münster, Germany. Received October 16, 1998; Revised Manuscript Received April 28, 1999

Coupling of a specific ligand to vaccines or drugs can be a powerful aid to route these compounds to a certain target cell population. However, if the targeted receptor is buried in a glycocalyx, binding of the ligand may be sterically hindered or even abolished, especially when the ligand is attached to bulky payloads. The antigen-transporting M cells that cover the gut-associated lymphoid tissue have a less pronounced glycocalyx than neighboring enterocytes. Such architectural differences might provide a possibility for targeting micro- or nanoparticulate vaccines to the mucosal immune system. To investigate the influence of the glycocalyx on the accessibility of cell surface receptors, we developed a system where a monolayer of ligand molecules is coupled in spatially aligned manner onto the surface of microparticles. On the basis of fluorescent carboxylate-modified particles of 1 μm diameter, different synthetic strategies were tested. Particles were first modified to display aldehyde functions on their surface, then protein ligands were coupled via Schiff base formation. The performance of the particles was tested on cultured mouse fibroblasts using the B subunit of cholera toxin as ligand and the plasma membrane glycolipid ganglioside G_{M1} as receptor. Cholera toxin B subunit-coated microparticles generated by one of our synthetic pathways exhibited specific binding to fibroblasts which could be blocked with soluble cholera toxin B subunit. As particles as small as 50 nm and any proteinaceous ligand may be used, this system provides a versatile means for monitoring receptor accessibilities in vitro and in vivo.

INTRODUCTION

Ligands which specifically bind to certain cell types are deemed proverbial "magic bullets" for delivering pharmaceuticals to their desired site of action. The concept of targeting a compound to a given cell type is of particular interest for the development of mucosal vaccines. The chief task of a mucosal vaccine is to induce a secretory immunoglobulin A response at the mucosal surfaces and thus intercept microbial pathogens in the run-up of infection (Kraehenbuhl and Neutra, 1992). Such a secretory immunoglobulin A response is induced only when the antigen is delivered to the mucosal immune system via the organized mucosa-associated lymphoid tissue, such as the Peyer's patches in the small intestine, the tonsils, and adenoids in the nasopharyngeal area or the appendix (Neutra et al., 1996b). At these sites, the antigen is taken up by M cells, a specialized epithelial cell type which is able to endocytose particulate antigens of up to 10 μm in diameter (Eldridge et al., 1989; Ermak et al., 1995) and translocate them to the underlying lymphoid tissue where an immune response is mounted (Kraehenbuhl and Neutra, 1992; Neutra et al., 1996b). M cells are therefore prime candidates for the targeted delivery of vaccines to the mucosal immune system. A major obstacle along that line, however, is the apparent lack of specific receptors on the apical M cell surface. No universal M-cell specific surface molecule has been identified as yet, and only a few cytoplasmic M cell markers have been described so far (Jepson et al., 1992; Gebert et al., 1994; Rautenberg et al., 1996). Nonetheless, M cells differ from the neighboring epithelial lining cells. For example, M cells lack an organized brush border and, in the gut, they display a less pronounced glycocalyx than the adjacent enterocytes (Kato, 1990; Gebert and Bartels, 1995; Frey et al., 1996; Neutra et al., 1996a). Consequently, plasma membrane receptors may be more accessible on M cells than on enterocytes. This opens up the possibility to target a ubiquitous receptor selectively on M cells simply because it may be shielded by the glycocalyx on neighboring enterocytes. We provided the proof of principle for this concept in a previous study in which we could demonstrate that binding of the B

* To whom correspondence should be addressed. Phone: +49-251-835-6477. Fax: +49-251-835-6467. E-mail: frey@uni-muenster.de.

[1] Abbreviations: CTB, cholera toxin B subunit; DMEM, Dulbecco's modified Eagle's medium; EDC, 1-ethyl-3-(3-dimethylaminopropyl) carbodiimide; Hepes, 4-(2-hydroxyethyl)-1-piperazineethanesulfonic acid; MES, 4-morpholinoethanesulfonic acid; OVA, ovalbumin; PBS, phosphate buffered saline (2.7 mM KCl, 1.5 mM KH_2PO_4, 136 mM NaCl, and 8.1 mM Na_2HPO_4); RT, room temperature; S-NHS, *N*-hydroxysulfonylsuccinimide; TEG-biotin, biotinyl-3,6,9-trioxaundecanediamine.

10.1021/bc980124p CCC: $18.00 © 1999 American Chemical Society
Published on Web 06/10/1999

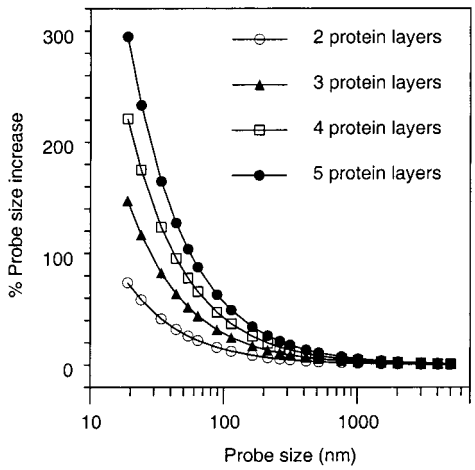


Figure 1. Influence of protein multilayers on probe size. Relative increase in total hydrodynamic diameter of a nano- or microparticulate probe caused by multilayers of an average protein (hydrodynamic diameter 7 nm) when compared to the hydrodynamic diameter of the same probe carrying a protein monolayer only.

subunit of cholera toxin (CTB)[1] to the plasma membrane glycolipid G_{M1} in the small intestine becomes M-cell specific when CTB is offered as a particulate probe of approximately 30 nm diameter (Frey et al., 1996). Soluble CTB of 7 nm hydrodynamic diameter bound ubiquitously, and CTB-coated particles exceeding 1 μm in diameter did not bind at all to the small intestinal epithelium. Consequently, there must be a size window in which selective ligand-mediated targeting of intestinal M cells is possible without the need for a specific receptor on the M-cell surface.

To define the exact size of this window, we were in demand of easy-to-detect, preferably fluorescent nanoparticulate probes on which a monolayer of proteinaceous ligands can be coupled covalently. The formation of a single ligand layer on the probe core is essential because the final probe size will be affected strongly by ligand multilayers or spikes consisting of ligand molecules which are coupled to each other (Figure 1).

Currently, there are only few companies who offer derivatizable fluorescent nanoparticles of a well-defined size. Most of these products carry carboxylate groups on their surface intended for attaching proteins via their amino functions by use of carbodiimides (Molday et al., 1975; Illum and Jones, 1985). A direct coupling of protein ligands to carboxylate-modified microparticles in the presence of carbodiimide cross-linker, however, also enables protein molecules to react with each other, thereby generating the undesired multilayers. We were therefore seeking alternative strategies in which the particles are preactivated such that they will react with ligand molecules without the need for additional cross-linkers.

In this report, we describe a system where a monolayer of proteinaceous ligands is coupled in a spatially aligned manner onto the surface of fluorescent microparticles. The resulting probes were shown to be versatile tools for assessing the accessibility of receptor molecules in complex biological settings.

MATERIALS AND METHODS

Materials and Cell Lines. Red and green fluorescent, carboxylate-modified microparticles of 1.0 μm nominal diameter (FluoSpheres) were from Molecular Probes Europe (Leiden, The Netherlands). These microparticles consist of a polystyrene core grafted with poly(acrylic acid) and acrylic acid. They possess a specific surface load of 0.1286 mequiv of carboxylate/g (corresponding to 7.76×10^{-14} mequiv of carboxylate/particle).

Cholera toxin B subunit (CTB) (low salt) was purchased from List Biological Laboratories (Campbell, CA; via Quadratech, Epsom, U.K.), avidin ($\geq$13.5 Units/mg) from Molecular Probes and chicken egg white ovalbumin (OVA) from Calbiochem-Novabiochem (Bad Soden, FRG). Biotinyl-3,6,9-trioxaundecanediamine (TEG-biotin) was obtained from Molecular Biosciences (Boulder, CO).

The BALB/c 3T3 fibroblast cell line clone A 31 was obtained from the American Type Culture Collection (Rockville, MD). Defined bovine calf serum (iron-supplemented) was from Hyclone (Logan, UT), Dulbecco's modified Eagle's medium (DMEM), glutamine, penicillin/streptomycin, and 4-(2-hydroxyethyl)-1-piperazineethanesulfonic acid (Hepes) were from PAA Laboratories (Linz, Austria). Round glass coverslips (13 mm diameter) were obtained from Bellco Glass (Vineland, NJ; via Dunn Labortechnik, Asbach, FRG).

Poly(vinyl formal) (Formvar 15/95) and 150 square mesh copper grids were purchased from Polysciences Europe (Eppelheim, FRG). Mowiol 4-88 was from Calbiochem-Novabiochem. FilterCount scintillation liquid was obtained from Canberra Packard (Dreieich, FRG), [^{14}C]ethanolamine was from Moravek Biochemicals (Brea, CA; via Hartmann Analytic, Braunschweig, FRG), and [^{14}C]biotin from Amersham Buchler (Braunschweig, FRG). Nitrocellulose filter membranes were from Schleicher & Schuell (Dassel, FRG). Micro BCA Protein Assay Reagent was from Pierce (Rockland, IL; via KMF, Sankt Augustin, FRG). Purpald and aminoacetaldehyde dimethylacetal were purchased from Aldrich (Deisenhofen, FRG). All other chemicals and solvents were from various sources in the highest quality commercially available.

Activation of Carboxylate-Modified Microparticles (1). A total of 1.29×10^9 carboxylate-modified microparticles (corresponding to 0.1 μmol of carboxylate groups according to the specific surface load given by the supplier) were washed twice by suspending in 1.8 mL of H_2O followed by two times 20 min centrifugation at 10000*g* and removal of the supernatant to less than 20 μL. The microparticles were suspended in 65 μL of H_2O before 100 μL of 10 mM 4-morpholinoethanesulfonic acid (MES)−NaOH, pH 6.0, 15 μL of 0.1 M *N*-hydroxysulfonylsuccinimide (S-NHS) (Staros et al., 1986), and 20 μL of 0.1 M 1-ethyl-3-(3-dimethylaminopropyl) carbodiimide (EDC) were added. The suspension was sonicated for 30 s in a Sonorex RK 510S sonifier (Bandelin Electronic, Berlin, FRG) and allowed to react for 20 min at room temperature (RT). The activated microparticles (**1**) were immediately used for the subsequent derivatization reactions without further purification.

Synthesis of Aldehyde-Derivatized Microparticles (2, 3). *Method A: via Aminoacetaldehyde Dimethylacetal*. To the suspension of activated microparticles (**1**) were added 200 μL of H_2O, 500 μL of 0.1 M Hepes−NaOH, pH 7.4, and 100 μL of 1 M aminoacetaldehyde dimethylacetal. The suspension was incubated for 16 h at RT in the dark on an end-over-end mixer rotating with 15 rpm. The particles (**2a**) were washed four times with 1.8 mL of H_2O each and resuspended in 1 mL of 1 M HCl. In some experiments, 0.1 M citric acid or 3.25 M TFA was used instead of 1 M HCl. The suspension was incubated for 4 h under rotation as described above, with 2×30 s sonication every 30 min. The aldehyde-deriva-

tized particles (**2**) were washed three times with 1.8 mL of H_2O and once with 1.8 mL of 50 mM Hepes−NaOH, pH 7.4.

Method B: via Ethylenediamine-Glutaraldehyde Bridge. To the suspension of activated microparticles (**1**) were added 200 μL of H_2O, 500 μL of 0.1 M Hepes−NaOH, pH 7.4, and 100 μL of 1 M ethylenediamine−HCl, pH 8. The suspension was incubated for 16 h under continuous rotation as described above. The particles (**3a**) were washed four times with 1.8 mL of H_2O each, suspended in 1 mL of 50 mM Hepes−NaOH, pH 7.4, and 0.1 M glutaraldehyde, sonicated 2 × 30 s, and rotated as described above for 4 h. The aldehyde-derivatized particles (**3**) were washed four times with 1.8 mL of H_2O and used immediately for subsequent coupling reactions.

Synthesis of Biotin-Derivatized Microparticles (4). To the suspension of activated microparticles (**1**) were added 275 μL of H_2O, 500 μL of 0.1 M Hepes−NaOH, pH 7.4, and 25 μL of 20 mM TEG-biotin. The suspension was incubated for 16 h under continuous rotation, and the biotinylated particles (**4**) were washed four times with 1.8 mL of H_2O as described above.

Protein Coupling to Aldehyde-Derivatized Microparticles. For the protein coupling reaction, 1.29×10^9 aldehyde-derivatized microparticles (**2** or **3**) were suspended in 500 μL of 0.1 M Hepes−NaOH, pH 7.4, and, in case of avidin coupling reactions, 100 μL of 5 M NaCl. To this suspension, 176 μL of 0.5 mg/mL (8.6 μM) CTB (1.51 nmol) or 88 μL of 1 mg/mL (22.2 μM) OVA (1.96 nmol) or 116 μL of 1 mg/mL (14.7 μM) avidin (1.70 nmol) were added, and the volume was adjusted to 1 mL with H_2O. The suspension was rotated at 4 °C for 1 h, then 50 μL of 1 M $NaCNBH_3$ was added, and the incubation was continued for 36 h under continuous rotation at 4 °C. The particles were washed three times with 1.8 mL of 10 mM Hepes−NaOH, pH 7.4, 0.2 M NaCl (avidin-derivatized particles: once with 10 mM Hepes−NaOH, pH 7.4, 0.2 M NaCl, twice with 250 mM sodium carbonate, pH 9.5, 0.5 M NaCl), with at least 30 min rotation at 4 °C for each washing step. For blocking of the remaining free aldehyde functions, the particles were suspended in 1 mL of 50 mM Hepes−NaOH, pH 7.4, containing 0.1 M ethanolamine (or 0.1 M glycine) and 50 mM $NaCNBH_3$, before they were incubated under continuous rotation at 4 °C for 16 h, washed three times with 1.8 mL of 10 mM Hepes−NaOH, pH 7.4, and stored in this buffer at 4 °C in the dark.

Determination of Maximum Ligand Load. The maximum number of protein molecules that can be bound to one individual microparticle in a monolayer was estimated with a model which assumes tight packing of globular protein molecules on the surface of a spherical core (Frey et al., 1996). The maximum ligand load in a protein monolayer is then given by eq 1:

$$n_{\text{molecules}} = \frac{2\pi}{\sqrt{3}}\left(\frac{d_{\text{particle}}}{d_{\text{protein}}} + 1\right)^2 \qquad (1)$$

where d_{particle} is the diameter of the microparticle and d_{protein} is the hydrodynamic diameter of the ligand. To determine the hydrodynamic diameters of CTB, avidin, and OVA, the respective diffusion coefficients were measured by dynamic light scattering as described before (Frey et al., 1996) and the hydrodynamic diameters d_h were calculated with the Stokes−Einstein eq 2:

$$d_h = \frac{2kT}{6\pi\eta D} \qquad (2)$$

Table 1. Maximum Protein Load of 1 μm Microparticle

protein	diffusion coefficient[a] (10^{-13} m^2/s)	diameter[b] (nm)	load[c] (molecules/particle)
CTB	634 ± 22	7.4	71 000
avidin	662 ± 17	7.0	80 000
ovalbumin	679 ± 6	6.4	92 000

[a] Diffusion coefficient at 24 °C in PBS as determined by dynamic light scattering. Data represent mean ± standard deviation of at least six independent experiments. [b] Hydrodynamic diameters were calculated from the mean diffusion coefficients using the Stokes−Einstein equation (see text). [c] The maximum number of protein molecules in a monolayer on the surface of one individual microparticle (diameter = 1030 nm) was calculated using eq 1 (see text).

where k is the Boltzmann constant, T is the absolute temperature, η is the viscosity of water, and D the diffusion coefficient. The diameter of the microparticles (1030 nm ± 2.3%) was provided by the manufacturer. The maximum ligand load for the proteins on the microparticles used in this study is given in Table 1.

Analytical Procedures. *Electron Micoscopy.* Carboxylate-modified microparticles were washed three times, suspended in H_2O to a concentration of 5×10^4 particles/μL, and sonicated for 30 s. Of these suspensions, 20 μL was placed on a Formvar-coated copper grid and allowed to settle for 90 min. Particles were contrasted with 4% (w/v) $U(OAc)_2$ for 2 min and photographed at 38000× and 69000× magnification in a Philips 401 transmisson electron microscope (Philips Electron Optics, Eindhoven, The Netherlands).

Determination of Coupling Yields. To determine the maximum number of derivatizable functional groups, 1.29×10^9 carboxylate-modified microparticles were activated with EDC and S-NHS to yield the active ester (**1**) as described above and incubated in 1 mL 50 mM Hepes−NaOH, pH 7.4, containing 2 mM/0.8 μCi/mL [^{14}C]-ethanolamine for 16 h at RT under continuous rotation. For quantitation of the product (**5**), aliquots of the reaction suspension were filtered through a glass frit equipped with a BA 85 nitrocellulose filter membrane (0.1 μm pore size) and washed extensively with 0.2 M NaCl under continuous suction. The filter membranes were air-dried, transferred into scintillation vials, and counted in a Beckman LS 6000 scintillation counter (Beckman, Fullerton, CA) 2 h after addition of 5 mL of FilterCount scintillation liquid.

The yields of acetal-derivatized (**2a**) and biotin-derivatized (**4**) particles were determined indirectly by coupling [^{14}C]ethanolamine to residual unreacted carboxylate groups in the presence of EDC and S-NHS as described above.

To determine the yield of aldehyde functionalization, the particles (**2**, **3**) were incubated at RT under continuous rotation in 1 mL of 50 mM Hepes−NaOH, pH 7.4, containing 2 mM/0.8 μCi/mL [^{14}C]ethanolamine. After 1 h of incubation, 2 μmol of $NaCNBH_3$ was added, and the incubation was continued for 16 h under rotation. The amount of radiolabel bound to the particles was determined as described above.

Determination of Protein Derivatization Yields. To determine the protein derivatization of microparticles in analytical assays, 1.29×10^9 microparticles either activated with EDC and S-NHS (**1**), or after aldehyde (**2**, **3**) or biotin derivatization (**4**) were incubated in 1 mL of 50 mM Hepes−NaOH, pH 7.4, 0.5 M NaCl, and 5 μM (5 nmol) avidin for 36 h at 4 °C under rotation. The particles were washed once with 10 mM Hepes−NaOH, pH 7.4,

0.2 M NaCl, and twice with 250 mM sodium carbonate, pH 9.5, 0.5 M NaCl. The avidin-derivatized particles (**6**, **7**, **8**, or **9**) were suspended in 1 mL of 50 mM Hepes−NaOH, pH 7.4, 5 μM/0.27 μCi/mL [^{14}C]biotin and incubated, processed, and counted as described above.

The protein load of particles derivatized with CTB, OVA, and avidin was also determined with the Micro BCA Protein Assay. The assay protocol provided by the supplier was modified to allow for determination of protein bound covalently to a particulate carrier (Stich, 1990). Suspensions of 1×10^9 particles in 500 μL of 10 mM Hepes−NaOH, pH 7.4, were mixed with 500 μL of Micro BCA working solution and incubated at 50 °C under continuous rotation (180 rpm) for 60 min. The suspensions were quickly cooled to 4 °C and centrifuged at this temperature for 10 min at 14000*g*. The supernatants were removed and their optical density at 562 nm was determined immediately. Protein solutions of known concentration were treated identically to the samples and used as standards.

Acetaldehyde Dimethylacetal Cleavage and Purpald Assay. Acetaldehyde dimethylacetal (final concentration 2 mM) was incubated for 2 h at RT in the following solutions: 3.25 M TFA (pH <0), 1 M HCl (pH 0); 0.1 M oxalic acid (pH 1.4); 0.1 M citric acid (pH 2.1); 0.1 M citric acid-NaOH (pH 2.5; pH 3.0; pH 3.5; pH 4.0; pH 5.0); 0.1 M MES−NaOH (pH 6.5); 0.1 M sodium phosphate (pH 7.0; pH 8.3). The amount of aldehyde released was determined spectrophotometrically (Watanabe et al., 1978) using acetaldehyde as standard. To 100 μL of the standard or the acetal reaction mixture were added 200 μL of 5 N NaOH and 150 μL of 5 mg/mL 4-amino-3-hydrazino-5-mercapto-1,2,4-triazole (Purpald) in 0.5 N HCl. The mixture was incubated for 20 min at RT, 150 μL of 7.5 mg/mL KIO_4 was added under vigorous shaking, and the absorbance at 550 nm was determined immediately.

Binding of Microparticles to BALB/c 3T3 Fibroblasts. BALB/c 3T3 fibroblasts were grown in high glucose (25 mM) DMEM supplemented with 10% (v/v) calf serum, 2 mM glutamine, 100 units/mL penicillin/100 μg/mL streptomycin, 25 mM Hepes, and 3.7 g/L $NaHCO_3$ at 37 °C in a humidified atmosphere containing 10% (v/v) CO_2. For particle-binding studies, the cells were seeded onto round glass cover slips in 24-well tissue culture plates and used on days 20−22 (=14−16 days post confluence). The cells were washed gently four times with 2 mL of prewarmed (37 °C) phosphate-buffered saline (PBS) containing 0.9 mM $CaCl_2$ and 0.5 mM $MgCl_2$, before 500 μL of DMEM containing a 1:1 mixture of 2.5×10^7 particles/mL each of CTB particles (or avidin particles) and OVA particles (in different color) were added. For competition with soluble CTB, cells were preincubated with 250 μL of 20 μg/mL CTB in DMEM for 15 min at 37 °C before 250 μL of a 1:1 mixture of 5×10^7 particles/mL each of CTB particles and OVA particles were added. After incubation for 60 min at 37 °C, the cells were washed again as above and fixed in 1 mL of 3% (w/v) *p*-formaldehyde in PBS for 90 min at RT in the dark. The coverslips were washed three times in PBS and once in H_2O and mounted on glass slides with Mowiol containing 2.5% (w/v) 1,4-diazabicyclo-[2.2.2]octane. Cell layers were examined and photographed en face with a Zeiss Axiophot microscope equipped for epifluorescence (Zeiss, Jena, FRG).

Data Collection and Statistical Analysis. For quantitative analysis of microparticle binding to the fibroblast monolayers, four randomly selected nonoverlapping regions of each coverslip were photographed with the Zeiss Axiophot microscope connected to an Intas Seescan Color LC 100C low light camera system (Intas, Göttingen, FRG) consisting of a Sony XC-003P Color Video Camera Module and a Seescan LC 100C control unit. Photographic documentation of microparticle binding was done with Kodak T-Max 400 film. Digitalized images were processed on a Power Macintosh G3 (Apple, Cupertino, CA) using Adobe Photoshop 4.0 (Adobe Systems, San Jose, CA) and Claris Draw 1.0v4 (Apple) software, printed on a HP Laserjet 4000 TN (Hewlett-Packard, Palo Alto, CA) and counted manually. Statistical analysis of particle binding and coupling yields was carried out with the StatView 4.5 program package (Abacus Concepts, Berkeley, CA). Mixed probes of test and control particles were considered paired samples, and the results of independent experiments were treated as unpaired samples. Results were considered significant only if $p < 0.05$.

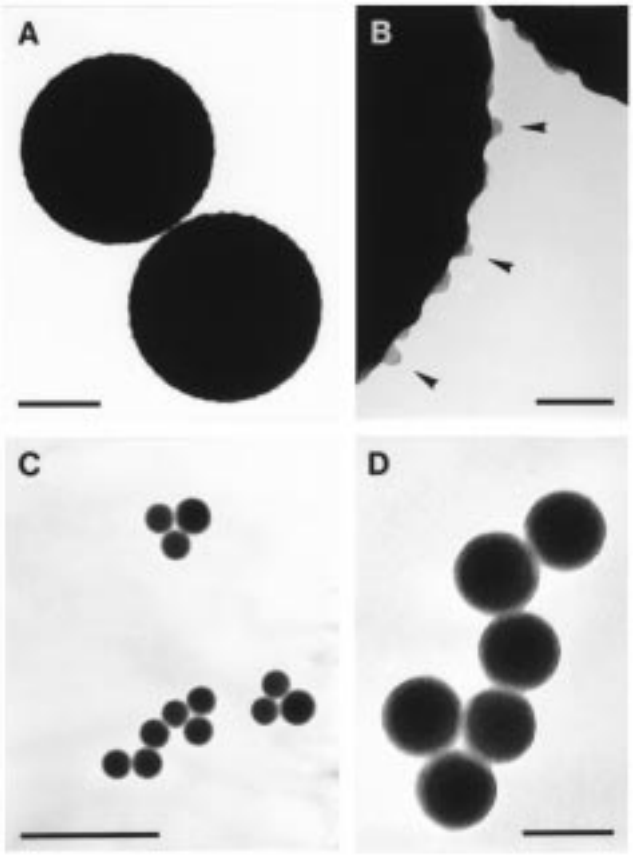


Figure 2. Electron microscopic analysis of carboxylate-modified particles. Particles of 1 μm (A, B) and 100 nm (C, D) nominal diameter were analyzed by transmission electron microscopy. While the majority of all 1 μm particles analyzed had small protrusions on their surface (B, arrowheads), 100 nm particles displayed a smooth surface texture (D). Bar, 400 nm (A, C), 100 nm (B, D).

RESULTS

Analysis of the Shape and Surface Texture of Carboxylate-Modified Microparticles. A uniform population of the core particles is a prerequisite for obtaining ligand-coated probes of well-defined size. For that reason, the red- and green-fluorescent carboxylate-modified microparticles were analyzed by transmission electron microscopy (Figure 2). The 1 μm particles were highly spherical in shape, but consisted of two subpopulations with respect to their surface texture. Approximately 20% of all red-fluorescent and 5−10% of all green-fluorescent

Table 2. Compatibility Chart for Carboxylate-Modified Polystyrene Microparticles

treatment	result[a]
2-propanol, 30 min, RT	stable
2-propanol, 4 h, RT	weak leaking of fluorophor
trifluoroethanol, 30 min, RT	stable
trifluoroethanol, 4 h, RT	weak leaking of fluorophor
hexafluoro-2-propanol, 30 min, RT	stable
hexafluoro-2-propanol, 4 h, RT	weak leaking of fluorophor
DMA, 15 min, RT	complete dissolution of particles
DMSO, 15 min, RT	complete dissolution of particles
CH_3CN, 15 min, RT	complete leaking of fluorophor
2-propanol/EDC/NHS, 2 h, RT	leaking of fluorophor, swelling of particles
1 M HCl, 4 h, RT	coagulation (reversible)[b], stable
3.25 M TFA, 3 h, RT	coagulation (reversible)[b], possibly swelling of particles, uncomplete sedimentation during centrifugation
0.1 M glutaraldehyde, 4 h, RT	stable
1 mM $NaIO_4$, 1 h, 4 °C	release of aldehyde[c]

[a] Carboxylate-modified polystyrene microparticles (diameter 1030 nm) were incubated with different chemicals for indicated times and analyzed visually (under the fluorescent microscope) for their integrity. [b] Particles tend to coagulate at acidic pH, but become again fully dispersed after neutralization and sonication. [c] Analyzed with Purpald.

particles analyzed by electron microscopy exhibited a smooth surface. The majority of all particles showed tiny, bell-shaped protrusions extending up to 20 nm from the spherical particle core (Figure 2, panels A and B). These protrusions clearly do not have any significant impact on the diameter of the 1 μm particles and, hence, the final probe size, but their presence must be taken into account when the particle surface is considered.

However, protrusions of this size would greatly influence the overall probe size of nanoparticles (see Figure 1). We therefore examined fluorescent, carboxylate-derivatized particles of 100 and 200 nm nominal diameter provided by the same supplier. Transmission electron microscopy at 38000× and 69000× magnification did not reveal any protrusions on the surface of the 200 nm and 100 nm particles (Figure 2, panels C and D). Thus, all particles examined in this study were suited for the development of size-defined ligand-coated fluorescent probes.

Derivatization of Fluorescent, Carboxylate-Modified Microparticles with Protein Monolayers. The demand for a ligand monolayer on the particle surface ruled out the use of carbodiimide-type cross-linkers in a one-pot reaction as proteinaceous ligand molecules may also get linked to each other. To overcome this problem, the particles had to be activated such that they displayed protein-reactive groups on their surface and then reacted with an excess of ligand molecules.

The polystyrene nature of the microparticle core precluded a synthetic procedure in organic solvents, even in lower alcohols (Table 2). Hence, reaction conditions were evaluated, which allowed particle activation and protein coupling in an aqueous system. Initial attempts to isolate N-hydroxysuccinimide or N-hydroxybenzotriazole esters of the particles before reacting them with a ligand resulted in very low yields (<2%) when tested with ^{14}C-labeled ethanolamine. Furthermore, satisfactory separation of the 1 μm particles from reactants was achieved only after several centrifugation steps consuming at least 40 min. Analogous procedures with smaller particles are anticipated to be even more time consuming and hence to lead to a substantial loss of the active ester by hydrolysis. This approach was therefore not pursued further. Subsequent experiments to generate an aldehyde derivative by oxidative fission of aminopropanediol that was coupled onto the particles failed as well because periodate caused damage to the particles, liberating some Purpald-reactive substance from the parent particles already.

Thus, alternative approaches to introduce aldehyde functions onto the particle surface were developed (Scheme 1). Activated carboxylate groups (**1**) were reacted in situ either with aminoacetaldehyde dimethylacetal followed by acidic cleavage of the protection group yielding **2**, or with ethylenediamine and glutaraldehyde resulting in **3**. Proteins were then reacted with the aldehyde functions under reducing conditions (**7**, **8**). In a completely different approach, a strategy via a biotin−avidin bridge was pursued (Scheme 1). First TEG-biotin was coupled to activated carboxylate groups yielding **4**, followed by binding of avidin to the biotin-derivatized microparticles (**9**). The resulting avidin-monolayer may serve as an anchor for any biotinylated ligand molecule. For comparison, direct coupling of avidin to carboxylate-modified microparticles in the presence of a carbodiimide cross-linker was also performed (**6**).

The efficacy of the individual pathways was evaluated by reacting [^{14}C]ethanolamine with each of the active intermediate compounds. Direct coupling to the active ester **1** showed that only approximately 14% of all carboxylate functions could be derivatized under these conditions (Table 3). After biotin derivatization, this value was reduced to 1.96 ± 0.22%, indicating that TEG-biotin had reacted with the majority of all accessible carboxylate groups. Derivatization of the carboxylate-modified microparticles with acetaldehyde dimethylacetal and subsequent determination of unreacted carboxylate functions gave a comparable result. After acidic cleavage of the acetal protection group, however, binding of ethanolamine to the aldehyde-modified microparticles occurred only with very low yields (Table 3). We therefore tried to optimize the reaction for the acetal cleavage of compound **2a** by assaying the aldehyde release from acetaldehyde dimethylacetal in the presence of different acids and at various pHs (Figure 3). Under all conditions applied in our synthesis (0.1 M citric acid, 1 M HCl, and 3.25 M TFA), aldehyde was released completely from the acetal in solution. In the heterogeneous reaction system involving the microparticles, however, yields could not be increased further even if incubation was prolonged (>12 h) or elevated temperatures (55 °C) or intense ultrasound treatment (2 × 30 min) were applied.

Nevertheless, the relatively low yield of aldehyde groups generated via both pathways was considered to be sufficient for the coupling of proteins, since a protein monolayer on the surface of 1 μm particles consists of only 70000−90000 protein molecules/microparticle, corresponding to 0.15−0.2 nmol of protein/0.1 μmol of

Scheme 1. Conjugation of Protein Monolayers onto Carboxylate-Modified Microparticles

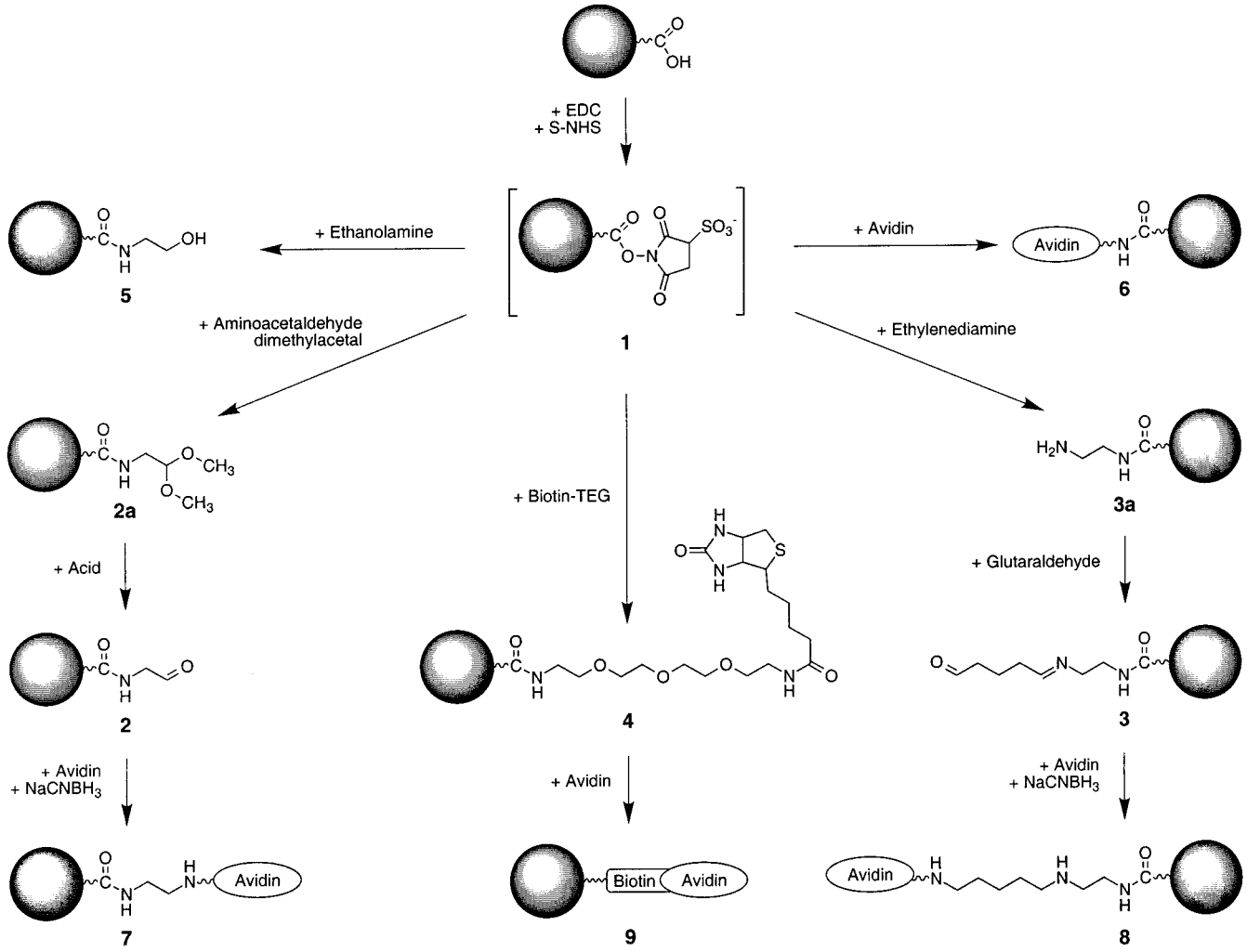


Table 3. Activated Binding Sites on Surface-Functionalized Carboxylate-Modified Microparticles[a]

conjugate	cleavage of aldehyde protective groups	% carboxylate functions activated
1	na	14.1 ± 2.7[b]
2	0.1 M citric acid	<2 (~0.0)
2	1 M HCl	<2 (~1.1 ± 0.4)
2	3.25 M TFA	2.4 ± 0.2[b]
3	na	<2 (~1.1 ± 0.3)
4	na	12.1 ± 2.7[b,c]

[a] Results refer to experiments with red-fluorescent carboxylate-modified microparticles (diameter 1030 nm). Each experiment was carried out at least in triplicate. Results are given as means ± standard deviation. [b] Yields differ significantly from nonspecific background binding ($p < 0.02$, two-tailed Student's unpaired *t*-test). [c] Yield determined indirectly; for details see text. na: not applicable.

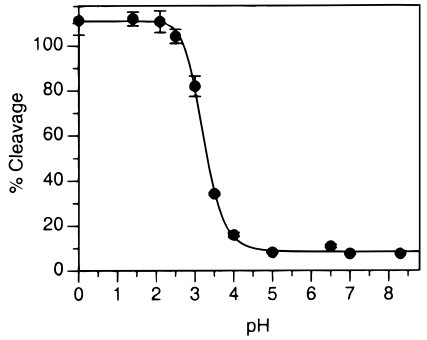


Figure 3. pH Dependence of acetal cleavage. Acetaldehyde dimethylacetal was incubated at different pH values, and the relative amount of aldehyde released was determined by Purpald assay. Data represent mean ± standard deviation of two independent experiments.

carboxylate functions (Table 1). For analytical purposes, the S-NHS/EDC/particle reaction mixture (**1**) and aldehydes **2** and **3**, as well as the biotinylated particles **4** were reacted with a 30-fold molar excess of avidin (relative to the protein amount sufficient to fill a complete monolayer) and coupling yields were determined by binding of [^{14}C]biotin (Table 4). A virtually complete avidin monolayer could be obtained with the aldehyde-derivatized particles generated either via aminoacetaldehyde dimethylacetal coupling followed by HCl cleavage or by an ethylendiamine−glutaraldehyde bridge. The binding of avidin via the TEG-biotin bridge was less efficient. As expected, direct coupling of avidin in the presence of EDC and S-NHS lead to the generation of multiple protein layers and/or multimeric avidin chains on the surface of the carboxylate-modified microparticles.

For the preparation of protein-coated microparticles, aldehyde-derivatized particles **2** (generated via HCl cleavage) and **3** were reacted with a 10-fold molar excess of CTB, OVA, or avidin. To reduce nonspecific reactions of remaining free aldehyde functions, the particles were finally incubated under reducing conditions with excess

Table 4. Avidin Binding to Surface-functionalized Carboxylate-Modified microparticles[a]

conjugate	cleavage of aldehyde protective groups	nmol of [^{14}C]biotin per 100 nmol carboxylate groups[b]	nmol of avidin[b,c] per 100 nmol carboxylate groups	% avidin monolayer formed[d]
6	na	2.32 ± 0.190[e]	0.580 ± 0.048	351 ± 29
7	1 M HCl	0.62 ± 0.008[e]	0.155 ± 0.002	94 ± 1
7	3.25 M TFA	0.34 ± 0.057[e]	0.085 ± 0.014	51 ± 9
8	na	0.76 ± 0.076[e]	0.19 ± 0.019	114 ± 11
9	na	0.08 ± 0.015[e]	0.027 ± 0.005	16 ± 3

[a] Results refer to experiments with red-fluorescent carboxylate-modified microparticles (diameter 1030 nm). Each experiment was carried out at least in triplicate. Results are given as means ± standard deviation. [b] Corrected for nonspecific background binding. Nonspecific adherence of avidin to nonactivated carboxylate-modified particles resulted in binding of 0.096 ± 0.017 nmol [^{14}C]biotin corresponding to 0.024 ± 0.004 nmol of avidin/100 nmol of carboxylate groups. [c] Assuming three accessible biotin binding sites per avidin molecule on compound 9 particles, four accessible biotin binding sites per avidin molecule on all other particles. [d] Calculated by using eq 1. [e] Significantly different from nonspecific background binding ($p < 0.005$, two-tailed Student's unpaired *t*-test). na, not applicable.

ethanolamine, introducing a hydrophilic function in addition to the secondary amine, or with excess glycine, which results in a zwitterionic blocking group.

To compare the protein coupling efficiency in the preparative reactions with the previous analytical setups, the protein load of various microparticle preparations was analyzed using the Micro BCA Protein Assay in a suspension reaction. Avidin coupling to red-fluorescent, aldehyde-derivatized particles in the preparative set up lead to the formation of a 89 ± 20% filled monolayer which is not statistically different from the value obtained in the analytical coupling procedure (94 ± 1%, as determined by [^{14}C]biotin binding). Coupling of CTB to red- and green-fluorescent microparticles by the same procedure resulted in a 93 ± 9% filled monolayer, while ovalbumin yielded a 33 ± 17% filled monolayer.

Binding of Protein-Coated Microparticles to Cultured BALB/c 3T3 Fibroblasts. To assess the biological functionality of our ligand-coated particles, we used fluorescent CTB-coated 1 μm particles to probe the accessibility of the plasma membrane receptor ganglioside G_{M1} on cultured BALB/c 3T3 fibroblasts, a cell line known to express ample amounts of receptor (Critchley et al., 1982) and to display a rudimentary glycocalyx only (Bailey and Gingell, 1988). In all experiments, confluent live 3T3 cell monolayers grown on glass coverslips were exposed to a 1:1 mixture of 2.5×10^7 particles for 1 h at 37 °C. CTB particles of two colors (red and green) generated via both synthetic pathways (via aldehyde **2** or **3**) and blocked with different aliphatic amines (ethanolamine and glycine) were examined in separate experiments. OVA particles of the respective other color served as internal background binding control (Figure 4, panels A−C). To verify the specificity of the binding, CTB particle binding was competed with 10 μg/mL soluble CTB (Figure 4, panels D−F).

Ethanolamine-quenched CTB particles generated via aminoacetaldehyde dimethylacetal coupling and HCl cleavage bound in a significantly higher number to the fibroblasts than did the respective OVA particles (Student's paired *t*-test, $p < 0.0001$) (Figure 5A). A total of 3.2 times (green particles) to 4.9 times (red particles) more CTB particles than OVA particles adhered to the confluent cell layers. By competition with soluble CTB, binding of red CTB particles could be reduced to 1.7 times that of the green OVA particles, while binding of green CTB particles did no longer differ from binding of red OVA particles (Figure 5A). Particles which had been synthesized by the same procedure but quenched with glycine showed similar binding characteristics (Figure 5A).

We also studied the binding behavior of avidin particles synthesized via the acetal route. Those particles exhibited

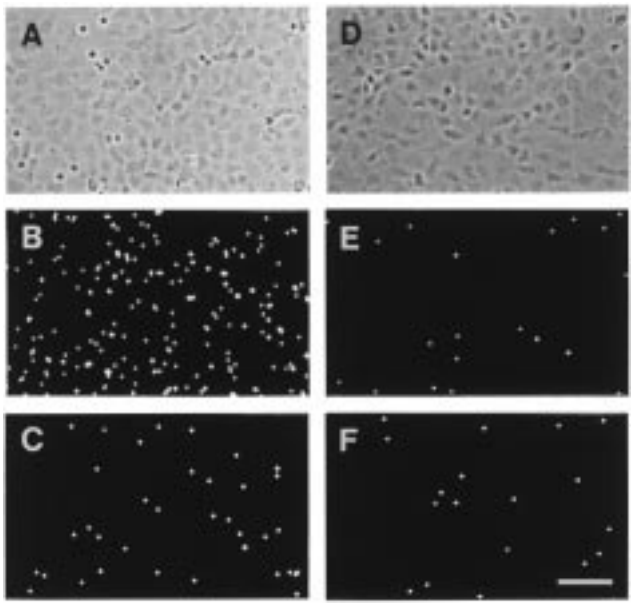


Figure 4. Binding of CTB particles to BALB/c 3T3 fibroblasts. Carboxylate-modified 1 μm particles were derivatized via aminoacetaldehyde dimethylacetal coupling and HCl cleavage and reacted with either CTB or OVA. Remaining aldehyde groups were quenched with ethanolamine/$NaCNBH_3$. BALB/c 3T3 fibroblasts grown on glass coverslips were incubated with 2.5×10^7 particles/mL each of red-fluorescent CTB particles and green-fluorescent OVA particles in the absence (A−C) or presence (D−F) of soluble CTB. Identical fields of the cell layers were photographed en face under phase contrast (A, D), under red fluorescence to visualize adherent CTB particles (B, E) and under green fluorescence to visualize adherent OVA particles (C, F). Bar, 100 μm.

a very strong binding to 3T3 fibroblasts, with 4.8−6.9 times more avidin than OVA particles bound (Figure 5B).

The binding of microparticles derivatized via the glutaraldehyde route was analyzed as well. Regardless of their protein load, all particles of this type showed a very high unspecific binding to 3T3 fibroblasts. Here, OVA particles bound approximately to the same extent as CTB particles (Figure 5B) which in turn bound as well (green particles) or even better (red particles) than those generated via the acetal pathway. Moreover, binding of CTB particles could not be reduced by competition with soluble CTB.

We also investigated whether the binding of the protein-coated microparticles (generated via the acetal pathway) was influenced by fluorophor color. Differences between the binding of red and green particles were detectable only when particle binding was low (less than 500 particles/mm^2). Significantly less green OVA particles

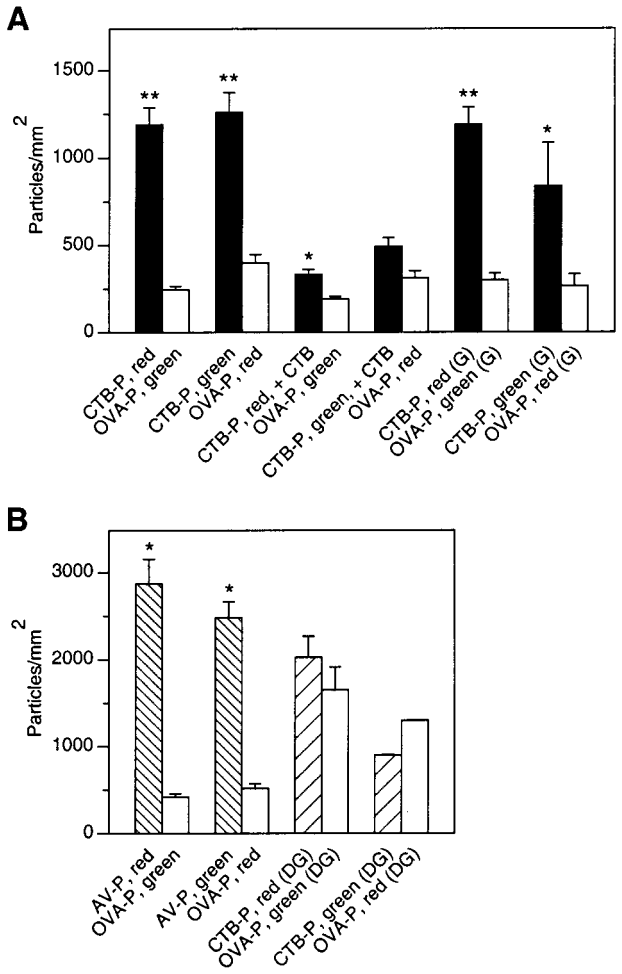


Figure 5. Quantitative analysis of microparticle binding to BALB/c 3T3 fibroblasts. BALB/c 3T3 fibroblasts grown on glass coverslips were incubated with 2.5×10^7 particles/mL each of CTB particles (CTB-P) (or avidin particles, AV-P) and OVA particles (OVA-P). Competition was done by addition of 10 μg/mL soluble CTB (+CTB). Bound particles were quantitated as described in Materials and Methods. Each bar represents the mean value and standard error of at least 3 independent experiments. (DG) Aldehyde particles synthesized via ethylenediamine and glutaraldehyde coupling, quenched with ethanolamine; (G) aldehyde particles synthesized via aminoacetaldehyde dimethylacetal coupling and HCl cleavage, quenched with glycine; (all others) aldehyde particles synthesized via aminoacetaldehyde dimethylacetal coupling and HCl cleavage, quenched with ethanolamine. (Asterisks) Binding significantly higher than that of the respective OVA particles [Student's paired *t*-test, $p < 0.001$ (two asterisks) or $p < 0.05$ (one asterisk)].

bound to the fibroblasts than red OVA particles, while in competition experiments with soluble CTB, less red CTB particles bound than green CTB particles (Student's unpaired *t*-test, $p < 0.02$). These differences became unsignificant for the binding of CTB particles (in the absence of competing soluble CTB) and of avidin particles, where high binding rates to fibroblasts were observed (more than 1000 particles/mm^2).

Taken together, we could demonstrate that carboxylate-modified microparticles which were aldehyde-derivatized by aminoacetaldehyde dimethylacetal-coupling and acid-deprotection bind protein ligands in a way that preserves their biological function. In addition, these probes show a low nonspecific binding which makes them useful tools to analyze the accessibility of cell surface receptors.

DISCUSSION

Affinity and specificity of ligand−receptor interactions are analyzed for the most part in biochemical or histological assays which assume a sterically unhindered contact, with affinities and specificities being solely due to endogenous features of the reaction partners themselves. However, the mere capacity to interact is a necessary but not always sufficient requirement for successful binding. In living systems, cell surface molecules were shown to modulate cell−cell binding by shielding certain receptor molecules (Manjunath et al., 1993; Wesseling et al., 1996) while other molecules evolved into rigid spikes which are purposely exposed to facilitate a certain type of interaction (Patel et al., 1995). The totality of the carbohydrate-rich cell surface molecules which form a continuous coat that covers the cell membrane, collectively termed glycocalyx, extends from 5 nm on erythrocytes (Linss et al., 1991) up to 1000 nm on intestinal epithelial lining cells (Frey et al., 1996; Neutra et al., 1996a). In a recent study, we could demonstrate that it might be possible to utilize such differences in the glycocalyx structure for targeting mucosal vaccines to Peyer's patch M cells (Frey et al., 1996). Plasma membrane ganglioside G_{M1}-specific CTB-probes of 30 nm diameter bound selectively to M cells, while soluble CTB of 7 nm diameter exhibited ubiquitous binding to the epithelium, and CTB probes of 1 μm diameter did not bind at all. To further define the size window for this M-cell tropism, we now have developed a conjugation procedure which enables us to synthesize CTB probes of a well-defined size range on the basis of commercially available fluorescent carboxylate-modified micro- and nanoparticles as a tool to probe the pore size and nanoarchitecture of the glycocalyx.

The key feature of this method is the controlled grafting of no more than one layer of ligand molecules onto the particle surface. Most current protocols for coupling proteins on microparticles are set up as one-pot reactions in which the protein is conjugated onto the particle by use of carbodiimides (Molday et al., 1975; Illum and Jones, 1985), conditions under which we observed the formation of protein multilayers. The main problem with those multilayers is that they are sterically undefined. Some areas of the particle may display the desired monolayer while in other regions multiple ligand molecules may be linked to each other forming thicker coats or even spike-like structures extending from the surface. Such an irregular, hairy surface will result in an increase of the hydrodynamic diameter of the probe and thus may reduce its advance to the cell membrane. On the other hand, long, thin spikes might be able to penetrate the glycocalyx which in fact may enhance access and binding to the plasma membrane receptor.

The three coupling procedures devised in this study overcome these problems by modifying the particulate probe core in such a way that chemically or biologically reactive functions are displayed on its surface. These functional groups are then able to react with respective counterparts of a ligand molecule without the need for an additional cross-linker. Our experiments started with fluorescent microparticles which carry a dense cage of carboxylate groups on their surface. Such microparticles are commercially available in different colors and in sizes ranging from 10 nm to several micrometers. For the sake of convenience, only 1 μm particles in two different colors were used to test and validate our coupling chemistry as those could be washed and separated from solute reactants simply by repeated centrifugation steps.

The most obvious approach to obtain protein-reactive particles was the conversion of the surface carboxylates into active esters followed by the removal of the unreacted activating agents and subsequent coupling of protein ligands via their amino functions. The lability of the carboxylate-modified polystyrene particles in organic solvents, however, necessitated the activation, washing, and final coupling steps to be performed in an aqueous environment. The coupling yields obtained following this approach were poor, probably due to the short half-life of active esters in aqueous solution (Jarret, 1987).

We therefore decided to introduce hydrolysis-resistant amine-reactive aldehyde functions or avidin-binding biotinyl groups onto the particle surface. In the latter case, an avidin or streptavidin bridge would be used to eventually attach a biotinylated ligand. Both strategies were evaluated in parallel. In all cases, the initial step was the reaction of the surface carboxylates with an excess of aliphatic amine in the presence of carbodiimide and *N*-hydroxysulfonylsuccinimide. The yield of these reactions was determined to be approximately 14% based on the number of carboxylate functions. Surprisingly, this yield could not be increased further by any means, such as longer reaction times, elevated temperatures, use of different buffers, higher excess of reactants, or sonication. We assume that this result represents the highest coupling rate achievable with these specific particles since their extremely high surface density of carboxylate functions (7 $Å^2$/charge group) may prevent complete derivatization by sterical hindrance.

The use of a water-soluble amino-biotin lead directly to the desired biotinylated particles. The formation of surface aldehyde groups required additional reaction steps. In case of the acetal-derivatized particles (**2a**), the protective groups had to be cleaved off in an acidic environment. Again, low reaction yields were obtained with dilute organic and mineral acids ($\leq$17% deprotection yield). In contrast to that, soluble acetaldehyde dimethylacetal performed as expected and was deprotected completely at pH $\leq$2. The meager reactivity of the immobilized acetal groups was paralleled in the second reaction step of the alternative pathway, where glutaraldehyde was coupled to the ethylenediamine-derivatized particles (**3a**) with a reaction yield of $\leq$8%. Yet, these moderate yields turned out to be ample for coupling proteinaceous ligands onto the particle surface. Both types of aldehyde-derivatized particles (**2**, **3**) bound a complete monolayer of avidin onto their surface, while avidin binding to the biotinylated particles fell short with only 16% surface coverage. Hence, we focused on the aldehyde-functionalized particles in the subsequent biological assays.

For these experiments, the B subunit of cholera toxin was chosen as ligand. CTB binds exclusively to the plasma membrane glycolipid ganglioside G_{M1}, a receptor that was shown to be accessible to 1 μm probes on BALB/c 3T3 fibroblasts (Frey et al., 1996). Ovalbumin and avidin served as control ligands. When using the particles prepared via the acetal route, the probes displayed a specific binding to fibroblast monolayers when coated with CTB and a low nonspecific background binding when covered with OVA. In contrast, protein-coated probes generated via the glutaraldehyde approach exhibited a high nonspecific background binding. The reasons for this behavior remain to be elucidated. It seems unlikely that the background binding was caused by aldehyde groups residing on the particle surface, since unreacted aldehyde functions were blocked with a more than 1000-fold excess of aliphatic amines in the presence of cyanoborohydride. Moreover, glutaraldehyde should not be able to span the protein layer. We rather attribute this phenomenon to the extra positive charges which we introduced along with the glutaraldehyde cross-linker after reduction of the Schiff bases. The impact of positive charges on the nonspecific binding was emphasized in experiments with avidin particles which had been prepared via the acetal route. The switch from OVA to avidin dramatically increased the nonspecific binding, most likely because of the high positive charge of avidin under assay conditions [pI_{Avidin} 10.5 (Green, 1975)]. OVA and CTB, on the other hand, have pIs of 4.9 (Salaman and Williamson, 1971) and 7.8 (Spangler, 1992) and are therefore less prone to interact with negatively charged cell surfaces at physiological pH. However, a negative charge on the particle surface does not necessarily preclude nonspecific background binding. In our hands, the carboxylate-modified parent particles showed a nonspecific binding similar to that of avidin-coated probes (data not shown).

Thus, an ideal probe core would consist of a fluorophor-loaded seed particle which is covered by a shell of uncharged hydrophilic molecules bearing terminal acetal functions that can be converted into aldehydes upon demand by acid deprotection. An aldehyde content of 1×10^{-7} mequiv/cm^2 should be sufficient for most applications. In a very recent publication, Búcsi et al. (1998) described the synthesis of poly(ethylene oxide)-coated latex nanoparticles with acetal functions terminating the poly(ethylene oxide) chains, an approach almost meeting the above demands. Unfortunately, the authors did not test their particles in biological settings, and shortcomings such as holes in the poly(ethylene oxide) shell were reported. If those problems can be fixed and an easily detectable label, such as a fluorophor, can be incorporated, these particles may provide an interesting alternative to the aldehyde-derivatized carboxylate-modified particles described in this report.

ACKNOWLEDGMENT

The authors thank Ms. Liselotte Greune for expert technical assistance with the electron microscopy and Dr. Winfried Weissenhorn for his help in the dynamic light scattering experiments. This work was supported by a personal grant from the Bundesministerium für Bildung, Wissenschaft, Forschung und Technologie and research grant FR 958/2-1 from the Deutsche Forschungsgemeinschaft to A.F.

LITERATURE CITED

Bailey, J., and Gingell, D. (1988) Contacts of chick fibroblasts on glass: results and limitations of quantitative interferometry. *J. Cell Sci. 90*, 215−224.

Búcsi, A., Forcada, J., Gibanel, S., Héroguez, V., Fontanille, M., and Gnanou, Y. (1998) Monodisperse polystyrene latex particles functionalized by the macromonomer technique. *Macromolecules 31*, 2087−2097.

Critchley, D. R., Streuli, C. H., Kellie, S., Ansell, S., and Patel, B. (1982) Characterization of the cholera toxin receptor on Balb/c 3T3 cells as a ganglioside similar to, or identical with, ganglioside G_{M1}. *Biochem. J. 204*, 209−214.

Eldridge, J. H., Gilley, R. M., Staas, J. K., Moldoveanu, Z., Meulbroek, J. A., and Tice, T. R. (1989) Biodegradable microspheres: vaccine delivery system for oral immunization. *Curr. Top. Microbiol. Immunol. 146*, 59−66.

Ermak, T. H., Dougherty, E. P., Bhagat, H. R., Kabok, Z., and Pappo, J. (1995) Uptake and transport of copolymer biodegradable microspheres by rabbit Peyer's patch M cells. *Cell Tissue Res. 279*, 433−436.

Frey, A., Giannasca, K. T., Weltzin, R., Giannasca, P. J., Reggio, H., Lencer, W. I., and Neutra, M. R. (1996) Role of the

glycocalyx in regulating access of microparticles to apical plasma membranes of intestinal epithelial cells: implications for microbial attachment and oral vaccine targeting. *J. Exp. Med. 184*, 1045−1059.

Gebert, A., and Bartels, H. (1995) Ultrastructure and protein transport of M cells in the rabbit cecal patch. *Anat. Rec. 241*, 487−495.

Gebert, A., Rothkötter, H.-J., and Pabst, R. (1994) Cytokeratin 18 is an M-cell marker in porcine Peyer's patches. *Cell Tissue Res. 276*, 213−221.

Green, N. M. (1975) Avidin. *Adv. Protein Chem. 29*, 85−133.

Illum, L., and Jones, P. D. E. (1985) Attachment of monoclonal antibodies to microspheres. *Methods Enzymol. 112*, 67−84.

Jarret, H. W. (1987) Development of N-hydroxysuccinimide ester silica, a novel support for high-performance affinity chromatography. *J. Chromatogr. 405*, 179−189.

Jepson, M. A., Mason, C. M., Bennett, M. K., Simmons, N. L., and Hirst, B. H. (1992) Coexpression of vimentin and cytokeratins in M cells of rabbit intestinal lymphoid follicle-associated epithelium. *Histochem. J. 24*, 33−39.

Kato, T. (1990) A study of secretory immunoglobulin A on membranous epithelial cells (M cells) and adjacent absorptive cells of rabbit Peyer's patches. *Gastroenterol. Jpn. 25*, 15−23.

Kraehenbuhl, J.-P., and Neutra, M. R. (1992) Molecular and cellular basis of immune protection of mucosal surfaces. *Physiol. Rev. 72*, 853−879.

Linss, W., Pilgrim, C., and Feuerstein, H. (1991) How thick is the glycocalyx of human erythrocytes? *Acta Histochem. 91*, 101−104.

Manjunath, N., Johnson, R. S., Staunton, D. E., Pasqualini, R., and Ardman, B. (1993) Targeted disruption of CD43 gene enhances T lymphocyte adhesion. *J. Immunol. 151*, 1528−1534.

Molday, R. S., Dreyer, W. J., Rembaum, A., and Yen, S. P. S. (1975) New immunolatex spheres: visual markers of antigens on lymphocytes for scanning electron microscopy. *J. Cell Biol. 64*, 75−88.

Neutra, M. R., Frey, A., and Kraehenbuhl, J.-P. (1996a) Epithelial M cells: gateways for mucosal infection and immunization. *Cell 86*, 345−348.

Neutra, M. R., Pringault, E., and Kraehenbuhl, J.-P. (1996b) Antigen sampling across epithelial barriers and induction of mucosal immune responses. *Annu. Rev. Immunol. 14*, 275−300.

Patel, K. D., Nollert, M. U., and McEver, R. P. (1995) P-selectin must extend a sufficient length from the plasma membrane to mediate rolling of neutrophils. *J. Cell Biol. 131*, 1893−1902.

Rautenberg, K., Cichon, C., Heyer, G., Demel, M., and Schmidt, M. A. (1996) Immunocytochemical characterization of the follicle-associated epithelium of Peyer's patches: anti-cytokeratin 8 antibody (clone 4.1.18) as a molecular marker for rat M cells. *Eur. J. Cell Biol. 71*, 363−370.

Salaman, M. R., and Williamson, A. R. (1971) Isoelectric focusing of proteins in the native and denatured states. *Biochem. J. 122*, 93−99.

Spangler, B. D. (1992) Structure and function of cholera toxin and the related *Escherichia coli* heat-labile enterotoxin. *Microbiol. Rev. 56*, 622−647.

Staros, J. V., Wright, R. W., and Swingle, D. M. (1986) Enhancement by N-hydroxysulfosuccinimide of water-soluble carbodiimide-mediated coupling reactions. *Anal. Biochem. 156*, 220−222.

Stich, T. M. (1990) Determination of protein covalently bound to agarose supports using bicinchoninic acid. *Anal. Biochem. 191*, 343−346.

Watanabe, T., Motomura, Y., and Suga, T. (1978) A new colorimetric determination of D-amino acid oxidase and urate oxidase activity. *Anal. Biochem. 86*, 310−315.

Wesseling, J., van der Valk, S. W., and Hilkins, J. (1996) A mechanism for inhibition of E-cadherin-mediated cell−cell adhesion by the membrane-associated mucin episialin/Muc1. *Mol. Biol. Cell 7*, 565−577.

BC980124P

A Psoralen-Conjugated Triplex-Forming Oligodeoxyribonucleotide Containing Alternating Methylphosphonate−Phosphodiester Linkages: Synthesis and Interactions with DNA

Paul S. Miller,* Sarah A. Kipp, and Cory McGill†

Department of Biochemistry, School of Public Health, Johns Hopkins University, 615 North Wolfe Street, Baltimore, Maryland 21205 . Received November 18, 1998; Revised Manuscript Received March 2, 1999

A psoralen-conjugated oligodeoxyribopyrimidine (1443), PS-pTTTT*C*TTTT*C*TT*C*TT, where PS is trimethylpsoralen and *C* is 5-methyl-2′-deoxycytidine, that contains alternating methylphosphonate-phosphodiester internucleotide linkages was synthesized. The ability of 1443 to form triple-stranded complexes with a purine tract in a synthetic DNA duplex was studied. Irradiation of solutions containing the DNA target and 10 μM 1443 or 0.25 μM of a similar psoralen-conjugated oligodeoxyribonucleotide that contained all phosphodiester linkages, (1193), with long-wavelength UV light resulted in approximately 80% formation of interstrand cross-links at pH 7.0, 37 °C, in the presence of 20 mM magnesium chloride. The extent of triplex formation as monitored by photo-cross-linking decreased over the pH range 5.5−8.0, and the apparent p*K* of the 5-methylcytosines (*C*) in 1443 was approximately one-half of a pH unit less than that of the 5-methylcytosines in 1193. Oligomer 1443 formed triplexes in the absence of magnesium, and maximum triplex formation was observed in solutions containing 2.5 mM magnesium, whereas maximal triplex formation by the fully charged 1193 was not observed until the magnesium concentration was 10 mM or higher. Unlike the all-phosphodiester backbone of 1193, the alternating methylphosphonate-phosphodiester backbone of 1193 is resistant to hydrolysis by exonucleases in fetal calf serum. The nuclease resistance of 1443 and its ability to form triplexes at very low magnesium concentrations suggests that triplex-forming oligomers with alternating methylphosphonate-phosphodiester backbones may be good candidates for use as antigene reagents in cell culture.

INTRODUCTION

Short oligonucleotides can bind to double-stranded DNA to form triple-stranded complexes. These triplex forming oligomers or TFOs[1] interact with homopurine tracts in DNA through the formation of Hoogsteen or reversed Hoogsteen hydrogen bonds. This observation has generated considerable interest in developing TFOs to suppress or manipulate gene expression (for reviews, see refs *1* and *2* and references therein). Most of the current studies on triplex formation have employed oligodeoxyribonucleotides. While certain oligodeoxyribonucleotides can form stable triplexes under physiological conditions, the phosphodiester linkages of these oligonucleotides are susceptible to nuclease hydrolysis, a property that can potentially limit their use in cell culture and in vivo.

This problem can be circumvented in principle by using nuclease-resistant oligonucleotide analogues. A number of nuclease-resistant oligonucleotide analogues have been shown to form triplexes with double-stranded DNA. These include oligodeoxyribonucleotide phosphorothioates (*3*−*6*), α-anomeric oligonucleotides (*7*−*9*), peptide nucleic acids (PNAs) (*10*, *11*), oligonucleotides with riboacetal internucleotide linkages (*12*), and oligonucleotides with methylphosphonate (*13*) or (aminoalkyl)-phosphonate internucleotide linkages (*14*, *15*).

Previous studies showed that a pyrimidine-containing oligodeoxyribonucleotide with methylphosphonate linkages could form a stable triplex, but only at low pH (*13*). In an effort to increase triplex stability while maintaining nuclease resistance, we have recently begun to explore triplex formation by chimeric oligodeoxyribonucleotides that contain alternating methylphosphonate-phosphodiester internucleotide linkages, d-AOMPs. In this paper, we describe the interaction of a psoralen-conjugated d-AOMP with double-stranded DNA.

MATERIALS AND METHODS

Nucleoside-derivatized controlled pore glass supports, protected deoxyribonucleoside-3′-*O*-(β-cyanoethyl-*N*,*N*-diisopropyl)phosphoramidites, and 2-[4′-(hydroxymethyl)-4,5′,8-trimethylpsoralen]hexyl-1-*O*-[β-cyanoethyl-(*N*,*N*-diisopropyl)]phosphoramidite were purchased from Glen Research, Inc, Sterling, VA. Protected deoxyribonucleoside-3′-*O*-(*N*,*N*-diisopropyl)methylphosphonamidites were obtained from JBL Scientific, San Luis Obispo, CA. All chemicals were of reagent grade or better. Phosphoramidite and phosphonamidite solutions were prepared using HPLC-grade acetonitrile stored over calcium hydride. Polyacrylamide gel electrophoresis was carried out on 20 × 20 × 0.75 cm gels containing 20% acrylamide and 7 M urea. The running buffer was TBE, which contained 89 mM Tris, 89 mM boric acid, and 0.2 mM

* To whom correspondence should be addressed. Phone: (410) 955-3489. Fax: (410) 955-2926. E-mail:pmiller@jhsph.edu.

† Summer Research Intern sponsored by the Leadership Alliance.

[1] Abbreviations: d-AOMP, oligodeoxyribonucleotide with alternating methylphosphonate-phosphodiester internucleotide linkages; d-*C*, 5-methyldeoxycytidine; HPLC, high-performance liquid chromatography; Mops, 3-(*N*-morpholino)propanesulfonic acid; *p*, methylphosphonate linkage; TFO, triplex-forming oligonucleotide.

10.1021/bc980140m CCC: $18.00 © 1999 American Chemical Society
Published on Web 05/13/1999

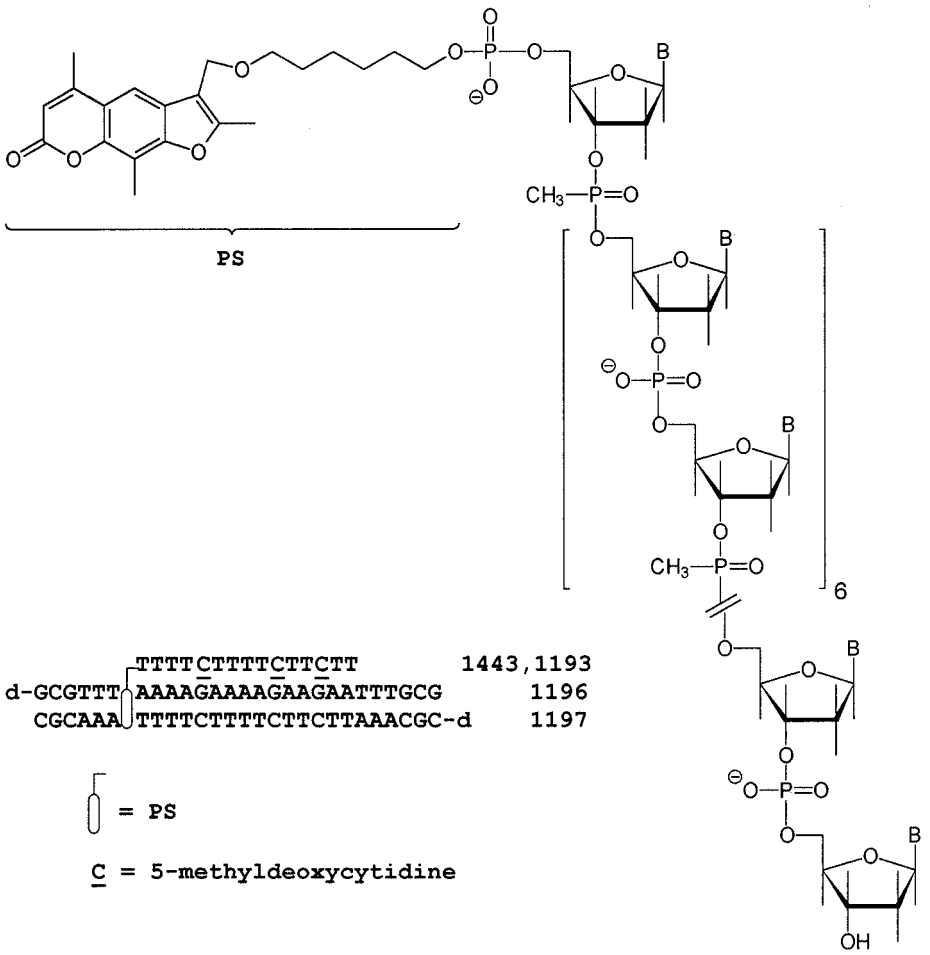


Figure 1. General structure of a psorlen conjugated oligodeoxyribonucleotide containing alternating methylphosphonate/phosphodiester internucleotide linkages, d-AOMP. The sequences of the triplex forming oligomers d-AOMP 1443 and all diester oligomer 1193 and the DNA target 1196/1197 are also shown.

ethylenediaminetetraacetate buffered at pH 8. The gel loading buffer contained 90% formamide, 0.05% xylene cyanol, and 0.05% bromophenol blue.

Syntheses of Oligodeoxyribonucleotides. Oligodeoxyribonucleotides 1196, 1197, psoralen derivatized oligodeoxyribonucleotide 1193, and psorlen-derivatized alternating methylphosphonate-phosphodiester oligonucleotide 1443 whose sequences are shown in Figure 1 were synthesized on nucleoside-derivatized controlled pore glass supports using an Applied Biosystems model 392 DNA/RNA synthesizer. The concentrations of the phosphoramidites or methylphosphonamidites were 0.15 M in anhydrous acetonitrile and the coupling time was 90 s. Tetrazole in acetonitrile was used as the activating agent. The coupling step was followed by a capping step, then iodine oxidation followed by a second capping step. Capping reagent B consisted of a solution of 2.54 g of (dimethylamino)pyridine in 50 mL of anhydrous pyridine. The synthesizer was programmed to remove the last dimethoxytrityl group from oligomers 1196 and 1197. Oligomers 1193 and 1443 were derivatized with psoralen using the psoralen phosphoramidite reagent.

Oligomers 1193, 1196, and 1197 were deprotected by treatment with solution of 50% concentrated ammonium hydroxide in pyridine at 55 °C for 6 h. Oligomer 1443 was deprotected by sequential treatment with ammonium hydroxide and ethylenediamine (*16*). Following deprotection, oligomers 1196 and 1197 were purified by strong anion-exchange HPLC. A 20 OD_{260} sample of each oligomer was injected onto the column, and the column was eluted with 18 mL of a linear gradient of 0 to 0.8 M ammonium sulfate in 20% acetonitrile buffered with 1 mM ammonium acetate at pH 6.2. The flow rate was 0.6 mL/min and the column was monitored at 290 nm. Psoralen-conjugated oligomers 1193 and 1443 were purified by reversed-phase HPLC on a C-18 column using a 20 mL gradient of 2 to 40% acetonitrile in 50 mM sodium phosphate buffered at pH 5.8. The flow rate was 1.0 mL/min, and the column was monitored at 290 nm. The oligomers were then desalted on SEP PAK C-18 cartridges.

Oligomer 1193 was completely degraded to pT and p−d*C* in the expected ratios when incubated with 2 μg of snake venom phosphodiesterase in 10 mM Tris, pH 8.1, and 2 mM magnesium chloride at 37 °C for 16 h. Similar treatment of oligomer 1443 produced d-pT*p*T, d−p*Cp*T, d-pT*pC* and pT, where *C* is 5-methyldeoxycytidine and *p* is methylphosphonate. The products of these enzyme digestions were analyzed by C-18 reversed-phase HPLC using a 20 mL gradient of 2 to 40% acetonitrile in 50 mM sodium phosphate buffered at pH 5.8. The extinction coefficients of the oligomers were determined by comparing the absorbances of a given amount of oligomer before and after digestion by snake venom phosphodiesterase as previously described (*17*). The ϵ_{260} values obtained were oligomer 1196, 225 000; oligomer 1197, 253 000; oligomer 1193, 107 000; and oligomer 1443, 96 500.

Triplex Formation and Photo-Cross-Linking Experiments The 5′-hydroxyl groups of oligomers 1196 and

1197 were each phosphorylated by polynucleotide kinase using γ-[^{32}P]ATP (specific activity 50−200 Ci/mmole). The labeled oligomers were purified on MicroSpin Sephadex G-25 columns (Amersham Pharmacia Biotech Inc). Duplexes were formed by mixing 1 equiv of labeled strand with 1.2 equiv of complementary unlabeled strand in a triplex buffer system containing 100 mM sodium chloride, 0−20 mM magnesium chloride, and 50 mM Mops buffered at the specified pH. The solution was heated at 65 °C for 2 min and then allowed to cool to room temperature.

Photo-cross-linking experiments were carried out as follows. Equal volumes of duplex solution and a solution of the triplex forming oligomer in triplex buffer were mixed, and the solution was incubated at a given temperature for 3−16 h. Ten microliter aliquots of the solution were then irradiated with 365 nm UV light for 10 min at 2 °C in borosilicate glass test tubes as previously described (*18*). The solvents were evaporated in a Speed Vac concentrator, and the residue was dissolved in 5−10 μL of gel loading buffer. The samples were electrophoresed on a 20% polyacrylamide gel run under denaturing conditions. Gels were run at 800 or 1000 V at room temperature until the bromophenol blue dye had migrated ∼15 cm on the gel. The wet gel was wrapped in Saran Wrap and imaged by autoradiography or by a FujiX BAS 1000 phosphorimager. Phosphorimages were quantitated using the Fuji software package to determine the amount of cross-linking. Control experiments showed that the same percentage of photoadduct formation was obtained regardless of whether the samples were irradiated at the temperature of incubation or at 2 °C. Thus, for example, when 0.1 μM 1193 was incubated with duplex 1196/1197 for 16 h at 22 °C and then irradiated for 10 min, 91% cross-linking was observed when irradiation was carried out at 2 °C and 91% cross-linking was observed when irradiation was carried out at 22 °C. Similarly, incubation of 2.5 μM 1443 and 1196/1197 for 16 h at 22 °C followed by irradiation gave 86% cross-linking when irradiation was carried out at 2 °C and 86% cross-linking when irradiation was carried out at 22 °C. The lower irradiation temperature was used in the experiments described here to minimize the possibility of evaporation and thus changes in concentration during irradiation.

RESULTS AND DISCUSSION

Synthesis and Stability of the Psoralen-Conjugated d-AOMP Oligomer 1443 whose general structure is shown in Figure 1, consists of thymidine and 5-methyldeoxycytidine linked by alternating methylphosphonate-phosphodiester internucleotide bonds. The oligomer is conjugated with trimethylpsoralen through a six carbon linker attached to the 5′-terminal phosphate group. The oligomer was prepared on a controlled pore glass using commercially available protected nucleoside β-cyanoethyl-*N*,*N*-(diisopropyl)phosphoramidites and protected nucleoside *N*,*N*-(diisopropyl)methylphosphonamidites. The amino group of 5-methyldeoxycytidine was protected with an isobutryl protecting group. The psoralen group was introduced as the phosphoramidite during the last coupling reaction. A control oligomer, 1193, that contains contiguous phosphodiester linkages was synthesized in a similar manner.

Protected oligomer 1443 was first treated with ammonium hydroxide for 30 min at room temperature. This treatment removes the isobutryl protecting groups from the 5-methyldeoxycytidines, partially removes the β-cyanoethyl groups, and partially cleaves the oligomer from the support. These conditions do not result in hydrolysis of the methylphosphonate linkages. The oligomer was then treated with 50% ethylenediamine for 6 h at room temperature to complete removal of the β-cyanoethyl groups and to completely cleave the oligomer from the support. This sequential deprotection scheme avoids transamination of the 5-methyldeoxycytidines by ethylenediamine (*16*).

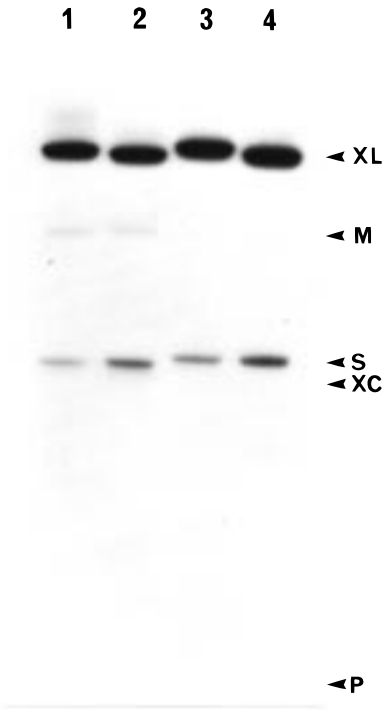
Previous studies have shown that the phosphodiester linkages of oligothymidine d-AOMPs can be hydrolyzed by an endonuclease activity found in snake venom phosphodiesterase (*19*). Similar results were observed for oligomer 1443. Thus, 1443 was incubated with snake venom phosphodiesterase for 18 h at 37 °C, and the products of the reaction analyzed by C-18 reversed-phase HPLC. In addition to the pT, which results from hydrolysis of the 3′-terminal phosphodiester linkage, three dimers, pT*p*T, p*Cp* T, and pT*pC* were observed. As expected, the methylphosphonate linkages of the oligomer were not hydrolyzed.

The stability of 1443 in cell culture medium containing 10% fetal calf serum was also studied. Because it was not possible to introduce a radioactive label into the oligomer, the fate of the oligomer was followed by C-18 reversed-phase HPLC. In contrast to the behavior observed with snake venom phosphodiesterase, the internal phosphodiester linkages of 1443 appear to be resistant to the 3′-exonuclease activity that is commonly found in most mammalian sera (*20*). Thus, only the 3′-terminal thymidine was hydrolyzed when 1443 was incubated with culture medium containing 10% fetal calf serum whereas similar incubation of the all phosphodiester oligomer 1193 resulted in approximately 40% hydrolysis of the oligomer after 1 h and complete hydrolysis after 4 h.

Interaction with Double-Stranded DNA. The interaction of 1443 and 1193 with double-stranded DNA was studied using the target system show in Figure 1. The target duplex, 1196/1197, which consists of 27 base pairs, contains a 15 nucleotide homopurine tract. The sugar−phosphate backbones of 1443 and 1193 have the same polarity as this purine tract, and both oligomers would be expected to interact with this tract via Hoogsteen hydrogen bonds with the formation of T·A−T and C^+·G−C triads (*21*). 5-Methyl-2′-deoxycytidine, *C*, was used instead of 2′-deoxycytidine because it has a higher apparent p*K* than dC and thus enables triplex formation to occur at higher pH. The 5′−T−A/5′−T−A sequence at the duplex/triplex junction would be expected to serve as a binding site for the psoralen group conjugated to the 5′-ends of either 1443 or 1193 (*22*−*24*).

The interaction of phosphodiester oligomer 1193 and duplex 1196/1197 could be detected by conventional melting experiments. Thus, a melting transition due to the dissociation of 1193 from the triplex was readily observable at pH 8.0 (T_m 24 °C) and a single melting transition (T_m 65 °C) due to dissociation of the triplex was observed at pH 6.2 (data not shown). The T_m of the duplex 1196/1197 was 65 °C at both pH 8.0 and 6.2. Similar melting experiments were carried out with methylphosphonate oligomer 1443 and duplex 1196/1197. In contrast to the results obtained with 1193, very broad transitions with small hypochromicity changes were observed for 1443. The midpoints of these transitions appeared to be approximately 45 °C at pH 6.2 and 16 °C at pH 8.0, although the breath the transitions precluded an accurate determination of the melting temperatures.

Triplex formation between 1443 or 1193 and duplex 1196/1197 was observed indirectly by irradiation of



Oligomer	% Cross-Link *p1197/1196	*p1196/1197
1443	80	82
1193	89	87

Figure 2. Triplex-mediated photoadduct formation. Solutions containing 0.7 μM 1193 (lane 1) or 2.5 μM 1443 (lane 2) and 100 nM *p1197/1196, or 0.7 μM 1193 (lane 3) or 2.5 μM 1443 (lane 4) and 100 nM *p1196/1197 in 100 mM sodium chloride, 20 mM magnesium chloride, 50 mM Mops, pH 7.0 were incubated for 16 h at 22 °C and then irradiated with 365 nm UV light at 2 °C for 10 min. The products of the reaction were analyzed by PAGE on a 20% gel. The mobilities of the labeled duplex strand (S), interstrand cross-linked products (XL), the monoadduct (M), xylene cyanol (XC) and bromophenol blue (P) are indicated at the side of the gel. The products were quantitated by phosphorimaging.

solutions containing the oligomer and [^{32}P]-labeled duplex with long wavelength (365 nm) UV light followed by analysis of the photoproducts by denaturing polyacrylamide gel electrophoresis. Under these conditions, photoproducts can arise only as a consequence of triplex formation between the oligomer and the duplex and only covalent adducts can give rise to mobility shifts on the gel.

Figure 2 is an autoradiogram of a gel from such an experiment. The experiment was carried out at 22 °C in the presence of 2.5 μM 1443 or 0.7 μM 1193 with a duplex whose upper, purine-rich strand or lower, pyrimidine-rich strand carried a 5′-terminal [^{32}P]phosphate. Both oligomers form triplexes as signaled by the presence of bands on the gel whose mobilities are less than those of single strands, *p1196 or *p1197. The bands of lowest mobility represent complexes formed by interstrand cross-links between the psoralen-conjugated oligomer and the duplex. The observation that essentially the same percentage of photoadduct is observed when either the upper or lower strand of the duplex is labeled is consistent with this interpretation. These interstrand cross-links most likely result from formation of photoadducts between the two thymidines at the 5′−T−A/5′−T−A duplex triplex junction and the furan and pyrone rings of the tethered psoralen (*24*). The bands of intermediate mobility result from monoadduct formation between the psoralen and the labeled strand of the duplex and represent less than 2% of the total photoadduct formation. The results of this experiment demonstrate that the alternating methylphosphonate-phosphodiester backbone is compatible with the formation of triple-stranded complexes.

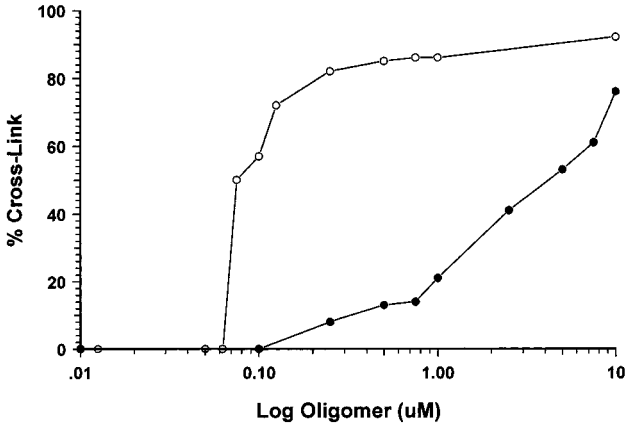


Figure 3. Effect of oligomer concentration on triplex formation. Solutions Mops containing 10 nM to 10 μM 1193 (○) or 1443 (●) and 2.5 nM *p1196/1197 in 100 mM sodium chloride, 20 mM magnesium chloride, 50 mM Mops, pH 7.0, were incubated at 37 °C for 3 h and then irradiated at 2 °C for 10 min and the products analyzed by gel electrophoresis. The percentage of interstrand cross-linked product was determined by phosphorimaging.

Effect of Oligomer Concentration on Triplex Formation. The dependence of triplex formation on oligomer concentration is shown in Figure 3. These experiments were carried out at pH 7.0 and 37 °C over a oligomer concentration range of 10 nM to 10 μM. Both oligomers undergo extensive triplex formation at 37 °C as monitored by photoadduct formation. However, an approximately seven times higher concentration of 1443 is required to achieve cross-linking comparable to that of 1193 under these conditions.

Photoadduct formation by 1193 is observed at nanomolar concentrations and the transition from no photoadduct formation to maximal photoadduct formation occurs over a relatively narrow concentration range. Thus, maximal photoadduct formation is observed by 0.25 μM oligomer and less than 1% photoadduct formation is seen below 0.07 μM 1193. Reduced photoadduct formation by 0.7 μM 1193 is observed at 37 °C (50%) as compared to that observed at 22 °C (88%, see Figure 2). This reduction most likely reflects the reduced stability of the triplex at the higher temperature.

The transition from no photoadduct formation to maximal photoadduct formation by 1443 is observed over a much broader concentration range, from 0.1 to 10 μM. Again, a lower percentage of photoadduct is observed at 37 °C (42%) than at 22 °C (81%) in the presence of 2.5 μM 1443.

The differences in the amounts of photoadduct formed by oligomers 1193 and 1443 most likely reflect differences in the stability of the triplexes formed by these two oligomers. Oligomer 1443 contains seven methylphosphonate linkages and thus consists of a mixture of 128 diastereoisomers. Molecular modeling experiments suggest that the Rp methylphosphonate linkage should not interfere with triplex formation (*25*). Preliminary results with a triplex forming oligomer that contains a single

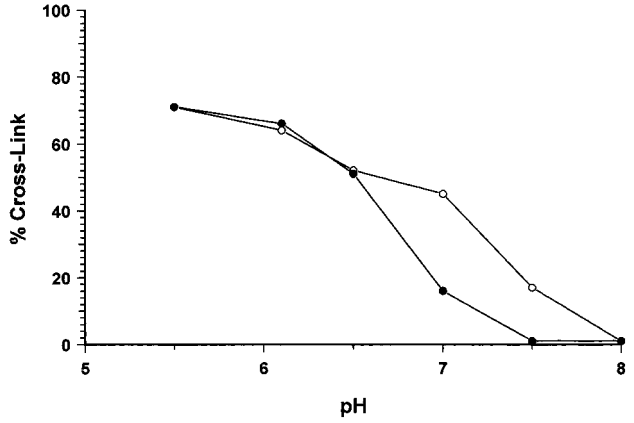


Figure 4. Effect of pH on triplex formation. Solutions containing 0.1 μM 1193 (○) or 2.5 μM 1443 (●) and 20 nM *p1196/1197 in 100 mM sodium chloride, 20 mM magnesium chloride and 50 mM Mops buffered at pH 5.5, 6.1, 6.5, 7.0, 7.5, or 8.0 were incubated at 37 °C for 3 h and then irradiated at 2 °C for 10 min and the products analyzed by gel electrophoresis. The percentage of interstrand cross-linked product was determined by phosphorimaging.

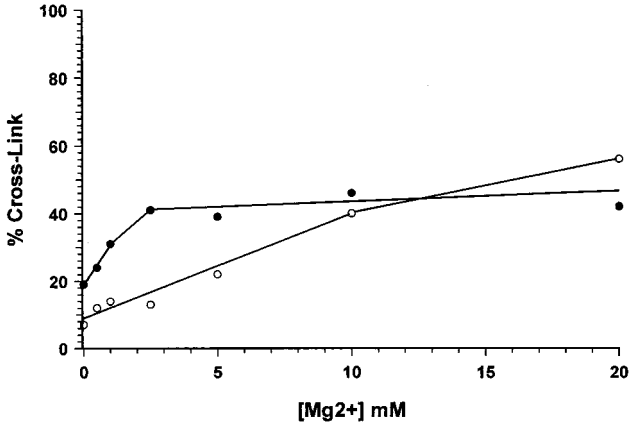


Figure 5. Effect of magnesium ion concentration on triplex formation. Solutions containing 0.1 μM 1193 (○) or 2.5 μM 1443 (●) and 20 nM *p1197/1196 in 100 mM sodium chloride, 50 mM Mops buffered at pH 7.0, and 0, 0,5, 1.0, 2.5, 5.0 10, or 20 mM magnesium chloride were incubated at 22 °C for 3 h and then irradiated at 2 °C for 10 min and the products analyzed by gel electrophoresis. The percentage of interstrand cross-linked product was determined by phosphorimaging.

methylphosphonate linkage suggest that the oligomer with an Rp methylphosphonate linkage forms a more stable triplex than does the oligomer with an Sp methylphosphonate linkage. Thus, the relatively higher concentrations of 1443 required for photoadduct formation may simply reflect the presence of diastereoisomers with high percentages of lower binding Sp methylphosphonate linkages.

Effect of pH on Triplex Formation. Formation of Hoogsteen bonded C^+·G−C triads requires protonation of 5-methylcytosine. Thus triplex formation and stability by oligomers that contain this base increases as pH decreases. The effects of pH on triplex formation by 1443 and 1193 were compared as shown in Figure 4. This experiment was carried out at 37 °C using oligomer concentrations which gave comparable levels of photoadduct formation at low pH. Both oligomers formed the same amount of photoadduct over the pH range 5.5−6.5. Above pH 6.5, photoadduct formation dropped off more rapidly for the triplex formed by 1443 and essentially no photoadduct formation was observed at pH 7.5 or higher under these conditions. In contrast, 1193 continued to form photoadducts at pH 7.5 with no photoadduct formation at pH 8.0.

Protonation of the three 5-methylcytosines of 1443 or 1193 introduces multiple positive charges into the oligomer. The resulting charge repulsion between the protonated 5-methylcytosines is probably compensated to some extent by the negatively charged phosphodiester groups in the oligomer backbone. The results of the experiment in Figure 4 suggest that the apparent p*K* of the 5-methylcytosines in oligomer 1443 is approximately a half pH unit less than the apparent p*K* of the 5-methylcytosines in oligomer 1193. This decrease in apparent p*K* is most likely the consequence of the decreased net negative charge of the alternating methylphosphonate backbone of 1443 versus that of the all phosphodiester backbone of 1193. This decreased net charge would therefore make it more difficult to protonate the 5-methylcytosines of 1443, resulting in reduced triplex stability as the pH of the medium is increased. Consistent with this explanation is the observation that apparent p*K* of cytosine bases in the all methylphosphonate oligomer d$(CT)_8$ is approximately 1.2 pH units less than that of the corresponding all phosphodiester oligomer when these oligomers form 2:1 d$(CT)_8$:d$(AG)_8$ triplexes (*13*).

Effect of Magnesium Concentration on Triplex Formation. Triplex stability is sensitive to ionic strength and is stabilized by divalent metal ions such as magnesium. The effect of magnesium ion concentration on photoadduct formation by 1443 and 1193 was examined as shown in Figure 5. These experiments were carried out at concentrations of 1443 and 1193 that gave comparable amounts of photoadduct in the presence of 20 mM magnesium ion. As shown in Figure 5, 1443 formed an appreciable amount of photoadduct even in the absence of magnesium. Maximal photoadduct formation was observed once the magnesium concentration reached 2.5 mM. In contrast to this behavior, very little photoadduct formation was observed for 1193 in the absence of magnesium and maximal photoadduct formation was not observed until the magnesium concentration reached 10 mM.

The differences in the dependence of triplex formation on magnesium concentration between the two oligomers can most reasonably be explained by the reduced number of phosphodiester linkages in the backbone of 1443. Because the sugar phosphate backbones of the triplex forming oligomer and the purine strand of the target are in close proximity, triplex formation would be expected to entail considerable charge repulsion between these two strands. This charge repulsion can be reduced by the presence of divalent metal ions or polycations such as spermine. Oligomer 1443 contains 7 negatively charged phosphodiester groups as opposed to the 14 negative charges in the backbone of oligomer 1193. Thus, charge repulsion between the backbone of 1443 and the purine strand of 1196/1197 would be expected to be considerably less than that in the triplex formed by 1193 and consequently the dependence of triplex stability on magnesium concentration is reduced.

CONCLUSION

The results of the experiments described above show that an oligopyrimidine with an alternating methylphosphonate-phosphodiester backbone can form stable triplexes with a duplex DNA target under physiological conditions of ionic strength and temperature. Triplex forming oligomers with this type of backbone may have distinct advantages over triplex forming oligodeoxyribonucleotides. Because the backbone of the d-AOMP is

resistant to nuclease hydrolysis, this type of oligomer may be particularly useful in cell culture experiments. The reduced dependence of triplex formation by this type of oligomer on divalent metal ion concentration may also promote triplex formation in the intracellular environment.

A potential drawback of pyrimidine containing TFOs is their pH dependence of triplex formation. This problem becomes more serious as the number of 5-methylcytosines in the oligomer increases and is particularly serious for oligomers that contain multiple contiguous 5-methylcytosines. The problem appears to be more serious for the partially charged d-AOMPs than fully charged oligodeoxyribonucleotides. This problem can in theory be circumvented by use of base analogues which do not require protonation or by employing other triplex motifs such as the antiparallel purine motif to form triplexes. Experiments to test these possibilities are currently in progress.

ACKNOWLEDGMENT

The research described in this paper was supported by a grant from the National Institutes of Health, GM57140. A portion of this work was also supported by a grant from the National Cancer Institute, CA42762.

LITERATURE CITED

(1) Svinarchuk, F., and Malvy, C. (1998) Gene-Targeted Triple-Helix-Forming Oligonucleotides. In *Applied Antisense Oligonucleotide Technology* (C. A. Stein, and A. M. Krieg, Eds.) pp 471−486, Wiley-Liss, New York.

(2) Faruqi, A. F., and Glazer, P. M. (1998) Triplex-Forming Oligonucleotides for Genetic Manipulation: An Alternative View. In *Applied Antisense Oligonucleotide Technology* (C. A. Stein, and A. M. Krieg, Eds.) pp 487−507, Wiley-Liss, New York.

(3) Kim, S. G., Tsukahara, S., Yokoyama, S., and Takaku, H. (1992) The Influence of Oligodeoxyribonucleotide Phosphorothioate Pyrimidine Strands on Triplex Formation. *FEBS Lett. 314*, 29−32.

(4) Hacia, J. G., Wold, B. J., and Dervan, P. B. (1994) Phosphorothioate Oligonucleotide-Directed Triple Helix Formation. *Biochemistry 33*, 5367−5369.

(5) Lacoste, J., Francois, J.-C., and Helene, C. (1997) Triple Helix Formation with Purine-Rich Phosphorothioate-Containing Oligonucleotides Covalently Linked to an Acridine Derivative. *Nucleic Acids Res. 25*, 1991−1998.

(6) Joseph, J., Kandala, J. C., Veerapane, D., Weber, K. T., and Guntaka, R. V. (1997) Antiparallel Polypurine Phosphorothioate Oligonucleotides form Stable Triplexes with the Rat α-1 Collagen Gene Promoter and Inhibit Transcription in Cultured Rat Fibroblasts. *Nucleic Acids Res. 25*, 2182−2188.

(7) Liquier, J., Letellier, R., Dagneaux, C., Ouali, M., Morvan, F., Raynier, B., Imbach, J. L., and Taillandier, E. (1993) Triple Helix Formation by alpha-Oligodeoxynucleotides: A Vibrational Spectroscopy and Molecular Modeling Study. *Biochemistry 32*, 10591−10598.

(8) Noonberg, S. B., Francois, J. C., Praseuth, D., Guieyssepeugeot, A. L., Lacoste, J., Garestier, T., and Helene, C. (1995) Triplex Formation with α Anomers of Purine-Rich and Pyrimidine-Rich Oligodeoxynucleotides. *Nucleic Acids Res. 23*, 4042−4049.

(9) Bates, P. J., Laughton, C. A., Jenkins, T. C., Capaldi, D. C., Roselt, P. D., Reese, C. D., and Neidle. S. (1996) Efficient Triple Helix Formation by Oligodeoxyribonucleotides Containing α- or *β*-2-Amino-5-(2-Deoxy-D-Ribofuranosyl)pyridine Residues. *Nucleic Acids Res. 24*, 4176−4184.

(10) Egholm, M., Buchardt, O., Nielsen, P. E., and Berg, R. H. (1992) Peptide Nucleic Acids (PNA)−Oligonucleotide Analogues with an Achiral Peptide Backbone. *J. Am. Chem. Soc. 114*, 1895−1897.

(11) Nielsen, P. E., Egholm, M., and Buchardt, O. (1994) Peptide Nucleic Acid (PNA)—A DNA Mimic with a Peptide Backbone. *Bioconjugate Chem. 5*, 3−7.

(12) Jones, R. J., Swaminathan, S., Milligan, J. F., Wadwani, S., Froehler, B. C., and Matteucci, M. K. (1993) Oligonucleotides Containing a Covalent Conformationally Restricted Phosphodiester Analogue for High-Affinity Triple Helix Formation: The Riboacetal Internucleotide Linkage. *J Am. Chem. Soc. 115*, 9816−9817.

(13) Callahan, D. E., Trapane, T. L., Miller, P. S., Ts'o, P. O. P., and Kan, L.-S. (1991) Comparative Circular Dichroism and Fluorescence Studies of Oligodeoxyribonucleotide and Oligodeoxyribonucleoside Methylphosphonate Pyrimidine Strands in Duplex and Triplex Formation. *Biochemistry 30*, 1650−1655.

(14) Fathi, R., Huang, Q., Syi, J.-L., Delany, W., and Cook, A. F. (1994) (Aminomethyl)phosphonate Derivatives of Oligonucleotides. *Bioconjugate Chem. 5*, 47−67.

(15) Fathi, R., Huang, Q., Coppola, G., Delaney, W., Teasdale, R., Krieg, A. M., and Cook, A. F. (1994) Oligonucleotides with Novel, Cationic Backbone Substituents: Aminoethylphosphonates *Nucleic Acids Res. 22*, 5416−5424.

(16) Hogrefe, R. I., Vaghefi, M. M., Reynolds, M. A., Young, K. M., and Arnold, L. J. (1993) Deprotection of Methylphosphonate Oligonucleotides using a Novel One-pot Procedure. *Nucleic Acids Res. 21*, 2031−2038.

(17) Miller, P. S., and Cushman, C. D. (1993) Triplex Formation by Oligodeoxyribonucleotides Involving the Formation of X• UA Triads. *Biochemistry 32*, 2999−3004.

(18) Kean, J. M., and Miller, P. S. (1994) Effect of Target Structure on Cross-Linking by Psoralen-Derivatized Oligonucleoside Methylphosphonates. *Biochemistry 33*, 9178−9186.

(19) Miller, P. S., Dreon, N., Pulford, S. M., and McParland, K. B. (1980) Oligothymidylate Analogues having Stereoregular, Alternating Methylphosphonate/Phosphodiester Backbones. Synthesis and Physical Studies *J. Biol. Chem. 255*, 9659−9665.

(20) Shaw, J.-P., Kent, K., Bird, J., Fishback, J., and Froehler, B. (1991) Modified Deoxyoligonucleotides Stable to Exonuclease Degradation in Serum. *Nucleic Acids Res. 19*, 747−750.

(21) Radhakrishnan, I., and Patel, D. J. (1994) DNA Triplexes: Solution Structures, Hydration Sites, Energetics, Interactions, and Function. *Biochemistry 33*, 11405−11416.

(22) Takasugi, M., Guendouz, A., Chassignol, M., Decout, J. L., Lhomme, J., Thuong, N. T., and Helene, C. (1991) Sequence-Specific Photoinduced Cross-Linking of the Two Strands of Double-Helical DNA by a Psoralen Covalently Linked to a Triple Helix-Forming Oligonucleotide. *Proc. Natl. Acad. Sci. U.S.A. 88*, 5602−5606.

(23) Gasparro, F. P., Havre, P. A., Olack, G. A., Gunther, E. J., and Glazer, P. M. (1994) Site-Specific Targeting of Psoralen Photoadducts with a Triplex-Forming Oligonucleotide: Characterization of Psoralen Monoadduct and Cross-link Formation. *Nucleic Acids Res. 22*, 2845−2852.

(24) Bates, P. J., Mcaulay, V. M., McLean, J. J., Jenkins, T. C., Reszka, A. P., Laughton, C. A., and Neidle, S. (1995) Characteristics of Triplex-Directed Photoadduct Formation by Psoralen-Linked Oligodeoxynucleotides. *Nucleic Acids Res. 23*, 4283−4289.

(25) Hausheer, F. H., Singh, U. C., Saxe, J. D., Colvin, O. M., and Ts'o, P. O. P. (1990) Can Oligonucleoside Methylphosphonates Form a Stable Triplet with a Double Stranded DNA Helix? *Cancer Drug Des. 5*, 159−167.

BC980140M

Synthesis and Application of Novel Bifunctional Spin Labels

Ralf M. Lösel,[†,‡] Reinhard Philipp,[†] Tamás Kálai,[§] Kálmán Hideg,[§] and Wolfgang E. Trommer*[,†]

Fachbereich Chemie, Universität Kaiserslautern, P.O. Box 3049, D-67653 Kaiserslautern, Germany, and Institute of Organic and Medicinal Chemistry, University of Pécs, H-7643 Pécs, P.O. Box 99, Hungary. Received November 18, 1998; Revised Manuscript Received February 22, 1999

The synthesis of new bifunctional spin-labeled cross-linking reagents is described. Covalent attachment to papain was achieved via a thiol-specific thiosulfonate residue and, for the second anchor point, via a nonspecific photoreactive azido function. The thiosulfonate formed a reversible disulfide linkage, which could be cleaved again reductively by dithiothreitol. The spin label, a pyrroline-1-oxyl radical, was highly immobilized after attachment to papain by both functional groups and showed little if any relative motion with respect to the protein.

INTRODUCTION

Spin labeling has widely been used for studies of structure−function relationships in proteins. ESR investigations using spin labels may yield information about local polarities, segmental mobilities, and the conformational changes correlated with these parameters (*1, 2*). Moreover, precise intramolecular distances have been obtained in special cases (*3*−*5*). Interpretation of the data may, however, be hampered due to relative mobility of the spin label with respect to the macromolecule to which it is attached. In case of distance measurements, the error increases from several tenths of an angstrom by more than an order of magnitude (*6, 7*). This problem pertains even more to motional studies of the protein. Relative motion of the spin label with respect the macromolecule can be minimized by the use of bifunctional probes which allow for cross-links within, e.g., the protein. Such compounds have first been described by Wenzel et al. (*8*), but they contain a rather long spacer between the nitroxide and the reactive groups which are also of low specificity with respect to protein side chains.

Intramolecular cross-linking of proteins with chemical reagents has become a well-established technique to give information on the proximity of amino acid residues. The reagents used for such purposes contain, separated by a spacer of defined length, two functional groups that may exhibit either equal (homobifunctional) or different (heterobifunctional) selectivity toward amino acid residues. Photoreactive groups are often favored as they remain silent, i.e., unreactive unless irradiated. Among the amino acids containing reactive side chains, amino and thiol (sulfhydryl) groups are most suitable for chemical derivatization as reactions usually take place under mild conditions. Whereas amino groups of lysines are quite abundant in most proteins, thiol-containing cysteines are usually present in small numbers, only. For this reason, the selective chemical modification of cysteines usually allows for rather precise determination of the site of attachment. There are, however, few reagents that are truly specific for thiols, as the commonly applied haloacetamides or maleimides may also react with other functional groups, particularly with amino groups of lysines. Among the specific sulfhydryl reagents are those forming disulfide bonds with the protein. This may be accomplished by disulfide exchange or by a substitution reaction with thiosulfonates (*9*). Cross-linking reagents with sulfhydryl-specific functionalities and additional photoreactive groups have been described (*10*−*13*).

A thiol-specific, reversible methanethiosulfonate spin label has been described earlier (*14*−*16*). On the basis of this compound (**1**), we have synthesized several derivatives containing a photoreactive moiety and applied them to the test system papain. The latter is a thiol protease consisting of 212 amino acids with a molecular weight of 23 406 (*17*). Its essential thiol located at Cys 25 is very reactive and easily modified. In the following, we demonstrate the application of the new compounds for spin labeling of papain under stepwise intramolecular cross-linking as shown in Figure 1.

EXPERIMENTAL PROCEDURES

Papain, twice crystallized (Sigma Lot no. 100H8075), was reductively activated at a concentration of 40 mg/mL by incubation with 50 mM dithiothreitol (DTT) in 0.1 M acetate, pH 4.5, for 1 h. There was no difference in final enzyme activity compared to longer incubation periods (up to 12 h). Activation did not cause significant autolytic degradation of papain as judged from SDS−PAGE (*18*). Activity measurements were done by photometric determination of liberated 4-nitroaniline from the substrate N_α-benzoyl-L-arginine-*p*-nitroanilide [L-BAPA (*19*), commercially available from Merck]. Briefly, the assay mixture contained 0.1 M Tris, 0.2 M KCl, 1 mM EDTA, pH 7.0, supplemented with 1 mM L-BAPA. Nitroaniline formation was followed at 410 nm ($\epsilon = 8800$ M^{-1} cm^{-1}) for 2 min using a Beckman DU 640 UV spectrometer operating in the kinetics mode. Protein concentration was estimated by the Bradford procedure (*20*) using defatted bovine serum albumin as a standard rather than by A_{280} determination, as the aromatic moiety of incorporated spin-labels interfered at this wavelength.

Photolysis was carried out by irradiating samples with 366 nm UV-light using a CAMAG source (254 or 366 nm, 4 W) or a Rayonet photoreactor (350 nm, 750 W).

* To whom correspondence should be addressed.
[†] Universität Kaiserslautern.
[‡] Present address: Labor Diagnostika Nord, PO Box 2180, D-48529 Nordhorn, Germany.
[§] University of Pécs.

10.1021/bc980138v CCC: $18.00 © 1999 American Chemical Society
Published on Web 06/11/1999

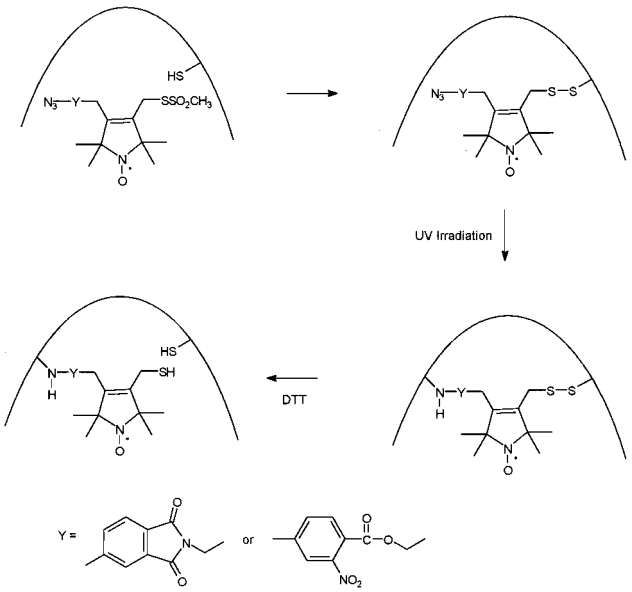


Figure 1. Principle of the method. After selective reaction of the reagent with the thiol group of the protein under disulfide formation, irradiation effects covalent binding via decomposition of the azide group (at the other terminus). Finally, the disulfide may be cleaved reductively. At each step, ESR spectra may be recorded.

ESR spectra were recorded at 25 °C on a BRUKER ESP 300E ESR spectrometer operating in the X-band mode and employing a 100 kHz modulation of 1 G amplitude.

To modify the enzyme, reductively activated aliquots (100 μL) were passed through centrifuge columns filled with Sephadex G25 (*21*) and equilibrated with the buffer used for activity measurements (0.1 M Tris, 0.2 M KCl, and 1 mM EDTA, pH 7.0). Some protein precipitated due to the different pH, but readily dissolved upon addition of an equal volume of buffer. To 100 μL of enzyme solution, 5 μL of the reagent stock solution (50 mM in dimethyl formamide) was added and thoroughly mixed. Reagents **2**, **3**, and **4** were not completely soluble under these conditions and formed turbid solutions. Samples were incubated for 1 h under exclusion of light and then separated from unbound reagent by column centrifugation over Sephadex G25 (*21*). Except for the thiosulfonate reagent **1**, this procedure was insufficient to completely remove unspecifically bound spin-label, as indicated by an intense ESR signal of freely mobile label. Therefore, microdialysis against the same buffer (16 h at room temperature) was used in addition.

Molecular modeling was performed using the QUANTA program running on a Silicon Graphics INDY. The structure data file used was 1pop found in the Protein Data Bank. Minimization was done in the CHARMm force field.

Synthesis of 1-Oxyl-3-[(*N*-phthalimido)ethyl]-4-methanethiosulfonylmethyl-2,5-dihydro-2,2,5,5-tetramethyl-1*H*-pyrrole (3). 1-Oxyl-3-[(*N*-phthalimido)-ethyl]-4-bromomethyl-2,5-dihydro-2,2,5,5-tetramethyl-1*H*-pyrrole (102 mg, 0.25 mmol), prepared analogously as described by Kálai et al. (*22*) for the 4-azido-*N*-phthalimido derivative, and $NaSSO_2CH_3$ (67 mg, 0.5 mmol) were dissolved in a mixture of dioxane (10 mL) and water (3 mL) and were refluxed for 30 min. Then the mixture was concentrated in vacuo, and the residue was dissolved in chloroform (20 mL), washed with brine (10 mL), dried over $MgSO_4$, filtered, evaporated and, purified by preparative TLC on a silica gel plate (hexane−ethyl acetate, 2:1). Yield 61 mg (56%); R_f 0.40 ($CHCl_3$-Et_2O 1:1); mp 128−129 °C. Anal. calcd for $C_{20}H_{25}N_2O_5S_2$ (437.54): C, 54.90; H, 5.76; N, 6.40; S, 14.65. Found: C, 54.73; H, 5.77; N, 6.27; S, 14.32 (Heraeus Micro U/E, sulfur titrimetrically by Schöniger's method). IR: 1700 cm^{-1} (C═O), 1610 cm^{-1} (C═C). MS *m/z* (rel int.%): 437 (M^+, 68), 407(36), 310(66), 160(100), carried out on a VG Trio 2 instrument, EI mode 70 eV, direct inlet.

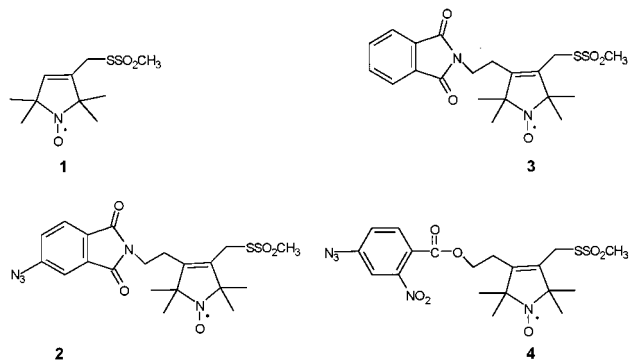


Figure 2. Chemical structures of reagents used in the modification experiments. (1) 1-Oxyl-4-methanethiosulfonylmethyl-2,5-dihydro-2,2,5,5-tetramethyl-1*H*-pyrrole, (2) 1-oxyl-3-(4-azido-*N*-phthalimido)ethyl-4-methanethiosulfonylmethyl-2,5-dihydro-2,2,5,5-tetramethyl-1*H*-pyrrole, (3) 1-oxyl-3-phthalimidoethyl-4-methanethiosulfonylmethyl-2,5-dihydro-2,2,5,5-tetra-methyl-1*H*-pyrrole, (4) 1-oxyl-3-(4-azido-2-nitrobenzoyloxy)ethyl-4-methanethiosulfonylmethyl-2,5-dihydro-2,2,5,5-tetra-methyl-1*H*-pyrrole.

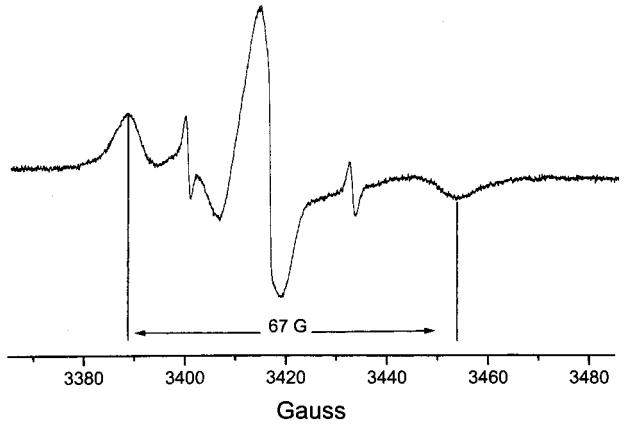


Figure 3. ESR spectrum obtained from papain modified with **2** as described in the Experimental Procedures. The protein concentration was 90 μM.

Synthesis of 1-Oxyl-3-[(4-azido-2-nitrobenzoyloxy)-ethyl]-4-methanethiosulfonylmethyl-2,5-dihydro-2,2,5,5-tetramethyl-1*H*-pyrrole (4). To a stirred solution of 1-oxyl-3-hydroxyethyl-4-methanethiosulfonylmethyl-2,5-dihydro-2,2,5,5-tetramethyl-1*H*-pyrrole (200 mg, 0.65 mmol) and pyridine (63 mg, 0.8 mmol) in dry CH_2Cl_2 (5 mL) was added 4-azido-2-nitrobenzoyl chloride [181 mg, 0.8 mmol, prepared according to Friebel et al. (*11*)], and the mixture was stirred for 3 h in the dark at room temperature. The mixture was washed with brine (5 mL), dried ($MgSO_4$), evaporated, and purified by preparative TLC (Merck Silica Gel GF_{254}, 20 × 20 × 0.2 cm), R_f 0.45 ($CHCl_3$/Et_2O 1:1), to give 1-oxyl-3-[(4-azido-2-nitrobenzoyloxy)ethyl]-4-methanethiosulfonylmethyl-2,5-dihydro-2,2,5,5-tetramethyl-1*H*-pyrrole (**4**), yield 48 mg (15%), as a thick oil, which solidified upon cooling. The reaction is accompanied by formation of the corresponding biradical, R_f 0.6 ($CHCl_3$/Et_2O 1:1). Anal. calcd for $C_{19}H_{24}N_5O_7S_2$ (498.55): C, 45.77; H, 4.85; N, 14.05; S, 12.86. Found:

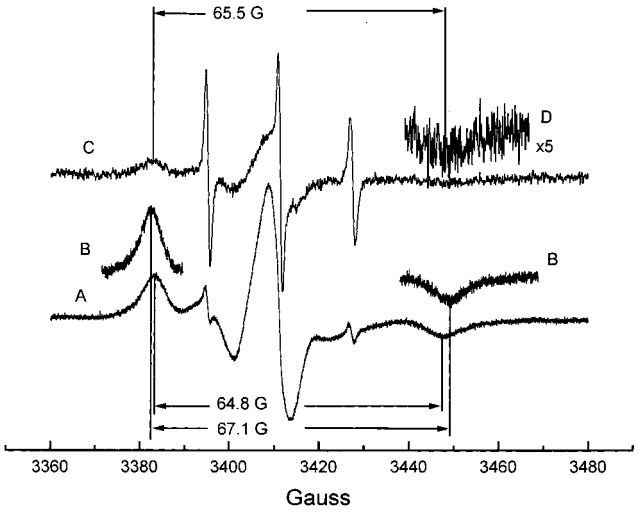


Figure 4. (A) Papain modified with reagent **4** in the dark, protein concentration 61 μM (17 scans, relative gain 1×10^6, resolution of *x*-axis 8192 points). (B) Rerecorded high and low-field region of the sample from trace A after 10 min irradiation at 350 nm (17 scans, relative gain 2×10^6, resolution of *x*-axis 8192 points). (C) Sample from trace B after addition of DTT and NEM and microdialysis, protein concentration 24 μM (17 scans, relative gain 2×10^6, resolution of *x*-axis 2048 points).

C, 45.58; H, 5.00; N, 14.12; S, 12.50. MS: *m*/*z* (rel int.%) 498 (M^+, 6), 468 (7), 442 (8), 196 (21), 165 (29), 134 (40), 65 (100). Compounds **1** and **2** were synthesized according to published procedures (*14*, *22*).

RESULTS

Papain was labeled at cysteine-25 with methanethiosulfonate spin label **1** under loss of activity and exhibited an ESR spectrum very similar to the one obtained by Berliner et al. (*14*) with the same reagent (data not shown). Likewise, the new spin-labeled reagents **2**, **3**, and **4** (structures shown in Figure 2) efficiently modified the active-site cysteine under complete inactivation of the enzyme.

The spectrum of the phthalimide **2** (Figure 3), when bound to the protein but before irradiation, however, was strikingly different from that of the simple thiosulfonate **1**. Whereas with **1**, a $2A_{zz}$ value of 52 G typical of weakly immobilized nitroxide radicals was observed, **2** exhibited a value of 67 G. Such large values are seen in highly immobilized radicals and are close to the rigid powder limit in a hydrophobic environment. Irradiation in a photoreactor at 350 nm for 10 min did not alter the spectrum, although **2** can be photolyzed readily in solution upon irradiation at 366 nm with a simple hand-held UV lamp (CAMAG) as demonstrated by concomitant changes in the UV spectrum (complete loss of absorbance at 261 and 344 nm within 15 min; isosbestic points at 231 and 375 nm). The almost identical, but not photoreactive label **3** after reaction with papain gave a spectrum that is indistinguishable from the one obtained with **2** (data not shown).

ESR spectra obtained with the azidonitrophenyl compound **4,** on the other hand, showed a significantly lower immobilization of the label ($2A_{zz} = 64.8 \pm 0.1$ G, Figure 4a) as compared to phthalimides **2** and **3**. After irradiation in a Rayonet photoreactor for 10 min, the maximum separation observed had increased to 67.1 ± 0.1 G (Figure 4b), thus, clearly indicating that an additional immobilization had occurred due to a second covalent linkage to the protein via the nitrene generated by photolysis. Upon addition of 3 mM DTT, the signal from freely tumbling radical increased, reaching equilibrium after about 30 min when *N*-ethyl maleimide in a final concentration of 20 mM was added to stop the disulfide

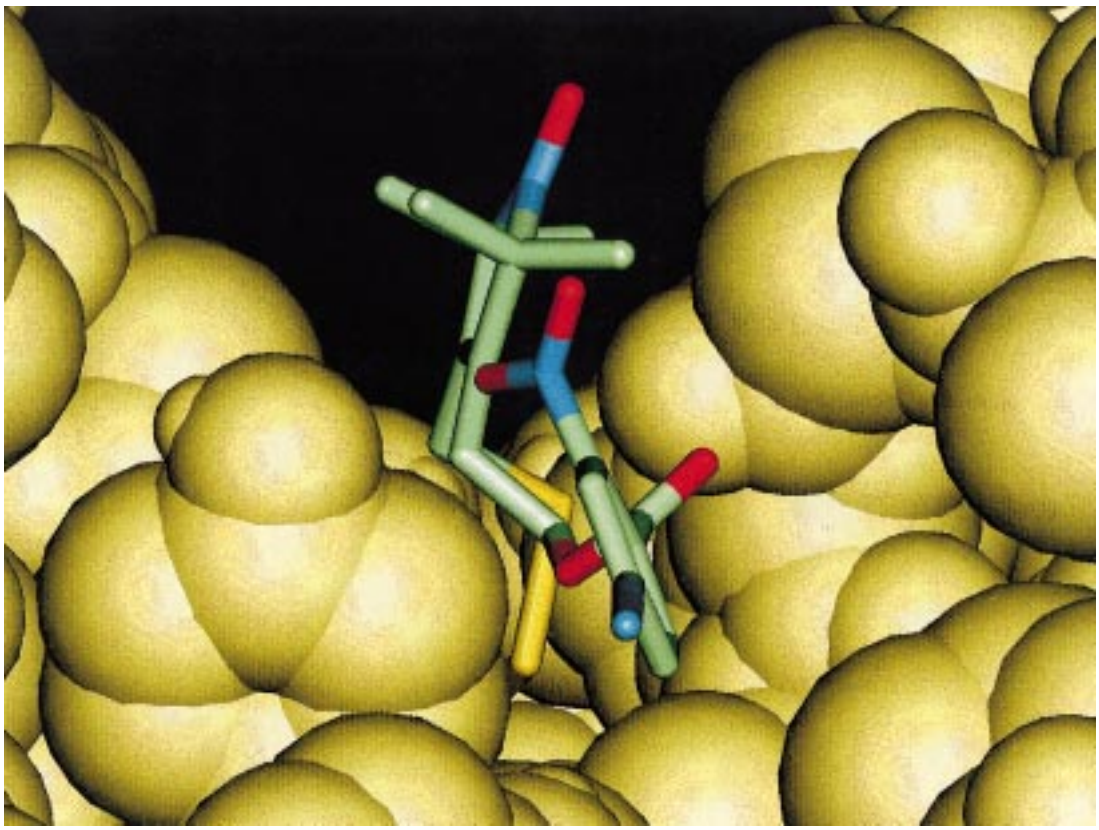


Figure 5. Molecular model of reagent **4** (liquorice model, colored by elements) bound in the substrate-binding cleft of papain (space-filling model, yellowish) as obtained from the CHARMm calculations.

reduction by DDT. At this point, the solution of modified protein was divided into two parts. One part was kept at room temperature without further treatment, while the other was dialyzed for 4 h against dialysis buffer as described in the Experimental Procedures. After this time, $2A_{zz}$ was 65.5 ± 0.2 G in the dialyzed sample (Figure 4c), whereas the spectrum of the reference sample had remained unchanged. The residual bound signal in several experiments accounted for at least 50% cross-linking. For comparison, in a control sample modified with thiosulfonate **1**, the reaction was complete in only 5 min, leaving no residual signal of immobilized radical.

Molecular modeling using the protein structure and the azidophenyl compound **4** with subsequent energy minimization in a force field by the program CHARMm gave an excellent fit for location of the aromatic group of **4** in the S_2 subsite of the protease (*23*) with the nitroxide moiety pointing outward, while the pyrroline ring to which the latter is attached is bound in the substrate-binding cleft (Figure 5).

DISCUSSION

The heterobifunctional spin label **4** was shown to react in a stepwise manner with papain under formation of a cross-link between the essential cysteine residue 25 and an amino acid located in the S_2 subsite. Modification of the thiol group of Cys-25 was accompanied by the loss of enzymic activity. That cross-linking (at least 50%) had indeed occurred upon irradiation was seen clearly by the increase in the $2A_{zz}$ value of the ESR spectrum of **4**. Subsequent reduction with DTT of the disulfide linkage lead again to a smaller $2A_{zz}$ value, indicating higher relative mobility. Upon double attachment, the label shows little if any relative motion with respect to papain ($2A_{zz} = 67.1$ G). According to Stoke's eq 1 and a radius of papain of about 25 Å the rotational correlation time τ_r at 25 °C is 1.41×10^{-8} s (eq 1). On the basis of the $2A'_{zz}$ value of **4** of 74 G in frozen solution at −25 °C (data not shown) a τ_r of 1.36×10^{-8} s can be calculated according to eq 2 for Brownian diffusion (*24*). Hence, **4** is well suited for motional studies of the protein by ESR and potentially, ST-ESR spectroscopy. The degree of cross-linking, however, is likely to vary from protein to protein.

$$\tau_r = 4\pi\eta r^3/3kT \quad (1)$$

$$\tau_r = 5.4 \times 10^{-10}\,(1 - A'_{zz}/A_{zz})^{-1.36} \quad (2)$$

Both reagents **2** and **3** exhibited highly immobilized ESR spectra after reaction with Cys-25 independent of subsequent irradiation. Apparently, the hydrophobic interaction of the aromatic moieties of these reagents with the S_2 subsite sufficiently immobilizes these compounds even without a second covalent linkage. Although the azido function in **2** can be converted to a reactive nitrene by irradiation as shown by UV spectroscopy, it did not form a stable bond with any of the amino acids in its vicinity as shown by almost complete release of the label upon reduction of the disulfide linkage by DTT. However, **2** should prove as useful for a stepwise and double attachment to appropriate proteins as was shown for reagent **4** in this study. Due to the strong hydrophobic interaction of the aromatic moieties in **2** and **3** with papain, motional studies, e.g. by means of ST-ESR, can be caried out even without the second attachment.

ACKNOWLEDGMENT

The authors express their gratitude to Anke Constantz and Elke Litmianski for excellent technical assistance. This work was supported by grants from the Hungarian National Research foundation (T017842) to K.H. and Fonds der Chemischen Industrie to W.E.T.

LITERATURE CITED

(1) Farrens, D. L., Altenbach, C., Yang, K., Hubbell, W. L., and Khorana, H. G. (1996) Requirement of rigid-body motion of transmembrane helices for light activation of rhodopsin. *Science 274*, 768−770.

(2) Morrisett, J. D. (1976) The use of spin labels for studying the structure and function of enzymes. In *Spin Labeling, Theory and Applications* (L. J. Berliner, Ed.) pp 273−338, Academic Press, New York.

(3) Beth, A. H., Robinson, B. H., Cobb, C. E., Dalton, L. R., Trommer, W. E., Birktoft, J. J., and Park, J. H. (1984) Interactions and spatial arrangement of spin-labeled NAD^+ bound to glyceraldehyde-3-phosphate dehydrogenase. *J. Biol. Chem. 259*, 9717−9728.

(4) Voss, J., Salwinski, L., Kaback, H. R., and Hubbell, W. L. (1995) A method for distance determination in proteins using a designed metal ion binding site and site-directed spin labeling: Evaluation with T4 lysozyme. *Proc. Natl. Acad. Sci. U.S.A. 92*, 12295−12299.

(5) Wilder, R. T., Venkataramu, S. D., Dalton, L. R., Birktoft, J. J., Trommer, W. E., and Park, J. H. (1989) Catalytic mechanism and interactions of NAD^+ with glyceraldehyde-3-phosphate dehydrogenase: Correlation of EPR data and enzymatic studies. *Biochim. Biophys. Acta 997*, 65−77.

(6) Hartmann, D., Philipp, R., Schmadel, K., Birktoft, J. J., Banaszak, L. J., and Trommer, W. E. (1991) Spatial arrangement of coenzyme and substrates bound to L-3-hydroxyacyl-CoA-dehydrogenase as studied by spin-labeled analogues of NAD and CoA. *Biochemistry 30*, 2782−2790.

(7) Vogel, P. D., Nett, J. H., Sauer, H. E., Schmadel, K., Cross, R. L., and Trommer, W. E. (1992) Nucleotide binding sites on mitochondrial F_1-ATPase. *J. Biol. Chem. 267*, 11982−11986.

(8) Wenzel, H. R., Becker, G., and von Goldammer, E. (1978) Synthese eines bifunktionellen Spin-labels zur Quervernetzung von Proteinen. *Chem. Ber. 111*, 2453−2454.

(9) Kenyon, G. L., and Bruice, T. W. (1977) Novel sulfhydryl reagents. *Methods Enzymol. 47*, 407−430.

(10) Chong, P. C., and Hodges, R. S. (1981) A new heterobifunctional cross-linking reagent for the study of biological interactions between proteins. I. Design, synthesis, and characterization. *J. Biol. Chem. 256*, 5064−5070.

(11) Friebel, K., Huth, H., Jany, K. D., and Trommer, W. E. (1981) Synthesis and application of a novel bifunctional reagent. *Hoppe-Seyler's Z. Physiol. Chem. 362*, 421−428.

(12) Trommer, W. E., Friebel, K, Kiltz, H.-H., and Kolkenbrock, H.-J. (1977) Synthesis and application of new bifunctional reagents. In *Protein Cross-Linking: Biochemical and Molecular Aspects* (M. Friedman, Ed.) pp 187−195, Plenum Press, New York.

(13) Huang, C.-K., and Richards, F. M. (1977) Reaction of a lipid-soluble, unsymmetrical, cleavable, cross-linking reagent with muscle aldolase and erythrocyte membrane proteins. *J. Biol. Chem. 252*, 5514−5521.

(14) Berliner, L. J., Grunwald, J., Hankovszky, O. H., and Hideg, K. (1982) A novel reversible thiol-specific spin label: papain active site labeling and inhibition. *Anal. Biochem. 119*, 450−455.

(15) Hideg, K., and Hankovszky, O. H. (1989) Chemistry of spin-labeled amino acids and peptides. Some new mono- and bifunctionalized nitroxide free radicals. In *Biological Magnetic Resonance, Vol. 8: Spin Labeling, Theory and Applications* (L. J. Berliner, and J. Reuben, Eds.) pp 427−488, Plenum Press, New York.

(16) Oh, J., Zhan, H., Cui, C., Hideg, K., Collier, R. J., and Hubbell, W. L. (1996) Organization of diphtheria toxin T domain in bilayers: a site-directed spin-labeling study. *Science 273*, 810−812.

(17) Mitchell, R. E., Chaiken, I. M., and Smith, E. L. (1970) The complete amino acid sequence of papain. *J. Biol. Chem. 245*, 3485−3492.

(18) Laemmli, U. K. (1970) Cleavage of structural proteins during the assembly of the head of bacteriophage T4. *Nature 227*, 680−685.

(19) Mole, J. E., and Horton, H. R. (1973) Kinetics of papain-catalyzed hydrolysis of α-*N*-Benzoyl-L-arginine-*p*-nitroanilide. *Biochemistry 12*, 816−822.

(20) Bradford, M. M. (1976) A rapid and sensitive method for the quantitation of microgram quantities of protein utilizing the principle of protein-dye binding. *Anal. Biochem. 72*, 248−254.

(21) Penefsky, H. S. (1977) Reversible binding of P_i by beef heart mitochondrial adenosine triphosphatase. *J. Biol. Chem. 252*, 2891−2899.

(22) Kálai, T., Rozsnyai, B., Jerkovich, Gy., and Hideg, K. (1994) Crosslinking 2,5-dihydro-1*H*-pyrrol-1-yloxyl spin-label reagents bifunctionalized with azidophthalimidyl and methylthiosulfonyloxy groups. *Synthesis 1994*, 1079−1082.

(23) Berger, A., and Schechter, I. (1970) Mapping the active site of papain with the aid of peptide substrates and inhibitors. *Philos. Trans. R. Soc. London, Ser. B 257*, 249−264.

(24) Freed, J. H. (1976) Theory of Slow Tumbling ESR Spectra for Nitroxides. In *Spin Labeling, Theory and Applications* (L. J. Berliner, Ed.) pp 53−132, Academic Press, New York.

BC980138V

Molecular Modeling of Hapten Structure and Relevance to Broad Specificity Immunoassay of Sulfonamide Antibiotics

C. A. Spinks,* G. M. Wyatt, H. A. Lee, and M. R. A. Morgan

Department of Biochemistry, Institute of Food Research, Norwich Research Park, Colney, Norwich, NR4 7UA, U.K. Received May 26, 1998; Revised Manuscript Received February 22, 1999

Molecular modeling of hapten structure was used to predict and influence, through appropriate synthetic work, the outcome of an immunization program. Examination of the structures of sulfonamide antibiotics led to the development of a hypothesis and the consequent synthesis of a sulfacetamide–protein immunogen aimed at the generation of broad specificity anti-sulfonamide antibodies. The antisera generated, alongside anti-sulfachlorpyradizine antisera generated at the same time, were characterized for cross-reactions against a range of sulfonamide drugs, and were found to exhibit good but not the desired broad specificity. Discussion is presented as to the reasons for the failure of the hypothesis. Further hypotheses are developed and speculation is made as to the future of molecular modeling in immunochemical research.

INTRODUCTION

Compounds of molecular masses less than about 1000–10000 Da are usually not intrinsically immunogenic. To generate antibodies to such compounds, it is required that they are covalently linked to a carrier of high molecular weight (almost always a protein) that is itself capable of stimulating the immune system. Of the many antibodies so produced, some are capable of recognizing the hapten molecule alone. On this basis, immunoassays have been established for many low molecular weight analytes, including mycotoxins (Wilkinson et al., 1992), pesticides (Van Emon et al., 1989) and vitamins (Finglas and Morgan, 1994). These reviews give an indication of the diversity and convenience of immunoassays for small molecules.

It has long been recognized that the manner of the linking of hapten to carrier protein for immunogen synthesis is critical in determining the nature of the antibody response; thus, antibody specificity is maximal for those sites distal to the point of conjugation (Landsteiner, 1945). With this knowledge, it has been possible to generate antibodies of very high specificities, capable of distinguishing very closely related structures. For example, high specificity has been particularly important in circumstances where close structural relationships do not reflect similar bioactivities. Wie and Hammock (1984) devised novel routes of synthesis in order to obtain maximum specificity for benzoylphenylurea insecticides.

However, it is sometimes also necessary to analyze a group of compounds of similar structure. This aim can often be achieved by judicious synthesis of the hapten–protein immunogen to expose maximally common features while minimizing the presentation of structural differences to the immune system. An example of this approach would be the immunoassay developed for quantification of the potato glycoalkaloids (Morgan et al., 1983). A further possibility is provided by monoclonal antibody technology, whereby low-frequency antibodies from the polyclonal population can be selected via the cloning and screening process. Accordingly, Ward et al. (1990) have described a surprisingly diverse population of anti-aflatoxin antibodies obtained through use of one immunogen.

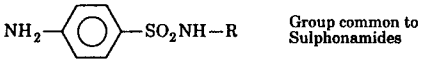
In past years, the development of high specificity antibodies has been a paramount consideration in the acceptance of immunoassay technology. However, the importance of broad specificity analysis is increasing, particularly in circumstances where a high proportion of samples will be negative, since economic and regulatory factors dictate that more resources are required for positive samples. Given their robustness, simplicity, high sample through-put, and low cost per sample, the immunoassays should be as well-suited to application in screening assays as they are in specific determinations. The limiting factor is the development of suitable antibodies.

The sulfonamide antibiotic drugs are analytes for which there is considerable demand for a broad specificity assay, detecting all members of the group and allowing the high proportion of negative samples to be rejected. The sulfonamides (used in pigs, cattle, and poultry, for example) seem to be particularly resistant to attempts to produce broad specificity antibodies. This is rather surprising since at first glance the general structure of the sulfonamides (Figure 1) with the comparatively large common aromatic ring moiety at one end of the molecule looks eminently suitable for broad specificity antibody generation. Indeed, Sheth and Sporns (1991) have described the production of antibodies using a sulfathiazole derivative linked through the variable R-group and exposing the common ring. The resultant antibodies were not as broadly specific as would be liked. Other groups of antibiotic drugs have proved easier to deal with (Kitagawa et al., 1983; Stanker et al., 1993; Brandon et al., 1994), but sulfonamide–protein immunogens have invariably generated antibodies of high specificity (Singh, et al., 1989; McCaughey, et al., 1990; Sheth and Sporns, 1990; Hoffmeister, et al., 1991; Martlbauer, et al., 1992; Garden and Sporns, 1994; Thomson and Sporns, 1995).

Molecular modeling of hapten structure has recently been used with some success in developing insight as to the reasons for the cross-reaction characteristics of

* To whom correspondence should be addressed.

10.1021/bc980054m CCC: $18.00 © 1999 American Chemical Society
Published on Web 05/11/1999



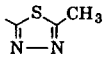
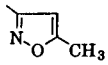
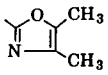
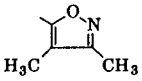
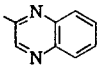
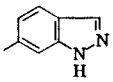
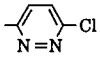
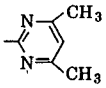
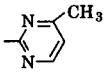
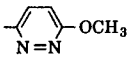
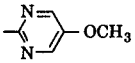
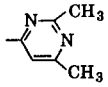
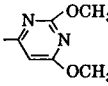
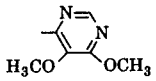
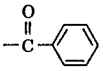
Drug	R-group	Abbreviation used in text
Sulfanilamide	– H	SAN
Sulfacetamide		SAM
Sulfaguanidine		SG
Sulfamethizole		SEZ
Sulfamethoxazole		SMX
Sulfamoxole		SOX
Sulfathiazole		STZ
Sulfisoxazole		SIX
Sulfaquinoxaline		SQ
Sulfanilamidoindazole		SAZ
Sulfachlorpyridazine		SCP
Sulfamethazine		SMZ
Sulfamerazine		SMR
Sulfamethoxypyridazine		SMP
Sulfameter		SME
Sulfapyridine		SP
Sulfisomidine		SID
Sulfadimethoxine		SDM
Sulfadoxine		SD
Sulfadiazine		SDZ
Sulfabenzamide		SBA

Figure 1. Sulfonamide drugs.

particular antibodies. There are clear advantages to looking at three-dimensional representations of structure, even without the further possibilities of investigating hydrophobic and electrostatic properties. Carlin et al. (1994) modeled the diuretic furosemide and related compounds and were able to explain the observed cross-reactions of a monoclonal anti-furosemide antibody. Elissalde et al. (1995) modeled the mycotoxin fumonisin and revealed unexpected folding within the structure with high significance for anyone interested in immunochemical studies on this compound.

Such studies and others have been carried out after the antibodies have been produced. In the present report, we describe the results of efforts to use molecular modeling in a predictive manner in order to enhance the possibility of developing a broad specificity anti-sulfonamide antibody.

MATERIALS AND METHODS

Chemicals. All starting materials for hapten synthesis and conjugation were obtained from Sigma Chemical Co. (Dorset, U.K.). All reagents were of the highest quality available.

Molecular Modeling. Modeling studies were carried out on a Silicon Graphics Workstation (Mountain View, CA) running QUANTA software (Molecular Simulations Inc., Burlington, MA). Twenty-two different sulfonamides were modeled. Minimum energy conformations of the compounds were calculated using the CHARMm force field. (CHARMm uses empirical energy functions to describe the forces on atoms in molecules, calculating conformational energies, local minima, barriers to rotation, energy surfaces, and time-dependent dynamic behavior).

Conformational searches were carried out by rotating all rotatable bonds through 360° in 30° increments and the lowest energy conformation computed. Electrostatic potentials were mapped across the surface of the structures by tumbling a positively charged particle over the surface of the molecule and calculating the energy for repulsion. Accordingly, high-energy regions correspond to a negative charge distribution within the molecule.

Synthesis of Drug–Protein Conjugates for Immunization. (i) Sulfacetamide Immunogen (SAM-BTG). Sulfacetamide (SAM) was reduced by sodium borohydride in a manner similar to the method described for triadimefon by Newsome (1986). SAM (400 mg) was dissolved in ethanol (20 mL) and mixed with sodium borohydride (700 mg in 12 mL ethanol). Frothing was observed, and the mixture was left overnight, after which concentrated HCl (4 mL) was added and the ethanol removed by rotary evaporation.

The SAM derivative (110 mg) was dissolved in pyridine (5 mL), to which succinic anhydride (500 mg) was added and left stirring gently for 3 days at room temperature. Pyridine was removed by rotary evaporation, and the residue dissolved in dichloromethane (6 mL). After washing with 1 M HCl (2 mL) followed by water (4 mL), the sample was again dried and the hemisuccinate product (52 mg) dissolved in dioxan (3 mL). The mixed anhydride method for conjugation to protein was then carried out (Erlanger et al., 1959) where isobutylchloroformate (4 μL)

and tributylamine (8 μL) was added to the SAM hemisuccinate solution and stirred for 30 min, ensuring that the temperature did not rise above 5 °C. In the meantime, bovine thyroglobulin (BTG; 45 mg) was dissolved in water (2 mL). Dioxan (2 mL) was added and mixed with half of the solution containing the activated SAM hemisuccinate, maintaining the pH at 9.0 with 1 M NaOH. After exhaustive dialysis against water, the conjugate was lyophilized.

(ii) Sulfachlorpyridazine (SCP) Immunogen (SCP−BTG). On the basis of the method described by Schlaeppi et al. (1989), SCP was derivatized by replacing the terminal chlorine atom with a hydroxyl group. SCP (0.5 g) was dissolved in 6 M HCl (10 mL) and stirred at room temperature for 4 h. The mixture was dried by rotary evaporation to give a brown syrup, half of which was dissolved in pyridine (4 mL). 2-Fluoro-1-methylpyridinium *p*-toluenesulfonate (FMP; 100 mg) was added and then stirred gently at room temperature for 1 h, after which BTG (86 mg) in carbonate buffer (pH 9.6; 10 mL) was added. After exhaustive dialysis against water, the conjugate was lyophilized.

Synthesis of Drug−Protein Conjugates for Coating Microtitration Plates. (i) SCP−BSA Conjugate. As with the immunogen, SCP was derivatized to produce a hydroxyl group. Succinic anhydride (500 mg) in pyridine (5 mL) was added to the derivative and gently stirred for 3 days at room temperature. The pyridine was removed by rotary evaporation, and half of the product was taken and added to 0.2 M phosphate buffer (pH 7.3; 1 mL) containing EDC (100 mg). After 30 min, BSA (75 mg) dissolved in 0.2 M phosphate buffer (pH 7.3; 2 mL) was added, and gently stirred for 1 h. After dialysis against water, the conjugate was lyophilized and stored at −20 °C.

(ii) SAM-BSA Conjugate. The SAM derivative (190 mg), used for the immunogen, was dissolved in pyridine (5 mL). Pyridine is necessary both as a solvent and scavenger. FMP (200 mg) was added to the solution and left for 30 min at room temperature. The solution turned dark red in color. Bovine serum albumin (BSA; 140 mg) was dissolved in 0.2 M carbonate buffer (pH 9.6; 5 mL), and this solution was added to the SAM derivative to cause fizzing and a change to a yellow/brown color. The whole mixture was stirred gently overnight, and then dialyzed exhaustively against water and lyophilized.

(iii) Diazo Conjugates. Several drug−protein conjugates were synthesized by the diazotization method and used as solid phases of the ELISA. This method links the drug to the protein via the para-amino benzene group of the common moiety. Essentially, the drug was dissolved in 1 M HCl (10 mL) with 0.1 M $NaNO_2$ added dropwise until a positive starch test was obtained. The solution was added to 0.1 M sodium borate buffer (10 mL) containing the protein carrier. The pH of the total mixture was maintained at pH 9.0 with 1 M NaOH and left gently stirring for 1 h at room temperature. The conjugation mixture was subsequently dialyzed against water and lyophilized. Amounts of drug and protein, respectively, used in diazo conjugate synthesis were for sulfachlorpyridazine, 23 mg and 100 mg of BSA; sulfaquinoxaline, 44 mg and 100 mg of keyhole limpet haemocyanin (KLH); sulfamethazine, 25 mg and 75 mg of KLH; sulfanilamide, 18 mg and 80 mg of BSA; 4-aminodibenzene-sulfonamide, 25 mg and 50 mg of KLH; 4-aminophenyl-4-methyl benzenesulfonamide, 25 mg and 50 mg of KLH.

(iv) Sulfabenzamide (SBA) Conjugate. Sulfabenzamide (SBA, 0.38 g) was dissolved in ethanol (15 mL) and mixed with sodium borohydride (0.2 g) in ethanol (15 mL). The mixture effervesced and a white precipitate formed. The ethanol was removed by rotary evaporation and the solid refluxed for 5 h with succinic anhydride (570 mg) in pyridine (10 mL). FMP (225 mg) was added, and the mixture left at room temperature for 30 min. KLH (75 mg) in carbonate buffer (pH 9.6, 15 mL) was added and left overnight at room temperature. The conjugation mixture was exhaustively dialyzed against water and then lyophilized.

Immunization of Rabbits. For each immunogen, two New Zealand White rabbits were immunized with 100 μg/animal of SCP−BTG or SAM−BTG conjugate emulsified in 1 mL of complete Freund's adjuvant and sterile physiological saline, 1:1 (v:v). The animals were immunized subcutaneously in multiple sites on the back. Subsequent monthly immunizations were carried out as above, except that incomplete Freund's adjuvant was used.

Blood (10 mL) was taken from the marginal ear vein of each animal 10 and 14 days after immunization. The blood was collected in heparinized tubes and centrifuged at 2500 rpm for 10 min. The supernatant was collected and stored frozen, with aliquots at 4 °C for use in ELISA.

Determination of Antibody Response. In 0.05 M sodium bicarbonate/carbonate buffer, pH 9.6, 96-well microtitration plates were coated with 1 μg mL^{-1} of the appropriate drug−protein conjugate. All wells were filled with 300 μL of the coating solution and incubated overnight at 2 °C, at which point they were washed 3 times with water using a Denley Wellwash 5000 microtitration plate washer (Denley Instruments Limited, Sussex, England). Plates were stored dry at room temperature until required for use.

A Beckman BioMek 1000 robotic pipetting workstation and side loader was programmed using BioMek software version 2.11 to carry out the liquid handling stages of the ELISAs. Each rabbit antiserum was diluted 1:1000 (v:v) in PBST and 200 μL added in triplicate to coated plates. A 10-fold serial dilution was carried out four times and the plates were incubated at 37 °C for 2 h. After washing and aspirating the plates five times with PBST, anti-rabbit IgG-HRP conjugate diluted 1:1000 (v:v; 200 μL) in PBST was added to each well and incubated for 1 h at 37 °C. After a further washing with PBST, to each well was added 200 μL of tetramethylbenzidine (TMB)-based substrate (Vetoquinol, Bicester, U.K.). After 10 min, the reaction was stopped using 50 μL/well of 2 M H_2SO_4. The absorbance of each well was measured at 450 nm using a Titertek Multiskan MCC plate reader.

Competitive ELISA. Since it was necessary to screen the antibodies raised against as many of the drugs as possible, the Beckman BioMek 1000 robotic system was programmed to perform all the liquid handling stages of the competitive ELISAs. The basic format of the assay involved the addition (in triplicate) of 100 mL of each standard at each concentration in PBST to drug−protein coated plate, followed by 100 mL of antiserum diluted in PBST to a concentration previously determined by ELISA. The concentrations of drug standards used were 1 mg mL^{-1}, 100 ng mL^{-1}, 1 ng mL^{-1}, and zero. The plates were incubated for 2 h at 37 °C, washed five times with PBST, and then 200 mL/well of anti-rabbit IgG-HRP diluted 1:1000 (v:v) in PBST was added to all wells. After a further incubation of 2 h at 37 °C the plates were washed and TMB substrate added (200 mL/well). After 10 min. the reaction was stopped with 2 M H_2SO_4 and absorbances of each well determined at 450 nm.

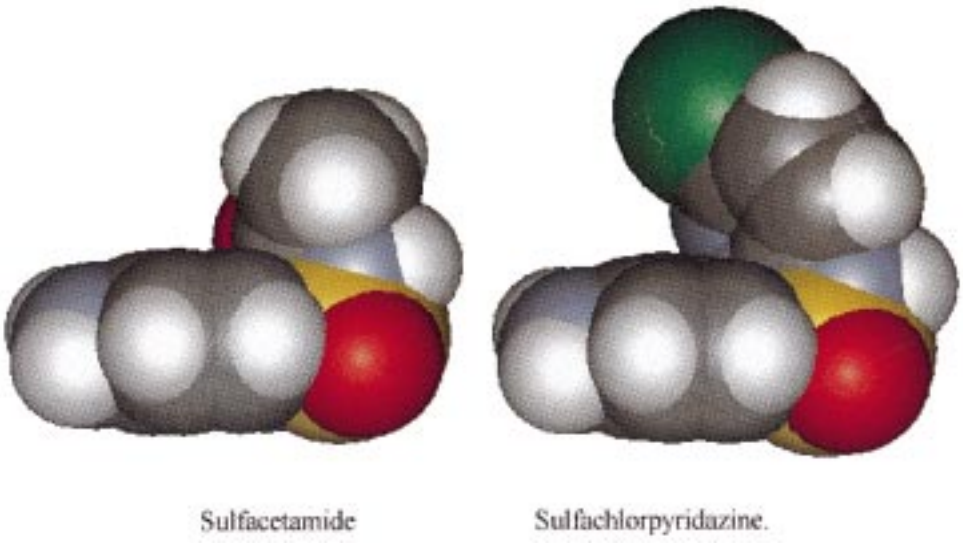


Figure 2. Van der Waals representation of the models of sulfacetamide and sulfachlorpyridazine.

Table 1. Spatial Information Obtained from Molecular Modeling

drug	angle of bend (deg)	distance between C1 and R-group (Å)
SCP	88.8	5.706
SMP	89.17	5.761
SEZ	97.1	6.502
SAM	86.6	5.847
SDM	90.64	6.394
SID	97.09	6.348
SDZ	92.88	6.504
SME	90.34	6.12
SD	95.93	6.651
SMZ	86.01	5.26
SMX	103.7	6.028
STZ	90.49	6.067
SQ	88.98	6.325
SAN	107.8	5.325
ADBS	95.21	9.088
SP	133.1	9.396

RESULTS AND DISCUSSION

The initial modeling studies carried out after performing a search rotating all torsions and energy minimizing for a number of different sulfonamides (Figure 2 shows only SCP and SAM) revealed that the drugs each had a characteristic "bend" around the tetrahedral $-SO_2-$ grouping. The bend varied considerably, being of least angle in SMZ (with the two halves of the drug almost folded back on each other) and of greatest angle in SP (where the drug is almost planar). The angles recorded are given in Table 1. Given the nature of the general structure of the sulfonamides, the differences are clearly due to the influence of the R-group alone.

Our initial hypothesis was based on the idea that maximal exposure of the common moiety was compromised in those drugs where the bend was of smallest angle. Consequently, recognition of the common moiety would be maximal in those drugs where the bend was of greatest angle. We synthesized two immunogens, the SAM−BTG and SCP−BTG conjugates, with the former being a more planar structure, the latter having a greater bend. Reasonable titers were obtained with both immunogens, and subsequent characterization was carried out by determining the ability of the antibodies to recognize different drug conjugates immobilized by passive adsorption to the wells of microtitration plates. Primary antiserum dilution was always 1:1,000 (v:v) for both anti-SAM and anti-SCP antisera. The results are summarized in Table 2. (The anti-SCP antiserum has been applied to the specific determination of the drug in food materials; Spinks et al., unpublished data).

Table 2. Summary of Antisera Binding to Different Hapten Conjugates[a]

coating conjugate based on:	immunogen based on: sulfachlor-pyridazine	sulf-acetamide
sulfachlorpyridazine (R-group linkage)	+++	++++
sulfamethazine (R-group linkage)	+++	++
sulfacetamide	+++	++++
acetyl sulfanilyl chloride	++	+++
sulfabenzamide	++	+++
sulfachlorpyridazine (common group linkage)	++++	−
4-aminodibenzene-sulfonamide	−	nt
4-aminophenyl-4-methyl benzenesulfonamide	+++	+++
sulfamethazine (common group linkage)	++++	++++
sulfaquinoxaline	−	−
sulfanilamide	+++	++++
sulfanillic acid	+++	+++
sulfasalazine	++	−

[a] Absorbance values obtained in ELISA of antiserum diluted 1:1000 v:v (++++ = >2.0; +++ = 1.5−2.0; ++ = 1.0−1.5; − = <0.5; nt = not tested).

Despite some recognition of the different immobilized sulfonamides, neither antisera showed useful broad specificity recognition of unconjugated sulfonamides by competitive ELISA (data not shown). Where recognition does occur (for example with the anti-SCP antiserum cross-reacting with SEZ and SMP), there are close structural similarities in the R-group. SEZ, SMP, and SCP all have an N−N structure within the R-group, and all have significant cross-reaction (1.9, 10.4, and 100%, respectively) as determined in the competitive ELISA. No cross-reactions were observed in the competitive ELISA for the anti-SAM antiserum.

Since the hypothesis based on maximal exposure of the common moiety by use of sulfonamide haptens with minimal bend was disproved, how can new hypotheses

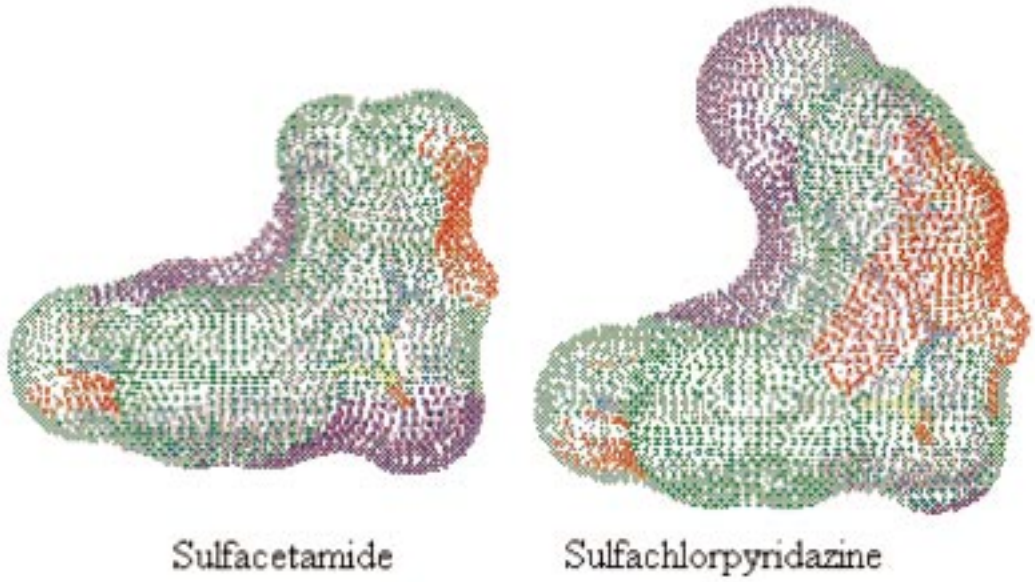


Figure 3. Electronic charge distribution across the surface of sulfacetamide and sulfachlorpyridazine. Blue = negatively charged; red = positively charged; green = relatively neutral.

be developed? It seems that there might be two possibilities. The first is that the $-SO_2-$ function provides a dominant recognition point for antibodies generated in vivo. Consequently, the antibody-binding sites would include some, if not all, of the variable R-group, and would always have a comparatively high degree of specificity. To overcome this problem, it might be possible to generate antibodies against "minimal" haptens such as sulfanilic acid, which does not contain the equivalent of an "R-group". However, antibodies generated against sulfanilic acid (data not presented) did not show any recognition of intact sulfonamides, again suggesting that the $-SO_2-$ moiety might be exerting disproportionate influence.

A second, and in our view more likely, explanation, lies in an examination of the charge distribution across the sulfonamide structures (Figure 3). We had anticipated that the R-group would not exert a significant effect on the charge distribution across the common group. However, it can be seen that this was not the case. Drugs such as SCP and SAM appear to be very different across the whole structure. Since so little is known about the molecular detail of recognition by antibodies of haptens, only speculation on the relative roles of different molecular attributes such as charge distribution or shape or hydrophobicity is possible. If charge distribution were the dominant force, then it would have to be the case that true broad specificity antibodies against sulfonamides would be impossible to generate in vivo.

In vitro generation of antibodies might offer hope of success, either through the use of artificial libraries of antibody genes (Hoogenboom and Winter, 1992), containing rare antibody functionalities not normally seen in nature or through the manipulation of antibody binding properties using the tools of molecular biology (Sharon et al., 1993). It is clear that recombinant antibodies offer considerable opportunities for future research (Nissim et al., 1994), though this has yet to be realized in terms of new applications. Molecular modeling of antibody-binding sites will be more widely utilized as rational manipulation of the binding site properties becomes an achievable goal for immunochemists. Part of this process will inevitably involve greater understanding of hapten structure at an earlier stage in proceedings than is currently the case. A limiting factor in the process will be the poor understanding of hapten-antibody interactions relative to protein-antibody interactions. It must also be remembered that interaction of antibodies with haptens is, if not an aberration, then at the extreme of a normal in vivo response. Given that the size of an amino acid side chain may be bigger than some haptens, then the degree of subtlety involved in bestowing specificity may be beyond current comprehension (and computing power). The involvement of antibody framework regions in the specificity of an anti-hapten response has previously been described (Kreissig et al., 1995). Mutations carried out on genes coding for those amino acids of the framework regions close to the complementarity-determining regions can have effects on antibody−antigen interactions since they may affect the conformation or stability of the binding site. Studies using anti-idiotype antibodies (Spinks et al. 1993) also suggest that framework regions may have some role in binding specificity.

In conclusion, molecular modeling of potential hapten structures has revealed an unexpected layer of complexity among a family of related structures, the sulfonamide drugs. While molecular modeling was, in this instance, unable to solve the problem of producing broad specificity antibodies, it has suggested new routes of experimentation. This, together with previous reports where molecular modeling was used to understand more about the interaction of antibody with target, suggests that modeling will become an increasingly used tool for the immunochemist.

ACKNOWLEDGMENT

The financial support of the Ministry of Agriculture, Fisheries and Food is gratefully acknowledged. We thank Dr. Steve Dixon (MAFF) for helpful discussion during the course of the research.

LITERATURE CITED

Brandon, D. L., Binder, R. G., Bates, A. H., and Montague, W. C., Jr. (1994) Monoclonal Antibody for Multiresidue ELISA of Benzimidazole Antihelmintics in Liver. *J. Agric. Food Chem. 42*, 1588−1594.

Bushway, R. J., and Fan, T. S. (1995) Detection of Pesticide & Drug Residues in Food by Immunoassay. *Food Technol. 49*, 108−115.

Carlin, R. J., Kamps-Holtzapple, C., and Stanker, L. H, (1994) Characterisation of Monoclonalanti-furosemide Antibodies and Molecular Modelling Studies of Cross-reactive Compounds. *Mol. Immunol. 31*, 153−164.

Elissalde, M. H., Kamps-Holtzapple, C., Beier, R. C., Plattner, R. D., Rowe, L. D., and Stanker, L. H. (1995) Development of an Improved Monoclonal Antibody-based ELISA for Fumonisin B-1−3 and the Use of Molecular Modelling to Explain Observed Detection Limits. *Food Agric. Immunol. 7*, 109−122.

Endoh, Y. S., Takahashi, Y., Hamamoto, S., Ishihara, Y., Nishikawa, M., and Nogawa, H. (1994) Usefulness of Enzyme Immunoassay (EIA) as an Analytical Method of Sulfamethoxazole Residues in Animal Tissues. *J. Food Hyg. Soc. Jpn.*

Erlanger, B. F., Borek, O. F., Beiser, S. M., and Liebermann, S. J. (1959) Steroid-protein Conjugates II. Preparation and Characterisation of Conjugates of Bovine Serum Albumin with Progesterone, Deoxycorticosterone and Estrone. *J. Biol. Chem. 234*, 1090−1094.

Finglas, P. M., and Morgan, M. R. A. (1994) Application of Biospecific Methods to the Determination of B − group Vitamins in Food − a Review. *J. Food Chem. 49*, 192−201 (Analytical Methods).

Garden, S. W., and Sporns, P. (1994) Development and Evaluation of an Enzyme Immunoassay for Sulfamerazine in Milk. *J. Agric. Food Chem. 42*, 1379−1391.

Goodrow, M. H., Harrison, R. O., and Hammock, B. D. (1990) Hapten Synthesis, Antibody Development and Competitive Inhibition Enzyme Immunoassay for s-Triazine Herbicides. *J. Ag. Food Chem. 38*, 990−996.

Griffiths A. D., Malniquist, M., Marks, J. D., Bye, J. M., Embleton, M. J., McCafferty, J., Baier, M., Holliger, K. P., Gorick, B. D., Hughes-Jones, N. C., Hoogenboom, H. R., and Winter, G. (1993) Human Anti-self-Antibodies with High Specificity from Phage Display Libraries. *EMBO J. 12*, 725−734.

Hoffmeister, A., Suhren, G., and Heeschen, W. (1991) Enzyme Immunoassays for Screening Sulfadimidine and Sulfanilamide Residues in Milk. *Milchwissenschaft 46* (11) 712−717.

Hoogenboom, H. R., and Winter, G. (1992) By-passing Immunisation, Human Antibodies from Synthetic Repertoires of Germline V_H Gene Segments Rearranged *in Vitro. J. Mol. Biol. 227*, 381−388.

Kitagawa, T., Fujiwara, K., Tomonoh, S., Takahashi, K., and Koida, M. (1983) Enzyme Immunoassays of Kanamycin Group Antibiotics with High Sensitivities Using Anti-Kanamycin as a Common Antiserum: Reasoning and Selection of a heterologous Enzyme Label. *J. Biochem. 94*, 1165−1172.

Kreissig, S. B., Ward, V. K., Hammock, B. D., and Choudary, P. V. (1995) Sequence Analysis of Individual Chains of Antibodies to Triazine Herbicides. In *Immunoanalysis of Agrochemicals, ACS Symposium Series 586* (J. O. Nelson, A. E. Karu, and R. B. Wong, Eds.) pp 31−49.

Landsteiner, K. (1945) *The Specificity of Serological Reactions*, Harvard University Press, Cambridge, MA.

Martlbauer, E., Meier, R., Usleber, E., and Terplan, G. (1992) Enzyme Immunoassays for the Detection of Sulfamethazine, Sulfadiazine, Sulfamethoxypyridazine and Trimethoprim in Milk. *Food Agric. Immunol. 4*, 219−228.

McCaughey, W. J., Elliott, C. T., and Crooks, S. R. H. (1990) Determination of Sulphadimidine in Animal Feedstuffs by an Enzyme-linked Immunoassay. *Food Addit. Contam. 7*, 259−264.

Morgan, M. R. A., McNerney, R., Matthew, J. A., Coxon, D. T., and Chan, H. W−S. (1983) An Enzyme-linked Immunosorbent Assay for Total Glycoalkaloids in Potato Tubers. *J. Sci. Food Agric. 34*, 593−598.

Newsome, W. H. (1986) Development of an Enzyme-Linked Immunosorbent Assay for Triadimefon in Foods. *Bull. Environ. Contam. Toxicol. 36*, 9−14.

Nissim, A., Hoogenboom, H. R., Tomlinson, I. M., Flynn, G., Midgley, C., Lane, D., and Winter, G. (1994) Antibody Fragments from a 'Single Pot' Phage Display Library as Immunochemical Reagents. *EMBO J. 13*, 692−698.

Schlaeppi, J.-M., Fory, W., and Ramsteiner, K. (1989) Hydroxyatrazine and Atrazine Determination in Soil and Water by Enzyme-Linked Immunosorbent Assay Using Specific Monoclonal Antibodies. *J. Agric. Food Chem. 37*, 1532−1538.

Sharon, J., Kao, C.-Y. Y., and Sompuram, S. R. (1993) Oligonucleotide-Directed Mutagenesis of Antibody Combining Sites. *Intern. Rev. Immunol. 10*, 113−127.

Sheth, H. B., and Sporns, P. (1990) Enzyme Immunoassay for Screening of Sulfathiazole in Honey. *J. Assoc. Off. Anal. Chem. Int. 73*, 871−874.

Sheth, H. B., and Sporns, P. (1991) Development of a Single ELISA for Detection of Sulfonamides. *J. Agric. Food Chem. 39*, 1696−1700.

Sheth, H. B., Yaylayan, V. A., Low, N. H., Stiles, M. E., and Sporns, P. (1990) Reaction of Reducing Sugars with Sulfathiazole and Importance of this Reaction to Sulfonamide Residue Analysis Using Chromatographic, Colorimetric, Microbiological, or ELISA Methods. *J. Agric. Food Chem. 38*, 1125−1130.

Singh, P., Ram, B. P., and Sharkov, N. (1989) Enzyme Immunoassay for Screening of Sulfamethazine in Swine. *J. Agric. Food Chem. 37*, 109−114.

Spinks, C. A., Wang, B., Mills, E. N. C., and Morgan, M. R. A. (1993). Production and Characterisation of Monoclonal Anti-idiotype Antibody Mimics for the Pyrethroid Insecticides and the Herbicide Paraquat. *Food Agric. Immunol. 5*, 13−25.

Stanker, L. H., McKeown, C., Watkins, B. E., Vanderlaan, M., Ellis, R., and Rajan, J. (1993) Detection of Dimetridazole and Other Nitroimidazole Residues in Turkey Using an Immunoassay. *J. Agric. Food Chem. 41*, 1332−1336.

Thomson, C. A., and Sporns, P. (1995) Variation in Enzyme-linked Immunosorbent Assay (ELISA) Components to Lower Sulfathiazole Detection Limits. *J. Food Sci. 60*, 872−879.

Van Emon, J. M., Seiber, J. N., and Hammock, B. D. (1989) Immunoassay Techniques for Pesticide Analysis. *Analytical Methods for Pesticides and Plant Growth Regulators 17*, 217−263.

Ward, C. M., Wilkinson, A. P., Bramham, S., Lee, H. A., Chan, H. W−S., Butcher, G. W., Hutchings, A., and Morgan, M. R. A. (1990) Production and characterisation of polyclonal and monoclonal antibodies against Aflatoxin B_1oxime-BSA in an enzyme-linked immunosorbent assay. *Mycotoxin Res. 6*, 73−83.

Wie, S. I., and Hammock, B. D. (1984) Comparison of coating and Immunizing Antigen Structure on the Sensitivity and Specificity of Immunoassays for Benzoylphenylurea Insecticides. *J. Agric. Food Chem. 32*, 1294−1301.

Wilkinson, A. P., Ward, C. M., and Morgan, M. R. A. (1992) Immunochemical Analysis of Mycotoxins. In *Modern Methods of Plant Analysis 13* (H. F. Linskens, and J. F. Jackson) Springer−Verlag, 185−218.

BC980054M

Structure−Activity Relationships of Water-Soluble Cationic Methacrylate/Methacrylamide Polymers for Nonviral Gene Delivery

Petra van de Wetering,[†] Ed E. Moret,[‡] Nancy M. E. Schuurmans-Nieuwenbroek,[†] Mies J. van Steenbergen,[†] and Wim E. Hennink*[,†]

Department of Pharmaceutics, Department of Medicinal Chemistry, Utrecht Institute for Pharmaceutical Sciences (UIPS), Faculty of Pharmacy, Utrecht University, Utrecht, The Netherlands. Received December 12, 1998; Revised Manuscript Received March 31, 1999

A number of water-soluble cationic carriers was evaluated as transfectant. Almost all studied cationic methacrylate/methacrylamide polymers were able to condense the structure of plasmid DNA, yielding polymer/plasmid complexes (polyplexes) with a size of 0.1−0.3 μm and a slightly positive ζ-potential, which can be taken up by cells, e.g., via endocytosis. However, the transfection efficiency and the cytotoxicity of the polymers differed widely: the highest transfection efficiency and cytotoxicity were observed for poly[2-(dimethylamino)ethyl methacrylate], p(DMAEMA). Assuming that polyplexes enter cells via endocytosis, p(DMAEMA) apparently has advantageous properties to escape the endosome. A possible explanation is that, due to its average pK_a value of 7.5, p(DMAEMA) is partially protonated at physiological pH and might behave as a proton sponge. This might cause a disruption of the endosome, which results in the release of both the polyplexes and cytotoxic endosomal/lysosomal enzymes into the cytosol. On the other hand, the analogues of p(DMAEMA) studied here have a higher average pK_a value and have, consequently, a higher degree of protonation and a lower buffering capacity. This might be associated with a lower tendency to destabilize the endosome, resulting in both a lower transfection efficiency and a lower cytotoxicity. Furthermore, molecular modeling showed that, of all studied polymers, p(DMAEMA) has the lowest number of interactions with DNA. We therefore hypothesized that the superior transfection efficiency of p(DMAEMA) containing polyplexes can be ascribed to an intrinsic property of p(DMAEMA) to destabilize endosomes combined with an easy dissociation of the polyplex once present in the cytosol and/or the nucleus.

INTRODUCTION

In previous studies, it has been shown that poly(2-(dimethylamino)ethyl methacrylate), p(DMAEMA), is able to bind plasmid DNA, yielding polymer/plasmid complexes (also called polyplexes) (*1*). The size and ζ-potential of the polyplexes were dependent on the polymer/plasmid ratio. We demonstrated that polyplexes with a slightly positive ζ-potential (25−30 mV) and a size around 0.2 μm possessed the highest transfection potential (*2*, *3*). However, as observed for many other polycationic compounds (*4*, *5*), e.g., the frequently used transfectant poly(l-lysine) (*6*), p(DMAEMA) is cytotoxic (*3*). We also reported, upon the synthesis and characterization of random copolymers of DMAEMA with hydrophilic, noncharged comonomers. These copolymers showed a better efficacy/cytotoxicity ratio as compared to p(DMAEMA) of comparable molecular mass (*7*).

In this study, the transfection capability of other water-soluble cationic polymers with structures closely related to p(DMAEMA) is evaluated to obtain insight into the relationship between their structure and activity. For cationic lipids, peptides, and cationic amphiphiles, a number of studies has been published concerning the relationship between structure and their transfection characteristics. For lipids, the effects of the nature of the lipid headgroup (*8*, *9*), the length of the hydrophobic tail (*10*), and the length of the head−tail linker (*11*) on their transfection characteristics have been studied. The influence of structural modifications in peptoids (*12*), peptides (*13*−*15*), and cationic facial amphiphiles (*16*) on transfection efficiency has been investigated. For synthetic cationic polymers, no systematic studies have been reported so far, to our knowledge.

The polymers in this study were evaluated on their ability to bind plasmid DNA using dynamic light scattering (DLS), and the resulting polyplexes were characterized by ζ-potential measurements. The transfection efficiency and the cytotoxicity of the polyplexes were studied in vitro in OVCAR-3 cells. Furthermore, molecular modeling was used to obtain insight into the characteristics of possible DNA−polymer interactions.

Polymer Selection. The structure of p(DMAEMA) is shown in Figure 1a. The effect of a propyl side chain instead of an ethyl side chain is studied with poly[3-(dimethylamino)propyl methacrylate] [p(DMAPMA), Figure 1b]. Substitution of the ester group in p(DMAEMA) by an amide group is evaluated with poly[2-(dimethylamino)ethyl methacrylamide] [p(DMAEMAm), Figure 1c]. The effect of both a longer side chain and an amide group is studied with poly[3-(dimethylamino)propyl methacrylamide] [p(DMAPMAm), Figure 1d]. P(DMAEMA) contains tertiary amino groups, with an average pK_a of 7.5, implying that around 50% of the side groups is positively charged at physiological pH. Poly[2-(trimethy-

* To whom correspondence should be addressed. Phone: +31 30 253 6964. Fax: +31 30 251 7839. E-mail: W.E.Hennink@pharm.uu.nl.

[†] Department of Pharmaceutics.

[‡] Department of Medicinal Chemistry.

10.1021/bc980148w CCC: $18.00 © 1999 American Chemical Society
Published on Web 06/04/1999

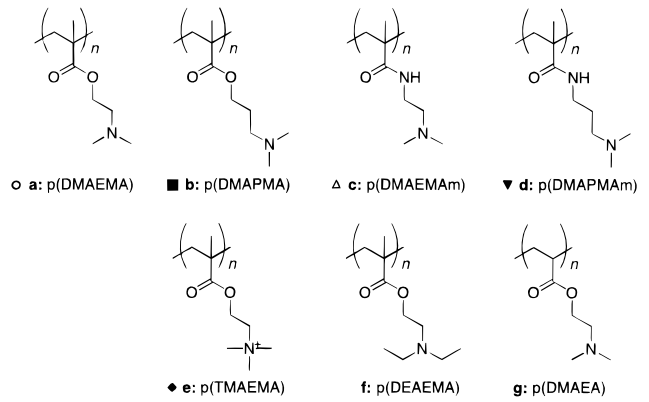


Figure 1. Chemical structure of (a) poly(2-(dimethylamino)-ethyl methacrylate), p(DMAEMA); (b) poly(3-(dimethylamino)-propyl methacrylate), p(DMAPMA); (c) poly(2-(dimethylamino)-ethyl methacrylamide), p(DMAEMAm); (d) poly(3-(dimethylamino)propyl methacrylamide), p(DMAPMAm); (e) poly(2-(trimethylamino)ethyl methacrylate chloride), p(TMAEMA); (f) poly(2-(diethylamino)ethyl methacrylate), p(DEAEMA); and (g) poly(2-(dimethylamino)ethyl acrylate), p(DMAEA).

lamino)ethyl methacrylate chloride] [p(TMAEMA), Figure 1e] is used to study the effect of structurally almost identical polymers with permanently positively charged side chains. Another modification of the amino group is studied with poly[2-(diethylamino)ethyl methacrylate] [p(DEAEMA), Figure 1f]. This polymer contains diethylamino groups instead of dimethylamino groups. Finally, the effect of a more hydrophilic, and probably more flexible, polymer backbone is investigated with poly[2-(dimethylamino)ethyl acrylate] [p(DMAEA), Figure 1g].

MATERIALS AND METHODS

Materials. The following compounds were used as received: 2-(dimethylamino)ethyl methacrylamide (DMAEMAm, Polysciences), 3-(dimethylamino)propyl methacrylamide (DMAPMAm, Aldrich, Bornem, Belgium), 2-(trimethylamino)ethyl methacrylate chloride (TMAEMA, Aldrich), 2-(dimethylamino)ethyl acrylate (DMAEA, Aldrich), 2,2′-azobisisobutyronitrile (AIBN, Fluka, Bornem, Belgium), and ammonium peroxodisulfate (APS, Fluka). All other chemicals were of analytical grade. Water purified by reversed osmosis was applied throughout the study.

2-(Dimethylamino)ethyl methacrylate (DMAEMA, Fluka) and 2-(diethylamino)ethyl methacrylate (DEAEMA, Aldrich) were purified by distillation under reduced pressure before use. 3-(Dimethylamino)propyl methacrylate (DMAPMA) was synthesized from methacryloyl chloride and 3-(dimethylamino)propanol as described elsewhere (*17*).

Cell culture flasks and microtiter plates were obtained from Falcon (Micronic, Lelystad, The Netherlands). Dulbecco's Modified Eagle's Medium (DMEM) and RPMI 1640 medium were from Gibco (Life technologies, Breda, The Netherlands). Fetal calf serum (FCS) was from Integro (Zaandam, The Netherlands). Biotinylated, methoxypsoralen inactivated adenovirus dl1014 (*18*, *19*) (stock solution 1.9×10^{11} particles/mL) was kindly provided by Dr. E. Wagner (Bender, Austria).

Hepes-buffered saline (HBS) was composed of 150 mM NaCl, 20 mM Hepes, pH 7.4. The plasmid pCMVLacZ containing a bacterial *LacZ* gene preceded by a nuclear localization signal under control of a CMV promoter was amplified and purified as reported before (*2*).

Synthesis and Characterization of Polymers. The polymers were synthesized by radical polymerization of the corresponding monomers essentially as described in detail previously for the synthesis of p(DMAEMA) (*3*). Polymers of DMAEMA, DMAEA, and DEAEMA were synthesized in toluene (20% w/v) using AIBN as initiator (M/I 100−250, mol/mol). After 22 h at 60 °C the polymers were isolated by precipitation in a 5−10-fold excess cold petroleum ether and dried in vacuo. The polymers were dissolved in water, dialyzed against water, and isolated by lyophilization. Polymers of DMAEMAm, DMAPMA·HCl, DMAPMAm·HCl, and TMAEMA were synthesized in aqueous hydrochloric acid (20% w/v) using APS as initiator (M/I 100−500, mol/mol). Polymerizations were stopped after 22 h at 60 °C, by transferring the reaction mixture into dialysis tubes. After extensive dialysis against water at 4 °C, the polymers were obtained by lyophilization.

The weight and number average molecular masses of the polymers were determined by gel permeation chromatography (GPC). The GPC measurements were performed with two thermostated (35 °C) columns in series (Shodex OHpak KB-802 and KB-80M, Showa Denko, Japan) equipped with a refractive index detector. The eluent was an aqueous solution of 0.7 M $NaNO_3$, 0.1 M Tris (pH 7.2), and the flow rate was 1 mL/min. The columns were calibrated using dextran standards of known molecular masses (Fluka).

pK_a Measurements. The pK_a values of monomers and polymers were determined by titration with a Metrohm combi-titrator, equipped with a 614 pulsomat. The compounds were dissolved in 0.9 w/v % NaCl solutions (to a final concentration of 0.2−0.3 w/v %), acidified with 0.1 M HCl and titrated with 0.25 M NaOH.

Particle Size and ζ-Potential Measurements. For dynamic light scattering (DLS) measurements, the stock solutions of the polymers (2 mg/mL in HBS) were diluted with "fake" RPMI medium (RPMI 1640 medium without phenol red and vitamins) to 2.4−78 μg/mL. The plasmid pCMV*LacZ* was diluted to 25 μg/mL in fake RPMI. Polymer solution (400 μL) was added to 100 μL of plasmid solution, resulting in 0.39/1 to 12.5/1 (w/w) polymer/plasmid ratio. After 30−45 min complex formation time, *Z*-average particle size and polydispersity index (PI) of the polyplexes were determined by dynamic light scattering (DLS) at 25 °C with a Malvern 4700 system using an argon-ion laser (488 nm) operating at 10.4 mW (Uniphase). The PCS (photon correlation spectrometry) software for Windows (version 1.34, Malvern, U.K.) was used. For the data analysis, the viscosity and refractive index of pure water at 25 °C were used. The instrument was checked with a polystyrene dispersion containing particles of 100 nm.

For the ζ-potential measurements, the polymer stock solutions were diluted with 20 mM Hepes. Next, 680 μL of polymer solution was added to 170 μL of plasmid solution (75 μg/mL in 20 mM Hepes), resulting in 0.39/1 to 12.5/1 (w/w) polymer/plasmid ratio. After 30−45 min of complex formation time, the ζ-potential was measured at a temperature of 25 °C in an aqueous DTS5001 cell with a Zetasizer 2000 (Malvern, U.K.) and PCS software for Windows (version 1.34, Malvern, U.K.). The instrument was checked using a polystyrene dispersion with a known ζ-potential.

Molecular Modeling. Molecular modeling was performed with Insight II 97.0 (*20*) on a Silicon Graphics workstation. Eight adenine-thymine (AT) basepairs were built in canonical B-conformation with Insight II. To choose a starting orientation of the flexible polymer backbone, either in the major or in the minor groove of octa(DNA), a Monte Carlo simulated annealing docking

was used. Therefore, the backbone of octa(DMAEMA) was docked flexibly five times to DNA with AutoDock 2.2 (*21*). The results were clustered and the best cluster was used as a starting conformation for building syndiotactic octa(DMAEMA). This was also done for the other polymers. The number of protonated side groups in the octamers was varied. To mimic the situation at pH 7.4, the fraction of protonated groups was calculated from the average pK_a values of the polymers. To exclude end effects, the outer groups of the octamers were protonated preferentially.

Minimization of the structure was performed with the CVFF force field and conjugate gradients in Discover 2.98. Minimization was stopped after 10^5 iterations or when the maximum derivative of the potential energy was less than 0.001 kcal/Å. Throughout the minimization and molecular dynamics, the DNA was held fixed, and the nonbonded energy (representing the hydrogen bonds) was computed within a cutoff radius of 12.5 Å at a default dielectric constant of 1. The minimized structure was subjected to 500 ps of molecular dynamics at 300 K with 1 fs steps. The number of hydrogen bonds formed during the simulation were counted every ps and used as a measure of binding. All simulations were performed at least twice.

Cell Culture. The human ovarian cancer cell line NIH:OVCAR-3 originated from Dr. Hamilton (National Cancer Institute, Bethesda, MD) (*22*). OVCAR-3 cells were cultured in DMEM supplemented with 10% (v/v) FCS, l-glutamine (2 mM), l-glucose (4.5 g/L), penicillin (100 IU/mL), streptomycin (100 μg/mL), and amphotericin B (0.25 μg/mL). Before performing a transfection experiment, the cells were grown to 60−80% confluency at 37 °C in a humidified atmosphere containing 5% CO_2.

Preparation of Polymer/Plasmid Complexes for Transfection Experiments. The stock solutions of the polymers (2 mg/mL in HBS) were diluted to 2.4−(6×10^{2}) μg/mL with plain RPMI medium. The plasmid pCMV-*LacZ* was diluted to 25 μg/mL in RPMI. Complexes of polymer and plasmid were prepared by adding 400 μL of polymer solution to 100 μL of plasmid solution, resulting in 0.39/1 to 100/1 (w/w) polymer/plasmid ratio. After 30−60 min complexation time, the complexes were added to the cells.

Transfection Studies. Transfection experiments were performed with OVCAR-3 cells using the plasmid pCMV*LacZ* as reporter gene essentially as described before (*2*, *3*, *7*). In brief, cells were seeded at a concentration of 3×10^4/cm^2 in 96-well plates 24 h before transfection. At the day of transfection, cells were rinsed and incubated for 1 h with 200 μL of polyplexes/well.

Transfection experiments in the presence of adenovirus were performed essentially as described above and analogous to Cotten et al. (*23*). Polyplexes were prepared by adding 5 μL (9.4×10^8 particles) of adenovirus and 50 μL of polymer solution (78 and 156 μg/mL) to 50 μL of plasmid solution (50 μg/mL). After 30 min, 400 μL of RPMI was added and the complexes were applied to the cells.

All transfection experiments were performed in two identical series in separate 96-well plates. After removal of the transfection complexes, 100 μL of fresh culture medium was added, and the cells were further cultured for about 48 h. Then, one series was tested for reporter gene expression (β-galactosidase) by histochemical staining with X-Gal (*24*). To determine the cytotoxic effect of polyplexes, the number of viable cells was measured using a XTT colorimetric assay (*25*).

Table 1. Molecular Masses of the Studied Cationic Polymers, and pK_a Values of the Polymers and Their Monomers

	polymer			
compd	M_w (kDa)	M_n (kDa)	average pK_a (±0.1)	monomer pK_a (±0.1)
DMAEMA	550 ± 200[a]	50 ± 30	7.4	8.3
DMAEMAm	120 ± 60[b]	27 ± 12	7.8	8.5
DMAPMA	275 ± 90[b]	27 ± 6	8.4	9.1
DMAPMAm	220 ± 180[b]	30 ± 19	8.8	9.2
DMAEA	25 ± 4[a]	7 ± 1	8.2	8.3
DEAEMA	90 ± 20[a]	8 ± 2	7.5	8.8
TMAEMA	845 ± 145[b]	70 ± 24	no pK_a	no pK_a

[a] Synthesized in toluene (M/I 100−250, mol/mol). [b] Synthesized in aqueous hydrochloric acid (M/I 100−500, mol/mol).

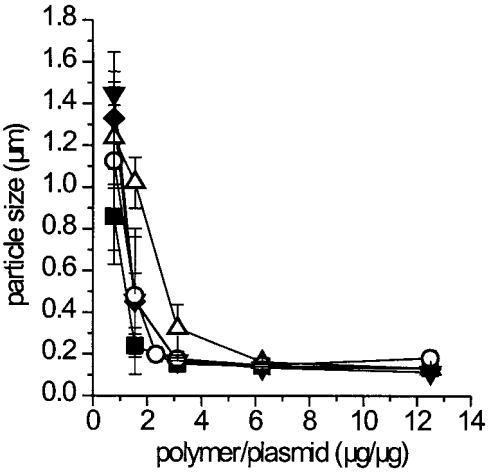


Figure 2. Particle size of complexes of plasmid (final concentration of 5 μg/mL) with different polymers as a function of the polymer/plasmid (w/w) ratio. The results are shown as mean values (±SD) of three experiments. (■) p(DMAPMA), (▼) p(DMAPMAm), (◆) p(TMAEMA), (△) p(DMAEMAm), (○) p(DMAEMA).

RESULTS

Polymer Characterization. The different (meth)acrylate/methacrylamide polymers (Figure 1) were synthesized by radical polymerization of the corresponding monomers. Since the transfection efficiency of p(DMAEMA) depended on the molecular mass (*3*), the aim was to synthesize high molecular mass polymers, which are also able to condense DNA to particles with a size of about 0.1−0.3 μm. Table 1 shows the molecular masses of the synthesized polymers. Except for p(DMAEA), polymers with a weight average molecular mass of ≥90 kDa were obtained. Further, Table 1 shows that the average pK_a (which is defined as the pH at which 50% of the amino groups in the polymers are protonated) is 0.1−1.3 pH units below the pK_a of the monomers. A likely explanation is that the presence of protonated side chains reduced the protonability of the remaining di(m)ethylamino groups; a phenomenon that has been reported before for other polymers (*26*).

Particle Size and ζ-Potential Measurements. The characteristics of the polyplexes in terms of particle size and ζ-potential were studied as a function of polymer/plasmid ratio. As reference polymer, p(DMAEMA) with good condensing properties (M_w 550 kDa) was used.

Like p(DMAEMA), polymers of DMAEMAm, DMAPMA, DMAPMAm, and TMAEMA were able to condense plasmid to particles with a size of 0.1−0.3 μm at a polymer/plasmid ratio of 1.5−3/1 (w/w) (Figure 2). P(DMAEA) (Figure 1g) was not able to condense plasmid to

Table 2. Results of the Molecular Dynamic Analysis of Octa(DNA) and the Octamers in 500 ps Using 1 fs Steps

poly- or octa-	pK_a[a]	calcd no. of H^+ at pH 7.4[b]	no. of H^+ in octamer[c]	DNA−polymer interactions		intrapolymer interactions	
				$(PO_4^-)_{DNA}$-$(amino)_{poly}$	$(NH)_{DNA}$-$(C{=}O)_{poly}$	$(amino)_{poly}$-$(C{=}O)_{poly}$	$(amide)_{poly}$-$(C{=}O)_{poly}$
DMAEMA	7.5	4.5	4	791 ± 28	74 ± 61	0 ± 0	
			5	961 ± 35	670 ± 180	0 ± 0	
			6	963 ± 87	103 ± 91	1 ± 1	
			7	984 ± 45	259 ± 153	31 ± 13	
			8	1174 ± 108	398 ± 103	3 ± 1	
DMAEMAm	7.8	5.5	6	1300 ± 5	147 ± 58	619 ± 22	406 ± 59
			8	1214 ± 151	55 ± 42	452 ± 128	141 ± 176
DMAPMA	8.4	7.3	7	2738 ± 766	1 ± 1	53 ± 92	
			8	2516 ± 52	1 ± 1	2 ± 3	
DMAPMAm	8.8	7.7	7	2874 ± 602	2 ± 1	10 ± 14	354 ± 15
			8	3869 ± 840	4 ± 4	0 ± 0	262 ± 370
DMAEA	8.2	6.9	4	1411 ± 308	3 ± 4	2 ± 2	
			7	1483 ± 317	173 ± 207	0 ± 0	
DEAEMA	7.5	4.5	4	1317 ± 3	294 ± 50	0 ± 0	
			5	1276 ± 118	622 ± 274	5 ± 7	

[a] Average pK_a values of the polymers. [b] Calculated number of protonated amino groups in the octamers at pH 7.4. [c] The number of protonated amino groups with which the modeling was performed.

Table 3. Maximum Value of the Zetapotential at Polymer/Plasmid (w/w) Ratio ≥2/1 and the IC_{50} Values (μg/mL) of the Different Polymers and of the Polyplexes (plasmid concentration 5 μg/mL)

polymer	ζ-potential max (mV)	IC_{50} polymer (mg/mL polymer)	IC_{50} polyplex (mg/mL polymer)
p(DMAEMA)	24 ± 2	4.5 ± 0.5	11.0 ± 0.5
p(DMAEMAm)	26 ± 2	14 ± 2	30 ± 2
p(DMAPMA)	28 ± 2	39 ± 1	58 ± 1
p(DMAPMAm)	30 ± 2	12 ± 1	20 ± 1
p(TMAEMA)	30 ± 2	21 ± 2	45 ± 2

small particles; a heterogeneous mixture (particle size 1−2 μm) with a high polydispersity was formed. This might be explained by the low molecular mass of this polymer (Table 1). At room temperature, only large aggregates were formed by incubation of p(DEAEMA) (Figure 1f) and plasmid. Particles with a relatively smaller size were obtained by incubation of p(DEAEMA) and plasmid at 4 °C (polymer/plasmid 6/1, particle size 0.6−0.7 μm). However, when the dispersion was brought at ambient temperature, aggregates of about 2 μm were formed within 5 min. The relatively low molecular mass of p(DEAEMA) combined with the low solubility of this polymer around pH 7 (*27*) could be the reason for the inability to form small complexes with DNA.

It was shown that at a polymer/plasmid ratio of ≥2/1 (w/w), the ζ-potential of the polyplexes composed of p(DMAEMAm), p(DMAPMA), p(DMAPMAm), or p(TMAEMA) and plasmid was 26−30 mV, which is comparable with the ζ-potential of polyplexes composed of p(DMAEMA) and plasmid (Table 3) and comparable with other systems [poly(l-lysine) (*28*), liposomes (*9*, *29*, *30*)].

Modeling. With molecular dynamics, the hydrogen bonding between octamers of all polymers [octa(repeating unit)] and a DNA octamer was studied. The octamers were built in a syndiotactic form, which is the preferred configuration for p(DMAEMA) prepared by radical polymerization (*31*). As an example, Figure 3 shows that the docking of octa(DMAEMA) to a DNA octamer resulted in a stable orientation in the major groove. Minimization and molecular dynamics performed on the complex showed that octa(DMAEMA) remained in the major groove, which was also observed for poly(N-vinyl pyrrolidone), PVP, by Mumper et al. (*32*). PVP was placed in a minimized conformation near a DNA oligomer. In their study, two kinds of interactions could be distinguished. The vinyl backbone of PVP provided a hydrophobic surface on DNA and hydrogen bonding was observed between the hydrophilic pyrrolidone groups and the base pairs of DNA.

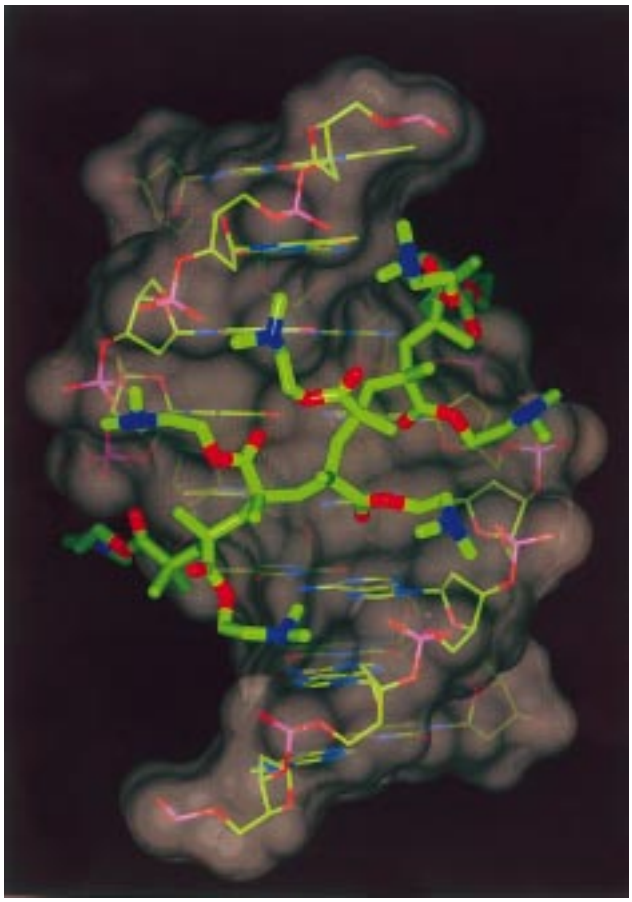


Figure 3. Octa(DMAEMA) docked into the major groove of octa(DNA).

In our study, using molecular dynamics, three (Figure 4) and four (Figure 5) types of interactions were observed between DNA and the methacrylate octamers and methacrylamide octamers, respectively. First, interaction occurred between the positively charged amino groups and the negatively charged phosphate groups in DNA: $(PO_4^-)_{DNA}$-$(amino)_{poly}$ interaction. Second, interaction between a NH of adenine and the C═O group of the polymers was observed ($(NH)_{DNA}$-$(C{=}O)_{poly}$, see Figure 6). Third, interaction between the positively charged amino

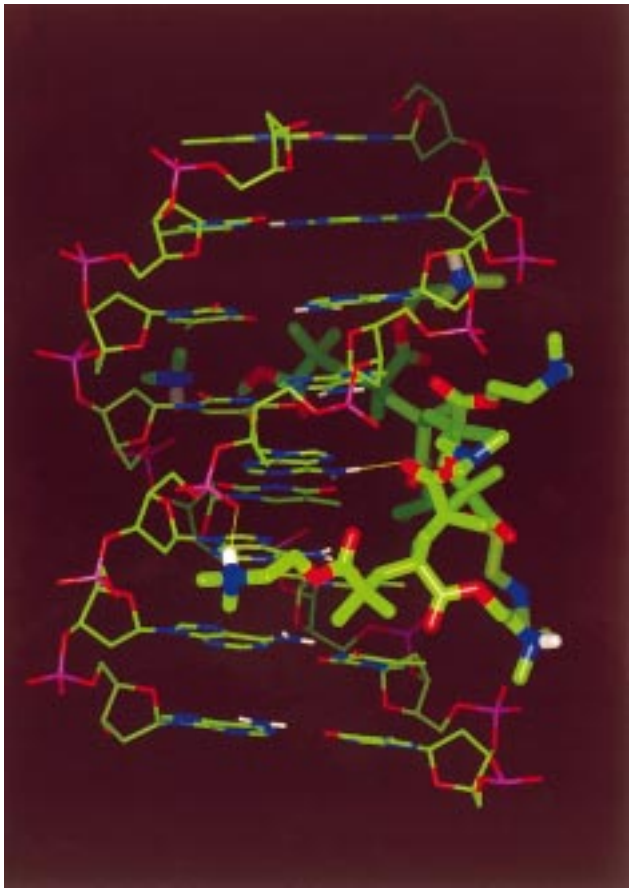


Figure 4. Interactions between a DNA octamer and octa(DMAEMA) $(PO_4^-)_{DNA}$-$(amino)_{poly}$ and $(NH)_{DNA}$-$(C{=}O)_{poly}$.

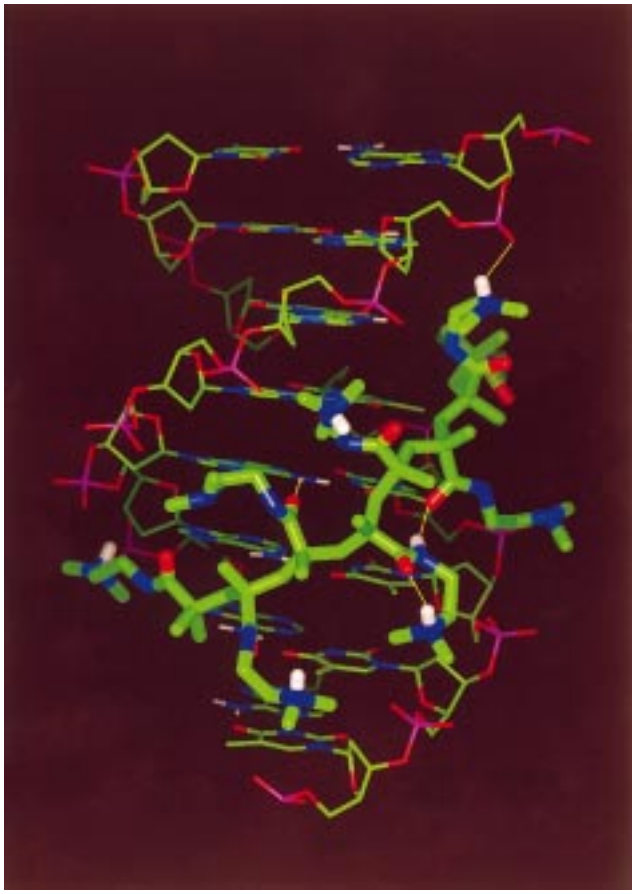


Figure 5. Interactions between a DNA octamer and octa(DMAEMAm) $(PO_4^-)_{DNA}$-$(amino)_{poly}$, $(NH)_{DNA}$-$(C{=}O)_{poly}$, $(amino)_{poly}$-$(C{=}O)_{poly}$, and $(amide)_{poly}$-$(C{=}O)_{poly}$.

group and the carbonyl group within a polymer chain occurred [intrapolymeric interaction: $(amino)_{poly}$-$(C{=}O)_{poly}$]. The fourth type of interaction could only occur between methacrylamide compounds, because it involved the interaction of the amide proton with the carbonyl: $(amide)_{poly}$-$(C{=}O)_{poly}$ interaction.

First, the effect of the degree of protonation of amino groups on the interaction with DNA was studied for octa(DMAEMA) (Figure 4). Table 2 shows that, with an increasing degree of protonation, the total number of $(PO_4^-)_{DNA}$-$(amino)_{poly}$ interactions increased. However, the number of these interactions per protonated group slightly decreased with an increasing degree of protonation. Besides $(PO_4^-)_{DNA}$-$(amino)_{poly}$ interactions, also $(NH)_{DNA}$-$(C{=}O)_{poly}$ interactions were observed. With exception of octa(DMAEMA) bearing five protonated groups, octa(DMAEMA)$^{5+}$, the number of interactions between the $(NH)_{DNA}$ and $(C{=}O)_{poly}$ increased with the degree of protonation. Taking both types of interactions together, it can be concluded that, with an increasing degree of protonation, the octamer comes into a more fixed position in the major groove of DNA.

Next, the number and types of interactions between the different fully protonated octamers and octa(DNA) were compared. Table 2 shows that replacement of the ester group in octa(DMAEMA)$^{8+}$ by an amide group, i.e. octa(DMAEMAm)$^{8+}$, had no significant effect on the number of interactions between $(PO_4^-)_{DNA}$ and $(amino)_{poly}$. Due to the presence of the amide group, octa(DMAEMAm)$^{8+}$ showed additional $(amide)_{poly}$-$(C{=}O)_{poly}$ interactions as well as an increased number of $(amino)_{poly}$-$(C{=}O)_{poly}$ interactions (Figure 5). In contrast, the number of interactions between $(C{=}O)_{poly}$ and $(NH)_{DNA}$ was lower in comparison with octa(DMAEMA)$^{8+}$, which might be due to the large increase in the number of $(amino)_{poly}$-$(C{=}O)_{poly}$ interactions. When the behavior of octa(DMAEMA)$^{8+}$ is compared with octa(DMAPMA)$^{8+}$, the number of interactions between $(PO_4^-)_{DNA}$ and $(amino)_{poly}$ was higher for octa(DMAPMA)$^{8+}$, whereas $(NH)_{DNA}$-$(C{=}O)_{poly}$ interactions were absent. As was observed for octa(DMAEMA)$^{8+}$, the number of intrapolymeric interactions within octa(DMAPMA)$^{8+}$ were marginal. Replacing the ester group in octa(DMAPMA)$^{8+}$ with an amide group, i.e. octa(DMAPMAm)$^{8+}$, resulted in an increase of $(PO_4^-)_{DNA}$-$(amino)_{poly}$ interactions while the number of $(NH)_{DNA}$-$(C{=}O)_{poly}$ and intrapolymer interactions remained very low. Similar as observed for octa(DMAEMAm)$^{8+}$, octa(DMAPMAm)$^{8+}$ also showed additional $(amide)_{poly}$-$(C{=}O)_{poly}$ interactions. However, in contrast to the ethyl compound octa(DMAEMAm)$^{8+}$, octa(DMAP-

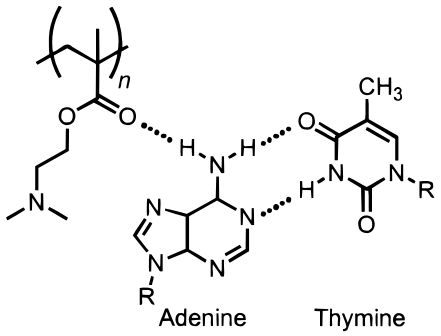


Figure 6. Interaction between an adenine-thymine base pair (R = sugar/phosphate backbone) and adenine and (the carbonyl group of) the polymer.

MAm)$^{8+}$ had no intrapolymeric $(amino)_{poly}$-$(C{=}O)_{poly}$ interactions.

Finally, we compared the types and the number of interactions at pH 7.4. For each octamer, the fraction protonated with amino groups was calculated from the average pK_a of the polymers (Table 2). Comparison of the interactions of the different octamers with DNA at pH 7.4 shows similar trends, as were observed for fully protonated octamers. However, the only observed difference is that for p(DMAEMA)$^{4-5+}$, the number of $(PO_4\text{-})_{DNA}$ and $(amino)_{poly}$ interactions, was 1.5, 2.8−3.5, and 4−5 times lower in comparison with octa(DMAEMAm)$^{6+}$, octa(DMAPMA)$^{7+}$, and octa(DMAPMAm)$^{8+}$, respectively.

For octa(TMAEMA), which permanently bears positively charged amino groups, interaction with DNA is expected. Because the $(PO_4\text{-})_{DNA}$-$(amino)_{poly}$ interaction does not involve hydrogen bonds, it was not possible to quantify the number of interactions between octa(DNA) and octa(TMAEMA). However, due to its permanent positive charge, relatively strong electrostatic interactions between octa(TMAEMA) and DNA can be expected.

Although complexing problems prevented evaluation in transfection, octa(DMAEA) and octa(DEAEMA) could be studied in terms of interaction with DNA. As can be seen in Table 2, for octa(DMAEA) and octa(DEAEMA), similar numbers of DNA−octamer interactions were observed. However, in comparison with the results of octa(DMAEMA), the number of $(PO_4^-)_{DNA}$-$(amino)_{poly}$ interactions was higher than the number of interactions found for octa(DMAEMA).

Transfection Efficiency and Influence on Cell Viability. The influence of the polymer concentration on the cell viability was evaluated in cell culture for the different polymers. From Figure 7a, which shows the effect of the polymer concentration on the cell viability, the IC_{50} values [defined as the concentration resulting in 50% inhibitory activity (cell-death)], which give an indication about the cytotoxicity, were determined (Table 3). Both Figure 7a and Table 3 show that all evaluated polymers had a lower cytotoxicity than p(DMAEMA). P(DMAEMAm) was about 3-fold less toxic than p(DMAEMA). The analogue with a propyl instead of an ethyl side chain, p(DMAPMA), was almost 9-fold less toxic than p(DMAEMA). Combination of both structural differences (amide and propylene side chain) in p(DMAPMAm) did not result in a synergistic reduction of the cytotoxicity: p(DMAPMAm) was only 3-fold less toxic than p(DMAEMA). Finally, the permanently positively charged p(TMAEMA) had about a 5-fold lower toxicity as compared to p(DMAEMA).

Next, the influence of the polymer/plasmid ratio on the cell viability and transfection efficiency was evaluated for the different polymers. Figure 7b shows the relation between the polymer/plasmid ratio and the cell viability. The same trend as found for the free polymers was observed (Figure 7a). The IC_{50} values, calculated from Figure 7b, give an indication about the cytotoxicity of the transfection mixture, consisting of polyplexes and free polymer which is likely present above a certain polymer/plasmid ratio. Comparison of the IC_{50} values of the polymers with the IC_{50} values of the polyplexes shows that the presence of plasmid masked part of the cytotoxic effect of the polymer. This phenomenon has also been reported for, e.g., α-helical peptides (*14*) and liposomes (*33*).

For p(DMAEMA), a bell-shaped relation between polymer/plasmid ratio and transfection efficiency was found (Figure 7c). At low polymer/plasmid ratios (<2/1, w/w), the polyplexes consisted of large aggregated particles (size around 1 μm), which obviously could not enter the cell easily. At a polymer/plasmid ratio 2−3/1 (w/w), the DNA was condensed by the polymer into small complexes (size 0.1−0.2 μm) with a positive ζ-potential. Here, about 10−20% of the cells was transfected. When the polymer/plasmid ratio was increased, the particles still had the

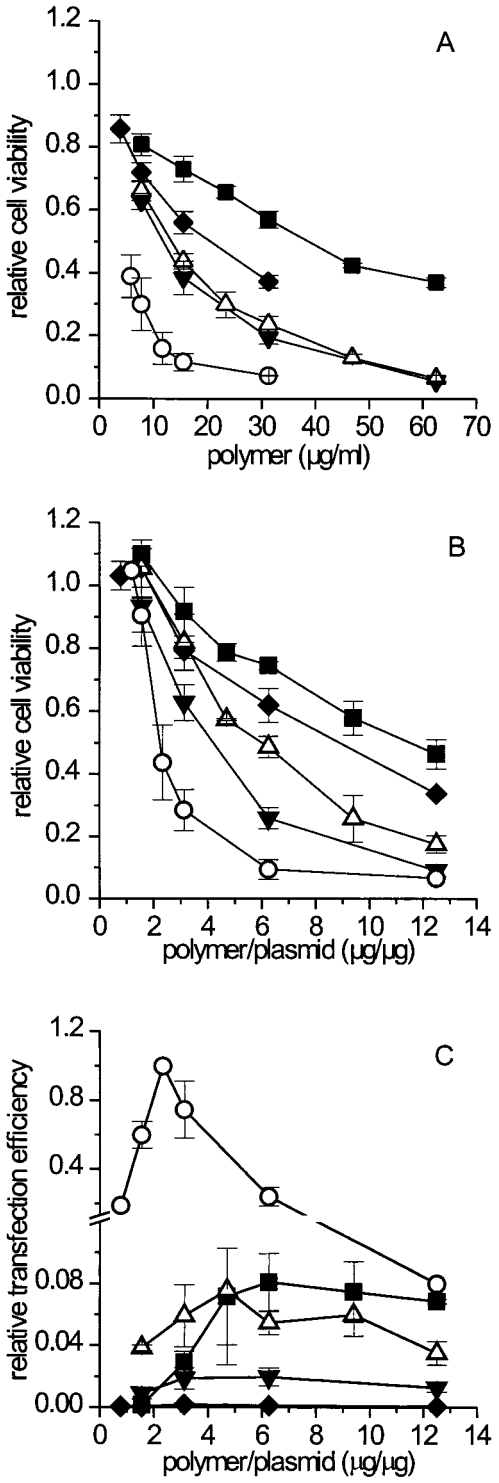


Figure 7. Effect of polymer concentration on the relative cell viability (a), effect of polymer/plasmid ratio on the relative cell viability (b), and transfection efficiency (c). The plasmid concentration was 5 μg/mL, the transfection time (incubation time of the complexes with OVCAR-3 cells) was 1 h. Transfection values are normalized to the maximum number of transfected cells after incubation with plasmid complexed to p(DMAEMA). The results are shown as mean values (±SEM) of three experiments. Symbols as in Figure 2.

Table 4. Relative Transfection Efficiency, Particle Size and Polydispersity (PI) of Polyplexes, Prepared at Two Different Polymer/Plasmid Ratios

	polymer/plasmid 3/1 (mg/mg)			polymer/plasmid 6/1 (mg/mg)		
polymer	relative transfection[a] (%)	particle size (mm)	PI	relative transfection[a] (%)	particle size (mm)	PI
p(DMAEMA)	75 ± 16	0.18 ± 0.04	0.2	24 ± 5	0.15 ± 0.02	0.2
p(DMAEMAm)	5.9 ± 2.0	0.32 ± 0.11	0.2	5.5 ± 0.7	0.16 ± 0.02	0.1
p(DMAPMA)	2.9 ± 0.7	0.15 ± 0.02	0.2	8.1 ± 1.8	0.14 ± 0.02	0.2
p(DMAPMAm)	1.9 ± 0.7	0.17 ± 0.03	0.1	2.0 ± 0.6	0.13 ± 0.02	0.2
p(TMAEMA)	0.19 ± 0.10	0.16 ± 0.02	0.1	0.12 ± 0.05	0.14 ± 0.01	0.2

[a] Transfection values are normalized to the maximum number of transfected cells obtained with p(DMAEMA)/plasmid complexes (resulting in an absolute transfection efficiency of 5−20%).

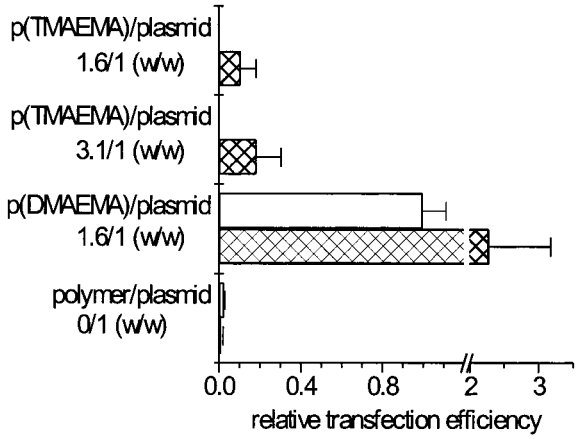


Figure 8. Influence of the presence of adenovirus during transfection on the relative transfection efficiency. Cells were incubated with polyplexes in the absence (open bars) or the presence (filled bars) of 1.9×10^9 adenovirus particles/mL. Transfection values are normalized to the maximum number of transfected cells after incubation with p(DMAEMA)/plasmid 1.6/1 (w/w) in absence of adenovirus. The plasmid concentration was 5 μg/mL. The results are shown as mean values (±SEM) of three experiments.

same physicochemical characteristics as observed at polymer/plasmid ratio 2−3/1 (w/w). However, at this high polymer/plasmid ratio, the transfection formulation contained besides polyplexes probably also free polymer. Due to the presence of an increasing amount of free polymer with an increasing polymer/plasmid ratio, the cell viability decreased resulting in a reduction of the transfection efficiency (*3*).

For the studied analogues of p(DMAEMA), the transfection efficiency was 5−400-fold lower than observed for p(DMAEMA). Moreover, the bell-shaped curve was less pronounced. Table 4 summarizes for two polymer/plasmid ratios, the particle size, the polydispersity index (PI) of the polyplexes and the relative transfection efficiency. Again, it can be seen that despite the fact that polyplexes with the same physicochemical characteristics are formed, the transfection efficiency of these polyplexes differed widely: p(DMAEMA) is far superior as transfectant in comparison with the other polymers investigated.

Figure 8 shows the effect of the presence of adenovirus during transfection with p(DMAEMA)/plasmid and p(TMAEMA)/plasmid complexes. In agreement with the results obtained with poly(l-lysine) (*23*), the transfection efficiency of p(DMAEMA)/plasmid complexes was enhanced in the presence of adenovirus. More interestingly, complexes of p(TMAEMA) and plasmid were also able to transfect at polymer/plasmid (w/w) ratios of 1.6/1 and 3.1/1, respectively, while in the absence of adenovirus, practically no cells were transfected. The cell viability was not significantly influenced by the presence of adenovirus.

DISCUSSION

To transfect cells, the polymer has to condense DNA to a particle of about 0.1−0.3 μm. After cellular entry via, e.g., endocytosis the plasmid has to be transported into the nucleus, which requires endosomal escape and dissociation of the polymer/plasmid complex. This study shows that relatively small changes in the structure of p(DMAEMA) do not have a large effect on the condensing properties of the polymer (Figure 2, Tables 3 and 4), while the effect on the cytotoxicity and transfection capability is substantial. For example, the presence of an amide group instead of an ester group in p(DMAEMAm) or a side chain with an extra methylene group in p(DMAPMA) resulted in a decrease in transfection capacity of the polymer (Table 4, Figure 7c). Since the polyplexes have comparable physicochemical characteristics, the reduced transfection efficiency cannot be ascribed to the formation of large complexes (*3*, *34*) or differences in ζ-potential (*9*) as was observed before.

The highest transfection efficiency was obtained with polyplexes containing p(DMAEMA). This superior transfection efficiency cannot be ascribed to the relatively high molecular mass of p(DMAEMA) as compared to the other polymers studied (Table 1) since we have demonstrated that both the DNA condensing properties and the transfection potential were independent of molecular mass of p(DMAEMA) above M_w 100−200 kDa (*3*, *7*). Assuming that all studied polymers are endocytosed in a comparable way, polyplexes containing p(DMAEMA) are apparently able to escape the endosome, and/or facilitate transport into the nucleus most efficiently. The more efficient endosomal escape of p(DMAEMA)-containing polyplexes might be explained by its (low) pK_a value. Due to a pK_a value of 7.5, p(DMAEMA) is only partially protonated at physiological pH, like poly(ethyleneimine) (PEI) (*35*) and poly(amidoamine) cascade polymers (*36*). Analogous to PEI and poly(amidoamine), p(DMAEMA) might also buffer the acidification in the endosomal/lysosomal vesicle and act as a so-called proton sponge, resulting in osmotic swelling and destabilization of the endosomal/lysosomal vesicle (*35*). This hypothesis is further supported by the observation that the presence of an endosome-disruptive agent (adenovirus) during the transfection resulted in a 2-fold increased transfection efficiency with p(DMAEMA)/plasmid complexes and in a substantially increased transfection efficiency with p(TMAEMA)/plasmid complexes. Although p(DEAEMA) and p(DMAEMAm) also have buffering capacity at physiological pH (pK_a 7.5 and 7.8, respectively (Table 1), the transfection efficiency was not evaluated for the p(DEAEMA)-containing complexes (because of severe aggregation) and was low for the p(DMAEMAm)-based polyplexes. The latter observation might be due to the lower buffering capacity of p(DMAEMAm) (Table 1), the greater size of the polyplexes (Table 4), and the higher

number of DNA-polymer interactions (Table 2) as compared to p(DMAEMA).

The relatively high cytotoxicity of p(DMAEMA) as compared to the other polymers (Table 3) might also be ascribed to its ability to destabilize endosomes. Disruption of endosomes is associated with the release of endosomal and/or lysosomal enzymes into the cytosol, which might exert a toxic effect to the cellular functions.

Once released from the endosome, the plasmid has to reach the nucleus. Therefore the polyplex has to dissociate, either in the cytosol or in the nucleus. Molecular modeling was used to obtain more insight into the interactions between polymer and plasmid DNA. Molecular modeling showed that elongation of the side group of octa(DMAEMA) resulted in an increase of the interactions between the cation and the DNA, due to a better fit of the propyl chain of octa(DMAPMA) into the major groove of octa(DNA). This also explains the high number of interactions between $(PO_4^-)_{DNA}$ and $(amino)_{poly}$ for the other propyl containing compound, octa(DMAPMAm). Furthermore, while the fit of the ethyl group in the major groove of DNA is similar for octa(DMAEMAm) and octa(DMAEMA), the presence of the amide group in octa(DMAEMAm) caused an increase in the number of intrapolymeric interactions, which can strengthen the conformation of the cation resulting in a more stable positioning in the major groove. An indication that a combination of a better fit and a rigid conformation could indeed result in an increase in the number of interactions with DNA was shown by octa(DMAPMAm). The higher number of interactions between DNA and the analogues of p(DMAEMA) can also explain the adequate condensing properties of p(DMAEMAm) with a relatively low molecular mass (120 kDa) in comparison with low molecular mass p(DMAEMA) (*3*). Molecular modeling suggests that p(DMAEMA) has the lowest number of interactions with DNA. This might be the reason for an easy dissociation of the polyplex, which is a prerequisite for the synthesis of the protein the plasmid encodes for. In a recent study using surface plasmon resonance (SPR) spectroscopy, the reversibility of p(DMAEMA)/plasmid interactions was indeed demonstrated (*37*).

Summarizing, we have shown that a combination of physicochemical, biological, and modeling techniques can shed light onto the factors determining the efficiency of polymeric transfectants.

LITERATURE CITED

(1) Felgner, P. L., Barenholz, Y., Behr, J. P., Cheng, S. H., Cullis, P., Huang, L., Jessee, J. A., Seymour, L., Szoka, F., Thierry, A. R., Wagner, E., and Wu, G. (1997) Nomenclature for synthetic gene delivery systems. *Hum. Gene Ther. 8*, 511−512.

(2) Cherng, J. Y., Van de Wetering, P., Talsma, H., Crommelin, D. J. A., and Hennink, W. E. (1996) Effect of size and serum proteins on transfection efficiency of poly(2-(dimethylamino)-ethyl methacrylate)-plasmid nanoparticles. *Pharm. Res. 13*, 1038−1042.

(3) Van de Wetering, P., Cherng, J. Y., Talsma, H., and Hennink, W. E. (1997) Relation between transfection efficiency and cytotoxicity of poly(2-(dimethylamino)ethyl methacrylate)/plasmid complexes. *J. Controlled Release 49*, 59−69.

(4) Morgan, D. M. L., Clover, J., and Pearsson, J. D. (1988) Effects of polycations on leucine incorporation, lactate dehydrogenase release, and morphology of human umbilical vein endothetlial cells. *J. Cell Sci. 91*, 231−238.

(5) Choksakulnimitr, S., Masuda, S., Tokuda, H., Takakura, Y., and Hashida, M. (1995) In vitro cytotoxicity of macromolecules in different cell culture systems. *J. Controlled Release 34*, 233−241.

(6) Santini, M. T., Cametti, C., Indovina, P. L., Morelli, G., and Donelli, G. (1997) Polylysine induces changes in membrane electrical properties of K562 cells. *J. Biomed. Mater. Res. 35*, 165−174.

(7) Van de Wetering, P., Cherng, J. Y., Talsma, H., Crommelin, D. J. A., and Hennink, W. E. (1998) 2-(Dimethylamino)ethyl methacrylate based (co)polymers as gene transfer agents. *J. Controlled Release 53*, 145−153.

(8) Wheeler, C. J., Sukhu, L., Yang, G., Tsai, Y., Bustamente, C., Felgner, P., Norman, J., and Manthorpe, M. (1996) Converting an alcohol to an amine in a cationic lipid dramatically alters the co-lipid requirement, cellular transfection activity and the ultrastructure of DNA-cytofectin complexes. *Biochim. Biophys. Acta 1280*, 1−11.

(9) Takeuchi, K. I., Ishihara, M., Kawaura, C., Noji, M., Furuno, T., and Nakanishi, M. (1996) Effect of zeta potential of cationic liposomes containing cationic cholesterol derivatives on gene transfection. *FEBS Lett. 397*, 207−209.

(10) Legendre, J. Y., Trzeciak, A., Bur, D., Deuschle, U., and Supersaxo, A. (1997) *N*-acyl-(α,γ diaminobutyric acid)n hydrazide as an efficient gene transfer vector in mammalian cells. *Pharm. Res. 14*, 619−624.

(11) Byk, G., Dubertret, C., Escriou, V., Frederic, M., Jaslin, G., Rangara, R., Pitard, B., Crouzet, J., Wils, P., Schwartz, B., and Scherman, D. (1998) Synthesis, activity, and structure−activity relationship studies of novel cationic lipids for DNA transfer. *J. Med. Chem. 41*, 224−235.

(12) Murphy, J. E., Uno, T., Hamer, J. D., Cohen, F. E., Dwarki, V., and Zuckermann, R. N. (1998) A combinatorial approach to the discovery of efficient cationic peptoid reagents for gene delivery. *Proc. Natl. Acad. Sci. U.S.A. 95*, 1517−1522.

(13) Ohmori, N., Niidome, T., Kiyota, T., Lee, S., Sugihara, G., Wada, A., Hirayama, T., and Aoyagi, H. (1998) Importance of hydrophobic region in amphiphilic structures of α-helical peptides for their gene transfer-ability into cells. *Biochem. Biophys. Res. Commun. 245*, 259−265.

(14) Niidome, T., Ohmori, N., Ichinose, A., Wada, A., Mihara, H., Hirayama, T., and Aoyagi, H. (1997) Binding of cationic α-helical peptides to plasmid DNA and their gene transfer abilities into cells. *J. Biol. Chem. 272*, 15307−15312.

(15) Wadhwa, M. S., Collard, W. T., Adami, R. C., McKenzie, D. L., and Rice, K. G. (1997) Peptide-mediated gene delivery: influence of peptide structure on gene expression. *Bioconjugate Chem. 8*, 81−88.

(16) Walker, S., Sofia, M. J., and Axelrod, H. R. (1998) Chemistry and cellular aspects of cationic facial amphiphiles. *Adv. Drug Delivery Rev. 30*, 61−71.

(17) Van de Wetering, P., Van Steenbergen, M. J., Van der Houwen, O. A. G. J., Underberg, W. J. M., and Hennink, W. E. (1998) A mechanistic study of the hydrolytic stability of poly(2-(dimethylamino)ethyl methacrylate). *Macromolecules 31*, 8063−8068.

(18) Bridge, E., and Ketner, G. (1989) Redundant control of adenovirus late gene expression by early region. *J. Virol. 63*, 631−638.

(19) Cotten, M., Saltik, M., Kursa, M., Wagner, E., Maass, G., and Birnstiel, M. L. (1994) Psoralen treatment of adenovirus particles eliminates virus replication and transcription while maintaining the endosomolytic activity of the virus capsid. *Virology 205*, 254−261.

(20) InsightII 97.0 (1997) Molecular Simulations, San Diego.

(21) Goodsell, D. S., and Olson, A. J. (1990) Automated docking of substrates to proteins by simulated annealing. *Proteins: Struct., Funct., Genet. 8*, 195−202.

(22) Hamilton, T. C., Young, R. C., McKoy, W. M., Grotzinger, K. R., Green, J. A., Chu, E. W., Whang-Penn, J., Rogan, A. M., Green, W. R., and Ozols, R. F. (1983) Characterization of a human ovarian carcinoma cell line (NIH OVCAR-3) with androgen and estrogen receptors. *Cancer Res. 43*, 5379−5389.

(23) Cotten, M., Wagner, E., Zatloukal, K., Phillips, S., Curiel, D. T., and Birnstiel, M. L. (1992) High-efficiency receptor-mediated delivery of small and large (48 kilobase) gene constructs using the endosome-disruption activity of defective

or chemically inactivated adenovirus particles. *Proc. Natl. Acad. Sci. U.S.A. 89*, 6094−6098.
(24) Lim, K., and Chae, C. B. (1989) A simple assay for DNA transfection by incubation of the cells in culture dishes with substrates for beta-galactosidase. *Biotechniques 7*, 576−579.
(25) Scudiero, D. A., Shoemaker, R. H., Paull, K. D., Monks, A., Tierney, S., Nofziger, T. H., Currens, M. J., Seniff, D., and Boyd,M. R. (1988) Evaluation of a soluble tetrazolium/formazan assay for cell growth and drug sensitivity in culture using human and other tumor cell lines. *Cancer Res. 48*, 4827−4833.
(26) Pradny, M., and Sevcik, S. (1987) Precursors of hydrophilic polymers, 7: Potentiometric properties and structure of copolymers of 2-dimethylaminoethyl methacrylate. *Makromol. Chem. 188*, 227−238.
(27) Asayama, S., Maruyama, A., Cho, C. S., and Akaike, T. (1997) Design of comb-type polyamine copolymers for a novel pH-sensitive DNA carrier. *Bioconjugate Chem. 8*, 833−838
(28) Pouton, C. W., Lucas, P., Thomas, B. J., Uduehi, A. N., Milroy, D. A., and Moss, S. H. (1998) Polycation−DNA complexes for gene delivery: a comparison of the biopharmaceutical properties of cationic polypeptides and cationic lipids. *J. Controlled Release 53*, 289−299.
(29) Schreier, H., Gagné, L., Bock, T., Erdos, G. W., Druzgala, P., Conary, J. T., and Müller, B. W. (1997) Physicochemical properties and in vitro toxicity of cationic liposome cDNA complexes. *Pharm. Acta Helv. 72*, 215−223.
(30) Szoka, F. C., and Tang, M. X. (1997) The influence of polymer structure on the interactions of cationic polymers with DNA and morphology of the resulting complexes. *Gene Ther. 4*, 823−832.
(31) Deboudt, K., Delporte, M., and Loucheux, C. (1995) Copolymers of *N*-vinyl-2-pyrrolidone and 2-(dimethylamino)-ethyl methacrylate, 1: synthesis, characterization, quaternization. *Macromol. Chem. Phys. 196*, 279−290.
(32) Mumper, R. J., Wang, J., Klakamp, S. L., Nitta, H., Anwer, K., Tagiaferri F., and Rolland, A. P. (1998) Protective interactive noncondensing (PINC) polymers for enhanced plasmid distribution and expression in rat skeletal muscle. *J. Controlled Release 52*, 191−203.
(33) Gao X., and Huang, L. (1991) A novel cationic liposome reagent for efficient transfection of mammalian cells. *Biochem. Biophys. Res. 179*, 280−285.
(34) Asayama, S., Maruyama, A., Cho, C. S., and Akaike, T. (1997) Design of comb-type polyamine copolymers for a novel pH-sensitive DNA carrier. *Bioconjugate Chem. 8*, 833−836.
(35) Boussif, O., Lezoualc'h, F., Zanta, M. A., Mergny, M. D., Scherman, D., Demeneix, B., and Behr, J. P. (1995) A versatile vector for gene and oligonucleotide transfer into cells in culture and in vivo: polyethyleneimine. *Proc. Natl. Acad. Sci. U.S.A. 92*, 7297−7301.
(36) Haensler, J., and Szoka, F. C., Jr. (1993) Polyamidoamine cascade polymers mediate efficient transfection of cells in culture. *Bioconjugate Chem. 4*, 372−379.
(37) Wink, Th., De Beer, J., Hennink, W. E., Bult, A., and Van Bennekom, W. P. (1999) Interaction between plasmid DNA and cationic polymers studied with surface plasmon resonance (SPR) spectroscopy. *Anal. Chem.* 71, 801−805.

BC980148W

Peptide−Oligonucleotide Phosphorothioate Conjugates with Membrane Translocation and Nuclear Localization Properties

Maxim Antopolsky,[†] Elena Azhayeva,[†] Unni Tengvall,[†] Seppo Auriola,[†] Ilpo Jääskeläinen,[‡] Seppo Rönkkö,[‡] Paavo Honkakoski,[‡] Arto Urtti,[‡] Harri Lönnberg,[§] and Alex Azhayev*[,†]

Departments of Pharmaceutical Chemistry and Pharmaceutics, University of Kuopio, FIN-70211 Kuopio, Finland, and Department of Chemistry, University of Turku, FIN-20014 Turku, Finland. Received November 6, 1998; Revised Manuscript Received April 19, 1999

Eighteen peptide−oligonucleotide phosphorothioate conjugates were prepared in good yield and thoroughly characterized with electrospray ionization mass spectra. When applied to the living cells, conjugates exhibiting membrane translocation and nuclear localization properties displayed efficient intracellular penetration but failed to show any serious antisense effect. Studies on the intracellular distribution of the fluorescein-labeled conjugates revealed their trapping in endosomes.

INTRODUCTION

Synthetic peptides having membrane translocation properties and those possessing additionally nuclear localization properties have been found to be useful vectors for efficient internalization of oligonucleotides into living cells. These peptides and their polylysine derivatives have been shown to complex with oligonucleotides and hence serve as carriers for cytoplasmic or nuclear delivery (*1, 2*). Covalent oligonucleotide−peptide conjugates have also received considerable attention as new potential antisense agents exhibiting potentially enhanced cellular uptake (*3*−*17*). The preparation of such conjugates has been accomplished by various methodologies, based either on postsynthetic conjugation of oligonucleotides and peptides, both bearing appropriate reactive groups (*3*−*8*, *10*, *11*, *13*, *14*, *16*, *17*) or on solid-phase assembly (9, *12*, *15*). Most of these methods concern the synthesis of conjugates of natural phosphodiester oligonucleotides, and only few papers describe the preparation of oligonucleotide phosphorothioates linked to peptides. Lebleu and co-workers have synthesized a 25-mer peptide-oligo-dC phosphorothioate conjugate in a 53% coupling yield, assessed from the HPLC trace (*8*), However, neither the yield of the isolated product nor characterization of this conjugate were reported. Heitz et al. have recently reported on successful use of a carrier peptide−oligonucleotide phosphorothioate conjugate (POPC) in transfer of an antisense sequence into living cells (*17*). Unfortunately, no experimental details concerning the synthesis, isolation, and characterization of this interesting compound were given. Since most peptides used as carriers for oligonucleotides possess relatively long hydrophobic sequences, the properties of their conjugates (e.g. solubility, chromatographic behavior, etc.) appear to differ considerably from those of oligonucleotide phosphorothioates, which, in turn, possess some restrictions to the methods that may be applied to synthesis of POPCs. We believe that appropriate synthetic procedures to obtain well-characterized POPCs are of considerable importance.

The present paper describes the synthesis of 18 POPCs. In these, the 3′-terminus of the oligonucleotide phosphorothioate is linked by a disulfide bond to the N- or C-terminus of either a 17-mer membrane permeable motif (MPM)—the hydrophobic region of signal peptide sequence of the Kaposi fibroblast growth factor, known to interact with lipid bilayers, or a 27-mer peptide (MPM-NLS), containing in addition to the above-mentioned MPM motiff a nuclear localization sequence (NLS) of the transcription nuclear factor *k*B (*18*). Furthermore, the cellular uptake and intracellular localization of fluorescein-labeled conjugates have been examined and inhibition of the luciferase gene expression in a cell-free model transcription-translation system and in living cells has been attempted.

EXPERIMENTAL PROCEDURES

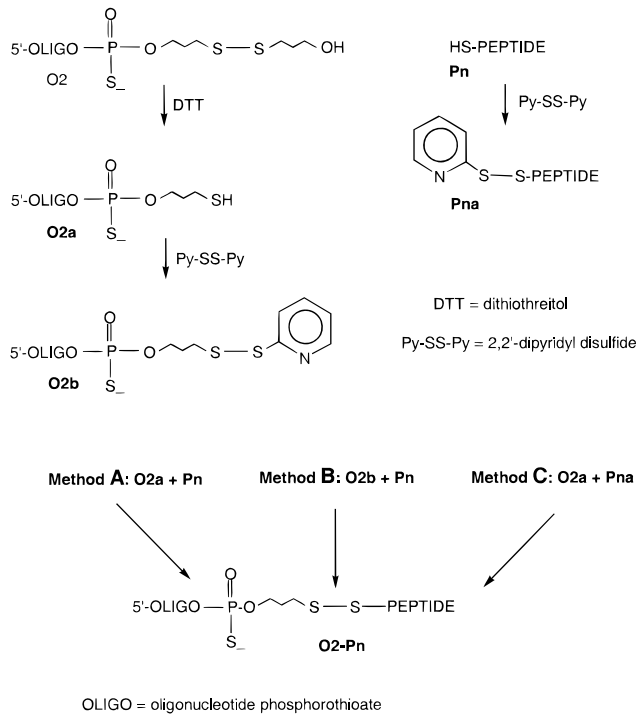
Peptide Synthesis. Fmoc-L-amino acids for peptide synthesis were purchased from Bachem and Novabiochem. Peptides **P1** and **P2** were synthesized on Fmoc-rink amide PEGA resin, peptide **P3** on Fmoc-Cys(Trt)-NovaSynPA500 resin, and peptide **P4** on Fmoc-Pro-NovaSynPA500 (Scheme 2), all from Novabiochem. The pyridinium salt of 3-tritylthiopropionic acid was obtained by the standard tritylation procedure and finally crystallized (ether/hexane); mp 175−177 °C. ^{1}H NMR ($CDCl_3$): δ 7.43−7.19 (m, 15H, arom.), 2.45 (t, 2H, J = 7.4 Hz, $-CH_2-$), 2.33 (t, 2H, J = 7.4 Hz, $-CH_2-$). The synthesis of all peptides was performed by a solid-phase method on a Milligen 9050 synthesizer. Standard protocols based on Fmoc/HBTU/TEA chemistry were used. 3-Tritylthiopropionic acid was introduced to the N-terminus of two peptides (**P2**, **P4**) directly on a synthesizer (HBTU/TEA condensation).

Oligonucleotide Synthesis. The oligonucleotide phosphorothioates were prepared on a solid support, bearing a disulfide linker (*19*). 2′-Deoxyribonucleoside 3′-phosphoramidites, fast-sulfurizing reagent, and fluorescein phosphoramidite were products of Glen Research. The solid-phase synthesis was performed on a PE Applied Biosystems 392 DNA synthesizer on a 1 μM scale.

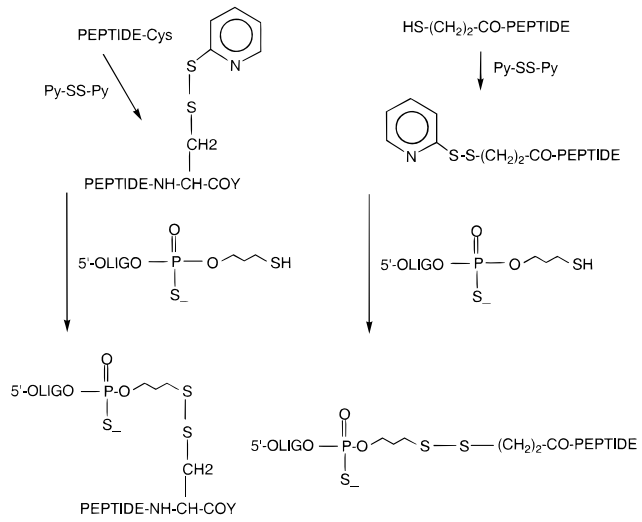
* To whom correspondence should be adressed. Phone: +358 17 162204. Fax: +358 17 162456. E-mail: Alex.Azhayev@uku.fi.
[†] Department of Pharmaceutical Chemistry.
[‡] Department of Pharmaceutics.
[§] Department of Chemistry.

10.1021/bc980133y CCC: $18.00 © 1999 American Chemical Society
Published on Web 06/30/1999

Scheme 1



Scheme 2



O1-P1; **O2-P1**; **O3-P1**; **O4-P1**; **O1-P3**; **O2-P3**; **O3-P3**; **O4-P3**; **O5-P3**.

O1-P2; **O2-P2**; **O3-P2**; **O4-P2**; **O1-P4**; **O2-P4**; **O3-P4**; **O4-P4**; **O5-P4.**

OLIGO = 5'-TGGCGTCTTCCATTT-3 ' (**O1**)

OLIGO = 5'-TTTACCTTCTGCGGT-3' (**O2**)

OLIGO = 5'-ACCGCAGAAGGTAAA-3' (**O3**)

OLIGO = 5'-XTGGCGTCTTCCATTT-3 ' (**O4**)

OLIGO = 5'-TTTTGGCGTCTTCCATTTTACCAAC-3 ' (**O5**)

X = Fluorescein

All oligonucleotides are phosphorothioates

PEPTIDE-Cys = H-AAVALLPAVLLALLAPC-NH_2 (**P1**)

HS-PEPTIDE = $HS(CH_2)_2$-CO-AAVALLPAVLLALLAP-NH_2 (**P2**)

PEPTIDE-Cys = H-AAVALLPAVLLALLAPVQRKRQKLMPC-OH (**P3**)

HS-PEPTIDE = $HS(CH_2)_2$-CO-AAVALLPAVLLALLAPVQRKRQKLMP-OH (**P4**)

Cationic Lipid Formulations. Formulations with Cytofectin GS (Glen Research) were prepared following the manufacturer's procedure.

HPLC Techniques. The peptides and their 2-pyridylsulfide derivatives were analyzed and isolated by reversed-phase chromatography (RP) (column, Genesis C4, 300 Å, 4 μm, 4.0 × 150 mm, Jones Ltd.; buffer A, 0.05 M triethylammonium acetate; buffer B, 0.05 M triethylammonium acetate in 80% MeCN; flow rate, 1.0 mL min^{-1}; a linear gradient from 40 to 100% B in 30 min was applied). The oligonucleotides containing disulfide tethers were analyzed and isolated by ion-exchange chromatography (IE) (column, PolyWax LP 300 Å, 4 μm, 4.6 × 100 mm, buffer A, 0.05 M KH_2PO_4 in 50% aqueous formamide, pH 6.7; buffer B, A + 1,5 M NaBr; flow rate, 1.0 mL min^{-1}; a linear gradient from 0 to 70% B in 30 min was applied) and RP [column, Genesis C18, 300 Å, 4 μm, 4.0 × 150 mm, Jones Ltd.; buffer A, 0.05 M triethylammonium acetate (TEAA); buffer B, 0.05 M TEAA in 80% MeCN; flow rate, 1.0 mL min^{-1}; a linear gradient from 0 to 50% B in 30 min was applied]. The conjugates were analyzed by IE as described for oligonucleotides. The final isolation and analysis of the conjugates were performed by RP HPLC similar to that described for oligonucleotides (a linear gradient from 0 to 100% B in 30 min was applied in this case).

Methods to Synthesize Disulfide Cross-Linked Conjugates. *Oligonucleotide **O2a***. A 5% triethylamine (TEA) in ethanol (40 μL) was added to a solution of oligonucleotide **O2** (20 OD) in 0.05 M TEAA buffer (1.5 mL). Dithiothreitol (3 mg) was then added, and the mixture was left for 3 h at rt and finally concentrated to a volume of 0.5 mL. The oligonucleotide bearing a free mercapto group was isolated by RP HPLC and used immediately.

*Oligonucleotide **O2b***. Oligomer **O2a** (20 OD) in 0.05 M TEAA buffer (1.5 mL) was diluted with an equal volume of ethanol. 2,2′-Bis(dipyridyl)disulfide (3 mg) was then added, and the mixture was left to stand for 1 h at rt. The corresponding 2-pyridyl sulfide derivative **O2b** was then concentrated to a volume of 0.5 mL and separated from the excess of 2,2′-bis(dipyridyl)disulfide and other byproducts with RP.

*Peptide **P2a***. Peptide (**P2**, 3 mg) was dissolved in a mixture of ethanol and formamide (1:1, 1 mL). 2,2′-Bis-(dipyridyl)disulfide (5 mg) was then added to a solution and the mixture was left for 1 h at rt. The pyridyl sulfide derivative was purified by RP HPLC. The appropriate peak (1.5 mL) was collected and diluted with formamide to a volume of 30 mL, followed by addition of 5% TEA in ethanol (300 μL).

Method A. Oligomer **O2a** (2 OD) in 0.05 M TEAA buffer (0.15 mL) was added to a solution of peptide **P2** (0.3 mg) in formamide-TEA (100:1, 3.03 mL) immediately after its separation. The mixture was kept overnight at rt and applied onto a DEAE-Toyopearl 650M column (10 × 80 mm, Br^-), equilibrated with 50% formamide. The column was washed with 50% formamide (50 mL), and the conjugate was eluted with 1 M NaBr and 0.05 M potassium phosphate buffer in 50% formamide (pH 6.5). Crude conjugate was finally analyzed, purified by RP HPLC, and desalted.

Method B. Oligomer **O2b** (2 OD) in 0.05 M TEAA buffer (0.15 mL) was added to a solution of peptide **P2** (0.3 mg) in formamide-TEA (100:1, 3.03 mL). The mixture was kept overnight at rt and the crude conjugate was analyzed and purified as in method A.

Method C. Oligomer **O2a** (2 OD) in 0.05 M TEAA buffer (0.15 mL) was added to a solution of peptide **P2a** (0.3 mg) in formamide-TEA (100:1, 3.03 mL). The mixture was kept overnight at rt and the crude conjugate was analyzed and purified as in method A.

Peptide–Oligonucleotide Phosphorothioate Conjugates. Each conjugate was synthesized according to method C, starting from 20 OD of initial oligonucleotide.

Electrospray Ionization Mass Spectrometry. Mass spectra were acquired using an LCQ quadrupole ion trap mass spectrometer equipped with an electrospray ionization source (Finnigan MAT, San Jose, CA). The spray needle was set to −3 kV. The nitrogen sheath gas flow rate was set to 70. The stainless steel inlet capillary was heated to 200 °C, and the capillary voltage was −39 V. The number of negative charges was maximized by calibrating the tube lens offset with a 15-mer oligonucleotide (data not shown). The value chosen was −10 V. The spectra were measured using 200 ms for collection of the ions in the trap, and 5−12 microscans were summed. The eluent consisted of 80% acetonitrile containing 25 mM TEA. The eluent flow rate was set to 10 μL/min, and 5 μL samples containing 1−20 pmol of conjugates were injected to the system. Positive ion mass spectra of the peptides were acquired by using 50% methanol as the eluent. The sample concentration was 10 μg/mL, and 5 μL was injected. The spray needle potential was set to 5 kV, capillary voltage 20 V, and tube lens 10 V. Other conditions were as in negative ion mode. The molecular weights of the compounds were calculated using computer program Gretas Carbos, created by Hines and Gibson (UCSF).

^{32}P-Labeling of Phosphorothioate Oligonucleotides and Oligonucleotide−Peptide Conjugates and Their Gel Electrophoresis. Oligonucleotides and conjugates were 5′-^{32}P-labeled with T4 polynucleotide kinase (Pharmacia), purified on the OPS cartridge (PE-Applied Biosystems). A 15% PAGE was employed to analyze the oligonucleotides and conjugates.

Development of Stable Cell Lines Expressing Luciferase Activity. CHO-AA8-Luc cells expressing luciferase activity were purchased from Clontech Inc. (Palo Alto, CA). Stable cell lines expressing tetracycline-regulated luciferase mRNA and activity were developed by the method of Gossen and Bujard (*20*) according to the instructions and plasmids from Clontech Inc (Palo Alto, CA). Briefly, monkey kidney fibroblast CV1-P and human retinal pigmented epithelium D407 cell lines were transfected with pTet-Off with calcium phosphate transfection (*21*), and cells with stably integrated plasmid DNA were selected in the presence of 0.4 mg/mL G418 (Calbiochem, La Jolla, CA) and tested for the expression of tetracycline-sensitive regulator by transient transfection of pTRE-luc and pCMV-beta-galactosidase plasmids, culturing in the presence or absence of 2 mg/L tetracycline and luciferase assays. Those cell lines displaying tetracycline-repressible luciferase activity were expanded and transfected with pTRE-luc plus pTK-hyg plasmids. Cells with stably integrated luciferase cDNA were selected in the presence of both 0.4 mg/mL G418 and 0.1 mg/mL hygromycin B (Calbiochem) and screened again for tetracycline-repressible luciferase activity. This procedure yielded derivatives indistinguishable from their parent CV1-P and D407 with respect to cell morphology and growth characteristics. The CV1-P derivatives CV-11 and CV-19 and D407 derivative 6-2 were used in this study.

Uptake of ^{32}P-Labeled Oligonucleotides and Conjugates. CV1-P cells were plated in Dulbecco's modified Eagle's medium (DMEM, Gibco) with 10% fetal bovine serum (FBS, Gibco) in 96-well plates, 2×10^5 cells/well, and grown for 24 h in a humidified cell incubator with 5% CO_2 at 37 °C. After washing the cells, medium was replaced with 180 μL of the serum-free medium containing a mixture of 5′-labeled (3.5×10^4 - 1.75×10^6 cpm) and unlabeled oligonucleotide or conjugate (0.1−5 μM). After 4 h of incubation at 37 °C, cells were washed several times with medium, phosphate buffer saline (PBS, Gibco), high salt-low pH buffer solution (0.4 M NaOAc, 1 M NaCl, pH 3.3), and finally with PBS (*22*, *23*). The cells were solubilized in 1% sodium dodecyl sulfate (SDS, Sigma) solution and the radioactivity was measured in the same plates with Micro Beta counter (Wallac). Aliquots of 20 μL from each well were taken for protein measurement. Background estimation experiments were conducted in parallel in separate plates without cells, where the corresponding amounts of cold and labeled oligonucleotides or conjugates were added. Both protein content data and background estimation experiments were taken into consideration while presenting the results of cellular uptake experiments. The stability of the oligonucleotides and conjugates in the cellular uptake experiments was controlled by PAGE electrophoresis which did not reveal any substantial degradation of the compounds.

Antisense Activity of the Oligonucleotides and Oligonucleotide−Peptide Conjugates. The luciferase-expressing cells were plated in 24-well plates at a density of $(4-5) \times 10^4$ cells/well and grown for 24 h to approximately 60−80% confluence. CV1-P cells were grown in DMEM with 10% of FBS, D 407 cells in DMEM with 5% of FBS, and CHO cells in α-modified Eagle's medium (α-MEM, Gibco) with 10% of FBS and medium before transfection was replaced by serum-free medium containing oligonucleotides, conjugates, or their Cytofectin GC formulation and incubated for 4 h. Cells were then grown in the normal medium for 12−20 h, washed with PBS, lysed, and tested for the luciferase activity as described earlier (*24*).

Luciferase Expression Assay. The influence of the compounds on the luciferase expression in vitro in the cell-free system was studied using TNT Coupled Wheat Germ Extract Systems kit (Promega) as described earlier (*24*).

RNase H Cleavage Experiments. Synthetic RNA fragment 5′-UACUGUUGGUAAAAUGGAAGACGCCA-AAAACAUA-3′ (**M**) was 5′ labeled with ^{32}P using T4 polynucleotide kinase (Pharmacia). One picomole of labeled matrix was annealed to 1 pmol of oligonucleotides or conjugates by heating to 70 °C and slowly decreasing the temperature to 25 °C overt 2 h. Annealed complexes were incubated with 1 unit of RNase H (USB−Amersham Pharmacia Biotech) in 20 mM Tris-HCl buffer, pH 7.5; containing 20 mM KCl, 10 mM $MgCl_2$, 0.1 mM EDTA, and 0.1 mM cystamine for 30 min at 37 °C. Products of the reaction were analyzed by 15% PAGE and subsequent autoradiography.

Confocal Fluorescence Microscopy. Luciferase-expressing cells were plated in glass Lab Tek 8-chamber slides (NUNC Inc.) at a density of $(6-10) \times 10^4$ cells/well and cultured for 36 h. The culture medium was discarded and after washing replaced by the serum-free medium containing fluorescein-labeled oligonucleotides, oligonucleotide−peptide conjugates, or their Cytofectin GC formulation. Cells were incubated for 4 h and washed twice with the serum-free medium and three times with PBS. After washing, cells were fixed with 0.1% glutaric dialdehyde in PBS for 5 min, washed with PBS, and mounted in 90% glycerol in PBS. Cells were examined under the confocal laser scanning microscope (Leica).

RESULTS AND DISCUSSION

Comparison of Methods To Synthesize Disulfide Cross-Linked Peptide-Oligonucleotide Phosphorothioate Conjugates. It is obvious that the yield of any reaction leading to the disulfide cross-linked POPC strongly depends on the spatial structures of the peptide

and the oligonucleotide in question. To develop a method of cross-linking that is as independent as possible of the structures of the molecules to be linked together, the composition of the solvent mixture and concentrations of the reacting components were first optimized. A large number of preliminary experiments demonstrated that the best yields were obtained when the resulting conjugation mixture contained about 90% of a chaotropic solvent, formamide, the concentration of peptides being about 0.09 mg/mL and that of oligonucleotides about 0.6 OD/mL. In principle, there are at least three straightforward routes to generate a disulfide bond between an oligonucleotide phosphorothioate tethered with a linker, bearing a mercapto group, and a synthetic peptide also having a mercapto function. This function may reside either in peptide's C-terminal cysteine or in a mercaptopropionic acid residue, attached to the N-terminus. We have investigated the applicability of these possible alternative procedures by binding peptides **P1**−**P4** to oligonucleotide **O2**: method A, the reaction of a thiol containing peptide with an oligonucleotide bearing mercaptoalkyl group [analogous to the approach mentioned in the literature (*17*)]; method B, the reaction of a thiol containing peptide with an oligonucleotide possessing a pyridyl disulfide function, similar to procedure reported by Lebleu et al (*8*); and, finally, method C, the reaction of a pyridyl disulfide containing peptide with an oligonucleotide having a mercaptoalkyl group (Scheme 1).

The results of these experiments have demonstrated that the yield of isolated conjugate strongly depends on the method of coupling and the peptide's structure. Method A gave yields ranging from 0.4 to 23%. Testing of method B has also revealed relatively low yields from 7 to 24%. Method C, however, have demonstrated the highest yields, ranging from 36 to 88%.

An additional experiment, employing method C, was carried out in order to demonstrate the absence of coupling between the peptide, activated by a pyridyl disulfide function and the phosphorothioate groups of the oligonucleotide. In this experiment, a control oligonucleotide phosphorothioate had the same sequence as **O1**, but contained no 3′-mercaptoalkyl function. After 12 h at rt, IE HPLC has revealed no formation of any conjugated structure. Oligonucleotide phosphorothioate appeared to be intact. RP HPLC, in turn, has demonstrated the formation of only 3% of peptide dimer, with the rest of the activated peptide remaining stable in the reaction mixture.

Thus, method C appears to be the procedure of choice for preparation of the disulfide cross-linked peptide−oligonucleotide phosphorothioate conjugates.

Synthesis and Characterization of Peptide−Oligonucleotide Phosphorothioate Conjugates. Method C was employed to synthesize 18 POPCs (Scheme 2). In all of these conjugates, the oligonucleotide moiety is a 15-mer (**O1**−**O4**) or 25-mer (**O5**) phosphorothioate. The peptide moiety is either a modified 17-mer hydrophobic MPM (**P1**, **P2**) or a modified 27-mer sequence, containing the above-mentioned 17-mer sequence and a the basic 10-mer NLS (**P3**, **P4**). The disulfide bridge was formed between the 3′-ends of **O1**−**O5** oligonucleotides and either the C-termini (**P1**, **P3**) or N-termini (**P2**, **P4**) of peptides. The yields of conjugates synthesized were 35−60%, and purity, as assessed from RP HPLC was higher than 95%. The 15% denaturing PAGE (data not shown) revealed good purity for all conjugates synthesized. The migration rate of the conjugates of peptides **P1** and **P2** was about 0.73−0.75 times, and that of peptides **P3** and **P4** conjugates 0.63−0.65 times that of the parent oligonucleotides. The final characterization of POPCs was achieved by electrospray ionization mass spectrometry (ESI-MS), which has proven to be a powerful method for the characterization of oligonucleotides (*25, 26*) as well as their peptide conjugates (*27*). In our study, the negative ion ESI mass spectra of the conjugates displayed a series of deprotonated molecules $(M - nH)^{n-}$ as major peaks, the charge states ranging from 4 to 9. Figure 1 demonstrates a typical ESI mass spectrum obtained after injection of 5 μL of conjugate **O4**−**P3**. Mass deconvulation program can be used for reconstruction of the molecular weight of the conjugate using the *m*/*z* values of the multiply deprotonated molecules (Figure 2). The measured and theoretically calculated average molecular weights of compounds reported here were in excellent agreement. The difference between the calculated and measured molecular masses was always less than 3.1 mass units (0.05%).

Attempted Inhibition of Luciferase Gene Expression in Vivo in Living Cells by Peptide−Oligonucleotide Phosphorothioate Conjugates. The peptide moiety of conjugates reported here contains membrane translocation and nuclear localization motives which are supposed to assist the oligonucleotide in passing through the cell membrane and reaching the nucleus. The oligonucleotide moiety is expected to display its antisense effect in the cytoplasm and nucleus, inhibiting the target gene expression (*28*).

We have attempted to influence the luciferase gene expression in stably transfected CV1-P, CHO-AA8-Luc, or D-407 luciferase producing cells with our conjugates. As in **O1**, the oligonucleotide sequence in the tested conjugates **O1**−**Pn** was complementary to the initiation codon region of firefly luciferase mRNA and was reported earlier to work as an effective antisense compound (*29*). The rest of the conjugates were used as controls containing either a reversed (**O2**−**Pn**) or a sense (**O3**−**Pn**) stretches. More than 10 identical experiments were performed in which the influence of these compounds on the reporter gene expression was compared to the inhibition of expression by the cationic lipid formulation of **O1** or **O1**−**P3** with the Cytofectin GC. These experiments have demonstrated the inability of the conjugate **O1**−**P3** alone to display any serious antisense effect. We have obtained more or less similar results for conjugates **O1**−**P1**, **O1**−**P2**, and **O1**−**P4** and conjugates **O5**−**P3** and **O5**−**P4**, which contain a longer antisense oligonucleotide sequence **O5** in comparison to **O1**. It is noteworthy that a substantial inhibition of luciferase expression was observed in all experiments with the Cytofectin formulation of **O1** or **O1**−**P3**. It appears that unlike the case where cationic lipid formulation was used, our conjugates alone fail to display reproducible antisense action.

Nevertheless, it was still interesting to find out which part of these conjugates (oligonucleotide or peptide) failed to play the desired role.

Cellular Uptake Studies with 5′-[^{32}P]-Oligonucleotide Phosphorothioates and Peptide−5′-[^{32}P]-Oligonucleotide Phosphorothioate Conjugates. Our unsuccessful attempt to inhibit the luciferase gene expression in cells raised some points of substance. First, it was necessary to verify if any of our conjugates were taken up by these cells. If some conjugates entered living cells, then it would be interesting to find out whether they remain intact throughout our experiment. Figure 3 demonstrates a typical result of cellular uptake experiments. One can see a relatively strong association of conjugate **O2**−**P3** with CV1-P cells in comparison to conjugates **O2**−**P1** and **O2**−**P2** and oligonucleotide **O2**.

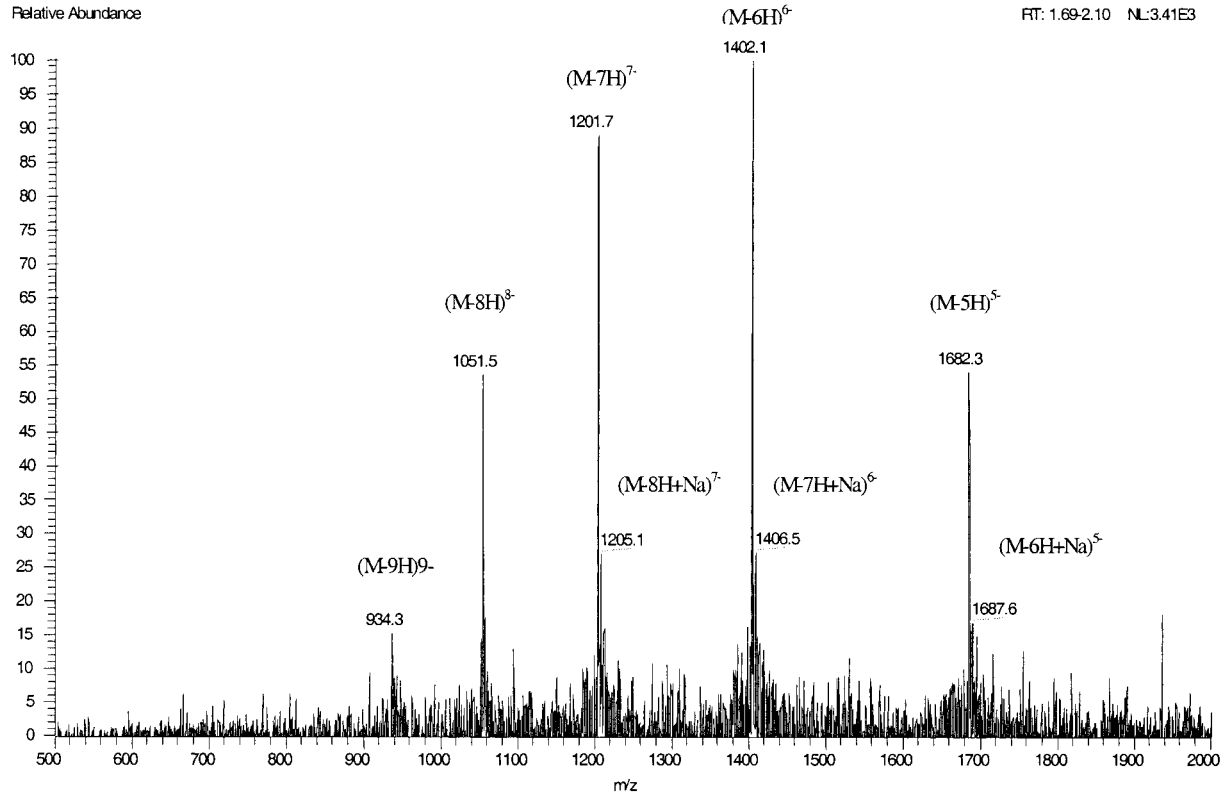


Figure 1. Negative ion ESI mass spectrum of conjugate **O4**−**P3**. The major multiply charged ions represent negative charge states from 5 to 9. Sample: 5 μL of conjugate **O4**−**P3**. Eluent: 10 μL/min of 80% acetonitrile with 25 mM triethylamine.

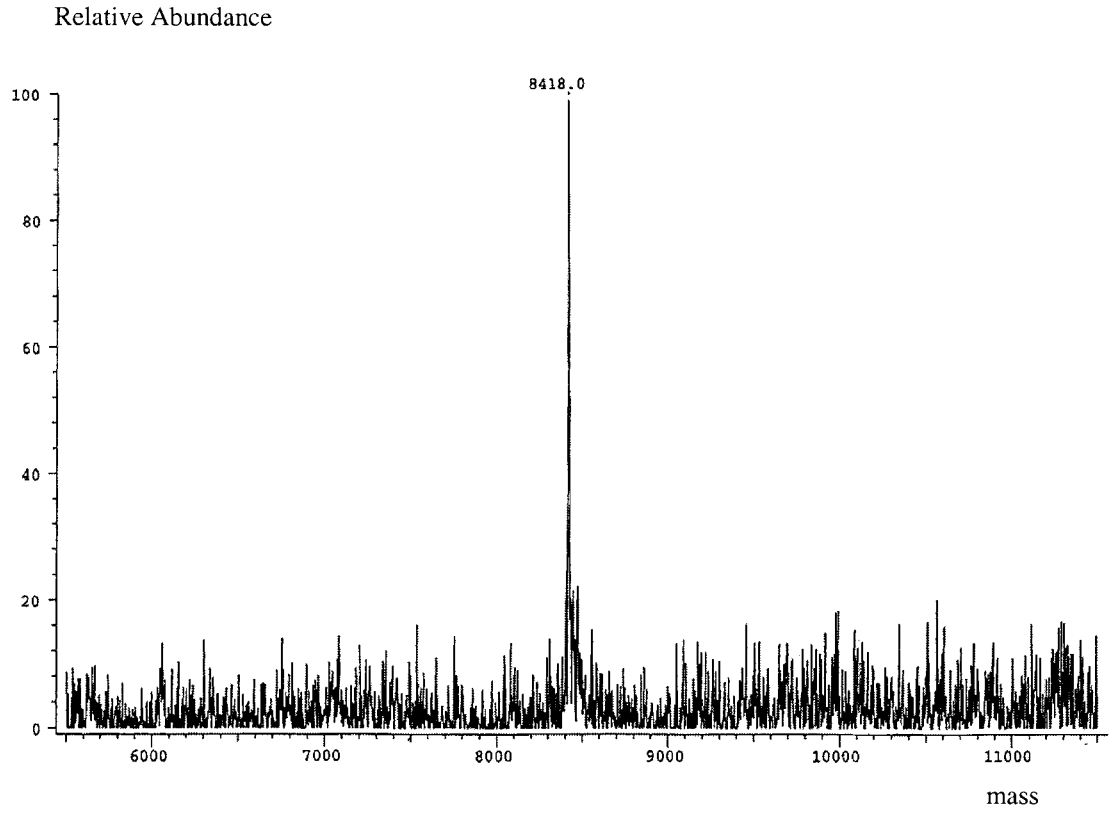


Figure 2. Reconstructed molecular weight spectrum of conjugate **O4**−**P3** (calculated mass 8418.1).

It is clear that the presence of the long 27-mer peptide with both membrane translocation and nuclear localization properties (**O2**−**P3**) is somehow responsible for this strong association, while the presence of mere membrane permeable motif (**O2**−**P1** and **O2**−**P2**) for some reason retards association even as compared to oligonucleotide **O2**. This conclusion received additional support from the stability test. Figure 4 shows the autoradiography of PAGE of cell lysates after incubation with ^{32}P-labeled conjugates and careful washing—standard procedure,

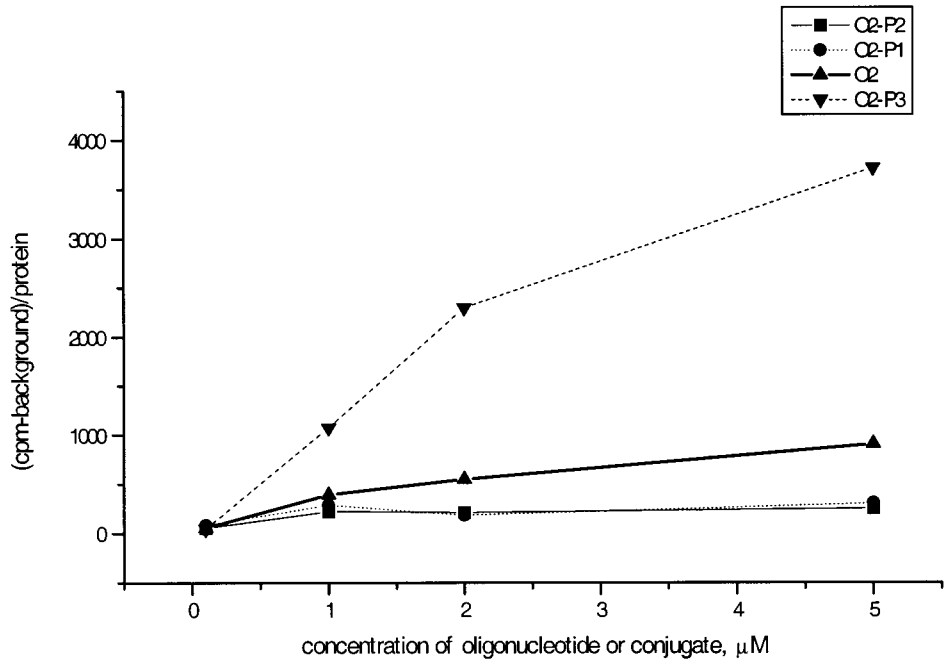


Figure 3. Uptake of the ^{32}P-labeled oligonucleotide and oligonucleotide–peptide conjugates by CV1-P cells. Dependence of cell associated radioactivity on the concentration of ^{32}P-labeled oligonucleotides and oligonucleotide–peptide conjugates in the incubation mixture. Cells were incubated with control substances for 4 h, washed and lysed as described in Experimental Procedures.

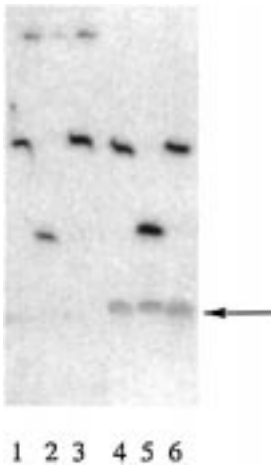


Figure 4. Stability of the oligonucleotide–peptide conjugates in the cells**.** Autoradiogram of 15% PAAG electrophoresis of the cell lysates and control ^{32}P-labeled conjugates: lines 1–3—cells incubated with mixtures of 5 μM unlabeled and 1.75×10^6 cpm of ^{32}P-labeled **O1**–**P3**, **O1**–**P1**, or **O2**–**P3** respectively; lines 4–6—^{32}P-labeled **O1**–**P3**, **O1**–**P1**, or **O2**–**P3**. The migration position of **O1** is indicated with arrow.

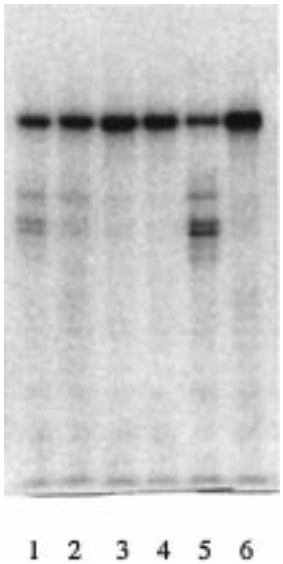


Figure 5. RNase H digestion of [^{32}P]**M** in the presence of oligonucleotides and conjugates: line 1—in the presence of **O1**–**P3**; line 2—in the presence of **O1**–**P4**; line 3—in the presence of **O3**–**P3**; line 4—in the presence of **O3**–**P4**; line 5—in the presence of **O1**; line 6—[^{32}P]**M**.

removing the noninternalized conjugates and dead cells, capable of accumulating labled compounds (*22*, *23*). Very little if any degradation was detected, demonstrating sufficient stability of the peptide–oligonucleotide phosphorothioate conjugates throughout our experiments with cells.

RNase H Mediated Cleavage of Synthetic RNA-Conjugate Complexes and Inhibition of Luciferase Gene Expression in an in Vitro Transcription-Translation System. The next question was whether our conjugates were capable of triggering the RNase H mediated cleavage of the target RNA. The answer to this question appears to be of significant importance since this type of mRNA degradation is believed to be the most common mechanism of the antisense action (*30*). To investigate this subject, we synthesized a 34-mer oligoribonucleotide (**M**), corresponding to the −13 to +21 fragment of the luciferase mRNA. This RNA fragment was 5′-^{32}P-labeled and subjected to the action of RNase H in the presence of oligonucleotide **O1** and conjugate **O1**–**P3** or **O1**–**P4**, all containing the 15-mer complementary sequence. Conjugates **O3**–**P3** and **O3**–**P4** containing the sense sequences were used as controls. The autoradiography of PAGE referring to these experiments is shown in Figure 5. One can see that while conjugates **O1**–**P3** or **O1**–**P4**, as well as oligonucleotide **O1**, clearly triggered the RNase H activity (Figure 5, lines 1, 2, and 5), control conjugates O3–P3 and O3–P4 were unable to recruit the enzyme for the RNA fragment digestion (Figure 5, lines 3 and 4). The observed effect of **O1**–**P3**

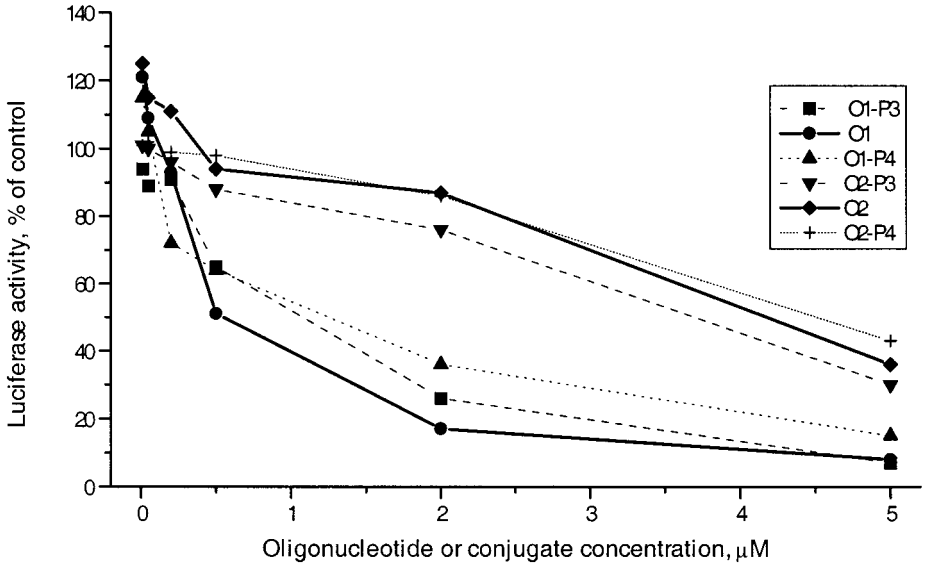


Figure 6. Influence of the antisense and control oligonucleotides and/or oligonucleotide−peptide conjugates on the luciferase reporter gene expression in cell-free system.

and **O1**−**P4** was noticably smaller than that of **O1**. This fact may be attributed to the reduced binding affinity of oligonucleotide part of conjugates to the target RNA, when compared to that of oligonucleotide phosphorothioate **O1**.

As indicated above, our conjugates contained sequences complementary to the initiation codon region of the firefly luciferase mRNA, and therefore, it was reasonable to probe their antisense properties in a cell-free luciferase gene expression system which proved to be a rather useful tool in our previous studies (*24*). In fact, this type of experiment would mimic the testing with living cells better than the enzymatic assay with RNase H, and it would hence better elucidate the potency of our conjugates as antisense agents. Figure 6 shows that conjugates **O1**−**P3** or **O1**−**P4**, as well as oligonucleotide **O1**, all containing the antisense sequence, were able to decrease the luciferase activity by 60−80% at 2 μM concentration, while the control conjugates **O2**−**P3**, **O2**−**P4**, and control oligonucleotide **O2**, all containing reversed sequence, showed inhibition of only 10−20% under the same conditions. Hence, it became obvious that our conjugates are taken up by the cells and they are in principle capable of showing the antisense properties. Their failure to demonstrate these features in the experiments with cells should be attributed to their "incorrect" intracellular distribution, i.e., absence from the cytoplasm and/or nucleus, where they have to be present in order to display antisense properties.

Cellular Localization of Peptide−Oligonucleotide Phosphorothioate Conjugate. To gain insight into localization of our conjugates in cells, we treated CV1-P cells with 5′-fluorescein-labeled oligonucleotide **O4**, conjugate **O4**−**P3**, and finally with **O4**−**P3** as a cationic lipid formulation with the Cytofectin GC, and examined the cells with confocal microscopy. Figure 7A demonstrates that while most of the conjugate **O4**−**P3** associated with cells is localized in endosomes, there is only faint fluorescence in cytoplasm and nucleus. Even lower level of nuclear fluorescence was detected when CV1-P cells were incubated with oligonucleotide **O4** (Figure 7B) alone. The cytoplasmic fluorescence detected in this case was much weaker than with conjugate **O4**−**P3**, and it may in all likelihood be attributed to very low level of oligonucleotide phosphorothioate internalization. In contrast to that, when the conjugate **O4**−**P3** was employed as a cationic lipid formulation, a very strong fluorescence was found within the nucleus (Figure 7C), indicating a different type of intracellular distribution as compared to results with pure conjugate (Figure 7A). Taken together, the microscopy results clearly show that although our conjugates as such indeed possess a clear affinity to cells they are trapped in the endosomes unlike the liposomal formulation. Therefore, the access of POPCs to their target in cytoplasm and nucleus is limited.

CONCLUSION

We have optimized the preparation of disulfide cross-linked POPCs. According to our results, the most efficient procedure makes use of a disulfide exchange reaction between an oligonucleotide phosphorothioate tethered with a mercaptoalkyl group and a peptide bearing a pyridyl disulfide function in 90% formamide. Eighteen compounds were prepared in a yield of 35−60% and thoroughly characterized by electrospray ionization mass spectroscopy.

The present work demonstrates that our POPCs are capable of inhibiting the luciferase gene expression in a cell-free model transcription-translation system. When applied to the living cells, some of conjugates with MPM-NLS peptide display the efficient intracellular penetration properties but fail to show any serious antisense effect. Studies on the intracellular distribution of the fluorescein-labeled conjugates have revealed their endosomal localization, thus indicating a failure to reach the cytoplasm and/or nucleus and hence to produce the antisense effect. On the contrary, when used as a cationic lipid formulation with the Cytofectin GC, our conjugates achieved effective and selective antisense inhibition of the reporter gene expression. All these data taken together brings over the conclusion that the structure of the conjugates of oligonucleotide phosphorothioates with peptides, exhibiting membrane translocation and nuclear localization properties, yet has to contain some additional feature to avoid endosomal trapping. It appears that mere conjugation of antisense oligonucleotides and peptides possessing membrane penetration and nuclear localization properties does not necessarily result in a reliable delivery system which works well with a number of cell types. However, the chemical methodology devel-

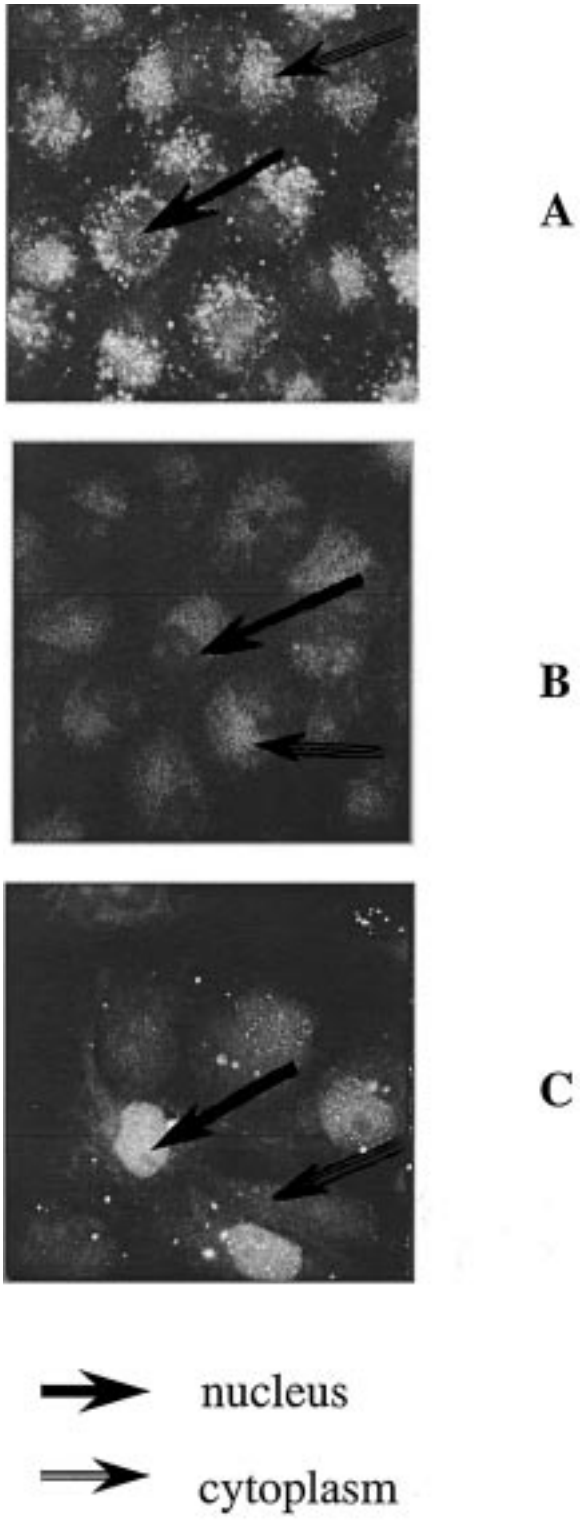


Figure 7. Confocal microscopy pictures of CV1-P cells after 4 h incubation with the fluoresceine-labeled antisense oligonucleotide and antisense oligonucleotide–peptide conjugate. Cells were incubated with (A) 0.5 μM of **O4**–**P3**, (B) 0.5 μM **O4**, (C) 0.5 μM **O4**–**P3** in the presence of 2.5 μg/mL of cytofectin.

oped by us allows conjugation of oligonucleotides also to peptide sequences enhancing endosomal escape and hence antisense activity.

ACKNOWLEDGMENT

Financial support from the Ministry of Education and Technology Development Center of Finland is gratefully acknowledged.

LITERATURE CITED

(1) Dokka, S., Toledo-Velasquez, D., Shi, X., Wang, L., and Rojanasakul, Y. (1997) Cellular delivery of oligonucleotides by synthetic import peptide carrier. *Pharm. Res. 14*, 1759–1764.

(2) Morris, M. C., Vidal, P., Chaloin, L., Heitz, F., and Divita, G. A. (1997) New peptide vector for efficient delivery of oligonucleotides into mammalian cells. *Nucleic Acids Res. 25*, 2730–2736.

(3) Eritja, R., Pons, A., Escarceller, M., Giralt, E., and Albericio, F. (1991) Synthesis of defined peptide–oligonucleotides hybrids containing a nuclear transport signal sequence. *Tetrahedron 47*, 4113–4120.

(4) Tung, C.-H., Rudolph, M. J., and Stein, S. (1991) Preparation of oligonucleotide–peptide conjugates. *Bioconjugate Chem. 2*, 464–465.

(5) Zhu, T., and Stein, S. (1994) Preparation of vitamin B_6-conjugated peptides at the amino terminus and of vitamin B_6-peptide–oligonucleotide conjugates. *Bioconjugate Chem. 5*, 312–315.

(6) Wei, Z., Tung, C.-H., Zhu, T., and Stein, S. (1994) Synthesis of oligoarginine-oligonucleotide conjugates and oligoarginine-bridged oligonucleotide pairs. *Bioconjugate Chem. 5*, 468–474.

(7) Edge, N. J., Tregear, G. W., and Haralambidis, J. (1994) Routine preparation of thiol oligonucleotides: application to the synthesis of oligonucleotide–peptide hybrids. *Bioconjugate Chem. 5*, 373–378.

(8) Bongartz, J.-P., Aubertin, A.-M., Milhaud, P. G., and Leblue, B. (1994) Improved biological activity of antisense oligonucleotides conjugated to a fusogenic peptide. *Nucleic Acids Res. 22*, 4681–4688.

(9) Robles, J., Pedroso, E., and Grandas, A. (1994) Stepwise solid-phase synthesis of the nucleopeptide Phac-Phe-Val-Ser-($p^{3'}$ACT)-Gly-OH. *J. Org. Chem. 59*, 2482–2486.

(10) Soukchareun, S., Tregear, G. W., and Haralambidis, J. (1995) Preparation and characterization of antisense oligonucleotide–peptide hybrids containing viral fusion peptides. *Bioconjugate Chem. 6*, 43–53.

(11) Tung, C.-H., Wang, J., Leibowitz, M., and Stein, S. (1995) Dual-specificity interaction of HIV-1 TAR RNA with Tat peptide–oligonucleotide conjugates. *Bioconjugate Chem. 6*, 292–295.

(12) Robles, J., Pedroso, E., and Grandas, A. (1995) Solid-phase synthesis of a nucleopeptide from the linking site of adenovirus-2 nucleoprotein, -Ser($p^{5'}$CATCAT)-Gly-Asp-. Convergent versus stepwise strategy. *Nucleic Acids Res. 23*, 4151–4161.

(13) Truffert, J.-C., Asseline, U., Brack, A., and Thuong, N. T. (1996) Synthesis, purification and characterization of two peptide–oligonucleotide conjugates as potential artificial nucleases. *Tetrahedron 53*, 3005–3016.

(14) Bruick, R. K., Dawson, P. E., Kent, S. BH., Usman, N., and Joyce, G. F. (1996) Template-directed ligation of peptides to oligonucleotides. *Chem. Biol. 3*, 49–56.

(15) Robles, J., Maseda, M., Concernau, M., Pedroso, E., and Grandas, A. (1997) Synthesis and enzymatic stability of phosphodiester-linked peptide–oligonucleotide hybrids. *Bioconjugate Chem. 8*, 785–788.

(16) Rajur, S. B., Roth, C. M., Morgan, J. R., and Yarmush, M. L. (1997) Covalent protein-oligonucleotide conjugates for effecient delivery of antisense molecules. *Bioconjugate Chem. 8*, 935–940.

(17) Chaloin, L., Vidal, P., Lory, P., Mery, J., Lautredou, N., Divita, G., and Heitz, F. (1998) Design of carrier peptide–oligonucleotide conjugates with rapid membrane translocation and nuclear localization properties. *Biochem. Biophys. Res. Commun. 243*, 601–608.

(18) Lin,Y–Z., Yao, S., Veach, R. A., Torgerso, T. R., and Hawiger, J. (1995) Inhibition of nuclear translocation of transcription factor NF-*k*B by a synthetic peptide containing a cell membrane-permeable motif and nuclear localization sequence. *J. Biol. Chem. 270*, 14255–14258.

(19) Azhayeva, E., Azhayev, A., Guzaev, A., Hovinen, J., and Lönnberg, H. (1995) Looped oligonucleotides form stable

hybrid complexes with a single-stranded DNA. *Nucleic Acids Res. 25*, 4954−4961.
(20) Gossen, M., and Bujard, H. (1992) Tight control of gene expression in mammalian cells by tetracycline responsive promoters. *Proc. Natl. Acad. Sci. U.S.A. 89*, 5547−5551.
(21) Chen, C., and Okayama, H. (1987) High-efficiency transformation of mammalian cells by plasmid DNA. *Mol. Cell Biol. 7*, 2745−2752.
(22) Basu. S., and Wickstrom, E. (1997) Synthesis and characterization of peptide nucleic acid conjugated to a D-peptide analogue of insulin-like growth factor 1 for encreased cellular uptake. *Bioconjugate Chem 8*, 481−488.
(23) Gray, G. D., Basu, S., and Wickstrom, E. (1997) Transformed and immortalized cellular uptake of oligonucleotide phosphorothioate conjugates, 3′-alkylamino oligonucleotides, 2′-*O*-methyl oligoribonucleotides, oligodeoxynucleotide methylphosphonates and peptide nucleic acids. *Biochem. Pharmocol. 48*, 1465−1476.
(24) Azhayeva, E., Azhayev, A., Auriola, S., Tengvall, U., Urtti, A., and Lönnberg, H. (1997) Inhibitory properties of double helix forming circular oligonucleotides. *Nucleic Acids Res. 25*, 4954−4961.
(25) Barry, J., Vouros P., Van Schepdael, A., and Law, S.-J. Mass and sequence verification of modified oligonucleotides using electrospray tandem mass spectrometry. (1995) *J. Mass Spectrom. 30*, 993−1006.
(26) Bothner, B., Chatham, K., Sarkisian, M., and Siuzdak, G. (1995) Liquid chromatography mass spectrometry of antisense oligonucleotides. *Bioorg. Med. Chem. Lett. 5*, 2863−2868.
(27) Jensen, O., Kulkarni, S., Aldrich, J., and Barofsky, D. (1996) Characterization of peptide−oligonucleotide heteroconjugates by mass spectrometry. *Nucleic Acids Res. 24*, 3866−3872.
(28) Marcusson, E. G., Bhat, B., Manohoran, M., Bennett, C. F., and Dean, N. M. (1998) Phosphorothioate oligodeoxyribonucleotides dissociate from cationic lipids before entering the nucleus. *Nucleic Acids Res. 26*, 2016−2023.
(29) Stull, R. A., Zon, G., and Szoka, F. C. (1996) An *in vitro* messenger RNA binding assay as tool for identifying hybridization-competent antisense oligonucleotides. *Antisense Nucleic Acid Drug Dev. 6*, 221−228.
(30) Toulme, J.-J. (1992) Artificial regulation of gene expression by complementary oligonucleotides-an overview. In *Antisense RNA and DNA* (J. A. H. Murray, Ed.) pp 175−194, Wiley-Liss, Inc., New York.

BC980133Y

Use of Heavy-Metal Clusters in the Design of N-Succinimidyl Ester Acylation Reagents for Side-Chain-Specific Labeling of Proteins

Domenico Osella,*,† Paola Pollone,† Mauro Ravera,† Michèle Salmain,‡ and Gérard Jaouen*,‡

Dipartimento di Scienze e Tecnologie Avanzate, Università del Piemonte Orientale "Amedeo Avogadro", Corso T. Borsalino, 54, I-15100 Alessandria, Italy, and Ecole Nationale Supérieure de Chimie de Paris, Laboratoire de Chimie Organométallique, UMR CNRS 7576, 11, rue Pierre et Marie Curie, F-75231 Paris Cedex 05, France . Received November 19, 1998; Revised Manuscript Received March 10, 1999

New heavy transition metal carbonyl markers for protein labeling, containing an "$M_n(CO)_{11}$" (M = Ru, Os, $n = 3$; M = Ir, $n = 4$) moiety, were prepared by reaction of "lightly stabilized" clusters with an N-succinimidyl ester functionalized phosphine, namely N-succinimidyl 3-diphenylphosphinepropionate (DPPS). The reaction of $Os_3(CO)_{11}$(DPPS) with the model amino acid β-alanine was performed and led to the expected amide. From the reaction of $M_n(CO)_{11}$(DPPS) with bovine serum albumin (BSA) in mixed organic/aqueous medium, conjugates bearing a fairly high number of metal carbonyl fragments were obtained, thus demonstrating the usefulness of this class of reagents for the selective and covalent graft of heavy metal clusters to side chain of proteins.

INTRODUCTION

Amine-reactive compounds are widely used in protein chemistry for probing protein structure and/or function or to introduce radioactive or cold reporter groups (Wong, 1991). Some examples of application of the resulting bioconjugates are immunoanalysis and immunohistochemistry. In these applications, the stability of the chemical bond between the marker and the biomolecule is particularly important.

The most widely used amine-reactive probes are reagents that form carboxamide, sulfonamide, urea, or thiourea bonds upon reaction with proteins amino groups (Means and Feeney, 1990). In particular, N-succinimidyl esters are able to acylate amines and lead to the formation of a peptide bond (Anderson et al., 1964). This family of reagents displays a high reactivity with protein amino groups (Brinkley, 1992). This is particularly interesting because virtually all proteins have lysine residues and, owing to their hydrophilic nature, most of them are located at the surface of proteins, readily accessible to reagents. Moreover, they have a very low reactivity toward tyrosine, serine, histidine, and cysteine residues (Anjaneyulu and Staros, 1987). Water-soluble N-sulfosuccinimidyl esters have also been described (Staros, 1982).

The prototypical compound of this category is the Bolton−Hunter reagent, *N*-succinimidyl 3-(4-hydroxy-5-iodophenyl)propionate (Bolton and Hunter, 1973), commercially available as labeled with ^{125}I. Proteins and peptides radiolabeled via the Bolton−Hunter reagent often exhibit a lower degree of deiodination compared with directly radioiodinated proteins and higher conjugation efficiencies are reached (Bolton et al., 1976; Vaidyanathan and Zalutsky, 1990).

Although radioisotopic labeling is a very sensitive method, owing to legal and technical problems associated with radioactivity, the implementation of "cold" labeling procedures has been an important goal (Gosling, 1990). Application of organotransition metal complexes containing biologically relevant ligands have attracted considerable attention in this field in recent years (*bioorganometallic chemistry*) (Severin et al., 1998). In this area, Jaouen et al. (1993) developed the so-called *carbonyl-metallo-immunoassay* (CMIA),[1] where biomolecules are labeled with metal carbonyl fragments and conjugates detected by FT-IR spectroscopy in the carbonyl ligands stretching vibration modes region (2150−1800 cm^{-1}), where proteins do not absorb. Transition metal carbonyl complexes containing an N-succinimidyl ester function (Varenne et al., 1993; Salmain et al., 1994; Gorfti et al., 1996), a pyrylium group (Salmain et al., 1994; Malisza et al., 1995), or an isothiocyanate (Kazimierczak et al., 1997), all reacting at the N-terminal position and/or the lysine residues of proteins, have been developed for this purpose.

In the same context, we covalently linked a third-row transition metal cluster fragment, namely "$Os_3(CO)_{10}$", to a model amine (i.e., benzylamine), to model amino acids (i.e., β-alanine and Nα-protected lysine), and finally to bovine serum albumin (BSA) by using *N*-succinimidyl-4-pentynoate as the linker. The average coupling ratio (CR) between the Os_3-marker and BSA was fairly high, i.e., around 20 (Osella et al., 1996). This was the first example of a marker containing a metal carbonyl cluster of predefinite nuclearity.

To make the Bolton−Hunter-like procedure more widely applicable to polymetallic carbonyl compounds, we have designed a new phosphine linker functionalized by an N-succinimidyl ester, namely *N*-succinimidyl 3-diphe-

* To whom correspondence should be addressed.
† Università del Piemonte Orientale "Amedeo Avogadro".
‡ Ecole Nationale Supérieure de Chimie.

[1] Abbreviations: BSA, bovine serum albumin; CMIA, carbonylmetallo-immunoassay; CR, coupling ratio; DCI-MS, desorption chemical ionization mass spectrometry; DPPS, *N*-succinimidyl 3-diphenylphosphinepropionate; FT-IR, Fourier transform infrared; RP-HPLC, reversed-phase high-performance liquid chromatography; STEM, scanning transmission electron microscopy; TFA, trifluoroacetic acid; THF, tetrahydrofuran.

10.1021/bc980139n CCC: $18.00 © 1999 American Chemical Society
Published on Web 06/19/1999

nylphosphine propionate (DPPS), **1**. In this paper, we report the synthesis of three polymetallic carbonyl complexes containing the DPPS ligand, namely $Ru_3(CO)_{11}$(DPPS), **5**, $Os_3(CO)_{11}$(DPPS), **6**, and $Ir_4(CO)_{11}$(DPPS), **7**, and their reactivity toward β-alanine and BSA.

Our goal is to label proteins with metal carbonyl clusters that we expect to be useful in scanning transmission electron microscopy (STEM) studies, owing to their electron-dense cores. In contrast to colloidal gold, derivatives **5**−**7** are not adsorbed but covalently linked to the target biomolecules, avoiding nonspecific interactions. An interesting precedent is the use of the rigid dimer $[Ir_4(CO)_{11}][Ph_2POC_6H_4{-}C_6H_4OPPh_2]$, which showed paired spots (ca. 6 Å in diameter) in STEM micrograph. The average separation between paired spots allowed the dimensions of molecular electronics structures to be established (Furuya et al., 1988).

Moreover, compounds **5**−**7** could be useful for the production of isomorphous heavy metal derivatives for protein X-ray crystallographic structure determination (Weinstein et al., 1989). Derivatization with heavy atom compounds at a unique lattice site is frequently used to obtain phase information and enable X-ray structure resolution of proteins (Branden and Tooze, 1991). This project may substantially contribute to the better understanding of the structure and role of proteins and other biomolecules.

EXPERIMENTAL PROCEDURES

Materials and Methods. Reactions were carried out under nitrogen using dried and prepurified solvents. Chromatographic separations were performed using microcrystalline cellulose (Merck Avicel). Routine FT-IR and FT-NMR spectra were recorded on a Bruker Equinox 55 and on a JEOL-EX 400 spectrometer, respectively. NMR chemical shifts are referenced to the internal standard tetramethylsilane (TMS) and 85% H_3PO_4 for ^1H and ^{31}P spectra, respectively. UV−vis spectra were recorded on a Safas UV/mc^2 spectrometer. DCI-MS spectra were recorded on a Finnigan-MAT 95Q instrument with magnetic and electrostatic analyzers. Isobutane was used as the reagent gas at 0.5 mbar pressure. The ion source temperature was kept at 50 °C, the electron emission current at 0.2 mA, and the electron energy at 200 eV. Positive ion spectra were collected. A computer program provided a digital readout of peak intensities and their comparison with the simulated isotopic pattern. The fit was satisfactory for all compounds under investigation. Quantitative FT-IR analyses were performed by depositing 10 mL samples on 9 mm diameter nitrocellulose membranes (Alltech), and recording spectra on a Bomem MB100 FT-spectrometer equipped with a liquid nitrogen-cooled MCT detector as described (Salmain et al., 1993).

N-Succinimidyl 3-diphenylphosphinepropionate, **1**, (DPPS) (Santimaria et al., 1995), lightly activated clusters **2** and **3** (Drake and Khattar, 1988), and **4** (Chini et al., 1978) were synthesized according to the literature methods and their purity checked by spectroscopic techniques.

Synthesis of $M_3(CO)_{11}$(DPPS) (M = Ru, 5, and Os, 6). Solid $M_3(CO)_{11}(NCCH_3)$ (M = Ru, **2**, and Os, **3**) (**2** 200 mg, 0.31 mmol; **3** 100 mg, ca. 0.11 mmol) was added to a freshly distilled THF solution (ca. 10 mL) of DPPS (1:1 ratio) at 0 °C in a Schlenk tube equipped with a magnetic stirring bar and an inlet arm for purging the solution with nitrogen. The color turned from yellow to orange. The mixture was allowed to reach room temperature and chromatographed on a cellulose column. Petroleum ether first eluted adventitious $M_3(CO)_{12}$, then mixtures containing petroleum ether and increasing amounts of CH_2Cl_2 eluted the monosubstituted compound (**5** or **6**) and then the higher substituted compounds. The polysubstituted compounds $M_3(CO)_{12-n}(DPPS)_n$ (n = 2, 3) were identified by comparison of their IR spectra with those of original samples (Bruce, 1987). The desired compounds were crystallized in petroleum ether/CH_2Cl_2 (1:1 v/v) at −10 °C, giving yellow or orange microcrystals.

Analytical Data for 5. IR (CH_2Cl_2): ν_{CO} 2097m, 2047vs, 2027sh, 2014vs, 1990sh, 1817w, 1790w, 1745ms cm^{-1}. UV−vis (absolute ethanol): λ_{max} 419 nm (ϵ = 5100). ^1H NMR (400 MHz, $CDCl_3$): δ 7.51 (m, 10H, Ph), ca. 2.9 (partially overlapped to the following signal, 2H, P−CH_2−CH_2), 2.83 (s, 4H, N-succinimidyl cycle), 2.50 (q, 2H, P−CH_2−CH_2-). ^{31}P NMR (161.9 MHz, $CDCl_3$): δ 27.6. MS (DCI, isobutane): $[M + H]^+ = 969$ m/z. Anal. Calcd. for $C_{30}H_{18}NO_{15}PRu_3$: C, 37.28; H, 1.88. Found: C, 37.06; H, 1.98.

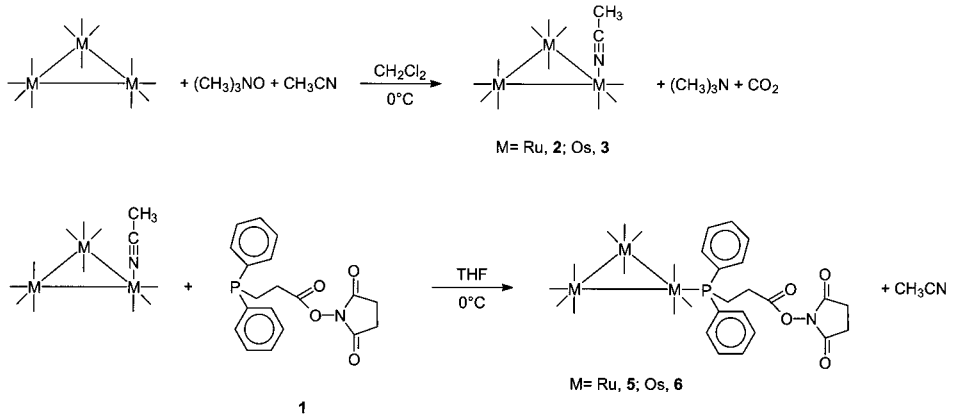
Analytical Data for 6. IR (CH_2Cl_2): ν_{CO} 2108m, 2055s, 2033ms, 2018vs, 2000ms, 1989ms, 1818w, 1789w, 1745ms cm^{-1}. UV−vis (absolute ethanol): λ_{max} 407 (ϵ = 4600), 345 (ϵ = 12000) nm. ^1H NMR (400 MHz, $CDCl_3$): δ 7.51 (m, 10H, Ph), 3.03 (q, 2H, P−CH_2−CH_2-), 2.83 (d?, 4H, N-succinimidyl cycle), 2.47 (q, 2H, P−CH_2−CH_2-). ^{31}P NMR (161.9 MHz, $CDCl_3$): δ −9.21. MS (DCI, isobutane): $[M + H]^+ = 1236$ m/z. Anal. Calcd for $C_{30}H_{18}NO_{15}POs_3$: C, 29.20; H, 1.47. Found: C, 29.01; H, 1.62.

Synthesis of $Ir_4(CO)_{11}$(DPPS), 7. $Ir_4(CO)_{12}$ (100 mg, 0.09 mmol) was added to a freshly distilled THF solution (ca. 20 mL) of $(C_2H_5)_4NBr$ (25 mg, 0.12 mmol) in a three-necked flask equipped with a magnetic stirring bar and an inlet arm for purging the solution with nitrogen. The solution was refluxed for 4 h, then DPPS (25 mg, 0.12 mmol) was added and refluxed for 1 h. The mixture was chromatographed on a cellulose column. Mixtures of petroleum ether and 10% CH_2Cl_2 first eluted **7**, then pure CH_2Cl_2 eluted the disubstituted compound $Ir_4(CO)_{10}$(DPPS)$_2$ in trace amounts. **7** was crystallized in dichloromethane/petroleum ether (1:1 v/v) at −10 °C, giving yellow microcrystals. The disubstituted compound $Ir_4(CO)_{10}(DPPS)_2$ was identified by comparison of its IR spectrum with that of an original sample of $Ir_4(CO)_{10}(PPh_3)_2$ (Darensbourg and Baldwin-Zuschke, 1982).

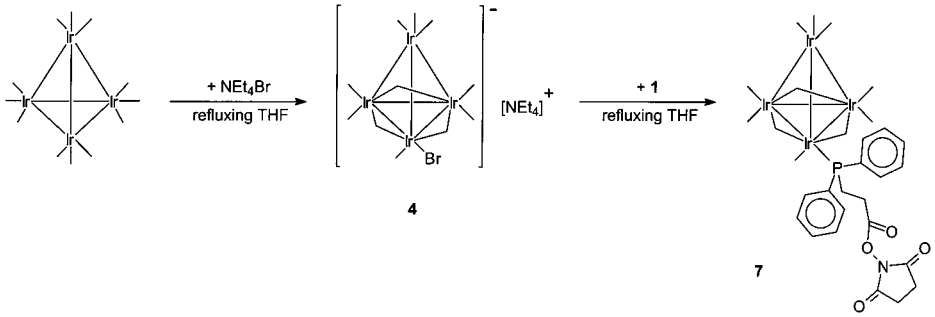
Analytical Data for 7. IR (CH_2Cl_2): ν_{CO} 2089m, 2057vs, 2020s, 1843m, 1819m, 1791w, 1745s cm^{-1}. ^1H NMR (400 MHz, $CDCl_3$): δ 7.50 (m, 10H, Ph), 2.83 (s, 4H, N-succinimidyl cycle), 2.73 (q, 2H, P−CH_2−CH_2−), 2.60 (q, 2H, P−CH_2−CH_2−). ^{31}P NMR (161.9 MHz, $CDCl_3$): δ −15.5. MS (DCI, isobutane): $[M + H]^+ = 1434$ m/z. Anal. Calcd. for $C_{30}H_{18}NO_{15}PIr_4$: C, 25.16; H, 1.27. Found: C, 24.80; H, 1.52.

Reaction of 6 with β-Alanine Ethyl Ester. β-Alanine ethyl ester hydrochloride, dissolved in CH_2Cl_2, was neutralized with a slight excess of triethylamine, then solid **6** was added in a 1:1 molecular ratio. The mixture was stirred overnight at room temperature, and chromatographed on a silica gel column. CH_2Cl_2 removed side-products, then acetone eluted the desired product $Os_3(CO)_{11}(Ph_2P(CH_2)_2C(O)NH(CH_2)_2COOEt)$, **8**, in 80% yield. IR (CH_2Cl_2): ν_{CO} 2107m, 2054s, 2033sh, 2017vs, 1999ms, 1990sh, 1730w, 1679w, 1607m, 1518w cm^{-1}. ^1H NMR (400 MHz, CD_2Cl_2): δ 7.61 (m, 10H, Ph), 6.07 (t, br, 1H, NH), 4.27 (m, 2H, −CH_2CH$_3$), 3.57 (m, 2H, −NH−CH_2CH$_2$−), 3.18 [m, 2H, −P−(CH_2)$_2$−], 2.62 (t, 2H, −NH−CH$_2$CH_2−), 2.17 [m, 2H, −P−(CH_2)$_2$−], 1.41 (t, 3H, −COOCH$_2$CH_3). ^{31}P NMR (161.9 MHz, $CDCl_3$): δ −9.01.

Scheme 1. Synthetic Steps for Preparing Clusters 2−3 and 5−6



Scheme 2. Synthetic Steps for Preparing Clusters 4 and 7



MS (DCI, isobutane): $[M + H]^+ = 1238$ *m/z*. Anal. Calcd for $C_{31}H_{24}NO_{14}POs_3$: C, 30.12; H, 1.96. Found: C, 29.98; H, 2.01.

Labeling of BSA with 5−7. Two stock solutions were prepared, the first being 10 μM in BSA (crystallized, Serva), dissolved in borate buffer (0.1 M pH 9.0 prepared from demineralized water), the second being 4 mM in **5**−**7** dissolved in DMF (**5** and **6**), or 2-propanol (**7**). To 0.45 mL of protein solution was added 0.05 mL of marker solution (the resulting solutions have a 10% v/v organic solvent content and a 45:1 marker-protein molar ratio). The solutions were stirred 5 h at room temperature, filtered on 0.2 μm porosity PVDF membranes, and chromatographed on a prepacked gel filtration column (Kwiksep 5 mL, Pierce) using NH_4HCO_3 10 mM as eluent. Twelve 0.5 mL fractions were collected and analyzed as described below.

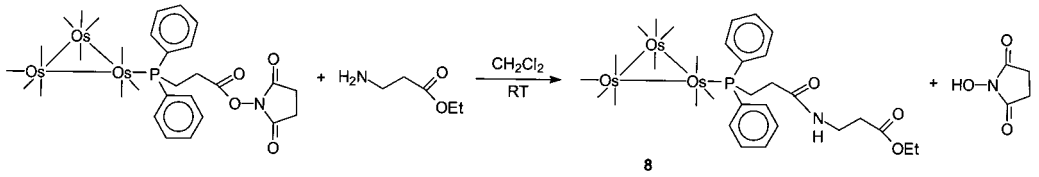
Analysis of the Conjugates. Protein concentration [P] was determined by the Coomassie blue method (Bradford, 1976) while marker concentration [M] was measured by UV−vis spectroscopy for **5** and **6** (**5** at $\lambda =$ 419 nm, $\epsilon = 5100$; **6** at $\lambda = 407$ nm, $\epsilon = 4600$) or by FT-IR spectroscopy of the ν_{CO} band at 2058 cm^{-1} ($k = 85$) for **7**, following a technique previously described (Salmain et al., 1993). The combination of these data provided the final ratio between marker and protein concentrations, namely the so-called coupling ratio CR = [M]/[P], and the coupling yield CY defined as $\{([M]/[P])_{final}/([M]/[P])_{initial}\} \times 100$. Reversed-phase HPLC of the conjugates was perfomed on a 4.6 × 150 mm Si-C4 column (Vydac 214 TP). Species were eluted by applying a linear gradient from 20 to 60% of 0.1% TFA-CH_3CN in 0.1% TFA-H_2O in 30 min (flow rate = 1 mL min^{-1}) and were detected at 280 nm.

RESULTS AND DISCUSSION

Synthesis and Characterization of Markers. Since the parent clusters $Ru_3(CO)_{12}$, $Os_3(CO)_{12}$, and $Ir_4(CO)_{12}$ are quite inert toward CO substitution, activated derivatives should be used. The "activated" $M_3(CO)_{11}(NCMe)$ (M = Ru, **2**, and Os, **3**) and $Ir_4(CO)_{11}Br$, **4**, have been prepared from the reaction of the parent clusters with trimethylamine-N-oxyde, $(CH_3)_3NO$ (Drake and Khattar, 1988) (Scheme 1), and tetraethylammonium bromide, $(C_2H_5)_4NBr$ (Chini et al., 1978) (Scheme 2), respectively. These intermediates are very convenient precursors in the preparation of the corresponding derivatives with a variety of phosphines in mild experimental conditions (Foulds et al., 1985; Ros et al. 1986). Hence, compounds **2**−**4** underwent fast reaction with **1** in THF giving $M_3(CO)_{11}(DPPS)$ (M = Ru, **5**, and Os, **6**) and $Ir_4(CO)_{11}(DPPS)$ (**7**) in excellent yields for Os and Ir (ca. 80%) (Schemes 1 and 2). Unfortunately, **5** was always obtained in low yield (ca. 15%) due to further substitution of CO ligands with DPPS, yielding the higher substituted $Ru_3(CO)_{10}(DPPS)_2$, and $Ru_3(CO)_9(DPPS)_3$, even when a low stoichiometric ratio between ligand and activated cluster was employed. Thermal reaction of $Ru_3(CO)_{12}$ with a wide variety of phosphines (L) led directly to the formation of trisubstituted $Ru_3(CO)_9(L)_3$, suggesting that replacement of carbonyl ligands by phosphorus ligands accelerates the rate of further substitution. This rate enhancement has been confirmed by a number of kinetic investigations (Muetterties et al., 1982). Alternative synthetic strategies have been attempted employing benzophenone ketyl (BPK) (Bruce, 1987) or [PPN^+] salts (PPN^+ = bis(triphenylphosphine)iminium) as catalysts (Lavigne and Kaesz, 1984). In both cases, the major product was again the disubstituted derivative.

Compounds **5**−**7** were characterized by elemental analysis, IR, ^1H and ^{13}C NMR spectroscopy, and DCI-MS (see Experimental Procedures). Noteworthy, compounds **5**−**7**, which have fairly high molecular weights and moderate to low polarity, were much more effectively characterized by the DCI technique than both electron impact (EI, ionizing energy = 70 eV) or fast-atom

Scheme 3. Coupling Reaction of 6 with β-Alanine Ethyl Ester



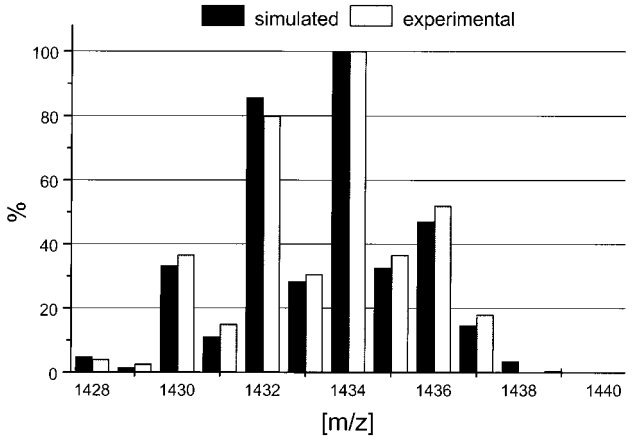


Figure 1. Experimental and simulated DCI mass spectra of **7** in the region corresponding to the $[M + H]^+$ peak. The two isotopic patterns have been compared by setting at 100% intensity the most abundant peaks at *m/z* 1434 in each spectrum.

bombardment (FAB, glycerol matrix) ionization methods. Among these techniques, only DCI-MS provided clean spectra, good sensitivity and well-defined isotopic patterns for the parent ions $[M + H]^+$ (Figure 1).

Coupling Reaction of 6 with β-Alanine Ethyl Ester. Once the synthesis and characterization of derivatives **5**−**7** was completed, it was still necessary to check that the coordination by metal fragments had not altered the acylating property of **1.** It was done by testing its reactivity with a model amino acid in dichloromethane. The reaction of **6** with β-alanine ethyl ester proceeded smoothly and completely within 24 h at ambient temperature giving the expected amide $Os_3(CO)_{11}[Ph_2P-(CH_2)_2C(O)N(H)(CH_2)_2C(O)OEt]$, **8**, in good yield (Scheme 3).

As already reported (Osella et al., 1996), the IR, in the ν_{CO} region, and UV−vis spectra of **6** and **8** are quite similar, representing good fingerprints for the presence of metallic markers in the conjugate.

Labeling Tests of BSA. Bovine serum albumin (BSA) is a very convenient and inexpensive model to test the binding capacity of newly developed amine reactive compounds. In particular, its contents in lysines is of 59 (i.e., a total of 60 amino groups), but in nondenaturating conditions (low temperature and low amount of organic cosolvent), 30−40 lysines are believed to be accessible to reagents (Erlanger, 1980).

Solutions of BSA at pH 9.0 were allowed to react with compounds **5**−**7** dissolved in DMF (**5** and **6**) or 2-propanol (**7**), so that the percentage of organic cosolvent was 10% and the initial reagent to protein molar ratio was 45. Reaction proceeded at room temperature for 5 h, and samples were submitted to gel filtration chromatography after filtration. The protein-containing fractions were analyzed by several spectroscopic methods in order to calculate the coupling ratio CR, corresponding to the final number of organometallic clusters bound per protein molecule. Results are reported in Table 1.

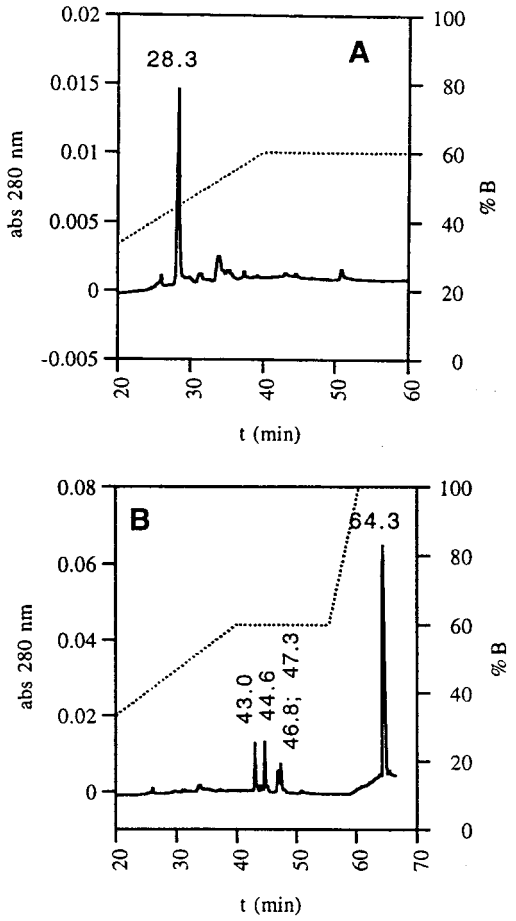


Figure 2. RP-HPLC of BSA (A) and BSA-**6** conjugate (B). For elution conditions, see the Experimental Procedures.

Table 1. Labeling of BSA with Compounds 5−7 (10% organic solvent in borate buffer pH 9.0, initial reagent to protein molar ratio = 45)

reagent	$[M]_{final}$ (M)	$[P]_{final}$ (M)	coupling ratio CR[a]	coupling yield CY[b]
5	48×10^{-6} [c]	4.2×10^{-6}	11.4	25%
6	88×10^{-6} [d]	6.5×10^{-6}	13.2	30%
7	59×10^{-6} [e]	6.1×10^{-6}	9.7	22%

[a] Coupling ratio CR = $[M]_{final}/[P]_{final}$. [b] Coupling yield CY = $[([M]/[P])_{final}/([M]/[P])_{initial}] \times 100$ = CR/45. [c] Measured by UV−vis spectroscopy at 419 nm. [d] Measured by UV−vis spectroscopy at 407 nm. [e] Measured by FT-IR spectroscopy at 2058 cm^{-1}.

Because of the high molecular weight of the reagents and their hydrophobic nature, we encountered some hurdles during the purification of the conjugates. Dialysis was unable to remove excess reagents (some part precipitated). Gel filtration chromatography of the reagents incubated in the same conditions without protein showed that some of them eluted in the same tubes as the protein while the rest precipitated in the column. We conclude that this means of purification is likely to lead to conjugates contaminated with noncovalently bound cluster.

The ultimate evidence of covalent binding of clusters **5**−**7** to BSA was brought by RP-HPLC. Chromatograms of BSA and BSA-**6** conjugates are displayed Figure 2. In the elution conditions chosen, BSA had a retention time of 28.3 min while BSA-**6** gave 4 major peaks at higher retention times ($43 < t_r < 47.3$ min), in agreement with the conjugation of several hydrophobic clusters to the protein. The presence of unbound cluster was detected by elution with 100% CH_3CN.

In summary, we observed a similar behavior of compounds **5**−**7** toward BSA; in particular, compound **6**, namely $Os_3(CO)_{11}$(DPPS), represents the best compromise between the moderate propensity toward hydrolysis showed by the isostructural compound **5** and the bulky hydrophobic character exhibited by the tetranuclear cluster **7**, so giving the highest CR and CY values.

CONCLUSIONS

Coordination of the ligand *N*-succinimidyl 3-diphenylphosphine propionate to activated triruthenium, triosmium, and tetrairidium clusters was achieved and the resulting complexes were shown to label BSA with yields in the range 22−30%. Within the Bolton−Hunter-like protocol for obtaining metallic-labeled acylating reagents for proteins, this phosphine ligand appears as a more widely applicable linker than the previously employed *N*-succinimidyl 4-pentynoate, since almost all metal carbonyl clusters react with phosphorus ligands and maintain their geometry. On the contrary, the coordination of the triple bond to clusters is not straightforward and often causes structural rearrangements (Osella and Raithby, 1989). By a similar strategy, it should also be possible to prepare derivatives targetted toward thiols (by introducing a maleimide function in place of the N-hydroxysuccinimide ester) or water-soluble compounds by exchanging some of the remaining CO ligands with water-soluble phosphines.

ACKNOWLEDGMENT

We thank Johnson Matthey for a generous loan of precious metals, European Union (EU) and MURST (COFIN 98) for financial support, and Dr. M. Vincenti (Department of Analytical Chemistry, University of Torino) for recording DCI-M.S. spectra. We are indebted with the two reviewers for valuable and constructive suggestions.

LITERATURE CITED

(1) Anderson, G. W., Zimmerman, J. E., and Callahan F. M. (1964) The use of esters of N-hydroxysuccinimide in peptide synthesis. *J. Am. Chem. Soc. 86*, 1839−1842.

(2) Anjaneyulu, P. S. R., and Staros, J. (1987) Reactions of N-hydroxysulfo-succinimide active esters. *Int. J. Pept. Protein Res. 30*, 117−124.

(3) Bolton, A. E., and Hunter, W. M. (1973) The labeling of proteins to high specific radioactivities by conjugation to a ^{125}I-containing acylating agent. *Biochem. J. 133*, 529−539.

(4) Bolton, A. E., Bennie, J. G., and Hunter, W. M. (1976) Innovations in labeling techniques for radiommunoassays. *Protides Biol. Fluids 24*, 687−693.

(5) Bradford, M. M. (1976) A rapid and sensitive method for the quantitation of microgram quantities of protein utilizing the principle of protein-dye binding. *Anal. Biochem. 72*, 248−254.

(6) Branden, C., and Tooze, J. (1991) *Introduction to protein structure*, Garland Publishing Inc., New York and London.

(7) Brinkley, M. (1992) A brief survey of methods for preparing protein conjugates with dyes, haptens and cross-linking reagents. *Bioconjugate Chem. 3*, 2−13.

(8) Bruce, M. I. (1987) Some reactions of ruthenium cluster carbonyls under mild conditions. *Coord. Chem. Rev. 76*, 1−43.

(9) Chini, P., Ciani, G., Garlaschelli, L., Manassero, M., Martinengo, S. and Sironi, A. (1978) New tetrahedral cluster compounds of iridium. Synthesis of the anions $[Ir_4(CO)_{11}X]^-$ (X = Cl, Br, I, CN, SCN) and X-ray structure of $[PPh_4][Ir_4(CO)_{11}Br]$. *J. Organomet. Chem. 152*, C35−C38.

(10) Darensbourg, D. J., and Baldwin-Zuschke, B. J. (1982) Ligand substitution processes in tetranuclear carbonyl clusters. 6. *J. Am. Chem. Soc. 104*, 3906−3910.

(11) Drake, S. R., and Khattar, R. (1988) Synthesis of activated clusters of $[M_3(CO)_{12}]$ (M = Ru or Os). *Organomet. Synth. 4*, 234−237.

(12) Erlanger, B. F. (1980) The preparation of antigenic hapten-carrier conjugates: a survey. *Methods Enzymol. 70*, 85−97.

(13) Furuya, F. R., Miller, L. L., Hainfield, J. F., Christophel, W. C., and Kenny, P. W. (1988) Use of $Ir_4(CO)_{11}$ to measure the length of organic molecules with a scanning transmission electron microscope. *J. Am. Chem. Soc. 110*, 641−642.

(14) Gorfti, A., Salmain, M., Jaouen, G., McGlinchey, M. J., Bennouna, A., and Mousser, A. (1996) Covalent and selective labeling of proteins with heavy metals. Synthesis, X-ray structure and reactivity studies of N-succinimidyl and N-sulfosuccinimidyl ester organotungsten complexes. *Organometallics 15*, 142−151.

(15) Gosling, J. P. (1990) A decade of development in immunoassay methodology. *Clin. Chem. 36*, 1408−1427.

(16) Jaouen, G., Vessières, A., and Butler I. S. (1993) Bioorganometallic chemistry: a future direction for transition metal organometallic chemistry? *Acc. Chem. Res. 26*, 361−369 and references therein.

(17) Kazimierczak, A., Zakrzewski, J., Salmain, M., and Jaouen, G. (1997) Cyclopentadienyl iron dicarbonyl (η^1-N-phthalimidato) complexes containing an isothiocyanate function: Synthesis and application to protein side-chain selective labeling. *Bioconjugate Chem. 8*, 489−494

(18) Lavigne, G., and Kaesz, H. D. (1984) Effects of highly dissociated salts in stoichiometric and catalytic reactions on ruthenium cluster complexes. *J. Am. Chem. Soc. 106*, 4647−4648.

(19) Malisza, K. L., Top, S., Vaissermann, J., Caro, B., Sénéchal-Tocquer, M.-C., Sénéchal, D., Saillard, J.-Y., Triki, S., Kahlal, S., Britten, J. F., McGlinchey, M. J., and Jaouen, G. (1995) Organometallics as potential protein labels: Pyrylium and pyridinium salts bearing $(C_6H_5)Cr(CO)_3$, $(C_5H_4)Mn(CO)_3$ and ferrocenyl substituents. *Organometallics 14*, 5273−5280.

(20) Means, G. E., and Feeney, R. E. (1990) Chemical modifications of proteins: History and applications. *Bioconjugate Chem. 1*, 2−12.

(21) Muetterties, E. L., Burch, R. R., and Stolzenberg, A. M. (1982) Molecular features of metal cluster reactions, *Annu. Rev. Phys. Chem. 33*, 89−118.

(22) Osella, D., and Raithby, P. R. (1989) Stereochemical aspects of organometallic clusters. A view of the polyhedral skeletal electron pair theory. In *Stereochemistry of Organometallic and Inorganic Compounds* (I. Bernal, Ed.) Vol. 3, pp 304−362, Elsevier, Amsterdam.

(23) Osella, D., Ravera, M., Vincenti, M., Salmain, M., and Jaouen, G. (1996) Labeling of proteins by a triosmium carbonyl cluster via a Bolton-Hunter-like procedure. *Organometallics 15*, 3037−3041.

(24) Ros, R., Scrivanti, A., Albano, V. G., Braga, D., and Garlaschelli, L. (1986) Chemistry of tetrairidium carbonyl clusters. Part 1. Synthesis, chemical characterization, and nuclear magnetic resonance study of mono- and di-substituted phosphine derivatives. X-ray crystal structure determination of the diaxial isomer of $[Ir_4(CO)_7(m\text{-}CO)_3(Me_2PCH_2CH_2PMe_2)]$. *J. Chem. Soc., Dalton. Trans.* 2411−2421.

(25) Salmain, M., Gunn, M., Gorfti, A., Top, S., and Jaouen, G. (1993) Labeling of proteins by organometallic complexes of rhenium (I). Synthesis and biological activity of the conjugates. *Bioconjugate Chem. 4*, 425−433.

(26) Salmain, M., Malisza, K. L., Top, S., Jaouen, G., Sénéchal-Tocquer, M.-C., Sénéchal, D., and Caro, B. (1994) [η^5-cyclopentadienyl] metal tricarbonyl pyrylium salts: Novel

reagents for the specific conjugation of proteins with transition organometallic labels. *Bioconjugate Chem. 5*, 655−659.

(27) Santimaria, M., Maina, T., Mazzi, U., and Nicolini, M. (1995) Preparation and characterization of a new rhenium (V) complex containing the 3-diphenylphosphinopropionyl-glycyl-L-(S-benzyl)-cysteinyl methyl ester ligand. *Inorg. Chim. Acta 240*, 291−297.

(28) Severin, K., Bergs, R., and Beck, W. (1998) Bioorganometallic chemistry—transition metal complexes with a-amino acids and peptides. *Angew. Chem., Int. Ed. Engl. 37*, 1634−1654.

(29) Staros, J. V. (1982) N-hydroxysulfosuccinimide active esters: Bis(N-hydroxy-succinimide) esters of two dicarboxylic acids are hydrophilic, membrane-impermeant, protein cross-linkers. *Biochemistry 21*, 3950−55.

(30) Vaidyanathan, G., and Zalutsky, M. R. (1990) Protein radiohalogenation: observations on the design of N-succinimidyl ester acylation agents. *Bioconjugate Chem. 1*, 269−273.

(31) Varenne, A., Salmain, M., Brisson, C., and Jaouen, G. (1992) Transition metal carbonyl labeling of proteins. A novel approach to a solid-phase two-site immunoassay using Fourier transform infrared spectroscopy. *Bioconjugate Chem. 3*, 471−476.

(32) Weinstein S., Jahn, W., Hanson, H., Wittmann, H. G., and Yonath, A. (1989) Novel procedures for derivatization of ribosomes for crystallographic studies. *J. Biol. Chem. 264*, 19138−42.

(33) Wong, S. S. (1991) *Chemistry of protein conjugation and cross-linking*, CRC Press, Boca Raton, Florida.

BC980139N

Conjugation, Immunoreactivity, and Immunogenicity of Calix[4]arenes; Model Study to Potential Calix[4]arene-Based Ac^{3+} Chelators

Marcel H. B. Grote Gansey,[†] Annemarie S. de Haan,[‡] Ebo S. Bos,[‡] Willem Verboom,[†] and David N. Reinhoudt*,[†]

Department of Supramolecular Chemistry and Technology, MESA+ Research Institute, University of Twente, P.O. Box 217, 7500 AE Enschede, The Netherlands, and Department of Analytical Chemistry for Research, N. V. Organon, P.O. Box 20, 5340 BH Oss, The Netherlands. Received December 10, 1998; Revised Manuscript Received April 9, 1999

For the development of calix[4]arene-based radiotherapeutic agents, the conjugation to biomolecules and immunogenicity in mice of potential $^{225}Ac^{3+}$-chelating calix[4]arenes were studied. A calix[4]arene triethyl ester isothiocyanate and a bis(calix[4]arene) hexacarboxylic acid, containing a masked thiol functionality, were used in conjugation experiments to a mouse monoclonal antibody and serum albumins. All characterization techniques indicate that only the calix[4]arene carboxylic acid is successfully conjugated to the biomolecules. The immunoreactivity of the conjugates is not impaired when up to 6 equiv of calixarene are bound to the monoclonal antibody. Animal tests indicated that the immunogenicity toward the calix[4]arene is strongly influenced by the nature of the carrier, the dosage, and the injection method. No immune response occurred when a homologous carrier was used or when a heterologous carrier was applied at a dosage of 10 μg per immunization via intravenous injection. Under all other conditions, the presence of antibodies directed against the calix[4]arene was demonstrated. Thus, for the application in radioimmunotherapy, the conjugation of a calix[4]-arene to a humanized antibody will probably not lead to an immune response, and the immunoreactivity will not be disturbed.

INTRODUCTION

Ionizing radiation is effective in the treatment of cancer. Radiolabeled agents that are selectively taken up by cancer cells confine the radiation specifically in the tumor, thereby minimizing damage to normal cells. For this purpose, tumor-selective mAbs or organ specific proteins are used (*1*−*7*). Crucial for the success of this approach are bifunctional ligands that can be attached to a protein and can bind a radioactive metal cation rapidly and selectively. The complex formed has to be kinetically inert with respect to dissociation either by acid or (serum) cation promoted pathways.

Calix[4]arene **1** is a cyclophane consisting of four phenolic units linked by methylene groups. It is widely used in supramolecular chemistry, e.g., in ionophores for cations and anions (*8*, *9*). We are interested in complexes of calix[4]arenes with cations in biological systems and have developed water-soluble derivatives (*10*) capable of sequestering luminescent trivalent lanthanide cations (*11*, *12*) as potential fluoroimmunoassays. This requires coupling of the ligand to biomolecules, such as mAbs and organ specific peptides. Kinetically inert ^{81}Rb complexes of calix[4]arene **2** were used to measure the renal blood flow (*13*, *14*).

Our ultimate goal is a calix[4]arene-based ionophore that irreversibly binds $^{225}Ac^{3+}$ (*15*), an α-emitting isotope with a half-life of 10 days and an attractive candidate for radiotherapy (*16*, *17*). Such a calix[4]arene should be conjugated to a mAb in order to convey the radiation source to the target. Very recently, Chen et al. (*18*) demonstrated the potential of calixarenes by performing extraction of $^{225}Ac^{3+}$ from an aqueous into an organic phase with a tetracarboxylic acid calix[4]arene.

The best position to connect a ligand to an antibody is at the Fc part, because it is positioned relatively distant from the variable region of the antibody, which is used for the recognition of and binding to the antigen. This is crucial for labeling antibodies in order to maintain a high degree of specific binding to target sites. Furthermore, the calix[4]arene−antibody conjugate should not elicit an immune response to the chelator, as this precludes repetitive administration of the therapeutic agent as has been described for DOTA[1] (*19*) and DTPA (*20*).

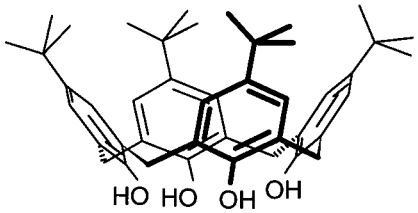
To the best of our knowledge, this paper describes the first study toward bioconjugation of calix[4]arenes that

* To whom correspondence should be addressed. Phone: +31 53 4892980. Fax: +31 53 4894645. E-mail: smct@ct.utwente.nl.
[†] University of Twente.
[‡] Department of Analytical Chemistry for Research.

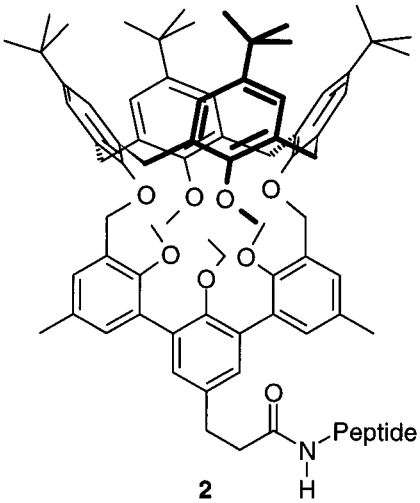
[1] Abbreviations: DOTA, 1,4,7,10-tetraazacyclododecane-*N*,*N*′,*N*″,*N*‴-tetraacetic acid; DTPA, diethylenetriaminepentaacetic acid; NBA, *m*-nitrobenzyl alcohol; THF, tetrahydrofuran; HSA, human serum albumin; MSA, mouse serum albumin; OVA, ovalbumin; hCG, human chorionic gonadotropin; DBU, 1,8-diazabicyclo[5.4.0]undec-7-ene; PBS, phosphate-buffered saline; DMF, *N*,*N*-dimethylformamide; EDTA, ethylenediaminetetraacetic acid; GMBS, γ-maleimido butyric acid *N*-hydroxysuccinimide ester; MALDI-ToF MS, matrix-absorbed laser desorption ionization time of flight mass spectrometry; HP-SEC, high performance−size exclusion chromatography; IEF, isoelectric focusing; SDS−PAGE, sodium dodecyl sulfate−polyacrylamide gel electrophoresis; ELISA, enzyme-linked immunosorbent assay; TMB, 3,3′,5,5′-tetramethylbenzidine; SPDP, 3-(2-pyridyldithio)propionic acid *N*-hydroxysuccinimide ester; DTT, dithiothreitol; HRP, horse radish peroxidase; Ig(G_1), immunoglobulin (G_1), i.p., intraperitoneal; s.c., subcutaneous; i.v., intravenous.

10.1021/bc9801474 CCC: $18.00 © 1999 American Chemical Society
Published on Web 06/23/1999

Chart 1. Calix[4]arenes



1



2

are potential chelators for $^{225}Ac^{3+}$. We will discuss the characterization of the conjugates and the important questions of whether the conjugation of calix[4]arenes alters the immunoreactivity of the antibody and whether it leads to an immune response reaction in mice.

MATERIALS AND METHODS

Melting points were determined with a Reichert melting point apparatus and are uncorrected. ^{1}H NMR (250 MHz) and ^{13}C NMR (62.9 MHz) spectra were recorded with a Bruker AC250F spectrometer in the absence of an internal standard. FAB mass spectra were obtained with a Finnigan MAT90 mass spectrometer using NBA as a matrix. The presence of solvent in the analytical samples was confirmed by ^{1}H NMR spectroscopy. CH_2Cl_2 was distilled from $CaCl_2$ and stored over molecular sieves (4 Å), EtOAc was distilled from K_2CO_3 and stored over molecular sieves (4 Å), THF was distilled over sodium benzophenone ketyl prior to use. All other solvents and chemicals were of reagent grade and were used without purification. Silica gel (particle size 0.040−0.063 mm, 230−400 mesh) was obtained from Merck, Darmstadt, Germany. All reactions were carried out under an argon atmosphere. For reasons of clarity and in order to reduce space, the name calix[4]arene was used instead of the original IUPAC name: pentacyclo-[19.3.1.1^{3,7}.1^{9,13}.1^{15,19}]octacosa-1(25),3,5,7(28),9,11,13(27),-15,17,19(26),21,23-dodecaene. HSA (M_w = 68 000 g/mol), MSA (M_w = 65 000 g/mol), and OVA (M_w = 46 000 g/mol) were purchased from Sigma, St. Louis, MO. MAb 506-A (M_w = 160 000 g/mol), directed against hCG, was prepared by standard hybridoma technology. PD-10 columns (purchased from Pharmacia Biotech) are prepackaged, disposable columns (bed volume 9.1 mL, bed height 5 cm) containing Sephadex G-25 M swollen in distilled water containing 0.15% Kathon CG/ICP Biocide (trademark of Röhm and Haas) as preservative.

Synthesis of Bifunctional Ligands. **25-[(Hydroxycarbonyl)methoxy]-26,27,28-tris[(ethoxycarbonyl)-methoxy]calix[4]arene (4)**. To a solution of calix[4]-arene **3** (*21*) (2.50 g, 3.25 mmol) in CH_2Cl_2 (75 mL) were added 100% HOAc (5.0 mL) and 65% HNO_3 (8.3 mL). The mixture was stirred at room temperature for 45 min and subsequently poured into a mixture of CH_2Cl_2 (125 mL) and water (750 mL). The organic layer was washed with water (2 × 750 mL). Evaporation of the solvent yielded pure **4** as a white solid. Yield 95%; mp 141−143 °C; ^{1}H NMR ($CDCl_3$) δ 7.1−6.9 (m, 6 H, ArH), 6.6−6.5 (m, 6 H, ArH), 4.99 (part of ABq, 2 H, J = 13.0 Hz, $ArCH_2Ar$), 4.92 [s, 2 H, $OCH_2C(O)$], 4.89 [d, 2 H, J = 15.0 Hz, $OCH_2C(O)$ proximal to carboxylic acid], 4.69 (part of ABq, 2 H, J = 13.3 Hz, $ArCH_2Ar$), 4.69 [s, 2 H, $OCH_2C(O)$], 4.41 [d, 2 H, J = 15.8 Hz, $OCH_2C(O)$ proximal to carboxylic acid], 4.3−4.2 (m, 6 H, OCH_2Me), 3.32 (part of ABq, 2 H, J = 13.3 Hz, $ArCH_2Ar$), 3.29 (part of ABq, 2 H, J = 13.3 Hz, $ArCH_2Ar$), 1.31 (t, 9 H, J = 7.1 Hz, CH_3); ^{13}C NMR ($CDCl_3$) δ 170.7, 170.0, and 169.5 (s, C=O), 157.0, 154.5, and 153.8 (s, ArC−O), 135.7, 135.3, 133.3, and 133.1 (s, Ar*C*-CH_2), 129.4, 129.2, 128.9, 128.5, 124.7, 124.0, and 123.7 (d, ArC−H), 73.0, 72.5 and 71.4 [t, O*C*H_2C(O)], 61.2 and 60.7 (t, OCH_2Me), 31.0 and 30.9 (t, $ArCH_2Ar$), 14.2 (q, CH_3); FAB-MS m/z 741.0 ([M + H]$^+$, calcd 741.3); Anal. ($C_{42}H_{44}O_{12}$) C, H.

25,26,27-Tris[(ethoxycarbonyl)methoxy]-28-[(4-nitrobenzylcarbamoyl)methoxy]calix[4]arene (5). Calix[4]arene monocarboxylic acid triethyl ester **4** (2.37 g, 3.20 mmol) was dissolved in oxalyl chloride (10 mL), and the solution was refluxed for 1 h. After evaporation of the excess of oxalyl chloride, the residue was dissolved in CH_2Cl_2 (50 mL) and slowly added to an ice-cooled solution of *p*-nitrobenzylamine hydrochloride (0.72 g, 3.84 mmol) and DBU (1.46 g, 9.60 mmol) in CH_2Cl_2 (25 mL). The mixture was stirred overnight at room temperature, CH_2Cl_2 (50 mL) was added, and the solution was washed with 0.2 N HCl (2 × 100 mL) and H_2O (100 mL). After evaporation of the solvent, the crude product was purified via column chromatography (SiO_2, CH_2Cl_2:EtOAc 9:1, R_f 0.4) to give pure **5** as a slightly yellow solid. Yield 73%; mp 63−65 °C; ^{1}H NMR ($CDCl_3$) δ 8.98 (t, 1 H, J = 6.3 Hz, NH), 8.11 (d, 2 H, J = 8.7 Hz, O_2N−ArH), 7.49 (d, 2 H, J = 8.7 Hz, O_2N−ArH), 6.85−6.7 (m, 6 H, ArH), 6.45−6.2 (m, 6 H, ArH), 4.87 (part of ABq, 2 H, J = 16.4 Hz, $ArCH_2Ar$), 4.7−4.4 [m, 12 H, $ArCH_2Ar$, $OCH_2C(O)$, and NCH_2Ar], 4.16 (q, 2 H, J = 7.2 Hz, OCH_2Me opposite of amide bond), 3.85−4.0 (m, 4 H, OCH_2Me next to amide bond), 3.21 (part of ABq, 2 H, J = 14.0 Hz, $ArCH_2Ar$), 3.19 (part of ABq, 2 H, J = 13.9 Hz, $ArCH_2Ar$), 1.22 (t, 3 H, J = 7.2 Hz, CH_3 opposite of amide bond), 1.08 (t, 6 H, J = 7.1 Hz, CH_3 next to amide bond); ^{13}C NMR ($CDCl_3$) δ 170.7, 170.1, and 169.5 (s, C=O), 156.6, 155.0, and 154.8 (s, ArC−O), 147.0 and 146.9 (s, O_2N−ArC), 135.2, 135.0, 133.5, and 133.3 (s, Ar*C*-CH_2), 132.7, 129.4, 129.2, 128.4, 127.8, 127.6, 123.7, 123.4, and 123.0 (d, ArC−H), 73.9, 71.5, and 71.3 [t, O*C*H_2C(O)], 60.9 and 60.7 (t, OCH_2Me), 42.3 (t, NCH_2Ar), 31.5 and 30.9 (t, $ArCH_2Ar$),

14.2 and 14.1 (q, CH_3); FAB-MS *m/z* 897.5 ($[M + Na]^+$, calcd 897.3); Anal. ($C_{49}H_{50}N_2O_{13}\cdot 0.3H_2O$) C, H, N.

Reduction of Nitrocalix[4]arene 5 to Aminocalix-[4]arene 6. Calix[4]arene monoamide **5** (0.53 g, 0.60 mmol) was dissolved in a mixture of EtOH (20 mL) and THF (5 mL) in a 250 mL pressure barrel. A catalytic amount of palladium on charcoal (10%) was added, and the mixture was stirred at room temperature for 3 h under a H_2 atmosphere. The mixture was filtered over Hyflo filter aid and the filter was rinsed with CH_2Cl_2 (100 mL). The solvent was evaporated, and the crude product (0.47 g) was immediately used in the reaction with thiophosgene. ^{1}H NMR spectroscopy of a crude sample shows a complete disappearance of the signals of the phenyl group bearing the nitro moiety, but also indicates that aminocalix[4]arene **6** has a tendency to oligomerize.

25,26,27-Tris[(ethoxycarbonyl)methoxy]-28-[(4-isothiocyanatobenzylcarbamoyl)methoxy]calix[4]-arene (7). To a solution of crude **6** (0.47 g) in CH_2Cl_2 (10 mL) was added 1 mL of a 0.61 M solution of thiophosgene in CH_2Cl_2. Subsequently, 1 mL of a 0.61 M solution of triethylamine in CH_2Cl_2 was added, and the mixture was stirred at room temperature for 4 h. After evaporation of the solvents, the crude product was taken up in CH_2Cl_2 (50 mL) and washed with H_2O (50 mL). The organic phase was evaporated and the crude product was purified with column chromatography (SiO_2, CH_2Cl_2:EtOAc 9:1, $R_f = 0.4$) to give pure **7** as a white solid. Yield 55% (based on nitro compound **5**); mp 58−60 °C; ^{1}H NMR ($CDCl_3$) δ 8.83 (t, 1 H, $J = 6.3$ Hz, NH), 7.30 (d, 2 H, $J = 8.4$ Hz, SCN−ArH), 7.10 (d, 2 H, $J = 8.4$ Hz, SCN−ArH), 6.8−6.7 (m, 6 H, ArH), 6.5−6.2 (m, 6 H, ArH), 4.83 (part of ABq, 2 H, $J = 16.4$ Hz, $ArCH_2$-Ar), 4.7−4.4 [m, 12 H, part of AB system of $ArCH_2Ar$, $OCH_2C(O)$, and NCH_2Ar], 4.16 (q, 2 H, $J = 7.2$ Hz, OCH_2-Me opposite of amide bond), 4.0−3.9 (m, 4 H, OCH_2Me next to amide bond), 3.19 (part of ABq, 2 H, $J = 14.0$ Hz, $ArCH_2Ar$), 3.18 (part of ABq, 2 H, $J = 13.9$ Hz, $ArCH_2$-Ar), 1.22 (t, 3 H, $J = 7.1$ Hz, CH_3 opposite of amide bond), 1.10 (t, 6 H, $J = 7.2$ Hz, CH_3 next to amide bond); ^{13}C NMR ($CDCl_3$) δ 170.6, 169.9, and 169.5 (s, C═O), 156.6 (s, ArC−O), 138.7(s, ArC), 135.2, 135.0, 133.6, and 133.3 (s, Ar*C*-CH_2), 129.8 (s, ArC), 129.3, 129.2, 128.4, 128.2, 125.7, 123.4, 123.3, and 123.0 (d, ArC−H), 74.0, 71.4, and 71.3 [t, O*C*H_2C(O)], 60.9 and 60.7 (t, OCH_2Me), 42.2 (t, NCH_2Ar), 31.5 and 30.9 (t, $ArCH_2Ar$), 14.2 and 14.1 (q, CH_3); FAB-MS *m/z* 887.2 ($[M + H]^+$, calcd 887.3); IR (KBr) ν 2099 (NCS), 1757 (C═O ester), 1680 (C═O amide) cm^{-1}; Anal. ($C_{50}H_{50}N_2O_{11}S\cdot 0.5H_2O$) C, H, N.

Bis[25,26,27-tris[(ethoxycarbonyl)methoxy]-28-[4-[(2-thioethyl-thioureido)benzylcarbamoyl]methoxy]-calix[4]arene] (8). To a solution of calix[4]arene isothiocyanate **7** (0.275 g, 0.325 mmol) in CH_2Cl_2 (10 mL) was added cystamine dihydrochloric acid salt (0.0366 g, 0.163 mmol) and triethylamine (45 μL, 0.325 mmol). The mixture was stirred at room temperature for 4 h and subsequently washed with water. After evaporation of the solvent, the crude product was purified with preparative thin-layer chromatography (SiO_2, CH_2Cl_2:EtOAc 1:1). Yield 73%; mp 101−103 °C; ^{1}H NMR ($CDCl_3$) δ 8.91 [t, 2 H, $J = 6.3$ Hz, C(O)NH], 8.03 (s, 2 H, ArNH), 7.34 (d, 4 H, $J = 8.3$ Hz, N−ArH), 7.15 (d, 4 H, $J = 8.3$ Hz, N−ArH), 6.8−6.65 [m, 14 H, CH_2−N*H*-C(S) and ArH], 6.5−6.2 (m, 12 H, ArH), 4.86 (d, 4 H, $J = 16.5$ Hz, $ArCH_2$-Ar), 4.7−4.4 [m, 24 H, $ArCH_2Ar$, $OCH_2C(O)$, and $ArCH_2N$], 4.2−3.8 (m, 16 H, OCH_2Me and NCH_2CH_2), 3.20 (d, 4 H, $J = 14.1$ Hz, $ArCH_2Ar$), 3.18 (d, 4 H, $J = 13.9$ Hz, $ArCH_2$-Ar), 2.82 (t, 4 H, $J = 6.2$ Hz, S−CH_2), 1.25−1.05 (m, 18 H, CH_3); ^{13}C NMR ($CDCl_3$) δ 181.0 (s, C═S), 170.7, 170.1, and 169.6 (s, C═O), 156.5, 155.1, and 155.0 (s, ArC−O), 137.9, 135.4, 135.1, 134.9, 133.7, and 133.3 (s, ArC), 129.3, 129.1, 128.4, 125.3, 123.3, and 123.0 (d, ArC−H), 74.0, 71.4, and 71.3 [t, O*C*H_2C(O)], 60.9 and 60.8 (t, OCH_2Me), 43.9 (t, $ArCH_2N$), 42.3 (t, NCH_2CH_2S), 37.2 (t, NCH_2CH_2S), 31.5 and 31.0 (t, $ArCH_2Ar$), 14.2 and 14.1 (q, CH_3); FAB-MS *m/z* 1948.5 ($[M + Na]^+$, calcd for $C_{104}H_{112}N_6O_{22}S_4$, 1948.6), 962.5 ($[1/2M + H]^+$, calcd for $C_{52}H_{56}N_3O_{11}S_2$, 962.3).

Table 1. Conjugation Experiments with Calix[4]arene Isothiocyanate 7

expt	vol of calix[4]arene stock solution (μL)	vol of HSA stock solution (μL)	vol of MoAb 506-A stock solution (μL)	molar ratio calix[4]arene: biomolecule
1	16.5	1000		5:1
2	32.5	1000		10:1
3	82	1000		25:1
4	164	1000		50:1
5	16.5		1000	12:1
6	32.5		1000	24:1
7	82		1000	59:1
8	164		1000	118:1

Bis[25,26,27-tris[(hydroxycarbonyl)methoxy]-28-[4-[(2-thioethyl-thioureido)benzylcarbamoyl]-methoxy]calix[4]arene] (9). A solution of K_2CO_3 (0.15 g, 1.09 mmol) in water (2 mL) was added to a refluxing solution of calix[4]arene **8** (0.107 g, 0.058 mmol) in MeOH (10 mL). After the mixture was refluxed for 30 min, it was poured into water (150 mL), after which the pH was adjusted to about 2 with 1 N HCl. The product was extracted with CH_2Cl_2 (3 × 50 mL) to give, after evaporation of the solvent, pure **9** as a white solid. Yield 92%; mp 169−171 °C; ^{1}H NMR[2] (THF-d_8) δ 9.07 (s, 2 H, ArNH), 8.57 [br t, 2 H, C(O)NH], 7.47 (d, 4 H, $J = 8.2$ Hz, N−ArH), 7.38 [s, 2 H, ArNHC(S)], 7.30 (d, 4 H, $J = 8.2$ Hz, N−ArH), 6.85−6.55 [m, 26 H, ArH and CH_2N*H*C-(S)], 5.0−4.6 [m, 28 H, $ArCH_2Ar$, $OCH_2C(O)$, and $ArCH_2N$], 3.92 (br q, 4 H, $NHCH_2CH_2$), 3.30 (d, 4 H, $J = 13.5$ Hz, $ArCH_2Ar$), 3.29 (d, 4 H, $J = 13.5$ Hz, $ArCH_2Ar$), 3.03 (t, 4 H, $J = 6.0$ Hz, CH_2S); FAB-MS *m/z* 1757.6 ($[M + H]^+$, calcd, 1757.5), 880.3 ($[1/2M + H]^+$, calcd, 879.3), 846.6 ($[1/2M - S]^+$, calcd, 846.3); Anal. ($C_{92}H_{88}N_6O_{22}S_4\cdot 4H_2O$) C, H, N.

Conjugation Experiments. *Conjugation of Calix[4]-arene Isothiocyanate **7** to mAb 506-A and HSA*. A 4.48 mM (3.97 mg/mL) stock solution of calix[4]arene isothiocyanate **7** in DMF was made. A 14.7 μM (1.00 mg/mL) stock solution of HSA in PBS was prepared, as was a 6.25 μM (1.00 mg/mL) stock solution of mAb 506-A in PBS. To a volume containing 1 mg of biomolecule were added different amounts of calix[4]arene **7**. Table 1 summarizes the performed experiments. After mixing the two volumes, the pH of the mixture was adjusted to approximately 9.0 with 0.1 M triethylamine in doubly distilled water and incubated at 37 °C for 2 h. In experiments 3, 4, 7, and 8, some additional DMF was added (up to 86 μL), because the mixtures became turbid. This did not result in improved clarity. Subsequently, the mixture was chromatographed on PD-10 columns equilibrated in PBS according to the manufacturers descriptions.

*Conjugation of Calix[4]arene Disulfide **9** to mAb 506-A, HSA, and MSA*. Two buffer solutions were prepared;

[2] Several signals in the ^{1}H NMR spectrum of bis-calixarene **9** are double, probably caused by hydrogen bonding of the thiourea hydrogen atoms to the oxygen atoms of carboxylic acid moieties.

Table 2. Conjugation Experiments with Calix[4]arene Disulfide 9

expt	vol of calix[4]arene solution (μL)	vol of HSA-GMBS solution (μL)	vol of MoAb-GMBS solution (μL)	molar ratio calix[4]arene: biomolecule
9	27	1600		5:1
10	55	1600		10:1
11	135	1600		25:1
12	270	1600		50:1
13	11.5		4400	5:1
14	23		4400	10:1
15	57		4400	25:1
16	115		4400	50:1

buffer A consisted of Na_2HPO_4 (50 mM) and EDTA (disodium salt, 1 mM) in milli Q water. The pH was adjusted to 7.5 with H_3PO_4. Buffer B consisted of Na_2HPO_4 (50 mM), EDTA (1 mM), and NaCl (100 mM) in milli Q water. The pH was adjusted to 6.0 with H_3PO_4. Nitrogen was bubbled through the solution in order to remove oxygen. PD-10 columns were equilibrated with buffer A. A solution of the biomolecule in PBS (1.0 mL of a 10 mg/mL HSA solution, 2 × 2.5 mL of a 2.7 mg/mL mAb 506-A solution) was chromatographed according to the manufacturers descriptions. The concentrations were determined by measuring the absorbance at 280 nm (3.9 mg/mL for HSA, 1.1 mg/mL for mAb 506-A). A 7.1 mM (2 mg/mL) stock solution of GMBS in DMF was freshly prepared. To 1.54 mL of the HSA solution (6.0 mg HSA) in buffer A was added 495 μL of the GMBS stock solution (molar ratio HSA:GMBS = 1:40). To 5.45 mL of the mAb 506-A solution (6.0 mg mAb 506-A) was added 79 μL of the GMBS stock solution (molar ratio mAb 506-A:GMBS = 1:15). The solutions were incubated at ambient temperature for 1 h in the dark. Subsequently, the solutions were chromatographed on PD-10 columns that were equilibrated with buffer B. The concentrations were determined spectrophotometrically (0.57 mg/mL for HSA, 0.23 mg/mL for mAb 506-A). A 1.42 mM (2.5 mg/mL) stock solution of calix[4]arene disulfide **9** in DMF was freshly prepared. Under a nitrogen atmosphere, 10 μL of tributylphosphine was diluted with 990 μL of 1-propanol to give a 36 mM solution of which 39.5 μL was added to 1 mL of the calix[4]arene **9** stock solution (molar ratio calix[4]arene **9**:PBu_3 = 1:1). The mixture was incubated at ambient temperature for 15 min. To a volume containing 1 mg of biomolecule were added different amounts of reduced calix[4]arene. Table 2 summarizes the performed experiments.

After incubation in the dark overnight at ambient temperature, to the HSA and mAb experiments were added 90 μL and 40 μL (24 equiv), respectively, of a 0.46 mg/mL cysteamine solution in water. Subsequently, the mixtures were chromatographed on PD-10 columns equilibrated with PBS.

The procedure for the MSA conjugates was comparable to the HSA conjugates.

Conjugation Characterization. *MALDI-ToF MS.* MALDI-ToF MS was carried out using a PerSeptive Biosystems Voyager-DE-RP MALDI-ToF mass spectrometer. A 337 nm UV Nitrogen laser producing 3 ns pulses was used in the reflection mode. The samples were prepared by mixing 10 μL of a 50% acetonitrile/water solution of the sample with 20 μL of a solution of 3 mg/L α-cyano-4-hydroxycinnamic acid or dihydroxybenzoic acid in water. Of that solution, 1 μL was loaded on the gold-sample plate.

HP−SEC. The conjugates were analyzed by HP−SEC on a Superdex 200 column. The system used was a Beckman System Gold HPLC system including an autosampler (type 507), a programmable solvent module (type 126), a column thermostat (Separations, type SPH99), a programmable detector module (type 166) or diode array detector module (type 168), and PC plus software (System Gold version 5.10). As the mobile phase, a filtered (0.45 μ type HA Millipore filter) 0.2 N Na_2HPO_4 solution of pH 6.8 was used at a rate of 0.4 mL/min and 60 min/run. A typical procedure consisted of equilibration of the column with the buffer solution, followed by a blank run (injection of 100 μL buffer solution), injection of 50 μL of a SEC-6 calibration mixture, and another blank run. The absorbance at 210 nm was monitored. Subsequently, 100 μL of protein solutions, diluted with the buffer solution to approximately 0.1 μg/μL, were injected. After the last sample, the column was tested by analysis of a calibration mixture and a blank run.

Table 3. MALDI-ToF MS Results of HSA-Calix[4]arene 9[a]

expt	molar ratio calix[4]arene: biomolecule	*m/z* maximum (no. of conjugated calix[4]arenes)
9	5:1	68.0×10^3 (1)
10	10:1	68.0×10^3 (1)
11	25:1	72.4×10^3 (5)
12	50:1	73.3×10^3 (6)

[a] The *m/z* ratio for the unmodified HSA was found to be 67.0×10^3. The *m/z* ratio for one calix[4]arene-GMBS moiety is 1042.

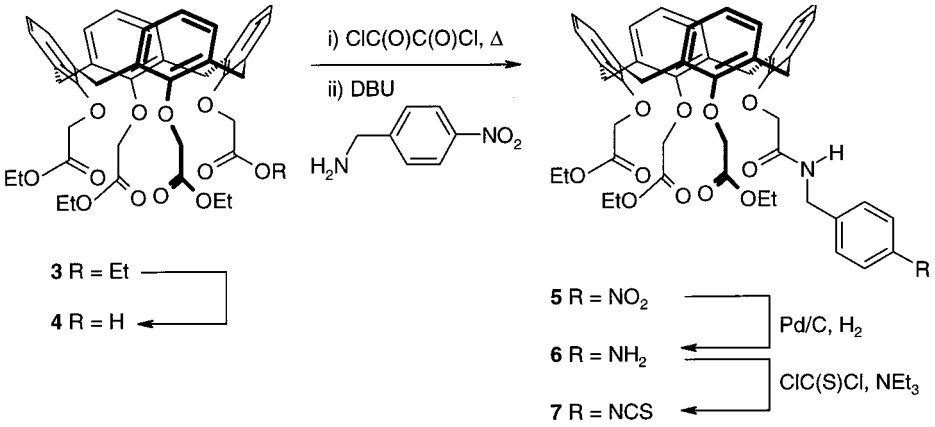
IEF. IEF of the calixarene conjugates was essentially carried out according to the procedures of Pham et al. (*22*).

SDS−PAGE. The conjugates were analyzed by SDS−PAGE on 4−26% T and 3% C gels using the discontinuous buffer system of Laemmli under reducing and nonreducing conditions as described by Hoes et al. (*23*).

ELISA. The immunoreactivity of the conjugates of mAb 506-A was determined in an ELISA. Microtitration plates were coated with 1 μg/mL β-hCG in PBS. After an overnight incubation at 4 °C, the contents of the wells were discarded and the plates were washed thoroughly with PBS-Tween. Then, the plates were incubated for 1 h with PBS-Tween at ambient temperature. A dilution series of the antibody and the conjugates starting at 10 μg/mL was pipetted into the wells. Incubation was performed for 1 h at ambient temperature. The plates were washed three times with PBS-Tween and then a goat anti mouse IgG_1−HRP conjugate of appropriate dilution in PBS-Tween was added. After a 1 h incubation at ambient temperature, the plates were washed three times with PBS-Tween and twice with distilled water. Subsequently, the TMB−H_2O_2 substrate solution was added. After the color had sufficiently developed, the reaction was stopped by the addition of 4 N H_2SO_4 and the absorbance at 450 nm was read in an ELISA-reader. The reduction of immunoreactivity was easily derived by comparing the reaction curves of the nonconjugated antibody and the immunoconjugates.

Immune Response Study. *Animal Tests.* Prior to use in the study, the HSA− and MSA−calix[4]arene conjugates were filtered over a 0.2 μm filter. Fifteen groups of five mice, which differed in injection method, antigen, and amount of antigen (see Table 4), were used. In the first method, the mice were injected i.p. at day 1 in the presence of Freund's Complete Adjuvant. At days 14, 28, and 42, an s.c. injection with Freund's Incomplete Adjuvant followed. The second method consisted of an i.p. injection without adjuvant at day 1, and an s.c. injection at days 14, 28, and 42. In the last method, only i.v. injections without adjuvant were applied at days 1, 14, 28, and 42. Prior to each injection blood was collected via an orbita punction. One week after the last series of

Scheme 1. Synthesis of Calix[4]arene Isothiocyanate 7



immunizations, all animals were bled by the intracardiac route. Three of the five mice that died during the study were replaced. All blood samples were centrifuged, and the sera were collected and stored at −20 °C.

Synthesis of OVA-Calix[4]arene Conjugate. A buffer solution consisting of Na_2HPO_4 (0.1 M) and NaCl (0.1 M) in milli Q water was prepared. The pH was adjusted to 7.5 with H_3PO_4. A 10 mg/mL solution of OVA in this buffer was prepared and chromatographed on a PD-10 column equilibrated with this buffer solution. The three 0.5 mL fractions with the highest absorbance at 280 nm were collected and diluted to give a final concentration of 5 mg/mL. To 1.4 mL of this solution, 190 μL of a 12.5 mg/mL solution of SPDP in 100% ethanol was added (molar ratio OVA:SPDP = 1:50) and incubated at ambient temperature for 30 min. The mixture was chromatographed (7 fractions of 0.5 mL were collected) on a PD-10 column equilibrated with the same buffer solution. The degree of substitution was determined by measuring the absorbance at 280 (A_{280}) and 343 nm (A_{343}) and of a 20-fold diluted sample, in the absence and presence of DTT. The degree of substitution is expressed by eq 1 and was 22.4 equiv of SPDP/molecule of OVA.

$$\text{degree of substitution} = \frac{\left(\frac{\Delta A_{343}}{8080}\right)}{\left(\frac{A_{280,\text{noDTT}} - 5100\frac{\Delta A_{343}}{8080}}{0.6 \times 46\,000}\right)} \quad (1)$$

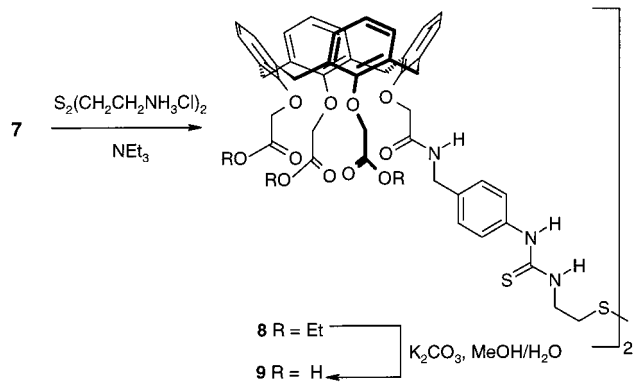
To a solution of 15 mg/mL of calix[4]arene **9** in DMF was added 103 μL of a 0.08 M solution of tributylphosphine in 1-propanol under a nitrogen atmosphere. After 15 min of incubation, 250 μL of this solution was added to the OVA-SPDP solution (molar ratio OVA:calix[4]-arene thiol = 1:44.8) and incubated for 90 min. The solution was chromatographed on PD-10 columns equilibrated in PBS. The conjugates were analyzed by UV measurements, IEF (which failed due to precipitation of the conjugate on the gel, whereas the unmodified protein can be applied without difficulties), and SDS−PAGE.

Analysis of Mouse Sera by ELISA (*Vide Supra).* Microtitration plates were coated with 1 μg/mL OVA−calix-[4]arene conjugate. The sera to be tested were diluted 10-fold with PBS-Tween. The second antibody [goat anti mouse Ig-HRP conjugate] was diluted 5000-fold with PBS-Tween.

RESULTS AND DISCUSSION

Synthesis of Bifunctional Ligands. Because of the frequent use of aryl isothiocyanate groups in coupling reactions to biomolecules (*17*, *24*−*26*), we decided to synthesize a calix[4]arene containing such a group at the *lower rim*. To obtain a binding site for cation complexation, e.g., a cavity consisting of the phenolic oxygen atoms and carboxylic acid groups or amides, as was shown to be useful for binding lanthanide ions (*11*, *27*), the synthesis route (Scheme 1) started with calix[4]arene tetraethyl ester **3** (*21*). Via selective monohydrolysis under acidic conditions (*28*), calix[4]arene monocarboxylic acid triethyl ester **4** was obtained. Activation of the carboxylic acid with oxalyl chloride afforded the corresponding acid chloride, which was reacted with *p*-nitrobenzylamine to give calix[4]arene monoamide **5** in 73% yield. Clearly distinguishable signals for the aromatic hydrogen atoms of the nitrophenyl moiety in the ^{1}H NMR spectrum indicated the successful introduction of this functionality. Aminocalix[4]arene **6** was obtained by reduction of the nitro group of calixarene **5** using H_2 and 10% palladium on charcoal in a mixture of ethanol and THF. Because of a tendency to oligomerize, due to a reaction between the amino group and the ethyl ester moieties, calix[4]arene **6** was immediately converted to calix[4]arene isothiocyanate **7** by reaction with thiophosgene and triethylamine as a base. After column chromatography, bifunctional calix[4]arene isothiocyanate **7** was obtained in 55% yield based on nitrocalix[4]arene **5**. The conversion of the nitro group was evidenced by a shift of the signals in the ^{1}H NMR spectrum of the aromatic hydrogen atoms of the isothiocyanate bearing phenyl ring and by the presence of a characteristic isothiocyanate peak at 2099 cm^{-1} in the infrared spectrum of calix[4]-arene isothiocyanate **7**. Calix[4]arene triethyl ester monoamide **7** may be regarded as a bifunctional ligand, because of its ability to complex cations in organic media and of the presence of a moiety with which it can be linked to biomolecules. However, for a strong binding to trivalent cations the ester groups of calix[4]arene **7** must be hydrolyzed to the corresponding calix[4]arene tricarboxylic acid monoamide. This was attempted by an acidic hydrolysis because of the sensitivity of isothiocyanate groups toward alkaline conditions and reactivity to refluxing methanol (*29*), in which solvent this reaction is usually accomplished (*27*). However, only partial hydrolysis was observed, probably because of inhibition of further hydrolysis by hydronium ion complexation, as was observed in the monohydrolysis of calix[4]arene tetraester **3** to calix[4]arene monocarboxylic acid triethyl ester **4** (*28*). Also, an attempt to enzymatically hydrolyze the ester groups did not result in the desired deprotection. Therefore, it was decided to further functionalize calix[4]arene **7** in such a way that a derivative stable to alkaline conditions was obtained.

Scheme 2. Synthesis of Calix[4]arene Dimer 9



Whereas an isothiocyanate functionality containing ligand can potentially be coupled directly to amino groups of the protein of choice, another method for the conjugation of bifunctional ligands is the coupling of the chelator to an engineered biomolecule. This is achieved by a reaction of the amino groups of the biomolecule with a so-called heterobifunctional linking agent containing two different functional groups, of which only one is reactive toward amino groups. The remaining functional group can subsequently be used in the coupling reaction with a bifunctional ligand. The ligand then has to be equipped with a reactive group, other than an amino group. For this purpose, a thiol functionality is frequently used. *S*-(2-pyridylthio)cysteamine (*30*) has been applied in our group as a precursor for a thiol group.[3] Calix[4]arene triethyl esters functionalized at the *lower rim* with this linking agent were converted to the corresponding calix[4]arene tricarboxylic acid by refluxing in a water/methanol mixture containing potassium carbonate (*27*). However, during this reaction, cleavage of the S−S bond occurred and this led to a dimer of calix[4]arene tricarboxylic acids linked by a newly formed disulfide bond. For the coupling to biomolecules, the disulfide bond is reduced, affording 2 equiv of calixarene thiols, which can be coupled to a biomolecule modified by reaction with a heterobifunctional linking agent.

Because of the scission of the disulfide bond, we decided to synthesize a calixarene dimer on purpose. Reaction of calix[4]arene isothiocyanate **7** with half an equivalent of cystamine afforded bis(calix[4]arene) thiourea disulfide **8** in 73% yield after preparative thin-layer chromatography. The bis-calix[4]arene was characterized by mass spectrometry and ^{1}H NMR spectroscopy, which proved the formation of a thiourea moiety. Selective basic hydrolysis of the ester groups (*27*) gave in 92% yield the corresponding bifunctional calix[4]arene hexacarboxylic acid **9** (Scheme 2). This gave a compound capable of binding cations in the cavity formed by the phenolic oxygen atoms, the carboxylate and the amide carbonyl groups.

Conjugation Experiments. Conjugation of bifunctional calix[4]arenes **7** and **9** was performed with two different types of biomolecules. MAb 506-A, directed against the pregnancy hormone hCG, was used as a model for the tumor specific mAbs to be applied as tools in radioimmunotherapy. HSA was used as a model for organ-specific proteins.

Conjugation of calix[4]arene isothiocyanate **7** was attempted by addition of different amounts of a solution of the calix[4]arene in DMF to aqueous solutions of the biomolecule in PBS and subsequent adjustment of the pH to 9. The mixtures in which the ratio calixarene: biomolecule was higher than 25:1 became turbid, but no precipitation occurred.

Reduction of the disulfide bond of bis-calix[4]arene **9** with 1 equiv of tributylphosphine afforded 2 equiv of a thiol-functionalized calix[4]arene. Modification of the biomolecule is necessary in this case because the biomolecule itself does not contain readily available groups to which the calixarene can be connected. The coupling was performed by reacting the proteins with the heterobifunctional linking agent GMBS, which contains an active ester moiety which reacts with the amino groups of the biomolecule to give a stable amide bond. Its maleimido functionality can be reacted in a Michael addition with a thiol like the reduced form of calix[4]arene **9**. In the first step, 15−40 equivalents of GMBS dissolved in DMF were added to a PBS solution of mAb 506-A and HSA, respectively. Subsequently, a solution of calix[4]arene thiol in DMF was added to oxygen-free solutions of the biomolecules in ratios varying from 5:1 up to 50:1, to allow the Michael addition to the maleimido group. After one night of incubation at ambient temperature in the dark, the remaining free maleimido groups were reacted with cysteamine in order to regain amino groups at positions that were not used in the conjugation to the calix[4]arene.

Conjugation Characterization. The mixtures obtained in the conjugation experiments were analyzed by MALDI-ToF MS, HP−SEC, IEF, and SDS−PAGE. All techniques indicated that the conjugation experiments with calix[4]arene isothiocyanate **7** were not successful. The reason is probably its low solubility in water. The biomolecules seem to solubilize the calix[4]arene by means of hydrophobic interactions, as was indicated by the turbidity of the mixtures and reflected by the strong aggregation that became apparent in the HP−SEC measurements.

On the other hand, the same techniques proved that the calix[4]arene thiol, obtained by reductive cleavage of the disulfide bond of calix[4]arene **9**, could be successfully linked to both mAb 506-A and HSA. MALDI-ToF MS experiments showed a clear shift to higher *m*/*z* values for the thiol derivative of calix[4]arene **9** conjugated to HSA. Upon addition of 50 equiv of the reduced calix[4]-arene to a solution of the GMBS-modified HSA, about six calix[4]arene molecules were conjugated to the protein. At a ratio of 25:1, approximately five calix[4]arene moieties are connected to the protein, and at lower ratios of 10 and 5:1, approximately only one calix[4]arene is bound (Table 3).

HP−SEC analysis of the calix[4]arene−antibody conjugate (Figure 1) shows a slight reduction in retention time as compared to the free antibody which is probably caused by the attachment of the chelator. A limited aggregation has occurred during the coupling reaction as is concluded from the UV-absorbing material in the void volume. However, the chromatographic profile shows that all contaminants can be easily removed by preparative gel permeation chromatography, leaving a homogeneous, monomeric immunoconjugate. The tendency to form aggregates was much less than observed for calix-[4]arene isothiocyanate **7**. This indicates that the enhanced solubility of calixarene **9** strongly improves its conjugation ability (data not shown).

Whenever the calix[4]arene thiol was involved in the IEF experiments (Figure 2, panels c and d), a clear anodal shift of the conjugate spots was observed (for reasons of

[3] Rudkevich, D. M., Verboom, W., and Reinhoudt, D. N., unpublished results.

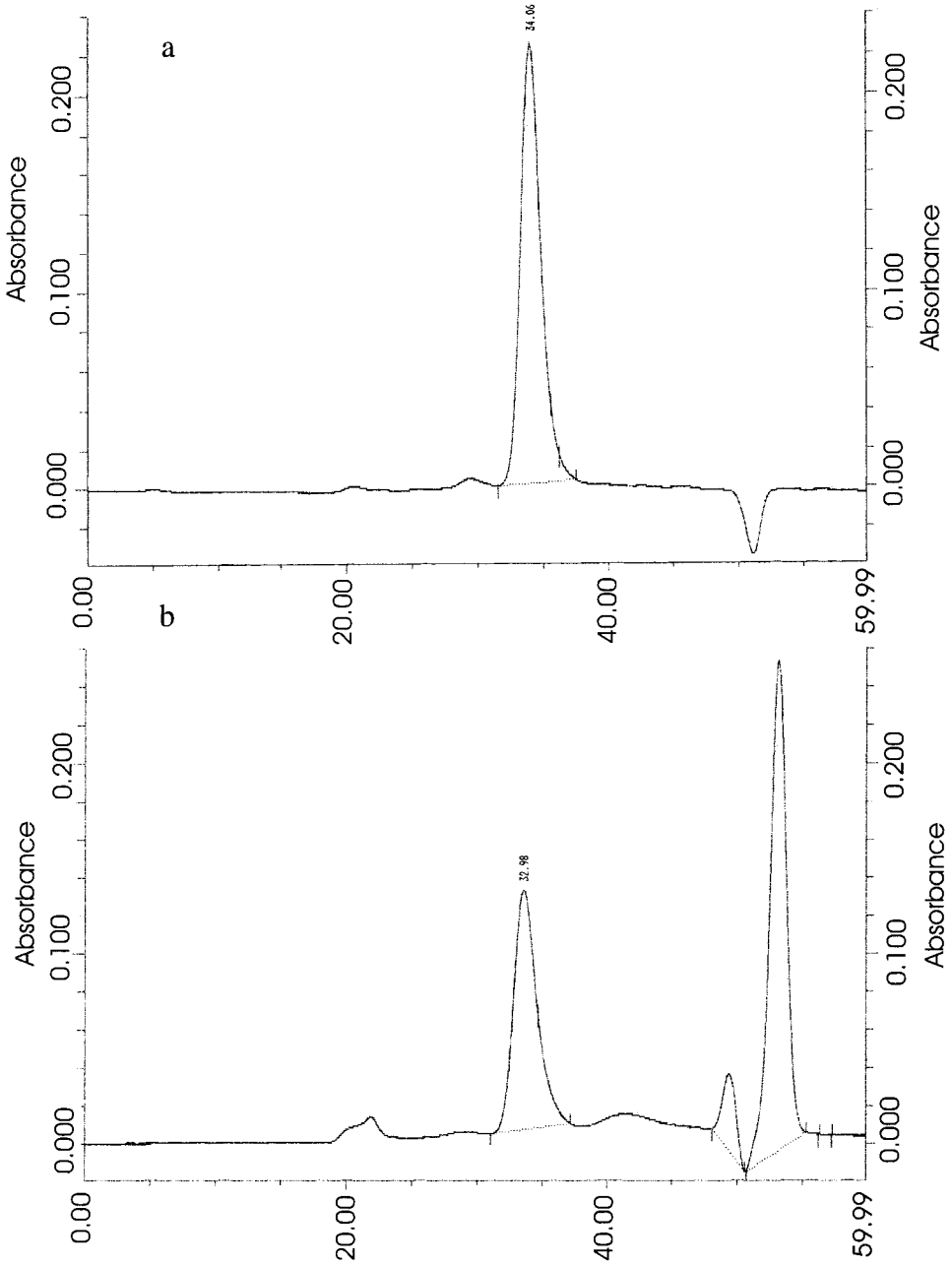


Figure 1. HP−SEC profiles of monoclonal antibody 506-A (a) and the (50:1) calix[4]arene disulfide immunoconjugate (b). Experimental details are described in the Materials and Methods.

comparison, the nonconjugated samples obtained with calix[4]arene isothiocyanate **7** are represented in Figure 2, panels a and b). These experiments indicate that the "acidity" of the calix[4]arene thiol conjugates is increased in comparison to the unmodified biomolecules due to the introduction of carboxylic acid groups.

When the calix[4]arene thiol was applied, in the SDS−PAGE experiments new bands appeared at positions corresponding to higher masses, indicative of a successful conjugation (Figure 3b). Also here, for reasons of comparison, the nonconjugated calix[4]arene **7** is presented in Figure 3a. Upon reduction of the disulfide bonds in the mAb conjugates, polypeptides with a molecular mass higher than that of the unmodified antibody were also observed.

Immunoreactivity Study. An important feature that has to be verified after conjugation of bifunctional ligands, in this case the thiol derivative of calix[4]arene **9**, to mAbs is the question whether the immunoreactivity, i.e., the binding of the antibody to its corresponding antigen, remains intact. The ELISA, described for the assessment of immunoreactivity, can be used for this purpose.

As can be concluded from Figure 4b, all conjugates tested show good immunoreactivity, indicating that this type of calix[4]arene can be coupled to mAbs without destroying the binding capabilities to antigens.

The immunoreactivity in the reaction mixtures with calix[4]arene isothiocyanate **7**, that could not be conjugated to the biomolecules, did not change significantly with the exception of the 118:1 mixture that showed no reaction at all (Figure 4a). Apparently, the binding sites of the mAb are involved in noncovalent interactions with the calix[4]arenes. It is possible that the calixarenes are kept in solution by means of hydrophobic interactions, leading to large structures which resulted in a turbid solution.

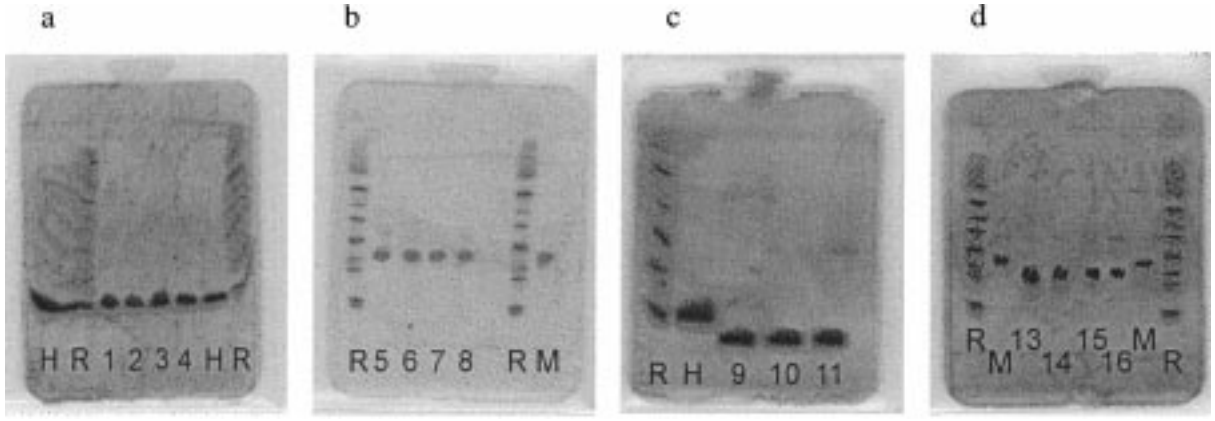


Figure 2. IEF analysis of the conjugation reactions. (a) HSA + calixarene **7**; (b) mAb 506-A + calixarene **7**; (c) HSA + calixarene **9**; (d) mAb 506-A + calixarene **9**. R represents the reference, H represents unmodified HSA, M represents unmodified mAb 506-A, the lane numbers correspond to the experiment numbers as mentioned in Tables 1 and 2.

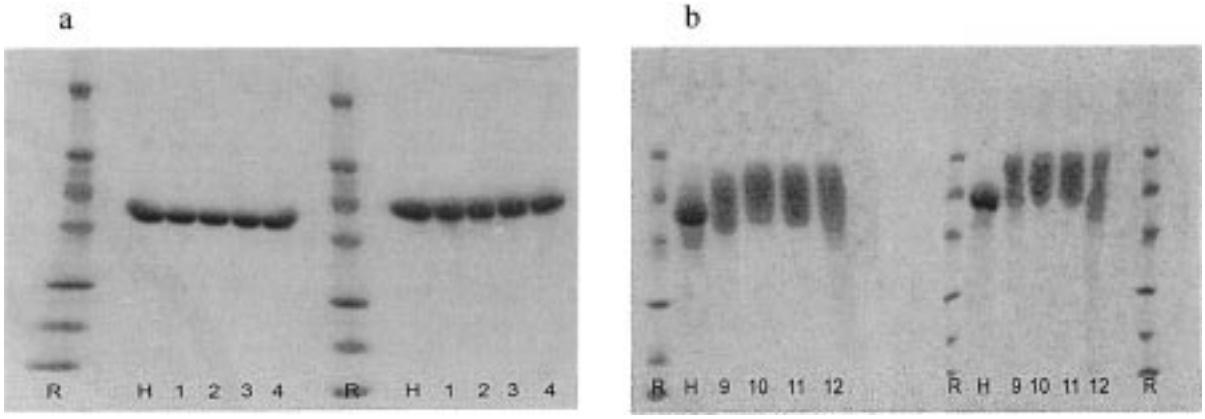


Figure 3. SDS−PAGE analysis of the conjugation reactions. (a) HSA + calix[4]arene **7**; (b) HSA + calix[4]arene **9**. R represents the reference, H represents unmodified HSA, the lane numbers correspond to the experiment numbers as mentioned in Tables 1 and 2. Reduced proteins are presented at the left side of the photograph; native proteins are presented at the right side of the photograph.

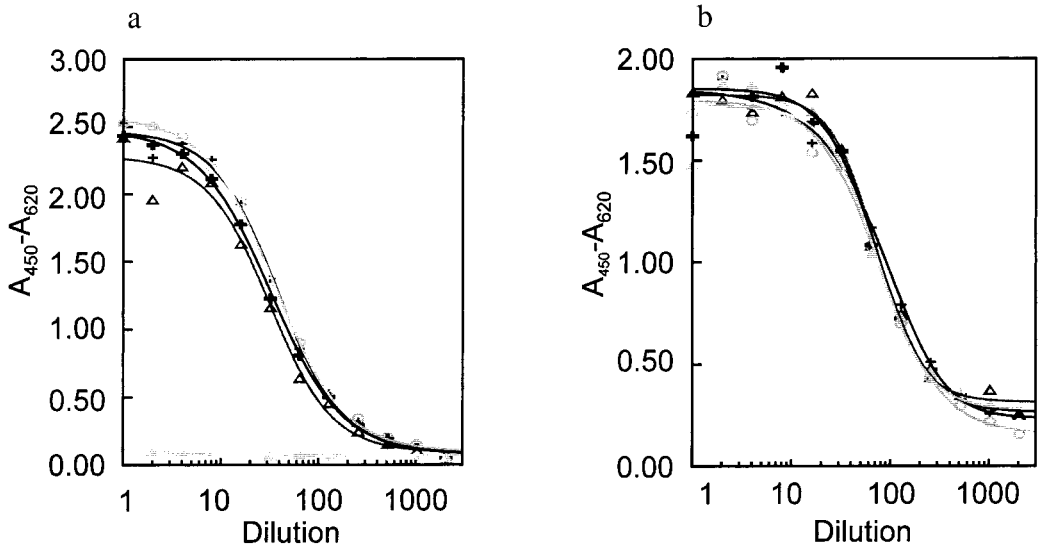


Figure 4. ELISA analysis of immunoreactivity. (a) calix[4]arene **7**: mAb 506-A; (+) unmodified mAB; (Δ) 5; (○) 6; (+) 7; (▲) 8. (b) Calix[4]arene **9**: mAb 506-A; (+) unmodified mAB; (Δ) 13; (○) 14; (+) 15; (▲) 16. The numbers correspond to the experiment numbers as mentioned in Tables 1 and 2.

Immunogenicity Study. The immunogenicity of protein bound calix[4]arene **9** was studied in mice. For this purpose (*31*), conjugates of the calix[4]arene with HSA and MSA were prepared as a heterologous and homologous immunogen, respectively. The study included five groups, each of 15 animals, schematically represented in Table 4. As can be seen from this table, regimen c can be compared in terms of doses and injection scheme with an immunotherapeutic or -diagnostic protocol in humans.

The sera were collected and assessed for the presence of antibodies directed against the calix[4]arene by ELISAs (Figure 5). For this purpose, a new conjugate had to be synthesized, which differed in carrier and cross-linker from the ones applied in immunization and which thus

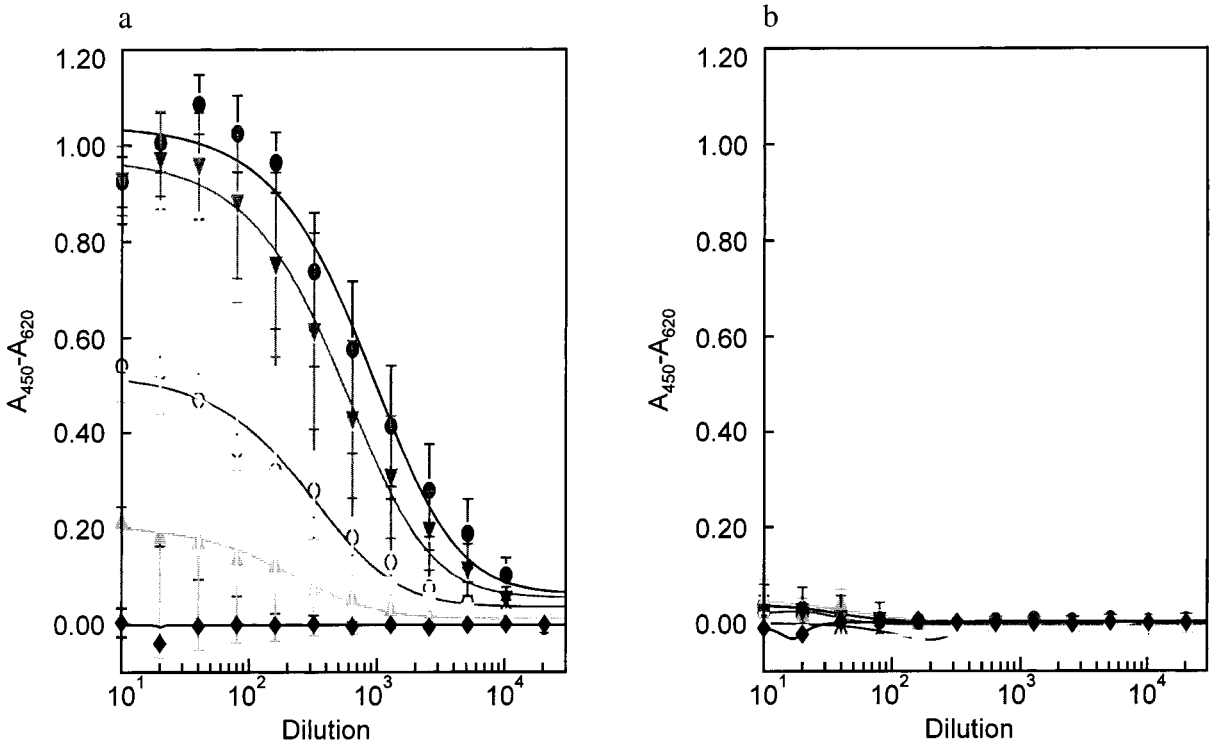


Figure 5. ELISA analysis of immunogenicity. (a) heterologous carrier; (●) group 1a; (○) group 1b; (▲) group 1c; (▼) group 2a; (■) group 2b; (◆) group 2c. (b) homologous carrier; (●) group 3a; (○) group 3b; (▲) group 3c; (▼) group 4a; (■) group 4b; (◆) group 4c. The group numbers correspond to those mentioned in Table 4.

Table 4. Experiments Performed in Immunogenicity Study[a]

group	antigen	amount of antigen (μg)
1a, b, c	HSA-calixarene	50
2a, b, c	HSA-calixarene	10
3a, b, c	MSA-calixarene	50
4a, b, c	MSA-calixarene	10
5a, b, c	− (PBS)	

[a] Each group of Table 4 was subdivided into three groups of five animals, which differed in injection method. In the first method the mice were injected i.p. at day 1 in the presence of Freund's Complete Adjuvant, an immunoresponse stimulating agent. At days 14, 28, and 42, an s.c. injection with Freund's Incomplete Adjuvant followed. The second method consisted of an i.p. injection without adjuvants on day 1 and an s.c. injection at days 14, 28, and 42. In the last method, only i.v. injections without adjuvants were applied at days 1, 14, 28, and 42. After approximately 1 week three mice of the same group died. No toxic effects of the antigen appeared, which makes it likely that the cause of death of these mice was not related to the injection with antigen. They were replaced by new mice, which were treated according to the original scheme. During the second immunization two mice, which were treated with the HSA-calix[4]arene conjugate by method 3 at both dosages, suffered from brain damage. These mice were not replaced due to shortage of antigen.

enables the selective detection of calixarene directed antibodies. OVA was selected as a carrier, which was reacted with the heterobifunctional linker SPDP (*32*). Subsequently, the calix[4]arene thiol, obtained by reduction of the disulfide bond of calix[4]arene **9**, was conjugated. UV measurements, IEF, and SDS−PAGE indicated that conjugation of the calix[4]arene was successfully performed.

The sera from mice that were injected intravenously with the homologous MSA−calix[4]arene (Figure 5b), a situation comparable to that during immunotherapy of humans with humanized mAbs (*33*), did not show a reaction against the calixarene. Neither did immunizations with MSA-calix[4]arene conjugates in the presence of adjuvants (method 1) evoke a humoral response to the chelator. However, in the experiments in which the heterologous HSA−calix[4]arene conjugates were involved, the formation of antibodies against the calix[4]arene was clearly demonstrated (Figure 5a). The adjuvants applied in injection method 1 clearly triggered the immune system. Injection method 2 gave a less severe reaction, but clearly, the presence of calix[4]arene directed antibodies in the sera was demonstrated. The results of the i.v. injection method 3 depended on the dosages. Application of 50 μg induced a response to some small degree, whereas the presence of antibodies was not demonstrated in the sera of mice that were given 10 μg of the antigen. This toxicity may be conjugate related. Although these effects were not observed with the syngeneic albumin conjugate and toxicity is considered to be beyond the scope of this study, it is a matter of serious concern and will be addressed in detail during the further development of the chelator.

The ELISAs of the sera obtained by taking a blood sample prior to each immunization were in good agreement with the results depicted in Figure 5. When the homologous systems were tested, no immune response was found, whereas there is a small response against the heterologous conjugate (except for the 10 μg dosage injected i.v.) after the first injection. In these cases, the response increased with subsequent injections.

These findings indicate that, for the future application in radioimmunotherapy in humans with humanized antibodies (*33*), an immune response against the calix[4]arene conjugate is unlikely to occur. Even after repeated administration of MSA−conjugate at a high dose, no immunoreaction was observed, which indicates that a therapeutic setting (e.g., injection method 3) with humanized mAbs is feasible. Recent studies of DeNardo et al. (*34*) show that a combination of a chimeric antibody and DOTA linked to it through a hydrolyzable peptide linker leads to an immunoconjugate that does not elicit

an antiglobulin response in humans despite five immunoconjugate infusions. Moreover, the biodegradable linker minimizes the radiation dose to critical normal tissues, thereby improving the therapeutic index. This study advocates additional attention to be focused on the introduction of biodegradable linkers in the development of novel, clinically applicable chelator molecules, which will be taken up in the studies on calix[4]arenes.

CONCLUSIONS

Bis(calix[4]arene) hexacarboxylic acid **9**, containing a masked thiol functionality, was conjugated to mAb 506-A and HSA. The immunoreactivity of the conjugates is not impaired when up to 6 equiv of calixarene are bound to the mAb. Animal tests indicated that the immunogenicity toward the calix[4]arene is strongly influenced by the nature of the carrier, the dosage, and the injection method. No reaction occurred when a homologous carrier was used or, when a heterologous carrier was applied, at a dosage of 10 μg/immunization via i.v. injection. Under all other conditions, the presence of antibodies directed against the calix[4]arene was demonstrated. Thus, for the application in radioimmunotherapy, the conjugation of a calix[4]arene to a humanized antibody will probably not lead to an immune response, while the immunoreactivity will not be disturbed.

It has already been shown that calix[4]arene tricarboxylic acids are able to chelate lanthanide cations in aqueous environments (*11*). Furthermore, Chen et al. (*18*) reported that calixarenes can be used to extract $^{225}Ac^{3+}$ from an aqueous into an organic phase. Experiments are now underway to investigate the $^{225}Ac^{3+}$ chelating properties of calix[4]arene **9**.

ACKNOWLEDGMENT

This study was in part supported by The Netherlands Foundation for Chemical Research (SON) with financial aid from The Netherlands Organization for Scientific Research (NWO) and the Technology Foundation STW in the framework of the SON/STW program Technical Chemistry (project number TST.3009).

LITERATURE CITED

(1) Parker, D. (1990) Tumour targeting with radiolabeled macrocycle-antibody conjugates. *Chem. Soc. Rev. 19*, 271.

(2) Goldenberg, D. M. (1991) Cancer imaging and therapy with radiolabeled antibodies. *Immunobiol. Proteins Pept. VI*, 107.

(3) Yuanfang, L., and Chuanchu, W. (1991) Radiolabeling of monoclonal antibodies with metal chelates. *Pure Appl. Chem. 63*, 427.

(4) Parker, D. (1990) Tumor targeting. *Chem. Brit.* 942.

(5) Suey, C. M., DeNardo, G. L., DeNardo, S. J., and Gobuty, A. H. (1990) Radioimmunotherapy with monoclonal antibodies. *J. Nucl. Med. Technol. 18*, 176.

(6) Meares, C. F., Diril, H., Kukis, D., McCall, M., Rana, T., Wellman, A., DeNardo, S. J., and DeNardo, G. L. (1991) Radiochemistry of antibodies: some recent advances. *Antibody, Immunoconj. Radiopharm. 4*, 389.

(7) Epperly, M. W., and Bloomer, W. D. (1991) Radiotherapy: the closer the better. *Chemtech* 744.

(8) Böhmer, V. (1995) Calixarenes, macrocycles with (almost) unlimited possibilities. *Angew. Chem., Int. Ed. Engl. 34*, 713, and references cited therein.

(9) Ikeda, A., and Shinkai, S. (1997) Novel cavity design using calix[n]arenes skeletons: toward molecular recognition and metal binding. *Chem. Rev. 97*, 1713, and references therein.

(10) Grote Gansey, M. H. B., Steemers, F. J., Verboom, W., and Reinhoudt, D. N. (1997) Synthesis of neutral, water-soluble calix[4]arenes. *Synthesis* 643.

(11) Steemers, F. J., Meuris, H. G., Verboom, W., Reinhoudt, D. N., Van der Tol, E. B., and Verhoeven, J. W. (1997) Water-soluble neutral calix[4]arene-lanthanide complexes. *J. Org. Chem. 62*, 4229.

(12) Steemers, F. J., Verboom, W., Reinhoudt, D. N., Van der Tol, E. B., and Verhoeven, J. W. (1995) New sensitizer-modified calix[4]arenes enabling near-UV excitation of complexed luminescent lanthanide ions. *J. Am. Chem. Soc. 117*, 9408.

(13) Iwema Bakker, W. I., Haas, M., Den Hertog, H. J., Jr., Verboom, W., De Zeeuw, D., Bruins, A. P., and Reinhoudt, D. N. (1994) Functionalized calixspherands: synthesis and peptide coupling. *J. Org. Chem. 59*, 972.

(14) Iwema Bakker, W. I., Haas, M., Khoo-Beattie, C., Ostaszewski, R., Franken, S. M., Den Hertog, H. J., Jr., Verboom, W., De Zeeuw, D., Harkema, S., and Reinhoudt, D. N. (1994) Kinetically stable complexes of alkali cations with calixspherands: an evaluation of shielding. *J. Am. Chem. Soc. 116*, 123.

(15) For a more detailed discussion about the use of calix[4]arenes in binding Ac^{3+}, see Grote Gansey, M. H. B., Verboom, W., Van Veggel, F. C. J. M., Vetrogon, V., Arnaud-Neu, F., Schwing-Weill, M.-J., and Reinhoudt, D. N. (1998) Model studies toward trivalent cation binding by appropriately functionalized calix[4]arenes. *J. Chem. Soc., Perkin Trans. 2*, 2351.

(16) Geerlings, M. W., Kaspersen, F. M., Apostolidis, C., and Van der Hout, R. (1993) The feasibility of ^{225}Ac as a source of α-particles in radioimmunotherapy. *Nucl. Med. Commun. 14*, 121.

(17) Kaspersen, F. M., Bos, E., Doornmalen, A. V., Geerlings, M. W., Apostolidis, C., and Molinet, R. (1995) Cytotoxicity of ^{213}Bi- and ^{225}Ac-immunoconjugates. *Nucl. Med. Commun. 16*, 468.

(18) Chen, X., Ji, M., Fisher, D. R., and Wai, C. M. (1998) Carboxylate-derived calixarenes with high selectivity for actinium-225. *Chem. Commun.* 377.

(19) Kosmas, C., Snook, D., Gooden, C. S., Courtenay-Luck, N. S., McCall, M. J., Meares, C. F., and Epenetos, A. A. (1992) Development of humoral immune responses against a macrocyclic chelating agent (DOTA) in cancer patients receiving radioimmunoconjugates for imaging and therapy. *Cancer Res. 52*, 904.

(20) Kosmas, C., Maraveyas, A., Gooden, C. S., Snook, D., and Epenetos, A. A. (1995) Anti-chelate antibodies after intraperitoneal yttrium-90-labeled monoclonal antibody immunoconjugates for ovarian cancer therapy. *J. Nucl. Med. 36*, 746.

(21) McKervey, M. A., Seward, E. M., Ferguson, G., Ruhl, B., and Harris, S. J. (1985) Synthesis, X-ray crystal structures, and cation transfer properties of alkyl calixaryl acetates, a new series of molecular receptors. *J. Chem. Soc., Chem. Commun.* 388.

(22) Pham, D. T., Kaspersen, F. M., and Bos, E. S. (1995) Electrophoretic method for the quantitative determination of a benzyl-DTPA ligand in DTPA monoclonal antibody conjugates. *Bioconjugate Chem. 6*, 313.

(23) Hoes, C. J. T., Grootoonk, J., Feijen, J., Boon, P. J., Kaspersen, F. M., Loeffen, P., Schlachter, I., Winters, M., and Bos, E. S. (1992) Synthesis and biodistribution of immunoconjugates of a human IgM and polymeric drug carriers. *J. Controlled Release 19*, 59.

(24) Westerberg, D. A., Carney, P. L., Rogers, P. E., Kline, S. J., and Johnson, D. K. (1989) Synthesis of novel bifunctional chelators and their use in preparing monoclonal antibody conjugates for tumor targeting. *J. Med. Chem. 32*, 236.

(25) Izard, M. E., Boniface, G. R., Hardiman, K. L., Brechbiel, M. W., Gansow, O. A., and Walker, K. Z. (1992) An improved method for labeling monoclonal antibodies with samarium-153: use of the bifunctional chelate 2-(*p*-isothiocyanatobenzyl)-6-methyldiethylenetriaminepentaacetic acid. *Bioconjugate Chem. 3*, 346.

(26) Li, M., Meares, C. F., Zhong, G.-R., Miers, L., Xiong, C.-Y., and DeNardo, S. J. (1994) Labeling monoclonal antibodies with ^{90}yttrium and ^{111}indium-DOTA chelates: a simple and efficient method. *Bioconjugate Chem. 5*, 101.

(27) Rudkevich, D. M., Verboom, W., Van der Tol, E. B., Van Staveren, C., Kaspersen, F. M., Verhoeven, J. W., and

Reinhoudt, D. N. (1995) Calix[4]arene-triacids as receptors for lanthanides; synthesis and luminescence of neutral Eu^{3+} and Tb^{3+} complexes. *J. Chem. Soc., Perkin Trans. 2* 131.

(28) Böhmer, V., Vogt, W., Harris, S. J., Raymond, G. L., Collins, E. M., Deasy, M., McKervey, M. A., and Owens, M. (1990) Selective monohydrolysis of a calix[4]arene tetraethyl ester with trifluoroacetic acid and its inhibition by Na^+ ion: evidence for hydronium ion complexation. *J. Chem. Soc., Perkin Trans. 1* 431.

(29) Drobnica, L., Kristián, P., and Augustín, J. (1977) *The Chemistry of the −NCS group*; *The Chemistry of Cyanates and Their Thio Derivatives*; *The Chemistry of Functional Groups*, John Wiley & Sons: Chichester.

(30) Ebright, Y. W., Chen, Y., Pendergrast, P. S., and Ebright, R. H. (1992) Incorporation of an EDTA-metal complex at a rationally selected site within a protein: application to EDTA-iron DNA affinity cleaving with catabolite gene activator protein (CAP) and Cro. *Biochemistry 31*, 10664.

(31) Roitt, I. M., Brostoff, J., and Male, D. K. (1989) *Immunology*, 2nd ed., Gower Medical Publishing: London.

(32) Carlsson, J., Drevin, H., and Axen, R. (1978) Protein thiolation and reversible protein−protein conjugation. *N*-Succinimidyl 3-(2-pyridyldithio)propionate, a new heterobifunctional reagent. *Biochem. J. 173*, 723.

(33) Schubiger, P. A., Alberto, R., and Smith, A. (1996) Vehicles, chelators, and radionuclides: choosing the "building blocks" of an effective therapeutic radioimmunoconjugate. *Bioconjugate Chem. 7*, 165.

(34) DeNardo, S. J., Richman, C. M., Goldstein, D. S., Shen, S., Salako, Q., Kukis, D. L., Meares, C. F., Yuan, A., Welborn, J. L., and Denardo, G. L. (1997) Yttrium-90/indium-111-DOTA-peptide-chimeric L6: Pharmacokinetics, dosimetry and initial results in patients with incurable breast cancer. *Anticancer Res. 17*, 1735.

BC9801474

Caged DNA Does Not Aggregate in High Ionic Strength Solutions

Vladimir S. Trubetskoy,*,† Aaron Loomis,† Paul M. Slattum,† James E. Hagstrom,† Vladimir G. Budker,‡ and Jon A. Wolff‡

Mirus Corporation, 545 Science Drive, Madison, Wisconsin 53711, and Departments of Pediatrics and Medical Genetics, Waisman Center, University of Wisconsin—Madison, Room 361, 1500 Highland Avenue, Madison, Wisconsin 53705. Received December 28, 1998; Revised Manuscript Received March 22, 1999

The assembly of DNA into compact particles that do not aggregate in physiologic salt solution occurs naturally in chromatin and viral particles but has been challenging to duplicate using artificial constructs. Cross-linking amino-containing polycations in the presence of DNA with bisimidoester cross-linker leads to the formation of caged DNA particles that are stable in salt solutions. This first demonstration of caged DNA provides insight into how natural condensation processes avoid aggregation and a promising avenue for developing nonviral gene therapy vectors.

INTRODUCTION

The condensation of DNA is an integral process of chromatin and viral assembly (*1*−*4*). These processes have been modeled by use of low molecular weight cations such as spermine and polycations such as polylysine which compact DNA into toroid and rod structures when the DNA's negative charge is more than 90% neutralized (*5*). These practices are also important for the preparation of nonviral vectors for gene therapy (*6*−*8*). In contrast to chromatin and viral particles, these artificial DNA particles aggregate in semidilute DNA solutions containing physiologic concentrations of NaCl (*9, 10*). The aggregation of large polycation/DNA complexes is not well understood and hampers the use of such condensates for gene therapy because they are rapidly cleared from the circulation (*11*). We now show that covalent cross-linking of polyamines in complexes with DNA increases the stability of the condensed DNA particles in salt.

MATERIALS AND METHODS

Reagents. Plasmid pCILuc encoding the firefly luciferase was used as DNA throughout the study (*12*). Sodium chloride, poly-L-lysine (PLL, molecular mass 34 and 210 kDa), histone H1 (type III-S) and dextran sulfate (DS, MW 500 kDa) were obtained from Sigma. Polyallylamine, (molecular mass 10 kDa) and fluorescein isothiocyanate (FITC) were purchased from Aldrich. Cross-linking reagent, dimethyl-3,3′-dithiobispropionimidate (DTBP), was a product of Pierce (Rockford, IL). Reagents for covalent labeling of DNA (*Label*IT Fluorescein and *Label*IT Rhodamine) were products of Mirus Corp.

Labeling of Polyions with Fluorescent Moieties. DNA was labeled using *Label*IT Rhodamine reagent (13) at 1:1 reagent/DNA w/w ratio to yield covalent rhodamine−DNA conjugate (Rh-DNA). DNA was incubated with the reagent at 1 mg/mL in Hepes buffer for 1 h at 37 °C and was purified by two ethanol precipitations and immediately redissolved in water at concentration 1 mg/mL. PLL was labeled with FITC at 1:100 fluorophore/lysine initial ratio to yield fluorescein-PLL (Fl-PLL). PLL (10 mg in 1 mL of 0.1 M sodium tetraborate, pH 9.0) was mixed with 0.18 mg of FITC dissolved in 50 μL of anhydrous methyl sulfoxide (Aldrich). After 1 h of incubation at room temperature, the polymer was precipitated with 2-propanol and redissolved in the same buffer supplemented with 0.5 M NaCl.

Preparation of DNA/Polycation Complexes and Their Cross-Linking. The complexes were prepared at different amine/phosphate charge ratios in 25 mM Hepes solution adjusted to pH 8.0 with 4N NaOH (Hepes buffer) by adding stock solution of polycation (typically 10 mg/mL in 6−30 μL of water) into 1 mL of Hepes solution of DNA (50 μg/mL) and vortexing for 30 s. Cross-linking of DNA/polycation DTBP occurred at a 2:1 molar ratio of DTBP to primary amine (e.g., lysine monomer for polylysine and histone). Reaction was conducted for 3 h at room temperature. Cleavage of DTBP was performed by treating cross-linked complexes with a final concentration of 20 mM dithiothreitol (DTT) (Sigma) for 30 min at 37 °C. To premodify PLL with DTBP, PLL (10 mg in 1 mL of Hepes buffer) and DTBP (15 mg as dry powder) were incubated for 3 h at room temperature. The reaction mixture was used without further purification.

Particle Sizing and ζ-Potential Measurements. Particle sizing and ζ-potential measurements were performed at 25 °C using a Zeta Plus Particle Analyzer (Brookhaven Instruments Corp., Holtsville, NY) with a laser wavelength of 532 nm.

Dialysis of DNA/Polycation Complexes. For dialysis experiments, Rh-DNA/Fl-PLL complexes were formed at 100 μg/mL DNA concentration with a charge ratio of DNA to PLL of 1:6. DTBP modification was then done for 3 h. Samples were loaded into Spectra/Por CE (Cellulose Ester) Membrane MWCO 300 000 (Spectrum Medical Industries, Houston TX) and then dialyzed against Hepes buffer for 48 h with two buffer exchanges.

Ultracentrifugation of Rh-DNA/Fl-PLL Complexes. For ultracentrifuge precipitation experiments, Rh-DNA/Fl-PLL complexes were prepared at [DNA] = 100 μg/mL in Hepes buffer at 1:2, 1:4, and 1:6 charge ratios. Within 1 h after mixing, the complexes (1 mL) were centrifuged in Beckman TX-100 benchtop ultracentrifuge at 60 000 rpm for 1 h using a Ti 100 rotor. Spectra of the complexes

* To whom correspondence should be addressed. Phone: (608) 238-4400. Fax: (608) 233-3007. E-mail: vladimirt@genetransfer.com.

† Mirus Corporation.

‡ University of Wisconsin—Madison.

10.1021/bc9801530 CCC: $18.00 © 1999 American Chemical Society
Published on Web 05/29/1999

were registered before and after centrifugation in a range of 400−700 nm using Beckman DU-7 spectrophotometer. Difference spectra were derived using the instrument's software to obtain spectra of precipitated complexes. Spectra of Rh-DNA and Fl-PLL were also registered separately in order to measure absorbance at 590 and 495 nm respectively for individual components.

Polycation exchange experiments. For polycation exchange experiments, Fl-PLL was used as a reporter molecule. Its fluorescence within DNA/Fl-PLL complex is decreased due to polyelectrolyte condensation. The addition of excess of nonlabeled PLL displaces Fl-PLL from the complex and leads to fluorescence increase. Complex was formed at an initial charge ratio (3:1) and at a DNA concentration of 20 μg/mL in Hepes buffer (total volume 0.5 mL). NaCl was added up to 50 mM in order to achieve the equilibrium quicker. After the signal was stable, nonlabeled PLL (20× molar excess) was added to displace Fl-PLL from the complex. The result was expressed as the percentage of nonexchangeable Fl-PLL in the complex: $(F_0 - F)/(F_0 - F_{min}) \times 100\%$ where F_0 is the initial fluorescence of Fl-PLL, F_{min} is the fluorescence of Fl-PLL/DNA complex, and F is the fluorescence after addition of 20× excess of nonlabeled PLL.

Release of Fl-DNA from Fl-DNA/PLL Complexes in Decondensation Conditions. Release of Fl-DNA from Fl-DNA/PLL complexes in decondensation conditions was assessed by monitoring the increase in Fl-DNA fluorescence (*13*) after interaction with dextran sulfate (DS, molecular mass 500 kDa, Sigma). Fl-DNA/PLL complexes (cross-linked and non-cross-linked) were mixed in 450 μL of Hepes buffer at [Fl-DNA] = 50 μg/mL with 50 μL of increasing amount of DS for 5 min at room temperature (PLL/DS ratio was varied from 0.15 to 16). Sample fluorescence (0.5 mL of total volume) was measured using a spectrofluorometer ($\lambda_{em} = 490$, $\lambda_{ex} = 530$) and expressed as % of uncondensed Fl-DNA fluorescence.

Electron Microscopy of Condensed DNA Samples. DNA complexes were placed onto glow-discharged Formvar-coated 200-mesh grids for 1 min followed by staining with 1% uranyl acetate for 30 s. The grids were blotted dry with filter paper and examined using a JEOL JEM 100S electron microscope.

Transfection with DTBP-Treated Plasmid DNA. A luciferase expression plasmid DNA/histone H1 complex was cross-linked with DTBP. After DTT treatment, the plasmid DNA was transfected into 3T3 cells using *Trans*IT LT-1 reagent (Mirus Corp.) and luciferase expression was similar to that of non-cross-linked plasmid DNA preparation.

RESULTS AND DISCUSSION

The salt stability of polycation complexes with plasmid DNA was assessed using dynamic light scattering (Figure 1) and further confirmed using static light scattering. For PLL complexes, raising the charge ratio of PLL/DNA from 2:1 to 6:1 increased salt stability but the complexes still aggregated in 50 mM NaCl (Figure 1a). The addition of DTBP, which cross-links the amines on the PLL, substantially increased the salt stability of the complexes. DTBP was chosen because its product with primary amino groups preserves positive charge upon coupling. The salt stabilization is reversed upon addition of dithiotreithol which cleaves DTBP, indicating that it is not due to the conversion of the amines to amidines and is dependent upon the cross-linking. DTBP also stabilized complexes of DNA and polyallylamine (Figure 1b). Remarkably, cross-linking of histone H1/DNA complexes

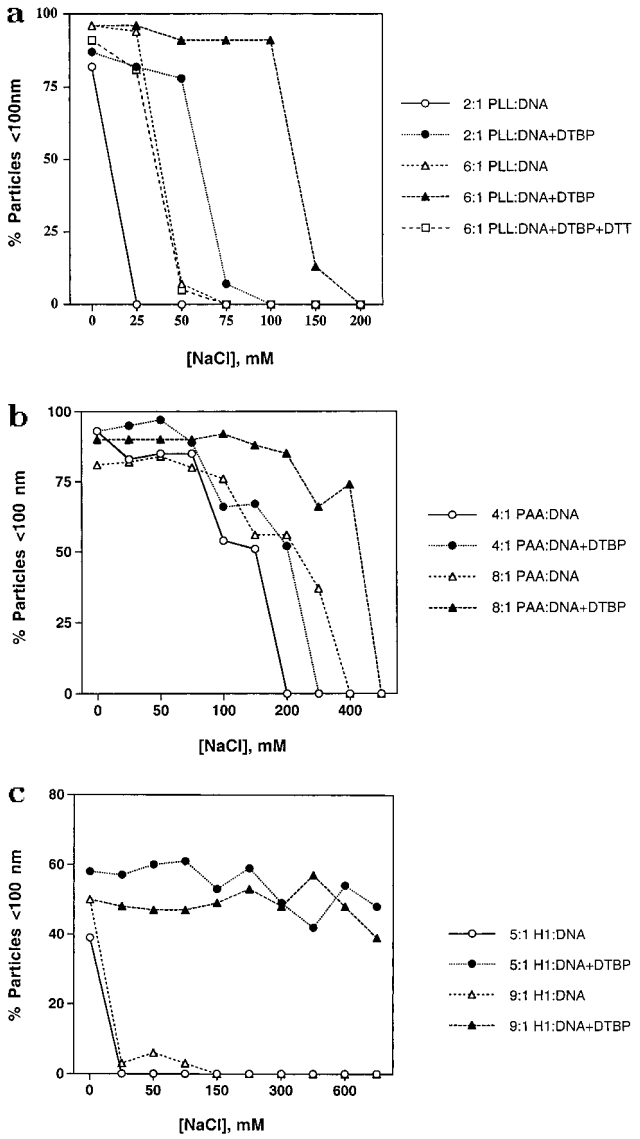


Figure 1. Relationship between particle size and NaCl concentration for polycation/DNA cross-linked complexes (filled symbols) and non-cross-linked ones (open symbols). (a) PLL (molecular mass = 34 kDa) and DNA were mixed at 2:1 and 6:1 charge ratios in low salt Hepes buffer following cross-linking of the complexes with DTBP. The 6:1 cross-linked complex was treated with 20 mM DTT. (b) PAA/DNA complex formation and cross-linking. (c) Histone H1/DNA complex formation and cross-linking. Charge ratios of polycation to DNA are indicated in the legends. The average size of all the PLL, PAA, and histone DNA particles under 100 nm with and without DTBP were ∼50, 60, and 75 nm in diameter, respectively.

created particles that were stable even in 800 mM NaCl (Figure 1c). Similar effects of cross-linking by DTBP on salt stabilization were evident when aggregation was assessed using static light scattering. The cross-linked particles did not aggregate for at least 7 days after the addition of salt. Taken together, these results suggest that the cross-linking of many polycations would stabilize their DNA complexes in salt.

The addition of the cross-linker DTBP could induce salt stabilization by either modifying the dispersion medium or the DNA-containing particles. If the DTBP was added to a concentrated solution of PLL first and this mixture is then added to DNA, no salt stabilization was observed. In addition, when the 6:1 PLL/DNA complexes (cross-linked and non-cross-linked) were dialyzed so as to reduce the net charge ratio of PLL/DNA to ∼1.7, the cross-linked

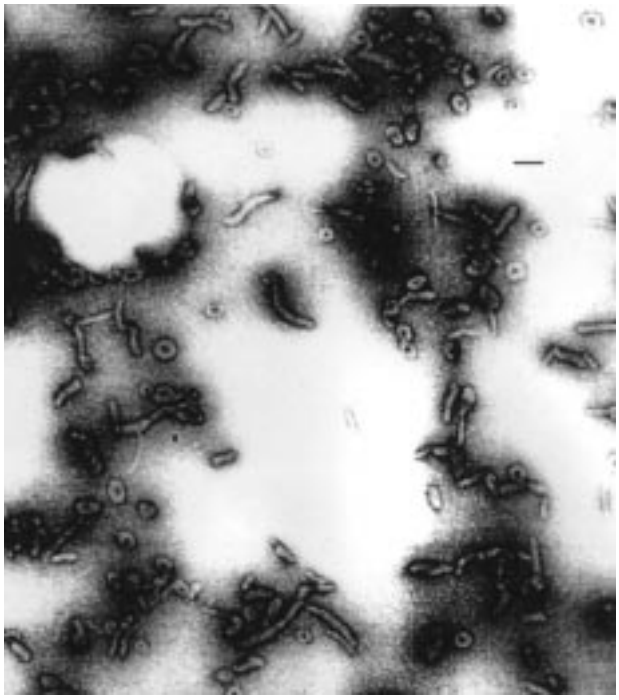


Figure 2. Transmission electron microscopy image of cross-linked PLL/DNA particles. The cross-linking reaction was carried at 6:1 PLL/DNA charge ratio. Bar length is 90 nm.

particles still had greater salt stability than the non-cross-linked complexes (data not shown). These results indicate that cross-linking increased salt stability by modifying the polyamine/DNA complex. It is noteworthy that the cross-linked DNA particles also did not aggregate in physiologic salt solutions that did not contain large amounts of excess polycation.

One possible mechanism by which cross-linking increases salt stability is by recruiting polycation to the particle thus providing electrosteric stabilization (*14*, *15*). Following cross-linking, neither ζ-potential nor particle size was significantly altered as compared to non-cross-linked DNA/PLL complexes. For example, particle size and ζ-potential for PLL/DNA 6:1 complex were found to be 61.6 nm and +59 mV for non-cross-linked vs 62.1 nm and + 53 mV for cross-linked complex, respectively. Similarly, electron microscopic analysis indicated that the cross-linked particles were toroids and rods that were similar in size and shape to non-cross-linked particles (Figure 2).

To directly determine the ratio of PLL to DNA in the complexes, the particles formed with fluorescently labeled Rh-DNA and Fl-PLL were pelleted by ultracentrifugation. The difference between the amount of PLL in solution before and after centrifugation indicates the amount of PLL in complexation with DNA. The non-cross-linked particles contained approximately a 1:1 ratio of amine/phosphate regardless of the initial ratios in the mixture (Figure 3). This is contrary to a common assumption in the polycation/DNA field, but is consistent with 1:1 charge ratios observed in some complexes of synthetic polyelectrolytes (*16*, *17*). Furthermore, cross-linking did not modify the ratio of PLL/DNA in the complexes (Figure 3). The ratio of PLL/DNA found in the precipitate was ~1:1 independent of both the initial PLL/DNA ratio and the addition of cross-linker. Similar results were obtained using analytical ultracentrifugation (data not shown). These studies indicate that cross-linking does not stabilize the DNA particles by recruiting additional polycations.

One hypothesis for the mechanism by which salt induces the aggregation of polycation/DNA complexes is by enabling the polycation on one particle to become bound to another particle by interparticle cross-bridging as it was proposed for both DNA condensates (*18*, *19*) and polyelectrolyte complexes in general (*20*, *21*). Cross-linking markedly decreases the exchange of unlabeled PLL in solution with Fl-PLL in 3:1 PLL/DNA complex. *The* percentage of nonexchangeable PLL in 3:1 complexes was found to decrease 3 times upon cross-linking (data not shown). Furthermore, cross-linking prevents high concentrations of NaCl and dextran sulfate (DS), a strong polyanion, from displacing the DNA in PLL complexes (Figure 4). DNA complexes containing larger PLL molecules of molecular mass 210 kDa were destabilized by DS (Figure 4b) and high salt (data not shown), which argues that the stabilization effect of DTBP is not merely due to increasing the size of PLL on the DNA. Taken together, these results suggest that cross-linking in fact "cages" condensed DNA inside the complexes. Even in the presence of high salt and DS, the "caged" DNA appears to be partially condensed. The cross-linked particles are more resistant to salt-induced aggregation

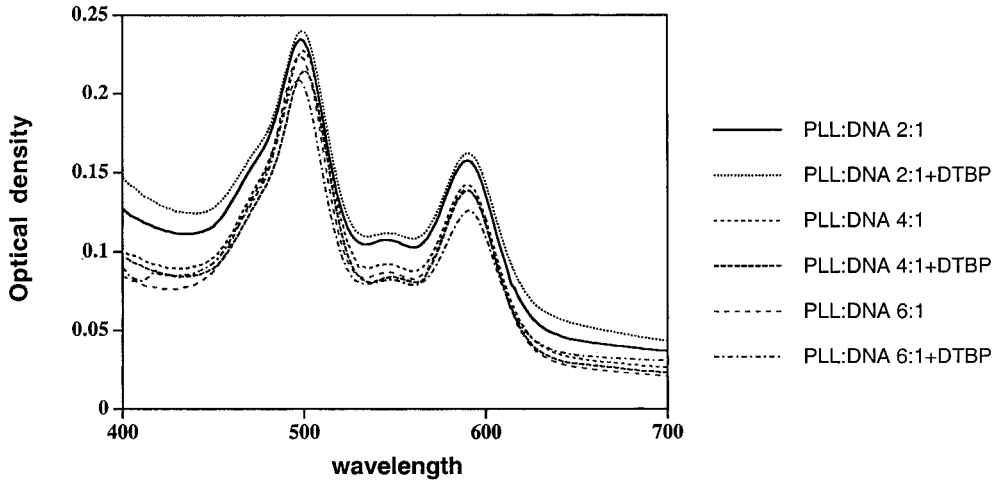


Figure 3. Difference spectra for precipitated portion of chromophore-labeled PLL/DNA cross-linked and non-cross-linked complexes with 2:1, 4:1, and 6:1 charge ratios. PLL and DNA were labeled with fluorescein isothiocyanate (λ_{max} = 495 nm) and rhodamine LabelIT (λ_{max} = 590 nm) reagent respectively (*15*). For stoichiometry measurements, the spectra were compared with the spectra of standard Fl-PLL and Rh-DNA solutions.

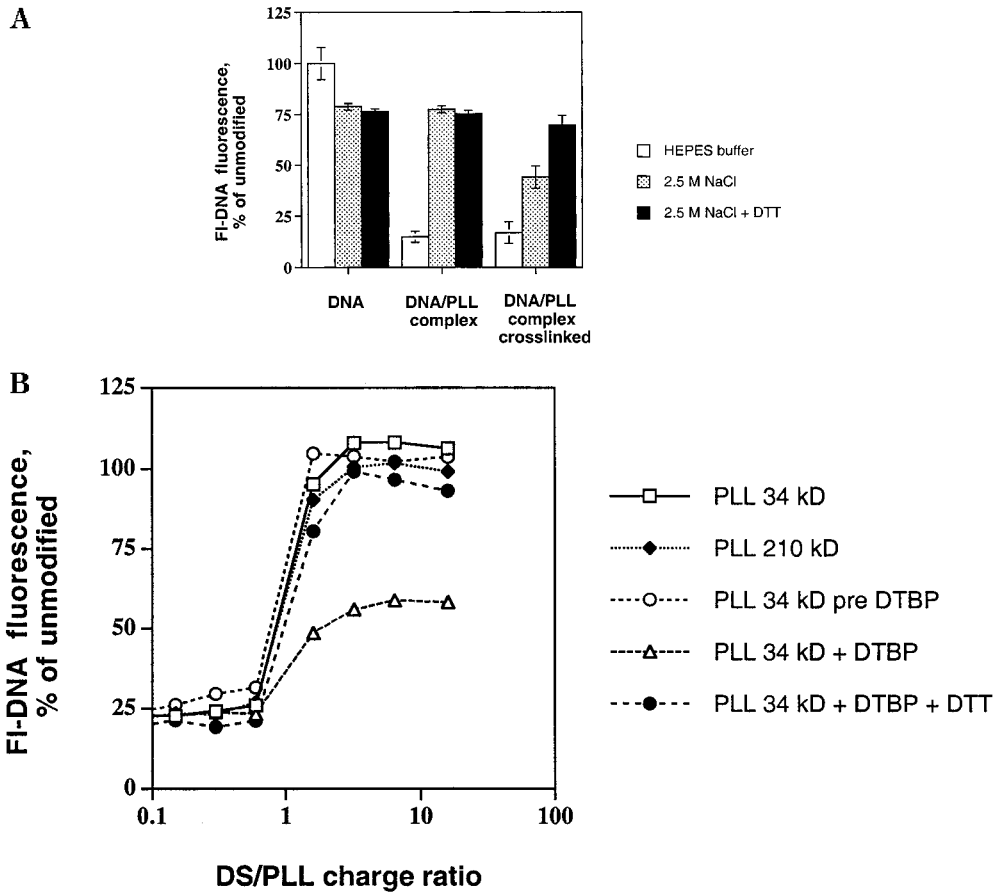


Figure 4. Decondensation of Fl-DNA in cross-linked and non-cross-linked PLL/DNA 6:1 complexes with different dissociative media. DNA covalently labeled with Fluorescein LabelIT reagent (3 fluorophore moieties per 100 base pairs) sustains considerable fluorescence quenching upon complexing with polycations. (A) Relative fluorescence of Fl-DNA and its cross-linked and non-cross-linked complexes with PLL upon decondensation in 2.5 M NaCl (*20*). (B) Decondensation of Fl-DNA with dextran sulfate. PLL (210 kDa) and pre-*cross*-linked PLL (34 kDa pre DTBP) were added as additional controls.

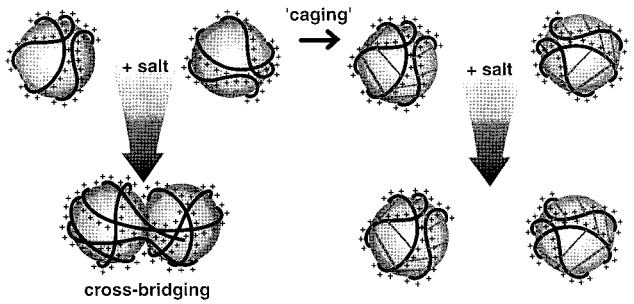


Figure 5. The model illustrates that salt induces the aggregation of polycation/DNA complexes by lowering the threshold for interparticle crossbridging with exchangeable polycations. Cross-linking of the polycation prevents this from occurring. Black, curving lines (+) indicate the polycations, and the gray, straight lines indicate the cross-links in the caged DNA.

because part of a polyamine molecule on one particle is less able to cross-bridge to another particle (Figure 5). In essence, cross-linking "freezes" the polycations on the particle.

Preliminary experiments indicated that caged complexes are inactive in gene transfer in vitro. On the other hand, experiments with cross-linked DNA/polycation (histone H1) complexes showed that DNA remains intact and expressable after reversing the cross-linking procedure with DTT treatment (data not shown). Considering intracellular reducing conditions (*22*, *23*), more labile cross-linkers may result in transfection-competent caged complexes.

Cross-linking of protein macromonomers accompanies the assembly of viral particles (*24*, *25*). Cross-linking of polyamine/DNA complexes mimics some aspects of viral particle assembly and provides a rationale for why it occurs during virus formation. The lack of aggregation of caged DNA particles in physiologic salt solutions presents an important advance in the development of nonviral vectors.

ACKNOWLEDGMENT

We would like to thank Dr. Grayson Scott for his assistance in obtaining electron microscopy images of caged DNA complexes and Dr. Darrell McCaslin for his expert advice in analytical ultracentrifugation experiments.

LITERATURE CITED

(1) Furlong, D., Swift, H., and Roizman, B. (1972) Arrangement of Herpesvirus Deoxyribonucleic Acid in the Core. *J. Virol. 10*, 1071−1074.

(2) Chattoraj, D., Gosule, L. C., and Schellman, J. A. (1978) DNA Condensation with Polyamines. II. Electron Microscopic Studies. *J. Mol. Biol. 121*, 327−337.

(3) Lepault, J., Dubochet, J., Baschong, W., and Kellenberger, E. (1987) Organization of double-stranded DNA in bacteriophages: a study by cryo-electron microscopy of vitrified samples. *EMBO J. 6*, 1507−1512.

(4) Hud, N. V. (1995) Double-Stranded DNA Organization in Bacteriophage Heads: An Alternative Toroid-Based Model. *Biophys. J. 69*, 1355−1362.

(5) Wilson R. W., and Bloomfield, V. A. (1979) Counterion-Induced Condensation of Deoxyribonucleic Acid. A Light-Scattering Study. *Biochemistry 18*, 2191−2196.

(6) Xu Y., and Szoka, F. C., Jr. (1996) Mechanism of DNA Release from Cationic Liposome/DNA Complexes Used in Cell Transfection. *Biochemistry 35*, 5616−5623.

(7) Cotton, M., and Wagner, E. (1993) Nonviral approaches to gene therapy. *Curr. Opin. Biotechnol. 4*, 705−710.

(8) Felgner, P. L., and Ringold, G. M. (1987) Cationic liposome-mediated transfection. *Nature 337*, 387−388.

(9) Tang, M. X., and Szoka, F. C., Jr. (1997) The influence of polymer structure on the interactions of cationic polymers with DNA and morphology of the resulting complexes. *Gene Ther. 4*, 823−832.

(10) Pouton, C. W., Lucas, P., Thomas, B. J., Uduehi, A. N., Milroy, D. A., and Moss, S. H. (1998) Polycation−DNA complexes for gene delivery: a comparison of the biopharmaceutical properties of cationic polypeptides and cationic lipids. *J. Controlled Release 53*, 289−299.

(11) Wolfert, M. A., Schacht, E. H., Toncheva, V., Ulbrich, K., Nazarova, O., and Seymour, L. W. (1996) Characterization of Vectors for Gene Therapy Formed by Self-Assembly of DNA with Synthetic Block Co−Polymers. *Human Gene Ther. 7*, 2123-2133.

(12) Zhang, G., Vargo, D., Budker, V., Armstrong, N., Knechtle, S., and Wolff, J. A. (1997) Expression of naked plasmid DNA injected into the afferent and efferent vessels of rodent and dog livers. *Human Gene Ther. 8*, 1763−1772.

(13) Trubetskoy, V. S., Budker, V. G., Slattum, P. M., Hagstrom, J. E., and Wolff, J. A. (1999) Quantitative Assessment of DNA Condensation by Quenching of Covalently-Bound Fluorescent Probes. *Anal. Biochem. 267*, 309−313.

(14) Peula, J. M., Fernandez-Barbero, A., Hidalgo-Alvarez, R., and de las Nieves, F. J. (1997) Comparative Study on the Colloidal Stability Mechanisms of Sulfonate Latexes. *Langmiur 13*, 3938−3943.

(15) Walker, H. W., and Grant, S. B. (1996) Role of Polymer Flexibility in the Stabilization of Colloidal Particles by Model Anionic Polyelectrolytes. *J. Colloid Interface Sci. 179*, 552−560.

(16) Dautzenberg, H. (1997) Polyelectrolyte Complex Formation in Highly Aggregating Systems. 1. Effect of Salt: Polyelectrolyte Complex Formation in the Presence of NaCl. *Macromolecules 30*, 7810−7815.

(17) Webster, L., Huglin, M. B., and Robb, I. D. (1997) Complex Formation Between Polyelectrolytes in Dilute Aqueous Solutions. *Polymer 38*, 1373−1380.

(18) Schellman, J. A., and Parthasarathy, N. (1984) X-ray Diffraction Studies on Cation-collapsed DNA. *J. Mol. Biol. 175*, 313−329.

(19) Olivera de la Cruz, M., Belloni, L., Delsanti, M., Dalbiez, J. P., Spalla, O., and Drifford, M. (1995) Precipitation of Highly Charged Polyelectrolyte Solutions in the Presence of Multivalent Salts. *J. Chem. Phys. 103*, 5781−5791.

(20) Hunter, R. J. (1995) *Foundations of Colloid Science*, vol. 1, pp 489−493, Clarendon Press, Oxford.

(21) Koetz, J., Koepke, H., Schmidt-Naake, G., Zarras, P., and Vogl, O. (1996) Polyanion-Polycation Complex Formation as a Function of the Position of the Functional Groups. *Polymer 13*, 2775−2781.

(22) Pisoni, R. L., Park, G. Y., Velilla, V. Q., and Thoene, J. G. (1995) Detection and Characterization of a Transport System Mediating Cysteamine Entry into Human Fibroblast Lysosomes. *J. Biol. Chem. 270*, 1179−1184.

(23) Collins, D. S., Unanue, E. R., and Harding, C. V. (1991) Reduction of Disulfide Bonds within Lysosomes is a Key Step in Antigen Processing. *J. Immunol. 147*, 4054−4059.

(24) McCarthy, M. P., White, W. I., Palmer-Hill, F., Koenig, S., and Suzich, J. A. (1998) Quantitative Dissasembly and Reassembly of Human Papillomavirus Type 11 Viruslike Particles in Vitro. *J. Virol. 72*, 32−41.

(25) Duda, R. L. (1998) Protein Chainmail: Catenated Protein in Viral Capsids. *Cell 94*, 55−60.

BC9801530

Novel Biotinylated Phenylarsonous Acids as Bifunctional Reagents for Spatially Close Thiols: Studies on Reduced Antibodies and the Agonist Binding Site of Reduced *Torpedo* Nicotinic Receptors

R. Moaddel, A. Sharma, T. Huseni, G. S. Jones, Jr.,† R. N. Hanson, and R. H. Loring*

Department of Pharmaceutical Sciences, Northeastern University, Boston, Massachusetts 02115. Received December 28, 1998; Revised Manuscript Received March 22, 1999

We synthesized three novel organoarsenicals as prototype bifunctional reagents for spatially close thiols, *N*-(4-arsenosophenyl) hexahydro-2-oxo-(3a*S*,4*S*,6a*R*)-1H-thieno[3,4-d]imidazole-4-pentamide (**1**), 2-[4-[(4-arsenosophenyl)amino]-1,4-dioxobutyl] hydrazide, (3a*S*,4*S*,6a*R*)-hexahydro-2-oxo- 1H-thieno-[3,4-d] imidazole-4-pentanoic acid (**2**), and [4-[[12-[[5-[(3a*S*,4*S*,6a*R*)-hexahydro-2-oxo-1H-thieno[3,4-d]imidazol-4-yl]-1-oxopentyl]amino]-1-oxododecyl]amino]phenyl]-arsonous acid (**3**) containing both biotin and arsenic with intervening varying length spacers extending from 2 to 15 Å beyond biotin bound to streptavidin. Conceptually, the arsenical group can form a stable, covalent ring structure with appropriately spaced thiols and thereby anchor the reagent to a macromolecule, while biotin allows for the detection of the reagent−macromolecule complex via avidin binding. Because the α-subunits of all characterized nicotinic receptors contain an easily reducible disulfide bond between adjacent cysteine residues, the reduced α-subunit is an attractive site for labeling. Compounds **1**−**3** all simultaneously bound streptavidin and dithiols, and all three decreased the number of [^{125}I]α-bungarotoxin-binding sites in reduced *Torpedo* nicotinic receptors (IC_{50s} 10−300 nM). Moreover, arsenylation of the receptors prevented their reoxidation with dithio-bis(nitrobenzoic acid), was reversible with 2,3-dimercaptopropanesulfonic acid, and protected the receptor from irreversible alkylation by bromoacetylcholine. However, in no case did **1**−**3** allow simultaneous binding to reduced nicotinic receptors and to [^{125}I]streptavidin, although **3** alone allowed simultaneous labeling of a spatially close dithiol located in reduced antibodies.

INTRODUCTION

Nicotinic receptors play an important role in vertebrate neuromuscular and ganglionic transmission and are believed to be important in the pharmacology of nicotine dependence (*1*). In addition, nicotinic agonists are currently being investigated for use as therapeutic agents in the treatment of Alzheimer's disease, Parkinson's disease, Tourette's syndrome, and ulcerative colitis (*1*). Muscle nicotinic receptors are pentameric membrane proteins consisting of two α1-subunits, and one *β*-, *γ*-, and *δ*-subunits. Multiple subtypes of neuronal nicotinic receptors are known, and all subtypes contain at least one kind of α-subunit. Currently, eight different neuronal α-subunits (α2−α9) and at least 3 neuronal *β*-subunits (*β*2−*β*4) are known (*2*). Since α-subunits from both muscle and nerve have an easily reducible disulfide bond between adjacent cysteine residues located within 0.9 nm of the agonist-binding site (*3*), the reduced α-subunit is an attractive site for labeling all known subtypes of nicotinic receptors. Bifunctional reagents that could label the agonist-binding site disulfide and give some spatial information relative to the rest of the receptor molecule would be very useful.

Of all multimeric receptors, the *Torpedo* nicotinic receptor is the best characterized, since it is so abundant in electroplax tissue. The *Torpedo* receptor has two agonist-binding sites located at the interface between the α−*δ* and the α−*γ* subunits (*4*, *5*). Both sites bind α-bungarotoxin (BGT), but a variety of evidence suggests that these two sites are not equivalent. The α−*γ* site binds D-tubocurarine with high affinity (*6*) and is easily reduced with dithiothreitol (DTT)[1] and alkylated with bromoacetylcholine (BAC), while the α−*δ* site shows low affinity for D-tubocurarine and is not as easily reduced or alkylated. Monoclonal antibodies are available from a variety of laboratories that discriminate between these two sites [referred to as the A and B sites, respectively (*7*)], indicating that the interfaces have different conformations. On the other hand, Unwin (*8*−*10*) has visualized *Torpedo* nicotinic receptors to a 9 Å resolution and suggests that two similar pits about 20 Å deep are the agonist-binding sites. Although one of those pits is located near the area mapped by an antibody against the α−*γ* binding site (*11*), there is no information as to where the corresponding disulfide bond is located relative to the three-dimensional structure of the receptor. The *Torpedo* nicotinic receptor is the best characterized, but there are still questions about the location and structure of the agonist-binding sites. Thus, we chose this receptor as our initial target.

We previously reported on the utility of simple trivalent organoarsenicals, which formed stable adducts with

* To whom correspondence should be addressed.
† Current address: RSP Amino Acid Analogues Inc., Worcester, MA 01605.

[1] Abbreviations: APA, *p*-aminophenylarsinedichloride hydrochloride; BAC, bromoacetylcholine; BGT, α-bungarotoxin; BSA, bovine serum albumin; DMPS, 2,3-dimercaptopropanesulfonic acid; DTNB, 5,5′-(dithiobis)-nitrobenzoic acid; DTT, dithiothreitol; IAA, iodoacetamide; MPB, maleimidopropionylbiocytin; NEM, *N*-ethylmaleimide; NHS, *N*-hydroxysuccinimide; SA-HRP, streptavidin-horseradish peroxidase conjugate.

10.1021/bc9801575 CCC: $18.00 © 1999 American Chemical Society
Published on Web 05/29/1999

reduced nicotinic receptors (*12*), from both *Torpedo* electroplax (ganglionic), and chick retina (neuronal). The findings were consistent with covalent As−S bond formation between trivalent arsenic and the adjacent cysteines generated upon reduction of the receptor. The decrease in [^{125}I]BGT binding upon arsenylation of receptors reduced with DTT was long-lasting but reversible upon treatment with the competitive dithiol, 2,3-dimercaptopropane sulfonic acid (DMPS). Monothiols such as 2-mercaptomethanesulfonic acid are not effective reagents to reverse the effects of arsenylation (*13*), and arsenylation prevented irreversible alkylation by BAC. Thus, our preliminary results suggested that trivalent arsenic could be used to anchor labeling groups in the *Torpedo* agonist-binding site. These novel bifunctional reagents would be potentially useful tools for receptor localization and quantification studies and mapping the nicotinic receptor and, thereby, provide a more rational basis for the design of agonists.

p-Aminophenylarsine oxide[2] was envisioned as a potentially useful starting material in our design strategies. The commercial sources were solubilized with HCl or could be freshly synthesized by reducing *p*-arsanilic acid (*14*). Here, we describe the synthesis of three novel biotinylated arsenical compounds with varying length spacers, demonstrate that these reagents are bifunctional for dithiols and streptavidin and that they each block [^{125}I]BGT binding when covalently attached to *Torpedo* nicotinic receptors. These compounds were then used to deduce information about the location of the disulfide in the *Torpedo* agonist-binding site, and one was found to be potentially useful as a labeling agent for antibodies.

MATERIALS AND METHODS

Chemicals and Reagents. *p*-Aminophenyl arsine oxide, *p*-arsanilic acid, and all other chemical precursors were obtained from Aldrich Chemical Co. (Milwaukee, WI) unless otherwise noted. Biotin, streptavidin, goat anti-rat IgG agarose beads, 4-chloro-1-naphthol, and β-galactosidase were purchased from Sigma Chemical (St. Louis, MO). Solvents and other materials, chemicals, and reagents were all analytically pure or of reagent grade and used without further purification. TLC (Whatman silica gel 60 F-254 plates; 0.25 mm layer thickness) and PTLC (Analtech Uniplate silica gel GF plates; 20 × 20 cm; 1 mm layer thickness) were used. Maleimidopropionylbiocytin (MPB) was purchased from Molecular Probes (Eugene, OR), streptavidin-horseradish peroxidase (SA-HRP) from Bio-Rad (Richmond, CA), and the peptide corresponding to residues 181−198 of the Torpedo nicotinic α-subunit (YRGWKHVYYTCCPDTPPY) obtained from Chiron Mimetopes (Raleigh, NC). Membranes rich in *Torpedo* nicotinic receptors were a generous gift of Dr. Jonathan Cohen, as was the monoclonal antibody mAb210 from Dr. Jon Lindstrom. α-Bungarotoxin (BGT; Biotoxins Inc., St. Cloud, FL) was radioiodinated using Iodogen (Pierce Chemical Co., Rockford IL) as previously described (*15*). ^{125}I-Labeled streptavidin was produced similarly, and specific activities of both radioligands ranged 300−500 Ci/mmol determined by isotope dilution (*16*).

Equipment. Melting points were determined with a Thomas−Hoover melting point apparatus. The NMR spectra were recorded with a Varian-300 spectrometer, and IR spectra (KBr) were recorded on a Perkin-Elmer 1600 FTIR spectrometer. MS and MS/MS data were obtained on a VG Quattro triple quadrupole mass spectrometer (Micromass Instruments, Beverly, MA) in the positive electrospray (ESI) mode. For product ion analyses by collision induced dissociation (CID), high-purity argon gas was used as the collision gas and a cell pressure of ≈1.0 X 10^{-3} mbar was maintained. A collision energy of 30 eV was employed for all product ion experiments. Elemental analyses were performed by Atlantic Microlab, Inc. (Norcross, GA).

Chemical Synthesis. *N-(4-Arsenosophenyl) hexahydro-2-oxo-(3aS,4S,6aR)-1H-thieno[3,4-d]imidazole-4-pentamide (**1**) (212391-23-6])*.[3] Commercial *p*-aminophenyl arsine oxide (92 mg, 0.5 mmol) was dissolved in water (1 mL) containing 1 M equiv of HCl. After filtration, the filtrate was diluted with 2 vol of acetone, followed by addition of sodium carbonate (3 M equiv). A suspension of biotinoyl chloride (0.5 mmol) in 3 mL of acetone was added dropwise to this solution. After 48 h, the white precipitate was collected by filtration and was purified by preparative TLC on silica gel using 10% methanol:dichloromethane as the eluant. The product (32 mg, 14% yield) tested positive for both biotin and the trivalent arsenic. mp 223−224 °C; TLC (10% methanol:dichloromethane) $R_{\times a6}$ = 0.6. Anal. Calcd for $C_{16}H_{22}AsN_3O_4S$, 0.5H_2O: C, 44.03; H, 5.31; N, 9.63. Found: C, 44.34; H, 5.33; N, 9.51. ^{1}H NMR (CH_3OH-d_4): δ 7.67 (d,2H; J = 8.5 Hz), 7.60 (d,2H; J = 8.6 Hz), 4.49 (m, 1H), 4.30 (m,1H), 2.93 (dd,-1H), 2.70 (d,1H), 2.41 (t,2H), 1.75 (m,4H), 1.66 (m,1H), 1.51 (m,2H). IR (KBr): 750−660 cm^{-1} (As−O−As); 1686 cm^{-1} (C═O, ureide, amide); 730, 640 cm^{-1} (As−O). Molecular weight was confirmed by electrospray mass spectrometry.[2] $C_{16}H_{22}AsN_3O_4S$ ($M + H^+$) Calcd: 428.1. Found: 428.

p-(N-Carbomethoxypropionyl) Aminophenyl Arsonous Acid (4). Commercial *p*-aminophenylarsine oxide (366 mg, 2 mmol) was placed in 8 mL of anhydrous DMF to which 1 M HCl in ether (2 mL, 1 equiv) was added. The precipitate was removed by filtration, and triethylamine was added (310 mg, 3 mmol) to the filtrate. The mixture was stirred, filtered, and 3-carbomethoxypropionyl chloride (150 mg, 1 mmol) in 1 mL of anhydrous DMF was added dropwise to the filtrate. After 24 h, the precipitated 3-carbomethoxy propionic acid was removed by filtration and the filtrate was evaporated to dryness under nitrogen. The oily residue was triturated with a small amount of water, and the precipitate was collected via filtration. The crude product was purified by column chromatography on silica gel using chloroform:methanol:triethylamine (95:5:2) as the eluant. The desired product was isolated as a yellow oil (41 mg, 13% yield). ^{1}H NMR (CH_3-OH-d_4): δ 7.66 (d,2H, J = 8.7 Hz) 7.57 (d,2H, J = 8.7

[2] The authors are aware that the terms arsine oxide/arsenoxide are archaic, and chemically incorrect, but these are the terms most widely used in the literature for this class of compounds which are sold as such commercially. The structures of members of this class of compounds reported in the literature, typically have not been convincingly established, but are probably not monomeric, particularly the commercial samples, since they are not soluble in the same solvents as the freshly synthesized compounds. For that reason, we distinguish between starting materials that were obtained commercially or freshly synthesized. See ref *36* for descriptions of oligomers. Also, in laser desorption MS of iodophenylarsine oxide, sodium adducts of various oligomeric species were observed (*37*). However, by all tests at our disposal including MS, the freshly synthesized products we made appear monomeric. Finally, *p*-aminophenylarsine oxide is no longer commercially available and now must be freshly made (*14*).

[3] The naming of compounds was provided by CAS services. CAS Registry Numbers: compound **1**, 212391-23-6; compound **2**, 212391-25-8; compound **3**, 212391-26-9.

Hz), 3.80 (s,3H), 2.70 (s,4H). Molecular weight was confirmed by electrospray mass spectrometry. $C_{11}H_{12}AsNO_4$ ($M + H^+$) Calcd: 297.9. Found: 297.8.

p-(N-Carbomethoxypropionyl) Aminophenyl Arsanilic Acid. *p*-Arsanilic acid (217 mg, 1 mmol) was placed in 3 mL of methanol and 1 mL of THF. To this solution, 3-carbomethoxypropionyl chloride (150 mg, 1 mmol) was added dropwise. After 24 h, the solution was taken to dryness. The residue was dissolved in methanol and purified by normal-phase preparative TLC with the eluant chloroform:methanol:ethyl acetate (65:5:5). The desired product was isolated as yellow crystals (222 mg, 67% yield). mp 179−180 °C. ^{1}H NMR (CH_3OH-d_4): δ 7.88 (d,2H; $J = 9.0$ Hz), 7.49 (d,2H; $J = 9.0$ Hz), 3.80 (s, 4H), 2.61 (s,3H). Molecular weight was confirmed by electrospray mass spectrometry. $C_{11}H_{13}O_6NAsNa^+$ (M^+H^+) Calcd: 354.0. Found: 354.7.

p-(N-Hydrazidopropionyl) Aminophenyl Arsonous Acid (5). A solution consisting of 12 mL of hydrazine hydrate (85%, 10.5 g, 0.2 mol) in 25 mL of ethanol was brought to a gentle reflux. A solution of *p*-(*N*-carbomethoxypropionyl) aminophenyl arsonous acid (60 mg, 0.20 mmol) in 4 mL of methanol was added dropwise to the stirred refluxing solution. After 2 h, the solution was concentrated and the resultant oil was purified by column chromatography on silica gel using chloroform:methanol: ethyl acetate (50:5:5) as the eluant (32 mg, 52% yield). IR (KBr) (C═O) amide 1652 cm^{-1}, (C═O) hydrazide 1588 cm^{-1}, N−H stretch(amide) 3290 cm^{-1}. Molecular weight was confirmed by electrospray mass spectrometry. $C_{10}H_{14}AsN_3O_4$ ($M + H^+$) Calcd: 316.2. Found: 316.4.

*2-[4-[(4-Arsenosophenyl)amino]-1,4-dioxobutyl] Hydrazide, (3aS,4S,6aR)-Hexahydro-2-oxo-1H−thieno[3,4-d]-imidazole-4-pentanoic Acid (**2**) (212391-25-8)*. *p*-(*N*-Hydrazidopropionyl) aminophenyl arsonous acid (93 mg, 0.3 mmol) was placed in a flask containing 1 mL of DMSO. Biotinyl-NHS (68 mg, 0.2 mmol) in 1 mL of DMF was added to this solution and stirred at ambient temperature for 16 h, and then the products were evaporated to dryness. The residue was triturated with methanol, and the precipitate was collected by filtration (23 mg, 21% yield). ^{1}H NMR (DMSO-d_6): δ 7.71 (d,2H, $J = 7.50$ Hz), 7.64 (d,2H, $J = 7.95$ Hz), 6.43 (d,1H; $J = 19.32$), 4.31 (m,1H), 4.12 (m,1H), 3.55(d,2H), 3.20 (s,2H), 3.11 (t,1H), 2.81 (dd,1H), 2.60 (m,2H), 2.50 (s,2H), 2.3 (m,1H), 2.13 (m,2H), 1.2−1.8 (m,5H). Molecular weight was confirmed by negative ion electrospray mass spectrometry. $C_{20}H_{28}AsN_5O_6S$ ($M - H^+$) Calcd: 540.5. Found: 540.6.

N-Biotinylaminododecanoic Acid (6). A solution of biotinyl-NHS (170 mg, 0.5 mmol) (*17*) in 10 mL of DMF was added dropwise to a heated solution (60 °C) of 12-aminododecanoic acid (129 mg, 0.6 mmol) in 6 mL of 0.2 M $NaHCO_3$. The resulting solution was stirred at 60 °C for 4 h and then at ambient temperature for 16 h. The resulting precipitate was collected, washed sequentially with water and 0.01 M HCl, and then dried under vacuum. 12-Biotinylaminododecanoic acid was obtained (61 mg, 0.16 mmol) in 28% yield. mp 216−217 °C (Lit. mp 217 °C) (*18*).

*[4-[[12-[[5-[(3aS,4S,6aR)-Hexahydro-2-oxo-1H-thieno-[3,4-d]imidazol-4-yl]-1-oxopentyl]amino]-1-oxododecyl]-amino]phenyl]-arsonous Acid (**3**) (212391-26-9)*. *N,N′*-Carbonyldiimidazole (32.4 mg, 0.2 mmol) was added to a solution of *N*-biotinyl-aminododecanoic acid (88 mg, 0.2 mmol) in 5 mL of DMF at 95 °C. The reaction was maintained at 95 °C until the evolution of carbon dioxide ceased. The solution was stirred for 1 h at ambient temperature, during which time a precipitate formed. A solution of freshly prepared *p*-aminophenyl arsine oxide (74 mg, 0.4 mmol) in 5 mL of acetone was added to the stirred reaction mixture. The solution was heated at 50 °C for 5 days, cooled to room temperature and filtered. The filtrate was evaporated to dryness and triturated with ether. The precipitate was collected by filtration and stirred in hot 2-propanol. The insoluble product was collected by filtration and dried to give 32 mg, 25% yield. mp 172−173 °C. Anal. Calcd for $C_{28}H_{43}AsN_4O_4S$·TEA: C, 57.77; H, 8.16; N, 10.34. Found: C, 57.77; H, 8.26; N, 9.9. ^{1}H NMR (DMSO-d_6): δ 7.63 (d,2H, $J = 7.4$ Hz), 7.54 (d,2H, $J = 7.8$ Hz), 6.40 (d,1H; $J = 20.52$), 4.30 (m,1H), 4.13 (m,1H), 2.9−3.2 (m,4H), 2.83 (dd,2H), 2.6 (d,1H), 2.29 (t,2H), 2.19 (t,1H), 2.04 (t,2H), 1.2−1.8 (m,24H). Molecular weight was confirmed by electrospray mass spectrometry. $C_{28}H_{43}AsN_4O_4S$ ($M + H^+$) Calcd: 607.6. Found: 607.4. TLC (75 $CHCl_3$:5CH_3OH:5EtOAc) $R_f = 0.1$.

Assays. *Quenching Effects of Compounds **1**−**3** on the Ellman Assay (19) of 2,3-Dimercaptopropanesulfonic Acid*. Varying concentrations (range 0−74 μM) of compounds **1**−**3** or *p*-aminophenyldichloro-arsine hydrochloride (APA) were incubated with DMPS (50 μM final concentration) for 10 min. Tris buffer (pH 8.1; 0.3 mM final concentration) and 5,5′-dithio-bis(2-nitrobenzoic acid) (DTNB; 200 μM final concentration) were added to a final volume of 1.5 mL, and absorbance at 412 nm was recorded.

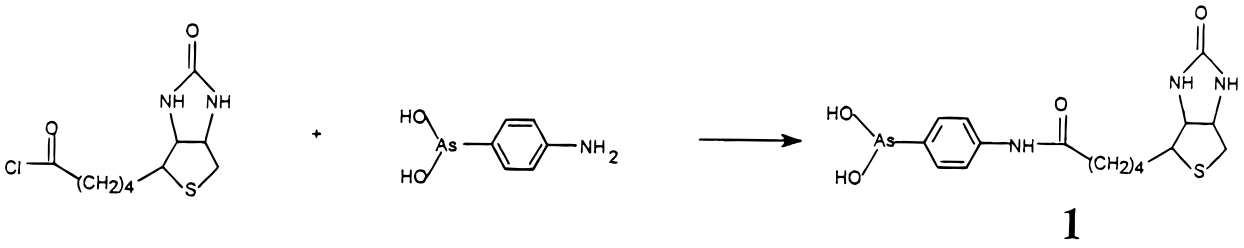
*Confirmation of the Biotin Moiety in Compounds **1**−**3***. Varying concentrations (range 0−1 mM) of **1**−**3** or d-biotin were added to avidin complexed with 4-hydroxyazobenzene-2-carboxylic acid (HABA). Absorbance at 500 nm was measured and plotted as the mean and range of duplicate samples, according to the method of Green (*20*). In addition, a dimethylaminocinnamaldehyde spray reagent (*21*) was used to qualitatively confirm the presence of biotin on TLC plates.

Displacement of [^{125}I]α-Bungarotoxin Binding from Torpedo Nicotinic Receptors. Solubilized *Torpedo* receptors were immunoprecipitated with mAb210 or mAb35 coupled to goat anti-rat IgG agarose beads in phosphate-buffered saline (PBS; 145 mM NaCl and 10 mM sodium phosphate, pH 7.2) containing 1% Triton X-100 (*13*). After reduction by 2 mM DTT for 20 min, receptors were treated with varying concentrations (range 1 nM−100 μM) of either the biotinylated arsenicals or APA or with 30 μM BAC. After reoxidation with 1 mM DTNB for 20 min, the remaining BGT-binding sites were assayed. Nonspecific binding was determined in the presence of 1 μM unlabeled BGT. In other experiments, receptors were treated with 1 mM DMPS for 20 min to remove bound arsenicals.

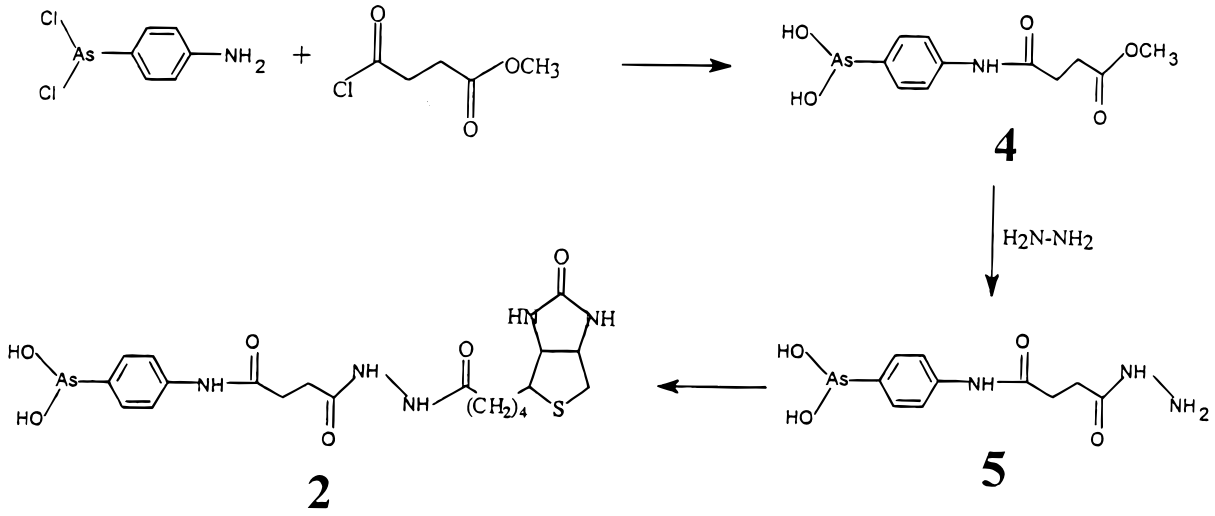
Staining of Dot-Blotted Torpedo Peptide and β-Galactosidase. Varying concentrations of *Torpedo* peptide or β-galactosidase in Burnette's buffer (*22*) (20 mM Tris, 150 mM glycine, and 20% methanol, pH 8.3) were applied under vacuum to PVDF membranes (Polyscreen, NEN-Dupont, Boston, MA) using a Schleicher and Schuell dot-blotter. PVDF membranes were cut into strips and blocked for 45 min at RT with 3% bovine serum albumin (BSA) in PBS. The individual strips were then treated with MPB or compounds **1** or **2** dissolved in PBS and then treated with SA-HRP and stained with 4-chloronaphthol as indicated by Bio-Rad. The strips were reassembled and digitally scanned using a UMAX Astra 1200 S scanner and Adobe Photoshop software.

[^{125}I]Streptavidin Binding. Quadruplicate goat anti-rat IgG-coated agarose beads were treated in 1.5 mL centrifuge tubes with 2 mM DTT in PBS, varying concentrations of compounds **1**−**3** (usually 10 μM), and then treated with 1 mM DTNB for 20 min each treatment.

Scheme 1



Scheme 2



The beads were washed between treatments and three times afterward by centrifuging for 5 s, aspirating the supernatant, and resuspending in 1 mL of PBS. [^{125}I]-Streptavidin (1 nM) was added to each sample in 0.1 mL of PBS with 1 mg/mL bovine serum albumin (BSA). After incubation at RT with mixing for 2 h, unbound streptavidin was removed by washing three times (1 mL at 4 °C) with PBS/BSA. Nonspecific binding was established by incubating with 100 nM streptavidin. Samples were counted in a Wizard γ-counter.

Molecular Modeling. Molecular modeling was performed on a Silicon Graphics O_2 system running Quanta 96 (Molecular Simulations, Inc.) to determine interatomic distances. Molecular structures of **1**−**3** were generated in their most extended conformation, and the length was measured from the carboxy group of the biotin to the arsenic group.

RESULTS AND DISCUSSION

The use of biotinylated bifunctional reagents to characterize macromolecules is well documented (*23*); however, the incorporation of a *p*-aminophenylarsonous acid moiety is unprecedented. Although this compound is isosteric to *p*-aminophenylboronic and *p*-aminobenzoic acid, which are well characterized, the presence of the arsonous acid group created unique synthetic challenges. Unlike the carboxylic and boronic acids, the arsonyl group can be oxidized to a higher valence which is unreactive toward the targeted vicinal dithiol moiety. Therefore, synthetic transformations and isolation methods required care to avoid oxidation. Second, the synthetic transformations required that the arsonous acid remain in its unprotected state as opposed to the boronate or carboxylate esters which could be hydrolyzed at a later stage of the synthesis. Consequently, the chemical transformations and isolation steps were performed in the presence of a polar, ionizable functionality that compromised the reactivity of the para-amino group and complicated chromatographic separations.

The syntheses of the target compounds are shown in Schemes 1−3. Preparation of the simplest biotinylated arsenical **1** was achieved using classical Schotten−Baumann chemistry. Although the isolated yield was low (14%), it was substantially better than methods employing the biotin-activated esters [*N*-hydroxysuccinimide (NHS), or pentafluorophenyl] or a diimide conjugating reagent [dicylohexylcarbodiimide, 1-[3-(dimethylamino) propyl]-3-ethylcarbodiimide]. The free arsonous acid exerted a dominating effect on the chromatographic behavior of the product, necessitating a polar solvent to elute it from the column. Compound **2** was prepared in three steps from *p*-aminophenylarsonous acid. Acylation of *p*-aminophenyl arsonous acid with 3-carbomethoxypropionyl chloride (13% yield) followed by hydrazinolysis (52%) and acylation with biotinyl NHS ester gave the final product (21%). The intermediates were purified by column chromatography and the final product by crystallization. Compound **3** was prepared in two steps beginning with the reaction of biotinyl NHS ester with 12-aminododecanoic acid. The intermediate was converted to its acyl imidazolide with 1,1′-carbonyldiimidazole and reacted with *p*-aminophenylarsonous acid (Scheme 3). The crude product was recrystallized to give the final derivative in a 25% yield.

Compounds **1**−**3** were characterized by various instrumental methods. In addition to the absorptions expected for the biotin-containing compounds, the infrared spectra contained strong absorptions in the 660−750 cm^{-1} region which were characteristic of the As−O stretching frequencies. The ^{1}H NMR spectra were consistent with the proposed structures, confirming the presence of biotin, phenyl, and spacer groups. The NMR data also corroborated the valence of the arsenic group. Comparison of the NMR spectra of *p*-(*N*-carbomethoxypropionyl)

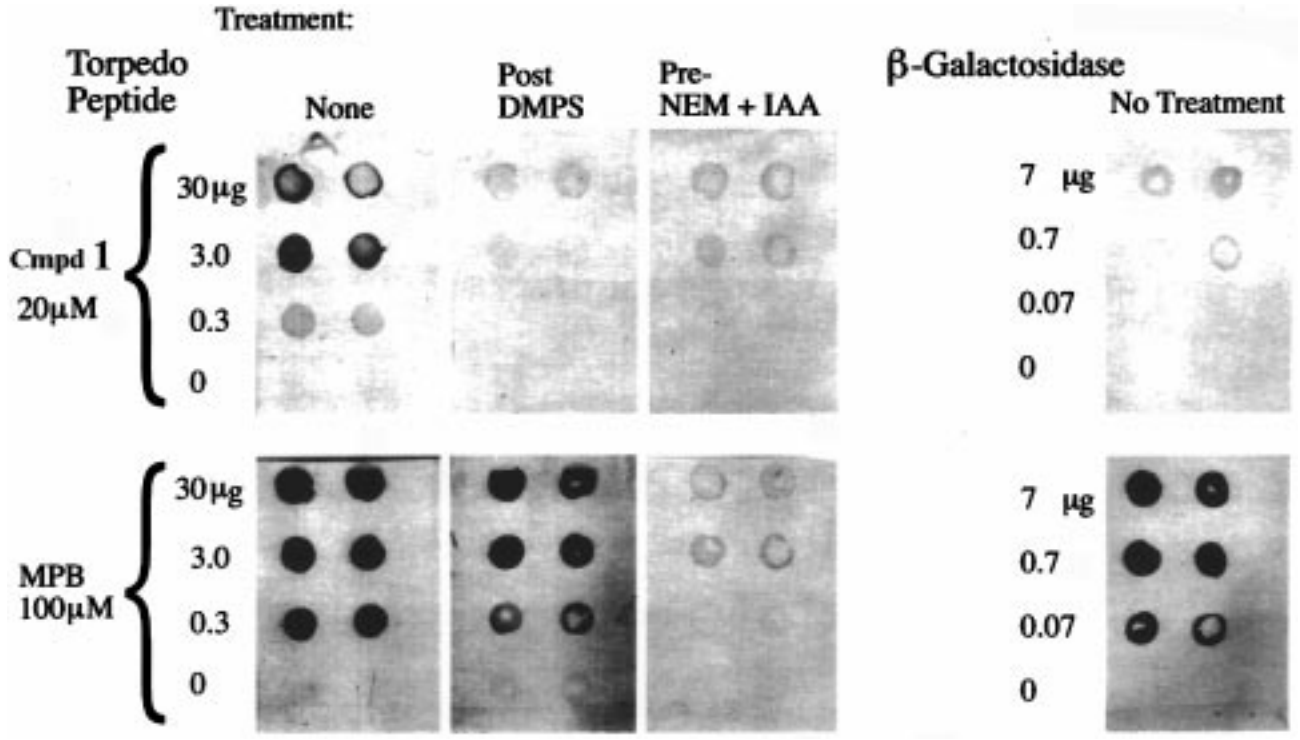
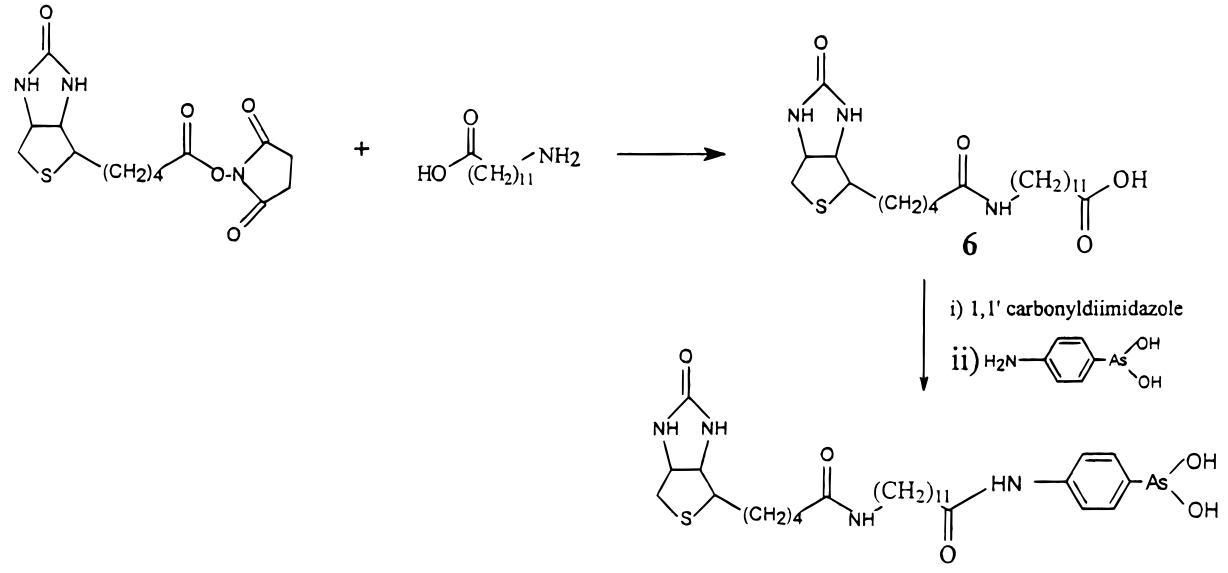


Figure 1. SA-HRP labeling with Compound **1** or MPB. Varying concentrations of *Torpedo* peptide (0−30 μg) or β-galactosidase (0−7 μg) in Burnette's buffer (*22*) were applied under vacuum to PVDF as described in the Materials and Methods. The individual strips were then treated with either 100 μM MPB or **1** (20 μM) in PBS, and then treated with SA-HRP and stained with 4-chloronaphthol and H_2O_2. The *Torpedo* peptide samples in the second column were further treated with 1 mM DMPS for 20 min, while the peptide samples in the third column were pretreated with 1 mM NEM and 1 mM IAA for 20 min. Compound **1** labeled only the untreated *Torpedo* peptide but did not bind with the thiols on β-galactosidase (fourth column). In contrast, MPB, which will react with single thiols and is irreversibly bound, labeled both β-galactosidase and *Torpedo* peptide that was posttreated with DMPS.

Scheme 3



aminophenyl arsonous acid and the corresponding arsanilic acid demonstrates a clear and distinctive difference in the chemical shift of the protons ortho to the arsenic group, occurring at 7.66 ppm in the former and 7.88 ppm in the latter.

Electrospray ionization mass spectrometry was also valuable in confirming the molecular structure of the products. The full-scale mass spectrum for **1** gave major ions at *m*/*z* 478, 464, 450 (100%), 428, 424, and 410. Assignments could be made for each ion and were consistent with the proposed structure. Mass spectra analysis for each of the other products were equally revealing. Elemental analyses also supported the proposed structure assignments.

Preliminary Characterization of the Compounds. The trivalent nature of arsenic in **1**−**3** was inferred from the results of an assay in which the Ellman response of DMPS to DTNB was quenched in a concentration-

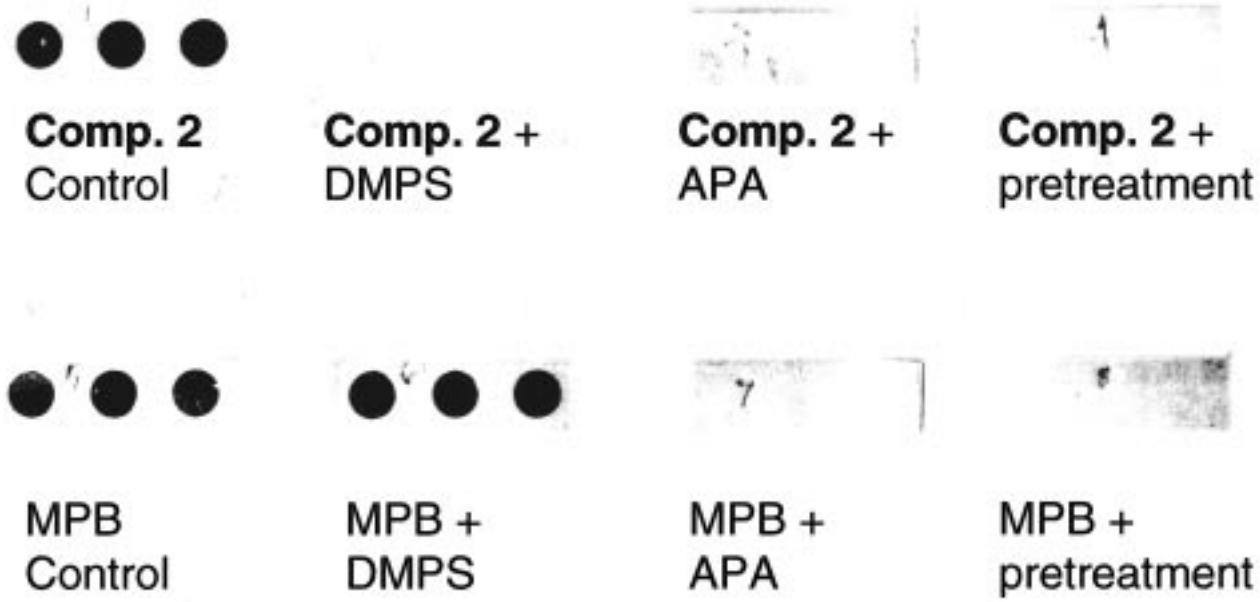


Figure 2. Compound **2** labels dot-blotted *Torpedo* peptides. Triplicate samples of 30 μg of *Torpedo* peptide blotted onto PVDF membranes were incubated for 20 min with either compound **2** (10 μM, top row) or MPB (100 μM, bottom row) and then stained. Further treatment with 1 mM DMPS for 20 min removed compound **2** but not MPB (second column), while prior treatment with either 1 mM APA (third column) or 1 mM NEM and 1 mM IAA (fourth column) blocked labeling by both compounds.

dependent fashion (not shown). Compounds **1**−**3** also gave a positive color reaction on TLC with *p*-dimethylaminocinnamaldehyde spray reagent, which has been used as a qualitative assay for the presence of biotin (*21*), and were equipotent with biotin in their ability to displace HABA from avidin (not shown). To demonstrate that compound **1** could simultaneously bind to streptavidin while covalently linked to a dithiol, reduced *Torpedo* peptide was blotted onto PVDF membranes at varying concentrations and then treated with either **1** (20 μM) or the sulfhydryl labeling agent MPB (100 μM) (Figure 1). Staining with compound **1** but not MPB was blocked if the samples were subsequently treated with the bissulfhydryl containing DMPS (1 mM). Pretreatment with 1 mM *N*-ethylmaleimide (NEM) and 1 mM iodoacetamide (IAA) substantially blocked the labeling of the peptide by both **1** and MPB. β-Galactosidase is a protein that binds well to PVDF membranes and has 14 free thiols per molecule, none of which are spatially close (*24*). MPB strongly stains β-galactosidase, while **1** shows no staining above the background seen for *Torpedo* peptide treated with NEM and IAA (Figure 1). This result demonstrates the selectivity of the arsenical for spatially close dithiols. The staining effects of **1** on *Torpedo* peptide are concentration dependent (data not shown) and the lowest concentration that stains peptide above background is 30 nM. Compound **2** also demonstrated labeling of *Torpedo* peptide that could be blocked by subsequent treatment with DMPS, simultaneous addition of 1 mM APA, or pretreatment with NEM and IAA (Figure 2). The simultaneous binding of **3** to spatially close dithiols and [^{125}I]streptavidin was demonstrated independently (see below).

Displacement of [^{125}I]α-Bungarotoxin Binding from Torpedo Nicotinic Receptor. In a previous study, we showed that aromatic trivalent arsenicals, e.g., *p*-APA, decreased the number of [^{125}I]BGT-binding sites in reduced *Torpedo* nicotinic receptors to the same level seen after alkylation with BAC (*12*). Furthermore, arsenylation of *Torpedo* receptors prevented their reoxidation with DTNB, was reversible with DMPS, and protected the receptor from irreversible alkylation by BAC. Compounds **1**−**3** displayed similar behavior and blocked [^{125}I]-BGT binding to DTT-treated *Torpedo* receptors to the same extent as alkylation with BAC (Figure 3). In other experiments (not shown), treatment of nonreduced receptors with **1**−**3** or reoxidation of DTT-treated receptors with DTNB before adding **1**−**3** prevented the blockade of [^{125}I]BGT binding by these compounds. As we previously demonstrated with APA (*12*, *13*), DMPS reverses the effects of **1**−**3** (Figure 4). Furthermore, adding compounds **1**−**3** to DTT-treated receptors before BAC and then treating with DMPS to remove the arsenicals restores [^{125}I]BGT binding. These data suggest that **1**−**3** and BAC are competing for the same site, and since BAC and other affinity-labeling agents attach to the reduced

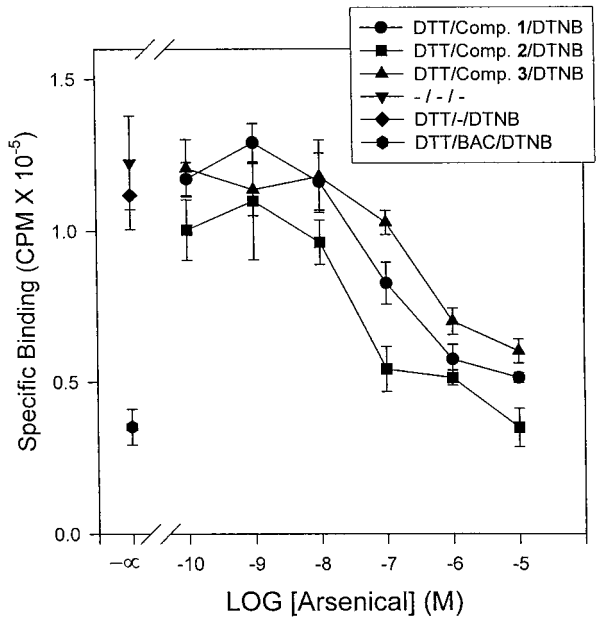


Figure 3. Effects of arsenylation on the binding of [^{125}I]BGT to reduced *Torpedo* nicotinic receptors: **1** (●); **2** (■); **3** (▲); control treatment (▼), DTT reduction followed by oxidation with DTNB (◆); DTT reduction, alkylation with 30 μM BAC, followed by oxidation with DTNB (⬢).

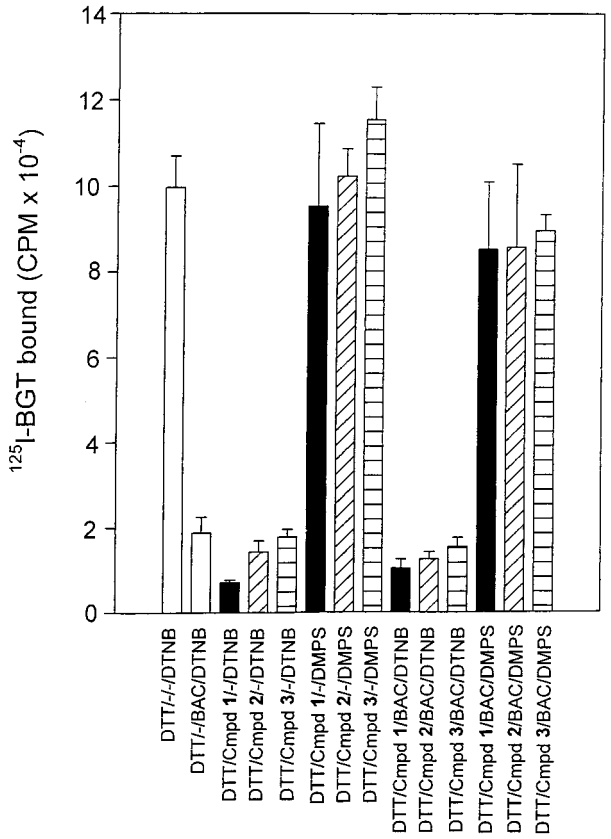


Figure 4. Compounds **1**−**3** are reversible with DMPS and protect [^{125}I]BGT binding sites against irreversible alkylation with BAC. Solubilized *Torpedo* receptors were immunoprecipitated using agarose beads as outlined in the Materials and Methods. After reduction with 2 mM DTT, 10 μM **1**−**3** (black bars, diagonally striped bars, and striped bars, respectively) all blocked [^{125}I]BGT binding to about the same extent as did 30 μM BAC. However, unlike BAC (not shown), the effects of **1**−**3** were completely reversed by treatment with 1 mM DMPS. Furthermore, DMPS reversed the effects of **1**−**3** even after the application of BAC.

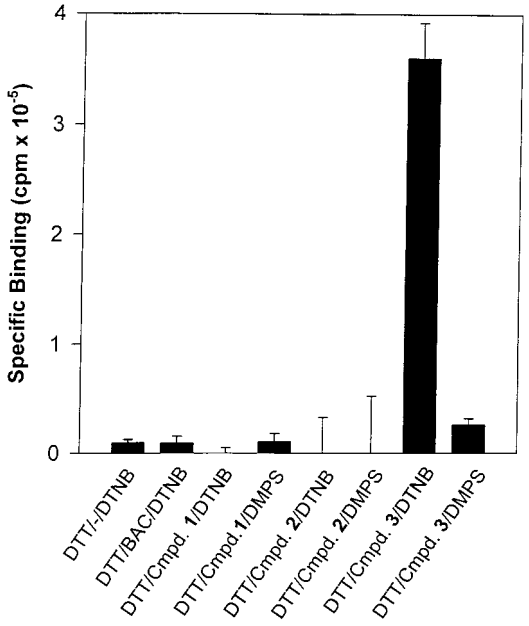


Figure 5. Compound **3**, but not **1** or **2**, labels DTT-treated antibody-coated beads. Quadruplicate samples (20 μL packed beads) of goat-anti rat IgG beads were treated for 10 min with 1 mM DTT before the DTT was removed, and then the beads were treated an additional 10 min with the compounds shown. All beads were then treated with 1 mM DTNB to oxidize any unreacted thiols. The beads were then incubated for 2 h in 1 nM [^{125}I]streptavidin and then washed three times in PBS before counting. Nonspecific binding was determined in quadruplicate samples incubated in the presence of 100 nM unlabeled streptavidin.

disulfide in the agonist binding site of nicotinic receptors (*25, 26*), we infer that **1**−**3** also react with the reduced disulfide in the agonist site.

[^{125}I]Streptavidin Binding to Arsenylated Macromolecules. In no case did **1**−**3** simultaneously block [^{125}I]BGT binding to *Torpedo* receptors and bind [^{125}I]-streptavidin (data not shown) if the arsenylating reagents were first added to DTT-reduced receptors and then the receptors were solubilized in Triton and immunoprecipitated. However, we observed significant [^{125}I]streptavidin binding to **3** reacted to DTT-treated antibody-coated beads. Figure 5 demonstrates that this effect is only observed for DTT-treated antibody-coated beads treated with **3** but not **1** or **2**, and that DMPS treatment significantly removes this binding. In other experiments (not shown), **3** did not label antibody-coated beads if the beads were not treated with DTT or if DTT-treated beads were reoxidized with DTNB before the addition of **3**. Since we had previously shown that APA forms a very stable complex with *Torpedo* receptors (*12*), we investigated the stability of **3** complexed with antibodies (Figure 6). We observed no change in the binding of [^{125}I]-streptavidin to beads treated with **3** over a period of 24 h, but DMPS could be used at any time to substantially remove the labeling agent.

The disulfide bonds located in the hinge regions of IgG isotypes are known to be important for the effector functions of these molecules, such as complement activation (*27*). It has been known for over 20 years that gentle reduction of the interheavy chain disulfides in the hinge region yields an antibody that can strongly bind antigen but not C1q (*28*), the trigger for the complement cascade. Furthermore, electron microscopic (*29*), gel filtration (*30*), and immunological and X-ray scattering data (*31*) all show conformational changes in immunoglobulins upon reduction of the interheavy chain disulfide bonds. This site is a well-established target for antibody-labeling agents, and we infer that this is the most likely site of labeling by **3** since Fab fragments are not labeled (data not shown). One potential advantage of arsenical-based labeling agents is that they could maintain the conformation of the immunoglobulins better than other reagents, since the arsenic interposes itself between spatially close dithiols and reestablishes an approximation of a disulfide bond. In addition, our data suggests that arsenical-based chromatography may be useful in purifying immunoglobulins (*32*).

Tsigelny et al. (*33*) modeled the extracellular domains of the nicotinic receptor based on homology with copper-binding proteins and current site-directed mutagenesis and affinity-labeling data. In their model, the disulfide bond in the agonist-binding site (Cys192−193) is highly exposed on the outer surface of the α-subunit. Unless glycosylation of the α-subunits prevents streptavidin binding to **3** due to unforseen steric block, the location of the disulfide in the agonist-binding site in that model does not seem to be very likely.

Our results might suggest that the disulfide bond in the agonist-binding site is located greater than 15 Å from the surface of the receptor. Two recent reports by Fairclough et al. (*11, 34*) appear to contradict that interpretation. They used a monoclonal antibody (mAb 383C) that binds to a peptide epitope corresponding to amino acids 187−199 on the *Torpedo* α-subunit, with

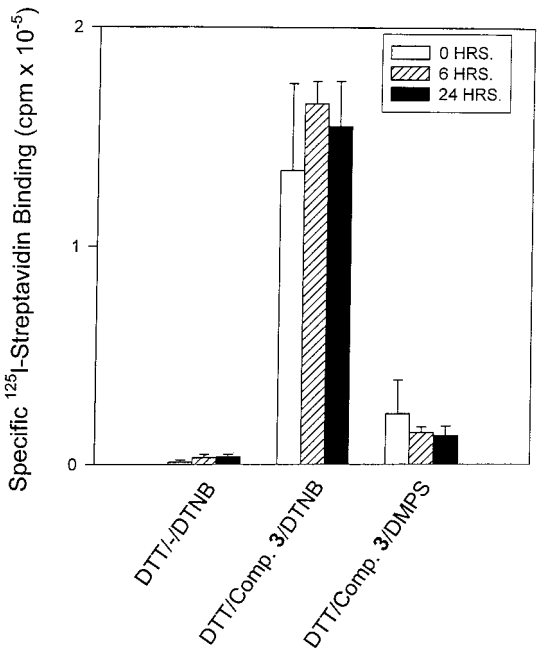


Figure 6. The complex of compound **3** and reduced antibodies is stable up to 24 h, but can be dissociated at any time by treating with DMPS. DTT-treated goat anti-rat IgG agarose beads were then either incubated with PBS [(−) left bars) or with 10 mM **3** (in PBS for 10 min, center and right bars) at time zero. At different times, immediately (clear bars), 6 (crosshatched bars) and 24 (reversed crosshatched bars) h later, the beads were then treated with either 1 mM DTNB (left and center bars) or 1 mM DMPS (right bars) for 10 min, and then assayed for specific [^{125}I]streptavidin binding. All samples were in quadruplicate with nonspecific binding determined in the presence of 100 nM unlabeled streptavidin.

specificity for the A site (the α−α interface). This antibody bound to intact receptors, and mapped to a site very near one of the two pits suggested by Unwin (*11*) to be the agonist-binding sites [but at some distance from where Tsigelny et al. place the disulfide bond in their model (*33*)]. We propose two possible explanations for this apparent difference in results using these two techniques.

First, monoclonal antibodies are well-known to induce conformational changes in the proteins to which they bind. For instance, a monoclonal antibody to avidin is reported to not only dissociate tetrameric avidin into monomers but also to cause the avidin to release bound biotin (*18*). Using fluorescence resonance energy transfer (FRET), Valenzuela et al. (*35*) report that binding of a different antibody [mAb A6 against the A site of *Torpedo* receptors (*7*)] induced the other agonist-binding site (the α−δ interface) to move about 30 Å closer to the membrane than observed for receptors without the bound antibody. This implies that monoclonal antibodies that selectively bind to one of the two agonist-binding sites can potentially induce major conformational changes. Also, the fact that an antibody binds suggests that the epitope is at least transiently exposed in one conformation of the receptor. It is possible that monoclonal antibodies can "trap" the receptor into a conformation that is relatively rare but in which the epitope including the disulfide bond is much more exposed than in other conformations. Second, our labeling method requires breaking the disulfide bond normally forming an eight-atom ring in the agonist binding site, and reforming a nine-atom ring structure including the arsenic atom. This could also induce an abnormal conformation. In addition, the protein folding could point our arsenicals with the biotin groups going into, rather than out of, the receptor molecule. If this is the case, then one might expect that arsenical-based reagents should abruptly stop working when some critical distance of the biotin spacer has been reached. Finally, the spacer groups are fairly hydrophobic, and it is possible that the biotin is too closely associated with hydrophobic groups in the receptor molecule to be recognized by streptavidin. We plan to address these last two issues, by using spacer groups that are longer, more rigid and hydrophilic. However, the data using **1**−**3** on antibody-coated beads clearly indicates that the length of the biotin spacer group is critical and that once the biotin group extends sufficiently far from the molecular surface, streptavidin binding ensues.

ACKNOWLEDGMENT

This work was supported by a grant from the Smokeless Tobacco Research Council, Inc., and by NIH NS22472. We thank John Lindstrom for the generous gift of mAb210, Jonathan Cohen for *Torpedo* membranes, and Ban-Ahn Khaw for a sample of Fab fragments. We thank Jack Cunniff and Jeannine Delaney for the mass spectra data and XiaoGong Zhang and Abdullah Baaj for some of the preliminary binding data. Igor Tsigelny generously provided us with a file specifying the atomic locations of his model for the extracellular domains of the *Torpedo* nicotinic receptor. We thank William N. Green for helpful discussions.

LITERATURE CITED

(1) Williams, M., Sullivan, J. P., and Arneric, S. P. (1994) Neuronal Nicotinic Acetylcholine Receptors. *Drug News Perspect. 7*, 205−223.

(2) McGehee, D. S., and Role, L. W. (1995) Physiological diversity of nicotinic acetylcholine receptors expressed by vertebrate neurons. *Annu. Rev. Physiol. 57*, 521−546.

(3) Karlin, A. (1993) Structure of nicotinic acetylcholine receptors. *Curr. Opin. Neurobiol. 3*, 299−309.

(4) Pedersen, S. E., and Cohen, J. B. (1990) *d*-Tubocurarine binding sites are located at α-gamma and α-δ subunit interfaces of the nicotinic acetylcholine receptor. *Proc. Natl. Acad. Sci. U.S.A. 87*, 2785−2789.

(5) Martin, M., Czajkowski, C., and Karlin, A. (1996) The contributions of aspartyl residues in the acetylcholine receptor gamma and δ subunits to the binding of agonists and competitive antagonists. *J. Biol. Chem. 271*, 13497−13503.

(6) Neubig, R. R., and Cohen, J. B. (1979) Equilibrium binding of ^{3}H-tubocurarine and ^{3}H-acetylcholine by *Torpedo* postsynaptic membranes: Stoichiometry and ligand interactions. *Biochemistry 18*, 5464−5475.

(7) Dowding, A. J., and Hall, Z. W. (1987) Monoclonal antibodies specific for each of the two toxin binding sites of *Torpedo* acetylcholine receptors. *Biochemistry 26*, 6372−6381.

(8) Unwin, N. (1993) Nicotinic acetylcholine receptor at 9 Å resolution. *J. Mol. Biol. 229*, 1101−1124.

(9) Unwin, N. (1995) Acetylcholine receptor channel imaged in the open state. *Nature 373*, 37−43.

(10) Unwin, N. (1996) Projection structure of the nicotinic acetylcholine receptor: Distinct conformations of the α subunits. *J. Mol. Biol. 257*, 586−596.

(11) Fairclough, R. H., Twaddle, G. M., Gudipati, E., Stone, R. J., Richman, D. P., Burkwall, D. A., and Josephs, R. (1998) Mapping the mAb 383C epitope to alpha 2(187−199) of the *Torpedo* acetylcholine receptor on the three-dimensional model. *J. Mol. Biol. 282*, 301−315.

(12) Loring, R. H., Dou, Y.-M., Lane, W., Jones, G. S., Jr., and Stevenson K. J. (1992) Aromatic trivalent arsenicals: Covalent yet reversible reagents for the agonist binding site of nicotinic receptors. *Mol. Brain Res. 15*, 113−120.

(13) Dou, Y., McHugh, T., Lane, W. V., Rossant, C. J., and Loring, R. H. (1994) Interactions of dithiols with *p*-aminophenyldichloroarsine and nicotinic acetylcholine receptors. *J. Biol. Chem. 269*, 20410−20416.

(14) Stevenson, K. J., Hale, G., and Perham, R. N. (1978) Inhibition of pyruvate dehydrogenase multienzyme complex from *Esherichia coli* with mono- and bifunctional arsenoxides. *Biochemistry 17*, 2189−2192.
(15) Loring, R. H., and Schulz, D. W. (1993) Autoradiographic localization of putative neuronal nicotinic receptors using snake venom neurotoxins. *Methods Neurosci. 12*, 324−341.
(16) Loring, R. H., Jones, S. W., Matthews-Bellinger, J. A., and Salpeter, M. M. (1982) ^{125}I-α-Bungarotoxin: Effects of radiodecomposition on specific activity. *J. Biol. Chem. 257*, 1418−1423.
(17) Jasiewicz, M. L., Schoenberg, D. R., and Mueller, G. C. (1976) Selective retrieval of biotin-labeled cells using immobilized avidin. *Exp. Cell Res. 100*, 213-217.
(18) Subramanian N., Subramanian, S., Karande, A. A., and Adiga, P. R. (1997) A monoclonal antibody to avidin dissociates quaternary structure and curtails biotin binding to avidin and streptavidin. *Arch. Biochem. Biophys. 344*, 281−288.
(19) Ellman, G. L. (1959) Tissue sulfhydryl groups. *Arch. Biochem. Biophys. 82*, 70−77.
(20) Green, N. M. (1965) A spectrophotmetric assay for avidin and biotin based on binding of dyes by avidin. *Biochem. J. 94*, 23c−24c.
(21) McCormick, D. B., and Roth, J. A. (1970) Colormetric determination of biotin and analogues. *Methods Enzymol. 18A*, 383−385.
(22) Burnette, W. M. (1981) "Western Blotting": Electorphoretic transfer of proteins from sodium dodecyl sulfate-polyacrylamide gels to unmodified nitrocellulose and radiographic detection with antibody and radioiodinated protein A. *Anal. Biochem. 112*, 195−203.
(23) Wolf, D. E., Valiant, J., and Folkers, K. (1993) Amides and amino acid derivatives of biotin. *Anal. Biochem. 212*, 325−334.
(24) Fowler, A. V., and Zabin, I. (1978) Amino acid sequence of beta-galactosidase. *J. Biol. Chem. 253*, 5521−5525.
(25) Damle, V. N., McLaughlin, M., and Karlin, A. (1978) Bromoacetylcholine as an affinity label of the acetylcholine receptor from torpedo californica. *Biochem. Biophys. Res. Commun. 84*, 845−851.
(26) Kao, P. N., Dwork, A. J., Kaldany, R. R. J., Silver, M. L., Wideman, J., Stein, S., and Karlin, A. (1984) Identification of the α subunit half-cystine specifically labeled by an affinity reagent for the acetylcholine receptor binding site. *J. Biol. Chem. 259*, 11662−11665.
(27) Brekke, O. H., Michaelsen, T. E., and Sandlie, I. (1995) The structural requirements for complement activation by IgG: does it hinge on the hinge? *Immunol. Today 16*, 85−90.
(28) Isenman, D. E., Dorrington, K. J., and Painter, R. H. (1975) The structure and function of immunological domains: II The importance of interchain disulfide bonds and the possible role of molecular flexibility in the interaction between immunoglobulin G and complement. *J. Immunol. 114*, 1726−1729.
(29) Seegan, G. W., Smith, C. A., Schumaker, V. N. (1979) Changes in quaternary structure of IgG upon reduction of the interheavy- chain disulfide bond. *Proc. Natl. Acad. Sci. U.S.A. 76*, 907−911.
(30) Michaelsen, T. E. (1988) Alteration of the conformation of human IgG subclasses by reduction of the hinge S−S bonds. *Mol. Immunol. 25*, 639−646.
(31) Ibraghimov, A., Jackubov, L., Kayushina, R., Mogilevsky, L., Maisurian, N., and Rokhlin, O. (1987) Appearance of neoantigen in mouse IgG1 upon reduction of interchain disulfide bridges: assessment of local and general conformational rearrangements using monoclonal antibody and small-angle X-ray scattering. *J. Biomol. Struct. Dyn. 5*, 177−185.
(32) Kalef, E., Walfish, P. G., and Gitler, C. (1993) Arsenical-based affinity chromatography of vicinal dithiol-containing proteins: Purification of L1210 leukemia cytoplasmic proteins and the recombinant rat c-erb Aβ_1 T_3 receptor. *Anal. Biochem. 212*, 325−334.
(33) Tsigelny, I., Sugiyama, N., Sine, S. M., and Taylor, P. (1997) A model of the nicotinic receptor extracellular domain based on sequence identity and residue location. *Biophys. J. 73*, 52−66.
(34) Fairclough, R. H., Twaddle, G. M., Gudipati, E., Lin, M. Y., and Richman, D. P. (1998) Differential surface accessibility of alpha(187−199) in the *Torpedo* acetylcholine receptor alpha subunits. *J. Mol. Biol. 282*, 317−330.
(35) Valenzuela, C. F., Dowding, A. J., Arias, H. R., and Johnson, D. A. (1994) Antibody-induced conformational changes in the *Torpedo* nicotinic acetylcholine receptor: A fluorescence study. *Biochemistry 33*, 6586−6594.
(36) Doak, G. O., and Freedman, L. D. (1970) Arsonous and arsinous acids, $RAs(OH)_2$ and R_2AsOH, and their derivatives. *Organometallic Compounds of Arsenic, Antimony and Bismuth*, Chapter 3, pp 63−119, John Wiley & Sons, New York.
(37) Hoffman, R. D., and Lane, M. D. (1992) Iodophenylarsine oxide and arsenical affinity chromatography: New probes for dithiol proteins. Application to tubulins and to components of the insulin receptor-glucose transporter transduction pathway. *J. Biol. Chem. 267*, 14005−14011.

BC9801575

Biopharmaceutical Properties of Uricase Conjugated to Neutral and Amphiphilic Polymers

Paolo Caliceti,* Oddone Schiavon, and Francesco M. Veronese

Department of Pharmaceutical Sciences, University of Padova, Via F. Marzolo 5, 35131 Padova, Italy.
Received December 29, 1998; Revised Manuscript Received March 30, 1999

A comparative pharmacokinetic and biodistribution investigation of polymer−protein conjugates prepared with various amphiphilic polymers was carried out using uricase as a model. Four polymer-uricase derivatives have been obtained by covalent binding of a similar number of polymer chains of (a) linear poly(ethylene glycol) (M_w 5000 Da); (b) branched poly(ethylene glycol) (M_w 10 000 Da); (c) poly(*N*-vinylpyrrolidone) (M_w 6000 Da); (d) poly(*N*-acryloilmorpholine) (M_w 6000 Da). By intravenous administration to Balb/c mice, the conjugates displayed different pharmacokinetic and organ distribution behaviors. (1) The unmodified enzyme and the poly(*N*-vinylpyrrolidone) conjugate were the enzyme forms with the shortest and the longest permanence in blood respectively (mean residence time 45 and 4378 min). (2*)* Native uricase was found to localize soon after administration significantly in heart, lungs, and liver from where it was also rapidly cleared. (3) The poly(*N*-acryloilmorpholine) derivative showed the highest concentration levels in liver (up to 25.5% of the dose) and considerable accumulation took also place in the other considered organs. (4) Poly(*N*-vinylpyrrolidone)-uricase displayed a relevant tropism for liver but low uptake indexes were found for the other organs. (5) The branched poly(ethylene glycol) derivative accumulated preferentially in liver and spleen. (6) The linear poly(ethylene glycol) conjugate was, among the various uricase forms, the species with the lowest distribution levels in all the examined organs. (7) Finally, all the enzyme forms slowly disposed in kidneys with higher levels for the poly(*N*-acryloilmorpholine) derivative (15% after 2880 min) and unmodified uricase (14% after 1440 min).

INTRODUCTION

The modification of protein and peptide drugs with soluble biocompatible polymers largely demonstrated to be a successful method to enhance their therapeutic performance. A number of studies report, in fact, that polymer-conjugated proteins usually present, as compared to the native counterparts, prolonged permanence in blood, lowered immunogenicity, improved physical, chemical, and enzymatic stability, and increased solubility.

To date, monomethoxypoly(ethylene glycol) (PEG) is receiving the lion's share in protein modification (*1*−*3*) and some PEG−protein conjugates are already in clinical use. However, despite the impressive results obtained with PEG, new synthetic and natural polymers are currently investigated for protein derivatization (*3*−*11*) in order to provide for macromolecules that, since their chemical and physical character, may dictate new properties and fate of the conjugate in the body. Indeed the polymeric portion, which often represents the major part of the construct, is more exposed than the protein to the biological environment and, therefore, can influence the interaction with biological structures and dictate body targeting and disposition.

Besides polymers designed for a selective recognition of biological receptors such as polysaccharides, antibodies, and neoglycoproteins (*12*−*14*), most of the macromolecules devised for protein modification do not mediate specific biological events or selective interactions. Anyhow, also, these polymers may possess tropism for organs and tissues that reflects in body disposition of their conjugates by passive mechanisms based on diffusion or by endocytosis.

Studies reported in the literature point out the effect of charge and molecular mass of macromolecular carriers on organ distribution of the conjugates (*15*−*18*). A typical example is the conjugation of an antitumor agent bound to a low molecular mass cationic dextran that showed a rapid disappearance from circulation due to accumulation in liver and spleen. High molecular mass cationic and anionic dextrans also promoted the localization of the conjugates in solid tumors (*17*, *18*). In addition proteins, peptides and antitumor agents covalently modified with negatively charged divinyl ether-maleic anhydride copolymer (DIVEMA) or styrene-maleic anhydride copolymer (SMA) showed tumoritropism, lymphotropism and captation by phagocytic cells (*6*, *19*).

Also, uncharged amphiphilic olygomers can passively interact with biological structures stimulating endocytosis (*20*−*24*). On the basis of these properties, several polymeric carriers have been developed for lysosomotropic delivery of antitumoral drugs and successful results have been obtained, for example, with poly(hydroxypropyl)methacrylamide and polyaspartamide-poly(oxyethylene) (*25*−*27*). Furthermore, poly(ethylene glycol)-derivatized proteins have been found to enter endothelial cells as well as blood cells (*28*, *29*), while conjugates of poly(vinyl alcohol) have been found to accumulate in small amounts in various organs (*30*).

All of these evidences indicate that biopharmaceutical properties of the conjugates must be carefully investigated since also slight differences in polymer structure may be reflected on different therapeutic performance of the conjugates (*31*−*33*).

* To whom correspondence should be addressed. Phone: 049-8275695. Fax: 049-8275366. E-mail: caliceti@dsfarm.unipd.it.

10.1021/bc980155k CCC: $18.00 © 1999 American Chemical Society
Published on Web 06/02/1999

To give a further contribution to understand the influence of the physicochemical and structural properties of neutral macromolecules on the biopharmaceutical properties of the conjugates, four different monofunctional soluble polymers have been considered: poly(*N*-vinylpyrrolidone) (PVP), poly(*N*-acryloilmorpholine) (PAcM), linear monomethoxypoly(ethylene glycol) (PEG), and branched monomethoxypoly(ethylene glycol) (PEG2). Uricase, an enzyme of potential therapeutic value in urea clearance, has been used as protein model (*34*, *35*) and a pharmacokinetic and biodistribution investigation of the native enzyme and its polymer conjugates was carried out in mice following intravenous administration. The concentration profiles in plasma, liver, kidney, spleen, heart, and lungs were evaluated and the main pharmacokinetic parameters have been calculated.

MATERIALS AND METHODS

Uricase from *Candida utilis* was obtained from Toyobo (Osaka, Japan). [^{3}H]succinimidyl propionate was from Amersham International (Amersham, U.K.) and Soluene 350, Instagel and Ionic Fluor were from Canberra Packard (Groninghen, The Netherlands). The Superose column and FPLC system were furnished by Pharmacia Biotech (Uppsala, Sweden), and the ultrafiltration system was from Amicon Inc. (Beverly, MA). All other reagents, of analytical grade, were purchased by Fluka (Buchs, Switzerland).

Male Balb/c mice, weighing 30 ± 2 g and fed ad libitum, obtained from Charles River (Calco, Italy), were used for "in vivo" experiments.

Polymer Preparation and Activation. Linear monomethoxypoly(ethylene glycol), M_w 5000 Da, obtained from Shearwater (Huntsville, AL), was end-carboxylated by introduction of a nor-leucine residue, and the free carboxylic group was activated as succinimidyl ester (*36*). Branched monomethoxypoly(ethylene glycol), M_w 10 000 Da, was prepared and activated as described in the literature (*37*). Carboxy-terminating poly(*N*-vinylpyrrolidone), M_w 6000 Da, and carboxy-terminating poly(*N*-acryloilmorpholine), M_w 6000 Da, were synthesized, fractionated, and activated according to the methods developed in our laboratory (*38*, *39*).

Preparation of Protein−Polymer Conjugates. Polymer activated as succinimidyl ester [15.4 μmol in the case of linear monomethoxypoly(ethylene glycol); 26.95 μmol of branched monomethoxypoly(ethylene glycol); 19.25 μmol of poly(*N*-vinylpyrrolidone); 23.1 μmol of poly(*N*-acryloilmorpholine)] was added under stirring to uricase (77 nmol) dissolved in 1 mL of 0.2 M borate buffer and 77 mM uric acid, pH 8.0. The reaction mixture was maintained under stirring at room temperature for 1 h, added to 9 mL of 0.1 M borate buffer, pH 8.0, and ultrafiltered using a membrane with 10 000 Da cut off to reach a volume of 1 mL. The remaining solution was diluted with 5 mL of the buffer reported above, and the ultrafiltration procedure was repeated three times. The ultrafiltered product was further purified by gel filtration chromatography using a Superose 12 preparative column eluted with 10 mM of phosphate buffer and 0.15 M NaCl, pH 7.2. The elution fractions were analyzed by OD at 280 nm for protein evaluation, by iodine assay for polymer determination (*40*) and by enzyme activity (*41*). The protein−polymer conjugate peak was concentrated by ultrafiltration. The protein concentration was finally determined by biuret method (*42*), the degree of modification by a trinitrobenzensulfonic acid colorimetric method (*43*) and by amino acid analysis on the basis of the nor-leucine content (*36*). The residual activity was assessed by enzyme assay.

Preparation of Tritium-Labeled Proteins. Native or polymer conjugated uricase (77 nmol) in 1 mL of borate buffer, pH 8.0, was added under vigorous stirring to 20 μL of toluene containing 1 nmol of succinimidyl [^{3}H]-propionate. After 30 min of reaction, the solution was chromatographied using a Superose 12 preparative column eluted with 10 mM of phosphate buffer and 0.15 M NaCl, pH 7.2. The protein peak was collected and radioactivity was assessed by β-counter and expressed as disintegrations per minute per protein milligram (DPM/protein mg).

Mouse serum albumin (144 nmol) was tritium-labeled following the procedure reported above for uricase.

The radioactivity of the ^{3}H-labeled derivatives was in the range of $0.6 \times 10^6 - 0.8 \times 10^6$ DPM/mg.

Pharmacokinetic and Biodistribution Studies. Animal treatments for the "in vivo" studies were performed according to institutional European guidelines.

Five groups of 10 Balb/c male mice (30 ± 2 g) each were separately treated by injection in the tail vein of the tritium-labeled compounds: native uricase, linear monomethoxypoly(ethylene glycol)-uricase, branched monomethoxypoly(ethylene glycol)-uricase, poly(*N*-vinylpyrrolidone)-uricase, and poly(*N*-acryloilmorpholine)-uricase (450 μg in 0.1 mL of 20 mM phosphate buffer, 0.15 M NaCl, pH 7.2). The animals were sacrificed at scheduled times, and blood samples, liver, spleen, lungs, heart, and kidneys were taken.

The blood samples were put in heparinized vials, centrifuged and the enzyme content in plasma was estimated by enzyme activity and by radioactivity evaluation after addition of 4 mL of Instagel cocktail to 50 μL of plasma.

The organs were carefully washed in saline solution, dried on paper, and weighted. Soluene 350 was added to the organs (10 mL/g tissue) and steeped at 100 °C for 2 h. Two hundred and fifty microliters of samples was added to 2.75 mL of Ionic Fluor, and the radioactivity was evaluated by β-counter.

Tritium-labeled mouse serum albumin (450 μg in 0.2 mL of sterile saline solution) was injected in the tail vein of 10 mice. The animals were sacrificed and blood samples and organs were taken and processed as described above for the estimation of the residual plasma in the organs.

Data Elaboration. The plasma concentration means and the standard deviations (±SD) of the native and conjugated uricase as well as the mouse serum albumin were estimated on the basis of the enzyme activity and the radioactivity obtained from the plasma samples.

The pharmacokinetic parameters were determined by computer elaboration of the enzyme concentrations in plasma obtained at the scheduled times according to the equation

$$C(t) = Ae^{-\alpha t} + Be^{-\beta t}$$

The concentration means and the standard deviations (±SD) of the native and conjugated uricase were determined on the basis of the values of the radioactivity obtained from the organ samples. The residual plasma volume in each organ was estimated by the [^{3}H]MSA levels, and the obtained data were used to correct the disposition levels of the various uricase forms in the organs (*22*).

The organ uptake indexes (CLin) were calculated, on the basis of the standard method reported in the litera-

Table 1. Protein/Polymer Molar Ratios Used in Conjugate Preparation and Main Properties of Native Uricase, PAcM-Uricase, PVP-Uricase, PEG2-Uricase, and PEG-Uricase

	protein NH_2/polymer molar ratio	extent of modification (% derivatized amino groups)	molecular mass (Da)
native uricase			130 000
PacM-uricase	1:3	47	400 000
PVP-uricase	1:2.5	43	380 000
PEG-uricase	1:3	44	350 000
PEG2-uricase	1:3.5	40	530 000

ture, according to the following expression:

$$\mathrm{CLin} = \frac{T(t)}{\int C(t)\,\mathrm{d}t} = \frac{T(t_1)}{\mathrm{AUC}_{0\rightarrow t1}}$$

where $T(t_1)$ is the percentage of dose per gram at 15 min and AUC_{0-t1} is the area under the curve in the range 0−15 min (*23*).

RESULTS

Polymer−Protein Conjugate Preparation. To carry out a comparative study, conjugates at similar molecular mass or degree of modification were prepared with the various polymers. This could be realized using polymers with close molecular masses (in the range 5000−6000 Da) and by attachment of a similar number of polymer molecules to the protein. To overcome the different reactivity of the activated polymers, proper protein NH_2/polymer molar ratios in the conjugation reaction were used. Table 1 reports the conjugate preparation conditions, degree of modification, and molecular mass of unmodified uricase and of the four polymer-uricase derivatives. The table shows that, in the case of PAcM, PVP, and PEG, molecular mass in the range 350000−400000 Da were obtained. The higher molecular mass of the PEG2 derivative (530 000 Da) is due to the fact that the reaching of the same degree of modification as the other conjugates was preferred to obtain a close overall mass.

The conjugation reaction was carried out in the presence of uric acid in order to prevent the dramatic loss in enzyme activity that the polymer binding can provoke in the absence of any active-site protection. Following this procedure, the conjugates could maintain enzyme activity in the range 20−80% of the unmodified uricase (*44*).

Pharmacokinetic Studies. The pharmacokinetic behaviors obtained by intravenous injection to mice of native and polymer conjugated uricases are depicted in Figure 1. The time course profiles were obtained by radioactivity determination of the enzyme concentration in plasma. For the radioactivity evaluation few amino groups of native and conjugated proteins were covalently labeled with [^{3}H]propionate, a method that prevents the "in vivo" release of the radioactive probe. Of note to report that in few samples the concentrations were also evaluated by enzyme activity and the values have been found in agreement with those obtained by radioactivity.

The patterns in plasma were found to fit a biexponential curve, indicating that the various enzyme forms are cleared from circulation following a bicompartimental pharmacokinetic model. Furthermore the figure shows that, although the performance of the conjugates deeply depends on the polymer, in any case they are eliminated from blood much more slowly with respect to the native enzyme.

The pharmacokinetic data reported in Table 2 point out that PVP-UC is, among the various uricase forms, the longest lasting in blood. The mean residence time (MRT) of PVP-UC is in fact about 10-fold of the native uricase, 3-fold of PAcM-UC, and 1.3-fold that of PEG-uricase and PEG2-uricase. The β phase half time ($t_{1/2}\beta$) and the elimination rate constants (k_e) also reflect the slow PVP-UC elimination from the body, followed in the order by PEG-UC and PEG2-UC, PAcM-UC and native uricase.

With regard to the distribution phase, the native uricase and the PAcM derivative show comparable α phase half times ($t_{1/2}\alpha$). These values that are about 10-fold shorter than the ones obtained with the other enzyme forms indicate that a rapid distribution process takes place. The high distribution rate constants (k_{12} and k_{21}) of native uricase and the PAcM derivative confirm

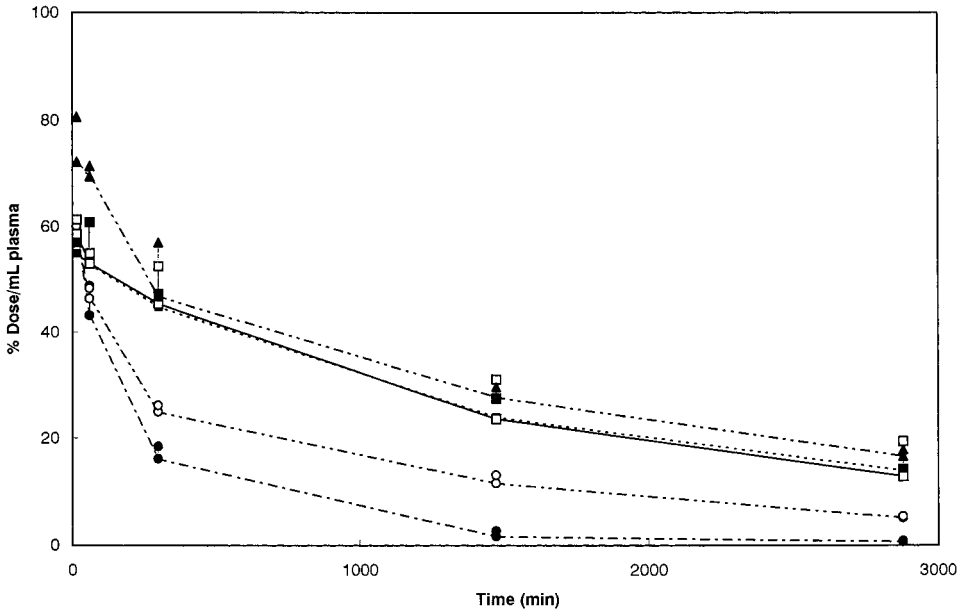


Figure 1. Time course profiles in plasma of radioactivity after intravenous administration to of native uricase (●), PAcM-uricase (○), PVP-uricase (■), PEG-uricase (□), and PEG2-uricase (▲); ±SD values are reported.

Table 2. Main Pharmacokinetic Parameters Obtained by Intravenous Injection in Mice of Native Uricase, PAcM-Uricase, PVP-Uricase, PEG2-Uricase, and PEG-Uricase

	native uricase	PAcM-uricase	PVP-uricase	PEG-uricase	PEG2-uricase
A	190.5	163.3	160.5	163.8	169.3
B	112.9	119.6	88.6	94.6	169.9
α	0.0118	0.0088	0.001	0.0011	0.0033
β	0.0018	0.0006	0.000 17	0.0002	0.000 27
$t_{1/2}\alpha$ (min)	58	79	685	617	206
$t_{1/2}\beta$ (min)	390	1190	4075	3384	2564
$AUC_{0-\infty}$ (μg/mL/min)	8×10^4	2.2×10^5	6.8×10^5	6.1×10^5	6.8×10^5
C_l (mL/min^{-1})	1.9×10^{-4}	7×10^{-5}	2×10^{-5}	2×10^{-5}	2×10^{-5}
V_c (mL)	1.48	1.59	1.8	1.74	1.32
MRT (min)	466	1585	4738	3926	3448
V_{ss} (mL)	2.6	3.18	3.1	2.9	2.3
k_{12}	1.2×10^{-2}	5.3×10^{-3}	4.7×10^{-6}	1×10^{-5}	0.5×10^{-3}
k_{21}	0.34	0.98×10^{-1}	2.7×10^{-2}	3.4×10^{-2}	4.7×10^{-2}
k_e	3.8×10^{-3}	1.3×10^{-3}	3.7×10^{-4}	4.3×10^{-4}	5×10^{-4}

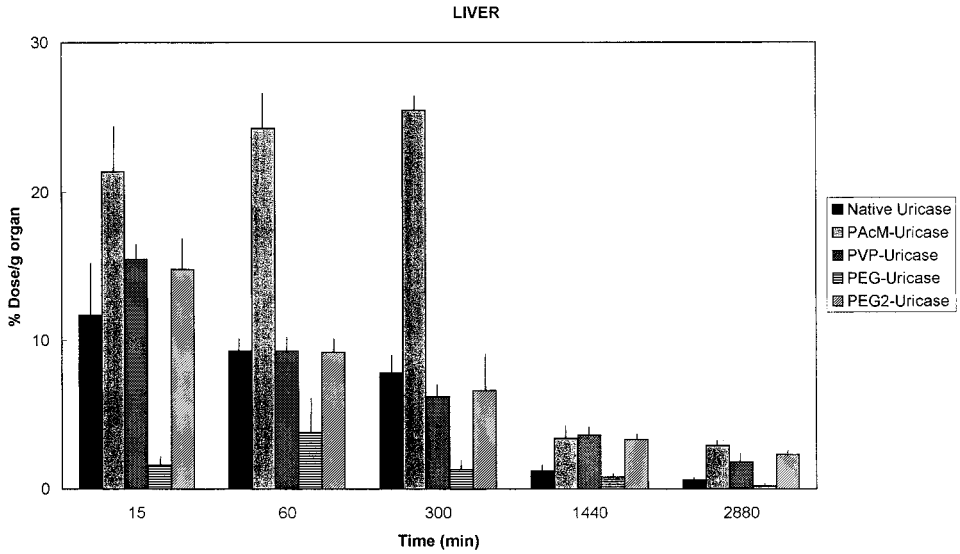


Figure 2. Disposition profiles in liver of native uricase, PAcM-uricase, PVP-uricase, PEG-uricase, and PEG2-uricase after intravenous administration to mice; ±SD values are reported.

the rapid equilibration of these enzyme forms with organs and peripheral tissues. On the other side PVP-UC, PEG-UC and PEG2-UC display high $t_{1/2}\alpha$ values and low k_{12} and k_{21} supporting that they slowly distributed in the peripheral tissues and slowly reach the equilibrium between blood and other tissues. In consideration of the $t_{1/2}\alpha$ and k_{12} and k_{21} values it is therefore possible to state that the peripheral distribution process follows the order native uricase > PAcM-UC > PEG2-UC > PEG-UC > PVP-UC.

Finally PVP-UC, PEG-UC, and PEG2-UC show similar high area under the curve (AUC), values indicating their significantly higher systemic availability, with respect to PAcM-UC and native enzyme.

Organ Disposition. The uricase accumulation levels in liver, kidneys, spleen, heart, and lungs, obtained after intravenous administration to mice of the native and polymer conjugated enzyme and expressed as a percentage of the dose per gram of tissue up to 48 h from the administration are depicted in Figures 2−6. After this time, low levels of enzyme accumulation have been observed in the tissues with exception of kidneys that displayed a prolonged retention of the various enzyme forms, in particular of PAcM-UC and PEG2-UC.

Liver. The distribution profiles reported in Figure 2 show an impressive amount of PAcM-UC in liver. The PAcM-UC disposition is practically instantaneous, and its concentration gradually increases by time to reach the maximal level of approximately 26% within 5 h. After 24 h from injection, the PAcM-UC concentration drastically drops to 4%. Native uricase, PVP-UC, and PEG2-UC also rapidly dispose in this organ and their distribution behaviors are very similar. Soon after administration these enzyme forms exhibit concentration levels ranging between 12 and 16%, but the clearance from this organ takes also place rapidly indicating a low affinity for the hepatic tissue. A different behaviour has instead been observed for PEG-UC that does not show any significant accumulation in liver in comparison to the other uricase forms. Levels below 4% of the dose were in fact found during the experiment.

Kidneys. PAcM-UC is the uricase species with the highest affinity for kidneys. Figure 3 shows that the disposition process in this organ is practically instantaneous and the concentration increases with the time reaching the level of about 15% in 5 h, a value constantly retained up to 48 h. The kidney distribution time courses during the first 24 h of native uricase and the PAcM derivative are very similar, but after this time, the native form is rapidly cleared. PVP-UC, PEG-UC, and PEG2-UC exhibit lower concentration values with respect to the native enzyme and the PAcM conjugate. Their accumulation is at the limit of detection after 15 min from injection and gradually rises to reach values of 3.3 and 4.8% after 24 h for the PVP and PEG2 derivatives, respectively, and of 5.6 after 48 h for the PEG one.

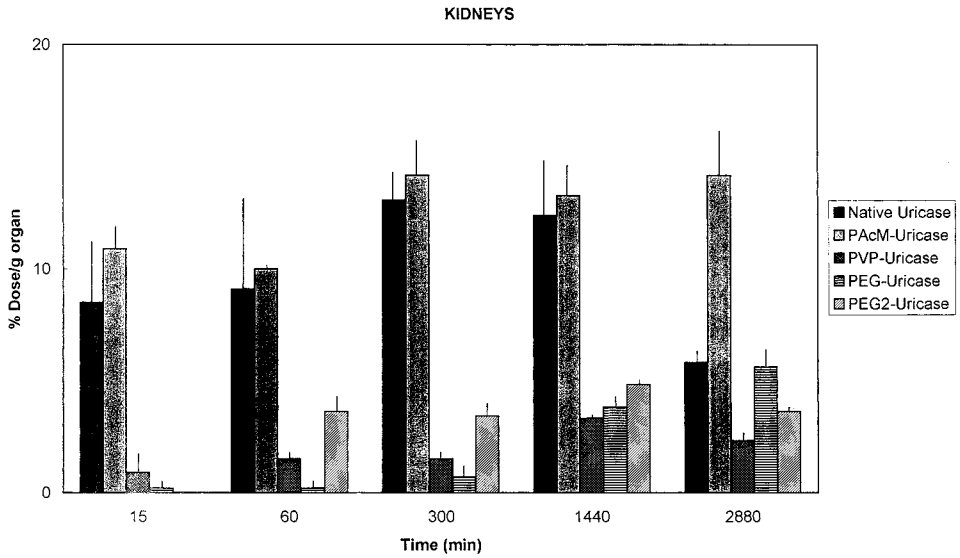


Figure 3. Disposition profiles in kidneys of native uricase, PAcM-uricase, PVP-uricase, PEG-uricase, and PEG2-uricase after intravenous administration to mice; ±SD values are reported.

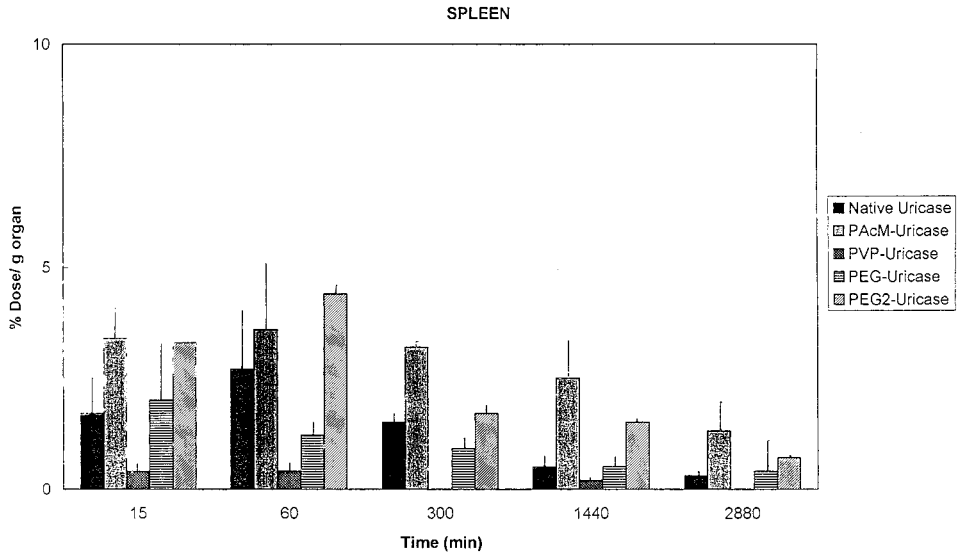


Figure 4. Disposition profiles in spleen of native uricase, PAcM-uricase, PVP-uricase, PEG-uricase, and PEG2-uricase after intravenous administration to mice; ±SD values are reported.

Spleen. The time courses of distribution in spleen depicted in Figure 4 indicate that PEG2-UC and PAcM-UC undergo a rapid accumulation in spleen that reaches the maximal concentration level after 1 h from administration: 4 and 5%, respectively. After this time, the PEG2 derivative concentration is reduced by 2/3, while the PAcM conjugate is cleared much more slowly. Native uricase and PEG derivative dispose in spleen at a lower extent with respect to the PEG2 and PAcM counterparts but with a similar trend, while PVP-UC accumulation is practically negligible.

Heart. Figure 5 describes the rapid and remarkable localization in heart of native uricase and PAcM-UC. In particular, the PAcM conjugate maintains constant concentration levels of about 3.5% for up to 5 h from the administration time, whereas the unmodified uricase is quickly cleared from this organ. Only a reduced localization in heart is instead found for PEG-UC and PEG2-UC. These conjugates, that present a similar behavior, have concentration levels constantly maintained below 1%. PVP-UC failed to accumulate in heart and its concentration levels are practically undetectable.

Lungs. The distribution patterns in lungs depicted in Figure 6 show that native uricase, PAcM-UC, and PVP-UC are rapidly localized in lungs and rapidly cleared from it. A high level of native enzyme is found after 15 min (13%). PEG-UC and PEG2-UC show, instead, a different disposition trend in comparison to the other uricase forms. Their concentrations gradually increase with time reaching a level of about 3% within 24−48 h.

Organ Uptake Index. Table 3 reports the organ uptake rate indexes that quantitatively define the differences in organ translocation of the various uricase forms.

Native uricase and PAcM-UC display, in the examined organs, the higher uptake rate values according to their consistent tissue disposition already observed in Figures 2−6. Interestingly the liver uptake of PAcM-UC is 1.3-fold of the native uricase one, while the latter presents higher lungs and heart uptake indexes. PVP-UC is rapidly taken up only by liver, which is the organ involved in polymer elimination (*45*). The data of the table point out a rapid translocation of the PEG2-UC in liver and spleen, two organs rich of reticulo-endothelial

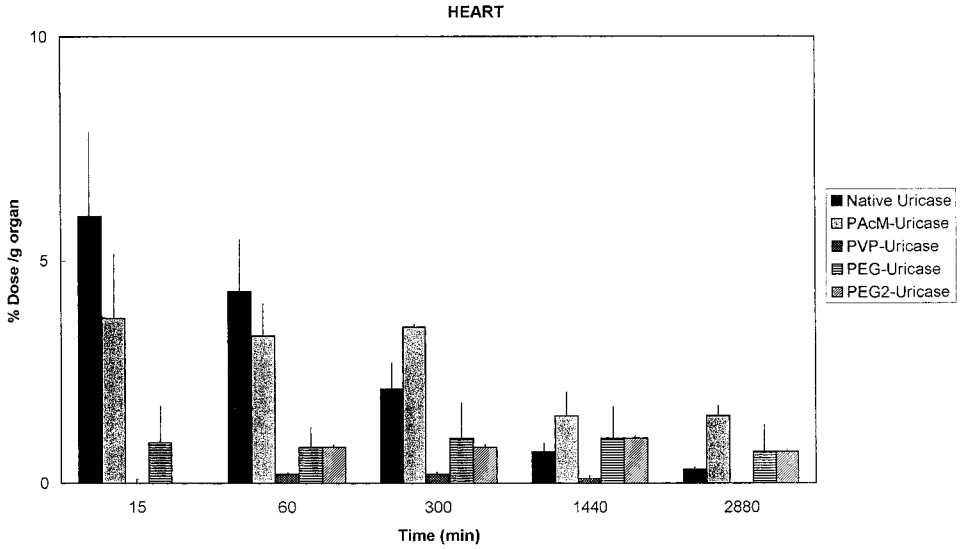


Figure 5. Disposition profiles in heart of native uricase, PAcM-uricase, PVP-uricase, PEG-uricase, and PEG2-uricase after intravenous administration to mice; ±SD values are reported.

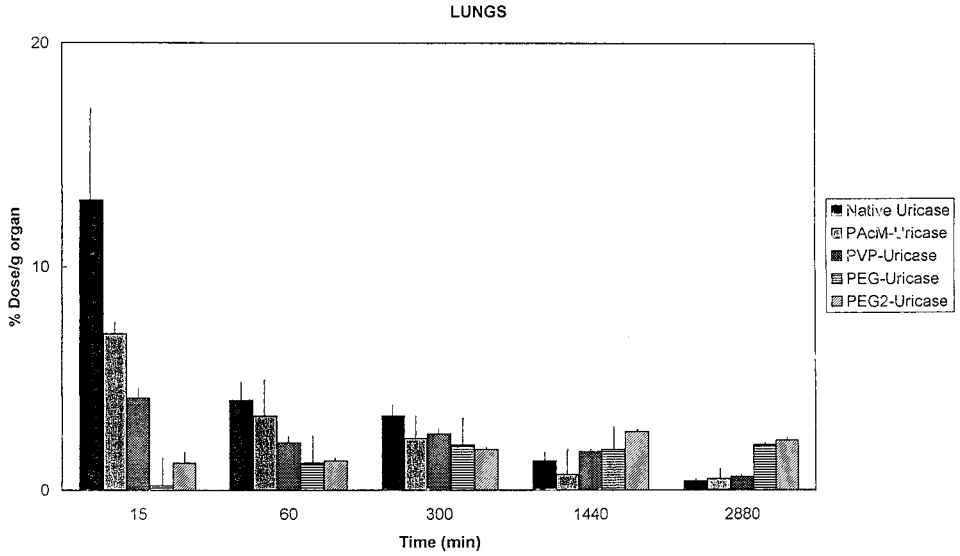


Figure 6. Disposition profiles in lungs of native uricase, PAcM-uricase, PVP-uricase, PEG-uricase, and PEG2-uricase after intravenous administration to mice; ±SD values are reported.

Table 3. Organ Uptake Rate Indexes Obtained with Native Uricase, PAcM-Uricase, PVP-Uricase, PEG2-Uricase, and PEG-Uricase

	CLin (μL/g/h)				
	native uricase	uricase-PAcM	uricase-PVP	uricase-PEG	uricase-PEG2
liver	816	1056	749	83.4	532
kidneys	624	762	45	9.6	0.9
spleen	128.4	241.6	19.8	108	120.2
heart	441	255	2.79	46.7	0
lungs	958	493	43.9	9.7	41.7

cells, while the linear PEG does not present significant index values in any studied organ. These results are in agreement with the enhanced uptake by Kuppfer cells observed with high molecular mass poly(ethylene glycol)s (*23*).

DISCUSSION

The present study was aimed at evaluating the influence of different neutral amphiphilic polymers on biopharmaceutical properties of polymer−protein conjugates. This is of primary importance in the choice of the polymer for protein modification because polymers with apparently similar physicochemical properties can affect in different way the biopharmaceutical properties of the conjugates.

Uricase was chosen for this investigation since its therapeutic value in the treatment of hyperuricemia-associated diseases such as nephropathologies and haematological malignancies and poly(ethylene glycol) and dextran conjugates have been recently prepared in order to overcome its considerable immunological and pharmacokinetic character (*15*, *34*, *35*).

The four polymers used in this study were selected because of their relevance in the preparation of protein conjugates for medical use. Indeed they have the prerequisites for medical use and possess similar properties such as good solubility in both aqueous and organic solvents, absence of charge, molecular shape, mass, and monofunctionality in reaction. Furthermore, previous studies carried out in our laboratories already demonstrated that monofunctional PVP, PAcM, and PEG2 provide for an excellent alternative to the most used linear PEG in protein modification (*37*−*39*, *46*−*48*).

The biopharmaceutical investigation reported here clearly indicates that the protein conjugation with these polymers yields derivatives with prolonged permanence in blood, although different clearance from circulation and organ distribution behaviors have been obtained.

With regard to the permanence in blood, we can say that the increased residence time of the conjugates, with respect to the native counterpart, can only partially be ascribed to reduction in renal ultrafiltration due to their high molecular volume, as often reported with other proteins. Native uricase "per se" has in fact a high molecular mass (128 000 Da) and Stokes' radius (42.7 Å) that overcome the renal filtration limit and therefore its main elimination route is by hepatic route (*15*). The organ disposition behaviors and uptake indexes of native uricase suggest that its rapid disappearance is by localization in organs, a behavior that is certainly followed by the uricase conjugates also. In particular, the high disposition of native uricase in reticulo-endotelial cell rich organs such as liver and lungs seems to suggest that its elimination takes place by phagocytic processes, followed by biliary excretion and/or degradation to low molecular mass peptides that can be cleared with urine. It is therefore worth noting that the changes in protein organ disposition determined by the polymer binding are accompanied by enhancing the uricase permanence in blood.

In addition, the resistance of the conjugates to proteolytic digestion and to recognition by the immunosystem already observed in our laboratories (*44*) also contribute to prevent the uricase conjugate disappearance from circulation. In this regard it may be of interest to remember the agreement between the enzyme activity and radioactivity levels in blood of the conjugated uricase a behavior that is in favor of the stability in blood of the conjugates despite their long permanence in it. This behavior points out that the protein degradation to inactive long circulating fragments does not take place.

If we now examine the "in vivo" performance of the four polymer conjugates, we can observe that PAcM promotes significantly the organ accumulation of the derivative in the main organs, in particular in liver, spleen, and kidneys. The high uptake rate indexes of these organs, and especially of liver, explains its rapid disappearance during the distribution phase (α phase). Nevertheless, the conjugate has a considerable higher permanence in blood (β phase) compared to the native enzyme probably due to a reduced degradation and a slow release from the tissues that guarantee sustained levels in blood.

For what the PVP derivative is concerned its long permanence in plasma reflects the low levels of tissue translocation. The conjugate in fact disposes significantly only in liver, in agreement with the data reported in the literature that indicate the hepatic uptake by endocytosis of this polymer as the main PVP elimination route (*24*).

Interesting results have been obtained with the PEG and PEG2 derivatives that show very different accumulation profiles in the examined organs. According to the literature data, the linear PEG derivative does not show specific localization in peripheral districts, and low amounts of its conjugate are found in all the tissues (*23*). On the other hand, the PEG2 adduct accumulates at significant extent in liver and spleen, two organs rich of reticulo-endothelial cells. These results suggest that the branched shape of this polymer can affect the cell/conjugate interaction process and the higher accumulation of the PEG2 derivative is probably related to the higher molecular volume of this conjugate that, with respect to the linear one, can more efficiently stimulate the cell phagocytic process.

The reasons that are at the basis of the differences in organ disposition among the conjugates are difficult to be understood. Differences in stability to proteolytic enzymes of the various enzyme forms, observed in "in vitro" experiments, seem not to be relevant in determining the disposition profiles of the various enzyme forms since all of them were found do not degrade in the experiment time. We can instead suggest that peculiar lipohilic/hydrophilic properties of the polymers can play a significant role in the interaction with the organ cell membranes indicating the importance of their amphiphilic character.

CONCLUSIONS

A careful choice of the polymer used for protein modification allows for controlling the "in vivo" fate of the conjugates. However, charge and molecular mass are not the only parameters playing a role in dictating the biopharmaceutical properties of the conjugates as often reported in the literature. The data reported here indicate that neutral polymers, with apparently similar physicochemical properties but different chemical composition and architecture, can confer to the conjugates peculiar biopharmaceutical properties. Therefore, the assumption that the covalent conjugation of uncharged and relatively low molecular mass polymers to proteins avoids the organ disposition of the conjugates, based on the low disposition properties of the most studied PEG derivatives, must be carefully reconsidered.

This suggests the possibility to use uncharged amphiphilic polymers for preparation of tailored conjugates that can preferentially accumulate in organs where their therapeutic effect is expected or from where they can be slowly released in the active form in order to ensure sustained concentrations in plasma.

Furthermore, in addition to the therapeutic value of the conjugates, also their toxicological aspect must be considered. Accumulation of the conjugates in organs where they can house for a long time can in fact represent a serious limit of their application, also in consideration of the usual high stability to degradation processes of the conjugates that prevents their elimination. However, it is important to observe that the non biodegradable polymers studied here do not induce any irreversible accumulation of the conjugates in organs that could cause toxicity problems.

LITERATURE CITED

(1) Delgado, C., Francis, G. E., and Fisher, D. (1992) The uses and properties of PEG-linked proteins. *Crit. Rev. Ther. Drugs Carrier Syst. 9*, 249−304.

(2) Veronese, F. M., Caliceti, P., Schiavon, O., and Sartore, L. (1991) In *Poly(ethylene glycol): chemistry, biochemical and biomedical applications* (J. M. Harris, Ed.) Plenum Publication Corp., New York.

(3) Kartre, K. (1993) The conjugation of proteins with poly(ethylene glycol) and other polymers. *Adv. Drug Deliv. Rev. 10*, 91−114.

(4) Caliceti, P., Schiavon, O., Hirano, T., Ohashi, S., and Veronese, F. M. (1996) Modification of physicochemical and biopharmaceutical properties of superoxide dismutase by conjugation to the polymer of divinyl ether and maleic anhydride. *J. Controlled Release 39*, 27−34.

(5) Ito, Y., Kotoura, M., Chung, D. J., and Imanishi, Y. (1993) Bioconjugate Chem. Trypsin modification by vinyl polymers with variable solubilities that responses to external signals, *4*, 358−361.

(6) In *Neocarzinostatin: the past, present and future of an anticancer drug* (1997) (H. Maeda, K. Edo, and N. Ishida, Eds.) Spinger-Verlag, Tokyo.

(7) Poznasky, M. J., Halford, J., and Taylar, D. (1988) Growth hormonealbumin conjugates reduced renal toxicity and altered clearance. *FEBS Lett. 239*, 18−22.
(8) Wileman, T. E. (1991) Properties of asparaginase-dextran conjugates. *Adv. Drug Del. Rev. 6*, 167−180.
(9) Von Specht, B. W., and Brendel, W. (1977) Preparation and properties of trypsin and chymotrypsin coupled covalently to poly(*N*-vinylpyrrolidone). BBA, *484*, 109−114.
(10) Kakimoto, K., Kojima, Y., Ishii, K., Onoue, K., and Maeda, H. (1993) The suppressive effect of gelatin-conjugated superoxide dismutase on disease development and severity of collagen-induced arthritis in mice. *Clin. Exp. Immunol. 94*, 241−246.
(11) Garman, A. J., and Kalindjian, S. B. (1987) The preparation and properties of novel reversible polymer-protein conjugates 2-omegamethoxypolyethylene (5000) glycoxymethylene-3-methylmaleyl conjugates of plasminogen activators. *FEBS Lett. 223*, 361−365.
(12) Bagshawe, K. D. (1994) Antibody-directed enzyme prodrug therapy (Adept). *J. Controlled Release 28*, 187−193.
(13) Rensen, P. C. N., Devrueh, R. L. A., and Vanberkel, T. J. C. (1996) Targeting hepatitis B therapy to the liver: clinical pharmacokinetic considerations. *Clin. Pharmacokinet. 31*, 131−155.
(14) Takakura, Y., and Hashida, M. (1996) Macromolecular carrier systems for targeted drug delivery: pharmacokinetic consideration on biodistribution. *Pharm. Res. 13*, 820−831.
(15) Fujita, T., Yasuda, Y., Takakura, Y., Hashida, M., and Sezaki, H. (1991) Tissue distribution of ^{111}In-labeled uricase conjugated with charged dextrans and poly(ethylene glycol). *J. Pharmacobio-Dyn. 14*, 623−629.
(16) Ekrami, H., Kennedy, A. R., and Shen, W−C. (1995) Disposition of positively charged Bowman-Birk protease inhibitor conjugates in mice: influence of protein conjugate charge density and size on lung targeting. *J. Pharm. Sci. 84*, 456−461.
(17) Bogdanov, A. A., Jr., Martin, C., Bogdanova, A. V., Brady, T. J., and Weissleder, R. (1996) An adduct of cis-diamminedichloroplatinum (II) and poly(ethylene glycol) poly(L-lysine)-succinate synthesis and cytotoxic properties. *Bioconjugate Chem. 7*, 144−149.
(18) Takakura, Y., Fujita, T., Hashida, M., and Sezaki, H. (1990) Disposition characteristics of macromolecules in tumor-bearing mice. *Pharm. Res. 7*, 339−346.
(19) Oda, T., Akaike, T., Hamamoto, S., Fujio, S., Hirano T., and Maeda, H. (1989) Oxygen radicals in influnza-induced pathogenesis and treatment with pyran polymer-conjugated SOD. *Science 244*, 974−976.
(20) Yamaoka, T., Tabata, Y., and Ikada, Y. (1995) Comparison of body distribution of poly(vinyl alcohol) with other water-soluble polymers after intravenous administration. *J. Pharm. Pharmacol. 47*, 479−486.
(21) Yamaoka, T., Tabata, Y., and Ikada, Y. (1995) Fate of water-soluble polymers administered via different routes. *J. Pharm. Sci. 50*, 349−354.
(22) Tabata, Y., Murakami Y., and Ikada, Y. (1998) Tumor accumulation of poly(vinyl alcohol) of different size after intravenous injection. *J. Controlled Release 50*, 123−133.
(23) Yamaoka, T., Tabata, Y., and Ikada, Y. (1994) Distribution and tissue uptake of poly(ethylene glycol) with different molecular weights after intravenous administration to mice. *J. Pharm. Sci. 83*, 601−606.
(24) Seale, S., Love, W. G., Amos, N., Williams, B. D., and Kellaway, I. W. (1992) Accumulation of poly(vinylpyrrolidone) within the inflamed paws of adjuvant arthritic rats. *J. Pharm. Pharmacol. 44*, 10−14.
(25) Pimm, M. V., Perkins, A. C., Strohalm, J., Ulrich, K., and Duncan, R. (1996) Gamma scintigraphy of a 123I-labeled N-(2-hydroxypropyl)methacrylamide. *J. Drug Target. 3*, 385−390.
(26) Flanagan, P. A., Kopeckova, P., Kopeck, J., and Duncan, R. (1989) Evaluation of protein-N-(2-hydroxypropyl)methacrylamide copolymer conjugates as targetable drug carriers. 1. Binding, pinocytic uptake and intracellular distribution of transferrin and anti transferrin receptor antibody conjugates. *Biochim. Biophys. Acta, 993*, 83−91.
(27) Kwon, G. S., Yokoyama, M., Okano, T., Sakurai, Y., and Kataoka, K. (1993) Biodistribution of micelle-forming polymer-drug conjugates. *Pharm. Res. 10*, 970−974.
(28) Munniksama, J., Noteborn, N., Kooistra, T., Steinstra, S., Bouma, J. M. W., Gruber, M., Brouwer, A., Dalenand, D. P. U., and Knook, D. L. (1980) Fluid endocytosis by rat liver and spleen. *Biochem. J. 192*, 613−621.
(29) Caliceti, P., Schiavon, O., Mocali, A., and Veronese, F. M. (1989) Evaluation of monomethoxypoly(ethylene glycol) derivatized superoxide dismutase in blood and evidence for its binding to blood cells. *Farmaco 44*, 711−720.
(30) Beckman, J. S., Minor, R. L., White, C. W., Repine, J. E., Rosen, G. M., and Freeman, B. A. (1988) Superoxide dismutase and catalase conjugated to poly(ethylene glycol) increases endothelial enzyme activity and oxidant resistance. *J. Biol. Chem. 263*, 6884−6892.
(31) Kojima, Y., and Maeda, H. (1993) Evaluation of poly(vinyl alcohol) for protein tailoring: improvements in pharmacokinetic properties of superoxide dismutase. *J. Bioact. Compat. Polym. 8*, 115−131.
(32) Brenner, B. M., Hostetter, T. H., and Humes, H. D. (1978) Glomerular permselectebility: barrier function based on discrimination of molecular size and charge. *Am. J. Physiol. 234*, F455−F460.
(33) Barrowcliffe, M. P, Zanelli, G. D., Ellison, D., and Jones, J. G. (1990) Clearance of charged and uncharged dextrans from normal and injured lungs. *J. Appl. Physiol. 68*, 341−347.
(34) Przybylski, M., Fell, E., and Ringsdorf, H. (1978) Synthesis and characterization of polymeric derivatives of the antitumour agent methotrexate. *Makromol. Chem. 179*, 1791−1733.
(35) Yasuda, Y., Fujita, T., Takakura, Y., Hashida, M., and Sezaki, H. (1990) Biochemical and biopharmaceutical properties of macromolecular conjugates of uricase with dextran and poly(ethylene glycol). *Chem. Pharm. Bull. 38*, 2053−2056.
(36) Chuna, C. C., Greenberg, M. L., Viau, A. T., Nucci, M., Brenckman, W. D., and Hershfield, M. S. (1988) Use of poly-(ethylene glycol)-modified uricase (PEG-uricase) to treat hyperuricemia in a patient with non-Hodgkin lymphoma. *Ann. Int. Med. 109*, 114−117.
(37) Sartore, L., Caliceti, P., Schiavon, O., and Veronese, F. M. (1991) Enzyme modification by MPEG with an amino acid or peptide as space arms. *Appl. Biochem. Biotechnol. 27*, 45−54.
(38) Monfardini, C., Schiavon, O., Caliceti, P., Morpurgo, M., Harris, J. M., and Veronese, F. M. (1995) A branched monometoxypoly(ethylene glycol) for protein modification. *Bioconjugate Chem. 6*, 62−69.
(39) Sartore, L., Ranucci, E., Ferruti, P., Caliceti, P., Schiavon, O., and Veronese, F. M. (1994) Low molecular weight end-functionalized PVP(*N*-vinylpyrrolidone) for the modification of polypeptide amino groups. *J. Bioact. Compat. Polym. 9*, 411−428.
(40) Ranucci, E., Spagnoli, G., Sartore, L., Ferruti, P., Caliceti, P., Schiavon, O., and Veronese, F. M. (1994) Synthesis and macromolecular weight characterization of low molecular weight end-functionalized poly(4-acryloilmorpholine). *Macromol. Chem. Phys. 195*, 3469−3479.
(41) Sims, G. E. C., and Snape, T. J. (1980) A method for estimation of poly(ethylene glycol) in plasma protein fractions. *Anal. Biochem. 107*, 60−63.
(42) Mahler, H. R. (1963) In *The Enzymes* (P. D. Boyer, Ed.) Vol III, 2nd ed., Academic Press, New York.
(43) Gornall, A G., Bardawill, C. J., and David, M. M. (1949) Determination of serum protein by means of biuret reaction. *J. Biol. Chem. 177*, 751−766.
(44) Habeeb, A. F. S. A. (1966) Determination of free amino groups in proteins by trinitrobenzensulfonic acid. *Anal. Biochem. 14*, 328−336.
(45) Schiavon, O., Caliceti, P., and Veronese, F. M., Uricase modification with amphiphilic polymers. *Farmaco* (in press).
(46) Caliceti, P., Schiavon, O., Morpurgo, M., and Veronese, F. M. (1995) Physisco-chemical and biological properties of

monofunctional hydroxy terminating poly(*N*-vinylpyrrolidone) conjugated superoxide dismutase. *J. Bioact. Compat. Polym. 10*, 103−120.
(47) Morpurgo, M., Schiavon, O., Caliceti, P., and Veronese, F. M. (1996) Covalent modification of mushroom tyrosinase with different amphiphilic polymers for pharmaceutical and biocatalysis applications. *Appl. Biochem. Biotechnol. 56*, 59−72.
(48) Veronese, F. M., Caliceti, P., Schiavon, O., Scrawen, M. D., and Beer, D. (1997) Branched and linear poly(ethylene glycol): influence of the polymer structure on enzymological, pharmacokinetic and immunological properties of protein conjugates. *J. Bioact. Compat. Polym. 12*, 196−207.

BC980155K

Bifunctional Phosphoramidite Reagents for the Introduction of Histidyl and Dihistidyl Residues into Oligonucleotides

Thomas H. Smith,* John V. LaTour, Dmitry Bochkariov, Grigoriy Chaga, and Paul S. Nelson

Nucleic Acids Chemistry Division, CLONTECH Laboratories, Inc., 1020 East Meadow Circle, Palo Alto, California 94303 . Received January 11, 1999; Revised Manuscript Received March 16, 1999

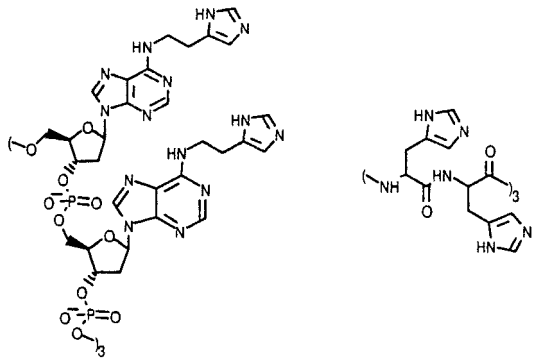
The synthesis and characterization of reagents for the incorporation of histidyl residues into oligonucleotides by automated chemical synthesis is described. Automated oligonucleotide synthesis utilizing a bifunctional reagent for the incorporation of a dihistidyl residue into oligonucleotides is described. Oligonucleotides incorporating one to three dihistidyl residues were prepared and characterized. The interaction of these oligonucleotides with a metal chelating IMAC matrix was explored.

INTRODUCTION

Oligonucleotides containing imidazole residues are of potential biological interest for a number of reasons. The metal complexing property of imidazole rings offers a potential handle for the purification of imidazole-tagged oligonucleotides and nucleic acids. Histidine- or imidazole-containing oligonucleotides can act as artificial nucleases due to the ability of imidazole rings to complex metal ions and cleave nucleic acid chains (*1*, *2*).

IMAC (immobilized metal affinity chromatography) is a widely used technique for the purification of recombinant proteins tagged with metal-coordinating peptide sequences (*3*, *4*) such as hexahistidine (*5*). Due to the binding strength and reversible nature of the imidazole-transition metal ion coordination, IMAC also has potential as a useful technique for nucleic acid applications. In 1995, Orum et al. reported the use of oligohistidine-PNA chimeras to purify cDNAs via an IMAC process (*6*). In 1996, Min and Verdine (*7*) reported the use of IMAC in a DNA application. In their work, the metal-coordinating peptide sequence was replaced by a tag composed of six consecutive 6-histaminylpurine nucleotide residues Figure 1 (1). This tag was constructed via automated incorporation into the oligonucleotide of O^6-phenyl-2′-deoxyinosine residues via phosphoramidite chemistry followed by postsynthesis reaction of the resulting oligonucleotide with aqueous histamine. This tag was shown to allow selective retention of a DNA strand to a Ni^{2+}-NTA (nitrilotriacetic acid)-agarose chromatography matrix (*8*).

The nature of the complex between the immobilized metal ion chromatography matrix and the polyhistine tag has never been fully understood. However, it has been shown that consecutive histidine residues are favored for optimal binding (*8*). With this in mind, we felt that the Min and Verdine structure **1**, with a 24-atom spacer between the imidazole rings versus the 6-atom distance between the imidazoles in a dihistidine peptide fragment **2**, may not be the optimal arrangement. We also wanted to introduce the metal-coordinating fragment in a single automated step on the DNA synthesizer without any postsynthetic manipulations. Our goal therefore became the design, synthesis, and evaluation of a reagent which meets these criteria. Herein we report the results of this study.



1 2

Figure 1. Structural comparison of IMAC active hexaimidazole fragment designed by Min and Verdine 1 with hexahistidine **2**.

EXPERIMENTAL PROCEDURES

General Methods. 2-Cyanoethoxy-*N*,*N*,*N*′,*N*′-tetraisopropylphosphoramidite was obtained from Dalton Laboratories (Toronto, Ontario). Tetrazole and diisopropylethylamine (DIPEA) were obtained from Chem-Impex (Wood Dale, IL). N^{α}-Fmoc-N^{im}-Boc-L-histidine cyclohexylamine (CHA) salt was obtained from Nova Biochem (LaJolla, CA). All other reagents were obtained from Aldrich Chemical Co. (Milwaukee, WI). All reactions were carried out under an Ar atmosphere. Solvent extracts of aqueous solutions were dried over anhydrous Na_2SO_4. Solutions were concentrated under reduced pressure using a rotary evaporator. Thin-layer chromatography (TLC) was done on Analtech Silica Gel GF (0.25 mm) plates. Chromatograms were visualized with either UV light or sulfuric acid. All compounds reported were homogeneous by TLC. HPLC analyses were performed on a Rainin (Emeryville, CA) Rabbit HPX system using either C18 Microsorb (4.6 × 150 mm, 5 μm) reversed-phase or Pharmacia (Piscataway, NJ) Mono Q HR 5/5 ion-exchange columns. UV measurements were obtained with a Perkin-Elmer Lambda 2 spectrophotometer

* To whom correspondence should be addressed. Phone: (650) 424-8222 ext. 4452. Fax: (650) 858-1239. E-mail: toms@clontech.com.

10.1021/bc990002c CCC: $18.00 © 1999 American Chemical Society
Published on Web 05/14/1999

equipped with a Peltier temperature controller and a six cell transport device. NMR spectra were obtained by Acorn NMR (Fremont, CA) at 360 MHz in $CDCl_3$. Mass spectra were obtained on a MALDI time-of-flight mass spectrometer from Ciphergen Biosystems, Inc. (Palo Alto, CA). Elemental analyses were obtained from the Microanalytical Laboratory of the Department of Chemistry, University of California, Berkeley.

***N*-(N^{α}-Fmoc-N^{im}-*t*-Boc-L-histidyl)-6-amino-2-hydroxymethyl-1-hexanol Dimethoxytrityl Ether (7)**. N^{α}-Fmoc-N^{im}-Boc-L-histidine CHA salt (35.0 g, 60.7 mmol) was placed in a separatory funnel containing EtOAc (800 mL) and 5% citric acid (800 mL) and shaken until the salt had fully dissolved. The organic layer was separated and the aqueous layer extracted with EtOAc (200 mL). The organic layers were combined, washed with water (200 mL) and brine (200 mL), dried, and evaporated to provide the free acid **5**. Separately, **3** (34.0 g, 50.6 mmol) was dissolved in 20% (v/v) piperidine in toluene (600 mL) and stirred at 22 °C for 2 h. The reaction mixture was evaporated, azeotroped with toluene (100 mL), redissolved in EtOAc (300 mL), washed with brine (2 × 100 mL), dried, evaporated, and azeotroped with toluene (100 mL) to afford the crude amine **4**. The residue was dissolved in DMF (80 mL) containing DIPEA (15 mL). The amino acid **5** from above was also dissolved in DMF (80 mL) containing DIPEA (16.7 mL) and combined with the solution of **4**. 1-Hydroxybenzotriazole (HOBT) (8.20 g, 60.7 mmol) was added followed by benzotriazol-1-yloxytripyrrolidinophosphonium hexafluorophosphate (PyBOP) (31.6 g, 60.7 mmol). The solution was stirred for 0.5 h at 22 °C, diluted with EtOAc (800 mL), washed with 10% Na_2CO_3 (2 × 800 mL), water (800 mL), and brine (800 mL), dried, evaporated, and azeotroped with toluene (100 mL). The residue was flash chromatographed on silica gel (1100 g) and eluted with 99:1 to 98:2 DCM/MeOH to afford 32.5 g (71%) of **7** as a diastereomeric mixture. ^{1}H NMR ($CDCl_3$): δ 8.02 (singlets, 1H), 7.76 (doublets, 2H), 7.59 (d, 2H), 7.35−7.45 (m, 4H), 7.13−7.34 (m, 10H), 6.83 (m, 4H, DMT), 6.77 (singlets, 1H), 6.45 (br, 1H), 4.32−4.50 (m, 3H), 4.09 (t, 1H), 3.78 (singlets, 6H), 3.74 (dd, 1H), 3.62 (m, 2H), 2.90−3.30 (m, 6H), 1.75 (br, 1H), 1.60 (singlets, 9H, Boc), 1.13−1.50 (m, 6H).

***N*-(N^{α}-Fmoc−N^{im}-*t*-Boc-L-histidyl)-6-amino-2-(*O*-DMT-hydroxymethyl)-1-hexanol (2-Cyanoethoxy)-*N*,*N*-diisopropylphosphoramidite (*12*)**. **7** (1.00 g, 1.1 mmol) was dissolved in dichloromethane (11 mL). Tetrazole (93 mg, 1.33 mmol) was added and the mixture stirred at 22 °C for 15 min. 2-Cyanoethoxy-*N*,*N*,*N*′,*N*′-tetraisopropylphosphoramidite (398 mg, 1.32 mmol) was added and the mixture stirred an additional 10 min at 22 °C. The mixture was filtered and the precipitate washed with EtOAc (10 mL). The combined filtrate and washing were diluted to 50 mL with EtOAc, washed with 10% Na_2CO_3 (2 × 15 mL) and brine (15 mL), dried, evaporated, and azeotroped with toluene. The residue was flash chromatographed on silica gel (40 g) and eluted with 70:30:3 to 50:50:3 hexane/EtOAc/TEA to afford 945 mg (78%) of **12** as a diastereomeric mixture. ^{1}H NMR ($CDCl_3$): δ 8.01 (s, 1H, His), 7.77 (d, 2H, Fmoc), 7.59 (d, 2H), 7.40 (m, 5H), 7.23−7.33 (m, 7H), 7.19 (m, 3H), 6.81 (dt, 4H, DMT), 6.42 (br, 1H, NH), 4.40 (m, 3H, His, Fmoc), 4.22 (t, 1H, Fmoc), 3.70 (s, 6H, DMT), 3.71 (m, 3H), 3.48−3.67 (m, 3H), 3.05−3.20 (m, 5H), 2.95 (dd, 1H), 2.53 (q, 2H, CH_2CN), 1.81 (septet, 1H), 1.57 (s, 9H, *t*-BOC), 1.30−1.42 (m, 4H), 1.60 (d, 8H), 1.11 (d, 6H). ^{31}P NMR ($CDCl_3$): δ 148.2 (singlets). Anal. Calcd for $C_{63}H_{77}N_6O_{10}P$: C, 68.21; H, 7.00; N, 7.58. Found: C, 68.33; H, 6.96; N, 7.80.

***N*-(N^{α}-Fmoc-N^{im}-*t*-Boc-L,L-dihistidyl)-6-amino-2-hydroxymethyl-1-hexanol Dimethoxytrityl Ether (9)**. **7** (1.37, 1.5 mmol) was dissolved in 20% (v/v) piperidine in toluene (15 mL) and stirred at 22 °C for 10 min. The reaction mixture was evaporated, azeotroped with toluene (15 mL), dissolved in EtOAc (100 mL), washed with brine (2 × 15 mL), dried, evaporated, and azeotroped with toluene (15 mL) to afford the crude amine **8**. N^{α}-Fmoc-N^{im}-Boc-L-histidine CHA salt (1.13 g, 2.25 mmol) was placed in a separatory funnel containing EtOAc (25 mL) and 5% citric acid (25 mL) and shaken until the salt had fully dissolved. The organic layer was separated, washed with water (25 mL) and brine (25 mL), dried, and evaporated to afford the free acid **5**. This was dissolved in DMF (6.9 mL). DIPEA (1.0 mL) was added, and this solution was added to the residue of the crude free amine **8**. When everything had been dissolved, PyBOP (1.02, 2.25 mmol) was added, and the solution was stirred at 22 °C for 30 min. The reaction mixture was diluted with EtOAc (50 mL), washed with 10% Na_2CO_3 (2 × 50 mL), water (50 mL), and brine (50 mL), dried and evaporated. The residue was flash chromatographed on silica gel (60 g) and eluted with 99:1 to 97.5:2.5 dichloromethane/MeOH to afford 1.35 g (78%) of **9** as a diastereomeric mixture. ^{1}H NMR ($CDCl_3$): 8.53 (br, 0.5H, NH), 8.40 (br, 0.5H), 7.98 (singlets, 1H), 7.76 (m, 3H), 7.59 (m, 3H), 7.13−7.44 (m, 14H), 6.82 (m, 4H), 6.75 (d, 1H), 6.58 (m, 1H), 4.71 (m, 1H, His), 4.26−4.44 (m, 3H), 4.22 (q, 1H, Fmoc), 3.78 (singlets, 6H, DMT), 3.70 (dt, 1H), 3.52−3.64 (m, 2H), 2.97−3.30 (m, 6H), 2.81 (m, 2H), 1.72 (m, 1H), 1.56 (singlets, 18H, *t*-BOC), 1.10−1.45 (m, 6H).

***N*-(N^{α}-Fmoc-N^{im}-*t*-Boc-L, L-dihistidyl)-6-amino-2-(*O*-DMT-hydroxymethyl)-1-hexanol (2-Cyanoethoxy)-*N*,*N*-diisopropylphosphoramidite (13)**. **9** (1.27 g, 1.1 mmol) was dissolved in dichloromethane (11 mL). Tetrazole (93 mg, 1.33 mmol) was added and the mixture was stirred at 22 °C for 20 min. 2-Cyanoethoxy-*N*,*N*,*N*′,*N*′-tetraisopropylphosphoramidite (398 mg, 1.32 mmol) was added, and the mixture stirred an additional 10 min at 22 °C. The mixture was filtered and the precipitate washed with EtOAc (10 mL). The combined filtrate and washing were diluted to 70 mL with EtOAc, washed with 10% Na_2CO_3 (2 × 50 mL) and brine (50 mL), dried, evaporated, and azeotroped with toluene. The residue was flash chromatographed on silica gel (40 g) and eluted with 50:50:3 to 30:70:3 hexane/EtOAc/TEA to afford 1.05 g (71%) of **13** as a diastereomeric mixture. ^{1}H NMR ($CDCl_3$): δ 8.28 (br d, 1H), 7.96 (s, 1H), 7.76 (d, 3H), 7.60 (t, 3H), 7.39 (t, 4H), 7.13−7.32 (m, 11H), 6.80 (d, 4H), 6.53 (br d, 1H), 4.69 (m, 1H), 4.35 (m, 3H), 3.22 (dd, 1H), 3.01−3.15 (m, 6H), 2.76 (m, 1H), 2.51 (q, 2H), 1.78 (m, 1H), 1.56 (d, 18H), 1.24−1.36 (m, 6H), 1.12 (doublets, 12H). ^{31}P NMR ($CDCl_3$): δ 148.0 (singlets). Anal. Calcd for $C_{72}H_{92}N_9O_{13}P$: C, 66.01; H, 6.89; N, 9.36. Found: C, 65.84; H, 6.93; N, 9.49.

N^{α}-TFA-N^{im}-*t*-Boc-L-histidine (6). L-Histidine (15.0 g, 96.7 mmol) was suspended in MeOH (500 mL). Triethylamine (66 mL) was added followed by ethyl trifluoroacetate (68 mL) over 30 min. The mixture was stirred at 22 °C for 15 h. The solvent was evaporated and the residue suspended in DMF (500 mL). DIPEA (20 mL) and di-*tert*-butyl dicarbonate (24 mL) were added, and the mixture was stirred at 22 °C for 1 h. The reaction mixture was diluted with EtOAc (1.4 L), washed with cold 10% citric acid (1.4 L), water (1.4 L), and brine (1.4 L), dried, and evaporated. The residue was recrystallized

from acetone to afford 27.5 g (81%) of **6**. mp 130−131 °C. ^{1}H NMR (DMSO-d_6): δ 13.08 (s, 1H), 9.65 (d, 1H), 8.12 (s, 11H), 7.24 (s, 1H), 4.55 (td, 1H), 3.05 (dd, 1H), 2.96 (dd, 1H), 1.54 (s, 9H). Anal. Calcd for $C_{13}H_{16}F_3N_3O_5$: C, 44.45; H, 4.59; N, 11.96. Found: C, 44.54; H, 4.65; N, 11.94.

***N*-(N^{α}-TFA-N^{im}-*t*-Boc-L,L-dihistidyl)-6-amino-2-hydroxymethyl-1-hexanol Dimethoxytrityl Ether (11).** *Method 1*. **9** (2.9 g, 2.5 mmol) was dissolved in 20% (v/v) piperidine in toluene (25 mL) and stirred at 22 °C for 10 min. The reaction mixture was evaporated, azeotroped with toluene (15 mL), dissolved in EtOAc (100 mL), washed with brine (2 × 15 mL), dried, evaporated, and azeotroped with toluene (15 mL) to afford the crude amine **10**. The residue was dissolved in dichloromethane (13 mL). Triethylamine (1.8 mL) and ethyl trifluoroacetate (1.5 mL) were added, and the solution was stirred at 22 °C for 16 h. Water (10 mL) was added, and stirring was continued for 1 h. The reaction mixture was diluted with EtOAc (20 mL) and 10% Na_2CO_3 (20 mL). The organic layer was separated, washed with 10% Na_2CO_3 (10 mL) and brine (10 mL), dried, evaporated, and azeotroped with toluene (10 mL). The residue was flash chromatographed on silica gel (90 g) and eluted with 99:1 to 95:5 dichloromethane/MeOH to afford 1.85 g (72%) of **11** as a diastereomeric mixture.

Method 2. **7** (20 g, 22 mmol) was dissolved in 20% (v/v) piperidine in toluene (220 mL) and stirred at 22 °C for 10 min. The reaction mixture was evaporated, azeotroped with toluene (150 mL), dissolved in EtOAc (500 mL), washed with brine (2 × 100 mL), dried, evaporated, and azeotroped with toluene (100 mL) to afford the crude amine **8**. Separately, **6** (9.27 g, 26.4 mmol) was dissolved in 5.5:1 dichloromethane/DMF (130 mL). *N*-Hydroxysuccinimide (NHS) (6.08 g, 52.8 mmol) was added and the mixture was cooled in an ice bath. Dicyclohexylcarbodiimide (DCC) (5.45 g, 26.4 mmol) was added, and the mixture stirred at 0 °C for 15 min. To this mixture was added a solution of **8** (prepared above) in dichloromethane (35 mL). This was stirred at 0 °C for 20 min. DIPEA (9 mL) was added, and stirring at 0 °C was continued for 10 min. The reaction mixture was filtered, and the filtrate concentrated to approximately 100 mL. This was diluted with EtOAc (400 mL) and washed with 10% Na_2CO_3 (2 × 100 mL). The carbonate washings were combined and extracted with EtOAc (200 mL). The organic layers were combined, washed with brine (100 mL), dried, evaporated, and azeotroped with toluene (50 mL). The residue was flash chromatographed on silica gel (1 kg) and eluted with 99:1 to 96:4 dichloromethane/MeOH to afford 16.1 g (72%) of **11** as a diastereomeric mixture. ^{1}H NMR: δ 8.52−8.72 (m, 2H, NH), 7.94 (doublets, 2H, His), 7.47 (br t, 1H, NH), 7.40 (m, 1H), 7.14−7.31 (m, 9H), 6.83 (m, 4H, DMT), 6.74 (d, 1H), 4.66 (m, 2H, His), 3.79 (singlets, 6H, DMT), 3.73 (m, 1H), 3.54−3.64 (m, 2H), 3.00−3.30 (m, 6H), 2.75 (m, 2H), 1.73 (m, 1H), 1.61 (singlets, 18H), 1.12−1.48 (m, 6H).

***N*-(N^{α}-TFA-N^{im}-*t*-Boc-L, L-dihistidyl)-6-amino-2-(*O*-DMT-hydroxymethyl)-1-hexanol (2-Cyanoethoxy)-*N*,*N*-diisopropylphosphoramidite (14).** **11** (14.2 g, 14 mmol) was dissolved in dichloromethane (140 mL). Tetrazole (1.17 g, 16.7 mmol) was added and the mixture stirred at 22 °C for 20 min. 2-Cyanoethoxy-*N*,*N*,*N*′,*N*′-tetraisopropylphosphoramidite (5.57 g, 18.5 mmol) was added, and the mixture stirred an additional 10 min at 22 °C. The mixture was filtered and the precipitate washed with EtOAc (100 mL). The combined filtrate and washing were diluted to 600 mL with EtOAc, washed with 10% Na_2CO_3 (2 × 400 mL) and brine (400 mL), dried, evaporated, and azeotroped with toluene. The residue was flash chromatographed on silica gel (500 g) and eluted with 50:50:3 to 30:70:3 hexane/EtOAc/TEA to afford 13.4 g (79%) of **14** as a diastereomeric mixture. ^{1}H NMR ($CDCl_3$): δ 8.57 (s, 1H, NH), 8.50 (d, 1H, NH), 7.94 (s, 1H, His), 7.90 (s, 1H, His), 7.40 (m, 3H), 7.12−7.33 (m, 9H, DMT), 6.80 (dt, 4H, DMT), 4.64 (m, 2H, His), 3.78 (s, 6H, DMT), 3.69 (m, 3H), 3.54 (m, 3H), 3.22 (d, 1H), 3.05 (m, 4H), 2.68 (dd, 1H), 2.52 (q, 2H, CH_2CN), 1.78 (m, 1H), 1.58 (singlets, 18H, *t*-BOC), 1.25−1.35 (m, 6H), 1.12 (singlets, 12H). ^{31}P NMR: δ 148.1 (singlets). Anal. Calcd for $C_{61}H_{81}F_3N_9O_{12}P$: C, 60.04; H, 6.69; N, 10.33. Found: C, 59.81; H, 6.72; N, 10.30.

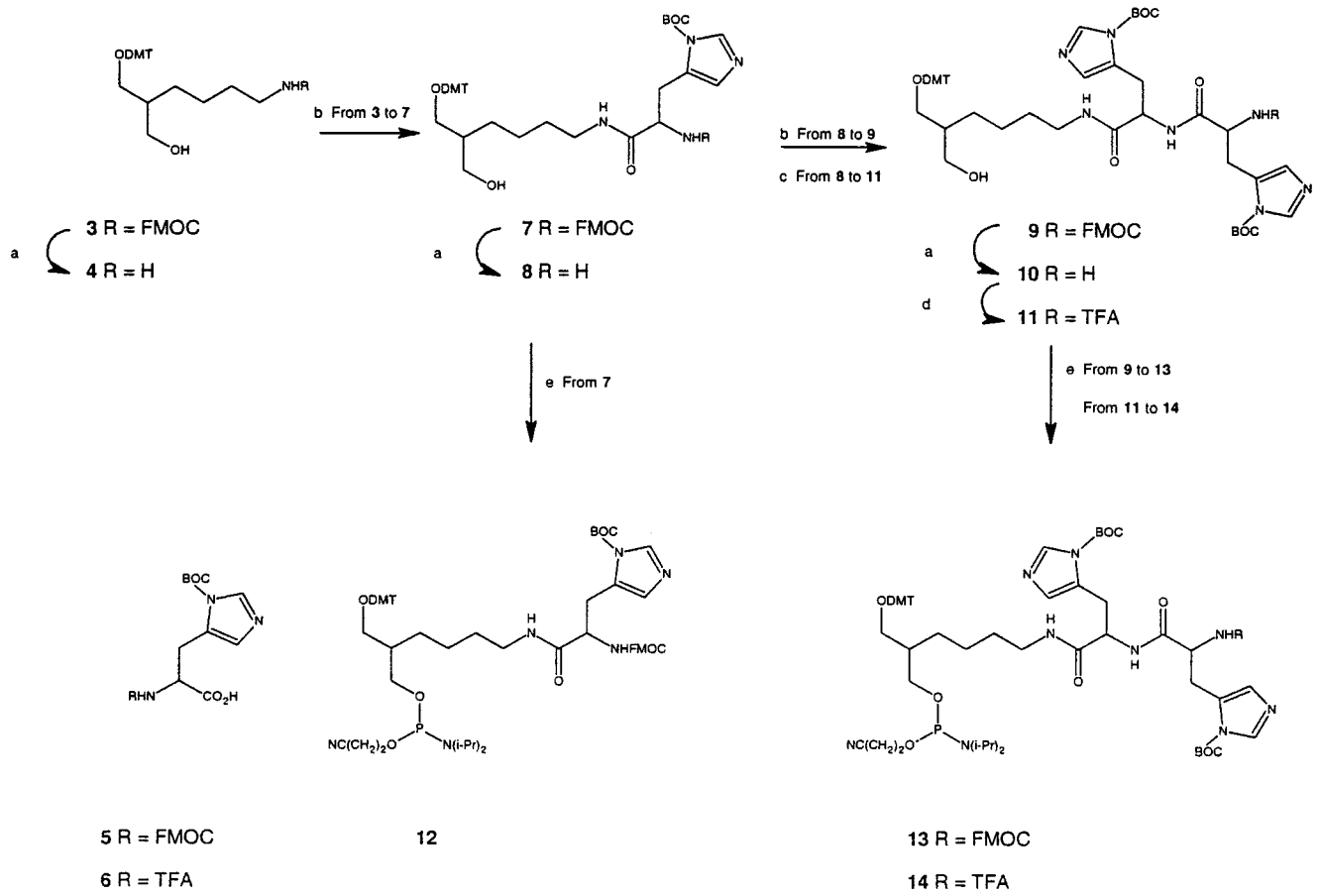
Oligonucleotide Synthesis. Phosphoramidites were used as 0.1 M solutions in acetonitrile in automated DNA synthesis using an Applied Biosystems 394 DNA/RNA synthesizer according to the manufacturer's suggested DNA synthesis protocols on a 1 μmol scale. Coupling efficiencies were measured by using the dimethoxytrityl cation concentration. Deprotection was accomplished with concentrated ammonium hydroxide at 55 °C for 16 h. Purification was accomplished using OPEC columns (CLONTECH Laboratories, Inc.) according to recommended procedures. Oligonucleotides were analyzed by gel electrophoresis (20% PAGE-denaturing) and ion-exchange HPLC (Mono Q column) and in every case demonstrated single band purity.

Ion-Exchange HPLC Analysis. The 5′-modified $(T)_7$ oligonucleotides **15a**−**c** synthesized from phosphoramidite **14** were analyzed by ion-exchange HPLC on a Pharmacia Mono Q HR 5/5 column (5 mm × 5 cm). The mobile phases employed were A = 50 mM Tris (pH 7.5) and B = 800 mM NaCl, 50 mM Tris (pH 7.5). A gradient of 5−45% B over 40 min at a flow rate of 1 mL/min was used.

RESULTS AND DISCUSSION

Reagent Design. A number of factors need to be taken into consideration in the design of an optimal labeling reagent to permit IMAC purification of DNA fragments. Several methods have been reported for the synthesis of oligonucleotide−peptide conjugates (*9*). However, we sought to avoid approaches which required both peptide and oligonucleotide couplings to prepare the desired conjugate. Therefore, we have designed a reagent which incorporates the peptidelike moiety in a form that can be directly utilized in oligonucleotide synthesis. Since introduction during the standard automated synthesis process without extraneous synthetic operations is clearly desirable, the reagent needs to be in the form of a suitably protected phosphoramidite. The nature of the chemical "backbone" which supports the labeling moiety must also be considered. While a 5′-labeling reagent based on 6-aminohexanol or a similar molecule would probably be suitable for many applications, added flexibility would be attained by a bifunctional scaffold which permitted multiple incorporations. For this purpose, we selected the 2-(4-aminobutyl)-1,3-propanediol backbone (*10*), although structures such as allonic acid (*11*, *12*) and others (*13*, *14*) could be considered. The number of imidazole moieties per reagent molecule is yet another issue. While a hexahistidine fragment is popular, and probably optimal (*5*), for protein purification, it has not been shown that the entire fragment is absolutely necessary. It is also unclear whether the optimal tag for protein purification would be the best choice for nucleic acid applications. Also, the molecular weight of a phosphoramidite reagent incorporating a suitably protected hexahistidine fragment

Scheme 1[a]



[a] Reagents: (a) 20% piperidine in toluene; (b) **5**, PyBOP, HOBt, DMF; (c) **6**, NHS, DCC, DCM; (d) $EtOCOCF_3$, TEA, DCM; (e) $NC(CH_2)_2OP(N(i\text{-}Pr)_2)_2$, tetrazole, DCM.

would be rather high, making its performance on the synthesizer and its cost-effective preparation questionable. The synthesis of a reagent incorporating one imidazole moiety should be fairly straightforward. However, in terms of mimicking the possible importance of consecutive histidines in transition metal coordination, such a reagent would offer no advantage over the method developed by Min and Verdine (*7*). We felt that a dihistidine fragment would best address these issues. The benefit of consecutive histidines is retained, and multiple couplings can be used to achieve the optimal number of histidine residues.

Chemistry. The chemistry utilized to prepare the tagging reagents used in this study is outlined in Scheme 1. A major chemical challenge in this problem is the identification of a suitable method for protection of the imidazole nitrogen. The protection of the imidazole ring has long been problematic in synthetic peptide chemistry (*15*). In addition to meeting the needs of peptide synthesis, suppression of side reactions, and racemization, the desired protecting group in this application must survive the conditions of phosphoramidite and oligonucleotide synthesis and yet be removable under mild conditions, preferably without requiring additional operations, after the completion of oligonucleotide synthesis. After considerable experimentation, *t*-butoxycarbonyl (BOC) was found to meet these criteria and appeared to be the best choice for our purposes. It survives the phosphoramidite and oligonucleotide synthesis conditions, and yet it is readily removed during the standard ammonium hydroxide cleavage and deprotection operation. Other possible protecting groups considered included fluorenylmethoxycarbonyl (Fmoc) and 2,4-dinitrophenyl (DNP) which were found to be too labile, and the trityl series which were either too labile as in the case of dimethoxytrityl or too difficult to remove as in the case of trityl.

The Fmoc group of the 2-(4-aminobutyl)-1,3-propanediol synthon **3** (*9*) was removed with piperidine and the resulting amine **4** coupled to N^{α}-Fmoc-N^{im}-Boc-L-His **(*5*)** via the BOP/HOBT procedure to afford **7** in 71% yield. Phosphitylation of this material with 2-cyanoethoxy-*N*,*N*,*N*′,*N*′-tetraisopropylphosphoramidite and tetrazole afforded the monoHis reagent **12** in 78% yield. **7** also serves as an intermediate in the preparation of the diHis reagents. Piperidine treatment to provide **8** followed by BOP-mediated coupling of **5** afforded **9** in 78% yield. Phosphitylation of **9** provided the diHis reagent **13**. Occasionally, we have observed instability with Fmoc-protected alkylamino oligonucleotide synthesis reagents. Such problems can be avoided by the use of N-trifluoroacetyl protection. Therefore, we designed **14**, the N-TFA protected version of the diHis reagent **13**. Exchange of the protecting group of **9** was readily achieved via piperidine Fmoc cleavage followed by reaction of the resulting amine **10** with ethyl trifluoroacetate to afford **11**. Phosphitylation of **11** provided the desired N-TFA-protected diHis reagent **14**. Alternatively, **11** can be obtained in good yield via NHS/DCC mediated coupling of **6** with **8**. The preparation of the protected histidine **6** was straightforward, involving sequential reaction of histidine with ethyl trifluoroacetate followed by di-*t*-butyl dicarbonate. The BOP-mediated coupling, which was successful with **5**, failed using **6** as substrate resulting in extensive racemization. This is not particularly sur-



Figure 2. Polyacrylamide gel electrophoresis analysis of oligonucleotides **16a**−**c** prepared with dihistidyl phosphoramidite **14**. Lane 1: standard 24-mer. Lane 2: 5′-GGCTCTCCAGAACATCCCTGC-3′. Lane 3: 5′-(2H) GGCTCTCCAGAACATCCCTGC-3′ **(16a)**. Lane 4: 5′-$(2H)_2$ GGCTCTCCAGAACATCCCTGC-3′ **(16b)**. Lane 5: 5′-$(2H)_3$ GGCTCTCCAGAACATCCCTGC-3′ **(16c)**.

Table 1. Summary of Ion-Exchange HPLC and MALDI-TOF Mass Spectroscopy Results

oligonucleotide	HPLC retention time (min)	mol. wt. calcd	mol. wt. actual
$(T)_7$	22.8		
15a	19.8	2549.9	2547.7
15b	20.5	3033.4	3032.2
15c	21.3	3516.9	3515.8

prising in view of the known propensity of TFA-protected amino acids to undergo racemization during coupling (*15*). Racemization when using **6** as a substrate was suppressed by utilizing the NHS/DCC coupling procedure.

Oligonucleotide Synthesis. Phosphoramidites **12**−**14** were successfully employed in automated DNA synthesis using a commercial instrument under standard conditions. The performance of the diHis reagents **13** and **14** was equivalent, and subsequent experiments were carried out with the more stable TFA-protected reagent **14**. A series of modified $(T)_7$ oligonucleotides **15a**−**c** were prepared incorporating 1, 2, or 3 additions of **14,** respectively, at the 5′-terminus. These oligos were assayed for purity by ion-exchange HPLC, and their identities confirmed by MALDI-TOF mass spectroscopy. These results are summarized in Table 1. Also prepared using **14** was a series, **16a**−**c**, of longer, 24-mer, mixed oligonucleotides incorporating 1, 2, and 3 additions of **14**. These syntheses also proceeded without incident. While the size of these molecules precluded acquisition of mass spectral data, the resulting oligonucleotides were analyzed by PAGE (Figure 2). This analysis demonstrates the effect of the introduction of multiple histidine residues on oligonucleotide gel mobility. Also demonstrated is the high efficiency with which dihistidyl residues can be incorporated into oligonucleotides with **14**.

IMAC Retention. The retention of the "His-tagged" oligonucleotides **16a**−**c** by a common IMAC matrix, Ni-IDA (iminodiacetic acid), was investigated, and the results were outlined in Figure 3. Samples were applied in denaturing phosphate buffer (pH 8), and the absorbed

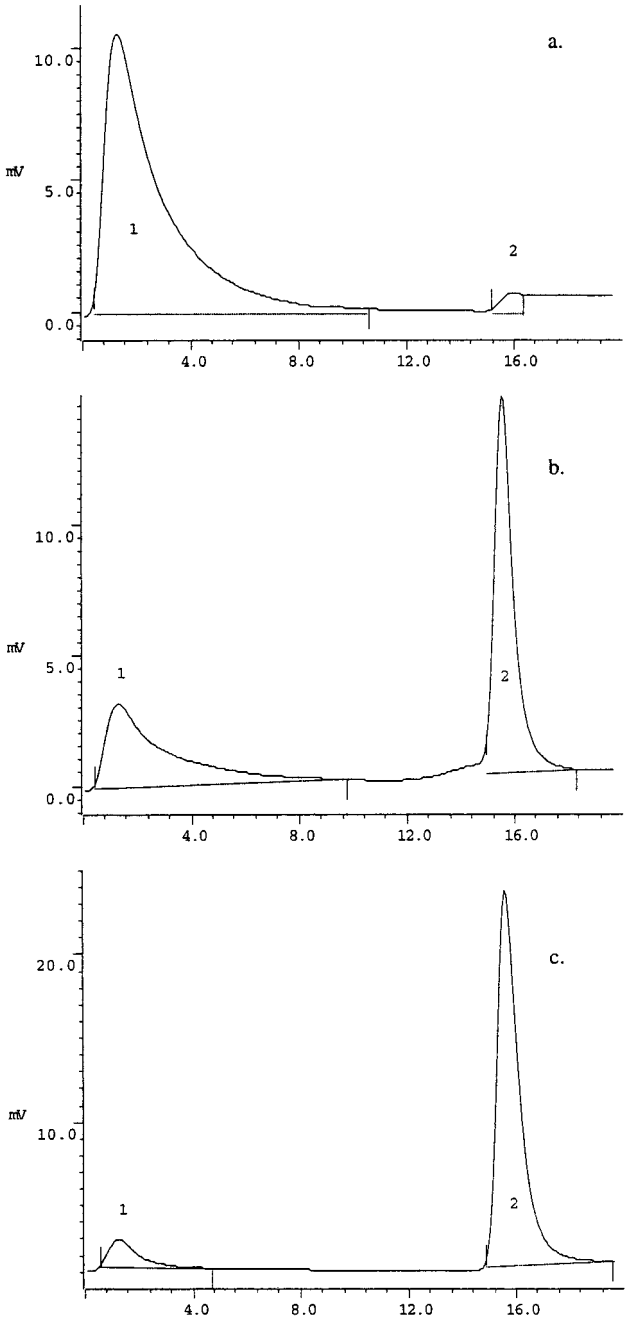


Figure 3. IMAC of 2-, 4-, and 6-His-Oligos (24-mer) (Figure 1) on Ni^{2+}-IDA-Superflow 6. Approximately 1.0 AU (254 nm) was loaded ona 5 × 1 cm.i.d. column packed with IDA-Superflow 6, charged with Ni^{2+} ions and equilibrated with 50 mM sodium phosphate; 0.25 M NaCl; 8.0 M Urea, pH 8.0, at a flow rate of 1 mL/min. The nonadsorbed material was washed out with the equilibration buffer and the adsorbed material was eluted with 150 mM imidazole in the equilibration buffer. a. 2-His-Oligo (24-mer) **16a**. b. 4-His-Oligo (24-mer) **16b**. c. 6-His-Oligo (24-mer) **16c**.

material eluted with 150 mM imidazole. Under these conditions, IMAC retentivity increased with increasing numbers of imidazole residues. Very little of oligonucleotide **16a**, with two His residues, was retained by the matrix while almost all of **16c**, with six His residues, was retained.

Summary. Synthesis of a bifunctional reagent for the incorporation of dihistidyl residues into oligonucleotides has been reported. Any number of dihistidyl residues can be incorporated at any position in the oligonucleotide. Preliminary experiments indicate feasibility of modifying

oligonucleotides with this reagent to permit their purification by IMAC methods. Histidine- or imidazole-containing oligonucleotides are also of interest as artificial nucleases due to the ability of imidazole rings to complex metal ions and cleave nucleic acid chains (*1*, *2*). The reagents reported herein provide a convenient and flexible way to introduce imidazole moieties into oligonucleotides.

LITERATURE CITED

(1) Hovinen, J., Guzaev, A., Azhayeva, E., Azhayev, A., and Lonnberg, H. (1995) Imidazole tethered oligodeoxyribonucleotide: Synthesis and RNA cleaving activity. *J. Org. Chem. 60*, 2205.

(2) Reynolds, M. A., Beck, T. A., Say, P. B., Schwartz, D. A., Dwyer, B. P., Daily, W. J., Vaghefi, M. M., Metzler, M. D., Klem, R. E., and Arnold, L. J. (1996) Antisense oligonucleotides containing an internal, nonnucleotide-based linker promote site-specific cleavage of RNA. *Nucleic Acids Res. 24*, 760.

(3) Porath, J. (1992) Immobilized metal ion affinity chromatography. *Protein Expression Purif. 3*, 263.

(4) Lopatin, S. A., and Varlamov, V. P. (1995) New trends in immobilized metal affinity chromatography of proteins. *App. Biochem. Microbiol. 31*, 221.

(5) Ford, C. F., Suominen, I., and Glatz, C. E. (1991) Fusion tails for the recovery and purification of recombinant proteins. *Protein Expression Purif. 2*, 95.

(6) Orum, H., Nielsen, P. E., Jorgensen, M., Larsson, C., Stanley, C., and Koch, T. (1995) Seauence-specific purification of nucleic acids by PNA-controlled hybrid selection. *BioTechniques 19*, 472.

(7) Min, C., and Verdine, G. L. (1996) Immobilized metal affinity chromatography of DNA. *Nucleic Acids Res. 24*, 3806.

(8) Hochuli, E., Dobeli, H., and Schacher, A. (1987) New metal chelate adsorbent selective for proteins and peptides containing neighbouring histidine residues. *J. Chromatogr. 411*, 177.

(9) Beltran, M., Pedroso, E., and Grandas, A. (1998) A comparison of histidine protecting groups in the synthesis of peptide−oligonucleotide conjugates. *Tetrahedrom Lett. 39*, 4115.

(10) Nelson, P. S., Kent, M., and Muthini, S. (1992) Oligonucleotide labeling methods 3. Direct Labeling of oligonucleotides employing a novel, nonnucleosidic, 2-aminobutyl-1,3-propanediol backbone. *Nucleic Acids Res. 20*, 6253.

(11) Smith, T. H., Kent, M. A., Muthini, S., Boone, S. J., and Nelson, P. S. (1996) Oligonucleotide labeling methods 4. Direct Labeling reagents with a novel, nonnucleosidic, chirally defined 2-deoxy-β-D-ribosyl backbone. *Nucleosides Nucleotides 15*, 1581.

(12) Hovinen, J., and Salo, H. (1997) C-Glycoside phosphoramidite building block for versatile functionalization of oligodeoxyribnucleotides. *J. Chem. Soc., Perkin Trans. 1*, 3017.

(13) Behrens, C., Petersen, K. H., Egholm, M., Nielsen, J., Buchardt, O., and Dahl, O. (1995) A new achiral reagent for the incorporation of multiple amino groups into oligonucleotides. *Bioorg. Med. Chem. Lett. 5*, 1785.

(14) Su, S.-H., Iyer, R. S., Aggarwal, S. K., and Kalra, K. L. (1997) Novel nonnucleosidic phosphoramidites for oligonucleotide modification and labeling. *Bioorg. Med. Chem. Lett. 7*, 1639.

(15) Bodanszky, M. (1993) *Principles of Peptide Synthesis*, 2nd ed. pp 152−157, Springer-Verlag, New York.

BC990002C

Application of Oligo-(14-amino-3,6,9,12-tetraoxatetradecanoic acid) Lipid Conjugates as Steric Barrier Molecules in Liposomal Formulations

Steven M. Ansell,* Ljiljana D. Kojic, Janet S. Hankins, Laura Sekirov, Anthony Boey, Dora K. Lee, Athena R. Bennett, Sandra K. Klimuk, Troy O. Harasym, Nancy Dos Santos, and Sean C. Semple

Inex Pharmaceuticals Corp., 100-8900 Glenlyon Parkway, Burnaby, B.C., V5J 5J8, Canada. Received January 12, 1999; Revised Manuscript Received April 14, 1999

Lipid conjugates of oligo-(14-amino-3,6,9,12-tetraoxatetradecanoic acid) (ATTA*n*) were synthesized as monodisperse analogues of poly(ethylene glycol) (PEG) derivatives used in liposomal drug delivery systems. The new lipids were shown to be at least equivalent to MePEGA-2000-DSPE in assays designed to evaluate the effectiveness of polymers as steric barrier molecules in liposomes. Liposomes containing 1−5% of ATTA8−DSPE (octamer) showed comparable long circulation behavior relative to PEG-2000-DSPE analogues. Surprisingly, the shorter ATTA4−DSPE (tetramer) appeared to be quite effective in reducing clearance. Liver enzyme levels and systemic single dose tolerability of ATTA8−DSPE liposomes were comparable to controls, suggesting that the new materials are nontoxic. Prolonged exposure of ATTA8−DSPE liposomes to splenocytes in vitro showed no evidence of mitogenicity relative to controls or MePEGA-2000-DSPE liposomes. ATTA8−DSPE was as effective as MePEGC-2000-DSPE in preventing complement activation by cationic liposome systems. Repeat dosage in vivo regimes in ICR mice using DSPC/cholesterol liposomes, with and without 5% ATTA8−DSPE and MePEGC-2000-DSPE, showed no evidence of enhanced clearance on successive doses. Splenocytes recovered after repeat doses showed no significant evidence of mitogenicity on restimulation with liposomes. Cellular differentiation and activation marker levels in splenocytes recovered after the fourth in vivo administration were at normal levels. These results suggest that ATTA*n* oligomers do not induce an immune response in isolation. It was demonstrated that ATTA8−DSPE could be used to replace PEG−lipids in the formulation of doxorubicin, plasmid DNA and oligonucleotides using a variety of formulation techniques. The study demonstrates that ATTA*n* oligomers can be safely and effectively used in place of poly(ethylene glycol) as well-defined biomaterials in liposomal applications where reproducible behavior is critical.

INTRODUCTION

Liposomes are currently being developed as drug delivery vehicles for a wide range of pharmaceutically active materials. These include conventional drugs, such as doxorubicin or vincristine, and genetic drugs, such as plasmid DNA or antisense molecules. In many cases, these formulations suffer from aggregation phenomena or rapid clearance in vivo. Poly(ethylene glycol) (PEG) lipid conjugates have been widely used to address some of these issues (*1*, *2*). Incorporation of small amounts of nonexchangeable PEG−lipids into bilayers has a marked effect on the clearance behavior of liposomes. This is believed to be due to a steric barrier effect on the part of the PEG molecules, which results in inhibition of adsorption of proteins to the membrane surface (*3*) and interactions with cells responsible for clearance in vivo (*4*, *5*). Other important applications of PEG−lipids in liposomes include the prevention of cross-linking when conjugating or adsorbing polyvalent entities, such as proteins (*6*) or nucleic acids (*7*), to vesicle surfaces and for attaching targeting vectors, such as proteins (*8*), peptides (*9*), oligosaccharides (*10*), and vitamins (*11*).

We are currently developing liposome drug delivery systems which depend on regulated exchange of PEG−lipids to reveal functional surfaces over time (*7*, *12*−*14*). Liposomes need to be able to release their contents either at the disease site or after cellular uptake in order to be effective as delivery vehicles. In the latter case, we are particularly interested in fusogenic liposomes which are capable of delivering their payloads into the cytoplasm. Much of our recent work has focused on plasmid DNA or antisense oligonucleotides, but similar strategies are also potentially useful for conventional drugs. These fusogenic systems, however, are typically cleared very rapidly in vivo and do not have time to accumulate at many tissue types of therapeutic interest. To address the problem, we include exchangeable PEG−lipids in these formulations that allow reasonable circulation lifetimes but which exchange out of the liposomes after accumulation in the disease tissue, thus allowing the fusogenic systems to function as designed. The PEG−lipids inhibit fusogenic activity and must be removed from the surface to restore functionality. Control of the PEG−lipid exchange process in these dynamic systems is therefore very important.

A major limitation of PEG is the fact that it is comprised of a set of oligomers with a wide range of molecular masses. The exchangeability and steric properties of PEG−lipids are dependent on the length of the PEG group; therefore, it is important that the polydispersity and size distribution be as narrow as possible so as to ensure that the pharmaceutical properties of PEGylated liposomal formulations are consistent. Most

* To whom correspondence should be addressed. E-mail: sansell@inexpharm.com. Phone: (604) 419-3200. Fax: (604) 419-3201.

10.1021/bc990005p CCC: $18.00 © 1999 American Chemical Society
Published on Web 05/29/1999

commercially available PEG has wide polydispersity and is available only in a few average molecular masses. Polydispersity generally results in the oligomer distribution being skewed to lower molecular masses. These factors make it difficult to determine the structural requirements of PEG−lipids for optimal liposome performance, particularly in applications where complete exchange of the PEG−lipid is required since residual low molecular mass oligomers are likely to exchange significantly more slowly than the mean. An additional problem relates to the inherent variability in the average molecular mass of each batch of polymer; for example, commercial PEG-2000 has been shown to comprise of a mixture of oligomers, of which 67% falls in the range 1600−2400 Da (*1*). The remaining material falls outside of this molecular mass range, most likely primarily at the lower end. This is an undesirable characteristic when trying to develop a reproducible pharmaceutical product based on our technology.−

We have recently developed a set of polyamide oligomers based on 14-amino-3,6,9,12-tetraoxatetradecanoic acid (ATTA*n*)[1] to address these issues (*15*). These compounds were designed to mimic the activity of PEG in liposomal formulations as well as in other applications. Our intent was to devise a process whereby we could rapidly generate a library of well-defined PEG mimics that might or might not incorporate additional functionality as the need arose. Since these compounds are not polymers, they can be used as tools (when suitably labeled) to determine the performance characteristics required to optimize a particular liposome application and will not cause batch variations when used in our applications.

This work describes the synthesis of some ATTA*n* lipid conjugates and evaluates their application in simple liposomal systems in comparison to existing PEG analogues. This was important since we first had to show that ATTA*n* was equivalent to PEG in current applications before we could develop more sophisticated applications based on ATTA*n*. Consequently, we have demonstrated that these new lipid conjugates are at least as effective as PEG−lipids as steric barrier molecules and could be used to replace PEG−lipids in current liposome based drug formulations. The toxicity and immunogenicity of ATTA*n*−lipid conjugates in liposomes is obviously critical. We show that these lipids do not induce an appreciable immune response, and do not cause any discernible gross toxicity.

EXPERIMENTAL METHODS

General. MePEGA-2000-DSPE (*16*) and **2**, **20**, and **25** (*15*) were synthesized as previously described. All reagents were obtained from Sigma-Aldrich, except for phospholipids (Northern Lipids, Vancouver); MePEGC-2000-DSPE (Avanti Polar Lipids, Alabaster); and Picogreen (Molecular Probes). AL-1 was purchased as the free base from Avanti (DODAP) and converted to the hydrochloride salt by a series of hydrochloric acid/saline washes. MePEGS-2000-Mcer and DODAC were obtained from Inex Pharmaceuticals Corp., Vancouver. [^{3}H]Cholesterylhexadecyl ether was obtained from NEN, Boston. Female Balb/c and ICR mice (6−8 weeks old) were obtained from Harlan Sprague Dewley (Indianopolis). Mice were provided food and water ad libidum. All studies involving animals were conducted in accordance with the guidelines established by the Canadian Council on Animal Care (CCAC).

***N*-(*ω*-Azido-tetra-(14′-amino-3′,6′,9′,12′-tetraoxatetradecanoyl))-1,2-distearoyl-sn-3-phosphoethanolamine 1.** Compound **1** was synthesized from **25** using the procedure described previously for **2** (*15*). Isolated as a colorless powder after lyophilization. ^{1}H NMR ($CDCl_3$): δ 5.17 (bs, 1H), 4.33 (dd, 1H), 4.12 (dd, 1H), 3.8−4.05 (m, 12H), 3.4−3.8 (m, 64H), 3.35 (t, J = 5 Hz, 2H), 2.26 (m, 4H), 1.55 (bs, 4H), 1.22 (s, 56H), 0.85 (t, J = 7.5 Hz, 6H).

Synthesis of Dimyristylamine 23. A solution of myristic acid (5 g) in benzene (40 mL) was treated with oxalyl chloride (2.5 mL) for 2 h. The solvent was removed on a rotovap and the residue dissolved in benzene (20 mL). A solution of tetradecylamine **21** (2.5 g) in benzene was added. The solution was warmed to 60 °C, stirred and treated with Et_3N (1 mL, slow addition). The reaction mixture was then allowed to stir at room-temperature overnight. The suspension was diluted with water, acidified and extracted with methylene chloride. The organic phase was dried over magnesium sulfate and the solvent removed under vacuum. The residue was passed down a silica gel column in order to remove any unreacted **21**, yielding **22** (2 g) as a colorless solid. The product was suspended in ether and treated with excess $LiAlH_4$ (added slowly until vigorous evolution of gas ceased). The mixture was stirred at room temperature for 1 h. Methanol was then slowly added, followed by water and finally enough dilute hydrochloric acid to acidify the mixture. The suspension was extracted with methylene chloride (the precipitate suspends in the organic phase) and the combined organic phases washed with aqueous sodium hydroxide. Column chromatography yielded **23** as a white powder (1.86 g). ^{1}H NMR ($CDCl_3$): δ 2.55 (t, J = 7.1 Hz, 6H), 1.45 (m, 4H), 1.23 (s, 44H), 0.85 (t, J = 6.7 Hz, 6H). Anal. ($C_{28}H_{58}N$) calcd: C; H; N, 14.30. Found: C; H; N, 13.72.

Synthesis of *N*-(*ω*-azido-octa-(14′-amino-3′,6′,9′,12′-tetraoxatetradecanoyl))-dimyristylamine 3. A solution of **20** (1.04 g) in methylene chloride (20 mL) was treated with NHS (0.10 g) and DCC (0.12 g) at room temprature for 1 h. The solution was filtered and added to a solution of **23** (0.30 g) in methylene chloride (20 mL). Triethylamine (10 drops) was added and the reaction mixture allowed to stir for half an hour. The solution was then washed with dilute hydrochloric acid. The combined organic fractions were dried under vacuum and the residue redissolved in water, filtered, and extracted with methylene chloride. Column chromatography yielded **3** as a colorless oil (0.62 g). ^{1}H NMR ($CDCl_3$): δ 7.2 (bs, ∼7H), 4.16 (s, 2H), 3.98 (s, 14H), 3.1−3.7 (m, 132H), 2.2 (bm, 10H), 1.49 (bs, 4H), 1.23 (s, 44H), 0.85 (t, J = 6.4 Hz, 6H). Anal. ($C_{108}H_{209}O_{40}N_{11}$) calcd: C, 56.35; H; N. Found: C, 55.43; H; N.

Dipalmitylamine 24. Compound **24** was synthesized from hexadecylamine using the method described for **23**. Isolated as a white powder. ^{1}H NMR ($CDCl_3$): δ 2.57 (t, J = 7.1 Hz, 6H), 1.47 (m, 4H), 1.23 (s, 52H), 0.86 (t, J =

[1] Abbreviations: VBS, veronal-buffered saline; HBS, Hepes-buffered saline; NHS, *N*-hydroxysuccinimide; DCC, *N*,*N*-dicyclohexylcarbodiimide; DSPC, 1,2-distearoyl-*sn*-glycero-3-phosphocholine; POPC, 1-oleoyl-2-palmitoyl-*sn*-glycero-3-phosphocholine; chol, cholesterol; MePEGA-2000-DSPE, *N*-(2′-*O*-(*ω*-monomethoxypoly(ethylene glycol)$_{2000}$)hydroxyacetoyl)-1,2-distearoyl-*sn*-glycero-3-phosphoethanolamine; MePEGC-2000-DSPE, *N*-(*ω*-monomethoxypoly(ethylene glycol$_{2000}$)carbonyl)-1,2-distearoyl-*sn*-glycero-3-phosphoethanolamine; SBL, steric barrier lipid; ATTA*n*, *ω*-azido-oligo(14-amino-3,6,9,12-tetraoxatetradecanoic acid); AL-1, *rac*-N, *N*-dimethyl-*N*-(2′,3′-dioleoyloxypropyl)-ammonium chloride.

6.6 Hz, 6H). Anal. ($C_{32}H_{66}N$) calcd: C, 83.04; H, 13.94; N. Found: C, 82.46; H, 14.79; N.

***N*-(*ω*-azido-octa-(14′-amino-3′,6′,9′,12′-tetraoxatetradecanoyl))di(hexadecyl)amine 4**. Compound **4** was synthesized from **24** using the method described for **3**. Obtained as a colorless oil. ^{1}H NMR ($CDCl_3$): δ 7.2 (bs), 4.17 (s, 2H), 3.99 (s, 14H), 3.1−3.7 (m, 132H), 1.49 (bm, 4H), 1.22 (s, 52H), 0.85 (t, J = 6.52 Hz, 6H). Anal. ($C_{112}H_{217}O_{40}N_{11}$) C; H; N.

Synthesis of rac-3-(*N*-BOC)-aminopropan-1,2-diol 13. *rac*-Glycidol **11** (15 g) was treated with concentrated ammonia (150 mL) overnight. The solvent was removed on a rotovap, and the residue dried by azeotropic removal of water using ethanol. A solution of the residue in ethanol was treated with *tert*-butoxypyrocarbonate (35 g) and thriethylamine (20 mL) for 4 h at room temperature. Workup followed by column chromatography yielded **13** as a colorless oil which slowly crystallized on standing. The resultant solid was dried under vacuum, yielding **13** as a colorless crystalline solid (22 g). ^{1}H NMR ($CDCl_3$): δ 5.39 (m, 1H), 4.08 (m, 1H), 3.94 (m, 1H), 3.70 (m, 1H), 3.52 (m, 2H), 3.17 (m, 2H), 1.40 (s, 9H).

Synthesis of *N*-*tert*-butoxycarbonyl-1,2-*rac*-dimyristoyloxypropyl-3-amine 14. A suspension of myristic acid (3.0 g) in benzene (50 mL) was treated with oxalyl chloride (1 mL), with occasional warming, until all of the solid was dissolved and gas evolution had largely ceased. The solvent and excess oxalyl chloride was removed on a rotovap. The residue was dissolved in benzene (50 mL) and treated with **13** (0.86 g), followed by triethylamine (1 mL). The mixture was then allowed to stir at room-temperature overnight. Workup, followed by column chromatography, yielded **14** (1.38 g) as a colorless powder. ^{1}H NMR ($CDCl_3$): δ 5.07 (m, 1H), 4.73 (m, 1H), 4.25 (dd, J = 4.1 Hz, J' = 11.9 Hz, 1H), 4.10 (dd, J = 5.7 Hz, J' = 11.9 Hz, 1H), 3.33 (bs, 2H), 2.29 (t, J = 7.3 Hz, 4H), 1.59 (bm, 4H), 1.42 (s, 9H), 1.24 (s, 44H), 0.86 (t, J = 6.5 Hz, 6H). Anal. ($C_{36}H_{69}O_6N$) calcd: C; H, 11.37; N. Found: C; H, 11.78; N.

***N*-*tert*-butoxycarbonyl-1,2-*rac*-dipalmitoyloxypropyl-3-amine 15**. A colorless powder (1.06 g) synthesized as for **14** from palmitic acid (3.28 g). ^{1}H NMR ($CDCl_3$): δ 5.07 (m, 1H), 4.73 (m, 1H), 4.25 (dd, J = 4.1 Hz, J' = 11.9 Hz, 1H), 4.10 (dd, J = 5.7 Hz, J' = 11.9 Hz, 1H), 3.33 (bs, 2H), 2.29 (t, J = 7.3 Hz, 4H), 1.59 (bm, 4H), 1.42 (s, 9H), 1.24 (s, 48H), 0.86 (t, J = 6.5 Hz, 6H). Anal. ($C_{40}H_{77}O_6N$) calcd: C; H, 11.62; N. Found: C; H, 12.07; N.

***N*-*tert*-butoxycarbonyl-1,2-*rac*-distearoyloxypropyl-3-amine 16**. A colorless powder (1.38 g) synthesized as for **14** from stearic acid (3.00 g). ^{1}H NMR ($CDCl_3$): δ 5.06 (m, 1H), 4.72 (m, 1H), 4.25 (dd, J = 4.1 Hz, J' = 11.9 Hz, 1H), 4.09 (dd, J = 5.6 Hz, J' = 11.9 Hz, 1H), 3.32 (bs, 2H), 2.28 (t, J = 7.4 Hz, 4H), 1.58 (bm, 4H), 1.41 (s, 9H), 1.24 (s, 56H), 0.85 (t, J = 6.5 Hz, 6H). Anal. ($C_{44}H_{85}O_6N$) calcd: C; H, 11.83; N. Found: C; H, 11.16; N.

General Synthesis of *N*-(*rac*-2′,3′-diacyoloxypropyl)ammonium Triflouroacetate 17−19. Compound **14−16** (∼0.90 g) was treated with neat TFA (5 mL) for 1 h. The solvent was removed on a rotovap and the residue recrystallized from ethanol, yielding **17−19** as fine colorless needles (84 g). **14** (0.90 g), **15** (0.90 g), and **16** (0.81 g) yielded **17** (0.84 g), **18** (0.85), and **19** (0.74 g), respectively.

Synthesis of *N*-(*ω*-azido-octa-(14′-amino-3′,6′,9′,12′-tetraoxatetradecanoyl))-*rac*-1′,2′-dimyristoyloxypropyl-3-amine 5. A solution of **20** (1.05 g) in methylene chloride was treated with NHS (0.136 g) and DCC (0.133 g) at room temperature for 1 h. The solution was filtered and treated with **17** (0.37 g) and triethylamine (0.5 mL) at room temperature for half an hour. Following workup, **5** was isolated as a colorless oil (0.65 g) after column chromatography. ^{1}H NMR ($CDCl_3$): δ 5.10 (m, 1H), 4.20 (dd, J = 3.4 Hz, J' = 12 Hz, 1H), 4.06 (dd, partially hidden, J = 6.1 Hz, J' = 12 Hz, 1H), 3.95 (s, 16H), 3.2−3.8 (m, 130H), 2.25 (t, J = 7.5 Hz, 4H), 1.44 (m, 4H), 1.20 (s, 40H), 0.82 (t, J = 6.6 Hz, 6H). Anal. ($C_{121}H_{211}O_{44}N_{11}$): C; H; N.

***N*-(*ω*-azido-octa-(14′-amino-3′,6′,9′,12′-tetraoxatetradecanoyl))-*rac*-1′,2′-dipalmitoyloxypropyl-3-amine 6**. Compound **6** was synthesized from **18** (0.39 g, 0.121 g NHS, 0.133 g of DCC, 1.01 g of **20**) in the same way as **5**, yielding **6** as a colorless oil (0.80 g). ^{1}H NMR ($CDCl_3$): δ 5.10 (m, 1H), 4.20 (dd, J = 3.4 Hz, J' = 12 Hz, 1H), 4.1 (dd, partially hidden, J = 6.1 Hz, J' = 12 Hz, 1H), 3.99 (s, 16H), 3.2−3.8 (m, 130H), 2.27 (t, J = 7.4 Hz, 4H), 1.57 (m, 4H), 1.22 (s, 48H), 0.84 (t, J = 6.2 Hz, 6H). Anal. ($C_{125}H_{219}O_{44}N_{11}$) C; H; N.

***N*-(*ω*-azido-octa-(14′-amino-3′,6′,9′,12′-tetraoxatetradecanoyl))-*rac*-1′,2′-distearoyloxypropyl-3-amine 7**. Compound **7** was synthesized from **19** (0.43 g, 0.113 g of NHS, 0.133 g of DCC, 1.07 g of **20**) in the same way as **5**, yielding **7** as a colorless wax (0.80 g). ^{1}H NMR ($CDCl_3$): δ 5.10 (m, 1H), 4.20 (dd, J = 3.4 Hz, J' = 12 Hz, 1H), 4.08 (dd, partially hidden, J = 6.0 Hz, J' = 12 Hz, 1H), 3.98 (s, 16H), 3.2−3.8 (m, 130H), 2.28 (t, J = 7.5 Hz, 4H), 1.57 (m, 4H), 1.22 (s, 56H), 0.85 (t, J = 6.5 Hz, 6H). Anal. ($C_{129}H_{227}O_{44}N_{11}$) C; H; N.

Preparation of Liposomes. Unless otherwise specified, liposomes were prepared as described by Hope et al. (*17*). Briefly, lipid mixtures of the appropriate composition were dissolved in chloroform and concentrated to a homogeneous film under a nitrogen stream in a warm water bath. The film was then dried overnight on a lyophilizer. The dried lipid was hydrated in HBS and extruded through stacked polycarbonate 100 nm filters (Nucleopore) using a previously dried extrusion press device (Lipex Biomembranes, Inc., Vancouver, Canada) at room temperature. The filters were inspected after extrusion to ensure that all of the lipid was in the liposome solution. Lipid concentrations were assumed by extrapolation from the original mass of lipid and volume of buffer.

In Vivo Immunogenicity. Female Balb/c mice (6−10 weeks old, 12 per group) were injected intravenously (i.v.) with 200 μL of 5 mM lipids [HBS control; DSPC/chol (55:45); DSPE/chol/MePEGA-2000-DSPE (50:14:5); DSPC/chol/ATTA8−DSPE (50:45:5)]. Four injections were given (at intervals of 7 days) over a period of 3 weeks. A group of mice injected with 200 μL of diluent over the course of administration served as a baseline control. Three mice from each group were sacrificed 24 h after each lipid administration. Spleens were harvested and assayed for lipid-specific clonal expansion (mitogenicity assay below) and cytokine release (ELISA assay below). The phenotypic profiles of the recovered cells were analyzed by measuring the expression of differentiation (CD22, CD4, CD8, and CD11b) and activation (CD25, CD54, CD86, Ly6A/E, MHC−II) markers. Spleen cells (1×10^6) were stained with appropriate PE-conjugated antibodies (PharMingen, CA), and phenotypic analysis was performed on a FACSsort flow cytometer (Becton Dickinson, CA).

Mitogenicity Assay. The mitogenicity of liposomes was evaluated by measuring the cellular immune response following stimulation of primary immune cells in vitro. Splenocytes from 8 week old Balb/c untreated mice

were used in the cell proliferation assay. Splenocytes were tested for their ability to proliferate upon in vitro stimulation with liposomes or with polyclonal activators for T (Concanavalin A; Con A) and B cells (Lipopolysaccharide, LPS). Single-cell suspensions of lymphocytes were prepared from whole spleens in complete RPMI medium, supplemented with 5% heat-inactivated fetal bovine serum (FBS). Viability of cells was examined by trypan blue dye exclusion and exceeded 95% viability. Cells were counted on a Coulter Counter and were adjusted to a density of 5×10^6/mL. Volumes 100 μL of the cell suspensions were placed into triplicate flat-bottom wells of 96-well plates along with equal volumes of the appropriate liposomes. Cells were labeled with 1 μCi/well of [^{3}H]thymidine for 48 h after incubation for 3 days with the test solutions (37 °C, 5% CO_2). Cells were harvested on glass filters (Skatron harvester) and levels of incorporated radioactivity were measured in a beta scintillation counter (Beckman, LS 6500). Appropriate controls (mitogens or medium alone) were set up on each plate.

Cytokine ELISA Assays. Splenocytes (1×10^6 cells/mL) were cultured in either the presence or the absence of various concentrations of lipids in 24-well plates. The supernatants were collected at different times after culture initiation (24 and 48 h), and the levels of cytokine release (Interleukin-2 and Interleukin-4) were determined by ELISA assays using antibodies provided by reagent mini-kit from Endogen (Endogen, MA.). Briefly, 96-well Immulon II plates were coated overnight with anti-IL-2 or anti-IL-4 antibody. Plates were washed with PBS-Tween 20 (0.05%) and blocked with PBS/BSA (2%) for 1 h at room temperature. Supernatant samples and standards (diluted in blocking buffer), were added and allowed to incubate overnight. Plates were washed and biotinylated anti-IL-2, or anti-IL-4 antibody, was added. After 2 h of incubation, the plates were washed, and HRP-extravidin, followed by TMB, was added to each well. Plates were read at OD_{450}. The amount of cytokine was determined by comparing the OD of test supernatants to a standard curve constructed from OD of serially diluted cytokine standards.

Complement Activation Assay. Activation of the complement system by cationic lipid vesicles was assessed using a two step complement consumption assay as previously described (*18*, *19*). Briefly, liposomes containing various SBL were prepared in VBS (20 mM, pH 7.50) and extruded through two stacked 100 nm polycarbonate filters using an extrusion apparatus (Lipex Biomembranes, Vancouver, Canada). Serial dilutions of the lipid vesicles (100 μL aliquoted volume) were added to an equal volume of 5×-diluted normal human serum and incubated for 30 min at 37 °C. Samples were subsequently diluted with 300 μL of ice-cold DGVB2+. Aliquots (100 μL) were incubated with an equal volume of hemolysin-sensitized sheep red blood cells (2×10^7 cells) for 30 min at 37 °C. At the end of the incubation, EDTA-GVB (1 mL) was added to the sample to inhibit further complement activity. Samples were centrifuged at 1500 rpm for 5 min at 4 °C to remove cells. The supernatant was then analyzed for hemoglobin content at 410 nm using a 96-well plate reader. All samples and reagents were maintained at 4 °C throughout the assay procedure unless otherwise noted. Hemolysin-sensitized sheep erythrocyte target cells and normal human serum pool, prepared from the blood of 10 healthy male and 10 healtlthy female donors, were prepared as previously described (*18*).

In Vitro Cytotoxicity. Various cell lines (all obtained from ATCC) were grown as monolayer cultures in T-75 flasks. The cells were subcultured twice a week at 37 °C in an atmosphere containing 5% CO_2 and maintained at a low passage number (5−10). The cells used in the assay were plated at 1×10^4 cells/well (inoculation volume, 100 μL/well) and left for 24 h at 37 °C to resume exponential growth. An equal volume (100 μL) of either complete culture medium (control wells) or test solution containing twice the final ATTA8 concentration diluted to volume with complete culture medium was added 24 h later. Final ATTA8 concentrations ranged from between 5 and 1000 μM. Eight replicate wells for each test concentration were used. Cytotoxicity was evaluated 24 h later by means of the Crystal Violet assay (*20*). Data were expressed as a percentage of control optical density.

In Vivo Tolerability of Polymer Modified Cationic Liposomes. Female, ICR mice, 6−8 weeks old, were used for tolerability studies. Each time group consisted of at least 4 mice. The plasma circulation levels of DSPC:CHOL:AL-1:ATTA8−DSPE (20:45:25:10) and DSPC:CHOL:AL-1:MePEGS-2000-Mcer (20:45:25:10) liposomes (prepared as described for in the *antisense formulation* section) containing a radiolabeled lipid marker, [^{3}H]cholesterylhexadecyl ether, were evaluated at 24 h post administration. Mice received a single bolus dose of liposomes up to 750 mg/kg via intravenous administration in the lateral tail vein. At 24 h, mice were anesthetized with halothane and blood was collected into EDTA tubes after cardiac puncture. Mice were then terminated by cervical dislocation. Plasma levels of lipid were determined by standard liquid scintillation techniques. Plasma volumes were estimated to be 5% of total body weight. Tolerability of increasing doses of DSPC:CHOL:AL-1:ATTA8−DSPE (20:45:25:10) and DSPC:CHOL:AL-1:MePEGS-2000-Mcer (20:45:25:10) was evaluated by monitoring changes in tissue weights and enzymes typically associated with liver damage. At 24 h postinjection, tissues were excised, trimmed of fat, and weighed on an analytical balance. An aliquot of the collected blood was placed in a serum tube and allowed to clot for 30 min at room temperature, and the serum was assayed kinetically for alanine aminotransferase (ALT), aspartate aminotransferase (AST), and lactate dehydrogenase (LDH) using a Vitros DT60II analyzer with a DTSCII module (Johnson & Johnson).

Encapsulation of Doxorubicin. Liposomes (25 mM) were prepared in citrate buffer (300 mM citric acid, pH 4.0). Aliquots (100 μL) were added to sodium citrate buffer (300 mM sodium citrate, pH 8.0; 356 μL). An aliquot (43.5 μL) from a stock solution of doxorubicin hydrochloride (10.0 mg/mL) was immediately added. Aliquots (10 μL) of potassium hydroxide solution (1 N) were added until the red color turned purple. The solutions were then warmed in a water bath at 60 °C for a few minutes with occasional shaking until the solutions turned dark red. The liposome suspensions were immediately passed down Sephadex G-50 columns (HBS, pH 7.4) to exchange buffer and remove any external doxorubicin. Doxorubicin content was assayed at 480 nm against a standard curve after lysis in 1% (net) Triton X-100. Lipid content was determined using a phosphate assay as previously described (*21*).

Picogreen Assay. A picogreen working solution was prepared by diluting 1 μL of stock solution/mL of HBS. A DNA standard solution was prepared at 20μg/mL in water. DNA standards (0−50 μL) and lipid/DNA samples (3 μL) were added to tubes. Picogreen working solution (3 mL) was added to each tube and the fluorescence

recorded (T_0) at 520 nm using excitation at 480 nm. Triton X-100 (10%, 30 μL) was then added, and the flourescence recorded again (T_f). Entrapped DNA was calculated using the standard curve or with the equation %DNA trapped = $100(1 - T_0/T_f)$.

Antisense Formulation. A stock solution of lipid (DSPC/chol/AL-1/SBL, 20:45:25:10 mol ratio, 13 μmol of total lipid) in ethanol (0.4 mL) was slowly added to a solution of 22 mer c-myc antisense DNA (0.6 mL, 2 mg/mL in citrate buffer, 300 mM, pH 4) at 65 °C with constant vortexing. The mixture was extruded through two 100 nm filters at 65 °C as described above. The liposomes were dialyzed (3500 MW cutoff SpectraPor membrane) against citrate buffer (300 mM citrate, pH 4.0, 4000 mL) for 1−2 h against HBS (pH 7.4, 4000 mL) overnight and then passed down a DEAE Sepharose CL-6B column (3 mL in HBS). The lipid content was analyzed by HPLC. Antisense DNA content was determined after dispersion in water/chloroform/methanol (10 μL of sample in 250 μL of water, followed by addition of 750 μL of 2:1 chloroform/methanol and 100 μL of methanol) at 260 nm using the equation [DNA] (mg/mL) = A_{260}/29.6. Vesicle sizes were determined using a Nicomp model 370 particle sizer. The formulation was scaled up on a proportional basis when larger quantities were required.

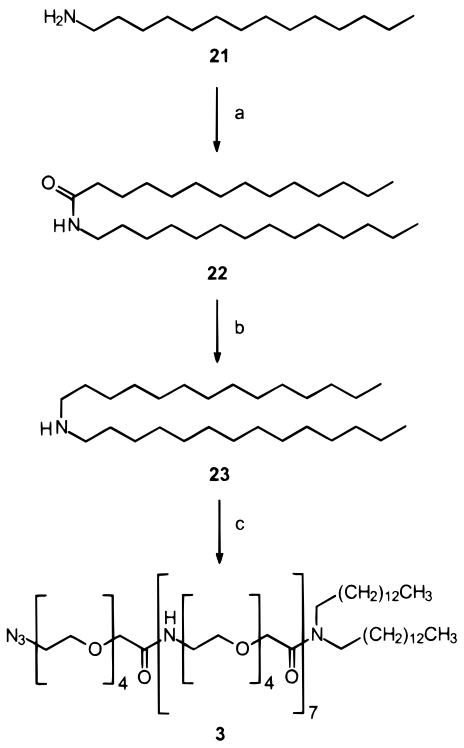
RESULTS AND DISCUSSION

Chemistry. The ATTA*n* oligomers (n = 4, 8) used to prepare the lipid conjugates in this study were synthesized as described elsewhere (*15*). The ethyl protecting group of ATTA*n* was deprotected by mild alkaline hydrolysis followed by acidification and extraction of the acid. It was necessary to ensure that the pH did not drop below 2 during the extraction step, since the amide bonds become protonated under very low pH conditions and the oligomer becomes too hydrophilic to extract into organic phases. The crude free acid was activated with DCC/NHS and conjugated to various amino lipids using procedures similar to those used in the preparation of PEG−lipids (*16*). The amino lipids included phosphatidylethanolamines (DSPE), dialkylamines (**23** and **24**), and 2,3-diacyloxypropylamines (**17**, **18**, and **19**).

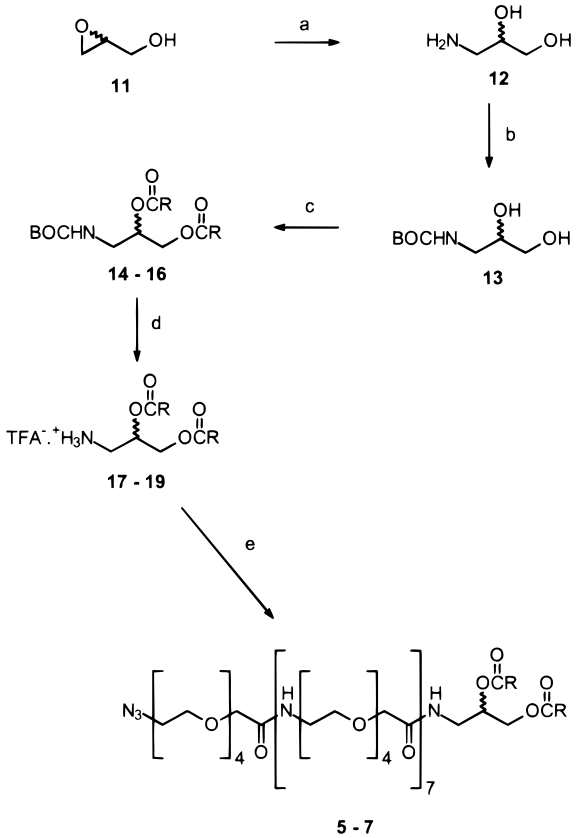
The dialkylamines were synthesized by acylating a primary alkylamine with the corresponding acyl chloride, followed by reduction with $LiAlH_4$ (Scheme 1). This procedure worked reasonably well in the synthesis of **23** and **24**, provided that any residual primary amine was removed prior to the reduction step. Difficulties were experienced when trying to prepare the C-18 analogue distearylamine. These appeared to stem primarily from the limited solubility of the saturated C-18 intermediates under the reaction conditions used. The problem can be solved by synthesizing dioleylamine instead and then hydrogenating it, either before or after conjugation to the ATTA*n* oligomer.

Compounds **17**−**19** were synthesized as shown in Scheme 2. Glycidol was ring opened using aqueous ammonia. Removal of water followed by BOC protection of **12** and column chromatography yielded the common precursor **13** in reasonable yield. The work was conducted using *rac*-glycidol, but we have prepared the R and S isomers as well since the relevant glycidol precursors are readily available from commercial sources. **13** was acylated with the appropriate acid chlorides and deprotected using neat TFA. The TFA salts had low solubility in most organic solvents at room temperature and could be purified easily by recrystalization. The amine should be stored as the salt form since the free base readily rearranges to the N-acyl analogue.

Scheme 1. Reagents: (a) Myristoyl Chloride, Et_3N; (b) $LiAlH_4$, Et_2O; (c) 20 NHS Ester, Et_3N, CH_2Cl_2



Scheme 2. Reagents: (a) Conc. NH_3; (b) *tert*-butoxypyrocarbonate, Et_3N, EtOH; (c) Acyl Chloride, Et_3N, CH_2Cl_2; (d) TFA; (e) 20 NHS Ester, Et_3N, CH_2Cl_2



Formulation Characteristics. We attempted to formulate the ATTA*n*−lipid derivatives in liposomes either

by inclusion in the lipid mixture prior to vesicle preparation or by exchange into preformed vesicles. Previous studies (*22*) have shown that PEG−lipid micelles undergo almost complete inclusion at subsaturation concentrations in vesicles at temperatures above the membrane phase transition after 1 h. The obvious advantage to the exchange approach is the short preparation time required to make a range of liposomes with various "steric barrier lipid" (SBL) concentrations. In addition, parameters such as vesicle size and lipid composition can be kept constant in this type of experiment. Experiments were also conducted using liposomes prepared with the polymer−lipid included prior to hydration. Incorporation before preparation results in vesicles with polymer associated with both leaflets whereas exchange results in association with the outer leaflet only. Obviously, this difference may cause problems at high polymer concentrations due to the induced asymmetry of the bilayer, however, these effects are likely to be minimal at the polymer−lipid levels used in most applications.

In practice the exchange method caused considerable problems since it appeared that the lipid did not always fully exchange into the vesicles. For example, aggregation was observed in antibody-coupling experiments, both for PEG−lipids and ATTA*n*−lipids. In addition, studies looking at the effect of polymer−lipid concentration (0−5% MePEGA-2000-DSPE; 0−5% ATTA8−DSPE or 0−10% ATTA4−DSPE) on liposome clearance yielded results which contradicted earlier studies (*15*) in that ATTA*n*−DSPE ($n = 4, 8$) was relatively ineffective compared to MePEGA-2000-DSPE. The difference between preformulated and exchanged ATTA*n*−DSPE was confirmed in this work when the experiments were repeated using the equivalent preformulated compositions. MePEGA-2000-DSPE behaved in much the same way in both sets of experiments, implying that the ATTA*n*−DSPE micelles were more stable in solution. The reasons for this behavior are not clear. All experiments reported in this work, unless denoted otherwise, were performed using preformulated compositions as a result of these observations. The term "steric barrier lipid" (SBL) is used in this work as a general term for the ATTA*n*−lipids and PEG−lipids.

Evaluation of Effectiveness as Steric Barriers. Polymers bound to the surface of liposomes act as steric barriers which inhibit interactions between the membrane surface and the environment. Many of the applications which use PEG−lipids rely on this property. For example, PEG bound to the membrane surface inhibits aggregation of liposomes during the preparation of protein−liposome conjugates (*6*) or polyanion−cationic lipid complexes (*13*). PEG also inhibits the adsorption of molecules, such as serum proteins, onto vesicle surfaces (*23*). The steric barrier effect is believed to be very important in protecting liposomes from rapid clearance in vivo (*24*). We therefore undertook a number of studies designed to evaluate the equivalence of the ATTA*n*−lipid and PEG−lipid conjugates in terms of their effectiveness as steric barrier molecules.

We are particularly interested in the development of cationic lipid based formulations of nucleic acids. Cationic liposomes are toxic to erythrocytes since the cationic lipids rapidly exchange into the anionic erythrocyte membrane on contact (*25*) and induce lysis (*26*). Polymers such as PEG inhibit this process when attached to the liposome surface as a result of steric interactions which prevent contact between the two membranes. The phenomena can be used as a crude assay to evaluate the potential of new SBLs under development as steric barrier molecules for situations where liposomes are exposed to cellular membranes in physiological ionic strength solutions.

DODAC/POPC (50:50) vesicles with and without 10% ATTA8−DSPE, MePEGA-2000-DSPE and MePEGS-2000-Mcer were incubated with erythrocytes at various concentrations (Figure 2). As expected, the unprotected vesicles induced lysis in a dose-dependent manner. Similar behavior was observed with MePEGS-2000-Mcer compositions, since that lipid undergoes rapid exchange when exposed to environmental membranes. This leaves the cationic membrane unprotected and capable of direct contact with the erythrocyte membrane. The liposomes containing the two DSPE-based SBLs do not induce lysis. Ionic lipid exchange in this case occurs primarily either through transient direct membrane-membrane contact events, which are unlikely at the SBL concentrations used, or by very slow monomer diffusion mechanisms. These results imply that ATTA8−DSPE is effective in preventing interactions with cell surfaces in a biological environment and does not undergo significant exchange on the time scale of the experiment.

PEG−lipid conjugates are known to inhibit the absorption of serum proteins in vivo (*23*). These proteins include complement (*18*), serum albumin, and other opsonins (*27*), and are believed to mediate enhanced clearance of liposomes in vivo (*28*). To assess the ability of ATTA*n*−lipids to protect liposomes from protein absorption, we used an adaption of a complement activation assay previously reported (*18*). Sheep erythrocytes sensitized with hemolysin activate complement in serum, causing lysis and release of hemoglobin. The hemoglobin levels can be assayed spectroscopically after removal of the cells by centrifugation. Pretreatment of the serum with some other particle which activates complement would decrease the available pool of protein, which in turn would result in lower levels of hemolysis when the treated serum was added to sensitized erythrocytes. In this particular case, we used DODAC/POPC (50:50) liposomes as the complement activating agent. The ability of these liposomes to inhibit complement induced lysis of sensitized sheep erythrocytes was compared against that for DODAC/POPC/SBL (50:40:10) liposomes (SBL = ATTA8−DSPE, MePEGS-2000-Mcer, or MePEGA-2000-DSPE; Figure 3). In all cases, the SBL caused significant inhibition of the ability of the cationic liposomes to consume complement. All SBLs tested were equally effective, suggesting that (a) ATTA8−DSPE inhibited protein binding to liposomes much like PEG−lipids, and (b) ATTA8−DSPE in itself did not bind or activate complement. Exchange phenomena are not relevant in the case of MePEGS-2000-Mcer in this experiment since the pretreatment with complement occurs before exposure to a membrane sink (the erythrocyte membranes).

Evaluation of in Vivo Clearance Behavior. The clearance of liposomes in vivo is dependent on a number of factors, including vesicle size (*29*), membrane outer leaflet composition (*30*, *31*), and lipid dose (*3*). In drug delivery applications, it is desirable to maintain the encapsulated drug in circulation for a reasonable length of time. In mice, however, even relatively innocuous compositions are largely removed from circulation within 24 h. The clearance rate can be reduced in a number of ways, the easiest of which is to simply increase the lipid dose. This is not always acceptable. In situations where low lipid doses are used, the circulation half-life can be increased by including nonexchangeable PEG−lipids in the composition (*2*, *32*). We therefore undertook a number

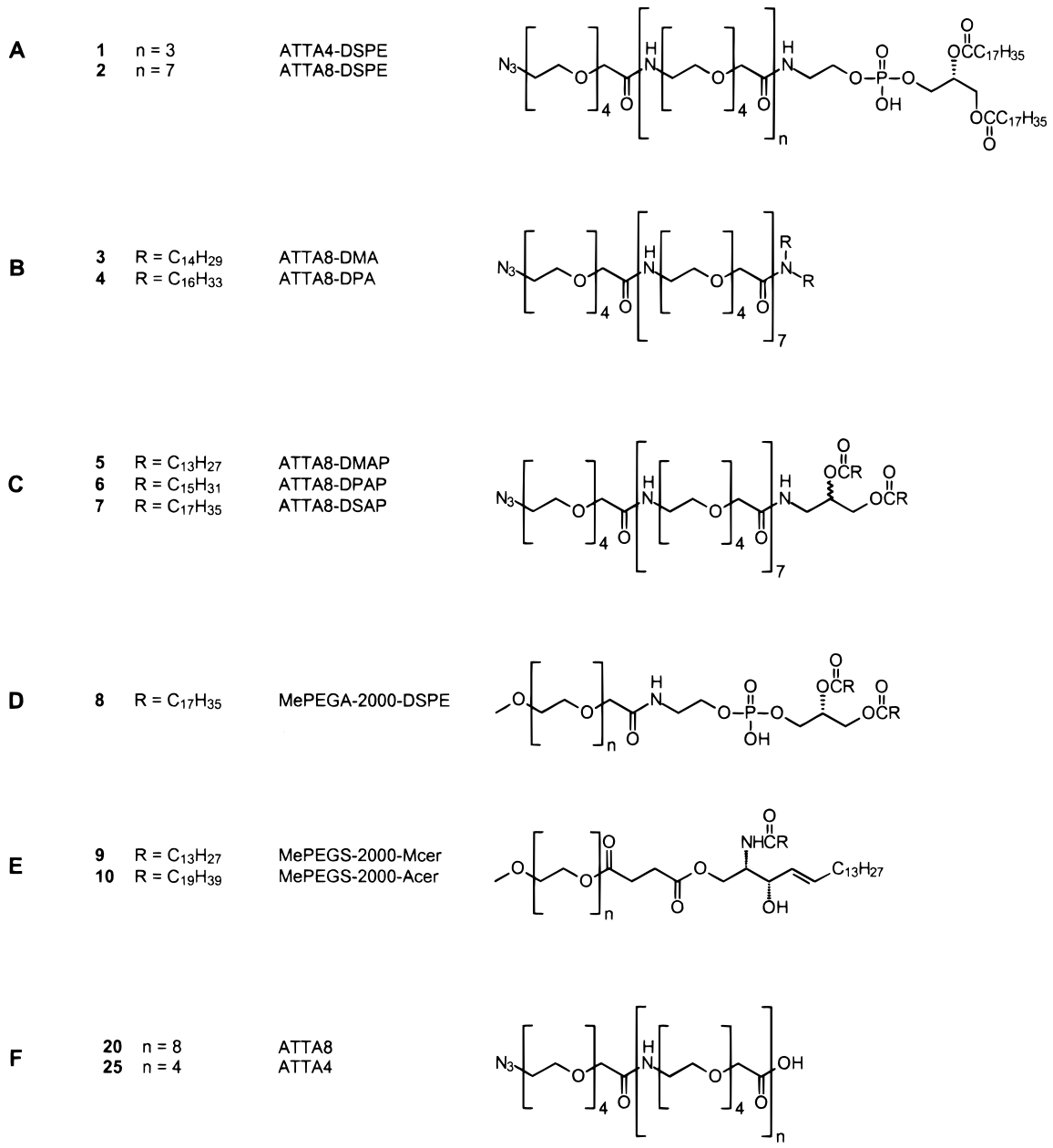


Figure 1. Structures of ATTA*n*–lipids and PEG–lipids: (A) ATTA*n*-DSPE; (B) ATTA8–D*x*A; (C) ATTA8–D*x*AP; (D) MePEGA-2000-D*x*PE; (E) MePEGS-2000-*x*cer; (F) ATTA*n* precursors.

of clearance studies to compare the performance of the ATTA*n*–lipids to PEG–lipids in this application.

We initially looked at the effects of SBL (MePEGA-2000-DSPE, ATTA8–DSPE and ATTA4–DSPE) concentration on the clearance of a single dose (30 mg/kg lipid) 20 h postadministration (Figure 4). The relative effects of an SBL in DSPC/cholesterol liposomes are most evident between 16 and 24 h since unprotected liposome levels fall (at this dose in mice) to ~2–3% whereas fully protected liposomes are still present at significant levels (25–30% initial dose). SBLs which exchange slowly out of the membrane in this time frame show intermediate clearance behavior, the magnitude of which depends on the exchange rate. MePEGA-2000-DSPE is an example of a widely used nonexchangeable SBL which fully protects the liposome surface at optimal concentrations and therefore was used as a control standard for optimal clearance inhibition behavior. The experiment was performed using 0–5% MePEGA-2000-DSPE or ATTA8–DSPE (1% steps) or 0–10% ATTA4–DSPE (2% steps). MePEGA-2000-DSPE and ATTA8–DSPE have similar sizes. The ATTA4–DSPE steps were chosen so that the bulk surface polymer load in the three systems was equivalent. The performance of ATTA8–DSPE and MePEGA-2000-DSPE were similar, achieving optimal clearance behavior at ~3 mol %. The ATTA8–DSPE showed slightly better performance at low concentrations ($P < 0.20$ at 1%; $P < 0.31$ at 2%), although these differences are probably due to small errors in the actual SBL concentration. We expected that ATTA4 would be equivalent to ATTA8 on a mass basis but were surprised to find that it compared well on a mole basis as well.

The effect of exchangeable SBL anchors was examined using a number of ATTA8 dialkylamine and 2,3-diacyloxypropylamine derivatives with different alkyl chain lengths. These particular lipids were designed as exchangeable neutral SBLs for applications involving cationic liposomes. SBLs based on DSPE are anionic and consequently form ion pairs with the cationic lipids in these formulations, greatly reducing the exchange rate.

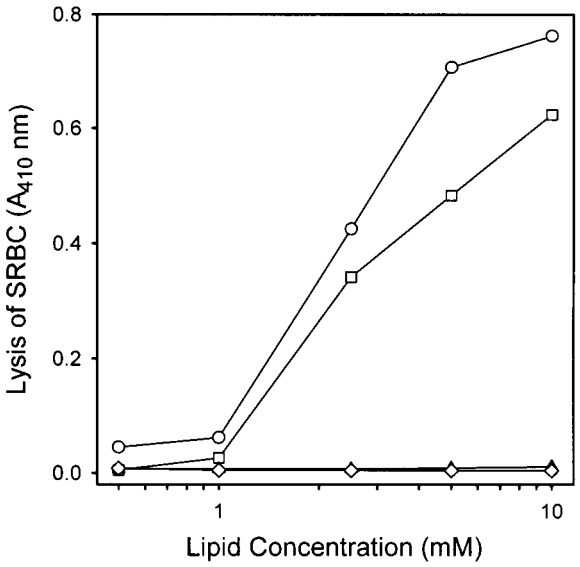


Figure 2. Inhibition of cationic lipid induced hemolysis of erythrocytes. Serial dilutions of DODAC/POPC (50:50, circles), DODAC/POPC/ATTA8−DSPE (50:40:10; diamonds), DODAC/POPC/MePEGA-2000-DSPE (50:40:10; triangles) and DODAC/POPC/MePEGS-2000-Mcer (50:40:10; squares) liposomes (all 20 mM in VBS, 100 μL) were incubated with an equal volume of sheep red blood cells (5×10^5 cells) for 30 min at 37 °C. The sample was diluted with 1.0 mL of EDTA-GVB, centrifuged at 1500 rpm for 5 min, and the absorbance of the supernatant analyzed at 410 nm.

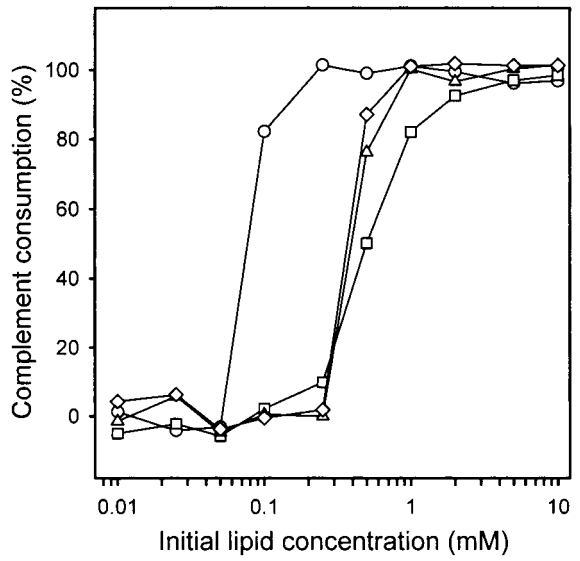


Figure 3. Inhibition of complement activation by DODAC/POPC/SBL vesicles. DODAC/POPC (50:50, circles), DODAC/POPC/ATTA8−DSPE (50:40:10; squares), DODAC/POPC/MePEGA-2000-DSPE (50:40:10; triangles) and DODAC/POPC/MePEGS-2000-Mcer (50:40:10; diamonds) vesicles were prepared and evaluated as described in the Experimental Methods.

The lipids were formulated at 5 mol % in POPC/cholesterol liposomes and circulation levels compared against ATTA8−DSPE, MePEGA-2000-DSPE, and unprotected vesicles, after 4 and 20 h (Figure 5). The di-C14 anchors (ATTA8−DMA and ATTA8−DMAP) showed little difference in clearance behavior compared to the unprotected control, suggesting that the SBLs rapidly exchange out of the bilayers in vivo and consequently do not inhibit clearance. Similar results have previously been observed for MePEGS-2000-Mcer (*33*), a SBL which has a lipid anchor that is equivalent to the di-C14 anchors used here in terms of hydrophobicity and size.

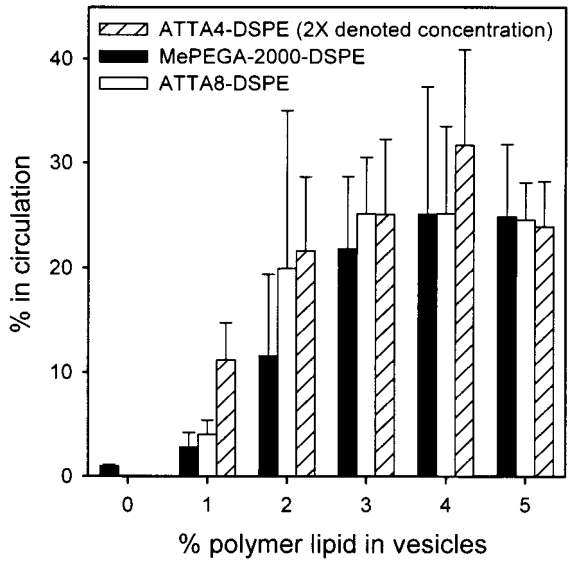


Figure 4. Clearance of sterically stabilized liposomes 20h post administration in female ICR mice (6−8 weeks old). [^{14}C]CHE labeled liposomes composed of POPC/chol/SBL (55-n:45:n; 5 mM) were prepared in HBS (25 mM Hepes, 150 mM NaCl, pH 7.4) and administered to mice (200 μL/animal) by intravenous tail vein injection. Serum was collected after 20 h and analyzed for radioactivity by liquid scintillation counting. SBL = MePEGA-2000-DSPE; ATTA8−DSPE; or ATTA4−DSPE. Error bars represent standard deviation for five animals.

Small but significant improvements in clearance behavior were observed for the pair of di-C16 derivatives (ATTA8−DPA and ATTA8−DPAP). The exchange rates of these lipids are significant on the time scale of the experiment but do not result in complete loss of the SBL, at least initially. This is particularly evident at the 4 h time point where the differences with the pair of DSPE-anchored SBLs is relatively small. The difference in clearance is larger at 20 h, presumably because most of the di-C16 SBL has exchanged out by then. An unexpected result was obtained with ATTA8−DSAP, a di-C18 analogue, in that it performed very much like the two di-C16 derivatives. The reason for this is not clear since we would have expected the C-18 analogue to be more securely anchored in the bilayer. These experiments were performed with the SBL formulated directly with the liposome. Experiments where the SBL was exchanged into preformed liposomes gave similar results.

Lipid dose plays an important role in the clearance behavior of liposomes. The process is believed to be mediated in part by the adsorption of serum proteins to liposomes in vivo. Increasing doses of lipid decrease the available pool of these proteins, resulting in decreases in the levels of bound proteins and reduced clearance. Nonexchangeable SBLs reduce the amount of adsorbed protein and thereby increase circulation levels. Direct inhibition of contact with the cells responsible for clearance probably also plays a significant role in the modulation of the clearance behavior. We compared the clearance behavior of ATTA8−DSPE vesicles comprised of DSPC/cholesterol/AL-1/SBL (20:45:25:10) with analogous MePEGS-2000-Mcer vesicles using a range of lipid doses (0−750 mg/kg) 24 h postinjection (Figure 6). We are currently using similar compositions to encapsulate antisense oligonucleotides. The MePEGS-2000-Mcer is required in these formulations to inhibit aggregation during the formulation process, but exchanges out rapidly in vivo and consequently has little or no effect on the clearance behavior. ATTA8−DSPE exchange rates would be negligible due to ion pair formation with the AL-1.

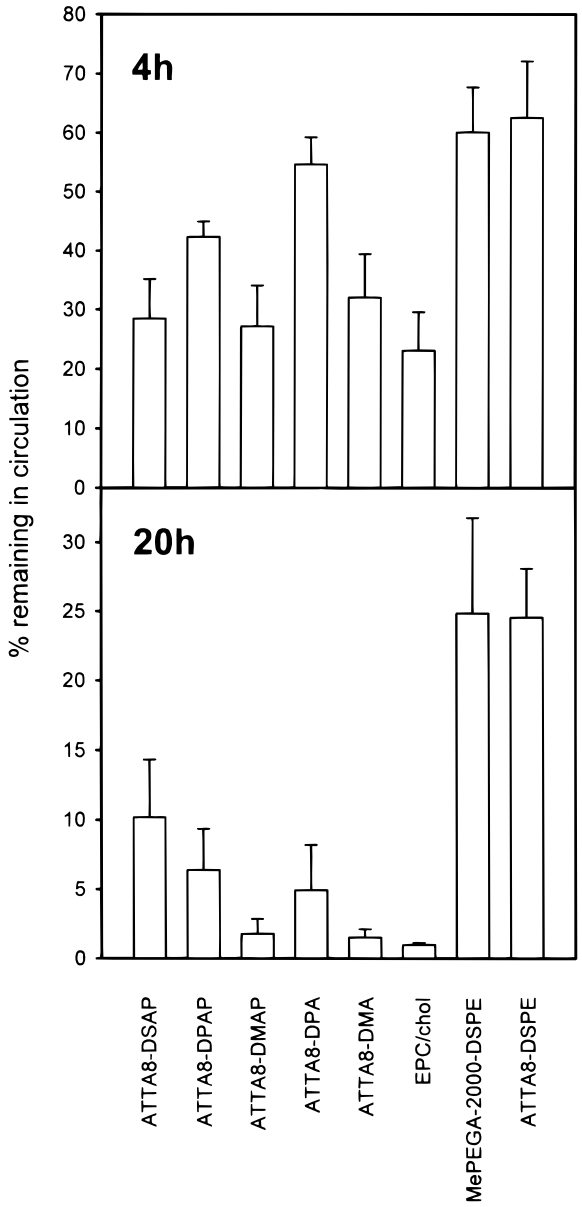


Figure 5. Clearance of sterically stabilized liposomes 4 h and 20 h post administration in female ICR mice (6−8 weeks old) using neutral SBL components. [^{14}C]CHE labeled liposomes composed of POPC/chol/SBL (50:45:5; 5 mM) were prepared in HBS (25 mM hepes, 150 mM NaCl, pH 7.4) and administered to mice (200 μL per animal) by intravenous tail vein injection. Blood (25 μL) was collected 4 h postinjection by tail nicks. Blood samples were digested in solvable and analyzed for radioactivity by liquid scintillation counting. Liposome levels were estimated based on estimated blood volume of 8%. Serum was collected after 20 h and analyzed for radioactivity by liquid scintillation counting. Liposome levels were estimated based on estimated serum volume of 4.55%. Error bars represent standard deviation for five animals.

The MePEGS-2000-Mcer vesicles are largely cleared from circulation at low doses after 24 h. Higher doses show significantly elevated liposome levels, but are still less than even the lowest dose of ATTA8−DSPE liposomes. Small increases in clearance behavior were observed as the ATTA8−DSPE liposome dose was increased. Depletion of the serum protein pool is likely not an issue in this case, so the observed minor increases either relate to saturation of other clearance mechanisms or are not significant. The result also implies that increasing the ATTA8−lipid dose does not in itself activate clearance mechanisms.

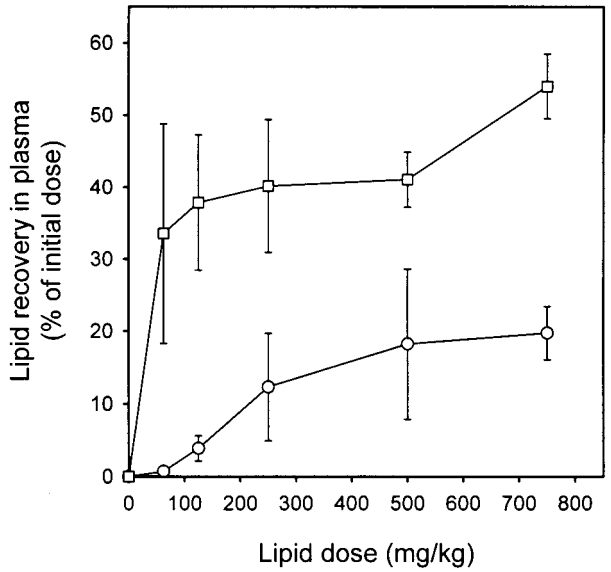


Figure 6. Effect of lipid dose on circulation levels of antisense encapsulated in DSPC/chol/AL-1/SBL (20:45:25:10) vesicles at 24 h. SBL = MePEGS-2000-Mcer, circles; ATTA8−DSPE, squares. Experiment conducted as described in the in vivo tolerability section of the experimental methods. Error bars represent standard deviation.

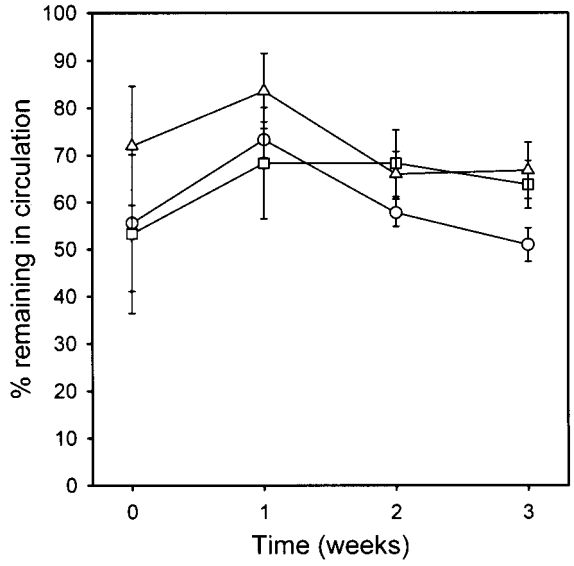


Figure 7. Clearance of liposomes 1 h postadministration in female ICR mice (6−8 weeks old) subjected to weekly administrations. Liposomes [DSPC/chol (55:45, circles); DSPC/chol/ATTA8−DSPE (50:45:5, triangles); DSPC/chol/MePEGC-2000-DSPE (50:45:5, squares)] labeled with [^{3}H]cholesteryl hexadecyl ether were prepared in HBS (Hepes-buffered saline; 20 mM Hepes, and 145 mM NaCl, pH 7.4) and diluted such that the injected lipid dose was 50 mg/kg/week. Lipid was administered by intravenous tail vein injections (200 μL) at weekly intervals for 3 weeks. Blood (50 μL) was collected 1 h postinjection by tail nicks. Mice were weighed at weekly intervals to estimate blood volume (8% body weight). Blood samples were digested in solvable and analyzed for radioactivity by liquid scintillation counting. Error bars represent standard deviation for six animals per time point.

The effect of repeat dosage regimes on clearance was evaluated using DSPC/cholesterol (55:45) or DSPC/cholesterol/SBL (50:45:5) liposomes at 50 mg/kg administered at weekly intervals. Blood was recovered 1 h postinjection and analyzed for liposome content (Figure 7). In the experiment, no significant difference was observed in the behavior of control, ATTA8−DSPE, and

Table 1. Phenotypic Profile of Spleen Cells Recovered from Mice after the fourth Injection Following Repeated Lipid Administration[a]

formulation	CD4	CD8	CD22	CD11b	CD25	CD54	CD86	MHC−II	Ly6A/E
HBS	25.67	12.93	52.45	13.78	1.27	18.51	10.46	57.92	7.75
DSPC/chol	22.2	11.92	57.72	13.23	1.11				
DSPC/chol/MePEGA-2000-DSPE	21.99	21.99	57.74	13.48	1.36				
DSPC/chol/ATTA8-DSPE	21.87	11.09	48.85	13.54	1.36	19.48	10.57	54.13	9.4

[a] Experiment performed as described in the in vivo immunogenicity section of the Experimental Methods. Values are expressed as the relative number of positive cells (%).

Table 2. Cell Proliferation and Cytokine Release Following in Vitro Restimulation of Spleen Cells with 0.62 mM Lipid Formulations[a]

in vivo treatment	in vitro stimulation	^{3}H incorporation, DPMs	cytokine release (OD_{450nm})	
			IL-2	IL-4
HBS	HBS	2544	0.816	0.588
HBS	DSPC/chol	6744	0.382	0.474
HBS	DSPC/chol/MePEGA-2000-DSPE	6085	0.333	0.328
HBS	DSPC/chol/ATTA8-DSPE	6916	0.67	0.321
DSPC/chol	DSPC/chol	2700	0.35	0.521
DSPC/chol/MePEGA-2000-DSPE	DSPC/chol/MePEGA-2000-DSPE	4144	0.44	0.44
DSPC/chol/ATTA8-DSPE	DSPC/chol/ATTA8-DSPE	4618	0.375	0.334
HBS	ConA	144 149	1.525	1.113
HBS	LPS	24 996		

[a] Cells were recovered from mice after the fourth injection following repeated weekly administrations of buffer or the listed liposome compositions. Restimulation was performed with the same compositions used for the treatment. Cells recovered from animals treated with buffer only were treated with all compositions as a control for non-specific effects. The animal protocol, cytokine ELISA assay and mitogenicity assays were performed as described in the in vivo immunogenicity section of the Experimental Methods.

MePEGC-2000-DSPE liposomes. DSPC/cholesterol liposomes are cleared more slowly than most liposome compositions and at 50 mg/kg are present at 60−80% of the injected dose 1 h postinjection. Liposomes with full steric protection are typically at similar levels. This behavior should remain the same after repeat administrations if there is no activation of some adaptive clearance mechanism, such as an immune response. An immune response would result in rapid clearance on repeat injection and very low levels of liposomes in circulation at 1 h postinjection (*34*). Obviously, this is very important if these materials are to be used in a practical pharmaceutical product. The results suggest that ATTA8−DSPE in isolation does not activate additional clearance mechanisms on repeat administration.

Evaluation of Immunogenicity. It is important that any polymer which has been designed for liposome applications in pharmaceutical products does not induce immune responses in vivo. The fact that ATTA8−DSPE liposome clearance in vivo does not change after repeat administration suggests that the conjugate is nonimmunogenic. To confirm this, we recovered spleens from mice 24 h after admininstration using a repeat dosage regime. Mice were administered up to four injections of DSPC/chol/ATTA8 (50:45:5), DSPC/chol/MePEGA-2000-DSPE (50:45:5), or DSPC/chol/ATTA8 (55:45) at weekly intervals for a total of 3 weeks. A control experiment using HBS buffer was run concurrently. Spleen cells were recovered after each time point and processed for analysis of phenotypic markers, mitogenic response after restimulation with liposomes, and cytokine release.

To analyze the expression of phenotypic markers, spleen cells from all groups were isolated, stained, and assayed within 5 h following isolation. Up-regulated expression of activation markers is associated with activation of immune cells. The analysis of phenotypic markers shows that there are no appreciable differences in the expression of differentiation (CD22, CD4, CD8, and CD11b) and activation (CD25, CD54, CD86, Ly6A/E, and MHC−II) markers between the control group and experimental groups receiving various lipid formulations (Table 1). The absence of any differences in expression of activation markers, between the control and experimental groups, suggests that in vivo treatment with ATTA8−DSPE formulations did not induce measurable activation of spleen cells.

Unseparated spleen cells from all experimental groups were tested in vitro for their ability to proliferate upon restimulation with the same lipid formulation [final concentration = 0.31 (data not shown), 0.62, or 1.25 (data not shown) mM] that was administered in vivo. Spleen cells from control mice (diluent treated group) were stimulated with the same set of liposomes in order to determine their mitogenic effect in vitro. Clones of memory cells would be generated if in vivo treatment with any of the lipid formulations had induced immunostimulation. In vitro restimulation of those cells with the same immunogen would then result in augmented cell proliferation. Our results show that when mice were primed with lipids, secondary responses to same formulations were practically undetectable, indicating that there was minimal immunostimulation (Table 2). Stimulation of splenocytes with polyclonal activators such as ConA and LPS induced strong mitogenic responses that were significantly different (5−10×) compared to those obtained from lipid-treated groups.

The recovered splenocytes were cultured in the presence of the various lipid formulations [final concentrations = 0.31 (data not shown), 0.62, and 1.25 (data not shown) mM]. Culture supernatants were collected at various times after culture initiation (24 or 48 h), and the levels of released cytokines (IL-2 and IL-4) measured. There was no significant difference in cytokine release between the groups that received the various lipid formulations or the buffer control.

The results show that following successive in vivo administration of DSPC/chol (55:45) or DSPC/chol/SBL (50:45:5; SBL = MePEGC-2000-DSPE or ATTA8−DSPE) liposomes, (a) there were no differences in expression of phenotypic and activation markers, (b) there was no induction of measurable cellular immune response (cell proliferation or cytokine release) to tested lipids, and (c)

lipid formulations were not mitogenic in control splenocytes stimulated in vitro. Together with the fact that repeated systemic administration of the liposomes did not result in rapid plasma clearance after subsequent injections, the results suggest that ATTA8 is nonimmunogenic in vivo, at least in terms of conjugates associated with normal liposome formulations.

Evaluation of Toxicity. The toxicity of any new polymer used in SBLs is obviously important. PEG is for the most part relatively nontoxic, although it is known to cause contact hypersensitivity under some circumstances (*35*). High concentrations of PEG−lipids will cause cell lysis through detergent action, although this should not be an issue at the concentrations typically used in liposome applications (otherwise the liposomes themselves would be dispersed). A full toxicity study of the ATTA*n* derivatives was beyond the scope of this work; however, some preliminary studies were performed to evaluate parameters that are potentially important in liposome applications.

ATTA8 was tested in various human (MB 231, HeLa, COLO 205, U87, SKOV-3, and MCF-7) and rodent (B16, 9L, and BHK-21) cell lines to evaluate any intrinsic cytotoxicity of the oligomer (Figure 8). Cell survival was determined using the crystal violet assay and expressed as a percentage of the optical density obtained after analysis of untreated cells. In most cases, the observed cytotoxic effects were negligible, although some cell lines showed significant falloff in survival at higher doses. Survival levels in all cell lines investigated, except SKOV-3 and 9L, exceeded those observed in the presence of cytostatic amounts of paclitaxel, indicating that cell growth continued at the highest ATTA8 doses used in the study.

Liposomes accumulate primarily in the liver and to a lesser extent in the spleen after clearance from circulation in vivo. Toxic effects from any consitituent lipids are therefore primarily associated with these organs. In the case of the liver, toxicity is associated with the release of enzymes, such as LDH, AST, and ALT, into the circulation. Levels of these enzymes can be assayed after recovery of serum and used as evidence of liver toxicity. We treated mice with a cationic liposome formulation normally used to encapsulate antisense DNA oligonucleotides (DSPC/chol/AL-1/SBL; 20:45:25:10; SBL = MePEGS-2000-Mcer or ATTA8−DSPE) at a range of lipid doses (50−750 mg of lipid/kg of body weight) and recovered plasma after 24 h. A SBL is required in these formulations to inhibit aggregation during the DNA formulation process. At least half of the MePEGS-2000-Mcer exchanges out of the formulation rapidly in vivo, however, much of it is still present when the vesicles accumulate in the liver. This model allowed us to assess the relative toxicity of ATTA8−DSPE in a real world situation. Analysis of LDH, AST, and ALT levels in recovered plasma samples indicated that there was no significant difference between the MePEGS-2000-Mcer and ATTA8−DSPE formulations (Figure 9). Slight increases in enzyme levels observed over the dose range are likely due to the encapsulated drug. Organs recovered (liver, kidney, lung an spleen) after the experiment (Figure 10) showed no evidence of change in weight or gross morphology over the dose range used. The data suggests that ATTA8−lipids do not result in significant gross toxicity to the organism and that the materials are well tolerated.

Evaluation of Utility. PEG−lipids are used for a variety of purposes in a wide range of liposomal drug formulations. Typical applications include reducing rates

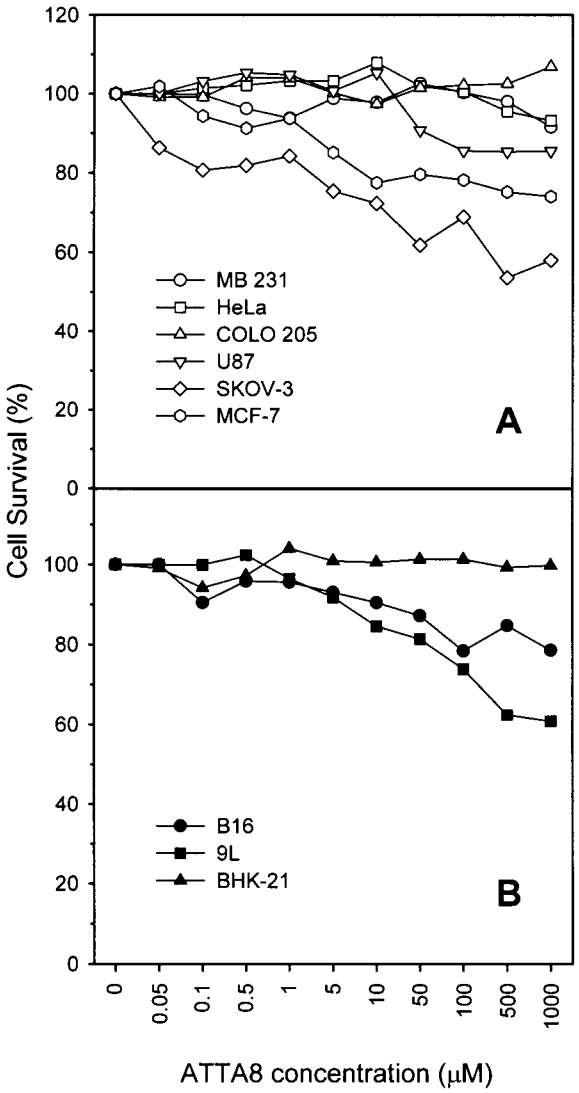


Figure 8. In vitro cytotoxicity of ATTA8. Panel A (human cell lines): MB 231, HeLa, Colo 205, U87, B16, 9L. Panel B (rodent cell lines): MCF-7, SKOV-3, and BHK-21. The experiments were performed in duplicate as described in the Experimental Methods. Error bars (standard deviation) have been omitted for clarity, but are available in the Supporting Information.

of clearance in vivo and inhibiting aggregation during the drug formulation process. In all of these applications, the PEG itself does not interact with the drug during the formulation process. Any molecule which is used in place of PEG would be required to behave in a similar manner. To evaluate the utility of ATTA*n*−lipids in drug formulation, we compared the performance of various ATTA8−lipids to PEG−lipids in the formulation of (a) doxorubicin using a pH gradient, (b) plasmid DNA, and (c) antisense DNA.

A commonly used procedure for encapsulating weak bases in liposomes involves generating vesicles with a pH gradient across the membrane. Typically, this involves an internal pH of ∼4. Neutral forms of the base cross the membrane and become trapped in the inner aqueous compartment in the protonated form. Many pharmaceutically useful drugs may be encapsulated in vesicles in this way (*36*). PEG−lipids are often included in these formulations in order to reduce rates of clearance in vivo. These SBLs can be exchanged into the membranes after drug loading but are more commonly incorporated prior to vesicle formation. Therefore, it is important that PEG, or any other polymer conjugate used

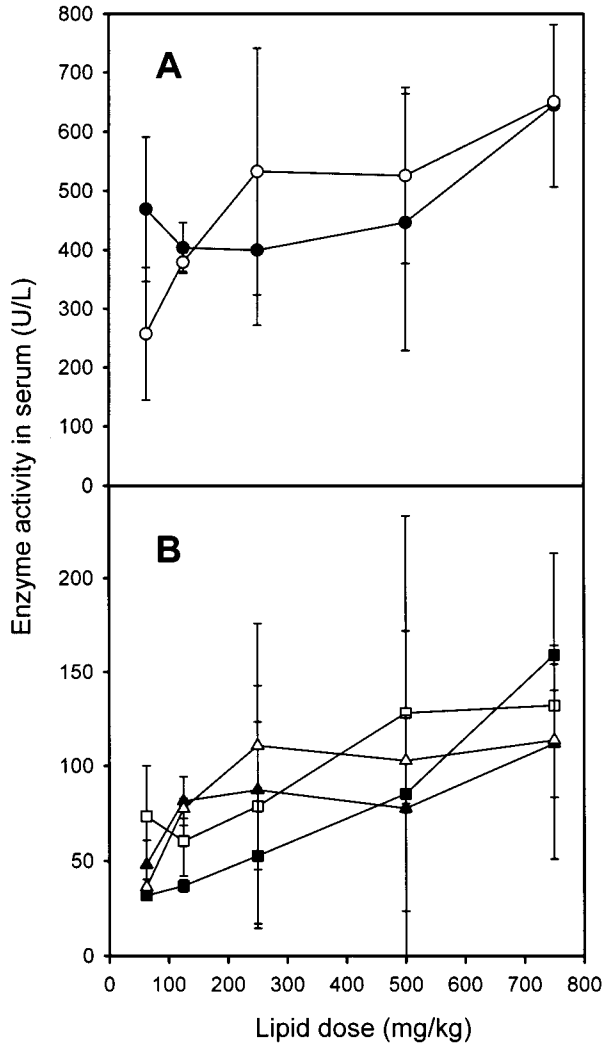


Figure 9. Liver enzyme levels after administration of antisense encapsulated in DSPC/chol/AL-1/SBL (20:45:25:10) vesicles. Shaded symbols represent SBL = MePEGS-2000-Mcer, open symbols represent SBL = ATTA8−DSPE. (A) LDH levels (circles); (B) AST levels (squares); ASL levels (triangles). Experiment conducted as described in the in vivo tolerability section of the Experimental Methods. Error bars represent standard deviation.

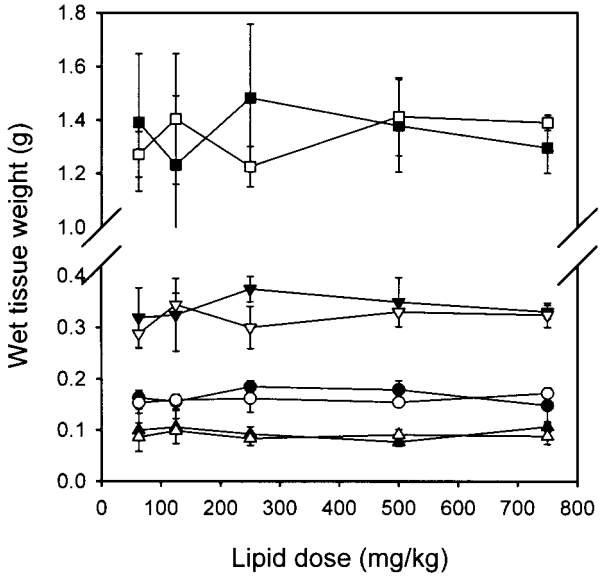


Figure 10. Single dose tolerability of encapsulated antisense oligonucleotide liposomes incorporating MePEGS-2000-Mcer (closed symbols) or ATTA8−DSPE (open symbols). Organs excised include liver (squares), kidney (inverted triangle), lung (circles) and spleen (triangle). Experiment conducted as described in the in vivo tolerability section of the Experimental Methods. Error bars represent standard deviation.

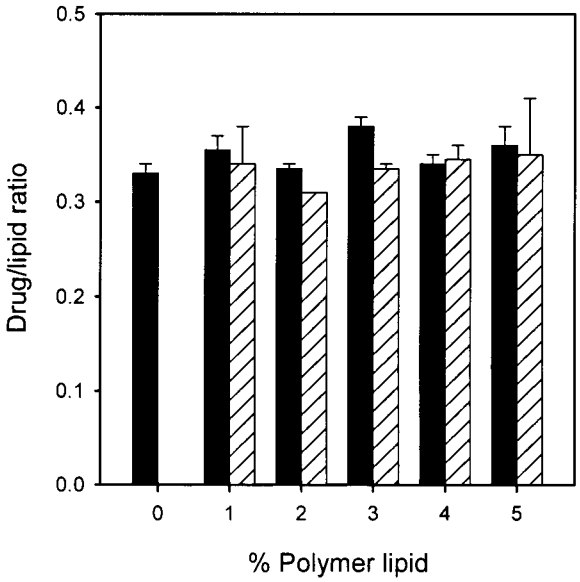


Figure 11. Effect of SBL on drug loading. Liposomes [POPC/chol/SBL (55-n:45:n; n = 0 to 5; SBL = MePEGA-2000-DSPE (solid bars) or ATTA8−DSPE (hatched bars); 25 mM] prepared in citrate buffer (300 mM, pH 4.0) were loaded with doxorubicin using an initial drug-to-lipid ratio of 0.3 as described in the Experimental Methods. Data represents the mean of two separate experiments. Error bars represent the range.

as a SBL, should not interact with the drug during the loading procedure or induce leakage of the internal contents after the creation of the pH gradient. Previous studies have shown that PEG−lipids do not affect drug loading across pH gradients (*37*).

In this study, we compared the effects of 0−5% of MePEGA-2000-DSPE or ATTA8−DSPE on the loading efficiency of doxorubicin into POPC/cholesterol (55-n:45) vesicles with a pH gradient of ∼Δ4 (internal pH 4.0, external pH ∼8). In all cases drug loading efficiency approached ∼100%, within the accuracy of the experiment (Figure 11). The results showed that ATTA8−DSPE does not adversely affect the stability of the vesicles or inhibit the drug loading process under the conditions of the experiment.

The formulation of plasmid DNA in cationic lipid vesicles is currently of great interest since the resultant complexes are potentially useful as gene therapy delivery vehicles. Traditionally, these complexes are formed by mixing cationic liposomes with free DNA to form aggregates which are capable of transfecting cells in vitro. These aggregates are typically large and suffer from very poor pharmacokinetics in vivo. Associates of ours have developed an elegant approach to address this problem (*13*). The DNA is encapsulated in vesicles comprised of neutral lipids, a cationic lipid, and an SBL, using a detergent dialysis procedure. The cationic lipid acts to catalyze the association of the DNA with the forming bilayer while the SBL prevents intervesicle cross-linking. The SBL may also induce asymmetric encapsulation of the DNA as a result of steric interactions between the polymer chains. Exchangeable and nonexchangeable SBLs may be used; however, transfection is adversely affected by the presence of SBLs, and as a result, we typically use a readily exchangeable SBL in these for-

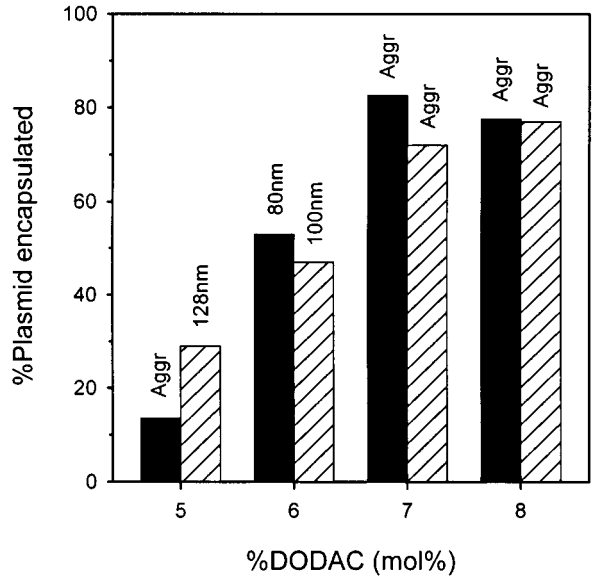


Figure 12. Effect of SBL on plasmid formulation. pINEXL018 was encapsulated in DODAC:DOPE:SBL [n:90-n:10; $n = 5-8\%$; SBL = ATTA8−DMAP (black bars) or ATTA8−DSAP (hatched bars)] vesicles by detergent dialysis as previously described [13]. Vesicle sizes were measured using a Nicomp Model 370 particle sizer. Encapsulation efficiency was determined using the PicoGreen assay as described in the Experimental Methods.

mulations. Formation of 100 nm vesicles with encapsulated DNA is critically dependent on the cationic lipid concentration. When MePEGS-2000-Mcer is used as an SBL in DOPE/DODAC formulations, the critical DODAC content is ~6%. Encapsulation efficiency falls off at lower concentrations while aggregation becomes a problem as DODAC levels increase. Similar behavior was observed when the MePEGS-2000-Mcer was replaced by ATTA8−DSAP or ATTA8−DMAP (Figure 12).

We have developed a similar procedure for encapsulating antisense DNA molecules (*7*). These drugs are much smaller than plasmid DNA. This results in many copies being encapsulated instead of one as is the case with plasmid DNA. In addition, antisense DNA oligomers associate with both leaflets of the bilayer rather than just the inner leaflet as with plasmid DNA. We resolved the problem by replacing the quaternary cationic lipid DODAC with the protonatable amine AL-1 (20%). This lipid is charged at low pH (~4) but is largely neutral at physiological pH (*38*). A SBL (typically MePEGS-2000-Mcer) is incorporated (10%) into these formulations to inhibit DNA induced cross-linking during vesicle formation. The vesicles themselves are formed at low pH using an ethanol dilution procedure followed by extrusion. The externally bound DNA was removed by replacement of the external buffer with HBS at pH 7.4 by dialysis followed by passage down a DEAE Sepharose CL-6B column. All versions of ATTA8−lipids (DSAP, DPAP, and DMAP) gave results similar to the MePEGS-2000-Mcer control formulation in terms of encapsulation efficiency, size, and stability against aggregation. Formulations prepared using ATTA4−DMAP and ATTA4−DLAP (the di-C12 analogue) were unstable and aggregated during preparation. We have preliminary data for formulations using novel MePEG-750-lipid derivatives which show similar behavior, suggesting that the polymer moiety of a SBL has to be larger than a minimum size to stabilize the liposomes against aggregation.

These results indicate that ATTA*n*−lipids may be used in most liposome drug formulations where PEG−lipids are currently employed. The only other major application of PEG−lipids in liposomes which we have not tested involves the use of the PEG as a cross-linker for attaching targeting ligands to the vesicle surface. We see no reason ATTA*n* lipids could not be used in this way, in fact, ATTA*n* may well be superior in these applications due to it's intrinsic heterobifunctionality and monodisperse nature.

CONCLUSION

In this work, we evaluated ATTA8−lipid conjugates as monodisperse replacements for PEG−lipids in most liposome applications. The ATTA*n* oligomers were conjugated to a range of amino lipids to form anionic (ATTA*n*−DSPE conjugates) or neutral species (ATTA*n*−DxAP or ATTA*n*−DxA conjugates). These conjugates were soluble in water and most organic solvents, allowing formulation in liposomes using a wide range of techniques commonly employed in the preparation of liposomes. The ATTA*n* liposomes showed no evidence of physical instability under normal circumstances. ATTA*n*−DSPE conjugates were shown to be at least as effective as PEG−lipids in assays designed to evaluate the ability of an SBL to inhibit interactions between liposomes and other membranes. Nonexchangeable ATTA*n*−lipids were effective in reducing the rate of liposome clearance in vivo, while exchangeable versions showed intermediate clearance behavior consistent with the predicted properties of the anchors used. There was no evidence that ATTA8−DSPE activated additional clearance mechanisms at high doses or on repeat administration, or activated any immune response in isolation. The lipids appeared to be relatively nontoxic in vitro and in vivo. On the basis of these results, we have concluded that ATTA*n*−lipids may be safely used in most liposome applications where PEG−lipids are currently used. We anticipate that the new compounds will facilitate the development of better defined and characterized SBL-liposome systems, particularly targeted liposomes, environmentally responsive systems, and those that undergo dynamic evolution in vivo based on loss of the SBL over time.

Supporting Information Available: Figures of clearance and ^{1}H NMR spectra and tables of elemental analysis data and standard deviations. This material is available free of charge via the Internet at http://pubs.acs.org.

LITERATURE CITED

(1) Lasic, D. D., and Needham, D. (1995) The "stealth" liposome: a prototypical biomaterial. *Chem. Rev. 95*, 2601−2628.

(2) Allen, T. (1994) The use of glycolipids and hydrophilic polymers in avoiding rapid uptake of liposomes by the mononuclear phagocyte system. *Adv. Drug. Delivery Rev. 13*, 285−309.

(3) Oja, C. D., Semple, S. C., Chonn, A., and Cullis, P. R. (1996) Influence of dose on liposome clearance: critical role of blood proteins. *Biochim. Biophys. Acta 1281*, 31−37.

(4) Klibanov, A. L., Maruyama, K., Beckerleg, A. M., Torchilin, V. P., and Huang, L. (1991) Activity of amphipathic poly(ethylene glycol) 5000 to prolong the circulation time of liposomes depends on the liposome size and is unfavourable for immunoliposome binding to target. *Biochim. Biophys. Acta 1062*, 142−148.

(5) Verut-Doi, A., Ishiwata, H., and Miyajima, K. (1996) Binding and uptake of liposomes containing a poly(ethylene glycol) derivative of cholesterol (stealth liposomes) by the macrophage cell line J774: influence of PEG content and its molecular weight. *Biochim. Biophys. Acta 1278*, 19−28.

(6) Harasym, T. O., Tardi, P., Longman, S. A., Ansell, S. M., Bally, M. B., Cullis, P. R., and Choi, L. S. L. (1995) Poly-(ethylene glycol)-modified phospholipids prevent aggregation during covalent conjugation of proteins to liposomes. *Bioconjugate Chem. 6*, 187−194.

(7) Semple, S. C., Klimuk, S. K., Harasym, T. O., Dos Santos, N., Sandhu, A., Ansell, S. M., Scherrer, P., and Hope, M. J. (1999) Stabilized antisense-lipid particles for sytemic applications: generation, characterization and in vivo activity. Manuscript in preparation.

(8) Kirpotin, D., Park, J. W., Hong, K., Zalipsky, S., Li, W. L., Carter, P., Benz, C. C., and Papahadjopoulos, D. (1997) Sterically stabilized anti-HER2 immunoliposomes: design and targeting to human breast cancer cells in vitro. *Biochemistry 36*, 66−75.

(9) Zalipsky, S., Puntambekar, B., Boulikas, P., Engbers, C. M., and Woodle, M. C. (1995) Peptide attachment to extremities of liposomal surface grafted PEG chains: preparation of the long-circulating form of laminin pentapeptide, YIGSR. *Bioconjugate Chem. 6*, 705−708.

(10) Murohara, T., Margiotta, J., Phillips, L. M., Paulson, J. C., DeFrees, S., Zalipsky, S., Guo, L. S., and Lefer, A. M. (1995) Cardioprotection by liposome-conjugated sialyl Lewisx-oligosaccharide in myocardial ischaemia and reperfusion injury. *Cardiovacular Res. 30*, 965−974.

(11) Wang, S., Lee, R. J., Cauchon, G., Gorenstein, D. G., and Low, P. S. (1995) Delivery of antisense oligodeoxyribonucleotides againste the human epidermal growth factor receptor into cultured KB cells with liposomes conjugated to folate via poly(ethylene glycol). *Proc. Nat. Acad. Sci. U.S.A. 92*, 3318−3322.

(12) Holland, J. W., Hui, C., Cullis, P. R., and Madden, T. D. (1996) Poly(ethylene glycol)-lipid conjugates regulate the calcium-induced fusion of liposomes composed of phosphatidylethanolamine and phosphatidylserine. *Biochemistry 35*, 2618−2624.

(13) Wheeler, J. J., Palmer, L., Ossanlou, M., MacLachlan, I., Graham, R. W., Zhang, Y. P., Hope, M. J., Scherrer, P., and Cullis, P. R. (1999) Stabilized plasmid-lipid particles: construction and characterization. *Gene Ther. 6*, 271−281.

(14) Adlakha-Hutcheon, G., Bally, M. B., Shew, C. R., and Madden, T. D. Controlled destabilization of a liposomal drug delivery system enhances mitoxantone antitumor activity. Manuscript in preparation.

(15) Dhawan, R., Kadijk, M. G. A., Joikinen, T. J., Feng M., and Ansell, S. M. (1999) Synthesis of polyamide oligomers based on 14-amino-3, 6, 9, 12-tetraoxatetradecanoic acid. Manuscript in preparation.

(16) Parr, M. J., Ansell, S. M., Choi, L. S., and Cullis, P. R. (1994) Factors influencing the retention and chemical stability of poly(ethyleneglycol)-lipid conjugates incorporated into large unilamellar vesicles. *Biochim. Biophys. Acta 1195*, 21−30.

(17) Hope, M. J., Bally, M. B., Webb, G., and Cullis, P. R. (1985) Production of large unilammelar vesicles by a rapid extrusion procedure. Characterization of size distribution, trapped volume and ability to maintain a membrane potential. *Biochim. Biophys. Acta 812*, 55−65.

(18) Chonn, A., Cullis, P. R. C., and Devine, D. V. (1991) The role of surface charge in the activation of the classical and alternative pathways of complement by liposomes. *J. Immunol. 146*, 4234−4241.

(19) Devine, D. V., Wong, K., Serrano, K., Chonn, A., and Cullis, P. R. (1994) Liposome complement interactions in rat serum: implications for liposome survival studies. *Biochim. Biophys. Acta 1191*, 43−51.

(20) Hogan, M. M. (1997) Measurement of tumor necrosis factor α and *β*. In *Current protocols in Immunology* (R. Coico, Ed.) Vol. 1, 6.10.2., John Wiley & Sons, Inc.

(21) Ansell, S. M., Tardi, P. G., and Buchkowsky, S. B. (1996) 3-(2-Pyridyldithio)propionic acid hydrazide as a cross-linker in the formation of liposome-antibody conjugates. *Bioconjugate Chem. 7*, 490−496.

(22) Uster, P. S., Allen, T. M., Daniel, B. E., Mendez, C. J., Newman, M. S., and Zhu, G. Z. (1996) Insertion of poly-(ethylene glycol) derivatized phospholipid into preformed liposomes results in prolonged in vivo circulation time. *FEBS Lett. 386*, 243−246.

(23) Oja, C. D. (1998) Studies on factors influencing the elimination of liposomes from the circulation. Ph.D. dissertation, UBC, Vancouver.

(24) Chonn, A., and Cullis, P. R. C., (1992) Ganglioside GM1 and hydrophilic polymers increase liposome circulation times by inhibiting the association of blood proteins. *J. Liposome Res. 2*, 397−410.

(25) Ansell, S. M., Dhawan, R., Chen, T., Joshi, P. B., Tam, P., and Lee, D. K. (1999) Effect of lipid composition on aggregation-disaggregation of cationic−anionic liposome systems: Implications for the design of lipid based gene delivery systems. Manuscript in preparation.

(26) Yoshihara, E., and Nakae, T. (1986) Cytolytic activity of liposomes containing stearylamine. *Biochim. Biophys. Acta 854*, 93−101.

(27) Chonn, A., Semple, S. C., and Cullis, P. R. C. (1995) *β*2-Glycoprotein I is a major protein associated with very rapidly cleared liposomes in vivo, suggesting a significant role in the immune clearance of "nonself" particles. *J. Biol. Chem. 270*, 25845−25849.

(28) Chonn, A., Semple, S. C., and Cullis, P. R. C. (1992) Association of blood proteins with large unilamellar liposomes in vivo. *J. Biol. Chem. 267*, 18759−18765.

(29) Litzinger, D. C., Buiting, A. M., van Rooijen, N., and Huang, L. (1994) Effect of liposome size on the circulation time and intraorgan distribution of amphipathic poly(ethylene glycol)-containing liposomes. *Biochim. Biophys. 1190*, 99−107.

(30) Semple, S. C., Chonn, A., and Cullis, P. R. (1996) Influence of cholesterol on the association of plasma proteins with liposomes. *Biochemistry 35*, 2521−2525.

(31) Chonn, A., Semple, S. C., and Cullis, P. R. (1992) Association of blood proteins with large unilamellar liposomes. *J. Biol. Chem. 267*, 18759−18765.

(32) Allen, T. M., Hansen, C., Martin, F., Redemann, C., and Yau-Yong, A. (1991) Liposomes containing synthetic derivatives of poly(ethylene glycol) show prolonged circulation half-lives in vivo. *Biochim. Biophys. Acta 1066*, 29−36.

(33) Webb, M. S., Saxon, D., Wong, F. M., Lim, H. J., Wang, Z., Bally, M. B., Choi, L. S., Cullis, P. R., and Mayer L. D. (1998) Comparison of different hydrophobic anchors conjugated to poly(ethylene glycol): effects on the pharmacokinetics of liposomal vincristine. *Biochim. Biophys. Acta 1372*, 272−282.

(34) Harding, J. A., Engbers, C. M., Newman, M. S., Goldstein, N. I., and Zalipsky, S. (1997) Immunogenicity and pharmacokinetic attributes of poly(ethylene glycol)-grafted immunoliposomes. *Biochim. Biophys. Acta 1327*, 181−192.

(35) Berch, M., Shao, L. P., Hagelthorn, G., Gafvert, E., Nilsson, J. L., and Karlberg, A. T. (1998) Contact allergens from surfactants. Atmospheric oxidation of polyoxyethylene alcohols, formation of ethoxylated aldehydes, and their allergenic activity. *J. Pharm. Sci. 87*, 276−282.

(36) Cullis, P. R., Hope, M. J., Bally, M. B., Madden, T. D., Mayer, L. D., and Fenske, D. B. (1998) Influence of pH gradients on the transbilayer transport of drugs, lipids, peptides and metal ions into large unilamellar vesicles. *Biochim. Biophys. Acta 1331*, 187−211.

(37) Tardi, P. G., Swartz, E. N., Harasym, T. O., Cullis, P. R., and Bally, M. B. (1997) An immune response to ovalbumin covalently coupled to liposomes is prevented when the liposomes used contain doxorubicin. *J. Immunol. Methods 210*, 137−148.

(38) Bailey, A. L., and Cullis, P. R. (1994) Modulation of membrane fusion by asymmetric transbilayer distributions of amino lipids. *Biochemistry 33*, 12573−12580.

BC990005P

© 1999 American Chemical Society, Bioconjugate Chem., Ansell bc990005p Supporting Info Page 1

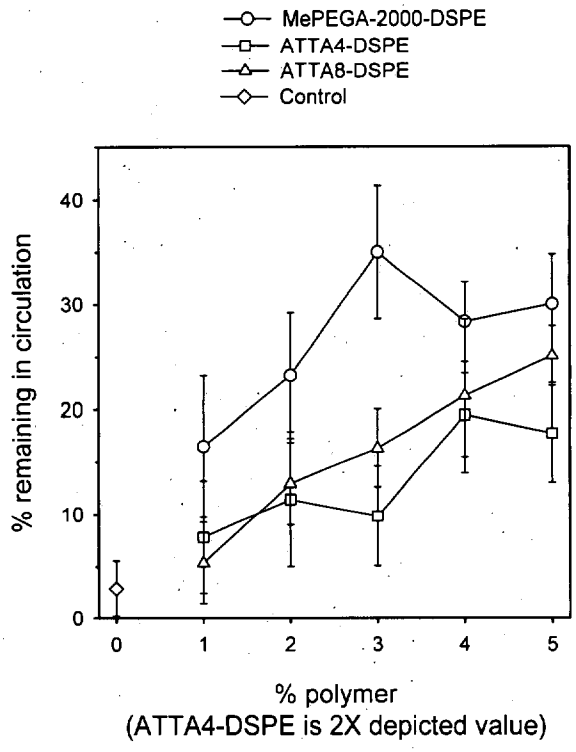


Figure 13. Clearance of sterically stabilized liposomes 20h post administration in female ICR mice (6-8 weeks old). [^{14}C]-CHE labeled liposomes composed of POPC/chol (55:45; 50mM) were prepared in HBS (25mM hepes, 150mM NaCl, pH7.4). Aliquots of the liposome solution were treated with aliquots from SBL stock solutions (0, 0.5, 1.0, 1.5, 2.0 and 2.5mol % of total lipid), diluted to 5mM lipid and incubated at 45°C for an hour. The liposomes were filtered through 0.22μm filters and administered to mice (200μl per animal) by intravenous tail vein injection. Serum was collected after 16h and analysed for radioactivity by liquid scintillation counting. SBL = MePEGA-2000-DSPE, circles; ATTA8-DSPE, triangles; ATTA4-DSPE, squares; no SBL, diamond. Error bars represent standard deviation for 5 animals.

These results demonstrate the effects of incomplete exchange of an SBL into preformed liposomes. The MePEGA-2000-DSPE data is comparable to that obtained using preformulated systems. The ATTA8-DSPE and particularly the ATTA4-DSPE systems, on the other hand, compare very poorly to their preformulated counterparts, suggesting that the ATTAn-DSPE micelles are stabilized against monomer exchange in some way.

© 1999 American Chemical Society, Bioconjugate Chem., Ansell bc990005p Supporting Info Page 2

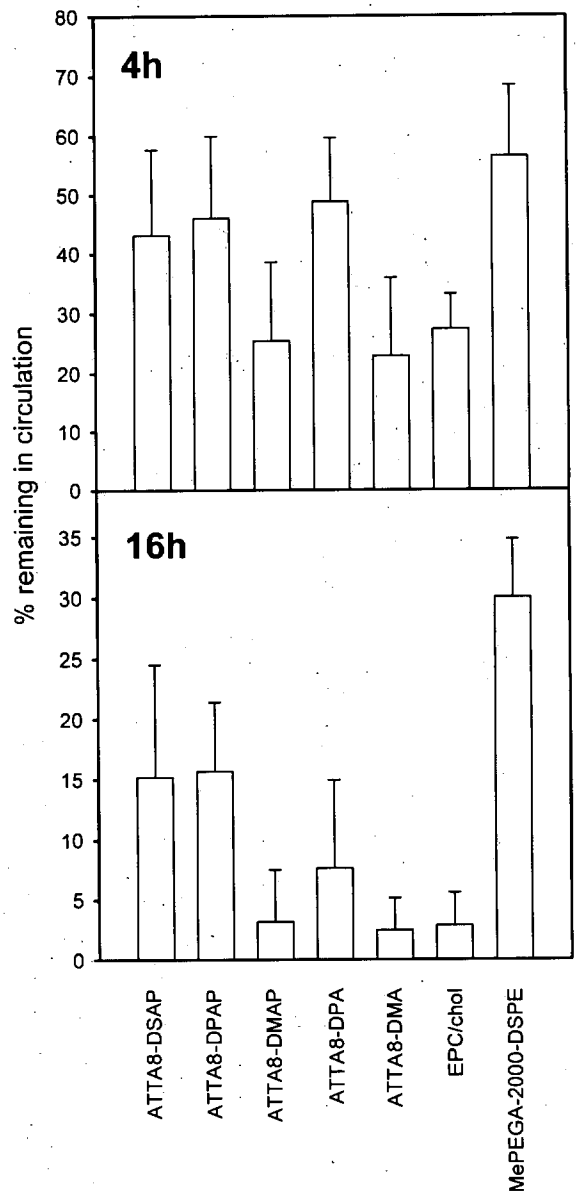
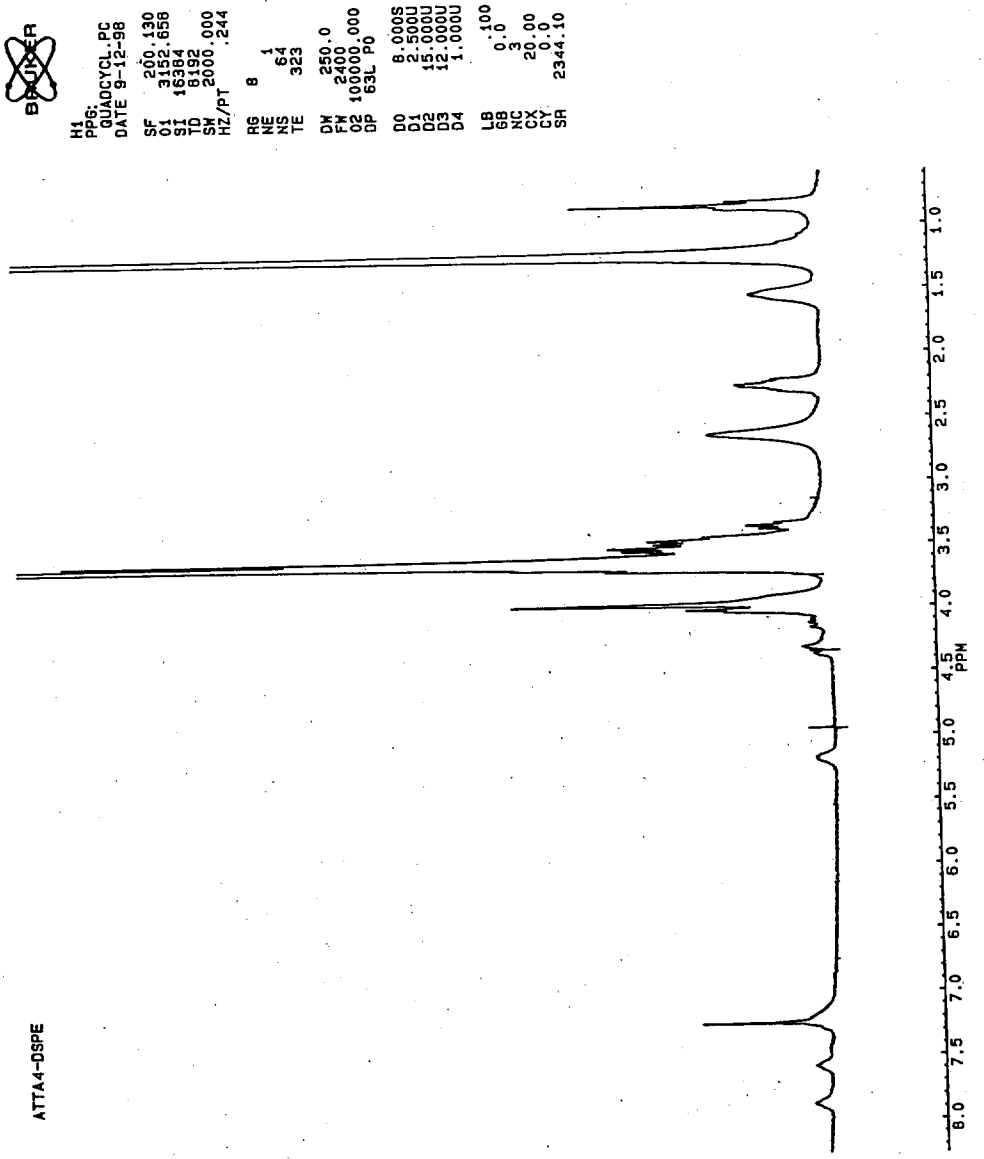


Figure 14. Clearance of sterically stabilized liposomes 4h and 20h post administration in female ICR mice (6-8 weeks old) using neutral SBL components. [^{14}C]-CHE labeled liposomes composed of POPC/chol (55:45; 50mM) were prepared in HBS (25mM hepes, 150mM NaCl, pH7.4). Aliquots of the liposome solution were treated with aliquots from SBL stock solutions (0, 0.5, 1.0, 1.5, 2.0 and 2.5mol % of total lipid), diluted to 5mM lipid and incubated at 45°C for an hour. The liposomes were filtered through 0.22μm filters and administered to mice (200μl per animal) by intravenous tail vein injection. Blood (25μl) was collected 4h post injection by tail nicks. Blood samples were digested in solvable and analyzed for radioactivity by liquid scintillation counting. Liposome levels were estimated based on estimated blood volume of 8%. Serum was collected after 16h and analysed for radioactivity by liquid scintillation counting. Liposome levels were estimated based on estimated serum volume of 4.55%. Error bars represent standard deviation for 5 animals.

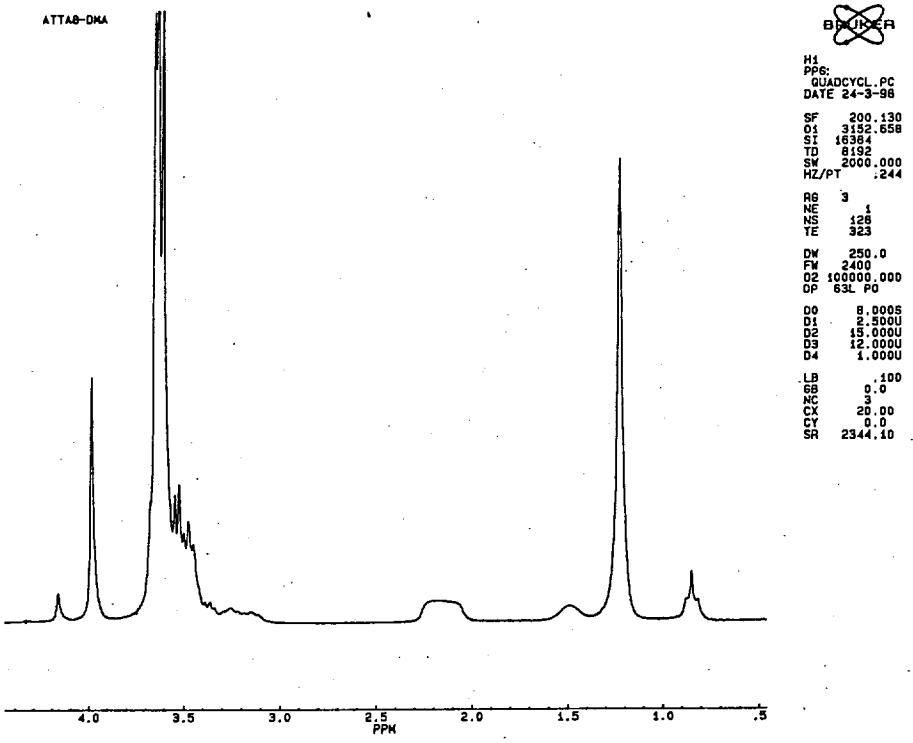
© 1999 American Chemical Society, Bioconjugate Chem., Ansell bc990005p Supporting Info Page 3

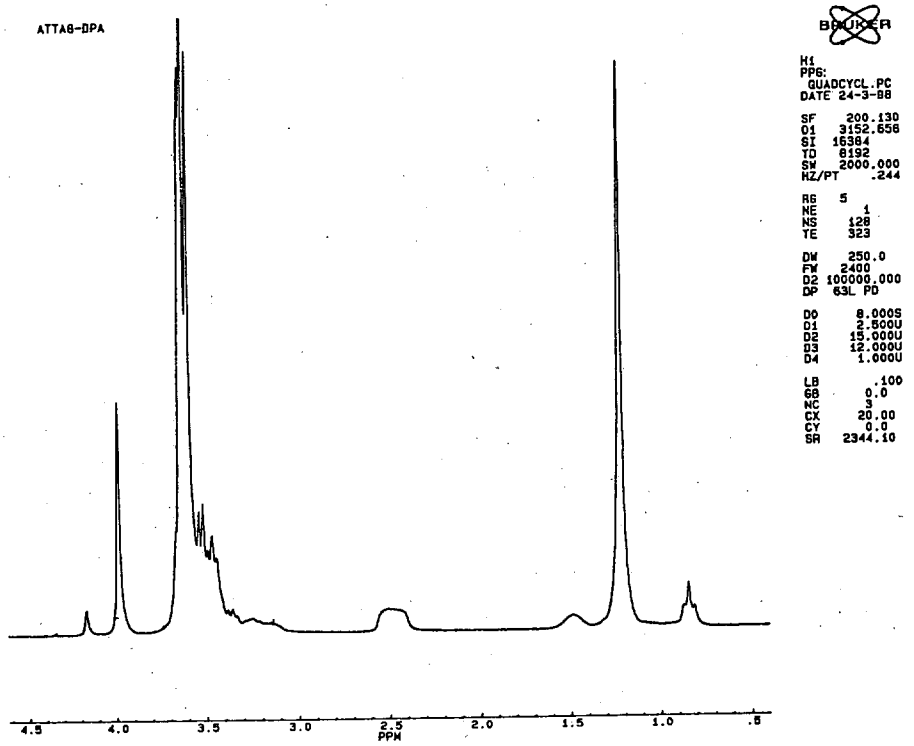
Figure 15. ^{1}H NMR spectra of ATTA4-DSPE



© 1999 American Chemical Society, Bioconjugate Chem., Ansell bc990005p Supporting Info Page 4

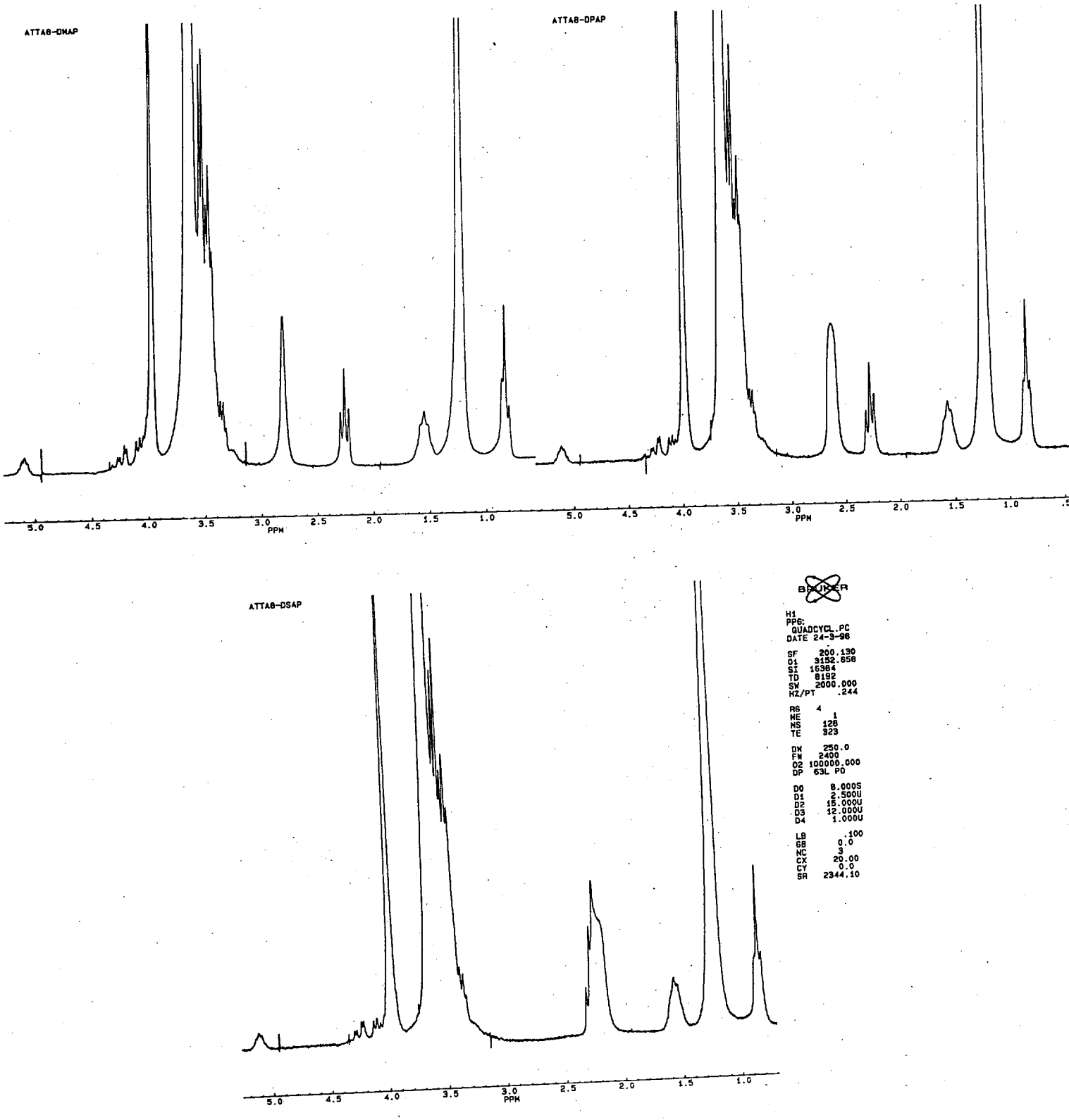
Figure 16. ^{1}H NMR spectra of ATTA8-DxA series





© 1999 American Chemical Society, Bioconjugate Chem., Ansell bc990005p Supporting Info Page 5

Figure 17. ^{1}H NMR spectra of ATTA8-DxAP



© 1999 American Chemical Society, Bioconjugate Chem., Ansell bc990005p Supporting Info Page 6

Elemental analysis

Sample	%C		%H		%N	
	found	calc.	found	calc.	found	calc.
ATTA8-DMAP	55.10	55.46	8.71	8.85	6.29	6.41
ATTA8-DPAP	55.93	56.15	9.09	8.97	6.05	6.26
ATTA8-DSAP	56.78	56.81	8.85	9.09	6.10	6.12
ATTA8-DMA	55.43	56.35	8.83	9.15	6.49	6.69
ATTA8-DPA	56.95	57.05	9.11	9.28	6.57	6.53
BOC-DMAP	70.94	70.65	11.78	11.37	2.20	2.29
BOC-DPAP	72.03	71.92	12.07	11.62	2.11	2.10
BOC-DSAP	73.18	72.98	11.16	11.83	1.92	1.93
DMA	82.15	82.27	13.72	14.30	3.45	3.43
DPA	82.46	83.04	14.79	13.94	2.99	3.03

© 1999 American Chemical Society, Bioconjugate Chem., Ansell bc990005p Supporting Info Page 7

Cytotoxicity profiles for ATTA8 through successive dilutions.

µM	MB 231 mean	SD	HeLa mean	SD	COLO 205 mean	SD	U87 mean	SD	B16 mean	SD	9L mean	SD
0	100	1	100	1	100	1	100	1	100	1	100	1
0.05	100	13.9	100.0	4.6	99.1	4.3	100.0	6.8	100.0	7.4	100.0	10.7
0.1	99.7	6.3	101.4	5.9	99.1	4.6	103.1	18.2	90.5	7.6	99.9	7.3
0.5	96.2	9.3	102.1	6.8	104.2	5.9	105.3	6.3	95.8	8.4	102.4	8.9
1	93.8	2.9	103.3	5.4	103.9	7.0	104.8	8.4	95.6	6.3	96.5	14.0
5	98.8	10.1	103.3	8.6	100.2	9.4	100.7	7.5	93.0	4.3	91.8	13.5
10	97.8	3.4	107.9	4.7	97.4	34.2	105.3	13.6	90.5	6.3	84.6	22.9
50	102.6	7.3	102.0	71.7	101.5	6.4	90.7	4.1	87.2	9.1	81.4	9.8
100	100.3	8.5	100.5	4.4	102.2	5.8	85.6	6.4	78.4	13.5	73.9	11.8
500	98.0	18.2	95.5	4.9	102.5	6.1	85.3	3.9	84.8	14.1	62.4	9.1
1000	91.6	10.6	93.2	5.1	106.9	5.5	85.5	3.4	78.6	7.9	60.9	10.1

µM	SKOV-3		MCF-7		BHK-21	
0	100	1	100	1	100	1
0.05	86.3	10.5	101.9	15.9	99.1	8.6
0.1	80.7	11.3	94.4	17.5	94.2	7.1
0.5	81.8	19.1	91.2	11.0	97.2	6.9
1	84.2	19.6	93.7	21.0	104.0	9.0
5	75.4	17.5	85.1	12.6	100.9	8.4
10	72.3	19.4	77.5	20.4	100.6	3.7
50	61.8	14.3	79.6	18.8	101.3	4.2
100	68.9	6.1	78.2	11.4	101.3	4.2
500	53.6	3.5	75.2	20.3	99.3	5.7
1000	58.0	13.6	74.1	14.9	99.8	7.2

n = 8

Functionalized Congeners of 1,4-Dihydropyridines as Antagonist Molecular Probes for A_3 Adenosine Receptors

An-Hu Li, Louis Chang, Xiao-duo Ji, Neli Melman, and Kenneth A. Jacobson*

Molecular Recognition Section, Laboratory of Bioorganic Chemistry, National Institute of Diabetes, Digestive and Kidney Diseases, National Institutes of Health, Building 8A, Room B1A-19, Bethesda, Maryland 20892-0810. Received February 4, 1999; Revised Manuscript Received March 26, 1999

4-Phenylethynyl-6-phenyl-1,4-dihydropyridine derivatives are selective antagonists at human A_3 adenosine receptors, with K_i values in a radioligand binding assay vs [^{125}I]AB-MECA [N^6-(4-amino-3-iodobenzyl)-5′-*N*-methylcarbamoyl-adenosine] in the submicromolar range. In this study, functionalized congeners of 1,4-dihydropyridines were designed as chemically reactive adenosine A_3 antagonists, for the purpose of synthesizing molecular probes for this receptor subtype. Selectivity of the new analogues for cloned human A_3 adenosine receptors was determined in radioligand binding in comparison to binding at rat brain A_1 and A_{2A} receptors. Benzyl ester groups at the 3- and/or 5-positions and phenyl groups at the 2- and/or 6-positions were introduced as potential sites for chain attachment. Structure−activity analysis at A_3 adenosine receptors indicated that 3,5-dibenzyl esters, but not 2,6-diphenyl groups, are tolerated in binding. Ring substitution of the 5-benzyl ester with a 4-fluorosulfonyl group provided enhanced A_3 receptor affinity resulting in a K_i value of 2.42 nM; however, a long-chain derivative containing terminal amine functionalization at the 4-position of the 5-benzyl ester showed only moderate affinity. This sulfonyl fluoride derivative appeared to bind irreversibly to the human A_3 receptor (1 h incubation at 100 nM resulting in the loss of 56% of the specific radioligand binding sites), while the binding of other potent dihydropyridines and other antagonists was generally reversible. At the 3-position of the dihydropyridine ring, an amine-functionalized chain attached at the 4-position of a benzyl ester provided higher A_3 receptor affinity than the corresponding 5-position isomer. This amine congener was also used as an intermediate in the synthesis of a biotin conjugate, which bound to A_3 receptors with a K_i value of 0.60 μM.

INTRODUCTION

Medicinal chemists are currently developing agonists and antagonists that interact selectively with adenosine receptors, of which A_1, A_{2A}, A_{2B}, and A_3 subtypes are known (*1*). As the only subtype identified through cloning (*2*, *3*), the A_3 adenosine receptor has demonstrated unique biological effects, SAR profile, and tissue distribution (*4*). Intense activation of A_3 receptors induces apoptosis (programmed cell death) (*4*). The A_3 receptor has also a cytoprotective action at low agonist concentrations (*4*). The first cytoprotective effects of an A_3 agonist [IB-MECA,[1] N^6-(3-iodobenzyl)-5′-*N*-methylcarbamoyladenosine] were shown following its chronic administration in gerbils in a model of stroke (*5*). The agonist was highly cerebroprotective and depressed nitric oxide synthase (*5*, *6*). In cultured chick cardiac myocytes, a brief prior exposure to nanomolar concentrations of the related 2-chloro derivative, Cl-IB-MECA, protected cells from damage induced by subsequent hypoxia (*7*), thus mimicking a phenomenon termed "preconditioning". The protective effects of an A_3 receptor agonist on cardiac myocytes were also evident when added during the prolonged ischemia (*8*). A_3 receptor agonists at micromolar concentrations were found to induce apoptosis a variety of cell types, including tumor cell lines (*9*) and rat cardiac myocytes (*10*). Thus, the varied effects of A_3 receptor agonists appear to be dual and opposite, i.e., either cytoprotective or cytotoxic, depending on the level of receptor activation and the system studied.

A_3 adenosine receptor antagonists, although only recently introduced (*11*−*16*), were previously hypothesized to act as potential antiasthmatic (*17*), antiinflammatory (*17*), or cerebroprotective agents (*18*).The most promising leads for A_3 receptor antagonists have appeared recently among chemically diverse nonxanthine heterocycles (Figure 1). For example, the 1,4-dihydropyridines, that are potent blockers of L-type calcium channels (*19*, *20*) and used widely in treating coronary heart disease, were found to bind with intermediate affinity to human A_3 receptors and consequently were structurally optimized for subtype selectivity (*12*). In the present and previous studies, we have used the 1,4-dihydropyridine (DHP) nucleus as a template for probing structure−activity relationships (SAR) at adenosine receptors. By careful

* To whom correspondence should be addressed. Phone: (301) 496-9024. Fax: (301) 480-8422. E-mail: kajacobs@helix.nih.gov.

[1] Abbreviations: [^{125}I]AB-MECA, [^{125}I]N^6-(4-amino-3-iodobenzyl)-5′-*N*-methylcarbamoyladenosine; CGS 21680, 2-[4-[(2-carboxyethyl)phenyl]ethyl-amino]-5′-*N*-ethylcarbamoyl-adenosine, CHAPS, 3-[(3-cholamidopropyl)dimethylammonio]−1-propanesulfonate; CHO cells, Chinese hamster ovary cells; DHP, 1,4-dihydropyridine; DMAP, *N*,*N*-dimethylaminopyridine; DMSO, dimethyl sulfoxide; DPPA, diphenylphosphoryl azide; EDAC, 1-ethyl-3-(3-dimethylaminopropyl)carbodiimide; HEK cells, human embryonic kidney cells; IB-MECA, N^6-(3-iodobenzyl)-5′-*N*-methylcarbamoyladenosine; K_i, equilibrium inhibition constant; MRS 1097, 3,5-diethyl 2-methyl-6-phenyl-4-[2-phenyl-(*E*)-vinyl]-1,4-(±)-dihydropyridine-3,5-dicarboxylate; MRS 1163, N^6-(3-isothiocyanatobenzyl)-5′-*N*-methylcarbamoyladenosine; MRS 1191, 3-ethyl 5-benzyl 2-methyl-6-phenyl-4-phenylethynyl-1,4-(±)-dihydropyridine-3,5-dicarboxylate; NBS, *N*-bromosuccinimide; *R*-PIA, *R*-N^6-phenylisopropyladenosine; SAR, structure−activity relationship; TBAF, tetrabutylammonium fluoride; TMS, tetramethylsilane; Tris, tris(hydroxymethyl)aminomethane.

10.1021/bc9900136 CCC: $18.00 © 1999 American Chemical Society
Published on Web 05/20/1999

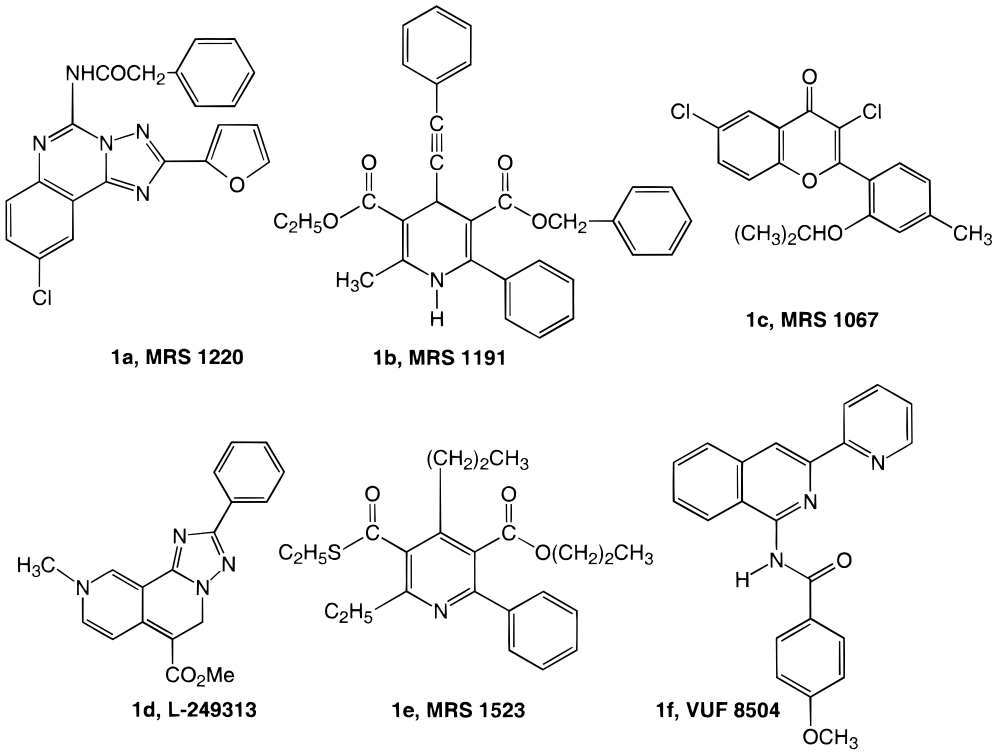


Figure 1. Structures of key A_3 adenosine receptor selective antagonists reported previously.

structural modification, it has been possible to select for affinity at adenosine receptors and deselect for affinity at L-type Ca^{2+}-channels.

The most potent antagonist of the human A_3 receptor yet reported is MRS 1220 (Figure 1, **1a**) (*16*), a derivative of the nonselective triazoloquinazoline antagonist CGS 15943. Within the series of DHP derivatives, affinity and selectivity for the human A_3 receptor were further enhanced in the trisubstituted analogue MRS 1191, 3-ethyl 5-benzyl 2-methyl-6-phenyl-4-phenylethynyl-1,4-(±)-dihydropyridine-3,5-dicarboxylate (Table 1, **1b**) (*12*). Other A_3 selective antagonists that have been recently reported include a flavonoid derivative (MRS 1067, **1c**) (*11*), a triazolonaphthyridine (L-249313, **1d**) (*13*), a pyridine (MRS 1523, **1e**) (*14*), and a pyridyl isoquinoline (VUF 8504, **1f**) (*15*).

In the present study, the SAR of 1,4-dihydropyridines as antagonist ligands for adenosine receptors has been expanded using a "functionalized congener approach" (*21*). By this approach, a chain substituent is attached to the pharmacophore at a strategic position, such that conjugation to other large molecules is made possible through an easily derivatized functional group, without losing the ability to bind to the receptor. This approach leads to increased flexibility of substitution and enhancement of potency/selectivity via distal interactions at the receptor. This approach has been developed for other selective adenosine receptor agonists and antagonists, such as the potent xanthine amine congener, XAC (8-[4-[[[[(2-aminoethyl)-amino]carbonyl]methyl]oxy]phenyl]-1,3-dipropylxanthine) (*34*), and ligands for other receptors (*35*), leading to irreversibly binding affinity probes, fluorescent probes, etc.

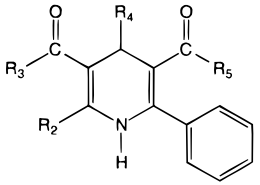
A typical means of derivatization in the design of functionalized congeners is to locate a position on the pharmacophore that may readily accommodate substitution with a phenyl group (*34*), without losing affinity for the receptor. In the present study, we have systematically explored the DHP template for additional sites of incorporation of phenyl substituents and various functional groups followed by chain extension. Fluorosulfonyl groups (*29*) were included in the analogues as an electrophilic group for potential covalent reaction with the receptor, which was indicated in binding experiments with one derivative. Finally, the incorporation of easily derivatizable amino groups at strategic positions was accomplished.

MATERIALS AND METHODS

Synthesis. *Materials and Instrumentation*. Phenylpropargyl aldehyde (**25**), benzyl acetoacetate (**26a**), ethyl benzoyl acetate (**26b**), 2-methoxyethyl acetoacetate (**26i**), 2,2,6-trimethyl-4*H*-1,3-dioxin-4-one (**27**), ethylene glycol (**28d**), 2-mercaptoethanol (**28e**), ethylene dithiol (**28f**), 2-trimethylsilylethanol (**28h**), *p*-nitrobenzyl alcohol (**29**), *p*-toluenesulfonyl fluoride (**30a**), *p*-toluenesulfonamide (**30b**), NBS, 2-(trimethylsilyl)ethanethiol, α-bromo-*p*-toluic acid, chloromethyl methyl ether, and 2-bromoethanol were purchased from Aldrich (St. Louis, MO). 2-Trimethylsilylethylthioethanol (**28g**) was prepared by reaction of 2-(trimethylsilyl)ethanethiol (1.1 mmol), 2-bromoethanol (1.0 mmol), and potassium hydroxide (1.5 mmol) in CH_3CN at room temperature for 4 h (yield, 78%). Compounds **1b**−**4** were prepared as described Jiang et al. (*12*). Dihydropyridines **21** [3-ethyl 5-[4-(2,2,2-trichloroethoxycarbonyl])benzyl] 2-methyl-4-phenylethynyl-6-phenyl-1,4(±)-dihydropyridine-3,5-dicarboxylate], **22** [3-ethyl 5-[4-(2-aminoethyl)aminocarbonyl-benzyl]-2-methyl-4-phenylethynyl-6-phenyl-1,4(±)-dihydropyridine-3,5-dicarbox-ylate], 1-(ethoxymethyl)-3-(ethoxycarbonyl)-2-methyl-4-(phenylethynyl)-6-phenyl-1,4-dihydropyridine-5-carboxylic acid (**32b**), compound **30c**, and bromide **31c** were prepared according to the method of Jiang et al. (*12*). Compounds **24a**, **24b**, and benzyl benzoyl acetate (**26c**) were prepared in our previous paper (*14*). All other materials were obtained from commercial sources.

Proton nuclear magnetic resonance spectroscopy was performed on a Varian GEMINI-300 spectrometer and

Table 1. Affinities of 1,4-Dihydropyridine Derivatives in Radioligand Binding Assays at A_1, A_{2A}, and A_3 Receptors[a−c]

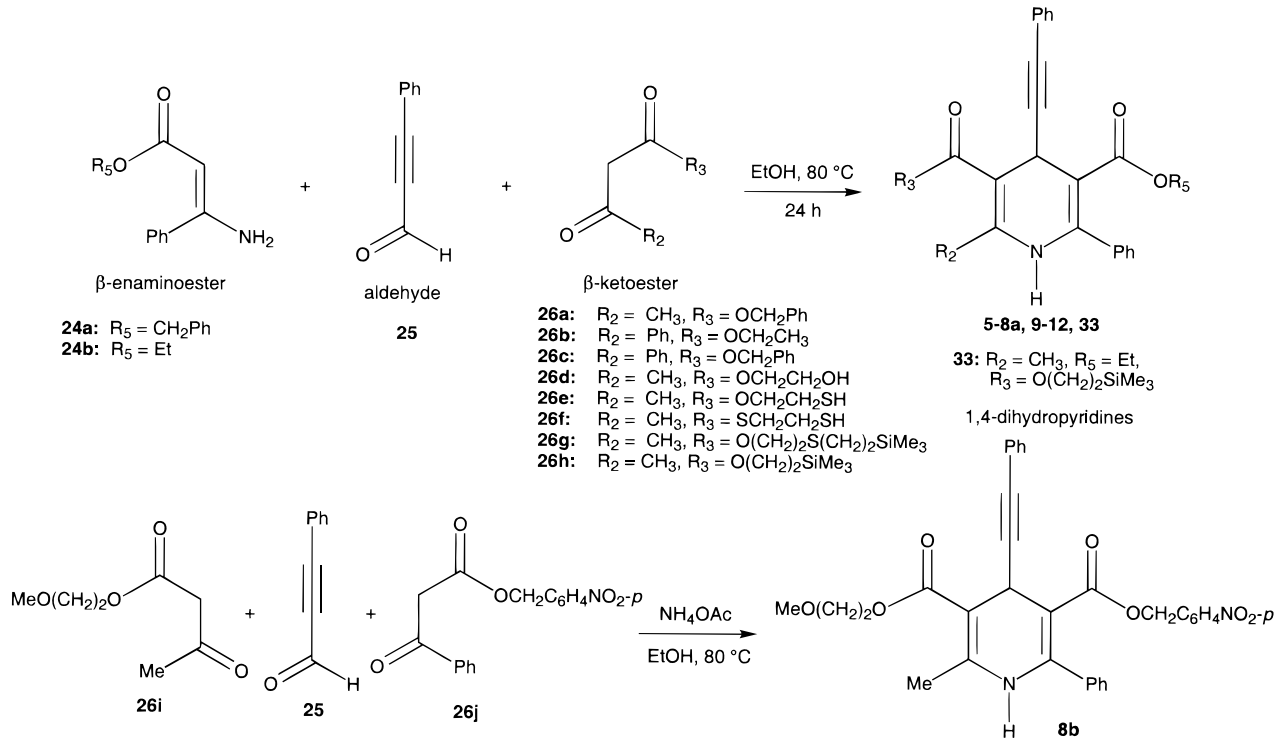


1 - 24, R_2 = Me, unless noted.

				K_i (μM) or % inhibition			
compd	R_3	R_4	R_5	rA_1[a]	rA_{2A}[b]	hA_3[c]	rA_1/hA_3
1b[e]	OCH_2CH_3	Ph-C≡C-	OCH_2Ph	40.1 ± 7.5	d (10^{-4})	0.0314 ± 0.0028	1300
2[e]	OCH_2CH_3	Ph-CH=CH- (trans)	OCH_2CH_3	5.93 ± 0.27	4.77 ± 0.29	0.108 ± 0.012	55
3[e]	OCH_2CH_3	Ph-C≡C-	OCH_2CH_3	11.0 ± 0.1	26 ± 12% (10^{-4})	0.0766 ± 0.0151	140
4[e]	OCH_2Ph	Ph-C≡C-	OCH_2CH_3	24 ± 4% (10^{-4})	d (10^{-4})	0.169 ± 0.026	>600
5	OCH_2Ph	Ph-C≡C-	OCH_2Ph	d (10^{-4})	d (10^{-4})	0.195 ± 0.038	>500
6, 2-Ph	OCH_2CH_3	Ph-C≡C-	OCH_2Ph	36 ± 11% (10^{-4})	d (10^{-4})	20% (10^{-5})	
7, 2-Ph	OCH_2Ph	Ph-C≡C-	OCH_{2Ph}	19 ± 8% (10^{-4})	d (10^{-4})	d (10^{-5})	
8a	$O(CH_2)_2OCH_3$	Ph-C≡C-	OCH_2Ph	48.7 ± 7.3	14 ± 7% (10^{-4})	0.001 91 ± 0.000 31	25 000
8b	$O(CH_2)_2OCH_3$	Ph-C≡C-	OCH_2Ph-4−NO_2	23.6 ± 9.1	d (10^{-4})	0.003 08 ± 0.001 22	7700
9	$O(CH_2)_2OH$	Ph-C≡C-	OCH_2Ph	10.6 ± 1.9	d (10^{-4})	0.002 07 ± 0.0012	5100
10	$O(CH_2)_2SH$	Ph-C≡C-	OCH_2Ph	d (10^{-4})	d (10^{-4})	0.197 ± 0.076	>500
11	$S(CH_2)_2SH$	Ph-C≡C-	OCH_2Ph	38 ± 11% (10^{-4})	d (10^{-4})	0.178 ± 0.018	>500
12	$O(CH_2)_2S(CH_2)_2$ $Si(CH_3)_3$	Ph-C≡C-	OCH_2Ph	13 ± 7% (10^{-4})	30% (10^{-4})	1.98 ± 0.64	>50
13	OCH_2(4-SO_2F)Ph	Ph-C≡C-	OCH_2CH_3	d (10^{-4})	18	0.341 ± 0.091	>300
14	OCH_2(4-SO_2NH_2)Ph	Ph-C≡C-	OCH_2CH_3	16.9 ± 5.0	13.5 ± 1.3	0.187 ± 0.033	90
15	OCH_2(4-$CO_2CH_2CCl_3$)Ph	Ph-C≡C-	OCH_2CH_3	19% (10^{-4})	5.99 ± 1.67	8.93 ± 5.63	>1
16	OCH_2Ph-4-CO−$NH(CH_2)_2NH2$	Ph-C≡C-	OCH_2CH_3	6.65 ± 1.35	7.85	0.128 ± 0.018	52
17	OCH_2(4-CO_2H)Ph	Ph-C≡C-	OCH_2CH_3	16.0 ± 2.1	<1 (shallow curves)	0.799 ± 0.297	20
18	OCH_2Ph-4-CO-$NH(CH_2)_2NH$-biotin	Ph-C≡C-	OCH_2CH_3	38 ± 2% (10^{-4})	16 ± 8% (10^{-4})	0.599 ± 0.151	>100
19[f]	OCH_2CH_3	Ph-C≡C-	OCH_2(4-SO_2F)Ph	41 ± 3% (10^{-4})	20% (10^{-4})	0.002 42 ± 0.000 32	>30 000
20	OCH_2CH_3	Ph-C≡C-	OCH_2(4-SO_2NH_2)Ph	14.4 ± 2.4	22.0 ± 6.1	0.292 ± 0.030	49
21	OCH_2CH_3	Ph-C≡C-	OCH_2 (4-$CO_2CH_2CCl_3$)Ph	33 ± 6% (10^{-4})	11% (10^{-4})	5.00	>20
22[g]	OCH_2CH_3	Ph-C≡C-	OCH_2Ph-4-CO-$NH(CH_2)_2NH_2$	3.0	39 ± 4% (10^{-4})	0.697 ± 0.259	4.3
23	OCH_2CH_3	Ph-C≡C-	OCH_2 (4-CO_2H)Ph	19.0 ± 5.3	8.22 ± 3.76	d (10^{-6})	

[a] Displacement of specific [^{3}H]*R*−PIA binding in rat brain membranes, expressed as K_i ± SEM (n = 2−5), or as a percentage of specific binding displaced at the indicated concentration (M). [b] Displacement of specific [^{3}H]CGS 21 680 binding in rat striatal membranes, expressed as K_i ± SEM (n = 2−6), or as a percentage of specific binding displaced at the indicated concentration (M). [c] Displacement of specific [^{125}I]AB-MECA binding at human A_3 receptors expressed in HEK cells, in membranes, expressed as K_i ± SEM (n = 2−4). [d] Displacement of ≤10% of specific binding at the indicated concentration (M). [e] Values taken from Jiang et al. (*12*) and references therein. [f] Bound to human A_3 receptors irreversibly (see Figure 2), K_i value is apparent. [g] Same as compound 25 in Jiang et al. (*12*) K_i values have been redetermined.

Scheme 1. Synthesis of 6-Phenyl-4-phenylethynyl-1,4-dihydropyridine Derivatives Using the Hantzsch Reaction[a]



[a] Silyl-, hydroxyl-, and thiol-containing ester groups are included. The 2-position contains either a methyl or a phenyl group.

all spectra were taken in $CDCl_3$. Chemical ionization (CI) mass spectrometry was performed with a Finnigan 4600 mass spectrometer and electron-impact (EI) mass spectrometry with a VG7070F mass spectrometer at 6 kV. Elemental analysis was performed either by Atlantic Microlab Inc. (Norcross, GA) or by Galbraith Laboratories, Inc. (Knoxville, TN).

General Procedure for Preparation of Substituted 1,4-Dihydropyridine (5−8a, 9−12, and 33, Scheme 1). Equimolar amounts (0.5−1.0 mmol) of the appropriate *β*-enaminoester (**24**), aldehyde (**25**), and *β*-ketoester (**26**) were dissolved in 2−5 mL of absolute ethanol. The mixture was sealed in a Pyrex tube and heated, with stirring, at 80 °C for 18−24 h. After cooled to room temperature, the solvent was evaporated and the residue was purified by preparative TLC [silica 60; 1000 or 2000 μm; Analtech, Newark, DE; petroleum ether-ethyl acetate (1:1−4:1)].

*3,5-Dibenzyl 2-Methyl-4-phenylethynyl-6-phenyl-1,4-(±)-dihydropyridine-3,5-dicarboxylate (**5**).* ^{1}H NMR ($CDCl_3$): 2.34 (s, 3 H, 2-CH_3), 5.01 (AB, 2 H, J = 12.6 Hz, 3-OCH_2Ph), 5.24 (s, 1 H, 4-H), 5.27 (AB, 2 H, J = 13.8 Hz, 5- OCH_2Ph), 6.05 (s, br, 1 H, NH), 7.04−7.11 (m, 2 H, aromatic H's), 7.15−7.30 (m, 9 H, aromatic H's), 7.33−7.40 (m, 7 H, aromatic H's), 7.44−7.47 (m, 2 H, aromatic H's). MS (EI): *m*/*z* 539 (M^+), 448 ($M^+ - CH_2$-Ph), 404 ($M^+ - CO_2CH_2Ph$), 91 ($^+CH_2Ph$, base).

*3-Ethyl 5-Benzyl 4-phenylethynyl-2,6-diphenyl-1,4-(±)-dihydropyridine-3,5-dicarboxylate (**6**).* ^{1}H NMR ($CDCl_3$): 1.10 (t, 3 H, J = 7.8 Hz, 3-OCH$_2CH_3$), 4.16 (q, 2 H, J = 7.8 Hz, 3- OCH_2CH$_3$), 5.11 (s, 1 H, 4-H), 5.14 (AB, 2 H, J = 12.9 Hz, 5-OCH_2Ph), 6.86−8.10 (m, 21 H, NH and aromatic H's). MS (EI): *m*/*z* 539 (M^+), 448 ($M^+ - CH_2$-Ph), 404 ($M^+ - CO_2CH_2Ph$), 91 ($^+CH_2Ph$, base).

*3,5-Dibenzyl 4-Phenylethynyl-2,6-diphenyl-1,4-(±)-dihydropyridine-3,5-dicarboxylate (**7**).* ^{1}H NMR ($CDCl_3$): 5.07 (AB, 4 H, J = 12.6 Hz, 3- and 5-OCH_2Ph), 5.35 (s, 1 H, 4-H), 6.15 (s, br, 1 H, NH), 7.07−7.45 (m, 25 H, aromatic H's). MS (EI): *m*/*z* 601 (M^+), 510 ($M^+ - CH_2$-Ph), 466 ($M^+ - CO_2CH_2Ph$), 91 ($^+CH_2Ph$, base). MS (CI−NH_3): *m*/*z* 619 ($M^+ + NH_4$), 602 ($M^+ + 1$). HRMS calcd: 601.2253. Found: 601.2255.

*3-(2-Methoxyethyl) 5-Benzyl 2-Methyl-4-phenylethynyl-6-phenyl-1,4-(±)-dihydropyridine-3,5-dicarboxylate (**8a**).* ^{1}H NMR ($CDCl_3$): 2.35 (s, 3 H, 2-CH_3), 3.37 (s, 3 H, 3-OCH$_2$CH$_2$OCH_3), 3.67 (s, 2 H, J = 5.7 Hz, 3-OCH$_2CH_2$-OCH$_3$), 4.34 (m, 2 H, 3-OCH_2CH$_2$OCH$_3$), 5.01 (AB, 2 H, J = 13.0 Hz, 5-OCH_2Ph), 5.18 (s, 1 H, 4-H), 6.06 (s, br, 1 H, NH), 7.05−7.09 (m, 2 H, aromatic H's), 7.17−7.22 (m, 3 H, aromatic H's), 7.24−7.26 (m, 3 H, aromatic H's), 7.31−7.39 (m, 7 H, aromatic H's). MS (EI): *m*/*z* 507 (M^+), 448 ($M^+ - CH_3OCH_2CH_2$), 416 ($M^+ - CH_2Ph$), 372 ($M^+ - CO_2CH_2Ph$), 268 ($M^+ + 1$-CO_2CH_2Ph-$CO_2CH_2CH_2OCH_3$, base). MS (CI−NH_3): *m*/*z* 525 ($M^+ + NH_4$), 508 ($M^+ + 1$).

*3-(2-Methoxyethyl) 5-(4-Nitrobenzyl) 2-Methyl-4-phenylethynyl-6-phenyl-1,4-(±)-dihydropyridine-3,5-dicarboxylate (**8b**).* 2-Methoxyethyl acetoacetate (**26i**, 160 mg, 1 mmol), phenylpropargyl aldehyde (**25**, 130 mg, 1 mmol), *p*-nitrobenzyl benzoyl acetate (**26j**, 299 mg, 1 mmol), and ammonium acetate (154 mg, 2 mmol) were dissolved in 3 mL of absolute ethanol. The mixture was stirred under N_2 at 95 °C for 24 h. After cooled to room temperature, the solvent was evaporated and the residue was purified by preparative TLC [silica 60; 1000 μm; Analtech, Newark, DE; petroleum ether-ethyl acetate (1:1)] to give 127 mg (yield = 23%) of the product. ^{1}H NMR ($CDCl_3$): 2.38 (s, 3 H, 2-CH_3), 3.40 (s, 3 H, 3-OCH$_2$CH$_2$OCH_3), 3.68 (m, 2 H, 3-OCH$_2CH_2$OCH$_3$), 4.37 (m, 2 H, 3-OCH_2CH$_2$-OCH$_3$), 5.12 (AB, 2 H, J = 13.5 Hz, 5-OCH_2Ph), 5.20 (s, 1 H, 4-H), 6.04 (s, br, 1 H, NH), 7.17−7.44 (m, 12 H, aromatic H's), 8.02 (m, 2 H, aromatic H's). MS (CI−NH_3): *m*/*z* 570 ($M^+ + NH_4$), 553 ($M^+ + 1$), 282 ($M^+ - CH_3$-$CO_2CH_2C_6H_4NO_2$-MeOCH$_2$CH$_2$O, base).

*3-(2-Hydroxyethyl) 5-Benzyl 2-Methyl-4-phenylethynyl-6-phenyl-1,4-(±)-dihydropyridine-3,5-dicarboxylate (**9**).* ^{1}H

NMR ($CDCl_3$): 2.35 (s, 3 H, 2-CH_3), 3.84 (m, 2 H, 3-OCH_2CH_2OH), 4.17 (m, 1 H, 3-OCH_2CH_2OH), 4.45 (m, 1 H, 3-OCH_2CH_2OH), 4.99 (AB, 2 H, J = 12.6 Hz, 5-OCH_2Ph), 5.17 (s, 1 H, 4-H), 6.20 (s, br, 1 H, NH), 7.02−7.39 (m, 15 H, aromatic H's). MS (EI): *m/z* 493 (M^+), 448 ($M^+ - HOCH_2CH_2$), 432 ($M^+ - HOCH_2CH_2O$), 404 ($M^+ - HOCH_2CH_2O_2C$), 402 ($M^+ - CH_2Ph$), 358 ($M^+ - CO_2CH_2Ph$), 91 ($^+CH_2Ph$, base).

*3-(2-Mercaptoethyl) 5-Benzyl 2-Methyl-4-phenylethynyl-6-phenyl-1,4-(±)-dihydropyridine-3,5-dicarboxylate (**10**).* ^1H NMR ($CDCl_3$): 1.77 (t, 1 H, J = 8.7 Hz, SH), 2.36 (s, 3 H, 2-CH_3), 2.82 (m, 2 H, 3-OCH_2CH_2SH), 4.23 (m, 1 H, 3-OCH_2CH_2SH), 4.42 (m, 1 H, 3-OCH_2CH_2SH), 5.01 (AB, 2 H, J = 12.6 Hz, 5-OCH_2Ph), 5.17 (s, 1 H, 4-H), 6.07 (s, br, 1 H, NH), 7.05−7.37 (m, 15 H, aromatic H's). MS (EI): *m/z* 509 (M^+), 448 ($M^+ - HSCH_2CH_2$), 419 ($MH^+ - CH_2Ph$), 404 ($M^+ - HSCH_2CH_2O_2C$), 374 ($M^+ - CO_2CH_2Ph$), 91 ($^+CH_2Ph$, base).

*3-(2-Mercaptoethylsulfanyl) 5-Benzyl 2-Methyl-4-phenylethynyl-6-phenyl-1,4-(±)-dihydropyridine-3,5-dicarboxylate (**11**).* ^1H NMR ($CDCl_3$): 1.69 (t, 1 H, J = 8.7 Hz, SH), 2.36 (s, 3 H, 2-CH_3), 2.75 (dt, 2 H, J = 8.7, 6.9 Hz, 3-SCH_2CH_2SH), 3.20 (t, 1 H, J = 6.9 Hz, 3-SCH_2CH_2SH), 5.04 (AB, 2 H, J = 12.6 Hz, 5-OCH_2Ph), 5.32 (s, 1 H, 4-H), 6.14 (s, br, 1 H, NH), 7.05−7.41 (m, 15 H, aromatic H's). MS (EI): *m/z* 525 (M^+), 432 ($M^+ - HSCH_2CH_2S$), 404 ($M^+ - HSCH_2CH_2SOC$), 330 ($MH^+ - CO_2CH_2Ph$-SCH_2CH_2SH, base), 91 ($^+CH_2Ph$). HRMS calcd for MH+: 526.1511. Found: 526.1466.

*3-(2-Trimethylsilylethylthioethyl) 5-Benzyl 2-Methyl-4-phenylethynyl-6-phenyl-1,4-(±)-dihydropyridine-3,5-dicarboxylate (**12**).* ^1H NMR ($CDCl_3$): 0.00 (m, 9 H, 3-$SiCH_3$), 0.85 (m, 2 H, 3-$SCH_2CH_2SiMe_3$), 2.34 (s, 3 H, 2-CH_3), 2.60 (m, 2 H, 3-$SCH_2CH_2SiMe_3$), 2.82 (m, 2 H, 3-$CO_2CH_2CH_2SCH_2CH_2SiMe_3$), 4.33 (m, 2 H, 3-$CO_2CH_2CH_2SCH_2CH_2SiMe_3$), 5.00 (AB, 2 H, J = 12.9 Hz, 5-OCH_2Ph), 5.15 (s, 1 H, 4-H), 6.03 (s, br, 1 H, NH), 7.04−7.40 (m, 15 H, aromatic H's). MS (CI−NH_3): *m/z* 609 (M^+), 518 ($M^+ - CH_2Ph$), 448 ($M^+ - CH_2CH_2SCH_2CH_2SiMe_3$, base).

*3-(2-Trimethylsilylethyl) 5-Ethyl 2-Methyl-4-phenylethynyl-6-phenyl-1,4-(±)-dihydropyridine-3,5-dicarboxylate (**33**).* ^1H NMR ($CDCl_3$): 0.00 (m, 9 H, 3-$SiCH_3$), 0.99 (t, 3 H, J = 7.8 Hz, 5-OCH_2CH_3), 1.12 (t, 2 H, J = 8.8 Hz, 3-$OCH_2CH_2SiMe_3$), 2.57 (s, 3 H, 2-CH_3), 4.02 (m, 2 H, 3-$CO_2CH_2CH_2SiMe_3$), 4.33 (t, 2 H, J = 7.8 Hz, 5-OCH_2CH_3), 5.13 (s, 1 H, 4-H), 5.87 (s, br, 1 H, NH), 7.25−7.44 (m, 10 H, aromatic H's).

General Procedure for Preparation of 1,4-Dihydropyridine-3,5-dicarboxylate Esters 13−15, 32c−d, and 19−20 (Scheme 3). (Condition a) Compound **32a** or **32b** (0.04 mmol) was dissolved in dry acetone (2 mL) and anhydrous potassium carbonate (0.1 g), and the appropriate benzyl bromide (**31a−d**, 5 equiv.) was added, and the mixture was refluxed for 2−6 h. After filtering the mixture, the solvent was evaporated in vacuo. The residue was separated by preparative TLC (4:1 hexanes/EtOAc), and the desired *N*-protected 3- or 5-benzyl ester DHP was isolated. (Condition b): Deprotection was achieved by dissolving these *N*-ethoxymethyl-protected DHPs in acetone (1 mL) and adding excess 1 N HCl (200 μL) and heating at 45 °C for 2−3 h. The solvent was evaporated followed by purification with preparative TLC (4:1 hexanes/EtOAc or 10:1 $CHCl_3$/MeOH) to afford the desired 3- or 5-benzyl ester DHP.

*3-(4-Fluorosulfonylbenzyl) 5-Ethyl 2-Methyl-4-phenylethynyl-6-phenyl-1,4(±)-dihydropyridine-3,5-dicarboxylate (**13**).* ^1H NMR ($CDCl_3$): δ 0.93 (t, 3H, J = 6.84 Hz, 5-CH_2CH_3), 2.39 (s, 3H, 2-CH_3), 4.12 (q, 2H, J = 6.83 Hz, 5-OCH_2), 5.20 & 5.58 (AB, 2H, J = 14.65 Hz, 3-OCH_2), 5.21 (s, 1H, H-4), 6.23 (br, 1H, NH), 7.28−7.44 (m, 10H, 4-C_6H_5 and 6-C_6H_5), 7.71−7.89 (m, 4H, 3-C_6H_4).

*3-(4-Sulfonylamidobenzyl) 5-Ethyl 2-Methyl-4-phenylethynyl-6-phenyl-1,4(±)-dihydropyridine-3,5-dicarboxylate (**14**).* ^1H NMR ($CDCl_3$): δ 0.93 (t, 3H, J = 6.84 Hz, 5-CH_2CH_3), 2.38 (s, 3H, 2-CH_3), 3.99 (m, 2H, 5-OCH_2), 4.77 (br, 2H, NH_2), 5.20 & 5.49 (AB, 2H, J = 13.67 Hz, 3-OCH_2), 5.19 (s, 1H, H-4), 5.97 (br, 1H, NH), 7.27−7.84 (m, 14H, 3-C_6H_4, 4-C_6H_5 and 6-C_6H_5). HPLC retention time: 7.66 min (> 95% purity) using solvent system 0.1 M TEAA (pH 5.0)/CH_3CN, 80:20 to 20:80, in 20 min with flow rate 1 mL/min.

*3-[4-(2,2,2-Trichloroethoxycarbonyl])benzyl] 5-ethyl 2-Methyl-4-phenylethynyl-6-phenyl-1,4(±)-dihydropyridine-3,5-dicarboxylate (**15**).* ^1H NMR ($CDCl_3$): δ 0.95 (t, 3H, J = 6.84 Hz, 5-CH_2CH_3), 2.38 (s, 3H, 2-CH_3), 4.00 (m, 2H, 5-OCH_2), 4.96 (s, 2H, CH_2CCl_3), 5.22 and 5.51 (AB, 2H, J = 14.65 Hz, 3-OCH_2), 5.21 (s, 1H, H-4), 5.97 (br, 1H, NH), 7.25−8.07 (m, 14H, 3-C_6H_4, 4-C_6H_5 and 6-C_6H_5).

*3-[4-(2-Aminoethyl)aminocarbonylbenzyl] 5-Ethyl 2-Methyl-4-phenylethynyl-6-phenyl-1,4(±)-dihydropyridine-3,5-dicarboxylate (**16**).* Compound **15** (13.4 mg, 0.02 mmol) was mixed with ethylenediamine (0.175 mL). After stirring at room temperature for 4 h, the ethylenediamine was evaporated and the product purified by preparative TLC (5:1 $CHCl_3$/MeOH) to yield 7.0 mg of a white solid (59%). Compound **16** (R_f = 0.68, EtOAc) was shown to be pure by TLC.

^1H NMR ($CDCl_3$): δ 0.95 (t, 3H, J = 6.84 Hz, 5-CH_2CH_3), 2.37 (s, 3H, 2-CH_3), 2.78 (s, 2H, NH_2), 2.96 (t, 2H, J = 5.86 Hz, $-CH_2$-), 3.50 (m, 2H, $-CH_2$-), 4.00 (m, 2H, 5-OCH_2), 5.21 and 5.45 (AB, 2H, J = 13.68 Hz, 3-OCH_2), 5.20 (s, 1H, H-4), 5.92 (br, 1H, NH), 6.75 (br, 1H, $-CH_2NH$-), 7.27−7.73 (m, 14H, 3-C_6H_4, 4-C_6H_5 and 6-C_6H_5).

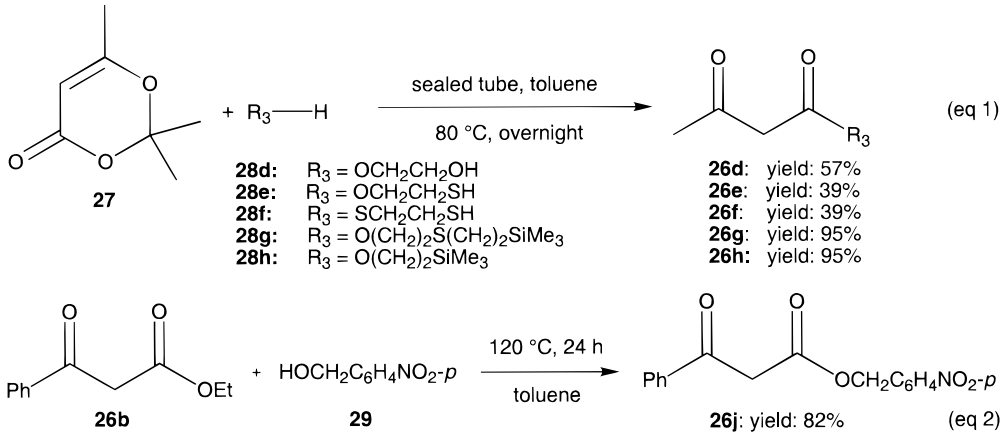
*3-(4-Carboxybenzyl) 5-Ethyl 2-Methyl-4-phenylethynyl-6-phenyl-1,4(±)-dihydropyridine-3,5-dicarboxylate (**17**).* Compound **32c** [3-(4-methoxyethoxycarbonylbenzyl) 5-ethyl 2-methyl-4-phenylethynyl-6-phenyl-1,4(±)-dihydropyridine-3,5-dicarboxylate] was prepared according to the general procedure using 30 mg of **32a** (0.067 mmol) and 86.8 mg of **31d** (0.335 mmol). The crude product was dissolved in 2 mL of acetone. To 1 mL of such acetone solution was added 0.2 mL of 1 N HCl. The mixture was stirred at 45 °C for 2 h. The solution was removed in vacuo and residue was purified by preparative TLC (silica 60; 1000 μM, 10:1 $CHCl_3$/MeOH) to give 13.2 mg of white solid, yield = 38%. Compound **17** (R_f = 0.17, MeOH) was shown to be pure by TLC.

^1H NMR ($CDCl_3$): δ 0.89 (t, 3H, J = 6.84 Hz, 5-CH_2CH_3), 2.38 (s, 3H, 2-CH_3), 4.01 (m, 2H, 5-OCH_2), 4.61 (s, 1H, OH), 5.21 and 5.49 (AB, 2H, J = 13.67 Hz, 3-OCH_2), 5.21 (s, 1H, H-4), 5.96 (br, 1H, NH), 7.35−8.04 (m, 14H, 3-C_6H_4, 4-C_6H_5 and 6-C_6H_5).

*3-[4-(2-D-biotinylaminoethyl)aminocarbonylbenzyl] 5-Ethyl 2-Methyl-4-phenylethynyl-6-phenyl-1,4(±)-dihydropyridine-3,5-dicarboxylate (**18**).* Compound **16** (6.1 mg, 0.01 mmol) and *N*-hydroxysuccinimide biotin (4.4 mg, 0.01 mmol) were dissolved in 0.5 mL of anhydrous DMF and stirred at room temperature overnight. The solvent was evaporated and the product was purified by preparative TLC [12:1 $CHCl_3$/MeOH followed by 6:1 $CHCl_3$/MeOH] to yield 5.6 mg of a yellow solid (64%). Compound **18** (R_f = 0.73, MeOH/EtOAc = 1/3) was shown to be pure by TLC.

^1H NMR ($CDCl_3$): δ 0.90 (t, 3H, J = 6.84 Hz, 5-CH_2CH_3), 1.32 (br, 1H, H-4′), 1.60 (t, 1H, J = 6.84 Hz, H-2′), 1.74 (br, 1H, H-3′), 2.17 (m, 4H, 2 X $-CH_2$-), 2.37

Scheme 2. Synthesis of β-Ketoesters



(s, 3H, 2-CH_3), 2.63 (d, 2H, J = 12.70 Hz, $-CH_2$-5′), 2.82 (m, 2H, $-CH_2$-), 2.97 (m, 2H, $-CH_2$-), 3.47 (br, 1H, NH), 3.55 (br, 1H, NH), 3.94 (q, 2H, J = 6.84 Hz, 5-OCH_2), 4.12 (br, 2H, $-CH_2$-), 4.39 (br, 2H, $-CH_2$-), 5.16 (s, 1H, H-4), 5.21 and 5.40 (AB, 2H, J = 13.67 Hz, 3-OCH_2), 5.60 (br, 1H, NH), 6.29 (br, 1H, NH), 6.54 (br, 1H, NH), 7.16−7.77 (m, 14H, 3-C_6H_4, 4-C_6H_5 and 6-C_6H_5).

*3-Ethyl 5-(4-Fluorosulfonylbenzyl) 2-Methyl-4-phenylethynyl-6-phenyl-1,4(±)-dihydropyridine-3,5-dicarboxylate (**19**).* ^{1}H NMR ($CDCl_3$): δ 1.36 (t, 3H, J = 6.83 Hz, 3-CH_2CH_3), 2.39 (s, 3H, 2-CH_3), 4.30 (m, 2H, 3-OCH_2), 5.04 and 5.13 (AB, 2H, J = 14.66 Hz, 5-OCH_2), 5.19 (s, 1H, 4-H), 6.32 (br, 1H, NH), 7.23−8.00 (m, 14H, 4-C_6H_5, 5-C_6H_4, and 6-C_6H_5).

*3-Ethyl 5-(4-Sulfonamidobenzyl) 2-Methyl-4-phenylethynyl-6-phenyl-1,4-(±)-dihydropyridine-3,5-dicarboxylate (**20**).* ^{1}H NMR ($CDCl_3$): δ 1.35 (t, 3H, J = 6.84 Hz, 3-CH_2CH_3), 2.38 (s, 3H, 2-CH_3), 4.29 (m, 2H, 3-OCH_2), 4.74 (br, 2H, NH_2), 5.10 and 5.18 (AB, 2H, J = 13.68 Hz, 5-OCH_2), 5.18 (s, 1H, 4-H), 5.93 (br, 1H, NH), 7.16−7.83 (m, 14H, 4-C_6H_5, 5-C_6H_4, and 6-C_6H_5). HPLC retention time: 7.42 min (>95% purity) using solvent system 0.1 M TEAA (pH 5.0)/CH_3CN, 80:20 to 20:80, in 20 min with flow rate 1 mL/min.

*3-Ethyl 5-(4-Carboxybenzyl) 2-Methyl-4-phenylethynyl-6-phenyl-1,4(±)-dihydropyridine-3,5-dicarboxylate (**23**).* Compound **32d** [3-ethyl 5-(4-methoxyethoxycarbonylbenzyl) 2-methyl-4-phenylethynyl-6-phenyl-1,4(±)-dihydropyridine-3,5-dicarboxylate] was prepared in quantitative yield according to the general procedure using 35 mg of **32b** (0.0786 mmol) and 102 mg of **31d** (0.392 mmol). An acetone solution (1 mL) of 25.3 mg (0.041 mmol) of **32d** was mixed with 1 N HCl (0.15 mL), and the mixture was stirred at 45 °C for 2 h. The solution was removed in vacuo and residue was purified by preparative TLC (silica 60; 1000 μM, 10:1 $CHCl_3$/MeOH) to give 10.9 mg of light yellow solid, yield = 51%.

^{1}H NMR ($CDCl_3$): δ 1.34 (t, 3H, J = 6.84 Hz, 3-CH_2CH_3), 2.37 (s, 3H, 2-CH_3), 4.26 (m, 2H, 3-OCH_2), 5.00 & 5.15 (AB, 2H, J = 13.68 Hz, 5-OCH_2), 5.17 (s, 1H, 4-H), 5.99 (br, 1H, NH), 7.07−7.92 (m, 14H, 4-C_6H_5, 5-C_6H_4, and 6-C_6H_5).

Synthesis of β-Ketoesters 26d−h (Scheme 2). β-Ketoesters **26d−h** were prepared by the reaction of 2,2,6-trimethyl-4*H*-1,3-dioxin-4-one (**27**) and an alcohol or a thiol (eq 1 in Scheme 2). Equimolar amounts (for example, 3 mmol) of compound **27** and an alcohol or a thiol were heated with a little toluene (1−2 mL) at 80 °C in a sealed tube overnight. After cooled to room temperature, the solvent was removed under reduced pressure and the residue was chromatographed to give desired products in satisfactory yields (57% for **26d**, 39% for **26e**, 39% for **26f**, 95% for **26g**, 95% for **26h**).

*2-Hydroxyethyl Acetoacetate (**26d**).* ^{1}H NMR ($CDCl_3$/TMS): δ 2.29 (s, 3 H, CH_3CO), 2.43 (s, br, 1 H, OH), 3.54 (s, 2 H, CH_3COCH_2CO), 3.84 (m, 2 H, $CO_2CH_2CH_2OH$), 4.31 (t, J = 4.8 Hz, 2 H, $CO_2CH_2CH_2OH$). MS (CI/NH_3): 164 ($M^+ + NH_4$, base), 147 ($M^+ + 1$), 129 ($M^+ - OH$).

*2-Mercaptoethyl Acetoacetate (**26e**).* ^{1}H NMR ($CDCl_3$/TMS): δ 1.54 (t, J = 8.7 Hz, 1 H, SH), 2.29 (s, 3 H, CH_3-CO), 2.78 (dt, J = 8.7, 6.9 Hz, 2 H, $CO_2CH_2CH_2SH$), 3.50 (s, 2 H, CH_3COCH_2CO), 4.28 (t, J = 6.9 Hz, 2 H, CO_2CH_2-CH_2SH). MS (CI/NH_3): 180 ($M^+ + NH_4$, base).

*S-(2-Mercaptoethyl) 3-Oxothiobutyrate (**26f**).* ^{1}H NMR ($CDCl_3$/TMS): δ 1.64 (t, J = 8.7 Hz, 1 H, SH), 2.28 (s, 3 H, CH_3CO), 2.74 (dt, J = 8.7, 6.9 Hz, 2 H, $COSCH_2CH_2$-SH), 3.16 (t, J = 6.9 Hz, 2 H, $COSCH_2CH_2SH$), 3.70 (s, 2 H, CH_3COCH_2CO). MS (CI/NH_3): 196 ($M^+ + NH_4$, base), 179 ($M^+ + 1$).

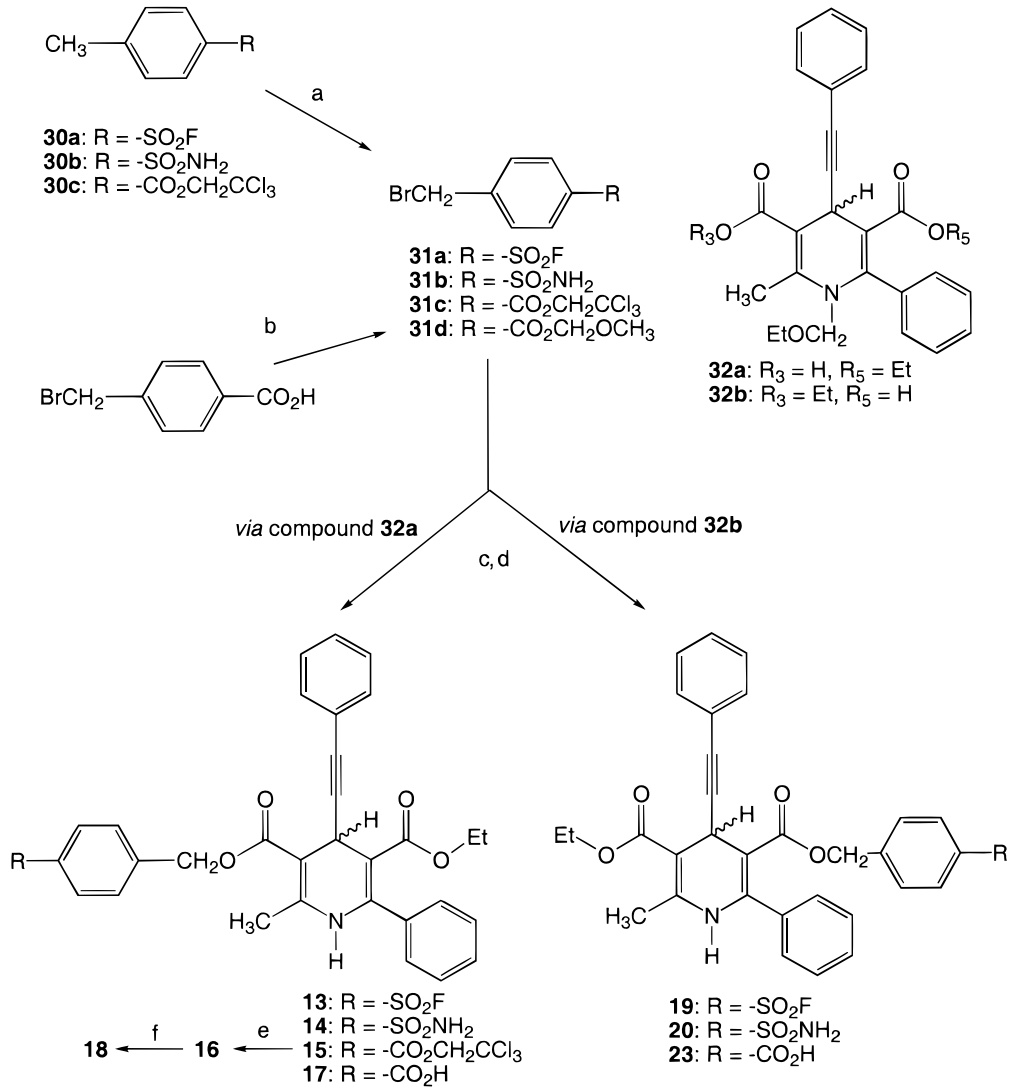
*(2-Trimethylsilylethylthio)ethyl Acetoacetate (**26g**).* ^{1}H NMR ($CDCl_3$/TMS): δ 0.03 (s, 9 H, $SiMe_3$), 0.86 (m, 2 H, $Me_3SiCH_2CH_2S$), 2.28 (s, 3 H, CH_3CO), 2.60 (m, 2 H, Me_3-$SiCH_2CH_2S$), 2.78 (t, J = 6.8 Hz, 2 H, $SCH_2CH_2O_2C$), 3.48 (s, 2 H, CH_3COCH_2CO), 4.29 (t, J = 6.8 Hz, 2 H, CO_2CH_2-CH_2S). MS (CI/NH_3): 280 ($M^+ + NH_4$), 161 ($M^+ - CH_2$-CH_2SiMe_3).

*2-Trimethylsilylethyl Acetoacetate (**26h**).* ^{1}H NMR ($CDCl_3$/TMS): δ 0.03 (s, 9 H, $SiMe_3$), 1.01 (m, 2 H, Me_3-$SiCH_2CH_2$), 2.26 (s, 3 H, CH_3CO), 3.43 (s, 2 H, $OCCH_2$-CO), 4.22 (m, 2 H, $Me_3SiCH_2CH_2O$).

Preparation of *p*-Nitrobenzyl Benzoyl Acetate (26j) (eq 2 in Scheme 2). Ethyl benzoyl acetate (**26b**, 1.92 g, 10 mmol) and *p*-nitrobenzyl alcohol (**29**, 1.53 g, 10 mmol) in toluene (10 mL) were heated with stirring for 24 h. The solvent was removed, and the residue was chromatographed [silica 60, petroleum ether-ethyl acetate (2:1)] to give **26j** (2.08 g, yield = 82%). ^{1}H NMR ($CDCl_3$/TMS): δ 4.11 (s, 2 H, $PhCOCH_2CO$), 5.30 (s, 2 H, $CH_2C_6H_4NO_2$-*p*), 7.47−7.65 (m, 5 H, aromatic H's), 7.94 (d, J = 9.0 Hz, 2 H, aromatic H's), 8.20 (d, J = 9.0 Hz, 2 H, aromatic H's). MS (CI/NH_3): 317 ($M^+ + NH_4$, base), 300 ($M^+ + 1$).

Preparation of Bromides 31a and 31b (Scheme 3) (*17*). A solution of *p*-toluenesulfonyl fluoride (**30a**, 1.0 equiv) or *p*-toluenesulfonamide (**30b**, 1.0 equiv), *N*-bromosuccinimide (1.0 equiv), and a catalytic amount of benzoyl peroxide dissolved in benzene (for example, 6 mmol of NBS using 10 mL of benzene) was stirred at 60 °C for 1 h. After the mixture cooled, the succinimide was filtered off and the filtrate chromatographed with pre-

Scheme 3. Synthesis of Sulfonyl-, Carboxy-, and Amine-Functionalized Congeners of the A_3 Adenosine Receptor Selective Antagonists Based on Dihydropyridines[a]



[a] Reagents: (a) NBS; (b) CH_3OCH_2Cl, Et_3N; (c) K_2CO_3, acetone, reflux; (d) 1 N HCl, acetone, 45 °C; (e) $H_2N(CH_2)2NH_2$, rt., 4 h; (f) N-hydroxysuccinimidyl biotin, DMF, rt.

parative TLC to yield the desired products (yield = 65% for **31a** and 62% for **31b**).

p-(Bromomethyl)benzenesulfonyl Fluoride (***31a***). ^{1}H NMR ($CDCl_3$/TMS): δ 4.52 (s, 2 H, CH_2), 7.65 (d, J = 7.8 Hz, 2 H, aromatic H's), 8.00 (d, J = 7.8 Hz, 2 H, aromatic H's).

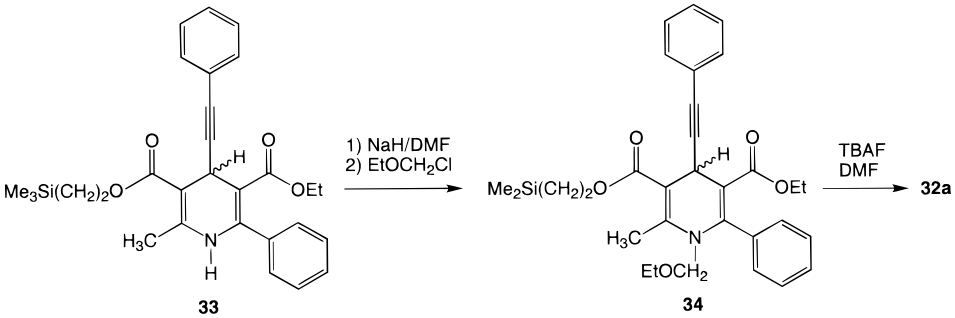
(p-Bromomethyl)benzenesulfonamide (***31b***). MS (EI): 249 and 251 (M^+).

Preparation of Methoxymethyl 4-(Bromomethyl)-benzoate (31d) (Scheme 3). α-Bromo-*p*-toluic acid (3.37 g, 15.7 mmol) was dissolved in DMF (10 mL). Chloromethyl methyl ether (1.26 g, 1.19 mL, 15.7 mmol) was then added, followed by adding triethylamine (1.9 g, 2.62 mL, 18.8 mmol). The reaction was stirred at room temperature overnight. Water (10 mL) was added, and the mixture was extracted with dichloromethane, washed with water, brine, and dried over $MgSO_4$. Column chromatography (hexanes/ethyl acetate = 5/1) gave 0.588 g of light yellowish oil, yield = 15%. ^{1}H NMR ($CDCl_3$/TMS): δ 3.55 (s, 3 H, OCH_3), 4.62 (s, 2 H, BrCH_2), 5.50 (s, 2 H, OCH_2O), 7.48 (d, J = 7.8 Hz, 2 H, aromatic H's), 8.08 (d, J = 7.8 Hz, 2 H, aromatic H's). MS (EI): 259 (M^+).

Preparation of 1-Ethoxymethyl-2-methyl-5-ethoxycarbonyl-4-phenylethynyl-6-phenyl-1,4-(±)-dihydropyridine-3-carboxylic acid (32a) (Scheme 4). Sodium hydride (60% in mineral oil, 107 mg, 4.46 mmol) was added to compound **33** in solution of DMF (10 mL). The mixture was stirred for 30 min, chloromethyl ethyl ether (422 mg, 0.414 mL, 4.46 mmol) was added slowly to the solution under N_2 at room temperature and stirred for 2h. The reaction was quenched by adding cold water (10 mL), extracted with ethyl acetate (10 mL x 2), the organic layer was washed with water (10 mL × 2), brine (10 mL × 2), dried with sodium sulfate. The solvent was evaporated and residue was purified with preparative TLC (silica gel 60, hexanes/EtOAc: 4/1) to give N-protected product **34** 497 mg, yield = 49%. ^{1}H NMR ($CDCl_3$): 0.00 (m, 9 H, 3-SiCH_3), 0.88 (t, 3 H, J = 6.8 Hz, 5-CH_2CH_3), 0.95 (t, 2 H, J = 6.8 Hz, 1-OCH_2CH_3), 1.12 (t, 2 H, J = 8.8 Hz, 3-OCH_2CH_2SiMe_3), 2.62 (s, 3 H, 2-CH_3), 3.15 (m, 1 H, 1-OCH_2CH$_3$), 3.69 (m, 1 H, 1-OCH_2CH$_3$), 3.92 (q, 2 H, J = 6.8 Hz, 5-OCH$_2$CH$_3$), 4.33 (t, 2 H, J = 6.8 Hz, 3-CO_2CH_2CH$_2$SiMe_3), 4.47 and 4.88 (AB, 2 H, J = 10.7 Hz, N-CH_2O), 5.09 (s, 1 H, 4-H), 7.24−7.42 (m, 10 H, aromatic H's). MS (CI−NH_3): m/z 563 ($M^+ + NH_4$), 546 ($M^+ + 1$).

TBAF (hydrate, 2.49 mmol, 1 M solution in THF) was added to a solution of **34** (340 mg, 0.623 mmol) in DMF

Scheme 4. Synthesis of a 3-Carboxylic Acid Dihydropyridine Intermediate for Alkylation, as Shown in Scheme 3



33 34

Table 2. Characterization of Dihydropyridine Derivatives

no	formula	MS	analysis	yield (%)
5	$C_{36}H_{29}NO_4$	539 (EI)	HRMS	11
6	$C_{36}H_{29}NO_4$	539 (EI)	HRMS	40
7	$C_{41}H_{31}NO_4 \cdot 0.5H_2O$	601 (EI)	C, H, N	50
8a	$C_{32}H_{29}NO_5$	507 (EI)	HRMS	15
8b	$C_{32}H_{28}N_2O_7$	570 (CI, $M^+ + NH_4$)	C, H, N	23
9	$C_{31}H_{27}NO_5$	493 (EI)	C, H, N	72
10	$C_{31}H_{27}NO_4S$	509 (EI)	C, H, N	22
11	$C_{31}H_{27}NO_3S_2 \cdot 1.0H_2O$	525 (EI)	C, H, N	16
12	$C_{36}H_{39}NO_4SSi$	609 (CI)	HRMS	28
13	$C_{31}H_{26}NFO_6S \cdot 0.71EtOAc$	559 (EI)	C, H, N	78
14	$C_{31}H_{28}N_2O_6S$	556 (EI)	HRMS(FAB)	49
15	$C_{34}H_{28}NCl_3O_6$	652 (CI)	C, H, N	89
16	$C_{34}H_{33}N_3O_5$	564 (FAB)	HRMS(FAB)	59
17	$C_{32}H_{27}NO_6$	521 (EI)	HRMS(FAB)	38
18	$C_{44}H_{47}N_5O_7S$	790 (CI)	HRMS(FAB)	64
19	$C_{31}H_{26}NFO_6S$	559 (EI)	C, H, N	75
20	$C_{31}H_{28}N_2O_6S$	556 (EI)	HRMS(FAB)	56
23	$C_{32}H_{27}NO_6 \cdot 0.92H_2O$	521 (EI)	C, H, N	51

(2 mL). The mixture was stirred under N_2 at room temperature for 2 h, diluted with ethyl acetate (20 mL), washed with 1 N HCl (5 mL), H_2O (20 mL × 2) and brine (20 mL × 2), and dried with magnesium sulfate. The solvent was evaporated, and residue was separated with preparative TLC to give 271 mg of compound **32a** as a yellow solid, yield = 98%. ^{1}H NMR ($CDCl_3$): δ 0.95 (m, 6 H, OCH_2CH_3x2), 2.67 (s, 3H, 2-CH_3), 3.16 and 3.69 (m, 2 H, N−$CH_2OCH_2CH_3$), 3.94 (q, 2 H, J = 6.8 Hz, 5-OCH_2), 4.50 and 4.90 (AB, 2 H, N-CH_2O), 5.13 (s, 1 H, 4-H), 7.18 (br, 1 H, COOH), 7.24−7.43 (m, 10 H, 2 x C_6H_5). MS (EI): m/z 445 (M^+).

Pharmacology. Radioligand Binding Studies. Binding of [^{3}H]*R*-*N*^{6}-phenylisopropyladenosine ([^{3}H]*R*-PIA) to A_1 receptors from rat cerebral cortex membranes and of [^{3}H]-2-[4-[(2-carboxyethyl)phenyl]ethylamino]-5′-*N*-ethylcarbamoyladenosine ([^{3}H]CGS 21680) to A_{2A} receptors from rat striatal membranes was performed as described previously (*22*, *23*). Adenosine deaminase (3 units/mL) was present during the preparation of the brain membranes, in a preincubation of 30 min at 30 °C and during the incubation with the radioligands.

Binding of [^{125}I]*N*^{6}-(4-amino-3-iodobenzyl)-5′-*N*-methylcarbamoyladenosine ([^{125}I]AB-MECA) to membranes prepared from HEK-293 cells stably expressing the human A_3 receptor (*2*), clone HS-21a (Receptor Biology, Inc., Beltsville, MD) or to membranes prepared from CHO cells stably expressing the rat A_3 receptor was performed as described (*11*, *24*). The assay medium consisted of a buffer containing 10 mM Mg^{2+}, 50 mM Tris, and 1 mM EDTA, at pH 8.0. The glass incubation tubes contained 100 μL of the membrane suspension (0.3 mg of protein/mL, stored at −80 °C in the same buffer), 50 μL of [^{125}I]AB-MECA (final concentration 0.3 nM), and 50 μL of a solution of the proposed antagonist. Nonspecific binding was determined in the presence of 100 μM *N*^{6}-phenylisopropyladenosine (*R*-PIA).

All nonradioactive compounds were initially dissolved in DMSO and diluted with buffer to the final concentration, where the amount of DMSO never exceeded 2%.

Incubations were terminated by rapid filtration over Whatman GF/B filters, using a Brandell cell harvester (Brandell, Gaithersburg, MD). The tubes were rinsed three times with 3 mL of buffer each.

At least five different concentrations of competitor, spanning 3 orders of magnitude adjusted appropriately for the IC_{50} of each compound, were used. IC_{50} values, calculated with the nonlinear regression method implemented in the Prism program (Graph-PAD, San Diego, CA), were converted to apparent K_i values using the Cheng−Prusoff equation (*25*) and K_d values of 1.0 and 14 nM for [^{3}H]*R*-PIA and [^{3}H]CGS 21680, respectively, and 0.59 nM for binding of [^{125}I]AB-MECA at human A_3 receptors, respectively.

For studies of irreversible binding, membranes were incubated with the indicated (Figure 2) concentration of ligand for 1 h at RT. Membranes were then washed 10 times by sequential resuspension and centrifugation with buffer (50 mM Tris, 10 mM Mg^{2+}, and 1 mM EDTA) at pH 7.4 containing 0.02% CHAPS. Adenosine deaminase (3 units/mL) was present during all steps. The final pellet was suspended in a fixed volume of the above buffer solution for the A_3 receptor binding assay as described.

RESULTS

Synthesis. The structures of the 1,4-dihydropyridines and related derivatives (**1b**−**23**) tested for affinity in

radioligand binding assays at adenosine receptors are shown in Table 1. As in the previous studies (*12*, *14*), the basic synthesis of the DHP nucleus consisted of the Hantzsch condensation (Scheme 1, reviewed in ref *19*). This method involves a three component reaction of a 3-amino-2-propenoate ester, such as benzyl 3-amino-3-phenyl-2-propenoate (Scheme 1), **24a**, an aldehyde, such as phenylpropargyl aldehyde, **25**, and a β-ketoester, such as benzyl acetoacetate, **26a**, that were dissolved in ethanol and refluxed. β-Ketoesters containing free hydroxyl and thio groups, **26d**−**f**, for use in the unprotected form in the condensation reaction, were synthesized as shown (Scheme 2). A silyl-protected thiol, **26g**, was also included.

The synthesis of DHP derivatives containing benzyl esters at the 3- and 5-positions, that were substituted with various acyl and sulfonyl groups, some of which were chemically reactive, was best approached through the alkylation of a free carboxylic acid using the corresponding benzyl bromide (Scheme 3). The benzyl bromides, **31a**−**c**, were synthesized by bromination of the corresponding toluene derivatives, **30a**−**c**, using *N*-bromosuccinimide. Use of compounds **30c** and **31c** in this context was described previously (*12*). The appropriate 3- or 5-carboxy derivative of the 6-phenyl-4-phenylethynyl-DHP was prepared by the methodology described (for the 5-carboxy derivative) in Jiang et al. (*12*). This approach incorporates a protecting group, a (2-trimethylsilylethyl)ester, at the 5-ester (*12*) or 3-ester (Scheme 4) position, that allows for facility of substitution of this ester and protection of the 1-position with the ethoxymethyl group (*12*). The 5-(2-trimethylsilylethyl)ester group was introduced at the stage of the Hantzsch condensation and subsequently removed using TBAF to provide **32b**. The resulting free carboxylic acid was then esterified in high yield by means of alkylation using the appropriate benzyl bromide, **31**, with potassium carbonate in acetone. The 1-ethoxymethyl group was finally removed upon heating at 45 °C for 1 h with 1 N HCl in acetone, to provide 5-position substituted benzyl esters, **19**−**21**, or 3-position esters, **13**−**15**.

Several additional modifications of functionality at the p-position of these benzyl esters were carried out. The 2,2,2-trichloroethyl derivatives (*12*), **15** and **21** (Scheme 3 and Table 1), were aminolyzed selectively using neat ethylenediamine at room temperature, to provide the amine functionalized congeners, **16** and **22**, respectively. As demonstrated by Jiang et al. (*12*), the ester groups at the 3- and 5-positions of the DHP were not susceptible to reaction with ethylenediamine under these conditions. Also, the methoxymethyl groups of **33** and **34** were removed using 1 N HCl to provide the corresponding carboxylic acid derivatives, **17** and **23** (Table 1). One of the primary amine congeners, **16**, was also acylated using a biotin-active ester to provide the biotin conjugate, **18**.

Pharmacology. Compounds **2** and **3** are 3,5-diethyl ester derivatives of 6-phenyl-1,4-dihydropyridines previously shown to act as selective A_3 receptor antagonists. Furthermore, the incorporation of a single benzyl ester at the 3- or 5-position was shown to enhance selectivity for the A_3 subtype. Several related benzyl esters, **4** and **5**, were included. As previously reported, the 3-benzyl ester, **4**, is >600-fold selective, although not as potent as the 3,5-diethyl ester, **3**, while the 5-benzyl ester, **1b**, is twice as potent at A_3 receptors as **3**. Combining both benzyl esters, in **5**, did not alter the receptor affinity of the 3-benzyl ester, **4**. However, at the 2- and 6-positions, double substitution with phenyl groups, as in compounds **6** and **7**, prevented binding to adenosine receptors.

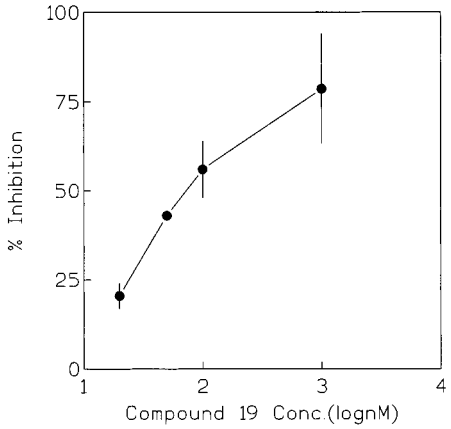


Figure 2. Irreversible inhibition of radioligand ([^{125}I]AB-MECA) binding to human A_3 adenosine receptors in HEK-293 cell membranes, following a 1 h incubation with the sulfonyl fluoride derivative, **19** (n = 2−6).

Transformation of the 3-ethyl ester of **1b** into a β-methoxyethyl ester, **8a**, enhanced affinity at A_3 receptors by ~15-fold. Incorporation of a p-nitro group in the 5-benzyl ester substituent, **8b**, which was shown previously to enhance A_3 receptor affinity by roughly an order of magnitude (*12*), had no further enhancing effect on the affinity of the β-methoxyethyl ester. Incorporation of a β-hydroxyl group in the 3-ethyl ester substituent, **9**, had an affinity-enhancing effect at A_3 adenosine receptors. Curiously, a thiol group at the same position was much less favorable for affinity at A_3 receptors, both for the 3-ester analogue, **10**, and the corresponding 3-thioester, **11**. A β-trimethylsilylethyl derivative, **12**, only weakly bound to adenosine A_3 receptors.

The structure activity relationships of p-substituted 3- and 5-ester positions were probed, as potential sites for attachment of functionalized chains. Ring substitution of the 5-benzyl ester with a 4-fluorosulfonyl group, **19**, provided enhanced selectivity of >30000-fold for the A_3 receptor, while similar substitution of the corresponding 3-benzyl ester, **13**, was not affinity enhancing. The corresponding sulfonamides, **14** and **20**, displayed only moderate potency and selectivity, with only minor affinity differences between 3- and 5-isomers. The corresponding 3- and 5- carboxylates, **17** and **23**, were prepared, and only **17** bound to A_3 receptors with moderate potency. A DHP containing a long amine-functionalized chain attached at the 3-position, **16**, displayed moderate affinity, while the corresponding 5-isomer, **22**, was 5-fold less potent at A_3 receptors and nonselective.

Since an amine-functionalized chain attached at the 4-position of a benzyl ester at the 3-position of the DHP ring provided higher affinity A_3 receptors, **16** was used as an intermediate in the synthesis of a biotin conjugate, **18**. The biotin derivative showed >100-fold selectivity for human A_3 receptors.

Unlike related derivatives not containing a reactive, electrophilic group, the sulfonyl fluoride derivative, **19**, appeared to irreversibly bind to the A_3 receptor in a concentration-dependent manner (Figure 2). A 1 h preincubation with this derivative resulted in the loss of binding in a subsequent experiment following exhaustive washing of the membranes. At 100 nM **19**, approximately 56% of human A_3 receptor radioligand binding sites in transfected HEK-293 cell membranes were irreversibly inhibited. As control experiments, similar preincubation with other A_3 receptor antagonists was carried out. Preincubation with 8-*p*-sulfophenyltheophylline (10 μM),

CGS 15943 (1 μM) (*16*), and MRS 1067 (1 μM) (*12*) failed to affect the level of subsequent A_3 receptor radioligand binding. Preincubation with compound **1b**, or its highly potent 4-nitrobenzyl derivative (*12*), at 100 nM did not significantly affect the level of subsequent A_3 receptor radioligand binding (loss of <10% of total binding). Compound **13**, another fluorosulfonyl derivative which bound considerably more weakly to human A_3 receptors, resulted in only 11 and 62% irreversible inhibition of radioligand binding at 1 and 5 μM, respectively.

DISCUSSION

Previously, we have applied a "functionalized congener approach" (*21*) to the design of ligands for G protein-coupled receptors, such as adenosine receptors (*12*), muscarinic receptors (*35*), and nucleotide receptors (*36*). By this approach, an easily derivatized functional group is incorporated at the end of a strategically designed and attached chain-substituent Several of the derivatives in Table 1, such as the amines, **16** and **22**, and the carboxylic acids, **17** and **23**, represent easily reacted functionalized congeners of dihydropyridines, derivatives of which would retain moderate affinity and/or selectivity as A_3 receptor antagonists.

The indication that the 5-ester position is the most flexible for substitution in relation to A_3 receptor affinity has suggested the design of the amine-functionalized congener, **22**. As in our previous studies of purines derivatized with long chains for the purpose of conjugating with other molecules while retaining the biological potency, this derivative may prove to be a key intermediate in the design of much higher molecular weight derivatives bearing "carrier" moieties, reporter groups, prosthetic groups, etc. The presence of the amino group in **22** also increased water solubility; unfortunately, it was not potent in binding at human A_3 receptors.

Irreversible inhibitors of binding of A_1 and A_{2A} subtypes of adenosine receptors have been reported (*26*−*29*). Furthermore, an irreversibly binding A_3 receptor agonist, MRS 1163, derived from IB-MECA was characterized (*30*). Among the pharmacological applications of such affinity labels are establishing the levels of spare receptors in native tissues, such as the heart (*31*−*33*). The irreversibly binding A_3 receptor antagonists presented in this study may prove to be useful tools in the characterization of this receptor subtype. Since the DHP antagonists (*12*) are selective for the human A_3 receptor vs other species, the design of irreversible ligands for A_3 receptors in rat (*14*) and other species remains to be accomplished.

ACKNOWLEDGMENT

We thank the Cystic Fibrosis Foundation (Silver Spring, MD) for financial support and Dr. Mark Olah and Dr. Gary L. Stiles of Duke University Medical Center for helpful discussions.

Supporting Information Available: Elemental analysis or HRMS data. This material is available free of charge via the Internet at http://pubs.acs.org.

LITERATURE CITED

(1) Jacobson, K. A., and Suzuki, F. (1997) Recent developments in selective agonists and antagonists acting at purine and pyrimidine receptors. *Drug Dev. Res. 39*, 289−300.

(2) Zhou, Q. Y., Li. C. Y., Olah, M. E., Johnson, R. A., Stiles, G. L., and Civelli, O. (1992) Molecular cloning and characterization of an adenosine receptor−The A_3 adenosine receptor. *Proc. Natl. Acad. Sci. U.S.A. 89*, 7432−7436.

(3) Salvatore, C. A., Jacobson, M. A., Taylor, H. E., Linden, J., and Johnson, R. G. (1993) Molecular cloning and characterization of the human A_3 adenosine receptor. *Proc. Natl. Acad. Sci. U.S.A. 90*, 10365−10369.

(4) Jacobson, K. A. (1998) A_3 adenosine receptors: Novel ligands and paradoxical effects. *Trends Pharmacol. Sci. 19*, 184−191.

(5) von Lubitz, D. K. J. E., Lin, R. C. S., Popik, P., Carter, M. F., and Jacobson, K. A. (1994) Adenosine A_3 receptor stimulation and cerebral ischemia. *Eur. J. Pharmacol. 263*, 59−67.

(6) von Lubitz, D. K. J. E., Lin, R.-C., Boyd, M., Bischofberger, N., and Jacobson, K. A. (1999) Chronic administration of adenosine A_3 receptor agonist and cerebral ischemia: neuronal and glial effects. *Eur. J. Pharmacol. 367*, 157−163.

(7) Strickler, J., Jacobson, K. A., and Liang, B. T. (1996) Direct preconditioning of cultured chick ventricular myocytes: novel functions of cardiac adenosine A_{2A} and A_3 receptors. *J. Clin. Invest. 98*, 1773−1779.

(8) Stambaugh, K., Jacobson, K. A., Jiang, J.-l., and Liang, B. T. (1997) A novel cardioprotective function of adenosine A_1 and A_3 receptors during prolonged stimulated ischemia. *Am. J. Physiol. 273*, H501−H505.

(9) Kohno, Y., Sei, Y., Koshiba, M., Kim, H. O., and Jacobson, K. A. (1996) Induction of apoptosis in HL-60 human promyelocytic leukemia cells by selective adenosine A_3 receptor agonists. *Biochem. Biophys. Res. Commun. 219*, 904−910.

(10) Shneyvays, V., Nawrath, H., Jacobson, K. A., and Shainberg, A. (1998) Induction of apoptosis in cardiac myocytes by an A_3 adenosine receptors agonist. *Exp. Cell Res. 243*, 383−397.

(11) Karton, Y., Jiang, J. L., Ji, X. D., Melman, N., Olah, M. E., Stiles, G. L., and Jacobson, K. A. (1996) Synthesis and biological-activities of flavonoid derivatives as as adenosine receptor antagonists. *J. Med. Chem. 39*, 2293−2301.

(12) Jiang, J.-l., van Rhee, A. M., Chang, L., Patchornik, A., Evans, P., Melman, N., and Jacobson, K. A. (1997) Structure activity relationships of 4-phenylethynyl-6-phenyl-1,4-dihydropyridines as highly selective A_3 adenosine receptor antagonists. *J. Med. Chem. 40*, 2596−2608.

(13) Jacobson, M. A., Chakravarty, P..K., Johnson, R. G., and Norton, R. (1996) Novel selective nonxanthine selective A_3 adenosine receptor antagonists. *Drug Dev. Res. 37*, 131.

(14) Li, A.-H., Moro, S., Melman, N., Ji, X.-d., and Jacobson, K. A. (1998) Structure activity relationships and molecular modeling of 3,5-diacyl-2,4-dialkylpyridine derivatives as selective A_3 adenosine receptor antagonists. *J. Med. Chem. 41*, 3186−3201.

(15) Van Muijlwijk-Koezen, J. E., Timmerman, H., Link, R., Van der Goot, H., and IJzerman, A. P. (1998) A novel class of adenosine A_3 receptor ligands. II. Structure affinity profile of a series of isoquinoline and quinazolinecompounds. *J. Med. Chem. 41*, 3994−4000.

(16) Kim, Y.-C., Ji, X.d., and Jacobson, K. A. (1996) Derivatives of the triazoloquinazoline adenosine antagonist (CGS15943) are selective for the human A_3 receptor subtype. *J. Med. Chem. 39*, 4142−4148.

(17) Beaven, M. A., Ramkumar, V., and Ali, H. (1994) Adenosine-A_3 receptors in mast-cells. *Trends Pharmacol. Sci. 15*, 13−14.

(18) von Lubitz, D. K. J. E., Lin, R. C. S., Sei, Y., Boyd, M., Abbracchio, M., Bischofberger, N., and Jacobson, K. A. (1996) A_3 adenosine receptors and ischemic brain injury: a hope or a disaster? *Drug Dev. Res. 37*, 140.

(19) Stout, D. M., and Myers, A. I. (1982) Recent advances in the chemistry of dihydropyridines. *Chem. Rev. 82*, 223−243.

(20) Goldmann, S., and Stoltefuss, J. (1991) 1,4-Dihydropyridines: Effect of chirality and conformation on the calcium antagonist and calcium agonist activities. *Angew. Chem., Int. Ed. Engl.* 1559−1578.

(21) Jacobson, K. A. (1990) Molecular probes for adenosine receptors. In *Purines in Cellular Signaling: Targets for New Drugs* (K. A. Jacobson, J. W. Daly, and V. Manganiello, Eds.) pp 54−64, Springer, New York.

(22) Schwabe, U., and Trost, T. (1980) Characterization of adenosine receptors in rat brain by (−) [^{3}H]N^6-phenylisopropyladenosine. *Naunyn-Schmiedeberg's Arch. Pharmacol. 313*, 179−187.

(23) Jarvis, M. F., Schutz, R., Hutchison, A. J., Do, E., Sills, M. A., and Williams, M. (1989) [^{3}H]CGS 21680, an A_2 selective adenosine receptor agonist directly labels A_2 receptors in rat brain tissue. *J. Pharmacol. Exp. Ther. 251*, 888−893.

(24) Olah, M. E., Gallo-Rodriguez, C., Jacobson, K. A., and Stiles, G. L. (1994) [^{125}I]AB-MECA, a high affinity radioligand for the rat A_3 adenosine receptor. *Mol. Pharmacol. 45*, 978−982.

(25) Cheng, Y. C., and Prusoff, W. H. (1973) Relationship between the inhibition constant (K_i) and the concentration of inhibitor which causes 50% inhibition (IC_{50}) of an enzyme reaction. *Biochem. Pharmacol. 22*, 3099−3108.

(26) Jacobson, K. A., Fischer, B., and Ji, X.-D. (1995) "Cleavable trifunctional" approach to receptor affinity labeling: regeneration of binding to A_1-adenosine receptors. *Bioconjugate Chem. 6*, 255−263.

(27) Niiya, K., Jacobson, K. A., Silvia, S. K., and Olsson, R. A. (1993) Covalent binding of a selective agonist irreversibly activates guinea pig coronary artery A_2 adenosine receptors. *Naunyn-Schmeideberg's Arch. Pharamacol. 347*, 521−526.

(28) Ji, X.-D., Gallo-Rodriguez, C., and Jacobson, K. A. (1993) 8-(3-Isothiocyanatostyryl)caffeine is a selective irreversible inhibitor of striatal A_2-adenosine receptors. *Drug Dev. Res. 29*, 292−298.

(29) Morey, T. E., Belardinelli, L., and Dennis, D. M. (1998) Validation of Furchgott's method to determine agonist-dependent A1-adenosine receptor reserve in guinea-pig atrium. *Br. J. Pharmacol 7*, 1425−1433.

(30) Ji, X.-D., Gallo-Rodriguez, C., and Jacobson, K. A. (1994) A selective affinity label for A_3 adenosine receptors. *Biochem. Biophys. Res. Commun. 203*, 570−576.

(31) Dennis, D., Jacobson, K., and Belardinelli, L. (1992) Evidence of spare A_1-adenosine in guinea pig atrioventricular node. *Am. J. Physiol. 262*, H661−H671.

(32) Zhang, J., Belardinelli, L., Jacobson, K. A., Otero, D. H., and Baker, S. P. (1997) Persistent activation of A_1 adenosine receptors by an acylating adenosine derivative and its receptor reserve in DDT_1 MF-2 cells and heart. *Mol. Pharmacol. 52*, 491−498.

(33) Shryock, J. C., Snowdy, S., Baraldi, P. G., Cacciari, B., Spalluto, G., Monopoli, A., Ongini, E., Baker, S. P., and Belardinelli, L. (1998) A_{2A}-adenosine receptor reserve for coronary vasodilation. *Circulation 7*, 711−718.

(34) Jacobson, K. A., Kirk, K. L., Padgett, W. L., and Daly, J. W. (1985) Functionalized congeners of 1,3-dialkylxanthines: preparation of analogues with high affinity for adenosine receptors. *J. Med. Chem. 28*, 1334−1340.

(35) Karton, Y., Baumgold, J., Handen, J. S., and Jacobson, K. A. (1992) Molecular probes for muscarinic receptors: Derivatives of the M_1-antagonist telenzepine. *Bioconjugate Chem. 3*, 234−240.

(36) Fischer, B., Boyer, J. L., Hoyle, C. H. V., Ziganshin, A. U., Brizzolara, A. L., Knight, G. E., Zimmet, J., Burnstock, G., Harden, T. K., and Jacobson, K. A. (1993) Identification of potent, selective P_{2Y}-purinoceptor agonists: Structure activity relationships for 2-thioether derivatives of adenosine-5′-triphosphate. *J. Med. Chem. 36*, 3937−3946.

BC9900136

Supplementary Table. Elemental Analysis or HRMS Data.

Compound No.	Formula	MW (anhyd)	Calculated (% or HRMS)	Found (% or HRMS)
5	$C_{36}H_{29}NO_4$	539.60	539.2097 (M^+)	539.2094
6	$C_{36}H_{29}NO_4$	539.60	539.2097 (M^+)	539.2076
7	$C_{41}H_{31}NO_4.0.5\ H_2O$	601.67	C80.63, H5.28, N2.29	C80.65, H5.34, N2.20
8a	$C_{32}H_{29}NO_5$	507.56	507.2046 (M^+)	507.2022
8b	$C_{32}H_{28}N_2O_7$	552.58	C69.55, H5.11, N5.07	C69.60, H5.42, N4.80
9	$C_{31}H_{27}NO_5$	493.55	C75.44, H5.51, N2.84	C75.64, H6.01, N2.40
10	$C_{31}H_{27}NO_4S$	509.61	C73.06, H5.34, N2.75	C72.81, H5.54, N2.50
11	$C_{31}H_{27}NO_3S_2.1.0\ H_2O$	525.68	C68.48, H5.38, N2.58	C68.45, H5.48, N2.30
12	$C_{36}H_{39}NO_4SSi$	609.85	609.2369	609.2353
13	$C_{31}H_{26}NFO_6S{\cdot}0.71$ EtOAc	559.60	C65.32, H5.13, N2.25	C65.59, H5.06, N2.22
14	$C_{31}H_{28}N_2O_6S$	556.63	FAB: 557.1746 (M+H)	FAB: 557.1709 (M+H)
15	$C_{34}H_{28}NCl_3O_6$	652.95	C62.54, H4.32, N2.15	C62.41, H4.45, N2.14
16	$C_{34}H_{33}N_3O_5$	563.65	FAB: 564.2498 (M+H)	FAB: 564.2493 (M+H)
17	$C_{32}H_{27}NO_6$	521.56	FAB: 522.1917 (M+H)	FAB: 522.1906 (M+H)
18	$C_{44}H_{47}N_5O_7S$	789.94	FAB: 790.3274 (M+H)	FAB: 790.3270 (M+H)
19	$C_{31}H_{26}NFO_6S$	559.60	C66.53, H4.68, N2.50	C66.28, H4.85, N2.40
20	$C_{31}H_{28}N_2O_6S$	556.63	FAB: 557.1746 (M+H)	FAB: 557.1748 (M+H)

© 1999 American Chemical Society, Bioconjugate Chem., Li bc990136 Supporting Info Page 1

2				
23	$C_{32}H_{27}NO_6 \cdot 0.92H_2O$	521.56	C71.42, H5.40, N2.60	C71.69, H5.46, N2.62

TECHNICAL NOTES

Bioactive Surfaces via Immobilization of Self-Assembling Polymers onto Hydrophobic Materials

Lev Bromberg* and Lawrence Salvati, Jr.

Abbott Laboratories, MediSense Products. Received August 5, 1998;
Revised Manuscript Received December 29, 1998

Conjugation of proteins to copolymers from poly(acrylic acid) grafted onto PEO−PPO−PEO backbone (Pluronic-PAA) following adsorption of the conjugates onto hydrophobic surfaces is reported. Insulin-Pluronic-PAA conjugates show negligible internalization of insulin into human uterine smooth muscle cells as well as enhancement of mitogenic activity. Glucose-induced release of glycated albumin complexed with a Pluronic-PAA-concanavalin conjugate and adsorbed onto polystyrene nanospheres may provide a model for a glucose-responsive protein delivery system or a heterogeneous diagnostic device.

INTRODUCTION

Immobilization of biomolecules such as enzymes, antibodies, and nucleic acids onto various particulates and films is a widespread method of producing bioactive surfaces for use in immunoassays, chromatography, cell proliferation, drug delivery, etc. (*1*). Hydrophobic polymers, and particularly polystyrene, are often quite useful as neutral carriers readily available in a variety of shapes and sizes. Since polystyrene causes nonspecific adsorption and also lacks functional groups, it is customary to modify it with hydrophilic polymers (*2*). This modification is usually accomplished by surface treatment, e.g., by glow discharge (*3*) or copolymerization (*4*). In this study, a novel strategy toward bioactive surfaces by adsorption of self-assembling copolymers modified by proteins and enzymes onto polystyrene was explored. The self-assembling copolymers possess sufficiently hydrophobic blocks that strongly interact with polystyrene and yet carry polyelectrolyte segments, which are accessible for modification. Recently, a novel class of hydrophobically modified polyelectrolytes was introduced whereby poly(propylene oxide) (PPO) group acts as a temperature-sensitive hydrophobe (*5*−*20*). Attachment of the PPO group onto a polyelectrolyte is a means of creating a dually responsive, self-assembling material by adding temperature sensitivity to an already pH- and ion-sensitive polymer. In the present work, ongoing study is continued that is concerned with a distinct species of such dually responsive polymers whereby multiple poly(acrylic acid) (PAA) segments are grafted onto Pluronic poly(ethylene oxide)-*b*-poly(propylene oxide)-*b*-poly(ethylene oxide) (PEO−PPO−PEO) block copolymers via C−C bonding (*10*). High molecular weights and extreme sensitivity to temperature distinguish these PEO−PPO−PEO−PAA copolymers. Above certain temperatures, their semidilute aqueous solutions can form reversible gels with significant elastic moduli (*9*). Gelation is due to appearance of micelle-like aggregates that serve as physical cross-links between Pluronic-PAA chains, as shown by rheological methods (*8*), probe solubilization (*17*), light scattering (*7*, *15*), NMR (*20*), SANS (*12*), SEC (*11*), and DSC (*11*) techniques. Herein, we have taken interest in the use of the self-assembling polymers as matrixes for conjugation of biomolecules. The conjugates appear to adsorb strongly onto hydrophobic surfaces, as described below.

EXPERIMENTAL SECTION

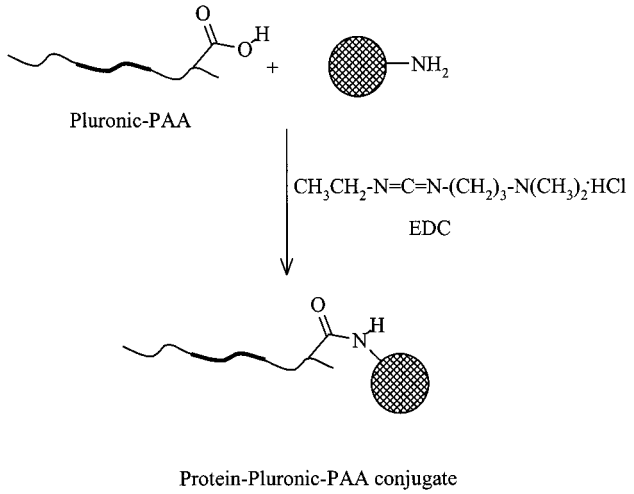
Unless stated otherwise, all chemicals were obtained from Sigma-Aldrich Co. and were used as received. Pluronic F127 NF ($EO_{100}PO_{65}EO_{100}$) was purchased from BASF Corp. (Parsippany, NJ). Poly(ethylene oxide)-*b*-poly(propylene oxide)-*b*-poly(ethylene oxide)-*g*-poly(acrylic acid) (PEO−PPO−PEO−PAA) (CAS no. 186810-81-1) was synthesized by dispersion/emulsion polymerization of acrylic acid along with simultaneous grafting of poly(acrylic acid) onto the Pluronic backbone using initiators lauroyl peroxide and 2,2′-azobis(2,4-dimethylpentanenitrile) (DuPont Specialty Chemicals) as described in detail elsewhere (*14*). Copolymer fraction used in this study had a M_w of 3.2×10^6 and PAA and Pluronic contents of 55 and 45%, respectively (*11*, *14*). Polystyrene (PS) nanospheres were obtained from Seradyn, Inc. (Indianapolis, IN) and had a nominal diameter of 69 nm. Albumin-2-amido-deoxy-D-glucose (bovine, ∼15−20 mol of glucose/mol of albumin) and α-D-glucosylated-FITC-albumin (bovine, ∼15−20 mol of glucopyranose and 2−3 mol of FITC/mol of protein) were obtained from Sigma and dissolved at 1:1 molar ratio in 10 mM phosphate buffer following lyophilization prior to use.

Conjugation of Proteins with Pluronic-PAA Copolymers. Conjugation of fluorescein isothiocyanate (FITC)-labeled concanavalin A (Con A, 1.5 mol of FITC/mol of protein, ∼95% protein) onto Pluronic-PAA was carried out by simultaneous activation and coupling with a water-soluble condensing agent, 1-ethyl-3-(3-dimethy-

* To whom correspondence should be addressed: 15 Sherwood Road, Swampscott, MA 01907. E-mail cpbrolev@aol.com.

10.1021/bc9800973 CCC: $18.00 © 1999 American Chemical Society
Published on Web 06/15/1999

Scheme 1. Conjugation of a Protein and Pluronic-PAA Copolymer



laminopropyl)carbodiimide (EDA) (Scheme 1). The Pluronic-PAA, FITC-Con A, and EDA components were dissolved in 10 mM phosphate buffer (pH 7.4) at 4 °C to result in final concentrations of 10 mg/mL, 2 mg/mL, and 2 mg/mL, respectively. The mixture was then gently shaken for 24 h at 4 °C. The resulting conjugate was precipitated by addition of 1 M HCl at pH 4.8, quickly filtered off, and redissolved in chilled 10 mM phosphate buffer. The conjugated FITC-Con A was assayed fluorometrically (typical λ_{ex} 490 nm, λ_{em} 520 nm). To verify that the FITC-Con A was covalently attached to Pluronic-PAA, a control experiment was conducted as follows. A mixture of FITC-Con A and the polymer was run without addition of the EDC activation reagent. After the same treatment as that with EDC, a negligible amount of protein and FITC-Con A was detected in the precipitate. Gel-permeation chromatography (GPC) of Pluronic-PAA and Con A-Pluronic-PAA conjugates was run at 15 °C on a Shimadzu LC-10A Series HPLC set up which included an RF-551 fluorescence HPLC detector, LC-10 AD solvent delivery unit, an SCL-10A system controller, and a Viscotek differential laser refractometer. An aliquot of 50 μL of 1.0 mg/g sample of conjugate solution in 0.05 M $NaNO_3$ was loaded onto a PL aquagel-OH analytical temperature-controlled 3-column system (particle size 8 or 15 μm; dimensions 300 × 7.5 mm, Polymer Laboratories, Inc.) and then eluted with 0.05 M $NaNO_3$ using a pump speed of 0.8 mL/min. Representative chromatograms of FITC-Con A-Pluronic-PAA conjugate are shown in Figure 1. GPC confirmed covalent binding of Con A and Pluronic-PAA. The conjugates were lyophilized and kept in sealed vials at 4 °C.

Zn^{2+}-insulin (from porcine pancreas, crystalline) and [^{125}I]insulin (porcine, 80−120 μCi/μg, NEN Life Science Products, Boston, MA) were conjugated to Pluronic-PAA copolymers as follows. Stock solution of Zn^{2+}-insulin and [^{125}I]insulin (50:1 mol ratio, total insulin concentration 500 μg/mL) was prepared in 10 mM phosphate buffer (pH 7.4). Pluronic-PAA and EDA were added to the stock solution at 4 °C to result in final concentrations of 10 and 2 mg/mL, respectively, and the mixture was gently shaken for 24 h at 4 °C. Then an equal volume of 10 mM glycine in phosphate buffer was added, and the solution was stirred at 4 °C for 6 h and filtered off using 0.45 μm membrane filter. The conjugate was then dialyzed against phosphate buffer at 4 °C for 24 h using Spectra/Por cellulose ester membrane (molecular weight cutoff 50 000, Spectrum, Laguna Hills, CA), lyophilized, and stored at

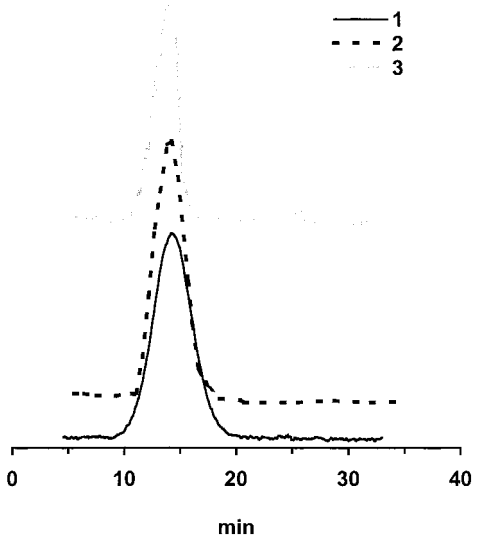


Figure 1. Gel-permeation chromatograms illustrating the conjugation of FITC-Con A with Pluronic-PAA copolymers. (1, 2) FITC-Con A-Pluronic-PAA; (3) FITC-Con A-Pluronic-PAA as in chromatogram 1 blended with FITC-Con A. Fluorescence at 515 nm (1 and 3) and refractive index (2) detection was used. Unbound FITC-Con A appears as a small peak in chromatogram 3.

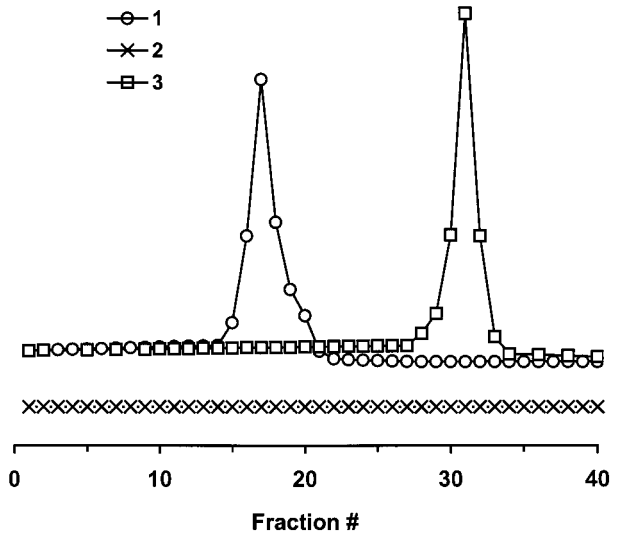


Figure 2. Gel-permeation chromatograms illustrating the conjugation of [^{125}I]insulin with Pluronic-PAA copolymers. (1) Insulin-Pluronic-PAA synthesized in the presence of EDA following dialysis; (2) Pluronic-PAA blended with [^{125}I]insulin without EDA following dialysis; (3) insulin.

4 °C in a sealed vial. To quantify conjugation of insulin onto Pluronic-PAA, identical synthetic procedure (but without EDA) was conducted followed by dialysis. A 0.01 mg/mL solution of the insulin-Pluronic-PAA conjugate or the initial mixture of [^{125}I]insulin and unlabeled insulin was passed through a TSK-gel G3000PW GPC column (600 × 7.5 mm, Toyo Soda) at 15 °C. The flow rate of 0.2 mL/min with 10 mM phosphate buffer as an eluent was used and a Gilson FC205 automatic fraction collector was applied. Collected fractions were kept in sealed vials at 4 °C and subjected to γ-radioactivity measurement. Figure 2 shows chromatograms pertaining to the insulin-Pluronic-PAA conjugate and Pluronic-PAA made with and without EDA, respectively, as well as insulin mixture. As can be seen, the polymer that participated in the control experiment without EDA did not contain detectable level of insulin, whereas the conjugate made

Table 1. Effect of Conjugate Adsorption on Surface Characteristics of Polystyrene Films

polystyrene	composition by XPS/ESCA (%) C	O	N	air-in-water contact angle (deg)
as received, bare surface	97.4	2.6	nd	86 ± 4 (6)
Pluronic-PAA	73.3	26.7	nd	33 ± 4 (10)
insulin-Pluronic-PAA	71.7	18.4	9.9	33 ± 6 (10)

with EDA exhibited well-defined peak clearly distinguishable from the original insulin. Fractions around the peak were collected and total radioactivity was measured. The yield of conjugation reaction of insulin onto Pluronic-PAA in the presence of EDA was estimated to be about 60%, based on relative radioactivity levels.

Conjugate Adsorption onto Polystyrene Surfaces. Polystyrene nanospheres were coated with FITC-Con A-Pluronic-PAA conjugates by first dispersing 2 mg/mL nanospheres in 10 mM chilled phosphate buffer following addition of equal volume of 2 mg/mL FITC-Con A-Pluronic-PAA conjugate. The resulting suspension was kept at 37 °C for 16 h, then snap-frozen and lyophilized. The resulting material was resuspended in 10 mM phosphate buffer (pH 7.4). The conjugate-coated particles were concentrated by centrifugation at 37 °C using Micropure Filtration Device (pore size 0.22 μm) (Millipore Co.), and the supernatant was removed. After resuspension in phosphate-buffered saline the particles were again concentrated and the supernatant collected for fluorescence measurement. Washing cycles were repeated until no FITC was detected in the washouts. Surface concentration of the conjugate was estimated spectrofluorometrically to be about 0.6 μg of FITC-Con A/cm^2. Adsorption of unconjugated FITC-Con A onto polystyrene particles under identical conditions was below 0.1 μg/cm^2.

Flat-well, polystyrene plates (Corning) with untreated surfaces were modified with insulin-Pluronic-PAA conjugates by placing 2 μL of 2 mg/mL conjugate solution in 10 mM phosphate buffer on the bottom of the well following evaporation of aqueous solution on air at 37 °C. A mixture of [^{125}I]insulin and unlabeled insulin was used for the conjugate preparation. Adsorption procedure was repeated up to 20 times for each well. The wells were gently rinsed by deionized water at 37 °C until γ-radioactivity in the washouts did not exceed that of a blank solution. In the control experiments, polystyrene surfaces were treated by identical Pluronic-PAA conjugate solutions without insulin or by insulin without conjugate. Insulin contents were calculated by comparing the radioactivity in the wells with that of [^{125}I]insulin per unit weight, as described elsewhere (*3*, *21*, *22*). The effect of conjugate adsorption on the properties of the polystyrene surfaces is presented in Table 1. Figure 3 shows adsorption isotherms (37 °C) of the insulin conjugated with Pluronic-PAA and that without conjugation. It can be seen that the amount of the adsorbed conjugated insulin at saturation by an order of magnitude exceeded that of unconjugated insulin.

Quantification of the Polymer Adsorption onto PS Particles. The mass of Pluronic-PAA conjugates and Pluronic F127 adsorbed on PS nanoparticles was determined by radioisotope method as follows (*23*, *24*). Amino-terminated Pluronic F127 was synthesized via the sequence of quantitative modifications (*25*):

$$\text{Pluronic-OH} \rightarrow \text{Pluronic-SO}_2\text{CH}_3 \rightarrow \text{Pluronic-N}_3 \rightarrow \text{Pluronic-NH}_2$$

with the amino group attached to one end of the Pluronic

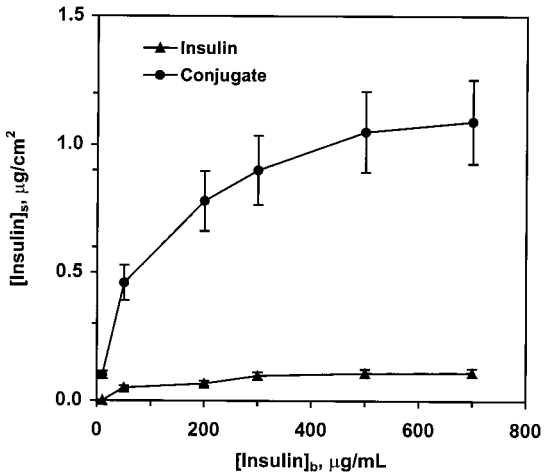


Figure 3. Adsorption isotherms (37 °C) of insulin and insulin-Pluronic-PAA conjugates onto polystyrene plate wells. Each point represents an average of six independent measurements.

molecule. Activation of only one terminal hydroxyl out of two present in a polyether is ensured by the proper ratio of equivalents of OH groups and an activation agent and is a commonly used technique (*25*−*27*). Marginal fractions with both end-groups modified are separated by HPLC (*27*). The 4-hydroxyphenyl moiety was then introduced into Pluronic-NH_2 by reaction with *N*-succinimidyl-3-[4-hydroxyphenyl]propionate (Bolton-Hunter reagent) (Pierce Chemical, Rockford, IL) in tetrahydrofuran following iodination reaction with Na^{125}I as described elsewhere (*28*).

For ^{125}I labeling, an aqueous solution of 3 w/v% Pluronic-PAA and 5 mg/mL *N*-hydroxysulfosuccinimidyl-4-azidosalicylic acid (sulfo-NHS-ASA) (Pierce) was deaerated under vacuum and illuminated by a Light-Welder 3010 EC UV spot/wand lamp (spectral output <500 nm and intensity of 600 mW/cm^2, Dymax Co., Torrington, CT) for 5 min. UV-irradiation results in formation of nitrenes of sulfo-NHS-ASA that attack tertiary H−C groups (*29*) thereby covalently binding the sulfo-NHS-ASA to Pluronic-PAA. The resulting solution (2 × 1 mL) was iodinated by using IODO-GEN solid-phase reagent kit (Pierce). IODO-GEN comprises 1,3,4,6-tetrachloro-3α,6 α-diphenylglycouril, a water-insoluble oxidizing agent that reacts with ^{125}I$^-$ to form a highly reactive mixed halogen species, ^{125}ICl. This intermediate adds radioactive iodine atoms to reagents possessing phenyl rings with electron-donating constituents, such as sulfo-NHS-ASA. The procedure of iodination using sulfo-NHS-ASA and IODO-GEN kit is recommended by Pierce Chemical Co. and is described in detail in Hermanson's monograph (*30*). Specific activity of ^{125}I-labeled Pluronic-PAA conjugate was in the range of 10^4 cpm/μg.

Aqueous solutions (3 w/v%) of labeled Pluronic or Pluronic-PAA conjugates mixed with their unlabeled counterparts at 1:20 weight ratios were used for adsorption onto PS nanospheres. Following a 24 h adsorption at 37 °C, the coated nanospheres were concentrated by centrifugation using Microcon-30 Microconcentrator (molecular weight cutoff 30 000) and Micropure Filtration Device (pore size 0.45 μm) (Millipore Co.) for Pluronic and Pluronic-PAA solutions, respectively, and the supernatant was removed. Due to high molecular weight of Pluronic-PAA, its (gelled) aqueous solutions could not be filtered with a pore size below 0.45 μm. Slurry of agglomerated polymer-coated PS particles was effectively concentrated by the filtration, without significant loss. After resuspension in phosphate-buffered saline, the

Table 2. Pluronic-PAA and Pluronic F127 Adsorption at 37 °C onto Polystyrene Nanoparticles

species	m_p (ag/particle)[a]	surface density (nm^2/molecule)
Pluronic-PAA	35 600 ± 6000 (5)	2.1 ± 0.4 (5)
Pluronic F127	25 ± 5 (3)	13 ± 3 (3)

[a] ag stands for attograms (10^{-18} g), as defined by SI.

particles were again concentrated and the supernatant was collected for radioactivity measurement. Washing cycles were repeated until supernatant radioactivity did not exceed that of a blank. Then the radioactivity of the separated solids was measured and related to the known amount of particles and known radioactivity per mass of the polymer. The value for the surface area occupiedper Pluronic or Pluronic-PAA molecule was calculated as (*24*)

$$\frac{\text{surface area}}{\text{molecule}} = \frac{\pi d^2 \times \text{MW}}{m_p N_A}$$

where $d = 69$ nm is the particle mean diameter, MW = 12 600 and 3×10^6 are molecular weights of the Pluronic and Pluronic-PAA conjugate, respectively, m_p is the mass of the adsorbed polymer, and N_A is Avogadro's number.

Results of quantification of polymer adsorption are collected in Table 2. Pluronic F127 adsorption correlated well with reported data on adsorption of other Pluronics onto the same particles (*23*).

In Vitro Protein Binding and Release Studies. A normal human uterine smooth muscle cell line from a single donor was used for conjugate−cell interaction studies. The cells were grown in 25 mL flasks at 37 °C, under 5% CO_2, in a minimum essential medium (MEM) supplemented with 10% fetal bovine serum, 50 mg/mL Gentamicin, and 50 μg/mL Amphotericin B. The cells of about 90% confluence were harvested using 0.025% trypsin/0.01% EDTA buffer solution at exponential growth phase (6−8 days after seeding), washed and incubated in 96-well plates at approximately 7200 cells/well. Four series of experiments were conducted where each well contained (i) a mixture of [^{125}I]insulin and Zn^{2+}-insulin (molar ratio 1:100) dissolved in MEM (dissolved insulin); (ii) a labeled insulin-Pluronic-PAA conjugate dissolved in MEM (dissolved conjugate); (iii) a mixture of [^{125}I]-insulin and Zn^{2+}-insulin adsorbed onto plate well (adsorbed insulin); and (iv) a labeled insulin-Pluronic-PAA conjugate adsorbed onto plate well (adsorbed conjugate). The insulin binding with the cells was measured after 3, 16, 24, and 48 h incubation following repeated cell washing with the binding buffer [15 mM Tris, 120 mM NaCl, 1.2 mM $MgSO_4$, 5 mM KCl, 10 mM glucose, 15 mM sodium acetate, 1% bovine serum albumin, 20 μg/mL bacitracin, and 50 μg/mL methiolate (*31*)]. The cells were detached from the plates by 0.025% trypsin/0.01% EDTA buffer solution. The fractions of bound and free insulin were separated by centrifugation. The cell pellet was resuspended in 200 μL of binding buffer. Insulin internalization was expressed as *Ins.In* (%) = $100 \times R_c/R_o$, where R_o (cpm) is the radioactivity of the well immediately after seeding, and R_c (cpm) is the radioactivity of the cells detached from the well. Cell growth was measured by the procedure of 6-[^{3}H]-thymidine uptake as described elsewhere (*32*−*34*). Confluent cells were incubated for 48 h and pulsed with ~1 μCi/well with [^{3}H]-thymidine for 3 h. The plates were then washed and DNA was precipitated by 10% trichloroacetic acid. The resulting precipitate was solubilized with 0.1% sodium dodecyl sulfate/0.1 M NaOH. The lysate was neutralized with 5 M HCl, and the incorporated radioactivity was assayed by β-liquid scintillation counting. Five series of experiments were conducted where a well contained one of the following: (i) Zn^{2+}-insulin dissolved in MEM (dissolved insulin); (ii) insulin-Pluronic-PAA conjugate dissolved in MEM (dissolved conjugate); (iii) Zn^{2+}-insulin adsorbed onto plate well (adsorbed insulin); and (iv) insulin-Pluronic-PAA conjugate adsorbed onto plate well (adsorbed conjugate). Relative cell growth rate [CGR (%)] was measured with and without (control) designated species and was calculated as an amount of DNA normalized to that in the control experiment. Quadruplicate CGR determinations were conducted for each insulin concentration.

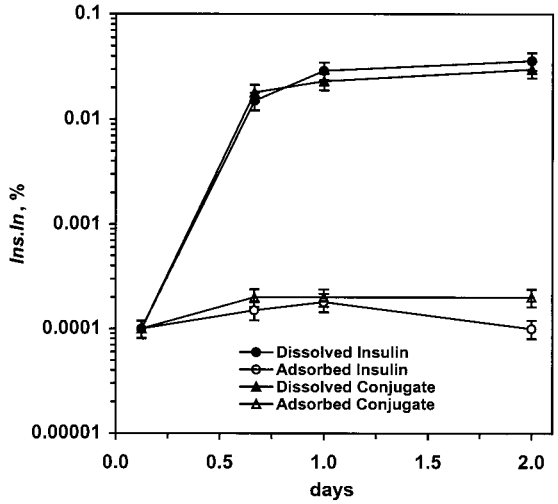


Figure 4. Internalization of different forms of insulin (*Ins.In*) into human uterine smooth muscle cells. For *Ins.In* definition, see the Experimental Section.

Glucosylated albumin binding to and release from FITC-Con A-Pluronic-PAA conjugates adsorbed onto PS nanoparticles was measured at 37 °C in 10 mM phosphate buffer at pH 7.4. A nanoparticle suspension (1 mL) with adsorbed concanavalin (effective Con A concentration 5 mg/mL, as measured by fluorescence) was mixed in a centrifuge tube with 1 mL of 1:1 mixture of albumin-2-amido-deoxy-D-glucose (G-Alb) and α-D-glucopyranosyl-FITC-albumin (G-FITC-Alb) (total glucosylated albumin concentration 0.2 mg/mL). The suspension was gently shaken at 37 °C for 8 h. The mixture was then centrifuged, and the pellet containing PS nanoparticles was separated from the supernatant and resuspended at 37 °C in 1 mL of 10 mM phosphate buffer. Total fluorescence of the G-Alb/G-FITC-Alb solution before contact with the conjugate-treated particles and of the supernatant after particle removal was measured. The weighted amount of particle suspension was mixed with 1 mL of either 10 mM phosphate buffer or 100 mg/dL glucose solution in the same buffer and the suspensions were gently shaken for 16 h at 37 °C. The suspensions were centrifuged and the fluorescence of the supernatant was measured. The procedure of loading and release was repeated. Identical experiments were conducted with nanoparticle suspension with 100 mg/dL glucose solution in 10 mM phosphate buffer without albumin.

Relative albumin release in the presence of glucose was expressed as R_g (%) = $100 \times (I_G - I_{wo})/(I_o - I_n)$, where I_G and I_{wo} is the maximum intensity of the supernatant with and without glucose, respectively (after corresponding cycle of albumin loading and release), and I_o and I_n is the maximum intensity of the FITC-Con A aqueous solution (corresponding to initial concentration of adsorbed Con A) and that of supernatant in the control experiment without albumin, respectively. Relative re-

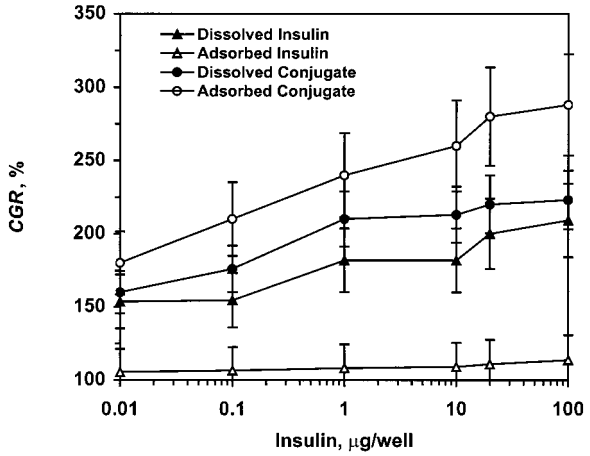


Figure 5. Relative cell growth rate (CGR) of human uterine smooth muscle cells in the presence of either native insulin or insulin conjugated onto Pluronic-PAA. Insulin or insulin-Pluronic-PAA conjugate were either dissolved in minimum essential medium or adsorbed onto plate wells as described in the Experimental Section.

lease without glucose was expressed by R_o (%) = 100 × $[I_{wo}/(I_o - I_n)]$. Cumulative desorption of Con A-Pluronic-PAA conjugates from nanoparticles was expressed as

$$z = 100\sum_{1}^{n}[1 - (I_o - I_n)/I_o]$$

Procedures. The β and γ radioactivity was determined using Wallac 1409 DSA liquid scintillation (EG&G Wallac) and COBRA gamma (Packard Instrument Co.) counters, respectively.

Fluorescence spectra were recorded on a SPEX FluoroMax spectrofluorometer applying 1 nm band-pass. Three scans were averaged and the spectra were corrected for scattering in blank solutions without FITC-Con A or G-FITC−Alb.

X-ray photoelectron spectroscopy (XPS/ESCA) was conducted using a 5000 Series spectrophotometer (Physical Electronics, Inc.). Air-in-water contact angles were measured using CAM-Micro optical device (KSV Instruments).

RESULTS

The binding/internalization of insulin into cells during culturing of human uterine smooth muscle cells for 2 days is depicted in Figure 4. It can be seen that either insulin or insulin-Pluronic-PAA conjugates exhibited almost identical association with the cells when dissolved in MEM, whereas adsorbed insulin or conjugate had negligible internalization. This result shows availability, in solution, of insulin conjugated with Pluronic-PAA, despite the high molecular weight of the conjugates.

Despite the lack of binding/internalization, adsorbed insulin-Pluronic-PAA conjugates appeared to stimulate the DNA synthesis to a higher degree (1.5−2.0-fold) when compared to free insulin (Figure 5). Although dissolved conjugates were less potent mitogenic agents than ad-

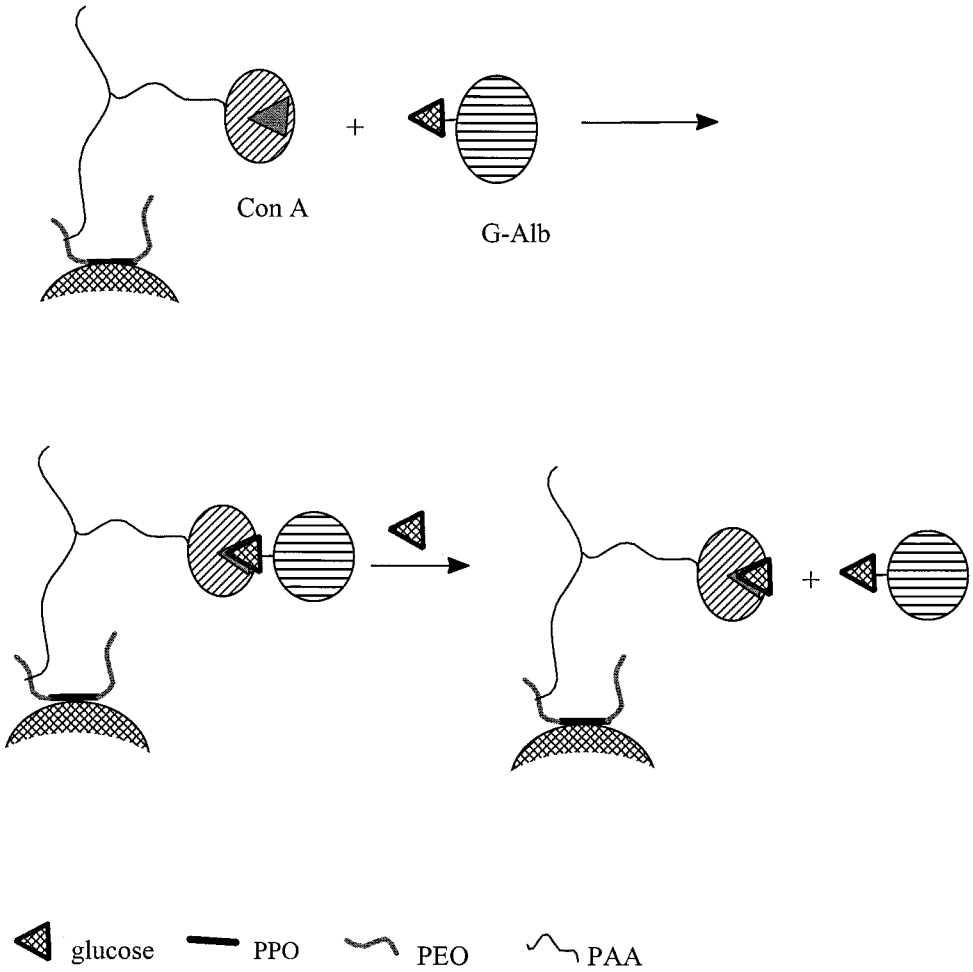


Figure 6. Scheme of interaction of glycosylated albumin (G-Alb) with Pluronic-PAA-Con A conjugates adsorbed onto polystyrene surfaces, followed by glucose-triggered G-Alb release.

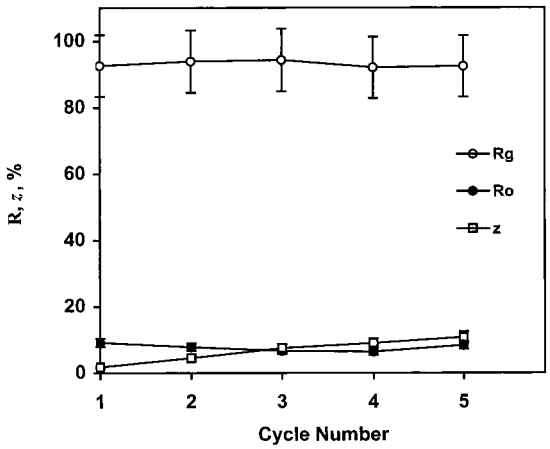


Figure 7. Relative release of glucosylated albumin in the presence (R_g, %) and absence (R_o, %) of glucose into 10 mM phosphate buffer (pH 7.4, pH 37 °C) from polystyrene nanoparticles treated by Con A-Pluronic-PAA conjugates. The R_g is found at 100 mg/dL glucose. Relative desorption of FITC-Con A-Pluronic-PAA conjugates from nanoparticles into 10 mM phosphate buffer at 37 °C is designated by *z*. Each point represents an average of 4 independent measurements. For parameter definition, see the Experimental Section.

sorbed ones, they exhibited 1.1−1.4-fold higher mitogenic activity than free insulin. Conversely, adsorbed insulin itself (without Pluronic-PAA) did not enhance the rate of DNA synthesis.

Glucose-stimulated release of glycosylated albumin (G-Alb) from complexes with Con A conjugated with Pluronic-PAA and adsorbed onto PS nanoparticles is shown schematically in Figure 6. The release was nearly complete, during at least five loading-desorption cycles (Figure 7). Cumulative desorption (*z*) of the FITC-Con A-Pluronic-PAA conjugates after same cycling was about 10% thereby demonstrating considerable stability of adsorbed conjugates on the PS particles under shear stresses applied due to handling. Release without glucose (R_o) was 10-fold lower than that with glucose and could be attributed to desorption of G-Alb-concanavalin complexes from the nanoparticles.

DISCUSSION

There have been numerous reports demonstrating applications of self-assembling poly(ethylene oxide)-*b*-poly(propylene oxide)-*b*-poly(ethylene oxide) (PEO−PPO−PEO) copolymers (Pluronic surfactants), for surface treatment. Pluronics are among a small number of surfactants approved by the U.S. Food and Drug Administration for the use in food and pharmaceuticals (*35*). The benign nature, lack of attractive interaction with proteins, and strong micelle-forming capability of Pluronics impart useful properties to Pluronic-modified surfaces, such as reduction of platelet adhesion (*36*), protein adsorption (*21*, *37*, *38*), bacterial adhesion (*39*), phagocytosis (*40*, *41*), and cell penetration enhancement in drug delivery (*7*). Conjugation of enzymes or antibodies to Pluronics following physical adsorption to hydrophobic surfaces is a means of tethering biomolecules to surfaces for use in heterogeneous assays (*28*). The tendency of many enzymes to denature on hydrophobic surfaces (*42*) may be overcome by tethering. The PPO block entropically interacts with the hydrophobic surface, while the hydrophilic PEO blocks extend to the hydration environment preventing direct exposure of the conjugated enzyme to the surface. Li et al. (*28*) developed a route of chemical modification of Pluronics via biomolecule conjugation to the OH end groups that produced robust coating for polystyrene surfaces. However, the end-group modification of Pluronics is inherently disadvantageous, if a high biomolecule loading is required. From this standpoint, recently developed copolymers of Pluronic and poly(acrylic acid) (Pluronic-PAA) (*5*−*20*) are attractive, as they combine spontaneous micellization capability of Pluronics and numerous carboxyl groups available for modification. An excess of carboxyl groups imparts an additional advantage to Pluronic-PAA conjugates such as mucoadhesive properties (*19*).

In this study, the concept of Pluronic-PAA copolymers conjugated with biomolecules for noncovalent surface modification is introduced. The grafting onto water-soluble polymers can alter biological activity of insulin (*34*, *43*−*45*). Insulin coupled with PEO possessed lower mitogenic activity than the native insulin, whereas PAA-insulin conjugates were shown to stimulate the growth of the mouse fibroblast cells more than the native insulin (*3*). It was intriguing to investigate mitogenic activity of the Pluronic-PAA copolymers, given their structure that combines PAA, PPO, and PEO segments. The overall enhancement of mitogenic activity observed for insulin conjugated to Pluronic-PAA (Figure 5) suggested that PAA-linked insulin might enhance receptor aggregation and formation of insulin conjugate−receptor complex. Conversely, lowering mitogenic activity by linking insulin to PEO (via A1-glycine and B29-lysine active sites) can be due to hindered access of the insulin-PEO to the receptor (*3*). Further enhancement of mitogenic activity by adsorption of the insulin-Pluronic-PAA complex (Figure 5) may be due to the lack of internalization and inhibited downregulation (*46*). Chen et al. (*3*) speculated that modification of polystyrene surface with PAA leaves no hydrophobic space available on PS for nonspecific interaction with insulin and reduces the roughness of the surface. On the basis of molecular weight and composition of Pluronic-PAA copolymers under study, their formula can be presented as $[EO_{100}PO_{65}EO_{100}AA_{132}]_{142}$ (*14*). The presence of ladder-like structures in these copolymers can be suggested (*9*) whereby PPO and PEO separate relatively long (over 10^2 units) PAA segments. Pluronic-PAA conjugates possess large area-per-molecule (~5.50 nm^2 at 20 °C and 4.0 nm^2 at 37 °C and pH 7.4) in dilute aqueous solutions (*8*). Using radioisotope method, we determined surface concentrations of Pluronic-PAA conjugates and Pluronic F127 on PS nanoparticles (Table 2). Surface concentration of Pluronic F127 correlated very well with that of other Pluronics (*23*). The area-per-molecule for various Pluronic surfactants at the air/water interface at 35 °C was reported to be in the range of 0.4-1.4 nm^2 (*47*). When compared with the surface density of 13−20 nm^2/molecule (Table 2 and ref *23*) this affords a conclusion that the surface density of Pluronic on nanoparticles is relatively low and no substantial adlayer is formed. The result is consistent with the observation of high mobility, in the absence of overlapping, of PEO segments of Pluronics on PS particles with $d = 69$ nm (*23*, *24*). More than 1400-fold higher m_p observed with Pluronic-PAA than with the parent Pluronic (Table 2) suggests large thickness of the adsorbed layer of the copolymer. The drastic difference between the adsorption of Pluronic and Pluronic-PAA copolymers can be understood based on the substantially different nature of their 3% solutions (*14*). Namely, the Pluronic solution at 3% and 37 °C exists in the form of micelles; no micellar cubic "gel" where PEO segments interpenetrate, is formed (*47*−*51*). At these same conditions, the Pluronic-PAA system forms a viscoelastic gel where large micellar aggregates are stabilized by domains of dense PPO segments (*8*−

11, 15). Most likely location of PS nanoparticles is within these domains (*15*). Low surface coverage in case of Pluronics causes the polymer chains to collapse into a "mushroom" conformation (*23, 24*), whereas Pluronic-PAA can form gellike layers on the PS surface (Figure 8). These relatively thick layers may completely maskthe roughness and hydrophobicity of the PS surface and reduce internalization/binding of insulin, "hidden" inside the layers (Figure 5). Low dissociation/internalization rate may explain increased mitogenic activity of the high molecular weight conjugates in viscous, gellike solutions. It has been argued (*52*) that enhanced mitogenicity of some insulin analogues is due to the longer association time with the insulin receptors. On the other hand, the gel layers of Pluronic-PAA are unlikely to inhibit diffusion of low molecular weight species (e.g., glucose) (*16, 20*). Hence, the complete recovery of G-Alb from Con A-Pluronic-PAA complexes was observed (Figure 7). This is the first encounter of a glucose-sensitive protein delivery system based on self-assembling Pluronic-PAA copolymer.

CONCLUSIONS

Applications of poly(acrylic acid) grafted onto PEO−PPO−PEO backbone (Pluronic-PAA) copolymers for polystyrene surface modification by adsorption were reported in this study. Insulin-Pluronic-PAA conjugates exhibited substantial association with the human uterine smooth muscle cells in solution, whereas the adsorbed conjugate had negligible internalization. It may be hypothesized that the lack of internalization contributed to the increase of mitogenic activity of the adsorbed Pluronic-PAA copolymers. Dramatic enhancement in the adsorption of Pluronic-PAA onto polystyrene nanospheres was observed when compared to that of the parent Pluronic due to adsorption of large domains of aggregated PPO segments. The glucose-induced release of glycated albumin complexed with concanavalin A conjugated with Pluronic-PAA and adsorbed onto polystyrene nanospheres may provide a model for a feedback-responsive protein delivery system or a heterogeneous detection device.

LITERATURE CITED

(1) Wojciechowski, P. W., and Brash, J. L. (1996) The role of interfacial phenomena in biotechnology: an overview. In *Interfacial Phenomena and Bioproducts* (P. W. Wojciechowski, and J. L. Brash, Eds.) Chapter 1, Marcel Dekker, New York.

(2) Riza, M., Tokura, S., Iwasaki, M., Yashima, E., Kishida, A., and Akashi, M. (1995) Graft copolymers having hydrophobic backbone and hydrophilic branches X. Preparation and properties of water-dispersible polyanionic microspheres having poly(methacrylic acid) branches on their surfaces. *J. Polym. Sci. Polym. Ed. 33,* 1219−1225.

(3) Chen, G., Ito, Y., and Imanishi, Y. (1997) Mitogenic activities of water-soluble and -insoluble insulin conjugates. *Bioconjugate Chem. 8,* 106−110.

(4) Akasi, M., Niikawa, T., Serizawa, T., Hayakawa, T., and Baba, M. (1998) Capture of HIV-1 gp120 and virions by lectin-immobilized polystyrene nanospheres. *Bioconjugate Chem. 9,* 50−53.

(5) Bromberg, L., Lupton, E. C., Schiller, M. E., Timm, M. J., McKinney, G. W., Orkisz, M., and Hand, B. (1997) Responsive polymer networks and methods of their use. Int. Patent Appl. WO 97/00275.

(6) Ron, E. S., Bromberg, L., Orkisz, M., Kearney, M., Luczak, S., Timm, M. J., and Wrobel, S. J. (1998) Composition for pharmaceutical applications. Int. Patent Appl. WO 98/06438.

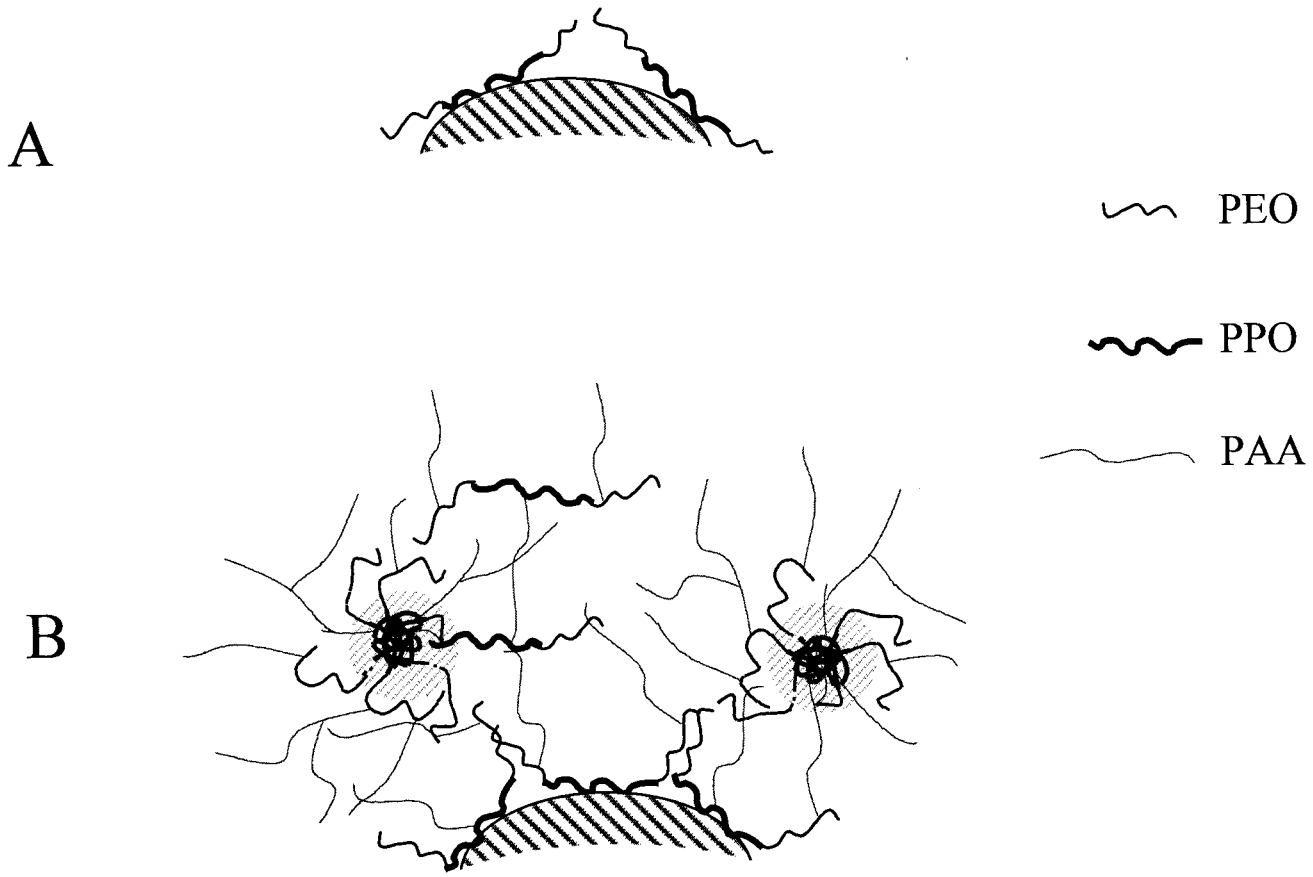


Figure 8. Scheme of Pluronic (A) and Pluronic-PAA (B) conjugates adsorbed onto polystyrene surfaces. (A) Low concentration allows for spreading on the surface; (B) electrostatic repulsion renders rodlike PAA conformation. In Pluronic-PAA conjugates, ladder-like structure is assumed whereby PAA is attached to PEO or PPO via C−C bonding (*33*). The Pluronic-PAA conjugates form micellar aggregates with PPO cores and PAA coronas (*12*). The aggregates are anchored on the surface by the PPO segments.

(7) Bromberg, L., and Ron, E. S. (1998) Protein and peptide release from temperature-responsive gels and thermogelling polymer matrices. *Adv. Drug Delivery Rev. 31*, 197−221.
(8) Bromberg, L. (1998) Self-assembly in aqueous solutions of polyether-modified poly(acrylic acid). *Langmuir 14*, 5806−5812.
(9) Bromberg, L. (1998) Scaling of rheological properties of hydrogels from associating polymers. *Macromolecules 31*, 6148−6156.
(10) Bromberg, L. (1998) A novel family of thermogelling materials via C−C bonding between poly(acrylic acid) and poly(ethylene oxide)-*b*-poly(propylene oxide)-*b*-poly(ethylene oxide). *J. Phys. Chem. B 102*, 1956−1963.
(11) Bromberg, L. (1998) Properties of aqueous solutions and gels of poly(ethylene oxide)-*b*-poly(propylene oxide)-*b*-poly-(ethylene oxide)-*g*-poly(acrylic acid) *J. Phys. Chem. B 102*, 10736−10744.
(12) Huibers, P. D. T., Bromberg, L. E., Robinson, B. H., Hatton, T. A. (1999) Reversible gelation in semidilute aqueous solutions of associative polymers: a small-angle neutron scattering study. *Macromolecules* (In press).
(13) Ron, E. S., Bromberg, L., Luszak, S., Kearney, M., Deaver, D. R., and Schiller, M. Smart Hydrogel: a novel mucosal delivery system. (1997) *Proc. Int. Symp. Control. Release Bioact. Mater. 24*, 407−408.
(14) Bromberg, L. (1998) Polyether-modified poly(acrylic acid): synthesis and applications. *Ind. Eng. Chem. Res. 37*, 4267−4274.
(15) Bromberg, L., Orkisz, M., Roos, E., Ron, E. S., and Schiller, M. (1997) Interpenetrating networks of Poloxamer copolymers and poly(acrylic acid) as vehicles in controlled drug delivery. *J. Controlled Release 48*, 305−308.
(16) Bromberg, L. E., Mendum, T. H. E., Orkisz, M. J., Lupton, E. C., and Ron, E. S. (1997) Polyoxyethylene-*b*-polyoxypropylene-*b*-polyoxyethylene-*g*-poly(acrylic acid) polymers (Smart Hydrogel) as a carrier in controlled delivery of proteins and peptides. *Polym. Prepr. 38*, 602−603.
(17) Bromberg, L. E., and Barr, D. P. (1999) Aggregation phenomena in aqueous solutions of hydrophobically modified polyelectrolytes. A probe solubilization study. *Macromolecules 32*, 3649−3657.
(18) Orkisz, M. J., Bromberg, L., Pike, R., Lupton, E. C., and Ron, E. S. (1997) Rheological properties of reverse thermogelling poly(acrylic acid)-*g*-poly(oxyethylene-*b*-oxypropylene-*b*-oxyethylene) polymers (Smart Hydrogel). *Proc. Polym. Mater. Sci. Eng. 76*, 276−277.
(19) Bromberg, L. E., Orkisz, M. J., and Ron, E. S. (1997) Bioadhesive properties of polyoxyethylene-*b*-polyoxypropylene-*b*-polyoxyethylene-*g*-poly(acrylic acid) polymers (Smart Hydrogel). *Polym. Prepr. 38*, 626.
(20) Bromberg, L. E., and Goldfeld, M. G. (1998) Self-assembly in aqueous solutions of hydrophobically modified poly(acrylic acid). *Polym. Prepr. 39*, 681−682.
(21) Lee, J. H., Kopecek, J., and Andrade, J. D. (1989) Protein-resistant surfaces prepared by PEO-containing block copolymer surfactants. *J. Biomed. Mater. Res. 23*, 351−368.
(22) Ito, Y., Liu, S. Q., and Imanishi, Y. (1991) Enhancement of cell growth on growth factor-immobilized polymer film. *Biomaterials 12*, 449−453.
(23) Li, J.-T., and Caldwell, K. D. (1991) Sedimentation field-flow fractionation in the determination of surface concentration of adsorbed materials. *Langmuir 7*, 2034−2039.
(24) Li, J.-T., Caldwell, K. D., and Rapoport, N. (1994) Surface properties of Pluronic-coated polymeric colloids. *Langmuir 10*, 4475−4482.
(25) Bromberg, L. (1999) Novel self-assembling polymers: poly-(ethylene oxide)-*b*-poly (propylene oxide)-*b*-poly(ethylene oxide)-*b*-poly(vinyl alcohol). Manuscript in preparation.
(26) Vinogradov, S., V., Bronich, T. K., and Kabanov, A. V. (1998) Self-assembly of polyamine-poly(ethylene glycol) copolymers with phosphorothioate oligonucleotides. *Bioconjugate Chem. 9*, 805−812.
(27) Chen, G., Hoffman, A. S., Kabra, B., and Randeri, K. (1997) Temperature-induced gelation Pluronic-*g*-poly(acrylic acid) graft copolymers for prolonged drug delivery to the eye. In *Poly(ethylene glycol) Chemistry and Biological Applications* (J. M. Harris, and S. Zalipsky, Eds.) Chapter 27, ACS Symp. Series 680, American Chemical Society, Washington, DC.
(28) Li, J.-T., Carlsson, J., Lin, J.-N., and Caldwell, K. D. (1996) Chemical modification of surface active poly(ethylene oxide)-poly(propylene oxide)-poly(ethylene oxide) triblock copolymers. *Bioconjugate Chem. 7*, 592−599.
(29) Bromberg, L. (1997) Zein-poly(N-isopropylacrylamide) conjugates. *J. Phys. Chem. B, 101*, 504−507.
(30) Hermanson, G. T. (1996) *Bioconjugate Techniques*, pp 407−410, Academic Press, San Diego.
(31) Baudyš, M., Letorneur, D., Liu, F., Mix, D., Jozefonvicz, J., and Kim, S. W. (1998) Extending insulin action in vivo by conjugation to carboxymethyl dextran. *Bioconjugate Chem. 9*, 176−183.
(32) Bornfeldt, K. E., Gidlöf, R. A., Wasteson, A., Lake, M., Skottner, A., and Arnquist, H. J. (1991) Binding and biological effects of insulin, insulin analogues and insulin-like growth factors in rat aortic smooth muscle cells. Comparison of maximal growth promoting activities. *Diabetologia 34*, 307−313.
(33) Frank, H. J. L., Levin, E. R., Hu, R.-M., and Pedram, A. (1993) Insulin stimulates endothelin binding and action on cultured vascular smooth muscle cells. *Endocrinology 133*, 1092−1097.
(34) Chytry, V., Letourneur, D., Baudyš, M., and Josefonvicz, J. (1996) Conjugates of insulin with copolymers of N−(2-hydroxypropyl) methacrylamide: effects on smooth muscle cell proliferation. *J. Biomed. Mater. Res. 31*, 265−272.
(35) *BASF Performance Chemicals. FDA and EPA status* (1993) BASF Corporation, North Mount Olive, New Jersey.
(36) Amiji, M., and Park, K. (1992) Prevention of protein adsorption and platelet adhesion on surfaces by PEO/PPO/PEO triblock copolymers. *Biomaterials 13*, 682−692.
(37) Tan, J. S., Butterfield, D. E., Voycheck, C. L., Caldwell, K. D., and Li, J.-T. (1993) Surface modification of nanoparticles by PEO/PPO block copolymers to minimize interactions with blood components and prolong blood circulation in rats. *Biomaterials 14*, 823−833.
(38) Lee, J., Martic, P. A., and Tan, J. S. (1989) Protein adsorption on Pluronic copolymer-coated polystyrene particles. *J. Colloid Interface Sci. 131*, 252−266.
(39) Bridgett, M. J., Davis, M. C., and Denyer, S. P. (1992) Control of staphylococcal adhesion to polystyrene surface by polymer surface modification with surfactants. *Biomaterials 13*, 411−416.
(40) Illum, L., Jacobsen, L. O., Müller, E. M., and Davis, S. S. (1987) Surface characteristics and the interaction of colloidal particles with mouse peritoneal macrophages. *Biomaterials 8*, 113−117.
(41) Watrous-Peltier, N., Uhl, J., Steel, V., Brophy, L., and Merisko-Liversidge, E. (1992) Direct suppression of phagocytosis by amphipatic polymeric surfactants. *Pharm. Res. 9*, 1177−1183.
(42) Sandwick, R. K., and Schray, K. J. (1987) Inactivation of enzymes upon interaction with a hydrophobic latex surface. *J. Colloid Interface Sci. 115*, 130−138.
(43) Mehvar, R. (1994) Preparative and analytical separation of insulin-dextran conjugates from native insulin. *Drug Dev. Indus. Pharm. 20*, 395−404.
(44) Ehrat, M., and Luisi, P. L. (1983) Synthesis and spectroscopic characterization of insulin derivatives containing one or two poly(ethylene oxide) chains at specific positions. *Biopolymers 22*, 569−573.
(45) Chytry, V., Vrana, A., and Kopecek, J. (1978) Synthesis and activity of a polymer which contains insulin covalently bound on a copolymer of N-(2-hydroxypropyl) methacrylamide and N-methacryloyldiglycidyl *p*-nitrophenyl ester. *Makromol. Chem. 179*, 329−336.
(46) Ito, Y., Zheng, J., Imanishi, Y., Yonezawa, K., and Kasuga, M. (1996) Protein-free cell culture on an artificial substrate with covalently immobilized insulin. *Proc. Natl. Acad. Sci. U.S.A. 93*, 3598−3601.
(47) Alexandridis, P., Athanassiou, V., Fukuda, S., and Hatton, T. A. (1994) Surface activity of poly(ethylene oxide)-*block*-poly(propylene oxide)-*block*-poly(ethylene oxide) copolymers. *Langmuir 10*, 2604−2612.

(48) Alexandridis, P., Nivaggioli, T., and Hatton, T. A. (1995) Temperature effects on structural properties of Pluronic P104 and F108 PEO−PPO−PEO block copolymer solutions. *Langmuir 11*, 1468−1476.

(49) Cau, F., and Lacelle, S. (1996) ^{1}H NMR Relaxation studies of the micellization of a poly(ethylene oxide)-poly(propylene oxide)-poly(ethylene oxide) triblock copolymer in aqueous solution. *Macromolecules 29*, 170−178.

(50) Nyström, B., and Walderhaug, H. (1996) Dynamic viscoelasticity of an aqueous system of a poly(ethylene oxide)-poly(propylene oxide)-poly(ethylene oxide) triblock copolymer during gelation. *J. Phys. Chem. 100*, 5433−5439.

(51) Alexandridis, P. (1997) Amphiphilic copolymers and their applications. *Curr. Opin. Colloid Interface Sci. 2*, 478−501.

(52) Ish-Shalom, D., Christoffersen, C. T., Vorwerk, P., Sacerdoti-Sierra, N., Shymko, R. M., Naor, D., and De Meyts, P. (1997) Mitogenic properties of insulin and insulin analogues mediated by the insulin receptor. *Diabetologia 40* (Suppl. 2), S25−S31.

BC9800973

A Versatile Method for the Conjugation of Proteins and Peptides to Poly[2-(dimethylamino)ethyl methacrylate]

W. N. E. van Dijk-Wolthuis,[†,‡] P. van de Wetering,[†] W. L. J. Hinrichs,[†] L. J. F. Hofmeyer,[§] R. M. J. Liskamp,[§] D. J. A. Crommelin,[†] and W. E. Hennink*[,†]

Department of Pharmaceutics, Sorbonnelaan 16, Department of Medicinal Chemistry, Utrecht Institute for Pharmaceutical Sciences (UIPS), Faculty of Pharmacy, Utrecht University, PO Box 80 082, 3508 TB Utrecht, The Netherlands, and OctoPlus BV, Niels Bohrweg 11-13, 2333 CA Leiden, The Netherlands.
Received October 28, 1998; Revised Manuscript Received March 29, 1999

Random copolymers of 2-(dimethylamino) ethyl methacrylate (DMAEMA) with aminoethyl methacrylate (AEMA) were synthesized by radical polymerization. The amount of incorporated primary amino groups could be controlled by the feed ratio of AEMA to DMAEMA, and was varied from 2 to 6 mol %. Subsequently, protected thiol groups were introduced in a derivatization step with *N*-succinimidyl 3-(2-pyridyldithio)propionate (SPDP) and subsequent treatment with dithiothreitol (DTT). The obtained thiolated p(DMAEMA-*co*-AEMA) was conjugated to transferrin (Tf) or the F(ab′) fragment of mAb 323/A3 via a disulfide linkage. Moreover, the maleimide derivative of the nuclear localization signal (NLS) decapeptide Gly-Pro-Lys-Lys-Lys-Arg-Lys-Val-Glu-Asp-NH_2 was coupled to the thiolated polymer via a thioether linkage. The coupling efficiency, as determined by GPC (Tf), SDS−PAGE [F(ab′)], or ^{1}H NMR (NLS peptide) was 90−95% for the Tf conjugate, and more than 95% for the F(ab′) conjugate and the NLS conjugate. The synthetic strategy described in this paper is a universal method for the preparation of conjugates of proteins and peptides with pDMAEMA in particular. This method can possibly be used to synthesize protein−polymethacrylate conjugates in general.

INTRODUCTION

Water-soluble methacrylate/methacrylamide polymers are presently under investigation for the delivery of anticancer drugs (*1*, *2*) and for the delivery of genetic material (*3*). These polymers can be easily synthesized by the radical polymerization of the corresponding monomers, and their molecular weight can be controlled by the polymerization conditions. To deliver the polymer-drug conjugates or polymer−DNA complexes selectively into the target cell, a homing device (protein, sugar moiety) is often required. These homing devices are covalently coupled to the polymer of interest via established conjugation reactions using functional groups in both the polymer and the protein. Functional groups are intrinsically present in the polymer or can be introduced by copolymerization. Jelinkova et al. reported on the synthesis of conjugates of poly(hydroxypropyl methacrylamide) (HPMA) with monoclonal antibodies (MAb) by reaction of active esters of HPMA with MAb in aqueous solution (*4*). Besides methods based on active esters, protein conjugates can also be synthesized using methods based on the formation of disulfide bridges. The SPDP method, as first described by Carlsson et al. (*5*), is successfully and frequently applied for the synthesis of protein−protein conjugates (e.g., α-amylase-urease and ribonuclease-albumin) as well as for the synthesis of polymer-protein conjugates, e.g., pLys−Tf[1] conjugates (*6*) and PEI-protein conjugates (*7*). Within our group, we are working on poly[2-(dimethylamino)ethyl methacrylate] (pDMAEMA) as polymeric gene transfer agent. This polymer has good transfection potential as compared to other nonviral systems (pLys, lipofectin) (*3*). We are therefore interested in the design of systems based on this polymer, which selectively deliver the plasmid DNA into the nucleus of the target cell. It can be anticipated that by using a homing device the cell selectivity will increase and that by introduction of a so-called nuclear localization signal (NLS) peptide, nuclear targeting can probably be accomplished.

For the synthesis of pDMAEMA-protein/peptide conjugates, the polymer has to be functionalized, since in pDMAEMA, no groups are available for the covalent linkage of a homing device. The aim of this research is to develop a universal method to couple proteins or peptides to pDMAEMA. Therefore, pDMAEMA was first functionalized with primary amino groups by copolymerization of DMAEMA with a limited amount of 2-aminoethyl methacrylate (AEMA). Next, (part of) the amino groups were translated into thiol groups, using the SPDP method, after which this thiolated polymer was coupled to three different homing devices. First, transferrin was selected as a homing device since this protein is predominantly taken up by proliferating cells (*8*). Second, a F(ab′) fragment of the mouse monoclonal antibody 323/A3 was

* To whom correspondence should be addressed. Phone: +31 30 253 6964. Fax: +31 30 251 7839. E-mail: W.E.Hennink@pharm.uu.nl.
† Department of Pharmaceutics.
‡ Department of Medicinal Chemistry.
§ OctoPlus BV.

[1]Abbreviations: AEMA, aminoethyl methacrylate; APS, ammonium peroxydisulfate; DMAEMA, 2-(dimethylamino) ethyl methacrylate; DTT, dithiothreitol; Fmoc, 9-fluorenylmethoxycarbonyl; GPC, gel permeation chromatography; NLS, nuclear localization signal; NMP, *N*-methylpyrrolidone; pDMAEMA, poly(2-(dimethylamino) ethyl methacrylate); p(DMAEMA-*co*-AEMA), poly(dimethylaminoethyl methacrylate-*co*-aminoethyl methacrylate); SPDP, *N*-succinimidyl 3-(2-pyridyldithio)propionate; Tf, transferrin.

10.1021/bc980126+ CCC: $18.00 © 1999 American Chemical Society
Published on Web 06/02/1999

coupled. This antibody is recognized by a M_r 43 kDa membrane glycoprotein, which is highly expressed on a variety of carcinomas (*9*). Last, thiolated pDMAEMA was coupled via a thioether linkage to a maleimide derivatized NLS peptide. As NLS sequence, the SV40 Slarge T antigen NLS sequence (Gly-Pro-Lys-Lys-Lys-Arg-Lys-Val-Glu-Asp-NH_2) was chosen because many NLS peptides contain (a variant of) this sequence (*10*, *11*).

MATERIALS AND METHODS

General. *Materials*. The following compounds were used as received: 2-aminoethyl methacrylate hydrochloride (AEMA, Polysciences Inc., Warrington, PA), ammonium peroxydisulfate (APS, Fluka, >98%), apotransferrin (*12*) (Sigma, low endotoxin, approximately 98%), dithiothreitol (DTT, Acros, 99%), 4-(2-hydroxyethyl)-1-piperazine-ethanesulfonic acid (Hepes, Acros, 99%), 1-hydroxybenzotriazole (HOBt), trifluoroacetic acid (TFA, peptide grade, Biosolve, The Netherlands), 9-fluorenylmethoxycarbonyl (Fmoc) protected amino acids, *N*-methylpyrrolidone (NMP, peptide grade Biosolve), succinimidyl 4-(p-maleimidophenyl butyrate) (SMPB, Pierce), N-succinimidyl 3-(2-pyridyldithio)propionate (SPDP, Pharmacia Biotech), and tris(hydroxymethyl)-aminomethane (TRIS, Acros, 99+ %).

N,*N*-Dimethylformamide (DMF, peptide synthesis grade, Biosolve, The Netherlands) was dried on molecular sieves before use. 2-(Dimethylamino)ethyl methacrylate (DMAEMA, Fluka, >98% by GC) was purified by distillation under reduced pressure just before use. All other chemicals were of analytical grade. Water was purified by reversed osmosis. The PBS used in this study contained 0.1 M phosphate, pH 7.5, with 0.1 M NaCl, whereas the HBS buffer was composed of 20 mM Hepes, pH 7.4, and 0.155 M NaCl.

Methods. Solid-phase peptide syntheses were carried out on an ABI 433A Peptide Synthesizer. The Fmoc-deprotection reaction was monitored at 301 nm. Tentagel S RAM resin was purchased from Rapp Polymere (Tübingen, Germany). Fast-atom bombardment (FAB) mass spectrometry (MS) was carried out on a JEOL JMS SX/SX 102A four-sector mass spectrometer, coupled with a HP-9000 data system. ^{1}H NMR spectra were recorded with a Gemini 300 MHz spectrometer (Varian Associates Inc. NMR Instruments, Palo Alto, CA). Approximately 30 mg of material was dissolved in 0.8 mL of ^2H_2O. The ^{2}HOH signal at 4.8 ppm was used as the reference line. A pulse length of 4.5 ms ($PW_{90} \approx 12$ ms) was used with a relaxation delay of 15 s. The molecular weights and molecular weight distributions of p(DMAEMA-*co*-AEMA) and its conjugates were determined by gel permeation chromatography (GPC) with an LC Module 1 Plus system (Waters Associates Inc., Milford, MA) and three thermostated (35 °C) columns in series (Shodex Ollpak KB-802 and KB-80, Showa Denko, Japan), equipped with a model 410 differential refractometer. The mobile phase was 0.1 M Tris (pH 7.2)/0.7 M $NaNO_3$, and the column was calibrated using dextran standards of known molecular weights (Fluka). The amount of free transferrin (Tf) in the p(DMAEMA-*co*-AEMA)-Tf conjugates was determined by GPC using a TSK 3000 column, eluted with 0.1 M phosphate (pH 6.7)/0.1 M Na_2SO_4. Conjugated Tf eluted in the void volume of the column (5 min), whereas the retention time of free Tf was 7 min and was quantified via a calibration curve (linear range 0.01−1.0 mg/mL Tf). Purification of derivatized polymer or protein was performed by gel filtration using Sephadex G-25 superfine columns with a void volume of 2.5 mL (PD-10, Pharmacia, Sweden). The intrinsic viscosity of p(DMAEMA-*co*-AEMA) was determined by measuring the specific viscosity of polymer solutions in 0.7 M $NaNO_3$/0.1 M Tris, pH 7.2, at 1.0, 0.66, and 0.33% w/v and extrapolating to zero concentration. The analysis was done with an Uhbelohde viscometer at 35 °C. The pDMAEMA concentration was quantified by Bio-Rad protein assay in water at 588 nm. The absorption was corrected for the protein present in the sample, and the calibration curve was linear from 0.5 to 4 mg/mL. SDS−PAGE was performed using the mini-PROTEAN II electrophoresis cell (Bio-Rad). The separating gel was 0.75 mm thick and contained 12.5% acrylamide. The gels were stained with Coomassie Blue.

Synthesis of Poly(dimethylaminoethyl methacrylate-*co*-aminoethyl methacrylate) [p(DMAEMA-*co*-AEMA)]. The DMAEMA-based copolymers were synthesized essentially according to Van de Wetering et al. (*3*). Freshly distilled 2-(dimethylamino)ethyl methacrylate (5.0 mL, 30 mmol) and varying amounts of aminoethyl methacrylate hydrochloride (0.75, 1.5 or 3 mmol) were dissolved in 25 mL of 1.3 M hydrochloric acid, and the pH was adjusted to 3. The solutions were deoxygenated by vacuum and nitrogen purging, and a calculated amount of APS (*M*/*I* 25, 50, or 100 mol/mol) was added. After polymerization in a water bath at 60 °C for 16 h, the polymers were purified by extensive dialysis against demineralized water and isolated by lyophilization. Yield: ca. 6 g (95−99%).

^{1}H NMR (^2H_2O): d 0.9−2.4 [5H, several bs, $-CH_2-CR(CH_3)-$], 3.0 [6H, bs, $-N(CH_3)_2$], 3.45 (small, bs, CH_2-NH_2), 3.6 [2H, bs, $(CH_3)_2NCH_2-$], 4.4 (2H, bs, $-OCH_2-$).

Thiolation of p(DMAEMA-*co*-AEMA). To a solution of p(DMAEMA-*co*-AEMA) (25 mg/mL in PBS) was added a calculated amount of SPDP (40 mM in ethanol) under vigorous mixing. After 30 min at room temperature, excess reagent and *N*-hydroxysuccinimide were removed by gel filtration (PD-10/PBS).

The pDMAEMA concentration was quantified by Bio-Rad protein assay in water at 588 nm. The amount of incorporated PDP groups was determined by quantifying 2-mercaptopyridine (pyrSH) at 343 nm, which was released from the PDP groups by treatment of 950 mL of PDP-derivatized polymer with 50 mL of 100 mM DTT in water (molar absorptivity of pyrSH: 8.08×10^3 M^{-1} cm^{-1}) (*5*). The thiol groups in p(DMAEMA-*co*-AEMA-PDP) were deprotected by treatment with excess dithiothreitol (DTT) (about 25 mg/100 mg of derivatized polymer) for 15−30 min at room temperature and subsequent gel filtration (PD-10/PBS), resulting in a solution of 11 mg/mL p(DMAEMA-*co*-AEMA)-SH (abbreviated as pol-SH).

Thiolation of Transferrin. To a solution of transferrin (10 mg/mL) was added a calculated amount of SPDP (40 mM in ethanol) under vigorous mixing. After 30 min at room temperature, excess reagent and *N*-hydroxysuccinimide were removed by gel filtration (PD-10/ PBS).

The transferrin concentration was quantified by UV absorbance at 280 nm. The amount of incorporated PDP-groups was determined as described for PDP-derivatized p(DMAEMA-*co*-AEMA).

Preparation of F(ab′) Fragments of the Mouse Monoclonal Antibody 323/A3. The mouse Mab 323/A3 was incubated with pepsin as described before (*13*) to yield $F(ab')_2$ fragments. It has been shown that under the selected conditions reduction of the disulfide bond between the heavy chains occurs, while the disulfide bond between the heavy and the light chain stayed intact (*13*).

The fragments were incubated at 3 mg/mL with 25 mM DTT in acetate buffer pH 5.5 (100 mM NaAc, 100 mM NaCl, and 1 mM EDTA) for 90 min at room temperature. DTT was removed by gel filtration (PD-10/deoxygenated HBS), yielding 2.1 mg/mL F(ab′) fragments in HBS. The F(ab′) fragments, which contain a thiol group, were used immediately for covalent coupling to PDP-derivatized p(DMAEMA-*co*-AEMA).

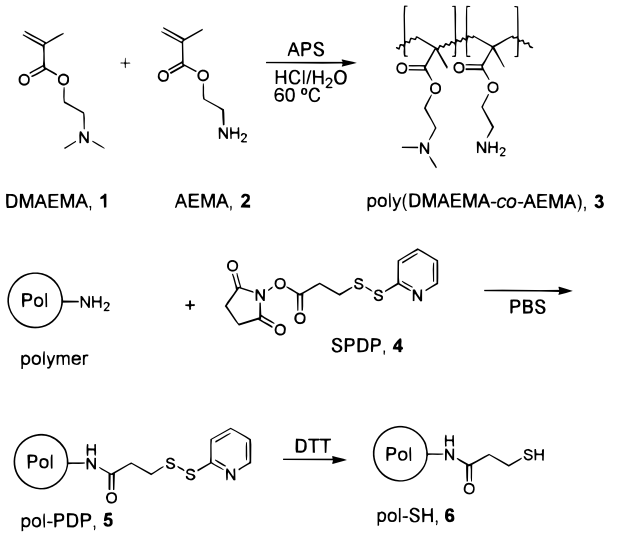
Synthesis of the 4-(4-Maleimidophenyl)butyrate Derivative of Gly-Pro-Lys-Lys-Lys-Arg-Lys-Val-Glu-Asp (NLS-MPB). The NLS decapeptide was synthesized by solid-phase synthesis. First, the amino acid Asp was attached to the resin (TentaGel S RAM). Coupling and deprotection cycles were carried out on a ABI 433A Peptide Synthesizer using ABI FastMoc 0.25 mmol protocols (*14*). Repetitive Fmoc cleavage was accomplished with 20% piperidine in NMP. Peptide couplings were performed using 4 molar equivalents of Fmoc-amino acid, BOP, and HOBt in the presence of DiPEA in NMP for 45 min. The Fmoc was removed by 20% piperidine in NMP. The Fmoc removal and formation of dibenzofulvene-piperidine adduct was followed by UV at 301 nm. A small portion of the resin was used for cleavage of the peptide by stirring in 95% TFA/H_2O for 2 h. The resin was removed by filtration, and the filtrate was lyophilized to give the deprotected peptide, which was characterized by HPLC, ^{1}H NMR, and FAB MS (*m*/*z* 1183.7 $[M + H]^+$).

The remaining peptide on resin (105 mg, 0.017 mmol of peptide) was weighed into a 10 mL flask, the Fmoc-group was removed using a 20% piperidine solution in NMP (stirred for 1 h at ambient temperature), after which the resin was washed with NMP (5×). The resin was suspended in NMP, after which 5 equiv (0.08 mmol) of SMPB, and 3 equiv of DiPEA were added. After 1.5 h stirring, the resin was filtered and washed with NMP. The product, containing a maleimide group, was cleaved from the resin by stirring with 95/5 TFA/water (v/v) for 2 h. The reaction mixture was filtered and the residue was washed with water. The total filtrate was lyophilized, yielding 0.039 g of peptide (0.018 mmol). ^{1}H NMR (^2H_2O): d 7.02 (s, 2H, maleimide), 7.25 (m, 2H, Ph), 7.40 (m, 2H, Ph). FAB MS: *m*/*z* 1424.8 $[MH]^+$.

Synthesis of Conjugates. *Conjugates of Transferrin with pDMAEMA*. The p(DMAEMA-*co*-AEMA)-Tf conjugate was prepared by addition of 0.67 mL of 15 mg/mL Tf-PDP (2.5 mol of PDP/mol of Tf) to 2.0 mL 10 mg/mL of pol-SH [1 mol of SH/150 mol of monomeric unit; p(DMAEMA-*co*-AEMA) with 6 mol % AEMA, M_n 30 kDa, M_w 785 kDa (relative to dextran)]. After incubation for 16 h, the low molecular mass compounds were removed from the reaction mixture by gel filtration (PD-10/HBS). The composition of the conjugate was determined by UV-analysis [A_{280} nm for Tf, Bio-Rad at 588 nm in water for p(DM)AEMA], whereas the conjugation efficiency was determined by quantification of free Tf by GPC chromatography.

Conjugates of F(ab′)-Fragment 323/A3 with pDMAEMA. The p(DMAEMA-*co*-AEMA)-F(ab′) conjugate was prepared by addition of 3.5 mL of 2.1 mg/mL F(ab′) in PBS to 0.88 mL of 17 mg/mL pol-PDP [1 PDP/140 monomeric units; p(DMAEMA-*co*-AEMA) with 6 mol % AEMA, M_n 30 kDa, M_w 785 kDa (relative to dextran)]. After incubation for 16 h, the low molecular mass compounds were removed from the reaction mixture by gel filtration (PD-10/HBS). The composition of the conjugate was determined by UV-analysis [A_{280} nm for F(ab′), Bio-Rad at 588 nm for p(DM)AEMA], whereas the conjugation efficiency was determined by SDS−PAGE analysis.

Scheme 1. Reaction Scheme of the Synthesis of Poly[2-(dimethylamino)ethyl Methacrylate-*co*-2-aminoethyl Methacrylate] and Subsequent Thiolation with *N*-Succinimidyl 3-(2-Pyridyldithio)propionate (SPDP)



Conjugation of NLS-MPB. To 3.5 mL of 12 mg/mL p(DMAEMA-*co*-AEMA)-SH in PBS [1 SH/50 monomeric units; 6 mol % AEMA, M_n 30 kDa, M_w 785 kDa (relative to dextran)], 0.011 g (0.0077 mmol) of NLS-MPB dissolved in 0.28 mL of water was added. After reacting for 18 h at room temperature, the polymer−peptide conjugate was obtained by gel filtration (PD-10/water) and subsequent lyophilization.

RESULTS AND DISCUSSION

Synthesis of pDMAEMA with Primary Amines. To obtain pDMAEMA with primary amino groups, which are necessary for the coupling of ligands, 2-(dimethylamino)-ethyl methacrylate (DMAEMA, Scheme 1-**1**) was copolymerized with aminoethyl methacrylate (AEMA, **2**). Since AEMA is only available as its HCl-salt, water was selected as solvent and ammonium peroxydisulfate (APS) as radical initiator (Scheme 1). The pH of the aqueous solution was set at 3−5 with hydrochloric acid in order to minimize saponification of DMAEMA (*15*) and to prevent reaction of the primary amino group with ester groups. The polymers were obtained in high yield (95−99%). The polymer was worked up by dialysis against water at pH 7 and subsequent lyophilization.

A ^{1}H NMR spectrum of the copolymer (Figure 1A) showed, besides the signals of the dimethylaminoethyl methacrylate signals, a small signal at 3.45 ppm, which can be ascribed to the methylene protons adjacent to the primary amino group in the aminoethyl methacrylate monomer. The intensity of this peak indeed increased with increasing amounts of AEMA in the feed of the polymerization. However, the amount of incorporated amino groups cannot be determined accurately by NMR, due to partly overlapping signals. For the determination of the amount of incorporated AEMA, the primary amines in the copolymer were quantitatively derivatized with an excess of the thiolating reagent SPDP. Subsequent spectrophotometric analysis of the incorporated amount of PDP-groups yielded an accurate determination of the primary amine content of p(DMAEMA-*co*-AEMA). Figure 2 shows the influence of the feed ratio of AEMA on the total methacrylate content of the copolymer. It can be seen that the incorporation efficiency of AEMA is about

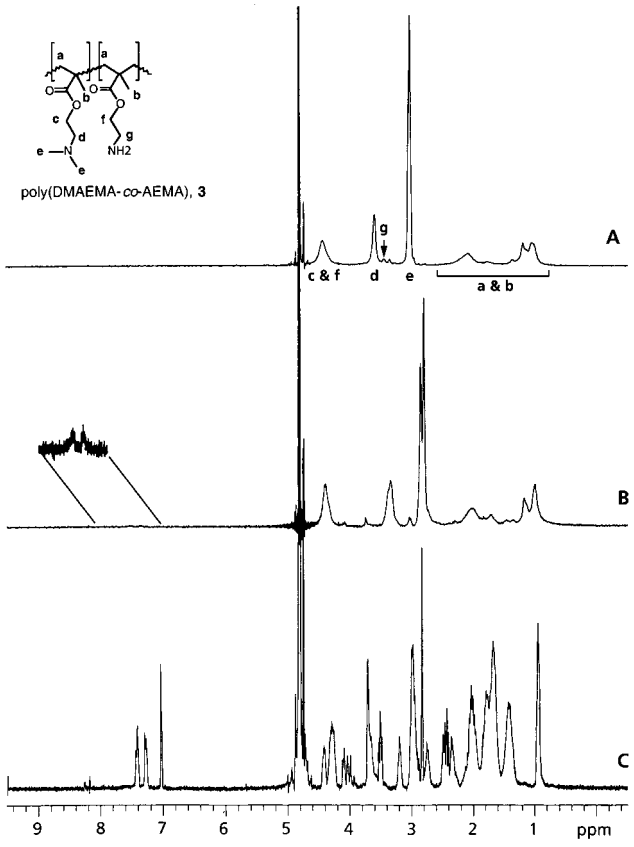


Figure 1. ^1H NMR spectrum in ^2H_2O of p(DMAEMA-*co*-AEMA) with 5.4 mol % AEMA (A), p(DMAEMA-*co*-AEMA)-NLS conjugate (B), and the MPB derivative of the NLS peptide (C).

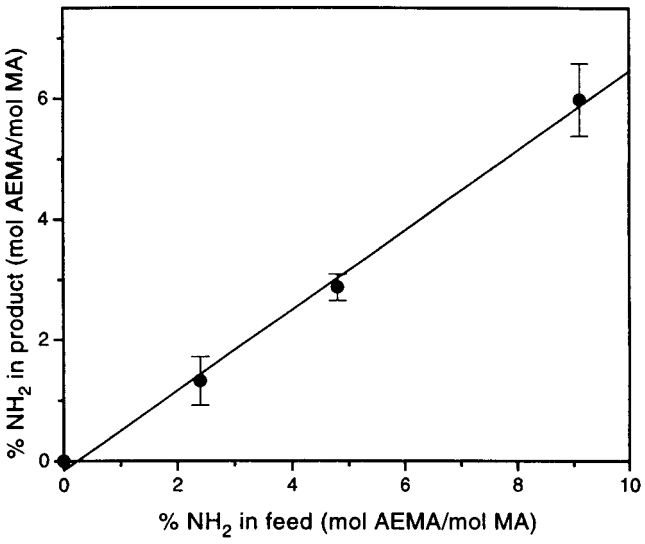


Figure 2. Correlation between feed ratio of AEMA to total methacrylate content and the incorporation of primary amines in p(DMAEMA-*co*-AEMA).

70% and the primary amine content can be tailored by the amount of AEMA in the feed.

The polymerization was carried out at varying ratios of monomer to initiator (*M*/*I* ratio). Figure 3 shows the influence of the *M*/*I* ratio on the molecular weight (GPC) of p(DMAEMA-*co*-AEMA) with 6 mol % AEMA. For comparison, the intrinsic viscosity of the polymer is also given. It can be concluded that, as expected, the molecular weight of p(DMAEMA-*co*-AEMA) increases with increasing *M*/*I* ratio.

Conjugation of Peptides and Proteins. p(DMAEMA-

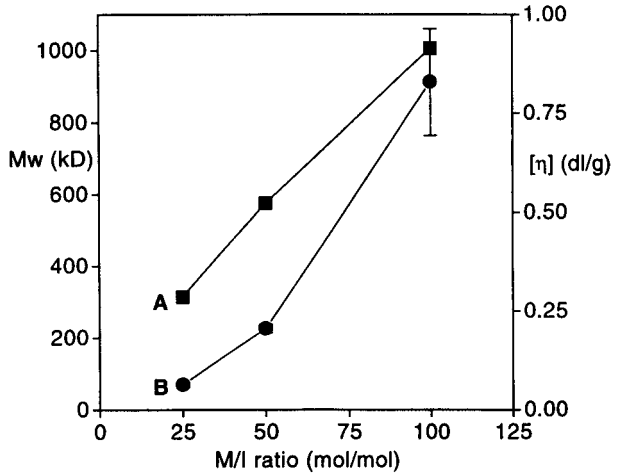


Figure 3. Molecular weight by intrinsic viscosity (A) and by GPC (relative to dextran, panel B) of p(DMAEMA-*co*-AEMA) as a function of the monomer/initiator ratio during synthesis.

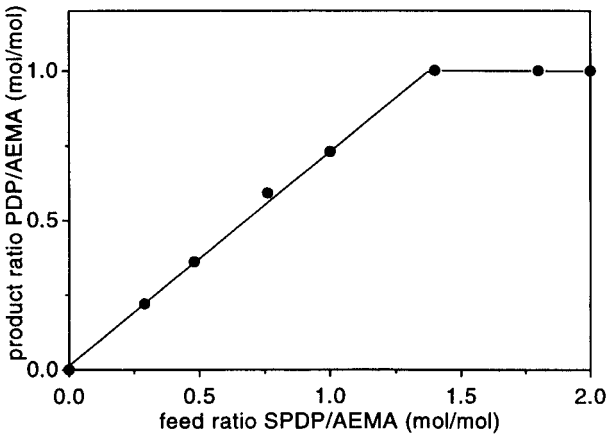


Figure 4. Correlation between feed ratio of SPDP/AEMA and the incorporation of thiol groups in p(DMAEMA-*co*-AEMA).

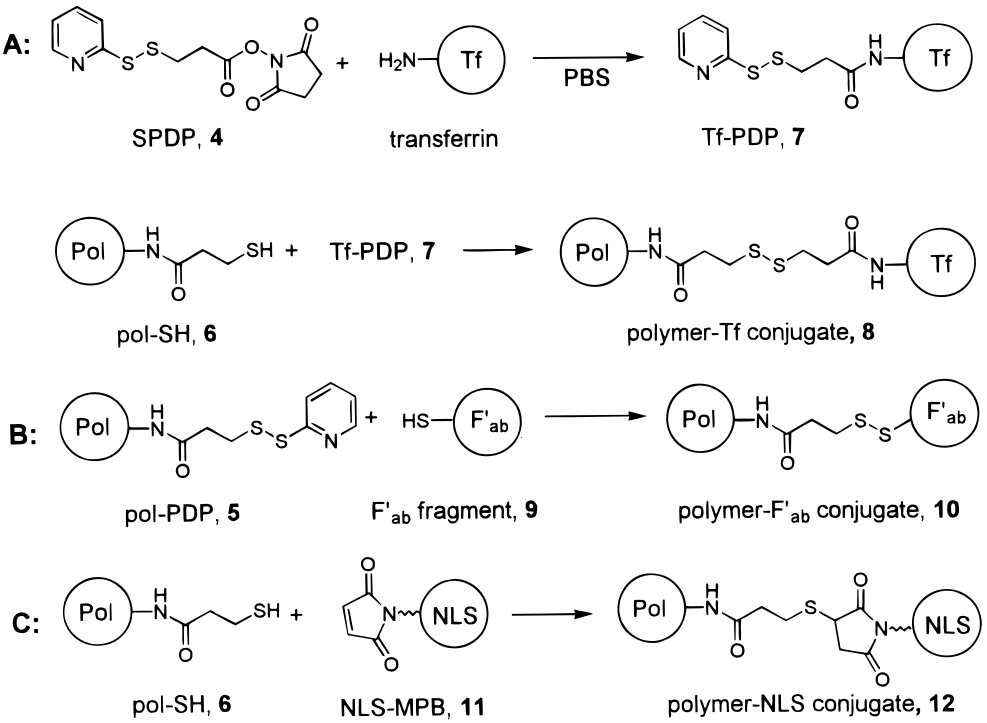
co-AEMA) contains primary amino groups which can be used to introduce (masked) thiol groups on the polymer backbone. These thiol groups can subsequently be used to couple a variety of compounds by a disulfide linkage. Therefore, p(DMAEMA-*co*-AEMA) is first derivatized with *N*-succinimidyl 3-(2-pyridyldithio)propionate (SPDP, Scheme 1, compd **4**) in PBS at pH 7.5, yielding p(DMAEMA-*co*-AEMA) with masked thiol groups (pol-PDP). Subsequent removal of the protecting thiopyridyl group by reaction with 1,4-dithio-2,3-dihydroxybutane (dithiothreitol, DTT) resulted in p(DMAEMA-*co*-AEMA) with free thiol groups (pol-SH, Scheme 1, compd **6**).

Figure 4 shows the amount of incorporated dithiopyridine groups as a function of the feed ratio of SPDP to AEMA residues. It can be concluded that the amount of incorporated PDP groups can be easily tailored by varying the ratio of SPDP to AEMA residues in the polymer, and that the incorporation efficiency of SPDP is about 70%. Above 1.4 molar equivalents of SPDP to amino groups, a plateau value was reached, indicating complete derivatization of the amino groups.

Both the polymer with the masked and the free thiol groups can be used for conjugation with compounds such as peptides and proteins via a variety of ways.

Transferrin can be easily conjugated to p(DMAEMA-*co*-AEMA) after introduction of PDP groups in Tf and subsequent reaction with pol-SH, yielding p(DM)AEMA-Tf conjugate (Scheme 2, compd **8**). For conjugation purposes with Tf, p(DMAEMA-*co*-AEMA) with a rela-

Scheme 2. Coupling of Transferrin (A), a F(ab′) Fragment (B), and NLS-MPB (C) to Derivatized p(DMAEMA-*co*-AEMA)



tively low amount of (masked) thiol groups [1 SH/150 (DM)AEMA units] was used to prevent possible cross-linking of polymer and protein. Incubation of underivatized Tf with thiolated p(DMAEMA-*co*-AEMA) did not result in the formation of pol-Tf conjugate, indicating that PDP groups are necessary for conjugation (results not shown). The degree of derivatization of Tf was dependent on the feed ratio of SPDP to Tf and could be tailored from 2.5 to 14 mol of PDP/mol of Tf. The higher the degree of derivatization, the more turbid the conjugation reaction mixture became, indicating the formation of cross-linked products. Therefore, Tf with a relatively low degree of derivatization (2.5 mol of PDP/mol of Tf) was used for conjugation. The conjugation efficiency could be determined by quantifying the amount of nonconjugated Tf by GPC chromatography. Above a ratio of 1:1 mol of PDP/mol of SH, the conjugation efficiency was 90−95% and was independent of the ratio of Tf-PDP to pol-SH. The conjugate contained 1.0 mg/mL p(DMAEMA-*co*-AEMA) and 0.41 mg/mL Tf.

Monoclonal antibody 323/A3, directed against the EGP-2 receptor on OVCAR-3 cells, was treated with pepsin to yield the corresponding $[F(ab')]_2$ molecule. After reaction with DTT, the F(ab′) fragment (Scheme 2, compd **9)** was subsequently coupled via its free thiol group to p(DMAEMA-coAEMA) with masked thiol groups [p(DM)-AEMA-PDP, Scheme 2, compd **5]** to yield the p(DM)-AEMA-F(ab′) conjugate (Scheme 2, compd **10**). The conjugate contained 2.1 mg/mL p(DMAEMA-*co*-AEMA) and 1.0 mg/mL F(ab′), with a coupling efficiency of more than 95% (SDS−PAGE analysis, results not shown).

After synthesis of the NLS peptide, analysis by HPLC, ^{1}H NMR, and FAB MS indicated that the expected product had been formed. A reaction between the immobilized NLS peptide and SMPB resulted in the formation of the maleimide derivative of the NLS peptide, which was analyzed by FAB MS and ^{1}H NMR. The MS analysis showed the expected mass for the derivatized peptide sequence *m*/*z* 1424.8 $[MH]^+$). Figure 1C shows the ^{1}H NMR of the NLS-MPB. Although the ^{1}H NMR spectrum was too complex for complete elucidation, some specific amino acids (e.g., Val at 0.9 ppm) and the maleimide group (at 7.0 ppm) could be distinguished.

The NLS-MPB (Scheme 2, compd **11**) was subsequently incubated with thiolated p(DMAEMA-*co*-AEMA) and purified by gel filtration (PD-10). The yield after lyophilization was 37 mg (70%), and the incorporation efficiency of NLS peptide, determined by ^{1}H NMR, was more than 95% based on SH groups, and 50% based on NLS-MPB. The isolated polymer-NLS conjugate (Scheme 2, compd **12**) was characterized with ^{1}H NMR (Figure 1B). Comparison of the NMR spectrum of NLS-MPB (Figure 1C) with the spectrum of the conjugate (Figure 1B) shows that the maleimide signal at 7.0 ppm has disappeared while the phenyl protons of the MPB group are still visible at 7.25 and 7.4 ppm. This and the presence of certain amino acid peaks in the spectrum indicates that the NLS peptide is covalently bound to the polymer. The incorporation efficiency of NLS peptide, estimated by ^{1}H NMR, was more than 95% based on thiol groups in the polymer, and 50% based on NLS-MPB.

It has been demonstrated that conjugates held together via disulfide bonds introduced via the SPDP method may be reduced in vivo (*16*). However, it can be envisaged that protein/polymer conjugates can be synthesized via a more stable thioether linkage essentially using the method described for the NLS−PDMAEMA conjugate. In addition, other methods described in the literature (e.g., as described in ref *17*) can also be applied to synthesize PDMAEMA-protein conjugates using essentially the same strategy as described in this paper.

CONCLUSIONS

pDMAEMA can be functionalized with primary amines by copolymerization of DMAEMA with low amount of AEMA. The molecular weight and the primary amine content of the resulting polymer can be tailored by the feed ratio of these monomers. Thiol groups can be

incorporated via a controlled derivatization step. Subsequently, proteins and peptides can be coupled to the polymer with high coupling efficiencies via a disulfide bond or a thioether linkage.

LITERATURE CITED

(1) Duncan, R. (1992) Drug-polymer conjugates: potential for improved chemotherapy. *Anti-Cancer Drugs 3*, 175−210.

(2) Flanagan, P. A., Duncan, R., Subr, V., Ulbrich, K., Kopeckova, P. and Kopecek, J. (1992) Evaluation of protein-N−(2-hydroxypropyl)methacylamide copolymer conjugates as targetable drug-carriers. 2. Body distribution of conjugates containing transferrin antitransferrin receptor antibody or anti-Thy 1.2 antibody and effectiveness of transferrin. *J. Controlled Release 18*, 25−38.

(3) Van de Wetering, P., Cherng, J.-Y., Talsma, H., and Hennink, W. E. (1997) Relation between the transfection efficiency and cytotoxicity of poly((2-dimethylamino)- ethyl methacrylate)-plasmid complexes. *J. Controlled Release 49*, 59−69.

(4) Jelinkova, M., Strohalm, J., Plocova, D., Subr, V., St′astny, M., Ulbrich, K., and Rihova, B. (1998) Targeting of human and mouse T-lymphocytes by monoclonal antibody-HPMA copolymer-doxorubicin conjugates directed against different T-cell surface antigen. *J. Controlled Release 52*, 253−270.

(5) Carlsson, J., Drevin, H., and Axen, R. (1978) Protein thiolation and reversible protein−protein conjugation. N-succinimidyl 3-(2-pyridyldithio)propionate, a new heterobifunctional reagent. *Biochem. J. 173*, 723−737.

(6) Wagner, E., Cotton, M., Mechtler, K., Kirlappos, H., and Birnsteil, M. (1991) DNA-binding transferrin conjugates as functional gene-delivery agents: synthesis by linkage of polylysine or ethidium homodimer to the transferrin carbohydrate moiety. *Bioconjugate Chem. 2*, 226−231.

(7) Kircheis, R., Kichler, A., Wallner, G., Kursa, M., Ogris, M, Felzmann, T., Buchberger, M., and Wagner, E. (1997) Coupling of cell-binding ligands to polyethylenimine for targeted gene delivery. *Gene Ther. 4*, 409−418.

(8) Wagner, E., Curiel, D., and Cotton, M. (1994) Delivery of drugs, proteins and genes into cells using transferrin as ligand for receptor-mediated endocytosis. *Adv. Drug Del. Rev. 14*, 113−136.

(9) Edwards, D. P., Grzyb, K. T., Dressler, L. G., Mansel, R. E., Zava, D. T., Sledge Jr., G. W., and McGuire, W. L. (1986) Monoclonal antibody identification and characterization of a Mr 43, 000 membrane glycoprotein associated with human breast cancer. *Cancer Res. 4*, 1306−1317.

(10) Garcia-Bustos, J., Heitman, J., and Hall, M. N. (1991) Nuclear protein localization. *Biochim. Biophys. Acta 1071*, 83−101.

(11) Boulikas, T. (1997) Nuclear localization signal peptides for import of plasmid DNA in gene therapy. *Int. J. Oncol. 10*, 301−309.

(12) Wherever transferrin (or Tf) is mentioned in the text, apotransferrin (i.e., not loaded with iron) is meant.

(13) Nässander, U.K., Steerenberg, P. A., de Jong, W. H., van Overveld, W. O. W. M., te Boekhorst, C. M. E., Poels, L. G., Jap, P. H. K., and Storm, G. (1995) Design of immunoliposomes directed against human ovarian carcinoma. *Biochim. Biophys. Acta 1235*, 126−139.

(14) *Applied Biosystems Model 433A Peptide Synthesizer User's Manual*, June 1993, version 1.0.

(15) Van de Wetering, P., Zuidam, N. J., Van Steenbergen, M. J., Van der Houwen, O. A. G. J., Underberg, W. J. M., and Hennink, W. E. (1998) A mechanistic Study of the Hydrolytic Stability of Poly(2-(dimethyl)aminoethyl methacrylate). *Macromolecules 31*, 8063−8068.

(16) Worrell, N. R., Cumber, A. J., Parnell, G. D., Ross, W. C., and Forrester, J. A. (1986) Fate of an antibody-ricin A Chain conjugate administered to normal rats. *Biochem. Pharmacol. 35*, 417−423.

(17) Arpicco, S., Dosio, F., Brusa, P., Crosasso, P., and Cattel, L. (1997) New coupling reagents for the preparation of disulfide cross-linked conjugates with increased stability. *Bioconjugate Chem. 8*, 327−337.

BC980126+

Characterization of Lysozyme-Estrone Glucuronide Conjugates. The Effect of the Coupling Reagent on the Substitution Level and Sites of Acylation

C. Mark Smales, Christopher H. Moore, and Leonard F. Blackwell*

Institute of Fundamental Sciences, Chemistry, Massey University, Private Bag 11 222, Palmerston North, New Zealand. Received January 27, 1999

Estrone glucuronide conjugates of hen egg white lysozyme were prepared by the mixed anhydride and active ester coupling procedures. Both methods gave good yields of conjugates, but the active ester procedure gave a more diverse range of products, making it less suitable for preparing conjugates for homogeneous enzyme immunoassay. Conjugation of lysozyme with estrone glucuronide by the mixed anhydride procedure gave one major derivative exclusively acylated at lysine residue 33 whereas conjugation by the active ester method gave six derivatives which were acylated at one or more of lysine residues 33, 97, and 116. None of the lysine residues 1, 13, and 96, or the N-terminal α-amino group, were acylated in any of the conjugates isolated. The correlation of the conjugate structures with the protein environments of the amino groups in the crystal structure of lysozyme suggested that the sites of acylation were determined not only by the chemical nature of the acylating reagent but also by the surface accessibility and nucleophilicity of the individual lysine residues.

INTRODUCTION

The Ovarian Monitor home test for measuring the levels of the metabolites of ovarian estradiol (estrone glucuronide, or E1G) and progesterone (pregnanediol glucuronide, or PdG) in urine (*1*−*5*) allows the daily monitoring of a woman's menstrual cycle and accurate identification of her fertile period. The basis of the home test is an homogeneous enzyme immunoassay, which has been used successfully for the determination of a variety of analytes in biological fluids (*6*, *7*). The attraction of the homogeneous enzyme immunoassay format lies in the fact that the enzyme activity of hapten conjugates of some enzymes (hen egg white lysozyme in this case) is extensively inhibited by anti-hapten antibodies in the immune complex. As a result, a simple kinetic measurement serves to differentiate between bound and free enzyme label (*8*) without the need for time-consuming and technically demanding physical separation procedures.

Hen egg white lysozyme is one of a limited number of enzymes which have been employed successfully in homogeneous enzyme immunoassays. It possesses an apparent specific activity with its bacterial substrate *Micrococcus lysodeikticus* which renders it ideal for the measurement of menstrual cycle levels of urinary E1G and PdG (*9*) without excessive dilution of the samples. Lysozyme possesses six lysine residues and a free α-NH_2 terminal amino group, all of which can be acylated by a variety of acylating reagents (*10*) to give stable conjugates which retain lytic activity providing that the total number of lysine residues acylated is less than four (*11*). However, the lytic activity of lysozyme is adversely affected whenever any of the amino groups are modified by moieties that result in the loss of positive charge from the surface of the enzyme (*12*). It has been proposed that this loss in activity reflects an alteration in the electrostatic interaction between the positively charged enzyme and the negatively charged *M. lysodeikticus* cell wall (*13*). Hence, in developing procedures for conjugation of lysozyme with steroid glucuronides, it is desirable to use conditions which maximize the concentration of conjugate(s) with low degrees of steroid substitution.

The estrone glucuronide−lysozyme conjugate mixtures utilized in the Ovarian Monitor assay system have been prepared with a mixed anhydride acylating reagent (*1*), but currently they are uncharacterized. Identification of the amino groups in a protein which are modified by various acylating reagents can be carried out by analysis of proteolytic digest patterns (*14*), mass spectrometric peptide mapping (*15*), and immunological studies (*16*). It has been suggested on the basis of these previous studies that the acylation position and orientation of haptens in enzyme conjugates is an important factor in determining the recognition and strength of binding of the hapten by antihapten antibodies (*17*). However, all of these studies have been undertaken on conjugates produced using a large excess of hapten to enzyme in the coupling procedure, therefore producing protein adducts with high levels of hapten substitution.

The present study was undertaken to characterize the preferred acylation positions in the E1G−lysozyme conjugates and hence to evaluate the effect of the acylation reagent on the acylation positions. The conjugates were characterized using proteolytic digestion and electrospray mass spectrometry to identify (1) the positions of acylation in the steroid glucuronide lysozyme conjugates and (2) the effect of the coupling procedure on the conjugate products and sites of acylation as a prerequisite to an understanding of the factors which are important in determining the mechanism of inhibition by anti-E1G antibodies.

* To whom correspondence should be addressd. Phone: 64-6-350 4783. Fax: 64-6-350 5682. E-mail: L.F.Blackwell@massey.ac.nz.

10.1021/bc9900441 CCC: $18.00 © 1999 American Chemical Society
Published on Web 05/29/1999

EXPERIMENTAL PROCEDURES

Reagents. The following reagents were obtained from the sources indicated: 17-oxoestra-1,3,5−3-β-yl-D-glucopyranosiduronic acid (estrone glucuronide or E1G[H]) was synthesized essentially according to Conrow and Bernstein (*18*) as described previously (*19*). Commercial hen egg white lysozyme (Grade 1, three times recrystallized and lyophilized, Sigma, St. Louis, MO) was further purified before use as described previously (*19*). Antisera were raised in sheep against thyroglobulin−estrone glucuronide conjugates. Trypsin (L-1-tosylamino-2-phenylethyl chloromethyl ketone treated) and *M. lysodeikticus* were obtained from Sigma. All other chemicals were analytical or reagent grade.

Preparation Of Estrone Glucuronide (E1G[H])−Lysozyme Conjugates. Conjugation of lysozyme with E1G[H] was achieved by both the mixed anhydride procedure of Erlanger et al. (*20*) and the *N*-hydroxysuccinimide/dicyclohexylcarbodiimide coupling method (*21*) at a 1.6:1 molar ratio of steroid glucuronide to lysozyme as described previously (*19*). The mixed anhydride reagent was prepared from E1G[H] (7.2 mg, 16.1 μmol) in dimethylformamide (116 μL) in a 0.5 mL glass reaction vial. The vial was placed in an aluminum block preequilibrated at 10 °C in a refrigerator and allowed to equilibrate for 3 h. Tri-*n*-butylamine (4.5 μL, 18.9 μmol), preequilibrated at 10 °C, was then added and the E1G[H] solution left for 5 min at 10 °C before the aluminum block was cooled to 0 °C. Once the aluminum block had cooled to 0 °C, it was removed from the freezer and placed in a cold room at 4 °C and left to equilibrate for 15 min. Isobutyl chloroformate (2.5 μL, 19.2 μmol) preequilibrated at 4 °C was then added and the resulting E1G[H] solution left to stand for 30 min. The mixed anhydride reagent was then stabilized by placing the aluminum block at the bottom of a refrigerated centrifuge preequilibrated at approximately −15 °C. Purified lysozyme (144 mg, 10.1 μmol) was dissolved in Milli-Q water (3.7 mL) with stirring and the pH adjusted to 8.00 with 0.5 M NaOH at room temperature. Ice was packed around the lysozyme reaction vessel, which was then placed in the cold room at 4 °C and left to equilibrate for 45 min with stirring while the pH was monitored. The temperature setting of the pH meter was set at 0 °C and stabilized at pH 8.54 after the equilibration period. After the solution stood at −15 °C for 1 h, the mixed anhydride reagent was added dropwise, with a dry 10 μL pipet at 4 °C, to the stirred lysozyme solution over 15 min. Associated with each addition of mixed anhydride reagent was a drop in the pH of the lysozyme solution which was readjusted back to approximately 8.54 with 0.5 M NaOH. The lysozyme solution was left with stirring for 2 h upon the final addition of mixed anhydride reagent (while 0.5 M NaOH was added as required to readjust the pH) after which time the reaction mixture, which appeared opaque, had stabilized at pH 8.39 and was stored at −10 °C until purified by cation-exchange chromatography.

In a typical active ester experiment, the reagent was prepared from E1G[H] (7.6 mg, 17.0 μmol) in dimethylformamide (52 μL). *N*-Hydroxysuccinimide (22.5 mg, 195 μmol) and dicyclohexylcarbodiimide (29.9 mg, 145 μmol) were each separately dissolved in dimethylformamide (100 μL). From these stock solutions, *N*-hydroxysuccinimide (20 μL, 39 μmol) was added to the E1G[H] solution followed by the addition of dicyclohexylcarbodiimide (20 μL, 29 μmol). After a stirred solution of purified lysozyme (152 mg, 10.7 μmol), dissolved in 1% aqueous sodium hydrogen carbonate (6 mL, pH 9.10) at 0 °C in an ice bath, stood at room temperature for 1 h, the active ester reagent was added dropwise. After standing overnight with stirring at 4 °C, the reaction mixture, which appeared opaque, was dialyzed against Milli-Q water (3 × 2 L) and then stored at −10 °C until purified by cation−exchange chromatography.

Purification of Estrone Glucuronide−Lysozyme Conjugates. The success of the conjugation experiments and purity of the derivatives was determined by analytical chromatography on a Mono-S cation-exchange column in 7 M urea buffers (*19*). Estrone glucuronide−lysozyme conjugates were purified from the conjugation reaction mixture by cation-exchange chromatography, also in 7 M urea buffers, on an S-Sepharose (fast flow) column (50 × 1.6 cm i.d.) connected to a Pharmacia Fast Protein Liquid Chromatography system. To the reaction mixture were added sufficient solid urea to give a 7 M solution and a calculated amount of solid sodium dihydrogen phosphate dihydrate to give a 50 mM phosphate solution. After the solution had been adjusted to pH 6.0 with 1 M NaOH, it was loaded, with a peristaltic pump, onto the column preequilibrated with 7 M urea/50 mM sodium dihydrogen phosphate dihydrate buffer (pH 6.0). The column was eluted with a linear salt gradient from 0 to 0.24 M NaCl in 792 min at a flow rate of 1.5 mL/min. The absorbance of the eluent fractions (6 mL) was read at 280 nm and the enzymic activities were determined from the rate of lysis of *M. lysodeikticus* using an Ovarian Monitor (*1*). Fractions from each peak were combined, dialyzed extensively against Milli-Q water, and freeze-dried before rechromatography on the same column. This procedure gave chromatographically homogeneous estrone glucuronide−lysozyme conjugates when analyzed by Mono-S cation-exchange chromatography (*19*). The purified conjugates were extensively dialyzed against Milli-Q water, freeze-dried, and then stored at −10 °C until required for digestion experiments.

Enzyme Assays for Lytic Activity of Chromatography Column Fractions. The assays for lytic activity of the various column fractions were performed in a plastic 1 mL cuvette (Adindas Plastics, Melbourne, Australia) designed specifically for the Ovarian Monitor (*1*). The appropriate volume from each fraction was added to a cuvette, 0.04 M tris-maleate buffer (pH 7.0) was added to make the volume up to 340 μL, and the solution was equilibrated at 40 °C. *M. lysodeikticus* (10 μL of a 7.5 mg/mL suspension in 75 mM tris-maleate buffer, pH 7.0) was then added with vortex mixing and the initial transmission noted. After 20 min, the final transmission was noted, and the lytic activity, expressed as the change in transmission (ΔT) per 20 min, was calculated. The volume of each fraction to be used in the assay was calculated from the concentration of the peak tube as determined by the absorbance at 280 nm. The dilution of this peak tube required to give an apparent change in transmission of 350 units in 20 min was determined. The same dilution was then used for all of the other fractions to measure their relative lytic activities. The inhibition of the lytic activity of each eluent fraction from the ion-exchange columns by anti-E1G antibodies was measured using the Ovarian Monitor assay by adding a slight excess of the antiserum to the assay mixture and comparing it with the appropriate control.

Reduction and Alkylation of Estrone Glucuronide−Lysozyme Conjugates with Iodoacetic Acid. Conjugates were reduced and alkylated with iodoacetic acid essentially as described by Rutherfurd et al. (*22, 23*). Typically, conjugate (5 mg) was dissolved in a mixture of 8 M urea and 0.25 M tris-HCl buffer (pH 8.75, 300

μL) containing 1 mM EDTA prior to the addition of dithiothreitol (0.84 mg, 5.4 μmol). The resulting solution was flushed with argon gas, and the reduction allowed to proceed at 37 °C for 3 h prior to the addition of iodoacetic acid (1.57 mg, 8.4 μmol). Alkylation was allowed to proceed in the dark at room temperature for 45 min. Excess β-mercaptoethanol was then added and the alkylated protein was dialyzed against 8 M urea (3 × 200 mL).

Tryptic Digestion. Tryptic digestion of the alkylated estrone glucuronide−lysozyme conjugates and unmodified lysozyme was carried out in 2 M urea solutions. After dialysis against 8 M urea, the alkylated protein solutions were diluted with 1% ammonium bicarbonate buffer (pH 8.50) to give 2 M urea solutions allowing for the volume of the trypsin solution. L-1-Tosylamino-2-phenylethyl chloromethyl ketone treated trypsin (2 mg) was dissolved in 330 μL of 1% ammonium bicarbonate (pH 8.50) and then the appropriate volume was added to the digest solution so that an enzyme-to-substrate ratio of 1.5:100 (w/w) was achieved. Digestion was allowed to proceed for 3.5 h at 37 °C after which the reaction mixture was stored at −10 °C until analysis by HPLC.

Separation of Trypsin Fragments. The separation of the tryptic fragments was carried out on a Vydak C18 reversed-phase column (4.6 × 250 mm) using a Spectra Physics SP8800 high-performance liquid chromatography (HPLC) system. Aliquots from the completed tryptic digests were loaded onto the column preequilibrated with deionized, distilled water (containing 0.1% TFA) and then eluted with a linear gradient from 0 to 40% acetonitrile (containing 0.08% TFA) in 80 min at a flow rate of 1 mL/min. Detection of the tryptic peptides was carried out at 220 nm with a Spectra Physics SP8490 detector and they were collected manually into 1 mL Eppendorf tubes. Peptides were concentrated on a Savant Speed Vac Concentrator to a volume of approximately 15 μL and then stored at −10 °C until analysis.

Analysis of Tryptic Peptides. Tryptic peptides were analyzed by both peptide sequencing and electrospray mass spectrometry. Peptide sequencing was undertaken on an Applied Biosystems Edman degrading gas phase 476A Protein Sequencer. Mass spectral analyses were obtained on a VG Platform II Electrospray Mass Spectrometer.

Immunochemical Analysis of Tryptic peptides. Peptides were screened for the presence of estrone glucuronide using the Ovarian Monitor (*1*). An assay mixture was prepared containing amounts of estrone glucuronide−lysozyme conjugate and E1G antibody such that a partially inhibited ΔT value of approximately 150 units in 40 min was obtained. To the assay mixture was added 5 μL of the concentrated peptide, and the change in transmission over 40 min was recorded. The difference between the ΔT value in the presence and absence of the peptide in the partially inhibited assay mixture was calculated as the immune reactivity.

RESULTS

Preparation and Purification of Estrone Glucuronide−Lysozyme Conjugates. Acylation of hen egg white lysozyme with estrone glucuronide by the mixed anhydride and *N*-hydroxysuccinimide/dicyclohexylcarbodiimide coupling procedures resulted in two distinctly different reaction mixtures (Figure 1). The mixed anhydride procedure produced two major chromatographically distinct peaks (Figure 1a) when passed though an S-Sepharose fast-flow column, the largest being unreacted

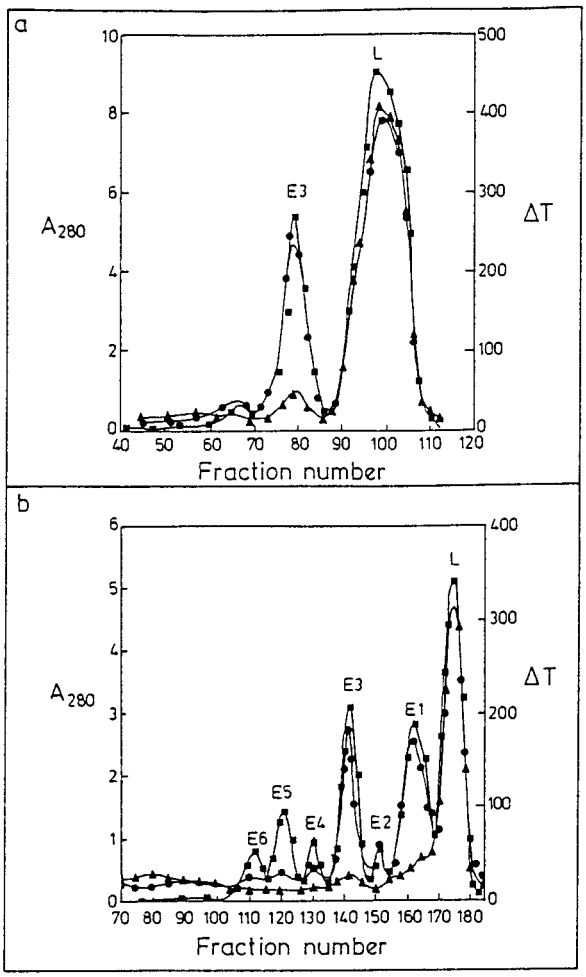


Figure 1. E1G−lysozyme reaction mixtures in 7 M urea on a S-Sepharose (fast flow) column. Mixed anhydride method (a), and active ester method (b). The profiles show A_{280} (■) and lytic activity profiles in the absence (● = ΔT) and presence (▲ = ΔT) of excess E1G antibody. L = lysozyme and E1-E6 are E1G−lysozyme conjugates. For conditions and details see text.

lysozyme (L). The material which eluted earlier consisted almost entirely of conjugate family E3. E refers to the nomenclature of Smales et al. (*19*) where E1 is the estrone glucuronide lysozyme peak which elutes next to lysozyme and E6 is the peak which elutes furthest from lysozyme (the first peak eluted). On the other hand, when lysozyme was conjugated by the *N*-hydroxysuccinimide/dicyclohexylcarbodiimide coupling procedure, seven chromatographically distinct peaks were obtained (Figure 1b). Again the largest peak was unreacted lysozyme and of the six conjugate peaks (E1−E6) which eluted earlier, E1 and E3 together comprised over half of the total conjugate yield. These six conjugate peaks were characteristic of acylation of lysozyme by steroid glucuronides at low concentrations of reagent, appearing in varying amounts in all conjugations. Even at a molar ratio of 3:1 for the active ester reagent the same six peaks were found but the amounts of E4, E5, and E6 were increased relative to E1, E2, and E3.

All of the conjugate families (E1−E6) and unreacted lysozyme from both conjugation procedures had lytic activities which paralleled their A_{280} profiles (Figure 1), and the conjugates were inhibited by 70−80% when excess E1G antibody was present in the assay mixture as reported previously (*19*). The unreacted lysozyme (designated L) was not affected by the anti-E1G antiserum as expected, and this was shown by the congruence

of the lytic activity in the presence and absence of the antiserum. Conjugate families E4, E5, and E6 had much lower specific activities relative to lysozyme (60.8, 57.6, and 42.3%, respectively) than the E1, E2, and E3 conjugate families (95.1, 88.2, and 94%, respectively) which had specific activities similar to that of native lysozyme. It was necessary to rechromatograph each conjugate family by passage twice through the S-Sepharose (fast flow) column to obtain chromatographically homogeneous derivatives.

Characterization of the E1G−Lysozyme Conjugate Families. The identities of the lysine residues acylated by estrone glucuronide in the chromatographically homogeneous conjugates were determined by tryptic digestion of the reduced, S-carboxymethylated derivatives in 2 M urea solutions at pH 8.5 and 37 °C. The resulting tryptic peptides were analyzed by reversed-phase chromatography (Figures 2, 3, and 4), peptide sequencing, and electrospray mass spectroscopy (Tables 1 and 2). The tryptic peptides from the native lysozyme digest are shown in Figure 2a and are numbered in their order of elution from the reversed-phase column. Twenty major peaks were observed in the digest of native lysozyme (Figure 2a) of which peaks 2 (T1 + 2, K1), 7−10 (T3 and T3 + 4, K13), 15 (T6, K33), 16−18 (T13 and T12 + 13, K97), and 20 (T11, K96) contained lysine residues as shown by amino acid sequencing. T refers to the nomenclature of Canfield (*24*) for the tryptic peptides of hen egg white lysozyme. The small lysine dipeptide T15 (K116) was not observed. The potential cleavage sites between T1 and T2 and between T17 and T18 (under peak 3) could not be hydrolyzed as was previously reported by Noda et al. (*25*) and Okazaki et al. (*26*) for S-carboxymethylated lysozyme derivatives in the absence of 2 M urea. The potential cleavage sites between T3 and T4 and T12 and T13 were only partially hydrolyzed. Peptide T13 appeared as two peaks in the present work, and Yamada et al. (*27*) have suggested that this is due to the presence of a monomer−dimer mixture which presumably persists also in 2 M urea.

In the tryptic maps for each conjugate family, certain lysine-containing peptides disappeared or diminished in height relative to the tryptic map of lysozyme. For example, it was found that peaks 6, 15, and 16−18, which contained the tryptic peptides T7 (6), T6 (15) and T13 + (T12 + 13) (*16*−*18*), respectively, were reduced in height in one or more of the conjugate digest profiles (see Figures 2−4 for examples). Associated with these changes, specific new peaks appeared later in the HPLC gradient than the native peptides (after peak 20 in Figure 2a). The amino acid sequence and mass of these later eluting lysine acylated peptides (c−m) were matched with the sequences and masses of the tryptic peptides from hen egg white lysozyme (*28*) (Table 2). By comparing the experimental data with the expected data, the acylated peptide, and thus the acylated lysine residue, could be assigned (Tables 1 and 2). Acylation with E1G could be readily determined in this way, and it was shown that conjugates resulting from both the active ester and mixed anhydride procedures, which eluted in the same place on the Mono S cation-exchange column (e.g., active ester E3 and mixed anhydride E3) were indeed equivalent (Table 1). For several of the acylated peptides, deamidation had occurred from glutamine to glutamic acid or asparagine to aspartic acid (as shown by amino acid sequencing, Table 2), while in other cases chymotryptic cleavage had occurred (Table 2). In all cases, the calculated and experimental mass spectral data were in good agreement and unambiguously identified the assigned

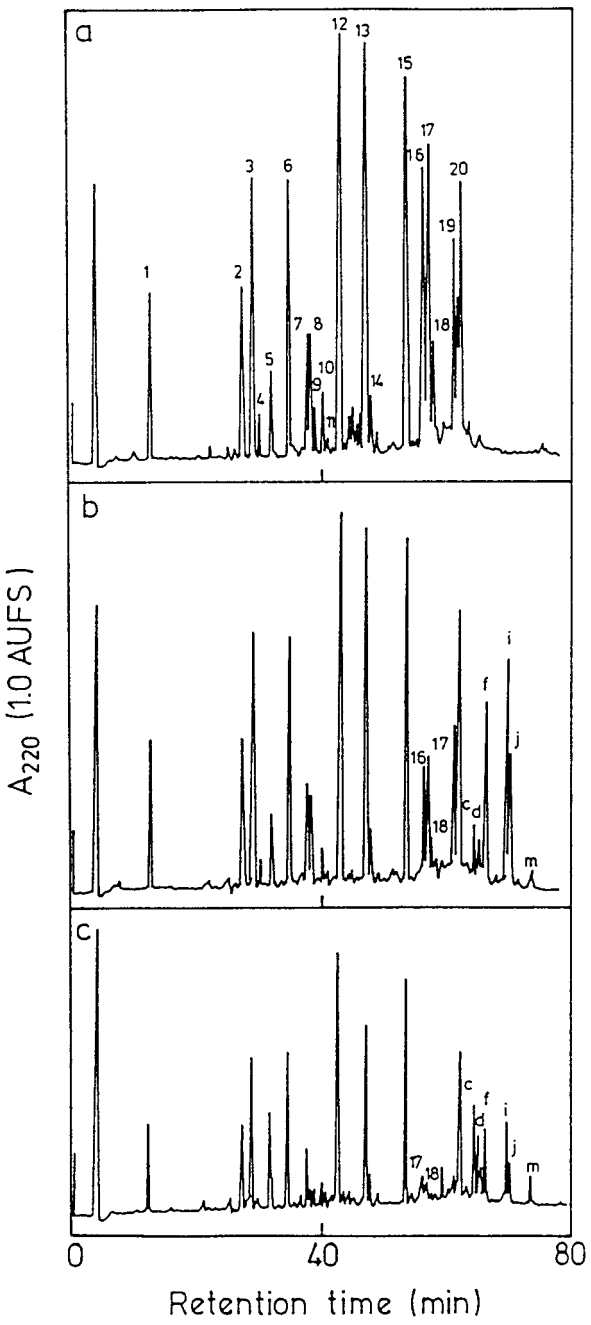


Figure 2. Reversed-phase HPLC separation of tryptic digests of unmodified lysozyme (a), and active ester E1G−lysozyme conjugates E1 (b), and E2 (c). The numbers refer to unmodified tryptic peptides and the letters to acylated tryptic peptides. For details see text.

peptide as confirmed by amino acid sequencing (Table 2). However, the acylated peptides did not exhibit a lysine peak where expected from the known tryptic peptide sequences during sequence analysis. Instead, a new peak was observed which eluted from the sequencer HPLC column after all of the other amino acid peaks. This peak was always present when sequencing the modified peptides and was presumably due to an estrone glucuronide acylated lysine residue. Since the new peak eluted last from the sequencer HPLC column, it did not interfere with detection of any of the other amino acids in the sequence. No evidence was found for acylation occurring via ester linkages as has been observed previously in conjugation experiments (*14*).

From the tryptic maps, it is evident that the N-terminal α-amino group and lysine residues 1, 13, and

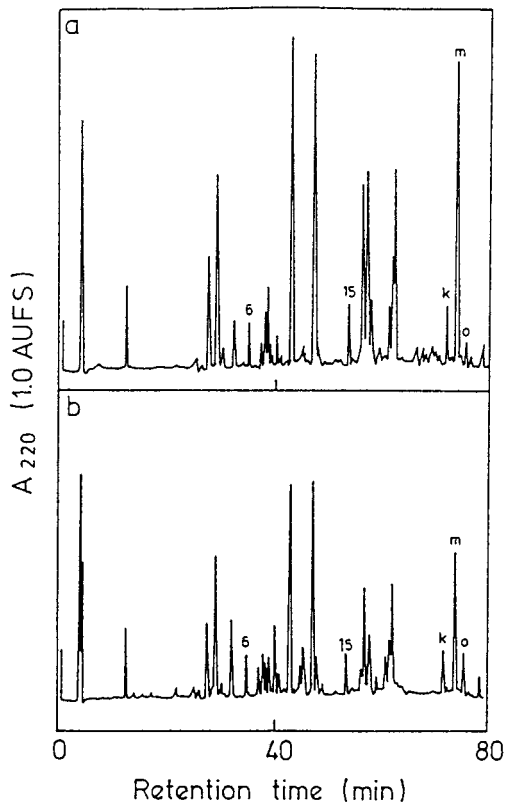


Figure 3. Reversed-phase HPLC separation of tryptic digests of active ester E1G−lysozyme conjugate E3 (a), and mixed anhydride E1G−lysozyme conjugate E3 (b). The numbers refer to unmodified tryptic peptides and the letters to acylated tryptic peptides. For details see text.

96 were unmodified in all of the conjugates since the peptide peaks T1 + 2 (residues 1−5, peak 2, Figure 2a), T3 + (T3 + 4) (residues 6−14, peaks 7−11, Figure 2a), and T11 (residues 74−96, peak 20 Figure 2a) remained unchanged in height and area relative to the tryptic map for the lysozyme control. Thus, acylation of lysozyme with estrone glucuronide was specific for the ϵ-amino groups of lysine residues at positions 33, 97, and 116 when using the active ester method and almost solely for the ϵ-amino group of lysine 33 when the mixed anhydride reagent was used (Table 1). Active ester conjugates E1 and E2 were found to be acylated at the same positions, lysines 97 and 116 (Table 1). However, E1 consisted of two monoacylated conjugates, one where acylation has occurred at lysine 97 and the other where acylation has occurred at lysine 116 (Table 1). Partial acylation at lysine residue 97 can be clearly seen as peptide peaks 16−18 had diminished in height by approximately 60% relative to the native digest (Figure 2b). On the other hand, conjugate E2 appears to be a disubstituted conjugate with both lysine residues 97 and 116 acylated on each lysozyme molecule. Peptide peaks 16−18 had almost disappeared in the tryptic digest of conjugate E2, indicating that residue 97 was almost completely acylated. Both active ester conjugate E3 and mixed anhydride conjugate E3 were acylated at lysine residue 33 (Table 1). Active ester conjugates E4 and E5 were disubstituted conjugates acylated at lysine residues 33 and 116 (E4) and 33 and 97 (E5), respectively (Table 1). The most highly substituted conjugate (active ester E6) was trisubstituted at lysine residues 33, 97, and 116 (Table 1).

Enzyme inhibition assays carried out in the presence of the native lysozyme tryptic peptides (peaks 1−20, Figure 2a) did not significantly increase the lytic activity

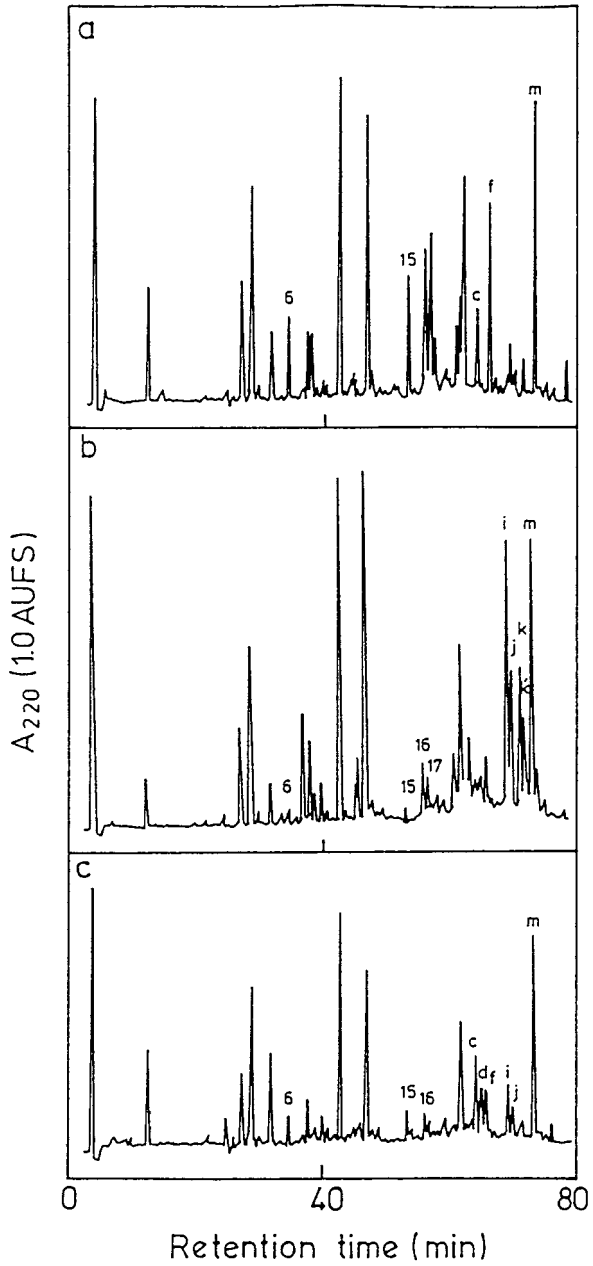


Figure 4. Reversed-phase HPLC separation of tryptic digests of active ester E1G−lysozyme conjugates E4 (a), E5 (b), and E6 (6). The numbers refer to unmodified tryptic peptides and the letters to acylated tryptic peptides. For details see text.

of the intact E1G−lysozyme mixed anhydride E3 conjugate in the inhibition assay (Figure 5a). The same result was obtained for peaks 1−20 obtained from the tryptic digest of E1 (Figure 5b) which therefore did not contain E1G after conjugation. However, inhibition assays carried out in the presence of the active ester E1 tryptic peptides f, i, and j increased the enzymic rates of lysis to approximately 350 units/40 min. This rate was the same as obtained for the control assay in the absence of the E1G antibody, thus the immune reactivities for these three peptides were high (Figure 5b), confirming the presence of at least one estrone glucuronide moiety.

DISCUSSION

Since the active ester methodology is easier to perform than the mixed anhydride method, it is used more often in protein conjugation reactions, especially in the hands of nonorganic chemists. However, close inspection of the

Table 1. Summary of Acylation Positions of Lysozyme-Estrone Glucuronide Conjugates

conjugate peak	E1G per lysozyme molecule[a]	acylated peptide(s)	corresponding peptide peaks[b]	location of acylation position
AE E1	1	T12 + 13	d, i, j	Lys 97
		T15 + 16	c, f	Lys 116
AE E2	1−1.5	T12 + 13	d, i, j	Lys 97
		T15 + 16	c, f	Lys 116
AE E3	1	T6 + 7	k, m, o	Lys 33
AE E4	2	T6 + 7	k, m, o	Lys 33
		T15 + 16	c, f	Lys 116
AE E5	2	T6 + 7	k, k′, o	Lys 33
		T12 + 13	i, j	Lys 97
AE E6	3	T6 + 7	k, k′, m	Lys 33
		T12 + 13	d, i, j	Lys 97
		T15 + 16	c, f	Lys 116
MA E3	1	T6 + 7	k, m, o	Lys 33

[a] Determined from proteolytic studies and titration of lysine groups (*19*). [b] See Figures 2, 3, and 4.

present data showed that there were significant differences between the two methods in terms of the conjugates they produced, and hence, careful consideration needs to be given to the choice of reagent depending on the aims of the study. The active ester reagent was more reactive and, hence, less selective than the mixed anhydride reagent as it gave a more diverse range of conjugate products at the same ratio of E1G to lysozyme (Figure 1). Hence, a greater overall yield of conjugate was obtained than with the mixed anhydride reagent, and the reaction was less time consuming. However, the complexity of the product mixtures made purification of the different conjugates more difficult. For immunoassays, the extra complexity of the less selective active ester reaction was undesirable since the relatively large amounts of the more highly substituted conjugates produced, E4, E5, and E6, had lower specific activities. A greater concentration of these conjugates was required, therefore, in the assays for a given rate of lysis than for the lower substituted conjugates. E4, E5, and E6 also required more antiserum to inhibit their lytic activities due to their higher substitution levels with E1G, hence, less sensitive standard curves were obtained, making them less suitable for homogeneous enzyme immunoassay. The mixed anhydride reagent is thus preferable to the active ester reagent as a source of conjugate for homogeneous enzyme immunoassay as it gives an almost pure mono E1G conjugate in good yield and with a high specific activity.

The difference between the two reagents is possibly due to the difference in their intrinsic reactivities. In support of this suggestion, the active ester reaction was almost instantaneous, as shown by the similarity of the FPLC traces for the reaction mixtures after 2, 5, 60, and 180 min and overnight when analyzed by chromatography on a Mono-S column in 7 M urea (*19*). On the other hand, the more selective mixed anhydride reagent reacted much more slowly, taking several hours as evidenced by the slow drop in pH as the reagent reacted with lysozyme. Under these conditions the estrone glucuronide moiety is more likely to react with the most reactive lysine residue having sufficient lifetime in solution to select among various possibilities.

The identification of the acylation positions in the conjugates obtained with both acylating reagents was relatively straightforward using tryptic digestion experiments. However, it was necessary to use 2 M urea to maintain the solubility of the hydrophobic reduced and S-carboxymethylated acylated conjugates and peptides. Under the 2 M urea conditions used for the digestion experiments, trypsin was active (*29*) and highly reproducible tryptic digests were obtained (Figures 2, 3, and 4). After calibration of the HPLC peaks by sequence data and mass analysis, visual inspection of the traces allowed ready identification of the major sites of acylation from a combination of the loss in amplitude of the lysine-containing tryptic peptides in the native digest and the appearance of new characteristic acylated peptides in the conjugate digest (peaks i, j, etc.).

As the coupling reactions were carried out under limiting conditions of reagent, the fact that conjugate E3 (lysine 33) was the major product of the mixed anhydride reaction indicates that lysine 33 is the most reactive residue at pH 8.5. The elution position of the mixed anhydride minor conjugate peak (Figure 1a) suggests that it is E5 with both lysines 33 and 97 acylated (Table 1) which in turn indicates that lysine 97 is the next in order of reactivity. This reactivity order suggested from the mixed anhydride reaction also holds for the active ester reaction. Conjugate E3 was still one of the major peaks, and of the two disubstituted conjugate fractions (E4 and E5 of Table 1), E5 was present in the greatest amount. Hence, the reactivity order suggested by the combined data is K33 > K97 > K116. Previous work involving the acylation and modification of the amino groups of hen egg white lysozyme has also shown a differential selectivity in the reactivity of the lysine residues (*14*−*15*). For example, when Suckau et al. (*15*) aminoacetylated lysozyme with acetic anhydride, the reactivities of the amino groups showed an order, K97 = K33 > K1 (ϵ-NH_2 and α-NH_2) > K13 = K116 > K96. The accessibility of the lysine side-chain ϵ-amino groups in hen egg white lysozyme as determined from their degree of extension in the crystal structure decreases in a similar order, K97 > K33 ≫ K1 (ϵ-NH_2) > K13 > K116 > K96 > α-NH_2 (*15*). Nuclear magnetic resonance studies have shown that the solution environments of the amino groups in lysozyme are similar to those in the crystalline protein (*30*), hence the difference in the reactivities of the lysine residues can be related to the different protein environments as revealed by crystallography. Thus, the reactivity data of Suckau et al. (*15*) shows that lysine availability or exposure is a major factor in determining chemical reactivity during acylation reactions.

The preferential acylation of lysozyme with estrone glucuronide at lysines 33 and 97 in the present work is consistent with the reactivity preference shown in the data of Suckau et al. (*15*) as lysines 33 and 97 are by far the most accessible of the seven having surface accessibilities of 40.1 and 47.4%, respectively. However, the preference for lysine 33 exhibited in the present work shows that other factors are involved. The p*K* value calculated for lysine 33 (9.7) is less than for lysine 97 (10.5) (*31*) which would result in an almost 10-fold higher concentration of the lysine 33 free base at pH 8.5 (relative to lysine 97) and, hence, could explain the greater reactivity. However, according to the results of Suckau et al. (*15*), acylation of lysine 116 with estrone glucuronide should not have occurred until after the acylation or partial acylation of lysine 1 (α and ϵ-NH_2) and lysine 13. The acylation of residue 116 with estrone glucuronide in preference to lysine 1 (α and ϵ-NH_2), lysine 13, or lysine 96 may be a result therefore of a relatively high local concentration of the E1G reagent in the vicinity of lysine 116. This could be achieved if E1G has an affinity for one or more of the sugar-binding sites in the active-site cleft since lysine 116 is situated just above this.

The present results show that the lysozyme molecule

Table 2. Sequence and Mass Spectral Data of E1G Acylated Tryptic Peptides

peptide peak	sequence data	calculated (*m*/*z*)	experimental (*m*/*z*)	acylation location
c	C[a]K[b]GTDVQAW[c]	1492.7	1493.0	Lys 116
d	K[b]IVSDGNGMNAW[c]	1718.9	1719.3	Lys 97
f	C[a]K[b]GTDVQAWIR	1762.7	1762.5	Lys 116
i	K[b]IVSDGNGMNAWVAWR	2231.9	2231.5	Lys 97
j	K[b]IVSDGNGMD[d]AWVAWR	2232.9	2233.5	Lys 97
k	[c]SLGNWVC[a]AAK[b]FESNFNTQ ATNR	2943.2	2943.9	Lys 33
k′	[c]SLGNWVC[a]AAK[b]FESNFNTE[e] ATNR	2944.2	2944.7	Lys 33
m	GYSLGNWVC[a]AAK[b]FESNFNTQ ATNR	3164.4	3163.6	Lys 33
o	GYSLGNWVC[a]AAK[b]FESNFNTE[e] ATNR	3165.2	3166.8	Lys 33

[a] S-carboxymethylated Cys. [b] Estrone glucuronide acylated lysine residue. [c] Chymotryptic cleavage at this site. [d] N → D amino acid interchange. [e] Q → E amino acid interchange.

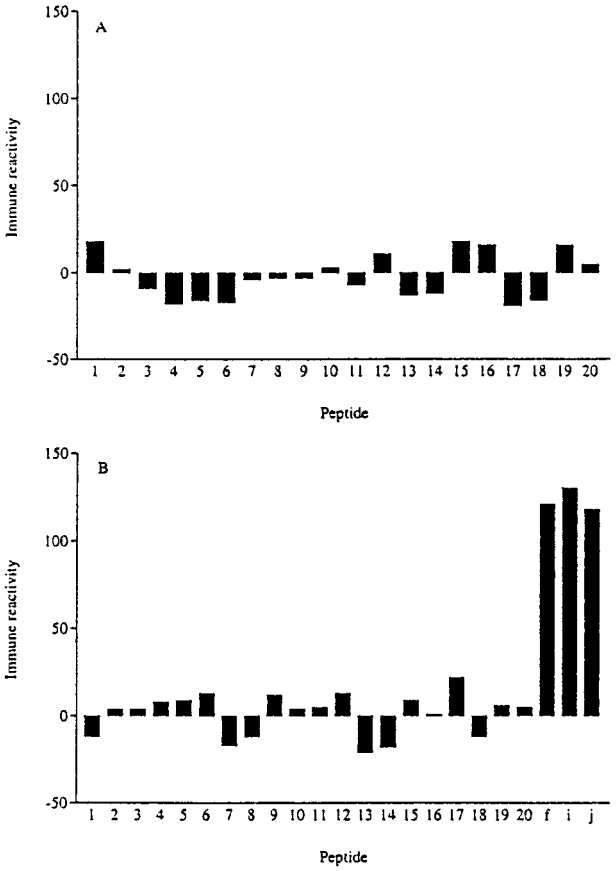


Figure 5. Immune reactivities of the tryptic peptides from unmodified lysozyme (A) and active ester E1G−lysozyme conjugate E1 (B) as measured using an Ovarian Monitor. The high immune reactivity of peptides f, i, and j (B) confirmed the presence of E1G.

is ideally constituted for homogeneous enzyme immunoassays for steroid glucuronides, since the most reactive lysine residues with respect to steroid glucuronide acylation are located near the active site. Steroid glucuronide conjugates of lysozyme, with low substitution levels and which are highly inhibited (>90%), can therefore be obtained using stoichiometric ratios of acylating reagent. Binding of the anti-hapten antibody to haptens attached at any of lysines 33, 97, or 116 results in a strong inhibitory effect on the lytic activity of the Ovarian Monitor conjugates, undoubtedly due to steric blocking of access of the *M. lysodeikticus* substrate to the active site. A combination of factors such as orientation of the hapten with respect to the active site (acylation position), the size of the substrate, the size of the enzyme itself, the length and rigidity of the link between the hapten and the enzyme and the binding kinetics are all important determinants of the degree of inhibition. A further understanding of the relative importance of these factors based on the structure and reactivity of the characterized conjugates E1-E6 is being carried out and may help in the rational design of other inhibitable enzyme conjugate systems.

ACKNOWLEDGMENT

We wish to thank the following people for their contributions: Associate Professor David Harding and Mr. Dick Poll for use of their chromatographic equipment, discussions, and suggestions; Dr. Brian Anderson for his help with computer graphics; and Dr. Keith Henderson for raising antibodies.

LITERATURE CITED

(1) Brown, J. B., Blackwell, L. F., Holmes, J., and Smyth, K. (1989) New Assays for Identifying the Fertile Phase. *Int. J. Gynecol. Obstet. Suppl. 1*, 111−122.

(2) Brown, J. B., Blackwell, L. F., Cox, R. I., Holmes, J. M., and Smith, M. A. (1988) Chemical and Homogeneous Enzyme Immunoassay Methods for the Measurement of Estrogens and Pregnanediol and their Glucuronides in Urine. *Prog. Biol. Clin. Res. 285*, 119−138.

(3) Brown, J. B., Blackwell, L. F., Billings, J. J., Conway, B., Cox, R. I., Garrett, G., Holmes, J. M., and Smith, M. A. (1987) Natural Family Planning. *Am. J. Obstet. Gynecol. 157*, 1082−1089.

(4) Thornton, S. J., Pepperell, R. J., and Brown, J. B. (1990) Home Monitoring of Gonadotrophin Ovulation Induction using the Ovarian Monitor. *Fertility and Sterility 54*, 1076−1082.

(5) Brown, J. B., Barker, G., and Holmes, J. (1991) Use of the Home Ovarian Monitor in Pregnancy Avoidance. *Am. J. Obstet. Gynecol. 165*, 2008−2011.

(6) Rubenstein, K. E., Schneider, R. S., and Ullman, E. F. (1972) "Homogeneous" Enzyme Immunoassay. A new Immunological Technique. *Biochim. Biophys. Res. Commun. 47*, 846−851.

(7) Dhar, T. K., Samanta, A. K., and Ali, E. (1988) Homogeneous Enzyme Immunoassay of Estradiol using Estradiol-3-O-Carboxymethyl Ether as Hapten. *Steroids 51*, 519−526.

(8) Schneider, R. S., Lindquist, P., Wong, E. T., Rubenstein, K. E., and Ullman, E. F. (1973) Homogeneous Enzyme Immunoassay for Opiates in Urine. *Clin. Chem. 19*, 821−825.

(9) Adlercreutz, H., Brown, J., Collins, W., Goebelsman, U., Kellie, A., Campbell, H., Spieler, J., and Braissand, G. (1982) The Measurement of Urinary Steroid Glucuronides as Indices of the Fertile Period in Women. World health organisation, Task Force on Methods for the Determination of the Fertile Period, Special Programme of Research, Development and Research Training in Human Reproduction. *J. Steroid Biochem. 17*, 695−702.

(10) Habeeb, A. F. S. A., and Atassi, M. Z. (1970) Enzymic and Immunochemical Properties of Lysozyme. Evaluation of Several Amino Group Reversible Blocking Reagents. *Biochemistry 9,* 4939−4944.

(11) Habeeb, A. F. S. A., and Atassi, M. Z. (1971) Enzymic and Immunochemical Properties of Lysozyme. V. Derivatives Modified at Lysine Residues by Guanidination, Acetylation, Succinylation, or Maleylation. *Immunochemistry 8,* 1047−1059.

(12) Patthy, L., and Smith, E. L. (1975) Identification of Functional Arginine Residues in Ribonuclease A and Lysozyme. *J. Biol. Chem. 250,* 565−569.

(13) Imoto, T., Johnson, L. N., North, A. C. T., Phillips, D. C., and Ruplet, J. A. (1972) Vertebrate Lysozymes. In *The Enzymes* (P. D. Boyer, Ed.) 3rd ed., Vol. VII, pp 781, Academic Press, New York.

(14) Lee, C., Atassi, M. Z., and Habeeb, A. F. S. A. (1975) Enzyme and Immunochemical Properties of Lysozyme. *Biochim. Biophys. Acta 400,* 423−432.

(15) Suckau, D., Mak, M., and Przybylski, M. (1992) Protein Surface Topology-Probing by Selective Chemical Modification and Mass Spectrometric Peptide Mapping. *Proc. Natl. Acad. Sci. U.S.A. 89,* 5630−5634.

(16) Burnens, A., Demotz, S., Corradin, G., Binz, H., and Bosshard, H. R. (1987) Epitope Mapping by Chemical Modification of Free and Antibody-Bound Protein Antigen. *Science 235,* 780−783.

(17) Gani, M., Coley, J., Piron, J., Humphreys, A. S., Arevalo, J., Wilson, I. A., and Taussig, M. J. (1994) Monoclonal Antibodies Against Progesterone. Effect of Steroid-Carrier Coupling Postion on Antibody Specificity. *J. Steroid Biochem. Mol. Biol. 48,* 277−282.

(18) Conrow, R. B., and Bernstein, S. (1971) Steroid conjugates. VI. An Improved Koenigs-Knorr Synthesis of Aryl Glucuronides using Cadmium Carbonate, a New and Effective Catalyst. *J. Org. Chem. 36,* 863−870.

(19) Smales, C. M., Cooke, D., and Blackwell, L. F. (1994) Use of Ion-Exchange and Hydrophobic-Interaction Chromatography for the Rapid Purification of Lysozyme-Estrone Glucuronide Conjugates. *J. Chromatogr. B 662,* 3−14.

(20) Erlanger, B. F., Borek, F., Beiser, S. M., and Lieberman, S. (1959) Steroid-Protein Conjugates II: Preparation and Characterisation of Conjugates of Bovine Serum Albumin and Progesterone Deoxycorticosterone and Estrone. *J. Biol. Chem.* 234, 1090−1094.

(21) Rajkowski, K. M., and Cittanova, N. (1981) The Efficiency of Different Coupling Procedures for the Linkage of Oestriol-16α-Glucuronide, Oestrone-3-Glucuronide and Pregnanediol-3α-Glucuronide to Four Different Enzymes. *J. Steroid Biochem. 14,* 861−866.

(22) Rutherfurd, K. J., Chen, S., and Shively, J. E. (1991) Isolation and Amino Acid Sequence Analysis of Bovine Adrenal 3β-Hydroxysteroid Dehydrogenase/Steroid Isomerase. *Biochemistry 30,* 8108−8116.

(23) Rutherfurd, K. J., Chen, S., and Shively, J. E. (1991) Affinity Labeling of Bovine Adrenal 3β-Hydroxysteroid Dehydrogenase/Steroid Isomerase by 5′-[p-(fluorosulfonyl)benzoyl] Adenosine. *Biochemistry 30,* 8116−8123.

(24) Canfield, R. E. (1963) Peptides Derived from Tryptic Digestion of Egg White Lysozyme. *J. Biol. Chem. 238,* 2691−2697.

(25) Noda, Y., Fujiwara, K., Yamamoto, K., Fukuno, T., and Segawa, S. (1994) Specificity of Trypsin Digestion and Conformational Flexibility at Different Sites of Unfolded Lysozyme. *Biopolymers 34,* 217−226.

(26) Okazaki, K., Imoto, T., Yamada, H., Kuroki, R., and Fujita, K. (1982) Specificity of Trypsin Cleavage of Aspartic Acid 101 Derivatives of Lysozyme by Trypsin. *J. Biol. Chem. 257,* 12559−12562.

(27) Yamada, H., Ueda, T., Kuroki, R., Fukumura, T., Yasukochi, T., Hirabayashi, T., Fujita, K., and Imoto, T. (1985) Isolation and Characterisation of 101-β-Lysozyme that Possesses the β-Aspartyl Sequence at Aspartic Acid-101. *Biochemistry 24,* 7953−7959.

(28) Canfield, R. E. (1963) The Amino Acid Sequence of Egg White Lysozyme. *J. Biol. Chem. 238,* 2698−2707.

(29) Winter, G. (1986) Manual Sequence Strategy—A Personal View. In *Practical Protein Chemistry-A Handbook* (A. Darbre, Ed.) pp 349, J. Wiley & Sons Ltd, New York.

(30) Gerken, T. A., Jentoft, J. E., Jentoft, N., and Dearborn, D. G. (1982) Intramolecular Interactions of Amino Groups in ^{13}C Reductively Methylated Hen Egg-White Lysozyme. *J. Biol. Chem. 257,* 2894−2900.

(31) Spassov, V. Z., Karshikov, A. D., and Atanisov, B. P. (1989) Electrostatic Interactions in Proteins. A Theoretical Analysis of Lysozyme Ionization. *Biochim. Biophys. Acta* 999, 1−6.

BC9900441

CORRECTIONS

Volume 10, Number 2, March/April 1999.

Silvio Aime,* Mauro Botta, Simonetta Geninatti Crich, Giovanni Giovenzana, Giovanni Palmisano, and Massimo Sisti

NOVEL PARAMAGNETIC MACROMOLECULAR COMPLEXES DERIVED FROM THE LINKAGE OF A MACROCYCLIC GD(III) COMPLEX TO POLYAMINO ACIDS THROUGH A SQUARIC ACID MOIETY

On page 195, the reaction arrows in Schemes 3 and 4 should be replaced with ↔. In addition, on page 195, right column, in the sixth sentence of the second full paragraph, the following change should be made. "Thus, the strong upfield shift of C-3 suggests a large decrease of its carbonylic character, which is consistent with a shift in the equilibrium represented in Scheme 4." should be changed to "Thus, the strong upfield shift of C-3 suggests a large decrease of its carbonylic character, which is indicative that A-2 contributes more to the resonance hybrid than A-1."

BC990056M

10.1021/bc990056m
Published on Web 06/25/1999

Volume 10, Number 3, May/June 1999.

Clemens Decristoforo and Stephen J. Mather*

PREPARATION, ^{99m}TC-LABELING, AND IN VITRO CHARACTERIZATION OF HYNIC AND N_3S MODIFIED RC-160 AND [TYR^3]OCTREOTIDE

On pages 437 and 438, the numbers were omitted from the corresponding references. The Literature Cited should appear as follows.

LITERATURE CITED

(1) Eising, E. G., Bier, D., Knust, E. J., and Reiners, C. (1996) Somatostatin-receptor scintigraphy. Methods, indications, results. *Radiologe 36*, 81−88.

(2) Lamberts, S. W., Chayvialle, J. A., and Krenning, E. P. (1993) The visualization of gastroenteropancreatic endocrine tumors. *Digestion 54* (Suppl. 1), 92−97.

(3) Vekemans, M. C., Urbain, J. L., and Charkes, D. (1995) Advances in radio-imaging of neuroendocrine tumors. *Curr. Opin. Oncol. 7,* 63−67.

(4) Krenning, E. P., Kwekkeboom, D. J., Bakker, W. H., Breeman, W. A., Kooij, P. P., Oei, H. Y., van Hangen, M., Postema, P. T., de Jong M., and Reubi J. C. (1993) Somatostatin receptor scintigraphy with [^{111}In-DTPA-D-Phe] and [^{123}I-Tyr]octreotide: The Rotterdam experience with more than 1000 patients. *Eur. J. Nucl. Med. 20,* 716−731.

(5) Srkalovic, G., Cai, R. Z., and Schally, A. V. (1990) Evaluation of receptors for somatostatin in various tumors using different analogues. *J. Clin. Endocrinol. Metab. 70,* 661−669.

(6) Liebow, C., Reilly, C., Serrano, M., and Schally, A. V. (1989) Somatostain analogues inhibit growth of pancreatic cancer by stimulating tyrosine phosphatase. *Proc. Natl. Acad. Sci. U.S.A.* 86, 2003−2007.

(7) Pinski, J., Milovanovic, T. Y., Yano, T., Hamaoui, A., Radulovic, S., Cai, R. Z., and Schally, A. V. (1992) Biological activity and receptor binding characteristics to various human tumors of acetylated somatostatin receptors. *Proc. Soc. Exp. Biol. Med. 200,* 49−56.

(8) Banks, W. A., Schally, A. V., Barrera, C. M., Fasold, M. B., Durham, D. A., Csernus, V. J., and Kastin, A. J. (1990) Permeability of the murine blood brain barrier to some octapeptide analogues of somatostatin. *Proc. Natl. Acad. Sci. U.S.A. 87*, 6762−6766.

(9) Breeman, W. A. P., Hofland, L. J., Bakker, W. H., van der Pluijm, M., van Koetsveld, P. M., de Jong, M., Setyono-Han, B., Kwekkeboom, D. J., Visser, T. J., Lamberts, S. W. J., and Krenning, E. P. (1993) Radioiodinated somatostatin analogue RC-160: preparation, biological activity, in vivo application in rats and comparison with [^{123}I-Tyr^3]octreotide. *Eur. J. Nucl. Med. 20,* 1089−1094.

(10) Breeman, W. A. P., Hofland, L. J., Pluijm, M.van-der, van Koetsveld, P. M., de Jong, M., Setyono-Han, B., Bakker, W. H., Kweekeboom, D. J., Visser, T. J., Lamberts, S. W. J., and Krenning, E. P. (1994) A new radiolabeled somatostatin analogue [^{111}In-DTPA-D-Phe^1]RC-160: preparation, biological activity, receptor scintigraphy in rats and comparison with [^{111}In-DTPA-D-Phe^1]octreotide. *Eur. J. Nucl. Med. 21,* 328−335.

(11) Zamora, P. O., Gulhke, S., Bender, H., Diekmann, D., Rhodes, B. A., Biersack, H. J., and Knapp, F. F., Jr. (1996) Experimental radiotherapy of receptor-positive human prostate adenocarcinoma with ^{188}Re-RC-160, a directly radiolabeled somatostatin analogue. *Int. J. Cancer 65,* 214−20.

(12) Liu, S., Edwards, D. S., and Barrett, J. A. (1997) ^{99m}Tc labeling of highly potent small peptides. *Bioconjugate Chem. 8,* 621−636.

(13) Vallabhajosula, S., Moyer, B. R., Lister-James, J., McBride, B. J., Lipszyk, H., Lee, H., Bastidas, D., and Dean, R. T. (1996) Preclinical evaluation of Technetium-99m-Labeled Somatostatin Receptor-Binding Peptides. *J. Nucl. Med. 37,* 1016−1022.

(14) Maina, T., Stolz, B., Albert, R., Bruns, C., Koch, P., and Mäcke, H. (1994). Synthesis and biological evaluation of a new somatostatin analogue (SDZ 219−387) labeled with technetium-99m. *Eur. J. Nucl. Med. 21,* 437−444.

(15) Maina, T., Stolz, B., Albert, R., Nock, B., Bruns, C., and Mäcke, H. (1995) Synthesis, radiochemistry and biological evaluation of ^{99m}Tc[N_4-(D)PHE$_1$]-octreotide, a new octreotide derivative with high affinity for somatostatin receptors. in *Technetium and Rhenium in Chemistry and Nuclear Medicine 4* (M. Nicolini, G. Banoli, and U. Mazzi, Eds.) pp 395−400, SG Editorali, Padova.

(16) Mäcke, H. R. and Behe, M. (1996) New octreotide derivatives labeled with technetium-99m. *J. Nucl. Med. 37,* 29P (abstr. 107).

(17) Thakur, M. L., Kolan, H., Wiaderkiewicz, R., Pallela, V. R., Duggaraju, R., and Schally, A. V. (1997) Radiolabeled Somatostatin analogues in Prostate Cancer. *Nucl. Med. Biol. 24,* 105−113.

(18) Kolan, H., Li, J., and Thakur, M. L. (1996) Sandostatin Labeled with ^{99m}Tc: In Vitro Stability, In Vivo Validity and Comparison with ^{111}In-DTPA-Octreotide. *Peptide Res. 9,* 144−150.

(19) Abrams, M. J., Juweid, M., tenKate, C. I., Schwartz, D. A., Hauser, M. M., Gaul, F. E., Fuccello, A. J., Rubin, R. H., Strauss, H. W., and Fischman, A. J. (1990) Technetium-99m-human polyclonal IgG radiolabeled via the hydrazino nicotinamide derivative for imaging focal sites of infection in rats. *J. Nucl. Med. 31,* 2022−2028.

(20) Kasina, S., Sanderson, J. A., Fitzner, J. N., Srinivasan, A., Rao, T. N., Hobson, L. J., Reno, J. M., Axworthy, D. B., Beaumier, P. L., and Fritzberg, A. R. (1998) Simplified preformed chelate protein radiolabeling with technetium-99m nercaptoacetamidoadipoylglycylglycine (N_3S-Adipate). *Bioconjugate Chem. 9,* 108−117.

(21) Hnatowich, D. J., Qu, T., Chang, F., Ley, A. C., Ladner, R. C., and Rusckowski, M. (1998) Labeling peptides with technetium-99m using a bifunctional chelator of a N-hydroxysuccinimide ester of mercaptoacetyltriglycine. *J. Nucl. Med. 39,* 56−64.

(22) Hnatowich, D. J., Virzi, F., Fogorasi, M., Rusckowski, M., and Winnard, P. (1994) Can a cysteine challenge assay predict the in vivo behavior of ^{99m}Tc-labeled antibodies. *Nucl. Med. Biol. 21,* 1035−1044.

(23) Stalteri, M. A., Bansal, S., Hider, R., and Mather, S. J. (1999) Comparison of the stability of technetium labeled peptides to challenge with cysteine. *Bioconjugate Chem. 10,* 130−136.

(24) Hofland, L. J., van Knoetsveld, P. M., Wouters, N., Waaijers, M., Reubi, J. C., and Lamberts, S. W. J. (1992) Dissociation of antiproliferative and antihormoral effects of somatostatin analogue octreotide on 7315b pituitary tumor cells. *Endocrinology 131,* 571−577.

(25) Hofland, L. J., van Knoetsveld, P. M., Waaijers, M., and Lamberts, S. W. (1996) Internalisation of isotope-coupled somatostatin analoges. *Digestion 57* (Suppl. 1), 2−6.

(26) Taylor, J. E., Theveniau, M. A., Bashirzadeh, R., Reisine, T., and Eden, P. A. (1994) Detection of somatostatin receptor subtype 2 (SSTR2) in established tumors and tumor cell lines: evidence for SST2 heterogeneity. *Peptides 15,* 1229−1236.

(27) Liu, S., Edwards, D. S., Looby, R. J., Harris, A. R., Poirier, M. J., Barrett, J. A., Heminway, S. J., and Carroll, T. R. (1996) Labeling a hydrazino nicotinamide-modified cyclic IIb/IIIa receptor antagonist with ^{99m}Tc using aminocarboxylates as coligands. *Bioconjugate Chem. 7,* 63−71.

(28) Edwards, D. S., Liu, S., Barrett, J. A., Harris, A. R., Looby, R. J., Ziegler, M. C., Heminway, S. J., and Carroll, T. R. (1997) New and versatile ternary ligand system for technetiumradiopharmaceuticals: water soluble phosphines and tricine as coligands in labeling a hydrazinonicotinamide-modifies cyclic glycoprotein IIb/IIIa receptor antagonist with ^{99m}Tc. *Bioconjugate Chem. 8,* 146−154.

(29) Liu, S., Edwards, D. S., and Harris, A. R. (1998) A novel tenary ligand system for ^{99m}Tc-labeling of hydrazio nicotinamide-modified biologically active molecules using imine-N-containing heterocycles as coligands, *Bioconjugate Chem. 9,* 583−595.

(30) Bormans, G., Cleynhens, B., Adriaens, P., Vanbilloen, H., de Roo M., and Verbruggen, A. (1995) Investigation of the labeling characteristics of ^{99m}Tc-Mercaptoacetyltriglycine. *Nucl. Med. Biol. 22,* 339−349.

(31) Millar, A. M. and O'Brien, L. M. (1990) An investigation of factors that might influence the radiochemical purity and stability of ^{99m}Tc-MAG3. *Eur. J. Nucl. Med. 16,* 615−619.

(32) Noll, B., Johannsen, B., and Spies, H. (1995) Sources of radiochemical impurities in the ^{99m}Tc/S-unprotected MAG3 system. *Nucl. Med. Biol. 22,* 1057−1062.

(33) Breeman, W. A. P., Van Hagen, P. M., Kwekkebroom, D. K., Visser, T. J., and Krenning, E. P. (1998) Somatostatin receptor scintigraphy using [^{111}In-DTPA^0]RC160 in humans: a comparison with [^{111}In-DTPA^0]octreotide. *Eur. J. Nucl. Med. 25,* 182−186.

BC9900688

10.1021/bc9900688
Published on Web 07/19/1999

SEPTEMBER/OCTOBER 1999
Volume 10, Number 5

© *Copyright 1999 by the American Chemical Society*

Bioconjugate Chemistry

COMMUNICATIONS

New Detachable Poly(ethylene glycol) Conjugates: Cysteine-Cleavable Lipopolymers Regenerating Natural Phospholipid, Diacyl Phosphatidylethanolamine

Samuel Zalipsky,* Masoud Qazen,† John A. Walker II,‡ Nasreen Mullah, Yolanda P. Quinn, and Shi Kun Huang

Alza Corporation, 1050 Hamilton Court, Menlo Park, California 94025. Received March 16, 1999

A new strategy for the reversible attachment of methoxypoly(ethylene glycol) (mPEG) to an amino-containing substrate is described. The strategy is based on formation of a benzyl carbamate linkage substituted with a disulfide in the para or ortho position. While being stable under nonreducing conditions, the dithiobenzyl (DTB) urethane linkage is susceptible to cleavage by mild thiolysis with cysteine resulting in release of the parent amino component of the conjugate in its original form. The method is exemplified by preparation of mPEG-DTB-alcohol, its activation and attachment to distearoylphosphatidylethanolamine (DSPE). The resulting lipopolymer incorporates into liposomes, which are capable of losing their polymer coating under conditions approximating those existing in vivo. Implications for drug delivery are briefly discussed.

Lipopolymers, polymer−lipid conjugates, have proven to be very useful in micellar and liposomal drug delivery systems (*1*). In particular, the use of poly(ethylene glycol)-lipid [usually distearoylphosphatidylethanolamine (DSPE)][1] conjugates (*2*) has become routine to convey favorable pharmacokinetic and in vivo distribution characteristics to various injectable particles. The presence of grafted PEG chains on the surface of particulates results in reduced nonspecific interactions with various biological cells and macromolecules. This is caused by the exclusion effect of the flexible, very mobile, well water solvated PEG chains. However, for a variety of applications interaction with target cells is desirable. These might include, for example, intracellular delivery of a liposomal drug payload, delivery of oligonucleotides, or delivery of genes. In these instances, it might be desirable to be able to facilitate a process of removal of the surface-grafted polymer chains. We recently demonstrated some of the useful properties of cleavable PEG-lipids in their liposomal formulations (*3*). The first generation of detachable PEG-bearing liposomes contained aliphatic di-

* To whom correspondence should be addresses. Phone: (650) 564-4651. Fax: (650) 617-3080. E-mail: samuelz@sequus.com.
† Current address: CellGate, Inc., 552 Del Rey Ave., Sunnyvale, CA 94086.
‡ Current address: Protogene Laboratories, 1454 Page Mill Road, Palo Alto, CA 94304.

[1] Abbreviations: PEG, poly(ethylene glycol); mPEG, methoxy-PEG; DTB, dithiobenzyl; DSPE, distearoylphosphatidylethanolamine; DOPE, dioleoylphosphatidylethanolamine; PHPC, partially hydrogenated phosphatidylcholine; MALDI-TOFMS, matrix-assisted laser desorption/ionization time-of-flight mass spectrometry.

10.1021/bc990031n CCC: $18.00 © 1999 American Chemical Society
Published on Web 08/05/1999

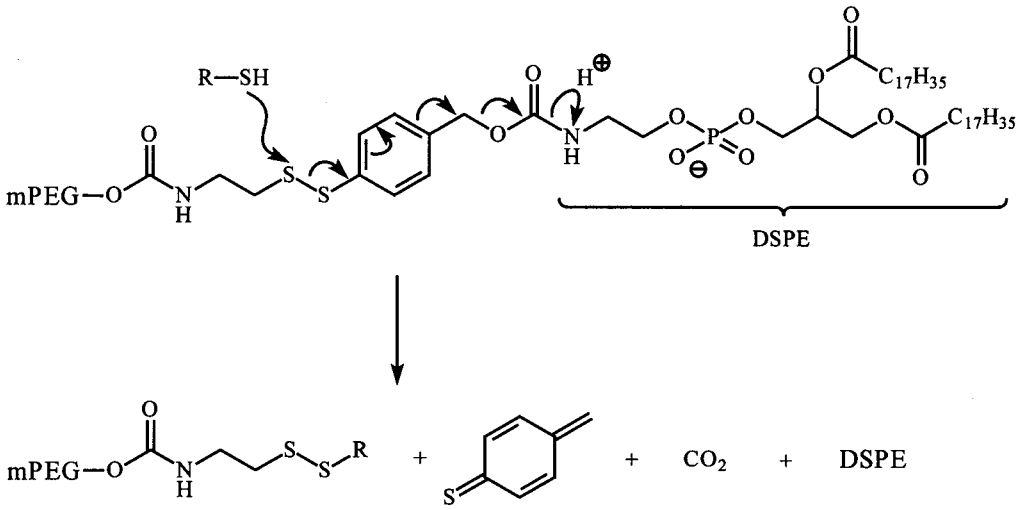


Figure 1. *p*-Dithiobenzyl urethane-linked mPEG-DSPE conjugate and its thiolytic cleavage. The *o*-DTB lipopolymer undergoes similar decomposition reaction. mPEG = $CH_3O(CH_2CH_2O)_{45}$-.

sulfide-linked conjugate with 3,3′-dithiodipropionate as the linking moiety. Consequently, cleavage of the mPEG grafts from these liposomes required a relatively potent thiolytic agent, 1,4-dithiothreitol, which is unacceptable for the in vivo use. Furthermore, a modified phospholipid, 3-mercaptopropionyl-DSPE product, was generated as a result of the disulfide cleavage (*3*). In this communication, we report the preparation and some of the properties of a new mPEG-DSPE conjugate, containing *o*- or *p*-ditiobenzyl carbamate (DTB-urethane) linkage moiety (Figure 1). In contrast to the earlier version of the disulfide-linked conjugate, these new lipopolymers are cleavable with cysteine, and as a result of this reaction, phosphatidylethanolamine lipid is regenerated in its natural, unmodified form. In essence in this application, the mPEG moiety is acting as a macromolecular protecting group, which is removable under mild thiolytic conditions achievable in vivo. To the best of our knowledge this is the first demonstration of this type of reversible PEGylation strategy applied to any substrate.

Thiolytic decomposition of benzyl urethane-linked drugs containing aromatic disulfides in the para or ortho positions has been utilized by Senter et al. as a basis for an elegant prodrug strategy (*4*). We decided to adapt the dithiobenzyl urethane as a linkage between the lipid, DSPE, and mPEG components of the cleavable lipopolymer. The main attraction of this linking strategy, as shown in Figure 1, lies in its ability to regenerate the amino component of the carbamate upon reaction with thiols. Moreover, cleavage of mixed aliphatic−aromatic disulfides is usually easier than of their symmetrical aliphatic counterparts. We anticipated that this would allow the use of a mild, nontoxic thiol such as cysteine as the cleaving reagent.

The syntheses of the polymer−lipid conjugates are schematically depicted in Figure 2. First, we prepared a novel mPEG-2000 derivative with a methoxycarbonyldithioalkyl end group. This was accomplished by reacting 2-(methoxycarbonyldithio)ethaneamine with mPEG-chloroformate. The former compound was obtained through the reaction of 2-aminoethanethiol hydrochloride with an equivalent amount of methoxycarbonylsulfenyl chloride[2] according to the previously published procedures (*6, 7*). The polymeric chloroformate was easily prepared by phosgenation of an anhydrous mPEG-OH solution (*8*). The methoxycarbonyldithio functionality, positioned in this instance at the end of mPEG, is known to be useful

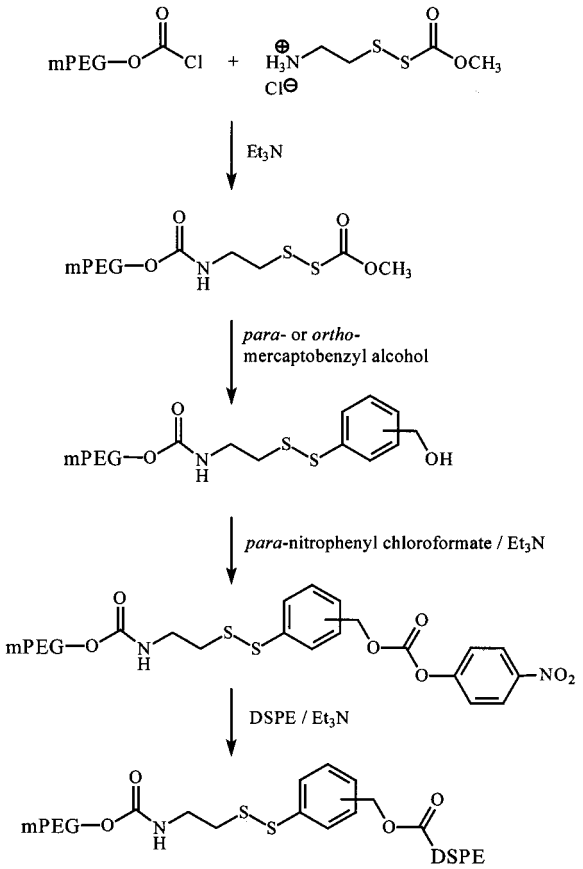


Figure 2. Schematic depiction of the synthesis of mPEG-DTB-DSPE.

for the formation of mixed disulfides (*6, 9, 10*). Furthermore, it is sufficiently active to react with even weakly nucleophilic aromatic thiols (*7*). Both para and ortho isomers of mercaptobenzyl alcohol (*11*) coupled cleanly with the polymeric acyl disulfide, yielding the mPEG-bearing dithiobenzyl alcohol end group. Active carbonate introduction proceeded as with the underivatized mPEG-

[2] To avoid complication due to various impurities potentially present in commercially available, aged methoxycarbonylsulfenyl chloride in some experiments, we used instead freshly prepared ethoxycarbonylsulfenyl chloride (*5*) with no bearing on the outcome of the syntheses.

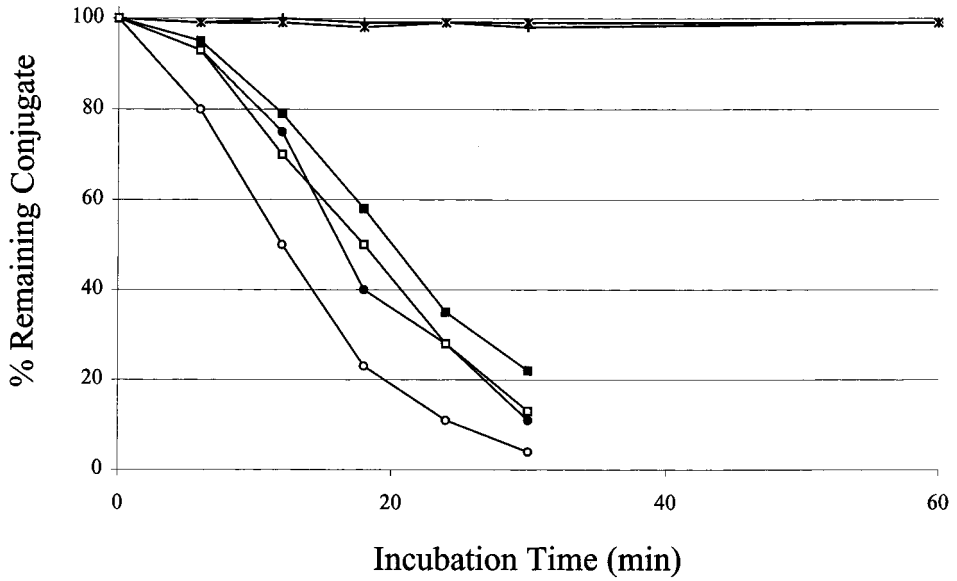


Figure 3. Cysteine-mediated cleavage of mPEG-DTB-DSPE conjugates (33 μM) in either micellar or liposomal (PHPC/cholesterol/lipopolymer at 95:5:3 mole ratio, ~120 nm diameter, closed symbols) solutions in PBS, pH 7.2, containing 5 mM EDTA at 37 °C with or without cysteine (150 μM). Disappearance of the conjugates was monitored by HPLC (Phenomenex C_8 Prodigy, 4.6 × 50 mm column, detection at 277 nm, mobile phase methanol/water 95:5 with 0.1% trifluoroacetic acid at 1 mL/min). Incubation in buffer only of ortho conjugate (*) and para conjugate (+). Incubations in cysteine-PBS of para conjugate (□), ortho conjugate (○); or liposomes containing para conjugate (■), ortho conjugate (●).

OH. We prepared both succinimidyl and *p*-nitrophenyl carbonates. However, most of the conjugation reactions with DSPE were performed with the latter derivatives, due to the ease of their preparation, shelf life stability, and avoidance of the potential side reactions associated with the succinimidyl carbonate chemistry (*12*). Both *o*- and *p*-DTB urethane linked lipopolymers were purified by silica gel chromatography (methanol gradient 0 to 10% in chloroform, ~70% isolated yield) and characterized by NMR[3] and MALDI-TOFMS. The latter technique confirmed the average molecular masses of the conjugates, 3127 and 3139 Da for para and ortho isomers, respectively (theoretical molecular mass ≈ 3100 Da). As was previously observed for various PEG conjugates (*13*, *14*), the spectra consisted of bell-shaped distributions of signals equally spaced at 44 Da, corresponding to the ethylene oxide repeating units. Consistent with the known tendency of MALDI-MS to, at least partially, cleave disulfides (*15*), separate distributions corresponding to mPEG-thiol, average molecular mass 2240 Da, were also observed.

The stabilities of both DTB-linked lipopolymers in buffered aqueous solution (pH 7.2) in the presence and absence of cysteine was monitored by HPLC. The results are illustrated in Figure 3. In these experiments, the *o*-DTB conjugate exhibited a slightly faster rate of decomposition than its para counterpart ($T_{1/2} \approx 12$ min vs ~18 min, at [Cys] = 150 μM). Both ortho and para conjugates were slightly more resistant to the thiolytic cleavage when incorporated into liposomes rather than in micellar solutions. In the absence of thiols, both conjugates appeared to be stable. Examination of completed thiolysis reactions of both para and ortho conjugates by TLC (silica gel G, chloroform/methanol/water 90:18:2) revealed the presence of DSPE as the sole lipid component (*16*) and another spot corresponding to a thiol-bearing, lipid-free mPEG derivative.

Due to the very large polar headgroup of PEG-lipid conjugates, they allow liposomal bilayer accommodation of lipids that normally do not form vesicles, e.g., DOPE, a hexagonal phase forming lipid. If a cleavable lipopolymer is used to facilitate the formation of this type of liposome, then chemical detachment of the grafted polymer chains would trigger decomposition of the vesicles and conversion of the lipids into the hexagonal phase. This, as was previously demonstrated (*3*), can be used for instant release of the liposomal contents and liposomal fusion. The content release characteristic of such liposomes, or the rate of the dequenching of the liberated fluorophores, provides for a convenient quantitative evaluation of the cleavable PEG-bearing liposomes. As illustrated in Figure 4, both dithiobenzyl-linked conjugates described here performed well in this assay, resulting in a cysteine-triggered release of encapsulated dyes. From these experiments, it is also apparent that the ortho conjugate was more susceptible to the thiolytic cleavage. For example, 300 μM cysteine liberates within 20 min most of the contents of DOPE liposomes stabilized by the *o*-DTB lipopolymer. Under the same conditions, only a very small fraction of the liposomes is decomposed when *p*-DTB-linked conjugate is used. After incubation for 20 min at 150 μM cysteine, half of the content release occurs by 20 min for *o*-DTB formulation, while only approximately 10% of the content release occurs in *p*-DTB liposomes even at the doubled cysteine concentration. Since we observed in Figure 3 that both ortho and para conjugates have half-lifetimes of less than 20 min, it is apparent that more than half of the original 3 mol % of PEG-lipids have to be cleaved in order to see a burst in the content release. Small, yet clearly not negligible, decomposition of the mPEG-DTB-DSPE/DOPE liposomes took place at 15 μM cysteine, which is the average plasma concentration in both humans and rodents (*17*), in the

[3] ^{1}H NMR for para conjugate: (d_6-DMSO, 360 MHz) δ 0.86 (t, CH_3, 6 H), 1.22 (s, CH_2 of lipid, 56H), 1.57 (m, $CH_2CH_2CO_2$, 4H), 2.50 (2xt, CH_2CO_2, 4H), 2.82 (t, CH_2S, 2H), 3.32 (s, OCH_3, 3H), 3.51 (m, PEG, ~180 H), 4.07 (t, PEG-CH_2OCONH, 2H), 4.11 and 4.28 (2 x dd CH_2CH of glycero, 2H), 4.98 (s, benzyl-CH_2, 2H), 5.09 (m, $CHCH_2$ of lipid), 7.35 and 7.53 (2 x d, aromatic, 4H) ppm. The ortho conjugate differed only in benzyl and aromatic signals at 5.11 (s, CH_2, 2H), and 7.31 (d, 1H), 7.39 (m, 2H) 7.75 (d, 1H) ppm.

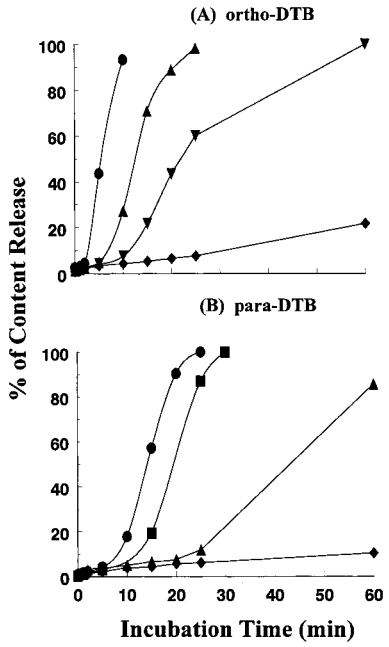


Figure 4. Fluorescent dequenching accompanying release of entrapped fluorophores (*p*-xylene-bis-pyridinium bromide, trisodium 8-hydroxypyrenetrisulfonate, 30 mM each) from liposomes (DOPE/mPEG-DTB-DSPE at 100: 3 molar ratio, ~100 nm diameter) incubated in HEPES buffer, pH 7.2, at 37 °C in the presence of cysteine (concentrations indicated for each curve). [Cys] = 15 μM (◆), 150 μM (▼), 300 μM (▲), 1 mM (■), 1.5 mM (●). The assays and calculations were performed according to the previously published procedures (*3*). Control experiments in the absence of reducing agents or with noncleavable urethane-linked mPEG-DSPE containing liposomes produced no content release.

time frame of these experiments (60 min). This suggests that DTB-linked lipopolymers should have sufficiently long lifetimes in plasma to allow the PEG-grafted vesicles to distribute systemically in vivo or to accumulate in a specific site either passively or through ligand-mediated targeting. Furthermore, these results suggest that a prolonged exposure to the natural plasma cysteine concentration (~15 μM) might be sufficient to decompose most of these lipopolymers. When faster cleavage is required, local or short-term increases in cysteine concentration can potentially be achieved by its intravenous or intraarterial administration.

The only example of the potential usefulness of in vivo reversible PEGylation was described by Garman and Kalindjian (*18*), who prepared acid-labile PEG-plasminogen activator by reacting mPEG-maleic anhydride reagent with amino groups of the protein. In this example, however, the conjugate was susceptible to cleavage not only under acidic conditions but even close to neutral pH and had to be stored frozen to minimize premature loss of the PEG attachments. Herein, we presented a new type of reversible PEGylation chemistry exemplified by preparation of mPEG-*o*/*p*-DTB-DSTE conjugates, which are rather stable in neutral pH in the absence of reducing agents. The linkages employed, *p*- or *o*-disulfide of a benzyl urethane, when subjected to mild thiolytic conditions can regenerate the original amine component, in this case DSPE, in its unmodified form. This is a very desirable outcome, since unnatural, modified lipids generated as a result of alternative cleavage strategies (see, for example, ref *3*) are more likely to have unpredictable, potentially negative in vivo effects. Since all the reactions shown in Figure 2 are clean high yielding transformations, the syntheses of mPEG-DTB reagents and their DSPE conjugates are of practical value. It is clear that DTB-linked PEG-lipids are cleavable with cysteine under mild conditions attainable in vivo. We are currently studying liposomes containing these cleavable lipopolymers in various biological systems. The results of these experiments will be reported in a due course. We anticipate that the new mPEG-DTB reagents and the described conjugation strategy will be of general applicability to a variety of amino-containing substrates including, peptides, proteins, aminoglycosides, and suitably functionalized biomaterials.

LITERATURE CITED

(1) Torchilin, V. P. (1997) Drug targeting by functional polymers: Targeting of polymer-coated liposomes. In *Desk Reference of Functionalized Polymers: synthesis and applications* (R. Arshady, Ed.) pp 769−788, American Chemical Society, Washington, DC.

(2) Zalipsky, S. (1995) Poly(ethylene glycol)-lipid conjugates. *Stealth Liposomes* (D. Lasic and F. Martin, Eds.) pp 93−102, CRC Press, Boca Raton, FL.

(3) Kirpotin, D., Hong, K., Mullah, N., Papahadjopoulos, D., and Zalipsky, S. (1996) Liposomes with detachable polymer coating: destabilization and fusion of dioleoylphosphatidylethanolamine vesicles triggered by cleavage of surface-grafted poly(ethylene glycol). *FEBS Lett. 388,* 115−118.

(4) Senter, P. D., Pearce, W. E., and Greenfield, R. S. (1990) Development of a drug-release strategy based on the reductive fragmentation of benzyl carbamate disulfides. *J. Org. Chem. 55,* 2975−2978.

(5) Barany, G., Schroll, A. L., Mott, A. W., and Halsrud, D. A. (1983) A general strategy for elaboration of the dithiocrbonyl functionality, -(C═O)SS-: Application of the synthesis of bis(chlorocarbonyl)disulfane and related derivatives of thiocarbonic acids. *J. Org. Chem. 48,* 4750−4761.

(6) Brois, S. J., Pilot, J. F., and Barnum, H. W. (1970) A new pathway to unsymmetrical disulfides. The thiol-induced fragmentation of sulfenylthiocarbonates. *J. Am. Chem. Soc. 92,* 7629−7631.

(7) Koneko, T., Willner, D., Minkovic, I., Knipe, J. O., Braslawsky, G. R., Greenfield, D. M., and Vyas, D. M. (1991) New hydrasone derivatives of adriamycin and their immunoconjugates—a correlation between acid stability and cytotoxisity. *Bioconjugate Chem. 2,* 133−141.

(8) Zalipsky, S., Seltzer, R., and Menon-Rudolph, S. (1992) Evaluation of a new reagent for covalent attachment of poly(ethylene glycol) to proteins. *Biotechnol. Appl. Biochem. 15,* 100−114.

(9) Chen, L., Zoulilova, I., Slaninova, J., and Barany, G. (1997) Synthesis and pharmacology of novel analogues of oxytocin and deaminooxytocin: Directed methods for the construction of disulfide and trisulfide bridges in peptides. *J. Med. Chem. 40,* 864−876.

(10) Le-Nguyen, D., and Rivier, J. (1986) Use of carboehoxysulfenyl chloride for disulfide bond formation. *Int. J. Pept. Protein Res. 27,* 285−292.

(11) Grice, R., and Owen, L. N. (1963) Cytotoxic compounds. Part IV. Substituted benzyl halides. *J. Chem. Soc.* 1947−1954.

(12) Zalipsky, S. (1998) Alkyl succinimidyl carbonates undergo Lossen rearrangement in basic buffers. *Chem. Commun.* 69−70.

(13) Zalipsky, S., Mullah, N., Harding, J. A., Gittelman, J., Guo, L., and DeFrees, S. A. (1997) Poly(ethylene glycol)-grafted liposomes with oligopeptide or oligosaccharide ligands appended to the termini of the polymer chains. *Bioconjugate Chem. 8,* 111−118.

(14) Zalipsky, S., Mullah, N., Dibble, A., and Flaherty, T. (1999) New chemoenzymatic approach to glyco-lipopolymers: practi-

cal preparation of functionally active galactose-poly(ethylene glycol)-distearoylphosphatidic acid conjugate. *Chem. Commun.* 653−654.

(15) Patterson, S. D., and Katta, V. (1994) Prompt fragmentation of disulfide-linked peptides during MALDI mass spectrometry. *Anal. Chem. 66,* 3727−3732.

(16) Dittmer, J. C., and Lester, R. L. (1964) A simple, specific spray for detection of phospholipids on thin-layer chromatography. *J. Lipid Res. 5,* 126−127.

(17) Lash, L. H., and Jones, D. P. (1985) Distribution of oxidized and reduced forms of glutathione and cysteine in rat plasma. *Arch. Biochem. Biophys. 240,* 583−592.

(18) Garman, A. J., and Kalindjian, S. B. (1987) The preparation and properties of novel reversible polymer-protein conjugates: 2-ω-methoxypolyethylene (5000) glycomethylene-3-methylmaleyl conjugates of plasminogen activators. *FEBS Lett. 223,* 361−365.

BC990031N

ARTICLES

Functionalization of Covalent DNA−Streptavidin Conjugates by Means of Biotinylated Modulator Components

Christof M. Niemeyer,*,† Bülent Ceyhan,† and Dietmar Blohm†

Universität Bremen, FB 2-UFT, Biotechnology and Molecular Genetics, Leobener Strasse, D-28359 Bremen, Germany . Received December 28, 1998; Revised Manuscript Received May 12, 1999

Covalent DNA−streptavidin conjugates are versatile biomolecular coupling reagents, since they have binding capacity for both a complementary nucleic acid and four molecules of biotin. The DNA−streptavidin hybrid molecules have been investigated for their capabilities to bind two different types of biotinylated components. Thus, (i) a functional biomolecule, e.g., a single-stranded DNA fragment or an enzyme and (ii) low-molecular weight biotin derivatives ("modulators") were coupled stepwise with the hybrid molecules. Modulators were D-biotin, aminobiotin, and biotin-fluorescein conjugate as well as a lysine-rich 10mer peptide, containing a biotin and a fluorescein substituent. These modulators were chosen to affected the hybridization properties of the DNA−streptavidin conjugates. As investigated by surface-plasmon resonance and microplate solid-phase hybridization measurements, D-biotin, biotin-fluorescein, and aminobiotin decreased the efficiency of hybridization with complementary, surface-bound oligonucleotides to a varying extent. The basic peptide increased the conjugate's hybridization efficiency. Moreover, it was demonstrated in two examples how modulators can be utilized as additional functional domains of streptavidin-based conjugates. First, fluorescein-containing modulators were used as hapten groups, allowing a sensitive detection by means of specific antibodies directed against the modulator. Second, the biotinylated peptide was used as a carrier molecule to attach multiple fluorogenic lanthanide-chelate groups to the streptavidin conjugate, enabling its sensitive detection by time-resolved fluorometry. The applicability of this kind of bioconjugation strategy to generate sensor-probes for gene detection assays was demonstrated.

INTRODUCTION

The exploration of biomolecular recognition systems and their utilization to fabricate novel biomaterials is a central goal of nanosciences-related biotechnology. Within this area of research, self-assembling strategies are increasingly becoming recognized as a way to generate nanometer-scaled structural and functional elements (*1*). For this purpose, nucleic acids appear to be a suitable construction material (*2*, *3*). DNA has been extensively used for the fabrication of nanostructured scaffolds (*2*, *4*), which have great potential for selective positioning of molecular components, such as conducting polymers (*5*), proteins (*6*, *7*), and nanocrystalline metal clusters (*7*−*10*). We have previously reported on the synthesis of covalent conjugates of single-stranded DNA and the tetrameric protein streptavidin (STV) (*6*). In these hybrid molecules, the proteins native binding capacity for four biotin molecules is extended with a specific binding site for complementary nucleic acids. Therefore, the conjugates can be utilized as biomolecular adaptors for the positioning of any biotin-containing functional component along a nucleic acid backbone, containing complementary sequence stretches. For example, stoichiometrically defined nanoscale assemblies can be generated from several DNA−STV hybrids (Figure 1a). Each of the hybrid adapters can be functionalized with a distinctive biotin-derivatized molecule such as enzymes and antibodies (*6*) but also metal nanoclusters (*7*). Another promising application of DNA−STV hybrids is their use as reagents for the reversible, site-selective and highly efficient attachment of biotinylated compounds to various surfaces, in particular, the immobilization of enzymes or binding proteins to DNA microarrays (*11*).

These applications, however, depend on the avoidance of undesired conjugates, formed from DNA−STV hybrids and excess biotinylated material. Thus, it is necessary to block the remaining free biotin-binding sites of the hybrids subsequently to the coupling with the biotinylated molecule of interest. For this purpose, typically D-biotin is used. To take advantage of the obligatory blocking, we here report on the examination of several low molecular weight biotin derivatives, "modulators", for their capability to modify and further functionalize the streptavidin conjugates. The strategy is schematically drawn in Figure 1b. A modification of the DNA−STV hybrids with two different biotinylated components is achieved by initial coupling with a macromolecular functional compound, such as an enzyme, and second, the remaining biotin-binding sites are saturated with low molecular weight modulators. We expected that a coupling of suitable modulators should affect and possibly fine-tune the bioconjugate's nucleic acid hybridization properties. Moreover, extra versatility should be obtain-

* To whom correspondence should be addressed. Phone: (49) 421 218-4911. Fax: (49) 421 218-7578. E-mail: CMN@biotec.uni-bremen.de.

† Universität Bremen.

10.1021/bc980150n CCC: $18.00 © 1999 American Chemical Society
Published on Web 07/30/1999

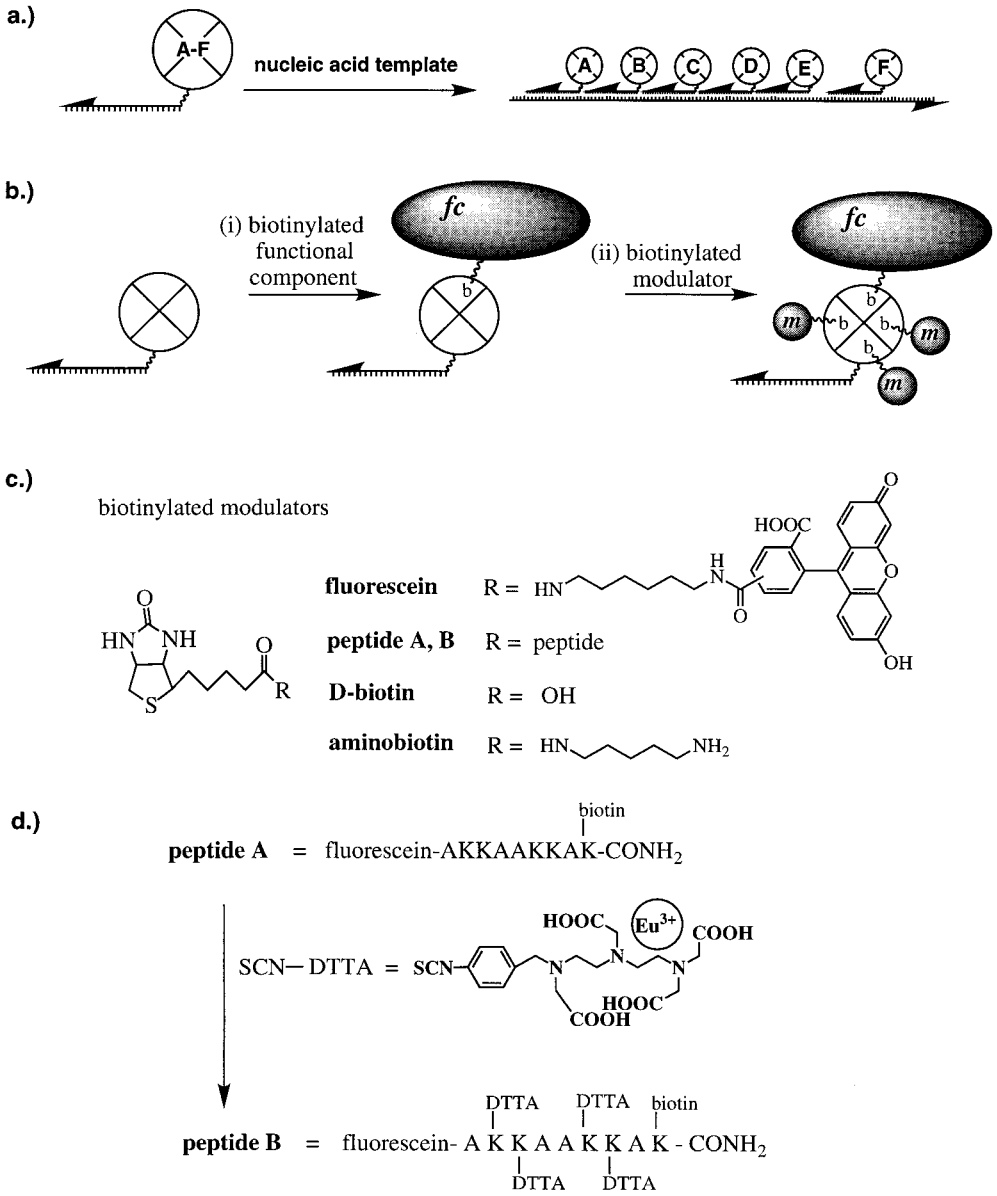


Figure 1. Schematic drawing of the bioconjugates investigated in this study. (a) Generation of supramolecular aggregates from six covalent DNA–STV hybrids, A–F, each containing an individual oligonucleotide sequence. The hybrids self-assemble in the presence of a complementary single-stranded nucleic acid template, e.g., an RNA molecule, to form supramolecular aggregates (*6*, *7*). Note that each of the six hybrids can be functionalized with individual biotinylated compounds. (b) Successive coupling of two different biotinylated compounds with a DNA–STV hybrid. In a first step, a macromolecular functional component (*fc*, represented by the shaded ellipse), such as a biotinylated enzyme or oligonucleotide, is coupled. In a second step, a biotinylated low molecular weight modulator (*m*, represented by the shaded sphere) is coupled to the remaining free biotin-binding sites. The modulator is used to modify the conjugate's hybridization properties or to enhance its functionality. (c) Chemical structure of the biotinylated modulators investigated in this study. (d) Chemical structure of the two peptides used as modulators.

able from the employment of modulators, if they contain additional functional moieties, such as chromophor or cofactor groups, chemically linked with the biotin. This should supplement the functionality of streptavidin bioconjugates, for instance, to exhibit high sensitivity as a detection tool or to enhance the catalytic turnover of enzymatic transformations.

The several modulators investigated in this study were D-biotin (bio), 5-aminopropyl-biotin (amb), fluorescein-biotin conjugate (fsc), and a biotinylated 10-mer peptide (peA), consisting of five lysine and five alanine residues in addition to a biotin substituent, attached to the carboxyl-terminal lysine, and a fluorescein substituent linked with the amino terminus (Figure 1, panels c and d). These modulators were chosen, to initially estimate any effects resulting from different molecular weights (e.g., biotin versus peptide A) or polarities of the biotin-attached side-chain groups (e.g., biotin versus aminobiotin, biotin versus fluorescein or aminobiotin versus peptide A). The stepwise modification of covalent DNA–STV conjugates, indicated in Figure 1b, was carried out by initial coupling of the DNA–STV hybrids with a biotinylated oligonucleotide (bDNA) or an enzyme as models for a macromolecular functional component. Subsequently, the low molecular weight modulators were bound. The effects of the these coupling steps have been studied with respect to the solid-phase hybridization capabilities of the conjugates. For this, a surface-plasmon resonance biosensor and also microplate measurements were used. Moreover, it was demonstrated in two examples that the binding of modulators provides additional functionality to the streptavidin conjugates.

Table 1. Oligonucleotides Used in This Study

name	description	sequence
tA	5′-thiolated 24-mer for synthesis of DNA-STV hybrid HA (**1**)	5′-thiol-TCC TGT GTG AAA TTG TTA TCC GCT-3′
FscA	5′-fluorescein labeled 24-mer for microplate assay in Figure 7	5′-fluorescein-TCC TGT GTG AAA TTG TTA TCC GCT-3′
bcA	5′-biotinylated 24-mer capture oligomer; complementary to sequence A	5′-biotin-AGC GGA TAA CAA TTT CAC ACA GGA-3′
tB	5′-thiolated 21-mer for synthesis of DNA-STV hybrid HB (**2**)	5′-thiol-GTA ATC ATG GTC ATA GCT GTT-3′
bB	5′-biotinylated 21-mer for coupling with DNA-STV hybrids	5′-biotin-GTA ATC ATG GTC ATA GCT GTT-3′
bcB	5′-biotinylated 21-mer capture oligomer; complementary to sequence B	5′-biotin-AAC AGC TAT GAC CAT GAT TAC-3′
tD	5′-thiolated 21-mer for synthesis of DNA-STV hybrid HD (**3**)	5′-thiol- CAG GTC GAC TCT AGA GGA TCC-3′
bD	5′-biotinylated 21-mer for coupling with DNA-STV hybrids	5′-biotin- CAG GTC GAC TCT AGA GGA TCC-3′
bcD	5′-biotinylated 21-mer capture oligomer; complementary to sequence D	5′-biotin- GGA TCC TCT AGA GTC GAC CTG-3′
tL	5′-thiolated 24-mer for synthesis of DNA-STV hybrid HL (**4**)	5′-thiol- GCG ACA CGG AAA TGT TGA ATA CTC-3′
bcL	5′-biotinylated 24-mer capture oligomer; complementary to sequence L	5′-biotin- GAG TAT TCA ACA TTT CCG TGT CGC-3′
bG	5′-biotinylated 18-mer for coupling with DNA-STV hybrids	5′-biotin- TTA AGT TGG GTA ACG CCA-3′
bK	5′-biotinylated 24-mer for coupling with DNA-STV hybrids	5′-biotin- CGC TCA TGA GAC AAT AAC CCT GAT-3′

First, modulators containing a fluorescein moiety were used as hapten groups, allowing for a sensitive detection by means of specific antibodies targeted against the chromophor. Second, peptide A was chemically derivatized with fluorogenic lanthanide-chelate DTTA groups to create a fluorogenic modulator, peptide B (Figure 1d). The coupling of this modulator with the DNA−STV hybrids allows a highly sensitive detection of the conjugates using time-resolved fluorometry (*12*). A potential application of this kind of bioconjugation strategy was demonstrated by generating biomolecular sensor probes, useful, e.g., in nucleic acid detection assays.

MATERIALS AND METHODS

Oligonucleotides and Covalent DNA−Streptavidin Hybrids. The sequences of the oligonucleotides used in this study are listed in Table 1. Various 5′-thiol-modified oligonucleotides, termed tA, tB, tD, and tL, were purchased from NAPS, Göttingen. These oligomers were used for the chemical synthesis of the DNA−STV hybrids described below. Biotinylated oligomer complements, termed bcA, bcB, bcD, and bcL (NAPS) were used as capture oligonucleotides in BIAcore and microplate hybridization measurements. Biotinylated oligomers, termed bB, bD, bG, and bK, were used for the coupling with DNA−STV conjugates (see Table 2).

Synthesis and purification of covalent DNA−STV hybrids, HA (**1**), HB (**2**), HD (**3**), and HL (**4**), were carried out from the corresponding thiolated oligonucleotides, tA through tL, respectively, and recombinant streptavidin (IBA, Göttingen), similar as previously described (*6*). In brief, STV (10 nmol) was derivatized with maleimido groups using a heterobispecific cross-linker, reacted with a 5′-thiolated oligonucleotide (10 nmol) and subsequently purified by anion-exchange chromatography. A 1:1 molar ratio of nucleic-acid and protein moiety of the hybrids was verified by gel-electrophoretic and photometric analysis, and concentrations of the preparations were determined by absorbance measurements (*6*).

Biotinylated Modulators. D-Biotin (bio) and biotin-fluorescein conjugate (fsc) were purchased from Sigma and Calbiochem, respectively. 5-Aminopropyl-biotin (amb) was synthesized from *N*-hydroxysuccinimidyl-biotin and 1,5-diaminopentane by the method of Sutoh et al. (*13*). The bifunctional modulator peptide A, containing four alanine and four lysine residues in addition to a biotin substituent, coupled to the carboxyl-terminal lysine side chain, and a fluorescein substituent, coupled to the amino terminus, was purchased from pepScan Immunoanalytik GmbH (Berlin). The peptide synthesis was carried by standard methods using Fmoc-protected amino acids. In an initial step, the ϵ-amino group of resin-bound lysine was deprotected and coupled with activated biotin. After removal of the Fmoc protection group, chain elongation of the peptide was carried out. Finally, the deprotected amino-terminus was derivatized with NHS-fluorescein, and the peptide was cleaved from the resin, yielding an amidated carboxyl-terminus. Full-length products were separated as a single peak by HPLC. MALDI-MS analysis of the product, however, revealed the presence of three major peaks at *m*/*z* 1305, 1531, and 1663. The peak at *m*/*z* 1531 corresponds to the desired peptide ($M = 1527$),

Table 2. Terminology of the Various Bioconjugates Investigated in This Report[a]

conjugate	acronyme	covalently attached DNA oligomer	biotinylated functional component	biotinylated modulator
1	HA	tA		
1a	HA_fsc	tA		fluorescein
1b	HA_peA	tA		peptide A
1c	HA_bio	tA		D-biotin
1d	HA_amb	tA		aminobiotin
1e	HA_peB	tA		peptide B
2	HB	tB		
2a	HB_fsc	tB		fluorescein
2b	HB_peA	tB		peptide A
2c	HB_bio	tB		D-biotin
2d	HB_amb	tB		aminobiotin
3	HD	tD		
3a	HD_fsc	tD		fluorescein
3b	HD_peA	tD		peptide A
4	HL	tL		
4a	HL_fsc	tL		fluorescein
4b	HL_peA	tL		peptide A
5	HB_bD	tB	oligomer bD	
5a	HB_bD_fsc	tB	oligomer bD	fluorescein
5b	HB_bD_peA	tB	oligomer bD	peptide A
5c	HB_bD_bio	tB	oligomer bD	D-biotin
5d	HB_bD_amb	tB	oligomer bD	aminobiotin
5e	HB_bB_fsc	tB	oligomer bB	fluorescein
5f	HB_bG_fsc	tB	oligomer bG	fluorescein
5g	HB_bK_fsc	tB	oligomer bK	fluorescein
6a	HD_bB_fsc	tD	oligomer bB	fluorescein
6b	HD_bD_fsc	tD	oligomer bD	fluorescein
7	HA_POD	tA	peroxidase	
7a	HA_POD_fsc	tA	peroxidase	fluorescein
7b	HA_POD_peA	tA	peroxidase	peptide A
7c	HA_POD_bio	tA	peroxidase	D-biotin
7d	HA_POD_amb	tA	peroxidase	aminobiotin

[a] The conjugates were generated by coupling of covalent DNA-STV hybrid molecules with biotinylated macromolecules and low-molecular weight modulators, as drawn in Figure 1b. The coupling through biotin-STV interaction is indicated by an underline dash.

while the peak at *m*/*z* 1305 likely corresponds to a product lacking the biotin moiety ($M = 227$). The presence of about 30% of this side product, possibly generated by incomplete coupling, was verified by chromatographic gel-filtration shift analysis after coupling with STV. The MALDI-MS peak at *m*/*z* 1663 likely corresponds to a biotinylated peptide containing an additional lysine residue ($M = 130$), possibly formed by elongation of deprotected lysine during the peptide synthesis.

Fluorogenic modulator peptide B was prepared from crude peptide A using Eu-labeling reagent, Eu^{3+}-N^1-(*p*-isothiocyanatobenzyl)-diethylentriamin-N^1,N^2,N^3,N^3-tetraacetic acid (DTTA, Wallac). The coupling was carried out according to manufacturer's instructions. As analyzed by MALDI-MS, all three peptides, present in the crude preparation of peptide A, gave coupling products, containing up to four DTTA moieties per peptide. An excess of the crude peptide B preparation was coupled with STV by 5 min of incubation at room temperature, and the conjugate was purified by gel filtration on a NAP-5 column (Pharmacia) and concentrated by ultrafiltration (Centricon 30, Millipore). The molar ratio of Eu^{3+} to STV was calculated from UV-vis photometry, time-resolved fluorometry, and MALDI-MS analysis.

Functionalization of DNA−STV Conjugates with Biotin Derivatives. Preconjugates of the DNA−STV hybrids and biotinylated modulators (**1a**−**4b** in Table 2) were prepared by mixing 1 mM stock solutions of the hybrids and a 16-fold molar excess (8 mM stock-solution) of biotinylated modulators in buffer A [20 mM Tris-Cl buffer, pH 7.5, 150 mM NaCl, 5 mM EDTA, and 0.01% (w/v) Tween-20]. After incubation for 30 min at room temperature, the mixtures were diluted to final concentrations, typically in the range of 200 to 5 nM of the hybrids, with buffer A. Conjugates of the DNA−STV hybrids and biotinylated oligonucleotides (**5**−**6b** in Table 2) were prepared from 0.1 mM stock solutions of the hybrids **2** and **3** and a 1−8-fold molar excess (1−8 mM stock solution) of biotinylated oligonucleotides in buffer A. After incubation for 30 min at room temperature, a 16-fold molar excess of biotinylated modulator was added, and the mixtures were diluted for BIAcore measurements as described below. Conjugates **7**−**7d** (Table 2) of the DNA−STV hybrids and biotinylated horseradish peroxidase (POD, Pierce) were prepared by mixing 0.1 mM stock solutions of the hybrid **1** and POD in buffer A. After incubation for 30 min at room temperature, a 16-fold excess of biotinylated modulator was added, the mixtures were incubated for additional 10 min and subsequently diluted to final concentrations, in the range 25 to 5 nM, with buffer A.

BIAcore Measurements. Biospecific interaction analysis was performed on a BIAcore 2000 Biosensor (Biacore AB, Upsala, Sweden) at a continuous flow of buffer B (150 mM NaCl, 30 mM sodium phosphate, 3 mM EDTA, and 0.25% Triton X-100, pH 7.4) at 10 μL/min and 25 °C, maintained throughout the entire analysis. The immobilization of capture oligonucleotides, bcA, bcB, bcD, bcL (Table 1), 10 μM in buffer B, was achieved by injection over STV-coated sensorchips (SA-Chips, Biacore AB) until an amount of about 1000 RU of the biotinylated oligomer complements was immobilized. Loosely attached material was removed by three cycles of 10 μL of 50 mM NaOH. To analyze the binding efficiencies of DNA−STV conjugates, previously modified with biotinylated compounds, various dilutions of typically 200−25 nM of the conjugates in buffer B were injected over the DNA-specific surface at 10 μL/min for 4 min. The interaction was monitored continuously as the change in SPR signal. Dissociation was affected by injecting buffer B only and was followed for 15 min. The surface was regenerated by injection of 10 μL of 50 mM NaOH. The entire process was automated, binding and dissociation curves were recorded automatically, and analytical cycles were preprogrammed. The data analysis was carried out using BIAcore Evaluation 2.1 software (Pharmacia).

Microplate Hybridization Assays. Microplate-based solid-phase hybridization assays were carried out on STV-coated microplates, prepared as previously described (*14*). Initially, 50 μL of a 240 nM solution of biotinylated capture oligomer bcA in buffer A were allowed to bind for 60 min to the STV-coated plates. After washing with buffer A containing 10 mM D-biotin, 50 μL of solutions of the conjugates **7**−**7d**, prepared as described above, were allowed to hybridize for 60 min at room temperature. Negative controls were run in parallel by applying conjugates to wells, coated with noncomplementary oligonucleotide bcB. After incubation and washing four times with buffer A and twice with buffer C (20 mM Tris, pH 7.5, and 150 mM NaCl) POD-substrate, ABTS (2,2'-azino-di-[3-ethylbenzthiazoline sulfonate], Boehringer Mannheim), prepared according to manufacturers instructions, was added and the absorbances at 405 nm were determined with a Victor 1420 Multilabel-Counter (Wallac) after incubation for 20 min at 37 °C. Standard deviations were calculated from the signal intensities of interest. Typically, duplicate determination of a particular sample revealed an error of about 10%.

Two-sided nucleic acid detection assays (see Figure 7) were carried out on microplates modified with capture oligonucleotide bB. Target DNA, prepared from M13mp18 vector as previously described (*6*), was heat denatured at 5 nM concentration in buffer A, and various dilutions ranging 2−0.005 nM were mixed with equal volumes of either oligonucleotide probe FscA (Table 1), HA_fsc (**1a**) or HA_peB (**1e**), 5 nM in buffer A. A total of 50 μL of the mixtures was allowed to hybridize to the microplate-bound capture oligomer for 60 min at room temperature. The plate was washed with buffer A, and the amount of probe **1e** immobilized was determined by time-resolved fluorometry with the Victor 1420 Multilabel-Counter after the addition of enhancement solution (Wallac). To detect probes FscA and **1a**, 50 μL of an anti-fluorescein immunoglobulin-alkaline phosphatase conjugate (Boehringer Mannheim, 1:3000 dilution in buffer A) were added to the wells and incubated for 30 min at room temperature. After washing, alkaline phosphatase-substrate, pNPP (4-nitrophenyl phosphate, Boehringer Mannheim), prepared according to manufacturers instructions, was added and the absorbance at 405 nm was determined with the Victor 1420 Multilabel-Counter after incubation for 30 min at 37 °C. Relative signal intensities were calculated by dividing signal intensities and background signals of negative controls in which no DNA target was present.

RESULTS AND DISCUSSION

Preparation of Bioconjugates. Covalent hybrids of DNA and streptavidin, HA (**1**), HB (**2**), HD (**3**), and HL (**4**), were synthesized from the analogous 5′-thiolated oligonucleotides, tA, tB, tD, and tL (for DNA sequences see Table 1) and recombinant streptavidin by chemical cross-linking as previously described (*6*). The chief products, hybrids containing a single oligonucleotide moiety per STV, were purified by chromatography (*6*).

To initially investigate the effects induced by the modulators, DNA−STV hybrids were exclusively coupled

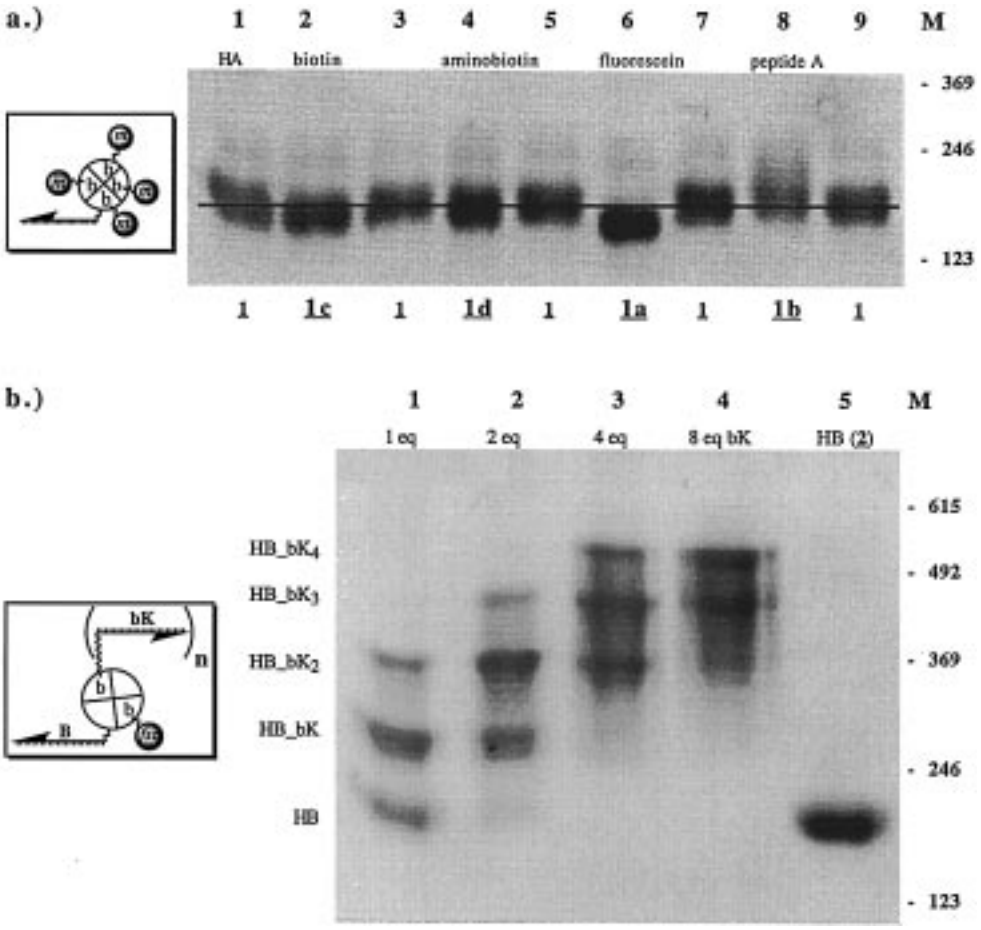


Figure 2. Analysis of DNA−STV conjugates by native 7.5% acrylamide gel-electrophoresis. (a) Influences of modulators on the conjugate's electrophoretic mobility. Conjugates **1a**−**d**, prepared from covalent DNA−STV hybrid HA (**1**) by coupling with 16 molar equivalents of the various biotinylated modulators, shown in Figure 1c. For comparison, unmodified **1** was applied to all odd-numbered lanes. (b) Analysis of bDNA conjugate **5g** prepared from DNA−STV hybrid HB (**2**) and 1, 2, 4, or 8 molar equivalents of biotinylated oligomer bK. Depending on their stoichiometric composition, HB_bK$_1$ through HB_bK$_4$ display a reduced electrophoretic mobility with increasing numbers of bK molecules bound to **2**. M: DNA molecular weight standards; the length is given in base pairs.

with the various modulators to yield conjugates **1a**−**4b** of Table 2. Gel-electrophoretic characterization was carried out with complexes prepared from DNA−STV hybrid HA (**1**) and 16 molar equivalents of the fluorescein (**1a**), peptide A (**1b**), biotin (**1c**), or aminobiotin modulator (**1d**) (Figure 2a). The coupling of the modulator caused only small changes in electrophoretic mobility. The most significant change was obtained from fluorescein, increasing the streptavidin's mobility. A faint decrease was observed for the peptide conjugate **1b**. These changes correlate with the polarity of the modulator's side chain (Figure 1c). The fluorescein affixes negative charges, while the amino groups of the lysine-rich peptide A append positive charges to the conjugates. Effects were even weaker when biotin (**1c**) or aminobiotin (**1d**) were used as modulators. However, a direct comparison of the bands suggests that the mobility of **1d** is similar to that of unmodified HA (**1**), while **1c** migrates somewhat faster than **1**. To demonstrate that the coupling of modulators is irreversible, conjugates **1a**−**d** were mixed with a biotinylated DNA oligomer. No additional bands were observed, similar as in Figure 2b (data not shown).

While conjugates of the DNA−STV hybrids and biotinylated enzymes, e.g., **7**, had previously been studied (*6*, *11*, *15*), conjugates of the hybrids with biotinylated DNA oligomers have not yet been investigated. Thus, several bDNA conjugates (**5**−**6b** in Table 2) were prepared from biotinylated oligonucleotides bB, bD, bG, and bK and covalent DNA−STV hybrids, HB (**2**) or HD (**3**). As an example, conjugate **5g** was analyzed by native gel electrophoresis. For conjugate preparation, DNA−STV hybrid **2** was mixed with increasing amounts of the biotinylated oligomer bK, incubated for 10 min, and subsequently, an excess of the fluorescein modulator was added. The resulting conjugates were analyzed on a nondenaturing acrylamide-gel (Figure 2b). The addition of 1 molar equivalent of bK oligomer already yielded the formation of several adducts. Depending on their stoichiometric composition, these adducts displayed significant differences in their electrophoretic mobility, which was reduced with increasing numbers of bK molecules bound to **2**. In the case of 1 equiv of bK, the major product was the expected monoadduct, HB_bK, formed in about 70% yield. Additional components were uncoupled **2** and also small amounts of a bis-adduct, HB_bK$_2$. The addition of 2, 3, or 8 equiv of bK led to the formation of adducts with a stoichiometry of HB_bK$_2$ and HB_bK$_3$ and also to the tetra-adduct HB_bK$_4$, containing four biotinylated oligonucleotide moieties, respectively. Further characterization of bDNA-containing conjugates, **5a** and **5e**−**g**, was carried out by BIAcore analysis described below.

To investigate whether a sequential coupling of two different biotinylated components can be achieved as proposed in Figure 1b, a series of doubly functionalized complexes (**5a**−**d** and **7a**−**d** in Table 2) was prepared from DNA−STV hybrids **2** and **1**, respectively. To prepare bDNA conjugates **5a**−**d**, **2** was initially coupled with biotinylated oligomer bD, and subsequently, the various

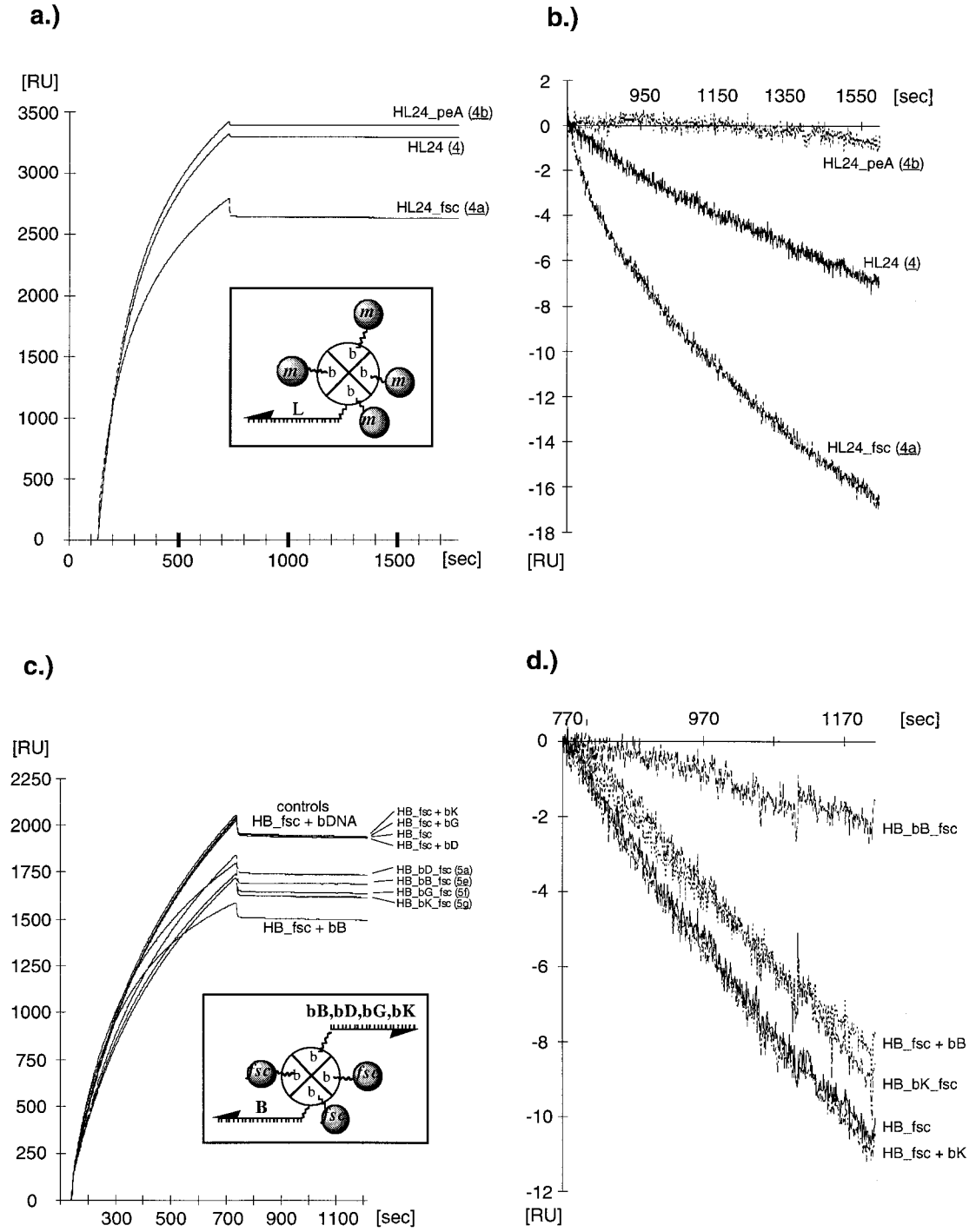


Figure 3. BIAcore analyses of solid-phase hybridization of DNA−STV conjugates. (a) Comparison of DNA−STV hybrid HL (**4**) (middle curve), and its conjugates with biotinylated fluorescein (**4a**) (lower curve) and biotinylated peptide A (**4b**) (upper curve). All analyte concentrations were 100 nM. (b) Overlay plot of the dissociation curves from Figure 3a. (c) Comparison of the binding curves of bDNA conjugates **5a** and **5e**−**g** obtained from DNA−STV conjugate HB (**2**), 1 molar equivalent of biotinylated oligonucleotides bB, bD, bG, or bK, and the fluorescein modulator. The upper set of curves was obtained from controls, in which (**2**) was saturated with fluorescein modulator prior to the addition of bDNA. The middle set of curves was obtained from the binding of conjugates **5a** and **5e**−**g**, the lower curve was obtained from the control in the presence of oligomer bB. All sample concentrations were 50 nM. (d) Overlay plot of selected dissociation curves from Figure 3c.

modulators were bound. Enzyme conjugates **7a**−**d** were prepared from DNA−STV hybrid **1** by stepwise coupling with 1 molar equivalent of biotinylated peroxidase, and the various modulators. The solid-phase hybridization capabilities of the double-functionalized streptavidin complexes were investigated using BIAcore or microplate analysis, as described below.

The fluorogenic modulator peptide B (Figure 1d) was synthesized to demonstrate how modulators can be used to extend the functionality of streptavidin complexes. To synthesize peptide B, Eu^{3+}-N^1-(*p*-isothiocyanatobenzyl)-diethylentriamin-N^1,N^2,N^3,N^3-tetraacetic acid was used as a reagent to chemically attach lanthanide-chelate (DTTA) groups to the lysine side chains of peptide A (see Figure 1d). This derivatization was carried out to obtain a modulator which is detectable with very high sensitivity by time-resolved measurement of Eu^{3+} fluorescence (*12*). The crude derivatization products were analyzed by

MALDI-MS. The spectra obtained showed peaks of peptide A coupled with two, three, or four DTTA groups. An excess of the crude peptide B was coupled with DNA−STV hybrid HA (**1**), and the resulting conjugate **1e** was purified by gel filtration chromatography and ultrafiltration. A ratio of about 10−11 Eu^{3+}/STV was calculated from UV-vis photometry and time-resolved fluorometry measurements. A similar ratio was obtained from MALDI-MS analysis of a conjugate prepared from native streptavidin and peptide B. The spectra revealed peaks at *m*/*z* 13 355 and *m*/*z* 16 438 (data not shown). The peaks were assigned to the masses of the STV subunit and its adduct with the peptide B, respectively. The difference in mass of about 3100 units suggests that on average three DTTA groups (M_r = 486 g/mol) are bound per peptide A moiety (M_r = 1527 g/mol). Conjugate **1e** was utilized as a sensor probe in the gene detection assay, described below.

Solid-Phase Hybridization Studies of the Conjugates. To study how biotinylated modulators influence the hybridization properties of DNA−STV conjugates, solid-phase hybridization studies were carried out using microplate analysis and biospecific interaction analysis (BIAcore) (*16*). The latter was performed using a biosensor based on surface plasmon resonance (SPR). With this technique, the refractive index within a gold sensor chip-immobilized dextran matrix is continuously monitored, plotted against time, and presented in a sensorgram. The change of SPR response, measured in resonance units (RU), allows a quantification of interaction between chip-immobilized and liquid-phase-diluted binding partners. Here, biotinylated oligomer complements were immobilized on streptavidin-coated sensor chips, and real-time measurements at several analyte concentrations were carried out with the various STV conjugates. A series of controls, carried out by injecting conjugates over sensor chips modified with noncomplementary capture oligomers gave no significant change in SPR response (not shown), indicating, that the binding observed is due exclusively to specific single-stranded DNA hybridization. BIAcore measurements were carried out in duplicate. Typically, the data obtained were highly reproducible, revealing errors of less than 3%. Unfortunately, kinetic analysis of the BIAcore data has not yet been achieved, although the determination of kinetic constants has previously been attained with similar analyte samples (*15*). In this study, highly irregular dissociation curves were observed (for instance see Figure 3b), suggesting that mass transport and rebinding phenomena occur which prohibit a detailed kinetic analysis (*17*). Since the signal intensities (RU values) at a given concentration directly correlate with the analyte's affinity, RU values were used instead of kinetic data to judge hybridization efficiency of the conjugates investigated.

Modulator-Induced Changes of Conjugate's Hybridization Capabilities. To initially study the influences of biotinylated modulators on the hybridization characteristics of the DNA−STV conjugates, BIAcore measurements were carried out with hybrids HA (**1**), HB (**2**), and HL (**4**) and compared with the modulator-modified analogous conjugates (Figure 3, panels a and b). The RU values obtained are summarized in Table 3. Compared to the unmodified hybrids **1**, **2**, and **4**, the hybridization efficiencies of fluorescein-modified conjugates, HA_fsc (**1a**), HB_fsc (**2a**), and HL_fsc (**4a**), were decreased by about −15, −24, and −20%, respectively. Note that these variations are well beyond the standard deviation of less than 3%. The decrease in hybridization efficiency is elucidated by a comparison of the BIAcore dissociation curves. As indicated from overlay plots (Figure 3b), the fluorescein-modified conjugates displayed an elevated dissociation, likely due to the additional negative charges introduced by the chromophor. The enhanced dissociation is probably the reason for the lower binding efficiencies observed.

Table 3. Influences of Biotinylated Modulators on the Solid-Phase Hybridization Efficiencies of DNA−STV Conjugates[a]

	conjugate/conc	50 nM	100 nM	200 nM	change [%]
1	HA	3742	4500	4973	
1a	HA_fsc	3099	3815	4411	−14.6 ± 2.2
2	HB	2566	3361	4057	
2a	HB_fsc	1955	2538	3135	−23.7 ± 0.6
control	HB_bio+fsc		2456		−26.9
2b	HB_peA	2941	3665	4433	11.6 ± 2.4
2c	HB_bio	1827	2413	2975	−27.9 ± 0.8
2d	HB_amb	2205	2906	3628	−12.7 ± 1.4
control	HB_bio+amb		2522		−25.0
3a	HD_fsc	431	709	1100	
3b	HD_peA	531	926	1527	30.9 ± 5.3
4	HL	2649	3300	3910	
4a	HL_fsc	2118	2643	3187	−19.5 ± 0.7
4b	HL_peA	2713	3393	4004	2.6 ± 0.2

[a] For terminology of the conjugates, see Table 2. The values are BIAcore resonance units (RU). All values are averaged from at least duplicate measurements with a typical standard deviation of about 3%. The values listed in the right column indicate the changes in hybridization efficiencies, averaged from the three different analyte concentrations and normalized as a percentage fraction of the signals obtained for unmodified DNA−STV hybrids.

The comparison of fluorescein- and peptide-A-modified complexes indicates that the coupling of the basic peptide increased the hybridization efficiencies of the bioconjugates (see Table 3). The increase was about 35 and 23% for HB conjugates **2a**/**2b** and HL conjugates **4a**/**4b**, respectively. The increase induced by peptide A was independent of the analyte concentration applied to the biosensor. In contrast, the increase observed from comparison of HD conjugates **3a**/**3b** was in the range of about 20−40%, depending on the analyte concentration applied. The coupling of four peptide A molecules increases the conjugate's masses by about 5% (2.8 kDa) compared to the coupling of four fluorescein modulators. Thus, the increased binding signals observed in BIAcore are not due to increased molecular weights, but rather due to enhanced hybridization capabilities of the peptide-containing conjugates. This is also evident from the comparison of BIAcore dissociation curves (Figure 3b). Overlay plots indicated that the coupling of the peptide A led to a remarkably reduced dissociation compared to fluorescein- and also to unmodified DNA−STV hybrids. This suggests that the higher binding of the peptide conjugates was due to reduced dissociation. The concentration dependency observed for HD-based conjugates **3a**/**3b** (see Table 3) is likely due to the sequence-specific hybridization properties of the D oligomer attached. HD hybridizes about 5-fold slower than HB or HL(*15*). Excess, uncoupled peptide A, which is present in the analyte solutions, can function as an intermolecular effector, accelerating nucleic acid hybridization due to its polyamine structure (*18*). This kind of intermolecular interaction is concentration dependent and more significant in slow hybridization reactions.

Further studies of modulator influences were carried out with the various HB conjugates **2a**−**d** (Table 3, see also the comparison of normalized data in Figure 5). Surprisingly, already the binding of D-biotin (**2c**) induces a significant decrease of about −28% in hybridization efficiency compared to unmodified HB (**2**). As a consequence, the signal intensity of 100 nM **2c** is similar to

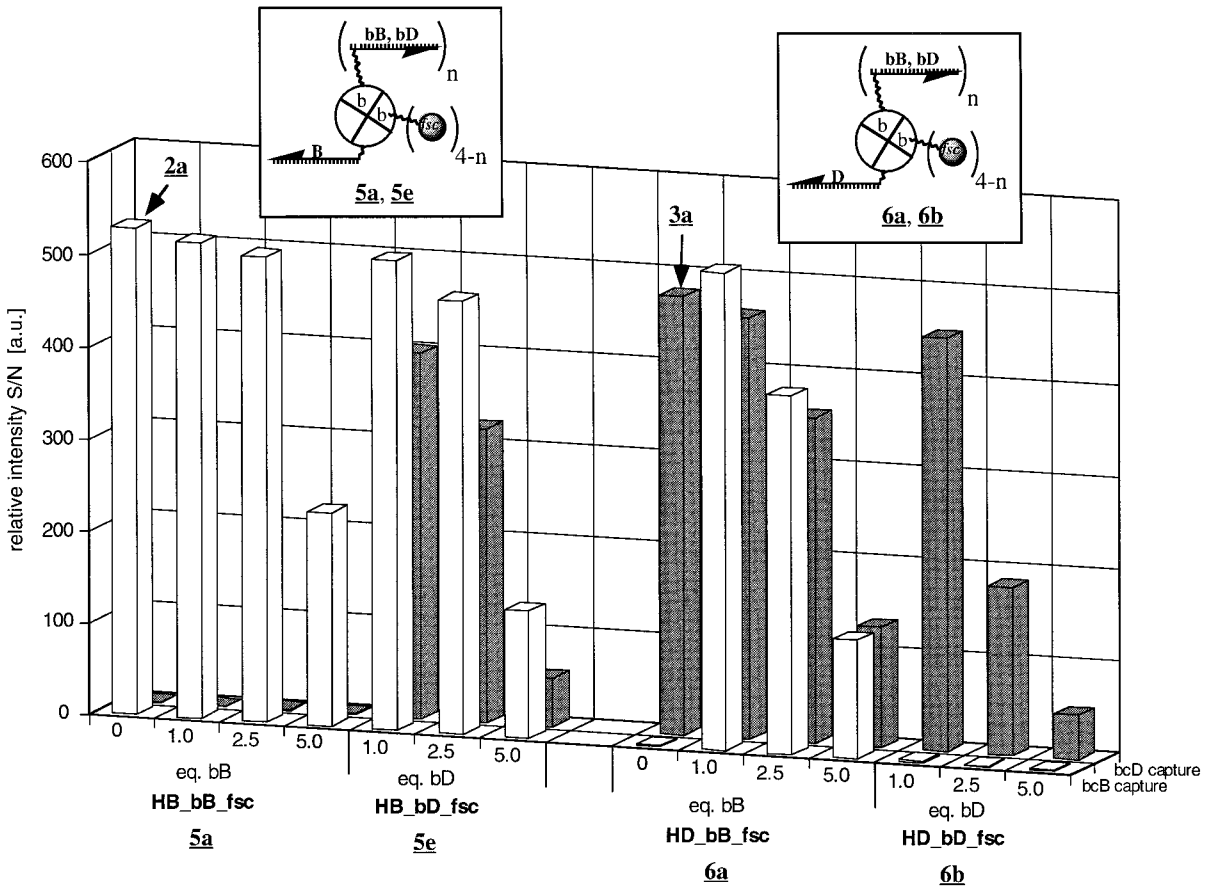


Figure 4. Microplate solid-phase hybridization of bDNA conjugates, prepared from DNA−STV hybrids HB or HD by successive coupling with either bB (**5a** and **6a**) or bD (**5e** and **6b**) oligonucleotide and the fluorescein modulator. The hybridization capabilities of the conjugates were tested in parallel with two microplate-bound capture oligomers, bcB and bcD. The detection of microplate-immobilized material was carried out using an anti-fluorescein-IgG-alkaline phosphatase conjugate and subsequent enzymatic color reaction. The height of the histograms represents relative signal intensities (*S*/*N*), obtained from the quotient of signal and background signals of the appropriate negative controls, in which the conjugates were incubated over noncomplementary capture oligomers.

Table 4. Influences of Biotinylated Modulators on the Hybridization Efficiency of HB Previously Coupled with Oligonucleotide bD[a]

	conjugate/conc	50 nM	100 nM	200 nM	change (%)
5	HB_bD	1998	2619	3221	
5a	HB_bD_fsc	1802	2307	2810	−11.5 ± 1.1
5b	HB_bD_PE	2075	2684	3280	2.7 ± 0.7
control	HB_bD_bio + PE	1755	2243	2771	−13.5 ± 0.9
5c	HB_bD_bio	1733	2208	2700	−15.1 ± 1.2
5d	HB_bD_amb	1840	2354	2867	−9.7 ± 1.2

[a] The numbers are BIAcore RU values, similar as indicated in Table 3.

that obtained from 50 nM of unmodified **2** (see Table 3). Thus, about a 2-fold reduced affinity of **2c** can be estimated. In contrast, the coupling with aminobiotin (**2d**) results in a significant smaller decrease in hybridization efficiency of about −13%, compared to unmodified **2**. Several controls were carried out by initial blocking of the biotin-binding sites with D-biotin and subsequent addition of modulators, e.g., fluorescein or aminobiotin (Table 3) or peptide A (Table 4). The controls indicated that the modulators only influence the hybridization when they are intramolecularly coupled with the streptavidin conjugate. Although systematic conclusions should not be drawn from these initial results, it seems reasonable that the biotin-binding induces conformational changes of the streptavidin molecule (*19*). The altered conformation causes altered intramolecular interactions between the surfaces of the protein and the nucleic acid moiety within the bioconjugate, and consequently, its hybridization capabilities are affected. Moreover, the results suggest that charged side chains, i.e., the carboxyl groups in D-biotin and fluorescein or the amino groups in aminobiotin and peptide A, significantly affect the hybridization properties of the bioconjugate's oligonucleotide domain. These observations are in agreement with extensive studies carried out by Corey and coworkers, who demonstrated that covalent oligolysine peptide−oligonucleotide conjugates display a significantly enhanced hybridization kinetics compared to the analogous unmodified oligonucleotides (*20*−*22*).

Conjugates Containing Biotinylated Oligonucleotides. To characterize conjugates consisting of covalent DNA−STV hybrids and biotinylated DNA oligomers (**5**−**6b** in Table 2), the binding capabilities of the two DNA domains within the complexes were initially investigated by a microplate-based hybridization assay (Figure 4). For this, the fluorescein modulator was incorporated into the conjugates to function as a hapten, allowing detection of the microplate-bound conjugates by a specific antibody directed against fluorescein. Four different bivalent complexes, **5a**, **5e** and **6a**, **6b**, were prepared from DNA−STV hybrids HB (**2**) or HD (**3**), respectively. This was achieved by initial coupling of the hybrids with various amounts of biotinylated oligonucleotides, bB or bD, followed by subsequent coupling with an excess of the fluorescein modulator. Following hybridization with microplate-immobilized, complementary capture oligonucleotides, bcB and bcD (see Table 1), the amounts of complexes bound to the plate were visualized by an anti-

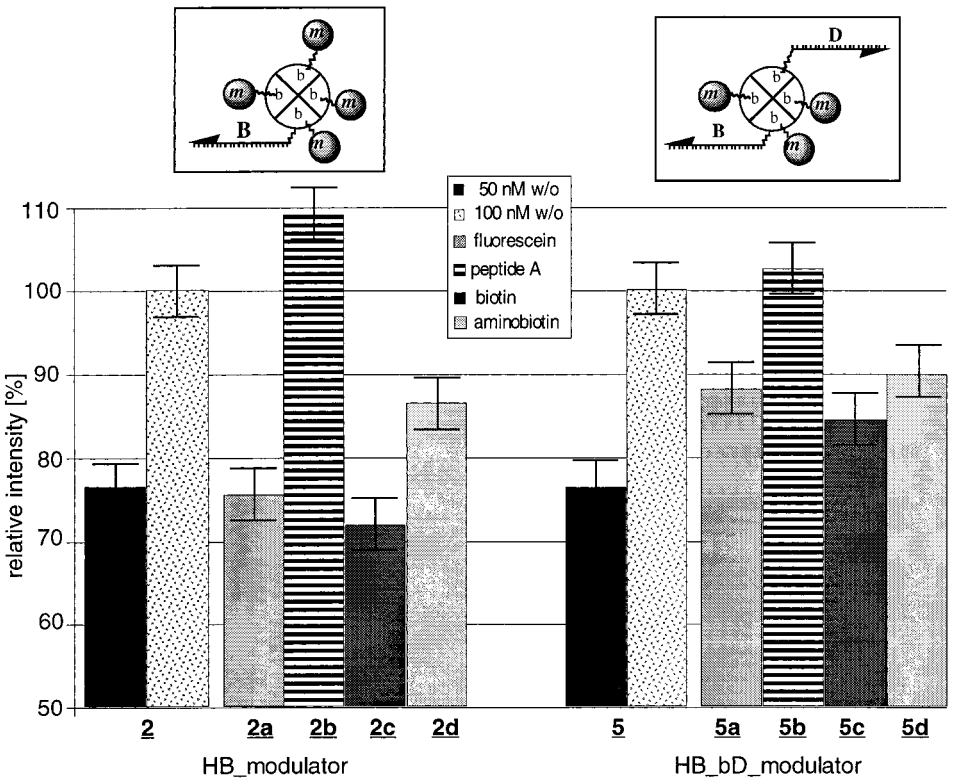


Figure 5. Comparison of modulator induced changes of the hybridization efficiency of HB conjugates **2a**−**d** (left set of bars) and bDNA conjugates **5a**−**d**, consisting of HB coupled with 1 molar equivalent of bD oligomer and the various modulators (right set of bars). The height of the histograms represents normalized binding efficiencies, obtained from the BIAcore analyses, indicated in Tables 3 and 4. The RU values obtained from 100 nM concentration of the various conjugates are normalized as a percentage fraction of the values obtained from the binding of 100 nM of **2** or **5**, respectively. Note that the coupling of fluorescein (**2a**) or D-biotin (**2c**) leads to a similar decrease in binding efficiency which is obtained from a reduction of the analyte's concentration of unmodified **2** to one-half (50 nM of **2**, left most bar).

fluorescein antibody-alkaline phosphatase conjugate and enzyme-dependent color reactions. As indicated in Figure 4, conjugates **5a**/**5e** and **6a**/**6b** displayed the bispecific binding capabilities expected, due to the presence of two DNA-binding sites coupled either covalently or through the STV−biotin interaction. A comparison of hybridization efficiencies obtained from binding of either of the two DNA domains, e.g., HB_bD_fsc (**5a**) versus HD_bB_fsc (**6a**) on bcB target oligomer, indicated that both domains have comparable hybridization capabilities which are independent of the coupling mode. The overall binding efficiency depended on the stoichiometric composition of the complexes. The comparison of signal intensities obtained from HB_fsc (**2a**) or HB_bD_fsc (**5a**) revealed that the coupling of bDNA only induced a small decrease in hybridization efficiency. It was similarly apparent for HD-based conjugates (**3a** versus **6b** in Figure 4). However, the hybridization efficiencies significantly decreased with increasing amounts of bDNA bound to the streptavidin complexes. For example, the use of 5 molar equivalents of bDNA led to a signal decrease of about 80−90% (Figure 4). This is likely due to the decreased hybridization capability of sterically hindered, highly bDNA conjugated complexes and also due to a reduced binding capacity for biotinylated fluorescein.

The hybridization properties of bDNA conjugates **5a** and **5e**−**g** (Table 2) have further been examined using the BIAcore method (Figure 3, panels c and d). **5a** and **5e**−**g** were prepared from DNA−STV hybrid HB (**2**) and 1 molar equivalent of biotinylated oligomers bB, bD, bG, or bK, respectively. The remaining free biotin-binding sites were subsequently blocked with an excess of biotinylated fluorescein. For comparison with the analogous conjugates, modified exclusively with the fluorescein modulator (e.g., **5a** versus **2a**), controls were prepared by initial coupling of biotinylated fluorescein and subsequent addition of the bDNA oligomers. As indicated in Figure 3c, hybridization measurements of the samples gave BIAcore signal intensities in the range of about 1500−2000 RU. All controls containing noncoupled bDNA led to signals, similar to that obtained from pure HB_fsc **2a** (1954 ± 3 RU). This indicated that a quantitative and irreversible blocking occurred with biotinylated fluorescein. In contrast, the binding of bDNA conjugates **5a** and **5e**−**g** gave signals, reduced by about 15% (1677 ± 48 RU). Thus, despite the high accumulation of negative charges, the coupling of bDNA affects the conjugate's hybridization properties only to an extent similar to the coupling of small biotinylated molecules, such as biotin or fluorescein (Tables 3 and 4). Similar results were obtained from the binding of HA_bDNA and HD_bDNA conjugates (data not shown).

The binding of bivalent, monospecific conjugate HB_bB_fsc (**5e**) gave interesting data. This conjugate contains two DNA-moieties of identical sequence B, bound either covalently or via biotin-STV interaction. As indicated in Figure 3c, BIAcore hybridization of the corresponding control, containing **2a** and uncoupled bB oligomer (HB_fsc + bB), led to a lower signal than controls containing bDNAs noncomplementary to surface-attached targets, for instance **2a** and uncoupled bK (1511 or 1954 RU, respectively). This can be attributed to a competition for surface-immobilized target strands of free, uncoupled bB oligomer and **2a**. The bivalent, monospecific conjugate **5e**, however, yielded similar signals

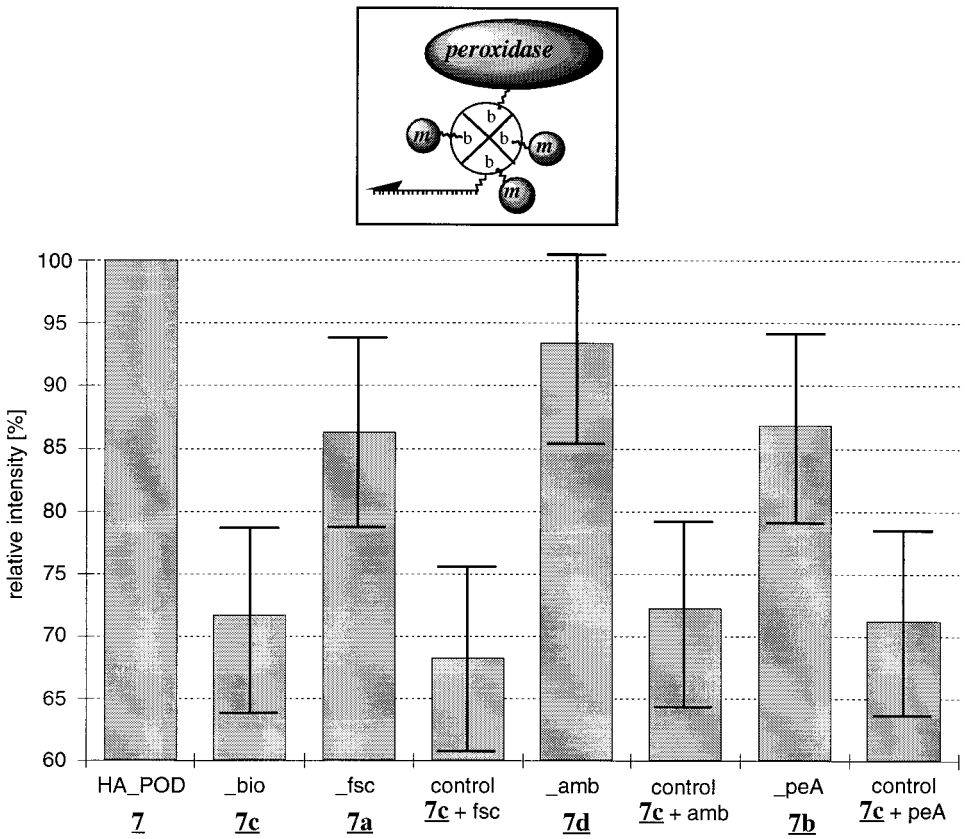


Figure 6. Influences of biotinylated modulators on the solid-phase hybridization of conjugates **7a**−**d**, generated from HA **1** and 1 molar equivalent of biotinylated peroxidase (HA_POD) which was subsequently coupled with the various modulators. The binding efficiencies of the conjugates were determined by microplate analysis. The height of the histograms represents absorbance readings obtained from POD-dependent color reactions.

than obtained for conjugates containing noncomplementary bDNAs, e.g., conjugate **5g** (1695 and 1677 RU, respectively). These observations suggest that the presence of two binding sites within a conjugate does not significantly improve its hybridization capabilities. Nevertheless, the comparison of dissociation curves indicated significant differences between **5e** and **5g**. As apparent from overlay plots in Figure 3d, a strong decrease in dissociation was observed for **5e**, suggesting that the presence of two binding sites caused enhanced rebinding with the surface-attached capture oligomers. Similar results were obtained from BIAcore analysis of conjugate **6b** (HD_bD_fsc, data not shown).

Modulator Effects in Double Functionalized Conjugates. To elucidate possible influences of modulators on the hybridization characteristics of double functionalized streptavidin conjugates (Figure 1b), a set of BIAcore measurements was carried out with bDNA conjugates **5a**−**d**. As indicated in Table 4, the modulators affected the conjugate's hybridization properties to a smaller extent than observed for nonfunctionalized DNA−STV conjugates **2a**−**d**. However, the comparison of the normalized data in Figure 5 indicated that similar effects were apparent. The binding of D-biotin and fluorescein induced a significant decrease in hybridization efficiency of about −15 and −12%, respectively. For aminobiotin, a reduction of about −10% was observed. The coupling of biotinylated peptide A, however, led to an increase in hybridization efficiency of about +3%. Controls, in which the biotin-binding sites had been blocked with D-biotin and the peptide A was subsequently added, revealed the typical, biotin-induced decrease in signal intensity (Table 4). This indicates that the peptide A acts as a hybridization promoter just in cases where it is intramolecularly coupled with the streptavidin conjugate.

The hybridization of enzyme-modified conjugates **7a**−**d** (Table 2) was investigated for modulator's influences by microplate solid-phase hybridization experiments. The conjugates were generated from DNA−STV hybrid HA (**1**) by sequential coupling of biotinylated peroxidase and the various biotinylated modulators. Additional controls were prepared from conjugate **7c** (in which the biotin-binding sites were already blocked with D-biotin) by addition of fluorescein, peptide A or the aminobiotin modulator. Samples of the conjugates were allowed to bind to microplates, previously coated with complementary capture oligomer. Following hybridization, the amount of streptavidin conjugate bound to the microplate was estimated from peroxidase activity. As shown in Figure 6, no effects were observed from the controls containing uncoupled biotinylated modulators. In contrast, distinct effects were observed for conjugates **7a**−**d**, containing modulators intramolecularly linked with the streptavidin. The effects observed were similar as described for bDNA conjugates **5a**−**d**. The enzyme complexes containing fluorescein (**7a**) and biotin (**7c**) as a modulator showed decreased hybridization efficiencies by about −14 and −28%, respectively. In contrast to the bDNA conjugates, the coupling of peptide A (**7b**) did not significantly increase the conjugate's binding compared to fluorescein (**7a**). However, the use of aminobiotin (**7d**) led to an almost unreduced hybridization efficiency compared to the HA_POD conjugate **7**, containing no modulator. Therefore, aminobiotin should be the modulator of choice to combine the obligatory saturation of the conjugate's biotin-binding capacity and high hybridization efficiency.

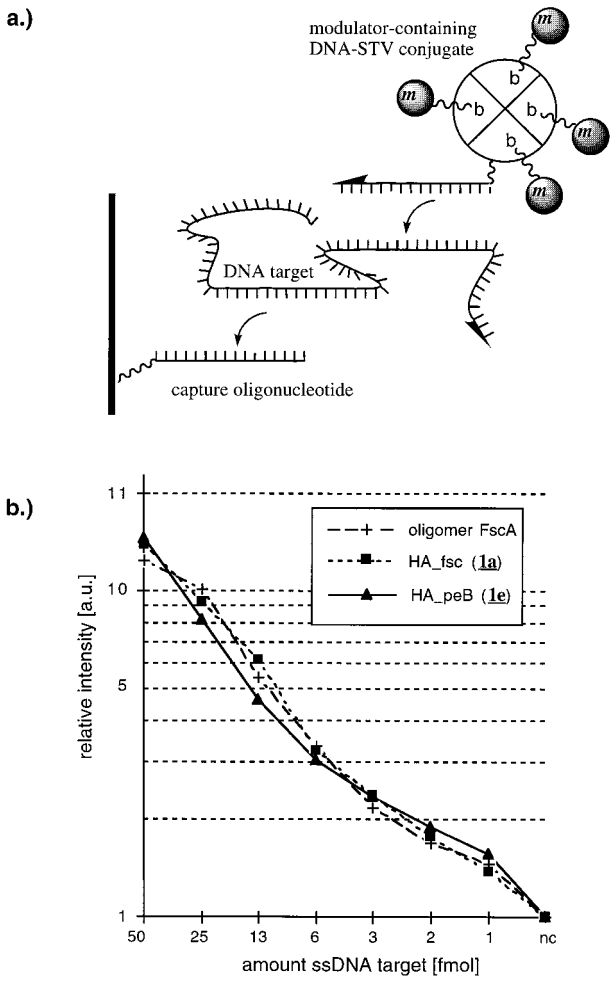


Figure 7. Utilization of streptavidin_modulator conjugates in a gene detection assay. (a) Schematic drawing of a two-sided nucleic-acid detection assay. A microplate-bound capture oligonucleotide is used for immobilization, and modulator-functionalized DNA−STV conjugates are employed as specific probes. The hapten-containing modulators fluorescein or peptide A were used. In these cases, surface-bound nucleic acid-target was detected using an anti-fluorescein antibody-alkaline phosphatase conjugate. Else, Eu^{3+}-chelate-derivatized peptide B was used as a modulator, enabling the direct detection by time-resolved fluorometry. (b) Comparison of the probe capabilities of fluorescein-labeled oligonucleotide (FscA), DNA−STV conjugate **1a** functionalized with the fluorescein modulator and conjugate **1e**, containing peptide B modulator. The curves represent relative signal intensities (*S*/*N*) obtained from alkaline phosphatase-dependent color reaction (FscA, **1a**) or time-resolved fluorometry (**1e**).

Extension of Bioconjugate's Functionality Using Modulators. To demonstrate how modulators can be utilized to extend the functionality of STV-based conjugates, the chromophor moiety of fluorescein and peptide A modulators was used as a hapten. As already shown in Figure 4, this allowed the specific and sensitive detection of the conjugate by means of an antibody directed against fluorescein. To further elucidate this approach, the probe capabilities for the detection of single-stranded DNA by fluorescein-modified HA (**1a**) were compared with an oligonucleotide directly conjugated with fluorescein through an alkyl chain linker (FscA, see Table 1). In a microplate-based, two-sided hybridization assay (Figure 7a), the surface-bound capture oligomer bB was employed for target immobilization. In addition, an oligonucleotide probe, **1a** or FscA, was used as a specific label for detecting the microplate-immobilized target. Following hybridization, the fluorescein-tagged DNA target was coupled with the commercially available anti-fluorescein antibody-alkaline phosphatase conjugate, and subsequently, alkaline phosphatase-dependent color reaction was carried out. As indicated in Figure 7b, DNA−STV conjugate **1a** functioned as a probe, equally efficient as oligomer FscA. This is remarkable since the hybridization kinetics of DNA−STV conjugates are reduced compared to their unmodified oligonucleotide analogues (*15*). Similar experiments, carried out with the fluorescein-containing peptide A modulator, led to comparable results, however, with lower signal-to-noise intensities due to elevated background signals (data not shown).

As an additional example of modulator-extended functionality, peptide B was used as a modulator. Peptide B was generated by covalently attaching Eu^{3+}-chelate (DTTA) groups to the ϵ-amino groups of the lysine residues of peptide A (Figure 1d), as described above. Due to the chemical modification, peptide B can be used as a fluorogenic modulator, since the lanthanide chelate groups enable the high sensitivity detection by time-resolved measurement of Eu^{3+}-fluorescence (*12*). DNA−STV hybrid **1** was coupled with peptide B to prepare conjugate **1e**, and the latter was tested as sensor probe in the nucleic acid detection assay, described above (Figure 7). Due to the extraordinary sensitivity of time-resolved fluorometry, detection limits of about 1 fmol of target DNA have been attained (Figure 7b). Thus, the incorporation of rare-earth chelate groups instead of hapten moieties into streptavidin conjugates not only allows high sensitivity detection without the necessity of enzymatic amplification, but it also simplifies the experimental protocol. Less reaction steps are required for signal generation and also, general drawbacks of enzymatic assays, such as batch-dependent changes in enzyme activity or possible inhibitory effects of analyte contaminants are avoided.

CONCLUSIONS

Taking advantage of streptavidin's tetravalent binding capacity for biotinylated compounds, both functional macromolecular biomolecules such as enzymes and oligonucleotides and also low-molecular weight modulator components, i.e., D-biotin, aminobiotin, and biotin-fluorescein as well as a biotin- and fluorescein-containing peptide, have been successively coupled with covalent DNA−STV conjugates. As demonstrated by solid-phase hybridization measurements, the incorporation of modulators allows a fine tuning of the hybridization properties. This is particularly useful, since many applications of the DNA−streptavidin conjugates depend on the blocking of the remaining biotin-binding sites subsequently to the coupling with a biotinylated compound of interest (*6*, *7*, *11*). As shown in this report, the use of D-biotin for this essential blocking step induces about a 2-fold decreased affinity for complementary nucleic acids. This decrease can be neutralized using biotin modulators containing amino groups.

Moreover, modulators can be used to expand the functionality of streptavidin conjugates. This was demonstrated with hapten and fluorophor-labeled modulators, enabling a highly sensitive detection of the conjugates, and thus, their utilization as probes for analytical purposes. Although the use of modulators will require further refinements for specific applications, the experiments demonstrate the advantageous applicability of low-molecular weight components for tailoring oligofunctional

bioconjugates. In particular, biotinylated peptide modulators should have great potential since they allow for convenient incorporation of basically any chemical group into streptavidin-based complexes. Besides a tuning of hybridization properties, potential applications of modulators include their use as enzyme-specific activator, cofactor, and antenna groups as well as optical or electrochemical mediator moieties. Moreover, DNA-directed assembly of molecular components can be extended to nonbiological macromolecules (*7*−*10*). Thus, DNA−STV conjugates may be anticipated as versatile building blocks in the fabrication of multifunctional supramolecular devices and also highly functionalized, nanostructured surface architectures (*23*) for applications in material sciences, enzyme process technology, biomedical analysis and also other fields of biotechnology and supramolecular chemistry.

ACKNOWLEDGMENT

We thank L. Boldt and R. Wieseke for experimental help with the microplate assays and M. Adler for critical reading of the manuscript and invaluable discussion. S. Hahner, Genom Analytik GmbH, is gratefully acknowledged for her help on MALDI-MS analysis. We also thank Biacore AB, Germany, for providing a BIAcore 2000 instrument. Financial support for this work was obtained from Deutsche Forschungsgemeinschaft, Fonds der Chemischen Industrie, and Tönjes-Vagt Stiftung Bremen.

LITERATURE CITED

(1) Whitesides, G. M., Mathias, J. P., and Seto, C. T. (1991) Molecular self-assembly and nanochemistry: a chemical strategy for the synthesis of nanostructures. *Science 254*, 1312−1319.
(2) Seeman, N. C. (1997) DNA components for molecular architecture. *Acc. Chem. Res. 30*, 357−363.
(3) Niemeyer, C. M. (1997) DNA as a Material for Nanotechnolgy. *Angew. Chem. Int. Ed. 36*, 585−587.
(4) Seeman, N. C. (1982) Nucleic acid junctions and lattices. *J. Theor. Biol. 99*, 237−247.
(5) Robinson, B. H., and Seeman, N. C. (1987) The design of a biochip: a self-assembling molecular-scale memory device. *Protein Eng. 1*, 295−300.
(6) Niemeyer, C. M., Sano, T., Smith, C. L., and Cantor, C. R. (1994) Oligonucleotide-directed self-assembly of proteins: Semisynthetic DNA-streptavidin hybrid molecules as connectors for the generation of macroscopic arrays and the construction of supramolecular bioconjugates. *Nucleic Acids Res. 22*, 5530−5539.
(7) Niemeyer, C. M., Bürger, W., and Peplies, J. (1998) Covalent DNA-streptavidin conjugates as building blocks for the fabrication of novel biometallic nanostructures. *Angew. Chem. Int. Ed. 37*, 2265−2268.
(8) Mirkin, C. A., Letsinger, R. L., Mucic, R. C., and Storhoff, J. J. (1996) A DNA-based method for rationally assembling nanoparticles into macroscopic materials. *Nature 382*, 607−609.
(9) Alivisatos, A. P., Johnsson, K. P., Peng, X., Wilson, T. E., Loweth, C. J., Bruchez Jr., M. P., and Schultz, P. G. (1996) Organization of 'nanocrystal molecules' using DNA. *Nature 382*, 609−611.
(10) Elghanian, R., Storhoff, J. J., Mucic, R. C., Letsinger, R. L., and Mirkin, C. A. (1997) Selective colorimetric detection of polynucleotides based on the distance-dependent optical properties of gold nanoparticles. *Science 277*, 1078−1081.
(11) Niemeyer, C. M., Boldt, L., Ceyhan, B., and Blohm, D. (1999) DNA-Directed Immobilization: Efficient, Reversible and Site-Selective Surface Binding of Proteins by Means of Covalent DNA-Streptavidin Conjugates. *Anal. Biochem. 268*, 54−63.
(12) Hemmilä, I., Dakubu, S., Mukkala, V.-M., Siitari, H., and Lövgren, T. (1984) Europium as a label in time-resolved immunofluorometric assays. *Anal. Biochem. 137*, 335−343.
(13) Sutoh, K., Yamamoto, K., and Wakabayashi, T. (1984) Electron microscopic visualization of the SH1 thiol of myosin by the use of an avidin−biotin system. *J. Mol. Biol. 178*, 323−339.
(14) Niemeyer, C. M., Adler, M., and Blohm, D. (1997) Fluorometric Polymerase Chain Reaction (PCR) Enzyme-Linked Immunosorbent Assay for Quantification of Immuno-PCR Products in Microplates *Anal. Biochem. 246*, 140−145.
(15) Niemeyer, C. M., Bürger, W., and Hoedemakers, R. M. J. (1998) Hybridization Characteristics of Biomolecular Adaptors, Covalent DNA-streptavidin Conjugates. *Bioconjugate Chem. 9*, 168−175.
(16) Malmquist, M. (1993) Biospecific interaction analysis using biosensor technology. *Nature 361*, 186−187.
(17) Nieba, L., Krebber, A., and Plückthun, A. (1996) Competition BIAcore for measuring true affinities: Large diffferences from values determined from binding kinetics. *Anal. Biochem. 234*, 155−165.
(18) Keller, G. H., and Manak, M. M. (1989) *DNA Probes*, Stockton, New York.
(19) Weber, P. C., Ohlendorf, D. H., Wendoloski, J. J., and Salemme, F. R. (1989) Structural origins of high-affinity biotin binding to streptavidin. *Science 243*, 85−88.
(20) Corey, D. R. (1995) 48000-fold Acceleration of Hybridization by chemically modified Oligonucleotides. *J. Am. Chem. Soc. 117*, 9373−9374.
(21) Iyer, M., Norton, J. C., and Corey, D. R. (1995) Accelerated Hybridization of Oligonucleotides to Duplex DNA. *J. Biol. Chem. 270*, 14712−14717.
(22) Smulevitch, S. V., Simmons, C. G., Norton, J. C., Wise, T. W., and Corey, D. R. (1996) Enhancement of strand invasion by oligonucleotides through manipulation of backbone charge. *Nat. Biotechnol. 14*, 1700−1704.
(23) Winfree, E., Furong, L., Wenzler, L. A., and Seeman, N. C. (1998) Design and self-assembly of two-dimensional DNA crystals. *Nature 394*, 539−544.

BC980150N

Thermoprecipitation of Streptavidin via Oligonucleotide-Mediated Self-Assembly with Poly(*N*-isopropylacrylamide)

Robin B. Fong, Zhongli Ding, Cynthia J. Long, Allan S. Hoffman,* and Patrick S. Stayton*

Department of Bioengineering, University of Washington, Seattle, Washington 98195

A versatile strategy has been developed for selectively and sequentially isolating targets in a liquid-phase affinity separation environment. The strategy uses a recently developed approach for joining together molecules in linkages that are defined by the complementary pairing of oligonucleotides conjugated to the different molecules [Niemeyer, C. M., Sano, T., Smith, C. L., and Cantor, C. R. (1994) *Nucleic Acids Res. 22,* 5530−9]. In the work presented here, streptavidin was noncovalently coupled with the temperature-responsive poly(*N*-isopropylacrylamide) [poly(NIPAAM)] through the sequence-specific hybridization of oligonucleotides conjugated to the protein and polymer. A 20-mer oligonucleotide was covalently linked through a heterobifunctional linker to a genetically engineered streptavidin variant that contained a unique cysteine residue at the solvent-accessible site Glu 116. The complementary DNA sequence was conjugated to the end of a linear ester-activated poly(NIPAAM). The two conjugates were allowed to self-assemble in solution via hybridization of their complementary DNA sequences. The streptavidin−poly(NIPAAM) complex could be used to affinity-precipitate radiolabeled biotin or biotinylated alkaline phosphatase above 32 °C through the thermally induced phase separation activity of the poly(NIPAAM). The streptavidin−oligo species could then be reversibly separated from the precipitated polymer−oligo conjugate and recycled by lowering the salt concentration, which results in denaturation of the short double-stranded DNA connection. The use of oligonucleotides to couple polymer to streptavidin allows for selective precipitation of different polymers and streptavidin complexes based on the sequence-specific hybridization of their oligonucleotide appendages.

INTRODUCTION

Affinity chromatography techniques which utilize matrix-immobilized ligands are the most widely used methods for specific isolation of molecules in separations and diagnostic technologies (*1*). There has been growing interest in developing liquid-phase separation techniques such as affinity partitioning and precipitation, which typically involve ligand-bearing polymers that can be phase separated after binding to complementary biomolecules (*2*−*6*). In affinity precipitation, the phase separation of polymer and polymer-bound species can be triggered by a small change in an environmental condition, such as pH, ionic strength, or temperature. Stimuli-responsive polymers have been employed in many applications in medicine and biotechnology (*7, 8*). One of the best examples is poly(NIPAAM),[1] a water-soluble, synthetic polymer which undergoes a phase transition to a hydrophobic state when the temperature is raised above its lower critical solution temperature (LCST) (*9*). Poly(NIPAAM) has been conjugated to immunoglobulin G, β-D-glucosidase, and trypsin to enable thermoprecipitation of these proteins (*10*−*13*). These alternative systems circumvent some of the shortcomings of chromatographic methods, because the ligand association step occurs in the solution phase. These systems exhibit fewer mass transport and steric limitations which exist with solid supports.

Another potential advantage of affinity precipitation strategies is the ability to selectively and sequentially separate different targets from complex mixtures. Polymers with responses that have been engineered for different temperature or pH ranges can be conjugated to different ligands and mixed together in order to sequentially pull targets out of solution under different conditions. Here we report a versatile strategy for sequentially separating selective components from complex mixtures using stimuli-responsive polymers and streptavidin. Streptavidin is a stable, tetrameric protein that binds as many as four biotin molecules with extraordinary affinity and is utilized widely in current separations and diagnostic applications (*14*−*23*). To reversibly conjugate poly(NIPAAM) to streptavidin, we have used a recently described strategy for selectively joining two molecular species through the self-assembly of complementary oligonucleotides. Niemeyer et al. showed that oligonucleotides can direct the assembly of bispecific and bifunctional supramolecular structures, and they used this clever strategy to make streptavidin conjugates

* To whom correspondence should be addressed. (A.S.H.) Department of Bioengineering, Box 352255. Phone: (206) 543-9423. Fax: (206) 543-6124. E-mail: hoffman@u.washington.edu. (P.S.S.) Department of Bioengineering, Box 352125. Phone: (206) 685-8148. Fax: (206) 685-8256. E-mail: stayton@u.washington.edu.

[1] Abbreviations: poly(NIPAAM), poly(*N*-isopropylacrylamide); LCST, lower critical solution temperature; STAV, streptavidin; STAV−nR, streptavidin conjugated to n number of oligonucleotide R; s-SMCC, sulfo-succinimidyl 4-(*N*-maleimidomethyl) cyclohexane-1-carboxylate; TCEP-HCl, Tris(2-carboxyethyl)-phosphine hydrochloride; NHS, *N*-hydroxysuccinimidyl; DEAE, diethylaminoethyl; SDS−PAGE, sodium dodecyl sulfate−polyacrylamide gel electrophoresis; EDTA, ethylenediaminetetracetic acid; DMF, dimethylformamide; PB75, 100 mM phosphate and 100 mM NaCl, pH 7.5, buffer; TB75, 10 mM Tris and 1 mM EDTA, pH 7.5, buffer; TB74, 50 mM Tris, 150 mM NaCl, and 0.05% bovine serum albumin, pH 7.4, buffer; BAP, biotinylated alkaline phosphatase; RT, room temperature.

10.1021/bc980151f CCC: $18.00 © 1999 American Chemical Society
Published on Web 08/25/1999

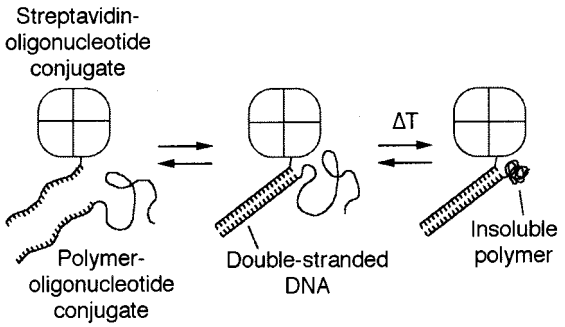


Figure 1. Schematic representation of reversible hybridization of a streptavidin−oligonucleotide conjugate and a temperature responsive polymer-oligonucleotide conjugate, and reversible phase separation of the resultant complex in response to a small temperature change.

(*24, 25*). Figure 1 illustrates the case of reversible self-assembly of streptavidin and a temperature-responsive polymer, followed by reversible phase separation of the complex. Because the assembly is DNA sequence specific, polymers with different stimuli responsiveness can be selectively attached to streptavidin conjugates that are similarly differentiated by their DNA sequences. Thus, different streptavidin−target complexes can be selectively and sequentially separated from a complex liquid mixture depending on which polymer response is triggered.

EXPERIMENTAL PROCEDURES

Materials. Oligodeoxyribonucleotide R (5′-GGACTCAGGCTTATAGCTGT-3′), modified at the 5′ end with a 6-carbon aliphatic amine, and complementary oligodeoxyribonucleotide RC (5′-ACAGCTATAAGCCTGAGTCC-3′), modified at the 3′ end with a 7-carbon aliphatic amine, were purchased from Integrated DNA Technologies (Coralville, IA). A melting temperature of ca. 65 °C for the renatured duplex R:RC (in 50 mM Tris and 150 mM NaCl, pH 7.4) was measured spectrophotometrically in our laboratory. Oligodeoxyribonucleotide S (5′-AGCGGATAACAATTTCACAC-3′), which shares no sequence complementarity with oligo R or RC, was used as a control sequence. The heterobifunctional linker sulfosuccinimidyl 4-(*N*-maleimidomethyl) cyclohexane-1-carboxylate (s-SMCC) and the disulfide reducing agent Tris(2-carboxyethyl) phosphine hydrochloride (TCEP-HCl) were obtained from Pierce (Rockford, IL). Tris-glycine and Tris-borate-EDTA-urea polyacrylamide gels and gel reagents were obtained from Novex (San Diego, CA). Sephadex gel (G25-medium and G50-fine) and DEAE Sepharose fast anion-exchange resin were from Pharmacia Biotech (Uppsala, Sweden). Centricon and Centriprep ultrafiltration concentrators were purchased from Amicon (Beverly, MA). D-[8,9-^{3}H]Biotin was from Amersham (Little Chalfont, England), and EcoLume liquid scintillation cocktail was from ICN (Costa Mesa, CA). Biotinylated calf intestine alkaline phosphatase was from Pierce, and *p*-nitrophenyl phosphate and diethanolamine were from Bio-Rad (Hercules, CA).

Streptavidin Production. The gene for streptavidin mutant E116C (cysteine in place of glutamic acid at amino acid position 116) was created by cassette mutagenesis, and the protein was expressed, purified, and characterized using previously described protocols (*26*).

Polymer Synthesis. Linear poly(NIPAAM), with one end having an *N*-hydroxysuccinimidyl (NHS) ester group, was produced according to the methods of Ding et al. (*13*). For the polymer used in this study, a mean molecular weight of 8500 was determined by vapor pressure osmometry (VPO, model OSV111, Knauer, Germany).

Streptavidin−Oligonucleotide Conjugation. Oligonucleotide R (∼200 nmol) was derivatized with a maleimido group by reacting it with 50-fold molar excess (4.2 mg) of s-SMCC in 1 mL of 100 mM phosphate and 100 mM NaCl, pH 7.5 (PB75). The reaction was incubated for 1 h at RT. Excess s-SMCC was removed using a Sephadex G25-medium gel filtration column (1.5 × 7 cm). Streptavidin mutant E116C (∼600 nmol) in 2 mL of PB75 was reduced by addition of 150 μL of 40 mM TCEP-HCl. The amount of streptavidin was determined using an extinction coefficient of 34 000 M^{-1} cm^{-1} for the monomer subunit (*27*). After 15 min at RT, the gel filtration fractions containing maleimide-derivatized oligonucleotide (1.5 mL total) were added. The reaction proceeded for 2 h at RT with a 50 μL addition of freshly made 40 mM TCEP-HCl at 1 h. Excess oligonucleotide was removed using Centricon-30 (30 000 MW cutoff) concentrators. The remaining unreacted oligonucleotide was removed using a Sephadex G50-fine gel filtration column (1.0 × 16 cm). Streptavidin conjugate was purified from unreacted streptavidin by anion-exchange perfusion chromatography using a BioCAD system (PerSeptive Biosystems, Farmington, MA). The sample was applied to a Poros HQ/M (PerSeptive Biosystems) 29 mL column and eluted with a salt gradient of 0.4 to 1.0 M NaCl in 20 mM Tris, pH 6.8. The fractions containing conjugate were concentrated using Centriprep-30 concentrators and analyzed by 10−20% Tris-glycine SDS−PAGE.

Poly(NIPAAM)−Oligonucleotide Conjugation. Oligonucleotide RC (∼1.5 μmol) was dissolved in 7.2 mL of 100 mM borate, 50 mM NaCl, and 5 mM EDTA, pH 9.5. A 50-fold molar excess of NHS ester-activated poly(NIPAAM) (96 mg) was dissolved in 800 μL of HPLC-grade DMF and added to the oligonucleotide solution. The reaction was gently mixed for 4 h at 4 °C, followed by 2 h at RT. To separate polymer from unreacted oligonucleotide, 100 μL of 5 M NaCl was added (to lower the LCST), and the temperature was raised to 37 °C, precipitating the polymer and conjugate. After 29000*g* centrifugation at 37 °C, the supernatant was decanted. The pellet was dissolved overnight in 4 mL of 10 mM Tris and 1 mM EDTA, pH 7.5 (TB75) at 4 °C, and the separation process was repeated twice. Polymer−oligonucleotide conjugate was purified from excess polymer by capturing it overnight with 10 μequiv of DEAE Sepharose fast anion-exchange resin at 4 °C in 4 mL of TB75. The resin-bound conjugate was washed three times with TB75 at 4 °C and eluted with 0.7 M NaCl. The conjugate was analyzed using 15% Tris-borate-EDTA-urea PAGE.

Precipitation of Biotin and Biotinylated Alkaline Phosphatase. Tritiated biotin (1.8 pmol) was incubated with an equimolar amount of STAV−1R (streptavidin with one attached oligonucleotide) and a 20-fold molar excess amount of poly(NIPAAM)−RC conjugate in 50 mM Tris, 150 mM NaCl, and 0.05% BSA, pH 7.4, buffer (TB74). Final concentrations of STAV−1R and poly(NIPAAM)−RC were 18 and 360 nM, respectively. After reaction for 1 h at RT, free poly(NIPAAM) (1 mg/mL final concentration) was added, and the sample was placed in a 37 °C bath for 10 min and then centrifuged at 16000*g* for 2 min. (Addition of the unmodified free polymer helped to enhance the precipitation.) The amount of biotin in the supernatant was measured by β-radiation counting (Beckman LS7000, Irvine, CA) using EcoLume scintillation cocktail. To show that hybridization was

occurring, oligonucleotides R, RC, or S were individually added at final concentrations ranging from 10^{-3} to 10^4 times that of STAV−1R. Recovery of pelleted STAV−1R (and bound biotin) was accomplished by overnight dissolution of the pellet in deionized water at 4 °C, followed by heating and centrifugation as described earlier.

Biotinylated alkaline phosphatase (BAP) and poly(NIPAAM)−RC were added to STAV−1R at a 1:20:400 molar ratio BAP:STAV−1R:poly(NIPAAM)−RC in TB74. Final concentrations of STAV−1R and poly(NIPAAM)−RC were 12 and 240 nM, respectively. The reaction was allowed to incubate for 1 h at RT. After addition of free poly(NIPAAM) (1 mg/mL final concentration), the sample was placed in a 37 °C bath for 10 min and then centrifuged at 16000*g* for 2 min. The supernatant activity was measured by reaction with *p*-nitrophenyl phosphate substrate in diethanolamine and UV absorbance at 405 nm.

Cloud Point Measurement. Cloud point data for poly(NIPAAM)−oligonucleotide conjugate, STAV/DNA/poly(NIPAAM) complex, and pure poly(NIPAAM) were taken using a UV−vis spectrophotometer with a jacketed cuvette holder. The heating rate was 0.2 °C/min. Polymer solutions were prepared by dissolving 8500 molecular weight poly(NIPAAM) in TB74 buffer at 0.005, 0.003, and 0.002 wt % polymer concentrations. The sample containing poly(NIPAAM)−RC (5 μM) was also prepared in TB74. The sample containing STAV/DNA/polymer complex (5 μM) was prepared by reacting equimolar quantities of STAV−1R conjugate and poly(NIPAAM)−RC conjugate in TB74 for 1 h at RT. The bioconjugate solutions were estimated to contain ca. 0.004 wt % poly(NIPAAM), assuming a molecular weight of 8500 for the conjugated polymer.

RESULTS

Preparation of Conjugates. Anion-exchange chromatography and PAGE analysis of the purified conjugation reaction products revealed three major species (Figure 2). Peaks I and II (combined in lanes 2 and 7) display only protein bands, and thus represent STAV and multimers of STAV. The bands migrated equivalently to a control sample of STAV (lane 1). Boiled samples displayed protein bands that were the correct size for streptavidin monomer subunits (lane 5). Peaks III and IV, however, displayed bands that stained positive for both protein (lanes 3 and 4, respectively) and DNA (lanes 8 and 9, respectively). These bands migrated faster than the STAV control, consistent with the increase in negative charge with the addition of a conjugated oligonucleotide. Because peak IV species migrated farther than peak III and because peak IV eluted off the cationic column under higher salt concentration compared to peak III, it is likely that peak IV represents a more highly conjugated STAV than peak III. Peak IV likely represents STAV with two oligonucleotide attachments (STAV−2R) and peak III represents STAV with one oligonucleotide attachment (STAV−1R). Secondary bands are oligomeric species which escaped disulfide reduction, e.g., STAV dimer conjugated to one oligonucleotide, or STAV dimer with a single oligonucleotide conjugated to each STAV.

Figure 3 demonstrated that the polymer−oligonucleotide conjugation reaction produced covalent poly(NIPAAM)−RC conjugates. After thermal precipitation, which removed excess oligonucleotide, the pellet was redissolved and subjected to anion exchange using DEAE-modified Sepharose beads. Poly(NIPAAM)−RC conjugate

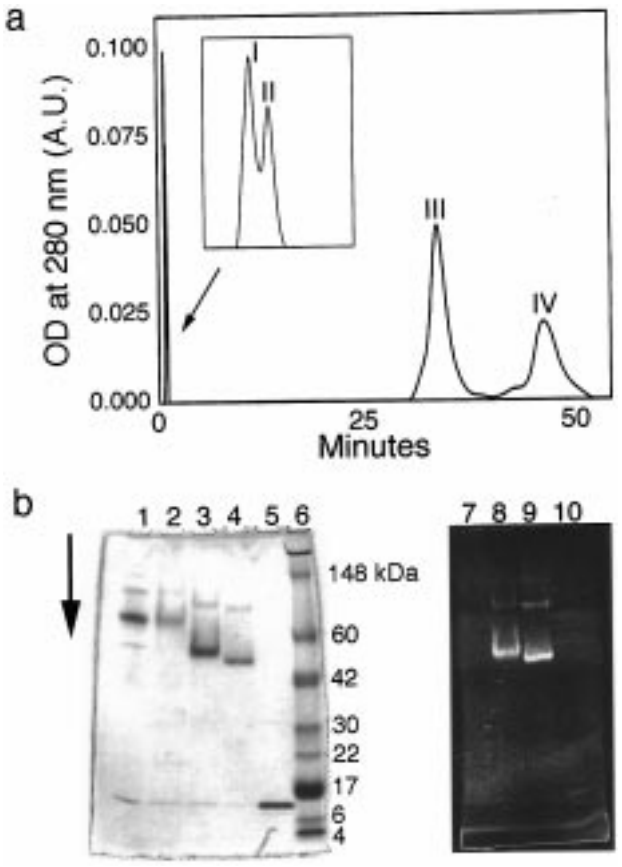


Figure 2. (a) Anion-exchange chromatography of the streptavidin−oligonucleotide conjugation reaction mixture on a PerSeptive Biosystems Poros HQ/M analytical column (4.6 × 100 mm, 1.7 mL). Four absorbance peaks (I−IV) were observed. The beginning of the chromatogram is magnified (inset) to show peaks I and II. (b) Electrophoretic analysis of the streptavidin−oligonucleotide conjugate chromatogram peaks using a 10−20% Tris-glycine-SDS polyacrylamide gel. Arrow indicates direction of migration. Samples were reduced by addition of β-mercaptoethanol to 5% volume. The gel on the left was stained for protein using Coomassie blue dye while the gel on the right was stained for DNA using ethidium bromide. Lanes 1 and 10: STAV control. Lanes 2 and 7: peaks I and II combined (STAV and multimers). Lane 5: peaks I and II combined, heated for 10 min at 99 °C to dissociate streptavidin into monomers. Lanes 3 and 8: peak III (STAV−1R conjugate). Lanes 4 and 9: peak IV (STAV−2R conjugate). Lane 6: Novex Multimark protein standard.

was expected to bind to the positively charged DEAE, while excess polymer remained in solution. The eluted product stained positive for DNA (lane 3), and gel migration was hindered compared to a control which contained oligonucleotide RC alone (lane 1). Free polymer did not impede migration of unmodified oligonucleotide (lane 2).

Precipitation of Biotin and Biotinylated Alkaline Phosphatase. Panels a and b of Figure 4 summarize the results of the [^{3}H]biotin and biotinylated alkaline phosphatase (BAP) separations, respectively. A control without poly(NIPAAM)−RC was included in each experiment to rule out nonspecific precipitation. The activity measurements were normalized against that of an internal reference composed of [^{3}H]biotin (or BAP) and STAV-1R in the same buffer, without free polymer. When poly(NIPAAM)−RC and STAV−1R were both present, most of the [^{3}H]biotin (∼76%) and BAP (∼85%) were removed from solution after heating. The pelleted [^{3}H]-biotin (and STAV−1R) could be subsequently redissolved



Figure 3. Electrophoretic analysis of the poly(NIPAAM)−oligonucleotide conjugation reaction using an ethidium bromide-stained 15% Tris-borate-EDTA-urea polyacrylamide gel. Arrow indicates direction of migration. Lane 1: oligonucleotide RC control. Lane 2: physical mixture of oligonucleotide RC and free poly(NIPAAM) (∼1 mg/mL). Lane 3: poly(NIPAAM)−RC conjugate.

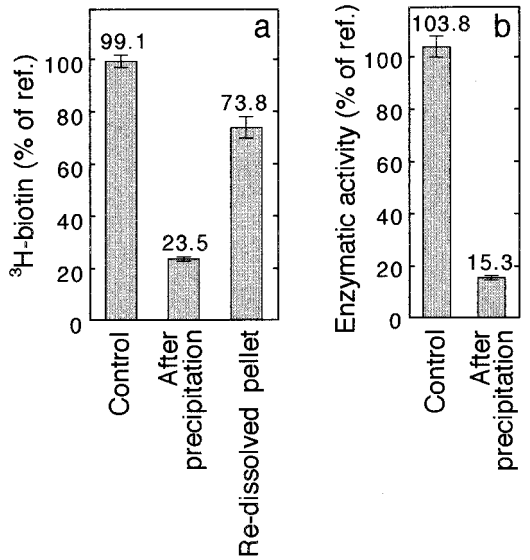


Figure 4. (a) Thermally induced affinity precipitation and recovery of [^{3}H]biotin. The solid bars represent the amount of [^{3}H]biotin in solution measured by β counting. (b) Thermally induced affinity precipitation of biotinylated alkaline phosphatase (BAP). The solid bars represent the BAP enzymatic activity in solution measured by colorimetric assay. Measurements were normalized against an appropriate reference sample (see Results). Data are the average of three different experiments. The error bars indicate standard deviations.

when the pellet was chilled in deionized water. STAV−1R is presumed to be separated from poly(NIPAAM)−RC under these conditions, which favor denaturation of the 20 base pair DNA.

The sequence-specificity of the self-assembling DNA was tested by addition of competing and noncompeting oligonucleotides in the [^{3}H]biotin experiment. In Figure 5, the free oligo RC begins to inhibit the precipitation of labeled biotin at a concentration equimolar to that of STAV−1R. Free oligo R inhibits the precipitation when its concentration is about 20 times that of STAV−1R. The inhibition curve for oligo R is shifted by a factor of about 20 relative to the curve for oligo RC, consistent with the 20:1 molar ratio of polymer−RC conjugate to STAV−1R conjugate in each of the experiments. Oligo S, which is not complementary in sequence to either R or RC, did not affect the precipitation. The results of this inhibition study indicate that a sequence-specific oligonucleotide

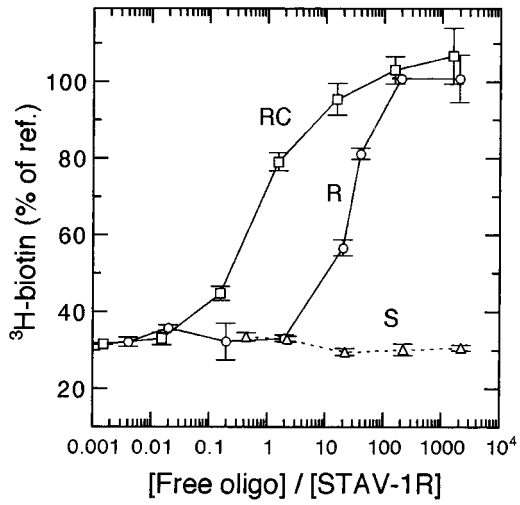


Figure 5. Free oligonucleotide inhibition curves for the thermally induced affinity precipitation of [^{3}H]biotin. Experiments were performed by adding varying amounts of a free oligonucleotide (R, RC, or S) to a solution containing a fixed amount of [^{3}H]biotin, STAV−1R, and poly(NIPAAM)−RC (molar ratio 1:1:20, respectively). The solution was allowed to react for 1 h at RT, prior to thermal precipitation. Oligo R is complementary to the sequence of RC; oligo RC is complementary to the sequence of R; and oligo S is not complementary to either R or RC. The vertical axis represents the amount (β count) of [^{3}H]-biotin remaining in the solution phase after precipitation. Measurements were normalized against a reference sample (see Results). Data are the average of three different experiments. The error bars indicate standard deviations.

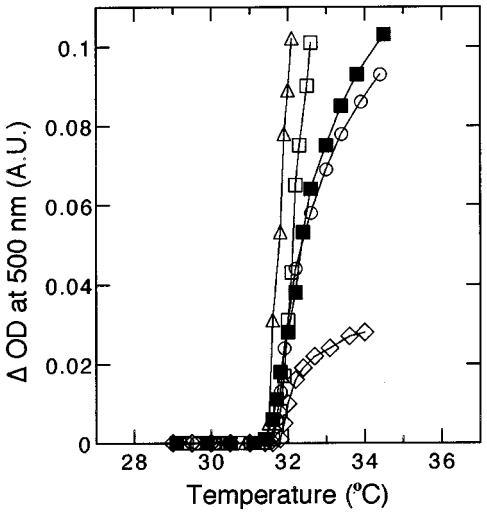


Figure 6. Cloud point curves for solutions containing 5 μM poly(NIPAAM)−RC (open squares); 5 μM STAV/DNA/poly-(NIPAAM) complex (darkened squares); and 0.005 wt % (open triangles), 0.003 wt % (open circles), and 0.002 wt % (open diamonds) pure poly(NIPAAM).

hybridization reaction occurs prior to thermal precipitation of the streptavidin−biotin complex.

Cloud Point Measurement. The reversible phase separation exhibited by poly(NIPAAM) as the solution temperature is raised above its LCST is characterized by an abrupt flocculation of the insoluble polymer chains (*28*). The thermally induced clouding of solutions containing either the poly(NIPAAM)−oligonucleotide conjugate or the STAV/DNA/poly(NIPAAM) complex was investigated and compared to solutions containing comparable concentrations of pure poly(NIPAAM) (Figure 6). The data demonstrate that the soluble-to-insoluble phase

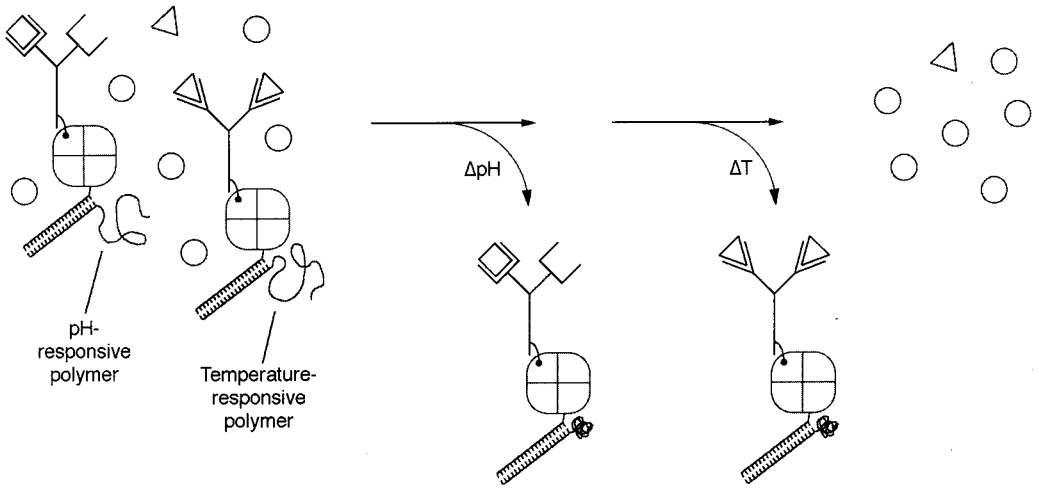


Figure 7. Proposed application of self-assembled streptavidin−DNA−polymer conjugates for sequential affinity precipitation of different target species. A complex composed of a pH responsive polymer, streptavidin, and an antibody against target 1 (open square) is mixed with a complex composed of a temperature responsive polymer, streptavidin, and an antibody against target 2 (open triangle). After binding to their respective ligand targets, the complexes can be sequentially retrieved from solution. Target 1 is coprecipitated with the pH responsive complex via a small pH change. Afterward, target 2 is coprecipitated with the temperature responsive complex via a small temperature change. A third target (open circle) does not precipitate because it shares no affinity with either complex.

transition of the polymer was not significantly affected by the conjugated biomolecules.

DISCUSSION

Chen and Hoffman introduced the concept of "smart" polymer affinity precipitation by using poly(NIPAAM)−protein A conjugates to purify IgG antibodies (*29*). Others have shown that DNA-binding proteins can be precipitated on the basis of their affinity to poly(NIPAAM)−DNA conjugates (*30, 31*). Related work has suggested that coprecipitation of hybridized poly(NIPAAM)−oligo(dT) conjugates may be a more efficient method for isolating polyadenylated mRNAs than conventional oligo(dT)-modified silica (*32*). While these strategies offer the advantages of liquid-phase binding steps, there are a number of parameters which require tailoring. For example, the activity of the conjugate may be affected depending on the number of polymer chains per biomolecule (*33*−*36*) and the location of these chains (*37*).

In the present work, we have developed a self-assembly system by which a defined polymer and a defined affinity connector, such as a biotinylated antibody, can be joined together from a mixture of polymers, connectors, and targets by using a strategy described by Niemeyer et al. to construct intermolecular linkages. Distinct target species can be separated in solution through either a direct interaction with a biotin group on the target or through a secondary interaction with a biotinylated connector. The new feature represented in this approach is the capability to sequentially separate a specific target-bound complex from a mixture. The specific stimuli-responsive polymer can be matched to a unique affinity complex, e.g., a streptavidin−antibody conjugate, by self-assembly in solution. The use of DNA tags on streptavidin and the polymer ensures conjugation of the appropriate smart polymer to the target-bound complex. For example, in step 1 a small pH change can be used to separate pH responsive polymer/antibody1/target1 complexes, while in step 2 a small temperature change can be used to separate temperature responsive polymer/antibody 2/target 2 complexes (Figure 7).

To demonstrate this technique, we have constructed a poly(NIPAAM)/DNA/streptavidin complex that self-assembles and binds biotinylated alkaline phosphatase. The entire assembly, including alkaline phosphatase (∼140 kDa), precipitates above the LCST of poly(NIPAAM) with high efficiency. Using radiolabeled biotin, we showed that the phase-separated streptavidin assembly could be fully resolubilized by lowering the temperature below the LCST of the poly(NIPAAM). If this is done under low salt conditions, the short double-stranded DNA melts, freeing the poly(NIPAAM)−DNA conjugate for recovery and recycling. Free oligonucleotides that were complementary to either the DNA tag on the streptavidin conjugate or the DNA tag on the poly(NIPAAM) conjugate could inhibit the affinity precipitation of radiolabeled biotin at stoichiometric ratios, whereas a random oligonucleotide had no effect.

Bispecific streptavidin−oligonucleotide conjugates may offer other possibilities for novel applications involving stimuli-responsive polymers. For example, we have shown that poly(NIPAAM) can reversibly manipulate the biotin-binding properties of streptavidin when it is site specifically attached near the binding pocket (*26, 38, 39*). A potential advantage of using oligonucleotide linkers is the ability to control the polymer attachment distance by ratcheting the site where the DNA sequence overlap is located. The use of polymer−oligonucleotide conjugates may also provide a convenient method for sequentially directing the adsorption of biomolecules to a surface. For the probing of genes, it may be possible to add smart polymer function to DNA targets using a pH responsive polymer−oligonucleotide conjugate that remains soluble under the thermal denaturation conditions needed to prepare the target for hybridization with the probe.

ACKNOWLEDGMENT

This work was supported by NIH Grant R01GM53771A, the Washington Technology Center, the Washington Research Foundation, and the Office of Technology Transfer. We gratefully acknowledge discussions with the Cantor group at Boston University for the initial suggestion of using oligonucleotides to assemble proteins and smart polymers.

LITERATURE CITED

(1) Jones, C., Patel, A., Griffin, S., Martin, J., Young, P., O'Donnell, K., Silverman, C., Porter, T., and Chaiken, I.

(1995) Current trends in molecular recognition and bioseparation. *J. Chromatogr. A 707*, 3−22.
(2) Diamond, A. D., and Hsu, J. T. (1992) Aqueous Two-Phase Systems for Biomolecule Separation. In *Advances in Biochemical Engineering/Biotechnology* (A. Feichter, Ed.) Vol. 47, pp 89−135, Springer-Verlag, Berlin.
(3) Luong, J. H. T., and Nguyen, A. L. (1992) Novel Separations Based on Affinity Interactions. In *Advances in Biochemical Engineering/Biotechnology* (A. Feichter, Ed.) Vol. 47, pp 137−58, Springer-Verlag, Berlin.
(4) Niederauer, M. Q., and Glatz, C. E. (1992) Selective Precipitation. *Advances in Biochemical Engineering/Biotechnology* (A. Feichter, Ed.) Vol. 47, pp 159−88, Springer-Verlag, Berlin.
(5) Irwin, J. A., and Tipton, K. F. (1995) Affinity precipitation: a novel approach to protein purification. *Essays Biochem. 29*, 137−56.
(6) Gupta, M. N., Kaul, R., Guoqiang, D., Dissing, U., and Mattiasson, B. (1996) Affinity precipitation of proteins. *J. Mol. Recognit. 9*, 356−9.
(7) Hoffman, A. S. (1995) "Intelligent" Polymers in Medicine and Biotechnology. *Macromol. Symp. 98*, 645−64.
(8) Galaev, I. Y., and Mattiasson, B. (1993) Thermoreactive water-soluble polymers, nonionic surfactants, and hydrogels as reagents in biotechnology. *Enzyme Microb. Technol. 15*, 354−66.
(9) Heskins, M., and Guillet, J. E. (1968) Solution Properties of Poly(*N*-isopropylacrylamide). *J. Macromol. Sci.-Chem. A2*, 1441−55.
(10) Monji, N., and Hoffman, A. S. (1987) A novel immunoassay system and bioseparation process based on thermal phase separating polymers. *Appl. Biochem. Biotech. 14*, 107−20.
(11) Takei, Y. G., Matsukata, M., Aoki, T., Sanui, K., Ogata, N., Kikuchi, A., Sakurai, Y., and Okano, T. (1994) Temperature-Responsive Bioconjugates. 3. Antibody−Poly(*N*-isopropylacrylamide) Conjugates for Temperature-Modulated Precipitations and Affinity Bioseparations. *Bioconjugate Chem. 5*, 577−82.
(12) Chen, G., and Hoffman, A. S. (1993) Preparation and properties of thermoreversible, phase-separating enzyme−oligo(*N*-isopropylacrylamide) conjugates. *Bioconjugate Chem. 4*, 509−14.
(13) Ding, Z., Chen, G., and Hoffman, A. S. (1996) Synthesis and purification of thermally sensitive oligomer−enzyme conjugates of poly(*N*-isopropylacrylamide)−trypsin. *Bioconjugate Chem. 7*, 121−6.
(14) Green, N. M. (1975) Avidin. *Adv. Protein Chem. 29*, 85−133.
(15) Green, N. M. (1990) Avidin and streptavidin. *Methods Enzymol. 184*, 51−67.
(16) Wilchek, M., and Bayer, E. A. (1990) Introduction to avidin−biotin technology. *Methods Enzymol. 184*, 5−13.
(17) Wilchek, M., and Bayer, E. A. (1990) Applications of avidin−biotin technology: literature survey. *Methods Enzymol. 184*, 14−45.
(18) Diamandis, E. P., and Christopoulos, T. K. (1991) The biotin−(strept)avidin system: principles and applications in biotechnology. *Clin. Chem. 37*, 625−36.
(19) Bayer, E. A., and Wilchek, M. (1990) Application of avidin−biotin technology to affinity-based separations. *J. Chromatogr. 510*, 3−11.
(20) Wilchek, M., and Bayer, E. A. (1990) Biotin-containing reagents. *Methods Enzymol. 184*, 123−38.
(21) Bayer, E. A., and Wilchek, M. (1990) Protein biotinylation. *Methods. Enzymol. 184*, 138−60.
(22) O'Shannessy, D. J. (1990) Antibodies biotinylated via sugar moieties. *Methods Enzymol. 184*, 162−6.
(23) Klevan, L., and Gebeyehu, G. (1990) Biotinylated nucleotides for labeling and detecting DNA. *Methods Enzymol. 184*, 561−77.
(24) Niemeyer, C. M., Sano, T., Smith, C. L., and Cantor, C. R. (1994) Oligonucleotide-directed self-assembly of proteins: semisynthetic DNA−streptavidin hybrid molecules as connectors for the generation of macroscopic arrays and the construction of supramolecular bioconjugates. *Nucleic Acids Res. 22*, 5530−9.
(25) Niemeyer, C. M., Burger, W., and Hoedemakers, R. M. (1998) Hybridization characteristics of biomolecular adaptors, covalent DNA−streptavidin conjugates. *Bioconjugate Chem. 9*, 168−75.
(26) Chilkoti, A., Tan, P. H., and Stayton, P. S. (1995) Site-directed mutagenesis studies of the high-affinity streptavidin−biotin complex: contributions of tryptophan residues 79, 108, and 120. *Proc. Natl. Acad. Sci. U.S.A. 92*, 1754−8.
(27) Sano, T., and Cantor, C. R. (1990) Expression of a cloned streptavidin gene in *Escherichia coli*. *Proc. Natl. Acad. Sci. U.S.A. 87*, 142−6.
(28) Chen, J. P., Yang, H. J., and Hoffman, A. S. (1990) Polymer−protein conjugates I. Effect of protein conjugation on the cloud point of poly(*N*-isopropylacrylamide). *Biomaterials 11*, 625−30.
(29) Chen, J. P., and Hoffman, A. S. (1990) Polymer−protein conjugates. II. Affinity precipitation separation of human immunogammaglobulin by a poly(*N*-isopropylacrylamide)−protein A conjugate. *Biomaterials 11*, 631−4.
(30) Maeda, M., Nishimura, C., Umeno, D., and Takagi, M. (1993) Modification of DNA with poly(*N*-isopropylacrylamide) for thermally induced affinity separation. *Reactive Polym. 21*, 27−35.
(31) Umeno, D., and Maeda, M. (1997) Poly(*N*-isopropylacrylamide) Carrying Double-Stranded DNA for Affinity Separation of Genotoxins. *Anal. Sci. 13*, 553−6.
(32) Umeno, D., Mori, T., and Maeda, M. (1998) Single stranded DNA−poly(*N*-isopropylacrylamide) conjugate for affinity separation of oligonucleotides. *Chem. Commun.* 1433−4.
(33) Park, T. G., and Hoffman, A. S. (1993) Synthesis and characterization of a soluble, temperature-sensitive polymer-conjugated enzyme. *J. Biomater. Sci. Polym. Ed. 4*, 493−504.
(34) Matsukata, M., Takei, Y., Aoki, T., Sanui, K., Ogata, N., Sakurai, Y., and Okano, T. (1994) Temperature modulated solubility-activity alterations for poly(*N*-isopropylacrylamide)−lipase conjugates. *J. Biochem. 116*, 682−6.
(35) Matsukata, M., Aoki, T., Sanui, K., Ogata, N., Kikuchi, A., Sakurai, Y., and Okano, T. (1996) Effect of molecular architecture of poly(*N*-isopropylacrylamide)−trypsin conjugates on their solution and enzymatic properties. *Bioconjugate Chem. 7*, 96−101.
(36) Ding, Z., Chen, G., and Hoffman, A. S. (1998) Unusual properties of thermally sensitive oligomer−enzyme conjugates of poly(*N*-isopropylacrylamide)−trypsin. *J. Biomed. Mater. Res. 39*, 498−505.
(37) Chilkoti, A., Chen, G., Stayton, P. S., and Hoffman, A. S. (1994) Site-specific conjugation of a temperature-sensitive polymer to a genetically engineered protein. *Bioconjugate Chem. 5*, 504−7.
(38) Stayton, P. S., Shimoboji, T., Long, C., Chilkoti, A., Chen, G., Harris, J. M., and Hoffman, A. S. (1995) Control of protein−ligand recognition using a stimuli-responsive polymer. *Nature 378*, 472−4.
(39) Sano, T., and Cantor, C. R. (1995) Intersubunit contacts made by tryptophan 120 with biotin are essential for both strong biotin binding and biotin-induced tighter subunit association of streptavidin. *Proc. Natl. Acad. Sci. U.S.A. 92*, 3180−4.

BC980151F

Preparation and Pharmacokinetics of Samarium(III)-153-Labeled DTPA-bis-Biotin. Characterization and Theoretical Studies of the Samarium(III)-152 Conjugate

Guillermina Ferro-Flores,*,† Flor De María Ramírez,‡ José I. Tendilla,† Gilmara Pimentel-González,§ Consuelo A. Murphy,|| Laura Meléndez-Alafort,|| Jorge A. Ascencio,⊥ and Barbara Y. Croft#

Instituto Nacional de Investigaciones Nucleares, México, Departamento de Materiales Radiactivos, Km. 36.5 Carretera México-Toluca, C.P. 52045, Departamento de Química, Departamento de Física Computacional, Salazar, Estado de México, México, Instituto de Oncología y Radiobiología, Habana, Cuba, Instituto Nacional de Nutrición Salvador Zubirán, México D. F., México, and National Institute of Health, Rockville, Maryland . Received January 19, 1999; Revised Manuscript Received May 24, 1999

The complex ^{153}Sm(III)DTPA-bis-biotin was prepared with a 99% radiochemical purity and a specific activity of 370 MBq/mg employing a molar ratio of DTPA-bis-biotin/Sm from 2 to 4 at pH 8.0. In vitro studies demonstrated that the complex is stable after dilution in saline and in human serum. Avidity of labeled biotin for avidin was not affected by the labeling procedure. Pharmacokinetic data of ^{153}Sm-(III)DTPA-bis-biotin in normal mice showed that blood clearance is biexponential during the time interval from 0 to 24 h and that 3 h postinjection 92 ± 4.32% of the dose is eliminated in the urine. To have further evidence which could sustain that ^{153}Sm(III)DTPA-bis-biotin is stable in solution as a real coordination complex, ^{152}Sm(III)DTPA-bis-biotin was obtained in macroscopic quantities and its characterization was done by IR, TGA, and conductivity measurements. The results indicated that the complex was chemically pure, where the Sm^{3+} ion is neutralized by three carboxylate groups of the DTPA-bis-biotin ligand and coordinated to it. Using the Force Field method followed by ab initio calculations, the DTPA-bis-biotin and the Sm(III)DTPA-bis-biotin molecules were done. Accordingly, the coordination sphere of Sm(III) was totally satisfied with nitrogen and oxygen donors; the best coordination number was 9. The conformation geometry of both compounds is presented.

INTRODUCTION

The localization of tumors using radiolabeled antibodies has been improved by an approach that utilizes the high avidity of both avidin and streptavidin for biotin (*1*−*5*). Biotin (*cis*-tetrahydro-2-oxothieno[3,4-d]imidazoline-4-valeric acid) is a 244 Da vitamin found in low concentration in blood and tissue (vitamin H). Avidin and streptavidin are tetrameric proteins, and each subunit binds one molecule of biotin. Because the noncovalently bound avidin/streptavidin−biotin conjugate has an extremely low dissociation constant (K_d of about 10^{-15} M), investigators have used these two molecules as binding pairs to bridge molecules that have no affinity for each other and also to target various radionuclides (*1*). So far, the avidin−biotin system has shown that target-to-nontarget radioactivity ratios and radioimaging scanning can be significantly improved by introducing a two-step or a three-step approach. In these, the antibody and the label are administered separately, delaying the delivery of the label to a time when the ratio tumor-bound to nontumor-bound antibody has reached its maximum value. The two-step approach is based on the administration of streptavidin conjugated to the antibody followed by a radioactive biotin conjugate or else biotinylated antibody is injected followed by radioactive streptavidin (*1*, *2*, *6*). In the three-step system, biotinylated antibody is injected followed by an excess of cold avidin or streptavidin and, as a third step, radioactive biotin is administered (*1*, *4*, *5*). Either approach shows enhancement of the tumor/background ratio and tumors are visualized 20 min postinjection avoiding the prolonged circulation and nonspecific accumulation of the radiolabeled antibody in metabolic organs.

Increased effort has been made to label mAbs with rhenium-188, samarium-153, yttrium-90, and lutetium-177 because of their potential role in the radioimmunotherapy of cancer (*7*−*13*). However, the radiolabeling of mAbs or $F(ab')_2$ fragments with Sm-153 by combination of avidin−biotin strategy has not been studied.

The coordination of lanthanides with ligand containing amino acids, amide functions, and related ligands such as the diethylenetriamine pentaacetic acid (DTPA) has been widely studied (*14*−*20*). This property is revealed in the spectroscopic, magnetic, and thermal behavior of the lanthanide compounds (*14*−*20*).

The aim of this work was the preparation of ^{153}Sm-(III)DTPA-bis-biotin, the analysis of the factors affecting radiochemical purity and stability of the complex and the study of its pharmacokinetics in normal mice. To understand the behavior of the complex in solution, spectro-

* To whom correspondence should be addressed. E-mail: gff@nuclear.inin.mx. Phone and Fax: (52-5) 3297306.
† Departamento de Materiales Radiactivos.
‡ Departamento de Química. Phone and Fax: (52-5) 3297301.
§ Instituto de Oncología y Radiobiología. Fax: (537) 328480.
|| Instituto Nacional de Nutrición Salvador Zubirán. Phone: (52-5) 5731200 ext. 2402. Fax: (52-5) 655 1076.
⊥ Departamento de Física Computacional. Phone and Fax: (52-5) 3297301.
National Institute of Health. Phone: (301) 496-9531. Fax: (301) 480-5785.

10.1021/bc9900082 CCC: $18.00 © 1999 American Chemical Society
Published on Web 09/03/1999

Table 1. Factorial Experimental Design Utilized in the Labeling of DTPA-bis-Biotin with Sm-153

Analysis of Variance Procedure[a], Class Level Information		
class	levels	values
molar ratio of DTPA-bis-biotin/Sm	3	1, 2, 4
pH	3	5.5, 7.4, 8
time (h), stability (295 K, without dilution)	2	2, 72

[a] Dependent variable: radiochemical purity.

scopic studies, thermal characterization, and theoretical calculations of ^{152}Sm(III)DTPA-bis-biotin were performed.

EXPERIMENTAL SECTION

Preparation of $^{153}SmCl_3$ Solution. Samarium-153 chloride was obtained by neutron irradiation of 10 mg of enriched Sm_2O_3 (^{152}Sm, 99.4%, from ISOTEC Inc.) in a TRIGA Mark III reactor at a flux in the central thimble of 3×10^{13} n cm^{-2} s^{-1} for 20 h. After irradiation, 100 μL of 12 N chloride acid was added to the irradiation vial and stirred for 1 min. To this solution was added 900 μL of injectable water, and it was also stirred for 2 min. The average radioactive concentration was 37 GBq/mL.

Preparation of Radiolabeled ^{153}Sm(III)DTPA-bis-Biotin Complex. The biotin used in this investigation was covalently conjugated to diethylenetriamine pentaacetic acid (DTPA) through the use of the cyclic anhydride and lysine conjugate to biotin (biocytin) to produce DTPA-α,ω-bis(biocytinamide) (DTPA-bis-biotin, Sigma Chemical Co.) as Hnatowich et al. reported (*21*).

Sterile and apyrogenic V-vials were prepared to contain 0.5 mg (4.8×10^{-4} mmol), 1.0 mg (9.7×10^{-4} mmol), and 2.0 mg (1.9×10^{-3} mmol) of the DTPA-bis-biotin compound in 1.0 mL of 0.05 M bicarbonate buffer (pH 8.0), or 1.0 mL of 0.05 M phosphate buffer solution (pH 7.4) or 1.0 mL of 0.05 M acetate buffer (pH 5.5). Then, 10 μL of $^{153}SmCl_3$ solution (4.9×10^{-4} mmol ^{153}Sm, 370 MBq) was added to each preparation. A factorial experimental design was applied as is shown in Table 1.

Radiochemical and Chemical Quality Control. *HPLC Chromatography.* Quality control of the labeled ^{153}Sm(III)DTPA-bis-biotin was performed by size-exclusion HPLC analysis employing a Protein Pak 300 SW gel filtration column (Waters), with photodiode array detector. As the mobile phase 0.1 M phosphate, pH 7.4, at a flow rate 1.0 mL/min was used with a Waters fraction collector. The radiochromatographic profile was determined by analyzing collected samples of 0.5 mL each one in an external NaI (Tl) detector (NML, Laboratories, Inc.).

TLC Chromatography. For thin layer chromatography, aluminum cellulose sheets (MercK) were utilized as the stationary phase and a ternary mixture of methanol: water:ammonium hydroxide (20:40:2) as the mobile phase. The procedure involved spotting a 5−10 μL sample of the radiopharmaceutical onto a chromatography strip 8 cm in length. ^{153}Sm(III)DTPA-bis-biotin traveled with the solvent front R_f 0.9−1.0 and the Sm^{3+} species remained at the origin ($R_f = 0$).

Avidity of ^{153}Sm(III)DTPA-bis-Biotin for Avidin. An aliquot of the labeled biotin conjugate (100 μL, 37 MBq) was loaded onto an immobilized avidin-agarose column and incubated for 10 min and washed with 60 mL of phosphate-buffered saline (PBS) at pH 7.4. The radioactivity of the eluted sample and of the column was assayed by using a dose calibrator (Capintec Radioisotope Calibrator, model CRC-7). The percentage of ^{153}Sm(III)-DTPA-bis-biotin bound to the avidin-agarose column was calculated by dividing column radioactivity over the total activity of both sample liquid fraction plus the column. To evaluate the nonspecific link of samarium-153 to the avidin column, the same procedure was performed but $^{153}SmCl_3$ was used instead of the ^{153}Sm(III)DTPA-bis-biotin.

In Vitro Stability of ^{153}Sm-DTPA-Biotin Complex. Stability studies against dilution were carried out by diluting the ^{153}Sm(III)DTPA-bis-biotin complex solution 2− 10^5 fold with saline solution and with human serum at 310 K. After 10 min and 24 h, the radiochemical purity of each ^{153}Sm complex solution was determined by TLC as mentioned earlier.

Biodistribution and Pharmacokinetic Studies. Female Balb-c mice (27−30 g) were used in these studies which were performed in accordance with the Mexican regulations regarding animal care and handling.

An intravenous injection of 50 ± 7 μg of ^{153}Sm(III)-DTPA-bis-biotin in a volume of 50 μL was given into the tail vein of the mice. Biodistributions were obtained as follows: the mice were killed 0.5, 1, 2, 3, 6, and 24 h postinjection, the blood samples and relevant organs (blood, kidney, stomach, intestine, liver, spleen, lung, heart, urine, and reminder body) were removed and weighted and then counted in a precalibrated NaI(Tl) detector system. The uptake in each organ was calculated and expressed as percent injected dose per gram (% ID/g). All sample counts were corrected for background and physical decay by using standards of comparable volume and the adequate geometry for blood and organs.

The counts per minute per milliliter (cpm/mL) serum obtained at different times were fed into the BIEXP (*22*) microcomputer program. The algorithm for this program is given by the following formula, which presents a biexponential curve:

$$C(t) = Ae^{-\alpha t} + Be^{-\beta t}$$

where $C(t)$ is the concentration at any given time, A and B are the intercept at the y-axis of the fast α and slow β slopes, and e is the base of the natural logarithms. By least-squares regression analysis, the program calculates points A and B on the y-axis and the constants k_α, rapid distribution constant, and k_β, slow elimination constant. With these four data, BIEXP calculates all the other parameters according to conventional equations for a two-compartment open model, which are extrapolated to the human volume of distribution at central compartment (V_{dcc}), extrapolated human volume of distribution at steady state (V_{dss}), total clearance, mean residence time, and elimination constant (k_{ss}).

Preparation of ^{152}Sm(III)DTPA-bis-Biotin Complex. A total of 6.0 mg (5.7×10^{-3} mmol) of the DTPA-bis-biotin compound was dissolved in 1.0 mL of 0.05 M bicarbonate buffer (pH 8.0) and the pH adjusted to 10.0 with 2.5 N NaOH. Then, 60 μL of Sm-152 solution (5.7×10^{-3} mmol in 1.0 N HCl of ^{152}Sm, 99.4%, from ISOTEC Inc.) was added. The reaction medium was kept at 295 K for 30 min, afterward the compound in solution was purified by size-exclusion HPLC (1.0 mL loop) employing a Protein Pak 300 SW gel filtration column (Waters), with photodiode array detector. HPLC water was used as mobile phase at a flow rate of 1.0 mL/min. The synthesis procedure was repeated three times, and the biotin conjugate collected from the HPLC was evaporated under vacuum. The solid residual was characterized by spectroscopic and thermal studies. The complex was obtained three times, and the analysis indicated its reproducibility.

Table 2. Effect of pH and DTPA-bis-Biotin/Sm Molar Ratios upon Radiochemical Purity (%) and Stability of ^{153}Sm(III)DTPA-bis-Biotin Complex (Results of the experimental design)[a]

molar ratio DTPA-bis-biotin/Sm	pH 5.5		pH 7.4		pH 8.0	
	2 h	72 h	2 h	72 h	2 h	72 h
1	67.63 ± 3.9	35.42 ± 6.4	95.43 ± 0.87	93.90 ± 1.30	97.36 ± 0.96	96.98 ± 1.10
2	*b*	*b*	97.20 ± 1.10	96.87 ± 0.97	99.43 ± 0.32	99.25 ± 0.41
4	*b*	*b*	97.56 ± 0.81	97.10 ± 1.20	99.56 ± 0.30	99.41 ± 0.32

[a] $n = 3$ for each data. [b] DTPA-bis-biotin was not dissolved.

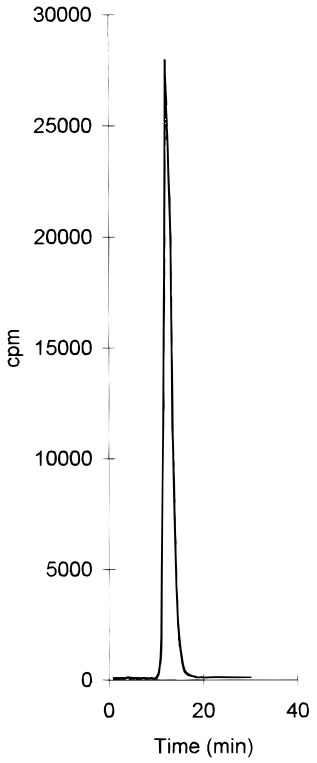


Figure 1. Radio-HPLC chromatogram of ^{153}Sm(III)DTPA-bis-biotin complex. Protein-Pak 300SW column, flow rate 1.0 mL/min, 0.1 M phosphate buffer (pH 7.4) as mobile phase.

Spectroscopic and Thermal Studies of ^{152}Sm-DTPA-Biotin. *IR Spectroscopy*. IR spectra of the reagents used for the synthesis of ^{152}Sm(III)DTPA-bis-biotin complex (97% enriched ^{152}Sm) and of the complex were recorded on a Nicolet Magna-IR Spectrometer 550 from 350 to 4000 cm^{-1} using KBr pellets.

Thermogravimetric Analyses (TGA). The TGA analyses of both the reagents and the complex were carried out in a Dupont 2000 TA Instrument with TGA 51 at 283 K min^{-1} (from 293 to 1273 K) under nitrogen flow.

Theoretical Methodology. The computational analysis was made on an Indigo 2 workstation with R10000 processor of Silicon Graphic Inc. and applying the Cerius^2 software of Molecular Simulation Inc. (*23*, *24*). A model was generated with all the corresponding conditions of hybridization bonding and atomic distribution for the free ligand DTPA-bis-biotin and for the complex, Sm(III)-DTPA-bis-biotin. A geometric analysis was done over the DTPA-bis-biotin molecule by energetic principles using the classic molecule mechanics (MM) method of force field (FF) and generated three configurations. The most stable and with the minimum potential energy was used to apply a quantum mechanics calculation and ab initio analysis to optimize the geometry configuration and to identify charge density distribution. The density functional theory (DFT) (*25*) and the local density approximation (LDA) (*26*) were applied.

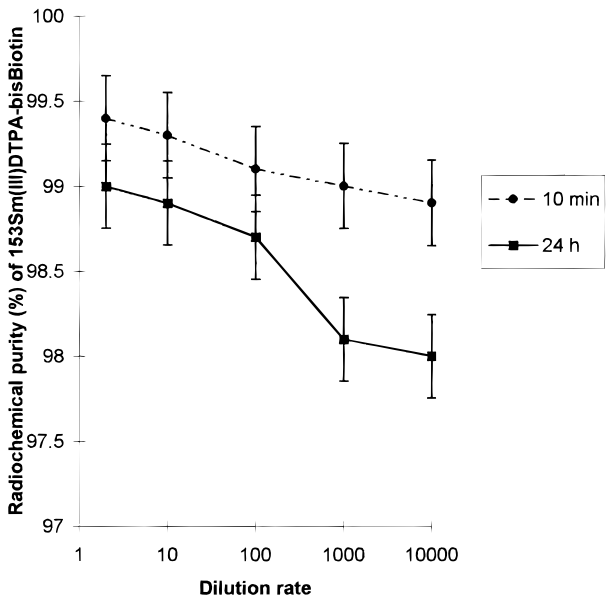


Figure 2. In vitro stability of ^{153}Sm(III)DTPA-bis-biotin in human serum dilution (10 min and 24 h after dilution, 310 K).

Table 3. Radiopharmacokinetic Data for ^{153}Sm(III)DTPA-bis-Biotin Complex in Normal Mice[a]

parameter	value
k_α (1/h)	1.5815 ± 0.1387
$t_{1/2} - \alpha$ (h)	0.4383 ± 0.0987
k_β (1/h)	0.0853 ± 0.0135
$t_{1/2} - \beta$ (h)	8.1240 ± 1.7125
V_{dcc} (L)	6.6923 ± 0.7854
V_{dss} (L)	18.0492 ± 3.8536
total clearance (L/h)	3.7675 ± 1.0235
mean residence time (h)	4.79 ± 0.8265
k_{ss} (1/h)	0.2087 ± 0.0196
3 h urine elimination (% dose)	92 ± 4.32

[a] *BIEXP* program. $n = 3$ for each data.

RESULTS

The ANOVA statistical analysis showed that the molar ratio DTPA-bis-biotin/Sm and pH have significant effect upon the radiochemical purity and stability of ^{153}Sm(III)-DTPA-bis-biotin ($p < 0.05$). As can be seen in Table 2, pH values from 7.4 to 8.0 can be considered satisfactory while pH 5.5 is definitively unsatisfactory. The mean of molar ratio values from 2 to 4 are not significantly different ($p > 0.05$).

The radio-HPLC analysis of ^{153}Sm(III)DTPA-bis-biotin solution showed a single peak with retention time of 12.1 ± 0.3 min (Figure 1).^{153}Sm-labeled biotin was 99 ± 0.5% bound to the avidin-agarose column, demonstrating that its biological properties were not affected by the radiolabeling procedure. The free $^{153}SmCl_3$ bound to the avidin-

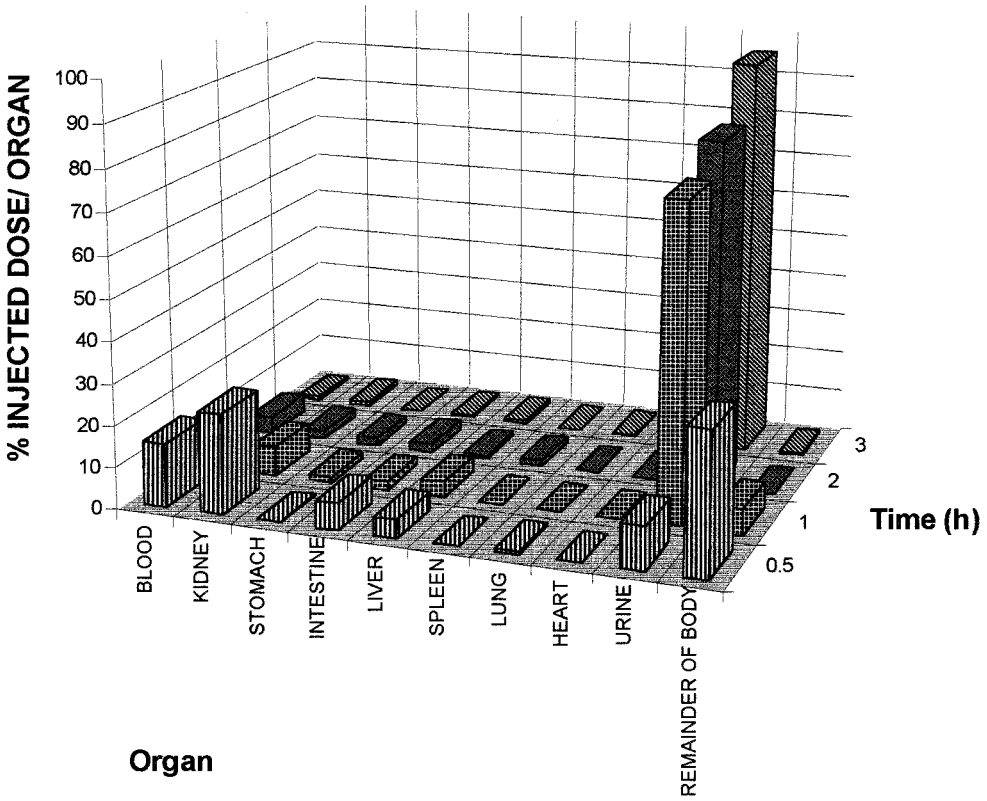


Figure 3. Average biodistribution in mice of ^{153}Sm(III)DTPA-bis-biotin complex (n = 4 for each time).

agarose column was less than 1%, and it represents the nonspecific bonding of samarium-153 to avidin column.

The results of the in vitro stability of ^{153}Sm(III)DTPA-bis-biotin in saline and human serum dilution showed that the complex was very stable since no significant change or decomposition (<2%) was detected by the TLC analyses (Figure 2).

Pharmacokinetic data show that blood clearance is biexponential during the time interval studied and that 3 h after the administration of ^{153}SmDTPA-bis-biotin, 87.68−96.32% of the dose was eliminated in the urine (Table 3).The biodistribution of ^{153}Sm-labeled Biotin is shown in Figure 3.

The IR spectra of the DTPA-bis-biotin ligand and the ^{152}Sm(III)DTPA-bis-biotin complex are shown in Figure 4. The substantial change of the spectrum of the free ligand after Sm^{3+} was bound is observed. The bending vibration frequencies corresponding to NH of the amides (−NH−CO− groups) between 3430 and 3075 cm^{-1} are shifted to lower energies (5 25 cm^{-1}). The bands observed between 2930 and 2840 cm^{-1}, which are normally assigned (*27*−*29*) to bending frequencies of $-CH_2-x$ (x = CO, NH, S, OH), are also shifted to lower energies (15−10 cm^{-1}). The Sm(III)DTPA-bis-botin complex (Figure 4b) seems to be pure because bands corresponding to free DTPA, biotin, or DTPA-bis-biotin ligands were not observed.

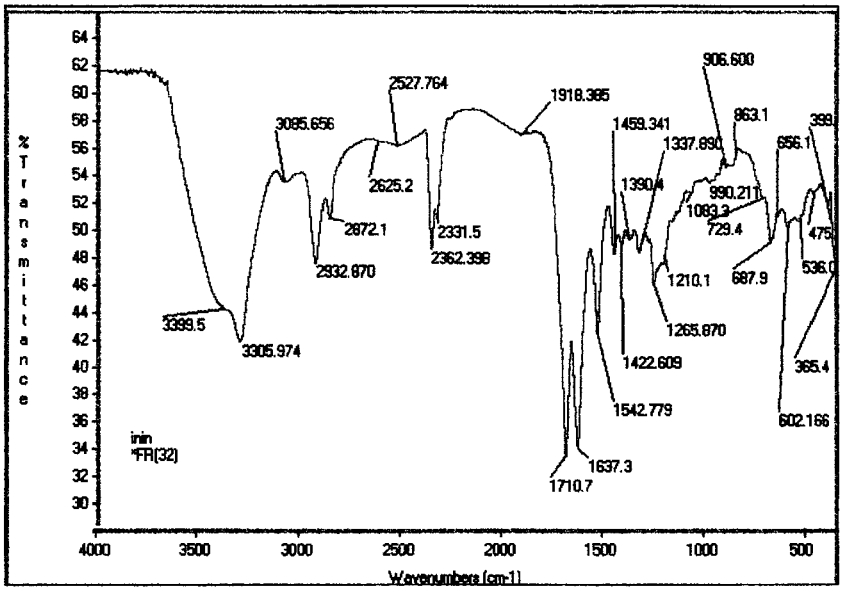
The thermograms indicated different thermal behavior of DTPA-bis-biotin and ^{152}Sm(III)DTPA-bis-botin. After heating from 293 to 1273 K, the former exhibited five decomposition steps and the latter six. The residue was 37.45% for the ligand and 23.56% for the complex.

DTPA-bis-biotin. At 444 K and at 574 K, the weight loss of about 1.79%, and 9.29% respectively, correspond to decomposition of methylenes as methane. The two hetero bicyclic biotin rings are decomposed at 646 K, since the weight loss was 23.79%. Two biamide components are eliminated at 953 and at 1035 K, respectively, since a total weight loss of 27.69% was found. At 1035 K, the residue consisting of 37.45% was found to be a mixture of a tertiary amino acid derivative and sulfur atoms.

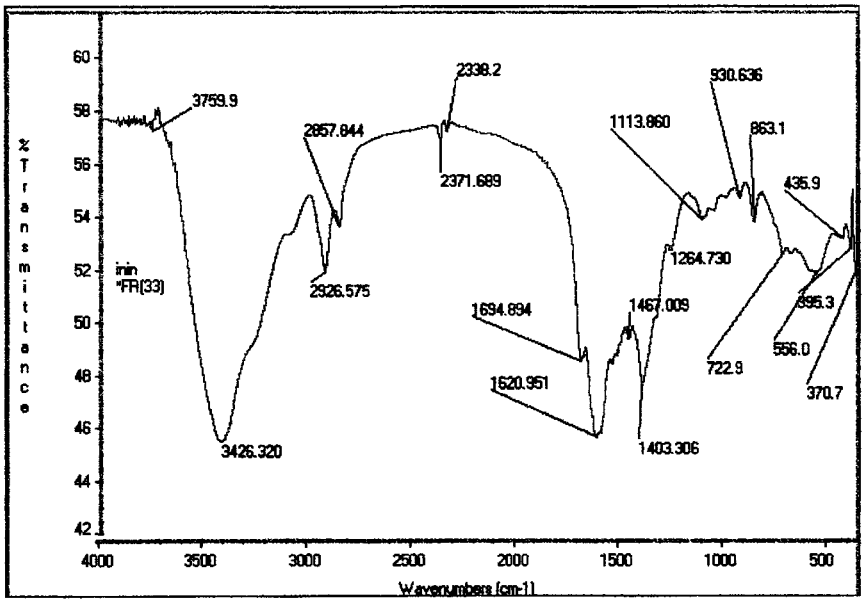
^{152}Sm(III)DTPA-bis-biotin complex. From 461 to 485 K, the weight loss of 2.03% is consistent with the elimination of two methylene groups. At 617 K the weight loss of 8.77%, was associated to the elimination of two groups of tetramethylenes. At 691 K, the weight loss was 3.28% and corresponds to the partial and asymmetric decomposition of the two heterocyclic biotin rings. At 828 K, the weight loss of 6.72%, reveals the total decomposition of one bicyclic ring. At 1066 K, the weight loss of 26.90% is consisting with the elimination of the remaining bicyclic rings, the partial destruction of the amino acid chain, and one of the amide group derivatives. At 1095 K, the carboxylic groups, the tertiary amines, and the another amide group derivative are decomposed and molecular oxygen is formed, the weight loss was 28.29%. The final residue was 23.56% and corresponds to O−Sm-(CO_3) + 2S.

The conductivity measurement of the complex in solution 1×10^{-4} M indicated a 1:1 electrolyte. The complex was surprisingly stable to hydrolysis, since after 24 h, the conductivity measurements did not change and it was not observed demetalation after 3 days under heating at 343 K.

On the basis of semiempirical (MM by FF) and theoretical (ab initio by DFT) calculations, the molecules of the free ligand and of the complex were built, and the best geometric arrangement acquired by the DTPA-bis-biotin ligand is shown in Figure 5. Three possible conformations with coordination number of nine were found for the ^{152}Sm(III)DTPA-bis-biotin complex, as a result of the high flexibility and multidonor characteristic of the ligand. The most stable is presented in Figure 6.



(a)



(b)

Figure 4. IR spectra recorded in KBr pellets of (a) DTPA-bis-biotin ligand and (b) Sm(III)DTPA-bis-biotin complex.

For every coordination number, a typical coordination polyhedron exists. Figure 7 is another representation of the molecule complex, and the coordinated central samarium ion is well shielded by the ligands. The heterocycle ring of the biotin groups is completely exposed to the medium (Figures 6 and 7). Final electronic densities (for the electronic configuration of each atom) and final charges (for the charge distribution of each atom) for the 150 atoms of the ligand and 148 of the complex were obtained. Changes of those parameters are observed after the coordination of the Sm(III) ion. The most important changes occur in the atoms of the amino, carboxylic, and carboxylate groups which are coordinated to the metal center. The final electronic densities and final charges of the donors N and O and of the C atoms of the ligand and of the samarium complex molecules are given in Table 4.

DISCUSSION

Preparation of ^{153}Sm(III)DTPA-bis-Biotin Complex. Results suggest that ^{153}Sm(III)DTPA-bis-biotin complex can be prepared with a specific activity of 370 MBq/mg and a radiochemical purity over 99% employing a molar ratio of DTPA-bis-biotin/Sm from 2 to 4 at pH 8.0. ^{153}Sm(III) is commercially available with specific activities up to 318.2 GBq/mg. Therefore, under the conditions described above, the samarium complex could be obtained with specific activity up to 3.2 GBq/mg for a therapeutic radiopharmaceutical, although radiolysis should be evaluated.

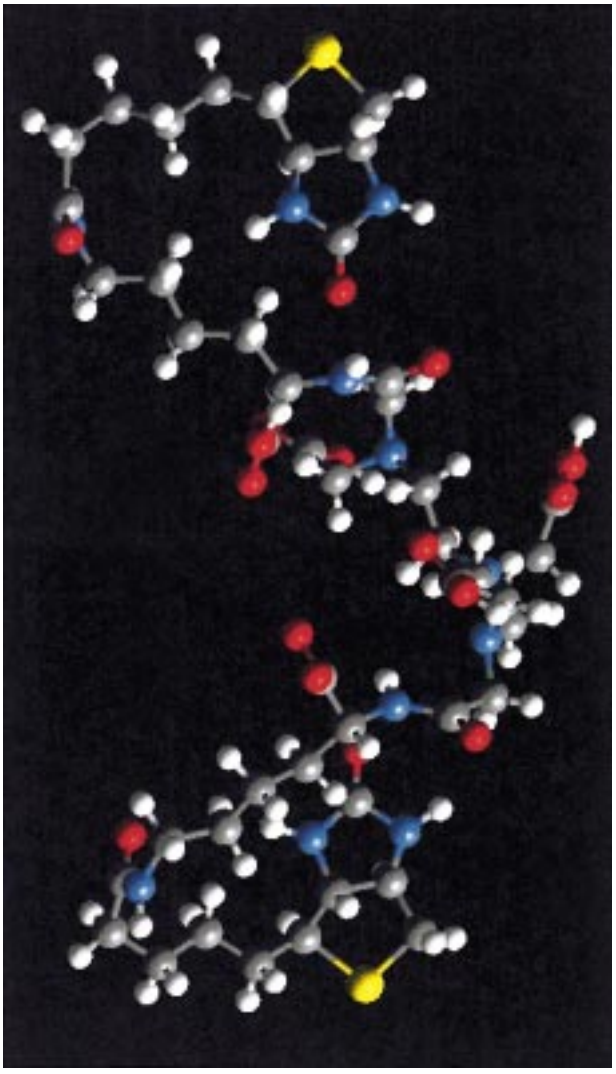


Figure 5. DTPA-bis-biotin ligand calculated by FF and DFT and simulated by Cerius[2].

The high in vitro stability of ^{153}Sm(III)DTPA-bis-biotin diluted in both saline and human serum, and taking into account its physicochemical behavior, we can propose that its stability constant has to be higher than that reported for the Sm(III)DTPA complex (log $K_f \approx 22$) (*15*).

Biodistribution and Pharmacokinetic Studies. Free samarium is captured almost in its entirety by the liver; therefore, the absence of hepatic uptake after the administration of ^{153}Sm(III)DTPA-bis-biotin demonstrates that samarium remains bound to the molecule in vivo. In this study, the tissue distribution of ^{153}Sm-(III)DTPA-bis-biotin (Figure 3) in normal mice is quite similar to that which would be expected for the renal agent ^{153}Sm(III)DTPA. As known, the biodistribution of labeled biotin depends on the chemical, and physicochemical properties of the chelating agents may be due to the action of biotinidase, which is present in high levels in murine serum (*1, 30*). Despite the effect produced by the biotinidase, Chinol et al. (*7*) have found tumor uptake of ^{90}Y-labeled biotins using three-step tumor targeting in mice and Nakamoto et al. (*4*) reported three-step tumor imaging with biotinylated mAb anti-CEA MLS128, streptavidin, and [^{111}In]DTPA-bis-biotin in mice. The use of three-step mAb tumor targeting in CEA positive patients employing [^{111}In]DTPA-bis-biotin for diagnosis was successfully applied by Paganelli (*5*). Chinol et al. (*7*) also studied the biodistribution of yttrium-90 bound to biotin through DTPA or DOTA (a polyaminemacrocycle) observing a higher stability in vivo for [^{90}Y]DOTA-biotin than for [^{90}Y(III)]DTPA-bis-biotin. However, tumor uptake was higher for the DTPA complex than for the DOTA complex which may be attributed to the presence of two biotin molecules in [^{90}Y(III)]DTPA-bis-biotin. Since it has been demonstrated that ^{153}Sm(III)DTPA-bis-biotin is highly stable, we could expect an appropriate tumor uptake because of the biotin dimeric structure.

In a pilot therapy trial (*31*), 11 patients were treated with yttrium-90-labeled DOTA-biotin by the pretargeting technique obtaining a mean absorbed dose in the tumor of 12.9 Gy. However, ^{90}Y is not a γ emitter and therefore unsuitable for scintigraphic imaging, restricting the in vivo absorbed dose calculation. Samarium-153 has favorable features as a radiotherapeutic agent: a 103 keV γ emission for scintigraphic imaging of its biological distribution, which allows the in vivo absorbed dose calculation, and it is easily handled from the point of view of radiation protection, its short half-life ($t_{1/2} = 1.8$ days) reduces the need for long patient isolation and facilitates the disposal of urine and other body fluid. Due to the absorption cross-section for thermal neutrons ($\sigma = 260$) of samarium-152, a reasonable high specific activity of samarium-153 can be produced even with fairly low flux nuclear reactors, which allows it to be applied in nuclear medicine.

IR Spectroscopy. As mentioned before, the IR spectrum of the DTPA-bis-biotin is substantially modified in the Sm(III)DTPA-bis-biotin complex. One important feature in the spectra is that the two broad signals centered at 2520 and 1910 cm^{-1} which are observed in the free ligand have been previously observed in ligands containing amino acids or amino acid derivative functions as the result of the formation of zwitterion (*28, 29*) $^{-}$OOC$-$(CH$_x$)$_y-$NH$_x^{+}$-, in KBr matrix, (*19*) and are gone in the complex, indicating that in the complex the COOH and the COO^{-} groups are strongly coordinated to the metal ion.

The stretching vibration frequencies of the carbonyls centered at 1690 cm^{-1} for the carboxylic (*CO*OH) and at 1630 cm^{-1} for the amide (*CO*NH) groups, respectively (*27*−*29*), in the free ligand, are shifted to lower energies 15 and 10 cm^{-1}, respectively, and their intensities diminish in the complex. Also the medium broad band centered at 1620 cm^{-1} is stronger than that at 1675, as a result of the coordination of the carboxylate groups (COO^{-}), since their band appear around 1620 cm^{-1} when they are coordinated. The band around 1675 cm^{-1} does not disappear at all, since two COOH remain.

The well-defined bands at 1530 cm^{-1} (*OC*NH) and at 3300 cm^{-1} (OC*NH*, *HN*CO*NH*) in the free ligand are shoulders in the complex, which is also evidence of the strong interaction between these functional groups and Sm^{3+} ion. Between 1480 and 1260 cm^{-1}, only one band survived, which is shifted to 1440 and assigned to, *CH*$_2-$N groups. The band at 1403 cm^{-1} (*−COOH*) is shifted to 1395 cm^{-1}. Moreover, the multiple bands between 1410 and 1260 cm^{-1} assigned to bending vibration frequencies of C*−OH*, which in this case are due to those of the carboxylic groups −CO*OH*, are not anymore present in the complex and only a centered medium band at 1395 with a shoulder at 1320 cm^{-1} is observed. The medium band at 1395 cm^{-1}, which is typical of coordinated carboxylate groups, is additional evidence of that the COO^{-} are not only neutralizing the charge of the metal ion but also coordinated. The C*−N* vibrations (1130−1150 cm^{-1}) of the $-CH_2-NH-CH_2-$ are clearly observed in the complex. The symmetry of the free ligand

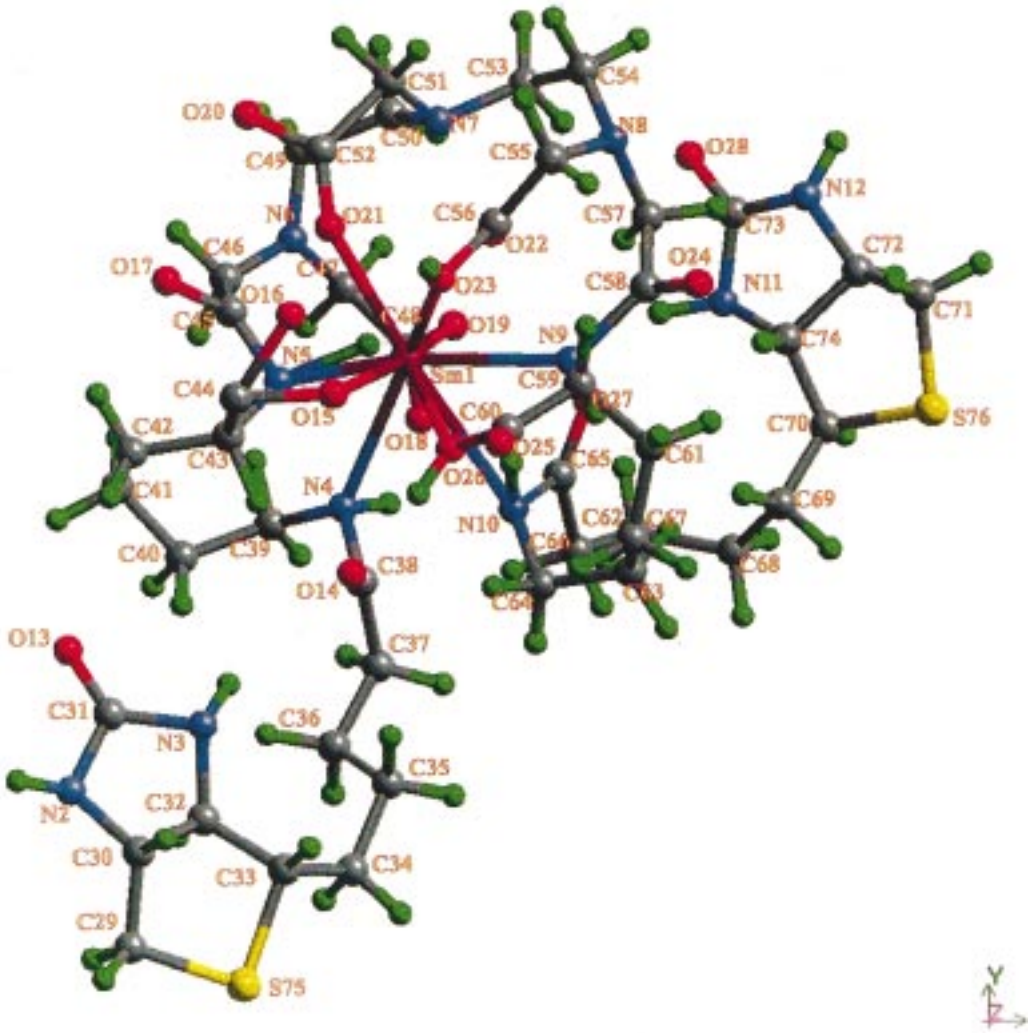


Figure 6. Sm(III)DTPA-bis-biotin calculated by FF and DFT and simulated by Cerius^2.

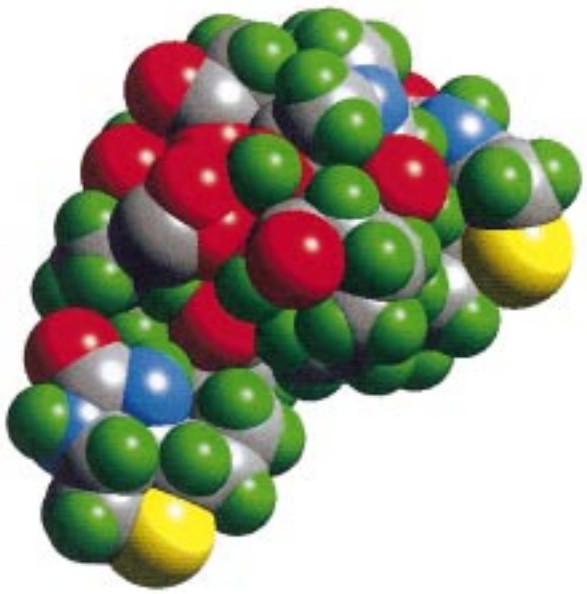


Figure 7. Sm(III)DTPA-bis-biotin calculated by FF and DFT and simulated by Cerius^2, bulky visualization.

is changed because of the coordination, as a result, the weak bands observed between 990 and 800 cm^{-1} in the free ligand and which are normally assigned to (CH_2−CH_2) groups are defined at 910 and 830 cm^{-1} in the complex and the two bands centered at 702 and 665 cm^{-1} which correspond to the rocking vibrations of the $(CH_{x=1-2})_n$ groups are shifted to lower energies, appearing at 690 and at 652 cm^{-1}, respectively. The fingerprint region between 650 and 450 cm^{-1}, where vibrations of the O−CO, C−C=O, OCN, the rock vibration of the COO^-, and the bending vibration of C−C−N− functional groups appear, is broadened in the complex (*27*). However, the broad band centered at 550 cm^{-1} fits well with the common observation of M−X vibration frequencies, when in complex interaction between N, O, and CO donors and M = lanthanide metal ion occurs (*14*−*20*).

Thus, IR spectroscopic study indicates that Sm^{3+} ion is coordinated to the DTPA-bis-biotin ligand through the three carboxylic groups of the tertiary amino acid functions, the carboxylic groups bound to the methylene of the secondary amide groups and to the amide function itself. On the basis of these results, we propose that the conformation of ligand changes by its coordination to the metal center and so the symmetry of the complex is remarkably different and, therefore, the transition vibration frequencies. Concerning the behavior of the donors (S, NH−CO−NH−) in the biheterocyclic rings of the biotins, there is no evidence which allows the proposition of the role of them in the complexation of Sm^{3+} ion. This result is important because the main contribution to the

Table 4. Summary of the Final Electronic Densities and Final Charge Distribution per Atom[a] of the DTPA-bis-Biotin and Sm(III)DTPA-bis-Biotin Applying the Density Functional Theory

	Sm(III)DTPA-bis-biotin		DTPA-bis-biotin			Sm(III)DTPA-bis-biotin		DTPA-bis-biotin	
atoms	final electronic densities	final charge distribution	final electronic densities	final charge distribution	atoms	final electronic densities	final charge distribution	final electronic densities	final charge distribution
75-S	5.7855	0.2145	5.8271	0.1729	21-O	6.3134	−0.3134	6.2439	−0.2439
32-C	4.0951	−0.0951	4.0984	−0.0984	20-O	6.1602	−0.1602	6.3135	−0.3135
2-N	5.3997	−0.3997	5.3767	−0.3767	76-S	5.8100	0.19	5.8132	0.1868
31-C	3.7053	0.2947	3.6717	0.3283	12-N	5.3897	−0.3897	5.3843	−0.3843
N3−N	5.3254	−0.3254	5.3589	−0.3588	73-C	3.6969	0.3031	3.6768	0.3232
13-O	6.2557	−0.2557	6.2909	−0.2909	11-N	5.3439	−0.3439	5.3655	−0.3655
38-C	3.6373	0.3627	3.7067	0.2933	28-O	6.2624	−0.2624	6.2837	−0.2837
4-N	5.3218	−0.3218	5.3577	−0.3576	65-C	3.6754	0.3241	3.6901	0.3099
14-O	6.2263	−0.2263	6.2553	−0.2553	10-N	5.3256	−0.3256	5.3411	−0.3411
44-C	4.0047	−0.0047	3.7000	0.3	27-O	6.2097	−0.2097	6.2569	−0.2569
5-N	5.0290	−0.029	5.3135	−0.3135	60-C	3.7315	0.2685	3.7112	0.2888
16-O	6.0287	−0.0287	6.3306	−0.3306	9-N	5.2589	−0.2589	5.3114	−0.3114
15-O	6.0146	−0.0146	6.2381	−0.2381	25-O	6.2586	−0.2586	6.3378	−0.3378
45-C	3.6130	0.387	3.7185	0.2815	26-O	6.2357	−0.2357	6.2436	−0.2436
46-C	4.4691	−0.4691	4.4375	−0.4375	58-C	3.7055	0.2945	3.7210	0.279
6-N	4.9215	0.0785	5.0042	−0.0042	57-C	4.4216	−0.4216	4.4892	−0.4892
17-O	6.2617	−0.2617	6.2710	−0.271	8-N	4.9835	0.0165	4.9687	0.0313
50-C	4.2710	−0.271	4.3291	−0.3291	24-O	6.2185	−0.2185	6.2606	−0.2606
7-N	4.9105	0.0895	5.0037	−0.0037	54-C	4.3185	−0.3185	4.3596	−0.3596
48-C	3.6666	0.3334	3.7007	0.2993	56-C	3.6050	0.395	3.6823	0.3177
19-O	6.1942	−0.1942	6.3204	−0.3204	22-O	6.2958	−0.2958	6.3191	−0.3191
18-O	6.3159	−0.3179	6.2375	−0.02375	23-O	6.0990	−0.099	6.2404	−0.2404
52-C	3.7074	0.2926	3.6767	0.3233	1-Sm	7.6586	0.3414		

[a] Final electronic densities and final charge distribution per atom have been calculated for the corresponding valence orbital.

binding of biotin to avidin is given by the aliphatic heterocycle including the ureido group (*1*).

Thermal Behavior (TGA). ^{153}Sm(III)DTPA-bis-biotin. The thermal decomposition pattern of this complex indicates that the Sm^{3+} was coordinated to the DTPA-bis-biotin since its thermal behavior is different from that of the free ligand.

Theoretical calculations. Semiempirical and theoretical investigation of complexes represent a valid tool for the characterization of their molecular properties. Recently, ab initio calculations by DFT for cobalt complexes (*32*) and FF and ab initio calculations for lanthanide complexes formed with polyamino carboxylate ligands (*33*) have been reported, and they were demonstrated to be useful for explaining the metal−ligand interactions and their conformational properties. In this work, molecular mechanics method as it is FF and ab initio calculations by DFT were applied to the ligand and the complex. These calculations allowed the obtaining of the best conformation for the Sm complex, that is the best geometric arrangement with the lower value of minimum potential energy (Figures 6 and 7), showing that the metal center is quite shielded by the ligand. The donors of the heterocyclic rings (N, S, and O donors) and the heterocyclic themselves do not have steric hindrance and are able to be linked to any substrate as for example the avidin.

Therefore, from these results we can establish that one of the factors which favored the high stability of the complex in solution is the shield effect which resulted from the geometrical arrangement of the molecule.

The electronic configuration or final electronic densities, and the final charge distribution (Table 4) for the atoms of the ligand compared with those of the complex revealed an important change which can be related with an important Sm−ligand interaction. The most important changes occur in the atoms of amino, carboxylic(COOH) and carboxylate groups(COO), which are coordinated to the metal center.

In general, it was observed that the final electronic densities of the donors bound to the metal ions diminished except the values of the 18-O and 21-O donors which increased. The same tendency was observed in their charge distribution. The increment in both atoms seems to be the result of retro-donation metal center- to ligand. Because of the high stability of the complex in solution, the increment cannot be assigned to no coordination of the two carboxylate groups which neutralized two positive charges of the metal center. These oxygens belong to two of the three tertiary aminocarboxylate groups. However the 15-O atoms of the third carboxylate group which belongs to a secondary aminocarboxylate derivative and which neutralized the remaining positive charge diminished, indicated that electron donation occurred. The parameters of the 4-N 5-N, 9-N, and 10-N atoms bound directly to the metal center diminished, but the most important effect is observed in the 5-N atom. The parameter values of the atoms of the carboxylic groups (COOH) diminished and indicate their coordination to the metal center. The same tendency is observed in the final charges. The general tendency to diminish the electronic densities and charge distribution of the donor atoms after the Sm(III) ion is joined to the ligand can be interpreted as the complex is a coordination compound where an important covalent character is also playing a role in the stability and inert of the complex. That is, seems that the chemical and physicochemical properties of the Sm(III)DTPA-bis-biotin is dominated by two effects: electronic and steric effects. The metal center is bound to the ligand and shielded from the medium therefore the complex is stable in vivo. It is quite probable that the two biotins are in the adequate spatial orientation to permit the molecule to be recognized by the corresponding avidin.

CONCLUSIONS

An easy preparation of a stable radiolabeled ^{153}Sm(III)-DTPA-bis-biotin complex was developed. This compound

is suitable for scintigraphic imaging and in vivo absorbed dose calculation because ^{153}Sm is a γ emitter, but in order to establish its therapeutic possibilities, it will be necessary to perform studies in normal and tumor-bearing mice.

Experimental results of radiolabeled ^{153}Sm(III)DTPA-bis-biotin and ^{152}Sm(III)DTPA-bis-biotin evidenced the high stability of the complex in solid and aqueous media (4.98×10^{-5}M) for 3 days and demetalation only occurred after heating at 363 K. Spectroscopic and thermal studies also supported the existence of a neutral high stable and chemically pure complex where three carboxylate anions are neutralizing the three positive charges of the samarium ion which is completely shielded by the ligands. These results suggest that the origin of such stability is thermodynamic and kinetic. It can be established that the conformation properties of ^{152}Sm(III)DTPA-bis-biotin complex determine its physicochemical behavior in vivo.

LITERATURE CITED

(1) Paganelli, G., Malcovati, M., and Fazio, F. (1991) Monoclonal antibody pretargeting techniques for tumor localization: The Avidin−Biotin. *Nucl. Med. Commun. 12*, 211−234.

(2) Paganelli, G., Magnani, P., and Fazio, F. (1993) Pretargeting of carcinomas with the avidin−biotin system. *Int. J. Biol. Markers 8*, 155−159.

(3) Paganelli, G., Stella, M., and Zito, F. (1994) Radioimmunoguided surgery using iodine-125-labeled biotinylated monoclonal antibodies and cold avidin. *J. Nucl. Med. 35*, 1970−1975.

(4) Nakamoto, Y., Saga, T., Sakahara, H., Yao, Z., Zhang, M., Sato, N., Zhao, S., Nakada, H., Yamashina, I., and Konishi, J. (1998) Three-step tumor imaging with biotinylated monoclonal antibody, streptavidin and ^{111}In-DTPA-Biotin. *Nucl. Med. Biol. 25*, 95−99.

(5) Paganelli, G., Magnani, P., Zito, F., Villa, E., Sudati, F., Lopalco, L., Rosseti, C., Malcovati, M., Chiolerio, F., Seccamani, E., Siccardi, A. G., and Fazio, F. (1991) Three-step monoclonal antibody tumor targeting in carcinoembryonic antigen-positive patients. *Cancer Res 51*, 5960−5966.

(6) Rosebrough, S. F. (1996) Two-step immunological approaches for imaging and therapy. *Q. J. Nucl. Med. 40*, 234−251.

(7) Chinol, M., Paganelli, G., Sudati, F., Meares, C., and Fazio, F. (1997) Biodistribution in tumor-bearing mice of two ^{90}Y-labeled biotins using three-step tumor targeting. *Nucl. Med. Commun. 18*, 176−182.

(8) Ferro-Flores, G., and Hashimoto, K. (1997) Direct labeling of monoclonal antibodies and antibody fragments with Re-188. *Radiochim. Acta 79*, 63−70.

(9) Ferro-Flores, G., Pimentel, G., González, M. A., Murphy, C. A., Meléndez L., Tendilla, J. I., and Croft, B. Y. (1999) Preparation, biodistribution and Dosimetry of ^{188}Re-labeled mAb ior cea1 and its F(ab′)$_2$ fragments by avidin−biotin strategy. *Nucl. Med. Biol. 26*, 57−62.

(10) Kraeber-Bodéré, F., Mishra, A., Thédrez, P., Faivre-Chauvet, A., Bardiès M., Imai, S., Le Boterff, J., and Chatal, J. F. (1996) Pharmacokinetic and biodistribution of samarium-153-labeled OC 125 antibody coupled to CITCDTPA in a xenograft model of ovarian cancer. *Eur. J. Nucl. Med. 23*, 560−567.

(11) Rhodes, B. A., Lambert, C. R., Marek, M. J., Knapp, F. F., and Harvey, E. B. (1996) Re-188 labeled antibodies. *Appl. Radiat. Isot. 47*, 7−14.

(12) Schott, M. E., Schol, J., Siler, K., Milenic, D. E., Eggensperger, D., Colcher, D., Cheng, R., Kruper, W. J., Fordyce, W., and Goeckeler, W. (1994) Biodistribution and preclinical radioimmunotherapy studies using radiolanthanide-labeled immunoconjugates. *Cancer 73*, 993−998.

(13) Winnard, P., Virzi, E., Fogarasi, M., Rusckowski, M., and Hnatowich, D. (1996) Investigations of directly labeling antibodies with rhenium-188. *Q. J. Nucl. Med. 40*, 151−160.

(14) Cotton, S. (1991) *Lanthanide and Actinides*, first edition, MacMillan Education LTD England.

(15) Huheey, J. E., Keiter, E. A., and Keiter, R. L. (1993) *Inorganic Chemistry "Principles, Structure and the Reactivity"*, fourth edition, Harper Collins College Publishers.

(16) Kumar, K., and Tweedle, M. F. (1993) Macrocyclic polyaminocarboxylate complexes of lanthanides as magnetic resonance imaging contrast agents. *Pure Appl. Chem. 65*, 515−520.

(17) Martínez, V., Ramírez, F. De M., and Padilla, J. (1994) Synthesis, Spectroscopic and magnetic behaviour of Dysprosium bis(tetraphenylporphyrinate and Bis(Dysprosium)tris-(tetraphenylporphyrinate). *Polyhedron, 13*, 965−973

(18) Alexander, V. (1995) Design and synthesis of macrocyclic ligands and their complexes of lanthanides and actinides. *Chem. Rev. 95*, 273−342

(19) Ramírez, F. De M., (1996) *Novel Lanthanide Complexes Formed with Tetraazamacrocyclic Ligands*, Ph.D. Thesis, F. Q. UNAM, Mexico.

(20) Ramírez, F. De M., Sosa-Torres, M. E., Castro, M., Basurto-Uribe, E., Zamorano-Ulloa, R., and Del Río-Portilla, F. (1997) Synthesis, ^{1}H, ^{13}C NMR and magnetic studies of the homodinuclear lanthanide(III) polymeric compounds formed with the 1,5,9,13-tetraazacyclohexadecane ligand, *J. Coord. Chem. 41*, 303−326.

(21) Hnatowich, D. J., Virzi, F., and Rusckowski, M. (1987) Investigations of avidin and biotin for imaging applications. *J. Nucl. Med. 28*, 1294−1302.

(22) Murphy, R. (1991) BIEXP Computer program, Instituto Nacional de Astrofísica, Optica y Electrónica INAOE, Tonantzintla, Puebla, México.

(23) *Cerius² Force Field Based Simulations* (1997) San Diego, Molecular Simulation Inc.

(24) Dinur, U., and Hagler, A. T. (1991) Approaches to empirical force fields. In *Reviews of Comput. Chemistry*, Vol. 2, Chapter 4 (K. B. Lipkwowitz and D. B. Boyd, Eds.) VCH, New York.

(25) Kohn, W., and Sham, L. J. (1965) Self-consistent equations including exchange and correlation effects. *Phys. Rev. A. 140*, 1133−1138.

(26) Rösch, N., Kruger, S., Mayer, M., and Nasluzov, V. A. (1996) In *Recent Developments and Applications of Modern Density Functional Theory* (J. M. Seminario) Elsevier, Amsterdam.

(27) Williams, H., and Fleming, I. (1980) *Spectroscopic methods in organic chemistry*, third edition, p 35, McGraw-Hill Book Company (U.K.) Limited, Great Britain.

(28) Nakamoto, K. (1986) *Infrared and Raman spectra of Inorganic and Coordination Compounds*, 4th ed., John Wiley and Sons, New York.

(29) Price, W. D., Jockusch, R. A., and Williams, E. R., (1997) Is Arginine a Zwitterion in the gas phase? *J. Am. Chem. Soc. 119*, 1188−1189.

(30) Foulon, C. F., Schoultz, B. W., and Zalutsky, M. R. (1997) Preparation and biological evaluation of an astatine-211 labeled biotin conjugate: Biotinyl-3-[^{211}At]astatoanilide. *Nucl. Med. Biol. 24*, 135−143.

(31) Paganelli, G., Chinol, M., Grana, C., Fiorenza, M., Cremonesi, M., Franceschini, R., Tarditi, L., Pecorale, A., Meares, C., Corti, A., and Siccardi, A. G. (1997) Therapy trial in cancer patients using an improved 3-step pretargeting approach. *Radioact. Isot. Clin. Med. Res. 22*, 513−517.

(32) Chan, J. C. C., Wilson, P. J, Au−Yeung, S. C. F., and Webb, G. A. (1997) Density Functional study of the electronic structures of $[Co(NH_3)_5X]^{(3+n)+}$ Complexes. Insight into the role of the 3d and 4s orbitals in metal−ligand interactions. *J. Phys. Chem. A, 101*, 4196−4201.

(33) Cosentino, U., Moro, G., Pitea, D., Villa, A., Fantucci, P. C., Maioccchi, A., and Uggeri, F. (1998) Ab initio investigation of gadolinium complexes with polyamino carboxylate ligands and Force Fields parametrization of metal−ligand interactions. *J. Phys. Chem. A, 102*, 4606−4614.

BC9900082

Solution Structure and Energy Calculation of Bis-Intercalation of Homodimeric Thiazole Orange Dye Derivatives in DNA: Effects of Modifying the Linker

Kent Bondensgaard and Jens Peter Jacobsen*

Department of Chemistry, Odense University, DK-5230 Odense M, Denmark. Received March 9, 1999; Revised Manuscript Received July 9, 1999

We have used two-dimensional ^{1}H NMR spectroscopy obtained at 750 MHz to determine a high-resolution solution structure of the double-stranded DNA oligonucleotide d(5′-CGCTAGCG-3′)$_2$ complexed with the bis-intercalating dye 1,1′-(5,5,9,9-tetramethyl-5,9-diazatridecamethylene)-bis-4-[3-ethyl-2,3-dihydro(benzo-1,3-thiazolyl)-2-methylidene]quino-linium tetraiodide (TOTO11Et). The determination of the structure was based on a complete relaxation matrix analysis of the NOESY cross-peaks followed by restrained molecular dynamics calculations. Forty final structures were generated for the TOTO11Et complex from A-form and B-form dsDNA starting structures. The root-mean-square (rms) deviation of the coordinates for the 40 structures of the complex was 0.52 Å. A conformational analysis of the deoxyribose rings based on coupling constants obtained from selective DQF-COSY spectra revealed that all ring conformations were almost pure S-type. The structure of the TOTO11Et complex was compared with the structure of a similar DNA complex with a dye containing a shorter linker (TOTOEt). Substantial differences were observed between the two structures because of the difference in the length of the linker. Most prominent was a large difference in the degree of unwinding of the dsDNA part in the two complexes. Unwinding of 73° and 22° relative to the free dsDNA was observed for the complexes with TOTOEt and TOTO11Et, respectively. The AMBER94 force field together with the GB/SA solvation model was used for energy calculations on both of the two complexes. In the calculations, the complex formation was divided into two steps: (i) unwinding of the free oligonucleotide and (ii) association of the bis-intercalators to the unwound oligonucleotide. The complex formation was in favor of TOTO11Et, mainly because the dsDNA is distorted less in the complex with TOTO11Et than in the complex with TOTOEt.

INTRODUCTION

Intercalation of small aromatic molecules (chromophores) in double-stranded DNA[1] (dsDNA) is an extremely efficient binding mode (Wakelin, 1986). Dimers with two intercalating chromophores linked with a chain of appropriate length (bis-intercalators) show high dsDNA binding affinities, greater by several orders of magnitude than those of the corresponding monomers (Wakelin, 1986).

Interest in nonradioactive detection of nucleic acids in gels has led to the synthesis and evaluation of bis-intercalating dyes that form highly fluorescent complexes with dsDNA. Glazer and co-workers (Benson et al., 1993a,b; Glazer and Rye, 1992) have synthesized and characterized a new family of high affinity fluorescent dyes for making dsDNA complexes. Among these, a homodimeric thiazole orange dye, 1,1′-(4,4,8,8-tetramethyl-4,8-diazaundecamethylene)-bis-4-(3-methyl-2,3-dihydro-(benzo-1,3-thiazolyl)-2-methylidene)-quinolinium tetraiodide (TOTO, Scheme 1), binds with an extremely high affinity and forms complexes that are stable to a variety of conditions, in particular, gel electrophoresis. This compound allows high sensitivity detection of dsDNA by fluorescence scanners (Rye et al., 1990, 1992, 1993a,b).

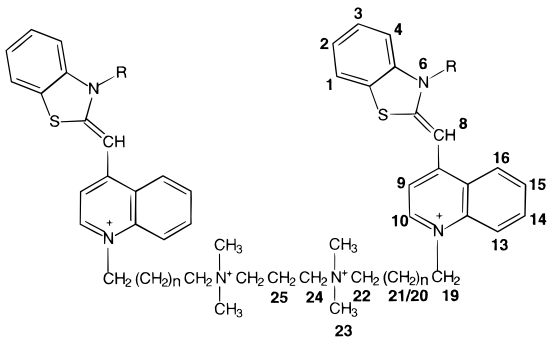
The charged polyamine linker of TOTO resembles spermidine and spermine and contributes to the binding mode by electrostatic interactions in the minor groove. The TOTO chromophores are flexible and can adapt to the propellor twist of the base pairs. The length of the linker can be varied without destroying the strong bis-intercalation in dsDNA. This makes it possible to synthesize TOTO analogues with different lengths of the linker and different substituents on the chromophore so to study the binding mode in detail.

* To whom correspondence should be addressed. E-mail: jpj@chem.ou.dk.

[1] Abbreviations: AMBER, assisted model building with energy refinement; CHEOPS, coupling constants from high-resolution NMR experiments by optimized parameter simulation; DNA, deoxyribose nucleic acid; DQF-COSY, double quantum filtered correlation spectroscopy; dsDNA, double-stranded DNA; DSS, 2,2-dimethyl-2-silapentane-5-sulfonate; E-BURP, excitation band-selective pulse with uniform response and pure phase; EDTA, ethylenediaminetetraacetic acid; GB/SA, generalized Born equation/solvent accessible surface area; HSQC, heteronuclear single quantum coherence; MARDIGRAS, matrix analysis of relaxation for discerning the geometry of an aqueous structure; NMR, nuclear magnetic resonance; NOE, nuclear Overhauser effect; NOESY, nuclear Overhauser effect spectroscopy; RANDMARDI, randomized MARDIGRAS; rMD, restrained molecular dynamics; TOCSY, total correlation spectroscopy; TOTO, 1,1′-(4,4,8,8-tetramethyl-4,8-diazaundecamethylene)-bis-4-(3-methyl-2,3-dihydro-(benzo-1,3-thiazolyl)-2-methylidene)-quinolinium tetraiodide; TOTO11, 1,1′-(5,5,9,9-tetramethyl-5,9-diazatridecamethylene)-bis-4-[3-methyl-2,3-dihydro(benzo-1,3-thiazolyl)-2-methylidene]quinolinium tetraiodide; TOTO11Et, 1,1′-(5,5,9,9-tetramethyl-5,9-diazatridecamethylene)-bis-4-[3-ethyl-2,3-dihydro(benzo-1,3-thiazolyl)-2-methylidene]-quinolinium tetraiodide; TOTOEt, 1,1′-(4,4,8,8-tetramethyl-4,8-diaza-undecamethylene)-bis-4-[3-ethyl-2,3-dihydro(benzo-1,3-thiazolyl)-2-methylidene]quinolinium tetraiodide.

10.1021/bc9900284 CCC: $18.00 © 1999 American Chemical Society
Published on Web 08/20/1999

Scheme 1



TOTO: R = CH_3 and n = 1
TOTO11: R = CH_3 and n = 2
TOTOEt: R = CH_2CH_3 and n = 1
TOTO11Et: R = CH_2CH_3 and n = 2

Recent research in our laboratory has shown that TOTO binds preferentially to 5′-pyrimidine-pyrimidine-purine-purine-3′ sequences (Jensen et al., 1998; Jacobsen et al., 1995; Hansen et al., 1996). Solution structures of the CTAG−TOTO and CTAG−TOTOEt complexes (Spielmann et al., 1995; Petersen and Jacobsen, 1998) place the benzothiazole moiety intercalated between the pyrimidine bases and the quinolinium part intercalated between the two purine bases. The optimal stacking displayed by these structures may explain the preference of TOTO for a 5′-pyrimidine-pyrimidine-purine-purine-3′ site (Hansen et al., 1996). The site selectivity of TOTO within the 5′-pyrimidine-pyrimidine-purine-purine-3′ sites is explained by a subtle interplay between optimal stacking of the chromophores with the nucleobases and electrostatic interactions of the polyamine linker with the minor groove (Jensen et al., 1998; Bunkenborg et al., 1998). When introducing the longer linker in TOTO11, the site selectivity is somewhat reduced (Bunkenborg et al., 1998).

To investigate the role of the linker in the site selectivity of TOTO further, we have used ^{1}H NMR spectroscopy to determine the high-resolution solution structure of the oligonucleotide **1** complexed with TOTO11Et [1,1′-(5,5,9,9-tetramethyl-5,9-diazatrideca-methylene)-bis-4-[3-ethyl-2,3-dihydro(benzo-1,3-thiazolyl)-2-methylidene]quinolinium tetraiodide, Scheme 1]. The insolubility of TOTO and TOTO analogues in water precludes any measurements of equilibrium constants for the complex formation. Instead, we have recoursed to force field calculations in analyzing the complex formation. The molecular modeling calculations were performed on the **1**-TOTOEt and the **1**-TOTO11Et structures to compare the energetics involved in the formation of the two complexes.

EXPERIMENTAL PROCEDURES

Sample Preparation. TOTO11Et was a gift from Dr. E. B. Pedersen (Department of Chemistry, Odense University, Denmark). The purified oligonucleotide d(CGCTAGCG) was purchased from DNA technology (Aarhus, Denmark). On the basis of an analytical HPLC run and the 1D ^{1}H NMR spectrum, the oligonucleotide was assessed to contain less than 5% impurities and was used without further purification. The numbering scheme for the double-stranded oligonucleotide **1** is the following:

		1	*2*	*3*	*4*	*5*	*6*	*7*	*8*		
5'	**-**	**C**	**G**	**C**	**T**	**A**	**G**	**C**	**G**	**-**	**3'**
3'	**-**	**G**	**C**	**G**	**A**	**T**	**C**	**G**	**C**	**-**	**5'**
		16	*15*	*14*	*13*	*12*	*11*	*10*	*9*		

TOTO11Et is almost insoluble in water, and the complexes with dsDNA were therefore made using the procedure described earlier (Jacobsen et al., 1995). The NMR samples were prepared by dissolving the complexes in 0.5 mL of 10 mM sodium phosphate buffer (ph 7.0), 0.05 mM NaEDTA, 0.01 mM NaN_3, and 0.1 mM DSS. For experiments carried out in D_2O, the solid complex was lyophilized twice from D_2O and redissolved in 99.96% D_2O (Cambridge Isotope Laboratories). A mixture of 90% H_2O and 10% D_2O (0.5 mL) was used for experiments examining exchangeable protons. The final concentration of the complex was 2 mM. The sample was kept in an NMR tube under nitrogen.

NMR Experiments. NOESY and TOCSY spectra of **1**-TOTO11Et in D_2O and H_2O were obtained on a Varian Unity 500 spectrometer at 25 °C with standard experimental parameters (Petersen and Jacobsen, 1998). A selective DQF-COSY spectrum was recorded using a pulse sequence in which the first pulse was replaced with an E-BURP type selective pulse (Geen and Freeman, 1991). The spectrum was recorded with a spectral width of 5000 Hz in F_2 and 2000 Hz in F_1 using the States phase cycling scheme with 2048 complex points in t_2 and 1024 t_1 experiments with 64 scans each.

A ^{1}H,^{13}C gradient enhanced HSQC spectrum was recorded on a Varian Inova 600 spectrometer at 25 °C.

NOE buildups were obtained on a Varian Inova 750 spectrometer at 27 °C. These NOESY spectra were acquired in D_2O using 2048 complex points in t_2 and a spectral width of 7500 Hz. A total of 512 t_1 experiments was recorded using the States phase cycling scheme. NOESY spectra with mixing times of 40, 80, 140, and 200 ms were obtained sequentially without removing the sample from the magnet. 64 scans were acquired for each t_1 value with a repetition delay of 3.8 s between each scan. The residual signal from HOD was removed by presaturation. Furthermore, a DQF-COSY spectrum was obtained on a Varian Inova 750 at 27 °C with a spectral width of 7500 Hz using the States phase cycling scheme with 1024 complex points in t_2 and 1024 t_1 experiments with 64 scans each.

The acquired data were processed using Felix (version 95.0, Bioym Technologies/ MSI, San Diego, Ca). All spectra were apodized by a skewed sine bell in F_1 and F_2. The four spectra used in the buildup were zero-filled in F_1 to 2K points and baseline corrected by a second-order polynomial fit in F_2 and a first-order polynomial fit in F_1. The NOESY spectrum recorded in H_2O was zero-filled in F_1 to 2K points and baseline corrected by a third-order polynomial fit in F_2.

Distance Restraints. The upper and lower diagonal part of each of the four NOESY buildup spectra were integrated separately with FELIX, yielding a total of eight peak intensity sets. The RANDMARDI procedure (Liu et al., 1995) of the complete relaxation matrix analysis method MARDIGRAS (Borgias and James, 1990; Borgias et al., 1990) was used to calculate interproton distance bounds from the eight intensity sets. In the calculations, an absolute noise level of the same order of magnitude as the smallest integrated cross-peak was used. A relative noise level for each integrated peak was set at 5% of the integrated peak intensity. The dynamic range of observed cross-peak intensities was 1000. In the RANDMARDI procedure, 30 different intensity sets were generated from each experimental data set based on the given noise levels and MARDIGRAS calculations were performed on all of them. Resulting distances from all 8 × 30 intensity sets were combined into a single bounds file from which the rMD restraint file was generated.

Upper and lower bounds in the bounds file were average interproton distances plus or minus one standard deviation calculated from all of the MARDIGRAS runs.

Restrained Molecular Dynamics. The obtained distance restraints were incorporated into an rMD procedure using DISCOVER (version 3.0, MSI, San Diego, Ca). The two starting models for structure refinement were obtained by manually docking TOTO11Et into a model of either A-form or B-form DNA in INSIGHTII (version 97, MSI, San Diego, Ca) followed by minimization using DISCOVER to relieve any strain in the models. During minimization, 22 distance restraints were included to mimic Watson−Crick hydrogen bonds. The TOTO11Et molecule was built using INSIGHTII and was geometry optimized to a minimum at the MNDO level using Gaussian94 (Frisch et al., 1995). Point charges were calculated at the HF/6-31G* level by fitting charges to the electrostatic potential at selected points (Breneman and Wiberg, 1990). The potentials for both DNA and TOTO11Et were assigned by the AMBER force field (Weiner et al., 1984, 1986), modified to accommodate the thiazole orange chromophore of TOTO11Et.

All the distance restraints were incorporated into an rMD procedure for structure refinement. An initial energy minimization was followed by 28 ps of restrained molecular dynamics at 600 K for 4 ps, followed by cooling to 200 K in 50 K steps of 3 ps each. The final structure was then energy minimized to a maximum derivative of 0.01 Å. A distance-dependent dielectric constant ($\epsilon = r$) was employed to account for solvent effects.

The pseudo-energy term used to enforce the distance restraints was

$$E_{NOE} = \begin{cases} k_1(r-r_1)^2 & \text{when } r_1 > r \\ 0 & \text{when } r_2 \geq r \geq r_1 \\ k_2(r-r_2)^2 & \text{when } r_2 > r \end{cases}$$

where r_1 and r_2 are the lower and upper distance bounds determined from cross-peak intensities and k_1 and k_2 are the force constants. A force constant of 50 kcal mol^{-1} Å^{-2} for lower and upper bounds was assigned to all distance restraints. DISCOVER uses a limit on the magnitude of the force a distance restraint can contribute with to the force field. This limit was set to 1000 kcal mol^{-1} Å^{-1}.

Helix parameters were calculated with the program CURVES 5.1 (Lavery and Sklenar, 1988, 1989).

Deoxyribose Ring Conformations. The H1′ to H2′ and H2″ region of a selective DQF-COSY spectrum was used as input to CHEOPS to obtain the values of the *J* coupling constants for the H1′, H2′, H2″, and H3′ deoxyribose ring protons (Macaya et al., 1992; Gochin et al., 1990).

The deoxyribose ring conformations were analyzed assuming a fast two-state equilibrium between N- and S-type conformations with a modified version of the program PSEUROT (de Leeuw and Altona, 1983). The standard version of PSEUROT applies a least-squares optimization routine to obtain the best fit of the parameters P_N, P_S, $\Theta_{max,N}$, $\Theta_{max,S}$, and X_S to the experimental coupling constants. In our randomized version of PSEUROT (RANDPSEUROT), we include the effect of uncertainties in the determined set of coupling constants. RANDPSEUROT generates 1000 sets of coupling constants by adding a random number to each experimentally determined coupling constant. The random numbers are generated according to a normal distribution (Press et al., 1986) where the dispersion is set according to the uncertainty of each determined coupling constant. Uncertainties of the coupling constants are carefully assessed by how well the back-calculated spectrum correlates with the experimental spectrum and by the response of the determined coupling constants to small changes in the simulation procedure. Subsequently, PSEUROT calculations are done on all the generated sets of coupling constants and RANDPSEUROT then calculates mean values and standard deviations of the parameters returned by PSEUROT. In the statistical analysis, N-type conformations are compared with N-types, and S-type conformations are compared with S-types based on the parameters returned by PSEUROT. In cases where PSEUROT returns either two N-type or two S-type conformations, the two conformations are sorted according to the major conformer.

Energy Calculations on the 1-TOTOEt and 1-TOTO11Et Complexes. The AMBER94 force field (Cornell et al., 1995) in MacroModel (version 6.0) (Mohamadi et al., 1990), modified to accommodate the thiazole orange chromophore, was used for the energy calculations together with the GB/SA solvation model (Still et al., 1990), which approximately includes the effects of solvent. Charges for the dsDNA were taken from the force field. For TOTOEt and TOTO11Et, charges were calculated by a restrained electrostatic potential (RESP) fit (Bay et al., 1993). The electrostatic potentials were calculated at the HF/6-31G* level with geometries optimized at the HF/3-21G* level using Gaussian94 (Frisch et al., 1995).

RESULTS

Spectral Analysis. The ^{1}H NMR spectrum of the **1**-TOTO11Et complex exhibits sharp lines (line widths of 7−9 Hz). These are as narrow as those observed for the **1**-TOTO and **1**-TOTOEt complexes. Observation of lines for just one DNA strand and one thiazole orange chromophore shows that **1**-TOTO11Et has dyad symmetry. The NOESY spectrum of this complex exhibits the characteristic features of bis-intercalation in the 5′-CTAG-3′ site (Stærk et al., 1997; Jacobsen et al., 1995; Spielmann et al., 1995; Petersen and Jacobsen, 1998; Hansen et al., 1996). A part of the NOESY spectrum is shown in the Supporting Information. The NOESY spectrum of the complex recorded in H_2O displays the normal Watson−Crick NOE connectivity pattern. The dsDNA and the thiazole orange chromophore resonances of the complex were assigned as previously described (Hansen et al., 1996; Jensen et al., 1998; Jacobsen et al., 1995; Spielmann et al., 1995). The DQF-COSY spectrum was used for the assignments of the proton resonances in the linker of TOTO11Et. Part of the DQF-COSY spectrum is shown in Figure 1. The chemical shift values of the TOTO11Et complex are given in the Supporting Information.

Structure Calculations. More than 550 NOE cross-peaks were observed in the NOESY spectrum obtained with a mixing time of 200 ms. Four sets of 458 NOE cross-peak intensities and four sets of 480 NOE cross-peak intensities, giving a total of 3752 integrated cross-peak intensities, were used in the MARDIGRAS calculations. Of these, 3480 corresponded to interproton distances that are not covalently fixed. Cross-peak integrals that corresponded to fixed distances in the dsDNA were used for internal calibrations in MARDIGRAS and, therefore, not converted into distance restraints for use in the rMD simulations. A correlation time of 3.75 ns was chosen for the calculations, based on experiments with dsDNA−drug complexes of a similar size (Spielmann et al., 1995; Petersen and Jacobsen, 1998). The RAND-

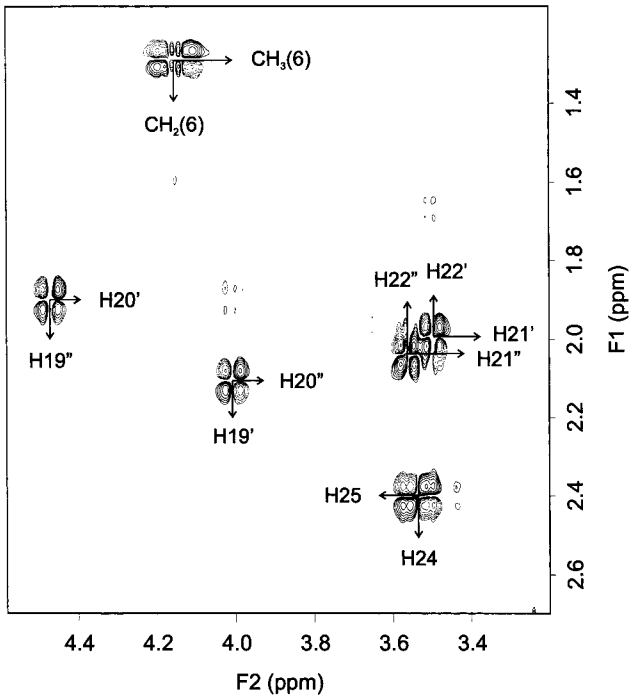


Figure 1. Part of the DQF-COSY spectrum of the **1**-TOTO11Et complex obtained at 750 MHz. Assignments of linker protons are shown together with the resonances of the N-ethyl protons of benzothiazole. The spectrum was used to make an unequivocal assignment of the linker protons. The cross-peak intensities between the H19′/H19″ and H20′/H20″ protons shows that H19′ is positioned trans to H20″ and gauche to H20′ and H19″ vice versa.

MARDI calculations returned 472 interproton distances based on the eight sets of NOE cross-peak intensities. The distribution of these is given in Table 1.

Covalently fixed distances within TOTO11Et were deliberately left out of the calibration in MARDIGRAS in order to provide a check on the performance of RANDMARDI. Good agreement between the covalently fixed distances and the corresponding distances derived from RANDMARDI indicated that the RANDMARDI procedure yielded accurate interproton distance bounds. The covalently fixed interproton distances within TOTO-11Et returned by RANDMARDI were not used in the rMD calculations. Unfortunately, no long covalently fixed interproton distances within TOTO11Et were calculated by RANDMARDI to provide a check on the performance of RANDMARDI for long interproton distances. Therefore, we decided to add 0.2 Å to all upper bounds so to compensate for any underestimated distances.

No symmetry was enforced during the RANDMARDI procedure. The bounds for symmetry-related restraints were calculated by averaging the symmetry-related upper and lower bounds for use in the rMD calculations.

Interproton distances involving exchangeable DNA amino and imino protons were derived from the NOESY spectrum of the complex recorded in H_2O. The normalized volume for the cross-peak between C7H5 and C7H6 was used as a reference for calculating the interproton distances involving exchangeable protons using the isolated spin pair approach (Borgias et al., 1990). Due to the inherent error in this approach, upper and lower bounds of ±1 Å were assigned to all distance restraints. Furthermore, 0.8 and 1.0 Å were added to the upper bounds for restraints involving methylene and methyl protons, respectively.

An additional 22 distance restraints were included to mimic Watson−Crick hydrogen bonds in the rMD calculations. Three hydrogen bonds were included for each of the six GC base pairs, and two hydrogen bonds were included for each of the two AT base pairs with upper and lower bounds of 1.7 and 2.1 Å, respectively.

Twenty final structures for each of the two starting structures were generated. All the structures converged to one family of conformations. The average all atom root-mean-square (rms) deviation of the coordinates of the 40 structures was 0.52 Å. The average sum of violations was 11.1 Å for both the A-form starting structures and the B-form starting structures. We observed two violations greater than 0.3 Å and none greater than 0.6 Å. Different views of the structure are presented in Figures 2 and 3.

The reliability of the structure calculations was carefully evaluated. rMD calculations were performed where the force constants of the distance restraints were varied between 25 and 100 kcal mol^{-1} $Å^{-2}$. All the calculations generated structures that converged to the same family of structures as with force constants of 50 kcal mol^{-1} $Å^{-2}$. A lower force constant resulted in a higher rms deviation and more violations. A higher force constant resulted in a lower rms deviation and fewer violations. The structure obtained is not strongly dependent on the exclusion of any of the restraints. In particular, calculations performed without the Watson−Crick restraints yielded exactly the same structure.

Helix Parameters. Helical parameters for the 40 final structures were analyzed with the program CURVES 5.1 (Lavery and Sklenar, 1988, 1989). Plots of some global helical parameters for the **1**-TOTO11Et complex are shown in Figure 4. The helical parameters for **1** (Spielmann, 1998a) along with the parameters for the **1**-TOTOEt complex (Petersen and Jacobsen, 1998) are included in Figure 4 for comparison.

Deoxyribose Ring Conformations. Due to the dyad symmetry of the **1**-TOTO11Et complex, only eight distinct deoxyribose residues are observed in the DQF-COSY

Table 1. Number of Distance Restraints Used in the rMD Calculations of the TOTO11Et Complex[a]

	intraresidue								
	sugar	base	total	interresidue		dye-DNA		dye-dye	
C1	10	6	16	C1-G2	11[b]	C3-TOTOEt	7(2)		31
G2	12	5	17	G2-C3	6	T4-TOTOEt	14(2)		
C3	4	2	6	C3-T4	4	A5-TOTOEt	27(1)		
T4	8	8	16	T4-A5	9	G6-TOTOEt	13(3)		
A5	13	6	19	A5-G6	4				
G6	6	5	11	G6-C7	5				
C7	6	5	11	C7-G8	4[b]				
G8	8	5	13	other	2(2)				
total	67	42	109	total	45	total	61	total	31

[a] The restraints were derived from MARDIGRAS calculations unless otherwise stated. Restraints derived from the NOESY spectrum recorded in H_2O are tabulated in parentheses. The 246 NOE connectivities gave a total of 492 symmetry related distance restraints; 22 distance restraints ensuring Watson−Crick base pairing were also included in the rMD calculations. [b] One restraint was derived directly from inspection of the spectra and used with loose bounds.

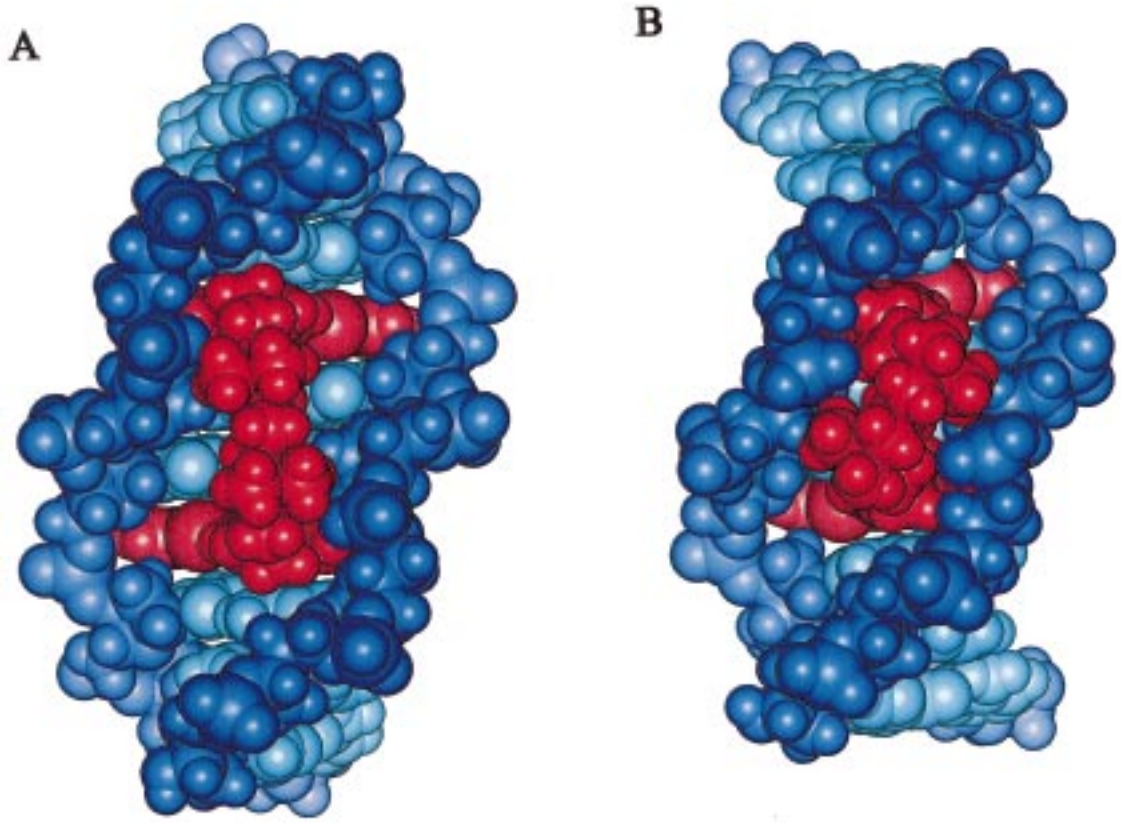


Figure 2. Structure of (A) **1**-TOTOEt and (B) **1**-TOTO11Et looking into the minor groove. The bis-intercalators are shown in red, the nucleobases are in light blue, and the sugar−phosphate backbones are in dark blue.

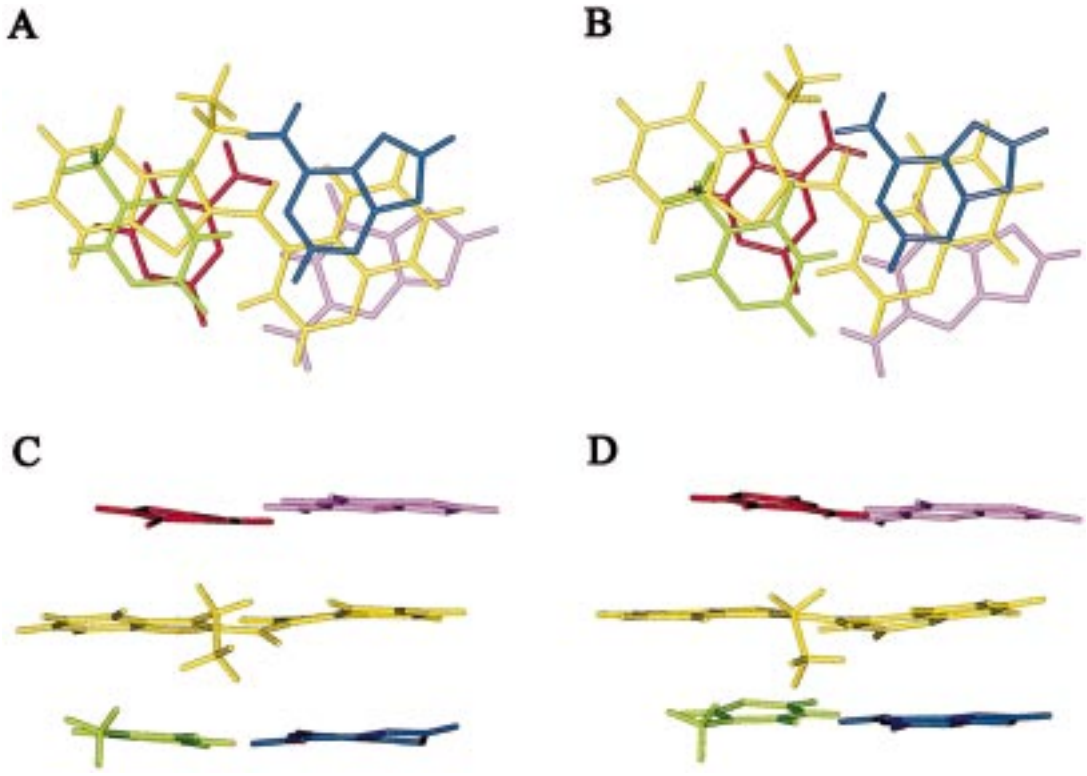


Figure 3. Stacking of the chromophore in the CpT·GpA binding site: (A) **1**-TOTOEt and (B) **1**-TOTO11Et viewed down the helix axis. (C) **1**-TOTOEt and (D) **1**-TOTO11Et viewed from the major groove side. Only nucleobases and chromophores are shown. It is evident that the chromophore in **1**-TOTO11Et is positioned toward the major groove compared with **1**-TOTOEt. The following coloring scheme is used: the chromophore, yellow; the adenine base, blue; the thymine base, green; the cytidine base, red; the guanine base, magenta.

spectrum. Simulation of G6 by CHEOPS was impossible due to severe overlap of the H2′ and H2″ resonances for this residue. For the remaining seven residues, the CHEOPS simulations of the DQF-COSY spectrum returned values that correlated rather well with the experimental spectrum (Macaya et al., 1992). The cou-

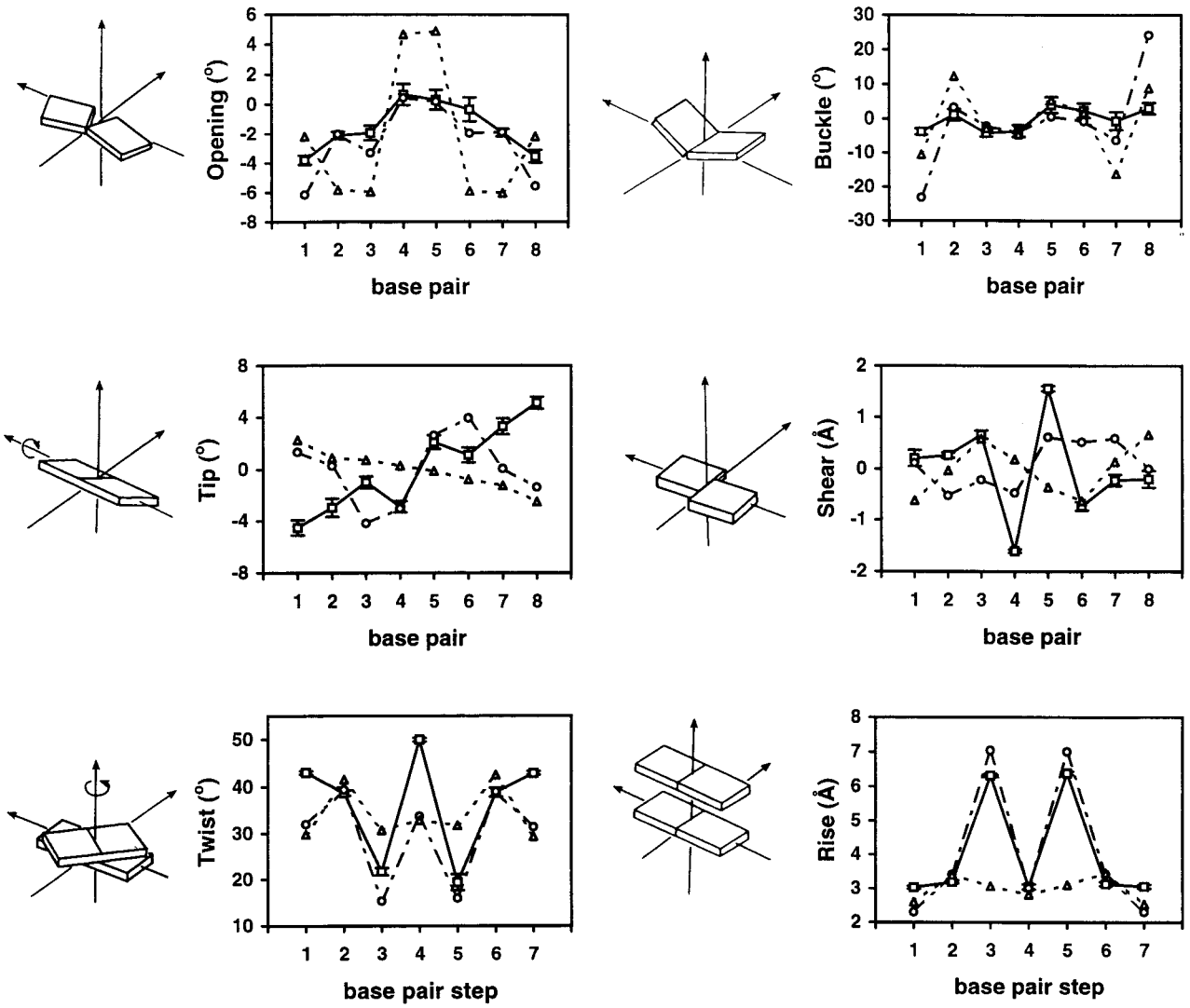


Figure 4. Helical parameters for **1**-TOTO11Et (□) calculated using CURVES and compared with **1** (△) and **1**-TOTOEt (○).

Table 2. Coupling Constants for the Sugar Protons in 1-TOTOEt and 1-TOTO11Et and the Derived Sugar Conformations[a]

	1-TOTO11ET							**1**-TOTOEt						
	$J_{1'2'}$	$J_{1'2''}$	$J_{2'3'}$	$J_{2''3'}$	%S	P_S	P_N[c]	$J_{1'2'}$	$J_{1'2''}$	$J_{2'3'}$	$J_{2''3'}$	%S	P_S	P_N[c]
C1	7.7	5.8	5.3	0.0	86(18)	178(32)	-	8.0	6.2	5.3	0.0	90(13)	146(21)	-
G2[b]	7.7	6.2	4.0	0.7	90(12)	189(17)	-	-	-	-	-	-	-	-
C3[d]	6.6	6.5	1.7	1.5			-	6.0	7.0	7.6	1.0	-	-	-
T4	9.8	5.2	6.5	1.0	90(12)	140(21)	-	9.6	4.5	6.7	2.8	84(8)	134(14)	-
A5	10.0	6.1	2.3	2.2	93(7)	176(9)	-	10.9	5.7	6.0	1.5	87(16)	181(31)	-
G6[b]	-	-	-	-	-	-	-	-	-	-	-	-	-	-
C7	8.1	6.1	4.9	0.0	90(15)	184(24)	-	7.8	6.4	7.0	0.0	83(19)	161(45)	-
G8	7.9	6.3	5.2	1.1	84(14)	180(26)	-	7.8	5.7	5.2	2.2	77(10)	167(21)	-

[a] The $J_{2'2''}$ coupling constants were fixed at −15 Hz in all CHEOPS simulations and the puckering amplitudes were fixed at 37 °C in PSEUROT calculations. The standard deviations are given in parentheses. [b] G6 in **1**-TOTO11Et and G2 and G6 in **1**-TOTOEt could not be analyzed due to spectral overlap. [c] If the mole fraction of the conformer was below 30% the *P* value was not considered to be determined with sufficient accuracy. [d] The coupling constants of C3 in **1**-TOTO11Et and **1**-TOTOEt could not be fitted to a two-state model.

pling constants returned by CHEOPS were used as input for RANDPSEUROT together with estimated uncertainties of the coupling constants. The coupling constants obtained along with the fraction of S-type sugar and pseudorotation angles calculated using RANDPSEUROT are given in Table 2. Corresponding values for **1**-TOTOEt are shown for comparison.

Energy Calculations. The noncovalent association of TOTOEt/TOTO11Et and dsDNA to form a complex was divided into two steps: (i) unwinding of the free dsDNA, **1**, to the dsDNA in the complex, **1***, and (ii) association of the bis-intercalator (B) to the unwound **1***. The first step describes the conformational distortion of the dsDNA to accommodate the bis-intercalator. In the second step, the bis-intercalator binds to the unwound dsDNA. To analyze the last step in more detail, TOTOEt and TOTO11Et were partitioned into a chromophore part (C) and a linker part (L) as indicated in Figure 5. Hydrogens were added where bonds were broken. The formation of the two complexes was evaluated by the following energies (Figure 5): ΔE_c (unwinding of **1** to **1***), ΔE_b (binding of **B** to **1***), ΔE_{bl} (binding of **L** to **1***), and ΔE_{bc} (binding

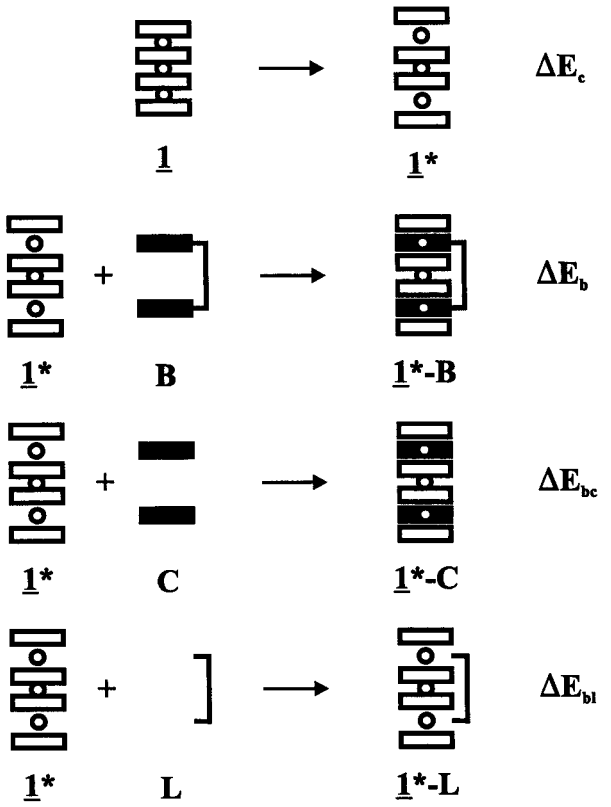


Figure 5. Schematic representation of the partition of the bis-intercalators TOTOEt and TOTO11Et (**B**) into a chromophore part (**C**) and a linker part (**L**) for energy calculations. **1** and **1*** represent free dsDNA and dsDNA in the complexes, respectively.

of **C** to **1***). We restricted the interpretation of the results only to include the calculated differences between the two complexes [e.g., $\Delta(\Delta E_c) = \Delta E_c$(TOTOEt) − ΔE_c-(TOTO11Et)] due to the approximative nature of the method.

The energies of **1***, **1***-C, **1***-L, and **1***-B for 1-TOTOEt and 1-TOTO11Et were evaluated using the structures determined by NMR spectroscopy in this work and earlier (Petersen and Jacobsen, 1998). Since the NMR structures are represented by an ensemble of 40 structures in each case, 10 structures were randomly chosen from the two ensembles and calculations were performed on all of them.

The energies of free TOTOEt, TOTO11Et, and the corresponding linkers were evaluated by finding the conformers with the lowest energy in each case. For the linkers, a systematic search through all torsional angles gave the global minimum. Unfortunately, the size of TOTOEt and TOTO11Et (18 and 20 variable torsion angles, respectively) precluded a systematic search. Instead, a number of systematic searches through subsets of torsion angles followed by 20 000 Monte Carlo steps were performed in each case. This led to more than 100 conformers with an energy within 1 kJ/mol of the lowest energy found. The conformers with the lowest energy were selected for each molecule. There is no guarantee that these conformers are the true lowest energy conformers, but due to the large number of conformers within 1 kJ/mol, it seems to be a reasonable choice. However, semiempirical PM3 calculations showed that the stacked geometry of the chromophores displayed by these lowest energy conformers of TOTOEt and TOTO11Et did not represent true energy minima, but were merely artifacts of the applied point charges. Consequently, a second set of force field calculations were done where stretched conformers of TOTOEt and TOTO11Et, optimized at the HF/3-21G* level, were used as reference geometries. The calculated energy differences with standard deviations are given in Table 3. It is important to notice that we obtain identical results for $\Delta(\Delta E_b)$ with the stacked and the stretched reference geometries of TOTOEt and TOTO11Et.

Table 3. Relative Energy Contributions to Complex Formation for TOTOEt and TOTO11Et

energy contribution	$\Delta(\Delta E)$ (kJ/mol)[a]	SD (kJ/mol)[d]
$\Delta(\Delta E_c)$	35.5	21.3
$\Delta(\Delta E_b)$	−9.4[b]	5.5
$\Delta(\Delta E_b)$	−8.6[c]	5.5
$\Delta(\Delta E_{bc})$	38.8	5.5
$\Delta(\Delta E_{bl})$	−33.8	4.1

[a] A positive value indicates more favorable reaction for TOTO-11Et compared with TOTOEt and vice versa. [b] Value with stacked reference geometries obtained by use of force field calculations guided by a Monte Carlo search (see text). [c] Value with stretched reference geometries obtained at the HF/3-21G* level (see text). [d] SD stands for standard deviation.

DISCUSSION

Description of the Structure. TOTO11Et bis-intercalates in the $(5'\text{-CTAG-}3')_2$ site. The benzothiazole moiety is intercalated between the pyrimidine bases, and the quinolinium system is intercalated between the two purine bases. The chromophore is positioned toward the edge of the major groove to optimize stacking with the nucleobases. The N-ethyl group on benzothiazole is centered in the major groove pointing toward the center of the oligonucleotide. The linker connecting the two chromophores is positioned in the minor groove. The N-methyl groups and the central part of the linker are positioned in the center of minor groove. Chemical shift values of the dsDNA protons at the binding site in TOTO11Et complex reflect intercalation similar to what was observed in the **1**-TOTO, **1**-TOTO11, and **1**-TOTOEt complexes (Spielmann et al., 1995; Stærk et al., 1997; Petersen and Jacobsen, 1998).

The structures of **1**-TOTOEt (Petersen and Jacobsen, 1998) and **1**-TOTO11Et exhibit the same overall features, but they are not identical. In fact, there are substantial differences between the two in both the dsDNA and the bis-intercalator part of the structures. These structural differences must be accredited to the longer linker in TOTO11Et. In both cases, the dsDNA part of the structures overall resembles B-DNA. The structural differences are analyzed with the aid of helical parameters and sugar conformations.

Helical Parameters. There are three major categories of helical parameters: Axis-base-pair, intra-base-pair, and inter-base-pair parameters (Dickerson et al., 1989). Plots of some of these parameters for **1**, **1**-TOTOEt and **1**-TOTO11Et are shown in Figure 4. The parameters reported for the terminal base pairs of the complex are not reliable because of the dynamic motions and are only included for completeness. Spectroscopically, the complexes were found to possess C_2 symmetry. The deviations of the structure and the calculated helical parameters from this symmetry reflect the level of uncertainty in the data.

Axis-Base-Pair Parameters. The global axes for the three structures are not completely straight but exhibit small overall bends of ∼2, ∼5, and ∼12° for **1**, **1**-TOTOEt, and **1**-TOTO11Et, respectively. The *x*-axis displacement, *y*-axis displacement, inclination, and tip are the param-

eters minimized to obtain the global helix axis (Lavery and Sklenar, 1988). The *x*-axis displacement, *y*-axis displacement, and inclination are not significantly different in the three structures, and in all cases they resemble the values for B-DNA. For **1**-TOTOEt and **1**-TOTO11Et, tip shows correlated changes from negative to positive going from C3 to G6, whereas with **1**, tip is essentially constant zero as in B-DNA. The correlated changes for **1**-TOTOEt and **1**-TOTO11Et are a consequence of a small kink in their helical axes (Petersen and Jacobsen, 1998).

Intra-Base-Pair Parameters. The values obtained for shear, stretch, stagger, and opening are partially determined by the constraints introduced to mimic Watson−Crick base pairing. However, for **1**-TOTOEt and **1**-TOTO11Et, the central part of the oligonucleotide is locked by the numerous NOEs between dsDNA and the bis-intercalators.

Shear shows large changes across the intercalation site compensating for the intercalation of the chromophores. The shear introduced is most pronounced with **1**-TOTO11Et. This is probable due to the relative position of the chromophores in the complexes (vide infra). An opening larger than for normal B-DNA narrows the minor groove essentially to the same degree for both complexes, probably due to van der Waals and electrostatic interactions between the linkers and minor groove.

The propeller twist and buckle are almost the same for the three structures, showing that the chromophore fits very well into the stacking pattern of the oligonucleotide without the introduction of propeller twist or buckle to maximize van der Waals contacts between the nucleobases and the chromophores.

Inter-Base-Pair Parameters. The twist and rise values reveal, as expected, that **1**-TOTOEt and **1**-TOTO11Et unwind relative to **1** in the C3·T4 and A5·G6 base pair steps to accommodate the chromophores. In these base pair steps, the twist is 31, 16, and 21° for **1**, **1**-TOTOEt, and **1**-TOTO11Et, respectively, showing that **1**-TOTOEt unwinds more than **1**-TOTO11Et. The twist in the central base pair step T4·A5 shows that **1**-TOTOEt does not unwind relative to **1** whereas **1**-TOTO11Et overwinds. However, the three structures have a similar rise in this base pair step, indicating that a rise smaller than ∼2.8−3.0 Å is unfavorable probably due to a large energy penalty from the exchange-repulsion contribution to the van der Waals interactions. Taking into account the five central base pair steps, **1**-TOTOEt and **1**-TOTO11Et are unwound by ∼73 and ∼22°, respectively, relative to **1**. This large structural difference between the **1**-TOTOEt and **1**-TOTO11Et complexes can be rationalized by considering the length of the linker (vide infra). The central part of minor groove in **1**-TOTO11Et is more narrow than in **1**-TOTOEt due to the larger degree of unwinding in the latter case.

Sugar Conformations. In B-DNA, the deoxyribose ring adopts an S-type conformation described by a pseudorotation angle *P* of 180 ± 90°, while the deoxyribose ring in A-DNA adopts an N-type conformation described by a pseudorotation angle *P* of 0 ± 90°. The RANDPSEUROT calculations resulted in almost pure S-type conformations (%S above ∼80%) for all residues analyzed in both **1**-TOTOEt and **1**-TOTO11Et. The analyzed sugar conformations in the two structures are nearly identical.

The inability of PSEUROT to describe C3 in **1**-TOTO11Et and **1**-TOTOEt with a two-state model shows that the dynamic behavior of these residues is complex. The $J_{2'3'}$ coupling constant in C3 is very different in **1**-TOTO11Et and **1**-TOTOEt. This is difficult to rationalize due to the inability of PSEUROT to describe these residues. However, this is in agreement with the unusual conformational properties observed by Spielmann (1998b) from NMR relaxation parameters of the **1**-TOTO complex.

Chromophore Part. The chromophore has virtually the same conformation in the two structures. In both cases, the relative conformation of the benzothiazole system and the quinolinium system is as indicated in Scheme 1. In both structures, the twist between the two flat aromatic ring systems is fairly small ∼5−10°. In **1**-TOTO11Et, the chromophore is moved toward the major groove compared with the position in the **1**-TOTOEt complex; this in turn leads to a diminution of the overlap between the chromophore and the flanking base pairs and a possible loss in stacking. In compensating for this loss, A5 is moved further into major groove to regain some overlap and by that introducing more shear in the central AT base pairs of **1**-TOTO11Et compared with **1**-TOTOEt. The separation of the chromophore and the flanking base pairs is smaller in **1**-TOTO11Et than in **1**-TOTOEt as reflected in the rise for the C3-T4 base pair step, which is ∼6.3 Å in **1**-TOTO11Et and ∼7.0 Å in **1**-TOTOEt. The relative orientation of the chromophores is ∼60 and ∼45° (C3-N11-N11′-C3′-dihedral) in **1**-TOTOEt and **1**-TOTO11ET, respectively, due to the different degree of unwinding in the two complexes.

Linker Part. The conformation of the two linkers is very different. In **1**-TOTOEt the short linker is stretched and crosses the minor groove between the two by symmetry related adenines in the oligonucleotide. The N-methyl groups are pointing toward the guanine phosphate, placing this positively charged group in an energetically favorable region caused by the negatively charged phosphate. The longer linker in **1**-TOTO11Et is curved in an S-form. The first 3−4 linker methylene groups guide the linker out into the minor groove, placing the middle part of the linker in the center of minor groove. In this complex the N-methyl groups are also positioned in the vicinity of a guanine phosphate, but now they are closest to the guanine phosphate on the other strand compared with **1**-TOTO11Et. In **1**-TOTO11Et, the linker has larger degree of van der Waals contacts to the walls of the narrow minor groove than with the **1**-TOTOEt complex.

The unwinding of **1**-TOTOEt creates a wide and shallow minor groove and enables the chromophores to be connected by a straight linker. On the other hand, **1**-TOTO11Et unwinds less, leading to a smaller vertical distance between the chromophores. At first this seems favorable for a short linker as in TOTOEt, but this is not the case because less unwinding also brings other structural changes along: the chromophore moves toward the major groove, probably due to a steric interference with the backbone, and the minor groove becomes more narrow and curved. This prevents the chromophores from being connected by a straight linker; this would lead to steric clashes between linker and backbone atoms. Instead, a longer linker as in TOTO11Et is needed to guide the linker from the chromophore out into minor groove and to follow the curved minor groove.

The dependence of unwinding of dsDNA on the linker length shows that with TOTO analogues the degree of unwinding displayed by the complexes can be controlled through the right choice of linker. An intermediate degree of unwinding compared to **1**-TOTOEt and **1**-TOTO11Et is likely obtained by choosing a linker length between the ones for **1**-TOTOEt and **1**-TOTO11Et.

Energetic. The positive value of $\Delta(\Delta E_c)$ indicates that the dsDNA is less distorted in **1**-TOTO11Et than in **1**-TOTOEt. This is probably due to the smaller degree of unwinding in the former case. The binding of the chromophores to the unwound dsDNA is more favorable for TOTO11Et than for TOTOEt as $\Delta(\Delta E_{bc}) > 0$. A closer look into the different contributions reveals that this is not due to a better stacking between the chromophores and the nucleobases in **1**-TOTO11Et. This would also be surprising considering that the position of the chromophores in terms of overlap with the nucleobases seems more favorable for TOTOEt (See above). Instead, a better electrostatic interaction with the solvent for TOTO11Et is the determining factor. Since $\Delta(\Delta E_{bl})$ is less than zero, the association of the linker to the unwound dsDNA is most favorable for TOTOEt probably due to the unfavorable curved conformation of the linker in **1**-TOTO11Et. If the linkers are preoptimized for binding (similar to the dsDNA), we find that there is a preference for binding in TOTO11Et. This indicates that the linker of TOTO11Et makes the best nonbonding contacts with dsDNA. In total, the binding of the bis-intercalators to the unwound dsDNA has a slight preference for TOTOEt over TOTO-11Et. The contributions from the linker and chromophore cancel each other partly.

Selectivity. The site selectivity of TOTO among 5′-pyrimidine-pyrimidine-purine-purine-3′ sites is explained by a subtle interplay between optimal stacking of the chromophores with the nucleobases and electrostatic interactions of the polyamine linker with the minor groove (Bunkenborg et al., 1998). The linker in **1**-TOTOEt is completely extended and therefore structurally restrictive. This makes TOTOEt prone to steric hindrance in minor groove. In **1**-TOTO11Et, the linker is curved and less restrictive on the structure. Steric hindrance in minor groove is therefore expected to more important for TOTO than for TOTO11. This is in agreement with the reduced site selectivity upon introduction of the longer linker in TOTO11 (Bunkenborg et al., 1998).

CONCLUSION

The longer linker introduced in **1**-TOTO11Et results in a much smaller degree of unwinding in **1**-TOTO11Et than in **1**-TOTOEt. This is explained by the inability of a short linker to connect the chromophores in a complex with a low degree of unwinding. In **1**-TOTO11Et, the chromophore is positioned toward the major groove compared with its position in **1**-TOTOEt. This is probably caused by a steric interference of the chromophore with the backbone in the former case. The position of the chromophore and the small degree of unwinding in **1**-TOTO11Et require a curved conformation of the linker here opposite to the extended conformation displayed by the linker in **1**-TOTOEt. The influence of the linker length on unwinding of dsDNA in complexes between dsDNA and TOTO analogues demonstrates that the degree of unwinding of dsDNA can be controlled through the choice of linker.

The binding of the bis-intercalators to the unwound dsDNA is slightly favorable for TOTOEt, but the complex formation is overall more favorable for **1**-TOTO11Et because dsDNA is distorted less upon complex formation in this case. This increase in affinity for TOTO11Et is followed by a likely decrease in site selectivity, because the linker in TOTO11Et is less restrictive on the structure than the linker in TOTOEt.

ACKNOWLEDGMENT

We thank The Instrument Center for NMR-Spectroscopy of Biological Macromolecules at The Carlsberg Laboratory, Copenhagen, granted by The Danish Natural Science Research Council for providing spectrometer time at the 750 MHz spectrometer. The authors are grateful to Dr. E. B. Pedersen for supplying the TOTO11Et and to Dr. F. Jensen for the use of MacroModel6.0 and many stimulating discussions.

Supporting Information Available: Table of chemical shift values and a figure of the NOESY spectrum of the TOTO11Et complex. This material is available free of charge via the Internet at http://pubs.acs.org.

LITERATURE CITED

Bay, C. I., Cieplak, P., Cornell, W. D., and Kollman, P. A. (1993) A Well-Behaved Electrostatic Potential Based Method Using Charge Restraints for Deriving Atimic Charges: The RESP Model. *J. Phys. Chem. 97*, 10269−10280.

Benson, S. C., Singh, P., and Glazer, A. N. (1993a) Heterodimeric DNA-Binding Dyes Designed for Energy Transfer: Synthesis and Spectroscopic Properties. *Nucleic Acids Res. 21*, 5727−5735.

Benson, S. C., Mathies, R. A., and Glazer, A. N. (1993b) Heterodimeric DNA-binding Dyes Designed for Energy Transfer: Stability and Applications of DNA Complexes. *Nucleic Acids Res. 21*, 5720−5726.

Borgias, B. A., and James, T. L. (1990) MARDIGRAS-A Procedure for Matrix Analysis of Relaxation for Discerning Geometry of an Aqueous Structure. *J. Magn. Reson. 87*, 475−487.

Borgias, B. A., Gochin, M., Kerwood, D., and James, T. L. (1990) Relaxation Matrix Analysis of 2D NMR Data. *Prog. NMR Spectrosc. 22*, 83−100.

Breneman, C. M., and Wiberg, K. B. (1990) Determinating Atom-Centered Monopoles from Molecular Electrostatic Potentials. The Need for High Sampling Density in Formamide Conformational Analysis. *J. Comput. Chem. 11*, 361−373.

Bunkenborg, J., Stidsen, M. M., and Jacobsen, J. P. (1999) On the Sequence Selective Bis-intercalation of a Homodimeric Thiazole Orange Dye in DNA. *Bioconjugate Chem*. (In press).

Cornell, W. D., Cieplak, P., Bayly, I., Gould, I. R., Merz, K. M., Ferguson, D. M., Spellmeyer, D. C., Fox, T., Caldwell, J. W., and Kollman, P. A. (1995) A Second Generation Force Field for the Simulation of Proteins, Nucleic Acids, and Organic Molecules. *J. Am. Chem. Soc. 117*, 5179−5197.

de Leeuw, F. A. A. M., and Altona, C. (1983) Computer-Assisted Pseudorotation Analysis of Five-Membered Rings by Means of Proton Spin−Spin Coupling Constants: Program PSEUROT. *J. Comput. Chem 4*, 428−437.

Dickerson, R. E., Bansal, M., Calladine, C. R., Diekmann, S., Hunter, W. N., Kennard, O., von Kitzing, E., Nelson, H. C. M., Lavery, R., Olson, W. K., Saenger, W., Shakked, Z., Soumpasis, D. M., Tung, C.-S., Sklenar, H., Wang, A. H. J., and Zhurkin, V. B. (1989) Definitions and Nomenclature of Nucleic Acid Structure Parameters. *EMBO J. 8*, 1−4.

Frisch, M. J., Trucks, G. W., Schlegel, H. B., Gill, P. M. W., Johnson, B. G., Robb, M. A., Cheeseman, J. R., Keith, T. A., Petersson, G. A., Montgomery, J. A., Raghavachari, K., Al-Laham, M. A., Zakrewski, V. G., Ortiz, J. V., Foresman, J. B., Cioslowski, J., Stefanov, B. B., Nanayakkara, A., Challacombe, M., Peng, C. Y., Ayala, P. Y., Chen, W., Wong, M. W., Andres, J. L., Replogle, E. S., Comperts, R., Martin, R. L., Fox, D. J., Binkley, J. S., Defrees, D. J., Baker, J., Stewart, J. P., Head-Gordon, M., Gonzalez, C., and Pople, J. A. (1995) *Gaussian94 (Rev D.3)*, Gaussian Inc, Pittsburgh, PA.

Geen, H., and Freeman, R. (1991) Band-Selective Radio frequency Pulses. *J. Magn. Reson. 93*, 93−141.

Glazer, A. N., and Rye, H. S. (1992) Stable Dye-DNA Intercalation Complexes as Reagents for High-Sensitivity Fluorescence Detection. *Nature 359*, 859−861.

Gochin, M., Zon, G., and James, T. L. (1990) Two-Dimensional COSY and Two-Dimensional NOE Spectroscopy of $d(AC)_4$: $d(AC)_4$: Extraction of Structural Constraints. *Biochemistry 29*, 11161−11171.

Hansen, L. F., Jensen, L. K., and Jacobsen, J. P. (1996) Bis-Intercalation of a Homodimeric Thiazole Orange Dye in DNA in Symmetrical Pyrimidine-Pyrimidine-Purine-Purine oligonucleotides. *Nucleic Acids Res. 24*, 859−867.

Jacobsen, J. P., Pedersen, J. B., Hansen, L. F., and Wemmer, D. E. (1995) Site Selective Bis- Intercalation of a Homodimeric Thiazole Orange Dye in DNA Oligonucleotides. *Nucleic Acids Res. 23*, 753−760.

Jensen, L. K., Gotfredsen, C. H., Bondensgaard, K., and Jacobsen, J. P. (1998) Bis-Intercalation of Homodimeric Thiazole Orange Dyes in Selective Binding Sites of DNA Studied by 1H NMR spectroscopy. *Acta Chem. Scand. 52*, 641−650.

Lavery, R., and Sklenar, H. (1988) The Definition af Generalized Helicoidal Parameters and for Axis Curvature of Irregular Nucleic Acids. *J. Biomol. Struct. Dyn. 6*, 63−91.

Lavery, R., and Sklenar, H. (1989) Defining the Structure of Irregular Nucleic Acids: Conventions and Principles. *J. Biomol. Struct. Dyn. 7*, 655−667.

Liu, H., Spielmann, H. P., Ulyanov, N. A., Wemmer, D. E., and James, T. L. (1995) Interproton Distances Bounds from 2D-NOE Intensities: Effect of Experimental Noise and Peak Integration Errors. *J. Bio. NMR 6*, 390−402.

Macaya, R. F., Schultze, P., and Feigon, J. (1992) Sugar Conformation in Intramolecular DNA Triplexes Determined by Coupling Constants Obtained by Automated Simulation of P.COSY Cross Peaks. *J. Am. Chem. Soc. 114*, 781−783.

Mohamadi, F., Richards, N. G. J., Guida, W. C., Liskamp, R., Lipton, M., Caufield, C., Chang, G., Hendrickson, T., and Still, W. C. (1990) MacroModel − An Integrated Software System for Modeling Organic and Bioorganic Molecules Using Molecular Mechanics. *J. Comput. Chem 11*, 440−452.

Petersen, M., and Jacobsen, J. P. (1998) Solution Structure of a DNA Complex with the Fluorescent Bis-Intercalator TOTO Modified on the Benzothiazole Ring. *Bioconjugate Chem. 9*, 331−340.

Press, W. H., Flannery, B. P., Teukolsky, S. A., and Vetterling, W. T. (1986) *Numerical Recipes*, Cambridge University Press, Cambridge.

Rye, H. S., Quesada, M. A., Peck, K., Mathies, R. A., and Glazer, A. N. (1990) High-Sensitivity Two-Color Detection of Double-Stranded DNA with a Confocal Fluorescence Gel Scanner using Ethidium Homodimer and Thiazole Orange. *Nucleic Acids Res. 19*, 327−333.

Rye, H. S., Yue, S., Wemmer, D. E., Quesada, M. A., Haugland, R. P., Mathies, R. A., and Glazer, A. N. (1992) Stable Fluorescent Complexes of Double-stranded DNA with Bis-Intervalating Asymmetric Cyanine Dyes: Properties and Applications. *Nucleic Acids Res. 20*, 2803−2812.

Rye, H. S., Yue, S., Quesada, M. A., Haugland, R. P., Mathies, R. A., and Glazer, A. N. (1993a) (30) Picogram Detection of Stable Dye-DNA Intercalation Complexes with Two-Color Laser-Excited Confocal Fluorescence Gel Scanner. *Methods in Enzymology 217*, 414−431.

Rye, H. S., Dabora, J. M., Quesada, M. A., Mathies, R. A., and Glazer, A. N. (1993b) Fluorometric Assay Using Dimeric Dyes for Double- and Single-Stranded DNA and RNA with Picogram Sensitivity. *Anal. Biochem. 208*, 144−150.

Spielmann, H. P. (1998a) Unpublished results.

Spielmann, H. P. (1998b) Dynamics of a Bis-Intercalator DNA Complex by ^{1}H-Detected Natural Abundance ^{13}C NMR Spectroscopy. *Biochemistry 37*, 16863−16876.

Spielmann, H. P., Wemmer, D. E., and Jacobsen, J. P. (1995) Solution Structure of a DNA Complex with the Fluorescent Bis-Intercalator TOTO Determined by NMR Spectroscopy. *Biochemistry 34*, 8542−8553.

Stærk, D., Hamed, A. A., Pedersen, E. B., and Jacobsen, J. P. (1997) Bis-Intercalation of Homodimeric Thiazole Orange Dyes in DNA: The Effect of Modifying the Linker. *Bioconjugate Chem. 8*, 869−877.

Still, W. C., Tempczyk, A., Hawley, R. C., and Hendrikson, T. (1990) Semianalytical Treatment of Solvation for Molecular Mechanics and Dynamics. *J. Am. Chem. Soc. 112*, 6127−6129.

Wakelin, L. P. G. (1986) Polyfunctional DNA intercalating agents. *Med. Res. Rev. 6*, 275−340.

Weiner, S. J., Kollman, P. A., Case, D. A., Singh, U. C., Ghio, C., Algona, G., Profeta, S., and Weiner, P. (1984) A New Force Field for Molecular Mechanical Simulation of Nucleic Acids and Proteins. *J. Am. Chem. Soc. 106*, 765−784.

Weiner, S. J., Kollman, P. A., Nguyen, C. H., and Case, D. A. (1986) An All Atom Force Field for Simulation of Proteins and Nucleic Acids. *J. Compt. Chem 7*, 230−252.

BC9900284

Table S1. Chemical Shifts Values (in Parts per Million) of the TOTO11Et Complex with d(CGCTAGCG)$_2$ at 27°C Compared to Those of the Free Oligonucleotide in parentheses[a]

	C1	G2	C3	T4	A5	G6	C7	G8
H8/H6	7.52(7.65)	7.74(7.99)	6.47(7.44)	7.07(7.41)	8.19(8.23)	7.79(7.70)	7.30(7.30)	7.88(7.93)
H5/CH_3/H2	5.75(5.92)		4.64(5.39)	0.76(1.70)	6.81(7.37)		5.30(5.34)	
H1'	5.67(5.81)	5.72(5.97)	5.99(5.98)	5.16(5.60)	5.72(6.02)	5.80(5.71)	5.76(5.76)	6.10(6.16)
H2'	1.89(2.00)	2.41(2.71)	1.83(2.07)	1.99(2.14)	2.80(2.74)	2.65(2.50)	1.87(1.87)	2.59(2.60)
H2"	2.31(2.45)	2.41(2.77)	2.46(2.51)	2.18(2.44)	2.74(2.88)	2.65(2.60)	2.31(2.33)	2.34(2.37)
H3'	4.63(4.76)	4.84(5.00)	4.64(4.78)	4.68(4.88)	5.14(5.05)	4.86(4.95)	4.79(4.79)	4.66(4.66)
H4'	4.01(4.09)	4.25(4.38)	4.06(4.24)	4.16(4.14)	4.39(4.40)	4.18(4.37)	4.19(4.14)	4.16(4.16)
H5'	3.68(3.74)	4.03(4.01)	4.22(4.26)	4.06(4.09)	4.16(4.06)	4.03(4.19)	4.12(4.19)	4.07(4.06)
H5"	3.68(3.74)	3.90(4.11)	4.17(4.18)	4.22(4.09)	4.06(4.15)	4.33(4.19)	4.12(4.10)	4.07(4.06)
H1/H3		12.76(13.02)		13.46(13.76)		12.03(12.76)		
H4/H6			8.02(8.27)		7.19(7.81)		8.17(8.34)	
H4/H6			6.56(6.58)		6.60(6.54)		6.39(6.47)	

© 1999 American Chemical Society, Bioconjugate Chem., Bondensgaard bc990284 Supporting Info Page 1

Table 1. .....continued

TOTO11Et		TOTO11Et		TOTO11Et		TOTO11Et	
H1	7.46	H9	6.46	H19'	4.02	H22"	3.56
H2	7.57	H10	7.95	H19"	4.48	CH_3(23')	3.23
H3	7.57	H13	6.84	H20'	1.90	CH_3(23")	3.28
H4	7.42	H14	6.84	H20"	2.10	H24'	3.55
CH_3(6)	1.28	H15	6.66	H21'	1.99	H24"	3.55
CH_2(6)	4.17	H16	7.49	H21"	2.04	H25'	2.39
H8	6.18			H22'	3.50	H25"	2.39

[a] The values are given relative to DSS. Hydrogen-bonded amino protons are underlined.

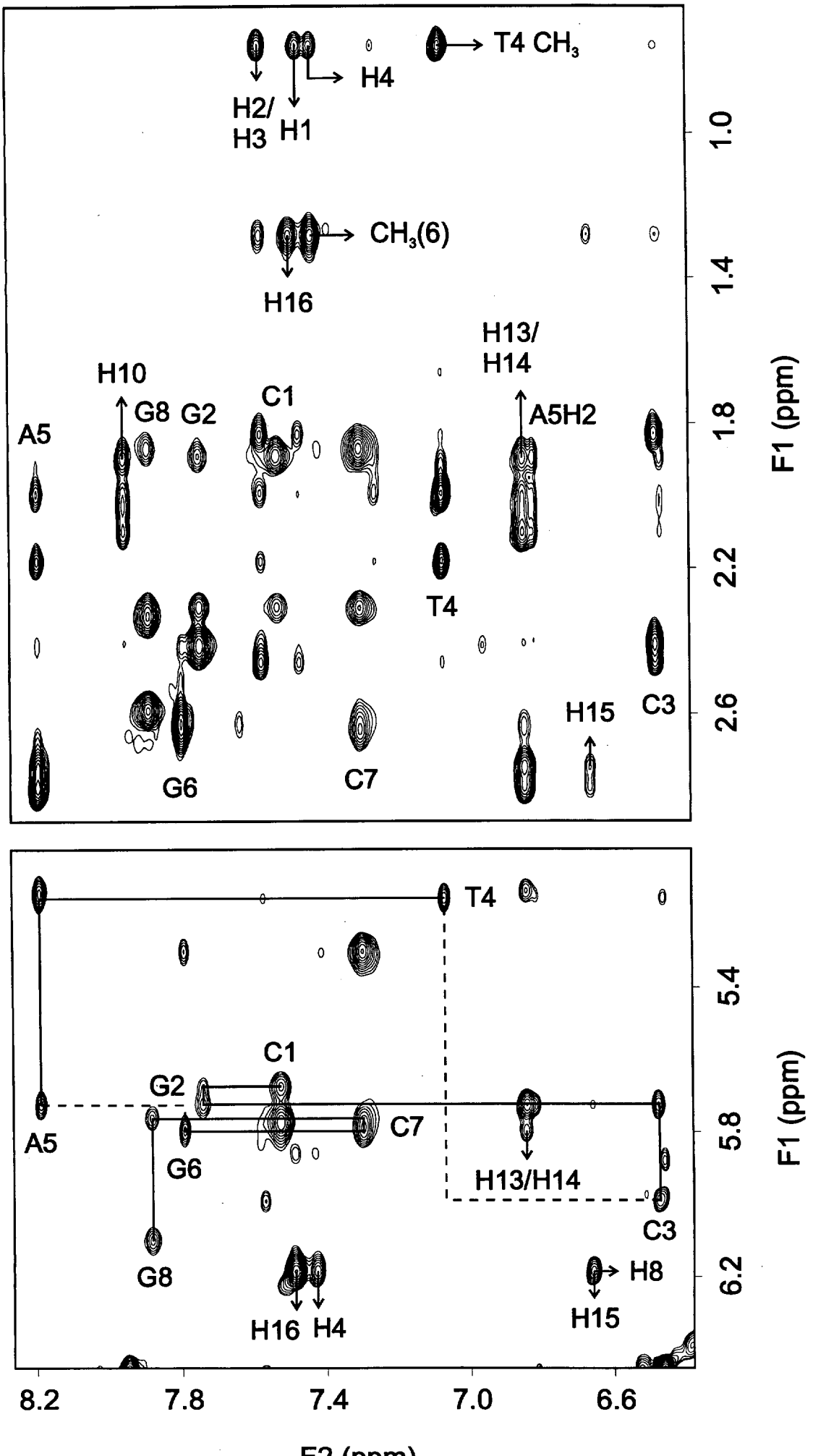
© 1999 American Chemical Society, Bioconjugate Chem., Bondensgaard bc9900284 Supporting Info Page 2

© 1999 American Chemical Society, Bioconjugate Chem., Bondensgaard bc9900284 Supporting Info Page 3

FIGURE LEGENDS

Figure S1. The H2'/H2" to aromatic part (top) and H1' to aromatic part (bottom) of the 200 ms NOESY spectrum of the TOTO11Et complex. The assignments of the H8/H6 resonances for the various nucleotides are indicated together with the resonances of the thymidine methyl protons and some of the TOTO protons (denoted by the letter H). The sequential H1'-H6/H8-H1' connectivity pathway is indicated by a solid line. The interrupted connectivities at the 5'-C3pT4-3' and 5'-A5pG6-3' base pair steps due to intercalation are indicated by dotted lines. A few of the observed cross peaks between TOTO11Et and the oligonucleotide are also marked.

© 1999 American Chemical Society, Bioconjugate Chem., Bondensgaard bc9900284 Supporting Info Page 4



Peptide-Based Intracellular Shuttle Able To Facilitate Gene Transfer in Mammalian Cells

Devender Singh,[‡] Stuart K. Bisland, Kim Kawamura, and Jean Gariépy[†]

Division of Molecular and Structural Biology, Department of Medical Biophysics, University of Toronto and the Ontario Cancer Institute, Princess Margaret Hospital, 610 University Avenue, Toronto, Canada M5G 2M9.
Received November 3, 1998; Revised Manuscript Received March 11, 1999

Loligomers are peptide-based intracellular vehicles able to penetrate cells and self-localize into distinct cellular compartments. Loligomers can be rapidly assembled by automated solid-phase approaches and were designed to act as nonviral, nonlipophilic intracellular shuttles. One nucleus-directed loligomer, termed loligomer 4, was evaluated for its ability to function as a transfection agent. Loligomer 4 readily associates with plasmids to form noncovalent complexes. The migration of loligomer 4−plasmid complexes into cells was monitored by flow cytometry and fluorescence microscopy. Populations of plasmids labeled with 7-AAD exist either free or in association with loligomer 4 inside cells and are visible throughout the cytosol and nucleus of chinese hamster ovary (CHO) cells. Loligomer 4−plasmid complexes were not cytotoxic to cells and were readily imported by most cells (>70%). CHO cells were transfected with complexes of loligomer 4 and plasmids harboring luciferase, green fluorescent protein or β-galactosidase reporter genes. The transfection efficiency of loligomer 4−plasmid DNA complexes was greater when cells were maintained as suspensions instead of monolayers. Transfections could be performed with cells suspended in serum-containing medium. The observed levels of transfection, however, were modest with 5−10% of CHO cells expressing either a green fluorescent protein or the enzyme β-galactosidase. Loligomers have recently been observed in vesicular compartments [Singh, D., Kiarash, R., Kawamura, K, LaCasse, E. C., and Gariépy, J. (1998) *Biochemistry 37*, 5798−5809] and differences between levels of cellular import and transfection efficiency may well reflect the need to optimize the release of loligomers and their complexes from these compartments in future designs. In summary, loligomer 4 behaves as a stable, soluble and effective transfection agent. These results demonstrate the feasibility of designing loligomers able to act as intracellular guided agents aimed at gene transfer applications.

INTRODUCTION

Transcription of exogenous genes in mammalian cells has proven invaluable in a wide variety of applications. These uses include the expression of foreign genes in mammalian cells, the production of proteins from cloned cDNAs, the analysis of transcriptional regulatory sequences, and the expression of molecules involved in the intracellular sorting and posttranslational processing of secreted polypeptides. A variety of methods has been developed to transfer genes into eukaryotic cells. These techniques involve the direct physical intake of DNA by the cell, either introduced in the context of a viral particle inside the cell (*1*, *2*), microinjected directly into the cell, or introduced through the use of receptor-mediated gene transfer strategies (*3*−*5*) or by utilizing nonviral gene-transfer methods in combination with a lysosomotropic agent such as chloroquine (*6*). The choice of a gene transfer technique is dependent on the cell line or cell type as well as the limitations of the experimental design. Most biochemical methods result in the disruption of cell membranes that allow the import of DNA (*7*), either through the formation of DNA complexes with inorganic salts and polycations (*8*) or with lipids (*9*, *10*). Recent examples of peptide− and polycations−DNA complexes able to act as efficient transfection agents have also been reported (*11*−*14*).

Nonviral DNA transfection techniques have historically resulted in a low efficiency transfer of the DNA into a cell population in comparison to virus-mediated transfer methods involving the use of SV40 vectors, vaccinia virus, adenovirus, and retroviruses. Although retroviral transduction can lead to a higher transfection efficiency in terms of gene transfer and integration (60−90%), the efficacy of retroviral infection itself remains limited by the titer associated with the helper-free packaging cell line, the time of infection, and its facilitated uptake with various chemical substrates (*2*, *15*). Calcium phosphate-mediated transfection (*16*) is one of the oldest approaches and is still the most popular transfection method (*17*). Other popular methods include DEAE-dextran mediated transfection (*18*), electroporation (*19*), liposome technology (*20*), lipid-mediated transfection (*21*), and electropermeabilization (*22*).

The need to design defined, guided intracellular vehicles able to act as efficient nonviral gene delivery agents is obvious and can potentially be addressed using solid-phase synthesis strategies. In particular, the concept of loligomers[1] (*23*, *24*) was recently developed as a design strategy for creating multitasking agents to target different organelles in cells. Loligomers contain functional domains presented on a tentacular scaffold. More precisely, lysine residues give rise to a branched peptide, which presents multiple domains that code for functions

* To whom correspondence should be addressed. Phone: (416) 946-2967. Fax: (416) 946-6529. E-mail: gariepy@oci.utoronto.ca.

[‡] Present address: Gemma Biotechnology, 620 University Avenue, Toronto, Canada M5G 2M9.

10.1021/bc980131d CCC: $18.00 © 1999 American Chemical Society
Published on Web 08/25/1999

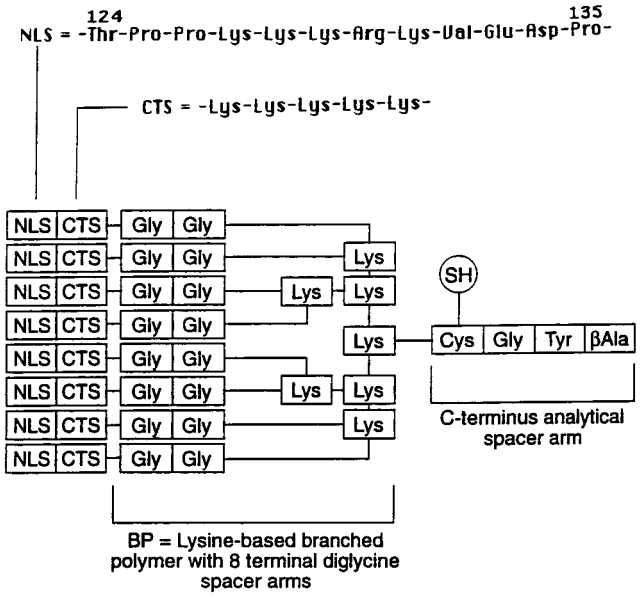


Figure 1. Structure of loligomer 4, a peptide-based intracellular vehicle (*23*, *24*). This construct consists of a 5-amino acid long, C-terminal region (analytical arm) and eight identical N-terminal arms linked together through a branched lysine polymer (BP). Each N-terminal arm contains a domain representing the nuclear localization signal of the SV40 large T-antigen (NLS; residues 124−135) and a lysine pentapeptide acting as a cytoplasmic translocation signal (CTS).

such as cellular delivery, cell signaling, and/or cytotoxicity. Prototypic loligomers have been generated that can self-localize in the nucleus of cells (*23*). The intracellular routing of a nucleus-directed loligomer was recently analyzed by microscopy and flow cytometry, indicating its presence in the cytosol, in endocytic vesicles, and in the nucleus of eukaryotic cells (*24*). In this report, we demonstrated the ability of one such loligomer, termed loligomer 4, to associate noncovalently with plasmids to form complexes that self-localize inside eukaryotic cells.

MATERIALS AND METHODS

Peptide Synthesis. The branched peptide (loligomer 4) was synthesized by classical solid phase peptide synthesis (*25*), on an Applied Biosystems 430A Synthesizer using *tert*-butoxycarbonyl (t-Boc) chemistry and phenylacetamidomethyl resin supports. The synthesis, coupling efficiencies, purification, and characterization procedures were described previously (*23*, *24*). Loligomer 4 was labeled with fluorescein via the free thiol group in the C-terminal arm of the molecule (Figure 1) as described previously (*23*, *24*). Fluorescein maleimide was purchased from Molecular Probes (Eugene, Oregon)

Gel Mobility Shift Assay. Plasmid DNA (1 μg; pGL2 Luciferase, Promega) was dispensed into microcentrifuge tubes and mixed with increasing amounts of loligomer 4 (5−1000 ηg). Aliquots of each loligomer 4−plasmid mixture (20 μL) were then incubated at room temperature for 5−10 min. A 3 μL volume of 6× loading buffer (0.25% bromophenol blue, 0.25% Xylene cyanol F. F., and 30% glycerol in water) was subsequently added to each tube. Samples were thereafter loaded into wells of a precast 0.8% agarose gel (1× TBE). Samples were electrophoresed on agarose gels for 1 h at 70 V in TBE buffer (0.09 M Tris-borate and 0.002 M EDTA). Bands corresponding to plasmid DNA were detected by staining the gel with ethidium bromide (10 μg/100 mL TBE buffer). Banding patterns were visualized under a UV light and photographed.

Cell Culture. Cells were maintained at 37 °C, 5% (v/v) CO_2, 90% humidity in Nunclon tissue culture plasticware (Gibco-BRL). CHO (Chinese hamster ovary cells subclone AUXB1; ref *26*), COS-7 (SV40 transformed African green monkey kidney cells; ref *27*), and MCF-7 cells (human breast carcinoma; ref *28*) were grown in a MEM supplemented with 10% (v/v) fetal calf serum (FCS; ImmunoCorp, Montreal, Canada), 1 unit/mL penicillin (Sigma), 100 μg/mL streptomycin sulfate (Sigma), and 1 mM L-glutamine (Gibco-BRL). Subconfluent cultures of cells were passaged by washing them with 10 mL of PBS, followed by a trypsinization step for 2 min at 37 °C with 1 mL Trypsin (Gibco-BRL). The reaction was stopped by adding growth medium once cells composing the monolayer were detached from the dish. Cells were then harvested by centrifugation for 5 min at 1500 rpm and grown either as adherent monolayers or as suspensions in plastic tubes (Nunc).

DNA Vectors. The following DNA plasmids were used in this study. The pGL2 luciferase (Ctrl) vector (Promega) contains both a SV40 promoter and an enhancer sequence inserted into the pGL2 basic vector, which harbors a luciferase gene. The pCMV β-gal vector consists of both a CMV promoter sequence and a β-galactosidase gene. The pCMV β-gal plasmid contains the major immediate early gene promoter and the enhancer region of the human cytomegalovirus (CMV) and LacZ genes (*29*). The pGFP vector (Clontech) incorporates a gene coding for a green fluorescent protein.

Transfection Methods. *Loligofection (Transfection with Loligomer 4-Plasmid Complexes).* Loligomer 4 (ranging in concentrations from 1 to 60 μg prepared in PBS) was mixed with 10 μg of either plasmids pGL2 luciferase (Promega), pGFP (Clontech), or pCMV β-gal (Clontech). Sample volumes were then adjusted to 50 μL with PBS, and the mixtures were incubated at room temperature for 10 min. Thereafter, the following methodologies were used for transfections.

Treatment of Cells as Monolayers. Two hundred thousand (2×10^5) cells were seeded in individual wells of 6-well plates and incubated overnight at 37 °C. A 50 μL sample of each loligomer 4−plasmid DNA mixture was adjusted to 500 μL with α-medium. The medium was removed from plates seeded with cells and replaced with medium containing a loligomer 4−plasmid mixture. The plates were incubated for 30 min at room temperature with occasional redistribution of the solution from the edges of the dish over the entire surface of the dish every 10 min. A 4.5 mL aliquot of fresh medium was then added and the cells were incubated at 37 °C for 48 h.

Treatment of Cells in Suspensions. Cells (2×10^5 cells) suspended in growth medium were mixed with loligomer 4−plasmid preparations giving a final volume of 500 μL. The resulting cell suspensions were incubated for up to 5 h at 37 °C in eppendorf tubes attached to a rotating shaker. The cells were subsequently plated in a 6-well dish for 48 h with an additional 4.5 mL of growth medium.

[1] Abbreviations: CTS, cytoplasmic translocation signal; GFP, green fluorescent protein; loligofection, process of transfecting cells with plasmid DNA-loligomer complexes; loligomer, a squid-like branched peptide construct that incorporates cell penetration and intracellular localization signals; loligomer 4, a loligomer harbouring 8 N-terminal arms that comprise of a pentalysine cytoplasmic translocation domain and the SV40 large T-antigen nuclear localization signal; NLS, nuclear localization signal; RLU, relative light unit.

Calcium Phosphate Method. Transfections were performed using the calcium phosphate method (*16*). Briefly, 15 μL of a 2 M $CaCl_2$ solution was added dropwise to 250 μL of DNA-HBS buffer. The cell suspension method described above was used and the medium was changed after 24 h. The cells were incubated for an additional 24 h period.

Other Methods. Superfect (Qiagen), Transfectam (Promega), Tfx-50 (Promega), and Lipofectamine (Gibco-BRL) reagents were used as described by their suppliers using cell suspensions described in the protocol for loligomer transfection (loligofection). Transfection with Lipofectamine was performed in a serum-free medium for the first 24 h. Superfect (Qiagen) is a specifically designed polycation based on dendrimer technology, Tfx-50 (Promega) consists of a synthetic cationic lipid molecule, *N*,*N*,*N*′,*N*′-tetramethyl-*N*-*N*′-bis(2-hydroxyethyl)-2−3,-dioleoyloxy-1,4-butane diammonium iodide and L-dioleoyl phosphatidyl ethanolamine (DOPE). Transfectam (Promega) contains dioctacylamidoglycyl spermine and Lipofectamine (Gibco-BRL) reagent contains 3:1 (w/w) liposome formulation of the polycationic lipid 2,3-dioleyloxy-*N*-[2-(spermine carboxamido) ethyl]-*N*,*N*-dimethyl-1-propaneminium trifluoroacetate (DOSPA) and L−α dioleoyl phosphatidylethanolamine (DOPE).

Preparation of Cell Extracts. Preparation of cell extracts was performed as described elsewhere (*30*). Briefly, cells were washed with PBS, incubated with 200 μL of a cell lysis solution (25 mM Tris, pH 7.8, with H_3PO_4; 2 mM EDTA; 2 mM DTT; 10% glycerol; 1% Triton X-100; Promega) for 5 min and finally scraped into an eppendorf tube. The cells were disrupted using one to two cycles of freezing in dry ice−ethanol or incubating at −70 °C for 30 min followed by a thawing step at 37 °C for 5 min. The extracts were centrifuged at 12 000 rpm for 5 min at 4 °C, and the resulting supernatants were transferred to new tubes. The protein concentration in cell lysates was determined using the Bradford (*31*) dye binding protein assay (Bio-Rad, Hercules, CA). The total amount of luciferase activity was reported in terms of light units per milligram of protein in the extracts.

Luciferase Assay. Luminescence was detected in cells transfected with a plasmid construct harboring a luciferase reporter gene (pGL2 luciferase control vector; Promega). The luciferase enzyme catalyzes the production of light in fireflies by oxidizing D-(−)-luciferin in the presence of ATP, Mg^{2+}, and O_2 (*32*). The reaction produces oxyluciferin, CO_2, and a photon. The level of light emitted during the reaction can be measured with a luminometer. A 20 μL aliquot of a cell extract was mixed with 100 μL of luciferase assay reagent [Promega; 20 mM tricine, 1.07 mM $(MgCO_3)_4$ $Mg(OH)_2{\cdot}5H_2O$, 2.67 mM $MgSO_4$, 0.1 mM EDTA, 33.3 mM DTT, 270 μM Coenzyme A (lithium salt), 470 μM luciferin, and 530 μM ATP; pH 7.8] maintained at room temperature. The test tube containing the reaction mixture was placed in a luminometer (Lumat LB 9507, Berthold, Princeton, NJ), and light produced (luminescence units) for 10 s was recorded.

Fluorescence Microscopy. The plasmid pGL2 Luciferase (10 μg) was incubated with the DNA 7-aminoactinomycin (7-AAD; 0.1 μg) for 5 min. The labeled plasmid was subsequently complexed with fluorescein-labeled loligomer 4 at a 2:1 loligomer 4:plasmid weight ratio. CHO cells (10^6 cells) grown in suspension were transfected with the dual-labeled complex following the procedure described in the section on transfection methods. Cells were examined by fluorescence microscopy (Leica DM-LB microscope) and photographed 4 h after transfection. Fluorescence excitation filters (fluorescein, EX filter 355/425, EM filter LP 470; 7-AAD, EX filter 530/595, EM filter LP615) were used to observe the migration of both fluorophores. The GFP fluorescence signal (EX filter 355/425, EM filter LP 470) emitted by CHO cells transfected with a plasmid harboring the gene coding for green fluorescent protein was stable and monitored directly in viable cells.

Flow Cytometry. CHO cells (10^6 cells) were transfected as described in the previous paragraph with the 7-AAD-labeled plasmid pGL2 or the complex of fluorescein-labeled-loligomer 4 and 7-AAD-labeled plasmid pGL2. Labeled cells were subsequently analyzed by flow cytometry on a FACScan unit (Becton Dickinson) to determine the extent of cell viability (forward scatter, FSC; side scatter, SSC) and the binding/internalization of 7-AAD into CHO cells (argon laser; excitation wavelength, 488 nm; emission signal, LP 650 nm filter). The dye 7-AAD is excluded by viable cells unless complexed to a molecule that is internalized by cells.

***β*-Galactosidase Staining.** The detection of β-galactosidase activity in situ in cultured cells was performed using a histochemical stain (*33*). The substrate, 5-bromo-4-chloro-3-indolyl-β-D-galactoside (X-Gal), is hydrolyzed by β-galactosidase to generate an indigo-colored precipitate which facilitates the subcellular localization of the β-galactosidase activity. A monolayer of cells was washed twice in PBS containing 2 mM $MgCl_2$. The cells were fixed in 0.75% (v/v) glutaraldehyde (Sigma) in PBS for 15 min at room temperature, and then washed with PBS/$MgCl_2$ for 5 min. A 1.5 mL volume of X-Gal (1 mg/mL) diluted in staining solution [5 mM $K_3Fe(CN)_6$, 5 mM $K_4Fe(CN)_6{\cdot}3H_2O$, 0.01% (w/v) sodium deoxycholate, 0.02% (v/v) Nonidet P40, and 2 mM $MgCl_2$ in PBS] was added to each one-chamber cover glass slide (LabTek borosilicate; Nunc). Cells were analyzed under a light microscope and photographs were taken.

RESULTS

Loligomers are intracellular vehicles able to import large cargos such as plasmids into cells. One of these constructs, loligomer 4, is a nucleus-directed vehicle. It is a structurally defined, synthetic peptide (Figure 1) which possesses properties expected of a transfection agent. Loligomer 4 is water soluble, heat stable and probably associates noncovalently with the phosphate backbone of nucleic acids. Its cellular import is insensitive to the presence of serum or medium. The ability of loligomer 4 to act as a transfection agent was analyzed using reporter plasmids.

Design and Synthesis of loligomer 4 Variants. Loligomers (*23*, *24*) are peptide-based multitasking shuttles, which are able to selectively deliver cytotoxic or therapeutic agents to the cytosol or inside cellular compartments. The term loligomer was derived from the latin root *loligo* referring to members of the squid family, thereby emphasizing the branched or "squid-like" nature of these peptides. In particular, loligomer 4 (Figure 1) contains eight nuclear localization signals (NLS) and eight pentalysine stretches acting as cytoplasmic translocation signals (CTS) which allow it to penetrate cells and relocate to their nucleus. Loligomer 4 (Figure 1) was synthesized by solid-phase peptide synthesis. Peptide branching was introduced following successive rounds of couplings of lysine derivatives harboring identical protecting groups on their α- and ϵ-amino groups (*23*). The concept of peptide branching originated from the work of Tam (*34*, *35*) dealing with the construction of multiple antigenic peptides. The thiol side chain located in the



Figure 2. A gel-retardation assay illustrating a shift in migration of plasmid DNA (pGL2 luciferase) in agarose gels when complexed with loligomer 4. Lane 1, banding pattern observed for 1 μg of pGL2 luciferase plasmid; lanes 2−11, banding patterns observed for 1 μg of pGL2 luciferase plasmid DNA complexed with increasing amounts of loligomer 4. Lane 2, 5 ng loligomer 4; lane 3, 10 ng; lane 4, 50 ng; lane 5, 100 ng; lane 6, 150 ng; lane 7, 200 ng; lane 8, 250 ng; lane 9, 500 ng; lane 10, 750 ng; lane 11, 1000 ng. Lane 12 was loaded with 0.5 μg of a 1 kb DNA ladder (Gibco BRL).

C-terminal arm of loligomer 4 (Figure 1) was modified with fluorescein maleimide to produce a fluorescein-labeled loligomer 4 for cell migration studies.

Loligomer 4 Forms a Complex with Plasmid DNA. The plasmid pGL2 luciferase was mixed at different ratios with loligomer 4 to generate noncovalently associated complexes. The resulting macromolecular aggregates were easily observed as large molecular weight species on agarose gels. Their noncovalent association is due to the fact that loligomer 4 is a cationic structure that can readily interact with the negatively charged phosphate backbone of plasmid DNA.

The migration of plasmid DNA (1μg) in agarose gels was retarded by the addition of loligomer 4, as detected with ethidium bromide (Figure 2). Plasmid DNA containing no loligomer migrated as a pair of bands representing both supercoiled and open circular forms of DNA (lane 1). The mobility of plasmid DNA (1 μg) was not altered by the presence of loligomer 4 ranging in concentrations between 5 and 100 ng (lanes 2−5). The presence of 150 ng of loligomer (lane 6) resulted in the appearance of a band migrating slightly above the supercoiled DNA plasmid band. Upon adding 200 ng of loligomer 4 (lane 7), the uncomplexed supercoiled DNA band disappeared with most of the plasmid DNA remaining in the sample well. The intensity of the plasmid DNA open circular form was further decreased by the addition of 250 ng of loligomer 4 (lane 8) and concentrations of the vehicle in the range 500−1000 ng (lanes 9−11) were sufficient to retard the migration of all the plasmid DNA. In summary, the mixing of loligomer 4 with the plasmid pGL2 luciferase at a minimal weight ratio of 0.5 resulted in an efficient complexation of all the available plasmid DNA as shown by the retardation of the DNA−peptide complex on agarose gels (Figure 2).

Complexes of Fluorescein-Labeled Loligomer 4 and 7-AAD-Labeled Plasmids Are Imported into CHO Cells. The migration of plasmids inside CHO cells occurs only in the presence of loligomer 4. The DNA intercalator 7-AAD does not enter cells that are viable and is typically used in flow cytometry to measure the extent of cell death in a cell population. This fluorescent intercalator was used to label plasmid DNA in an effort to follow the migration of plasmid inside CHO cells. Loligomer 4 was labeled with fluorescein in order to track its intracellular movement in relation to the 7-AAD-labeled plasmid. A typical distribution pattern of plasmid (red color) and loligomer 4 (green color) inside CHO cells after 4 h is presented in Figure 3 (Panel A). Zones of yellow color inside cells highlight areas of comigration of the 7-AAD and fluorescein chromophores and suggest that a significant fraction of labeled plasmid exists as complexes with loligomer 4. The overall cellular distribution of 7-AAD fluorescence (red color) also suggests the occurrence of either free plasmid inside these cells or the rapid exchange of 7-AAD originally associated with the plasmid with intracellular pools of DNA. The flow cytometric patterns of CHO cells exposed to a 7-AAD-labeled plasmid for 4 h indicate that the plasmid alone is not imported by these cells (Figure 3, panel B, right side, relative fluorescence signal less than 10 units). In contrast, CHO cells transfected with a complex of loligomer 4 and 7-AAD-labeled plasmid bind and internalize the complex rapidly (in less than a hour) with >70% of cells being labeled with the plasmid harboring the 7-AAD label (Figure 3, panel C, right side, relative fluorescence signal greater than 10). All cells analyzed for the binding and internalization of the 7-AAD-labeled plasmid were viable (gated cell population [R1] based on forward and side scatter properties, Figure 3, panels B and C, left sides), indicating that unbound 7-AAD was not responsible for the fluorescence signal observed. The viability of CHO cells also confirms that loligomer 4 at a concentration of 3 μM is not toxic to these cells when the peptide is associated with a plasmid (30 μg of loligomer 4 and 10 μg of plasmid in 500 μL).

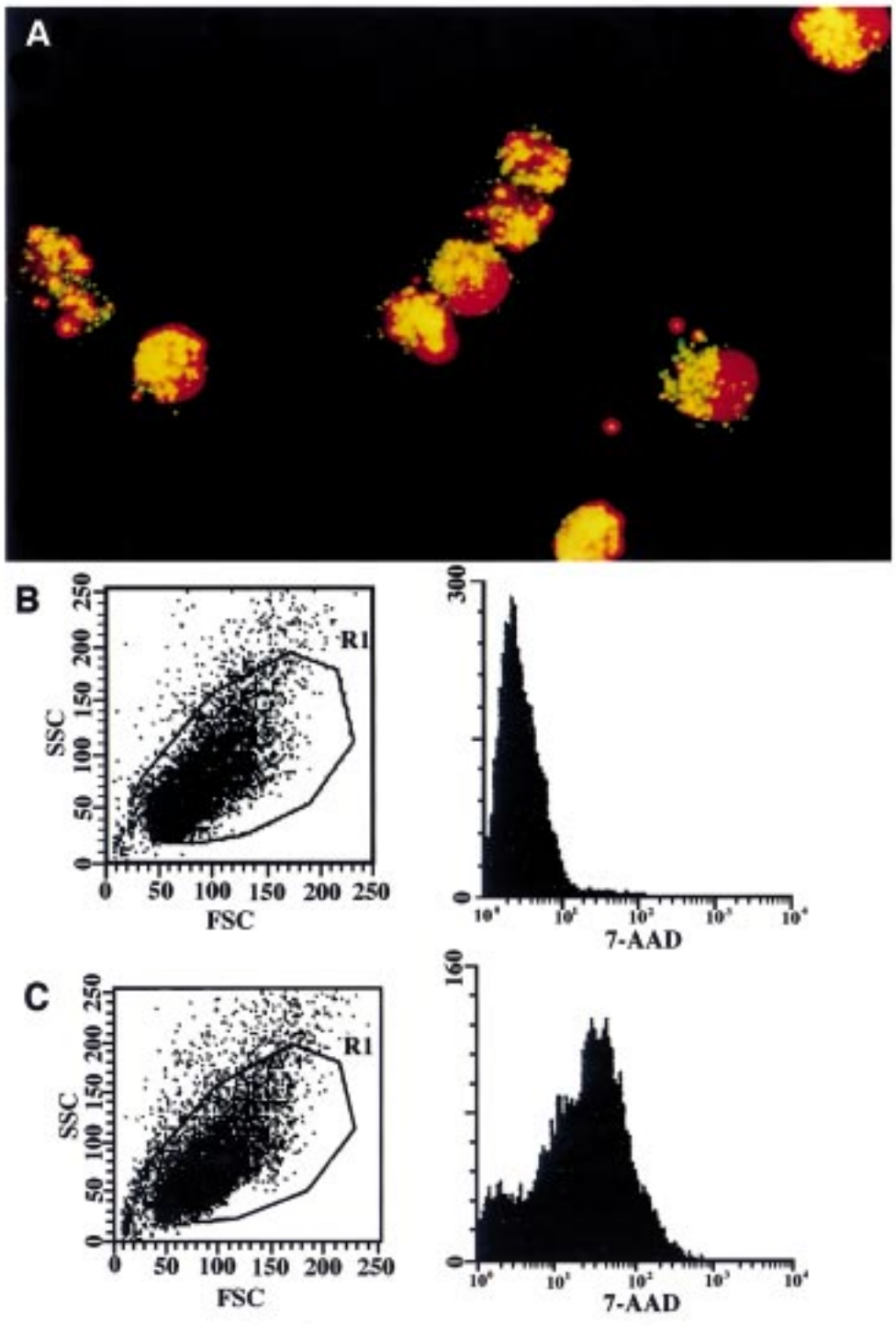


Figure 3. Localization of loligomer 4−plasmid complexes in CHO cells. (A) Photograph of an unfixed preparation of viable CHO cells after a 4 h exposure to loligomer 4−plasmid complexes depicting the intracellular distribution of fluorescein-labeled loligomer 4 (green color) complexed with 7-AAD-labeled plasmid pGL2 (red color) in CHO cells. The comigration of labeled loligomer 4 and 7-AAD-labeled plasmid gives rise to intracellular areas of yellow fluorescence. (B) FACS analysis of CHO cells after a 4 h exposure to 7-AAD labeled plasmid. (Panel B, left side) Flow cytometric pattern (forward scatter and side scatter properties) indicating that most CHO cells remained viable following this treatment. (Panel B, right side) Histogram of viable cells (R1) labeled with the 7-AAD labeled plasmid. Most cells do not bind or internalize 7-AAD (autofluorescence). (C) FACS analysis of CHO cells after a 4-hour exposure to loligomer 4- complexed with the 7-AAD labeled plasmid. (Panel C, left side) Flow cytometric pattern (forward scatter and side scatter properties) indicating that most CHO cells remained viable following their exposure to these complexes. (Panel C, right side) Histogram of viable cells (R1) labeled with the peptide- 7-AAD labeled plasmid complex. Most cells (>70%) bind and internalize 7-AAD (panel A) suggesting that the plasmid requires the presence of loligomer 4 to effectively be imported inside CHO cells.

Micromolar Concentrations of Loligomer 4 Facilitate Efficient Gene Transfer. The transfection efficiency of the pGL2 luciferase vector complexed to loligomer 4 into CHO cells was confirmed by monitoring the extent of luciferase activity present in the cytosol of CHO transfected cells. The histogram presented in Figure 3A highlights the level of luciferase activity (per milligram of protein) in CHO cell extracts as a function

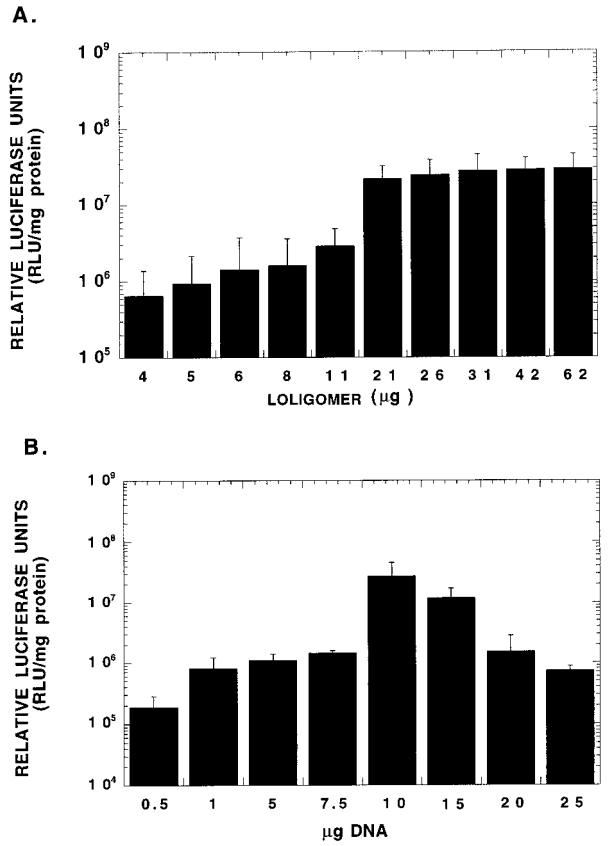


Figure 4. Levels of luciferase activity detected in extracts of CHO cells transfected with loligomer 4-pGL2 plasmid complexes. The luciferase activity present in cell lysates is reported as relative light units per milligram of protein (RLU/mg of protein). It represents a late stage measurement of the transfection efficiency of loligomer-plasmid complexes in CHO cells. (A) Effect of loligomer 4 concentration on recorded luciferase activity. The pGL2 luciferase plasmid (10 μg) was complexed with increasing amounts of loligomer 4 (4−62 μg). (B) Plasmid concentration on recorded luciferase activity. Loligomer 4 (31 μg) was complexed with increasing amounts of pGL2 luciferase plasmid (0.5−25 μg). Luciferase activity was not observed in CHO cells transfected with naked DNA only.

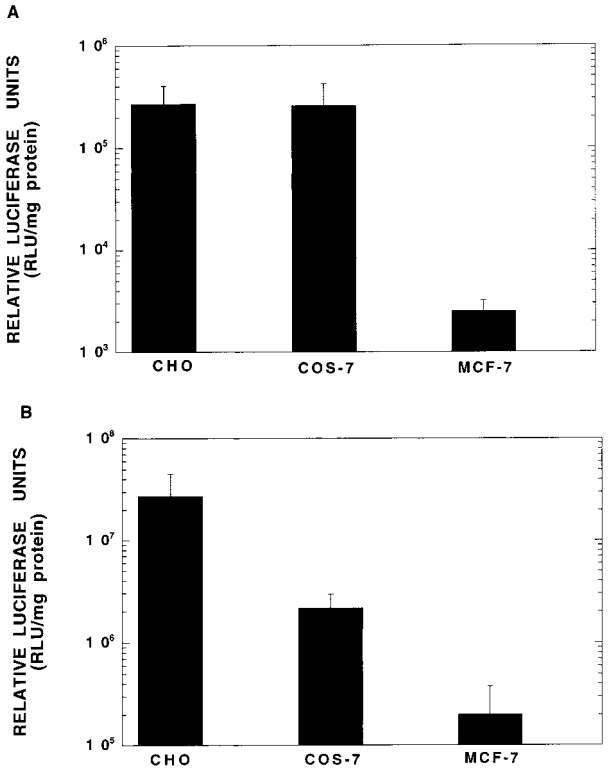


Figure 5. Comparison of transfection efficiencies for loligofection in CHO, COS-7, and MCF-7 cells. Transfections were performed on cells grown as monolayers (Panel A) or maintained in suspension (Panel B) with loligomer 4−plasmid complexes. Transfection efficiency is reported in terms of luciferase activity (RLU/mg of protein) present in cell lysates. A 31 μg aliquot of loligomer 4 was complexed with the plasmid pGL2 luciferase (10 μg). Transfection with naked DNA did not result in any luciferase activity.

of the weight ratio of loligomer 4 to plasmid used to initially transfect CHO cells. A 10 μg aliquot of the plasmid pGL2 luciferase was mixed with increasing amounts of loligomer 4. Significant levels of loligofection yielding (0.06−0.3) $\times$ 10^7 relative luciferase unit (RLU)/mg of protein were observed at loligomer 4 concentrations ranging in values from 4 to 11 μg. However, a 7-fold increase in luciferase units (2.1 $\times$ 10^7 RLU/mg of protein) was obtained when 21 μg of loligomer 4 (1.1 μmol; loligomer 4-to-plasmid weight ratio, 2.1) was used in the transfection procedure. The magnitude of the luciferase signal then reached a plateau between 21 and 62 μg of loligomer 4 (loligomer 4 to plasmid weight ratios between 2.1 and 6.2) with RLU values leveling to between 2.4 $\times$ 10^7 and 2.8 $\times$ 10^7 RLU /mg of protein.

Loligomer 4 to Plasmid Weight Ratio of 3 Is Optimal To Achieve Maximal Transfection Efficiency. A fixed concentration of loligomer 4 (31 μg; 1.67 μmol) was mixed with increasing amounts of pGL2 luciferase plasmid DNA ranging 0.5−25 μg (Figure 4B; log scale units). A low level of relative luciferase activity (1.9 $\times$ 10^5 RLU/mg of protein) could be detected in CHO cells transfected with a mixture containing 0.5 μg of plasmid DNA, reaching a maximal value of 2.7 $\times$ 10^7 RLU/mg of protein at a plasmid content of 10.0 μg (loligomer 4 to plasmid weight ratio of 3.1). Further increase in plasmid DNA content in relation to loligomer 4 resulted in a decreased transfection efficiency down to 1.2 $\times$ 10^7 RLU/mg of protein at 15 μg of pGL2 luciferase plasmid and 0.07 $\times$ 10^7 RLU/mg of protein at 25 μg of plasmid.

Transfection Efficiency of Loligomer 4 Is Greater When Cell Suspensions Are Treated with Loligomer:Plasmid Complexes Rather Than Cell Monolayers. Three cell lines (CHO, COS-7, and MCF-7) were used to evaluate the transfection efficiency of our loligomer 4−plasmid complexes. Cell lines maintained as monolayers, then transfected with 10 μg of pGL2 luciferase plasmid DNA and 31 μg of loligomer 4, exhibited very low transfection efficiency as monitored by the resulting levels of luciferase activity (Figure 5 A; log scale units). Recorded light emissions ranged in values between 2.6 and 2.7 $\times$ 10^5 RLU/mg of protein for COS-7 and CHO cells and 2.5 $\times$ 10^3 RLUs with MCF-7 cells. The transfection efficiency was found to be more prominent and efficient (up to 100-fold increases) when cells were transfected as suspensions (Figure 5B), where luciferase activity values of 2.7 $\times$ 10^7 and 0.2 $\times$ 10^7 RLUs were recorded for CHO and COS-7 cells, respectively. Finally, a value of only 2 $\times$ 10^5 RLU/mg of protein was registered when MCF-7 cells were transfected as suspension cells, suggesting that the efficiency of this procedure remains dependent on the cell line.

Comparing Loligomer 4 to Other Transfection Agents in the Context of Cells Maintained in Suspension. The efficacy of loligomer 4 as a prototypic transfection agent is significant only in the context of cells presented as suspensions. The relative ability of

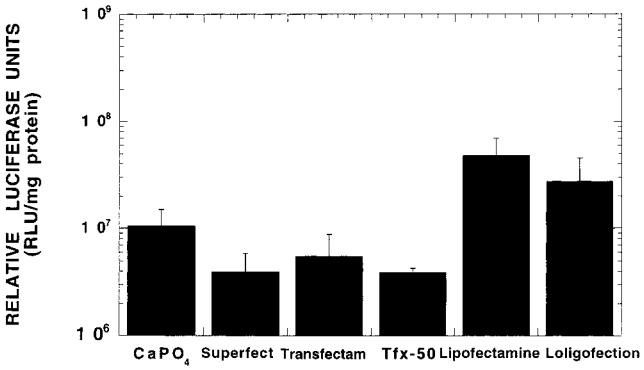


Figure 6. Comparison of transfection efficiencies (luciferase activity) in CHO cells for loligofection in relation to other established nonviral transfection methods. The luciferase activity present in cell lysates is reported as relative light units per milligram of protein (RLU/mg of protein). The luciferase activity was monitored using 10 μg of pGL2 luciferase and 31 μg of loligomer 4. Other transfection methods including calcium phosphate and commercially available agents such as Superfect (Qiagen), Transfectam (Promega), Tfx-50 (Promega), and Lipofectamine (Gibco-BRL) were compared to loligofection. No luciferase activity was observed in CHO cells transfected with naked DNA only.

loligomer 4−plasmid complexes to transfect CHO cells in suspension was compared to other available methods (Figure 6) in order to highlight their comparable potential as nonviral transfection strategies. Agents such as Superfect (Qiagen), Transfectam (Promega), and Tfx-50 (Promega) all facilitated the transfection of the pGL2 luciferase plasmid into CHO cells maintained in suspension with RLU/mg of protein values ranging between 0.4 $\times$ 10^7 and 0.6 $\times$ 10^7. Similarly, luciferase activities of the order of 1.0 $\times$ 10^7 RLU/mg of protein were recorded with the calcium phosphate method. Higher values [(2.7−4.8) $\times$ 10^7 RLU/mg of protein) were observed with Lipofectamine (Gibco-BRL) and loligomer 4. All differences in transfection efficiencies must be contrasted with the fact that none of the previous established methods were optimized for transfecting cells in suspension. Nevertheless, there is a clear indication that the loligomer 4 construct represents a useful template for designing alternate classes of transfection agents.

***β*-Galactosidase and Green Fluorescent Protein Are Expressed in Transfected CHO Cells.** CHO cells were transfected with 10 μg of pCMV β-gal or pGFP complexed to 31 μg of loligomer 4. The reporter plasmid pCMV β-gal incorporates a β-galactosidase gene. The production of β-galactosidase was monitored by the cleavage of its substrate, 5-bromo-4-chloro-3-indolyl-β-D-galactoside (X-gal), which resulted in an indigo color precipitate present in CHO cells successfully transfected with the loligomer 4−plasmid complex (Figure 7B). In contrast, no color was observed for cells exposed to the plasmid alone (Figure 7A). The plasmid pGFP harbors a gene coding for a green fluorescent protein (GFP). The transfection and expression of this plasmid in CHO cells occurs only when complexed to loligomer 4 (Figure 7C). The transfection efficiency of loligomer 4−plasmid complexes in CHO cells in terms of the percentage of cells expressing the reporter proteins ranges in value from 5 to 10% of cells.

DISCUSSION

The transfection of eukaryotic cells has become an important technique for the study of cellular genes and for the development of gene transfer studies. Advances in gene therapy depend in large part on the development of delivery systems capable of introducing DNA into a target cell or tissue. These approaches include the use of carrier molecules, such as liposomes or chemical precipitates, to self-replicating systems, such as viruses (*36*). In this study, a peptide-based, intracellular vehicle, termed loligomer 4 (*23*, *24*), was tested for its ability to form complexes with plasmid DNA and facilitate their transport into cells. Loligomer 4 contains eight copies of the SV40 large T antigen nuclear localization signal (*37*) as well as eight pentalysines sequences that act as a cytoplasmic translocation signal (CTS; ref *23*) (Figure 1).

The branched nature of loligomers is derived from a synthetic approach initially developed for the creation of multiple antigenic peptides (*34*, *35*). This tentacular geometry affords several distinct advantages in terms of incorporating tissue-targeting sequences and cytotoxic moieties. First, branching reduces the impact of proteolytic degradation on loligomers (*23*, *24*) since the cleavage of one or more arms does not destroy the overall localization properties of the construct. Second, multivalency represents an important feature of loligomers and other recent delivery strategies involving dendrimers (*14*, *38*) and peptabodies (*39*) in terms of enhancing the avidity of such constructs for a cell surface receptor or to promote their localization properties inside cells. For example, it has been demonstrated that, in the case of protein conjugates, the efficiency of their nuclear targeting property increases with the number of NLS sequences coupled to them (*40*). The attachment of the SV40 Large T antigen nuclear localization signal peptide induced the nuclear accumulation of the conjugated DNA in digitonin-permeabilized cells (*41*). In the case of loligomers, the display of eight pentalysine sequences dramatically enhances its cellular uptake (*23*).

The cellular uptake and intracellular routing of loligomer 4 has recently been studied by flow cytometry and microscopy (*24*). Loligomer 4 was shown to be irreversibly retained inside cells when its intracellular routing leads to its accumulation into the nucleus (*24*).

The major objective of this study was to determine if loligomer 4 is able to act as a vehicle in terms of delivering large molecular cargos such as plasmids inside cells. Loligomer 4 is a branched cationic peptide with a theoretical net charge of +71. This construct was thus expected to interact noncovalently with the negatively charged phosphate backbone of plasmid DNA. Loligomer 4 retarded the electrophoretic migration of plasmid DNA in agarose gels (Figure 2) starting at a 1:2 peptide:DNA weight ratio. The minimal theoretical charge ratio ($\pm$) necessary for loligomer 4 to complex plasmid DNA was calculated to be $\sim$6.5. In contrast, the optimal level of transfection in CHO cells observed for these peptide−DNA complexes occurs at a loligomer 4:plasmid DNA weight ratio of 3: 1 (Figure 4). The efficiency of this transfection approach was monitored using a plasmid incorporating a luciferase reporter gene. Overall, these results suggest that a range of peptide−DNA complexes exist in solution and that efficient levels of transfection are achieved with complexes presenting a charge ratio between 30 and 70 (loligomer 4:plasmid DNA weight ratios between 2:1 and 6:1; Figure 4). Previous studies have shown that the interaction of plasmid DNA with cationic substrates results in a marked condensation of DNA molecules into 80−100 nm diameter toroid structures (*8*). The ratio of loligomer 4 to DNA may thus regulate the fraction of "packaged" plasmid complexes optimally suited to their penetration into cells and intracellular routing.

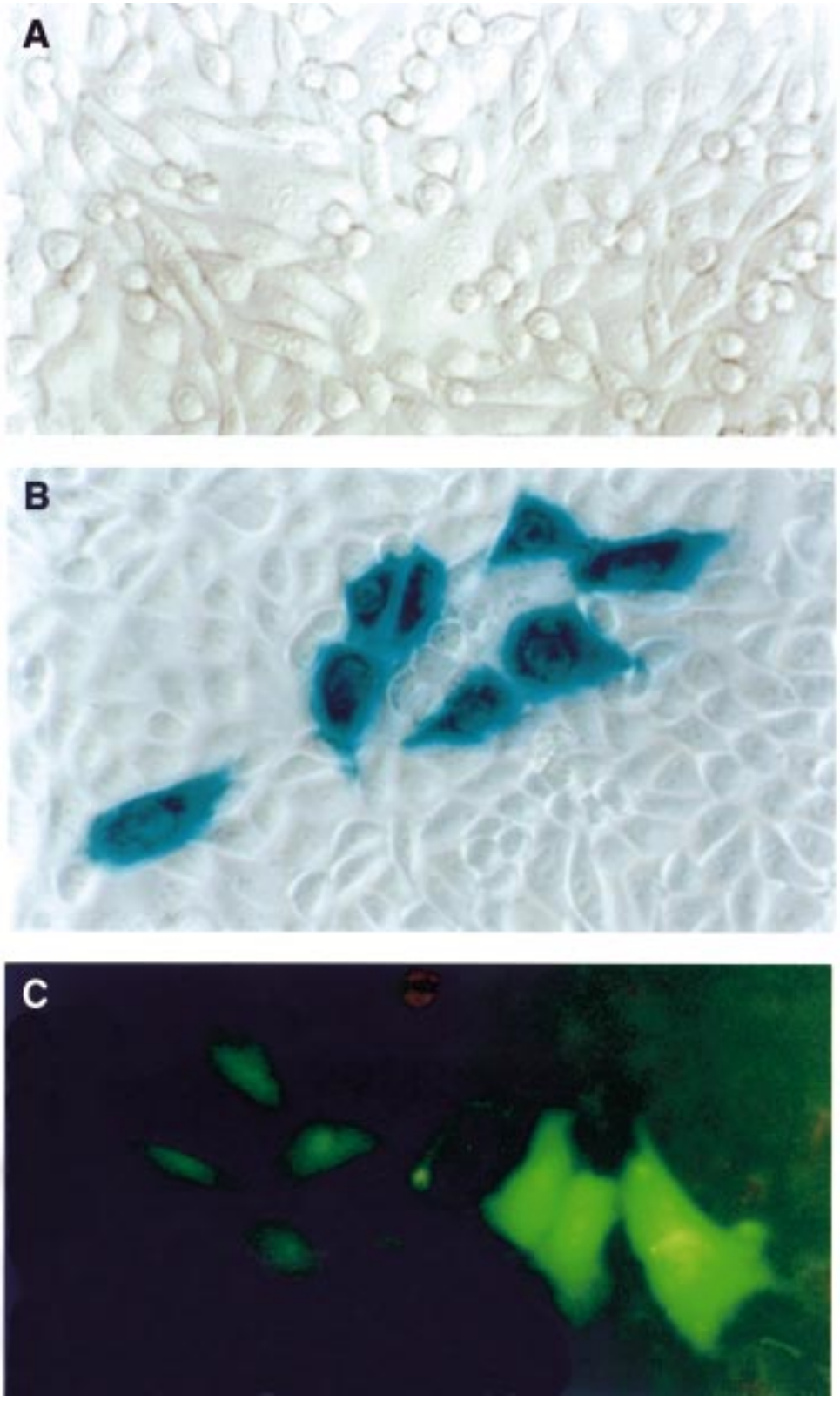


Figure 7. Expression of β-galactosidase and GFP in CHO cells. (A) CHO cells transfected with the naked plasmid pCMV β-gal showing no indigo staining of cells. (B) Indigo-colored cells are observed in this preparation of CHO cells transfected with loligomer 4-pCMV β-gal plasmid. (C) Fluorescent green cells were visualized in a field of CHO cells transfected with loligomer 4-pGFP plasmid.

The import of loligomer 4 into CHO cells occurs through absorptive endocytosis (*23*, *24*). One-arm peptide or loligomer constructs lacking the cytoplasmic translocation domains were either poorly endocytosed or unable to enter cells (*23*). Loligomer 4 is typically observed in vesicular compartments as well as in the cytosol of CHO cells within the first 30 min of exposing cells to this construct. After a few hours, a significant fraction of internalized loligomer 4 accumulates in the cell nucleus (*23*, *24*). Free loligomer 4 and loligomer 4−plasmid DNA complexes represent two (or more) distinct presentations of this peptide vehicle. The presentation of loligomer 4 as part of a peptide−DNA complex may alter its ability to enter cells. In addition, plasmid DNA may not be

routed through the same intracellular pathway as loligomer 4. The migration of loligomer 4−plasmid DNA complexes was thus analyzed by fluorescence microscopy and flow cytometry. The migration of the reporter plasmid was monitored by marking the plasmid with the fluorescent DNA intercalator 7-AAD, a dye that does not enter into viable cells. Loligomer 4 was labeled with fluorescein, and dual-labeled complexes of loligomer 4−plasmid DNA were created by mixing both fluorescent entities together. The majority of CHO cells (>70%) rapidly imported the labeled complex (Figure 3, panel A and panel C, right side) while the labeled plasmid alone was not endocytosed by cells (Figure 3, panel B, right side). An image depicting the distribution of the two fluorophores inside CHO cells after 4 h is presented in Figure 3A. No fluorescence signal was observed for cells exposed to the labeled plasmid alone (results not shown). Yellow areas in Figure 3A represent zones where plasmids (7-AAD, red fluorescence) and loligomer 4 (green fluorescence) comigrated inside CHO cells. The intracellular distribution of yellow fluorescence is reminiscent of previous patterns observed for loligomer 4 alone (*23*, *24*), suggesting that its complexation with plasmid DNA has not altered its properties as an intracellular shuttle. Intracellular regions of red fluorescence highlight areas where the labeled plasmid is not complexed to loligomer 4. Alternatively, 7-AAD may rapidly exchange between plasmid DNA and intracellular pools of DNA. Overall, these results suggest the comigration of a significant population of peptide−plasmid DNA complexes inside CHO cells and the possible dissociation of a large fraction of these complexes inside cells yielding free plasmid or the exchange of 7-AAD. The relatively global distribution of fluorescein-labeled loligomer and 7-AAD in these viable CHO cells suggests that both the cytosol and nucleus have been targeted by these agents.

The uptake of loligomer 4 into cells is greater for cells either maintained in suspension or gently trypsinized to generate a cell suspension than for cells presented as monolayers (*24*). This difference in cellular uptake is less significant, however, in the case of nonadherent cell lines such as Daudi and EL4 (*24*). It was thus predicted that the levels of transfection efficiencies observed for loligomer 4−plasmid DNA complexes would be greater for CHO, COS-7, and MCF-7 cells grown in suspension rather than monolayers. Results presented in Figure 5 confirmed this hypothesis and support the view that the import of plasmid DNA as part of a loligomer 4−plasmid complex follows the internalization mechanism proposed for loligomer 4 itself. The reason the import mechanism is enhanced by cells presented as suspensions remains unclear although effects due to cytoskeletal components have now been ruled out (*24*). No differences in transfection efficiency were observed for cells grown in spinner flasks as opposed to suspension cells arising from trypsinizing cell monolayers.

The value of loligomer 4 as a transfection agent was evaluated using two approaches. The efficiency of transfection of loligomer 4 complexed to a reporter plasmid harboring the luciferase gene was initially compared to other nonviral transfections methods. The major limitation of such an analysis stems from the fact that transfections were performed on cell suspensions (significant levels of transfection for loligomer 4−plasmid complexes are only achieved for cells presented as suspensions; Figure 5). Since other transfection strategies are typically performed on cell monolayers, the resulting transfection conditions for these methods were not optimal. Nevertheless, the transfection efficiency observed in CHO cells with loligomer 4−plasmid DNA complexes was comparable to results observed for lipofectamine and better than results obtained for other transfection agents used in this study (Figure 6). Comparable results (using luciferase as a reporter protein) have been reported for other recently developed cationic agents (*13*, *42*). A more conclusive method of evaluating the value of loligomer 4−plasmid complexes in transfecting cells is to simply tabulate the percentage of cells that either produce β-galatosidase (reporter plasmid, pCMV β-gal) or GFP (reporter plasmid, pGFP) within a field of cells. Calculated percentages for CHO cells transfected with loligomer 4−plasmid DNA complexes ranged in values from 5 to 10% depending on the vector used. Images of CHO cells expressing these reporter proteins are presented in Figure 7 (panels B and C).

Finally, a clear difference exists between the level of import of loligomer 4−plasmid complexes by cells (>70% of viable cells take up the constructs; Figure 3) and the maximal level of transfection observed (∼10% of cells). Reasons for this discrepancy probably lie in the design of loligomer 4 itself. For example, a large fraction of this construct remains trapped in vesicular compartments (*24*) since we have not yet introduced a signal in this construct to favor its escape from such compartments. Their release from cytoplasmic vesicles is at best inefficient but does occur as demonstrated in this report as well as in previous studies (*23*, *24*). Nevertheless, the fact that a prototypic peptide design such as loligomer 4 can already act as a transfection agent demonstrates the potential of creating biologically effective, multitasking peptide constructs using simple solid-phase strategies. Loligomers may thus represent useful vehicles for gene transfer experiments (*43*), antisense technologies (*38*), DNA-based immunization strategies (*44*), as well as photodynamic therapy (*45*).

ACKNOWLEDGMENT

The authors thank Jim Ferguson for synthesizing peptides. This work was supported by a grant from the National Cancer Institute of Canada with funds from the Canadian Cancer Society. D.S. was the recipient of successive AMGEN and George Knudson Foundation fellowships during the tenure of this project.

LITERATURE CITED

(1) Chen, D. S., Zhu, Nian-Ling, Hung, G., Skotzko, M. J., Hinton, D. R., Tolo, V., Hall, F. L., Anderson, W. F., and Gordon, E. M. (1997) Retroviral vector-mediated transfer of an antisense cyclin G1 construct inhibits osteosarcoma tumor growth in nude mice. *Human Gene Ther. 8*, 1667−1674.

(2) Singh, D., and Rigby, P. W. J. (1996) The use of histone as a facilitator to improve the efficiency of retroviral gene transfer. *Nucleic Acid Res. 24* (15), 3113−3114.

(3) Fisher, K. J., And Wilson, J. M. (1997) The transmembrane domain of diptheria toxin improves molecular conjugate gene transfer. *Biochem J. 321*, 49−58.

(4) Perales, J. C., Grossmann, G. A., Molas, M., Liu, G., Ferkol, T., Harpst, J., Oda, H., and Hanson, R. W. (1997) Biochemical and functional characterization of DNA complexes capable of targeting genes to hepatocytes via the asialoglycoprotein receptor. *J. Biol. Chem. 272*, 7398−7407.

(5) Sobolev, A. S., Rosenkranz, A. A., Smirnova, O. A., Nikitin, V. A., Neugodova, G. L., Naroditsky, B. S., Shilov, I. N., Shatski, I. N., and Ernst, L. K. (1998) Receptor mediated transfection of murine and bovine mammary glands in vivo. *J. Biol. Chem. 273* (14), 7928−7933.

(6) Cotten, M, Langle-Rouault, F., Kirlappos, H., Wagner, E., Mechtler, K., Zenke, M., Beug, H., and Birnstiel, M. L. (1990) Transferrin-polycation-mediated introduction of DNA into human leukemic cells: Stimulation by agents that affect the

survival of transfected DNA or modulate transferrin receptor levels. *Proc. Natl. Acad. Sci. U.S.A. 87*, 4033−4037.
(7) Yang, N. S., Burkholder, J., Roberts, B., Martinell, B., and McCabe, D. (1990) In vivo and in vitro gene transfer to mammalian somatic cells by particle bombardment. *Proc. Natl. Acad. Sci. U.S.A. 87*, 9568−9572.
(8) Wagner, E., Cotten, M., Foisner, R., and Birnstiel, M. (1991) Transferrin-polycation- DNA complexes: The effect of polycations on the structure of the complex and DNA delivery to cells. *Proc. Natl. Acad. Sci. U.S.A. 88*, 4255−4259.
(9) Legendre, J. Y., Trzeciak, A., Bohrmann, B., Deuschle, U., Kitas, E., and Supersaxo, A. (1997) Dioleoylmelittin as a novel serum insensitive reagent for efficient transfection of mammalian cells. *Bioconjugate Chem. 8*, 57−63.
(10) Templeton, N. S., Lasic, D. D., Frederik, P. M., Stry, H. H., Roberts, D. D., and Pavlakis, G. N. (1997) Improved DNA: Liposome complexes for increased systematic delivery and gene expression. *Nat. Biotech. 15*, 647−652.
(11) Budker, V., Gurevich, V., Hagstrom, J. E., Bortzov, F., and Wolff, J. A. (1996) pH sensitive cationic liposomes: A new synthetic virus such as vector. *Nat. Biotech. 14*, 760−764.
(12) Georgiev, O., Bourquin, J. P., Gstaiger, M., Knoepfel, L., Schaffner, W., and Hovens, C. (1996) Two versatile eukaryotic expression vectors permitting epitope tapping, radiolabeling and nuclear localisation of expressed proteins. *Gene 168*, 165−167.
(13) Goldman, C. K., Soroceanu, L., Smith, N., Gillespie, G. Y., Shaw, W., Burgess, S., Bilbao, G., and Curiel, D. T. (1997) In vitro and in vivo gene delivery mediated by a synthetic polycationic amino polymer. *Nat. Biotech. 15*, 462−466.
(14) Kukowska-Latallo, J. F., Bielinska, A. U., Johnson, J., Spindler, R., Tomalia, D. A., and Baker, J. R., Jr. (1996) Efficient transfer of genetic material into mammalian cells using starburst polyamidoamine dendrimers. *Proc. Natl. Acad. Sci. U.S.A. 93*, 4897−4902.
(15) Miller, A. D. (1992) Human gene therapy comes of age. *Nature 357*, 455−460.
(16) Graham, F. L., and Van der Eb, A. J. (1973) A new technique for the assay of infectivity of human adenovirus 5′ DNA. *Virology 52*, 456−467.
(17) Seelos, C. (1997) A critical parameter determining the aging of DNA-calcium phosphate precipitates. *Anal. Biochem. 245*, 109−111.
(18) McCutchan, J. H., and Pagano, J. S. (1968) Enhancement of the infectivity of Simian virus 40 DNA with diethyl -aminoethyldextran. *J. Natl. Cancer Inst. 41*, 351−357.
(19) Dagher, S. F., Conrad, S. E., Werner, E. A., and Patterson, R. J. (1991) Phenotypic conversion of Tk deficient cells following electroporation of functional Tk enzyme. *Exp. Cell Res. 198*, 36−42.
(20) Schaffer-Ridder, M., Wong, Y., and Hofschneider, P. H. (1982) Liposomes as gene carriers: Efficient transformations of mouse cells by Thymidine Kinase gene. *Science 215*, 166−168.
(21) Felgner, P. L., Gadek, T. R., Holm, M., Roman, R. Chan, H. W., Wenz, M., Northrop, J. P., Ringold, G. M., and Danielson, M. (1987) Lipofection: A highly efficient, lipid-mediated DNA-transfection procedure. *Proc. Natl. Acad. Sci. U.S.A. 84*, 7413−7417.
(22) Rols, Marie-Pierre, Dilteil, C., Golzio, M., Dumond, P., Cros, S., and Teissie, J. (1998) *in vivo* electrically mediated protein and gene transfer in murine melanoma. *Nat. Biotech. 16*, 168−171.
(23) Sheldon, K., Liu, D., Ferguson, J., and Gariépy, J. (1995) Loligomers: Design of *de novo* peptide-based intracellular vehicles. *Proc. Natl. Acad. Sci. U.S.A. 92*, 2056−2060.
(24) Singh, D., Kiarash, R., Kawamura, K., Lacasse, E. C., and Gariépy, J. (1998) Penetration and intracellular routing of nucleus-directed peptide-based shuttles (loligomers) in eukaryotic cells. *Biochemistry 37*, 5798−5809.
(25) Stewart, J. M., and Young, J. D. (1984) *Solid-Phase peptide Synthesis*, 2nd ed., Pierce, Rockford, IL.
(26) McBurney, M. W., and Whitmore, G. F. (1974) Isolation and biochemical characterization of Folate Deficient mutants of Chinese Hamster Cells. *Cell 2* (3), 173−182.
(27) Gluzman, Y. (1981) SV40 Transformed Simian cells support the replication of Early SV40 mutants. *Cell 23*, 175−182.
(28) Soule, H. D., Vazquez, J., Long, A., Albert, S., and Brennan, M. (1973) Human cell line from a pleural effusion derived from a breast carcinoma. *J. Natl. Cancer Inst. 51*, 1409−16.
(29) Wenger, R. H., Moreau, H., and Nielsen, P. J. (1994) A comparison of different promoter enhancer and cell type combinations in transient transfections. *Anal. Biochem. 221*, 416−418.
(30) Sambrook, J., Fritsch E. F., and Maniatis, T. (1989) *Molecular Cloning: A laboratory Manual*, vol. 3, Cold Spring Harbor Laboratory press, Plainview, NY.
(31) Bradford, M. (1976) A rapid and sensitive method for the quantitation of microgram quantities of protein utilizing the principle of protein dye binding. *Anal. Biochem. 72*, 248−254.
(32) Bronstein, I., Fortin, J., Stanley, P. E., Stewart, G. S. A. B., and Kricka, L. J. (1994) Chemiluminiscent and bioluminescent reporter gene assays. *Anal. Biochem. 219*, 169−181.
(33) MacGregor, G. R., Nolan, G. P., Fiering, S., Roerderer, M., and Herzenberg, L. A. (1991) In *Methods in Molecular Biology -Gene Transfer and Expression Protocols* (E. J. Murray, Ed.) pp 217−235, The Humana Press, Clifton, NJ.
(34) Tam, J. P. (1988) Synthetic peptide vaccine design: Synthesis and properties of a high-density multiple antigenic antigenic peptide system. *Proc. Natl. Acad. Sci. U.S.A. 85*, 5409−5413.
(35) Tam, J. P. (1989) High-Density Multiple antigen peptide system for preparation of antipeptide antibodies. Hormone Action. *Methods Enzymol.* (P. M. Conn, Ed.) Vol. 168, pp 7−15, Academic Press, San Diego.
(36) Curiel, D. T., Agarwal, S., Wagner, E., and Cotten, M. (1991) Adenovirus enhancement of transferrin-polylysine mediated gene delivery. *Proc. Natl. Acad. Sci. U.S.A. 88*, 8850−8854.
(37) Kalderon, D., Richardson, W. D., Markham, A. F., and Smith, A. E. (1984) Sequence requirements for nuclear location of Simian virus 40 large T-antigen. *Nature 311*, 33−38.
(38) Bielinska, A., Kukowska-Latallo, J. F., Johnson, J., Tomalia, D. A., and Baker, J. R., Jr. (1996) Regulation of in vitro gene expression using antisense oligonucleotides or antisense expression plasmids transfected using starburst PAMAM dendrimers. *Nucleic Acid. Res. 24* (11), 2176−2182.
(39) Terskikh, A. V., Le Doussal, Jean-Marc, Crameri, R., Fisch, I., Mach, Jean-Pierre, and Kajava, A. V. (1997) "Peptabody": A new type of high avidity binding protein. *Proc. Natl. Acad. Sci. U.S.A. 94*, 1663−1668.
(40) Dworetzky, S. I., Lanford, R. E., and Feldherr, C. M. (1988) The Effects of variations in the number and sequence of targeting signals on nuclear uptake. *J. Cell Biol. 107*, 1279−1287.
(41) Sebestyen, M. G., Ludtke, J. J., Bassik, M. C., Zhang, G., Budker, V., Lukhtanov, E. A., Hagstrom, J. E., and Wolff, J. A. (1998). DNA vector chemistry: The covalent attachment of signal peptides to plasmid DNA. *Nat. Biotech. 16*, 80−85.
(42) Wadhwa, M. S., Collard, W. T., Adami, R. C., McKenzie, D. L., and Rice, K. G. (1997) Peptide-mediated gene delivery: Influence of peptide structure on gene expression. *Bioconjugate Chem. 8*, 81−88.
(43) Dietrich, G., Bubert, A., Gentschev, I., Sokolovic, Z., Simm, A., Catic, A., Kaufmann, S. H. E., Hess, J., Szalay, A. A., and Goebel, W. (1998) Delivery of antigen-encoding plasmid DNA into the cytosol of macrophages by attenuated suicide Listeria monocytogenes. *Nat. Biotech. 16*, 181−185.
(44) Condon, C., Watkins, S. C., Celluzzi, C. M., Thompson, K., and Falo, L. D., Jr. (1996) DNA based immunization by in vivo transfection of dendritic cells. *Nat. Med. 2* (10), 1122−1128.
(45) Akhlynina, T. A., Jans, D. A., Rosenkranz, A. A., Statsyuk, N. V., Balashova, I. Y., Toth, G., Pavo, I., Rubin, A. B., and Sobolev, A. S. (1997). Nuclear targeting of Chlorin e_6 enhances its photosensitizing activity. *J. Biol. Chem. 272* (33), 20328−20331.

BC980131D

Synthesis and Selective Cytotoxicity of a Hyaluronic Acid–Antitumor Bioconjugate

Yi Luo and Glenn D. Prestwich*

Department of Medicinal Chemistry, The University of Utah, 30 South 2000 East, Room 201, Salt Lake City, Utah 84112-5820. Received March 18, 1999; Revised Manuscript Received May 21, 1999

A cell-targeted prodrug was developed for the anti-cancer drug Taxol, using hyaluronic acid (HA) as the drug carrier. HA–Taxol bioconjugates were synthesized by linking the Taxol 2′-OH via a succinate ester to adipic dihydrazide-modified HA (HA-ADH). The coupling of Taxol-NHS ester and HA-ADH provided several HA bioconjugates with different levels of ADH modification and different Taxol loadings. A fluorescent BODIPY–HA was also synthesized to illustrate cell targeting and uptake of chemically modified HA using confocal microscopy. HA–Taxol conjugates showed selective toxicity toward the human cancer cell lines (breast, colon, and ovarian) that are known to overexpress HA receptors, while no toxicity was observed toward a mouse fibroblast cell line at the same concentrations used with the cancer cells. The drug carrier HA-ADH was completely nontoxic. The selective cytotoxicity is consistent with the results from confocal microscopy, which demonstrated that BODIPY–HA only entered the cancer cell lines.

INTRODUCTION

Hyaluronic acid (HA)[1] (Figure 1), a linear polysaccharide of alternating D-glucuronic acid (GlcUA) and *N*-acetyl-D-glucosamine (GlcNAc) units, adopts a three-dimensional structure in solution that shows extensive intramolecular hydrogen bonding. This restricts the conformational flexibility of the polymer chains and induces distinctive secondary (helical) and tertiary (coiled coil) interactions (*1*). HA is one of several glycosaminoglycan components of the extracellular matrix (ECM), the synovial fluid of joints, and the scaffolding comprising cartilage (*2*). The remarkable viscoelastic properties of HA and commercial cross-linked derivatives (*3*) account for their usefulness in joint lubrication. HA–protein interactions play crucial roles in cell adhesion, growth, and migration (*4*–*6*), and HA acts as a signaling molecule in cell motility, in inflammation, wound healing, and cancer metastasis (*7*). The immunoneutrality of HA makes it an excellent building block for the development of novel biocompatible and biodegradable biomaterials used in tissue engineering and drug delivery systems (*8*–*10*). For example, HA has been employed as both a vehicle and angiostatic agent in cancer therapy (*11*–*13*).

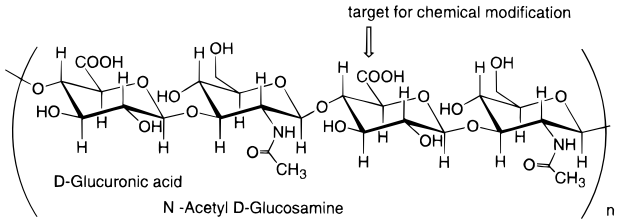


Figure 1. Tetrasaccharide fragment of HA showing the disaccharide repeat units.

The use of biocompatible polymers in the treatment of various ailments has expanded rapidly in the last two decades (*14*). Moreover, derivatization of such polymers with reporter groups (*15*) and drugs (*16*, *17*) has emerged as a powerful method for controlling delivery and release of a variety of compounds. Small drug molecules can be linked to the polymer that allows controlled release of the free bioactive group. In general, coupling of antitumor agents to biopolymers provides advantages in drug solubilization, stabilization, localization, and controlled release (*18*). For example, the linking of a cytotoxic small molecule such as adriamycin to poly(hydroxymethyl)-acrylamide (HPMA) gives a new material with improved in vitro tumor retention, a higher therapeutic ratio, avoidance of multidrug resistance (*19*), and encouraging clinical results. In work with a naturally occurring biocompatible polymer, mitomycin C and epirubicin were coupled to HA by carbodiimide chemistry; the former adduct was selectively taken up by, and toxic to, a lung carcinoma xenograft (*20*).

HA is overexpressed at sites of tumor attachment (*21*) to the mesentery and provides a matrix that facilitates invasion (*22*). HA is an important signal for activating kinase pathways (*23*, *24*) and regulating angiogenesis in tumors (*25*). Moreover, several types of cellular HA receptors respond to HA as a signal. These include CD44, a family of glycoproteins originally associated with lymphocyte activation; RHAMM, the receptors for HA-mediated cell motility (*26*, *27*); and HARLEC, responsible

* To whom correspondence should be addressed. Phone: (801) 585-9051. Fax: (801) 585-9053. E-mail: gprestwich@deans.pharm.utah.edu.

[1] Abbreviations: α-MEM, Minimal Essential Medium, Eagle; ADH, adipic dihydrazide; BODIPY-FL, 4,4-difluoro-5,7-dimethyl-4-bora-3a, 4a-diaza-*s*-indacene-3-propionic acid; D-MEM, Dulbecco's Modified Eagle Medium; DPPC, diphenylphosphoryl chloride; ECM, extracellular matrix; EDCI, 1-ethyl-3-[3-(dimethylamino)-propyl]carbodiimide; FBS, fetal bovine serum; GlcNAc, *N*-acetyl-D-glucosamine; GlcUA, D-glucuronic acid; GPC, gel permeation chromatography; HA, hyaluronic acid; HA-ADH, adipic dihydrazide-modified HA; HAse, hyaluronidase; HMPA, poly(hydroxymethyl)acrylamide; LMW, low molecular weight; MTT, thiazoyl blue; SDPP, *N*-hydroxysuccinimido diphenyl phosphate.

10.1021/bc9900338 CCC: $18.00 © 1999 American Chemical Society
Published on Web 07/27/1999

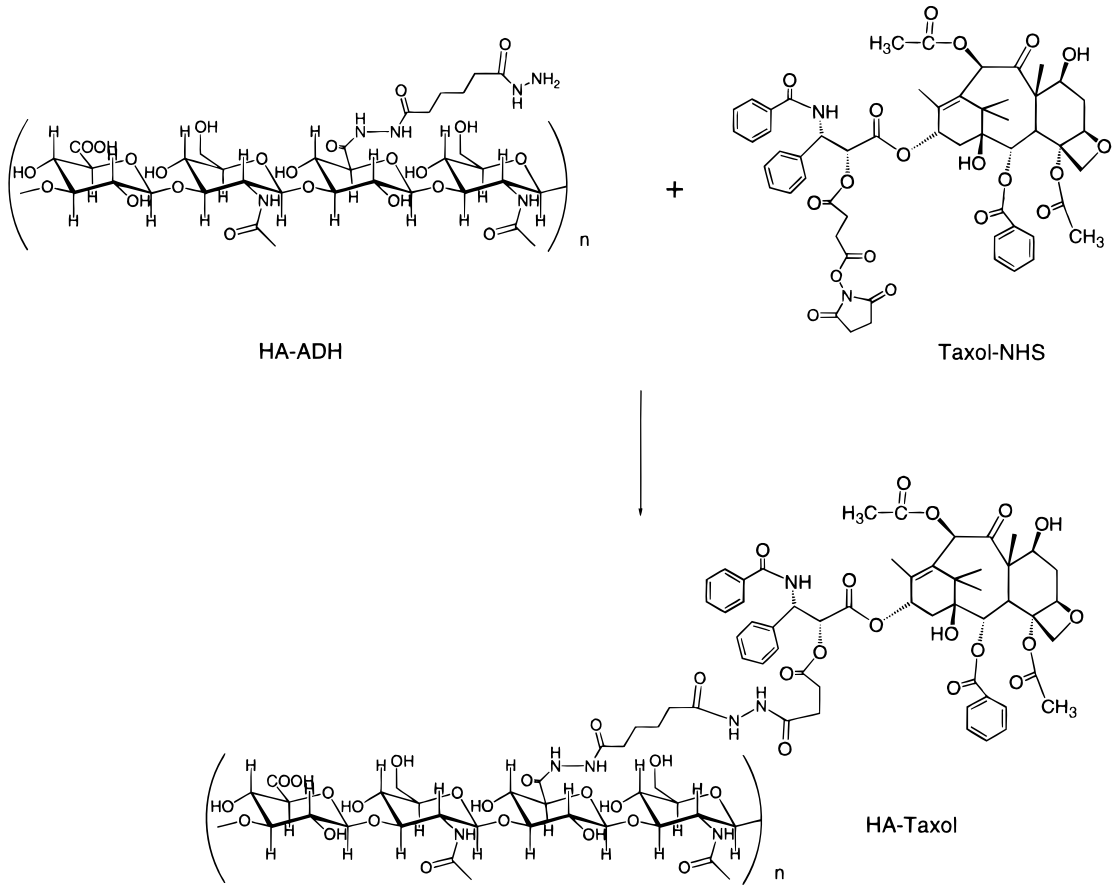


Figure 2. Synthesis of HA−Taxol.

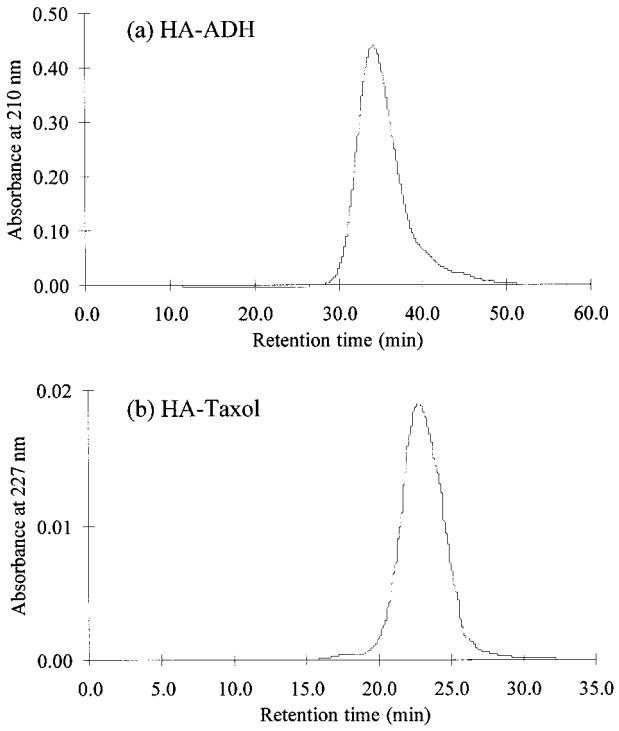


Figure 3. GPC profile. (a) Purified HA-ADH detection at λ = 210 nm. Waters Ultrahydrogel 250, 2000 columns (7.8 mm ID × 30 cm) were used in the analysis. (b) Purified HA−Taxol conjugate detection at λ = 227 nm. Only the Ultrahydrogel 250 column was employed. Eluent was 150 mM, pH 6.5, phosphate buffer/MeOH = 80:20 (v/v); the flow rate was 0.5 mL/min.

for receptor-mediated uptake of HA in liver. Using radiolabeled HA analogues and HA-coupled prodrugs, it

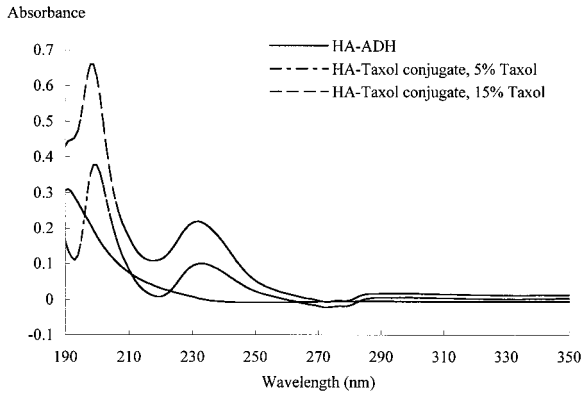


Figure 4. UV spectra of HA−Taxol conjugates.

was possible to selectively target tumor cells and tumor metastases through the use of chondroitin sulfate to block "housekeeping" receptors in the liver without affecting specific HA receptors of tumor cells (*28*−*31*). Targeting of anti-cancer agents to tumor cells and tumor metastases can be accomplished by receptor-mediated uptake of bioconjugates of these agents to HA (*20*). Since HA receptors (CD44, RHAMM) are overexpressed in transformed human breast epithelial cells and other cancers (*32*), selectivity for cancerous cells is markedly enhanced and overall dosages may be reduced. Moreover, coupling of antitumor agents to biopolymers can provide advantages in drug solubilization, stabilization, localization, and controlled release (*18*). Our methodology (*33*) for coupling antitumor agents to HA adds further value by specifically targeting the bioconjugate to aggressively growing cancers that overexpress HA receptors.

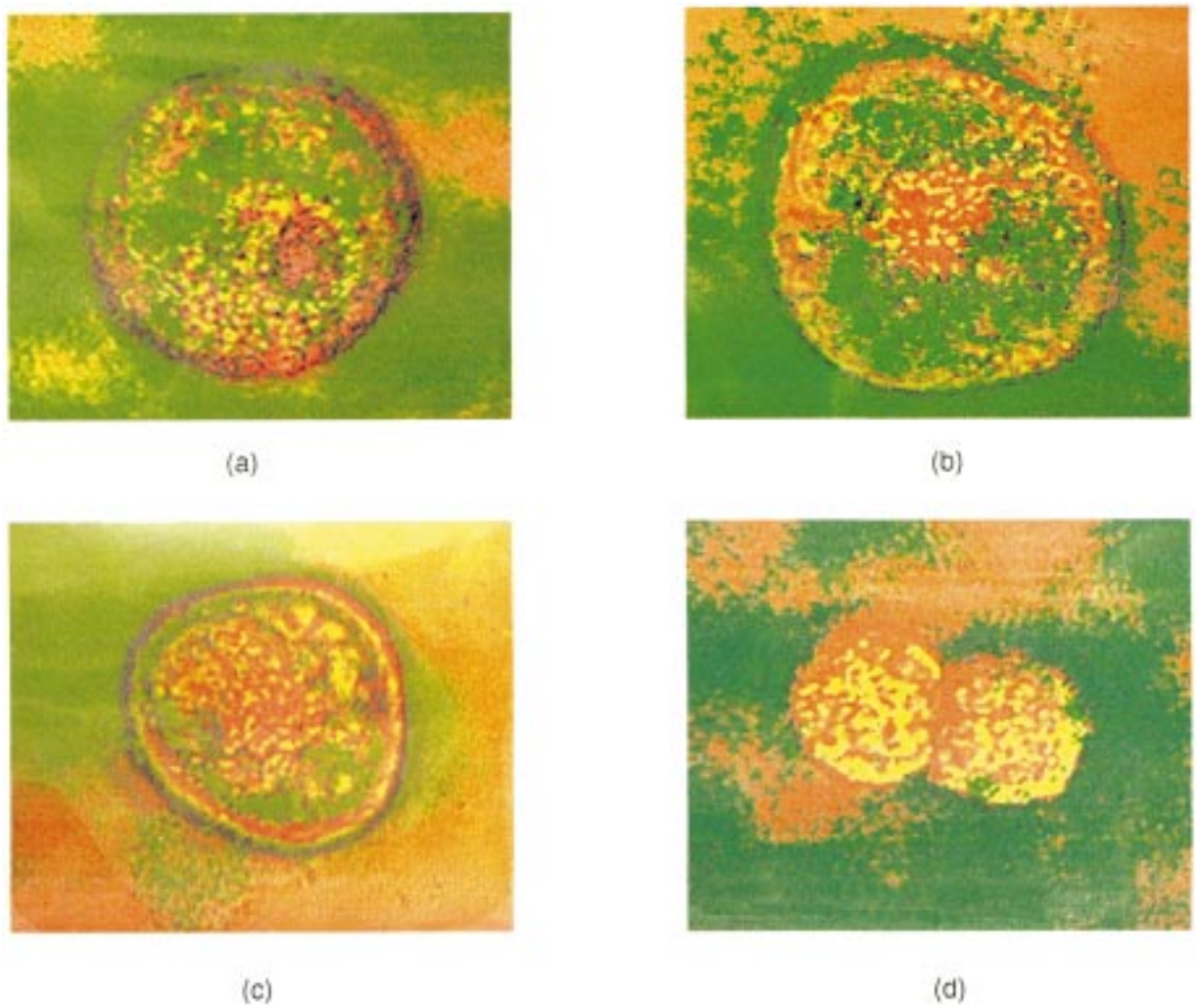


Figure 5. Targeting human breast cancer HBL-100 cells with HA-BODIPY. Panel a fluorescence image shows HA binding to cell surfaces in 3 min. Panels b and c show HA accumulation in the nucleus after 6 and 9 min. In panel d, after 20 min HA, has been completely taken up and fluorescence is dispersed throughout the cells.

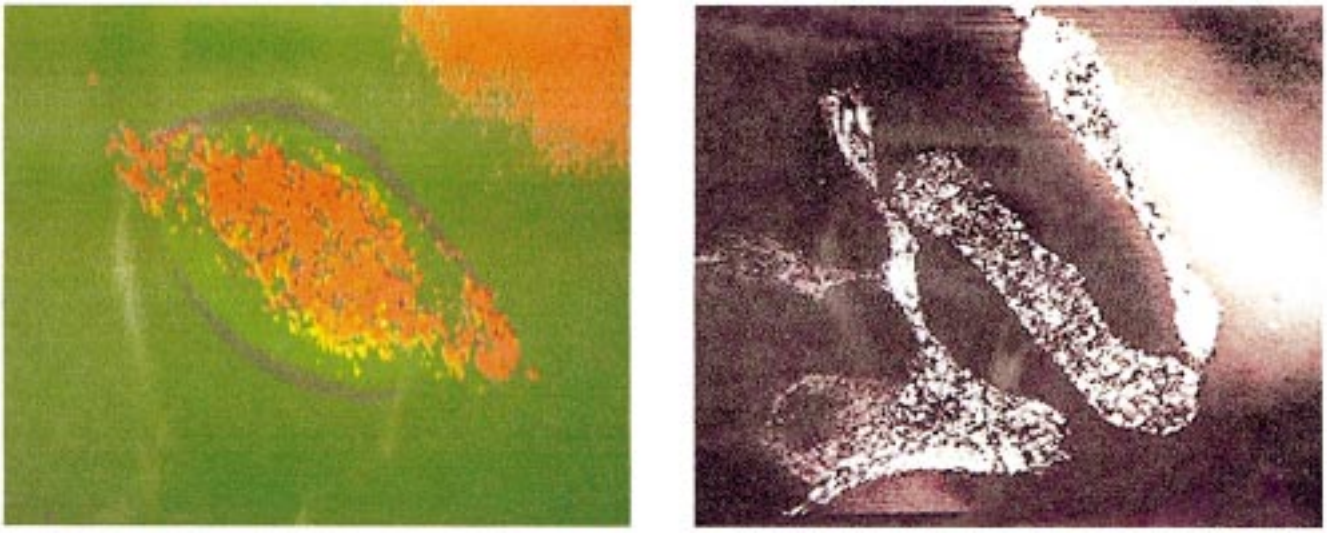


Figure 6. Targeting ovarian cancer SK-OV-3 cells with HA-BODIPY. Panel a shows HA uptake by cells in 15 min. Panel b shows HA uptake by cells in 60 min.

Paclitaxel (Taxol) (*34*), a diterpenoid originally isolated from the bark of the Pacific yew, *Taxus brevifolia*, is a powerful anti-mitotic agent that acts by promoting tubulin assembly into stable aggregated structures. It binds to microtubules and inhibits their depolymerization into tubulin. Although Taxol has shown tremendous potential as an anti-cancer compound, its use as an anti-cancer drug is compromised by its poor aqueous solubility. One attempt to address this involved preparation of 2′-OH linked water-soluble poly(ethylene glycol) derivatives

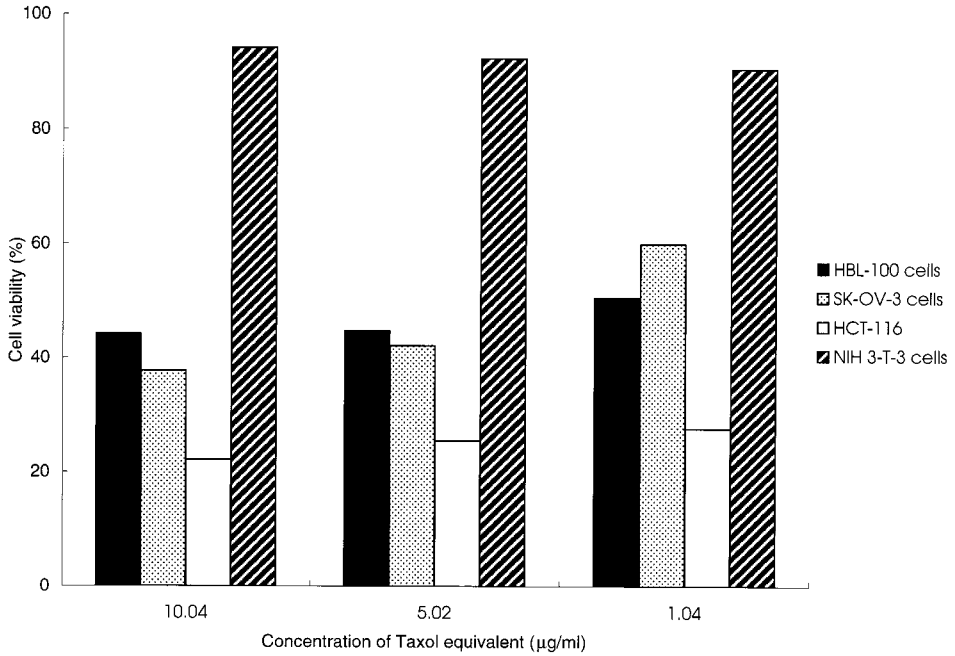


Figure 7. Cytotoxicity of HA−Taxol conjugate with 5% Taxol loading against HBL-100, SK-OV-3, HCT-116, and NIH 3-T-3 cells.

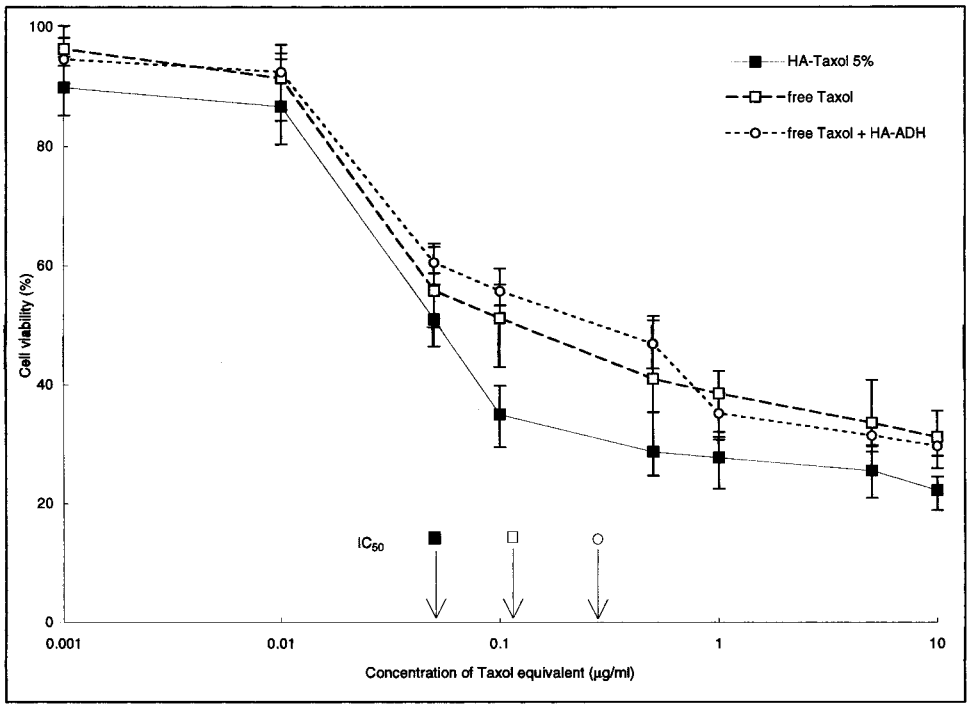


Figure 8. In vitro cytotoxicity of HA−Taxol conjugate with 5% Taxol loading against colon tumor HCT-116 cells.

(*35*). In this paper, we have taken a different approach that uses a prodrug strategy to both increase water solubility and provide cellular targeting. Thus, we selected Taxol as a model anti-cancer drug for covalent attachment to HA that had been modified with adipic dihydrazide (ADH) (*36*−*38*). The coupling of Taxol-2′-hemisuccinate NHS ester to HA-ADH was optimized to give HA−Taxol conjugates with a variety of ADH and Taxol loadings (Figure 2). Selective in vitro cell cytotoxicity was studied with an untransformed mouse fibroblast cell line (NIH 3-T-3) and with three human cell lines: HCT-116 colon tumor cells, HBL-100 breast cancer cells, and SK-OV-3 ovarian cancer cells. In addition, a fluorescent (BODIPY)-labeled HA bioconjugate was prepared and employed to visualize selective uptake of HA by confocal microscopy.

MATERIALS AND METHODS

General. Fermentation-derived HA (sodium salt, M_w 1.5 MDa) was provided by Clear Solutions Biotechnology, Inc. (Stony Brook, NY). 1-Ethyl-3-[3-(dimethylamino)-propyl]carbodiimide (EDCI), ADH, succinic anhydride, diphenylphosphoryl chloride (DPPC), *N*-hydroxysuccinimide, and triethylamine were purchased from Aldrich Chemical Co. (Milwaukee, WI). Bovine testicular hyaluronidase (HAse, 880 units/mg) was obtained from Sigma Chemical Co. (St. Louis, MO). Paclitaxel (Taxol) was purchased from CBI Tech, Inc. (Cambridge, MA). 4,4-

Difluoro-5,7-dimethyl-4-bora-3a,4a-diaza-*s*-indacene-3-propionic acid, hydrazide (BODIPY-FL hydrazide) was obtained from Molecular Probes, Inc. (Portland, OR). All solvents were of reagent grade or HPLC grade (Fisher Scientific Co., Santa Clara, CA). CH_2Cl_2 and acetonitrile were distilled from CaH_2.

Analytical Instrumentation. All ^{1}H NMR spectral data were obtained using an NR-200 FT-NMR spectrometer at 200 MHz (IBM Instruments Inc.). UV−Vis spectra were recorded on a Hewlett-Packard 8453 UV−Vis diode array spectrophotometer (Palo Alto, CA). Gel permeation chromatography (GPC) analysis was carried out on the following system: Waters 515 HPLC pump, Waters 410 differential refractometer, Waters 486 tunable absorbance detector, Waters Ultrahydrogel 250 and 2000 columns (7.8 mm ID × 30 cm) (Milford, MA). The GPC eluent was 150 mM phosphate buffer, pH 6.5:MeOH = 80:20 (v/v), and the flow rate was 0.5 mL/min. The system was calibrated with HA standards supplied by Dr. S. Gustafson (University of Uppsala, Sweden), and thus the molecular sizes of each HA oligosaccharide and the corresponding bioconjugates were calculated from the standard samples. Confocal fluorescence images of HA-BODIPY binding and uptake by cells were recorded using a Zeiss Microscope (Carl Zeiss, Inc., Germany). Coulter Counter was from Coulter Electronics, Inc. (Hialeah, FL). Cell viability was determined by thiazoyl blue (MTT) dye uptake protocols at 540 nm, which was recorded on a Bio-Rad M-450 microplate reader (Hercules, CA).

Synthesis of Taxol-NHS Ester. To a stirred solution of 270 mg of Taxol and 38 mg (1.2 equiv) of succinic anhydride in 13 mL of CH_2Cl_2 at room temperature was added 36 μL (10-fold molar excess) of dry pyridine. The reaction mixture was stirred for 3 days at room temperature and then concentrated in vacuo. The residue was dissolved in 5 mL of CH_2Cl_2, and Taxol-2′-hemisuccinate was purified on silica gel (wash with hexane; elute with ethyl acetate) to give 258 mg of product (86%). FAB-MS calcd for $C_{51}H_{55}NO_{17}$: 953.99. Found: 954.4 (MH^+).

Next, *N*-hydroxysuccinimido diphenyl phosphate (SDPP) was prepared from 10 mmol of diphenylphosphoryl chloride, 10 mmol of *N*-hydroxysuccinimide, and 10 mmol of triethylamine in 6 mL of CH_2Cl_2 as previously described (*39*). Crude SDPP was triturated with ether, dissolved in ethyl acetate, washed (2 × 10 mL H_2O), dried ($MgSO_4$), and concentrated in vacuo to give SDPP with mp 89−90 °C (85%). To a solution of 150 mg of Taxol-hemisuccinate and 82 mg (1.5 equiv) of SDPP in 5 mL of acetonitrile was added with 88 μL (4 equiv) of triethylamine. The reaction was stirred for 6 h at room temperature, and then concentrated in vacuo. The residue was dissolved in 5 mL of ethyl acetate and 2 mL of hexane and purified on silica gel. SDPP gave superior yields in less time and under milder conditions than did any carbodiimide coupling reagent. The purified Taxol-NHS ester was dried for 24 h in vacuo at room temperature to give 134 mg (80%). FAB-MS calcd for $C_{55}H_{58}N_2O_{19}$: 1051.07. Found: 1051.5 (MH^+).

Preparation of Low Molecular Weight (LMW) HA. To a solution of 2.0 g of high molecular mass HA (1.5 MDa) in pH 6.5 PBS buffer (4 mg/mL) was added hyaluronidase (HAse) (10 units/mg of HA). The degradation was carried out at 37 °C, 190 rpm stirring for 1 h, then 95 °C for 20 min. Dialysis tubing (M_w cutoff 3 500 Da) was prepared by soaking the membrane in water at room temperature for 3−4 h and subsequently rinsing it with water. The solution was dialyzed against water for 4 days using this washed membrane tubing. The retained material was filtered through a 0.2 μm cellulose acetate membrane (Corning) and lyophilized to give 1.12 g of LMW HA (56%).

Adipic Dihydrazido-Functionalized HA (HA-ADH). HA-ADH was prepared as described previously (*37*, *38*, *40*). In a representative example, LMW HA (50 mg) was dissolved in water to give a concentration of 4 mg/mL, and then a 5-fold excess of ADH was added into the solution. The pH of the reaction mixture was adjusted to 4.75 by addition of 0.1 N HCl. Next, 1 equiv of EDCI was added in solid form. The pH of the reaction mixture was maintained at 4.75 by addition of 0.1 N HCl. The reaction was quenched by addition of 0.1 N NaOH to adjust the pH of reaction mixture to 7.0. The reaction mixture was then transferred to pretreated dialysis tubing (Mw cutoff 3 500) and dialyzed exhaustively against 100 mM NaCl, then 25% EtOH/H_2O and finally H_2O. The solution was then filtered through 0.2 μm cellulose acetate membrane, flash frozen, and lyophilized. The purity of HA-ADH was measured by GPC. The substitution degree of ADH was determined by the ratio of methylene hydrogens to acetyl methyl protons as measured by ^{1}H NMR. In this example, 37 mg of HA-ADH was obtained with an 18% loading based on available carboxylates modified.

HA−Taxol. Several loadings were prepared following a general protocol (Figure 2). In a representative example, HA-ADH with 18% ADH loading (10 mg, 4.4 μmole hydrazide) was dissolved in 3 mM, pH 6.5, phosphate buffer to give a concentration of 1 mg/mL. To this mixture was added Taxol-NHS ester dissolved in sufficient DMF (DMF:H_2O = 2:1, v/v) to give a homogeneous solution, and the reaction mixture was stirred at room temperature for 24 h. The reaction mixture was dialyzed successively against 50% acetone/H_2O and water (membrane tubing, Mw cutoff 3 500). The solution was then filtered through a 0.2 μm membrane and then lyophilized. The purity of HA−Taxol conjugate was measured by GPC analysis. Taxol loading was determined by UV absorbance (λ_{max} = 227 nm, $\epsilon = 2.8 \times 10^4$) in 80:20 CH_3CN:H_2O.

BODIPY-FL-Labeled HA. In a representative reaction, 100 mg of LMW HA was dissolved in 10 mL of H_2O, and 10 mL of an acetone solution (0.8 mg/mL) of BODIPY−FL hydrazide was added. The pH was adjusted to 4.75 with 0.1 N HCl, and then 51.5 mg (3 molar equiv) of EDCI was added in solid form into the mixture. The reaction was stirred overnight at room temperature at pH 4.75. The HA-BODIPY was purified by dialysis against H_2O, and its purity was characterized by GPC with detection at 210 nm (HA) and 502 nm (BODIPY).

In Vitro Cell Culture Cytotoxicity. The cytotoxicity of HA−Taxol conjugates was determined using a 96-well plate format in quadruplicate with increasing doses: 0.001, 0.01, 0.1, 0.5, 1, 5, 10, 50, and 100 μg/mL. Each well contained approximately 20 000 cells in 200 μL of cell culture media. Cells were cultured in the following media: HBL-100 cells, high glucose D-MEM (Dulbecco's Modified Eagle Medium) + 10% FBS (fetal bovine serum) + 1% sodium pyruvate; SK-OV-3 cells, D-MEM/F12 + 10% FBS; HCT-116 cells, α-MEM (Minimal Essential Medium, Eagle) + 10% FBS; NIH 3-T-3 cells, high glucose D-MEM + 10% FBS.

HA−Taxol conjugates and HA-ADH control were added as stock solutions in DMSO:H_2O = 1:1 (v/v); free Taxol was added as a DMSO stock solution. A 2 μL aliquot of the stock solution was added to each well of the cell culture plate. Cells were incubated at 37 °C for 3 days with the test material, and cell viability was determined using MTT dye uptake by reading plates at 540 nm.

Table 1. Optimization of ADH Modification of HA and the Reaction Condition

molar ratio of HA:ADH:EDCI	reaction time (min)	ADH loading (%)
	5	28.3
	10	31.2
	15	31.4
1:40:4	30	32.2
	60	38.6
	120	45.7
	240[a]	44.0
1:5:0.5	15	9.0
1:5:1	15	17.5
1:10:1	15	18.0
1:20:1	15	19.0
1:10:0.2	180	19.3

[a] No 0.1 N HCl was used to maintain the pH of the reaction mixture.

Response was graded as percent live cells compared to untreated controls (*41*).

RESULTS

Degradation and Modification of HA. LMW HA was generated by degradation of high molecular mass HA (1.5 MDa) with testicular HAse. This enzyme degrades HA to generate a series of even-numbered HA oligosaccharides with the *N*-acetylglucosamine moiety at the reducing terminus (*42*). Thus, incubation of a solution of high molecular mass HA in pH 6.5 PBS buffer with testicular HAse at 37 °C provided partially degraded HA. Small fragments, HA oligosaccharides, and buffer salts were removed by dialysis against H_2O (four changes per day). The final LMW HA product was lyophilized, and an aliquot was analyzed by GPC analysis: $M_n = 3883$, $M_w = 11\,199$, and molecular dispersity (DP) = 2.88. This corresponds to an average of 28 disaccharide repeats/LMW HA molecule. This preparation is quite reproducible as time, temperature, and concentrations of HA and HAse are controlled.

The use of the mild and versatile hydrazide method for preparation of chemically modified HA derivatives (*36*, *37*) allows attachment of reporter molecules, drugs, cross-linkers, and any combination of the above moieties to HA (*10*, *33*, *40*). Covalent attachment of ADH to the carboxylic acid groups of HA provides a controlled loading of pendant hydrazide functionalities arrayed along the hyaluronate backbone, used herein for the attachment of an antitumor agent. We selected LMW HA for modification in this study for four main reasons. First, it was possible to perform reproducible chemical modifications and to monitor the extent of modification by simple proton NMR methods. Second, LMW HA can be cleared from the body via ultrafiltration by the kidney. Third, the LMW HA bioconjugates were expected to provide a readily injectable nonviscous solution at concentrations up to 10 mg/mL, and the LMW materials should suffer minimal further degradation in plasma and would be rapidly taken up by cells. Finally, with LMW HA bioconjugates, we were confident that future efforts to cross-link the material into a hydrogel could also be easily controlled.

Thus, LMW HA (4 mg/mL) was mixed with ADH at several concentrations (Table 1). The pH of the reaction mixture was adjusted to 4.75, and then different quantities of solid EDCI were added in solid form to initiate the reaction. An increase in pH was observed immediately corresponding to proton uptake in the coupling reaction. The pH of the reaction mixture was maintained at 4.75 by addition of 0.1 N HCl. Preliminary studies had provided guidelines as to ratios of HA:ADH:EDCI suitable to achieve a given percentage modification of the glucuronate functions of HA. The reaction was stopped by addition of 0.1 N NaOH to adjust the pH of reaction mixture to 7.0. The HA-ADH was purified by sequential dialysis against 100 mM NaCl, 25% EtOH/H_2O, and H_2O. The dialyzed solutions were filtered through a 0.2 μm membrane, and then lyophilized to give HA-ADH in yields ranging 50−70%.

Table 2. Optimization of Taxol Loading. Both the Total ADH Modification of HA and the Molar Ratio of ADH to Taxol-NHS Ester during the Conjugation Reaction Were Varied

$(HA)_x(HA\text{-}ADH)_y(HA\text{-}ADH\text{-}Taxol)_z$

	composition of HA−Taxol conjugates				
preparation	HA (x) (%)	HA-ADH (y) (%)	HA-ADH-Taxol (z) (%)	solubility in H_2O	ADH%: Taxol-NHS[a]
	A. ADH loading = 9%[b]				
1	91	7.8	1.2	yes	9:5
2	91	7.7	1.3	yes	9:9
3	91	3.8	5.2	yes	9:18
	B. ADH loading = 18%				
4	82	16.4	1.6	yes	18:5
5	82	16.1	1.9	yes	18:10
6	82	15.8	2.2	yes	18:15
7	82	3.1	14.9	partially[c]	18:36
	C. ADH loading = 45%				
8	55	30	15	no	45:90

[a] The molar ratio used in the grafting reaction of HA-ADH and Taxol-NHS that resulted in the composition of the HA−Taxol conjugates. [b] Total ADH loading for modified HA = $y + z$. [c] Limited solubility; only soluble below 0.1 mg/mL due to high loading of Taxol.

The purity and molecular size distribution of the HA-ADH was measured by GPC. The narrow single-peak GPC profile detected by UV (210 nm) (Figure 3a) and RI indicated that both large and small impurities had been completely removed. It is essential to establish this fact rigorously to ensure that all subsequent molecules added also become covalently attached, rather than remaining noncovalently associated. In addition, the GPC results showed that there was virtually no molecular weight decrease due to further HA degradation or increase due to bifunctional cross-linking during the modification reaction. The loading of ADH on the polymer backbone was determined by ^1H NMR spectroscopy studies with D_2O as a solvent. The degree of substitution could be calculated by integration of the ADH methylene signals using the methyl resonance ($\delta = 1.95-2.00$ ppm) of the acetamido moiety of the GlcNAc residues of HA as an internal standard (*37*). Thus, ^1H NMR integration confirmed that different ADH loadings occurred with different ratios of reactants and for different reaction times. The relationship between the degree of substitution of ADH and the reaction conditions, i.e., molar ratio of HA:ADH:EDCI, and reaction time was optimized. The results are shown in Table 1. Importantly, the degree of ADH substitution on HA was influenced primarily by the HA:EDCI ratio, with the amount of excess ADH varying from 5 to 25-fold having little effect. The carbodiimide quantity is thus the controlling factor for determining ADH loading on HA.

Taxol (paclitaxel) is a taxane natural product that promotes polymerization of tubulin and stabilizes the structure of intracellular microtubules. This process has the effect of inhibiting the normal dynamics reorganization of the microtubules, which is necessary for inter-

Table 3. In Vitro Cytotoxcity of HA−Taxol Conjugates against Different Cell Lines

HA−Taxol preparations	IC_{50} (μg/mL)[d]					
	HBL-100[e]		SK-OV-3[e]		HCT-116[e]	
	conjugate[b]	Taxol equivalents[c]	conjugate	Taxol equivalent	conjugate	Taxol equivalent
1	48.0 (118 μM)	1.21 (1.42 nM)	21.5 (53 μM)	0.54 (0.64 nM)	7.20 (17.8 μM)	0.18 (0.21 nM)
3	16.4 (37 μM)	1.65 (1.93 nM)	8.0 (18.2 μM)	0.80 (0.94 nM)	0.52 (1.2 μM)	0.052 (0.061 nM)
7	6.8 (12.4 μM)	1.58 (1.85 nM)	0.37 (0.68 μM)	0.086 (0.10 nM)	0.11 (0.20 μM)	0.026 (0.030 nM)
8[a]	68.0 (115 μM)	1.48 (17.3 nM)	7.2 (17.3 nM)	1.56 (1.83 nM)	2.15 (3.65 μM)	0.47 (0.55 nM)

[a] Dissolved in 3:1 DMSO/H_2O. [b] The data in these columns show the IC_{50} of HA−Taxol conjugates against the tumor cell line. [c] The data in these columns are calculated as the Taxol equivalents present in the HA−Taxol bioconjugate using the molar ratios in Table 2. This calculation allows comparison of conjugated and free Taxol. [d] The IC_{50} value is the molarity at which 50% of tumor cell death was observed after 72 h under standard tissue culture conditions. [e] Cell type.

phase and mitotic functions. Because of the problems in administering emulsified forms of this water-insoluble drug, Taxol was selected as the model anti-cancer drug in our study. Taxol was first converted to its 2′-hemisuccinate derivative by standard methods (*43*), and its structure was confirmed spectroscopically. Second, the activated Taxol-NHS ester was prepared by coupling with SDPP. Taxol-NHS was then coupled to HA-ADH in 3 mM phosphate buffer at pH 6.50 using DMF as a cosolvent to maintain a homogeneous solution. The purification of HA−Taxol bioconjugate was carried out by dialysis of the reaction mixture against 50% acetone/H_2O. The purity of the HA−Taxol conjugate was determined by GPC analysis, monitoring absorbance at 227 nm (Figure 3b) and RI. The single symmetrical GPC peak showed that no free Taxol or other small molecular impurities remained in this preparation. The Taxol was quantified by UV absorbance at 227 nm (Figure 4) in 80% acetonitrile: H_2O. To obtain the optimal modification on HA for anticancer ability, HA−Taxol conjugates with different Taxol loading were synthesized. Table 2 shows the optimization of Taxol loading and the molar ratio of HA-ADH to Taxol-NHS during the conjugation reaction. These data demonstrate that the molar ratio of ADH to Taxol-NHS during the grafting reaction is critical in determining the Taxol loading of the bioconjugate.

Fluorescently labeled HA has been prepared with several chemistries and used in other studies of receptor-mediated uptake. Most recently, RHAMM-mediated uptake and trafficking of HA by transformed fibroblasts (*44*) was observed with Texas Red-HA. Previously, fluorescein-HA was employed to study HA uptake in a variety of systems, e.g., cells expressing CD44 variants (*21*, *45*−*48*), uptake by tumor cells for correlation with metastatic potential (*49*, *50*), internalization by chondrocytes (*51*), and as a measure of liver endothelial cell function (*52*). In this study and in the Texas Red study, hydrazide derivatives of the dyes were used to form covalent bishydrazide linkages to the HA carboxylic acid functions under the mild all-aqueous conditions employed for other hydrazide modifications of HA (*33*).

To study the binding ability of HA to tumor cells and uptake by cells, a variety of fluorescently labeled HA derivatives were prepared. Of those evaluated for use with cancer cells, we obtained the best results with the BODIPY fluorophore (Y. Luo, M. R. Ziebell, unpublished results). Thus, BODIPY−FL hydrazide was coupled to LMW HA using EDCI as the condensing agent to give HA-BODIPY, which was purified by dialysis against H_2O; the loading of GPC-homogeneous HA-BODIPY was determined spectrophotometrically to be 1.8% (based on available glucuronates).

Cell-Based Assays for Uptake and Toxicity. An aliquot (2 μL) of a 1.5 mg/mL aqueous stock solution HA-BODIPY was added to 100 μL cell culture media with tumor cells cultured on cover slips. Confocal images of HA-BODIPY uptake by HBL-100 cells can be seen in Figure 5. Initially, the HA-BODIPY can be seen on cell membrane; over the course of several minutes, it is taken up into the cell and then gradually begins to accumulate in the nucleus. After 20 min, cells showed HA-BODIPY in most compartments. Uptake of HA-BODIPY into SK-OV-3 cells occurred with a similar appearance and time course (Figure 6). These data suggest that HA binds readily to tumor cell surface and is rapidly taken up via HA receptor-mediated pathways. This supports the notion that HA should be a good targeting polymer for selective delivery of anti-cancer drugs to tumor cells. Similar results were observed independently with HA−Texas Red uptake by transformed fibroblasts (*44*). Importantly, nontransformed cells, such as the NIH 3-T-3 fibroblasts, did not show this binding and rapid uptake of HA-BODIPY.

Next, the cytotoxicity of HA−Taxol conjugates was measured using a 96-well plate format in quadruplicate with increasing doses from 0.001 to 100 μg/mL. The cytotoxicity of HA−Taxol conjugates was studied by using the MTT assay to identify cells still active in respiration (*41*). HA−Taxol conjugates showed effective cytotoxicity against SK-OV-3, HBL-100, and HCT-116 cell lines, while no cytotoxicity against NIH 3-T-3 cells was observed at concentrations up to 10 μg/mL of Taxol equivalents (Figure 7). These results confirm the selective toxicity of HA−Taxol toward different cells lines, and the known overexpression of CD44 by HBL-100 (*53*) and SK-OV-3 cells (*54*) suggests that this selective toxicity is due to receptor-mediated binding and uptake of the HA−Taxol bioconjugate.

The HA-BODIPY binding and uptake results support the hypothesis that selective toxicity of HA−Taxol is due to receptor-mediated events. This was further explored by investigating the relative toxicity of polymer-bound and free Taxol, as well as examining the effect of the polymeric carrier itself on the toxicity of the drug. Thus, Figure 8 summarizes the cytotoxicity data for HA−Taxol (5% Taxol loading) with HCT-116 colon cancer cells. The bioconjugate showed increased cytotoxicity, e.g., lower IC_{50}, relative to free Taxol or free Taxol mixed with the HA-ADH carrier. In a further control experiment, we had established that HA-ADH alone elicited no detectable change in cell viability at a concentration 10 times higher than the maximal concentration of HA−Taxol conjugate used. These data support the notion that the increased cytotoxicity of HA−Taxol conjugates requires cellular uptake of the complex followed by hydrolytic release of the active Taxol by cleavage of the labile 2′ ester linkage.

The in vitro cytotoxicity results of HA−Taxol conjugates with different modifications against different cell lines are shown in Table 3. For the least-modified HA (9% ADH modification), higher cytotoxicity was observed

as Taxol loading increased. However, the cytotoxicity of highly modified HA actually decreased at the highest Taxol loading. Apparently, high loading of Taxol decreased the solubility of HA−Taxol conjugate, masked the HA receptor recognition elements of HA, caused aggregation of the polymeric conjugate, and thus limited the toxicity of the conjugate relative to that of free drug. Clearly, the cytotoxicity of HA−Taxol conjugates depends on a balance between minimal HA modification and maximal Taxol loading.

ACKNOWLEDGMENT

Financial support for this work was provided by Department of Army (DAMD 17-9A-1-8254) and by the Huntsman Cancer Foundation at The University of Utah. Initial studies of HA modification and degradation were performed with M.R. Ziebell (UUtah) and we thank Drs. D.M. Marecak and C.M. Amann (UUtah) for assistance with Taxol modification. We are grateful to D. Schmehl and Dr. L. R. Barrows (UUtah) for assistance with cell cytotoxicity experiments and Mr. Ziebell and Dr. W. G. Pitt (Brigham Young University, Provo, UT) for assistance with confocal microscopy. We thank Dr. L. Y.-W. Bourguignon (University of Miami Medical School, Miami, FL) for providing HBL-100 and SK-OV-3 cells. We are grateful to Clear Solutions Biotech, Inc. (Stony Brook, NY) for providing HA and the Center for Cell Signaling (UUtah) for equipment and facilities.

LITERATURE CITED

(1) Scott, J. E., Secondary structures in hyaluronan solutions: chemical and biological implications; In *The Biology of Hyaluronan*; C. Foundation, Ed.; J. Wiley & Sons, Ltd.: Chichester, UK, 1989; pp 6−20.

(2) Laurent, T. C., Laurent, U. B. G., and Fraser, J. R. E. (1995) Functions of hyaluronan. *Ann. Rheum. Dis. 54*, 429−432.

(3) Larsen, N. E., Leshchiner, E., and Balazs, E. A. (1995) Biocompatibility of Hylan polymers in various tissue compartments. *Mater. Res. Soc. Symp. Proc. 394*, 149−153.

(4) Knudson, C. B., and Knudson, W. (1993) Hyaluronan-Binding proteins in development, tissue homeostasis, and disease. *FASEB J. 7*, 1233−1241.

(5) Turley, E. A., The role of a cell-associated hyaluronan binding protein in fibroblast behavior; In *The Biology of Hyaluronan*; C. Foundation, Ed.; J. Wiley & Sons, Ltd.: Chichester, UK, 1989; pp 121−137.

(6) Underhill, C. B., The interaction of hyaluronate with the cell surface: the hyaluronate receptor and the core protein; In *The Biology of Hyaluronan*; C. Foundation, Ed.; J. Wiley & Sons, Ltd.: Chichester, UK, 1989; pp 87−106.

(7) Entwistle, J., Hall, C. L., and Turley, E. A. (1996) Hyaluronan receptors: regulators of signaling to the cytoskeleton. *J. Cell Biochem. 61*, 569−577.

(8) Vercruysse, K. P., and Prestwich, G. D. (1998) Hyaluronate derivatives in drug delivery. *Crit. Rev. Ther. Drug Carr. Syst. 15*, 513−555.

(9) Freed, L. E., Vunjak-Novakovic, G., Biron, R. J., Eagles, D. B., Lesnoy, D. C., Barlow, S. K., and Langer, R. (1994) Biodegradable polymer scaffolds for tissue engineering. *Bio/Technology 12*, 689−693.

(10) Prestwich, G. D., Marecak, D. M., Marecek, J. F., Vercruysse, K. P., and Ziebell, M. R., Chemical modification of hyaluronic acid for drug delivery, biomaterials, and biochemical probes; In *The Chemistry, Biology, and Medical Applications of Hyaluronan and its Derivatives*; T. C. Laurent, Ed.; Portland Press: London, 1998; pp 43−65.

(11) Alam, C. A. S., Seed, M. P., and Willoughby, D. A. (1995) Angiostasis and vascular regression in chronic granulomatous inflammation induced by diclofenac in combination with hyaluronan in mice. *J. Pharm. Pharmacol. 47*, 407−411.

(12) Ziegler, J. (1996) Hyaluronan seeps into cancer treatment trials. *J. Nat. Cancer Inst. 88*, 397−399.

(13) Falk, R. E. In *PCT Int. Appl. WO 9740841*; 1997.

(14) Duncan, R., Dimitrijevic, S., and Evagorou, E. G. (1996) The role of polymer conjugates in the diagnosis and treatment of cancer. *J. Therap. Polymers Pharmaceut. Sci. 6*, 237−263.

(15) Brinkley, M. (1992) A brief survey of methods for preparing protein conjugates with dyes, haptens, and cross-linking agents. *Bioconjugate Chem. 3*, 2−13.

(16) Puttnam, D., and Kopecek, J. (1995) Polymer conjugates with anticancer activity. *Adv. Polym. Sci. 122*, 55−123.

(17) Krinick, N. L., and Kopecek, J., Soluble polymers as targetable drug carriers; In *Targeted Drug Delivery. Handbook of Experimental Pharmacology*; R. L. Juliano, Ed.; Springer-Verlag: Berlin, 1991; pp 105−179.

(18) Maeda, H., Seymour, L., and Miyamoto, Y. (1992) Conjugates of anticancer agents and polymers: advantages of macromolecular therapeutics in vivo. *Bioconjugate Chem. 3*, 351−362.

(19) Minko, T., Kopeckova, P., Pozharov, V., and Kopecek, J. (1998) HPMA copolymer bound adriamycin overcomes MDR1 gene encoded resistance in a human ovarian carcinoma cell line. *J. Controlled Release 54*, 223−233.

(20) Akima, K., Ito, H., Iwata, Y., Matsuo, K., Watari, N., Yanagi, M., Hagi, H., Oshima, K., Yagita, A., Atomi, Y., and Tatekawa, I. (1996) Evaluation of antitumor activities of hyaluronate binding antitumor drugs: synthesis, characterization and antitumor activity. *J. Drug Targeting 4*, 1.

(21) Yeo, T. K., Nagy, J. A., Yeo, K. T., Dvorak, H. F., and Toole, B. P. (1996) Increased hyaluronan at sites of attachment to mesentery by CD44-positive mouse ovarian and breast tumor cells. *Am. J. Pathol. 148*, 1733−1740.

(22) Knudson, W. (1996) Tumor-associated hyaluronan: providing an extracellular matrix that facilitates invasion. *Am. J. Pathol. 148*, 1721−1726.

(23) Nelson, R. M., Venot, A., Bevilacqua, M. P., Linhardt, R. J., and Stamenkovic, I. (1995) Carbohydrate-protein interactions in vascular biology. *Annu. Rev. Cell Dev. Biol. 11*, 601−631.

(24) Hall, C. L., Yang, B. H., Yang, X. W., Zhang, S. W., Turley, M., Samuel, S., Lange, L. A., Wang, C., Curpen, G. D., Savani, R. C., Greenberg, A. H., and Turley, E. A. (1995) Overexpression of the hyaluronan receptor RHAMM is transforming and is also required for h-ras transformation. *Cell 82*, 19−28.

(25) Rooney, P., Kumar, S., Ponting, J., and Wang, M. (1995) The role of hyaluronan in tumour neovascularization (review). *Int. J. Cancer 60*, 632−636.

(26) Hoare, K., Savani, R. C., Wang, C., Yang, B., and Turley, E. A. (1993) Identification of hyaluronan binding proteins using a biotinylated hyaluronan probe. *Connect. Tissue Res. 30*, 117−126.

(27) Turley, E. A., Belch, A. J., Poppema, S., and Pilarski, L. M. (1993) Expression and function of a receptor for hyaluronan-mediated motility on normal and malignant lymphocytes-B. *Blood 81*, 446−453.

(28) Gustafson, S., Bjorkman, T., and Westlin, J. E. (1994) Labeling of high molecular weight hyaluronan with I-125-tyrosine: studies in vitro and in vivo in the rat. *Glycoconjugate J. 11*, 608−613.

(29) Gustafson, S., Hyaluronan in drug delivery; In *The Chemistry, Biology, and Medical Applications of Hyaluronan and its Derivatives*; T. C. Laurent and E. A. Balazs, Ed.; Portland Press: UK, 1997.

(30) Gustafson, S., and Bjorkman, T. (1997) Circulating hyaluronan, chondroitin sulphate and dextran sulphate bind to a liver receptor that does not recognize heparin. *Glycoconjugate J. 14*, 561−568.

(31) Samuelsson, C., and Gustafson, S. (1998) Studies on the interaction between hyaluronan and a rat colon cancer cell line. *Glycoconjugate J. 15*, 169−175.

(32) Culty, M., Nguyen, H. A., and Underhill, C. B. (1992) The hyaluronan receptor (CD44) participates in the uptake and degradation of hyaluronan. *J. Cell Biol. 116*, 1055−1062.

(33) Prestwich, G. D., D. M., M., Marecek, J. F., Vercruysse, K. P., and Ziebell, M. R. (1998) Controlled chemical modification of hyaluronic acid: synthesis, applications and biodegradation of hydrazide derivatives. *J. Controlled Release* 93−103.

(34) Teicher, B. A. *Cancer Therapeutics: Experimental and Clinical Agents*; Humana Press: Totowa, New Jersey, 1997; p 451.
(35) Greenwald, R. B., Gilbert, C. W., Pendri, A., Conover, C. D., Xia, J., and Martinez, A. (1996) Drug delivery systems: water soluble taxol 2′-poly(ethylene glycol) ester prodrugs - - design and in vivo effectiveness. *J. Med. Chem. 39*, 424−431.
(36) Pouyani, T., and Prestwich, G. D. In *US Patent 5,616, 568*; Research Foundation of SUNY: USA, 1997.
(37) Pouyani, T., and Prestwich, G. D. (1994) Functionalized derivatives of hyaluronic acid oligosaccharides − drug carriers and novel biomaterials. *Bioconjugate Chem. 5*, 339−347.
(38) Pouyani, T., Harbison, G. S., and Prestwich, G. D. (1994) Novel hydrogels of hyaluronic acid: synthesis, surface morphology, and solid-state NMR. *J. Am. Chem. Soc. 116*, 7515−7522.
(39) Ogura, H., Nagai, S., and Takeda, K. (1980) A novel reagent (N-succinimidyl diphenyl phosphate) for synthesis of active ester and peptide. *Tetrahedron Lett. 21*, 1467−1468.
(40) Vercruysse, K. P., Marecak, D. M., Marecek, J. F., and Prestwich, G. D. (1997) Synthesis and in vitro degradation of new polyvalent hydrazide cross-linked hydrogels of hyaluronic acid. *Bioconjugate Chem. 8*, 686−694.
(41) Kokoshka, J. M., Ireland, C. M., and Barrows, L. R. (1996) Cell-based screen for identification of inhibitors of tubulin polymerization. *J. Nat. Prod. 59*, 1179−1182.
(42) Kreil, G. (1995) Hyaluronidases − a group of neglected enzymes. *Protein Sci. 4*, 1666−1669.
(43) Nicolaou, K. C., Riemer, C., Kerr, M. A., Rideout, D., and Wrasidlo, W. (1993) Design, synthesis and biological activity of protaxols. *Nature 364*, 464−466.
(44) Collis, L., Hall, C., Lange, L., Ziebell, M., Prestwich, G., and Turley, E. (1998) Rapid hyaluronan uptake is associated with enhanced motility: implications for an intracellular mode of action. *FEBS Lett. 440*, 444−449.
(45) Chow, G., Knudson, C. B., Homandberg, G., and Knudson, W. (1995) Increased expression of CD44 in bovine articular chondrocytes by catabolic cellular mediators. *J. Biol. Chem. 270*, 27734−27741.
(46) Lesley, J., and Hyman, R. (1992) CD44 Can be activated to function as an hyaluronic acid receptor in normal murine T-cells. *Eur. J. Immunol. 22*, 2719−2723.
(47) Lesley, J., English, N., Perschl, A., Gregoroff, J., and Hyman, R. (1995) Variant cell lines selected for alterations in the function of the hyaluronan receptor CD44 show differences in glycosylation. *J. Exp. Med. 182*, 431−437.
(48) Perschl, A., Lesley, J., English, N., Trowbridge, I., and Hyman, R. (1995) Role of CD44 cytoplasmic domain in hyaluronan binding. *Eur. J. Immunol. 25*, 495−501.
(49) Asplund, T., and Heldin, P. (1994) Hyaluronan receptors are expressed on human malignant mesothelioma cells but not on normal mesothelial cells. *Cancer Res. 54*, 4516−4523.
(50) Culty, M., Shizari, M., Thompson, E. W., and Underhill, C. B. (1994) Binding and degradation of hyaluronan by human breast cancer cell lines expressing different forms of CD44: correlation with invasive potential. *J. Cell. Physiol. 160*, 275−286.
(51) Hua, Q., Knudson, C. B., and Knudson, W. (1993) Internalization of hyaluronan by chondrocytes occurs via Receptor-Mediated endocytosis. *J. Cell Sci. 106*, 365−375.
(52) Nakabayashi, H., Tsujii, H., Okamoto, Y., and Nakano, H. (1996) Fluorescence-labeled-hyaluronan loading test as an index of hepatic sinusoidal endothelial cell function in the rat. *Int. Hepatol. Commun. 5*, 345−353.
(53) Iida, N., and Bourguignon, L. Y. W. (1997) Coexpression of CD44 variant (v10/ex14) and CD44S in human mammary epithelial cells promotes tumorigenesis. *J. Cell. Physiol. 171*, 152−160.
(54) Bourguignon, L. Y.-W., Zhu, H. B., Chu, A., Iida, N., Zhang, L., and Hung, M. C. (1997) Interaction between the adhesion receptor, CD44, and the oncogene product, p185(HER2), promotes human ovarian tumor cell activation. *J. Biol. Chem. 272*, 27913−27918.

BC9900338

Effect of Albumin and Polyanion on the Structure of DNA Complexes with Polycation Containing Hydrophilic Nonionic Block

David Oupický,*,† Čestmír Koňák,† Philip R. Dash,‡ Leonard W. Seymour,‡ and Karel Ulbrich†

Institute of Macromolecular Chemistry, Academy of Sciences of the Czech Republic, Heyrovsky Sq. 2, 162 06 Prague 6, Czech Republic, and CRC Institute for Cancer Studies, University of Birmingham, Birmingham B15 2TA, U.K. Received January 15, 1999; Revised Manuscript Received April 29, 1999

Self-assembling systems based on ionic complexes of DNA with block copolymer of *N*-(2-hydroxypropyl)-methacrylamide with 2-(trimethylammonio)ethyl methacrylate were studied as systems suitable for gene delivery. In this study, the influence of albumin and polyanion on parameters of the DNA polyelectrolyte complexes in aqueous solutions was investigated. Static and dynamic light-scattering methods were used as a main tool for characterizing these interactions. It was found that albumin is not able to release free DNA, but it can rather bind to the complexes forming ternary DNA−polycation−albumin complexes with increased hydrodynamic radii of about 10 nm. Polyanion tested, sodium poly(styrenesulfonate), was able to release free DNA in the presence of a low-molecular-weight electrolyte. In the absence of a low-molecular-weight electrolyte, only formation of ternary complexes and no DNA release was observed. The in vivo biodistribution analysis of DNA complexes showed no effect of the presence of hydrophilic nonionic poly(HPMA) on the circulatory time or organ distribution. The interaction of DNA complexes with albumin and other plasma proteins was suggested to be a major reason for the short circulatory times.

INTRODUCTION

The concept of using diblock or graft copolymers of cationic and hydrophilic nonionic monomers has been introduced as a potential way in development of nonviral gene delivery vectors (*1, 2*). So far, several different polycations have been used in combination with hydrophilic nonionic polymers to produce complexes with DNA. These include block copolymers of poly(ethylene glycol) (PEG) with poly(L-lysine) (PLL) (*3, 4*) (studied most widely) and with spermine (*5*), poly[*N*-(2-hydroxypropyl)-methacrylamide] [poly(HPMA)] with poly[2-(trimethylammonio)ethyl methacrylate chloride] [poly(TMAEM)] (*2, 6*) or graft copolymers of PEG with PLL, dextran with PLL, poly(HPMA) with PLL and poly(TMAEM) (*7, 8*).

Most of the above-mentioned block and graft copolymers have shown improved solution properties of their complexes with DNA (*2*−*4*). Block and graft copolymers offer the possibility of improving the solubility of the DNA complexes due to solubilization by the hydrophilic blocks. It has been shown in our previous papers (*6, 8, 9*) that using block or graft copolymers of *N*-(2-hydroxypropyl)-methacrylamide (HPMA) with 2-(trimethylammonio)-ethyl methacrylate chloride (TMAEM) offered such improvement in solubility of stoichiometric complexes with DNA. There was a clear relation between the content of poly(HPMA) in the copolymers and the molecular weight and size of their complexes with DNA. High contents of poly(HPMA) suppressed more efficiently aggregation of the complexed DNA through hydrophobic interactions and thus the complexes were smaller and had lower molecular weight, approaching that of the complexes containing only one DNA molecule. The effect of the presence of poly(HPMA) was even more pronounced if the complexes were formed by slow titration of polycation into DNA solution, in contrast to the complexes formed by rapid titration. While DNA complexes of poly(TMAEM) formed in water by slow titration have precipitated from the solution when the charge ratio close to unity was reached, the complexes formed by the same method using both the block and the graft copolymers of TMAEM were fully soluble. Although DNA complexes of poly(TMAEM) formed in water by the rapid titration were soluble at all the charge ratios studied (0−2), the complexes formed at charge ratios close to unity showed high degrees of aggregation. We have assumed that the solubility of the DNA−poly(TMAEM) complexes formed by the rapid titration was caused by imperfect compensation of DNA phosphate groups; the slow titration method facilitates their better compensation and thus formation of more hydrophobic and insoluble complexes.

It has also been shown (*8*) that the presence of NaCl considerably influences solution properties of the formed complexes. The complexes formed in 0.15 M NaCl solution exhibited significantly higher sizes and molecular weights than those formed in water. The formation of the complexes in distilled water resulted in small complexes, which were relatively stable when transferred into 0.15 M NaCl solution. The study showed that a relatively high content of HPMA in block or graft copolymers with TMAEM was a necessary prerequisite for achieving good stability in 0.15 M NaCl. Complexes of DNA with poly(TMAEM) and block copolymers with low contents of HPMA precipitated shortly after NaCl addition, thus, not fulfilling basic requirements for gene delivery vector intended for the in vivo use. Whereas the stability in NaCl solution and parameters of the DNA complexes (molecular weight, hydrodynamic radius) were strongly affected by the presence of hydrophilic blocks in copolymers, the ability of the polycationic part of block

* To whom correspondence should be addressed. Phone: 420-2-20403212. Fax: 420-2-367981. E-mail: oupicky@imc.cas.cz.
† Institute of Macromolecular Chemistry.
‡ University of Birmingham.

10.1021/bc990007+ CCC: $18.00 © 1999 American Chemical Society
Published on Web 07/27/1999

or graft copolymer to interact with DNA was unaffected (*8*). Analysis of the complexes by atomic force microscopy revealed that whereas most block copolymers produce common spherical complexes, PEG−PLL complexes showed a mixture of extended toroidal and linear strands and spherical structures (*10*).

It has been shown that complexation of DNA with PLL can protect it from degradation by nucleases (*11*); however, in the presence of mung bean nucleases, Dash (*3*) found partial degradation of DNA−PLL complexes, while DNA−PEG−*b*-PLL complexes remained completely intact.

The ability to transfect cells in vitro was shown for most of the above-mentioned block and graft copolymers, although the transfection efficiency could vary considerably depending on the type of the copolymer used. DNA−PEG−*b*-PLL complexes showed an impressive ability to transfect *293* cells, the effect thought to result from the ability of PEG to dehydrate cell membranes (*2*). Presumably, the clusters of PEG exposed in closed juxtaposition can cause local permeability of the cell membrane of 293 cells. On the other hand, DNA complexes formed with poly(HPMA)-*b*-poly(TMAEM) mediated only limited transfection efficiency compared with that of DNA−PEG−*b*-PLL complexes (*2*). The low level of transfection in the case of DNA complexes with poly(HPMA)-*b*-poly(TMAEM) suggests that they do not enter the cell in such a nonspecific manner as PEG-based systems and thus this type of copolymer could be a good candidate for in vivo applicable targeted gene delivery systems after attachment of specific targeting moieties into the poly(HPMA) blocks.

The complexes of DNA, similarly to other colloidal particles (like liposomes), show very low stability in the bloodstream (*12, 13*). They are rapidly removed from the bloodstream, which decreases their potential for specific targeting in vivo. It has been proposed that interaction of the complexes with plasma proteins (either adsorption or breaking of the complexes by proteins) can be the major obstacle for their successful in vivo use. In analogy with STEALTH liposomes (*14*), it was suggested that incorporation of hydrophilic, nonionic polymer onto the surface of the complexes can help to solve this problem (*2, 7*). The concept of using block or graft copolymers, having been developed in our laboratories for several years, seems to offer that possibility. It was suggested that the complex formation may proceed with a degree of orientation, leaving the hydrophilic blocks on the surface of the complex free to provide a protective layer (*7*).

In this work, we have studied the interactions of the polyelectrolyte complexes of DNA with poly(TMAEM) containing hydrophilic poly(HPMA) block with albumin and synthetic polyanion. The interactions were studied by combination of several methods, including dynamic and static light-scattering and measurements of ζ-potential. The ability of albumin and polyanions to release free DNA from the complexes was tested using dynamic light scattering and agarose gel electrophoresis. Finally, the body distribution analysis was performed in order to obtain more information on the effect of the hydrophilic poly(HPMA) block on biological properties of complexes.

EXPERIMENTAL PROCEDURES

Chemicals. Calf-thymus DNA and bovine serum albumin were purchased from Sigma. Sodium poly(styrenesulfonate) (PSS) (M_w = 74 000) was from PolySciences. All other chemicals were of analytical grade.

Synthesis of Polymers. Block copolymer was prepared by the reaction of active succinimidyl esters of carboxylic end groups in semitelechelic poly(HPMA) with semitelechelic poly(TMAEM) containing terminal amino group.

Synthesis of Poly(HPMA) with Carboxylic Acid End Group [Poly(HPMA)-COOH]. Precipitation polymerization of HPMA in acetone was carried out in the presence of a chain transfer agent 3-sulfanylpropionic acid (SPA) at 50 °C for 24 h. The concentrations were as follows: initiator 2,2′-azobisisobutytonitrile (AIBN) 3×10^{-3} M, HPMA 0.8 M and SPA 7.6×10^{-3}. The polymer was purified by double precipitation from methanol solution into 20-fold excess of a mixture of acetone and diethyl ether (3:1). Yield 45%. Weight (M_w)- and number-average (M_n) molecular weights determined by size-exclusion chromatography (SEC) were M_w = 14 700 and M_n = 8400. Molecular weight calculated from the content of end carboxylic acid group was M_n = 8500.

Synthesis of Poly(TMAEM) with Amino End Group [Poly(TMAEM)-NH_2]. The polymer was prepared by a solution radical polymerization in methanol in the presence of 2-aminoethanethiol hydrochloride (AET.HCl) at 50 °C for 24 h. The concentrations were as follows: initiator AIBN, 4.8×10^{-3} M; TMAEM, 0.6 M; and AET·HCl, 8.5×10^{-2} M. The polymer poly(TMAEM)-NH_2 was isolated by precipitation into acetone, purified by dialysis (dialyzing tubing with molecular weight cutoff 3500), and freeze-dried. Yield 35%. Molecular weights determined by SEC using poly(HPMA) calibration were: M_w = 10 600; M_n = 7470. Molecular weight calculated from the content of end amino groups was M_n = 5000.

Synthesis of Active Succinimidyl Ester of Poly(HPMA)-COOH. The end carboxylic acid group was converted into succinimidyl ester by the reaction common in peptide synthesis. Poly(HPMA)-COOH (0.17 mmol) and *N*-hydroxysuccinimide (HOSu) (1.70 mmol) were dissolved in 6 mL of dimethylformamide (DMF) (dried with P_2O_5, freshly distilled before use) and cooled to −20 °C; to this solution was added a solution of *N*,*N*′-dicyclohexylcarbodiimide (1.70 mmol) and 4-(dimethylamino)pyridine (0.33 mmol) in 5 mL of DMF. The solution was left overnight at 0 °C. The *N*,*N*′-dicyclohexylurea precipitated during the reaction was removed by filtration and polymer was isolated by precipitation into 15-fold excess of a mixture of dry acetone and diethyl ether (3:1). The succinimidyl ester of poly(HPMA)-COOH [poly(HPMA)-COOSu] in quantitative yield was dried and used directly in the subsequent reaction.

Synthesis of Block Copolymer [Poly(HPMA)-block-poly(TMAEM)]. Poly(HPMA)-COOSu was dissolved in dimethyl sulfoxide (10 wt % solution) and added to a solution of poly(TMAEM)-NH_2. Molar ratio of polymer end groups COOSu:NH_2 was 1.2:1. The mixture was stirred at room temperature for 8 h and polymer was isolated by precipitation into 40-fold volume excess of acetone. The polymer (BLOCK-1) was dried in vacuo, excess of poly(HPMA) was removed from dry copolymer by extraction with DMF, and the product was washed with acetone and dried in vacuo. Molecular weight of the copolymer BLOCK-1 determined by SEC using poly(HPMA) calibration was M_w = 21 000. The content of HPMA block determined by elemental analysis was 63 wt %.

Formation of Polyelectrolyte Complexes. The complexes were formed in deionized water by titration of DNA solution (concentration 20 μg/mL, concentration of phosphate groups 0.0615 mM) with polycation stock

solution (positive charge concentration 0.012 M). Two modes of preparation were used in this study.

(1) Rapid titration: a polycation stock solution was added as quickly as possible (typically in 1 s) to 3 mL of a stirred DNA solution.

(2) Slow titration: a polycation stock solution was slowly added using a programmable syringe pump to 3 mL of a stirred DNA solution, the rate of addition being 30 μL/h (full compensation of negative DNA phosphate groups was achieved in 30 min).

Calf-thymus DNA was used in all experiments, unless otherwise stated.

Characterization of Polymers. Molecular weights of poly(HPMA)-COOH and poly(TMAEM)-NH_2 were determined by size-exclusion chromatography (SEC) in 0.05 M Tris buffer (pH 8.1) on a Superose 12 column (Pharmacia). Number-average molecular weights (M_n) were also calculated from the content of the end functional carboxylic or amino groups, assuming one functional end group per macromolecule. The content of the end carboxylic groups of poly(HPMA)-COOH was determined by titration with 0.05 M NaOH using automatic titrator (Radiometer). The amount of amino end groups of poly(TMAEM)-NH_2 was determined by the 2,4,6-trinitrobenzenesulfonic acid assay using molar absorption coefficient 10 500 L/(mol cm).

Agarose Gel Electrophoresis. The ability of albumin or polyanion to release free DNA from the complexes was also determined by agarose gel electrophoresis. DNA complexes in water in the presence of various concentrations of albumin or polyanion were electrophoresed on agarose gel (0.5%) in 0.05 M Tris buffer, pH 7.5, for 30 min at 90 V. Ethidium bromide (1 μg/mL of gel) was incorporated in the gel to show the location of DNA using UV detection (254 nm).

Analysis of ζ-Potential. The charge of the calf-thymus DNA complexes was determined by using a Zetamaster system (Malvern Instruments). The system was calibrated using a −55 mV standard. Solutions of the complexes (5 mL) were measured five times for 30 s at 1000 Hz with zero field correction.

Static Light Scattering (SLS). Static light-scattering measurements were performed with a commercial Fica 40 apparatus in vertically polarized light at wavelength $\lambda_0 = 632.8$ nm, angle $\theta = 90°$, and temperature 25 °C. The apparatus was calibrated with benzene at $\theta = 90°$. The data are expressed as the scattered light intensity at 90 ° normalized with intensity scattered by benzene.

Dynamic Light Scattering (DLS). Polarized DLS measurements were made in the angular range 30−130° using a light-scattering apparatus equipped with an He−Ne (632.8 nm) and Ar-ion laser (514.5 nm) and an ALV 5000, multibit, multi-tau autocorrelator covering approximately 10 decades in delay time τ. The time autocorrelation functions were fitted assuming the Pearson distribution of characteristic relaxation times, τ_c:

$$z(\tau_c) = \tau_o^{\,p} p \tau_c^{\,-p-1} \exp(-\tau_c/\tau_o)/\Gamma(p) \qquad (1)$$

where τ_o and p are parameters, and $\Gamma(p)$ is the gamma function of parameter p. The Pearson distribution was chosen for the simplicity of its mathematical treatment. The apparent hydrodynamic radius, R_h, was calculated from the zero angle limit of apparent collective diffusion coefficient, D^a, using the Stokes−Einstein equation:

$$R_h = kT/6\pi\eta D^a \qquad (2)$$

where k is the Boltzmann constant, T is absolute temperature, and η (0.894 cP) is the viscosity of water at 25 °C.

The experimental error of the aggregate size determination was typically about 3%.

Radiolabeling of DNA. The linearized plasmid pCMV-β-Gal was radiolabeled using the Ready-to-Go DNA Labeling Kit (-dCTP) from Pharmacia Biotech. The DNA was purified from unincorporated nucleotides using MicroSpin DNA purification columns from Pharmacia Biotech.

Body Distribution Analysis. Radiolabeled DNA (50 ng/mL) was added to a calf-thymus DNA solution (20 μg/mL), and the complexes were formed using different polycations and various charge ratios. The complex solutions were diluted with PBS buffer to balance the solution osmotically prior to injecting 100 μL into the tail vein of BALB/c mice. After 30 min, the animals were killed and their liver, kidneys, intestines, heart, and lungs were removed. The blood and tissue samples were analyzed for radioactivity in a Packard Scintillation Counter. The total amount of radioactivity in blood was determined by assuming that the volume of blood in a mouse is 8.64 mL/100 g. In all cases, the tails of the mice were removed prior to dissolution and were not assayed for radioactivity. The percentage of radioactivity in each organ is given as a percentage of the recovered dose.

RESULTS

Good candidate for in vivo delivery of DNA should exhibit prolonged circulation times in the bloodstream in order to accomplish targeting. In analogy with other particulate systems (liposomes, nanoparticles), the use of cationic block copolymers containing hydrophilic blocks is thought to reduce the removal of polyelectrolyte DNA complexes by the immune system. Since hydrophobic forces are thought to be the main driving force in phagocytosis of nanoparticles and liposomes, the presence of hydrophilic polymers decreases hydrophobic nature of these delivery systems. Particles containing hydrophilic polymers usually display reduced protein adsorption and consequently increased circulation times and altered body distribution (*15*).

We have evaluated several block and graft copolymers of HPMA and TMAEM (*8*, *9*). We have chosen the block copolymer BLOCK-1 as a polymer that can form polyelectrolyte complexes with DNA that are relatively small and are sufficiently stable in saline solution. Before testing the biodistribution of its complexes with DNA, we have studied the interaction of these complexes with albumin.

Proteins can interact with DNA complexes among others by electrostatic and hydrophobic interactions. To investigate electrostatic interactions, it is important to measure the charge of the complexes, and in order to suppress these interactions, it is reasonable to attempt to form them charge-neutral. The charge of the complexes was evaluated by measuring their ζ-potentials. Figure 1A shows the dependencies of ζ on the ratio of positive charges of polycation and negative charges of DNA (φ) for poly(TMAEM)-NH_2 and block copolymer BLOCK-1 used for the formation of DNA complexes by the rapid titration method. In both cases, ζ monotonically increases and crosses zero between charge ratios 0.7 and 0.8. The complexes gain positive charge at higher charge ratios ($\varphi > 0.8$). Since the ζ-potential is related to the sum of all charges of complexes, the shift of complete neutralization of charges to φ values lower than 1 might be due to

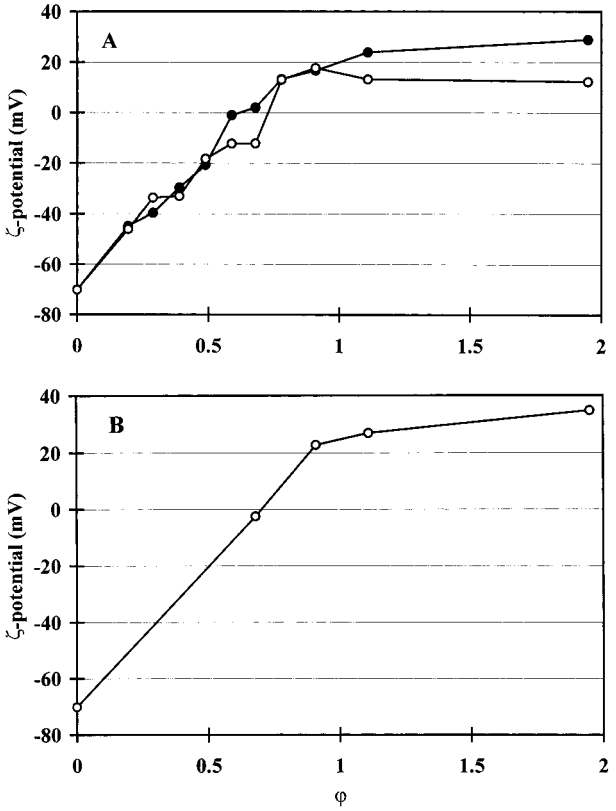


Figure 1. Dependence of ζ-potential on the ratio between positive charges of polycation and negative charges of DNA (φ). (A) complexes formed by rapid titration using poly(TMAEM)-NH_2 (●) and BLOCK-1 (○); (B) complexes formed by slow titration using BLOCK-1.

positive counterions entrapped inside the complexes by electrostatic interactions with DNA. It has been shown by Manning (*16*) that when DNA is neutralized by polycations to the critical φ (0.88), the hydrophobicity of DNA is so high that it cannot stay in its extended form and collapses. The collapse then may cause entrapping of remaining free phosphate groups inside the complex. The incorporation of excess block copolymer to the complexes at $\varphi > 0.8$ manifested in positive ζ-potential values is probably caused by partly neutralized copolymer molecules on the surface of the complexes. Similar behavior was already observed by several other authors (*2, 7, 17*). On the contrary, formation of DNA complexes with almost neutral charge was reported by Kataoka using PEG−*b*-PLL (*4*). The point of zero ζ-potential around $\varphi \approx 0.8$ also well corresponds to a maximum in the size and molecular weight dependencies observed in our previous paper (*9*). This confirms that these maxima are caused by the hydrophobically driven aggregation, which most easily proceeds if the complexes are uncharged ($\zeta = 0$). To our surprise, there was no significant difference in ζ-potential between complexes formed by slow or rapid titration (Figure 1B). On the basis of our previous data, we have intuitively anticipated that the slow titration method facilitates formation of complexes with better compensated DNA negative charges. In such case, the recharging of the complexes after reaching zero ζ-potential could be avoided, and as a consequence, neutral complexes could be easily obtained. Since this assumption was not justified, we have attempted to obtain neutral complexes by finding the exact charge ratio of neutrality (Figure 2). The change from the negatively to positively charged complexes occurs suddenly in a very narrow interval of charge ratios and thus,

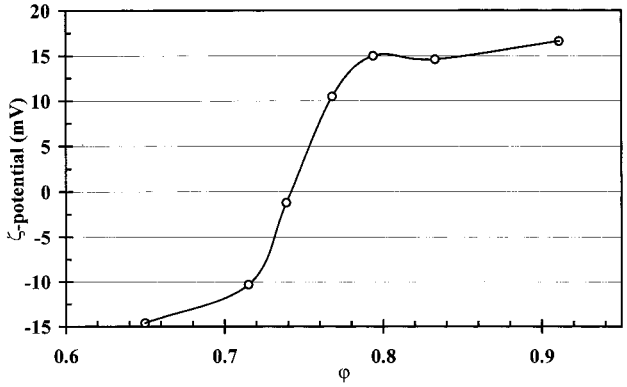


Figure 2. Dependence of ζ-potential on the ratio between positive charges of polycation and negative charges of DNA (φ) for DNA−BLOCK-1 complexes. The complexes were formed at $\varphi = 0.65$ by rapid titration and the aliquots of BLOCK-1 solution were added up to $\varphi = 0.9$.

from the practical point of view, charge-neutral complexes cannot be easily obtained. Since the recharging of the complexes coincides with the maxima of molecular weight and size of the complexes and with sudden repulsion of intercalated ethidium bromide from DNA (*8*), the dramatic conformation change (coil−globule transition) of DNA structure (collapse) is assumed to occur in this charge ratio interval.

To induce collapse of the extended DNA structure, it is necessary to use charge ratios higher than 0.8. Then, the positive charge of the complexes (Figures 1 and 2) has to be considered when evaluating their interactions with proteins. After interaction with proteins, positive charges of the complexes could promote binding of negatively charged proteins. In certain cases, negatively charged protein could possibly replace DNA in the complex, and free DNA may be released. Since the major protein with negative net charge occurring in blood plasma in high concentrations is albumin, we have used it in this study. A possible release of free DNA from the complexes was assessed by agarose gel electrophoresis.

We have shown by electrophoresis that albumin is not able to destroy the complexes and release free DNA, but it could probably interact with positively charged complexes and form ternary albumin−DNA−polycation complexes. In that case, some parameters of the DNA complexes, such as charge, molecular weight, and hydrodynamic radius, have to be changed. To verify this possibility, we have used static and dynamic light-scattering and ζ-potential techniques. DNA complexes with BLOCK-1 were first formed in water at $\varphi = 0.9$, and then increments of albumin solution were added. The dependence of ζ-potential of the complexes on the concentration of albumin is shown in Figure 3A. The increasing concentration of albumin causes gradual change in ζ from positive to negative values. Reaching constant negative ζ above 1 mg/mL of albumin suggests possible saturation of the complexes with albumin. Almost all the positively charged complexes of BLOCK-1 formed at different charge ratios altered their ζ-potential to negative in the presence of 1 mg/mL of albumin (Figure 3B). The complexes formed with high excess of polycation ($\varphi = 6$) are an exception. In this case, substantial quantity of polycation is free in solution and forms additional complexes with albumin having hydrodynamic radii in the range 10−100 nm and ζ varying from negative to positive values depending on the polycation/albumin ratio. In consequence, polycation−albumin complexes may interfere with DNA complexes and distort the

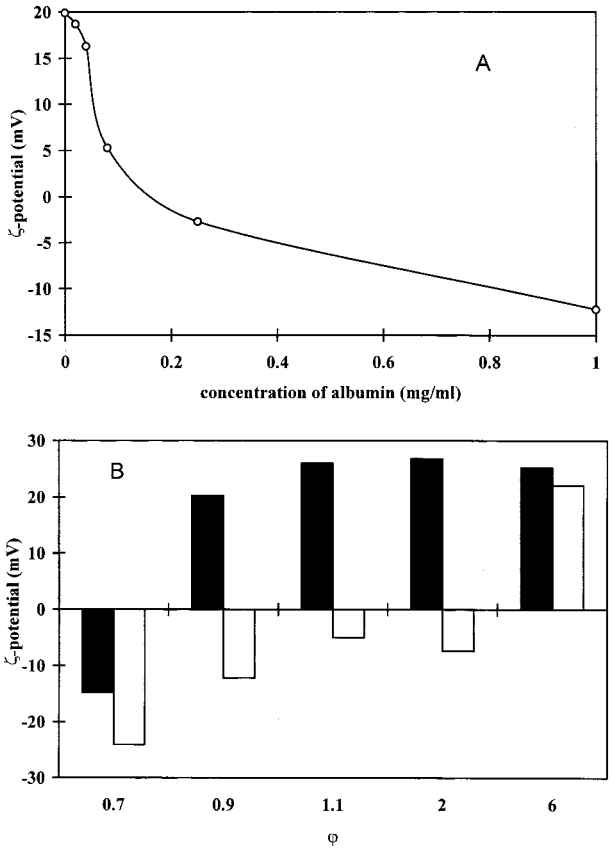


Figure 3. Effect of albumin on ζ-potential of DNA complexes. (A) DNA−BLOCK-1 complexes were formed at $\varphi = 0.9$ and effect of increasing albumin concentration on ζ-potential was monitored. (B) DNA−BLOCK-1 complexes were formed at $\varphi =$ 0.7, 0.9, 1.1, 2, and 6, their ζ-potential was measured (■) and then effect of 1 mg/mL of added albumin on ζ-potential was monitored (□).

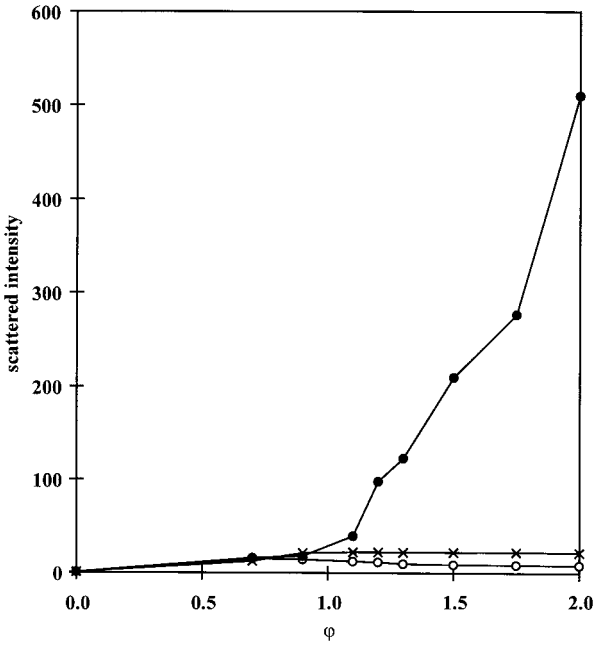


Figure 4. Effect of the addition of 1 mg/mL of albumin to DNA−BLOCK-1 complexes formed at different φ on the scattering intensity at 90°. The complexes were formed in water, scattering intensity was measured (○), then albumin was added and scattering intensity of the solution was again measured (●). The scattering intensity of the DNA−BLOCK-1 complexes in the presence of 1 mg/mL of albumin on addition of 0.15 M NaCl was finally measured (×).

results of ζ-potential measurements as in the case of the complexes formed at $\varphi = 6$ (Figure 3B). Polycation−albumin complexes are positively charged at high φ values and most albumin is probably consumed in the formation of the complexes with free polycation. As a consequence, the overall measured ζ-potential remains positive.

Light-scattering techniques can contribute to better understanding of the effect of albumin on the DNA complexes. Figure 4 demonstrates the effect of an addition of albumin (1 mg/mL) on the normalized intensity of scattered light (the scattered light intensity at 90 ° normalized with intensity scattered by benzene) of complexes formed at different charge ratios in water. Scattering intensity is used instead of customary molecular weights because the concentration of albumin built in DNA complexes is unknown. A minor increase in the scattering intensity is observed after albumin addition to the complexes at $\varphi = 0.9$. This corresponds well with the observed positive ζ of the complexes formed at $\varphi =$ 0.9 (Figure 1). The increase in scattering intensity suggests an increase in molecular weight of the complexes due to their interaction with albumin. In addition, an abrupt break above the charge ratio 1.1 is observed. We suppose that the abrupt break is provoked mostly by the interaction of albumin with free polycation. The polycation−albumin complexes bring additional scattering to that of DNA complexes. The scattering intensity is again decreased if NaCl is added (Figure 4) to the complexes in the presence of albumin. A markedly dramatic decrease is observed for the complexes formed at $\varphi > 1.2$. We assume that this decrease is mainly caused by break-up of the polycation−albumin complexes. The polycation−albumin complexes are not stable in the presence of a low-molecular-weight electrolyte (NaCl) due to only weak interactions. This is in contrast to the complexes of DNA with polycations, where a strong cooperative effect induces high stability. The decrease in scattering intensity after NaCl addition is significant but yet it has not reached the scattering intensity of DNA−BLOCK-1 complexes. This observation suggests that some albumin could be possibly entrapped inside the DNA complex (by hydrophobic interactions) increasing thus molecular weight of the complex (manifested by increased scattering intensity).

The static light-scattering methods require precise knowledge of particle concentrations in solution to calculate their molecular weights. Dynamic light scattering, on the contrary, offers the possibility of determining directly the hydrodynamic radii of the complexes without precise knowledge of the particle concentration. The effect of increasing concentration of albumin on the distribution of hydrodynamic radii [$A(R_h)$] of the complexes (DNA−BLOCK-1) formed in water by slow titration ($\varphi = 0.9$) is demonstrated in Figure 5. An addition of albumin causes a shift of radii distribution to higher values. Saturation of the complexes with albumin was observed above 0.7 mg/mL of albumin where the hydrodynamic radius of the complexes was found to be almost independent of albumin concentration. We assume that the shift of the size distribution is caused predominantly by albumin binding on the surface of the complexes forming there a "protein layer" (hydrodynamic radius of albumin $\approx$ 4 nm). The average hydrodynamic radius of the complexes in the presence of 1 mg/mL of albumin increased by about 10 nm compared with the original complex.

The complexes formed at $\varphi = 2$ exhibited considerably higher shifts of the hydrodynamic radii distributions after

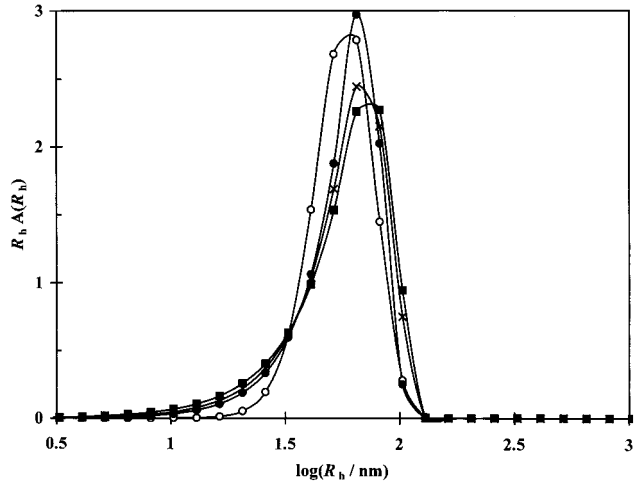


Figure 5. Effect of increasing concentration of albumin on the distribution of hydrodynamic radii of DNA−BLOCK-1 complexes. The complexes were formed at $\varphi = 0.9$ (○), and then the distribution of hydrodynamic radii of DNA−BLOCK-1 complexes was measured after albumin addition [final concentrations of albumin: 0.4 (●), 0.7 (×), and 1 mg/mL albumin (■)].

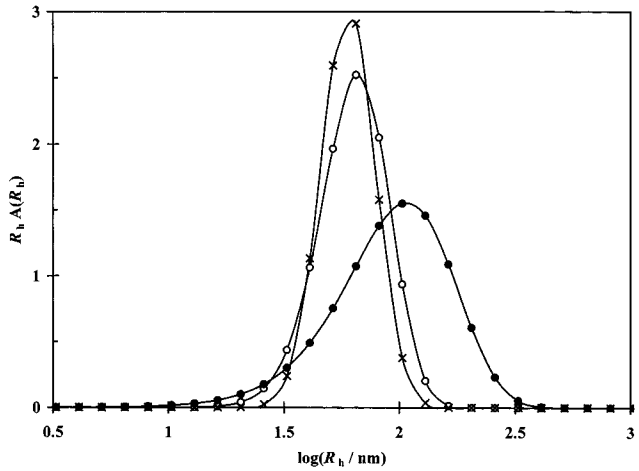


Figure 6. Effect of 1 mg/mL albumin and 0.15 M NaCl on the distribution of hydrodynamic radii of DNA−BLOCK-1 complexes. The complexes were formed at $\varphi = 2$ (○). Effect of albumin (●) and subsequent addition of NaCl (×) on the distribution of hydrodynamic radii of the complexes is shown.

albumin addition (1 mg/mL) (Figure 6) in water, compared with the complexes formed at $\varphi = 0.9$ (Figure 5). A significant increase in average hydrodynamic radius and polydispersity was observed after albumin addition due to the formation of polycation/albumin complexes. In agreement with our previous results, large complexes formed mostly between albumin and free polycation have broken after addition of NaCl to their solutions (final concentration 0.15 M) (Figure 6). The solution then contained DNA−BLOCK-1 complex particles similar to those prior to the albumin addition. Corresponding experiment with the complex formed at the 0.9 charge ratio showed that a slight increase in the complex size only slightly decreased in 0.15 M NaCl, suggesting that the interaction of albumin with the complexes is relatively more stable than that with free polycations. This is in agreement with the static light-scattering experiments (Figure 4), which indicate that some albumin could be bound to the complexes even in 0.15 M NaCl. The complexes in the presence of albumin were stable over a period of hours, but after 24 h, the starting aggregation was observed. From the practical standpoint, the complexes should remain in circulation until they reach their target site; as the required half-life in the bloodstream is several hours (*13*), the observed stability could be sufficient.

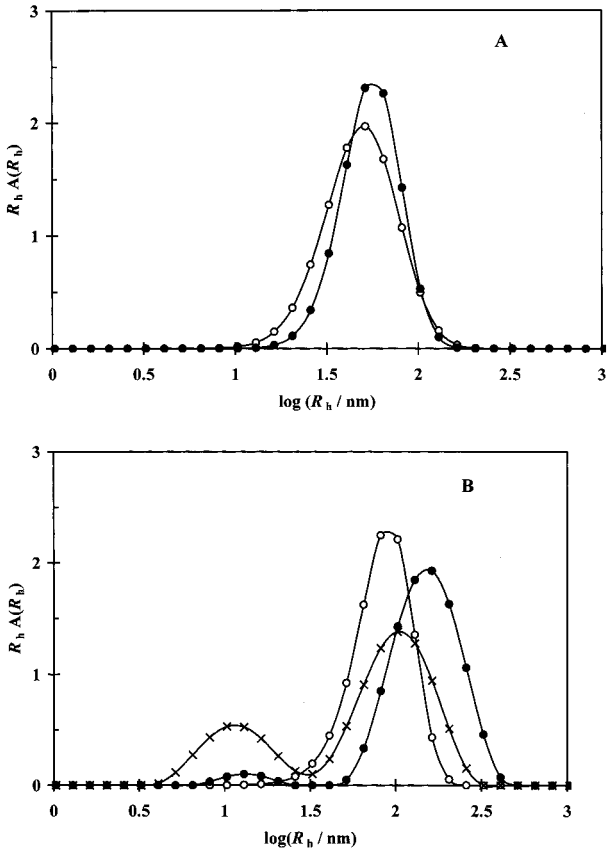


Figure 7. Effect of PSS on the distribution of hydrodynamic radii of DNA−BLOCK-1 complexes. (A) The complexes were formed at $\varphi = 1.1$ in distilled water (○), effect of an addition of PSS is shown (●). (B) The complexes were formed at $\varphi = 1.1$ in 0.15 M NaCl (○), effect of an addition of PSS is shown 30 min (●) and 3 days (×) after addition.

It has been shown that certain polyanions (polyaspartic acid, heparin) can release free DNA from the complexes (*3*). This reaction can also possibly account for the low stability of the complexes in the bloodstream. We have studied the ability of synthetic polyanion sodium poly(styrenesulfonate) (PSS) to release free DNA from its complexes with BLOCK-1 by agarose gel electrophoresis and dynamic light scattering.

To compare the effect of PSS on DNA complexes in water and in 0.15 M NaCl, we have used a high concentration of PSS. The ratio of positive charges of BLOCK-1 used for complex formation and negative charges of PSS was 1:25. The use of a high excess of PSS should ensure that in the case of exchange polyelectrolyte reaction between DNA and PSS in DNA complexes with BLOCK-1, the possibly formed complexes PSS-BLOCK-1 have relatively small size and thus do not interfere with the DNA complexes. Figure 7 shows the distribution of hydrodynamic radii of the DNA−BLOCK-1 complexes prior to and after addition of PSS. The complexes in water (Figure 7A) showed only a small increase in the hydrodynamic radius. Similarly to the interaction of complexes with albumin, a shift of the size distribution to higher values was observed. The hydrodynamic radius of these complexes virtually did not change during the 3 days of observation. The same experiment in 0.15 M NaCl (graph B) showed a similar increase in R_h and shift of the R_h

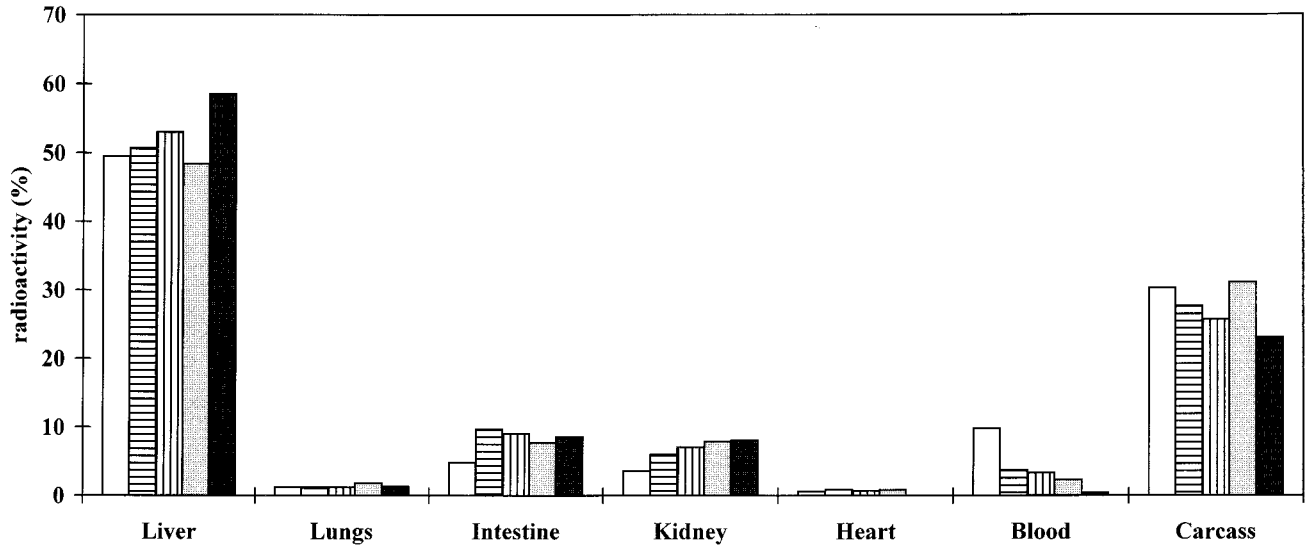


Figure 8. Body distribution of radiolabeled DNA (■) and of the complexes of radiolabeled DNA with poly(TMAEM)-NH_2 (□) or BLOCK-1. The latter complexes were formed in water at $\varphi = 0.7$ (□), 0.9 (□), and 1.1 (□). The complex or DNA solutions were diluted with PBS buffer prior to injecting. The mice were killed after 30 min, and the blood and tissue samples were analyzed for radioactivity.

distribution immediately after a PSS addition. From the very beginning, a second population of small particles with the hydrodynamic radius around 10 nm was apparent. The proportion of these particles increased with time at the expense of the DNA complexes. Together with the alteration of the relative content of these two populations, the intensity of the scattered light of the solution at 90° decreased, indicating dissociation of the DNA complexes. This means that large, highly scattering particles slowly disappear. We suppose that, in the absence of NaCl, the exchange polyelectrolyte reaction virtually does not take place and only formation of ternary complexes DNA−BLOCK-1−PSS occurs, as manifested by a minor increase in the mean hydrodynamic radius. In the presence of 0.15 M NaCl, the exchange reaction can take place. This is manifested by an increasing quantity of 10 nm particles and by a decrease in intensity of scattered light. These observations agree with the results published in ref *18*. They have demonstrated that the exchange polyelectrolyte reactions can take place only in the presence of a low-molecular-weight electrolyte. We suppose that the particles with $R_h = 10$ nm correspond to complexes PSS−BLOCK-1. The exchange reaction is relatively slow and thus the interaction of DNA complexes in the bloodstream with possibly present polyanions does not have to be an obstacle in successful in vivo gene delivery.

Agarose gel electrophoresis was used in order to observe release of free DNA from the complexes. Since DNA complexes do not migrate in the gel, the released free DNA can be easily monitored by this method. PSS was able to release free DNA from the complexes and the amount of DNA released from the complexes increases with increasing concentration of PSS in solution.

We have studied the organ distribution of different DNA complexes 30 min after an i.v. tail vein injection (Figure 8). The figure compares the organ distribution of DNA−BLOCK-1 complexes formed at three different φ (0.7, 0.9, 1.1) and that of the complex DNA−poly(TMAEM)-NH_2 ($\varphi = 0.9$). To our surprise, the DNA−BLOCK-1 complexes have manifested almost no difference in their biodistribution compared with DNA−poly(TMAEM)-NH_2 complexes. Unlike STEALTH liposomes, the presence of poly(HPMA) in the complexes has apparently no effect on the prolongation of circulation times of the complexes. Neither did exhibit the effect of varying charge ratio in the complex formation and any significant difference in the organ distribution, although the complexes formed at $\varphi = 0.7$ had a negative ζ-potential. No explanation for such an observation was available until now. The accumulation of the complexes in the liver could be probably a consequence of both the charge and relatively high hydrodynamic radius of the complexes (*19*).

DISCUSSION

It has been shown that DNA−PLL complexes are rapidly cleared from the bloodstream, with a half-life of less than 5 min. The interaction of the complexes with albumin was proposed to have a major impact on the circulation of the complexes in blood (*13*). It was suggested that the main reason could be an increase in the size of the complexes. To test this hypothesis we have studied the interaction of DNA complexes with albumin by combination of several analytical techniques.

As we have shown above, albumin is able to interact with DNA−BLOCK-1 complexes and increase their hydrodynamic radii, nevertheless, the increase was not so significant to explain the observed biodistribution.

The exchange reaction between DNA and polyanions which caused a release of free DNA is relatively slow, and thus the interaction of DNA complexes in the bloodstream with possibly present polyanions does not have to be an obstacle in successful in vivo gene delivery.

On the basis of these promising observations, we have expected prolonged plasma circulation of DNA complexes with block copolymers. In analogy with STEALTH liposomes, we have expected the hydrophilic poly(HPMA) block to increase the circulatory times of the complexes. To explain the fact, that using block copolymers we have observed no significant improvement of the biodistribution of the complexes, it is necessary to review the analogy with STEALTH liposomes. In our previous physicochemical study (*9*), we have shown that increasing relative HPMA content in both the block and graft copolymers used for the formation of DNA complexes resulted in decreasing density of the complexes. In the case of a graft copolymer containing 80% of HPMA, the

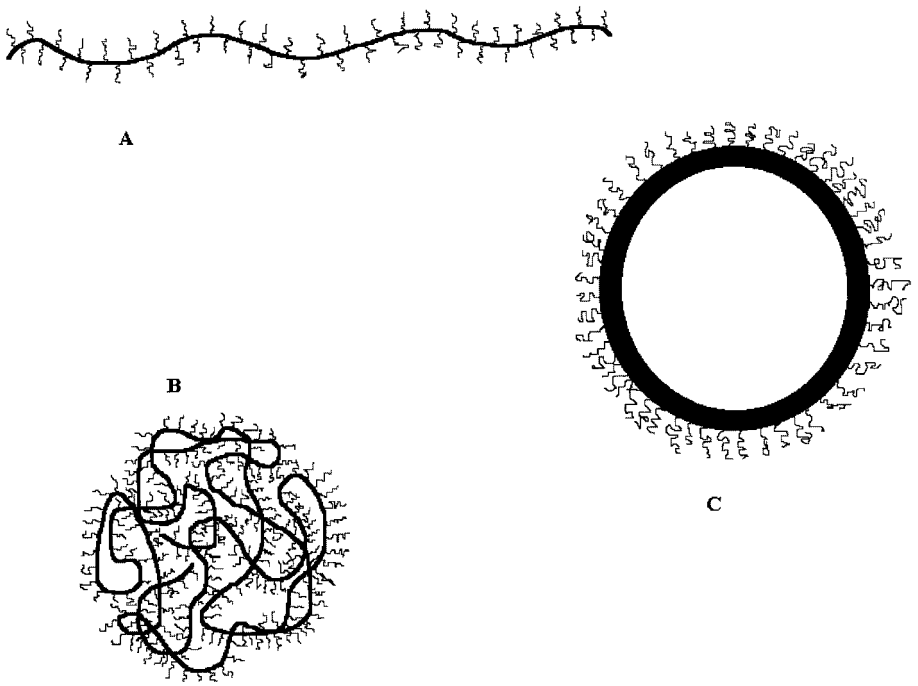


Figure 9. (A) structure of brush polymer (DNA fully compensated with block copolymers). (B) Proposed structure of DNA complexes with block or graft copolymers in solution. (C) Structure of STEALTH liposome.

complexes displayed an expanded structure that was very close to that of a flexible polymer coil, as assessed by the ratio of radius of gyration and hydrodynamic radius of the complexes. Then, the complexes have "swollen and expanded" structure, where their hydrophobic parts might tend to concentrate in the central core of the complex and hydrophilic poly(HPMA) blocks on the surface, but microphase separation of the hydrophobic and hydrophilic parts is virtually impossible. The frequently suggested micelle-like structure with hydrophobic core surrounded by hydrophilic poly(HPMA) or PEG shell seems to be not fully realistic (*4*, *7*) in case for high-molecular-weight DNA. To better explain a possible structure of the DNA complexes with block or graft copolymers, it is necessary to realize that full compensation of DNA with molecular weight of almost 7 million requires several hundreds of polycation macromolecules (molecular weight $\approx$ 20 000). Then the complexes have the structure of so-called brush polymers (Figure 9A). The DNA complexes are usually about 100 nm in diameter, and thus it is not possible for poly(HPMA) blocks located on the DNA parts in the center of the complex to reach the surface and they must be also located in the core of the complex, where they cause an internal swelling (Figure 9B). In STEALTH liposomes, the protecting polymer layer is located on the surface (Figure 9C), where it sterically stabilizes the liposome due to osmotic and entropic effects of an inert, nonionic, hydrophilic, and flexible polymer coating, which increases repulsive pressure above these surfaces (*20*). The complexes with the structure closer to STEALTH liposomes, i.e., those with hydrophobic DNA−polycation core surrounded by hydrophilic protecting surface layer, would be more stable in the bloodstream, due to the ability of the compact surface layer to sterically stabilize the particle. We could conclude that a compact surface layer of hydrophilic nonionic polymer is probably required to efficiently decrease interaction with proteins and, consequently, to achieve good stability in the bloodstream. The absence of such compact continuous layer of poly(HPMA) in the DNA complexes studied in this work results in facile binding of albumin or other proteins to the complexes. The complexes then may have a structure of "large albumin spheres" with positive or negative surface charge dependent on the amount of bound albumin. Then, other plasma proteins (opsonins) could bind and also promote removal of the DNA complexes from the bloodstream, preferably by the liver.

A potential way of obtaining the DNA complexes with poly(HPMA) chains located only on their surface might be the chemical modification of the preformed complexes containing surface reactive groups with a reactive poly(HPMA) derivative.

ACKNOWLEDGMENT

The support of the EU by Grant ERBIC20CT97005 and of the Grant Agency of the Czech Republic by Grant 307/96/K226 is gratefully acknowledged.

LITERATURE CITED

(1) Seymour, L. W., Kataoka, K., and Kabanov, A. V. (1998) Cationic block copolymers as self-assembling vectors for gene delivery. In *Self-assembling Complexes for Gene Delivery: From Laboratory to Clinical Trials* (K. V. Kabanov, P. L. Felgner, and L. W. Seymour, Eds.) pp 219−239, John Wiley & Sons, New York.

(2) Wolfert, M. A., Schacht, E. H., Toncheva, V., Ulbrich, K., Nazarova, O., and Seymour, L. W. (1996) Characterization of vectors for gene therapy formed by self-assembly of DNA with synthetic block copolymers. *Hum. Gene Ther. 7*, 2123−2133.

(3) Dash, P. R., Toncheva, V., Schacht, E. H., and Seymour, L. W. (1997) Synthetic polymers for vectorial delivery of DNA: characterization of polymer-DNA complexes by photon correlation spectroscopy and stability to nuclease degradation and disruption by polyanions in vitro. *J. Controlled Release 48*, 269−276.

(4) Katayose, S., and Kataoka, K. (1997) Water-Soluble Polyion Complex Associates of DNA and Poly(ethylene glycol)-Poly(L-lysine) Block Copolymer. *Bioconjugate Chem. 8*, 702−707.

(5) Kabanov, A. V., Vinogradov, S. V., Suzdaltseva, Y. G., and Alakhov, V. Y. (1995) Water-Soluble Block Polycations as Carriers for Oligonucleotide Delivery. *Bioconjugate Chem. 6*, 639−643.

(6) Koňák, Č., Mrkvičková, L., Nazarova, O., Ulbrich, K., and Seymour, L. W. (1998) Formation of DNA complexes with diblock copolymers of poly(*N*-(2-hydroxypropyl) methacrylamide) and polycations. *Supramol. Sci. 5*, 67−74.

(7) Toncheva, V., Wolfert, M. A., Dash, P. R., Oupický, D., Ulbrich, K., Seymour, L. W., and Schacht, E. H. (1998) Novel vectors for gene delivery formed by self-assembly of DNA with poly(L-lysine) grafted with hydrophilic polymers. *Biochim. Biophys. Acta 1380*, 354−368.

(8) Oupický, D., Koňák, Č., and Ulbrich, K. (1998) DNA Complexes with Block and Graft Copolymers of *N*-(2-Hydroxypropyl)methacrylamide and 2-(Trimethylammonio)ethyl methacrylate. *J. Biomater. Sci., Polym. Ed.* (in press).

(9) Oupický, D., Koňák, Č., and Ulbrich, K. (1999) Preparation of DNA Complexes with Diblock Copolymers of Poly[N−(2-Hydroxypropyl)methacrylamide] and Polycations. *Mater. Sci. Eng. C* (in press).

(10) Wolfert, M. A., and Seymour, L. W. (1996) Atomic Force Microscopy of the influence of the molecular weight of poly(L-lysine) on the size of polyelectrolyte complexes formed with DNA. *Gene Ther. 3*, 269−273.

(11) Chion, H. C., Tangco, M. V., Levine, S. M., Robertson, D., Karmisk, L., Wu, C. H., and Wu, G. Y. (1994) Enhanced resistance to nuclease degradation of nucleic acids complexed to asialoglycoproteins-polylysine carriers. *Nucleic Acids Res. 22*, 5439−5446.

(12) Oja, C. D., Semple, S. C., Chonn, A., and Cullis, P. R. (1996) Influence of dose on liposome clearance: critical role of blood proteins. *Biochim. Biophys. Acta 1281*, 31−37.

(13) Dash, P. R. (1998) The Development of Polymer-based Synthetic Vectors for Use in Gene Therapy. Ph.D. Thesis, University of Birmingham.

(14) Lasic, D. D., and Needham, D. (1995) The "stealth" liposome: A prototypical biomaterial. *Chem. Rev. 95*, 2601−2628.

(15) Moghimi, S. M. (1995) Mechanisms regulating body distribution of nanospheres conditioned with pluronic and tetronic block copolymers. *Adv. Drug Delivery Rev. 16*, 183−193.

(16) Manning, G. S. (1969) Limiting laws and counterion condensation in polyelectrolyte solutions. I. Colligative properties. *J. Chem. Phys. 51*, 924−938.

(17) Wolfert, M. A. Self-assembling systems based on synthetic polymers for gene delivery. (1998) Ph.D. Thesis, University of Birmingham.

(18) Bakeev, K. N., Izumrudov, V. A., Kuchanov, S. I., Zezin, A. B., and Kabanov, V. A. (1992) Kinetics and Mechanism of Interpolyelectrolyte Exchange and Addition Reactions. *Macromolecules 25*, 4249−4254.

(19) Takakura, Y., and Hashida, M. (1998) Pharmacokinetics of macromolecules and synthetic gene delivery systems. In *Self-assembling complexes for gene delivery: From laboratory to clinical trial* (A. V. Kabanov, P. L. Felgner, and L. W. Seymour, Eds.), pp 295−306, John Wiley & Sons, New York.

(20) Lasic, D. D. (1997) Recent developments in medical applications of liposomes: sterically stabilized liposomes in cancer therapy and gene delivery in vivo. *J. Controlled Release 48*, 203−222.

BC990007+

Chain Length of Cationic α-Helical Peptide Sufficient for Gene Delivery into Cells

Takuro Niidome,*,† Keiko Takaji,† Mamiko Urakawa,† Naoya Ohmori,† Akihiro Wada,‡ Toshiya Hirayama,‡ and Haruhiko Aoyagi†

Department of Applied Chemistry, Faculty of Engineering, Nagasaki University, Nagasaki 852-8521, Japan, and Department of Bacteriology, Institute of Tropical Medicine, Nagasaki University, Nagasaki 852-8523, Japan.
Received February 4, 1999; Revised Manuscript Received May 19, 1999

To define the minimal peptide length needed for gene delivery into mammalian cells, we synthesized several peptides with shortened chain lengths from the amino-termini of the original amphiphilic peptides (4_6, Ac-LARL-LARL-LARL-LRAL-LRAL-LRAL-NH_2, and Hel 11-7, KLLK-LLLK-LWKK-LLKL-LK), which have been known to have gene transfer abilities into cells. Each synthetic peptide was studied for its ability to bind and aggregate with plasmid DNA and the structural change of the peptide caused by binding with the DNA to establish a relative in vitro gene transfection efficiency in COS-7 cells. As a result, the deletion of eight amino acid residues of 4_6 had little influence on their ability, whereas that of 12 amino acid residues remarkably reduced the abilities to make aggregates and transfer the DNA into the cell. In the case of the Hel 11-7 series peptides, deletion of amino acid residues caused a considerable reduction in abilities to bind and form aggregates with DNA and to transfer the DNA into cell in due order. In summary, 16 and 17 amino acid residues were sufficient to form aggregates with the DNA and transfer the DNA into the cells in the deletion series of 4_6 and Hel 11-7, respectively. Furthermore, it was indicated that reduction of membrane perturbation activity of the peptide−DNA complex due to deletion of the peptide chain length caused suppression of the transfection efficiency even if the complex was incorporated into the cells. Transfer of the complex to cytosol mediated by membrane perturbation activity of the peptide is an important step for efficient protein expression from its cDNA. The results of this study will make it easy to design and synthesize a functional gene carrier molecule such as a carbohydrate-modified peptide used in targeted gene delivery.

INTRODUCTION

An efficient gene-transfer technique is necessary for the development of gene therapy. Various methods are being developed to transfect mammalian cells with foreign genes. In these situations, nonviral gene delivery systems are expected to introduce genes into cells without several problems, which are pointed out in transfection methods using viral vectors, such as endogenous virus recombinations, oncogenic effects and immunogenic reactions (*1*, *2*). Nonviral delivery systems generally consist of a cationic polymer such as polylysine delivartives (*3*−*5*), polyethyleneimines (*6*) and polyamidoamine dendrimers (*7*), or cationic lipids (*8*) that electrostatically form a complex with the negatively charged DNA that can be taken up by the cells. Furthermore, Gottschalk et al. and Wadhwa et al. reported that synthetic peptides containing several cationic amino acids are useful as a gene carrier molecule (*9, 10*). The low molecular and homogeneous peptides are expected to easily construct a functional carrier molecule by attaching to a receptor ligand such as a carbohydride or peptide.

Recently, novel gene transfer techniques, in which an amphiphilic α-helical peptide containing cationic amino acids is used as a gene carrier into cells, have been reported. Wyman et al. employed a peptide, KALA (WEAK-LAKA-LAKA-LAKH-LAKA-LAKA-LKAC-EA), which is derived from the sequence of the amino-terminal segment of the HA-2 subunit of the influenza virus hemagglutinin involved in the fusion of the viral envelope with the endosomal membrane (*11*). This peptide showed several functions in the transfection process, e.g., condensing DNA and causing an endosome−membrane perturbation, which enables it to deliver the incorporated DNA to the cytosol, which is essential for efficient transfection. Similarly, we have also reported the transfection technique, which is mediated by some amphiphilic α-helical peptides consisting of 24 amino acids, including six arginines (e.g., Ac-LARL-LARL-LARL-LRAL-LRAL-LRAL-$NHCH_3$, 4_6) (*12*, *13*). Furthermore, to clarify in detail the importance of the hydrophobic region in the amphiphilic peptide in relation to its transfection efficiency, we have employed the Hel series peptides (e.g., KLLK-LLLK-LWLK-LLKL-LL, Hel 13−5), which consist of 18 residues and have systematically varied the hydrophobic−hydrophilic balance in the amphiphilic structures (*14*, *15*). As a result, the peptide with a large hydrophobic region could strongly bind to the plasmid DNA and form large aggregates with the DNA. In addition, it could be said that the hydrophobic region of the peptides plays an important role in the disruption of the endosomal membrane in the targeted cell, which can transfer the incorporated DNA to cytosol and prevent the degradation of the DNA in the lysosomal vesicles.

As is well-known, a peptide is readily synthesized due to the development of an automatic peptide synthesis

* To whom correspondence should be addressed. Phone and Fax: 81-95-843-7306. E-mail: tanido@net.nagasaki-u.ac.jp.
† Department of Applied Chemistry.
‡ Department of Bacteriology.

10.1021/bc990012d CCC: $18.00 © 1999 American Chemical Society
Published on Web 07/30/1999

apparatus and reagents for synthesis. From this point of view, it is expected that the transfection method mediated by the peptide is easily accepted by many researchers taking part in a gene therapy study. Development of an efficient gene transfer system using peptide with simple structure will cause many applications to gene therapy.

In this paper, for the purpose of refining of the peptide structure, we investigated the influence of the peptide chain length on gene transfer ability. We synthesized several peptides with shortened chain lengths from the amino-termini of amphiphilic peptides 4_6 and Hel 11-7, which have transfection abilities (*13*, *15*), and then evaluated the DNA-binding, aggregate-forming, and transfection abilities into cultivated cells.

MATERIALS AND METHODS

Chemicals and Instruments. Reagents used for the synthesis and analysis were of reagent grade. All amino acid derivatives and reagents for peptide synthesis were purchased from Watanabe Chemical (Hiroshima, Japan). Ethidium bromide and alamer Blue were purchased from Wako chemicals (Osaka, Japan). Egg yolk phosphatidylcholine, bovine brain phosphatidylserine, and bovine brain sphingomyeline were purchased from Sigma (St. Louis, MO).

Peptide purification was carried out on a Hitachi L7100 system (Tokyo, Japan) with a semipreparative RP-HPLC[1] column, YMC-Pack ODS column (10 × 250 mm, Kyoto, Japan) using the following solvent system: 0.1% trifluoroacetic acid (TFA)−0.08% TFA in acetonitrile. Flow rate was 3.0 mL/min, and elution was monitored at 220 nm. Mass spectra were obtained by fast-atom bombardment mass spectrometry (FAB-MS) using a JEOL JMS-DX303 mass spectrometer (Tokyo, Japan) or by matrix-assisted time-of-flight mass spectrometry (MALDI TOF-MS) using a Shimadzu Kratos Kompact MALDI III apparatus (Kyoto, Japan). Plasmid DNA which contains a luciferase gene and SV40 promoter (PicaGene control vector, PGV-C) was purchased from Toyo Ink (Tokyo, Japan). Closed circular plasmid DNA was purified by ultracentrifugation in CsCl gradients. The plasmid preparations showed a major band of closed circular DNA and minor amount (<20%) of nicked plasmid. COS-7 cells (a monkey kidney cell line, RCB accession no. RCB0539), HeLa cells (a human cervix, RCB accession no. RCB0271), and CHO cells (a chinese hamster ovary, RCB accession no. RCB0285) were purchased from RIKEN Cell Bank (Tsukuba, Japan). HuH-7 cells (a human hepatoma cell line, JCRB accession no. JCRB0403) were purchased from Health Science Research Resources Bank (Osaka, Japan). DMEM, RPMI1640, media supplements, and heat inactivated FCS were from IWAKI GLASS (Chiba, Japan).

Peptides Synthesis. Peptides were synthesized by the stepwise elongation of Fmoc-amino acid on Rink amide resin [4-(2′,4′-dimethoxyphenyl-Fmoc-aminomethyl)-phenoxy resin, 0.43 mmol/g resin] or Wang resin (*p*-benzoyloxy alcohol resin, 0.70 mmol/g resin) on a 0.05 mmol scale. The Fmoc amino acid derivatives used were as follows: Ala, Arg(Mtr), Leu, Lys(Boc), and Trp. The coupling protocol was as follows: 1, wash, DCM (x3); 2, wash, DMF (x3); 3, wash, 20% piperidine/DMF (x1); 4, deprotection, 20% piperidine/DMF (15 min); 5, wash, DMF (x5); 6, coupling Fmoc-amino acid (0.15 mmol), HBTU (0.15 mmol), HOBt (0.15 mmol), and DIEA (0.3 mmol) (15 min); 7, wash, DMF (x3); and 8, Kaiser Test (*16*). When the coupling was incomplete, the protocol was repeated from step 6. In the case of modifying by acetyl group to amino-terminal of peptide, the Fmoc-deprotected peptide resin was treated with acetic anhydride (10 equiv) in DMF for 20 min. The protecting groups and the resin were removed with TFA (1.0 mL) in the presence of *m*-cresol (30 μL), ethandithiol (90 μL) and thioanisole (180 μL) at room temperature for 60 min. In the case of the peptides containing Arg(Mtr), the filtered solution was shaken with trimethylbromosilane (350 μL) at 0 °C for 1 h (*17*). The crude peptides were precipitated by diethyl ether and then purified by RP-HPLC on a YMC-Pack ODS column (10 × 250 mm). The purified peptides were identified by the amino acid analysis and FAB-MS or MALDI TOF-MS.

Agarose Gel Electrophoresis. The peptide−DNA complex formation was examined by the electrophoretic mobility of the complex on an agarose gel stained with ethidium bromide at the various ratios of peptide to a double stranded DNA. The tests were performed by mixing 0.1 μg of the plasmid DNA (PGV-C) with the peptides in 10 μL of HBS (21 mM Hepes-NaOH buffer containing 135 mM NaCl, 5.0 mM KCl, and 0.76 mM Na_2HPO_4 pH 7.4), in which the positive (peptide)/negative (DNA) charge ratios were 0, 0.10, 0.25, 0.50, 1.0, 2.0, 4.0, and 8.0, respectively. Gel electorophoresis sample buffer was added to each sample, and it was electrophoresed on 1% (w/v) agarose gel for 40 min at 100 V. TBE (45 mM Tris-Borate and 1 mM EDTA, pH 8.0) buffer was used as electrophoresis buffer. The gel was stained with ethidium bromide (0.5 μg/mL) for 30 min and illuminated with a UV illuminator to show the location of the DNA.

Fluorescence Titration Assay. Binding abilities of the peptides were monitored by a fluorescent titration assay (*18*). A total of 10 μg of the plasmid DNA was mixed with the peptides in 980 μL of HBS, in which the positive (peptide)/negative (DNA) charge ratios were 0, 0.25, 0.50, 0.75, 1.0, 1.25, 1.5, 1.75, 2.0, 2.5, 3.0, and 4.0, respectively. After the solution stood for 20 min at room temperature, 20 μL of 20 μg/mL of ethidium bromide solution was added to the peptides−DNA mixtures. The fluorescence of the intercalated dye was measured on a spectrofluorometer F-3010 (Hitachi, Japan) by exciting at 530 nm while monitoring emmision at 590 nm, with the slits set at 20 nm. Fluorescence intensity blanks were subtracted from all values before data analysis.

Circular Dichroism. Circular dichroism (CD) spectra were recorded on a JASCO J-720W spectropolarimeter using a quartz cell of 1.0 mm path length. The peptides were dissolved at the concentration of 10 μM in HBS. Measurements were performed in the presence of the plasmid DNA at peptide/DNA charge ratio of 2.0 and in the absence of the plasmid DNA at 25 °C.

Particle Size Analysis. Samples were prepared by mixing 0.5 μg of the plasmid DNA with the peptides at peptide/DNA charge ratio of 2.0 in 50 μL of HBS and analyzed using a Nicomp submicron particle sizer model 370 in the solid particle mode. The mean diameter and population distribution were computed from the diffusion coefficient using functions supplied by the instrument.

[1] Abbreviations: Fmoc, 9-fluorenylmethoxycarbonyl; HBTU, *O*-benzotriazolyl-*N*,*N*,*N*′,*N*′-tetramethyluronium hexafluorophosphate; HOBt, 1-hydroxybenzotriazol; RP-HPLC, reversed-phase high-performance liquid chromatography; DCM, dichloromethane; DIEA, ethyldiisopropylamine; DMF, *N*,*N*-dimethylformamide; TFA, trifluoroacetic acid; FAB-MS, fast-atom bombard mass spectrometry; MALDI TOF-MS, matrix-assisted time-of-flight mass spectrometry; HBS, 21 mM Hepes-NaOH buffer (pH 7.4) containing 135 mM NaCl, 5.0 mM KCl; CD, circular dichroism; DMEM, Dulbecco's modified Eagle's medium; FCS, fetal calf serum.

Transmission Electron Microscopy. Samples were prepared by mixing 0.5 μg of the plasmid DNA with the peptides at peptide/DNA charge ratio of 2.0 in 50 μL of HBS. These were then left standing for 20 min at room temperature. Peptide−DNA complexes were processed for transmission electron microscopy (TEM) using a negative stain technique. Fifteen microliter drops of aliquot of the mixture was placed on glow-discharged carbon-coated 200-mesh copper grids for 3 min. Solution was wicked off with filter paper and replaced with 1% aqueous uranyl acetate for 30 s. After removal of the solution, grids were rinsed in distilled water and allowed to dry. Grids were imaged in a JEOL JEM-100S transmission electron microscope.

Peptide-Mediated Gene Transfer. COS-7 cells, a simian kidney cell line transformed with simian virus 40 (SV40), were grown to just before confluence in 16 mm dishes in Dulbecco's modified Eagle's medium (DMEM) with 10% fetal calf serum (FCS) and 50 μg/mL kanamycin in an atmosphere of 5% CO_2 at 37 °C, and washed twice with 1 mL of HBS. Mixture of peptide and DNA was prepared by mixing 2.5 μg of the plasmid DNA (PGV-C) with the peptides at peptide/DNA charge ratio of 2.0 in 250 μL of HBS and allowed to stand for 20 min at room temperature. The mixture was poured gently to the cells in 250 μL of serum free DMEM. After incubation for 3 h at 37 °C, 1 mL of DMEM with 10% FCS was added. After incubation for 24 h, the medium was replaced with 1 mL of a fresh medium and the cells were furthermore incubated for 24 h. Treatment of the cells with chloroquine was performed at 50 μM during transfection procedure. Harvesting of cells and luciferase assays were performed as described in the protocol of PicaGene luminescence kit (Toyo Ink; Tokyo, Japan). Luciferase relative light units (RLU) were analyzed by luminometer (Maltibiolumat LB9505, Berthold, Germany). The protein concentrations of the cell lysates were measured by Bradford assay using bovine serum albumin as a standard (*19*). The light unit values shown in the figures represent the specific luciferase activity (RLU/mg of protein) which is standardized for total protein content of the cell lysate. The measurement of gene transfer efficiency was performed in triplicate. In the case of other cell lines, the same protocol was applied except for the case of HuH-7 cells, in which RPMI1640 with 5% FCS was used instead of DMEM with 10% FCS as a medium.

Cytotoxic Activities of Peptides. Cytotoxic activities of the peptides were evaluated using alamer Blue. COS-7 cells were plated at 1×10^4 cells/well in a 96-well tray and incubated for 12 h at 37 °C. Mixture of peptide and DNA was prepared by mixing 0.25 μg of the plasmid DNA with the peptides at a charge ratio of 2.0 in 25 μL of HBS and allowed to stand for 20 min at room temperature. The mixture was poured gently to the cells in 25 μL of serum-free DMEM. After incubation for 3 h at 37 °C, 100 μL of DMEM with 10% FCS was added. After incubation for 24 h, the medium was replaced with 100 μL of a fresh medium and the cells were furthermore incubated for 24 h. The medium was removed and replaced by 10 μL of the alamer Blue solution. After incubation for 3 h, fluorescence at 590 nm (excitation wavelength, 544 nm) of each well was measured using a Labsystems Fluoroskan II (Helsinki, Finland). Results are expressed as the percentage of fluorescence reduction in cells treated according to the transfection protocol to fluorescence reduction in cells treated with HBS. The measurement was performed in duplicate.

Dye Leakage from Phospholipid Vesicles by the Action of Peptides. The dye-leakage experiment was carried out as reported by Suenaga et al. (*20*). The tests were performed by mixing 25 μL of the complex solution containing the peptide and the plasmid DNA with 975 μL of the small unilamellar vesicle suspension containing 100 μM calcein to give a vesicle solution with a final concentration of 70 μM lipid, which consists of egg phosphatidylcholine, phosphatidylserine, and bovine brain sphingomyeline at molar ratio of 7, 1, and 2, respectively, in HBS (pH 7.4) or 20 mM sodium citrate buffer (pH 5.0) containing 150 mM NaCl. The complex of the peptide and the plasmid DNA was prepared mixing peptide at a final concentration of 400 μM with the plasmid DNA in 25 μL of HBS, in which charge ratio was 2.0. The fluorescence intensities of calcein were monitored at 515 nm (excitation wavelength, 495 nm) and measured 2 min after the addition of the peptides. To measure the fluorescence intensity for 100% dye release, 10 μL of Triton X-100 (10% in H_2O) was added to dissolve the vesicles. The percentage of the dye release caused by the peptides was evaluated by the equation $100 \times (F - F_0)/(F_t - F_0)$, where F is the fluorescence intensity achieved by the peptides, and F_0 and F_t are intensities observed without the peptides and after Triton X-100 treatment, respectively.

Table 1. Structures of Peptides Deleted from Amino Termini of Gene Carrier Peptides, 4_6, and Hel 11-7

peptide	sequence	chain length	cationic charge
4_6	Ac-LARL-LARL-LARL-LRAL-LRAL-LRAL-NH_2	24	6
$4_6\Delta_4$	Ac-LARL-LARL-LRAL-LRAL-LRAL-NH_2	20	5
$4_6\Delta_8$	Ac-LARL-LRAL-LRAL-LRAL-NH_2	16	4
$4_6\Delta_{12}$	Ac-LRAL-LRAL-LRAL-NH_2	12	3
Hel 11-7	KLLK-LLLK-LWKK-LLKL-LK	18	7
Hel 11-7Δ1	LLK-LLLK-LWKK-LLKL-LK	17	6
Hel 11-7Δ2	LK-LLLK-LWKK-LLKL-LK	16	6
Hel 11-7Δ3	K-LLLK-LWKK-LLKL-LK	15	6
Hel 11-7Δ8	LWKK-LLKL-LK	10	4

RESULTS AND DISCUSSION

Peptide Design. Cationic α-helical peptides were designed to probe the minimal size needed to mediate efficient gene transfer into mammalian cells. As shown in Table 1, we synthesized several peptides with shortened chain lengths from the amino-termini of amphiphilic peptides, 4_6, and Hel 11-7, which have transfection abilities (*13*, *15*). The deletion of 4_6 was done with tetrapeptide-repeat units up to 12 residues (3 repeat units) ($4_6\Delta4$, Δ8, and Δ12). The number of cationic charges (arginine residues) of the 4_6 series peptides was reduced one by one by deletion of one unit of the repeat. In the case of Hel 11-7, the amino acids were deleted one by one up to three residues (Hel 11-7Δ1, Δ2, and Δ3). In addition, a peptide deleted with eight amino acid residues (Hel 11-7Δ8) was also prepared. As the amino- and carboxyl-terminals of the Hel series peptides are not protected, the net charge of the peptides also corresponded to the number of the lysine residues. Therefore, Hel 11-7Δ1 to Δ3 and Δ8 has six and four cationic charges, respectively. All peptides were synthesized by stepwise elongation using Fmoc-amino acid. However, a sufficient amount of $4_6\Delta4$ could not be obtained due to its poor solubility in buffer solution. It is likely that $4_6\Delta4$ accidentally forms a strong aggregation. The purified peptides except for $4_6\Delta4$ were identified by FAB-MS or MALDI TOF-MS.

Binding Ability of Peptide to DNA. The formation of peptide−plasmid DNA complexes was examined by

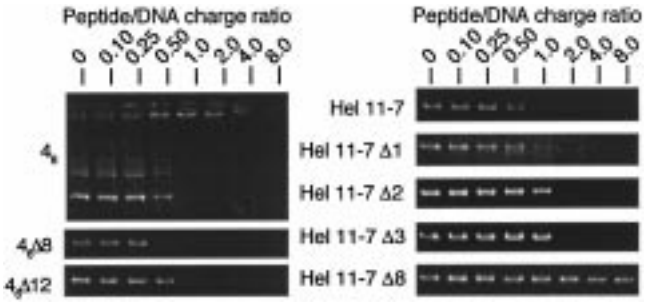


Figure 1. Agarose gel electrophoresis of the complexes of the peptides and the plasmid DNA. The plasmid DNA (100 ng) and several amounts of the peptides were mixed, followed by electrophoresis on an agarose gel (1% w/v) stained with ethidium bromide. The charge ratio (peptide:DNA) is indicated *above* each *lane*. Bands of the migrated DNA are indicated except for the case of 4_6.

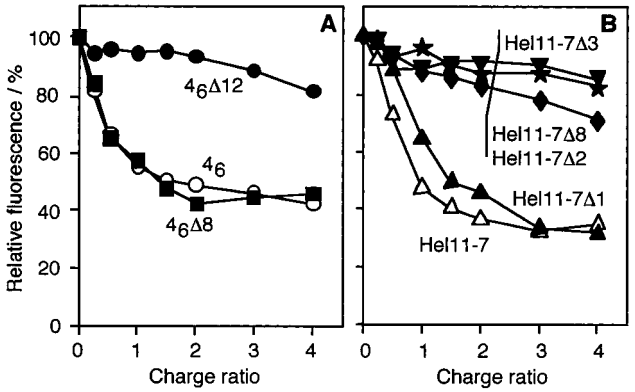


Figure 2. Fluorescence titration assay. A total of 10 μg of the plasmid DNA was mixed with the peptides in 980 μL of HBS at various charge ratios. After the solution stood for 20 min at room temperature, 20 μL of 20 μg/mL of ethidium bromide solution was added to the peptide−DNA mixtures. The fluorescence was measured on a spectrofluorometer by exciting at 530 nm while monitoring emmision at 590 nm. (A) 4_6 series peptides; 4_6 (○), $4_6\Delta8$ (■), and $4_6\Delta12$ (●). (B) Hel series peptides; Hel 11-7 (△), Hel 11-7Δ1 (▲), Hel 11-7Δ2 (◆), Hel 11-7Δ3 (▼), and Hel 11-7Δ8 (★×9a).

their electrophoretic mobility on an agarose gel stained with ethidium bromide at the various charge ratios of the peptide to a plasmid DNA (Figure 1). In the case of the 4_6 series peptides, no migration of the plasmid DNA band occurred at charge ratios of 1.0, 0.5, and 1.0 for 4_6, $4_6\Delta8$, and $4_6\Delta12$, respectively. This lack of migration was due to neutralization of the nucleic acid by the cationic peptide and/or formation of a large complex between the peptide and the DNA. This result indicated that $4_6\Delta8$ had a slightly stronger DNA-binding ability compared to 4_6 and $4_6\Delta12$. On the other hand, in the case of the Hel 11-7 series peptides, the charge ratio at which no migration of the plasmid DNA occurred was increased by increasing the number of deleted amino acids in the peptide. The deletion of amino acids of Hel 11-7 clearly decreased the binding abilities of the peptides. Especially, Hel 11-7Δ8 with four cationic charges similar to $4_6\Delta8$, which has DNA-binding ability, could not bind to the plasmid DNA even if the charge ratio of the peptide/DNA increased to 8.0. This result indicates that not only the number of cationic amino acids but also the structural feature of the peptide such as chain length or width of the hydrophobic region in the amphiphilic structure is necessary for binding to the DNA.

The binding ability was also estimated by the ethidium bromide-titration assay (*18*). Peptides bound to DNA leads to exclusion of ethidium bromide intercalation and a decrease in fluorescence. Increasing the amount of 4_6 or $4_6\Delta8$ caused a reduction in the fluorescence to about 40% at a charge ratio of 2.0. The fluorescence intensities versus charge ratio flatten out at charge ratios above 2.0 (Figure 2A). This result indicated that these peptides are not highly efficient DNA-compacting agents. On the other hand, little reduction of the fluorescence was observed by the addition of $4_6\Delta12$, whereas this peptide inhibited the migration of the plasmid DNA on agarose gel. It is also likely that binding of $4_6\Delta12$ to the DNA could not cause compaction of the DNA. The titration of Hel 11-7 and Hel 11-7Δ1 with DNA led to a reduction within the charge ratio of 2.0 and 3.0, respectively (Figure 2B). These fluorescences also reached plateaus at 30%. Hel 11-7Δ2 showed moderate exclusion of the ethidium bromide from DNA compared with Hel 11-7Δ3 and Δ8, which caused only a slight reduction in fluorescence. These data from the ethidium bromide titrations for the Hel series peptides correspond to those from the agarose gel shift assay.

Structural Change in Peptide. To analyze the structural changes in the peptides by binding to the plasmid DNA, the CD spectra of the peptides were measured. As shown in Figure 3, panels A-C, the 4_6 series peptides showed a typical α-helix CD pattern with double minima at 208 and 222 nm in the HBS. The ellipticity at 222 nm indicated that these peptides took α-helical structures with helical contents of 73, 81, and 62% for 4_6, $4_6\Delta8$, and $4_6\Delta12$, respectively (*21*). Among the 4_6 series peptides, $4_6\Delta8$, which showed the strongest DNA-binding ability as already described, strongly formed α-helical structures compared with 4_6 and $4_6\Delta12$. In the presence of the plasmid DNA at a charge ratio of 2.0, 4_6 and $4_6\Delta8$ showed a large valley at 222 nm, and another valley at 208 nm became shallower. This result would mean aggregation of the peptide with DNA (*13*, *22*). The CD spectrum of peptide $4_6\Delta12$, which showed no ability to exclude the ethidium bromide from the DNA, was only slightly influenced by the addition of the plasmid DNA.

These changes in ellipticities at 208 nm by the addition of the plasmid DNA are summarized in Figure 3D. It is clear that a larger change in spectra was observed for $4_6\Delta8$ versus 4_6. In the case of the Hel series peptides, longer peptides such as Hel 11-7, Hel 11-7Δ1, and Hel 11-7Δ2 took α-helical structures with helical contents of 46, 37, and 8% in the absence of the plasmid DNA, respectively. On the other hand, shorter peptides such as Hel 11-7Δ3 and Hel 11-7Δ8 took mainly a random coil structure in HBS (data not shown). With the addition of the plasmid DNA, changes in the spectra were observed for the longer peptides and the differences decreased depending on the deleted number of amino acids residues.

Particle Size and Distribution of Peptide-DNA Complex. The size distribution of the peptide-plasmid DNA complexes at a charge ratio of 2.0 was compared using the dynamic light-scattering data (Table 2). A population of particles with a mean diameter of 0.5−9.6 μm was determined for these peptides except for $4_6\Delta12$ and Hel 11-7Δ8, of which the sizes could not be estimated due to the little light scattering of its complex with the DNA. Especially, $4_6\Delta8$ and Hel 11-7 formed aggregates of 5.3 and 9.6 μm, respectively, along with a large standard deviation of the average particle size. Although these values already exceeded the precisely measurable range by this method, it can be considered that the peptides with strong binding abilities induced larger aggregates with wider particle size distributions than the peptides with moderate binding abilities to DNA. Among

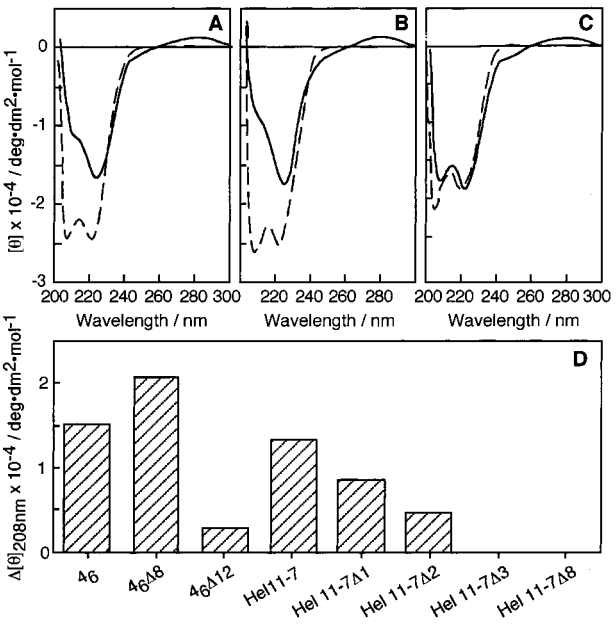


Figure 3. Circular dichroism spectra of the peptides with or without the plasmid DNA. The peptide was dissolved at 10 μM in HBS. Measurement was performed in the absence (*broken line*) or in the presence (*solid line*) of the plasmid DNA at 25 °C. Panels A, B, and C show the spectra of 4_6, $4_6\Delta8$, and $4_6\Delta12$, respectively. Panel D shows the difference between the mean residue ellipticities at 208 nm in the absence and presence of the plasmid DNA.

Table 2. Size Distribution of Peptide−Plasmid DNA Complexes

	particle size population	
peptide−DNA condensate[a]	diameter (nm)[b]	σ (nm)[c]
4_6	2330	1640
$4_6\Delta_8$	5300	4080
$4_6\Delta_{12}$	nd[d]	nd[d]
Hel 11-7	9610	9030
Hel 11-7Δ1	3050	1810
Hel 11-7Δ2	1810	1020
Hel 11-7Δ3	574	315
Hel 11-7Δ8	nd[d]	nd[d]

[a] Peptide DNA condensates were prepared by mixing 0.5 μg of the plasmid DNA with the peptides at peptide/DNA charge ratio of 2.0 in 50 μL of HBS. [b] Represents the mean diameter of particles. [c] Standard deviation of the population. [d] Correct values could not be determined due to little light scattering of the complex.

the Hel series peptides, the mean diameter of the peptide−DNA complex was decreased with decreasing chain length of the peptide. The chain length of the peptide plays an important role in the formation of aggregates between the peptide and DNA. It is likely that the hydrophobic interaction among the peptides is increased by extending its chain length.

Particle sizes determined by dynamic light scattering were also confirmed by observation of the peptide−DNA complexes using transmission electron microscopy with negative staining. As a result, all the peptides formed several sizes of aggregates, and twisted fiberlike structures were common, except for $4_6\Delta12$ and Hel 11-7Δ8, of which the aggregates could not be observed (*13*, *15*). Large DNA aggregates for $4_6\Delta8$ and Hel 11-7 were observed with diameters of approximately 1−10 μm. In the case of 4_6 and Hel 11-7Δ1 to Δ3, DNA aggregates were also observed within the ranges of the size distributions determined using dynamic light scattering (data not shown).

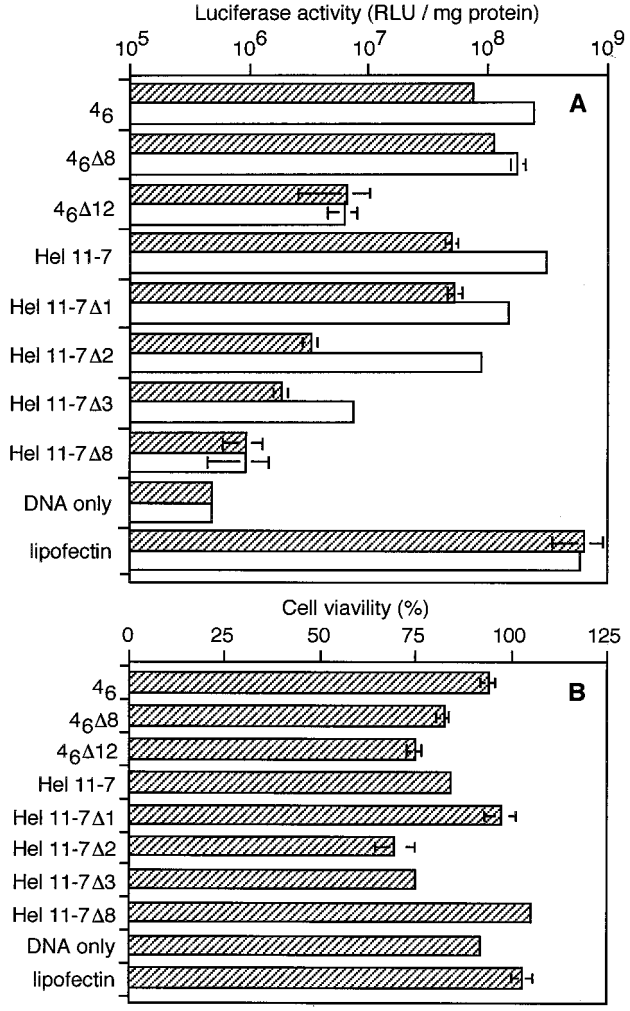


Figure 4. Transfection efficiencies of the peptides into COS-7 cells, and the cytotoxic activities of the peptides and their complexes with the plasmid DNA. (A) COS-7 cells were incubated with peptide-DNA complexes containing 2.5 μg of the plasmid DNA (PGV-C) and the peptides at peptide/DNA charge ratio of 2.0 for 3 h at 37 °C. Harvesting of the cells and luciferase assays were performed 48 h after transfection as described in the Materials and Methods. *Crosshatched bars* indicate the efficiency without chloroquine treatment. *Open bars* indicate the efficiency with chloroquine treatment. (B) Cytotoxitic activities of the peptides−DNA complexes evaluated using alamer Blue.

Gene Transfer Efficiency of Peptide in Vitro. The transfection efficiencies of these peptides into COS-7 cells were tested with the plasmid DNA, which contains a reporter gene encoding firefly luciferase. In Figure 4A, the *crosshatched bar* shows the gene transfer efficiency of the peptides when the peptides were mixed with 2.5 μg of the plasmid DNA at a charge ratio of 2.0 without chloroquine treatment. In these cases, 4_6, $4_6\Delta8$, Hel 11-7, and Hel 11-7Δ1 had remarkable abilities. These observations indicated that the transfection ability of the peptide was correlated to its ability to form aggregates with the DNA.

Furthermore, current treatment of the cells with chloroquine, which inhibits the degradation of the DNA by lysosomal hydrolases, made the efficiencies of 4_6, $4_6\Delta8$, Hel 11-7, and Hel 11-7Δ1 to Δ3 increase (Figure 4A, *open bar*). Particularly, the enhanced efficiency of Hel 11-7Δ2 by chloroquine was 30-fold higher than that in the absence of chloroquine and reached the efficiency of Hel 11-7 and Hel 11-7Δ1. This result suggested that the DNA complexes of Hel 11-7Δ2 could be well incorporated into

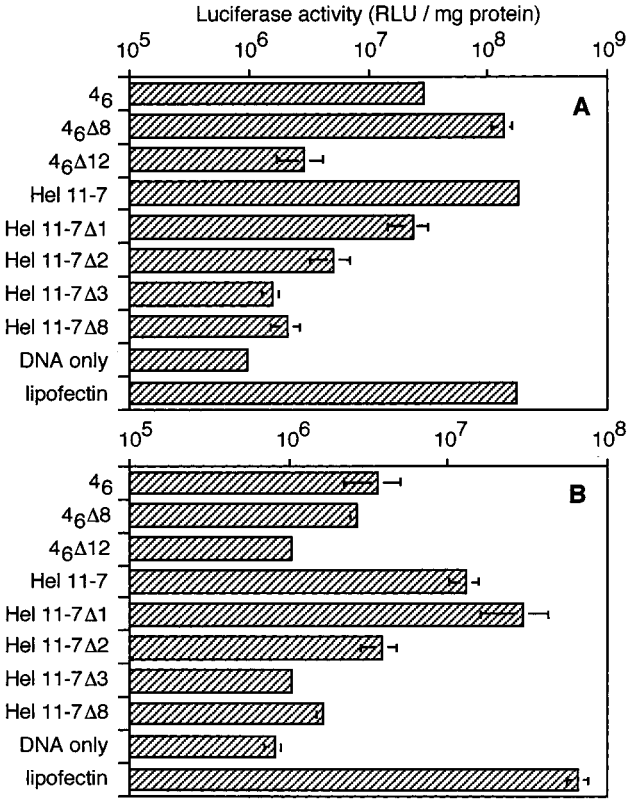


Figure 5. Transfection efficiencies of the peptides into several cell lines. Panels A and B show the efficiencies into HuH-7 and HeLa cells, respectively.

cells mediated by the endocytosis pathway, but most complexes would be transferred to the lysosome and digested in the absence of chloroquine.

Cytotoxic activities of the peptides−DNA complexes were evaluated using alamer Blue under the same conditions as those in the transfection procedure. As shown in Figure 4B, considerable cytotoxic activities of the complexes could not be observed except for Hel 11-7Δ2, of which the complex with the DNA had moderateactivity (70% cell viability). At this stage, we cannot explain the cytotoxic activity of Hel 11-7Δ2.

To prove the universality of the transfection efficiencies, we also tested the efficiencies of the peptides into several cell lines. As shown in Figure 5A, in the case of HuH-7 cells (a human hepatoma cell line), 4_6, $4_6\Delta8$, Hel 11-7, and Hel 11-7Δ1 showed remarkable efficiencies. The result in the case of CHO cells (a chinese hamster ovary) was also similar to that of HuH-7 cells (data not shown). In the case of HeLa cells (a human cervix), high efficiencies were also observed in 4_6, $4_6\Delta8$, and then Hel 11-7 and Hel 11-7Δ1 Hel series peptides were more advantageous than 4_6 series peptides (Figure 5B). From these results, although there were the some differences in transfection efficiencies of the peptides depending on several cell lines, the general tendencies were common, that is, high efficiencies were observed in the peptides with 16 or 17 residues.

Membrane Perturbation Activity of the Peptide−DNA Complex. The reason the efficiency of Hel 11-7Δ2, of which the DNA complex would be incorporated into cells, was low in the absence of chloroquine might be explained by the result that this peptide had a lower membrane perturbation activity, which would be considered to contribute to the transfer of the complex from the endosomal compartment to cytosol, compared with Hel 11-7 and Hel 11-7Δ1. To clarify this point, the membrane

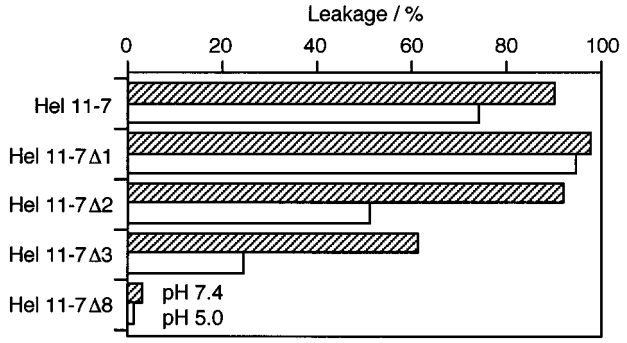


Figure 6. Dye-leakage from phospholipid vesicles by the action of peptides. The tests were performed by mixing the peptide−DNA complex with small unilamellar vesicle suspension, which consists of egg phosphatidylcholine, phosphatidylserine and bovine brain sphingomyeline at molar ratios of 7, 1, and 2, respectively, in HBS (pH 7.4; *crosshatched bars*) or 20 mM sodium citrate buffer containing 150 mM NaCl (pH 5.0; *open bars*) as described in the Materials and Methods.

perturbation activities of the Hel series peptide−DNA complexes were measured in neutral (pH 7.4) and acidic (pH 5.0) conditions (Figure 6). As the lipid membrane, we employed small unilamellar vesicles composed of phosphatidylcholine, phosphatidylserine, and sphingomyeline at molar ratios of 7, 1, and 2, respectively, which mimicked the endosomal membrane (*23*). As a result, DNA complexes of Hel 11-7 and Hel 11-7Δ1 showed strong membrane perturbation activities under both the neutral and acidic conditions. However, the DNA complex of Hel 11-7Δ2 showed a significantly weaker membrane perturbation activity compared with that of Hel 11-7 and Hel 11-7Δ1 under the acidic conditions, whereas a strong activity was observed under the neutral conditions. We speculate that, in the absence of chloroquine, the DNA complex of Hel 11-7Δ2 could not be transferred from acidic endosomal compartment to cytosol due to its weak membrane perturbation activity under the acidic conditions, even if the complex was incorporated into the cells. In the presence of the chloroquine, which inhibits the acidification of the endosome, the incorporated complex could be transferred to cytosol because the complex was continuously exposed in neutral condition. These findings strongly suggest that the perturbation activity of the peptide complexed with DNA plays an important role for delivery to cytosol in the cells, and consequently, leads the efficiently gene expression.

CONCLUSIONS

The results reported in this paper demonstrate that 16 amino acid residues including four cationic amino acids and 17 amino acid residues including six cationic amino acids were sufficient to form aggregates with the DNA and then transfer DNA into the cells in the deletion series of 4_6 and Hel 11-7, respectively. From the standpoint of the chain length and number of cationic amino acids, the 4_6 series peptides were advantageous. It is reasonable to postulate that the arginine residues as cationic amino acids in the peptide were favorable for efficient transfection. Practically, we have confirmed that the substitution of arginine residues for all lysine residues of Hel 11-7 enhanced its transfection efficiency by about five times (unpublished data).

Furthermore, in the deletion process, the 4_6 and Hel series peptide showed different behavior. A reasonable correlation between the chain length of the peptide, DNA binding, aggregate formation, and transfection efficiency was found in the case of the Hel series peptides. On the

other hand, although deletion of the 4_6 series peptide by 12 amino acid residues had little influence on their binding abilities for the gel retardation assay, a remarkable reduction in abilities to form aggregates with DNA and the transfection efficiencies occurred. The result from the 4_6 series peptides indicated that the binding to the DNA does not necessarily result in the formation of transfection-competent aggregates. Peptides 4_6 and $4_6\Delta8$, which have transfection abilities, showed high α-helical contents in HBS compared with $4_6\Delta12$ (Figure 1), indicating that stable oligomers of the peptides were formed with a well-defined number of monomers by self-association with their hydrophobic faces (*12*, *14*, *15*). In contrast, $4_6\Delta12$ could not compact the DNA and form large aggregates, although this peptide could bind to the DNA. It is, therefore, likely that the formation of some stable oligomer of the peptides plays an important role in transfection.

Finally, such as in the case of Hel 11-7Δ2, deletion of the peptide chain length caused a reduction in the membrane perturbation activity of the peptide−DNA complex under the acidic conditions. Simultaneously, suppression of the transfection efficiency was observed in the absence of chloroquine, whereas the complex could be incorporated into the cells. This suggests that transfer of the complex to cytosol mediated by the membrane perturbation activity of the peptide is an important step for efficient protein expression from cDNA encoded in the plasmid DNA.

We could minimize the peptide for gene transfer into cells to 16−17 amino acids residues in this study. It is considered that the result that we could achieve shortening the chain length to this size was due to use of the α-helical peptides with an amphiphilic structure, which have been known to show various interesting multibehaviors such as forming an oligomer, membrane perturbation, etc. The results obtained in this study allow us to easily design and synthesize the functional gene carrier molecule such as the carbohydrate modified peptide for targeted gene delivery.

ACKNOWLEDGMENT

This research was supported in part by a Grant-in-aid (09772027) from the Ministry of Education, Science, Sports and Culture of Japan. We acknowledge technical support in performing particle size analysis by Drs. Tohru Inoue and Sannamu Lee in the Department of Chemistry, Faculty of Science, Fukuoka University, Fukuoka, Japan. MALDI TOF-MS was performed by Dr. Hisakazu Mihara in the Department of Bioengineering, Faculty of Bioscience and Biotechnology, Tokyo Institute of Technology, Yokohama, Japan; his help is greatly appreciated.

LITERATURE CITED

(1) Ross, G., Erickson, R., Knorr, D., Motulsky, A. G., Parkman, R., Samulski, J., Straus, S. E., and Smith, B. R. (1996) Gene Therapy in the United States: a Five-year Status Report. *Hum. Gene Ther. 7*, 1781−1790.

(2) Temin, H. M. (1990) Safety Considerations in Somatic Gene Therapy of Human Disease with Retrovirus Vectors. *Hum. Gene Ther. 1*, 111−123.

(3) Wu, G. Y., and Wu, C. H. (1987) Receptor-Mediated in Vitro Gene Transformation by a Soluble DNA Carrier System. *J. Biol. Chem. 262*, 4429−4432.

(4) Wagner, E., Cotton, M., Foiser, R., and Birnstiel, M. L. (1991) Transferrin-Polycation DNA Complexes: the Effect of Polycation on the Structure of the Complex and DNA Delivery to Cells. *Proc. Natl. Acad. Sci. U.S.A. 88*, 4255−4259.

(5) Stankovics, J., Crane, A. M., Andrews, E., Wu, C., Wu, G. Y., and Ledley, F. D. (1994) Overexpression of Human Methylmalonyl CoA Mutase in Mice after in Vivo Gene Transfer with Asialoglycoprotein/Polylysine/DNA Complexes. *Hum. Gene Ther. 5*, 1095−1104.

(6) Boussif, O., Lezoualc'h, F., Zanta, M. A., Mergny, M. D., Scherman, D., Demeneix, B., and Berh, J.-P. (1995) A Sersatile Vector for Gene and Oligonucleitide Transfer into cells in Culture and in Vivo: Polyethyleneimine. *Proc. Natl. Acad. Sci. U.S.A. 92*, 7297−7301.

(7) Tang, M. T., Redemann, C. T., and Szoka, F. C., Jr. (1996) In Vitro Gene Delivery by Degraded Polyamidoamine dendrimers. *Bioconjugate Chem. 7*, 703−714.

(8) Felgner, P. L., Tsai, Y. J., Sukhu, L., Wheeler, C. J., Manthorpe, M., Marshall, J., and Cheng, S. H. (1995) Improved Cationic lipid Formulations for in Vivo Gene Therapy. *Ann. N. Y. Acad. Sci. 772*, 126−139.

(9) Gottschalk, S., Sparrow, J. T., Hauer, J., Mims, M. P., Leland, F. E., Woo, S. L. C., and Smith. L. C. (1996) A Novel DNA-Peptide Complex for Efficient Gene Transfer and Expression in Mammalian Cells. *Gene Ther. 3*, 448−457.

(10) Wadha, M. S., Collard, W. T., Adami, R. C., Mckenzie, D. L., and Rice, K. G. (1997) Peptide-Mediated Gene Delivery: Influence of Peptide Structure on Gene Expression. *Bioconjugate Chem. 8*, 81−88.

(11) Wyman, T. B., Nicol, F., Zelphati, O., Scaria, P. V., Plank, C., and Szoka, F. C. (1997) Design, Synthesis, and Characterization of a Cationic Peptide that Binds to Nucleic Acids and Permeabilizes Bilayers. *Biochemistry 36*, 3008−3017.

(12) Ohmori, N., Niidome, T., Hatakeyama, T., Mihara, H., and Aoyagi, H. (1998) Interaction of α-Helical Peptides with Phospholipid Membrane: Effects of Chain Length and Hydrophobicity of Peptides. *J. Pept. Res. 51*, 103−109.

(13) Niidome, T., Ohmori, N., Ichinose, A., Wada, A., Mihara, H., Hirayama, T., and Aoyagi, H. (1997) Binding of Cationic α-Helical Peptides to Plasmid DNA and Their Gene Transfer Abilities into Cells. *J. Biol. Chem. 272*, 15307−15312.

(14) Kiyota, T., Lee, S., and Sugihara, G. (1996) Design and Synthesis of Amphiphilic α-Helical Model Peptides with Systematically Varied Hydrophobic−Hydrophilic Balance and Their Interaction with Lipid- and Bio-Membranes. *Biochemistry 35*, 13196−13204.

(15) Ohmori, N., Niidome, T., Kiyota, T., Lee, S., Sugihara, G., Wada, A., Hirayama, T., and Aoyagi, H. (1998) Importance of Hydrophobic Region in Amphiphilic Structures of α-Helical Peptides for Their Gene Transfer-Ability into Cells. *Biochem. Biophys. Res. Commun. 245*, 259−265.

(16) Kaiser, E., Colescott, R. L., and Bossinger, C. D. (1970) Color Test for Detection of Free Terminal Amino Groups in the Solid-Phase Synthesis of Peptides. *Anal. Biochem. 34*, 595−598.

(17) Fujii, N., Otaka, A., Sugiyama, N., Hatano, M., and Yajima, H. (1987) Studies on Peptides. CLV. Evaluation of Trimethylsilyl Bromide as a Hard-Acid Deprotecting Reagent in Peptide Synthesis. *Chem. Pharm. Bull. (Tokyo) 35*, 3880−3883.

(18) Wadhwa, M. S., Collard, W. T., Adami, R. C., McKenzie, D. L., and Rice, K. G, (1997) Peptide-Mediated Gene Delivery: Influence of Peptide Structure on Gene Expression. *Bioconjugate Chem. 8*, 81−88.

(19) Bradford, M. M. (1976) A Rapid and Sensitive Method for the Quantitation of Microgram Quantities of Protein Utilizing the Principle of Protein-Dye Binding. *Anal. Biochem. 72*, 248−254.

(20) Suenaga, M., Lee, S., Park, N. G., Aoyagi, H., Kato, T., Umeda, A., and Amako, K. (1989) Basic Amphipathic Helical Peptides Induce Destabilization and Fusion of Acidic and Neutral Liposomes. *Biochim. Biophys. Acta 981*, 143−150.

(21) Scholtz, J. M., Qian, H., York, E. J., Stewart, J. M., and Baldwin, R. L. (1991) Parameters of Helix-Coil Transition Theory for Alanine-Based Peptides of Varying Chain Lengths in Water. *Biopolymers 31*, 1463−1470.

(22) Yoshimura, T., Goto, Y., and Aimoto, S. (1992) Fusion of Phospholipid Vesicles Induced by an Amphiphilic Model Peptide: Close Correlation Between Fusogenicity and Hydrophobicity of the Peptide in an α-helix. *Biochemistry 31*, 6119−6126.

(23) Evans, W. H., and Hardison, W. G. (1985) Phospholipid Cholesterol, Polypeptide and Glycoprotein Composition of Hepatic Endosome Subfractions. *Biochem. J. 232*, 33−36.

BC990012D

Carrier Design: New Generation of Polycationic Branched Polypeptides Containing OH Groups with Prolonged Blood Survival and Diminished in Vitro Cytotoxicity

Ferenc Hudecz,*,† Malcolm V. Pimm,‡ Éva Rajnavölgyi,§ Gábor Mező,† Angels Fabra,|| Dezső Gaál,⊥ Attila L.Kovács,# Attila Horváth,§ and Mária Szekerke†

Research Group of Peptide Chemistry, Hungarian Academy of Sciences, Budapest 112, POB 32, H-1518, Budapest, Hungary, Cancer Research Laboratory, University of Nottingham, Nottingham NG7 2RD, U.K., Department of Immunology, Eötvös L. University, Göd, Hungary, Cancer Research Institute, Hospital Duran I Reynals, Barcelona, Spain, National Institute of Oncology, Budapest, Hungary, and Department of General Zoology, Eötvös L. University, Budapest, Hungary. Received February 10, 1999; Revised Manuscript Received May 12, 1999

For the construction of macromolecule−drug conjugates, it is important to provide rational basis to the selection of proper carrier. With respect to the importance of the side-chain structure and charge of the branched polypeptides in biological properties, we have prepared a new class of branched polypeptides with single or multiple hydroxyl groups and studied their solution conformation, in vitro cytotoxicity, biodistribution, and immunoreactivity. For comparative studies, polypeptides were designed to contain serine at various positions of the side chains, varying also the number. Ser was attached to the end of oligo(DL-Ala) side chains grafted to polylysine resulting polypeptides with the general formula poly[Lys(Ser$_i$-DL-Ala$_m$)], (SAK). Ser was also coupled directly to the polylysine backbone poly[Lys(Ser$_i$)] (S$_i$K) and then elongated by polymerization of *N*-carboxy-DL-Ala anhydride resulting poly[Lys(DL-Ala$_m$-Ser$_i$)] (ASK). An additional polymer was also prepared, but instead of the oligo(DL-Ala) branches, oligo(DL-Ser) side chains were introduced (poly[Lys(DL-Ser$_m$)], SK). The presence of hydroxyl groups resulted in compounds with improved of water solubility. CD spectra of polypeptides showed significant differences correlating with the position and numbers of Ser residues in the side chains. Under physiological conditions, polycationic polypeptides assumed ordered secondary structure (S$_i$K and LSK) or partially unordered conformation (SK, SAK, and ASK). Data of selected polymers demonstrate that these polycationic compounds are essentially nontoxic in vitro on normal rat liver or mouse spleen cells and have no cytostatic effect on mouse colorectal carcinoma C26 cells. The blood clearance and biodistribution of these derivatives were greatly dependent on the position and number of Ser residues in the branches and possess a rather extended blood survival in mice. Polypeptides were taken up predominantly by the liver and kidney (S$_i$K, LSK, and ASK) or kidney and lung (SK and SAK). The best survival in the blood was found with SAK, representing the first polycationic branched polypeptide, which show extended blood clearance. The relative position of Ser residue had also a marked influence on the immunogenicity of polypeptides. The characteristics of the antibody response to polypeptide containing Ser at the end of the branches (SAK) or adjacent to the polylysine backbone (ASK) was also dependent on the genetic background of the mouse strains. We also found that these compounds have no effect on to the SRBC-specific humoral immune response, indicating the lack of nonspecific immunostimulatory potential. In conclusion, these studies suggest that synthetic branched polypeptides with Ser can be considered as candidates for constructing suitable conjugates for drug/epitope delivery. It is not only due to the presence of hydroxyl group to be used for oxime chemistry but also to their beneficial biological features.

INTRODUCTION

There is an increasing interest in the development of target-specific delivery systems for various drugs and isotopes as well as preparation of long-acting drug−macromolecule conjugates (*1*−*3*). Appropriate carrier molecules are required also for the construction of synthetic antigens for vaccination and/or for the production of conventional or monoclonal hapten specific antibodies (*4*, *5*).

In our laboratory different types of branched polypeptide have been synthesized to establish structure−function relationship (*6*, *7*). The synthetic branched polymeric polypeptides were characterized by their chemical (size, primary structure, and conformation) and biological (toxicity, pyrogenicity, biodegradation, immunoreactivity, and biodistribution) properties. Correlation has been demonstrated between the side-chain structure of polymers and some biological activities such as biodistribution (*8*) or in vitro cytotoxicity (*9*).

Branched polypeptides were also used successfully as carriers for peptide epitopes of glycoprotein D of Herpes

* To whom correspondence should be addressed. Fax: 36-1-2090602. Phone: 36-1-2090555. E-mail: fhudecz@ludens.elte.hu.
† Hungarian Academy of Sciences.
‡ University of Nottingham.
§ Department of Immunology, Eötvös L. University.
|| Cancer Research Institute.
⊥ National Institute of Oncology.
Department of General Zoology, Eötvös L. University.

10.1021/bc990015q CCC: $18.00 © 1999 American Chemical Society
Published on Web 08/28/1999

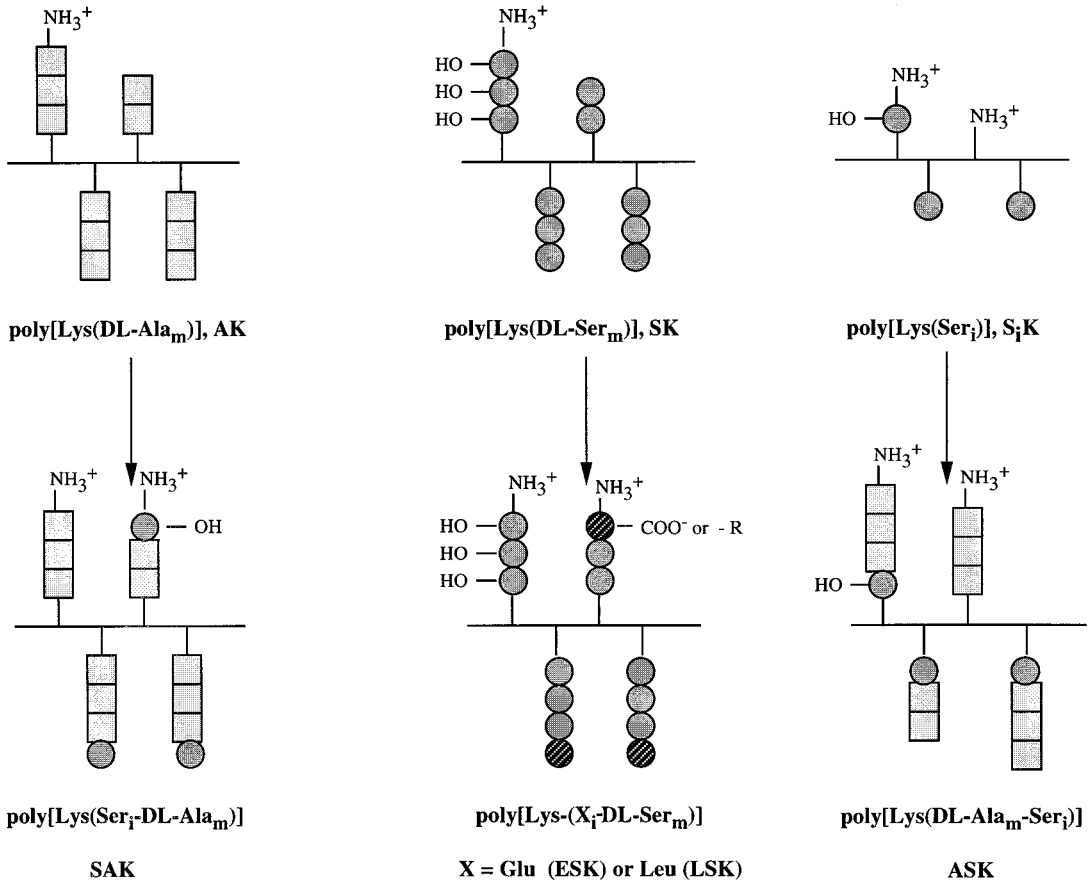


Figure 1. Schematic presentation of branched polypeptides.

Simplex virus (*10*), mucin 1 glycoprotein (*11*), and of *M. tuberculosis* proteins (*12*). Antitumor activity of daunomycin-EAK[1] conjugate (*13*, *14*) or Ac-[D-Trp$^{1-3}$, D-Cpa^2, D-Lys^6, D-Ala^{10}]-GnRH-AcEAK conjugate (*15*, *16*) has shown very promising results. These studies have also demonstrated that the biological properties (e.g., epitope-related immunogenicity or drug-related antitumor effect) and pharmacokinetics (e.g., blood survival, tissue distribution) of conjugates are greatly influenced by the chemical structure of the carrier.

Several authors have reported the application of poly(ethyleneglycol) (PEG) or PEG-containing polymers as water soluble drug carriers (*17*, *18*). It has been reported that PEG attached to proteins or synthetic polymers can increase their water solubility, blood survival, and/or lower the immunogenicity.

In view of these observations published in the literature, we have designed and synthesized a new class of branched polypeptides with single or multiple hydroxyl groups (*19*). For comparative biodistribution, in vitro cytotoxicity and immunological studies, these polypeptides were designed to contain serine at various positions of the side chains, varying also the number of the Ser residues (Figure 1). Serine was attached to the end of oligo(DL-Ala) side chains grafted to polylysine resulting polypeptides with the general formula poly[Lys(Ser$_i$-DL-Ala$_m$)] (SAK). Ser was also coupled directly to the polylysine backbone poly[Lys(Ser$_i$)], (S$_i$K) and then elongated by polymerization of *N*-carboxy-DL-Ala anhydride-resulting poly[Lys(DL-Ala$_m$-Ser$_i$)], (ASK). An additional polymer was also prepared, but instead of the above used oligo(DL-Ala) branches, oligo(DL-Ser) side chains were introduced (poly[Lys(DL-Ser$_m$)], SK) (*19*). The presence of hydroxyl functional groups could provide a new feature for oxime-based conjugation (*20*, *21*) of branched polypeptides with appropriate biologically active molecules leading to compounds with improved water solubility.

In this communication, we describe new branched polypeptides with a rather extended blood survival in mice. Data of selected polymers demonstrate that these compounds are essentially nontoxic in vitro on normal rat liver or mouse spleen cells and have no cytostatic features on mouse colorectal carcinoma C26 cells. The results of immunological experiments presented in this paper indicate that the position of Ser residue in the branches influences markedly the immunoreactivity of these polymers.

EXPERIMENTAL SECTION

Abbreviations. Abbreviations for amino acids and their derivatives follow the revised recommendation of the IUPAC-IUB Committee on Biochemical Nomenclature, entitled "Nomenclature and Symbolism for Amino Acids and Peptides" (*22*). The nomenclature of branched polypeptides is used in accordance with the recommended nomenclature of graft polymers (*23*). For the sake of

[1] Abbreviations: AXK, poly[Lys(DL-Ala$_m$-X$_i$)]; ASK, poly[Lys-(DL-Ala$_{6.5}$-Ser$_{0.88}$)]; AK, poly[Lys(DL-Ala$_m$)]; AUC, area under the curve; CD, circular dicroism; DMSO, dimethyl sulfoxide; DP$_n$, number average of the degree of polymerization; EAK, poly[Lys-(Glu$_i$-DL-Ala$_m$)]; ESK, poly[Lys(Glu$_{0.96}$-DL-Ser$_3$)]; FCS, foetal calf serum; LAK, poly[Lys(Leu$_i$-DL-Ala$_m$)]; MTT 3-(4,5 dimethylthiazol-2-yl)2,5-diphenyltetrazolium bromide; NCA, *N*-carboxy-anhydride; PBS, phosphate-buffered saline; PEG, poly(ethyleneglycol); PFC, plaque forming cell; RPMI, Roswell Park Memorial Institute; SAK, poly[Lys(Ser$_{0.96}$-DL-Ala$_{3.1}$)]; SK, poly-[Lys(DL-Ser$_{3.1}$)]; S$_i$K, poly[Lys(DL-Ser$_{0.96}$)]; SRBC, sheep red blood cell; XAK, poly[Lys-(X$_i$-DL-Ala$_m$)].

Table 1. Characteristics of Branched Polypeptides

polypeptide	code[a]	amino acid composition[b] Lys	Ala	Ser	X[c]	$\bar{M}_w$[d]
poly[Lys(Ser$_i$-DL-Ala$_m$)]	SAK	1.00	6.58	1.00		191 200
poly[Lys(Ser$_i$)]	S$_i$K	1.00		0.93		58 600
poly[Lys(DL-Ala$_m$-Ser$_i$)]	ASK	1.00	6.50	0.88		186 700
poly[Lys(DL-Ser$_m$)]	SK	1.00		2.93		107 300
poly[Lys(Leu$_i$-DL-Ser$_m$)]	LSK	1.00		3.11	1.0	149 300
poly[Lys(Glu$_i$-DL-Ser$_m$)]	ESK	1.00		3.0	0.93	142 700

[a] Code of branched polypeptides, based on one letter symbol of amino acids. [b] Determined by amino acid analysis after hydrolysis in 6 M HCl at 105 °C for 24 h. [c] X = Leu or Glu. [d] Calculated from the number average degree of polymerization of polylysine ($\overline{DP}_n$ = 280) and from the amino acid composition of the branches.

brevity, codes of branched polypeptides were constructed by us using the one-letter symbols of amino acids (Table 1). All amino acids are of the L configuration unless otherwise stated.

Polypeptides. Branched polypeptides containing Ser residues were prepared in our laboratory by previously (*19*) published methods. Briefly, poly(L-Lys) was produced by the polymerization of N^{α}-carboxy-N^{ϵ}-(benzyloxycarbonyl)-lysine anhydride under conditions that allowed an average degree of polymerization of ~300. After cleavage of the protecting groups with HBr in glacial acetic acid, poly[Lys(DL-Ala$_{6.5}$)] (AK), or poly[Lys(Ser$_{2.9}$)] (SK) were formed by grafting of short oligomeric DL-Ala or DL-Ser side chains onto the ϵ-amino groups of polylysine using the respective *N*-carboxy-DL-amino acid anhydride (NCA). The side chain of DL-Ser was protected by the benzyl group, which was removed with HBr/glacial acetic acid. For poly[Lys(Ser$_i$-DL-Ala$_m$)] (SAK), attachment of suitably protected and activated Ser residues to AK was carried out by the active ester method. Similarly, SK was reacted with *Z*-Leu-OPcp or with *Z*-Glu(OBzl)-OPcp to produce poly[Lys(Leu$_i$-DL-Ser$_m$)] (LSK) or poly[Lys(Glu$_i$-DL-Ser$_m$)] (ESK), respectively. Poly[Lys(Ser$_i$)] (S$_i$K) was prepared by the attachment of protected and activated Ser residue to the ϵ-amino groups of polylysine followed by the removal of protecting groups, while poly[Lys(DL-Ala$_m$−Ser$_i$)] (ASK) was synthesized from S$_i$K by polymerization of DL-Ala-NCA. After the deblocking, branched polypeptide samples were purified by extensive dialysis using Visking tubing followed by lyophilization. The removal of blocking groups was verified by UV spectroscopy (*19*). The average molar mass of the branched polypeptides was estimated from the number average degree of polymerization ($\overline{DP}_n$) of polylysine backbone (*24*) and from the amino acid composition of the side chains determined by quantitative amino acid analysis (Table 1). The synthesis of LSK and ESK is described in detail.

Synthesis of Poly[Lys(Leu$_i$-DL-Ser$_m$)] and poly-[Lys(Glu$_i$-DL-Ser$_m$)] (LSK and ESK). One and a half grams of DL-Ser(Bzl)-NCA (7.3 mmol) was dissolved in 3 mL dioxan, and it was added to 300 mg of polylysine·HBr (1.4 mmol) dissolved in 3 mL of deionized water and neutralized with 200 μL of triethylamine. The reaction mixture was stirred for 45 min and then allowed to stand for 24 h. The poly[Lys(DL-Ser(Bzl)$_m$)] sample was dialyzed for 2 days and freeze-dried. The product was dried over P_2O_5 for 24 h, and then the Bzl-protecting groups were removed by 35% HBr/acetic acid (50 mL) in an overnight reaction at 4 °C. The product was precipitated by addition of dry ether (100 mL). The precipitate was washed with ether several times and dried over P_2O_5 and KOH. The poly[Lys(DL-Ser$_m$)] (SK) sample dissolved in deionized water was dialyzed in Visking tube (cutoff 8000−12000) against deionized water for 2 days and freeze-dried.

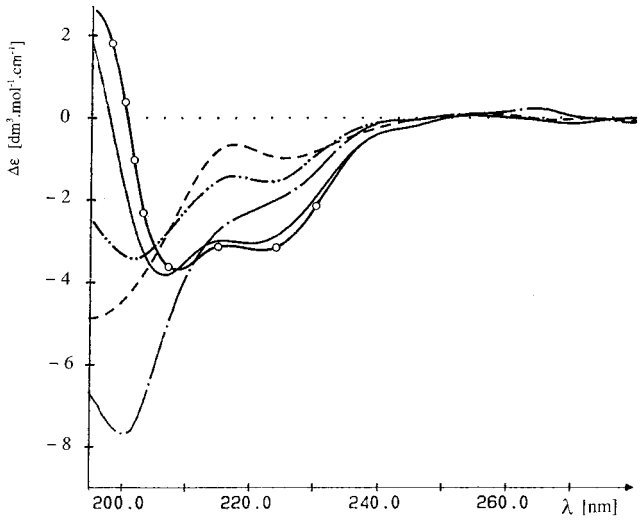


Figure 2. CD spectra of branched polypeptides at pH 7.3 in PBS: S$_i$K (—), SAK (- - -), ASK (-·-·), SK (-··-··), and LSK (○).

A total of 115 mg (0.25 mmol) of SK was dissolved in 1 mL of deionized water, and then the solution was diluted with 5 mL of DMF. One and the half equivalent amount of *Z*-Leu-OPcp (193 mg; 0.375 mmol) or *Z*-Glu-(OBzl)-OPcp (233 mg; 0.375 mmol) dissolved in 3 mL of DMF was added to the polymer solution. Equivalent amount of HOBt (61 mg, 20% water content) calculated according to the active ester derivatives was added in 1 mL of DMF to the reaction mixture. Finally, the pH of the solutions was adjusted to 7.5−8.0 with *N*-methylmorpholine. The mixture was stirred at RT for overnight, then the solvent was removed by evaporation. The remaining oil was solidified with ether, and the precipitate was washed several times with 10% DCM/ether, respectively. The dried product was suspended in 2 mL of abs. acetic acid and was treated with 20 mL of 35% HBr/acetic acid for overnight at 4 °C. The deprotected polymer samples were precipitated by addition of dry ether. The products were worked up as described above in case of SK polymer.

Amino Acid Analysis. The amino acid composition of polypeptides was investigated by amino acid analysis using a Beckman (Fullerton, CA) model 6300 amino acid analyzer. Prior to analysis, samples were hydrolyzed in 6 M HCl in sealed and evacuated tubes at 110 °C for 24 h.

Circular Dichroism Spectroscopy. Circular dichroism (CD) was measured with a Jobin-Yvon Mark VI dichrograph (Jobin-Yvon, Longjumean, France). CD spectra from 195 to 260 nm were recorded in a quartz cell with optical path of 0.02 cm at room temperature under constant nitrogen flush. The dichrograph was calibrated with D-(−)-pantoyllactone at 220 nm (*25*). CD spectra were recorded in PBS solution at pH 7.3, the concentrations of solutions being about 0.5 mg/mL (Figure 2.). The data of CD in the figure are expressed in terms of $\Delta\epsilon$, calculated for one Lys residue in the polypeptide backbone carrying an average side chain. The interpretation of CD spectra was based on the CD curves of polylysine (*26*), from which the branched polypeptides have been derived. The CD spectrum characterized by negative maxima at 208 and 221 nm of about the same intensity were considered helical, while the unordered structure is indicated with a strong negative maximum at 199 nm,

a weak negative maximum at 234 nm, and a weak positive maximum at 218 nm (*7*).

In Vitro Cytotoxicity Assays. In vitro toxicity was evaluated by measuring the viability of isolated rat liver (method A) or mouse spleen (method B) cells after incubation with various amount of polypeptides.

Method A. Isolated rat liver cells were prepared by the collagenase perfusion method of Seglen (*27*). Cells were incubated with varying amounts of polymers in rapidly shaking centrifuge tubes in suspension buffer (*28*) for 1 h at 37 °C. Controls were incubated with buffer alone. Viability of liver cells was measured by the trypan blue exclusion test. Three parallel samples were incubated for each polymer at each concentration, and 200−300 cells were counted for staining with trypan blue. Percentage viability was calculated from the mean of the three measurements (*28*).

Method B. Spleen cells were prepared from spleens of six 10−11 week old 22−24 g female BDF1 mice and resuspended in RPMI medium (*28*). Cells were taken at 3 mL (6×10^7 cells/mL) and incubated at 37 °C for 1 or 4 h. Polypeptides dissolved in PBS were diluted with RPMI. Each dilution was added in 100 μL to triplicate culture tubes, the concentration stated in the Results being the final concentration in the test tube. Control culture tubes were treated with 100 μL of RPMI alone. Viability of spleen cells was measured by the trypan blue exclusion test. Three parallel experiments were carried out with each polypeptide at each concentration. Percentage viability was calculated from the mean of the three measurements. Values for cell samples are given as percentage of mean of control samples incubated without any compound.

Cytostatic Assay. In vitro cytostatic properties were evaluated by measuring the viability of mouse colorectal carcinoma C26 cells after incubation with various amount of polypeptides. C26 cells were grown in tissue culture flasks at 37 °C in a humidified atmosphere in DMEM: Ham F12 medium and supplemented with 10% (v/v) heat inactivated foetal bovine serum (Biological Industries, Israel). Routine test showed the cells to be free of Mycoplasma.

C26 cells in logarithmic growth were trypsinized, resuspended in medium, and adjusted to a concentration of 1.5×10^4 cell/mL. A total of 200 μL of cell suspension was plated in a 96-well-flat-bottom tissue culture grade microtiter plates (Costar, Cambridge MA) and incubated at 37 °C for 24 h. A total of 100 μL of polymer solutions in serum-free medium at different concentrations was added in quadruplicate. After incubation at 37 °C for 3 h, medium was removed by aspiration, the cells were washed twice, and 200 μL of fresh complete medium containing FCS was added. Incubation for an additional 72 h was followed by the viability measurements using MTT assay (*29*). The absorbance was measured at $\lambda =$ 540 nm using a microplate reader (Titertek Multiskan). Absorbance of treated wells was compared to the control wells corresponding to the metabolically active cells. Cytostasis was calculated as a measure of growth inhibition, expressed as percentage of controls and calculated by the formula (100 − absorbance of treated wells) x 100/ absorbance of control wells.

Labeling with ^{125}I. ^{125}I labeling of polypeptides was carried out with *N*-succinimidyl 3-(4-hydroxy-phenyl)-propionate prelabeled with ^{125}I (Amersham International plc, Amersham, U.K.) as described before (*3*). The labeled polypeptides were purified of unreacted [^{125}I]sodium iodide by passage through Sephadex G-25, elution being in PBS at pH 7.2, using prepacked PD-10 columns (Pharmacia, Milton Keynes, U.K.). Electrophoresis on native polyacrylamide gel with a continuous 8 to 25% gradient was applied to assess the low molecular weight labeled product content of the preparation. The labeling efficacy was 35−40%. Specific activities of the final products were ∼2 MBq/mg.

Blood Clearance and Biodistribution Studies. All in vivo studies were carried out in adult (∼20 g) female BALB/c mice (Biomedical Services Unit, University of Nottingham) with appropriate licenses from the U.K. Home Office and with due consideration for animal welfare. Groups of mice ($n = 4$) were injected intravenously via a tail vein 5−10 mg of labeled polypeptides in 0.2 mL of PBS. Serial blood samples (10 mL) were taken from the tail tip at 1, 10, and 30 min and at 1, 2, and 3 h after injection directly into microcapillary pipets (Drummond Microcaps, Drummond Scientific Co., Broomhall, PA).

Blood clearance curves were constructed of the percent of the total initially injected count rates in the total blood volumes against time. The total intravascular blood volumes were calculated assuming the blood volume of the mice (in milliliters) to be 11.2% of the body weight (in grams). Areas under curves (AUC), as percent dose per hour, were calculated using the trapezoidal rule. At 4 h after injection, mice were killed, and weighed samples of blood, visceral organs, and residual carcass were assayed for radioactivity. Earlier comparative studies with ^{125}I, ^{111}In, and ^{51}Cr labeled branched polypeptides showed no significant differences in radioactivity in tissue samples (*31*). On the basis of these data, we assumed that ^{125}I-labeled marker is associated with the polypeptide during the study period. Results of the tissue-distribution analysis were expressed as a percentage of the total initially injected count rate recovered per gram of tissue.

Immunization. C57/Bl/6 (H-2^b, Igh-1^b), CBA (H-2^k, Igh-1^e), and BALB/c (H-2^d, Igh-1^a) mouse strains (LATI, Gödöllö, Hungary) were used for immunization. One experimental group consisted of six 10−12-week old male mice. Twenty micrograms of synthetic polypeptide dissolved in sterile saline (50 μL, 2 mg/mL) was emulsified in complete Freund's adjuvant (1:1, v/v) and injected sc into the backpaws and also ip. Serum samples were taken 7 and 14 days after antigen administration and titrated for IgM and IgG type antibodies and for IgG subclasses. Four weeks later the primed mice were boosted with the same amount of antigen emulsified in incomplete Freund's adjuvant (1:1, v/v) and administered as before. Serum samples were collected 20 days after the injection. A third challenge was given ip in PBS on day 55, and blood samples were taken 14 days after antigen administration.

Measurements of Antibody Titers by Solid-Phase Indirect Enzyme Immunoassay. Detection of the antigen-specific serum antibodies was performed by solid-phase indirect enzyme immunoassay using antigen-coated plates as described previously (*9*). SAK or ASK were coated on the surface of PVC plates (Propilén, Pécs, Hungary) at 5 μg/mL. After the washing and blocking procedures, various dilutions of the immune sera of mice were added. The bound antibodies were detected by horseradish-peroxidase-labeled anti-mouse IgM or IgG antibodies (Sigma, St. Louis, MO). Antibody titers were characterized by serum dilution corresponding to a fixed OD value (∼30%) chosen from the linear phase of the binding curve. For specificity studies, SAK or ASK were coated to the surface of the plates at graded concentrations (0.1−10 μg/mL) and a pretitrated dilution of pooled sera were added. For titration of IgG subclasses antibody

binding was developed by biotin-labeled subclass specific antibodies (Southern Biotechnology Associates Inc., Birmingham, AL). Titers were calculated from four or five independent titrations and mean values ±SD were given. Results of separate experiments were compared on the basis of reference sera used in all tests.

Immunomodulatory activity. Sheep red blood cells (SRBC) as immunogen were injected at 10^8 cell/0.2 mL of sterile saline ip into 10−12 week old mice. Control mice were injected with 0.2 mL of saline. The branched polypeptides and levamisole as potential immunomodulators were used at 0.2 and 1.0 mg/kg of body weight and were administered simultaneously with SRBC.

The hemolytic plaque-forming cell (PFC) assay, first described by Jerne and Nordin (*32*) and modified by Behling and Nowotny (*33*), was applied for the assessment of immunomodulatory ability of polypeptides. Spleens from each treatment group of five mice were obtained 4 days after immunization with SRBC and pooled. The washed spleen cells were resuspended in TC-199 medium, filtered, and adjusted to concentrations of 1:10 and 1:100 (v/v) for plating. Two milliliters of a 0.7% Noble agar solution, containing 0.1 mL of 1% DEAE dextran, 0.1 mL of a 10% suspension of freshly washed SRBC, and 0.1 mL of any of the various spleen cell concentrates were carefully mixed at 45 °C and layered on plates covered with 4 mL of 1.4% solidified but prewarmed agar. The plates were incubated for 60 min at 37 °C, and 2.5 mL of guinea pig complement diluted with 1:10 (v/v) balanced salt solution was added. The plates were incubated for an additional 30 min. Hemolyzed plaques in the agar were counted in triplicate and analyzed blind.

RESULTS AND DISCUSSION

In the present study, the development of a new series of branched polypeptides, which contain hydroxyl groups in their side chains, is reported. Ser was attached by HOBt-catalyzed active ester method to the N-terminals of oligo(DL-Ala) chains grafted to a polylysine backbone resulted poly[Lys(Ser_i-DL-Ala_m)] (SAK). Ser was coupled also directly to the ϵ-amino groups of polylysine followed by polymerization of DL-Ala NCA resulting oligo(DL-Ala) chain terminals. In this way, a reverse sequence was built up in the side chains corresponding to the poly[Lys(DL-Ala_m Ser_i)] (ASK). The number of hydroxyl groups in the polymer was increased by oligo(DL-Ser) branches instead of oligo(DL-Ala) ones [poly[Lys-(DL- Ser_m)] (SK)] (Figure 1).

Solution Conformation. Classification of solution conformations as an important property of branched polypeptides was carried out by CD spectroscopy. The CD curves of S_iK, SK, SAK, ASK, and LSK in PBS at pH 7.3 are shown in Figure 2. In the 190−250 nm wavelength region, the circular dichroic spectra, originated from the optical activity of amide bonds, indicate the formation of a helical secondary structure for S_iK and LSK, but only partially ordered conformation for SAK, ASK, and SK (Figure 2). It should be noted that the CD spectrum of polypeptide AK corresponds to a disordered conformation (*35*).

The incorporation of hydroxyl groups in side chains of branched polypeptides resulted in slightly more ordered conformation than observed with oligo(DL-Ala) side chains. In line with the hydrophilic character of the Ser residue(s), the aggregation of polymers was not detectable neither in solution nor after storage in solid state. Branched polypeptides with a number of hydroxyl groups described in this paper represent a new class of polycationic biodegradable polymers (*36*) with significantly increased water solubility. Polycationic polypeptide, LSK, assumed essentially ordered (helical) secondary structure (Figure 2).

Effect of Polypeptides on the Viability of Isolated Liver and Spleen Cells. In vitro cytotoxicity against isolated rat liver and mouse spleen cells was investigated and compared with data obtained earlier using the same cellular assays (*28*). Polypeptides at various concentrations (1.5−50.0 μg/mL) were incubated with rat liver cells or with mouse spleen cells, and the percentage of cell viability was determined (Figure 3, panels A and B). As reported previously, poly(L-Lys) proved to be rather toxic to the liver cells in the above concentration range (*28*). The present set of data indicate that the attachment of a single Ser residue to the ϵ-amino group of polylysine resulted in an essentially nontoxic polypeptide, S_iK. Cell toxicity of AK for spleen or liver cells was also reported earlier at $c = 50$ μg/mL concentration (*28*). In contrast, treatment with SK containing oligo(DL-Ser) instead of oligo(DL-Ala) did not reduce the viability of liver or spleen cells (Figure 3, panels A and B). ASK on spleen cells and LSK on liver cells were marginally toxic (5% decrease), while in case of other polypeptides, the number of viable liver or mouse cells even after 4 h incubation period was almost identical to the controls.

Effect on Growth of C26 Cells. Estimation of cytotoxicity was extended to the evaluation of the growth of C26 mouse colorectal carcinoma cells in the presence of various amounts of polycationic polymers. Cytostatic effect of polymers was determined by MTT assay (*29*). Results are demonstrated in Figure 3C. As described previously, poly[L-Lys] was shown to retard the growth of various tumor cells (*9*, *34*). The treatment of C26 cells with poly[L-Lys] resulted in a similar effect. Elongation at the ϵ-amino groups by oligo(DL-Ala) branches in AK reduced the cytostatic effect by more then 1 order of magnitude. Similar effect was observed with ASK. Interestingly, S_iK the backbone of ASK exhibit greatly reduced cytostatic effect as compared to poly[L-Lys], but the extension of Ser with oligo(DL-Ala) resulted in an elevated growth (Figure 3C). In contrast to ASK, much diminished cytostatic effect could be demonstrated with polypeptide SAK containing one Ser residue attached to oligo(DL-Ala) side chains. Poly[Lys(DL-Ser_m)], comprising only oligo(DL-Ser) branches exhibited no cytostatic effect in the concentration range studied.

Our data summarized in Figure 3 clearly suggest that there is a correlation between the number and location of Ser residues and cell killing activity of branched polypeptides. The incorporation of hydroxyl amino acid(s) could reduce markedly the in vitro cytotoxic effect of polycationic polypeptides.

Biodistribution of Polymeric Polypeptides. ^{125}I-labeled polypeptides were prepared by introduction of *N*-succinimidyl 3-(4-hydroxyphenyl)propionate containing ^{125}I onto the α-amino groups of the side-chain terminals as described before (*30*). The blood clearance profile and tissue distribution of polypeptides after iv administration are depicted in Figure 4 and Table 2. We found no significant difference in the area under the curve (AUC 0−4 h) for polypeptides prepared with either single Ser residue (S_iK) adjacent to the polylysine backbone or its oligo(DL-Ala) elongated version (ASK) (Figure 4A). Percentage of the total injected dose 4 h after injection was somewhat elevated for S_iK (38.3 ± 3.1% injected dose vs 27.8 ± 3.6% injected dose for ASK). Besides an increased kidney uptake of S_iK, the tissue distribution profiles of

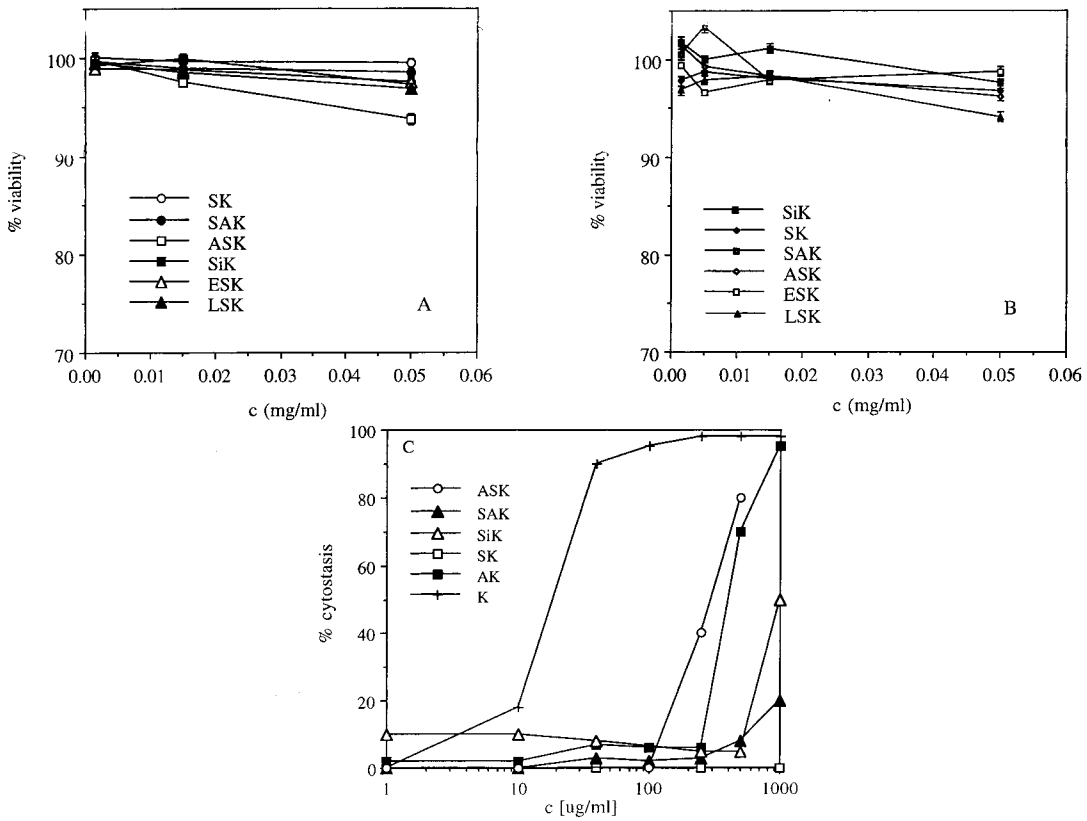


Figure 3. Effect of branched polypeptides on viability of isolated rat liver cells (A), of isolated mouse spleen cells (B) or on C26 carcinoma cell growth (C).

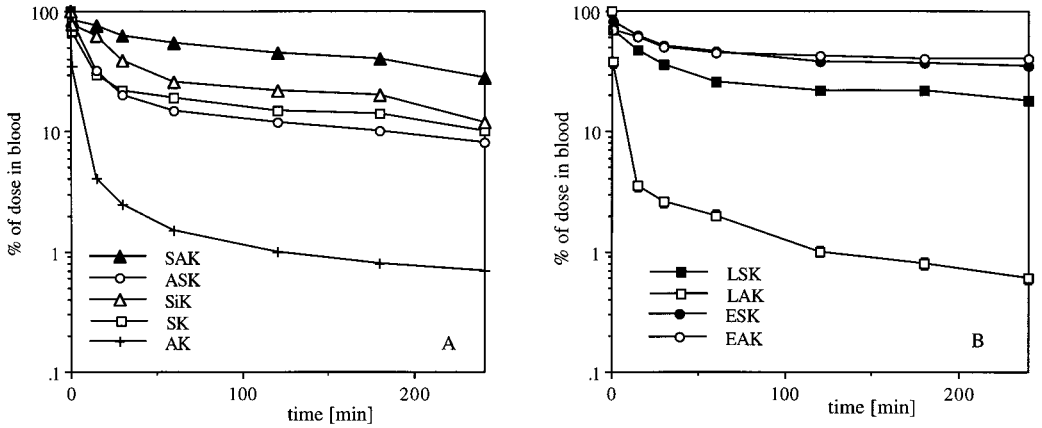


Figure 4. Blood clearance curves of ^{125}I labeled branched polypeptides. (A) S$_i$K, SK, AK, SAK, ASK; (B) LSK, LAK, ESK, EAK. Four mice/group. The areas under these time: activity curves are shown in Table 2.

Table 2. Biodistribution Data of Branched Polypeptides

code	AUC; 0−4 h (% dose h ± SD)	percent of the total injected dose at 4 h (% dose ± SD)	percent of the total injected dose (± SD)/gram of					
			blood	spleen	kidney	liver	lung	carcass
SAK	177.5 ± 7.6	32.9 ± 4.2	11.0 ± 0.8	1.8 ± 0.3	5.9 ± 0.9	2.3 ± 0.3	3.9 ± 0.4	1.4 ± 0.2
ASK	58.7 ± 6.3	34.6 ± 3.7	2.6 ± 0.1	3.1 ± 0.5	4.6 ± 0.5	8.7 ± 1.1	1.4 ± 0.3	0.9 ± 0.3
SK	97.1 ± 2.6	27.8 ± 3.6	3.7 ± 0.3	1.0 ± 0.2	3.2 ± 0.2	1.5 ± 0.1	3.0 ± 1.0	1.2 ± 0.1
S$_i$K	66.3 ± 4.0	38.3 ± 3.1	3.3 ± 0.3	2.7 ± 1.4	13.0 ± 1.9	9.3 ± 1.1	3.1 ± 1.2	0.9 ± 1.2
LSK	95.8 ± 1.6	47.7 ± 2.7	6.0 ± 0.3	5.7 ± 0.7	19.5 ± 1.5	14.5 ± 0.7	3.8 ± 0.4	1.0 ± 0.8
ESK	161.8 ± 3.0	41.4 ± 1.2	13.9 ± 0.7	4.0 ± 0.3	11.8 ± 0.7	11.5 ± 0.5	4.8 ± 0.3	1.2 ± 0.1

these polymers were similar (Table 2.), both compounds being taken up predominantly by kidney and liver. The presence of multiple Ser residues in the branches (SK) resulted in significantly increased blood survival (Figure 4A) with an AUC of 97.1% dose/h (Table 2). Interestingly, branched polypeptide with oligo(DL-Ala) branches (AK) in accord with earlier published data was cleared rapidly from circulation with an AUC of only 17.8% dose/h (*8*). Elongation of the side chains of AK by a single Ser residue led to a dramatic increase in blood survival (AUC of 177.5% dose/h). The major sites of retention of ^{125}I-labeled SAK at the 4 h dissection time were the kidney with about 6% of the injected dose/g and the lung with about 4% (Table 2).

As described earlier, the branched polypeptide containing Leu at the end of the oligo(DL-Ala) branches (LAK)

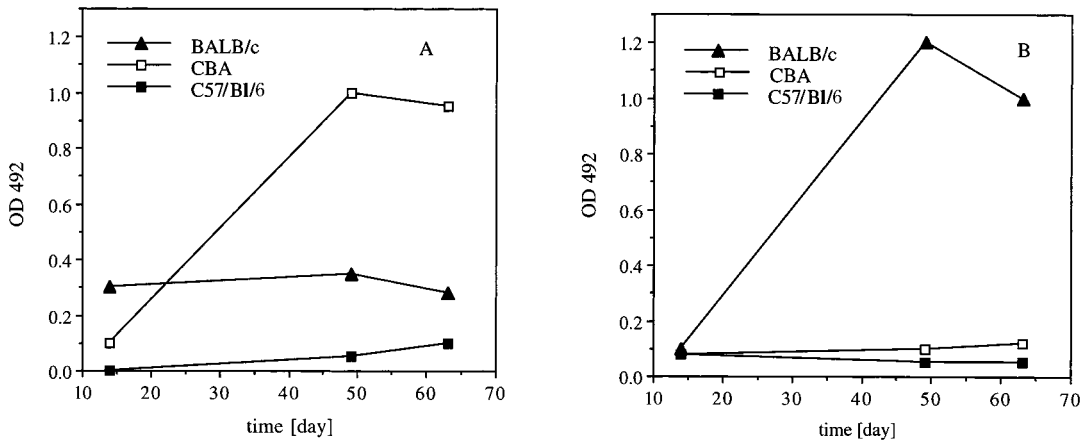


Figure 5. Magnitude of the IgG type memory antibody responses C57/BL/6, CBA and BALB/c mice to synthetic branched polypeptides SAK (A) or ASK (B).

Table 3. Antibody Responses Induced by Branched Polypeptides in Inbred Mouse Strains

	SAK			ASK		
strain	IgM	IgG (primary)	IgG (memory)	IgM	IgG (primary)	IgG (memory)
C57/Bl/6	457 ± 86[a]	111 ± 18	107 ± 4	247 ± 42	143 ± 6	125 ± 7
CBA	583 ± 47	2210 ± 459	>20 000	222 ± 47	147 ± 6	145 ± 10
BALB/c	667 ± 51	1122 ± 8	1459 ± 5	3119 ± 190	10 321 ± 1651	19 688 ± 2473

[a] Antibody titer ± SD. Pooled serum samples taken at different points of time were titrated using solid-phase indirect immunoassay as described in the Experimental Section. Mean values ± SD of three parallel titrations are given.

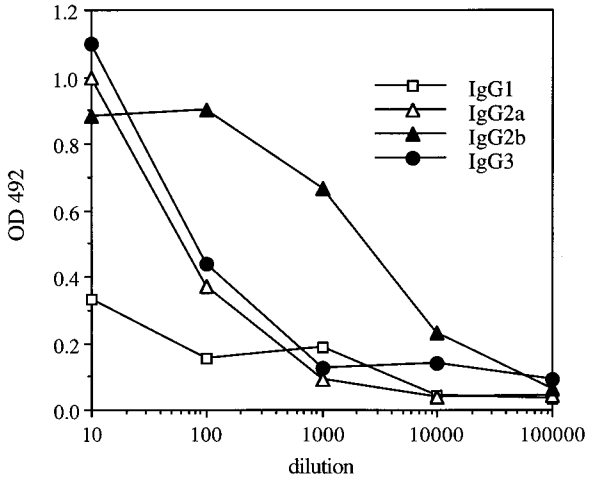


Figure 6. The distribution of different IgG subclasses during the memory antibody response of BALB/c mice immunized with ASK. The relative levels of specific antibody isotypes was determined as described in the Experimental Section.

was cleared rapidly from circulation (*8*). In contrast, LSK with oligo(DL-Ser) showed a longer blood survival (Figure 4B) with an AUC of 95.8% dose/h and the whole body retention was the highest value observed among polypeptides with Ser residue (47.7% dose/h) (Table 2). The blood clearance curve and AUC of amphoteric [^{125}I]EAK (*8*) was virtually identical to that of the labeled polypeptide ESK with oligo(DL-Ser) in the branches (Figure 4B, Table 2). It should be noted that the amphoteric ESK displayed greater blood survival than its polycationic counterpart LSK (Figure 4B). There was also a different pattern of tissue biodistribution, with reduced levels in the lung (3.8% for LSK vs 4.8% for ESK) but higher levels in spleen and liver (19.5% and 14.5% for LSK vs 11.8% and 11.5% for ESK) (Table 2.)

The results of this comparative study suggest that the survival of polycationic polypeptides is prolonged, and their tissue distribution is altered by the incorporation of Ser residue into the side chains. The substitution of Ala residues by Ser ones (AK vs SK, LAK vs LSK) elevated significantly the blood circulation time. Interestingly enough, the relative position of Ser in the branches influenced markedly the biodistribution of the polycationic polypeptides. The most favorable blood clearance profile and tissue distribution were obtained with SAK in which Ser is situated at the end of the side chain. For the evaluation of these findings, it should be borne in mind that this is the first branched polypeptide reported in the literature which is capable to circulate in the blood for an extended period of time despite its polycationic feature. This observation has to be taken in consideration for the design of future conjugates.

Immunoreactivity of branched polypeptides. The immunoreactivity of two representatives of polycationic Ser-containing polypeptides was characterized by their immunogenicity and immunomodulatory properties. In the first set of experiments SAK and ASK were used as immunogen and their capability of provoking antibody responses was investigated. In another assay we studied the effect of these polypeptides on sheep red blood cell (SRBC) antigen-induced immune responses.

Antibody Response. The immune response induced by the branched polypeptides was studied in three inbred mouse strains of different H-2 haplotype and Igh-1 allotype (*37*). The qualitative and quantitative features of the antibody response of polycationic polypeptides were characterized by IgM- and IgG-type antibody levels (Figure 5., Table 3), IgG isotype distribution (Figure 6), and fine specificity of antibodies (Figure 7) produced during the primary and memory response of BALB/c, CBA, and C57/Bl/6 mice.

The magnitude of the IgM and IgG type antibody response was measured at different points of time. As summarized in Table 3 and in Figure 5, SAK and ASK induced negligible level of IgM or IgG type antibodies in C57/Bl/6 mice even after the secondary antigen challenge. After repeated immunization of BALB/c mice with SAK or CBA mice with ASK, the antibody titers were rela-

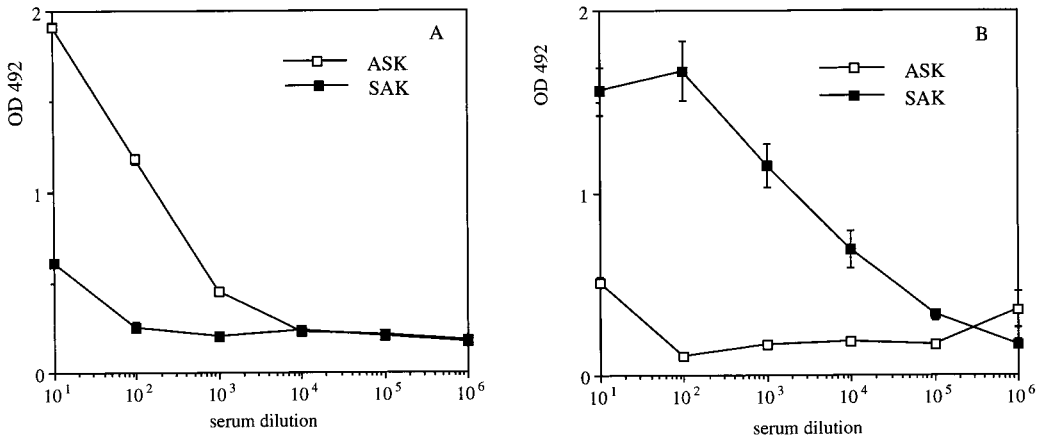


Figure 7. Cross reactivity pattern of antibodies induced by ASK in BALB/c mice (A) and by SAK in CBA mice (B). Mean antibody titers ±SD measured in the serum of immunized mice taken 14 days after antigen challenge on ASK- or SAK-coated plates.

tively low. Increased levels of IgG-type antibodies could be only detected after the third injection of ASK to BALB/c and of SAK to CBA mice (Figure 5). These findings indicate that the immunogenicity of branched polypeptides is highly dependent on the responsiveness of the inbred mouse strain (e.g., SAK is capable to elicit antibody response in CBA, but this compound is nonimmunogenic in C57/Bl/6 and poor immunogen in BALB/c) as well as on the amino acid sequence of the branches (e.g., SAK is not immunogenic, while ASK induced antibody response in BALB/c). The elevated level of ASK- and SAK-specific IgG isotypes in memory response of BALB/c and CBA mice of different MHC class II haplotypes (H-2^d vs H-2^k) point to a helper T-cell-dependent antibody response against these antigens (Figure 6).

Fine specificity of the polyclonal IgG type antibodies after hyperimmunization with ASK in BALB/c or with SAK in CBA was also studied (Figure 7). We found that the ASK-induced antibodies of BALB/c mice react with ASK but do not recognize SAK adsorbed to the solid phase (Figure 7A). Similarly, antibodies raised by SAK in CBA mice react with the immunizing antigen, but do not bind to ASK (Figure 7B). The recognition pattern of ASK- and SAK-specific antibodies demonstrate the lack of significant cross-reactivity between the two analogues, indicating that their antigenic determinants are different.

Immunomodulatory Effect. In a separate experiment the ability of SAK and ASK of modulating the ongoing immune response of BDF1 mice against sheep red blood cells (SRBC) was tested by the hemolytic direct PFC assay. On the basis of earlier data obtained from branched polypeptide studies in the same assay (*28*), the immunomodulatory activity of these polypeptides was studied at two concentrations (0.2 mg/kg and 1.0 mg/kg). The results are presented in Figure 8. Polypeptides administered in aqueous solution simultaneously with primary SRBC immunization have no pronounced effect on PFC levels expressed as adjuvant index. Small but concentration-independent enhancement could be detected in PFC formation after administration of ASK (AI $= 1.2 \pm 0.1$) Treatment with levamisol used as positive control increased PFC formation (AI $= 3.2 \pm 0.4$). These data indicated that the polypeptides had apparently no effect on the SRBC specific immune responses under the conditions studied.

CONCLUSION

For the construction of macromolecule−drug conjugates, it is important to provide rational basis for the selection of a proper carrier. With respect to the importance of the side-chain structure and charge of the branched polypeptides in various chemical and biological properties (*6*, *7*), we have studied the conformation, the immunoreactivity, the biodistribution, and in vitro cytotoxicity of a new set of branched polypeptides containing Ser residue. We found that the water solubility of these polycationic compounds with single or multiple OH group(s) was higher than of those containing only amino groups at the end of the branches.

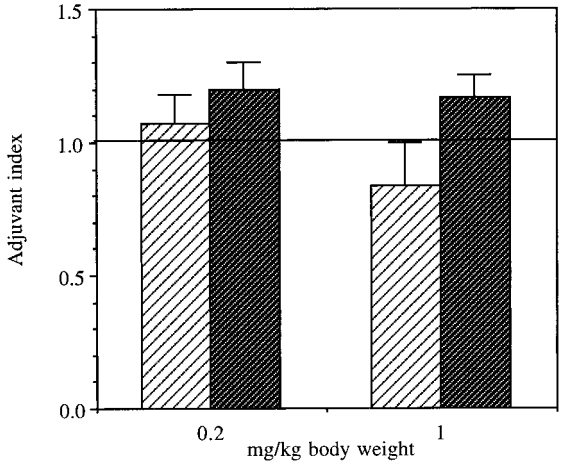


Figure 8. Dose-dependent effect of branched polypeptide ASK (dark bars) and SAK (light bars) on the PFC immune response to SRBC in BDF1 mice. Polypeptides and SRBC were applied simultaneously, ip, in saline.

CD spectra of polypeptides showed significant differences correlating with the position and numbers of Ser residues in the side chains (*19*). Under physiological conditions, polycationic polypeptides assumed ordered (helical) secondary structure (S_iK and LSK) or partially unordered conformation (SK, SAK, and ASK). It should be noted that in case of Ala-containing polypeptides an expressed tendency could be demonstrated in the formation of more ordered structure as compared to the respective serine analogues (SK vs AK and LSK vs LAK) (*7*). Consequently, the incorporation of even a single Ser could have an effect on the solution conformation by promoting its transition toward unordered secondary structure. The data summarized in this report indicate that these new compounds under in vitro conditions are essentially nontoxic on rat liver or mouse spleen cells up to a concentration of 50 μg/mL.

The blood clearance, biodistribution, and immunogenicity of these derivatives were dependent on the position

and number of Ser residues in the branches. The polypeptides investigated were taken up predominantly by the liver and kidney (S_iK, LSK, and ASK) or kidney and lung (SK and SAK). The best survival in the blood was found with SAK, representing the first polycationic branched polypeptide which show extended blood clearance similar to various proteins or the amphotheric polypeptide EAK (*8*, *37*). The investigation of the immunostimulatory capacity of the new analogues indicate that these compounds have no effect on to the SRBC specific humoral immune response in the dose interval investigated.

In contrast to the high pK_a value of the ϵ-NH_2 groups of polylysine, branched polypeptides, including compounds described in this paper, possess α-NH_2 groups with lower pK_a. The introduction of Ser residue(s) does not change the number of amino functional group in the polypeptides; therefore, the reduced cytotoxicity and prolonged blood circulation observed could mainly be attributed to the presence of OH groups, which might iniciate a further acidic shift in the pK_a of the free α-NH_2 groups positioned at the end of the branches.

In conclusion, these studies have indicated that synthetic branched polypeptides with Ser can be considered as potential candidates for constructing suitable conjugates for drug/epitope delivery. It is not only due to the presence of hydroxyl functional group to be used for oxime chemistry, but also to their beneficial biological features. Data summarized here indicate that the incorporation a single Ser residue preferably at the N-terminal position of the side chain provide optimal biological properties. No additional improvements were observed in case of polypeptides possessing oligo(DL-Ser) branches. These polypeptides are essentially nontoxic, nonimmunomodulatory under conditions studied and can be present in the circulation for a much longer period of time than previously described polycationic polymers.

ACKNOWLEDGMENT

These studies were supported by grants from the Hungarian Research Fund, (OTKA T 014964), from the Ministry of Health (ETT 115/1996), from PECO-COST SPIDER program (CIPA 4031), and from the Association for International Cancer Research (UK). M.V.P. is supported by the Cancer Research Campaign, London, UK.

LITERATURE CITED

(1) Duncan, R. (1992) Drug-polymer conjugates; potential for improved chemotherepy. *Anti-Cancer Drugs 3*, 153−156.

(2) Maeda, H., Seymour, L. W., and Miyamoto, Y. (1992) Conjugates of anticancer agents and polymers: advantages of macromolecular therapeutics in vivo. *Bioconjugate Chem. 3*, 351−362.

(3) Takakura, Y., and Hashida, M. (1995) Macromolecular drug carrier systems in cancer chemotherapy: macromolecular prodrugs. *Crit. Rev. Oncol./Haematol. 18*, 207−231.

(4) Del Giudice, G. (1992) New carriers and adjuvants in the development of vaccines. *Curr. Opin. Immunol. 4*, 454−459.

(5) Hudecz, F., and Tóth, G. K. (1994) Synthetic peptide constructs to increase the immunogenicity of B-cell epitopes. In *Synthetic peptides in the search for B-and T-cell epitopes* (E. Rajnavölgyi, Ed.) pp 97−119, R. G. Landes Company, Austin.

(6) Hudecz, F., Votavova, H., Gaál, D., Sponar, J., Kajtár, J., Blaha, K., and Szekerke, M. (1985) Branched polypeptides with a poly(L-lysine) backbone: synthesis, conformation and immunomodulation. In *Polymeric Materials in Medication* (Ch. G. Gebelein and Ch. E. Carraher, Eds.) pp 265−289, Plenum Press, New York.

(7) Hudecz, F. (1995) Design of synthetic branched-chain polypeptides as carriers for bioactive molecules. *Anti-Cancer Drugs 6*, 171−193.

(8) Clegg, J. A., Hudecz, F., Mező, G., Pimm, M. V., Szekerke, M., and Baldwin, R. W. (1990) Carrier design: biodistribution of branched polypeptides with poly-(L-lysine) backbone. *Bioconjugate Chem. 2*, 425−430.

(9) Hudecz, F., Gaál, D., Kurucz, I., Lányi, S., Kovács, A. L., Mező, G., Rajnavölgyi, É., and Szekerke, M. (1992) Carrier design: cytotoxicity and immunogenicity of synthetic branched polypeptides with poly(L-lysine) backbone. *J. Controlled Release 19*, 231−243.

(10) Hudecz, F., Hilbert, Á., Mező, G., Kajtár, J., and Rajnavölgyi, É. (1994) B-cell epitopes in Herpes simplex Virus- (HSV-1) glycoprotein D (gD). In *Synthetic peptides in the search for B-and T-cell epitopes* (É. Rajnavölgyi, Ed.) pp 157−169, R. G. Landes Company, Austin.

(11) Hudecz, F., and Price, M. R. (1992) Monoclonal antibody binding to peptide epitopes conjugated to synthetic branched polypeptide carriers. Influence of the carrier upon antibody recognition. *J. Immunol. Methods 147*, 201−210.

(12) Wilkinson, K. A., Vordermeier, M. H., Wilkinson, R., Iványi, J., and Hudecz, F. (1998) Synthesis and in vitro T cell immunogenicity of conjugates with dual specificities: attachment of epitope peptides of 16 kDa and 38 kDa proteins from M.tuberculosis to branched polypeptide. *Bioconjugate Chem. 9*, 539−547.

(13) Hudecz, F., Clegg, J. A., Kajtár, J., Embleton, M. J., Szekerke, M., and Baldwin, R. W. (1992) Synthesis, conformation, biodistribution and in vitro cytotoxicity of daunomycin-branched polypeptide conjugates. *Bioconjugate Chem. 3*, 49−57.

(14) Gaál, D., and Hudecz, F. (1998) Low toxicity and high antitumour activity of daunomycin by conjugation to immunpotential amphoteric branched polypeptide. *Eur. J. Cancer 34*, 155−161.

(15) Vincze, B., Pályi, I., Daubner, D., Kálnay, A., Mező, G., Hudecz, F., Szekerke, M., Teplán, I., and Mező, I. (1994) Antitumor effect of a GnRH antagonist and its conjugate on human breast cancer cells and their xenografts. *J. Cancer Res. Clin. Oncol. 120*, 578−584.

(16) Mező, G., Mező, I., Seprődi, A., Teplán, I., Kovács, M., Vincze, B., Pályi, I., Kajtár, J., Szekerke, M., and Hudecz, F. (1996) Synthesis, conformation, biodistribution and hormon related in vitro antitumor effect of a GnRH antagonist-branched polypeptide conjugate. *Bioconjugate Chem. 7*, 642−650.

(17) Hershfield, M. S., and Mitchell, B. S. (1995) In *The Metabolic and Molecular bases of Inherited Disease* (C. R. Scriver, A. L. Beaduet, W. S. Sly, and D. Valle, Eds.) pp 1725−1768, McGraw-Hill, New York.

(18) Nucci, M. L., Shorr, R., and Abuchowski, A. (1991) The therapeutic values of poly(ethylene glycol)-modified proteins. *Adv. Drug Deliv. Rev. 6*, 133−151.

(19) Mező, G., Kajtár, J., Nagy, I., Majer, Zs., Szekerke, M., and Hudecz, F. (1997) Carrier design: Synthesis and conformational studies of poly[L-lysine] based branched polypeptides with hydroxyl groups. *Biopolymers 42*, 719−730.

(20) Rose, K. (1994) Facile synthesis of homogeneous artificial proteins. *J. Am. Chem. Soc. 116*, 30−33.

(21) Tuchscherer, G. (1993) Template assembled synthetic proteins. *Tetrahedron Lett. 34*, 8419−8430.

(22) IUPAC-IUB Commission on Biochemical Nomenclature (1972) *Biochem. J. 127*, 753−756.

(23) IUPAC-IUB Commission on Biochemical Nomenclature (1984) *Eur. J. Biochem. 138*, 9−37.

(24) Hudecz, F., Kovács, P., Kutassi-Kovács, S., and Kajtár, J. (1984) GPC, CD and sedimentation analysis of poly-Lys and branched chain poly-Lys-poly-DL-Ala polypeptides. *Colloid Polymer Sci. 262*, 208−212.

(25) Schippers, P. H., and Dekkers, H. P. J. (1981) Direct determination of absolute circular dichroism data and calibration of commercial instruments. *Anal. Chem. 53*, 778−782.

(26) Greenfield, N., and Fasman, G. D. (1969) Computed circular dichroism spectra for the evaluation of protein conformation. *Biochemistry 8*, 4108−4116.
(27) Seglen, P. O. (1976) Preparation of isolated rat liver cells. *Methods Cell Biol. 13*, 29−33.
(28) Gaál, D., Hudecz, F., Kovács, A. L., and Szekerke, M. (1986) Immunomodulatory effect of synthetic branched polypeptides. II. *J. Biol. Response Modif. 5*, 148−159.
(29) Scudiero, D. A., Shoemaker, R. H., and Paull, K. D., et al. (1988) Evaluation of a soluble tetrazolium/formazan assay for cell growth and drug sensitivity in culture using human and other tumor cell lines. *Cancer Res. 48*, 4827−4833.
(30) Pimm, M. V., Gribben, S. J., Mező, G., and Hudecz, F. (1995) Strategies for labeling branched polypeptides with a poly(L-lysine) backbone with radioiodines (^{123}I, ^{125}I, ^{131}I) and radiometals (^{111}In, ^{51}Cr) for biodistribution studies and radiopharmaceutical development. *J. Labelled Compd. Radiopharm. 36*, 157−172.
(31) Pimm, M. V., Gribben, S. J., Bogdán, K., and Hudecz, F. (1995) The effect of charge on the biodistribution in mice of branched polypeptides with poly(L-lysine) backbone labeled with ^{125}I, ^{111}In or ^{51}Cr in mice. *J. Controlled Release 37*, 161−172.
(32) Jerne, N. K., and Nordin, A. A. (1963) Plaque formation in agar by single anti-body-producing cells. *Science 140*, 405−409.
(33) Behling, U. H., and Nowotny, A. (1978) Long-term adjuvant effect of bacterial endotoxin in prevention and restoration of radiation-caused immunosuppression. *Proc. Soc. Exp. Biol. Med. 157*, 348−353.
(34) Arnold, L. J., Gutheil, I., and Kaplan, N. O. (1979) Antineoplastic activity of poly(l-lysine) with some ascites tumor cells. *Proc. Natl. Acad. Sci U.S.A. 76*, 3246−3250.
(35) Votavova, H., Hudecz, F., Kajtár, J., Szekerke, M., Sponar, J., and Blaha, K. (1980) Conformation of branched polypeptides based on poly(L-lysine): circular dichroism study. *Collect. Czech. Chem. Commun. 45*, 941−949.
(36) Hudecz, F., Kutassi-Kovács, S., Mező, G., and Szekerke, M. (1989) Biodegradability of synthetic branched polypeptide with poly(L-lysine) backbone. *Biol. Chem. Hoppe-Seyler 370*, 1019−1026.
(37) Rajnavölgyi, É., Hudecz, F., Mező, G., Szekerke, M., and Gergely, J. (1986). Isotype distribution and fine specificity of the antibody response of inbred mouse strains to four compounds belonging to a new group of synthetic branched polypeptides. *Mol. Immunol. 23*, 27−37.

BC990015Q

Use of Dithiodiglycolic Acid as a Tether for Cationic Lipids Decreases the Cytotoxicity and Increases Transgene Expression of Plasmid DNA in Vitro

Fuxing Tang and Jeffrey A. Hughes*

Department of Pharmaceutics, College of Pharmacy, University of Florida, P.O. Box 100494, Gainesville, Florida 32610. Received February 12, 1999; Revised Manuscript Received May 16, 1999

Two major barriers that limit cationic lipids in gene delivery are low transfection efficiency and toxicity. In the present studies, we used dithiodiglycolic acid as a new tether for the polar and hydrophobic domains of a cationic lipid, cholesteryl hemidithiodiglycolyl tris(aminoethyl)amine (CHDTAEA). We compared the transfection activity and toxicity of CHDTAEA with its nondisulfide analogue and cholesteryl *N*-(dimethylaminoethyl) carbamate (DC-Chol). The liposomes of CHDTAEA had more than 2 orders of magnitude greater transfection activity than DC-Chol in CHO cells and 7 times greater transfection activity in SKnSH cells. CHDTAEA also demonstrated much less toxicity than the other two lipids. Dithiodiglycolic acid may act as an excellent linker in the application of cationic lipid syntheses.

INTRODUCTION

Cationic lipids are popular nonviral gene transfer vectors (Felgner et al., 1995; Gao and Huang, 1995; Rolland, 1998). However, two major barriers for cationic lipid-mediated gene transfer limit the application of cationic lipids. First, the low transfection efficiency compared to the virus system, and second, the toxicity. Since Felgner et al. first reported application of *N*-[1-(2,3-dioleyloxy)propyl]-*N*,*N*,*N*-trimethylammonium chloride (DOTMA) in transfection of plasmid DNA in 1987 (Felgner et al., 1987), many cationic lipids have been synthesized and used in plasmid DNA delivery (Gao and Huang, 1995; Lee and Huang, 1997; Rolland, 1998). Most of these efforts have been focusing on improving the transfection activity and decreasing the cytotoxicity. The uses of ester, amide, and carbamate linkages to tether polar and hydrophobic domains are common strategies to lower the toxicity. However, no intracellular degradation studies have been conducted for any cationic transfection lipid (Aberle et al., 1998). 3-β-[*N*-(*N*′,*N*′-dimethyl amino ethane) carbamoyl] cholesterol (DC-Chol)[1] was the first lipid used in clinical trials because of its combined properties of transfection efficiency, stability, and low toxicity (Gao and Huang, 1995). Recently, Nantz et al. reported a novel tetraester construct that reduced the cationic lipid-associated cytotoxicity compared to DC-Chol (Aberle et al., 1998). However, the introduction of the ester bond may also decrease the stability of liposome in systemic circulation when the liposomes are used in clinical trials. We proposed a strategy of taking advantage of the high intracellular reductive environment to make a disulfide linker-containing cationic lipid, which is stable outside cells whereas it can be reduced in cells by intracellular reductive substance (Tang and Hughes, 1998). The reduction of the disulfide bond will enhance the release of DNA from DNA−liposomes complexes. Dissociation of DNA from DNA−liposomes complexes is one of the major barriers for cationic liposome-mediated gene transfection (Escriou et al., 1998; Rolland, 1998; Zabner et al., 1995). Previously, we reported that a disulfide lipid—1′,2′-dioleoyl-*sn*-glycero-3′-succinyl-2-hydroxyetheyl disulfide ornithine conjugate (DOGSDSO)—could increase the plasmid gene transfection compared to its nondisulfide cationic lipid. However, the toxicity of the lipid was not significantly altered by the addition of disulfide bond (Tang and Hughes, 1998). We demonstrated that dithiothreitol (DTT) could reduce the part of disulfide cationic lipid and help to release part of DNA from DNA−liposomes complexes. However, DTT is not a cellular substance. When we tried to use a cellular reductive substance (e.g., glutathione) in the same experiment, no DNA was released. DTT is a stronger reductive reagent than glutathione since it forms a stable six member ring product (Hermanson, 1996). We hypothesized that the disulfide linker in DOGSDSO might be too strong so that it could not be degraded fast enough to significantly decrease the cytotoxicity. Since the disulfide bond of dithiodiglycolic acid is weakened by the strong electric withdrawing effects of two carboxyl groups which are symmetrically connected to the two α-carbons of disulfide bond (Figure 1), we hypothesized that introduction of dithiodiglycolic acid to tether the polar group and lipophilic domains will increase the transfection activity and decrease the toxicity of cationic lipid. Also the favorable results obtained with DC-Chol in vivo demonstrated that cholesterol is a suitable backbone as a starting reagent for cationic lipids. We synthesized cholesteryl hemidithiodiglycolyl tris(aminoethyl)amine (CHDTAEA) with a dithiodiglycolyl linker, its nondisulfide analogue cholesteryl hemisuccinyl tris(aminoethyl)-amine (CHSTAEA). We compared their transfection activities and cytotoxicity of CHDTAEA, CHSTAEA, and DC-Chol in mammalian cells. The results demonstrated

* To whom correspondence should be addressed. E-mail: hughes@cop.ufl.edu. Fax: 352-392-4447. Phone: 352-846-2725.

[1] Abbreviation: CHDTAEA, cholesteryl hemidithiodiglycolyl tris(aminoethyl)amine; CHSTAEA, cholesteryl hemisuccinyl tris(aminoethyl)amine; DC-Chol, cholesteryl *N*-(dimethylaminoethyl)carbamate; DOPE, L-dioleoyl phosphatidylethanolamine; DTT, dithiothreitol; Calcein-AM, acetoxymethyl ester of calcein; RLU, relative light unit.

10.1021/bc990016i CCC: $18.00 © 1999 American Chemical Society
Published on Web 07/30/1999

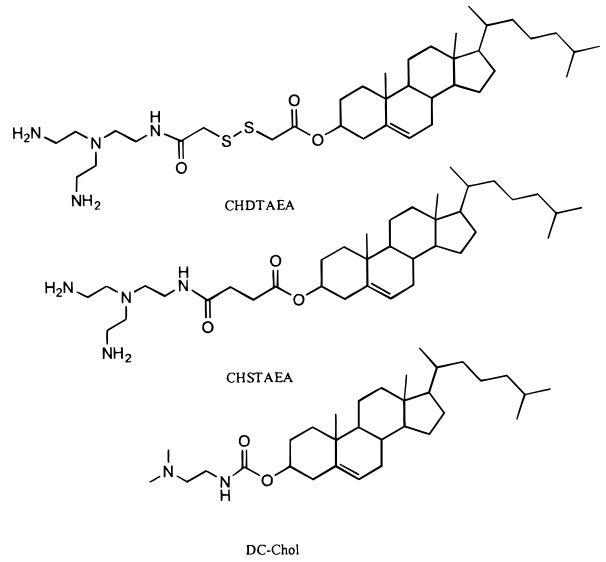


Figure 1. Structures of cholesteryl *N*-(dimethylaminoethyl)-carbamate (DC-Chol), cholesteryl hemidithiodiglycolyl tris-(aminoethyl)amine (CHDTAEA), and cholesteryl hemisuccinyl tris(aminoethyl)amine (CHSTAEA).

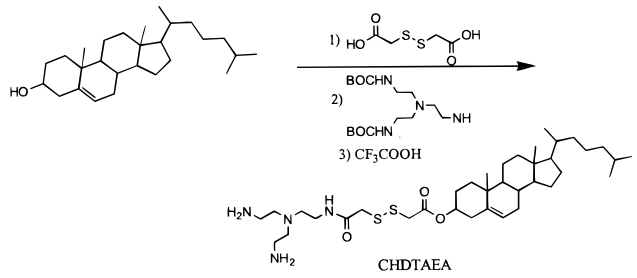


Figure 2. Scheme of synthesis of cholesteryl hemidithiodiglycolyl tris(aminoethyl)amine (CHDTAEA).

dithiodiglycolic acid as a linker in cationic lipid can greatly increase the transfection activity and decrease the toxicity of cationic lipids.

MATERIALS AND METHODS

Syntheses of CHDTAEA and CHSTAEA. CHDTAEA was synthesized as outlined in Figure 2. A total of 2.0 g (6 mmol) of cholesterol and 1.9 g of dithiodiglycolic acid (12 mmol) was dissolved in 30 mL of ethyl acetate under nitrogen. A total of 12 mmol of 1,3-dicyclohexylcarbodiimide (DCC), 0.19 g of 4-pyrrolidinopridine (1.2 mmol), and 1.43 mL of triethylamine (12 mmol) were added at 0 °C. The mixture was warmed to room temperature naturally and stirred under nitrogen at room temperature overnight. The reaction mixture was filtered and washed by 5% citric acid followed by brine three times. The organic layer was separated and dried over anhydrous sodium sulfate. The organic solvent was evaporated. The product cholesteryl hemidithiodiglycolate was purified on silica gel with a developer of hexane:ethyl acetate:acetic acid (30:10:1) (R_f = 0.3, 2.4 g, yield = 80%). *N*,*N*-BOC_2-tris (2-aminoethyl) amine was prepared by treating tris(2-aminoethyl)amine with 2 equiv of 2-(*tert*-butoxycarbonyloxyimino)-2-phenylacetonitrile (BOC-ON) in wet THF. A total of 0.30 g (0.5 mmol) of cholesteryl hemidithiodiglycolate, 0.24 g of *N*,*N*-BOC_2-tris(2-aminoethyl)amine (0.65 mmol), and 0.007 g of 4-pyrrolidinopridine (0.005 mmol) was dissolved in 20 mL of dichloromethane. A total of 0.6 mmol of DCC in dicholormethane and 0.06 mL of triethylamine was added dropwise at 0 °C. The mixture was stirred under nitrogen at room temperature overnight. The product *N*,*N*-BOC_2-[cholesteryl hemidithiodiglycolyl tris(aminoethyl)amine] was separated and purified on silica with a developer of dichlorometnae:methanol (10:1) (R_f = 0.35, 0.37 g, yield = 85%). The molecular weight was determined by a Micromass Quattro-LC-Z triple quadrupole mass spectrometer equipped with an atmospheric pressure chemical ionization (APCI) ion source (Beverly, MA). $M + H^+$= 881.5 (calculated, 881.3 for $C_{47}H_{82}N_4O_7S_2+H^+$). ^{1}H NMR ($CDCl_3$, 300 MHZ): 0.69 (s, CH_3), 0.830−2.04 [m, 3× (CH_3), 10× (CH_2), and 6× (CH)], 1.02 (s, CH_3), 1.42 [s, 2× $(CH_3)_3CO$], 2.38 [m, CH_2C═C], 2.52−2.68 [m, $(CH_2)_3N$], 3.28 [m, 2× (CH_2NCO)], 3.35 (m, CH_2NCO), 3.50 (s, CH_2-SS), 3.60 (s, CH_2SS), 4.68 (m, CHO), 4.99−5.32 (m, 3× NHCO), 5.38 (m, C═CH). BOC groups were detached (CF_3COOH, 0 °C, 15 min), and excessive trifluoroacetic acid was dried under high vacuum to produce CHDTAEA. This step is quantitative as reported by Behr (Behr et al., 1989). After the reaction, the purity was checked by TLC, and CHATAEA were used to prepare liposomes without further purification. Similar synthesis strategy was used to synthesize the nondisulfide analogue CHSTAEA (Figure 1) with slight modifications. Commercial available cholesteryl hemisuccinate was directly used to conjugate with *N*,*N*-BOC_2-tris (2-aminoethyl)amine to obtained the BOC protected CHSTAEA. $M + H^+$= 817.5 (calculated, 817.2 for $C_{47}H_{82}N_4O_7 + H^+$). ^{1}H NMR ($CDCl_3$, 300 MHZ): 0.69 (s, CH_3), 0.830−2.04 [m, 3× (CH_3), 10× (CH_2), and 6× (CH)], 1.02 (s, CH_3), 1.44 [s, 2× $(CH_3)_3$-CO], 2.30 (m, CH_2C═C), 2.48−2.70 [m, $(CH_2)_3N$], 3.15 [m, 2× (CH_2NCO)], 3.29 (m, CH_2NCO), 4.61 (m, CHO), 4.99−5.32 (m, 3× NHCO), 5.35 (m, C═CH). The same method was applied to detach the BOC group as mentioned above.

Liposome Preparation. CHDTAEA or CHSTAEA was dissolved in chloroform and mixed with a neutral helper lipid DOPE [1:1 molar ratio, which was optimized (data not shown)] (Felgner et al., 1994). DC-Chol was dissolved in chloroform and mixed with DOPE at the optimal molar ratio of 6:4 according to Gao and Huang (1991). The mixtures were evaporated to dryness in a round-bottomed flask using a rotary evaporator at room temperature. The lipid film was dried by nitrogen for a further 10 min to evaporate residual chloroform, and the lipid film was resuspended in sterile water to a concentration of 1 mg/mL based on the weight of cationic lipids. The resultant mixtures were shaken in a water bath at 30 °C for 30 min. The liposomes were hydrated at 4 °C overnight. The suspensions were sonicated using a Sonic Dismembrator (Fisher Scientific) for 2 min at 4 °C to form homogenized liposomes. The particle size distribution and ζ-potential of liposomes were measured using a NICOMP 380 ZLS instrument (Santa Babara, CA). The diameters were expressed by the volume-weight distribution parameter. The average diameters of CHDTAEA/DOPE, CHSTAEA/DOPE, and DC-Chol/DOPE were 121.7 ± 14.2, 154.7± 19.8, and 165.8± 19.9 nm, respectively. The ζ-potentials were +8.04, +7.68, and +6.98 mV, respectively. Liposomes were stored at 4 °C and used in 3 months.

Gel Electrophoretic Analysis of Release of DNA from DNA−Liposome Complexes by Glutathione. One microgram of plasmid DNA was dissolved in 10 μL of phosphate-buffered saline (PBS). Cationic liposomes CHATAEA/DOPE or CHSTAEA/DOPE were added to pDNA solution at the increasing weight ratios of 2/1, respectively. All calculations of the weight of liposomes in this paper were based on the weight of cationic lipids only. After the complexes were incubated for 30 min at

room temperature, 10 μL of 20 mM of glutathione in PBS (pH = 7.3) was added to the mixture to reach a final concentration of glutathione of 10 mM. The mixtures were incubated at 37 °C for 20 h. Released DNA was visualized by 1% agarose gel electrophoresis.

Cell Culture and Luciferase Gene Transfection. Chinese hamster ovary (CHO) and SKnSH cells were obtained from American Tissue Type Collection (Rockville, MD). The cells were maintained in RPMI 1640 or α-MEM media, respectively. All cells were kept in 5% CO_2 and at 37 °C in humidified air. Cells of same passage from same flask were cultured and seeded in three 24 well plates (2×10^5 cells/well) and grown to 60−80% confluence in 1 mL of serum-containing media. pGL3 luciferase DNA−liposome complexes were made and incubated at room temperature in serum free media for 30 min and used for transfection. The plasmid was isolated as previously described (Tang and Hughes, 1998). Before transfection, growth media containing serum was changed to 400 μL of serum free media. DNA−liposome complexes in 100 μL of serum free media were added to each well and incubated for 4.5 h. After the 4.5 h transfection time, the transfection media were changed to growth media and cells were incubated for another 24 h. Luciferase activity was measured using a standard luciferase assay (Thierry et al., 1997). Luciferase activity in transfected cells was expressed as RLU per well. All conditions for transfection were strictly kept the same for each different kind of liposomes. Experiments were repeated at least twice, and experiments were done in triplicate within a given series.

Toxicity Assay. The toxicity of CHDTAEA/DOPE, CHSTAEA/DOPE, and DC-Chol/DOPE in the CHO and SKnSH cell line was determined using a CARE-LASS (a calcein release assay) (Lichtenfels et al., 1994). Before the assay, cells were plated in a 96 well plate (1×10^5-cells/well) and grown to 60−80% confluence overnight. To test the toxicity of the DNA−liposome complexes, a fixed amount of DNA (1 μg/well) was used to complex with increasing amount of liposomes. The ratios of DNA to liposome of different treatments were the same as the ratios used in transfection studies. The cytotoxicity of three liposomes were measured and expressed according to our previous procedure (Tang and Hughes, 1998). Each experiment was performed in triplicate and repeated at least twice.

Flow Cytometry Analysis of the Delivery of Fluorescein (FITC)-Labeled pDNA into CHO Cells. The nucleic acid fluorescein labeling kit was purchased from PanVera Corporation (Madison, WI), and pDNA was labeled according to the product directions. One microgram per well of fluorescein-labeled pDNA was complexed with CHDTAEA/DOPE, CHSTAEA/DOPE, or DC-Chol/DOPE with the weight ratio of cationic lipid to DNA of 2/1, respectively. The complexes were used for transfection as stated in preceding methods in CHO cells. After a 4.5 h transfection period, the cells were quickly washed with PBS three times. One hundred microliters of trypsin-EDTA was added to each well. The cells were trypsinized for 2−3 min, and the reaction was stopped by 200 μL of 1% of bovine serum albumin (BSA) in PBS. The cells were collected and centrifuged at 250 g for 10 min. The supernatant was decanted, and the cell pellet was resuspended in 500 μL of 1% BSA and centrifuged for another 10 min to further wash phenol red and possible residue FITC-DNA. After the BSA solution was discharged, the cell pellet was resuspended in 500 μL of PBS followed by 500 μL of 2% of paraformaldehyde PBS solution. The cells were fixed at 0 °C for 15 min then stored at 4 °C overnight. Cell fluorescence was measured using a Becton Dickinson FACSort flow cytometer (San Jose, CA). A total of 10 000 cells were counted for each treatment. Cells, which were treated with nonlabeled DNA−liposome complexes, were used in compensation experiments. Cells were gated with their morphological properties. The mean fluorescence intensity of the cells was measured in terms of arbitrary units using a LYSYS II software program (Becton Dickinson, San Jose, CA). Each experiment was performed in triplicate and repeated twice.

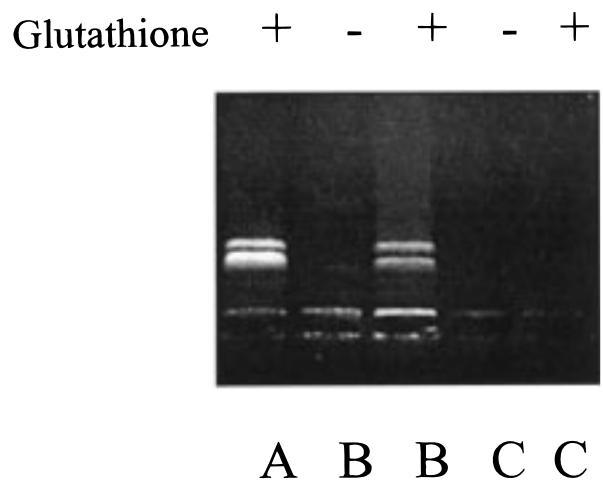


Figure 3. Gel electrophoretic analysis of the release of pDNA from cationic liposomes−DNA complexes in 10 mM glutathione in phosphate-buffered saline. (A) DNA, (B) CHDTAEA/DOPE + DNA (2/1, w/w), (C) CHSTAEA/DOPE + DNA (2/1, w/w).

Statistical Analysis. Statistical analyses were performed using one way ANOVA (Stat View 4.53, Abacus Concepts, Inc., Berkeley, CA). A probability of less than 0.05 was considered significantly different.

RESULTS

Release of DNA from Disulfide Cationic Liposomes−DNA Complexes by Glutathione. In this experiment, DNA was complexed with a disulfide cationic liposome CHDTAEA/DOPE or its nondisulfide cationic liposome analogue CHSTAEA/DOPE at the cationic lipid to DNA ratio of 2/1. As indicated in Figure 3, DNA was tightly complexed by both cationic liposomes. In the absence of glutathione, disulfide liposomes/DNA complexes did not release DNA after a 20 h incubation in PBS at 37 °C. In the presence of 10 mM of glutathione, >50% of DNA was released from complexes after the incubation. In both reductive and nonreductive environments, nondisulfide liposome CHSTAEA−DNA complexes did not release any DNA. The results suggested cationic liposome−DNA complexes were fairly stable and that cellular reductive substance (i.e., glutathione) can destabilize the complexes and help DNA to dissociate from liposomes. The complexes with the ratios of cationic liposome−DNA from 3/1 to 5/1 were also used to do the release assay with similar same results (data not shown).

Transfection of pGL3-Luciferase Plasmid in Mammalian Cells. Transfection activities of liposomes of CHDTAEA/DOPE, CHSTAED/DOPE, and DC-Chol/DOPE were compared in CHO and SKnSH cells (Figure 4). The experiment conditions were strictly controlled. The same cell lines with the same passage number and from the same flask were plated in three plates. The cells were transfected and the transgene expression was analyzed at the same time. We found the data was

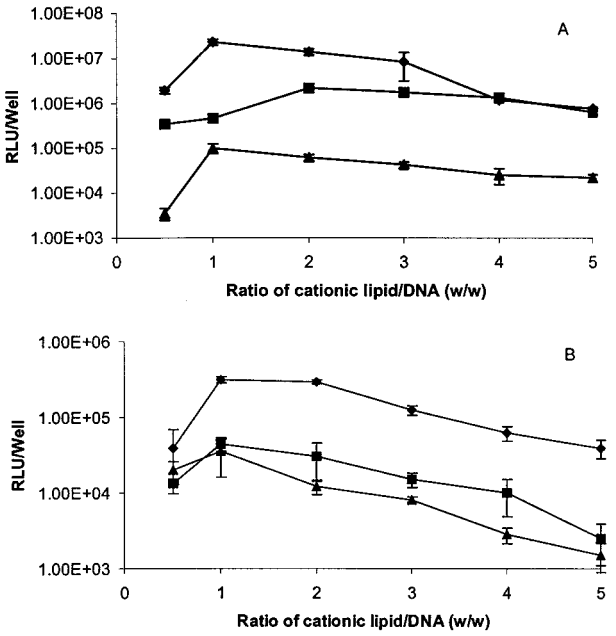


Figure 4. Comparison of the transfection of pGL3-luciferase plasmid by CHDTAEA/DOPE, CHSTAEA/DOPE, and DC-Chol in CHO and SKnSH cells. A fixed dose 2 μg/well of pGL3 DNA was mixed with increasing weight ratios of cationic liposomes (calculation based on cationic lipid) and used for transfection. Experiments were repeated at least twice. The trends were consistent in all experiments and the absolute values of transgene expression (RLU/well) were variable. (A) Transfection in CHO cells, (B) transfection in SKnSH cells. (◆) CHDTAEA/DOPE, (■) CHSTAEA/DOPE; (▲) DC-Chol/DOPE. Data are shown as mean ± SD (n = 3).

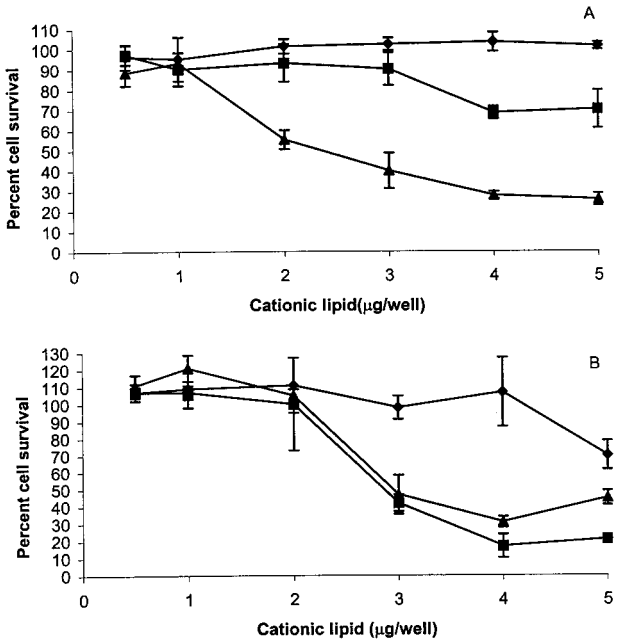


Figure 5. Toxicity assays. Cytotoxicity of the liposome−DNA complexes was studied in CHO and SKnSH cells. A fixed dose of 1 μg/well of pDNA was mixed with increasing amount of cationic liposomes and used in the toxicity assay. Cell viability was calculated as percentage of survival cells as stated in the Materials and Methods. (A) Toxicity in CHO cells. (B) Toxicity in SKnSH cells. (◆) CHDTAEA/DOPE, (■) CHSTAEA/DOPE; (▲) DC-Chol/DOPE. Data are shown as mean ± SD (n = 3).

variable from time to time although the same cell line, the same liposomes, and the same transfection period were used. It is safe to compare the transfection activities of different liposomes only in the same experiments. However, although the values from different experiments were variable, the trends were consistent. For example, the results that CHDTAEA had more than 100 times higher transfection activities were consistent in all experiments whereas the absolute value of RLU/well for each liposome in different experiments would fluctuate. In CHO cells, the transfection activities of liposomes CHDTAEA/DOPE and DC-Chol/DOPE peaked at the weight ratio of cationic lipid to DNA of 1/1, and CHSTAEA/DOPE peaked at the weight ratio of 2/1 (Figure 4A). At the optimal ratios of each liposome, CHDTAEA/DOPE had more than 100 times higher transfection activities than DC-Chol/DOPE, and 7 times higher transfection activities than its nondisulfide analogue CHSTAEA/DOPE. In SKnSH cells, all three transfection agents peaked at weight ratio of 1/1. CHDTAEA/DOPE had 7 times greater transfection activities than both CHSTAEA/DOPE and DC-CHOL/DOPE (Figure 4B).

Cytotoxicity of Liposome−DNA Complexes. The cytotoxicity of DNA−liposome complexes was tested in both CHO and SKnSH cells. Cell viability was variable between CHO cells and SKnSH cells (Figure 5). As indicated in Figure 5A, CHDTAEA/DOPE was not toxic to CHO cells up to the dose of 5 μg/well ($p > 0.05$) (Figure 5A). The nondisulfide analogue CHSTAEA/DOPE had higher toxicity than CHDTAEA/DOPE at the doses of 4 μg/well and 5 μg/well ($p < 0.05$). DC-Chol/DOPE had only about 30% cell survival at the dose of 5 μg/well. In SKnSH cells, CHDTAEA/DOPE also demonstrated lower toxicity, and it did not show significant toxicity until to the dose of 5 μg/well ($p > 0.05$). At the dose of 5 μg/well, about 70% of cells survived for the toxicity of CHDTAEA/DOPE. CHSTAEA/DOPE and DC-Chol/DOPE had much higher toxicity than CHDTAEA/DOPE at the doses of 3, 4, and 5 μg/well ($p < 0.05$). In both cell lines, the data suggested that application of dithiodiglycolic acid as a linker could greatly decrease the toxicity of cationic liposomes.

Cellular Associated DNA by Different Liposomes. To investigate if the greater transgene expression by CHDTAEA/DOPE liposomes resulted from greater amount of delivered pDNA by the liposomes, cell-associated fluorescein-pDNA after a 4.5 h transfection period was analyzed by using flow cytometric analysis. The relative amount of FITC-pDNA associated with cells after transfection period in CHO cells was measured by relative fluorescence intensity by using flow cytometry. The weight ratio of cationic lipid to DNA of 2/1 was used for each liposome (i.e., CHDTAEA/DOPE, CHSTAEA/DOPE, and DC-Chol/DOPE) (Figure 6). It was suprising to find that CHDTAEA/DOPE liposomes delivered less DNA to cells than either the CHSTAEA/DOPE or DC-Chol/DOPE liposomes, even though it had more that 100 times higher transgene expression than DC-Chol/DOPE and 7 times higher than CHSTAEA/DOPE at the weight ratio (i.e., 2/1) (Figure 4 A). It is also worth noting that the cell-associated pDNA of CHSTAEA/DOPE liposome and DC-Chol/DOPE liposome treatments were not significantly different, whereas the transfection activity of CHSTAEA/DOPE was higher than that of DC-Chol/DOPE (Figure 4A).

DISCUSSION

The use of ester, amide, and carbamate linkages to tether polar and hydrophobic domains is a common strategy to lower the toxicity of cationic lipids. However, the introduction of an ester also sacrifices the stability of cationic lipids because of hydrolysis reaction in the aqueous extracellular environment. The application of

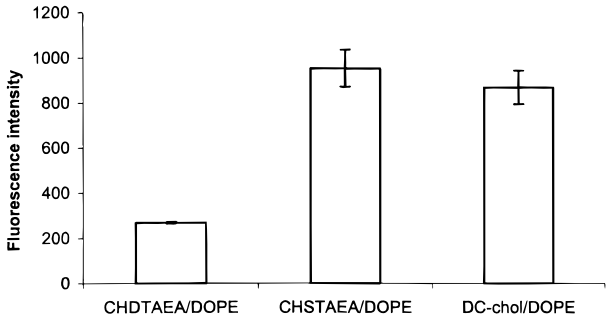


Figure 6. Comparison of the delivery of pDNA by CHDTAEA/DOPE, CHSTAEA/DOPE, and DC-Chol/DOPE in CHO cells. One microgram per well of fluorescein-labeled pDNA was complexed with CHDTAEA/DOPE, CHSTAEA/DOPE, or DC-Chol/DOPE with the weight ratio of cationic lipid to DNA of 2/1, respectively. The relative amount of pDNA, which was delivered into cells by different cationic liposomes, was measured as relative mean fluorescence intensity of cells as indicated in the Materials and Methods. Data are shown as mean ± SD ($n = 3$).

disulfide as a linker in cationic lipid is an alternative strategy to decrease the toxicity and increase the transfection activity of cationic lipids. The disulfide is stable at nonreductive extracellular environments and is unstable in the presence of high concentration of reductive intracellular substance, e.g., the concentration of glututhione in human tissue such as liver and lens is up to 10 mM (Halliwell, 1988). Disulfide conjugate techniques have widely been used in drug delivery to achieve high delivery efficiency (Boutorine and Kostina, 1993; Legendre et al., 1997; Trail et al., 1997) in the development of treatments for cancer. The normal method used involves crossing-linking or modification reactions using disulfide exchange processes to form disulfide linkage with sulfhydryl-containing molecules (Boutorine and Kostina, 1993; Legendre et al., 1997; Trail et al., 1997). This method will result in the more stable disulfide compound. A reductive substance such as dithiothreitol (DTT) is usually used to prove the hypothesis that the disulfide conjugate linker can be broken after delivery of conjugated drug in vivo. However, DTT is not a cellular substance. In this study, we used a cellular reductive substance (i.e., glutathione) to reduce the disulfide and release the complexed DNA. In CHDTAEA lipid, the disulfide bond is weakened by the strong electric withdrawing effects of two carboxyl groups, which is symmetrically connected to the two α-carbons of disulfide bond (Figure 1). CHDTAEA liposomes released more than half of complexed DNA in the presence of glutathione (Figure 3). As shown in Figure 3, CHDTAEA was as stable as its nondisulfide analogue CHSTAEA in a nonreductive environment since DNA/CHDTAEA/DOPE liposomes did not release any pDNA after incubation. Therefore, the introduction of this weak disulfide bond did not sacrifice the stability of DNA−liposome complexes outside cells. Without a disulfide bond, its analogue CHSTAEA did not release DNA at any conditions after incubation for 20 h. The release of DNA from DNA/liposomes complexes is a major barrier for cationic lipid-mediated gene transfection (Escriou et al., 1998, Rolland, 1998, Zabner et al., 1995). An interesting finding was observed during this study, very little DNA was released at the early time points of incubation until about 20 h (data not shown), after this time a large portion of the DNA was released. This result implies that a certain fraction of the liposome has to be degraded before the plasmid is released. More DNA released from the delivery system should result in greater transgene expression if the transcription machine has not been saturated.

The results of transgene expression demonstrated that CHDTAEA liposomes had greater transfection activity than its nondisulfide analogue CHSTAEA in both CHO and SKnSH cells. A second major concern is the toxicity of the delivery system. Common sense dictates that less toxic agent should have greater transfection. An optimal cationic lipid should be able to complex DNA and deliver DNA into cells, then release DNA from complexes for transcription (Pollard et al., 1998, Zabner et al., 1995). Finally, cationic liposome should be quickly degraded, otherwise freed liposome will fuse with cell membrane and result in cytotoxicity. In a dithioglcolyic acid linker, the disulfide is relatively weak and can be easily degraded by cellular substance such as glutathione. This facet of the lipid should lower toxicity, increase the amount of free plasmid DNA within the cell, and ultimately both of these events should increase transfection. As shown in Figure 5, in CHO cells, complexes of DNA/CHDTAEA/DOPE did not show cytotoxicity at all tested concentrations ($p > 0.05$). In SKnSH cells, it did not show cytotoxicity until at the concentration of 5 μg/well. Without the dithiodiglycolic acid linker, CHSTAEA and DC-Chol had much greater cytotoxicity (Figure 5). To investigate whether the greater gene transfection of CHDTAEA/DOPE liposomes resulted from more DNA delivered into cell instead of released into the cytosol, we investigated the cell-associated DNA after transfection period. Although CHDTAEA/DOPE had greater transfection activity, it had less cellular associated DNA than CHSTAEA/DOPE and DC-Chol ($p < 0.05$). More work is needed to understand the reason CHDTAEA delivered less DNA than its analogue CHSTAEA. On the other hand, the results supported the previous hypothesis that the association of DNA from DNA/cationic liposomes is a one of the majors barrier for gene delivery.

In summary, the application of dithiodiglycolic acid as a linker to tether polar domain of lipophilic domain of cationic lipid can enhance the transfection activity and decrease the cytotoxicity of cationic lipids. Dithiodiglycolic acid may be used in synthesizing new cationic lipids and may also be used as a drug conjugation linker. In the future, we will continue our work in CHDTAEA-mediated gene transfection in animal trials.

ACKNOWLEDGMENT

The authors thank the National Institutes of Health R29-HL 55779-04 and PO1-AG10485-08 for financial support and the University of Florida Gene Therapy Center and the Center for Neurobiology of Aging. The technical help of Sriram Krishnaswami in obtaining mass spectrum of the compounds was also greatly appreciated.

LITERATURE CITED

(1) Aberle, A. M., Tablin, F., Zhu, J., Walker, N. J., Gruenert, D. C., and Nantz, M. H. (1998) A novel tetraester construct that reduces cationic lipid-associated cytotoxicity. Implications for the onset of cytotoxicity. *Biochemistry 37*, 6533−40.

(2) Behr, J. P., Demeneix, B., Loeffler, J. P., and Perez-Mutul, J. (1989) Efficient gene transfer into mammalian primary endocrine cells with lipopolyamine-coated DNA. *Proc. Natl. Acad. Sci. U.S.A. 86*, 6982−6.

(3) Boutorine, A. S., and Kostina, E. V. (1993) Reversible covalent attachment of cholesterol to oligodeoxyribonucleotides for studies of the mechanisms of their penetration into eucaryotic cells. *Biochimie 75*, 35−41.

(4) Escriou, V., Ciolina, C., Helbling-Leclerc, A., Wils, P., and Scherman, D. (1998) Cationic lipid-mediated gene transfer:

analysis of cellular uptake and nuclear import of plasmid DNA. *Cell Biol. Toxicol. 14*, 95−104.
(5) Felgner, J. H., Kumar, R., Sridhar, C. N., Wheeler, C. J., Tsai, Y. J., Border, R., Ramsey, P., Martin, M., and Felgner, P. L. (1994) Enhanced gene delivery and mechanism studies with a novel series of cationic lipid formulations. *J. Biol. Chem. 269*, 2550−61.
(6) Felgner, P. L., Gadek, T. R., Holm, M., Roman, R., Chan, H. W., Wenz, M., Northrop, J. P., Ringold, G. M., and Danielsen, M. (1987) Lipofection: a highly efficient, lipid-mediated DNA-transfection procedure. *Proc. Natl. Acad. Sci. U.S.A. 84*, 7413−7.
(7) Felgner, P. L., Tsai, Y. J., Sukhu, L., Wheeler, C. J., Manthorpe, M., Marshall, J., and Cheng, S. H. (1995) Improved cationic lipid formulations for in vivo gene therapy. *Ann. N. Y. Acad. Sci. 772*, 126−39.
(8) Gao, X., and Huang, L. (1991) A novel cationic liposome reagent for efficient transfection of mammalian cells. *Biochem. Biophys. Res. Commun. 179*, 280−5.
(9) Gao, X., and Huang, L. (1995) Cationic liposome-mediated gene transfer. *Gene Ther. 2*, 710−22.
(10) Halliwell, B., Gutteridge, J. M. C. (1988) *Free Radicals in Biology and Medicine*, Oxford, London.
(11) Hermanson, G. T. (1996) *Bioconjugate Techniques*, Academic Press, Inc, San Diego.
(12) Lee, R. J., and Huang, L. (1997) Lipidic vector systems for gene transfer. *Crit. Rev. Ther. Drug Carrier Syst. 14*, 173−206.
(13) Legendre, J. Y., Trzeciak, A., Bohrmann, B., Deuschle, U., Kitas, E., and Supersaxo, A. (1997) Dioleoylmelittin as a novel serum-insensitive reagent for efficient transfection of mammalian cells. *Bioconjugate Chem. 8*, 57−63.
(14) Lichtenfels, R., Biddison, W. E., Schulz, H., Vogt, A. B., and Martin, R. (1994) CARE-LASS (calcein-release-assay), an improved fluorescence-based test system to measure cytotoxic T lymphocyte activity. *J. Immunol. Methods 172*, 227−39.
(15) Pollard, H., Remy, J. S., Loussouarn, G., Demolombe, S., Behr, J. P., and Escande, D. (1998) Polyethylenimine but not cationic lipids promotes transgene delivery to the nucleus in mammalian cells. *J. Biol. Chem. 273*, 7507−11.
(16) Rolland, A. P. (1998) From genes to gene medicines: recent advances in nonviral gene delivery. *Crit. Rev. Ther. Drug Carrier Syst. 15*, 143−98.
(17) Tang, F., and Hughes, J. A. (1998) Introduction of a disulfide bond into a cationic lipid enhances transgene expression of plasmid DNA. *Biochem. Biophys. Res. Commun. 242*, 141−5.
(18) Thierry, A. R., Rabinovich, P., Peng, B., Mahan, L. C., Bryant, J. L., and Gallo, R. C. (1997) Characterization of liposome-mediated gene delivery: expression, stability and pharmacokinetics of plasmid DNA. *Gene Ther. 4*, 226−37.
(19) Trail, P. A., Willner, D., Knipe, J., Henderson, A. J., Lasch, S. J., Zoeckler, M. E., TrailSmith, M. D., Doyle, T. W., King, H. D., Casazza, A. M., Braslawsky, G. R., Brown, J., Hofstead, S. J., Greenfield, R. S., Firestone, R. A., Mosure, K., Kadow, K. F., Yang, M. B., Hellstrom, K. E., and Hellstrom, I. (1997) Effect of linker variation on the stability, potency, and efficacy of carcinoma-reactive BR64-doxorubicin immunoconjugates. *Cancer Res. 57*, 100−5.
(20) Zabner, J., Fasbender, A. J., Moninger, T., Poellinger, K. A., and Welsh, M. J. (1995) Cellular and molecular barriers to gene transfer by a cationic lipid. *J. Biol. Chem. 270*, 18997−9007.

BC990016I

Human Serum Albumin Incorporating Tetrakis(*o*-pivalamido) phenylporphinatoiron(II) Derivative as a Totally Synthetic O_2-Carrying Hemoprotein

Eishun Tsuchida,* Teruyuki Komatsu, Yasuko Matsukawa, Kazuyoshi Hamamatsu, and Jian Wu

Department of Polymer Chemistry, Advanced Research Institute for Science & Engineering, Waseda University Tokyo 169-8555, Japan. Received February 22, 1999; Revised Manuscript Received May 24, 1999

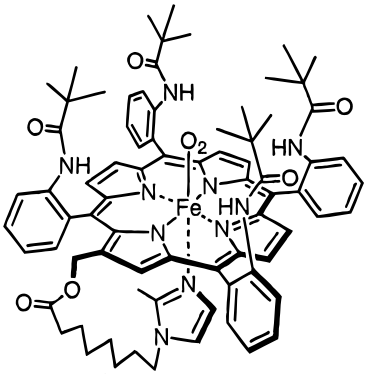
2-[8-{*N*-(2-Methylimidazolyl)}octanoyloxymethyl]-5,10,15,20-tetrakis(*o*-pivalamido)phenylporphinatoiron(II)s (FePs) were incorporated into hydrophobic cavities of recombinant human serum albumin (rHSA), providing a totally synthetic O_2-carrying hemoprotein (rHSA-FeP). An rHSA host absorbs maximally eight FeP molecules. Solution properties of the obtained albumin hybrid [[rHSA] = 5 wt %; FeP/HSA = 1−8 (mol/mol)] are almost identical to those of the rHSA itself; the specific gravity is 1.013 and the viscosity is 1.1 cP. Circular dichroism spectroscopy and isoelectric focusing measurement revealed that the second-order structure and surface charge distribution of rHSA were always constant independent of the binding numbers of FeP. Hydrophobic interaction is probably a major molecular force of the incorporation of this synthetic heme. rHSA-FeP can bind and release dioxygen reversibly under physiological conditions (in aqueous media, pH 7.3, 37 °C) like hemoglobin and myoglobin. Its O_2-coordination structure was evaluated by resonance Raman spectroscopy. The O_2 rebinding after the laser flash photolysis showed three-phases decay, which were analyzed by triple-exponential kinetics. The O_2-binding affinity and O_2-association and -dissociation rate constants of rHSA-FeP satisfy the initial clinical requirements for O_2 infusion as a red cell substitute.

INTRODUCTION

In the blood stream of the mammals, serum albumin is the major transport protein and binds a great variety of metabolites and organic compounds (Kragh-Hansen, 1981; Peters, 1985, 1997). Employing this nonspecific binding ability, it has been used in sustaining the release of therapeutic drugs injected into the blood stream. For example, the circulation time of the antitumor agent, *Adriamycin*, is prolonged by coupling to albumin (Gupta et al., 1990). The binding properties of porphyrin derivatives to serum albumin have also been widely studied, because they are the most attractive chromophores in biological systems (Little et al., 1960; Beaven et al., 1974; Muller-Eberhand et al., 1975; Adams et al., 1980). However, little attention has been paid to the clinical application of these albumin−porphyrin conjugates (Marden et al., 1989; Bonaventura et al., 1994).

Despite numerous researches on ligand bindings, there are only a few reports on the crystal structure of human serum albumin (HSA). Therefore, there is current interest in the three-dimensional structure of this very usual protein. The Protein Data Bank (Brookhaven) contains only three entries of HSA (PDB ID codes 1uor, 1ao6, and1bj5). The 585 amino acids consist of a unique heart-shaped structure, which is made of three repeating domains I−III (He et al., 1992; Carter et al., 1989, 1994). The majority of the ligands is bound at one or both sites within special hydrophobic cavities of the subdomains IIA and IIIA with typical equilibrium constants (*K*) ranging 10^6−10^4 M^{-1} (Kragh-Hansen, 1981). The crystal structure of the rHSA hybrid with five myristate molecules was resolved at 2.5 Å resolution (Curry et al., 1998). The five binding sites of the fatty acid were distributed asymmetrically throughout the rHSA molecules: one in subdomain IB, one between IA and IIA, two in IIIA, and one in IIIB.

More recently, we have found that a tetraphenylporphinatoiron(II) derivative with a covalently linked axial base, 2-[8-{*N*-(2-methylimidazolyl)}octanoyloxymethyl]-5,10,15,20-tetrakis(α,α,α,α-*o*-pivalamido)phenylporphinatoiron(II) (FeP) is efficiently incorporated into recombinant HSA, which is manufactured on a large scale by expression in *Pichia pastoris* (Sumi et al., 1993). The obtained rHSA-FeP hybrid can bind and release dioxygen reversibly under physiological conditions (in aqueous media, pH 7.3, 37 °C) in a fashion similar to hemoglobin and myoglobin. We report for the first time the physicochemical properties and O_2-coordination behavior of this *totally synthetic hemoprotein*, rHSA-FeP, as a new type of red cell substitute.



* To whom the correspondence should be addressed, CREST investigator, JST. Phone: +81 3-5286-3120. Fax: +81 3-3205-4740. E-mail: eishun@mn.waseda.ac.jp.

10.1021/bc990019v CCC: $18.00 © 1999 American Chemical Society
Published on Web 08/12/1999

EXPERIMENTAL PROCEDURES

Materials and Methods. FeP was synthesized according to our previously reported procedures (Tsuchida et al., 1995). An rHSA (25 wt %) was provided from Yoshitomi Pharmaceutical Ind., Ltd. and a natural plasma HSA was purchased from Bayer Co., Ltd. (Albumin Cutter, 5 wt %). Ethanol (>99.5%, Kanto Chemical Co., Ltd.) was used for the solvent of FeP. The preparation of rHSA-FeP was carried out as follows. Aqueous ascorbic acid (0.15 mM, 10 mL) was added to an ethanol solution of Fe(III)P (0.15 mM, 400 mL) under carbon monoxide atmosphere to reduce the central iron of Fe(III)P, affording a bright red carbonyl Fe(II)P complex. This Fe(II)P(CO) in ethanol was slowly added dropwise to the phosphate buffer solution (10 mM, pH 7.3) of rHSA (18.8 μM, pH 7.3, 400 mL) and ethanol was evaporated by a rotary evaporator. In this step, pH adjustment was essential. If the pH value was not 7.3, red precipitation was immediately formed after mixing with the ethanol solution of FeP. This is very different from the case of plasma HSA (Albumin Cutter). The mixture was then ultrafiltrated (ADVANTEC ultrafilter, cut off M_w, 50 000, 4 kg cm^{-2}) and dialyzed with cellulose membrane against phosphate buffer (pH 7.3) for 2 h and another 15 h, giving rHSA-FeP(CO) solution ([rHSA] = 5 wt %; FeP/rHSA = 4 mol/mol, 10 mL). UV−vis absorption spectra were obtained on a Shimadzu V-570 spectrometer.

Binding Numbers of FeP into rHSA. During the course of preparation of the rHSA-FeP hybrid with different FeP/rHSA mixing ratios, the precipitated carbonyl FeP [FeP(CO)] was extracted with $CHCl_3$, and its concentration was assayed by the absorption spectrum (ϵ_{max} at 427 nm, 2×10^5 M^{-1}cm^{-1}). On the basis of the quantitative analysis of this free FeP(CO) molecule, the binding numbers of FeP were determined (Komatsu et al., 1999).

Solution and Physicochemical Properties. The viscosity and density of the rHSA-FeP solution were measured at 37 °C according to the previously reported procedures (Komatsu et al., 1999). For optical microscopy observation, an OLYMPUS BX60 equipped with an OLYMPUS PM-10AK camera was used. Isoelectric points and molecular weights were measured by a Pharmacia Phastsystem using isoelectric focusing (IEF) in pH 3−9 Phast Gel IEF 3-9 and native PAGE in Phast Gel Gradient 8-25, respectively (Komatsu et al., 1999). Colloid osmotic pressure was measured by a Wescor 4420 colloidosmometer at 25 °C.

Circular dichroism (CD) spectra were obtained by a JASCO J-725 spectropolarimeter. The rHSA concentration was 1 μM (FeP/HSA = 1, 4, 8 mol/mol), and quartz cuvettes with 1 and 10 mm thickness were used for measurements over the range 190−250 and 250−700 nm, respectively.

Resonance Raman (RR) Spectroscopy. RR spectra were obtained on a JASCO NRS-2000 laser Raman spectrometer equipped with a CCD multichannel detector. Excitation was carried out by the 457.9 nm line of an NEC GLG2162 Ar^+ ion laser at 25 °C. The details of the measurements were reported elsewhere (Komatsu et al., 1999).

O_2-Binding Equilibrium and Kinetics. O_2-binding to the FeP was expressed by

$$\mathrm{FeP} + \mathrm{O_2} \underset{k_{off}}{\overset{k_{on}}{\rightleftharpoons}} \mathrm{FeP(O_2)} \qquad (1)$$

$$(K = k_{on}/k_{off})$$

The O_2-binding affinity (gaseous pressure at half O_2 binding for FeP, $P_{1/2} = 1/K$) was determined by spectral changes at various partial pressure of O_2 as in previous literatures (Tsuchida et al., 1993; Collman et al., 1983). FeP concentrations of 20 μM were normally used for UV−vis absorption spectroscopy. The spectra were recorded within the range 350−700 nm. The thermodynamic parameters for O_2 binding (ΔH, ΔS) were determined by van't Hoff plots of K. The O_2-association and -dissociation rate constants (k_{on}, k_{off}) were measured by a competitive rebinding technique using a Unisoku TSP-600 laser flash photolysis apparatus (Tsuchida et al., 1993; Collman et al., 1983; Traylor et al., 1985). The absorption decays accompanied O_2 association to FeP in rHSA obeyed triphases of the first-order kinetics. We employed triple-exponential rebinding kinetics to analyze the absorption decays, $\Delta A(t)$,

$$\Delta A(t) = C_1 \exp(-k_1 t) + C_2 \exp(-k_2 t) + C_3 \exp(-k_3 t) \qquad (2)$$

where k_1, k_2, and k_3 are apparent rate constants for the each reaction. The data were fit to this equation using a Solver in Excel 5.0.

RESULTS AND DISCUSSION

FeP Binding to rHSA. A maximum of eight FeP molecules were incorporated into certain domains of human serum albumin with binding constants from 10^6 to 10^4 M^{-1} (Tsuchida et al., 1997; Komatsu et al., 1999). FeP was expected to bind to rHSA in a similar manner, and the association sites would also be identical, namely, subdomains IB-IIA, IIA, and IIIB, etc. From the quantitative analyses of the free FeP(CO) in the prepared rHSA-FeP solution, the binding ratios were calculated to be 99% for FeP/rHSA = 8 and 70% for 9. Thus, the maximum binding numbers of FeP to an rHSA were determined to be eight, the same as that of HSA-FeP.

Solution and Physicochemical Properties. The red solution of rHSA-FeP was stored for more than 3 months at 4 °C without any aggregation and precipitation. The long-term stability and absence of a specific blood type are great advantages for O_2 infusion as a red cell substitute.

The solution properties of rHSA-FeP satisfy the physiological requirements. Specific gravities were 1.013 (FeP/rHSA = 1−8 mol/mol). The viscosity of 1.1 cP (at a high shear rate of 230 s^{-1}) was much lower than that of human blood (4.0 cP) and exhibited Newtonian type shear rate dependence just as such as as rHSA itself (Figure 1). Furthermore, rHSA-FeP possessed good compatibility with human blood [1/1 (v/v)]; the viscosity of the mixed dispersion with freshly drawn human whole blood showed 1.8 cP (at 230 s^{-1}). Optical microscopic observation also revealed that the homogeneous morphology of the red cells were not affected by mixing with the whole blood (Figure 2).

The isoelectric points (pI) of the rHSA-FeP [FeP/rHSA = 1−8 (mol/mol)] were 4.8, exactly the same as those of rHSA (Figure 3). Fatty acid binding, for example, induced the significant reduction of the pI value due to partial neutralization of the surface charge. The FeP molecule without any ionic residue interacts nonspecifically with a hydrophobic cavity of rHSA, such that its surface charge distributions are not changed. The colloid osmotic pressure (COP) of the rHSA-FeP solution ([rHSA] = 5 wt %) showed 18 Torr, which is also identical to the 5 wt % rHSA. Consequently, the essential biologi-

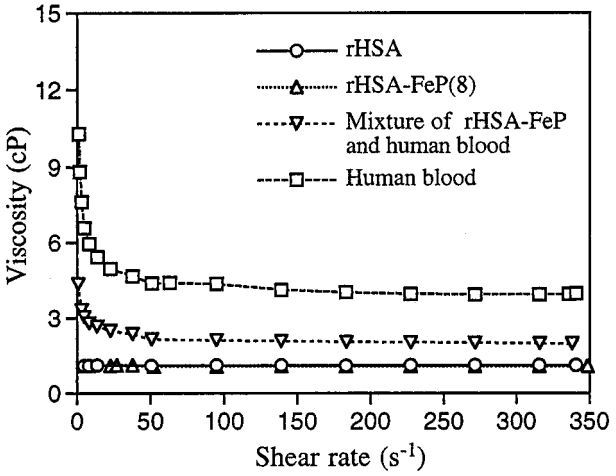


Figure 1. Shear rate dependence of the viscosity of rHSA-FeP solution at 37 °C.

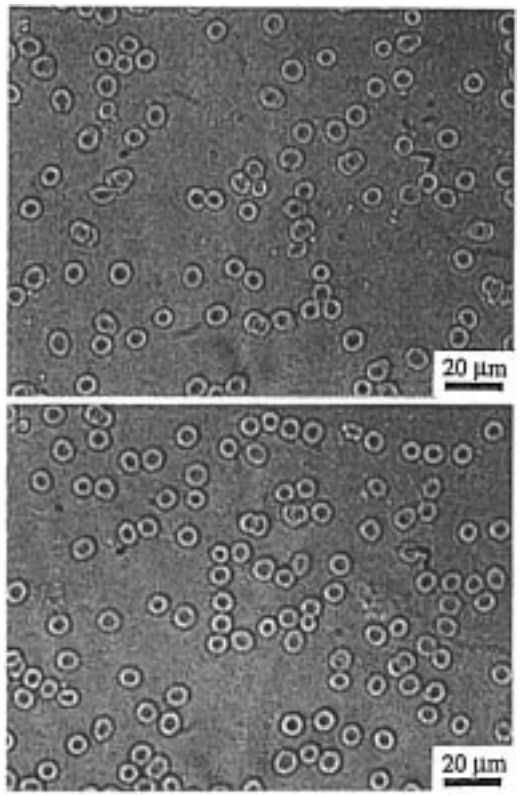


Figure 2. Optical microscopic observation of (a) rHSA + human whole blood and (b) rHSA-FeP(8) + human whole blood.

cal roles as serum albumin, i.e., control of COP and plasma expansion, are completely sustained after incorporation of FeP.

The secondary and tertiary structures of rHSA and the deformation upon the FeP binding were measured by circular dichroism (CD) spectroscopy. The spectral pattern showed typical double-minimum negative peaks in the UV region independent of the binding numbers of FeP. There were no differences when compared to that of rHSA (Figure 4). The estimated α-helix content was approximately 60%, suggesting that the FeP association did not cause any high-ordered structural change of rHSA. Moreover, rHSA-FeP showed no CD peaks in the Soret region (400−500 nm). The porphyrinatoiron binding to the serum albumin is accompanied by a rise to an extrinsic negative Cotton effect in the Soret region, because it binds to an albumin through a coordination

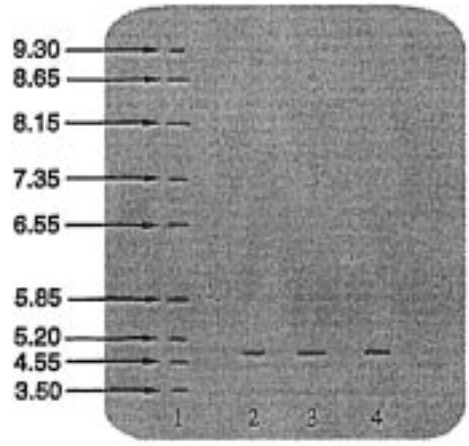


Figure 3. IEF patterns of rHSA and rHSA-FeP solutions. Lane 1, markers; lane 2, rHSA; lane 3, rHSA-FeP(4); lane 4, rHSA-FeP(8) from the left.

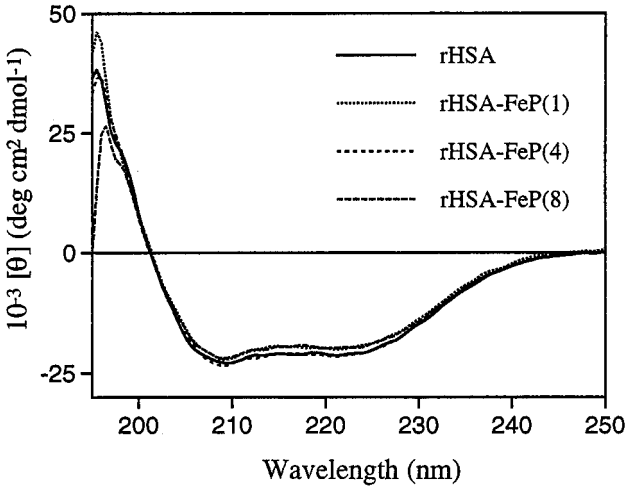


Figure 4. Circular dichroism spectra of the rHSA-FeP in phosphate buffer solution (pH 7.3) at 25 °C.

between the imidazole of histidine and the central iron, allowing a high degree of immobilization (Beaven et al., 1974; Casella et al., 1993). We concluded that hydrophobic interaction is the major molecular force of the FeP binding to rHSA, and its incorporation does not induce any changes in the highly ordered structure and surface charge distribution of the host albumin.

O_2-Coordination Properties of rHSA-FeP. The UV−vis absorption spectrum of the aqueous rHSA including carbonyl FeP complex [FeP(CO)] displayed a typical CO-coordinated low-spin tetraphenylporphinatoiron(II) derivative (λ_{max} = 427 and 539 nm) (Figure 5). Light irradiation with 500 W incandescent lamp on this solution under flowing O_2 led to CO dissociation, giving the dioxygenated species (λ_{max} = 426 and 552 nm). Upon exposure of rHSA-FeP(O_2) to argon, the UV−vis absorption spectrum changed to that of a five-N-coordinated species (λ_{max} = 443, 542, and 567 nm). This dioxygenation was reversible and kinetically stable under physiological conditions (pH 7.3, 37 °C). The HSA hybrid incorporating tetrakis (α,α,α,α-*o*-pivalamido)phenylporphinatoiron(II) without axial imidazole showed a similar spectrum under an argon atmosphere like HSA-FeP, but the ferrous complex immediately oxidized after exposure of dioxygen. This result suggested that the covalently bound imidazole arm is necessary for O_2-adduct formation.

Resonance Raman spectroscopy was then employed to characterize the coordination structure of the FeP com-

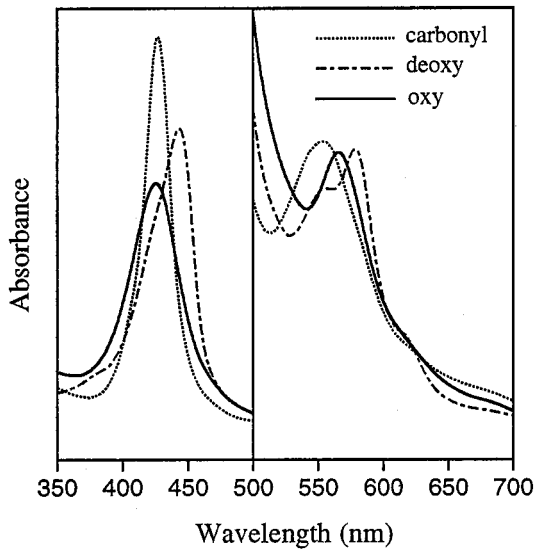


Figure 5. UV−vis absorption spectral changes of the rHSA-FeP in phosphate buffer solution (pH 7.3) at 25 °C.

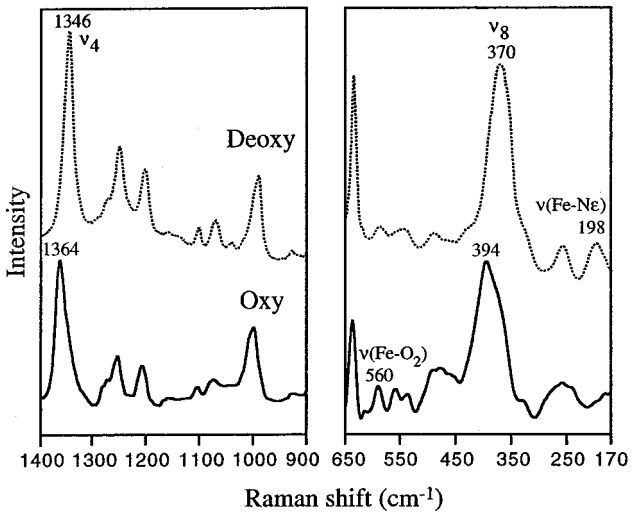


Figure 6. Resonance Raman spectra of the rHSA-FeP phosphate buffer solution (pH 7.3) at 25 °C.

plex in rHSA. Under argon, a medium band at 198 cm^{-1} was assigned to the Fe(II)-N(imidazole) stretching mode, $\nu(Fe-N_\epsilon)$, based on a similar assignment for other porphyrinatoiron(II) systems (Figure 6) (Hori et al., 1980). The covalently linked imidazole moiety coordinates to the central iron(II) of the porphyrin in rHSA. After exposure to O_2, a new $\nu(Fe-O_2)$ vibration of dioxygenated FeP appeared at 560 cm^{-1}. This frequency suggests a typical end-on type O_2 coordination to the porphyrinatoiron(II) (Hirota et al., 1996; Wu et al., 1998). The deformation modes of the porphyrin ring (ν_8 and ν_4) were also upshifted from 370 and 1346 cm^{-1} to 394 and 1364 cm^{-1}, respectively. These observations indicate the conversion of the five-coordinated high-spin state to the six-coordinated low-spin state of FeP (Desobois et al., 1989; Hori et al., 1980). All the observed shifts were reversibly dependent on the O_2 concentration. We conclude that the rHSA-FeP definitely binds and releases O_2 molecule in aqueous solution.

The autoxidation reaction of the oxy state (λ_{max} = 552 nm), however, occurred, and the absorption band of 552 nm almost disappeared after 24 h, leading to the formation of inactive Fe(III)P. The half-life of the dioxygenated species ($\tau_{1/2}$) was 8 h at 25 °C and 2 h at 37 °C (pH 7.3, [NaCl] = 150 mM). The relatively low stability of dioxygenated rHSA-FeP seems insufficient to meet clinical requirements, however, the $\tau_{1/2}$ was significantly prolonged in the bloodstream (Tsuchida et al., 1999). This observation preliminary shows that some plasma contents, i.e., ascorbic acid, contribute to the apparent long-lifetime of the dioxygenated FeP in vivo.

Table 1. O_2-Association and -Dissociation Rate Constants of rHSA-FeP at 25 °C (pH 7.3, [NaCl] = 150 mM)

	10^{-7} k_{on} (M^{-1} s^{-1})	10^{-6} k'_{on} (M^{-1} s^{-1})	10^{-2} k_{off} (s^{-1})	10^{-2} k'_{off} (s^{-1})
rHSA-FeP(4)	3.2	10	7.2	2.2
rHSA-FeP(8)	3.4	9.5	7.5	2.0
Hb(T-state)α[a]	0.29		1.8	

[a] pH 7, 20 °C, Sawicki et al. (1977).

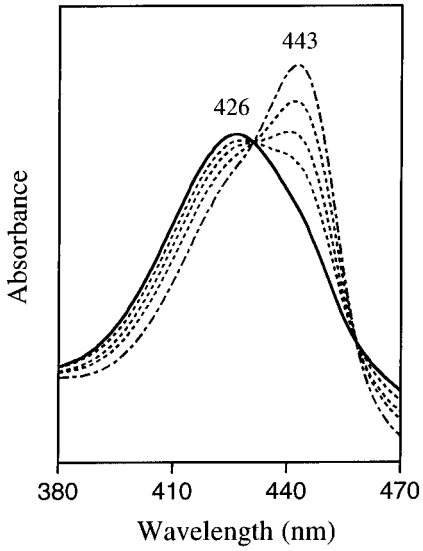


Figure 7. UV−vis absorption spectral changes of the rHSA-FeP(4) on O_2 titration in phosphate buffer solution (pH 7.3) at 37 °C.

The O_2-association and -dissociation rate constants (k_{on}, k_{off}) were explored by laser flash photolysis. The absorption decays accompanied O_2 recombination were composed of three-phases of the first-order kinetics, the curves were therefore fit by triple-exponential equation. The minor, less than 10%, component k_1, which is the fastest rate constant, was always independent of the O_2 concentration. It is presumably correlated with a base elimination reaction (Geibel et al., 1979). From the slope of linear plots of k_2 and k_3 versus O_2 concentration, two association rate constants for the fast O_2 rebinding (k_{on}) and the slow O_2 rebinding (k'_{on}) were obtained (Table 1). The k_{on} values are 3-fold larger than k'_{on}. The ratio of the fast reaction and the slow reaction was approximately 2 for rHSA-FeP(4) and 3 for rHSA-FeP(8). In the case of rHSA-FeP(1), k_{on} (3.2×10^7 M^{-1} s^{-1}) was only major ingredient. Thus, we concluded that the O_2 association to FePs incorporated into the certain domains of serum albumin are largely influenced by the molecular microenvironments around the each FeP, for example, steric hindrance by the protein residues and polarity.

The O_2-binding affinities [$P_{1/2}$, gaseous pressure at half O_2 binding for the porphyrinatoiron(II)] of the rHSA-FeP were determined on the basis of the UV−vis spectral changes by O_2 titration. The isosbestic points were maintained in all cases (Figure 7). According to the results of the kinetics experiments, the $P_{1/2}$ values were divided by two components using eq 3,

Table 2. O_2-Binding Affinities of rHSA-FeP at 25 °C and the Thermodynamic Parameters (pH 7.3, [NaCl] = 150 mM)

	O_2-binding affinities (Torr)		ΔH (kJ mol^{-1})	ΔS (J K^{-1} mol^{-1})
rHSA-FeP(4)	$P_{1/2}$	13	−60	−114
	$P'_{1/2}$	13	−61	−116
rHSA-FeP(8)	$P_{1/2}$	14	−60	−112
	$P'_{1/2}$	13	−61	−101
red blood cell	$P_{1/2}$	9		
Hb(T-state)α[a]	$P_{1/2}$	40[a]	−57 to −65[b]	−116 to −133[b]

[a] pH 7, 20 °C, Sawicki et al. (1977). [b] pH 7.4, Imai et al. (1975).

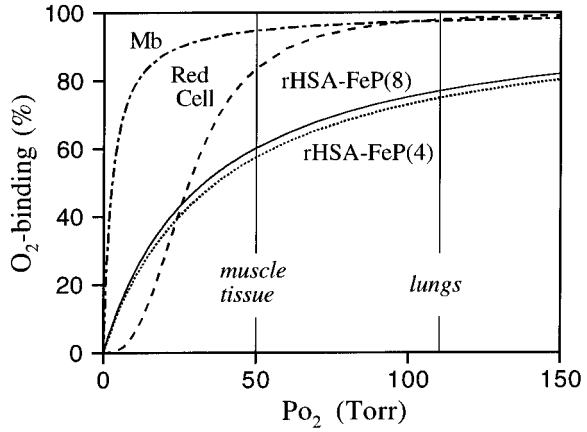


Figure 8. O_2-binding equilibrium curves of rHSA-FeP at 37 °C. The O_2-binding affinities of rHSA-FeP represented are averages of the two components.

$$Y = A[K[O_2]/(1 + K[O_2])] + B[K'[O_2]/(1 + K'[O_2])] \quad (3)$$

where Y is total O_2 saturation of FeP in rHSA, $K = (P_{1/2})^{-1}$, and $K' = (P'_{1/2})^{-1}$. The values A and B determined from the kinetic experiments were used. The obtained $P_{1/2}$ and $P'_{1/2}$ are relatively close, and the thermodynamic parameters for each O_2 binding are nearly identical for rHSA-FeP(4) and rHSA-FeP(8) (Table 2). The O_2-dissociation rate constants were also calculated by k_{on}/K (Table 1). 2-Methyl-substituted imidazole covalently bound to the parent porphyrin plays a role for adjustment of the $P_{1/2}$ value suitable for picking up dioxygen in the lungs and releasing it to the myoglobin in the tissues, namely T-state model (Collman et al., 1978; Geibel et al., 1979). The CO-binding affinity of rHSA-FeP(4) was ca. 0.1 Torr at 25 °C; therefore, the active ferrous porphyrins may be partially poisoned by the small amount of CO at the cellular level.

As expected, monomeric FeP in rHSA did not show a cooperative O_2-binding profile like that seen in hemoglobin; the Hill coefficient was 1.0 (Figure 8). Although the $P_{1/2}$ at 37 °C is slightly lower than that of hemoglobin, the O_2-transporting efficiency (OTE) of rHSA-FeP between the lungs (P_{O_2} = 110 Torr) and muscle tissue (P_{O_2} = 40 Torr) becomes 22%, which is nearly the same value (23%) as that of the red cells.

In conclusion, recombinant human serum albumin incorporating tetraphenylporphinatoiron(II) derivatives as O_2-binding sites provides a totally synthetic O_2-carrying hemoprotein. The FeP binding is a hydrophobic interaction, that did not lead to a change in the physicochemical properties of the rHSA molecule, e.g., surface charge, highly ordered structure, as well as the solution properties. All eight Fe(II)P complexes, in which the imidazolyl group is intramolecularly coordinated to the central iron(II), form reversible dioxygen adducts in the albumin. The O_2-binding ability (O_2-binding affinities = 31−37 Torr, OTE = 22% at 37 °C, etc.) satisfies the initial clinical requirements for O_2 infusion as red cell substitutes.

ACKNOWLEDGMENT

This work was partially supported by the Core Research for Evolution Science and Technology, JST, the Health Science Research Grants (Artificial Blood Project), of the Ministry of Health and Welfare, Japan, and a Grant-in-Aid for Scientific Research (no. 11650935) from the Ministry of Education, Science, Culture and Sports, Japan.

LITERATURE CITED

(1) Adams, P. A., and Berman, M. C. (1980) Kinetics and Mechanism of the Interaction Between Human Serum Albumin and Monomeric Haemin, *Biochem. J. 191*, 95−102.
(2) Beaven, G. H., Chen, S.-H., D'Albis, A., and Gratzer, W. B. (1974) A Spectroscopic Study of the Haemin-Human-Serum-Albumin System. *Eur. J. Biochem. 41*, 539−546.
(3) Bonaventura, J., Brouwer, M., Brouwer, T., Cashon, B., and Cameron, S. (July 1994) Presented in part at the 11th Congress ISABI, Boston.
(4) Carter, D. C., He, X.-M., Munson, S. H., Twigg, P. D., Gernert, K. M., Broom, M. B., and Miller, T. R. (1989) Three-Dimensional Structure of Human Serum Albumin. *Science 244*, 1195−1198.
(5) Carter, D. C., and Ho, J. X. (1994) Structure of Serum Albumin. *Adv. Protein Chem. 45*, 153−203.
(6) Casella, L., Gullotti, M., Poli, S., and De Gioia, L. (1993) Haem-Protein Interactions. The Binding of Haem Complexes to Serum Albumin. *Gazz. Chim. Ital. 123*, 149−154.
(7) Collman, J. P., Brauman, J. I., Doxsee, K. M. Halbert, T. R., and Suslick, K. S. (1978) Model Compounds for the T State of Hemoglobin. *Proc. Natl. Acad. Sci. U.S.A. 75*, 564−568.
(8) Collman, J. P., Brauman, J. I., Iverson, B. L., Sessler, J. L., Morris, R. M., and Gibson, Q. H. (1983) O_2 and CO Binding to Iron(II) Porphyrins: A Comparison of the "Picket Fence" and "Pocket" Porphyrins. *J. Am. Chem. Soc. 105*, 3052−3064.
(9) Curry, S., Mandelkow, H., Brick, P., and Franks, N. (1998) Crystal Structure of Human Serum Albumin Complexed with Fatty Acid Reveals an Asymmetric Distribution of Binding Sites. *Nat. Struct. Biol. 5*, 827−835.
(10) Desobois, A., Momenteau, M., and Lutz, M. (1989) Resonance Raman Spectroscopy of Iron(II) Super Structured Porphyrins: Influence of Porphyrin Distortion on CO and O_2 Ligand Dissociation. *Inorg. Chem. 28*, 825−834.
(11) Geibel, J., Cannon, J., Campbell, D., and Traylor, T. G. (1978) Model Compounds for R−State and T-State Hemoglobins. *J. Am. Chem. Soc. 100*, 3575−3585.
(12) Gupta, P. K., Hung, C. T., and Lam, F. C. (1990) Application of Regression Analysis in the Evaluation of Tumor Response Following the Administration of Adriamycin Either as a Solution or via Albumin Microsphere to the Rat. *J. Pharm. Sci. 79*, 634−637.
(13) He, X. M., and Carter, D. C. (1992) Atomic Structure and Chemistry of Human Serum Albumin. *Nature 356*, 209−215.
(14) Hirota, S., Li, T., Philips, G. N., Jr., Olson, J. S., Mukai, M., and Kitagawa, T. (1996) Pertubation of the Fe−O_2 Bond by Nearby Residues in Heme Pocket: Observation of νFe−O_2 Raman Bands for Oxymyoglobin Mutants. *J. Am. Chem. Soc. 118*, 7845−7846.
(15) Hori, H., and Kitagawa, T. (1980) Iron-Ligand Stretching Band in the Resonance Raman Spectra of Ferrous Iron Porphyrin Derivatives. Importance as a Probe Band for Quaternary Structure of Hemoglobin. *J. Am. Chem. Soc. 102*, 3608−3613.
(16) Imai, K., Yonetani, T. (1975) Thermodynamical Studies of Oxygen Equilibrium of Hemoglobin *J. Biol. Chem. 250*, 7093−7098.
(17) Komatsu, T., Hamamatsu, K., Wu, J., and Tsuchida, E. (1999) Physicochemical Properties and O_2−Coordination Structure of Human Serum Albumin Incorporating Tetrakis-

(*o*-pivalamido)phenylporphyrinatoiron(II) Derivatives. *Bioconjugate Chem. 10,* 82−86.
(18) Kragh-Hansen, U. (1981) Molecular Aspects of Ligand Binding to Serum Albumin. *Pharmacol. Rev. 33,* 17−53.
(19) Little, H. N., and Nelands, J. B. (1960) Binding of Hematin by Human Serum Albumin. *Nature 170,* 913−915.
(20) Marden, M. C., Hazard, E. S., Leclerc, L., and Gibson, Q. H. (1989) Flash Photolysis of the Serum Albumin-Heme-CO Complex. *Biochemistry 28,* 4422−4426.
(21) Muller-Eberhand, U., and Morgan, W. T. (1975) Porphyrin-Binding Proteins in Plasma. *Ann. N. Y. Acad. Sci. 244,* 625−650.
(22) Peters, T., Jr. (1985) Serum Albumin. *Adv. Protein Chem. 37,* 161−245.
(23) Peters, T., Jr. (1997) All about Albumin, Biochemistry, Genetics, and Medical Applications, Academic Press, San Diego.
(24) Sawicki, C. A., and Gibson, Q. H. (1977) Properties of the T State of Human Oxyhemoglobin Studied by Laser Photolysis. *J. Biol. Chem., 252,* 7538−7547.
(25) Sumi, A., Ohtani, W., Kobayashi, K., Ohmura, T., Yokoyama, K., Nishida, M., and Suyama, T. (1993) Purification and Physicochemical Properties of Recombinant Human Serum Albumin. In *Biotechnology of Blood Proteins* (C. Rivat and J.-F. Stoltz, Eds.) Vol. 227, pp 293−298, John Libbey Eurotext, Montrouge.
(26) Traylor, T. G., Tsuchiya, S., Campbell, D., Mitchell, M., Stynes, D., and Koga, N. (1985) Anthracene Heme Cyclophanes. Steric Effects in CO, O_2, and RNC Binding. *J. Am. Chem. Soc. 107,* 604−614.
(27) Tsuchida, E., Komatsu, T., Arai, K., and Nishide, H. (1993) Synthesis and Dioxygen-Binding Properties of Doble-sided Porphyrinatoiron(II) Complexes Bearing Covalently Bound Axial Imidazole. *J. Chem. Soc., Dalton Trans. 1993,* 2465−2469.
(28) Tsuchida, E., Komatsu, T., Kumamoto, S., Ando, K., and Nishide, H. (1995) Synthesis and O_2−Binding Properties of Tetraphenylporphyrinatoiron(II) Derivatives Bearing a Proximal Imidazole Covalently Bound at the β-pyrrolic Position. *J. Chem. Soc., Perkin Trans. 2 1995,* 747−753.
(29) Tsuchida, E., Ando, K., Maejima, H., Kawai, N., Komatsu, T., Tekeoka, S., and Nishide, H. (1997) Properties of and Oxygen Binding by Albumin-Tetraphenylporphinatoiron(II) Derivative Complexes. *Bioconjugate Chem. 8,* 534−538.
(30) Tsuchida, E., and Komatsu, T., et al. (1999) Exchange Transfusion with Albumin-Heme as an Artificial O_2-Infusion into Hemorrhagic Shock Rats: Physiological Responses, O_2-Delivery and Reduction of the Oxidized Hemin Sites by Red Blood Cells. *Bioconjugate Chem. 10* (submitted for publication).
(31) Wu, J., Komatsu, T., and Tsuchida, E. (1998) Resonance Raman Studies of O_2−Binding to *ortho*-Substituted Tetraphenyl- and Tetranaphthyl-Porphyrinatoiron(II) Derivatives with a Covalently Linked Axial Imidazole. *J. Chem. Soc., Dalton Trans. 1998,* 2503−2506.

BC990019V

^{99m}Tc-Labeling of Hydrazones of a Hydrazinonicotinamide Conjugated Cyclic Peptide

D. Scott Edwards, Shuang Liu,* Anthony R. Harris, Michael J. Poirier, and Barbara A. Ewels

DuPont Pharmaceuticals Company, Medical Imaging Division, 331 Treble Cove Road, North Billerica, Massachusetts 01862. Received February 24, 1999; Revised Manuscript Received April 9, 1999

Eight HYNICtide hydrazones (three with aliphatic substituents and five with aromatic groups) were studied for their potential use as the final intermediate for preparation of RP444, a new radiopharmaceutical under development for imaging thrombosis. The goal of this study is to screen various hydrazones through stability testing and radiolabeling and find those which are able to remain stable without significant degradation in the manufacturing process and at the same time are reactive to produce enough free hydrazine in situ for successful ^{99m}Tc-labeling. In an initial screening study, only hydrazones **6** and **8**, which contain aliphatic substitients, gave satisfactory (≥90%) yields of RP444 using 50 °C and 30 min of heating. However, their solution instability excludes them from being used as commercial reagents. Hydrazones **1** and **4** gave ≥90% yields when the reaction mixtures were heated at 80 °C for 30 min. Both hydrazone **1** and hydrazone **4** can be used as the final intermediate for preparation of RP444. The combination of 40 mg of tricine, 1−10 mg of TPPTS, 20−40 μg of hydrazone **1** or **4** for 50 mCi of [^{99m}Tc]pertechnetate, 20−50 μg of stannous chloride, pH 4.5 ± 0.5, and heating at 80 °C for 30 min gives the best yield for RP444. It is surprising that hydrazones **1** and **4** have both the solution stablity with respect to decomposition and to reaction with aldehydes and ketones and yet are able to hydrolyze in situ to produce enough free HYNICtide for the ^{99m}Tc-labeling.

INTRODUCTION

Recently, Abrams and co-workers (*1*−*3*) reported the use of organic hydrazines such as hydrazinonicotinamide (HYNIC) in labeling polyclonal IgG with ^{99m}Tc for imaging focal sites of infection. This technology has also been used for the ^{99m}Tc-labeling of a variety of biologically active molecules. These include chemotactic peptides (*4*−*7*) for infection imaging, somatostatin analogues (*8*, *9*), and antisense DNA oligonucleotides (*10*−*12*) for tumor imaging.

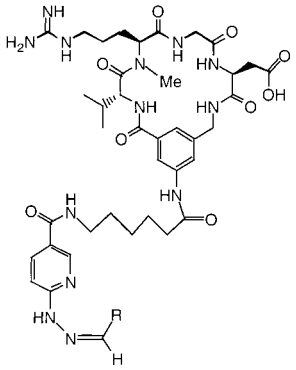
We are interested in the ^{99m}Tc-labeling of glycoprotein IIb/IIIa (GPIIb/IIIa) receptor antagonists for the development of thrombosis imaging agents (*13*−*20*). Recently, we labeled an HYNIC-derivatized cyclic peptide [HYNICtide, cyclo(D-Val-NMeArg-Gly-Asp-Mamb(5-(6-(6-hydrazinonicotinamido)hexanamide)))] using tricine and TPPTS (trisodium triphenylphosphine-3,3′,3″-trisulfonate) as coligands (*19*). The combination of HYNICtide with tricine and phosphine produces a new ternary ligand system which forms stable technetium complexes, [^{99m}Tc(HYNICtide)(tricine)(TPPTS)] (RP444) in high yield and high specific activity (≥20 000 Ci/mmol). In the canine arteriovenous (AV) and deep vein thrombosis (DVT) models, RP444 has been shown to be able to detect rapidly growing arterial and venous thrombi (*20*). The phase I clinical trials demonstrated an excellent safety profile and acceptable dosimetry. Preliminary results from phase II trials showed that RP444 can detect DVT within 60 min with 93% sensitivity, 75% specificity, and 82% accuracy (*21*).

* To whom correspondence should be addressed: Phone: 978-671-8696. Fax: 978-436-7500. E-mail: shuang.liu@dupontpharma.com.

In the manufacturing process, we found that the final intermediate HYNICtide itself is not stable in aqueous solution, particularly under basic conditions, and reacts readily with aldehydes or ketones. The presence of aldehydes and ketones in small quantities is unavoidable in a commercial pharmaceutical manufacturing setting, because they can be extracted from various plastic and rubber materials, and are also found in common disinfectants. In a recent patent application (*22*), Schwartz et al. disclosed the use of a lower alkyl hydrazone (propylaldehyde hydrazone) to stabilize HYNIC-modified proteins. Although its use can prevent the cross-reaction of the hydrazine with other reactive groups on the proteins, it can also be displaced by other aldehydes, formaldehyde in particular, and ketones to form different hydrazones. This presents a significant problem in maintaining the purity of the final intermediate and, thus, renders lower alkyl hydrazones unattractive as commercial reagents. To prevent the decomposition or degradation of the HYNICtide in the manufacturing process, several stable hydrazones have been synthesized (*23*, *24*) and studied for their solution stability in the presence of formaldehyde. It was found that for a hydrazone to be stable in aqueous solution there must be a conjugated π-system (*23*, *24*).

The radiolabeling efficiency of the HYNICtide is dependent on the availability of the free hydrazine group, relative component levels, and reaction conditions. The formation of hydrazones stabilizes HYNICtide and prevents its degradation or decomposition, but it reduces the availability of the free hydrazine group for ^{99m}Tc-labeling. To assess the impact of hydrazone formation on the ^{99m}Tc-labeling of the HYNICtide, we performed a series of radiolabeling studies and explored the factors influencing the ^{99m}Tc-labeling kinetics of several stable hydrazones (Figure 1). The results are described in this report.

10.1021/bc990022e CCC: $18.00 © 1999 American Chemical Society
Published on Web 07/08/1999



Hydrazone	Aldehyde	R
1	Benzaldehyde	C_6H_5
2	4-Dimethylaminobenzaldehyde	4-NMe_2-C_6H_4
3	4-Carboxybenzaldehyde	4-HO_2C-C_6H_4
4	2-Sulfonatobenzaldehyde	2-NaO_3S-C_6H_4
5	4-Pyridinecarboxaldehyde	4-C_5H_4N
6	Propyladehyde	C_2H_5
7	Crotonadehyde	CH_3CH=CH-
8	Glyoxylic Acid	COOH

Figure 1. Hydrazones of the HYNICtide.

EXPERIMENTAL SECTION

Materials. TPPTS (trisodium triphenylphosphine-3,3′,3″-trisulfonate) and tricine were purchased from Aldrich Chemical Co. TPPTS was purified according to the literature method (*25*) before use for the radiolabeling. $Na^{99m}TcO_4$ was obtained from a commercial DuPont Pharma $^{99}Mo/^{99m}Tc$ generator, N. Billerica, MA. The syntheses of hydrazones **1**−**8** of the HYNICtide with benzaldehyde, 4-(*N*,*N*-dimethylamino)benzaldehyde, 4-carboxy-benzaldehyde, sodium 2-formylbenzenesulfonate, 4-pyridinecarboxaldehyde, propylaldehyde, crotonaldehyde, and glyoxylic acid will be reported as a separate communication (*24*).

General Procedure for the ^{99m}Tc-Labeling of Hydrazones. To a clean 10 mL vial were added 0.4 mL of tricine solution (100 mg/mL in H_2O), 0.2 mL of the hydrazone solution (50 μg/mL in H_2O), 0.1 mL of phosphine coligand solution (10 mg/mL in H_2O), 0.5 mL of $Na^{99m}TcO_4$ solution (100 mCi/mL in saline), and 20 μL of $SnCl_2 \cdot 2H_2O$ solution (1.0 mg/mL in 0.1 N HCl). The pH was adjusted to 4.5 ± 0.5, if necessary. The reaction mixture was heated at 50 or 80 °C for 30 min. After cooling at room temperature, the reaction mixture was analyzed by radio-HPLC and ITLC.

The HPLC method used a heated (50 °C) Zorbax C_{18} column (4.6 mm × 250 mm, 80 Å pore size) at a flow rate of 1 mL/min. The mobile phase is isocratic from 0 to 14 min using 100% mobile phase A [90:10 (0.025 M phosphate buffer, pH 8):acetonitrile] and from 14 to 25 min using 100% mobile phase B [50:50 (0.025 M phosphate buffer, pH 8):acetonitrile]. The ITLC method used Gelman Sciences silica gel ITLC paper strips and 1:1 mixture of acetone and saline as eluant. Using this ITLC method, RP444 and [^{99m}Tc]pertechnetate migrate while the [^{99m}Tc]-colloid remains at the origin.

RESULTS AND DISCUSSION

In the development of a new ^{99m}Tc-based radiopharmaceutical, several factors need to be considered. These include biological efficacy (high target uptake, high target-to-background ratio, and favorable pharmacokinetics), high radiochemical purity (RCP ≥ 90%), and high solution stability (≥6 h). In addition, a kit formulation is often required due to the 6 h half-life of ^{99m}Tc. A kit contains the final drug intermediate (a chelator−peptide conjugate for peptide-based radiopharmaceuticals), a reducing agent such as stannous chloride, if necessary, and other components such as a bulking agent or a weak transfer ligand. Kits can be purchased and stored for daily preparation. In many cases, the ^{99m}Tc-labeling can be accomplished simply by adding [^{99m}Tc]pertechnetate to the kit.

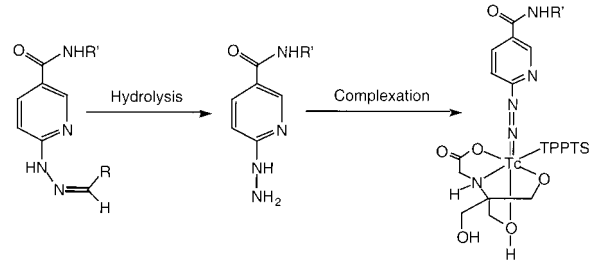


Figure 2. Synthesis of RP444 from HYNICtide hydrazones.

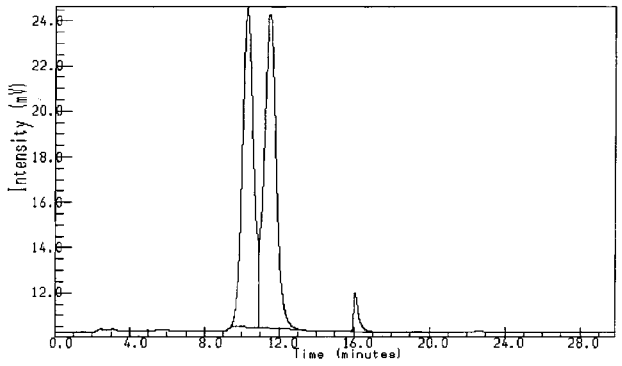


Figure 3. HPLC chromatogram of RP444 prepared from hydrazone **4**.

RP444 contains three different ligands (HYNICtide, TPPTS, and tricine) in the technetium chelate. All of them are considered as active ingredients or final intermediates. Tricine and TPPTS are relatively stable to oxidation and inert to reactions with chemicals often found in commercial pharmaceutical manufacturing settings. The free hydrazine group of the HYNICtide is not stable to oxidation, particularly under basic conditions, and reacts readily with aldehydes or ketones, which are extracted from various plastic and rubber materials. This makes it very difficult to maintain the purity and the stability of the HYNICtide. To solve the problem, several aromatic aldehydes have been used to form stable hydrazones with the HYNICtide. These hydrazones were found to be stable to the challenge of 10-fold excess formaldehyde (*23*, *24*).

Hydrazones are used only as protecting groups for the HYNICtide. In the radiolabeling process, the hydrazones must hydrolyze (Figure 2) to produce sufficient quantity of the hydrazine that binds to the technetium via either a Tc−hydrazino or Tc−diazenido bond. However, the hydrolysis does not need to go to completion since there are typically 50−100 equiv of the hydrazone to total Tc in each reaction. All the hydrazones react with [^{99m}Tc]-pertechnetate in the presence of stannous chloride, excess tricine, and TPPTS coligands to form the same ternary ligand complex RP444 as that prepared from the unprotected HYNICtide. Figure 3 shows a representative radio-HPLC chromatogram of RP444 prepared from hydrazone **4**. The presence of two radiometric peaks in the radio-HPLC chromatogram is due to the resolution of diaster-

Table 1. Radiolabeling Yields of RP444 Using Hydrazones at 50 °C

hydrazone	RCP (%)[a]	*n*	hydrazone	RCP (%)[a]	*n*
1	85.7 ± 2.5	4	**5**	31.3 ± 5.5	3
2	79.0 ± 1.0	3	**6**	94.5	1
3	74.5 ± 0.7	3	**7**	81.0 ± 7.9	3
4	79.7 ± 1.5	5	**8**	91.3 ± 0.6	3

[a] Calculated by subtracting the percent peak area for the [^{99m}Tc]colloid determined by ITLC from the percent peak area of RP444 in the radio-HPLC. In all the cases, the [^{99m}Tc]colloid was less that 2%.

eomers, which result from the presence of chiral cyclic peptide and the formation of two enantiomers of the technetium chelate (*19*, *26*). The small peak at ~16 min is from a combination of several radioimpurities. To develop an accurate RCP method for RP444, we intentionally "squeezed" these radioimpurities into a single peak using the chromatographic conditions described in the experimental. Since these radioimpurities are less than 1.0%, no further characterization was performed.

The yield of RP444 depends largely on the kinetics of hydrolysis, as well as the total concentration of the unprotected HYNICtide in the reaction mixture. The higher degree of the hydrolysis of the hydrazone, the more free hydrazine groups available for Tc-binding, and the higher the radiolabeling yield of RP444, within certain limits. The goal of this study was to screen various hydrazones through stability testing and radiolabeling and find those which are able to remain stable without significant degradation in the manufacturing process and at the same time are reactive to produce enough free hydrazine in situ for successful ^{99m}Tc-labeling.

There are several factors influencing the hydrolysis of these hydrazones. These include the type of hydrazone, the heating temperature, the reaction time, and the pH of the reaction mixture. The initial labeling study was focused on the screening of hydrazones. The hydrazones screened included three with aliphatic substituents and five with aromatic groups functionalized by electron withdrawing or electron donating substituents. In this study, we fixed the amount of hydrazone (10 μg), tricine (40 mg), TPPTS (1 mg), $^{99m}TcO_4$- (50 mCi), and stannous chloride (25 μg). The total volume for each radiolabeling kit was ~1.2 mL. The pH was adjusted to 4.0 ± 0.5. After heating in a 50 °C water bath for 30 min, the reaction mixtures were analyzed by HPLC and ITLC. The RCP of RP444 was corrected for the contribution from [^{99m}Tc]-colloid. The results are summarized in Table 1. It is obvious that the type of hydrazone has dramatic impact on the yield of RP444.

The hydrazones **6** and **8** contain aliphatic substituents and gave highest yield (>90%) of RP444 because they can be easily hydrolyzed in situ to produce the free HYNICtide for the ^{99m}Tc-labeling. However, both of them were found to be unstable to the challenge of 10-fold excess formaldehyde (*23*, *24*). Therefore, they were not suitable as commercial reagents for the preparation of RP444. Hydrazone **5** contains a substituted pyridine ring and gave very low yield (~30%) of RP444 probably because it is too stable in aqueous solution to produce enough free HYNICtide for the ^{99m}Tc-labeling. Therefore, it is not suitable to be used as a commercial reagent either. Hydrazones **1**−**4** contain an aromatic benzene ring with various substituents, while the hydrazone **7** has propenyl substituent (Figure 1). These five hydrazones gave yields between 75 and 85% and were studied in the next radiolabeling experiment using higher heating temperature to see if the yield of RP444 could be improved.

Table 2. Radiolabeling Yields of RP444 Using Hydrazones at 80 °C

hydrazone	RCP (%)	*n*	hydrazone	RCP (%)	*n*
1 (TFA salt)	94.0 ± 1.4	4	**3**	79.5	1
1 (mesylate salt)	92.0 ± 1.0	3	**4**	91.0 ± 2.0	5
2	86.0 ± 1.7	3	**7**	83.3 ± 1.5	3

[a] Calculated by subtracting the percent peak area for the [^{99m}Tc]colloid determined by ITLC from the percent peak area of RP444 in the radio-HPLC. In all the cases, the [^{99m}Tc]colloid was less that 2%.

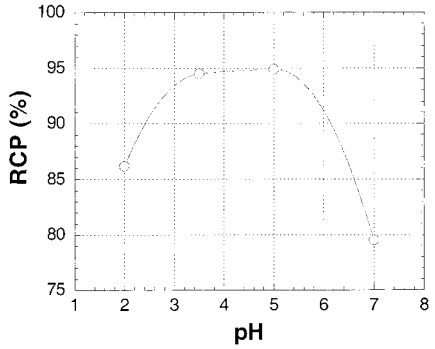


Figure 4. Plot of RCP of RP444 versus pH. Each vial contains 12.5 μg of hydrazone **4**, 3.5 mg of TPPTS, 40 mg of tricine, and 40 μg of $SnCl_2 \cdot 2H_2O$ with pH varying from 2.0 to 7.0.

In this experiment, all the component levels and reaction conditions remain the same as those used in the screening study except that the reaction mixtures were heated at 80 °C for 30 min. After radiolabeling, the reaction mixtures were analyzed by HPLC and ITLC. The RCP of RP444 was corrected for the contribution from [^{99m}Tc]colloid. The results are shown in Table 2. In general, the higher temperature and longer reaction time gave better yield for RP444, probably due to faster hydrolysis at higher temperatures.

Hydrazones **1** and **4** gave yields of RP444 higher than 90% using 80 °C and 30 min heating. Different salt forms (trifluoroacetate and mesylate) of hydrazone **1** did not have a detectable effect on the yield of RP444. The remaining three hydrazones did not give significantly higher yields than those obtained at 50 °C. On the basis of these data, it was concluded that hydrazones **1** and **4** can be used as the final intermediate for preparation of RP444 under the radiolabeling conditions descibed in the Experimental Section. It should be noted that these conditions are not optimized. Under more forcing conditions (such as heating at 100 °C), hydrazones **2** and **7** may also give ≥90% yields.

We also explored the effect of varying pH and the component levels on the yield of RP444 using hydrazone **4**. The component levels are shown in Figures 4−7. Vials containing these components were reconstituted by adding 0.5 mL of [^{99m}Tc]pertechnetate solution (100 mCi/mL). The prior elution time for the generator was 24 ± 2 h, and the eluate age was 0−2 h. The total volume of the reaction mixture was ~1.5 mL. The stannous chloride concentration was fixed at 40 μg/vial. The pH of the reaction mixture was adjusted using 1.0 N HCl. Reactions were carried out in duplicate by heating reaction mixtures at 80 °C for 30 min. The resulting solutions were analyzed by radio-HPLC and ITLC. The RCP was corrected for the contribution from [^{99m}Tc]colloid.

pH Effect. The pH of the reaction mixture has a dramatic impact on the RCP of RP444 (Figure 4). At pH

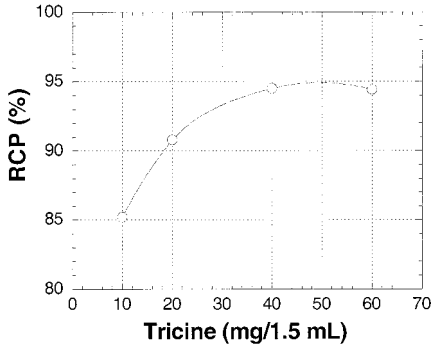


Figure 5. Plot of RCP of RP444 versus tricine concentration. Each vial contains 12.5 μg of hydrazone **4**, 3.5 mg of TPPTS, 40 μg of $SnCl_2 \cdot 2H_2O$, and various amounts of tricine with pH 3.5.

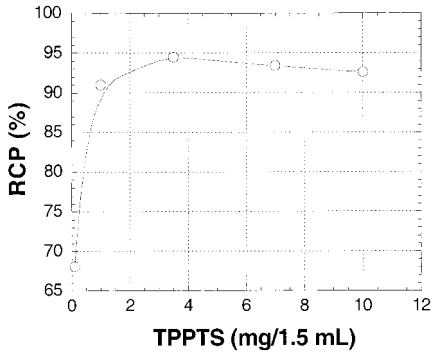


Figure 6. Plot of RCP of RP444 versus TPPTS concentration. Each vial contains 12.5 μg of hydrazone **4**, 40 mg of tricine, 40 μg of $SnCl_2 \cdot 2H_2O$, and various amounts of TPPTS with pH 3.5.

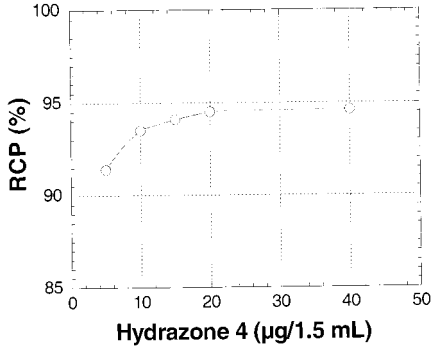


Figure 7. Plot of RCP of RP444 versus HYNICtide concentration. Each vial contains 3.5 mg of TPPTS, 40 mg of tricine, 40 μg of $SnCl_2 \cdot 2H_2O$, and various amounts of hydrazone **4** with pH 5.0.

≤3.5, the tricine coligand may become protonated, and is not able to stabilize the [^{99m}Tc]tricine intermediate. This may lead to decomposition of the [^{99m}Tc]tricine intermediate, and formation of a significant amount of [^{99m}Tc]pertechnetate. At pH ≥5.0, the hydrazone remains highly stable in solution. There is not enough hydrolyzed free hydrazine for ^{99m}Tc-labeling. Therefore, the yield of RP444 was also low. The ideal pH range for successful radiolabeling is 3.5−5.0.

Tricine Concentration. Tricine is both a stabilizing agent for the [^{99m}Tc]tricine intermediate and a coligand in the ternary ligand system at the same time. Increasing the amount of tricine from 40 to 60 mg did not have significant impact on the yield of RP444 (Figure 5). At a lower tricine level (≤20 mg), [^{99m}Tc]colloid formation became significant, and resulted in lower yield for RP444. The optimum concentration for tricine is 40−60 mg/vial.

TPPTS Concentration. In the reaction mixture, TPPTS reacts with the binary complex [^{99m}Tc(HYNICtide)(tricine)$_2$] to form RP444. Figure 6 shows the effect of TPPTS concentration on the RCP of RP444. If the amount of TPPTS was lower than 1.0 mg/1.5 mL, the yield of RP444 was dramatically reduced. Increasing the amount of TPPTS from 1.0 mg/1.5 mL to 10.0 mg/1.5 mL had no significant effect on the yield of RP444 within the experimental error. Under ideal radiolabeling conditions, the TPPTS concentration could be varied from 1.0 mg/1.5 mL to 10 mg/1.5 mL.

Hydrazone Concentration. Hydrazone concentration also affects the RCP of RP444. When the hydrazone is in large excess over the total Tc (^{99m}Tc and ^{99}Tc) in each reaction vial, hydrolysis of a small percentage of hydrazone should produce enough free HYNICtide for radiolabeling. Thus, it is not surprising that increasing the amount of hydrazone **4** from 10 to 40 μg did not have a significant effect on the yield of RP444 (Figure 7). The optimum concentration for hydrazone **4** is 20−40 μg/1.5 mL for 50 mCi of [^{99m}Tc]pertechnetate.

It should be noted that the purity of hydrazones also has dramatic impact on the yield of RP444. HYNICtide hydrazones are prepared by conjugation of cyclic peptide with slight excess succinimidyl 6-(2-aldehydehydrazino)-nicotinate (*23*, *24*). The excess succinimidyl ester is then converted to 6-(2-aldehyde-hydrazino)nicotinamide for the purpose of easy separation. Hydrazones used in this study often contain a small amount of the HYNIC-amide hydrazone as impurities. For example, hydrazone **1** contains a trace amount of 6-(2-benzaldehydehydrazino)-nicotinamide. Since the molecular weight of 6-(2-benzaldehydehydrazino)nicotinamide is only ∼1/5 of that of hydrazone **1**, one percent of it will cause at least a 5% decrease in the yield of RP444.

Stannous chloride is a reducing agent for [^{99m}Tc]-pertechnetate. If the stannous chloride level is too low (≤5 μg/mL), [^{99m}Tc]pertechnetate is often not completely reduced, and the yield of RP444 is low. If a large amount (≥100 μg/vial) is used, [^{99m}Tc]colloid formation becomes a major problem, and the corrected yield of RP444 is also low. During these radiolabeling studies, we found that the optimum range of stannous chloride is 20−50 μg/mL.

CONCLUSION

In conclusion, eight HYNICtide hydrazones (three with aliphatic substituents and five with aromatic groups functionalized by electron withdrawing or electron donating substituents) were screened and studied for their potential use as the final intermediate for preparation of RP444. It was found that using 50 °C and 30 min, heating only hydrazones **6** and **8** gave satisfactory (≥90%) yields of RP444. However, their solution instability excludes them from being used as commercial reagents. Hydrazones **1** and **4** gave ≥90% yields when reaction mixtures were heated at 80 °C for 30 min. The salt forms (trifluoroacetate and mesylate) of hydrazone **1** did not show a detectable effect on the yield of RP444. Both hydrazone **1** and hydrazone **4** can be used as the final intermediate for preparation of RP444. It seems that the combination of 40 mg tricine, 1−10 mg of TPPTS, 10−40 μg of hydrazone for 50 mCi of [^{99m}Tc]pertechnetate, 20−50 μg of stannous chloride, pH 4.5 ± 0.5, and heating at 80 °C for 30 min gives best yield of RP444. Under more forcing conditions (such as heating at 100 °C for 30 min), hydrazones **2** and **7** may also be used as the final intermediate for RP444 and give ≥90% yields.

Both hydrazones **1** and **4** have demonstrated their solution stability. They do not react with other aldehydes

and ketones (*23*, *24*). It is surprising that both hydrazones are stable enough to withstand a 10-fold excess of formaldehyde, and at the same time are reactive enough to hydrolyze in situ producing free HYNICtide for successful ^{99m}Tc-labeling.

LITERATURE CITED

(1) Schwartz, D. A., Abrams, M. J., Hauser, M. M., Gaul, F. E., Larsen, S. K., Rauh, D., and Zubieta, J. A. (1991) Preparation of hydrazino-modified proteins and their use for the synthesis of ^{99m}Tc-protein conjugates. *Bioconjugate Chem. 2*, 334−336.

(2) Abrams, M. J., Juweid, M., tenKate, C. I., Schwartz, D. A., Hauser, M. M., Gaul, F. E., Fuccello, A. J., Rubin, R. H., Strauss, H. W., and Fischman, A. J. (1990) Technetium-99m-human polyclonal IgG radiolabeled via the hydrazino nicotinamide derivative for imaging focal sites of infection in rats. *J. Nucl. Med. 31*, 2022−2028.

(3) Larson, S. K., Solomon, H. F., Caldwell, G., and Abrams, M. J. (1995) [^{99m}Tc]Tricine: a useful precursor complex for the radiolabeling of hydrazinonicotinate protein conjugates. *Bioconjugate Chem. 6*, 635−638.

(4) Edwards, D. S., Barrett, J. A., Liu, S., Ziegler, M. C., Mazaika, T., Vining, M., Bridger, G., Higgins, J., III, and Abrams, M. J. (1996) A stabilized Tc-99m complex of a chemotactic peptide-HYNIC conjugate for imaging infection. *Eur. J. Nucl. Med. 23*, 1142 (abstr. Omo440).

(5) Babich, J. W., Solomon, H., Pike, M. C., Kroon, D., Graham, W., Abrams, M. J., Tompkins, R. G., Rubin, R. H., and Fischman, A. J. (1993) Technetium-99m-labeled hydrazino nicotinamide derivatized chemotactic peptide analogues for imaging focal sites of bacterial infection. *J. Nucl. Med. 34*, 1967−1974.

(6) Babich, J. W., and Fischman, A. J. (1995) Effect of "coligand" on the biodistribution of ^{99m}Tc-labeled hydrazino nicotinic acid derivatized chemotactic peptides. *Nucl. Med. Biol. 22*, 25−30.

(7) Fischman, A. J., Babich, J. W., and Rubin, R. H. (1994) Infection imaging with technetium-99m-labeled chemotactic peptide analogues. *Semin. Nucl. Med. 24*, 154−168, references therein.

(8) Mäcke, H. R., and Behe, M. (1996) New octreotide derivatives labelled with technetium-99m. *J. Nucl. Med. 37*, 29P (abstr. 107).

(9) Behe, M., and Mäcke, H. R. (1995) New somatostatin analogues labelled with technetium-99m. *Eur. J. Nucl. Med. 22*, 791 (abstr. 267).

(10) Dewanjee, M. K., Ghalfouripour, A. K., Subramanian, M., Hanna, M., Kapadvanjwala, M., Serafini, A. N., Ezuddin, S., Lopez, D., and Sfakianakis, G. N. (1994) Labeling antisense deoxyoligonucleotide with Tc-99m and hybridation with c-myc oncogene mRNA in P388 leukemic cells. *J. Labeled Compds Radiopharm. 35*, 40−42.

(11) Dewanjee, M. K., Abrams, M. J., Wu, S. M., Kapadvanjwala, M., Serafini, A. N., and Sfakianakis, G. N. (1995) Technetium-99m labeled single-strand DNA probe for imaging thrombin in viscera formed during cardiopulmonary bypass. *J. Nucl. Med. 36*, 16P (abstr. 54).

(12) Hnatowich, D. J., Winnard, P., Jr., Virzi, F., Fogarsi, M., Sano, T., Smith, C. L., Cantor, C. L., and Rusckowski, M. (1995) Technetium-99m labeling of DNA oligonucleotides. *J. Nucl. Med. 36*, 2306−2314.

(13) Liu, S., Edwards, D. S., and Barrett, J. A. (1997) ^{99m}Tc-labeling of highly potent small peptides. *Bioconjugate Chem. 8*, 621−636.

(14) Edwards, D. S., and Liu, S. (1997) ^{99m}Tc-labeling of hydrazino nicotinamide (HYNIC) modified highly potent small molecules: problems and solutions. *Transition Metal Chem. 22*, 425−426.

(15) Liu, S., and Edwards, D. S. (1995) New N_2S_2 diamidedithiol and N_3S triamidethiols as bifunctional chelating agents for labeling small peptides with technetium-99m. In *Technetium and Rhenium in Chemistry and Nuclear Medicine* (M. Nicolini, G. Banoli, and U. Mazzi, Eds.) Vol. 4, pp 383−393, SGEditorali, Padova.

(16) Liu, S., Edwards, D. S., Looby, R. J., Harris, A. R., Poirier, M. J., Barrett, J. A., Heminway, S. J., and Carroll, T. R (1996) Labeling a hydrazino nicotinamide-modified cyclic IIb/IIIa receptor antagonist with ^{99m}Tc using aminocarboxylates as coligands. *Bioconjugate Chem. 7*, 63−71.

(17) Liu, S., Edwards, D. S., Looby, R. J., Harris, A. R., Poirier, M. J., Rajopadhye, M., and Bourque, J. P. (1996) Labeling cyclic IIb/IIIa receptor antagonists with ^{99m}Tc by the preformed chelate approach: effects of chelators on properties of [^{99m}Tc]chelator-peptide conjugate. *Bioconjugate Chem. 7*, 196−202.

(18) Barrett, J. A., Damphousse, D. J., Heminway, S. J, Liu, S., Edwards, D. S., Looby, R. J., and Carroll, T. R. (1996) Biological evaluation of ^{99m}Tc-labeled cyclic GPIIb/IIIa receptor antagonists in the canine arteriovenous shunt and deep vein thrombosis models: effects of chelators on biological properties of [^{99m}Tc]chelator-peptide conjugates. *Bioconjugate Chem. 7*, 203−208.

(19) Edwards, D. S., Liu, S., Harris, A. R., Looby, R. J., Ziegler, M. C., Heminway, S. J., Barrett, J. A., and Carroll, T. R. (1997) A new and versatile ternary ligand system for technetium radiopharmaceuticals: water soluble phosphines and tricine as coligands in labeling a hydrazinonicotinamide-modified cyclic glycoprotein IIb/IIIa receptor antagonist with ^{99m}Tc. *Bioconjugate Chem. 8*, 146−154.

(20) Barrett, J. A., Crocker, A. C., Damphousse, D. J., Heminway, S. J., Liu, S., Edwards, D. S., Harris, A. R., Looby, R. J., Lazewatsky, J. L., Kagan, M., Mazaika, T. J., and Carroll, T. R. (1997) Biological evaluation of thrombus imaging agents utilizing water soluble phosphines and tricine as coligands to label a hydrazinonicotinamide-modified cyclic glycoprotein IIb/IIIa receptor antagonist with ^{99m}Tc. *Bioconjuate Chem. 8*, 155−160.

(21) Line, B. R., Seabold, J. E., Edell, S. L., Weiland, F. L., Heit, J. A., Crane, P. D., Widner, P. L., and Haber, S. J. (1998) Preliminary diagnostic results with DMP444, a new thrombus imaging agent. *J. Nucl. Med. 39*, 218P (abstr. 969).

(22) Schwartz, D. A., Abrams, M. J., Gladomenico, C. M., and Zubieta, J. A. (1993) Certain pyridyl hydrazines and hydrazides useful for protein labeling. U.S. Patent 5,206,370.

(23) Sworin, M., Rajopadhye, M., Harris, T. D., Edwards, D. S., Cheesman, E. H., and Liu, S. (1998) Stable hydrazones linked to a peptide moiety as reagents for the preparation of radiopharmaceuticals. U.S. Patent 5,750,088.

(24) Harris, T. D., Rajopadhye, M., Sworin, M., and Cheesman, E. H. Synthesis of stable hydrazones of a hydrazinonicotinyl-modified peptide for the preparation of ^{99m}Tc-labeled radiopharmaceuticals. *Bioconjugate Chem.* (submitted for publication).

(25) Bartik, T., Bartik, B., Hanson, B. E., Glass, T., and Bebout, W. E. (1992) Comments on the synthesis of trisulfonated triphenylphosphine: reaction monitoring by NMR spectroscopy. *Inorg. Chem. 31*, 2667−2670.

(26) Liu, S., Edwards, D. S., Harris, A. R., Heminway, S. J., and Barrett, J. A. (1999) Technetium complexes of a hydrazinonicotinamide-conjugated cyclic peptide and 2-hydrazinopyridine: synthesis and characterization. *Inorg. Chem.* 38, 1326−1335.

BC990022E

Synthesis of Stable Hydrazones of a Hydrazinonicotinyl-Modified Peptide for the Preparation of ^{99m}Tc-Labeled Radiopharmaceuticals

Thomas D. Harris,*,† Michael Sworin,† Neal Williams,† Milind Rajopadhye,† Paul R. Damphousse,† Danuta Glowacka,† Michael J. Poirier,‡ and Karmine Yu†

DuPont Pharmaceutical Co., 331 Treble Cove Road, North Billerica, Massachusetts 01862, and Upsher-Smith Laboratories, Inc., 14905 23rd Avenue North, Minneapolis, Minnesota 55447. Received February 25, 1999; Revised Manuscript Received May 10, 1999

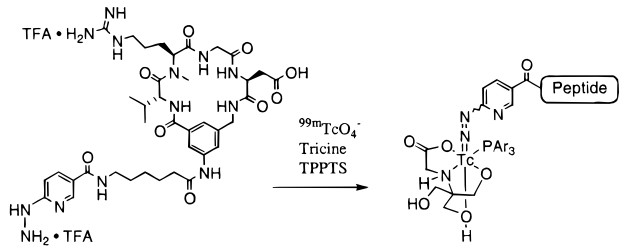
Hydrazones of a 6-hydrazinonicotinyl-modified cyclic peptide IIb/IIIa receptor antagonist were prepared in order to protect the hydrazine moiety from reaction with trace aldehyde and ketone impurities encountered during the process of manufacturing and compounding lyophilized kits used in radiolabeling with ^{99m}Tc. Hydrazones were prepared by either a direct reaction of the 6-hydrazinonicotinyl-modified cyclic peptide with carbonyl compounds or by conjugation of the cyclic peptide with hydrazones of succinimidyl 6-hydrazinonicotinate. Stability of the hydrazones was evaluated by treatment with formaldehyde. Hydrazones derived from simple aliphatic aldehydes underwent an exchange reaction with formaldehyde, while hydrazones of aromatic aldehydes and ketones provided the greatest level of stability when challenged with formaldehyde. We have been successful in protecting 6-hydrazinonicotinyl-modified cyclic peptides from reacting with formaldehyde, while still allowing sufficient reactivity for radiolabeling with ^{99m}Tc. The hydrazones of succinimidyl 6-hydrazinonicotinate are convenient and general reagents for forming 6-hydrazinonicotinyl conjugates with amino-functionalized bioactive molecules.

INTRODUCTION

There is currently a great need for new methods for the noninvasive diagnosis of a variety of diseases such as thromboembolic disease, infection, and cancer. Radiopharmaceuticals comprised of biomolecules labeled with gamma-ray emitting radionuclides have shown promise in fulfilling this need. The biomolecule serves to selectively localize the radionuclides at sites of disease and thus allow the sites to be visualized by gamma scintigraphy. The preferred method of introducing the radiolabel is by the use of a heterobifunctional molecule containing a moiety for coordination of the radionuclide and a moiety for covalent attachment to the biomolecule.

Abrams and co-workers have recently described the modification of polyclonal IgG with the 6-hydrazinonicotinyl group (Hynic) for labeling with ^{99m}Tc and subsequent imaging of focal sites of infection (*1*−*3*). Focal infections have also been imaged using Hynic-modified chemotactic peptides (*4*−*6*) and Hynic-modified LTB4 antagonists (*7*−*9*). Hynic derivatives of somatostatin and monoclonal antibody fragments have shown promise as tumor imaging agents (*10*−*11*). We recently reported the synthesis of a Hynic-modified cyclic peptide glycoprotein IIb/IIIa receptor antagonist (**1**) containing the N-Me-Arg-Gly-Asp motif, as shown in Scheme 1 (*12*). Hynic is tethered to the meta-aminobenzoic acid (Mamb) group via a 5-aminocaproic acid (5-Aca) spacer. For labeling with ^{99m}Tc, the Hynic-modified cyclic peptide is reacted with ^{99m}Tc pertechnetate in the presence of tricine and trisodium triphenylphosphine-3,3′,3″-trisulfonate (TPPTS).

Scheme 1. Synthesis of Ternary Ligand Complex RP444



1 **RP444**, Ar = 3-sulfonatophenyl

This forms the ternary ligand system **RP444** (Scheme 1) in which the technetium is bound to Hynic through a diazenido linkage with the coordination sphere of technetium completed by the tricine and TPPTS ancillary ligands (*13*). The combination of tricine, TPPTS, and Hynic−peptide conjugate **1** can be rapidly labeled with 25 mCi of ^{99m}Tc to >90% radiochemical purity using as little as 0.02 μmol of conjugate **1**. Evaluation of **RP444** in the canine arteriovenous and deep vein thrombosis models has demonstrated its ability to rapidly detect growing thrombi under both mixed arterial and venous conditions (*12*). **RP444** is a developmental candidate currently in clinical trials for the rapid detection of thromboembolic events.

During the process of manufacturing and compounding the lyophilized kit used in the preparation of **RP444**, we discovered that Hynic−peptide conjugate **1** reacts readily with aldehydes and ketones to form various hydrazone impurities. The presence of aldehyde and ketone impurities is unavoidable in a commercial pharmaceutical manufacturing setting, because they are extracted from various rubber and plastic materials and are also used in common disinfectants. Formaldehyde is particularly

* To whom correspondence should be addressed. E-mail: thomas.d.harris@dupontpharma.com. Phone: 978-671-8266. Fax: 978-436-7500.

† DuPont Pharmaceutical Co.

‡ Upsher-Smith Laboratories, Inc.

10.1021/bc9900237 CCC: $18.00 © 1999 American Chemical Society
Published on Web 07/14/1999

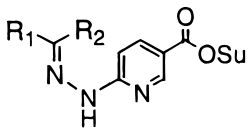


Figure 1. General structure of succinimidyl hydrazononicotinates.

ubiquitous. Given the very small quantity of Hynic−peptide conjugate **1** present in a single-dosage vial (∼20 μg), the low level of aldehyde and ketone-derived impurities became significant. We began a search for a hydrazine-protecting group which would block the reaction of the hydrazine moiety of **1** with aldehyde and ketone impurities present during the manufacturing process, but which would be sufficiently labile to form a free hydrazine during labeling with ^{99m}Tc. Schwartz et al. have described the use of lower alkyl hydrazone protecting groups to prevent cross-reaction between the hydrazine moiety and protein-reactive substituents during Hynic modification (*14*). While these alkyl hydrazones prevent the formation of hydrazone-modified protein, they undergo an exchange reaction with other aldehydes and ketones, especially formaldehyde, to form different hydrazones. Thus, the lower alkyl hydrazones are unsuitable for the protection of the hydrazine moiety of Hynic during the manufacturing process. In this paper, we describe the synthesis of several stable hydrazones of Hynic−peptide conjugate **1**, and examine their solution stability in the presence of formaldehyde. The majority of these hydrazones do not react appreciably with formaldehyde under simulated manufacturing conditions, but are still reactive enough to form ternary ligand complexes with ^{99m}Tc. The radiolabeling of these hydrazones with ^{99m}Tc to form **RP444** is reported in a companion paper in this issue. We have also demonstrated the use of succinimidyl esters of Hynic hydrazones (Figure 1) as general reagents for forming stable Hynic hydrazone conjugates with amino-functionalized bioactive molecules.

EXPERIMENTAL PROCEDURES

General. ^{1}H NMR spectra were obtained on a Varian 270 MHz spectrometer in the indicated solvent. Chemical shifts are expressed in δ units downfield from TMS. Low-resolution MS data were obtained on a VG Trio 2000 spectrometer using the indicated ionization method. High-resolution MS data were obtained on a VG 70-VSE spectrometer using the indicated ionization method. Analytical HPLC separations were accomplished on a Zorbax-Rx C18 column, 4.6 × 250 mm, operated at 50 °C using a 2.0%/min gradient of 10−50% ACN containing 50 mM ammonium acetate at a flow rate of 1.5 mL/min. UV detection was set at 240 nm. Preparative HPLC separations were accomplished at ambient temperatures using the column and gradient conditions indicated in individual procedures. UV detection was set at 220 nm. Products were isolated from HPLC eluant by freeze-drying. Cyclo-[D-Val-NMeArg-Gly-Asp-Mamb(5-Aca)] and cyclo-(D-Val-NMeArg-Gly-Asp-Mamb(Hynic-5-Aca)] were synthesized as previously described (*12, 15*). Succinimidyl 6-(2-propenylhydrazone)nicotinate was prepared as previously described (*14*). Deionized water was obtained from a Milli-Q Water System and was of >18 MΩ quality. HPLC-grade ACN was obtained from J. T. Baker. All other reagents and solvents were obtained from Aldrich Chemical Co. and Fluka Chemical Corp.

General Procedure for the Preparation of Hynic Hydrazone Succinimidyl Esters 3−9. To a suspension of 6-hydrazinonicotinic acid (6.5 mmol) in DMF (40 mL) was added the aldehyde or ketone (6.9 mmol), and the reaction mixture was allowed to stir at room temperature for 3 h. To the homogeneous reaction solution was added N-hydroxysuccinimide (748 mg, 6.5 mmol) and DCC (2.76 g, 13.4 mmol), and the reaction was allowed to stir at room temperature for 18 h. The DCU precipitate was removed by filtration. The filtrate was concentrated, diluted with EtOAc (50 mL), and the mixture was heated at reflux for 1 h. Filtration of the hot mixture provided the hydrazone as a pale yellow powder. This material was used without further purification.

Succinimidyl 6-(2-Benzaldehydehydrazono)nicotinate (3). Benzaldehyde provided 1.78 g (81%) of the title compound. ^{1}H NMR (D_6-DMSO): 11.86 (s, NH), 8.82 (dd, Py-H), 8.20 (dd, Py-H), 8.20 (s, =CH), 7.75 (dd, 2 Ar−H), 7.43 (m, Py-H & 3 Ar−H), 2.89 (s, 2 CH_2). DCI(NH_3)-MS calcd for $C_{17}H_{15}N_4O_4$ [M+H]: 339.1093. Found: 339.1084.

Succinimidyl 6-[2-(2-Sulfo)benzaldehydehydrazono]nicotinate Sodium Salt (4). Sodium 2-formylbenzenesulfonate provided 1.63 g (85%) of the title compound. ^{1}H NMR (D_6-DMSO): 11.91 (s, NH), 9.16 (s, =CH), 8.79 (dd, Py-H), 8.16 (dd, Py-H), 8.03 (dd, Ar−H), 7.79 (dd, Ar−H), 7.35 (m, Py-H & 2 Ar−H), 2.88 (s, 2 CH_2). FAB(NBA)-MS calcd for $C_{17}H_{15}N_4O_7S$ [M + H]: 419.0661. Found: 419.0654. Anal. calcd for $C_{17}H_{14}N_4NaO_7S\cdot(H_2O)_{1.5}$: C, 43.69; H, 3.45; N, 11.99; Na, 4.92; S, 6.86. Found: C, 43.66; H, 3.62; N, 12.10; Na, 4.75; S, 6.43.

Succinimidyl 6-[2-(4-Dimethylamino)benzaldehydehydrazono]nicotinate (5). 4-Dimethylaminobenzaldehyde provided 1.20 g (48%) of the title compound. ^{1}H NMR (D_6-DMSO): 11.58 (s, NH), 8.76 (dd, Py-H), 8.13 (dd, Py-H), 8.07 (s, =CH), 7.54 (d, 2 Ar−H), 7.29 (d, Py-H), 6.75 (d, 2 Ar−H), 2.97 (s, 2 NCH_3), 2.88 (s, 2 CH_2). DCI(NH_3)-MS calcd for $C_{19}H_{20}N_5O_4$ [M + H]: 382.1515. Found: 382.1513.

Succinimidyl 6-(2-Cyclopentanonehydrazono)nicotinate (6). Cyclopentanone provided 1.78 g (86%) of the title compound. ^{1}H NMR (D_6-DMSO): 10.33 (s, NH), 8.76 (dd, Py-H), 8.11 (dd, Py-H), 7.15 (d, Py-H), 2.88 (s, 2 CH_2), 2.41 (q, 2 CH_2), 1.75 (m, 2 CH_2). DCI(NH_3)-MS calcd for $C_{15}H_{17}N_4O_4$ [M + H]: 317.1250. Found: 317.1259.

Succinimidyl 6-(2-Acetophenonehydrazono)nicotinate (7). Acetophenone provided 2.11 g (92%) of the title compound. ^{1}H NMR (D_6-DMSO): 10.86 (s, NH), 8.84 (dd, Py-H), 8.21 (dd, Py-H), 7.86 (dd, 2 Ar−H), 7.41 (m, Py-H and 3 Ar−H), 2.89 (s, 2 CH_2), 2.39 (s, CH_3). DCI(NH_3)-MS calcd for $C_{18}H_{17}N_4O_4$ [M + H]: 353.1250. Found: 353.1244.

Succinimidyl 6-[2-(1-Methoxycarbonyl)acetaldehydehydrazono]nicotinate (8). Methyl pyruvate provided 0.90 g (41%) of the title compound. ^{1}H NMR (D_6-DMSO): 11.21 (s, NH), 8.91 (dd, Py-H), 8.33 (dd, Py-H), 7.42 (d, Py-H), 3.78 (s, OCH_3), 2.89 (s, 2 CH_2), 2.18 (s, CH_3). DCI(NH_3)-MS calcd for $C_{14}H_{15}N_4O_6$ [M + H]: 335.0991. Found: 335.1004.

Succinimidyl 6-[2-(2-Methoxycarbonyl)cyclopentanonehydrazono]nicotinate (9). 2-Methoxycarbonylcyclopentanone provided 1.80 g (74%) of the title compound. ^{1}H NMR (D_6-DMSO): 10.56 (s, NH), 8.79 (dd, Py-H), 8.15 (dd, Py-H), 7.11 (d, Py-H), 3.67 (s, OCH_3), 3.55 (t, CH), 2.88 (s, 2 CH_2), 2.50 (m, CH_2), 1.90 (m, 2 CH_2). DCI(NH_3)-MS calcd for $C_{17}H_{19}N_4O_6$ [M + H]: 375.1304. Found: 375.1310.

Synthesis of the 2-Formylbenzenesulfonic Acid Hydrazone of Cyclo-(D-Val-NMeArg-Gly-Asp-Mamb-[hydrazinonicotinyl-5-Aca)] (10). *Method A*. A solution of succinimidyl 6-[2-(2-sulfo)benzaldehydehydrazono]nicotinate sodium salt (**4**) (220 mg, 0.50 mmol), cyclo-[D-

Val-NMeArg-Gly-Asp-Mamb(5-Aca)]·2 TFA (465 mg, 0.50 mmol), and TEA 0.208 mL, 1.50 mmol) in anhydrous DMF (3 mL) was stirred at ambient temperatures under nitrogen for 18 h. The DMF was removed under vacuum, and the residue was triturated with EtOAc to give crude product as a pale yellow powder (0.54 g). A 36 mg sample was purified by reversed-phase HPLC on a Vydac C18 Protein and Peptide column (22 × 250 mm) at a flow rate of 15 mL/min using a 0.30%/min gradient of 18 to 27% ACN containing 50 mM ammonium acetate. The product fraction (retention time 20.6 min) was lyophilized to give the title compound as a fluffy colorless solid (20 mg, 66%). Analytical HPLC indicated a product purity of 97.7%. DCI(NH_3)-MS calcd for $C_{45}H_{59}N_{13}O_{12}S$ [M + H]: 1006.4205. Found: 1006.4200.

Method B. Sodium 2-formylbenzenesulfonate (3.9 mg, 0.019 mmol) and cyclo-[D-Val-NMeArg-Gly-Asp-Mamb-(hydrazinonicotinyl-5-Aca)] (10 mg, 0.0094 mmol) were dissolved in 0.05 M sodium phosphate buffer, pH 7.0 (1.0 mL) and allowed to stand at ambient temperatures for 1.5 h, at which time the entire reaction had turned to a gel. The gel was dissolved in 90:10 0.1M ammonium acetate:ACN (1.0 mL) and purified using reversed-phase HPLC on a Zorbax-RX C18 column (21.2 × 250 mm) at a flow rate of 15 mL/min using 10% ACN containing 0.1 M ammonium acetate for 2 min, followed by a 2.22%/min gradient of 10 to 50% ACN containing 0.1 M ammonium acetate. The product fraction (retention time 12.9 min) was lyophilized to give the title compound as a fluffy colorless solid (7 mg, 74%). Analytical HPLC indicated a product purity of 97.3%. DCI(NH_3)-MS: [M + H] = 1006.3.

General Procedure for the Synthesis of Cyclo-[D-Val-NMeArg-Gly-Asp-Mamb(hydrazinonicotinyl-5-Aca)] Hydrazones 11−17 from Succinimidyl Hydrazononicotinates. To an equimolar solution of cyclo-[D-Val-NMeArg-Gly-Asp-Mamb(5-Aca)]·2 TFA and succinimidyl hydrazononicotinate in DMF (1 mL) was added 4 equiv of TEA, and the reaction mixture was allowed to stir at ambient temperatures for 42 h. The reaction mixture was concentrated, dissolved in 50% ACN, and lyophilized to provide the crude title compound as an off-white powder. Purification was accomplished by reversed-phase HPLC on a Vydac C18 Protein & Peptide column (22 × 250 mm) using the specified ACN gradient containing 0.1% TFA at a flow rate of 15 mL/min to give the TFA salt of the title compound as a colorless fluffy solid.

Benzaldehyde Hydrazone of Cyclo-[D-Val-NMeArg-Gly-Asp-Mamb(hydrazinonicotinyl-5-Aca)] (11). Succinimidyl 6-(2-benzaldehydehydrazono)nicotinate (**3**) (7.5 mg, 0.022 mmol) provided 17.5 mg (71%) of the title compound after HPLC purification (1.65%/min gradient of 6 to 72%, retention time 30.9 min). ^{1}H NMR (D_6-DMSO): 11.30 (br s, OH), 10.02 (s, NH), 8.94 (d, 1H), 8.61 (d, 1H), 8.55 (d, 1H), 8.41 (m, 2H), 8.10 (s, =CH), 8.09 (m, 1H), 7.70 (m, 4H), 7.61 (m, 1H), 7.52 (t, 1H), 7.42 (m, 3H), 7.27 (d, 1H), 7.07 (s, 1H), 5.18 (dd, 1H), 4.53 (m, 2H), 4.34 (dd, 1H), 4.20 (dd, 1H), 4.02 (dd, 1H), 3.25 (q, 2H), 3.13 (q, 2H), 2.99 (s, NCH_3), 2.72 (dd, 1H), 2.50 (m, 1H), 2.33 (t, 2H), 2.10 (m, 2H), 1.60 (m, 5H), 1.35 (m, 4H), 1.10 (d, CH_3), 0.92 (d, CH_3). FAB(NBA)-MS calcd for $C_{45}H_{60}N_{13}O_9$ [M + H]: 926.4637. Found: 926.4625.

4-Dimethylaminobenzaldehyde Hydrazone of Cyclo-[D-Val-NMeArg-Gly-Asp-Mamb(hydrazinonicotinyl-5-Aca)] (12). Succinimidyl 6-[2-(4-dimethylamino)-benzaldehydehydrazono]nicotinate (**5**) (13.5 mg, 0.034 mmol) provided 29.7 mg (72%) of the title compound after HPLC purification (2.2%/min gradient of 6 to 72%, retention time 26.2 min). ^{1}H NMR (D_6-DMSO): 10.03 (s, NH), 8.94 (d, 1H), 8.55 (d, 1H), 8.50 (s, 1H), 8.42 (t, 1H), 8.15 (br s, 1H), 8.06 (s, 1H), 7.70 (d, 2H), 7.61 (m, 4H), 7.16 (d, 1H), 7.07 (s, 1H), 7.00 (br s, 2H), 6.76 (d, 2H), 5.17 (dd, 1H), 4.52 (m, 2H), 4.33 (dd, 1H), 4.20 (dd, 1H), 3.25 (q, 2H), 3.12 (q, 2H), 2.98 (s, 3 NCH_3), 2.72 (dd, 1H), 2.50 (m, 1H), 2.33 (t, 2H), 2.10 (m, 2H), 1.60 (m, 5H), 1.35 (m, 4H), 1.10 (d, CH_3), 0.92 (d, CH_3). FAB(NBA)-MS calcd for $C_{47}H_{65}N_{14}O_9$ [M + H]: 969.5059. Found: 969.5043.

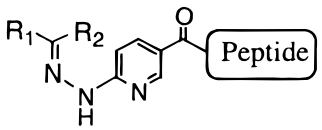
Cyclopentanone Hydrazone of Cyclo-[D-Val-NMeArg-Gly-Asp-Mamb(hydrazinonicotinyl-5-Aca)] (13). Succinimidyl 6-(2-cyclopentanonehydrazono)nicotinate (**6**) (35 mg. 0.108 mmol) provided the crude title compound (131 mg) as a pale yellow powder. HPLC purification (2.2%/min gradient of 2 to 90%, retention time 24.1 min) of a portion of this material gave pure title compound. ^{1}H NMR (D_6-DMSO): 10.02 (s, NH), 8.93 (d, 1H), 8.61 (d, 1H), 8.55 (d, 1H), 8.51 (s, 1H), 8.41 (t, 1H), 8.10 (m, 1H), 7.70 (s, 2H), 7.55 (m, 1H), 7.52 (t, 1H), 7.10 (br s, 3H), 7.06 (s, 1H), 5.17 (dd, 1H), 4.52 (m, 2H), 4.33 (dd, 1H), 4.19 (dd, 1H), 4.02 (dd, 1H), 3.62 (d, 1H), 3.24 (q, 2H), 3.12 (q, 2H), 2.99 (s, NCH_3), 2.72 (dd, 1H), 2.50 (m, 1H), 2.41 (m, 4H), 2.33 (t, 2H), 2.10 (m, 2H), 1.75 (m, 3H), 1.68 (m, 4H), 1.34 (m, 4H), 1.10 (d, CH_3), 0.92 (d, CH_3). FAB(NBA/TFA)-MS calcd for $C_{43}H_{62}N_{13}O_9$ [M + H]: 904.4793. Found: 904.5136.

Acetophenone Hydrazone of Cyclo-[D-Val-NMeArg-Gly-Asp-Mamb(hydrazinonicotinyl-5-Aca)] (14). Succinimidyl 6-(2-acetophenonehydrazono)nicotinate (**7**) (38 mg, 0.108 mmol) provided the crude title compound (30 mg) as a colorless powder. HPLC purification (2.2%/min gradient of 2 to 90%, retention time 31.1 min) gave pure title compound. ^{1}H NMR (D_6-DMSO): 10.03 (s, NH), 8.93 (d, 1H), 8.62 (s, 1H), 8.55 (d, 1H), 8.42 (m, 2H), 8.13 (br s, 1H), 7.87 (d, 2H), 7.70 (m, 2H), 7.55 (m, 2H), 7.40 (m, 4H), 7.07 (s, 1H), 5.17 (dd, 1H), 4.52 (m, 2H), 4.33 (dd, 1H), 4.20 (dd, 1H), 4.02 (dd, 1H), 3.63 (dd, 1H), 3.26 (q, 2H), 3.12 (q, 2H), 2.98 (s, NCH_3), 2.72 (dd, 1H), 2.50 (m, 1H), 2.35 (s, CH_3), 2.33 (m, 2H), 2.10 (m, 2H), 1.60 (m, 5H), 1.35 (m, 4H), 1.10 (d, CH_3), 0.92 (d, CH_3). FAB-(NBA)-MS calcd for $C_{46}H_{62}N_{13}O_9$ [M + H]: 940.4793. Found: 940.4818.

Methyl Pyruvate Hydrazone of Cyclo-[D-Val-N-MeArg-Gly-Asp-Mamb(hydrazinonicotinyl-5-Aca)] (15). Succinimidyl 6-[2-(1-methoxy-carbonyl)acetaldehydehydrazono]nicotinate (**8**) (36 mg, 0.108 mmol) provided the crude title compound (123 mg) as a pale yellow powder. HPLC purification (2.2%/min gradient of 2 to 90%, retention time 22.3 min) gave pure title compound. ^{1}H NMR (D_6-DMSO) 10.69 (s, NH), 10.02 (s, NH), 8.92 (d, 1H), 8.70 (d, 1H), 8.55 (d, 1H), 8.44 (m, 2H), 8.14 (dd, 1H), 7.70 (s, 2H), 7.56 (m, 2H), 7.28 (d, 1H), 7.07 (s, 1H), 5.17 (dd, 1H), 4.52 (m, 2H), 4.33 (dd, 1H), 4.19 (dd, 1H), 4.04 (m, 1H), 3.76 (s, OCH_3), 3.63 (dd, 1H), 3.26 (q, 2H), 3.13 (q, 2H), 2.99 (s, NCH_3), 2.72 (dd, 1H), 2.50 (m, 1H), 2.33 (t, 2H), 2.13 (s, CH_3), 1.60 (m, 5H), 1.35 (m, 4H), 1.10 (d, CH_3), 0.92 (d, CH_3). FAB(NBA)-MS calcd for $C_{42}H_{60}N_{13}O_{11}$ [M + H]: 922.4535. Found: 922.4539.

2-(Methoxycarbonyl)cyclopentanone Hydrazone of Cyclo-[D-Val-NMeArg-Gly-Asp-Mamb(Hynic-5-Aca)] (16). Succinimidyl 6-(2-(2-methoxycarbonyl)cyclopentanonehydrazono)nicotinate (**9**) (41 mg, 0.108 mmol) provided the crude title compound (138 mg) as a pale yellow powder. HPLC purification (2.2%/min gradient of 2 to 90%, retention time 24.9 min) of a portion of this material gave pure title compound. ^{1}H NMR (D_6-DMSO): 10.01 (s, NH), 8.90 (m, 1H), 8.57 (m, 2H), 8.39 (m, 2H), 8.07 (d, 1H), 7.71 (s, 2H), 7.59 (m, 2H), 7.09 (m,

Table 1. Stability of Hynic Hydrazones in the Presence of 1 equiv of Formaldehyde



Hynic Hydrazones **10-27**

hydrazone	carbonyl compound	R_1	R_2	% hydrazone remaining at 2 h
10	2-formylbenzenesulfonic acid	2-$NaO_3S-C_6H_4$	H	100
11	benzaldehyde	C_6H_5	H	100/100[a]
12	4-dimethylaminobenzaldehyde	4-$Me_2N-C_6H_4$	H	100
13	cyclopentanone	-$CH_2CH_2CH_2CH_2$-		100
17	propionaldehyde	CH_3CH_2	H	23
18	4-carboxybenzaldehyde	4-$HO_2C-C_6H_4$	H	100
19	crotonaldehyde	$CH_3CH{=}CH$	H	100
20	5-nitro-2-furaldehyde	5-$NO_2-C_4H_2O$	H	100
21	glyoxylic acid	COOH	H	>99
22	4-pyridinecarboxaldehyde	4-C_5H_4N	H	100
23[b]	phenylacetaldehyde	$C_6H_5-CH_2$	H	75
24[b]	glycolaldehyde	$HOCH_2$	H	60
25[c]	benzaldehyde-2,4-disulfonic acid	2,4-$(NaO_3S)-C_6H_3$	H	
26[c]	3-pyridinecarboxaldehyde methiodide	I^- 3-$(Me-C_5H_3N)^+$	H	
27[c]	4-pyridinecarboxaldehyde methiodide	I^- 4-$(Me-C_5H_3N)^+$	H	

[a] Also tested with 10 equiv of formaldehyde and found to be completely stable. [b] Hydrazone formed in situ by treatment with 1 equiv of aldehyde. [c] Hydrazone failed to form in situ.

2H), 5.17 (dd, 1H), 4.52 (m, 2H), 4.34 (dd, 1H), 4.20 (dd, 1H), 4.02 (d, 1H), 3.67 (s, OCH_3), 3.24 (q, 2H), 3.12 (m, 2H), 2.99 (s, NCH_3), 2.71 (dd, 1H), 2.50 (m, 1H), 2.34 (t, 2H), 2.10 (m, 4H), 1.60 (m, 5H), 1.34 (m, 3H), 1.25 (m, 2H), 1.10 (d, CH_3), 0.93 (d, CH_3). ESI-MS: 962.5 [M + H].

Propionaldehyde Hydrazone of Cyclo-[D-Val-NMeArg-Gly-Asp-Mamb(Hynic-5-Aca)] (17). Succinimidyl 6-(2-propionaldehydehydrazono)nicotinate (7.0 mg, 0.022 mmol) provided 8.4 mg (39%) of the title compound after HPLC purification (2.2%/min gradient of 2 to 90%, retention time 22.3 min). FAB(NBA)-MS calcd for $C_{41}H_{60}N_{13}O_9$ [M + H]: 878.4640. Found: 878.4622.

General Procedure for the Synthesis of Cyclo-[D-Val-NMeArg-Gly-Asp-Mamb(hydrazinonicotinyl-5-Aca)] Hydrazones 18−21 Directly from the Peptide−Hynic Conjugates. A mixture of cyclo-[D-Val-NMeArg-Gly-Asp-Mamb(hydrazinonicotinyl-5-Aca)]·2 HBr (50 mg, 0.05 mmol) and aldehyde or ketone (0.70 mmol) in DMF (1 mL) was stirred at ambient temperature under nitrogen for 4 h. The solvent was removed under vacuum, the residue was dissolved in 50% ACN, and lyophilized to dryness. The crude mixture was purified by reversed-phase HPLC on a Zorbax-RX C18 column (21.2 × 250 mm) at a flow rate of 15 mL/min using 10% ACN containing 50 mM ammonium acetate for 2 min followed by the specified ACN gradient containing 50 mM ammonium acetate to give the title compound as a colorless fluffy solid.

4-Carboxybenzaldehyde Hydrazone of Cyclo-[D-Val-NMeArg-Gly-Asp-Mamb(hydrazinonicotinyl-5-Aca)] (18). 4-Carboxybenzaldehyde gave 7.0 mg (14%) of the title compound after HPLC purification (0.54%/min gradient of 10 to 25%, retention time 22.5 min). DCI-(NH_3)-MS calcd for $C_{46}H_{60}N_{13}O_{11}$ [M + H]: 970.4535. Found: 970.4535.

Crotonaldehyde Hydrazone of Cyclo-[D-Val-NMeArg-Gly-Asp-Mamb(hydrazinonicotinyl-5-Aca)] (19). Crotonaldehyde gave 4.5 mg (10%) of the title compound after HPLC purification (6.0%/min gradient of 10 to 28%, followed by a 0.28%/min gradient of 28 to 35%, retention time 12.6 min). DCI(NH_3)-MS calcd for $C_{42}H_{60}N_{13}O_9$ [M + H]: 890.4636. Found: 890.4637.

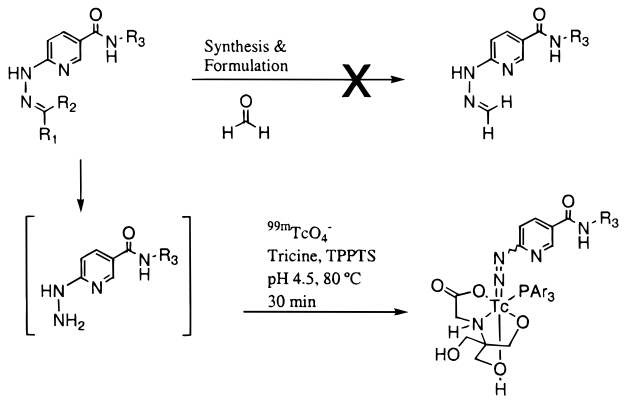
5-Nitro-2-furaldehyde Hydrazone of Cyclo-[D-Val-NMeArg-Gly-Asp-Mamb(hydrazinonicotinyl-5-Aca)] (20). 5-Nitro-2-furaldehyde gave 2.0 mg (4.2%) of the title compound after HPLC purification (6.0%/min gradient of 10 to 28%, followed by a 0.08%/min gradient of 28 to 30%, retention time 11.9 min). DCI(NH_3)-MS calcd for $C_{43}H_{57}N_{14}O_{12}$ [M + H]: 961.4280. Found: 961.4280.

Glyoxylic Acid Hydrazone of Cyclo-[D-Val-NMeArg-Gly-Asp-Mamb(hydrazinonicotinyl-5-Aca)] (21). Glyoxylic acid gave 4.6 mg (10%) of the title compound after HPLC purification (0.43%/min gradient of 10 to 25%, retention time 21.1 min). DCI(NH_3)-MS calcd for $C_{40}H_{56}N_{13}O_{11}$ [M + H]: 894.4222. Found: 894.4225.

Synthesis of the 4-Pyridinecarboxaldehyde Hydrazone of Cyclo-[D-Val-NMeArg-Gly-Asp-Mamb(hydrazinonicotinyl-5-Aca)] (22). 4-Pyridinecarboxaldehyde (1.14 mg, 0.011 mmol) and cyclo-[D-Val-NMeArg-Gly-Asp-Mamb(Hynic-5-Aca)] (10 mg, 0.0094 mmol) were dissolved in 0.05 M sodium phosphate buffer, pH 7.0 (5.0 mL) and allowed to stand at ambient temperature for 72 h. The now slightly yellow solution was lyophilized to dryness, and the resulting solid was purified using reversed-phase HPLC with a preparative Zorbax-RX C18 column (21.2 × 250 mm) at a flow rate of 15 mL/min using 10% ACN containing 0.1 M ammonium acetate for 2 min, followed by a 2.22%/min gradient of 10 to 50% ACN containing 0.1 M ammonium acetate. The product fraction (retention time 10.9 min) was lyophilized to give the title compound as a fluffy colorless solid (8 mg, 74%). Analytical HPLC indicated a product purity of 100%.

Hydrazone Stability Testing. Hydrazones were dissolved in 50 mM phosphate, pH 7.0, at ambient temperatures and a concentration of 0.1 mg/mL, and treated with 1 equiv of formaldehyde. The solutions were evaluated at 2 h using HPLC. Other hydrazones were generated in situ by reacting cyclo-[D-Val-NMeArg-Gly-Asp-Mamb(Hynic-5-Aca)] with 1 equiv of the aldehyde or ketone to be tested. The solutions were monitored by

Scheme 2. Reactivity Requirements of the Hydrazone Protecting Group[a]



[a] R_3 = bioactive targeting group.

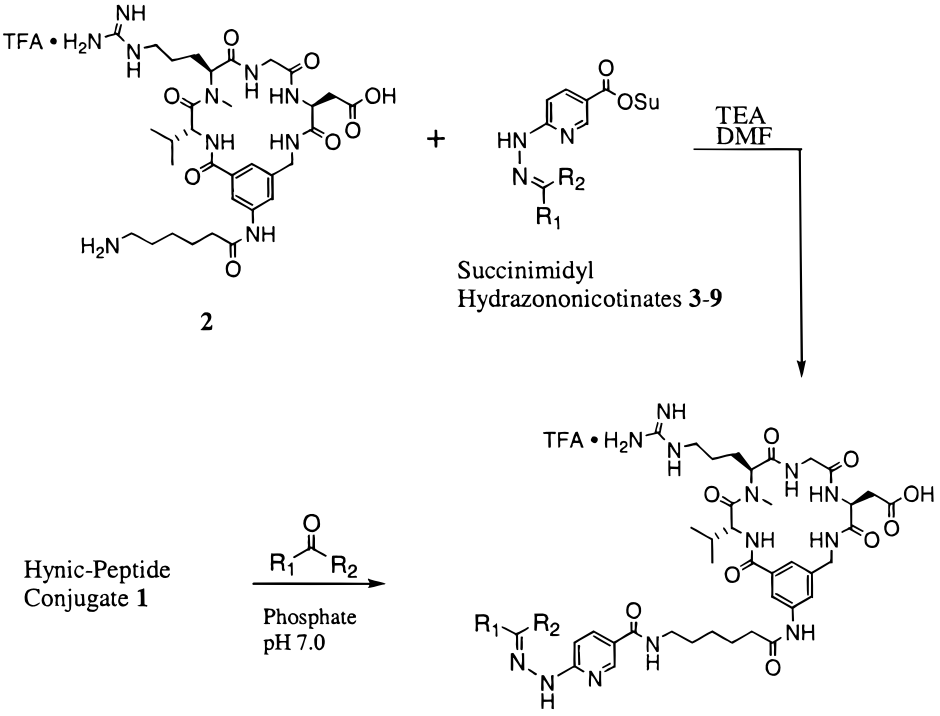
HPLC until the hydrazone-forming reaction was complete and then treated with 1 equiv of formaldehyde and monitored for reaction by HPLC. As a further test of hydrazone stability, benzaldehyde hydrazone **11** was dissolved in 50 mM phosphate, pH 7.0, at ambient temperatures and a concentration of 0.1 mg/mL, and treated with 10 equivalents of formaldehyde. The resulting solution was analyzed by HPLC at 2 h. The results of these tests are shown in Table 1.

RESULTS AND DISCUSSION

Thrombus imaging agent **RP444** is a ternary ligand complex prepared from Hynic−peptide conjugate **1**, tricine, TPPTS, and ^{99m}Tc pertechnetate, as shown in Scheme 1. Early formulation work using Hynic−peptide conjugate **1** revealed the presence of hydrazone impurities resulting from the reaction of **1** with trace aldehyde and ketone impurities present in the manufacturing environment. Because of the very small amount of Hynic−peptide conjugate **1** present in a single-dosage vial (20 μg), this presented a serious manufacturing problem. We sought to prevent the formation of these impurities by protecting the hydrazine moiety as a stable hydrazone which would not undergo an exchange reaction with other aldehydes or ketones, such as formaldehyde, as shown in Scheme 2. However, efficient formation of ^{99m}Tc complex **RP444** requires an unprotected hydrazine moiety. Thus, the hydrazone protecting group must be sufficiently labile to undergo hydrolysis during the labeling procedure to form a free hydrazine (Scheme 2). This hydrolysis need not be a high-yield reaction, for the Hynic−peptide conjugate is present in large excess relative to the total amount of technetium added to each kit. In addition to stability issues, we were also concerned with the physical properties of the active drug substance in the formulation. Therefore, we were especially interested in hydrazones having polar and ionic groups that would increase water solubility and crystallinity.

The Hynic hydrazone conjugates used in this study were prepared by two different methods as shown in Scheme 3. Reaction of cyclic RGD peptide **2** with succinimidyl hydrazononicotinates (**3**−**9**) gave Hynic hydrazone conjugates **10**-**16** in good yields and in high purity after HPLC purification. The maximum purity achieved with propionaldehyde hydrazone **17** was 80% due to hydrolysis of the hydrazone during lyophilization of the HPLC eluant. Not surprisingly, of the hydrazones tested in this study, **17** showed the least stability toward formaldehyde. Succinimidyl hydrazononicotinates **3**−**9** were prepared in a one-pot, two-step sequence of reactions by treatment with the carbonyl compound to form the hydrazone, followed by treatment with DCC and N-hydroxysuccinimide to form the active ester. Hynic hydrazone conjugates **18**−**22** were synthesized directly from Hynic−peptide conjugate **1** by reaction with an excess of the corresponding aldehyde in either DMF or phosphate buffer, pH 7.0. These hydrazones were isolated, purified, and characterized prior to the formaldehyde stability

Scheme 3. Synthesis of Hynic Hydrazone Conjugates



studies. Two additional hydrazones (**23** and **24** in Table 1) were not isolated, but prepared in situ by reaction with 1 equiv of aldehyde, using HPLC to monitor the completeness of the reaction. The solutions were then used directly in the formaldehyde stability studies. Three other hydrazones (**25**−**27** in Table 1) failed to form by this latter method. In all three cases, the carbonyl compound was a strongly electron-deficient aromatic aldehyde.

Of the large number of carbonyl compounds which are potential trace contaminants in a pharmaceutical manufacturing setting, formaldehyde is the most ubiquitous. It is also likely to be the most reactive, and surviving a formaldehyde challenge therefore became our minimum requirement for hydrazone stability. The stability studies were carried out at ambient temperatures in phosphate buffer, pH 7.0 at a Hynic hydrazone conjugate concentration of 0.1 mg/mL, and using 1 equiv of formaldehyde. This level of formaldehyde is far in excess of anything likely to be encountered in a real-world manufacturing setting. The results of these studies are shown in Table 1. All of the hydrazones derived from aromatic aldehydes (entries **10**−**12**, **18**, **20**, and **22**) are completely stable to the formaldehyde challenge. It appears not to matter if the ring is unsubstituted (entry **11**), electron rich (entry **12**), or electron deficient (entries **10**, **18**, **20**, and **22**). Conjugation of the hydrazone moiety to an olefin (entry **19**) or carbonyl group (entry **21**) also confers stability toward formaldehyde. Three aldehyde-derived hydrazones without such conjugation (entries **17**, **23**, and **24**) showed significant reactivity toward formaldehyde, with the simple alkyl hydrazone of propionaldehyde being the most reactive. Only one ketone-derived hydrazone was examined (entry **13**), and it was completely stable to formaldehyde, despite the fact that there is no unsaturated group in conjugation with the hydrazone. Hydrazone **11** was also challenged with 10 equiv of formaldehyde and found to be completely stable at this higher concentration.

CONCLUSIONS

We have shown that the hydrazine moiety of Hynic-modified peptides can be protected from undergoing hydrazone-forming reactions with formaldehyde by the use of stable hydrazones. Conjugation of the hydrazone with the unsaturation of an aromatic ring, an olefin, or a carbonyl group greatly enhanced its stability. Hydrazones lacking such conjugation readily underwent a hydrazone exchange reaction with formaldehyde. We also developed general methods for the preparation of the hydrazone-protected Hynic−peptide conjugates. The hydrazone protecting group can be introduced directly by reaction of the Hynic-peptide conjugate with a carbonyl compound. Alternatively, Hynic can be introduced with the hydrazone protecting group in place via its NHS ester.

The ability to prevent the formation of hydrazone impurities during the manufacturing process will greatly simplify the commercialization of radiopharmaceuticals containing the Hynic bifunctional coupling agent. The stability we have demonstrated here is, however, only half of the picture. While resisting reaction with formaldehyde and other carbonyl impurities, the hydrazones must be reactive enough to undergo hydrolysis to the free hydrazine during labeling with ^{99m}Tc. Several of the hydrazones described here have shown this balance of reactivity and can be used as the final intermediate for the preparation of **RP444**. The preferred method of preparing **RP444** is via Hynic hydrazone conjugate **10**, which is prepared by the use of NHS ester **4**. The hydrazone of 2-formylbenzenesulfonic acid provides the best combination of stability toward formaldehyde, lability during ^{99m}Tc labeling, ease of preparation, and water solubility. A full description of the ^{99m}Tc work is reported in the preceding paper in this issue.

ACKNOWLEDGMENT

The authors wish to thank John Pietryka and Maria Toler for analytical support.

LITERATURE CITED

(1) Abrams, M. J., Juweid, M., tenKate, C. I., Schwartz, D. A., Hauser, M. M., Gaul, F. E., Fuccello, A. J., Rubin, R. H., Strauss, H. W., and Fischman, A. J. (1990) Technetium-99m-Human Polyclonal IgG Radiolabeled via the Hydazino Nicotinamide Derivative for Imaging Focal Sites of Infection in Rats. *J. Nucl. Med. 31*, 2022−2028.

(2) Schwartz, D. A., Abrams, M. J., Hauser, M. M., Gaul, F. E., Larsen, S. K., Rauh, D., and Zubieta J. A. (1991) Preparation of Hydrazino-Modified Proteins and Their Use for the Synthesis of ^{99m}Tc-Protein Conjugates. *Bioconjugate Chem. 2*, 333−336.

(3) Larson, S. K., Solomon, H. F., Caldwell, G., and Abrams, M. J. (1995) [^{99m}Tc]Tricine: A Useful Precursor Complex for the Radiolabeling of Hydrazinonicotinate Protein Conjugates. *Bioconjugate Chem. 6*, 635−638.

(4) Babich, J. W., Solomon, H., Pike, M. C., Kroon, D., Graham, W., Abrams, M. J., Tompkins, R. G., Rubin, R. H., and Fischman, A. J. (1993) Technetium-99m-Labeled Hydrazino Nicotinamide Derivatized Chemotactic Peptide Analogues for Imaging Focal Sites of Bacterial Infection. *J. Nucl. Med. 34*, 1964−1974.

(5) Babich, J. W., Graham, W., Barrow, S. A., Dragotakes, S. C., Tompkins, R. G., Rubin, R. H., and Fischman, A. J. (1993) Technetium-99m-Labeled Chemotactic Peptides: Comparison with Indium-111-Labeled White Blood Cells for Localizing Acute Bacterial Infection in the Rabbit. *J. Nucl. Med. 34*, 2176−2181.

(6) van der Laken, C. J., Boerman, O. C., Oyen, W. J. G., van de Ven, M. T. P., Edwards, D. S., Barrett, J. A., van der Meer, F. W. M., and Corstens, F. H. M. (1997) Technetium-99m-Labeled Chemotactic Peptides in Acute Infection and Sterile Inflammation. *J. Nucl. Med. 38*, 1310−1315.

(7) Harris, T. D., Glowacka, D., Kalogeropoulos, S. A., Edwards, D. S., Liu, S., Barrett, J. A., and Heminway, S. J. (1998) Synthesis and Evaluation of ^{99m}Tc-Labeled LTB4 Antagonists as Potential Infection/Inflammation Imaging Agents. *Abstracts of Papers*, 216th National Meeting of the American Chemical Society, MEDI 35, Boston, MA.

(8) Cheesman, E. H., Looby, R. J., and Sworin, M. (1998) Using Catalyst® to Design Labeled LTB4 Antagonists for use in Imaging Infection and Inflammation. *Abstracts of Papers*, 216th National Meeting of the American Chemical Society, MEDI 34, Boston, MA.

(9) Rajopadhye, M., Overoye, K. L., Nguyen, H. M., Barrett, J. A., Heminway, S. J., Liu, S., and Edwards, D. S. (1998) Leukotriene B4 Antagonists with Amino Acid "East Ends" Designed for the Detection of Sites of Inflammation/Infection. *Abstracts of Papers*, 216th National Meeting of the American Chemical Society, MEDI 5, Boston, MA.

(10) Mäcke, H. R., and Behe, M. (1996) Octreotide Derivatives Labeled with Technetium-99m. *J. Nucl. Med. 37*, 29P.

(11) Bridger, G. J., Abrams, M. J., Padmanabhan, S., Gaul, F. E., Larsen, S. K., Henson, G. W., Schwartz, D. A., CLongley, C. B., Burton, C. A., and Ultee, M. E. (1996) A Comparison of Cleavable and Noncleavable Hydrazinopyridine Linkers for the ^{99m}Tc Labeling of Fab′ Monoclonal Antibody Fragments. *Bioconjugate Chem. 7*, 255−264.

(12) Rajopadhye, M., Harris, T. D., Yu, K., Glowacka, D., Damphousse, P. R., Barrett, J. A., Heminway, S. J., Edwards, D. S., and Carroll, T. R. (1997) Synthesis, Evaluation and Tc-99m Complexation of a Hydrazinonicotinyl Conjugate of a GP IIb/IIIa Antagonist Cyclic Peptide for the Detection of Deep Vein Thrombosis. *Bioorg. Med. Chem. Lett. 7*, 955−960.

(13) Edwards, D. S., Liu, S., Harris, A. R., Looby, R. J., Ziegler, M. C., Heminway, S. J., Barrett, J. A., and Carroll, T. R. (1997) A New and Versatile Ternary Ligand System for Technetium Radiopharmaceuticals: Water Soluble Phosphines and Tricine as Coligands in Labeling a Hydrazinonicotinamide-Modified Cyclic Glycoprotein IIb/IIIa Receptor Antagonist with ^{99m}Tc. *Bioconjugate Chem. 8*, 146−154.

(14) Schwartz, D. A., Abrams, M. J., Giadomenico, C. M., and Zubieta, J. A. (1993) *Certain Pyridyl Hydrazines and Hydrazides Useful for Protein Labeling*, U.S. Patent 5,206,370.

(15) Harris, T. D., Rajopadhye, M., Damphousse, P. R., Glowacka, D., Yu, K., Bourque, J. P., Barrett, J. A., Damphousse, D. J., Heminway, S. J., Lazewatsky, J., Mazaika, T., and Carroll, T. R. (1996) Tc-99m-Labeled Fibrinogen Receptor Antagonists: Design and Synthesis of Cyclic RGD Peptides for the Detection of Thrombi. *Bioorg. Med. Chem. Lett. 6*, 1741−1746.

BC9900237

Aminooxy Functionalized Oligonucleotides: Preparation, On-Support Derivatization, and Postsynthetic Attachment to Polymer Support

Harri Salo,*,† Pasi Virta,† Harri Hakala,† Thazha P. Prakash,‡ Andrei M. Kawasaki,‡ Muthiah Manoharan,‡ and Harri Lönnberg†

Department of Chemistry, University of Turku, FIN-20014 Turku, Finland, and Department of Medicinal Chemistry, Isis Pharmaceuticals, 2292 Faraday Avenue, Carlsbad, California 92008. Received February 25, 1999; Revised Manuscript Received June 29, 1999

Three novel phosphoramidites, each bearing a phthaloyl-protected aminooxy tail, were prepared and applied in automated oligonucleotide synthesis. After chain assembly, the phthaloyl protection was removed with hydrazinium acetate. Normal succinyl linker turned to be stable under these conditions, and hence the support-bound oligonucleotide could be converted to a pyrene oxime conjugates by reacting with pyrene carbaldehyde or *cis*-retinal. Standard ammonolytic deprotection then released the deprotected conjugate in solution. Alternatively, the crude aminooxy-tethered oligonucleotide was immobilized to microscopic polymer particles by reacting the aminooxy function with the particle-bound aldehyde or epoxide groups. These immobilized oligonuceotides were shown to serve properly as probes in a mixed phase hybridization assay.

INTRODUCTION

The expanding use of mixed-phase hydridization assays for the detection of specific nucleic acid sequences has made the covalent immobilization of oligonucleotides to solid supports an object of increasing interest (*1*−*19*). Although the oligonucleotide probes may be assembled in situ on the support employed in the assay (*5*−*7*, *12*, *20*−*26*), postsynthetic attachment of purified oligonucleotide conjugates to the support may still be advantageous for some applications. A variety of methods for tethering of oligonucleotides to solid supports have been reported. Most of the methods are based on reactions of 5′-aminoalkyl conjugates of oligonucleotides with various functional groups on the support. Accordingly, oligonucleotides bearing a 5′-terminal amino function have been attached (i) to carboxyalkylated polymer supports by carbodiimide assisted acylation (*27*, *28*), (ii) to aminoalkylated polymer supports by activation with 2,4,6-trichloro-1,3,5-triazine and subsequent displacement of one of the remaining chloro substituents with a resin bound amino group (*29*), (iii) to aldehyde-derivatized surfaces by reductive amination (*30*), and (iv) to phenyldiisothiocyanate-activated (*8*) or epoxide-derivatized glass (*31*) surfaces by direct nucleophilic substitution. 5′-Phosphorylated oligonucleotides have been immobilized to aminoalkylated supports by carbodiimide-assisted phosphoramidate coupling (*27*), and 5′-mercapto-functionalized oligonucleotides to mercaptoalkyl supports by disulfide formation (*32*). The latter oligonucleotides have also been successfully immobilized to iodoacetamido-derivatized supports by nucleophilic α-substitution (*33*). Oligonucleotides bearing a 5′-terminal aldehyde function have been attached to aminoalkylated supports by reductive amination (*30*) and to latex microspheres bearing hydrazine residues (*34*). 2,4,6-Trichloro-1,3,5-triazine activation and disulfide bond formation have also been exploited in immobilization of 3′-amino and 3′-mercapto functionalized oligonucleotides, respectively (*35*). Homopolymer-tailed oligomers have been attached to a nylon membrane by UV irradiation (*3*).

The aminooxy group, NH_2O, is more nucleophilic than the primary amino group, the enhanced nucleophilicity being usually attributed to the so-called α-effect (*36*). Moreover, it is well-known that the *O*-alkyl oximes formed upon the reaction of *O*-alkylhydroxylamines with carbonyl compounds are much more stable than the imines derived from primary amines (*37*). Accordingly, one might assume that the aminooxy conjugates of oligonucleotides react more rapidly than their amino counterparts with support-bound aldehyde functions and give oxime-type linkers which tether the oligonucleotides to the support in a virtually irreversible manner without any additional reduction step. Aminooxy chemistry has not been previously applied to oligonucleotide immobilization, although several related conjugations in solution have been described. For example, 5′-*O*-amino-2′-deoxyribonucleosides have been prepared and used in hammerhead ribozyme studies (*38*) and in construction of non-phosphorus analogues of dinucleoside 3′,5′-monophosphates (*39*). Oligonucleotides have also been tethered with aminooxy-functionalized probes, reacting either at the apurinic sites (*40*−*42*) or at aldehydic sites generated in modified base residues (*43*). Furthermore, aminooxy linkers have been attached to oligonucleotides by transamination with the cytosine 4-amino group (*44*).

We now report on incorporation of three phosphoramidites (**1**−**3**), bearing a masked aminooxy group, into oligodeoxyribonucleotides. These building blocks enable tethering of the aminooxy group either at the 5′-terminus of the oligonucleotide (**1**) or at any desired position within the sequence (**2** and **3**). The protected aminooxy functionality was introduced into the building blocks by displacing a hydroxy group with *N*-hydroxyphthalimide

* To whom correspondence should be addressed. Phone: +358 2 333 8092. Fax: +358 2 333 8050. E-mail: harri.salo@utu.fi.
† University of Turku, Finland.
‡ Isis Pharmaceuticals, California.

10.1021/bc990021m CCC: $18.00 © 1999 American Chemical Society
Published on Web 08/27/1999

under Mitsunobu reaction conditions (*45*). The phthaloyl protection was removed from the aminooxy functions of the assembled oligonucleotide conjugates with hydrazinium acetate. The normal succinyl linker is not cleaved by this treatment, and hence the support-bound oligonucleotides may be converted, when desired, to more stable oxime conjugates before the conventional ammonolytical base moiety deprotection and release from the support. The deprotected aminooxy-tethered oligonucleotides were finally immobilized to polymer microparticles bearing either aldehyde or epoxide functions. The oligonucleotide-coated particles obtained were shown to behave in mixed-phase hybridization assays (*19*, *25*, *35*) in exactly the same manner as those prepared by methods established previously for postsynthetic immobilization.

EXPERIMENTAL SECTION

General. The reagents for oligonucleotide synthesis were products of Glen Research. The aldehyde-derivatized Tentagel supports were from Rapp Polymere Gmbh (Tübingen, Germany), and the epoxy-modified microparticles were from SINTEF Applied Chemistry (Trondheim, Norway). All the other reagents were from Aldrich Chemical Co. Adsorption chromatography was performed on silica gel 60 (Merck). NMR spectra were recorded on JEOL GX-400 spectrometer operating at 399.8 and 100.5 MHz for ^{1}H and ^{13}C, respectively, and 161.9 MHz for ^{31}P. $CDCl_3$ and DMSO-d_6 were used as solvents, and TMS as an internal (^{1}H) and H_3PO_4 as an external (^{31}P) standard. Electron spray ionization mass spectra were recorded with PE SCIEX API 365 LC/ESI-MS/MS. UV measurements were carried out on a Perkin-Elmer Lambda 2 UV−vis spectrometer.

TLC. Analytical TLC was conducted on silica gel 60 F_{254} plates (Merck). Eluent systems: A (1/19, MeOH/CH_2Cl_2, v/v); B (1/9, MeOH/CH_2Cl_2, v/v); C (17/34/49, Et_3N/MeOH/CH_2Cl_2, v/v/v).

HPLC Techniques. The oligonucleotides were analyzed by ion-exchange chromatography (column, Synchropak AX-300, 4.0 × 250 mm, 6 μm), flow rate 1 mL min^{-1}, buffer A = 0.05 KH_2PO_4 in 50% (v/v) formamide, pH 5.6; buffer B = buffer A + 0.6 mol L^{-1} $(NH_4)_2SO_4$, linear gradient from 10 to 80% B in 30 min. The reversed-phase conditions (also LC/ESI-MS/MS) were as follows: column Nucleosil C18 (300, 4.6 × 250 mm, 5 μm), linear gradient from 5 to 60% B in 30 min and from 60 to 100% B from 30 to 50 min, flow rate 1 mL min^{-1}, buffer A = 0.05 M NH_4OAc(aq), buffer B = buffer A in 65% MeCN.

Oligonucleotide synthesis. The protected oligonucleotides were assembled on an Applied Biosystems 392 DNA Synthesizer in 0.2 and 1.0 μmol scales using commercial solid supports and phosphoramidite chemistry. Phosphoramidites **1** and **2** were used as 0.1 mol L^{-1} solution in dry MeCN, with 600 s coupling time, otherwise unaltered and recommended synthesis protocols were used. After synthesis, the support-bound oligonucleotides were first treated with 0.5 mol L^{-1} hydrazine hydrate in Pyr/AcOH (4:1 v/v) for 30 min and then with ammonia for 8 h at 55 °C.

11-(4,4′-Dimethoxytrityloxy)-3,6,9-trioxaundecanol (4). Tetraethyleneglycol (14.0 g, 72 mmol) was coevaporated with dry pyridine (2 × 50 mL), dissolved in dry dioxane, and 4,4′-dimethoxytrityl chloride (8.0 g, 23.6 mmol) was added portionwise to the stirred solution. The reaction was followed by TLC. After overnight stirring at ambient temperature, the reaction mixture was evaporated and dissolved in dichloromethane (200 mL), washed with saturated $NaHCO_3$(aq) (3 × 100 mL) and brine (100 mL). The organic phase was dried over Na_2SO_4 and concentrated. Purification on silica gel column using a stepwise gradient of MeOH (0 to 10%) in CH_2Cl_2 containing 0.2% pyridine yielded 8.5 g (73%) of **4**. ^{1}H NMR ($CDCl_3$; δ, ppm): 7.25−7.45 (9H, m, DMTr), 6.81 (4H, d, J = 8.8, DMTr), 3.77 (6H, s, 2×OMe), 3.70−3.65 (12H, m, 3×OCH_2CH_2), 3.59 (2H, m, HOCH_2), 3.23 (2H, t, J = 5.4, DMTrOCH_2). ^{13}C NMR ($CDCl_3$; δ, ppm): 158.3, 145.0, 136.3, 130.0, 129.0, 128.2, 127.7, 126.6, 125.2, 113.0, 85.9, 72.5, 70.3−70.7 (5×C), 63.1, 61.7, 55.1 (2×C). TLC: R_f(A) = 0.4.

***N*-[11-(4,4′-Dimethoxytrityloxy)-3,6,9-trioxaundecanyloxy]phthalimide (5)**. *N*-Hydroxyphthalimide (0.7 g, 4.3 mmol) and triphenylphosphine (1.1 g, 4.2 mmol) were added to a solution of **4** (2.0 g, 4.0 mmol) in THF (60 mL). Diethylazodicarboxylate (DEAD, 0.7 mL, 3.6 mmol) was added dropwise, and the stirring was continued overnight at ambient temperature. The reaction mixture was evaporated to oil, applied onto a silica gel column, and eluted with a linear gradient from neat CH_2Cl_2 to a 97:3 (v/v) mixture of CH_2Cl_2 and MeOH. The purification was repeated to yield 2.1 g (80%) of **5**. ^{1}H NMR ($CDCl_3$; δ, ppm): 7.70−7.85 (4H, m, phthaloyl), 7.45−7.25 (9H, m, DMTr), 6.80 (4H, d, J = 9.0, DMTr), 4.35 (2H, t, J = 4.6, DMTrOCH_2), 3.84 (2H, t, J = 4.6, DMTrOCH$_2$CH_2), 3.77 (6H, s, 2×OMe), 3.70−3.55 (10H, m, 5×CH_2), 3.21 (2H, t, J = 5.4, CH_2ON). ^{13}C NMR ($CDCl_3$; δ, ppm): 163.41, 158.38, 149.82, 145.10, 137.85, 136.35, 134.39, 130.06, 129.00, 182.22, 127.73, 126.64, 125.29, 123.45, 113.03, 85.91, 77.17, 70.81, 70.70, 70.66, 70.58, 69.34, 63.13, 55.19, TLC: R_f(A) = 0.9.

***O*-(11-Phthalimidooxy-3,6,9-trioxaundecyl)-*O*-(2-cyanoethyl)-(*N*,*N*-diisopropyl)phosphoramidite (1)**. A solution of dichloroacetic acid in dichloromethane (100 mL, 3:97, v/v) and 20 mL of methanol was added to **5** (2.3 g, 3.6 mmol), and the reaction mixture was stirred for 18 h. All volatile material was evaporated in vacuo, and the residue was dissolved in CH_2Cl_2 (10 mL). Silica gel column purification using an eluent system with a stepwise gradient of acetic acid in CH_2Cl_2 (0−4%) gave 0.88 g (72%) of 11-(phthalimidooxy)-3,6,9-trioxaundecan-1-ol after coevaporation of the pooled fractions with water and pyridine. ^{1}H NMR ($CDCl_3$; δ, ppm): 7.90−7.75 (4H, m, phthaloyl), 4.39 (2H, t, J = 4.6, *H*-11), 3.87 (2H, t, J = 4.6, *H*-10), 3.90−3.50 (12H, m, 3×OCH_2CH_2). TLC: R_f(A) = 0.3. The alcohol (0.37 g,1.09 mmol) was further dried with coevaporation with dry MeCN and finally in vacuo. 2-Cyanoethyl-*N*,*N*,*N*′,*N*′-tetraisopropylphosphorodiamidite (0.45 mL, 1.42 mmol), MeCN (1.0 mL) and 1*H*-tetrazole (0.45 mol L^{-1}, 2.43 mL, and 1.10 mmol) were added, and the reaction mixture was stirred at ambient temperature. After 60 min, 100 mL of saturated $NaHCO_3$(aq) solution was added and the mixture was extracted with ethyl acetate (3 × 50 mL). The organic phase was dried with Na_2SO_4, and evaporated. The crude product was almost pure, the yield being 0.58 g (98%). ^{1}H NMR ($CDCl_3$; δ, ppm): 7.90−7.75 (4H, m, phthaloyl), 4.38 (2H, t, J = 4.6, *H*-11), 3.87 (2H, t, J = 4.6, *H*-10), 3.90−3.50 (16H, 3×OCH_2CH_2, POCH_2, and 2×PNC*H*), 2.66 (2H, t, J = 6.6, CH_2CN), 1.30−1.10 (12H, 4×CH_3CHN). ^{31}P NMR($CDCl_3$): 147.63. TLC: R_f(A) = 0.3.

***N*^{4}-Benzoyl-2′-deoxy-5′-*O*-(4,4′-dimethoxytrityl)cytidine (6)**. 2′-Deoxycytidine (5.82 g, 25.6 mmol) was dried by evaporation with dry pyridine (2 × 50 mL) and taken up in dry pyridine (100 mL). To this suspension was added trimethylsilyl chloride (11.5 mL, 90.6 mmol), and

the mixture was stirred at ambient temperature for 2 h. The reaction mixture was cooled on an ice−water bath, and benzoyl chloride (4.60 mL, 39.6 mmol) was slowly introduced. The ice−water bath was removed, and the mixture was stirred at room temperature for additional 2 h. The reaction was quenched by adding methanol (15 mL), concentrated to one-half of the original volume and filtered. To the filtrate was added water (30 mL), and the solution was evaporated to oil. Additional evaporations with water (3 × 30 mL) were performed to remove pyridine, and the resulting residue was partitioned between water and ethyl acetate. After vigorous stirring, the product crystallized from the aqueous layer. The crystals were washed with cold water and ethyl acetate, and they were used in the next step without further purification. TLC: R_f(A) = 0.7. Crude N^4-benzoyl-2′-deoxycytidine was dried by evaporation with dry pyridine (3 × 50 mL) and then dissolved in the same solvent (100 mL). 4,4′-Dimethoxytrityl chloride (7.4 g, 22 mmol) was added portionwise to the reaction mixture, and the stirring was continued overnight at ambient temperature. The reaction mixture was evaporated to oil and dissolved in dichloromethane (100 mL). The organic phase was washed with saturated $NaHCO_3$(aq) (50 mL) and water (3 × 100 mL) and dried with anhydrous Na_2SO_4. After coevaporation with toluene, the residue was applied onto a silica gel column and eluted with a gradient of MeOH in CH_2Cl_2 (0 to 8% MeOH). The product (**6**) was obtained in 65% yield (9.0 g) starting from 2′-deoxycytidine. ^{1}H NMR ($CDCl_3$; δ, ppm): 8.30 (1H, d, J = 7.6, *H*-6), 7.45−7.10 (9H, m, DMTr), 6.84 (4H, m, DMTr), 7.90−7.40 (5H, m, benzoyl), 6.31 (1H, t, J = 5.9, *H*-1′), 4.55 (1H, m, *H*-3′), 4.19 (1H, m, *H*-4′), 3.78 (6H, s, 2×OMe), 3.49 (1H, dd, J = 3.2 and 11.0, *H*-5′), 3.42 (1H, dd, J = 3.9 and 10.8, *H*-5″), 2.77 (1H, m, *H*-2″). TLC: R_f(B) = 0.85.

2′-Deoxy-N^4-(5-hydroxypentyl)-5′-*O*−(4,4′-dimethoxytrityl)cytidine (7). A solution of 5-aminopentanol (10.0 g, 96.9 mmol) in 2-propanol (10 mL) was added to **6** (2.61 g, 4.12 mmol) and stirred until the mixture was clear. 1,5,7-Triazabicyclo[4.4.0]dec-5-ene (TBD, 2.40 g, 17.2 mmol) was added and the reaction mixture was stirred at ambient temperature for 48 h. The reaction mixture was evaporated to oil with an oil pump, dissolved in $CHCl_3$ (100 mL), extracted with 0.1 mol L^{-1} NaOH(aq) (2 × 50 mL) and water (4 × 50 mL). The organic phase was dried with anhydrous Na_2SO_4, evaporated, and dissolved in CH_2Cl_2. Silica gel column purification (eluents: 2/4/94 Et_3N/MeOH/CH_2Cl_2 and 2.5/5/92.5 Et_3N/MeOH/CH_2Cl_2; v/v/v) was hampered by the presence of 2′-deoxy-5′-O-(4,4′-dimethoxytrityl)-cytidine, formed as a side product, and that is why the separation had to be repeated until a reasonably pure product was obtained. The yield was 18% (0.53 g). ^{1}H NMR ($CDCl_3$; δ, ppm): 7.75 (1H, d, J = 7.3, *H*-6), 7.45−7.15 (9H, m, DMTr), 6.82 (4H, d, J = 8.5, DMTr), 6.33 (1H, t, J = 5.9, *H*-1′), 5.40 (1H, d, J = 7.3, *H*-5), 4.49 (1H, m, *H*-3′), 4.05 (1H, dd, J = 3.7, *H*-4′), 3.77 (6H, s, 2×OMe), 3.60 (2H, t, J = 5.9, CH_2OH), 3.50−3.30 (4H, m, H-5′, H-5″, HNCH_2), 2.17 (1H, m, H-2′), 1.57 (4H, m, 2×CH_2), 1.40 (2H, m, CH_2). TLC: R_f(C) = 0.7.

2′-Deoxy-5′-*O*-(4,4′-dimethoxytrityl-N^4-(5- phthalimidooxypentyl)cytidine (8). Compound **7** was dried by evaporation with dry pyridine (2 × 20 mL). *N*-Hydroxyphthalimide (0.17 g, 1.04 mmol) and triphenylphosphine (0.14 g, 0.53 mmol) were added, and the mixture was dissolved in dry THF (30 mL). Diethylazodicarboxylate (DEAD, 0.089 mL, 0.57 mmol) was added dropwise, and the reaction mixture was stirred at ambient temperature for 18 h. All volatile material was evaporated in vacuo, and the residue was dissolved in a small volume of dichloromethane and applied onto a silica gel column. Triphenylphosphine oxide was eluted first from the column with a mixture of ^{i}PrOH and CH_2Cl_2 (1/19, v/v) and the product with a mixture of MeOH and CH_2Cl_2 (1/9, v/v). The purification afforded 0.24 g of compound **8** (40%). ^{1}H NMR ($CDCl_3$; δ, ppm): 8.61 (1H, m, N*H*), 7.85−7.65 (4H, m, phthaloyl), 7.45−7.15 (9H, m, DMTr), 6.83 (4H, m, DMTr), 6.30 (1H, t, *H*-1′), 5.47 (1H, d, J = 7.3, *H*-5), 4.51 (1H, m, *H*-3′), 4.21 (2H, t, J = 5.9, CH_2ON), 4.05 (1H, m, *H*-4′), 3.78 (6H, s, 2×OMe), 3.60−3.10 (4H, m, H-5′,H-5″, CH_2N), 2.60 (1H, m, *H*-2′), 2.20 (1H, m, *H*-2″), 1.79 (2H, m, CH_2), 1.70−1.40 (4H, m, 2×CH_2). TLC: R_f(B) = 0.5.

2′-Deoxy-5′-*O*-(4,4′-dimethoxytrityl)-N^4-(5-phthalimidooxypentyl)cytidine 3′-[*O*-(2-cyanoethyl)-*N*,*N*-diisopropyl)]phosphoramidite (2). Compound **8** (0.22 g, 0.29 mmol) was dried by evaporation with dry acetonitrile (3 × 20 mL) and finally in vacuo for 30 min. 2-Cyanoethyl-*N*,*N*,*N*′,*N*′-tetraisopropylphosphorodiamidite (0.12 mL, 0.38 mmol) and dry acetonitrile (1.0 mL) were added, and the mixture was stirred until all material dissolved. 1*H*-Tetrazole (0.45 mol L^{-1} in MeCN, 0.64 mL, 0.29 mmol) was added, and the reaction mixture was shaken. After 1 h at ambient temperature, 100 mL of saturated $NaHCO_3$(aq) solution was added to the reaction mixture, and the resulting solution was extracted with ethyl acetate (2 × 40 mL). The organic phase was dried with anhydrous Na_2SO_4 and evaporated to dryness, affording 0.24 g (97%) of almost pure compound **2**. ^{1}H NMR ($CDCl_3$; δ, ppm): 7.75−7.70 (4H, m, phthaloyl), 7.45−7.20 (9H, m, DMTr), 6.83 (4H, m, DMTr), 6.36 (1H, m, *H*-1′), 5.41 (1H, d, J = 5.6, *H*-5), 4.60 (1H, m, *H*-3′), 4.22 (2H, t, J = 5.4, CH_2ON), 4.10 (1H, m, *H*-4′), 3.78 (6H, s, 2×OMe), 3.65−3.30 (8H, m, *H*-5′,*H*-5″, CH_2N, POCH_2, 2×PONC*H*), 2.63 (2H, m, CH_2CN), 2.60 (1H, m, *H*-2′), 2.25 (1H, m, *H*-2″), 1.85−1.50 (6H, m, 3×CH_2), 1.30−1.00 (12H, m, 4×CH_3). ^{31}P NMR ($CDCl_3$, δ, ppm): 149.2 and 148.7.

5′-*O*-(4,4′-Dimethoxytrityl)-2′-*O*-(2-phthalimidooxyethyl)-5-methyluridine 3′-[*O*-(2-cyanoethyl)-*N*,*N*-diisopropyl)]phosphoramidite (3). The compound was synthesized as published previously (*46*).

Immobilization of Oligodeoxyribonucleotide Conjugates to Microparticles. The ODN conjugates 5′-d(NH_2O-TEG-ACACCAAAGATGATAT)-3′ (**9**) and 5′-d[ACACCAAAGATGATATmC(ONH_2)T]-3′ (**10**) [TEG stands for tetraethyleneglycol and mC for N^4-(5-hydroxypentyl)-2′-deoxycytidine] were assembled according to the phosphoramidite protocol, using building blocks **1** and **2** to obtain **9** and **10**, respectively. A modified coupling time of 600 s was used to insert **1** and **2**. Deprotection and cleavage were performed with a double syringe method employing a 0.5 mol L^{-1} hydrazine acetate solution (0.124/4/1 H_2NNH_2·H_2O/pyridine/AcOH, v/v/v) for 30 min, followed by ammonolysis with concentrated ammonia at 55 °C for 8 h. The crude ODN conjugates (**9** and **10**) were evaporated to dryness and dissolved in 1.0 mL of water and mixed immediately with the aldehyde derivatized microparticles (90 nmol of **9** and 2.8 mg of Tentagel, 0.6 μmol of CHO groups, or 80 nmol of **10** and 3.5 mg of Tentagel, 0.8 μmol of CHO groups). ODN conjugate **10** (1.0 mL, 80 nmol) was also mixed with epoxide-modified microparticles (3.0 mg, 0.3 μmol epoxide groups). The progress of the reactions was followed by UV absorbance change at 260 nm. According to the observed decrease in the absorbance, a loading of 1 μmol of oligonucleotides in 1 g of the microparticles was obtained. After reaction,

Table 1. Properties of the Oligonucleotide Conjugates

oligonucleotide	retention time (min)[a]	observed mass	calculated mass	product ratio (%)
18a	27.9	2246.4	2246.6	41
18b	41.8	2301.2	2300.8	51
19a	36.7/37.4[b]	2352.6	2356.9	70
19b	38.3	2104.4	2104.8	52

[a] RP-HPLC, for detailed chromatografic conditions, see Experimental Section. [b] E/Z isomers, both peaks exhibited same molecular mass (Figure 4).

the derivatized microparticles were washed with water, dried, and used in hybridization assays.

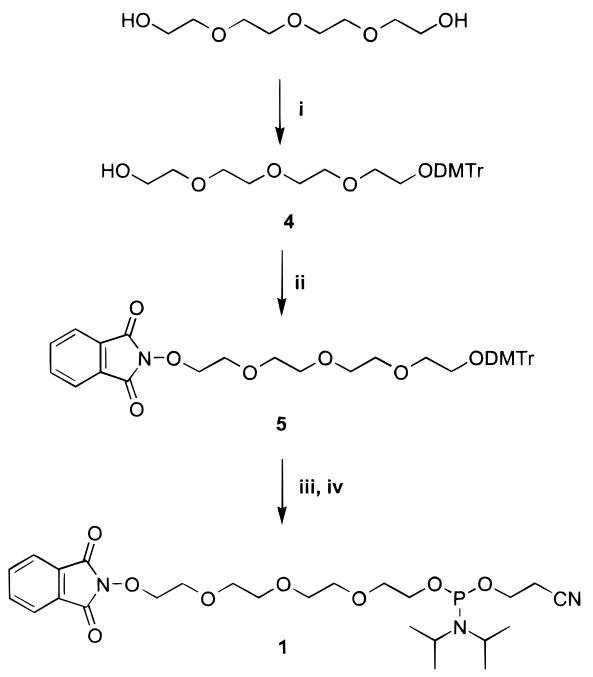
Hybridization Assays. The ODNs attached to microparticles were used as capture probes for a complementary 16-mer sequence, 5′-d(X_5ATATCATCTTTGGTGT)-3′ (**11**), where X stands for N^4-(6-aminohexyl)-2′-deoxycytidine tethered to a photoluminescent europium(III) chelate, {2,2′,2″,2‴-{{4′-{4‴-[(4,6-dichloro-1,3,5-triazin-2-yl)amino]phenyl}-2,2′:6′,2″-terpyridine-6,6″-diyl}bis(methylenenitrilo)}-tetrakis(acetato)}europium(III) (*47*). To evaluate the contribution of unspecific binding to the solid phase, a sequence 5′-d(X_5TCATGAGTCAAGTCTA)-3′(**12**) was used instead of **11**. The signal intensity of time-resolved fluorescence of europium from one microparticle was measured with a microfluorometer as a function of added **11** or **12**. A detailed description of the measuring system and the hybridization conditions has been described previously (*19*, *35*, *48*). With the aldehyde-derivatized Tentagel, a slightly modified mode of measurement was applied. Instead of capillary tubing, the microparticles were collected on a filter and the signal was collected from one bead with the microfluorometer.

Labeling of Aminooxy Functionalized Oligonucleotides with Aldehydes on Solid Support. Oligonucleotide sequences 5′-(PhthNO-TEG-T_6)-3′ (**16**) and 5′-(PhthNOEt-MeU-T_5)-3′ (**17**), where PhthNOEt-MeU stands for a 2′-*O*-(2-phthalimidooxyethyl)-5-methyluridine (**3**) unit, were synthesized on standard CPG-succinyl-thymidine support as described previously for **9**, with the exception that a standard 30 s coupling time was used to introduce **3** into **17**. The support-bound oligonucleotides were treated with 0.5 mol L^{-1} hydrazine acetate solution (0.124/4/1 $H_2NNH_2 \cdot H_2O$/pyridine/AcOH, v/v/v) for 30 min and washed with pyridine, methanol, acetonitrile, and dried. The supports (2.0 mg/sample, 50 nmol of ODN) were transferred to microcentrifuge tubes, and a solution of either pyrenecarbaldehyde (100 μL, 40 μmol in DMF) or *cis*-retinal (100 μL, 3.5 μmol in MeCN) was added, and the mixture was shaken 16 h at ambient temperature in dark. The excess of reagents was washed with several portions of DMF and MeCN until no color was released from the supports. The supports were then dried and finally treated with concentrated ammonia at ambient temperature for 24 h to release the resulting oligonucleotide−oxime conjugates: **18a** (reaction of **16** with pyrenecarbaldehyde), **18b** (reaction of **16** with *cis*-retinal), **19a** (reaction of **17** with pyrenecarbaldehyde), and **19b** (reaction of **17** with *cis*-retinal). Evaporation, dissolution in water and analysis by HPLC/ESI-MS/MS verified the formation of the expected oligonucleotide conjugates and complete disappearance of the starting material (see Table 1).

RESULTS AND DISCUSSION

Synthesis of the Phosphoramidites. The synthesis of phosphoramidite **1** is described in Scheme 1. One of the hydroxy functions of tetraethyleneglycol was initially

Scheme 1[a]



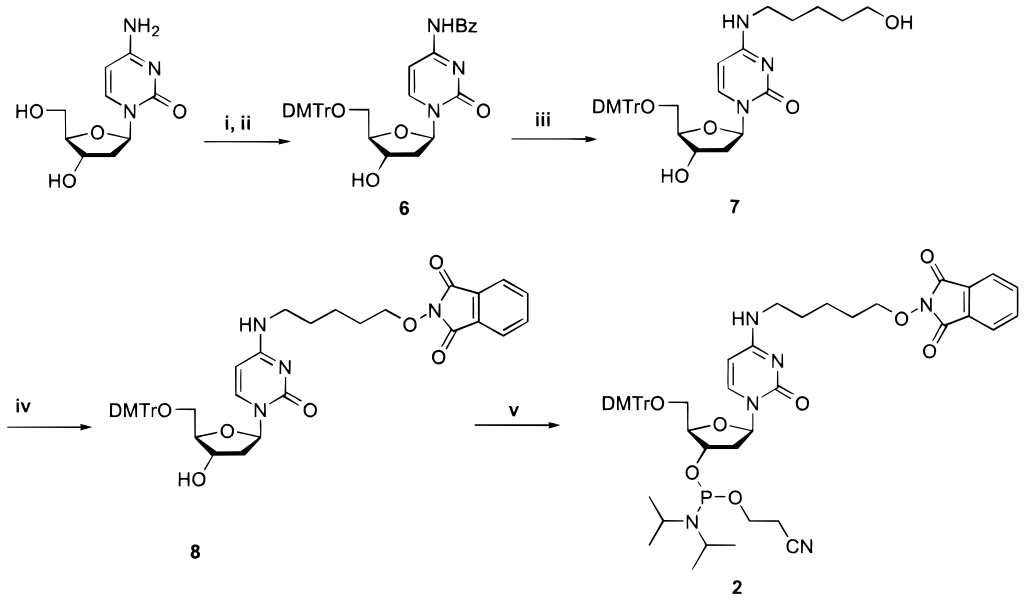
[a] (i) DMTrCl/dioxane/Pyr; (ii) *N*-hydroxyphthalimide/Ph_3P/DEAD/THF; (iii) dichloroacetic acid/CH_2Cl_2/MeOH; (iv) 2-cyanoethyl-*N*,*N*,*N*′,*N*′-tetraisopropylphosphorodiamidite/1-*H*-tetrazole/MeCN. Ph_3P: triphenylphosphine.

dimethoxytritylated (to get **4**) by treating an excess of the glycol with 4,4′-dimethoxytrityl chloride in a mixture of pyridine and dioxane. The remaining hydroxy function of **4** was then subjected to Mitsunobu reaction (*45*), using *N*-hydroxyphthalimide as a nucleophile and diethyldiazodicarboxylate (DEAD) and triphenylphosphine as activators. The desired *O*-phthalimido derivative **5** was obtained in 80% yield. Detritylation of **5** with dichloroacetic acid afforded the corresponding alcohol in 72% yield. Subsequent reaction with *N*,*N*,*N*′,*N*′-tetraisopropyl-2-cyanoethylphosphorodiamidite in the presence of 1-*H*-tetrazole then gave **1** in excellent yield (98%).

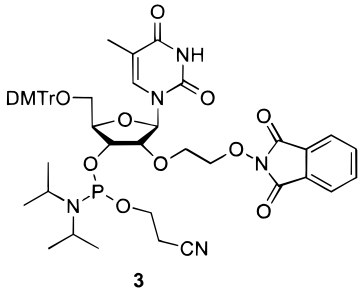
The synthesis of phosphoramidite **2** is described in Scheme 2. 2′-Deoxycytidine was first N^4-benzoylated according to the method of Jones (*49*) and the 5′-oxygen was then dimethoxytritylated, affording **6** in a 65% overall yield. The product was subjected to transamination reaction using 5-aminopentanol as the entering amine and TBD as a catalyst (*50*). The reaction was not optimized, and the yield of the product, 2′-deoxy-N^4-(5-hydroxypentyl)-5′-*O*-(4,4′-dimethoxytrityl)cytidine (**7**) was low (18%). The major product formed was debenzoylated 5′-*O*-(4,4′-dimethoxytrityl)cytidine, which could be collected and recycled. No other side products were detected. Application of Mitsunobu reaction to **7** gave **8** in 40% yield, and the latter was finally converted to **2** (97%). The amidite **3** (Figure 1) was synthesized as described previously (*46*).

Synthesis of Oligodeoxyribonucleotide Conjugates (9, 10), and Their Immobilization. To test the coupling efficiency of phosphoramidites **1** and **2** and the removal of the phthaloyl group with hydrazine acetate, a T_6 sequence was first assembled and elongated with **1**. On the basis of HPLC analysis and DMTr-cation assay (data not shown), a reaction time of 600 s was selected for the coupling and a 30 min treatment with 0.5 mol L^{-1} hydrazinium acetate followed by standard ammonolysis at 55 °C for the deprotection. Although this treatment has previously been used in solid-phase oligonucleotide

Scheme 2[a]



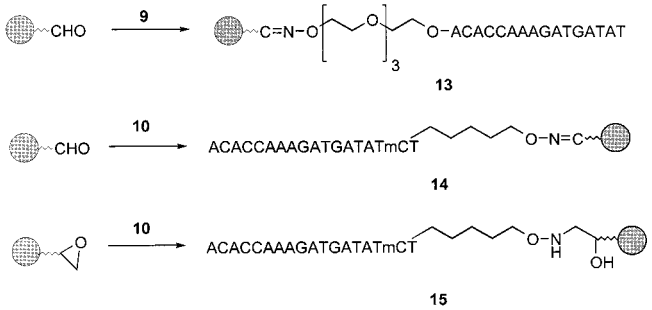
[a] (i) TMSCl/Pyr/BzCl; (ii) DMTrCl/Pyr; (iii) 5-aminopentanol/TBD/i-PrOH; (iv) *N*-hydroxyphthalimide/Ph_3P/DEAD/THF; (v) 2-cyanoethyl-*N*,*N*,*N*′,*N*′-tetraisopropylphosphorodiamidite/1-*H*-tetrazole/MeCN. TBD: 1,5,7-triazabicyclo[4.4.0]dec-5-ene.



3

Figure 1. The structure of phosphoramidite **3**.

Scheme 3. A Schematic View of the Attachment of ODNs 9 and 10 to the Microparticles Forming the Particle-Bound Conjugates 13, 14, and 15

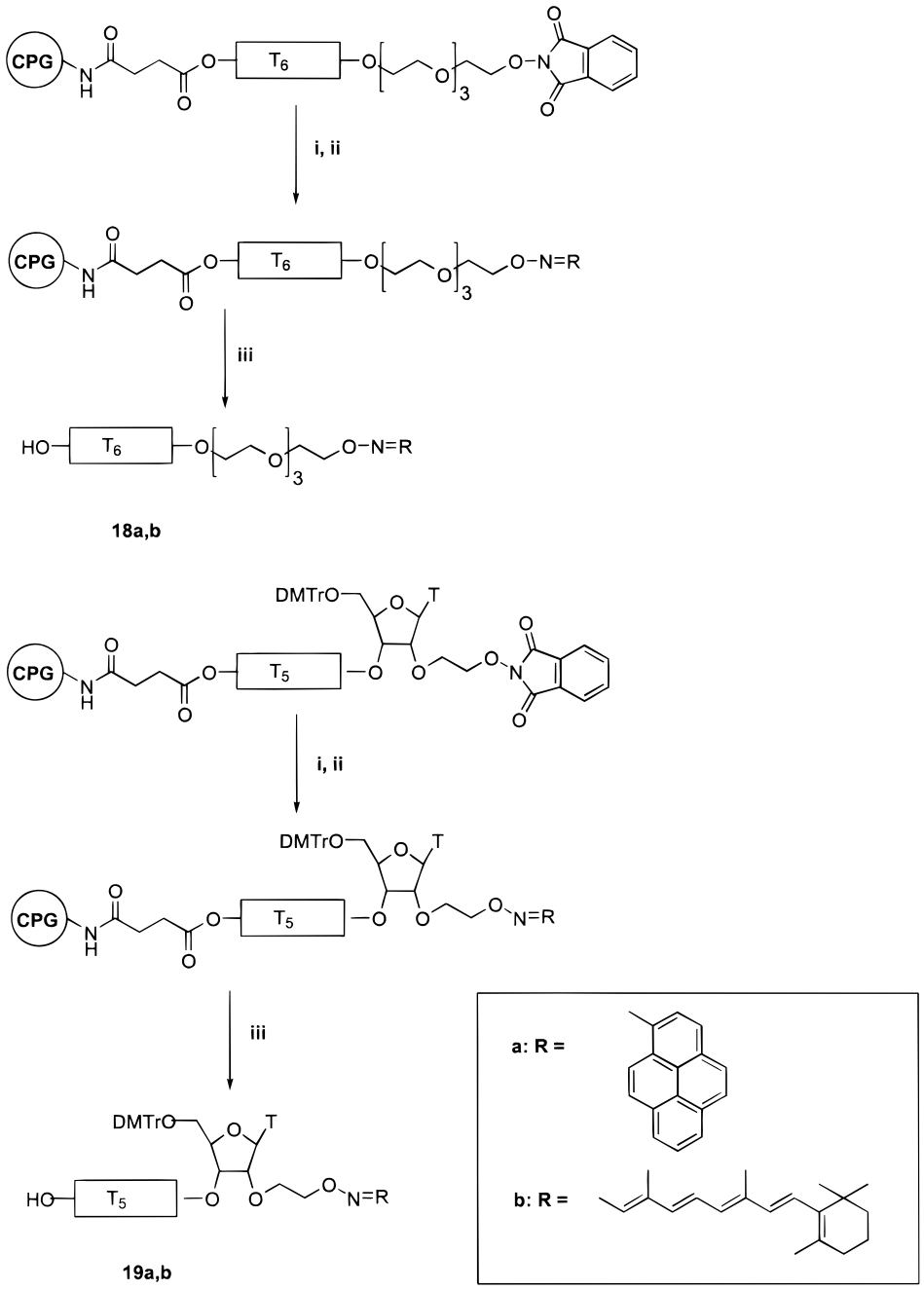


synthesis (*51*), we checked the effect on each nucleoside separately. A sample of each CPG-bound nucleoside (dA, dG, dC, and T) was treated according to the deprotection protocol and analyzed by RP-HPLC. No additional peaks were detected in the chromatograms of the hydrazine-treated nucleosides compared to those referring to nucleosides released from the support by mere ammonolysis.

The applicability of the developed protocol was verified by synthesis of two 16mer heterosequences, **9** and **10,** using phosphoramidites **1** and **2**, respectively (see Scheme 3). All attempts to isolate the oligonucleotide conjugates by RP-HPLC after deprotection of the aminooxy group failed, in all likelihood owing to the high nucleophilicity of the aminooxy function. For this reason, the crude deprotected conjugate was used for immobilization without any purification. The ammoniacal solution containing the deprotected conjugate was simply evaporated to dryness, and the residue was dissolved in water. Tentagel or polyacrylate particles bearing aldehyde or epoxide groups were then immediately added to the resulting solution, and the mixture was gently stirred at room temperature. The disappearance of **9** and **10** from the solution phase was monitored by UV absorbance decrease at 260 nm. According to these observations, less than 10% of the ODN conjugate became immobilized, the loading achieved being of the order of 1 μmol g^{-1}. With the aldehyde supports and epoxy supports, the immobilization took place for 24 h.

Hybridization Assays. The success of immobilization of **9** and **10** to the microparticles was verified by showing that the oligonucleotide-coated particles obtained were able to bind highly selectively the complementary sequence (**11**) from solution. The measurements were carried out by our previously reported (*19*) method that is based on time-resolved detection of a fluorescently tagged oligonucleotide directly from the surface of a single particle. According to these measurements, the intensity of the fluorescence emission signal obtained on treating the particles with a complementary fluorescently tagged oligonucleotide (**11**) was always more than 2 orders of magnitude higher than that resulting from unspecific binding of a noncomplementary fluorescently labeled oligonucleotide (**12**) to the particles. The following systems were tested: (i) oligonucleotide conjugate **9** immobilized to aldehyde-coated Tentagel (**13**), (ii) conjugate **10** immobilized to aldehyde-coated Tentagel (**14**), and (iii) conjugate **10** immobilized to epoxide-coated polyacrylate particles (**15**) (Scheme 3). As illustrative examples, the signals of specific and unspecific binding of oligonucleotides to particles **14** and **15** are shown in Figures 2 and 3 as a function of the oligonucleotide concentration in solution (**11** or **12**). As seen, the epoxide-modified microparticles exhibit a somewhat higher ratio of specific to unspecific binding signal than the aldehyde-derivatized Tentagel particles. These results and our previous findings using this hybridization assay indicate that, first, the amount of oligonucleotide immobilized on the particles was sufficient for efficient and specific

Scheme 4[a]



[a] (i) Hydrazinium hydrate/Pyr/AcOH (0.124/4/7); (ii) RCHO in DMF or MeCN; (iii) NH_3(aq).

hybridization. Second, the use of crude oligomer in the immobilization step did not result in loss of selectivity in the hybridization, which is in good agreement with our previous results. (*19*, *25*)

Labeling Oligonucleotides with Aldehydes on the Support. To verify the authentity of the aminooxy functionalized oligomers (**9**, **10**) and to illustrate more general applicability of aminooxy tethering in the field of oligonucleotide chemistry, some additional experiments with the aminooxy-derivatized oligonucleotides were conducted. Since the aminooxy functionality could be deprotected with a pyridine-buffered hydrazinium-acetate solution without cleaving the succinyl linker, the support-bound aminooxy oligonucleotide conjugates could be converted to oxime conjugates by reacting them with aldehydes. Very recently, the methodology of on-column conjugation with amino-tethered oligonucleotides and acids via PyBOP mediated amide bond formation has been successfully exploited by Greenberg et al. (*52*, *53*). To show the applicability of oxime bond formation, model sequences T_6 and T_5 elongated at the 5′-end with building blocks **1** and **3**, respectively, were reacted both with pyrenecarbaldehyde and *cis*-retinal, forming the corresponding oxime conjugates (Scheme 4). Excess of reagents was washed and ammonolytic treatment of the supports released the crude oxime conjugate in solution. Analysis of the reaction mixtures revealed clearly the formation of E/Z isomers, especially in the case of **19a** (Figure 4). The conjugates were then characterized with ESI-MS, which definitely proved the formation of correct products. According to the areas of the HPLC signals, the total amount of products in the crude ammonolysis mixtures could be estimated to fall in the range 40−70% (Table 1).

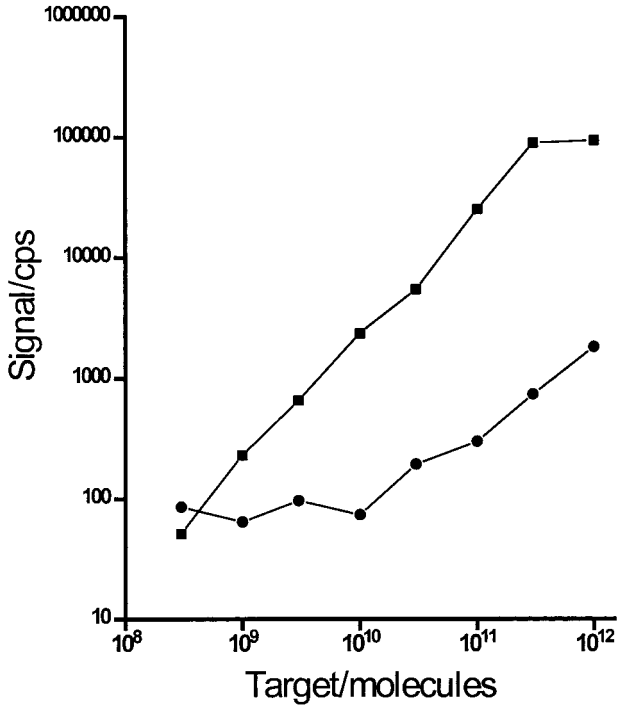


Figure 2. Hybridization of an aminooxy oligonucleotide immobilized to an aldehyde functionalized particle (**14**) with a fluorescently tagged complementary (**11**) and noncomplementary (**12**) sequence. The signal intensity measured from the surface of **14** plotted against the concentration of **11** (squares) or **12** (circles).

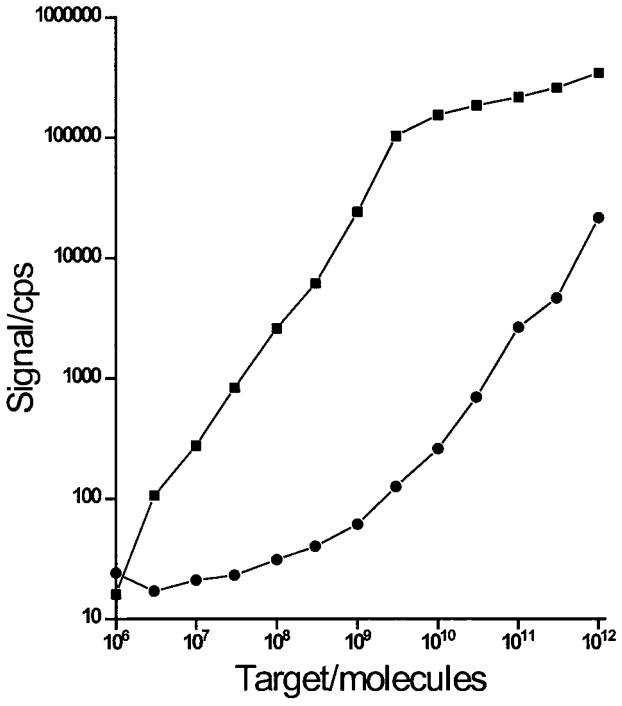


Figure 3. Hybridization of an aminooxy oligonucleotide immobilized to an epoxide functionalized particle (**15**) with a fluorescently tagged complementary (**11**) and noncomplementary (**12**) sequence. The signal intensity measured from the surface of **15** plotted against the concentration of **11** (squares) or **12** (circles).

CONCLUSIONS

Three phosphoramidites that allow tethering of an oligonucleotide with a phthalimidooxy moiety have been prepared and introduced in oligodeoxyribonucleotides. Treatment with hydrazinium acetate have been shown to convert the phthalimidooxy group to an aminooxy group, which as a powerful nucleophile may be exploited in immobilization of oligonucleotides to aldehyde or epoxide modified polymer particles. The immobilized oligonucleotides are shown to serve properly as capture probes in mixed phase hybridization assays. In addition, the aminooxy functionalized oligonucleotides may conveniently be conjugated with aldehydes on solid support, giving oxime conjugates of oligonucleotides.

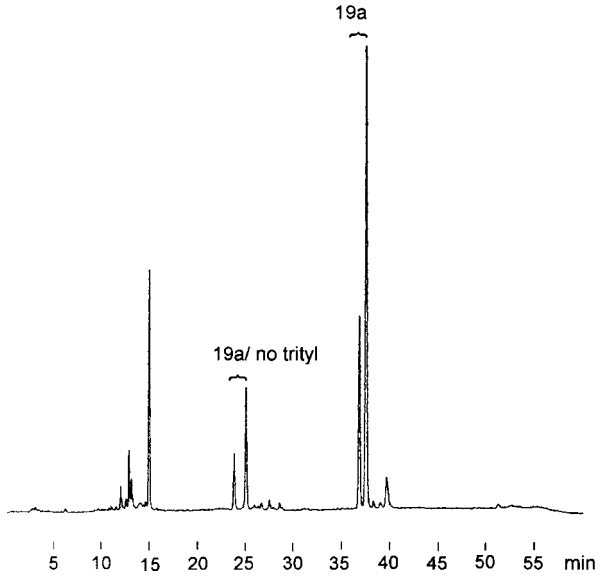


Figure 4. The HPLC profile of an oligonucleotide conjugate (**19a**) obtained by labeling with pyrenecarbaldehyde on support and subsequent ammonolytical release in solution. The product shows two peaks referring to the E/Z isomers of both tritylated and detritylated compounds. For the conditions, see Experimental Section.

ACKNOWLEDGMENT

Financial support from the Research Council for Techniques and Natural Sciences, the Academy of Finland, is gratefully acknowledged.

LITERATURE CITED

(1) Gingeras, T. R., Kwoh, D. Y., and Davis, G. R. (1987) Hybridization properties of immobilized nucleic acids *Nucleic Acids Res. 15*, 5373−90.

(2) Lund, V., Schmid, R., Rickwood, D., and Hornes, E. (1988) Assessment of methods for covalent binding of nucleic acids to magnetic beads, Dynabeads, and the characteristics of the bound nucleic acids in hybridization reactions. *Nucleic Acids Res. 16*, 10861−80.

(3) Saiki, R. K., Walsh, P. S., Levenson, C. H., and Ehrlich, H. A. (1989) Genetic analysis of amplified DNA with immobilized sequence-specific oligonucleotide probes. *Proc. Natl. Acad. Sci. U.S.A. 86*, 6230−34.

(4) Albretsen, C., Kalland, K.-H., Haukanes, B.-I., Håvarstein, L.-S., and Kleppe, K. (1990) Applications of magnetic beads with covalently attached oligonucleotides in hybridization: isolation and detection of specific measles virus mRNA from a crude cell lysate. *Anal. Biochem. 189*, 40−50.

(5) Southern, E. M., Maskos, U., and Elder, J. K. (1992) Analyzing and comparing nucleic acid sequences by hybridization to arrays of oligonucleotides: evaluation using experimental models. *Genomics 13*, 1008−17.

(6) Williams, J. C., Case-Green, S. C., Mir, K. U., and Southern, E. M. (1994) Studies of oligonucleotide interactions by hybridization to arrays: the influence of dangling ends on duplex yield. *Nucleic Acids. Res. 22*, 1365−67.

(7) Southern, E. M. Case-Green, S. C., Elder, J. K., Johnson, M., Mir, K. U., Wang, L., and Williams, J. C. (1994) Arrays

of complementary oligonucleotides for analysing the hybridisation behaviour of nucleic acids. *Nucleic Acids Res. 22*, 1368−73.

(8) Guo, Z., Guilfoyle, R. A., Thiel, A. J., Wang, R., and Smith, L. M. (1994) Direct fluorescence analysis of genetic polymorphisms by hybridization with oligonucleotide arrays on glass supports. *Nucleic Acids Res. 22*, 5456−65.

(9) Stimpson, D. I., Hoijer, J. V., Hsieh, W. T., Jou, C., Gordon, J., Theriault, T., Gamble, R., and Baldeschwieler, J. D. (1995) Real-time detection of DNA hybridization and melting on oligonucleotide arrays by using optical waveguides. *Proc. Natl. Acad. Sci. U.S.A. 92*, 6379−83.

(10) Chee, M., Yang, R., Hubbell, E., Berno, A., Huang, X. C., Stern, D., Winkler, J., Lockhardt, D. J., Morris, M. S., and Fodor, S. P. A. (1996) Accessing genetic information with high-density DNA arrays. *Science 267*, 5287.

(11) Erout, M.-N., Troesch, A., Pichot, C., and Cros, P. (1996) Preparation of conjugates between oligonucleotides and N-vinylpyrrolidone/N-acryloxysuccinimide copolymers and applications in nucleic acid assays to improve sensitivity. *Bioconjugate Chem. 7*, 568−75.

(12) O'Donnell-Maloney, M. J., Smith, C. L., and Cantor, C. R. (1996) The development of microfabricated arrays for DNA sequencing and analysis. *Trends Biotechnol. 14*, 401−7.

(13) Yershov, G., Barsky, V., Belgovskiy, A., Kirillov, E., Kreindlin, E., Ivanov, I., Parinov, S., Gushin, D., Drobishev, A., Dubiley, S., and Mirzabekov, A. (1996) DNA analysis and diagnostics on oligonucleotide microchips. *Proc. Natl. Acad. Sci. U.S.A. 93*, 4913−8.

(14) Seliger, H., Bader, R., Hinz, M., Rotte, B., Astriab, A., Markiewicz, M., and Markiewicz, W. T. (1997) Synthetic oligonucleotide combinatorial libraries: tools for studying nucleic acid interactions. *Nucleosides Nucleotides 16*, 703−10.

(15) Peterlinz, K. A., and Georgiadis, R. M. (1997) Observation of hybridization and dehybridization of thiol-tethered DNA using two-color surface plasmon resonance spectroscopy. *J. Am. Chem. Soc. 119*, 3401−2.

(16) Pastinen, T., Kurg, A., Metspalu, A., Peltonen, L., and Syvänen, A.-C. (1997) Minisequencing: a specific tool for DNA analysis and diagnostics on oligonucleotide arrays. *Genome Res. 7*, 606−14.

(17) Dubiley, S., Kirillov, E., Lysov, Y., and Mirzabekov, A. (1997) Fractionation, phosphorylation and ligation on oligonucleotide microchips to enhance sequencing by hybridization. *Nucleic Acids Res. 25*, 2259−65.

(18) Wallraff, G., Labadie, J., Brock, P., Dipietro, R., Nguyen, T., Huynh, T., Hinsberg, W., and McGall, G. (1997) DNA sequencing on a chip. *Chemtech 27*, 22−32.

(19) Hakala, H., Mäki, E., and Lönnberg, H. (1998) Detection of oligonucleotide hybridization on a single microparticle by time-resolved fluorometry: quantitation and optimization of a sandwich type assay. *Bioconjugate Chem. 9*, 316−321.

(20) Maskos, U., and Southern, E. M. (1992) Oligonucleotide hybridizations on glass supports: a novel linker for oligonucleotide synthesis and hybridization properties of oligonucleotides synthesized in situ. *Nucleic Acids Res. 20*, 1679−84.

(21) Pirrung, M. C. And Bradley, J.-C. (1995) Comparison of methods for photochemical phosphoramidite-based DNA synthesis. *J. Org. Chem. 60*, 6270−76.

(22) Cohen, G., Deutsch, J., Fineberg, J., and Levine, A. (1997) Covalent attachment of DNA oligonucleotides to glass. *Nucleic Acids Res. 25*, 911−2.

(23) Bader, R., Hinz, M., Schu, B., and Seliger, H. (1997) Oligonucleotide microsynthesis of a 200-mer and of one-dimensional arrays on a surface of hydroxylated polypropylene tape. *Nucleosides Nucleotides 16*, 829−33.

(24) Weiler, J., and Hoheisel, J. D. (1997) Picomole syntheses of high quality oligonucleotide primers in combination with the preparation of oligonucleotide arrays. *Nucleosides Nucleotides 16*, 1793−6.

(25) Hakala, H., Heinonen, P., Iitiä, A., and Lönnberg, H. (1997) Detection of oligonucleotide hybridization on a single microparticle by time-resolved fluorometry: hybridization assays on polymer particles obtained by direct solid phase assembly of the oligonucleotide probes. *Bioconjugate Chem. 8*, 378−84.

(26) Kumar, A. (1994) Development of a suitable linkage for oligonucleotide synthesis and preliminary hybridization studies on oligonucleotides synthesized in situ. *Nucleosides Nucleotides 13*, 2125−34.

(27) Ghosh, S., and Musso, G. (1987) Covalent attachment of oligonucleotides to solid supports. *Nucleic Acids Res. 15*, 5353−72.

(28) Zhang, Y., Coyne, M. Y., Will, S. G., Levenson, C. H., and Kawasaki, E. S. (1991) Single-base mutational analysis of cancer and genetic diseases using membrane bound modified oligonucleotides. *Nucleic Acids Res. 19*, 3929−33.

(29) Van Ness, J., Kalbfleisch, S., Petrie, C. R., Reed, M. W., Tabone, J. C., and Vermeulen, N. M. J. (1991) A versatile solid support system for oligodeoxynucleotide probe-based hybridization assays. *Nucleic Acids Res. 19*, 3345−50.

(30) Timofeev, E. N., Kochetkova, S. V., Mirzabekov, A. D., and Florentiev, V. L. (1996) Regioselective immobilization of short oligonucleotides to acrylic copolymer gels. *Nucleic Acids Res. 24*, 3142−8.

(31) Lamture, J., Beattie, K., Burke, B., Eggers, M., Ehrlich, D., Fowler, R., Hollis, M., Kosicki, B., Reich, R., Smith, S., Varma, R., and Hogan, M. (1994) Direct detection of nucleic acid hybridization on the surface of a charge coupled device. *Nucleic Acids Res. 22*, 2121−5.

(32) Bischoff, R., Coull, J., and Regnier, F. (1987) Introduction of 5′-terminal functional groups into synthetic oligonucleotides for selective immobilization. *Anal. Biochem. 164*, 336−44.

(33) O′Donnell, M., Tang, K., Köster, H., Smith, C., and Cantor, C. (1997) High-density, covalent attachment of DNA to silicon wafers for analysis by MALDI-TOF mass spectrometry. *Anal. Chem. 69*, 2438−43.

(34) Kremsky, J. N., Wooter, J. L., Dougherty, J. P., Meyers, R. E., Collins, M., and Brown, E. L. (1987) Immobilization of DNA via oligonucleotides containing an aldehyde or carboxylic acid group at the 5′-terminus. *Nucleic Acids Res. 15*, 2891−909.

(35) Hakala, H., and Lönnberg, H. (1997) Time-resolved fluorescence detection of oligonucleotide hybridization on a single microparticle: covalent immobilization of oligonucleotides and quantitation of a model system. *Bioconjugate Chem. 8*, 232−7.

(36) Isaacs, N.(1995) *Physical Organic Chemistry*, 2nd ed., Longman, Essex, pp 276−7.

(37) Jencks, W. P. (1964) Mechanism and catalysis of simple carbonyl group reactions. *Prog. Phys. Org. Chem. 2*, 63−128.

(38) Karpeisky, A., Gonzalez, C., Burgin, A., B., and Beigelman, L. (1998) Highly efficient synthesis of 2′-*O*-amino nucleosides and their incorporation in hammerhead ribozymes. *Tetrahedron Lett. 39*, 1131−4.

(39) Perbost, M., Hoshiko, T., Morvan, F., Swayze, E., Griffey, R., and Sanghvi, Y. (1995) Synthesis of 5′-O-amino-2′-deoxypyrimidine and purine nucleosides: building blocks for antisense oligonucleosides. *J. Org. Chem. 60*, 5150−6.

(40) Kubo, K., Ide, H., Wallace, S. S., and Kow, Y. W. (1992) A novel, sensitive, and specific assay for abasic sites, the most commonly produced DNA lesion. *Biochemistry 31*, 3703−8.

(41) Ide, H., Akamatsu, K., Kimura, Y., Michiue, K., Makino, K., Asaeda, A., Takamori, Y., and Kubo, K. (1993) Synthesis and damage sensitivity of a novel probe for the detection of abasic sites of DNA. *Biochemistry 32*, 8276−83.

(42) Boturyn, D., Boudali, A., Constant, J., Defrancq, E., and Lhomme, J. (1997) Synthesis of fluorescent probes for the detection of abasic sites in DNA. *Tetrahedron 53*, 5485−92.

(43) Trevisiol, E., Renard, A., Defrancq, E., and Lhomme, J. (1997) The oxyamino-aldehyde coupling reaction: an efficient method for the derivatization of oligonucleotides. *Tetrahedron Lett. 38*, 8687−90.

(44) Adarichev, V. A., Kalachikov, S. M., Kiseliova, A. V., and Dymshits, G. M. (1998) Molecular hybridization probes prepared with 4-aminooxybutylamine. *Bioconjugate Chem. 9*, 671−5.

(45) Mitsunobu, O. (1981) The use of diethyl azodicarboxylate and triphenylphosphine in synthesis and transformation of natural products. *Synthesis*, 1−28.

(46) Kawasaki, A. M., Casper, M. D., Prakash, T. P., Manalili, S., Sasmor, H., Manoharan, M., and Cook, P. D. (1999) Synthesis, hybridization and nuclease resistance properties of 2′-O-aminooxyethyl (2′-*O*-AOE) modified oligonucleotides. *Tetrahedron Lett. 40*, 661−4.

(47) Mukkala, V.-M., Helenius, M., Hemmilä, I., Kankare, J., and Takalo, H. (1993) Development of luminescent europium-(III) and terbium(III) chelates of 2,2′:6′,2″-terpyridine derivatives for protein labeling. *Helv. Chim. Acta 76*, 1361−78.

(48) Lövgren, T., Heinonen, P., Lehtinen, P., Hakala, H., Heinola, J., Harju, R., Takalo, H., Mukkala, V.-M., Schmid, R., Lönnberg, H., Pettersson, K., and Iitiä, A. (1997) Sensitive bioaffinity assays with individual microparticles and time-resolved fluorometry. *Clin. Chem. 43*, 1937−43.

(49) Jones, R. A. (1984) Preparation of protected deoxyribonucleosides. In *Oligonucleotide Synthesis: A Practical Approach* (M. J. Gait, Ed.) p 23, IRL Press, Oxford.

(50) Hovinen, J. (1998) A Simple synthesis of N^4-(6-aminohexyl)-2′-deoxy-5′-*O*-(4, 4′-dimethoxytrityl)cytidine. *Nucleosides, Nucleotides 17*, 1209−13.

(51) Azhayev, A., Guzaev, A., Hovinen, J., Azhayeva, E., and Lönnberg, H. (1993) Analogues of oligonucleotides containing 3′-deoxy-β-**D**-psicothymidine. *Tetrahedron Lett. 34*, 6435−8.

(52) Kahl, J. D., and Greenberg, M. M. (1999) Introducing structural diversity in oligonucleotides via photolabile, convertible C5-substituted nucleotides. *J. Am. Chem. Soc. 121*, 597−604.

(53) Kahl, J. D., McMinn, D. L., and Greenberg, M. M. (1998) High-yielding method for on-column derivatization of protected oligodeoxynucleotides and its application to the convergent synthesis of 5′,3′-bis-conjugates. *J. Org. Chem. 63*, 4870−1.

BC990021M

On the Sequence Selective Bis-Intercalation of a Homodimeric Thiazole Orange Dye in DNA

Jakob Bunkenborg, Maria Munch Stidsen, and Jens Peter Jacobsen*

Department of Chemistry, Odense University, DK-5230 Odense M, Denmark. Received March 15, 1999; Revised Manuscript Received June 24, 1999

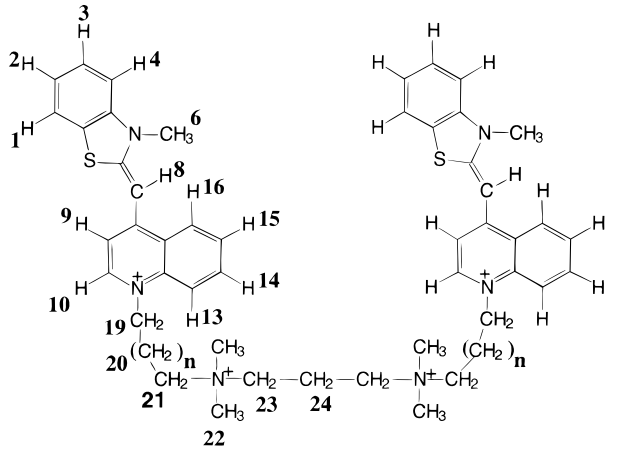
The thiazole orange dye 1,1′-(4,4,8,8-tetramethyl-4,8-diazaundecamethylene)-bis-4-[(3-methyl-2,3-dihydro(benzo-1,3-thiazolyl)-2-methylidene]quinolinium tetraiodide (TOTO) binds sequence selectively to double-stranded DNA (dsDNA) by bis-intercalation. Each chromophore is sandwiched between two base pairs in a d(5′-py-p-py-3′):d(5′-pu-p-pu-3′) site, and the linker spans over two base pairs in the minor groove. We have examined the binding of TOTO to various dsDNA oligonucleotides containing variations of the 5′-CTAG-3′ binding motif by introducing inosine (I = inosine, 2-desaminoguanosine) and 5-methylcytosine (^{me}C). A one- and two-dimensional NMR spectroscopy characterization yielded detailed structural information on the binding mode and for the well-defined TOTO-complexes competition experiments allowed determination of the relative binding strengths resulting from the various structural alterations. The experimentally observed base pair preference of TOTO in the palindromic sequences investigated is ^{me}CG > CG > CI > TA for the flanking base pair and ^{me}CI > CI > TA > CG > UA for the central base pair. The best binding site observed so far is the d(5-C^{me}CIG-3′)$_2$ site. This site is much more favorable than the d(5′-CTAG-3′)$_2$ site formerly believed to be the best binding site. The present paper discusses these results in terms of different contributions to the binding affinity and offers some explanations for the site selectivity of TOTO.

INTRODUCTION

DNA[1]-intercalating agents (Denny, 1989) have attracted much attention since Lerman (Lerman, 1961) first described the intercalation binding motif as the insertion of a flat, aromatic chromophore between two base pairs, and many compounds have been found to interact with DNA in this way (Denny, 1989). The noncovalent binding of small molecules to DNA may occur with high affinity and varied sequence selectivity. Much of the affinity and specificity is derived from the small molecules having a structure capable of forming hydrogen bonds with DNA. However, several other factors influence the affinity and selectivity such as steric complementarity, base stacking ability, and electrostatic properties.

Recent work in our laboratory has concerned the binding properties and sequence selectivity of the homodimeric bis-intercalating cyanine dye TOTO [1,1′-(4,4,8,8-tetramethyl-4,8-diazaundecamethylene)-bis-4-[(3-methyl-2,3-dihydro-2(3H)-benzo-1,3-thiazolylidene]-methyl]quinolinium tetraiodide; Scheme 1), which was developed by Glazer and co-workers (Glazer and Rye, 1992) as a flourescent probe for DNA detection. On the basis of a linear relationship between fluorescence intensity and DNA concentration in base pairs, Glazer concluded that TOTO does not show strong sequence specificity. However, we have shown (Jensen et al., 1998; Hansen et al., 1996) that TOTO binds preferentially to 5′-pyrimidine-pyrimidine-purine-purine-3′ (5′-py-py-pu-pu-3′) sequences with 5′-CTAG-3′ as the preferred binding site. The binding of TOTO to various symmetric double-stranded DNA sequences was found to be quite sensitive to changes in the base sequence (Jensen et al., 1998; Hansen et al., 1996). TOTO certainly binds to all the oligonucleotides investigated as evidenced by the

Scheme 1. Chemical Structure of the Bis-Intercalating TOTO and TOTO11 and the Atomic Numbering Scheme for TOTO



TOTO: n = 1

TOTO11: n = 2

* To whom correspondence should be addressed. E-mail: jpj@chem.ou.dk.

[1] Abbreviations: DMSO, dimethyl sulfoxide; DNA, deoxyribose nucleic acid; dsDNA, double-stranded DNA; DSS, 2,2-dimethyl-2-silapentane-5-sulfonate; EDTA, ethylenediaminetetraacetic acid; I, inosine; ^{me}C, 5-methylcytosine; NMR, nuclear magnetic resonance; NOESY, nuclear Overhauser effect spectroscopy; p, phosphate; pu, purine; py, pyrimidine; TOCSY, total correlation spectroscopy; TOTO, 1,1′-(4,4,8,8-tetramethyl-4,8-diazaundecamethylene)-bis-4-[(3-methyl-2,3-dihydro(benzo-1,3-thiazolyl)-2-methylidene]-quinolinium tetraiodide; TOTO11, 1,1′-(5,5,9,9-tetramethyl-5,9-diazatridecamethylene)-bis-4-[(3-methyl-2,3-dihydro(benzo-1,3-thiazolyl)-2-methylidene]quinolinium tetraiodide; TOTO11Et, 1,1′-(5,5,9,9-tetramethyl-5,9-diazatridecamethylene)-bis-4-[(3-methyl-2,3-dihydro(benzo-1,3-thiazolyl)-2-methylidene]quinolinium tetraiodide; TPPI, time proportional phase incrementation.

10.1021/bc990030v CCC: $18.00 © 1999 American Chemical Society
Published on Web 08/05/1999

disappearance of NMR resonances from the free dsDNA, but TOTO does not always form well-defined complexes that permits spectral assignments and thus NMR characterization. The main reasons for this are line broadening arising from exchange of TOTO between different sites or from different binding modes. Previous studies have shown that there is at least a 100-fold preference for bis-intercalating in the (5′-CTAG-3′)$_2$ site over any other site contained in the d(5′-CGCTAGCG-3′)$_2$ sequence. This site selectivity seems somewhat surprising in view of the rather nonspecific intercalator and electrostatic binder motif, neither of which are capable of forming hydrogen bonds, that is combined into the TOTO molecule. On the basis of the solution structure of the TOTO−CTAG complex (Spielmann et al., 1995), it was suggested that the sequence selectivity is influenced by the ability of the thiazole orange chromophores to adapt to the propeller twist of the bases in the binding step. The benzothiazole moiety of the chromophore is intercalated between the two pyrimidine bases and the quinolinium part is intercalated between the two purine bases. The optimal stacking displayed by this structure may explain why TOTO prefers a 5′-py-py-pu-pu-3′ site but does not explain the selectivity within this type of sequences.

NMR studies of polyamines (Padmanabhan et al., 1988; Wemmer et al., 1985; Padmanabhan et al., 1991) indicate a nonselective, electrostatic binding mode to DNA. Consequently, it was concluded that although adding significantly to the binding strength, the polyamine linker of TOTO is only a spectator with respect to the sequence selectivity. Thus, the sequence selectivity seems to be governed by the interaction of the intercalated thiazole orange chromophores with the bases. It is not really well understood what causes the preference of TOTO for the 5′-CTAG-3′ site, but several contributions have been suggested. The solution structure indicates that the 5′-py-py-pu-pu-3′ binding motif offers the best stacking of the chromophores. Competition experiments have shown that the substitution of thymine with uracil (Jensen et al., 1998) causes a weaker binding of TOTO, leading to the conclusion that the methyl group on thymine causes some stabilization of the complex. This stabilization could be attributed to dispersion attractions between the methyl group and the benzene moiety of the benzothiazole ring, or to hydrophobic interactions between the two. The lack of the methyl group could also explain why 5′-CCGG-3′ is a worse site, but is certainly not sufficient to explain why neither d(5′-CGTCGACG-3′)$_2$ nor d(5′-CGTTAACG-3′)$_2$ form well-defined complexes with TOTO.

Theoretical (Sponer et al., 1996) and experimental (Joireman et al., 1998) studies on aromatic−aromatic interactions suggest that there are three major components in determining the geometry and strength of the stacking interaction. The exchange repulsion is the short-range interaction that determines how close two nonbonding atoms can get. The dispersion attraction is an attractive electron correlation phenomenon that favors the close contact between nonbonding atoms, while the electrostatic interactions can be both attractive and repulsive and show a strong orientational dependence. The exchange repulsion and the dispersion attraction are often collectively referred to as van der Waals forces. The electrostatic and van der Waals forces often have conflicting demands on the optimum structure of an intermolecular complex leading to different binding motifs when either dispersion or electrostatic interactions dominate.

Scheme 2. Palindromic DNA Sequences Studied and Their Numbering Schemes

CTAG:

```
          1 2 3 4 5 6 7 8
5' - C G C T A G C G - 3'
3' - G C G A T C G C - 5'
```

CCIG:

```
5' - C G C C I G C G - 3'
3' - G C G I C C G C - 5'
```

CCII:

```
5' - C G C C I I C G - 3'
3' - G C I I C C G C - 5'
```

CCGI:

```
5' - C G C C G I C G - 3'
3' - G C I G C C G C - 5'
```

^{me}CTAG:

```
5' - C G mC T A G C G - 3'
3' - G C G A T mC G C - 5'
```

C ^{me}CIG:

```
5' - C G C mC I G C G - 3'
3' - G C G I mC C G C - 5'
```

To investigate the structural basis of the site selectivity of TOTO, we have studied some variations of the 5′-CTAG-3′ binding motif by introducing inosine (I = inosine, 2-desaminoguanosine) and 5-methylcytosine (^{me}C). The NMR characterization by the NOESY spectra yields detailed structural information on the binding mode, and for the well-defined TOTO complexes, the competition experiments allow a determination of the binding strength as a result of the various structural alterations. While replacement of the outer guanosine with inosine destabilized the complex, replacement of the central T−A base pairs with C−I improved the stability. The best binding site observed so far was obtained with the d(5′-C^{me}CIG-3′) site. Our new results indicate that the linker is not altogether a passive spectator to the sequence selectivity, and we therefore included a TOTO analogue with a longer linker into the study. This analogue contained two more methylene groups in the linker and is named TOTO11 [1,1′-(5,5,9,9-tetramethyl-5,9-diazatridecamethylene)-bis-4-[(3-methyl-2,3-dihydro(benzo-1,3-thiazolyl)-2-methylidene]quinolinium tetraiodide; Scheme 1]. Combined with earlier results, the present study offers some elucidation of TOTO's site selectivity.

EXPERIMENTAL SECTION

Materials. TOTO and TOTO11 were kindly provided by Dr. E. B. Pedersen (Department of Chemistry, Odense University, Denmark). The self-complementary oligonucleotides shown in Scheme 2 were purchased from DNA-Technology, Aarhus, Denmark, and were delivered redissolved in doubly distilled H_2O after being ethanol precipitated from 500 mM NaCl buffer, pH 8.0. The purity of the oligonucleotides was assessed by 1-D H NMR spectroscopy, and they were used without further purification. The complexes of TOTO with the oligonucleotides were prepared by the procedure described earlier (Jacobsen et al., 1995). The NMR samples were prepared by dissolving the complexes in 500 μL of 10 mM sodium phosphate buffer (pH 7.0) containing 50 μM EDTA, 10 μM NaN_3, and 100 μM DSS. For experiments carried out in D_2O, the solid complex lyophilized twice from D_2O was redissolved in 99.96% D_2O (Cambridge Isotope Laboratories). A mixture of 90% H_2O and 10% D_2O was used

for experiments examining exchangeable protons. The samples were kept in NMR tubes under nitrogen. The final concentrations of the complexes ranged 1.7−2.0 mM.

Methods. NMR experiments were performed on a 500 MHz Varian Unity 500 spectrometer. NOESY spectra in D_2O were acquired with a 200 ms mixing time using 1024 complex points in t_2 and a spectral width of 5000 Hz. A total of 512 t_1 experiments were recorded using the States phase cycling scheme with 64 scans for each t_1 value. The residual signal from HOD was removed by presaturation. TOCSY spectra with mixing times of 30 and 90 ms were obtained in the TPPI mode using 1024 complex points in t_2 and 512 t_1 experiments with 64 scans each. The NOESY spectra in H_2O were acquired with a spectral width of 12.000 Hz for the inosine containing oligonucleotides and 10.000 Hz for the rest using 2048 complex points and a pulse sequence where the last 90° pulse is replaced with a shaped 90° pulse containing a notch to avoid excitation of the solvent signal (Stein et al., 1995). This ensured suppression of the water signal together with a linear excitation profile over the whole spectral width. Most spectra were acquired at 298 K, but the oligonucleotide sequences containing a central inosine formed a hairpin minor form, and to minimize the hairpin-concentration, the spectra were acquired at low temperature (either 274 or 283 K). The acquired data were processed using either FELIX (version 95.0 or 97.0, MSI/Biosym Technologies, San Diego). For the competition experiments, at least 2048 scans were acquired at 283 K and the integration of the imino resonances was done using the line fitting procedure in FELIX. The spectra were analyzed by conventional methods (Boelens et al., 1985; Feigon et al., 1983; Hare et al., 1983; Scheek et al., 1984; Wüthrich, 1986).

RESULTS

Spectral Analysis. The DNA complexes formed by TOTO with the oligonucleotides listed in Scheme 2 yielded proton resonances with line widths ranging 6−15 Hz. Narrow lines are certainly indicative of a well-defined complex, but broad lines may result from a slight overtitration of TOTO. Except for CCGI, all the complexes of TOTO with the palindromic oligonucleotides exhibit dyad symmetry as evidenced by the occurrence of resonances from only one dsDNA strand and half of the TOTO resonances expected for an asymmetric complex. CCGI and TOTO formed a symmetric major form and an asymmetric minor form, for the other sequences, there were no discernible minor forms.

Figure 1 shows the aromatic to aromatic and H1′ region of the NOESY spectra of the C^{me}CIG−TOTO complex, which is spectroscopically representative for the complexes included in this study. The NOESY spectra of the TOTO complexes exhibit the characteristic dsDNA sequential connectivities, but the sequential pathway is disconnected in the 5′-C3-p-^{me}C4-3′ and 5′-I5-p-G6-3′ base pair step. Several of the C3 and ^{me}C4 resonances are shifted upfield compared to the position in the free oligonucleotide and there are a number of cross-peaks between the TOTO chromophores and the surrounding DNA residues. All these observations unambiguously place each thiazole orange chromophore sandwiched between two base pairs in an overall symmetric bis-intercalative binding mode. The spectra were assigned as previously described (Jacobsen et al., 1995; Spielmann et al., 1995). The cross-peaks between the purine H8 and the protons H13, H14, and H15 of the quinoline moiety position the quinoline ring between the two purine bases. Cross-peaks between I5H2 and H9/H10 place the H9/H10 end of the quinoline ring above the purine base at the center of the minor groove. The cross-peaks between the methyl group of the central pyrimidine and H1−H4 of the benzothiazole part indicates that the benzene ring is situated between the pyrimidines and pointing toward the pyrimidine side of the major groove. Although minor changes in the structure are to be expected, all these NOE contacts are in rough accordance with the CTAG−TOTO solution structure. It therefore seems reasonable to make inferences about the substitution of new bases on the basis of this structure. The poly(propylenamine) linker is without doubt placed in the minor groove for all the well-defined complexes. Cross-peaks (not shown) between the H2 proton of inosine and the H21, H22, and H23 linker protons and between the H1′ of I5 and the H19, H20, and H21 linker protons unambiguously locate the linker in the minor groove. The NOESY spectra recorded in H_2O exhibit the normal Watson−Crick NOE connectivities for the exchangeable protons with an interruption at the 3−4 and 5−6 base pair steps where the chromophores are inserted.

Site Selectivity of TOTO. To gain insight into the causes of the site selectivity of TOTO, we performed NMR competition studies between various oligonucleotides containing the (5′-py-py-pu-pu-3′)$_2$ binding motif. In the competition experiments, the distribution of TOTO between almost equal amounts of two oligonucleotides was measured by the intensities of the imino proton resonances from both the two free oligonucleotides and the two complexes. This procedure requires one isolated imino proton resonance for each species. The oligonucleotides CCGI, CCIG, CCII, and C^{me}CIG competed against CTAG, but due to the similarity of CTAG and ^{me}CTAG and the resulting spectral overlap, ^{me}CTAG competed against CCII. The imino region of the competition experiment between C^{me}CIG and CTAG is displayed in Figure 2, where the resonances in the mixture are unambiguously identified by the single species assignments of the free oligonucleotides and TOTO complexes. The equilibrium

$$\text{CTAG-TOTO} + \text{C}^{me}\text{CIG(free)} \rightleftarrows \text{CTAG(free)} + \text{C}^{me}\text{CIG-TOTO}$$

is established very fast and has an equilibrium constant given by

$$K = \frac{[\text{CTAG(free)}][\text{C}^{me}\text{CIG-TOTO}]}{[\text{CTAG-TOTO}][\text{C}^{me}\text{CIG(free)}]}$$

The values of K measured from the integral of the imino resonances at 10 °C are given in Table 1 together with the results from previous studies (Jensen et al., 1998; Hansen et al., 1996). The results have been normalized with the CTAG sequence as the reference. A general problem with this approach is that only the relative affinity between two different well-defined sites having nonoverlapping resonances can be measured, and therefore, the affinity of the ill-defined sites cannot be measured. It is therefore not possible to establish an affinity scale that encompasses all the possible sites. Furthermore, there is a large uncertainty when comparing sequences with very disparate affinities.

The present study has yielded a new binding sequence for TOTO that is much better than the previously best

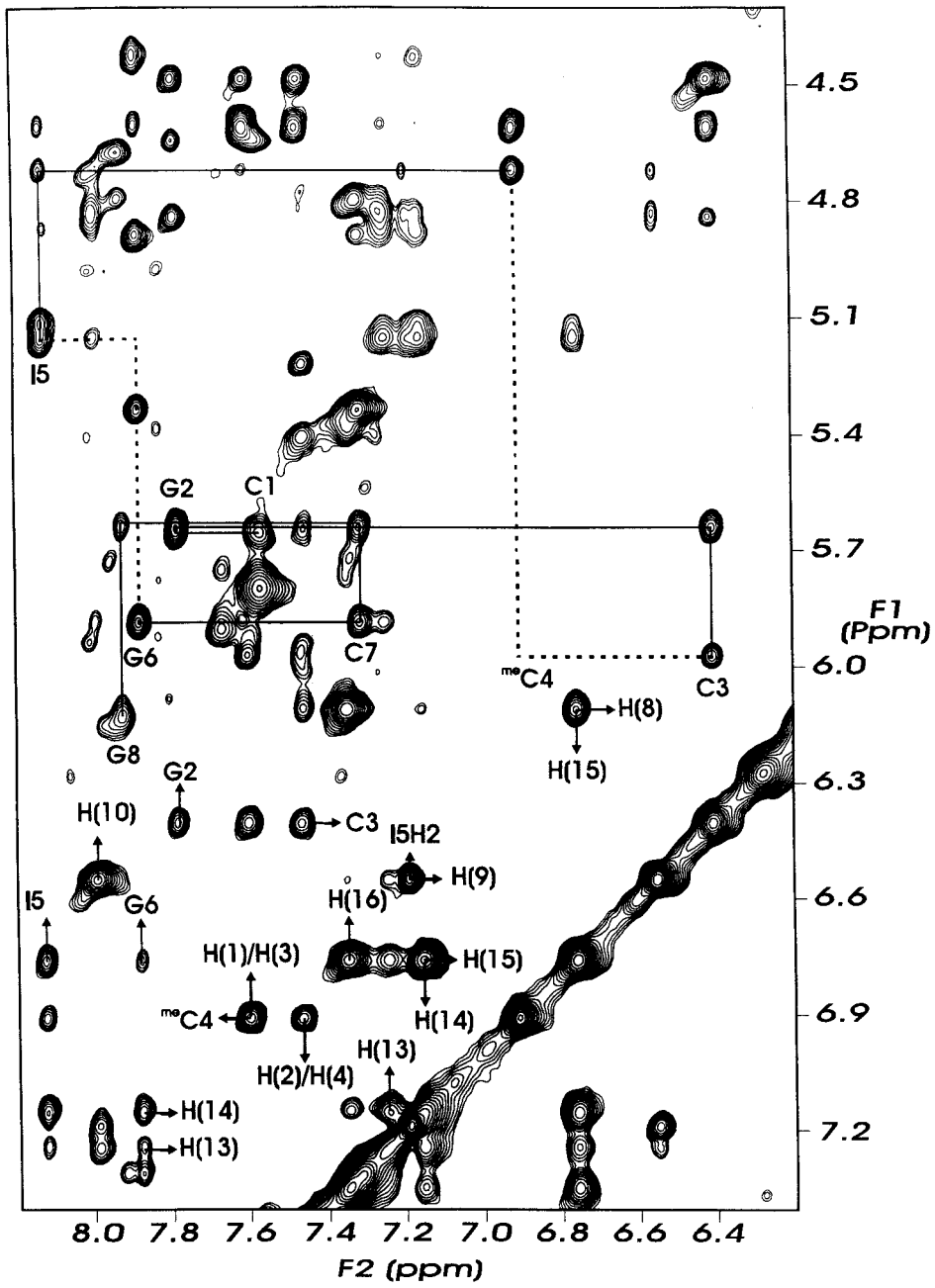


Figure 1. The aromatic to H1′ and aromatic part of the 200 ms NOESY spectrum of the C^{me}CIG−TOTO complex. The sequential H1′−H6/H8−H1′ connectivity pathway is indicated by a solid line. The interrupted connectivities at the 5′-C3-p-^{me}C4-3′ and 5′-I5-p-G6-3′ base pair steps due to intercalation sites are indicated by dotted lines. Some of the observed cross-peaks between TOTO and the oligonucleotide are also marked. The connectivities between H(8)−H(16)-H(15)−H(14)-H(13) have been indicated together with the connectivities between the two H(9) and H(10) protons.

sequence d(5′-CTAG-3′)$_2$ by a factor of about 68—namely d(5′-C^{me}CIG-3′)$_2$. The new competition experiments have also augmented the number of well-defined TOTO-binding sites, with a number of new sites including several superior to d(5′-CTAG-3′)$_2$. Within the 5′-py-py-pu-pu-3′ (and here only substitutions that retain Watson−Crick base pairing have been included), our data yield the following preferences: The preferred flanking purine is guanine followed by inosine both base pairing with cytosine, all of which are better than an AT pair. For the central base pair, inosine is the favorite choice for purine followed by adenine and then guanine. The pyrimidine ^{me}C is better than cytosine in accordance with the earlier result that thymine (5-methyl uracil) is better than uracil. Thus, the experimentally observed base pair preference from Table 1 may be summarized for the palindromic sequences:

Flanking base pair: ^{me}CG > CG > CI > TA

central base pair: ^{me}CI > CI > TA > CG > UA

DISCUSSION

The binding strength of TOTO is largely determined by the intercalation of the chromophores and by the interactions of the cationic charges of TOTO and the anionic phosphate backbone of DNA. Thus, the site selectivity obviously must stem from an interplay of the binding contributions from the linker and the chromophores.

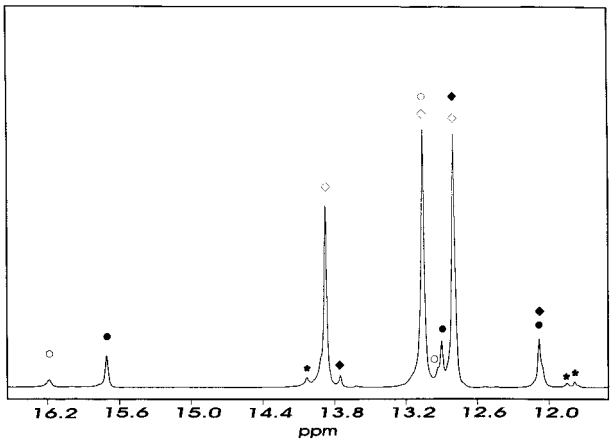


Figure 2. The imino proton region of the 1D spectrum obtained in 90% H_2O/10% D_2O of the mixture of C^{me}CIG, CTAG, and TOTO in the ratio 1.1:4.3:1.0. Resonances from the C^{me}CIG−TOTO (●), CTAG−TOTO (◆) complexes and the free oligonucleotides C^{me}CIG(F) and CTAG (◇) are observed. (★) These resonances were not assigned.

Table 1. the Affinity of TOTO and TOTO11 to 5′-py-py-pu-pu-3′ Sites Relative to the CTAG Sequence[a]

	TOTO	TOTO11
TCGA	more	
TTAA	than one	
CTGA	complex	
CCGI	is formed	
CUAG	0.15	
CCGG	0.16	0.70
CTAI	0.55	
CTAG	1.00	1.00
^{me}CTAG	1.4	
CCII	5.6	3.3
CCIG	12	
C^{me}CIG	68	

[a] The values are given as the ratio of the values of the equilibriums constant at 10 °C. The values given for the TOTO and TOTO11 cannot be compared directly since it is not possible to determine the relative affinity af these two drugs.

Chromophores. The site selectivity of TOTO is to some extent governed by the interactions of the intercalated chromophores with the bases. Simple planar intercalators exhibit little or no sequence selectivity. Footprinting studies indicate that intercalators are relatively excluded from runs of A and T (Fox and Waring, 1987) while differential dialysis experiments show that there is some preference for GC base pairs (Müller and Crothers, 1975), and the ellipticine chromophore has been shown to prefer GC regions (Bailly et al., 1990). However, these preferences are only weak and to our knowledge there have not been reports on any simple intercalator preferences for a (5′-CT-3′):(5′-AG-3′) site. The diversity and general low specificity of intercalators makes it quite difficult to make any inferences of the specificity of the thiazole orange chromophore on the basis of other intercalative compound. Therefore, the properties of the thiazole orange chromophore will be considered from a more theoretical point of view.

Some of the changes in binding site affinity on base pair replacement may be rationalized by considering the dipole moments and polarizabilities of the nucleobases involved to reflect the strength of the electrostatic interactions, the induction, and the dispersion attractions, respectively. The close relationship between the strength of the base-stacking interactions for pyrimidines and the molecular polarizability in an aqueous environment has been experimentally shown by Sowers et al.

Table 2. Dipole Moments (μ) and Dipole Polarizabilities (α) of Nucleobases[a]

	U	T	C	^{me}C	A	I	G
μ	1.71	1.7	2.49	2.67	1.06	2.02	2.52
α	71.3	83.7	79.3	91.3	97.4	91.3	103.3

[a] The size of the dipole moments and dipole polarizabilities are given in atomic units. These MP2\[5s3p2d]\[3s2p]\\MP2\6-31G(d,p) results are taken from Johnson et al. (1996).

(Sowers et al., 1987). Qualitatively, we may assume that the electrostatic interactions are dominated by the ion−dipole interaction, the induction interaction by the ion polarizability interaction and the dispersion attraction is by the polarizability (viz., induced dipole−induced dipole). MP2 calculations on nucleobases by Johnson et al. (Johnson et al., 1996) yield the dipole moments and polarizabilities shown in Table 2.

For the flanking bases of the intercalation site, the position of the linker is of little consequence and guanine with the largest polarizability and dipole moment is the preferred flanking base followed by inosine with intermediate dipole moment and low polarizability both base pairing with cytosine (with the largest dipole moment). The methylation of cytosine enhances the dipole moment and polarizability, and this leads to an enhanced affinity. The TA flanking base pair is the least favored with relatively small dipole moments. Earlier, we proposed that the low affinity of (5′-TTAA-3′)$_2$ probably was due to steric hindrance caused by the methyl groups of the flanking thymine (Hansen et al., 1996), but the very similar ^{me}CTAG forms a well-defined complex, suggesting that the steric hindrance due to the methyl groups is not the cause of the low affinity.

There are two contributions to be considered when discussing the central base pairs: the minor groove environment experienced by the linker and the stacking of the chromophores. Although the CG base pair following the above lines of thought should be the best central base pair, the amino group protruding into the minor groove interacts detrimentally with the linker as described below. Replacing thymine with uracil lowers the affinity because the removal of the methyl group reduces the dispersion attraction. Substituting the central TpA with CpI enhances the affinity (due to larger dipole moments), which may be further enhanced by the introduction of ^{me}C facilitating better dispersion attraction.

The enhanced affinity of the methylated pyrimidines could also stem from hydrophobic interactions between the benzothiazole moiety and the methyl group. The simple relationship between polarizability and base stacking for the nucleobases is obviously a bit too crude when applied to DNA, because the sugar−phosphate backbone and hydrogen-bonding demands on the optimal geometry are not identical to those of base stacking. The NMR solution structure does offer some explanation why the methylation of the flanking pyrimidine (leading to higher polarizability) doesn't lead to as large an affinity enhancement as exhibited by the central pyrimidines. The methyl group of the central pyrimidine is situated right above the benzene moiety of the benzothiazole ring, thereby making contact with the whole ring. The CTAG−TOTO solution structure suggests that a methyl group on the flanking pyrimidine would be positioned above the N-methyl group of TOTO. The dispersion attraction favors geometries that maximize the number of close contacts with as many atoms as possible, and the methyl group of the flanking pyrimidine does not have as good van der Waals contacts with the thiazole chromophore as the central pyrimidine.

Linker. The polyamine linker of TOTO is analogous to a family of linear positively charged molecules (including spermine and spermidine) that has been intensely studied but, unfortunately, has proven quite elusive to most spectroscopic techniques and there seems to be little consensus on the binding mode of these polycationic polyamines. NMR studies by Wemmer (1985) of spermine binding to the Dickerson−Drew dodecamer have shown that the spermine molecule does not form a tight well-defined complex with DNA and its mobility is effectively independent of that of DNA. These data suggested a nonselective electrostatic binding mode, and therefore it was proposed that the polyamine linker of TOTO only contributes to the binding strength and not to the sequence selectivity (Jacobsen et al., 1995). However, photoaffinity cleavage with polyaminobenzene-diazonium salts and competition experiments with the minor groove binder distamycin (Schmid and Behr, 1991) have shown that polyamines have a strong preference for the minor groove and a weak 2−3-fold preference for AT-rich regions. Spermine blocking of both mechloroethamine (nitrogen mustard) guanine N7 alkylation (Hartley et al., 1990) and 5′-GC interstrand cross linking by 2,5-diaziridinylbenzoquinone (Yuki et al., 1996) indicate that the major groove is preferred for GC sequences. It has recently been proposed that the linker of N^1-(acridin-9-ylcarbonyl)spermine interacts with the phosphate backbone (Blackbrough et al., 1998), but this phosphate strand binding is claimed to be ruled out by the results of Schmid (Schmid and Behr, 1991).

Before drawing any conclusions from the somewhat bewildering material presented above, it should be made clear that the polyamine linker of TOTO differs in several respects from spermine and spermidine. The alkylated polyamine chain rules out any possibility of hydrogen bond formation, but a study on the affinity of several polyamines has shown that the affinity of the alkylated linear polyamines generally lie only a little under that of the protonated polyamines (Schneider and Blatter, 1992). The intercalation of the chromophores also puts some restrictions on the mobility and binding possibilities of the linker. The linker cannot interact with the phosphate backbone in the way described by Blackbrough (1998). Furthermore, the alkylated polyamine is more hydrophobic than its nonalkylated analogues, and the narrow minor groove offers protection from the solvent and van der Waals contacts with the walls of the groove.

The electrostatic environment created by DNA may be represented by an electrostatic potential map as shown by Pullman (Lavery and Pullmann, 1981). The electrostatic potential maps for the Watson−Crick base paired AT and GC in Figure 3 show that the two base pairs offer different binding possibilities. While the GC base pair has a very negative electrostatic region in the major groove, the AT base pair has two negative contact points in the minor groove. The NOESY cross-peaks between TOTO and the oligonucleotide unambiguously place the linker in the minor groove for all the assigned 5′-py-py-pu-pu-3′ complexes. The structure of the CTAG−TOTO complex (Spielmann et al., 1995) positions the linker dimethyl nitrogens in the vicinity of the adenine N3. The electrostatic potential maps also lend some credibility to this position, since it must be energetically favorable to position the charged group in a region with negative electrostatic potential. The guanine amino group protruding into the minor groove does hamper this interaction, and on removing the amino group by the introduction of inosine the affinity is enhanced. Thus, to some extent the linker does affect the site selectivity of TOTO.

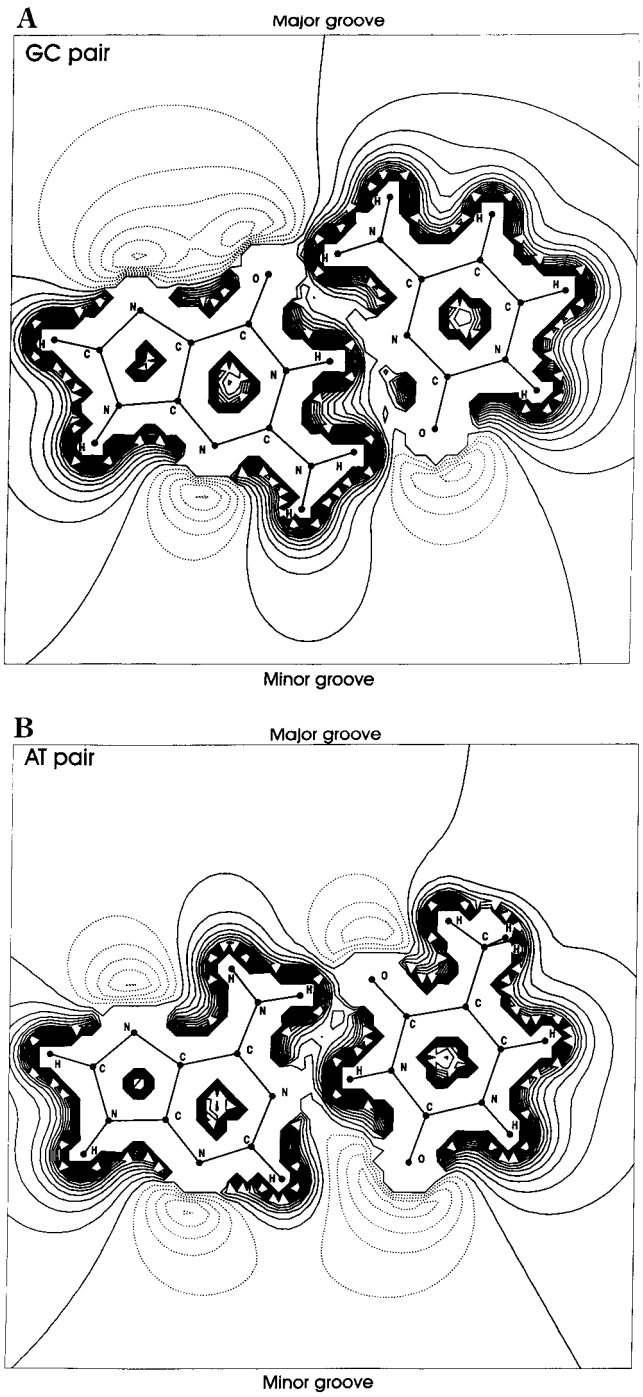


Figure 3. The liniarly spaced electrostatic potential contours around the GC (A) and AT (B) base pairs. Negative contours are dashed. The base pair geometries were taken as the standard B-DNA base pair in InsightII, and the electrostatic potential was calculated and displayed by MOLDEN (Schaftenaar, 1991) on the basis of a Gaussian94 (Frisch et al., 1995) RHF[\]6-31G single point calculation.

To investigate how the position and length of the linker affected the affinity, we performed two competition experiments with TOTO11. The site selectivity was diminished in the sense that the affinity for CCGG is less reduced while the affinity for CCII is less enhanced. This could indicate that the steric hindrance by the amino groups is also an important factor together with the minor groove electrostatic potential. However, a high-

resolution NMR structure of the TOTO11Et−CTAG complex (Bondensgaard and Jacobsen, 1998) shows that the longer linker shifts the position of the dimethyl nitrogens toward the thymine minor groove oxygen making any inference on the relative size of the two factors quite difficult.

CONCLUSION

The affinity pattern of the various complexes indicates that the site selectivity of TOTO is not solely due to an absolute preference of the thiazole orange chromophores for the CT base step. Actually, the chromophore seems to prefer the CC base step among the binding sites offered by the four common DNA bases, but the restraints imposed by the favorable positioning of the polyamine linker in the minor groove results in a compromise that utilizes the favorable ion−dipole interactions between the flanking CG pair and the chromophore, while the charged linker benefits from the electrostatic potential of the AT minor groove. Thus, the removal of the guanosine amino group by the introduction of inosine partly offers the electrostatic benefits of guanosine while having a minor groove wall very similar to that of the TA pair. The affinity can be enhanced by introducing methyl groups on the pyrimidines thereby enhancing the dispersion attraction/hydrophobic interaction. This enhancement is much more pronounced for the central pyrimidines where the methyl group is able to make van der Waals contacts with the benzene part of the benzothiazole than the flanking base pairs, where the methyl group seems mainly to interact with the N-methyl group of TOTO.

LITERATURE CITED

Bailly, C., OhUigin, C., Rivalle, C., Bisagni, E., Hénichart, J. P., and Waring, M. J. (1990) Sequence-Selective Binding of an Ellipticine Derivative to DNA. *Nucleic Acids Res. 18*, 6283−6291.

Blackbrough, I. S., Taylor, S., Carpenter, M. L., Novoselskiy, V., Shamma, T., and Haworth, I. S. (1998) Asymmetric Intercalation of N^1-(Acridin-9-ylcarbonyl)spermine at Homopurine Sites of Duplex DNA. *Chem. Commun.* 929−930.

Boelens, R., Scheek, R. M., Dijkstra, K., and Kaptein, R. (1985) Sequential Assigment of Imino- and Amino-Proton Resonances in 1H NMR Spectra of Oligonucleotides by Two-Dimensional NMR Spectroscopy. Application to lac Operator Fragment. *J. Magn. Reson. 62*, 378−386.

Bondensgaard, K., and Jacobsen, J. P. (1999) Solution Structure and Energy Calculation of Bis-Intercalation of Homodimeric Thiazole Orange Dye Derivaties in DNA: Effects of Modifying the Linker. Submitted for publication.

Denny, W. A. (1989) DNA-Intercalating Ligands as Anti-Cancer Drugs: Prospects for Future Design. *Anti-Cancer Drug Des. 4*, 241−263.

Feigon, J., Leupin, W., Denny, W. A., and Kearns, D. R. (1983) Two-Dimensional Proton Nuclear Magnetic Resonance Investigation of the Synthetic Deoxyribonucleic Acid Decamer $d(ATATCGATAT)_2$. *Biochemistry 22*, 5943−5951.

Fox, K. R., and Waring, M. J. (1987) Footprinting at Low Temperatures: Evidence that Ethidium and Other Simple Intercalators can discriminate between Different Nucleotide Sequences. *Nucleic Acids Res. 15*, 491−507.

Frisch, M. J., Trucks, G. W., Schlegel, H. B., Gill, P. M. W., Johnson, B. G., Robb, M. A., Cheeseman, J. R., Keith, T. A., Petersson, G. A., Montgomery, J. A., Raghavachari, K., Al-Laham, M. A., Zakrewski, V. G., Ortiz, J. V., Foresman, J. B., Cioslowski, J., Stefanov, B. B., Nanayakkara, A., Challacombe, M., Peng, C. Y., Ayala, P. Y., Chen, W., Wong, M. W., Andres, J. L., Replogle, E. S., Comperts, R., Martin, R. L., Fox, D. J., Binkley, J. S., Defrees, D. J., Baker, J., Stewart, J. P., Head-Gordon, M., Gonzalez, C., and Pople, J. A. (1995) *Gaussian94 (Rev D.3)*, Gaussian Inc, Pittsburgh, PA.

Glazer, A. N., and Rye, H. S. (1992) Stable Dye-DNA Intercalation Complexes as Reagents for High-Sensitivity Fluorescence Detection. *Nature 359*, 859−861.

Hansen, L. F., Jensen, L. K., and Jacobsen, J. P. (1996) Bis-Intercalation of a Homodimeric Thiazole Orange Dye in DNA in Symmetrical Pyrimidine-Pyrimidine-Purine-Purine Oligonucleotides. *Nucleic Acids Res. 24*, 859−867.

Hare, D. R., Wemmer, D. E., Chou, S.-H., Drobny, G., and Reid, B. R. (1983) Assignment of the Non-Exchangeable Proton Resonances of d(C-G-C-G-A-A-T-T-C-G-C-G) using Two-dimensional Nuclear Magnetic Resonance Methods. *J. Mol. Biol. 171*, 319−336.

Hartley, J. A., Forrow, S. M., and Souhami, R. L. (1990) Effect of Ionic Strength and Cationic DNA Affinity Binders on the DNA Sequence Selective Alkylation of Guanine N7−Positions by Nitrogen Mustards. *Biochemistry 29*, 2985−2991.

Jacobsen, J. P., Pedersen, J. B., Hansen, L. F., and Wemmer, D. E. (1995) Site Selective Bis- Intercalation of a Homodimeric Thiazole Orange Dye in DNA Oligonucleotides. *Nucleic Acids Res. 23*, 753−760.

Jensen, L. K., Gotfredsen, C. H., Bondensgaard, K., and Jacobsen, J. P. (1998) Bis-intercalation of Homodimeric Thiazole Orange Dyes in Selective Binding Sites of DNA studied by ^{1}H NMR Spectroscopy. *Acta Chem. Scand. 52*, 641−650.

Johnson, R. C., Power, T. D., Holt, J. S., Immaraporn, B., Monat, J. E., Sissoko, A. A., Yanik, M. M., Zagorodny, A. V., and Cybulski, S. M. (1996) Electron-Correlated Calculations of Electric Properties of Nucleic Acid Bases. *J. Phys. Chem. 100*, 18875−18881.

Joireman, P. W., Ohline, S. M., and Felker, P. M. (1998) Structural Characterization of Aromatic−Aromatic Complexes by Rotational Coherence Spectroscopy. *J. Phys. Chem. A 102*, 4481−4494.

Lavery, R., and Pullman, B. (1981) Molecular Electrostatic Potential on the Surface Envelopes of Macromolecules: B-DNA. *Int. J. Quantum Chem. 20*, 259−272.

Lerman, L. S. (1961) Structural Considerations in the Interaction of DNA and Acridines. *J. Mol. Biol. 3*, 18−30.

Müller, W., and Crothers, D. M. (1975) Interactions of Heteroaromatic Compounds with Nucleic Acids. *Eur. J. Biochem. 54*, 267−277.

Padmanabhan, S., Brushaber, V. M., Anderson, C. F., and Record, M. T. J. (1991) Relative Affinities of Divalent Polyamines and of Their N-Methylated Analogues for Helical DNA Determined by ^{23}Na NMR. *Biochemistry 30*, 7550−7559.

Padmanabhan, S., Richey, B., Anderson, C. F., and Record, M. T. J. (1988) Interaction of an N-methylated Polyamine Analogue, Hexamethonium(2+), with NaDNA: Quantitative ^{14}N and ^{23}Na NMR Relaxation Rate Studies of the Cation-Exchange Process. *Biochemistry 27*, 4367−4376.

Schaftenaar, G. (1991) *Molden*, CAOS/CAMM Center, Neijmegen, The Netherlands.

Scheek, R. M., Boelens, R., Russo, N., Van Boom, J. H., and Kaptein, R. (1984) Sequential Resonance Assigments in 1H NMR Spectra of Oligonucleotides by Two-Dimensional NMR Spectroscopy. *Biochemistry 23*, 1371−1376.

Schmid, N., and Behr, J. P. (1991) Location of Spermine and Other Polyamines on DNA As Revealed by Photoaffinity Cleavage with Polyaminobenzenediazonium Salts. *Biochemistry 30*, 4357−4361.

Schneider, H. J., and Blatter, T. (1992) Interactions Between Acyclic and Cyclic Peralkylammonium Compounds and DNA. *Angew. Chem., Int. Ed. Engl. 31*, 1207−1208.

Sowers, L. C., Shaw, B. R., and Sedwick, W. D. (1987) Base Stacking and Molecular Polarizability: Effect of a Methyl Group in the 5-position of Pyrimidines. *Biochem. Biophys. Res. Commun. 148*, 790−794.

Spielmann, H. P., Wemmer, D. E., and Jacobsen, J. P. (1995) Solution Structure of a DNA Complex with the Fluorescent Bis- Intercalator TOTO Determined by NMR Spectroscopy. *Biochemistry 34*, 8542−8553.

Sponer, J., Leszczynski, J., and Hobza, P. (1996) Hydrogen Bonding and Stacking of DNA Bases: A Review of Quantum-chemical ab initio Studies. *J. Biomol. Struct. Dyn. 14*, 117−135.

Stein, P. C., Jacobsen, J. P., and Spielmann, H. P. (1995) Design and Implementation of a Simple Shaped Notch Filter. *J. Magn. Res., Ser. B 109*, 93−96.

Wemmer, D. E., Srivenugopal, K. S., Reid, B. R., and Morris, D. R. (1985) Nuclear Magnetic Resonance Studies of Polyamine Binding to a Defined DNA Sequence. *J. Mol. Biol. 185*, 457−459.

Wüthrich, K. (1986) *NMR of Proteins and Nucleic Acids*, John Wiley & Sons, New York.

Yuki, M., Grukhin, V., Lee, C. S., and Haworth, I. S. (1996) Spermine Binding to GC−Rich DNA: Experimental and Theoretical Studies. *Arch. Biochem. Biophys. 325*, 39−46.

BC990030V

Convenient Preparation of No-Carrier-Added Technetium-99m Radiopharmaceuticals Using Solid-Phase Technology

Robert Dunn-Dufault,[†,‡] Alfred Pollak,[†] John R. Thornback,*[,†] and James R. Ballinger[‡,§]

Resolution Pharmaceuticals Inc., 6850 Goreway Drive, Mississauga, Ontario, Canada, L4V 1V7, Faculty of Pharmacy, University of Toronto, Ontario, Canada, Division of Experimental Therapeutics, Ontario Cancer Institute, Toronto, Ontario, Canada, and Division of Nuclear Medicine, University Medical Imaging Centre, Toronto, Ontario, Canada . Received March 17, 1999; Revised Manuscript Received June 14, 1999

A solid-phase technetium chelation chemistry was developed as a means of preparing ^{99m}Tc radiopharmaceuticals at high effective specific activity (HSA). Three peptidic N_3S ^{99m}Tc ligands [mercaptoacetyl-Gly-Gly-Gly (MAG3), picolinyl-Ser-Cys-Gly-Thr-Lys-Pro-Pro-Arg (RP063), and dimethyl-Gly-Ser-Cys-Gly-Thr-Lys-Pro-Pro-Arg (RP128)] were used. The free thiol of Cys in each was attached to a series of commercially available amine-functionalized supports in a two-step process. The amine groups on the solid supports were converted to maleimide groups followed by the attachment of the ^{99m}Tc chelators through a thiol ether linkage with Cys. The optimized loading of the supports ranged 6−122 μmol/g support as determined by amino acid analysis. Each of the peptide-loaded supports (50−100 mg) was placed in either glass syringe vessels or disposable chromatography columns. Labeling with [^{99m}Tc]pertechnetate (200−800 MBq) in the presence of stannous gluconate was achieved at room temperature for 30−60 min or in a 100 °C water bath for 10 min. Up to 80% of the activity was eluted from the column with saline to give products with purity up to 99.8% as determined by HPLC. Amino acid analysis indicated as little as 100 pmol of peptide present in the ^{99m}Tc products, demonstrating that extremely high effective specific activity can be achieved without the need for purification.

INTRODUCTION

Most radiopharmaceutical kits contain a quantity of the ligand which is in vast excess of the amount of ^{99m}Tc complex formed (i.e. the effective specific activity is low), but this quantity of ligand is safe for administration to patients. For example, a kit for the preparation of a bone-scanning agent might contain 10 mg of diphosphonate; thus, each dose would contain on the order of 1 mg, but this presents no hazard. However, with newer radiopharmaceuticals, such as bioactive peptides and receptor-binding agents, administration of milligram or in some cases even microgram quantities could produce pharmacological or toxic effects or could saturate the receptor sites of interest. A purification step may be required to separate the ^{99m}Tc chelate from the excess free ligand. Purification can be as simple as a syringe column or as complex as high-pressure liquid chromatography (HPLC). Alternatively, it may be possible to prepare the ^{99m}Tc chelate at sufficiently high effective specific activity (HSA) by starting with extremely large amounts of pertechnetate. Babich et al. have prepared ^{99m}Tc-labeled chemotactic peptides by both approaches (*1*). However, all of these procedures are unsuitable for routine use, being labor intensive, time consuming, and inefficient in yield with respect to the radiotracer, requiring special equipment, and involving higher radiation exposure.

The term "specific activity" refers to the ^{99m}Tc content of a product relative to the total technetium present (i.e., ^{99m}Tc plus ^{99}Tc). Specific activity is determined by ingrowth time between elutions of the generator and decay time since elution. "Effective specific activity" refers to the ^{99m}Tc content per total mass present and is determined by the amount of ligand, ^{99m}Tc-labeled and free, in solution.

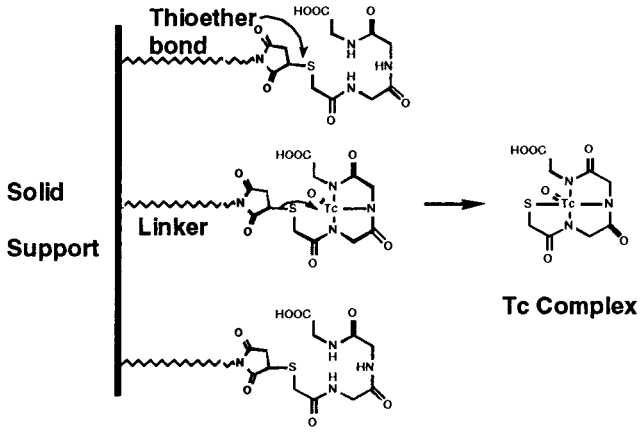


Figure 1. Release of an N_3S HSA ^{99m}Tc radiopharmaceutical from a solid phase. Unreacted ligand remains covalently bound.

We have developed a simple method of preparing ^{99m}Tc chelates at extremely high effective specific activities by making use of a solid-phase technology (Figure 1). Many of the new N_2S_2 and N_3S chelators require that the sulfur atom(s) be protected prior to labeling. If the protecting group is attached to a solid support, only molecules which have been released by chelating ^{99m}Tc will be present in solution while the excess precursor remains covalently attached to the support. This labeling technology can be incorporated into a kit from which an

* To whom correspondence should be addressed. Phone: (905) 677-0831. Fax: (905) 677-9595. E-mail: jthornbk@respharm.com.
† Resolution Pharmaceuticals.
‡ University of Toronto.
§ Ontario Cancer Institute and University Medical Imaging Centre

10.1021/bc990032f CCC: $18.00 © 1999 American Chemical Society
Published on Web 08/03/1999

Table 1. Amine Functionalization of the Various Commercial Solid Supports

type of support	abbreviation	amino groups (μmol/g)
controlled pore glass	CPG	100
silica	SIL	200
acrylic copolymer	ACR	50
agarose	AGR	300
glass	GLA	50
argogel	ARG	400

HSA product can be eluted simply and safely in a process amenable to preparation of a sterile product. We have evaluated this approach using a variety of solid supports and demonstrated its utility in the preparation of three ^{99m}Tc radiopharmaceuticals: the renal imaging agent MAG3 (*2*) and two peptides for imaging inflammation, RP063 and RP128 (*3, 4*).

EXPERIMENTAL PROCEDURES

Materials. Affi-Gel 102 (amine-functionalized cross-linked agarose) and Affi-Prep (N-hydroxysuccinimide-functionalized acrylic polymer), Bio-Spin polypropylene chromatography columns (sterile with filter, 1.5 mL capacity) and accessories were purchased from Bio-Rad Laboratories (Hercules, CA). 3-Aminopropyl-functionalized silica and glass were purchased from Sigma-Aldrich Canada (Oakville, ON). Amine-functionalized controlled-pore glass was purchased from CPG Inc. (Fairfield, NJ). Argogel [amine-functionalized poly(ethylene glycol)-grafted polystyrene] was obtained from Argonaut Technologies Inc. (San Carlos, CA). The amine functionalization of each support is reported in Table 1.

Radioactivity was measured in a Capintec CRC-15R dose calibrator using the ^{99m}Tc setting. ^{1}H/^{13}C NMR spectra were recorded on a Bruker 300AC spectrometer. Electrospray mass spectra (ESMS) were obtained on a Sciex API#3 mass spectrometer in the positive ion mode. Amino acid analysis (AAA) was conducted on a Waters Picotag system at the Banting Institute (Toronto, ON). Analytical RP-HPLC of each of the ^{99m}Tc-labeled products was run on a Vydac reversed-phase C-18 protein and peptide column (5 μm, 0.46 cm $\times$ 25 cm) using a Beckman Instruments (Fullerton, CA) system employing both radiometric detection set on a ^{99m}Tc window (Beckman 171 radioisotope detector with a modified yttrium silicate scintillant) and UV absorbance detection (Beckman 168 UV detector set at 215 nm wavelength). The column was eluted using a linear gradient of 100% A to 90% B over 20 min at a flow rate of 1.5 mL/min where solvent A was 0.1% trifluoroacetic acid (TFA) in water and solvent B was 0.1% TFA in acetonitrile.

Reagents for peptide synthesis including solvents, resins, and protected amino acids were obtained from Applied Bioresearch Inc. (Foster City, CA) and Bachem Biosciences Inc. (Philadelphia, PA). Buffers, inorganic salts, and reagent chemicals were purchased from Sigma-Aldrich Canada. HPLC-grade acetonitrile was purchased from BDH Inc. (Toronto, ON). Solutions of stannous chloride (90 mM, 20 mg/mL in 1 N HCl) and sodium gluconate (60 mM, 13 mg/mL in Milli-Q water) used for radiolabeling were prepared in advance and were stored frozen until use. ^{99m}Tc in the form of sodium pertechnetate solution was obtained from Mallinckrodt Medical Inc. (Mississauga, ON) or from a DuPont ^{99}Mo/^{99m}Tc generator.

Syntheses of Peptides. Three different peptidic N_3S technetium chelators were prepared to explore the universality of the solid-phase labeling method outlined. MAG3 (mercaptoacetyl-Gly-Gly-Gly-COOH) was synthesized with a benzoyl-protected sulfur whereas RP063 (picolyl-Ser-Cys-Gly-Thr-Lys-Pro-Pro-Arg-COOH) and RP128 (*N*,*N*-dimethyl-Gly-Ser-Cys-Gly-Thr-Lys-Pro-Pro-Arg-COOH) were prepared with acetamidomethyl (Acm) protection on the Cys. Each was synthesized using standard 9-fluorenylmethoxycarbonyl (Fmoc) chemistry starting with the carboxy-terminal amino acid (Fmoc-Gly or Fmoc-Arg) preloaded on Sasrin resin (Bachem Biosciences Inc.) using an ABI 433A automated peptide synthesizer. The products were cleaved from the resin in 95% TFA (100 mg of resin/mL) at room temperature for 2 h. The resin was removed by filtration and the peptides were precipitated by dripping the supernatant into 50 mL of *tert*-butyl methyl ether at 5 °C. The solids were centrifuged to a pellet, the ether decanted, and the pellet dried in vacuo. The pellets were dissolved in water and lyophilized to white powders.

MAG3, RP063, and RP128 were purified by reversed-phase HPLC on a Beckman Instruments HPLC system (System Gold) using a Millipore-Waters radial compression module (RCM, 0.8 cm $\times$ 10 cm) C-18 column with 0.1% TFA in water as solvent A and 0.1% TFA in acetonitrile as solvent B. The column was eluted using a linear gradient of 100% A to 100% B over 25 min at a flow rate of 1 mL/min. For each peptide, the fractions containing the correct species were pooled and lyophilized to a white powder. The authenticity of each product was confirmed by mass spectral analysis. benzoyl-MAG3: MW 367.0. ESMS: 368.0 (MH^+). RP063: MW 1020.1. ESMS: 1021.1 (MH^+). RP128: MW 1000.2. ESMS: 1001.0 (MH^+).

Free-thiol MAG3 was obtained by hydrolysis of the benzoyl sulfur-protecting group. Care was taken to exclude oxygen where possible. Free-thiol RP063 and RP128 were prepared by removal of the Acm protecting group. To the Acm-protected peptide (120 mmol) in aqueous acetic acid (30%, 2 mL) purged with argon was added mercuric acetate (180 mmol). The reaction was stirred under argon for 2.5 h at room temperature. Water (10 mL) was added and hydrogen sulfide gas was bubbled through the solution where a black precipitate formed. The black suspension was centrifuged to a clear solution and a black pellet. Each solution was decanted and filtered through a 0.2 μm PVDF syringe filter. The solutions were frozen in liquid nitrogen and lyophilized to white powders. Products were analyzed by HPLC and were typically >95% pure with traces of the Acm-protected species. Correct species were also identified by mass spectral analysis.

Loading of Supports. Each of the supports, Affi-Gel 102 (AGR), silica (SIL), controlled-pore glass (CPG), glass (GLA), and Argogel (ARG) were commercially available with amine functionalization. Affi-Prep 10 acrylic polymer (ACR) was obtained N-hydroxysuccinimide-functionalized and required conversion to amine functionalization by reaction with 1,4-diaminobutane in DMF. Carbethoxymaleimide was synthesized by a literature method (*5*).

The maleimide-functionalized supports were prepared as follows. To the amine-functionalized support (1 g) in saturated sodium bicarbonate (4 mL) at 0 °C was added powdered carbethoxymaleimide (100 mg). The reaction was shaken for 15 min after which water (15 mL) was added. The reaction was continued at room temperature for 15 min. The support was filtered and washed copiously with water.

The MAG3- and RP063-loaded supports were prepared by reacting the corresponding maleimide-functionalized

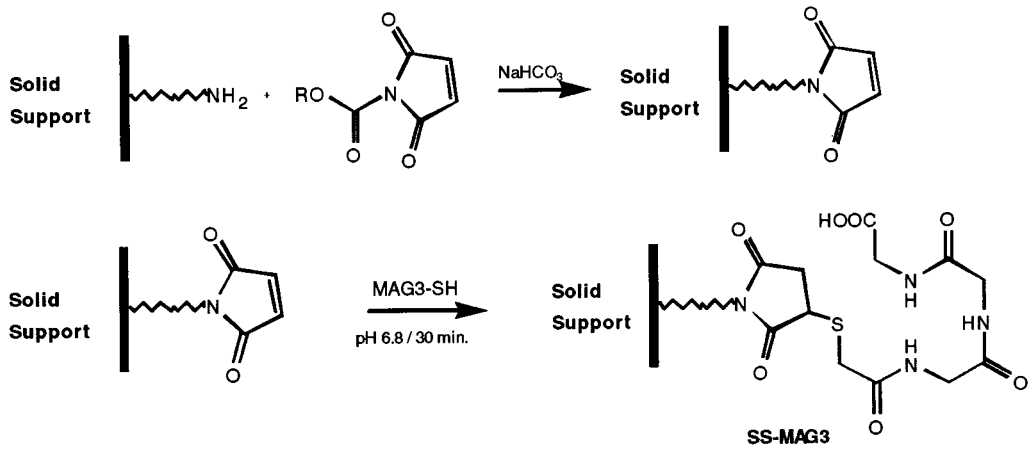


Figure 2. Synthetic scheme for loading MAG3 to a solid support. R = ethyl or methyl.

Table 2. Loading of MAG3, RP063, and RP128 to Solid Supports and ^{99m}Tc-Labeling Results

support type	N_3S	N_3S loading (μmol/g)	radiochemical yield (%)	radiochemical purity (%)
CPG	MAG3	9	56	93
	RP063	9	13	60
	RP128	12	37	87
AGR	MAG3	122	60	81
	RP063	100	41	86
	RP128	55	76	99
ACR	MAG3	21	33	97
	RP063	29	20	85
	RP128	6	40	75
SIL	MAG3	78	81	97
	RP063	7	52	45
	RP128	19	25	8
GLA	RP128	14	69	99
ARG	RP128	28	65	97

support (1 g) at 0 °C with an argon-purged solution of MAG3-SH (15 mg) or RP063−SH (25 mg) in sodium bicarbonate (0.2 N, 4 mL). After 30 min of shaking the solution, the reaction was allowed to warm to room temperature. The reaction was shaken for 3−16 h, after which the support was filtered, washed copiously with water and then an organic solvent (acetone, chloroform, dichloromethane, or diethyl ether), and dried in vacuo. Loading was determined by AAA, and the results are presented in Table 2.

The RP128-loaded supports were prepared by a slightly different procedure. To each amine-functionalized support (1 g) in saturated sodium bicarbonate (3 mL) at 0 °C was added powdered carbethoxymaleimide (30 mg). The reaction mixture was shaken for 30 min and then water (5 mL) was added. The shaking was continued at room temperature for 30 min. The support was then filtered and washed copiously with water and methanol and dried in vacuo. To each support (300 mg) was added an argon-purged solution of RP1280-SH (10 mg) in phosphate-buffered saline (PBS, 0.02 N, 1 mL). After 1 h at room temperature, each support was filtered, washed with copious water and then methanol, and dried in vacuo. Each was analyzed by AAA, and results are reported in Table 2.

^{99m}Tc Labeling of Supports. Typically, to each peptide-loaded support (50−100 mg) in a glass syringe barrel or a Bio-Spin disposable chromatography column were added saline (100 μL), [^{99m}Tc]pertechnetate (200−800 MBq, 100 μL), and aqueous stannous gluconate (100 μL) containing 20 μg of stannous chloride and 1.3 mg of sodium gluconate. The reaction mixture was capped, swirled, and left to proceed for 30−60 min at room temperature or for 10 min in a 100 °C water bath. The cap was removed and the column was fitted with a luer-lock stopcock and needle. Three portions of saline (300 μL, 1 mL, and 1 mL) were added sequentially, and the dose eluted from the column into three evacuated vials. The activity of each was measured in a dose calibrator. An aliquot from fraction 1 was analyzed by HPLC. The balance of fraction 1 of each labeling was submitted for AAA in order to confirm that the dose liberated from the support was free of excess unlabeled peptide. For comparison, standard solution-phase low effective specific activity (LSA) labeling was performed as described elsewhere (*2*−*4*), and the products were analyzed by HPLC.

RESULTS

Each of the support types used in this study was loaded with the free-thiol peptides by the methods outlined for MAG3 in Figure 2. Each of the three peptides was conveniently synthesized by an automated solid-phase peptide synthesizer in high yields and with typical purity of >95% based on HPLC analysis of the cleaved products. As appropriate, the sulfur-protecting groups were removed in preparation for loading to the supports. The supports were first rapidly functionalized with maleimide under mild conditions in buffered aqueous solutions, typically for 1 h. The maleimide-functionalized supports were then quenched with the thiol-containing peptides, again under mild aqueous conditions. The loading of each, reported in Table 2, was determined by AAA and ranged 6−122 μmol/g. These values represent the final loading of the peptides but do not indicate at which step the variability occurred.

The final evaluation of the technology is the labeling step with ^{99m}Tc. The labeling of MAG3, RP063, and RP128 from each of the solid supports was evaluated with respect to three parameters: radiochemical yield, radiochemical purity, and the level to which the eluted fractions were free of excess unlabeled peptides. Optimal labeling was observed with RP128 loaded to Argogel and is shown in Figure 3, where it can be seen that >96% of the injected radioactivity elutes in a peak at 8.5 min (solid line) and that there is no UV absorbance associated with this peak (dotted line).

To confirm that the dose liberated from the support was free of excess unlabeled peptide, the first eluted fraction from each support was tested by amino acid analysis. In each case, AAA showed only background levels of the amino acids found in MAG3, RP063, or

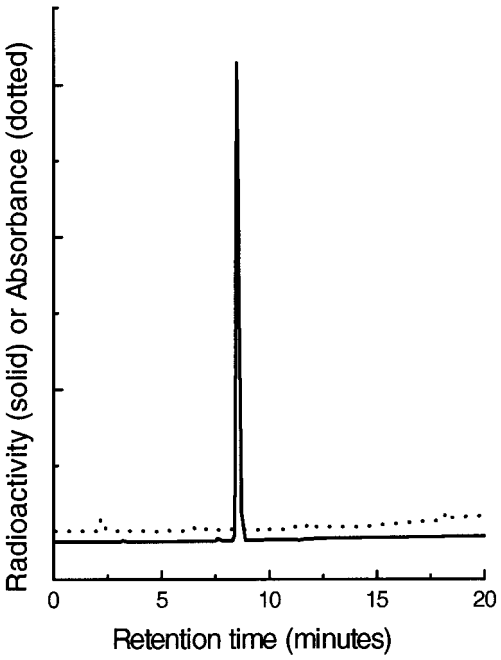


Figure 3. HPLC radiometric trace of a HSA [^{99m}Tc]RP128 labeling from Argogel support. Injection of 50 μL onto a C-18 column (5 μm, 0.46 cm × 25 cm). The column was eluted using a linear gradient of 100% A to 90% B over 20 min at a flow rate of 1.5 mL/min where solvent A was 0.1% TFA in water and solvent B was 0.1% TFA in acetonitrile. The system was run with dual detection: ^{99m}Tc (solid line), UV detection at 215 nm (dotted line).

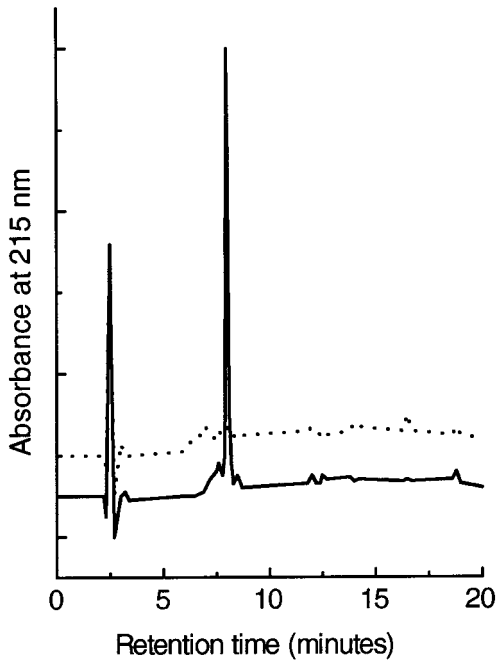


Figure 4. A comparison of the HPLC UV traces of HSA [^{99m}Tc]RP128 (dotted line) labeled from Argogel and LSA [^{99m}Tc]-RP128 (solid line) labeled in solution. The major peak in the LSA trace corresponds to unlabeled Acm-protected RP128. HPLC conditions as in Figure 3.

RP128. These values ranged from 100 pmol to 1 nmol per sample and were a function of contaminants on the detection column. Accordingly, these background levels were used in estimation of effective specific activity. Since the various supports have different adsorption properties, each was washed thoroughly to minimize any noncovalent peptide binding to the support. As supporting evidence, the UV traces of the HPLC-analyzed products showed essentially no peak corresponding to unlabeled ligands. Typical UV traces of LSA and HSA formulations of [^{99m}Tc]RP128 are shown in Figure 4, where it can be seen that the major peak at 8.0 min in the LSA preparation (solid line), representing unlabeled Acm-protected RP128, is absent in the HSA product (dotted line).

The radiochemical yield and radiochemical purity of the three peptides on each of the supports is shown in Table 2. For most of these measurements, $n = 1$; however, in subsequent work, the yield and purity were found to be reproducible, with a typical coefficient of variation of <5% for five determinations. Low yield represents loss of ^{99m}Tc through adsorption onto the support, while low purity represents inefficient reaction between [^{99m}Tc]-gluconate and the immobilized peptide. The purity of the released products eluted in fraction 1 as determined by HPLC ranged from a modest 8.1% for RP128 loaded to silica to as high as 99.8% for the same peptide loaded to agarose. The yield of total activity used in each labeling recovered in these first fractions also ranged greatly from 13.3% for RP063 loaded on control pore glass to 80.8% for MAG3 loaded on silica.

DISCUSSION

The theoretical specific activity of carrier-free ^{99m}Tc is ~20 000 TBq/mmol (520 000 Ci/mmol). However, ^{99m}Tc obtained from a ^{99}Mo/^{99m}Tc generator is never truly carrier free, since 13% of the decays of ^{99}Mo form ^{99}Tc directly. On the basis of the equations developed by Lamson et al. (*6*), the maximum mole fraction of ^{99m}Tc obtained from a generator 30 min after the previous elution is 0.84, and after the usual 24 h of in growth, the mole fraction is 0.28. Thus, maximization of the specific activity of ^{99m}Tc by repeated elutions produces a net gain of only a factor of 3 in specific activity and is of importance only with purified materials. In any procedure which does not use purification, the effect of the remaining excess ligand is far greater. For example, 3700 MBq of a ^{99m}Tc radiopharmaceutical containing 10 μg of a ligand with a molecular weight of 1000 (i.e. 10 nmol) represents an effective specific activity of 370 TBq/mmol (10 000 Ci/mmol). Thus, even 10 μg of ligand reduces the specific activity by 50-fold. Therefore, a method of avoiding excess ligand has been developed.

The need for a simple preparation of HSA ^{99m}Tc radiopharmaceuticals is an immediate one. Widespread clinical application of agents which show toxicity or which are designed to target specific receptor populations would require simple preparation of HSA formulations (*7*−*15*). Efforts to improve specific activity by reducing the amount of ligand in the labeling or by using extremely high quantities of pertechnetate have been demonstrated to improve imaging but are not practical where a routine kit is to be developed (*1*). A recent report of post-labeling purification is applicable to ligands having a free thiol (*16*), though for most agents HPLC or solid-phase cartridge purification is still required. The present solid-phase technology developed has been shown to be an effective means of generating some peptidic ^{99m}Tc agents in high specific activity without the need for postlabeling purification. This is analogous to the use of immobilized precursors for radioiodination (*17*, *18*).

The peptide content of the HSA products obtained using amino acid analysis ranged from 100 pmol to 1 nmol of the total decayed doses. To some extent this directly reflects the specific activity of the HSA products, but the values obtained approach the detection limits of

AAA under the conditions used for testing. For this reason, a modest estimate of the typical effective specific activities of the radiolabeled products is 1850 TBq/mmol (50 000 Ci/mmol), though the true effective specific activity may be far higher.

From the data, it is clear that not all supports were equally effective at generating high radiochemical yield and purity of the three ^{99m}Tc-labeled agents (Table 2). This is in part a function of the efficiency of the ligand to coordinate ^{99m}Tc as well as the labeling environment. Of the two parameters, radiochemical purity is more important since it determines whether the eluate is suitable for use (generally >90% purity is required) while a yield which is only moderate may still be acceptable. The preparation of the supports involves a two-step loading process which results in a loading value for each ligand loaded to each support type tested. The loading of the ligand to the supports varied greatly, from 6 to 122 μmol/g, despite similar loading conditions. The loading differences are in part due to differences in the level of amine functionalization on the supports (Figure 2) and in the reactivity of the amines with carbethoxymaleimide under the given conditions in the first step.

Discrepancies between the loading levels of the ligands and their effective labeling suggests that simple AAA indicates the amount of total ligand bound to the support but not necessarily the amount of ligand that is structurally available to coordinate ^{99m}Tc. For example, RP128-loaded silica gave 19 μmol/g loading but a meager 8% radiochemical purity upon ^{99m}Tc labeling, whereas RP063 loaded to silica showed only 7 μmol/g loading with a 45% radiochemical purity of [^{99m}Tc]RP063. This indicates the interaction of the ligand with the support greatly affects the success of the labeling.

In addition, the data show a large variation in the recovered yields from the supports, ranging from 13% to as high as 81% of the dose in the collected fractions. The loss of a high percentage of the dose is undesirable in that the use of higher activities would be required to generate a suitable dose for patient use. This binding to the supports was found to be partly physical trapping of colloids, partly ionic interaction of ^{99m}Tc species with the support, and potentially some weak coordination with the vast excess of ligand still covalently attached to the supports. Recoveries from agarose and Argogel were both influenced by the length of time the supports were soaked in saline before elution, indicating diffusion out of the beads played a role in dose recovery. Ultimately, it appears that the interaction of the ligand with the supports during loading and both of these with ^{99m}Tc species during coordination with ^{99m}Tc dictates the purity of the ^{99m}Tc complex and the yield recovered.

Optimization of the loading of each ligand to each type of support would be required in order to make strong evaluative comparisons. However, in general, supports with the highest amine functionalization, with the least possibility for unwanted charge interaction, and which best approximate solution-like conditions, should provide the best labeling results with the highest recovered yields. For these reasons, Argogel or a similar PEGylated support shows great potential, provided that there is no release of PEG.

Initially, the supports studied were chosen for their commercial availability with amine functionalization. The mechanical and surface properties of the supports vary greatly. Silica, glass, and acrylic are rigid supports. Silica and glass have charged surfaces where acrylic is neutral. Cross-linked agarose and PEG Argogel are flexible and have gel characteristics. Agarose is 95% water when swollen, has moderate mechanical stability, and completely dissolves in extremes of pH, whereas Argogel swells slightly and equally well in aqueous and organic solvents, with high mechanical and chemical stability, although release of trace amounts of PEG may be a problem.

With the rapid pace of developments in solid-phase chemistry, the type and quality of supports are becoming broader and the tailoring of supports to specific needs is or will soon be a possibility. The ability to use supports with high mechanical and chemical stability, coupled with a diversity of commercially available linking groups, makes a solid-phase radiopharmaceutical kit design a very real possibility.

ACKNOWLEDGMENT

We thank Tam Nguyen for assistance in peptide synthesis and Resolution Pharmaceuticals Inc. for supporting this work.

LITERATURE CITED

(1) Babich, J. W., Solomon, H., Pike, M. C., Kroon, D., Graham, W., Abrams, M. J., Tompkins, R. G., Rubin, R. H., and Fishman, A. J. (1993) Technetium-99m-labeled hydrazino nicotinamide derivatized chemotactic peptide analogs for imaging focal sites of bacterial infection. *J. Nucl. Med. 34*, 1964−1974.

(2) Fritzberg, A. R., Kasina, S., Eshima, D., and Johnson, D. L. (1986) Synthesis and biological evaluation of technetium-99m MAG3 as a hippuran replacement. *J. Nucl. Med. 27*, 111−116.

(3) Goodbody, A., Ballinger, J., Tran, L., Sumner-Smith, M., Lau, F., Meghi, K., and Pollak, A. (1994) A new Tc-99m labelled penta-peptide inflammation imaging agent. *Eur. J. Nucl. Med. 21*, 870.

(4) Caveliers, V., Goodbody, A., Tran, L., Bossuyt, A., and Thornback, J. (1996) Human dosimetry of TC99m-RP128, a potential inflammation imaging agent. *Eur. J. Nucl. Med. 23*, 1131.

(5) Bodanszky, M., and Bodanszky, A. (1984) *The Practice of Peptide Synthesis*, Springer-Verlag, New York.

(6) Lamson, M. L., Kirschner, A. S., Hotte, C. E., Lipsitz, E. L., and Ice, R. D. (1975) Generator-produced $^{99m}TcO_4^-$: carrier free? *J. Nucl. Med. 16*, 639−641.

(7) Del Rosario R. B., Jung, Y. W., Baidoo, K. E., Lever, S. Z., and Wieland, D. M. (1994) Synthesis and in vivo evaluation of a $^{99m/99}$Tc-DADT-benzovesamicol: a potential marker for cholinergic neurons. *Nucl. Med. Biol. 21*, 197−203.

(8) DiZio, J. P., Fiaschi, R., Davison, A., Jones, A. G., and Katzenellenbogen, J. A. (1991) Progestin−rhenium complexes: metal-labeled steroids with high receptor binding affinity, potential receptor-directed agents for diagnostic imaging or therapy. *Bioconjugate Chem. 2*, 353−66.

(9) DiZio, J. P., Anderson, C. J., Davison, A., Ehrhardt, G. J., Carlson, K. E., Welch, M. J., and Katzenellenbogen, J. A. (1992) Technetium- and rhenium-labeled progestins: synthesis, receptor binding and in vivo distribution of an 11 beta-substituted progestin labeled with technetium-99 and rhenium-186. *J. Nucl. Med. 33*, 558−569.

(10) Hirai, H. (1990) Use of tumor receptors for diagnostic imaging. A review. *Acta Radiol.* (Suppl.) *374*, 57−64.

(11) Kung, H. F., Kim, H. J., Kung, M. P., Meegalla, S. K., Plossl, K., and Lee, H. K. (1996) Imaging of dopamine transporters in humans with technetium-99m TRODAT-1. *Eur. J. Nucl. Med. 23*, 1527−1530.

(12) Kung, H. F. (1991) Overview of radiopharmaceuticals for diagnosis of central nervous disorders. *Crit. Rev. Clin. Lab. Sci. 28*, 269−86.

(13) O'Neil, J. P., Carlson, K. E., Anderson, C. J., Welch, M. J., and Katzenellenbogen, J. A. (1994) Progestin radiopharmaceuticals labeled with technetium and rhenium: synthesis, binding affinity, and in vivo distribution of a new progestin N_2S_2-metal conjugate. *Bioconjugate Chem. 5*, 182−193.

(14) Pearson, D. A., Lister-James, J., McBride, W. J., Wilson, D. M., Martel, L. J., Civitello, E. R., and Dean, R. T. (1996) Thrombus imaging using technetium-99m-labeled high-potency GPIIb/IIIa receptor antagonists. Chemistry and initial biological studies. *J. Med. Chem. 39*, 1372−1382.

(15) Lever, S. Z., Baidoo, K. E., Mahmood, A., Matsumura, K., Scheffel, U., and Wagner, H. N. (1994) Novel technetium ligands with affinity for the muscarinic cholinergic receptor. *Nucl. Med. Biol. 21*, 157−164.

(16) Kao, C. H., Baidoo, K. E., and Lever, S. Z. (1997) Validation and application of a solid-phase chemistry method for preparation of high effective specific activity technetium-99m radiopharmaceuticals. *Nucl. Med. Biol. 24*, 499−505.

(17) Flanagan, R. J., Wilson, J. S., and Wiebe, L. I. (1986) A high speed, no-carrier-added radiochemical reactor for the synthesis of halogenated radiopharmaceuticals. *J. Labelled Compd. Radiopharm. 23*, 1242−1243.

(18) Zhu, X., Gobi, J., and Hunter, D. H. (1998) A convenient preparation of no-carrier-added MIBG via solid-phase organic chemistry. *J. Nucl. Med. 39*, 143P.

BC990032F

Conversion of Proteins to Diazeniumdiolate-Based Nitric Oxide Donors

Joseph A. Hrabie,*,† Joseph E. Saavedra,‡ Peter P. Roller,§ Garry J. Southan,‡ and Larry K. Keefer||

Chemical Synthesis and Analysis Laboratory and Intramural Research Support Program, SAIC Frederick, NCI-FCRDC, Frederick, Maryland 21702, Chemistry Section, Laboratory of Comparative Carcinogenesis, National Cancer Institute-Frederick Cancer Research and Development Center, Frederick, Maryland 21702, and Laboratory of Medicinal Chemistry, National Cancer Institute, Bethesda, Maryland 20892. Received March 19, 1999; Revised Manuscript Received April 29, 1999

Michael reaction of the methoxymethyl-protected monodiazeniumdiolate of piperazine (MOM-PIPERAZI/NO) with 4-maleimidobutyric acid followed by its conversion to the N-hydroxy-succinimido ester produces a reagent capable of transferring the nitric oxide (NO)-donating diazeniumdiolate group to the terminal amines of the lysine residues contained in proteins. The reagent has been used to produce diazeniumdiolated bovine serum albumin (D-BSA) and diazeniumdiolated human serum albumin (D-HSA) containing 22 and 19 modified lysyl groups, respectively. Upon dissolution in pH 7.4 phosphate buffer at 37 °C, these albumin derivatives gradually released all of their contained NO (approximately 40 mol/mol of protein) with initial rates of about 30−40 pmol/min/mg and half-lives on the order of 3 weeks. This methodology is now available for use in exploiting the unique specific metabolic interactions of proteins to target NO therapy to specific physiological processes in vivo.

INTRODUCTION

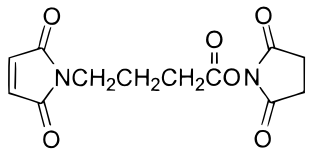
Every new discovery of yet another bioregulatory role for nitric oxide (NO) presents both a promising opportunity for the development of novel therapeutic agents and another barrier to be overcome in any attempt to target any such agents to a specific physiological process. Given the ever increasing number of such processes known to involve NO as well as the possible harmful effects (*1*) of this toxic chemical, it is apparent that, in those instances where an input of NO is necessary to achieve a desired clinical result, one of the key attributes of any pharmaceutical will be the ability to deliver the molecule to a highly specific site. Fortunately, virtually every life process presents a potential solution to this specificity problem in the form of the molecular recognition inherent in protein function.

This report describes the development of a method for converting proteins into NO donors via the attachment of methoxymethylated diazeniumdiolates. The process employs several modifications of the chemistry involved in the use of the traditional cross-linking reagent *N*-(γ-maleimido-butyryloxy)succinimide (GMBS) (*2*) as well as the judicious use of protecting groups both to assemble the protein-derivatizing reagent and to regulate NO release from the resulting conjugate. The method has been used to prepare serum albumin conjugates which have been studied by mass spectrometry and by analysis of their NO-releasing properties.

RESULTS AND DISCUSSION

Reagent for Diazeniumdiolate Protein Conjugation. Despite the short half-lives and acid-labile nature of most diazeniumdiolates (*3*), it has proven possible to prepare versions suitable for linkage to protein-reactive reagents. As shown in Scheme 1, monoprotected piperazine can be reacted with nitric oxide to afford bifunctional compound **1**. The nitrogen in this compound remains protected by the ethoxycarbonyl group while the diazeniumdiolate is available for alkylation by previously described methods (*4*). We chose reaction with chloromethyl methyl ether to produce the methoxymethyl (MOM) derivative **2** since this protecting group was found to hydrolyze slowly in aqueous solution at physiological pH. Removal of the ethoxycarbonyl group in refluxing ethanolic sodium hydroxide afforded amine **3**. These reactions have been described in detail elsewhere (*5*).

We envisioned a reagent which would link our diazeniumdiolate **3** to the ϵ-amino group of the lysines since this would be the best way to guarantee that hydrolysis to release NO would not be impeded by close proximity to the bulky protein. The widely used heterobifunctional cross-linking reagent **6** (GMBS) (*2*) is usually utilized to



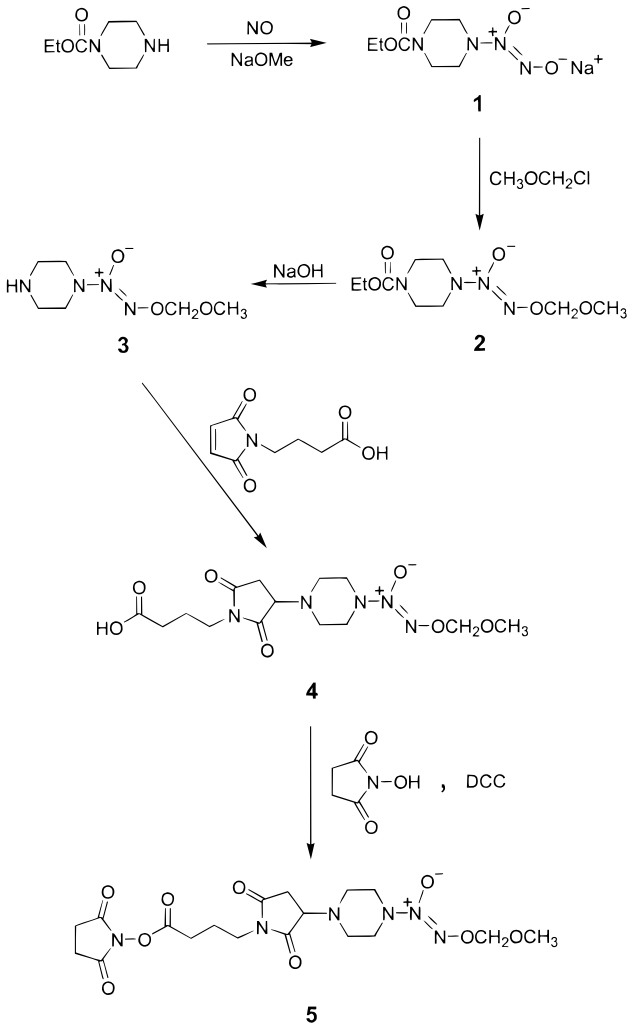
6

link the lysyl groups of proteins (via the reaction of the ϵ-amines with the *N*-hydroxysuccinimidyl ester) with the sulfhydryl group of the same or another protein (via reaction of the thiol with the maleimide). While the reaction of the ester with the free amines of a protein is conducted without interference from the maleimide in aqueous solution at carefully controlled pH, the Michael reaction of amines with maleimides in organic solvents is well-known (*6*). We used this method to prepare acid

* To whom correspondence should be addressed. Phone: (301) 846-1226. Fax: (301) 846-1438. E-mail: hrabie@mail.ncifcrf.gov.
† Chemical Synthesis and Analysis Laboratory.
‡ Intramural Research Support Program.
§ Laboratory of Medicinal Chemistry.
|| Laboratory of Comparative Carcinogenesis.

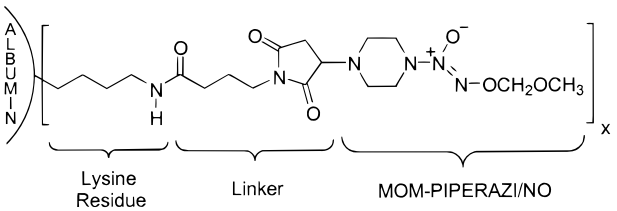
10.1021/bc990035s CCC: $18.00 © 1999 American Chemical Society
Published on Web 07/15/1999

Scheme 1. Synthesis of Protein Diazeniumdiolation Reagent



4, which was then esterified to yield a diazeniumdiolated GMBS derivative, N-hydroxysuccinimide ester **5**.

Serum Albumin Conjugates. As a demonstration of the usefulness of reagent **5** and to gain information about the properties of diazeniumdiolated proteins, we prepared diazeniumdiolated bovine serum albumin (D-BSA, **7**) and human serum albumin (D-HSA, **8**).



7: D-BSA x = ~22
8: D-HSA x = ~19

Matrix-assisted laser desorption ionization time-of-flight (MALDI-TOF) mass spectrometry was used to compare the initial molecular mass (M_r) to that of the conjugate as a means of determining the number of lysines which had reacted with the ester. Figure 1 shows the result for D-HSA. The initial M_r of HSA (66.4 kDa) (*7*) was raised by 6.7 kDa, which shows that an average of 19 diazeniumdiolate-bearing side chains (the M_r of each side chain is 356) have been added to each albumin molecule. As is customary, we employed a large excess

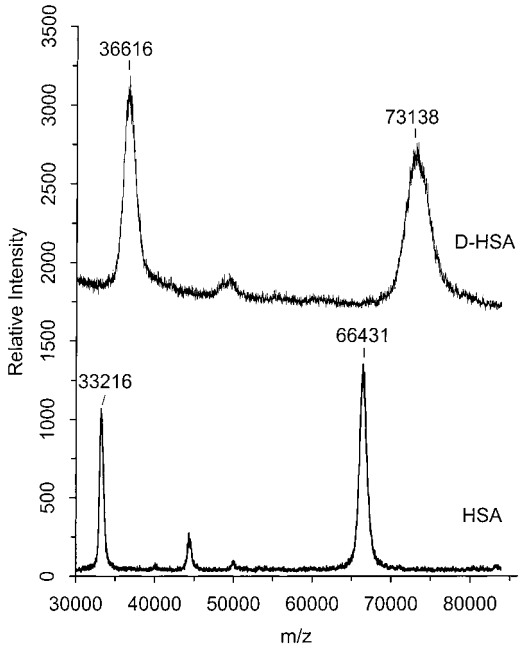
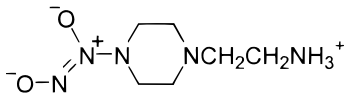


Figure 1. MALDI-TOF mass spectra of HSA and D-HSA compared.

(250 molar equiv) of **5** in these conjugations to compensate for the hydrolysis of the reagent which competes with the desired protein reaction. It is interesting to note that while both HSA (*8*) and BSA (*9*) contain 59 lysine residues, our reagent derivatizes an average of 22 of these in the latter but only 19 in the former. We assume that the higher reactivity of the lysyl residues in BSA is in some way related to their increased degree of exposure to the proteins' surface.

Our exploration of the NO-releasing characteristics of D-BSA was begun with several assumptions based upon the small molecule chemistry already known. While the synthesis conditions required for the preparation of both reagent **5** and the protein conjugates themselves prevent the isolation of the corresponding unprotected diazeniumdiolates, the half-life of NO release in pH 7.4 phosphate buffer for the closely related piperazine **9** has been



9

reported to be short (5.0 min at 22 °C) (*10*). In contrast, the rate of hydrolytic cleavage of the methoxymethyl protecting group attached to the diazeniumdiolate of compound **3** has been reported to be very slow (>17 days at pH 7.4 and 37 °C, consistent with expectations for an acetal) (*5*). This tremendous contrast in rates caused us to believe that we could observe the release of NO from these protein conjugates as a relatively simple pseudo-first-order process uncomplicated by the formation of significant concentrations of intermediates. This belief was further supported by the knowledge that diazeniumdiolates such as **9** release two full equivalents of NO on decomposition with no apparent byproducts other than the original amino compound (*10*). In fact, pseudo-first-order kinetics has been observed even when some nitrosamine does form during diazeniumdiolate decomposition (*11*). While reports that S-nitros(yl)ation of proteins may serve as a transport mechanism for NO in vivo (*12*) are cause for some concern to anyone interested in analytical

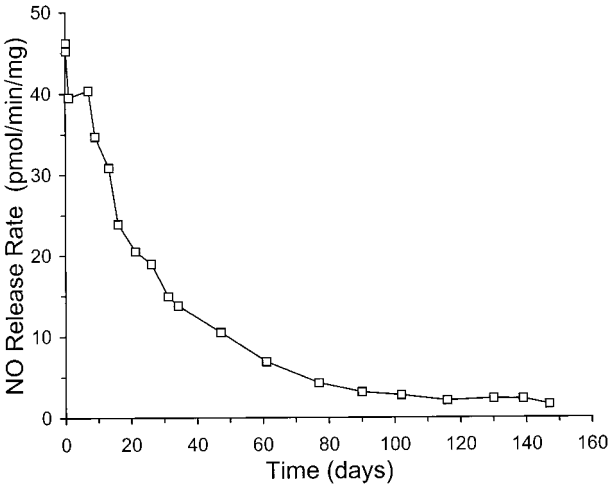


Figure 2. Release of NO from D-BSA as a solution in pH 7.4 phosphate buffer at 37 °C.

measurements of NO in their presence, our selection of serum albumin, a robust globular material in which all but one of the cysteine thiols are usually tied up in disulfide bonds, suggested that all of the initially released NO could be detected successfully.

With these considerations in mind, we selected an assay based upon the detection of NO by chemiluminescence which we had previously employed in a study of synthetic polymers (*13*). The release of NO was not monitored continually but rather a solution of D-BSA (**7**) in phosphate buffer at pH 7.4 was maintained at 37 °C, and periodically all of the accumulated NO gas was flushed from the sample so that the rate of NO release could be measured for a period of time after the chemiluminescence trace became stabilized. Figure 2 shows the result of monitoring the NO production of a sample of D-BSA for almost half a year. This experiment indicates that the half-life for NO release from D-BSA is on the order of 20 days. While a sample of D-HSA (**8**) has not as yet been studied over the same lengthy interval, preliminary results suggest a similar, though perhaps somewhat shorter, half-life for that protein as well as a release profile similar to Figure 2. The area under the curve shown in Figure 2 suggests that essentially all of the 44 equiv of NO that one would expect to be produced by hydrolytic breakdown of all 22 of the attached diazeniumdiolated piperazines are released during this experiment. Since this type of study does not lend itself conveniently to any statistical analysis to remove what can be significant variations in any single analysis for NO, we also measured the initial NO generation rate using fresh samples of D-BSA and D-HSA dissolved in the same buffer system at 37 °C. The slightly lower degree of substitution (19 vs 22) of D-HSA vs D-BSA was reflected in a slightly slower initial NO release rate [30 $\pm$ 5 pmol/min/mg for D-HSA ($n = 2$) vs 40 $\pm$ 5 pmol/min/mg for D-BSA ($n = 4$)].

It should be noted that the requirement that the methoxymethyl protecting group undergo an acid-catalyzed hydrolysis as the first step toward NO release means that these protein conjugates should generate 1 equiv each of formaldehyde and methanol for every 2 mol of NO. We have verified the increase in formaldehyde concentration with time in a solution of decomposing D-BSA but have made no attempts to quantify the production of this chemical which is both highly reactive and a ubiquitous contaminant of most laboratory equipment.

Significance. The diazeniumdiolates have emerged as an important class of NO donor compounds (*14*). The successful conjugation of these prodrugs to serum albumin will serve as a guide in the development of NO-releasing derivatives of peptide hormones, antibodies, and other proteins whose receptor-mediated interactions may be used to target NO delivery to specific points in the body. This study shows that relatively large numbers of diazeniumdiolate-containing groups can be introduced into a typical protein without causing fragmentation or denaturation (although some conformational changes undoubtedly occur and the consequences of these will have to be investigated for each protein on a case-by-case basis) and that the material can be stored for long periods of time (so far up to one year) as a solid in a freezer with no apparent decrease in activity upon reconstitution in phosphate buffer. The procedures reported herein should be applicable to diazeniumdiolates derivatized with a large variety of protecting groups which may be devised as an additional mechanism for introducing specificity into possible clinical agents based on these compounds.

Very importantly, D-HSA itself may prove to be an important clinical agent. The cardiovascular system offers many targets for NO-based therapeutic intervention (*15*), and as a principal component of that system, serum albumin is an obvious candidate for exploitation as a drug carrier. Previous studies have shown that diazeniumdiolate-based NO donation can inhibit thrombosis (*16*, *17*), and D-BSA has been shown to reduce thickening of the arterial wall following coronary angioplasty in the pig (*18*). Accordingly, D-HSA may offer an excellent treatment for those cardiovascular problems that can be rectified by addition of excess NO even though it does not provide the types of targeting opportunities offered by other proteins which we hope to exploit in the future.

EXPERIMENTAL SECTION

Nitric oxide was obtained from Matheson Gas Products (Montgomeryville, PA) and used as received. Unless noted otherwise, reagents and solvents were obtained from Aldrich Chemical Co. (Milwaukee, WI). A suitable apparatus for NO reactions has been described previously (*10*) as has the preparation of compounds **1**−**3** (*5*). Nuclear magnetic resonance (NMR) spectra were recorded at 300 MHz with a Varian Unity INOVA 300WB spectrometer. Ultraviolet spectra were recorded on a Hewlett-Packard model 8451A diode array spectrophotometer. Melting points were obtained on a hot stage and are uncorrected. Elemental analyses were performed by Atlantic Microlab, Inc. (Norcross, GA). General procedures for the handling of diazeniumdiolates have been described elsewhere (*3*) and all compounds containing this functional group are routinely stored in a freezer. Routine mass spectra were obtained with a VG Micromass 70-OPUS double focusing mass spectrometer. Protein mass spectra were obtained with a Bruker Reflex 2 MALDI-TOF mass spectrometer using a 2-mercaptobenzothiazole matrix. Nitric oxide release rates were measured as previously described for polymeric diazeniumdiolates (*13*) except that the proteins give homogeneous solutions. This NO analysis method employs a Thermal Energy Analyzer, thermostated reaction vessel, and flow system as described by Feelisch and Noack (*19*).

***O*^{2}-(Methoxymethyl) 1-[4-(3′-ω-Succinimidylbutyric acid)piperazin-1-yl]diazen-1-ium-1,2-diolate (*4*)**. A solution of 6.23 g (32.7 mmol) of **3** in 30 mL of

benzene was treated with 6.00 g (32.7 mmol) of 4-maleimidobutyric acid and allowed to stir at room temperature for 18 h. The product precipitated as an off-white solid which was isolated by filtration, washed with cold benzene and then ether, and dried under vacuum. Yield 9.04 g (75%); mp 139−140 °C dec. ^{1}H NMR (CD_3OD): δ 1.8−1.9 (2H, m), 2.28−2.34 (2H, m), 2.69 (1H, dd, J_1 = 5.2 Hz, J_2 = 18.2 Hz), 2.87 (1H, dd, J_1 = 8.8 Hz, J_2 = 18.2 Hz), 3.0−3.1 (2H, m), 3.45 (3H, s), 3.4−3.5 (4H, m), 3.5−3.6 (4H, m), 3.95 (1H, dd, J_1 = 5.2 Hz, J_2 = 8.8 Hz), 5.21 (2H, s). UV λ_{max} (0.1 M NaOH): 234 nm (ϵ = 8.28 mM^{-1} cm^{-1}). Exact mass calcd for $C_{14}H_{24}N_5O_7$ (MH^+): 374.1676. Found: 374.1680.

Anal. calcd for $C_{14}H_{23}N_5O_7$: C, 45.04; H, 6.21; N, 18.76. Found: C, 45.83; H, 6.18; N, 18.27.

***O*^{2}-(Methoxymethyl) 1-[4-(3′-ω-Succinimidylbutyric acid)piperazin-1-yl]diazen-1-ium-1,2-diolate, *N*-Hydroxysuccinimide Ester (*5*)**. A solution of 1.617 g (14.1 mmol) of *N*-hydroxysuccinimide in 500 mL of dry ethyl acetate was heated to just below reflux. The heat was removed and 5.25 g (14.1 mmol) of **4** was added followed by 3.20 g (15.5 mmol) of dicyclohexylcarbodiimide. The resulting mixture was stirred for 18 h, filtered, and concentrated, and the residual oil was dried under vacuum. Yield 6.60 g (100%); mp 56−57 °C. ^{1}H NMR ($CDCl_3$): δ 1.9−2.1 (4H, m), 2.5−2.8 (5H, m), 2.83 (4H, s), 2.8−3.1 (3H, m), 3.49 (3H, s), 3.5−3.7 (4H, m), 3.78−3.87 (1H, m), 5.22 (2H, s). UV λ_{max} (CH_3CN): 234 nm (ϵ = 7.67 mM^{-1} cm^{-1}).

Anal. calcd for $C_{18}H_{26}N_6O_9$: C, 45.96; H, 5.57; N, 17.86. Found: C, 46.09; H, 6.08; N, 17.90.

Diazeniumdiolated Bovine Serum Albumin. A solution of 4.00 g (0.0597 mmol) of bovine serum albumin (Calbiochem, LaJolla, CA) in 265 mL of 50 mM, pH 8.5, borate buffer was treated with a solution of 6.18 g (13.1 mmol) of N-hydroxysuccinimide ester **5** in 23 mL of tetrahydrofuran. After stirring for 2 h, the solution was loaded into SpectraPor 4 dialysis tubing (Spectrum, Houston, TX) and dialyzed against distilled water for a total of 7 h at 0 °C, during which time the 4 L reservoir of distilled water was changed five times. The resulting material was centrifuged to remove ca. 20 mg of residue and then freeze-dried to yield 4.8 g of puffy white product. MALDI-TOF MS showed this material to have a M_r of 74.2 kDa.

Sample purity was checked by capillary zone electrophoresis (CZE) employing a Beckman Model P/ACE System 5500 instrument fitted with a 50 μm ID 10% polyacrylamide-coated fused silica column with a total length of 47 cm (operative length was 40 cm). Using a mobile phase of 50 mM phosphoric acid adjusted to pH 2.5 with triethylamine and a voltage of 12 kV (current: 16 μA), underivatized BSA eluted at 10.8 min, while D-BSA eluted at 12.3 min. The D-BSA sample contained neither underivatized BSA nor any other impurity detectable by UV at 214 nm and produced a clean Gaussian-shaped peak.

Diazeniumdiolated Human Serum Albumin. A solution of 3.00 g (0.0457 mmol) of human serum albumin (Calbiochem, LaJolla, CA) in 200 mL of 50 mM pH 8.5 borate buffer was treated with a solution of 5.35 g (11.4 mmol) of N-hydroxysuccinimide ester **5** in 15 mL of tetrahydrofuran. After stirring for 2 h, the solution was loaded into SpectraPor 4 dialysis tubing (Spectrum, Houston, TX) and dialyzed against 50 mM, pH 8.5, borate buffer for a total of 7 h at room temperature, during which time the 3 L reservoir of buffer was changed five times. The resulting solution was centrifuged to remove ca. 20 mg of residue. The total volume of this solution was 270 mL. The solution was freeze-dried to yield 4.42 g of puffy white product calculated to contain 3.24 g of diazeniumdiolated HSA and 1.18 g (26.6%) of buffer salts. MALDI-TOF MS showed this material to have a M_r of 73.1 kDa.

ACKNOWLEDGMENT

We thank Terry Sumpter for obtaining the mass spectra and George Janini for the CZE analysis. This project has been funded in part with Federal funds from the National Cancer Institute, National Institutes of Health, under Contract NO1-CO-56000.

LITERATURE CITED

(1) Ohshima, H., and Bartsch, H. (1994) Chronic infections and inflammatory processes as cancer risk factors: possible role of nitric oxide in carcinogenesis. *Mutat. Res. 305*, 253−264.

(2) Partis, M. D., Griffiths, D. G., Roberts, G. C., and Beechey, R. B. (1983) Cross-linking of protein by ω-maleimido alkanoyl *N*-hydroxysuccinimido esters. *J. Protein Chem. 2*, 263−277.

(3) Keefer, L. K., Nims, R. W., Davies, K. M., and Wink, D. A. (1996) "NONOates" (1-substituted diazen-1-ium-1,2-diolates) as nitric oxide donors: convenient nitric oxide dosage forms. *Methods Enzymol. 268*, 281−293.

(4) Saavedra, J. E., Dunams, T. M., Flippen-Anderson, J. L., and Keefer, L. K. (1992) Secondary amine/nitric oxide complex ions, $R_2N[N(O)NO]^-$. O-Functionalization chemistry. *J. Org. Chem. 57*, 6134−6138.

(5) Saavedra, J. E., Booth, M. N., Hrabie, J. A., Davies, K. M., and Keefer, L. K. (1999) Piperazine as a linker for incorporating the nitric oxide-releasing diazeniumdiolate group into other biomedically relevant functional molecules. *J. Org. Chem. 64* (in press).

(6) Mustafa, A., Asker, W., Khattab, S., and Zayed, S. M. A. D. (1961) On the reactivity of the unsaturated system in *N*-arylmaleimides. *J. Org. Chem. 26*, 787−789.

(7) Smith, R. D., Loo, J. A., Edmonds, C. G., Barinaga, C. J., and Udseth, H. R. (1990) New developments in biochemical mass spectrometry: electrospray ionization. *Anal. Chem. 62*, 882−899.

(8) Minghetti, P. P., Ruffner, D. E., Kuang, W.-J., Dennison, O. E., Hawkins, J. W., Beattie, W. G., and Dugaiczyk, A. (1986) Molecular structure of the human albumin gene is revealed by nucleotide sequence within q11-22 of chromosome 4. *J. Biol. Chem. 261*, 6747−6757.

(9) Hirayama, K., Akashi, S., Furuya, M., and Fukuhara, K.-i. (1990) Rapid confirmation and revision of the primary structure of bovine serum albumin by ESIMS and Frit-FAB LC/MS. *Biochem. Biophys. Res. Commun. 173*, 639−646.

(10) Hrabie, J. A., Klose, J. R., Wink, D. A., and Keefer, L. K. (1993) New nitric oxide-releasing zwitterions derived from polyamines. *J. Org. Chem. 58*, 1472−1476.

(11) Hrabie, J. A., Saavedra, J. E., Davies, K. M., and Keefer, L. K. (1999) Adducts of piperazine with nitric oxide. *Org. Prep. Proced. Int. 31*, 189−192.

(12) Stamler, J. S., Simon, D. I., Osborne, J. A., Mullins, M. E., Jaraki, O., Michel, T., Singel, D. J., and Loscalzo, J. (1992) S-Nitrosylation of proteins with nitric oxide: synthesis and characterization of biologically active compounds. *Proc. Natl. Acad. Sci. U.S.A. 89*, 444−448.

(13) Smith, D. J., Chakravarthy, D., Pulfer, S., Simmons, M. L., Hrabie, J. A., Citro, M. L., Saavedra, J. E., Davies, K. M., Hutsell, T. C., Mooradian, D. L., Hanson, S. R., and Keefer, L. K. (1996) Nitric oxide-releasing polymers containing the $[N(O)N(O)]^-$ group. *J. Med. Chem. 39*, 1148−1156.

(14) Feelisch, M., and Stamler, J. S. (1996) Donors of Nitrogen Oxides. *Methods in Nitric Oxide Research* (Feelisch, M., and Stamler, J. S., Eds.) pp 71−115, John Wiley & Sons, Chichester.

(15) Pörsti, I., and Paakkari, I. (1995) Nitric oxide-based possibilities for pharmacotherapy. *Ann. Med. (Helsinki) 27*, 407−420.

(16) Kaul, S., Makkar, R. R., Nakamura, M., Litvack, F. I., Shah, P. K., Forrester, J. S., Hutsell, T. C., and Eigler, N. L. (1996) Inhibition of acute stent thrombosis under high-shear flow conditions by a nitric oxide donor, DMHD/NO. An ex vivo porcine arteriovenous shunt study. *Circulation 94*, 2228−2234.

(17) Saavedra, J. E., Southan, G. J., Davies, K. M., Lundell, A., Markou, C., Hanson, S. R., Adrie, C., Hurford, W. E., Zapol, W. M., and Keefer, L. K. (1996) Localizing antithrombotic and vasodilatory activity with a novel, ultrafast nitric oxide donor. *J. Med. Chem. 39*, 4361−4365.

(18) Baek, S. H., Keefer, L. K., Mehdi, K., and March, K. L. (1997) Intrapericardial nitric oxide donor reduces neointimal and adventitial thickening following porcine coronary overstretch. *J. Am. Coll. Cardiol. 29* (Suppl. A), 51A (Abstract 701-1).

(19) Feelisch, M., and Noack, E. A. (1987) Correlation between nitric oxide formation during degradation of organic nitrates and activation of guanylate cyclase. *Eur. J. Pharmacol. 139*, 19−30.

BC990035S

DNA Complexing with Polyamidoamine Dendrimers: Implications for Transfection

Anna U. Bielinska,[†] Chunling Chen,[†] Jennifer Johnson,[†] and James R. Baker, Jr.*[,†]

Department of Internal Medicine and Center for Biologic Nanotechnology, University of Michigan Medical School, 9220 MSRB III, 1150 West Medical Center Drive, Ann Arbor, Michigan 48109. Received March 22, 1999; Revised Manuscript Received June 11, 1999

DNA and polyamidamine (PAMAM) dendrimers form complexes on the basis of the electrostatic interactions between negatively charged phosphate groups of the nucleic acid and protonated (positively charged) amino groups of the polymers. Charge neutralization of both components and subsequent increases of the net positive charge of the complex result in changes in the physicochemistry and biological properties of the complexes. The formation of soluble, low-density and insoluble, high-density complexes was analyzed using UV light absorption and measurements of radioactive labeled DNA. Formation of high molecular weight and high-density complexes depended mainly on the DNA concentration and was enhanced by increasing the dendrimer−DNA charge ratio. Electrostatic charge related effects (attraction or repulsion of charged particles) appeared to be modulated by the generation of dendrimer (size of the polymer). With the progressive increases in the dendrimer−DNA charge ratio (above 20), an increase in the amount of low-density, soluble complexes was observed. Functional analysis revealed that the great majority (>90%) of transfection is carried by low-density, soluble, complexes which only represent approximately 10−20% of total complexed DNA. The ability of the dendrimer to complex and form aggregates with DNA is crucial for efficient transfection and the function of the complexed DNA.

INTRODUCTION

Formation of a complex between DNA and a synthetic carrier appears to be the initial and possibly the critical parameter for nonviral gene delivery. A number of synthetic vector systems, including polylysines, cationic liposomes, cationic polymers, or various types of block copolymers, have been utilized for the transfer of DNA molecules into cells (*1*−*3*). All these cationic systems have been shown to self-assemble with plasmid DNA expression vectors. In certain conditions, the interaction of DNA with polyvalent cations results in compaction of extended DNA structures, that then aggregate and precipitate from the solution (*4*−*6*). Physicochemical properties of the formed complexes depend mainly on the type of cationic agent used (*7*−*9*). Among cationic polymers, dendrimers have recently emerged as a novel synthetic carrier for DNA transfer (*10*−*12*). Starburst PAMAM dendrimers are nanoscopic polyamidoamine polymers with a molecular architecture characterized by the regular dendritic branching and radial symmetry (*10*, *13*, *14*). The perfectly spheric topological structure and homogeneity of these polymers is achieved by the ordered assembly of polymer subunits in concentric, dendritic tiers surrounding an initiator core. Physical and chemical properties of dendrimers are an outgrowth of their shape as well as the presence of charged groups on the surface. High positive charge density in these molecules is due to the presence of protonized primary amine groups on the surface of the molecules. Together with high solubility in water, these characteristics have led to the use of these polyamines to mediate efficient DNA transfer. Dendrimers appear to be highly efficient for in vitro transfection and are not cytotoxic (*12*, *15*). Other evidence suggests that these polymers are not immunogenic or carcinogenic, enhancing their potential as vectors for an in vivo gene transfer system (*16*).

The alterations of DNA structure caused by complexation with dendrimers and the function of the complexed genetic material are yet to be clarified. In other trivalent or higher valency cationic polyamines, nucleic acid complexation affects DNA structure and physicochemical properties both in vitro (*17*−*19*) and in vivo (*20*, *21*). In particular, high molecular weight cationic polymers such as polylysine, protamine, spermidine, spermine, and histones are known to complex and condense DNA and alter transcription efficiency in vivo (*17*, *22*−*24*). Complexing DNA with dendrimers leads to changes in transcription efficiency in vitro, but also increases DNA survival upon delivery in vitro and in vivo (*15*, *25*). Thus, the physicochemical properties and biological function of dendrimer−DNA complexes appear to be an important issue for the development of artificial, self-assembling systems for gene transfer (*17*, *26*).

Our previous studies suggested that transfection efficiency and functionality of DNA complexed with dendrimers may depend on the structure, size, and charge density of the polymer (*12*, *17*). The defined structure of dendrimers and the ability to alter a single parameter in the structure of the molecule make these polymers unique reagents to study the interaction between DNA and polycations. Structural studies on dendrimer-complexed condensed DNA may reveal the geometric and stoichiometric interactions relevant for the in vivo function. We therefore set out to examine the interactions occurring during DNA−dendrimer complex formation for use in in vitro transfections. This focused our work on

* To whom correspondence should be addressed.
[†] Department of Internal Medicine.

10.1021/bc990036k CCC: $18.00 © 1999 American Chemical Society
Published on Web 08/11/1999

complexes formed in DNA concentrations up to 1 mg/mL and in salt-free, water solutions. In the present studies, we characterize the processes involved with the formation of DNA−dendrimer complexes and the implications of this phenomenon for gene transfer.

MATERIAL AND METHODS

Dendrimers. The synthesis of Starburst PAMAM dendrimers has been previously described in detail (*10*, *11*). In these studies we have used dendrimeres with ethylenediamine (EDA) as a tetravalent polymerization initiator core. Generations (G) 4, 5, 6, 7, and 9 EDA core dendrimers have molar masses of 14 215, 28 826, 58 048, 116 493, and 467 162 kDa, respectively; the number of surface charges (amine groups) is 64, 128, 256, 512, and 2048.

Preparation of Polycation−DNA Complexes. Methyl alcohol stocks of dendrimers were diluted to an appropriate concentration in water and stored at 4 °C. Dendrimer−DNA complexes were formed by incubating the two components together in 100 μL of double distilled water for a minimum of 10 min at room temperature (RT) unless indicated otherwise. Ratios of dendrimer to nucleic acids were based on the calculation of the electrostatic charge present on each component, the number of terminal amine groups on a dendrimer vs the number of phosphate groups in the nucleic acid. For example, a G7 EDA dendrimer has approximately 2.65×10^{15} positive charges (protonized surface amine groups $NH3^{+}$)/μg (1 μg); the number of bases in a microgram (1 μg) of DNA is 1.71×10^{15}, resulting in approximately 1.71×10^{15} negative charges (ionized P, of phosphodiester groups, in pH 7)/1 μg of DNA. To obtain the theoretical charge ratio equal 1 (neutralizing conditions), 0.65 μg of this dendrimer is mixed with 1 μg of DNA. Similar calculations and mixing were used to make DNA complexes with the spermidine and spermine (1.8×10^{24} and 2.4×10^{24} positive charges/ mol, respectively). Charge ratios are presented as positive equivalents of the cationic component to negative charge equivalents of the nucleic acid components, as recommended in Nomenclature for Synthetic Gene Delivery Systems (*27*).

DNA for Precipitation Studies. Herring sperm DNA (from Promega or Gibco BRL-LifeTechnologies) preparations of sonicated double stranded DNA with a particle size ranging 100−1000 kb, where the majority of DNA fragments ranged 600−800 bp, were utilized in most of the precipitation studies. Plasmids pGL-2 control (Promega, 6 kb), pBK-RSV (Stratagene, 4.4 kb) and pCMV-Luc (*11*) were amplified in *E. coli* XL1Blue cells and isolated by double cesium chloride gradient (*28*) to ensure the purity of the DNA preparation. Single-stranded deoxyribonucleotide 27 base long oligonucleotide was synthesized using a DNA/RNA synthesizer (Model 394, Applied Biosystems) and purified by HPLC in the Biomedical Core Facility of the University of Michigan.

Analysis of Polycations−DNA Interactions. A number of polycations, such as dendrimers, spermidine, or spermine, were mixed with DNA samples in double distilled water, gently vortexed, incubated for 10 min RT and centrifuged at 11750*g* in an Eppendorf centrifuge for 5−7 min unless indicated otherwise. The supernatant and pellet were separated and the amount of DNA present in supernatant, denoted as "low density", was analyzed by spectrophotometry of DNA absorption at 260 nm or by measurement of the radioactivity of ^{32}P-labeled DNA. For UV absorbance measurement, an aliquot (100 μL) of the supernatant was diluted in water up to 400 μL. For the radioactive assay, 2.0−5.0 ng of tracer DNA, either 27 bp oligonucleotide or herring sperm DNA 5′-end labeled with ^{32}P, was added to the nonlabeled DNA. After centrifugation the radioactivity in supernatants was determined by counting in a Wallac 1409 Liquid Scintillation Counter.

Cells and Media. COS-1 and Rat2 cells were maintained in D-MEM medium (Gibco BRL) with 5% −10% FCS (Hyclone), 1% penicillin-streptomycin and 2 mM L-glutamine. D5 cells were cultivated in RPMI 1640 (Life Technologies) supplemented with 10% fetal calf serum, 1% penicillin-streptomycin, 2 mM L-glutamine, 50 μM 2-mercaptoethanol, 1 mM nonessential amino acids). All cell lines were incubated at 37 °C in 5% CO_2.

Transfection Methods. Transfections with dendrimer−plasmid DNA complexes were performed and analyzed using assays for luciferase activity expression from pCMV-Luc reporter plasmid (*15*). Indicated amounts of pCMV-Luc DNA were mixed with dendrimers at a variety of dendrimer to DNA charge ratios (ranging 1−50) and were then allowed to complex for 5−10 min at RT. The 24-well plates seeded 24 h before the transfection with approximately 2×10^4 cells/well, were washed once with serum-free media. The dendrimer−DNA complexes were then added, and transfection was carried for 3 h at 37 °C. After transfection, mix containing the complexes was washed out of the cells and standard growth media was added for incubation. The cells were harvested 24 h later and assayed for the expression of luciferase. To further analyze transfectional properties of complexes, dendrimer-complexed DNA was fractionated by centrifugation at 8160−11750*g* in water or using 0 to 2% and 0 to 5% step glycerol gradients. For the transfections 25 μL of the solution containing DNA−dendrimer complexes either not fractionated (suspension) or after centrifugation (low density) was added to 200 μL of serum-free media in each well of cells. Transfections and posttransfectional incubations proceeded as above. Luciferase activity was determined by measuring the light emission from 10 μL of cell lysate incubated with 2.35×10^{-2} μmol of luciferin substrate (Promega, Technical Bulletin no. 101). Light emission was measured in a relative light units (RLU) using chemiluminometer LB96P (EG&G Berthold), and adjusted to the protein concentration of the sample. The protein concentration in the cell lysates was measured in a standard protein assay (DC protein assay, Bio-Rad Richmond, CA).

Statistical Analysis. Statistical analysis was performed using Systat 5.2 software for Macintosh. Mean and standard deviations of the samples were determined and differences between them were analyzed by ANOVA.

RESULTS

Complexing with Dendrimers Results in DNA Precipitation. Formation of dendrimer complexes with supercoiled plasmid DNA, single- and double-stranded oligonucleotides, and linear forms of high molecular weight DNA has been previously demonstrated by retardation of electrophoretic mobility as well as by electronmicroscopy. Binding of DNA to dendrimer changes the molecular structure of DNA and results in condensation and aggregation of DNA particles (*12*, *15*, *17*). To examine the general physicochemical properties of dendrimer−DNA complexes and the changes in solubility of DNA upon interaction with dendrimers, several studies were performed. Complexes of dendrimer/herring sperm DNA at charge ratios ranging 0.01−100 were formed in 100 μL of water containing 10 μg of DNA (concentration

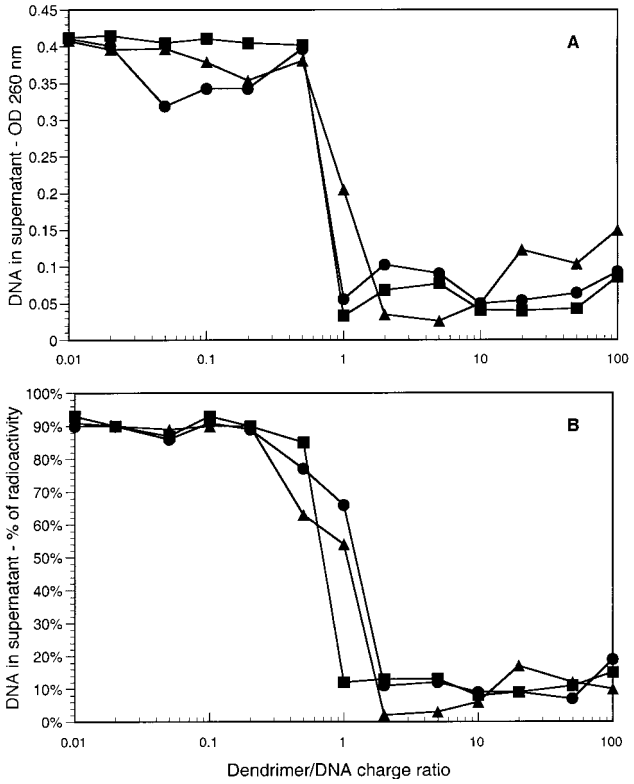


Figure 1. The formation of insoluble DNA aggregates with different generations of EDA core dendrimers. Comparison of the data obtained with spectrophotometric assay of DNA absorption at 260 nm (A) and measurement of radioactive DNA (B) present in supernatants after separation of precipitated complexes and soluble DNA fractions. EDA dendrimers G5 (■), G7 (●), and G9 (▲).

0.1 μg/μL) and increasing amounts of G 5, 7, and 9 EDA dendrimers. All complexing was performed in the absence of other ions in double-distilled water. DNA remaining in supernatant after centrifugation was analyzed using DNA absorption at 260 nm (Figure 1A) and by measuring the presence of radioactivity in the supernatant (Figure 1B). A simple spectrophotometric assay was possible because dendrimers, in the concentrations used in the experiments, have very low absorption across the broad spectrum of wavelengths (including the 260 nm maximum of DNA absorption; data not shown). The course of the precipitation curves in Figure 1 illustrates that both methods of measurement can accurately reflect formation of DNA precipitate. At 0.1 μg/μL concentration, DNA is completely neutralized at dendrimer−DNA charge ratio of 1 when complexed with three different generations of EDA core dendrimer (*12*, *17*). Approximately 95% of these complexes precipitate and the transition of DNA from soluble to condensed form seemed to be abrupt. Charge ratios lower than 1 (e.g., 0.5), did not result in a significant formation of the precipitate, and increasing of the dendrimer−DNA charge ratio (to 10−15) did not further enhance the precipitate formation. However, complexing at a charge ratio of 20 or greater resulted in higher DNA content in the soluble fractions reaching approximately 10−20% (of the total DNA). This phenomenon seems to be somewhat dependent on the generation of dendrimer used (Figure 1B). We also observed increased UV light absorption at these ratios (up to 25−30%), suggesting the generation of low-density particles containing both DNA and dendrimers (Figure 1A).

DNA Concentration Effects. We have studied the effect of DNA concentration on the formation of dendrimers−DNA complexes using plasmid pGL-2 DNA and G7 EDA. A broad range of DNA concentrations (from 0.01 to 1 μg/μL) was mixed with dendrimer at increasing concentrations from 0.0065 to 26 μg/μL (Figure 2). Plasmid DNA at the lowest concentration of 0.01 μg/μL did not form insoluble complexes with G7 EDA dendrimers at any polycation concentration or charge ratio (for this DNA concentration, analyzed dendrimer−DNA charge ratios are 1−4000). Increasing the DNA concentration to 0.1−1 μg/μL and complexing with 3.25 μg/μL of G7 EDA resulted in a 50% of DNA present in precipitates. Complexing DNA at a concentration of 1 μg/μL with G7 EDA at the charge ratio of 10 (concentration 6.5 μg/μL) resulted in the formation of 95% aggregated dendrimer−DNA complexes. The formation of the precipitate increased as the DNA concentration grew from 0.01 to 1 μg/μL, and less dendrimer and a lower dendrimer−DNA charge ratio were sufficient to generate insoluble aggregates in this conditions (Figure 2). We have observed that further increases of DNA concentration resulted in resolubization of the complexes, particularly at greater than 10 dendrimer−DNA charge ratios (data not shown).

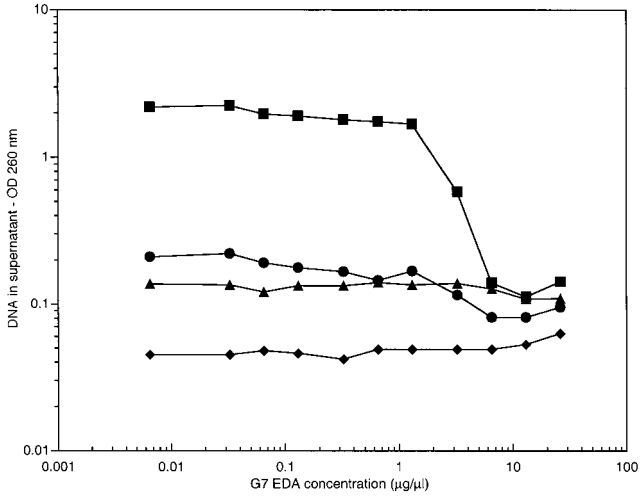


Figure 2. Effect of DNA concentration on the formation of aggregated dendrimer−DNA complexes. Note that a logarithmic scale is used for dendrimer concentration (μg/μL). DNA concentrations: (■) 1 μg/μL, (●) 0.1 μg/μL, (▲) 0.05 μg/μL, (◆) 0.01 μg/μL.

Dendrimers Form Complexes with Various Forms of Nucleic Acid. G7 EDA dendrimer formed complexes with 27 base oligonucleotides, herring sperm DNA (average length of DNA particle 600−800 bp) or pGL2—the latter, a supercoiled, covalently closed 6 kb plasmid (Figure 3). All DNA preparations were prepared at 0.1 μg/μL concentration and mixed at the appropriate charge ratio with G7 EDA. To increase the capability to detect differences in dendrimer−DNA complex formation with various forms of nucleic acids, the separation of the low- and high-density fractions was performed by centrifugation at 5220*g* instead of the standard conditions (Materials and Methods). All three types of DNA formed insoluble complexes when mixed with G7 EDA at increasing dendrimer−DNA charge ratios. However, 50% of 0.1 μg/μL plasmid DNA remained in supernatant when complexed with G7 EDA dendrimer at a dendrimer−DNA charge ratio of 5 (Figure 3A). In contrast, the oligonucleotides or herring sperm DNA complexed at the same charge ratio resulted in approximately 20% of the total DNA remaining in the supernatant. While similar patterns of the precipitation curves were obtained with all three forms of DNA, aggregation of plasmid DNA proceeded at higher G7 EDA/DNA charge ratio.

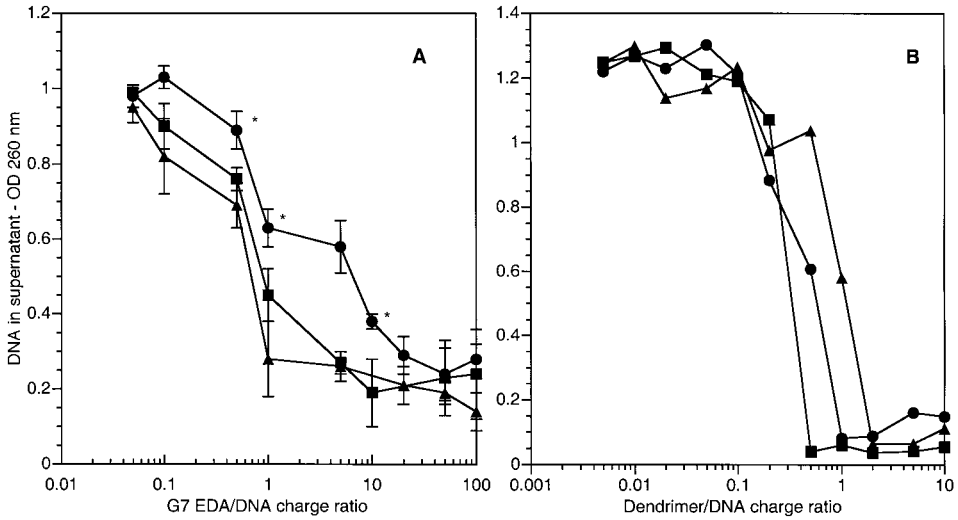


Figure 3. Formation of the aggregates with various types of nucleic acids. (A) G7 EDA complexed with 0.1 μg/μL of the different types of DNA: (■) low molecular weight, single-stranded 27 base DNA (oligo); (●) heterogeneous population of double stranded sonicated herring sperm DNA (hs DNA); and (▲) uniform population of covalently closed plasmid DNA (pGL-2). [The asterisk (*) indicates data points where $p < 0.05$ for herring sperm DNA or oligo and plasmid DNA]. (B) Plasmid DNA (pBK RSV) at 1 μg/μL complexed with EDA dendrimers. EDA dendrimers G5 (■), G7 (●), and G9 (▲).

Soluble dendrimer−plasmid DNA complexes were not observed with higher concentrations of plasmid DNA (Figure 3B). When 100 μg of pBK RSV plasmid DNA (4 kb) at a final concentration of 1 μg/μL was complexed with G5, G7, and G9 EDA in dendrimer−DNA (charge ratios ranging 0.05−1), the precipitation curves indicated that at this DNA concentration and at a dendrimer−DNA charge ratio equal to 1, all generations of dendrimers precipitated >95% of plasmid DNA. The profiles of the precipitation curves are similar, but there are subtle differences in maximum of complexation with different generations of dendrimers. Smaller dendrimers, G5 and G7 EDA, tend to form insoluble DNA complexes at lower charge ratios (~0.5) than the larger G9 EDA dendrimer (Figure 3B). This result may suggest that the electrostatic process of complexing and aggregation of DNA may be uniquely affected by the size of the dendrimer.

To further analyze the effect of size, surface charge, and molar concentration of dendrimer on complex formation, herring sperm DNA at 0.025 μg/μL was incubated with increasing concentrations of G4, G5, G6, G7, and G9 EDA dendrimers (Figure 4). As previously observed with plasmid, at a charge ratio of 1, 95% of DNA complexed with dendrimers was found in the insoluble fractions. The efficiency of precipitation with dendrimers, defined here by the lowest molar concentration of polymer in which the maximum precipitation of DNA occurs, was proportional to the increase in size of the dendrimer. This is not unexpected given the primarily electrostatic nature of dendrimer−DNA interaction, since larger dendrimers carry higher surface charge than smaller ones (*10*). Maximum formation of insoluble complex with 0.025 μg/μL of herring sperm occurs in 0.054 μM G9 EDA, 0.215 μM G7 EDA, 0.429 μM G6 EDA, 0.57 μM G5 EDA, and 0.86 μM G4 EDA dendrimers. Consequently, calculations of the ratios between molar concentrations of G6/G7 (~2), G7/G9 (~4), and G6/G9 (~8) generations reflect the inverse correlation of surface charge ratios between these dendrimers. Interestingly, the molar concentrations of larger G9, G7, and G6 EDA dendrimers most effective in the precipitation of DNA are ~1.5 times higher than those required for neutralizating of the DNA (dendrimer−DNA charge ratio equal 1). In contrast, for the G5 and G4 EDA dendrimers, these concentrations are ~1.3 times lower than expected for charge neutralization

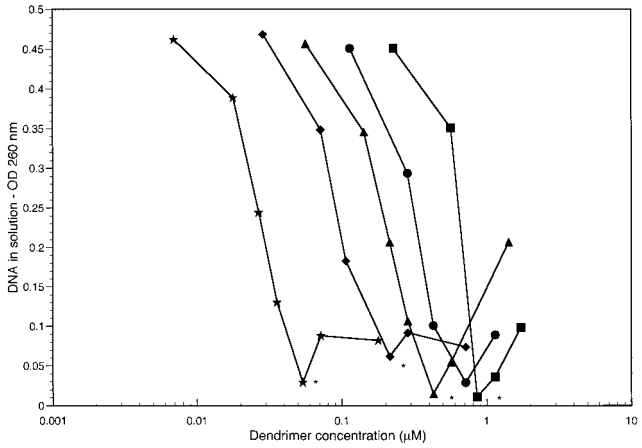


Figure 4. Effect of the size of dendrimer on the formation of aggregated dendrimer DNA complexes. Complexes were formed in a constant DNA concentration (0.025 μg/μL) with increasing concentrations of various generations of dendrimers. Data from dendrimers G4 (■), G5 (●), G6 (▲), G7 (◆), and G9 EDA (★) is described. Differences (*) between molar concentrations of dendrimers were significant with $p < 0.02$.

(Figure 4). These subtle differences in the threshold formation of an insoluble complex again suggest that the overall process of DNA aggregation is not strictly electrostatic, but also involves the size and, consequently, amount of dendrimer particles in the complex.

Efficiency of DNA Precipitation with Dendrimers and Polyamines. Spermidine and spermine are multivalent cations with charges of +3 and +4 per molecule, respectively. Both are known to induce condensation of DNA in aqueous solutions (*5*, *19*, *29*, *30*). To compare the condensation and precipitation with dendrimers, spermidine, and spermine 1 μg/μL of herring sperm DNA with radiolabeled DNA tracer was mixed with the increasing concentrations of each of the polycations. As has been reported previously, 10 mM spermine and spermidine precipitate the majority 80−90% of DNA. When the concentration reaches 100 mM, both polycations resolubilize the DNA pellet, and this transition is significantly enhanced by the presence of 25 mM NaCl (*5*). In contrast, G7 EDA at 1.12 μM (charge ratio 1) precipitates almost 90% of DNA and at 27.7 μM resolubilizes approximately

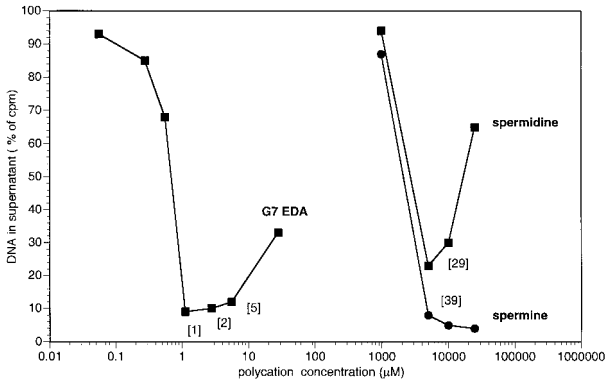


Figure 5. Comparison of DNA complex formation with G7 EDA dendrimer vs polyamines spermidine and spermine. Polycation/DNA charge ratios at the maximum of the DNA aggregation are indicated in the brackets.

30% of dendrimer−DNA complexes. Approximate polycation−DNA charge ratios of the most precipitation-effective molar concentrations of polymers are 1−5 for G7 EDA, 29 for spermidine, and above 39 for spermine (Figure 5). This indicates that spermidine and spermine require 30−40 times higher charge ratios and (5−10) × 10^3 higher molar concentrations than dendrimer to induce a similar degree of DNA condensation.

Transfection Studies with Fractionated DNA−Dendrimer Complexes. To test transfection efficiency of soluble and insoluble complexes, 100 μL of mix containing 4 μg of pCMV-Luc plasmid (0.04 μg/μL) and increasing amounts of G9 EDA dendrimer were fractionated by centrifugation at 5220*g*. Two cell lines, Rat2 and D5, were transfected with either 25 μL of whole complex suspension or 25 μL of supernatant from the centrifuged samples. In all dendrimer−DNA charge ratios the majority of in vitro transfection appears to be mediated by the supernatant fractions of DNA−dendrimer complexes (Figure 6). Analysis of DNA distribution using radioactive tracer DNA, indicated that from 11% (at a charge ratio of 1) to 26% (at a charge ratio of 50) of total dendrimer−DNA complexes is in the supernatant fractions (Figure 6, insert). Although the amount of DNA in supernatant samples at charge ratios 1 and 50 differs approximately 2.5-fold, the efficiency of transfection is 5−6 orders of magnitude higher at the 20 and 50 charge ratios as compared to a charge ratio of 1. This result may suggest that the composition of the complexes is the most important factor for the efficient in vitro transfection and not simply the amount of complexed, compacted, and neutralized DNA. Transfections performed with complexes from the resuspended pellets yielded various degrees of reporter gene expression. This indicates that highly aggregated insoluble dendrimer−DNA complexes can be reconstituted to a functional form for transfection. By comparison, the efficiency of transfections performed using DNA complexed with spermidine or spermine was not better than transfections with DNA alone (data not shown).

To further analyze the nature of the most effective for transfection dendrimer−DNA complexes, G7 EDA dendrimer complexed with pCMVLuc plasmid DNA at 0.02μg/μL (charge ratio 10) was fractionated using 0 to 5% step glycerol gradient. The 100 μL samples of fractionated complexes were used in transfection of Rat2 cells. Control cells were transfected with 100 μL of regular transfection mix prepared in 2.5% glycerol solution. Transfection was augmented with 50 μM chloroquine in medium. Most efficient transfection complexes were found in the two least-dense fractions (Figure 7). Calculation of glycerol density (Sigma catalog, 1998) of these fractions enabled estimation of equilibrium density for dendrimer−DNA complexes. Lowest density fractions 1 and 2 contained complexes of density of 1.000−1.004 g/mL. Radioactive tracing of the fractionated DNA indicated almost uniform distribution across the density gradient, reflecting the polydyspersed, nonuniform nature of the dendrimer−DNA complex population (Figure 7). The approximately 30% of total DNA present in the two lowest density fractions transfeced Rat2 cells twice as effectively as unfractionated control preparations.

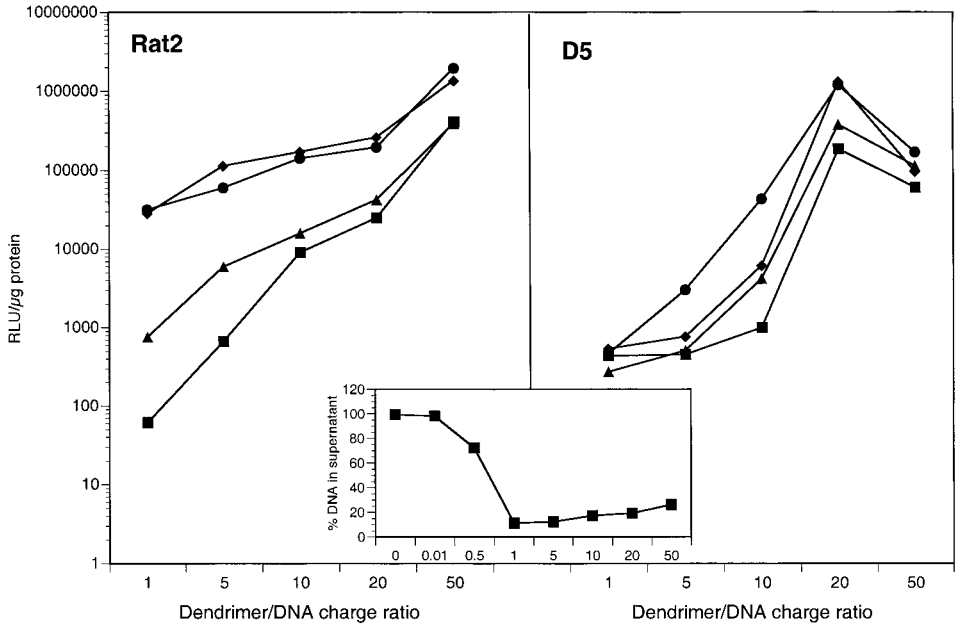


Figure 6. In vitro transfection of Rat2 and D5 cells with unfractionated dendrimer−DNA complexes vs low-density fractionated complexes. Transfection of cells with a suspension of dendrimer−DNA complexes performed either without (■) or with (●) 0.5 μM DEAE-dextran. Transfection with supernatant fractions containing soluble dendrimer−DNA complexes without (▲) and with (◆) augmentation with DEAE-dextran. Insert illustrates data obtained from radioactive tracing of fractionated G7 EDA/pCMV-Luc DNA complexes.

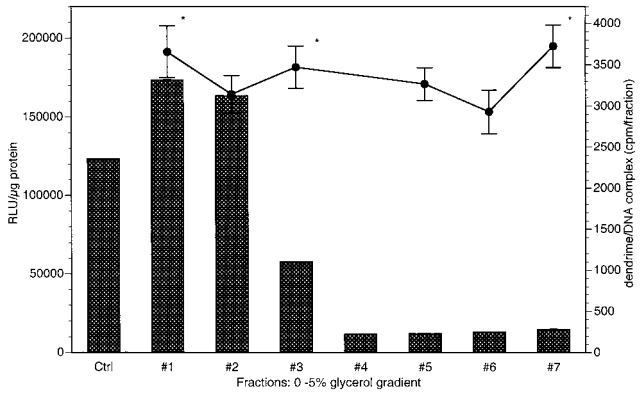


Figure 7. In vitro transfection of Rat2 cells with G7 EDA/DNA complexes. Complexes were fractionated by centrifugation on 0−5% glycerol gradient. Line (●) represents the distribution of the radioactively labeled dendrimer−DNA complexes in the gradient (right side axis). (*) $p > 0.5$ (± S.D.). The columns represent luciferase expression after transfection with unfractionated complexes vs the fractions 1−7 (left side axis).

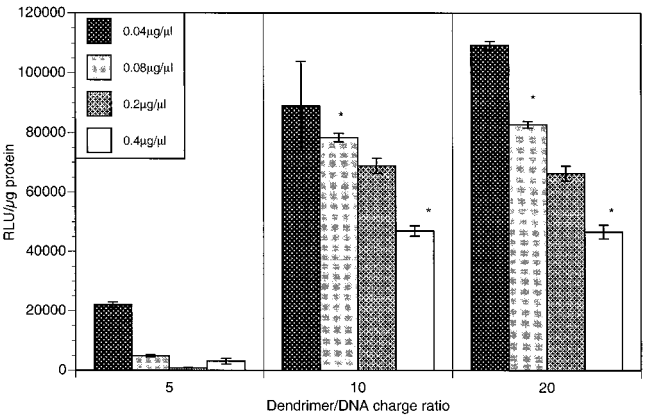


Figure 8. Effect of DNA concentration on the efficiency of in vitro transfection. COS-1 cells transfection with 1 μg of pCMV-luc plasmid DNA. DNA concentrations during complex formation with dendrimers (from 0.04 to 0.4 μg/μL) are indicated in the legend. (*) $p < 0.05$ (mean ± S.D.).

Figure 8 illustrates another approach to analyze the effect of DNA concentration-dependent compacting and aggregation on the efficiency of transfection in vitro. The G9 EDA dendrimer−DNA complexes were prepared with constant amount (1 μg) of pCMVLuc DNA at concentrations of 0.04, 0.08, 0.2, and 0.4 μg/μL and at the varying dendrimer−DNA charge ratios. The most efficient transfection of COS-1 cells occurred at the lowest DNA concentrations during complex formation, particularly in the high dendrimer−DNA charge ratios 10 and 20 (Figure 8). The precipitation experiments (Figures 2 and 3A) indicated that complexing dendrimers with DNA at lower concentrations (e.g., 0.05 μg/μL) resulted in the generation of lower density complexes which did not form precipitates. This type of complex mediated at least 2.5 times more efficient transfection of COS-1 cells than the higher density (less soluble) complexes obtained at higher DNA concentrations.

DISCUSSION

Various types of cationic molecules, including cationic lipids, polylysines, recombinant histones, and, recently, PAMAM dendrimers, have been employed as nonviral vectors for gene transfer into eukaryotic cells (*1*−*12*, *31*, *32*). These diverse materials have in common the ability to bind DNA binding via charge-based interactions, this property appearing to be necessary for transfection (*17*, *33*). The subsequent processes involved in the transfer and expression of the genetic material are not fully understood, but the compaction of DNA into condensed structures is also thought to play an important role in the cellular internalization of the genetic material. Alterations in the structure of the DNA polycation complex appear to affect the transfer and expression of the genetic material in cells and may be a critical issue in the development of nonviral gene transfer systems.

PAMAM dendrimers are an interesting new class of highly defined, spherical, cationic polymers (*10*, *14*). Recent studies have shown that these polymers can bind genetic material and facilitate gene transfer to a wide variety of cells (*11*, *12*, *15*, *26*). The characterization of the physiochemical properties of the DNA−dendrimer complex, including aggregation and precipitation are documented for the first time in this paper. We have identified that in DNA concentrations ranging 0.01−1 μg/μL, complexation with dendrimers may result in the formation of aggregates and precipitation. The primary mechanism of this process involves the electrostatic interaction between DNA and dendrimer molecules (*17*). This is illustrated in Figures 1, 3, and 4 by the generally identical shape of precipitation curves observed with dendrimers of different generations (sizes). However, the shift in the position of the curve indicates there is an influence of other parameters such as size and concentration of both dendrimers and DNA. Although all generations of PAMAM dendrimers have the same surface charge density, the interaction of smaller dendrimers G5 and G7 EDA with DNA led to formation of insoluble DNA complexes at lower charge ratios than with larger G9 EDA dendrimers. While dendrimers will form complexes with various forms of nucleic acid, including single-stranded oligonucleotides, larger fragments of salmon sperm DNA, or circular plasmid DNA, aggregation of plasmid DNA required higher dendrimer−DNA charge ratios. This indicates that average density of particles in populations of complexes formed at a specific charge ratio may differ depending on the type of DNA.

Various forms of synthetic and natural polyamines, spermidine, spermine, cobalthexamine, or polylysine interact physicochemically with DNA. Our data revealed similarities between the dendrimer mediated aggregation of DNA and that observed with other polycationic polymers (*5*, *6*, *11*, *13*, *20*, *34*). All these compounds bind various forms of DNA through charge−charge interactions, and efficiency of precipitation is dependent on the concentrations and charge ratios of both components as well as chemical structure of polycation (*5*, *26*). However, some specific differences are observed. Although the actual binding constants of large polyvalent compounds such as DNA and dendrimers are not readily determined (*5*, *8*, *35*) the high-density surface charge of the dendrimer molecules, the molar concentrations and dendrimer−DNA charge ratios that yield maximum DNA complexing are much lower for dendrimers than for other polycations. Another interesting difference is observed when comparing concentrations of DNA involved in complex formation. Spermidine and spermine seem to be most effective at forming insoluble complexes at lower DNA concentrations up to 0.01 μg/μL (*5*), while all generations of dendrimers are most effective at forming aggregates with higher DNA concentrations ranging from 0.04 to 1 μg/μL.

It is important to note that all experimental conditions tested correspond to those used for transfection in vitro and are not associated with cytotoxic effects. The excess of dendrimer provides DNA complexes with a positive net

charge. This is necessary for the efficient cellular uptake of dendrimer−DNA complexes through both energy-dependent and -independent mechanisms, as well as prolongs the survival of the transfected DNA (*12*, *17*, *25*).

In light of the precipitation studies, we have considered the link between compacting DNA and transfection in vitro. As other high molecular weight polycations, dendrimers form neutralized complexes with DNA at a charge ratio equal to 1. If compacting DNA is a crucial feature for the gene transfer as has been suggested (*1*, *2*, *9*, *32*), then one could expect that most efficient transfection with dendrimer−DNA complexes would be obtained with this conditions. Our results indicate otherwise and suggest in general that the transfection efficiency of complexes increase with an excess of cationic dendrimer (*12*). Such complexes display several unique properties in comparison to complexes formed at neutralizing concentrations of dendrimers. In particular, the appearance of the populations of low-density particles occurs only at these ratios. These low-density complexes, not yet fully characterized for structure and stoichiometry, seem to be important for achieving gene transfer since the transfection activity is contained in these soluble fractions. The complexity of polymeric polyelectrolite theories currently prevents a reliable theoretical calculation of complex stoichiometry (*5*, *34*, *35*). However, our results indicate that the conditions of complex formation (e.g., DNA concentration) define the transfection efficiency of the complex and in turn suggest that the initial complex formation may determine the final functionality of complexed DNA.

Naturally occurring polyamines are involved in numerous cellular processes (*21*) and are often used for in vitro studies of the functional properties of DNA (*18*). The correlation between condensation and aggregation of DNA and the stimulatory effect on DNA replication and transcription (*21*, *36*, *37*) have lead to the suggestion that these aggregates are fluid (*5*, *38*). Some forms of polyamine-condensed DNA are known to acquire liquid crystalline structure (*5*, *39*), and it is possible that dendrimer−DNA complexes may display properties of liquid crystals (*5*). The generation of the low-density particles at high DNA concentrations and high charge ratios closely resembles the resolubilization of DNA, which has been documented for spermidine, spermine, cobalthexamine (*5*, *29*), and other polyamines (*40*). However, the relevance of this phenomenon for gene transfer is not clear, since none of the these low molecular weight polycations is effective by itself for transfection even if they are frequently used as modifying moieties for lipid, liposome or polylysine based synthetic gene carriers (*30*−*33*).

In conclusion, the dendrimer−DNA interactions described in this study offer several insights into how these complexes form and mediate transfection. They also provide structural possibilities to enhance these polycations as carriers for cellular delivery of DNA and other genetic materials. Further characterization of the dendrimers with possible modifications of the charge and structure will clarify which properties of DNA−dendrimer complex absolutely determine its biological activity.

ACKNOWLEDGMENT

We thank Dr. Jolanta Kukowska-Latallo, Clara Verweij, and Carolyn Wurster for assistance in preparation of this manuscript.

LITERATURE CITED

(1) Wagner, E., Cotten, M., Foisner, R., and Birnstiel, M. L. (1991) Transferrin-polycation DNA complexes: the effect of polycations on the structure of the complex and DNA delivery to cells. *Proc. Natl. Acad. Sci. U.S.A. 88*, 4255−4268.

(2) Zhou, X., and Huang, L. (1994) DNA transfection mediated by cationic liposomes containing lipopolylysine: characterization and mechanism of action. *Biochim. Biophys. Acta 1189*, 195−203.

(3) Wolfert, M. A., Schacht E. T., Toncheva V., Ulbrich K., Nazarova O., and Seymur L. (1996) Characterization of vectors for gene therapy formed by self-assembly of DNA with synthetic block copolymers. *Human Gene Ther. 7*, 2123−2133.

(4) Eickbush, T. H., and Moudrianakis, E. N. (1978) The compaction of DNA helices into either continuous supercoils or folded-fiber rods and toroids. *Cell 13*, 295−306.

(5) Pelta, J., Livolant, F., and Sikorav, J. L. (1996) DNA aggregation induced by polyamines and cobalthexamine. *J. Biol. Chem. 271*, 5656−5662.

(6) Post, C. B., and Zimm, B. H. (1982) Theory of DNA condensation: collapse versus aggregation. Biopolymers *Biopolymers 21*, 123−137.

(7) Radler, J. O., Koltover, I., Salditt, T., and Safinya, C. R. (1997) Structure of DNA-cationic liposome complexes: DNA intercalation in multilamellar membranes in distinct interhelical packing regimes. *Science 275*, 810−814.

(8) Wilson, R. W., and Bloomfield, V. A. (1979) Counterion-induced condesation of deoxyribonucleic acid; a light-scattering study. *Biochemistry 18*, 2192−2196.

(9) Dunlap, D. D., Maggi, A., Soria, M. R., and Monaco, L. (1997) Nanoscopic structure of DNA condensed for gene delivery. *Nucleic Acids Res. 25*, 3095−3101.

(10) Tomalia, D. A., Naylor, A. N., and Goddard, W. A., III (1990) Starburst dendrimers: Molecular level control of size, shape, surface, chemistry and topology. *Angew. Chem., Int. Ed. Engl. 29*, 138−175.

(11) Haensler, J., and Szoka, F. C., Jr. (1993) Polyamidoamine cascade polymers mediate efficient transfection of cells in culture. *Bioconjugate Chem. 4*, 372−379.

(12) Kukowska-Latallo, J. F., Bielinska, A. U., Johnson, J., Spindler, R., Tomalia, D. A., and Baker, J. R., Jr., (1996) Efficient transfer of genetic material into mammalian cells using Starburst polyamidoamine dendrimers. *Proc. Natl. Acad. Sci. U.S.A. 93*, 4897−4902.

(13) Fritz, J. D., Herweijer, H., Zhang, G., and Wolff, J. A. (1996) Gene transfer into mammalian cells using histone-condensed plasmid DNA. *Human Gene Ther. 7*, 1395−1404.

(14) Frechet, J. M. (1994) Functional polymers and dendrimers: reactivity, molecular architecture, and interfacial energy. *Science 263*, 1710−1715.

(15) Bielinska, A., Kukowska-Latallo, J., Johnson, J., Tomalia, D. A., and Baker, J. R., Jr., (1996) Regulation of in vitro gene expression using antisense oligonucleotides or antisense expression plasmids transfected using Starburst PAMAM dendrimers. *Nucleic Acids Res. 24*, 2176−2182.

(16) Roberts, J. C., Bhalgat, M. K., and Zera, R. T. (1996) Preliminary biological evaluation of polyamidoamine (PAMAM) Starburst dendrimers. *J. Biomed. Mater. Res. 30*, 53−65.

(17) Bielinska, A. U., Kukowska-Latallo, J. F., Baker J. R., Jr., (1997) The interaction of plasmid DNA with polyamidoamine dendrimers: mechanism of complex formation and analysis of alteration induced in nuclease sensitivity and transcriptional activity of the complex DNA. *Biochim. Biophys. Acta 1353*, 180−190.

(18) Baeza, I., Gariglio, P., Rangel, L. M., Chavez, P., Cervantes, L., Arguello, C., Wong, C., and Montanez, C. (1987) Electron microscopy and biochemical properties of polyamine-compacted DNA. *Biochemistry 26*, 6387−6392.

(19) Gosule, L. C., and Schellman, J. A. (1976) Compact form of DNA induced by spermidine. *Nature 259*, 333−335.

(20) Zimmerman, S. B., and Harrison, B. (1987) Macromolecular crowding increases binding of DNA polymerase to DNA: an adaptive effect. *Proc. Natl. Acad. Sci. U.S.A. 84*, 1871−1875.

(21) Matthews, H. R. (1993) Polyamines, chromatin structure and transcription. *Bioessays 15*, 561−566.
(22) Oller, A. R., Vanden Broek, W., Conrad, M., and Topal, M. D. (1991) Ability of DNA and spermidine to affect the activity of restriction endonucleases from several bacterial species. *Biochemistry 30*, 2543−2549.
(23) Post, C. B., and Zimm, B. H. (1982) Light-scattering study of DNA condensation: competition between collapse and aggregation. *Biopolymers 21*, 2139−2160.
(24) Celano, P., Baylin, S. B., and Casero, R. A., Jr., (1989) Polyamines differentially modulate the transcription of growth-associated genes in human colon carcinoma cells. *J. Biol. Chem. 264*, 8922−8927.
(25) Raczka, E., Kukowska-Latallo, J. F., Rymaszewski, M., Chen, C., and Baker, J. R., Jr., (1998) The effect of synthetic surfactant Exosurf on gene transfer in mouse lung in vivo. *Gene Ther. 5*, 1333−1339.
(26) Tang, M., Redemann, C. T., and Szoka, F. C., Jr., (1996) In vitro gene delivery by degraded polyamidoamine dendrimers. *Bioconjugate Chem. 7*, 703−714.
(27) Felgner, P. L., Barenholtz, Y., Behr, J.-P., Cheng, S. H., Cullis, P., Jesse, J. A., Seymor, L., Szoka, F., Thierry, A. R., Wagner, E., and Wu, G. (1997) Nomenclature for synthetic gene delivery systems. *Human Gene Ther. 8*, 511−512.
(28) Ausubel, F. A., Breut, R., Kingston, R. E., Moore, D. D., Seidman, J. G., Smith, Y. A., Strubl, K., Eds. (1994) *Current protocols in molecular biology*, John Wiley & Sons, Inc. 1.7.6−1.7.7., 1.7.13.
(29) Srivenugopal, K. S., Wemmer, D. E., and Morris, D. R. (1987) Aggregation of DNA by analogues of spermidine; enzymatic and structural studies. *Nucleic Acids Res. 15*, 2563−2580.
(30) Gao, X., and Huang, L. (1996) Potentiation of cationic liposome-mediated gene delivery by polycations. *Biochemistry 35*, 1027−1036.
(31) Curiel, D. T., Agarwal, S., Wagner, E., and Cotten, M. (1991) Adenovirus enhancement of transferrin-polylysine-mediated gene delivery. *Proc. Natl. Acad. Sci. U.S.A. 88*, 8850−8863.
(32) Wadhwa, M. S., Knoell, D. L., Young, A. P., and Rice, K. G. (1995) Targeted gene delivery with a low molecular weight glycopeptide carrier. *Bioconjugate Chem. 6*, 283−291.
(33) Singh, A. K., Kasinath, B. S., and Lewis, E. J. (1992) Interaction of polycations with cell-surface negative charges of epithelial cells. *Biochim. Biophys. Acta 1120*, 37−42.
(34) Sakai, T. T., Torget, R. I. J., Freda, C. E., and Cohen, S. S. (1975) The binding of polyamines and of ethidium bromide to tRNA. *Nucleic Acids Res. 2*, 1005−1022.
(35) Bloomfield, V. A., Ma, C., and Arscott, P. G. (1994) in *Macro-Ion Characterization from Dilute Solutions to Complex Fluids* (K. S. Schmitz, Ed.) American Chemical Society Symposium Series, Volume 548, pp 195−209, American Chemical Society, Washington, DC.
(36) Krajewski, W. A., Panin, V. M., and Razin S. V. (1993) Dynamics of unfolded nucleosomal fiber. *J. Biomol. Struct. Dyn. 10*, 1013−1022.
(37) Zimmerman, S. B. (1993) Macromolecular crowding effects on macromolecular interactions: some implications for genome structure and function. *Biochim. Biophys. Acta 1216*, 175−185.
(38) Rau, D. C., and Parsegian, V. A. (1992) Direct measurement of the intermolecular forces between counterion-condensed DNA double helices. Evidence for long-range attractivehydration forces. *Biophys. J. 61*, 246−259.
(39) Shapiro, J. T., Leng, M., and Felsenfeld, G. (1969) Deoxyribonucleic acid−polylysine complexes. Structure and nucleotide specificity. *Biochemistry 8*, 3219−3232.
(40) Delsanti, M., Dalbiez, J. P., Spalla, O., Belloni, L., and Drifford, M. (1994) In *Macro-Ion Characterization from Dilute Solutions to Complex Fluids* (K. S. Schmitz, Ed.) American Chemical Society Symposium Series, Volume 548, pp 381−391, American Chemical Society, Washington, DC.

BC990036K

Polyion Complex Micelles with Protein-Modified Corona for Receptor-Mediated Delivery of Oligonucleotides into Cells

Serguei Vinogradov, Elena Batrakova, Shu Li, and Alexander Kabanov*

Department of Pharmaceutical Sciences, College of Pharmacy, 986025 Nebraska Medical Center Omaha, Nebraska 68198-6025. Received March 22, 1999; Revised Manuscript Received July 6, 1999

Graft-copolymers, containing poly(ethylene glycol) (PEG) and polyethyleneimine (PEI) chains have been proposed as carriers for delivery of phosphorothioate oligonucleotides (SODNs). Complexes of such copolymers with SODN self-assemble into particles having a core of neutralized PEI and SODN and a corona of PEG. Transferrin molecules are attached to the PEG corona using avidin/biotin construct. For this purpose, biotin moieties are covalently linked to the free ends of the PEG chains in the PEG-*g*-PEI copolymer. SODNs are reacted with mixtures of biotinylated and biotin-free PEG-*g*-PEI copolymers of various compositions to adjust the number of the biotin moieties in the complex. Resulting complexes have small size (ca. 40 nm) and do not aggregate in aqueous solutions for at least several days. To attach transferrin, they are supplemented first with avidin and then with biotin−transferrin conjugate. This increases the effective diameter of the particles to ca. 75−103 nm, depending on the composition of the complex. Cellular accumulation and fluorescence microscopy studies characterize the effects of these modifications on interaction of fluorescently labeled SODNs with KBv cell monolayers. The data suggest significant enhancement of SODN association with cells resulting from modification of the complex with transferrin. SODN complimentary to the site 546−565 of human *mdr 1*-mRNA was used to inhibit expression of the drug efflux transporter, P-glycoprotein (P-gp), in multiple drug resistant (MDR) cancer cells (KBv, MCF-7 ADR). Accumulation of a P-gp specific probe, rhodamine 123, in the cell monolayers is used to characterize the effects on P-gp efflux system following the treatment of the cells with antisense SODN or its complexes. This study suggests that antisense SODN incorporated in the complexes retain the ability to inhibit P-gp efflux system, while complexes of the randomized control SODN are inactive. Therefore, the antisense SODN is released from the complex and interacts with its intracellular target upon interaction of the complexes with the cells. Furthermore, modification of the complexes with transferrin leads to a significant increase of the effects of the antisense SODN on the P-gp efflux system in the cells. Overall, this study suggests that polyion complex micelles with protein-modified corona are promising tools for the delivery of antisense SODN.

INTRODUCTION

Development of efficient delivery systems for oligonucleotides (ODN) has been a major challenge in practical application of antisense therapeutics (*1*, *2*). The set of properties required from these systems is quite complex, and not surprisingly, only limited successes were achieved with simple delivery systems such as cationic liposomes and polymers (*2*). A novel class of cationic carriers has recently been proposed which might advance the field of ODN delivery (*3*). These carriers have block or graft copolymer architecture and consist of a polycation linked to a nonionic water-soluble polymer, most commonly, poly(ethylene glycol) (PEG). Examples of such carriers include PEG-*b*-polyspermine (*4*), PEG-*b*-poly(L-lysine) (*5*), and PEG-*g*-polyethyleneimine (PEG-*g*-PEI) (*6*). All these carriers bind with ODNs due to electrostatic interaction of the polycation and ODN chains. The complexes self-assemble into small, micelle-like aggregates termed "polyion complex micelles" (*5*), which have a hydrophobic core from neutralized polycation and ODN chains and hydrophilic corona from PEG chains. One clear advantage of such systems is their improved solubility compared to most other cationic carriers, which commonly aggregate after interaction with ODNs (*3*). Also, prevention of binding of ODN with serum proteins and digestion of ODN by nucleases as a result of incorporation of ODN into such complexes has recently been demonstrated (*6*). Furthermore, increased activity of antisense ODNs incorporated into such systems has been reported based on in vitro and in vivo studies (*7*, *8*).

This work examines complexes of ODN and cationic copolymers displaying transferrin at the surface of the complex that can promote uptake of ODN in the cell and increase transfection. The complexes were prepared using biotin-modified PEG-*g*-PEI copolymer. As a result, biotin moieties linked to the free ends of PEG chains became incorporated in the PEG corona. These moieties were then used to anchor biotinylated transferrin at the surface of the complex using avidin as a linker. Both the increased binding of phosphorothioate ODN (SODN) with cells and increased sequence-specific activity of the SODN were observed as a result of such modification. Fluorescently labeled SODN was used to examine transport and localization of SODN in the cells. 20-mer phosphodiester sequence directed to the human *mdr1*-mRNA was used to characterize effects of SODN on expression of P-glycoprotein (P-gp) in multiple drug

* To whom correspondence should be addressed. E-mail: akabanov@unmc.edu.

10.1021/bc990037c CCC: $18.00 © 1999 American Chemical Society
Published on Web 08/18/1999

resistant (MDR) cancer cells: human oral epidermoid carcinoma (KBv) and human breast carcinoma (MCF-7 ADR).

MATERIALS AND METHODS

Materials. PEG, 8 kDa (as determined by viscometry) (lot no. 01925EG); PEI, 2 kDa (M_w, $M_w/M_n = 1.1$) (lot no. 40870-0), other reagents for copolymer synthesis, and fluorescent labels were obtained from Sigma-Aldrich Chemical Co. (St Louis, MO). PEG(8K)-*g*-PEI(2K) and dimethoxytrityl-PEG, 8 kDa (DMT-PEG), were synthesized in our laboratory as previously described (*6*). FITC-avidin (10−15 units/mg of protein; 1 unit binds 1 μg of d-biotin) and biotinylated human transferrin (biotin-transferrin) (6.7 biotin moieties/protein molecule) were purchased from Sigma-Aldrich Chemical Co. (St Louis, MO).

Synthesis of Monoamino-PEG. A total of 0.18 mmol of DMT-PEG was coevaporated twice in vacuo with anhydrous acetonitrile (10 mL), treated with 0.54 mmol of 1,1′-carbonyldiimidazole in 10 mL of anhydrous acetonitrile for 4 h at 40 °C, and then reacted with 10.5 mmol of ethylenediamine for 18 h at 25 °C. Thin-layer chromatography (TLC) using Silicagel and dichloromethane-methanol (9:1) (product R_f 0.3, DMT-PEG Rf 0.45) showed that the reaction was complete. Colorimetric reactions of the product with ninhydrine and 1% trifluoroacetic acid showed presence of amino groups and DMT groups, respectively. An excess of ethylenediamine was removed in vacuo, the product was treated with 30 mL of 2% trifluoroacetic acid in dichloromethane (5 min, 25 °C) to remove DMT group, the solvents were evaporated and the residue was dissolved in 15 mL of 40% ethanol containing 1% of triethylamine. This solution was filtered and dialyzed (Membra-Cel dialysis tubes with cutoff 3500) against 40% ethanol for 24 h, and the solvents were evaporated again. Finally, the product was redissolved in methanol (15 mL), precipitated into ether (300 mL), filtered, and dried in vacuo. The yield of monoamino-PEG was 1.20 g. Primary amine content in the product was 93% as shown using fluorescamine titration (*9*).

Synthesis of Biotin-PEG. A total of 0.145 mmol of monoamino-PEG was reacted with 0.145 mmol of d-biotin *p*-nitrophenyl ester in 5 mL of dimethylformamide containing 1% (v/v) of triethylamine for 18 h at 40 °C. TLC (using the same solvent as above) revealed appearance of a new product with R_f 0.25. This product showed no reaction with ninhydrine in contrast to the initial monoamino-PEG (Rf 0.1). It was purified by gel-permeation chromatography (GPC) using a column (3 × 30 cm) with Sephadex LH-20 (Pharmacia Biotech, Piscataway, NJ) and 50% methanol as an eluent (elution rate 2 mL/min, fractions 6 mL). After lyophilization, 0.79 g of biotinylated PEG (biotin-PEG) was obtained.

Synthesis of 1,1′-Carbonyldiimidazole-Activated Biotin-PEG. A total of 0.75 g of biotin-PEG was dried by coevaporation with anhydrous acetonitrile (10 mL) and then treated at 25 °C with an excess of 1,1′-carbonyldiimidazole (1 mmol) in 5 mL of anhydrous acetonitrile. The reaction was terminated after 18 h by addition of 0.2 mL of water, and the reaction mixture was dialyzed as previously described against 20% ethanol for 2 days and lyophilized. This produced 1,1′-carbonyldiimidazole activated biotin-PEG with the quantitative yield.

Synthesis of Biotin-PEG(8K)-*g*-PEI(2K). A total of 0.04 mmol of activated biotin-PEG in 5 mL of 80% ethanol was added dropwise under vigorious stirring to 5% solution of PEI, 2 kDa in 80% ethanol (10 mL). Reaction mixture was allowed to stand for 18 h at 25 °C then was diluted twice by water and dialyzed as previously described against 20% ethanol for 2 days. After solvent evaporation the product was twice precipitated from methanol into ether and dried in vacuo yielding 0.27 g of slightly yellow solid.

Molecular Mass Determination. Molecular masses of the cationic copolymers were determined by GPC analysis (M_{GPC}) using the SigmaChrom GFC-1300 column (7 mm × 30 cm) and 20% ethanol in 50 mM aqueous ammonium, pH 10.0, as a mobile phase. The column was calibrated using PEG and PEI with the molecular mass ranging 0.9−200 kDa, obtained from Shearwater Polymers Inc. (Huntsville, AL), Monomer-Polymer Dajac Laboratories Inc. (Feasterville, PA), and Sigma-Aldrich Chemical Co. (St Louis, MO).

PEG and PEI Ratio. The ratio of PEG and PEI in the copolymer samples was determined from ^{1}H NMR spectra using integral values obtained for the CH_2CH_2O protons of PEG and CH_2NH protons of PEI. Prior to NMR measurements all copolymers were purified from admixtures of nonconjugated PEG by preparative thin-layer chromatography on Silicagel using dichloromethane-methanol mixture (6:4) for elution.

Determination of the Nitrogen Groups. The total content of the nitrogen in the copolymers was determined by elemental microanalysis. The ratios of primary, secondary and tertiary amino groups were determined from ^{1}H NMR spectra.

Determination of the Biotin Content. The ratio of the biotin moieties and PEI chains in the biotin-PEG-(8K)-*g*-PEI(2K) copolymer was determined by elemental microanalysis from the sulfur and nitrogen contents. Also, biotin content in the biotin-PEG(8K)-*g*-PEI(2K) copolymer was determined using competitive displacement of 2-anilinonaphthalene-6-sulfonic acid in avidin (*10*). In a typical experiment, 20 μL of white egg avidin solution (14 units/mg of protein, 93 units/mL) were diluted with phosphate buffered saline (PBS), pH 7.4, to a total volume of 1 mL, and then supplemented with 15 μL of 5 mM 2-anilinonaphthalene-6-sulfonic acid in dimethyl sulfoxide. The resulting solution was shaken thoroughly and mixed with various amounts of the copolymer. Fluorescence of the mixture was measured at λ_{ex} = 328 nm and λ_{em} = 408 nm using Shimadzu RF5000 fluorescent spectrophotometer. The dependence of the fluorescence intensity on the amount of the copolymer added revealed a break indicating saturation of biotin binding sites in avidin, which was used to determine the biotin content in the copolymer.

Polynucleotides. Oligonucleotides and their 3′-aminolinker derivatives were synthesized at the Oligonucleotide Core Facility, UNMC (Omaha, NE). To introduce fluorescent label, fluorescein isothiocyanate (FITC) or rhodamine isothiocyanate (RITC) were taken into reaction with 3′-amino-modified SODN using manufacturer's protocol. All oligonucleotides were purified by precipitation from 0.3 M NaCl solutions into 2-propanol. In the experiments on *mdr1*-gene inhibition, the following SODNs were used: GTCAAGCCAATTTGAATAGC (**S4**) complementary to *mdr1*-mRNA binding site 546−565, and randomized control SODN, CGATATAGATTGC-CTAAAACG (**RS4**). For RT-PCR procedure, two sets of PCR-primers were used: GGGACCGCAATGGAGGAG and CAGATTCATGAAGAACCCTG to amplify *mdr1*-gene fragment of 308 bp (*439*−*746*) (*11*), as well as ACCCCCACTGAAAAAGATGA and ATCTTCAAACCTC-

Table 1. Characteristics of Synthesized Cationic Copolymers

	molecular characteristics of the synthesized copolymers				
copolymer name[a]	*N* (μmol/mg)[b]	biotin content (mg/g)[c]	PEG:PEI[d]	biotin:PEI[e]	molecular mass (kDa)[f]
PEG(8K)-*g*-PEI(2K)	2.2	0	1.7	0	15.5
Biotin-PEG(8K)-*g*-PEI(2K)	2.1	26	2.3	2.5	18.5

[a] The nomenclature for PEG and PEI copolymers accounts for the molecular masses of the PEG and PEI fragments [i.e., "PEG(8K) for PEG, 8 kDa or "PEI(2K)" for PEI, 2 kDa]. [b] Nitrogen concentration as determined by elemental analysis. [c] Milligrams of biotin per gram of copolymer as determined by avidin titration. [d] As determined by ^{1}H NMR analysis of the copolymer samples. [e] As determined by elemental analysis. [f] M_{GPC}.

CATGATG to synthesize β-microglobulin (*bmg*) gene fragment of 120 bp (*12*).

Preparation of the Complexes of SODN and Cationic Copolymers. Solutions of cationic copolymers and SODNs were prepared in 50 mM phosphate buffer, pH 7.4, filtered through 0.22 μm sterile filters, and mixed with each other to obtain desired *N*/*P* ratio (molar ratio of total nitrogen in cationic copolymers to thiophosphate groups in SODN). After incubation for 1 h at 25 °C, these mixtures were supplemented with the solution (8 mg/mL) of egg white avidin in phosphate buffer, pH 7.4, at avidin/biotin molar ratio 1. These mixtures were incubated for additional 1 h at 25 °C and then supplemented with the solution (8 mg/mL) of human biotinylated transferrin in phosphate buffer, pH 7.4, at transferrin/avidin molar ratio 1. The final system was equilibrated for at least 2 h at 25 °C prior to further use.

Particle Size Determination. Effective hydrodynamic diameter of particles was measured by photon correlation spectroscopy as described elsewhere (*6*).

Cell cultures. KBv and KB cells were provided by Dr. D. W. Miller (UNMC, Omaha, NE) while MCF7 and MCF7 ADR cells were provided by Dr. V. Yu, Alakhov (Supratek Pharma Inc., Laval, Canada). Cells were seeded at a density 5×10^4 cells/well and maintained in DMEM medium supplemented with 10% FBS in 5% CO_2 incubator.

Interaction of FITC−SODN with Cells. Cells were grown in 24-well plates (Falcon Co., Becton Dickenson, Lincoln Park, NJ) for 24 h prior to the treatment. After 30 min preincubation with the serum-free assay buffer (122 mM sodium chloride, 25 mM sodium bicarbonate, 10 mM glucose, 10 mM Hepes, 3mM potassium chloride, 1.2 mM magnesium sulfate, 1.4 mM calcium chloride, and 0.4 mM potassium phosphate dibasic), cells were exposed to 10 μM FITC−SODN or FITC−SODN complexes with cationic copolymers in serum-free media for 6 h at 37 °C. Thereafter, cells were washed three times with ice-cold PBS and solubilized in 1% Triton X-100 solution. Fluorescence was measured at $\lambda_{ex} = 488$ nm and $\lambda_{em} = 520$ nm using a Shimadzu RF5000 fluorescent spectrophotometer and normalized by protein content in each sample determined by Pierce BCA method. All experiments were carried out in four repeats.

Fluorescence Microscopy. KBv cells grown on chamber slides (Fisher Sci., Pittsburgh, PA) were exposed to 5 μM free RITC−SODN or complexes of RITC−SODN with cationic copolymers for 3 h at 37 °C in serum-free media. After that, cellular accumulation of RITC-labeled SODN was examined using fluorescent Nikon Microphot FXA microscope equipped with CCD camera (Photometrics, Tucson, AZ) and Rhodamine filter set (Omega Optical).

Cell Exposure to Antisense SODN. KBv or MCF-7/ADR cells were seeded in 24-well plates at a density of 50 000 cells/well, grown for 24 h, and then exposed to 0.5n 5 μM free SODN or SODN complexes in cell culture medium containing 10% FBS for 2 days. The treatment solutions were replaced for the fresh ones after first 24 h of exposure. Thereafter, the cells were further incubated in the fresh DMEM medium containing 10% FBS for 24 h before harvesting for analysis.

Accumulation of Rhodamine 123 (R123) in Cells. Following exposure of cells to SODNs rhodamine 123 (R123), accumulation studies were performed as previously described (*13*).

Quantitation of mdr1-mRNA by RT-PCR. Total RNA was isolated from cell lysates using an RNA isolation system, RNAgents (Promega, Madison, WI). Access RT-PCR system with Tfl DNA polymerase (Promega, Madison, WI) was used for quantitative RT-PCR. PCR reagent mixture was prepared as follows: (i) 21.5 μL of RNase-free water, (ii) 10 μL of 5× reaction buffer, (iii) 1 μL of 1/8x RNasin RNase Inhibitor, (iv) 3 μL of primer mixture 1 (50 pmol each of *mdr1*-specific ODNs), (v) 3 μL of primer mixture 2 (50 pmol each of *bmg*-specific ODNs), (vi) 1 μL of 10 mM nucleoside triphosphates mixture, (vii) 2 μL of 25 mM magnesium sulfate, (viii) 1 μL of AMV reverse transcriptase, and (ix) 1μL of Tfl DNA polymerase. A total of 43 μL of this solution was added to cellular RNA solution, and the mixture was incubated for 45 min at 48 °C. DNA fragments were amplified during 27 cycles: 0.5 min at 94 °C, 1 min at 60 °C, 2 min at 68 °C, using Perkin-Elmer PCR amplificator. PCR products were analyzed by electrophoresis in 2% low-melting agarose gels. PCR markers (Promega, Madison, WI) were used to determine the size of DNA fragments. Bands at 308 bp (*mdr1*-gene) and 120 bp (*bmg*-gene) were cut, and DNA was extracted from agarose in 1 mL of 20 mM tris-EDTA buffer for 15 min at 80 °C. The amount of the extracted DNA was quantified using PicoGreen solution (Molecular Probes, Eugene, OR) as described elsewhere (*14*).

Western Blot Experiment. Western blot analysis of P-gp was done as described previously (*15*).

RESULTS

Synthesis of Cationic Copolymers. The nomenclature and characteristics of the cationic copolymers synthesized are presented in Table 1. PEG(8K)-*g*-PEI(2K) copolymer was synthesized by grafting PEG chains to the amino groups of PEI as previously described (*6*). The scheme of synthesis of biotin-PEG(8K)-*g*-PEI(2K) copolymer is presented in Figure 1. According to this scheme, PEG was initially converted to monoamino-PEG (stages a, b, c, d), which was then modified with biotin *p*-nitrophenyl ester yielding biotin-PEG (stage e). After that, the free end hydroxyl group of the biotin-PEG was activated by 1,1′-carbonyldiimidazole (stage f), and then activated biotin-PEG was conjugated to the PEI (stage g). The product was separated by precipitation into ether and further analyzed by GPC on SigmaChrom GFC-1300 column in 20% ethanol. This analysis showed no significant impurities of the initial reaction components (less that 5% total).

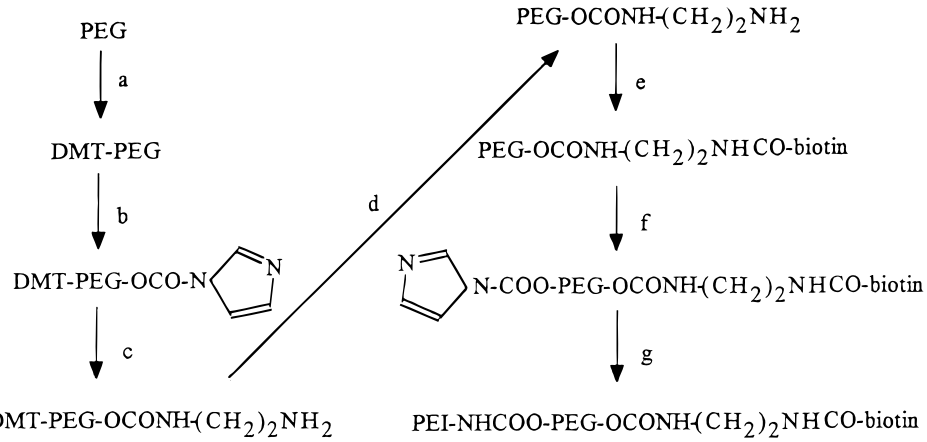


Figure 1. Synthesis of biotinylated copolymers. (a) Dimetoxytrityl chloride, pyridine, 4 h; (b) 1,1′-carbonyldiimidazole, acetonitrile, 18 h; (c) ethylenediamine, ethanol, 18 h; (d) 2% trifluoroacetic acid, dichloromethane, 5 min; (e) biotin *p*-nitrophenyl ester/triethylamine, dimethylformamide, 18 h; (f) 1,1′-carbonyldiimidazole, acetonitrile, 18 h; (g) PEI, ethanol, 18 h.

The ratios of the PEG and PEI chains in the copolymer samples were determined from ^{1}H NMR spectra using integral values obtained for the CH_2CH_2O protons (PEG) and CH_2NH protons (PEI). The molecular masses (M_{GPC}) of these copolymers were determined by GPC analysis. For both copolymer samples used in this work, PEG(8K)-*g*-PEI(2K) and biotin-PEG(8K)-*g*-PEI(2K), the molecular masses were in reasonable agreement with the ^{1}H NMR analysis of the contents of the PEG and PEI fragments in these copolymers (Table 1).

Comparison of the PEG:PEI ratio 2.3 obtained from ^{1}H NMR with biotin:PEI ratio 2.5 obtained from the elemental analysis suggests that within the margin of the experimental error, every PEG chain in the biotin-PEG(8K)-*g*-PEI(2K) copolymer contains approximately one biotin moiety (Table 1). The biotin content in this copolymer determined using the functional assay based on displacement of the fluorescent probe 2-anilinonaphthalene-6-sulfonic acid in avidin binding centers was 26 mg/g of the copolymer (Table 1). This amount corresponds to ca. 2.0 functionally active biotin groups in the biotin-PEG(8K)-*g*-PEI(2K) molecule, suggesting that at least 80% of biotin groups in this copolymer can interact with the avidin.

Coupling of Biotinylated Copolymers with Biotin-Transferrin through Avidin. Binding of (*1*) the biotin-PEG(8K)-*g*-PEI(2K) copolymer with avidin and (*2*) the biotin-PEG(8K)-*g*-PEI(2K)/avidin complexes with biotin-transferrin conjugate was further studied by analytical chromatography using Sephadex G-100 column. An example of the typical result obtained during chromatography experiments is presented in Figure 2. In this example, the retention time of the biotin-PEG(8K)-*g*-PEI(2K) copolymer is decreased when avidin is added to the copolymer at 1 mol equiv of avidin/1 mol equiv of biotin. There were no peaks corresponding to either free biotin-PEG(8K)-*g*-PEI(2K) copolymer or free avidin in the mixture, suggesting that binding of the biotinylated copolymer and avidin is complete. Further addition of biotin-transferrin to the preformed biotin-PEG(8K)-*g*-PEI(2K)/avidin complex altered the chromatographic profile of the mixture, suggesting that the three component biotin-PEG(8K)-*g*-PEI(2K)/avidin/biotin-transferrin complex is formed. The resulting complex was eluted in the free volume of the column. This experiment demonstrates that biotin-PEG(8K)-*g*-PEI(2K) copolymer can be effectively linked to biotin-transferrin using the avidin "bridge".

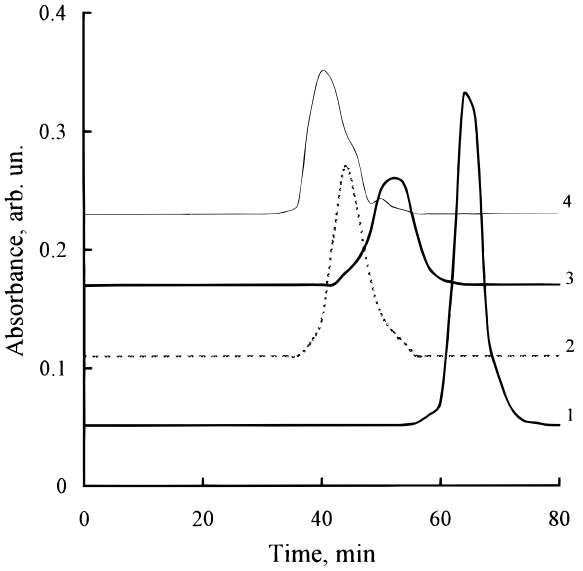


Figure 2. Chromatographic profiles of biotin-PEG(8K)-*g*-PEI(2K) alone (**1**), biotin-PEG(8K)-*g*-PEI(2K) and FITC-avidin mixture (**2**); FITC-avidin alone (**3**), and biotin-PEG(8K)-*g*-PEI(2K)/FITC-avidin complex mixed with biotin-transferrin (**4**). Biotin-PEG(8K)-*g*-PEI(2K) and FITC-avidin were mixed at 1 equiv of avidin per 1 equiv of biotin and incubated for 1 h at 25 °C; biotin-transferrin was added to this mixture at 1 equiv of biotin-transferrin per 1 equiv of avidin and incubated 2.5 h. Chromatography: Sephadex G-75 (fine) column (1 × 30 cm), eluent PBS, pH 7.4, elution rate 0.2 mL/min, UV-light absorption at 230 nm.

Incorporation of SODN in the Complexes. SODNs were mixed with the cationic copolymers to prepare SODN−copolymer complexes. At this stage mixtures of biotin-free PEG(8K)-*g*-PEI(2K) (*F*) and biotin-PEG(8K)-*g*-PEI(2K) (*B*) copolymers at various weight ratios (*F*/*B*, w/w) were used to adjust the number of the biotin moieties linked at the surface of the SODN−copolymer complex. The ratio of the amounts of total nitrogen groups (N) in the copolymers and thiophosphate groups (P) in SODN was kept constant at $N/P = 4$ based on the results of the previous report (*6*) to ensure complete incorporation of the SODN in the complexes. As is seen in Table 2, the sizes of particles formed by SODN and PEG(8K)-*g*-PEI(2K)/biotin-PEG(8K)-*g*-PEI(2K) mixtures practically did not depend on the *F*/*B* ratio and were ca. 40 nm. After addition of avidin to these complexes, the sizes were increased reaching from ca. 57 to 62 nm,

Table 2. Effective Diameters of Particles Formed by S4 SODN and PEG(8K)-*g*-PEI(2K)/Biotin-PEG(8K)-*g*-PEI(2K) Mixtures at Various *F*/*B* Ratios without Avidin and Biotin-Transferrin and in the Presence of Avidin and Biotin-Transferrin

system studied[a]	effective diameter (nm)[b]		
	F/*B* = 24	*F*/*B* = 11.5	*F*/*B* = 7.3
S4/copolymer complex alone	39.9 ± 0.1	40.5 ± 0.5	39.1 ± 0.2
S4/copolymer complex + avidin	62.6 ± 2.9	59.4 ± 0.5	57.0 ± 3.3
S4/copolymer complex + avidin + biotin-transferrin	75.5 ± 0.8	103 ± 1	91.6 ± 0.2

[a] Complexes were prepared as described in the Materials and Methods in 50 mM phosphate buffer, pH 7.4, at **S4** concentration 5 μM and total *N*/*P* ratio 4. [b] Means ± SD, $n = 3$.

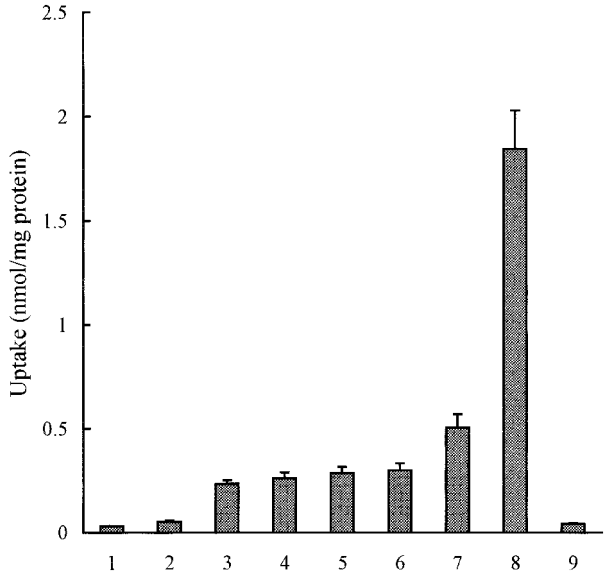


Figure 3. Cellular accumulation of FITC−SODN following exposure of KBv cells to free FITC−SODN (column 1), avidin- and transferrin-free complex FITC-SODN/PEG(8K)-*g*-PEI(2K)/biotin-PEG(8K)-*g*-PEI(2K) (column 2), transferrin-free complexes FITC-SODN/PEG(8K)-*g*-PEI(2K)/biotin-PEG(8K)-*g*-PEI(2K)/avidin (columns 3, 4, 5), transferrin-containing complexes FITC−SODN/PEG(8K)-*g*-PEI(2K)/biotin-PEG(8K)-*g*-PEI(2K)/avidin/biotin-transferrin (columns 6, 7, 8), avidin-free mixtures of biotin-transferrin and FITC−SODN/PEG(8K)-*g*-PEI(2K)/biotin-PEG(8K)-*g*-PEI(2K) complex (column 9). In the cases of complexes containing mixtures of the biotin-free and biotin-modified copolymers *F*/*B* ratios were 24 (columns 3, 6), 11.5 (columns 4, 7), and 7.3 (columns 2, 5, 8, 9) and *N*/*P* ratios were fixed at 4. In all cases, SODN concentration in the treatment solution was 10 μM. Data are mean ± SEM, $n = 4$.

suggesting that avidin became incorporated into the complex. Finally, the sizes were further increased upon addition of the biotin−transferrin conjugate to this complex and reached from 75 to 103 nm depending on the *F*/*B* ratios, suggesting that tranferrin became incorporated in the complex particles. No aggregation was observed with all these complexes stored at 4 °C for at least several days.

Cellular Accumulation of SODN. For the cellular accumulation studies, KBv cell monolayers were exposed for 6 h to free SODN or various complexes. After that, the cellular levels of FITC−SODN were determined as described in Materials and Methods. As shown in Figure 3 binding of SODN incorporated into complexes containing avidin (columns 3, 4, and 5) was 5- and 9-times higher than that in the cases of avidin-free complex (column 2) and free SODN (column 1), respectively. Cellular levels of SODN in avidin-modified complexes revealed no apparent dependency on the *F*/*B* ratio that determines the number of the biotin residues in the complex. In contrast, complete constructs containing both transferrin and avidin exhibited strong dependency of the SODN levels in cells on the *F*/*B* ratio (columns 6, 7, and 8). At *F*/*B* ratio 7.3 (corresponding to the highest studied content of biotin moieties), the cellular levels of SODN were ca. 80 times higher that those of the free SODN. At the same time, biotin-transferrin conjugate added to the complex in the absence of avidin had no effect on the cellular levels of SODN, which remained the same as in the case of both avidin- and transferrin-free complex (line 9). Therefore, the presence of avidin is essential for exhibition of the transferrin effects in the studied system, presumably, because avidin is necessary for bridging the SODN/copolymer complex with transferrin moieties.

In a separate experiment, SODN localization in the cells was characterized by fluorescent microscopy following a 2 h incubation of KBv cells with SODN−copolymer complexes. For this study, a different fluorescent label, RITC, was used with SODN to decrease the bleaching of the label upon examination of the cells in the fluorescent microscope. As is seen in Figure 4, incorporation of the RITC−SODN in the transferrin-modified complex resulted in increased fluorescence staining of the cells, suggesting stronger cellular accumulation of SODN compared to that observed with the transferrin-free complex. Further localization studies are needed to confirm cytoplasmic and nuclear localization of the SODN, which are apparent in microphotographs in the case of the transferrin-modified complex.

Mdr1 Inhibition by SODNs and Their Complexes. Specific activity of antisense SODN incorporated in the complexes with cationic copolymers was evaluated using MDR cancer cells, KBv, and MCF-7 ADR, expressing P-gp efflux transport protein. To inhibit the expression of P-gp in these cells, antisense SODN **S4** complimentary to the site 546−565 of human *mdr 1*-mRNA was used. This sequence was determined using a computer search for loop-forming sites downstream of the start codon in the *mdr1*-mRNA nucleotide sequence. To confirm that **S4** SODN is able to inhibit the expression of mRNA responsible for the P-gp synthesis in MDR cells, *mdr1*-mRNA levels were quantified by RT-PCR technique following exposure of the cells to SODN as described in Materials and Methods. Two sets of primers were used in the RT-PCR reaction, one set flanking the SODN binding site in the *mdr1*-mRNA and another set specific to the sequence of *bmg*-mRNA. The *bmg*-mRNA was used as an internal standard, and the quantities of *mdr-1*-mRNA fragments were normalized by the quantities of *bmg*-mRNA fragments determined by the RT-PCR reaction in the same mixture. As is shown in Table 3, treatment of the cells with 5 μM **S4** SODN alone decreases the *mdr-1*-mRNA expression level to ca. 51% of that observed in the untreated control. In the same experiment, the effect of the **S4**/PEG(8K)-*g*-PEI(2K) complex on the *mdr-1*-mRNA expression was assessed. As is seen in Table 3, cells treated with this complex expressed ca. 30% of *mdr-1*-mRNA observed in the untreated control groups. Reduction in P-gp expression

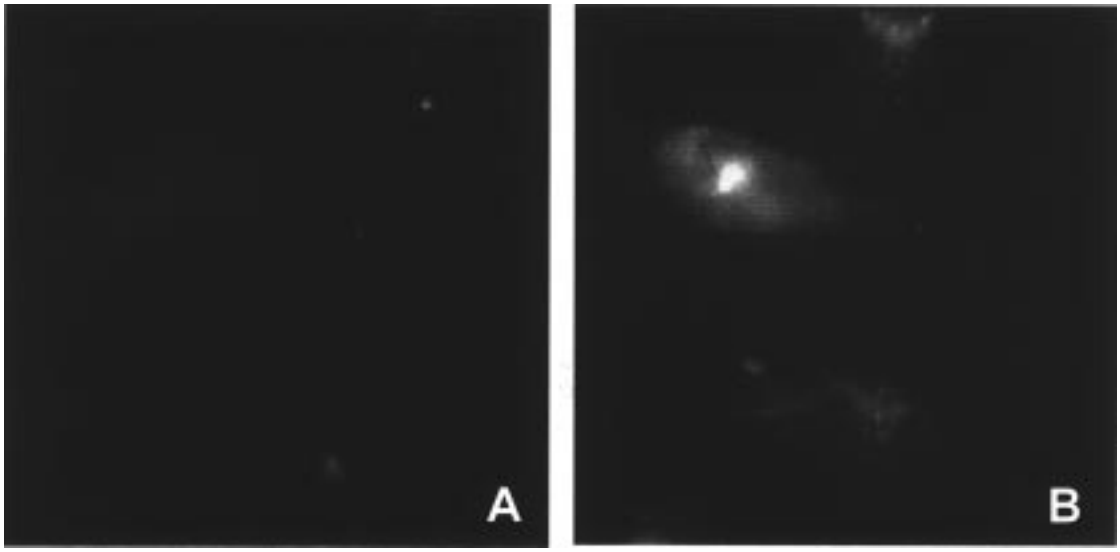


Figure 4. Fluorescent microphotographs of the monolayers of KBv cells following 3 h exposure to (A) RITC-SODN/PEG(8K)-*g*-PEI(2K) complex or (B) RITC-SODN/PEG(8K)-*g*-PEI(2K)/biotin-PEG(8K)-*g*-PEI(2K)/avidin/biotin-tranferrin complex at *N*/*P* ratio 4 and *F*/*B* ratio 9. RITC-SODN concentration in the treatment solution was 5 μM.

Table 3. Inhibition of *mdr-1* mRNA Levels in KBv Cells Following Treatment with S4 SODN or S4/Peg(8K)-*g*-PEI(2K) Complex

treatment[a]	*mdr-1* mRNA, arb. un.[b]	P-gp expression, arb. un.[c]
untreated control	1.58 ± 0.12	90
S4 SODN	0.80 ± 0.03	97
S4/PEG(8K)-*g*-PEI(2K) complex	0.49 ± 0.06	58
PEG(8K)-*g*-PEI(2K)	nd	100

[a] **S4** concentration in the treatment solution was 5 μM (RT PCR) or 4 μM (Western blot); **S4**/PEG(8K)-*g*-PEI(2K) complex was prepared at N/P ratio 4. [b] Levels of *mdr-1* mRNA fragments are normalized by the quantities of *bmg*-MNA fragments determined by the RT-PCR reaction in the same mixture. Data are means ± SD, $n = 4$. [c] Levels of P-gp expression are presented based on the densitometry of the Western blot film presented in Figure 5.

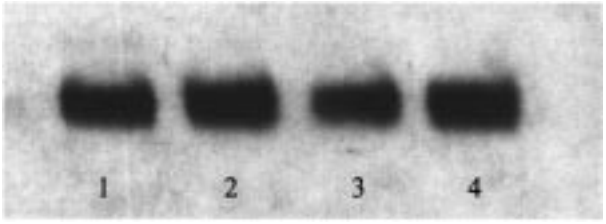


Figure 5. Western blot analysis of P-gp expression in untreated KBv cells (lane 1) and KBv cells treated with free **S4** SODN (lane 2), **S4**/PEG(8K)-*g*-PEI(2K) complex (lane 3) and free PEG(8K)-*g*-PEI(2K) (lane 4). SODN concentration in the treatment solutions was 4 μM (lanes 1−3); PEG(8K)-*g*-PEI(2K) concentration was 0.15 mg/mL (lanes 3, 4) and SODN/PEG(8K)-*g*-PEI(2K) complexes were prepared at *N*/*P* ratio 4 (lane 3).

following exposure of the cells to the **S4**/PEG(8K)-*g*-PEI(2K) complex was demonstrated in the independent Western blot experiment (Figure 5 and Table 3). Western blot shows no changes in the P-gp expression following cell exposure to the PEG(8K)-*g*-PEI(2K) carrier alone. The results of the RT PCR and Western blot experiments suggest that (i) SODN can be released from the complex and reach its molecular target inside the cell, (ii) the specific activity of SODN is increased as a result of its incorporation into the complex. The magnitudes of reduction in the message and protein levels observed in these experiments are consistent with the previous reports describing antisense oligonucleotide inhibition of *mdr1* gene in MDR cells (*16*, *17*).

These conclusions were further validated in the experiments measuring the P-gp functional activity following the exposure of the cell monolayers to the treating solutions containing SODN and various SODN complexes. In these experiments, the functional activity of the P-gp was assessed by accumulation of the P-gp-specific substrate R123 in the cell monolayers. Increased R123 accumulation in the MDR cells is indicative of the inhibition of the P-gp efflux system (*18*, *19*). On the basis of the studies of the kinetics of R123 accumulation in the KBv and MCF-7 ADR cells used in these studies, changes in R123 cellular levels at 60−120 min are indicative of the effects on the P-gp functional activity in these cells (*19*). The R123 accumulation enhancement factors were calculated at the 90 min time point as ratios of R123 accumulation in the treated cells to those in the nontreated cells:

$$\text{enhancement factor} = \frac{\text{R123 accumulation in the treated cells}}{\text{R123 accumulation in the nontreated cells}}$$

Figure 6 presents R123 accumulation factors measured in KBv cell monolayers following treatment of the cell monolayers by **S4** SODN or **S4**/PEG(8K)-*g*-PEI(2K) complex at SODN doses varying from 0.5 to 2 μM. Free SODN at 0.5 and 1 μM practically did not affect R123 accumulation levels (columns 1 and 3). At 2 μM of the free SODN, the treatment resulted in a two times increase in R123 accumulation (column 5). When the **S4**/PEG(8K)-*g*-PEI(2K) complex was used instead of the free SODN, the R123 accumulation was increased at all doses studied reaching ca. two times at 2 μM SODN (columns 2, 4, and 6). It is noteworthy that the complex of the randomized SODN, **RS4**/PEG(8K)-*g*-PEI(2K) at 2 μM was practically inactive (column 7). This suggests that the effects of SODN complexes on R123 accumulation were sequence specific.

The final experiment reported here characterizes the effects of transferrin bound to the SODN−copolymer complexes on the activity of antisense SODN incorporated into these complexes. To incorporate transferrin, the complexes displaying biotin groups were supple-

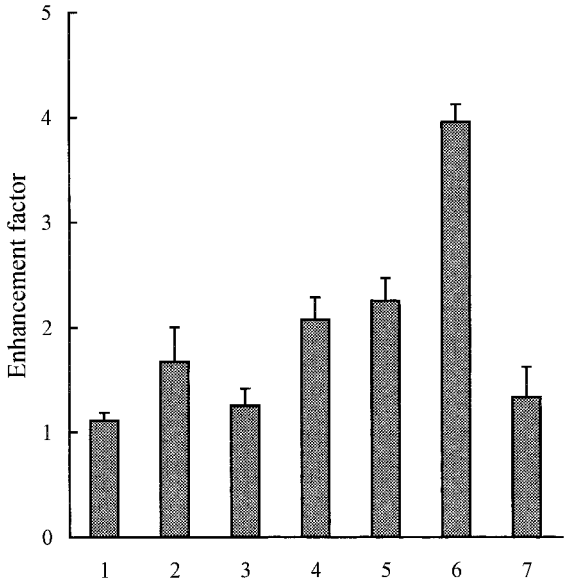


Figure 6. Enhancement of R123 accumulation in KBv cell monolayers following treatment of the cells with free **S4** SODN (columns 1, 3, 5), **S4**/PEG(8K)-*g*-PEI(2K) complex (columns 2, 4, 6) and **RS4**/PEG(8K)-*g*-PEI(2K) (column 7). SODN concentrations in the treatment solutions were 0.5 μM (columns 1, 2), 1 μM (columns 3, 4), and 2 μM (columns 5, 6, 7). SODN/PEG(8K)-*g*-PEI(2K) complexes were prepared at *N*/*P* ratio 4. Data are mean ± SEM, $n = 3$.

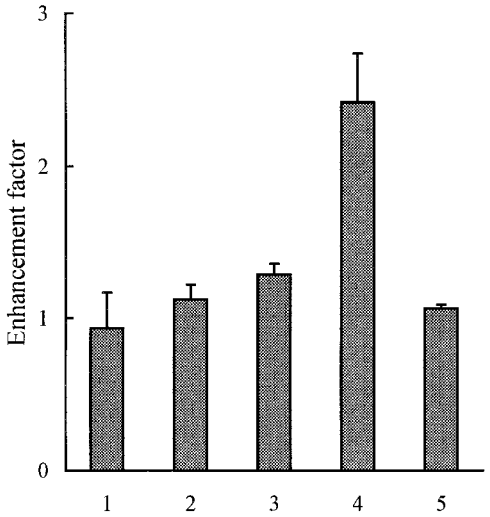


Figure 7. Enhancement of R123 accumulation in MCF-7 ADR monolayers following treatment of the cells with free **S4** SODN (column 1), **S4**/PEG(8K)-*g*-PEI(2K)/biotin-PEG(8K)-*g*-PEI(2K) complex (column 2), **S4**/PEG(8K)-*g*-PEI(2K)/biotin-PEG(8K)-*g*-PEI(2K)/avidin/biotin-transferrin complexes (columns 3, 4) and **RS4**/PEG(8K)-*g*-PEI(2K)/biotin-PEG(8K)-*g*-PEI(2K)/avidin/biotin-transferrin complexes (column 5). In the cases of complexes containing mixtures of the biotin-free and biotin-modified copolymers *F*/*B* ratios were 9 (columns 2, 4, 5) and 19 (column 3) and *N*/*P* ratios were fixed at 4. In all cases, SODN concentration in the treatment solution was 0.5 μM. Data are mean ± SEM, $n = 3$.

mented first by avidin and then by biotin−transferrin conjugate. The monolayers of MCF-7 ADR cells were treated with 0.5 μM SODN or its complexes of various composition and the P-gp activity was determined in the R123 accumulation experiment. As is seen in Figure 7, the free **S4** SODN or its complex with cationic copolymers without avidin and transferrin did not affect R123 accumulation in the cells under conditions studied (columns 1 and 2). Also transferrin-containing complex of

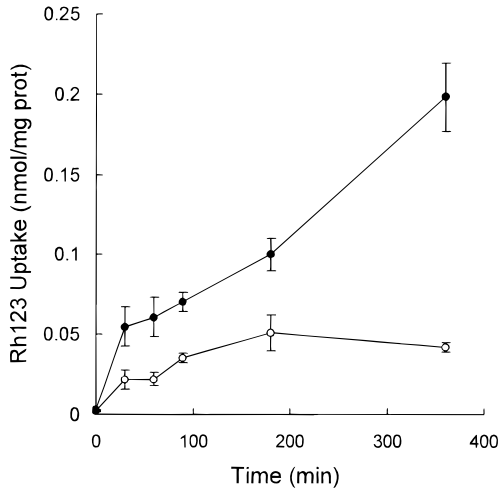


Figure 8. Kinetics of R123 accumulation in MCF-7 ADR cell monolayers following treatment of the cells with free **S4**/PEG(8K)-*g*-PEI(2K) complex (empty circles) and **S4**/PEG(8K)-*g*-PEI(2K)/biotin-PEG(8K)-*g*-PEI(2K)/avidin/biotin-transferrin complex (filled circles). Complexes were prepared at *N*/*P* ratio 4 and *F*/*B* ratio 9 (transferrin-containing system). SODN concentration in the treatment solution was 0.5 μM. Data are mean ± SEM, $n = 3$.

S4 prepared at *F*/*B* ratio 19 appeared to be practically inactive (column 3). At the same time, there was a significant increase in R123 accumulation following treatment of the cells with transferrin-containing complex of **S4** prepared at *F*/*B* ratio 9 corresponding to higher transferrin content (column 4). In contrast, the transferrin-containing complex of nonspecific oligomer **RS4** with the same content of transferrin practically did not affect the R123 accumulation, which suggests that the effects observed with the **S4** complex were sequence specific. The kinetics of R123 accumulation in MCF-7 ADR cell monolayers following treatment of the cells with transferrin-modified and transferrin-free complexes of antisense SODN are shown in Figure 8. It is noteworthy that no effect on R123 accumulation was observed in non-MDR cells, KB, and MCF-7, following cell exposure to **S4** or its various complexes described in this work (data not shown).

DISCUSSION

Previous work reported a novel type of polycationic carrier for delivery of antisense SODNs on the base of PEG and PEI graft copolymers (*6*). PEG(8K)-*g*-PEI(2K) copolymer was shown to form spontaneously electrostatic complexes with SODN in aqueous solutions at physiological pH and ionic strengths. These complexes self-assemble in small supramolecular particles with a core from neutralized PEI and SODN chains and a corona from PEG. Due to the effect of the PEG corona, these particles are stable in aqueous solution for apparently unlimited amounts of time. Thermodynamic stability of such complexes in aqueous solutions appears to be an intrinsic property of the whole class of polyion complex micelles (also termed "block ionomer complexes") to which such systems belong (*20*, *21*). From, the drug delivery standpoint, it is important that SODNs incorporated in the complex with PEG(8K)-*g*-PEI(2K) are resistant against digestion by nucleases (*6*). Furthermore, these complexes were shown to be stable in the presence of serum proteins, such as negatively charged bovine serum albumin, which does not displace the SODN in the complex

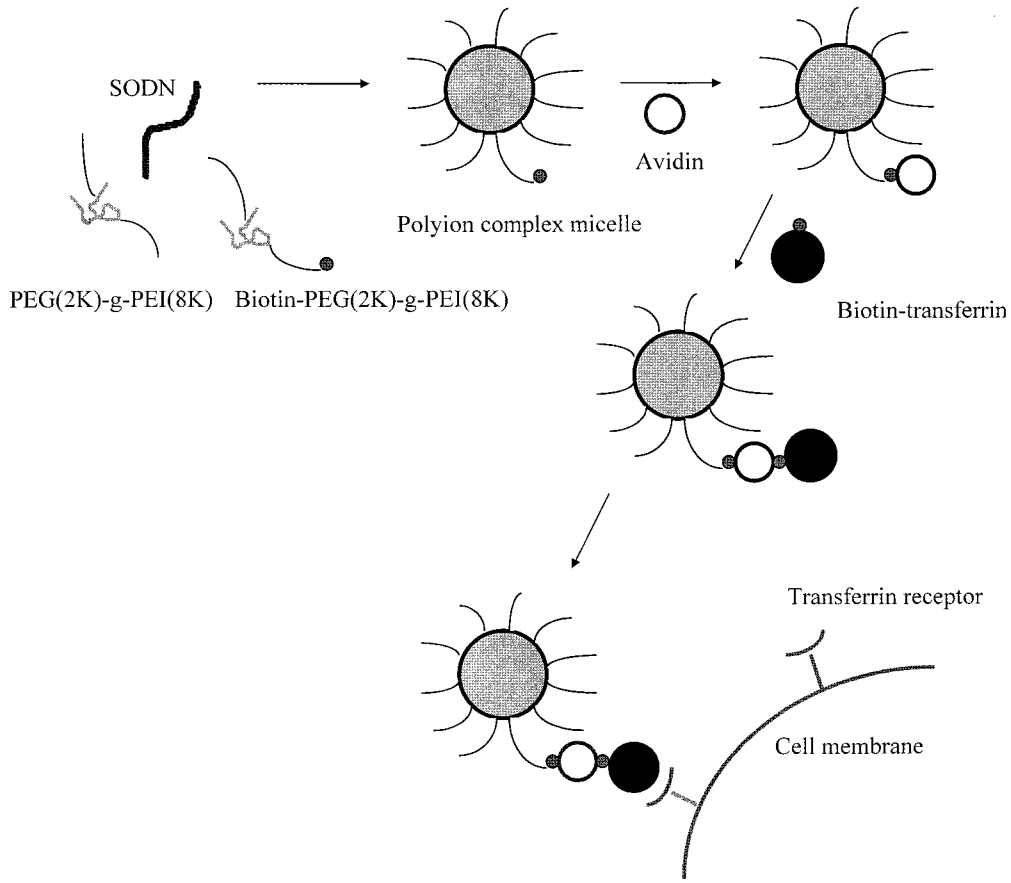


Figure 9. Schematic illustrating formation of transferrin-modified polyion complex micelle using avidin/biotin construct and its binding to transferrin receptor at the cell surface.

with PEG(8K)-*g*-PEI(2K), although it can bind electrostatically to the copolymer in the absence of the SODN (*6*).

The results of the study for the first time show that SODN incorporated in the complex with PEG(8K)-*g*-PEI-(2K) exhibit significant activity in inhibition of *mdr 1* gene expression in cells. This means that despite high stability of the SODN/PEG(8K)-*g*-PEI(2K) complex the SODN is released from this complex upon interaction with a cell and reaches its molecular target inside a cell. Further, this study shows that the polyion complex micelles from SODN and PEG-*g*-PEI copolymers can be additionally modified by transferrin that promotes uptake of the complex in the cell and increases transfection. The modification is carried out in this work using avidin/biotin construct. The biotin moieties are introduced at the free ends of the PEG chain in the PEG-*g*-PEI copolymer. Molecular characteristics of the resulting biotin-PEG(8K)-*g*-PEI(2K) copolymer (molecular mass, PEG:PEI ratio, nitrogen content) are relatively close to those of the PEG(8K)-*g*-PEI(2K) copolymer. The complexes formed between SODN and PEG(8K)-*g*-PEI(2K)/biotin-PEG(8K)-*g*-PEI(2K) mixtures are stable in solution and have small sizes of ca. 40 nm, appearing to be very similar to SODN/PEG(8K)-*g*-PEI(2K) complexes. These complexes, however, contain biotin moieties in the corona, which was used to attach transferrin through the biotin/avidin construct as is schematically shown in Figure 9. For this purpose, the particles of the complex were first supplemented with avidin and then supplemented with biotin−transferrin conjugate. Egg white avidin contains four biotin-binding sites and serves in this construct as a linker between biotin containing complex and biotin−transferrin conjugate.

Interestingly enough, cellular accumulation studies using fluorescently labeled SODN suggest that avidin alone (without transferrin) attached to the surface of the complex increases the uptake of the SODN into cells. A marked enhancement of cellular uptake of biotinylated ODN in the presence of avidin has previously been reported (*22*). This effect was explained by the binding of avidin, a cationic protein, with the cell membrane stimulating the adsorption-mediated endocytosis of the biotinylated ODN−avidin complex. It is likely that similar reason underlies the enhanced uptake of the avidin-modified polyion complex micelles observed in this work. Attachment of transferrin to such complexes further enhances the uptake of the SODN into cells. Furthermore, transferrin-modified complexes carrying antisense SODN targeted to human *mdr1* gene were shown to be the most effective in inhibition of the P-gp functional activity in MDR cancer cells. Transferrin conjugates with polylysine have previously been described as efficient carriers for DNA delivery into cells (*23*). These conjugates promote DNA uptake and transfection as a result of transferrin interaction with the transferrin receptor at the cell surface. We hypothesize that the effects of surface modificatioin of the polyion complex micelles with transferrin on cell accumulation and activity of SODNs incorporated in the complex are due to a similar mechanism involving binding of transferrin with a cell receptor (Figure 9).

In conclusion, this work provides a method for incorporation of the protein molecules in the PEG corona of the polyion complex micelles using avidin/biotin construct. The use of biotinylated copolymers described in this work provides a universal and convenient way to modify the surface of the DNA−copolymer complexes

with various peptides, which can be applied to screen peptide sequences to enhance gene transfer. One promising candidate for future studies using such complexes is the peptide containing R-G-D sequence, which binds to α_v integrin (*24*). Attachment of this peptide to the plasmid DNA−lipofectin complex was shown to improve gene transfer in several cell lines, which was mediated by the interaction of this peptide with integrin. Another promising candidate is 30 amino acid long peptide P3, derived from monoclonal anti-DNA auto-antibodies that were shown to spontaneously penetrate into cells and accumulate into nucleus (*25*). This peptide conjugated to a polylysine sequence was shown recently to be an efficient vector for gene transfer in several cell lines. While conjugates of polycations with peptides has been evaluated as carriers for nonviral gene delivery, there has been a concern about immunological reactions and related side effects during administration of such conjugates in vivo. It is known that conjugation of natural or synthetic haptene with a polycation dramatically enhances the immune response of an organism with respect to that haptene (*26*). In contrast, modification of peptides with PEG chains is known to decrease the immune response with respect to these peptides (*27*). Therefore, using specific peptides linked to cationic copolymers via PEG chains might have practical significance in the future by decreasing the side effect problem for the in vivo applications.

ACKNOWLEDGMENT

The National Science Foundation (BES-9712657) and Nebraska Research Initiative (Gene Therapy Initiative) supported this work. Supratek Pharma Inc. sponsored the synthesis and characterization of the cationic copolymers. Dr. Kabanov serves as a consultant to this company. M-H-W Laboratories (Phoenix, AZ) did elemental analysis. Core laboratories at the University of Nebraska Medical Center (Omaha, NE) carried out the NMR measurements and SODN synthesis. The authors thank Dr. Valery Alakhov (Supratek Pharma Inc.) for very useful discussions of the block copolymer based gene delivery systems. Dr. Tatiana Bronich (UNMC) is acknowledged for determining the molecular masses of the copolymers. Dr. Ludmila Chystiakova (Supratek Pharma Inc.) is provided helpful advice on RT-PCR experiment.

LITERATURE CITED

(1) Crooke, S. T. (1995) Oligonucleotides as potential therapeutic agents. In *Trends and Future Perspectives in Peptide and Protein Drug Delivery* (V. H. L. Lee, M. Hashida, and Y. Mizushima, Eds.) pp 297−320, Harwood Academic Publishers GmbH, Chur, Switzerland.

(2) Gewirtz, A. M., Stein, C. A., and Glazer, P. M. (1996) Facilitating oligonucleotide delivery: helping antisense deliver on its promise. *Proc. Natl. Acad. Sci. U.S.A. 93*, 3161−3163.

(3) Seymour, L. W., Kataoka, K., and Kabanov, A. V. (1998) Cationic block copolymers as self-assembling vectors for gene delivery. In *Self-Assembling Complexes for Gene Delivery. From Laboratory to Clinical Trial (*A. V. Kabanov, L. W. Seymour, and P. Felgner, Eds.) pp 219−239, John Wiley, Chichester.

(4) Kabanov, A. V., Vinogradov, S. V., Suzdaltseva, Yu. S., and Alakhov, V. Yu. (1995) Water-soluble block polycations as carriers for oligonucleotide delivery. *Bioconjugate Chem. 6*, 639−643.

(5) Kataoka, K., Togawa, H., Harada, A., Yasugi, K., Matsumoto, T., and Katayose S. (1996) Spontaneous formation of polyion complex micelles with narrow distribution from antisense oligonucleotide and cationic block copolymers in physiological saline. *Macromolecules 29*, 8556−8557.

(6) Vinogradov, S. V., Bronich, T. K., and Kabanov A. V. (1998) Self-assembly of polyamine-poly(ethylene glycol) copolymers with phosphorothioate oligonucleotides. *Bioconjugate Chem. 9*, 805−812.

(7) Mundigl, O., Ochoa, G.-C., Slepnev, V. I., Kabanov, A. V., and DeCamilli, P. (1998) The role of amphiphysin in neurite outgrowth. *J. Neurosci. 18*, 93−103.

(8) Roy, S., Zhang, K., Roth, T., Vinogradov, S., and Kabanov, A. (1999) Reduction of specific gene expression by intravitreal administration of antisense oligonucleotides in rat retina. *Nat. Biotechnol. 17*, 476−479.

(9) Udenfriend, S., Stein, S., Bohlen, P., Dairman, W., Leimgruber, W., and Weigele, M. (1972) Fluorescamine: a reagent for assay of amino acids, peptides, proteins, and primary amines in the picomole range. *Science 178*, 871−872.

(10) Mock, D. M., Lankford, G., and Horowitz, P. (1988) A study of the interaction of avidin with 2-anilinonaphthalene-6-sulfonic acid as a probe of the biotin binding site. *Biochim. Biophys. Acta 956*, 23−29.

(11) Sugawara, I., Watanabe, M., Masunaga, A., Itoyama, S., and Ueda, K. (1992) Primer-dependent amplification of *mdr1* mRNA by polymerase chain reaction. *Japan J. Cancer Res. 83*, 131−133.

(12) Noonan, K. E., Beck, C., Holzmayer, T. A., Chin, J. E., Wunder, J. S., Andrulis, I. L., Gazdar, A. F., Willman, C. L., Griffith, B., von Hoff, D. D., and Roninson, I. B. (1994) Quantitative analysis of MDR1 (multidrug resistance) gene expression in human tumors by polymerase chain reaction. *Proc. Natl. Acad. Sci. U.S.A. 91*, 13033−13037.

(13) Batrakova, E. V., Han, H.-Y., Alakhov, V. Yu., Miller, D. W., and Kabanov, A. V. (1998) Effects of Pluronic block copolymers on drug absorption in Caco-2 cell monolayers. *Pharm. Res. 15*, 850−855.

(14) Enger, O. (1996) Use of the fluorescent dye PicoGreen for quantitation of PCR products after agarose gel electrophoresis. *BioTechniques 21*, 372−374.

(15) Miller, D. W., Fontaine, M., Kolar, C., and Lawson, T. (1996) The expression of multidrug resistance associated protein (MRP) in pancreatic adenocarcinoma cell lines. *Cancer Lett. 107*, 301−306.

(16) Alahari, S. K., Dean, N. M., Fisher, M. H., Delong, R., Manoharan, M., Tivel, K. L., and Juliano, R. L. (1996) Inhibition of expression of the multidrug resistance-associated P-glycoprotein of by phosphorothioate and 5′ cholesterol-conjugated phosphorothioate antisense oligonucleotides. *Mol. Pharmacol. 50*, 808−819.

(17) Alahari, S. K., Dean, N. M., Fisher, M. H., Delong, R., Manoharan, M., Tivel, K. L., and Juliano, R. L. (1998) Novel chemically modified oligonucleotides provide potent inhibition of P-glycoprotein expression. *J. Pharmacol. Exp. Ther. 286*, 419−428.

(18) Batrakova, E. V., Han, H.-Y., Alakhov, V. Y., Miller, D. W., and Kabanov, A. V. (1998) Effects of Pluronic block copolymers on drug absorption in Caco-2 cell monolayers. *Pharm. Res. 15*, 850−855.

(19) Batrakova, E., Lee, S., Li, S., Venne, A., Alakhov, V., and Kabanov A (1998) Fundamental relationships between the composition of Pluronic block copolymers and their hypersensitization effect in MDR cancer cells. *Pharm. Res.* In press.

(20) Harada, A., and Kataoka, K. (1995) Formation of polyion complex micelles in an aqueous milieu from a pair of oppositely charged block copolymers with poly(ethylene glycol) segments. *Macromolecules 28*, 5294−5299.

(21) Kabanov, A. V., Bronich, T. K., Kabanov, V. A., Yu, K., and Eisenberg, A. (1996) Soluble stoichiometric complexes from poly(*N*-ethyl-4-vinylpyridinium) cations and poly(ethylene oxide)-*block*-poly(methacrylate) anions. *Macromolecules 29*, 6797−6802.

(22) Pardridge, W. M., and Boado, R. J. (1991) Enhanced cellular uptake of biotinylated antisense oligonucleotide or peptide mediated by avidin, a cationic protein. *FEBS Lett. 288*, 30−32.

(23) Wagner, E., Zenke, M., Cotton, M., Beug, H., and Birnstiel, M. L. (1990) Transferrin-polycation conjugates as carriers for DNA uptake into cells. *Proc. Natl. Acad. Sci. U.S.A. 87*, 3410−3414.

(24) Hart S. L., Arancibia-Carcama, C. V., Wolfert, M. A., Mailhos, C., O′Reilly, N. J., Ali, R. R., Coutelle, C., George, A. J., Harbottle, R. P., Knight, A. M., Larkin, D. F., Levinsky, R. J., Seymour, L. W., Thrasher, A. J., and Kinnon, C. (1998) Lipid-mediated enhancement of transfection by a nonviral integrin-targeting vector. *Human Gene Ther. 9*, 575−585.

(25) Avrameas, A., Ternynck, T., Gasmi, L., and Buttin, G. (1999) Efficient gene delivery by a peptide derived from a monoclonal anti-DNA antibody. *Bioconjugate Chem. 10*, 87−98.

(26) Kabanov, V. A., Petrov, R. V., and Khaitov, R. M. (1984) Artificial antigens and vaccines based on nonnatural polyelectrolytes. In *Sov. Sci. Rev. D. Physicochem. Biol.* (V. P. Skulachev, Ed.) Vol. 5, pp 277−322, Harwood Academic Publishers, Glasgow.

(27) Chinol, M., Casalini, P., Maggiolo, M., Canevari, S., Omodeo, E. S., Caliceti, P., Veronese, F. M., Cremonesi, M., Chiolerio, F., Nardone, E., Siccardi, A. G., and Paganelli, G. (1998) Biochemical modifications of avidin improve pharmacokinetics and biodistribution, and reduce immunogenicity. *Br. J. Cancer. 78*, 189−197.

BC990037C

Identification of Fluorescein-5′-Isothiocyanate-Modification Sites in Proteins by Electrospray-Ionization Mass Spectrometry

Volker Schnaible and Michael Przybylski*

Fakultät für Chemie, Universität Konstanz, 78457 Konstanz, Germany. Received April 9, 1999; Revised Manuscript Received June 1, 1999

Model peptides and proteins, such as hen eggwhite lysozyme, have been modified with fluorescein-5′-isothiocyanate (FITC) to yield the corresponding fluorescein-thiocarbamoyl (FTC) conjugates (*N,N′*-disubstituted thiourea and dithiourethane adducts). The extent of FITC incorporation, i.e., number of modified residues, has been identified by direct molecular weight determination using matrix-assisted laser desorption−ionization and electrospray-ionization mass spectrometry (MALDI-MS; ESI-MS). A specific fragmentation by cleavage of the FTC moiety from modified residues occurs by nozzle-skimmer dissociation in ESI mass spectra at increased declustering potential. This fragmentation pathway is easily obtained and renders ESI-MS an efficient tool for the characterization of FITC-modified proteins, and identification of modification sites in FTC−peptide mixtures.

INTRODUCTION

The modification of proteins by fluorescein-5′-isothiocyanate (FITC)[1] is an established method to generate fluorescent proteins, e.g., in antibodies (*1*), which then can be detected in low quantities according to the number of FITC molecules incorporated into the protein. FITC reacts with amino and thiol groups of proteins to yield fluorescein-5′-thiocarbamoyl (FTC) conjugates, *N,N′*-disubstituted thiourea and dithiourethane adducts (as shown in the reaction scheme in Figure 1) (*2, 3*). According to the general pathway of the Edman coupling with aryl-isothiocyanate, only the thiourea adducts are stable at alkaline pH and in the presence of nucleophiles such as β-mercaptoethanol (*4*).

Eukaryotic ATPases (*5*) and recombinant partial ATPase sequences have been specifically modified by FITC at the ATP-binding region (*6, 7*). To obtain structural information about FITC modified ATPases, e.g., by fluorescence energy transfer (*8*), the molecular characterization of the number and the precise location of FITC-modified amino acid residues are crucial. To determine the sites modified by FITC, enzymatic digestion of the modified proteins is usually carried out, and the proteolytic peptide mixture separated by HPLC. FITC-labeled peptides are then identified by Edman degradation (*9*) or mass spectrometry (*10, 11*). However, pure peptide samples for Edman degradation are frequently difficult to obtain (*11*). The direct analysis of proteolytic peptides from complex mixtures, e.g., upon enzymatic digestion has been employed by mass spectrometric peptide mapping with both electrospray-ionization and matrix-assisted laser desorption−ionization mass spectrometry (ESI-MS, MALDI-MS) (*12*−*15*). As shown in several recent studies, mass spectrometric peptide mapping provides the exact information of the number and distribution of covalent modification sites in the protein (*16, 17*). Furthermore, it has been shown that peptide backbone fragmentation in ESI-MS can be induced at increased declustering potential (*18, 19*) (ΔCS), normally used to assist the desolvation of the initial charged microdroplets. This fragmentation occurs in the nozzle-skimmer region of the electrospray ion source, and is therefore readily observed, e.g., with single quadrupole instruments (*18, 20*). In the present study, a specific fragmentation of FITC-modified side chains at increased declustering potential has been investigated and used for the identification of FITC-modification sites. This is illustrated by an FITC-modified model peptide (LGYLGYL-$CONH_2$), hen eggwhite lysozyme (HEL) as a well characterized model protein, and by peptides of FITC modified HEL following trypsin digestion.

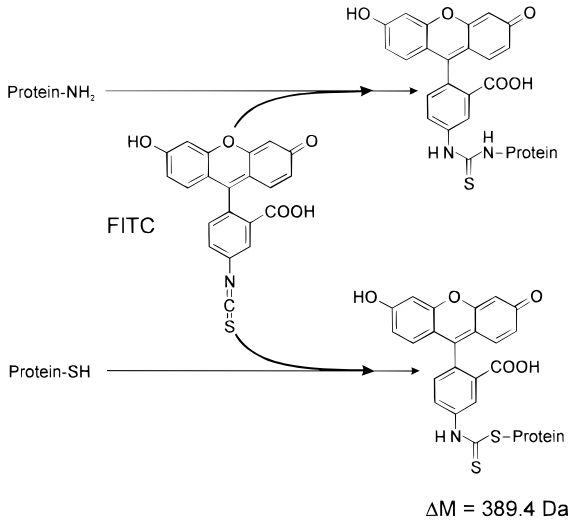


Figure 1. Scheme for the reaction of FITC with thiol and amino groups.

* To whom correspondence should be addressed. Phone: +49 7531 88 2249. Fax: +49 7531 88 3097. E-mail: Michael.Przybylski@uni-konstanz.de.

[1] Abbreviations: DMF, dimethylformamide; DMSO, dimethyl sulfoxide; DTT, 1,4-dithiothreitol; ESI, electrospray-ionization; FITC, fluorescein-5′-isothiocyanate; FTC, fluorescein-5′-thiocarbamoyl; HCCA, α-cyano-4-hydroxy cinnamic acid; HEL, hen eggwhite lysozyme; MALDI, matrix assisted laser desorption−ionization; PTFE, poly(tetrafluoroethylene); TFA, trifluoroacetic acid; TPCK, L-1-tosylamido-2-phenylethyl chloromethyl ketone.

10.1021/bc990039x CCC: $18.00 © 1999 American Chemical Society
Published on Web 09/01/1999

EXPERIMENTAL PROCEDURES

Materials. Solvents and reagents were of highest available purity from Merck (Darmstadt, Germany). The following reagents and proteins were obtained from Sigma (St. Louis, MO): DTT, FITC Isomer I, HCCA, hen eggwhite lysozyme (HEL), and trypsin (TPCK treated). The model peptide LGYLGYL-$CONH_2$ was synthesized by solid-phase peptide synthesis (SPPS) using the Fmoc strategy on a semiautomatic peptide synthesizer EPS 221 from Abimed (Langenfeld, Germany). The synthesis product was purified by HPLC. Homogeneity of the peptide was ascertained by MALDI and ESI-MS.

FITC Modification of HEL. (a) A total of 100 μg of HEL was dissolved in 100 μL of 50 mM NaH_2PO_4 buffer, pH 8. A total of 39 μg of FITC was added using a freshly prepared stock solution (c = 1.95 μg/μL) in DMSO. The molar ratio of FITC:HEL is 14 under these conditions. The reaction was carried out for 17 h at 25 °C in the dark and quenched by addition of 400 μL of acetone at −20 °C followed by centrifugation (5 min at 13000*g*) after storage at −20 °C for 1 h. The supernatant containing free excess FITC was discarded and the pellet washed twice with 500 μL of acetone at −20 °C. The pelleted protein was then redissolved in 200 μL of acetonitrile/aqueous 0.1% TFA (v/v = 2:1) and purified by HPLC. (b) A total of 3 mg of HEL were dissolved in 1.08 mL of 50 mM NaH_2PO_4-buffer, pH 8. A total of 480 μg of FITC were added using a freshly prepared stock solution in (c = 3.9 μg/μL) 120 μL of DMF. The molar ratio FITC:HEL is 6 under these conditions. The reaction was carried out at 25 °C. A total of 200 μL samples were taken from the reaction mixture after 0, 30, 60, 120, and 300 min and 55 h reaction time. The reaction was quenched by the addition of 800μL of −20 °C cold acetone to the 200 μL samples. The protein was pelleted after 1 h storage at −20 °C by centrifugation (5 min at 13000*g*). The supernatant was discarded and the pellet washed twice with 500 μL of −20 °C cold acetone. The pelleted protein then was subjected to trypsin digestion.

FITC Modification of Synthetic Peptide LGYL-GYL-$CONH_2$. FITC modification of the synthetic peptide, LGYLGYL-$CONH_2$, was carried out with 90 μg of the peptide dissolved in 280 μL of 100 mM sodium borate buffer, pH 9. A total of 20 μL of a freshly prepared 20 mM solution of FITC in DMF was added. The reaction was terminated after 12 h. The reaction mixture was purified by HPLC, since the removal of unbound reagent by acetone precipitation was not possible. The HPLC fraction containing FITC-derivatized peptide was analyzed by ESI-MS.

Trypsin Digestion of FITC-Modified HEL. A 500 μg sample of FITC-modified HEL, prepared by a reaction time of 55 h, was redissolved in 50 mM NH_4HCO_3 buffer, pH 8, containing 30% methanol (*21*) to yield a final protein concentration of 1 μg/μL. The high methanol content is crucial to achieve digestion of HEL, which is highly resistant to proteolysis in the native state. A solution of freshly prepared trypsin in 50 mM NH_4HCO_3 was added to yield an enzyme-to-substrate ratio of 1:30. The digestion was carried out for 18 h at 37 °C. A 10-fold excess of DTT per cysteine residue was added, the reduction was carried out for 1 h, and then stopped by addition of 10 μL of 10% TFA. A 1 μL aliquot of the reaction mixture was taken for mixture analysis by MALDI-MS. The digestion mixture was centrifuged for 5 min at 13000*g* in order to remove partially digested protein which precipitates upon DTT reduction. The supernatant was subjected to HPLC separation and subsequently analyzed by MALDI-MS. A complete coverage of the HEL-sequence was achieved, although some of the protein is lost due to the precipitation.

HPLC Separation. All HPLC separations were performed with a Waters/Millipore solvent delivery system (high-pressure pumps model M 510 and M 45) using a binary gradient of 0.1% TFA in water and 0.07% TFA in acetonitrile. Separation was carried out on a (250 × 8 mm) Macherey & Nagel C_8-Nucleosil RP-HPLC column using linear gradients of 45 min (1% acetonitrile/min from 40 to 60%) for the FITC-modified HEL and of 80 min (1% acetonitrile/min from 5 to 55%) for the tryptic digestion mixtures. Peak detection was performed with a Waters 490 E multiwavelength detector system at a wavelength of 220 nm. FITC-modified peptides were also detected with a Shimadzu RF-551 fluorescence detector with the excitation wavelength set to 447 nm and the emission wavelength set to 514 nm. All fractions were manually collected and characterized by MALDI-MS.

Mass Spectrometry. MALDI-MS analyses were carried out with a Bruker Biflex linear time-of-flight spectrometer (Bruker-Franzen, Bremen, Germany) equipped with a UV nitrogen laser (λ = 337 nm) and a dual microchannel plate detector. The acceleration voltage was set to 25 kV. Lyophilized HPLC fractions were redissolved in acetonitrile/aqueous 0.1% TFA (v/v = 2:1) and 1 μL of the solution was mixed with 1 μL of a saturated HCCA solution in acetonitrile/aqueous 0.1% TFA (v/v = 2:1). The digestion mixture of HEL was prepared by mixing 1 μL of the DTT-containing digestion mixture solution with 1 μL of saturated HCCA solution. The dried sample spot was washed with 3 μL of 0.1% TFA, redissolved in acetonitrile/0.1% TFA (v/v = 2:1) and spotted again on the target. Spectra were recorded after evaporation of the solvent and processed by means of the X-MASS data system. Peptide spectra were calibrated internally with insulin and HCCA reference ions. Protein spectra were calibrated externally with the singly and doubly charged molecular ions of HEL.

Nano-ESI-MS (*22, 23*) was carried out with a Vestec A201 single-quadrupole mass spectrometer (Vestec, Houston, TX) fitted with a 10 kV conversion dynode and a 2000 m/z mass range. A home-built nano-ESI source was used (*24*). Borosilicate glass capillaries of the type GC120F-10 from Clark Electromedical Instruments (Pangbourne, U.K.) were used for preparation of the microcapillaries. Capillaries were pulled with a capillary puller model P-97 from Sutter Instruments (Novato, CA) in a two-step cycle. The capillaries were then coated with a thin layer of a gold/palladium alloy using a Polaron SC7610 sputter coater (VG Microtech, Uckfield, U.K.), for providing the high voltage connection. Protein and peptide samples were dissolved in 2% aqueous acetic acid:methanol mixtures (v/v = 9:1 unless otherwise stated). An aliquot of 1−4 μL of the sample solution was loaded by dipping the capillary tip into the sample solution. In case of plugging, the capillary was reopened by briefly touching a glass plate. The loaded capillary was fixed via a PTFE screw in a metal mounting and then pushed forward into the ion source region. The voltage at the capillary tip was set to 1.4−1.5 kV. To obtain a stable spray the capillary was manually adjusted to the nozzle of the ion source. The declustering potential between nozzle and skimmer was adjusted in a range of 10−120 V for recording ESI-MS spectra of intact and fragmented peptides and proteins.

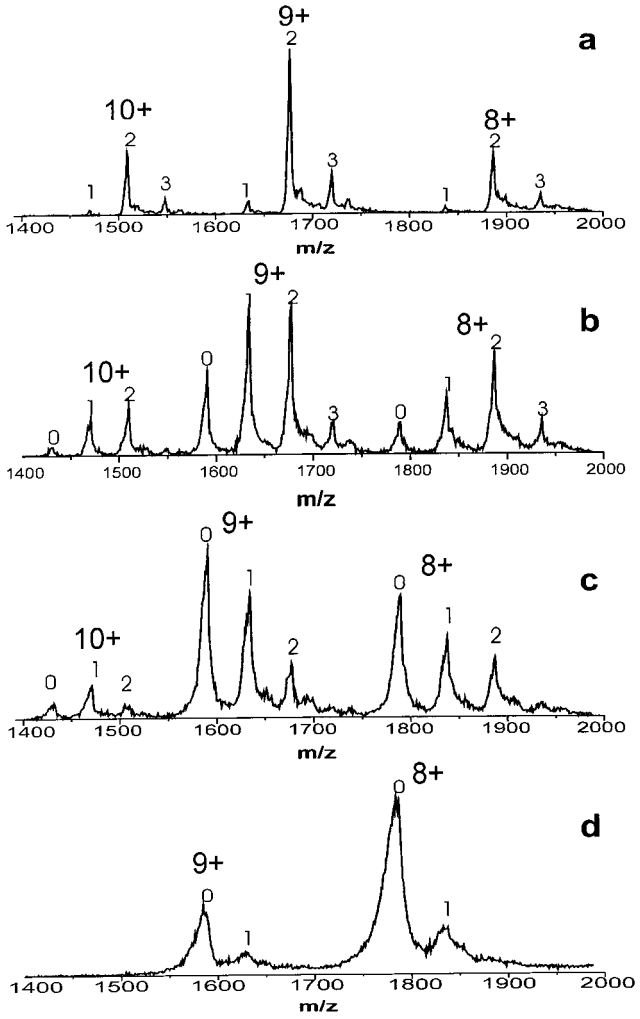


Figure 2. ESI spectra of HPLC purified HEL containing predominantly two FITC groups. Spectra were recorded with different declustering potentials. (a) 10 V; (b) 60 V; (c) 80 V; (d) 120 V. Numbers at the peaks indicate the number of FITC molecules incorporated.

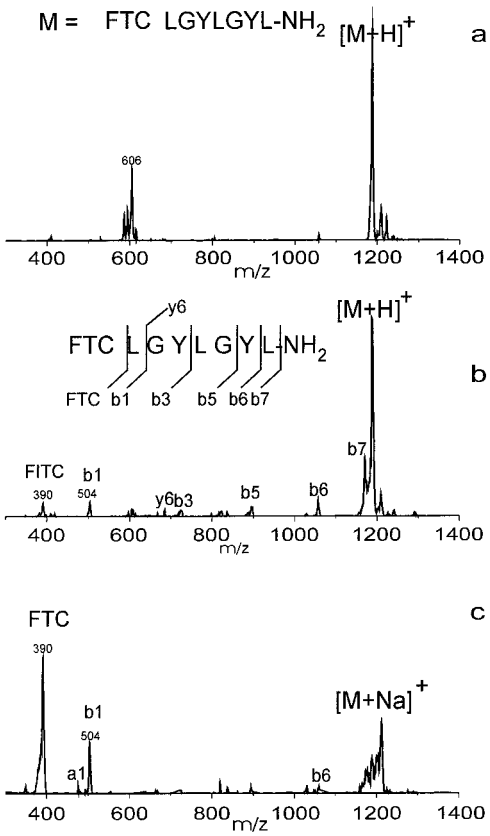


Figure 3. ESI-mass spectra of the FITC modified model peptide LGYLGYL-$CONH_2$ recorded at three different declustering potentials. (a) 10 V; (b) 40 V; (c) 80 V.

RESULTS

HEL was modified for 17 h at 25 °C at pH 8 using a molar ratio of FITC:HEL of 14. After the removal of unbound FITC by acetone precipitation, MALDI-MS was used to ascertain the number of FITC molecules incorporated into the protein. The MALDI-MS spectrum indicated an average incorporation of two FITC groups into the protein. It also revealed that the extent of FITC incorporation is heterogeneous. To isolate homogeneous protein derivatives, FITC-treated HEL was subjected to HPLC separation on a C_8-RP-HPLC column. HEL species with one to four FITC groups were isolated, although the isolation of a single, homogeneous HEL derivative was not achieved. ESI-mass spectra of a HPLC fraction of modified HEL containing predominantly two FTC groups were recorded by application of different declustering potentials as shown in Figure 2. With a declustering potential of 10 V (Figure 2a), the main protein species is 2-fold FITC-modified HEL (molecular mass 15 083 Da). An increase of the declustering potential of the ESI-ion source to 60 V revealed significant fragmentation at the FTC residues of HEL as shown in Figure 2b. The base peak at *m*/*z* 1677 is still corresponding to the $[M + 9H]^{9+}$ molecular ion of a HEL derivative containing two FTC groups, but in addition intense ions of mono-FTC-HEL (molecular mass 14 694 Da) and free HEL (molecular mass 14 305 Da) are detected. At a declustering potential of 80 V (Figure 2c), the $[M + 9H]^{9+}$ molecular ion of unmodified HEL (i.e., removal of all FTC groups) at *m*/*z* 1591 is the base peak of the spectrum. A further increase of the declustering potential up to 120 V (Figure 2d) resulted in a spectrum with broad signals showing complete removal of all FTC residues.

To test whether the nozzle skimmer fragmentation of FTC residues occurs also with FITC-modified peptides, a synthetic model peptide (LGYLGYL-$CONH_2$), (molecular mass 797 Da) was investigated. The N-terminus is the only amino group in this peptide. Since the removal of excess FITC was not possible by acetone precipitation, the reaction mixture was purified by HPLC. The HPLC fraction containing the FITC-modified peptide was subjected to ESI-MS analysis. Figure 3 shows ESI spectra of the modified peptide (molecular mass 1186 Da). Under standard conditions (declustering potential set to 10 V, Figure 3a), the singly and doubly charged molecular ions of the peptide carrying one FTC group are detected. A doubly charged species representing the sodium adduct of the modified peptide was additionally found. With the declustering potential set to 40 V (Figure 3b) sequence fragments of the modified peptide belonging to the b series (*25*), still containing the FTC group and the $[M + H]^+$ ion of the free FTC moiety were observed. With the declustering potential set to 80 V (Figure 3c), predominantly, the $[M + H]^+$ ion of the free FTC moiety was found at *m*/*z* 390. This result with the model peptide confirmed the predominant fragmentation of the FTC-N bond by release of the FTC moiety.

Tryptic digest mixtures of FITC-modified HEL were analyzed by MALDI-MS. Figure 4 shows the MALDI-MS spectrum of a reduced digestion mixture of HEL after

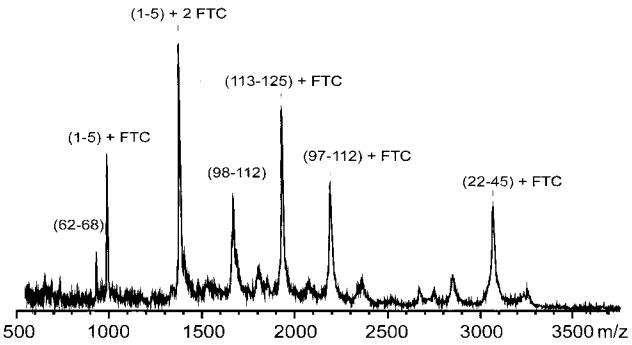


Figure 4. MALDI mass spectrum of a reduced tryptic digest mixture of HEL treated 55 h with 1 mM FITC. Partial tryptic sequences and the number of incorporated FITC labels are assigned.

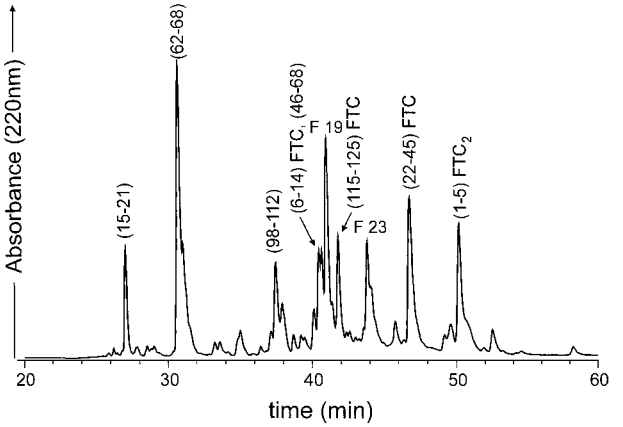


Figure 5. RP-HPLC chromatogram of a reduced tryptic digest mixture of HEL treated 55 h with 1 mM FITC. Partial peptides of HEL are assigned. Fractions 19 and 23 were subjected to ESI-MS (see Figure 6 and Figure 7).

Table 1. Localization of FTC-Residues in HPLC Separated HEL Derivatives

molecular ion with highest intensity (MALDI-MS)	number of FTC-residues incorporated	major modification sites identified by tryptic MALDI-MS peptide mapping
14 693	1	α-NH_2, K-33, K-97
15 110	2	α-NH_2, K-33 K-97
15 503	3	α-NH_2, K-1, K-33, K-97, K-116
15 890	4	α-NH_2, K-1, K-33, K-97, K-116

modification for 55 h at pH 8 at a molar ratio FITC:HEL of 6. The peptide fragments and the number of FITC groups incorporated are assigned to the molecular ions. These results (summarized in Table 1 for HEL derivatives with different degrees of modification) revealed that α-NH_2, K-1, K-33, K-97, and K-116 amino groups were predominantly modified by FITC. The digestion mixture was subsequently separated by RP-HPLC on a C_8 column; the corresponding chromatogram is shown in Figure 5. The isolated peptides were analyzed by MALDI-MS, which showed that K-13 was detected as an additional modification site. No modification was found at K-96, which is consistent with previous results of the amino-acylation of HEL (*26*, *27*). This lysine residue has a particularly low accesibility to chemical modification due the hydrogen bonding to the carbonyl oxygen of H-15.

The HPLC-separated tryptic peptides of FITC-modified HEL were also analyzed by ESI-MS. The effect of different declustering potentials on FTC peptides is illustrated in Figure 6 and Figure 7. Spectra of the homogeneous peptide (97−112) modified with FITC at K-97 (molecular mass 2193 Da) are shown in Figure 6.

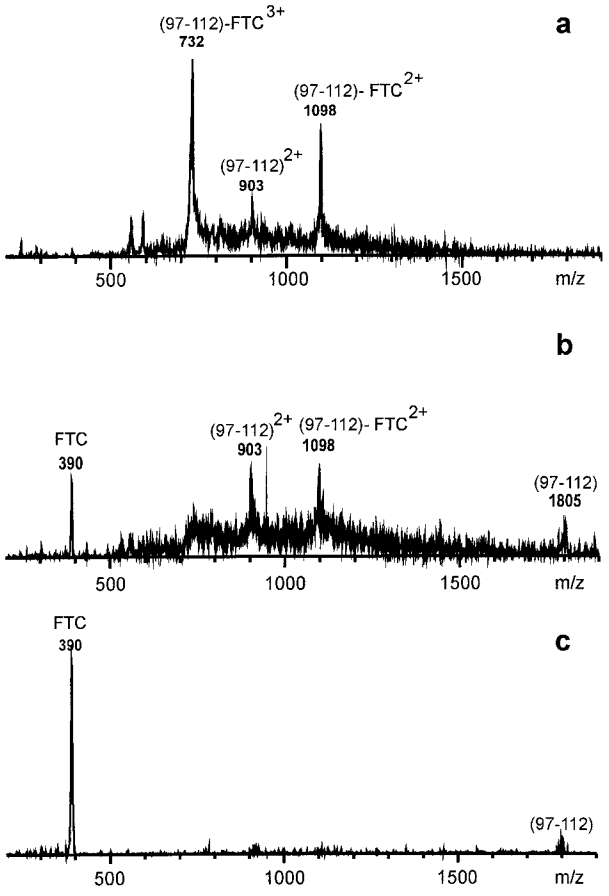


Figure 6. ESI mass spectrum of HPLC fraction 23 (see Figure 5) containing the peptide (97−112) carrying a FITC group at K-97. The sample was dissolved in 2% acetic acid/methanol (v/v = 8/2). Spectra were recorded with declustering potentials of (a) 20 V, (b) 40 V, and (c) 80 V.

The spectrum recorded with a declustering potential of 20 V (Figure 6a) is dominated by signals of the intact FTC peptide. Upon increasing the declustering potential to 40 V (Figure 6b), the signal intensity of the unmodified peptide (97−112) is comparable to the intensity of the FTC peptide, and the free FTC moiety is detected at *m/z* 390. Upon further increase of the declustering potential up to 80 V (Figure 6c), the molecular ions of the FTC peptide had disappeared and only an intense $[M + H]^+$ signal of the FTC moiety together with a weak $[M + H]^+$ signal of the unmodified peptide were observed.

Further studies were carried out to identify FITC-modified peptides from more complex mixtures. Figure 7a shows a spectrum from an HPLC fraction containing several peptides at a declustering potential of 20 V. The abundant signal at *m/z* 1168 (indicated by an asterisk) is due to a trimer of FITC, formed during lyophilization and storage of the HPLC fractions (*28*). (In MALDI-MS spectra recorded directly after HPLC separation, no signal at *m/z* 1168 was detected.) The triply charged molecular ion of the FTC peptide (1−5) (molecular mass 995 Da; B) at *m/z* 333 and the doubly and triply charged molecular ions of the FTC peptide (113−125) (molecular mass 1936 Da; A) at *m/z* 969 and 647 were identified. The unmodified peptide (74−97) (molecular mass 2466 Da; C) was found as doubly and triply charged ions. The $[M + H]^+$ ions of the FTC moiety (*m/z* 390) strongly increased by increasing the declustering potential to 50 V (Figure 7b), and a strong signal at *m/z* 775 corresponding to the doubly charged molecular ion of unmodified peptide (113−125) (molecular mass 1547 Da) was now

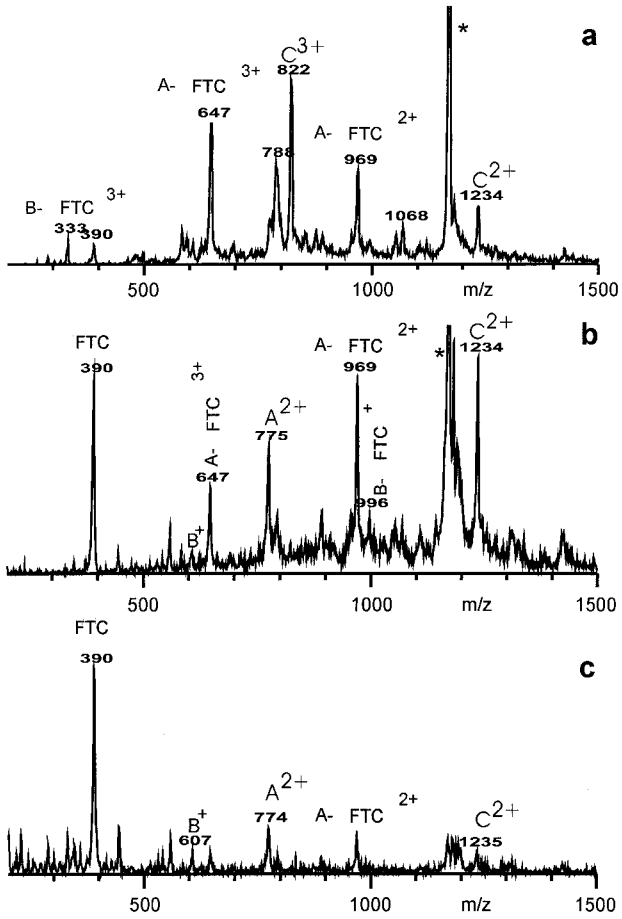


Figure 7. ESI mass spectrum of HPLC fraction 19 (see Figure 5) containing a complex mixture of peptides. The sample was dissolved in 2% acetic acid/methanol (v/v = 8/2). Spectra were recorded with declustering potentials of (a) 20 V, (b) 50 V, and (c) 80 V. A corresponds to the peptide (113−125) (molecular mass 1547 Da). B corresponds to the peptide (1−5) (molecular mass 606 Da). C corresponds to the peptide (74−97) (molecular mass 2466 Da).

observed. The intensity of these ions was further increased at a declustering potential of 80 V (Figure 7c). The identification of the FTC peptide (1−5) was somewhat more difficult since the ion intensities of these signals were very low in all spectra.

DISCUSSION

The results of this study show that the FITC modification provides a broad, inhomogeneous distribution of FTC groups at lysine residues at the conditions employed, as shown for the FITC modification of HEL. For example, the modification of the highly reactive K-97 (*26*) is not quantitative as shown by the intense ions for the peptide (98−112) (molecular mass 1676 Da) in the digestion mixture (see Figure 4); the quantitative modification of K-97 would have abolished the tryptic cleavage at this site. Furthermore, signals of the peptide (1−5) as singly (molecular mass 995 Da) and doubly modified species (molecular mass 1384 Da) were detectable with high intensity, indicating partial modification of the amino groups of K-1. These results are consistent with the MALDI-MS data of the intact, modified proteins where 2−5-fold modified species were found (see Table 1).

The ESI-MS spectra of FITC-modified peptides and proteins show that covalently bound FITC is specifically removed by simple increase of the declustering potential in the ESI ion source. This fragmentation is equally occurring with peptide and protein derivatives, and for α- and ϵ-FTC-amino groups. The site of each FITC modification can be readily assigned by this specific fragmentation.

The direct identification of FITC-labeling sites is possible even when other molecular ions of different intensities are present, as shown by the ESI spectra of a peptide mixture (see Figure 7). Thus, the identification of the number of FTC groups by MALDI-MS and the facile characterization of the specific modification sites by peptide mapping using ESI-MS with increased declustering potentials applied should render this approach an efficient tool for the molecular characterization of fluorescence labeled peptides and proteins, even from complex mixtures.

ACKNOWLEDGMENT

We thank Klaus Hägele for expert assistance in ESI-mass spectrometric procedures. This work has been supported by the Deutsche Forschungsgemeinschaft, Bonn, Germany ("Struktur und Funktionssteuerung an zellulären Oberflächen"), the EU network "Peptide and Protein Structure Elucidation by Mass Spectrometry", and the Fonds der chemischen Industrie, Germany.

LITERATURE CITED

(1) Coons, A. H., Creech, H. J., Jones, R. N., and E, B. (1942) The demonstration of pneumococcal antigen in tissues by the use of fluorescent antibody. *J. Immunol. 45,* 159−70.

(2) Swoboda, G., and Hasselbach, W. (1985) Reaction of fluorescein isothiocyanate with thiol and amino groups of sarcoplasmic ATPase. *Z. Naturforsch. 40c,* 863−75.

(3) Hucho, F., and Tsetlin, V. I. (1998) Modifizierung als Mittel zur Einführung von Reportergruppen. In *Bioanalytik* (F. Lottspeich and H. Zorbas, Eds.) pp 113−8, Spektrum Akademischer Verlag GmbH, Heidelberg, Berlin.

(4) Breier, A., Ziegelhoffer, A., Famulsky, K., Michalak, M., and Slezak, J. (1996) Is cysteine residue important in FITC-sensitive ATP-binding site of P-type ATPases? A commentary to the state of the art. *Mol. Cell Biochem. 160,* 89−93.

(5) Kirley, T. L., Wang, T., Wallick, E. T., and Lane, L. K. (1985) Homology of ATP binding sites from Ca2+ and (Na,K)-ATPases: comparison of the amino acid sequences of fluorescein isothiocyanate labeled peptides. *Biochem. Biophys. Res. Commun. 130,* 732−8.

(6) Gatto, C., Wang, A. X., and Kaplan, J. H. (1998) The M4M5 cytoplasmic loop of the Na,K-ATPase, overexpressed in *Escherichia coli*, binds nucleoside triphosphates with the same selectivity as the intact native protein. *J. Biol. Chem. 273,* 10578−85.

(7) Moutin, M. J., Rapin, C., Miras, R., Vincon, M., Dupont, Y., and McIntosh, D. B. (1998) Autonomous folding of the recombinant large cytoplasmic loop of sarcoplasmic reticulum Ca2+-ATPase probed by affinity labeling and trypsin digestion. *Eur. J. Biochem. 251,* 682−90.

(8) Corbalan-Garcia, S., Teruel, J. A., and Gomez-Fernandez, J. C. (1993) Intramolecular distances within the Ca(2+)-ATPase from sarcoplasmic reticulum as estimated through fluorescence energy transfer between probes. *Eur. J. Biochem. 217,* 737−44.

(9) Ohta, T., Morohashi, M., Kawamura, M., and Yoshida, M. (1985) The amino acid sequence of the fluorescein-labeled peptides of electric ray and brine shrimp (Na,K)-ATPase. *Biochem. Biophys. Res. Commun. 130,* 221−8.

(10) Hentz, N. G., Richardson, J. M., Sportsman, J. R., Daijo, J., and Sittampalam, G. S. (1997) Synthesis and characterization of insulin-fluorescein derivatives for bioanalytical applications. *Anal. Chem. 69,* 4994−5000.

(11) Pavela-Vrancic, M., Pfeifer, E., Schroder, W., von Dohren, H., and Kleinkauf, H. (1994) Identification of the ATP binding site in tyrocidine synthetase 1 by selective modification with fluorescein 5′-isothiocyanate. *J. Biol. Chem. 269,* 14962−6.

(12) Vorm, O., Roeppstorff, P., and Mann, M. (1994) Improved resolution and very high sensitivity in MALDI TOF of matrix surfaces made by fast evaporation. *Anal. Chem. 66,* 3281−7.
(13) Spengler, B., and Kaufmann, R. (1992) Gentle probe for tough molecules: matrix assisted laser desorption mass spectrometry. *Analysis 20,* 91−101.
(14) Denzinger, T., Przybylski, M., Savoca, R., and Sonderegger, P. (1997) Mass spectrometric characterisation of primary structure, sequence heterogeneity, and intramolecular disulfide loops of the cell adhesion protein axonin-1 from chicken. *Eur. Mass Spectrom. 3,* 379−89.
(15) Macht, M., Fiedler, W., Kürzinger, K., and Przybylski, M. (1996) Mass Spectrometric Mapping of Protein Epitope Structures of Myocardial Infarct Markers Myoglobin and Troponin T. *Biochemistry 35,* 15633−9.
(16) Glocker, M. O., Nock, S., Sprinzl, M., and Przybylski, M. (1998) Characterization of Surface Topology and Binding Area in Complexes of the Elongation Factor Proteins EF-Ts and EF-Tu*GDP form Thermus thermophilus: A Study by Protein Chemical Modification and Mass Spectrometry. *Chem. Eur. J. 4,* 707−15.
(17) Fiedler, W., Borchers, C., Macht, M., Deininger, S. O., and Przybylski, M. (1998) Molecular Characterization of a Conformational Epitope of Hen Egg White Lysozyme by Differential Chemical Modification of Immune Complexes and Mass Spectrometric Peptide Mapping. *Bioconjugate Chem. 9,* 236−41.
(18) Allen, M. H., and Vestal, M. L. (1992) Design and performance of a novel electrospray interface. *J. Am. Soc. Mass Spectrom. 3,* 18−26.
(19) Huddleston, M. J., Annan, R. S., Bean, M. F., and Carr, S. A. (1993) Selective detection of phosphopeptides in complex mixtures by electrospray liquid chromatography/mass spectrometry. *J. Am. Soc. Mass Spectrom. 4,* 710−7.
(20) Lehmann, W. D. (1996) Vergleich zwischen API−CID und Kollisionszellen-CID *Massenspektrometrie in der Biochemie,* pp 282−6, Spektrum Akademischer Verlag, Heidelberg, Berlin, Oxford.
(21) Glocker, M. O., Kalkum, M., Yamamoto, R., and Schreurs, J. (1996) Selective Biochemical Modification of Functional Residues in Recombinant Human Macrophage Colony-Stimulationg Factor β (rhM-CSF β): Identification by Mass Spectrometry. *Biochemistry 35,* 14625−33.
(22) Wilm, M. S., and Mann, M. (1994) Electrospray and Taylor-Cone theory, Dole's beam of macromolecules at last? *Int. J. Mass Spec. Ion Proc. 136,* 167−80.
(23) Wilm, M. S., and Mann, M. (1996) Analytical properties of the nanoelectrospray ion source. *Anal. Chem. 68,* 1−8.
(24) Fligge, T. A., Bruns, K., and Przybylski, M. (1998) Analytical development of electrospray and nanoelectrospray mass spectrometry in combination with liquid chromatography for the characterization of proteins. *J. Chromatogr. B 706,* 91−100.
(25) Roepstorff, P., and Fohlmann, J. (1984) Proposal for a Common Nomenclature for Sequence Ions in Mass Spectra of Peptides. *Biomed. Mass Spectrom. 11,* 601.
(26) Suckau, D., Mak, M., and Przybylski, M. (1992) Protein surface topology probing by selective chemical modification and mass spectrometric peptide mapping. *Proc. Natl. Acad. Sci. U.S.A. 89,* 5630−4.
(27) Glocker, M. O., Borchers, C., Fiedler, W., Suckau, D., and Przybylski, M. (1994) Molecular characterization of surface topology in protein tertiary structures by amino-acylation and mass spectrometric peptide mapping. *Bioconjugate Chem. 5,* 583−90.
(28) Richter, R., and Ulrich, H. (1977) Oligomerization and polymerization of isocyanates. In *The chemistry of cyanates and their thio derivatives* (S. Patai, Ed.) Vol. 2, pp 667−80, John Wiley & Sons, Chichester.

BC990039X

Preparation and Characterization of Anti-Tenascin Monoclonal Antibody−Streptavidin Conjugates for Pretargeting Applications

Catherine F. Foulon,* Darell D. Bigner, and Michael R. Zalutsky

Departments of Radiology and Pathology, Duke University Medical Center, DUMC 3808, Durham, North Carolina 27710. Received April 12, 1999; Revised Manuscript Received June 17, 1999

Radioimmunopretargeting is based on the separate injection of a modified mAb and the radionuclide and most frequently exploits the very high avidity of biotin for streptavidin (SA). Currently, we are evaluating the therapeutic potential of directly labeled monoclonal antibody (mAb) 81C6, reactive with the extracellular matrix protein tenascin, in surgically created glioma resection cavity patients. To be able to investigate pretargeting in this setting, the synthesis of 81C6 mAb−SA conjugates was required. In the current study, we have evaluated five methods for preparing both murine 81C6 (m81C6) and human/mouse chimeric 81C6 (c81C6) SA conjugates with regard to yield, biotin-binding capacity, immunoreactivity, and molecular weight. The 81C6 mAb and SA were coupled by covalent interaction between sulfhydryl groups generated on the mAb via *N*-succinimidyl-*S*-acetylthioacetate, dithiothreitol or 2-iminothiolane (2IT), and maleimido-derivatized SA, prepared via sulfosuccinimidyl 4-(*N*-maleimidomethyl)cyclohexane-1-carboxylate (SMCC) or *N*-succinimidyl-3-(2-pyridyldithio)-propionate. A noncovalent approach involving reaction of a biotinylated mAb, prepared using biotin caproate, and SA also was studied. The evaluation criteria were yield of mAb−SA 215 kDa monomer, as well as conjugate biotin-binding capacity and immunoreactive fraction. The optimal procedure involved activation of m81C6 or c81C6 with 30 equiv of 2IT and reaction of SA with 10 equiv of SMCC and yielded a conjugate with excellent biotin-binding capacity and immunoreactivity. The (^{125}I-labeled m81C6)-2IT-SMCC-SA was stable and did not lose biotin-binding capacity after a 72 h incubation in human glioma cyst fluid in vitro. Although the conjugate was stable in murine serum in vivo, its biotin-binding capacity declined rapidly, consistent with high endogenous biotin levels in the mouse. After injection of the radioiodinated conjugate into athymic mice with subcutaneous D-54 MG human glioma xenografts, high tumor uptake (36.0 ± 10.7% ID/g at 3 days) and excellent tumor:normal tissue ratios were observed.

INTRODUCTION

One of the most significant limitations of monoclonal antibodies (mAbs)[1] for radioimmunotherapeutic application is that their large molecular mass impedes homogeneous tumor uptake and clearance from normal tissues. To circumvent this problem, pretargeting strategies have been pursued in which the mAb and the radiolabel are injected separately. In such a protocol, a modified mAb conjugate is injected, and once optimal tumor-to-normal tissue ratios have been achieved (usually, within 2−4 days), a low molecular mass radiolabeled ligand that exhibits high-affinity binding to the conjugate is administered (*1*).

Most pretargeting investigations have attempted to exploit the high-affinity binding of biotin, a 244 Da vitamin, for 65 kDa avidin or 54 kDa streptavidin (SA). Although many different approaches have been described (*2*−*4*), theoretical calculations predict that administration of mAb−SA conjugates, followed by a radiolabeled biotin derivative, should provide optimal tumor targeting (*5*). Indeed, some of the most promising clinical results to date have been achieved with pretargeting protocols that utilize biotin as the radionuclide carrier (*6*, *7*).

Monoclonal antibodies directed against tenascin, an extracellular matrix protein found on gliomas, melanomas, and breast carcinomas (*8*−*10*), might be useful for pretargeting because they do not internalize after antigen binding. Currently, we are investigating the therapeutic potential of the ^{131}I-labeled anti-tenascin mAb m81C6 administered into surgically created glioma resection cavities and via the intrathecal route in patients with neoplastic meningitis (*11*, *12*). Encouraging results have been obtained in many patients with these directly labeled mAbs; however, pretargeting approaches using 81C6-SA conjugates and radiolabeled biotin molecules might offer significant advantages. Recent results suggest that it might be possible to deliver high radiation doses to intracranial malignancies using pretargeting, even when reagents are administered intravenously (*7*). In addition, by labeling biotin instead of the mAb, radiotherapy with promising short half-life radionuclides, such as the 7.2 h half-life α-emitter ^{211}At, should be facilitated.

Prior to initiating clinical investigations, methodologies for the preparation, purification, and characterization of reagents with optimal properties for pretargeting must

* To whom correspondence should be addressed. Phone: (919) 684-7705. Fax: (919) 684-7122. E-mail: cfoulon@duke.edu.

[1] Abbreviations: mAb, monoclonal antibody; SA, streptavidin; m81C6, murine 81C6, c81C6, human/mouse chimeric 81C6; IBA, biotinyl-3-iodoanilide; IBB, (3-iodobenzoyl)norbiotinamide; BnLCsNHS, biotinamidocaproic acid 3-sulfo-*N*-hydroxysuccinimide; BSA, bovine serum albumin; SATA, *N*-succinimidyl-S-acetylthioacetate; DTT, dithiothreitol; 2IT, 2-iminothiolane; SMCC, sulfosuccinimidyl 4-(*N*-maleimidomethyl)cyclohexane-1-carboxylate; SPDP, *N*-succinimidyl-3-(2-pyridyldithio)-propionate; SDS−PAGE, sodium dodecyl sulfate−polyacrylamide gel electrophoresis; HPLC, high-performance liquid chromatography; ITLC, instant thin-layer chromatography.

10.1021/bc990040w CCC: $18.00 © 1999 American Chemical Society
Published on Web 08/03/1999

be developed. We have recently described the synthesis of radiohalogenated biotin conjugates including (3-[$^{125/131}$I]-iodobenzoyl)norbiotinamide (IBB) and its ^{211}At-labeled analogue and documented their resistance to degradation by biotinidase (*13*, *14*). In the current study, we have investigated several methods for preparing anti-tenascin 81C6-SA conjugates and evaluated them with regard to yield, biotin-binding capacity, immunoreactivity and molecular mass. Approaches involving the noncovalent interaction between biotinylated 81C6 (via sulfo-NHS-BnLC) and SA, as well as covalent binding between SA and thiolated mAb, were investigated. Variables that were studied included SA maleimido-activation (SMCC and SPDP), mAb thiolation (reduction of existing disulfide bonds via DTT, addition of sulfhydryl groups using 2IT or SATA), and mAb (m81C6 and c81C6). Our results indicate that using covalent approaches, a 215 kDa mAb−SA monomer, consisting of one SA molecule and one mAb molecule, can be prepared in reasonable yield and with excellent biotin and antigen binding capacities. Furthermore, (^{125}I-labeled m81C6)-2IT-SMCC-SA exhibited excellent in vitro stability in human glioma tumor cyst fluid and a tissue distribution in athymic mice with subcutaneous D-54 MG human glioma xenografts that compares favorable with that of directly radioiodinated m81C6.

MATERIALS AND METHODS

Materials. Murine 81C6 (m81C6) is an IgG_{2b} that binds to domain 12 of alternatively spliced fibronectin type III repeats of tenascin (*8*, *15*). Details concerning the generation and characterization of human/mouse chimeric 81C6 (c81C6), consisting of human IgG_2 constant regions and m81C6 variable regions, can be found in a previous publication (*16*). Both mAbs were purified using Protein A Sepharose and an ion-exchange method compatible with mAb isoelectric point (*17*). Streptavidin, 2-IT, iodoacetamide, and BnLCsNHS were purchased from Sigma Chemical Co. (St. Louis, MO); all other reagents were purchased from Pierce (Rockford, IL). Radioiodine ($Na^{125}I$ or $Na^{131}I$) in 0.1 N NaOH was obtained from Dupont-NEN (Boston, MA). The radioiodinated biotin conjugates [^{131}I]IBA and [$^{131/125}$I]IBB were prepared as described elsewhere (*13*, *18*).

General. For spin column purification, Sephadex G-25 (Pharmacia, Pistacaway, NJ) was reconstituted in PBS containing 0.05 M EDTA and added to a 3 mL syringe fitted with a cotton ball. The column was conditioned with 200 μL of 0.1% BSA and washed with 3 mL of the above buffer. The column was spun at 1000 rpm for 3 min, the sample (<250 μL) was added, and the column was spun again at 1000 rpm for 3 min in tandem with a 2 mL conical receiving tube. HPLC was conducted on a Beckman system (126 pumps, 168 UV detector set at 280 nm, 170 radioactivity detector, 406 Analogue Interface Module) using either an analytical (60 × 7.5 cm) or semipreparative (60 × 21.5 cm) gel filtration TSK 3000 column (TosoHaas, Montgomeryville, PA), fitted with an appropriate guard column. The eluent recommended by the manufacturer was filtered through a 0.22 μm membrane prior to use and run at flow rates of 1 and 5 mL/min for the analytical and semipreparative columns, respectively. Amicon Centriplus-100 Concentrators were supplied by Millipore (Bedford, MA). Protein quantification was performed at 595 nm using the Bio-Rad Protein Assay based on the method of Bradford (Bio-Rad, Hercules, CA). The extinction coefficient measured for IgG and SA were 71 000 and 1600, respectively. Silica-gel-impregnated glass fiber instant TLC (ITLC) plates were purchased from Gelman Science (Ann Arbor, MI) and cut into 1.5 × 8 cm strips. SDS−PAGE (7.5% polyacrylamide) was run under nonreducing and nonboiling conditions (150 V, 1.5 h) to minimize SA degradation. Nonradioactive materials were analyzed by silver staining while radioactive bands were analyzed by phosphoimaging with a Molecular Dynamics Storm 360 system (Sunnyvalle, CA). Radioactivity was quantified using a LKB 1282 Compugamma automated γ counter run in either single- or dual-channel mode. Higher levels of activity were measured using a Capintec CRC-7R radioisotope calibrator.

Activation of m81C6 with BnLCsNHS. m81C6 (16 mg/mL PBS) was dialyzed overnight in 0.1 M borate buffer, pH 8.5. Biotinylation was carried out by mixing m81C6 (2 mg, 125 μL of borate buffer) and 10 equiv of BnLCsNHS (72 μL, 1 mg/mL 0.9% saline) at room temperature for 30 min. The biotinylated mAb was purified with a Sephadex G-25 spin column.

Activation of m81C6 with SATA and $HONH_2$. m81C6 (16 mg/mL PBS) was dialyzed overnight in 0.1 M borate buffer, pH 8.5, and 2 mg of m81C6 and 10 equiv of SATA (31 μL, 1 mg/mL DMSO) were incubated at room temperature for 30 min. The activated mAb was purified with a Sephadex G-25 spin column and incubated with hydroxylamine (10 μL, 10 mg/mL PBS containing 0.05M EDTA) at room temperature for 1 h. The thiolated mAb was purified by Sephadex G-25 spin column prior to reaction with activated SA.

Activation of 81C6 with DTT. m81C6 or c81C6 (16 mg/mL PBS) was dialyzed overnight in 0.1 M borate buffer, pH 8.5, and 2 mg of m81C6 or c81C6 were incubated at room temperature for 30 min with 10 equiv of DTT (21 μL, 1 mg/mL PBS). After Sephadex G-25 spin-column purification, the thiolated mAb was ready for reaction with activated SA.

Activation of 81C6 with 2IT. c81C6, m81C6, or radioiodinated m81C6 (125 μL, 2 mg) in PBS and 2IT (18 μL, 1 or 3 mg/mL 0.9% saline, 10 or 30 equiv, respectively) were incubated at room temperature for 30 min. The thiolated mAb was purified by Sephadex G-25 spin column prior to reaction with activated SA.

Activation of SA with SMCC. SA (80 μL, 10 mg/mL) in 0.1 M borate buffer pH 8.5 and 10 equiv of SMCC (29 μL, 2 mg/mL 0.9% saline) were incubated at room temperature for 30 min. The maleimido-derivatized SA was purified by Sephadex G-25 spin column prior to reaction with the thiolated mAb.

Activation of SA with SPDP. SA (80 μL, 10 mg/mL 0.1 M borate buffer, pH 8.5) and 10 equiv of SPDP (5 μL, 8 mg/mL DMSO) were incubated at room temperature for 30 min. Prior to reaction with thiolated mAb, the maleimido-derivatized SA was purified using a Sephadex G-25 spin column.

Preparation and Purification of 81C6-SA Conjugates. These reactions were performed on an equimolar basis; generally, 2 mg of mAb and 0.8 mg of SA were used. For mAb−BnLC-SA conjugates, biotinylated m81C6 and SA were incubated at room temperature for 45 min. Preparation of covalent mAb−SA conjugates involved incubation of thiolated 81C6 (unlabeled m81C6, c81C6 or radiolabeled m81C6) and maleimido-derivatized SA at room temperature for 45 min. The reaction was quenched by addition of iodoacetamide (5 μL, 100 mg/mL PBS containing 0.05 M EDTA). All reaction mixtures were purified on the analytical-scale TSK 3000 gel filtration column at a flow rate of 1 mL/min. On this system, m81C6, SA, and iodoacetamide eluted at 15.5, 20.1, and 25.5 min, respectively. Comparison to molecular mass

standards (Bio-Rad) indicated that the peak at 11−12 min was consistent with the presence of the 215 kDa mAb−SA monomer.

When upscaling the preparation of m81C6-2IT-SMCC-SA for the biodistribution study, the reaction mixture was purified by four injections of 11.2 mg of protein on the semipreparative TSK 3000 at a 5 mL/min flow rate. In this system, the conjugate, m81C6 and SA eluted at 17, 22.5, and 29 min, respectively. Excess solvent was removed by concentration over Centriplus 100 (5000 rpm, 40 min), to reach the concentration required (150 μg/200 μL) for the animal experiment.

Analysis of the Conjugates. After HPLC purification, each isolated fraction was subjected to protein assay and SDS−PAGE to determine the molecular mass profile of the species present after the reaction of mAb and SA. HPLC fractions also were evaluated with regard to binding capacity for radiolabeled IBB and immunoreactive fraction.

Radiolabeled Biotin Binding Potency. Aliquots (50 μL) from HPLC fractions of interest were incubated with [^{125}I]IBB or [^{131}I]IBB (4 μCi, 10 μL) in 100 μL of saline for 1 h at room temperature. An aliquot (3 μL) was analyzed on ITLC using saline:ethanol (95:5) as the solvent and the fraction of input counts bound to protein was calculated as described (*18*).

Immunoreactivity. SA-coated MPG magnetic beads (5 μm) were obtained from CPG (Lincoln Park, NJ). The beads (1 mL) were mixed with biotinylated recombinant tenascin TnFn 6-12 (positive) or TnFn 6-11 (negative) fragments (100−150 μL, 1 mg/mL) for 3 h at room temperature and rinsed with 115 mM phosphate buffer, pH 7.4, containing 0.05% BSA and 0.05% Brij 35 to remove nonbound proteins. The beads were resuspended in 1 mL of this buffer and stored at 4 °C. Prior to use, beads were incubated with biotin (100 μL, 5 mg/mL saline) for 1 h at room temperature to block any free SA on the beads. Likewise, each mAb−SA conjugate was incubated with an excess of biotin (100 μL, 5 mg/mL saline) to avoid binding of mAb−SA to any free biotin on the tenascin fragments. The immunoreactive fraction was determined by incubating 50 μL of mAb−SA conjugate, labeled with [$^{131/125}$I]IBB as described above, or (^{125}I-labeled mAb)-SA, in triplicate with increasing volumes of beads (10, 20, or 40 μL) in 500 μL of 115 mM phosphate buffer. After 45 min agitation at room temperature, beads were isolated from the supernatant using a magnetic separator, and beads and supernatant assayed for radioactivity on the gamma counter. The specific binding was determined by subtracting nonspecific binding to TnFn 6-11 beads from the binding to TnFn 6-12 beads. The immunoreactive fraction was calculated according to the method of Lindmo et al. (*19*) by plotting the inverse of % specific binding versus the inverse of bead concentration.

Preparation of ^{125}I-Labeled m81C6-2IT-SMCC-SA Conjugate. To a vial coated with Iodogen (10 μg) was added m81C6 (62.5 μL, 16 mg/mL) in PBS and Na^{125}I (∼1 mCi). The vial was placed on an orbital shaker at room temperature for 5 min, and the mixture purified on a Sephadex G-25 spin column. Cold m81C6 (1 mg) was then added, and the m81C6-2IT-SMCC-SA conjugate was prepared by reacting the labeled mAb with 30 equiv of 2IT, followed by a 1:1 reaction with SMCC-SA.

In Vivo Stability of the Conjugate in Normal Mice. Five normal Balb/c mice weighing 20−25 g were injected intravenously with (^{125}I-labeled m81C6)-2IT-SMCC-SA (150 μg, 4 μCi). Blood samples were obtained by retro-orbital bleed 2, 6, 24, and 48 h later. Serum was separated by centrifugation, incubated in triplicate with [^{131}I]IBA (10 μL in saline, 2 μCi) for 30 min at room temperature, and biotin binding monitored by ITLC as described above. Serum samples also were analyzed by SDS−PAGE.

Tissue Distribution Measurements. The HPLC fractions containing the ∼215 kDa peak were pooled and administered intravenously to athymic mice weighing 25−30 g and bearing subcutaneous D-54 MG human glioma xenografts (*20*). Groups of five animals received 150 μg/4 μCi of (^{125}I-labeled m81C6)-2IT-SMCC-SA and were killed by halothane overdose 2, 3, or 4 days later. Organs were harvested, weighed and the ^{125}I activity levels were measured in the gamma counter. The percentage of injected dose per gram of tissue was calculated by comparison to injection standards of appropriate count rate.

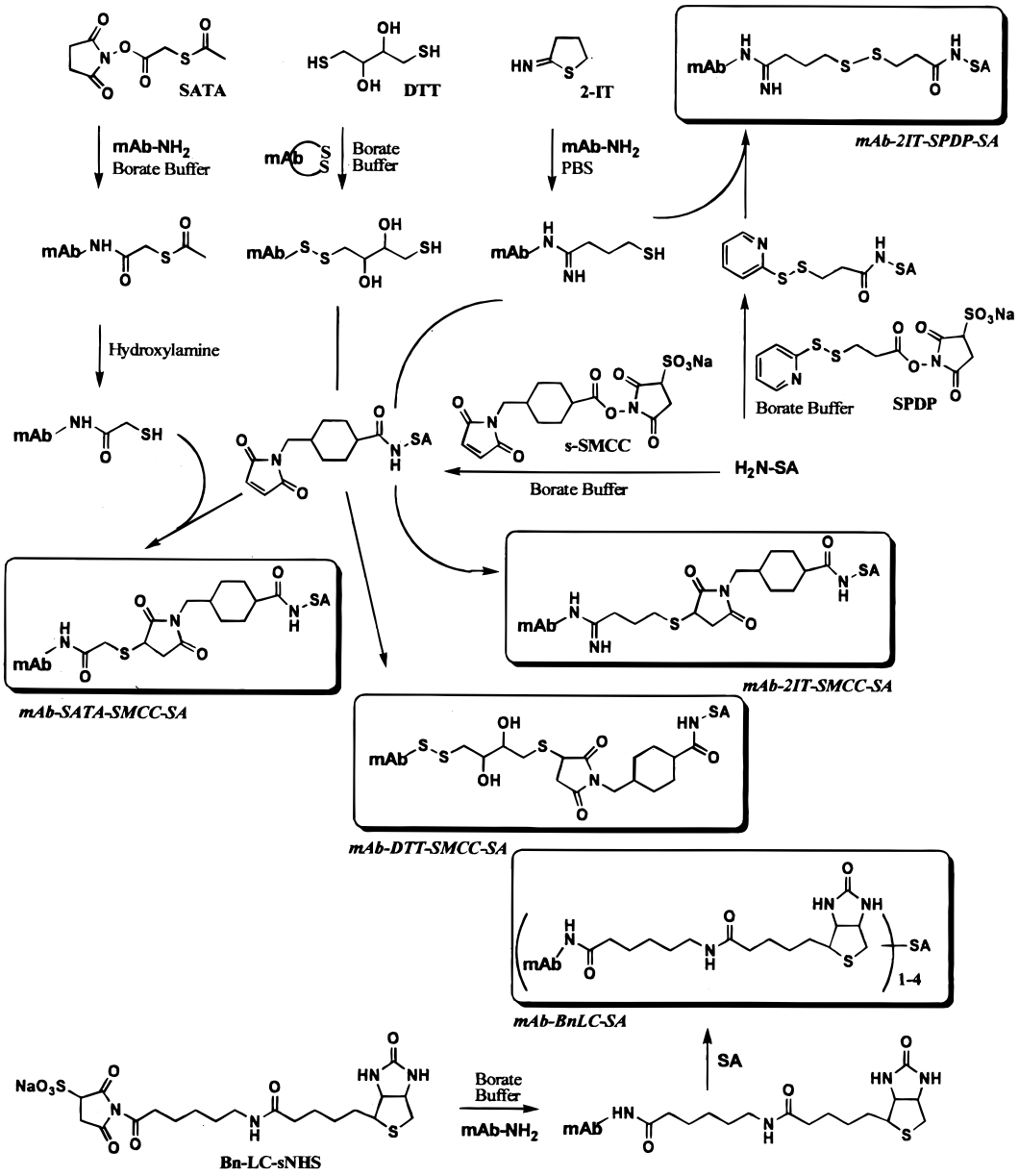
In Vitro Stability of mAb−SA Conjugate in Tumor Cyst Fluid. Tumor cyst fluid was obtained from a patient with a surgically created glioma resection cavity and stored at −170 °C. Aliquots of tumor cyst fluid (20 μL) were mixed with saline (50 μL) and incubated at 37 °C with (a) (^{125}I-labeled m81C6)-2IT-SMCC-SA (20 μL, 1.16 mg/mL), (b) SA (20 μL, 1 mg/mL) as a positive control, or (c) saline (20 μL) as a negative control. At various time intervals (2, 8.5, 19, 31, 48, and 72 h), [^{131}I]-IBA (10 μL, 1 μCi) was added in duplicate. The biotin-binding capacity was monitored by ITLC after a 30 min incubation at room temperature, as described above. In addition, the molecular mass profile of (^{125}I-labeled m81C6)-2IT-SMCC-SA in tumor cyst fluid (in the absence of [^{131}I]IBA) was monitored as a function of time by SDS−PAGE.

RESULTS

Preparation and Characterization of the mAb−SA Conjugates. In Scheme 1, the synthetic approaches utilized for preparing 81C6 mAb−SA conjugates are illustrated. Reaction mixtures were analyzed by size-exclusion HPLC and SDS−PAGE, and biotin-binding capacity and immunoreactive fraction also were determined. The goal was to maximize yield and binding capacity of the desired monomeric mAb_1-SA_1 ∼215 kDa species and determine the presence and binding profile of other macromolecular contaminants. Conjugation yields were calculated by dividing the protein concentration in the 215 kDa peak, isolated by HPLC, by the initial amount of mAb added to the reaction mixture. This approach was taken because of the more than 40-fold lower extinction coefficient of SA compared with mAb in the protein assay. No corrections were applied for transfer losses during the multistep procedure.

Figure 1 illustrates the type of analyses that were performed for evaluating the mAb−SA conjugates. These are the results of a preliminary experiment in which c81C6 was activated with 10 equiv of DTT, SA was activated with 10 equiv of SMCC, and the two proteins reacted at an equimolar ratio. As shown in Figure 1A, size-exclusion HPLC indicated the presence of multiple peaks in the reaction mixture including those with retention times corresponding to authentic samples of c81C6 (15.5 min) and SA (20.2 min). Comparison to molecular mass standards indicated that the peak eluting at 11.9 min was consistent with the desired mAb−SA monomer. Aliquots from fractions eluting at 12, 13.5, 15.7, 16.6, 17.3, and 20.2 min were analyzed for biotin-binding capacity and immunoreactive fraction (Figure

Scheme 1. Synthetic Schemes for the Five Methods Used to Prepare 81C6 mAb-SA Conjugates

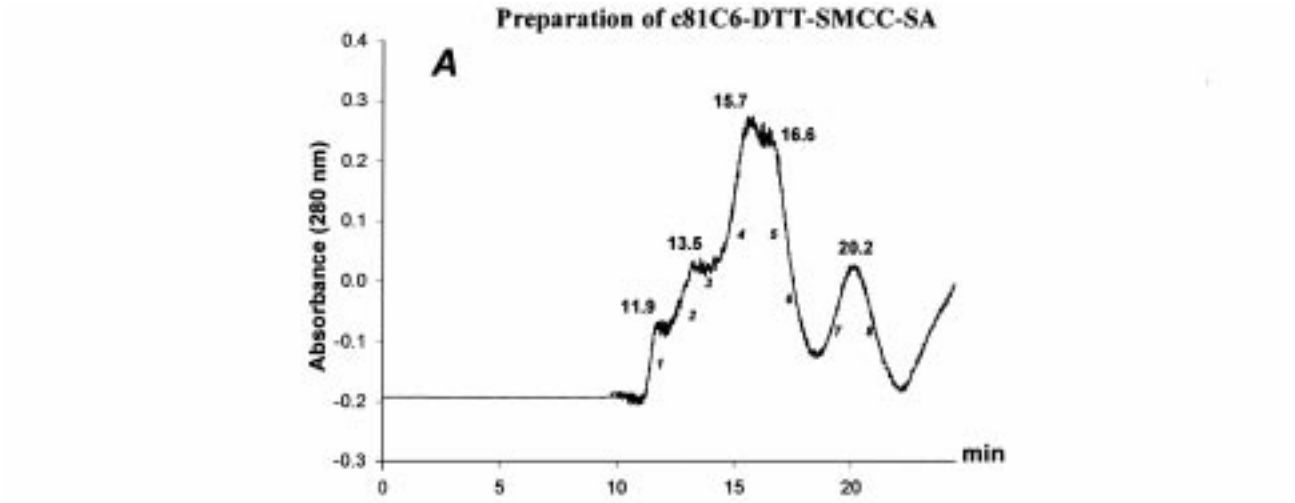


1B), SDS−PAGE with silver staining (Figure 1C) and after incubation with [^{131}I]IBB, by autoradiography (Figure 1D).

On SDS−PAGE, the HPLC fraction eluting at 11.9 min consisted of a major band at the desired ~215 kDa, as well as a minor band at 230 kDa. Protein quantification of this fraction indicated formation of the desired conjugate in 23% yield. Biotin-binding capacity (87%) and immunoreactive fraction (100%) for this fraction were excellent, consistent with the formation of a functional mAb−SA monomer. The SDS−PAGE autoradiograph obtained after incubation with [^{131}I]IBB indicated that the band at 230 kDa did not bind biotin, suggesting that it did not contain a functional SA subunit. These analyses also demonstrated that HPLC fractions eluting at 13.5, 15.7, and 16.6 min were capable of binding to both biotin and tenascin, and included species with molecular masses of 140, 165, and 180 kDa.

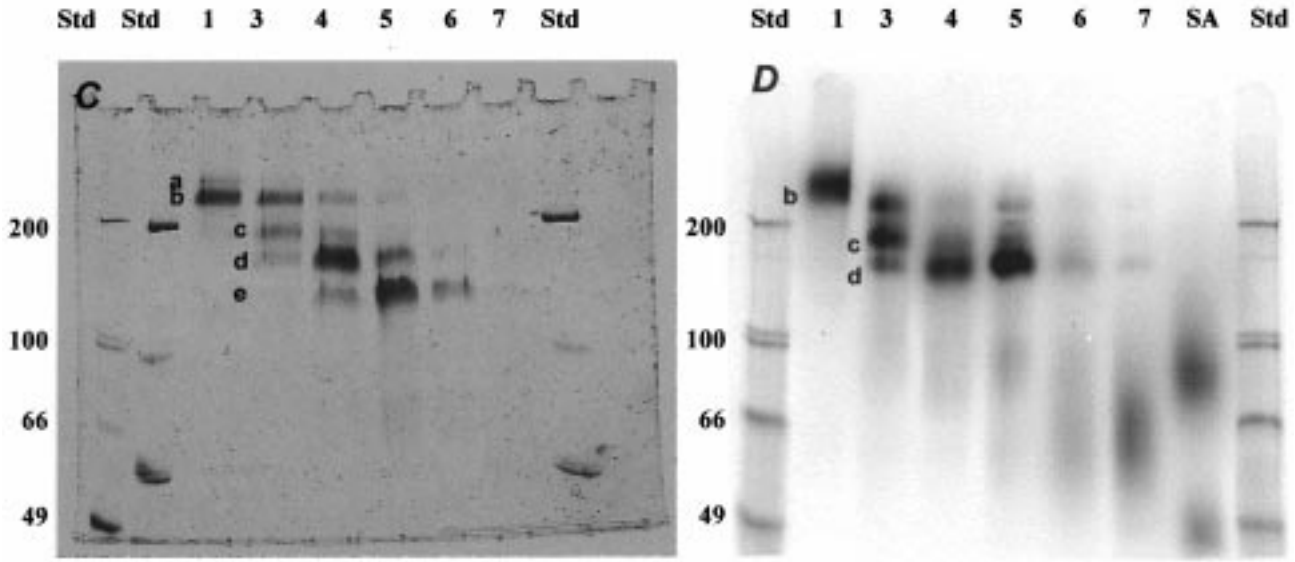
Although the above set of reaction conditions provided a mAb−SA conjugate with excellent binding properties, yields of this product were less than ideal. To improve recovered yield while maintaining conjugate function, a series of experiments was then performed with m81C6 using the methods outlined in Scheme 1. A representative analytical HPLC profile for the standards (HPLC-isolated and SDS−PAGE-confirmed mAb-2IT-SMCC-SA, mAb, and SA) is shown in Figure 2A and chromatograms for mAb-BnLC-SA, mAb-DTT-SMCC-SA, mAb-SATA-SMCC-SA, mAb-2IT-SMCC-SA, and mAb-2IT-SPDP−SA prepared at 10:1 activating agent:mAb and reagent:SA ratios are shown in Figure 2, panels B−F. Conjugation yields, biotin-binding capacities, and immunoreactive fractions for these and other reactions carried out at 30:1 activating agent:mAb ratios, and with c81C6, are summarized in Table 1. The HPLC fraction eluting at 12 min was incubated with [^{131}I]IBB and analyzed by SDS−PAGE. Silver-staining and autoradiography of this gel were performed, and the results are presented in Figure 3.

All five methods yielded 81C6 mAb−SA conjugate; however, results with the noncovalent approach involving reaction of biotinylated mAb with SA were least favorable (Figure 2, Table 1). The immunoreactive fraction for conjugate prepared by this approach was only 49%, presumably due to continuing polymerization due to the



B

Fraction #	1	3	4	5	6	7	Control	
Fraction (min)	12	13.5	15.7	16.6	17.3	20.2	SA	c81C6
% ^{131}IBB binding	87	88	89	91	88	80	93	<3
% IRF	100	84	100	94	14	<5	<5	85



Approx. MW (kDa): a = 230, b = 215, c = 180, d = 165, e = 140

Figure 1. Analysis of the species produced following the (1:1) reaction of c81C6-DTT (prepared at a 1:10 molar ratio) with SMCC-SA (prepared at a 10:1 molar ratio). (A) TSK 3000 size-exclusion HPLC elution profile (UV absorbance at 280 nm); (B) percent biotin-binding capacity and immunoreactive fraction for different HPLC fractions, identified by fraction number (elution position shown in panel A) and retention time (min), as well as for SA and c81C6 controls; (C) silver-stain SDS−PAGE of [^{14}C]molecular mass standards (lane 1), molecular mass standards (lanes 2 and 9) and samples from HPLC fractions 1, 3−7 (lanes 3−8); and (D) autoradiograph SDS−PAGE of samples from HPLC fractions 1, 3−7 (lanes 2−7) after incubation with [^{131}I]IBB, [^{14}C]molecular mass standards in lanes 1 and 9, SA in lane 8. Approximate molecular masses of bands in SDS−PAGE, a = 230 kDa, b = 215 kDa, c = 180 kDa, d = 165 kDa, e = 140 kDa.

lack of appropriate quenching method for this type of coupling. In comparison, immunoreactive fractions for conjugate prepared by the covalent coupling approaches were >68% for m81C6 and >79% for c81C6, values comparable to those for native mAbs. In addition, SDS−PAGE indicated the presence of a single ~215 kDa peak capable of biotin binding. The exception was the reaction run at a 30:1 DTT:mAb molar ratio where a 75 kDa species that did not bind biotin, as well as multiple 150−180 kDa species that did bind biotin, was observed. On the basis of ease of synthesis, yield, and binding properties of the resultant conjugate, the method selected for further study involved activation of mAb with 30 equiv of 2IT followed by reaction with SMCC-SA (prepared at 10:1 molar ratio). Representative size-exclusion HPLC chromatograms obtained using this procedure with m81C6

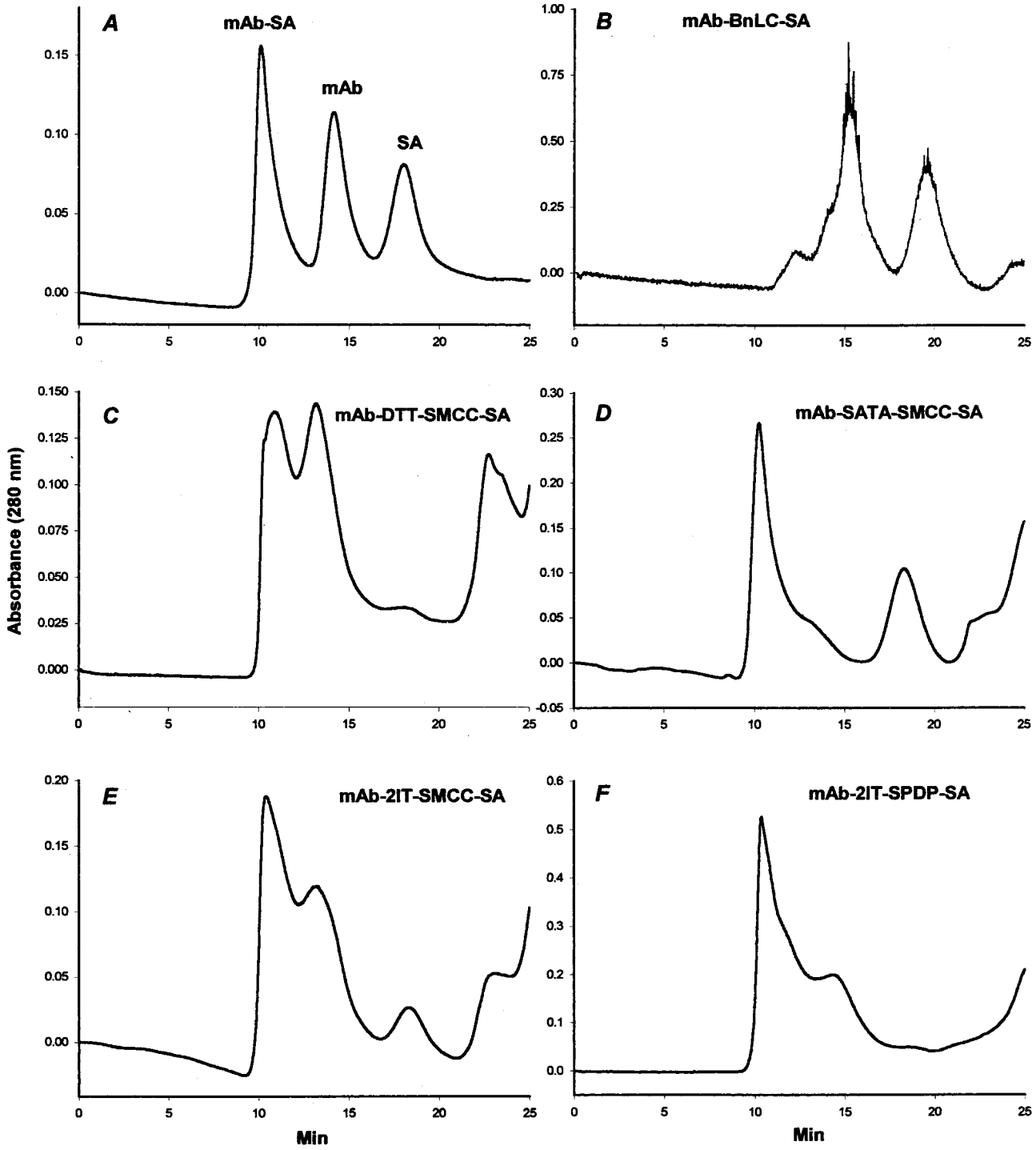


Figure 2. Size-exclusion TSK 3000 profile (UV absorbance at 280 nm) of (A) monomeric mAb−SA, mAb, and SA standards, and (B−F) conjugate reaction mixtures prepared at 10:1 reagent:mAb and reagent:SA molar ratios. Peak at approximately 25 min corresponds to iodoacetamide.

and c81C6 are illustrated in Figure 4. Even though the mAbs had different elution times on this column (m81C6, 15.5 min; c81C6, 16.5 min), with both mAbs, the predominant peak in the reaction mixture eluted at 12 min, corresponding to the desired mAb−SA conjugate.

In Vivo Stability of (^{125}I-Labeled m81C6)-2IT-SMCC-SA in Normal Mice. The in vivo stability of (^{125}I-labeled m81C6)-2IT-SMCC-SA was investigated after injection of the conjugate to normal mice. Figure 5 presents an SDS−PAGE autoradiograph comparing the molecular mass profile of the conjugate to those present in murine serum samples obtained 2−48 h after injection. The only radioactive band observed in serum had a molecular mass of ∼215 kDa with no evidence for the generation of lower molecular mass labeled catabolites. The biotin-binding capacity of the mAb−SA conjugate in serum, measured using [^{131}I]IBA, was 92.1 ± 3.1% at 2 h, 32.4 ± 4.0% at 6 h, 11.5 ± 0.5% at 24 h, and 16.6 ± 1.1% at 24 h.

In Vivo Distribution of (^{125}I-Labeled m81C6)-2IT-SMCC-SA. Murine 81C6 was labeled with ^{125}I, thiolated using 2IT, and reacted with SMCC-SA. Table 2 summarizes the tissue distribution of this conjugate in athymic mice bearing subcutaneous D-54 MG human glioma xenografts. The radioiodinated mAb−SA conjugate exhibited high tumor uptake, reaching a maximum

Table 1. Coupling Yields, Biotin-Binding Capacities, and Immunoreactive Fractions for Anti-Tenascin 81C6 mAb−Streptavidin Conjugates

mAb	mAb activation[a]	SA activation[b]	yield (%)[c]	biotin binding (%)[d]	IRF (%)[e]
m81C6	BnLC (10:1)	none	13	79	49
m81C6	DTT	SMCC	5	96	71
c81C6	DTT (10:1)	SMCC	4	87	83
m81C6	DTT (30:1)	SMCC	4	95	68
m81C6	SATA (10:1)	SMCC	9	95	69
m81C6	SATA (30:1)	SMCC	15	95	79
m81C6	2IT (10:1)	SPDP	13	99	86
m81C6	2IT (10:1)	SMCC	8	96	76
m81C6	2IT (30:1)	SMCC	28	96	73
c81C6	2IT (30:1)	SMCC	31	79	74

[a] Reagent used for mAb modification (reagent:mAb molar ratio). [b] Reagent used for SA modification (reagent:SA molar raito). [c] Yield of 215 kDa product calculated based on initial mAb concentration. [d] Percentage of labeled biotin counts bound in vitro. [e] Immunoreative fraction.

of 36.04 ± 10.69% ID/g at 3 days. Deiodination of the conjugate was reflected by the fact that about 3% of the injected dose was taken up by the thyroid at all three time points. Three days after injection, tumor-to-blood ratios were 3.6:1, while tumor-to-normal organ ratios were greater than 10:1, demonstrating that this SA coupling method did not compromise the tumor localizing capacity and normal tissue clearance of m81C6.

In Vitro Stability of (^{125}I-Labeled m81C6)-2IT-SMCC-SA in Tumor Cyst Fluid. No evidence for degradation of the conjugate was observed on SDS−PAGE autoradiographs during the 72 h incubation period. Incubation in glioma resection cyst fluid had no effect on the biotin-binding capacity of the conjugate. The percentage of [^{131}I]IBA bound decreased only slightly, from 98.8% after 2 h to 94.3% after 72 h. For comparison, after incubation of SA in cyst fluid, [^{131}I]IBA binding ranged 98.9−94.7% from 2 to 72 h. As a control, the binding of [^{131}I]IBA to cyst fluid alone was measured and, as expected, was less than 1−5% during the 72 h incubation period.

DISCUSSION

Our ongoing radioimmunotherapy trials for the treatment of brain tumors involve direct administration of radiolabeled anti-tenascin mAbs into surgically created glioma resection cavities (*12*). As one of our second-generation strategies, we envision investigating a two-step pretargeted approach in which the 81C6-SA conjugate would be injected into the cavity in order to saturate tenascin-binding sites on the tumor. The radiolabeled biotin derivative would be delivered about 2 days later, also into the resection cavity. By associating the radiolabel with a small molecule instead of the mAb, we hope to increase the diffusion of the labeled moiety into the tumor and extend the zone of effective treatment beyond the regions adjacent to the cavity interface.

With this goal in mind, we have previously designed a series of biotin conjugates derivatives, including [^{131}I]IBA, [^{131}I]IBB, and their ^{211}At-labeled analogues (*13*, *14*, *18*, *21*) with varying degrees of resistance to biotinidase degradation. Herein, we have attempted to optimize the production of the other reagent needed for pretargeting, the anti-tenascin mAb−SA conjugate. Some of the methods that were investigated have been described in the literature; however, evaluation of their relative merit is complicated by the fact that different mAbs, reagent amounts, reaction times, and conjugate isolation methods were used. In addition, to the best of our knowledge, the use of SATA and SPDP for the preparation of mAb−SA conjugates has not been reported.

The simplest method for preparing mAb−SA conjugates is by reaction between a biotinylated mAb and SA, thereby exploiting the SA-biotin reaction itself to form the conjugate. This approach is attractive because several activated biotin agents are commercially available, and it can be used for generating the conjugate in vivo by preinjection of the biotinylated mAb, followed by intravenous injection of SA (*22*, *23*). Furthermore, biotinylation results in negligible structural modification of the protein with retention of immunoreactivity (*24*). On the other hand, a limitation of this approach, when used in vitro, is that no form of quenching is available, and polymerization and cross linkage can take place, resulting in high molecular mass proteins with compromised binding properties and tissue distribution.

The results that we obtained with m81C6-BnLC-SA were consistent with the formation of higher molecular mass species than the desired 215 kDa mAb_1-SA_1 conjugate. The immunoreactive fraction of m81C6-BnLC-SA was less than 50%, considerably lower than that observed with other conjugate formation methods. In addition, this conjugation method makes use of the highest affinity SA biotin-binding site in the conjugation process and decreases the binding capacity of the conjugate for subsequently administered radiolabeled biotin. For these reasons, we decided to focus our efforts on covalent methods for coupling mAb and SA.

Covalently linked mAb−SA have been generated using classical cross-linking chemistry involving the high reactivity of sulfhydryl residues with maleimido groups. Typically, free thiols are generated on one protein by direct reduction of existing disulfide bridges using mercaptoethylamine (MEA) or DTT, or by addition of sulfhydryl groups on the lysyl residues with 2IT or SATA. Maleimido groups are substituted on the lysyl residues of the other protein using sulfo-SMCC or SPDP. Several of the possible combinations have been applied to the coupling of mAb and SA including mAb-SMCC-2IT-SA (*25*, *26*), mAb-2IT-SMCC-SA (*27*), mAb-MEA-SMCC-SA (*25*, *27*), and mAb-DTT-SMCC-SA (*28*). In addition, site-specific biotinylation of thiolated mAbs also has been described (*29*, *30*).

Our goals were to identify a covalent approach for producing anti-tenascin mAb−SA conjugates with high biotin-binding capacity and immunoreactivity, and good yield of the 215 kDa mAb−SA monomer. We decided to focus on this molecule because it is the smallest product containing both intact mAb and SA, and thus should diffuse more rapidly through the tumor than larger conjugates. Only limited information is available concerning the molecular mass profiles of mAb−SA conjugates. After reaction of a disulfide-reduced mAb with SMCC-SA, FPLC analysis indicated the formation of a single ∼210 kDa species capable of binding biotin (*25*). However, in a subsequent study using similar reaction conditions, the molecular mass of the mAb−SA conjugate was determined to be about 350 kDa by size-exclusion HPLC (*31*). SA−mAb conjugates in the 440−600 kDa range also have been reported (*32*).

Initially, we attempted covalent synthesis of mAb−SA conjugates using the approach described by NeoRx Corporation (*28*). This procedure involves thiolation of the mAb with 10 equiv of DTT, activation of SA with 10 equiv of SMCC, and reaction of the proteins at an equimolar ratio. Although biologically active 81C6 mAb−SA conjugates were obtained, yields of the 215 kDa

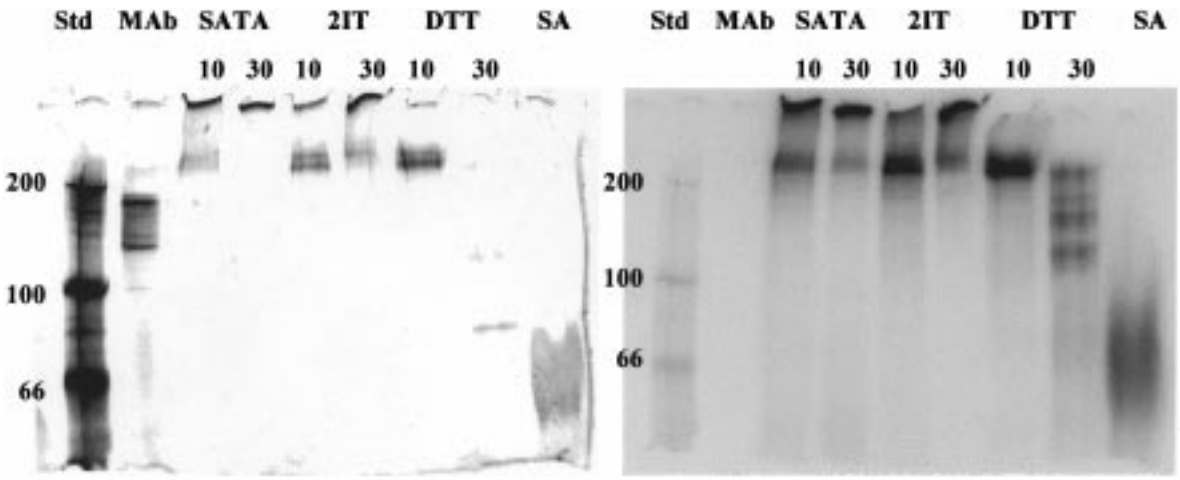


Figure 3. SDS−PAGE of size-exclusion-HPLC-purified m81C6-SA; silver stain on left, autoradiograph after exposure of reaction mixture to [^{125}I]IBB on right, of the same gel. Lane 1, molecular mass standards; lane 2, murine mAb; lane 3, SATA:mAb 10:1; lane 4, SATA:mAb 30:1, lane 5, 2IT:mAb 10:1, lane 6, 2IT:mAb 30:1; lane 7, DTT:mAb 10:1; lane 8, DTT:mAb 30:1; lane 9, streptavidin.

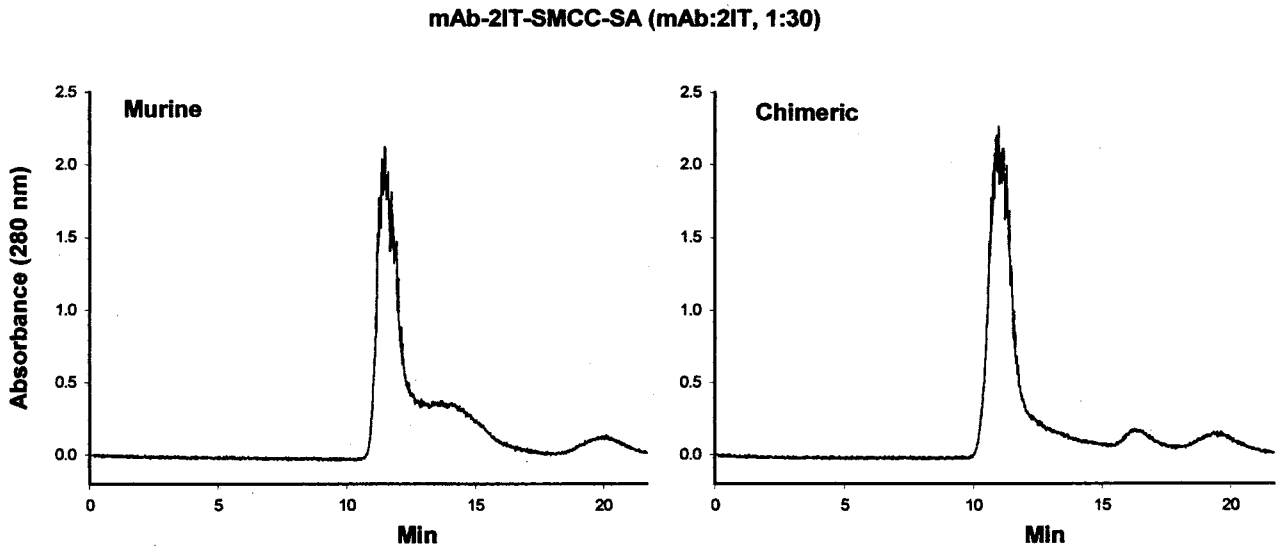


Figure 4. Size-exclusion TSK 3000 profile (UV absorbance at 280 nm) of (A) murine and (B) chimeric 81C6-streptavidin conjugate prepared at 30:1 2IT:mAb molar ratio.

monomer were less than 5% in our hands. Interestingly, the c81C6 reaction mixture contained higher levels of unreacted SA and mAb while, with m81C6, prominent peaks in the 170−200 kDa and <50 kDa range were observed. At higher DTT:m81C6 molar ratios, nearly complete fragmentation of the mAb was observed. The average number of free sulfhydryl groups on the mAb determined using Ellman's reagent was higher for m81C6 (4.5 SH, 10:1; 6.9 SH, 30:1) than for c81C6 (3.4 SH, 10:1; 4.9 SH, 30:1) (data not shown). Thus, even though there are four intrachain disulfides on human IgG_2 compared with three on murine IgG_{2b}, treatment of m81C6 with DTT yielded more free SH groups, presumably resulting in the generation of more lower molecular mass degradation products. These differences also are consistent with the increased in vivo stability of c81C6 compared with m81C6, which appears to be related to differences in reduction of hinge-region disulfides (*33*).

As summarized in Table 1, the other covalent methods could be used to produce 81C6 mAb−SA conjugates in reasonable yield, biotin-binding capacities equivalent to native SA, and immunoreactive fractions comparable to those obtained with native m81C6 and c81C6 (*17*, *34*). Coupling efficiencies were similar to those reported previously by Karacay et al. (*27*) but lower than those

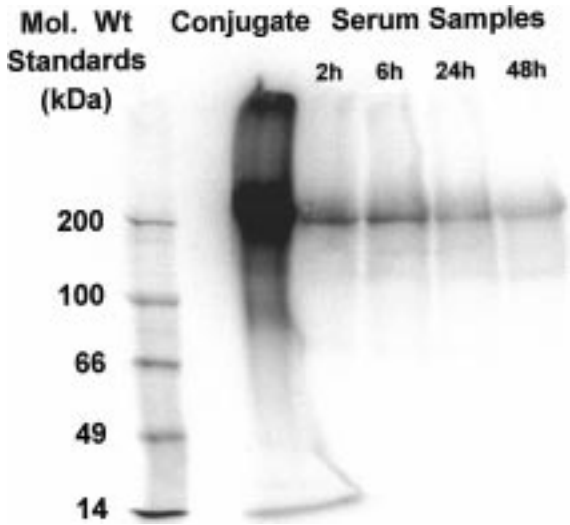


Figure 5. SDS−PAGE autoradiograph of serum samples (Lanes 3−6) obtained 2−48 h after injection of (^{125}I-labeled m81C6)-2IT-SMCC-SA in normal mice. Band at approximately 215 kDa corresponds to monomeric mAb−SA conjugate. Molecular mass standards and preinjection sample of conjugate shown in lanes 1 and 2 for comparison.

Table 2. Tissue Distribution of Radioactivity after Injection of(^{125}I-Labeled M81C6)-2IT-SMCC-SA in Tumor Bearing Mice

	% injected dose per gram of tissue[a]		
organ	day 2	day 3	day 4
liver	2.45 ± 0.04	1.97 ± 0.30	1.53 ± 0.43
spleen	2.35 ± 0.04	1.97 ± 0.59	1.59 ± 0.31
lungs	6.22 ± 1.91	3.33 ± 0.59	3.62 ± 1.03
heart	2.41 ± 0.31	1.87 ± 0.19	1.58 ± 0.22
kidneys	2.90 ± 0.16	2.66 ± 0.32	1.83 ± 0.34
bladder	2.24 ± 0.51	2.78 ± 1.16	2.28 ± 0.18
stomach	1.24 ± 0.31	1.00 ± 0.25	0.73 ± 0.09
sm. intestine	0.50 ± 0.11	0.60 ± 0.14	0.43 ± 0.08
lg. intestine	0.43 ± 0.04	0.31 ± 0.05	0.27 ± 0.06
thyroid[a]	3.11 ± 1.04	3.42 ± 0.92	3.07 ± 1.07
muscle	0.95 ± 0.07	0.73 ± 0.12	0.59 ± 0.07
blood	11.64 ± 0.59	9.97 ± 1.65	7.31 ± 1.15
urine	1.51 ± 3.38	10.50 ± 16.51	6.04 ± 2.18
tumor	30.98 ± 4.98	36.04 ± 10.69	24.34 ± 5.19
bone	2.41 ± 0.20	2.14 ± 0.30	2.11 ± 0.47
brain	0.28 ± 0.03	0.24 ± 0.04	0.20 ± 0.02

[a] %ID per organ for thyroid. IV injection, mean ± standard deviation of five animals.

obtained by Ngai et al. (*25*) using similar methods. However, it should be noted that in the later study, yields were based on levels of unreacted SA remaining in the reaction mixture, and the principal product had a molecular mass greater than 350 kDa.

Size-exclusion HPLC analysis of conjugation reaction mixtures (Figures 1A, 2, and 4) indicated the presence of multiple peaks including those with retention times corresponding to the desired ~215 kDa mAb−SA conjugate as well as unreacted mAb and SA. When iodoacetamide was used to terminate the reaction, an additional peak was observed at about 24−25 min corresponding to this species. Although these HPLC chromatograms suggested the existence of other products, the resolution was not sufficient to make reasonable molecular mass assignments. For this reason, SDS−PAGE analyses also were performed. Gels were not subjected to reducing and boiling conditions in order to minimize degradation of SA; however, this may have contributed to incomplete entry of the samples into the gel. As illustrated in Figure 1, panels C and D, multiple bands between 140 and 180 kDa were observed. We speculate that those at about 165 and 180 kDa, and capable of binding radiolabeled biotin, could represent mAb coupled to 1 or more SA subunits. In most cases, SDS−PAGE indicated that the HPLC peak eluting at about 12 min contained both the anticipated 215 kDa product as well as an unidentified 230 kDa product that did not possess biotin-binding capacity. One possibility is that this peak is the reaction product between intact IgG and an 75 kDa Fab/Fc monomer, a species observed previously in the catabolism of this mAb (*33*).

The procedure involving thiolation of mAb using 30 equiv of 2IT, and reaction of SA with 10 equiv of SMCC, gave the highest yield of 81C6 mAb−SA monomer. In more recent runs, the overall yield of 81C6 mAb-2IT-SMCC-SA has been increased to 75−80% by using Bio-Rad Poly-Prep columns (catalog no. 731-1550) as spin columns. Compared with SATA, use of 2IT is advantageous from a practical perspective because it is a one-step instead of a two-step procedure and does not require a buffer exchange dialysis. Although use of SPDP for SA modification might result in slightly higher conjugation yields, the resultant mAb−SA conjugate is formed via a disulfide bond that might be susceptible to rapid degradation in vivo.

Because of our interest in applying pretargeting strategies to the treatment of surgically created glioma resection cavities (*12*) the effect of human glioma cyst fluid on the integrity of (^{125}I-labeled m81C6)-2IT-SMCC-SA was investigated in vitro. Biotin-binding capacity was greater than 94% over a 72 h incubation period indicating that the conjugate remained functional in this environment. No evidence for degradation of the conjugate in tumor cyst fluid was observed by SDS−PAGE (data not shown). In contrast, the results of a similar assay indicated ~20% degradation of m81C6 after only 4 h in this milieu (*33*). The enhanced stability of the m81C6-SA conjugate compared with mAb alone warrants further investigation.

The in vivo properties of (^{125}I-labeled m81C6)-2IT-SMCC-SA were investigated in normal mice and athymic mice bearing subcutaneous D-54 MG human glioma xenografts. SDS−PAGE autoradiographs of serum samples obtained from normal mice demonstrated that the conjugate was quite stable in vivo. The biotin-binding capacity of the conjugate decreased rapidly with time (Figure 5), an observation that likely reflects saturation of the conjugate due to the high endogenous concentration of biotin in murine serum (*35*). Indeed, subsequent experiments have shown that when mice are placed on a biotin-deficient diet, the biotin-binding capacity of the conjugate is retained in vivo (C.F.F. and M.R.Z., manuscript in preparation). The tissue distribution of (^{125}I-labeled m81C6)-2IT-SMCC-SA was similar to that reported previously in this animal model for m81C6 radioiodinated using the Iodogen method (*16*, *34*). Three days after injection, tumor:blood ratios were 3.6:1 and greater than 10:1 for all other organs. These results compare favorably with those reported for an anti-CEA mAb−SA conjugate prepared via a procedure involving reduction of mAb sulfhydryls with (2-mercaptoethyl)-amine (*27*).

In summary, m81C6 and c81C6 mAb−SA monomeric conjugates could be prepared in good yield by thiolation of the mAb with 30 equiv of 2IT and formation of maleimido groups on SA by reaction with 10 equiv of SMCC. Conjugates retained the biotin-binding capacity and immunoreactivity of unmodified SA and 81C6, respectively. Further evaluation of (^{125}I-labeled m81C6)-2IT-SMCC-SA revealed that this conjugate possessed excellent in vitro and in vivo stability and tumor localizing capacity. This conjugate, in tandem with our radiohalogenated biotin derivatives, will now be evaluated for use in pretargeted radioimmunotherapy.

ACKNOWLEDGMENT

The excellent technical assistance of Susan Slade (animal experiments) and Phil Welsh (gel electrophoresis) is gratefully appreciated. This work was supported by the National Institutes of Health (CA42324, NS20023, and CA14236) and the Department of Energy (95ER62021).

LITERATURE CITED

(1) Goldenberg, D. M. (1994) New developments in monoclonal antibodies for cancer detection and therapy. *CA Cancer J. 44*, 43−64.

(2) Hnatowich, D. J., Virzi, F., and Rusckowski, M. (1987) Investigation of avidin and biotin for imaging applications. *J. Nucl. Med. 28*, 1294−1302.

(3) Paganelli, G., Magnani, P., Zito F., Villa, E., Sudati, F., Lopalco, L., Rossetti, C., Malcovati, M., Chiolerio, F., Seccamani, E., Siccardi, A. G., and Fazio, F. (1991) Three-step

monoclonal antibody tumor targeting in carcinoembryonic antigen-positive patients. *Cancer Res. 51*, 5960−5966.
(4) Stoldt, H. S., Aftab, F., Chinol, M., Paganelli, G., Luca, F., Testori, A., and Geraghty, J. G. (1997) Pretargeting strategies for radio-immunoguided tumour localization and therapy. *Eur. J. Cancer 33*, 186−192.
(5) Sung, C. and van Osdol, W. (1995) Pharmacokinetic comparison of direct antibody targeting with pretargeting protocols based on streptavidin−biotin binding. *J. Nucl. Med. 36*, 867−876.
(6) Breitz, H., Knox, S., Weiden, P., Goris, M., Murtha, A., Bryan, J., Axworthy, D., Seiler, C., Su, F.-M., Beaumier, and P., Reno, J. (1998) Pretargeted radioimmunotherapy with antibody-streptavidin and Y-90 DOTA-biotin (Avicidin): result of a dose escalation study. *J. Nucl. Med. 39*, 71P (abstr.).
(7) Paganelli, G., Grana, C., Chinol, M., Cremonesci, M., Cicco, C. De., Braud, F. De., Maggiolo, M. Robertson, C., Zurrida, S., Casadio, C., Siccardi, A. G., and Veronisi, U. (1998) Antibody guided three-step therapy for high grade glioma with ^{90}Y-biotin. *J. Nucl. Med.* 39, 70P (abstr.).
(8) Bourdon, M. A., Wikstrand, C. J., Furthmayr, H., Matthews, T. J., and Bigner, D. D. (1983) Human glioma-mesenchymal extracellular matrix antigen defined by monoclonal antibody. *Cancer Res. 43*, 2796−2805.
(9) Howeedy, A. A., Virtanen, I., Laitinen, L., Gould, N. S., Koukoulis, G. K., and Gould, V. E. (1990) Differential distribution of tenascin in the normal, hyperplastic, and neoplastic breast. *Lab. Invest. 63*, 798−806.
(10) Mackie, E. J., Chiquet-Ehrismann, R., Pearson, C. A., Inaguma, Y., Taya, K., Kawarada, Y., and Sakakura, T. (1987) Tenascin is a stromal marker for epithelial malignancy in the mammary gland. *Proc. Natl. Acad. Sci. U.S.A. 84*, 4621−4625.
(11) Brown, M. T., Coleman, R. E., Friedman, A. H. Friedman, H. S., McLendon, R. E. Reiman, R., Felsberg, G. J., Tien, R. D. Bigner, S. H., Zalutsky, M. R., Zhao, X. G., Wikstrand, C. J., Pegram, C. N., Herndon II, J. E., Vick, N. A., Paleologos, N., Fredericks, R. K., Schold, S. C., Jr., and Bigner, D. D. (1996) Intrathecal ^{131}I-labeled anti-tenascin monoclonal antibody 81C6 treatment of patients with leptomeningeal neoplasm or primary brain tumor resection cavities with subarachnoid communication: Phase I trial results. *Clin. Cancer Res. 2*, 963−972.
(12) Bigner, D. D., Brown, M. T., Friedman, A. H., Coleman, R. E., Akabani, G., Friedman, H. S., Thorstad, W. L., McLendon, R. E., Bigner, S. H., Zhao, X.-G., Pegram, C. N., Wikstrand, C. J., Herndon, J. E., II, Vick, N. A., Paleologos, N., Cokgor, I., and Zalutsky, M. R. (1998) Iodine-131-labeled anti-tenascin monoclonal antidoby 81C6 treatment of patients with recurrent malignant gliomas: Phase I trial results. *J. Clin. Oncol. 16*, 2202−2212.
(13) Foulon, C. F., Alston, K. L., and Zalutsky, M. R. (1997) Synthesis and preliminary evaluation of (3-iodobenzoyl)-norbiotinamide and (5-iodo-3-pyridine)carbonyl norbiotinamide: Two radioiodinated conjugates with improved stability. *Bioconjugate Chem. 8*, 179−186.
(14) Foulon, C. F., Alston, K. L., and Zalutsky, M. R. (1998) Astatine-211 labeled biotin conjugates resistant to biotinidase for use in pretargeted radioimmunotherapy. *Nucl. Med. Biol. 25*, 81−88.
(15) Murphy-Ullrich, J. E., Lightner, V. A., Aukhil, I., Yan, Y. Z., Erickson, H. P., and Höök, M. (1991) Focal adhesion interity is downregulated by the alternatively spliced domain of human tenascin. *J. Cell Biol. 115*, 1127−1136.
(16) He, X., Archer, G. E., Wikstrand, C. J., Morrison, S. L., Zalutsky, M. R., Bigner, D. D., and Batra, S. K. (1994) Generation and characterization of a mouse/human chimeric antibody directed against extracellular matrix protein tenascin. *J. Neuroimmunol. 52*, 127−137.
(17) Zalutsky, M. R., Schuster, J. M., Garg, P. K., Archer, Jr., G. E., Dewhirst, M. W., and Bigner, D. D. (1996) Two approaches for enhancing radioimmunotherapy: alpha emitters and hyperthermia. *Recent Results Cancer Res. 141*, 101−122.
(18) Foulon, C. F., Adelstein, S. J., and Kassis, A. I. (1996) One-step synthesis of radiolabeled biotin derivatives. *Bioorg. Med. Chem. Let. 6*, 779−784.
(19) Lindmo, T., Boven, E., Cuttitta, F., Fedoroko, J., and Bunn, P. A., Jr. (1984) Determination of the immunoreactive fraction of radiolabeled monoclonal antibodies by linear extrapolation to binding at infinite antigen excess. *J. Immunol. Methods 72*, 77−89.
(20) Bullard, D. E., Schold, S. C., Jr., Bigner, S. H., and Bigner, D. D. (1981) Growth and chemotherapeutic response in athymic mice of tumors arising from human glioma-derived cell lines. *J. Neuropathol. Exp. Neurol. 40*, 410−427.
(21) Foulon, C. F., Schoulzt, B. W., and Zalutsky, M. R. (1997) Preparation and biological characterization of an astatine-211 labeled biotin conjugate: biotinyl-3[^{211}At]astatoanilide. *Nucl. Med. Biol. 24*, 135−143.
(22) Kassis, A. I., Jones, P. L., Matalka, K. Z., and Adelsein, S. J. (1996) Antibody-dependent signal amplification in tumor xenografts after pretreatment with biotinylated monoclonal antibody and avidin or streptavidin. *J. Nucl. Med. 37*, 343−352.
(23) Chinol, M., Casalini, P., Maggiolo, M., Canervari, S. Omodeo, E. S., Caliceti, P., Veronese, F. M., Cremonesi, M., Chiolerio, F., Nardone, E., Siccardi, A. G., and Paganelli, G. (1998) Biochemical modifications of avidin improve pharamacokinetics and biodistribution, and reduce immunogenicity. *Br. J. Cancer 78*, 189−197.
(24) Khawli, L. A., Alauddin, M. M., Miller, G. K., and Epstein, A. L. (1993) Improved immunotargeting of tumors with biotinylated monoclonal antibodies and radiolabeled streptavidin. *Antibody, Immunoconjugates, Radiopharm. 6*, 13−27.
(25) Ngai, W. M., Reilly, R. M., Polihronis, J., and Shpitz, B. (1995) In vitro and in vivo evaluation of streptavidin immunoconjugates of the second generation TAG-72 monoclonal antibody CC49. *Nucl. Med. Biol. 22*, 77−86.
(26) Sheldon, K., Baumal, R., and Marks, A. (1992) Targeting of [^{111}In]biocytin to cultured ovarian adenocarcinoma cells using covalent monoclonal antibody-streptavidin conjugates. *Appl. Radiat. Isot. 43*, 1399−1402.
(27) Karacay, H., Sharkey, R. M., Govindan, S. V., McBride, W. J., Goldenberg, D. M., Hansen, H. J., and Griffiths, G. L. (1997) Development of a streptavidin-anti-carcinoembryonic antigen antibody, radiolabeled biotin pretargeting method for radioimmunotherapy of colorectal cancer. Reagent development. *Bioconjugate Chem. 8*, 585−594.
(28) Reno, J. M., Theodore, L. J., and Gustavson, L. M. (1997) Two-step pretargeting methods using improved biotin-active agent conjugates. U.S. Patent 5,630,996.
(29) Del Rosario, R. B., Baron, L.-A., Lawton, R. G., and Wahl, R. L. (1992) Streptavidin−biotinylated IgG conjugates: a simple procedure for reducing polymer formation. *Nucl. Med. Biol. 19*, 417−421.
(30) Wilbur, D. S., Hamlin, D. K., Vessella, R. L., Stray, J. E., Buhler, K. R., Stayton, P. S., Klumb, L. A., Pathare, P. M., and Weerawarna, S. A. (1996) Antibody fragments in tumor pretargeting. Evaluation of biotinylated Fab, colocalization with recombinant streptavidin and avidin. *Bioconjugate Chem. 7*, 689−702.
(31) Alvarez-Diez, T. M., Polihronis, J., and Reilly, R. M. (1996) Pretargeted tumor imaging with streptavidin immunoconjugates of monoclonal antibody CC49 and ^{111}In-DTPA-biocytin. *Nucl. Med. Biol. 23*, 459−466.
(32) Del Rosario, R. B., and Wahl, R. L. (1989) Site-specific radiolabeling of monoclonal antibodies with biotin/streptavidin. *Nucl. Med. Biol. 16*, 525, 529.
(33) Reist, C. J., Bigner, D. D., and Zalutsky, M. R. (1998) Human IgG2 constant region enhances in vivo stability of anti-tenascin antibody 81C6 compared with its murin parent. *Clin. Cancer Res. 4*, 2495−2502.
(34) Zalutsky, M. R., Moseley, R. P., Coakham, H. B., Coleman, R. E., and Bigner, D. D. (1989) Pharmacokinetics, and tumor localization of ^{131}I-labeled anti-tenascin monoclonal antibody 81C6 in patients with gliomas and other intracranial malignancies. *Cancer Res. 49*, 2807−2813.
(35) Wolf, B., Hymes, J., and Heard, G. S. (1990) Biotinidase. *Methods Enzymol. 184*, 103−111.

BC990040W

Synthesis of Polyallylamine Derivatives and Their Use as Gene Transfer Vectors in Vitro

Otmane Boussif,*,† Thierry Delair,‡ Catherine Brua,† Laurent Veron,‡ Andrea Pavirani,† and Hanno V. J. Kolbe†

TRANSGENE S.A., 11 rue de Molsheim, 67082 Strasbourg Cedex, France, and Unité Mixte CNRS-BioMérieux, ENS de Lyon, 46, allée d'Italie, 69364 Lyon Cedex 07, France. Received April 12, 1999; Revised Manuscript Received June 24, 1999

Cationic polymers possessing primary amine groups are inefficient in transferring nucleic acids into eukaryotic cells. With appropriate chemical modification, namely glycolylation of the amine groups of polylysine and polyallylamine, the actual number of free amino groups was decreased, hydrophilic residues were introduced, and the cytotoxicity of both polymers decreased significantly. Furthermore, in the case of polyallylamine, its ability to mediate gene transfer into cells increased by several orders of magnitude. Transfection efficiency was found to be dependent on the substitution level of amino groups and reached highest levels in the presence of lysosomotropic and/or fusogenic agents. At optimal conditions, glycolylated PAM was shown to be as efficient as the linear polyethylenimine of 22 kDa.

INTRODUCTION

Viral and synthetic gene transfer methods for applications in gene therapy are one of the major developing domains of biological research. The fact that selective gene delivery to target tissues still needs improvement with respect to transfer efficiency and expression persistence is a limiting factor for this approach to become routine therapy.

Various types of cationic polymers have been shown to be efficient agents for gene delivery into eukaryotic cells (Haensler and Szoka, 1993; Kabanov and Kabanov, 1995; Boussif et al., 1995; Boussif, 1996). Polyethylenimines (PEI)[1] and polyamidoamine dendrimers (PAMAM), which possess buffering capacity below physiological pH, are efficient carriers per se (Boussif et al.,1995; Behr, 1996). On the other hand, cationic polymers such as poly(L-lysine) are inefficient except when conjugated to specific ligands which lead to receptor-mediated endocytosis and when used in the presence of lysosomotropic and/or fusogenic agents (Zenke et al., 1990; Wagner et al., 1992; Midoux et al., 1993; Zauner et al., 1996). The aim of our work is to develop new cationic polymer families for efficient gene transfer. Rather than synthesizing new types of polymers, we have taken the approach of studying whether appropriate chemical modification of otherwise relatively cytotoxic polymers, e.g., poly-L-lysine (PLL) or polyallylamine (PAM), can reduce their toxicity and, at the same time, retain their capability to efficiently condense DNA. In this context, it has been shown that the transfection capacity of PLL could be improved by substituting to a certain extent the ϵNH_2 groups of the polypeptide with δ-gluconoyl (Erbacher et al., 1997) or poly(ethylene glycol) (Choi et al., 1998) moieties.

PAM contains, regularily spaced along its polymeric hydrocarbon backbone, a high density of primary amino groups existing either as free amine or as cationic ammonium salt. Here we report the successful modification of PAM and PLL by transamidification with methylglycolate leading to the decrease of their toxicity. Further glycolylation was shown to increase drastically the efficiency of PAM to mediate gene transfer. PAM at different degrees of glycolylation was compared to nonmodified or glycolylated PLL in in vitro cell transfection assays.

EXPERIMENTAL PROCEDURES

Chemicals. Polyallylamines (PAM x HC1, 50−65 kDa and 8.5−11 kDa), poly-L-lysine (PLL × HC1, 30−70 kDa) and triethylamine were purchased from Aldrich (France). Methylglycolate and methoxymethyl acetate were from Fluka (France). MTT [3-(4,5-dimethylthiazol-2-yl)- 2,5-diphenyltetrazolium bromide], chloroquine, and dimethyl sulfoxide (DMSO) were from Sigma. ExGen500, a linear PEI of 22 kDa (polyethylenimine), was purchased from Euromedex (Souffelweyersheim, France).

Cell Lines and Cell Culture. A549 human lung carcinoma, MRC-5 human fetal lung epithelium, HepG2 human hepatocarcinoma, and HeLa human cervix carcinoma cell lines were purchased from ATCC (Rockville, MD) and grown in Dulbecco's modified Eagle medium (DMEM, Gibco BRL, Cergy-Pontoise, France). Cell culture medium was supplemented with 10% FCS (fetal calf serum, Sigma) and 2 mM L-glutamine (Gibco BRL). Cells were maintained at 37 °C in a 5% CO_2 humidified atmosphere.

Cell Transfection. Cells were seeded (in 48 multiwell plates) 18 h before transfection to reach ~70% confluence at the time of transfection. Before adding the transfecting complexes, the medium (DMEM, Gibco BRL) was removed and replaced by 0.5 mL of serum-free medium or medium supplemented with 10% serum.

The polymer−DNA complexes were obtained as follows: 2 μg of plasmid pTG11033 (encoding the *Photinus pyralis* luciferase gene under the control of the cytome-

* To whom correspondence should be addressed. Fax: (33)3-88-22-58-07. Phone: (33) 3-88-27-91-14. E-mail: boussif@transgene.fr.

† Transgene S.A.

‡ Unite Mixte CNRS-BioMérieux.

[1] Abbreviations: PAM, polyallylamine; PLL, poly(L-lysine); PEI, polyethylenimine; Chlq, chloroquine.

10.1021/bc9900439 CCC: $18.00 © 1999 American Chemical Society
Published on Web 08/26/1999

galovirus immediate early enhancer/promoter) and the desired amount of cationic polymer [from 10 mM stock solutions in terms of protonated amine, in water at pH 7.4; 1 *N*/*P* equivalent corresponds to the amount of polymer necessary to have one amino group per phosphate of nucleic acid (330 Da mean M_W) (Zanta et al., 1997)] were each diluted in 50 μL (or 10 μL) of Hepes buffer (20 mM, pH 7.4) and vortexed. The two solutions were then mixed and gently vortexed. After 30 min of incubation at room temperature, the polyplexes were added to the cells. The plate was immediately centrifuged for 5 min at 1500 rpm [~280 g (Boussif et al., 1996)]. After 3−4 h, the medium was replaced by 0.5 mL of medium supplemented with 10% fetal calf serum. When transfection was performed in the presence of 100 μM chloroquine, 5 μL of 10 mM chloroquine solution was added to the medium immediately before the addition of the polyplexes. After 48 h, the medium was removed, cells were washed twice with PBS (Gibco), 100 μL of lysis buffer (Promega) were added and cells were frozen at −80 °C until analysis for luciferase activity. A total of 20 μL of supernatant was analyzed using the luciferase assay system (Promega) in 96 multiwell plates (Biolumat LB 9500, Berthold, Wilbach, Germany). Each transfection was done in triplicate. Values are given as mean relative light units (RLU) per milligram of cell protein (BCA assay, Pierce).

MTT Assay. Evaluation of cytotoxicity was performed by the MTT assay (Mossman, 1983). The cells were incubated with increasing amounts of the desired polymer in serum-free medium. After 4 h, the medium was replaced by 1 mL of medium supplemented with 10% fetal calf serum, and cells were incubated for an additional 24 h. MTT in PBS (20 μL/well of a 5 mg/mL MTT solution) was added 5 h before the end of the incubation period (Sgouras and Duncan, 1990). The medium was then removed, and the cells were carefully washed twice with PBS. The insoluble blue formazan crystals were dissolved in 200 μL of DMSO, and the absorbance was measured at 550 nm. Untreated cells were used as control (100% viability).

Synthesis of 0.5G-PAM. (Approximately 50% of primary amines was substituted with glycolate.) A total of 898 mg of PAM × HCI, 50−65 kDa (9.6 mmol NH_3^+) was dissolved in 1 mL of MilliQ water. A total of 540 mg (6 mmol, i.e., 0.625 equiv) of methylglycolate was added at room temperature followed by addition of 2.7 mL triethylamine (19.4 mmol, i.e, 2 equiv). After 72 h, the mixture was evaporated, and the obtained residue was redissolved in 35% ammonia/water (50:50 v/v). This treatment was repeated twice followed each time by evaporation under vacuum to completely eliminate triethylamine. The residue was dissolved in water at pH 1 (adjusted with 6 N HCl) and then precipitated in acetone. The precipitate was filtered and redissolved in water for lyophilization. A total of 858 mg of 0.5G-PAM was obtained as a white powder, with a yield of 86%. The ^{1}H NMR spectrum was recorded in D_2O containing 10 μL of 4 N NaOH with trimethylsilyl deuterated propionic acid (TSPD4) as an internal reference: δ (ppm) 4.09 (-CH_2-OH); 3.22 (-CH_2-NH-CO-); 2.81 (-CH_2-NH_2); 1.77−1.25 (aliphatic protons).

Synthesis of 0.68G-PAM. A similar protocol was used for the synthesis of 0.68G-PAM (approximately 68% of primary amines substituted with glycolate) with minor modifications. Briefly, 500 mg of PAM × HCl, 50−65 kDa (5.37 mmol of NH_3^+) was dissolved at room temperature in 1.75 mL of MilliQ water. A total of 418 mg (4.57 mmol, i.e., 0.85 equiv) of methylglycolate was added at room temperature followed by addition of 1.5 mL of triethylamine (10.7 mmol, i.e 2 equiv). The subsequent steps were similar to those described above. This synthesis was reproduced three times; modification levels were 68.7, 68.2, and 67.4%, respectively, as determined by ^{1}H NMR integration.

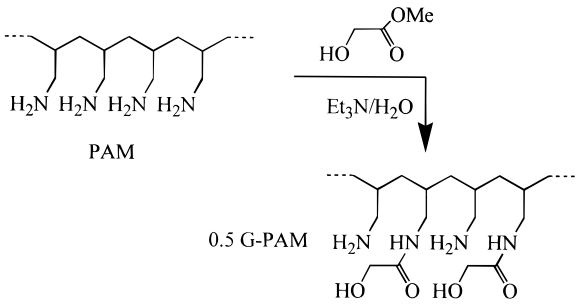


Figure 1. Scheme of the synthesis of glycolylated PAM.

Synthesis of 0.7G-PLL. A total of 108 mg of PLL × HCl (0.4 mmol of NH_3^+) was dissolved in 3 mL of MilliQ water. After addition of 3 mL of triethylamine (21.5 mmol, i.e 54 equiv), 237 mg (2.59 mmol, i.e., 6.48 equiv) of methylglycolate was added at room temperature in four portions over 4 days. The reaction mixture was then diluted with 16% ammonia in water and concentrated under reduced pressure. This dilution−concentration process was repeated twice. The mixture was then acidified with concentrated HCl, and the polymer was precipitated in 400 mL of acetone. The precipitate was dissolved in water and lyophilized. The polymer was analyzed by ^{1}H NMR in D_2O, containing traces of sodium hydroxide (reference: trimethylsilyl propionic acid, TSPD4): δ 4.25 ppm, 1H; 4.07 (-CH_2-OH); 3.25 (-CH_2-NH-CO-); 2.96 (-CH_2-NH_2); 2−1.2 (6H). The level of derivatization (69.6%) was determined by the ratio of the integration of the peak at 3.25 ppm versus the integration of the peaks at 3.25 and 2.96 ppm corresponding to the methylene group bearing the primary amine.

Amidation of PAM with Methylmethoxyacetate. The synthesis was carried out in analogy to the protocol using methylglycolate. ^{1}H NMR, D_2O: δ 4.01 ppm, 2H (CH_2-O-CH_3), 3.43 3H (CH_2-O-CH_3), 3.22 2H (CH_2NH-CO), 2.78 2H (C$H_2$$NH_2$), 1.77−1.28 (aliphatic protons).

RESULTS

We have derivatized the amino groups of PAM and PLL with methylglycolate to study its effect on their cytotoxicity and cell transfection efficiency in vitro. Below, the influence of various parameters such as degree of polymerization, level of glycolylation, ratio of polymer amino groups to DNA phosphate groups (*N*/*P* ratio), amount of DNA used in the assay, and the presence of serum or helper agent is described.

Synthesis of Glycolylated PAM. A series of derivatives of PAM was synthesized by random substitution of the primary amino groups with methylglycolate residues (Figure 1). Such a modification reduces the intrinsic charge of the polymer and introduces hydrophilic residues (hydroxyl groups) which may increase the solubility of the polymer−DNA complex. Glycolylated PAM products were characterized by ^{1}H NMR in D_2O with 10 μL of NaOH as solvent (signal at 4.6−4.7 ppm). The percentage of glycolyl group derivatization was estimated from the peak area of the amido methylene group (3.22 ppm) divided by the sum of the peak areas of the amido methylene and the amino methylene groups (3.22 and 2.81 ppm, respectively). In the case of 0.68G-PAM,

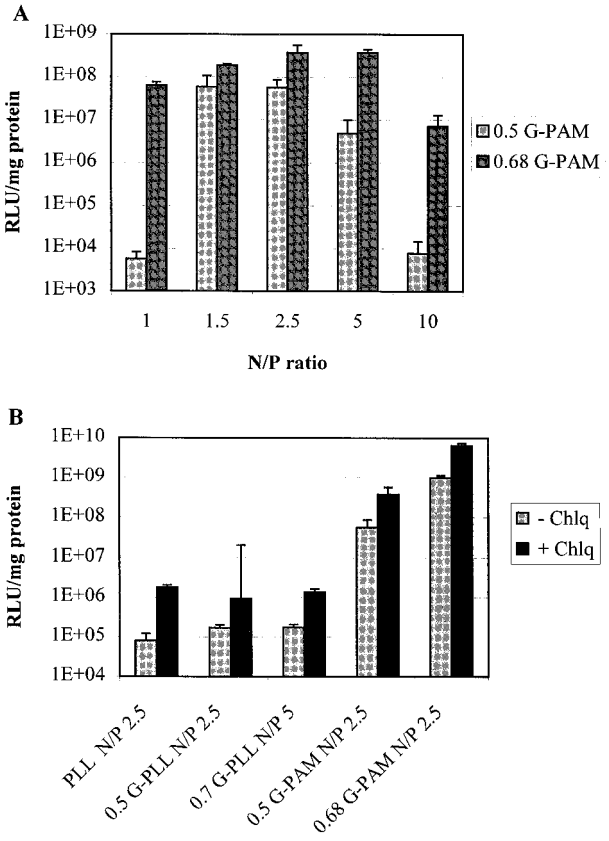


Figure 2. (A) Polyfection with Glycolylated PAM vs *N/P* ratio. A549 cells were transfected with 2 μg of pTG11033 and increasing amounts of polymer. (B) Polyfection with glycolylated PLL and chlorocuine effect. A549 cells were incubated in the presence or absence of chloroquine (100 μM) with pTG11033 (2.9 μg) formulated with the desired polymer at *N/P* 2.5 or 5. Transgene expression was measured 48 h posttransfection. Each point was determined in triplicate and results are expressed as mean values ± SD.

repeated synthesis yielded three different batches of 0.68G-PAM with 68.1 ± 0.66% of glycolylation. This attests to the relatively high reproducibility of such chemistry. Two glycolylated PAMs, 0.5GPAM and 0.68G-PAM (50.3 and 68.7%, respectively, of amino groups converted to amidylglycolate) were thus obtained and used to define the optimal conditions to reach high transfection efficacy.

Transfection Efficiency of Glycolylated PLL and PAM vs *N/P* Ratio. In vitro studies, with both lipoplexes and polyplexes (Felgner et al., 1997), have shown that electrostatic interactions between the negatively charged cell membranes and the positively charged DNA complexes are enhanced by increasing the overall charge of the complexes, which in turn is achieved by increasing the ratio of carrier to DNA. We wanted to study the relationship between the level of transgene expression and *N/P* ratio. 0.5G-PAM and 0.68G-PAM polyplexes were tested on A549 human lung carcinoma cells at different *N/P* ratios. Indeed, it is believed that for efficient gene delivery polycation−DNA complexes must bear a net positive charge (Behr, 1994; Boussif et al., 1995). A series of experiments was performed in the presence or absence of 100 μM chloroquine, an endosomolytic agent which leads to an enhancement of transfection with PLL carrier systems. The results are shown in Figure 2. Both polymers, 0.5G-PAM and 0.68G-PAM, showed transfection activity at all *N/P* ratios tested (Figure 2A). Luciferase expression after 48 h was high even in cells transfected with complexes at low *N/P* ratios: at a ratio

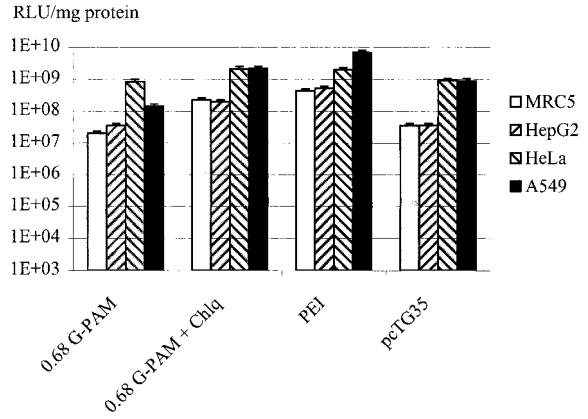


Figure 3. Polyfection of various cell lines with glycolylated PAM. Cells were transfected with 2 μg of pTG11033 complexed to 0.68 G-PAM, PEI, or pcTG35 at *N/P* 2.5, 5, and 5, respectively. Transgene expression was measured 48 h posttransfection. Values are the mean of three independent experiments made in triplicate.

of 2.5, the expression levels reached 10^8-10^9 RLU/mg of protein. The transfection efficiency was always higher when experiments were performed in the presence of 100 μM chloroquine (Figure 2B). Using 0.5- and 0.7G-PLL, the expression levels were variable, even in the presence of chloroquine, and in the same order of magnitude as those obtained with nonmodified PLL (Figure 2B). Importantly, in all cases, the levels of expression were approximately 100- to 1000-fold lower than those obtained with the corresponding 0.68G-PAM, indicating the importance of the hydrophobic backbone of PAM for efficient gene transfer.

Transfection efficiency of synthetic gene delivery systems also depends on the cell type (Boussif et al., 1996). We therefore performed transfection in three widely used cell types, MRC-5 (human fetal lung epithelium), HepG2 (human hepatocarcinoma), and HeLa (human cervix carcinoma) cells. Different cationic polymers at different *N/P* ratios were used to define optimized transfection conditions. As shown in Figure 3, a high level of luciferase expression (at least 5×10^7 RLU/mg of protein) was achieved with glycolylated PAM. A significant increase of efficiency was observed in the presence of 100 μM chloroquine (Figure 3) or 14% glycerol (not shown). At optimal conditions, transgene expression levels were similar to or even higher than those obtained with PEI and the cationic glycerolipid pcTG35 (Schughart et al., 1999).

Dose Response Study. DNA dose dependency was analyzed by observing the transfection efficiency of 0.68G-PAM as a function of the amount of DNA polyplexes at *N/P* ratio 2.5. Again, the transfection was performed in the presence or absence of chloroquine. Although transfection efficiency decreased with decreasing amount of polyplexes, at low amounts of DNA, e.g., 0.1 μg, significant transgene expression was still obtained (Figure 4). However, like other synthetic vectors, transfection efficiency decreased more than 2 orders of magnitude when less than 0.5 μg of DNA was used. It should be noted that using 4 μg of plasmid and 0.68G-PAM/DNA polyplexes at *N/P* ratio 5, no chloroquine was required to achieve optimal transfection, and by increasing the amount of DNA up to 6 μg, no cell damage was seen reflecting the low toxicity of the modified PAM (see also below).

Cytotoxicity of Glycolylated PAM. We examined the effect of glycolylation on cytotoxicity on A549 cells

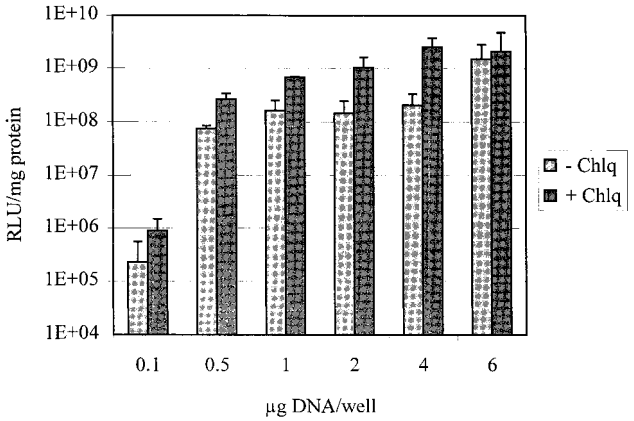


Figure 4. DNA dose−response effect on polyfected cells. A549 cells were transfected in the presence or absence of chloroquine (100 μM) with various amounts of pTG11033 (0.1−6 μg) complexed with 0.68 G-PAM at *N*/*P* 2.5. Transgene expression was measured 48 h posttransfection. Each point was realized in triplicate and results are expressed as mean values ± SD.

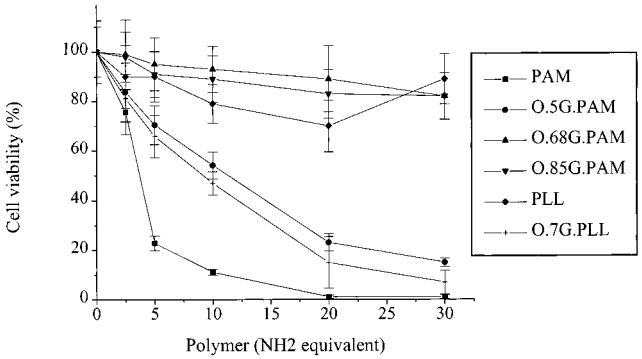


Figure 5. Glycolylation effect on cytotoxicity of PLL and PAM. A549 cells were incubated in the absence of serum with increasing amounts of polymer for 4 h. After replacing medium with fresh one supplemented with 10% serum, the cells were grown for another 40 h. Each point was realized in triplicate and results are expressed as mean values ± SD.

by using a tetrazolium-based MTT colorimetric assay (Sgouras and Duncan, 1990). Cells were incubated for 4 h with increasing amounts of polymer (corresponding to the amount of the polymer needed for 4 μg of plasmid to obtain *N*/*P* ratios ranging 2.5−30) in the absence of serum. The results are expressed as percentage of cell viability relative to nontreated cells.

Modified PLL and PAM showed a better biocompatibility than the corresponding non-modified polymers (Figure 5). 0.5G-PAM was less toxic than PAM but a residual toxicity comparable to that of nonmodified PLL was still detectable. When the level of glycolylation was increased to above 70%, glycolylated PAM exhibited only very slight cytoxicity even at high concentrations (more than 75% cell viability with *N*/*P* ratio 30).

A similar assay was carried out with polymer−DNA complexes (polyplexes). A549 cells were polyfected with 4 μg of plasmid complexed to increasing amounts of 0.5G-PAM, 0.68G-PAM, PLL, or 0.7G-PLL. The general behavior of polymers alone or polyplexes was similar: nonmodified polymers were relatively toxic and their biocompatibility increased with increasing degree of glycolylation (data not shown).

Transfection Efficiency Depends on the Degree of Glycolylation. To study the influence of the degree of substitution of amino groups, we synthesized several PAM derivatives differing by their degree of glycolylation (50−85%) according to the protocol described above by

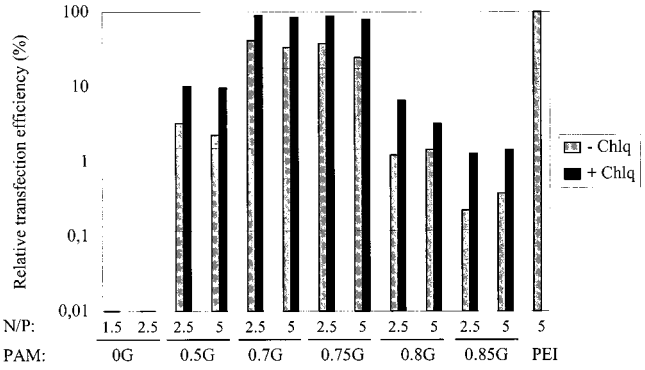


Figure 6. Effect of glycolylation level on transfection efficiency. A549 cells were transfected with 2 μg of pTG11033 complexed with different glycolylated PAM (0−85%; see legend) at *N*/*P* of 2.5 or 5. Luciferase activity was measured 48 h after transfection. Values are given as relative transfection efficiency to PEI (100%). Results represent the mean of four independent experiments.

adjusting the ratio of methylglycolate. Transfection of A549 cells with polyplexes was performed at *N*/*P* ratio 2.5 and 5; agarose gel electrophoresis of polyplexes was carried out in parallel to the in vitro assays to verify that DNA was completely retarded by interaction with the polymer (data not shown). Figure 6 summarizes the mean transfection efficiencies of four independent experiments. The results are presented as relative activity as compared to the value obtained with PEI (100%). The substitution levels from 70% to about 75% gave the highest luciferase expression. Beyond this substitution level, the transfection efficiency decreased gradually. As assessed by agarose gel retardation assay (data not shown), this phenomenon is not due to a partial complexation of the DNA with highly modified polymer. It may be due to a decreased affinity of the polymer for DNA leading to a faster decomplexation by interaction of the polyplex with constituents present in the culture medium or in the target cell.

Influence of Polymer Size. It has been shown that transfection efficiency of cationic polymers such as polylysine or PAMAM dendrimers depends on their degree of polymerization (Haensler and Szoka, 1993; Boussif, 1996; Erbacher et al., 1995). To see whether the size of polyallylamine may influence its transfection ability, polyallylamines with different degrees of polymerization were glycolylated to the same extent. The resulting transfection efficiencies were compared under various conditions. 0.74G-PAM (∼10 kDa) and 0.68G-PAM (∼60 kDa) gave similar results. Both polymers showed high levels of expression even at low *N*/*P* ratio (Figure 7A). Their transfection efficiencies in the presence of serum were affected to about the same extent (Figure 7B). Therefore, the size of the polymer, at least within the range 10−60 kDa, does not interfere with its ability to mediate gene transfer into cells in vitro.

Requirement of Glycolate Hydroxyl Residue for Efficient Polyfection. To examine whether the presence of free glycolate hydroxyl groups influences the transfection efficiency, we substituted the hydroxyl group with a methoxy group. Thus, referring to the protocol described for the synthesis of glycolylated polymers, two methoxyacetylated PAMs were prepared (0.45MeG-PAM, and 0.65MeG-PAM: 45% and 65% of amino groups of PAM substituted with methoxyacetate, respectively). Transfections of A549 cells were performed with these polymers complexed to 2 μg of DNA in the absence and presence of 100 μM chloroquine. Methoxyacetylated PAM

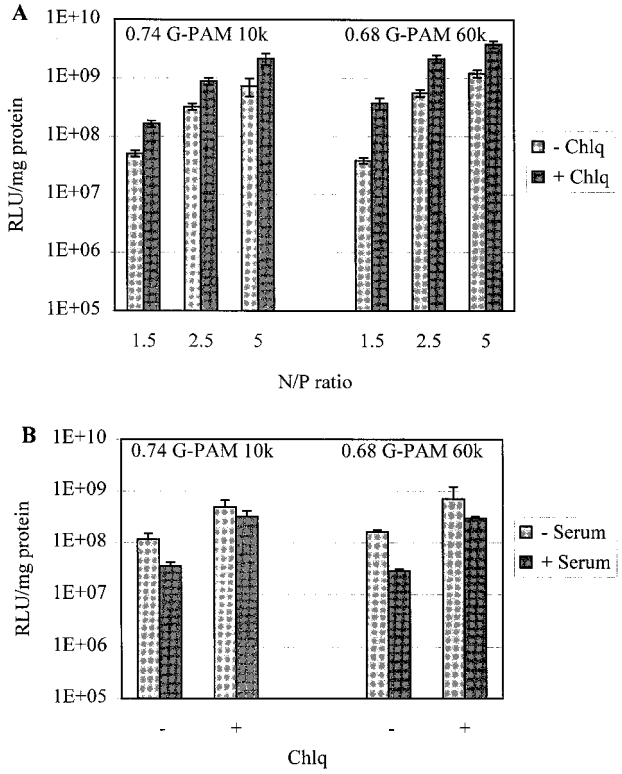


Figure 7. Effect of polymer size on transfection efficiency. (A) Effect of *N*/*P* ratio. A549 cells were transfected with 2 μg of pTG11033 and the amount of the desired polymer (0.74G-PAM or 0.68G-PAM). Expression was stopped 48 h later. Values are the mean ± SD of triplicate. (B) Serum effect on polyfection with glycolylated PAM. A549 cells were incubated in the presence or absence of serum (10%) with pTG11033 (2 μg) complexed with the desired polymer (0.74G-PAM or 0.68G-PAM) at *N*/*P* 2.5. Experiment was performed with and without chloroquine (100 μM). Results are the mean values ± SD of triplicate.

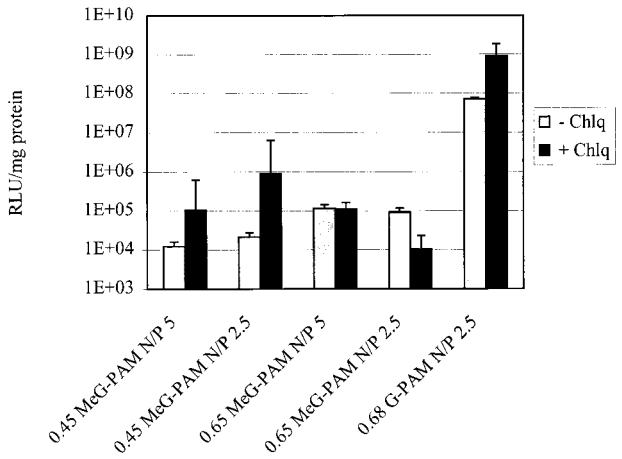


Figure 8. Effect of the substitution of glycolyl-hydroxyl group with methoxyl on glycolylated PAM transfection efficiency. A549 cells were transfected with 2 μg of pTG11033 complexed to the desired amount of polymer tested. Transgene expression was measured 48 h posttransfection. Each point was determined in triplicate and results are expressed as mean values ± SD.

efficiencies were found to be irreproducible and at least 100−1000-fold lower than those obtained with glycolylated PAM (Figure 8), demonstrating that the hydroxyl group is required to achieve high and reproductible gene transfer and expression. However, it should be noted that methoxyacethylated PAMs were more efficient than the native polymer, showing that reducing free primary amines of the polymer is also required.

DISCUSSION

Several cationic polymers have been used for in vitro and in vivo gene transfer (Kabanov et al., 1991; Wu et al., 1987; Wu and Wu, 1988; Boussif et al., 1995; Haensler and Szoka 1993; Cherng et al., 1996). Cationic polymers such as PLL and PAM possessing only primary amines are relatively toxic (Sgours and Duncan, 1990) and are, when complexed to DNA, inefficient transfection agents (Boussif, 1996). PLL, when conjugated to specific ligands (Wagner, 1998) and/or substituted with δ-gluconoyl (Erbacher et al., 1997) or poly(ethylene glycol) residues (Choi et al., 1998) to a certain extent, becomes more efficient especially when transfection is performed in the presence of lysosomotropic and/or fusogenic agents (Zenke et al., 1990; Wagner et al., 1992; Erbacher et al., 1997; Zauner et al., 1996).

We hypothesized that, by reducing the density of primary amino groups and by introducing hydrophilic groups, such polymers could be detoxified and their ability to mediate transfection of eukaryotic cells could be enhanced. Thus, glycolylated PAMs and PLLs were synthesized. First, the modified molecules were significantly less toxic than the original polymers (Figure 5). Second, in the case of PAM, transfection efficiency increased by several orders of magnitude (Figure 2). Below 75% modification, polymers reached high levels of transgene expression, similar to those obtained with the linear PEI of 22 kDa (Boussif, 1996) and the cationic glycerolipid pcTG35 (Schughart et al., 1999) (Figure 6). Efficient transfection was achieved even at low *N*/*P* ratios (Figure 2). According to a potentiometric study with nonmodified PAM reported by Suh et al. (1994), polyplexes in the range of the *N*/*P* ratio used (1.5−5) should have an overall negative charge or at most a slightly positive charge. Indeed, at about pH 7 only ∼14% of amino groups are protonated showing that the ammonium ions of PAM are sufficiently proximal to enhance mutual deprotonation (Suh et al., 1994). This is a relevant feature as it was shown that lipoplexes as well as polyplexes activate the complement system, but the activation decreases when a low charge ratio is used (Plank et al., 1996). Further glycolated PAM polyplexes, in contrast to PAM polyplexes, could be easly formulated at high DNA concentration (at least 0.25 g/L), and as measured by laser light scattering (Coulter N4plus), their sizes were relatively small (∼200 nm).

As endocytosis is the main route for polyplexes to enter the cell, they should escape the endosomal pathway as rapidly as possible to avoid DNA degradation and, therefore, increase their probability of reaching the nucleus. Thus, the presence of 100 μM chloroquine (Zenke et al., 1990; Midoux et al., 1993) or 14% glycerol (Zauner et al., 1996) (data not shown) enhanced significantly the expression levels of reporter gene in the various cell types tested. Furthermore, it was reported that chloroquine could participate in the dissociation of polyplex in the endosomes (Erbacher et al., 1996), allowing the release of DNA into the cytosol.

The comparison of glycolylated PAMs of different degrees of derivatization showed that the highest transgene expression was obtained between 70 and 75% (Figure 6). Beyond 75% glycolylation, the transfection efficiency decreased rapidly. As assessed by gel retardation, in contrast to PLL (Plank et al., 1992; Erbacher et al., 1995), even highly substituted PAM (>80%) is still able to complex DNA. The decrease of efficiency is not likely to be due to a difference in DNA complexation. It may be due to a decrease in the polymer−DNA interac-

tion leading to decomplexation by interaction of the polyplex with constituents of the culture medium or the cellular membrane followed by faster degradation of plasmid DNA.

Using two PAMs of different size, the in vitro transfection efficiency was found to depend neither on the *N*/*P* ratio nor on the amount of polyplex within the molecular mass range 10−60 kDa. Indeed, the results obtained with 0.74G-PAM, 10 kDa, and 0.68G-PAM, 60 kDa, were quite similar under all conditions tested (Figure 7).

One factor which strongly influences transfection efficiency is the presence of the glycolate hydroxyl group. Transamidification of PAM with methoxymethyl acetate (methoxyl group) instead of methyl glycolate (hydroxyl residue) led to low and irreproducible expression levels of the reporter gene (Figure 8). This could be due to the higher viscosity of ether functions leading to more hydrophobic and/or rigid polyplexes. In fact, Tang and Szoka (1996) reported that transfection efficiency is related to the flexibility of the polymer.

In contrast, although complete gel retardation of DNA was achieved at low polymer/DNA ratios with all modified PLLs (0.7 G-PLL), they showed rather weak gene delivery into A549 cells (Figure 2). Expression levels obtained in the presence of 100 μM chloroquine were still 100−1000-fold lower than those of glycolylated PAM and were comparable to those of unmodified PLL ($\sim 10^5-10^6$ RLU/mg of protein). According to our cell viability studies, this is not be due to residual cytotoxicity (Figure 5). Improvement of PLL efficiency may require extended hydrophilic moieties (Erbacher et al., 1997; Choi et al., 1998). The differences between PLL and PAM seem to underline the importance of the nature of the backbone of the polymer: PLL being less hydrophobic than PAM. A good hydrophilic/lipophilic balance could facilitate the trafficking of DNA into the cytoplasm and/or toward the nucleus.

Because glycolylated PLLs are less cytotoxic than unmodified PLL and although their transfection efficiency is low, it would be interesting to study whether glycolylated PLL conjugated to a ligand for receptor-mediating endocytosis could achieve efficient gene transfer to permissive cells.

Chloroquine was recently used to enhance in vivo gene delivery (Baru et al., 1995; Merwin et al., 1994), but this approach would not be suitable in the development of gene delivery systems for use in humans. Thus, we plan to substitute the chloroquine function by additional chemical modifications of PAM such as the generation of secondary amino leading, hopefully, to an intrinsic buffering capacity of the polymer and/or even enhancing its solubility and flexibility. Further presence of primary and secondary amines could modulate favorably the interactions between the polymer and DNA.

In conclusion, the detoxification of cationic polymers seems to be a feasible approach to develop new polymer-based synthetic gene delivery systems. Although detoxification is not sufficient to systematically improve the capacity of the polymer to mediate gene transfer, it will be interesting to investigate glycolylation of other polymers used for gene transfer to determine if the phenomenon of detoxification can be applied in general terms.

ACKNOWLEDGMENT

We would like to thank Dr. Bruno Cavallini and Isabelle Renardet for providing us with plasmid DNA. We are grateful to Dr. Michael Courtney for critical reading of the manuscript. This work was partially supported by the Association Francaise contre les Myopathies (AFM) and the Association Française contre La Mucoviscidose (AFLM).

LITERATURE CITED

Baru, M., Axelrod, J. H., and Nur, I. (1995) Liposome-encapsulated DNA-mediated gene transfer and synthesis of human factor IX in mice. *Gene 161*, 143−150.

Behr, J. P. (1994) Gene transfer with synthetic cationic amphiphiles: prospects for gene therapy. *Bioconjugate Chem. 5*, 382−389.

Behr, J. P. (1996) L′éponge ā protons: un moyen d′entrer dans une cellule auquel les virus n′ont pas pensé. *Med. Sci. 12*, 5−59.

Boussif, O. (1996) *Gene transfer mediated by cationic polymers*, Ph.D. Thesis, p 166, Louis Pasteur University, Strasbourg, France.

Boussif, O., Lezoualc′h, F., Zanta, M. A., Mergny, M. D., Scherman, D., Demeneix, B., and Behr, J. P. (1995) A versatile vector for gene and oligonucleotide transfer into cells in culture and in vivo: polyethylenimine. *Proc. Natl. Acad. Sci. U.S.A. 92*, 7297−7301.

Boussif, O., Zanta, M. A., and Behr, J. P. (1996) Optimized galenics improve in vitro gene transfer with cationic molecules up to 1000-fold. *Gene Ther. 3*, 1010−1017.

Cherng, J. Y., van de Wetering, P., Talsma, H., Crommelin, D. J., and Hennink W. E. (1996) Effect of size and serum proteins on transfection efficiency of poly ((2-dimethylamino)ethyl methacrylate)-plasmid nanoparticles. *Pharm Res. 13*, 1038−1042.

Choi, Y. H., Liu, F., Kim, J. S., Choi, Y. K., Park, J. S., and Kim, S. W. (1998) Poly(ethylene glycol)-grafted poly-L-Lysine as polymeric gene carrier. *J. Controlled Release 54*, 39−48.

Erbacher, P., Roche, A. C., Monsigny, M., and Midoux, P. (1995) Glycosylated polylysine/DNA complexes: gene transfer efficiency in relation with the size and the sugar substitution level of glycosylated polylysines and with the plasmid size. *Bioconjugate Chem. 6*, 401−410.

Erbacher, P., Roche, A. C., Monsigny, M., and Midoux, P. (1996) Putative role of chloroquine in gene transfer into a human hepatoma cell line by DNA lactosylated PLL complexes. *Exp. Cell Res. 225*, 186−194.

Erbacher, P., Roche, A. C., Monsigny, M., and Midoux, P. (1997) The reduction of positive charges of polylysine by partial gluconylation increases the transfection efficiency of polylysine/DNA complexes. *Biochim. Biophys. Acta 1324*, 27−36.

Felgner, P. L., Barenholz, Y., Behr, J. P., Cheng, S. H., Cullis, P., Huang, L., Jessee, J.A., Seymour, L., Szoka, F., Thierry, A. R., Wagner, E., and Wu, G. (1997) Nomenclature for synthetic gene delivery systems. *Hum. Gene Ther. 8*, 511−512.

Haensler, J., and Szoka., F. C. (1993) Polyamidoamine cascade polymers mediate efficient transfection of cells in culture. *Bioconjugate Chem. 4*, 372−379.

Kabanov, A.V., and Kabanov., V. A. (1995) DNA complexes with polycations for the delivery of genetic material into cells. *Bioconjugate Chem. 6*, 7−20.

Kabanov, A.V., Astafyeva, I. V., Chikindas, M. L., Rosenblat, G. F., Kiselev, V. I., Severin, E. S., and Kabanov., V. A. (1991) DNA interpolyelectrolyte complexes as a tool for efficient cell transformation. *Biopolymers 31*, 1437−1443.

Merwin, J. R., Noell, G. S., Thomas, W. L., Chiou, H. C., DeRome, M. E., McKee, T. D.,Spitalny, G. L., and Findeis, M. A. (1994) Targeted delivery of DNA using YEE(GalNAcAH)3, a synthetic glycopeptide ligand for the asialoglycoprotein receptor. *Bioconjugate Chem. 5*, 612−620.

Midoux, P., Mendes, C., Legrand, A., Raimond, J., Mayer, R., Monsigny, M., and Roche,A. C. (1993) Specific gene transfer mediated by lactosylated poly-L-lysine into hepatoma cells. *Nucleic Acid Res. 21*, 871−878.

Mossman, T. (1983) Rapid colorimetric assay for cellular growth and survival: application to proliferation and cytotoxicity assays. *J. Immunol. Methods 65*, 55−63.

Plank, C., Mechtler, K., Szoka, F. C., and Wagner, E. (1996) Activation of the complement system by synthetic DNA complexes: a potential barrier for intravenous gene delivery. *Hum. Gene Ther. 7*, 1437−1446.

Plank, C., Zatloukal, K., Cotten, M., Mechtler, K., and Wagner, E. (1992) Gene transfer into hepatocytes using asialoglycoprotein receptor mediated endocytosis of DNA complexed with an artificial tetra-antennary galactose ligand. *Bioconjugate Chem. 3*, 533−539.

Plank., C., Oberhauser., B., Mechtler., K., Koch., C., and Wagner, E. (1994) The influence of endosome-disruptive peptides on gene transfer using synthetic virus-like gene transfer systems. *J. Biol. Chem. 269*, 12918−12924.

Schughart, K., Bischoff, R., Ali Hadji, D., Boussif, O., Perraud, F., Accart, N., Rassmussen,U. B., Pavirani, A., Van Rooijen, N., and Kolbe, H. V. J. (1999) Effect of liposome- encapsulated clodronate pretreatment on synthetic vector-mediated gene expression in mice. *Gene Ther.* 6, 448−453.

Sgours, D., and Duncan, R. (1990) Methods for the evaluation of biocompatibility of soluble synthetic polymers which have potential for biomedical use: 1-Use of the tetrazolium-based colorimetric assay (MTT) as a preliminary screen for evaluation of in vitro cytotoxicity. *J. Mater. Sci.: Mater. Med. 1*, 61−68.

Suh, J., Paik, H.J., and Hwang., B. K. (1994) Ionization of poly(ethylenimine) and poly(allylamine) at various pH's. *Bioorg. Chem. 22*, 318−327.

Tang, M. X., and Szoka F. C. (1997) The influence of polymer structure on the interactions of cationic polymers with DNA and morphology of the resulting complexes. *Gene Ther. 4*, 823−832.

Tang, M. X., Redemann, C. T., and Szoka, F.C. (1996) In vitro gene delivery by degraded polyamidoamine dendrimers. *Bioconjugate Chem. 7*, 703−714.

Wagner, E., Plank, C., Zatloukal, K., Cotten, M.,and Bimstiel, M. L. (1992) Influenza virus hemagglutinin HA-2 N-terminal fusogenic peptides augment gene transfer by transferrin-polylysine-DNA complexes: toward a synthetic virus-like gene-transfer vehicle. *Proc. Natl. Acad. Sci. U.S.A. 89*, 7934−7938.

Wagner, E. (1998) Receptor-mediated delivery of plasmid DNA. *Biogenic Amines 14*, 519−536.

Wu, G.Y., and Wu, C. H. (1988) Receptor-mediated gene delivery and expression *in vivo. J. Biol. Chem. 263*, 14621−14624.

Zanta, M. A., Boussif, O., Adib, A., and Behr, J.P. (1997) In vitro gene delivery to hepatocytes with galactosylated polyethylenimine. *Bioconjugate Chem. 8*, 839−844.

Zenke, M., Steinlein, P., Wagner, E., Cotten, M., Beug, H., and Birnstiel, M. L. (1990) Receptor-mediated endocytosis of transferrin-polycation conjugates: an efficient way to introduce DNA into hematopoietic cells. *Proc. Natl. Acad. Sci. U.S.A. 87*, 3655−3659

Zauner, W., Kichler, A., Schmidt, W., Sinski, A., and Wagner, E. (1996) Glycerol enhancement of ligand-polylysine/DNA transfection. *Biotechniques 20*, 905−913.

BC9900439

RP463: A Stabilized Technetium-99m Complex of a Hydrazino Nicotinamide Derivatized Chemotactic Peptide for Infection Imaging

D. Scott Edwards, Shuang Liu,* Marisa C. Ziegler, Anthony R. Harris, Andrew C. Crocker, Stuart J. Heminway, and John A. Barrett

DuPont Pharmaceuticals Company, Medical Imaging Division, 331 Treble Cove Road, North Billerica, Massachusetts 01862

Gary J. Bridger and Michael J. Abrams

AnorMed Inc., 200-20353 64th Avenue, Langley BC V2Y 1N5, Canada

John D. Higgins III

McNeil Consumers Products, 7050 Camp Hill Road, Fort Washington, Pennsylvania 19034. Received April 28, 1999; Revised Manuscript Received June 8, 1999

A HYNIC-conjugated chemotactic peptide (fMLFK-HYNIC) was labeled with ^{99m}Tc using tricine and TPPTS as coligands. The combination of fMLFK-HYNIC, tricine, and TPPTS with ^{99m}Tc produced a ternary ligand complex [^{99m}Tc(fMLFK-HYNIC)(tricine)(TPPTS)] (RP463). RP463 was synthesized either in two steps, in which the binary ligand complex [^{99m}Tc(fMLFK-HYNIC)(tricine)$_2$] (RP469) was formed first and then reacted with TPPTS, or in one step by direct reduction of [^{99m}Tc]pertechnetate with stannous chloride in the presence of fMLFK-HYNIC, tricine, and TPPTS. The radiolabeling yield for RP463 was usually ≥90% using 10 μg of fMLFK-HYNIC and 100 mCi of [^{99m}Tc]pertechnetate. Unlike RP469, which decomposed rapidly in the absence of excess tricine coligand, RP463 was stable in solution for at least 6 h. [^{99}Tc]RP463 was prepared and characterized by HPLC and electrospray mass spectrometry. In an in vitro assay, [^{99}Tc]RP463 showed an IC_{50} of 2 nM against binding of [^{3}H]fMLF to receptors on PMNs. [^{99}Tc]RP463 also induces effectively the superoxide release of polymorphonuclear leukocytes (PMNs) with an EC_{50} value of 0.2 ± 0.2 nM. The localization of RP463 in the infection foci was assessed in a rabbit infection model. RP463 was cleared from the blood faster than RP469 and was excreted mainly through the renal system. As a result of rapid blood clearance and increased uptake, the target-to-background ratios continuously increased from 1.5 ± 0.2 at 15 min postinjection to 7.5 ± 0.4 at 4 h postinjection. Visualization of the infected area could be as early as 2 h. A transient decrease in white blood cell count of 35% was observed during the first 30 min after injection of the HPLC-purified RP463 in the infected rabbit. This suggests that future research in this area should focus on developing highly potent antagonists for chemotactic peptide receptor or other receptors on PMNs and monocytes.

INTRODUCTION

Accurate and rapid localization of infectious and inflammatory foci facilitate elucidation of the cause of disease, and the implementation of a tailored therapeutic regiment. Numerous diagnostic imaging procedures have been developed in the past three decades. Morphological imaging modalities such as X-ray-computed tomography (CT), ultrasound (US), conventional radiography, and magnetic resonance imaging (MRI) rely primarily on focal changes in tissue density to define lesions. In the early stage of an inflammatory lesion, however, lesion localization using these procedures may be difficult because the tissue changes associated with necrosis have not occurred (*1*).

White blood cells (WBCs), particularly polymorphonuclear leukocytes (PMNs) and monocytes, accumulate in high concentrations at the site of infection. Therefore, recent attention has been directed toward radiolabeling small molecules that bind to both circulating granulocytes and leukocytes. These include chemotactic peptides, analogues of *N*-formyl-methionyl-leucyl-phenylalanine (fMLF) (*1*−*8*), small peptides based on platelet factor 4 (*9*), and tuftsin receptor antagonists (*10*−*12*).

The chemotactic peptide, fMLF, is a bacterial product. It binds with high affinity to a specific receptor expressed on the surface of WBCs, stimulates chemotaxis of granulocytes, upregulates expression of adhesion molecules, and increases vascular permeability. In 1991, Fischman and co-workers (*13*) first reported the potential diagnostic use of ^{111}In-labeled chemotactic peptide analogues of fMLF. Since then, they have studied a series of radiolabeled chemotactic peptides as infection/inflammation imaging agents (*1, 3*−*8*). These peptides were modified with either HYNIC (for ^{99m}Tc) or DTPA (for ^{111}In) at the C-terminus. The ^{99m}Tc labeling of HYNIC-modified chemotactic peptides (such as fMLFK-HYNIC) can be achieved

* To whom correspondence should be addressed. Phone: (978) 671-8696. Fax: (978) 436-7500. E-mail: shuang.liu@dupontpharma.com.

10.1021/bc990049y CCC: $18.00 © 1999 American Chemical Society
Published on Web 07/20/1999

using coligands such as glucoheptonate, mannitol, and glucamine (*4*). It was reported that very high specific activity (≥20 000 mCi/μmol) could be achieved using glucoheptonate as the coligand. Different biodistributions were observed using different coligands (*4*). Recently, van der Laken and co-workers (*14*) also reported the use of a ^{99m}Tc-labeled chemotactic peptide fMLFK-HYNIC for imaging acute infection and sterile inflammation. Animal studies have shown evidence of binding to leukocytes in vivo and localization at the infection site (*1, 5*−*8, 15*).

Recently, we found that both tricine and glucoheptonate form binary technetium complexes, [^{99m}Tc(fMLFK-HYNIC)(L)$_2$] (L = tricine and glucoheptonate), which exist in many isomeric forms and are not stable in solution in the absence of excess coligand (*16*). Although the biological data from animal studies show that these agents are able to localize at the infection site (*14*−*16*), it would still be difficult to develop them for routine clinical use, due to solution instability and the presence of many isomers.

In this study, a ternary ligand system was used to prepare the stabilized complex [^{99m}Tc(fMLFK-HYNIC)-(tricine)(TPPTS)] (RP463). The goal was to minimize the number of isomeric forms and increase the solution stability of the ^{99m}Tc complex. RP463 was prepared, and its solution stability was compared to that of the binary ligand complex, [^{99m}Tc(fMLFK-HYNIC)(tricine)$_2$] (RP469). RP463 was evaluated in a rabbit focal infection model for its potential use as an infection imaging agent.

EXPERIMENTAL SECTION

Materials. TPPTS (trisodium triphenylphosphine-3,3′,3″-trisulfonate) and tricine were purchased from Aldrich Chemical Co. Na^{99m}TcO$_4$ was obtained from a Technelite ^{99}Mo/^{99m}Tc generator, DuPont Pharmaceuticals Co., North Billerica, MA. Deionized water was obtained from a Millipore MilliQ Water System and was of >18 MΩ quality. The peptide fMLFK was synthesized and conjugated to 6-hydrazinonicotinic acid (HYNIC) according to the literature procedure (*3*).

Instruments and Methods. The electrospray mass spectrum of [^{99}Tc]RP463 was obtained using a HP 1100 Series LC/MSD (G1946A) mass spectrometer and 0.1% formic acid/acetonitrile as the mobile phase. The HPLC methods used a Hewlett-Packard model 1050 instrument with a NaI radiometric detector. The ITLC method used Gelman Sciences silica gel strips and a 1:1 mixture of acetone and saline as the eluant.

HPLC method 1 used a Zorbax C_{18} reversed-phase column (4.6 mm × 250 mm, 80 Å pore size) at a flow rate of 1 mL/min. Solvent A contained 90% 25 mM phosphate buffer (pH 8) and 10% acetonitrile while solvent B was a 50:50 (v:v) mixture of acetonitrile and 25 mM phosphate buffer (pH 8). A linear gradient from 0% B to 20% B over 40 min was used.

HPLC method 2 used a Zorbax C_{18} reversed-phase column (4.6 mm × 250 mm, 80 Å pore size) and a Rainin Dynamax UV−vis detector (model UV-C, λ = 230 nm). The flow rate was 1 mL/min with a gradient from 90% solvent A (0.01 M phosphate buffer, pH 6) and 10% solvent B (acetonitrile) to 70% solvent A and 30% solvent B at 30 min.

Synthesis of RP463. *Two-Step Labeling Using Stannous Chloride*. To a 10 mL vial were added 0.2 mL of fMLFK-HYNIC solution (50 μg/mL in H_2O), 0.4 mL, of tricine solution (100 mg/mL in H_2O), 0.5 mL of Na^{99m}TcO$_4$ solution (100 mCi/mL in saline), and 25 μL of $SnCl_2 \cdot 2H_2O$ solution (1.0 mg/mL in 0.1 N HCl). The reaction mixture was allowed to stand at room temperature for 30 min. The labeling yield for the resulting complex RP469 was usually ≥90%. To the solution above was added 0.3 mL of TPPTS solution (50 mg/mL in H_2O). The reaction mixture was heated at 50 °C for 30 min and then analyzed by radio-HPLC (method 1). ITLC was used to determine the amount of [^{99m}Tc]colloid. The product RP463 migrated while the [^{99m}Tc]colloid remained at the origin.

One-Step Labeling Using Stannous Chloride. To a shielded 10 mL vial was added 0.5 mL of Na^{99m}TcO$_4$ solution (100 mCi/mL in saline), 0.4 mL of tricine solution (100 mg/mL in H_2O), 0.2 mL of the fMLFK-HYNIC solution (50 μg/mL in H_2O), 0.3 mL of TPPTS solution (50 mg/mL in H_2O), and 25 μL of $SnCl_2 \cdot 2H_2O$ solution (1.0 mg/mL in 0.1 N HCl). The reaction mixture was heated at 80 °C for 30 min and then analyzed by radio-HPLC (method 1) and ITLC. RP463 prepared by this method was shown by HPLC to be identical to that prepared according to the two-step synthesis. The radiolabeling yield was ≥90%.

RP463 was purified by HPLC (method 1) to remove excess reactants, particularly unlabeled fMLFK-HYNIC. The fraction at 10−12 min was collected into a 25 mL round-bottom flask. Volatiles were removed under reduced pressure. The residue was dissolved in saline at a concentration of 1.5 mCi/mL for animal studies. The resulting solution was reanalyzed by radio-HPLC.

One-Step Labeling without Stannous Chloride. To a shielded 10 mL vial were added 0.5 mL of Na^{99m}TcO$_4$ solution (100 mCi/mL in saline), 0.1 mL of tricine solution (100 mg/mL in H_2O), 0.2 mL of the fMLFK-HYNIC solution (50 μg/mL in H_2O), and 0.2 mL of TPPTS solution (50 mg/mL in H_2O). The reaction mixture was heated at 80 °C for 30 min and then analyzed by radio-HPLC (method 1). RP463 prepared by this method was shown by HPLC to be identical to that prepared using the stannous formulation.

Solution Stability Studies. Complexes RP463 and RP469 were prepared and separated from the kit matrix by HPLC (method 1). Fractions of interest were collected into a 25 mL round-bottom flask. Volatiles in the collected fractions were removed under reduced pressure. The residue was dissolved in saline to give a concentration of 1.5 mCi/mL. The stability of RP463 and RP469 was monitored by HPLC (method 1) over ∼6 h.

Synthesis of [^{99}Tc]RP463. To a 10 mL vial were added tricine (41.7 mg, 0.230 mmol), followed by [NH_4]-[^{99}TcO$_4$] (3.7 mg, 0.021 mmol) in water (1 mL), fMLFK-HYNIC (16.5 mg, 0.022 mmol) in methanol (1 mL), and TPPTS (50 mg, 0.088 mmol). The vial was crimped and heated in a boiling water bath for 30 min. The product [^{99}Tc]RP463 was separated from the reaction mixture by HPLC (method 2). The product fraction was collected, and volatiles were removed under reduced pressure. Analysis of the product by HPLC (method 2, λ = 230 nm) showed no residual starting peptide.

Receptor Binding Assays. Human PMNs were isolated from heparinized venous blood obtained from healthy donors. Blood samples of 40 mL were mixed with an equal volume of Hanks' balanced salt solution (HBSS), layered on a Ficoll−Hypaque gradient and centrifuged at 10 °C and 1300 rpm for 30 min. The supernatant was discarded, and the PMN-rich pellet was resuspended in cold HBSS, to which cold 2% dextran solution (in saline) was added to remove residual red blood cells. After 25 min of sedimentation at room temperature, the suspended cells were removed and centrifuged at 10 °C and 1300 rpm for 10 min. The supernatant was discarded,

and the pellet was resuspended in 10 mL of cold hypotonic lysing buffer for a 5-min lysis of residual RBC. After lysis, cold HBSS (40 mL) was added, and the cells were centrifuged at 10 °C and 1300 rpm for 10 min. This final PMN pellet was washed once and resuspended to the desired cell concentration in phosphate incubation buffer containing 140 mM NaCl, 1.0 mM KH_2PO_4, 5 mM Na_2HPO_4, 0.5 mM $MgCl_2$, 0.15 mM $CaCl_2$, and 0.5% BSA (pH 7.4) for fMLF binding assays. For the cytochrome *c* reduction assays, cells were resuspended in HBSS.

fMLF Binding Assay. [^{3}H]fMLF (10 nM), [^{99}Tc]RP463, and 100 μL of PMN solution (8×10^6 PMNs/mL) were added to a 96-well microplate with filters (0.65 μm pore size). The microplate was incubated for 60 min at room temperature with gentle agitation. The microtiter plate was then placed on a filtration system. The wells were washed with incubation buffer three times and dried. The filters were removed from the microplate, placed into scintillation vials, and agitated for 1 h at room temperature in the presence of scintillation fluid. Percentage inhibition of [^{3}H]fMLF binding to PMNs was calculated by dividing the specific binding (total binding -nonspecific binding) obtained in the presence of technetium complex by that obtained in the absence of the technetium complex. IC_{50} values were calculated by fitting the percentage inhibition values to a regression line.

Cytochrome c PMN Free Radical Release Assay. The biological activity of [^{99}Tc]RP463 was determined by measuring superoxide release of PMNs after they are exposed to the technetium complex. Typically, the PMN solution (1 mL, 1×10^6 PMNs/mL) was incubated with cytochalasin B (10 μM) and 100 μL of cytochrome *c* (40 μM) for 10 min at 37 °C. Then [^{99}Tc]RP463 was added, and the tubes were incubated for 10 min at room temperature. After centrifugation (200 × g, for 10 min at 10 °C), the supernatants were transferred to cuvettes for spectrophotometric analysis to measure reduction of cytochrome *c*, reflecting the amount of superoxide release by PMNs. Superoxide release in the presence of [^{99}Tc]-RP463 was expressed as a percentage of maximal response. EC_{50} values were calculated by fitting a curve to the data generated.

Animal Studies. Absesses were induced in the left thigh muscle of female New Zealand rabbits (2.2−2.8 kg) with 1.5×10^{10} colony forming units of *Escherichia coli* in 0.5 mL. During the procedure, the rabbits were anesthetized with subcutaneous injection of a 0.5 mL mixture of 0.315 mg/mL fentanyl and 10 mg/mL fluanisone. After 24 h, when swelling of the muscle was apparent, groups of four rabbits were immobilized, and were placed prone on the gamma camera.

RP463 was administered (1.0 mCi/kg, i.v.) in the lateral ear vein. Serial images were acquired using a gamma camera (Digital Dyna Camera, Picker International, Cleveland, OH) every 15 min for 4 h. The scintigraphic results were analyzed quantitatively by drawing regions of interest over the abscess, the uninfected contralateral thigh muscle (background), and the whole body. Abscess-to-background ratios and percentage residual activity in the abscess (abscess-to-whole body ratio × 100%) were calculated. Arterial blood was withdrawn prior to administration and every 30 min thereafter for determination of blood clearance. At the end of the protocol, the animal was euthanized with an overdose of pentobarbital. Samples of blood, infected thigh muscle, uninfected contralateral thigh muscle, bone, bone marrow, lung, spleen, liver, kidneys, and intestines were collected. The dissected tissues were weighed and counted in a gamma well counter (LKB 1282, Wallac Inc., Gaithersburg, MD).

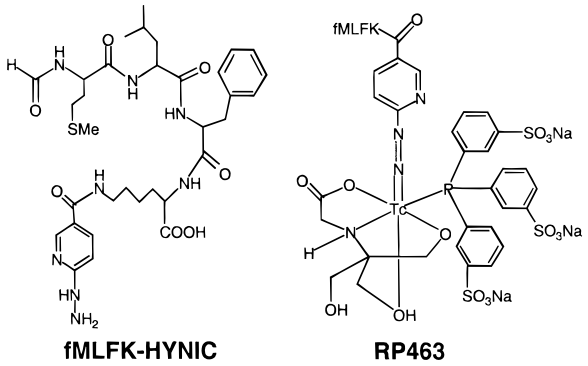
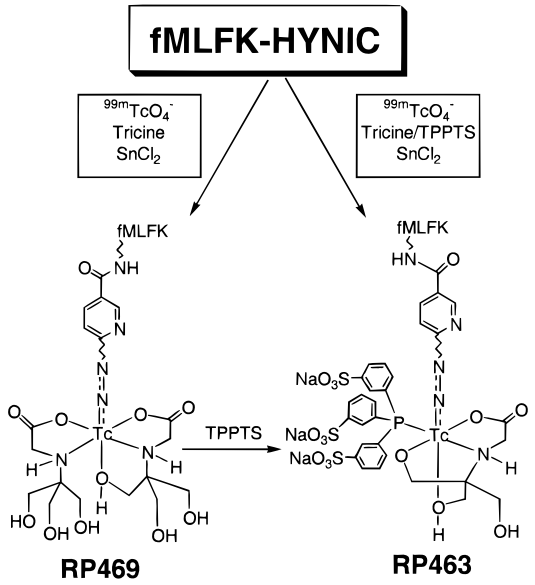


Figure 1. Structures of fMLFK-HYNIC and RP463.

Chart 1. Synthesis of RP463



To correct for radioactive decay, injection standards were counted simultaneously. The measured activity in samples was expressed as injected dose per gram (% ID/g). Abscess-to-contralateral muscle ratios and abscess-to-blood ratios were calculated.

RESULTS

Synthesis of RP463. RP463 was synthesized either in two steps, in which the binary ligand complex RP469 is formed first and then reacts with TPPTS, or in one step by direct reduction of [^{99m}Tc]pertechnetate with stannous chloride in the presence of fMLFK-HYNIC, tricine, and TPPTS (Chart 1). The radiolabeling yield for the complex RP463 is usually ≥90% using 10 μg of fMLFK-HYNIC and 100 mCi of [^{99m}Tc]pertechnetate. The formation of [^{99m}Tc]colloid is minimal. Since the radiolabeled kit contains excess unlabeled peptide (fMLFK-HYNIC), which has been shown to be a strong agonist (*3*, *14*), RP463 has to be purified by HPLC before animal studies.

HPLC Characterization RP463 and RP469. RP463 and RP469 were characterized using the same reversed-phase HPLC method. Figure 2 shows the chromatograms (method 1) for the binary ligand complex RP469 (top) and the ternary ligand complex RP463 (bottom). There are several radiometric peaks for RP469 at retention times between 20 and 45 min, suggesting that there are many ^{99m}Tc-species in solution. The ratios of the peak areas in the radio-HPLC chromatograms change with time, reaction temperature, and pH. Using the same method, the

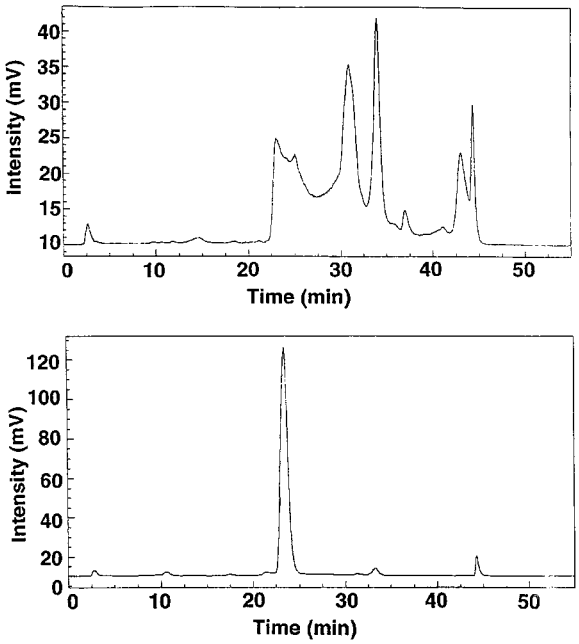


Figure 2. Radio-HPLC chromatograms (method 1) for RP469 (top) and RP463 (bottom).

chromatogram of RP463 showed only one peak at 23 min (bottom in Figure 2). RP463 prepared by the two-step synthesis was found to be exactly the same as that prepared by the one-step synthesis.

The technetium chelate moiety is chiral, due to the tricine ligand being pro-chiral, and should be formed in an equal mixture of D and L enantiomers. These enantiomers in combination with the chiral centers on the peptide backbone should result in two diastereomers, DLLLL and LLLLL. Theoretically, these two diastereomers should be separable under ideal conditions. We tried several different reversed-phase HPLC methods under either gradient or isocratic conditions and were unable to resolve these two diastereomers, probably due to the high flexibility of the linear peptide.

Solution Stability Studies. The solution stability of HPLC-purified RP463 was examined, and was compared to that of RP469. Both complexes were separated from the kit matrix. Their solution stability in saline (pH ~6) was monitored by HPLC (method 1) for 6 h. Figure 3 shows the plot of RCP vs time for RP463 and RP469. It is clear that the HPLC-purified RP469 was not stable in solution. The RCP dropped to ~50% at 6 h post HPLC purification. The ternary ligand complex RP463 remained relatively unchanged in solution. The RCP only dropped slightly from 94% to 91% at 6 h post HPLC purification.

[^{99}Tc]463. [^{99}Tc]RP463 was prepared in one step by reacting fMLFK-HYNIC with [NH_4][$^{99}TcO_4$], in the presence of excess tricine and TPPTS. It was isolated by HPLC purification (method 2). The HPLC concordance (Figure 4) of RP463 and [^{99}Tc]RP463 showed that the same complexes were prepared at the tracer (^{99m}Tc) and macroscopic (^{99}Tc) levels. Electrospray mass spectrometry gave m/z 1476 for [^{99}Tc]RP463 ([$C_{57}H_{72}N_9O_{21}S_4Tc]^+$) in its acid form.

In Vitro Studies. The binding of [^{3}H]fMLF to receptors on PMNs could be completely inhibited by [^{99}Tc]-RP463. The concentration of [^{99}Tc]RP463 required for 50% inhibition against [^{3}H]fMLF binding to PMNs (IC_{50}) was 2 nM. Nonspecific binding on average was less than 15%. Like the unlabeled peptide (fMLFK-HYNIC), [^{99}Tc]-

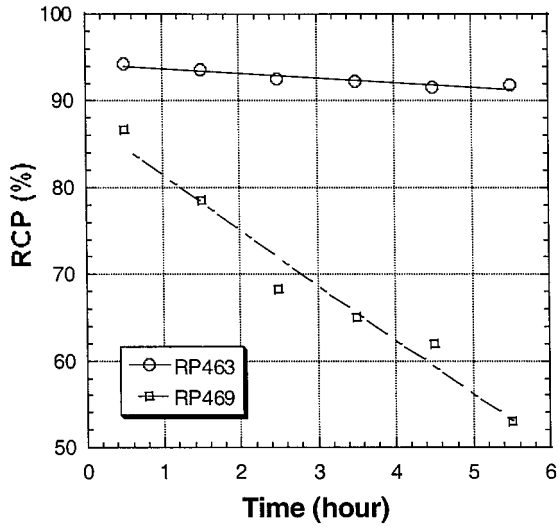


Figure 3. Solution stability of HPLC purified RP463 and RP469.

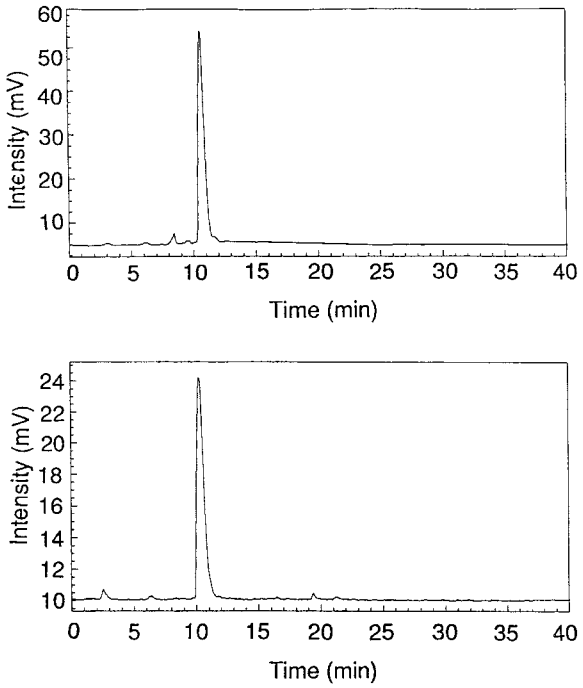


Figure 4. HPLC concordance (method 2) for RP463 (top, NaI radio-detector) and [^{99}Tc]RP463 (bottom, UV detector).

RP463 is also an effective inducer of superoxide release of PMN, with an EC_{50} value of 0.2 ± 0.2 nM (n = 3).

In Vivo Animal Studies. RP463 was evaluated in rabbits infected with *E. coli*. After injection of RP463 into infected rabbits, a minimal transient reduction in peripheral leukocyte levels was observed. Immediately after injection, the WBC count decreased to 65% of the initial level and then returned to 90−95% within 30 min postinjection (Figure 5). Similar phenomena were observed for the complex RP469 in both the healthy and the infected rabbit (*14*). RP463 cleared from the blood rapidly (Figure 6). The biodistribution data (Figure 7) at 4 h postinjection showed that RP463 excreted via both the renal and hepatobillary systems and were consistent with the imaging data. Compared with RP469, RP463 showed comparable renal excretion and less blood residence. Despite fast blood clearance, images clearly showed rapid accumulation of RP463 in the infected site, and the

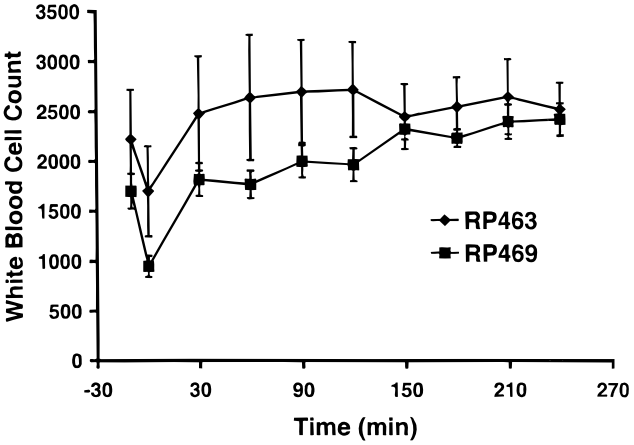


Figure 5. White blood cell counts in blood of the infected rabbits after injection of the HPLC purified RP463 and RP469.

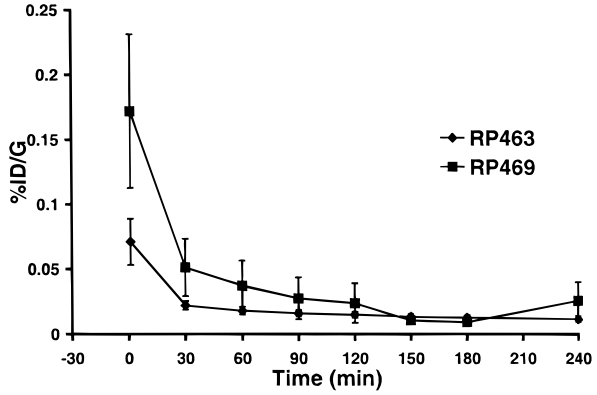


Figure 6. Blood clearance of RP463 and RP469 in the infected rabbits. Data expressed as percentage of the injected dose per gram (% ID/g, mean values ± sem).

uptake at the infection site increased with time (Figure 8). The infection foci could be clearly visualized at 2 h postinjection. As a result of rapid blood clearance and increased uptake, the target-to-background ratios continuously increased from 1.5 ± 0.2 at 15 min postinjection to 3.5 ± 0.4 at 2 h postinjection and to 7.5 ± 0.4 at 4 h postinjection (Figure 9).

DISCUSSION

In the development of a new receptor-based ^{99m}Tc infection imaging agent, several factors need to be considered to satisfy the clinical requirements. The agent has to demonstrate the biological efficacy, including high specificity and high uptake at the infection site. It should also have favorable pharmacokinetics, show rapid blood clearance, and be renally excreted. A kit formulation is often required due to the 6 h half-life of ^{99m}Tc. Injection of the whole or part of the reconstituted kit should not cause any significant biological effect such as neutropenia. The agent should have high radiochemical purity (RCP = 90%) and high solution stability with a shelf life of preferably 6 h. Finally, the ^{99m}Tc labeling should be accomplished in 10−30 min, preferably at room temperature.

Development of a specific agent for imaging focal infection remains a major challenge for investigators in nuclear medicine. For a number of years, imaging inflammation and infection has been performed using [^{67}Ga]citrate. But the specificity is low and the exact mechanism of localization is still not well understood. ^{111}In- and ^{99m}Tc-labeled nonspecific polyclonal IgGs were also used for detection of infection foci (*17*−*24*). However, it usually takes 24 h to obtain diagnostically useful images due to their slow clearance from the blood pool. [^{99m}Tc]HMPAO-WBCs (*25*−*27*), and [^{99m}Tc]albumin colloid-WBCs (*28*) have specificity for the infected foci since WBCs, particularly PMNLs and monocytes, accumulate at the site of acute infection as part of the inflammatory response induced by bacteria. Imaging using both agents can be completed on the same day, but these procedures may impose significant risks to laboratory personnel and patients, particular with the increasing prevalence of human immunodeficiency virus in the population (*29*, *30*).

^{99m}Tc labeling of biologically active small peptides is of current interest because small peptides are necessary elements in many biological processes and, in some cases, have affinities significantly higher than those of antibodies or antibody fragments (*5*). Small peptides are easy to synthesize and modify, are less likely to be immunogenic, and can have rapid blood clearance. The faster blood clearance results in adequate *T*/*B* ratios earlier so that it is practical to use ^{99m}Tc, which is the preferred radionuclide for diagnostic nuclear medicine. Examples

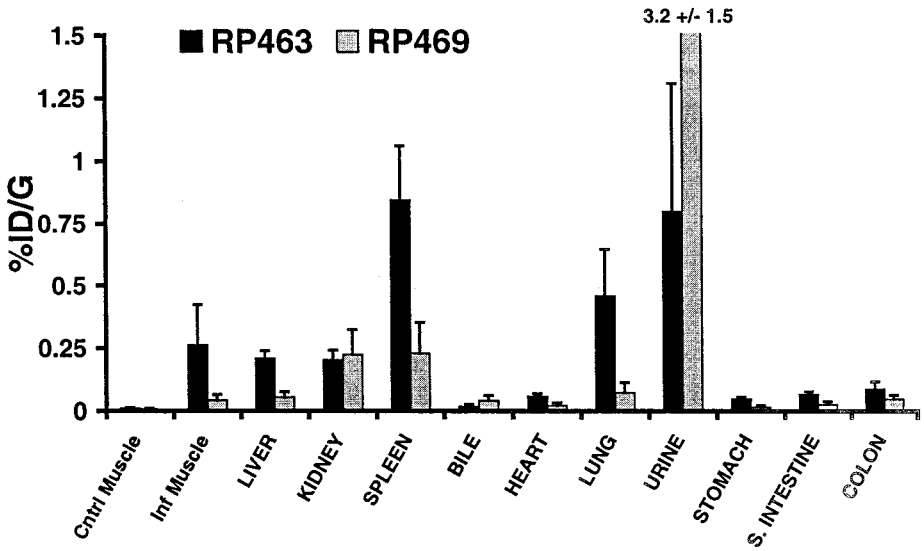


Figure 7. Biodistribution of RP463 versus RP469 in the infected rabbits. Data expressed as percentage of the injected dose per gram (% ID/g, mean values ± sem).

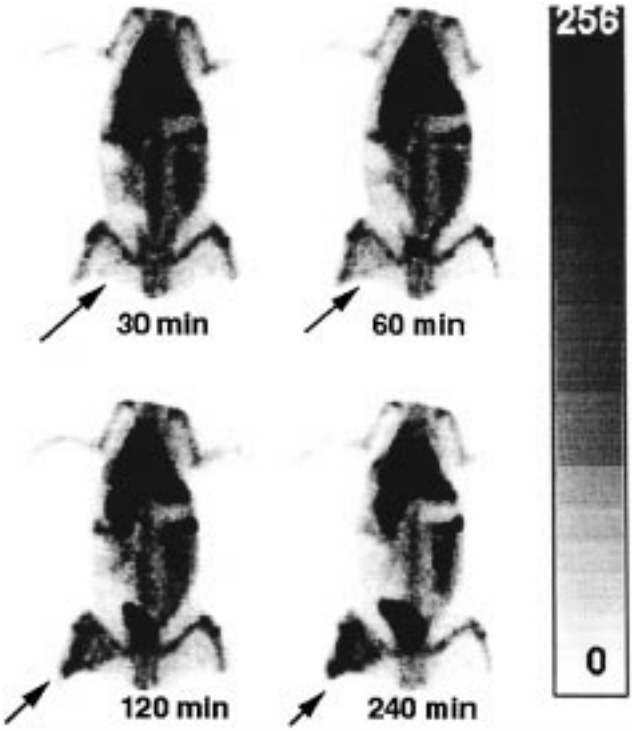


Figure 8. Representative images (anterior view) of rabbits infected with *E. coli* at 30, 60, 120, and 240 min after injection of the HPLC purified RP463. Arrows indicate location of the infected thigh.

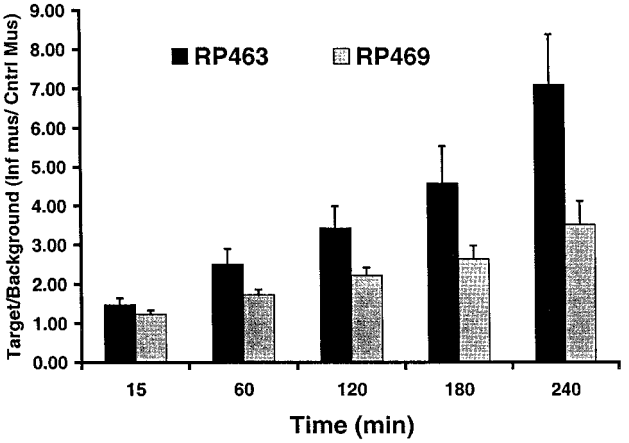


Figure 9. Target-to-background (infected muscle to contralateral muscle) ratios, calculated from rabbits infected with *E. coli* at 15, 60, 120, 180, and 240 min after injection of HPLC-purified RP463 and RP469.

of ^{99m}Tc-labeled small peptides for imaging infection or inflammation include chemotactic peptides (*1*−*8*), small peptides based on platelet factor 4 (*9*), and tuftsin receptor antagonists (*10*−*12*).

The ^{99m}Tc-labeled fMLFK-HYNIC has been studied for infection imaging using several different animal models (*3*, *4*, *6*−*8*, *15*). Various coligands such as glucoheptonate, mannitol, and glucamine have been used for the ^{99m}Tc labeling. Different biodistributions were observed depending on the coligand (*4*). However, these studies did not address problems associated with the presence of multiple species of the binary ligand complexes such as RP469 and the solution stability of the ^{99m}Tc-labeled peptides.

In this study, it has been clearly demonstrated by a reversed-phase HPLC method that the binary ligand complex RP469 exists in solution as a mixture of several isomeric forms. Similar results were obtained for the complex [^{99m}Tc(fMLFK-HYNIC)(glucoheptonate)$_2$] (*16*) and for the ^{99m}Tc complex of a HYNIC-conjugated cyclic platelet GPIIb/IIIa receptor antagonist (*31*). In addition, RP469 was found to be unstable in the absence of excess tricine coligand (Figure 3). Thus, it would be difficult to develop RP469 into a product for routine clinical use because of the solution instability and the presence of the many isomeric forms even though animal studies showed that the agent was able to localize at the site of infection (*1*−*8*, *14*, *15*).

To minimize the formation of various isomeric forms and increase the solution stability of the ^{99m}Tc complex, a ternary ligand system was used to prepare RP463. This new ligand system has been successfully used for the ^{99m}Tc labeling of an HYNIC-conjugated cyclic GPIIb/IIIa antagonist for the development of a thrombus imaging agent, RP444 (*32*, *33*). Using the combination of fMLFK-HYNIC, tricine, and TPPTS, RP463 can be synthesized in high yield and high specific activity (>10 000 mCi/μmol fMLFK-HYNIC) without HPLC purification. It was found that RP463 was stable for up to 6 h in solution. Apparently, the addition of TPPTS coligand dramatically reduces the number of isomeric forms and significantly increases the solution stability of ^{99m}Tc-labeled peptide. The composition of RP463 and the 1:1:1:1 ratio for Tc:fMLFK-HYNIC:tricine:TPPTS was confirmed by mass spectral data of [^{99}Tc]RP463.

In an in vitro binding assay, [^{99}Tc]RP463 was able to effectively compete with [^{3}H]fMLF for receptors on PMNs, with an IC_{50} value of 2 nM. Like the unlabeled peptide, fMLFK-HYNIC ($IC_{50} = 3 \pm 2$ nM; $EC_{50} = 0.8 \pm 0.4$ nM) (*14*), [^{99}Tc]RP463 also induces superoxide release of PMN with an EC_{50} value of 0.2 ± 0.2 nM. These data clearly show that RP463 is a high affinty agonist of the fMLF receptors on PMNs, and the ^{99m}Tc-labeling did not significantly alter the binding affinity even though the molecular weight after radiolabeling is more than doubled.

After injection of RP463 in the rabbit, a transient reduction in peripheral leukocyte levels was observed. Since RP463 was purified by HPLC, it should be free of unlabeled fMLFK-HYNIC. The injected dose for the rabbit was 1 mCi/kg. For a generator with 24 h prior elution time, the total amount of Tc (^{99m}Tc + ^{99}Tc) in 1 mCi of activity is $\sim 7 \times 10^{-12}$ mol. The total amount of technetium complex (RP463 + [^{99}Tc]RP463) injected into each infected rabbit (~2.5 kg) is ~25 ng (MW = 1542 for [^{99}Tc]RP463 in its sodium salt form). A study in primates showed that the minimal amount of peptide causing decrease of white blood cells is 10 ng/kg for fNleLFNleYK-DTPA (*6*). Therefore, it is not surprising that even the HPLC purified RP463 could cause the biological effect at a dose of 1 mCi/kg.

The use of ^{99m}Tc-labeled highly potent agonists as radiopharmaceuticals suffers a major drawback: severe reduction of peripheral leukocyte count. In general, there are three approaches to avoid this problem. The first approach is to separate the radiolabeled peptide from the excess unlabeled peptide using HPLC. This results in a product almost at its theoretical specific activity but is inconvenient for routine clinical use. The results described in this study clearly show that even the HPLC purified ^{99m}Tc-labeled peptide can cause a neutropenic effect if the ^{99m}Tc complex itself is a very potent agonist. The second approach involves using less active agonists with similar binding characteristics (*15*). However, lower binding affinity may result in less accumulation of the radioactivity at the receptor sites. The third approach is

to use antagonist peptides, which bind to the receptor but do not cause any neutropenic response, as targeting molecules. Unfortunately, the receptor binding affinity of the antagonists tested to date appear to be much lower than that of the agonists (*34*).

Recently, van der Laken and co-workers (*14*) have demonstrated that accumulation of the ^{99m}Tc-labeled fMLFK-HYNIC (RP469) in acute infection and sterile inflammation took place by virtue of binding to receptors on locally present PMNs and monocytes. Both the scintigraphic and biodistribution data showed that RP469 was cleared via both the kidneys and the liver. The high blood activity is probably related to the instability of RP469 and plasma protein binding. This assumption is supported by the fact that imine-N containing heterocycles can act as coligands and form stable ternary ligand complexes with the ^{99m}Tc-labeled HYNIC-peptide conjugate (*35*). The use of TPPTS coligand significantly increases the solution stability and hydrophilicity of the radiolabeled fMLFK-HYNIC. As a result, the excretion route for RP463 is mainly the renal system. The fast accumulation of RP463 at the infection site in combination with its rapid clearance results in continuously improving target-to-background ratios over 4 h.

Traditionally, modification of pharmacokinetics of a radiopharmaceutical is achieved either by attaching a pharmacokinetic modifier on the targeting biomolecule or by using a linker between the targeting biomolecule and the technetium chelate. The lipophilicity of the linker depends on pharmacokinetic requirements for the radiopharmaceutical. Results from this study and others (*4*) clearly show that the coligand of the technetium chelate can also be used for modifying pharmacokinetics and biodistribution of the radiopharmaceutical. As a matter of fact, one of the advantages using HYNIC as BFCA is that various coligands can be used for synthesis of ternary ligand technetium chelates.

CONCLUSION

The HYNIC-conjugated chemotactic peptide (fMLFK-HYNIC) has been labeled with ^{99m}Tc using a ternary ligand system (fMLFK-HYNIC, tricine and TPPTS). The complex [^{99m}Tc(fMLFK-HYNIC)(tricine)(TPPTS)] (RP463) was prepared in high yield (≥90%) and high specific activity (10 000 mCi/μmol fMLFK-HYNIC). The use of TPPTS as a coligand dramatically reduced the number of ^{99m}Tc species in the radiolabeled kit and increased the solution stability of the radiolabeled peptide. Compared to the unlabeled fMLFK-HYNIC ($IC_{50} = 3 \pm 2$ nM against binding of [^{3}H]fMLF to receptors on PMNs; $EC_{50} = 0.8 \pm 0.4$ nM), RP463 remains to be a strong agonist for the chemotactic receptor ($IC_{50} = 2$ nM against binding of [^{3}H]-fMLF to receptors on PMNs; $EC_{50} = 0.2 \pm 0.2$ nM) even though the molecular weight of RP463 is more than twice that of fMLFK-HYNIC.

The localization of RP463 in the infection foci was assessed in the rabbit infection model. Visualization of the infected foci could be as early as 2 h postinjection with the target-to-background ratio increasing from 1.5 ± 0.2 at 15 min postinjection to 7.5 ± 0.4 at 4 h postinjection as a result of a faster blood clearance mainly through the renal system. However, a 35% transient decrease in WBC count was observed during the first 30 min after injection of the HPLC-purified RP463. Because of this limitation, further research in this area should focus on the development of ^{99m}Tc-labeled antagonists with similar binding affinity for chemotactic peptide receptor or other receptors on PMNs and monocytes.

LITERATURE CITED

(1) Fischman, A. J., Babich, J. W., and Rubin, R. H. (1994) Infection imaging with technetium-99m-labeled chemotactic peptide analogues. *Semin. Nucl. Med. 24*, 154−168.

(2) Baidoo, K. E., Scheffel, U., Stathis, M., Finley, P., Lever, S. Z., Zhan, Y., and Wagner, H. N., Jr. (1998) High affinity no-carrier-added ^{99m}Tc-labeled chemotactic peptides for studies of inflammation in vivo. *Bioconjugate Chem. 9*, 208−217.

(3) Babich, J. W., Solomon, H., Pike, M. C., Kroon, D., Graham, W., Abrams, M. J., Tompkins, R. G., Rubin, R. H., and Fischman, A. J. (1993) Technetium-99m-labeled hydrazino nicotinamide derivatized chemotactic peptide analogues for imaging focal sites of bacterial infection. *J. Nucl. Med. 34*, 1964−1974.

(4) Babich, J. W., and Fischman, A. J. (1995) Effect of "co-ligand" on the biodistribution of ^{99m}Tc-labeled hydrazino nicotinic acid derivatized chemotactic peptides. *Nucl. Med. Biol. 22*, 25−30.

(5) Fischman, A. J., Babich, J. W., and Strauss, H. W. (1993) A ticket to ride: peptide radiopharmaceuticals. *J. Nucl. Med. 34*, 2253−2263.

(6) Fischman, A. J., Rauh, D., Solomon, H., Babich, J. W., Tompkins, R. G., Kroon, D., Strauss, H. W., and Rubin, H. R. (1993) In vivo bioactivity and biodistribution of chemotactic peptide analogues in nonhuman primates. *J Nucl. Med. 34*, 2130−2134.

(7) Babich, J. W., Graham, W., Barrow, S. A., and Fischman, A. J. (1995) Comparison of the infection imaging properties of a ^{99m}Tc labeled chemotactic peptide with ^{111}In IgG. *Nucl. Med. Biol. 22*, 643−648.

(8) Babich, J. W., Graham, W., Barrow, S. A., Dragotakes, S. C., Tompkins, R. H., Rubin, R. H., and Fischman, A. J. (1993) Technetium-labeled chemotactic peptides: comparison with Indium-111-labeled white blood cells for localizing acute bacterial infection in the rabbit. *J. Nucl. Med. 34*, 2176−2181.

(9) Moyer, B. R., Vallabhajosula, S., Lister-James, J., Bush, L. R., Cyr, J. E., Snow, D. A., Bastidas, D., Lipszyc, H., and Dean, R. T. (1996) Technetium-99m-white blood cell-specific imaging agent developed from platelet factor 4 to detect infection. *J. Nucl. Med. 37*, 673−679.

(10) Goodbody, A. E., Ballinger, J., Tran, L. L., Sumner-Smith, M., Lau, F., Meghji, K., and Pollak, A. (1994) A new Tc-99m labeled peptide inflammation imaging agent. *Eur. J. Nucl. Med. 21*, 790 (abstr. 262).

(11) Cavelier, V., Goodbody, A. E., Tran, L. L., Bossuyt, A., and Thornback, J. (1996) Human dosimetry of Tc99m-RP128, a potential inflammation imaging agent. *Eur. J. Nucl. Med. 23*, 1131 (abstr. OMo398).

(12) Peers, S. H., Tran, L. L., Eriksson, S. J., Ballinger, J., and Goodbody, A. E. (1995) Imaging a model of colitis with RP128, a Tc-99m-chelated tuftsin antagonist. *J. Nucl. Med. 36*, 114P (abstr. 465).

(13) Fischman, A. J., Pike, M. C., Kroon, D., Fuccello, A. J., Rexinger, D., tenKate, C., Wilkinson, R., Rubin, R. H., and Strauss, H. W. (1991) Imaging focal sites of bacterial infection in rats with indium-111-labeled chemotactic peptide analogues. *J. Nucl. Med. 32*, 483−491.

(14) van der Laken, C. J., Boerman, O. C., Oyen, W. J. G., van den Ven, M. T. J., Edwards, D. S., Barrett, J. A., van der Meer, J. W. M., and Corstens, F. H. M. (1997) Technetium-99m-labeled chemotactic peptides in acute infection and sterile inflammation. *J. Nucl. Med. 38*, 1310−1315.

(15) Babich, J. W., Tompkins, R. H., Graham, W., Barrow, S. A., and Fischman, A. J. (1997) Localization of radiolabeled chemotactic peptide at focal site of *Eschrichia coli* infection in rabbits: evidence for a receptor-specific mechanism. *J. Nucl. Med. 38*, 1316−1322.

(16) Edwards, D. S., Barrett, J. A., Liu, S., Ziegler, M. C., Mazaika, T., Vining, M., Bridger, G., Higgins, J., III, and Abrams, M. J. (1996) A stabilized Tc-99m complex of a chemotactic peptide-HYNIC conjugate for imaging infection. *Eur. J. Nucl. Med. 23*, 1142 (abstr. Omo440).

(17) Abrams, M. J., Juweid, M., tenKate, C. I., Schwartz, D. A., Hauser, M. M., Gaul, F. E., Fuccello, A. J., Rubin, R. H., Strauss, H. W., and Fischman, A. J. (1990) Technetium-99m-

human polyclonal IgG radiolabeled via the hydrazino nicotinamide derivative for imaging focal sites of infection in rats. *J. Nucl. Med. 31*, 2022−2028.
(18) Schwartz, D. A., Abrams, M. J., Hauser, M. M, Gaul, F. E., Larsen, S. K., Rauh, D., and Zubieta, J. A. (1991) Preparation of hydrazino-modified proteins and their use for the synthesis of ^{99m}Tc-protein conjugates. *Bioconjugate Chem. 2*, 334−336.
(19) McAfee, J. G. (1990) What is the best method for imaging focal infections? *J. Nucl. Med. 31*, 413−416 (Editorial).
(20) Claessens, R. A. M. J., Koenders, E. B., Oyen, W. J. G., and Corstens, F. H. M. (1996) Retention of technetium-99m in infectious foci in rats after release from technetium-99m labeled human nonspecific polyclonal immunoglobulin G: a dual-label study with hydrazino-nicotinamido and iminothiolano immunoglobulin. *Eur. J. Nucl. Med. 23*, 1536−1539.
(21) Buscombe, J. R., Lui, D., Ensing, G., de Jong, R., and Ell, P. J. (1990) ^{99m}Tc-human immunoglobulin (HIG)-first results of a new agent for the localization of infection and inflammation. *Eur. J. Nucl. Med. 16*, 649−655.
(22) Barrow, S. A., Graham, W., Jyawook, S., Dragotakes, S. C., Solomon, H. F, Babich, J. W., Rubin, R. H., and Fischman, A. J. (1993) Localization of indium-111-immunoglobulin G, technetium-99m-immunoglobulin G and indium-111-labeled white blood cells at sites of acute bacterial infection in rabbits. *J. Nucl. Med. 34*, 1975−1979.
(23) Callahan, R. J., Barrow, S. A., Abrams, M. J., Rubin, R. H., and Fischman, A. J. (1996) Biodistribution and dosimetry of technetium-99m-hydrazinonicotinamide IgG: comparison with indium-111-DTPA-IgG. *J. Nucl. Med. 37*, 843−846.
(24) Fischman, A. J., Solomon, H. F., Babich, J. W., Abrams, M. J., Callahan, R. J., and Strauss, H. W. (1994) Imaging of focal sites of inflammation in rhesus monkeys with ^{99m}Tc-labeled human polyclonal IgG. *Nucl. Med. Biol. 21*, 111−116.
(25) Peters, A. M., Danpure, H. J., Osman, S., Halker, R. J, Henderson, B. L., Hodgson, H. J., Kelly, J. D., Neirinckx, R. D., and Lavender, J. P. (1986) Clinical experience with ^{99m}Tc-hexamethylpropyleneamineoxime for labeling leukocytes and imaging inflammation. *Lancet 2*, 946−949.
(26) Vorne, M., Soini, I., Lantto, T., and Paakkinen, S. (1989) Technetium-99m-HM-PAO-labeled leukocytes in detection of inflammatory lesions: comparison with gallium-67 citrate. *J. Nucl. Med. 30*, 1332−1336.
(27) Charron, M., Orenstein, S. R., and Bhargava, S. (1994) Detection of inflammatory bowel disease in pediatric patients with technetium-99m-HMPAO-labeled leukocytes. *J. Nucl. Med. 35*, 451−455.
(28) Peters, A. M. (1996) The choice of an appropriate agent for imaging inflammation. *Nucl. Med. Commun. 17*, 455−458.
(29) Lange, J. M. A., Boucher, C. A. B., Hollak, C. E. M., Wiltink, E. H. H., Reiss, P., van Royen, E. A., Roos, M., Danner, S. D., and Goudsmit, J. (1990) Failure of zidovudine prophylaxis after accidental exposure to HIV-1. *N. Eng. J. Med. 322*, 1375−1377.
(30) Rojas-Burke, J. (1990) Health officials reacting to infection mishaps. *J. Nucl. Med. 33*, 13−27.
(31) Liu, S., Edwards, D. S., Looby, R. J., Harris, A. R., Poirier, M. J., Barrett, J. A., Heminway, S. J., and Carroll, T. R. (1996) Labeling a hydrazinonicotinamide-modified cyclic IIb/IIIa receptor antagonist with ^{99m}Tc using aminocarboxylates as coligands. *Bioconjugate Chem. 7*, 63−71.
(32) Edwards, D. S., Liu, S., Harris, A. R., Looby, R. J., Ziegler, M. C, Heminway, S. J., Barrett, J. A., and Carroll, T. R. (1997) A new and versatile ternary ligand system for technetium radiopharmaceuticals: water soluble phosphines and tricine as coligands in labeling a hydrazinonicotinamide-modified cyclic glycoprotein IIb/IIIa receptor antagonist with ^{99m}Tc. *Bioconjugate Chem. 8*, 146−154.
(33) Barrett, J. A., Crocker, A. C., Damphousse, D. J., Heminway, S. J., Liu, S., Edwards, D. S., Harris, A. R., Looby, R. J., Lazewatsky, J. L., Kagan, M., Mazaika, T. J., and Carroll, T. R. (1997) Biological evaluation of thrombus imaging agents utilizing water soluble phosphines and tricine as coligands to label a hydrazinonicotinamide-modified cyclic glycoprotein IIb/IIIa receptor antagonist with ^{99m}Tc. *Bioconjugate Chem. 8*, 155−160.
(34) Solomon, H. F., Derlan, C. K., Beblavy, M., Jester, D., Santulll, R., Pike, M., Kroon, D., Hoey, K., and Fischman, A. J. (1994) Focal infection imaging using an In-111 labeled antagonist chemotactic peptide. *J. Nucl. Med. 35*, 45P (abstr. 172).
(35) Liu, S., Edwards, D. S., and Harris, A. R. (1998) A novel ternary ligand system for ^{99m}Tc-labeling of hydrazino nicotinamide-modified biologically active molecules using imine-N-containing heterocycles as coligands. *Bioconjugate Chem. 9*, 583−595.

BC990049Y

Preparation of a Cathepsin D Sensitive Near-Infrared Fluorescence Probe for Imaging

Ching-Hsuan Tung,* Sebastian Bredow, Umar Mahmood, and Ralph Weissleder

Center for Molecular Imaging Research, Massachusetts General Hospital, Harvard Medical School, 149, 13th Street, Room 5406, Boston, Massachusetts 02129-2060. Received April 28, 1999; Revised Manuscript Received June 28, 1999

A variety of proteases are overexpressed or activated during pathogenesis and represent important targets for therapeutic drugs. We have previously shown that optical imaging probes sensitive in the near-infrared fluorescence (NIRF) spectrum can be used for in vivo imaging of enzyme activity. In the current study, we show that these probes can be designed with specificity for specific enzymes, for example, cathepsin D which is known to be overexpressed in many tumors. A NIR cyanine fluorochrome served as the optical reporter and was attached to the amino terminal of an 11 amino acid peptide sequence with specificity for cathepsin D. The peptides were subsequently attached to a synthetic graft copolymer for efficient tumoral delivery. The close spatial proximity of the multiple fluorochromes resulted in quenching of fluorescence in the bound state. A 350-fold signal amplification was observed post cleavage during in vitro testing. Cell culture experiments using a rodent tumor cell line stably transfected with human cathepsin D confirmed enzyme specific activation within cells. This sequence but not a scrambled control sequence showed enzyme specificity in vitro. We conclude that activatable NIRF optical probes can be synthesized to potentially probe for specific enzymes in living organisms.

INTRODUCTION

Cathepsin D (EC 3.4.23.5) (CaD) is an aspartic proteinase that is normally localized in lysosomes of various mammalian tissues. Its main function is in protein catabolism; however, a 2−50-fold increase in enzyme levels has been reported in breast cancers, demonstrated by immunohistochemistry (*1*) and in situ hybridization (*2*). High cathepsin D levels in tumors have also been associated with higher metastatic potential (*3*), invasion (*4, 5*), angiogenesis and degradation of basement membrane (*6*), and activation of other proteolytic enzymes (*4, 7*) as part of the metastatic cascade. Given its central role in different tumor pathways, cathepsins may represent unique targets for therapeutic (*4, 8*) or imaging applications (*9*).

We have recently reported a novel near-infrared fluorescence (NIRF)[1] probe for in vivo imaging of enzyme activity (*9*). The generic probes were designed to (1) have a long circulation time (*10*), (2) have high tumoral accumulation (*11*), and (3) contain quenched fluorescent markers which become fluorescent in the near-infrared spectrum after enzyme activation. The delivery vehicle consisted of a synthetic graft copolymer [partially methoxy poly(ethylene glycol) modified poly-L-lysine] onto which multiple NIR fluorochromes were attached to free poly-L-lysine residues. The graft copolymer has been used as delivery vehicle in several applications (*11*−*13*). Among them, ^{99m}Tc chelated graft copolymer used in blood pool imaging has been tested in phase I clinical trials (*14*). More recently, we also applied it to deliver NIRF probe for in vivo optical imaging of other lysosomal enzymes (*9*).

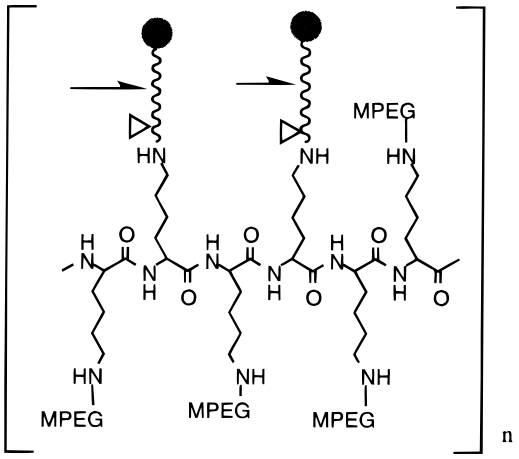


Figure 1. Schematic structure of NIRF probes. The undulating line represents the enzyme specific substrate peptide. The Cy5.5 fluorochrome is depicted as a dark circle and FITC as an open triangle. The cleavage position by target protease is indicated by the arrows.

The hypothesis underlying the current study was that cathepsin D sensitive peptide sequences could be used as linkers between the protected graft copolymer (PGC) and the NIRF fluorochrome and would act as substrates releasing fluorochrome after enzyme activation (Figure 1). Following optimization of reaction conditions, a CaD

* To whom correspondence should be addressed. Office: (617) 726-5788. Fax: (617) 726-5708. E-mail: tung@helix.mgh.harvard.edu.

[1] Abbreviations: CaD, cathepsin D; FITC, fluorescein isothiocyanate; HBTU, 2-(1H-benzotriazole-1-yl)-1,1,3,3-tetramethyluronium hexafluorophosphate; HOBt, *N*-hydroxybenzotriazole; MPEG, methoxy poly(ethylene glycol); NIR, near-infrared; NIRF, near-infrared fluorescence; PGC, protected graft copolymer; PL, poly-L-lysine; TNBS, trinitrobenzene sulfonic acid; CDF, CaD sensitive peptide [Gly-Pro-Ile-Cys(Et)-Phe-Phe-Arg-Leu-Gly-Lys(FITC)-Cys-NH_2]; SCDF, scrambled control peptide [Gly-Pro-Phe-Cys(Et)-Ile-Arg-Phe-Leu-Gly-Lys(FITC)-Cys-NH_2].

10.1021/bc990052h CCC: $18.00 © 1999 American Chemical Society
Published on Web 09/20/1999

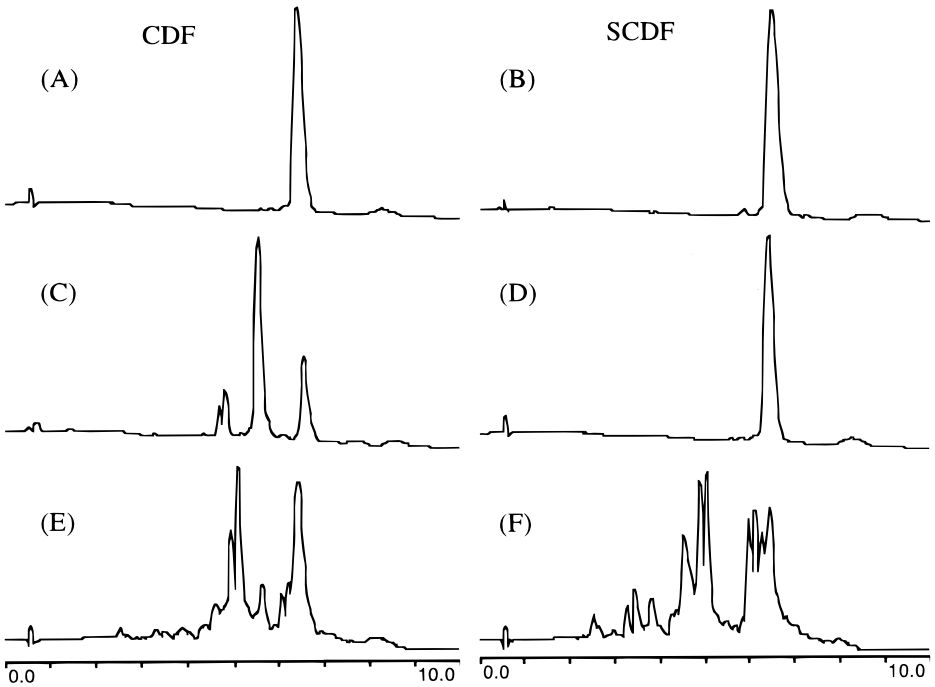


Figure 2. HPLC chromatogram of CDF (A) and SCDF (B) and their digested products by CaD (C, D) and Chymotrypsin (E, F).

sensitive probe and a scrambled nonsense control probe were synthesized and tested in vitro.

MATERIALS AND METHODS

Peptide Synthesis. A peptide with cathepsin D substrate specificity was synthesized on an automatic synthesizer (PS3, Rainin, Woburn, MA) by Fmoc chemistry using 2-(1H-benzotriazole-1-yl)-1,1,3,3-tetramethyluronium hexafluorophosphate (HBTU)/*N*-hydroxybenzotriazole (HOBt) as the activating agent. All amino acids, resin, and reagents for peptide synthesis were purchased from Calbiochem-NovaBiochem (San Diego, CA), except Fmoc-Cys(Et) was obtained from Bachem (King of Prussia, PA). The sequences are Gly-*Pro-Ile-Cys(Et)-Phe-Phe-Arg-Leu*-Gly-Lys(FITC)-Cys-NH_2 [the italicized amino acids correspond to cathepsin D substrate (*15*)] for the CaD sensitive peptide (CDF), and Gly-Pro-Phe-Cys(Et)-Ile-Arg-Phe-Leu-Gly-Lys(FITC)-Cys-NH_2 for the scrambled control peptide (SCDF). Fmoc-Cys(Trt) was anchored to 0.1 mmol of Rink amide MBHA and followed with other amino acids, i.e., Fmoc-Lys(Dde), Fmoc-Gly, Fmoc-Leu, Fmoc-Arg(Pbf), Fmoc-Phe, Fmoc-Cys(Et), Fmoc-Ile, and Fmoc-Pro. The N-terminal was finally capped with t-Boc-Gly. Thereafter, the lysine side-chain protecting group, Dde, was selectively removed with 10 mL of 2% hydrazine in DMF (2 × 3 min), and the deprotected amino group was reacted with 0.4 mmol of fluorescein isothiocyanate (FITC) (Aldrich, Milwaukee, WI) in 5 mL of DMSO/diisopropylethylamine (20% v/v) overnight. The peptide was cleaved by 5 mL of TFA/thioanisole/ethandithiol/anisole (90/5/3/2) and purified by C18 reversed-phase HPLC using 0.1% TFA and acetonitrile as elution buffers. MALDI-MS $(M + H)^+$: CDF peptide, 1658.5 (calcd), 1658.2 (found); SCDF peptide 1658.5 (calcd), 1659.1 (found).

Specificity of Peptide Substrate. CDF or SCDF peptide (0.5 μmol) was incubated with 1 unit of CaD or positive control protease, chymotrypsin, in 200 μL of buffer and 20 μL of acetonitrile for 15 min (Sigma, St Louis, MO). PBS and 50 mM Gly-HCl, pH 3.5, buffers were used in chymotrypsin and CaD assays, respectively. The degradation was analyzed by reversed-phase HPLC (Brownlee, Spheri-5, ODS, 30 × 4.6 mm), using 0.1% TFA and acetonitrile as elution buffers.

Synthesis of NIRF Probes. Protected graft copolymer (PGC) consisting of a poly-L-lysine (PL) backbone and methoxy poly(ethylene glycol) (MPEG) side chains was prepared as described (*12*). The available amino groups for chemical conjugation is quantitated using TNBS (trinitrobenzene sulfonic acid) assay (*16*). There were 55 free amino groups per PGC molecule. The PGC (1 mg, MW = 450 000) in 200 μL of 50 mM $NaHCO_3$ was iodoacetylated by reaction with excess of iodoacetic anhydride (3.5 mg, 10 μmol) in 100 μL of DMF for 3 h. A microconcentrator, 50 kDa cutoff (Amicon, Beverly, MA), was used to separate the product from excess reagents, byproducts, and solvents. No free amino group on PGC was detected using TNBS assay.

The iodoacetylated PGC was then coupled to 3.2 mg (2 μmol) of CDF or SCDF through thiol specific reaction in 200 μL of acetonitrile and 200 μL of 0.1 M sodium acetate, pH 6.5, buffer for 3 h. Excess peptide and byproducts was separated from peptide−PGC conjugate by P-10 Bio-gel (Bio-Rad, Hercules, CA) size-exclusion chromatography. The coupling efficiency of peptide to PGC was determined by measuring fluorescein absorption at 494 nm ($\epsilon = 7.3 \times 10^4\ M^{-1}\ cm^{-1}$) divided by initial available amino groups. A total of 42 CDF or 44 SCDF peptide chains were coupled per PGC molecule.

Monoactivated near-infrared dye Cy5.5 (Amersham-Pharmacia, Piscataway, NJ), 1 μmol, was reacted to the N-termini of the peptide-PGC (0.5 mg) in 2 mL of 50 mM $NaHCO_3$. The reaction mixture was incubated at room temperature for 1 h, and products were purified using a 50 kDa cutoff Microcon concentrators. The loading efficiency of Cy5.5 was determined by dividing molarity of Cy5.5 to FITC. Extension coefficients $250 \times 10^3\ M^{-1}\ cm^{-1}$ and $73 \times 10^3\ M^{-1}\ cm^{-1}$ of Cy 5.5 at 675 nm and FITC at 494 nm were used. The average loading percentage was 50−60% for both probes.

Enzyme Activation. Fluorescence activation of the Cy-CDF-PGC probe (containing 0.5 nmol of Cy5.5 in 2

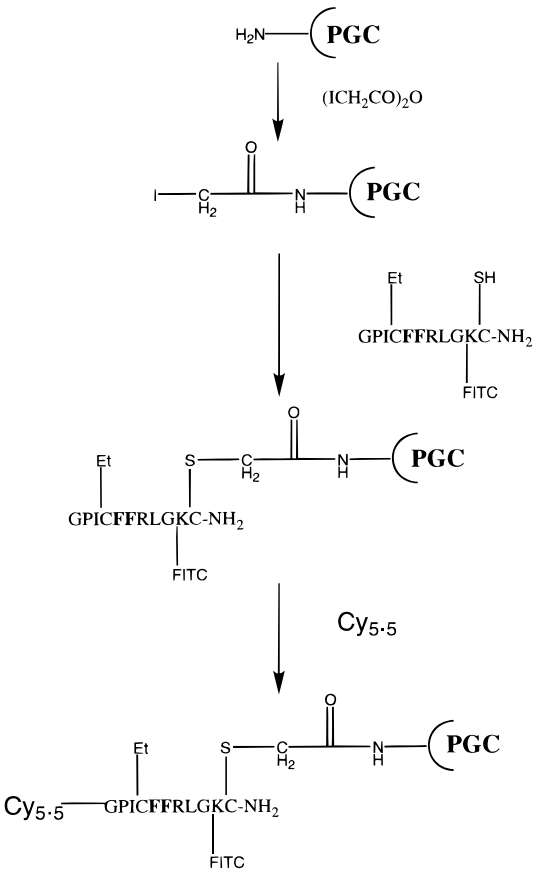


Figure 3. Synthetic scheme of the Cy-CDF-PGC probe.

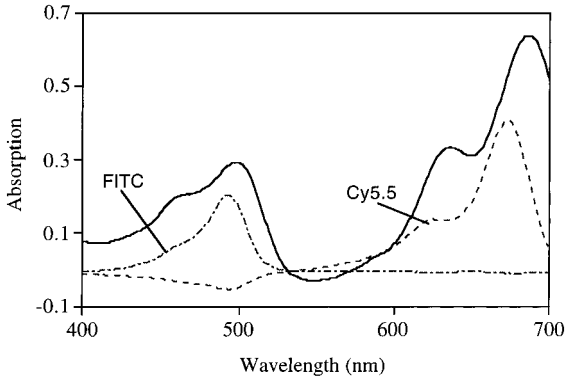


Figure 4. Absorption spectrum of Cy-CDF-PGC probe (solid line), free FITC and free Cy5.5. Absorption maximum for bound FITC and Cy5.5 are 498 and 687 nm, respectively.

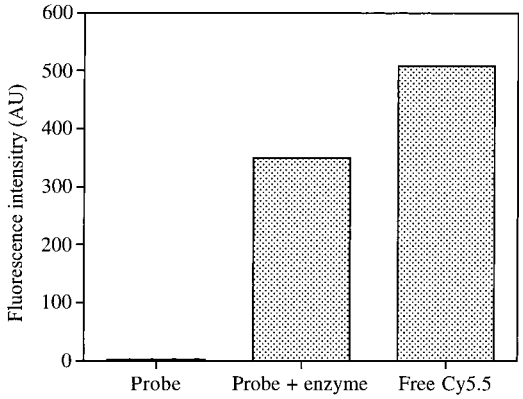


Figure 5. NIRF activation of Cy-CDF-PGC (ex = 675 nm and em = 694 nm). Initially, the Cy-CDF-PGC probe was completed quenched. At same concentration of Cy5.5, the fluorescence intensity of Cy-CDF-PGC, Cy-CDF-PGC with chymotrypsin and free Cy5.5 is 1 AU, 350 AU, and 509 AU, respectively.

mL of previously described buffer) with CaD or chymotrypsin was determined at different time point using a fluorescence spectrophotometer (Hitachi, U4500, Tokyo, Japan). Fluorescence intensity was measured at λ_{ex} 675 nm/λ_{em} 694 nm. The same concentration of free Cy5.5 fluorochrome solution was prepared, and its fluorescence intensity was collected as a reference.

Cell Culture Experiments. The NIRF probe was subsequently tested in cell culture using a rodent cell line stably transfected with human cathepsin (Cath D-1), which was kindly provided by Dr. Henri Rochefort (INSERM, Montpellier, France) (*7*). Cath D-1 cells were cultured in RPMI medium containing 10% FCS and 400 μg/mL G418 on glass cover slips in a 12-well plate (Becton Dickinson, Bedford, MA). CaD expression was confirmed by RT-PCR and Western blotting (*17*). Culture medium was then replaced with 500 μL of fresh medium containing 1 nmol of the NIRF probe. After 1 h at 37 °C, the cells were washed three times and analyzed by fluorescence microscopy. Cells were viewed in phase contrast or fluorescence mode using an inverted epifluorescence microscope (Zeiss, Axiovert, Thornwood, NY) with a cooled charged coupled device (CCD) camera (Sensys, Photometrics, Tuscon, Az) interfaced to a Power Macintosh 7600/120 computer. The microscope was equipped with appropriate excitation and emission filters for FITC (485/530 nm) and Cy5.5 (670/700 nm) (Omega Optical, Brattleboro, VT). Images were analyzed using Spectrum Analysis software, and images were fused using Adobe Photoshop software.

RESULTS AND DISCUSSION

NIRF Probe Preparation. To impart enzyme specificity onto the optical probe, a CaD substrate spacer was used to link the NIR fluorochrome to the PGC backbone (Figure 1). The CaD-specific substrate, Pro-Ile-Cys(Et)-Phe-Phe-Arg-Leu, was selected from published literature (*15*). This peptide has a K_m and k_{cat} of 27.5 μM and 196 S^{-1}, respectively. Glycine residues were added to both termini as spacers. The peptide was furthermore modified to accommodate fluorescein isothiocyanate (FITC) as a tracing tag during conjugation and for quantitation. A cysteine amide residue was then incorporated to obtain a mono reactive sulfhydryl group. The overall sequence of this CaD fluorescein (CDF) peptide is Gly-Pro-Ile-Cys(Et)-Phe-Phe-Arg-Leu-Gly-Lys(FITC)-Cys-NH_2. In addition, a scrambled peptide (SCDF), Gly-Pro-Phe-Cys(Et)-Ile-Arg-Phe-Leu-Gly-Lys(FITC)-Cys-NH_2, was prepared as a control.

Before synthesizing the NIRF probe, the specificity of the peptide substrates was determined with CaD and a nonspecific endoprotease, chymotrypsin (Figure 2). The latter served as an in vitro positive control; in vivo, chymotrypsin is exclusively present in exocrine pancreas but not in other solid organs, tumors, muscle, or fat or within the vasculature. As expected, CaD recognized the CDF and cleaved the peptide between two phenylalanine residues. The HPLC elution chromatogram indicates one major cut of the CDF peptide. Two fragments were eluted at 4.8 and 5.5 min (Figure 2C). Since the scrambled control peptide SCDF was not a substrate of CaD, the peptide remained intact and eluted at the original time, 6.4 min (Figure 2, panels B and D). In contrast, chymotrypsin, a nonspecific endoprotease, recognized and cleaved the C-termini of hydrophobic amino acids, e.g., Phe and

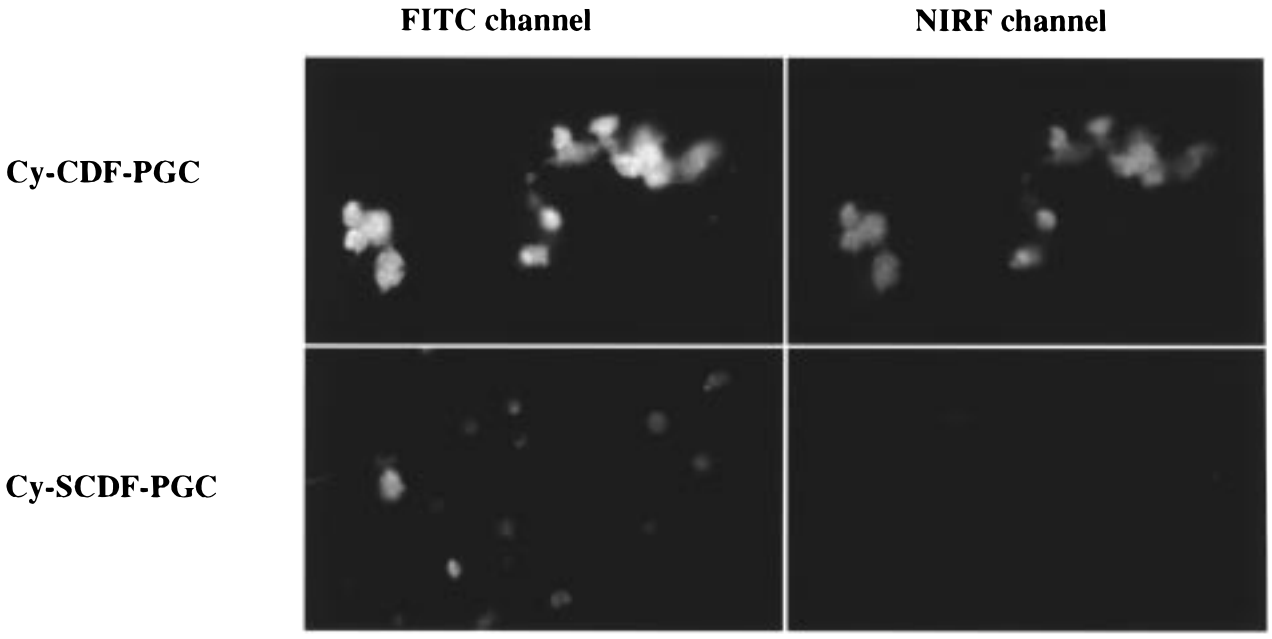


Figure 6. Testing of Cy-CDF-PGC and control Cy-SCDF-PGC probes in rodent tumor cells stable transfected with human cathepsin D. Cellular internalization of the probes is monitored in the FITC channel while probe activation through CaD is observed in the NIRF channel.

Leu in these peptides, resulting in complex chromatograms for both peptides (Figure 2, panels E and F).

The conjugation of the peptide to PGC was initiated by iodoacetylation of PGC (Figure 3) using a large excess of iodoacetic anhydride. All free amino groups on PGC were converted into iodoacetyl group. CDF or SCDF was then coupled to functionlized PGC in 50% acetonitrile and 50% sodium acetate buffer, 0.1 M, pH 6.5. Due to the relative hydrophobicity of the peptides, higher loading of PGC caused precipitation of the entire complex. The achieved loading of the peptide to PGC was 42 peptide chains per PGC molecule, i.e., 80%.

A monoreactive activated ester of the NIR fluorochrome, Cy5.5, was subsequently attached to the N-terminus of the peptide under a basic condition. Since Cy5.5 and FITC have their absorption and emission at different wavelengths, no energy transfer was observed between these two fluorochromes (Figure 4). Wavelength shifts of the fluorescein and Cy5.5 were observed; the absorption maximum shift ranged from 493 to 498 nm and 674 to 687 nm, respectively. The loading efficiency of Cy5.5 was determined by absorption at 675 nm, compared to the absorption of FITC at 494 nm. Approximately 60% of the peptide chain was labeled with Cy5.5, which is equivalent to 24 Cy5.5 fluorochromes/PGC molecule. A larger excess of Cy5.5 was also used to achieve more complete loading, however, precipitation was observed, despite the excellent aqueous solubility of Cy5.5. The prepared NIRF probes were named Cy-CDF-PGC and Cy-SCDF-PGC.

Quenching and Dequencing Effect. The NIRF probe was designed to have minimal fluorescent signal while in circulation, important for in vivo use. Ideally, only specific proteases under investigation would activate the probe and initiate NIR fluorescence. The quenching effect of the prepared NIRF probes was examined using fluorescent spectroscopy. In PBS, a solution of free Cy5.5 fluorochrome had a fluorescence intensity of 509 AU, while an equimolar solution of Cy-CDF-PGC had an emission signal of only 1 AU at 694 nm (i.e., more than 99% quenching) (Figure 5). Although we only achieved 60% loading of the peptide-PGC, the local density of fluorochrome was sufficiently high for autoquenching to occur.

The activation of the fluorescence signal of the NIRF probe was tested with CaD at its optimal condition, a 50 mM Gly-HCl, pH 3.5, buffer (*15*). Surprisingly, neither Cy-CDF-PGC nor Cy-SCDF-PGC was activatable under this experimental condition. The reason of inactivation of NIRF probe with pure CaD at acidic condition in vitro is somewhat unclear. One possibility is that the intramolecular interaction between peptides or fluorochromes causes collapse of the macromolecule.

However, when Cy-CDF-PGC was incubated with the in vitro positive control protease, chymotrypsin, a 350-fold NIRF signal increase was obtained within 8 h of incubation (Figure 5). The regained NIRF signal is equal to 70% of theoretical signal of free Cy5.5 fluorochrome. In contrast, a previously described probe, which had the same Cy5.5 fluorochrome directly attached to the backbone of PGC without any peptide spacer between, had only a 15-fold increase in NIRF signal recovery. However, this was sufficient for in vivo selective imaging of tumors (*9*). The improved ratio of signal generation compared with background of the quenched state in the new probe is due to the increased number of fluorochromes attached per PGC, resulting in more complete quenching, as well as a better release of fluorochromes from each backbone.

Activation in Cell Culture. The usefulness of the NIRF probe for imaging was subsequently evaluated in cell culture. We utilized murine 3Y1-AD12 embryonic tumor cells which were stably transfected with human CaD (CathD-1) (*7*). In tissue culture, the CathD-1 cells were incubated with 1 nmol of Cy-CDF-PGC at 37 °C for 1 h. Subsequently, the live cells were studied by fluorescence microscopy at FITC and Cy5.5 channels with appropriate filter sets. The fluorescein signal indicated internalization of the probe, and the Cy5.5 signal indicated the cellular CaD activity. When Cy-CDF-PGC was applied, the fluorescein signal correlated with NIR signal in the CathD-1 cells. In contradistinction, only fluorescein

signal was observed in Cy-SCDF-PGC; no NIR signal was detected at the Cy5.5 channel (Figure 6).

These results indicate that cellular internalization of the Cy-CDF-PGC probe occurs presumably into the lysosomal compartment, and NIRF is generated due to CaD activity. The specificity was confirmed when virtually no NIRF signal was recovered using the Cy-SCDF-PGC probe. These data from cellular activation assays suggest potential usage of this CaD sensitive probe for in vivo optical imaging.

CONCLUSION

The developed biocompatible, enzyme activatable NIRF imaging probe represents a critical link toward development of in vivo molecular optical imaging (*9*). The enzyme specific probe could potentially be used to image exogenous or endogenous enzyme expression. Whereas the former has far reaching applications in gene therapy and developing marker genes detectable by imaging, the latter can be used to probe for enzyme activities in various disease states. One specific application is to use the probe for tumor detection based on overexpressed proteolytic enzymes involved in tumorigenesis, angiogeneis, or matastagenesis. Ultimately, the technique can be extended to other enzymes, for example matrix metaloproteinases, caspases, or prostate specific antigen among others.

ACKNOWLEDGMENT

We would like to thank Dr. Alexei Bogdanov for providing PGC and Dr. H. Rochefort for Cathepsin D cell lines. This study was supported in part by grants from NIH (RO1 NS35258) and the MGH Center for Innovative Minimally Invasive Therapy (CIMIT).

LITERATURE CITED

(1) Escot, C., Zhao, Y., Puech, C., and Rochefort, H. (1996) Cellular localisation by in situ hybridisation of cathepsin D, stromelysin 3, and urokinase plasminogen activator RNAs in breast cancer. *Breast Cancer Res. Treat. 38,* 217−26.

(2) Roger, P., Montcourrier, P., Maudelonde, T., Brouillet, J. P., Pages, A., Laffargue, F., and Rochefort, H. (1994) Cathepsin D immunostaining in paraffin-embedded breast cancer cells and macrophages: correlation with cytosolic assay. *Hum. Pathol. 25,* 863−71.

(3) Garcia, M., Derocq, D., Pujol, P., and Rochefort, H. (1990) Overexpression of transfected cathepsin D in transformed cells increases their malignant phenotype and metastatic potency. *Oncogene 5,* 1809−14.

(4) Leto, G., Gebbia, N., Rausa, L., and Tumminello, F. (1992) Cathepsin D in the malignant progression of neoplastic diseases. *Anticancer Res. 12,* 235−40.

(5) Tedone, T., Correale, M., Barbarossa, G., Casavola, V., Paradiso, A., and Reshkin, S. J. (1997) Release of the aspartyl protease cathepsin D is associated with and facilitates human breast cancer cell invasion. *FASEB J. 11,* 785−92.

(6) Keppler, D., Sameni, M., Moin, K., Mikkelsen, T., Diglio, C., and Sloane, B. (1996) Tumor progression and angiogenesis: Cathepsin B & Co. *Biochem. Cell. Biol. 74,* 799−810.

(7) Liaudet, E., Derocq, D., Rochefort, H., and Garcia, M. (1995) Transfected cathepsin D stimulates high-density cancer cell growth by inactivating secreted growth inhibitors. *Cell Growth Differ. 6,* 1045−52.

(8) Peterson, J. J., and Meares, C. F. (1998) Cathepsin substrates as cleavable peptide linkers in bioconjugates, selected from a fluorescence quench combinatorial library. *Bioconjugate Chem. 9,* 618−26.

(9) Weissleder, R., Tung, C. H., Mahmood, U., and Bogdanov, A. (1999) In vivo imaging of tumors with protease-activated near-infrared fluorescent probes. *Nat. Biotech. 17,* 375−8.

(10) Bogdanov, A., Jr., Wright, S. C., Marecos, E. M., Bogdanova, A., Martin, C., Petherick, P., and Weissleder, R. (1997) A long-circulating copolymer in "passive targeting" to solid tumors. *J. Drug Target. 4,* 321−30.

(11) Marecos, E., Weissleder, R., and Bogdanov, A., Jr. (1998) Antibody-mediated versus nontargeted delivery in a human small cell lung carcinoma model. *Bioconjugate Chem. 9,* 184−91.

(12) Bogdanov, A., Martin, C., Bogdanova, A. V., Brady, T. J., and Weissleder, R. (1996) An adduct of cis-diamminedichloroplatinum(II) and poly(ethylene glycol)poly(L-lysine)-succinate: synthesis and cytotoxic properties. *Bioconjugate Chem. 7,* 144−9.

(13) Bogdanov, A., Weissleder, R., and Brady, T. (1995) Long-circulating blood pool imaging agents. *Adv. Drug Deliv. Rev. 16,* 335−48.

(14) Callahan, R., Bogdanov, A., Fischman, A., Brady, T., and Weissleder, R. (1998) Preclinical evaluation and phase I clinical trial of a 99mTc labeled synthetic polymer used in blood pool imaging. *Am. J. Roentgenol. 171,* 137−43.

(15) Gulnik, S., Suvorov, L., Majer, P., Collins, J., Kane, B., Johnson, D. G, and Erickson, J. (1997) Design of sensitive fluorogenic substrates for human cathepsin D. *FEBS Lett. 413,* 379−84.

(16) Hancock, W. S., and Battersby, J. E. (1976) A new microtest for the detection of incomplete coupling reactions in solid-phase peptide synthesis using 2,4,6-trinitrobenzenesulphonic acid. *Anal. Biochem. 71,* 260−4.

(17) Sambrook, J., Fritsch, E. F., and Maniatis, T. (1989) Molecular cloning: a laboratory manual, 2nd ed., Cold Spring Harbor Laboratory, Plainview, NY.

BC990052H

Synthesis and Evaluation of Two Technetium-99m-Labeled Peptidic 2-Nitroimidazoles for Imaging Hypoxia

Zi-Fen Su,[†,‡] Xiuguo Zhang,[†,‡] James R. Ballinger,[‡,§] A. M. Rauth,*[,†,‡] Alfred Pollak,[||] and John R. Thornback[||]

Departments of Medical Biophysics and Pharmaceutical Sciences, University of Toronto, 610 University Avenue, Toronto, Ontario M5G 2M9, Canada, Division of Experimental Therapeutics, Ontario Cancer Institute, 610 University Avenue, Toronto, Ontario M5G 2M9, Canada, Division of Nuclear Medicine, University Medical Imaging Centre, 600 University Avenue, Toronto, Ontario M5G 1X5, Canada, and Resolution Pharmaceuticals Inc., 6850 Goreway Drive, Mississauga, Ontario L4V 1V7, Canada. Received May 4, 1999; Revised Manuscript Received June 29, 1999

The presence of hypoxic cells in solid tumors is a marker for therapy-resistant, aggressive disease. The noninvasive detection of hypoxic cells in tumors by radiolabeled 2-nitroimidazoles is a diagnostic technique under current evaluation. Two peptidic agents, dimethylglycyl-L-seryl-L-cysteinyl-lysyl{N_ϵ-[1-(2-nitro-1*H*-imidazolyl)acetamido]}glycine (RP435) and dimethylglycyl-*tert*-butylglycyl-L-cysteinyl-glycine-[2-(2-nitro-1*H*-imidazolyl)ethyl]amide (RP535) have been synthesized. Both agents contain an N_3S class chelator for ^{99m}Tc and Re and a 2-nitroimidazole group which can be enzymatically reduced and selectively trapped in cells under hypoxic conditions. Two isomers of ^{99m}TcO-RP435, which are assumed to be syn and anti conformations, were observed on HPLC analysis. The interconversion of the two isomers in aqueous solution was investigated. In contrast, RP535 chelated ^{99m}Tc to form a single isomer and no conversion to its counterpart has been observed on HPLC analysis. The *tert*-butyl group on the chelator may inhibit the formation and interconversion of the syn and anti isomers of ^{99m}TcO-RP535. Both tracers showed a significant degree of hypoxia-specific accumulation in an in vitro assay, with ^{99m}TcO-RP535 showing higher selectivity for hypoxic cells than ^{99m}TcO-RP435. These results suggest that ^{99m}TcO-RP535 represents a lead compound worthy of further investigation as an agent for imaging hypoxia in tumors.

INTRODUCTION

Detection of regions of hypoxia is important in several medical conditions. It is important to delineate hypoxic but viable tissue following interruption of blood flow in cerebral or myocardial infarction (*1*). Furthermore, it has recently been recognized that hypoxia in tumors plays a role not only in response to radiation, through the oxygen effect in fixation of DNA damage, but also in metastatic potential and response to other forms of therapy (*2*−*4*). However, hypoxia is heterogeneous, and tumors which appear identical by all other clinical measures can vary greatly in their proportion of hypoxic cells. At present, hypoxia is measured clinically with a polarographic oxygen electrode inserted into tumors; however, this is invasive, operator dependent, limited to accessible tumors, and not readily repeatable (*2, 4*). In recent years, several radiopharmaceuticals have been developed which are targeted to hypoxic tissues via a 2-nitroimidazole (2-NI) moiety (*1, 5*). 2-NIs are electron-affinic compounds which undergo an enzyme-mediated one-electron reduction; in normoxic tissue, the resultant radical anion is immediately oxidized back to the starting compound, whereas under hypoxic conditions there is further reduction to products which are trapped by binding to macromolecules (*6*). A radiolabeled 2-NI would therefore be selectively trapped in hypoxic tissues.

Clinical studies have been performed with several radiolabeled 2-NIs, including [^{18}F]fluoromisonidazole (FMISO) (*7*, *8*) and [^{123}I]iodoazomycin arabinoside (IAZA) (*9, 10*). However, the search continues for a ^{99m}Tc-labeled analogue that would be more widely applicable. BMS181-321, a 2-NI linked to a PnAO chelator, has been evaluated in several model systems and shows promise, but its high lipophilicity and metabolic instability result in high background levels of radioactivity (*11*−*14*). BRU59-21 (previously known as BMS194796) appears to possess improved biodistribution characteristics, but only limited information is available about it (*15, 16*). In addition, butyleneamine oxime (BnAO or HL91; Prognox, Nycomed-Amersham) is a nonnitro ^{99m}Tc complex that shows localization in hypoxic myocardium and tumors via an undetermined mechanism (*17*−*20*).

Recent work involving radioiodinated sugar derivatives of 2-NI has suggested that an octanol/water partition coefficient (PC) of ∼1 confers optimal biodistribution properties for tumor imaging (*5*). BMS181321 and BRU59-21 have PCs which are much higher (40 and 12, respectively) and cannot be readily modified to achieve a lower PC. As part of our radiopharmaceutical development program, we designed two compounds in which peptidic chelators for ^{99m}Tc were linked to 2-NI and evaluated the complexes in an in vitro model of tumor hypoxia. Dimethylglycyl-L-seryl-L-cysteinyl-glycinamide (RP294, Figure 1), which contains a sulfur atom (protected by an acetoamidomethyl group), one amine nitrogen atom, and two

* To whom correspondence should be addressed. Phone: (416) 946-2977. Fax: (416) 946-2984. E-mail: rauth@oci.utoronto.ca.
[†] Department of Medical Biophysics.
[‡] Ontario Cancer Institute.
[§] Pharmaceutical Sciences and University Medical Imaging Centre.
[||] Resolution Pharmaceuticals Inc.

10.1021/bc9900542 CCC: $18.00 © 1999 American Chemical Society
Published on Web 08/27/1999

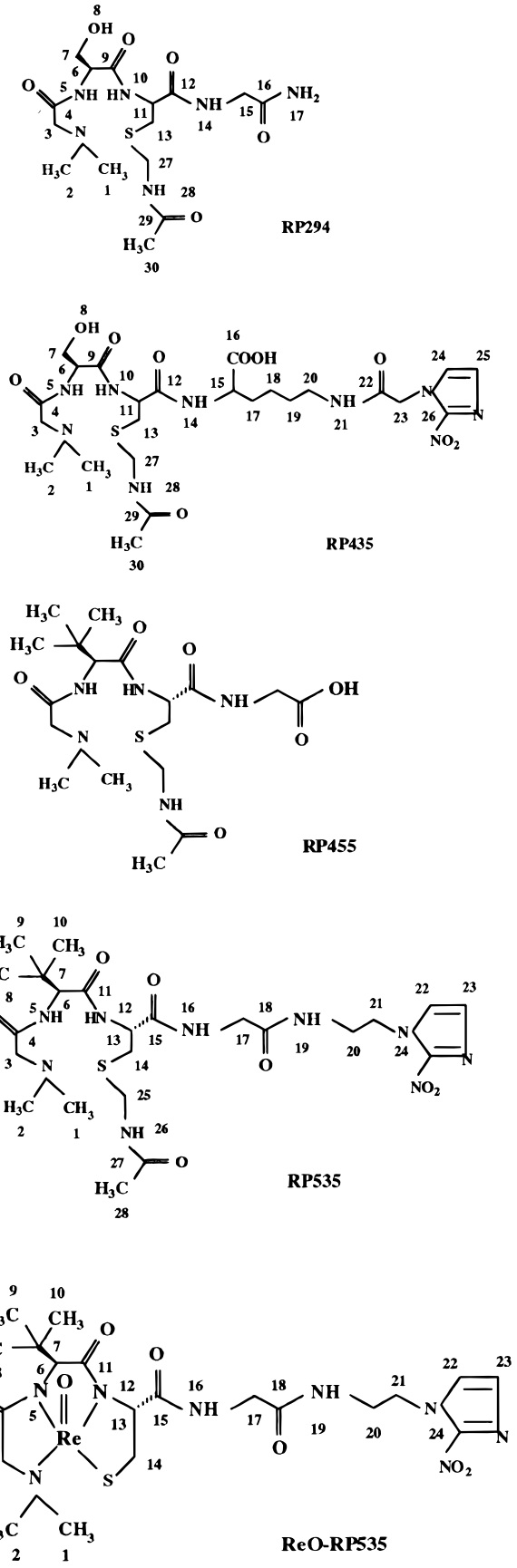


Figure 1. Chemical structures of two peptidic N_3S chelators, their 2-nitroimidazole-linked derivatives, and the ReO complex of RP535. Numbers refer to proton assignments.

amide nitrogen atoms, is an N_3S class chelator for $^{99m}Tc^{v}O$ and $Re^{v}O$ in a distorted square pyramidal geometry with the oxo moiety in the apical position. The metal complexes exist in syn and anti isomers with respect to the position of the metal−oxo bond and serine hydroxymethyl side chain. Interconversion of the two isomers in aqueous solution at room temperature has been observed (*21*).

In the present work, *N*,*N*-dimethylglycyl-L-seryl-L-cysteinyl-lysyl{N_ϵ-[1-(2-nitro-1*H*-imidazolyl)acetamido]}-glycine (RP435, Figure 1) was prepared by attaching 2-NI-acetic acid to a lysine linker connected to the RP294 chelator. RP435 chelates ^{99m}Tc at room temperature, and two peaks, assumed to be the syn and anti isomers, were detected by HPLC. However, the PC of ^{99m}TcO-RP435 is far lower than what is believed to be the optimum value. Accordingly, a new N_3S class peptide, *N*,*N*-dimethylglycyl-L-*tert*-butylglycyl-L-cysteinyl-glycin[2-(2-nitro-1*H*-imidazolyl)ethyl]amide (RP535, Figure 1) was designed and synthesized. The chelator (RP455, Figure 1) contains a *tert*-butyl group, which should increase the lipophilicity of the corresponding ^{99m}Tc complex and inhibit the interconversion of syn and anti isomers. The labeling, stability, and in vitro cellular accumulation of these compounds was studied.

EXPERIMENTAL PROCEDURES

2-Nitroimidazole, 2-bromoethylphthalimide, *N*,*N*-dimethylformamide (DMF), 1-(3-dimethylaminopropyl)-3-ethylcarbodiimide hydrochloride (DECI), 2,3,5,6-tetrafluorophenol (TFP), and trifluoroacetic acid (TFA) were purchased from Aldrich Chemical Co. (Milwaukee, WI). *N*,*N*-Dimethylglycyl-L-*tert*-butylglycyl-L-cysteinyl-glycine (RP455) was custom synthesized by Bachem Bioscience Inc. (Philadelphia, PA). *N*,*N*-Dimethylglycyl-L-seryl-L-cysteinyl-glycinamide (RP294) and ReO-RP455 precursor were provided by Resolution Pharmaceuticals Inc. (Mississauga, ON). Sodium $^{99m}TcO_4$ in saline was obtained from a ^{99}Mo/^{99m}Tc generator (DuPont Pharma, Billerica, MA). α-MEM and fetal bovine serum were purchased from Sigma Chemical Co. (St. Louis, MO).

NMR data (^{1}H, ^{13}C, COSY, HSQC, HMQC, TOCSY) were recorded on a Varian UNITYplus-500 spectrometer (500 MHz) with TMS as external standard. Electrospray mass spectra were obtained on a Sciex API#3 spectrometer in the positive ion mode. Reversed-phase high-pressure liquid chromatography (HPLC) analyses of peptide and ^{99m}Tc−peptide complexes were carried out on a Beckman model 125 System Gold (Fullerton, CA), with Zorbax SB or Beckman ODS 4.6 × 250 mm 5 μm C_{18} columns. Purification of peptides was accomplished by HPLC with a Waters C_{18} RCM 8 × 10 semipreparative column. UV and radiometric detectors were connected in series. Two mobile phases were used for HPLC analysis of ^{99m}Tc tracers. Mobile phase I was composed of H_2O/ACN containing 0.1% TFA, whereas mobile phase II was 0.02 M, pH 4.6, NH_4OAc buffer/MeOH; both were run as gradients. The flow rate was 1.0 mL/min for analysis and 2.0 mL/min for purification.

Synthesis of 2-Nitroimidazole Acetic Acid. To 1.0 g (8.8 mmol) 2-nitroimidazole and 2.0 g (14.5 mmol) potassium carbonate in 10 mL dry acetonitrile was added 1.20 mL (10.6 mmol) of bromoethyl acetate. The reaction mixture was stirred for 24 h at room temperature followed by filtration and washing of the solid product with acetone. Evaporation of the pooled filtrates under reduced pressure yielded 2.29 g of crude 2-nitroimidazole ethyl acetate as a yellow oil. To the crude oil was added a solution of NaOH (4 N, 2.5 mL), water (10 mL), and MeOH (10 mL). The solution was stirred and monitored

by thin-layer chromatography (silica gel; CH_2Cl_2:MeOH:NH_3, 50:7:1) until none of the ester remained (~30 min). The solution was acidified by addition of a cation-exchange resin (Bio-Rad, 4 g), which had been converted to the protonated form by washing with H_2SO_4 (1 N, 60 mL). Following filtration and evaporation of MeOH, the concentrated solution was lyophilized for 4 days to yield 1.16 g (6.8 mmol, 77%) of 2-nitroimidazole acetic acid. ^{1}H NMR (275 MHz, DMSO): δ 7.5 (s, 1H), 7.1 (s, 1H), 4.8 (s, 2H).

Synthesis of *N*,*N*-Dimethylglycyl-L-seryl-L-cysteinyl-lysyl{N_ϵ-[1-(2-nitro-1*H*-imidazolyl)acetamido]}-glycine (RP435). The peptide backbone was prepared on an automated peptide synthesizer (Applied Biosystems Inc., model 433A, Foster City, CA) using Sasrin resin and 9-fluorenylmethoxycarbonyl-protected amino acids. When the backbone was complete, the 1-(4,4-dimethyl-2,6-dioxocyclohexylidine)-ethyl protecting group on the ϵ-amine of lysine was cleaved with 2% hydrazine and the free amine was coupled with 2-nitroimidazole acetic acid. The peptide was cleaved from the resin by stirring with 95% aqueous TFA at 0 °C for 30 min and then at room temperature for 60 min. The resin was filtered, and the filtrate was evaporated under vacuum. The residue was washed with a minimum amount of *tert*-butyl methyl ether, which caused the precipitation of the peptide. The ether was removed, and the residue was dissolved in a minimum amount of water and then lyophilized to yield 190 mg of crude product, of which 110 mg was further purified by HPLC, yielding 35 mg (31%) pure RP435. ^{1}H NMR (500 MHz, d_6-DMSO): δ 1.33 [m, 2H, H(18)], 1.43 [m, 2H, H(19)], 1.59 [m, 1H, H(17a)], 1.72 [m, 1H, H(17b)], 1.86 [s, 3H, H(30)], 2.58 [broad, 6H, H(1, 2)], 2.68 [dd, 1H, H(13a), $J_{H13a-H11}$ = 9.89 Hz, $J_{H13a-H13b}$ = 14.04 Hz], 2.95 [dd, 1H, H(13b), $J_{H13b-H11}$ = 3.91 Hz, $J_{H13b-H13a}$ = 13.92 Hz], 3.05 [m, 2H, H(20)], 3.61 [m, 2H, H(7)], 4.13 [m, 1H, H(15)], 4.20 [dd, 1H, H(27a), $J_{H27a-H28}$ = 5.86 Hz, $J_{H27a-H27b}$ = 13.67 Hz], 4.32 [dd, 1H, H(27b), $J_{H27b-H28}$ = 5.13 Hz, $J_{H27b-H27a}$ = 13.67 Hz], 4.44 [m, 1H, H(6)], 4.56 [m, 1H, H(11)], 5.07 [s, 2H, H(23)], 5.09 [broad, 1H, H(8)], 7.18 [d, 1H, H(25), $J_{H25-H24}$ = 0.97 Hz], 7.61 [d, 1H, H(24), $J_{H24-H25}$ = 0.98 Hz], 8.0 [d, 1H, H(14), J_{H14-15} = 7.57 Hz], 8.31 [m, 2H, H(*10, 21*)], 8.56 [t, 1H, H(28), $J_{H28-H27}$ = 6.47 Hz]. Electrospray mass spectrum: *m*/*z* 646.15 ([M + H]$^+$, $C_{24}H_{40}N_9O_{10}S$, calculated = 645.69).

Synthesis of 2-(2-nitro-1*H*-imidazolyl)ethylamine hydrochloride was accomplished by minor modification of a published method (*22*). A total of 0.56 g (5.0 mmol) of 2-nitroimidazole, 1.33 g (5.2 mmol) of *N*-(2-bromoethyl)phthalimide, and 0.72 g (5.2 mmol) of potassium carbonate was mixed in 15 mL of DMF and heated at 110 °C for 2 h. After removing the solvents, water was added to the residue to dissolve the salts. The precipitate was collected, washed by water, and dried under vacuum to yield 0.8 g (2.8 mmol, yield 56%) of raw product. The raw product was refluxed with 0.28 g (5.6 mmol) hydrazine monohydrate in 20 mL of EtOH for 2 h and then cooled to 4 °C, filtered, and evaporated to dryness. The residue was dissolved in 20 mL of 1 N HCl, filtered, and brought to dryness again. The residue was recrystallized from MeOH/EtOAc to yield 240 mg (1.25 mmol, 44%) of product.

Synthesis of *N*,*N*-Dimethylglycyl-L-*tert*-butylglycyl-L-cysteinylglycin[2-(2-nitro-1*H*-imidazolyl)ethyl]amide (RP535). A total of 80 mg (0.18 mmol) of RP455, 55.4 mg (0.29 mmol) of DECI, and 48 mg (0.29 mmol) of TFP was dissolved in 1 mL of DMF. The mixture was stirred in an ice bath for 10 min, followed by 30 min at room temperature, and then in a 45 °C oil bath for 60 min. A total of 37.2 mg (0.19 mmol) of 2-(2-nitro-1*H*-imidazolyl)ethylamine hydrochloride was added to the mixture which was set in an ice bath. To the mixture was added dropwise 74.7 mg (0.58 mmol) of diisopropyl ethylamine (DIEA) in 1 mL of DMF. The mixture was stirred at 45 °C for 1 h. The solvent was removed after the reaction was completed. About 2 mL of water was added and then removed. The crude product was purified by HPLC, yielding 50 mg (0.085 mmol, 47%) of pure RP535. ^{1}H NMR (500 MHz, d_6-DMSO): δ 0.93 [s, 9H, H(8, 9, 10)], 1.86 [s, 3H, H(28)], 2.71 [dd, 1H, H(14a), $J_{H14a-H13}$ = 9.3 Hz, $J_{H14a-H14b}$ = 13.9 Hz], 2.79 [t, 6H, H(1, 2), J = 4.0 Hz], 2.90 [dd, 1H, H(14b), $J_{H14b-H13}$ = 4.6 Hz, $J_{H14b-H14a}$ = 13.9 Hz], 4.25 [d, 1H, H(25a), $J_{H25a-H26}$ = 6.59 Hz], 4.27 [d, 1H, H(25b), $J_{H25b-H26}$ = 6.59 Hz], 4.37 [d, 1H, H(6), J_{H6-H5} = 9.27 Hz], 4.47 [m, 1H, H(13)], 7.16 [d, 1H, H(23), $J_{H23-H22}$ = 1.2], 7.51 [d, 1H, H(22), $J_{H22-H23}$ = 0.98 Hz], 7.89 [t, 1H, H(19), $J_{H19-H20}$ = 5.98 Hz], 8.14 [t, 1H, H(16), $J_{H16-H17}$ = 5.6 Hz], 8.39 [d, 1H, H(12), $J_{H12-H13}$ = 7.57 Hz], 8.45 [t, 1H, H(26), $J_{H26-H25}$ = 6.59 Hz], 8.61 [d, 1H, H(5), J_{H5-H6} = 9.27 Hz]. Electrospray mass spectrum: *m*/*z* 586.11 ([M+H]$^+$, $C_{23}H_{40}N_9O_7S$, calculated = 585.69).

Synthesis of ^{99m}TcO-RP294, ^{99m}TcO-RP435, ^{99m}TcO-RP455, and ^{99m}TcO-RP535. To a 3 mL tube were added RP294, RP435, RP455, or RP535 (100−200 μg), $Na^{99m}TcO_4$ solution (2−10 mCi in 200 μL of saline), and 100 μL of stannous gluconate solution (which contained 10−40 μg of $SnCl_2$ and 0.25−1.0 mg of sodium gluconate). The mixture was incubated at 20−100 °C for 15−30 min. The ^{99m}Tc complexes were analyzed by HPLC (Zorbax SB column, H_2O/ACN containing 0.1% TFA; gradient 100 to 90% H_2O over 45 min for ^{99m}TcO-RP294, 100 to 70% H_2O for ^{99m}TcO-RP435, and 100 to 50% H_2O for ^{99m}TcO-RP455 and ^{99m}TcO-RP535). UV detection at 320 nm was used to monitor the disappearance of the 2-NI absorption peak of the ligand. The radiochemical yields were ^{99m}TcO-RP294, >97%; ^{99m}TcO-RP435, >68%; ^{99m}TcO-RP455, >99%; and ^{99m}TcO-RP535, >78%. Formation of ^{99m}Tc-colloid was <6%. ^{99m}TcO-RP435 and ^{99m}TcO-RP535 were purified for further experiments by HPLC using the same conditions stated above.

Synthesis of ReO-RP535. A total of 10 mg (0.017 mmol) of ReO-RP455 and 13.3 mg (0.070 mmol) of DECI were dissolved in 0.6 mL of ACN solution, which contained 20% 0.01 M NaOAc/HOAc. To the mixture was added 2.89 mg (0.017 mmol) of TFP dissolved in 0.3 mL of ACN-acetate solution. The mixture was stirred at room temperature for 30 min and then at 45 °C for 1 h. To the mixture was added 3.34 mg (0.017 mmol) of 2-(2-nitro-1*H*-imidazolyl)ethylamine HCl in 0.5 mL of ACN-acetate solution, followed by 2.6 mg (0.20 mmol) of DIEA. After stirring at 45−50 °C for 2 h, the solvent was removed, and the crude product was purified by HPLC (Zorbax SB column, H_2O/ACN containing 0.1% TFA, flow rate 1.0 mL/min; gradient 100 to 50% H_2O in 45 min). The fraction with a retention time of 11.62 min was collected and lyophilized. ^{1}H NMR (500 MHz, d_6-DMSO): δ 1.03 [s, 9H, H(8, 9, 10)], 2.44 [s, 3H, H(1)], 3.55 [s, 3H, H(2)], 3.83 [d, 1H, H(14a), $J_{H14a-H13}$ = 12.2 Hz], 4.02 [d, 1H, H(3a), $J_{H3a-H3b}$ = 14.9 Hz], 4.40 [t, 1H, H(21a), $J_{H21a-H20}$ = 5.62 Hz], 4.41 [t, 1H, H(21b), $J_{H21b-H20}$ = 5.6 Hz], 4.46 [s, 1H, H(6)], 4.82 [d, 1H, H(3b), $J_{H3b-H3a}$ = 14.9 Hz], 5.08 [d, 1H, H(14b), $J_{H14b-H13}$ = 6.84 Hz], 6.99 [d, 1H, H(23), $J_{H23-H22}$ = 1.22 Hz], 7.44 [d, 1H, H(22), $J_{H22-H23}$ = 1.22 Hz], 7.72 [t, 1H, H(19), $J_{H19-H20}$ = 5.86 Hz], 8.19 [t, 1H, H(16), $J_{H16-H17}$ = 5.62 Hz]. ES-MS: *m*/*z* 712.93 ([M + H]$^+$, $C_{20}H_{32}N_8O_7{}^{185}ReS$, calculated = 712.58) and *m*/*z* 714.94

([M + H]$^+$, $C_{20}H_{32}N_8O_7{}^{187}ReS$, calculated = 714.58), confirming a 1:1 ratio of ligand to metal ion.

Partition Coefficient (*n*-Octanol/PBS) Determination for ^{99m}TcO-RP435 and ^{99m}TcO-RP535. A total of 10 μL of HPLC purified ^{99m}TcO-RP435 or ^{99m}TcO-RP535 was added to a tube which contained 1.0 mL of *n*-octanol and 1.0 mL of 0.1 M, pH 7.4, PBS. The tube was shaken for 1 min. After partial separation of the phases by gravity, 0.7 mL of each phase was transferred to a tube and centrifuged at 12000*g* for 5 min. Duplicate 0.2 mL aliquots of each phase were taken for γ-radioactivity counting.

Cellular Accumulation in an in Vitro Model. Each complex was evaluated in an in vitro model which has been used in the study of other tracers of hypoxia (*14, 16, 20, 23*). Suspensions of Chinese hamster ovary (CHO) cells were incubated at 37 °C with stirring under an atmosphere of air or nitrogen (both containing 5% CO_2) to generate aerobic or hypoxic conditions, respectively. The tracer was added and aliquots were removed over the course of 4 h and centrifuged, and the radioactivity associated with the cell pellet was measured in a γ well counter. The results were expressed as the ratio of concentration of radioactivity in the cell pellet to that in an equivalent volume of supernatant medium (C_{in}/C_{out}) as a function of time, as described previously (*14*). To demonstrate the involvement of the 2-NI group in localization, experiments were performed in which 5 mM misonidazole or 8 mM metronidazole were added 30 min before the tracer. We have demonstrated previously that an unlabeled 2-NI, such as misonidazole, can inhibit the hypoxic accumulation of ^{99m}Tc-labeled 2-NI, and that an unlabeled 5-NI, such as metronidazole, which has a lower electron affinity than 2-NI, can enhance the cellular accumulation of ^{99m}Tc-labeled 2-NI (*24*).

RESULTS

Synthesis of RP435 and RP535. RP435 was prepared by attaching 2-NI-acetic acid to a lysine connected to a peptidic N_3S chelator (Figure 1). After being cleaved from the resin, RP435 was purified by reversed-phase HPLC. The purity was shown to be >98%. RP535 was prepared by coupling 2-(2-nitro-1*H*-imidazolyl)ethylamine to RP455 (Figure 1). The purity of RP535 was analyzed by two HPLC gradients (100 to 70% H_2O and 100 to 50% H_2O over 45 min) and shown to be >97% based on UV detection at 214 and 320 nm.

The molecular weight of RP435 determined by mass spectrometry was consistent with the proposed structure. The ^{1}H NMR (500 MHz) spectrum of RP435 revealed the two protons of the 2-nitroimidazole at 7.19 and 7.61 ppm with a weak mutual coupling (J = 0.97 Hz). The proton of the hydroxyl H(8) appeared at 5.09 ppm as a broad peak. Four of the five amide protons of RP435, H(10), H(14), H(21), and H(28), were identified. H(10) and H(21) overlapped each other at 8.31 ppm. The six protons of H(1) and H(2) formed a broad peak at 2.57 ppm, while the two protons of H(3) were merged in the solvent peak ranging from 3.26 to 3.36 ppm.

MS analysis of RP535 showed the molecular ion signal at the expected mass. The ^{1}H NMR spectrum of RP535 exhibited signals of all five amide protons (Figure 1), with H(5) at 8.61 ppm, H(26) at 8.45 ppm, H(12) at 8.39 ppm, H(16) at 8.13 ppm, and H(19) at 7.89 ppm, respectively. Similar to RP435, the two protons of the 2-nitroimidazole of RP535 showed a weak mutual coupling ($J_{H22-H23}$ = 1.1 Hz). The nine protons of the *tert*-butyl group, H(8, 9, 10), appeared as a singlet peak at 0.91 ppm. It is interesting to note that the six protons, H(1, 2), of the two methyl groups of dimethylglycine produced triplet peaks, instead of a singlet peak, at 2.80 ppm. The signals of H(3), H(17), and H(20) were partly merged in the solvent peak ranging from 3.50 to 3.66 ppm, while H(13) and H(21) overlapped each other at 4.45 ppm (m, 3H). These data indicated that RP535 contained the N_3S chelator, a 2-nitroimidazole group, and the acetamidomethyl protecting group for the sulfur atom of cysteine.

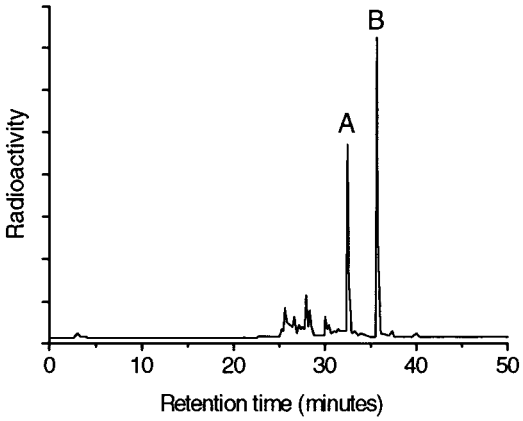


Figure 2. HPLC analysis of ^{99m}Tc labeling of RP435 demonstrating formation of two main products, peak A and peak B, in a total yield of ~70%. Zorbax C_{18} column eluted with H_2O/ACN containing 0.1% TFA; gradient 100% to 70% H_2O over 45 min; flow rate 1 mL/min.

^{99m}Tc Labeling of RP294, RP455, and RP435. ^{99m}Tc labeling of RP294 and RP435, which have the same N_3S chelator, can be carried out at room temperature via transchelation from ^{99m}Tc-gluconate. However, ^{99m}Tc labeling of RP455, which has a *tert*-butyl group on the chelator, requires heating in a boiling water bath for 10−15 min. ^{99m}TcO-RP294 showed two peaks on HPLC in 0.1% aqueous TFA/ACN in a total yield >97%. In contrast, ^{99m}TcO-RP455 showed one single peak (yield >99%). When analyzed in acetate/MeOH, ^{99m}Tc-RP294 showed two major peaks, at 33.69 min (39.6%) and 36.81 min (59.3%), with a gradient of 100% to 10% acetate over 45 min, while ^{99m}Tc-RP455 showed a major peak at 35.55 min (84.8%) with the same gradient (data not shown).

Stannous gluconate was used as reducing agent for $Na^{99m}TcO_4$ in the presence of 100−200 μg of RP435. Two main peaks (peak A: 32.42 min, yield 26.4%; peak B: 35.59 min, yield 42.5%) were detected on HPLC (Figure 2) with aqueous TFA/ACN (gradient: 100% to 70% H_2O over 45 min). The ratio of peaks A and B in the reaction mixture varied with time, while their retention times remained unchanged. The difference in retention times of peaks A and B of ^{99m}TcO-RP435 was 3.1 min, while that of the two peaks from ^{99m}TcO-RP294 was 0.7 min.

Stability of ^{99m}TcO-RP435. Peaks A and B of ^{99m}TcO-RP435, after being separated, were reanalyzed by HPLC after different time intervals. A slow interconversion of the two isomers in aqueous solution containing 0.1% TFA was observed. For example, 4.2% of B was detected 103 min after the isolation of A from the labeling mixture, and 4.0% of A was detected 118 min after isolation of B (data not shown). The interconversion of A and B could be greatly accelerated when they were mixed with an equal volume of 0.25 M pH 7.4 phosphate buffer (PB). Figure 3 shows the interconversion of purified A to B and of purified B to A, and it is evident that an approximate 1:1 equilibrium was reached within 1 h.

^{99m}Tc Labeling of RP535. RP535 (100−200 μg) was labeled with 2−10 mCi ^{99m}Tc with stannous gluconate

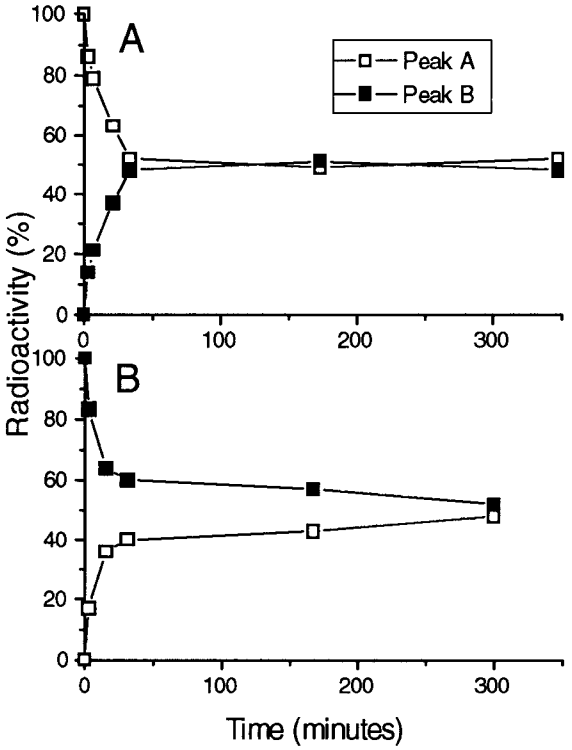


Figure 3. Time course of interconversion of syn and anti conformations of ^{99m}TcO-RP435 in phosphate buffer (PB). The isomers (peak A and peak B) were isolated by HPLC, mixed with an equal volume of PB, and aliquots reanalyzed after different time intervals. (A) Conversion of peak A to peak B. (B) Conversion of peak B to peak A.

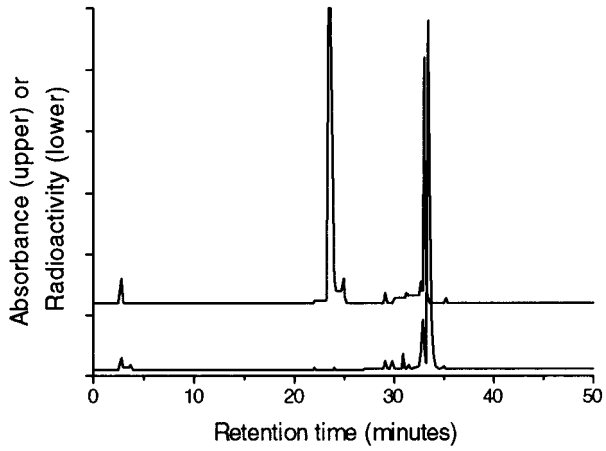


Figure 4. HPLC analysis of co-injection of ^{99m}TcO-RP535 and ReO-RP535. ^{99m}TcO-RP535 was monitored by radiometric detector (lower trace) and ReO-RP535 by UV detector at 320 nm (upper trace). The UV peak at 23.4 min is free RP535 while the peak at 33.0 min is ReO-RP535. ^{99m}TcO-RP535 eluted at 33.4 min. Zorbax C_{18} column eluted with H_2O/ACN containing 0.1% TFA; gradient 100 to 30% H_2O over 45 min; flow rate 1 mL/min.

as reducing agent. Higher temperatures (60−100 °C) were required to label the compound. One major labeled peak (yield >78%) was obtained when the reaction mixture was incubated in a boiling water bath for 30 min (Figure 4, lower trace). Varying the pH from 2 to 7 did not significantly affect the labeling yield. Although the nitroimidazole group of RP535 was stable under the labeling conditions, significant reduction was noted (analyzed by HPLC and monitored by the UV detector at 320 nm) when larger amounts of $SnCl_2$ were added, resulting in a dramatic decrease in the yield of ^{99m}TcO-RP535. For example, the yield of ^{99m}TcO-RP535 dropped to less than 5% of the total detected radioactivity on HPLC when 100 μg of $SnCl_2$ was used, and no intact RP535 remained when 600 μg of $SnCl_2$ was added.

Determination of Octanol/Water Partition Coefficients (PC) of ^{99m}TcO-RP435 and ^{99m}TcO-RP535. The PC values obtained were ^{99m}TcO-RP435, peak A, 0.0009 ± 0.0001; ^{99m}TcO-RP435, peak B, 0.0011 ± 0.0001; and ^{99m}TcO-RP535, 2.8 ± 0.1, $n = 4$. Thus, the difference in partition coefficients of ^{99m}TcO-RP535 and ^{99m}TcO-RP435 is over 2000-fold.

Preparation of ReO-RP535 and Co-Injection with ^{99m}TcO-RP535. It is difficult to determine directly the structure of a ^{99m}Tc complex because of the extremely small amount of the compound present. ^{99}Tc is a long-lived radioactive isotope ($t_{1/2} = 2.1 \times 10^5$ years) which restricts its application. However, the composition and structure of ^{99m}TcO-RP535 could be indirectly determined by comparison with ReO-RP535, which can be prepared in weighable quantities and characterized. Re belongs to the same group (VIIb) of the periodic table as Tc and thus possesses similar chemical properties; furthermore, Re and Tc are similar in size because of the lanthanide contraction.

ReO-RP535 was prepared by coupling 2-(2-nitro-1*H*-imidazolyl)ethylamine with ReO-RP455. The compound was purified by HPLC. ^{1}H NMR data showed that the two amide protons, H(5) and H(12), disappeared after the chelation of RP535 to ReO^{3+}, while those of H(16) and H(19) of the uncoordinated RP535 (Figure 1) remained. The protons of the acetamidomethyl protecting group also disappeared, indicating the involvement of sulfur in the coordination with ReO. The two methyl groups and the methylene group of dimethylglycine could no longer freely rotate around the C(3)−N_{amine} bond in ReO-RP535, which made the protons of these groups become chemically nonequivalent. For example, the protons of H(1) shifted from 2.80 to 2.44 ppm, and H(2) shifted from 2.80 to 3.55 ppm upon the formation of ReO-RP535. This indicated that the N atom of the dimethylglycine was coordinated with the ReO^{3+} core. The two protons of H(3) of ReO-RP535 were in a chemically nonequivalent environment as well. H(3a) appeared at 4.02 ppm and H(3b) at 4.82 ppm with a coupling constant $J_{H3a-H3b}$ at 14.9 Hz. H(14a) coupled H(13) with $J_{H14a-H13}$ for 6.8 Hz, while H(14b) coupled H(13) with $J_{H14a-H13}$ for 12.2 Hz. However, no signals of H(14a) coupling with H(14b) were found. Taken together, this evidence supported the assumption that the ReO^{3+} core was complexed with the N_3S chelator.

No evidence of the coexistence of the syn and anti isomers of ReO-RP535 was found in the ^{1}H NMR spectrum. The prepared ReO-RP535 could be either a syn or anti isomer. The electrospray mass spectrum exhibited the characteristic two molecular ions at *m*/*z* 712.93 ([M + H]$^+$), which corresponded to a 1:1 ^{185}ReO to RP535 complex, and *m*/*z* 714.94 ([M + H]$^+$), which corresponded to another 1:1 ^{187}ReO to RP535 complex. Moreover, the relative abundances of the two peaks (36.5 and 63.5%) are consistent with the natural abundances of ^{185}Re and ^{187}Re (37.4 and 62.6%).

An aqueous solution of ReO-RP535 was mixed with the ^{99m}TcO-RP535 labeling mixture and co-injected into the HPLC for analysis. Two gradients of aqueous TFA/ACN were used: 100 to 30% and 100 to 50% water over 45 min. Two detectors, UV and radiometric, were connected in series with the eluent entering the UV detector first and then the radiometric detector. There was a time delay of 0.3−0.4 min for signal response between the UV and radiometric detectors. Figure 4 shows the chromato-

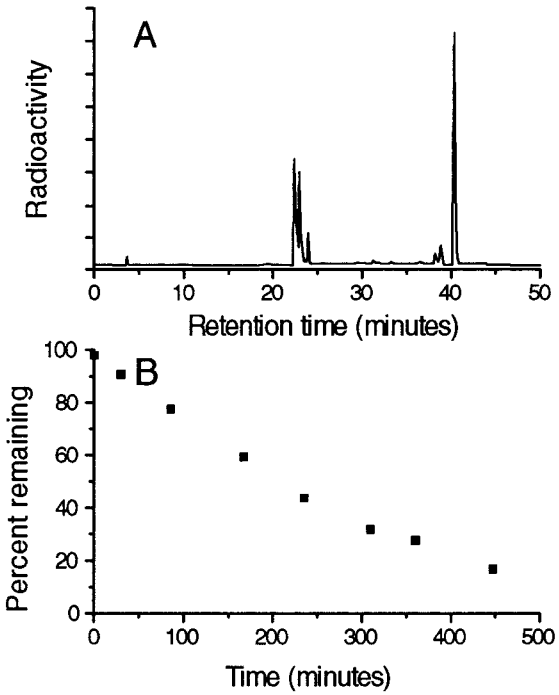


Figure 5. Stability of ^{99m}TcO-RP535 diluted in an equal volume of phosphate buffer (PB). (A) HPLC analysis of sample obtained 235 min after mixing demonstrates appearance of decomplexation products with retention times of 22−24 min but little release of free pertechnetate (retention time 3 min). Zorbax C_{18} column eluted with H_2O/ACN containing 0.1% TFA; gradient 100 to 50% H_2O over 45 min; flow rate 1 mL/min. (B) Time course of stability of ^{99m}TcO-RP535 diluted in PB.

gram of the co-injection of ReO-RP535 with ^{99m}TcO-RP535 with the 100 to 30% water gradient. The retention time of ReO-RP535 was 33.04 min (upper trace), while that of ^{99m}TcO-RP535 was 33.35 min (lower trace). The UV peak at 23.37 min was free RP535 (upper trace). The retention times of ReO-RP535 and ^{99m}TcO-RP535 became 39.91 and 40.51 min, respectively, when a 100 to 50% water gradient was used. The retention times of ReO-RP535 and ^{99m}TcO-RP535 are the same when the time delay in signal response is taken into account. This implies that ^{99m}TcO-RP535 has the same composition and structure as ReO-RP535, i.e., ^{99m}Tc is coordinated by the N_3S chelator of RP535, there is a ^{99m}Tc═O core, and the ratio of ^{99m}Tc to RP535 is 1:1.

Stability of ^{99m}TcO-RP535. ^{99m}TcO-RP535 was isolated by HPLC, and the collected ^{99m}TcO-RP535 in aqueous TFA/ACN was reinjected into the HPLC for analysis after different time intervals at room temperature. It was evident that ^{99m}TcO-RP535 was more stable than ^{99m}TcO-RP435 in aqueous solution, which contained 0.1% TFA, because neither decomplexation nor change in the radioactive peak was seen over 26 h.

Theoretically, the formation of syn and anti isomers of ^{99m}TcO-RP535 is possible, when the *tert*-butyl side chain on the N_3S chelator is in the syn and anti conformations with respect to the ^{99m}Tc═O core. When the isolated ^{99m}TcO-RP535 was mixed with an equal volume of 0.25 M, pH 7.4, phosphate buffer (PB) and reinjected after different time intervals, a decomplexation of the complex, instead of interconversion of syn and anti isomers, was observed (Figure 5A). ^{99m}TcO-RP535 (retention time 40.27 min) decomplexed in PB and formed three products, which appeared in the region of 22.1−23.7 min on the HPLC. These decomplexed compounds cannot be the isomers of ^{99m}TcO-RP535 because they did not exist

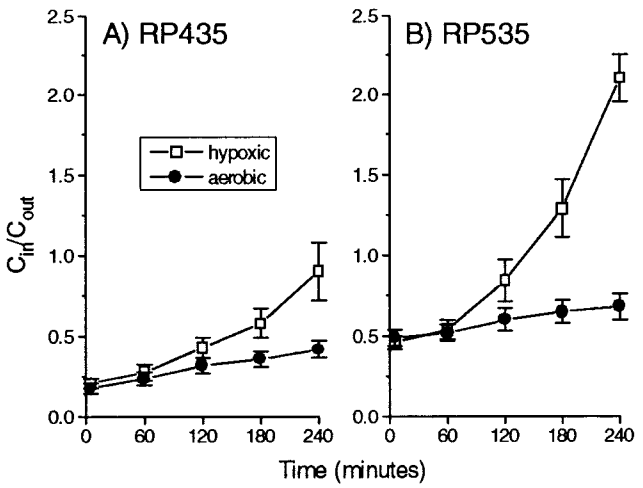


Figure 6. Time course of accumulation of ^{99m}TcO-RP435 and ^{99m}TcO-RP535 in Chinese hamster ovary cells under aerobic and hypoxic conditions. Ordinate is ratio of radioactivity concentration inside cells (C_{in}) to that in supernatant (C_{out}). Each point is mean of eight or nine experiments and error bars are SEM.

in the labeling mixture (Figure 4, lower trace; note different gradient) and they did not reach any fixed equilibrium with ^{99m}TcO-RP535 over time. The decomplexation might occur when one or more coordination bonds of the ^{99m}TcO-RP535 complex are broken. No free pertechnetate (retention time 3 min) was detected from the decomplexation of ^{99m}TcO-RP535. The half-time for decomplexation was about 200 min (Figure 5B). Interestingly, ^{99m}TcO-RP535 decomposed immediately with release of pertechnetate when mixed with 0.01 N NaOH.

To summarize, ^{99m}TcO-RP535 with its *tert*-butyl group on the N_3S chelator, is more difficult to label than ^{99m}TcO-RP435 and does not interconvert to another isomer. This suggests that the *tert*-butyl group acts as an important steric hindrant that inhibits the coexistence and interconversion of syn and anti isomers of ^{99m}TcO-RP535 and indeed forces the complex into a single conformation. However, the configuration of ^{99m}TcO-RP535 remains to be determined.

In Vitro Tests of ^{99m}TcO-RP294, ^{99m}TcO-RP455, ^{99m}TcO-RP435, and ^{99m}TcO-RP535. The ability of these ^{99m}Tc-labeled compounds to be taken up by mammalian cells under aerobic or hypoxic conditions was tested using CHO cells in suspension culture in equilibrium with air or nitrogen gas mixtures. Samples were removed as a function of time and ratios of cell-associated radioactivity (C_{in}) to that in the medium (C_{out}) were calculated. The control compounds, ^{99m}TcO-RP294 and ^{99m}TcO-RP455, which do not contain 2-NI groups, did not show selective accumulation in hypoxic CHO cells. In contrast, ^{99m}TcO-RP435 showed differential accumulation between hypoxic and aerobic cells. The C_{in}/C_{out} for aerobic cells at 4 h was 0.42, while that of hypoxic cells was 0.90 (Figure 6A), for a hypoxic/aerobic differential of 2.1 ± 0.4 (mean ± SEM, n = 8). In comparison, ^{99m}TcO-RP535 revealed a greater differential accumulation between hypoxic and aerobic cells than ^{99m}TcO-RP435. When ^{99m}TcO-RP535 was added to a suspension of CHO cells in vitro, there was a modest accumulation of radioactivity in the cells under aerobic conditions, reaching a C_{in}/C_{out} value of 0.68 at 4 h (Figure 6B). In contrast, under hypoxic conditions, there was a further increase to a C_{in}/C_{out} value of 2.10, for a 3.1 ± 0.4 (n = 9) fold hypoxic/aerobic differential.

Previous work (*24*) with the ^{99m}Tc-labeled 2-NI BMS181-321, using the same cell line and in vitro system, showed

that a large molar excess of the 2-NI compound misonidazole prevented selective accumulation in hypoxic cells while the 5-nitroimidazole metronidazole stimulated it. In the present work, addition of 5 mM misonidazole abolished the hypoxia-specific accumulation of ^{99m}TcO-RP535, whereas 8 mM metronidazole selectively increased hypoxic accumulation to 130% of the control value.

DISCUSSION

On the basis of promising results obtained with [^{18}F]-FMISO and [^{123}I]IAZA (*7*−*10*), there has been great interest in the development of ^{99m}Tc-labeled markers of hypoxia which would be convenient to prepare and widely applicable. However, the standard ^{99m}Tc-chelation systems have not all proved to be useful. The first attempt using the BATO approach resulted in a complex which was not efficiently reduced and trapped, and which showed inadequate permeability to lipophilic membranes (*25*). A bis(amine-phenol) complex similarly failed to cross cell membranes (*26*). Greatest success thus far has been obtained with amineoxime-type chelators, specifically BMS181321 (*11*), BRU59-21 (*27*), and BnAO (*17*); however, each has its limitations. BMS181321 has a PC of 40, which results in slow clearance from the blood and background tissues and extensive elimination via the gastrointestinal tract (*14*). BRU59-21 has a lower PC of 12 with resultant improved clearance from the blood, but the extent of hepatobiliary excretion remains high (*15, 16*). In contrast, BnAO undergoes extensive renal elimination, but lacking a nitro group, its mechanism of hypoxia-specific localization is unclear (*20*). BnAO has a low PC of 0.1, although this does not appear to limit its penetration of tissue (*20*). Work in the radioiodinated sugar 2-NI series has suggested an optimum PC of ∼1 (*5*).

The RP294 chelation system for ^{99m}Tc was developed by Resolution Pharmaceuticals Inc. (*21*) and is used in RP128, a peptide for imaging inflammation (*28*). Acetamidomethyl was selected as the thiol-protecting group because it can be cleaved at room temperature. The free carboxylic acid group of the molecule contributes to the hydrophilicity of the complex and RP435, the 2-NI-containing derivative of RP294, has an extremely low PC of 0.001. Therefore, an analogue containing *tert*-butylglycine in place of serine was developed. In the present work, the utility of this chelator on a 2-NI compound targeted to hypoxic tumor cells was evaluated. The partition coefficient of ^{99m}TcO-RP535 was 2.8, which is similar to that reported for IAZA (*9*).

Although the presence of the *tert*-butyl group was desirable to increase the PC of the complex, it made the chelator more difficult to label. While ^{99m}Tc labeling of RP294 and RP435 by transchelation from gluconate proceeded efficiently at room temperature, the *tert*-butyl analogues RP455 and RP535 required heating. Radiochemical yields obtained were 26 and 43% for the two peaks of ^{99m}TcO-RP435 (Figure 2) and 78% for ^{99m}TcO-RP535 (Figure 4, lower trace). It was shown that the nitro group was not reduced by the typical quantities of stannous chloride used in ^{99m}Tc labeling, but that it could be reduced by excessive amounts.

The structure of RP294 was determined by ^{13}C and ^{1}H NMR, except the assignments of the amide protons (*21*). In addition, ReO-RP294 and ^{99}TcO-RP294 have been structurally confirmed by ^{1}H NMR and X-ray crystallography, which indicated that the metal ions were coordinated by the N_3S chelator. RP435, containing the same N_3S chelator as RP294, can be presumed to chelate the $^{99m}TcO^{3+}$ core in the same manner. As has been shown previously for ^{99m}TcO-RP294 (*21*), two complexes of ^{99m}TcO-RP435 were formed, presumably syn and anti isomers (Figure 2). Following separation by HPLC, these were quite stable in acidic aqueous solution (4% interconversion in 2 h) but equilibrated in 0.25 M, pH 7.4, phosphate buffer with a half-time of ∼1 h (Figure 3), suggesting that the rate of interconversion is a function of hydroxide concentration. In contrast, ^{99m}TcO-RP535 existed as a single isomer (Figure 4, lower trace), confirmed by co-injection with its Re analogue (Figure 4, upper trace), which was extremely stable in acidic aqueous medium. When diluted in PB, ^{99m}TcO-RP535 decomplexed with a half-time of ∼3 h, resulting in the formation of several hydrophilic species but no release of free pertechnetate (Figure 5). However, when ^{99m}TcO-RP535 was diluted in 0.01 N NaOH it decomposed rapidly to pertechnetate. These results with ^{99m}TcO-RP535 also implicate the concentration of hydroxide in the decomposition process.

Following HPLC purification, ^{99m}TcO-RP435 and ^{99m}TcO-RP535 were evaluated in an in vitro model of cellular hypoxia that has been used extensively in radiation biology and investigation of bioreductive drugs, including other ^{99m}Tc-, ^{123}I-, and ^{18}F-labeled hypoxia tracers (*14, 16, 20, 23*). Both tracers showed a modest level of uptake in aerobic CHO cells, which increased slightly over the course of 4 h. In contrast, hypoxic cells accumulated 2−3 times as much radioactivity over that time period, a significant degree of hypoxia-specific accumulation (Figure 6). Moreover, the selective accumulation of ^{99m}TcO-RP535 could be modulated by coincubation with millimolar concentrations of unlabeled nitro compounds (data not shown). The 2-NI misonidazole abolished the hypoxia-specific accumulation of ^{99m}TcO-RP535 while metronidazole, a 5-NI of lower electron affinity, enhanced this accumulation. The same effects have been reported previously with the 2-NI ^{99m}Tc-BMS181321 and suggest a bioreductive mechanism of localization of the tracer (*24*).

CONCLUSIONS

RP435 and RP535 have a similar N_3S chelator in structure, but their ability to form chelates with ^{99m}Tc is different. The ^{99m}TcO-RP435 chelate could be prepared at room temperature, and showed interconversion of syn and anti isomers in aqueous solution. The interconversion of the two isomers was much faster in neutral than in acidic medium. In contrast, the *tert*-butyl group on the backbone of the N_3S chelator of RP535 hindered the chelation with ^{99m}Tc, presumably by steric effects, and blocked the formation and interconversion of the theoretically existing syn and anti isomers of ^{99m}TcO-RP535 in acidic and neutral aqueous solution at room temperature. However, the *tert*-butyl group of RP535 did have the desired effect of significantly increasing the lipophilicity of the corresponding ^{99m}Tc chelate. Both ^{99m}TcO-RP435 and ^{99m}TcO-RP535 showed selective uptake in hypoxic cells, suggesting that ^{99m}TcO-peptidic complexes containing the 2-nitroimidazole group can be a new class of hypoxia imaging agents.

ACKNOWLEDGMENT

We would like to thank Dr. Ernest Wong, Tam Nguyen, Linda Lu, and Dr. Susan Peers of Resolution Pharmaceuticals Inc. for their support and suggestions. This work was funded by the University-Industry program of the

Medical Research Council of Canada in conjunction with Resolution Pharmaceuticals Inc. (Grant UI-13558).

LITERATURE CITED

(1) Nunn, A., Linder, K., and Strauss, H. W. (1995) Nitroimidazoles and hypoxia imaging. *Eur. J. Nucl. Med. 22*, 265−280.

(2) Hockel, M., Knoop, C., Schlenger, K., Vorndran, B., Baussmann, E., Mitze, M., Knapstein, P. G., and Vaupel, P. (1993) Intratumoral pO_2 predicts survival in advanced cancer of the uterine cervix. *Radiother. Oncol. 26*, 45−50.

(3) Graeber, T. G., Osmanian, C., Jacks, T., Housman, D. E., Koch, C. J., Lowe, S. W., and Giaccia, A. J. (1996) Hypoxia mediated selection of cells with diminished apoptotic potential in solid tumors. *Nature 379*, 88−91.

(4) Brizel, D. M., Scully, S. P., Harrelson, J. M., Layfield, J. M., Bean, J. M., Prosnitz, L. R., and Dewhirst, M. W. (1996) Tumor oxygenation predicts for likelihood of distant metastases in human soft tissue sacroma. *Cancer Res. 56*, 941−943.

(5) Chapman, J. D., Engelhardt, E. L., Stobbe, C. C., Schneider, R. F., and Hanks, G. E. (1998) Measuring hypoxia and predicting tumor radioresistance with nuclear medicine assays. *Radiother. Oncol. 46*, 229−237.

(6) Rauth, A. M. (1984) Pharmacology and toxicology of sensitizers. *Int. J. Radiat. Oncol. Biol. Phys. 10*, 1293−1300.

(7) Grierson, J. R., Link, J. M., Mathis, C. A., Rasey, J. S., and Krohn, K. A. (1989) A radiosynthesis of fluorine-18 fluoromisonidazole. *J. Nucl. Med. 30*, 343−350.

(8) Koh, W. J., Rasey, J. S., Evans, M. L., Grierson, J. R., Lewellen, T. K., Graham, M. M., Krohn, K. A., and Griffin, T. W. (1992) Imaging of hypoxia in human tumors with [^{18}F]-fluoromisonidazole. *Int. J. Radiat. Oncol. Biol. Phys. 22*, 199−212.

(9) Mannan, R. H., Somayaji, V. V., Lee, J., Mercer, J. R., Chapman, J. D., and Wiebe, L. I. (1991) Radioiodinated 1-(5-iodo-5-deoxy-beta-D-arabinofuranosyl)-2-nitroimidazole (Iodoazomycin arabinoside: IAZA): a novel marker of tissue hypoxia. *J. Nucl. Med. 32*, 1764−1770.

(10) Parliament, M. B., Chapman, J. D., Urtasun, R. C., McEwan, A. J., Golberg, L., Mercer, J. R., Mannan, R. H., and Wiebe, L. I. (1992) Noninvasive assessment of human tumor hypoxia with ^{123}I-iodoazomycin arabinoside: preliminary report of a clinical study. *Br. J. Cancer 65*, 90−95.

(11) Linder, K. E., Chan, Y. W., Cyr, J. E., Malley, M. F., Nowotnik, D. P., and Nunn, A. D. (1994) TcO(PnAO-1-(2-nitroimidazole)) [BMS-181321], a new technetium-containing nitroimidazole complex for imaging hypoxia: synthesis, characterization, and xanthine oxidase-catalyzed reduction. *J. Med. Chem. 37*, 9−17.

(12) Di Rocco, R. J., Bauer, A. A., Pirro, J. P., Kuczynski, B. L., Belnavis, L., Chan, Y. W., Linder, K. E., Narra, R. K., Nowotnik, D. P., and Nunn, A. D. (1997) Delineation of the border zone of ischemic rabbit myocardium by a technetium-labeled nitroimidazole. *Nucl. Med. Biol. 24*, 201−207.

(13) Barron, B., Grotta, J., Lamki, L., Villar, C., Ephron, V., Patel, D., Linder, K. E., and Nunn, A. D. (1996) Preliminary experience with technetium-99m BMS-181321, a nitroimidazole, in the detection of cerebral ischemia associated with acute stroke. *J. Nucl. Med. 37*, 272P−273P.

(14) Ballinger, J. R., Kee, J. W., and Rauth, A. M. (1996) In vitro and in vivo evaluation of a technetium-99m-labeled 2-nitroimidazole (BMS181321) as a marker of tumor hypoxia. *J. Nucl. Med. 37*, 1023−1031.

(15) Johnson, L. L., Schofield, L., Mastrofrancesco, P., Donahay, T., and Nott, L. (1998) Technetium-99m-nitroimadazole uptake in a swine model of demand ischemia. *J. Nucl. Med. 39*, 1468−1475.

(16) Melo, T., Duncan, J., Ballinger, J. R., and Rauth, A. M. (1998) BRU59−21, a second-generation technetium-99m-labeled 2-nitroimidazole for imaging hypoxia in tumors. *J. Nucl. Med. 39*, 219P.

(17) Archer, C. M., Edwards, B., Kelly, J. D., King, A. C., Burke, J. F., and Riley, A. L. M. (1995) Technetium labeled agents for imaging tissue hypoxia in vivo. In *Technetium and rhenium in chemistry and nuclear medicine* (M. Nicolini, G. Bandoli, and U. Mazzi, Eds.) pp 535−539, S G Editorali, Padova.

(18) Okada, R. D., Johnson, G., Nguyen, K. N., Edwards, B., Archer, C. M., and Kelly, J. D. (1997) ^{99m}Tc-HL91: Effects of low flow and hypoxia on a new ischemia-avid myocardial imaging agent. *Circulation 95*, 1892−1899.

(19) Cook, G. J., Houston, S., Barrington, S. F., and Fogelman, I. (1998) Technetium-99m-labeled HL91 to identify tumor hypoxia: correlation with fluorine-18-FDG. *J. Nucl. Med. 39*, 99−103.

(20) Zhang, X., Melo, T., Ballinger, J. R., and Rauth, A. M. (1998) Studies of ^{99m}Tc−BnAO (HL-91): a nonnitroaromatic compound for hypoxic cell detection. *Int. J. Radiat. Oncol. Biol. Phys. 42*, 737−740.

(21) Wong, E., Fauconnier, T., Bennett, S., Valiant, J., Nguyen, T., Lau, F., Lu, L. F. L., Pollak, A., Bell, R. A., and Thornback, J. R. (1997) Rhenium(V) and technetium(V) oxo complexes of an $N_2N'S$ peptidic chelator: evidence of interconversion between syn and anti conformations. *Inorg. Chem. 36*, 5799−5808.

(22) Hay, M. P., Wilson, W. R., Moselen, J. W., Palmer, B. D., and Denny, W. A. (1994) Hypoxia-selective antitumor agents. 8. Bis(nitroimidazolyl)alkanecarboxamides: A new class of hypoxia-selective cytotoxins and hypoxic cell radiosensitizers. *J. Med. Chem. 37*, 381−391.

(23) Ballinger, J. R., Cowan, D. S., Boxen, I., Zhang, Z. M., and Rauth, A. M. (1993) Effect of hypoxia on the accumulation of technetium-99m-glucarate and technetium-99m-gluconate by Chinese hamster ovary cells in vitro. *J. Nucl. Med. 34*, 242−245.

(24) Melo, T., Hua, H. A., Ballinger, J. R., and Rauth, A. M. (1997) Modifying the in vitro accumulation of BMS181321, a technetium-99m-nitroimidazole, with unlabeled nitroaromatics. *Biochem. Pharmacol. 54*, 685−693.

(25) Linder, K. E., Chan, Y. W., Cyr, J. E., Nowotnik, D. P., Eckelman, W. C., and Nunn, A. D. (1993) Synthesis, characterization, and in vitro evaluation of nitroimidazole-BATO complexes: new technetium compounds designed for imaging hypoxic tissue. *Bioconjugate Chem. 4*, 326−333.

(26) Ramalingam, K., Raju, N., Nanjappan, P., Linder, K. E., Pirro, J., Zeng, W., Rumsey, W., Nowotnik, D. P., and Nunn, A. D. (1994) The synthesis and in vitro evaluation of a ^{99m}technetium-nitroimidazole complex based on a bis(amine-phenol) ligand: comparison to BMS-181321. *J. Med. Chem. 37*, 4155−4163.

(27) Wedeking, P., Yost, F., Wen, M., Patel, B., Eaton, S., Romero, V., Linder, K. E., Rumsey, W., and Nunn, A. D. (1995) Comparison of the biologic activity of the isomers of Tc-99m-nitroimidazole complex BMS-194796. *J. Nucl. Med. 36*, 17P.

(28) Caveliers, V., Goodbody, A. E., Tran, L. L., Bossuyt, A., and Thornback, J. R. (1996) Human dosimetry of Tc99m-RP128, a potential inflammation imaging agent. *Eur. J. Nucl. Med. 23*, 1131.

BC9900542

TECHNICAL NOTES

Boron-Enriched Streptavidin Potentially Useful as a Component of Boron Carriers for Neutron Capture Therapy of Cancer

Takeshi Sano*

Center for Molecular Imaging Diagnosis and Therapy, and Basic Science Laboratory, Department of Radiology, Beth Israel Deaconess Medical Center, Harvard Medical School, Boston, Massachusetts 02215.
Received March 10, 1999; Revised Manuscript Received June 24, 1999

A boron-enriched streptavidin has been prepared by chemical conjugation of a boron-rich compound, $B_{12}H_{11}SH^{2-}$ (BSH), to a genetically engineered streptavidin variant. The streptavidin variant used has 20 cysteine residues per molecule, derived from a C-terminal cysteine stretch consisting of five cysteine residues per subunit. Because natural streptavidin has no cysteine residues, the reactive sulfhydryl groups of the cysteine stretch serve as unique conjugation sites for sulfhydryl chemistry. BSH was conjugated irreversibly to the sulfhydryl groups of the streptavidin variant via a sulfhydryl-specific homobifunctional chemical cross-linker. Quantitative boron analysis indicates that the resulting streptavidin−BSH conjugate carries approximately 230 boron atoms/molecule. This indicates that the chemical conjugation of BSH to the streptavidin variant was highly specific and efficient because this method should allow the conjugation of a maximum of 240 boron atoms/streptavidin molecule. This boron-enriched streptavidin retained both full biotin-binding ability and tetrameric structure, suggesting that the conjugation of BSH has little, if any, effect on the fundamental properties of streptavidin. This boron-enriched streptavidin should be very useful as a component of targetable boron carriers for neutron capture therapy of cancer. For example, a monoclonal antibody against a tumor-associated antigen can be attached tightly to the boron-enriched streptavidin upon simple biotinylation, and the resulting conjugate could be used to target boron to tumor cells on which the tumor-associated antigen is overexpressed.

INTRODUCTION

Boron neutron capture therapy (BNCT)[1] is potentially a useful therapeutic modality for cancer [for recent reviews, see Barth and Soloway (1994), Barth et al. (1996), Coderre and Morris (1999), Gahbauer et al. (1998), Hawthorne (1993, 1998), and Soloway et al. (1997, 1998)]. BNCT uses the nuclear capture and fission reactions of a stable (nonradioactive) boron isotope species, ^{10}B, which occur when ^{10}B is irradiated by thermal neutrons. This process releases approximately 2.8 MeV of kinetic energy, which is distributed between $^4He^{2+}$ (α-particle) and $^7Li^{3+}$, plus weak γ-radiation (480 keV). BNCT uses this kinetic energy to kill target cancer cells where boron has accumulated. The most attractive characteristic of BNCT is that $^4He^{2+}$ and $^7Li^{3+}$ have mean ionization tracks of only 7 and 4 μm, respectively. Thus, most of the kinetic energy is deposited within about one cell diameter, minimizing radiation doses to surrounding normal tissues. Another feature of BNCT is that it is a binary method; the occurrence of two independent, relatively nontoxic events, i.e., accumulation of ^{10}B and irradiation by thermal neutrons, is needed to activate the killing reaction. These two distinct characteristics offer potential for BNCT to become an effective therapeutic modality for cancer.

For successful BNCT, selective, high-level accumulation of ^{10}B in target tumor cells (at least 25−35 μg of ^{10}B/gram tissue or 10^9 ^{10}B atoms/cell) is essential. Large amounts of ^{10}B must accumulate in target cells to minimize radiation doses to normal tissues. Thus, many current BNCT efforts are directed toward the preparation of boron-containing reagents and the development of boron-targeting strategies that allow selective, high-level accumulation of boron in target cells. Although relatively small boron-containing reagents, such as BSH and *p*-boronophenylalanine, have primarily been used in BNCT, macromolecular boron carriers are potentially very useful. For example, certain macromolecules, such as antibodies against tumor-associated antigens (antitumor antibodies), have the natural ability to bind, specifically, to the tumor cells. Such macromolecules could be used as specific boron carriers to deliver boron to the target tumor cell. In addition, such macromolecules could be attached or fused to other molecules which do no have selectivity to tumor cells but can carry large amounts of

* To whom correspondence should be addressed.

[1]Abbreviations: BNCT, boron neutron capture therapy; BSH, borocaptate or mercaptoundecahydro-*closo*-dodecaborate ($B_{12}H_{11}SH^{2-}$); DTT, dithiothreitol; EDTA, ethylenediaminetetraacetic acid; FPLC, fast protein liquid chromatography; ICP-AES, inductively coupled plasma atomic emission spectrometry; MPHPD, *N,N′*-bis(3-maleimidopropionyl)-2-hydroxy-1,3-propanediamine; PAGE, polyacrylamide gel electrophoresis; PBS, phosphate-buffered saline; SDS, sodium dodecyl sulfate; Stv-28, a recombinant streptavidin encoded in the plasmid pTSA-28; TBS, Tris-buffered saline; TCEP-HCl, tris(2-carboxyethyl)-phosphine hydrochloride; Tris, tris(hydroxymethyl)aminomethane.

10.1021/bc990029w CCC: $18.00 © 1999 American Chemical Society
Published on Web 08/17/1999

boron. This should allow the generation of the boron-enriched molecules with specific binding affinity for target tumor cells. Thus, boronated macromolecules, such as antitumor antibodies and the ligands for cell surface receptors overexpressed on target tumor cells, have been produced and tested as potential boron carriers for BNCT [for reviews, see Barth et al. (1996), Gahbauer et al. (1998), Hawthorne (1993, 1998), Soloway et al. (1997, 1998)]. However, the properties and biological activities of such macromolecules are often altered or even lost by conjugation of large amounts of boron or by the chemical conjugation methods used. If large amounts of boron could be attached indirectly to these macromolecules, changes in their biological activities and functions could be minimized, allowing the resulting boronated macromolecules to become effective boron carriers for BNCT.

Streptavidin, a tetrameric protein produced by *Streptomyces avidinii*, binds a water-soluble vitamin, D-biotin (vitamin H), with a remarkably high affinity ($K_d \approx 10^{-14}$–10^{-15} M) (Chaiet et al., 1963; Chaiet and Wolf, 1964; Green, 1970, 1990). The extremely tight biotin binding by streptavidin and the ability of biotin to be incorporated easily into various biological materials have made the streptavidin−biotin system one of the most useful tools in the biological and medical sciences (Bayer and Wilchek, 1980; Wilchek and Bayer, 1988, 1990). Streptavidin could also be very useful as a component of macromolecular boron carriers for BNCT. For example, streptavidin carrying a large amount of boron could be conjugated easily and tightly to a macromolecular tumor-targeting reagent, such as an antitumor antibody, upon simple biotinylation. Indirect conjugation of boron to macromolecular targeting reagents via streptavidin could allow the maintenance of their biological functions and activities. The exceptionally high structural stability of streptavidin should allow a variety of chemistries to be used for conjugation of large amounts of boron without disturbing the fundamental properties of streptavidin.

In this work, a boron-enriched streptavidin was produced by chemical conjugation of a boron-rich compound to a genetically engineered streptavidin. The resulting boron-enriched streptavidin carries approximately 230 boron atoms/molecule, and it retains both full biotin-binding ability and tetrameric structure. The preparation and characterization of this boron-enriched streptavidin are described, along with its potential use as a component of macromolecular boron carriers for BNCT of cancer.

EXPERIMENTAL PROCEDURES

Materials. Disodium BSH ($Na_2B_{12}H_{11}SH$) was obtained from Boron Biologicals, Inc., Raleigh, NC. TCEP-HCl was from Pierce Chemical. MPHPD, 2-iminobiotin agarose, iodoaceticacid, and iodoacetamide were from Sigma Chemical. D-[*carbonyl*-^{14}C]Biotin (53 mCi/mmol), a sulfur-labeling reagent (*t*-butoxycarbonyl-[^{35}S]methionine *N*-succinimidyl ester; >800 Ci/mmol), and a fluorography reagent, Amplify, were from Amersham. Superdex 75 HR 10/30 and PD-10 columns were from Pharmacia Biotech.

Preparation of a Streptavidin Variant, Stv-28. A streptavidin variant containing a C-terminal cysteine stretch, Stv-28, was expressed in *Escherichia coli* strain BL21(DE3)(pLysE) carrying the expression vector pTSA-28 (Sano et al., 1993) by using the bacteriophage T7 expression system (Studier et al., 1990). Expressed Stv-28 was purified to homogeneity by the method previously described (Sano and Cantor, 1990; Sano et al., 1993). Purified Stv-28 was stored frozen at −85 °C in Tris-buffered saline (TBS; 150 mM NaCl, 20 mM Tris-Cl, pH 7.4, and 0.02% NaN_3) containing 5 mM DTT (TBS/DTT) until used.

Chemical Conjugation of BSH to Stv-28. Chemical conjugation of BSH to Stv-28 was carried out by using a two-step procedure (Figure 1). All solutions used during chemical conjugation had been equilibrated with argon gas to prevent oxidation of sulfhydryl groups. Stv-28 in TBS/DTT was dialyzed against phosphate-buffered saline (PBS; 150 mM NaCl and 50 mM sodium phosphate, pH 6.8) containing 5 mM EDTA and 2 mM TCEP-HCl (Rüegg and Rudinger, 1977) (PBS/EDTA/TCEP). The dialyzed protein (410 μg; 2.5 mL) was mixed with 7.6 μmol of MPHPD dissolved in 300 μL of PBS/EDTA/TCEP (molar ratio of MPHPD to cysteine, ∼50), and the mixture (2.8 mL) was allowed to stand at 30 °C for 30 min. Then, BSH (90 μmol), dissolved in 500 μL of PBS/EDTA/TCEP, was added, and the mixture was incubated at 30 °C for 30 min. The mixture was dialyzed against PBS/EDTA at 4 °C, and the dialyzed protein was filtered through a 0.22-μm polyvinylidene fluoride filter unit (Millex-GV; Millipore).

Purification of functional conjugates was performed at 4 °C by 2-iminobiotin affinity chromatography (Hoffman et al., 1980). The filtered protein fraction was dialyzed against 1.0 M NaCl and 100 mM Na_2CO_3, pH 11.0, and applied to a 2-iminobiotin-agarose column which had been equilibrated with the same solution. The column was washed with the same solution to remove unbound protein, and then bound protein was eluted with 2 M urea and 100 mM ammonium acetate (pH 4.0). The eluate was dialyzed against TBS and used in subsequent experiments.

Serum Stability Analysis. A boron-enriched streptavidin was labeled with ^{35}S using a sulfur labeling reagent (*t*-butoxycarbonyl-[^{35}S]methionine *N*-succinimidyl ester) to facilitate the serum stability analysis. Briefly, a boron-enriched streptavidin in 0.1 M sodium borate (pH 8.5) (protein concentration, 7.8 μg/mL; total volume, 500 μL) was mixed with approximately 10 pmol (8 μCi) of the sulfur-labeling reagent that had been lyophilized, and the mixture was incubated at room temperature (∼22 °C) for 30 min with occasional mixing. The reaction was terminated by the addition of 20 μL of 0.2 M glycine dissolved in 0.1 M sodium borate (pH 8.5), and the mixture was dialyzed against water. The dialyzed protein was filtered through a 0.22 μm polyvinylidene fluoride filter unit (Millex-GV) and lyophilized.

The lyophilized ^{35}S-labeled boron-enriched streptavidin (specific activity, approximately 90 nCi/μg) was dissolved in fetal bovine serum (Gibco-BRL) at a final streptavidin concentration of 16 μg/mL. The mixture was incubated at 37 °C, and aliquots were collected periodically. The collected samples were subjected to SDS−PAGE analysis, followed by detection of proteins by fluorography, as described below. The gel was also analyzed by using a PhosphorImager (Molecular Dynamics) for quantitation of radioactivity.

S-Alkylation of Stv-28. S-Alkylation of Stv-28 with iodoacetic acid and iodoacetamide was done by standard methods (Gurd, 1967, 1972) to block the highly reactive sulfhydryl groups which cause the aggregation of Stv-28 upon oxidation. All solutions used during S-alkylation had been equilibrated with argon gas. Stv-28 (434 μg; 2.0 mL) in PBS/EDTA containing 350 μM DTT was mixed with 5.4 μmol of iodoacetic acid or iodoacetamide dissolved in PBS/EDTA, and the mixture was incubated at 30 °C for 30 min in the dark. 2-Mercaptoethanol (56 μmol) was added to the mixture to terminate the S-alkylation

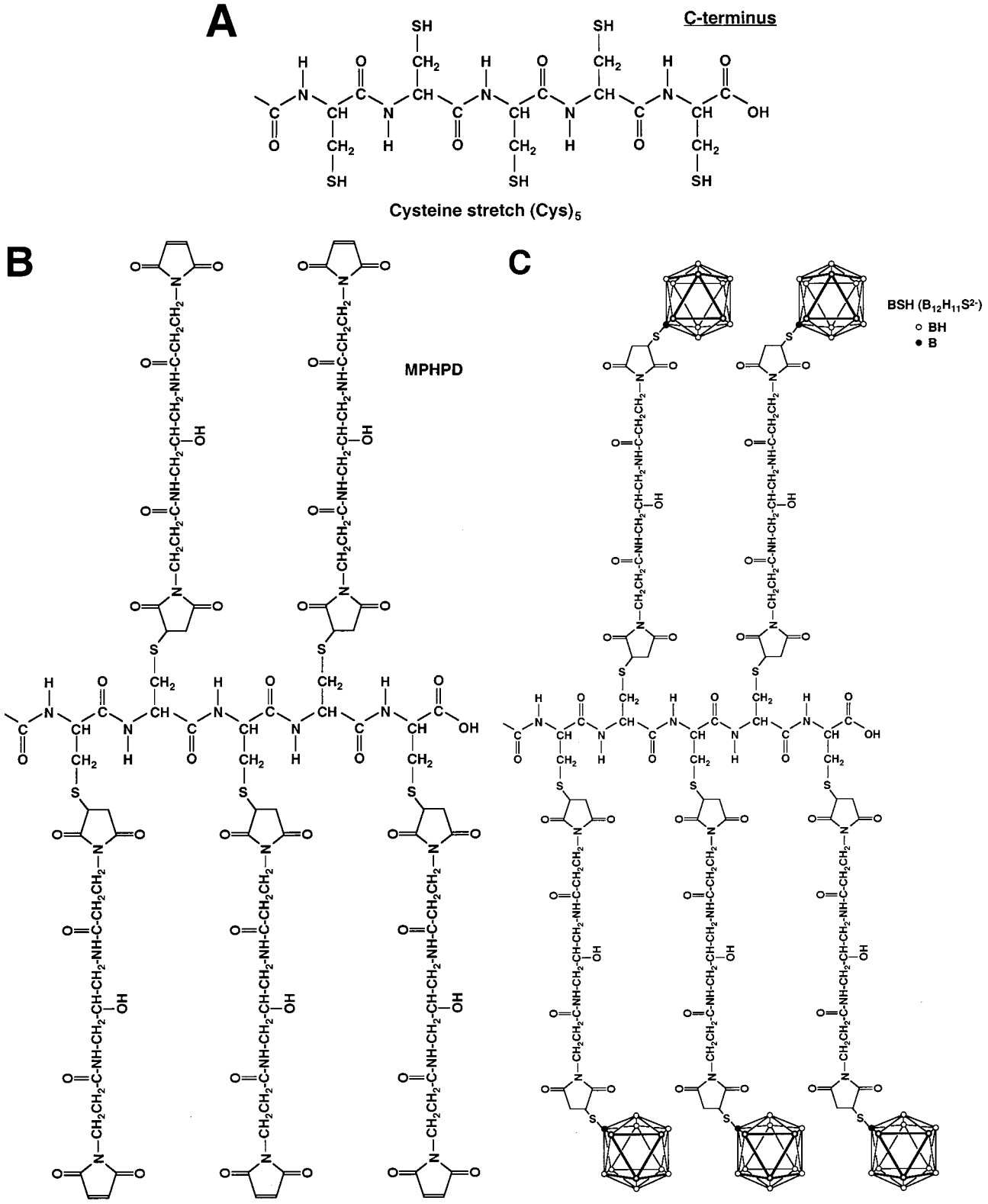


Figure 1. Chemical conjugation of a boron-rich compound, BSH, to a genetically engineered streptavidin, Stv-28, using a sulfhydryl-specific homobifunctional chemical cross linker, MPHPD. (A) Cysteine stretch of Stv-28; (B) after the addition of excess MPHPD to Stv-28; (C) after the addition of excess BSH. Not drawn to scale.

reaction. Then, the mixture was dialyzed against TBS in the dark, and the dialyzed protein was filtered through a 0.22 μm polyvinylidene fluoride filter unit (Millex-GV). The resulting S-alkylated streptavidin preparations were stored frozen at −85 °C until used.

Quantitative Boron Analysis. Quantitative boron analysis was performed by ICP-AES (inductively coupled plasma atomic emission spectrometry) using a Perkin-Elmer Optima 3000, following the method described by Tamat et al. (1987). The 249.77 nm line for boron was used with calibration using a boric acid standard solution for atomic absorption.

Biotin-Binding Assays. Biotin-binding ability was

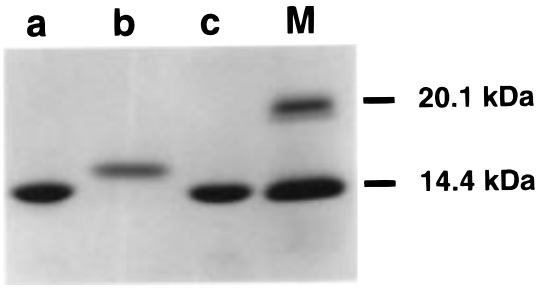


Figure 2. SDS−PAGE analysis of a boron-enriched streptavidin. Lane a, Stv-28 S-alkylated with iodoacetic acid; b, a boron-enriched streptavidin prepared from Stv-28 and BSH; c, Stv-28 S-alkylated with iodoacetamide; M, molecular mass standard proteins (soybean trypsin inhibitor, 20.1 kDa; bovine α-lactalbumin, 14.4 kDa) (Pharmacia Biotech). SDS−PAGE was carried out using a 10−20% polyacrylamide gradient gel with a Tris/tricine buffer system (Schägger and von Jagow, 1987). Approximately 2 μg of protein was applied to each lane. Proteins were stained with Coomassie brilliant blue R.

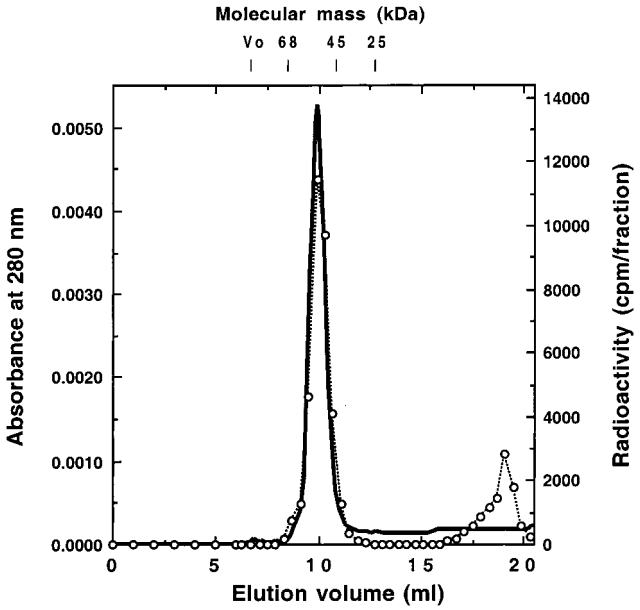


Figure 3. Gel filtration chromatography of a boron-enriched streptavidin. A boron-enriched streptavidin (approximately 3.8 μg) was mixed with excess D-[*carbonyl*-^{14}C]biotin, and the mixture was applied to a Superdex 75 HR 10/30 column (1.0 × 30 cm), which had been equilibrated with TBS. Proteins were eluted at room temperature with TBS at a flow rate of 500 μL/min, and absorbance at 280 nm (—) was monitored during elution. Eluate was collected in 400 μL fractions, and the radioactivity of each fraction (○) was determined by liquid scintillation counting. The positions where the molecular mass standard proteins (bovine serum albumin, 68 kDa; ovalbumin, 45 kDa; chymotrypsinogen A, 25 kDa; Boehringer Mannheim) eluted are indicated at the top.

determined by a gel filtration method (Wei, 1970) using D-[*carbonyl*-^{14}C]biotin and PD-10 columns.

Gel Filtration Chromatography. Gel filtration chromatography was performed using a Superdex 75HR 10/30 column with an FPLC system (Pharmacia). Detailed conditions are given in the legend to Figure 3.

SDS−PAGE Analysis. SDS−PAGE was carried out by a Tris-tricine buffer system (Schägger and von Jagow, 1987) using 10 to 20% polyacrylamide gradient gels. Proteins were stained with Coomassie brilliant blue R. For fluorography, gels were incubated at room temperature for 30 min in 25% methanol, 10% acetic acid, and 2% glycerol, followed by incubation at room temperature for 30 min in 60% Amplify, 25% methanol, and 2% glycerol. Then, the gels were dried in vacuo and exposed to Kodak BioMax MR film.

RESULTS

Chemical Conjugation of a Boron-Rich Compound to a Streptavidin Variant. The genetically engineered streptavidin Stv-28 (Sano et al., 1993) was used to prepare a boron-enriched streptavidin. Like natural streptavidin, Stv-28 is tetrameric (13.2 kDa/subunit), and each subunit has a C-terminal cysteine stretch consisting of five cysteine residues; hence, each Stv-28 molecule has 20 cysteines. Because natural streptavidin has no cysteine (Argaraña et al., 1986; Green 1990), the reactive sulfhydryl groups of the cysteine stretch can be used as specific conjugation sites for sulfhydryl chemistry. The known three-dimensional structure of natural streptavidin (Hendrickson et al., 1989; Weber et al., 19989) shows that the C-termini of streptavidin are located on the surface of the molecule and that they are distant from the biotin-binding sites and the subunit−subunit interfaces. Thus, conjugation of partner molecules to the cysteine stretch should have little, if any, effect on the fundamental properties of streptavidin, such as the biotin-binding ability and subunit association. This has previously been shown by making a radiolabeled streptavidin and a fluorescent streptavidin, in each of which either a radiolabel or a fluorescent marker, respectively, was attached covalently to the cysteine stretch of Stv-28 using sulfhydryl chemistry without disturbing the properties of streptavidin (Sano et al., 1993).

To prepare a boron-enriched streptavidin using Stv-28, a polyhedral sulfhydryl borane, BSH ($B_{12}H_{11}SH^{2-}$), was used. BSH has a reactive sulfhydryl group that can be used as a conjugation site. BSH could be attached to the sulfhydryl groups of Stv-28 by disulfide bond formation. However, it is possible that disulfide bonds between Stv-28 and BSH would be reduced or exchanged with other sulfhydryl-containing materials when used in vivo, diminishing the effectiveness of the conjugate as a boron carrier for BNCT. Thus, a water-soluble sulfhydryl-specific homobifunctional chemical cross-linker, MPHPD, was used to attach BSH irreversibly to Stv-28. MPHPD is a bis-maleimide (Weston, 1980; Wong, 1993), each moiety of which reacts with a sulfhydryl group. MPHPD has a 17 Å spacer between the two maleimide moieties. This relatively long spacer may help to avoid steric hindrance generated by conjugation of five BSH molecules to each cysteine stretch.

Chemical conjugation of BSH to Stv-28 was carried out by using a two-step procedure (Figure 1). First, MPHPD was attached to the sulfhydryl groups of the cysteine stretch of Stv-28 (Figure 1A). To avoid intra- and intermolecular cross-linking between sulfhydryl groups of Stv-28 by MPHPD, excess MPHPD was added to Stv-28 to allow only one maleimide moiety of each MPHPD molecule to react with a sulfhydryl group of Stv-28 (Figure 1B). A reducing agent, TCEP-HCl (Rüegg and Rudinger, 1977), that is not reactive with maleimide, was included in the reaction mixture to avoid disulfide formation. Then, excess BSH was added to the reaction mixture to allow the sulfhydryl group of BSH to react with the unreacted maleimide group of MPHPD which had been attached to Stv-28 (Figure 1C). The resulting mixture was dialyzed against a neutral solution to remove MPHPD−BSH complexes and unreacted MPHPD and BSH that were present in large quantities. The

dialyzed streptavidin conjugates retained at least 90% of the original biotin-binding ability, analyzed by biotin-binding assays. These conjugates showed a sharp peak with a molecular mass slightly greater than S-alkylated Stv-28 preparations on gel filtration chromatography (data not shown). No appreciable changes in solubility were seen by conjugation of BSH to Stv-28 under the conditions used. These suggest that functional conjugates between Stv-28 and BSH had been produced. However, relatively large amounts of MPHPD−BSH complexes and unreacted MPHPD and BSH were seen in the final conjugate solution, suggesting inefficient removal of these compounds by dialysis. To remove these compounds, chemical conjugates between Stv-28 and BSH were purified by 2-iminobiotin affinity chromatography (Hofmann et al., 1970). This affinity chromatography step should remove not only MPHPD−BSH complexes and unreacted MPHPD and BSH but also streptavidin conjugates which had lost the biotin-binding ability due to the chemical conjugation of BSH, if any.

Characterization of a Boron-Enriched Streptavidin. The conjugate between Stv-28 and BSH, purified by 2-iminobiotin affinity chromatography, was analyzed by SDS−PAGE for the subunit molecular mass and structural homogeneity. The conjugate showed a single band on SDS−PAGE (Figure 2), indicating its high structural homogeneity. The migration of the subunit of this conjugate is slower than those of Stv-28 molecules, which had been S-alkylated with iodoacetic acid (subunit molecular mass, 13.5 kDa) and with iodoacetamide (13.5 kDa). The subunit molecular mass of this conjugate was estimated at approximately 16 kDa by calibration with the S-alkylated Stv-28 preparations, recombinant core streptavidins (Stv-13 and Stv-25 with subunit molecular masses of 12.6 and 13.2 kDa, respectively) (Sano et al., 1995), and molecular mass standard proteins (Pharmacia Biotech). If the sulfhydryl groups of Stv-28 are saturated with BSH, the subunit molecular mass of the resulting conjugate should be 16.1 kDa. This suggests that the sulfhydryl groups of Stv-28 are fully saturated with BSH.

Quantitative boron analysis by ICP-AES (Tamat et al., 1987) shows that this conjugate contains 230 ± 15 boron atoms/streptavidin molecule. Since a maximum of 240 boron atoms (20 BSH molecules) can be attached to each Stv-28 molecule by this chemical conjugation method, the result reveals that the sulfhydryl groups of Stv-28 are fully saturated with BSH, as also suggested by SDS−PAGE analysis. This also demonstrates that the chemical conjugation, the method used to attach BSH to the sulfhydryl groups of Stv-28, was highly efficient and specific.

The biotin-binding ability and subunit association of this boron-enriched streptavidin were analyzed by biotin-binding assays and gel filtration chromatography, respectively. This boron-enriched streptavidin binds greater than 0.97 molecules of biotin/subunit, indicating that it has full biotin-binding ability. No appreciable changes in biotin-binding affinity were seen. On gel filtration chromatography (Figure 3), this boron-enriched streptavidin had a sharp peak, indicating its high structural homogeneity, and no changes in subunit association were seen. The molecular mass of the boron-enriched streptavidin was estimated to be 53 kDa by calibration with molecular mass standard proteins (Boehringer Mannheim). This reveals that this boron-enriched streptavidin is tetrameric, like natural streptavidin, suggesting that the conjugation of BSH has no apparent effect on the subunit association of streptavidin.

The serum stability of the boron-enriched streptavidin was analyzed in vitro. The boron-enriched streptavidin was labeled with ^{35}S, and the resulting radiolabeled protein was incubated at 37 °C in fetal bovine serum. Aliquots were collected periodically and analyzed by SDS−PAGE. Proteins were detected by fluorography for the changes in subunit molecular mass and structural homogeneity. In this assay, dissociation of BSH from streptavidin and degradation of streptavidin are shown by shifts to smaller molecular masses (subunit molecular mass of intact boron-enriched streptavidin, 16 kDa) and by reduction in radioactivity of the 16 kDa band. Fluorography of the gel (Figure 4) shows no apparent change of the subunit molecular mass of the radiolabeled boron-enriched streptavidin (16 kDa), and no degradation products with smaller molecular masses were seen. Quantitation of radioactivity by a PhosphorImager also showed no appreciable change in radioactivity of the 16 kDa band.

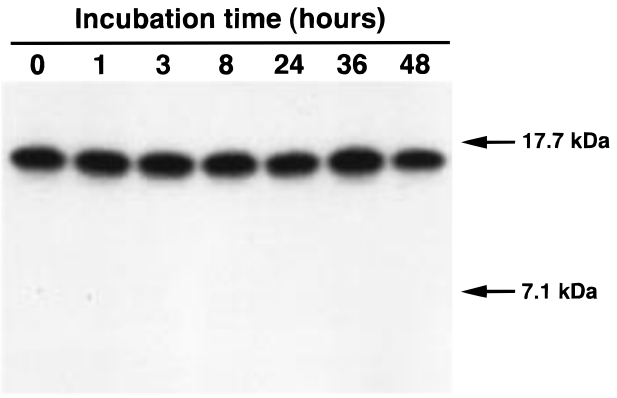


Figure 4. Serum stability of a boron-enriched streptavidin. A boron-enriched streptavidin was labeled with ^{35}S by using a sulfur labeling reagent (Amersham). The radiolabeled boron-enriched streptavidin was incubated at 37 °C in fetal bovine serum at a final streptavidin concentration of 16 μg/mL. Aliquots were collected periodically and analyzed by SDS−PAGE using a 10−20% polyacrylamide gradient gel. Proteins were visualized by fluorography. The number above each lane is the incubation time in hours. The positions of prestained molecular mass standard proteins (lysozyme, 17.7 kDa; aprotinin, 7.1 kDa; Kaleidoscope Prestained Standards, Bio-Rad) are shown by arrows.

These results reveal that the chemical conjugation of BSH to the C-terminal cysteine stretch of Stv-28 has little, if any, effect on the fundamental properties of streptavidin, such as biotin-binding ability and subunit association. They also indicate that the chemical conjugation method used is highly specific and efficient and that the resulting boron-enriched streptavidin has high structural homogeneity. In addition, the boron-enriched streptavidin has high stability in serum, suggesting that the linkage between Stv-28 and BSH may be sufficiently stable for in vivo uses. Additional analysis indicated that 2-iminobiotin affinity chromatography is not necessary to obtain functional conjugates without contaminating BSH-MPHPD complexes and unreacted BSH and MPHPD. Since the chemical conjugation of BSH is quite efficient and it does not alter the fundamental properties of streptavidin, only the removal of small compounds, i.e., BSH−MPHPD complexes and unreacted BSH and MPHPD, is needed to obtain purified boron-enriched streptavidin preparations. For example, simple gel filtration chromatography using desalting columns, such as PD-10, has shown to be sufficient to obtain pure boron-enriched streptavidin preparations. Other means, such as ultrafiltration and dialysis using membrane with larger pore sizes than that used in this study, should also

be useful for removal of these compounds. Use of these methods should facilitate the production of this boron-enriched streptavidin in large quantities due to their simplicity, as compared to that of 2-iminobiotin affinity chromatography.

DISCUSSION

A boron-enriched streptavidin has been produced by chemical conjugation of a boron-rich compound to a genetically engineered streptavidin using sulfhydryl chemistry. This boron-enriched streptavidin should be very useful as a component of boron carriers for BNCT of cancer. For example, a monoclonal antibody against a tumor-associated antigen (antitumor antibody) could be attached specifically and tightly to this boron-enriched streptavidin upon simple biotinylation. The resulting conjugate between the biotinylated antitumor antibody and the boron-enriched streptavidin could be used to deliver boron to target tumor cells which overexpress the tumor-associated antigen on their surface. Similarly, the boron-enriched streptavidin could be attached to a ligand, such as a growth factor, upon biotinylation, and the resulting conjugate could be used to target boron to tumor cells on which the cell surface receptor of the ligand is overexpressed. In these boron-targeting schemes, the extreme biotin-binding affinity of streptavidin precludes the dissociation of the boron-enriched streptavidin from biotinylated partner macromolecules, such as biotinylated antitumor antibodies and biotinylated ligands. As shown experimentally, the dissociation of BSH from streptavidin, caused by degradation of streptavidin or cleavage of the linkage between streptavidin and BSH, is also negligible. Similar targeting strategies have been tested by using monoclonal antibodies and ligands to which large amounts of boron are directly conjugated. However, the biological activities and functions of these macromolecules are often altered or even lost by either direct conjugation of large amounts of boron or the conditions used for chemical conjugation. This problem may be solved by attaching large amounts of boron indirectly to these macromolecules, for which streptavidin serves as a linker or spacer between the macromolecules and boron. The availability of a variety of biotinylation methods (Wilchek and Bayer, 1990) should allow this indirect boronation scheme applicable to a wide range of macromolecular tumor targeting reagents.

In this work, only one boron-enriched streptavidin species was produced which carries approximately 230 boron atoms/molecule. However, the length of the C-terminal cysteine stretch can easily be varied by simple genetic engineering. Thus, the number of boron atoms attached to each streptavidin molecule can be maximized, if needed, by conjugating BSH to a streptavidin variant containing a longer cysteine stretch using the same chemical conjugation method.

ACKNOWLEDGMENT

The author thanks David Friedman, Ilhan Olmez, Gordon Korse, Kent Riley, and Otto Harling at the Nuclear Reactor Laboratory, Massachusetts Institute of Technology, for their help in quantitative boron analysis using ICP-AES. The author also thanks Rolf Barth and Albert Soloway at the Ohio State University for helpful suggestions and discussions and Mark Pandori for critical reading of the manuscript. This work was supported by Research Grant Awards from the Brain Tumor Society.

LITERATURE CITED

Argaraña, C. E., Kuntz, I. D., Birken, S., Axel, R., and Cantor, C. R. (1986) Molecular cloning and nucleotide sequence of the streptavidin gene. *Nucleic Acids Res. 14*, 1871−1881.

Barth, R. F., and Soloway, A. H. (1994) Boron neutron capture therapy of primary and metastatic brain tumors. *Mol. Chem. Neuropathol. 21*, 139−154.

Barth, R. F., Soloway, A. H., and Brugger, R. M. (1996) Boron neutron capture therapy of brain tumors: Past history, current status, and future potential. *Cancer Inv. 14*, 534−550.

Bayer, E. A., and Wilchek, M. (1980) The use of the avidin−biotin complex as a tool in molecular biology. *Methods Biochem. Anal. 26*, 1−46.

Chaiet, L., and Wolf, F. J. (1964) The properties of streptavidin, a biotin-binding protein produced by Streptomycetes. *Arch. Biochem. Biophys. 106*, 1−5.

Chaiet, L. Miller, T. W., Tausing, F., and Wolf, F. J. (1963) Antibiotic MSD-235. II. Separation of purification of synergistic components. *Antimicrob. Agents Chemother. 3*, 28−32.

Coderre, J. A., and Morris, G. M. (1999) The radiation biology of boron neutron capture therapy. *Radiat. Res. 151*, 1−18.

Gahbauer, R., Gupta, N., Blue, T., Goodman, J., Barth, R., Grecula, J., Soloway, A. H., Sauerwein, W., and Wambersie, A. (1998) Boron neutron capture therapy: principles and potential. *Recent Results Cancer Res. 150*, 183−209.

Green, N. M. (1970) Avidin. *Adv. Protein Chem. 29*, 85−133.

Green, N. M. (1990) Avidin and streptavidin. *Methods Enzymol. 184*, 51−67.

Gurd, F. R. N. (1967) Carboxymethylation. *Methods Enzymol. 11*, 532−541.

Gurd, F. R. N. (1972) Carboxymethylation. *Methods Enzymol. 25*, 424−438.

Hermanson, G. T. (1995) *Bioconjugate Techniques*, Academic Press, New York, NY.

Hawthorne, M. F. (1993) The role of chemistry in the development of boron neutron capture therapy of cancer. *Angew. Chem., Int. Ed. Engl. 32*, 950−984.

Hawthorne, M. F. (1998) New horizons for therapy based on the boron neutron capture reaction. *Mol. Med. Today 4*, 174−81.

Hendrickson, W. A., Pähler, A., Smith J. L., Satow, Y., Merritt, E. A., and Phizackerley, R. P. (1989) Crystal structure of core streptavidin determined from multiwavelength anomalous diffraction of synchrotron radiation. *Proc. Natl. Acad. Sci. U.S.A. 86*, 2190−2194.

Hofmann, K., Wood, S. W., Brinton, C. C., Montibeller, J. A., and Finn, F. M. (1980) Iminobiotin affinity columns and their application to retrieval of streptavidin. *Proc. Natl. Acad. Sci. U.S.A. 77*, 4666−4668.

Rüegg, U. T., and Rudinger, J. (1977) Reductive cleavage of cysteine disulfides with tributylphosphine. *Methods Enzymol. 47*, 111−116.

Sano, T., and Cantor, C. R. (1990) Expression of a cloned streptavidin gene in *Escherichia coli*. *Proc. Natl. Acad. Sci. U.S.A. 87*, 142−146.

Sano, T., and Cantor, C. R. (1991) Expression vectors for streptavidin-containing chimeric proteins. *Biochem. Biophys. Res. Commun. 176*, 571−577.

Sano, T., Smith, C. L., and Cantor, C. R. (1993) A streptavidin mutant containing a cysteine stretch that allows production of a variety of specific streptavidin conjugates. *BioTechnology 11*, 201−206.

Sano, T., Pandori, M. W., Chen, X., Smith, C. L., and Cantor, C. R. (1995) Recombinant core streptavidins. A minimum-sized core streptavidin has enhanced structural stability and higher accessibility to biotinylated macromolecules. *J. Biol. Chem. 270*, 28204−28209.

Schägger, H., and von Jagow, G. (1987) Tricine-sodium dodecyl sulfate-polyacrylamide gel electrophoresis for the separation of proteins in the range from 1 to 100 kDa. *Anal. Biochem. 166*, 368−379.

Soloway, A. H., Barth, R. F., Gahbauer, R. A., Blue, T. E., and Goodman, J. H. (1997) The rationale and requirements for the development of boron neutron capture therapy of brain tumors. *J. Neuro-Oncol. 33*, 9−18.

Soloway, A. H., Tjarks, W., Barnum, B. A., Rong, F.-G., Barth, R. F., Codogni, I. M., and Wilson, J. G. (1998) The chemistry of neutron capture therapy. *Chem. Rev. 98*, 1515−1562.

Studier, F. W., Rosenberg, A. H., Dunn, J. J., and Dubendorff, J. W. (1990) Use of T7 RNA polymerase to direct expression of cloned genes. *Methods Enzymol. 185*, 60−89.

Tamat, S. R., Moore, D. E., and Allen, B. J. (1987) Determination of boron in biological tissues by inductively coupled plasma atomic emission spectrometry. *Anal. Chem. 59*, 2161−2164.

Weber, P. C., Ohlendorf, D. H., Wendroski, J. J., and Salemme, F. R. (1989) Structural origins of high-affinity biotin binding to streptavidin. *Science 243*, 85−88.

Wei, R.-D. (1970) Assay of avidin. *Methods Enzymol. 18A*, 424−427.

Weston, P. D., Devries, J. A., and Wrigglesworth, R. (1980) Conjugation of enzymes to immunoglobulins using dimaleimide. *Biochim. Biophys. Acta 612*, 40−49.

Wilchek, M., and Bayer, E. A. (1988) The avidin−biotin complex in bioanalytical applications. *Anal. Biochem. 171*, 1−32.

Wilchek, M., and Bayer, E. A. (ed.) (1990) Avidin−biotin technology, *Methods in Enzymology*, Volume 184, Academic Press, San Diego, CA.

Wong, S. S. (1991) *Chemistry of Protein Conjugation and Cross-linking*, CRC Press, Boca Raton, FL.

BC990029W

Radioiodination of Cyanocobalamin Conjugates Containing Hydrophilic Linkers: Preparation of a Radioiodinated Cyanocobalamin Monomer and Two Dimers, and Assessment of Their Binding with Transcobalamin II

D. Scott Wilbur,*,† Pradip M. Pathare,† Donald K. Hamlin,† Sheldon P. Rothenberg,‡ and Edward V. Quadros‡

Department of Radiation Oncology, University of Washington, Seattle, Washington 98195, and SUNY-Downstate Medical Center, Brooklyn, New York 11203. Received March 18, 1999; Revised Manuscript Received June 3, 1999

This report describes an investigation aimed at preparation of radioiodinated cyanocobalamin (CN-Cbl) monomers and dimers with improved water solubility and decreased nonspecific binding. In the investigation, synthesis and radioiodination reactions of one monomeric and two dimeric CN-Cbl derivatives were conducted. The initial step in the synthesis of the CN-Cbl derivatives was mild acid hydrolysis of CN-Cbl, **1**, followed by separation of the resultant corrin ring *b*-, *d*-, and *e*-monocarboxylate isomers. The investigation was limited to preparation of conjugates of CN-Cbl-*e*-carboxylate, **2**, as earlier studies had shown binding of that isomer with recombinant human transcobalamin II (rhTCII) was similar to CN-Cbl. In a second synthetic step, the hydrophilic linker moiety, 4,7,10-trioxa-1,13-tridecandiamine, **3**, was conjugated with **2** to form the adduct, **4**. The synthesis of a monomeric CN-Cbl derivative, **6a**, which can be used for radioiodination, was accomplished by reaction of **4** with *p*-tri-*n*-butylstannylbenzoate tetrafluorophenyl (TFP) ester, **5a**. Two CN-Cbl dimers containing the arylstannane radioiodination moiety were also synthesized. The first dimer, **8a**, was synthesized by cross-linking **4** with a stannylbenzoyl-aminoisophthalate di-TFP ester, **7a**. The second dimer, **11a**, was synthesized by reacting benzene tricarboxylate tri-TFP ester, **10**, in a stepwise manner with 1 equiv of the adduct of **5a** and **3** (forming **9a**), followed by 2 equiv of **4**. Iodobenzoate HPLC standards, **6b**, **8b**, and **11b**, used in the radioiodination studies, were prepared in a manner similar to that of the stannylbenzoate derivatives. Radioiodinations were performed by reacting **6a**, **8a**, or **11a** with *N*-chlorosuccinimide and Na[^{125}I]I in methanol under neutral conditions. Radiochemical yields of 17−42% were obtained. Evaluation of the binding properties of radiolabeled CN-Cbl conjugates with rhTCII showed that the dimer of CN-Cbl, **11b**, bound more avidly than the monomer, **6b**, and that the binding affinity of the dimer is essentially equivalent to that of unmodified CN-Cbl. Incubation of radioiodinated monomer, [^{125}I]**6b**, and dimer, [^{125}I]**11b**, with rhTCII followed by size-exclusion chromatographic analysis provided data that the monomer bound one rhTCII molecule whereas two rhTCII molecules were bound to approximately 30% of the dimer.

INTRODUCTION

Cobalamins (Cbl) function as coenzymes in two mammalian enzymes, methionine synthase and L-methylmalonyl-CoA mutase (*1*, *2*). Although an essential nutrient, mammalian cells do not synthesize the basic Cbl structure, rather it is a vitamin (vitamin B_{12}) obtained from microorganisms (*2*) and purified in its cyanocobalamin (CN-Cbl)[1] form (*3*). The adsorption, transport, cellular uptake, and storage of cobalamins is highly regulated (*4*−*8*). Abnormalities in various aspects of this regulated process can result in hematological and neurologic disease (*6*, *9*−*11*). Elucidation of the biochemical pathways and associated abnormalities of cobalamins have been aided greatly by the use of radiolabeled cobalamins (*9*, *12*).

The radiolabel widely used with cobalamins is ^{57}Co, but other radionuclides of cobalt (e.g., ^{58}Co and ^{60}Co) and tritium have also been used (*13*−*17*). While the cobalamins that contain ^{57}Co have many applications, cobalamins labeled with other radionuclides may offer advantages in some applications. One important advantage that can be obtained with certain radionuclides is higher specific activities of CN-Cbl derivatives. Introduction of ^{57}Co into CN-Cbl is obtained by microbial synthesis, and the specific activity can be variable due to differences in growth conditions. Once incorporated, the ^{57}Co-labeled product must be extracted and subjected to extensive purification. Tritium and ^{14}C can be used but the specific activity of the product is inadequate for most applications. Recently, high specific activity ^{99m}Tc- and ^{111}In-

* To whom correspondence should be addressed. Phone: 206-685-3085. Fax: 206-685-9630. E-mail: dswilbur@u.washington.edu.

† University of Washington.

‡ SUNY-Downstate Medical Center.

[1]Abbreviations: BSA, bovine serum albumin; ca, carrier-added; Cbl, cobalamin; CN-Cbl, cyanocobalamin; cpm, counts per minute; DMIX, thioglycerol/dimethyl sulfoxide/trifluoroacetic acid mixture; DTPA, diethylenetriaminepentaacetic acid; EDC, 1-(3-dimethylaminopropyl)-3-ethylcarbodiimide; HOAc, acetic acid; HSA, human serum albumin; ES, electrospray; Et_3N, triethylamine; FAB, fast-atom bombardment; LC, liquid chromatography; NaOAc, sodium acetate; *nca*, no-carrier-added NCS, *N*-chlorosuccinimide; NHS, *N*-hydroxysuccinimide; PBS, phosphate-buffered saline; rt, room temperature; Rxn, reaction; TCII, transcobalamin II; rhTCII, recombinant human transcobalamin II; TFP, tetrafluorophenyl; TFP-OH, tetrafluorophenol.

10.1021/bc9900340 CCC: $18.00 © 1999 American Chemical Society
Published on Web 07/23/1999

labeled cobalamins have been described for in vivo imaging of the transcobalamin II (TCII) receptors (*18*). In those studies, the chelating agent DTPA was conjugated to the corrin ring via a short lipophilic linker molecule. We have also described a method for labeling cobalamins with iodine radionuclides utilizing a pendant group attached to the corrin ring (*19*). While the attachment of a pendant group to cobalamins for radiolabeling alters the structure, if the attachment is made in specific locations, the binding with TCII is only minimally affected (*20*). The radioiodinated CN-Cbl derivatives prepared bound with TCII nearly as avidly as unaltered CN-Cbl and had specific activities nearly three times that of commercially available ^{57}Co-labeled CN-Cbl (*19*).

Several CN-Cbl derivatives previously prepared in our laboratory are under investigation as new anti-neoplastic therapeutics for AIDS related lymphoma (*19*−*21*). The cobalamin derivatives initially prepared contained the lipophilic linker moiety 1,12-diaminododecane. This linker was used as a 16 Å spacer between the CN-Cbl moiety and conjugated molecules to provide adequate distance such that binding with carrier proteins (e.g., TCII) is not affected. To obtain radioiodinated CN-Cbl derivatives, an arylstannyl moiety, *p*-tri-*n*-butylstannylhippuric acid, which serves as a penultimate precursor to radioiodination (*22*), was conjugated using the lipophilic diaminododecane linker. Radioiodination of the resultant cobalamin-stannylhippurate conjugates produced compounds with high specific activities, but the compounds bound nonspecifically to glassware and syringe needles. Although the nonspecific binding was reduced by addition of bovine serum albumin (BSA), this property made the radioiodinated CN-Cbls of limited use. Dimers of CN-Cbl were also produced using similar chemistry; however, attempted iodination and radioiodination of the CN-Cbl dimers containing arylstannyl moieties were unsuccessful.

Our desire to decrease the nonspecific binding of monomeric radioiodinated CN-Cbl derivatives and to develop a method for radioiodination of CN-Cbl dimers led to an investigation of CN-Cbl derivatives that incorporate a more hydrophilic linker, 4,7,10-trioxa-1,13-tridecandiamine, of similar length (i.e., 17 Å) in the place of 1,12-diaminododecane. Only the corrin ring *e*-monocarboxylate conjugates were prepared as that regioisomer had been previously shown to bind more avidly than conjugates of the other regioisomeric corrin ring carboxylates (*20*). The CN-Cbl derivatives were prepared in sets of two similar compounds, the arylstannane used for radioiodination and the corresponding aryliodide. Thus, two monomeric CN-Cbl derivatives and four dimeric CN-Cbl derivatives were prepared. The primary difference in the CN-Cbl dimers was that in one set of compounds two trioxatridecanediamines were incorporated whereas three of the same linkers were incorporated into the second set of dimers. Once prepared, the CN-Cbl conjugates containing arylstannane moieties were evaluated in radioiodination reactions, and their binding with recombinant human transcobalamin II (rhTCII) was assessed.

EXPERIMENTAL PROCEDURES

Materials. All chemicals purchased from commercial sources were of analytical grade or better and were used without further purification. Cyanocobalamin (vitamin B_{12}) was purchased from Sigma Chemical Co. (St. Louis, MO). *N*-Hydroxysuccinimide was purchased from Lancaster Synthesis Inc. (Windham, NH). All other reagents were obtained from Aldrich Chemical Co. (Milwaukee, WI). Solvents for HPLC analysis were obtained as HPLC grade and were filtered (0.2 μm) prior to use. Human serum albumin was obtained from Miles, Inc. (Elkhart, IN). Strongly basic anion exchange matrix, 2% crosslinked Dowex 1 chloride form, 200−400 mesh, Amberlite XAD-2 nonionic polymeric adsorbent, and octadecyl functionalized silica gel for column chromatography were obtained from Sigma-Aldrich (St Louis, MO). Bio-Sil NH_2 (aminopropyl bonded silica) (40−63 μm) for column packing was purchased from Bio-Rad Laboratories (Hercules, CA).

Radioactivity. [^{57}Co]Cyanocobalamin was obtained from Amersham Corp. (Amersham, U.K.) at a specific activity of 200 μCi/μg. Na[^{125}I] was purchased from NEN/Dupont (Billerica, MA) as high concentration/high specific activity radioiodide in 0.1 N NaOH. Samples containing ^{57}Co were measured in a Beckman 300 gamma counter or Wallac 1480 gamma counter, and those containing ^{125}I were measured in a Capintec CRC-15R or a Capintec CRC-6A radioisotope calibrator. Procedures for safe handling of radioactive materials were followed in the manner previously described (*19*).

Spectroscopic Analysis. ^{1}H NMR spectra were obtained on a Bruker AC-500 (500 MHz) or a Bruker AC-750 (750 MHz) instrument. The chemical shifts are expressed as parts per million using tetramethylsilane as an internal standard (δ = 0.0 ppm). IR data were obtained on a Perkin-Elmer 1420 infrared spectrophotometer. Mass spectral data were obtained on a VG 70SEQ mass spectrometer with 11250J data system. Fast-atom bombardment (FAB) mass spectral data were obtained at 8 kV using a matrix of MeOH/DMIX (thioglycerol/DMSO/TFAA, 90/9/1). Electrospray (ES) mass spectra were acquired on a Sciex API III triple quadrapole spectrometer fitted with a nebulization assisted electrospray source (PE/Sciex, Thornhill, Ontario).

Chromatography. Separation of compounds (nonradioactive) by HPLC was done on a Hewlett-Packard quaternary 1050 gradient pumping system with a variable wavelength UV detector (360 nm) and a Varex ELSD MKIII evaporative light-scattering detector. The HPLC data were analyzed using Hewlett-Packard HPLC ChemStation software. The compounds were separated by reversed-phase HPLC on an Alltech Altima C-18 column (5 μm, 4.6 × 250 mm) using one of two different gradient solvent systems at a flow rate of 1 mL/min. Gradient I used methanol as solvent A and aqueous 1% HOAc as solvent B. Starting with 40% A, the initial solvent mixture was held for 2 min, then the gradient was increased to 100% A over the next 10 min and then held at 100% A for 5 min. Retention times, t_R, under these conditions were (min) **1** = 2.7; **2** = 5.1; **4** = 2.3; **6a** = 15.7; **6b** = 10.8; **8a** = 14.8; **8b** = 10.5; **9a** = 18.4; **9b** = 10.5; **11a** = 14.8; **11b** = 10.3 . The starting solvent mixture for gradient II was 70% A, and all other parameters were the same as for gradient I. Retention times, t_R, under these conditions were (min) **5a** = 13.8; **5b** = 20.7. Preparative scale purifications of CN-Cbl conjugates **6a**, **8a**, and **11a** for use in radioiodination reactions were conducted with a gradient of MeOH/H_2O (no HOAc).

Chromatographic separation of radiolabeled cobalamins was carried out on a system consisting of two Beckman model 110B pumps, a Beckman 420 controller, a Beckman model 153 UV detector (254 nm), and a Beckman model 170 radioisotope detector. The compounds were separated on a Hamilton PRP-1 column (10 μm, 4.6 mm × 250 mm; Alltech) using one of two gradient

solvent systems at a flow rate of 1 mL/min. The first solvent system consisted of 50% MeOH as solvent A and 50% water as solvent B. The initial solvent mixture was held for 2 min, then the gradient was increased to 100% A over the next 10 min, and 100% A was held for 5 min. Retention times, t_R, under these conditions were **6b** = 13.8; **11b** = 13.4. In the second gradient, the starting solvent mixture was 60% A, the initial solvent mixture was held for 2 min, then the gradient was increased to 100% A over next 13 min and held there for 10 min. Retention time, t_R, under these conditions was **8b** = 12.8 min.

A preparative LC system containing a Rainin Rabbit-plus peristaltic pumping system, a Dynamax (model UV-1) UV-vis absorbance detector, and a Dynamax model FC1 fraction collector were used to obtain pure samples of **6a**, **6b**, **8a**, **8b**, **11a**, and **11b**. A glass column (150 psi, C_{18}, 25 mm × 500 mm) packed with either Bio-Sil NH_2 (for separation of CN-Cbl-carboxylates) or reversed-phase C_{18} was used. The eluant solvents and gradients were the same as above. Fractions were collected and evaluated by analytical HPLC before combining those containing only the desired compound.

Synthesis of CN-Cbl-*e*-carboxylic acid, 2. The CN-Cbl corrin ring *e*-carboxylate, **2**, was prepared by acid hydrolysis of CN-Cbl, **1**, and purified by preparative LC on Bio-Sil NH_2 as previously described (*20*).

Synthesis of 4. Conjugation of the CN-Cbl-*e*-carboxylate, **2**, with trioxatridecanediamine, **3**, to form the adduct **4** was accomplished as previously described (*21*).

Synthesis of *p*-Tri-*n*-butylstannylbenzoyltrioxatridecanediamine-CN-Cbl Conjugate, 6a. To a solution containing 0.3 g (0.193 mmol) of **4** in 20 mL of DMF and 27 μL of Et_3N was added 0.108 g (0.193 mmol) of *p*-tri-*n*-butylstannylbenzoate TFP ester, **5a**, over a 5−10 min period. The reaction mixture was stirred at room temperature for 2 h (HPLC monitored) and then evaporated to dryness. The resultant solid residue was dissolved in 10 mL of 60% methanol/H_2O, loaded on a preparative C_{18} reversed-phase LC column, and eluted with the same solvent mixture as used for loading the column. The fractions containing the final product were evaporated to dryness to yield 42% of **6a**, mp 170−172 °C. ^{1}H NMR (MeOH-d_4, 750 MHz): δ 0.35 (s, 2H); 0.7−2.6 (m, 80H); 2.76 (m, 2H); 3.0−3.65 (m, 38H); 3.8 (m, 1H); 3.95−4.1 (m, 3H); 4.2 (m, 1H); 4.4 (m, 1H); 4.6 (m, 1H); 5.95 (s, 1H); 6.18 (s, 1H); 6.47 (s, 1H); 7.02 (s, 1H); 7.16 (s, 1H); 7.45 (m, 2H); 7.65 (m, 2H). MS (FAB$^+$) mass calcd for $C_{92}H_{139}N_{15}O_{18}CoPSn$: 1952. Found: 1953 (M + H). IR (KBr): 3300, 3200, 2900, 1640, 1570, 1200, 1070.

Synthesis of *p*-Iodobenzoyltrioxatridecanediamine-CN-Cbl Conjugate, 6b. The same procedure as described for the synthesis of **6a** was used, except 0.076 g (0.193 mmol) of *p*-iodobenzoate TFP ester, **5b**, was added in place of **5a**. The product was isolated in 35% yield, mp 161−163 °C. ^{1}H NMR (MeOH-d_4, 750 MHz): δ 0.44 (s, 2H); 1.05−1.5 (m, 13H); 1.65−2.7 (m, 40H); 2.84 (m, 2H); 3.15−3.75 (m, 40H); 3.88 (m, 1H); 4.05−4.2 (m, 2H); 4.3 (m, 1H); 4.54 (m, 1H); 4.65 (m, 1H); 6.04 (s, 1H); 6.27 (s, 1H); 6.56 (s, 1H); 7.11 (s, 1H); 7.25 (s, 1H); 7.56 (m, 2H); 7.82 (m, 2H). MS (FAB$^+$) mass calcd for $C_{80}H_{112}N_{15}O_{18}CoPI$: 1787. Found: 1788 (M + H). IR (KBr): 3300, 3200, 2900, 1640, 1570, 1200, 1070.

4′-(Tri-*n*-butylstannyl)benzoyl-5-aminoisophthalate DiTFP Ester, 7a, and 4′-Iodobenzoyl-5-aminoisophthalate DiTFP Ester, 7b. These compounds were synthesized as described previously (*21*).

Synthesis of 8a. To a solution containing 0.3 g (0.193 mmol) of **4** in 20 mL of DMF was added 30 μL of Et_3N followed by 0.084 g (0.096 mmol) of **7a**. The reaction mixture was stirred at room temperature for 3 h and then evaporated to dryness. The resultant solid residue was dissolved in 10 mL of 80% methanol/H_2O, loaded on a preparative C_{18} reversed-phase LC column, and eluted with the same solvent mixture as used for loading the column. The fractions containing the final product were evaporated to dryness to yield 43% of **8a**, mp 238−241 °C (dec). ^{1}H NMR (MeOH-d_4, 500 MHz): δ 0.45 (s, 4H); 0.9−2.7 (m, 140H); 2.8−2.9 (m, 5H); 3.1−3.8 (m, 64H); 3.88 (m, 4H); 4.08−4.2 (m, 6H); 4.34 (m, 3H); 4.48 (m, 4H); 4.68 (m, 4H); 6.05 (s, 2H); 6.28 (s, 2H); 6.57 (s, 2H); 7.14 (s, 2H); 7.26 (s, 2H); 7.6−7.8 (m, 3H); 7.9−8.01 (m, 3H); 8.33 (s, 1H). MS (ES) mass calcd for $C_{173}H_{251}N_{31}O_{37}Co_2P_2Sn$: 3654. Found: 3655 (M + H). IR (KBr): 3300, 3200, 2900, 1640, 1570, 1200, 1070.

Synthesis of 8b. The same procedure was used as described for the synthesis of **8a**, except 0.067 g (0.096 mmol) of **7b** was added in place of **7a**. The product was isolated in 45% yield, mp 210−213 °C (dec). ^{1}H NMR (MeOH-d_4, 500 MHz): δ 0.44 (s, 4H); 1.0−2.65 (m, 115H); 2.8−2.9 (m, 5H); 3.1−3.8 (m, 62H); 3.88 (m, 4H); 4.04−4.2 (m, 6H); 4.34 (m, 3H); 4.48 (m, 4H); 4.67 (m, 4H); 6.04 (d, J = 5.5 Hz, 2H); 6.26 (s, 2H); 6.56 (d, J = 6.5 Hz, 2H); 7.13 (d, J = 4 Hz, 2H); 7.24 (d, J = 3.5 Hz, 2H); 7.73−7.79 (m, 3H); 7.88−8.01 (m, 3H); 8.3 (s, 1H). MS (ES) mass calcd for $C_{161}H_{224}N_{31}O_{37}Co_2P_2I$: 3491. Found: 3492 (M + H). IR (KBr): 3300, 3200, 2900, 1640, 1570, 1200, 1070.

***N*-(13′-Amino-4′,7′,10′-trioxatridecanyl)-4-tributylstannylbenzamide, 9a, and *N*-(13′-Amino-4′,7′,10′-trioxatridecanyl)-4-iodobenzamide, 9b**. Compounds **9a** and **9b** were synthesized as described previously (*23*).

Synthesis of 11a. A solution of **9a** (0.058 g, 0.095 mmol) in 25 mL of anhydrous DMF was added dropwise over 1 h to a solution of **10** (0.062 g, 0.095 mmol) and Et_3N (40 μL) in 15 mL of DMF. The reaction was stirred at room temperature for 30 min and a solution of **4** (0.190 mmol, 0.296 g) in 10 mL of DMF was added. The reaction mixture was stirred at room temperature for 24 h and then evaporated to dryness. The resultant solid residue was dissolved in 10 mL of 70% methanol/H_2O, loaded on a preparative C_{18} reversed-phase LC column, and eluted with the same solvent mixture as used for loading the column. The fractions containing the product were evaporated to dryness to obtain **11a** in 30% yield, mp 285−290 °C. ^{1}H NMR (MeOH-d_4, 750 MHz): δ 0.44 (s, 4H); 0.85−2.7 (m, 138H); 2.85 (m, 5H); 3.15−3.8 (m, 88H); 3.87 (m, 3H); 4.05−4.2 (m, 6H); 4.3 (m, 3H); 4.45−4.7 (m, 10H); 6.03 (s, 2H); 6.27 (s, 2H); 6.56 (s, 2H); 7.11 (s, 2H); 7.25 (s, 2H); 7.54 (d, J = 7.5 Hz, 2H); 7.73 (d, J = 8.5 Hz, 2H); 8.39 (s, 3H). MS (ES) mass calcd for $C_{184}H_{274}N_{32}O_{41}Co_2P_2Sn$: 3887. Found: 3886 (M − H). IR (KBr): 3300, 3200, 2900, 1640, 1570, 1200, 1070.

Synthesis of 11b. The same procedure was used as described for the synthesis of **11a**, except 0.043 g (0.095 mmol) of **9b**, which was added in place of **9a**. The product was isolated in 26% yield, mp 215−218 °C (dec). ^{1}H NMR (MeOH-d_4, 750 MHz): δ 0.49 (s, 4H); 1.15−1.55 (m, 8H); 1.7−2.75 (m, 80H); 2.9 (m, 5H); 3.2−3.85 (m, 112H); 3.96 (m, 4H); 4.1−4.27 (m, 6H); 4.4 (m, 3H); 4.55−4.75 (m, 8H); 6.1 (s, 2H); 6.34 (s, 2H); 6.63 (s, 2H); 7.18 (s, 2H); 7.31 (s, 2H); 7.6 (d, J = 8.0 Hz, 2H); 7.87 (d, J = 8.5 Hz, 2H); 8.45 (s, 3H). MS (ES) mass calcd for $C_{172}H_{247}N_{32}O_{41}Co_2P_2I$: 3724. Found: 3723 (M − H). IR (KBr): 3300, 3200, 2900, 1640, 1570, 1200, 1070.

Synthesis of CN-Cbl-*p*-[^{125}I]Iodobenzamide Derivatives [^{125}I]6b, [^{125}I]8b, and [^{125}I]11b. *Purification of **6a**, **8a**, and **11a** by HPLC.* A saturated solution of a CN-Cbl derivative was prepared in methanol. This solution was passed through a 45 μm filter and three to five 20 μL aliquots were injected on the HPLC (C_{18} column). The product peak from each injection was collected, and the collected fractions were combined. The concentration of the cobalamin derivative in the combined fractions was calculated from the UV absorbance at 360 nm. The cobalamin-containing solution was then divided into aliquots containing 0.5 mg each, dried under a stream of argon, and stored at 4 °C.

*Preparation of nca [^{125}I]**6b***. The HPLC-purified **6a** was dissolved in methanol at a concentration of 1 mg/mL and 50 μL of that solution was placed in a small vial. To the solution was added 1 μL (92 μCi) of Na[^{125}I]I in 0.1 N NaOH, followed by addition of 2 μL of 0.1 N HOAc. To the resulting solution was added 25 μL of a 1 mg/mL solution of NCS in MeOH. After 15 min, 25 μL of a 1.0 mg/mL solution of sodium metabisulfite in H_2O was added to quench the reaction. A total of 87 μCi in approximately 75 μL of solution was removed from the reaction vessel by syringe and injected on an HPLC column (PRP-1 column). The iodinated product was collected from the HPLC effluent (13.8 min), yielding 24 μCi (28%) of [^{125}I]**6b**. The radioiodinated product was evaluated by HPLC and stored at 4 °C.

*Preparation of nca [^{125}I]**8b***. A 3.5 μL (1.0 mCi) aliquot of Na[^{125}I]I in 0.1 N NaOH was added to 50 μL of a 1 mg/mL solution of **8a**, followed by the addition of 4.0 μL of 0.1 N HOAc. To the resulting solution was added 10 μL of a solution containing 1 mg/mL NCS in methanol. After 15 min, the entire reaction mixture (990 μCi) was drawn into a syringe and injected onto an HPLC column (PRP-1 column). The collected fraction (12.7 min) yielded 168 μCi (17%) of **8b**.

*Preparation of ca [^{125}I]**11b***. A 1 μL (253 μCi) aliquot of Na[^{125}I]I in 0.1 N NaOH was added to 50 μL of a 1 mg/mL solution of **11a**, followed by addition of 2 μL of 0.095 mg/mL solution of NaI. To the resulting solution was added 10 μL of solution containing 1 mg/mL NCS in methanol. After 15 min, the entire reaction mixture (245 μCi) was drawn into a syringe and injected onto an HPLC column (PRP-1). The collected fraction (13.5 min) yielded 103 μCi (42%) of **11b**.

Determination of Specific Activity of [^{125}I]6b and [^{125}I]11b. Specific activities of the [^{125}I]**6b** and [^{125}I]**11b** were determined by calculation (theoretical) and by TCII-binding assay. The calculation of specific activities was adjusted for time between preparation and when binding assays were run (45 days; 59% remaining) and adjusted for added NaI (ca reaction only).

In the TCII-binding assay, increasing amounts of radiolabeled CN-Cbl were incubated for 1 h with aliquots of human serum which had a predetermined Cbl-binding capacity. Protein bound and free radiolabeled compound were separated by adsorption of unbound radiolabeled CN-Cbl to hemoglobin-coated charcoal. The cpm for saturation of TCII with radiolabeled CN-Cbl provided cpm per picogram of compound. The cpm were corrected for efficiency of the counter (80%), and the values were converted into microcurie to obtain a specific activity in microcurie per microgram.

Binding of CN-Cbl-[^{125}I]iodobenzoate Derivatives with Recombinant Human Transcobalamin II (rhTCII). rhTCII was produced and partially purified as previously reported (*24*). The rhTCII was diluted in 0.025% HSA/PBS/0.1% Triton x-100 to bind approximately 1 pmol of CN-Cbl/100 μL. The [^{125}I]**6b** and [^{125}I]-**11b** were diluted respectively to 100 000 and 60 000 cpm/mL in 0.05% HSA/PBS/0.1% Triton x-100. The binding of **6b** and **11b** to rhTCII was measured in a competitive binding assay in which 100 μL of each ^{125}I-labeled or ^{57}Co-labeled CN-Cbl was mixed with 0.1−8 pmol of unlabeled CN-Cbl, followed by addition of 100 μL of rhTCII solution to each tube. The volume was adjusted to 1 mL with PBS and incubated for 1 h at room temperature. The protein-bound fraction was determined by adsorption of the free fraction to hemoglobin-coated charcoal (2.5% charcoal/0.25% hemoglobin in PBS). The amount of compound bound as a function of concentration in the reaction was calculated and plotted.

Size-Exclusion Chromatography of ^{125}I-Labeled 6b and 11b Bound to rhTCII. The quantities of 1 pmol of [^{125}I]**6b** and 2 pmol of [^{125}I]**11b** were separately incubated for 1 h at room temperature with a 10-fold molar excess of rhTCII in a 0.75 mL solution containing 20 mM tris/200 mM NaCl/0.1% Triton x-100. Blue dextran (0.25 mL, 10 mg/mL) was added to each sample to mark the void volume of the column. The sample was layered on a 1.5 × 90 cm Sephacryl S-200 column. The column was equilibrated and eluted in the same buffer at a flow rate of 1 mL/min, and 2 mL fractions were collected. The radioactivity in each fraction was determined in a gamma counter, and the elution profile of TCII-bound compound was plotted.

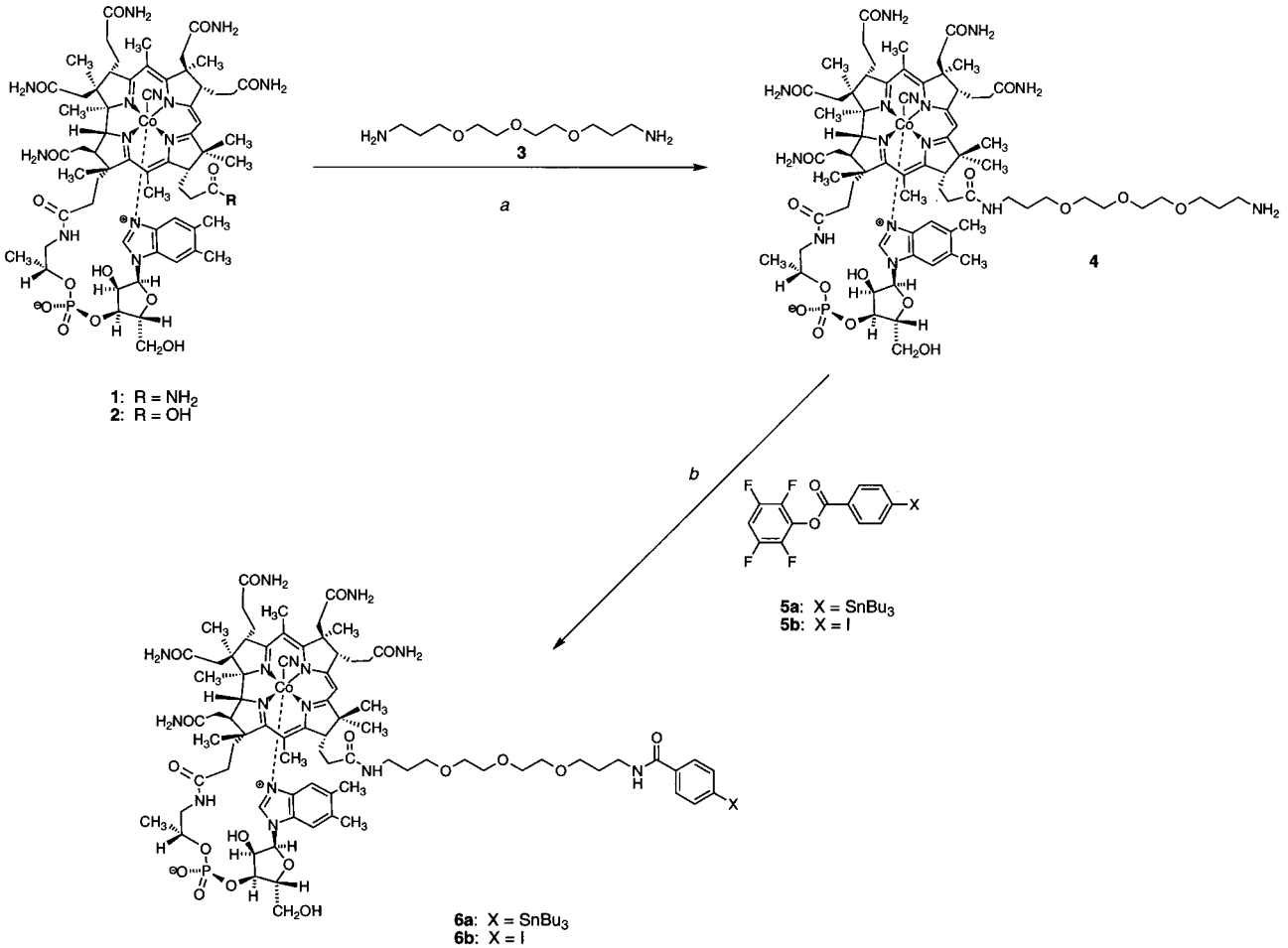
RESULTS

Synthesis of CN-Cbl Conjugates. The CN-Cbl corrin ring *e*-carboxylate, **2**, was obtained by preparative LC separation of the mixture of CN-Cbl monocarboxylic acids produced by acid hydrolysis of CN-Cbl, **1** (*20*). The isolated CN-Cbl-*e*-carboxylate, **2**, was conjugated with 4,7,10-trioxa-1,13-tridecandiamine, **3**, by reaction with a carbodiimide (EDC) in water containing NaCN/NHS to yield compound **4** as shown in Scheme 1. The stannylbenzoate conjugate, **6a**, and iodobenzoate conjugate, **6b**, were prepared by the reaction of **4** with either the TFP ester of *p*-tri-*n*-butylstannylbenzoic acid, **5a**, or the TFP ester of *p*-iodobenzoic acid, **5b**. Compounds **6a** and **6b** were isolated pure from the conjugation reaction in 42 and 35% yield, respectively.

The approaches taken to synthesize the hydrophilic CN-Cbl dimers are shown in Schemes 2 and 3. As in previous syntheses of CN-Cbl dimers (*21*), each synthesis utilized a trifunctional cross-linking reagent to couple two CN-Cbl moieties. In one synthesis (Scheme 2), the reagent used to cross-link the two CN-Cbl moieties contained an arylstannane or aryliodide moiety such that the CN-Cbl dimer could be formed in one step. Thus, reaction of **4** with either the di-TFP ester of *p*-(tri-*n*-butylstannyl)benzoylaminoisophthalate, **7a**, or the di-TFP ester of *p*-iodobenzoyl-aminoisophthalate, **7b**, provided the desired CN-Cbl dimers, **8a** and **8b** in 43 and 45% yields, respectively, after purification. The requisite aminoisophthaloyl derivative, **7b**, was prepared by conjugation of *p*-iodobenzoyl chloride with 5-aminoisophthalic acid followed by preparation of the di-TFP ester using EDC and TFP−OH in ethyl acetate (*21*). Conversion of the aryl iodide, **7b**, into the aryl stannane, **7a**, was accomplished in 62% yield using bis(tributyl)tin and palladium catalyst.

The synthesis of the second set of CN-Cbl dimers, **11a** and **11b**, was accomplished by the reaction shown in Scheme 3. In a stepwise manner, 1 equiv of either the trioxatridecanediamine-conjugated arylstannane, **9a**, or

Scheme 1. Synthetic Route Used to Prepare CN−Cbl Conjugates 6a and 6b



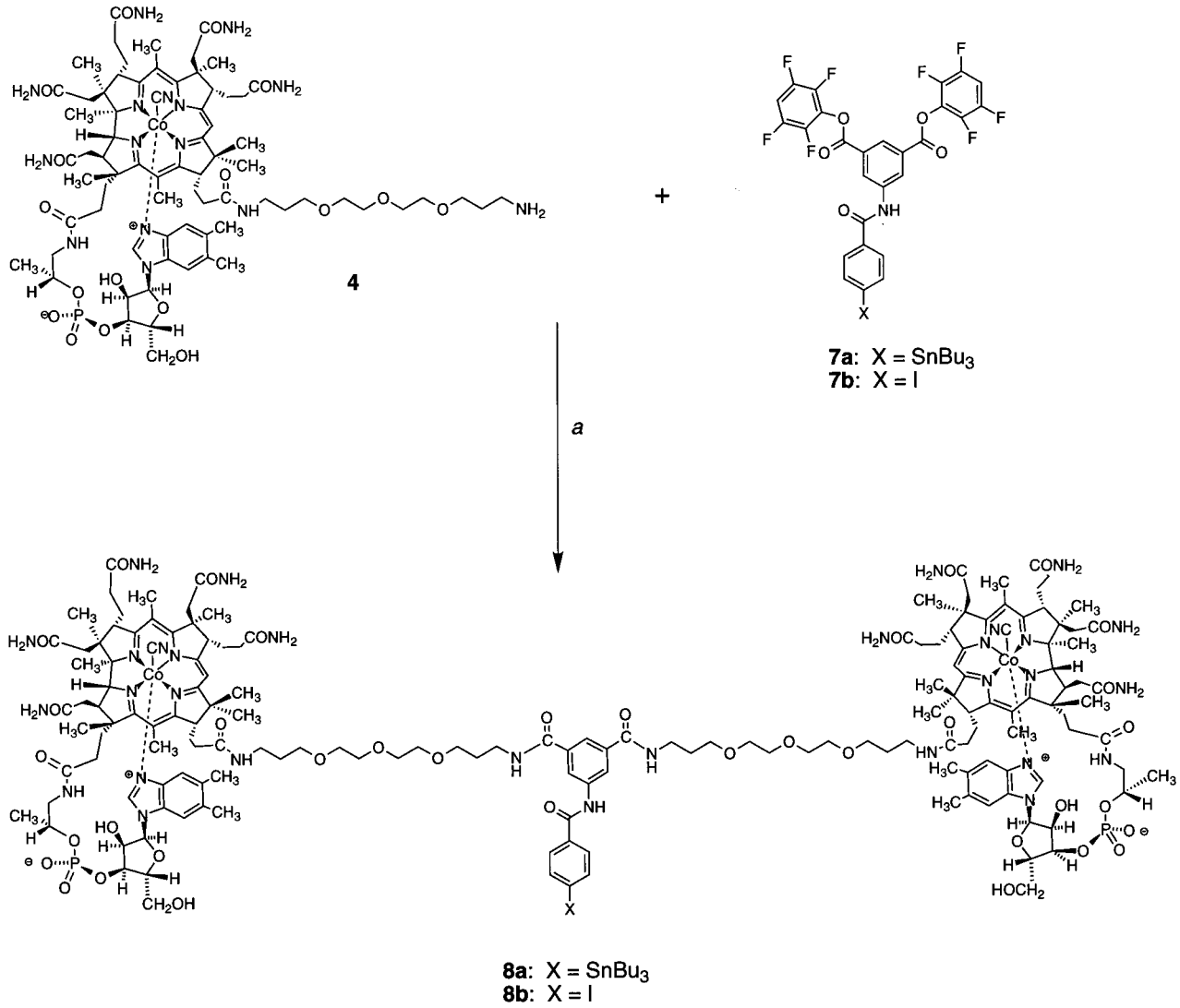
[a] NHS/NaCN/H_2O/**3**/HCl/EDC/rt/4 days. [b] DMF/Et_3N/**5a** or **5b**/rt/2 h

aryliodide, **9b**, was reacted with the tri-TFP ester of benzenetricarboxylic acid, **10**, followed by addition of 2 equiv of the trioxatridecanediamine adduct of CN-Cbl-*e*-carboxylate, **4**. The progress of the reaction after each addition was followed by HPLC analysis. Preparation of **9a** and **9b** was accomplished by reaction of the TFP ester of *p*-tri-*n*-butylstannylbenzoic acid or the TFP ester of *p*-iodobenzoic acid with trioxatridecanediamine, **3**, as previously described (*23*). Following this procedure, and purification by HPLC, the CN-Cbl dimers **11a** and **11b** were obtained in 30 and 26% yields, respectively.

Iodination Reactions. Although the isolated arylstannanes **6a**, **8a**, and **11a** were >95% pure by HPLC analysis, the starting material was further purified by preparative HPLC prior to radioiodination to ensure that reactive minor impurities would not compete in *nca*-radioiodinations. Initial radioiodination of **6a** was carried out in MeOH employing NCS/Na[^{125}I]I. The HPLC retention time for the new radioiodinated species indicated that the arylstannane was not substituted by iodine, suggesting that the radioiodide may have undergone another reaction, such as displacement of the cyano group on the cobalt. Radioiodination in aqueous 1% AcOH provided the desired radioiodinated product, but the yield was low (20−30%), and an additional radioiodinated species which was similar in lipophilicity to the starting arylstannane was also formed. Addition of just enough HOAc to neutralize the NaOH in the added Na[^{125}I]I gave only the desired radioiodinated product, albeit again in low yields (17−42%). Although there are a number of possible causes for the low radiochemical yields, one explanation for the low yields is that recovery of the radioiodinated compound from the HPLC column did not reflect the actual yields. This statement is made since it was observed that a large proportion of the radioactivity was retained on the HPLC column even after extended elution times. Radioiodination of **11a** under the same conditions as used to prepare [^{125}I]**6b** and [^{125}I]**8b** failed to give the desired *nca* product, [^{125}I]**11b**. However, when the reaction was carried out with a small quantity of carrier NaI, the radioiodinated ca product was obtained in 42% yield. The in vitro stability of [^{125}I]**6b**, [^{125}I]**8b** (*20*), and [^{125}I]**11b** was evaluated by reexamining the radioiodinated CN-Cbl conjugates after storage at 4 °C for over 3 months. Radiochromatographic peaks of the isolated products were unchanged (peak areas were corrected for decay) after storage for 1 h, 24 h, and 3 months.

Specific activities for [^{125}I]**6b** and [^{125}I]**11b** were estimated by calculation and by measurement of the quantity of radioactivity that it takes to saturate TCII in serum which has a known binding capacity for CN-Cbl. The specific activity value for [^{125}I]**6b** obtained by calculation is 720 μCi/μg and that obtained by the binding assay was 625 μCi/μg. These numbers are very close, but the lower specific activity measured by binding is most likely closer to the actual value as one would expect some decrease in specific activity (from theoretical) due to the introduction of stable iodide in solvents and reagents. The specific activity for the carrier added [^{125}I]**11b** was calculated to be 12 μCi/μg. In contrast, the specific activity measured by TCII binding in serum was 38 μCi/μg. It is not known why there is a 3 times difference in these numbers, but

Scheme 2. Synthetic Route Used to Prepare CN-Cbl Conjugates 8a and 8b



[a] 2 equiv of **4**/DMF/Et_3N/**7a** or **7b**/rt/3 h.

they are fairly close considering the two different methods of obtaining them.

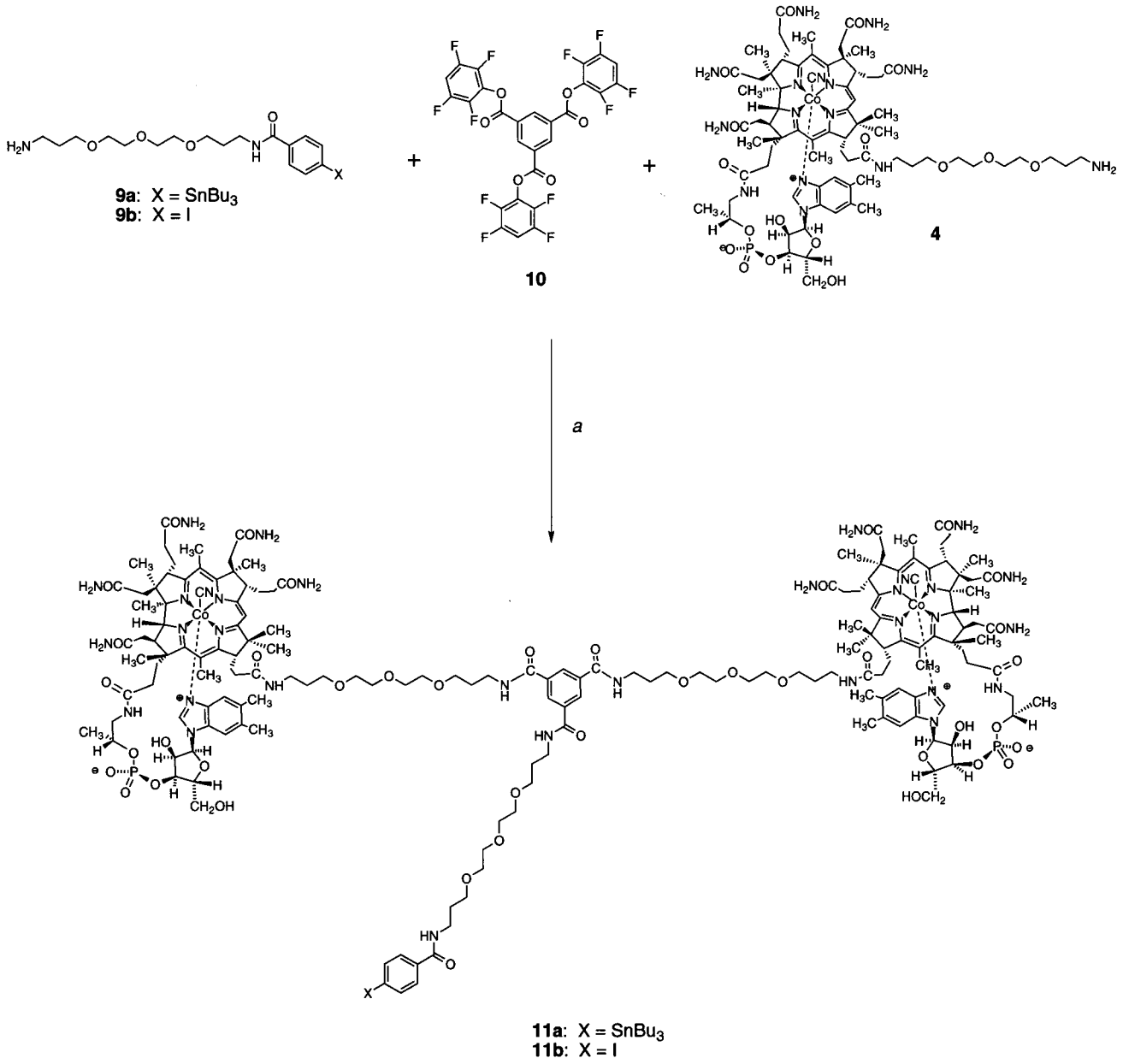
Competitive Binding with rhTCII. The CN-Cbl monomer [^{125}I]**6b** and CN-Cbl dimer [^{125}I]**11b** were evaluated for their competitive binding to (partially purified) rhTCII relative to CN-Cbl. The assay was set up such that a quantity of rhTCII that would bind approximately 1 pmol of [^{57}Co]CN-Cbl was used in each evaluation. Trace quantities of [^{57}Co]CN-Cbl, [^{125}I]**6b**, or [^{125}I]**11b** were mixed with 0.1−8 pmol of unlabeled CN-Cbl, then mixed with rhTCII. The percent radioactivity bound relative to the picomoles of unlabeled CN-Cbl was measured. The results obtained are provided in Figure 1 and show that the binding of radioiodinated monomer **6b** as well as the dimer **11b** to rhTCII is essentially unaltered and is similar to that of CN-Cbl. The initial flat portion of the graph representing 100% binding is due to having less than saturating quantities CN-Cbl present.

Evaluation of [^{125}I]6b and [^{125}I]11b Binding to rhTCII. A 1 pmol quantity of monomer [^{125}I]**6b** and 2 pmol of dimer [^{125}I]**11b** were incubated with 10-fold molar excess of rhTCII at room temperature, and the resulting adducts were examined by size-exclusion gel chromatography (Sephacryl S-200). Fractions were collected from the column and the radioactivity in each fraction was determined. The elution profile of the binding of [^{125}I]-**6b**, [^{125}I]**11b**, and [^{57}Co]CN-Cbl with rhTCII is plotted in Figure 2. The [^{57}Co]CN-Cbl, the [^{125}I]**6b** monomer, and approximately 70% of the[^{125}I]**11b** dimer eluted from the column as a single peak corresponding to ∼40 kDa, the size of the monomeric rhTCII. A second peak of ∼80 kDa was only observed with the dimer **11b** and accounted for ∼30% of the rhTCII-bound radiolabel.

DISCUSSION

This investigation was undertaken because our previous attempts to synthesize radioiodinated CN-Cbl derivatives produced compounds that were not optimal for our needs due to their poor solubility in aqueous medium and their propensity to adhere to glass and metal (needle) surfaces. Furthermore, we were unsuccessful in preparing a radioiodinated CN-Cbl dimer. Although the cause of the nonspecific binding is uncertain, we thought that this property could be due, at least in part, to the hydrophobic linker molecule, 1,12-diaminododecane. It was apparent that the hydrophobic linker made the CN-Cbl conjugates very lipophilic and resulted in their having low water solubility. Also, NMR data from the CN-Cbl dimers suggested that the tri-*n*-butylstannylbenzoate moiety was affected by the lipophilic nature of the linker, perhaps resulting in shielding it from reacting

Scheme 3. Synthetic Route Used to Prepare CN-Cbl Conjugates 11a and 11b



[a] **9a** or **9b**/DMF/Et_3N/rt/30 min; 2 equiv **4**/rt/24 h

with radioiodination reagents. Therefore, we reasoned that using a more hydrophilic linker might provide CN-Cbl derivatives with more favorable characteristics.

We have previously used the ether-containing linker 4,7,10-trioxa-1,13-tridecandiamine to increase water solubility of biotin derivatives (*23*, *25*) and CN-Cbl dimers (*21*). This linker increases the solubility of the compound greatly over that of an aliphatic linker moiety. Accordingly, we observed a marked improvement in water solubility of the radioiodinated CN-Cbl derivatives and found that, in contrast to the more aliphatic CN-Cbl derivatives, these compounds did not adhere to glass or metal (syringe needle) surfaces. Previously prepared CN-Cbl dimers which were cross-linked using aliphatic diaminododecane linkers required dissolution in DMSO and dilution with water (2−10% DMSO solutions) to prepare 1 mg/mL solutions. In contrast, 1 mg of **8b** or **11b** was found to be soluble in only 10 μL of water, indicating that the compounds have a solubility of >100 mg/mL. The reason for including three trioxatridecanediamine linkers in the CN-Cbl dimer **11b** was primarily to evaluate whether providing a greater distance between the arylstannane moiety and the cross-linking aminoisophthalate moiety would improve the radiochemical yield. Unfortunately, it appears to have done just the opposite as no radioiodinated product was obtained when the reaction was conducted under *nca* conditions. Despite this, we have been successful in obtaining radioiodinated CN-Cbl dimers, and the new radioiodinated CN-Cbl conjugates can be formulated in aqueous solution without difficulty.

To date there have been few evaluations to determine the in vitro and in vivo characteristics of the radioiodinated CN-Cbl derivatives. As in our previous studies, comparison of the binding of the corrin ring *e*-carboxylate conjugates (Figure 1) indicate that their binding with rhTCII is similar to that of unaltered CN-Cbl. It is interesting to note that the CN-Cbl monomer [^{125}I]**6b** binds with a slightly lower avidity than CN-Cbl, but binding of [^{125}I]**11b** appears to be essentially equivalent to CN-Cbl. The CN-Cbl dimers were designed to bind with two rhTCII moieties, which in turn may alter

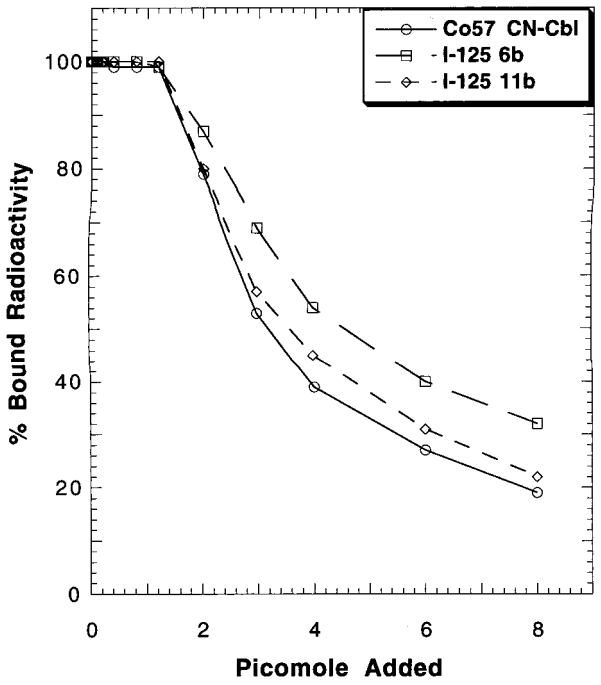


Figure 1. Competitive binding curves for [^{57}Co]CN-Cbl, **1**, and iodobenzoyl-CN-Cbl derivatives, **6b** and **11b**, with rhTCII. [^{57}Co]CN-Cbl (0.01 pmol) was mixed with increasing concentrations of **1** or Cbl derivatives **6b** or **11b**. Diluted rhTCII (100 μL) with a binding capacity of approximately 1 pmol of **1** was then added to each tube. The volume was adjusted to 1 mL with PBS and incubated at room temperature for 1 h. Free and protein bound radioactivity was separated by adsorption to hemoglobin coated charcoal, and the radioactivity in each fraction was determined and plotted.

binding with the cell surface receptor for TCII−Cbl. We hypothesized that CN-Cbl dimer cross-linked with the aminoisophthalate moiety and two trioxatridecanediamine linkers would have adequate space between the two CN-Cbl moieties (41 Å linker, fully extended) to permit binding with two rhTCII molecules. In this study, the question of whether the CN-Cbl dimer can bind with two rhTCII molecules was addressed successfully for the first time. The results obtained by size-exclusion separation of complexes formed with the CN-Cbl monomer **6b** and the CN-Cbl dimer **11b** (Figure 2) appear to indicate that at least a fraction of the CN-Cbl dimer binds with two rhTCII molecules. Additional studies need to be conducted to determine if what appears to be an equilibrium mixture can be shifted to having mostly two TCII bound and to determine if there is a difference in binding affinity between the first TCII bound and the second TCII bound. It also remains to be determined if the two TCII molecules bound to the same CN-Cbl dimer can interact with two TCII-receptors on the cell surface, and if this should occur, what effect it would have on TCII−Cbl internalization.

Summary. Three CN-Cbl conjugates containing arylstannane moieties for radioiodination have been synthesized. Use of the hydrophilic linker molecule, 4,7,-10-trioxa-1,13-tridecandiamine, in the place of 1,12-diaminododedane that was previously employed, resulted in radioiodinated CN-Cbl derivatives that are water soluble and do not have the propensity to adhere to glass and metal surfaces. From our earlier studies, it was demonstrated that the corrin ring *e*-monocarboxylate isomer bound more tightly with TCII than the other regioisomers. Therefore, in this investigation we used only *e*-carboxylate isomer. One Cbl monomer and two Cbl dimers were prepared using conjugates of CN-Cbl-*e*-carboxylate and the hydrophilic linker trioxatridecanediamine. Arylstannane CN-Cbl conjugates were prepared as reactive compounds for site-specific radioiodination, and the corresponding aryliodides were prepared as HPLC standards. Following the syntheses, attempts to develop optimal conditions for radioiodination of CN-Cbl-arylstannane conjugates were fraught with difficulties. In our earlier investigation we showed that good radiochemical yields (40−65%) could be obtained under neutral reaction conditions. In this study, the radiochemical yields ranged 17−42%. High specific activity was obtained in radioiodination of CN-Cbl monomer **6b** and CN-Cbl dimer **8b**. Radioiodination of dimer **11b** with *nca* radioiodine failed, but ca radioiodination was successful. The binding of radioiodinated CN-Cbl derivatives to rhTCII was similar to that observed with unmodified CN-Cbl. The results obtained indicate that the dimer of CN-

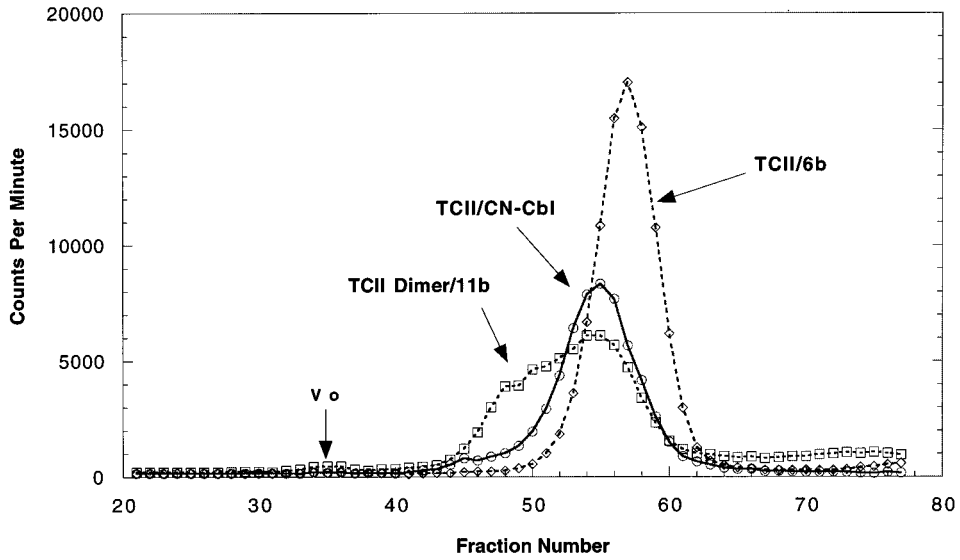


Figure 2. Elution profile of radioactivity in fractions from size exclusion chromatography of [^{57}Co]CN-Cbl, [^{125}I]**6b**, and [^{125}I]**11b** bound to rhTCII. In the experiment, 1 pmol of [^{125}I]**6b** and 2 pmol of [^{125}I]**11b** were each incubated with a 10-fold molar excess rhTCII for 1 h at room temperature. Blue dextran (0.25 mL, 10 mg/mL) was added to each sample to mark the void volume for the column. The sample was layered on a 1.5 × 90 cm Sephacryl S-200 column. The column was equilibrated and eluted in the same buffer at a flow rate of 1 mL/min and 2 mL fractions were collected. The radioactivity in each fraction was determined and plotted.

Cbl **11b** binds more avidly with rhTCII than the monomer of CN-Cbl, **6b**, and its binding affinity is essentially equivalent to that of CN-Cbl. Size-exclusion chromatographic analysis of [^{125}I]**11b** binding with TCII indicated that approximately 30% bound with two TCII molecules.

ACKNOWLEDGMENT

We thank Dr. Ross Lawrence (Medicinal Chemistry Department, University of Washington) for efforts in obtaining mass spectral data. This work was supported in part by the Department of Radiation Oncology at the University of Washington and by an NIH grant (DK 28561) to S.P.R.

Supporting Information Available: HPLC chromatograms, 1H NMR, and mass spectra for CN-Cbl derivatives **6a**, **6b**, **8a**, **8b**, **11a**, and **11b** are provided. This material is available free of charge via the Internet at http://pubs.acs.org.

LITERATURE CITED

(1) Banerjee, R. (1997) The Yin-Yang of Cobalamin Biochemistry. *Chem. Biol. 4*, 175−186.

(2) Roth, J. R., Lawrence, J. G., and Bobik, T. A. (1996) Cobalamin (Coenzyme B_{12}): Synthesis and Biological Significance. *Annu. Rev. Microbiol. 50*, 137−181.

(3) Wagner, A. F., and Folkers, K. (1964) Cyanocobalamin and the Cobamide Coenzymes. *Vitamins and Coenzymes*, pp 194−243, Interscience Publishers, New York.

(4) Ellenbogen, L. (1975) Absorption and Transport of Cobalamin. Intrinsic Factor and the Transcobalamins. In *Cobalamin. Biochemistry and Pathophysiology* (B. M. Babior, Ed.) pp 215−286, Wiley-Interscience, New York.

(5) Allen, R. H. (1975) Human Vitamin B_{12} Transport Proteins. *Prog. Hematol. 9*, 57−84.

(6) Seetharam, B. (1994) Gastrointestinal Absorption and Transport of Cobalamin (Vitamin B_{12}). In *Physiology of the Gastrointestinal Tract.* (L. R. Johnson, Ed.) pp 1997−2026, Raven Press, New York.

(7) Rothenberg, S. P., and Quadros, E. V. (1995) Transcobalamin II and the membrane receptor for the transcobalamin II-cobalamin complex. *Baillieres Clin. Haematol. 8*, 499−514.

(8) Nicolas, J. P., and Gueant, J. L. (1995) Gastric intrinsic factor and its receptor. *Baillieres Clin. Haematol. 8*, 515−531.

(9) Linnell, J. C. (1975) The Fate of Cobalamins in vivo. In *Cobalamin. Biochemistry and Pathophysiology* (B. M. Babior, Ed.) pp 287−333, Wiley-Interscience, New York.

(10) Mahoney, M. J., and Rosenberg, L. E. (1975) Inborn Errors of Cobalamin Metabolism. In *Cobalamin. Biochemistry and Pathophysiology* (B. M. Babior, Ed.) pp 369−402, Wiley-Interscience, New York.

(11) Beck, W. S. (1975) Metabolic Features of Cobalamin Deficiency in Man. In *Cobalamin. Biochemistry and Pathophysiology* (Babior, B. M., Ed.) pp 403−450, Wiley-Interscience, New York.

(12) Quadros, E. V., Jackson, B., Joffbrand, A. V., and Linnell, J. C. (1979) Interconversion of Cobalamins in Human Lymphocytes in Vitro and the Influence of Nitrous Oxide on Synthesis of Cobalamin Coenzymes. In *Vitamin B_{12}* (B. Zagalak and W. Friedrich, Eds.) pp 1045−1054, Walter de Gruyter & Co., Berlin.

(13) Smith, E. L., Hockenhull, D. J. D., and Quilter, A. R. J. (1952) Tracer Studies with the B_{12} Vitamins. *Biochem. J. 52*, 387−388.

(14) Maddock, A. G., and Coelho, F. P. (1954) The Retention of Cobalt-60 in Vitamin B_{12}. *J. Chem. Soc.* 4702−4704.

(15) Bradley, J. E., Smith, L. E., Baker, S. J., and Mollin, D. L. (1954) The use of the radioactive isotope of Cobalt Co^{58} for the preparation of labeled vitamin B_{12}. *Lancet 267*, 476−477.

(16) Smith, E. L., Fantes, K. H., Ball, S., Waller, J. G., Emery, W. B., Anslow, W. K., and Walker, A. D. (1952) B_{12} Vitamins (Cobalamins) 1. Vitamins B_{12c} and B_{12d}. *Biochem. J. 52*, 389−395.

(17) Toraya, T., Ohashi, K., Ueno, H., and Fukui, S. (1975) Preparation, Properties and Biological Activities of Succinyl Derivatives of Vitamin B_{12}. *Bioinorg. Chem. 4*, 245−255.

(18) Collins, D. A., and Hogenkamp, H. P. C. (1996) Synthesis and Biological Activity of Radiolabeled DTPA-Cobalamin Analogues. *J. Nucl. Med. 37*, 350P.

(19) Wilbur, D. S., Hamlin, D. K., Pathare, P. M., Heusser, S., Vessella, R. L., Buhler, K. R., Stray, J. E., Daniel, J., Quadros, E. V., McLoughlin, P., and Morgan, A. C. (1996) Synthesis and *nca*-radioiodination of arylstannylcobalamin conjugates. Evaluation of aryliodocobalamin conjugate binding to transcobalamin II and biodistribution in mice. *Bioconjugate Chem. 7*, 461−474.

(20) Pathare, P. M., Wilbur, D. S., Heusser, S., Quadros, E. V., McLoughlin, P., and Morgan, A. C. (1996) Synthesis of cobalamin-biotin conjugates that vary in the position of cobalamin coupling. Evaluation of cobalamin derivative binding to transcobalamin II. *Bioconjugate Chem. 7*, 217−232.

(21) Pathare, P. M., Wilbur, D. S., Hamlin, D. K., Heusser, S., Quadros, E. V., McLoughlin, P., and Morgan, A. C. (1997) Synthesis of cobalamin dimers using isophthalate crosslinking of corrin ring carboxylates and evaluation of their binding to transcobalamin II. *Bioconjugate Chem 8*, 161−172.

(22) Wilbur, D. S. (1992) Radiohalogenation of Proteins: An Overview of Radionuclides, Labeling Methods, and Reagents for Conjugate Labeling. *Bioconjugate Chem. 3*, 433−470.

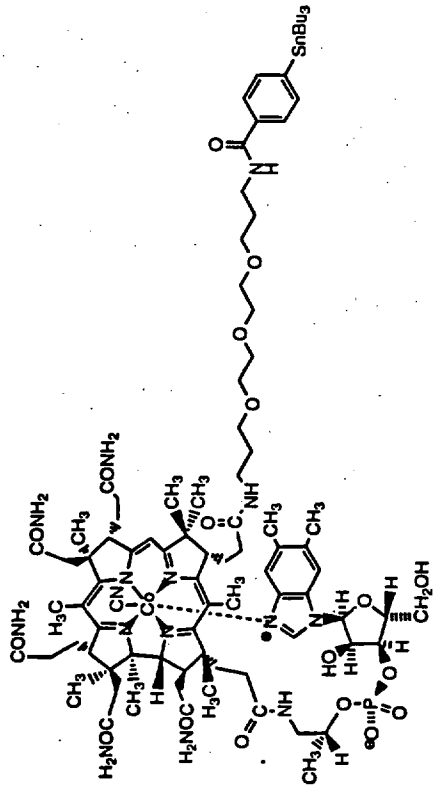
(23) Wilbur, D. S., Hamlin, D. K., Pathare, P. M., and Weerawarna, S. A. (1997) Biotin Reagents for Antibody Pretargeting. Synthesis, Radioiodination and In Vitro Evaluation of Water Soluble, Biotinidase Resistant Biotin Derivatives. *Bioconjugate Chem. 8*, 572−584.

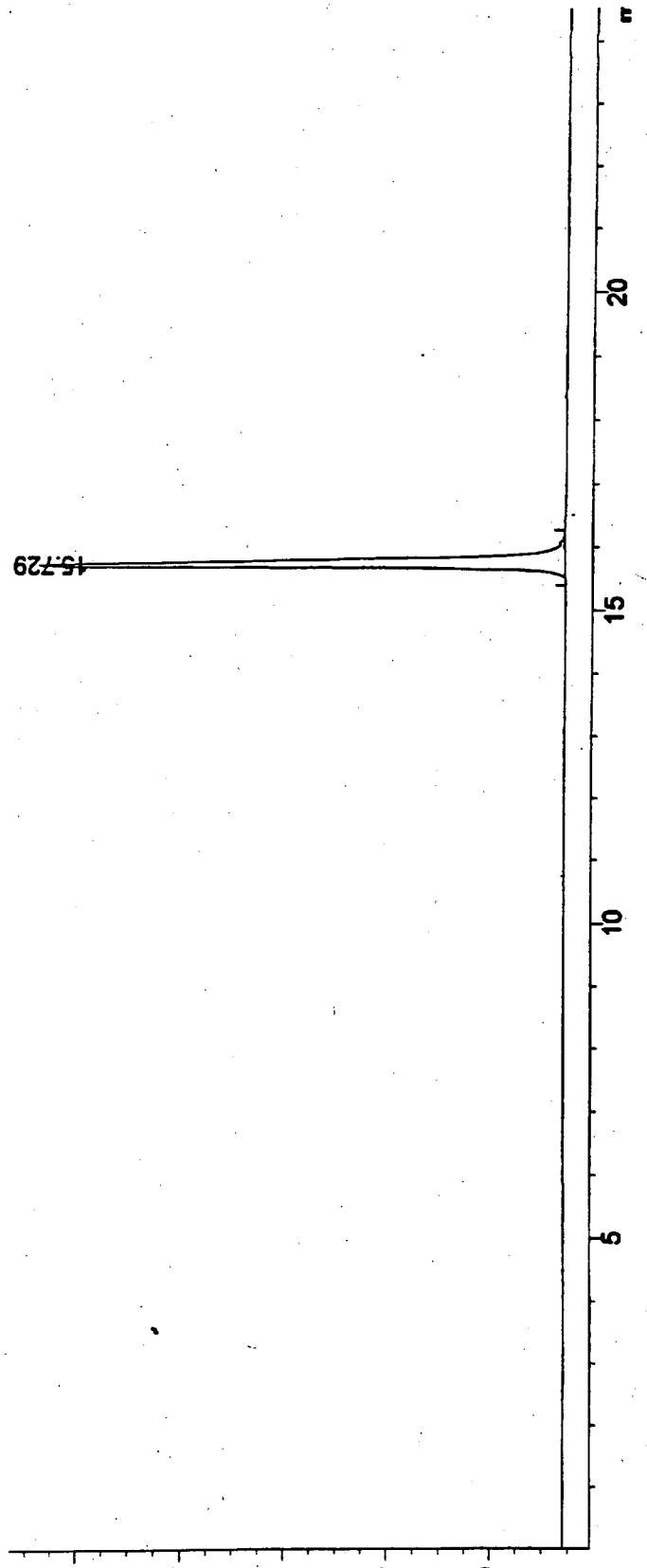
(24) Quadros, E. V., Sai, P., and Rothenberg, S. P. (1993) Functional Human Transcobalamin II Isoproteins Are Secreted by Insect Cells Using the baculovirus Expression System. *Blood 81*, 1239−1245.

(25) Wilbur, D. S., Hamlin, D. K., Pathare, P. M., and Weerawarna, S. A. (1997) Biotin Reagents for Antibody Pretargeting. 2. Synthesis and In Vitro Evaluation of Biotin Dimers and Trimers for Cross Linking of Streptavidin. *Bioconjugate Chem. 8*, 819−832.

BC9900340

© 1999 American Chemical Society, Bioconjugate Chem., Wilbur bc9900340 Supporting Info Page 1

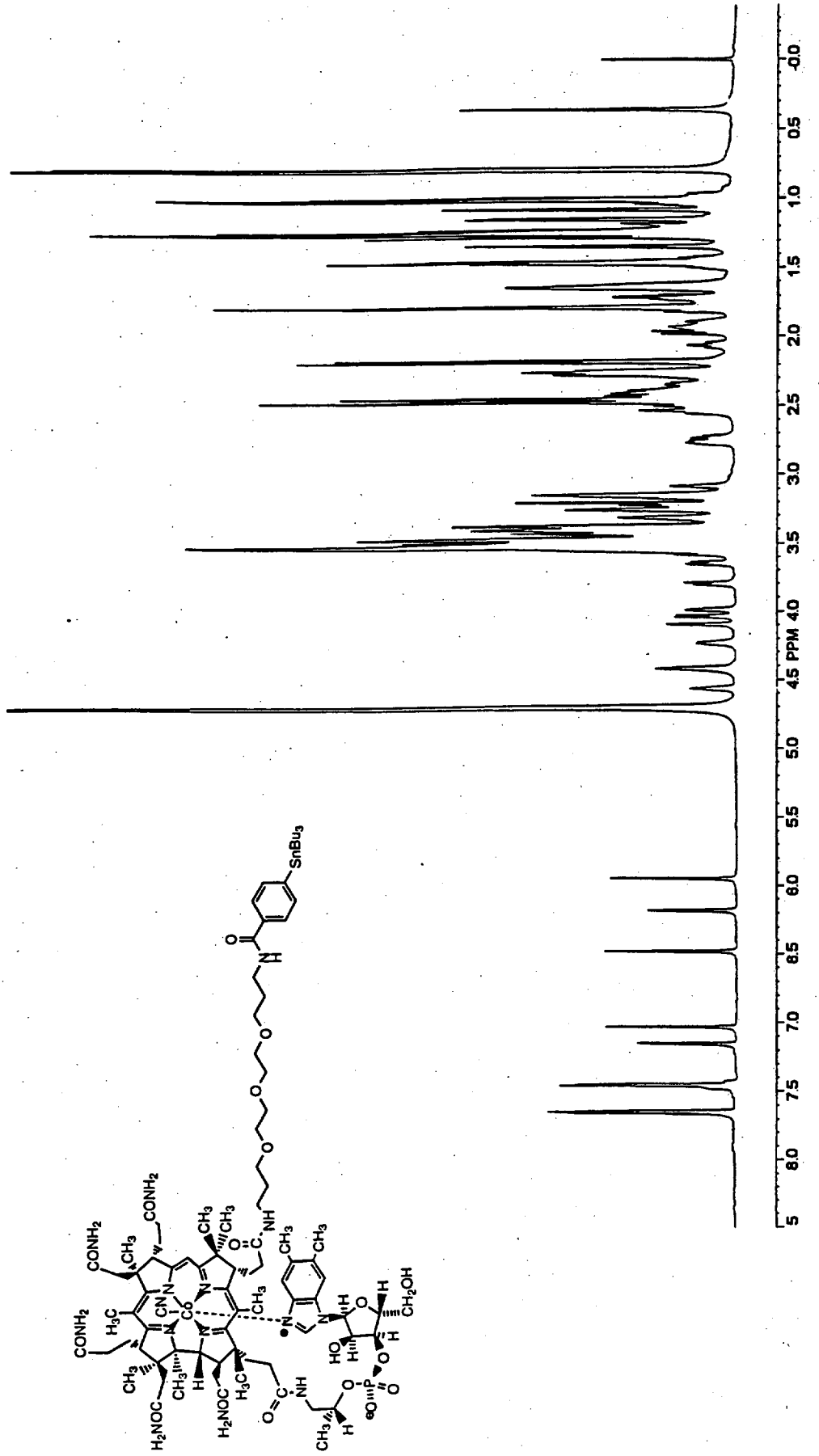




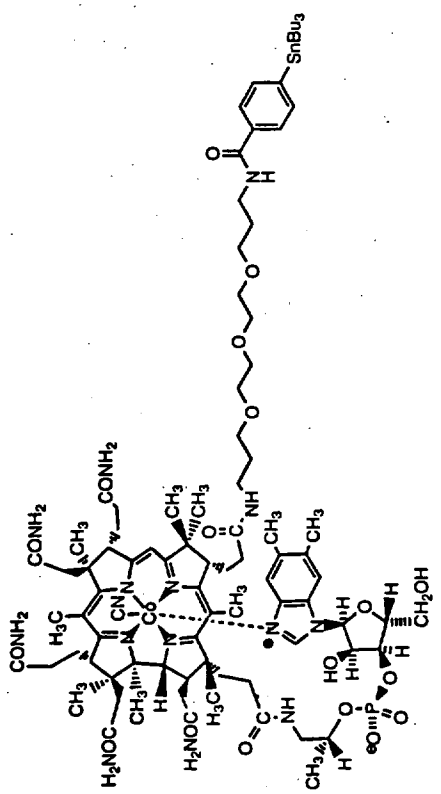
Analytical Reversed-Phase HPLC of 6a

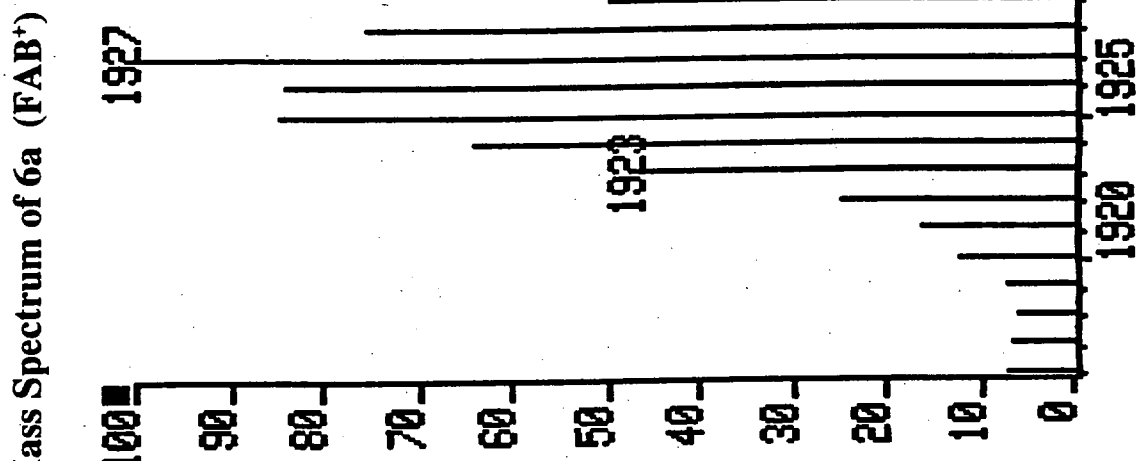
© 1999 American Chemical Society, Bioconjugate Chem., Wilbur bc9900340 Supporting Info Page 2

^{1}H NMR of 6a (750 MHz, MeOH-d_4)

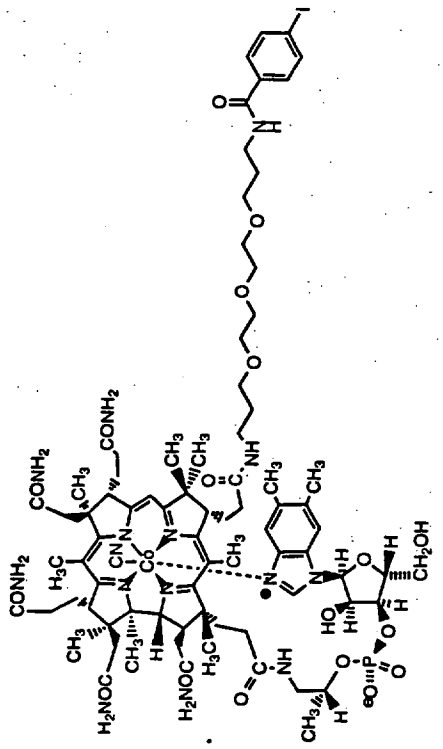


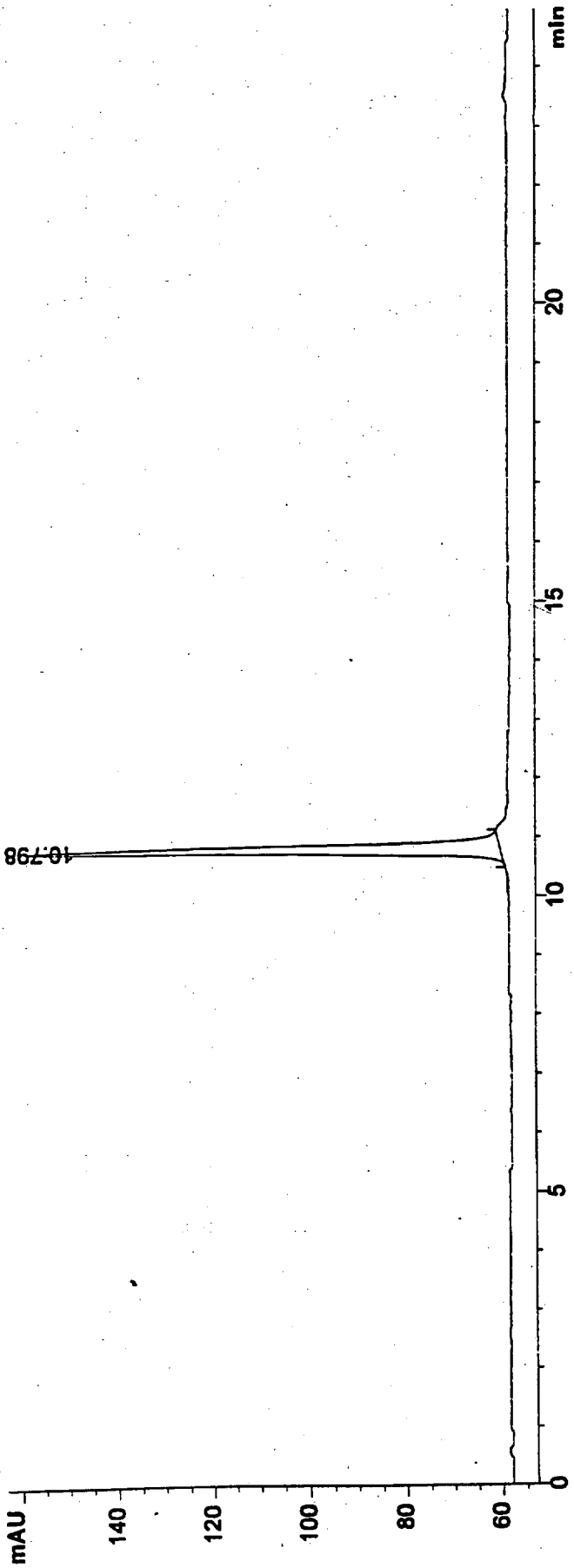
© 1999 American Chemical Society, Bioconjugate Chem., Wilbur bc9900340 Supporting Info Page 3





© 1999 American Chemical Society, Bioconjugate Chem., Wilbur bc9900340 Supporting Info Page 4

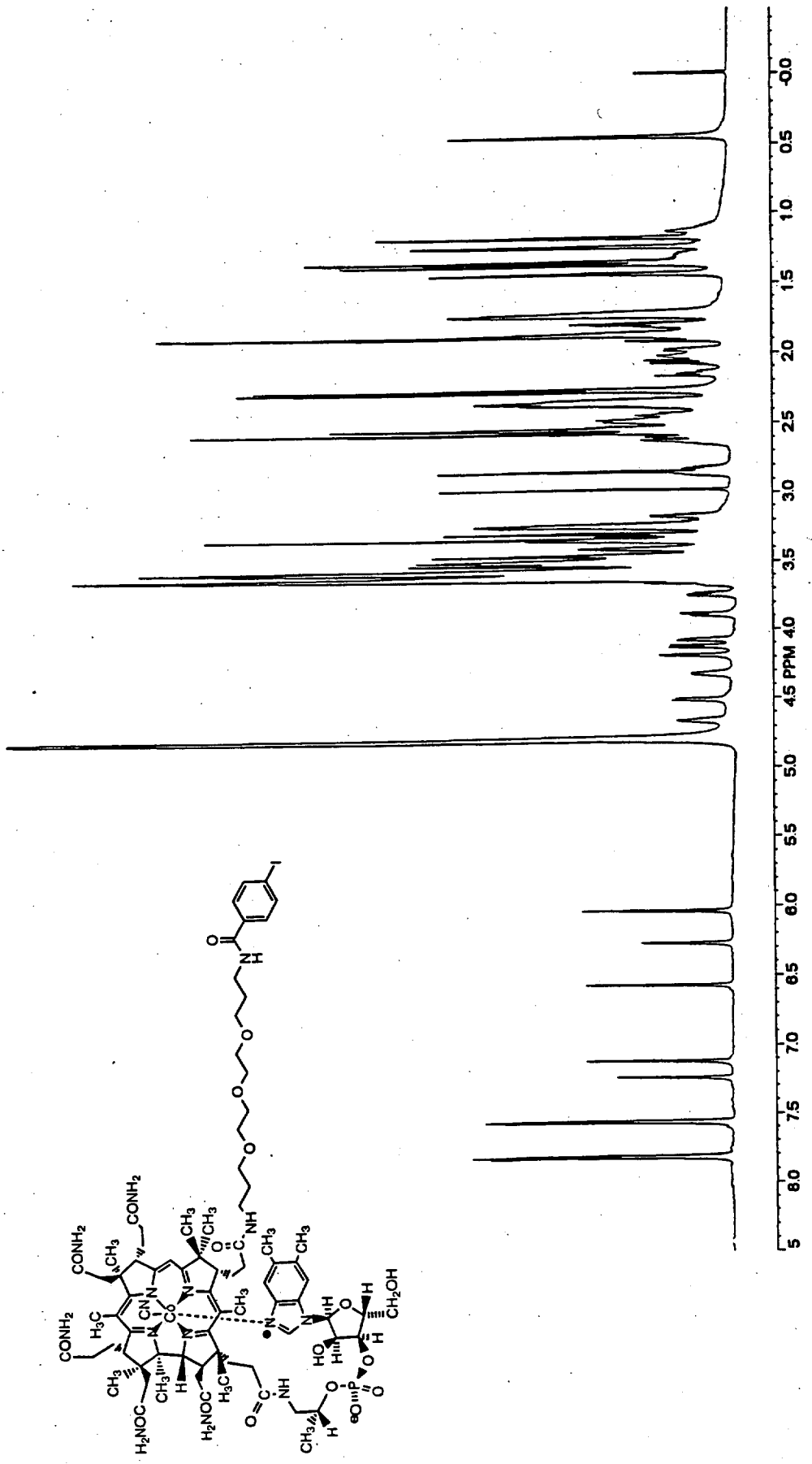




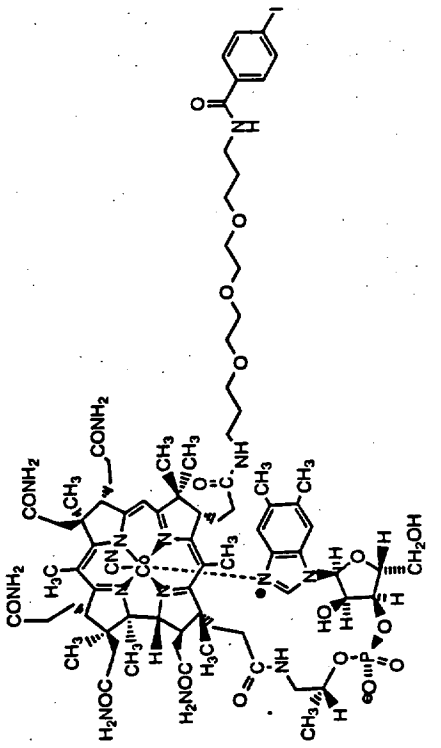
Analytical Reversed-Phase HPLC of 6b

© 1999 American Chemical Society, Bioconjugate Chem., Wilbur bc9900340 Supporting Info Page 5

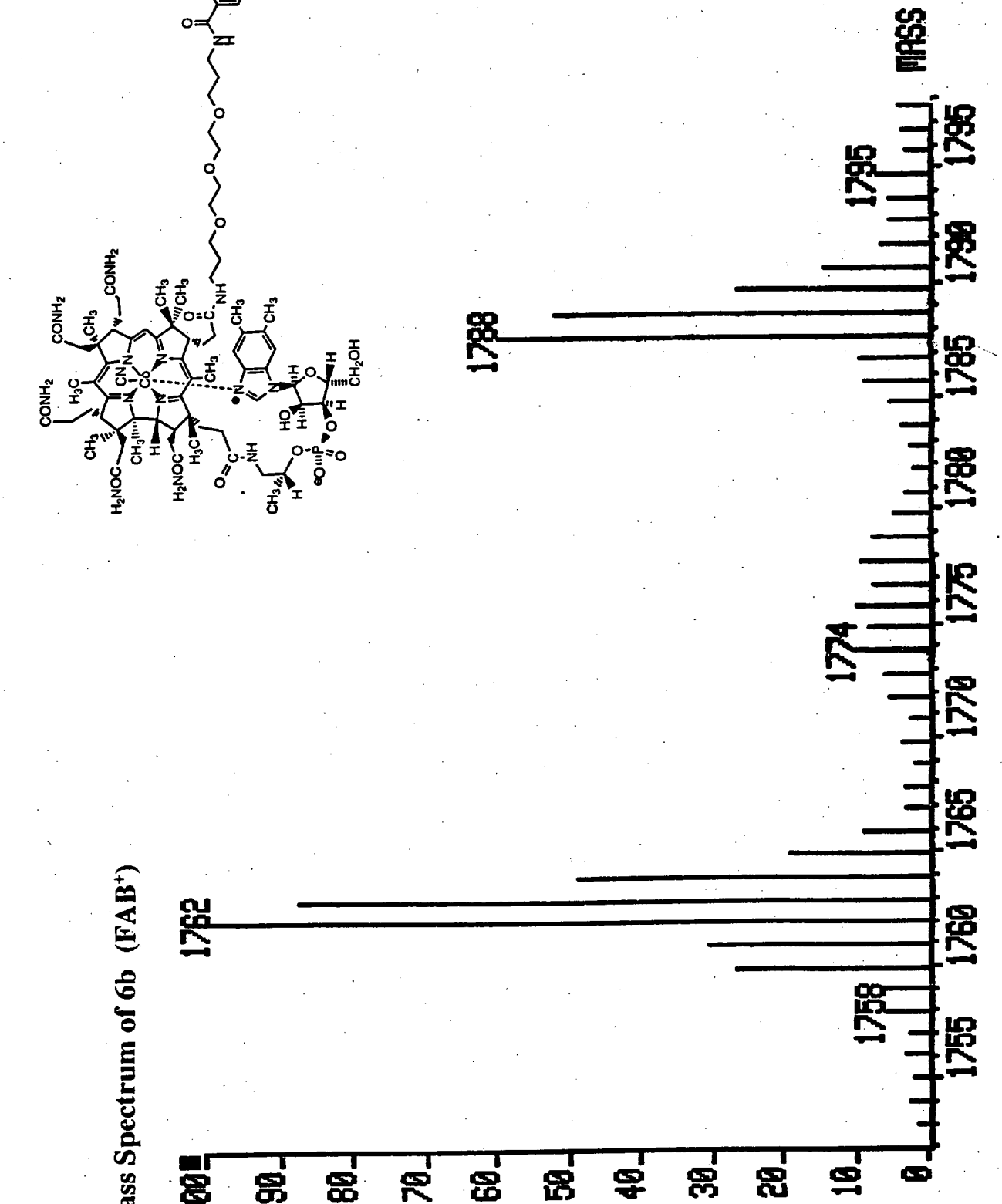
^{1}H NMR of 6b (750 MHz, MeOH-d_4)



© 1999 American Chemical Society, Bioconjugate Chem., Wilbur bc9900340 Supporting Info Page 6

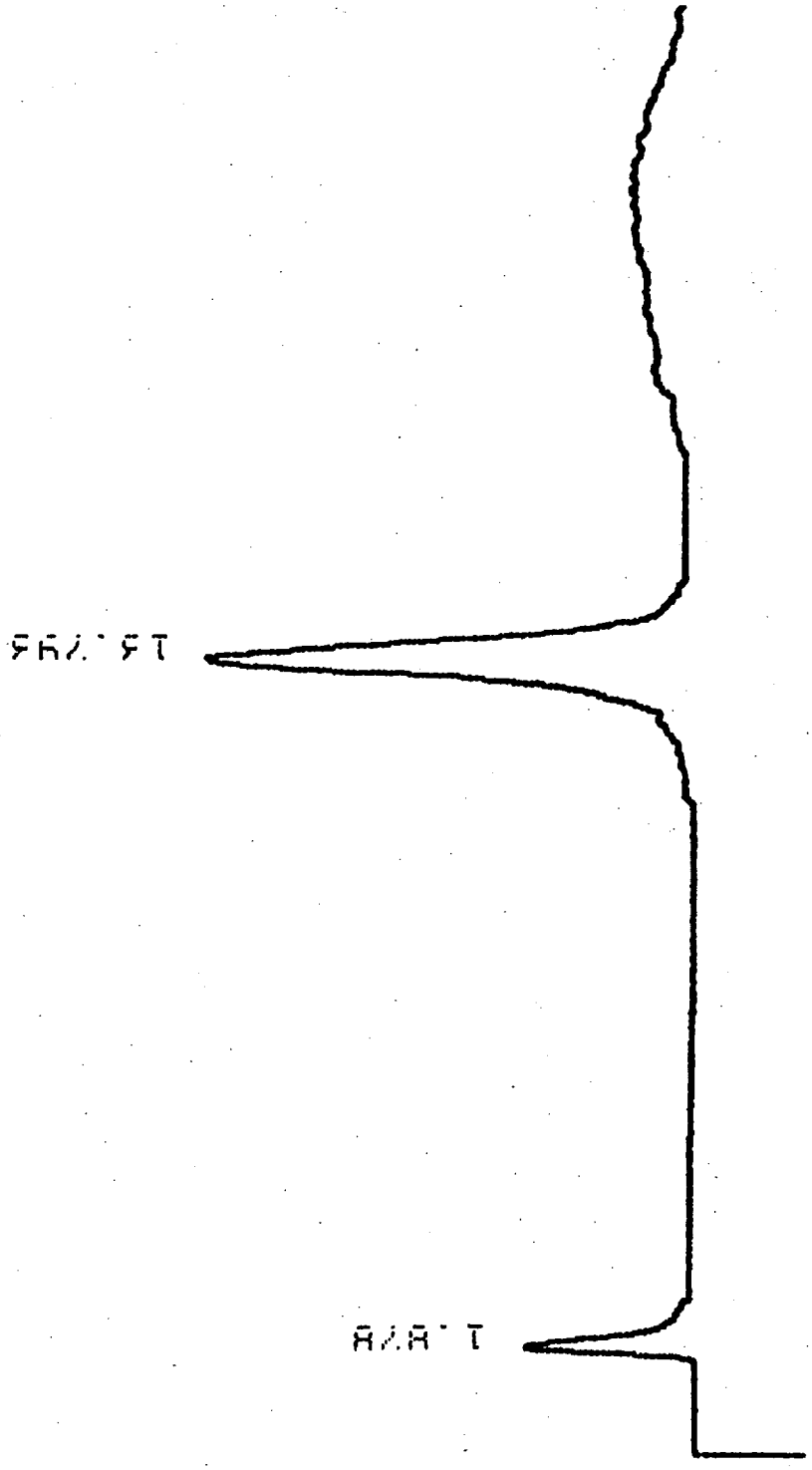


Mass Spectrum of 6b (FAB+)

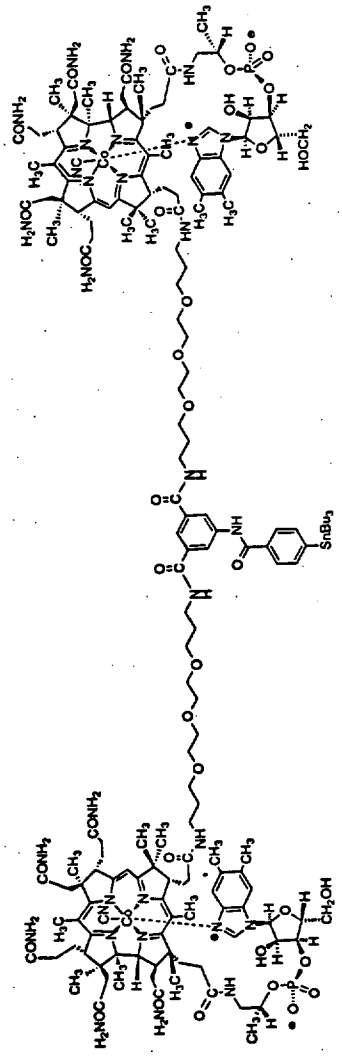


© 1999 American Chemical Society, Bioconjugate Chem., Wilbur bc9900340 Supporting Info Page 7

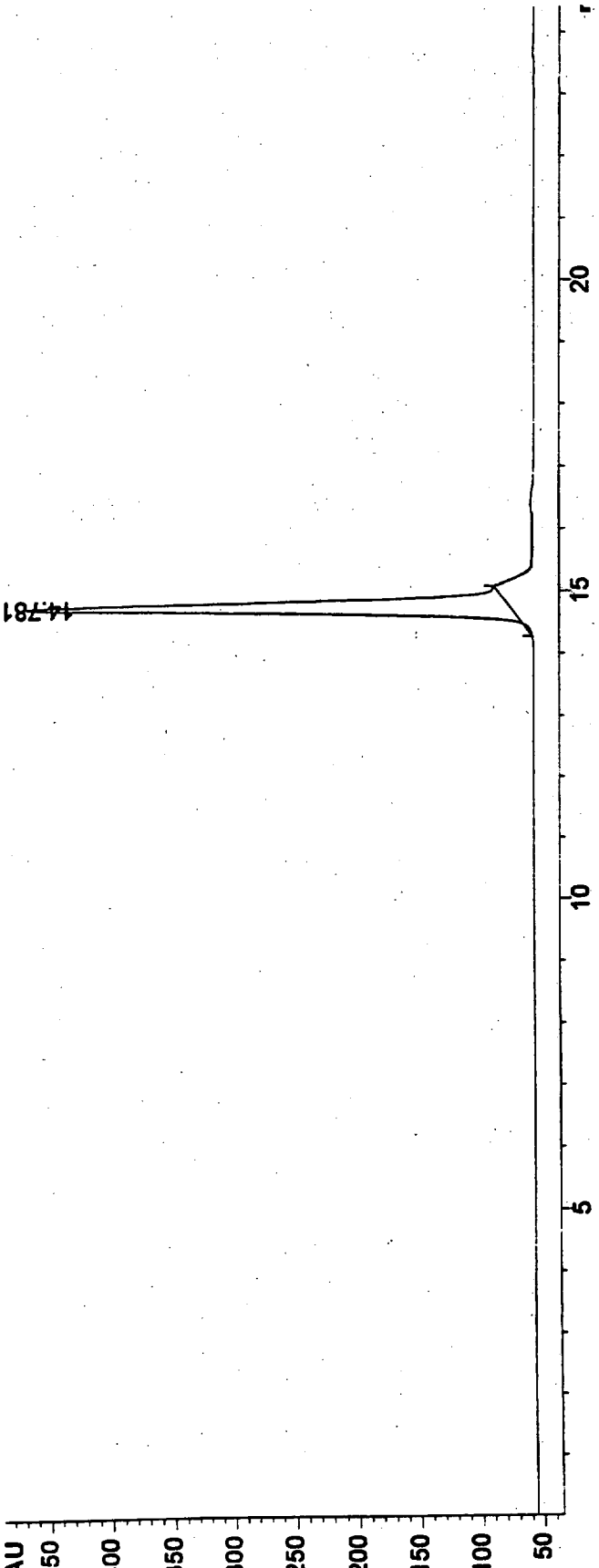
Radiochromatogram of Purified 6b (Radioactivity at solvent front from previous injection)



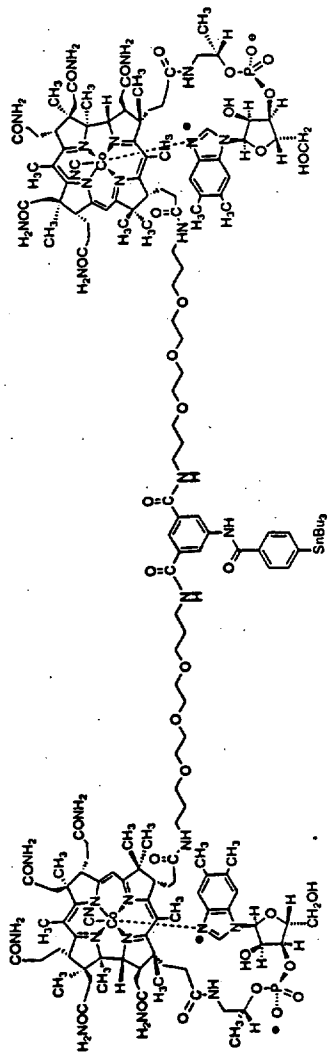
© 1999 American Chemical Society, Bioconjugate Chem., Wilbur bc9900340 Supporting Info Page 8

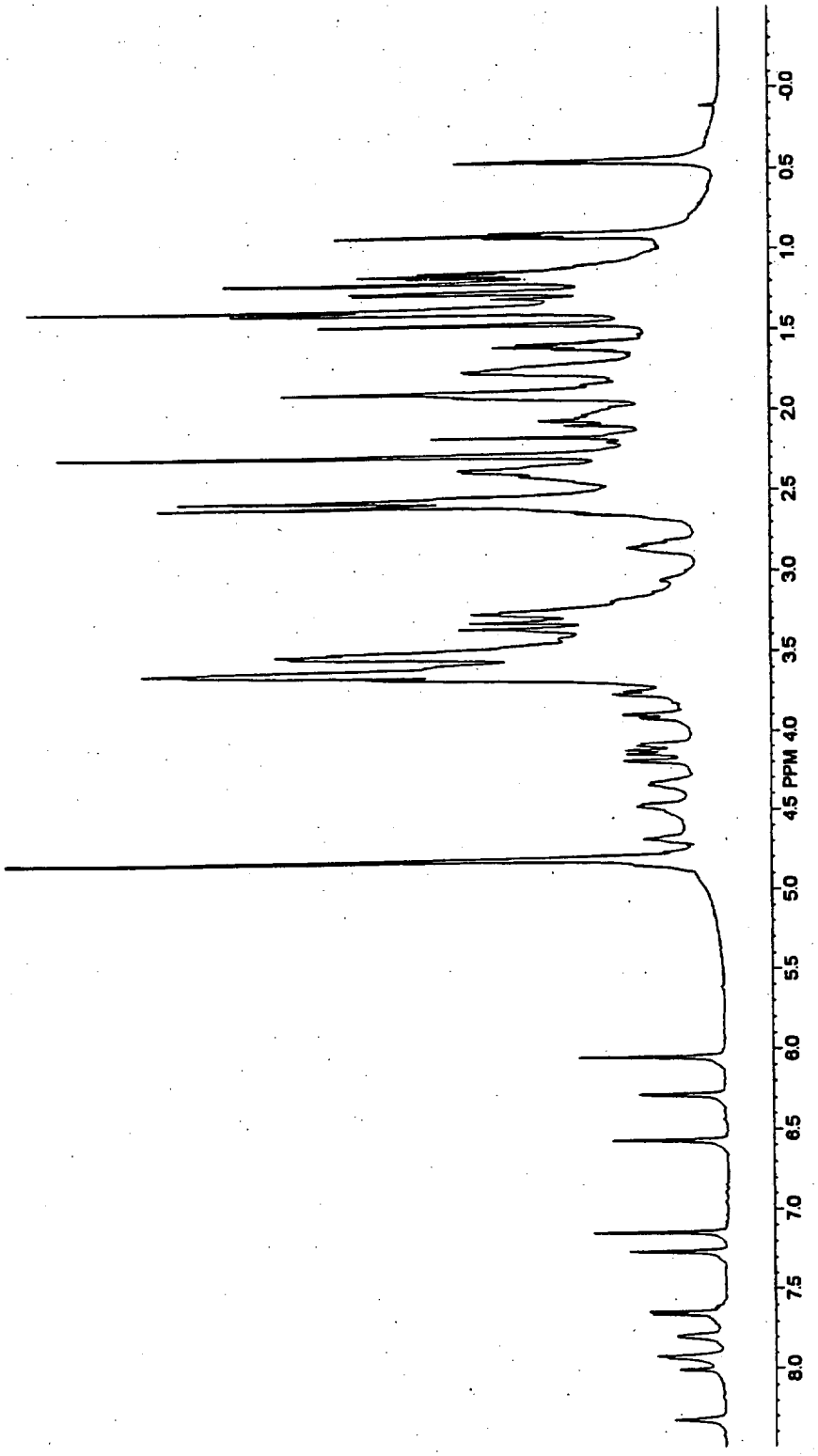


Analytical Reversed-Phase HPLC of 8a



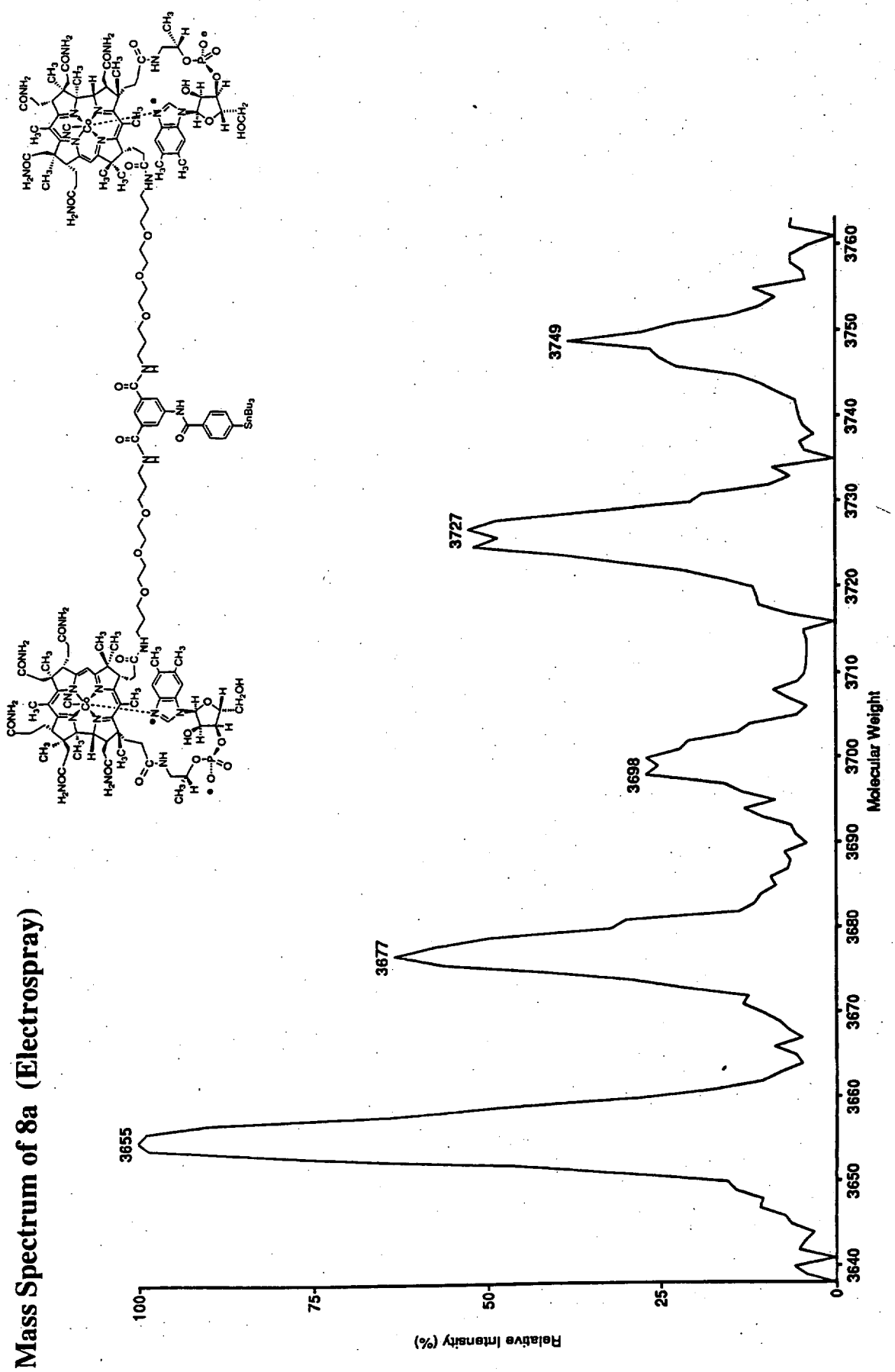
© 1999 American Chemical Society, Bioconjugate Chem., Wilbur bc9900340 Supporting Info Page 9



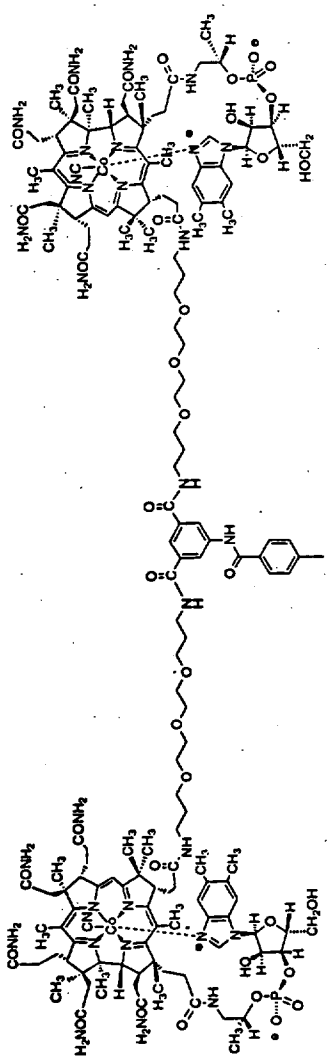


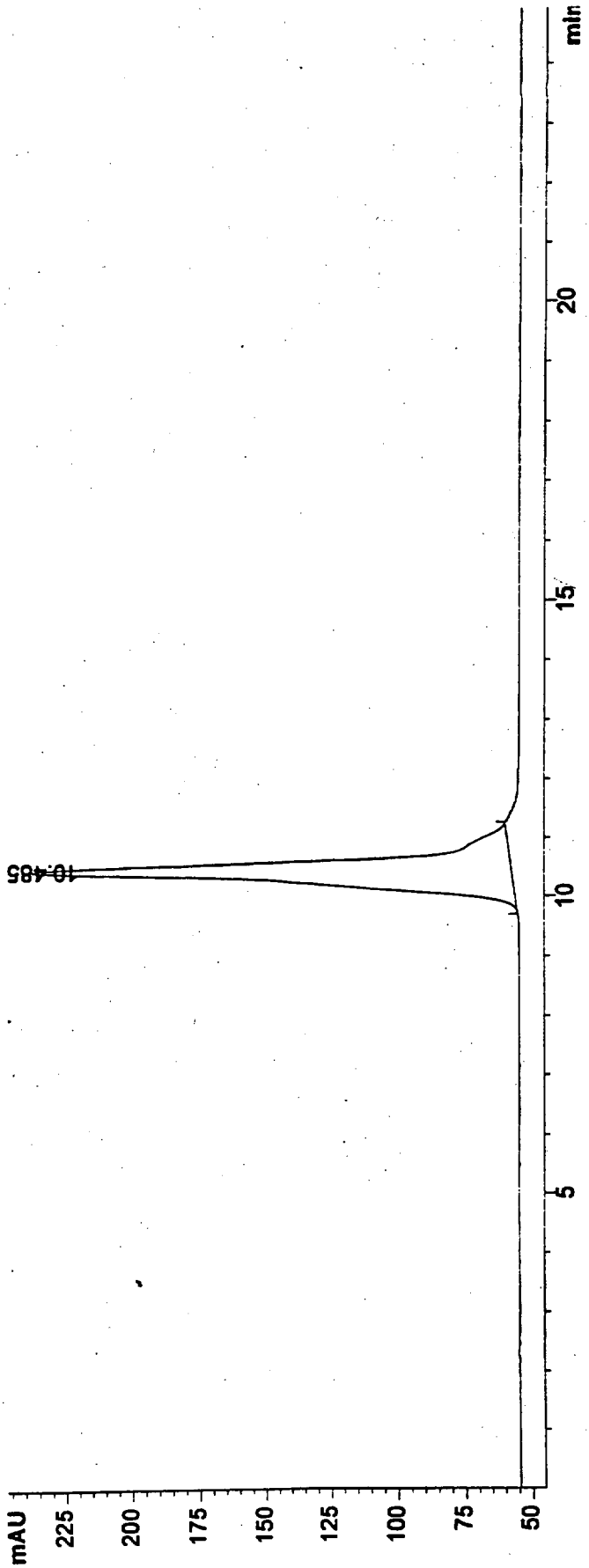
^{1}H NMR of 8a (500 MHz, MeOH-d_4)

© 1999 American Chemical Society, Bioconjugate Chem., Wilbur bc9900340 Supporting Info Page 10



© 1999 American Chemical Society, Bioconjugate Chem., Wilbur bc9900340 Supporting Info Page 11

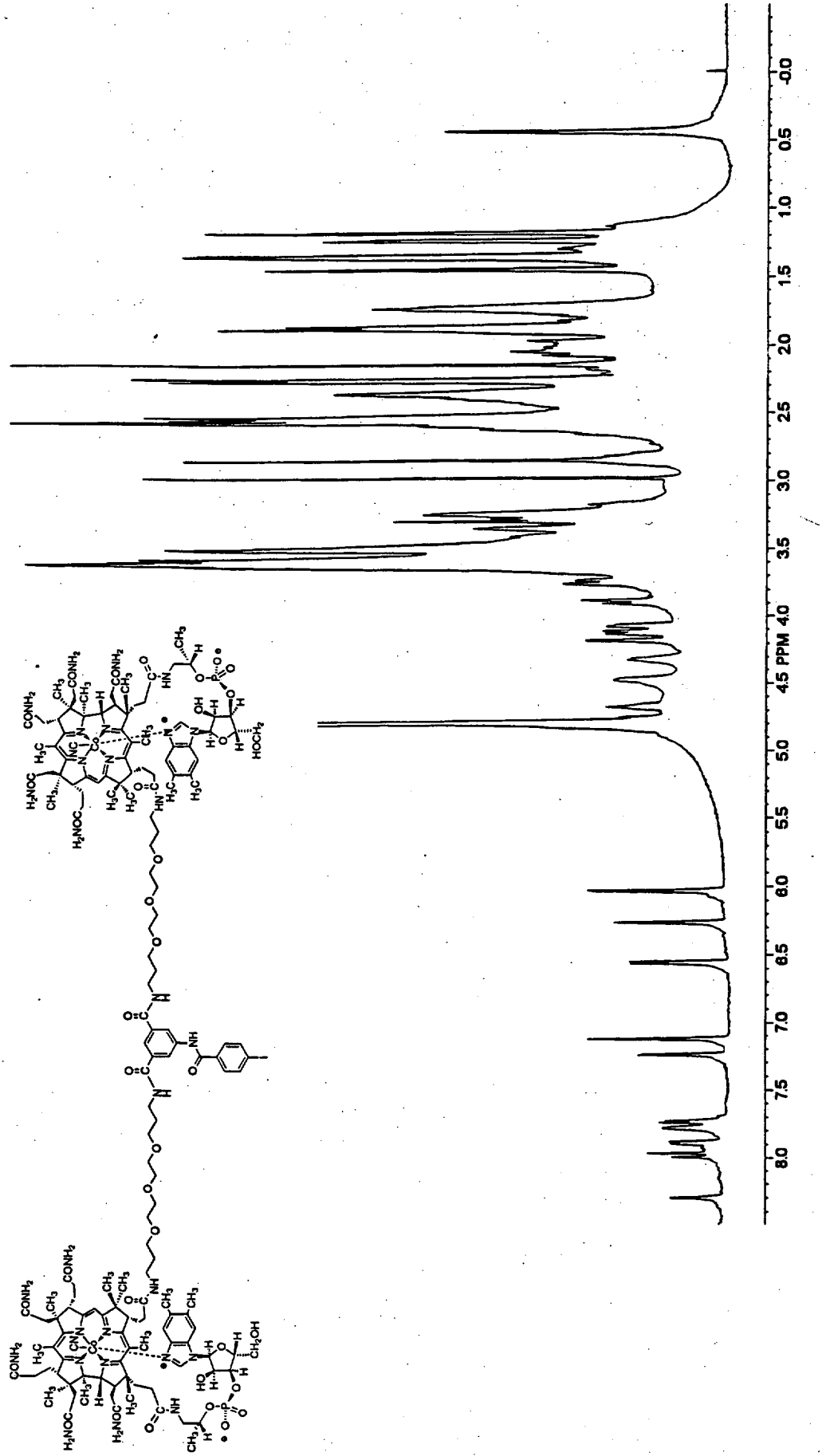




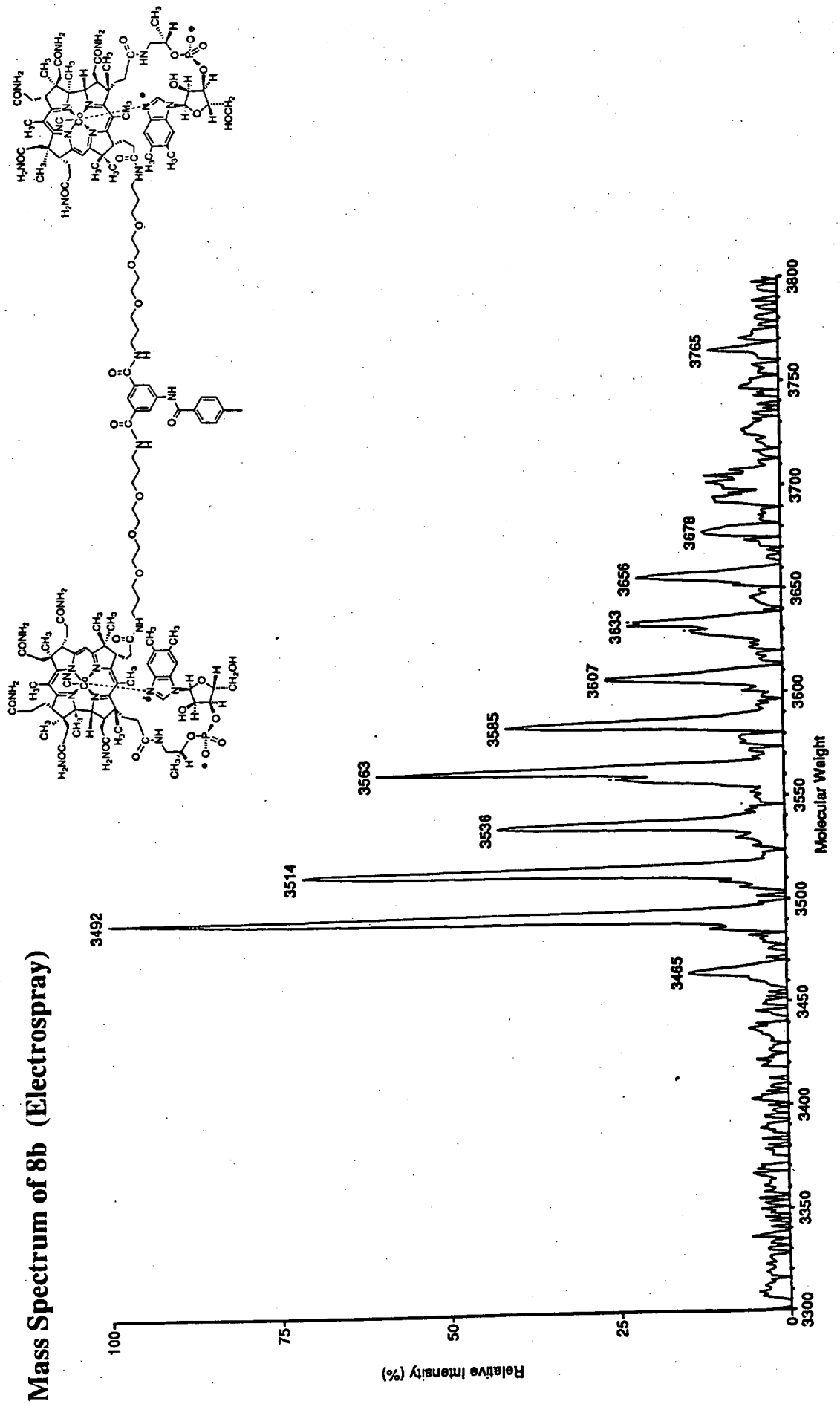
Analytical Reversed-Phase HPLC of 8b

© 1999 American Chemical Society, Bioconjugate Chem., Wilbur bc9900340 Supporting Info Page 12

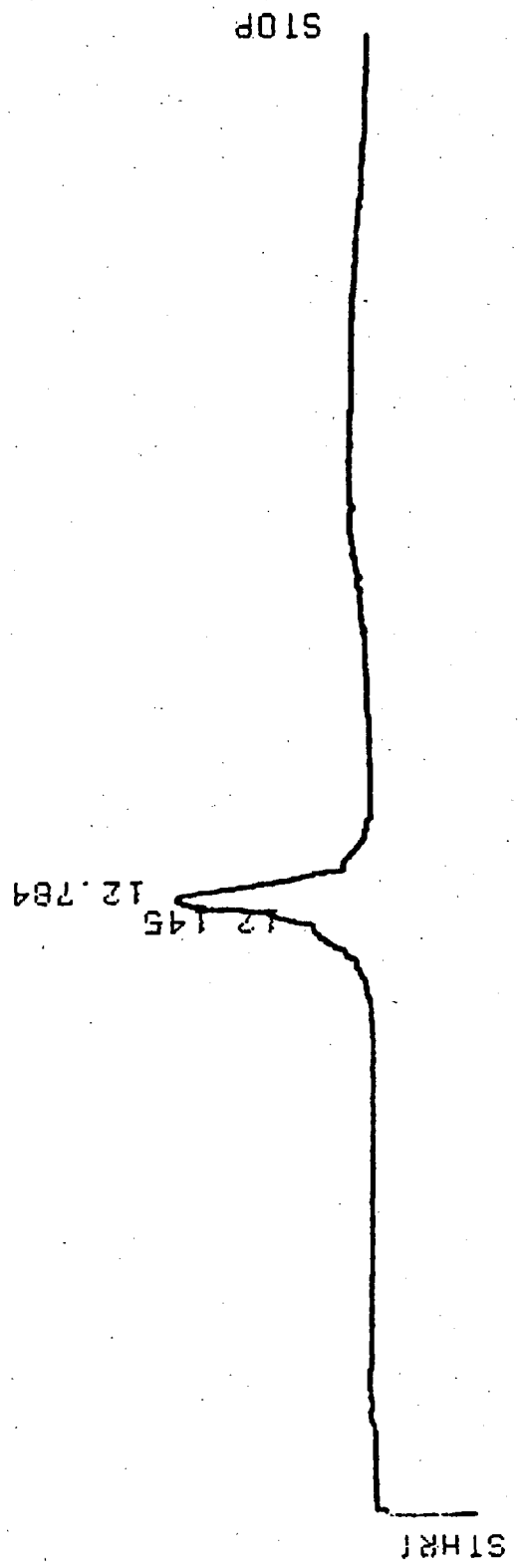
^{1}H NMR of 8b (500 MHz, MeOH-d_4)



© 1999 American Chemical Society, Bioconjugate Chem., Wilbur bc9900340 Supporting Info Page 13

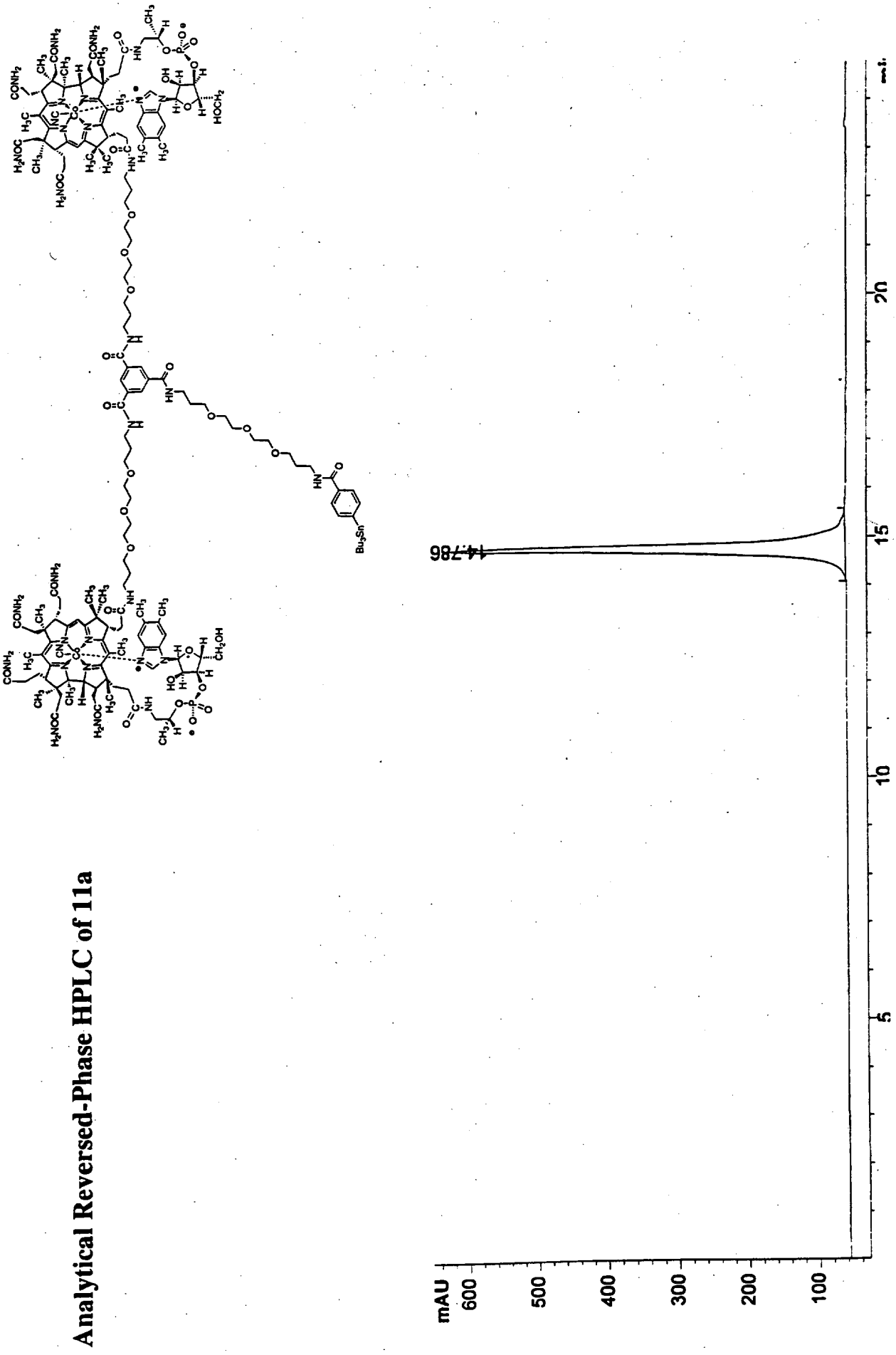


© 1999 American Chemical Society, Bioconjugate Chem., Wilbur bc9900340 Supporting Info Page 14



Radiochromatogram of Purified 8b

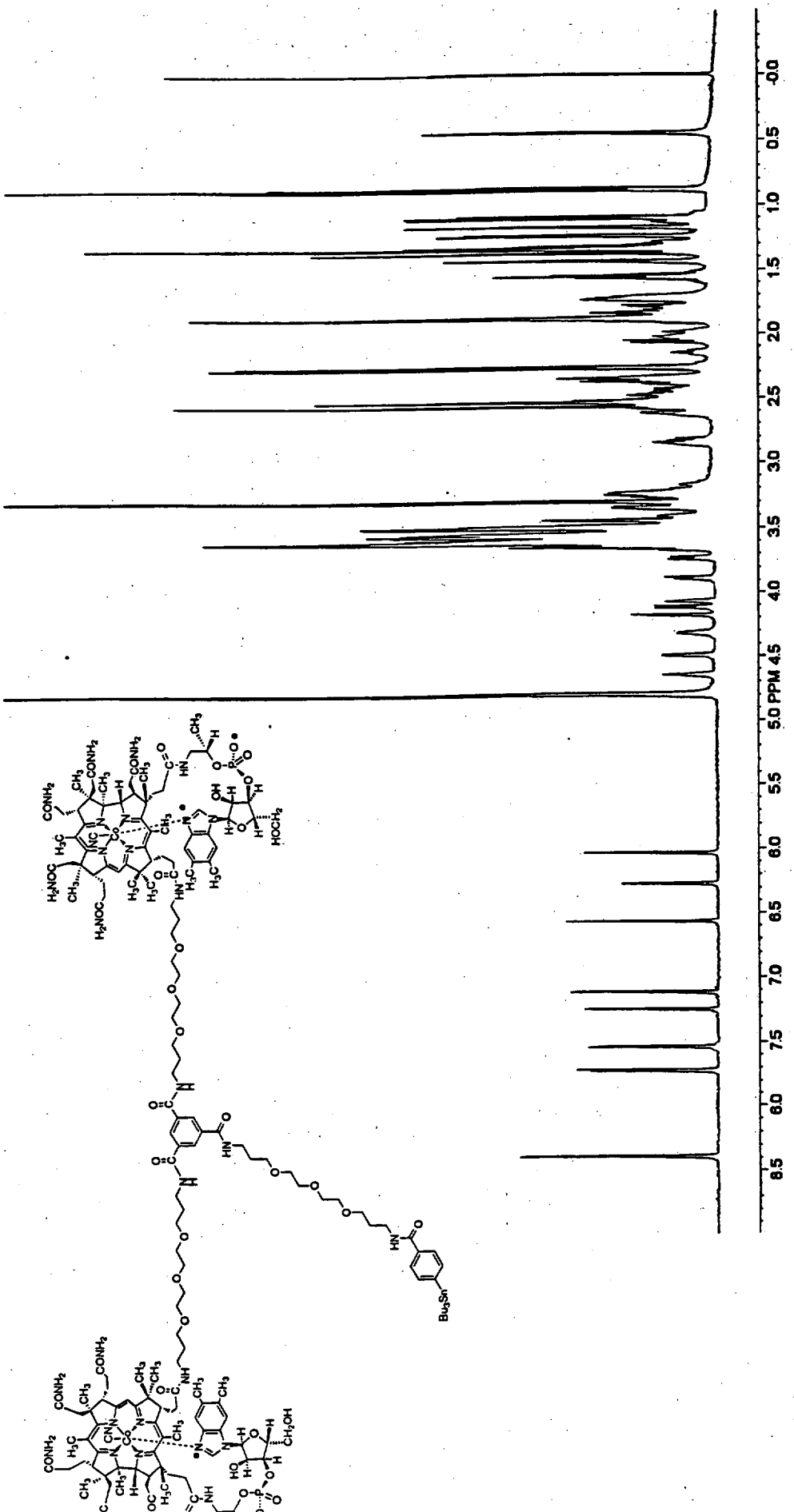
© 1999 American Chemical Society, Bioconjugate Chem., Wilbur bc9900340 Supporting Info Page 15



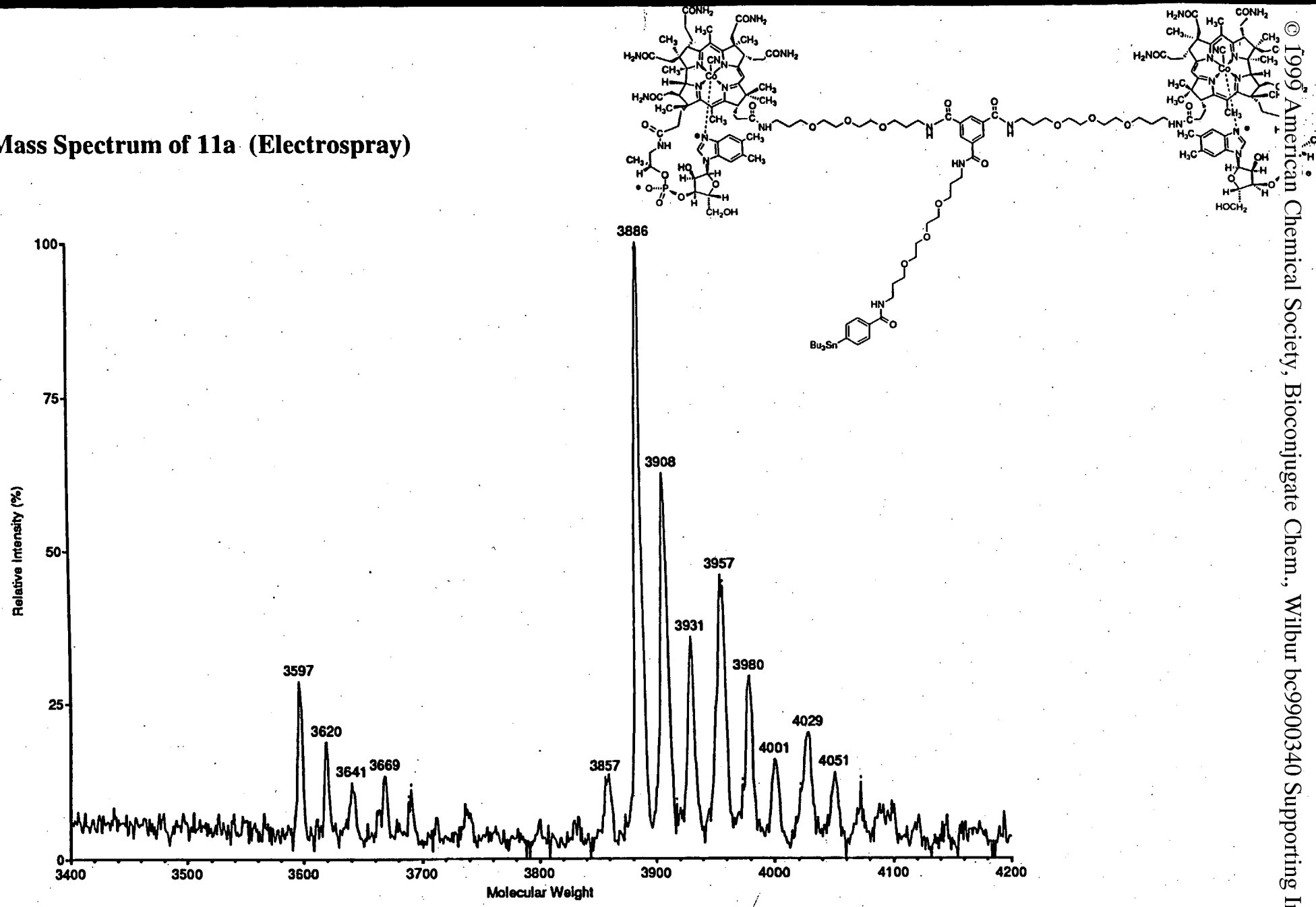
Analytical Reversed-Phase HPLC of 11a

© 1999 American Chemical Society, Bioconjugate Chem., Wilbur bc9900340 Supporting Info Page 16

^{1}H NMR of 11a (750 MHz, MeOH-d_4)

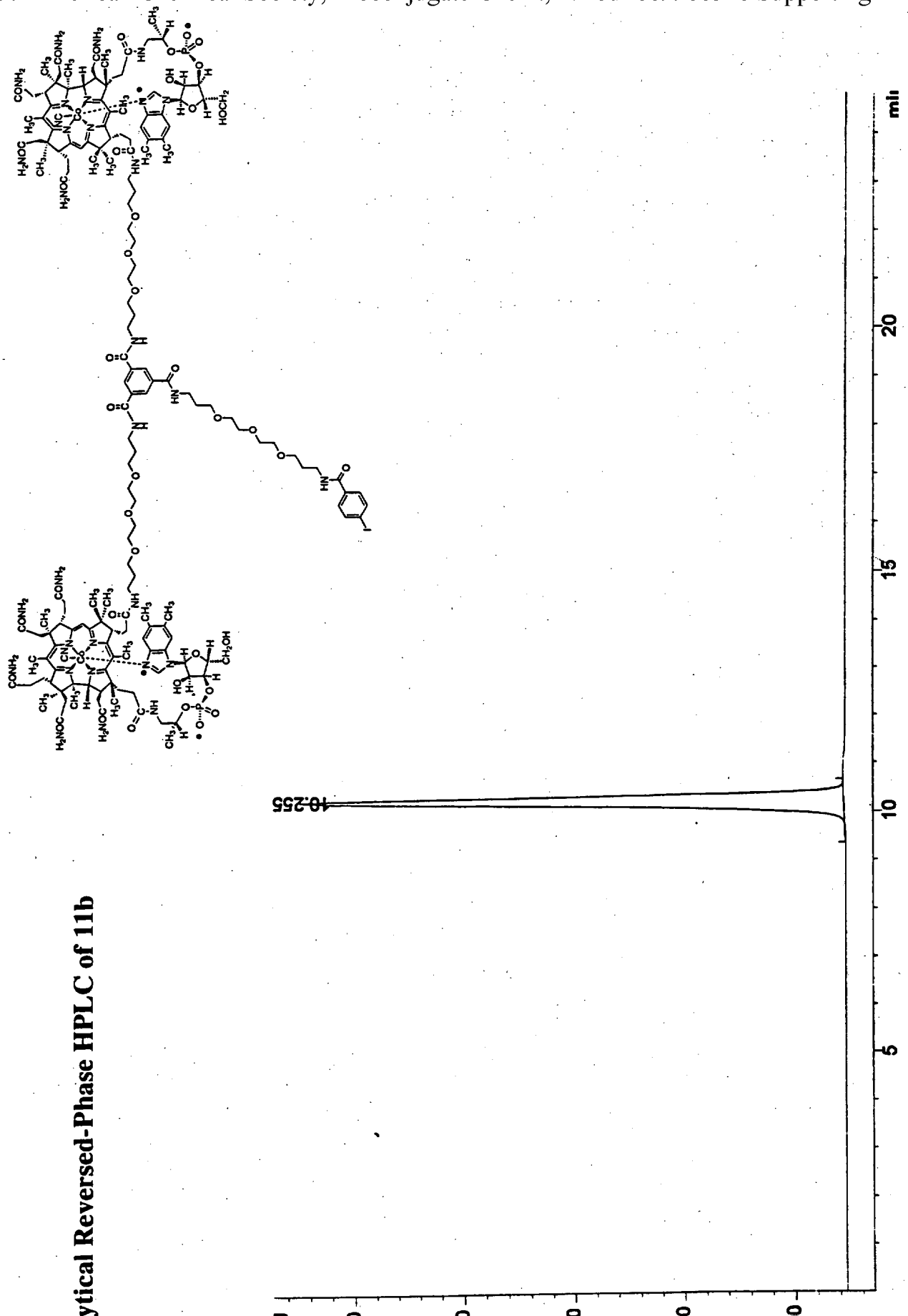


Mass Spectrum of 11a (Electrospray)



© 1999 American Chemical Society, Bioconjugate Chem., Wilbur bc990340 Supporting Info Page 17

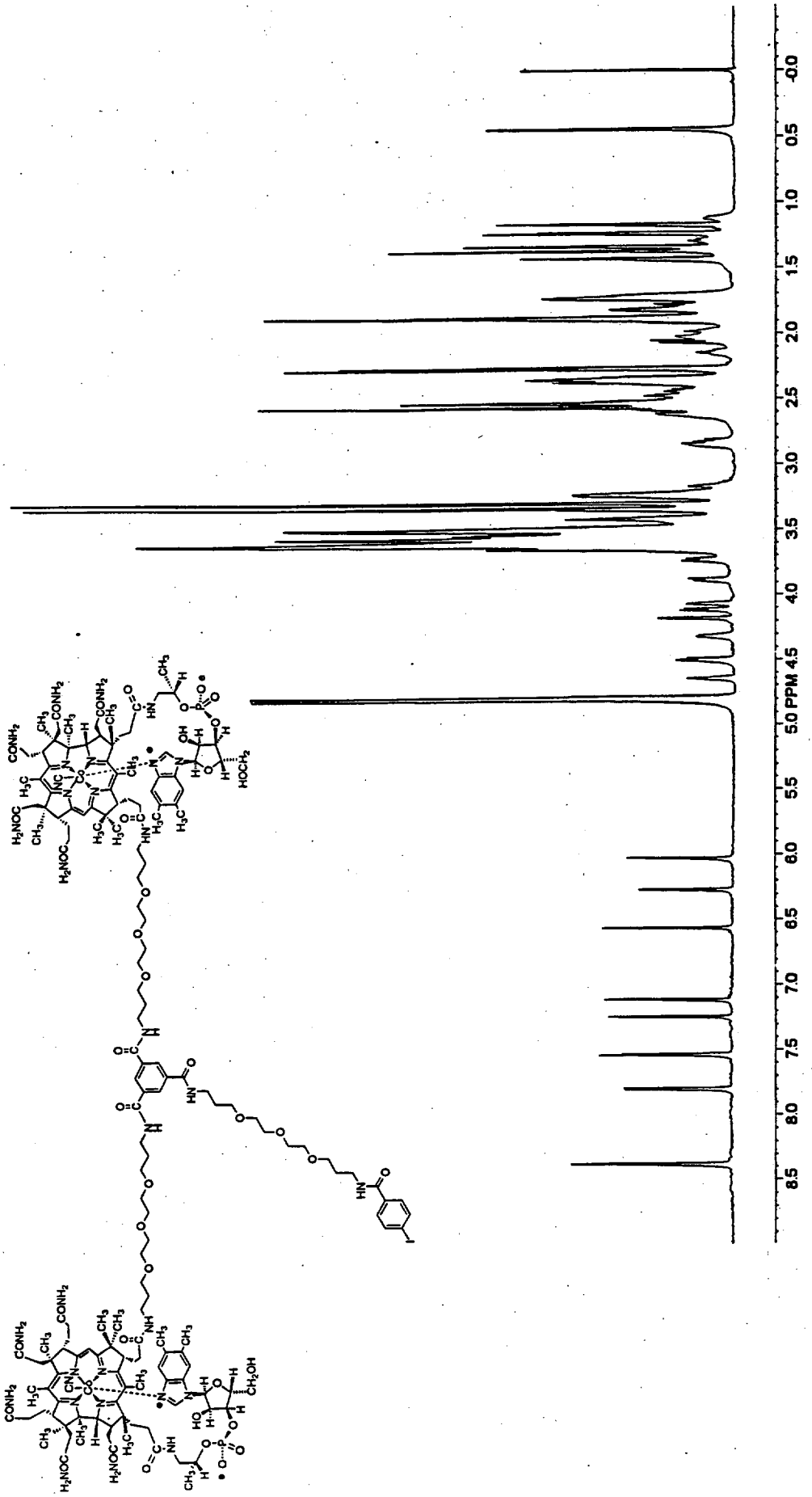
© 1999 American Chemical Society, Bioconjugate Chem., Wilbur bc9900340 Supporting Info Page 18



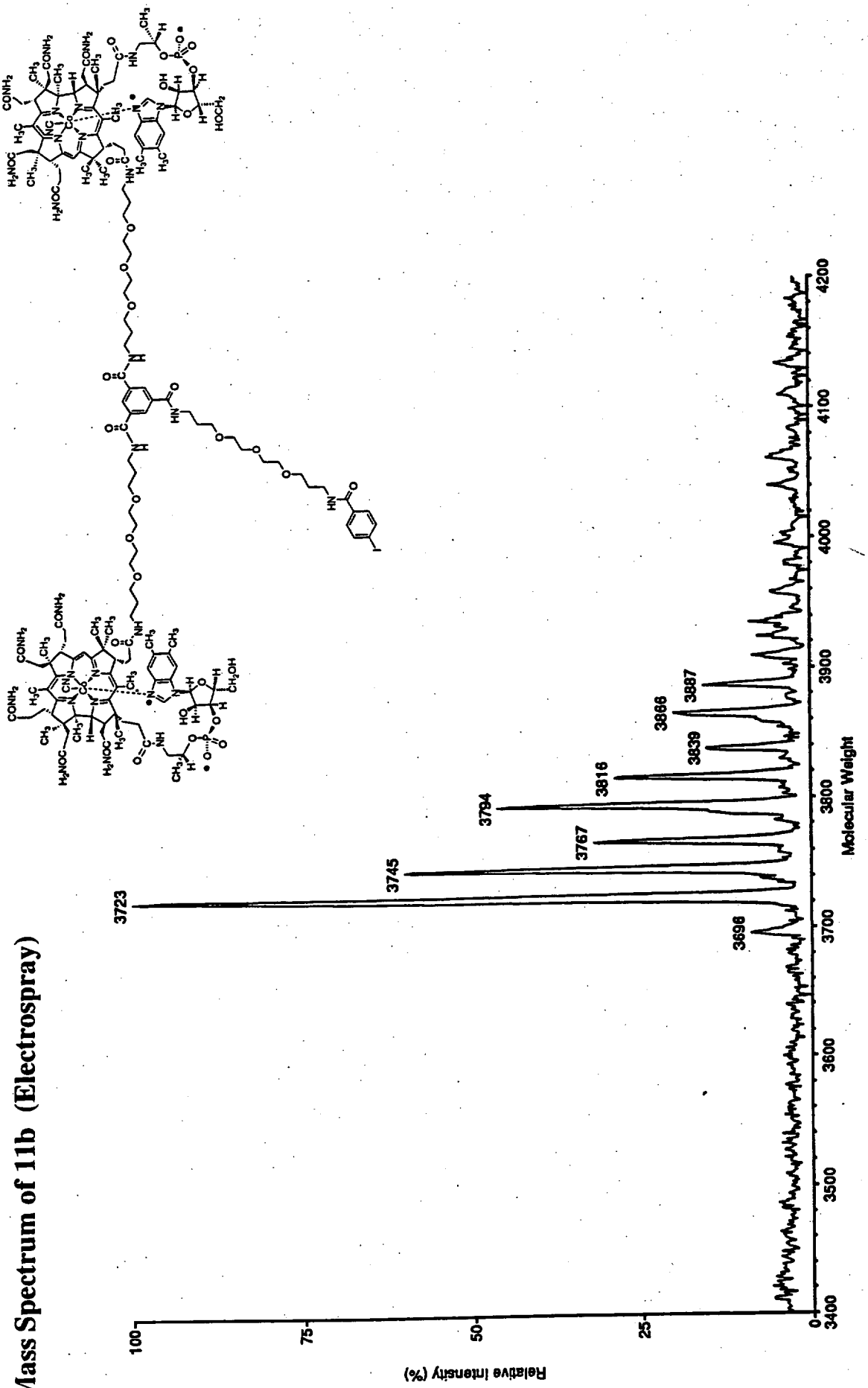
Analytical Reversed-Phase HPLC of 11b

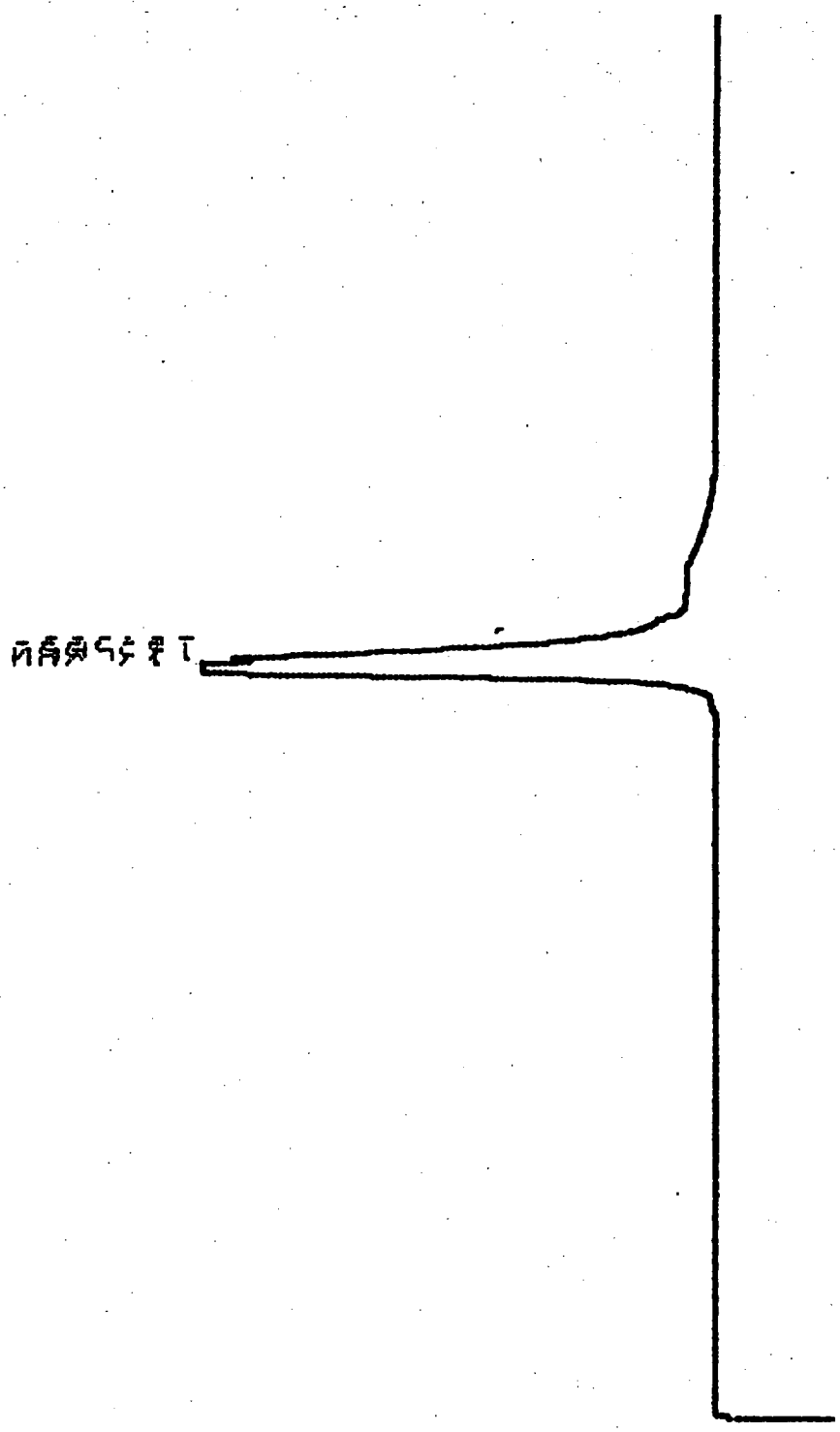
© 1999 American Chemical Society, Bioconjugate Chem., Wilbur bc9900340 Supporting Info Page 19

^{1}H NMR of 11b (750 MHz, MeOH-d_4)



© 1999 American Chemical Society, Bioconjugate Chem., Wilbur bc9900340 Supporting Info Page 20





Radiochromatogram of Purified 11b

NOVEMBER/DECEMBER 1999
Volume 10, Number 6

© *Copyright 1999 by the American Chemical Society*

Bioconjugate Chemistry

COMMUNICATIONS

Functionalization of the Sugar Moiety of Oligoribonucleotides on Solid Support

Xiaolin Wu and Stefan Pitsch*

Organisch-chemisches Laboratorium der Eidgenössischen Technischen Hochschule, Universitätstrasse 16, CH-8092 Zürich, Switzerland. Received June 24, 1999

A solid-phase method for the introduction of a variety of different side chains into oligoribonucleotides is presented. It is based on a β-D-allofuranosyl phosphoramidite with a bromopentyl-substituent tethered to the 6′-O position. After its incorporation into fully protected, immobilized RNA sequences, the bromine was substituted with a variety of soft nucleophiles which, in some cases, allowed further transformations. After deprotection and detachment, the corresponding functionalized oligoribonucleotides were purified and characterized. Incorporation of such side chains led to a slight lowering of transition temperatures, but some of them led to a significant enthalpic stabilization of an A-type RNA duplex.

Oligonucleotide conjugates are prepared routinely to create molecular probes and to attach specific reporter groups. A great, not yet exploited potential lies in the development of modified ribozymes with more functional groups able to recognize organic molecules and to catalyze organic reactions (*1*−*4*). Additional substituents are usually added to the ends of oligonucleotides and often carry an unspecific functionality which allows the postsynthetic formation of conjugates (*5*−*7*). Among the reasons for the relatively small number of base and sugar modified nucleic acid analogues (*8*−*11*) are the lengthy syntheses of corresponding building blocks which have usually to be carried out separately for every new modification. This drawback has been overcome partially by the development of building blocks containing reactive nucleobases, which during deprotection can be substituted with a variety of nucleophiles (*12*−*15*) or prior to deprotection with a variety of electrophiles (*16*).

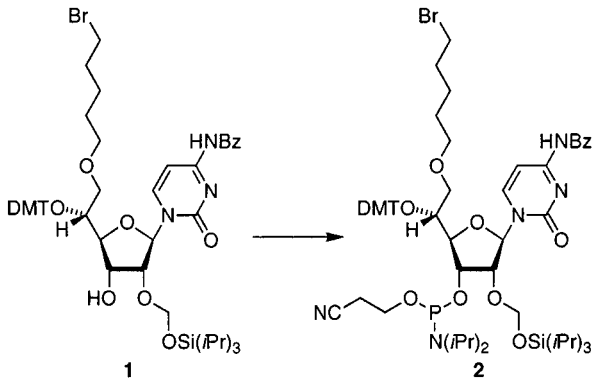


Figure 1. Conditions: $(i\text{Pr})_2\text{NP(Cl)OCH}_2\text{CH}_2\text{CN}$, $(i\text{Pr})_2\text{NEt}$, CH_2Cl_2; 89%; Bz = benzoyl, DMT = 4,4′-dimethoxytrityl.

* To whom correspondence should be addressed. Phone: (++411) 632 45 01. Fax: (++411) 632 36 11. E-mail: wu@org.chem.ethz.ch.

10.1021/bc9900901 CCC: $18.00 © 1999 American Chemical Society
Published on Web 10/22/1999

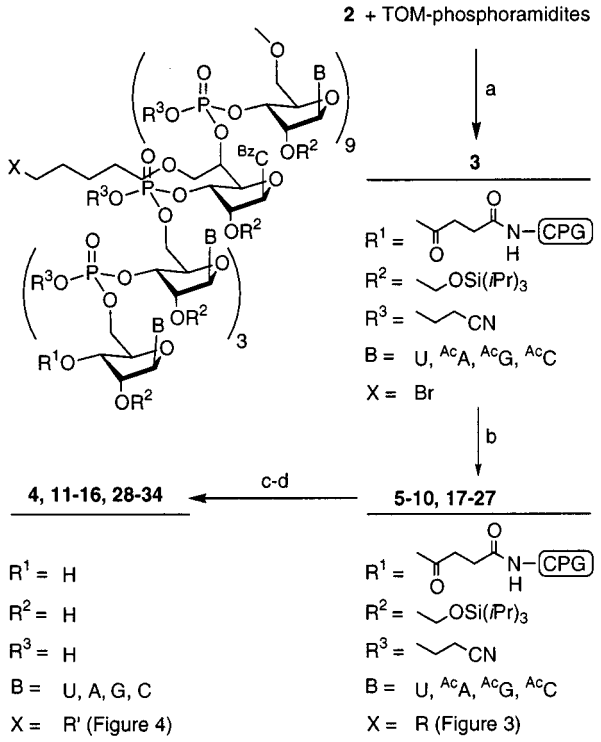


Figure 2. Conditions: (a) automated 20 μmol synthesis (500 mg of CPG, loading 40 μmol g^{-1}) on a Pharmacia Gene Assembler; detritylation with 4% $CHCl_2COOH/(CH_2Cl)_2$. Coupling: 7 min (360 μL 0.1 M TOM-phosphoramidites (*17, 19*), 360 μL of 0.12 M **2**/600 μL 0.35 M benzylthio-1*H*-tetrazol in MeCN), coupling yields >99%. Capping/oxidation: under standard conditions (*20*). (b) See Figure 3. (c) 10 M $MeNH_2$, EtOH/H_2O 1:1, 25 °C, 2 h. (d) 1 M $NBu_4F{\cdot}3H_2O$, THF, 25 °C, 3−12 h. Ac = acetyl.

In the context of our investigations toward the synthesis and the properties of hexofuranosyl oligonucleotides, we have developed fully protected nucleosides, containing reactive groups at the sugar moiety that can be substituted with additional functionalities at a very late stage of the synthesis (*17*). Extending this concept, we have now prepared the 6′-*O*-bromopentyl-substituted allofuranosyl-cytosine phosphoramidite **2** (Figure 1)[1] from

[1] **2**: A solution of **1** (*17*) (204 mg, 0.2 mmol) in CH_2Cl_2 was treated with $(iPr)_2NEt$ (85 μL, 0.5 mmol) and $(iPr)_2NP(Cl)OCH_2CH_2CN$ (62 mg, 0.26 mmol), stirred 1h at 25 °C and purified on Al_2O_3 (Act. III; hexane/EtOAc 3:2 → 3:7), 217 mg (89%) of **2** as colorless foam (2 diastereoisomers). TLC (SiO_2, hexane/EtOAc 1:1) R_f 0.67; UV (MeCN): $\lambda_{max/min}$ (ϵ) = 259 (29 600), 239 (31 500), 224 (29 700). ^{1}H NMR (300 MHz, $CDCl_3$): δ 0.97−1.07 (m, 21H), 1.17−1.25 (m, 12H), 1.37−1.41 (m, 4H), 1.77−1.82 (m, 2H), 2.54 and 2.61 (2t, J = 5.5, 2H), 3.03−3.18 (m, 3H), 3.35−3.40 (m, 2H), 3.42−3.53 (m, 2H), 3.60−3.75 (m, 4H), 3.81 (s, 6H), 4.32−4.44 (m, 2H), 4.65−4.80 (m, 1H), 4.98−5.06 (m, 2H), 6.05 and 6.07 (2d, J = 5.1, 1H), 6.83−6.91 (m, 4H), 7.21−7.63 (m, 14H), 7.80−7.87 (m, 2H), 8.65 (s, 1H). ^{31}P NMR (121 MHz, $CDCl_3$): δ 148.8, 150.2. Pos. FAB MS (NOBA): *m/z* (%) 1216/1214 (13/15) [M$^+$], 1115/1113 (26/23), 1001 (59), 303 (100) Anal. calcd for $C_{62}H_{85}N_5O_{11}BrPSi$: C, 61.27; H, 7.05; N, 5.76. Found: C, 61.38; H, 7.10; N, 5.84.

[2] Preparation and isolation of the functionalized sequences: 5 mg of the solid support (Figure 2) was shaken with 0.5 mL of the reaction solution (Figure 3). After centrifugation, the pellet was washed twice with DMF and EtOH and mixed with 0.5 mL of 10 M $MeNH_2$ (EtOH/H_2O 1:1). After 2 h at 25 °C, the supernatant was evaporated and the residue dissolved in 0.5 mL 1 M $Bu_4NF{\cdot}3H_2O$ (THF). After 3−12 h at 25 °C, 0.5 mL of aqueous Tris-HCl (1 M, pH 7.4) was added. The mixture was desalted on Sephadex G-10 and purified by HPLC.

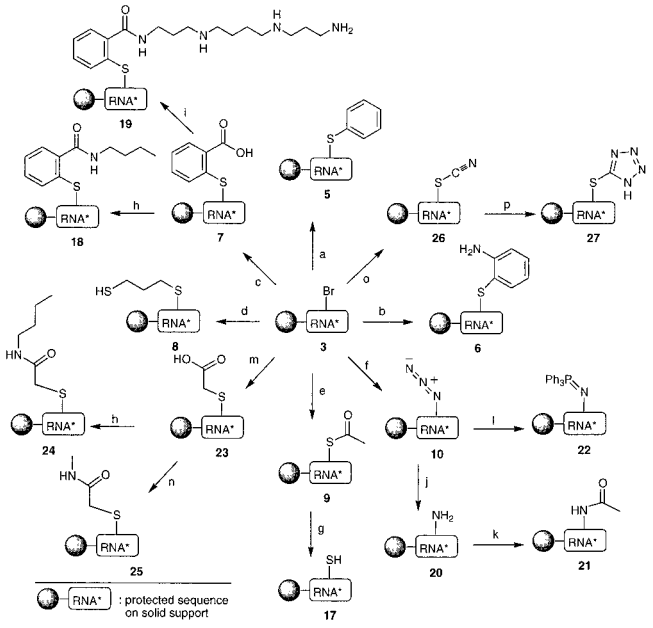


Figure 3. Conditions: (a) 2 M thiophenol, 1 M NaH, DMF, 4 h. (b) 0.2 M 2-amino thiophenol, 0.2 M $(iPr)_2NEt$, DMF, 5 h. (c) 0.2 M thiosalicylic acid, 0.4 M $(iPr)_2NEt$, DMF, 12h. (d) 1 M propane dithiole, 0.5 M $(iPr)_2NEt$, DMF, 4 h. (e) 1 M AcSNa, 2 M AcSH, DMF/H_2O 1:1, 4 h. (f) 1 M NaN_3, DMF/H_2O 4:1, 15 h. (g) 0.2 M $(NH_2NH_3)OAc$, DMF, 2 h. (h) 0.1 M TBTU, 0.1 M HOBT, 0.2 M $(iPr)_2NEt$, 0.2 M $BuNH_2$, DMF, 2 h. (i) 0.2 M TBTU, 0.2 M HOBT, 0.4 M spermine, 2 h. (j) 0.15 M $SnCl_2$, 0.6 M thiophenol, 0.45 M Et_3N, CH_3CN, 6 h, then 0.8 M $NaHCO_3$, H_2O, 5 min (*21*). (k) pyridine/Ac_2O 4:1, 1 h. (l) 0.5 M PPh_3, pyridine, 12 h. (m) 1 M thioglyolic acid, 2 M $(iPr)_2NEt$, DMF, 12 h. (n) 0.1 M TBTU, 0.1 M HOBT, 0.2 M $(iPr)_2NEt$, 0.2 M $MeNH_2$, DMF, 2 h. (o) 1 M $Bu_4N(SCN)$, DMF, 50 °C, 12 h. (p) 0.5 M NaN_3, 1 M NH_4Cl, DMF/H_2O 1:1, 85 °C, 6 h.

R → R' (a-b)			Product ratio[b] %	T_m[c] °C	MS[d] *m/z* found	MS[d] *m/z* calc.
5 →	11	R' = R[a]	95	63.3	4615	4614
6 →	12	"	95	62.7	4629	4629
7 →	13	"	90	64.4	4658	4658
8 →	14	"	70	63.9	4612	4612
10 →	16	"	90	64.0	4548	4546
17 →	15	"	80	64.9	4538	4538
18 →	28	"	60	62.6	4714	4715
19 →	29	"	40	61.9	4842	4842
21 →	30	"	60	63.6	4562	4563
24 →	32	"	45	62.4	4652	4651
25 →	33	"	70	64.0	4608	4609
27 →	34	"	75	63.1	4607	4606
3 →	4	R' = −NH(CH$_3$)	95	63.9	4535	4534
9 →	15	R' = −SH	80	64.9	4538	4538
22 →	31	R' = −NH$_2$	75	63.5	4520	4521

Figure 4. (a, b) Deprotection (Figure 2). [a]R: Figure 3. [b]Area % (HPLC) of product signal, yields after purification: 15−35%. [c]1 μM functionalized sequence + 1 μM **35** (Figure 6) in 150 mM NaCl, 10 mM Tris-HCl (pH 7.4), measured according to ref *17*; the T_m-value of the unfunctionalized sequence **36** was 65.8 °C. [d]MALDI-TOF MS, [M − H]$^-$, measured according to ref *22*.

the earlier described nucleoside **1** (*17*) incorporated it into a tetradecamer sequence **3** (Figure 2, Figure 6) and investigated its functionalization on solid support (Figure 3). The sequence r(5′-CUAUCGAGC**X**UACG-3′) (**X**, vari-

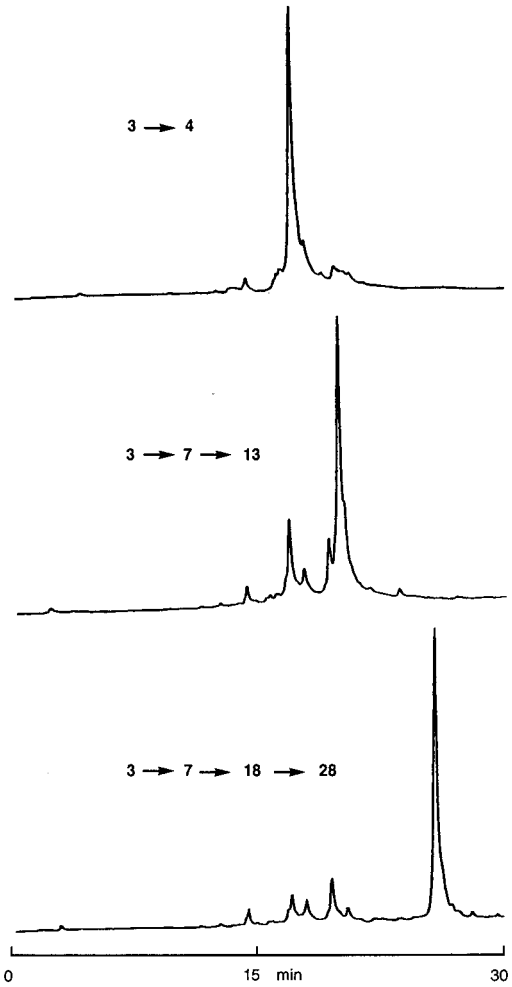


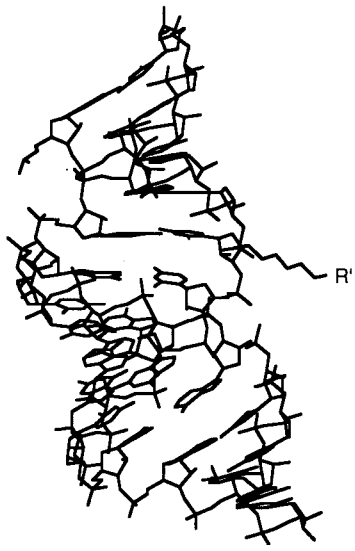
Figure 5. HPLC of crude products. Reaction conditions: Figures 2 and 3. HPLC conditions: Nucleosil 100-5 C18HD, 4.6 × 220 mm, 1 mL/min, elution (30 min) with 0.1 M (Et_3NH)OAc (H_2O, pH 7) → 0.1 M (Et_3NH)OAc (H_2O/MeCN 4:1, pH 7), detection at 260 nm.

able, from phosphoramidite **2**) was chosen, because its pairing behavior was already well documented (*17*, *18*). Molecular modeling revealed that additional functional groups connected to the side chain of the allofuranosyl nucleoside are located above the major groove of a corresponding duplex (Figure 6).

Each modification of the prefunctionalized, fully protected and immobilized sequence **3** was carried out with 5 mg (0.2 μmol sequence) of the solid support. Finally, detachment from the solid support, deprotection of the base and phosphate protecting groups and removal of the 2′-*O*-(triisopropylsilyloxy)methyl (TOM) groups (*17*, *19*) was carried out (Figure 2). The crude products were analyzed by HPLC (Figure 5), and the main products isolated in pure form and characterized by MALDI-TOF MS.

First, sequence **3** was deprotected without prior modification ($MeNH_2$, followed by Bu_4NF). The HPLC of the crude product showed a dominating main product; its MS agreeing with the methylamino substituted sequence **4**. These results reflected a clean overall process including good coupling yields, complete removal of all protecting groups, and a quantitative substitution of bromine during deprotection (Figure 2, Figure 5). Next, the solid-phase nucleophilic substitution of bromine was investigated (Figure 3). According to our analysis, almost quantitative displacement occurred with the soft nucleophiles thiophenol, 2-amino-thiophenol, thiosalicylic acid (Figure 5), propane dithiole, thioacetic acid, and sodium azide. After deprotection of the corresponding intermediates **5**−**10**, products **11**−**16** could be isolated in satisfying yields (Figure 4). These substitutions were best carried out at 25 °C in the presence of base or buffer, with concentrated solutions of the nucleophiles (0.1−1 M) in DMF or DMF/H_2O.[2]

Additional solid-phase functionalizations were carried out with some of the intermediates (Figure 3). Thioacetate **9** was transformed to thiole **17** with H_2NNH_3(OAc). From the acid **7**, amide **18** (Figure 5) and the spermine derivative **19** were obtained under peptide coupling conditions. Azide **10** was reduced with $SnCl_2$ according



3′ G A U A G C U C G G A U G C 5′ : **35**
5′ C U A U C G A G C C U A C G 3′ : **4, 11-16, 28-34**
R'

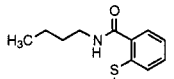
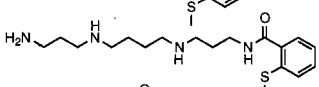
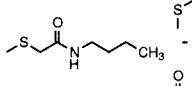
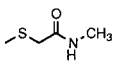
R' =	Duplex[a]	ΔH°	ΔS°	ΔG°$_{37°C}$
	35 ·	kcalmol^{-1}	calmol^{-1}K^{-1}	kcalmol^{-1}
—NH(CH$_3$) ----	**4**	-128.4	-333.2	-20.6
 ----------	**12**	-139.9	-387.4	-19.8
 ----	**13**	-147.6	-409.3	-20.8
 ----------	**28**	-151.1	-420.7	-21.7
 ----	**29**	-171.1	-481.9	-20.4
 ----------	**32**	-230.2	-657.7	-26.3
 ----	**33**	-231.8	-659.6	-27.3
	36[b]	-123.1	-333.2	-19.8

Figure 6. Schematic representation of the functionalized duplexes. [a]Thermodynamic data measured in 150 mM NaCl, 10 mM Tris-HCl (pH 7.4) according to ref *23*. [b]Values of the unfunctionalized duplex **35·36**.

to ref *21*, and the resulting amine **20** was transformed to the amide **21** with Ac_2O/pyridine. Reaction of azide **10** with PPh_3 in pyridine gave the phosphoimine **22**. Substitution of **3** with thioglycolic acid, followed by condensation with $MeNH_2$ and $BuNH_2$ led to amides **24** and **25**, respectively. The thiocyanate **26** was transformed into tetrazole **27** by cycloaddition with NaN_3/NH_4Cl. After deprotection of the sequences **17**−**19**, **21**, **22**, **24**, **25**, and **27**, oligonucleotides **15** and **28**−**34** were obtained in satisfying yields of 15−35% after purification (Figure 4, Figure 5).

The transition curves from the functionalized sequences and the complementary sequence **35** revealed T_m-values which were between 0.9 and 3.9 °C lower than the values obtained from the unfunctionalized duplex **36·35** (Figure 4, Figure 6). The thermodynamic parameters of duplex formation (at 37 °C) of selected functionalized sequences showed similar or even greater negative $\Delta G°$ values than for the unfunctionalized duplex **36·35** (Figure 6). The favorable $\Delta G°$ values of for the amide-containing duplexes **32·35** and **33·35** (relative to the parent duplex **36·35**) is the consequence of a more favorable $\Delta H°$ term, which compensates for the less favorable $\Delta S°$ term.

The phosphoramidite **2** allows an efficient preparation of sugar-modified RNA sequences which can be further functionalized in solution or on solid support. The new functionalization site allows site-specific incorporation of additional substituents and labels into the major groove (of corresponding RNA duplexes). The demonstrated concept is also suited for the use in combinatorial syntheses. We meanwhile have prepared the analogous building blocks with the three other canonical nucleobases and are about to prepare and to characterize functionalized ribozymes.

ACKNOWLEDGMENT

This work was supported by the ETH Zürich and the "Alfred Werner Stipendium". We thank Patrick A. Weiss (Xeragon AG, Switzerland) for providing us with reagents and TOM-phosphoramidites.

LITERATURE CITED

(1) Joyce, G. F. (1998) Nucleic acid enzymes: Playing with a fuller deck. *Proc. Natl. Acad. Sci. U.S.A. 95*, 5845−5847.

(2) Frauendorf, C., and Jäschke, A. (1998) Catalysis of organic reactions by RNA. *Angew. Chem., Int. Ed. Engl. 37*, 1378−1381.

(3) Hausch, F., and Jäschke, A. (1997) Libraries of multifunctional RNA conjugates for the selection of new RNA catalysts. *Bioconjugate Chem. 8*, 885−890.

(4) Hovinen, J. (1998) Synthesis of carbon-3-substituted 1,5,9-triazacyclodecanes, RNA cleavage agent suitable for oligonucleotide tethering. *Bioconjugate Chem. 9*, 132−136.

(5) Tyagi, S., and Kramer, F. R. (1996) Molecular beacons: Probes that fluoresce upon hybridization. *Nat. Biotechnol. 14*, 303−308.

(6) Telser, J., Cruickshank, K. A., Morrison, L. E., and Netzel, T. L. (1989) Synthesis and characterization of DNA oligomers and duplexes containing covalently attached molecular labels: Comparison of biotin, fluorescein and pyrene labels by thermodynamic and optical spectroscopic measurements. *J. Am. Chem. Soc. 111*, 6966−6976.

(7) Jäschke, A. (1997) Oligonucleotide-poly(ethylene glycol) conjugates: Synthesis, properties, and applications. In *Poly(ethylene glycol). Chemistry and Biological Applications* (J. M. Harris and S. Zalipsky, Eds.) ACS Symp. Ser., pp 265−284, American Chemical Society, Washington DC.

(8) Goodwin, J. T., Osborne, S. E., Scholle, E. J., and Glick, G. D. (1996) Design, synthesis and analysis of yeast $tRNA^{Phe}$ analogues possessing intra- and interhelical disufide cross-links. *J. Am. Chem. Soc. 118*, 5207−5215.

(9) Karpeisky, A., Gonzalez, C., Burgin, A. B., and Beigelman, L. (1998) Highly efficient synthesis of 2′-*O*-amino nucleosides and their incorporation in hammerhead ribozymes. *Tetrahedron Lett. 39*, 1131−1134.

(10) Cuenoud, B., Casset, F., Hüsken, D., Natt, F., Wolf, R. M., Altmann, K.-H., Martin, P., and Moser, H. E. (1998) Dual recognition of double-stranded DNA by 2′-aminoethoxy-modified oligonucleotides. *Angew. Chem., Int. Ed. Engl. 37*, 1288−1291.

(11) Salo, H., Guzaev, A., and Lönnberg H. (1998) Disulfide-tethered solid supports for synthesis of photoluminescent olignucleotide conjugates: Hydrolytic stability and labeling on the support. *Bioconjugate Chem. 9*, 365.

(12) Allerson, C. R., Chen, S. L., and Verdine, G. L. (1997) A chemical method for site-specific modification of RNA: The convertible nucleoside approach. *J. Am. Chem. Soc. 119*, 7423−7433.

(13) Allerson, C. R., and Verdine, G. L. (1995) Synthesis and biochemical evaluation of RNA containing an intrahelical disulfide cross-link. *Chem. Biol. 2*, 667−675.

(14) Xu, Y.-Z. (1996) Postsynthetic introduction of labile functionalities onto purine residues via 6-methylthiopurines in oligodeoxyribonucleotides. *Tetrahedron 52*, 10737−10750.

(15) Schmid, N., and Behr, J.-P. (1995) Recognition of DNA Sequences by Strand Replacement with Polyamino-oligonucleotides. *Tetrahedron Lett. 36*, 1447−1450.

(16) Kahl, J. D., and Greenberg, M. M. (1999) Introducing structural diversity in oligonucleotides via photolabile, convertible C5-substituted nucleotides. *J. Am. Chem. Soc. 121*, 597−604.

(17) Wu, X., and Pitsch, S. (1998) Synthesis and pairing properties of oligonucleotide analogues containing a metal-binding site attached to β-D-allofuranosyl cytosine. *Nucleic Acids Res. 26*, 4315−4323.

(18) Pitsch, S. (1997) Towards the Synthesis of Functionalized Ribonucleic Acids. *Chimia 51*, 242−243.

(19) Pitsch, S., Weiss, P. A., Wu, X., Ackermann, D., and Honegger, T. (1999) Fast and reliable automated synthesis of RNA and partially 2′-*O*-protected precursors ("caged RNA") based on two novel, orthogonal 2′-*O*-protecting groups. *Helv. Chim. Acta 82*, 1753−1761.

(20) Gait, M. J., Pritchard, G., and Slim, G. (1991) In *Oligonucleotides and analogues, a practical approach* (F. Eckstein, Eds.) Oxford University Press, pp 25−49.

(21) Bartra, M., Romea, P., Urpí, F., and Vilarrasa, J. (1990) A fast procedure for the reduction of azides and nitro compounds based on the reducing ability of $Sn(SR)_3$- species. *Tetrahedron 46*, 587−594.

(22) Pieles, U., Zürcher, W., Schär, M., and Moser, H. E. (1993) Matrix-assisted laser desorption ionization time-of-flight mass spectrometry: a powerful tool for the mass and sequence analysis of natural and modified oligonucleotides. *Nucleic Acids Res. 21*, 3191−3196.

(23) Marky, L. A., and Breslauer, K. J. (1987) Calculating Thermodynamic Data for Transitions of any Molecularity from Equilibrium Melting Curves. *Biopolymers 26*, 1601−1620.

BC9900901

ARTICLES

Synthesis, Spectral Properties, and Detection Limits of Reactive Squaraine Dyes, a New Class of Diode Laser Compatible Fluorescent Protein Labels

Bernhard Oswald,[†] Leonid Patsenker,[†] Josef Duschl,[†] Henryk Szmacinski,[‡] Otto S. Wolfbeis,[†] and Ewald Terpetschnig*[,†,§]

University of Regensburg, Institute of Analytical Chemistry, Chemo- and Biosensors, 93040 Regensburg, Germany, and FluorRx Inc., 979 Keystone Way, Carmel, Indiana 46032. Received August 31, 1998; Revised Manuscript Received March 11, 1999

We describe the synthesis and spectral characterization of two reactive long-wavelength fluorescence labels (Sq635-m and Sq635-b), having either one or two *N*-hydroxysuccinimidyl esters. Both are squaraine derivatives and consist of a cyanine-type chromophore and a central squarate bridge. To improve water solubility, we introduced two sulfonic acid groups into the heterocyclic ring systems, and for covalent attachment to proteins, a reactive *N*-hydroxy-succinimide ester (NHS ester) was synthesized. The squaraine markers exhibit low quantum yields in water ($\phi = 0.15$) and high quantum yields ($\phi = 0.6-0.7$) when bound to proteins. The absorption maxima at 635 nm in water and at approximately 645 nm when bound to proteins allow excitation with commercially available diode lasers. The detection limit of a representative squaraine dye in blood was estimated to be half that of a commonly used fluorophore.

INTRODUCTION

Fluorescence detection is widely used in immunoassays, hybridization assays, enzymatic reactions and other analytical procedures (*1*−*3*). The advantages of fluorescence detection at long-wavelength excitation are the decreased autofluorescence from cells and tissues and the use of inexpensive laser light sources such as diode lasers operating at 635, 645, and 650 nm. It is well-known that the autofluorescence of biological samples decreases with increasing wavelength, particularly beyond 600 nm. Only a few fluorescent probes exist which absorb in the red or near-infrared (NIR) region and even fewer of them are available in a reactive form (*4*−*8*). Amine-reactive functionalities such as isothiocyanate and *N*-hydroxysuccinimide esters and thiol-reactive iodoacetamide and maleimide groups can be used to covalently attach marker molecules to drugs, DNA, or antibodies (*5*, *6*).

The synthesis and spectral characterization of a squaraine derivative for covalent attachment to biomolecules was already reported (*4*). Squaraines, which are 1,3-disubstituted squaric acid derivatives, show high-absorption coefficients ($\epsilon > 200.000$ L mol^{-1} cm^{-1}) in the red region, display a high photostability, and allow the introduction of reactive functional groups such as NHS[1] esters. These dyes exhibit good quantum yields on binding to proteins but insufficient water solubility. The protein conjugates precipitate, in particular at higher dye-to-protein ratios (*4*, *9*). The water solubility of dyes can be improved by introducing sulfonic acid groups (*4*).

Reactive squaraines developed by Mank et al. were used as precolumn derivatization reagents for trace analysis of small molecules (e.g., drugs) in combination with diode laser induced fluorescence and allowed detection of analyte concentrations as low as 50−100 nmol L^{-1} (*6*). We now introduce the second generation of squaraine dyes with improved spectral and chemical properties. Specifically, we report the synthesis of a symmetrical, "bis-reactive" (Sq635-b), and an unsymmetrical, "monoreactive" (Sq635-m), water-soluble, squaraine-dye, and their conjugation to BSA, HSA, and anti-HSA. We also discuss their absorption and fluorescence spectral properties and compare the detection limit of one representative dye to CY5 in blood.

EXPERIMENTAL PROCEDURES

Chemicals, Proteins, and Media. Squaric acid, squaric acid dibutyl ester, and 6-bromohexanoic acid were

* To whom correspondence should be addressed. Phone: (408) 541 4110. Fax (408) 548 0571. E-mail: eterpetschnig@ljlbio.com.
[†] University of Regensburg.
[‡] Fluorrx Inc.
[§] Present address: LjL BioSystems, 404 Tasman Drive, Sunnyvale, CA 94089.

[1] Abbreviations: BSA, bovine serum albumin; DCC, dicyclohexylcarbodiimide; DMF, dimethylformamide; DMSO, dimethyl sulfoxide; *D*/*P*, dye-to-protein ratio; HSA, human serum albumin; hCG, human chorionic gonadotropin; mp, melting point; NHS, *N*-hydroxysuccinimide; Sq635-b, 2,4-bis[*N*−(ϵ-butoxycarbonylpentanyl)-3,3-dimethyl-5-sulfo-2-indolinylidenemethyl]cyclobutenediylium-1,3-diolate; Sq635-m, 2-[*N*-(ϵ-butoxycarbonylpentanyl)-3,3-dimethyl-5-sulfo-2-indolinylidenemethyl]-4-[3,3-dimethyl-5-sulfo-2-indolinylidenemethyl] cyclobutenediylium-1,3-diolate; TMS, tetramethylsilane; TSTU, *N*,*N*,*N*′,*N*′-tetramethyl(succinimido)uronium tetrafluoroborate.

10.1021/bc9801023 CCC: $18.00 © 1999 American Chemical Society
Published on Web 10/21/1999

purchased from Aldrich. Cy5 was obtained from Amersham Life Science, Pittsburgh. BSA was purchased from Serva Feinchemica, Heidelberg. HSA and anti-HSA were obtained from Sigma. All other chemicals and solvents were obtained from Merck. All chemicals were used as received. Phosphate buffer of pH 7.3, 0.1 M, 3.17 g of NaH_2PO_4 and 13.7 g of Na_2HPO_4, was dissolved in 1 L of doubly distilled water. Bicarbonate buffer of pH 9, 0.05 M, 2.1 g of $NaHCO_3$, was dissolved in 500 mL of doubly distilled water.

Purification and Spectroscopic Analysis. Analytical and preparative thin-layer chromatography was carried out on RP-18 F_{254} silica plates from Merck. Ion-exchange chromatography was performed using a weakly acidic cation exchanger Amberlite IRC-50. Gel permeation chromatography was carried out using Sephadex G50 as the stationary phase (0.5 × 20 cm column) and a 100 mM phosphate buffer solution (pH 7.3) as eluent. Melting points were measured with apparatus SMP-20 from Büchi and are not corrected. pH values were measured at room temperature with a pH meter WTW 538.

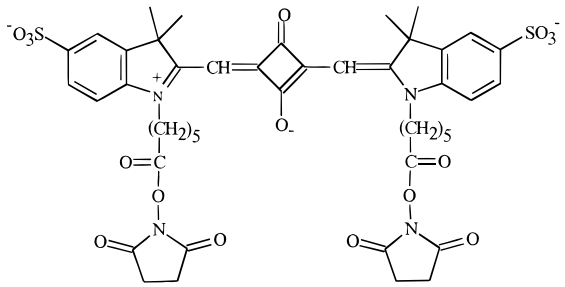
UV spectra were recorded with a U-3000 spectrophotometer (Hitachi). Emission spectra were acquired with a luminescence spectrometer from Aminco (Series 2, from SLM) with a standard 150 W xenon lamp as the excitation source. ^{1}H NMR spectra were recorded with a 250 MHz PFT-NMR spectrometer (AC 250, from Bruker). The internal standard was TMS. The chemical shifts are given in parts per million. The following abbreviations were used to describe the signals: s = singlet, d = doublet, dd = double of doubletts, t = triplet, m = multiplet. Mass spectral analysis was performed at the Central Analytical Department at the University of Regensburg, Germany.

The BSA concentration was determined using the BCA Protein Assay Reagent Kit from Pierce (Rockford, IL). Quantum yields were determined relative to Cy5 assuming a quantum yield of 0.25 for λ_{exc} = 650 nm for Cy5 using the formula $\Phi = \Phi_{Cy5}(F/F_{cy5})$, where F is $\int I(\lambda)\, d\lambda$.

Syntheses. Synthesis of *p*-hydrazinobenzenesulfonic acid (*10*), 2,3,3-trimethylindole-5-sulfonic acid potassium salt (*4*, *5*, *11*), and 1-(ϵ-carboxypentanyl)-2,3,3-trimethylindolenium-5-sulfonic acid potassium salt **(1)** (*5*) was carried out using literature procedures.

Synthesis of Sq635-b-butylester (2) (*4*). To 1 g (2.17 mmol) of 1-(ϵ-carboxypentanyl)-2,3,3-trimethylindolenium-5-sulfonic acid potassium salt (**1**) was added 120 mg (1.03 mmol) of squaric acid, and the mixture was refluxed in 50 mL of a 1-butanol:toluene (1:1, v/v) mixture for 22 h using a Dean−Stark trap filled with 4A molecular sieve. After cooling, the solvent was removed, and the product purified by preparative thin-layer chromatography using RP-18 glass plates and methanol:water (2:1, v/v) as eluent to give 90 mg (22%) of **2**. R_f: 0.47 (RP-C18, methanol:water 2:1); mp >300 °C: FAB-MS, *m/e* (M^+, dianion) for $C_{46}H_{58}N_2O_{12}S_2K_2$, calcd 895.1, found 894.8. ^{1}H NMR (D_2O): δ 7.7−7.1 (m, 6H), 5.7 (s, 2H), 3.7 (t, 4H, J = 6.5), 2.0 (t, 4H, J = 7 Hz), 1.55−0.9 (m, 24H), 1.45 (s, 12H), 0.5 (t, 6H, J = 7 Hz).

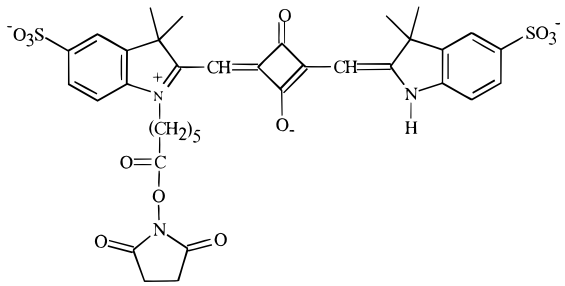
*Synthesis of Sq635-b-acid (**3**).* To 50 mg (0.05 mmol) of Sq635-b-butylester (**2**) was added 1 mL of water and 20 mL of 1 M HCl. The mixture is heated to 100 °C for 80 min. At the end of the reaction, 5 mL of 1 mol/L HCl was added. After cooling, the solvent was removed and the product vacuum dried. The product was used without further purification (43 mg, 99%). R_f: 0.75 (RP-C18, methanol:water 2:1), mp >300 °C, FAB-MS, *m/e* (M^+, dianion) for $C_{38}H_{42}N_2O_{12}S_2K_2$, calcd 782.9, found 783.0.



Sq635-b-NHS-ester

λ_{max}(abs.): 634 nm, λ_{max}(em.): 648 nm

ε = 140,000 [l mol^{-1} cm^{-1}]

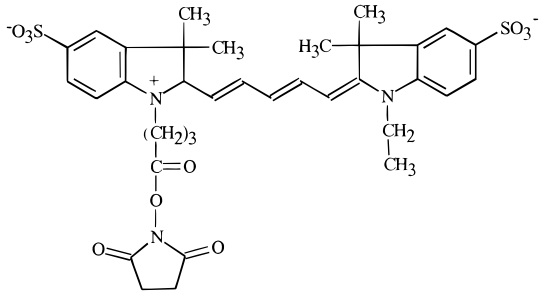


Sq635-m-NHS-ester

λ_{max}(abs.): 634 nm, λ_{max}(em.): 646 nm

ε = 120,000 [l mol^{-1} cm^{-1}]

Figure 1. Chemical structure of the Sq635-b- and Sq635-m-NHS ester.



Cy5

λ_{max}(abs.): 647 nm, λ_{max}(em.): 664 nm

ε = 250,000 [l mol^{-1} cm^{-1}]

Figure 2. Chemical structure of the Cy5-NHS ester.

^{1}H NMR (D_2O): δ 7.8−7.3 (m, 6H), 5.9 (s, 2H), 4.2 (t, 4H, J = 6.5 Hz), 2.4 (t, 4H, J = 7 Hz), 1.95−1.3 (m, 12H), 1.77 (s, 12H).

*Synthesis of Sq635-b-NHS-ester (**4**) (a) with TSTU [N,N,N′,N′-tetramethyl(succinimido)uronium tetrafluoroborate] (12).* To 43 mg (0.05 mmol) of Sq635-b-acid (**3**) in 1 mL of DMF, 1 mL of dioxane, and 0.5 mL of water were added 26 μL (0.15 mmol) of diisopropylethylamine and 38 mg (0.126 mmol) of TSTU. After 30 min, the mixture was filtered, and the solvents were removed in a vacuum. The product was dried over P_2O_5 and used without further purification. Yield: 40 mg (76%). R_f: 0.82 (RP-C18, methanol:water 2:1); mp >300 °C; FAB-MS, *m/e* (M^+, dianion) for $C_{46}H_{48}N_4O_{16}S_2K_2$, calcd 977.0, found 977.1. ^{1}H NMR (d_6-DMSO): δ 7.65−7.2 (m, 6H), 5.8 (s, 2H), 4.2 (t, 4H, J = 6.5 Hz), 2.9−2.6 (m, 12H), 1.65−1.4 (m, 12H), 1.75 (s, 12H).

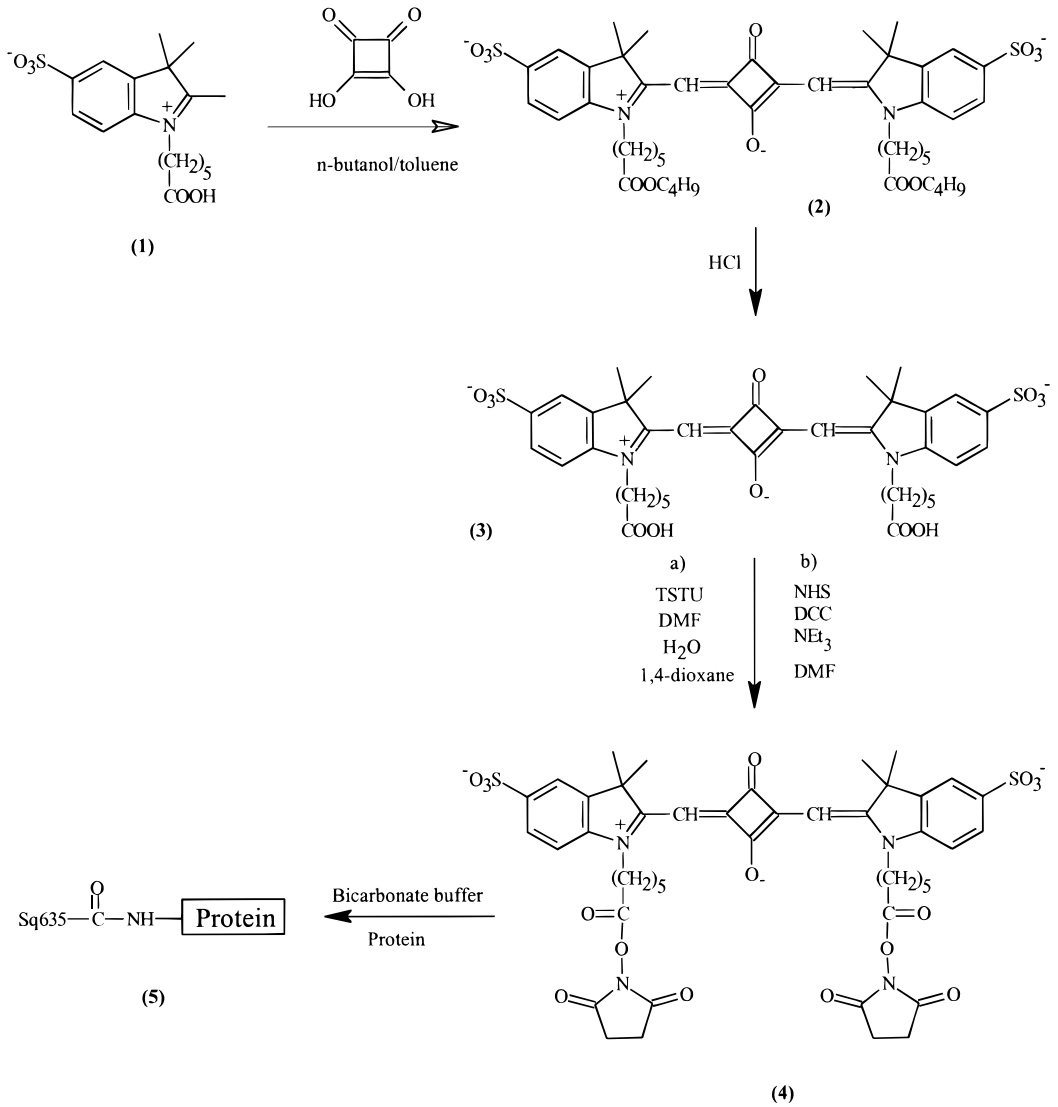


Figure 3. Synthetic pathway for the bis-functional squaraine-NHS ester.

Synthesis of Sq635-b-NHS-ester (4) (b) with NHS/DCC. A total of 14 mg (0.069 mmol) of dicyclohexylcarbodiimide (DCC) and 8 mg (0.069 mmol) of *N*-hydroxysuccinimide (NHS) was added to 20 mg (0.023 mmol) of Sq635-b-acid **(3)** in 1 mL of anhydrous DMF. The solution was stirred for 24 h at room temperature and filtered. The solvent was removed under reduced pressure, and the remaining solid was triturated with ether and dried over P_2O_5 (22 mg, 91%). R_f: 0.82 (RP-C18, methanol: water 2:1); mp >300 °C; FAB-MS, *m/e* (M^+, dianion) for $C_{46}H_{48}N_4O_{16}S_2K_2$, calcd 977.0, found 977.2. ^{1}H NMR (d_6-DMSO): δ 7.65−7.2 (m, 6H), 5.8 (s, 2H), 4.2 (t, 4H, J = 6.5 Hz), 2.9−2.6 (m, 12H), 1.65−1.4 (m, 12H), 1.75 (s, 12H).

Synthesis of Sq635-m-acid (8). To 47 mg (0.1 mmol) of 1-(ϵ-carboxypentanyl)-2,3,3-trimethylindolenium-5-sulfonic acid potassium salt **(1)** was added 22 μL (0.1 mmol) of squaric acid dibutyl ester, and the mixture was refluxed in 8 mL of ethanol with 140 μL of triethylamine for 30 min. Subsequemtly, 220 μL of 1 M aqueous NaOH was added, and the mixture was refluxed for 30 min. After cooling to room temperature, 2.3 mL of 1 M hydrochloric acid was added, and the solvent was removed under reduced pressure to obtain the monosubstituted squaraine derivative **(7)**.

The residue was refluxed with 24 mg (0.09 mmol) of 2,3,3-trimethylindole-5-sulfonic acid potassium salt in a butanol:toluene mixture (1:1 v/v) for 1 h. Water was removed as an azeotrope using a Dean−Stark trap. After cooling, the solvents were removed using a rotary evaporator. The product was treated with 100 μL of methanol, collected under reduced pressure, and purified on preparative TLC (RP-18 F_{254S}) using methanol:water (2:1 v/v) as the eluent. Yield: 31 mg (33%). R_f: 0.50 (RP-C18, methanol:water 2:1); mp >300 °C. FAB-MS, *m/e* (M^+, dianion) for $C_{32}H_{32}N_2O_{10}S_2K_2$, calcd 668.1, found 668.5. ^{1}H NMR (D_2O): δ 7.75−7.5 (m, 4H), 7.15−6.95 (m, 2H), 5.55 (s, 1H), 5.35 (s, 1H), 4.55 (t, 2H, J = 6.5 Hz), 2.05−2.3 (m, 2H), 1.5−1.2 (m, 6H), 1.25 (t, 12H).

The activation to the NHS-ester was carried out analogous to Sq635-b-acid (**3**) using procedure b. R_f: 0.55 (RP-C18, methanol:water 2:1), mp >300 °C. FAB-MS, *m/e* (M^+, dianion) for $C_{36}H_{35}N_3O_{12}S_2K_2$, calcd 766.1, found 766.4. ^{1}H NMR (D_2O): δ 7.85−7.5 (m, 4H), 7.15−6.9 (m, 2H), 5.55 (s, 1H), 5.35 (s, 1H), 4.45 (t, 2H, J = 6.5 Hz), 2.7 (s, 4H) 2.05−2.35 (m, 2H), 1.5−1.2 (m, 6H), 1.25 (t, 12H).

General Protein Labeling Procedures and Determination of Dye-to-Protein Ratios. Protein labeling reactions were carried out using 50 mM bicarbonate buffer (pH 9.0). A stock solution of 1 mg of dye in 100 μL of anhydrous DMF was prepared; 10 mg of protein was dissolved in 1 mL of a 100 mM bicarbonate buffer, pH 9.1, and various amounts of dye from the stock solution

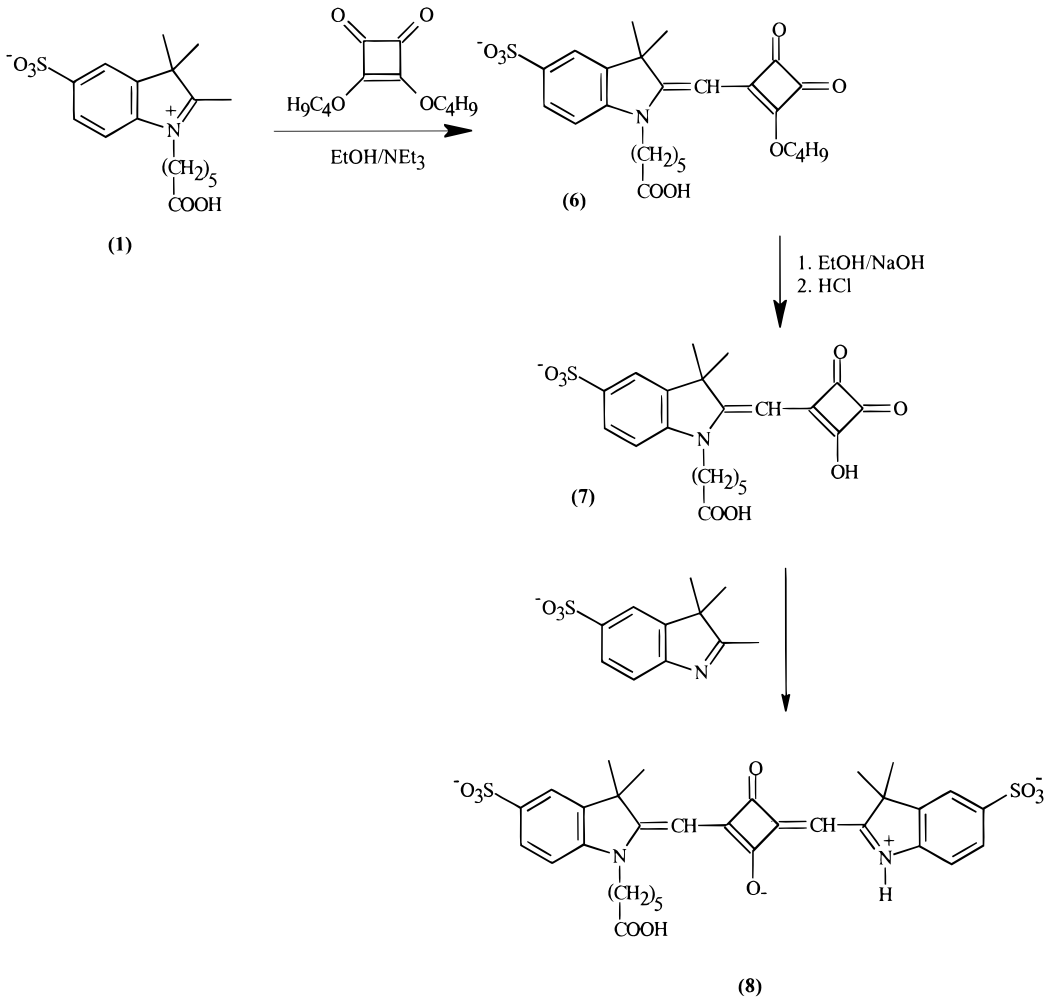


Figure 4. Synthetic pathway for the monofunctional squaraine-NHS ester.

were added, and the mixture was allowed to stir for 24 h at room temperature.

Unconjugated dye was separated from the labeled proteins using gel permeation chromatography with Sephadex G50 (0.5 cm × 20 cm column) and a 22 mM phosphate buffer solution of pH 7.3 as the eluent. The first colored band contained the dye−protein conjugate, while the blue band with a much higher retention time contained the separated free dye. A series of labeling reactions as described above was set up to obtain different dye-to-protein ratios. Compared to the free forms, the protein-bound forms of the dyes show distinct changes in their spectral properties.

The molar dye-to-protein ratio (degree of labeling) for each dye conjugate was calculated as the molarity of dye divided by the molarity of protein. The dye concentration of the conjugate was determined according to Lambert−Beer's Law from the absorbance of the dye at the absorption maximum. The protein concentration was determined using the BCA Protein Assay Reagent Kit from Pierce (Rockford, IL). The dye-to-protein ratio (*D*/*P*) gives the number of dye molecules covalently bound to the protein.

Determination of the Extinction Coefficients. Sq635-b-butylester (**2**) was purified on preparative TLC. The K^+ ions were replaced by H^+ ions by ion-exchange chromatography using Amberlite IRC-50 as the stationary phase and methanol as the eluent. Sq635-b-butylester (**2**) (0.55 mg) was dissolved in 100 mL of doubly distilled water. From this stock solution, three dilutions (1:20, 1:50, and 1:100) were made, and the absorbances were measured. The extinction coefficient was calculated according to Lambert−Beer's law and was found to be 140 000 L/(mol cm) for Sq635-b-butylester (**2**). In an analogous way the extinction coefficient for Sq635-m-acid (**8**) was determined to be 120 000 L/(mol cm). Both values refer to 634 nm.

Determination of the Detection Limits in Blood. Human blood was diluted 1:20 with phosphate buffer solution (pH 7.2). The absorbances of 50 nmol/L solutions of Sq635-b-NHS-ester (**4**), Sq635-b-anti-HSA, Cy5-NHS-ester, and Cy5-HSA were measured, and the concentrations were determined via Lambert−Beer's law assuming an extinction coefficient of 140 000 L/(mol cm) for Sq635-b-NHS-ester (**4**) and 250 000 L/(mol cm) for Cy5-NHS-ester. The emission spectra (Figure 6) of the solutions were measured by exciting at 600 nm using a standard xenon lamp (150 W) as the excitation source. The dye-to-protein ratios for Sq635-b-anti-HSA and Cy5-HSA are 0.49 and 1.1, respectively.

RESULTS

The synthetic pathway and the structures of the squaraine dyes are shown in Figures 1−4. While the synthesis of the symmetrical Sq635-b-acid (**3**) was achieved in a direct procedure (Figure 3), the synthesis of the unsymmetrical dye required the synthesis of a monosubstituted key intermediate (**6**) (Figure 4) that was hydrolyzed to the intermediate (**7**) and subsequently reacted

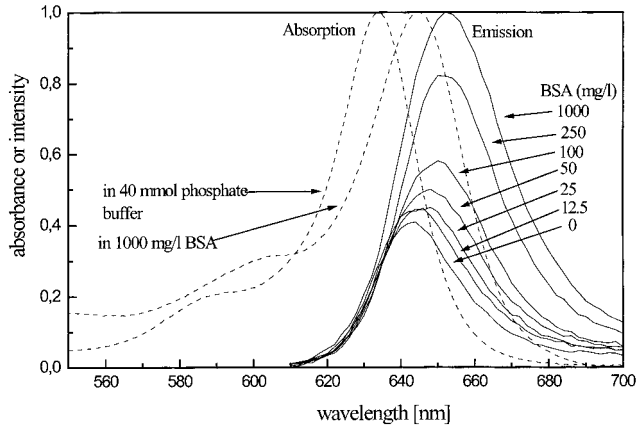


Figure 5. Absorption and relative emission spectra of Sq635-b-butylester in buffer and at various concentrations of BSA (λ_{ex} = 600 nm).

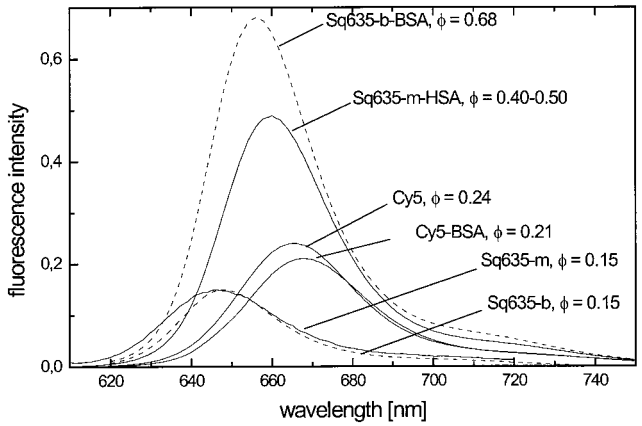


Figure 6. Relative emission spectra of Sq635-b, Sq635-m, and Cy5, free (NHS-ester) and conjugated to protein in buffer. The excitation wavelength was 600 nm using a standard 150 W xenon lamp.

with a second nonidentical methylene base to give the unsymmetrical Sq635-m-acid (**8**).

Two approaches were used to evaluate the potential of the squaraine dyes as protein labels. In the first, a nonreactive dye was mixed with increasing amounts of BSA. The extent of noncovalent binding of dyes to BSA was estimated by an increase of the relative fluorescence intensity (Figure 5). In the second approach, a reactive derivative of the dye was used for a covalent attachment procedure. In this case, the unlabeled dye was removed from the dye conjuagate using standard methods such as size-exclusion chromatography or dialysis.

The absorption and emission spectra of Sq635-b-butylester (**2**) at various concentrations of BSA are shown in Figure 5. The absorption maximum of the Sq635-b-butylester (**2**) at 635 nm shifts to 645 nm upon noncovalent binding to BSA, which makes the dye suitable for excitation with a 635 or 645 nm diode laser source. Compared to water, the emission maximum of (**2**) exhibits a small bathochromic shift of 14 nm on noncovalent binding to BSA, and the fluorescence intensity increases about two and a half times on addition of 1000 mg/L BSA. This suggests that sulfonated squaraines are suitable as fluorescent labels and would display good quantum yields when covalently bound to proteins.

Figure 6 shows a comparison of the relative emission spectra of Sq635-b, Sq635-m, and Cy5 both in free (NHS-ester) and protein-conjugated form in phosphate buffer of pH 7.3. The emission maximum of free Sq635-b-NHS-ester (**4**) at 648 nm shifts to 656 nm when covalently bound to protein. Similarly, the emission maximum of free Sq635-m-NHS-ester (**9**) at 646 nm shifts to 660 nm when bound to protein. The emission maximum of free Cy5-NHS-ester at 664 nm shifts to 668 nm when covalently linked to BSA. Importantly, the quantum yield of Sq635-b-NHS-ester (**4**) and of the Sq635-m-NHS-ester (**9**) increases on covalent attachment to protein from 0.15 to 0.68 and from 0.15 to 0.50, respectively. In contrast to the squaraine dyes, Cy5 shows a decrease in its quantum yield when bound to proteins, which lowers the ultimate sensitiviy of an assay using such dye conjugates.

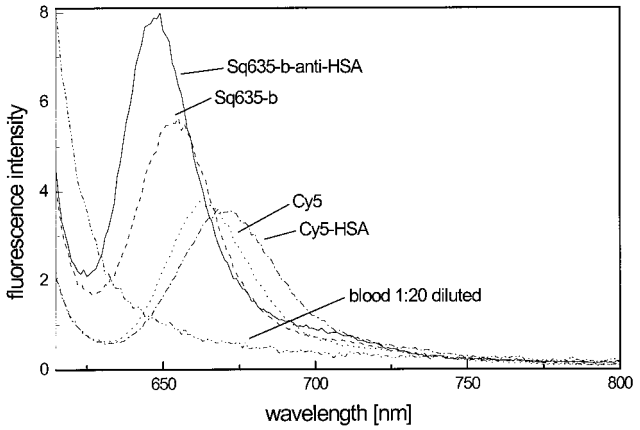


Figure 7. Comparison of the detection limits of free and protein-labeled Sq635-b and Cy5 in blood. Dye concentrations are 50 nmol l^{-1} in whole blood (dilution 1:20). λ_{ex} = 600 nm, using a standard 150 W xenon lamp. (ϵ_{600}Cy5 ≈ ϵ_{600}Sq635-b).

In Figure 7, the detection limits of free and anti-HSA labeled Sq635-b-NHS-ester (**4**) are compared to those of free and HSA-labeled Cy5-NHS-ester. The concentrations of the dyes are 50 nmol/L. At 600 nm, the Cy5-NHS-ester and the Sq635-b-NHS-ester (**4**) have similar extinction coefficients. This wavelength was used for excitation of the blood samples. The data show that the detection limit of the squaraine dye can be as much as twice that of Cy5 due to the higher quantum yields of (**4**).

Lifetime-based sensing applications (*13*−*15*) using long-wavelength probes have gained increased attention in the last couple of years since convenient and inexpensive light sources and detection systems are available in the wavelength range beyond 600 nm. There are two widely used methods for the measurement of fluorescent lifetimes: the time domain and the frequency domain method. The frequency domain method uses sinusoidally modulated light for excitation of a fluorophore, and the phase shift (phase angle) and demodulation (modulation) of the emission (Figure 8), relative to the incident light, is used to calculate the lifetime or decay time (*16*).

Table 1 summarizes the intensity decays for the Sq635-b-butylester (**2**), Sq635-b-NHS-ester (**4**), Sq635-b-BSA, and Cy5 as presented in Figure 8. The free dyes (**2** and **4**) display two similar decay times. The mean lifetime of the NHS-ester **2** appears to be longer which is due to the higher fractional intensity of its longer component (Table 1).

On binding to BSA, the mean lifetime of the Sq635-b-NHS-ester (**4**) increased more than 4-fold due to the long decay time of 2.81 ns of the major component with a fractional intensity of 0.76. In addition, the intensity of the BSA-bound form became more heterogeneous. The increase of the mean lifetime from 0.43 to 2.26 ns is in good agreement with the 4-fold increase in the quantum yield for the free and BSA-bound forms of the squaraine

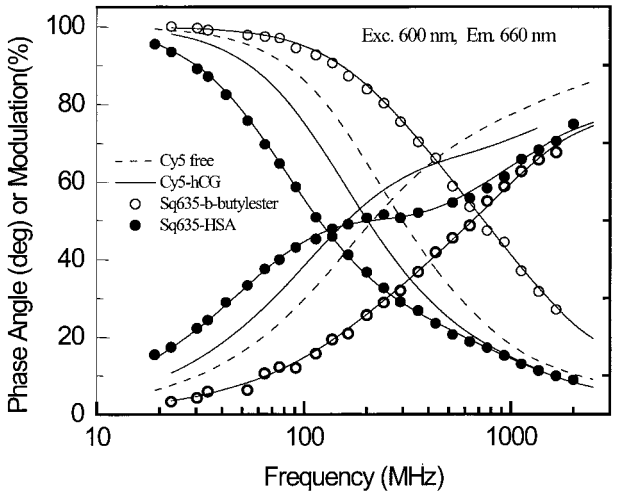


Figure 8. Frequency responses (phase angle and modulation) of Sq635-b-butylester, Sq635-b-HSA, Cy5, and Cy5-hCG, λ_{max} (exc) = 600 nm, λ_{max} (em) = 660 nm.

Table 1. Fluorescence Decay Times of Sq635-b-butylester (2), Sq635-b-NHS-ester (4), Sq635-b-HSA, Cy5, and Cy5-hCG[a]

sample	decay time (ns)	amplitude	fractional intensity	mean lifetime (ns)	χ^2
Sq635-*b*-butylester (2)	0.21	0.752	0.496	0.43	3.7
	0.65	0.248	0.504		
Sq635-*b*-NHS-ester (4)	0.20	0.558	0.286	0.51	3.8
	0.64	0.442	0.714		
Sq635-*b*-HSA	0.18	0.676	0.142		
	0.96	0.089	0.097	2.26	1.7
	2.81	0.235	0.761		
Cy5	1.01	1	1	1.01	2.1
Cy5-hCG	0.16	0.408	0.071	1.33	2.8
	1.41	0.592	0.929		

[a] Experimental conditions: excitation at 600 nm (rhodamine B dye laser), emission observed through interference filter at 660 nm with 10 nm band; 20 °C (1) The quantum yield of Cy5-avidin (D/P = 2.3) was found to be reduce by 55% on addition of biotinylated BSA.

dye. Figure 8 also reveals the distinct nature of the intensity decays of the free and BSA-bound forms for the squaraine dye and Cy5. The intensity decays of the free and covalently bound Cy5 to hCG (human chorionic gonadropin) are shown for comparison.

DISCUSSION

The synthesized squaraine dyes are highly water soluble, and their conjugates are not likely to precipitate even at high dye-to-protein ratios. The reactive derivatives Sq635-b-NHS-ester (**4**) and Sq635-m-NHS-ester (**9**) exhibit useful fluorescence characteristics and are well suited for covalent attachment to amino groups of proteins. In addition, the new squaraine derivatives can be excited with a laser diode at 635 nm. Their conjugates exhibit high quantum yields relative to the quantum yield of the free dye in water (0.15). This is in contrast to Cy5, a commonly used commercially available protein marker, whose quantum yields are sometimes reduced dramatically in the presence of protein.[2] These features make Sq635-b-NHS-ester (**4**) and Sq635-m-NHS-ester (**9**) attractive alternatives as fluorescent labels in biological assays or biophysical studies of proteins. The high extinction coefficient and quantum yield of the squaraine dye allowed measurements in whole blood with a detection limit twice as low as Cy5.

We also did an analysis of the frequency domain data for the free and the protein-bound dyes (Table 1). After covalent binding to the protein, the mean fluorescence decay time of the squaraine dye (**2**) increases five times from 0.43 to 2.26 ns. The intensity decay of Sq635-b-butylester (**2**) and Sq635-b-NHS-ester (**4**) measured in water can best be described by two-exponential decays, since the three-exponential models only result in moderate improvement in χ^2 (Table 1). The intensity decay of Sq635-b-BSA is well distinct from those of the free dyes (**2** or **4**). The long component of 2.8 ns contributes 76% to the total fluorescence intensity and thus increases the mean lifetime to 2.26 ns for the protein-bound form. The lifetime increase of the squaraine dyes when covalently bound to proteins can be explained by a shielding effect of the protein. In extreme cases, the dye quasi hides in the hydrophobic pockets of the protein and is protected from the water molecules. In contrast, the mean lifetime of Cy5 increased only from 1.01 to 1.33 ns upon covalent binding to protein (Table 1). These two intensity decays are less distinct as observed for the squaraine dyes (Figure 8) and indicate that Cy5 is less sensitive to the environment than the related squaraine dyes.

CONCLUSION

The synthesis of two reactive water-soluble dyes for derivatization of primary amines and their conjugation procedure to proteins is described. The dyes show absorption and emission maxima in the red region of the visible spectra, which allows the use of inexpensive excitation sources such as diode lasers and avalanche photodiodes as detectors. Long-wavelength absorption and emission is preferred because of the reduced autofluorescence from biological samples in the red region. The dyes also exhibit lower quantum yields and shorter lifetimes in water and improved properties when bound to proteins. We are currently exploring the use of these dyes in lifetime and polarization based immunoassays.

ACKNOWLEDGMENT

The authors thank the Center for Fluorescence Spectroscopy at the University of Maryland at Baltimore for the measurement of the lifetimes of the squaraine dyes.

LITERATURE CITED

(1) Daehne, S., Resch-Genger, U., and Wolfbeis, O. S., Eds. (1998) *Near-Infrared Dyes for High Technology Applications*, NATO ASI Ser. 3 (High Technology), Vol. 53, Kluwer Acad. Publ., Dordrecht.

(2) Wolfbeis, O. S., Ed. (1993) *Fluorescence Spectroscopy: New Methods and Applications*, Springer-Verlag, Berlin.

(3) Wolfbeis, O. S. (1987) Fibre-optic sensors in biomedical sciences. *Pure Appl. Chem. 59*, 663−672.

(4) Terpetschnig, E., Szmacinski H., Ozinskas A., and Lakowicz J. R. (1994) Synthesis of Squaraine-*N*-Hydroxysuccinimide Esters and Their Biological Application as Long-Wavelength Fluorescent Labels. *Anal. Biochem. 217*, 197−204.

(5) Mujumdar, R. B., Ernst, L. A., Mujumdar, S. R., Lewis, C. J., and Waggoner, A. S. (1993) Cyanine Dye Labeling Reagents: Sulfoindocyanine Succinimidyl Esters. *Bioconjugate Chem. 4*, 105−111.

(6) Mank, A. J. G., van der Laan, H. T. C., Lingeman, H., Gooijer, C., Brinkmann, U. A. Th., and Velthorst, N. H. (1995) Visible Diode Laser-Induced Fluorescence Detection in Liquid Chromatography after Precolumn Derivatization of Amines. *Anal. Chem. 67*, 1742−1748.

[2] The quantum yield of Cy5-avidin (D/P = 2.3) was found to be reduced by 55% on addition of biotinylated BSA.

(7) Patonay, G., and Antoine, M. D. (1991) Near-Infrared Fluorogenic Labels: New Approach to an Old Problem. *Anal. Chem. 63*, 321−327.
(8) Terpetschnig, E., and Lakowicz., J. R. (1993) Synthesis and Characterization of Unsymmetrical Squaraines: A New Class of Cyanine Dyes. *Dyes Pigment 21*, 227−229.
(9) Terpetschnig, E., Szmacinski, H., and Lakowicz J. R. (1993) Synthesis, Spectral Properties and Photostabilities of Symmetrical and Unsymmetrical Squaraines: A New Class of Fluorophores with Long-Wavelength Excitation and Emission. *Anal. Chim. Acta 282*, 633−641.
(10) Fierz-David, H. E., and Blangey, L. (1943) Grundlegende Operationen der Farbenchemie, pp 123−124, Springer-Verlag, Wien.
(11) Illy, H., and Funderburk, L. (1968) Fischer Indole Synthesis. Direction of Cyclization of Isopropylmethyl Ketone Phenylhydrazone. *J. Org. Chem. 33*, 4283−4285.
(12) Bannwarth, H., and Knorr, R (1991) Formation of Carboxamides with N,N,N′,N′-Tetramethyl(Succinimido)Uronium Tetrafluoroborate in Aqueous/Organic Solvent Systems. *Tetrahedron Lett. 32*, 1157−1160.
(13) Bambot, S. B., Holavanahali, R., Lakowicz, J. R., Carter, G., and Rao, G. (1994) Phase Fluorometric Sterilizable Optical Oxygen Sensor. *Biotechnol. Bioeng. 43*, 1139−1145.
(14) Lakowicz, J. R., and Maliwal, B. P. (1993) Optical Sensing of Glucose Using Phase-Modulation Fluorometry. *Anal. Chim. Acta 271*, 155−164.
(15) Bambot, S. B., Romauld, M., Sipior, J., Carter, G. M., Terpetschnig, E., Lakowicz, J. R., and Rao, G. (1995), Sensing Oxygen Through Skin Using a Red Diode Laser and Fluorescence Lifetimes. *Biosensors Biotechn. 10* (6/7), 643−652.
(16) Lakowicz, J. R. (1986) *Principles of Fluorescence Spectroscopy*, 3rd ed., Plenum Press, New York, London.

BC9801023

Volume 10, Number 6, November/December

Bernhard Oswald, Leonid Patsenker, Josef Duschl, Henryk Szmacinski, Otto S. Wolfbeis, and Ewald Terpetsching*

SYNTHESIS, SPECTRAL PROPERTIES, AND DETECTION LIMITS OF REACTIVE SQUARAINE DYES, A NEW CLASS OF DIODE LASER COMPATIBLE FLUORESCENT PROTEIN LABELS

Page 925. In the address byline, FluorRx Inc., 979 Keystone Way, Carmel, Indiana 46032 should be University of Maryland School of Medicine, 725 West Lombard Street, Baltimore, Maryland 21201. In addition, in the footnotes at the lower left, ‡Fluorrx Inc. should be ‡Present address: FluorRx Inc., 979 Keystone Way, Carmel, IN 46032.

BC000019R

10.1021/bc000019r
Published on Web 05/15/2000

Synthesis and Biological Activity of Polyethylene Glycol−Mouse Nerve Growth Factor Conjugate

Nadya Belcheva, Kim Woodrow-Mumford, Melissa J. Mahoney, and W. Mark Saltzman*

School of Chemical Engineering, Cornell University, 120 Olin Hall, Ithaca, New York 14853. Received January 8, 1999; Revised Manuscript Received June 14, 1999

Conjugation of poly(ethylene glycol) derivatives with therapeutic proteins is a promising approach for enhancing protein stability and, therefore, effectiveness. An N-hydroxysuccinimidyl ester of fluorescein-PEG 2000 was used for chemical modification of mouse nerve growth factor (mNGF), a dimeric protein with therapeutic potential for Alzheimer's disease. The mNGF-PEG2000-fluorescein conjugate was characterized by RP-HPLC, spectrofluorometry, and SDS−PAGE and was biologically active, as determined by two independent NGF-specific assays (enhancement of ChAT activity in fetal neurons and neurite outgrowth in PC12 cells). The conjugate was not detectable by a standard NGF ELISA, suggesting a fortuitous reduction in protein recognition by antibodies.

INTRODUCTION

Nerve growth factor (NGF),[1] the prototypic member of the neurotrophin family of proteins, is known to be involved in the survival and maintenance of function of cholinergic basal forebrain neurons (Charles et al., 1996; Yuen et al., 1996). Mouse nerve growth factor 2.5S (mNGF) consists of two polypeptide subunits with 118 and 110 residues, respectively, in which the shorter chain has eight fewer amino acids near the NH_2-terminus (Wlodawer et al., 1975). Studies in animals suggest that NGF can reverse, halt, or slow the progression of Alzheimer's disease related atrophy (Scott and Crutcher, 1994) so there has been considerable interest in NGF as a therapeutic agent. However, NGF does not enter the brain after systemic administration, so its use in the treatment of neurological disorders is problematic. Therefore, novel protein delivery systems are needed.

A number of recent studies suggest that chemical modification of NGF can preserve biological activity, while enhancing stability and altering biodistribution. Conjugation to an antibody directed against transferrin receptor (OX-26) promoted transport across the blood-brain barrier, permitting delivery of NGF to the brain after peripheral injection (Friden et al., 1993; Kordower et al., 1994; Charles et al., 1996; Bäckman et al., 1996). Biotinylated NGF retained full binding and biological activity, as determined by a competitive radioreceptor assay and stimulation of neurite outgrowth from PC12 cells (Rosenberg et al., 1986, 1987). A highly fluorescent, biologically active rhodamine conjugate of NGF was synthesized and used to probe mobility and distribution of NGF receptors in cultured cells (Levi et al., 1980). Similar conjugates have been described for BDNF (Pardridge et al., 1998; Sakane and Pardridge, 1997), another neurotrophin with ∼50% sequence homology to NGF (Robinson et al., 1995).

The pharmacokinetic characteristics of therapeutic proteins can be altered by conjugation with synthetic polymers. Among the synthetic polymers that have been tested for protein modification, PEGs are frequently used (Zalipsky, 1995), due to their nontoxicity, biocompatiblity, high solubility in aqueous media and nonimmunogenicity (Harris and Zalipsky, 1997). Functionalized PEG derivatives are available (Shearwater Polymers, Inc.), which greatly facilitates conjugate synthesis. In this study, we sought to develop procedures for the covalent modification of mNGF using functionalized PEG derivatives.

EXPERIMENTAL PROCEDURES

Materials and Methods. All starting materials were used as received. Mouse nerve growth factor 2.5 S, grade II (mNGF 2.5S), was purchased from Boehringer Mannheim (Indianapolis, IN). Methoxy-PEG5000-amine (M-NH2-5000), *N*-hydroxysuccinimidyl ester of methoxy-PEG5000 (M-SSA-5000), *N*-hydroxysuccinimidyl ester of fluorescein-PEG2000 (Fluor-NHS-2000) were purchased from Shearwater Polymers, Inc. (Huntsville, AL).

PEGylation of mNGF. In preliminary studies, we attempted to conjugate PEG to NGF via carboxylic groups (in MES buffer) and via animo groups (in DMSO). The condensation reaction in MES was performed in 0.1 M buffer (pH 6.2−6.4) on ice. The reactants were added as follows: 50 μg (1.9 nM) of mNGF was reconstituted in 200 μL of 0.1 M MES buffer. Methoxy-PEG5000-amine, 2.5 mg (0.5 mM) dissolved in 320 μL of MES, was added to this solution in a molar ratio of PEG/carboxylic groups (24/mNGF) = 10/1. Separately, 2 mg of NHS (17.4 μM) (Aldrich) and 2 mg of EDC (10.4 μM) (Sigma) were

* To whom correspondence should be addressed. Phone: (607) 255-2657. Fax: (607) 255-1136. E-mail: saltzman@cheme.cornell.edu.

[1] Abbreviations: ChAT activity, choline acetyltransferase activity; DMSO, dimethyl sulfoxide; DTT, dithiothreitol; EDC, 1-ethyl-3-(3-dimethylaminopropyl)-carbodiimide; Fluorescein-PEG2000-NHS, *N*-hydroxysuccinimidyl ester of fluorescein-poly(ethylene glycol) with MW = 2000; MALDI-TOF mass spectrometry, matrix-assisted laser desorption ionization−time of flight mass spectrometry; MES, (4-morpholineethanesulfonic acid); Methoxy-PEG5000-amine, amino-methoxy-poly(ethylene glycol) with MW = 5000; Methoxy-PEG5000-NHS, *N*-hydroxysuccinimidyl ester of methoxy-poly(ethylene glycol) with MW = 5000; mNGF, mouse nerve growth factor; mNGF-PEG2000-fluorescein, mouse nerve growth factor, poly(ethylene glycol) 2000, fluorescein conjugate; NHS, *N*-hydroxysuccinimide; PC12, pheochromocytoma cell line; PEGs, poly(ethylene glycol)s; RP-HPLC, reversed-phase−high-performance liquid chromatography; SDS, sodium dodecyl sulfate; SDS−PAGE, sodium dodecyl sulfate−polyacrylamide gel electrophoresis.

10.1021/bc990001k CCC: $18.00 © 1999 American Chemical Society
Published on Web 08/31/1999

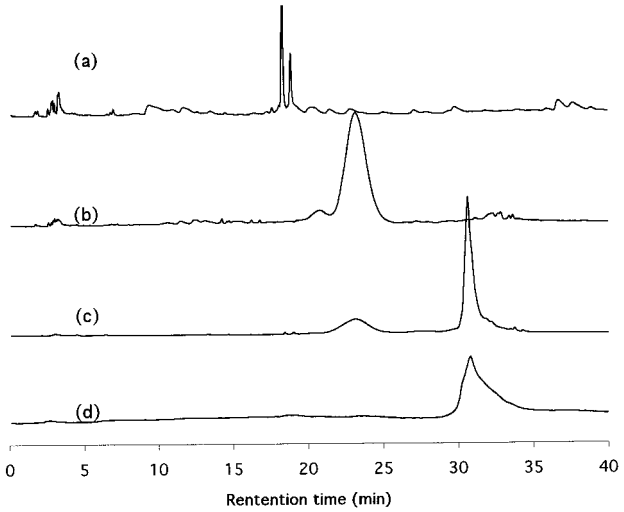


Figure 1. RP−HPLC of (a) mNGF in borate buffer (pH 8.0); (b) fluorescein-PEG2000-glycine in borate buffer (pH 8.0) after 24 h; (c) reaction mixture of mNGF with fluorescein-PEG2000-NHS in borate buffer (pH 8.0) after 24 h; (d) purifiaed mNGF-PEG2000-fluorescein conjugate after dialysis against 10 mM PBS (pH 7.4). A gradient/isocratic method was performed, 0 to 15 gradient/15 to 25 isocratic/25 to 50 gradient: gradient 0 to 80% acetonitrile (0.1% trifluoroacetic acid) for 50 min at flow rate 1 mL/min and column temperature 25 °C, monitoring at λ = 275 nm, using a Zorbax 300SB-CN 4.6 mm × 250 mm separation column.

dissolved in 200 μL of MES and added to the reaction mixture. The condensation reaction was carried out for 7 days at 4 °C under shaking. After dialysis against PBS (10 mM, pH 7.4) (MWCO = 10 000) for 7 days at 4 °C, the solution was lyophilized.

The condensation reaction in DMSO was carried out at 20 °C under stirring. In a typical procedure, 25 μg of mNGF (0.96 nM) was dissolved in 500 μL of DMSO. To this solution was added 48 μL of a methoxy-PEG5000-NHS solution in DMSO (1 mg/mL) (48 μg, 9.6 nM) in a molar ratio of PEG/mNGF = 10/1. The reaction mixture was stirred for 10 days at 20 °C, after which a 10% solution of glycine in PBS (pH 7.4) was added to deactivate the excess of methoxy-PEG5000-NHS. The reaction mixture was dialyzed (MWCO = 10 000) against PBS (pH 7.4) for 7 days.

The synthesis of mNGF-PEG2000-fluorescein conjugate was performed with mono-*N*-hydroxysuccinimidyl ester of PEG2000-fluorescein in borate buffer (pH 8.0) in a molar ratio of PEG/mNGF = 10/1. In a typical reaction, 250 μg (9.62 nM) of mNGF was reconstituted in 2.5 mL of borate buffer (pH 8.0). Fluorescein-PEG2000-NHS (192.3 μg, 96.2 nM), dissolved in DMSO (42.7 μL), was added, and the reaction mixture was stored for 24 h at 4 °C under shaking. Before dialyzing against 10 mM PBS (pH 7.4), 10 mg of BSA was added. Dialysis tubing (MWCO = 10 000) was used for purifying the conjugate from unreacted fluorescein-PEG2000-NHS as well as from the low molecular side product of the condensation reaction, NHS. The conjugation yield was estimated by RP-HPLC. The purified product was analyzed by SDS−PAGE and tested for biological activity by neurite outgrowth using PC12 cells and ChAT activity of fetal neurons.

Reversed-Phase−High-Performance Liquid Chromatography (RP-HPLC). The conjugation reaction was followed by RP-HPLC using Waters 2690 Alliance Separations Module, including Waters 996 PDA detector, on a Zorbax 300SB-CN 4.6 mm × 250 mm separation column.

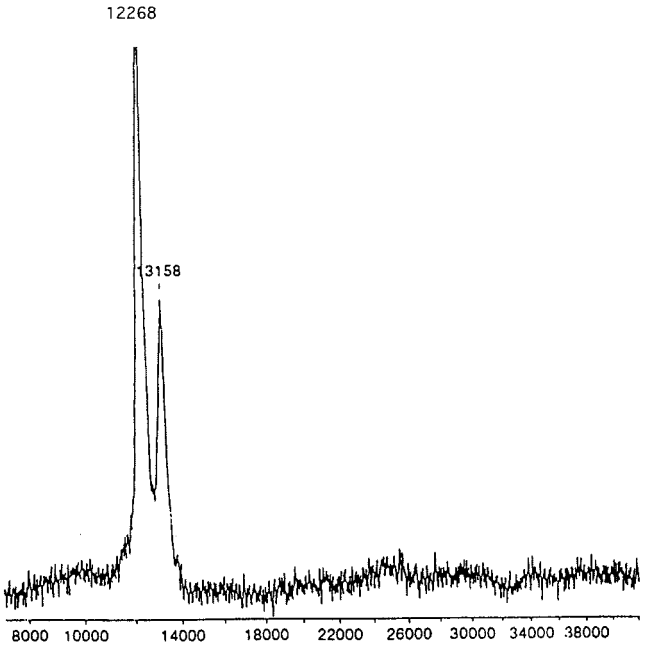


Figure 2. MALDI mass spectrum of mNGF.

An appropriate aqueous mobile phase for mNGF was found to be a gradient 0 to 80% acetonitrile (0.1% trifluoroacetic acid) at a flow rate of 1 mL/min and column temperature of 25 °C with PDA monitoring at 275 nm. A gradient/isocratic method was developed for separation of the conjugate: 0 to 15 gradient/15 to 25 isocratic/25 to 50 gradient; gradient 0 to 80% acetonitrile (0.1% trifluoroacetic acid) at a flow rate of 1 mL/min and column temperature of 25 °C, monitoring at 275 nm.

Spectrofluorometry Measurements. Fluorescence of mNGF-PEG2000-fluorescein conjugate was studied in buffered saline and supernatant of brain homogenate. Brains were retrieved from Fischer 344 rats 8−10 weeks old. The tissue was sonicated in phosphate buffer (pH 7.4) supplemented with 0.0117 g/mL NaCl and 0.5% Triton X-100. After sonication, samples were centrifuged at 14 000 rpm for 20 min at 4 °C, and the supernatant was collected. Spectra were recorded on FluoroMax-2 spectrofluorometer equipped with 150 W continuous ozone-free xenon lamp and modified Czerny-Turner spectrometers under control of DataMax spectroscopy software. Excitation (λ = 488 nm) and emission (λ = 530 nm) maxima were determined using fluorescein-PEG-NHS standard solutions for calibration. All procedures with animals were performed according to NIH guidelines and were approved by the Cornell University Institutional Animal Care and Use Committee.

Conjugate Characterization. MALDI-TOF mass spectra were obtained on a ThermoBIOANALYSIS Laser-MAT 2000 system using nitrogen laser at 337 nm and 4-hydroxy-α-cyano-cinnamic acid as a matrix (10 mg/mL in 70% acetonitrile/water).

SDS−PAGE was performed on a 18% Tris-HCl gel at room temperature for 2 h at 150 V using Mini-PROTEIN II cell (Bio-Rad) system and Bio-Rad reagents (Laemmli, 1970). Protein samples (30 mL) were solubilized and denaturated by boiling with 15 mL of SDS and DTT solution, and loaded into the wells (44 mL of each sample). Bands were visualized by silver staining.

Biological Assays for mNGF Activity. PC12 cells (pheochromocytoma cell line) were suspended in medium (85% RPMI 1640, 5% fetal bovine serum, and 10% horse serum) that was supplemented with either the conjugate

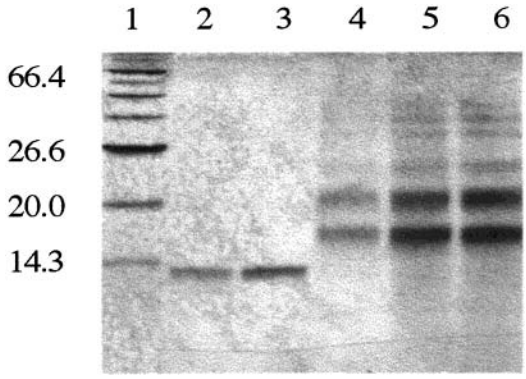


Figure 3. SDS−PAGE of (1) protein markers (each 200−400 ng); (2) mNGF (200 ng); (3) mNGF (300 ng); (4) mNGF-PEG2000-fluorescein conjugate, reaction mixture after 1 day (based on 100 ng of mNGF); 5) mNGF-PEG2000-fluorescein conjugate, reaction mixture after 1 day (based on 200 ng mNGF); and (6) mNGF-PEG2000-fluorescein conjugate, reaction mixture after 1 day (based on 300 ng mNGF).

or unmodified mNGF at concentrations in the range 0.1−800 ng/mL (based on mNGF). Twelve-well tissue culture polystyrene plates, coated with collagen (5 μg/cm^2), were seeded with the cells at a density of 5×10^4 cells/well. After 2 and 4 days of incubation, cells were examined for neurite expression.

Neural cells were retrieved from fetal rat brains at 17 days gestation as previously described (Mahoney and Saltzman, 1999). Briefly, cells were plated on poly-lysine (Collaborative Biomedical)-coated Petri dishes (2 μg/cm^2) and incubated for 24 h in sBME + 5% FBS. After this initial incubation, cells were cultured in sBME + 1% penicillin streptomycin. Medium was changed every 2−3 days. Cells were sacrificed after 4 days of culture and prepared for ChAT analysis as described previously (Mahoney and Saltzman, 1999).

The reagents and protocol for the NGF ELISA were obtained from Boehringer Mannheim Biochemicals. The wells of a microtiter plate were first coated with a monoclonal antibody directred against the subunit of mNGF and subsequently washed. Blocking buffer was added, and the wells were washed again. Samples containing the NGF conjugate were incubated on the plate at concentrations between 0.03 and 2 ng/mL (based on mass of mNGF) and mNGF standards were prepared in the concentration range 0.03 ng/mL−1 ng/mL. After incubation, the wells were treated with a secondary monoclonal antibody conjugated to β-galactosidase. CPRG, the substrate for β-galactosidase, was added to each well. Optical density measurements were obtained at 575 nm using a Thermomax plate reader with Softmax Software (Molecular Devices, Menlo Park, CA).

RESULTS

To select an appropriate reaction medium, we tested the stability of mNGF in distilled water, DMSO, MES buffer (pH 6.2−6.4) and borate buffer (pH 8.0). Using RP-HPLC, two peaks were resolved at retention time (RT) 18.5 and 19.6 min (Figure 1a), corresponding to the two polypeptide chains of mNGF. MALDI-TOF mass spectrometry confirmed the presence of two molecules with molecular mass peaks (M) at 12 268 and 13 158, respectively (Figure 2). Mouse NGF solutions were stable in MES (pH 6.2−6.4) at 4 °C for 7 days, while a 20−30% decrease in the peak area (RP-HPLC) was found for samples maintained in distilled water and borate buffer (pH 8.0) for the same period. A similar decrease in the peak area was observed with mNGF solutions in distilled water when kept frozen for 20 days at −20 °C. Chromatographic changes of mNGF in DMSO solution were complex: in addition to the usual peaks at RT = 18.5 and 19.6 min, new peaks (RT = 32.6 and 36.0 min) were detected over a period of 2 days, simultaneously with a decrease in the NGF peaks. We suspect that this sequence of changes represents slow solubilization followed by aggregation in DMSO; in any case, these changes made it difficult to identify the products of reactions, so use of DMSO was abandoned.

In preliminary studies, we attempted to react NGF with amino-PEG derivatives via activation of the carboxylic groups of the protein using water-soluble carbodiimide. Unfortunately, we could not identify experimen-

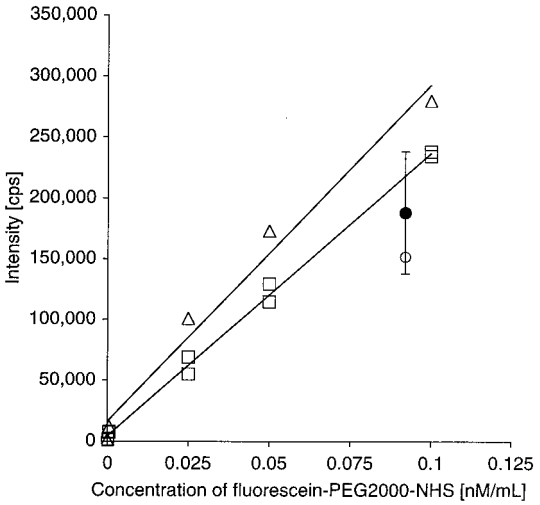


Figure 4. Fluorescence intensity (cps) of standard solutions of fluorescein-PEG2000-NHS in brain homogenate media: (□) fluorescein-PEG2000-NHS added directly to the brain sample prior to sonication and centrifugation at 14 000 rpm; (△) fluorescein-PEG2000-NHS dissolved in brain homogenate supernatant after sonication and ultracentrifugation at 14 000 rpm; (○) experimentally detected intensity of mNGF-PEG2000-fluorescein conjugate dissolved in brain homogenate prior to sonication and ultracentrifugation at a concentration of 0.046 nmol/mL (based on mNGF); (●) theoretically calculated intensity (based on the calibration) of mNGF-PEG2000-fluorescein conjugate sample dissolved in brain homogenate prior to sonication and ultracentrifugation at a concentration of 0.046 nmol/mL (based on mNGF). (Example: The theoretically calculated concentration of the tested conjugate was 0.046 nmol/mL, based on mNGF, or 0.092 nmol/mL, based on protomer chain.)

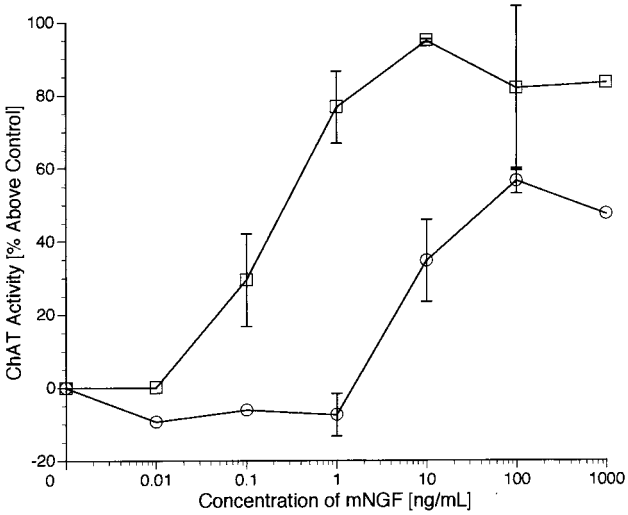


Figure 5. ChAT activity as a function of dose of mNGF (□) and mNGF-PEG2000-fluorescein conjugate (○).

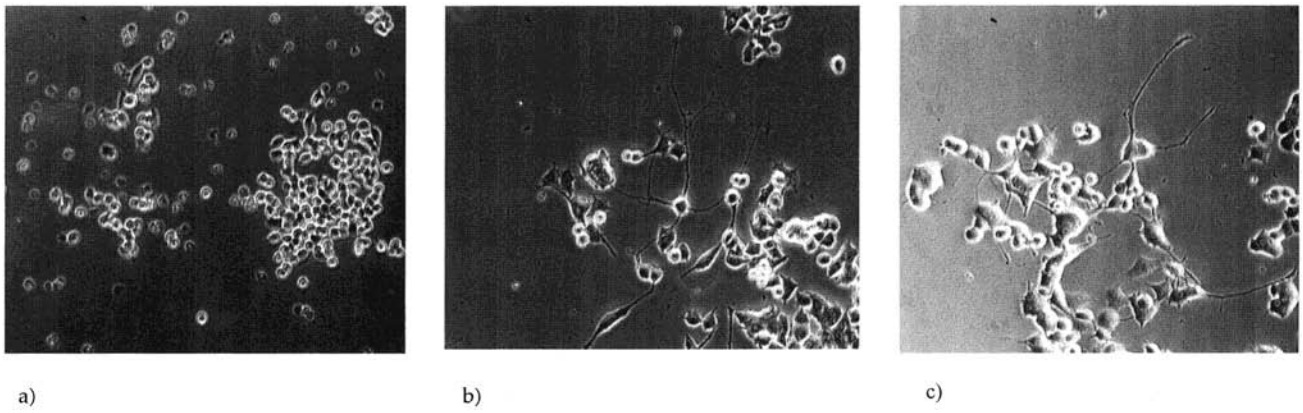


Figure 6. PC12 assay of (a) untreated cells; (b) cells exposed to native mNGF at a concentration 0.1−0.2 ng/mL; (c) cells exposed to mNGF-PEG2000-fluorescein conjugate at a concentration 3.0 ng/mL.

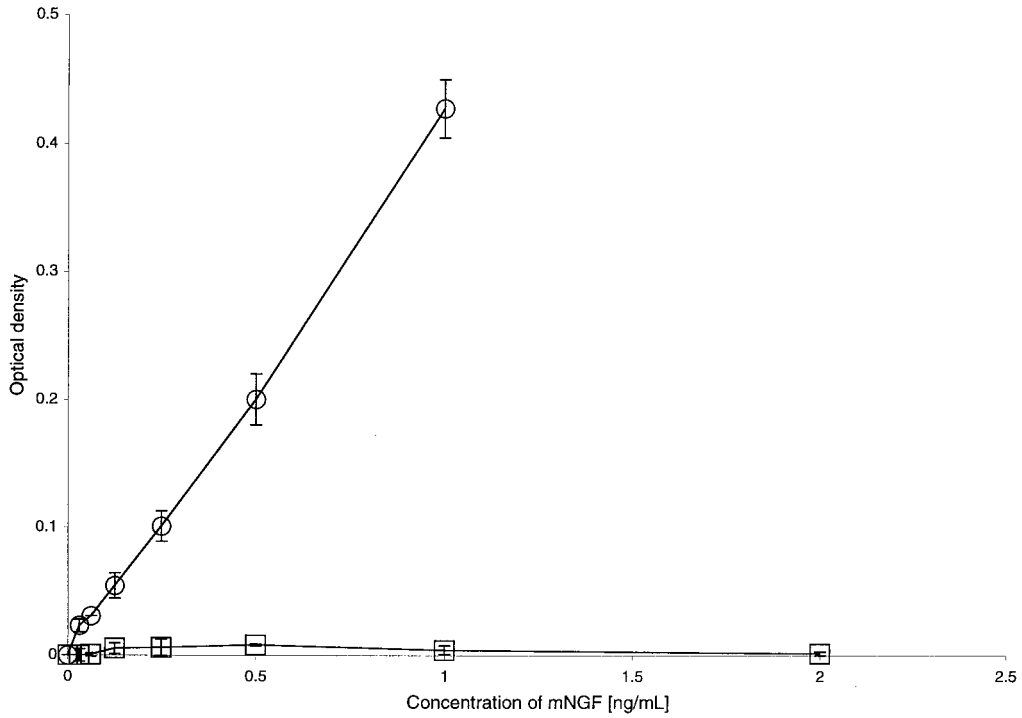


Figure 7. ELISA for mNGF (○) and mNGF-PEG2000-fluorescein conjugate (□).

tal conditions that avoided significant cross-linking of the activated protein chains. To eliminate this problem, PEGylation via protein amino groups using fluorescein-PEG2000-NHS was considered in all subsequent experiments.

Our stability data indicated that mNGF was more stable at pH 6 and that substantial degradation (up to 30%) could occur upon incubation in distilled water or borate buffer (pH 8.0). However, the higher pH was preferable for activation of the amino groups during condensation reactions with NHS esters. To identify the optimal synthetic approach, three buffer systems—10 mM PBS (pH 7.4), borate buffer (pH 8.0), and borate buffer (pH 8.5)—were tested in model reactions with fluorescein-PEG2000-NHS and glycine. Borate buffer with pH 8.0 allowed a reasonable rate of conversion and relatively low deactivation of the active ester. The presence of the fluorophore on PEG permitted simultaneous monitoring of mNGF, fluorescein-PEG2000 derivatives and the resulting conjugate (Figure 1). In a typical reaction, fluorescein-PEG-NHS was added in a 10 molar excess to mNGF. The reaction was performed for 24 h; decrease in NGF peaks suggested 95−98% conversion (Figure 1c). The new peak (RT = 30.8 min) was related to the formation of mNGF-PEG2000-fluorescein conjugate; no such peak was detected in the model systems. Excess BSA was added to the reaction mixture (to stabilize NGF conjugates), and the mixture was dialyzed against 10 mM PBS (pH 7.4) at 4 °C. The progress of purification by dialysis was monitored by following the disappearance of the fluorescein-PEG2000-glycine peak (RT = 23.0, Figure 1d).

The dialyzed conjugate was subjected to SDS−PAGE, which revealed new protein bands with molecular masses of ∼20 kDa (Figure 3, lanes 4−6). These bands were clearly different than those observed with unmodified NGF (Figure 3, lanes 2 and 3), implying that the predominant fraction consisted of mono-PEGmers of the two different mNGF chains. The formation of multi-PEGmers with higher molecular masses was also detected although their yields were much lower.

The presence of fluorophor in the purified conjugate provided a convenient marker for analysis; we measured the fluorescence in brain homogenate supernatant of known quantities of conjugate, assuming 1:1 ratio of PEG and mNGF protomer. A slight decrease in the fluores-

cence intensity was observed for the conjugate extracted from the brain tissue, implying some quenching or incomplete extraction (Figure 4). Nevertheless, the experimental results supported the assumption that the average number of PEG molecules per protein chain was 1:1.

The conjugates were biologically active. Addition of conjugate to fetal brain cell cultures stimulated ChAT activity in a dose-dependent manner (Figure 5). The conjugate was active at higher doses of mNGF (~ 10 ng/mL), suggesting that conjugation with poly(ethylene glycol) results in a slight reduction in bioactivity. Unmodified mNGF elicited neurite growth from PC12 cells at concentrations as low as 0.1−0.2 ng/mL; the mNGF-PEG2000-fluorescein conjugate stimulated neurite outgrowth at concentrations above 3ng/mL (Figure 6). Interestingly, the mNGF-PEG2000-fluorescein conjugate was not detected by a widely used NGF ELISA, suggesting that mNGF-PEG2000-fluorescein could not bind monoclonal antibodies directed against specific epitopes of unmodified mNGF (Figure 7).

DISCUSSION

NGF is a basic protein with a pI of 9.3 (Kasaian, 1994). The amino acid sequence of the NGF subunit contains 11 carboxylic and 17 basic side groups (McDonald, 1991). Carboxylic groups originate from L-glutamic acid (pK_a = 3.9) and L-aspartic acid (pK_a = 4.3); while basic groups come from L-histidine (imidazole group, pK_a=6.0), L-lysine (primary amine, pK_a=10.5), and L-arginine (guanidine group, pK_a=12.5). Decreasing the pH of the reaction medium is known to promote both the activation of the carboxylic groups and the reactivity of the water-soluble carbodiimides (Nakajima and Ikada, 1995; Hermanson, 1996). In our hands, however, activation of mNGF by this method produced substantial cross-linking of the polypeptide chains and no detectable reactivity to amino-PEG derivatives.

The crystal structure of the mNGF dimer suggests highly flexible domains at the amino terminus (residues 1−10) and the carboxy terminus (residues 112−118). These regions are likely to be solvent accessible and, therefore, susceptible to proteolytic modification (McDonald et al., 1991; Shamovsky et al., 1996). The relative reactivity of the amino- and carboxy-terminal ends is still unknown. Rosenberg et al. reported a dose-dependent loss of receptor binding activity after biotinylation of NGF via amino groups, suggesting that carboxyl end groups were accessible to modification and not critically involved in biological activity (Rosenberg et al., 1986). However, Drinkwater et al. found that the seven most carboxyl-terminal amino acids were crucial in mediating receptor recognition and ligand binding (Drinkwater, 1993).

By varying the reaction conditions, we formed conjugate from mNGF and fluorescein-PEG2000-NHS in pH 8.0 borate buffer. The conjugate was identified by RP-HPLC and purified by extensive dialysis. On the basis of the fluorescence intensity of conjugate solutions, we estimated that approximately one fluorescein-PEG2000 chain was attached to each of the polypeptide chains of mNGF.

In summary, reaction of mNGF with fluorescein-PEG2000-NHS led to the formation of mNGF-PEG conjugate. The new fluorescein-labeled conjugate was biologically active in two NGF specific assays, yet undetected by mNGF specific antibodies in an ELISA. This new compound, mNGF-PEG2000-fluorescein, may have future applications in treatment of neurodegenerative diseases.

ACKNOWLEDGMENT

The authors thank Dr. Dan Luo for useful discussions concerning SDS-PAGE results. Financial support was provided by a grant from NASA (NAG-9-654).

LITERATURE CITED

Bäckman, C., Rose, G., Hoffer, B., Henry, M., Bartus, R., Frieden, P., and Granholm, A. (1996) Systemic administration of a nerve growth factor conjugate reverses age-related cognitive dysfunction and prevents cholinergic neuron atrophy. *J. Neurosci. 16* (17), 5437−5442.

Charles, V., Mufson, E., Frieden, P., Bartus, R., and Kordower, J. (1996) Atrophy of cholinergic basal forewbrain neurons following excitotoxic cortical lesions is reversed by intravenous administration of an NGF conjugate. *Brain Res. 728*, 193−203.

Drinkwater, C., Barker, P., Suter, U., and Shooter, E. (1993) The carboxyl terminus of nerve growth factor is required for biological activity. *J. Biol. Chem. 268* (31), 23202−23207.

Frieden, P., Walus, L., Watson, P., Doctrow, S., Kozarich, J., Bäckman, C., Bergman, H., Hoffer, B., Bloom, F., and Granholm, A. (1993) Blood-brain barrier penetration and in vivo activity of an NGF conjugate. *Science 259* (15 January), 373−377.

Harris, M., and Zalipsky, S. (1997) Poly(ethylene glycol) chemistry and biological applications. *ACS Symp. Ser. 680.*

Hermanson, G., (1996) Zero-length Cross-linkers; Tags and Probes. *Bioconjugate techniques*, pp 169−186, 297−416, Academic Press, Inc.

Kasaian, M., Jacobberger J., and Neet K. (1994) Flow cytometric analysis of fluorescein-labeled nerve growth factor binding to A875 human melanoma cells. *Exp. Cell Res. 210*, 77−85.

Kordower, J., Charles, V., Bayer, R., Bartus, R., Putney, S., Walus, L., and Frieden, P. (1994) Intravenous administration of a transferrin receptor antibody-nerve growth factor conjugate prevents the degeneration of cholinergic striatal neurons in a model of Huntington disease. *Proc. Natl. Acad. Sci. U.S.A. 91*, 9077−9080.

Laemmli, U.K. (1970) Cleavage of structural proteins during the assembly of the head of bacteriophage T4. *Nature 227* (259), 680−685.

Levi, A., Shechter, Y., Neufeld, E., and Schlessinger, J. (1980) Mobility, clustering, and transport of nerve growth factor in embryonal sensory cells and in a sympathetic neuronal cell line. *Proc. Natl. Acad. Sci. U.S.A. 77* (6), 3469−3473.

Mahoney, M., and W. M. Saltzman (1999) Cultures of cells from fetal rat brain: methods to control composition, morphology, and biochemical activity. *Biotechnol. Bioeng. 62* (4), 461−467.

McDonald, N., Lapatto, R., Rust, J., Gunning, J., Wlodawer, A., and Blundell, T. (1991) New protein fold reveald by a 2.3-Ä resolution crystal structure of nerve growth factor. *Nature 354*, 411−414.

Nakajima, N., and Ikada, Y. (1995) Mechanism of amide formation by carbodiimide for bioconjugation in aqueous media. *Bioconjugate Chem. 6*, 123−130.

Olson, L. (1993) NGF and the treatment of Alzheimer's disease. *Exp. Neurol. 124*, 5−15.

Pardridge, W. M., Wu, D., and Sakane, T. (1998) Combined use of carboxyl-directed protein pegylation and vector-mediated blood-brain barrier drug delivery system optimizes brain uptake of brain-derived neurotrophic factor following intravenous administration. *Pharm. Res. 15* (4), 576−582.

Robinson, R., Radziejewski, C., Stuart, D., and Jones, Y. (1995) Structure of the brain-derived neutrophic factor/neutrophin 3 heterodimer. *Biochemistry 34* (13), 4139−4146.

Rosenberg, M., Hawrot, E., and Breakefield, X. (1986) Receptor binding activities of biotinylated derivatives of β-nerve growth factor. *J. Neurochemistry 46* (2), 641−647.

Rosenberg, M., Breakefield, X., and Hawrot, E. (1987) Targeting of liposomes to cells bearing nerve growth factor receptors

mediated by biotinylated nerve growth factor. *J. Neurochem. 48* (3), 865−875.

Sakane, T., and Pardridge, W. M. (1997) Carboxyl-directed pegylation of brain-derived neurotrophic factor markedly reduces systemic clearance with minimal loss of biologic activity. *Pharm. Res. 14* (8), 1085−1091.

Scott, S. A., and Crutcher, K. A. (1994) Nerve growth factor and Alzheimer's disease. *Rev. Neurosci. 5* (3), 179−211.

Shamovsky, I., Ross, G., Riopelle, R., and Weaver, D. (1996) Theoretical studies on the bioactive conformation of nerve growth factor using VBMC−a novel variable basis Monte Carlo simulated annealing algorithm for peptides. *J. Am. Chem. Soc. 118,* 9743−9749.

Shearwater Polymers, Inc., Polyethylene Glycol derivatives, technical data.

Wlodawer, A., Hodgson, K., and Shooter, E. (1975) Crystallization of nerve growth factor from mouse submaxillary glands. *Proc. Natl. Acad. Sci. U.S.A. 72* (3), 777−779.

Yuen, E., Howe, C., Li, Y., Holtzman, D., and Mobley, W. (1996) Nerve growth factor and the neurotrophic factor hypothesis. *Brain Dev. 18,* 362−368.

Zalipsky, S. (1995) Chemistry of poly(ethylene glycol) conjugates with biologically active molecules. *Adv. Drug Deliv. Rev. 16,* 157−182.

BC990001K

Effects of Dextranation on the Pharmacokinetics of Short Peptides. A PET Study on mEGF

Qinghai Zhao,[†] Vladimir Tolmachev,*[,†] Jörgen Carlsson,[†] Hans Lundqvist,[†] Johanna Sundin,[†,‡] Jan-Christer Janson,[§,||] and Anders Sundin[‡]

Biomedical Radiation Sciences, Box 535, Uppsala University, S-751 21 Uppsala, Sweden, Department of Diagnostic Radiology, Uppsala University and Uppsala University PET-Centre, Uppsala University Hospital, S-751 85 Uppsala, Sweden, Pharmacia Biotech AB, S-751 82 Uppsala, Sweden, and Centre of Surface Biotechnology, Uppsala Biomedical Centre, Box 577,S- 751 23 Uppsala, Sweden. Received January 27, 1999; Revised Manuscript Received June 1, 1999

The effects of dextranation on the biodistribution of mouse epidermal growth factor (mEGF, 6 kDa) were assessed. By reductive amination, mEGF was coupled to 13 and 46 kDa dextran. The two dextranated conjugates and free mEGF were labeled with the positron-emitting nuclide ^{76}Br ($T_{1/2}$ = 16 h). After intravenous administration to Sprague Dawley rats, the radioactivity biodistribution was evaluated by positron emission tomography (PET) and by measurements of dissected tissues. The dextranation prolonged the retention time in blood, especially when the dextran chain was long. [^{76}Br]-mEGF−dextran conjugates were shown to have significantly, more than 5 times, lower kidney accumulation than the nonconjugated [^{76}Br]mEGF. In conclusion, dextranation affects the biodistribution of mEGF in vivo giving a prolonged circulation time, a decreased uptake in kidney, and an increased spleen accumulation.

INTRODUCTION

Epidermal growth factor (EGF) is a short (53 residues, 6 kDa) regulatory protein, which is involved in growth and maturation of epithelial tissues in homeostasis as well as wound healing. The binding of EGF to the extracellular part of the EGF−receptor, EGFR, induces the signal pathway, ultimately leading to DNA replication and cell proliferation (*13*). The EGFR is overexpressed in some tumors and may therefore serve as a potential diagnostic and therapeutic target in some malignancies such as gliomas, bladder cancers, squamous cell carcinomas, and some forms of adenocarcinomas (*14*−*18*).

EGF injected intravenously (iv) has a fast blood clearance. Only 7% of the radioactivity remained in blood 2.5 min after iv administration of [^{125}I]EGF (*20*). Intravenously injected EGF is taken up by the liver. It is also to a high extent accumulated in the kidney, which is typical for short peptides such as octreotide, vasoactive intestinal peptide (VIP), or single chain Fv (*19*−*23*). Even in animals with tumors expressing high numbers of EGF receptors, the dominating EGF uptake is in the liver and kidney (*21*). Studies of human lung cancer have, however, shown a higher uptake in tumors expressing EGF receptors than in receptor negative tumors (*34*).

Glycosylation has been shown to improve the stability and prolong the retention time of proteins in vivo in mice after iv injection (*24, 25*). In this study, we used dextran for protein glycosylation. Dextran is a glucose polymer in which glucose units are bound to each other by α1−6 linkages. The branching of the dextran structure is approximately 5% and comprises mostly α1−3 linkages. By sequential degradation, which quantitatively removes nonreducing end groups, it has been found that about 40% of the side chains are only one glucose (*1, 2*). For clinical application, dextran is usually produced by fermentation using the microbes *Leuconostoc mesenteroides* NRRL B-512 (F) or the B-512 strain (*1, 3, 4*).

In the clinic, dextran is used worldwide as the plasma volume expander of choice, applied to treat shock caused by hemorrhage, burns, surgery, or trauma (*3*−*5*). An interesting application of dextran is its conjugation to biologically active substances with the aim to prolong their biological half-life and to increase their stability in vivo (*6, 7*). Dextran may also act as a carrier for various cytotoxic drugs and radioisotopes in targeted therapy and may, in addition, reduce the antigenicity of biomolecules (*8*−*12*).

The primary aim of this paper was to study general changes in the kinetics of dextranated molecules. However, a secondary interest was to see if dextranated EGF could be modified to increase the circulation time and to lower the normal tissue uptake, thus improving the targeting properties. EGF was chosen as a suitable biomolecule since it is known to have a dominating and fast receptor-mediated liver uptake and that small changes in the uptake kinetic should be possible to perceive fairly easily. The mEGF−dextran conjugates were prepared by reductive amination, in which the end aldehyde group of dextran reacted with the only amino group on the N terminal of mEGF (*26*). A positron-emitting nuclide, ^{76}Br ($T_{1/2}$ =16 h), was used to label mEGF and the mEGF−dextran conjugates in order to apply positron emission tomography (PET) for the assessment. PET was used since it can follow fast kinetic changes in vivo. It also has a spatial resolution, which

* To whom correspondence should be addressed. Phone: (46) 18-4713840. Fax: (46) 18-4713432. E-mail: Vladimir.Tolmachev@bms.uu.se.
[†] Biomedical Radiation Sciences.
[‡] Department of Diagnostic Radiology.
[§] Pharmacia Biotech AB.
[||] Centre of Surface Biotechnology.

10.1021/bc990011l CCC: $18.00 © 1999 American Chemical Society
Published on Web 09/24/1999

makes it possible to distinguish the liver uptake from any other organ in the rat. Excised tissues were also measured for radioactivity content in the body.

MATERIAL AND METHODS

Conjugation. Freeze-dried dextran weighting of 13 kDa (D13) and 46 kDa (D46) was obtained by fractionation of Dextran T10 or T40 (Pharmacia Biotech AB, Sweden) by gel filtration on Sephacryl 100 HR (Pharmacia Biotech AB, Sweden). Sodium cyanoboronhydride ($NaCNBH_3$, Merck-Schuchardt, Germany), mEGF (tissue culture grade, Janssen Biochimica, Belgium), and ^{125}I (Amersham Laboratories, England) were used as received from the manufacturer.

The mEGF−dextran conjugates were produced by reductive amination as previously reported (*26*). Dextran D13 or D46 (20 mg, 1.54 and 0.43 μmol, respectively) was dissolved in 100 μL mEGF (25 μg, 4.17 nmol) in 0.05 M phosphate buffer solution, pH 8.0. To this, $NaCNBH_3$ (8 mg, 127 μmol) was added and the reaction was allowed to continue for 24 h at room temperature during continuous stirring. The reductive amination reaction mixture was applied to a Sephadex G-50 Fine (Pharmacia HR 10/30) column (Pharmacia Biotech AB, Sweden), and the conjugate was eluted with distilled water at a flow rate of 0.25 mL/min and a fraction volume of 0.5 mL. The fractions containing conjugate were pooled and freeze dried.

Bromination. Br-76 was produced at the Uppsala PET Centre, Uppsala, Sweden, by the $^{76}Se(p,n)^{76}Br$ reaction using ^{76}Se-enriched Cu_2Se as target. Radiobromine was separated from target material by dry distillation (*27*). About 150−200 MBq ^{76}Br was obtained in 100 μL of ethanol after separation. The ethanol was evaporated, and freeze-dried mEGF−dextran conjugate (15−20 μg) or mEGF (20 μg) dissolved in 30 μL of citrate-phosphate buffer (pH 4, 0.05 M) was added. Adding 10 μL of Chloramine-T (4 mg/mL in 0.05 M citrate-phosphate buffer, pH 4.0) started labeling. After the solution was mixed for 3 min, the reaction was quenched with 20 μL of sodium bisulfite (4 mg/mL in 0.05 M citrate-phosphate buffer, pH 4.0). Purification was performed on a NAP-5 column (Sephadex G-25, Pharmacia Biotech AB, Sweden) equilibrated and eluted with PBS. Fractions of 0.2 mL were collected and measured for radioactivity. The high-molecular-weight fractions were pooled and used in the cell test and animal experiment.

Cell Test. A subclone (U-343MGaC12:6) of a glioma cell line U-343 was grown in HAM'S F-10 culture media (Kebo, Stockholm, Sweden), supplemented with FCS, L-glutamine, penicillin, and streptomycin, in culture dishes. Brominated mEGF−dextran conjugates and mEGF, respectively, were mixed in culture media or in the culture media containing 1 μg/mL mEGF. The incubation experiments were carried out in triplicates. After 90 min of incubation at 37 °C, the cultures were washed 6 × 1 min with HAM'S F-10 media and trypsinized. The number of cells was determined in a cell counter (Coulter ZM, Coulter Electronics Ltd, U.K.) and analyzed for cell-associated radioactivity in a γ-counter (1480 Wizard γ-counter, Wallac, Finland).

Animals. Fourteen Sprague Dawley male rats weighing 350 ± 120 g (mean ± SD) from BK Universal AB (Stockholm, Sweden) were used. After arrival at the animal department, the rats were allowed to condition for 10 days before the experiment. For anesthesia, the rats were injected intraperitoneally with 0.24−0.3 mL/100 g body weight of thiobutabarbital sodium salt 5 mg/mL (Inactin, RBI, MA).

PET Imaging. Through a groin incision, the right femoral vein was isolated and cannulated with a plastic catheter to ensure iv injection of the tracers. The rats, placed in a plastic multicompartment holder, were positioned in a Scanditronix GE 2048 PET scanner (Scanditronix, Uppsala, Sweden), which simultaneously produces 15 contiguous 6.5 mm tomographic slices and has an in-plane resolution of 5−6 mm. Before injection, a 10 min transmission scan was performed to enable attenuation corrections of the emission scan. After a rapid iv bolus of 3−10 MBq of [^{76}Br]mEGF and [^{76}Br]mEGF−dextran conjugates, a dynamic sequence was started and continued for 1 or 2 h, respectively. Tomograms were reconstructed using a 128 × 128 image matrix and a 6 mm Hanning filter. Data were corrected for attenuation and scattered radiation. The regional radioactivity concentration measured by PET was divided by injected radioactivity per gram of body weight to provide images of standardized uptake values (SUV). Regions of interest (ROI), representing liver, heart, blood, kidney, muscle, and urinary bladder, were drawn manually in the SUV images and time−activity curves were calculated and plotted.

Pharmacokinetic Analysis. Clearance of radioactivity from blood was analyzed by fitting a dual exponential function to data, $SUV = Ae^{-at} + Be^{-bt}$, using the least-squares method where A and B are constants, a and b are clearance rates, and t is time after injection.

The impact of dextranation to the blood kinetics was tested statistically. To accentuate the early, rapidly changing blood kinetics, a constant steady-state radioactivity level appearing in all the blood curves was subtracted. The time integral of the resulting radioactivity curve, divided by the maximum value, was calculated for each animal. The obtained values, the transit times, for each experimental group were tested by a two-samples Student's t-test.

The early uptake phase in the liver, i.e., the first minutes after injection, was analyzed by a simple two compartment model assuming that all radioactivity passing the liver was trapped in the liver. This can mathematically be described as

$$C_L(t) = k_1 * \int_0^t C_b(S)\, dS + \epsilon C_b(t)$$

where C_L is the radioactivity concentration in liver, C_b is the radioactivity concentration in blood, k_1 is the rate constant (min^{-1}), and ϵ is the blood volume.

The late phase of the liver uptake, i.e., the part where the liver starts to lose radioactivity was analyzed by fitting data by the least-squares method to a simple exponential function, $SUV = Ae^{-at}$, where A is a constant, a is the clearance rate of radioactivity, and t is the time after injection.

Kinetic analysis was also performed according to Patlak et al. (*28*) where the transport rate of ligand into the tissues, generated on a pixel by pixel basis was presented as images. The radioactivity concentration in blood obtained from a ROI over the heart blood pool was used as the input function. In the Patlak graphs, $Y = C_i/C_b$ was plotted against $X = \int C_b(t)\, dt/C_b(t)$, where C_i = tissue radioactivity concentration and C_b = radioactivity concentration in the blood at time t. This graphical representation is, after onset of a dynamic equilibrium, equivalent to a situation, where the blood radioactivity concentration is constant throughout the examination. For a radiolabeled compound that is trapped in the tissue, the graph shows a linear increase over time, whereas a

Table 1: Receptor Binging Test for [^{76}Br]mEGF and [^{76}Br]mEGF-Dextran Conjugate[a]

	cell associated radioactivity (cpm/10^5 cells)	
	presaturated receptors	not presaturated receptors
76Br-mEGF	3130 (410)	22 630 (1400)
76Br-mEGF-dextran	5570 (310)	12 240 (920)

[a] Test was performed on a glioma cell line U-343. For presaturation of the EGFR, 1 μg/mL mEGF was added. Cell were incubated with labeled compounds during 90 min, than washed three times. Data are presented as mean values from three dishes and maximum errors.

compound equilibrating in the tissue gives a constant value after a while. In a situation where the compound is heavily degraded and the radioactivity concentration in blood, at later times, may be dominated by labeled metabolites, the graphical presentation can show a negative slope after the initial equilibrium.

Tissue Measurements. After PET scanning, the animals were killed at different times after tracer injection. Samples of blood and urine were collected and various organs were excised, weighed, and measured for radioactivity in the γ-counter. The accumulation index (AI) of each tissue was calculated, after decay correction, according to the formula

$$\mathrm{AI} = \frac{(\text{tissue radioactivity/tissue weight})}{(\text{injected radioactivity/body weight})}$$

Assuming a tissue density of 1 g/cm^3, AI corresponds to the SUV. The use of AI for studies of biodistribution of small molecules enables comparison of data obtained from animals with different body weight and, to a certain extent, even between different species, e.g., mice and rats.

Chromatography. Serum and urine were analyzed by gel filtration with a Sephadex G-50 Fine (1 × 50 cm) column coupled with a FPLC system (Pharmacia Biotech AB, Uppsala, Sweden). The column was eluted with PBS with a flow rate of 0.5 mL/min. Fractions of 1 mL were collected and measured for radioactivity content. By calibrating the column with a conjugate (>10 kDa), mEGF (6 kDa) and salt, the high-molecular-weight (HMW) position, the mEGF position, and the low-molecular-weight (LMW) position, respectively, were defined in the chromatogram. Since the conjugates were desalted before the animal experiment and the fractionation range for globular protein with Sephadex G-50 Fine is within $(1.5 \times 10^3)-(3 \times 10^4)$ kDa, the radioactivity eluted at the salt position was considered to represent degraded fragments of mEGF.

RESULTS

Radiolabeled Conjugates. The labeling yield of bromination varied from 15 to 30%. To ensure that the EGF−receptor binding ability of the different preparations was retained before starting the biodistribution experiments, each batch was tested by incubating the [^{76}Br]mEGF and [^{76}Br]mEGF−dextran conjugates with U343 cells as described in the Material and Methods. The data concerning cell-binding tests are given in Table 1. The results of the tests demonstrated specific binding of conjugates to EGF−receptor-expressing cells, since it can be displaced by nonradioactive mEGF.

PET Pharmacokinetics. The *blood* pharmacokinetics of the different preparations measured by PET are presented in Figure 1 for the first 10 min of the experiments. All curves showed a marked two-phase behavior with an early rapid phase (mean rate constant $a = 2.28$, 1.85, and 0.58 min^{-1} for the [^{76}Br]mEGF, [^{76}Br]mEGF-D13, and [^{76}Br]mEGF-D46, respectively) and a slow phase (mean clearance rate $b = 0$, 0.06, and 0.01 min^{-1} for the [^{76}Br]mEGF, [^{76}Br]mEGF-D13, and [^{76}Br]mEGF-D46, respectively).

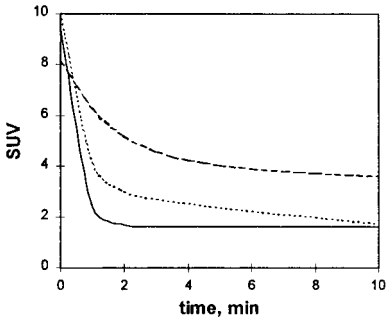


Figure 1. The kinetic standard uptake values (SUVs) of [^{76}Br]-mEGF (solid line), [^{76}Br]mEGF−dextran D13 (dotted line), and [^{76}Br]r-mEGF−dextran D46 (dashed line) in blood evaluated by PET. The experiment animals were Sprague Dawley male rats. The curve fittings were done with a formula $\mathrm{SUV} = Ae^{at} + Be^{bt}$ to evaluate the uptake within 10 min PI. [^{76}Br]mEGF, [^{76}Br]-mEGF D13, and [^{76}Br]mEGF D46 have designated b values of 0, −0.06, and −0.01, respectively. Each curve represents the result of one rat.

The transit times in blood for [^{76}Br]mEGF, [^{76}Br]-mEGF-D13, and [^{76}Br]mEGF-D46 were found to be 0.68 ± 0.18, 1.97 ± 0.37, and 5.14 ± 1.15 min (mean ± standard deviation), respectively. The differences between the different values were proved to be statistically significant in a paired t-test, giving the results [^{76}Br]-mEGF minus [^{76}Br]mEGF-D13 ($p < 0.007$), [^{76}Br]mEGF minus [^{76}Br]mEGF-D46 ($p < 0.01$), and [^{76}Br]mEGF-D13 minus [^{76}Br]mEGF-D46 ($p < 0.02$).

The liver pharmacokinetics of the three brominated compounds measured by PET are shown in Figure 2. There was a fast radioactivity uptake in the liver, which leveled out after a few minutes. After 20 min, there was a pronounced decrease in the SUV values indicating a loss of radioactivity from the liver for all three ligands although the loss was most rapid for the mEGF. The mean clearance rate of this radioactivity between 20 and 60 min was calculated to be 0.01, 0.007, and 0.006 min^{-1} for [^{76}Br]mEGF, [^{76}Br]mEGF-D13, and [^{76}Br]mEGF-D46, respectively.

The liver pharmacokinetics plotted according to the Patlak method is seen in Figure 3. All three plots show a pronounced decrease after a few minutes, which indicated a considerable influence of labeled metabolites in the analyzes. The first half-minute was analyzed using a simple linear model to compare the initial liver increase of the three ligands. The mean increase was found to be 2.14, 1.84, and 2.23 min^{-1} for [^{76}Br]mEGF, [^{76}Br]mEGF-D13, and [^{76}Br]mEGF-D46, respectively.

The uptake in the kidneys was also rapid and rather high for all three ligands. However, the variation in the pharmacokinetic pattern varied considerably between animals. The uptake of [^{76}Br]mEGF reached rapidly a plateau but showed no significant decrease with time. Radioactivity appeared in the urinary bladder 20−40 min PI for all three [^{76}Br]compounds. The kinetic pattern was similar for all three ligands although uptake values varied greatly (Figure 4).

Table 2 summarizes the PET results of the kinetic studies in which different mathematical models have been applied.

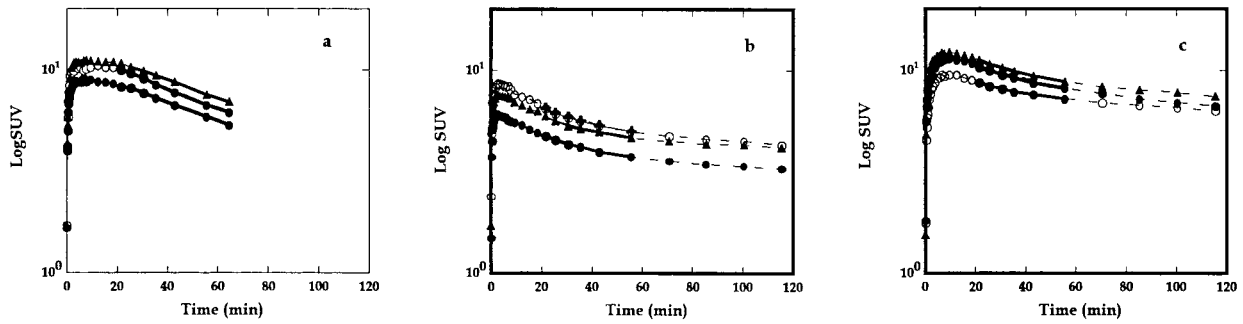


Figure 2. The kinetic standard uptake values (SUVs) of [^{76}Br]mEGF (a), [^{76}Br]mEGF−dextran D13 (b), and [^{76}Br]mEGF−dextran D46 (c) in liver evaluated by PET. The experiment animals are Sprague Dawley rats. The curve fittings were done with a formula $SUV = Ae^{at}$ between 20 and 60 min PI to evaluate the clearance after 20 min PI. Each curve represents the result of one rat.

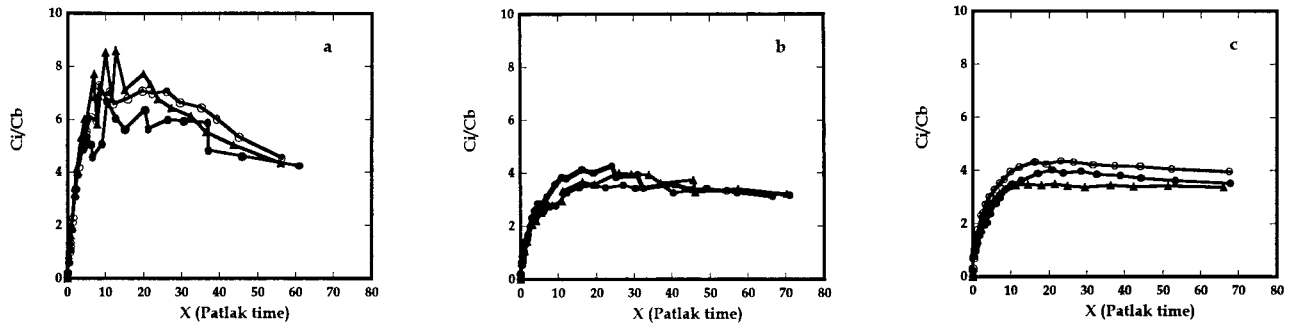


Figure 3. Patlak plot of [^{76}Br]mEGF (a), [^{76}Br]mEGF−dextran D13 (b), and [^{76}Br]mEGF−dextran D46 (c) in liver of PET study according to a two-compartment model. The experiment animals are Sprague Dawley rats. The curve fittings were done with the formula $C_i/C_b = A + BX$ between 0 and 0.5 Patlak time where $X = \int C_b(t)\, dt/C_b(t)$. Each curve represents the result of one rat.

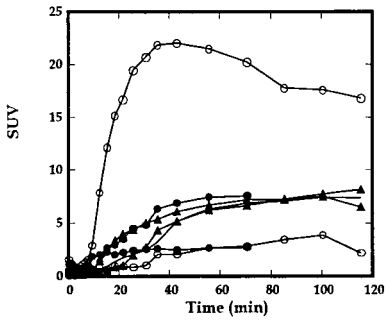


Figure 4. The kinetic standard uptake values (SUVs) of [^{76}Br]-mEGF (filled circles), [^{76}Br]mEGF−dextran D13 (open circles), and [^{76}Br]mEGF−dextran D46 (filled triangles)in urinary bladder evaluated by PET. The experiment animals are Sprague Dawley male rats. Each curve represents the result of one rat.

Measurements on Excised Tissues. The ^{76}Br accumulation at different times postinjection (PI) was measured in excised organs and tissues after intravenous injection of [^{76}Br]mEGF, [^{76}Br]mEGF−dextran D13, and [^{76}Br]mEGF−dextran D46 (Table 3). High radioactivity concentrations were measured in the urine. At 1 h PI, the dextranated conjugates were compared with mEGF. The AI for all three compounds was found to be high in the liver. The spleen showed high AI values for the dextranated compounds only, whereas the opposite was true for the kidney. In blood, AI ranged 1.4−2.4 with the lowest value for [^{76}Br]mEGF. The small intestine and colon showed higher AI for [^{76}Br]mEGF than for the dextranated compounds. In all other tissues the AI was low for all three preparations.

Chromatographic Analysis. The chromatograms of serum and urine sample are shown in Figure 5. Two hours PI, the ratio of LMW to HMW in serum was significantly lower for [^{76}Br]mEGF−dextran D46 than for [^{76}Br]mEGF−dextran D13 and [^{76}Br]mEGF. No radioactive peaks corresponding to the mEGF position were found in the serum chromatograms (Figure 5, panels a−c), not even when mEGF without dextran was administered. A radioactivity peak corresponding to mEGF was found in urine after the injection of [^{76}Br]mEGF. This was not the case for the dextranated compounds (Figure 5, panels d−f).

DISCUSSION

The aim of this study was to investigate if dextranation of a peptide changed its in vivo pharmacokinetics and biodistribution. EGF administered iv into rats was expected to be a sensitive test system since EGF is known to be effectively removed from the circulation by receptor-mediated trapping in the liver and through kidney excretion. Even a small change in the pharmacokinetic pattern due to dextranation should thus be detected. Due to the fast pharmacokinetics of mEGF, PET was used since this technique allows measurements with high temporal and spatial resolution. During the first minutes PI when free intact ligand still circulated in plasma, the measuring time was 10 s/time frame. The spatial resolution of about 6−7 mm made it possible to study the pharmacokinetics separately in liver and kidney in the rat. However, due to the limited spatial resolution, PET generally tends to underestimate the radioactivity uptake in small organs (*30*). Also, the 6.5 mm tomographic slice may only include a part of an organ, which also will change the absolute value of the measurements due to partial volume effect. In the measurements of kidney radioactivity in vivo, the spatial resolution of PET is insufficient to discriminate the radioactivity related to urine from that related to renal tissue. Thus, PET allows accurate pharmacokinetic measurements although absolute quantification of tracer uptake in the small organs of the rat may be less dependable.

Human EGF and mEGF are both 53 amino acid long peptides, with 37 amino acids in common, and with three

Table 2: Pharmacokinetics Evaluation by PET of Intravenous Administered [^{76}Br]mEGF, [^{76}Br]mEGF−dextran (D13), and [^{76}Br]mEGF-Dextran (D46) Conjugates in Sprague Dawley Rats[a]

tissue/conjugate	time	formula	*A*	*a*	*B*	*b*
blood						
[^{76}Br]mEGF	0−10 min PI	$SUV = Ae^{-at} + Be^{-bt}$	7.9	2.28	1.6	0
[^{76}Br]mEGF-D13			6.8	1.85	3.2	0.06
[^{76}Br]mEGF-D46			4.1	0.58	4.0	0.01
liver						
[^{76}Br]mEGF	20−60 min PI	$SUV = Ae^{-at}$	12.2	0.01		
[^{76}Br]mEGF-D13			6.5	0.007		
[^{76}Br]mEGF-D46			11.3	0.006		
liver						
[^{76}Br]mEGF	0−0.5 *P* time*	$C_i/C_b = A + BX$	0.006		2.14	
[^{76}Br]mEGF-D13			0.009		1.84	
[^{76}Br]mEGF-D46			0.074		2.23	

[a] *P* time is Patlak time; *X* is Patlak time, $X = \int C_b(t)\, dt/C_b(t)$. Data represent the mean values of three curve fittings for each compound.

Table 3: Accumulation Index (AI) for [^{76}Br]mEGF and [^{76}Br]mEGF-Dextran Conjugates 1 h after Intravenous Administration in Sprague Dawley Rats[a]

	[^{76}Br]mEGF	[^{76}Br]mEGF-D13	[^{76}Br]mEGF-D46
blood	2.4 (0.2)	1.4 (0.1)	2.0 (0.0)
urinary bladder	3.0 (0.4)	2.1 (0.4)	1.0 (0.4)
kidney	8.7 (1.5)	0.1 (0.1)	1.6 (0.1)
spleen	1.5 (0.1)	7.3 (1.6)	7.6 (0.0)
pancreas	1.8 (0.2)	0.5 (0.1)	0.5 (0.0)
liver	5.6 (0.2)	6.2 (0.1)	6.0 (0.4)
stomach	1.8 (0.2)	0.6 (0.0)	0.5 (0.0)
small intestine	2.9 (0.6)	0.7 (0.1)	1.1 (0.2)
colon	1.5 (0.1)	0.4 (0.0)	0.4 (0.0)
heart	1.0 (0.1)	0.5 (0.0)	0.6 (0.1)
lung	1.9 (0.1)	1.5 (0.7)	0.9 (0.0)
muscle	0.5 (0.0)	0.2 (0.0)	0.2 (0.0)
bone	1.2 (0.1)	0.6 (0.2)	0.5 (0.0)
skin	1.2 (0.1)	0.5 (0.0)	0.5 (0.1)
testicle	0.8 (0.0)	0.3 (0.0)	0.3 (0.0)
brain	0.4 (0.1)	0.1 (0.0)	0.1 (0.0)
thyroid	1.4 (0.2)	0.4 (0.1)	0.4 (0.1)
submandibular gland	1.8 (0.1)	0.5 (0.0)	

[a] Data are presented as mean values and maximum errors. Values lower than 0.05 are shown as zero. The number of rats killed and measured was two, four and three for [^{76}Br]mEGF, [^{76}Br]mEGF-dextran D13 ([^{76}Br]mEGF-D13), and [^{76}Br]mEGF-dextran D46 ([^{76}Br]mEGF-D46), respectively.

disulfide bonds in the same relative positions. Also, they both have approximately the same binding affinity to the human EGF−receptor (*29*). In the present study, mEGF was used since it has one single free amino group, the amino terminus (no lysine residues), which can be coupled by reductive amination to a unique position on dextran, the aldehyde group on the reducing end of the dextran chain. This yielded a well-defined complex with a 1:1 ratio of mEGF to dextran. After bromination, mEGF and conjugates retained their binding ability to the human glioma cancer cell line U343.

PET Pharmacokinetics of [^{76}Br]mEGF. The analysis of the blood clearance indicated a rapid mEGF turnover (Figure 1), in good agreement with the fast accumulation of radioactivity in liver (Figure 2a). The liver pharmacokinetics during this early phase was just an integral of the blood curve. The liver uptake reached a plateau 2−3 min PI. After this time point, the radioactivity in the blood probably represented merely labeled metabolites and not mEGF. This is also supported by the liver Patlak-plot, which after leveling out showed a pronounced decrease (Figure 3a). The liver uptake plateau, which probably lasted for about 20 min, reflects the receptor binding and the internalization process. After about 20 min, an exponential radioactivity decrease probably reflected the excretion of labeled metabolites from the liver.

The kidney also showed a rapidly increasing radioactivity uptake, which after a few minutes leveled out to a plateau and decreased only slightly during the next hour. Since the mEGF most likely was trapped quantitatively in the liver and in kidney, the high uptakes in these organs reflect their high blood perfusion.

The findings of a rapid clearance from the circulation and a high accumulation in liver and kidney of [^{76}Br]-mEGF are in agreement with previous results. It has been reported that, 2.5 min after iv injection of [^{125}I]EGF into rats, 52% was found in liver and 14% in kidney (*31*). This high accumulation of EGF in liver and kidney was also shown in a study using iv injected [^{76}Br]/[^{125}I]EGF into rats (*23*). In this latter study it was claimed that the liver and kidney were the major organs responsible for the elimination and metabolism of hEGF from the plasma. The contribution of the liver and kidney to the total body clearance was estimated to approximately 70 and 20%, respectively (*32*). Moreover, in tumor-bearing mice, ^{125}I-labeled EGF accumulated in receptor-positive tumors, but to a much lesser extent than in the liver. One hour after iv injection, the tumor-to-liver ratio was less than 0.5 (*21*).

Pharmacokinetic Analyses of Dextranated mEGF. Compared with free mEGF, dextranation somewhat prolonged the retention time of the conjugates in the circulation (Figure 1). The conjugate with the longer dextran chain also showed the longest retention time, indicating a relation between the dextran chain length and blood residence time.

The liver uptake of dextranated ligands was equally fast for all three compounds, and the maximal uptake was reached within 2−3 min (Figure 2). The rate constants obtained in the detailed analysis of the first minute were equally high and probably just reflected the blood perfusion of the liver. We concluded that the extraction of the ligand from blood to liver is close to 100% for all three ligands. The dextranated ligands thus retain their receptor binding ability although small changes in receptor affinity cannot be excluded. More refined studies with preparations of different specific radioactivity might show if such changes occur.

After the maximal liver uptake, the accumulation pattern varied. The dextranated ligands showed not an extended plateau as for native EGF but a two-phase exponential decrease in radioactivity. The first phase might represent dextranated ligand returning into circulation, which is supported by the prolonged retention times in blood. Thus, it is possible that the dextranation may prevent some of the ligand being internalized. The

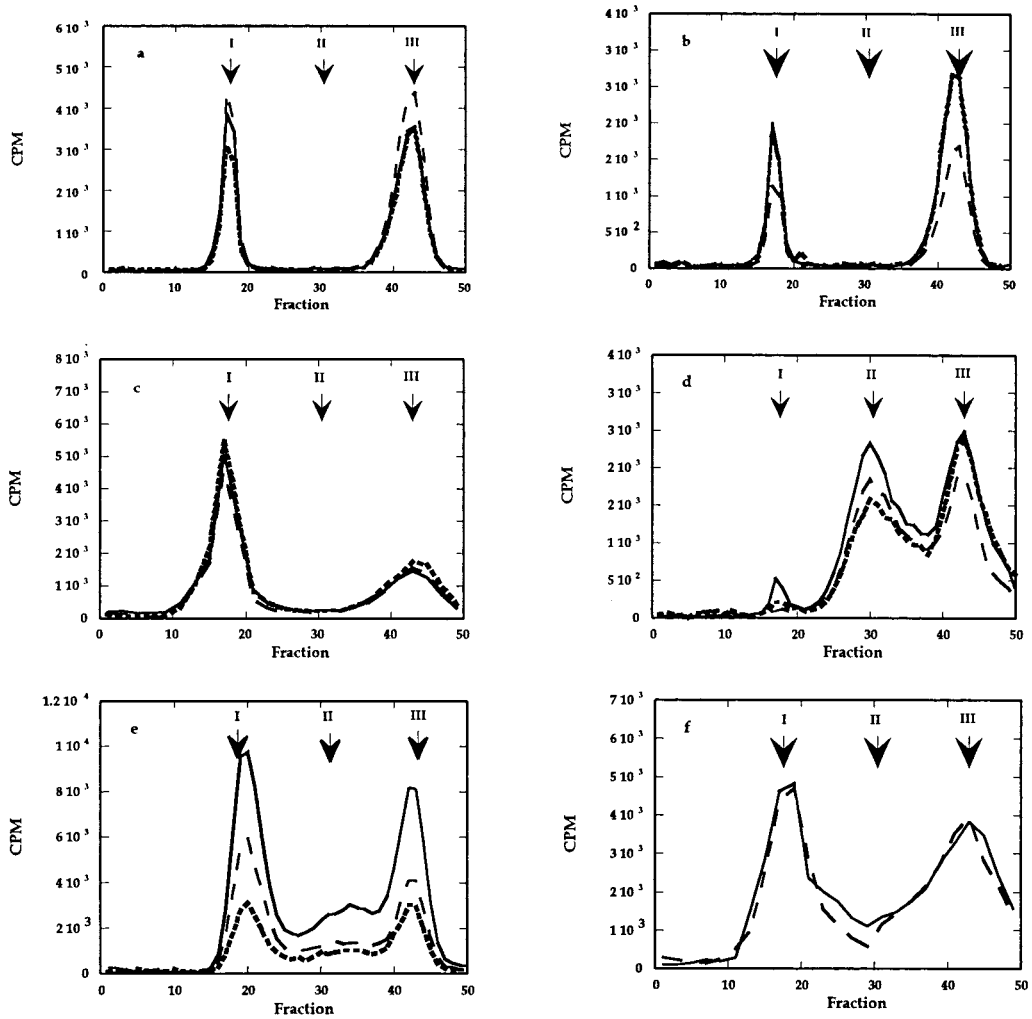


Figure 5. The chromatograms obtained by eluting serum and urine samples through Sephadex G-50 Fine column (1 × 50 cm) were shown. I, II, and III represent high molecular weight (conjugate), mEGF, and low molecular weight (salt) elution positions. The serum (a, b, and c) and urine (d, e, and f) samples from the rats administered with [^{76}Br]mEGF (a, d), [^{76}Br]mEGF−dextran D13 (b, e), and [^{76}Br]mEGF−dextran D46 (c, f) were analyzed by gel filtration. Each dotted, dashed, or solid line in the chromatogram represents the sample from one rat.

second phase may represent ligand, which was internalized and undergoing degradation. However, the rate of radioactivity loss here was less than that of free mEGF, which indicates that dextran can partly protect an internalized molecule from degradation.

Earlier, we studied the influence of dextranation of EGF on in vitro binding to EGFR-expressing tumor cells (*41*). It was shown that dextranation somewhat decreases the binding affinity to EGFR (dissociation constants were 6.6×10^{-10} and 7.1×10^{-9} for [^{125}I]mEGF and [^{125}I]-mEGF-D14, respectively). Still, the affinity after dextranation remained high. It was also noticed that dextranation slows down the internalization, but the mechanism for this process is not fully understood. We propose the following model. It is known that the activation of EGFR-associated protein kinase required dimerization of receptors (*42*). According to the model presented by Heldin and Östman (*41*), one EGF molecule binds to one receptor with one epitope and to the second receptor with another epitope. The other EGF molecule would then bind in a reciprocal manner. The presence of bulky dextran moiety might preclude the binding to the second receptor or to complicate the binding of the second EGF molecule. Thus, the internalization might be hampered. On the other hand, it has been shown for antibodies that a bivalent attachment to antigens is essential to make a binding nearly irreversible while a monovalent lead to dissociation (*43*). This might be also the truth for binding of EGF to its receptors. Such a model can explain both the delay of internalization and the release of a part of the conjugate back into blood stream.

At least a part of the ligand returning into circulation may have lost its receptor-binding ability since the plasma chromatography showed labeled high molecular complexes (Figure 5, panels b and c). The nature of this inactivation will be discussed in the chapter dealing with the results of chromatographic analysis.

The observation that the release of radioactivity associated with dextranated EGF is slower that in the case of free ligand is worth attention. Peptides and proteins are after internalization rapidly degraded in the lysosomes (*29*). The radioactivity, mainly in the form of halogenated tyrosine, leaks out from the cells. This will reduce the tumor-to-background ratio in diagnostic procedures and the tumor dose during targeted therapy. It has been demonstrated earlier in vitro that conjugation to dextran improves intracellular retention of mEGF-associated radioactivity (*12*). The results in this PET study indicate that this protective effect of dextran was true also in vivo. However, an even better retention effect can be obtained if the dextran part of the molecule is

radiohalogenated since dextran will remain intracellularly for a longer time (*35*).

Due to the fast liver uptake, the fast blood clearance and the rapid appearance of labeled metabolites in blood, the Patlak graphical analysis was not applied to calculate the transport rate constants, but used in order to make a normalized qualitative comparison between the different labeled compounds. For the liver, the Patlak plot during the first minute showed the same slope for all three ligands, indicating a similar receptor-binding rate. After reaching equilibrium, free EGF showed a more pronounced negative slope (Figure 3) and was probably more affected by the influence of labeled metabolites than that of the dextranated ligands. However, the [^{76}Br]-mEGF curve still reached a higher level than the curves for the conjugates. This was probably due to the faster release of receptor-bound dextranated ligands, which was also seen in the direct comparison of SUV in the PET measurements.

Well Counter Measurements. Consistent with the PET results, the well counter measurements showed high accumulation of radioactivity in liver, spleen, kidney, and urine, whereas the accumulation in the other organs was low (Table 3). An interesting finding of this study was that the dextranation of EGF decreased the uptake in the kidney. This result may have implications for future studies on EGF and targeted radiotherapy since the kidney is one of the dose-limiting critical organs. It is assumed nowadays that renal uptake of short proteins is facilitated by positively charged amino acids reacting with negative "receptors" on the surface of proximal tubuli (*36*). The most successful attempts to decrease renal uptake of short peptides are associated with the use of lysine and its derivatives to block these negative patches (*37*−*39*). However, it has been reported that similar reduction of labeled protein uptake in kidney may be achieved by acetylation of free amino groups (*40*), which dramatically decreases an isoelectric point of antibody fragment. The coupling of a bulky dextran to the mEGF might have reduced the binding of this molecule, due to the sterical hindrance, to the negative regions of renal tubuli. Another possible explanation to the reduced reabsorption by the kidney could be an increased hydrophilicity of the conjugate.

By contrast, in the spleen, the dextranation of mEGF resulted in increased AI values. This was most likely explained by phagocytosis of the [^{76}Br]mEGF−dextran by the reticular endothelial system cells in the spleen, a phenomenon that has previously been shown for non-conjugated dextran (*31*). The finding is consistent with the PET measurements where the spleen could only be visualized when using the D46 conjugate.

Size-Exclusion Chromatography. The serum from the rats administered with [^{76}Br]mEGF did not show any peak corresponding to the mEGF itself. Surprisingly, there was a peak found at the high-molecular-weight position in the chromatogram (Figure 5a). It has earlier been not shown that EGF binds to some component in plasma but the chromatogram suggests that such a complex was formed. The possibility of mEGF aggregation during bromination may be excluded since [^{76}Br]-mEGF showed a single peak corresponding to the mEGF position by gel filtration on Sephadex G-50 Fine (data now shown). A high-molecular-weight peak in the same position was found as well when [^{125}I]mEGF was incubated with blood plasma, taken from Sprague Dawley rats. When separated, the substance in this peak did not bind to EGFR expressing cells in vitro. It is possible that binding of EGF to some of blood component should limit the action of the growth factor to paracrine mode and prevent the activation of cell division far away from the site where it is required. It is also possible that the high-molecular-weight peaks obtained after chromatography of blood samples after injection of [^{76}Br]mEGF−dextran conjugates rather belong to such complex than free conjugate. The size-exclusion system, which was used for the analysis, is not able to resolve such high-molecular-weight compounds. A formation of a nonactive complex can explain why nonbound conjugate remains in the circulation. We believe that the formation of high-molecular weight complex of EGF with blood components deserves a thorough study in a future.

In urine, a main peak corresponding to mEGF was seen, but the high-molecular-weight peak seen in plasma was usually not present, i.e., it was only seen to a small extent in some animals. Since the urine content was integrated over the whole experiment, this can be interpreted as that mEGF was excreted in urine early, but the compound corresponding to the high-molecular-weight peak was not. The small high-molecular-weight peaks seen in some urine samples were probably caused by leakage of blood into the urinary bladder during dissection. Other possible explanations may include extreme extension of the urinary bladder during prolonged anesthesia during PET scanning or bleeding in connection with intraperitoneal anesthesia.

In urine from rats administered with [^{76}Br]mEGF−dextran conjugates, the main peaks were still of high-molecular-weight indicating that the kidneys excreted the intact ligand. Probably, longer dextran chains (>70 kDa) have to be used in order to prevent or considerably decrease the urinary excretion and thus prolong the circulation time of the conjugates even more.

To conclude, dextranation affects the biodistribution of mEGF in vivo giving a prolonged circulation time, decreased uptake in kidney, and increased spleen accumulation.

ACKNOWLEDGMENT

The authors thank laboratory engineers Veronika Asplund and Ulla Johansson and the staff at the Uppsala University PET center for valuable technical assistance. Financial support was given by the Swedish Cancer Society, the Swedish Medical Research Council and the Swedish Institute.

LITERATURE CITED

(1) Cote, G. L., and Robyt, J. F. (1982) Isolation and partial characterization of an extracellular glucansucrase from *Leuconostoc mesenteroides* NRRL B-1355 that synthesizes an alternating (1 goes to 6), (1 goes to 3)-alpha-D-glucan. *Carbohydr. Res. 101*, 57−74.

(2) Larm, O., Lindberg, B., and Svensson, S. (1971) Studies on the length of the side chains of the dextran elaborated by *Leuconostoc mesenteroides* NRRL B-512. *Carbohydr. Res. 20*, 39−48.

(3) Steinmann, E., Duckert, F., and Gruber, U. F. (1975) The value of dextran 70 in the prevention of thromboembolism in general surgery, orthopedics, urology and gynecology. A review of the literature. *Schweiz. Med. Wochenschr. 105*, 1637−1649.

(4) Atik, M. (1967) Dextran 40 and dextran 70. A review. *Arch. Surg. 94*, 664−672.

(5) Dubick, M. A., and Wade, C. E. (1994) A review of the efficacy and safety of 7.5% NaCl/6% dextran 70 in experimental animals and in humans. *J. Trauma. 36*, 323−330.

(6) Baudys, M., Letourneur, D., Liu, F., Mix, D., Jozefonvicz, J., and Kim S. W. (1998) Extending insulin action in vivo by conjugation to carboxymethyl dextran. *Bioconjugate Chem. 9*, 176−183.

(7) Takakura, Y., Fujita, T., Hashida, M., Maeda, H., and Sezaki, H. (1989) Control of pharmaceutical properties of soybean trypsin inhibitor by conjugation with dextran. II: Biopharmaceutical and pharmacological properties. *J. Pharm. Sci. 78*, 219.

(8) Sjostrom, A., Bue, P., Malmstrom, P. U., Nilsson, S., and Carlsson, J. (1997) Binding, internalization and degradation of EGF-dextran conjugates in two human bladder-cancer cell lines. *Int. J. Cancer. 70*, 383−389.

(9) Lindstrom, A., and Carlsson, J. (1993) Penetration and binding of epidermal growth factor-dextran conjugates in spheroids of human glioma origin. *Cancer Biother. 8*, 145−158.

(10) Gedda, L., Olsson, P., Ponten, J., and Carlsson, J. (1996) Development and in vitro studies of epidermal growth factor-dextran conjugates for boron neutron capture therapy. *Bioconjugate Chem. 7*, 584−591.

(11) Carlsson, J., Gedda, L., Gronvik, C., Hartman, T., Lindstrom, A., Lindstrom, P., Lundqvist, H., Lovqvist, A., Malmqvist, J., and Olsson, P., et al. (1994) Strategy for boron neutron capture therapy against tumor cells with overexpression of the epidermal growth factor-receptor. *Int. J. Radiat. Oncol. Biol. Phys. 30*, 105−115.

(12) Olsson, P., Lindstrom, A., and Carlsson, J. (1994) Internalization and excretion of epidermal growth factor-dextran-associated radioactivity in cultured human squamous-carcinoma cells. *Int. J. Cancer. 56*, 529−537.

(13) Carpenter, G., and Cohen, S. (1990) Epidermal growth factor. *J. Biol. Chem. 265*, 7709−7712.

(14) Libermann, T. A., Nusbaum, H. R., Razon, N., Kris, R., Lax, I., Soreq, H., Whittle, N., Waterfield, M. D., Ullrich, A., and Schlessinger, J. (1985) Amplification and overexpression of the EGF receptor gene in primary human glioblastomas. *J. Cell. Sci. Suppl. 3*, 161−172.

(15) Messing, E. M., and Reznikoff, C. A. (1992) Epidermal growth factor and its receptor: markers of-and targets for-chemoprevention of bladder cancer. *J. Cell. Biochem. Suppl. 16I*, 56−62.

(16) Sauter, G., Haley, J., Chew, K., Kerschmann, R., Moore, D., Carroll, P., Moch, H., Gudat, F., Mihatsch, M. J., and Waldman, F. (1994) Epidermal-growth-factor-receptor expression is associated with rapid tumor proliferation in bladder cancer. *Int. J. Cancer 57*, 508−514.

(17) Filmus, J., Trent, J. M., Pollak, M. N., and Buick, R. N. (1987) Epidermal growth factor receptor gene-amplified MDA-468 breast cancer cell line and its nonamplified variants. *Mol. Cell. Biol. 7*, 251−257.

(18) Hernandez Sotomayor, S. M., Arteaga, C. L., Soler, C., and Carpenter, G. (1993) Epidermal growth factor stimulates substrate-selective protein-tyrosine-phosphatase activity. *Proc. Natl. Acad. Sci. U.S.A. 90*, 7691−7695.

(19) Burwen, S. J., Barker, M. E., Goldman, I. S., Hradek, G. T., Raper, S. E., and Jones, A. L. (1984) Transport of epidermal growth factor by rat liver: evidence for a nonlysosomal pathway. *J. Cell Biol. 99*, 1259−1265.

(20) Jorgensen, P. E., Poulsen, S. S., and Nexo, E. (1988) Distribution of iv administered epidermal growth factor in the rat. *Regul. Pept. 23*, 161−169.

(21) Mateo de Acosta, C., Justiz, E., Skoog, L., and Lage, A. (1989) Biodistribution of radioactive epidermal growth factor in normal and tumor bearing mice. *Anticancer Res. 9*, 87−92.

(22) Yanai, S., Sugiyama, Y., Iga, T., Fuwa, T., and Hanano, M. (1990) Kinetic analysis of the downregulation of epidermal growth factor receptors in rats in vivo. *Am. J. Physiol. 258*, C593−598.

(23) Scott Robson, S., Capala, J., Carlsson, J., Malmborg, P., and Lundqvist, H. (1991) Distribution and stability in the rat of a 76Br/125I-labeled polypeptide, epidermal growth factor. *Int. J. Rad. Appl. Instrum. B 18*, 241−246.

(24) Fujita, T., Nishikawa, M., Tamaki, C., Takakura, Y., Hashida, M., and Sezaki, H. (1992) Targeted delivery of human recombinant superoxide dismutase by chemical modification with mono- and polysaccharide derivatives. *J. Pharmacol. Exp. Ther. 263*, 971−978.

(25) Mikolajczyk, S. D., Meyer, D. L., Fagnani, R., Hagan, M. S., Law, K. L., and Starling, J. J. (1996) Dextran modification of a Fab′-β-lactamase conjugate modulated by variable pretreatment of Fab′ with amine-blocking reagents. *Bioconjugate Chem. 7*, 150−158.

(26) Zhao, Q., Gottschalk, I., Carlsson, J., Arvidsson, L.-E., Oscarsson, S., Medin, A., Ersson, B., and Janson, J.-C. (1997) Preparation and Purification of an End to End coupled mEGF-dextran conjugate. *Bioconjugate Chem. 8*, 927−934.

(27) Tolmachev, V., Lövqvist, A., Einarsson, L., Schultz, J., and Lundqvist, H. Production of ^{76}Br by a low-energy cyclotron. *Appl. Radiat. Isot. 49*, 1537−1540.

(28) Patlak, C., Blasberg, R., and Fenstermacher, J. (1983) Graphic evaluation of blood-to-brain transfer constants from multiple-time uptake data. *J. Cerebr. Blood. Flow. Metab. 3*, 1−7.

(29) Carpenter, G., and Cohen, S. (1976) 125-I labeled human growth factor. *J. Cell Biol. 71*, 159−171.

(30) Bergstrom, M., Litton, J., Eriksson, L., Bohm, C., and Blomqvist, G. (1982) Determination of object contour from projections for attenuation correction in cranial positron emission tomography. *J. Comput. Assist. Tomogr. 6*, 365−372.

(31) Jorgensen, P. E., Rasmussen, T. N., Skov Olsen, P., Raaberg, L., Seier Poulsen, S., and Nexo, E. (1990) Renal uptake and excretion of epidermal growth factor from plasma in the rat. *Regul. Pept. 28*, 273−281.

(32) Kim, D., Sugiyama, Y., Fuwa, T., Sakamatomo, S., Iga, T., and Hanano, M. (1989) Kinetic analysis of the elimination process of human epidermal growth factor (hEGF) in rats. *Biochem. Pharm. 38*, 241−249.

(33) Renfrew, C. A., and Hubbard, A. L. (1991) Sequental Processing of epidermal growth factor in early and late endosomas of rat liver. *J. Biol. Chem. 266*, 4348−4356.

(34) Cuartero-Plaza, A., Martinez-Miralles, E., Rossel, R., Vadell-Nadal, C., Farre., Magi., and Real., F. R. (1996) Radiolocalization of suamous lund carcinoma with 131I-labeled epidermal growth factor. *Clin. Cancer Res. 2*, 13−20.

(35) Zhao, Q., Blomquist, E., Bolander, H., Gedda, L., Hartvig, P., Janson, J.-C., Lundqvist, H., Mellstedt, H., Nilsson, S., Nister, M., Sundin, A., Tolmachev, V., Westlin, J.-E., and Carlsson, J. (1998) Conjugate chemistry, iodination and cellular binding of mEGF-dextran-tyrosine: preclinical tests in preparation for clincal trials. *Int. J. Mol. Med. 1*, 693−702.

(36) Behr, T. M., Goldenberg, D. M., and Becker, W. (1998) Reducing the renal uptake of radiolabeled antibody fragments and peptides for diagnosis and therapy: present status, future prospects and limitations. *Eur. J. Nucl. Med. 25*, 201−212.

(37) Bernard, B. F., Krenning, E. P., Breeman, W. A., Rolleman, E. J., Bakker, W. H., Visser, T. J., Macke, H., and de Jong, M. J. (1997) D-lysine reduction of indium-111 octreotide and yttrium-90 octreotide renal uptake. *J. Nucl. Med. 38*, 1929−1933.

(38) De Jong, M., Bakker, W. H., Breeman, W. A., Bernard, B. F., Hofland, L. J., Visser, T. J., Srinivasan, A., Schmidt, M., Behe, M., Macke, H. R., and Krenning, E. P. (1998) Preclinical comparison of [DTPA0] octreotide, [DTPA0, Tyr3] octreotide and [DOTA0, Tyr3] octreotide as carriers for somatostatin receptor-targeted scintigraphy and radionuclide therapy. *Int. J. Cancer 7*, 406−411.

(39) Behr, T. M., Becker, W. S., Sharkey, R. M., Juweid, M. E., Dunn, R. M., Bair, H. J., Wolf, F. G., and Goldenberg, D. M. (1996) Reduction of renal uptake of monoclonal antibody fragments by amino acid infusion. *J. Nucl. Med. 37*, 829−833.

(40) Tarburton, J. P., Halpern, S. E., Hagan, P. L., Sudora, E., Chen, A., Fridman, D. M., and Pfaff, A. E. (1990) Effect of acetylation on monoclonal antibody ZCE−025 Fab′: distribution in normal and tumor-bearing mice. *J. Biol. Response Modif. 9*, 221−230.

(41) Zhao, Q., and Carlsson, J. (1997) In vitro characterization of an end-end coupled mEGF-dextran conjugate using a cultured human glioma cell line. *Int. J. Oncol. 11*, 1263−1269.
(42) Heldin, C.-H., and Östman, A. (1996) Ligand-induced dimerization of growth factor receptors: variation on the theme. *Cytokine Growth Factor Rev. 7*, 3−10.
(43) Kyriakos, R. J., Shih, L. B., Ong, G. L., Patel, K., Goldenberg, D. M., and Mattes, M. J. (1992) The fate of antibodies bound to the surface of tumor cells in vitro. *Cancer Res 52*, 835−842.

BC990011L

Folate Copolymer-Mediated Transfection of Cultured Cells

Christopher P. Leamon,*,† Debra Weigl,† and R. Wayne Hendren†

Department of Oligomer Development, GlaxoWellcome Research Institute, 5 Moore Drive, Research Triangle Park, North Carolina 27709. Received May 27, 1999; Revised Manuscript Received August 3, 1999

Poly(ethylene glycol) of various sizes was used as a molecular spacer to separate the cell-targeting ligand, folate, from the surface of poly-L-lysine. The resulting ternary macromolecule (pLys-PEG-folate) was investigated in various formulations for its ability to transfect reporter plasmids into receptor-bearing HeLa and IGROV cell lines. Formulations were optimized with respect to DNA content, ± charge ratio, and the size and amount of PEG substitution off the pLys backbone. Transfection activity was highest 48 h after sample introduction, and PEG 3400 was determined to be the most favorable spacer size tested. pLys-PEG-folate:DNA transfection was also found to be both concentration dependent and saturable; plus, it was blocked by the addition of excess-free folate, indicative of a specific mechanism of uptake. Transfection activity was virtually identical for complexes formed in 10% serum-supplemented media, deionized water, or Hepes buffer. And, cell viability remained greater than 85% at the highest concentrations of pLys-PEG-folate:DNA complexes tested (4.8 μg/mL pLys 331 000; 12 μg/mL DNA). Taken together, these observations provide evidence that pLys-PEG-folate:DNA complexes are taken up specifically by the folate endocytosis pathway, and that the intramolecular spatial distance of the ligand from the pLys backbone dramatically influences transfection.

INTRODUCTION

Poly-L-lysine (pLys)[1] is one of many polycations used to condense plasmid DNA through electrostatic interactions (*1*, *2*). Electron microscopic examination of pLys:DNA complexes has revealed that nanometer-sized particles, either as solid or toroidal conformations, form as the result of electrostatic complexation (*3*). Because these diameters closely approximate the diameter of coated pits found on the plasma membrane of endocytosing cells, pLys condensation of plasmid DNA became a popular technique for use in DNA transfection studies (*3*, *4*). Unfortunately, DNA (or oligonucleotide) condensation with pLys alone did not necessarily ensure successful transfection (*4*−*6*), probably because pLys complexes relied on nonspecific adsorptive pinocytosis mechanisms for cellular entry (*7*, *8*).

To overcome the problems associated with poor cellular uptake of pLys:DNA complexes, a portion of the ϵ-amino side chains on the pLys backbone has been derivatized with cell-specific targeting ligands. Thus, following condensation with DNA, externally oriented ligands on the pLys backbone became available for binding to specific cell surface receptors. Transferrin, insulin, asialoglycoprotein, monoclonal antibodies, mannose, lactose, and folic acid have all been shown to improve cellular uptake of pLys:DNA (or pLys:oligonucleotide complexes) into cells (*3*, *4*, *6*, *8*−*19*). However, the majority of the delivered DNA was believed to remain sequestered within endosomes/lysosomes, hence, unavailable for transfection (*7*, *8*). Fortunately, improvements such as the incorporation of fusogenic peptides (*20*), perfringolysin O (*21*), or replication-incompetent adenovirus (*13*, *14*, *17*, *22*, *23*) into the overall pLys:DNA delivery vehicle have greatly enhanced transfection levels.

Despite these improvements, the orientation of the ligand on the pLys backbone has never been optimized. Conceptually, the ligand should be (i) firmly anchored to the pLys backbone (preferably via a covalent bond), (ii) anchored in an orientation that does not destroy its affinity for its receptor, and (iii) positioned far enough away from the pLys backbone to allow good penetration into the binding pocket of its cell surface receptor. Interestingly, the latter concern may be of little importance when very large ligands (like insulin, transferrin, asialoglycoprotein, etc.) are employed for targeted pLys:DNA delivery. However, smaller ligands attached to pLys (folates, mannose, etc.) may not be effectively presented in an orientation that permits optimal receptor binding, especially when DNA is present and the overall complex is highly condensed.

In this publication we describe a method for transfecting plasmid DNA into cultured cells using a pLys-based delivery vehicle that contains an extended ligand spacer arm. The technique involves the use of a poly(ethylene glycol) (PEG) "spacer" which is derivatized with a ligand to one end and pLys to the other end. Folate was chosen as the ligand of choice for this investigation owing to its relative ease of chemical derivatization and remarkable ability to deliver covalently attached macromolecules and/or delivery systems into receptor-bearing cells (*6*, *17*, *24*−

* To whom correspondence should be addressed. Endocyte Pharmaceuticals, Inc., 1205 Kent Ave., West Lafayette, IN 47906. Phone: (765) 463-7175. Fax: (765) 463-9271. E-mail: Leamon@Endocyte.com.

† GlaxoWellcome Research Institute.

[1] Abbreviations: FFMEM, folate-free Dulbecco's modified Eagles medium; Hepes, *N*-2-hydroxyethylpiperazine-*N*′-2-ethanesulfonic acid; NHS-PEG-MAL, *N*-hydroxysuccinimidyl-poly(ethylene glycol)-maleiimide; MTT, 3-(4,5-dimethylthiazol-2-yl)-2,5-diphenyltetrazolium; NHS, *N*-hydroxysuccinimide; PBS, phosphate-buffered saline; pLys, poly-L-lysine; PEG, poly(ethylene glycol).

10.1021/bc990066n CCC: $18.00 © 1999 American Chemical Society
Published on Web 11/15/1999

38). Using a plasmid containing a luciferase reporter gene, we were able to quantitatively evaluate transfections mediated by various pLys-PEG-folate:DNA complexes. Importantly, this technique was further optimized by carefully evaluating the effect of complexation charge ratios, complexation medias, PEG size, and the extent of pLys derivatization.

EXPERIMENTAL PROCEDURES

Preparation of Folate-γ-Cysteine. Folate-γ-cysteine (pteroyl-γGlu-Cys) was synthesized as previously described.[2] Briefly, an Applied Biosystems Inc. 433A peptide synthesizer equipped with conductivity monitoring was used to prepare folate-γ-cysteine at 0.25 mmol scale. The compound was formed by the stepwise addition of Fmoc-Glu-OtBu followed by N^{10}-trifluoracetylpteroic acid onto a cysteine-modified *p*-hydroxymethylphenoxymethyl polystyrene resin. Following a wash with excess dichloromethane, the resin was repeatedly treated with 0.1 M aqueous piperidine (to remove the N^{10}-trifluoracetyl group) and then with a cleavage/deprotection cocktail consisting of 750 mg of phenol, 10 mL of trifluoroacetic acid, 0.5 mL of water, 0.25 mL of dithioethane, and 0.5 mL of thioanisol for 2 h at room temperature. The freely soluble compound was separated from the resin by filtration through a medium pore fritted funnel. The filtrate was then diluted with 4 vol of diethyl ether to precipitate the folate-γ-cysteine product. Following multiple ether washes, the precipitate was dried in vacuo. Barring no further purification, folate-γ-cysteine produced in this manner was typically 70−85% pure, as determined by the A_{280} peak area generated from C_{18} reversed-phase HPLC analyses, with the primary impurity being the dimerized (disulfide-linked) species. An Ellman's assay (*39*) on the crude material confirmed that the solid contained 70−85% free sulfhydryls.

Preparation of NHS-PEG-γ-Folate. A total of 5.9 μmol of commercially available or custom-synthesized *N*-hydroxysuccinimidyl-poly(ethylene glycol)-maleiimide (NHS-PEG-Mal; all of these PEG reagents along with their analytical characterization data were provided by Shearwater Polymers, Huntsville, AL) were dissolved in 1 mL of dry dichloromethane within a 10 mL round-bottom flask. A 3-fold molar excess of solid folate-γ-cysteine was added to the flask. While stirring, a 5-fold molar excess (relative to folate-γ-cysteine) of neat triethylamine was added to the flask, and the solution was stirred continuously for a minimum of 18 h at room temperature. Under these conditions, thiols can add to maleiimide groups in organic solvents (*40*).[3] Unreacted folate-γ-cysteine remained a solid while NHS-PEG-γ-folate had completely dissolved. Samples were centrifuged for 5 min at 15000*g*, and the yellow supernatants were diluted with 50 mL of diethyl ether to precipitate the NHS-PEG-γ-folate product. Samples were spun at 2500 rpm for 10 min, the supernatants were decanted, and the yellow pellets were redissolved in 1 mL of dichloromethane. The ether precipitation step was repeated two more times, and the final yellow pellet was dissolved in 1 mL of chloroform and stored at −20 °C. The concentration of NHS-PEG-γ-folate was determined as follows. A 10 μL aliquot of the chloroform sample was placed in a 1 mL eppendorf tube and dried using a Savant tabletop speedvac. The dried residue was dissolved in 1 mL of phosphate-buffered saline (PBS), and the absorbance at 362 nm was measured. Molar concentrations were determined using the extinction coefficient for folate at 362 nm ($\epsilon_{362} = 6100\ M^{-1}\ cm^{-1}$).

Preparation of pLys-PEG-γ-Folate. Stock solutions of poly-L-lysine hydrobromide (Sigma Chemical, St. Louis, MO) with an average molecular weight of 331 000 were prepared in 100 mM *N*-2-hydroxyethylpiperazine-*N*′-3-propanesulfonic acid, pH 8.0. Typically, 3 nmol of pLys were added to a 1.5 mL eppendorf tube, and additional buffer was added to give a final volume of 450 μL. An aliquot of NHS-PEG-γ-folate (in $CHCl_3$) was added to a 1.5 mL eppendorf tube. The $CHCl_3$ was removed using a speedvac, and the remaining residue was hydrated in 50 μL of deionized water. The entire volume of NHS−PEG-γ-folate solution was then mixed with the pLys sample (while vortexing), and the sample was left to react at room temperature for a minimum of 2 h. Unreacted NHS-PEG-γ-folate was removed from pLys-PEG-γ-folate by exhaustive dialysis through a 30 000 molecular weight cutoff membrane using 20 mM *N*-2-hydroxyethylpiperazine-*N*′-2-ethanesulfonic acid (Hepes) and 100 mM NaCl, pH 7.30. Alternatively, conjugates were purified by using a Mono S 5/5 column (buffer = 50 mM Hepes, pH 7.9, and a NaCl gradient from 0 to 3 M over 30 min) followed by overnight dialysis against 20 mM Hepes and 100 mM NaCl, pH 7.3. Samples were filtered with a 0.22 μm membrane prior to characterization (vide infra).

Characterization of pLys-PEG-γ-Folate Conjugates. Poly-L-lysine content was measured using a modified trypan blue precipitation assay (*41*). Aliquots from a stock 1.0 mg/mL solution of pLys (mw 331 000) in deionized water were dispensed into 1.5 mL eppendorf tubes. PBS was added to each tube to bring the final volume to 990 μL. Similarly, sample aliquots estimated to contain approximately 5 μg of pLys were added to eppendorf tubes and diluted with PBS to 990 μL. A total of 10 μL of a 4 mg/mL trypan blue solution was added to each tube followed by vortexing for 5 s each. Tubes were heated to 60 °C and shaken for a minimum of 1 h. Following immersion in ice for 5 min, tubes were then spun for 5 min at 15000*g*. The absorbance at 580 nm of each supernatant was measured, and the concentrations of pLys were calculated from a standard curve.[4] Since each PEG moiety present in the pLys-PEG-folate conjugate contains one folate moiety, the PEG content from each sample was determined by measuring the absorbance due to folate at 362 nm.[5] An estimate of the degree of PEG substitution on the pLys molecule was calculated by simply dividing the concentration of PEG by the concentration of pLys.

Cell Culture. HeLa and IGROV-1 cells were grown continuously as a monolayer using folate-free Dulbecco's modified Eagles medium (FFMEM) containing 10% heat-inactivated fetal calf serum and 2 mM L-glutamine at 37 °C in a 5% CO_2/95% air humidified atmosphere. Because the heat-inactivated serum contained its normal complement of endogenous folates, the cells could be maintained indefinitely in the folate-deficient medium (*24*).

Supercoiled Plasmid DNAs. Plasmids pGL3 (for luciferase gene expression; Promega, Madison, WI) and pSV-βgal (for β-galactosidase expression; Promega) were transformed and propagated in *Escherichia coli* strain

[2] *J. Drug Targeting* (1999) (in press).

[3] We have also successfully prepared this reagent in dimethyl sulfoxide; however, an additional ether precipitation step and selective solvation in DCM is needed prior to the final workup.

[4] Neither folic acid nor PEG_{3400} caused Trypan Blue to precipitate under similar conditions.

[5] At the concentrations measured, pLys does not appreciably absorb at 362 nm.

JM109. Milligram quantities of super-coiled plasmids were prepared using Quiagen plasmid preparation kits, as suggested by the manufacturer.

Formation of pLys-PEG-folate:DNA Complexes. Complexes were formed in either polypropylene tubes or polystyrene plates. Briefly, pLys was dissolved in half the final volume of either reagent-grade water, Hepes, or 10% serum-supplemented FFMEM. Plasmid DNA was then dissolved in the second half of water, Hepes, or serum-supplemented FFMEM, and the entire solution was mixed with the pLys solution. Plasmid DNA concentrations were typically 20 μg/mL at this step. Following a 5 s vortex mix, the solution was left to complex at room temperature for 1 h. The solution was later diluted with additional serum-containing FFMEM and added to cells without further purification.

Time-Dependent Transfection. Cells were added to 96-well plates in a total volume of 100 μL of 10% serum-supplemented FFMEM, and the plates were incubated at 37 °C for 18−24 h. Spent incubation media was replaced with 100 μL of sample-containing media per well (four wells per sample), and cells were incubated at 37 °C for the indicated times. Each well was vacuum aspirated, and 20 μL of 1× Cell Lysis Buffer (Promega) was added per well. Plates were then stored overnight at −70 °C. Following a 30 min thaw at room temperature on a rocker platform, cell lysates were quantitatively transferred to wells of Dynatech Microlite plates. A Dynatech ML3000 luminometer was used to autodispense 100 μL of luciferase assay reagent (Promega)/well and to sum the relative luminescence units over a 30 s period.

Ratio Study. Cells were added to 96-well plates in a total volume of 100 μL of the media described above, and the plates were incubated at 37 °C for 18−24 h. Spent incubation media was replaced with 100 μL of sample-containing media/well (three wells per sample), and cells were incubated at 37 °C for 48 h. Importantly, the quantity of plasmid DNA was held constant at 1 μg/mL in each well, whereas the quantity of pLys or pLys-PEG_{3400}-folate was varied from 0 to 4 μg/mL to account for the various ±ratios examined. Following the incubation, cells were harvested and the luminescence activity was measured according to the procedure detailed above.

Concentration-Dependent Transfection and Related cytotoxicity. A total of 2000 HeLa cells in 100 μL of serum-supplemented FFMEM was added to each well of duplicate 96-well plates and then incubated at 37 °C for 18−24 h. Aliquots from a master pLys-PEG-folate:DNA complex mix (20 μg/mL as DNA) were added to individual polypropylene tubes and diluted with serum-supplemented FFMEM to the indicated concentrations. Spent incubation media in each well was replaced with 100 μL of the appropriately diluted complex (four wells per sample), and the cells were incubated for 48 h at 37 °C. Cells from one plate were harvested and the luminescence activity was measured according to the procedure detailed above.

Cells in the duplicate plate were used in a cytotoxicity assay (two wells per sample). Briefly, 10 μL of a 5 mg/mL 3-[4,5-dimethylthiazol-2-yl]-2,5-diphenyltetrazolium bromide (MTT) solution in PBS was added to each well 2 h prior to the end of the 37 °C incubation. At the end of the incubation, spent media was aspirated from each well, and 100 μL of dimethyl sulfoxide plus 10 μL of 0.1 M glycine, pH 9.0, was added per well. The absorbance at 580 nm was read for each well, and the percent cytotoxicity was calculated based on the absorbance values measured in wells that had contained untreated cells.

Cytochemical Staining for β-Galactosidase. Approximately 50 000 cells in 2.5 mL of serum-supplemented media were added to each well of a Falcon 6-well plate and then incubated for 24 h at 37 °C. Using pSV-βgal as the DNA source, pLys-PEG-folate:DNA complexes were prepared 1 h prior to the experiment according to the protocol described above. Spent incubation media was removed from each well and replaced with 1 mL of sample-containing, serum-supplemented media. Following a 48 h incubation at 37 °C, monolayers were rinsed twice with PBS and then stained for β-galactosidase activity using the protocol and reagents supplied in the β-galactosidase Staining Kit (In Vitrogen; San Diego, CA). Cells were stained for a maximum of 24 h and then photographed at 200× magnification using Kodak color slide film.

Comparison of pLys-PEG-Folate:DNA Transfection to Cationic Liposome Transfection. A total of 2000 HeLa cells in 100 μL of serum-supplemented FFMEM was added to each well of a 96-well plate and then incubated at 37 °C for 18−24 h. pLys-PEG_{3400}-folate:pGL3 complexes were formed per the method detailed above using 10% serum-supplemented FFMEM. The cationic liposomes were complexed with pGL3 in 10% serum-supplemented FFMEM using the average of the vendor-recommended quantity of liposome per unit DNA. Thus, 10 μg of Lipofectin (Life Technologies, Gaithersburg, MD), 12.5 μg of LipofectAmine (Life Technologies), 6 μg of DOTAP (Boehringer Mannheim, Indianapolis, IN), 3 μg of DOPSER (Boehringer Mannheim), 5 μg of Transfectam (Promega), or 4.7 μg of TFx-50 (Promega) were complexed/μg of pGL3. Spent incubation media in each well was replaced with 100 μL of the appropriately diluted complex (8 wells/sample; 100 ng of DNA/well), and the cells were incubated for 48 h at 37 °C. Following the incubation, cells were harvested and the luminescence activity in two-thirds of the cell lysate was measured according to the procedure detailed above. The remaining cell lysate was used to perform a DotMetric protein assay (GenoTechnologies, St. Louis, MO), per the manufacturers instructions. Luminescent activity was normalized by the protein content for each sample, and the results were expressed as relative luminescence units per milligram of cell protein.

RESULTS

Proposed Structure of pLys-PEG-Folate:DNA Complexes. Figure 1 depicts a proposed structure for pLys-PEG-folate:DNA complexes. Here we assume that polyanionic DNA will electrostatically complex with polycationic pLys to form a charge-neutral hydrophobic core, and despite a covalent linkage to pLys, we further believe that the hydrophilic PEG-folate moieties should naturally orient outward from the core and into the aqueous milieu, thus forming a targetable micelle-like DNA delivery vehicle. Interestingly, a similar micellar structure has previously been proposed for oligonucleotide-polyoxyethylene derivatives (*42*); however, that particular delivery system lacked a cell-targeting ligand component.

Time-Dependent Transfection. The first transfection parameters we examined were the effect of folate-copolymer transfection with respect to the plated cell density and the length of incubation (exposure) time. Cells were plated at increasing densities into the wells

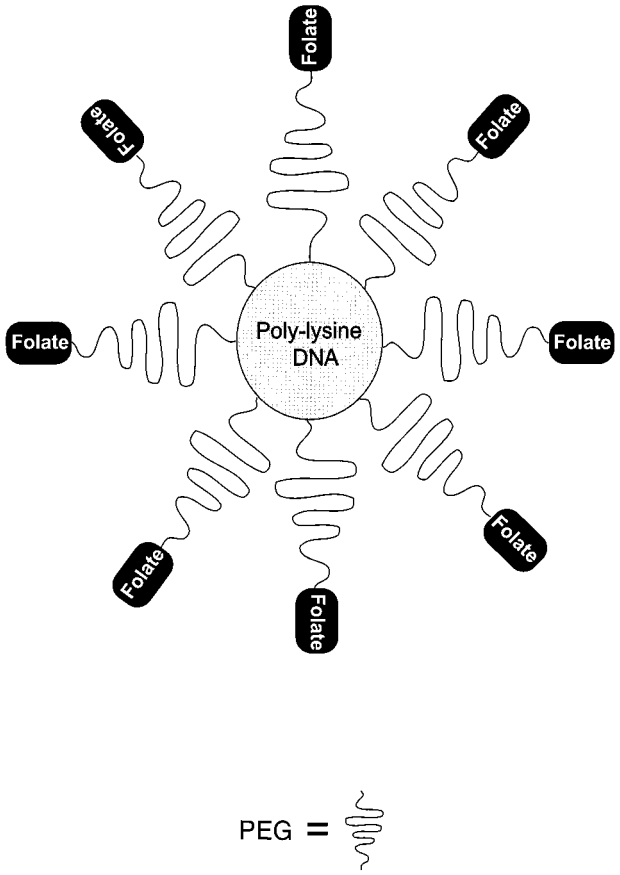


Figure 1. Proposed structure of pLys-PEG-folate:DNA complexes. Polyanionic DNA is assumed to electrostatically complex with polycationic pLys to form an electrically neutral, or hydrophobic core. The hydrophilic PEG-folate moieties naturally orient outward from this core into the bulk aqueous milieu, thus creating a targetable micelle-like DNA delivery vehicle.

of tissue-culture-treated microtitier plates and incubated for 18−24 h. Complexes between pLys-PEG_{3400}-folate (72 PEG-folates/pLys chain) and plasmid DNA (1:1 ± charge ratio) were preformed in 10% serum-supplemented FFMEM, and 100 ng of the complex (relative to DNA) was added to the wells. Following a 37 °C incubation for various time intervals, cells were harvested and assayed for luciferase activity. As shown in Figure 2, luciferase activity was not detected until >12 h of incubation, and this phenomenon was independent of cell density. However, the time of maximal luciferase expression did appear to be dependent on cell density. For example, at cell densities of >2000/well maximal luciferase activity was detected after 48 h of incubation. In contrast, maximal luciferase activity was reached and transiently sustained after 72 h for cells plated at the lower cell densities, suggesting that the extent of transfection (luciferase activity levels) was directly related to the degree of cell confluency within the wells. Interestingly, no luciferase activity was measured from cells treated with pLys:DNA (Figure 2) or pLys-PEG control complexes (not shown). Thus, for the remainder of the experiments described below, we chose to test cells plated at an initial density of 2000 cells/100 μL/well and to assess the levels of transfection 48 h later.

Charge Ratio Optimization. Theoretically, an electrostatic complex between a polycation and polyanion would carry a net neutral charge if the ± charge ratio were unity. A neutral complex would be desirable to incorporate into a ligand-targeted nucleic acid delivery vehicle, such as the one proposed here (see Figure 1), because it would eliminate the opportunity for nonspecific, adsorptive binding and uptake to nontarget cells. Unfortunately, interactions with buffer-associated ions and/or component proteins (e.g., from the serum) may alter the thermodynamically optimal ± charge ratio that would promote the formation of a neutral particle. Therefore, we elected to experimentally determine the optimal ± complexation ratios for pLys-PEG-folate and plasmid DNA, while simultaneously exploring the effect of the complexation media.

Complexes were prepared between pGL3 (5256 base pair) and increasing charge equivalents of pLys or pLys-PEG_{3400}-folate (72 PEG-folates per pLys chain), thereby spanning a large ± charge ratio spectrum.[6] Cells were exposed to the complexes for 48 h, and luciferase activity

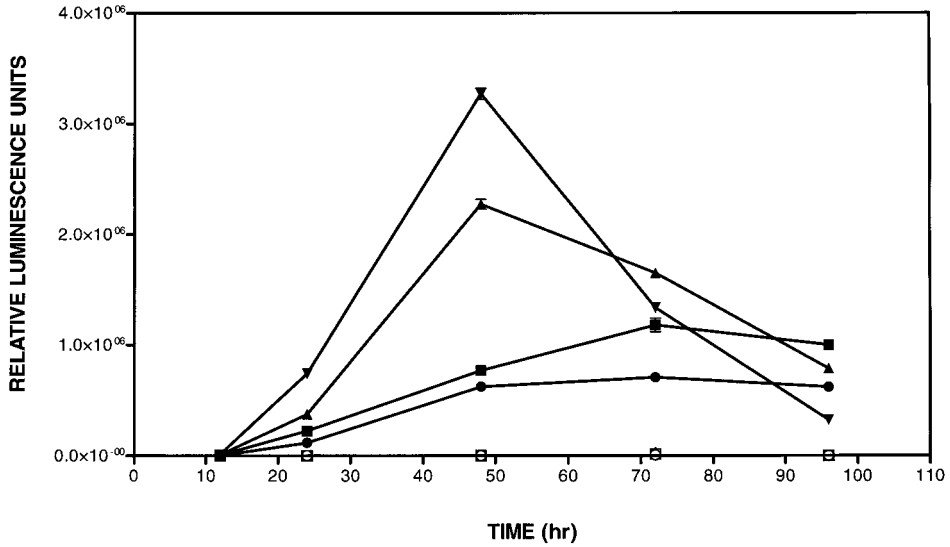


Figure 2. Effect of cell density and exposure time on pLys-PEG-folate:DNA transfection. A total of 100 μL of 10% serum-supplemented FFMEM containing pLys-PEG_{3400}-folate:DNA complexes (72 PEG-folates per pLys chain) was added to HeLa monolayers of increasing cell densities in 96 well plates. Cells were incubated at 37 °C for the indicated times. Spent incubation media was removed, and cells were assayed for endogenous luciferase activity as described in the Experimental Procedures. Number of cells originally seeded per well of a 96 well plate: (●, ○) 500 cells; (■, □) 1000 cells; (▲, △) 2000 cells; (▼, ▽) 4000 cells. Solid symbols represent pLys-PEG-folate:DNA complexes, while open symbols represent pLys:DNA complexes. *Error bars* represent one standard deviation ($n = 4$).

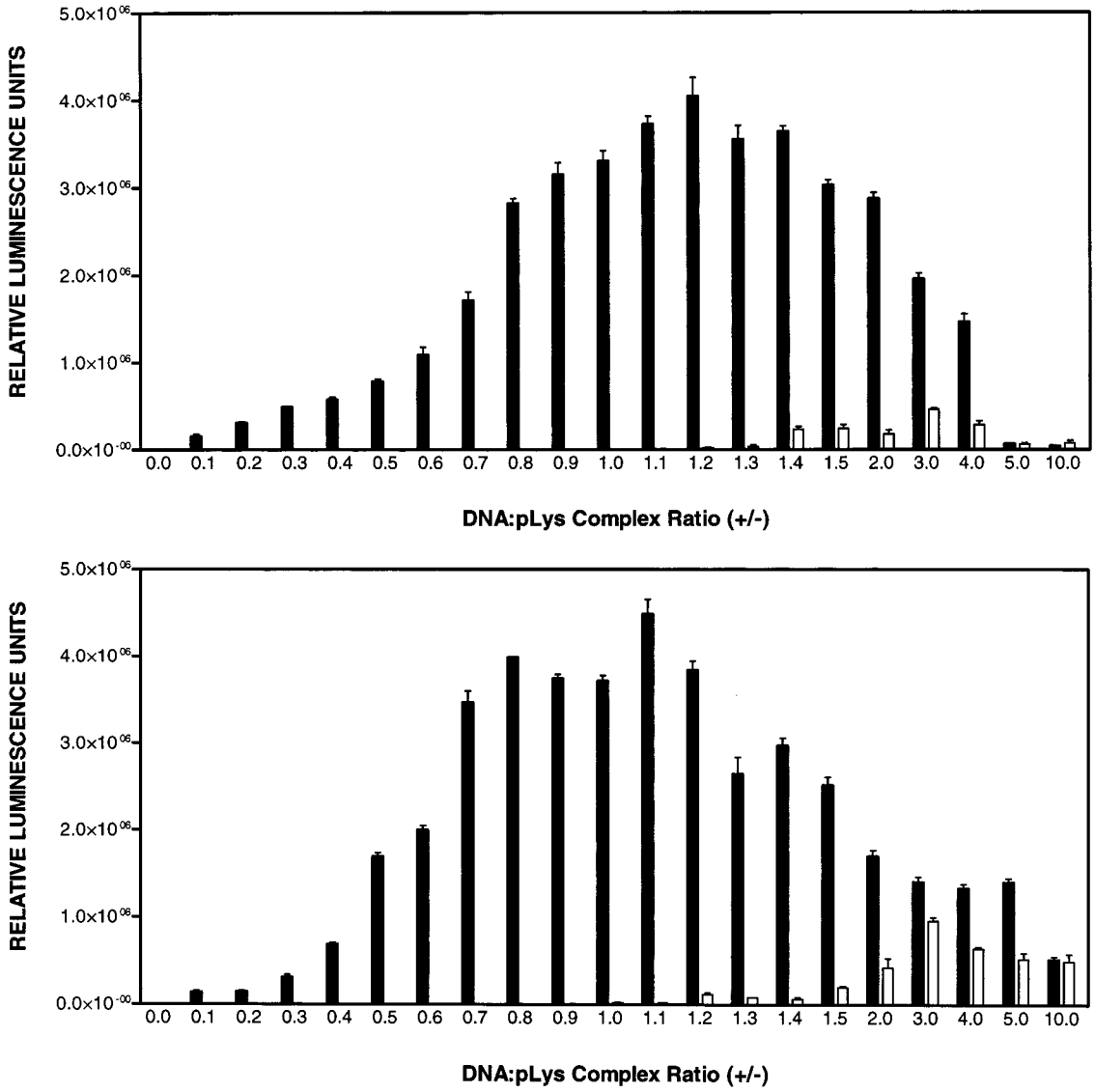


Figure 3. Effect of ± charge ratio and complexation medium on pLys-PEG-folate:DNA transfection. Complexes were prepared between pGL3 and increasing charge equivalents of pLys-PEG_{3400}-folate (72 PEG-folates per pLys chain). The quantity of plasmid DNA was held constant at 1 μg/mL in each well, whereas the quantity of pLys varied from 0 to 4 μg/mL to account for the various ± ratios examined. Cells were exposed to these complexes for 48 h, and endogenous luciferase activity was measured according to Experimental Procedures. (Solid bars) pLys-PEG-folate:DNA complexes; (open bars) pLys:DNA complexes. (A) Complexes formed in FFMEM supplemented with 10% heat-inactivated fetal calf serum; (B) Complexes formed in double deionized water. *Error bars* represent one standard deviation ($n = 3$).

was then measured. The results in Figure 3A show that luciferase activity levels gradually increased with respect to an increasing ± charge ratio until a maximum was reached at a near-neutral ratio. Beyond this optimum, the luciferase activity decreased as the charge ratio was further raised. In contrast, pGL3 titrated with unmodified pLys produced relatively large particles (easily observed at 250× magnification floating in the media) that were very ineffective transfection agents. This may partly explain why only minimal transfection activity was measured with these particles and only at the higher ± ratios (Figure 3).

All of the data presented thus far have been generated using complexes formed in 10% serum-supplemented media. This was initially done to optimize our experimental conditions for future cell studies that were intended to be performed in the presence of serum. However, we decided to determine if complexes preformed in nonserum-containing solutions were more efficient mediators of transfection. Thus, we chose to titrate pGL3 with increasing charge equivalents of pLys-PEG-folate in deionized water. As shown in Figure 3B, maximal levels of luciferase activity were achieved with a charge ratio near unity, similar to the results obtained from complexes formed in the presence of 10% serum. Interestingly, identical results were obtained when complexes preformed in Hepes-buffered saline solution were used in a similar assay (data not shown). Taken together, we interpret these results to suggest that optimal pLys-PEG-folate:DNA complexes are formed when the ± charge ratio is near unity and that the complexation process is not significantly influenced by the composition of the complexation buffer.

Effect of Increasing PEG Size. Figure 1 depicts a cartoon of a possible organizational structure formed between pLys-PEG-folate and nucleic acids. The PEG

[6] Approximately four pLys chains or four pLys-PEG_{3400}-folate copolymer units are needed to charge-neutralize 1 plasmid molecule.

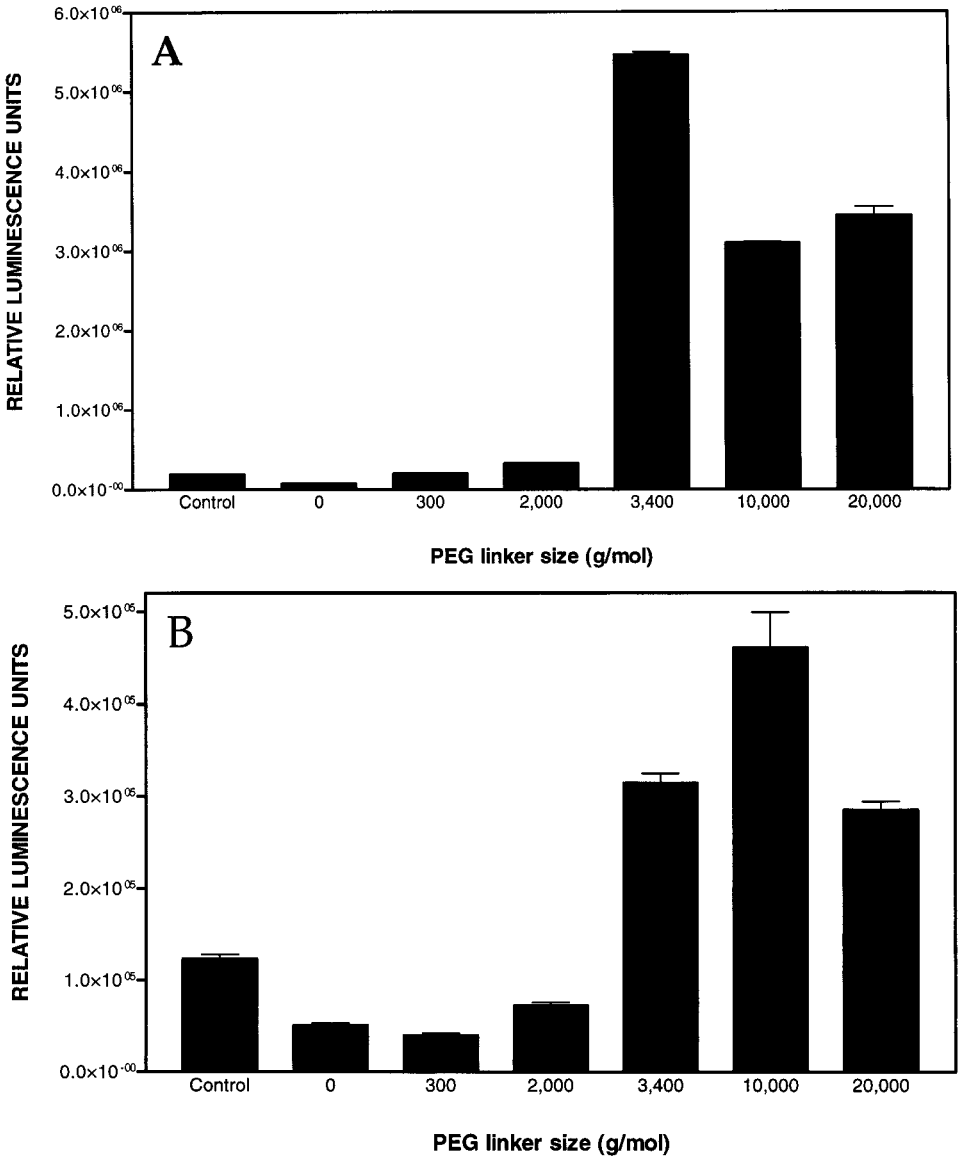


Figure 4. Effect of PEG size on pLys-PEG-folate:DNA transfection. Cells were incubated for 48 h at 37 °C in the presence of various pLys-PEG-folate:pGL3 complexes (1 μg/mL as DNA). Following the incubation, cells were harvested and the endogenous luminescence activity was measured according to Experimental Procedures. Control represents a pLys:DNA complex (no folate). Values 0−20000 represent the average molecular weight of PEG used in the particular pLys-PEG-folate conjugate assayed. (A) HeLa cells. (B) IGROV-1 cells. *Error bars* represent one standard deviation ($n = 4$).

component is assumed to orient on the outermost shell of the complex and to interact with the external aqueous environment, similar to the PEG component of Stealth liposomes (*43*, *44*). However, it is not known if transfection via pLys-PEG-folate:DNA complexes is dependent on the length of the PEG chain utilized. To evaluate this effect, we derivatized pLys with folate attached to PEG of various sizes ranging 0−20000 in average molecular weight. Complexes formed between this collection of pLys-PEG-folates and pGL3 were incubated with cultured cells for 48 h, and the levels of luciferase activity were measured. As shown in Figure 4A, very low levels of luciferase activity were measured in HeLa cells treated with complexes containing PEG components of 2000 molecular weight and smaller. However, significant luciferase activity was measured from cells transfected with PEG_{3400}-containing complexes. There was also no apparent advantage using the higher molecular weight PEG components (i.e., PEG_{10000} or PEG_{20000}). Interestingly, a similar PEG molecular weight trend was observed when a second cell type (IGROV-1) was used in this assay (see Figure 4B). This phenomenon is likely related to the observation that PEG forms "mushroom-like", or compacted, conformations at higher molecular weights (*44*), indicating that steric protection of the pLys:DNA core is a desirable property for transfection (see Figure 1). Notably, the remainder of the experiments described below was completed using pLys-PEG_{3400}-folate.

Effect of PEG-Folate Substitution. In addition to determining a favored PEG size for pLys-PEG-folate:pGL3 transfection, we investigated the effect of increasing the number of PEG-folate units conjugated per pLys chain. Thus, pLys was conjugated with increasing amounts of NHS−PEG_{3400}-folate, and following purification, the extent of PEG_{3400}-folate derivatization was determined. Complexes were formed with pGL3 and then added to HeLa cells for 48 h. As shown in Figure 5, a conjugate constructed with an average of 72 PEG_{3400}-folates per pLys chain (2.8% of the ~2586 lysine units derivatized) produced the highest measured level of luciferase activity in HeLa cells. Although no further attempt was made to determine the exact derivatization optimum, we believe

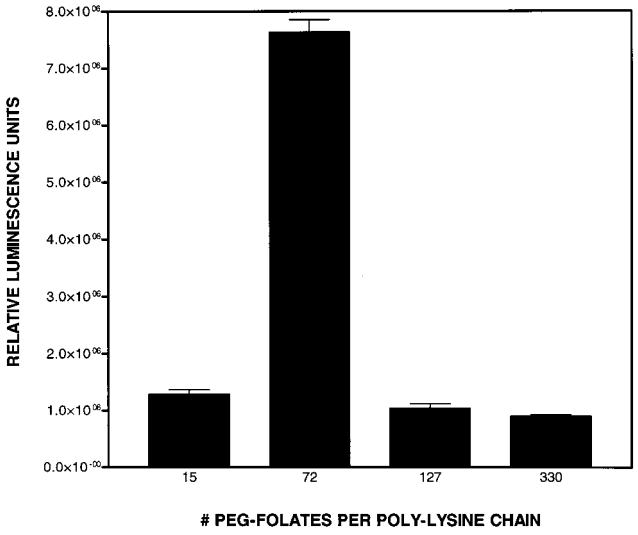


Figure 5. Effect of PEG substitution on pLys-PEG_{3400}-folate:DNA transfection. pLys (MW ≈ 331 000) was derivatized with increasing amounts of PEG_{3400}-folate and complexed to pGL3. Cells were incubated for 48 h at 37 °C in the presence of 1 μg/mL complex (as DNA). Following the incubation, cells were harvested and the endogenous luminescence activity was measured according to Experimental Procedures. *Error bars* represent 1 standard deviation ($n = 4$).

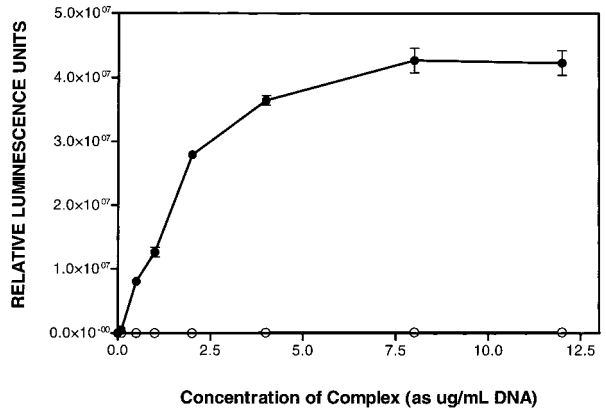


Figure 6. Concentration-dependent transfection. pLys-PEG_{3400}-folate:pGL3 complexes (72 PEG-folates/pLys chain) were formed and diluted in serum-supplemented FFMEM and then added at increasing concentrations to HeLa cell monolayers. Following a 48 h 37 °C incubation, cells were harvested and the endogenous luminescence activity was measured according to Experimental Procedures. (●) pLys-PEG_{3400}-folate:pGL3 complex; (○) pLys:pGL3 complex. *Error bars* represent 1 standard deviation ($n = 4$).

one clearly exists. Furthermore, the optimum PEG derivatization number may likely dictate the overall three-dimensional structure (and transfection potency) of these pLys-PEG-folate:DNA complexes.

Concentration-Dependent Transfection and Related Cytotoxicity. The folate moiety within the pLys-PEG-folate:DNA complex should effectively bind to external folate binding protein receptors on HeLa cells as well as mediate uptake via endocytosis. Because receptor-mediated endocytosis is a saturable process, we elected to determine the concentration dependence of pLys-PEG-folate:DNA transfection. As shown in Figure 6, luciferase activity reached a plateau at pLys-PEG_{3400}-folate:DNA concentrations of 8 μg/mL and higher (relative to DNA). Similar to what we observed in Figure 3 above, complexes formed with pLys had absolutely no transfection capability, even with concentrations as high as 12 μg/mL. Plus,

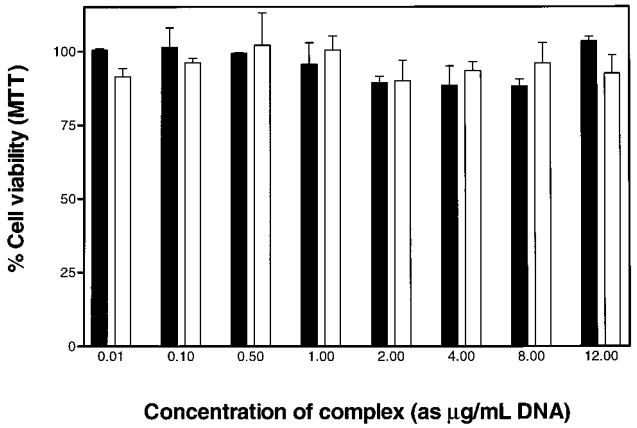


Figure 7. Cytotoxicity of pLys-$PE2G_{3400}$-folate:pGL3 complexes. Cells in a duplicate 96 well plate to that described in the legend to Figure 6 were used to evaluate the cytotoxicity of pLys-PEG_{3400}-folate:pGL3 complexes. Thus, complexes were formed and diluted in serum-supplemented FFMEM and then added at increasing concentrations to HeLa cell monolayers. Following a 46 h 37 °C incubation, cells were incubated for an additional 2 h at 37 °C in the presence of the MTT viability stain. Cells were harvested, and the percent cytotoxicity was calculated based on the viability values measured in wells that had contained untreated cells, as detailed in the Experimental Procedures. (Solid bars) pLys-PEG_{3400}-folate:pGL3 complexes; (open bars) pLys:pGL3 complexes. *Error bars* represent 1 standard deviation ($n = 2$).

a 100-fold excess of free folic acid nearly abolished (activity reduced by 95% at 5 μg/mL complex; not shown) pLys-PEG_{3400}-folate:DNA transfection, thus confirming the involvement of a receptor-mediated process.

Because there are reports that pLys:DNA complexes are toxic to some cells (*45*, *46*), we chose to examine the extent of cell toxicity on cells treated with increasing concentrations of pLys-PEG_{3400}-folate:pGL3 complexes. As shown in Figure 7, no significant cytotoxicity was measured in our HeLa cells treated with complexes up to 4.8 μg/mL pLys 331 000 molecular weight (or 12 μg/mL DNA).

Cytochemical Staining for β-Galactosidase. To better assess the extent to which treated cells are transfected by pLys-PEG-folate:DNA complexes, we elected to quantify the number of transfected cells in a population by using a β-galactosidase reporter plasmid and chromogenic staining. Complexes between pSV-βgal and pLys-PEG_{3400}-folate (72 PEG-folates/pLys chain) were formed in 10% serum-containing FFMEM per the usual protocol detailed above. A saturable concentration of the complex (9 μg, relative to DNA) was introduced to adherent cells in a 6-well Falcon culture dish, and the plate was incubated at 37 °C for 48 h. Using a commercially available kit, functionally transfected (i.e., β-galactosidase expressing) cells were detected by the visual appearance of a blue stain. Figure 8 shows a representative field of cells treated in this manner. Interestingly, positive blue staining varied among the cells. Some cells stained very heavily, and the stain was diffuse throughout the entire cell body. Other cells, however, limited their display of blue staining to vacuolar compartments. By summing the total number of cells containing blue stain (both vacuolar and diffuse) within any given field of view, we estimated that approximately 6% of the exposed cells were functionally transfected by pLys-PEG_{3400}-folate:pSV-βgal complexes (see Discussion).

Comparison of pLys-PEG-Folate:DNA Transfection to Cationic Liposome Transfection. Cationic liposomes have been widely used to transfect plasmid

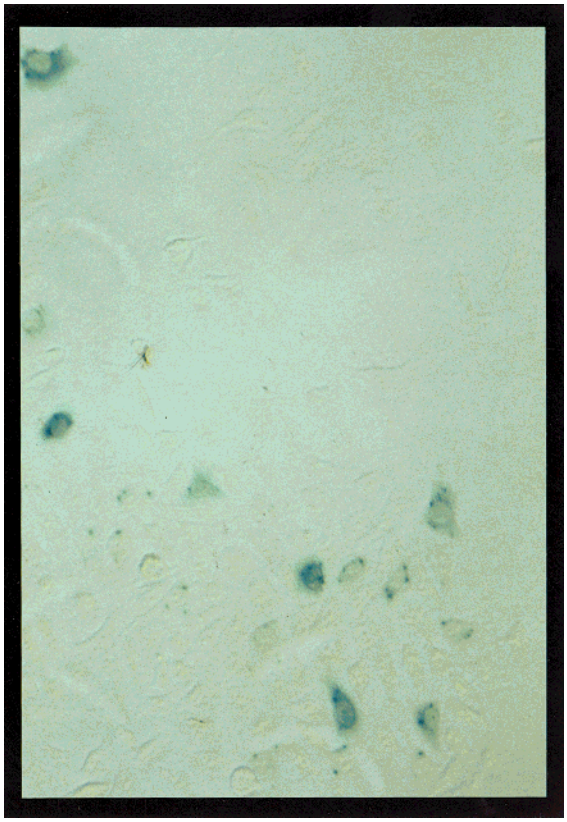


Figure 8. Cytochemical staining for β-galactosidase activity. Complexes of pSV-βgal and pLys-PEG$_{3400}$-folate (72 PEG-folates/pLys chain) were formed in 10% serum-containing FFMEM for 1 h, as described in Experimental Procedures and were then added to plated cells at saturable levels (9 μg with respect to DNA). Following 48 h of incubation at 37 °C, cells were developed using a commercially available β-galactosidase staining kit. Functionally transfected cells (blue color) were identified using bright-field microscopy. The transfection efficiency was calculated by counting the number of stained cells in a random microscope field viewed at 200× and then dividing by the total number of cells in that same field. Four fields were counted and averaged to give an overall transfection efficiency of ~6%.

DNA into cells both in vitro and in vivo (*47*−*50*). Unfortunately, cationic liposome-mediated transfection has not worked well in the presence of serum (*50*, *51*). Because our pLys-PEG-folate conjugates are typically complexed to plasmid DNA in the presence of serum, we elected to evaluate the levels of cellular transfection achieved by pLys-PEG-folate:DNA complexes to that obtained with cationic liposome:DNA complexes also prepared in the presence of 10% serum. The results in Figure 9 show that pLys-PEG$_{3400}$-folate (72 PEG-folates/pLys chain) produced equal to or greater levels of transfection relative to that of six popular commercially available cationic liposome formulations, each tested using their vendor-recommended optimal complexation ratios (~2.5−5 ± ratios; see Experimental Procedures). Importantly, the data in this figure were normalized with respect to the amount of residual cellular protein present at the end of the experiment. Many of the cationic liposome formulations produced significant cell killing (which was evident from the lower total cell protein values), whereas pLys-PEG$_{3400}$-folate complexes did not affect cell number (see Figure 7). Considering the added benefit of cell targeting via folate endocytosis, pLys-PEG$_{3400}$-folate was obviously the preferred transfection reagent for use in these studies that employed serum-containing medias.

DISCUSSION

We developed a method for transfecting plasmid DNA into cultured cells using a targetable pLys-based delivery vehicle that contains an extended poly(ethylene glycol) "spacer" arm strategically placed between the ligand and the pLys backbone. Using a luciferase reporter gene plasmid, we quantitatively evaluated transfections mediated by various pLys-PEG-folate:DNA complexes and carefully optimized this technique by studying the influence of complexation charge ratios, complexation medias, PEG size, and the extent of pLys derivatization.

We discovered that a finite lag period exists between the time that pLys-PEG-folate:DNA complexes enter the cells and the time that endogenous luciferase activity is detected (Figure 2). This latency period is crudely estimated to fall within 12−24 h postexposure to cells. Interestingly, folate−toxin conjugates have been shown to gain access to the cytosol after only a 2−8 h delay following entry into cells via receptor-mediated endocytosis (*25*, *27*). Perhaps the longer lag phase seen with our pLys-PEG-folate:DNA complexes is due to (i) the larger size of the "payload" (i.e., condensed plasmid) and (ii) the fact that this payload must further enter the nucleus, become transcribed and then translated prior to the detection of transfection activity.

Another interesting observation is that the time of maximal luciferase expression appeared to be dependent on cell density (see Figure 2). Cells in the most heavily seeded wells displayed maximal luciferase activity at the earlier time points, while cells in the lower seeded wells reached maximal luciferase activity at the later time points. Interestingly, this phenomenon may be related to a recent observation that wild-type folate receptors failed to deliver externally bound folate molecules into the cytoplasm of confluent, nondividing cells (*52*). Assuming this physiological effect occurred in our HeLa cells, one might have predicted that the more heavily seeded wells (4000 cells/well; Figure 2) would have reached confluency, or folate-endocytosis incompetentcy, faster than the lesser-seeded wells; this, in turn, would have negatively affected the luciferase activity levels (especially at the later time points). Overall, this cell-density effect may have ramifications for comparing similar results of different studies and, therefore, should be cautiously noted.

During the course of this study, we discovered that the size of PEG used to construct the pLys-PEG-folate conjugate was critical for successful mediation of DNA transfection into target cells. Thus, the results in Figure 4 show that no enhancement of DNA transfection was detected until the PEG size within the pLys-PEG-folate conjugate was increased to 3400 in molecular weight. PEGs larger than 3400 molecular weight added little (if any) benefit to the overall transfection activity, and that effect varied among the two cell types tested within this study. This linker or "cushion" effect has also been seen with Stealth liposomes, where lipids modified with PEG of molecular weights >2000 had diminished protective properties (*44*). We believe, however, that the PEG within pLys-PEG-folate conjugates serves not only to provide a hydrophilic barrier to protect the pLys-condensed DNA but that it also acts as an extended linker arm to allow the folate ligand to optimally bind to its cell-surface receptor (see Figure 1). Notably, extended linker arms have also been shown to be critically beneficial for the successful targeting of folate liposomes (*30*). In particular, folate anchored to the phospholipid headgroup by a one- or two-amino acid "spacer" failed to promote targeted

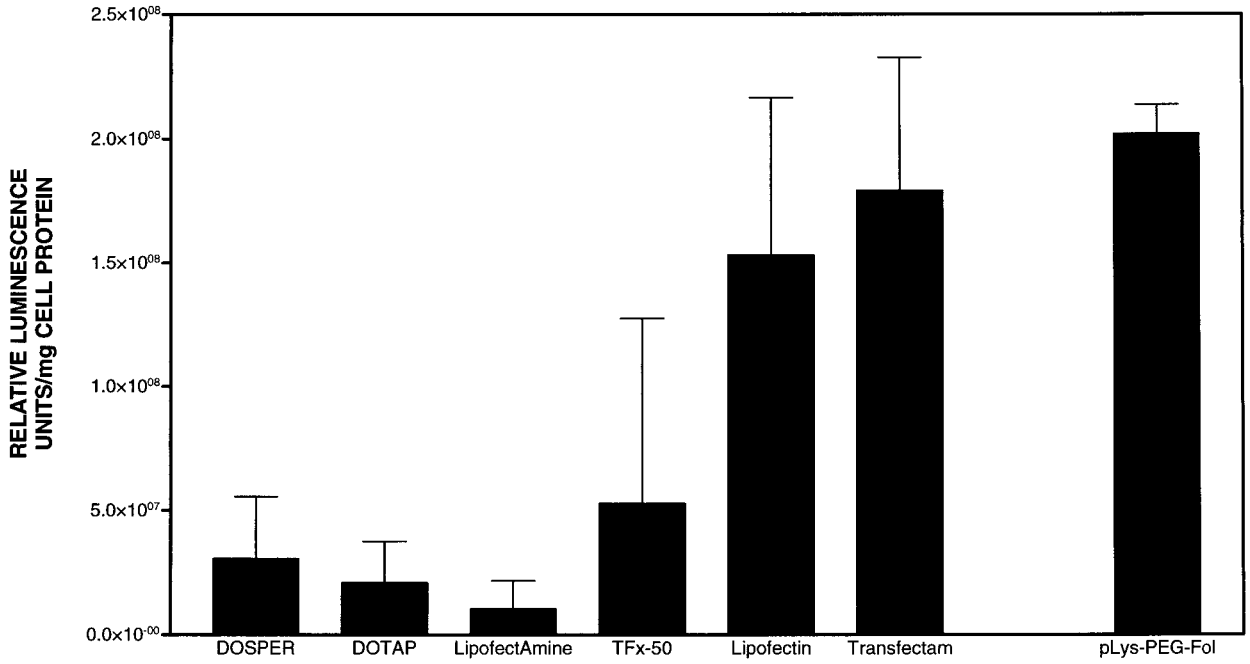


Figure 9. Comparison of pLys-PEG_{3400}-folate and cationic liposome mediated DNA transfection. pGL3 was complexed to pLys-PEG_{3400}-folate (72 PEG-folates/pLys chain) or to preformed cationic liposomes in 10% serum-supplemented FFMEM for 10−30 min at room temperature. Complexes were added to cells (1 μg/mL as DNA) and incubated for 48 h at 37 °C. Spent incubation media was removed, and cells were assayed for endogenous luciferase activity as described in Experimental Procedures. *Error bars* represent 1 standard deviation ($n = 8$).

liposome delivery to cells, whereas a ~3400 molecular weight PEG spacer produced fully targetable liposomes (*30*). Interestingly, this present study revealed that a useful PEG size for the pLys-PEG-folate transfection is also 3400 in molecular weight. And although we do not yet fully understand why the PEG 2000 spacer (or shorter) failed to mediate folate-targetable transfection, it is possible that steric constraints between the folate receptor and our pLys-PEG-folate:DNA particles prevented effective ligand binding. However, this parameter should be investigated further.

The value of including the PEG spacer within a targeted pLys:DNA complex was further revealed when we tested the ability of pLys-folate to transfect cells in parallel with pLys-PEG_{3400}-folate. The data presented in Figure 4 shows that pLys-folate is an inferior transfection agent. The simple addition of a PEG spacer afforded a 74-fold enhancement of transfection in HeLa cells and a 10-fold enhancement in IGROV-1 cells, relative to transfection levels mediated by pLys-folate. Presumably, the distinct levels of transfection enhancement between these two cell lines is due to their distinct levels of folate receptor expression ($>15 \times 10^6$ folate binding sites/HeLa cell versus $\sim 5 \times 10^5$ sites/IGROV-1 cell) (*26*, *53*). Interestingly, others have reported that transfection via pLys-folate:DNA complexes could be enhanced by co-treatment of cells with lysosomotropic agents (*8*) or adenoviral particles (*17*). Although not tested here, these techniques may also improve upon the transfection mediated by pLys-PEG-folate.

The proposed structure of pLys-PEG-folate:DNA complexes shown in Figure 1 represents what we conceive to be an effective transfection particle. It seemed logical to assume that polycationic and polyanionic polymers can, under charge neutral conditions, complex together to form a hydrophobic "core". Indeed, such a hypothesis has recently been proposed for oligonucleotide−polyoxyethylene complexes (*42*). And in a related way, it seemed logical to assume that the hydrophilic PEG-folate moiety would orient itself outward toward the bulk solution. This is evidenced by the observations that (i) free folic acid blocks the cell-association of the pLys-PEG_{3400}-folate:DNA complex and (ii) the transfection process mediated by pLys-PEG_{3400}-folate is saturable, suggesting that transfection occurs by a receptor-mediated process. Obviously, further biochemical analyses as well as electron microscopic characterization of these complexes is needed to confirm the proposed structure and to determine the effect of varying the size of the pLys component within the complex (*54*).

All of the studies presented above were conducted on cultured cells previously determined to express folate binding protein receptors. Assuming that each cell in the culture bears this receptor, one might expect that each cell would become transfected by pLys-PEG_{3400}-folate:DNA complexes. However, when we attempted to stain for transfection following the delivery of a plasmid containing a β-galactosidase gene, only 6% of these treated cells stained positively (see Figure 9). It is very unlikely that 94% of the cell population was incompetent to bind and internalize these complexes, since delivery of folate−toxin conjugates into the identical cell line effectively killed the entire population (*25*, *27*). Instead, we believe that the majority of the cells either expressed very low levels (staining not visually detectable) of β-galactosidase, or that the majority of DNA plasmid within these cells remained entrapped within organellar structures. Unlike protein toxins, plasmid DNA must breach not only the endosomal barrier but also the nuclear membrane barrier prior to eliciting an effect. Although access to the cytosol is difficult in itself, that alone would not guarantee successful translocation of DNA into the nucleus (*55*). Clearly, these results indicate that transfection mediated by pLys-PEG_{3400}-folate may be further enhanced, possibly with the co-incorporation of endosome-disrupting agents (*14*, *20*, *21*).

LITERATURE CITED

(1) Shapiro, J. T., Leng, M., and Felsenfeld, G. (1969) Deoxyribonucleic acid−polylysine complexes. Structure and nucleotide specificity. *Biochemistry 8*, 3219−3232.

(2) Haynes, M., Garrett, R. A., and Gratzer, W. B. (1970) Structure of Nucleic Acid-Poly Base Complexes. *Biochemistry 9*, 4410−4416.

(3) Wagner, E., Cotten, M., Foisner, R., and Birnstiel, M. L. (1991) Transferrin-polycation−DNA complexes: The effect of polycations on the structure of the complex and DNA delivery to cells. *Proc. Natl. Acad. Sci., U.S.A. 88*, 4255−4259.

(4) Wu, G. Y., and Wu, C. H. (1988) Evidence for targeted Gene Delivery to Hep G2 Hepatoma Cells in vitro. *Biochemistry 27*, 887−892.

(5) Clarenc, J. P., Degols, G., Leonetti, J. P., Milhaud, P., and Lebleu, B. (1993) Delivery of antisense oligonucleotides by poly(L-lysine) conjugation and liposome encapsulation. *Anti-Cancer Drug Des. 8*, 81−94.

(6) Citro, G., Szczylik, C., Ginobbi, P., Zupi, G., and Calabretta, B. (1994) Inhibition of leukaemia cell proliferation by folic acid−polylysine-mediated introduction of c-myb antisense oligodeoxynucleotides into HL-60 cells. *Br. J. Cancer 69*, 463−467.

(7) Kabanov, A. V., and Kabanov, V. A. (1995) DNA complexes with polycations for the delivery of genetic material into cells. *Bioconjugate Chem. 6*, 7−20.

(8) Mislick, K. A., Baldeschwieler, J. D., Kayyem, J. F., and Meade, T. J. (1995) Transfection of folate-polylysine DNA complexes: Evidence for lysosomal delivery. *Bioconjugate Chem. 6*, 512−515.

(9) Zenke, M., Steinlein, P., Wagner, E., Cotten, M., Beug, H., and Birnstiel, M. L. (1990) Receptor-mediated Endocytosis of Transferrin-Polycation Conjugates: An Efficient Way to Introduce DNA into Hematopoietic Cells. *Proc. Natl. Acad. Sci. U.S.A. 87*, 3655−3659.

(10) Wagner, E., Zenke, M., Cotten, M., Beug, H., and Birnstiel, M. L. (1990) Transferrin-polycation Conjugates as Carriers for DNA Uptake into Cells. *Proc. Natl. Acad. Sci. U.S.A. 87*, 3410−3414.

(11) Cotten, M., Langle-Rouault, F., Kirlappos, H., Wagner, E., Mechtler, K., Zenke, M., Beug, H., and Birnstiel, M. L. (1990) Transferrin-Polycation-mediated Introduction of DNA into Human Leukemic Cells: Stimulation by Agents that Affect the Survival of Transfected DNA or Modulate Transferrin Receptor Levels *Proc. Natl. Acad. Sci. U.S.A. 87*, 4033−4037.

(12) Trubetskoy, V. S., Torchilin, V. P., Kennel, S. J., and Huang, L. (1992) Use of N−Terminal Modified Poly(L-lysine)-Antibody Conjugate as a Carrier for Targeted Gene Delivery in Mouse Lung Endothelial Cells. *Bioconjugate Chem. 3*, 323−327.

(13) Wagner, E., Zatloukal, K., Cotten, M., Kirlappos, H., Mechtler, K., Curiel, D. T., and Birnsteil, M. L. (1992) Coupling of adenovirus to transferrin-polylysine/DNA complexes greatly enhances receptor-mediated gene delivery and expression of transfected genes. *Proc. Natl. Acad. Sci. U.S.A. 89*, 6099−6103.

(14) Curiel, D. T., Agarwal, S., Wagner, E., and Cotten, M. (1991) Adenovirus Enhancement of Transferrin-Polylysine-mediated Gene Delivery. *Proc. Natl. Acad. Sci. U.S.A. 88*, 8850−8854.

(15) Wu, G. Y., and Wu, C. H. (1993) Liver-directed gene therapy. *Adv. Drug Delivery Rev. 12*, 159−167.

(16) Midoux, P., Mendes, C., Legrand, A., Raimond, J., Mayer, R., Monsigny, M., and Roche, A. C. (1993) Specific gene transfer mediated by lactosylated pol-L-lysine into hepatoma cells. *Nucleic Acids Res. 21*, 871−878.

(17) Gottschalk, S., Cristiano, R. J., Smith, L. C., and Woo, S. L. C. (1994) Folate receptor mediated DNA delivery into tumor cells: potosomal disruption results in enhanced gene expression. *Gene Ther. 1*, 185−191.

(18) Liang, W. W., Shi, X., Deshpande, D., Malanga, C. J., and Rojanasakul, Y. (1996) Oligonucleotide targeting to aveolar macrophages by mannose receptor-mediated endocytosis. *Biochim. Biophys. Acta 1279*, 227−234.

(19) Rojanasakul, Y., Weissman, D. N., Shi, X., Castranova, V., Ma, J. K. H., and Liang, W. (1997) Antisense inhibition of silica-induced tumor necrosis factor in alveolar macrophages. *J. Biol. Chem. 272*, 3910−3914.

(20) Wagner, E., Plank, C., Zatloukal, K., Cotten, M., and Birnstiel, M. L. (1992) Influenza virus hemagglutinin HA-2 N-terminal fusogenic peptides augment gene transfer by transferrin-ploylysine-DNA complexes: Toward a synthetic virus-like gene-transfer vehicle. *Proc. Natl. Acad. Sci. U.S.A. 89*, 7934−7938.

(21) Gottschalk, S., Tweten, R. K., Smith, L. C., and Woo, S. L. C. (1995) Efficient gene delivery and expression in mammalian cells using DNA coupled with perfringolysin O. *Gene Ther. 2*, 498−503.

(22) Curiel, D. T., Wagner, E., Cotten, M., Birnstiel, M. L., Agarwal, S., Li, C. M., Loechel, S., and Hu, P. C. (1992) High-Efficiency Gene Transfer Mediated by Adenovirus Coupled to DNA−Polylysine Complexes. *Human Gene Ther. 3*, 147−154.

(23) Cotten, M., Wagner, E., Zatloukal, K., Phillips, S., Curiel, D. T., and Birnsteil, M. L. (1992) High-efficiency receptor-mediated delivery of small and large (48 kilobase) gene constructs using the endosome-disruption activity of defective or chemically inactivated adenovirus particles. *Proc. Natl. Acad. Sci. U.S.A. 89*, 6094−6098.

(24) Leamon, C. P., and Low, P. S. (1991) Delivery of macromolecules into living cells: A method that exploits folate receptor endocytosis. *Proc. Natl. Acad. Sci. U.S.A. 88*, 5572−5576.

(25) Leamon, C. P., and Low, P. S. (1992) Cytotoxicity of momordin-folate conjugates in cultured human cells. *J. Biol. Chem. 267*, 24966−24971.

(26) Leamon, C. P., and Low, P. S. (1993) Membrane folate-binding proteins are responsible for folate-protein conjugate endocytosis into cultured cells. *Biochem. J. 291*, 855−860.

(27) Leamon, C. P., Pastan, I., and Low, P. S. (1993) Cytotoxicity of folate-*Pseudomonas* exotoxin conjugates toward tumor cells. *J. Biol. Chem. 268*, 24847−24854.

(28) Turek, J. J., Leamon, C. P., and Low, P. S. (1993) Endocytosis of folate-protein conjugates: ultrastructural localization in KB cells. *J. Cell Sci. 106*, 423−430.

(29) Leamon, C. P., and Low, P. S. (1994) Selective targeting of malignant cells with cytotoxin-folate conjugates. *J. Drug Targeting 2*, 101−112.

(30) Lee, R. J., and Low, P. S. (1994) Delivery of liposomes into cultured KB cells via folate receptor-mediated endocytosis. *J. Biol. Chem. 269*, 3198−3204.

(31) Lee, R. J., and Low, P. S. (1995) Folate-mediated tumor cell targeting of liposome-entrapped doxorubicin in vitro. *Biochim. Biophys. Acta 1233*, 134−144.

(32) Wang, S., Lee, R. J., Cauchon, G., Gorenstein, D. G., and Low, P. S. (1995) Delivery of antisense oligodeoxyribonucleotides against the human epidermal growth factor receptor into cultured KB cells with liposomes conjugated to folate via poly(ethylene glycol). *Proc. Natl. Acad. Sci. U.S.A. 92*, 3318−3322.

(33) Wang, S., Lee, R. J., Mathias, C. J., Green, M. A., and Low, P. S. (1996) Synthesis, purification, and tumor cell uptake of ^{67}Ga-deferoxamine-folate, a potential radiopharmaceutical for tumor imaging. *Bioconjugate Chem. 7*, 56−62.

(34) Vogel, K., Wang, S., Lee, R. J., Chmielewski, J., and Low, P. S. (1996) Peptide-mediated release of folate-targeted liposome contents from endosomal compartments. *J. Am. Chem. Soc. 118*, 1581−1586.

(35) Mathias, C. J., Wang, S., Lee, R. J., Waters, D. J., Low, P. S., and Green, M. A. (1996) Tumor-selective radiopharmaceutical targeting via receptor-mediated endocytosis of Gallium-67-deferoxamine-folate. *J. Nuc. Med. 37*, 1003−1008.

(36) Lee, R. J., and Huang, L. (1996) Folate-targeted, anionic liposome-entrapped polylysine-condensed DNA for tumor cell-specific gene transfer. *J. Biol. Chem. 271*, 8481−8487.

(37) Lee, R. J., Wang, S., and Low, P. S. (1996) Measurement of endosome pH following folate receptor-mediated endocytosis. *Biochim. Biophys. Acta 1312*, 237−242.

(38) Li, S., and Huang, L. (1997) Targeted delivery of antisense oligodeoxynucleotides by LPDII. *J. Liposome Res. 7*, 63−75.

(39) Riddles, P. W., Blakeley, R. L., and Zerner, B. (1979) Ellman's reagent: 5, 5′-dithiobis(2-nitrobenzoic acid)-a reexamination. *Anal. Biochem. 94*, 75−81.

(40) Dix, L. R., Ebdon, J. R., and Hodge, P. (1995) Chain extension and cross-linking of telechelic oligomers-II. Michael additions of bisthiols to bismaleiimides, bismaleates and bis-(acetylene ketone)s to give linear and cross-linked polymers. *Eur. Polym. J. 31*, 653−658.

(41) Shen, W. C., Yang, and Ryser, H. J. P. (1984) Colorimetric determination of microgram quantities of polylysine by trypan blue precipitation. *Anal. Biochem. 142*, 521−524.

(42) Kabanov, A. V., Vinogradov, S. V., Suzdaltseva, Y. G., and Alakhov, V. Y. (1995) Water-soluble Block Polycations as Carriers for Oligonucleotide Delivery. *Bioconjugate Chem. 6*, 639−643.

(43) Evans, E., and Needham, D. (1988) Attraction between lipid bilayer membranes in concentrated solutions of nonadsorbing polymers: comparison of mean field theory with measurements of adhesion energy. *Macromolecules 21*, 1822−1831.

(44) Hristova, K. and Needham, D. (1995) Physical properties of polymer-grafted bilayers. In *Stealth Liposomes* (D. Lasic and F. Martin, Eds.) pp 35−49. CRC Press, Boca Raton.

(45) Yamaoka, T., Iwata, H., Hamada, N., Ide, H., and Kimura, Y. (1994) Transfection of foreign gene to mammalian cells using low-toxic cationic polymers. *Nucleic Acids Sym. Ser. 31*, 229−230.

(46) Ekrami, H. M., and Shen, W.-C. (1995) Carbamylation decreases the cytotoxicity but not the drug-carrier properties of polylysines. *J. Drug Targeting 2*, 469−475.

(47) Philip, R., Liggitt, D., Philip, M., Dazin, P., and Debs, R. (1993) In Vivo Gene Delivery: Efficient transfection of T lymphocytes in adult mice. *J. Biol. Chem. 268* (22), 16087−16090.

(48) Felgner, J. H., Kumar, R., Sridhar, C. N., Wheeler, C. J., Tsai, Y. J., Border, R., Ramsey, P., Martin, M., and Felgner, P. L. (1994) Enhanced Gene Delivery and Mechanism Studies with a Novel Series of Cationic Lipid Formulations. *J. Biol. Chem. 269*, 2550−2561.

(49) Gao, X., and Huang, L. (1995) Cationic liposome-mediated gene transfer. *Gene Ther. 2*, 710−722.

(50) Lewis, J. G., Lin, K.-Y., Kothavale, A., Flanagan, W. M., Matteucci, M. D., DePrince, R. B., Mook, R. A., Hendren, R. W., and Wagner, R. W. (1996) A serum-resistant cytofectin for cellular delivery of antisense oligodeoxynucleotides and plasmid DNA. *Proc. Natl. Acad. Sci. U.S.A. 93*, 3176−3181.

(51) Vitiello, L., Chonn, A., Wasserman, J. D., Duff, C., and Worton, R. G. (1996) Condensation of plasmid DNA with polylysine improves liposome-mediated gene transfer into established and primary muscle cells. *Gene Ther. 3*, 396−404.

(52) Ritter, T. E., Fajardo, O., Matsue, H., Anderson, R. G. W., and Lacey, S. W. (1995) Folate receptors targeted to clathrin-coated pits cannot regulate vitamin uptake. *Proc. Natl. Acad. Sci. U.S.A. 92*, 3824−3828.

(53) Miotti, S., Facheris, P., Tomassetti, A., Bottero, F., Bottini, C., Ottone, F., Colnaghi, M. I., Bunni, M. A., Priest, D. G., and Canevari, S. (1995) Growth of ovarian-carcinoma cell lines at physiological folate concentration: Effect on folate-binding protein expression *in vitro* and *in vivo*. *Int. J. Cancer 63*, 395−401.

(54) Wolfert, M. A., and Seymour, L. W. (1996) Atomic force microscopic analysis of the influence of the molecular weight of poly(L)lysine on the size of the polyelectrolyte complexes formed with DNA. *Gene Ther. 3*, 269−273.

(55) Capecchi, M. R. (1980) High efficiency transformation by direct microinjection of DNA into cultured Mammalian cells. *Cell 22*, 479−488.

BC990066N

Prediction of *q*-Values and Conformations of Gadolinium Chelates for Magnetic Resonance Imaging

L. A. Castonguay,*,† A. M. Treasurywala,†,‡ T. J. Caulfield,§ E. P. Jaeger,†,|| and K. E. Kellar⊥

Departments of Biophysics and Computational Chemistry, Medicinal, and Analytical Chemistry, Sterling Winthrop Pharmaceutical Research Division, 1250 S. Collegeville Road, P.O. Box 5000, Collegeville, Pennsylvania 19426-0900. Received March 8, 1999; Revised Manuscript Received August 11, 1999

For gadolinium chelates, we determined that there is a linear correlation between calculated solvent-accessible surface area and *q*-value, the number of rapidly exchanging water molecules directly bound to the gadolinium ion. A calibration curve was developed to predict *q*-value based on the solvent-accessible surface area of gadolinium. This predictive method was validated with the following gadolinium crystal structures: (ethylenediaminetetraacetic acid)-gadolinium(III) [Gd(EDTA)] [Templeton, L. K., Templeton, D. H., Zalkin, A., and Ruben, H. W. (1982) Anomalous Scattering by Praseodymium, Samarium, and Gadolinium and Structures of their Thylenediaminetetraacetate (EDTA) Salts. *Acta Crystallogr., Sect. B 38*, 2155], (1,4,7,10-tetraazacyclododecane-*N*,*N*′,*N*″,*N*‴-tetraacetic acid)-gadolinium(III) [Gd(DOTA)] [Dubost, J.-P., Leger, J.-M., Langlois, M.-H., Meyer, D., and Schaefer, M. (1991) Structure of a Magnetic Resonance Imaging Agent - The Gadolinium-DOTA Complex $C_{16}H_{24}N_4O_8NaGd$, $5H_2O$. *C. R. Acad. Sci., Ser. 2 312*, 349], (diethylenetriaminepentaacetic acid)-gadolinium(III) [Gd(DTPA)] [Stezowski, J. J., and Hoard, J. L. (1984) Heavy Metal Ionophores - Correlations Among Structural Parameters of Complexed Nonpeptide Polyamino Acids. *Isr. J. Chem. 24*, 323], (diethylenepenta-acetato)-gadolinium(III) [Gd(DTPA-BEA)] [Smith, P. H., Brainard, J. R., Morris, D. E., Jarvinen, G. D., and Ryan, R. R. (1989) Solution and Solid-State Characterization of Europium and Gadolinium Schiff-Base Complexes and Assessment of their Potential as Contrast Agents in Magnetic Resonance Imaging. *J. Am. Chem. Soc. 111*, 7437], and (1,7,13-triaza-4,10,16-trioxacyclo-octadecane-*N*,*N*′,*N*″-triacetato)-gadolinium(III) [Gd(TTTA)] [Chen, D., Squattrito, P. J., Martell, A. E., and Clearfield, A. (1990) Synthesis and Crystal Structure of a 9-Coordinate Gadolinium-(III) Complex of 1,7,13-Triaza-4,10,16-Trioxacyclooctadecane-N,N′,N″-Tri-Acetic Acid. *Inorg. Chem. 29*, 4366]. Predicted *q*-values were in complete agreement with experimentally determined *q*-values. A genetic algorithm-based conformational search method was developed to generate valid 3D models for gadolinium chelates. The method was successfully tested on the following gadolinium chelates: Gd(EDTA) (Templeton et al., 1982), Gd(DOTA) (Dubost et al., 1991), Gd(DTPA-BEA) (Smith et al., 1989), Gd(TTTA) (Chen et al., 1990), Gd(triethylene glycol) [Rogers, R. D., Voss, E. J., and Etzenhouser, R. D. (1988) F-Element Crown Ether Complexes. 17. Synthetic and Structural Survey of Lanthanide Chloride Tiethylene Glycol Complexes. *Inorg. Chem. 27*, 533], and Gd(tetraethylene glycol) [Rogers, R. D., Etzenhouser, R. D., Murdoch, J. S., and Reyes, E. (1991) Macrocycle Complexation Chemistry. 35. Survey of the Complexation of the Open-Chain 15-Crown-5 Analogue tetraethylene Glycol with the Lanthanide Chlorides. *Inorg. Chem. 30*, 1445].

INTRODUCTION

The importance of intravenously administered contrast agents for magnetic resonance imaging (MRI) is evidenced by the fact that approximately one-half of all routine clinical MRI procedures involve the use of contrast agents (*8*). Particularly, small water-soluble chelates of Gd(III) such as $[Gd(DTPA)]^{2-}$ and $[Gd(DOTA)]^{-}$ have found widespread clinical application as MRI contrast agents due to their favorable characteristics of high chemical stability, low toxicity, and rapid clearance. The effectiveness of a contrast agent is determined by the ability of the complex to increase the relaxation rate of bulk water protons, or relaxivity in vivo.

For small water soluble polyaminocarboxylate gadolinium chelates at field strengths pertinent to MRI, the magnitude of the relaxivity is determined mainly by four parameters: (1) t_R, the rotational correlation time of the chelate; (2) *r*, the distance between the centers of the gadolinium ion and the protons of the coordinated water molecules; (3) *q*, the number of water molecules bound in the inner coordination sphere of the gadolinium ion; and (4) τ_M, the residence lifetime of water molecules in the inner coordination sphere of the gadolinium ion. For most gadolinium chelates reported in the literature (*9*−*11*), the values of t_R, *r*, and τ_M affect the relaxivity to a minor extent as compared to the value of *q*. Indeed,

* To whom correspondence should be addressed. Current address: Merck Research Laboratories, P.O. Box 2000, RY50SW-100, Rahway, NJ 07065. E-mail: castong@merck.com.

† Department of Biophysics and Computational Chemistry.

‡ Current address: Pfizer Central Research, Groton, CT 06340.

§ Department of Medicinal Chemistry. Current address: Rhone-Poulenc Rorer, 500 Arcola Rd., P.O. Box 1200 Collegeville, PA 19426.

|| Current address: 3D Pharmaceuticals, 665 Stockton Dr., Suite 104, Exton, PA 19341.

⊥ Department of Analytical Cheimisty. Current address: Nycomed Amersham Imaging, 466 Devon Park Dr., Wayne, PA 19087.

10.1021/bc990027b CCC: $18.00 © 1999 American Chemical Society
Published on Web 10/09/1999

previous work has established a linear relationship between integer *q*-value and relaxivity at 1.2 T, a field-strength typical of clinical MRI (*10*).

Due to the toxicity of free lanthanide ions, the biological tolerance of contrast agents is largely determined by the ability of the gadolinium complex to remain intact in vivo. The acute toxicity of a number of polyaminocarboxylate gadolinium complexes has been demonstrated to be inversely proportional to the conditional binding constants of the ligands. Despite a 50-fold range of LD_{50} values for four Gd(III) complexes, all become lethally toxic to mice at dosages where 13−15 mM of Gd(III) is released in vivo (*12*). The authors propose that release of Gd(III) from the complex is responsible for the toxicity and that this appears to be a consequence of Zn(II), Cu(II), and Ca(II) transmetalation in vivo. In general, the stability of metal−ligand complexes increases with the number of potential coordination sites which are occupied.

The goal in designing improved MRI contrast agents is to maximize both the biological tolerance (conditional stability) and efficacy (*q*-value) of the gadolinium chelate. Therefore, predictive methods for determining both conditional stability constants and *q*-value for gadolinium chelates would help facilitate the discovery of improved contrast agents. Previously, molecular mechanics calculations and dynamics simulations, based on the AMBER force field (*13*), were used to examine the structure and stabilities of gadolinium complexes (*14*). However, no predictive methods for the determination the *q*-values has been reported. Herein, we would like to report a computational method to predict the *q*-values and structures of gadolinium chelates for magnetic resonance imaging.

COMPUTATIONAL DETAILS

***q*-Value Calculation and Validation.** The Connolly surface is the area traced out by rolling a defined probe (a sphere of 1.4 Å which represents a water molecule) over the gadolinium ion. A calibration curve for translating calculated Connolly surface area to *q*-value was developed using the crystal structure of $Gd(H_2O)_9$ (*15*). If one water is removed, then there is one vacancy to which a water molecule can bind; in other words, eight of the nine coordination sites are already occupied. This is analogous to a $q = 1$ system where there is space for one solvent water molecule to coordinate to the gadolinium ion, and the rest of the "solvent sites" are involved in complexation to the chelate. Therefore, for $q = 1$, one water is removed from the structure and the Connolly surface area is calculated for the gadolinium using SYBYL software (*16*). There are nine possible ways to remove one water molecule, each of the nine possible Connolly surface areas are calculated, and the average, maximum, and minimum values are recorded. This same procedure was repeated for $q = 0$ to $q = 9$ and the resultant data plotted as a calibration curve, Figure 1. For $q = 2$, 3, 4, 5, 6, 7, and 8, only contiguous waters were removed. This restriction was applied to prevent "partial sites" from being mistakenly counted. For example, if one and a half sites were available on the top of the molecule and half a site was available on the bottom, there would not actually be room for two solvent water molecules to bind since the sites are not contiguous.

Since the structures generated during conformational analysis will be minimized structures, a new calibration curve was developed using the same procedure for the $Gd(H_2O)_9$ crystal structure after minimization. Gadolinium nonahydrate was minimized in SYBYL using the parameters and conditions listed below. The data were plotted as before and the same linear calibration curve was observed.

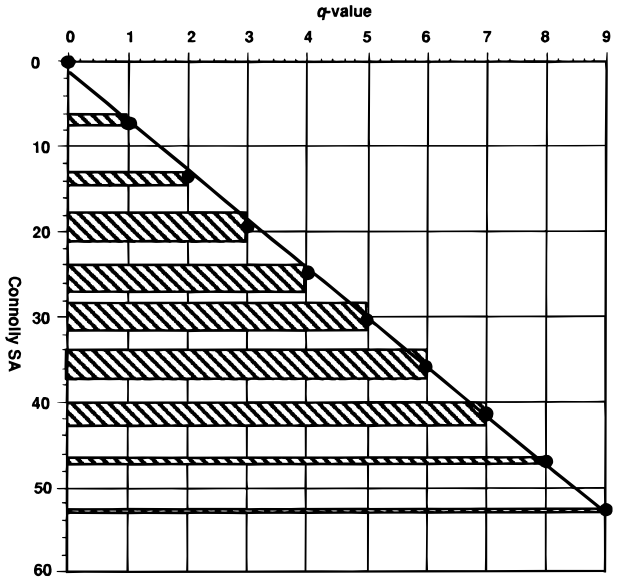


Figure 1. Graph of *q*-value vs calculated Connolly surface area for the crystal structure of $Gd(H_2O)_9$. The dots denote the average value of Connolly surface area for each *q*-value. The shaded bar denotes the data spread between highest and lowest calculated Connolly surface area for each *q*-value. Note no bands overlap.

Gadolinium Parameter Development. The SYBYL force field was extended in this work to include an atom type for Gd(III). The parameters for the remaining atoms are taken directly from the published SYBYL force field (*17*). Since the gadolinium is not covalently bonded to the chelates, only nonbonded parameters needed to be developed. The van der Waals energy term used in the SYBYL force field is as follows:

$$E_{\mathrm{vdw}} = \sum_{\substack{i=1 \\ \text{nonbonded}}}^{\text{Natoms}} \sum_{j>1} E_{ij} \left(1/a_{ij}^{12} - 2/a_{ij}^{6}\right)$$

where E_{ij} is the van der Waals constant, a_{ij} equals $r_{ij}/(R_i + R_j)$, r_{ij} is the distance between atoms i and j, R_i is the van der Waals radius of the ith atom, and R_j is the van der Waals radius of the jth atom.

These parameters were developed empirically by varying E_{ij} and R_i for a database of gadolinium complex crystal structures. The optimal parameters being the ones that fit the structural data obtained from the crystal structures.

Crystal structures from the Cambridge Structural Database (CSD) (*18*) were used to construct this database. A search of the CSD resulted in 76 structures containing gadolinium and carbon. Structures were eliminated if they were duplicates, contained more than one gadolinium, were diagnostic imaging agents that would be used later to test these methods, contained uncomplexed gadolinium with the ligand, contained just gadolinium and solvent, or contained other metals as part of the ligand. A total of 59 structures were eliminated, leaving 17 structures in the database.

The database contained the following structures: (18-crown-6)-ethanol-dichloro-gadolinium(III) chloride (*19*),

nona-aqua-gadolinium(III) tris(trifluoromethanesulfonate) (*14*), tris(acetylacetonato)-diaqua-gadolinium(III) monohydrate (*20*), tris(acetylacetonato-*O*,*O*′)-bis(acetylacetoniminato)-gadolinium(III) acetylacetonimine solvate (*21*), chloro-diaqua-(*18*−*crown*−*6*)-gadolinium(III) dichloride dihydrate (*22*), bis(η-1,3,5-tri-*tert*-butylbenzene)-gadolinium(0) (*23*), penta-aqua-(triethylene glycol-*O*,*O*′,*O*″,*O*‴)-gadolinium(III) trichloride (6), cis-trichloro-tris(2, 6-dimethyl-4-pyrone)-gadolinium(III) (*24*), aqua-tris(nitrato-*O*,*O*′)-bis[di-isopropyl(1, 2-bis(diethylcarbamoyl)ethyl) phosphonato-*O*]gadolinium(III) (*25*), tris[(3-aza-4-methylhept-4-en-6-on-1-yl)amine-*O*,*O*′,*O*″]-tris(nitrato-*O*,*O*′)-gadolinium(III) (*26*), triaqua-chloro-(tetraethylene glycol)-gadolinium(III) dichloride monohydrate (*7*), [10-(2-((2-hydroxy-1-(hydroxymethyl)ethyl) amino]-1-[(phenylmethoxy)methyl]-2-oxo-ethyl)-1,4,7,10-tetra-azacyclododecane-1,4,7-triacetic acid)-gadolinium(III) trihydrate (*27*), pentasodium tris(oxy-diacetato-*O*,*O*′,*O*″)gadolinium-(III) diperchlorate hexahydrate (*28*), trinitrato-1, 2-bis-(pyridine-2-aldimino)ethane-gadolinium(III) (*29*), acidic gadolinium tetrakis(benzoylacetonate) piperidine (*30*), bis[diaqua-(2-formyl-4-methyl-6-(4-(2-pyridyl)-2-azonia-but-1-enyl)phenolato-*O*,*O*′)-gadolinium(III)] diperchlorate chloride hydrate (*31*), and trichloro-bis(dimethoxyethane-*O*,*O*′)-gadolinium(III) (*32*).

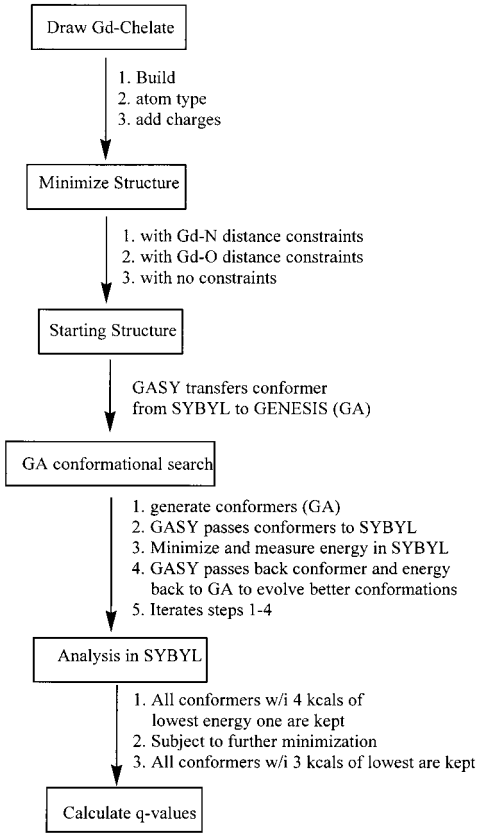
All structures in the database were subjected to the following protocol after extraction from the CSD. The crystal structures were imported into SYBYL, and counterions and water molecules were removed. Atoms were atom typed, and bonding was fixed if necessary. Hydrogens were added and minimized, holding the rest of the molecule fixed (default conditions: simplex method (*33*), 20 steps for any atom with a force above 1000 kcal/mol Å^2 followed by the Powell method of conjugate gradient minimization (*34*) to a convergence 0.05 kcal/molÅ^2 RMS (root-mean-square gradient). Gasteiger charges were calculated setting the charge on gadolinium to +3.0.

The R_i of Gd was varied from 1.8 to 2.3 Å in increments of 0.1 Å, the database was minimized (default conditions) using the default E_{ij} (van der Waals constant or well depth) value of 0.1. The resulting minimized structures were saved in a new database, and the total RMS deviations (no hydrogen atoms) from original crystal structures were used as a measure of "goodness" of parameter fit. The following four structures were eliminated since the RMS deviation (no hydrogen atoms) was very poor (>1) for all values of R_i: cis-trichloro-tris(2,6-dimethyl-4-pyrone)-gadolinium(III) (*24*), bis(diethylcarbamoyl)ethyl-phosphonato-*O*-gadolinium(III) (*25*), acidic gadolinium tetrakis(benzoylacetonate)piperidine (*30*), and bis[diaqua-(2-formyl-4-methyl-6-(4-(2-pyridyl)-2-azonia-but-1-enyl)phenolato-*O*,*O*′)-gadolinium(III)] diperchlorate chloride hydrate (*31*).

A narrower range of suitable R_i was obtained by graphing the sum of the total RMS deviations (no hydrogen atoms) for each run vs R_i. An approximately parabolic curve was obtained with the best radius range in the well being 1.9−2.1. Using a similar procedure as before, both R_i (1.9−2.1 with increments of 0.05) and E_{ij} (0.001, 0.01, 0.05, 0.1, 0.2, 1.0) were varied. The best parameters found were $R_i = 2.0$ and $E_{ij} = 0.2$.

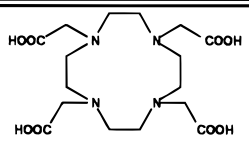
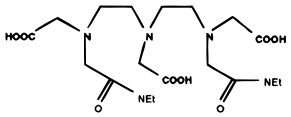
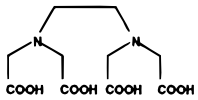
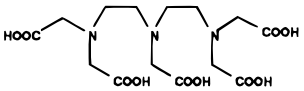
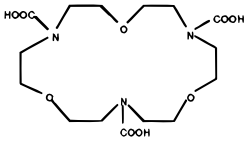
Genetic Algorithm Conformational Search Method. A flow chart representation of this method is shown in Scheme 1. Initially in SYBYL, the gadolinium chelate is built, then atom typed and charged using Gasteiger charges, setting the charge on Gd to +3.0. To go from a 2D drawing to a reasonable starting gadolinium chelate complex, initial constraints are applied. Distance constraints of 2.6 Å are applied to all gadolinium−nitrogen pairs, and the structure is minimized [Powell method of conjugate gradient minimization (*34*) until a convergence of 0.01 energy gradient tolerance is reached]. Then additional distance constraints of 2.4 Å are added for the gadolinium−oxygen pairs (one constraint for each carboxylate group, arbitrarily picking just one of the oxygens in the COO^- group), and the chelate is minimized. Then all constraints are removed, and the structure is minimized. The structure is output in SYBYL's mol2 format. This conformation is used as the starting structure for the genetic algorithm conformational searching technique described below.

Scheme 1. Flowchart of Gd-Chelate Conformation Generation and *q*-Value Prediction



A genetic algorithm (GA) search method was used to identify favorable binding conformation for the gadolinium ligand system. This search was performed using a hybrid system known as GASY which linked the genetic algorithm package GENESIS (*35*) with the molecular-modeling package SYBYL, hence the name GASY (GA linked through the SYBYL software). The GENESIS package was configured to generate lists of floating point numbers whose values had a possible range of −180 to 180. These lists were passed to SYBYL via named pipes. SYBYL was configured using SYBYL programming language (SPL) procedures to retrieve the sets of floating point numbers from the incoming pipe and interpret them as strings of torsional values. GASY then used the values to set a conformation of the molecular system, minimize the conformation [simplex method (*33*), 20 steps for any atom with a force above 1000 kcal/molÅ^2 followed by the Powell method of conjugate gradient minimization (*34*), 200 steps or a minimum energy change of 0.05kcal/mol], and measure the energy of this binding conformation. The energy value was then passed to the GENESIS program via a second pipe where it was treated as a measure of the fitness of the set of floating point numbers. This completed the evaluation loop and allowed

Table 1. Gd Chelates Used to Test the Predictive Capability of This Method[a]

Gd Chelate	Chelate	Connolly SA	Predicted q-value	Exptl. q-value
DOTA		5.9	1	1
DTPA-BEA		6.1	1	1
EDTA		18.6	3	3
DTPA		6.5	1	1
TTTA		0	0	0

[a] Connolly surface area was calculated for each of these known crystal structures, and the calibration curve shown in Figure 1 was used to predict the *q*-value. The predicted and experimental *q*-values are in agreement.

the GA to evolve better conformations. For cyclic chelates, a bond must be broken before the GA run and then reestablished before the SYBYL minimization and energy evaluation.

The messaging scheme used by GASY was necessary because both programs are designed to be in control of the sequence of operations and there is no easy way to make either program a subprogram of the other. GASY is a general modeling optimization tool. It allows the easy optimization of any number of problems where a string of numbers can be encoded into a molecular system and a fitness evaluation of the resulting system can be performed.

Analysis of Genetic Algorithm Searches. The analysis of the conformations that were generated by the method outlined above was performed within SYBYL using a macro that had been created in SYBYL Programming Language (SPL) (see Scheme 1.). This macro reads a file that was generated by the Genetic Algorithm that contains an ordered list of the values of the torsions of each of the rotatable bonds. All energetically acceptable conformations were defined as those that were less than or equal to the minimum energy found over the entire run, plus 4 kcals. The program creates a table in SYBYL whose rows represent the conformations and whose columns represent a rotatable bond. Atom numbers of the four atoms which define each of the torsions from the GA initialization file are determined. Lastly, the program generates each of the conformations in the 4 kcal set and reports their energies as calculated in the SYBYL package. The resulting conformations are minimized with another SPL and deposited into a SYBYL database along with their corresponding calculated energies. All low-energy structures (within 3 kcal of lowest) are considered valid models, and their *q*-values are calculated using the above-described method. The Connolly surface of the gadolinium for each model is calculated in SYBYL, and the calibration curve is used to convert Connolly surface area to corresponding q-value.

RESULTS AND DISCUSSION

Our hypothesis was that *q*-value would be proportional to the solvent-accessible surface area of the gadolinium ion. Typically, calculated Connolly surface area has been used to estimate the solvent accessible surface area of proteins. Using the crystal structure of gadolinium nonahydrate (*15*), it was shown that a linear correlation exists between calculated Connolly surface area of the gadolinium ion and *q*-value (see Figure 1). This calibration curve was developed by iteratively removing waters from the crystal structure of gadolinium nonahydrate and calculating Connolly surface area. To test the predictive capability of this method, this calibration curve was used to determine the *q*-values of the following gadolinium crystal structures: Gd(EDTA) (*1*), Gd(DOTA) (*2*), Gd(DTPA) (*3*), Gd(DTPA-BEA) (*4*), and Gd(TTTA) (*5*) (see Table 1). The predicted *q*-values were in total agreement with the experimentally determined values (*36*).

To develop this as a tool for novel agent design, where no prior structural information exists, we needed to develop a method to generate valid 3D structures for the gadolinium chelates. Since any computationally generated model would be a minimized structure, the force field used had to be augmented to include gadolinium. Nonbonded force field parameters for Gd(III) were developed empirically within SYBYL. A new calibration curve was developed for minimized structures using the minimized gadolinium nonahydrate crystal structure (vide infra). The predictive capability was again tested using the minimized crystal structures listed above. Again, the predicted *q*-values were in complete agreement with the experimentally determined values (*36*).

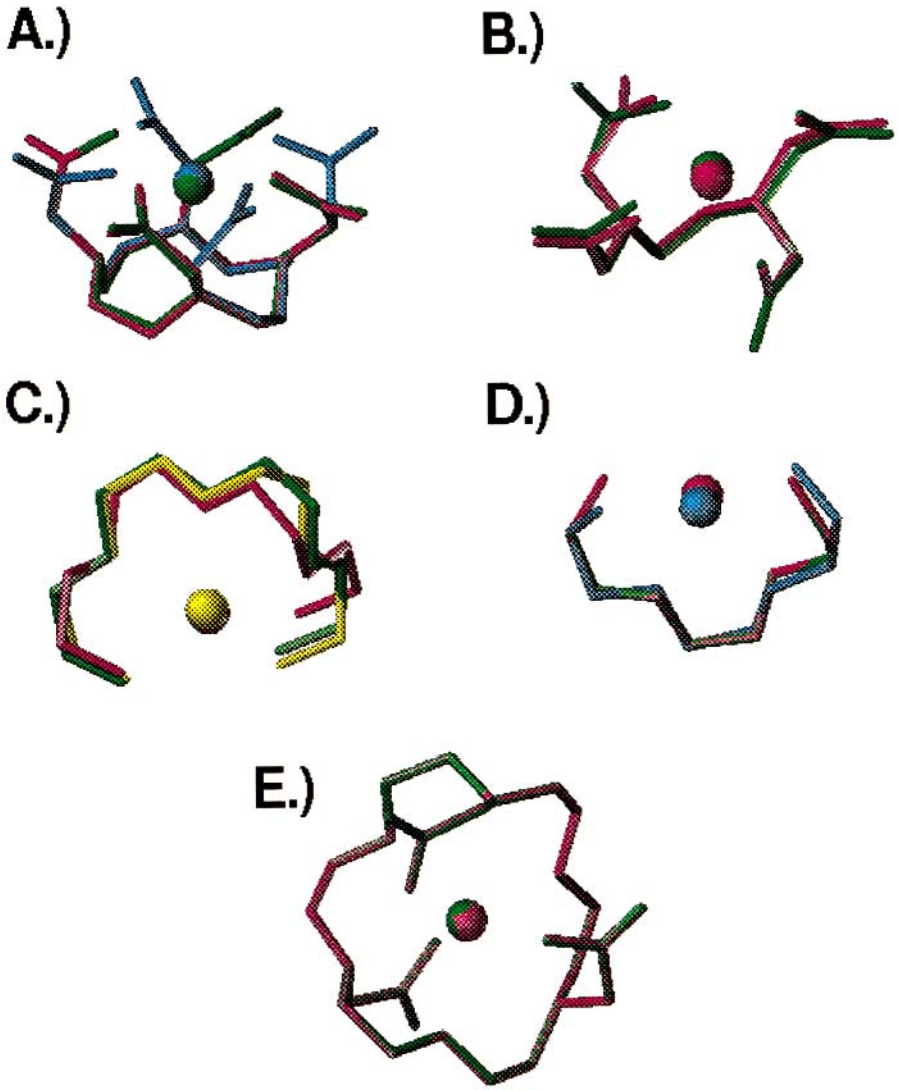


Figure 2. Superposition of minimized crystal structures (green) and the GA generated conformations (magenta) for (A) Gd(DOTA), second unique GA generated conformation shown in blue; (B) Gd(EDTA); (C) Gd(tetraethylene glycol), two crystal structures are reported for this molecule and the second minimized crystal strucure is shown in yellow; (D) Gd(triethylene glycol), the second unique GA generated conformation is shown in blue; (E) Gd(TTTA).

A genetic algorithm based conformational search method (vide infra) was used to generate 3D models for the following chelates: Gd(EDTA) (*1*), Gd(DOTA) (*2*), Gd(DTPA-BEA) (*4*), Gd(TTTA) (*5*), Gd(tetraethylene glycol) (*7*), and Gd(triethylene glycol) (*6*). For Gd(EDTA) and Gd(tetraethylene glycol), one unique low-energy structure was generated (see Figure 2, panels B and C). Two unique equivalent energy structures were generated for Gd(DOTA) and for Gd(triethylene glycol). For Gd(DOTA), one structure is a diastereomer of the minimized crystal structure differing only in the rotation about the $N-CH_2$ bond and the other is the enantiomer of the crystal structure (see Figure 2A). For Gd(triethylene glycol), one structure is the same as the minimized crystal structure and the other is a slightly lower energy structure which is similar in conformation to the minimized crystal structure (see Figure 2D). Two families of structures are generated for Gd(TTTA); one is the same as the minimized crystal structure and the other is the enantiomer of the minimized crystal structure (see Figure 2E). All the GA-generated structures are similar to the minimized crystal structures and have the same *q*-value and number of metal coordinating ligands as the minimized crystal structures. For Gd(DTPA-BEA), two families of structures were generated. Within the families, the structures are very similar and only differ by end methyl rotations. Both structures are similar in energy to the minimized crystal structure, but are inverted at one nitrogen (see Figure 3). These two models still yield the correctly predicted *q*-value and number of metal coordinating ligands and, therefore, are reasonable models to use for design purposes.

Water molecules that exchange rapidly between the inner coordination sphere of the gadolinium ion and the bulk solvent dominate the relaxivity. Despite the fact that our calculations do not take water exchange rates ($1/\tau_M$) into account, the exchange rates for all gadolinium chelates reported thus far are sufficiently rapid to contribute to the relaxivity. In a recent study, the exchange rates [298 K, units of inverse seconds (s^{-1})] ranged from 8.3×10^8 to 4.3×10^5 for a series of gadolinium compounds (*11*). Although this range of exchange rates spans 4 orders of magnitude, the exchange rates are sufficiently rapid to make the value of the relaxivity insensitive to the precise value of the exchange rate for small gadolinium complexes (*37*). Consequently for small gadolinium complexes, the water molecules in the inner coordination sphere may be considered in rapid exchange with the bulk.

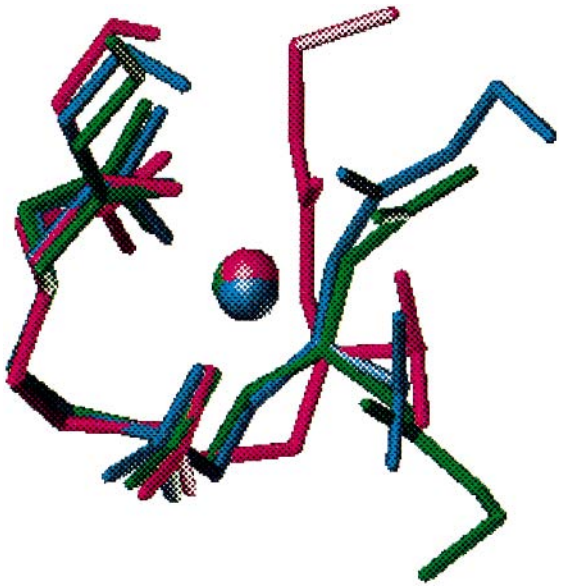


Figure 3. Superposition of minimized crystal structure (green) and the two GA generated conformations (magenta and blue) for Gd(DTPA-BEA).

SUMMARY AND CONCLUSIONS

A quick computational method for predicting integer *q*-value of small molecule gadolinium chelates has been developed. Using the crystal structure of gadolinium nonahydrate, a calibration curve to predict *q*-value from solvent accessible surface area of the gadolinium ion was developed. The calibration curve was tested using the crystal structures of gadolinium chelates obtained from the CSD, thus establishing a linear relationship between the calculated Connolly surface area of the gadolinium ion and experimental *q*-value. Furthermore, a genetic algorithm based protocol which generates valid three-dimensional structures of known gadolinium chelates has been developed. The combination of the genetic algorithm conformational search method and *q*-value calibration curve produce literature consistent *q*-values and structures for selected MRI contrast agents. Use of the described method will help facilitate the discovery of novel MRI contrast agents.

LITERATURE CITED

(1) Templeton, L. K., Templeton, D. H., Zalkin, A., and Ruben, H. W. (1982) Anomalous Scattering by Praseodymium, Samarium, and Gadolinium and Structures of their Thylenediaminetetraacetate (EDTA) Salts. *Acta Crystallogr., Sect. B 38*, 2155.

(2) Dubost, J.-P., Leger, J.-M., Langlois, M.-H., Meyer, D., and Schaefer, M. (1991) Structure of a Magnetic Resonance Imaging Agent - The Gadolinium-DOTA Complex $C_{16}H_{24}N_4O_8$-NaGd, $5H_2O$. *CR Acad. Sci., Ser. 2 312*, 349.

(3) Stezowski, J. J., and Hoard, J. L. (1984) Heavy Metal Ionophores - Correlations Among Structural Parameters of Complexed Nonpeptide Polyamino Acids. *Isr. J. Chem. 24*, 323.

(4) Smith, P. H., Brainard, J. R., Morris, D. E., Jarvinen, G. D., and Ryan, R. R. (1989) Solution and Solid-State Characterization of Europium and Gadolinium Schiff-Base Complexes and Assessment of their Potential as Contrast Agents in Magnetic Resonance Imaging. *J. Am. Chem. Soc. 111*, 7437.

(5) Chen, D., Squattrito, P. J., Martell, A. E., and Clearfield, A. (1990) Synthesis and Crystal Structure of a 9-Coordinate Gadolinium(III) Complex of 1,7,13-Triaza-4,10,16-Trioxacyclooctadecane-N,N′,N"-Tri-Acetic Acid. *Inorg. Chem. 29*, 4366.

(6) Rogers, R. D., Voss, E. J., and Etzenhouser, R. D. (1988) F-Element Crown Ether Complexes. 17. Synthetic and Structural Survey of Lanthanide Chloride Tiethylene Glycol Complexes. *Inorg. Chem. 27*, 533.

(7) Rogers, R. D., Etzenhouser, R. D., Murdoch, J. S., and Reyes, E. (1991) Macrocycle Complexation Chemistry. 35. Survey of the Complexation of the Open-Chain 15-Crown-5 Analogue tetraethylene Glycol with the Lanthanide Chlorides. *Inorg. Chem. 30*, 1445.

(8) Koenig, S. H., and Brown, R. D. (1990) Field-Cycling Relaxometry of Protein Solutions and Tissue-Implications for MRI. *Progr. NMR Spectrosc. 22*, 487.

(9) Geraldes, C. F. G. C., Sherry A. D., Cacheris, W. P., Kuan, K.-T., Brown, R. D., Koenig, S. H., and Spiller, M. (1988) Number of Inner-Sphere Water Molecules in Gd^{3+} and Eu^{3+} Complexes of DTPA-Amide and DTPA-Ester Conjugates. *Magn. Reson. Med. 8*, 191.

(10) Geraldes, C. F. G. C., Brown, R. D., Brucher, E., Koenig, S. H., Sherry A. D., and Spiller, M. (1992) Nuclear Magnetic Relaxation Dispersion Profiles of Aqueous Solutions of a Series of Gd(NOTA) Analogues. *Magn. Reson. Med. 27*, 284.

(11) Gonzalez, G., Powell, D. H., Tissieres, V., and Merbach, A. E. (1994) Water Exchange, Electronic Relaxation, and Rotational Dynamics of the MRI Contrast Agent [Gd(DTPA-BMA)(H2O)} in Aqueous Solution - A Variable Pressure, Temperature, and Magnetic Field O17 NMR Study. *J. Phys. Chem. 98*, 53.

(12) Cacheris, W. P., Quay, S. C., and Rocklage, S. M. (1990) The Relationship between Thermodynamics and the Toxicity of Gadolinium Complexes. *Magn. Reson. Imaging 8*, 467.

(13) Weiner, S. J., Kollman, P. A., Nguyen, D. T., and Case, D. A. (1986) An All Atom Force Field for Simulations of Proteins and Nucleic Acids. *J. Comput. Chem. 7*, 230.

(14) a) Fossheim, R., Dugstadt, H., and Dahl, S. G. (1991) Structure Stability Relationships of Gd(III) Ion Complexes for Magnetic Resonance Imaging. *J. Med. Chem. 34*, 819. (b) Fossheim, R., and Dahl, S. G. (1990) Molecular Structure and Dynamics of Aminopolycarboxylates and their Lanthanide Ion Complexes. *Acta Chem. Scand. 44*, 698.

(15) Chatterjee, A., Maslen, E. N., and Watson, K. J. The Effect of the Lanthanoid (1988) Contraction on the Nonaaqualanthanoid(III) Tris(Trifluoromethanesulfonates). *Acta Crystallogr., Sect. B 44*, 381.

(16) SYBYL, Version 6.0, TRIPOS Assoc. Inc., St. Louis, Mo. 63144.

(17) Clark, M., Cramer, R. D., III, and Van Opdenbosch, N. (1989) Validation of the General Purpose Tripos 5.2 Force-Field. *J. Comput. Chem. 10*, 982.

(18) Cambridge Crystallographic Data Center, 12 Union Road, Cambridge CB2 1EZ, U.K.

(19) Forsellini, E., Benetollo, F., Bombieri, G., Cassol, A., and De Paoli, G. (1985) Preparation, Crystal and Molecular Structure of GdCl3(18-Crown-6)EtOH. *Inorg. Chim. Acta 109*, 167.

(20) Cheng, S., Yuguo, F., Guofa, L., Yutian, W., and Pinzhe, L. (1983) *Gaodeng Xuexiao Huaxue Xuebao (Chem. J. Chin. Univ.) 4*, 769.

(21) Batsanov, A. S., Struchkov, Y. T., Trembovetskii, G. V., Martynenko, L. I., and Muraveva, I. A. (1986) Crystal Structure of Tris(Acetylacetonato)Bis(O-Acetylacetoneimino)-Gadolinium(III) (1-2) Solvate with Acetylacetoneimine. *Zh. Neorg. Khim. 31*, 345.

(22) Rogers, R. D., and Kurihara, L. K. (1987) F-Element Crown Ether Complexes. 4. Synthesis and Crystal and Molecular Structures of $[SmCl(OH_2)_2(18\text{-Crown-6})Cl_2.2H_2O$, $(GdCl(OH_2)_2$-$(18\text{-Crown-6}))Cl_2.2H_20$, $(TbCl(OH_2)_2(18\text{-Crown-6}))Cl_2.2H_2O$. *Inorg. Chem. 26*, 1498.

(23) Brennan, J. G., Cloke, F. G. N., Sameh, A. A., and Zalkin, A. (1987) Synthesis of Bis(Eta-1,3,5-Tri-*tert*-Butylbenzene) Sandwich Complexes of Yttrium(0) and Gadolinium(0) - the X-ray Crystal Structure of the 1st Aunthentic Lanthanide(0) Complex, $[Gd(ETA\text{-}But_3C_6H_3)_2]$. *J. Chem. Soc., Chem. Commun.* 1668.

(24) Castellani, C. B., and Tazzoli, V. (1984) Cis-Trichlorotris-(2,6-Dimethyl-4-Pyrone)Gadolinoum(III), $[GdCl_3(C_7H_8O_2)_3]$ *Acta Crystallogr., Sect. C 40*, 183.

(25) McCabe, D. J., Duesler, E. N., and Paine, R. T. (1988) Synthesis and Coordination Chemistry of Tripodal Dialkyl-

[1,2-Bis(Diethylcarbamoyl)Ethyl]Phosphonates with Lanthanide Nitrates. *Inorg. Chim. Acta 147*, 265.
(26) Smith, A., Rettig, S. J., and Orvig, C. (1988) Lanthanide Complexes of Potentially Heptadentate Ligands Including the Structure of [Tris(3-Aza-4-Methylhept-4-Ene-6-On-1-Yl)-Amine]Tris(Nitrato)Gadolinium(III). *Inorg. Chem. 27*, 3929.
(27) Aime, S., Anelli, P. L., Botta, M., Fedeli, F., Grandi, M., Paoli, P., and Uggeri, F. (1992) Synthesis, Characterization, and 1/T(1) NMRD Profiles of Gadolinium(III) Complexes of Monoamide Derivatives of DOTA-like Ligands - X-ray Structure of the 10-[-[[2-Hydroxy-1-(Hydroxymethyl)Ethyl]Amino]-1-[(Phenylmethoxy) Methyl]-2-Oxo-Ethyl]-1,4,7-Triacetic Acid Gadolinium(III) Complex. *Inorg. Chem. 31*, 2422.
(28) Albertson, J. (1968) Structural Studies on the Rare Earth Carboxylates. I. Crystal and Molecular Structure of $Na_3(M(O_2CCH_2OCH_2CO_2)_3).2NaClO_4.6H_20$; M= Neodynium, Gadolinium, and Ytterbium. *Acta Chem. Scand. 22*, 1563.
(29) Smith, G. D., Caughlan, C. N., Haque, M., and Hart, F. A. (1973) Crystal and Molecular Structure of Trinitrato-1,2-Bis-(Pyridine-2-Aldimino)Ethanegadolinium(III). *Inorg. Chem. 12*, 2654.
(30) Butman, L. A., Aslanov, L. A., and Porai-Koshits, M. A. (1970) Crystal and Molecular Structure of Acidic Gadolinium Tetrakis(benzoylacetonate). *Zh. Strukt. Khim. 11*, 46.
(31) Bakalbassis, E., Kahn, O., Sainton, J., Trombe, J. C., and Galy, J. (1991) Synthesis of Dissymmetric Schiff-Base Ligands Through Gadolinium(III) Coordination. *J. Chem. Soc., Chem. Commun. 1991*, 755.
(32) Gecheng, W., Hanrong, G., Zhongsheng, J., and Qi, S. (1989) *Jiegou Huaxue (J. Struct. Chem.) 8*, 61.
(33) Press, W. H., Teukolsky, S. A., Vetterling, W. T., and Flannery, B. P. (1995) *Numerical Recipes in C*, 2nd ed., Cambridge University Press.
(34) Powell, M. J. D. (1981) *Approximation Theory and Methods*, Cambridge University Press.
(35) Grefenstette, J. J., and Schraudolph, N. N. *GENESIS 1.2ucsd*, available via anonymous ftp from ftp.aic.nrl.navy.mil in /pub/galist/source-code/gasource/gaucsd12.tar.
(36) Lauffer, R. B. (1987) Paramagnetic Metal Complexes as Water Proton Relaxation Agents for NMR Imaging: Theory and Design. *Chem. Rev. 87*, 901.
(37) Koenig, S. H. (1994) The Need for Electron Paramagnetic Resonance and Water Exchange-Rate Data for Understanding Small Magnetic Imaging Contrast Agents and their Macromolecular Complexes. *Invest. Radiol. 29* (Suppl. 2), S127.

BC990027B

Cellular Uptake of Adamantyl Conjugated Peptide Nucleic Acids

Trine Ljungstrøm, Helle Knudsen, and Peter E. Nielsen*

Center for Biomolecular Recognition, Department of Medical Biochemistry & Genetics, Biochemistry Laboratory B, The Panum Institute, Blegdamsvej 3c, 2200 Copenhagen N, Denmark. Received April 30, 1999; Revised Manuscript Received August 30, 1999

Peptide nucleic acids (PNA) (15-mers) conjugated to adamantyl acetic acid and labeled with fluorescein have been prepared, and their (liposome mediated) uptake in human cells in culture (HeLa, IMR-90 and MDA-MB-453) has been studied by confocal fluorescence microscopy. It is found that adamantyl-PNAs show greatly improved (endosomal) cellular uptake, but that this uptake is dependent on the cell line. Cellular uptake of such lipophilic PNAs is further mediated by cationic liposomes, and in some cases, the intracellular localization is diffuse cytoplasmic or nuclear, again cell-type dependent. The results show that this simple PNA modification can indeed greatly improve cellular uptake, but the effect appears strongly cell-type as well as PNA-sequence dependent.

INTRODUCTION

Short synthetic oligonucleotides as highly specific inhibitors of translation or transcription have shown great promise as antisense (and antigene) gene therapeutic drugs (Agrawal, 1996; Altmann et al., 1996; Sharma and Narayanan 1995; Wagner and Flanagan, 1997; Bennet, 1998). The quest for oligonucleotide analogues and mimics with improved properties in terms of nuclease resistance and target affinity have led to the development of a large number of DNA analogues (Agrawal and Iyer, 1995; De Mesmaeker et al., 1995; Freier and Altmann, 1997).One of the more promising of these mimics is peptide nucleic acid (PNA), which contains a pseudo-peptide backbone composed of uncharged *N*-(2-aminoethyl)glycine units to which the nucleobases are attached via methylene carbonyl linkers (Nielsen et al., 1991; Egholm et al., 1992a,b; Egholm et al., 1993; Hyrup and Nielsen, 1996; Good and Nielsen, 1997). PNA hybridizes with high affinity and sequence selectivity to complementary DNA or RNA oligomers by normal Watson−Crick base pairing (Egholm et al., 1993; Leijon et al., 1994; Brown et al., 1994; Jensen et al., 1997; Eriksson and Nielsen, 1996a,b). Notably, homopyrimidine PNAs binds to sequence complementary targets in double-stranded DNA by forming a strand displacement complex where two PNAs bind to the target strand, forming a triplex, and the nontarget strand is looped out (Cherny et al., 1993; Nielsen et al., 1994a). Such complexes are extremely stable and can efficiently block transcription and replication elongation (Hanvey et al., 1992; Nielsen et al., 1994b; Taylor et al., 1997). Likewise, homopyrimidine PNAs form thermally extremly stable PNA_2−RNA triplexes with targets in RNA (Egholm et al., 1992a,b; Kim et al., 1993). PNA is resistant to degradation by nucleases and proteases and show high stability in cellular extracts (Demidov et al., 1994). They are conveniently synthesized by solid-phase peptide chemistry (Christensen et al., 1995). Taken together, these properties make PNA a promising candidate for development of gene-specific drugs. Indeed, PNA has been shown in vitro to have antisense activity against interleukin-2 receptor α (IL-2Rα) (Hanvey et al., 1992), chloramphenicol acetyltransferase (CAT) (Knudsen and Nielsen, 1996) and promyelocytic leukemia/retinoic acid receptor α (PML/RARα) (Gambacorti-Passerini et al., 1996; Mologni et al., 1998).

Table 1: List of the PNAs Used in the Study[a]

PNA or S-ON	sequence	target
960	Fl-TTT AGC TTC CTT AGC-LysNH_2	CAT
1118	Ada-Fl-TTT AGC TTC CTT AGC-LysNH_2	CAT
1196	Ada-Fl-TTT GGG CGG CAT GAC-LysNH_2	Rb
1252	Fl-GGT GCT CAC TGC GGC-LysNH_2	Her-2
1253	Ada-Fl-GGT GCT CAC TGC GGC-LysNH_2	Her-2
1401	Ada-Fl-GGT_{Lys} GCT_{Lys} CAC T_{Lys}GC GGC-LysNH_2	Her-2
1402	Fl-GGT_{Lys}GCT_{Lys}CAC T_{Lys}GC GGC-LysNH_2	Her-2
1662	Ada-Fl-ACT TGC GGC TCC GGC C-LysNH_2	Her-2
S-ON	Fl-GGT GCT CAC TGC GGC	Her-2

[a] Ada is adamantyl acetic acid, Fl is fluoresceinated PNA monomer, and T_{Lys} is a thymine PNA monomer with a lysine residue.

However, simple PNAs show very poor cellular uptake when studied in cell culture (Bonham et al., 1995; Gray et al., 1997). Previous experiments with anionic oligonucleotides have shown that their cellular uptake can be greatly improved by covalent attachment of lipophilic groups, such as cholesterol (Letsinger et al., 1989; Stein et al., 1991; Boutorine et al., 1993) or aliphatic chains of different lengths (Kabanov et al., 1990; Saison-Behmoaras et al., 1991; Svinarchuk et al., 1993; Hubus et al., 1995; Mishra et al., 1995). However, the only general solution for delivery of oligonucleotides to cells in culture has been employment of cationic liposomes as vehicles (Bennett et al., 1992; Thierry and Dritschillo, 1992; Zelphati and Szoka, 1996; Wielbo et al., 1997).

Recently, various small peptides have been used to transport PNA into cultured cells. For instance, PNA conjugated to the insulin-like growth factor 1 peptide was reported to be taken up if the cognate receptor was expressed on the cell surface (BALB/c 3T3 cells) (Basu and Wickstrom, 1997). Hybrids between PNAs and cationic peptides, such as the third helix of the homeodomain of Antennapedia, were reported to cross through cell membranes and enter immortal human prostate

* To whom correspondence should be addressed. Phone: (+45) 35327762. Fax: (+45) 35396042. E-mail: pen@imbg.ku.dk.

10.1021/bc990053+ CCC: $18.00 © 1999 American Chemical Society
Published on Web 10/29/1999

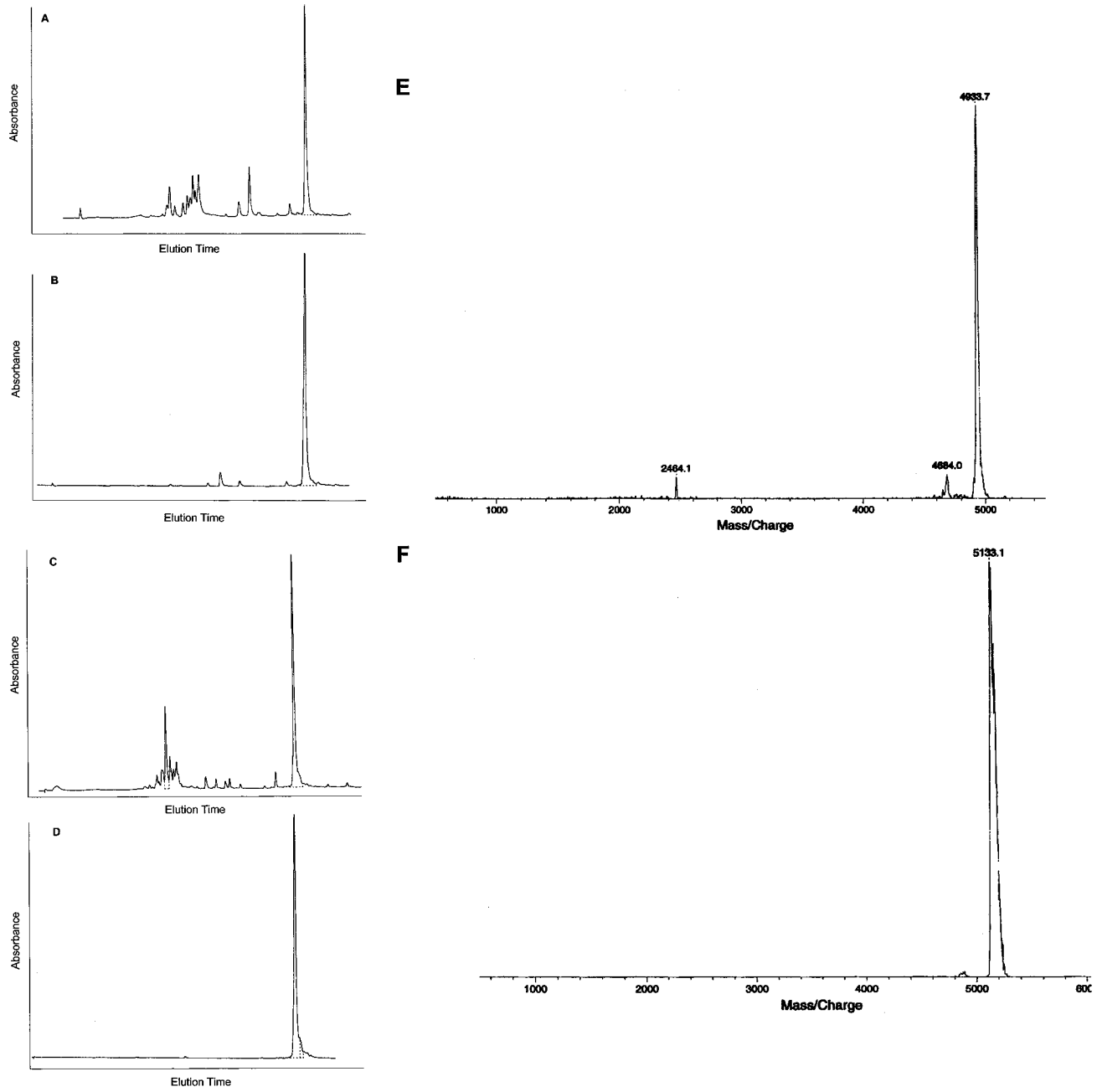


Figure 1. HPLC chromatographs of raw and purified PNA 1253 (A and B, respectively) and 1401 (C and D, respectively). The gradient (35 min) was 0 to 100% (0−30 min, 0 to 50%; 30−33 min, 50%; 33−35 min, 50 to 100%) CH_3CN in H_2O, 0.1% CF_3COOH, and the PNA oligomers eluted at 28 min. MALDI-TOF mass spectra (Kratos Maldi-II) of PNAs 1253 (E) and 1401 (D). The found (and calculated) masses are 4933.7 (4928.8) (PNA1253) and 5133.1 (5141) (PNA1401), respectively. The signal from PNA 1401 was weak and, thus, rather broad and less accurate.

tumor-derived D4145 cells (Simmons et al., 1997). This peptide (or its retro-inverso analogue) was also recently used as a vehicle to carry PNA into mammalian cells (Pooga et al., 1998; Aldrian-Herrada et al., 1998), and in one case, down regulation of an antisense targeted neural receptor was reported using a PNA conjugated to "penetratin" (Pooga et al., 1998).

As PNAs are inherently charge neutral oligomers, these will not spontaneously associate with cationic liposomes as do the anionic oligonucleotides, and liposome delivery of PNAs is therefore impeded by inefficient liposome loading. Others have used cationic oligonucleotides either conjugated to the PNA (Uhlmann et al., 1996) or just complexed by hybridization (Hamilton et al., 1999) to increase the efficiency of liposomal loading. We reasoned that supplying PNAs with a lipophilic tail

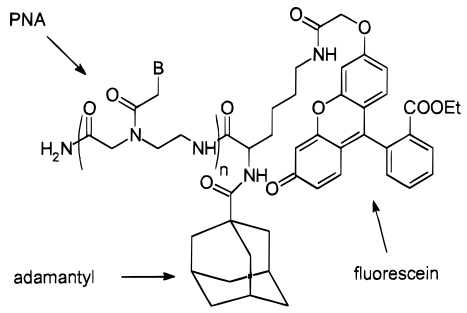


Figure 2. Chemical structure of adamantyl conjugated, fluoresceinated PNA. For regular PNA units R = H and B = adenine, cytosine, guanine or thymine; for T_{lys} modified PNA units R = $-(CH_2)_4-NH_2$ and B = thymine.

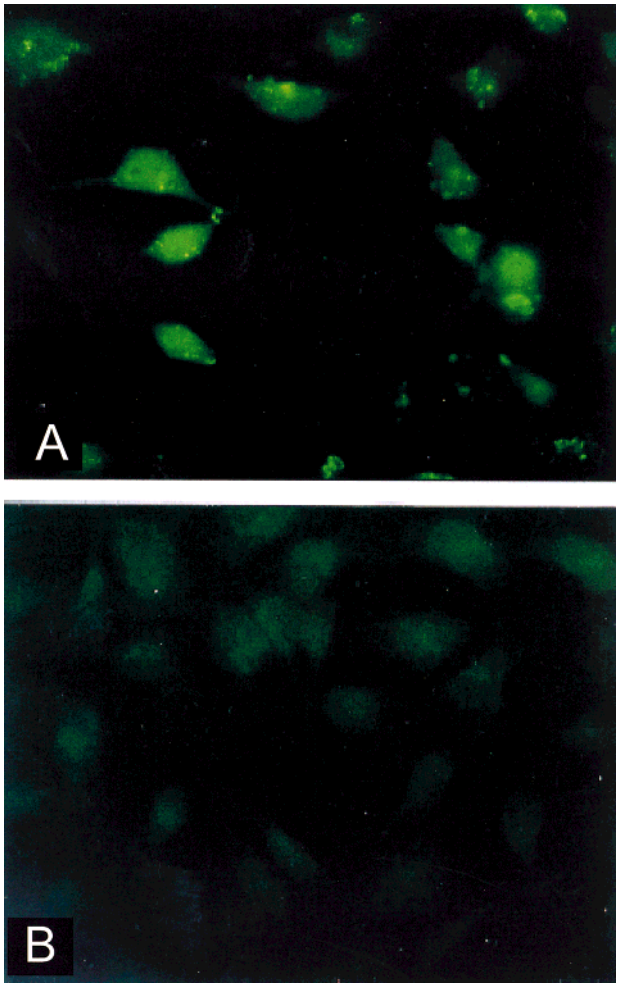


Figure 3. Fluorescence microscopic images of HeLa cells incubated with PNA 1118/DOPE/DDAB (A) or PNA 1118 (B).

should greatly increase their affinity toward liposomes and could even confer spontaneous incorporation upon liposome assembly. Furthermore, such PNA−lipid conjugates could by themselves exhibit improved cellular uptake by initial membrane association and subsequent internalization. We therefore set out to synthesize lipid-PNA conjugates and study their (liposome mediated) cellular uptake.

The cellular uptake of five PNAs was investigated in three different cell lines, HeLa, IMR-90, and MDA-MB-453. Fluorescein-labeled adamantyl-conjugated PNAs were added to cell cultures either alone or in combination with cationic DOPE/DDAB liposomes, and the uptake was observed by fluorescence (confocal) microscopy. We find that the pattern of uptake varies with the type of cells used. Furthermore, the behavior of the PNAs in the cell culture is highly dependent on their sequence as well as the chemical modification.

EXPERIMENTAL PROCEDURES

Synthesis of PNAs and S−ON. PNAs were synthesized and purified as described previously (Christensen et al., 1995). The sequences of the employed PNAs and their gene targets are outlined in Table 1. Conjugation of fatty acids was done using the normal coupling procedure (Christensen et al., 1995). T_{Lys} monomer (D-form) was synthesized and incorporated into PNA oligomers as described (Haaima et al., 1996). As for standard PNA Boc-synthesis, the procedure yielded PNA oligomers of good purity that were further purified by reversed-phase HPLC and characterized by MALDI-TOF mass spectrometry (Figure 1). Typically, the yield of purified PNA was 1−2 μmol from a 10 μmol (50 mg of resin) synthesis. Phosphorothioate oligonucleotides were synthesized by standard procedures and were kindly provided by Dr. Otto Dahl, University of Copenhagen.

Preparation of DOPE/DDAB Liposomes. DOPE/DDAB liposomes were prepared by a modification of the ethanol injection method described by Campbell (Campbell, 1995). Briefly, 13.4 μmol of DOPE (dioleyl-L-α-phosphatidylethanolamine) and 6.6 μmol of DDAB (dimethyldioctadecylammonium bromide) were dissolved in 1 mL of 96% ethanol. Then 40 μL of this solution was combined with 10 μL of a 2.5 mM PNA solution in DMSO. The resulting 50 μL of PNA/lipid mix was added rapidly to 950 μL of sterile distilled water while vortex mixing. The PNA concentration in the liposome solution was thus 25 μM.

Uptake Experiments. The cells were maintained at 37 °C in a humidified atmosphere containing 5% CO_2. The human breast cancer cell line MDA-MB-453 and HeLa cells were grown in RPMI 1640 medium containing Glutamax, penicillin/streptomycin (10 μg/mL), and 10% fetal calf serum. The human fibroblast cell line IMR-90 was grown in DMEM containing the same supplements. On day 0, the cells were plated at the appropriate density in 35 mm dishes containing a glass coverslip. On day 1, the semiconfluent cells were washed twice with Opti-MEM (Life Technologies: modified Eagle medium with L-glutamine, $NaHCO_3$, Hepes, sodium-pyruvate, hypoxanthine, thymidine, trace elements, and growth factors) and given 1 mL of OptiMEM containing either PNA or DNA alone or PNA combined with DOPE/DDAB liposomes or DNA combined with LipofectAMINE. On day 3, the cells were washed three times with PBS and fixed for 15 min on ice in 3% formaldehyde/0.2% glutaraldehyde. The coverslips were then mounted on objective glasses and the cells examined by fluorescence microscopy on a Leitz Diaplan microscope. Micrographs were taken using a Kodak Ektachrome 1600 ASA film. Confocal microscopy was performed on a Nicon DIAPHOT 200 controlled by a Silicon Graphics Computer.

RESULTS AND DISCUSSION

Initially, we synthesized PNAs conjugated to various fatty acids (heptanoic acid, decanoic acid, dodecanoic acid, and adamantyl acetic acid) by coupling of this acid to the terminal amine of a PNA on the solid support using conventional in situ activation, followed by deprotection and cleavage from the solid support by the low/high TFMSA procedure routinely used for PNA synthesis (Christensen et al., 1995). However, upon purification by RP-HPLC, only the heptyl and adamantyl derivatives eluted off the column as sharp peaks, and since these in initial cellular experiments appeared to behave identical, we focused on the adamantyl derivatives which could be purified and handled without special precautions.

Four different 15-mer PNAs (1118, 1196, 1253, and 1662) as listed in Table 1 were conjugated to adamantyl and a fluorescein monomer (Lohse et al., 1997) was included as well as a marker for cellular uptake. Furthermore, a derivative of PNA 1253 containing three T_{Lys}-monomers (having a lysine replacing the glycine in the backbone) was made (PNA 1401) to increase the aqueous solubility of the PNA (Haaima et al., 1996). Finally, control PNAs without adamantyl were made (PNAs 960, 1252, and 1402) as well as a phosphorothioate corresponding to PNAs 1253, 1401, and 1402.

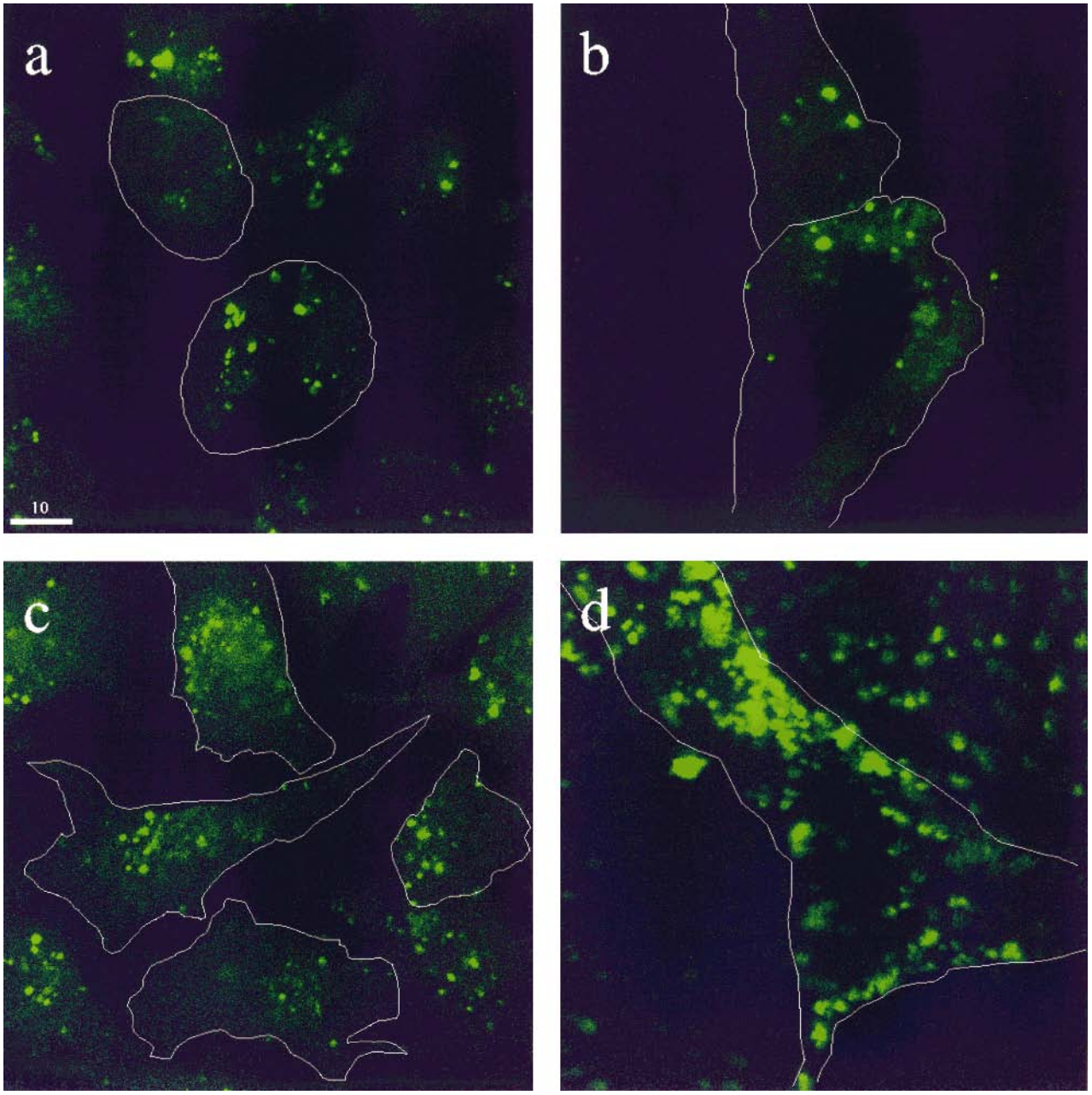


Figure 4. Confocal images of cells incubated overnight with 1 μM fluorescein labeled adamantyl-PNA. (a) HeLa cells incubated with PNA 1118. (b) IMR-90 cells incubated with PNA 1118. (c) HeLa cells incubated with PNA 1196. (d) IMR-90 cells incubated with PNA 1196. The scale-bar is 10 μm. The contour of the cells are indicated by white lines.

Uptake of Adamantyl-Conjugated PNAs. To avoid possible interfering interactions between PNA and serum proteins, the PNAs were added to the cells in serum-free medium. Generally, the uptake was evaluated after an overnight incubation (16−18 h).

Three different monolayer cell lines were used for the uptake studies (HeLa, IMR-90, and MDA-MB-453) and the PNA was delivered either in pure water (added to the serum free medium) or as a liposome preparation (in serum free medium). Selected and representative fluorescence images are presented in Figures3−6 and schematically the results are compiled in Table 2. At first sight, these data may appear confusing since the uptake apart from being strongly influenced by the presence of the lipophilic adamantyl group as well as the use of a cationic liposome vehicle (Figure 3), is also strongly dependent both on the cell type and on the PNA (sequence). Nonetheless, some trends can easily be extracted.

First of all, no significant cellular uptake was found for any of the simple PNAs (960 and 1252) even with the help of liposomes. Furthermore, the attachment of the adamantyl group clearly increased the spontaneous uptake (PNA 1118 and 1196), although PNA 1118 was not taken up by the MDA-MB-453 cells. This uptake appeared, however, exclusively endosomal as concluded from a distinctly punctuated appearance by (confocal) fluorescence microscopy (Figure 4). Employment of cationic liposomes to mediate the uptake of the adamantyl PNAs 1118 and 1196 clearly increased the uptake (Figure 5). However, more interestingly a qualitatively different intracellular distribution of the PNA was obtained at least with some cells. In HeLa cells PNA 1118 showed clear nuclear as well as diffuse cytoplasmic localization (Figure 6a), whereas diffuse cytoplasmic localization was obtained with PNA 1196 in IMR-90 cells (Figure 5b).

PNAs 1253 and 1662, which are both relatively purine (and especially guanine) rich, aggregated easily and,

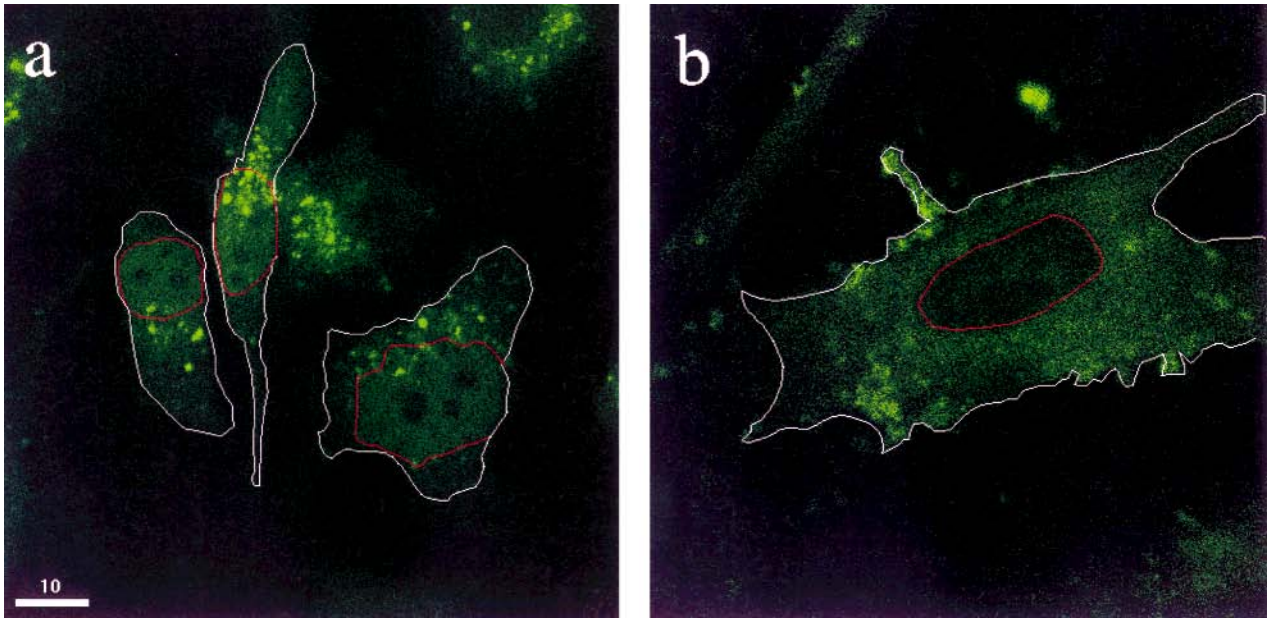


Figure 5. Confocal images of cells incubated overnight with 1 μM fluorescein labeled ada-PNA in DOPE/DDAB complexes. (a) HeLa cells incubated with PNA 1118/DOPE/DDAB. (b) IMR-90 cells incubated with PNA 1196/DOPE/DDAB. The contour of the cells are indicated by white lines and that of the nuclei by red lines.

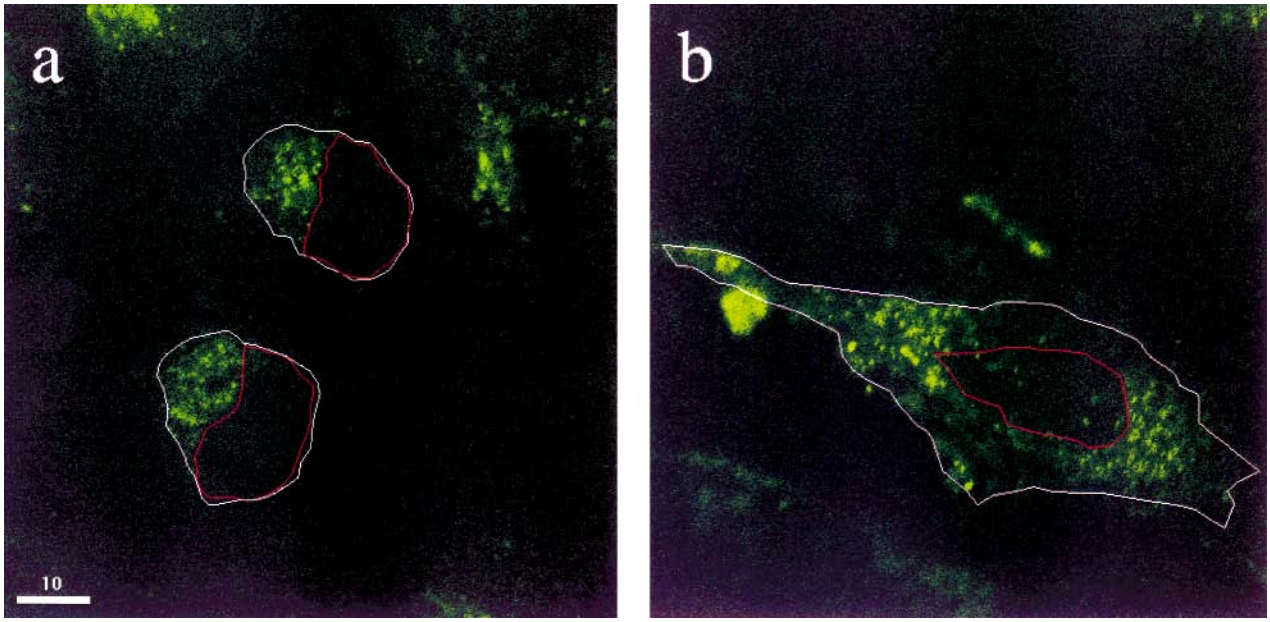


Figure 6. Confocal images of cells incubated overnight with 1 μM PNA 1401. (a) HeLa cells. (b) IMR-90 cells. The contour of the cells are indicated by white lines and that of the nuclei by red lines.

therefore, could not be handled in terms of cellular uptake experiments. To produce a more water-soluble derivative of PNA 1253, we included three T_{Lys} monomers in the PNA (1401), which introduces three positive charges and which we have previously found to confer significantly increased aqueous solubility (Haaima et al., 1996). As a control, we also tested such a PNA (1402) lacking the adamantyl group. Quite interestingly, membrane association as well as some endosomal uptake was observed with this PNA—in contrast to the normal PNA (1252)—indicating that simply equipping the PNA with positive charges may significantly facilitate cellular uptake. This mechanism could be analogous to that responsible for the effect of, e.g. the Antennapedia peptide which is also cationic, as well as the use as polyethylenimine as carrier in DNA transfection. The introduction of the lysine backbone modification also significantly increased the aqueous solubility of the corresponding adamantyl conjugated PNA (1401) which showed spontaneous endosomal uptake (Figure 6). This uptake was, however, not facilitated further by liposomes. Instead aggregation was observed. Possibly, the positive charges of the PNA are interfering with the incorporation into the also cationic liposomes.

Finally, uptake of the PNAs were compared with the uptake of a phosphorothioate having the same sequence as PNA 1253 (and 1401 and 1402). The phosphorothioate was added to HeLa and IMR-90 cells either alone or combined with commercial liposomes (LipofectAMINE) and to MDA-MB-453 cells combined with LipofectAMINE. The S−ON alone showed clear endosomal uptake in HeLa and IMR-90 cells, whereas in combination with LipofectAMINE strongly fluorescent nuclei were observed in all three cell lines (Figure 7).

Table 2: Summary of Uptake Patterns of the PNAs in the Three Cell Lines Studied

PNA or S-ON	treatment	HeLa	IMR-90	MDA-MB-453
960	alone	no uptake	nd[a]	nd
	DOPE + DDAB	no uptake	nd	nd
1118	alone	endosomal	endosomal	no uptake
	DOPE + DDAB	nuclear	no uptake	no uptake
1196	alone	endosomal	endosomal/aggregation	endosomal
	DOPE + DDAB	endosomal	diffuse, cytoplasmic	endosomal
1252	alone	nd	no uptake	nd
	DOPE + DDAB	nd	no uptake	nd
1253	alone	aggregation	aggregation	aggregation
	DOPE + DDAB	aggregation	aggregation	aggregation
1662	alone	aggregation	aggregation	aggregaton
	DOPE + DDAB	aggregation	aggregation	aggregation
1401	alone	endosomal	endosomal	membrane-association
	DOPE/DDAB	aggregation	aggregation	aggregation
1402	alone	nd	membrane-association and endosomal	membrane-association and endosomal
	DOPE/DDAB	nd	endosomal	endosomal
S-ON	alone	endosomal	endosomal	nd
	LipofectAMINE	nuclear	nuclear	nuclear

[a] nd, not done.

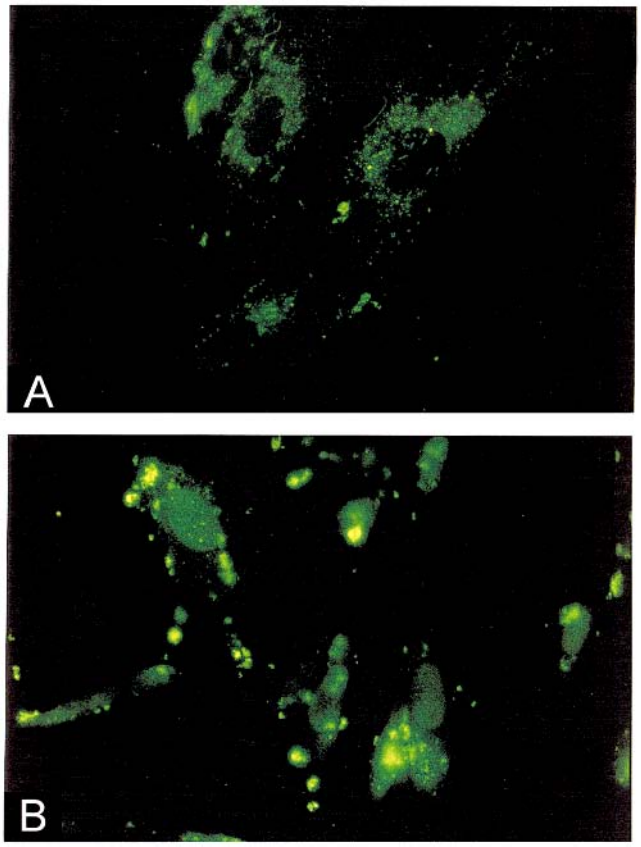


Figure 7. Fluorescence images of IMR-90 cells incubated overnight with 1 μM fluorescein labeled S-ON. (A) Alone or (B) in combination with LipofectAMINE.

CONCLUSION

The present results clearly demonstrate that conjugation of PNAs to a simple lipophilic ligand, such as an adamantyl group, can confer dramatically increased cellular uptake properties, especially when mediated by cationic liposomes. The results also show that increased cellular uptake may be attained by using a lysine backbone modification. However, the results just as clearly show that the cellular uptake by any of these schemes is highly dependent on the cell-type as well as on the PNA sequence. The limited data, unfortunately, does not yet allow us to deduce guidelines as to which modification to be used with which cells and PNA sequences, but it should eventually be possible to arrive at such more general guidelines. Nonetheless, the adamantyl and backbone lysine modifications represent significant improvements toward more efficient PNA antisense reagents. Naturally, the real test of such PNAs will be antisense efficacy and such experiments are now in progress.

ACKNOWLEDGMENT

This work was supported by the Danish Cancer Society, the European Commission (contract no BMH4-CT96-0848) and the Danish National Research Foundation. We thank Peter Walmod from the Protein Laboratory, University of Copenhagen, for doing the confocal microscopy.

LITERATURE CITED

Agrawal, S. (1996) Antisense oligonucleotides: towards clinical trials. *Trends Biotechnol. 14*, 376−387.

Agrawal, S., and Iyer, R. P. (1995) Modified oligonucleotides as therapeutic and diagnostic agents. *Curr. Biol. 6*, 12−19.

Aldrian-Herrada, G., Desarménien, M. G., Orcel, H., Boissin-Agasse, L., Méry, J., Brugidou, J., and Rabie, A. (1998) A peptide nucleic acid (PNA) is more rapidly internalized in cultured neurons when coupled to a *retro-inverso* delivery peptide. The antisense activity depresses the target mRNA and protein in magnocellular oxytocin neurons. *Nucleic Acids Res. 26* (21), 4910−4916.

Altmann, K. H., Dean, N. M., Fabbro, D., Freier, S. M., Geiger, T., Häner, R., Hüsken, D., Martin, P., Monia, B. P., Müller, M., Natt, F., Nicklin, P., Phillips, J., Piels, U., Sasmor, H., and Moser, H. E. (1996) Second generation of antisense oligonucleotides: From nuclease resistance to biological efficacy in animals. *Chimia 50*, 168−176.

Basu, S., and Wickstrom, E. (1997) Synthesis and Characterization of a Peptide Nucleic Acid Conjugated to a D-Peptide Analogue of Insulin-like Growth Factor 1 for Increased Cellular Uptake. *Bioconjugate Chem. 8*, 481−488.

Bennet, C. F. (1998) Antisense Oligonucleotides: Is the Glass Half Full or Half Empty? *Biochem. Pharmacol. 55*, 9−19.

Bennett, C. F., Chiang, M. Y., Chan, H., Shoemaker, J. E. E., and Mirabelli, C. K. (1992) Cationic lipids enhance cellular uptake and activity of phosphorothioate antisense oligonucleotides. *Mol. Pharmacol. 41*, 1023−1033.

Bonham, M. A., Brown, S., Boyd, A. L., Brown, P. H., Bruckenstein, D. A., Hanvey, J. C., Thomson, S. A., Pipe, A., Hassman, F., Bisi, J. E., Froehler, B. C., Matteucci, M. D., Wagner, R. W., Noble, S. A., and Babiss, L. E. (1995) An assessment of the antisense properties of RNase H-competent and steric-blocking oligomers. *Nucleic Acids Res. 23*, 1197−1203.

Boutorine, A. S., and Kostina, E. V. (1993) Reversible covalent attachment of cholesterol to oligodeoxyribonucleotides for studies of the mechanisms of their penetration into eukaryotic cells. *Biochimie 75*, 35−41.

Brown, S. C., Thomson, S. A., Veal, J. M., and Davis, D. G. (1994) NMR solution structure of a peptide nucleic acid complexed with RNA. *Science 265*, 777−780.

Campbell, M. J. (1995) Lipofection reagents prepared by a simple ethanol injection technique. *Biotechniques 18*, 1027−1032.

Cherny, D. Y., Belotserkovskii, B. P., Frank-Kamenetskii, M. D., Egholm, M., Buchardt, O., Berg, R., and Nielsen, P. E. (1993) DNA unwinding upon strand-displacement binding of a thymine-substituted polyamide to double-stranded DNA. *Proc. Natl. Acad. Sci. U.S.A. 90*, 1667−1670.

Christensen, L., Fitzpatrick, R., Gildea, B., Petersen, K. H., Hansen, H. F., Koch, T., Egholm, M., Buchardt, O., Nielsen, P. E., Coull, J., and Berg, R. H. (1995) Solid-phase synthesis of peptide nucleic acids (PNA) *J. Pept. Sci. 3*, 175−183.

De Mesmaeker, A., Altmann, K. H., Waldner, A., and Wendeborn, S. (1995) Backbone modifications in oligonucleotides and peptide nucleic acid systems. *Curr. Opin. Struct. Biol. 5*, 343−355.

Demidov, V., Potaman, V. N., Franck-Kamenetskii, M. D., Egholm, M., Buchardt, O., Sönnichsen, S. H., and Nielsen, P. E. (1994) Stability of peptide nucleic acids in serum and cellular extracts. *Biochem. Pharmacol. 48*, 1309−1313.

Egholm, M., Nielsen, P. E., Buchardt, O., and Berg, R. H. (1992a) Recognition of guanine and adenine in DNA by cytosine and thymine containing peptide nucleic acids (PNA). *J. Am. Chem. Soc. 114*, 9677−9678.

Egholm, M., Buchardt, O., Nielsen, P. E., and Berg, R. H. (1992b) Peptide nucleic acids (PNA). Oligonucleotide analogues with an achiral peptide backbone. *J. Am. Chem. Soc. 114*, 1895−1897.

Egholm, M., Buchardt, O., Christensen, L., Behrens, C., Freier, S. M., Driver, D. A., Berg, R. H., Kim, S. K., Norden, B., and Nielsen, P. E. (1993) PNA hybridizes to complementary oligonucleotides obeying the Watson−Crick hydrogen-bonding rules. *Nature 365*, 566−568.

Eriksson, M., and Nielsen, P. E. (1996a) Solution Structure of a Peptide Nucleic Acid-DNA Duplex. *Nat. Struct. Biol. 3*, 410−413.

Eriksson, M., and Nielsen, P. E. (1996b) PNA-nucleic acid complexes. Structure, stability and dynamics *Q. Rev. Biocphys. 29*, 369−394.

Freier, S. M., and Altmann, K. H. (1997) The ups and downs of nucleic acid duplex stability: structure−stability studies on chemically modified DNA: RNA duplexes. *Nucleic Acids Res. 25*, 4429−4443,

Gambacorti-Passerini, C., Mologni, L., Bertazzoli, C., Marchesi, E., Grignani, F., and Nielsen, P. E. (1996) In vitro transcription and translation inhibition by anti-Promyelocytic Leukemia (PML)/Retinoic acid receptor α and anti-PML peptide nucleic acid. *Blood 88*, 1411−1417.

Good, L., and Nielsen, P. E. (1997) Progress in developing PNA as gene targeted drugs. *Antisense Nucleic Acid Drug Dev. 7*, 431−437.

Gray, G. D., Basu, S., and Wickstrom, E. (1997) Transformed and immortalized cellular uptake of oligodeoxynucleoside phosphorothioates, 3′-alkylamino oligonucleotides, 2′−O-methyl oligonucleotides, oligodeoxynucleoside methylphosphonates and peptide nucleic acids. *Biochem. Pharmacol. 53*, 1465−1476.

Haaima, G., Lohse, A., Buchardt, O., and Nielsen, P. E. (1996) Peptide Nucleic Acids (PNA) containing thymine monomers derived from chiral amino acids.: Hybridization and solubility properties of d-lysine PNA. *Angew. Chem. 35*, 1939−1941.

Hamilton, S. E., Simmons, C. G:, Kathiriya, I. S., and Corey, D. R. (1999) Cellular delivery of peptide nucleic acids and inhibition of human telomerase. *Chem. Biol. 6*, 343−351.

Hanvey, J. C., Peffer, N. J., Bisi, J. E. Thomson, S. A., Cadilla, R., Josey, J. A., Ricca, D. J., Hassman, C. F., Bonham, M. A., Au, K. G., Carter, S. G., Bruckenstein, D. A., Boyd, A. L., Noble, S. A., and Babiss, L. E. (1992) Antisense and antigene properties of peptide nucleic acids. *Science 258*, 1481−1485.

Hubus, I., Zhao, Q., and Agrawal, S. (1995) Synthesis, Hybdridization properties, nuclease stability, and cellular uptake of oligonucleotide-amino-*b*-cyclodextrins and adamantane conjugates. *Bioconjugate Chem. 6*, 327−331.

Hyrup, B., and Nielsen, P. E. (1996) Peptide Nucleic Acids (PNA). Synthesis, Properties and Potential Applications (review). *Bioorg. Biomed. Chem. 4*, 5−23.

Jensen, K. K., Ørum, H., Nielsen, P. E., and Norden, B. (1997) Hybridization Kinetics of Peptide Nucleic Acids (PNA) with DNA and RNA Studied with BIAcore Technique. *Biochemistry 36*, 5072−5077.

Kabanov, A. V., Vinogradov, S. V., Ovcharenco, A. V., Krivonos, A, V, Melik-Nubarov, N. S., Vsevolod, I., and Severin, E. S. (1990) A new cass of antivirals: antisense oligonucleotides combined with a hydrophobic substituent efficiently inhibit influenza virus reproduction and synthesis of virus-specific proteins in MDCK cells. *FEBS Lett. 259*, 327−330.

Kim, S. K., Nielsen, P. E., Egholm, M., Buchardt, O., Berg, R. H., and Norden, B. (1993) Right-handed triplex formed between peptide nucleic acid PNA-T8 and poly(dA) shown by linear and circular dichroism spectroscopy. *J. Am. Chem. Soc. 115*, 6477−6481.

Knudsen, H., and Nielsen, P. E. (1996) Antisense properties of duplex- and triplex-forming PNAs. *Nucleic Acids Res. 24*, 494−500.

Leijon, M., Graslund, A., Nielsen, P. E., Buchardt, O., Norden, B., Kristensen, S. M., and Eriksson, M. (1994) Structural characterization of PNA-DNA duplexes by NMR. Evidence for DNA in a B-like conformation. *Biochemistry 33*, 9820−9825.

Letsinger, R. L., Zhang, G. R., Sun, D. K., Ikeuchi, T., and Sarin, P. S. (1989) Cholesteryl-conjugated oligonucleotides: synthesis, properties and activity as inhibitors of replication of human immunodeficiency virus in cell culture. *Proc. Natl. Acad. Sci. U.S.A. 86*, 6553−6556.

Lohse, J., Nielsen, P. E., Harrit, N., and Dahl, O.(1997) Fluorescein-conjugated lysine monomers for solid-phase synthesis of fluorescent peptides and PNA oligomers. *Bioconjugate Chem. 8*, 503−509.

Mishra, R. K., Moreau, C., Ramazeilles, C., Moreau, S., Bonnet, J., and Toulme, J. J. (1995) Improved leishmanical effect of phosphorothioate antisense oligonucleotides by LDL-mediated delivery. *Biochim. Biophys. Acta 1264*, 229−237.

Mologni, L., LeCoutre, P., Nielsen, P. E., and Gambacorti-Passerini, C. (1998) Additive antisense effects of different PNAs on the in vitro translation of the PML/RAR α-gene. *Nucleic Acids Res. 26*, 1934−1938.

Nielsen, P. E., Egholm, M., Berg, R. H., and Buchardt, O. (1991) Sequence-selective recognition of PNA by strand displacement with a thymine-substituted polyamide. *Science 254*, 1497−1500.

Nielsen, P. E., Egholm, M., and Buchardt, O. (1994a) Evidence for $(PNA)_2$/DNA triplex structure upon binding of PNA to dsDNA by strand displacement. *J. Mol. Recognit. 7*, 165−170.

Nielsen, P. E., Egholm, M., and Buchardt, O. (1994b) Sequence-specific transcription arrest by nucleic acid bound to the DNA template strand. *Gene 149*, 139−145.

Pooga, H., Soomets, U., Hällbrink, M., Valkna, A, Saar, K, Rezaei, K., Kahl, U, Hao, J.-X, Xu, X.-J., Wiesenfeld-Hallin, Z., Hökfelt, T., Bartfai, T., and Langel, Ü. (1998) Cell penetrating PNA constructs regulate galanin receptor levels and modify pain transmission in vivo. *Nat. Biotechnol. 16*, 857−861.

Saison-Behmoaras, T., Tocqué, B., Rey, I., Chassignol, M., Thuong, N. T., and Hélène, C. (1991) Short modified antisense oligonucleotides directed against Ha-*ras* point mutation induce selective cleavage of the mRNA and inhibit T24 cells proliferation. *EMBO J. 10*, 1111−1118.

Sharma, H. W., and Narayanan, R. (1995) The therapeutic potential of antisense oligonucleotides. *BioAssays 17*, 1055−1063.

Simmons, C. G., Pitts, A. E., Mayfield, L. D., Shay, J. W., and Corey, D. R. (1997) Synthesis and Membrane Permeability of PNA-Peptide Conjugates. *Bioorg. Med. Chem. Lett. 7* (23), 3001−3006.

Stein, C. A., Pal, R., DeVico, A. L., Hoke, G., Mumbauer, S., Kinstler, O., Sarngadharan, M. G., and Letsinger, R. L. (1991) Mode of action of 5′-linked cholesteryl phosphorothio-ate

oligodeoxynucleotides in inhibiting syncytia formation and infection by HIV-1 and HIV-2 in vitro. *Biochemistry 30*, 2439−2444.

Svinarchuk, F. P., Konevetz, D. A., Pliasunova, O. A., Pokrovsky, A. G., and Vlassov, V. V. (1993) Inhibition of HIV proliferation in MT-4 cells by antisense oligonucleotide conjugated to lipophilic groups. *Biochimie 75*, 49−54.

Taylor, R. W., Chinnery, P. F., Turnbull, D. M., and Lightowlers, R. N. (1997) Selective inhibition of mutant human mitochondrial DNA replication in vitro by peptide nucleic acids. *Nat. Genet. 15*, 212−215.

Thierry, A. R., and Dritschillo, A. (1992) Intracellular availability of unmodified, phosphorothioated and liposomally encapsulated oligodeoxynucleotides for antisense activity. *Nucleic Acids Res. 20*, 5691−5698.

Uhlmann, E., Will, D. W., Breipohl, G., Langner, D., and Ryte, A. (1996) Synthesis and properties of PNA/DNA chimeras. *Angew. Chem., Int. Ed. Engl. 35*, 2632−2633.

Wagner, R. W., and Flanagan, M. (1997) Antisense technology and prospects for therapy of viral infections and cancer. *Mol. Med. Today 1*, 31−38.

Wielbo, D., Shi, N., and Serina, C. (1997) Antisense inhibition of angiotensinogen in hepatoma cell culture is enhanced by cationic liposome delivery. *Biochem. Biophys. Res. Commun. 232*, 794−799.

Zelpathy, O., and Szoka, F. C., Jr. (1996) Intracellular distribution and mechanism of delivery of oligonucleotides by cationic lipids. *Pharm. Res. 13*, 1367−1372.

BC990053+

Prolonged Circulating Lives of Single-Chain Fv Proteins Conjugated with Polyethylene Glycol: A Comparison of Conjugation Chemistries and Compounds

L. Stanford Lee,* Charles Conover, Celine Shi, Marc Whitlow,† and David Filpula*

Enzon Inc./SCA Ventures, 20 Kingsbridge Road, Piscataway, New Jersey 08854-3969. Received June 14, 1999; Revised Manuscript Received August 16, 1999

The utility of single-chain Fv proteins as therapeutic agents would be substantially broadened if the circulating lives of these minimal antigen-binding polypeptides were both prolonged and adjustable. Poly(ethylene glycol) (PEG) bioconjugate derivatives of the model single-chain Fv, CC49/218 sFv, were constructed using six different linker chemistries that selectively conjugate either primary amines or carboxylic acid groups. Activated PEG polymers with molecular weights of 2000, 5000, 10 000, 12 000, and 20 000 were included in the sFv bioconjugate evaluation. Additionally, the influence of PEG conjugate geometry in branched PEG strands (U-PEG) and the effect of multimeric PEG-sFv bioconjugates on circulating life and affinity were examined. Although random and extensive PEG polymer conjugations have been achievable in highly active derivatives of the prototypical PEG-enzymes, PEGylation of CC49/218 sFv required stringent adjustment of reaction conditions in order to preserve antigen-binding affinity as measured in either mucin-specific or whole cell immunoassays. Purified bioconjugates with PEG:sFv ratios of 1:1 through 2:1 were identified as promising candidates which exhibit sFv affinity (K_d) values within 2-fold of the unmodified sFv protein. Interestingly, PEG conjugation to carboxylic acid moieties, using a PEG-hydrazide chemistry, achieved significant activity retention in bioconjugates at a higher PEG:sFv ratio (5:1) than with any of the amine-reactive activated PEG polymers. Prolonged circulating life in mice was demonstrated for each of the PEG conjugates. An increase in PEG polymer length was found to be more effective for serum half-life extension than a corresponding increase in total PEG mass. For example, CC49/218 sFv conjugated to either one strand of PEG-20000, or four strands of PEG-5000, displayed about 20- or 14-fold increased serum half-life, respectively, relative to the unmodified sFv. The demonstrated suitability of established random conjugation chemistries for PEGylation of sFv proteins, in conjunction with innovative site-specific conjugation methods, indicates that production of a panoply of sFv proteins with both engineered affinity and tailored circulating life may now be achievable.

INTRODUCTION

The immunoglobulin repertoires in vertebrates consist of antigen-binding domains—the Fv modules—which may be employed within the animal in a limited number of Fc formats corresponding to IgG, IgM, IgA, IgE, and IgD isotypes. The utility of antibody derived therapeutics has been confined by the restrictive circulating lives and associated Fc effector functions of mAbs. It has been the goal of antibody engineers to greatly extend the versatility of antigen-binding proteins by tailoring the binding properties, valency, effector functions, and pharmacokinetic behavior of immunomolecules through protein engineering and bioconjugate strategies. The single gene, single polypeptide design of single-chain Fv proteins provides a minimal antigen-binding format which has been extensively explored by antibody engineers in the past decade (*1*−*3*). Early clinical trials are employing sFv derived therapeutics as immunotoxins, imaging agents, antagonists, targeting agents, and intracellular antigen-binding compounds (*4*−*7*). The clinical versatility and therapeutic efficacy of sFv proteins may be expanded by drug delivery technologies that provide control over the rate at which these small protein compounds are cleared from circulation via renal filtration. The use of very high-affinity human sFv molecules or multivalent/multi-specific formats are promising solutions to this challenge (*8*−*13*). However, to provide a more general approach to controlling the circulating lives of sFv proteins, we wished to investigate the potential of a bioconjugate strategy that is clinically well established for enhancing the efficacy of other protein drugs.

Two FDA licensed therapeutics and several compounds undergoing clinical trials employ PEGylation,[1] the conjugation of compounds with poly(ethylene glycol) polymers, to prolong circulating life and reduce immunogenicity. In general, activated PEG polymers reactive with primary amines have been employed and PEG conjugation of the majority of available lysine residues on enzyme therapeutics such as adenosine deaminase and asparaginase has provided extensively modified derivatives which still maintain specific activities similar to the unmodified enzymes (*14*−*16*). In comparison, PEGylation of cytokines, hormones, and other small protein ligands generally represents a greater challenge in enhancing the clinical potency of the PEG derivatives due to the opposing effects of (1) a reduction in receptor binding affinity versus (2) a prolonged circulating life relative to the unmodified protein (*17*−*23*). The antigen-binding site may constitute about one-third of the Fv

* To whom correspondence should be addressed. Phone: (732) 980-4500. Fax: (732) 885-2950.

† Present address: Berlex Biosciences, 15049 San Pablo Ave., PO Box 4099, Richmond CA 94804-0099.

10.1021/bc990076o CCC: $18.00 © 1999 American Chemical Society
Published on Web 09/30/1999

surface area (*24*) and reactive amines or carboxyls are prevalent surface moieties on the hypervariable and framework regions of essentially all Fv sequences (*25*). Consequently, extensive random conjugations may be inactivating either through direct attachments to antigen-binding contact residues or as a result of transient steric hindrance and diffusional constraints from the long polymer strands.

We have previously reported the successful construction of sFv variants with engineered cysteine or N-glycan sites which retain binding activity following site-specific single or multiple PEG attachments (*4*, *26*). However, these structural adjustments are not suitable for all therapeutic sFv applications. In this report, we describe the controlled application of conventional random PEGylation chemistries in production of delimited PEG-CC49/218 sFv compounds which have binding affinities comparable to the parent compound, yet display markedly extended circulating lives that correlate with the mass and length of the attached polymers. We also demonstrate the capacity of homobifunctional PEG polymers to generate multivalent sFv compounds that display increased functional affinity (avidity) and may simulate the long circulating life and multivalency of antibodies.

EXPERIMENTAL PROCEDURES

Materials. The *Escherichia coli* GX9251 expression strain for production of CC49/218 sFv protein has been described (*27*). Precast polyacrylamide slab gels (4−20%) were obtained from Novex (San Diego, CA). Bovine submaxillary mucin type I was purchased from Sigma (St. Louis, MO). Superdex 75 was obtained from Pharmacia Biotech (Piscataway, NJ). POROS HS was purchased from PerSeptive Biosystems (Framingham, MA). Rabbit anti-CC49/218 sFv polyclonal antibody was obtained from HRP (Denver, PA). Mouse anti-CC49/218 polyclonal antibody was supplied by Enzon. PEG-hydrazide hydrochloride (Hz-PEG-5000), PEG-trichlorophenyl carbonate (TPC-PEG-5000), and *N*-hydroxysuccinimide PEG-biotin (NHS-PEG-3400-biotin) were obtained from Shearwater Polymers (Huntsville, AL). Succinimidyl carbonate PEG (SC-PEG), Thiazolidine-2-thione PEG (T-PEG), branched SC-PEG (U-PEG), and bifunctional SC-PEG (BSC-PEG) were synthesized by Enzon as previously reported (*16*, *28*−*30*). Calibrated PEG-protein molecular mass standards were obtained from Enzon.

Purification and Characterization of CC49/218 sFv Protein. The purification of clinical-grade CC49/218 sFv from *E. coli* expression strain GX9251 by refolding and cation-exchange chromatography has been described in detail (*27*). Purified sFv was further characterized by SE-HPLC and RP-HPLC as previously reported (*10*, *27*, *31*). Protein determination employed the BCA (bicinchoninic acid) procedure according to the vendor's instructions (Pierce Chemical Co., Rockford, IL).

Molecular Modeling. The model of 4-4-20/212 sFv was constructed on an Evans & Sutherland PS330 using Frodo, starting from the 4-4-20 Fab structure (PDB entry 1FLR). Poly(ethylene glycol) strands were modeled on surface accessible lysine residues, L112, and H78 (*26*), using the program Add_PEG (written by M. Whitlow). Add_PEG builds the PEG polymer one atom at a time, checking each for unfavorable contacts. Each atom is added using a random procedure that generates trans, gauche+, and gauche− in the ratios of 0.68:0.16:0.16.

Chemical Analysis of PEG-sFv Derivatives. Three methods were employed for determination of the stoichiometry of PEG attachment on sFv proteins. First, the TNBS method of Habeeb (*32*) was performed for quantitation of free primary amines. Second, the molecular mass of individual PEG-sFv compounds was examined by SDS−PAGE and compared to calibrated PEG-protein standards with known PEG:protein stoichiometry. Proteins were electrophoresed on precast 4−20% slab gels and protein bands were visualized with Coomassie brilliant blue G-250. Area quantitation of stained bands was performed using a Molecular Dynamics PD-SI laser scanner. PEGylated polypeptides exhibit reduced mobility on SDS−PAGE compared to unmodified polypeptides of equivalent molecular mass. For example, PEG-sFv molecules containing one PEG-5000 linear unbranched polymer per protein display an increased molecular mass of approximately 10 000 compared to the unmodified sFv. Area quantitation of stained bands was also used to estimate the percentage of each PEG derivative if the conjugation reaction produced multiple fractions. The PEG/sFv stoichiometric values are reported as the average for the integrated distribution. Third, size-exclusion HPLC was performed on selected PEG-sFv samples to analyze the molecular size of the derivatives compared to PEG-proteins with calibrated polymer numbers.

PEG Modification of Primary Amines. The model CC49/218 sFv protein contains 19 primary amine groups including lysines and the N-terminus. The amine-reactive PEG polymers examined in this study included SC-PEG with molecular masses of 2000, 5000, 10 000, 12 000, and 20 000; U-PEG-10000; NHS-PEG-3400-biotin; T-PEG-5000; T-PEG-12000; and TPC-PEG-5000. Chemical conjugation chemistries for these polymers have been published (*16*, *28*−*30*). While phosphate buffers are commonly employed in these protocols, the choice of borate buffers may beneficially influence the PEGylation reaction rates and resulting products. As an example, for derivatives modified with SC-PEG-5000, the CC49/218 sFv (2 mg/mL) in 0.1 M sodium borate buffer, pH 8.0, was reacted with SC-PEG at the designated molar ratios for 1 h at 25 °C. The reaction was quenched by the addition of 50 mM glycine and the product was purified by Superdex 75 SE-HPLC.

PEG Modification of Carboxyl Sites. The CC49/218 sFv protein sequence includes 19 aspartic acid/glutamic acid groups in addition to the carboxyl terminus of the polypeptide. The utility of PEG-hydrazide in selective modification of carbodiimide-activated protein carboxyl groups under acidic conditions has been described (*16*, *33*). CC49/218 sFv protein (2 mg/mL) in 50 mM NaCl was adjusted to pH 4.75 by addition of HCl. PEG-hydrazide powder was added to a final molar excess of 200-fold. The reaction was initiated with the addition of EDC in 100:1

[1] Abbreviations: AUC, area under the curve; BSA, bovine serum albumin; BSC-PEG, bifunctional SC-PEG; CDR, complementarity determining region; DTT, dithiothreitol; EDC, 1-ethyl-3-[3-(dimethylamino) propyl] carbodiimide hydrochloride; ELISA, enzyme-linked immunosorbent assay; HRP, horseradish peroxidase; Hz, hydrazide; mAb, monoclonal antibody; mFv, multivalent sFv; MRT, mean retention time; MTT, (3-[4,5-dimethylthiazol-2-yl]-2,5-diphenyltetrazolium) bromide; NHS, *N*-hydroxysuccinimide; PBS, phosphate-buffered saline; PEG, poly(ethylene glycol); SC, succinimidyl carbonate; SDS−PAGE, sodium dodecyl sulfate−polyacrylamide gel electrophoresis; SE-HPLC, size-exclusion−high-performance liquid chromatography; sFv, single-chain Fv protein; $t_{1/2}$, serum half-life; TAG, tumor-associated glycoprotein; TMB, 3,3′,5,5′-tetramethylbenzidine; TNBS, 2,4,6-trinitrobenzene sulfonic acid; TPC, trichlorophenyl carbonate; T-PEG, thiazolidine-2-thione PEG; Tris, tris(hydroxymethyl)aminomethane; U-PEG, branched PEG polymer with central SC linker.

molar quantities relative to the sFv protein. The reaction was allowed to proceed for 45 min, while maintaining the pH (4.75−5.0). The reaction product was chromatographed on size-exclusion−HPLC and high molecular weight fractions were isolated.

Bifunctional PEG Modification of CC49/218 sFv. The homobifunctional activated PEG polymer BSC-PEG-5000, which includes one activated SC group at each of the two polymer termini, was utilized in cross-linking reactions to produce multimeric Fv (mFv). BSC-PEG-5000 (1.89 mg) was dissolved in 0.1 mL of 25 mM Mops (3-[*N*-morpholino]propane-sulfonic acid) buffer, pH 7.3. Within 10 s of dissolution, the PEG solution was added to CC49/218 sFv protein (1.5 mg/mL) in 2 mL of PBS (25 mM sodium phosphate, pH 7.3, 0.15 M NaCl). The mixture was stirred for 1 h at 24 °C. The reaction was terminated by addition of solid guanidine hydrochloride (GuHCl) to a final concentration of 0.6 M. The material was immediately applied to a 2 cm × 60 cm Superdex 75 SE-HPLC column previously equilibrated in 50 mM Tris-HCl, pH 7.3, 1 mM $CaCl_2$, 0.1 mM PMSF (phenylmethanesulfonyl fluoride), 50 mM KCl, and 60 mM GuHCl. Following fractionation of heterogeneous multimers by gel filtration chromatography, monomer, dimer, and trimer fractions were identified from comparisons to calibrated PEG-sFv standards by SDS−PAGE and SE-HPLC.

ELISA for sFv Binding Activity. Immunoassay procedures were performed using modifications of previously published procedures (*10*, *34*−*36*). Bovine submaxillary mucin (1 μg/100 μL well) was used to coat microtiter plate wells (MaxiSorp, Nunc, VWR Scientific, Boston, MA). The purified CC49/218 sFv protein or PEGylated sFv derivatives were diluted serially in PBS containing 1% BSA and incubated in the coated wells at 22° C for 1 h. After the plate had been washed with PBS containing 0.05% Tween 20 (PBS-T), the bound sFv was detected by a 1 h incubation with a secondary anti-CC49/218 sFv rabbit serum (1:2000) followed by a PBS-T wash and a 1 h incubation with an HRP-conjugated goat anti-rabbit serum (1:2000 dilution) at 22 °C. The plates were washed three times with PBS-T. After addition of 50 μL of 3,3′,5,5′-tetramethylbenzidine (TMB) and 50 μL of 1 M H_2SO_4 as described by Harlow and Lane (*34*), the plate was read at 450 nm using a Molecular Devices (Sunnyvale, CA) plate reader.

Competition ELISA. The apparent affinity constants (K_d) of the PEGylated sFv derivatives were determined using biotin-labeled CC49/218 sFv in competition immunoassays as reported previously (*26*, *35*). HRP-conjugated streptavidin (Pierce) was employed as the detection agent.

ELISA for Relative Affinity of Multimeric Fv. The method of Friguet et al. (*36*) was used for comparison of the relative affinities of mFv derivatives. PEGylated CC49/218 sFv compounds were incubated at varied molar ratios with bovine submaxillary mucin in PBS for 24 h at 4° C. ELISA determinations of the unbound and bound sFv fractions were performed as described above.

Circulating Life in Mice. Pharmacokinetics of sFv and PEGylated sFv derivatives were measured in ICR (CD-1) 7−8 week-old mice supplied by Harlan Sprague Dawley (Madison, WI). A single injection (200 μL) with 60 μg of protein of PEG-sFv derivatives was performed via the tail vein. After compound administration, sampling of blood (100 μL) via the recta orbital sinus was undertaken following anesthetization with 0.09% Avertine. In the minimal standard protocol ($N = 6$): three mice were bled at 2 min and 1, 4, and 8 h; three other mice were bled at 15 min, and 2 and 6 h; all six mice were bled at 24 h. Blood was allowed to clot and then processed for serum and immediately frozen. The concentrations of the modified, active sFv were measured by ELISA. The circulatory half-life, area under the curve, and mean residence time for the sFv compounds were calculated using a one-compartment i.v. bolus model (WinNonlin software package, Scientific Consulting, Apex, NC). The correlation between the observed and predicted model time points was ≥95%.

RESULTS AND DISCUSSION

Characterization of Purified CC49/218 sFv. The detailed purification protocol for clinical-grade CC49/218 sFv, which recognizes the human pancarcinoma antigen TAG-72, has been reported (*27*). Vialed CC49/218 sFv protein (*37*) was determined by SDS−PAGE and RP-HPLC to exhibit ≥99% homogeneity. We have previously reported that CC49 sFv with the 18 residue "218" linker maintains a monomeric rather than multimeric structure (*31*). SE-HPLC characterization of CC49/218 sFv demonstrated that multimeric Fv species constitute less than 1% of the freshly purified protein preparation. Mucin-binding activity of the sFv protein was characterized by ELISA and competition ELISA as previously described (*35*) and the apparent dissociation constant, $K_d = 4.5 \times 10^{-9}$ M, was determined as previously reported (*26*).

Molecular Modeling of PEGylated sFv. Covalent attachment of poly(ethylene glycol) polymers is a proven drug delivery strategy which is employed in established FDA-licensed protein therapeutics and several ongoing clinical trials of experimental medicines (*14*, *15*). Initial success in the use of random and extensive PEGylation of enzyme therapeutics having small molecule substrates demonstrated the capacity of many such enzymes to tolerate PEG conjugation on the majority of the surface lysines while maintaining suitable enzymatic specific activity. In contrast to this global conjugation approach for enzymes, a more parsimonious PEGylation strategy is mandated for small protein ligands such as cytokines, hormones, and peptides (*17*, *18*, *22*) by utilizing either site-specific conjugations or controlled and limited conjugations. The goal of these studies is to introduce the benefits of prolonged circulating life and diminished clearance by PEGylation, while maintaining acceptable biological activity for the bioconjugate. As shown in Figure 1, single-chain Fv molecules constitute a family of small proteins with six hypervariable antigen-binding loops (CDRs) within a conserved β-sheet framework architecture. We have shown previously (*4*, *26*) that the use of site-specific sFv conjugations to engineered cysteines or *N*-glycans is a promising approach for selected applications. However, it would also be desirable to develop sFv PEGylation methodologies that employ clinically explored linker chemistries, which also do not require an alteration of the primary sequence of the sFv of interest. Molecular modeling of a representative sFv protein conjugated at two exposed lysines to PEG-12000 polymers is illustrated in Figure 2. The model sFv protein is derived from the available crystal structure of 4-4-20 anti-fluorescein Fab (*26*).

The degree of surface exposure of lysine, aspartic acid, and glutamic acid residues for 34 Fv structures is shown in Table 1. These three amino acid moieties are partially to completely exposed for most Fv residue assignments. About 21% percent of the surface-exposed lysines and 27% of the exposed carboxyls occur within the CDR segments, though not necessarily in antigen contacts. In

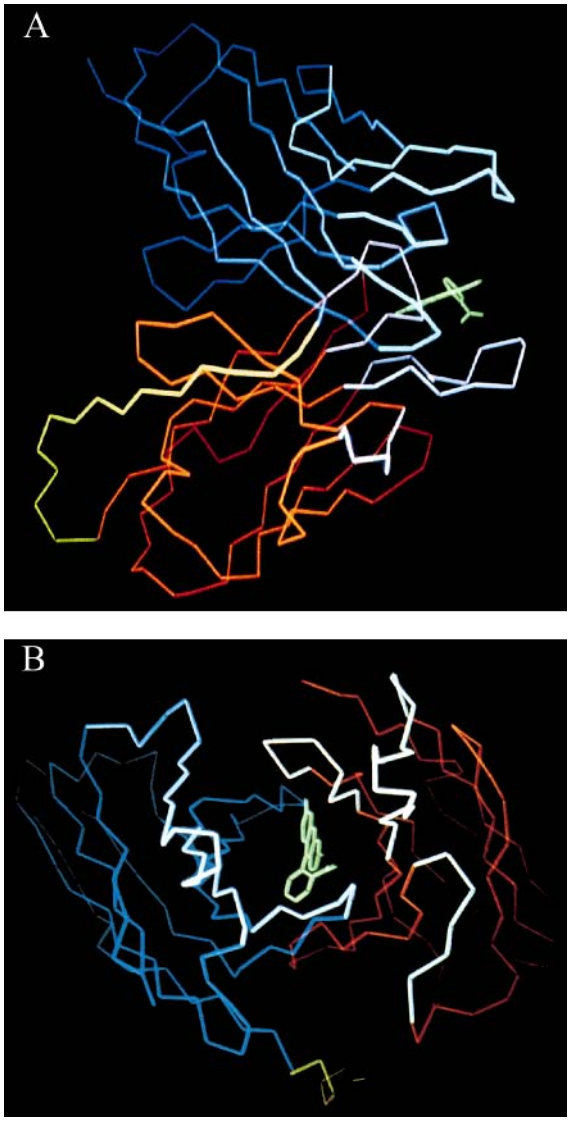


Figure 1. Two views of the V_L-linker-V_H anti-fluorescein 4-4-20/212 sFv model based on the Fab crystal structure. The V_L is shown in red, the V_H in blue, the linker in yellow and the antigen in green. The CDRs have been highlighted in light shades. (A) Antigen-binding site is at right in the α-carbon tracing model. (B) The molecule shown in panel A is rotated 90° on two axes placing the antigen-binding site in the center of the sFv model.

addition, single-chain Fv proteins have an exposed amine at the N-terminus and an exposed carboxyl group at the C-terminus plus additional target residues within the engineered linker peptide (Figure 1). While the correlation of the degree of surface exposure of these residues and their reactivity to conjugation will also be influenced by regional chemical and steric factors, the prevalence and dispersity of these three amino acids on Fv surfaces suggest that optimal PEGylation chemistries for these target residues may need to be carefully tailored for individual sFv. We chose as a model protein, CC49/218 sFv, which was recently investigated clinically as an imaging agent for metastatic colorectal carcinoma (*37*). The sFv exhibited rapid blood and whole body clearance, almost exclusively via renal clearance. As shown in Figure 3, we have chosen a fairly challenging model murine sFv wherein four of the total 18 lysines are within designated CDR regions while five of the total 19 aspartic/glutamic acid residues are within CDR loops. In comparison, the Kabat consensus sequence for a prototypical human V_kI/218/V_HIII sFv contains 11 lysines (two in CDRs) and 17 aspartic/glutamic acids (five in CDRs) if the most commonly occurring amino acids at each position are represented (*25*).

PEGylations of sFv Primary Amines. Two critical parameters, (a) relative binding affinity and (b) circulatory retention in mice, were evaluated for PEGylated sFv compounds using five different activated PEG linker chemistries. In addition, PEGylated sFv conjugates were evaluated by SDS−PAGE, SE-HPLC, and chemical analysis in order to estimate the polymer:protein stoichiometry and heterogeneity of the compounds. The PEGylation reaction conditions (see Experimental Procedures) require an excess of activated PEG relative to sFv protein, and the relative stoichiometry and reaction times were adjusted to optimize the polymer number on the bioconjugate while also maintaining acceptable binding activity. The five amine reactive linker chemistries included succinimidyl carbonate (SC-PEG), thiazolidine-2-thione (T-PEG), *N*-hydroxysuccinimide (NHS-PEG), trichlorophenyl carbonate (TPC-PEG), and branched SC-PEG (U-PEG). Incremental PEG polymer lengths of 2, 5, 12, and 20 kDa were additionally investigated for the SC-PEG linker chemistry. PEGylated sFv proteins were purified by SE-HPLC and cation-exchange chromatography to completely separate bioconjugates from any remaining unmodified sFv protein. Our initial ELISA results indicated that attachment of greater than four PEG polymers per sFv using any of these five methods resulted in diminution of sFv apparent affinity by 30−100-fold (data not shown). Consequently, we focused our attention on the goal of producing minimally PEGylated sFv, which displayed apparent binding affinities within one log value of the unmodified protein. Figure 4 shows an SDS−PAGE analysis of the bioconjugate preparations used in the subsequent ELISA and pharmacokinetic studies. While random conjugation chemistries are expected to produce heterogeneous mixtures of bioconjugates that correspond to differences in the number of modified amines, the overall dispersity in bioconjugate masses under our optimized reaction conditions was relatively limited as seen in Figure 4. For most reactions, the production of a single predominant molecular size of PEG-sFv was observed, which may be accompanied by a subpopulation of bioconjugates of larger molecular size. This simplified the estimation of the average PEG number per sFv protein in the purified preparations. Under the selected reaction conditions, one major molecular mass constituted the majority of the total PEGylated sFv product using all of the amine-reactive PEG polymers except SC-PEG-2000 and SC-PEG-5000. Competition ELISA demonstrated excellent retention of apparent binding affinity (K_d) in representative minimally PEGylated sFv proteins as shown in Table 2. The PEG-20000 sFv bioconjugate exhibited the greatest difference in apparent K_d (7.5×10^{-9}) when compared to the unmodified CC49 sFv (4.5×10^{-9}). We have previously reported an increase in apparent K_d of 2- and 12-fold for glycosylated sFv and multiply PEGylated, glycosylated CC49/218 sFv, respectively (*26*). While identification of the most reactive primary amine sites for each individual sFv protein and for each individual activated PEG polymer would require peptide mapping and other chemical analyses, the demonstrated capability of randomly attaching one or two polymers to active sFv molecules suggests that the lysines within, or very near, the antigen-binding site may not be the most reactive moieties using these reaction conditions.

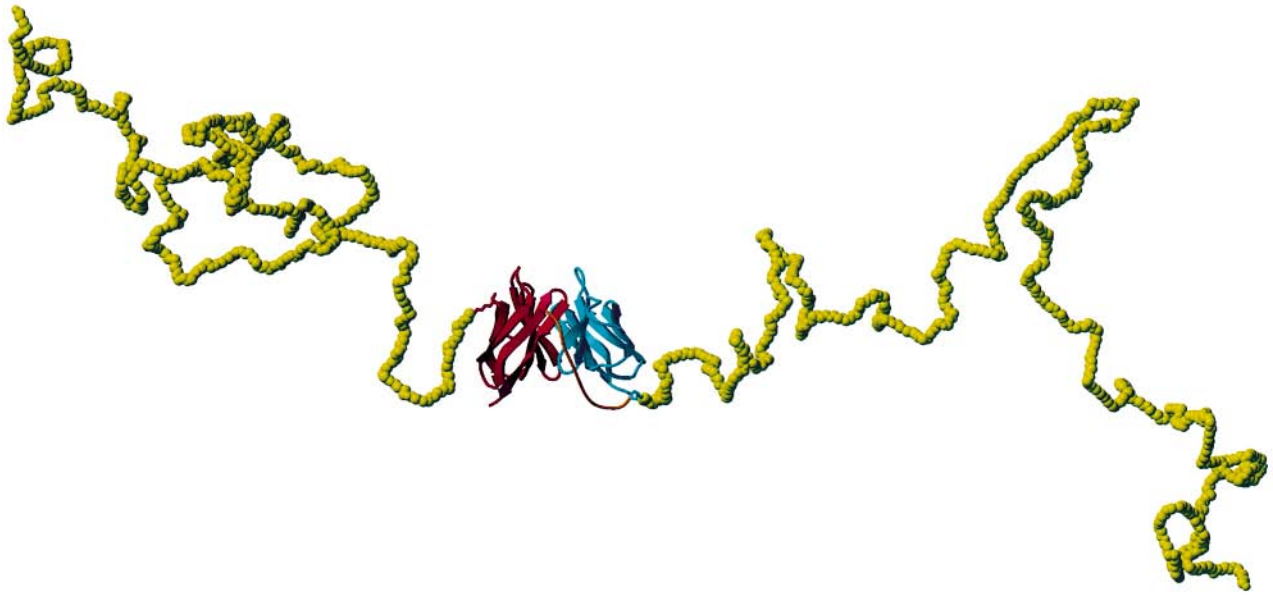


Figure 2. Molecular model of PEGylated V_L-linker-V_H 4-4-20/212 sFv. The PEG-12000 polymers attached to surface lysines L112 (blue) and H78 (red) are shown as yellow CPK models. The 4-4-20/212 sFv is shown as a ribbon diagram, with the light chain in blue; the linker in orange; and the heavy chain in red. The figure was produced using MolScript (45) and Raster3D (46).

Table 1. Exposure Patterns of CDR and Framework Residues in 34 Fv Structures[a]

amino acid	Bu	mB	pB	mE	Ex	totals
CDR residues						
lysine	0	5	13	32	28	78
aspartic acid	14	21	21	28	37	121
glutamic acid	7	6	10	12	8	43
framework residues						
lysine	9	11	39	128	109	296
aspartic acid	59	13	22	45	69	208
glutamic acid	20	4	37	92	85	238
totals	109	60	142	337	336	984

[a] Data adapted from compilation by Padlan (*24*) for 34 human and mouse Fv regions of known three-dimensional structures, which were analyzed for fractional solvent accessibilities of residues within CDR and framework sequences. The five categories of relative solvent exposure are defined from the following range of fractional accessibility values: 0.00−0.20, completely buried (Bu); 0.20−0.40, mostly buried (mB); 0.40−0.60, partly buried/partly exposed (pB); 0.60−0.80, mostly exposed (mE); ≥0.80, completely exposed (Ex).

```
*                    * #         #              #
DVVMSQSPSSLPVSVGEKVTLSCKSSQSLLYSGNQKNYL      39
CC49 VL                    CDR 1
        #    #              *    *         *
AWYQQKPGQSPKLLIYWASARESGVPDRFTGSGSGTDFT      78
              CDR 2
      #  * *                      #    #
LSISSVKTEDLAVYYCQQYYSYPLTFGAGTKLVLKGSTSG     118
              CDR 3                  218-linker
   #     *     #          *  *     #    #
SGKPGSGEGSTKGQVQLQQSDAELVKPGASVKISCKASG      157
                CC49 VH
    *         #    *    *           * *  #   *   #
YTFTDHAIHWVKQNPEQGLEWIGYFSPGNDDFKYNERFK      196
      CDR 1                CDR 2
  #      * #                * *
GKATLTADKSSSTAYVQLNSLTSEDSAVYFCTRSLNMAY      235
                                      CDR 3

WGQGTSVTVS                                    245
```

Figure 3. Amino acid sequence of CC49/218 sFv protein. Lysine (K) residues are indicated (#). The amino acids aspartic acid (D) and glutamic acid (E) are also highlighted (*). CDR sequences are underlined and the 218 linker is in italics.

Carboxyl-Reactive PEGylation and Branched PEG. Charged amino acid residues, including lysine, aspartic acid, and glutamic acid, have a marked tendency to be solvent accessible on protein surfaces (Table 1). Conjugation to carboxylic acid groups of proteins is a less frequently explored approach for production of protein bioconjugates. However, the hydrazide/EDC chemistry described by Zalipsky and colleagues (*16*, *33*) offers a practical method of linking PEG polymers to protein carboxylic sites. For example, this alternate conjugation chemistry has been shown to be superior to amine linkages for PEGylation of brain-derived neurotrophic factor (BDNF) while retaining biological activity (*38*). Maeda and colleagues have also found carboxyl-targeted PEGylation to be the preferred approach for bilirubin oxidase conjugations (*39*). Two significant observations from our investigations of the conjugation reactions of Hz-PEG-5000 with CC49 sFv are as follows: (a) the employment of much higher PEG concentrations in the PEGylation reactions was possible in generation of active PEG-sFv compounds and (b) the retention of antigen-binding activity in PEG-sFv compounds was possible with increased numbers of PEG polymers on the bioconjugates. Specifically, antigen-binding activity was lost by PEGylation of CC49 sFv with a 14-fold or greater molar excess of activated PEG polymer using any of the amine chemistries with straight-chain polymers; whereas the activity was well preserved when the SC-PEG per sFv molar reaction ratio was below 4. An exception to this rule occurred for the branched SC-activated PEG (U-PEG) for which PEG:sFv reaction ratios of 14 produced a predominately monoPEGylated sFv compound (Figure 4, panels C and D) that demonstrated an equivalent apparent affinity when compared to the unmodified sFv. These results illustrate the influence of steric factors in the reaction rates of the polymer conjugation. The development of U-PEG by Greenwald and colleagues (*29*) has provided significant geometric adaptability for PEGylation strategies, and is shown here to substantially modulate the reaction kinetics of conjugation as well.

In contrast to the linear amine-reactive PEG polymers, PEGylation reactions employing a 200-fold molar excess of Hz-PEG-5000 relative to sFv protein were demonstrated to produce active PEG-sFv compounds with an average PEG number of 4.8 (Figure 4D and Table 3). Although this Hz-PEG-sFv preparation displayed a 10−15-fold diminished binding affinity by competition ELISA, the retention of significant antigen-binding activity in

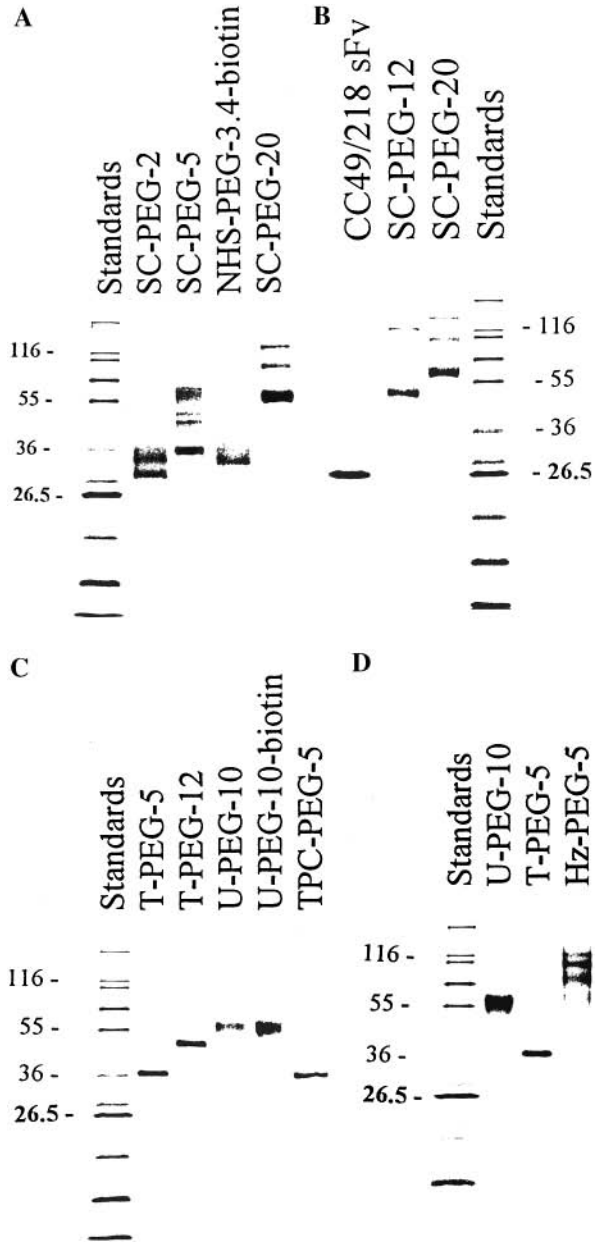


Figure 4. SDS−PAGE analysis of PEGylated CC49/218 sFv formulations. Coomassie blue stained proteins and conjugates were analyzed by 4−20% SDS−PAGE. Highlighted standard markers (kDa × 10^{-3}) within the Novex Mark12 series (Experimental Procedures) are unmodified CC49/218 sFv (26.5); lactate dehydrogenase (36); glutamic dehydrogenase (55); and β-galactosidase (116). (A) SC-PEG-2000, SC-PEG-5000, NHS-PEG-3400-biotin, SC-PEG-20000; (B) CC49/218 sFv, SC-PEG-12000, SC-PEG-20000; (C) T-PEG-5000, T-PEG-12000, U-PEG-10000, U-PEG-10000-biotin, TPC-PEG-5000; (D) U-PEG-10000, T-PEG-5000, Hz-PEG-5000.

Table 2. Dissociation Constants (K_d) of sFv Compounds

sFv formulation	PEG/sFv[a]	K_d (×10^{-9} M)
native CC49/218	0	4.5
SC-PEG-2000	2.1	4.6
NHS-PEG-3400-biotin	2.0	6.1
SC-PEG-12000	1.3	5.8
SC-PEG-20000	1.1	7.5
T-PEG-5000	1.0	7.0

[a] Ratio of PEG polymer per sFv.

this moderately PEGylated sFv provides a very attractive alternative conjugation strategy which may be employed when amine chemistries are not suitable. Remarkably,

Table 3. Pharmacokinetics of sFv and PEG-sFv Conjugates

sFv compd			PEG/	circulating half-life (h)		area under the curve (μg h/mL)		mean residence time (h)	
MW	linker	label	sFv	mean	std error	mean	std error	mean	std error
CC49/ 218 sFv			0	0.7	0.4	54	27	1.0	0.6
2000	SC		2.1	3.4	0.4	135	13	4.9	0.6
3400	NHS	biotin	2.0	2.5	0.4	95	14	3.6	0.6
5000	T		1.0	1.8	0.4	67	14	2.6	0.6
5000	SC		1.7	4.1	1.0	147	32	5.9	1.6
5000	TPC		1.4	3.4	1.0	120	28	5.0	1.4
5000	Hz		4.8	9.8	1.6	395	56	14	2.3
10 000	U	biotin	1.5	10.4	1.3	415	47	15	2.0
12 000	T		1.2	13.9	1.7	583	64	20	2.5
12 000	SC		1.3	13.2	1.5	586	58	19	2.2
20 000	SC		1.1	12.8	0.7	1110	56	18	1.0

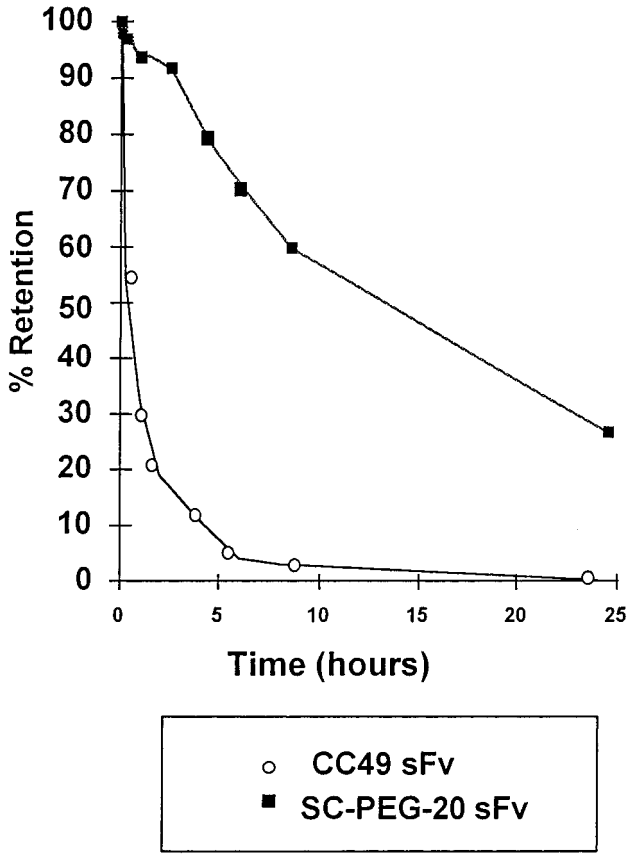


Figure 5. Pharmacokinetics of plasma retention of CC49/218 sFv and SC-PEG-20 conjugate. Plasma retention studies of the unmodified sFv (open circles) and the PEGylated compound (closed boxes) were performed in mice (six per group) as described in Experimental Procedures.

SE-HPLC purified, Hz-PEG-5000-modified sFv compounds with PEG numbers as high as 11 demonstrated detectable antigen-binding activity (data not shown). The observed capacity of carboxyl-directed conjugations of the sFv protein to preserve binding activity at higher PEG numbers plausibly correlates with the locations for the most reactive moieties in this category at sites distal to the CDRs; in this connection, surface exposure of carboxyls is not as predominant as for lysines in Fv structures (Table 1). Ultimately, Hz-PEG polymers of higher molecular weight and/or with branched U-PEG geometry may provide further benefits. Since the V_L and V_H immunoglobulin families have inherent sequence variability, the availability of alternate conjugation

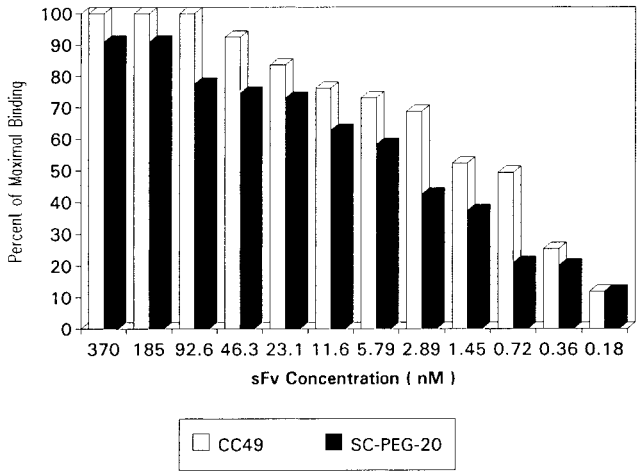


Figure 6. ELISA showing equilibrium binding of CC49/218 sFv (open bars) and SC-PEG-20 conjugate (filled bars) using LS-174-T whole cell preparations. Control compounds (10 mg/mL) BSA and 4-4-20 sFv did not exhibit binding activity. Each starting sFv compound was analyzed in 1:2 serial dilutions.

chemistries provides the antibody engineer with options for construction of individual PEG-sFv immunomolecules. The eventual biochemical characterization of therapeutic PEG-sFv-lead candidates with regard to the specific residue modifications and degree of heterogeneity will provide a more detailed understanding of these bioconjugates.

Circulating Lives of PEGylated sFv. Table 3 presents the pharmacokinetic profiles of 10 PEGylated sFv compounds which differ in linker chemistry, polymer length, and polymer geometry. Included in Table 3 is the estimated stoichiometry (PEG/sFv) in these compounds. Each of these minimally modified preparations demonstrated an average PEG number (n) of $1.0 \leq n \leq 2.1$ except the Hz-PEG-sFv conjugate. Groups of six mice were injected intravenously with unmodified CC49/218 sFv or one of the PEGylated sFv compounds, and circulatory half-life, area under the curve (AUC), and mean residence time were calculated using a one compartment model as described in Experimental Procedures. Unmodified sFv protein cleared rapidly from the plasma with a circulating half-life of 0.7 ± 0.4 h. Renal clearance has previously been established as the predominant, if not exclusive, mechanism responsible for sFv protein elimination (*35*, *37*). All PEGylated sFv compounds demonstrated markedly increased circulating lives which extend the $t_{1/2}$ values from 2.6-fold (T-PEG-5000) up to 20.3-fold (T-PEG-12000). Three significant observations may be drawn from these pharmacokinetic data. First, PEGylated sFv compounds having both similar PEG numbers and polymer sizes also had similar circulating lives.

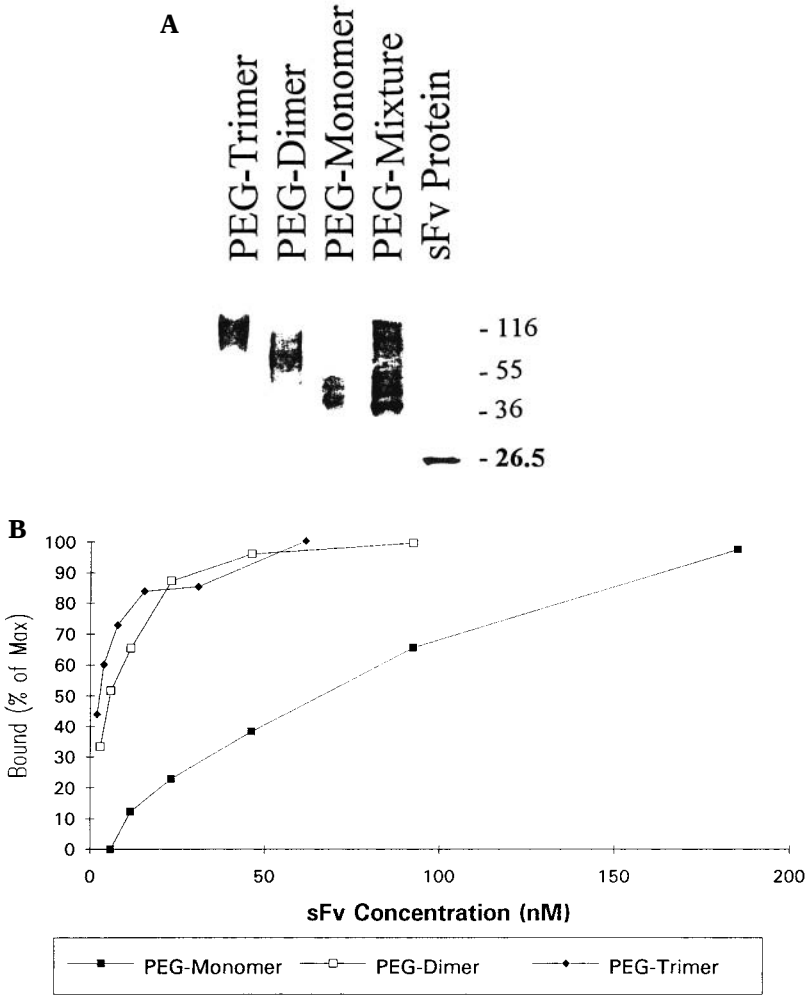


Figure 7. Production and functional affinity of multivalent cross-linked PEG-sFv compounds. (A) Purified CC49/218 sFv compounds corresponding to monomer, dimer, and trimer valencies were generated with homobifunctional cross-linking BSC-PEG-5000 and analyzed on Coomassie blue stained SDS−PAGE 4−20% slab gels. The initial product mixture of the PEGylation reaction is also shown. (B) ELISA of monomer, dimer, and trimer PEG-sFv compounds for mucin-binding activity versus sFv protein concentration.

Second, the employment of PEG polymers of longer lengths extended circulating lives to a greater degree than multiple shorter polymers of equivalent total mass. For example, Hz-PEG-5000-sFv with a PEG number of 4.8 exhibited a $t_{1/2} = 9.8 \pm 1.6$ h, while SC-PEG-20000-sFv with a PEG number of 1.1 demonstrated a $t_{1/2} = 12.8 \pm 0.7$ h. Third, the extension of AUC by as much as 20-fold, such as in the SC-PEG-20000 sFv compound, without substantially compromising sFv antigen-binding activity, bodes well for the potential of PEGylation for systematically extending the bioavailability of sFv protein therapeutics. Figure 5 shows the blood clearance kinetics of the PEG-20000 sFv compound, and Table 2 includes the calculated K_d for this compound for the validated surrogate antigen, bovine submaxillary mucin. As an independent confirmation of binding activity for this compound to the tumor-associated mucin target, a modified ELISA analysis of equilibrium binding using the TAG-72-expressing LS-174-T carcinoma cell line as capture antigen was performed as previously described (*35*). As shown in Figure 6, the PEG-20000-modifed sFv also maintained specific cell-binding activity comparable to the unmodified sFv protein.

In the context of our observations on the benefits of employing PEG polymers of longer length, as opposed to multiple short-chain conjugations, we anticipate that clearance rates for succeeding sFv bioconjugate formulations may be further optimized. The overall selection of PEG modifications will ultimately relate to the individual targeting goal for the sFv, and verification of PEG-sFv efficacy can only be fully validated by in vivo studies. Although the attached polymers may have a temporal influence on the rapid tissue penetration of sFv proteins, the described "enhanced permeability and retention effect" (*40*−*43*) of polymers such as PEG may provide interesting dual targeting modalities utilizing both passive (PEG) and active (sFv) targeting strategies for tumors or other tissues.

PEGylated Multivalent sFv. Multivalency is another intrinsic property of natural human antibodies of any class. Recent success in engineering multivalent and multifunctional forms of sFv proteins (*1*, *9*−*12*, *44*) has established the single-chain Fv format as a comprehensive antibody technology. Conceptually, multivalent Fv may also be engineered through polymer-based bioconjugates, which simulate the functional affinity advantages of multivalency for repetitive epitopes. In a pilot study to evaluate the valency and activity of multimeric PEG-cross-linked sFv proteins, we utilized a bifunctional PEG-5000 polymer having activated SC moieties (BSC-PEG) on both termini of the linear strand (*16*). Our selected reaction conditions did not produce substantial amounts of PEG-sFv monomers, and multimeric PEG-sFv (PEG-mFv) could be readily purified from monomeric sFv forms by Superdex 75 chromatography. As with most homobifunctional reagent linkages, the cross-linked sFv proteins are expected to be heterogeneous with regard to valency (i.e., dimers, trimers, and tetramers) and also with respect to surface linkage sites. However, for antigen-binding molecules such as CC49 sFv which recognizes a repetitive Sialyl-Tn epitope on mucin, a parameter which may be investigated in formulations of cross-linked sFv is the relative degree of functional affinity in these compounds. Two SE-HPLC fractions of PEG-mFv were isolated, which, according to molecular mass estimates, correspond to dimeric and trimeric sFv species. Monomer, dimer, and trimer are defined here as having either one, two, or three sFv proteins, respectively, incorporated in the heterogeneous PEGylated conjugates. Figure 7A shows the SDS−PAGE analysis of these preparations. As described in Experimental Procedures, a solution-binding assay was developed to compare the relative functional affinity of the monomeric SC-PEG-5000 sFv and multimeric PEG-sFv compounds. As shown in Figure 7B, a marked increase in apparent affinity was observed in the PEG-mFv conjugates when compared to the PEG-sFv monomer. A comparable increase in apparent affinity was previously reported in immunoassays of the dimeric CC49 mAb when compared to the monovalent CC49 sFv (*10*, *31*). Further improvements of this approach may be anticipated by employing site-specific heterobifunctional activated PEG polymers of selected length to achieve well-defined cross-linked sFv protein compounds, which may be highly adjustable with respect to the critical circulating life parameters.

In conclusion, we report the applicability of established random PEGylation procedures for generating highly active PEG-sFv compounds exhibiting substantial extensions of circulating lives in mice. The potential to create designed antibody derived drugs with tailored pharmacokinetic properties provides numerous practical applications in immunotherapy.

ACKNOWLEDGMENT

We thank Jeng-Dar Yang, Anna Nepomich, and Maoliang Wang for technical assistance in the ELISA data collection and the purification of bioconjugates. We are also grateful to Jeff McGuire, Jo Bossart, Rich Greenwald, Kwok Shum, and Chyi Lee for support and helpful discussions on PEGylation and pharmacokinetic analysis.

LITERATURE CITED

(1) Hudson, P. J. (1998) Recombinant antibody fragments. *Curr. Opin. Biotechnol. 9*, 395−402.

(2) Dall'Acqua, W., and Carter, P. (1998) Antibody engineering. *Curr. Opin. Struct. Biol. 8*, 443−450.

(3) De Haard, H., Henderikx, P., and Hoogenboom, H. R. (1998) Creating and engineering human antibodies for immunotherapy. *Adv. Drug Deliv. Rev. 31*, 5−31.

(4) Filpula, D., and McGuire, J. (1999) Single-chain Fv designs for protein, cell, and gene therapeutics. *Exp. Opin. Ther. Patents 9*, 231−245.

(5) Kreitman, R. J., and Pastan, I. (1998) Immunotoxins for targeted cancer therapy. *Adv. Drug Deliv. Rev. 31*, 53−88.

(6) Pelegrin, M., Marin, M., Noel, D., and Piechaczyk, M. (1998) Genetically engineered antibodies in gene transfer and gene therapy. *Hum. Gene Ther. 9*, 2165−2175.

(7) Begent, R. H. J., Verhaar, M. J., Chester, K. A., Casey, J. L., Green, A. J., Napier, M. P., Hope-Stone, L. D., Cushen, N., Keep, P. A., Johnson, C. J., Hawkins, R. E., Hilson, A. J. W., and Robson, L. (1996) Clinical evidence of efficient tumor targeting based on single-chain Fv antibody selected from a combinatorial library. *Nat. Med. 2*, 979−984.

(8) Fitch, J. C. K., Elefteriades, J. A., Rinder, H. M., Matis, L. A., Evans, M. J., Rollins, S. A., Alford, B. L., and Hines, R. L. (1996) Safety, pharmacokinetics, and immunogenicity of intravenous administration of H5G1.1-SCFV in humans. *Blood 88*, 654a.

(9) Holliger, P., Wing, M., Pound, J. D., Bohlen, H., and Winter, G. (1997) Retargeting serum immunoglobulin with bispecific diabodies. *Nat. Biotechnol. 15*, 632−636.

(10) Whitlow, M., Filpula, D., Rollence, M. L., Feng, S.-L., and Wood, J. F. (1994) Multivalent Fvs: characterization of single-chain Fv oligomers and preparation of a bispecific Fv. *Protein Eng. 7*, 1017−1026.

(11) Adams, G. P., Schier, R., McCall, A. M., Crawford, R. S., Wolf, E. J., Weiner, L. M., and Marks, J. D. (1998) Prolonged in vivo tumour retention of a human diabody targeting the extracellular domain of human HER2/*neu*. *Br. J. Cancer 77*, 1405−1412.

(12) Wang, D., Berven, E., Li, Q., Uckun, F., and Kersey, J. H. (1997) Optimization of conditions for formation and analysis of anti-CD19 FVS191 single-chain Fv homodimer $(scFv')_2$. *Bioconjugate Chem. 8*, 64−70.
(13) Cao, Y., and Suresh, M. R. (1998) Bispecific antibodies as novel bioconjugates. *Bioconjugate Chem. 9*, 635−644.
(14) Nucci, M. L., Shorr, R., and Abuchowski, A. (1991) The therapeutic value of poly(ethylene glycol)-modified proteins. *Adv. Drug Deliv. Rev. 6*, 133−151.
(15) Francis, G. E., Delgado, C., Fisher, D., Malik, F., and Agrawal, A. K. (1996) Poly(ethylene glycol) modification: Relevance of improved methodology to tumour targeting. *J. Drug Targeting 3*, 321−340.
(16) Zalipsky, S. (1995) Functionalized poly(ethylene glycol) for preparation of biologically relevant conjugates. *Bioconjugate Chem. 6*, 150−165.
(17) Clark, R., Olson, K., Fuh, G., Marian, M., Mortensen, D., Teshima, G., Chang, S., Chu, H., Mukku, V., Canova-Davis, E., Somers, T., Cronin, M., Winkler, M., and Wells, J. A. (1996) Long-acting growth hormones produced by conjugation with poly(ethylene glycol). *J. Biol. Chem. 271*, 21969−21977.
(18) Pettit, D. K., Bonnert, T. P., Eisenman, J., Srinivasan, S., Paxton, R., Beers, C., Lynch, D., Miller, B., Yost, J., Grabstein, K. H., and Gombotz, W. R. (1997) Structure−function studies of interleukin 15 using site-specific mutagenesis, poly(ethylene glycol) conjugation, and homology modeling. *J. Biol. Chem. 272*, 2312−2318.
(19) Delgado, C., Pedley, R. B., Herraez, A., Boden, R., Boden, J. A., Keep, P. A., Chester, K. A., Fisher, D., Begent, R. H. J., and Francis, G. E. (1996) Enhanced tumour specificity of an anti-carcinoembrionic antigen Fab′ fragment by poly(ethylene glycol) (PEG) modification. *Br. J. Cancer 73*, 175−182.
(20) Benhar, I., Brinkmann, U., Webber, K. O., and Pastan, I. (1994) Mutations of two lysine residues in the CDR loops of a recombinant immunotoxin that reduce its sensitivity to chemical derivatization. *Bioconjugate Chem. 5*, 321−326.
(21) Benhar, I., Wang, Q.-c., FitzGerald, D., and Pastan, I. (1994) *Pseudomonas* exotoxin A mutants. Replacement of surface-exposed residues in domain III with cysteine residues that can be modified with poly(ethylene glycol) in a site-specific manner. *J. Biol. Chem. 269*, 13398−13404.
(22) Wang, Q.-c., Pai, L. H., Debinski, W., FitzGerald, D. J., and Pastan, I. (1993) Poly(ethylene glycol)-modified chimeric toxin composed of transforming growth factor alpha and *Pseudomonas* exotoxin. *Cancer Res. 53*, 4588−4594.
(23) Kinstler, O. B., Brems, D. N., Lauren, S. L., Paige, A. G., Hamburger, J. B., and Treuheit, M. J. (1996) Characterization and stability of *N*-terminally PEGylated rhG-CSF. *Pharm. Res. 13*, 996−1002.
(24) Padlan, E. A. (1994) The structure of antibodies. *Molecular Biology Intelligence Unit: Antibody−antigen complexes*, pp 17−30, R. G. Landes Company, Austin, TX.
(25) Kabat, E. A., Wu, T. T., Perry, H. M., Gottesman, K. S., and Foeller, C. (1991) *Sequences of proteins of immunological interest*, 5th ed., U.S. Department of Health and Human Services, Bethesda, MD.
(26) Wang, M., Lee, L. S., Nepomich, A., Yang, J.-D., Conover, C., Whitlow, M., and Filpula, D. (1998) Single-chain Fv with manifold *N*-glycans as bifunctional scaffolds for immunomolecules. *Protein Eng. 11*, 1277−1283.
(27) Filpula, D., McGuire, J., and Whitlow, M. (1996) Production of single-chain Fv monomers and multimers. In *Antibody Engineering: a Practical Approach* (J. McCafferty, H. R. Hoogenboom, and D. J. Chiswell, Eds.) pp 253−268, Oxford University Press, Oxford.
(28) Greenwald, R. B., Pendri, A., Martinez, A., Gilbert, C., and Bradley P. (1996) PEG thiazolidine-2-thione, a novel reagent for facile protein modification: Conjugation of bovine hemoglobin. *Bioconjugate Chem. 7*, 638−641.
(29) Martinez, A., Pendri, A., Xia, J., and Greenwald, R. B. (1997) Branched poly(ethylene glycol) linkers. *Macromol. Chem. Phys. 198*, 2489−2498.
(30) Hermanson, G. T. (1996) Modification with synthetic polymers. *Bioconjugate Techniques*, pp 605−618, Academic Press, San Diego CA.
(31) Whitlow, M., Bell, B. A., Feng, S.-L., Filpula, D., Hardman, K. D., Hubert, S. L., Rollence, M. L., Wood, J. F., Schott, M. E., Milenic, D. E., Yokota, T., and Schlom, J. (1993) An improved linker for single-chain Fv with reduced aggregation and enhanced proteolytic stability. *Protein Eng. 6*, 989−995.
(32) Habeeb, A. F. S. A. (1966) Determination of free amino groups in proteins by trinitrobenzenesulfonic acid. *Anal. Biochem. 14*, 328−336.
(33) Zalipsky, S., and Menon-Rudolph, S. (1997) Hydrazide derivatives of poly(ethylene glycol) and their bioconjugates. In *Poly(ethyleneglycol) Chemistry and Biological Applications* (J. M. Harris and S. Zalipsky, Eds.) pp 318−341, American Chemical Society, Washington DC.
(34) Harlow, E., and Lane, D. (1988) Immunoassays. *Antibodies: a Laboratory Manual*, pp 553−612, Cold Spring Harbor Laboratory, Plainview, NY.
(35) Milenic, D. E., Yokota, T., Filpula, D. R., Finkelman, M. A. J., Dodd, S. W., Wood, J. F., Whitlow, M., Snoy, P., and Schlom, J. (1991) Construction, binding properties, metabolism, and tumor targeting of a single-chain Fv derived from the pancarcinoma monoclonal antibody CC49. *Cancer Res. 51*, 6363−6371.
(36) Friguet, B., Chaffotte, A. F., Djavadi-Ohaniance, and Goldberg, M. E. (1985) Measurements of the true affinity constant in solution of antigen−antibody complexes by enzyme-linked immunosorbent assay. *J. Immunol. Methods 77*, 305−319.
(37) Larson, S. M., El-Shirbiny, A. M., Divgi, C. R., Sgouros, G., Finn, R. D., Tschmelitsch, J., Picon, A., Whitlow, M., Schlom, J., Zhang, J., and Cohen, A. M. (1997) Single chain antigen binding protein (sFv CC49). First human studies in colorectal carcinoma metastatic to liver. *Cancer 80*, 2458−2468.
(38) Wu, D., and Pardridge, W. M. (1999) Neuroprotection with noninvasive neurotrophin delivery to the brain. *Proc. Natl. Acad. Sci. U.S.A. 96*, 254−259.
(39) Maeda, H., Kimura, M., Sasaki, I., Hirose, Y., and Konno, T. (1992) Toxicity of bilirubin and detoxification by PEG-bilirubin oxidase conjugate. In *Poly(ethylene glycol) Chemistry. Biotechnical and Biomedical Applications* (J. M. Harris, Ed.) pp 153−169, Plenum Press, New York.
(40) Maeda, H., and Matsumura, Y. (1989) Tumoritropic and lymphotropic principles of macromolecular drugs. *Crit. Rev. Ther. Drug Carrier Syst. 6*, 193−210.
(41) Maeda, H., Seymour, L. W., and Miyamoto, Y. (1992) Conjugates of anticancer agents and polymers: advantages of macromolecular therapeutics in vivo. *Bioconjugate Chem. 3*, 351−362.
(42) Murakami, Y., Tabata., Y., and Ikada, Y. (1997) Tumor accumulation of poly(ethylene glycol) with different molecular weights after intravenous injection. *Drug Deliv. 4*, 23−31.
(43) Marecos, E., Weissleder, R., and Bogdanov, A., Jr. (1998) Antibody-mediated versus nontargeted delivery in a human small cell lung carcinoma model. *Bioconjugate Chem. 9*, 184−191.
(44) Siemers, N. O., Kerr, D. E., Yarnold, S., Stebbins, M. R., Vrudhula, V. M., Hellström, I., Hellström, K. E., and Senter, P. D. Construction, expression, and activities of L49-sFv-β-lactamase, a single-chain antibody fusion protein for anticancer prodrug activation. *Bioconjugate Chem. 8*, 510−519.
(45) Kraulis, P. J. (1991) MOLSCRIPT: a program to produce both detailed and schematic plots of protein structures. *J. Appl. Crystallogr. 24*, 946−950.
(46) Merritt, E. A., and Bacon, D. J. (1997) Raster3D: Photorealistic molecular graphics. *Methods Enzymol. 277*, 505−524.

BC990076O

Potentiation of Chlorin e6 Photodynamic Activity in Vitro with Peptide-Based Intracellular Vehicles

Stuart K. Bisland, Devender Singh,† and Jean Gariépy*

Department of Medical Biophysics, University of Toronto and the Division of Molecular and Structural Biology, Ontario Cancer Institute, Princess Margaret Hospital, 610 University Avenue, Toronto, Ontario, Canada M5G 2M9. Received February 23, 1999; Revised Manuscript Received August 20, 1999

Photodynamic therapy (PDT) is a targeted treatment modality where photosensitizers accumulate into cells and are selectively activated by light leading to the production of toxic species and cell death. Focusing the action of photosensitizers to a unique intracellular target may enhance their cytotoxicity. In this study, we demonstrate that the routing of the porphyrin-based photosensitizer chlorin e_6, to the nucleus of cells can significantly alter its toxicity profile. The cellular localization of chlorin e_6 was achieved by coupling the chromophore during solid-phase synthesis to a nucleus-directed linear peptide (Ce6-peptide) or a branched peptide (Ce6-loligomer) composed of eight identical arms displaying the sequence of the Ce6-peptide. These constructs incorporated signals guiding their cytoplasmic uptake and nuclear localization. Ce6-peptide and Ce6-loligomer displayed an enhanced photodynamic activity compared to unconjugated chlorin e_6, lowering the observed CD_{50} values for CHO and RIF-1 cells by 1 or more orders of magnitude. The intracellular accumulation of Ce6-peptide and Ce6-loligomer was assessed by electron and confocal microscopy as well as by flow cytometry. Constructs were internalized by cells within an hour and by 6 h, the release of active oxygen species could be observed within the nucleus of cells pretreated with Ce6-loligomer. These results highlight the utility of designing peptides as vehicles for regulating the intracellular distribution of photosensitizers such as chlorin e_6 in order to maximize their efficacy in PDT.

INTRODUCTION

The dynamic use of light to selectively kill proliferating cells is termed photodynamic therapy (PDT). PDT represents a noninvasive procedure requiring the use of a photosensitizer (a photosensitive compound) to generate cytotoxic oxygen radicals within a diseased tissue. This approach has recently been popularized by the introduction of Photofrin, a porphyrin derivative, presently being evaluated in clinical trials (*1*). Photofrin, a clinically effective first-generation photosensitizer, is characterized by a low absorbance in the red region of the spectrum and displays side effects such as prolonged skin photosensitivity (*2*). Recent animal studies found chlorin e_6, a related porphyrin-based agent, to be a useful photosensitizer in vivo, with low toxicity and preferential tumor localization (*3*−*5*). The efficiency of photosensitizers in situ is ultimately dependent on their selective uptake into tissues and on their cellular accumulation within tissues. This finding is supported by the fact that singlet oxygen ($^1O_2$)-induced photodamage incurred upon porphyrin activation is usually localized to within 0.1 μm of its site of release (*6*). The toxicity of photodynamic drugs could potentially be enhanced by delivering high amounts of a photosensitizer into subcellular organelles such as the nucleus where nucleic acids represent target molecules sensitive to photodamage (*7*). The photodynamic potential of unbound chlorin e_6 is limited as a result of its tendency to localize largely at the plasma membrane (*8*). Bovine serum albumin (BSA) conjugates incorporating chlorin e_6 and nuclear localization sequences have recently been assembled to guide their cellular localization (*11*). These PDT-labeled conjugates have an enhanced phototoxicity in relation to free chlorin e_6 (*9*−*12*). In particular, BSA conjugates incorporating insulin have been reported to target the insulin receptor in an effort to create cell-specific constructs (*11*). The composition of these BSA constructs, however, remains approximate and had to be inferred from the average ratio of each component present in these conjugates as estimated from polyacrylamide gel electrophoresis and by absorbance measurements based on the incorporation of chlorin e_6 molecules (*11*). The engineering and characterization of defined, optimal delivery agents based on the chemical cross-linking of multiple components remain a challenging and difficult task.

Our group has recently designed branched peptides that act as multitasking intracellular vehicles (*13*−*15*). This first generation of vehicles incorporates eight identical peptide arms coding for two functional domains, namely a pentalysine domain acting as a cytoplasmic transport sequence (CTS)[1] and the simian virus SV40 large T antigen nuclear localization signal (NLS) which

* To whom correspondence should be addressed at the Ontario Cancer Institute. Phone: (416) 946-2967. Fax: (416) 946-6529. E-mail: gariepy@oci.utoronto.ca.

† Present address: Gemma Biotechnology, 620 University Avenue, Toronto, Canada M5G 2M9.

[1] Abbreviations: A^{124}SV40LTa (124−135), residues 124−135 of the SV40 large T antigen with a threonine to alanine substitution at position 124; C6-peptide, a linear peptide composed of a chlorin e_6 group linked to a nuclear localization signal and a pentalysine cytoplasmic translocation domain; C6-loligomer, a loligomer harbouring 8 N-terminal arms that comprise of a chlorin e_6 group followed by a nuclear localization signal and a pentalysine cytoplasmic translocation domain; CTS, cytoplasmic translocation signal; loligomer, a squid-like branched peptide construct that incorporates cell penetration and intracellular localization signals; NLS, nuclear localization signal.

10.1021/bc990020u CCC: $18.00 © 1999 American Chemical Society
Published on Web 10/16/1999

guide their nuclear uptake (*13*−*15*). These squid-like, intracellular vehicles are referred to as loligomers (derived from the Latin root *loligo* referring to members of the squid family). This study describes the assembly and application of a nucleus-directed linear peptide and a loligomer incorporating the photosensitizer chlorin e_6. The chromophore was introduced during solid-phase peptide synthesis and the resulting constructs display a photodynamic activity that exceeded the toxicity of free chlorin e_6.

MATERIALS AND METHODS

Synthesis of Chlorin e_6 Peptides and Their Derivatives. Peptides were assembled using *tert*-butoxycarbonyl (t-Boc) chemistry and phenylacetamidomethyl (PAM) resin supports as described elsewhere (*13*, *14*). Chlorin e_6 was coupled to the N-terminus of the peptide and the loligomer by first activating its carboxylic groups with 0.5 molar equivalent of dicyclohexylcarbodiimide and *N*-methyl-2-pyrrolidone at 23 °C for 40 min. The activated chlorin e_6 (4 molar excess in relation to the number of N-terminal amino groups) was then added to the reaction vessel containing the peptide resins. The coupling reaction was left to proceed in the dark for 24 h at room temperature. Both chlorin e_6-containing peptides were desalted using Sephadex G10 (Ce6-peptide) or G25 size-exclusion columns (Ce6-loligomer), respectively. Columns were preequilibrated in phosphate-buffered saline (PBS; pH 7.2). Ce6-peptide was further purified by reversed-phase HPLC (Lichrosorb C_{18}) using a linear gradient of acetonitrile in water (20 to 60%) containing 0.1% (v/v) trifluoroacetic acid. The peptide eluted at 40% acetonitrile:water. The mass of Ce6-peptide was established by ionization mass spectroscopy. (MH+ ion: calculated, 2889; observed, 2888). The amino acid composition of both peptides were confirmed by amino acid analysis. The calculated and expected (parentheses) number of residues comprising each peptide construct are listed in accordance with the three-letter code for each amino acid. Ce6-peptide: Arg, 1.0 (1); Asp, 0.9 (1); Glu, 1.0 (1); Gly, 1.9 (2); Lys, 8.3 (9); Pro, 3.0 (3); Ala, 0.9 (1); Tyr, 1.0 (1); Val, 1.0 (1). Ce6-loligomer: Arg, 8.0 (8); Asp, 6.6 (8); Glu, 9.8 (8); Gly, 19.8 (17); Lys, 81.4 (79); Pro, 22.5 (24); Ala, 8.3 (8); Tyr, 2.4 (1); Val, 8.3 (8). The absorption spectra of either chlorin e_6, Ce6-peptide, or Ce6-loligomer displayed a characteristic Soret band (maximum at ∼401 nm) and Q-band (maxima at 654, 656 and 664 nm), respectively (data not shown). Using chlorin e_6 as a standard, extinction coefficients were calculated at 401 nm [Ce6-peptide (17 000 M^{-1} cm^{-1}) and Ce6-loligomer (129 000 M^{-1} cm^{-1})] and at 664 nm [chlorin e_6 (10 000 M^{-1} cm^{-1}), Ce6-peptide (12 000 M^{-1} cm^{-1}), and Ce6-loligomer (40 000 M^{-1} cm^{-1})]. The calculated number of chlorin e_6 molecules attached to Ce6-loligomer based on amino acid analysis and spectral properties (410 nm) was 7.6 or 0.95 mol of chlorin e_6/mol of loligomer arm (7.6/8). A cysteine residue was included within the C-terminus (analytical arm) of each peptide to allow the attachment of either a maleimido-containing fluorescent probe or a biotin moiety. Texas red or fluorescein were incorporated by dispensing 1 mg of Ce6-peptide or Ce6-loligomer in 1 mL of PBS, pH 7.4 into a glass vial and by adding dropwise a solution of 0.1 mg of either Texas red C_2 maleimide or fluorescein-5-maleimide dissolved in 100 μL of dimethylformamide (Molecular Probes, Eugene, OR). The coupling reactions were left to proceed with constant stirring for 4 h at 4 °C in the dark. The molar ratio of each incorporated fluorochrome was <1. Biotin maleimide (0.5 mg; Molecular Probes) was dissolved in 100 μL of dimethylformamide before being added to a 1 mg solution of either Ce6-peptide or Ce6-loligomer. The pH of the resulting solutions was adjusted to pH 6.5 with 1 M NaOH. The solutions were mixed for 4 h at 4 °C in the dark. Unreacted fluorochrome or biotin reagent was removed by size-exclusion chromatography (as described above). The incorporation of biotin into peptides was established by ELISA using a streptavidin-horseradish peroxidase conjugate, as described elsewhere (*14*). Aliquots of Ce6-peptide and Ce6-loligomer were lyophilized and stored in the dark at −70 °C.

Cell Lines and Cell Cultures. The Chinese hamster ovary (CHO) cell subclone, AUXB1 (*16*), was purchased from the American Type Culture Collection. The radiation-induced fibroblast cell line (RIF-1) was obtained from Dr. Brian Wilson (Ontario Cancer Institute). Cells were grown as monolayers in α-minimal essential medium (α-MEM) supplemented with 10% (v/v) fetal calf serum (FCS; ImmunoCorp., Montreal, Canada), penicillin (1 units/mL) streptomycin (100 μg/mL), and 1 mM glutamine and maintained at 37 °C and 5% CO_2 in a humidified incubator.

Intracellular Uptake. Aliquots of 5×10^5 cells were pipetted into microcentrifuge tubes and suspended in 1 mL of medium containing a noncytotoxic dose (0.01 μM) of either fluorescein-labeled Ce6-peptide (Ce6-peptide-FL5) or Ce6-loligomer (Ce6-loligomer-FL5). Control samples were also prepared which were not exposed to chlorin e_6 and related peptides in order to assess the background level of autofluorescence. The cells were maintained in suspension using a gentle rocking motion and incubated at 37 °C in the dark. At time intervals of 0, 1, 2, 4, 6, and 8 h, samples from each treated cell suspension were placed on ice for 5 min and the cells recovered by centrifugation, washed with PBS (three times), and finally resuspended in aliquots of 0.5 mL of PBS. Cytometric analyses were recorded on a FACScan instrument (Becton Dickinson, San Jose, CA) gating on viable cell populations assessed using 7-amino-actinomycin D (7-AAD; Sigma, St. Louis, MO) (*17*). Samples were prepared in duplicate with 10 000 events recorded for each and experiments repeated 3 or 4 times.

Confocal Microscopy. Aliquots of 5×10^2 cells suspended in 1 mL of medium were plated onto sterile borosilicate coverglass slides (Lab-Tek Nunc, Napierville, IL) and incubated at 37 °C for 16 h to allow time for cells to adhere. Cells were then treated with a nontoxic concentration (0.01 μM) of either fluorescein-labeled Ce6-peptide (Ce6 peptide-FL5) or Ce6-loligomer (Ce6-loligomer-FL5). At selected time intervals, labeled cells were washed five times with sterile PBS to remove any excess construct from the extracellular space and examined by confocal microscopy (Zeiss LSM510 instrument). The signal from chlorin e_6 linked to the N-terminus of our peptide vehicles was observed directly upon UV excitation (Argon laser; Nikon, 364/585 LP filter) while a Nikon 488/520 BP filter was used to visualize the fluorescein signal associated with the C-terminal arm of both peptide constructs.

Electron Microscopy. RIF-1 and CHO cells were harvested from monolayer cultures and dispensed as suspensions (10^6 cells/mL) into medium containing Ce6-peptide-biotin or Ce6-loligomer-biotin (final concentration of biotinylated peptides; 0.01 μM). Cells were incubated at 37 °C without light, and samples collected at 1, 2, 4, 6, or 24 h. Cells were prepared and analyzed using electron microscopy, as previously described (*14*). The accumulation and distribution of gold particles (colloidal gold streptavidin conjugate, 21.7μg/mL; British Biocell

International, Cardiff, U.K.) within cells was quantified using electron micrographs analyzed using a software program (NIH Image; version 1.61). A total of six cells were analyzed for two time points (1 and 6 h) following the exposure of cells to either peptide constructs. Cells were randomly chosen from over 10 electron micrographs.

Photodynamic Treatment. Aliquots of 5×10^3 cells of either CHO or RIF-1 cells suspended in 200 μL growth medium were seeded into wells of blackened 96 well plates with clear bottoms (Corning Costar Corp., Cambridge, MA) and cultured for 6 h at 37 °C in the presence of 5% CO_2. Cells (as quadruplicate cultures) were treated with PBS or increasing concentrations of either chlorin e_6, Ce6-peptide, or Ce6-loligomer followed by light activation treatments. Control samples were also prepared and kept from light. The concentration range of peptides differed for each cell line. CHO cells were treated with chlorin e_6, $(1 \times 10^{-6})-(5 \times 10^{-4})$ M, Ce6-peptide, $(5 \times 10^{-9})-(2 \times 10^{-5})$ M, and Ce6-loligomer, $(2 \times 10^{-11})-(5 \times 10^{-8})$ M, while RIF-1 cells were treated with chlorin e6, $(1 \times 10^{-6})-(5 \times 10^{-4})$ M, Ce6-peptide, $(2 \times 10^{-8})-(1 \times 10^{-4})$ M, and Ce6-loligomer, $(5 \times 10^{-10})-(2 \times 10^{-6})$ M. Wells were irradiated with 664 nm light from above using an optic fiber coupled to a dye laser source (Spectra Physics model 375B), applying a radiant exposure of 12 J/cm^2 at a fluence rate of 20−30 mW/cm^2. The photoinduced thermal effect was measured in individual wells using a thermovision camera. The increase in temperature was found to be less than 3 °C (23.5−26 °C). Once irradiated, cells were incubated with fresh growth medium for an additional 48 h at 37 °C in the dark.

Photoinduced Oxidative Burst. RIF-1 cells (2×10^4 cells) were suspended in 1 mL of growth medium containing 0.01 μM Ce6-loligomer-TxRd and incubated (37 °C, 5% CO_2) for 6 h in the dark and then washed with PBS (three times). Two subsequent incubations were performed. Cells were exposed for 25 min at 37 °C in medium containing 5 μM 5 (and 6)-chloromethyl-2,′7′-dichlorodihydrofluorescein diacetate (CM-H_2 DFDA) followed by a second incubation for 5 min at 23 °C in medium containing 5 μM AcrO. Cells were washed twice with PBS between incubation periods, resuspended in fresh medium, and seeded into chamber slides (Nunc Inc. Naperville, IL). Slides remained at room temperature in the dark until analyzed by confocal microscopy. Single cells were visualized before and after the activation of chlorin e_6 and Ce6-loligomer-TxRd and AcrO signals recorded using a scanning confocal imaging system (Argon-ion laser; 488/514.5 nm; MRC 600, Bio-Rad Laboratories Ltd., Ont., Canada). Both signals were viewed through a ×40/0.55 Nikon water-immersible objective lens. Chlorin e_6 was subsequently activated using a helium cadmium (HeCd) laser (omNichrome series 56). The fluorescence signal from CM-H_2 DFDA was simultaneously recorded using a green filter.

Cell Viability. The toxicity of chlorin e_6, Ce6-peptide, or Ce6-loligomer toward CHO and RIF-1 cells was measured using a tetrazolium salt-based cell viability assay (*18*). Following a 6 h exposure to chlorin e_6 and related peptide constructs, identical groups of cell samples were treated either with light (photoirradiation) or kept in the dark. The assay was performed on cells 48 h after the photoirradiation treatment (±photoirradiation). Cells were incubated in the presence of the tetrazolium salt WST-1 [10 μL/well; 4-[3{4-iodophenyl}-2-{4-nitrophenyl}-2H-5-tetrazolio]-1−3-benzene disulfonate; Boehringer Mannheim, Montreal, Canada] for 1 h, and the resulting orange formazan product was quantified by measuring the optical density of the cell extracts at 450 nm. Percent

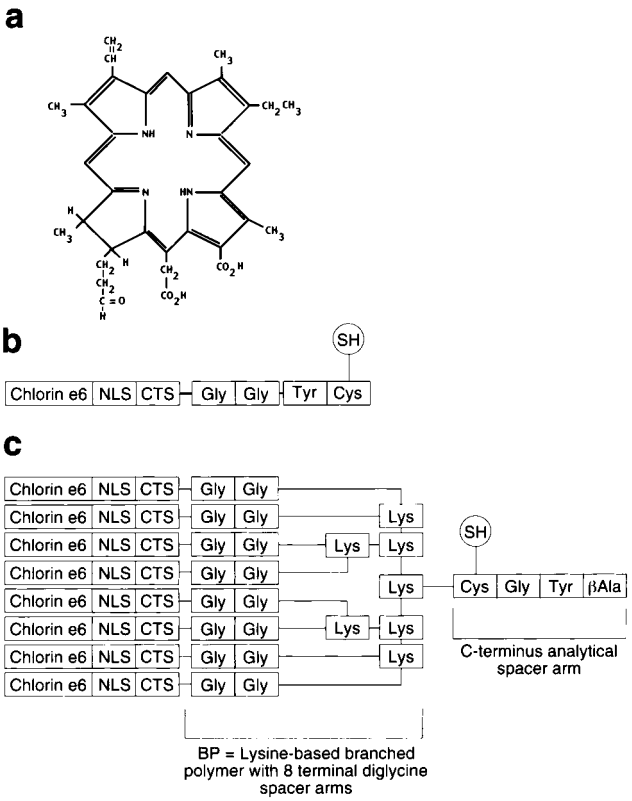


Figure 1. Structures of chlorin e_6-derived constructs. (a) Chlorin e_6 (*8*). (b) Ce6-peptide. The N-terminal region of Ce6-peptide consists of a single chlorin e_6 molecule followed by the simian virus (SV40) large-T-antigen nuclear localization signal residues 124−135 [NLS; A^{124}SV40LTa(124−135), Ala-Pro-Pro-Lys-Lys-Lys-Arg-Lys-Val-Glu-Asp-Pro harboring a threonine to alanine substitution at position 124] and a pentalysine sequence representing a cytoplasmic translocation signal (CTS). This region is linked via a diglycine spacer arm to a C-terminal region (analytical arm) consisting of tyrosine and cysteine residues. (c) Ce6-loligomer. This construct represents a branched version of the Ce6-peptide with eight N-terminal branches linked to a lysine scaffold (BP). The construct incorporates a C-terminal analytical arm also containing a cysteine residue. Each N-terminal arm consists of a chlorin e_6 group, a NLS and a CTS sequence. The unique thiol side chain of the cysteine residue within the C-terminal region of each construct was derivatized with either Texas red, fluorescein or a biotin moiety.

cell viability was defined by the equation

$$[\text{Abs(drug/light)} - \text{Abs(no cells)}/\text{Abs(absence of drug/light)} - \text{Abs(no cells)} \times 100]$$

and represented the average of duplicate cell cultures within a group. Experiments were repeated at least three times. The morphological characteristics of healthy and apoptotic CHO cells were also discerned visually by light microscopy.

RESULTS

Design and Characterization of Chlorin e_6 Conjugates. Chlorin e_6 (Figure 1A) was initially coupled via solid-phase synthesis to a single arm peptide incorporating an homologue of the SV40 large T antigen nuclear localization sequence (NLS; A^{124}SV40LTa(124−135), Ala-Pro-Pro-Lys-Lys-Lys-Arg-Lys-Val-Glu-Asp-Pro) (*19*), a pentalysine cytoplasmic transport sequence (CTS) and a C-terminus analytical arm. Kalderon and co-workers (*19*) had defined residues 127−133 of the SV40 large T antigen as the minimal region responsible for the nuclear import of this protein. It was subsequently shown by one

of us (*20*) as well as others (*21)* that peptides containing the minimal sequences 126−135 or 126−132 could be coupled to carrier proteins and effectively routed to the nucleus of cells. The kinetics of nuclear import with the minimal length peptide 126−135 (*20*) have proven to be comparable to values observed with longer analogues of this NLS domain shown by Rihs and co-workers to cause a 2-fold improvement in nuclear uptake (*22*). Since the length of the NLS sequence incorporated into our peptide and loligomer designs represents an important issue in terms of the limitations of solid-phase peptide synthesis, it was decided that residues 125− 135 of the SV40 large T antigen would be introduced into our constructs. An alanine residue (position 124) was added at the N-terminus to avoid ending the peptide arms with a terminal proline imino group. Alanine was selected over the naturally occuring threonine residue since this latter residue is a site of phosphorylation known to modulate in the level of nuclear import (*23*). As for the cytoplasmic uptake of our constructs, it is well established that most eukaryotic cells tend to harbor a net negative charge on their surface and, as a result, will bind linear chains of polycationic amino acids such as poly(L-lysine). These cationic peptides are rapidly internalized by cells through a process termed adsorptive endocytosis and are able to enhance the cytoplasmic transport of macromolecules such as albumin and horseradish peroxidase (*24*−*27*). A pentalysine sequence (CTS) was thus introduced into each arm of our peptide vehicles as a strategy to have these constructs routed into cells. This design strategy has proven to be an effective approach to import loligomers into cells (*13*−*15*).

A schematic representation of the resulting chlorin e_6-peptide construct (Ce6-peptide) is shown in Figure 1B. The loligomer used in this study (Figure 1C; referred to as Ce6-loligomer) incorporates eight arms containing NLS and CTS domains. The arms are linked to a branched lysine structure using a peptide synthesis strategy developed by Tam (*28*). This branched peptide has been shown in the past to act as a nucleus-directed peptide shuttle (*13, 14*). Three variants of the Ce6-peptide and Ce6-loligomer were created by derivatizing the unique thiol group (cysteine side chain; C-terminus region) with either fluorescein (FL-5), Texas red, or a biotin group. Texas red was introduced for analyzing cellular uptake of constructs by confocal microscopy, while fluorescein derivatives were used for flow cytometry. The biotinylated constructs, Ce6-peptide-biotin and Ce6-loligomer-biotin, were designed for electron microscopic studies.

Intracellular Uptake of Chlorin e_6-Constructs into CHO and RIF-1 Cells. The time-dependent internalization of Ce6-peptide-FL5 and Ce6-loligomer-FL5 (0.01 μM) into CHO and RIF-1 cells at 37 °C is represented by the mean fluorescence intensity for a given cell population. Ce6-peptide-FL5 and Ce6-loligomer-FL5 were initially associated with the cell surface and subsequently internalized at similar rates by both cell lines (Figure 2). The mean fluorescence signal associated with Ce6-peptide-FL5 and Ce6-loligomer-FL5 gradually increases as a function of time reaching a plateau after 6 h. Flow cytometric histograms depicting cell number as a function of fluorescence intensity reveal that all cells show an increase in fluorescence intensity over time (results not shown; see Figure 3), suggesting that the entire cell population is targeted by the constructs.

Visualization of Chlorin e_6-Construct Internalization and Intracellular Distribution. The uptake and distribution of Ce6-loligomer-FL5 into RIF-1 and

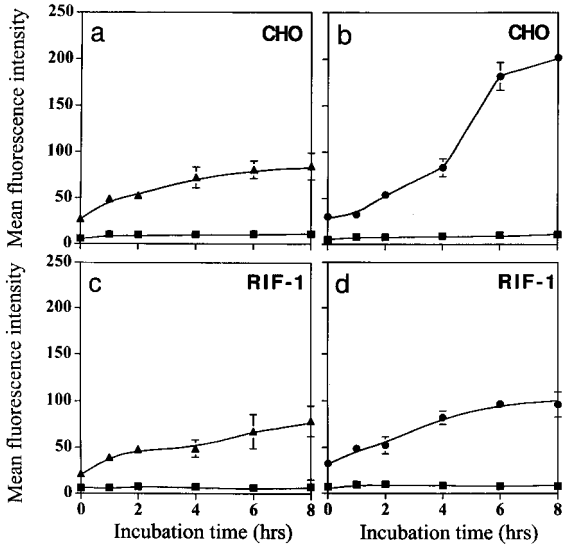


Figure 2. Uptake of chlorin e_6-constructs by CHO cells (panels a and b) and RIF-1 cells (panels c and d) as a function of time. Cells suspensions maintained at 37 °C were exposed to a 0.01 μM solution of either Ce6-peptide-FL5 (▲) or Ce6-loligomer-FL5 (●). Mean fluorescence intensities were recorded by flow cytometry over a period of 8 h. The autofluorescence of cells (■) which had not been exposed to a construct were also analyzed for each experiment.

CHO cell lines was monitored as a function of time by confocal microscopy (Figure 3). The emission fluorescence of conjugated chlorin e_6 was visualized directly (red fluorescence) and shown to colocalize with the fluorescein label attached to the C-terminal arm of the loligomer (green fluorescence). The combination of phase contrast and fluorescence images suggests that all cells import the chlorin e_6 construct, a result confirmed by flow cytometric analyses (not shown). After a 1 h incubation period, Ce6-loligomer-FL5 was mainly localized to the cytoplasm of RIF-1 or CHO cells, with only a small amount observed in the nucleus (Figure 3 panels A and D). By 6 h, the Ce6-loligomer-FL5 construct was clearly visible within the nucleus of RIF-1 and CHO cells (Figure 3, panels B and E) and was still observed at 24 h (Figure 3, panels C and F).

The migration of Ce6-peptide-biotin and Ce6-loligomer-biotin into RIF-1 cells was analyzed by electron microscopy using streptavidin-conjugated gold particles (see Figure 4). Micrographs revealed that while both constructs were initially internalized into RIF-1 cells within endocytic vesicles, their subsequent patterns of cellular distribution clearly differ. Vesicular compartments were saturated with Ce6-peptide-biotin after 1 h of exposing cells to the construct (Figure 4a). At 6 h, Ce6-peptide-biotin remained primarily confined to these vesicles with some of the construct reaching the cytosol (Figure 4c, see arrows). A small fraction of the Ce6-peptide-biotin population was also seen in the nucleus of cells by 24 h (results not shown). In contrast, Ce6-loligomer-biotin accumulates in the nucleus of RIF-1 cells within 6 h of exposure (Figure 4d). In the case of both chlorin e_6 constructs, peptide-loaded vesicles accumulated at the perimeter of the nucleus by 24 h (not shown). Electron microscopy allowed the events leading to cellular uptake to be visualized where small aggregates of Ce6-loligomer-biotin became enveloped by invaginations in the plasma membrane (Figure 5a; see arrow) and vesicles formed within 1 h of being exposed to the construct (Figure 5b). Endocytic vesicles were evident throughout the cytoplasm of cells at differing distances from the nucleus (Figure

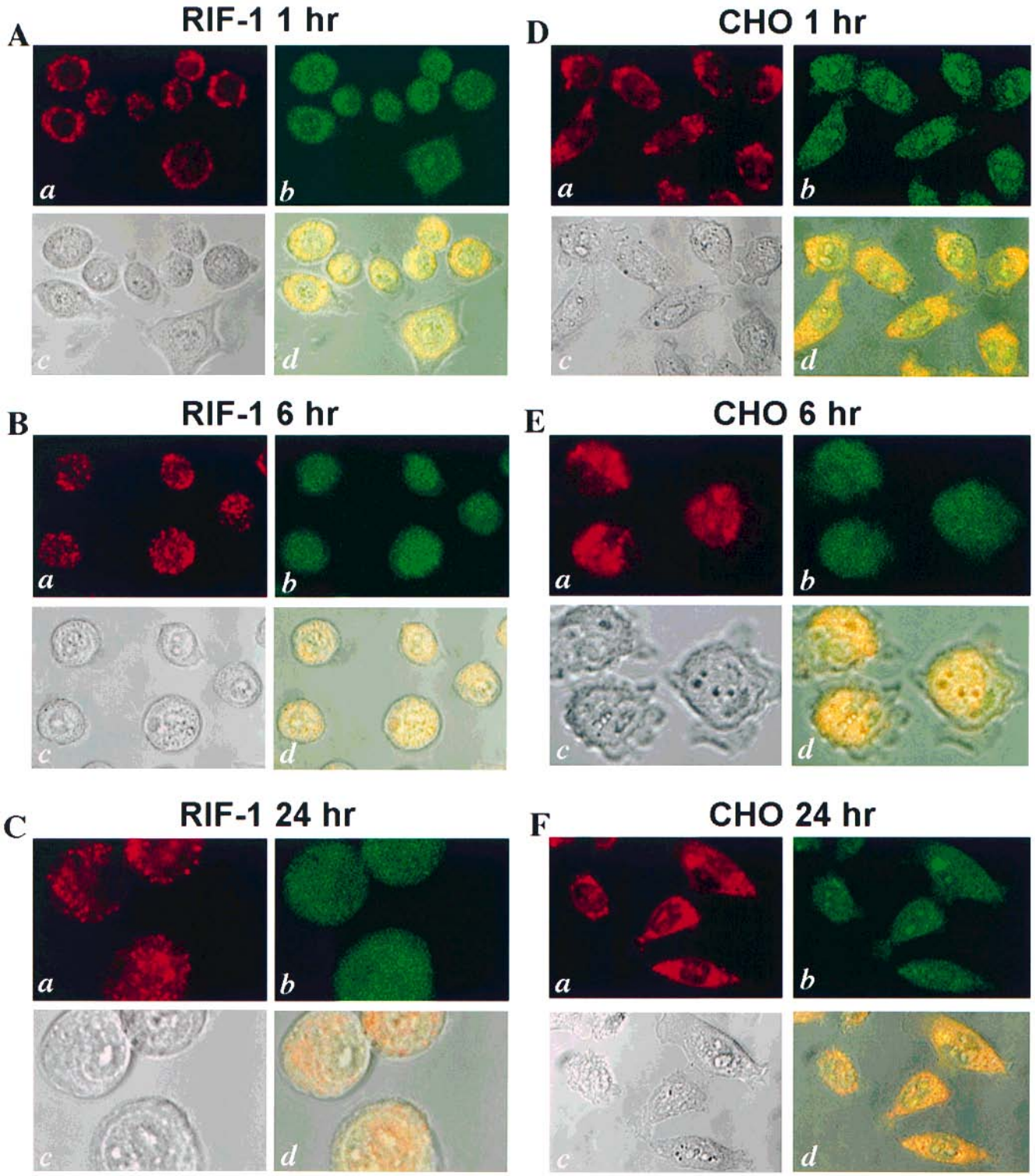


Figure 3. Confocal images of Ce6-loligomer-FL5 (0.01 μM) inside RIF-1 or CHO cells recorded after 1 h (panels A and D), 6 h (panels B and E), or 24 h (panels C and F) of exposure to the construct. Images of fluorescence signals in RIF-1 cells from chlorin e_6 (images labeled *a*) and fluorescein-labeled loligomer (images labeled *b*) indicate that all cells (as shown in the matched phase contrast images labeled *c*) import the construct. Composite images of both fluorescence signals and phase contrast images are presented in panels labeled *d*. The yellow fluorescence in these images emphasizes the comigration of chlorin e_6 (red fluorescence) linked to the loligomer (green fluorescence) over a period of 24 h.

5c). Constructs appear to be released from their endocytic compartments prior to nuclear uptake. A number of steps which characterize the endocytic pathway are shown in Figure 5d. Quantitative analysis of gold particle accumulation provided an estimate of the distribution of each construct within RIF-1 cells. The quantity of gold particles within an individual cell exposed to Ce6-loligomer-biotin or Ce6-peptide-biotin for 1 or 6 h was calculated in terms of gold particles present per square micron (μm^2) unit area (Table 1). Similar analyses were also conducted for cells which had not been exposed to the constructs. Background levels of gold particle accumulation never exceeded 5% of the values obtained for treated cells (data not shown). In RIF-1 cells, Ce6-

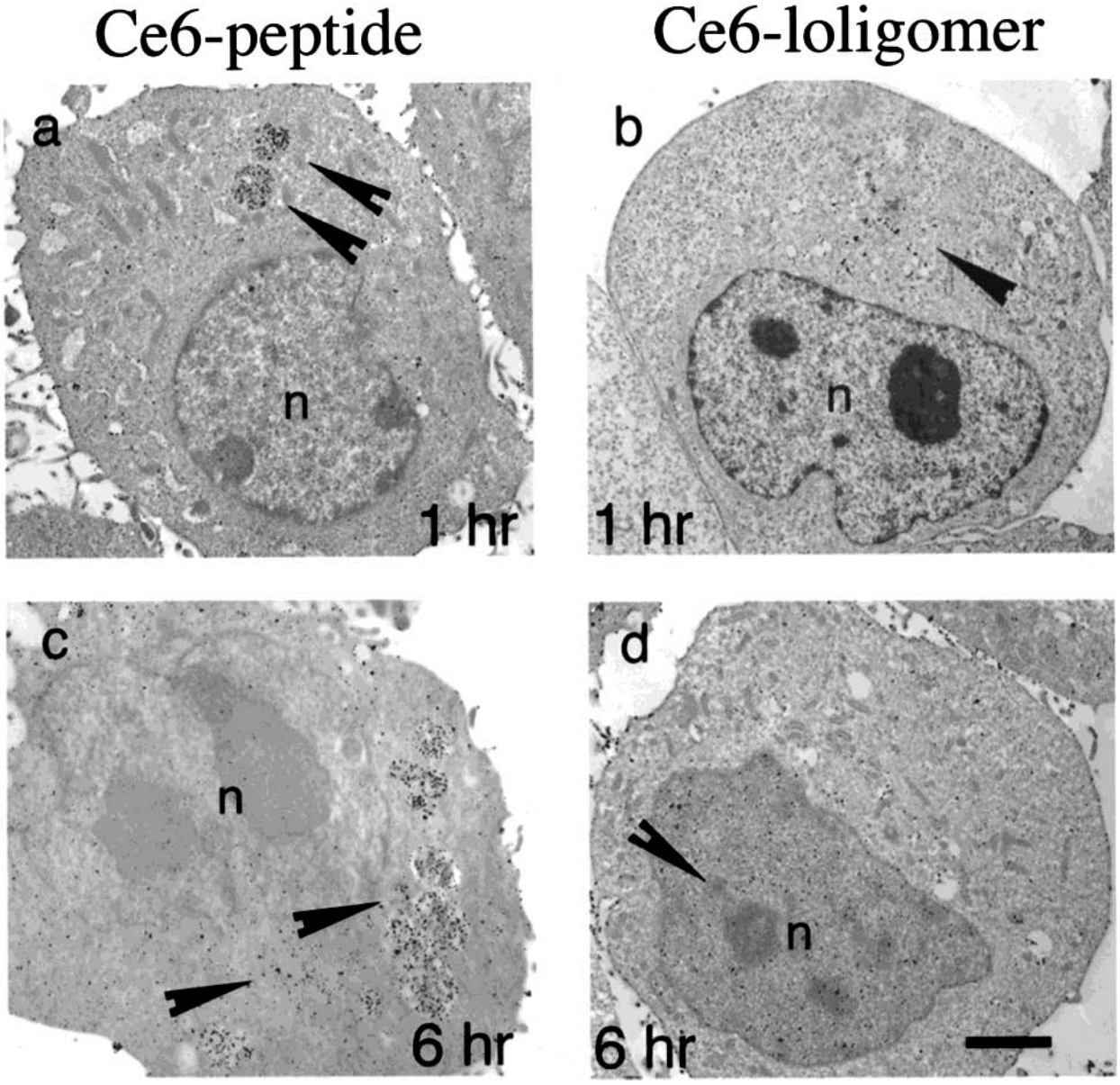


Figure 4. Electron micrographs showing the distribution of Ce6-peptide-biotin (0.1 μM) or Ce6-loligomer-biotin (0.1 μM) inside RIF-1 cells after 1 h (panels a and b) or 6 h (panels c and d) of exposure to either construct. Vesicular compartments containing the construct can be observed within the cytosol of cells by 1 h (panel a; see arrows). By 6 h, Ce6-peptide-biotin is still largely confined to vesicules (panel c), while Ce6-loligomer-biotin accumulates within the nucleus (panel d; see arrow). Scale bar represents 6 μm.

loligomer-biotin accumulated within the nucleus to a greater extent (1.5 times; 19.2 ± 1.9 particles/μm^2) after a 1 h incubation period than Ce6-peptide-biotin (12.4 ± 2.2 particles/μm^2). This difference is further augmented after 6 h where the extent of nuclear uptake by Ce6-loligomer-biotin was >3-fold (3.3 times; 49.9 ± 12.1 particles/μm^2) higher than the level of Ce6-peptide-biotin (15.3 ± 5.4 particles/μm^2). In contrast, the amount of Ce6-loligomer-biotin in the cytoplasm of RIF-1 cells after 1 and 6 h incubations was 0.5 (12.8 ± 1.9 vs 27.9 ± 9.3 particles/μm^2) and 0.7 (46.1 ± 16.4 vs 34.3 ± 4.9particles/μm^2) times that of Ce6-peptide-biotin, respectively. Analysis for individual cells demonstrated that after an incubation period of 1 or 6 h, Ce6-peptide-biotin preferentially localized within the cytoplasm of RIF-1 cells with less than half of the total amount of biotinylated peptide within the cell being present in the nucleus (0.4, 12.4 ± 2.2 vs 27.9 ± 9.3 particles/μm^2, and 0.3, 15.3 ± 5.4 vs 46.1 ± 16.4 particles/μm^2, respectively). Meanwhile, the amount of Ce6-loligomer-biotin within the nucleus of RIF-1 cells was 1.5 times (19.2 ± 1.9 vs 12.8 ± 1.9 particles/μm^2) and 1.4 times (49.9 ± 12.1 vs 34.3 ± 4.9 particles/μm^2) the amount in the cytoplasm after a 1 or 6 h incubation, respectively. These results confirm the enhanced nuclear localization properties of Ce6-loligomer-biotin compared with Ce6-peptide-biotin.

Photodynamic Action of Nucleus-Targeted Chlorin e_6-Peptide Constructs. The viability of CHO and RIF-1 cells was determined as a function of exposure to increasing concentrations of chlorin e_6 or the two peptide constructs using an established cell viability assay (WST-1 tetrazolium salt assay). Dose response curves (Figure 6) indicate that both constructs were moderately cytotoxic toward CHO and RIF-1 cells in the absence of photoirradiation (Figure 6, panels a and b). CD_{50} values determined for chlorin e_6 and the related peptide conjugates following photoirradiation (Figure 6, panels c and d), revealed that the photodynamic activity of Ce6-loligomer against CHO cells (CD_{50}; 20 nM) was 400 times higher than that of chlorin e_6 alone (CD_{50}; 8 μM), whereas the activity of Ce6-peptide (CD_{50}; 200 nM) was 40 times that of chlorin e_6. The photodynamic activity of Ce6-

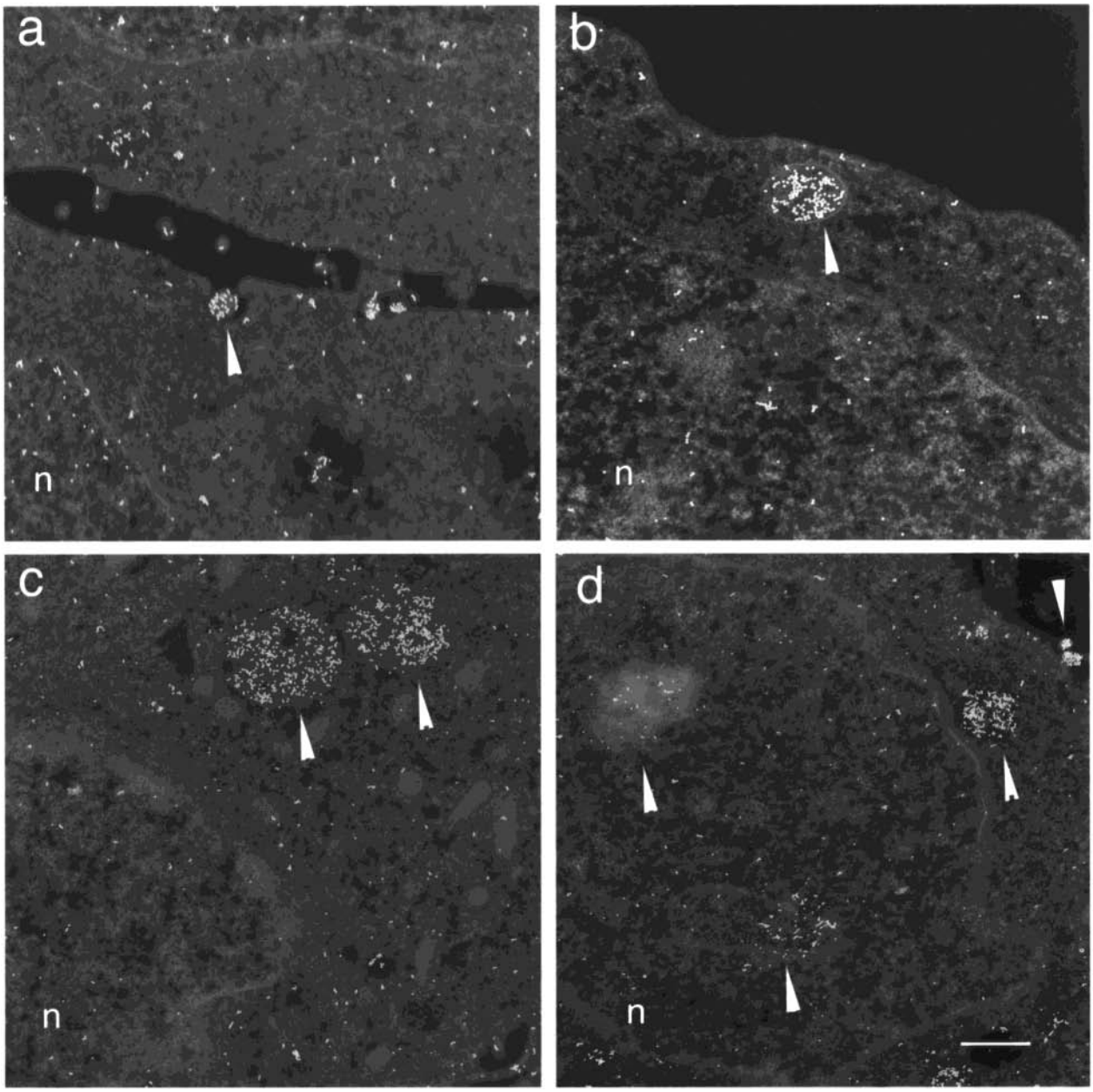


Figure 5. Electron micrographs (negative prints) detailing the endocytic uptake and migration of Ce6-loligomer-biotin (0.1 μM) in RIF-1 cells. The loligomer construct was initially internalized through the plasma membrane by absorptive endocytosis (panel a; arrow) and subsequently encapsulated within a membrane-bound endocytic vesicle (panel b). Within 1 h of exposure to Ce6-loligomer-biotin, RIF-1 cells contained large cytoplasmic vesicles densely packed with gold particle-associated Ce6-loligomer-biotin (panel c). The construct accumulated within regions of the nucleus (n) after 6 h (panel d). Scale bar represents 0.88 μm (panels a and b), 0.94 μm (panel c) or 1.85 μm (panel d).

Table 1. Quantification of Gold Particles in Electron Micrographs of RIF-1 Cells Exposed to Biotinylated Ce6-Peptide and Ce6-Loligomer

peptide construct	biotinylated Ce6−peptide[a]		biotinylated Ce6-loligomer[a]	
time (h)	1	6	1	6
nucleus (N)	12.4 ± 2.2	15.3 ± 5.4	19.2 ± 1.9	49.9 ± 12.1
cytoplasm (C)	27.9 ± 9.3	46.1 ± 16.4	12.8 ± 1.9	34.3 ± 4.9
total cellular uptake ($N + C$)	40.4 ± 11.5	61.4 ± 21.8	32 ± 3.8	84.2 ± 17
N/C ratio	0.4	0.3	1.5	1.4

[a] Biotinylated peptide constructs were labeled with streptavidin-conjugated gold particles. Values are expressed as the number of gold particles per square micron area (μm^2) of cell.

loligomer against RIF-1 cells (CD_{50}; 1.6 μM) was less than that for CHO cells although significantly enhanced (~40-fold) in relation to chlorin e_6 (CD_{50}; 63 μM). The phototoxicity of Ce6-peptide toward RIF-1 cells (CD_{50}; 6.3 μM) as in the case of CHO cells, was less than the effects of Ce6-loligomer and showed a 10-fold killing enhancement relative to chlorin e_6. The enhanced phototoxicity of our Ce6 peptide conjugates thus depends in part on the nature of the cell line targeted.

Generation of Reactive Oxygen Species within the Nucleus of RIF-1 Cells by Chlorin e_6-Loligomer Construct. To establish the precise subcellular sites of photoactivation/photooxidation of chlorin e_6 and to confirm that the conjugation of chlorin e_6 to the loligomer did not interfere with its activity, RIF-1 cells which had previously been treated with Ce6-loligomer-TxRd (0.01 μM) for 6 h were subsequently treated with CM-H_2 DFDA (5 μM). CM-H_2 DFDA passively diffuses into cells, where the acetates are cleaved by intracellular esterases to form reduced 2′,7′-dichlorofluorescin. The subsequent produc-

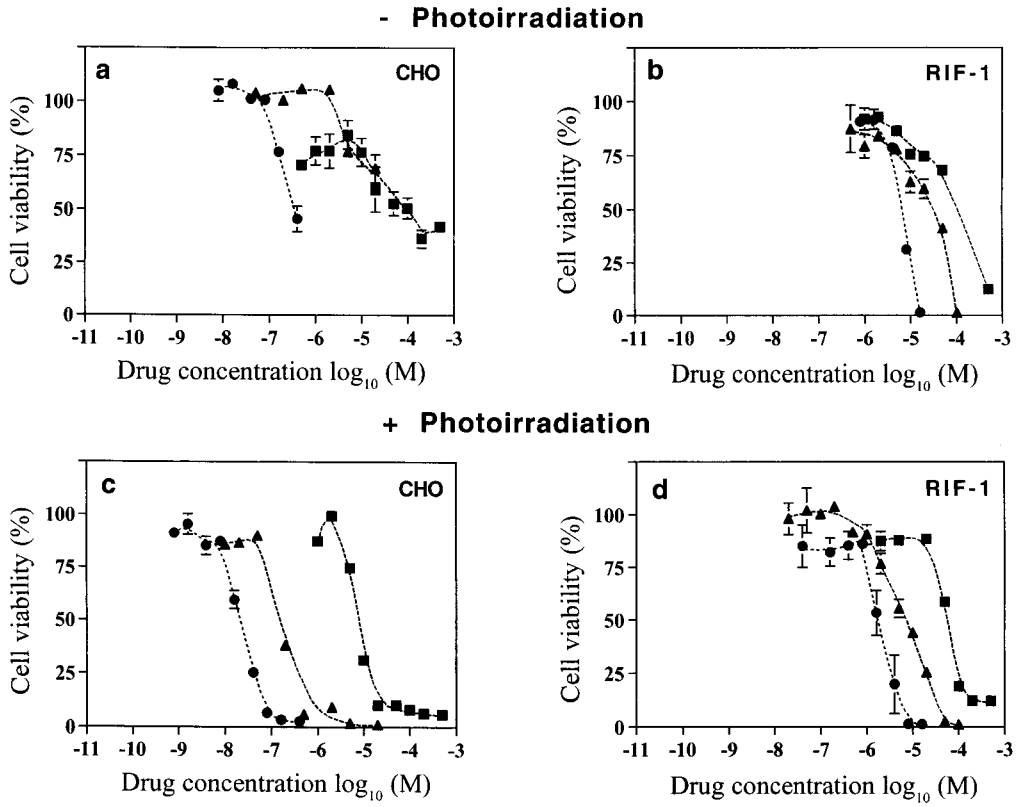


Figure 6. Cell viability curves for CHO and RIF-1 cells incubated (6 h) in the presence of increasing concentrations of chlorin e_6 (■), Ce6-peptide (▲), or Ce6-loligomer (●). Cell viability was determined for cells exposed (+) or not (−) to photoirradiation. Cell viability was reported as the percentage of surviving cells measured using the WST-1 assay (ref *17*; see Materials and Methods). The term drug concentration represents the molar concentration of chlorin e_6 either free or attached to the peptide constructs.

tion of active oxygen species induced by photoirradiation oxidizes 2′,7′-dichlorofluorescin to a highly fluorescent product, dichlorofluorescein (*28*). The thiol-reactive chloromethyl groups of CM-H_2 DFDA potentially interact with intracellular thiols to form adducts that prolong its retention within cells. This event allows the observation of reactive oxygen for several seconds after chlorin e_6 activation (Figure 7). Cells were either treated in the presence (Figure 7f) or absence (Figure 7b) of AcrO (5 μM) to indicate the position of the cell nucleus. The fluorescent signal generated by Ce6-loligomer-TxRd was recorded prior to the activation of chlorin e_6 (Figure 7, panels a and e) as well as after chlorin e_6 activation (Figure 7, panels c and g). CM-H_2 DFDA-associated fluorescence was undetectable prior to the activation of chlorin e_6 (Figure 7, panels b and f). Photoirradiation of the cells and the subsequent activation of intracellular chlorin e_6 resulted in a delay of ∼10−20 s before the generation of reactive oxygen species within RIF-1 cells, an event that was confirmed by a strong fluorescence burst which persisted for 1−2 min. The release of reactive oxygen species colocalizes exactly with the site of Ce6-loligomer accumulation (see Figure 7, panels a and d, or Figure 7, panels e and h). AcrO staining provided evidence of its release in the nucleus of these cells (see Figure 7, panels f and h).

DISCUSSION

Photodynamic therapy has emerged within the past decade as a promising treatment modality for certain malignancies, offering the possibility of guided therapies which restrict phototoxicity to the tumor site. PDT is currently used in the treatment of early and late stage cancers including bladder, esophageal, lung, gastric, and cervical cancers and is either in use or being evaluated in clinical trials for early stage oesophageal and lung cancer (*30*). The phototoxicity of photosensitizers is associated with the production of singlet oxygen species ($^1O_2$), which has a lifetime of several microseconds in aqueous environments and a limited cellular diffusion [∼20 nm (*31*, *32*)]. The sphere of influence of $^1O_2$ is thus very small, and only intracellular regions with both a high $^1O_2$ concentration and a high photosensitizer concentration are susceptible to photooxidative damage. Therefore, the location of the photosensitizer within cells governs the areas subjected to its photodynamic action. Potential targets of $^1O_2$-mediated toxicity include cellular membranes which may undergo lipid peroxidation, protein cross-linking and loss of ionic homeostasis (*33*), lysosomes which can release acidic hydrolases into the cytosol (*34*), mitochondria as well as the endoplasmic reticulum (*35*).$^1O_2$ is also known to cause single-strand breaks and alkali-labile lesions in DNA (*36*) as well as inactivate enzymes involved in DNA repair (*37*). Consequently, the nucleus represents an attractive target for photooxidative damage. Unfortunately, photosensitizers tend to accumulate to the perinuclear region of the cell cytoplasm. As a result, DNA is not usually subjected to photoinduced toxicity. The realization that certain sites within a cell display enhanced sensitivity to photooxidative damage justifies the design of delivery strategies which target photosensitizers to these sensitive sites. One strategy would be to use intracellular vehicles such as linear and branched peptides (*13*−*15*) to shuttle photosensitizers to specific cellular loci. The results of this study demonstrate that peptide constructs can be used to traffic the photodynamic drug chlorin e_6 to the nucleus of cells and, in doing so, can potentiate its cytotoxicity.

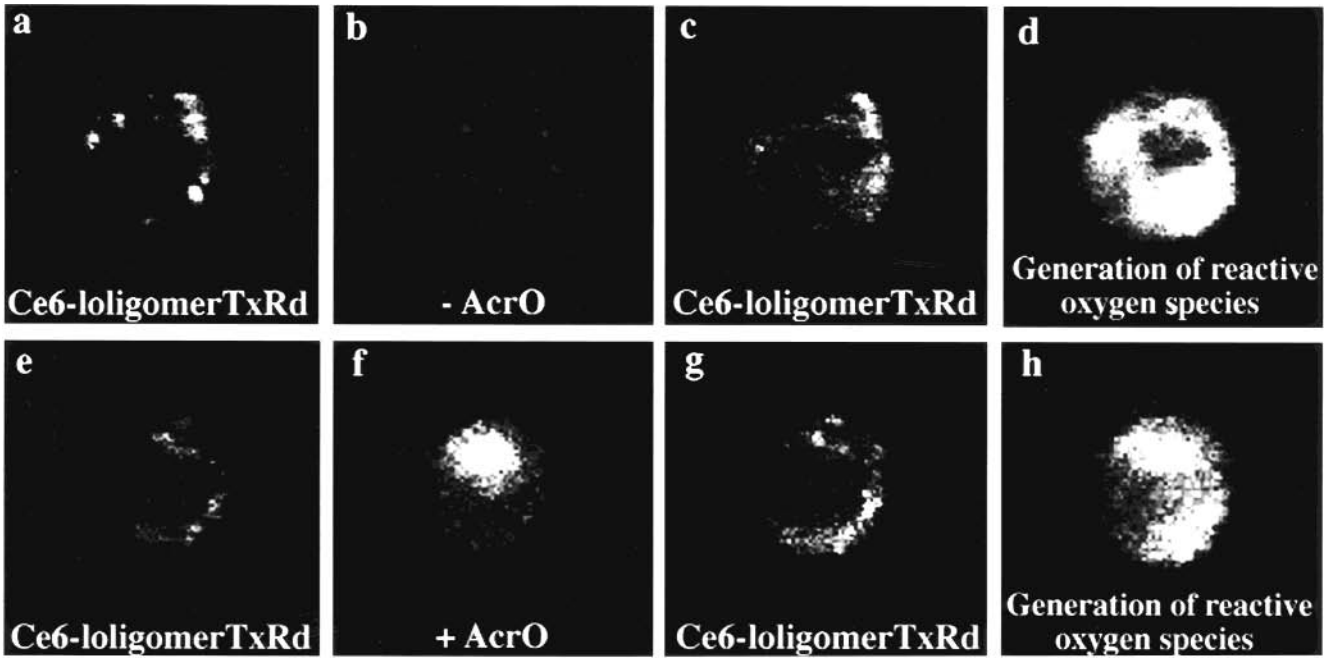


Figure 7. Light activation of chlorin e_6 in RIF-1 cells as monitored by fluorescence microscopy. Photoinduced generation of reactive oxygen species within two individual RIF-1 cells (cell 1, panels a−d; cell 2, panels e−h) following their treatment with Ce6-loligomer-TxRd for 6 h. Panels a, b, e, and f depict fluorescence images recorded prior to light exposure and panels c, d, g, and h are images taken following light activation. Cell 2 was stained with AcrO to identify areas within the cell containing DNA (panel f). CM-H_2-DCFDA was used to visualize the generation of reactive oxygen species in cells following the activation of chlorin e_6 (panels d and h). The fluorescent signal of CM-H_2DCFDA colocalizes with the signal of Ce6-loligomer-TxRd in both cells.

Chlorin e_6 was coupled to either a nucleus-directed loligomer (Ce6-loligomer; Figure 1C) or a peptide corresponding to one arm of this construct (Ce6-peptide; Figure 1B) in an effort to guide the intracellular uptake and nucleus routing of this photosensitizer. The endocytosis and subsequent localization of these constructs within cell nuclei could be visualized using fluorescently tagged constructs with confocal microscopy and by following the migration of biotinylated constructs inside cells using electron microscopy. The time course and extent of intracellular accumulation of fluorescently tagged constructs were also assessed by flow cytometry. Cellular uptake studies were conducted with CHO and RIF-1 cells maintained in suspension.

Loligomers have been shown in the past to be internalized rapidly into eukaryotic cells by absorptive endocytosis, with their maximal uptake occurring between 6 and 8 h of incubation (*13, 14*). In contrast, unconjugated chlorin e_6 is taken up by passive membrane diffusion (*38, 39*). The interaction between photosensitizers and cells is ultimately governed by their chemical properties. Negatively charged hydrophobic photosensitizers such as chlorin e_6 tend to concentrate at the surface of membranes with minimal electrostatic drive to actually traverse them (*7*). In contrast, cationic dyes such as rhodamines and kryptocyanines, are subject to electrochemical gradients which promote their interaction with anionic sites and subsequent translocation across cellular membranes, in particular, across mitochondrial membranes (*40*). Ce6-loligomer and Ce6-peptide were rapidly imported inside CHO cells (Figures 2 and 3). Furthermore, Ce6-peptide uptake into CHO cells was considerably greater than the level of import previously observed for a similar linear peptide which lacked chlorin e_6 (*13*), suggesting a role for the porphyrin group in promoting the internalization of the construct. Another factor which may influence intracellular uptake is the net negative charge of the cell membrane which varies depending on cell type and cell function (*41*).

All cells (CHO and RIF-1) were targeted by the constructs as confirmed by flow cytometry (results not shown) and by confocal microscopy (Figure 3). However, the distribution of biotinylated constructs inside cells as revealed by electron microscopy indicate that nuclear uptake is only significant for the Ce6-loligomer constructs (Figure 4, panels c and d). Electron microscopy also provided evidence suggesting that biotinylated variants of both peptide (Figure 4, panels a and c) and loligomer (Figure 4, panels b and d) constructs enter the cytosol of target cells in a similar fashion. To reach the cell nucleus, these constructs must first escape their vesicular compartments with their NLS sequences still intact (*13−15*). The precise mechanism underlying this translocation event of constructs across endosomal membranes is presently unknown. Zauner et al. (*42*) suggested that polylysine may under certain circumstances promote lysis of internal vesicles. The distribution of biotinylated Ce6-peptide and Ce6-loligomer constructs inside cells was monitored with colloidal gold particles conjugated to steptavidin. The constructs were released from endocytic vesicles into the cytoplasm and subsequently routed to the nucleus (Figure 5). Dual labeling of loligomers with distinct fluorochromes attached to the N-terminus and C-terminus arms have indicated that both probes remain at least partly associated following their release from vesicular compartments (Sheldon and Gariépy, unpublished results) and that 80% of the intracellular pool of loligomer is retained within CHO cells (*14*). These results suggest that the degradation of signals on loligomers is not extensive within the time scale of our measurements (hours) and that cycling of such constructs back to the cell surface does not represent a dominant cellular pathway. This result was confirmed in the present study where the fluorescence signal associated with both chlorin e_6 linked to the N-terminus and a fluorescein label attached to the C-terminal end of Ce6-loligomer-FL5 were shown to co-localize in cells over a period of at least 24 h (Figure 3). The branching design of loligomers with

multiple SV40 NLS sequences was also shown to enhance nuclear localization (ref *13*; see also Figures 3−5 and Table 1). The quantitation of gold particles present in the cytosol and nucleus of RIF-1 cells indicated that the amount of Ce6-loligomer in their nuclei at 6 h was more than three times that of Ce6-peptide (Table 1). Once inside the nucleus, biotinylated loligomer constructs appear to localize in areas of high DNA content. It has previously been documented that cationic photosensitizers (e.g., methylene blue) have a greater affinity for nucleic acid interactions compared with noncationic photosensitizers (*43*).

The incorporation of eight chlorin e_6 molecules into a single loligomer construct (Ce6-loligomer) was found to enhance its toxicity by 400-fold in CHO cells and by 40-fold in RIF-1 cells when compared on a mole-to-mole basis with chlorin e_6 alone (Figure 6). Similarly, the phototoxicity of the single arm construct Ce6-peptide, although modest in relation to Ce6-loligomer, was greater than the toxicity level observed for chlorin e_6. A comparison of CD_{50} values for Ce6-loligomer with values obtained for loligomer without the photosensitizer (*14*) reveals a shift in CD_{50} values of almost 4 log units. These results point out that the level of enhanced phototoxicity observed using our chlorin e_6-containing peptide constructs is dependent on the cell line targeted. The present study supports results published recently by Akhlynina et al. (*11*) describing the construction and delivery of macromolecular conjugates composed of insulin, chlorin e_6, and NLS peptides chemically cross-linked to bovine serum albumin into cells. The insulin-containing BSA constructs were shown to enhance the photodynamic activity of chlorin e_6 by >2000-fold. A comparison of the levels of enhancement in phototoxicity observed between our compounds and these BSA conjugates is difficult to establish since the basal toxicity of the insulin-containing BSA constructs in the absence of photoirradiation was not reported and the cell lines tested by Akhlynina's group were different from the ones used in our studies. The BSA conjugates incorporating insulin do target the insulin receptor and as such may represent constructs affording a more guided delivery. However, this past study did not provide phototoxicity data of these constructs toward a control cell line that did not express the insulin receptor. Akhlynina et al. (*11*) suggested that the enhanced PDT activity of their constructs could be partly linked to the number of NLS peptides attached to the conjugates, rather than the number of chlorin e_6 molecules. In the present study, the introduction of multiple NLS sequences in the structure of Ce6-loligomer also resulted in the enhanced nuclear localization potential and cytotoxicity profile of this construct in relation to Ce6-peptide. From the perspective of designing intracellular vehicles, the simplicity and directed assembly of Ce6-peptide and Ce6-loligomer can be contrasted with the preparation of the reported BSA conjugates (*11*). More precisely, the average ratio of components in these BSA conjugates had to be inferred from molecular weight estimates derived from polyacrylamide gel electrophoresis and optical density measurements of chlorin e_6. The present study demonstrates that peptide-based vehicles such as Ce6-peptide and Ce6-loligomer represent simple and easily constructed synthetic assemblies able to deliver PDT agents into specific areas of a cell which display heightened photosensitivity in order to improve the photodynamic efficiency of these agents.

The mechanism of Ce6-loligomer-mediated toxicity was shown to involve the generation of reactive oxygen species, confirming that the activation of chlorin e_6 is not hindered upon its attachment to the loligomer (Figure 7). Although it was demonstrated that Ce6-loligomer reaches the cytosol and accumulates in the nucleus of CHO and RIF-1 cells (Figures 3−5 and Table 1), it remains unclear if the enhanced phototoxicity observed is predominantly due to singlet oxygen events occurring in the nucleus of cells as a result of nuclear localization or a simple consequence of the improved cellular uptake of chlorin e_6 when attached to this peptide construct. The sites of production of reactive singlet oxygen species as reported using CM-H2-DFDA (Figure 7) suggest a diffuse distribution of the reactive $^1O_2$ species throughout the cytosol and nucleus of RIF-1 cells. Preliminary results from flow cytometry studies also confirmed that PDT-induced cell death following treatment with uncoupled chlorin e_6 or related constructs occurred via an apoptotic pathway for CHO and RIF-1 cell lines (results not shown). Morphological signs of apoptotic cell death were apparent as cytoplasmic blebbing and shrunken nuclei.

In summary, the cytotoxicity of photosensitizers such as chlorin e_6, in the context of photodynamic therapy, is dependent on the intracellular localization of these agents. The incorporation of chlorin e_6 into peptide-based intracellular vehicles will dictate its toxicity. In particular, the routing of chlorin e_6 to the cytoplasm and nucleus of CHO and RIF-1 cells using intracellular peptide shuttles can alter its phototoxicity.

ACKNOWLEDGMENT

The authors thank Drs. Lothar Lilge and Eric LaCasse for their assistance with experimental apparatus and protocol, Battista Calvieri, Steven Doyle, and Trudy Franklin for their kind help with electron and confocal microscopy, Juliet Sheldon for her technical assistance in operating the flow cytometer and Jim Ferguson for synthesizing peptides. This work was supported by a grant from the National Cancer Institute of Canada with funds from the Canadian Cancer Society.

LITERATURE CITED

(1) Boyle, R. W., and Dolphin, D. (1996) Structure and biodistribution relationships of photodynamic sensitizers. *Photochem. Photobiol. 64*, 469−485.

(2) Bellnier, D. A., Ho, Y.-K., Pandey, R. K., Missert, J. R., and Dougherty, T. J. (1989) Distribution and elimination of Photofrin II in mice. *Photobiol. 50*, 221−228.

(3) Kostenich, G. A., Zhuravkin, I. N., Furmanchuk, A. V., and Zhavrid, E. A. (1991) Photodynamic therapy with chlorin e_6. A morphologic study of tumor damage efficiency in experiment. *J. Photochem. Photobiol., B 11*, 307−318.

(4) Kostenich, G. A., Zhuravkin, I. N., Furmanchuk, A. V., and Zhavrid, E. A. (1993) Sensitivity of different rat tumour strains to photodynamic treatment with chlorin e_6. *J. Photochem. Photobiol., B 17*, 187−194.

(5) Kostenich, G. A., Zhuravkin, I. N., and Zhavrid, E. A. (1994) Experimental grounds for using chlorin e_6 in the photodynamic therapy of malignant tumours. *J. Photochem. Photobiol., B 22*, 211−217.

(6) Henderson, B. W., and Dougherty, T. J. (1992) How does photodynamic therapy work? *J. Photochem. Photobiol. 55*, 145−157.

(7) Peng, Q., Moan, J., and Nesland, J. M. (1996) Correlation of subcellular and intratumoral photosensitizer localization with ultrastructural features after photodynamic therapy. *Ultrastruct. Pathol. 20*, 109−129.

(8) Bachor, R., Shea, C. R., Gillies, R., and Hasan, T. (1991) Photosensitized destruction of human bladder carcinoma cells treated with chlorin e_6-conjugated microspheres. *Proc. Natl. Acad. Sci. U.S.A 88*, 1580−1584.

(9) Akhlynina, T. V., Rosenkranz, A. A., Jans, D. A., Gulak, P. V., Serebryakova, N. V., and Sobolev, A. S. (1993) The use of

internalizable derivatives of chlorin e_6 for increasing its photosensitizing activity. *Photochem. Photobiol. 58*, 45−48.
(10) Akhlynina, T. V., Rosenkranz, A. A., Jans, D. A., and Sobolev, A. S. (1995) Insulin-mediated intracellular targeting enhances the photodynamic activity of chlorin e_6. *Cancer Res. 55*, 1014−1019.
(11) Akhlynina, T. V., Jans, D. A., Rosenkranz, A. A., Statsyuk, N. V., Balashova, I. Y., Toth, G., Pavo, I., Rubin, A. B., and Sobolev, A. S. (1997) Nuclear targeting of chlorin e_6 enhances its photosensitizing activity. *J. Biol. Chem. 272*, 20328−20331.
(12) Sobolev, A. S., Akhlynina, T. V., Yachmenev, S. V., Rosenkranz, A. A., and Severin, E. S. (1992) Internalizable insulin-BSA-chlorin e_6 conjugate is a more effective photosensitizer than chlorin e_6 alone. *Biochem. Int. 26*, 445−450.
(13) Sheldon, K., Liu, D., Ferguson, J., and Gariépy, J. (1995) Loligomers: Design of *de novo* peptide-based intracellular vehicles. *Proc. Natl. Acad. Sci. U.S.A 92*, 2056−2060.
(14) Singh, D., Kiarash R., Kawamura K., LaCasse E. C., and Gariépy J. (1998) Penetration and intracellular routing of nucleus-directed peptide-based shuttles (Loligomers) in eukaryotic cells. *Biochemistry 37*, 5798−5809.
(15) Singh, D., Bisland, S. K., Kawamura, K., and Gariépy, J. (1999) Peptide-based intracellular shuttle able to facilitate gene transfer in mammalian cells. *Bioconjugate Chem. 10*, 745−754.
(16) McBurney, M. W., and Whitmore, G. F. (1974) Isolation and biochemical characterization of folate deficient mutants of chinese hamster cells. *Cell 2*, 173−182.
(17) Schmid, I., Krall, W. A., Uittenbogaart, C. H., Braun, J., and Giorgi, J. V. (1992) Sensitive method for measuring apoptosis and cell surface phenotype in human thymocytes by flow cytometry. *Cytometry 13*, 204−208.
(18) Mosmann, T. J. (1983) Rapid colorimetric assay for cellular growth and survival: application to proliferation and cytotoxicity assays. *Immunol. Methods 65*, 55−63.
(19) Kalderon, D., Richardson, W. D., Markham, A. F., and Smith A. E. (1984) Sequence requirements for nuclear location of simian virus 40 large-T antigen. *Nature 311*, 33−38.
(20) Goldfarb, D., Gariépy, J., Schoolnik, G., and Kornberg, R. D. (1986) Synthetic peptides as nuclear localization signals. *Nature 322*, 641−644.
(21) Lanford, R. E., Kanda, P., and Kennedy, R. C. (1986) Induction of nuclear transport with a synthetic peptide homologous to the SV40 T antigen transport signal. *Cell 46*, 575−582.
(22) Rihs, H. P., Jans, D. A., Fan, H., and Peters, R. (1991) The rate of nuclear cytoplasmic protein transport is determined by the casein kinase II site flanking the nuclear localization sequence of the SV40 T-antigen. *EMBO J. 10*, 633−639.
(23) Jans, D. A., Ackermann, M. J., Bischoff, J. R., Beach, D. H., and Peters, R. (1991) p34cdc2-mediated phosphorylation at T124 inhibits nuclear import of SV-40 T antigen proteins. *J. Cell Biol. 115*, 1203−1212.
(24) Ryser, H. J.-P., and Shen, W. C. (1978) Conjugation of methotrexate to poly (L-lysine) increases drug transport and overcomes drug resistance in cultured cells. *Proc. Natl. Acad. Sci. U.S.A. 75*, 3867−3870.
(25) Shen, W.-C., and Ryser, H. J.-P. (1978) Conjugation of poly (L-lysine) to albumin and horseradish peroxidaase: a novel method of enhancing the cellular uptake of proteins. *Proc. Natl. Acad. Sci. U.S.A. 75*, 1872−1876.
(26) Shen, W. C., and Ryser, H. J.-P. (1979) Poly (L-lysine) and poly (D-lysine) conjugates of methotrexate: different inhibitory effect on drug resistant cells. *Mol. Pharmacol. 16*, 614−622.
(27) Arnold, L. J., Jr., Dagan, A., Gutheil, J., and Kaplan, N. O. (1979) Antineoplastic activity of poly (L-lysine) with some acsites tumor cells. *Proc. Natl. Acad. Sci. U.S.A. 76*, 3246−3250.
(28) Tam, J. P. (1988) Synthetic peptide vaccine design: synthesis and properties of a high-density multiple antigenic peptide system. *Proc. Natl. Acad. Sci. U.S.A. 85*, 5409−5413.
(29) Patel, A. K., Hallet, M. B., and Campbell, A. K. (1987) Threshold responses in production of reactive oxygen metabolites in individual neutrophils detected by flow cytometry and microfluorimetry. *Biochem. J. 248*, 173−180.
(30) Schuitmaker, J. J., Baas, P., van Leengoed, H. L. L. M., van der M., Star, W. M., and van Zandwijk, N. (1996) Photodynamic therapy: a promising new modality for the treatment of cancer. *J. Photochem. Photobiol., B 34*, 3−12.
(31) Moan, J. (1990) On the diffusion length of singlet oxygen in cells and tissue. *J. Photochem. Photobiol., B 6*, 343−344.
(32) Moan, J., and Berg, K. (1991) The photodegradation of porphyrins in cells can be used to estimate the lifetime of singlet oxygen. *Photochem. Photobiol. 53*, 549−553.
(33) Kessel, D. (1977) Effects of photoactivated porphyrins at the cell surface of L1210 cells. *Biochemistry 16*, 3443−3449.
(34) Jori, G., and Spikes, J. D. (1984) Photobiochemistry of porphyrins. In *Topics in Photomedicine* (K. C. Smith, Ed.) pp 183−318.
(35) Moan, J., Johannessen, J. V., Christensen, T., Espevik, T., and Mcghie, J. B. (1982) Porphyrin-sensitized photoactivation of human cells in vitro. *Am. J. Pathol. 109*, 184−192.
(36) Gomer, C. J. (1980) DNA damage and repair in CHO cells following hematoporphyrin photoradiation. *Cancer Lett. 11*, 161−167.
(37) Boegheim, J. P., Scholte, H., Dubbelman, T. M. A. R., Beems, E., Raap, A. K., and van Steveninck, J. (1987) Photodynamic effects of hematoporphyrin-derivative on enzyme activities of murine L929 fibroblasts. *J. Photochem. Photobiol. B. Biol. 1*, 61−73.
(38) Spikes, J. D. (1990) Chlorins as photosensitizers in biology and medicine. *J. Photochem. Photobiol., B 6*, 259−274.
(39) Schmidt-Erfurth, U., Diddens, H., Birngruber, R., and Hasan, T. (1997) Photodynamic targeting of human retinoblastoma cells using covalent low-density lipoprotein conjugates. *Br. J. Cancer 75*, 54−61.
(40) Oseroff, A. R., Ohuoha, D., Ara, G., McAuliffe, D., Foley, J., and Cincotta, L. (1986) Intramitochondrial dyes allow selective in vitro photolysis of carcinoma cells. *Proc. Natl. Acad. Sci. U.S.A 83*, 9729−9733.
(41) Bauer, J. (1987) Electrophoretic separation of cells. *J. Chromatogr. 418*, 359−383.
(42) Zauner, W., Kichler, A., Schmidt, W., Mechtler, K., and Wagner, E. (1997) Glycerol and polylysine synergize in their ability to rupture vesicular membranes: a mechanism for increased transferrin-polylysine-mediated gene transfer. *Exp. Cell Res. 232*, 137−145.
(43) Gomer, C. J., Rucker, N., Ferrario, A., and Wong, S. (1989) Properties and applications of photodynamic therapy. *Radiation Res. 120*, 1−18.

BC990020U

Polyelectrolyte Vectors for Gene Delivery: Influence of Cationic Polymer on Biophysical Properties of Complexes Formed with DNA

Margreet A. Wolfert, Philip R. Dash, Ola Nazarova,† David Oupicky,† Leonard W. Seymour,* Sarah Smart, Jiri Strohalm,† and Karel Ulbrich†

CRC Institute for Cancer Studies, University of Birmingham, B15 2TA, U.K., and Institute of Macromolecular Chemistry, Academy of Sciences of the Czech Republic, Prague 6, The Czech Republic. Received March 2, 1999; Revised Manuscript Received August 13, 1999

Cationic polymer/DNA complexes are widely used for gene delivery, although the influence of the cationic polymer on the biophysical properties of the resulting complex is poorly understood. Here, several series of cationic polymers have been used to evaluate the influence of structural parameters on properties of DNA complexes. Parameters studied included the length of side chain, charge type (primary versus tertiary and quaternary), polymer molecular weight, and charge spacing along the polymer backbone. Cationic polymers with short side chains (such as polyvinylamine) formed small complexes, resistant to destabilization by polyanions, with low surface charge, limited transfection activity, and efficient intranuclear transcription. Conversely, cationic polymers with long side chains (e.g., poly[methacryloyl-Gly-Gly-NH-$(CH_2)_6$-NH_2)] showed inefficient complex formation, high positive surface charge, and better transfection activity. The effects of molecular weight varied between polymers, for example, low molecular weight poly(L-lysine) produced relatively small complexes, whereas low molecular weight poly[2-(trimethylammonio)ethyl methacrylate chloride] produced large aggregates. Polymers containing quaternary ammonium groups showed efficient complex formation but poor transfection. Finally, spreading charges widely on the polymer structure inhibited their ability to condense DNA. In summary, to achieve small, stable complexes, the use of cationic polymers with short side chains bearing primary amino groups is suggested.

INTRODUCTION

The successful application of gene therapy can lead in principle to significant improvements in the treatment of several diseases (*1*). However, studies to date have highlighted the difficulty of achieving efficient transfection of target cells and tissues, both in vitro and in vivo. Indeed, inadequate transgene expression currently comprises a major factor limiting therapeutic application of sophisticated molecular treatment strategies (*2, 3*). Most existing gene delivery vectors are relatively inefficient when applied in vivo, requiring administration directly to the target tissue to attain useful levels of therapeutic gene expression (*4*). For useful deployment of gene therapy protocols, there is an urgent need for development of more efficient and biocompatible vectors (*5*). Ideally, these should ideally be capable of remote targeting and efficient transfection of specific cells and tissues following intravenous injection (*6*).

We are developing novel vectors for gene delivery based on self-assembly of DNA with synthetic polymers. Although the final vectors are expected to contain several functional groups, the core of the complex will be formed by binding and condensation of DNA expression plasmids by cationic polymers, producing discrete polyelectrolyte particles (*7, 8*). There are several biophysical requirements of such polyelectrolyte particles. Chief among these are requirements that the particles should be small, to facilitate good biodistribution and extravasation properties (*9*), and also be capable of undergoing efficient transcription following arrival in the nucleus of the target cell (*10*). In addition, resistance of complexes to destabilization by serum proteins is desirable, since there is increasing evidence that the rapid clearance of such polyelectrolyte complexes from the circulation follows their interaction with serum proteins (*11*).

The principles of particle formation following cooperative binding of polycations to DNA have been widely studied, although several details of the process remain to be elucidated (*12*−*16*). Most of the work performed so far on formation of interpolyelectrolyte complexes has made use of the simple cationic polymer poly(L-lysine) (pLL), and there has been very little systematic study of the influence of polycation structure on self-assembly with DNA and the properties of the resulting complexes.

In this study, we have examined a range of synthetic linear cationic polymers, selected to permit systematic evaluation of the influence of individual parameters on the biophysical properties of complexes formed by self-assembly with DNA. Specific molecular parameters selected for study are the distance of cationic charge from polymer backbone (length of side chain), order of cationic charge, influence of charge density along the polymer backbone, and polycation molecular weight. The ability of the cationic polymers to bind and condense DNA into particles has been assessed using gel electrophoresis and fluorescence inhibition assays. Physical properties of the particles formed have been characterized using atomic force microscopy (AFM)[1] and ζ-potential (a measurement of charge at the surface of the particle). Their stability has been assessed using a polyanion-disruption assay, and finally, their biological properties have been assessed

* To whom correspondence should be addressed at the University of Birmingham. Phone: 44-121-414-3289. Fax: 44-121-414-3263. E-mail: L.Seymour@bham.ac.uk.

† Institute of Macromolecular Chemistry.

10.1021/bc990025r CCC: $18.00 © 1999 American Chemical Society
Published on Web 10/23/1999

by monitoring transfection of cells in vitro and measuring transcriptional activity directly following microinjection into the nucleus of Xenopus oocytes. In this way, we aim to identify molecular parameters of cationic polymers influencing properties of the complexes formed with DNA, providing information that should allow us to begin the design and development of polyelectrolyte complexes with properties selected for specific applications.

EXPERIMENTAL PROCEDURES

DNA Purchase and Preparation. A circular 6 kb expression vector containing a CMV promoter-driven β-galactosidase reporter and ampicillin resistance was used for the atomic force microscopy, electrophoresis, and all studies of biological properties. This was prepared by growth in *Escherichia coli* DH5α and purified by standard technology. Following the final ethanol precipitation, the purity of the DNA was checked by agarose gel electrophoresis. The ethidium bromide fluorescence quenching and ζ-potential assays were performed using calf thymus DNA (Sigma Chemical Co.), with average molecular size determined to be 8 kb. For calculation of the N-to-P ratio of polyelectrolyte complexes, a mass per charge of 325 Da was used for DNA.

Cationic Polymers Studied. The polymers described below were purchased or synthesized for systematic examination of the influence of individual parameters on the properties of complexes formed by self-assembly with DNA. Chemical structures of all cationic polymers examined are shown in Figure 1.

(1) Influence of Length of Side Chain Bearing Cationic Residue. Several poly-(methacrylate)-based homopolymers with differing side chains bearing primary amino groups were synthesized as described below. These were poly[methacryloyl-Gly-Gly-NH-$(CH_2)_6$-NH_2] hydrochloride (pMADGHDA.HCl), mass per primary amino group, 334.6 Da; poly[methacryloyl-Gly-NH-$(CH_2)_2$-NH_2] hydrochloride (pMAGEDA.HCl), mass per primary amino group, 221.6 Da, and poly[methacryloyl-NH-$(CH_2)_2$-NH_2] hydrochloride (pMAEDA.HCl), mass per primary amino group, 164.5 Da, together with poly(L-lysine) hydrobromide (pLL.HBr), mass per primary amino group, 209 Da; poly(allylamine) hydrochloride (pAA.HCl), mass per primary amino group, 57 Da; and poly(vinylamine) hydrochloride (pVA.HCl), mass per primary amino group, 79 Da. They were allowed to form complexes with DNA, using cationic polymer preparations of roughly similar molecular weight distribution in each case, and properties of the resulting complexes were determined and compared as described below.

(2) Primary, Tertiary, and Quaternary Amino Groups. The influence of order of cationic charge on the properties of complexes formed with DNA was examined. The tertiary amino group-containing polymer poly(2-dimethylaminoethyl methacrylamide) (in free base form, pDMAEMam, mass per amino group 157 Da) was synthesized and properties of its DNA complexes were compared with those of the quaternized ester poly[2-(trimethylammonio)ethyl methacrylate chloride] (pTMAEM.Cl, mass per charge 208 Da) and also with those formed by polymers bearing primary amino groups, mentioned above.

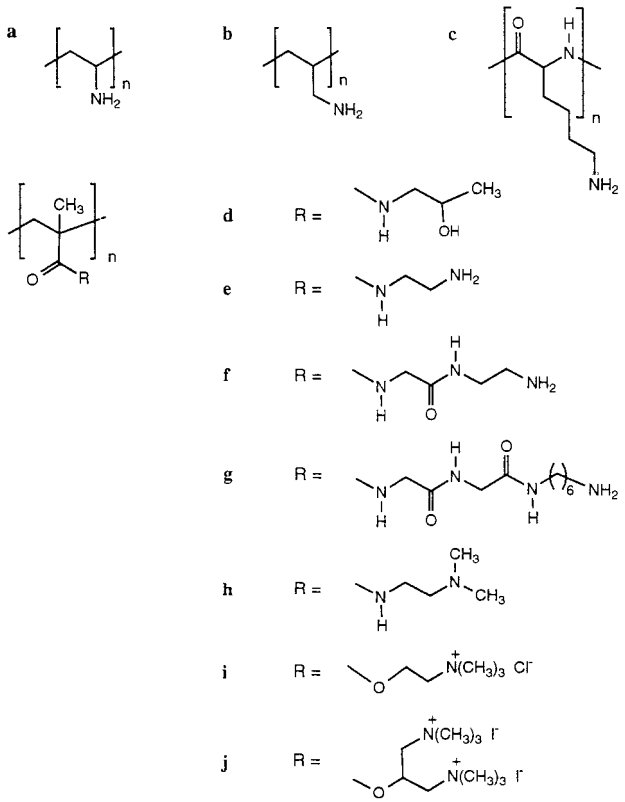


Figure 1. Structure of synthetic polymers used in this study. For simplicity, primary cationic monomers are shown as free bases. Panels a–c represent simple monomers as follows: a, pVA; b, pAA; c, pLL. Panels d–j show the side chains based on the methacrylate backbone shown, as follows: d, pHPMA; e, pMAEDA; f, pMAGEDA; g, pMADGHDA; h, pDMAEMam; i, pTMAEM.Cl; j, pBTMAIP.I_2. Systematic names, together with full details of molecular weight averages, counterions, etc., are given in the text.

(3) Influence of Charge Spacing along the Polymer Chain. Charge spacing was varied by synthesising statistical copolymers containing *N*-(2-hydroxypropyl)-methacrylamide (HPMA) and 2-(trimethylammonio)ethyl methacrylate chloride (TMAEM.Cl), with TMAEM.Cl present at monomer ratios of 5, 15, 50, 75, and 100 mol %, masses per charge 2925, 1019, 351, 255, and 208 Da, respectively. In addition, poly[1,3-bis-(trimethylammonio)isopropyl methacrylate iodide] (pBTMAIPM.I_2), which bears two cationic groups per monomer, was examined. It had a mass per charge of 249 Da.

(4) Influence of Molecular Weight or Degree of Polymerization. Several families of polymers were compared to evaluate the influence of molecular weight on properties of complexes formed with DNA. pLL.HBr was purchased with weight average molecular masses, 4, 10, 24, 54, and 224 kDa (manufacturer's specifications). Several polymers were synthesized (described below), including pTMAEM.Cl, weight average molecular masses, 5, 8, 21, 34, and 413 kDa; pMADGHDA.HCl, weight average molecular masses, 38, 74, and 330 kDa; pMAGEDA.HCl, weight average molecular masses, 29, 82, and 323 kDa; and pMAEDA.HCl, weight average molecular masses 19

[1] Abbreviations: HPMA, (2-hydroxypropyl)methacrylamide; pMADGHDA.HCl, poly[methacryloyl-Gly-Gly-NH-$(CH_2)_6$-NH_2] hydrochloride; pMAGEDA.HCl, poly[methacryloyl-Gly-NH-$(CH_2)_2$-NH_2] hydrochloride; pMAEDA.HCl, poly[methacryloyl-NH-$(CH_2)_2$-NH_2] hydrochloride; pLL.HBr, poly(L-lysine) hydrobromide; pAA.HCl, poly(allylamine) hydrochloride; pVA.HCl, poly(vinylamine) hydrochloride; pDMAEMam, poly(2-dimethylaminoethyl methacrylamide); pTMAEM.Cl, poly[2-(trimethylammonio)ethyl methacrylate chloride]; pBTMAIPM.I_2, poly[1,3-bis-(trimethylammonio)isopropyl methacrylate iodide]; DCC, *N*,*N*′-dicyclohexylcarbodiimide; AIBN, azobisisobutyronitrile; IVA, 4,4′-azobis(4-cyanovaleric acid); DMSO, dimethyl sulfoxide; DMF, *N*,*N*-dimethyl formamide; BOC, di-*tert*-butyl dicarbonate; pVFA, poly(*N*-vinylformamide).

and 42 kDa. Degrees of polymerization (DPn) are given in Table 1.

Chemicals. 1-Amino-2-propanol, methacryloyl chloride (freshly distilled), glycine, glycylglycine, 4-nitrophenol, *N*,*N*′-dicyclohexylcarbodiimide (DCC), azobisisobutyronitrile (AIBN), 4,4′-azobis(4-cyanovaleric acid) (IVA), 3-mercaptopropionic acid, cysteamine, cysteamine hydrochloride, *N*,*N*-dimethyl ethylenediamine, 1,2-diaminoethane, di-*tert*-butyl dicarbonate, *N*-BOC-1,6-diaminohexane hydrochloride, 4-(dimethylamino)pyridine, tetramethylammonium chloride, dimethyl sulfoxide (DMSO), *N*,*N*-dimethyl formamide (DMF), trifluoracetic acid, and triethylamine were from Fluka A.G., Switzerland. *N*-Vinylformamide was from Aldrich, Germany, and poly(L-aspartic acid, sodium salt) and pLL.HBr preparations were from Sigma, U.K. Solvents (all used after distillation) and other chemicals were of analytical grade quality, Lachema Brno, Czech Republic.

Synthesis of Cationic Polymers. Cationic monomers and polymers were synthesized as described below. In each case, the composition of the monomers was checked by elemental analysis prior to polymerization and found to be within 0.5% of the theoretical values. In most cases, ^{1}H NMR was used as an additional technique to characterize the monomers and some of the polymers. In addition, the polymer products were routinely characterized by GPC for weight and number average molecular weights. The polydispersity of most of the polycations was about 1.8.

Poly[*N*′-{2-[(*tert*-butyloxycarbonyl) amino]ethyl}-methacryl amide] [MA-NH-$(CH_2)_2$-NH-BOC] was prepared as follows. A solution of di-*tert*-butyl dicarbonate (2.45 g, 0.011 mol) in dioxane (30 mL) was added dropwise to a solution of 1,2-diamino-ethane (5.25 g, 0.087 mol) in dioxane (30 mL). The mixture was stirred for 22 h at room temperature. The dioxane was evaporated in vacuo and the crude product triturated with 50 mL of water. The insoluble bis-substituted diamine was removed by filtration. The filtrate was extracted three times with methylene chloride (150 mL), the organic layer was separated and the solution was dried over Na_2SO_4. Methylene chloride was evaporated, and the yield of oily BOC-NH-$(CH_2)_2$-NH_2 was 1.29 g (72%). Contamination of the product with free diamine was checked by TLC, but none could be determined. The oily product was used for the synthesis of MA-Gly-NH-$(CH_2)_2$-NH-BOC and MA-NH-$(CH_2)_2$-NH-BOC without further purification.

N-BOC-1,2-diamino-ethane (1 g, 0.00625 mol) and triethylamine (5.5 mL) were dissolved in 50 mL of freshly distilled chloroform. The mixture was cooled to −5 °C and methacryloyl chloride (0.68 g, 0.0065 mol) was added dropwise under stirring within 3 h. Reaction mixture was extracted four times with 20 mL of water and then a chloroform layer was dried with Na_2SO_4. Chloroform was evaporated, and after trituration in diethyl ether, the yellow crude product was obtained. This product was purified by recrystallization from the benzene−hexane mixture and characterized by elemental analysis and ^{1}H NMR ($CDCl_3$). Yield was 1.2 g (81%). Melting point: 73−76 °C. The monomer and initiator of polymerization (AIBN) were dissolved in methanol to form a solution containing 7−30 wt % of monomer and 0.1−2 wt % of AIBN related to polymerization mixture. The solution was introduced into an ampule and bubbled through with nitrogen. The ampule was sealed, and polymerization was carried out at 50 or 60 °C for 24 h. The polymer was precipitated into diethyl ether and reprecipitated from methanol into diethyl ether. The precipitated polymer was filtered off, washed with diethyl ether, and dried in vacuo. Molecular weight of polymers was controlled by varying the monomer concentration, the initiator concentration, or the temperature. BOC protecting group was removed by dissolution of the polymer in a solution of dry hydrochloric acid in methanol (15 wt % of HCl in methanol and 20 wt % of polymer in solution) and stirring for 1 h. The deprotected polymer was diluted with methanol, evaporated in vacuo to remove the excess of hydrochloric acid, and precipitated into diethyl ether. The precipitated polymer was filtered off, washed with diethyl ether and dried in vacuo. The quantitative removal of the protecting BOC groups was confirmed by the absence of the BOC signal (1.4 ppm) in the ^{1}H NMR spectrum of the polymer.

Poly[*N*′-{2-[(*tert*-butyloxycarbonyl)amino]ethyl}-methacryloylglycinamide] [MA-Gly-NH-$(CH_2)_2$-NH-BOC] was prepared as follows: BOC-NH-$(CH_2)_2$-NH_2 (1.1 g, 0.0068 mol) was dissolved in 2 mL of DMSO. MA-Gly-ONp (1.6 g, 0.0061 mol) was dissolved in 3.5 mL of DMSO and added dropwise to the solution of amine. Reaction mixture was stirred for 2 h at room temperature. DMSO was evaporated in vacuo (bp 55 °C) and an oily residue was dissolved in 50 mL of chloroform. An organic layer was extracted three times with 20 mL of distilled water. Organic layer was dried over Na_2SO_4. Chloroform was evaporated, and MA-Gly-NH-$(CH_2)_2$-NH-BOC was crystallized from ethyl acetate. Melting point: 136−38 °C. Polymerization and deprotection of the amino group were carried out according to the polymerization of MA-NH-$(CH_2)_2$-NH-BOC with subsequent deprotection of the BOC-containing polymer and NMR check of the BOC group removal.

Poly[*N*′-{(6-*tert*-butyloxycarbonyl)amino]hexyl}-methacryloylglycylglycin amide] [MA-GlyGly-NH-$(CH_2)_6$-NH-BOC] was prepared as follows. MA-GlyGly-ONp (3 g, 0.0093 mol) and *N*-BOC-1,6-diamino-hexane hydrochloride were dissolved in 15 mL of DMF. Triethylamine (1.3 mL) was added in three portions, and reaction mixture was stirred 24 h at room temperature. The precipitated triethylamine hydrochloride was filtered off, and the filtrate was evaporated in vacuo to dryness. A crude product was dissolved in chloroform and extracted three times with 15 mL of water. An organic layer was dried with Na_2SO_4 and evaporated in vacuo. The product was crystallized from a chloroform−diethyl ether mixture. Melting point: 122−124 °C. Yield was 1.98 g (54%). Polymerization and deprotection of the amino group were carried out according to the polymerization of MA-NH-$(CH_2)_2$-NH-BOC with subsequent deprotection of the BOC-containing polymer and NMR check of the BOC group removal.

DMAEMam was prepared as follows. *N*,*N*-Dimethyl ethylenediamine (8.22 g, 0.093 mol) was diluted with 30 mL of dichlormethane, and the solution was cooled to −15 °C. The solution of methacryloyl chloride (5.0 g, 0.047 mol) in dichloromethane (5 mL) was added dropwise under stirring within 2 h. The precipitate (*N*,*N*-dimethylethylenediamine hydrochloride) was filtered off, and dichlormethane was evaporated from the reaction mixture. The product was purified by rectification at reduced pressure. Polymerization of DMAEMam was carried out according to the polymerization of MA-NH-$(CH_2)_2$-NH-BOC. Briefly, a polymerization mixture consisting of 13 wt % methanol solution containing 0.6 wt % AIBN was introduced into an ampule and bubbled through with nitrogen. The ampule was sealed and polymerization was carried out at 60 °C for 20 h. A mixture of acetone and

Table 1. Physical and Biological Properties of Complexes Formed by Self-Assembly of DNA with Cationic Polymers

cationic polymer	molecular weight average (Mw, unless indicated)	degree of polymerization (DPn)	min *F* (%)	IF_{50} (N-to-P ratio)	RFI_{50} poly(L-aspartic acid) (μg/mL) and (aspartic acid/cation molar ratio)	AFM average X−Y diameter (nm) and (diameter of equivalent sphere, nm)	ζ-potential (mV) $n = 5$	transfection 293 cells (l.u./μg) $n = 3$	Intranuclear injection (oocytes) (% of free DNA control)
	3000 (Mn)	38	nd	nd	55.0 ± 5.0 (3.2)	nd	nd	$(6.9 \pm 2.6) \times 10^1$	nd
	8 000 (Mn)	101	13.2 ± 1.3	0.75	nd	aggregated	−2 ± 1	$(1.3 \pm 1.6) \times 10^1$	nd
	60 000 (Mn)	760	nd	nd	402 ± 54.4 (23.4)	no images possible	−1 ± 0	$(2.12 \pm 0.14) \times 10^2$	64
pAA.HCl	54 700	960	13.6 ± 1.4	1.10	204 ± 79.1 (11.9)	78 ± 9 (38)	−1 ± 0	$(1.81 \pm 1.15) \times 10^4$	63
pLL.HBr	4000	19	22.1 ± 1.0	1.28 ± 0.05	46 ± 5.4 (2.7)	25 ± 5 (19)	16 ± 0	0 ± 175	64
	10 000	48	19.9 ± 0.4	0.73 ± 0.15	57 ± 3.2 (3.3)	73 ± 13 (49)	nd	63	
	24 000	114	12.5 ± 0.2	0.68 ± 0.18	58 ± 1.6 (3.4)	88 ± 20 (54)	36 ± 1	$(3.39 \pm 1.41) \times 10^4$	59
	54 000	258	22.5 ± 2.5	0.85 ± 0.05	55 ± 3.5 (3.2)	145 ± 42 (80)	36 ± 1	$(3.61 \pm 0.52) \times 10^5$	61
	224 000	1072	20.9 ± 0.9	1.10 ± 0.05	55 ± 4.5 (3.2)	210 ± 90 (105)	33 ± 1	$(3.16 \pm 0.11) \times 10^5$	63
pMAEDA.HCl	18 500	112	34.2 ± 3.5	9	17.0 ± 7.2 (1.0)	129 ± 25 (53)	−1 ± 0	$(1.21 \pm 1.69) \times 10^4$	nd
	41 900	255	16.6 ± 0.6	0.95	14.1 ± 1.1	91 ± 20 (42)	14 ± 3	$(9.37 \pm 3.62) \times 10^4$	77
pMAGEDA.HCl	29 400	133	29.8 ± 4.1	nd	nd	100 ± 10 (45)	nd	nd	nd
	82 000	370	25.9 ± 7.2	2.23	7.5 ± 1.7 (0.4)	106 ± 23 (44)	1 ± 2	$(2.69 \pm 0.21) \times 10^4$	63
	322 800	1457	27.9 ± 2.6	1.10	nd	74 ± 18 (43)	nd	$(3.68 \pm 3.00) \times 10^5$	nd
pMADGHDA.HCl	38 400	115	nd	nd	nd	75 ± 19 (35)	42 ± 2	nd	nd
	73 700	220	nd	2.1	nd	76 ± 16 (37)	36 ± 1	$(1.83 \pm 0.47) \times 10^5$	25
	333 500	997	26 ± 5.2	2.1	nd	73 ± 9 (36)	27 ± 1	nd	nd
pDMAEMam	54 700	348	85.8 ± 13	>4.0	not applicable	78 ± 16 (42)	−15 ± 1	$(4.67 \pm 0.77) \times 10^4$	71
pTMAEM.Cl	5000 (Mn)	24	nd	nd	nd	nd	31 ± 2	$(4.01 \pm 0.56) \times 10^2$	46
	8470	41	21.2 ± 0.3	0.75	nd	363 ± 93 (137)	nd	nd	nd
	21 240	102	23.9 ± 0.4	0.73	nd	80 ± 25 (44)	29 ± 1	$(5.63 \pm 3.61) \times 10^2$	nd
	34 150	164	24.2 ± 1.1	0.80	26.9 ± 1.7 (1.6)	94 ± 28 (43)	30 ± 2	$(7.23 \pm 3.78) \times 10^2$	40
	413 000	1986	23.9 ± 0.8	0.78	nd	88 ± 18 (41)	20 ± 2	$(9.61 \pm 4.54) \times 10^2$	3
$pBTMAIPM.I_2$	93 100	374	25.8 ± 2.4	1.08	19.9 ± 0.7 (1.2)	86 ± 17 (51)	41 ± 1	$(8.85 \pm 1.39) \times 10^2$	22
$pHPMA_{25}$-$pTMAEM_{75}$	16 000	63	41.6 ± 2.5	2.2	nd	79 ± 14 (45)	nd	$(1.16 \pm 0.32) \times 10^3$	14
$pHPMA_{50}$-$pTMAEM_{50}$	13 000	37	84.8 ± 8.1	>5.0	nd	83 ± 25 (45)	17 ± 5	$(9.45 \pm 8.53) \times 10^2$	20
$pHPMA_{85}$-$pTMAEM_{15}$	41 000	40	95.8 ± 1.2	>5.0	nd	no particles	31 ± 2	$(1.01 \pm 1.38) \times 10^4$	30
$pHPMA_{95}$-$pTMAEM_5$	35 000	12	100 ± 0	>5.0	nd	no particles	13 ± 3	$(1.73 \pm 1.40) \times 10^3$	nd

diethyl ether was used for deprotection and reprecipitation of the polymer.

pTMAEM.Cl was prepared as follows. TMAEM.Cl was prepared by quaternization of 75 g dimethylaminoethyl methacrylate with gaseous methyl chloride in 200 mL of acetone in the presence of 5 mL of *N,N*-dimethylformamide at room temperature. The crystalline precipitate was isolated by filtration, washed three times with acetone, and dried in vacuo. Melting point: 174 °C. Polymerization was carried out as described elsewhere (*17*).

pBTMAIPM.I_2 was prepared by radical polymerization of 1,3-bis-(trimethylammonio)isopropyl methacrylate iodide (10 wt %) in DMF using IVA (0.3%) as initiator. Polymerization was carried out at 70 °C for 40 h in a sealed ampule under nitrogen atmosphere. The polymer was precipitated into dry acetone-diethyl ether mixture, washed with dry acetone, and dried in a vacuum.

pVA.HCl was prepared by alkaline hydrolysis of poly(*N*-vinylformamide) (pVFA). pVFA was prepared by radical precipitation polymerization of 4 g of *N*-vinylformamide dissolved in methanol, using 0.38 g of initiator (AIBN) and 2-mercaptoethanol as a chain transfer agent for regulation of molecular weight. Polymerization was carried out at 60 °C for 24 h. Precipitated polymer was washed with methanol, dissolved in 28 mL of NaOH (1.7 M), and hydrolyzed at 80 °C for 6 h. The polymer solution was acidified by concentrated HCl solution. Precipitated pVA.HCl was washed with methanol, acetone, and dried in vacuo.

Synthesis of statistical copolymers of TMAEM.Cl with HPMA. HPMA was prepared by the reaction of methacryloyl chloride with 1-amino-2-propanol, as described earlier (*18*). Copolymers were prepared by radical copolymerization of TMAEM.Cl with HPMA in methanol using AIBN as initiator. Monomers in various molar ratio (25−95% HPMA) were dissolved in methanol to obtain 20 wt % solution. Concentration of AIBN was 0.6 wt %, polymerization temperature 60 °C, and polymerization time 24 h. Polymerization was conducted in sealed ampules under nitrogen atmosphere. Copolymers were isolated by precipitation into diethyl ether−acetone and purified on GPC (Sephadex LH-20, methanol). The composition of copolymers was calculated using data of elemental analysis (chlorine content).

The molecular weight distribution (weight average molecular weight M_w and polydispersity M_w/M_n) of cationic polymers was determined either by FPLC on Sepharose 12 using 0.25 M sodium acetate buffer, pH 6.6, containing 0.5 M NaCl and 0.028 M tetramethylammonium chloride, or using Catsec 300 column (Micra Scientific) with an aqueous solution of $NaNO_3$ (0.2 M, adjusted to pH 2 using trifluoroacetic acid) as mobile phase. The columns were calibrated with fractionated low-polydispersity polyHPMA standards with molecular weights in a range 18000−300000 g/mol. The molecular weights of polyHPMA standards were determined by static laser light scattering. Weight average of molecular weight (M_w) of selected polycations was determined using light scattering (Fica 40).

Formation of Cationic Polymer/DNA Complexes. The conditions of complex formation were standardized to permit comparison of different properties. DNA was dissolved in water at 20 μg/mL, and then cationic polymers were added in a small volume of concentrated (5 mg/mL) solution in water. Samples were mixed very gently and then allowed to stand for at least 1 h at room temperature before more thorough mixing. To permit comparison of different cationic polymers, containing amino groups with different pK_a values, complexes were formed at defined molar ratios of highly charged amino groups to DNA phosphate (N-to-P ratios), and no correction was made for different levels of protonation.

Inhibition of Ethidium Bromide/DNA Fluorescence by Cationic Polymers. Decreased ethidium bromide-DNA fluorescence can be used to indicate condensation of the DNA (*13*). The influence of N-to-P ratio on DNA condensation by each polymer was determined by loss of ethidium bromide fluorescence in aqueous solution using a fluorimeter ($\lambda_{ex} = 366$ nm, $\lambda_{em} = 590$ nm). DNA (20 μg/mL) was incubated in water in the presence of ethidium bromide (400 ng/mL) before sequential addition of small volumes of the cationic polymer (5 mg/mL), each addition accounting for increased N-to-P ratio of 0.1. The parameters deduced for each interaction were the N-to-P ratio of polymer causing 50% fall in measured fluorescence (IF_{50}) and the lowest fluorescence level achieved at any N-to-P ratio (Min F), expressed as a % the fluorescence of equivalent free DNA.

Ethidium Bromide/DNA Fluorescence Restoration by Poly(L-aspartic acid). Polyelectrolyte complexes containing 20 μg/mL DNA were formed at an N-to-P ratio of 2 in the presence of ethidium bromide (400 ng/mL). Poly(L-aspartic acid) was then added in sequential aliquot portions in water. After each addition, solutions were mixed and ethidium bromide/DNA fluorescence was monitored as above. Poly(L-aspartic acid) was added in small portions until fluorescence was restored to 50% of its original value (the RFI_{50} concentration; Figure 3).

Agarose Gel Electrophoresis. Polymer/DNA complexes in water were electrophoresed on agarose gel (0.8% w/v) (BRL) for 45 min at 90 V. Ethidium bromide was included in the gel to show the location of DNA using a UV transilluminator.

Atomic Force Microscopy (AFM). Samples containing complexes in water (1−2 μL) with final DNA concentration of 20 μg/mL were deposited onto the center of a freshly split untreated mica disk (Agar Scientific). Following adsorption for 1−2 min at room temperature, excess fluid was taken off by absorption onto filter paper. The mica surface was dried at room temperature before imaging using an AFM-2, part of the NanoScope II system (Digital Instruments). A 200 μm long Si_3N_4 cantilever with a spring constant of 0.12 N/m and a D scanner head (AFM 351) with 12 μm scan range were used. The image mode was set to constant force mode, hence the images obtained are height images of the sample surface. The scanning speed varied between 2.48 and 8.68 Hz.

Analysis of ζ-Potential. The surface charge of the polymer/DNA complexes was assessed by using a Zetamaster system (Malvern Instruments). The system was routinely calibrated using a −55 mV standard. Experimental samples (5 mL) contained a final calf thymus DNA concentration of 20 μg/mL and were measured 5 times for 30 s at 1000 Hz with zero field correction.

Microinjection of DNA Complexes into *Xenopus oocytes*. Reporter gene activity was determined following injection of polymer/DNA complexes directly into the nucleus of Xenopus oocytes. Mature female frogs were killed by benzocaine overdose, and oocytes were individually examined in a Petri dish containing Modified Barth's Solution (MBS, pH 7.6). Only oocytes at developmental stage IV were used, and complexes were microinjected using a Drummond Auto Oocyte Injector (Drummond Scientific Company). The injection volume was 13.8 nL/oocyte and DNA concentration 22 pg/nL (either free DNA

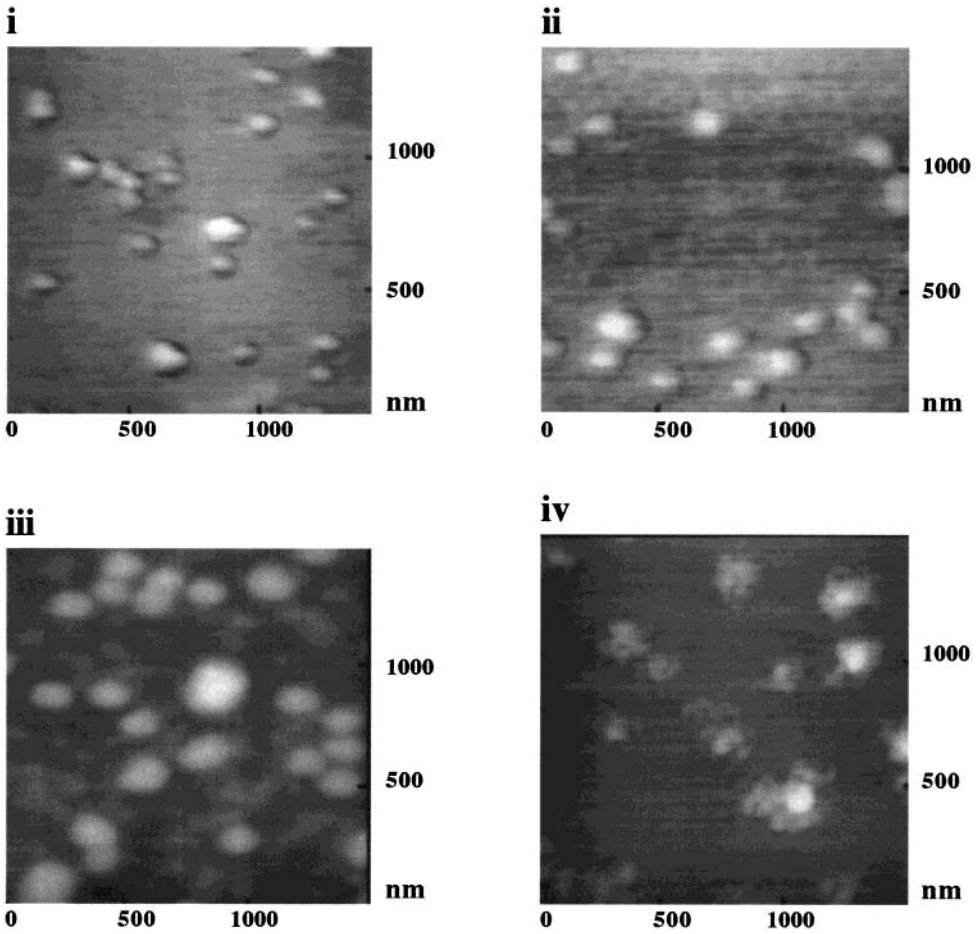


Figure 2. Influence of side-chain length on structure of complexes formed with DNA, viewed by AFM. Polymer/DNA complexes were formed at an N-to-P ratio of 2.0. The images show conjugates formed using (i) pAA.HCl (54 700 Mw; DPn 960), (ii) pMAEDA.HCl (41 900 Mw; DPn 255), (iii) pMAGEDA.HCl (82 000 Mw; DPn 370), and (iv) pMADGHDA.HCl (73 700 Mw; DPn 220). The height of the AFM image is represented by a graded black-white scale, with white indicating a height of 30 nm above the mica surface. The *x* and *y* dimensions are scaled as shown. The images are typical of the results of multiple evaluations performed on separate days.

or as polymer/DNA complexes). Oocytes were maintained in MBS for a further 48 h in small Petri dishes at 18−20 °C (individually grouped for specific studies), at which time healthy looking oocytes were pooled together (10 oocytes/mL) in lysis solution (100 mM potassium phosphate, 0.2% vol/vol Triton X-100, and 1 mM dithithreitol, pH 7.8). Oocytes were lysed by pipetting them up and down, and samples were centrifuged at 13 000 rpm (MicroCentaur, 10 min). The clear supernatant (20 μL) was then assayed for β-galactosidase activity by Galactolight, as described below.

Efficiency of Transfection in Vitro. Polymer/DNA complexes were prepared in water at an N-to-P ratio of 2 and with a DNA concentration of 20 μg/mL. Complexes were added to 293 cells and incubated for 4 h at a final DNA concentration of 2.6 μg/mL in serum-free medium containing chloroquine (100 μM). Cells were washed after exposure and reincubated in the presence of serum (10%). After 48 h, medium was removed from the culture and the cells were washed once with PBS (100 μL). Aliquots of lysis buffer (100 mM potassium phosphate, pH 7.8, and 0.2% Triton X-100) (100 μL) were added, and the plates were left for 40 min at room temperature until the lysis was complete. After centrifugation, the cell lysates were assayed for gene expression and total protein content (see below).

Evaluation of Gene Expression. Total β-galactosidase activity was quantified using the chemiluminescent reporter assay system Galacto-Light Plus (Tropix, Cam-

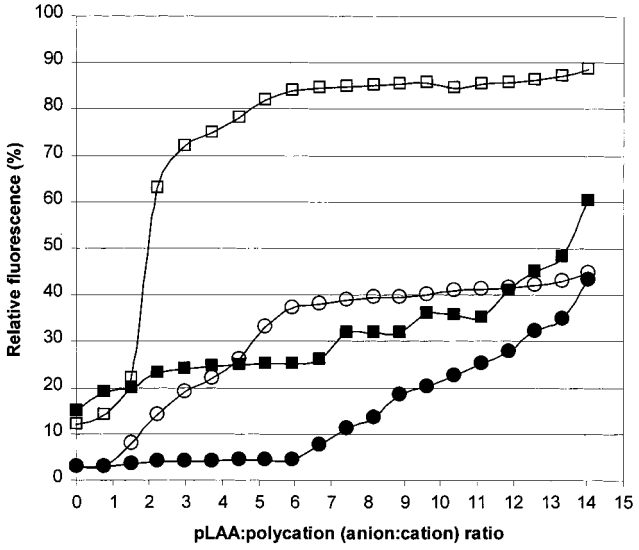


Figure 3. Restoration of ethidium bromide/DNA fluorescence by addition of poly(L-aspartic acid) to preformed polymer/DNA complexes. Complexes were formed at an N-to-P ratio of 2.0, in the presence of ethidium bromide (400 ng/mL), and allowed to stabilize for 2 h, and then poly(L-aspartic acid) was added in small portions, with fluorescence determined at λ_{ex} 366 and λ_{em} 590 nm. The behavior of DNA complexes formed with pVA.HCl [60 000 Mw, DPn 760 (●)], pAA.HCl [54 000 Mw, DPn 960 (○)], pMAEDA,HCl [41 900 Mw, DPn 255 (■)], and pMAGEDA.HCl [82 000 Mw, DPn 370 (□)] is shown.

bridge, U.K.). Cell lysates were diluted 1:1 with lysis buffer containing 2 mM dithiothreitol. After centrifugation, 50 μL of the supernatant was then added to 200 μL of chemiluminescent substrate solution (Galacton-Plus in 100 mM sodium phosphate, pH 8.0, and 1 mM magnesium chloride). After incubation for 1 h, 300 μL of luminescence accelerator reagent was added, and the sample was assayed on a monolight luminometer (Lumat LB9501, Berthold) by counting emitted light units for 10 s. Transfection was quantified as β-galactosidase activity measured per μg of protein (light units/μg). The total protein content was measured in the absence of dithiothreitol using the bicinchonninic acid (BCA) assay for protein.

RESULTS

Influence of Length of Polycation Side Chain on Properties of Complexes Formed with DNA. Different distance of cationic charge from the polymer backbone had an important influence on the properties of complexes formed with DNA. Polymers with charges close to the backbone (e.g., pVA.HCl) showed generally efficient condensation, with relatively low values of IF_{50} and Min F (Table 1). Conversely, polymers with long lateral side chains (e.g., pMADGHDA.HCl) showed poor condensation. It is important throughout these studies comparing different side chains to consider the influence of DPn, since polymers based on small monomers have more charges per polymer of the same molecular weight compared with polymers based on larger monomers. However, even bearing this in mind, it is clear that polymers with long side chains tend to be less efficient at condensing DNA than polymers with short side chains (Table 1). Nonetheless, the influence of side-chain length is not simple as some polymers with intermediate length side chains, such as pLL.HBr, also achieved efficient DNA condensation judged by inhibition of ethidium bromide/DNA fluorescence.

AFM was used to measure sizes of polymer/DNA complexes. However, pVA.HCl/DNA complexes tended to flocculate in water, particularly with lower molecular weight pVA.HCl, and no AFM images were possible. pAA.HCl and cationic polymers with side chains of intermediate length produced discrete, well-defined complexes with DNA, typical diameter about 100 nm. DNA complexes produced with cationic polymers with long side chains (pMADGHDA.HCl) were often loose with structural irregularities, and there was still DNA protruding from the complexes even several hours following initial mixing of pMADGHDA.HCl with DNA (Figure 2).

The influence of side-chain length was also evident when complexes were subject to interaction with pLAA, and restoration of ethidium bromide/DNA fluorescence was monitored. Although complexes based on all other polymers showed fluorescence restoration (RFI_{50}) at concentrations of pLAA less than 60 μg/mL (a molar ratio of aspartic acid to cation of 3.5), those based on polymers with shortest side chains (pVA.HCl and pAA.HCl) showed much greater resistance to pLAA, pVA.HCl achieving RFI_{50} values even over 400 μg/mL (aspartic acid/cation ratios over 20; Table 1 and Figure 3). This does not appear to be strongly influenced by the DPn and may reflect high stability of DNA complexes formed with cationic polymers such as pAA.HCl and pVA.HCl.

When the surface charge of complexes was monitored (using N-to-P ratio of 2.0), DNA complexes formed with pVA.HCl or pAA.HCl were found to have ζ-potentials of approximately zero (Table 1), perhaps contributing to the tendency of pVA.HCl complexes to flocculate in water. Comparing complexes formed with medium molecular mass (40−80 kDa) cationic polymers, most of the cationic polymers with medium or long pendent side chains produced positive ζ-potential values, for example, pMADGHDA.HCl, 36 mV; pLL.HBr, 36 mV; pTMAEM.Cl, 9 mV. Although it is intuitively attractive to consider that longer side chains may result in a surface layer of nonneutralized positive charges, any such proposal is compromised by the low value of ζ-potential (1 mV) produced by pMAGEDA.HCl and the higher value (14 mV) produced by the shorter side chain pMAEDA.HCl.

DNA complexes formed using the short side-chain PVA.HCl gave no significant spontaneous transfection when applied to 293 cells in vitro, and pAA.HCl also produced only slight increases compared with DNA alone. Complexes based on all the other nonquaternized cationic homopolymers examined produced higher levels of gene expression, and this may relate to the known positive ζ-potential of the latter complexes, possibly mediating greater membrane adsorption. Complexes formed using pMADGHDA.HCl, known from AFM studies to be incompletely condensed, also mediated high levels of transgene expression, similar to the levels achieved using high molecular weight pLL.HBr (Table 1).

Following direct inoculation into Xenopus *oocytes*, complexes based on most homopolymers produced levels of gene expression comparable to that following injection of free DNA. pAA.HCl and pVA.HCl complexes showed over 60% expression, suggesting that despite their high stability to polyanions they are still suitable for intranuclear transcription. The only indication of the influence of side-chain length was from the long side-chain pMADGHDA.HCl polymer, which gave relatively low gene expression (25%) (Table 1).

Influence of Charge Strength on Properties of Complexes Formed with DNA. Comparison of similar molecular weight poly(methacrylamide)-based polymers containing primary (pMAEDA.HCl), tertiary (pDMAEMam), or quaternary (pTMAEM.Cl) amino groups permitted examination of the influence of these different types of charge on properties of complexes formed with DNA.

Quaternary charged pTMAEM.Cl was relatively efficient at DNA condensation, achieving low IF_{50} values (Table 1). In contrast, the tertiary amino-based pDMAEMam was very poor at DNA condensation, and failed to decrease ethidium bromide/DNA fluorescence to 50% of the starting value even at N-to-P ratios of 4.0. This poor ability of pDMAEMam to form complexes with DNA was probably due to its presence in free base form, leading to lower levels of protonation in water than with the other cationic polymers which were salts.

When poly(L-aspartic acid) was added to complexes to restore fluorescence of ethidium bromide/DNA, complexes based on pTMAEM.Cl/DNA required greater levels of poly(L-aspartic acid) than DNA complexes formed using methacrylate polymers containing primary amino groups (Table 1). AFM showed no obvious differences between DNA complexes formed using methacrylate-based polymers of different order of charge, with all polymers capable of producing discrete complexes of about 100 nm diameter. Similarly, there were no trends in ζ-potential determined for the complexes, except that DNA complexes formed with the tertiary amino-containing pDMAEMam displayed negative values of ζ-potential (Table 1).

Spontaneous transfection of 293 cells in vitro could be achieved to levels of about 10^5 l.u./μg protein by DNA

complexes formed using the methacrylate based primary amino polymer pMAEDA.HCl, and also by the tertiary amino pDMAEMam. These levels were comparable with those achieved using pLL.HBr. Complexes based on quaternary pTMAEM.Cl, however, showed much lower levels of spontaneous transfection, achieving maximal levels of 10^3 l.u./μg protein. This was only marginally increased compared with the intrinsic transfection activity of free DNA. Following direct intranuclear injection in Xenopus oocytes, complexes based on primary amino-bearing pMAEDA.HCl showed transgene expression at a level of 77% that of the equivalent dose of free DNA. pDMAEMam/DNA complexes achieved 71%, and pTMAEM.Cl/DNA complexes 40%. However, the 2-fold decreased intranuclear activity of the quaternary pTMAEM.Cl-based complexes is not sufficient to explain their very low levels of spontaneous cell transfection, suggesting that cellular transfection by pTMAEM.Cl/DNA complexes may be subject to particular problems of gaining access to the cytoplasm or nucleus (Table 1).

Influence of Charge Spacing along Polymer Backbone on Properties of Complexes Formed with DNA. A series of random copolymers of TMAEM.Cl and HPMA permitted examination of the influence of charge spacing on the properties of complexes formed with DNA. To permit comparison, all copolymers were used at standard concentrations of charge, which for some materials (particularly the 5% TMAEM.Cl copolymer) necessitated use of very high total concentrations of copolymer. Copolymers containing 50% pHPMA were unable to mediate 50% inhibition of ethidium bromide/DNA fluorescence at any N-to-P ratio examined (Figure 4a). Interestingly, agarose gel electrophoresis showed that all random copolymers, including the material containing 95% HPMA (where each positively charged TMAEM.Cl group is surrounded by an average 19 noncharged HPMA groups) was capable of binding DNA and mediating a gel-shift assay (Figure 4b). At N-to-P ratio of 1.0, there was still some electrophoretic mobility of DNA condensed with the 5% TMAEM.Cl copolymer, although at N-to-P ratio of 2.0, this had disappeared. In addition, fluorescence of DNA complexes retained in the wells was lower using polymers with greater TMAEM.Cl content, corresponding with data in Figure 4a, and suggesting formation of tighter complexes. AFM analysis showed that the higher charge density cationic polymers was capable of forming discrete complexes, while copolymers containing 50% or less TMAEM.Cl produced images of extended structures, probably representing DNA/cationic polymer complexes which are not subject to charge neutralization-driven particle self-assembly (Figure 5).

Measurement of ζ-potential also showed that every copolymer was capable of binding DNA, with all ζ-potentials measured in the range 10−50 mV, compared with the ζ-potential of free DNA (−80 mV, approximately). Although all copolymer complexes showed some activity in spontaneous transfection of 293 cells, levels were very low compared with pLL.HBr/DNA complexes, similar to the level achieved using complexes formed using pTMAEM.Cl homopolymer. After direct intranuclear injection to Xenopus oocytes, copolymer/DNA complexes showed low levels of gene expression (14−30% of DNA control), although again this is comparable with the activity of pTMAEM.Cl/DNA complexes (Table 1).

pBTMAIPM.I_2 is a polymer bearing two quaternary positive charges per methacrylate-based monomer, and hence the charge density of the polymer is relatively high. Properties of the complexes formed between pBTMAIPM.I_2 and DNA were very similar to pTMAEM/DNA complexes, showing similar condensation parameters and poor ability to transfect cells despite positive surface charge. This may reflect the poor transcriptional ability of pBTMAIPM.I_2/DNA complexes observed following intranuclear injection, similar to that observed for complexes based on high molecular weight pTMAEM.Cl.

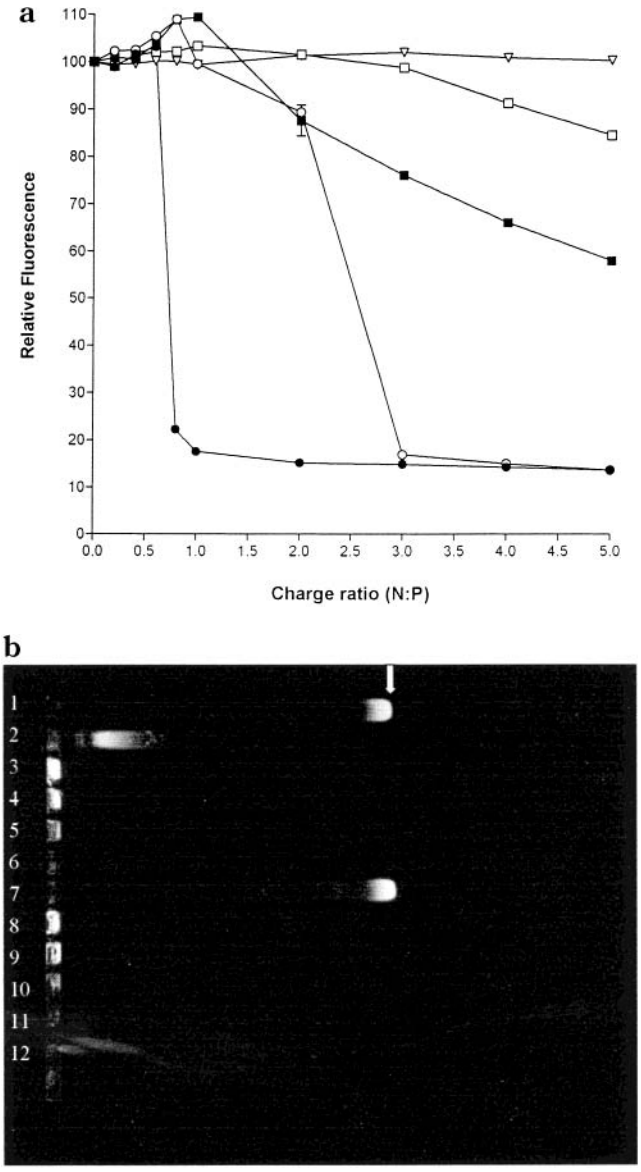


Figure 4. Assessment of DNA condensation by TMAEM.Cl-*co*-HPMA random copolymers. (a) Fluorescence of ethidium bromide allowed to integrate into the DNA before addition of the cationic polymers, as described in the text. The lines represent sequential addition of copolymers of different composition: 100 mol % TMAEM.Cl (Mw 21 240; DPn 102; ●), 75 mol % TMAEM.Cl (Mw 16 000; DPn 63; ○), 50 mol % TMAEM.Cl (Mw 13 000, DPn 37; ■), 15 mol % TMAEM.Cl (Mw 41 000, DPn 40; □), 5 mol % TMAEM.Cl (Mw 35 000, DPn 12, ▽). (b) Agarose gel shift assay. Complexes were formed by addition of precise amounts of TMAEM.Cl-*co*-HPMA random copolymers to DNA. After 2 h, samples were analyzed by agarose gel electrophoresis, with ethidium bromide present in the gel to permit visualization of DNA. Samples applied are as follows: lanes 1 and 7, free DNA; lanes 2 and 8, 5 mol % TMAEM.Cl (Mw 35 000); lanes 3 and 9, 15 mol % TMAEM.Cl (Mw 41 000); lanes 4 and 10, 50 mol % TMAEM.Cl (Mw 13 000); lanes 5 and 11, 75 mol % TMAEM.Cl (Mw 16 000); lanes 6 and 12, 100 moly TMAEM.Cl (Mw 34 150). Complexes were formed at an N-to-P ratio of 1.0 (lanes 2−6) or 2.0 (lanes 8−12). The gel was photographed using a UV transilluminator, and the arrow marks the position of free DNA running into the gel.

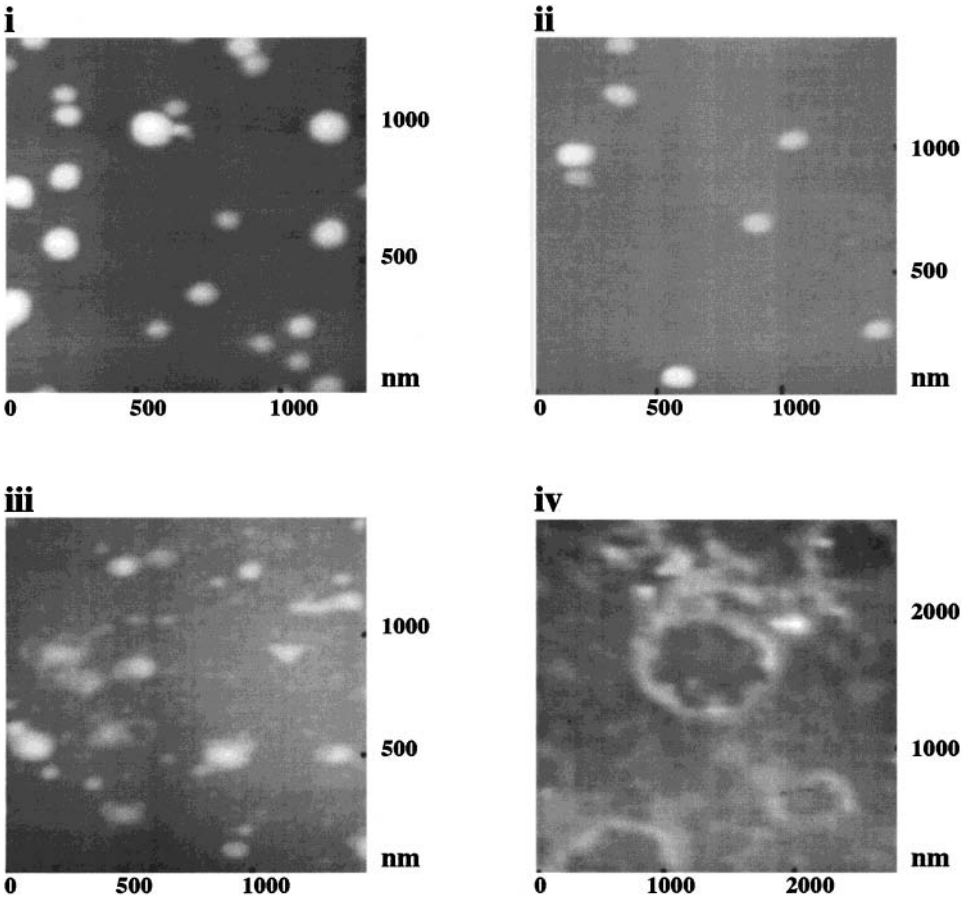


Figure 5. Influence of charge spacing in TMAEM.Cl-*co*-HPMA random copolymers on complexes formed with DNA, visualized by AFM. Complexes were formed at an N-to-P ratio of 2.0. The images show conjugates formed using (i) 100 mol % TMAEM.Cl (Mw 21 240), (ii) 75 mol % TMAEM.Cl (Mw 16 000), (iii) 50 mol % TMAEM.Cl (Mw 13 000), and (iv) 15 mol % TMAEM.Cl (Mw 41 000). The height of the AFM image is represented by a graded black-white scale, with white indicating a height of 30 nm above the mica surface. The *x* and *y* dimensions are scaled as shown. The images are typical of the results of multiple evaluations performed on separate days.

Influence of Cationic Polymer Molecular Weight or DPn on Properties of Complexes Formed with DNA. Self-assembly of cationic polymers with DNA, measured by inhibition of ethidium bromide/DNA fluorescence, showed molecular weight (or DPn) effects that varied from polymer to polymer. The simplest methacrylate-based polymer, pMAEDA.HCl, showed much better DNA condensation using a higher molecular weight preparation, achieving lower values of IF_{50} and Min F. Similar results were obtained using the longer side chain pMAGEDA.HCl. With the quaternary pTMAEM.Cl, no real effects of molecular weight were seen, and all polymer fractions showed similar condensation abilities. In contrast, pLL.HBr showed clear effects of molecular mass, with medium molecular mass pLL (24 kDa) mediating more efficient condensation of DNA than high or low molecular mass preparations.

Sizes of complexes formed by self-assembly with DNA, measured by AFM, showed molecular weight influences that varied between polymers. There were no reproducible effects for the polymer pMAEDA.HCl, although pMAGEDA.HCl and pMADGHDA.HCl both seemed to give better defined complexes at higher molecular weight, with lower molecular weight preparations yielding more extended structures. pTMAEM.Cl showed a clear effect of molecular weight, with complexes based on low molecular weight polymer showing a larger size, probably due to aggregation. pLL.HBr also showed a clear molecular weight effect that was effectively the opposite, namely significantly smaller complexes formed using lower molecular weight polycation. This phenomenon has been observed before (*7*).

ζ-Potential of complexes formed between DNA and polycations showed no trends with molecular weight for any of the cationic polymers examined except pLL.HBr. In the case of pLL.HBr, low molecular weight polycations yielded lower values of ζ-potential, with pLL.HBr 4 kDa showing a relatively low positive value (16 mV). Smaller preparations (e.g. pLL.HBr 1 kDa) showed further decreased ζ-potential, perhaps reflecting incomplete condensation, but also a tendency to flocculate.

Following microinjection of complexes into the nucleus of Xenopus oocytes, complexes based on high molecular weight pTMAEM.Cl showed much lower levels of gene expression than even those based on midrange pTMAEM.Cl. This may reflect relatively high stability of these complexes and protection of DNA from polymerase enzymes, or could reflect other effects, possibly toxicological, of this high molecular weight polycation. Complexes based on pLL.HBr show no such effects of molecular weight, with even complexes based on very high molecular weight pLL.HBr showing roughly the same levels of transcription as all other pLL.HBr/DNA complexes. This was in sharp contrast to the levels of gene expression achieved by simple transfection, where the use of complexes based on high molecular weight pLL.HBr achieved much greater levels of gene expression (Figure 6). The other polymers examined also showed the same trend in transfection, with complexes based on larger polymers mediating higher levels of transgene expres-

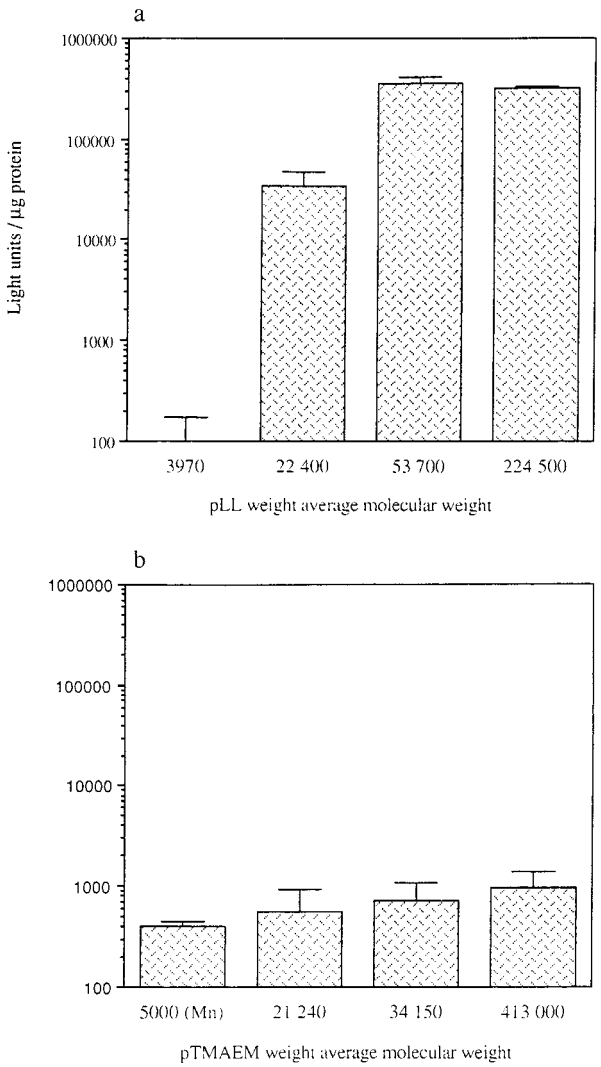


Figure 6. Influence of molecular weight of cationic polymers on transfection activity against 293 cells. (a) Influence of molecular weight of pLL.HBr, while panel b shows the influence of molecular weight of pTMAEM.Cl. Complexes were formed, cells were transfected, and expression of the β-galactosidase gene delivered was assayed as described in the text.

sion, although the effect was not always statistically significant.

DISCUSSION

Several techniques have been employed in this study to characterize the biological and physical properties of complexes formed spontaneously between cationic polymers and DNA. Some of the techniques are still under development, however, and results must be interpreted cautiously. For example, it is not clear whether loss of ethidium bromide/DNA fluorescence upon complex formation (*13*, *19*) results from expulsion or quenching of the fluorophore, and in the case of expulsion, whether the motive force is physical compression or electrostatic repulsion of the ethidium bromide from the complex.

Subject to these qualifications, the techniques employed have yielded considerable information on the interaction of cationic polymers with DNA. Considering first the influence of side-chain length, polymers studied with long side chains (e.g., pMADGHDA.HCl) were incapable of efficient complex formation with DNA. The resulting complexes maintained considerable residual fluorescence and high ζ-potential and showed loops of nonincorporated DNA protruding from the structure when viewed by AFM. They did show considerable transfection activity, however, despite poor gene expression following direct intranuclear injection. At the other extreme were complexes formed using pVA.HCl and pAA.HCl, both with very short side chains. These polymers were efficient at complex formation, yielding complexes that displayed little residual fluorescence and no appreciable surface charge. They appeared to form complexes efficiently with DNA, showing remarkable stability to subsequent polyanion-mediated disruption. Efficient charge neutralization may also explain their lack of surface charge, which probably underlies their tendency to aggregate. Their low transfection activity may also reflect their low surface charge, but their ability to undergo efficient intranuclear transcription is perhaps surprising in light of their stability to polyanions. The ability of cells to transcribe DNA bound even relatively firmly to cationic polymers may increase the opportunities for design of complexes combining good extracellular stability with efficient transcription following arrival within the nucleus (*20*).

The next parameter studied in depth was the influence of cationic charge strength, using primary, tertiary, or quaternary amino groups, on the properties of complexes formed with DNA. Quaternary amino groups (pTMAEM.Cl) seemed to form complexes relatively efficiently with DNA, perhaps reflecting a stronger bond than with primary amino groups. Perhaps the most striking observation was the very poor transfection activity associated with the quaternarized polycation, pTMAEM.Cl, being 10−100-fold less active than complexes based on most other cationic polymers. It did undergo reasonably efficient intranuclear transcription, however, (except at high molecular weights) and the reason for its poor transfection activity may involve relatively poor access to the nucleus. Complexes formed using cationic polymers with pK_a values in the endosomal range [e.g. poly(ethylene imine), Starburst dendrimers] are thought to mediate selective membrane activity on the endosome, perhaps via the so-called proton sponge mechanism (*21*), and this leads to extremely high transfectional activity. Hence, it seems possible that the complete absence of pH responsiveness in the quaternized polycation may restrict its ability to enter the cytoplasm/nucleus of target cells.

The tertiary amine-containing pDMAEMam was less effective at DNA condensation in water, probably reflecting low protonation of its free base form, and complexes displayed a low ζ-potential (−15 mV). However, AFM showed that discrete complexes were formed and there was efficient transcription following their injection into the nuclei of Xenopus oocytes. These complexes also demonstrated reasonably high levels of transfection of 293 cells in vitro, compatible with the suggestions of good transfection activity associated with polymers with pK_a in the endosomal range (*21*, outlined above). It should be noted that the pDMAEMam polymer is based on a methacrylamide backbone, while most of the other polymers are methacrylate-based; however, this difference is thought unlikely to affect properties of the complexes formed. Indeed, the corresponding methacrylate-based polymer has been studied in great detail (*22*), and high molecular weight forms are reported to have particularly good activity as in vitro transfection agents (*23*).

The influence of the density of positive charge along the cationic polymer on the properties of complexes formed with DNA was examined by comparing pTMAEM.Cl with pBTMAIPM.I_2, which bears two quater-

nary ammonio groups per monomer. Properties of complexes were remarkably similar, suggesting that a high density of positive charges does not adversely affect the interaction with DNA, although neither were any significant benefits observed. The effect of charge dilution was addressed by spreading out the positive charges using random copolymers containing TMAEM.Cl and HPMA as monomers. All copolymers were capable of binding DNA, according to ζ-potential and effects on electrophoretic mobility of the DNA, although copolymers with greater than 50% TMAEM.Cl content were not capable of forming particulate complexes, judged by AFM. Hence, it seems likely that these copolymers cannot drive hydrophobic self-assembly of polymer/DNA complexes even at charge neutrality; instead they form extended structures which can even display greater ethidium bromide/DNA fluorescence than untreated DNA controls (Figure 4a). It seems likely that the effects noted using these copolymers are mediated more by the presence of the hydrophilic HPMA component than directly by the spreading of the positive charges.

In terms of biological activity, complexes based on the random copolymers showed low levels of transfection similar to the parent pTMAEM.Cl quaternary homopolymer. However, they also showed particularly poor ability to undergo transcription following intranuclear injection. Although the reasons for this are not clear, it may involve steric protection of the DNA from polymerases by the presence of the hydrophilic polymer.

Finally, the influence of cationic polymer molecular weight average on properties of complexes formed with DNA has been examined. With DNA complexes based on pLL.HBr, polycation molecular weight is known to influence several properties (*7*). For example, complexes based on larger pLL.HBr are significantly bigger, more resistant to disruption by poly(L-aspartic acid), show a higher ζ-potential and are more active in transfecting cells (Figure 6). One explanation may be that, during complex formation, binding of small pLL.HBr to DNA is essentially reversible and leads to formation of thermodynamically stable complexes based on single DNA molecules. Such small complexes are efficiently charge neutralized and can often flocculate. Binding of larger pLL.HBr can be irreversible, however, and often proceeds inefficiently due to the inability of the polyelectrolytes to rearrange themselves. This leads to regions of excess positive charge, cross-linking of DNA molecules, and eventually to formation of complexes which are stable kinetically but thermodynamically locked in an unstable configuration. However, despite the simplicity of this hypothesis, it remains unsubstantiated when the same principles do not seem to govern self-assembly of DNA with other polymers such as pTMAEM.Cl.

There were some indications of effects of molecular weight on transfection activity against 293 cells for many of the polymers examined in this study, including pVA.HCl, pLL.HBr, pMAEDA.HCl, pMAGEDA.HCl, and pTMAEM.Cl. With these polymers, DNA complexes formed with higher molecular weight cationic polymer preparations often showed greater expression of reporter genes. This was generally parallel with increased cytotoxicity of preparations based on larger cationic polymers, and it is not clear whether the cationic polymer which is free in solution at these N-to-P ratios is exerting an important effect in either cytotoxicity or transfection.

The observations made in this study permit us to begin identifying parameters of cationic polymers that may affect the properties of the complexes they form with DNA. Many people working in this field are searching for complexes with improved transfectional activity. It is clear from the above that polymer/DNA complexes formed using high molecular weight polymers are generally more transfection active, although the involvement of quaternary charges may lead to less efficient passage through the target cell to the nucleus.

In contrast, targeted gene delivery for systemic application requires DNA complexes that are stable in the circulation, small enough to undergo extravasation into target tissues, able to recognize and enter target cells, including translocation into the nucleus, and suitable for efficient transcription within the nucleus of the target cell. One key issue is stability of complexes in the plasma, where they may interact with many different biological components (*24*−*27*). This area is the subject of several related studies, and at present, it is uncertain whether all of these requirements can be fulfilled by a simple self-assembling polycation/DNA system. We are therefore presently developing means of postassembly modification of complexes to mediate some of the objectives specified, using the self-assembling system as the core of the final complex (*27*−*29*). Chief requirements of the core complex are therefore small size, formation of monodisperse complexes, and the ability to permit efficient transcription within the nucleus of target cells. Consideration of the information generated in this analysis leads us to believe that the most appropriate complexes will be based on cationic polymers with a high charge density, containing nonquaternary amino groups, short side chains, and medium-to-low molecular weight distribution.

ACKNOWLEDGMENT

This work was supported in part by the European Biotechnology Program 972334, PECO project Grant IC20CT970005, Grant Agency of the Czech Republic (307/96/K226), British Heart Foundation, and the Cancer Research Campaign.

LITERATURE CITED

(1) Dalgleish, A. G. (1997) Why: Gene therapy? *Gene Ther. 4*, 629−630.

(2) Wright, M. J., Rosenthal, E., Stewart, L., Wightman, L. M. L., Miller, A. D., Latchman, D. S., and Marber, M. S. (1998) Beta-galactosidase staining following intracoronary infusion of cationic liposomes in the in vivo rabbit heart is produced by microinfarction rather than effective gene transfer: a cautionary tale. *Gene Ther. 5*, 301−308.

(3) Bosch, A., McCray, P. B., Walters, K. S., Bodner, M., Jolly, D. J., Van Es, H. H. G., Nakamura, T., Matsumoto, K., and Davidson, B. L. (1998) Effects of keratinocyte and hepatocyte growth factor in vivo: Implications for retrovirus-mediated gene transfer to liver, *Hum. Gene Ther. 9*, 1747−1754.

(4) Kong, H. L., Hecht, D., Song, W., Kovesdi, I., Hackett, N. R., Yayon, A., and Crystal, R. G. (1998) Regional suppression of tumor growth by in vivo transfer of a cDNA encoding a secreted form of the extracellular domain of the flt-1 vascular endothelial growth factor receptor. *Hum. Gene Ther. 9*, 823−833.

(5) Velu, P. T. (1997) Publication of the European Commission ETD/94/B5−3000/M1/11.

(6) Marshall, E. (1995) The trouble with vectors. *Science 269*, 1052−1053.

(7) Wolfert, M. A., and Seymour, L. W. (1996) Atomic force microscopic analysis of the influence of the molecular weight of poly(L)lysine on the size of polyelectrolyte complexes formed with DNA. *Gene Ther. 3*, 269−273.

(8) Wolfert, M. A., Schacht, E. H., Toncheva, V., Ulbrich, K., Nazarova, O., and Seymour, L. W. (1996) Characterisation of vectors for gene therapy formed by self-assembly of DNA with synthetic block copolymers. *Hum. Gene Ther. 7*, 2123−2133.

(9) Seymour, L. W. (1992) Passive tumour targeting of soluble macromolecules and drug conjugates. *CRC Crit. Rev. Therapeut. Drug Carr. Syst. 9*, 135−187.

(10) Wolfert, M. A., and Seymour, L. W. (1998) Chloroquine and amphipathic peptide helices show synergistic transfection in vitro. *Gene Ther. 5*, 409−414.

(11) Dash, P. R., Wolfert, M. A, and Seymour, L. W. (1998b) *Gene Ther.* (in press).

(12) Kabanov, A. V., and Kabanov, V. A. (1995) DNA complexes with polycations for the delivery of genetic material into cells. *Bioconjugate Chem. 6*, 7−20.

(13) Dash, P. R., Toncheva, V., Schacht, E. H., and Seymour, L. W. (1997) Synthetic polymers for vectorial delivery of DNA: characterisation of polymer/DNA complexes by photon correlation spectroscopy and stability to nuclease degradation and disruption by polyanions in vitro. *J. Controlled Release 48*, 269−276.

(14) Tang, M. X., and Szoka, F. C. (1998) Structure of polycation/DNA complexes and theories of compaction. In *Self-Assembling Complexes for Gene Delivery; from laboratory to clinical trial* (A. V. Kabanov, P. L. Felgner, and L. W. Seymour, Eds.) pp 27−50, John Wiley and Sons Ltd., Chichester, U.K.

(15) Tang, M. X., and Szoka, F. C. (1998) Characterisation of polycation complexes with DNA. In *Self-Assembling Complexes for Gene Delivery; from laboratory to clinical trial* (A. V. Kabanov, P. L. Felgner, and L. W. Seymour, Eds.) pp 169−196, John Wiley and Sons Ltd., Chichester U.K.

(16) Wagner, E., Cotten, M., Foisner, R., and Birnstiel, M. L (1991) Transferrin-polycation−DNA complexes − The effect of polycations on the structure of the complex and DNA delivery to cells. *Proc. Natl. Acad. Sci. 88*, 4255−4259.

(17) Konak, C., Mrkvickova, L., Nazarova, O., Ulbrich, K., and Seymour, L. W. (1998) Formation of DNA complexes with diblock copolymers of poly(N−(2-hydroxypropyl)methacrylamide) and polycations, *Supramol. Sci. 5*, 67−74.

(18) Kopecek, J., Rejmanova, P., and Chytry, V. (1981) Polymers containing enzymatically degradable bonds 0.1. Chymotrypsin catalyzed-hydrolysis of para-nitroanilides of phenylalanine and tyrosine attached to side-chains of copolymers of N−(2-hydroxypropyl)methacrylamide. *Makromol. Chem. 182*, 799−809.

(19) Pouton, C. W., Lucas, P., Thomas, B. J., Uduehi, A. N., Milroy, D. A., and Moss, S. H. (1998) Polycation/DNA complexes for gene delivery: A comparison of the biopharmaceutical properties of cationic polypeptides and cationic lipids. *J. Controlled Release 53*, 289−299.

(20) Pollard, H., Remy, J. S., Loussouarn, G., Demolombe, S., Behr, J. P., and Escande, D. (1998) Polyethylenimine but not cationic lipids promotes transgene delivery to the nucleus in mammalian cells, *J. Biol. Chem. 273*, 7507−7511.

(21) Behr, J. P. (1997) The proton sponge: A trick to enter cells the viruses did not exploit. *Chimia 51*, 34−36.

(22) Cherng, J. Y., VandeWetering, P., Talsma, H., Crommelin, D. J. A., and Hennink, W. E. (1996) Effect of size and serum proteins on transfection efficiency of poly((2-dimethylamino)-ethyl methacrylate)-plasmid nanoparticles. *Pharm. Res. 13*, 1038−1042.

(23) VendeWetering, P., Cherng, J. Y., Talsma, H., Crommelin, D. J. A., and Hennink, W. E. (1998) 2-(Dimethylamino)ethyl methacrylate based (co)polymers as gene transfer agents *J. Controlled Release 53*, 145−153.

(24) Dash, P. R., Read, M. L., Barrett, L. B., Wolfert, M. A., and Seymour, L. W. (1999) Protein binding by polyelectrolyte complexes for gene delivery, *Gene Ther. 6*, 643−650.

(25) Oupicky, D., Konac, C., Dash, P., Seymour, L. W., and Ulbrich, K. Effect of albumin and polyanions on the structure of DNA complexes with polycation-containing hydrophilic nonionic blocks. *Bioconjugate Chem. 10*, 764−772.

(26) Ward, C. M., Ogris, M., Howard, K., and Seymour, L. W. Increased stability and prolonged plasma circulation of polyelectrolyte complexes containing DNA and high molecular weight poly(L-lysine) (manuscript in preparation).

(27) Ogris, M., Brunner, S., Schuller, S., Kircheis, R., and Wagner, E. (1999) PEGylated DNA/transferrin-PEI complexes: reduced interaction with blood components, extended circulation in blood and potential for systemic gene delivery. *Gene Ther. 6*, 595−605.

(28) Dash, P. R., Read, M. L., Fisher, K. D., Wolfert, M. A., Oupicky, D., Subr, V., Strohalm, J., Ulbrich, K., and Seymour, L. W., Decreased binding to proteins and cells of polymeric gene delivery vectors surface-modified with a multivalent hydrophilic polymer (submitted for publication).

(29) Fisher, K. D., Ulbrich, K., Strohalm, J., Ward, C. M., Mautner, V., Blakey, D., and Seymour, L. W. (1999) A versatile system for receptor-mediated gene delivery permits increased entry of DNA into target cells, enhanced delivery to the nucleus and elevated rates of transgene expression (submitted for publication).

BC990025R

Synthesis and Binding Properties of Oligonucleotides Carrying Nuclear Localization Sequences

Beatriz García de la Torre, Fernando Albericio,[†] Ester Saison-Behmoaras,[‡] Angela Bachi,[§] and Ramon Eritja*[,§]

Centro de Investigación y Desarrollo, C.S.I.C. Jordi Girona 18-26, E-08034 Barcelona, Spain, Department of Organic Chemistry, Universitat de Barcelona, Martí i Franquès 1-11, E-08028 Barcelona, Spain, Museum National d'Histoire Naturelle, 43 rue Cuvier Paris Cedex, France, and European Molecular Biology Laboratory, Meyerhofstrasse 1, D-69117 Heidelberg, Germany. Received April 20, 1999; Revised Manuscript Received August 5, 1999

The synthesis of oligonucleotides carrying nuclear localization peptide sequences is described using two strategies: first, oligonucleotides carrying a thiol group at the 5′ end were reacted with maleimido peptides; second, peptide and oligonucleotide were prepared stepwise on the same support, yielding oligonucleotide-3′-peptide conjugates. This second approach was thoroughly studied. Using amino acids and small peptides as model compounds, some side reactions were analyzed, detected, and minimized. Oligonucleotides complementary to Ha-*ras* gene and carrying nuclear localization peptides at the 3′ and 5′ ends were prepared. Melting temperature studies showed that duplexes containing nuclear localization peptides were more stable than duplexes with unmodified oligonucleotides. Moreover, oligonucleotide−peptide conjugates maintain a good mismatch discrimination when they bind to their target RNA.

INTRODUCTION

A large interest in oligonucleotide−peptide conjugates has arised. These conjugates are chimeric molecules constituted by oligonucleotides connected to peptide sequences and they are produced to add some of the biological and/or biophysical properties of peptides to synthetic oligonucleotides. They were first used to introduce multiple nonradioactive labels (Haralambidis et al., 1987, 1990) and as artificial sequence-specific nucleases (Corey and Schultz, 1987). Later, they were used as antisense oligonucleotides (Crooke and LeBleu, 1994). Conjugation of oligonucleotides to polylysine (Lamaitre et al., 1987), basic (Vivès and LeBleu, 1997), hydrophobic (Juby et al., 1991), fusogenic (Bongartz et al., 1994; Soukchareun et al., 1995), and signal peptides (Arar et al., 1993; Ede et al., 1994; Reed et al., 1995; Zanta et al., 1999) and penetratin (Allinquant et al., 1995) has been performed in order to increase the cellular uptake or the intracellular delivery of antisense oligonucleotides. Moreover, binding oligonucleotides to certain peptide sequences improves the binding to complementary DNA (Tung et al., 1996), the hybridization speed (Corey, 1995), the binding to RNA (Tung et al., 1995) and proteins (Lin et al., 1995), and the resistance to nucleases (Robles et al., 1997). Finally, peptide sequences have been used for encoded combinatorial libraries (Tetzlaff et al., 1998).

Two strategies can be followed to synthesize oligonucleotide−peptide hybrids. In the postsynthetic conjugation approach, the two moieties are independently prepared and thiols and maleimido groups are especially incorporated to link both molecules (Eritja et al., 1991a; Arar et al., 1993; Ede et al., 1994). In the stepwise approach, oligonucleotide−peptide conjugates are prepared by stepwise addition of amino acids and nucleobases in solid phase on the same solid support (de la Torre et al., 1994; Bergmann and Bannwarth, 1995; Soukchareun et al., 1995; Robles et al., 1997). In this case, the problem to be solved is the incompatibility of the standard schemes of protection. For example, at the end of the solid-phase peptide synthesis, a treatment with acid is usually required and can provoke partial depurination of DNA. In the synthesis of oligonucleotide 3′-peptides, this effect could be prevented using Boc-protected amino acids with Fm or Fmoc groups for the protection of side chains, a base-labile linker, and standard phosphoramidites (de la Torre et al., 1994; Bergmann and Bannwarth, 1995; Soukchareun et al., 1995; Robles et al., 1997). Moreover, protected peptide fragments (Peyrottes et al., 1998) and protected oligonucleotide (McMinn and Greenberg, 1998, 1999) fragments have been used.

In the present communication, we describe the synthesis of oligonucleotides carrying nuclear localization peptide sequences following two strategies and the binding properties of these conjugates. Our target oligonucleotide sequence is the dodecamer R5, complementary to a mutated Ha-*ras* oncogene (Duroux et al., 1995). The specific binding to mutated mRNA and not to the wild-type sequence accounts for the antiproliferative activity of R5 (Duroux et al., 1995). Thus, the discriminatory properties of the conjugates were analyzed.

EXPERIMENTAL SECTION

Peptide syntheses. The maleimido peptide carrying the SV40 nuclear localization sequence (maleimidoben-

* To whom correspondence should be addressed, Centro de Investigación y Desarrollo. Phone: 34-93-4006145. Fax: 34-93-2045904. E-mail: recgma@cid.csic.es.

[†] Universitat de Barcelona.

[‡] Museum National d'Histoire Naturelle.

[§] European Molecular Biology Laboratory.

10.1021/bc990046l CCC: $18.00 © 1999 American Chemical Society
Published on Web 09/28/1999

zoyl-Ala-Ala-Pro-Lys-Lys-Lys-Arg-Lys-Val-$CONH_2$) was prepared on polystyrene supports using Fmoc amino acids, as described in Eritja et al. (1991a). Other peptide sequences were synthesized in a homemade manual synthesizer using PEG-PS functionalized with amino groups (PerSeptive Biosystems) as starting solid support. The NPE[1] handle 2,4,5-trichlorophenyl 4-hydroxyethyl-3-nitrobenzoate [3-fold excess, Eritja et al. (1991b)] was anchored in excellent yields to the amino-PEG-PS resin when HOBt was added (3-fold excess) using DMF as solvent. The Fm handle (Rabanal et al., 1992) was coupled to the amino-PEG-PS resin following Rabanal et al. (1995). The C-terminal-protected Boc amino acid derivative (5 equiv) was reacted with the hydroxyethyl group of the NPE and Fm resins with DCC (5 equiv), DMAP (0.5 equiv) and DMF as solvent. After 2 h of coupling, unreacted hydroxyl groups were acetylated with 10% acetic anhydride in pyridine. The aminohexyl handle MMT-NH-hexyl hemisuccinate (Will et al., 1995) was coupled to the amino-PEG-PS following Gupta et al. (1995). The elongation of peptide chains was performed in DMF using 5-fold excess of amino acid Boc-protected and 5-fold excess of PyBOP for 1 h. The peptide sequences were (A) Gln-Ala-[Lys(Fmoc)]$_4$-Leu-Asp(Fm)-Lys(Fmoc) and (B) Ala-[Lys(Fmoc)]$_4$-Leu-Asp(Fm)-Lys(Fmoc). For the incorporation of Boc-Gln-OH, DIPCI and HOBt (5-fold excess) were used to avoid the formation of the nitrile.

Synthesis and Solid-Phase Coupling of the Spacer. *p*-Nitrophenyl 6-(4,4′-dimethoxytrityloxy)hexanoate was prepared as has been described for the hydroxybutyrate derivative (Haralambidis et al., 1990).

The Boc-peptide supports described above were treated with 50% TFA in DCM to remove the Boc protecting group of the last amino acid and were neutralized (5% DIEA in DCM). The resulting resins were swelled in DMF for 10 min, and then 5-fold excess of spacer dissolved in DMF was added. After 2 h, the support was washed with DMF five times, twice with DCM and once with MeOH. Finally, it was dried and stored for further use in oligonucleotide synthesis. Small aliquots of the supports carrying the peptide and the spacer were detritylated and treated with concentrated ammonia at 55 °C overnight. The resulting products were purified by reversed-phase HPLC, and the major products were collected and analyzed by MALDI-TOF mass spectrometry: HO-spacer-$AK_4LDK-CONH-(CH_2)_6$-OH, MS (MALDI-TOF) [M] = 1171.6 g/mol (M= 1171.4 g/mol calculated for $C_{55}H_{106}N_{14}O_{13}$); HO-spacer-$QAK_4LDK-CONH-(CH_2)_6$-OH, MS (MALDI-TOF) [M] = 1299.7 g/mol (M= 1299.5 g/mol calculated for $C_{60}H_{114}N_{16}O_{15}$).

Synthesis and Purification of Oligonucleotide−Peptide Conjugates. The conjugate carrying the SV40 nuclear localization sequence was prepared by conjugation of maleimido-benzoyl-Ala-Ala-Pro-Lys-Lys-Lys-Arg-Lys-Val-$CONH_2$ with 5′-thiolhexyl phosphate-CACCGACGGCGC (Eritja et al., 1991a). The thiol group at the 5′ end of the oligonucleotide was incorporated by addition of the available (Glen Research) phosphoramidite of DMT-protected bis-(6-hydroxyhexyl) disulfide. The oligonucleotide was deprotected with a solution (1 mL) of 0.1 M DTT in concentrated ammonia at 55 °C overnight as described in Gottschling et al. (1998). The desired product was characterized by amino acid analysis and enzymatic digestion. VKRKKKPAA-maleimidobenzoyl-hexylthio-CACCGACGGCGC. Amino acid analysis: Arg 1.22 (1), Ala 1.81 (2), Pro 1.04 (1), Val 1.00 (1), Lys 3.89 (4). Enzymatic analysis: dC 5.6 (6), dG 4.0 (4), dA 2.3 (2). Yield (1 μmol scale synthesis): 14 OD units at 260 nm.

The conjugates with the nucleoplasmine nuclear localization sequence were synthesized following a stepwise method. The sequences were (I) 5′ T_5-spacer-QAK_4LDK, (II) 5′ T_5-spacer-AK_4LDK, (III) 5′ CAC CGA CGG CGC-spacer-QAK_4LDK, and (IV) 5′ CAC CGA CGG CGC-spacer-AK_4LDK. Oligonucleotides were synthesized by a DNA synthesizer (Applied Biosystems 392) using standard 2-cyanoethyl phosphoramidites on 1 μmol scale. The phosphoramidites were dissolved in dry DCM (0.1 M), and a modified cycle was used. Coupling time was increased to 5 min, capping and oxidation times to 1 min, and detritylation time to 2 min (4 × 30 s). The last DMT-protecting group was not removed. The average coupling yield was >98%/step. The solid supports containing the oligonucleotide−peptide conjugates were washed with acetonitrile, treated with a 0.5 M DBU solution in acetonitrile for 5 min, washed with acetonitrile and dried. The resulting supports were finally treated with concentrated aqueous ammonia-dioxane 10:1 overnight at 55 °C. After filtration of the solid supports, the solutions were evaporated to dryness, the residues dissolved in water, and the hybrids purified using a standard two-step HPLC purification. HPLC conditions were as follows: column, Nucleosil 120-10 C_{18} (250 × 4 mm); 20 min linear gradient from 15 to 80% B and 5 min 80% B (DMT on conditions); 20 min linear gradient from 0 to 60% B (DMT off conditions); flow rate 1 mL/min; mobile phase A was 20 mM TEAA in water and B (1:1) acetonitrile: water. In the first step, truncated sequences were separated from the product containing DMT, and in the second step the desired conjugates were isolated after removal of the DMT with 80% acetic acid. Characterization of the conjugates was made by amino acid analysis after 6 N HCl hydrolysis and nucleoside analysis after enzyme digestion. Moreover, the purified products were analyzed by electrospray and MALDI-TOF mass spectrometry: T_5-spacer-$AK_4LDK-CONH-(CH_2)_6$-OH, MS (MALDI-TOF) [M] = 2692.3 g/mol (M= 2692.2 g/mol calculated for $C_{105}H_{171}N_{24}O_{48}P_5$); T_5-spacer-$QAK_4LDK-CONH-(CH_2)_6$-OH, MS (MALDI-TOF) [M] = 2820.3 g/mol (M = 2820.3 g/mol calculated for $C_{110}H_{179}N_{26}O_{50}P_5$); R5 dodecamer-spacer-$AK_4LDK-CONH-(CH_2)_6$-OH, MS (electrospray) [M] = 4848.5 g/mol (M= 4851.3 g/mol calculated for $C_{169}H_{252}N_{62}O_{83}P_{12}$); R5 dodecamer-spacer-$QAK_4LDK-CONH-(CH_2)_6$-OH, MS (electrospray) [M] = 4979.0 g/mol (M= 4979.4 g/mol calculated for $C_{174}H_{260}N_{64}O_{85}P_{12}$). Amino acid analysis of the R5 dodecamer-spacer-$QAK_4LDK-CONH-(CH_2)_6$-OH: Leu 1.00 (1), Asp 1.07 (1), Glu 1.23 (1), Lys 5.48 (5), Ala 0.86 (1). Nucleoside composition for R5 dodecamer-spacer-$QAK_4LDK-CONH-(CH_2)_6$-OH: dC 5.5 (6), dG 4.0 (4), dA 2.2 (2). The average yield of the R5 dodecamer conjugates synthesis (1 μmol scale synthesis) was 12 OD units at 260 nm.

Mass Spectrometry Analysis. Mass measurements were performed on a Bruker REFLEX MALDI time-of-

[1] Abbreviations: AmHex, 6-aminohexylsuccinyl; Boc, *t*-butoxycarbonyl; DBU, 1,8-diazabicyclo[5.4.0]undec-7-ene; DCC, *N*,*N*-dicyclohexylcarbodiimide; DCM, dichloromethane; DIEA, *N*,*N*-diisopropylethylamine; DIPCI, *N*,*N*′-diisopropylcarbodiimide; DMAP, *N*,*N*-(dimethylamino)pyridine DMF, *N*,*N*-dimethylformamide; DMT, dimethoxytrityl; DTT, dithiothreitol; Fm, fluorenylmethyl; Fmoc, fluorenylmethoxycarbonyl; HOBt, 1-hydroxybenzotriazol; MBS, *N*-succinimidyl 3-maleimido benzoate; MeOH, methanol; MMT, monomethoxytrityl; NPE, 2-(4-nitrophenyl)ethyl; PEG-PS, poly(ethylene glycol)-polystyrene; PyBOP, (benzotriazol-1-yloxy)trispyrrolidinophosphonium hexafluorophosphate, TEAA, triethylammonium acetate; TFA, trifluoroacetic acid.

flight mass spectrometer (Bruker-Franzen, Bremen, Germany) using α-cyano-4-hydroxy-cinnamic acid as matrix and the fast evaporation technique for sample preparation (Jensen et al., 1997).

Alternatively, the samples were dissolved in 50% acetonitrile and analyzed by nano electrospray on a triple quadrupole mass spectrometer on negative mode (API III, PE-Sciex, Ontario, Canada).

Evaluation of the Optical Purity of the Amino Acids. Boc amino acids were anchored on NPE-PEG-PS as described above. After removal of the Boc-protecting group, resins were treated with concentrated aqueous ammonia-dioxane 10:1 and left overnight at 50 °C. After filtration of the solid supports, the solutions were evaporated to dryness. A total of 0.2 mL of the residue was dissolved in 0.1 M $NaHCO_3$ and added to 0.2 mL of 1-fluoro-2,4-dinitrophenyl-5-L-alanine amide (FDAA) 10 mM in acetone freshly prepared. The mixture was kept for 1 h at 40 °C with frequent shaking. After cooling, 0.2 mL of 0.2 N HCl was added, and the resulting solution was analyzed by HPLC on a Nucleosil 120-10 C_{18} column (250 × 4 mm) using a 30 min gradient from 10 to100% B at a flow rate of 1 mL/min, detection at $\lambda = 340$ nm. The mobile phase A was 20 mM TEAA in water and B acetonitrile:water (1:1). Standards were prepared following the same procedure using commercially available unprotected amino acids in L- and D-form. The amino acids studied were Phe, Leu, Val, and the dipeptide Gly-Val.

Carboxylic Acid versus Carboxamide Formation during Treatment of NPE and Fm Solid Supports with Ammonia. To study the formation of carboxylic acid and/or amide at the C-terminal position of peptides when NPE and Fm supports were used, model pentapeptides (H-Tyr-Gly-Gly-Phe-Leu-OH and H-Tyr-Gly-Gly-Phe-Leu-NH_2) were prepared following standard Fmoc methodology. The same sequence (H−Phe-Gly-Gly-Phe-Leu) was assembled on PEG-PS supports carrying the NPE and Fm linkers using Boc amino acids as described above. Aliquots of the peptide supports were treated with several solutions: (a) concentrated ammonia at 55 °C, (b) 20% piperidine in DMF at room temperature, and (c) 0.1 M tetrabutylammonium fluoride in tetrahydrofuran at room temperature. At different times, the supports were filtered out and the resulting solutions were evaporated to dryness. The residues were dissolved in water and analyzed by HPLC using the same conditions as for the racemization studies. The retention time of H-Tyr-Gly-Gly-Phe-Leu-OH was 20 min and the peptide amide eluted at 24 min.

Stability of the Side Chain of Trifunctional Amino Acids during Oligonucleotide Synthesis Conditions. Dipeptides Boc-Gln-Phe, Boc-Asp(Fm)-Phe, and Boc-Lys(Fmoc)-Phe were synthesized on PEG-PS supports with the AmHex linker as described above. Aliquots of these supports were treated for 1 h at room temperature with the following solutions: (a) a 1:1 mixture of the oligonucleotide synthesis capping solutions [Cap A, acetic anhydride/lutidine/tetrahydrofuran (1:1:8) and Cap B: 0.1M *N*-methylimidazole in tetrahydrofuran]; (b) 0.05 M iodine solution in tetrahydrofuran, H_2O/pyridine (7:2:1); and (c) a 1:1 mixture of 0.1 M solution of A phosphoramidite in acetonitrile and 0.4 M tetrazol in acetonitrile. Thereafter, the supports were washed with acetonitrile, treated with a 0.5 M DBU solution in acetonitrile for 5 min, washed again with acetonitrile, and dried. The resulting supports were finally treated with concentrated ammonia at 55 °C overnight. The supernatants were concentrated to dryness and the residues were analyzed by HPLC and mass spectrometry. The desired dipeptide was obtained and no side products were found. Boc-Gln-Phe-CONH-$(CH_2)_6$-OH MS (electrospray) [M + H] = 493.4 g/mol (M = 492.6 g/mol calculated for $C_{25}H_{40}N_4O_6$); Boc-Asp-Phe-CONH-$(CH_2)_6$-OH MS (electrospray) [M] = 479.3 g/mol (M = 479.5 g/mol calculated for $C_{24}H_{37}N_3O_7$); Boc-Lys-Phe-CONH-$(CH_2)_6$-OH MS (electrospray) [M+H] = 493.5 g/mol (M= 492.6 g/mol calculated for $C_{26}H_{44}N_4O_5$).

Melting Studies. Melting experiments were carried out by mixing equimolar amounts of two dodecamer strands dissolved in a solution containing 0.15 M NaCl and 0.05 N Tris-HCl buffer, pH 7.5. Duplexes were annealed by slow cooling from 80 to 4 °C. UV absorption spectra and melting curves (absorbance vs temperature) were recorded in 1 cm path-length cells using a Varian Cary 13 spectrophotometer with a temperature controller and a programmed increase of 0.5 °C/min. Melts were run on duplex concentrations of 4 μM at 260 nm.

Binding of Oligonucleotide−Peptide Conjugates to Ha-*ras* RNA (Gel Shift Assay). 27-mer RNA (4 nM) carrying the sequence complementary to the R5 dodecamer (5′ GUG GUG GGC GCC GUC GGU GUG GGC AAG 3′) and wild-type RNA sequence (5′ GUG GUG GGC GCC GGC GGU GUG GGC AAG 3′) were radioactively labeled and incubated with unlabeled oligonucleotides in a buffer containing 40 mM Tris (pH 7.9) and 100 mM KCl. After preincubation for 15 min at 37 °C, glycerol loading buffer (80% glycerol, 0.1% xylene cyanol, 0.1% bromophenol blue) was added, and samples were electrophoresed on a 15% native polyacrylamide gel at 37 °C, using 0.05 M Tris-borate (pH 9). Hybridization to the 5′-end-labeled 27 mer (^{32}P) RNA was analyzed by quantitation of gel shifts using particle detection (Phosphorimager). The fraction of duplex is the ratio of particle counts of the double-stranded oligonucleotide−RNA complex (arrow) referred to the total (single and double stranded).

RESULTS

Synthesis of Oligonucleotide−Peptide Conjugates Using the Postsynthetic Conjugation Approach. Two types of oligonucleotide−peptide conjugates were prepared. The conjugate carrying the SV40 nuclear localization sequence was synthesized by conjugation of maleimido-benzoyl-AAPKKKRKV-$CONH_2$ with 5′-thiol-hexyl phosphate-CACCGACGGCGC, as described in Eritja et al. (1991a) (see Figure 1). The thiol group at the 5′ end of the oligonucleotide was incorporated by addition of a phosphoramidite derivative of bis-(6-hydroxyhexyl) disulfide. The maleimido peptide carrying the SV40 nuclear localization sequence (maleimidobenzoyl-AAPKKKRKV-$CONH_2$) was prepared on polystyrene supports using Fmoc amino acids (Eritja et al., 1991a).

Preliminary Studies on the Synthesis of Oligonucleotide−Peptide Conjugates Using the Stepwise Approach. Oligonucleotide−peptide conjugates carrying the nucleoplasmine nuclear localization sequence (QAKKKKLDK) were synthesized by the stepwise approach. Polyethylenglycol-polystyrene (PEG-PS) was selected as solid support since it gave the best results for the coupling of both amino acids and nucleoside phosphoramidites (de la Torre et al., 1994). Figure 2 shows the pathway followed to synthesize oligonucleotide−peptide conjugates on the same support (de la Torre et al., 1994). To avoid the use of strong acids in the presence of the oligonucleotide, the peptide part was first synthesized using the acid-labile Boc group to protect the α-amino function. The protective groups of the side

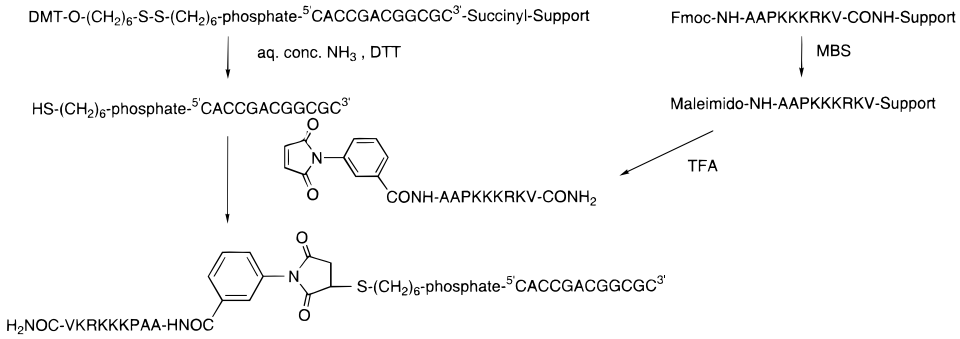


Figure 1. Synthesis of oligonucleotide−peptide conjugates following the postsynthetic conjugation approach.

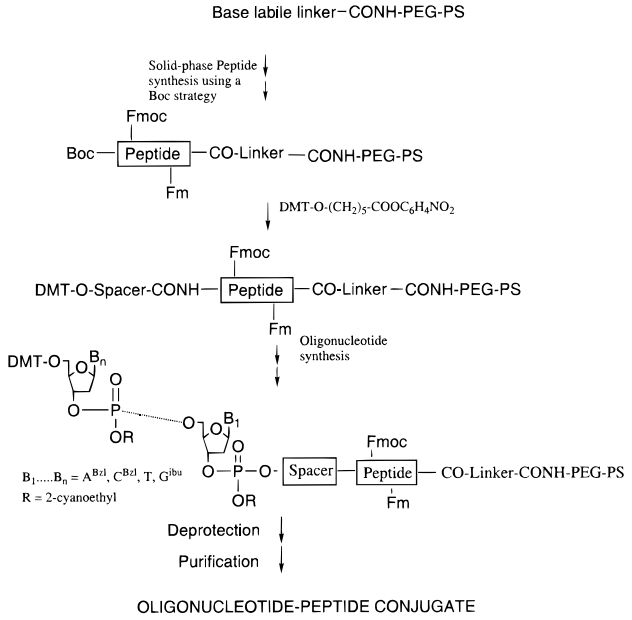


Figure 2. Synthesis of oligonucleotide−peptide conjugates following the stepwise conjugation approach.

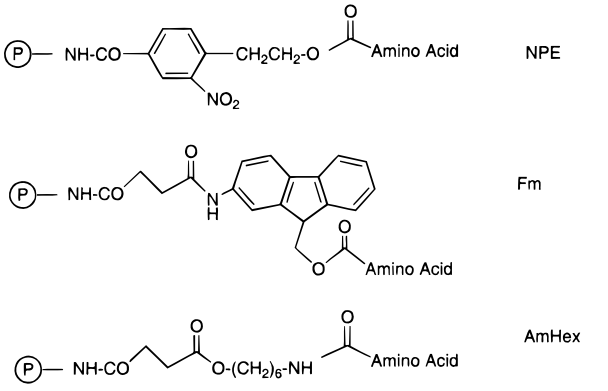


Figure 3. Base labile linker molecules used to connect the first amino acid to the solid support. P, polymer [poly(ethylene glycol)-polystyrene]; NPE, 2-(2-nitrophenyl)ethyl linker; Fm, fluorenylmethyl linker; AmHex, 6-aminohexylsuccinyl linker.

chain of the amino acids (Fmoc for Lys and Fm for Asp) and the linker of the first amino acid to the support were base labile so that they would be removed at the same time as the protective groups of the nucleobases. To that end, three base-labile linkers (see Figure 3) were examined: the 2-(2-nitrophenyl)ethyl (NPE, Eritja et al., 1991b), the fluorenylmethyl [Fm, Rabanal et al. (1992, 1995)], and the 6-aminohexylsuccinyl [AmHex, Will et al. (1995)]. The linkage between the amino acid and the NPE and the Fm linkers is excised by strong bases such

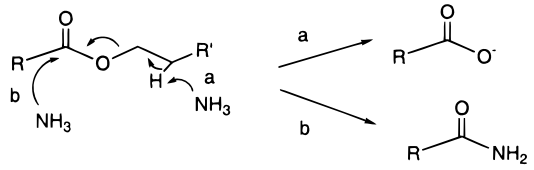


Figure 4. Ammonolysis of 2-substituted ethyl esters: Nucleophillic attack versus β-elimination mechanisms yielding peptides with carboxylic acid or carboxamide group at the C-terminus.

as piperidine or DBU following a β-elimination reaction which releases the free carboxylic function of the amino acid or peptide. In the AmHex linker, the excised bond is a succinyl ester which yields the amino acid or peptide with an aminohexylamide group at the C-terminal. Prior to the synthesis of oligonucleotide−peptide conjugates, racemization of the C-terminal amino acid was studied.

Racemization Studies on the C-Terminal Amino Acid in Base Deprotection Conditions. The synthetic protocol implies the use of basic conditions in the removal of the protective groups. Oligonucleotides are usually treated with concentrated aqueous ammonia for 16 h at 55 °C. To check the stability of the peptide part in such conditions, several amino acids and a dipeptide were attached to the support and analyzed after ammonia treatment. The possible racemization of the C-terminal amino acid due to the anchoring method or the cleavage conditions was carefully studied.

Boc-valine, Boc-leucine, and Boc-phenylalanine were incorporated to the NPE support (Albericio et al., 1991). After removal of the Boc group, the amino acyl-NPE supports were treated with concentrated ammonia. The resulting amino acids were reacted with Marfey's reagent (Adamson et al., 1992) to obtain the diastereoisomers, which were analyzed by HPLC. The free L-amino acids were obtained and no racemization was found (detection limit 0.1%), in agreement with Bray et al., who showed that there was no racemization when deblocking peptides with ammonia vapors (Bray et al., 1994). Moreover, the dipeptide Gly-L-Val was prepared on the NPE-resin, the support was treated with concentrated ammonia, and the product was reacted with Marfey's reagent. Likewise, no racemization was found, but a second product, thought to be, the dipeptideamide (Gly-L-Val-NH_2), was detected. This side product coeluted with a synthetic sample of the peptide amide. In addition to the expected β-elimination reaction of the ester, there was direct nucleophillic attack of ammonia to the ester, which resulted in the formation of the amide (Figure 4).

Carboxylic Acid vs Carboxamide Formation during Deprotection. The sequence H-Tyr-Gly-Gly-Phe-Leu (Leu-enkephaline) was selected in order to study this reaction and, therefore, synthesized on NPE and Fm handles. Independently, H-Tyr-Gly-Gly-Phe-Leu-OH and H-Tyr-

Gly-Gly-Phe-Leu-NH_2, used as controls, were synthesized following conventional solid-phase peptide protocols. Aliquots of the pentapeptide-NPE and Fm supports were treated with concentrated ammonia, 20% piperidine in DMF, and 0.1 M tetrabutylammonium fluoride. The resulting solutions were analyzed by HPLC. When concentrated ammonia at 55 °C was used, the ratio carboxylic acid:carboxamide was 50:50 on the NPE support and 75:25 on the Fm support. When 20% piperidine in DMF and 0.1 M tetrabutylammonium fluoride in tetrahydrofuran were used, only the carboxylic acid was found. In the deprotection of larger molecules, such as oligonucleotide−peptide conjugates, treatments with piperidine and, especially, fluoride were less efficient than treatment with ammonia. These results are not consistent with those described by Robles et al. (1997), who found that in fluoride solutions, oligonucleotide−peptide conjugates were released. Here, poly(ethylene glycol)-polystyrene was used as solid support, whereas Robles et al. (1997) used polystyrene. Therefore, poly(ethylene glycol) may inhibit the fluoride-catalyzed reaction. As poly(ethylene glycol) improves the coupling of phosphoramidites (de la Torre et al., 1994), we focused on the linker AmHex (Figure 3), which has been used in the synthesis of peptide nucleic acid chimeras on poly(ethylene glycol)-polystyrene supports (Will et al., 1995). The succinate bond is easily cleaved by concentrated ammonia, yielding the peptide with the *N*-(6-hydroxyhexyl)amide group at the C-terminus. This linker also allows the removal of the Fm (Asp), Fmoc (Lys), and cyanoethyl (phosphate) groups with a nonnucleophillic base (such as DBU) before ammonia deprotection. At this stage, a DBU treatment will minimize or prevent the formation of Asn from Asp(Fm) and the alkylation of lysine residues by the acrylonitrile formed during the phosphate deprotection described by Tetzlaff (Tetzlaff et al., 1998).

Stability of the Side Chains of Trifunctional Amino Acids in Oligonucleotide Synthesis Conditions. The stability of the peptide moiety in oligonucleotide synthesis conditions was also studied. Hydrophobic amino acids are stable in oligonucleotide synthesis conditions (Soukchareun et al., 1995; Robles et al., 1997; Tetzlaff et al., 1998), but to our knowledge, the behavior of trifunctional amino acids has not been thoroughly studied. To test the stability of the trifunctional amino acids belonging to the nucleoplasmine sequence, Boc-[Gln, Asp(Fm) and Lys(Fmoc)]-Phe dipeptides were prepared on PEG-PS supports with the AmHex linker. The Boc-dipeptide supports were treated with oligonucleotide synthesis reagents such as capping (acetic anhydride, *N*-methylimidazol), oxidation (iodine), and coupling (phosphoramidite and tetrazol) solutions for 1 h at room temperature. After DBU treatment and ammonia deprotection, the products were analyzed by HPLC and mass spectrometry. Only the expected dipeptides were found. To determine whether activated phosphoramidites can react with peptide bonds and/or with the primary amide group of Gln., aliquots treated with phosphoramidite and tetrazole were also treated with iodine and 2% trichloroacetic acid in DCM between the phosphoramidite treatment and deprotection. A small amount of phosphoramidite may react with peptides, as, after treatment with 2% trichloroacetic acid, a red solution was observed. The amount of DMT released from the peptide supports was 12, 15, and 14% for Boc-Lys(Fmoc)-Phe, Boc-Asp(Fm)-Phe, and Boc-Gln-Phe, respectively. No extra peak was observed on HPLC or MS analysis. Thus, the small amount of phosphoramidite addition on the peptide supports does not yield detectable side products.

Synthesis of the Oligonucleotide−Peptide Conjugates Using the Stepwise Approach. The following molecules were prepared: (I) 5′ TTTTT-spacer-Gln-Ala-Lys-Lys-Lys-Lys-Leu-Asp-Lys, (II) 5′ TTTTT-spacer-Ala-Lys-Lys-Lys-Lys-Leu-Asp-Lys, (III) 5′ CACCGACGGCGC-spacer-Gln-Ala-Lys-Lys-Lys-Lys-Leu-Asp-Lys, and (IV) 5′ CACCGACGGCGC-spacer-Ala-Lys-Lys-Lys-Lys-Leu-Asp-Lys. The pentanucleotide sequence was used to find the optimal coupling conditions. The dodecamer sequence is complementary to the mutated Ha-*ras* oncogene. The peptide sequence is the nuclear localization sequence found in nucleoplasmine. In one set of experiments (II and IV), the last glutamine was not included so that the influence of unprotected glutamine in the purity of the oligonucleotide−peptide conjugates could be studied. Although our results on model dipeptides (see above) indicated that there were no side-reactions on glutamine, the formation of N-acyl phosphoramidates has been described as side reaction of glutamine and chlorophosphines (Robles et al., 1995). First, peptide sequences were prepared on the PEG-PS support containing the aminohexyl linker (AmHex, Figure 3). Once the peptide was synthesized, a spacer molecule was added to connect the oligonucleotide by conversion of the last amino group of the peptide into an hydroxyl group protected with a DMT group. For this purpose, we used the active ester of the *O*-DMT protected derivative of the 6-hydroxy hexanoic acid [Figure 2, Haralambidis et al. (1990)]. After the addition of the linker, oligonucleotide synthesis was studied in the pentathymidine sequence I. Unexpectedly, the addition of the phosphoramidites was strongly influenced by the solvent used during the coupling reaction. We tried different combinations of acetonitrile, pyridine, DMF, and DCM. The highest coupling efficiencies (<98%) were reached when DMT-T phosphoramidite was dissolved in DCM and tetrazol was dissolved in acetonitrile or THF. We used acetonitrile for dissolving tetrazol and DCM for dissolving phosphoramidites as tetrazol dissolved in acetonitrile is available and thus, the only change required was to dissolve phosphoramidites in dry DCM instead of dry acetonitrile. From the results obtained in the manual synthesis, a new cycle for the automatic synthesizer was developed for 1 μmol scale. The following changes were applied: coupling time was increased from 25 s to 5 min; capping and oxidation times were increased to 1 min; detritylation was increased to 2 min (4 × 30 s). The detritylation rate with PEG-PS was clearly lower than with CPG because of the polyethylenglycol matrix. After these changes, the coupling yield was similar to the one found in standard conditions. For cleavage and deprotection, two consecutive treatments were applied: first a 0.5 M DBU solution in acetonitrile for 5 min and second, concentrate aqueous ammonia-dioxane 10:1 at 55 °C overnight. Oligonucleotide−peptide conjugates (I−IV) were separated from truncated sequences as DMT protected compounds (Figure 5a). After removing the DMT group with 80% acetic acid, a major product was obtained (Figure 5b) that was characterized by (i) amino acid analysis after hydrolysis 6 N HCl, (ii) nucleoside analysis after digestion with snake venom phosphodiesterase and alkaline phosphatase, and (iii) mass spectrometry (MALDI-TOF, electrospray). By mass spectroscopy, the pentanucleotides I and II were easily characterized by MALDI-TOF, whereas dodecamers III and IV only gave the correct mass on electrospray (Figure 5c). The MALDI-TOF spectra of dodecamers III and IV gave a mass corresponding to the peptide part, the spacer and a phosphate (data not shown), which was not found by electrospray. During the acquisition of the MALDI-

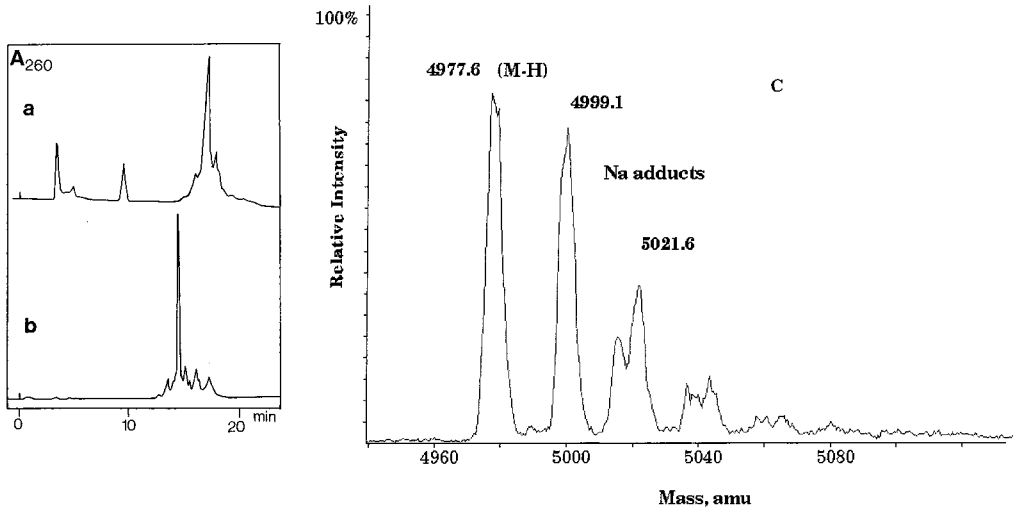


Figure 5. Purification and characterization of the dodecamer R5-QAK$_4$LDK synthesized following the stepwise approach. (a) HPLC profile of the conjugate containing the DMT group. (b) HPLC profile after removal of the DMT group. (c) Mass spectrum of the purified compound (deconvolution of the electrospray spectrum).

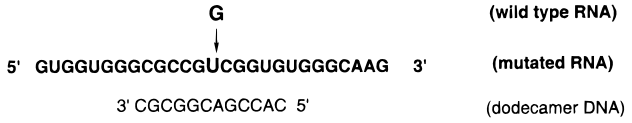


Figure 6. Sequence of 27-mer RNA and dodecamer R5.

TOF mass spectra, the phosphate bond between oligonucleotide and peptide breaks and the peptide fragment is easier to detect than the conjugate. As for pentamers I and II and dodecamers III and IV, no differences were observed, and we concluded that the presence of unprotected glutamine does not affect the purity of the oligonucleotide−peptide conjugates. Average yield for the stepwise synthesis of the R5 dodecamer conjugates was 12 OD units at 260 nm (1 μmol scale synthesis). Using the postsynthetic approach 14 OD units of the conjugate (1 μmol synthesis) were obtained.

Properties of Oligonucleotide−Peptide Conjugates. Hybridization of oligonucleotide−peptide conjugates to their complementary DNA sequence was evaluated spectrophotometrically. Melting temperatures (Tm) of dodecamer duplexes at 0.15 M NaCl, 0.05 M Tris·HCl, pH 7.5, 1 mM EDTA were as follows: unmodified R5 dodecamer (5′ CACCGACGGCGC3′) with its complementray strand (5′GCGCCGTCGGTG3′), 61.5 °C; 5′-peptide (VKRKKKPAA-R5 dodecamer), 63.5 °C; 3′-peptide (R5 dodecamer- AKKKKLDK), 62.6 °C; 3′-peptide (R5 dodecamer-QAKKKKLDK), 63.6 °C. All the oligonucleotide−peptide conjugates carrying nuclear localization sequences show a slightly higher melting temperature. The higher stability, related to the presence of positive charges of lysine and arginine side chains in the peptides, is in agreement with data on conjugates carrying basic amino acids (Eritja et al., 1991; Harrison and Balasubramanian, 1998; Zhu et al., 1993).

Binding of peptide modified dodecamers to their target RNA was analyzed by gel shift experiments. Target RNA (27 mer, Figure 6) carrying the Ha-*ras* sequence complementary to the dodecamers was radioactively labeled and incubated with dodecamers carrying the SV40 (5′-peptide) and nucleoplasmine (3′-peptide) sequences. Single-stranded RNA and dodecamer−RNA complexes were separated by polyacrylamide native gel electrophoresis (see Figure 7). One or two bands with less mobility revealed that there had been duplex formation. Double bands (especially with the 5′-peptide) indicated the presence of RNA: dodecamer−peptide complexes with different mobility. We have compared the affinity of dodecamers for the mutated Ha-*ras* and for the wild-type Ha-*ras* gene to analyze the mismatch discrimination of oligonucleotide−peptide conjugates. The dodecamer R5 is a perfect match to mutated RNA (A·U) but contains a mismatch to wild-type RNA (A·G misspair). Titration curves of unmodified and peptide-modified dodecamers with both mutated and wild type 27-mer RNA were performed (data not shown). The concentration of antisense oligonucleotide (μM) required to complex 50% of the target RNA is shown in Table 1. Peptide-modified dodecamers elicit approximately 10-fold less affinity for target RNA than the unmodified dodecamer but oligonucleotide−peptide conjugates discriminate mutated RNA from wild-type RNA.

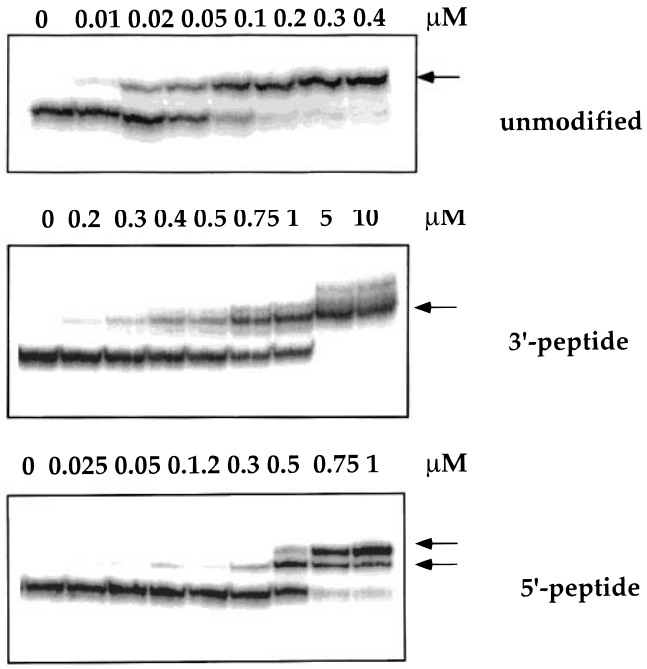


Figure 7. Binding of oligonucleotide−peptide conjugates carrying nuclear localization sequences to target 27-mer RNA by gel-shift experiments (see conditions in Experimental Section). The arrows show the position of the complex between the RNA target and the conjugate.

Table 1. Concentration of Oligonucleotide (μM) Required to Complex 50% of the RNA Target (4 nM)[a]

modification	RNA 27-mer (mutated)	RNA 27-mer (wild-type)
no	0.07	>10
5′-peptide	0.5	7.2
3′-peptide	0.7	9

[a] In the modification column: no = unmodified R5 dodecamer, 5′-peptide = VKRKKKPAA-R5 dodecamer and 3′-peptide = R5 dodecamer-QAKKKKLDK.

DISCUSSION

There is a growing interest in oligonucleotide−peptide conjugates, due to their potential use as oligonucleotide probes and antisense inhibitors of gene expression. The incorporation of peptide sequences opens the possibility of enhancing some of the biophysical and biological properties of oligonucleotides. Signal sequences (Arar et al., 1993), penetratin (Allinquant et al., 1995), and fusogenic peptides (Bongartz et al., 1994) are among the most interesting peptide sequences introduced into oligonucleotides because of their biological properties.

The aim of this study is the synthesis of oligonucleotide−peptide conjugates carrying nuclear localization sequences. Previously, oligonucleotide−peptide conjugates carrying nuclear localization sequences were found, inactive, in the freshwater ciliate *Paremecium* (Reed, 1995). Recently, it has been shown that a single nuclear localization signal sequence in a 3.3 kbp luciferase gene induces a strong transfection enhancement (Zanta, 1999). We studied the effect of the peptide sequence upon the binding properties of oligonucleotides, especially in mismatch discrimination.

Nuclear localization sequences are rich on basic amino acids, especially lysine, that may hinder the synthesis of oligonucleotide−peptide conjugates (Tetzlaff et al., 1998). For the synthesis of the conjugates, we used two approaches. First, we prepared the oligonucleotide and the peptide on separate supports following well-known methods. A thiol group was introduced at the 5′ end of the oligonucleotide and a maleimido group at the *N*-terminal position of the peptide to ensure the formation of a defined oligonucleotide−peptide conjugate (Eritja et al., 1991; Arar et al., 1993; Ede et al., 1994). Such conjugates carry the peptide moiety at the 5′ end of the oligonucleotide, which is attached to the N-terminal residue of the peptide. Likewise, other conjugates can be prepared by changing the position of the thiol and the maleimido group. Nevertheless, the most common connection between peptide and oligonucleotide in the postsynthetic conjugation approach is the N-terminus → 5′ end connection since the connecting molecules are coupled at the end of the synthesis preventing the exposure of the connecting molecules to peptide and oligonucleotide synthesis conditions. Most of the oligonucleotide−peptide conjugates described in the literature are prepared following the postsynthetic conjugation approach, which allows the use of standard conditions in the assembly of both polymers.

The synthesis of oligonucleotide−peptide conjugates following the stepwise approach is an attractive choice in the large-scale production of conjugates. In this approach, the building blocks are not the standard Boc/Bzl or Fmoc/*t*Bu-protected amino acids and the connection between peptide and oligonucleotide is N-terminus to the 3′ end because of the normal C → N and 3′ → 5′ sense of synthesis. It is also easier to assemble first the peptide using Boc chemistry without the oligonucleotide since oligonucleotides can undergo depurination during the TFA treatments needed for the removal of the Boc group. To avoid further acid treatments in the presence of oligonucleotides, the side chains of the amino acids are protected with base-labile groups. Whether the conditions used during oligonucleotide synthesis and deprotection provoke side reactions in the peptide part was also studied. To that end, we used model compounds and exhaustive characterization to analyze the possibility of racemization and the modification of the side chain of trifunctional amino acids in synthesis and deprotection conditions. The use of a special 6-aminohexyl linked prevented the formation of a mixture of products containing carboxylic acid/carboxamide at the C-terminus. This side reaction may also take place on Fm protected Asp and Glu. Moreover, alkylation of lysine residues by acrylonitrile (Telzlaff, 1998) is avoided by a two-step deprotection protocol that removes acrylonitrile before ammonia treatment, but does not prevent small amounts of several products eluting near the desired product (see Figure 5b). Nevertheless, these products can be easily separated from the desired compound. In agreement with several authors (Bermann and Bannwarth 1995, Souckchareun et al., 1995; Robles et al., 1997), we found that both postsynthetic conjugation and stepwise approaches produce the desired oligonucleotide−peptide conjugates with similar yields and purity.

All oligonucleotide−peptide conjugates carrying nuclear localization sequences hybridized with complementary sequences with a slightly higher stability than unmodified sequences. This is in agreement with the results obtained with conjugates carrying basic amino acids (Harrison and Balasubramanian, 1998; Zhu et al., 1993). On the contrary, the binding of conjugates carrying nuclear localization sequences to the target 27-mer RNA was 10-fold less efficient (see Table 1) and several complexes were found. This indicates that melting studies, although they are needed to screen high-affinity compounds, cannot be used for predicting RNA binding because of the secondary structure of RNA. To understand the binding of oligonucleotide analogues to their target RNA, further structural studies ahould be carried out. However, and despite the less efficient binding, conjugates carrying the nuclear localization sequence discriminate single-mutated RNA from wild-type RNA.

CONCLUSION

In summary, we showed that oligonucleotide−peptide conjugates carrying nuclear localization peptides can be synthesized using either a postsynthetic conjugation or a stepwise approach. These conjugates show a slightly higher affinity to complementary DNA but a lower affinity to target RNA than ummodified oligonucleotides, although they maintain a good mismatch discrimination.

ACKNOWLEDGMENT

This work was supported by funds from CICYT (PB 92-0043) and E.E.C.C. Biomed and Health Program (BMH1-CT93-1669).

LITERATURE CITED

(1) Adamson, J. G., Hoang, T., Crivici, A., and Lajoie, G. A. (1992) Use of Marfey's reagent to quantitate racemization upon anchoring of amino acids to solid supports for peptide synthesis *Anal. Biochem. 202*, 210−214.

(2) Albericio, F., Giralt, E., and Eritja, R. (1991) NPE-resin, a new approach for the solid-phase synthesis of protected

peptides and oligonucleotides. II Synthesis of protected peptides. *Tetrahedron Lett. 32*, 1515−1518.
(3) Allinquant, B., Hantraye, P., Mailleux, P., Moya, K., Bouillot, C., and Prochiantz, A., (1995) Downregulation of amyloid precursor protein inhibits neurite outgrowth in vitro *J. Cell. Biol. 128*, 919−927.
(4) Arar, K., Monsigny, M., and Mayer, R. (1993) Synthesis of oligonucleotide−peptide conjugates containing a KDEL signal sequence. *Tetrahedron Lett. 34*, 8087−8090.
(5) Bergmann, F., and Bannwarth, W. (1995) Solid phase synthesis of directly linked peptide-oligodeoxynucleotide hybrids using standard synthesis protocols. *Tetrahedron Lett. 36*, 1839−1842.
(6) Bongartz, J. P., Aubertin, A. M., Milhaud, P. G., and Lebleu, B. (1994) Improved biological activity of antisense oligonucleotides conjugated to a fusogenic peptide. *Nucleic Acids Res. 22*, 4681−4688.
(7) Bray, A. M., Jhingran, A. G., Valerio, R. M., and Maeji, N. J. (1994) Simultaneous multiple synthesis of peptide amides by the multipin method. Application of vapor-phase ammonolysis *J. Org. Chem. 59*, 2197−2203.
(8) Corey, D. R. (1995) 4800-fold acceleration of hybridization by chemically modified oligonucleotides. *J. Am. Chem. Soc. 117*, 9373−9374.
(9) Corey, D. R., and Schultz, P. G. (1987) Generation of a hybrid sequence-specific single-stranded deoxyribonuclease *Science 238*, 1401−1403.
(10) Crooke, S. T., and Lebleu, B. (1993) *Antisense Research and Applications*, CRC Press Inc., Boca Raton, FL.
(11) Duroux, I., Godard, G., Boidot-Forget, M., Schwab, G., Hélène, C., and Saison-Behmoaras, T. (1995) Rational design of point mutation-selective antisense DNA targeted to codon 12 of Ha-*ras* mRNA in human cells. *Nucleic Acids Res. 23*, 3411−3418.
(12) de la Torre, B. G., Aviñó, A., Tarrasón, G., Piulats, J., Albericio, F., and Eritja, R., (1994) Stepwise solid-phase synthesis of oligonucleotide−peptide hybrids. *Tetrahedron Lett. 35*, 2733−2736.
(13) Ede, N. J., Tregear, G. W., and Haralambidis, J. (1994) Routine preparation of thiol oligonucleotides: application to the synthesis of oligonucleotide−peptide hybrids. *Bioconjugate Chem. 5*, 373−378.
(14) Eritja, R., Pons, A., Escarceller, M., Giralt, E., and Albericio, F. (1991a) Synthesis of defined peptide−oligonucleotide hybrids containing a nuclear transport signal sequence. *Tetrahedron 47*, 4113−4120.
(15) Eritja, R., Robles, J., Fernández-Forner, D., Albericio, F., Giralt, E., and Pedroso, E. (1991b) NPE-resin, a new approach for the solid-phase synthesis of protected peptides and oligonucleotides. I Synthesis of the supports and their application to oligonucleotide synthesis. *Tetrahedron Lett. 32*, 1511−1514.
(16) Gottschling, D., Seliger, H., Tarrasón, G., Piulats, J., and Eritja, R. (1998) Synthesis of oligodeoxynucleotides containing N^4-mercaptoethylcytosine and their use in the preparation of oligonucleotide−peptide conjugates carrying c-*myc* Tag-sequence. *Bioconjugate Chem. 9*, 831−837.
(17) Gupta, K. C., Kumar, P., Bhatia, D., and Sharma, A. K. (1995) A rapid method for the functionalisation of polymer supports for solid-phase oligonucleotide synthesis. *Nucleosides Nucleotides 14*, 829−832.
(18) Haralambidis, J., Duncan, L., and Tregear, G. W. (1987) The solid-phase synthesis of oligonucleotides containing a 3′-peptide moiety. *Tetrahedron Lett. 28*, 5199−5202.
(19) Haralambidis, J., Duncan, L., Angus, K., and Tregear, G. W. (1990) The synthesis of polyamide-oligonucleotide conjugate molecules. *Nucleic Acids Res. 18*, 493−499.
(20) Harrison, J. G., and Balasubramanian, S. (1998) Synthesis and hybridization analysis of a small library of peptide−oligonucleotide conjugates. *Nucleic Acids Res. 26*, 3136−3145.
(21) Jensen, O. N., Mortensen, P., and Mann, M. (1997) Identification of the components of simple protein misxture by high-accuracy peptide mass mapping and database searching. *Anal. Chem. 69*, 4741−4750.
(22) Juby, C. D., Richardson, C. D., and Brousseau, R. (1991) Facile preparation of 3′ oligonucleotide−peptide conjugates *Tetrahedron Lett. 32*, 879−882.
(23) Lemaitre, M., Bayard, B., and LeBleu, B. (1987) Specific antiviral activity of a poly(L-Lys) conjugated oligodeoxyribonucleotide sequence complementary to vesicular stomatitis virus N protein mRNA initiation site. *Proc. Natl. Acad. Sci. U.S.A. 84*, 648−652.
(24) Lin, Y., Padmapriya, A., Morden, K. M., and Jayasena, S. D. (1995) Peptide conjugation to an in vitro-selected DNA ligand improves enzyme inhibition. *Proc. Natl. Acad. Sci. U.S.A. 92*, 11044−11048.
(25) McMinn, D. L., and Greenberg, M. M. (1998) Postsynthetic conjugation of protected oligonucleotides containing 3′-alkylamines. *J. Am. Chem. Soc. 120*, 3289−3294.
(26) McMinn, D. L., and Greenberg, M. M. (1999) Convergent solution-phase synthesis of a nucleopeptide using a protected oligonucleotide. *Bioorg. Med. Chem. Lett. 9*, 547−550.
(27) Peyrottes, S., Mestre, B., Burlina, F., and Gait, M. J. (1998) The synthesis of peptide−oligonucleotide conjugates by a fragment coupling approach. *Tetrahedron 54*, 12513−12522.
(28) Rabanal, F., Giralt, E., and Albericio, F. (1992) A new fluorene-derived anchor for solid-phase synthesis of protected peptides. *Tetrahedron Lett. 33*, 1775−1778.
(29) Rabanal, F., Giralt, E., and Albericio, F. (1995) *Tetrahedron 51*, 1449−1458.
(30) Reed, M. W., Fraga, D., Schwartz, D. E., Scholler, J., and Hinrichsen, R. D. (1995) Synthesis and evaluation of nuclear targeting peptide-antisense oligodeoxynucleotide conjugates. *Bioconjugate Chem. 6*, 101−108.
(31) Robles, J., Pedroso, E., and Grandas, A. (1995) Peptide−oligonucleotide hybrids with N-acylphosphoramidate linkages. *J. Org. Chem. 60*, 4856−4861.
(32) Robles, J., Maseda, M., Beltrán, M., Concernau, M., Pedroso, E., and Grandas, A. (1997) Synthesis and enzymatic stability of phosphodiester-linked peptide−oligonucleotide hybrids. *Bioconjugate Chem. 8*, 785−788.
(33) Soukchareun, S., Tregear, G. W., and Haralambidis, J. (1995) Preparation and characterization of antisense oligonucleotide−peptide hybrids containing viral fusion peptides. *Bioconjugate Chem 6*, 43−53.
(34) Tetzlaff, C. N., Schwope, I., Bleczinski, C. F., Steinberg, J. A., and Richert, C. (1998) A convenient synthesis of 5′-amino-5′-deoxythymidine and preparation of peptide-DNA hybrids. *Tetrahedron Lett. 39*, 4215−4218.
(35) Tung, C. H., Wang, J., Leibowitz, M. J., and Stein, S. (1995) Dual-specificity interaction of HIV-1 TAR RNA with Tat peptide−oligonucleotide conjugates. *Bioconjugate Chem. 6*, 292−295.
(36) Tung, C. H., Breslauer, K. J., and Stein, S. (1996) Stabilization of DNA triple-helix formation by appended caitonic peptides. *Bioconjugate Chem. 7*, 529−531.
(37) Vivès, E., and LeBleu, B. (1997) Selective coupling of a highly basic peptide to an oligonucleotide. *Tetrahedron Lett. 38*, 1183−1186.
(38) Will, D. W., Breipohl, G., Langner, D., Knolle, G., and Uhlmann, E. (1995) The synthesis of polyamide nucleic acids using a novel monomethoxytrityl protecting-group strategy. *Tetrahedron 51*, 12069−12082.
(39) Zanta, M. A., Belguise-Valladier, P., and Behr, J. P. (1999) Gene delivery: A single nuclear localization signal peptide is sufficient to carry DNA to the cell nucleus. *Proc. Natl. Acad. Sci. U.S.A. 96*, 91−96.
(40) Zhu, T., Wei, Z., Tung, C.-H, Dickerhof, W. A., Breslauer, K. J., Georgopoulos, D. E., Leibowitz, M. J., and Stein, S. (1993) Oligonucleotide-poly-L-ornithine conjugates: binding to complementary DNA and RNA. *Antisense Res. Dev. 3*, 265−275.

BC990046L

Polymerization of Diaspirin Cross-Linked Hemoglobin (DCLHb) with Water-Soluble, Nonimmunogenic Polyamide Cross-Linking Agents

Ton T. Hai,* David E. Pereira, Deanna J. Nelson,† Ana Srnak, and James Catarello

Corporate Research and Technical Services, Baxter Healthcare Corporation, 25212 West State Route 120, Round Lake, Illinois 60073-9799 . Received April 28, 1999; Revised Manuscript Received August 17, 1999

Diaspirin cross-linked hemoglobin (DCLHb), a human hemoglobin that is intramolecularly cross-linked between the α chains (lysine $99_{\alpha1}$−lysine $99_{\alpha2}$), was polymerized with a number of water-soluble, nonimmunogenic polyamide cross-linking agents. The degree of polymerization and the oxygen-carrying capacity depended upon the polyamide reagent, the starting concentration of DCLHb, the molar ratio of the polyamide reagent to DCLHb used, the reaction pH, and whether oxy- or deoxy-DCLHb was used in the polymerization reaction.

INTRODUCTION

It is generally accepted in the blood substitutes community that increasing the size of hemoglobin by polymerization or surface modification offers the benefits of reduced renal clearance, reduced rate of metabolism, and increased duration in the vascular circulation (*1*−*3*). Historically, this was accomplished by using reagents such as glutaraldehyde (*4*), poly(ethylene glycol) (*5*), or dextran (*6, 7*). The polymerized products were mixtures of hemoglobin, oligomers of hemoglobin, and polymers of hemoglobin having a spectrum of sizes and molecular weights. If a product in a specific size range was desired, it had to be separated from the bulk product mixture by chromatographic or ultrafiltration methods.

Because the separation of such product mixtures into the various size ranges on a commercial scale is technically difficult, time consuming, and costly, our goal was to control the product composition of hemoglobin polymerization using water-soluble, nonimmunogenic polyamide cross-linking agents (*8, 9*). These novel cross-linking agents were used to effect the polymerization of diaspirin cross-linked hemoglobin (DCLHb), a human hemoglobin that is intramolecularly cross-linked between the α chains (lysine $99_{\alpha1}$−lysine $99_{\alpha2}$) (*10, 11*). The goal of the research was to obtain a polymerized DCLHb (poly-DCLHb) product that would meet the following requirements (a) The polyDCLHb would be an oxygen-delivering solution suitable for large-volume infusions. (b) It would have a longer half-life in the systemic circulation as oxyhemoglobin than DCLHb. (c) It would have an enhanced safety profile relative to DCLHb. (d) It would have a stability profile at least equivalent to that of DCLHb.

Objectives a−c appeared to be related to the size of the polyDCLHb. We recognized that, in general, larger hemoglobins are retained longer in the vascular system. Moreover, we also recognized those polyhemoglobin molecules that are too large are prone to aggregation and/or precipitation. With this in mind, polyDCLHb synthesis was directed to obtain a polymerized DCLHb product having hemoglobin molecules with molecular mass in the range 130000−260000 Da (equivalent to dimers to tetramers of DCLHb).

To this end, we have tried various synthetic approaches in an attempt to produce a polyDCLHb solution that contained neither residual DCLHb nor high molecular mass polymer (defined as any product having a molecular mass exceeding the exclusion limit of 1×10^6 Da of a TSK G4000SW column). These experiments included the assessment of a spectrum of polyamide reagents with varying molecular masses and terminal reactive functional groups, using various concentrations of DCLHb, varying the number of molar equivalents of the polyamide reagent, and altering the reaction pH.

EXPERIMENTAL PROCEDURES

General. Diaspirin cross-linked hemoglobin (DCLHb), Plasma Lyte A, and Lactated Ringer's irrigation solution were obtained from Baxter Healthcare Corporation, Deerfield, IL. The polyamide cross-linking agents were prepared as previously described (*8*). All other commercial reagents were of the highest purity available. All solvents used were of HPLC grade.

Analytical Methods. Analytical RP-HPLC was carried out on a Vydac Protein C_4 column (5 μm, 4.6 × 250 mm). The mobile phase was delivered at 1 mL/min as a linear gradient of B (CH_3CN:H_2O:TFA, 60:40:0.1, by volume) in A (CH_3CN:H_2O:TFA, 20:80:0.1, by volume) as follows: (1) 50% B to 55% B over 20 min, (2) 55% B to 75% B over 10 min, and (3) 75% B to 85% B over 10 min. Analytes were detected by measuring the absorbance at 220 nm.

Size-exclusion chromatography (SEC) was performed using TSK G4000SW and TSK G3000SW columns (7.5 × 300 mm, TosoHaas) connected in series. Analytes were eluted with a binary mobile phase (50 mM phosphate, pH 6.5/2-propanol, 9:1 by volume) delivered at a flow rate of 1 mL/min. Analytes were detected by measuring the absorbance at 280 nm.

Oxygen equilibrium curves were recorded by reoxygenation of nitrogen equilibrated deoxyhemoglobin in 0.1 M Bis-Tris buffer (pH 7.4 at 37 °C) in the spectral cuvette of a Hemox Analyzer (TCS Medical Products Co., Huntington Valley, PA). The oxygen pressure at which

* To whom correspondence should be addressed. Phone: (847) 270-5837. Fax: (847) 270-5897. E-mail: ton_hait@baxter.com.

† Current address: Magellan Laboratories Inc., P.O. Box 13341, Research Triangle Park, NC 27709.

10.1021/bc9900486 CCC: $18.00 © 1999 American Chemical Society
Published on Web 10/15/1999

hemoglobin is half saturated (P_{50}) and the subunit cooperativity (n_{40-60}) were calculated from the oxygen equilibrium curves.

The concentrations of oxy-, deoxy-, and methemoglobin were calculated from their absorbances at three wavelengths (630, 576, and 560 nm) and the reported molar extinction coefficients (*12*). Total hemoglobin concentration was calculated by summation of the concentrations of these components, and percent methemoglobin (MetHb) was calculated as its portion of the total hemoglobin concentration. The number of reactive thiols on the polyDCLHb molecules was determined by the method of Neis et al. (*13*).

Polymerization of DCLHb with Activated Esters (1a, 1b, and 2a Reagents). *Method 1.* DCLHb polymerizations with activated esters of the polyamides were completed as follows. A solution of DCLHb in 0.1 M Hepes, pH 7, or DCLHb in Lactated Ringer's solution was deoxygenated by successive vacuum/nitrogen cycles at room temperature for 1.5 h. In some experiments, 15 molar equivalents of sodium tripolyphosphate (STP) were added to facilitate hemoglobin deoxygenation. A solution of the activated ester in deoxygenated water was added quickly to the deoxyDCLHb solution, and the resulting reaction solution was stirred at room temperature under nitrogen. The course of the reaction was monitored by SEC. When a suitable SEC profile was observed or the reaction was complete (the point at which the SEC profile no longer changed), the reaction mixture was cooled to 5 °C, and a solution of 1 M *N*-acetyl-L-cysteine (NAC), pH 9, was added (i.e., NAC/**1a**, **1b,** or **2a** molar ratio of 4:1). The solution was stirred at 5 °C under nitrogen overnight, and then the solution was dialyzed against Lactated Ringer's solution to give the final product.

Method 2. A solution of the **1a**, **1b**, or **2a** in cold, sterile water was added through a 0.2 μm pore-size filter to a deoxygenated DCLHb solution in 0.1 M Hepes, pH 8 at 5 °C. In some experiments, 15 molar equivalents of sodium tripolyphosphate were added to facilitate the hemoglobin deoxygenation. After the addition of the polyamide solution, the reaction mixture was stirred at 5 °C under nitrogen, and the course of the polymerization was monitored by SEC. When the reaction was complete, the polyDCLHb solution was reoxygenated, concentrated to 7−7.5 g/dL, and diafiltered into PlasmaLyte A solution.

Effects of DCLHb Concentration. Polymerizations of DCLHb with **1a** (MW 4200) were completed under the conditions described in method 1. In these reactions, the DCLHb concentration was varied from 3 to 15 g/dL, and the effects of DCLHb concentration on the degree of polymerization were monitored by SEC. The experimental data are summarized in Table 1 and Figure 2.

Effects of Increased Polyamide Molecular Mass. Polymerizations of DCLHb (15 g/dL) with **1a** (MW 4200) and **1a** (MW 7600) were completed as described in method 1. The polymerization was complete in about 1 h for **1a** (MW 7600) and in about 4 h for **1a** (MW 4200). The experimental data are summarized in Supporting Information, Table S-1, and Figure 3.

Effects of Changes in Reaction pH. The polymerization of DCLHb in 0.1 M Hepes, pH 8, or in 0.1 M borate buffer, pH 9, with **1a** (MW 5600) or **1b** (MW 5200) was performed as follows. A solution of DCLHb (3 g/dL) in 0.1 M borate buffer, pH 9, containing 15 equiv of STP was deoxygenated by vacuum/nitrogen cycles at room temperature for 1.5 h. The deoxygenated hemoglobin solution was cooled to 5 °C, and a deoxygenated solution of **1a** (MW 5600) or **1b** (MW 5200) in deoxygenated water was added. The solution was stirred at 5 °C under nitrogen, and the reaction was monitored by SEC. The polymerization was complete in about 3.0 h. The reaction mixture was dialyzed against PlasmaLyte A solution to give the final product. The experimental results are summarized in Supporting Information, Table S-2.

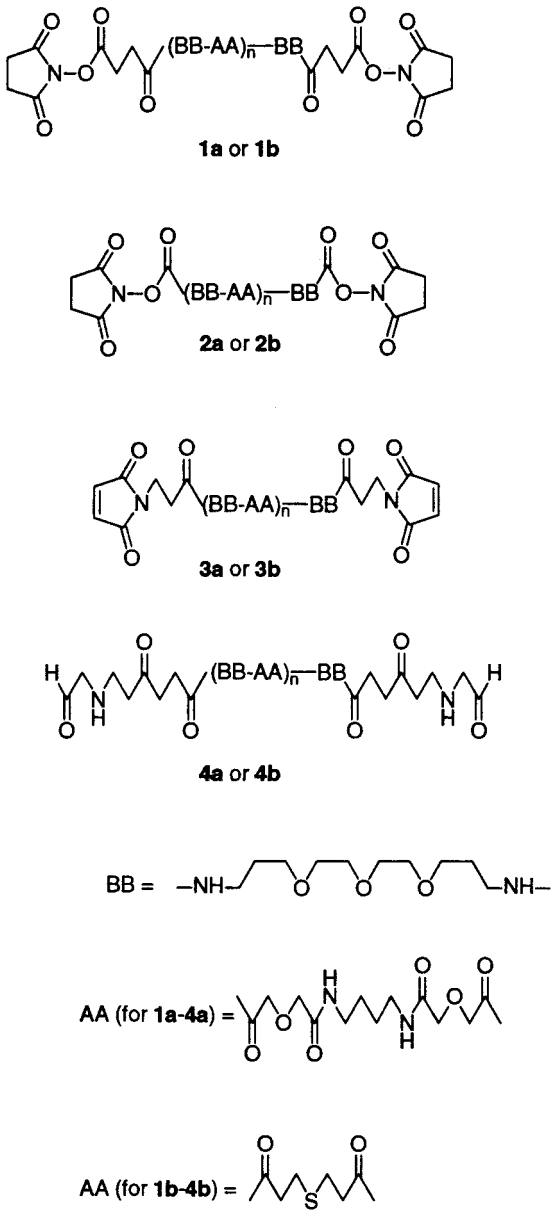


Figure 1. Polyamide reagent structures.

Polymerization of DCLHb with Maleimides [3a (MW 4080)]. A solution of DCLHb (20 g/dL) was deoxygenated by successive vacuum/nitrogen cycles for 1.5 h at room temperature. A solution of the maleimide-terminated polyamide reagent **3a** (MW 4080) in deoxygenated water was added immediately to the deoxy-DCLHb solution, and the reaction mixture was stirred at room temperature under nitrogen. The course of the reaction was followed by SEC. After 15 h, the reaction was complete. The reaction mixture was cooled to 5 °C and a solution of 1 M *N*-acetyl-L-cysteine, pH 9 [molar ratio NAC to **3a** (MW 4080) of 5] was added. The solution was stirred at 5 °C under nitrogen overnight and then dialyzed against Lactated Ringer's solution to give the final product. The experimental data are presented in Supporting Information, Table S-3.

Polymerization of DCLHb with Aldehydes (4a). A solution of DCLHb (15 g/dL) in 0.1 M Hepes, pH 7,

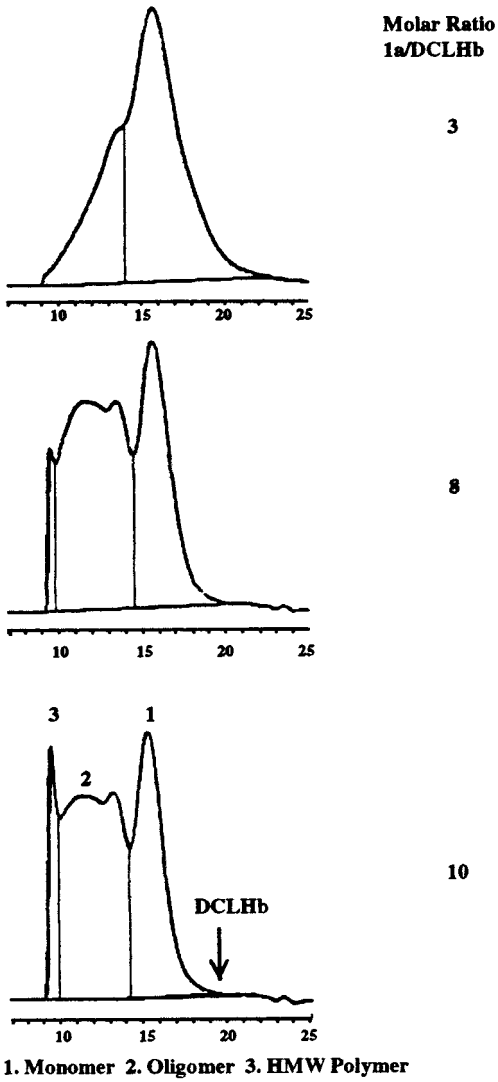


Figure 2. SEC profiles of **1a** (MW 4200) polymerized DCLHb.

was deoxygenated by successive vacuum/nitrogen cycles for 1.5 h at room temperature. A solution of **4a** (MW 4000) and a reducing agent (in a molar ratio of reducing agent to **4a** of 10) was added. When sodium borohydride was used as the reducing agent, it was added after 20 h to allow time for imine formation and to avoid reducing the aldehyde groups of **4a**. After 24 h, the reaction mixture was cooled to 5 °C, and 1.0 M glycine, pH 9 (molar ratio of glycine to **4a** of 4), and 1.0 M NAC, pH 9 (molar ratio NAC to DCLHb of 8), were added to quench the polymerization and to reduce methemoglobin, respectively. The solution was stirred under nitrogen at 5 °C overnight and then dialyzed against Lactated Ringer's solution to give the final products. The experimental results are summarized in Supporting Information, Table S-3.

Effects of Polymerization with OxyDCLHb. A solution of oxy- or deoxy-DCLHb in 0.1 M Hepes, pH 8, in the presence of 15 molar equivalents of STP was employed. The reactions were generally conducted as described in method 1. Experimental results are summarized in Supporting Information, Table S-4.

RESULTS AND DISCUSSION

Polymerization of DCLHb with Polyamide Cross-Linking Agents. All of the polyamide cross-linking agents employed in these studies were bifunctional reagents. The activated bis(*N*-oxysuccinimidyl) diesters **1a** and **1b** can react with the ϵ-amino groups of lysine residues or the N-terminal amino groups of hemoglobin to form amide linkages between the polyamide and the protein. Maleimide derivatives, such as **3a** and **3b**, can react with lysine or cysteine residues of hemoglobin to form C−N and C−S linkages, respectively. **2a** and **2b** (that contain succinimidyl-N-oxycarbonyl end groups) can react with lysine residues or the N-terminal amino groups of hemoglobin to form urea linkages. The polyamide bis(aldehyde) **4a** and **4b** can polymerize DCLHb via reductive amination reactions, to yield DCLHb molecules linked by covalent C−N bonds.

If both reactive end groups of a polyamide react with different DCLHb molecules, an intermolecularly cross-linked polyDCLHb is produced, and the SEC retention time is decreased. In contrast, if only one reactive terminus reacts with a DCLHb molecule and the other reactive terminus is deactivated (i.e., via hydrolysis), surface modification of DCLHb will result. As is true of a polyDCLHb, the SEC retention time of a surface-modified DCLHb is decreased, but not as greatly as when DCLHb is polymerized.

Historically, the size of hemoglobin derivatives has been assessed using size-exclusion chromatography (SEC). A series of protein standards having known molecular weights typically are used to calibrate the chromatographic conditions, so that retention times may be correlated with the molecular weight. A shortcoming of this relationship is that its rigor depends on the similarity of the test articles to the protein standards. The polyDCLHb derivatives we have evaluated have been modified using polyamides that both modify the surface and polymerize the protein. This type of modification renders them different from the protein standards. Therefore, the chromatographic retention time does reflect the relative size of the polyDCLHb molecules being separated, but it cannot be used to vigorously establish molecular weights.

The targeted polymerized DCLHb product would be devoid of monomer (DCLHb) and high molecular mass polymers (defined as products having with molecular masses that exceed the exclusion limit of 1×10^6 Da a of TSK G4000SW column). With this objective in mind, the molecular mass of the polyamide, the polyamide reactive end groups, the DCLHb concentration, the number of molar equivalents of polyamide used (relative to DCLHb), and the reaction pH were varied. In addition to these reaction parameters, the effects of sodium tripolyphosphate (STP) on the polymerization of DCLHb were studied. In general, the methemoglobin content increased from 3 to 10% during the polymerization reaction. Methemoglobin is the oxidized form (Fe^{2+} to Fe^{3+}) of hemoglobin and is nonfunctional, that is, does not transport oxygen. Therefore, to minimize the methemoglobin content of the polyDCLHb molecules, *N*-acetyl L-cysteine was added to the deoxygenated product. The reduction of methemoglobin was allowed to take place over a 12−24 h period prior to product workup.

The effects of the DCLHb concentration on the course of polymerization were studied using **1a** (MW 4200) (Table 1 and Figure 2). In general, polymerization of DCLHb with this polyamide gave a product mixture having a SEC profile consisting of three peaks. These peaks were identified as "monomer" (DCLHb and surfaced modified DCLHb), "oligomers" of DCLHb, and "high molecular weight (HMW) polymers" of DCLHb that eluted in the excluded volume of the column.

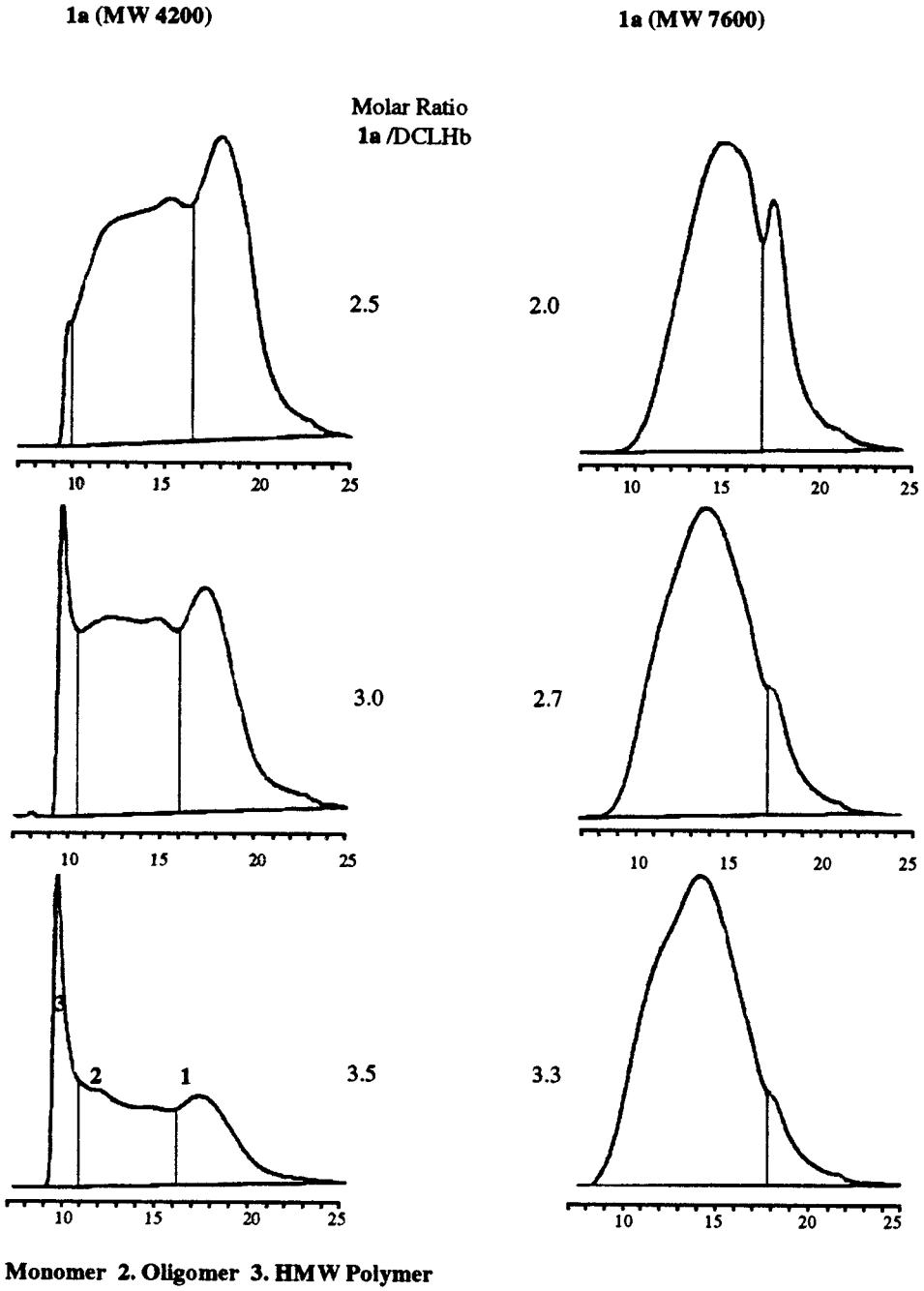


Figure 3. Comparison of the SEC profiles of **1a** (MW 4200) and **1a** (MW 7600) polymerized DCLHb.

As expected, the data indicate that high DCLHb concentrations favor the formation of polymeric products, even when low molar ratios of the cross-linker to DCLHb were used. Thus, when the DCLHb concentration was 15 g/dL, the use of 3 molar equivalents of **1a** (MW 4200) gave a product in which 60% of the DCLHb had been polymerized. In contrast, when the DCLHb concentration was 6 or 3 g/dL, the use of 3 molar equivalents of **1a** (MW 4200) gave only 37 and 22% polymerized hemoglobin, respectively.

The polymerization of DCLHb at higher DCLHb concentrations was difficult to control. The use of 2.5 molar equivalents of **1a** (MW 4200) and a DCLHb concentration of 15 g/dL yielded a product mixture containing 2% of the undesired HMW polymers. The data are presented in Table 1. If the number of molar equivalents of the cross-linker was increased in an attempt to increase the extent of polymerization, the percentage of undesired HMW polymers increased rapidly. However, if the DCLHb concentration was 3 g/dL (the lowest concentration that is practical for commercial manufacture), as many as 7 molar equivalents of **1a** (MW 4200) could be used for polymerization. These conditions provided a product that was 50% polymerized and contained no HMW polymers. Moreover, the shift in retention times of the monomers indicated that the product was extensively surface modified. Surface modification of DCLHb may enhance the longevity in the systemic circulation and the biocompatibility of the polyDCLHb. Thus, the degree of polymerization and product composition could be controlled by altering the concentration of DCLHb and the molar ratio of the polyamide reagent to DCLHb.

The molecular mass of the polyamide reagent played a key role in maximizing the efficiency of the polymerization reaction. DCLHb is a globular protein having a diameter of about 60 Å. Because of this relative bulki-

Table 1. Effect of DCLHb Concentration on the Polymerization Profile Obtained with 1a (MW 4200)

molar ratio of PA to DCLHb	SEC profile: % monomer (RT)[a]	SEC profile: % oligomer	SEC profile: % HMW polymer	P_{50} (mmHg) (*n*)
DCLHb				
0	100 (19.9)	0	0	32 (2.6)
[DCLHb] = 15 g/dL, no STP				
2.5	44 (18.1)	54	2	27 (1.7)
3	39 (17.3)	48	13	29 (1.6)
3.5	55 (17.4)	34	33	32 (1.7)
4	gel			
[DCLHb] = 10 g/dL, no STP				
1	100 (18.9)	0	0	30 (1.9)
1.5	54 (18.2)	46	0	33 (1.8)
2	41 (18.3)	58	1	30 (1.7)
2.5	33 (18.0)	60	7	31 (1.6)
3	23 (17.4)	50	27	36 (1.7)
[DCLHb] = 6 g/dL, no STP				
2	72 (18.3)	28	0	ND
3	63 (17.5)	37	0	38 (1.9)
4	47 (16.9)	50	3	42 (1.9)
5	38 (16.5)	46	16	42 (1.6)
6	27 (16.0)	33	40	44 (1.7)
[DCLHb] = 3 g/dL, no STP				
3	78 (17.3)	22	0	39 (1.9)
4	72 (17.0)	28	0	40 (1.8)
5	68 (16.6)	32	0	44 (1.9)
6	51 (16.0)	49	0	49 (1.8)
7	49 (15.6)	51	0	50 (1.7)
8	37 (15.9)	58	5	46 (1.5)
10	35 (15.4)	54	11	52 (1.6)
[DCLHb] = 3 g/dL, 15 molar equivalents STP (relative to DCLHb)				
3	64 (17.2)	36	0	30 (1.9)
4	49 (16.5)	51	0	30 (1.8)
5	41 (16.3)	59	0	29 (1.8)
6	36 (15.9)	62	2	32 (1.7)
7	36 (16.3)	58	6	28 (1.6)
8	30 (16.5)	59	11	30 (1.7)

[a] Number in parentheses is the elution time in minutes of the corresponding peak maximum.

ness, a longer chain polyamide would be expected to facilitate intermolecular linking of DCLHb molecules; thus, the efficiency of polymerization was expected to increase with the chain length of the cross-linker. This was indeed the case. A comparison of the extent of DCLHb polymerization with **1a** (MW 4200) and (the longer) **1a** (MW 7600) shows that as much as 90% polymerization could be obtained with **1a** (MW 7600). Moreover, no HMW polymers formed when the higher molecular weight (longer chain) **1a** (MW 7600) was used (Table S-1). Thus, a shorter chain cross-linking agent is more useful for surface modification and polymerizing DCLHb, while a polyamide with a longer chain provides a higher degree of polymerization**.** Representative SEC profiles are shown in Figure 3.

The polyamide cross-linking agents **1a** and **1b** contain reactive end groups that can be hydrolyzed; therefore, the reaction pH can affect the extent of polymerization. In a solution that contains DCLHb, the reagents **1a** or **1b** can react either with the amino groups on DCLHb to form amide bonds or can be hydrolyzed by water to carboxylic acids that can no longer react with DCLHb. Therefore, if one of the end groups of the polyamide reagent reacts with DCLHb via aminolysis and the end group under goes hydrolysis, surface modification of DCLHb will result. Thus, the reaction of a **1a** or **1b** derivative with DCLHb affords a mixture of polyDCLHb and surface-modified DCLHb molecules in which the ratio of polymerized to surface-modified DCLHb molecules is dependent on the relative rates of aminolysis and hydrolysis of the activated end groups of the polyamides. Because the nucleophilicity of the amino groups of DCLHb depends on their lack of protonation, the rate of aminolysis will depend on the buffer pH.

The effect of the buffer pH on the degree of polymerization was evaluated by performing DCLHb polymerizations at pH 8 (0.1 M Hepes) and pH 9 (0.1 M borate) and comparing the product profiles. The product distribution of the polymerization of deoxyDCLHb (3 g/dL) at 5 °C in 0.1 M Hepes, pH 8, or 0.1 M borate, pH 9, containing 15 molar equivalents of STP were compared using both **1b** (MW 5200) and **1a** (MW 5600). The data presented in Table S-2 illustrate several points. First, using the same Polyamide/DCLHb molar ratio, reactions performed at pH 9 gave polyDCLHb containing less surface-modified DCLHb (monomer) and more oligomers than those performed at pH 8. For example, at pH 8, polymerization of DCLHb (3 g/dL) with 3.5 molar equivalents of **1b** yielded a product mixture containing 8% surface modified DCLHb and 90% oligomers, about 1/4 of which were the higher molecular weight Oligomer II fraction, defined as molecules with peak maxima having retention times of 11.0−14.7 min. At pH 9, oligomerization was almost quantitative; the corresponding product mixture contained at most traces of surface-modified DCLHb, and approximately a third was the Oligomer II fraction.

Similar results were obtained with **1a** (MW 5600). For example, with a **1a**/DCLHb molar ratio of 3, at pH 8, polymerization with **1a** (MW 5600) yielded a product mixture containing 10% surface-modified DCLHb and 90% oligomers, about 1/3 of which were the higher molecular weight Oligomer II fraction. In contrast, at pH 9, the corresponding product mixture contained 5% surface-modified DCLHb and 95% oligomers, approximately half of which are the Oligomer II fraction. Second, similar polyDCLHb profiles could be obtained by using lower polyamide/DCLHb molar ratios if the reaction was performed at pH 9 rather than at pH 8. For example, the polyDCLHb obtained from **1b** (MW5200) at pH 9 using a 3:1 molar ratio of **1b**/DCLHb had a similar SEC profile to that obtained at pH 8 using a 3.5:1 molar ratio of **1b**/DCLHb. Finally, the P_{50} and n values of Poly-DCLHb derived from **1b** were not extensively affected by the reaction pH.

The effect that competitive hydrolysis of a reactive end group of a polyamide has on the extent of polymerization was demonstrated by the comparison of the polymerization of DCLHb with **1a** (MW 4200) (a cross-linking agent subject to hydrolysis) with the polymerization observed using **3a** (MW 4080), a maleimide-terminated cross-linker of comparable length that will not hydrolyze under the reaction conditions. The reactions of the two cross-linkers were similar in two respects: (a) the yield of the oligomer increased with the number of molar equivalents of cross-linker used and (b) the elution times of the monomer decreased with the number of molar equivalents of cross-linker used, indicating that surface modification of DCLHb had occurred. The data are presented in Tables S-2 and S-3.

The reactions of these two cross-linkers also differed in two other respects. First, the RP-HPLC profiles (Figure 4) suggest that **3a** (MW 4080) reacted specifically with DCLHb. A new peak, the β_1 peak, was detected at all ratios of **3a** (MW 4080) tested. Maleimide reagents, such as **3a**, are expected to bind specifically to cysteine-β 93 residues, and this modification would shift the retention time of the β-subunit. Specific reaction of the β-chain was also supported by the decrease in titratable thiol residues (Figure 5); about 65 and 90% of the titratable thiol groups are modified when 1 and 2 equiv of **3a** (MW 4080) are used, respectively. Second, thiol modification by **3a** (MW 4080) resulted in a decrease in the P_{50} values of the polymerized products to 18−20 mmHg, whereas modification by **1a** did not effect the P_{50} values under similar reaction conditions. A decrease in the P_{50} value is an expected consequence of cysteine-β 93 modification (*14*, *15*).

Finally, the effectiveness of two other types of polyamide cross-linking agents was assessed. DCLHb was polymerized with **4a** (MW 4000), a polyamide containing aldehyde end groups, via reductive amination. The reductive amination reactions were performed in 0.1 M Hepes, pH 7.0, in the presence of either sodium cyanoborohydride, borane-pyridine, sodium borohydride, or borane-dimethylamine. The data are presented in Table S-3. Unexpectedly, we found that reduction of the imine with borane-dimethylamine or sodium borohydride did not produce polyDCLHb, although other investigators have reported that these are useful reducing agents for reductive amination reactions (*16*). In contrast, when either sodium cyanoborohydride or borane-pyridine was used, **4a** (MW4000) provided both surface-modified and polymerized DCLHb, although the efficiency of the latter was modest. Under the best conditions found, the polymerized products still contain 38−48% of modified

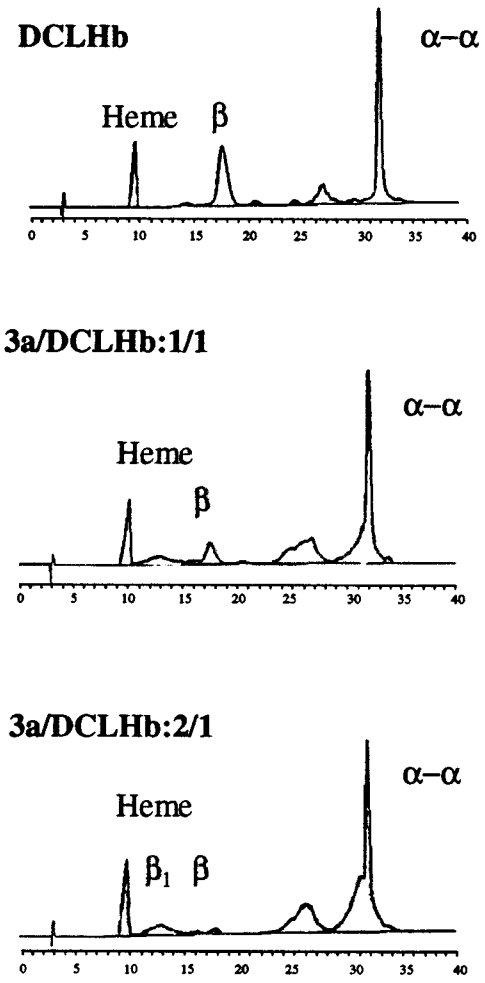


Figure 4. Reversed-phase HPLC profiles of **3a** (MW 4800) polymerized DCLHb.

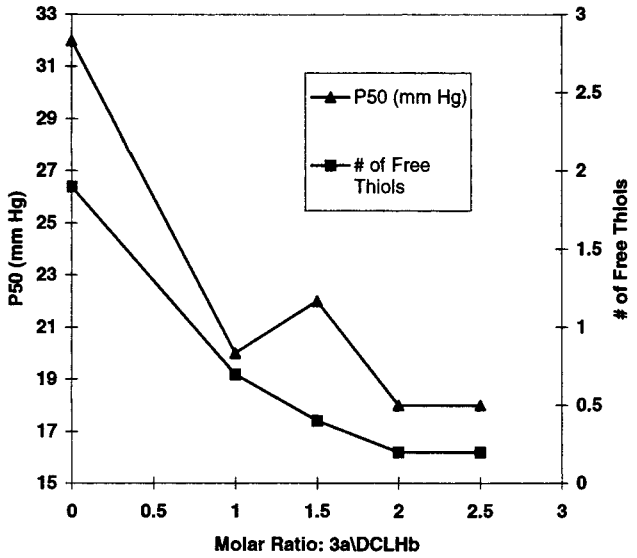


Figure 5. Relationship between the number of free thiols and the P_{50} value of **3a** polymerized DCLHb.

monomer. Reduction with borane-pyridine produced a polyDCLHb having values of P_{50} and n in the range 33−36 mmHg and 1.9−2.1, respectively. Thus, the polymerization of DCLHb by reductive amination maintained the P_{50} value and cooperativity of DCLHb.

DCLHb was also polymerized with **2a** (MW 2800) and **2a** (MW 5600), polyamides having succinimidyl-*N*-oxy-

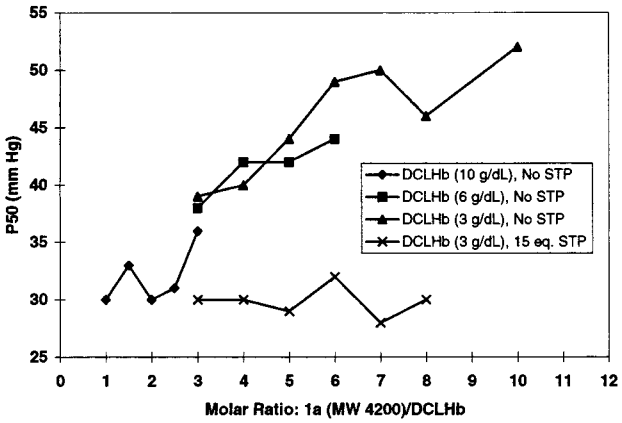


Figure 6. Relationship between the P_{50} value of polymerized DCLHb and the concentration of DCLHb.

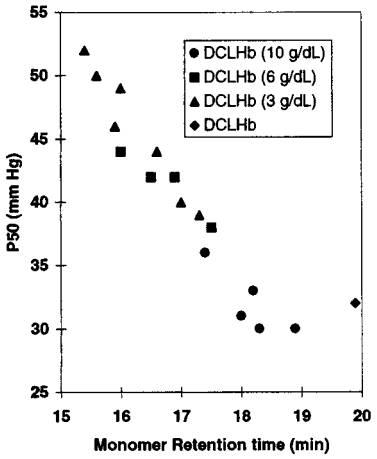


Figure 7. Relationship between the P_{50} value and the retention time of the monomer peak of **1a** (MW 4200) polymerized DCLHb.

carbonyl (activated urethane) termini. In each case, a 3 g/dL deoxyDCLHb solution in 0.1 M Hepes, pH 8, was allowed to react at 5 °C. Six molar equivalents of **2a** (MW 2800) and 4 molar equivalents of the longer **2a** (MW 5600) were used in the respective polymerizations. Both polyDCLHbs had acceptable SEC profiles and appeared to be suitable for additional biological screening. However, the SEC profiles changed during refrigerated storage of the products, suggesting that the resulting urea linkages were unstable.

Controlling the Oxygen-Binding Characteristics of the PolyDCLHbs. Three means for controlling the oxygen-binding characteristics of the polyDCLHb products were studied. First, the polymerization reaction was performed in the presence of STP. Under these conditions, the P_{50} of the product was maintained in the range 27−36 mmHg, the same range as that of DCLHb. However in the absence of STP, the P_{50} of the product was dependent upon the starting concentration of DCLHb used in the polymerization and the molar equivalents of the polyamide reagent used. The data are presented in Figure 6. For each concentration of DCLHb used, the P_{50} increased with an increase in the molar equivalents of the polyamide used in the reaction. The highest P_{50} values were obtained with dilute starting concentrations of DCLHb. It was also noted, as the graph in Figure 7 illustrates, that there is an approximately linear relationship between the P_{50} value of the polyDCLHb solution and the SEC retention time of the monomer. The data suggest that an increase in the extent of surface modification of DCLHb correlates with an increase in the P_{50} value of the polymerized product.

A comparison of the SEC profiles of the polymerized products indicates that STP has no detectable effect on the product composition despite the effect on the P_{50} value. Since STP is known to bind to hemoglobin at the 2,3-diphosphoglycerate (DPG) binding site (*17*, *18*), one reasonable interpretation of this observation is that the presence of STP in the DPG-binding site protects the amino acid residues in that region from modification by **1a** (MW 4200).

Altering the reactive end group provided a second means for controlling the oxygen-binding characteristics of the polyDCLHb products. A P_{50} value of about 20 mmHg and a decrease of the cooperativity value to 1.7 (n_{40-60}) were obtained by polymerization with a polyamide containing a maleimide end group such as **3a** (MW 4080). As shown in Figure 5**,** the alkylation of the thiols of cys β93 has a profound effect on the oxygen binding characteristics of the polymerized products.

Last, the oxygen-binding characteristics of the poly-DCLHb products could be modified by polymerization of either oxyDCLHb or deoxyDCLHb. Other investigators have shown that polymerization in the T-conformation of hemoglobin (deoxyHb) or in the R-conformation (oxyHb) yields polymerized hemoglobins that are partially locked in the T- or R-conformation, respectively (*2*). The oxygen affinity of a polyHb prepared from a T-state Hb is expected to be different from that prepared from a R-state Hb. To demonstrate that this also applied to the polyamide-polymerized DCLHb, deoxyDCLHb (3 g/dL or 6 g/dL) or oxyDCLHb (3 g/dL or 6 g/dL) in 0.1 M Hepes, pH 8, was polymerized with **1a** (MW 5600) in the presence of 15 molar equivalents of STP at 5 °C. In general, SEC profiles of the polyDCLHbs produced under these conditions gave four SEC bands: monomer band, oligomer I band (defined as molecules having peak maxima with retention times of 15.2−17.2 min), oligomer II band (defined as molecules having peak maxima with retention times of 11.0−14.7 min), and HMW polymer band (defined as molecules having molecular sizes exceeding the exclusion limit of the columns) (see Table S-4). When oxyDCLHb was polymerized with **1a** (MW 5600), the polyDCLHb products had P_{50} and n values in the range of 18−27 mmHg and 1.5−2.3 (n_{40-60}), respectively. In contrast, when deoxyDCLHb was polymerized, these values were in the range of 23−36 mmHg and 1.8−2.5(n_{40-60}), respectively.

In summary, we have demonstrated the ability to control the polymerization of DCLHb and the oxygen-binding properties of the polyDCLHb product. This was accomplished by either altering the polyamide cross-linking reagent, the reaction pH, the DCLHb concentration, the molar equivalents of the polyamide reagent, or by conducting the polymerization with either oxy- or deoxyDCLHb.

Supporting Information Available: Data describing the polymerized DCLHb products are presented in Tables S-1−S-4. This material is available free of charge via the Internet at http://pubs.acs.org.

LITERATURE CITED

(1) Bolin, R., and DeVenuto, F. (1983) Hemoglobin solution as a blood substitute. *Adv. Blood Res.* 1−7.

(2) Labrude, P., Chaillot, B., Dellacherie, E., Stoltz, J. F., and Vigneron, C. (1986) Hemoglobin solutions as oxygen carriers: Ligands and other molecules interactions with hemoglobin. *Adv. Biosci. 54*, 161−172.

(3) Leonard, M., Neel, J., and Dellacherie, E. (1984) Synthesis of monomethoxypolyethylene-bovine hemoglobins. *Tetrahedron 40*, 1581−1584.

(4) Sehgal, L. R., Rosen, A. L., Gould, S. A., Sehgal, H. L., and Moss, G. S. (1983) Preparation and in vitro characteristics of polymerized pyridoxylated hemoglobin. *Transfusion 23*, 158−162.

(5) Iwasaki, K., Iwashita, Y., and Okami, T. (1987) *Hemoglobin combined with a poly(alkylene oxide)*, U.S. Patent 4,670,417.

(6) Tam, S. C, Blumenstein, J., and Wong, T. F. (1976) Soluble dextran-hemoglobin complex as potential blood substitute. *Proc. Natl. Acad. Sci. U.S.A. 73*, 2128−2131.

(7) Chang, J. E., and Wong, T. F. (1977) Soluble dextran-hemoglobin complexes of different molecular sizes. *Can J. Chem. 55*, 398−403.

(8) Hai, T. T., Pereira, D. E., and Nelson, D. J. (1998) Synthesis of water soluble, non immunogenic polyamide cross-linking agents. *Bioconjugate Chem. 9*, 645−654.

(9) Hai, T. T., and Nelson, D. J. (1994) Water soluble, non immunogenic polyamide cross-linking agents. *PTC Int. Appl.* WO 94/12220.

(10) Hai, T. T., Nelson, D. J., and Srnak, A. (1992) *Process for the production of cross-linked hemoglobin in the presence of sodium tripolyphosphate*, U.S. Patent 5,128,452.

(11) Chatterjee, R., Welty, E. V., Walder, R. Y., Pruitt, S. L., Roger, P. H., Arnone, A., and Walder, J. A. (1986) Isolation and characterization of a new hemoglobin derivative cross-linked between the α chains (Lysine $99_{\alpha 1}$-Lysine $99_{\alpha 2}$). *J. Biol. Chem. 261*, 9929−9937.

(12) Van Assendelft, O. W., and Zijlstra, W. G. (1975) Extinction coefficients for use in equations for the spectrophotometric analysis of hemoglobin mixtures. *Anal. Biochem. 69*, 43−48.

(13) Neis, J. M., Van Gemert, P. J. L., Roelofs, H. M. J., and Henderson, P. T. H. (1984) Disappearance of free SH-groups in hemoglobin of man, rat and rabbit after exposure to alkylating agents in vitro. *Toxicology 31*, 319−327.

(14) Riggs, A. (1961) The binding of *N*-Ethylmaleimide by human hemoglobin and its effect upon the oxygen equilibrium. *J. Biol. Chem. 236*, 1948−1954.

(15) Garel, M. G., Beuzard, Y., Domenget, C., Martin, J., Galacteros, F., and Rosa, J. (1982) Binding of 21 thiol reagents to human hemoglobin in solution and intact cells. *Eur. J. Biochem. 123*, 513−519.

(16) Geoghegan, K. F., Cabacungan, J. C., Dixon, H. B. F., Feeney, R. E. (1981) Alternative reducing agents for reductive methylation of amino groups in proteins. *Int. J. Pept. Protein Res. 17*, 345−352.

(17) Chanutin, A., and Herman, E. (1969) The interaction of organic and inorganic phosphates with hemoglobin. *Arch. Biochem. Biophys. 131*, 180−184.

(18) Chanutin, A., and Curnish, R. R. (1967) Effect of organic and inorganic phosphates of the oxygen equilibrium of human erythrocytes. *Arch. Biochem. Biophys. 121*, 96−102.

BC9900486

© 1999 American Chemical Society, Bioconjugate Chem., Hai bc9900486 Supporting Info Page 1

Polymerization of Diaspirin Crosslinked Hemoglobin (DCLHb) with Water Soluble, Non Immunogenic Polyamide Crosslinking Agents.

Ton T. Hai*, David E. Pereira, Deanna J. Nelson, Ana Srnak and James Catarello.
Corporate Research and Technical Services, Baxter Healthcare Corporation
25212 West State Route 120, Round Lake, IL 60073-9799 USA

Supporting Information

Table S-1. Effect of Polyamide Chain Length on the Course of Polymerization

Molar ratio of PA to DCLHb	SEC Profile			P_{50}, mm Hg (n)
	% Monomer (RT)[a]	% Oligomer	% HMW Polymer	
DCLHb				
0	100 (19.9)	0	0	32 (2.6)
1a (MW 4200), [DCLHb] = 15 g/dL				
2.5	44 (18.1)	54	2	27 (1.7)
3	39 (17.3)	48	13	29 (1.6)
3.5	55 (17.4)	34	33	32 (1.7)
4	gel	-	-	
1a (MW 7600), [DCLHb] = 15 g/dL				
2.0	57 (19.5)	43	0	28 (2.2)
2.7	24 (19.3)	76	0	29 (1.9)
3.3	9 (19.1)	91	0	29 (1.9)

[a] Number in parentheses is the elution time in minutes of the corresponding peak maximum.

© 1999 American Chemical Society, Bioconjugate Chem., Hai bc9900486 Supporting Info Page 2

Table S-2. Effect of pH on the Polymerization Profile of DCLHb

Molar ratio of PA to DCLHb	SEC Profile[a]			P_{50}, mm Hg (n)
	% Monomer (RT)	% Oligomer I	% Oligomer II	
DCLHb				
0	100 (19.9)	0	0	32 (2.6)
1b (MW 5200), 0.1 M HEPES, pH 8				
2	33 (19.4)	58 (18.1)	8 (shoulder)	ND
2.5	21 (19.3)	67 (18.1)	11 (shoulder)	31 (2.3)
3	13 (19.1)	69 (17.5)	17 (shoulder)	31 (2.2)
3.5	8 (19.0)	69 (17.2)	21 (shoulder)	32 (2.1)
4	4 (shoulder)	70 (16.8)	24 (14.2)	33 (2.1)
4.5	-	72 (16.7)	27 (14.0)	33 (2.1)
1b (MW 5200), 0.1 M Borate, pH 9				
2	19 (19.1)	60 (18.1)	20 (shoulder)	30 (2.2)
2.5	10 (shoulder)	71 (17.5)	17 (14.9)	30 (2.1)
3	6 (shoulder)	66 (17.2)	27 (14.6)	29 (2.1)
3.5	-	66 (16.9)	33 (14.6)	32 (1.9)
4	-	64 (16.8)	35 (14.3)	31 (1.9)
1a (MW 5600), 0.1 HEPES, pH 8				
2.5	15 (19.4)	66 (17.1)	17 (shoulder)	30 (2.4)
3	10 (19.3)	65 (16.1)	25 (shoulder)	29 (2.3)
3.5	6 (19.3)	64 (16.4)	29 (shoulder)	28 (2.3)
4	3 (19.3)	61 (15.8)	34 (shoulder)	30 (2.3)
1a (MW 5600), 0.1 Borate, pH 9				
2	13 (19.3)	52 (17.3)	35 (shoulder)	30 (2.3)
2.5	8 (19.3)	54 (16.9)	36 (14.0)	29 (2.4)
3	5 (18.9)	50 (16.5)	44 (13.8)	29 (2.3)
3.5	3 (18.9)	48 (16.1)	48 (13.4)	25 (2.0)

[a] Number in parentheses is the elution time in minutes of the corresponding peak maximum.

© 1999 American Chemical Society, Bioconjugate Chem., Hai bc9900486 Supporting Info Page 3

Table S-3. Polymerization Profile of DCLHb Polymerized with Maleimides and Aldehydes

Molar ratio of PA to DCLHb	SEC Profile[a]			P_{50}, mm Hg (n)
	% Monomer (RT)	% Oligomer	% HMW Polymer	
DCLHb				
0	100 (19.9)	0	0	32 (2.6)
4a (MW 4000), [DCLHb] = 15 g/dL (Reducing Agent: Sodium Cyanborohydride)				
2	69 (18.6)	31	0	ND
3	59 (17.6)	41	1	ND
4	55 (17.4)	40	5	ND
5	48 (16.9)	37	15	ND
4a (MW 4000), [DCLHb] = 15 g/dL (Reducing Agent: Borane-Pyridine)				
2	53 (18.8)	47	0	33 (1.9)
3	38 (18.5)	54	8	35 (2.0)
4	36 (17.9)	40	24	36 (2.1)
3a (MW 4080), [DCLHb] = 20 g/dL				
1	50 (19.6)	50	0	20 (1.7)
1.5	45 (18.9)	55	0	22 (1.6)
2	32 (18.7)	58	0	18 (1.7)
2.5	28 (18.3)	54	18	18 (1.7)

[a] Number in parentheses is the elution time in minutes of the corresponding peak maximum.

© 1999 American Chemical Society, Bioconjugate Chem., Hai bc9900486 Supporting Info Page 4

Table S-4. Polymerization of OxyDCLHb or DeoxyDCLHb With **1a** (MW 5600)

	SEC Profile[a]				
Molar ratio of PA to DCLHb	% Monomer	% Oligomer I	% Oligomer II	% HMW Polymer	P_{50}, mm Hg (n)
[DeoxyDCLHb] = 6 g/dL					
2	16	40 (18.2)	44 (15.4)	0	30 (2.5)
2.5	3	22 (16.5)	63 (11.4)	0	31 (2.4)
3	2	25 (16.0)	46 (11.5)	26	29 (2.2)
3.5	1	22 (16.5)	40 (11.5)	36	31 (2.4)
[DeoxyDCLHb] = 3 g/dL					
5.5	0	38 (15.4)	62 (11.6)	0	36 (2.0)
6	0	32 (15.2)	61 (11.6)	7	34 (1.8)
[OxyDCLHb] = 6 g/dL					
2	18	37 (18.2)	44 (15.3)	0	27 (2.3)
2.5	6	31 (17.5)	62 (12.0)	0	25 (2.0)
[OxyDCLHb] = 3 g/dL					
3	6	69 (16.8)	25 (14.7)	0	23 (1.8)
3.5	2	63 (16.4)	35 (14.2)	0	25 (1.9)
4	0	54 (16.0)	36 (13.7)	0	22 (1.8)
5	0	45 (15.6)	55 (12.2)	0	21 (1.6)
5.5	0	39 (15.5)	61 (11.7)	0	19 (1.5)
6	0	34 (15.2)	61 (11.4)	0	18 (1.5)

[a] Number in parentheses is the elution time in minutes of the corresponding peak maximum.

Synthesis of Biotinylated Glycoconjugates and Their Use in a Novel ELISA for Direct Comparison of HIV-1 Gp120 Recognition of GalCer and Related Carbohydrate Analogues

Katherine D. McReynolds, Michael J. Hadd, and Jacquelyn Gervay-Hague*

The University of Arizona, Department of Chemistry, Tucson, Arizona 85721. Received April 28, 1999; Revised Manuscript Received September 16, 1999

As part of our program directed toward the design and synthesis of high-affinity ligands for the GalCer-binding site on the HIV cell surface glycoprotein, gp120, we required a reliable method for qualitatively assessing relative binding affinities for related analogues. Due to the hydrophilic nature of these synthetic conjugates, difficulties were encountered with typical ELISA methods, which rely upon hydrophobic interactions to anchor the ligand to a microtiter plate. Other types of assays were also problematic due to nonspecific binding of gp120. Therefore, we developed a general method for plating water-soluble ligands on microtiter plates using biotin/NeutrAvidin recognition for adhesion. A water-soluble GalCer analogue was prepared by conjugating psychosine to biotin using a novel tetraethylene glycol linker. In a similar manner, LacCer and GlcCer analogues were prepared and these conjugates were plated into microtiter wells containing NeutrAvidin. Unoccupied sites were blocked using biotin functionalized as a primary amide. Gp120 binding to galactosyl sphingosine, GalSph (**19**), GlcSph (**22**), and LacSph (**23**) conjugates was assessed through incubation with recombinant HRP-gp120. It was determined that LacSph has the strongest interaction with gp120. The binding affinities of GalSph and GlcSph were similar to each other and less strong than LacSph. These data contradict earlier studies where HPTLC showed that LacCer and GlcCer do not significantly bind gp120. They also contradict liposome-based assays that reported psychosine is not recognized by gp120. The extent of plating for each biotinylated molecule was quantified using HRP-biotin, allowing direct comparison of ligand plating efficiencies for the first time. Several other synthetic biotin conjugates were prepared and tested, demonstrating the feasibility of performing ELISA on water-soluble ligands.

INTRODUCTION

HIV entry into host cells is a complex process. The primary mode of host cell recognition and infection involves the CD4 receptor on the surface of helper T cells and is mediated by the viral envelope glycoproteins, gp120 and gp41. In 1991, Harouse and co-workers reported that there is an alternate mode of viral entry, based upon the susceptibility of CD4 negative cell lines to infectivity (*1*). Instead of using CD4 as a receptor, gp120 is able to recognize and bind a glycolipid, galactosyl ceramide (GalCer, **1**), and infect cells that do not express CD4. GalCer is present on the surfaces of neuronal and glial cells in the brain, in addition to some colorectal cell lines, vaginal epithelial cells, and primary macrophages (*2*). The ability of HIV to infect these CD4-negative cell lines represents a possible mode of infection through sexual transmission.

A primary goal of our research is to develop target-specific drug delivery systems that prevent HIV entry into both CD4-positive and CD4-negative host cells. As a part of this program, we are developing new carbohydrate-based drug candidates designed to block the GalCer-binding domain. Our design process requires a functional screening assay to determine the extent to which these water-soluble compounds bind to gp120 in comparison to GalCer. Although several binding studies of GalCer analogues have been reported, there are contradicting conclusions (vide infra). This is partly due to the fact that, until this report, there was not a uniform method available for directly comparing the binding of new synthetic conjugates to gp120 in the same assay.

Harouse and co-workers utilized high-performance thin-layer chromatography (HPTLC) to determine that GalCer is a receptor for gp120 (*1*). In their study, glycolipids such as GalCer (**1**), GalCer sulfatide (GalS (**2**)), psychosine (**3**), glucosyl ceramide (GlcCer (**4**)), lactosyl ceramide (LacCer (**5**)), and ceramide (**6**) and a mixture of neutral glycolipids from human erythrocytes including ceramide, trihexose, and globoside were plated on HPTLC plates (Figure 1). After separation and washing, the plates were incubated with ^{125}I-labeled recombinant gp120, then washed and counted. Upon development, it was found that gp120 bound only to GalCer (**1**) and GalS (**2**). A second experiment confirmed that antibodies against GalCer inhibited both the infectivity of susceptible cell lines and internalization of the virus. Table 1 summarizes the binding profiles of several bioconjugates compared to GalCer (*3*).

Interestingly, similar studies by Latov et al. utilizing ELISA, an immunospot assay on nitrocellulose, and HPTLC contradict the results by Harouse and co-workers (*4*). Specifically, Latov determined that GalS bound to gp120, but GalCer did not, in both an immunospot assay and ELISA. However, in HPTLC, GalCer was found to bind. They attributed this discrepancy to a lower specificity of the TLC assay because the binding on the plates can be altered by the polyisobutyl methacrylate coating.

Binding studies were also performed using liposomes doped with glycoconjugates (*5*). Mixtures of phosphatidyl ethanolamine (PE), phosphatidyl choline (PC), cholesterol, and various glycosphingolipids (GalCer, GalS, psychosine, GlcCer, LacCer, and sphingomyelin) were

10.1021/bc990050x CCC: $18.00 © 1999 American Chemical Society
Published on Web 10/27/1999

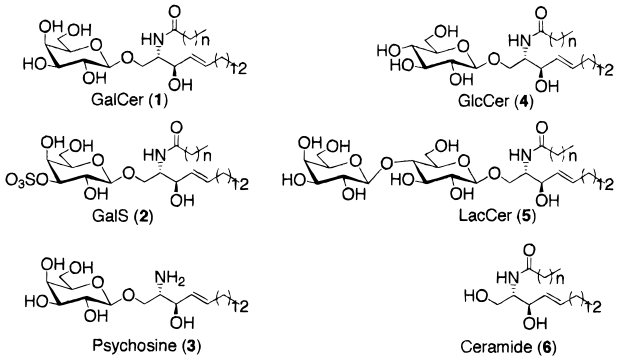


Figure 1. Representative bioconjugates assayed for HIV-1 gp120 affinity using various techniques.

Table 1. Assays of Various Bioconjugates Affinity for HIV-1 gp120 Using HPTLC and Doped-Liposomes

bioconjugate	percent binding (HLTLC) (*1*)	percent Gp120 bound (liposomes) (*4*)
GalCer (**1**)	100	95
GalS (**2**)	109 ± 11	30−60
psychosine (**3**)	95 ± 14	<5
GlcCer (**4**)	5 ± 2	25−55
LacCer (**5**)	19 ± 2	60−90
ceramide (**6**)	9 ± 3	not assayed

used to make liposomes. The assay consisted of incubating gp120 with the liposomes, then allowing binding to occur before a series of steps were performed to isolate the bound gp120-liposomal components. The isolated media was subjected to SDS−PAGE electrophoresis and Western blotting to detect the presence of gp120. Using this methodology, the researchers determined that GalS (**2**), GlcCer (**4**), and LacCer (**5**) have significant activity, while psychosine (**3**) does not (Table 1).

Because the presentation geometry of the ligands may differ dramatically between the aforementioned assays, drawing conclusions about relative binding affinities from comparative data is problematic. To enable the direct comparison of several different carbohydrate analogues, we developed a new ELISA wherein various ligands are conjugated to a water-soluble linker possessing a biotin moiety. These conjugates are then irreversibly adhered to NeutrAvidin-coated microtiter plates, ensuring that all ligands are bound in a similar manner and allowing direct comparison of binding affinity data.

Utilization of the water-soluble chemical linker is a critical factor in this ELISA. There are commercially available biotin linkers that can be conjugated to various ligands, however, they are typically comprised of hydrophobic caproic acid segments (*6*). In addition to creating solubility problems in plating, our studies showed that the commercial hydrophobic linkers obscured important interactions between gp120 and carbohydrate analogues through nonspecific binding. Both of these problems are alleviated with hydrophilic linkers. We have synthesized a water-soluble linker with bifunctionality bearing amino and carboxylic acid termini. The amino side is used for biotinylation, and the carboxylic acid is used to covalently attach carbohydrates with amine functionality. Both the linker and carbohydrate are hydrophilic. The linker can thus effectively extend the carbohydrate out into solution, maximizing the carbohydrate/protein interaction. Although the use of biotin/streptavidin for carbohydrate assays has been reported (*7*), to our knowledge, this is the first report of a water-soluble chemical linker for use in gp120 binding ELISA (*8*). We have also developed a unique method for quantifying the plating efficiency of individual ligands. This report focuses on the synthetic preparation of various bioconjugates and the determination of their binding affinity for recombinant HRP-gp120 using a novel ELISA construct. This assay provides a powerful tool for studying the binding of hydrophilic carbohydrate-based ligands.

EXPERIMENTAL SECTION

General Procedures. All materials were obtained from commercial sources and used without additional purification, unless otherwise noted. Solvents were all distilled prior to use as reaction media. All glassware utilized in water-sensitive reactions was flame-dried before use. ^{1}H NMR spectra were recorded at 250 or 500 MHz on Bruker superconducting FT spectrometers. ^{13}C NMR spectra were recorded at 62.5 or 125 MHz and were proton decoupled. All spectra are reported as ppm downfield of tetramethylsilane.

***tert*-Butyl-4,7,10-trioxadodecyl-12-*p*-toluenesulfonate (8).** A total of 2.0 g (7.19 mmol) **7** (prepared by the method of Seitz and Kunz) (*9*) was weighed directly into an oven-dried flask. The flask was placed in an ice bath upon addition of 40 mL of pyridine, and the solution was allowed to cool to 0 °C under argon gas. A total of 2.74 g (14.38 mmol) of purified TsCl (recrystallized from petroleum ether) was added, and the reaction was stirred under argon from 0 °C to room temperature for 4.5 h. The reaction was quenched by the addition of 80 mL of deionized H_2O and extracted three times with ethyl acetate. The combined organic layers were washed with brine and dried over anhydrous sodium sulfate. Purification of the crude product was achieved by silica gel chromatography with 9:1 toluene/acetone. A total of 2.42 g (75%) of a clear yellow oil was obtained. ^{1}H NMR (250 MHz, $CDCl_3$) δ 1.51 (s, 9H), 2.51−2.59 (m, 5H), 3.64−3.66 (app d, 8H, J = 3.0), 3.76 (app q, 4H, J = 6.6, 13.0), 4.22 (t, 2H, J = 4.3), 7.42 (d, 2H, J = 8.1), 7.86 (d, 2H, J = 8.2). ^{13}C NMR (62.5 MHz, $CDCl_3$) δ 21.56, 28.02, 36.19, 66.80, 68.57, 69.27, 70.27, 70.44, 70.63, 80.35, 127.89, 129.81, 132.91, 144.78, 170.79. High-resolution mass spectrum (FAB^+) calcd for $C_{20}H_{33}SO_8$ $(MH)^+$: 433.1896. Found: 433.1895.

***tert*-Butyl-12-azido-4,7,10-trioxadodecylate (9).** A total of 2.12 g (4.91 mmol) of compound **8** was transferred to a flask as a solution in dichloromethane, then evaporated and weighed. A total of 29.5 mL of DMF was added to a flask under argon and stirred. A total of 958 mg (14.73 mmol) of NaN_3 was added, and the reaction was stirred at room temperature under argon for 1.5 h. The reaction was quenched by the addition of 50 mL of deionized H_2O and extracted three times with diethyl ether. The combined organic layers were washed with brine and dried over anhydrous sodium sulfate. Purification of the crude product was achieved by silica gel chromatography using 3:1 hexanes/ethyl acetate. A total of 1.35 g (91%) of a clear, colorless oil was obtained. The product contained a slight impurity by TLC. ^{1}H NMR revealed that the product was ~95% pure. IR (thin film) 2978, 2864, 2104, 1719 cm^{-1}. ^{1}H NMR (250 MHz, $CDCl_3$) δ 1.39 (s, 9H), 2.45 (t, 2H, J = 6.6), 3.33 (t, 2H, J = 5.0), 3.54−3.68 (m, 12H). ^{13}C NMR (62.5 MHz, $CDCl_3$) δ 27.89, 36.09, 50.48, 66.70, 69.88, 70.20, 70.41, 70.49, 70.56, 80.17, 170.64. High-resolution mass spectrum (FAB^+) calcd for $C_{13}H_{26}N_3O_5$ $(MH)^+$: 304.1872. Found: 304.1865.

***tert*-Butyl-12-amino-4,7,10-trioxadodecylate (10).** A total of THF was added to a flask containing 539 mg (1.78 mmol) of compound **9**. 64.1 mL (3.56 mmol) of deionized H_2O was added, followed by 512 mg (1.95

mmol) of triphenylphosphine (*10*). The reaction was stirred at room temperature for 80 h, and then evaporated. A solution of 1:1 ether/petroleum ether was added to the flask, then placed on ice (*11*). The solution was filtered through Celite, then filter paper, to remove the precipitated triphenylphosphine oxide. The filtrate was then evaporated. Purification of the crude product was achieved by silica gel chromatography with 90:10:0.1 chloroform/methanol/triethylamine. A total of 405 mg (82%) of a clear yellow oil was obtained. ^{1}H NMR (250 MHz, $CDCl_3$) δ 1.37 (s, 9H), 2.43 (t, 2H, $J = 6.5$), 2.80 (t, 2H, $J = 5.1$), 3.45 (t, 2H, $J = 5.2$), 3.56 (s, 8H), 3.64 (t, 2H, $J = 6.5$). ^{13}C NMR (62.5 MHz, $CDCl_3$) δ 28.09, 36.25, 41.72, 66.89, 70.27, 70.38, 70.51, 70.57, 73.23, 80.47, 170.8. High-resolution mass spectrum (FAB^+) calcd for $C_{13}H_{28}NO_5$ $(MH)^+$: 278.1967. Found: 278.1960.

D-Biotin-*tert*-butyl-12-amido-4,7,10-trioxadodecylate (12). A total of 205 mg (0.74 mmol) of compound **10** was transferred to the reaction flask as a solution in dichloromethane, then evaporated and weighed. A total of 11.6 mL of DMF was added, followed by 309 μL (2.22 mmol) of TEA, with the flask under nitrogen. The solution was stirred, and 290 mg (0.74 mmol) of D-biotin-2,3,5,6-tetrafluorobenzoate (**11**) was added. The reaction was stirred at room temperature, under nitrogen, for 24 h, then evaporated. The resultant crude product was purified using silica gel chromatography with a gradient of 16:1 to 8:1 chloroform/methanol. A total of 369 mg (99%) of a clear amorphous solid was obtained. ^{1}H NMR (250 MHz, $CDCl_3$) δ 1.38 (app s, 11H), 1.46−1.75 (m, 4H), 2.16 (t, 2H, $J = 7.2$), 2.43 (t, 2H, $J = 6.4$), 2.67 (d, 1H, $J = 13.7$), 2.83 (dd, 1H, $J = 4.5, 12.9$), 3.07 (app d, 1H, $J = 4.4$), 3.36 (app t, 2H, $J = 4.6$), 3.50 (app t, 2H, $J = 5.1$), 3.55 (app s, 8H), 3.64 (app t, 2H, $J = 6.5$), 4.25 (m, 1H), 4.43 (m, 1H), 6.02 (s, 1H), 6.87 (m, 2H). ^{13}C NMR (62.5 MHz, $CDCl_3$) δ 25.79, 28.28, 28.40, 36.15, 36.41, 39.33, 40.72, 55.81, 60.42, 61.96, 67.07, 70.15, 70.29, 70.56, 80.80, 164.2, 171.1, 173.58. High-resolution mass spectrum (FAB^+) calcd for $C_{23}H_{42}N_3SO_7$ $(MH)^+$: 504.2743. Found: 504.2754.

D-Biotin-12-amido-4,7,10-trioxadodecanoic acid (13). Reagent K (*12*) was prepared in a separate glass-stoppered flask and contained the following: 1.65 mL of TFA (85% v/v), 100 μL of thioanisole (5% v/v), 50 μL of 1,2-ethanedithiol (2.5% v/v), 100 μL of deionized H_2O (5% v/v), and a small amount of phenol (~5% w/v). A total of 42.4 mg (0.079 mmol) of compound **12** was transferred to the reaction flask as a solution in dichloromethane, then evaporated and weighed. Reagent K was transferred to the reaction flask, stoppered with glass, stirred at room temperature for 1.5 h, then evaporated. Purification of the crude acid was achieved using silica gel chromatography with a gradient of chloroform/methanol/glacial acetic acid from 20:1:0.1 to 8:1:0.1. A total of 31 mg (89%) of a powdery white solid was obtained. ^{1}H NMR (250 MHz, DMSO-d_6) δ 1.23−1.62 (m, 6H), 2.06 (t, 2H, $J = 7.1$), 2.43 (t, 2H, $J = 6.2$), 2.57 (d, 1H, $J = 12.4$), 2.81 (dd, 1H, $J = 5.1, 12.4$), 3.05−3.14 (m, 1H), 3.18 (app t, 2H, $J = 5.5$), 3.38 (t, 2H), $J = 6.0$), 3.49 (s, 8H), 3.59 (t, 2H, $J = 6.3$), 4.13 (m, 1H), 4.30 (m, 1H), 6.38 (s, 1H), 6.44 (s, 1H), 7.85 (t, 1H, $J = 5.5$). ^{13}C NMR (62.5 MHz, DMSO-d_6) δ 25.28, 28.05, 28.21, 34.79, 35.10, 38.46, 55.44, 59.10, 59.21, 60.95, 61.05, 66.29, 69.18, 69.58, 69.65, 69.72, 162.75, 172.15, 172.79. High-resolution mass spectrum (FAB^+) calcd for $C_{19}H_{34}N_3SO_7$ $(MH)^+$: 448.2117. Found: 448.2117.

D-Biotin-12-amido-4,7,10,-trioxadodecyl-1-(2,3,5,6-tetrafluoro)benzoate (14). A total of 13.6 mg (0.03 mmol) of compound **13** was transferred to the reaction flask as a solution in dichloromethane, then evaporated and weighed. Next, 272 μL of 70 °C DMF was added to the flask under argon. This was then allowed to cool to room temperature, followed by the addition of 8.5 μL (0.061 mmol) of TEA and 15.7 μL (0.091 mmol) of 2,3,5,6-tetrafluorophenyl trifluoroacetate (prepared by the method of Gamper et al.) (*13*). Upon the addition of the last reagent, opaque white fumes filled the flask. These fumes dissipated with time. The reaction was stirred at room temperature under argon overnight, then evaporated. The crude product was purified using silica gel chromatography in 12:1 chloroform/methanol. A total of 15 mg (86%) of pure compound was obtained as a clear yellow amorphous solid. ^{1}H NMR (250 MHz, DMSO-d_6) δ 1.14−1.64 (m, 6H), 2.05 (t, 2H, $J = 7.2$), 2.57 (d, 1H, $J = 12.5$), 2.81 (dd, 1H, $J = 5.0, 12.4$), 3.02 (app t, 2H, $J = 5.9$), 3.07−3.20 (m, 2H), 3.38 (t, 2H, $J = 6.0$), 3.50−3.61 (m, 9H), 3.77 (t, 2H, $J = 5.9$), 4.12 (m, 1H), 4.29 (m, 1H), 6.38 (s, 1H), 6.44 (s, 1H), 7.85 (t, 1H, $J = 6.2$), 7.95 (m, 1H). ^{13}C NMR (62.5 MHz, DMSO-d_6) δ 25.27, 28.05, 28.20, 34.02, 35.10, 38.44, 55.43, 59.21, 61.05, 65.61, 69.18, 69.56, 69.71, 69.75, 69.83, 104.11, 104.48, 104.86, 162.73, 167.95, 172.13. High-resolution mass spectrum (FAB^+) calcd for $C_{25}H_{34}N_3F_4SO_7$ $(MH)^+$: 596.2054. Found: 596.2054.

D-Biotinamide (15). A total of 21.2 mg (0.054 mmol) of D-biotin-1-(2,3,5,6-tetrafluoro)benzoate (compound **11**) was dissolved in 2.0 mL of THF. NH_3(g) was then bubbled into the reaction solution for 30 min. After the NH_3(g) was removed, the reaction was stirred for an additional 15 min before evaporating. A total of 15.4 mg of crude product was obtained. This was used without further purification. ^{1}H NMR (500 MHz, DMSO-d_6) δ 1.28−1.35 (m, 2H), 1.42−1.49 (m, 3H), 1.58−1.63 (m, 1H), 2.03 (t, 2H, $J = 7.4$), 2.57 (d, 1H, $J = 12.4$), 2.82 (dd, 1H, $J = 5.1, 12.4$), 3.10 (m, 1H), 4.13 (m, 1H), 4.30 (m, 1H), 6.35 (s, 1H), 6.43 (s, 1H), 6.69 (s, 1H), 7.23 (s, 1H). ^{13}C NMR (125 MHz, DMSO-d_6) δ 25.07, 28.05, 28.24, 34.90, 40.01, 55.41, 59.17, 61.03, 162.69, 174.21. High-resolution mass spectrum (FAB^+) calcd for $C_{10}H_{18}N_3SO_2$ $(MH)^+$: 244.1120. Found: 244.1127.

D-Biotin-12-amido-4,7,10-trioxadodecyl Cyclohexylamide (16). A total of 10 mg (0.0168 mmol) of compound **14** was dissolved in 400 μL of DMF. Next, 8 μL (0.057 mmol) of TEA was added, followed by 3.8 μL (0.034 mmol) of cyclohexylamine. The reaction mixture was stirred at room temperature under nitrogen overnight, then evaporated. The crude compound was purified by silica gel chromatography using a gradient from 95:5 to 8:2 chloroform/methanol. A total of 8.2 mg (92%) of a clear yellow amorphous solid was obtained. ^{1}H NMR (250 MHz, $CDCl_3$) δ 1.05−1.48 (m, 7H), 1.56−1.69 (m, 7H), 1.83−1.88 (m, 2H), 2.21 (t, 2H, $J = 7.5$), 2.42 (t, 2H, $J = 5.9$), 2.72 (d, 1H, $J = 12.6$), 2.88 (dd, 1H, $J = 4.7, 12.8$), 3.12 (app q, 1H, $J = 7.1, 11.4$), 3.39−3.46 (m, 2H), 3.54 (t, 2H, $J = 4.8$), 3.61 (s, 8H), 3.72 (app t, 3H, $J = 5.9$), 4.30 (m, 1H), 4.48 (m, 1H), 5.44 (s, 1H), 6.29 (d, 1H, $J = 7.7$), 6.43 (s, 1H), 6.75 (app t, 1H). ^{13}C NMR (62.5 MHz, $CDCl_3$) δ 25.04, 25.79, 28.30, 29.90, 33.27, 36.11, 37.37, 39.34, 40.74, 48.22, 55.75, 60.39, 62.00, 67.75, 70.20, 70.28, 70.49, 70.60, 77.43, 164.03, 170.66, 173.50. High-resolution mass spectrum (FAB^+), calcd for $C_{25}H_{45}N_4SO_6$ $(MH)^+$: 529.3060. Found: 529.3078.

D-Biotin-12-amido-4,7,10-trioxadodecyl Sphingosinamide (18). A total of 5 mg (0.017 mmol) of D-sphingosine (**17**) (Avanti Polar Lipids, Inc.) was dissolved in 266 μL of DMF. Next, 7.1 μL (0.051 mmol) of TEA was added, followed by 11.1 mg (0.019 mmol) of compound **14**. The reaction was stirred at room-temperature

overnight under argon, then evaporated. The crude product was purified using silica gel chromatography in 9:1 chloroform/methanol. A total of 12 mg (100%) of an off-white powder was obtained. ^{1}H NMR indicated the presence of a minor impurity. ^{1}H NMR (250 MHz, DMSO-d_6) δ 0.85 (m, 5H), 1.14−1.59 (m, 39H), 1.94 (m, 2H), 2.06 (t, 2H, J = 7.4), 2.32 (t, 2H, J = 6.6), 2.57 (d, 1H, J = 12.7), 2.81 (dd, 1H, J = 5.0, 14.9), 3.09−3.21 (m, 5H), 3.33−3.65 (m, 17H), 3.87 (m, 1H), 4.12 (m, 1H), 4.49 (t, 1H, J = 7.7), 4.83 (d, 1H, J = 5.4), 5.34−5.60 (m, 2H), 6.37 (s, 1H), 6.44 (s, 1H), 7.54 (d, 1H, J = 8.7), 7.86 (t, 1H, J = 5.3). ^{13}C NMR NMR (62.5 MHz, DMSO-d_6) δ 13.97, 22.11, 25.26, 28.04, 28.20, 28.60, 28.72, 28.83, 28.99, 29.07, 31.31, 31.73, 35.09, 36.18, 55.43, 59.19, 60.31, 61.03, 66.97, 69.19, 69.52, 69.56, 69.72, 71.19, 130.81, 131.24, 162.71, 169.90, 172.12. High-resolution mass spectrum (FAB$^+$), calcd for $C_{37}H_{69}N_4SO_8$ $(MH)^+$: 729.4836. Found: 729.4814.

D-Biotin-12-amido-4,7,10-trioxadodecyl Psychosinamide (19). A total of 9 mg (0.015 mmol) of compound **14** was dissolved in dichloromethane, transferred to reaction flask, then evaporated and weighed. A total of 356 μL of DMF was then added to the reaction flask, followed by 7.1 μL (0.051 mmol) of TEA. Psychosine (**3**) (Sigma) (7.6 mg, 0.016 mmol) was added next. The reaction was stirred at room temperature under argon overnight, then evaporated. The purification method was the same as that for compound **18**. A total of 10 mg (74%) of a pale yellow amorphous solid was obtained. ^{1}H NMR (500 MHz, DMSO-d_6) δ 0.85 (t, 4H, J = 6.6), 1.15−1.31 (m, 27H), 1.40−1.56 (m, 4H), 1.58−1.65 (m, 1H), 1.95 (app. d, 2H, J = 7.0), 2.06 (t, 2H, J = 7.4), 2.32 (m, 2H), 2.57 (d, 1H, J = 12.4), 2.82 (dd, 1H, J = 5.0, 12.5), 3.09 (m, 1H), 3.18 (app. q, 2H, J = 5.8, 11.6), 3.26−3.62 (m, 39H, incl. HOD), 3.78 (m, 1H), 3.93 (m, 2H), 4.03 (d, 1H, J = 7.2), 4.12 (m, 1H), 4.30 (m, 1H), 4.36 (d, 1H, J = 4.5), 4.56 (app. t, 1H, J = 5.7), 4.71 (d, 1H, J = 5.3), 4.87 (m, 2H), 5.39 (dd, 1H, J = 6.9, 15.4), 5.55 (m, 1H), 6.35 (s, 1H), 6.41 (s, 1H), 7.62 (d, 1H, J = 9.0), 7.83 (t, 1H, J = 5.5). ^{13}C NMR (125 MHz, DMSO-d_6) δ 13.91, 22.05, 25.21, 28.00, 28.15, 28.58, 28.66, 28.78, 28.94, 28.97, 29.02, 31.25, 31.67, 35.06, 36.19, 38.40, 40.01, 53.19, 55.37, 59.16, 60.37, 61.00, 66.86, 68.04, 68.50, 69.15, 69.46, 69.52, 69.69, 70.61, 70.73, 72.20, 73.12, 75.20, 104.30, 131.12, 131.28, 162.66, 169.75, 172.09. High-resolution mass spectrum (FAB$^+$) calcd for $C_{43}H_{79}N_4SO_{13}$ $(MH)^+$: 891.5364. Found: 891.5351.

2,3,4,6-Tetra-*O*-acetyl-β-D-glucopyranosyl-(1→1)-(2S,3R,4E)-3-hydroxy-2-*N*-(12-D-biotinamide-4,7,10-trioxadodecyl)-sphingenine (20). 1-Hydroxy-2,3,4,6-tetra-*O*-acetyl-D-glucopyranose was prepared by method of Flandor et al. (*14*), starting with 1,2,3,4,6-penta-*O*-acetyl-β-D-glucopyranose (Aldrich). A 74% yield resulted after purification of the crude product by silica gel chromatography. This product was converted to the α-trichloroacetimidate, utilizing a procedure by Schmidt and co-worker (*15*). A 48% yield of the α-anomer was obtained after silica gel chromatography. The spectral data for both of the above precursors matches that of the literature precedence. The α-trichloroacetimidate-derivatized glucose was weighed dry into the reaction flask (19 mg, 0.038 mmol), as was compound **18** (35 mg, 0.048 mmol). These constituents were dissolved in 1.20 mL of 1,2-dichloroethane and stirred over AW-300 powdered molecular sieves at −10 °C. $BF_3{\cdot}Et_2O$ (9.7 μL, 0.077 mmol) was introduced last and the reaction stirred at 0 °C. After 16 h, an additional equivalent of $BF_3{\cdot}Et_2O$ was added. At 22 h, the reaction mixture was filtered through Celite, then washed with saturated $NaHCO_3$, followed by water. The organic layer was dried over anhydrous $MgSO_4$, filtered, then evaporated. The crude product was purified by silica gel chromatography in 9:1 chloroform/methanol. A total of 9.6 mg (24%) of an amorphous light yellow solid resulted. ^{1}H NMR (500 MHz, $CDCl_3$) δ 0.85 (t, 3H, J = 7.1), 1.23 (app s, 22H), 1.44 (m, 2H), 1.67 (m, 5H), 2.00 (m, 17H), 2.20 (t, 2H, J = 7.4), 2.46 (m, 2H), 2.73 (d, 1H, J = 12.7), 2.88 (dd, 1H, J = 4.9, 12.8), 3.13 (app q, 1H, J = 7.1, 11.9), 3.41 (app s, 2H), 3.53 (t, 2H, J = 5.0), 3.59−3.73 (m, 15H), 3.97−4.05 (m, 2H), 4.10 (app d, 1H, J = 2.3), 4.13 (m, 1H), 4.24 (dd, 1H, J = 4.7, 12.2), 4.30 (m, 1H), 4.46−4.48 (m, 2H), 4.94 (q, 1H, J = 8.1, 9.4), 5.04 (t, 1H, J = 9.5), 5.17 (app s, 2H), 5.44 (dd, 1H, J = 6.3, 15.4), 5.70 (m, 1H), 6.14 (s, 1H), 6.70 (t, 1H, J = 5.4), 6.78 (d, 1H, J = 7.8). ^{13}C NMR (125 MHz, $CDCl_3$) δ 14.32, 20.80, 20.92, 20.93, 22.89, 25.75, 28.29, 28.36, 29.49, 29.53, 29.56, 29.69, 29.75, 29.87, 29.88, 29.91, 32.13, 32.60, 36.05, 37.24, 39.36, 40.70, 53.59, 55.69, 60.37, 62.02, 62.09, 67.49, 68.60, 68.65, 70.19, 70.27, 70.50, 70.62, 71.50, 72.12, 72.83, 72.95, 100.94, 128.71, 133.99, 163.83, 169.66, 169.84, 170.34, 170.86, 171.87, 173.49. High-resolution mass spectrum (FAB$^+$) calcd for $C_{51}H_{87}N_4SO_{17}$ $(MH)^+$: 1059.5787. Found: 1059.5801.

2,3,4,6-Tetra-*O*-acetyl-β-D-galactopyranosyl-(1→4)-*O*-(2,3,6-tri-*O*-acetyl-β-D-glucopyranosyl)−(1→ 1)−(2S,3R,4E)-3-hydroxy-2-*N*-(12-D-biotinamide-4,7,10-trioxadodecyl)-sphingenine (21). The reducing end 1-hydroxy derivative of hepta-*O*-acetyl lactose was prepared using the techniques of Flandor et al. (*14*), starting with octa-*O*-acetyl lactose (Aldrich). An 80% yield resulted upon purification by column chromatography. This product was subsequently converted to the α-trichloroacetimidate utilizing a procedure by Schmidt and coworker (*15*). Silica gel chromatography of the crude product yielded 42% of the desired α-trichloroacetimidate. This α-trichloroacetimidate-derivatized lactose was weighed into a reaction flask dry (25 mg, 0.033 mmol), along with compound **18** (26 mg, 0.036 mmol). These components were dissolved in 1.03 mL of 1,2-dichloroethane and stirred over AW-300 powdered molecular sieves at −10 °C. $BF_3{\cdot}Et_2O$ (8.4 μl, 0.066 mmol) was introduced last, and the reaction was stirred overnight at 0 °C. At this time, an additional equivalent of $BF_3{\cdot}Et_2O$ was added, and the reaction stirred at between 5 and 10 °C. After 48 h, the reaction solution was filtered through Celite and evaporated. The crude product was purified by column chromatography using a gradient from 15:1 to 12:1 chloroform/methanol. An amorphous yellowish solid resulted (5.4 mg, 12%). ^{1}H NMR (500 MHz, $CDCl_3$) δ 0.85 (t, 3H, J = 6.9), 1.23 (app s, 22H), 1.43 (m, 2H), 1.53−1.68 (m, 5H), 1.95−2.12 (m, 23H), 2.20 (t, 2H, J = 7.4), 2.46 (t, 2H, J = 5.9), 2.72 (d, 1H, J = 12.7), 2.89 (dd, 1H, J = 4.8, 12.6), 3.13 (app q, 1H, J = 7.1, 11.9), 3.41 (app t, 2H, J = 5.1), 3.53 (app t, 2H, J = 4.8), 3.62 (s, 5H), 3.61−3.79 (m, 22H), 3.86 (m, 1H), 3.95 (app dd, 1H, J = 5.6, 10.6), 4.00−4.16 (m, 6H), 4.30 (m, 1H), 4.43−4.52 (m, 5H), 4.85 (app t, 1H), 4.95 (dd, 1H, J = 3.4, 10.4), 5.07 (dd, 1H, J = 7.9, 10.3), 5.16 (t, 1H, J = 9.1), 5.20 (app s, 1H), 5.32 (d, 1H, J = 11.2), 5.43 (dd, 1H, J = 6.5, 15.4), 5.69 (dt, 1H, J = 6.9, 15.4), 6.04 (s, 1H), 6.70 (d, 2H, J = 7.7). ^{13}C NMR (125 MHz, $CDCl_3$) δ 14.31, 20.84, 20.85, 20.95, 21.00, 21.05, 22.89, 25.72, 28.27, 28.33, 29.50, 29.53, 29.56, 29.69, 29.75, 29.87, 29.91, 32.12, 32.61, 36.01, 37.20, 39.34, 40.71, 53.57, 55.67, 60.35, 60.99, 61.99, 62.14, 66.85, 67.49, 68.71, 69.33, 70.19, 70.24, 70.49, 70.58, 70.60, 70.88, 71.17, 71.84, 72.83, 72.87, 72.99, 76.40, 100.76, 101.25, 128.65, 134.05, 163.73, 169.28, 169.87, 170.08, 170.26, 170.32, 170.56, 170.68, 171.82, 173.48. High-resolution mass spectrum

(FAB$^+$) calcd for $C_{63}H_{103}N_4SO_{25}$ (MH)$^+$: 1347.6632. Found: 1347.6605.

***β*-D-Glucopyranosyl-(1→1)−(2S,3R,4E)-3-hydroxy-2-*N*-(12-D-biotinamide-4,7,10-trioxadodecyl)-sphingenine (22).** A total of 9.6 mg (0.009 mmol) of compound **20** was dissolved in 1 mL of methanol, and a catalytic quantity of sodium methoxide (Avocado) was added. The reaction was allowed to stir at room temperature for 1 day. After TLC in 9:1 chloroform/methanol indicated that reaction was complete, Dowex H$^+$ resin was added and the solution stirred for 45 min until the pH was neutral. The solution was filtered through glass paper and evaporated. The compound was then taken up into a small quantity of water and freeze-dried. A total of 6.3 mg (78%) of an off-white fluffy solid resulted. ^{1}H NMR (500 MHz, 4:1 $CDCl_3$/MeOD mixture, using internal $CDCl_3$ as a reference) δ 0.72 (t, 3H, $J = 6.7$), 1.10 (s, 22H), 1.28 (m, 2H), 1.43−1.58 (m, 6H), 1.87 (m, 3H), 2.07 (t, 3H, $J = 7.3$), 2.33 (t, 2H, $J = 5.8$), 2.58 (d, 1H, $J = 12.8$), 2.77 (dd, 1H, $J = 4.9, 12.8$), 3.01 (app q, 1H), 3.09−3.14 (m, 2H), 3.20−3.31 (m, 6H, includes MeOD signal), 3.40 (t, 2H, $J = 4.9$), 3.47−3.60 (m, 14H), 3.70 (app d, 2H), 3.87 (br s, 1H), 4.11 (d, 1H, $J = 7.7$), 4.16 (m, 1H), 4.35 (dd, 1H, $J = 4.9, 7.5$), 5.31 (dd, 1H, $J = 7.1, 15.3$), 5.55 (m, 1H). ^{13}C NMR NMR (125 MHz, 4:1 $CDCl_3$/MeOD mixture, using internal $CDCl_3$ as a reference) δ 13.94, 22.61, 25.45, 28.07, 28.34, 29.25, 29.28, 29.30, 29.50, 29.60, 29.64, 31.87, 32.35, 35.62, 36.57, 39.10, 40.28, 53.50, 55.58, 60.16, 61.47, 61.93, 67.21, 68.46, 69.78, 69.86, 69.94, 70.05, 70.14, 70.26, 72.17, 73.53, 76.17, 76.26, 103.21, 128.92, 134.05, 164.27, 172.17, 174.40. High-resolution mass spectrum (FAB$^+$) calcd for $C_{43}H_{78}N_4SO_{14}Na$ (MNa)$^+$: 913.5184. Found: 913.5156.

***β*-D-Galactopyranosyl-(1→4)-*O*-(*β*-D-glucopyranosyl)−(1→1)−(2S,3R,4E)-3-hydroxy-2-*N*-(12-D-biotinamide-4,7,10-trioxadodecyl)-sphingenine (23).** A total of 13.4 mg (0.010 mmol) of compound **21** was dissolved in 2 mL of methanol and a catalytic quantity of sodium methoxide (Avocado) was added. The reaction was allowed to stir overnight at room temperature. At this time, TLC in 12:1 chloroform/methanol indicated a complete reaction. Dowex H$^+$ resin was added to the reaction solution, and stirring was continued until neutral pH was achieved. The solution was filtered through glass paper and evaporated. The residue was dissolved in a small quantity of water, then freeze-dried. A total of 9.9 mg (94%) of an off-white fluffy solid resulted. ^{1}H NMR (500 MHz, 4:1 $CDCl_3$/MeOD mixture, using internal $CDCl_3$ as a reference) δ 0.73 (t, 3H, $J = 6.8$), 1.11 (s, 22H), 1.29 (m, 3H), 1.43−1.60 (m, 5H), 1.87 (app q, 2H, $J = 7.0, 14.2$), 2.07 (t, 2H, $J = 7.6$), 2.33 (t, 2H, $J = 6.1$), 2.59 (d, 1H, $J = 12.8$), 2.77 (dd, 1H, $J = 5.0, 12.9$), 3.02 (m, 1H), 3.16−3.26 (m, 5H, includes MeOD signal), 3.35−3.50 (m, 18H), 3.53−3.62 (m, 3H), 3.67−3.76 (m, 4H), 3.87 (m, 1H), 3.98 (app dd, 1H), 4.14 (d, 1H, $J = 7.8$), 4.17 (m, 1H), 4.21 (d, 1H, $J = 7.8$), 4.36 (app q, 1H, $J = 4.9, 7.8$), 5.31 (dd, 1H, $J = 7.0, 15.3$), 5.55 (dt, 1H, $J = 6.8, 15.1$). ^{13}C NMR (125 MHz, 4:1 $CDCl_3$/MeOD mixture, using internal $CDCl_3$ as a reference) δ 13.95, 22.62, 25.50, 28.12, 28.42, 29.27, 29.30, 29.50, 29.61, 29.65, 31.87, 32.35, 35.68, 36.56, 39.11, 40.28, 53.41, 55.63, 60.17, 60.88, 61.57, 61.97, 67.18, 68.53, 69.12, 69.71, 69.85, 69.96, 70.118, 70.29, 71.04, 72.11, 73.21, 73.42, 74.66, 74.97, 75.41, 79.58, 103.08, 103.71, 128.99, 134.06, 164.28, 172.11, 174.41. High-resolution mass spectrum (FAB$^+$) calcd for $C_{49}H_{89}N_4SO_{18}$ (MH)$^+$: 1053.5893. Found: 1053.5885.

1-(Trichloroacetamide)-2-(2,3,4,6-tetra-*O*-acetyl-*β*-D-galactopyranoside)-ethanolamine (25). To a solution of 1,2,3,4,6-penta-*O*-acetyl-galactopyanoside (300 mg, 0.77 mmol) in 3 mL of dichloromethane with 3 Å molecular sieves was added iodotrimethylsilane (120 μL, 0.85 mmol). This solution was allowed to stand at room temperature for 1 h. The solvent was then removed in vacuo, and 2 mL of toluene was added and again removed in vacuo. A solution of the trichloroacetamide of ethanolamine (238 mg, 1.15 mmol) was added as a solution in 4 mL of acetonitrile and refluxed for 3 h. Sodium bicarbonate (70 mg) was then added and the solvent was removed in vacuo. The resultant oil was subjected to column chromatography (2:1 hexanes:ethyl acetate) twice to yield 26 mg (6%) of the target compound. ^{1}H NMR (250 MHz, $CDCl_3$) δ 1.96 (s, 3H), 2.02 (s, 3H), 2.03 (s, 3H), 2.13 (s, 3H), 3.42−3.63 (m 2H), 3.72−3.80 (m, 1H), 3.88−3.96 (m, 2H), 4.05−4.13 (m, 2H), 4.49 (d, 1H, $J = 7.9$ Hz), 4.99 (dd, 1H, $J = 10.5, 4.20$ Hz), 5.17 (dd, 1H, $J = 10.5, 7.8$ Hz), 5.37 (dd, 1H, $J = 3.3, 1.0$ Hz); ^{13}C NMR (62.5 MHz, $CDCl_3$) δ 20.5, 20.6, 20.8, 41.2, 61.3, 66.9, 67.3, 68.7, 70.7, 70.9, 101.0, 170.0, 170.1, 170.3. High-resolution mass spectrum (FAB$^+$) calcd for $C_{18}H_{25}NO_{11}Cl_3$: 536.0493 (MH)$^+$. Found: 536.0474. $[\alpha]_D = +12.0$ ($c = 0.04$ $CDCl_3$).

1-(Trichloroacetamide)-2-(2,3,4,6-tetra-*O*-acetyl-*β*-D-glucopyranoside)-ethanolamine (27a/b). To a solution of 1,2,3,4,6-penta-*O*-acetyl-glucopyanoside (400 mg, 1.02 mmol) in 3 mL of acetonitrile was added iodotrimethylsilane (120 μL, 0.85 mmol). This solution was allowed to stand at room temperature for 20 min. The solvent was removed in vacuo, and 2 mL of toluene was added and again removed in vacuo. A solution of the trichloroacetamide of ethanolamine (317 mg, 1.53 mmol) was added as a solution in 4 mL of acetonitrile and refluxed for 2.5 h. Diisopropylethylamine (500 μL) was then added, the solution filtered, and the solvent then removed in vacuo. Acetic anhydride (5 mL) was then added followed by diisopropylethylamine (500 mL) and a catalytic amount of DMAP. The solution was stirred for 20 min, and then the solvent was removed in vacuo. The resulting oil was subjected to column chromatography (2:1 hexanes: ethyl acetate) to yield 160 mg (29%) of a 2:1 β: α ratio of glycosides. This mixture was carried forward without further purification. High-resolution mass spectrum (FAB$^+$) calcd for $C_{18}H_{25}NO_{11}Cl_3$: 536.0493 (MH)$^+$. Found: 536.0512.

Deacetylation Conditions (28, 29a/b). The above glycosides (Compounds **25** and **27a/b**) were dissolved in methanol and a catalytic amount of sodium methoxide was added. The solution was stirred overnight. Dowex H$^+$ resin was added, the solution filtered, and the solvent then removed in vacuo. This yielded the fully deprotected 1-ethanolamine-2-*β*-D-galactopyranoside (**28**) and 1-ethanolamine-2-α/*β*-D-glucopyranoside (**29a/b**).

D-Biotin-12-amido-4,7,10-trioxadodecyl-1-(2-*β*-D-galactopyranosyl)-ethanolamide (30). A total of 4.0 mg (0.018 mmol) of 1-ethanolamine-2-*β*-D-galactopyranoside (compound **28**) was dissolved in methanol and transferred to the reaction flask, then evaporated and weighed. Next, 187 μL of DMF and 4.9 μL (0.035 mmol) of TEA were added. This was followed by the addition of 7 mg (0.012 mmol) of compound **14** to the reaction mixture as a solution in dichloromethane. The reaction was stirred overnight at room temperature under nitrogen and then evaporated. The crude product was dissolved in 2 mL of 0.03 M ammonium bicarbonate buffer and purified by low-pressure chromatography in a 1.5 × 50 cm column packed with Biogel P-2. The product was detected at 222 nm via the use of an Isco V3 UV−vis detector. A total of 6 mg (73%) of a light yellow grainy powder resulted. ^{1}H NMR (500 MHz, DMSO-d_6)

δ 1.20−1.35 (m, 2H), 1.40−1.52 (m, 3H), 1.55−1.65 (m, 1H), 2.06 (t, 2H, J = 7.3), 2.32 (t, 2H, J = 6.4), 2.57 (d, 1H, J = 12.4), 2.82 (dd, 1H, J = 5.1, 12.4), 3.09 (m, 1H), 3.17−3.62 (m, 28H, incl. HOD), 3.69 (m, 1H), 4.07 (d, 1H, J = 7.0), 4.13 (m, 1H), 4.30 (m, 1H), 6.36 (s, 1H), 6.42 (s, 1H), 7.85 (m, 2H). ^{13}C NMR (125 MHz, DMSO-d_6) δ 25.24, 28.02, 28.18, 35.08, 36.04, 38.43, 38.73, 55.41, 59.18, 60.44, 61.03, 66.76, 67.74, 68.10, 69.15, 69.55, 70.55, 73.24, 75.23, 103.73, 162.71, 170.14, 172.14. High-resolution mass spectrum (FAB$^+$) calcd for $C_{27}H_{49}N_4SO_{12}$ $(MH)^+$: 653.3068. Found: 653.3081.

D-Biotin-12-amido-4,7,10-trioxadodecyl-1-(2-α/β-D-glucopyranosyl)-ethanolamide (31a/b). 1-Ethanolamine-2-α/β-D-glucopyranosyl ethanolamine (compound **29a/b**) was dissolved in enough methanol to yield a 10 mg/mL solution. Some of this volume was transferred to the reaction flask, then evaporated and weighed (24.5 mg, 0.103 mmol). Compound **29a/b** was then dissolved in 532 μL of DMF, followed by the addition of 14.2 μL TEA (0.102 mmol). Compound **14** was then introduced to reaction flask as a solid. The reaction was stirred at room-temperature overnight under argon, then evaporated. The crude product was purified in the manner described for compound **30**. A total of 15.8 mg (72%) of a light yellow grainy powder was obtained. The ratio of α- to β-anomers was found to be roughly 12:1 by ^{1}H NMR. ^{1}H NMR (250 MHz, DMSO-d_6) δ 1.22−1.67 (m, 6H), 2.06 (t, 2H, J = 6.6), 2.24−2.36 (m, 2H), 1.53 (app s, 1H), 2.82 (dd, 1H, J = 5.2, 12.8), 2.93−3.78 (m, 38H, incl. HOD), 4.12 (m, 2H), 4.30 (m, 1H), 4.57 (m, 1H), 4.99 (br. s, 2H), 6.37 (s, 1H), 6.44 (s, 1H), 6.82 (s, 1H), 7.10 (br. s, 2H), 7.30 (s, 1H), 7.86 (app s, 2H). ^{13}C NMR (62.5 MHz, DMSO-d_6) δ 22.60, 25.26, 28.04, 28.20, 35.09, 35.84, 36.04, 55.43, 59.19, 60.92, 61.04, 66.77, 67.99, 69.17, 69.51, 69.56, 69.71, 70.03, 73.44, 76.51, 76.88, 98.82, 103.14, 162.73, 170.18, 172.16, 172.25. High-resolution mass spectrum (FAB$^+$) calcd for $C_{27}H_{49}N_4SO_{12}$ $(MH)^+$: 653.3068. Found: 653.3050.

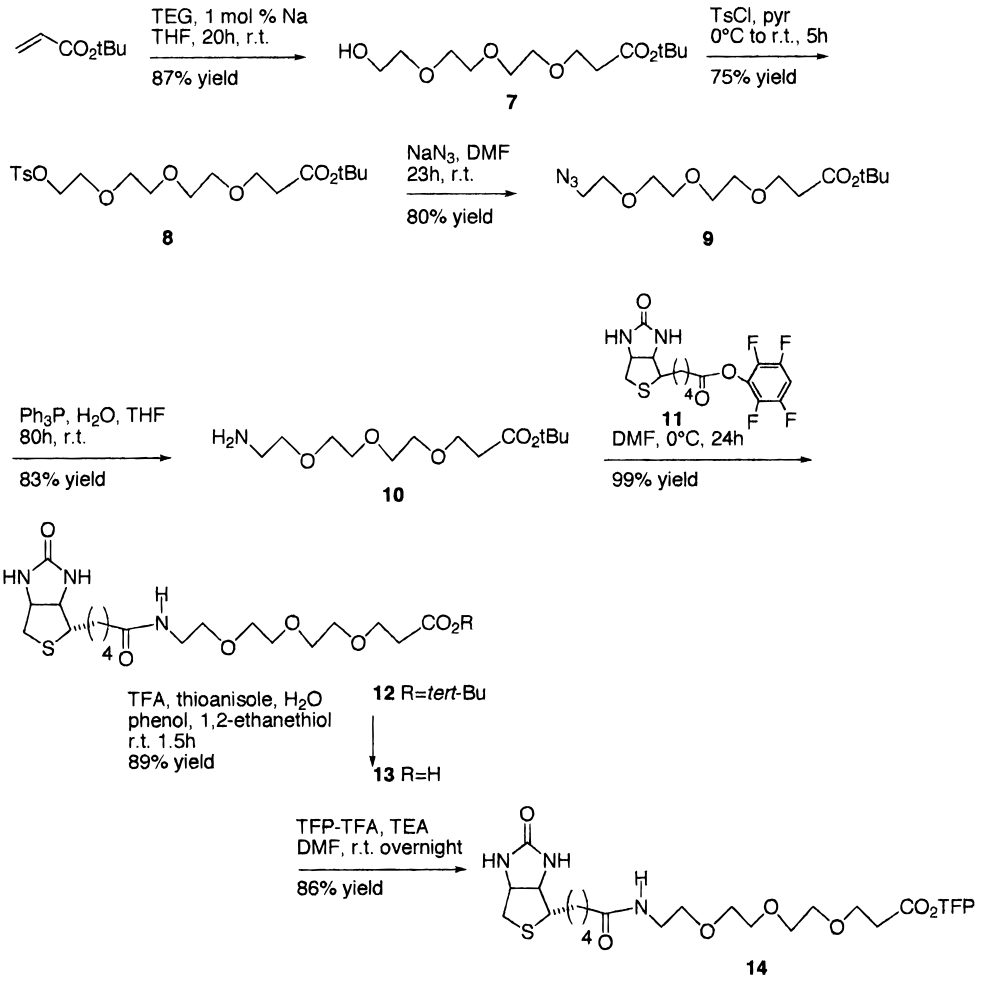
ELISA Ligand Dilutions. Freeze-dried biotinylated analytes (compounds **12**, **15**, **16**, **18**, **19**, **22**, **23**, **30**, **31a/b**) were weighed out to the tenth of a microgram using a Cahn 21 Automatic Electrobalance. Stock solutions of these compounds were prepared at 1 mg/mL concentrations in 20% DMSO/80% PBS buffer. DMSO was first added, and the compounds allowed to fully dissolve prior to addition of PBS buffer. The solutions were thoroughly mixed prior to further dilution in PBS for assaying, and they were stored at −20 °C between uses. The dilution concentration of all compounds utilized in the assays was 20 μg/mL, unless otherwise noted.

Testing of Blocking Reagents. Compounds **12**, **15**, and **16** were evaluated as potential blocking reagents for ELISA using NeutrAvidin coated 8-well strip plates (Pierce). Each compound was plated into four wells each at a volume of 150 μL and incubated for 1 h at 25 °C at 1000 rpm on a Jitterbug microplate incubator (Boekel). An additional eight wells were incubated in this step with 150 μL/well of PBS buffer. After the incubation, the wells were rinsed 3 × 200 μL of PBS. Next, all wells, with the exception of four PBS-incubated wells of the first incubation, were incubated with 100 μL each of a 1:4000 dilution of HRP-biotin (Pierce Biochemicals) for 1 h at 25 °C and 1000 rpm. The four wells without HRP-biotin were incubated with 100 μL each of PBS and would serve as the TMB blank. The wells were rinsed as before. A TMB (3,3′,5,5′-tetramethylbenzidine, Sigma) solution was prepared (1 mg of TMB in 500 μL of DMSO and 9.5 mL of 0.05 M phosphate-citrate buffer with sodium perborate). The TMB solution was added to each well, including the blanks, at a volume of 100 μL/well. The plate was immediately read on a Bio-Rad model 550 microplate reader every minute for 20 min at 630 nm, with a reference wavelength of 490 nm, and 5 s of shaking between each reading. All wells for each analyte were averaged, and had the TMB blank automatically subtracted through the use of the Bio-Rad Microplate Manager software package. The standard deviations for all data points were determined using Excel. The four wells containing only HRP-biotin at its absorbance maximum served as a 100% measure of the sites filled by HRP-biotin. All other blocking reagent wells were compared to the HRP-biotin wells at the same reference point. Upon the basis of these results, the percentage of NeutrAvidin sites filled was determined for each compound. The results given for this assay are representative of several trials performed.

Plating Efficiency Assay. The plating efficiency of each compound (see ELISA Ligand Dilutions) was tested to ensure comparable coverage on NeutrAvidin-coated eight-well strip plates (Pierce Biochemicals). In this assay, each compound was plated into two wells at 150 μL each and incubated for 4 h at 25 °C and 1000 rpm in a Jitterbug microplate incubator (Boekel). Two blank wells were incubated with 150 μL of PBS, and four wells were incubated with 150 μL of PBS each for HRP-biotin determination in the second incubation. After four h, each well was rinsed 3 × 200 μL of PBS. Next, a 1:4000 dilution of HRP−biotin was added to all wells excluding the blanks in 100 μL quantities. The blank wells were incubated with 100 μL of PBS. The second incubation was for one h at 25 °C and 1000 rpm. After the incubation, the wells were rinsed as before. A TMB (3,3′,5,5′-tetramethylbenzidine, Sigma) solution was prepared (1 mg of TMB in 500 μL of DMSO and 9.5 mL of 0.05 M phosphate-citrate buffer with sodium perborate). The TMB solution was added to each well, including the blanks, at a volume of 100 μL/well. The plate was immediately read on a Bio-Rad model 550 microplate reader every min for 20 min at 630 nm, with a reference wavelength of 490 nm and 5 s of shaking between each reading. All wells for each analyte were averaged and had the TMB blank automatically subtracted through the use of the Bio-Rad Microplate Manager software package. The standard deviations for all data points were determined using Excel. The four wells containing only HRP-biotin at its absorbance maximum served as a 100% measure of the sites filled by HRP-biotin. All other analyte wells were compared to the HRP-biotin wells at the same reference point. Upon the basis of these results, the percentage of NeutrAvidin sites filled was determined for each compound. The results given for this assay are representative of multiple assay trials.

ELISA Assay. The compounds (see ELISA Ligand Dilutions) were plated in 150 μL volumes into four wells each of NeutrAvidin-coated eight-well strip plates (Pierce Biochemicals). The plate was incubated for 4 h at 25 °C and 1000 rpm on a Jitterbug microplate incubator (Boekel). An additional four wells each of both a TMB blank (see Plating Efficiency Assay) and a gp120 blank were incubated with 150 μL of PBS in this incubation. Following the first incubation, the wells were rinsed 3 × 200 μL of PBS. Next, 150 μL/well, excluding the TMB and gp120 wells, of compound **15** was incubated for 1 h at 25 °C and 1000 rpm, to ensure that all remaining open NeutrAvidin sites were blocked. The TMB and gp120 wells were incubated instead with 150 μL of PBS, as before. After the second incubation, the wells were rinsed as in the first incubation. The third incubation comprised

Scheme 1



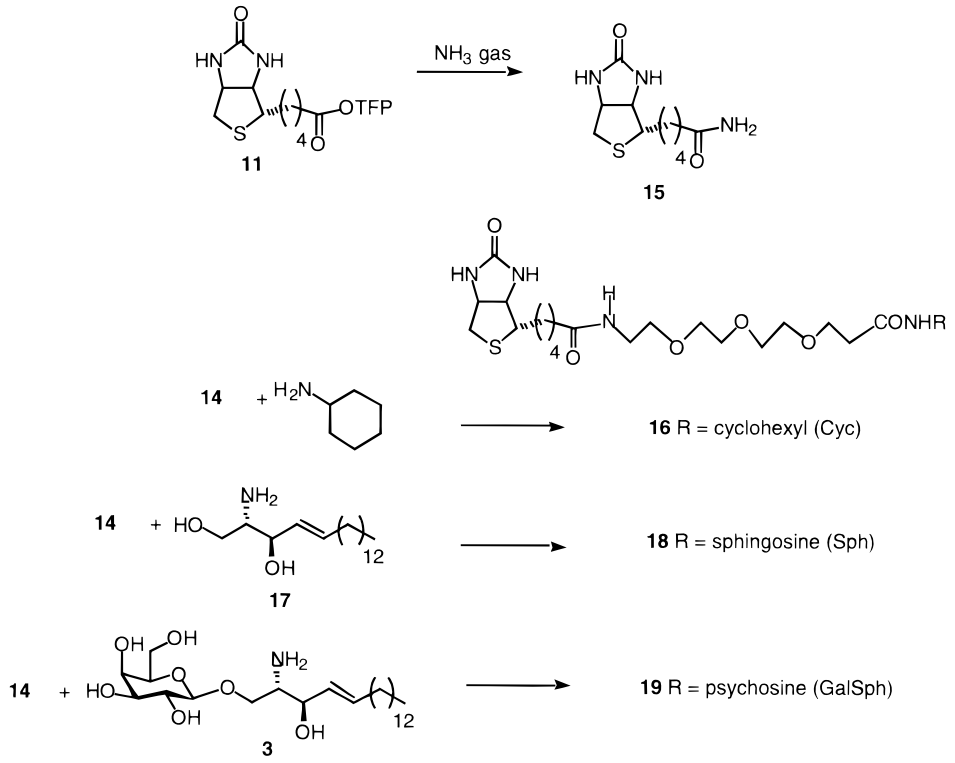
of adding 100 μL of a 1:4 dilution (from a 500 μL vial containing 0.333 μg of gp120) of gp120-HRP (Intracel) into every well, except the TMB wells. The TMB wells were incubated with 100 μL of PBS each. The incubation was for 1 h at 25 °C at 1000 rpm. The wells were then rinsed with 5 × 200 μL of PBS. A solution of TMB reagent (1 mg tablet) was prepared in 500 μL of DMSO and 9.5 mL of phosphate-citrate buffer containing sodium perborate. A total of 100 μL of the TMB reagent was added to each well. The plate absorbances were read every min for 20 min at a test wavelength of 630 nm, a reference wavelength of 490 nm, with a 5 s shake between each reading, on a Bio-Rad model 550 microplate reader. All wells for each analyte were averaged and had the TMB blank automatically subtracted through the use of the Bio-Rad Microplate Manager software package. The standard deviations for all values were determined using Excel. The wells containing only gp120 served as a measure of nonspecific binding interactions between the glycoprotein and the plate and were minimal. This assay was repeated several times, with a representative experiment reported. The error bars reflect the standard deviation between these experiments.

RESULTS

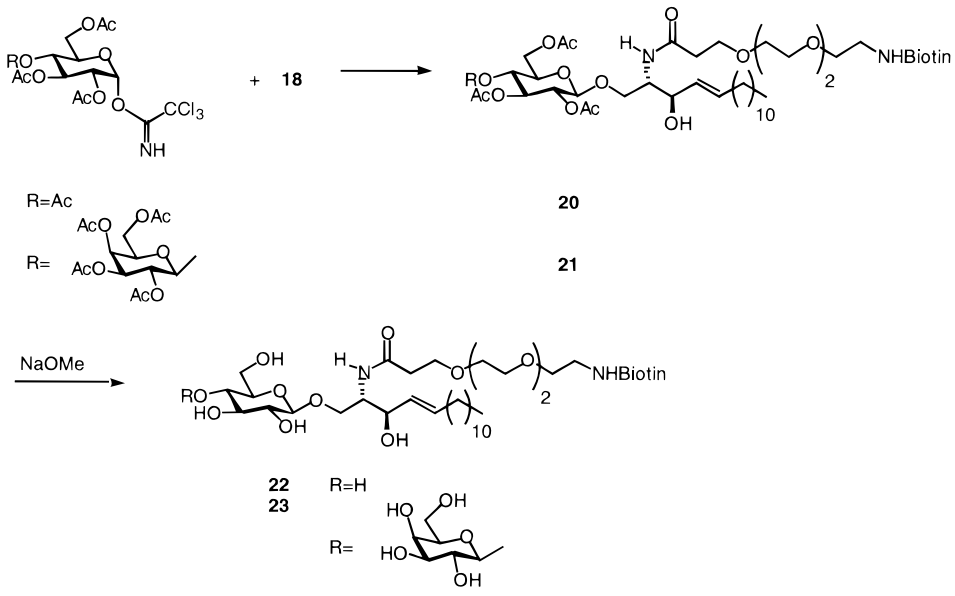
The water-soluble linker was prepared by reacting *tert*-butyl acrylate with tetraethylene glycol (TEG) in the presence of sodium to give **7** (Scheme 1) (*9*). Conversion of the primary alcohol to an azide was accomplished by tosylation (**8**) with subsequent azide displacement to give **9**. Direct incorporation of the azide under Mitsunobu conditions (***16***) was also possible; however, the yield was not as high as the two-step approach. Azide reduction under Staudinger conditions provided the amine **10 (***10*), which was reacted with the tetrafluorophenyl ester of biotin (compound **11**) (*17*) to give **12** in 99% yield. The *tert*-butyl ester was removed under the action of trifluoroacetic acid (TFA) in the presence of thioanisole, 1,2-ethanedithiol, water, and phenol to prevent degradation of the biotin thioether (*12*). The acid (compound **13**) was activated by reaction with tetrafluorophenyl trifluoroacetate (*13*) to give the activated water-soluble linker **14**. Several ligands containing amine functionalities were conjugated to **14** providing a panel of ligands for subsequent ELISA screening.

A simple amide analogue of biotin was prepared by reacting **11** with ammonia to give **15** (Scheme 2). A cyclohexyl analogue, **16**, was prepared by reacting **14** with cyclohexylamine. Sphingosine (**17**) was reacted with **14** to give Sph (**18**), which is a semi-water-soluble analogue of ceramide. In a similar fashion, reaction of **14** with psychosine (**3**) afforded a hydrophilic derivative of GalCer (GalSph, **19**). Synthesis of the GlcSph (**22**) and LacSph (**23**) analogues was more involved since the sphingosine derivatives of Glc and Lac were not commercially available (Scheme 3). Nonetheless, sufficient quantities of these compounds were prepared through reaction of the corresponding peracetylated trichloroacetimidates (*15*) with **18** according to the method of Ogawa (*18*), to give the conjugates **20** and **21**, which when deprotected, afforded **22** and **23**.

Scheme 2

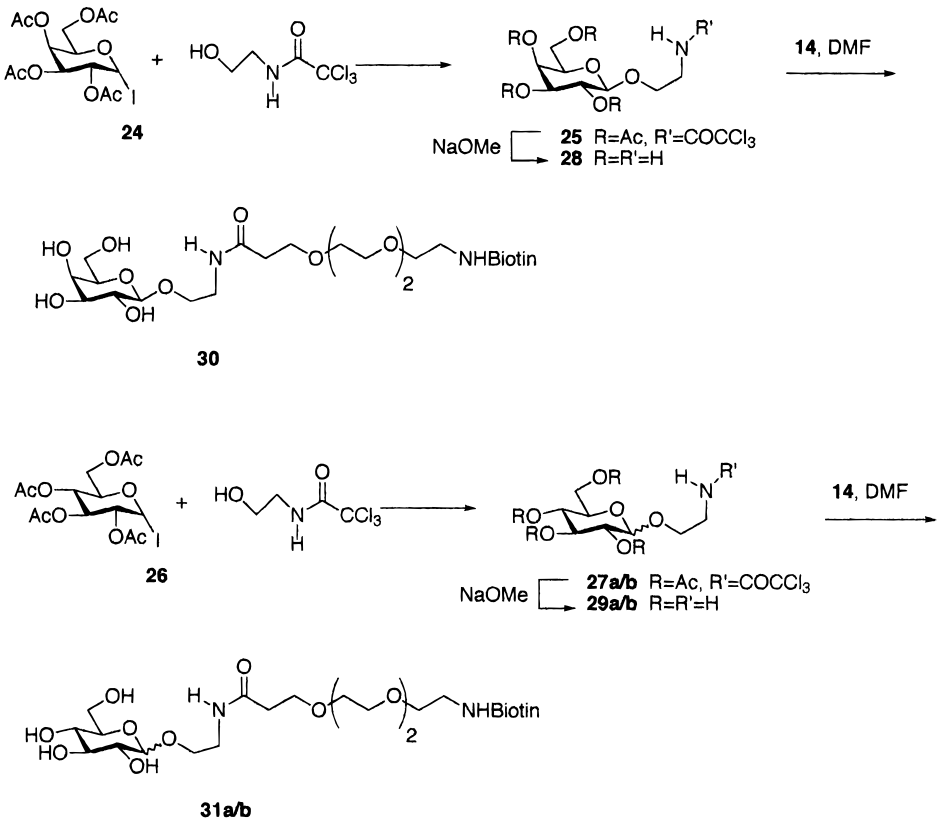


Scheme 3



To probe the importance of the sphingosine component, simple amino analogues of Glc and Gal were prepared (Scheme 4). Reaction of 2,3,4,6-tetra-*O*-acetyl galactosyl iodide **24** with 2-*N*-trichloroacetyl ethanol gave **25**. In a similar fashion, the glucosyl iodide **26** was reacted with 2-*N*-trichloroacetyl ethanol to give an inseparable mixture of anomers **27a/b**. These analogues were deprotected to give GalEA **28** and GlcEA **29a/b**. Subsequent conjugation to **14** afforded the water-s**o**luble Gal and Glc ethanolamine derivatives (WSGalEA, **30**) and (WSGlcEA, **31a**/**b**), respectively. Filling the maximum number of NeutrAvidin binding sites is essential and is done to ensure minimization of nonspecific gp120 binding. We had previously determined that common blocking agents, such as Tween and BSA, led to significant interference due to nonspecific binding of gp120. A series of ELISA were performed in order to determine which of the ligands would best serve as blocking agents. The simple biotin amide **15**, cyclohexyl amide **16**, and *tert*-butyl ester **12** conjugates were screened. Compound **15** was thought to be a good choice as a blocking reagent because of its small size, increased hydrophilicity over biotin, and the lack of an interfering anionic functionality, known to bind the V3 loop region of gp120. Compounds **12** and **16** were tested as blocking reagents because of the presence of the hydrophilic linker that would resemble the analyte ligand and possibly plate more favorably than compound **15**. Compounds **12** and **16** were also tested because of their inability to bind gp120. The extent of blocking was determined by incubating the blocked wells with HRP-biotin. The magnitude of HRP-biotin plating can be monitored by colorimetric measurements, where the

Scheme 4



amount bound is directly proportional to increased absorbance. An efficient blocking agent would prevent HRP-biotin from binding to the plate and result in lower absorbance readings. As can be seen in Figure 2, the simple amide (**15**) was most effective at preventing HRP-biotin binding and was therefore used as the blocking agent in all subsequent assays.

The efficiency of plating for each bioconjugate could be determined by first incubating the microtiter plate with the analyte, followed by incubation with HRP-biotin. NeutrAvidin sites left unoccupied by ligand become saturated with HRP-biotin, analogous to the situation given in the blocking reagent assays. The efficiency of plating is shown in Table 2. Using the maximum absorbance value generated by filling all available NeutrAvidin sites with HRP-biotin as our 100% estimate, relative measurements of the percentage of sites filled by each ligand were generated at the same reference point. It was critical to ensure that all ligands filled approximately the same number of protein sites in the well. If they did not, the gp120 binding events could not be attributed solely to differences in affinity for each bioconjugate, but instead might be a consequence of variable plating efficiency. Table 2 illustrates that all of the bioconjugates tested fill 75−93% of the NeutrAvidin sites available, when compared to the 100% HRP-biotin value. The standard deviations for each data point in four separate experiments were calculated as a measure of the error for each ligand. These plating efficiencies were used to normalize the data obtained from subsequent ELISA with recombinant HRP gp120.

After the best blocking agent and the efficiency of plating were determined, the panel of ligands was subjected to screening with recombinant HRPgp120. The proof of the ELISA validity as a new method to test hydrophilic compounds for gp120 binding was evidenced by the results of the known positive GalCer analogue,

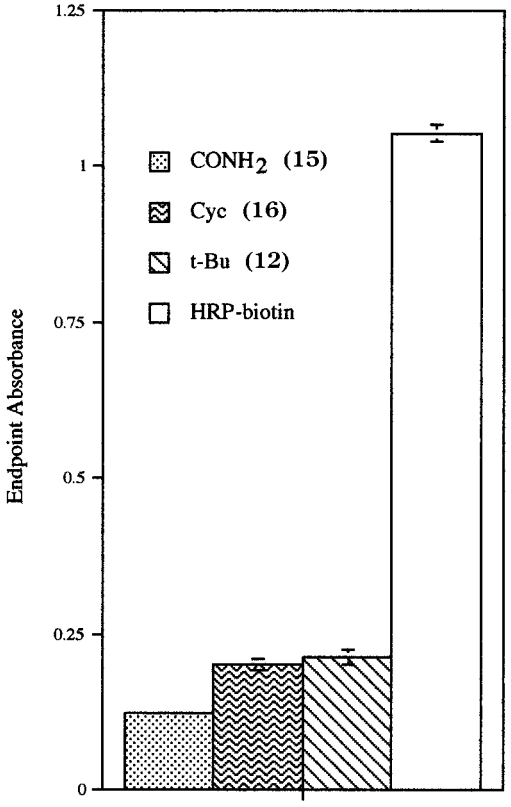


Figure 2. Determination of the optimal blocking reagent for ELISA. The endpoint determination for each ligand at the maximum absorbance of HRPbiotin is graphed. The error was calculated from the standard deviation in data from four different experiments. These data are representative of two separate trials.

compound **19**, and also by the negative test, compound **16**. Compound **16** was initially synthesized as a negative

Table 2. Absorbance Data Was Determined from End Point Reading at Maximum Absorbance for HRP-Biotin and the Corresponding Ligands at the Same Point[a]

compound	absorbance	standard deviation	% of filled sites
HRP−biotin	1.088	0.031	100
WSGalEA (**30**)	0.079	0.010	93
$CONH_2$ (**15**)	0.159	0.018	85
Sph (**18**)	0.173	0.000	84
LacSph (**23**)	0.177	0.006	84
GlcSph (**22**)	0.217	0.012	80
WSGlcEA (**31a/b**)	0.235	0.087	78
GalSph (**19**)	0.243	0.017	78
Cyc (**16**)	0.272	0.000	75

[a] The standard deviation was calculated from the data in four different experiments. These data are representative of three separate trials.

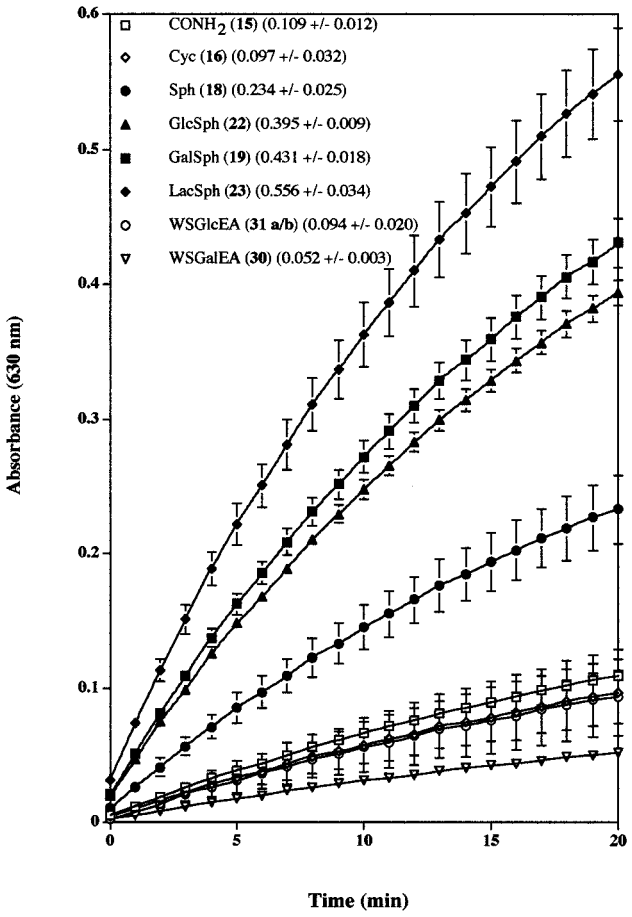


Figure 3. The gp120 ELISA binding profiles of all ligands tested. The absorbance as a function of time is plotted after it was normalized to reflect plating efficiencies. The error was calculated from the standard deviation in data from four different experiments. These data are representative of multiple trials.

test reagent because it had a six-membered ring, much like a carbohydrate. It was suspected that it would not bind to gp120 because it lacks the carbohydrate component present in GalCer. As shown in Figure 3, GalSph, (**19**) did have significant binding to gp120, whereas **16** showed only background levels of gp120 binding activity. GalSph (**19**) and GlcSph (**22**) had similar binding affinities for gp120, while the binding affinity of LacSph (**23**) was higher. These observations contradict previously reported results, where GalCer binds with the highest affinity and GlcCer and LacCer do not bind at all. (*1*,*2*,*3*)

DISCUSSION

There are a number of possible explanations for the similar binding profiles of GalSph and GlcSph, and enhanced binding of LacSph. One possibility is that the monosaccharides are not spatially far enough away from the lipid-linker portion of the molecule and interfere with full protein interaction, while the disaccharide is further removed. It may also be that the presentation geometries of the monosaccharides versus the disaccharide are significantly different, affecting the protein-binding event. A third possibility is that gp120 recognition of cell-surface glycoconjugates is mediated by a combination of hydrophobic and hydrophilic interactions and LacSph (**23**) may fulfill the requirements better than GlcSph (**22**) and GalSph (**19**). We are currently investigating these possibilities.

Interestingly, we have found that Sph (**18**) interacts moderately well with gp120, suggesting that the lipid component is important, as had been demonstrated in earlier work (*19*). The WSGalEA (**30**) and WSGlcEA (**31a/b**) ligands do not bind gp120, indicating that while the carbohydrate component is important, it is not sufficient to achieve full gp120 binding. Perhaps, the lipid portion of the glycoconjugate forms the first contact point with gp120 and the second interaction with the carbohydrate affords strength and specificity to the interaction. Alternatively, the lipid/gp120 interaction could cause a conformational change in the protein, facilitating access to the binding region for the carbohydrate.

In summary, we have prepared water-soluble analogues of GalCer, GlcCer, and LacCer and determined their relative binding affinities for recombinant HIV-1 gp120 using a novel ELISA construct. To our knowledge, this ELISA is the only known method to directly compare gp120 recognition of various bioconjugates that yields both consistent and reproducible results. The assay has the added advantage that the analyte plating efficiency can be determined, which is not possible with the existing lipid-based assays. This assay is a powerful screening tool for obtaining qualitative binding measurements. To obtain accurate binding affinities, more sensitive techniques will be required. The hydrophilic nature of the reported synthetic bioconjugates may uniquely position us to study their binding using biosensors, where both on and off rates, as well as quantitative binding affinities, could be measured.

ACKNOWLEDGMENT

We are indebted to Dr. Arpad Somogyi, director of the UA Mass Spectrometry Facility. Financial support for this research was gratefully received from NIH (AI40359-02), Eli Lilly, Alfred P. Sloan Foundation, and The National Science Foundation Early Career Award (CHE9623583). K.D.M. gratefully acknowledges receipt of the University of Arizona Dean's Fellowship and the Department of Chemistry Carl S. Marvel Fellowship. We would also like to thank the reviewers for their helpful comments. We are also indebted to Dr. Javier Enriquez for facilitating ELISA measurements.

LITERATURE CITED

(1) Harouse, J. M., Bhat, S., Spitalnik, S. L., Laughlin, M., Stefano, K., Silberberg, D. H., and Gonzalez-Scarano, F. (1991) Inhibition of Entry of HIV-1 in Neural Cell Lines by Antibodies Against Galactosyl Ceramide. *Science 253*, 320−323.

(2) Clapham, P. R., McKnight, A., Talbot, S., and Wilkinson, D. (1996) HIV Entry into Cells by CD4-Independent Mechanisms. *Perspect. Drug Discovery Des. 5*, 83−92; Delezay, O.,

Yahi, N., Fantini, J. (1996) Detection of Functional Galactosylceramide (GalCer) Receptors on CD4-Negative HIV-1 Target Cells. *Perspect. Drug Discovery Drug Des. 5*, 192−202.

(3) Bhat, S., Spitalnik, S. L., Gonzalez-Scarano, F., and Silberberg, D. H. (1991) Galactosyl Ceramide or a Molecule Derived from it is an Essential Component of the Neural Receptor for HIV-1 Envelope Glycoprotein gp120. *Proc. Natl. Acad. Sci. U.S.A. 88*, 7131−7134.

(4) McAlarney, T., Apostolski, S., Lederman, S., and Latov, N. (1994) Characteristics of HIV-1 gp120 Glycoprotein Binding to Glycolipids. *J. Neurosci. Res. 37*, 453−460.

(5) Long, D., Berson, J. F., Cook, D. G., and Doms, R. W. (1994) Characterization of Human Immunodeficiency Virus Type 1 gp120 Binding to Liposomes Containing Galactosylceramide. *J. Virol. 68*, 5890−5898.

(6) Several linker molecules for use in bioconjugate chemistry are commercially available. At the time we began our studies, only hydrophobic linkers were available. Recently, several new hydrophilic ethylene-glycol based linkers have been marketed.

(7) Shao, M.-C. (1992) The use of streptavidin−biotinylglycans as a tool for characterization of oligosaccharide-binding specificity of lectin. *J. Immunol. Methods 205*, 77−82.

(8) Gervay, J., and McReynolds, K. D. (1999) Utilization of ELISA technology to measure biological interactions of carbohydrates relevant in disease states. *Curr. Med. Chem. 6*, 129−153. While this manuscript was in preparation, and the review article containing our linker synthetic strategy was at press, a similar *N*-methyl amide linker synthesis was reported. Wilbur, D. S., Pathare, P. M., Hamlin, D. K., Buhler, K. R., and Vessella, R. L. (1998) Biotin reagents for antibody pre-targeting. 3. Synthesis, radioiodination, and evaluation of biotinylated starburst dendrimers. *Bioconjugate Chem. 9*, 813−825.

(9) Seitz, O., and Kunz, H. (1997) HYCRON, an allylic anchor for high-efficiency solid-phase synthesis of protected peptides and glycopeptides *J. Org. Chem. 62*, 813−826.

(10) Nagarajan, S., and Ganem, B. (1987) Chemistry of naturally occurring polyamines. 11. Unsaturated spermidine and spermine derivatives. *J. Org. Chem. 52*, 5044−5046.

(11) Knouzi, N., Vaultier, M., and Carrie, R. (1985) Reduction d'azides par la triphenylphosphine en presence d'eau: Une methode generale et chemioselective d'acces aux amines primaries. *Bull. Soc. Chim. France 5*, 815−819.

(12) King, D. S., and Fields, G. B. (1990) A cleavage method which minimizes side reactions following Fmoc solid-phase synthesis. *Int. J. Pept. Protein Res. 36*, 255−266.

(13) Gamper, H. B., Reed, M. W., Cox, T., Virosco, J. S., Adams, A. D., Gall, A. A., Scholler, J. K., and Meyer, R. B., Jr. (1993) Facile preparation of nuclease resistant 3′ modified oligodeoxynucleotides. *Nucleic Acids Res. 21*, 145−150.

(14) Flandor, J., Garcia-Lopez, M. T., de las Heras, F. G., and Mendez-Castrillon, P. P. (1985) A facile regioselective 1-*O*-deacylation of peracetylated glycopyranoses. *Synthesis* 1121−1123

(15) Schmidt, R. R., and Michel, J. (1980) Facile synthesis of α- and *β*-*O*-glycosyl imidates; preparation of glycosides and disaccharides. *Angew. Chem., Int. Ed. Engl. 19*, 731−732.

(16) (a) Lal, B., Pramanik, B. N., Manhas, M. S., and Bose, A. K. (1977) Diphenylphosphoryl azide a novel reagent for the stereospecific synthesis of azides from alcohols. *Tetrahedron Lett. 23*, 1977−1980. (b) Pearson, W. H., Lin, K.-C. (1990) The intramolecular cycloaddition of azides with *ω*-chloroalkenes. A facile route to (−)-swainsonine and other indolizidine alkaloids. *Tetrahedron Lett. 31*, 7571−7574.

(17) Wilbur, D. S., Hamlin, D. K., Vessella, R. L., Stray, J. E., Buhler, K. R., Stayton, P. S., Klumb, L. A., Pathare, P. M., and Weerawarna, S. A. (1996) Antibody fragments in tumor pretargeting. Evaluation of biotinylated Fab′ colocalization with recombinant streptavidin and avidin. *Bioconjugate Chem., 7*, 689−702.

(18) Numata, M., Sugimoto, M., Shibayama, S., and Ogawa, T. (1988) A total synthesis of hematoside, α-NeuGc-(2→3)-*β*-Gal-(1→4)-*β*-Glc-(1→1)-Cer. *Carbohydrate Res. 174*, 73−85.

(19) Fantini, J., Hammache, D., Delézay, O., Yahi, N., André-Barres, C., Rico-Lattes, I., and Lattes, A. (1997) Synthetic Soluble Analogues of Galactosylceramide (GalCer) Bind to the V3 Domain of HIV-1 gp120 and Inhibit HIV-1-induced Fusion and Entry. *J. Biol. Chem. 272*, 7245−7252.

BC990050X

Surface Plasmon Resonance (SPR) as a Tool for Antibody Conjugate Analysis

Maciej Adamczyk,* Phillip G. Mattingly, Kevin Shreder, and Zhiguang Yu

Abbott Laboratories, Diagnostics Division, Department of Chemistry D9NM, Building AP 20, 100 Abbott Park Road, Abbott Park, Illinois, 60064-6016. Received May 20, 1999; Revised Manuscript Received August 12, 1999

Surface plasmon resonance (SPR) analysis was used to assess the immunoreactivity of anti-biotin (**4**) and anti-fluorescein (**5**) monoclonal antibody after conjugation with the *N*-hydroxysuccinimide ester of acridinium-9-carboxamide **1**. Only minor changes in the apparent equilibrium dissociation constants of the antibody conjugates for their ligands resulted from the conjugation process. However, comparison of the initial binding rate of the conjugates with their ligands with those of the unmodified antibodies over a range of concentrations showed that the antibody conjugates were partially inactivated. The anti-fluorescein conjugates retained at least 90% of their immunoreactivity over the range of modification tested, while anti-biotin conjugates showed a progressive loss of reactivity with increased substitution by the label.

INTRODUCTION

Surface plasmon resonance (SPR) is a phenomenon that is measured by the change in the refractive index at a surface as a function of the mass of the material bound to the surface. As commercialized on the BIAcore instrument, SPR allows for the real-time measurement of the kinetics of noncovalent interactions between a ligand and a binding partner (*1*−*3*). We have recently highlighted surface plasmon resonance on the BIAcore system as a valuable tool that can be used to characterize immunoreagents utilized in immunoassays (*4*−*8*). The previous reports have detailed the utility of SPR in evaluating how the structural variations in a library of small molecule haptens affected the kinetics and thermodynamics of binding to anti-hapten antibodies or Fab fragments. In one study, each analogue in the library was immobilized on a separate biosensor chip and evaluated individually with the antibody or Fab (*7*). The association and dissociation rates for each analogue were determined from the generated sensorgrams, and the affinity constants were calculated and compared. In this *direct* SPR method, it was necessary to optimize the surface density of the ligand at a low level on the biosensor chip to *minimize* rebinding events and mass transport limitations. Other studies have taken a different approach in which a single biosensor was used to determine the affinity constants of each member of the library with the Fab in solution at equilibrium (*5*, *8*). The technique is based on the observation that under mass transport limited conditions the initial binding rate of the antibody with the biosensor is proportional to the concentration of the antibody and independent of the affinity of the antibody for the ligand on the biosensor chip (*9*). Plotting initial binding rate versus antibody concentration produces a calibration curve from which concentrations of free antibody in an unknown sample at equilibrium can be determined. For this experiment, the surface density of the ligand on the biosensor must be *high* enough to *ensure* mass transport limited kinetics.

Both types of studies were particularly applicable to characterizing the reagents used in assay formats in which the antibody would be unmodified by labeling or immobilization. It is often the case, however, that the antibody component of the immunoassay is modified by conjugation to a detectable tag, ligand, or solid support [see, for example, Abraham et al. (*10*)]. SPR has only recently been reported to study the effect of the biotinylation of anti-LH mAbs on binding to LH in an immunometric format (*11*). The degree of biotinylation of the mAbs was not determined, but the authors offered the qualitative observation that the conjugation procedure had a marked effect on the sensor-bound antibody binding to LH. In general, chemical modifications to any antibody may vary from lot to lot and unpredictably change the conjugate's binding properties with the analyte ligand, which in turn would affect assay performance. SPR provides a convenient tool for assessing the changes in antibody binding characteristics in a reproducible, automated fashion using a minimal amount of the antibody conjugate.

In this report, a series of conjugates between anti-biotin (**4**) and anti-fluorescein (**5**) monoclonal antibodies and a new chemiluminescent *N*-sulfonylacridinium-9-carboxamide derivative (**1**) was prepared and evaluated by SPR on the BIAcore system using the solution competition method.

MATERIALS AND METHODS

Anti-biotin (**4**, IgG2a) and anti-fluorescein (**5**, IgG1) monoclonal antibodies, obtained from the Abbott cell culture facility (Abbott Laboratories, Abbott Park, IL), were dialyzed exhaustively against PBS (100 mM sodium phosphate and 150 mM sodium chloride, pH 7.2) using a 10 000 MW cutoff membrane dialysis cassette (Slide-A-Lyzer, Pierce Chemical Co., Rockford, IL). The acridinium-9-carboxamide label **1** (*12*, *13*) and *O*-(6-fluoresceinylmethyl)hydroxylamine **2** (6-OFMHA) (*14*, *15*) were prepared as previously described. 5-(Biotinamido)pentylamine **3** was obtained from Pierce Chemical Co. UV−vis spectroscopy was performed on a Beckman DU 640 spectrophotometer (Fullerton, CA). Preparative HPLC

* Author to whom correspondence should be addressed. Phone: (847) 938-8927. E-mail: maciej.adamczyk@abbott.com.

10.1021/bc990057e CCC: $18.00 © 1999 American Chemical Society
Published on Web 10/14/1999

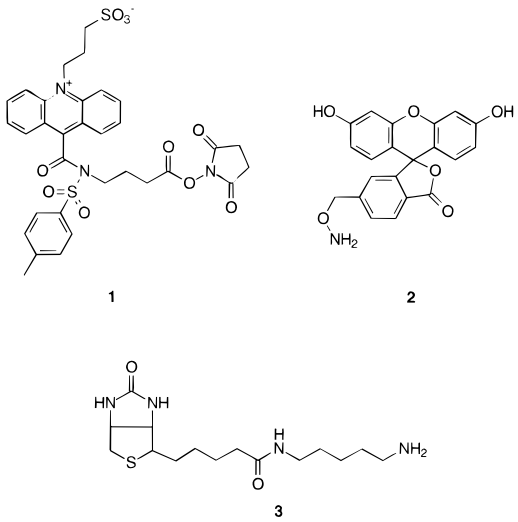


Figure 1. Structures of the active ester of the acridinium label (**1**), *O*-(fluoresceinylmethyl)hydroxylamine (**2,** 6-OFMHA), and 5-(biotinamido)pentylamine (**3**).

was performed using a Waters (Milford, MA) 600E system controller and pumps and a model 486 tunable absorbance detector set to 280 nm. Surface plasmon resonance measurements were carried out at 25 °C on a BIAcore 2000 (BIAcore, Inc., Piscataway, NJ) automated system using research-grade CM-5 four-channel sensor chips. Reagents for the BIAcore instrument consisted of HBS running buffer [10 mM Hepes (pH 7.4), 150 mM NaCl, 3.4 mM EDTA, and 0.05% surfactant P-20], a biosensor chip activation kit containing *N*-hydroxysuccinimide (0.5 M, NHS), *N*-ethyl-*N*′-(3-dimethylaminopropyl)carbodiimide hydrochloride (0.2 M, EDC), and a capping solution of ethanolamine hydrochloride (1 M, pH 8.5), all from BIAcore, Inc.

Preparation of Antibody-acridinium-9-carboxamide Conjugates. *General Procedure.* To each antibody (3.0 mg mAb in 1.4 mL of PBS, pH 8.0) was added (a) 4, (b) 8, or (c) 16 molar equivalents of the acridinium-9-carboxamide active ester **1** (Figure 1) in DMF (0.2 mL). Upon addition, the solutions were rapidly vortexed then allowed to stand for 18 h in the dark. Each reaction was purified by preparative HPLC using a Bio-Rad (Hercules, CA) SEC-250-5 gel permeation chromatography column eluting with PBS [pH 6.3, containing CHAPS (0.1%), 1.0 mL/min] and subsequently stored at 2−8 °C in the dark. Labeled antibody ($R_t \approx 8.3$ min) and unconjugated acridinium-9-carboxamide label ($R_t = 11.1$ min) were readily separated under these conditions.

The concentration of antibody conjugate was determined by UV−vis spectroscopy using the following formula:

$$[\text{conjugate}] = [A_{280} - (A_{369}/4.1)]/\epsilon_{280}$$

where A_{280} and A_{369} are the absorbance readings of the acridinium-9-carboxamide-antibody conjugates at the corresponding wavelengths; 4.1 is the A_{369}/A_{280} of the free carboxylic acid form of **1**, and ϵ_{280} (210 000 M^{-1} cm^{-1}) is the extinction coefficient of the IgG antibody at 280 nm. The ratio of acridinium label to antibody (**r**) conjugate was determined by UV−vis spectroscopy using the following formula:

$$r = \frac{A_{369}/\epsilon_{369}}{[A_{280} - (A_{369}/4.1)]/\epsilon_{280}}$$

where ϵ_{369} (14 700 M^{-1} cm^{-1}) is the extinction coefficient of the label free carboxylic acid form of **1** at 369 nm. For the acridinium-9-carboxamide-anti-biotin conjugates **4a**−**c**, label-to-antibody ratios of 2.1, 4.0, and 7.5 were obtained, respectively. For the acridinium-9-carboxamide-anti-fluorescein conjugates **5a**−**c**, label-to-antibody ratios of 2.2, 3.6, and 7.4 were obtained, respectively.

Preparation of Biotin and Fluorescein Biosensors. Biosensors were prepared under the conditions listed in Table 1. In general, CM-5 chips were equilibrated with running buffer (10 μL/min), then activated with NHS/EDC. A solution of 5-(biotinamido)pentylamine (**3**) or 6-OFMHA (**2**) was injected over the cell. Reactive sites remaining on the biosensor chip were blocked with ethanolamine (70 μL, 1.0 M). The binding capacities of the resulting biosensors were estimated using unlabeled anti-biotin mAb (**4**) or unlabeled anti-fluorescein mAb (**5**). Control surfaces for each sensor were generated at the same conditions, omitting the ligand immobilization step.

Antibody Conjugate Analysis by the Solution Competition Method. *(A) Calibration Curve.* Stock solutions of the native antibodies (**4** and **5**) and antibody conjugates (**4a**−**c** and **5a**−**c**) in PBS were serially diluted into HBS buffer to obtain 11 solutions in concentrations ranging 2−22 nM. The diluted solutions of known concentration were injected over the corresponding biosensors (5 μL/min, 2.0 min). The biotin biosensor was regenerated after each run with formic acid (1.0 M, 1 min), then guanidine·HCl (6.0 M, 1 min; 1.5 M, 1 min). The fluorescein biosensor surface was regenerated by consecutive pulses of guanidine·HCl (6.0 M, 2 × 1 min; 1.5 M, 1 min). The initial binding rate was obtained from each sensorgram by linear fitting of a 15 s window, starting 20 s after injection. Calibration curves were generated for either the native antibodies or their conjugates by plotting the initial binding rate vs antibody (or conjugate) concentration.

(B) Determination of Apparent Solution Equilibrium Dissociation Constants (K_D). 5-(Biotinamido)pentylamine (**3**) and 6-OFMHA (**2**) were each serially diluted with HBS buffer to give 11 solutions ranging 8−100 nM for **3** and 40−1000 nM for **2**. Stock solutions of the native antibodies (**4** and **5**) and antibody conjugates (**4a**−**c** and **5a**−**c**) in PBS buffer were diluted into HBS buffer to obtain 40 nM solutions. Each ligand solution was mixed with the corresponding antibody or conjugate solution (1:1 v/v). Once equilibration was reached after 1 h at ambient temperature, the concentration of free antibody or antibody conjugate in each sample was assayed using a biosensor chip and the corresponding calibration curve. Nonlinear least-squares regression analysis supplied with the BIAevaluation software (version 3.0) was used to fit a plot of the concentrations of free antibody versus the concentrations of the competitor and determine the apparent solution affinity. The formula used in the software is shown below:

$$A_{\text{Free}} = (A_T - L_T - K_D)/2 + [(A_T + L_T + K_D)^2/4 - L_T A_T]^{1/2}$$

where A_{Free} is the concentration of free antibody in equilibrated solution with the competitor ligand, A_T is the total concentration of antibody, L_T is the total concentration of ligand, and K_D is the apparent equilibrium dissociation constant for the binding between the ligand and the antibody.

Determination of Retained Antibody Conjugate Activity. Solutions of antibody conjugates (**4a**−**c** and

Table 1. Experimental Conditions for the Preparation and Regeneration of Biotin and Fluorescein Biosensors

type of sensor	sensor activation, 0.5 M NHS/0.2 M EDC (μL)	ligand immobilization,[a] ligand (vol, concn)	sensor surface capacity (RU)	sensor regeneration
biotin	120	**3**[b] (100 μL, 10 mM)	11 000	*c*
fluorescein	200	**2**[d] (200 μL, 1.0 mM)	>30 000	*e*

[a] Any reactive sites remaining on the sensor chip after ligand immobilization were reacted with ethanolamine (70 μL, 1.0 M). [b] In HBS buffer, pH 7.4 [c] 1 min, 1.0 M formic acid; 1 min, 6.0 M guanidine hydrochloride; 1 min, 1.5 M guanidine hydrochloride. [d] In acetate buffer (10 mM NaOAc and 0.1 M NaCl), pH 5.5. [e] 2 × 1 min, 6.0 M guanidine hydrochloride; 1 min, 1.5 M guaninine hydrochloride.

5a−**c**) ranging 2−22 nM were injected over the corresponding biosensors (5 μL/min), and the initial binding rate was determined from each sensorgram. The activity of each conjugate (**4a**−**c** and **5a**−**c**) was compared to the unmodified antibody (**4** or **5**, respectively) using the formula

$$\% \text{ active antibody conjugate} = k/k_0$$

k_0 is the slope in the calibration curve of the unmodified antibody (**4** or **5**) and k is the slope observed for the antibody conjugates (**4a-c** and **5a-c)**.

RESULTS

Preparation of Antibody-acridinium-9-carboxamide Conjugates. The antibodies **4** and **5** were conjugated with the acridinium-9-carboxamide active ester **1** at three stoichiometries (4:1, 8:1, and 16:1) in buffer/DMF (7:1, pH 8.0). The antibodies and labeling reagent were completely soluble during the course of the reaction and throughout purification. Purification of the conjugates by gel permeation chromatography removed unreacted or hydrolyzed **1**. The efficiency of the coupling reaction between both antibodies and the active ester **1** ranged from 53 to 47% based on incorporated **1**. There was no significant difference in the coupling efficiency between the three stoichiometries.

Preparation of Biosensors. *Anti-Biotin mAb Sensor.* Biotin containing a pentanediamine linker (**3**) was immobilized on a NHS/EDC-activated carboxymethylated dextran surface of a CM-5 sensor chip to afford a biosensor. Using a ligand concentration of 10 mM for 10 min produced a biosensor with an anti-biotin antibody (**4**) binding capacity of 11 000 RU (Table 1).

Anti-Fluorescein mAb Sensor. Immobilization of 5(6)-fluoresceinamine, 4′-aminomethylfluorescein or 5(6)-aminomethylfluorescein (data not shown) under the conditions that were successful for the biotin series, proved to be insufficient to generate the ligand density necessary to achieve mass transport limitation. It was reasoned that at pH 8 the negatively charged fluorescein molecule is electrostatically repulsed from the carboxylated sensor surface. 6-OFMHA (**2**) was immobilized on the sensor chip under acidic conditions that circumvented this problem. Thus, a 1 mM solution of **2** buffered at pH 5.5 reacted with the activated CM-5 chip over 20 min to afford a suitable ligand surface with a binding capacity for anti-fluorescein mAb **5** of 30 000 RU (Table 1).

Mass transport limited conditions were reached when biotin and fluorescein surfaces were prepared to have antibody capacities of 11 000 and 30 000 resonance units (RU), respectively. Injection of native antibodies on sensor chips with slightly less antibody capacities yielded the same initial binding rates, which confirmed that mass transport limited conditions had been reached. Fluorescein surfaces were regenerated by two consecutive pulses of 6.0 M guanidine·HCl and one pulse of 1.5 M guanidine·HCl, each lasting for 1.0 min. In contrast, regeneration of biotin surfaces was found to be more difficult. To clean the latter surface thoroughly, a 1 min pulse of 1.0 M formic acid was needed prior to washing the surface with 6.0 and 1.5 M guanidine·HCl (Table 1).

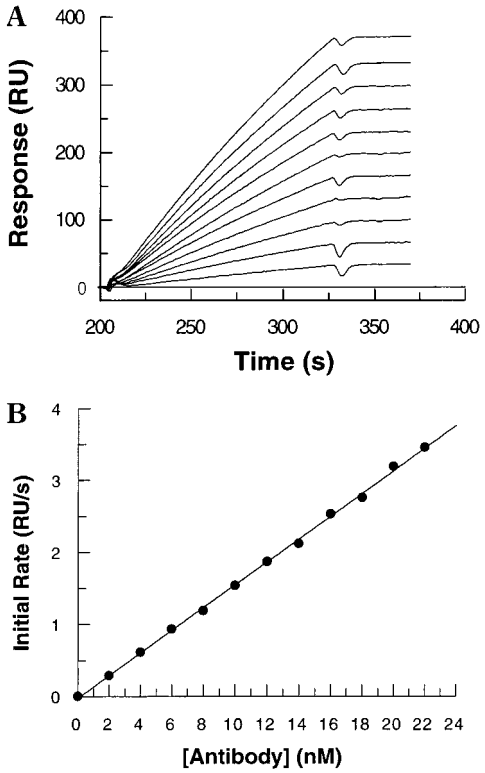


Figure 2. Calibration curve for anti-biotin mAb **4.** (A) Sensorgrams (**4,** 2−22 nM). (B) The initial rate at each concentration was calculated using a 15 s window, starting 20 s after the injection.

Antibody Conjugate Analysis by the Solution Competition Method. The required calibration curves of initial binding rate vs antibody (or conjugate) concentration were constructed using the corresponding biotin or fluorescein biosensors. Thus, the sensorgrams obtained for different concentrations of anti-biotin mAb (**4**) under mass transport limiting conditions are typical (Figure 2A). Both the initial binding rates and the total response units obtained during the binding phase of the sensorgrams increase proportionally to the increase in binding protein concentration within the range examined (2−22 nM). The initial binding rate for each concentration of **4** was obtained by analyzing the sensorgram over a 15 s window beginning 20 s postinjection. Data from the first 20 s of each sensorgram was omitted due to sample dispersion effects at the start of injections. A plot of initial binding rate versus concentration of **4** yielded the calibration curve (Figure 2B).

To determine the apparent solution equilibrium dissociation constant of anti-biotin antibody **4** with biotin ligand **3**, a stock solution of **3** was serially diluted into HBS buffer to obtain solutions ranging 6.6−67 nM. These diluted ligand solutions were mixed with the anti-biotin antibody **4** (40 nM) in equal volumes. After equilibrium

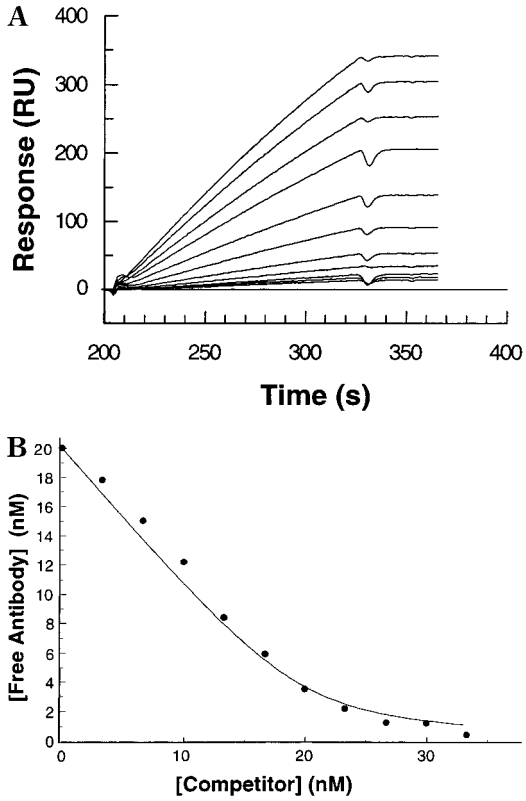


Figure 3. Solution competition of anti-biotin mAb **4** and biotin ligand **3**. (A) Sensorgrams using **4** (20 nM) and **3** (0−33.3 nM). (B) Competition curve derived from A.

Table 2. Effect of Acridinium Conjugation on Antibody Activity and Apparent Affinity

antibody	incorporation ratio of acridinium:Ab	active antibody (%)	apparent dissociation constant K_D (nM)
anti-biotin (**4**)		100	5.2
4a	2.1	95	5.5
4b	4.0	91	5.5
4c	7.5	77	6.4
anti-fluorescein (**5**)		100	81
5a	2.2	100	77
5b	3.6	96	72
5c	7.4	90	85

was reached (>1 h), the resulting solutions were injected over the biotin surface to produce the sensorgrams shown in Figure 3A. The initial slope of each sensorgram was converted to concentration of free native antibody based on the calibration curve. The apparent equilibrium dissociation constant of anti-biotin antibody **4** with ligand **3** was determined after plotting the free concentrations of antibody vs concentrations of the ligand **3** (Figure 3B) using BIAevaluation 3.0 software. Conjugates **4a**−**c** were evaluated analogously using the corresponding calibration curves. Apparent equilibrium dissociation constants of anti-fluorescein mAb **5** and its acridinium-9-carboxamide conjugates (**5a-c**) were measured in a similar fashion using solutions of 6-OFMHA (**2**), ranging from 40 to 1000 nM as the competing ligand.

Table 2 shows the apparent equilibrium dissociation constants of anti-biotin antibody **4**, anti-fluorescein antibody **5**, and their acridinium-9-carboxamide conjugates at different labeling ratios. Within a set, the affinities were very similar. For **4** and **4a**−**c**, the apparent equilibrium dissociation constants ranged 5.2−6.4 nM. For **5** and **5a**−**c**, the apparent equilibrium dissociation constants ranged 72−81 nM.

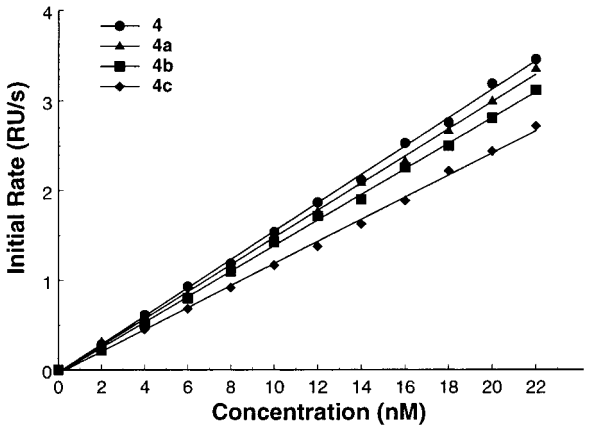


Figure 4. Comparison of the calibration curves of anti-biotin mAb **4** and conjugates **4a**−**c**.

Determination of Retained Antibody Conjugate Activity. To evaluate the extent to which the conjugation procedure deactivated the antibodies **4** and **5**, conjugates **4a**−**c** and **5a**−**c** (2−22 nM) were injected over the corresponding ligand-bearing biosensors under mass transfer limiting conditions. Plotting the initial binding rate from the resulting sensorgrams versus the concentration of the antibody (conjugate) produced a series of calibration curves (Figure 4). The slope (k) of the calibration curve of each conjugate was compared to the slope (k_0) of the native antibody and the ratio was taken as a measure of the immunoreactive fraction of the conjugate. As shown in Table 2, relatively little anti-fluorescein antibody was deactivated during the conjugation process. Even at a high loading ratio of acridinium to anti-fluorescein antibody (7.4:1), more than 90% of the antibody retains activity similar to the native antibody. By contrast, a larger percentage of the anti-biotin conjugates lost their binding ability at higher label-to-antibody ratios. Approximately 23% of the anti-biotin conjugates were effectively inactive when the coupling ratio of acridinium to antibody reached 7.5.

DISCUSSION

There are several advantages to using SPR as a technique to characterize antibody conjugates. First, with the advent of commercially available instrumentation, characterization of the binding parameters of antibody conjugates can be performed in an automated and reproducible fashion. Because antigen bearing sensor chips can be regenerated and reused, a single and controllable surface can be created to test the binding parameters among different lots of antibody conjugates. This advantage can be especially useful when comparing antibodies utilized in different diagnostic platforms. Second, SPR is an efficient method of analysis. Real-time monitoring of the antibody-binding event eliminates time-consuming secondary methods (e.g., enzyme or colorimetric based assays) to detect the bound antibody. Dangerous radioactivity, as might be used in immunoassay-based analyses, is also avoided. Because SPR instrumentation is accompanied by software capable of commanding automated routines, once the immobilization of ligand to a sensor chip has been optimized, samples can be analyzed in a high-throughput manner within minutes for a typical antibody. Third, the quantity of materials needed is minimal using SPR analysis. For each passover, the amount of antibody required ranges from roughly 0.0005 to 0.05 mg, depending on the nature of the antibody. This minimal amount of material allows

for multiple runs to be performed within an experiment or over time without the large expenditure of conjugate. If an antibody lot is destined for commercial development, the nonconsumptive nature of the method is a plus for both reasons of production and cost.

As in any analysis of antibody binding, the bivalency of the antibody must be considered in determining true equilibrium affinity or dissociation constants. Often the study can be simplified by preparing monovalent Fab fragments of the antibody (*7*). This alternative is not practical in the evaluation of antibody conjugates that will be used as such in an assay. The added manipulation to form and purify the Fab fragment may itself alter the binding properties of the protein. In previous studies using the BIAcore, it has been shown that the binding data obtained from intact antibodies actually fits the equation for a one to one binding interaction better than the equation that takes bivalency into consideration (*9*). The binding constants from both equations were quite close in that case.

The present study utilizes Karlsson's simplified model to determine apparent equilibrium dissociation constants useful in the comparison of the relative avidity of antibodies covalently modified with a low molecular weight label. For the two antibodies studied here, SPR analysis demonstrated that conjugation with a chemiluminescent acridinium label did not significantly affect the antibody conjugates' ability to bind ligand in solution (Table 2). With these data alone, one would conclude that the immunoreactivity of the conjugate was not compromised during the conjugation procedure. However, comparison of the calibration curves generated for each conjugate with those of the native antibodies revealed a discrepancy.

In the anti-biotin mAb series (Figure 4), the calibration curve of each conjugate differed from the unmodified antibody by showing a progressively shallower slope that correlated with the degree of hapten substitution. Conjugate **4c** had a slope that was 23% less than the unmodified **4**. In the anti-fluorescein mAb series, this effect was much less pronounced; the most highly substituted anti-fluorescein conjugate, **5c** was still within 10% of the native mAb. Under the mass transport limiting conditions of these experiments, the initial binding rate depends only on the concentration of the antibody (conjugate), the bivalency of the antibody is not an issue. The initial rates were calculated for the antibody and conjugates at the same protein concentrations, thus, the calibration curves should be nearly identical. Any deviation could be due to inactivation of some percentage of the conjugate during the conjugation process. Because the apparent equilibrium dissociation constants within a set of conjugates and their parent antibody were similar, the deactivation of the conjugates appears to be an all-or-nothing effect; conjugation either completely disrupts binding or does not change the affinity of the antibody. In addition, anti-fluorescein antibody was clearly less sensitive to the process of label conjugation than the anti-biotin antibody. For the anti-biotin antibody, this difference may point to a higher susceptibility of key residues in the CDR to acylation by the label, a lowered resistance to denaturation imposed by the covalent attachment of the label, or a combination of both.

The use of the BIAcore instrument to measure active protein concentration is not new. Indeed, Karlsson et al. have measured the concentration of active, unmodified antibodies under mass transport limiting conditions (*16*). They observed that the initial rate versus antibody concentration calibration curves to be identical for a variety of IgGs (monoclonal, monoclonal mixtures, and polyclonal) and thus valid as a general method with the caveat that the association rate of the antibodies had to be at or above 10^5 M^{-1} s^{-1}. Others have modified the procedure to measure the concentration of lower affinity, unmodified binding proteins under partial mass transport limiting conditions (*17*, *18*). Neither group had exploited their methods to characterize antibodies that have been covalently modified.

In summary, our past studies have shown that SPR can be useful in determining the optimal structure of small molecule ligands for binding to a given antibody whether the ligand is in solution or bound to a solid support (*4*−*8*). While that was a significant advance in the design of immunoassay components, it also set the basis for monitoring lot to lot variations in the binding properties of the antibody. Until now, SPR had not been used to systematically examine the affect of covalent modification on antibody immunoreactivity. The present study demonstrated that random coupling of the activated ester of acridinium-9-carboxamide **1** to anti-biotin (**4**) and anti-fluorescein (**5**) monoclonal antibodies was chemically efficient based on UV analysis. Surface plasmon resonance of the purified conjugates indicated only minor variations in the apparent equilibrium dissociation constants of these antibody conjugates as a result of the conjugation process, which was a welcome result. In addition, and more importantly, SPR provided a means of detecting the ratio of active to inactive antibody-conjugate present in the preparation. While the anti-fluorescein conjugates retained at least 90% of their immunoreactivity over the extent of modification tested, anti-biotin conjugates showed a progressive loss of reactivity. The ultimate goal is to match the conjugation procedure to the antibody to minimize losses of immunoreactive conjugate. The reasons for the loss of active antibody is, of course, still speculation, but SPR proved to be a very convenient method for observing the effect.

LITERATURE CITED

(1) Malmqvist, M. (1993) Surface plasmon resonance for detection and measurement of antibody−antigen affinity and kinetics. *Curr. Opin. Immunol. 5*, 282−286.

(2) O'Shannessy, D. J. (1993) Determination of kinetic rate and equilibrium binding constants for macromolecular interactions: a critique of the surface plasmon resonance literature. *Curr. Opin. Biotechnol. 5*, 65−71.

(3) Schuck, P. (1997) Reliable determination of binding affinity and kinetics using surface plasmon resonance biosensors. *Curr. Opin. Biotechnol. 8*, 498−502.

(4) Adamczyk, M., Moore, J. A., and Yu, Z. Application of surface plasmon resonance toward studies of low molecular weight antigen−antibody binding interactions. *Methods* (in press).

(5) Adamczyk, M., Grote, J., Moore, J. A., Rege, S. D., and Yu, Z. (1999) Structure-binding relationships for the interaction between a vancomycin monoclonal antibody Fab fragment and a library of vancomycin analogs and tracers. *Bioconjugate Chem. 10*, 176−185.

(6) Adamczyk, M., Chen, Y.-Y., Moore, J. A., and Mattingly, P. G. (1998) Estradiol-mimetic probes. Preparation of 17α-(6-aminohexynyl)estradiol biotin, fluorescein and acridinium conjugates. *Bioorg. Med. Chem. Lett. 8*, 1281−1284.

(7) Adamczyk, M., Gebler, J. C., Gunasekera, A. H., Mattingly, P. G., and Pan, Y. (1997) Immunoassay reagents for thyroid testing. 2. Binding properties and energetic parameters of a T_4 monoclonal antibody and its Fab fragment with a library of thyroxine analog biosensors using surface plasmon resonance. *Bioconjugate Chem. 8*, 133−145.

(8) Adamczyk, M., Johnson, D. D., Mattingly, P. G., Moore, J. A., and Pan, Y. (1998) Immunoassay reagents for thyroid testing. 3. Determination of the solution binding affinities of a T_4 monoclonal-antibody Fab fragment for a library of thyroxine analogs using surface plasmon resonance. *Bioconjugate Chem. 9*, 23−32.

(9) Karlsson, R. (1994) Real-time competitive kinetic analysis of interactions between low-molecular-weight ligands in solution and surface-immobilized receptors. *Anal. Biochem. 221*, 142−151.

(10) Abraham, R., Moller, D., Gabel, D., Senter, P., Hellström, I., and Hellström, K. E. (1991) The influence of periodate oxidation on monoclonal antibody avidity and immunoreactivity. *J. Immunol. Methods 144*, 77−86.

(11) Pearson, J. E., Kane, J. W., Petraki-Kallioti, I., Gill, A., and Vadgama, P. (1998) Surface plasmon resonance: a study of the effect of biotinylation on the selection of antibodies for use in immunoassays. *J. Immunol. Methods 221*, 87−94.

(12) Adamczyk, M., Fishpaugh, J., Mattingly, P. G., and Shreder, K. (1998) Tracermer (TM) signal generators: An arborescent approach to the incorporation of multiple chemiluminescent labels. *Bioorg. Med. Chem. Lett. 8*, 3595−3598.

(13) Adamczyk, M., Chen, Y.-Y., Mattingly, P. G., and Pan, Y. (1998) Neopentyl 3-triflyloxypropanesulfonate. A reactive sulfopropylation reagent for the preparation of chemiluminescent labels. *J. Org. Chem. 63*, 5636−5639.

(14) Adamczyk, M., Chen, Y.-Y., Grote, J., and Mattingly, P. G. (1999) *O*-(Fluoresceinylmethyl)hydroxylamine (OFMHA): A reagent for the preparation of fluorescent *O*-(fluoresceinylmethyl)oxime (FMO)-steroid conjugates. *Steroids 64*, 283−290.

(15) Adamczyk, M., Mattingly, P. G., and Moore, J. A. (1998) *O*-(Fluoresceinylmethyl)hydroxylamine (OFMHA): a fluorescent reagent for detection of damaged nucleic acids. *Bioorg. Med. Chem. Lett. 8*, 3599−3602.

(16) Karlsson, R., Fägerstam, L., Nilshans, H., and Persson, B. (1993) Analysis of active antibody concentration. Separation of affinity and concentration parameters. *J. Immunol. Methods 166*, 75−84.

(17) Christensen, L. L. (1997) Theoretical analysis of protein concentration determination using biosensor technology under conditions of partial mass transport limitation. *Anal. Biochem. 249*, 153−164.

(18) Richalet-Sécordel, P. M., Rauffer-Bruyère, N., Christensen, L. L., Ofenloch-Haehnle, B., Seidel, C., and Van Regenmortel, M. H. (1997) Concentration measurement of unpurified proteins using biosensor technology under conditions of partial mass transport limitation. *Anal. Biochem. 249*, 165−173.

BC990057E

New Cyclization Reaction at the Amino Terminus of Peptides and Proteins

Keith Rose,*,† Jianhua Chen,† Marina Dragovic,† Weiguang Zeng,† Damien Jeannerat,‡ Philippe Kamalaprija,‡ and Ulrich Burger‡

Department of Medical Biochemistry, University Medical Center and Department of Organic Chemistry, University of Geneva, CH-1211 Geneva 4, Switzerland. Received May 20, 1999; Revised Manuscript Received September 8, 1999

Mild oxidation with periodate of the 1-amino-2-ol moiety of N-terminal seryl or threonyl peptides and proteins leads to a terminal aldehyde function O=CH−CO− which usually may be exploited for bioconjugate formation (e.g., via oximation with an O-alkyl hydroxylamine). We report that, when followed by a prolyl residue, the O=CH−CO− group can undergo a rapid cyclization and dehydration reaction through nucleophilic attack by the amide nitrogen of the third amino acid residue of the chain. We have characterized the resulting heterocycle, which is stable in aqueous acid, by mass spectrometry and NMR. Quantitative oximation can nevertheless be achieved in such cases by performing a one-pot oxidation-oximation without isolation of the intermediate aldehyde, as is demonstrated with cholera toxin B subunit.

INTRODUCTION

The oxidation by periodate of N-terminal 1,2-amino alcohols Ser (R = CH_2OH) or Thr [R = $CH(OH)CH_3$] residues NH_2−CHR−CO− of a polypeptide to an aldehyde function O=CH−CO− has been known for many years (*1*). More recently, this mild oxidation reaction has been exploited for the synthesis of bioconjugates through formation of hydrazone, thiazolidine, or oxime (−ON=CH−CO-) bonds (e.g., refs *2*−*8*). Usually, the polypeptide aldehyde is stable in aqueous solution at pH values between 2 and 5 and may be lyophilized and stored as a powder at −20 °C (*4*). In some cases, however, the aldehyde can undergo side reactions. For example, formation of a 1,3,4-oxadiazolino peptide containing two peptide aldehyde units has been observed during attempted hydrazone formation (*9*).

We have observed that some polypeptides and proteins, including Cholera toxin B subunit (CTB), undergo rapid and quantitative oxidation to yield a compound which may be isolated and has the mass calculated for the expected O=CH−CO-polypeptide species, but oximation occurs very slowly indeed (half time estimated in weeks under conditions where normally the half time is of the order of very few minutes). The first protein which gave such difficulties was a β-lactamase (*5*), and in that case, the problem was solved by careful optimization of the conditions of oxidation of the N-terminus and storage of the aldehyde, but such an approach was not successful with CTB. We were able to reproduce the phenomenon of oxidation followed by very slow oximation using a small synthetic peptide consisting of the first six residues of the β-lactamase, Thr-Pro-Val-Ser-Glu-Lys-amide. In this article, we show that, when followed by a prolyl residue, the O=CH−CO− group formed by oxidation of N-terminal Ser or Thr can undergo a rapid cyclization and dehydration reaction through nucleophilic attack by the amide nitrogen of the third amino acid residue of the chain. The resulting heterocycle, which is stable in aqueous acid, was characterized by mass spectrometry and NMR. To achieve quantitative oximation in such cases, we developed a one-pot oxidation-oximation without isolation of the intermediate aldehyde and demonstrate here with CTB that it is possible to prepare in good yield a hybrid construct of which 60% of the mass is the B subunit and 40% is totally synthetic. CTB conjugates are potentially useful as vaccines: CTB can supply T helper epitopes and, if the construct assembles as its noncovalent pentamer, such constructs would be expected to elicit a mucosal immune response (e.g., refs *10* and *11*).

EXPERIMENTAL PROCEDURES

Materials. Synthetic peptides were prepared using Boc chemistry on a model 430A synthesizer (Applied Biosystems Inc.) modified according to Kent (*12*). ^{15}N (99 atom %) N^t-Boc-L-valine was purchased from Isotec. Methylbenzhydrylamine resin (NovaBiochem, Switzerland) was used to obtain peptide amides directly upon cleavage with HF. Synthetic peptides were purified by high-pressure liquid chromatography (HPLC), acetonitrile was removed by rotary evaporation at room temperature, and product was recovered by lyophilization. Purified peptides gave a single peak on analytical HPLC and the expected mass spectrum. The aminooxyacetyl peptide NH_2OCH_2CO-Gly_3[Lys(Ser)]$_5$Gly-OH was prepared as previously described (*13*). Cholera toxin B subunit (CTB, Inaba strain) was obtained from the Swiss Serum and Vaccine Institute, Berne, Switzerland. Sodium metaperiodate and guanidine hydrochloride (MicroSelect grade) were purchased from Fluka, Buchs, Switzerland. Boc-aminooxyacetic acid was from Calbiochem-NovaBiochem, Läufelfingen, Switzerland.

Chromatography. High-pressure liquid chromatography was performed using a column of Nucleosil 300A 5 μm C_8 (Macherey Nagel, Oensingen, Switzerland), 250

* To whom correspondence should be addressed. Phone: +41 22 702 5523. Fax: +41 22 346 8758. E-mail: rose@cmu.unige.ch.
† Department of Medical Biochemistry.
‡ Department of Organic Chemistry.

10.1021/bc9900587 CCC: $18.00 © 1999 American Chemical Society
Published on Web 10/21/1999

× 4 mm id for analytical work (0.6 mL/min, 2 mL loop) and a radial compression system (210 × 25 mm id, Nova-Pak HR 60A 6 μm C_{18}, 20 mL/min, 50 mL loop) for preparative work, monitoring at 214 or 229 nm for analytical or preparative work, respectively. Linear gradients were established between solvent A [1 g of trifluoroacetic acid (TFA) added to 1 L of HPLC grade water and then vacuum filtered and degassed] and solvent B (1 g of TFA added to 100 mL of water, brought to 1 L with gradient grade acetonitrile then vacuum filtered and degassed). Gel filtration was performed on a Superdex 75 HR 10/30 column (Pharmacia, Uppsala, Sweden) at a flow rate of 0.4 mL/min using 0.25 M phosphate buffer, pH 7.0 (counterion sodium), which was 1 mM in EDTA, monitoring at 280 nm.

Mass Spectrometry. Spectra were obtained using electrospray ionization on either a Trio 2000 (infused at 2 μL/min) or Platform II instrument (infused at 7 μL/min); both machines were from Micromass, Altrincham, U.K. Samples of synthetic peptides were dissolved in water/acetonitrile 1:1 by volume, whereas protein samples were dissolved in water/acetonitrile/acetic acid (49.5:49.5:1 by volume).

NMR spectroscopy (*14*) was performed on a Bruker AMX-2−600 spectrometer operating at 14.1 T. Peptide samples were dissolved in D_2O at pD 4.7 (DCl). After acquisition of all data, samples were reanalyzed by HPLC to check for possible decomposition. Two-dimensional experiments were performed at 298 K. $^1H/^1H$-DQF−COSY spectra were acquired using 512 × 16K data points and a spectral width of 12 ppm in both dimensions. A shifted sine bell function was applied to the indirectly detected dimension during data processing. The heteronuclear HSQC (*15*−*17*) and HMBC experiments (*18*−*19*) were performed with 128 × 4K data points and spectral widths of 90 × 10.69 ppm in the carbon and proton dimension, respectively. Folded signals could easily be identified as such. For the processing, sine bells were applied in both dimensions.

Oxidation of TPVSEK-amide. To a solution of purified hexapeptide amide (17.6 mg, 26.8 μmol of peptide, 28 mL of water, 2.8 mL of 10% ammonium bicarbonate solution) was added 5.6 mL of sodium metaperiodate solution (0.184 g/L in water, 4.8 μmol) with vortex mixing. As soon as possible, the reaction was quenched by mixing in 5.6 mL of ethyleneglycol (10 M in water) and injecting the reaction mixture onto preparative HPLC. After a 5 min isocratic period, a linear gradient of 1% B/min was established. Once the three components had eluted (within 30 min), the column was washed briefly at 50% B then reequilibrated at 100% A. Organic solvent was removed by rotary evaporation at room temperature and product recovered by lyophilization. From 85 mg of peptide, we isolated 39 mg of peak 1, 4.6 mg of peak 2 and 4.6 mg of peak 3.

Oximation of Oxidized TPVSEK-amide. For the study at pH 4.6, the buffer was 0.1 M acetate, counterion sodium. In separate experiments, both forms of the oxidized hexapeptide amide (peaks 2 and 3, 0.3 mg in 60 μL buffer) were treated with aminooxyacetic acid (60 μL, 5 mM in buffer). For the study at pH 7.0, a phosphate buffer was used (0.1 M, counterion sodium) in place of acetate. The oximation reactions were monitored by HPLC, injecting 10 μL volumes with a gradient from 0 to 35% B over 30 min.

Oxidation and Oximation of CTB. CTB was supplied as a lyophilized powder in the presence of buffer salts, including Tris which might be expected to react with periodate. Vial contents (1 mg of protein) were therefore dissolved in 1 mL of water, and the protein was isolated by gel filtration as the noncovalent pentamer. The protein was concentrated by ultrafiltration (Centricon, Amicon, Beverly, MA, 10000 molecular weight cutoff, precentrifuged twice with 1 mL of phosphate chromatography buffer to remove glycerol which interferes with the oxidation step) to 400 μL. Methionine (50 μL, 0.2 M in the phosphate buffer) was added to protect against thioether oxidation, then oxidation of the N-terminal Thr residue was initiated by addition of sodium periodate (25 μL, 40 mM in the phosphate buffer). After 5 min in the dark, excess periodate was quenched with ethyleneglycol (60 μL, 0.5 M in water), then 4 min later, 27.8 mg of aminooxyacetyl peptide NH_2OCH_2CO-$Gly_3[Lys(Ser)]_5$Gly-OH was added, followed by 50 μL of acetic acid. An aliquot (15 μL) was removed for HPLC and mass spectrometric analysis after 30 min, whereupon the sample was placed at −20 °C overnight. The next day, 500 mg of guanidine hydrochloride was added and the protein oxime isolated by gel filtration and ultrafiltration to a volume of about 400 μL. Oxidation of the Ser residues on the Lys side chains of the peptide attached to CTB was achieved by adding methionine (150 μL, 0.2 M in phosphate buffer) followed by periodate (62.5 μL, 80 mM in phosphate buffer). After 5 min in the dark, the reaction was quenched with 1,3-diamino-2-propanol (Fluka, 300 μL, 0.5 M in water adjusted to pH 7.8 with acetic acid). Four minutes later, 500 mg of guanidine hydrochloride was added, and the oxidized protein isolated again by gel filtration and concentrated by ultrafiltration to about 400 μL. A second 400 μL sample (from a separate experiment) was pooled at this stage. To the pool (800 μL), aminooxyacetyl peptide CH_3CO-$DC(CH_2CONH_2)$-TLIDALLGDPHK$(COCH_2ONH_2)$-NH_2 was added (5.7 mg), and the solution made 4% in acetic acid. For every microliter of this solution, 1 mg of guanidine hydrochloride was added and the oximation left overnight. Final product was isolated by semipreparative HPLC (1 mg after lyophilization) and characterized by mass spectrometry.

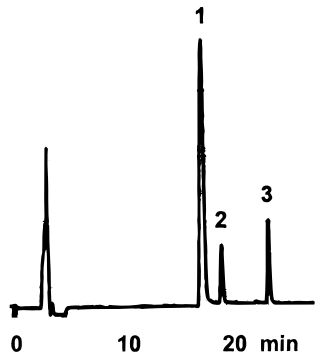


Figure 1. Preparative HPLC chromatogram of the oxidation of TPVSEK-amide with a limited quantity of periodate. After a 5 min isocratic period at 100% A, a gradient of 1%/min solvent B was applied, monitoring at 229 nm. Mass spectrometry and NMR identified components as peak 1, unmodified peptide; peak 2, hydrated glyoxylyl peptide $(HO)_2CHCO$−PVSEK-amide; peak 3, cyclic isomer of the expected O=CHCO−PVSEK-amide.

RESULTS AND DISCUSSION

Oxidation of TPVSEK-amide. To study the rapid oxidation of the terminal 1-amino-2-ol moiety of **1**, oxidation with periodate was performed with limiting amounts of periodate and a reaction time of a few seconds (to allow mixing). This allowed isolation of three components by HPLC (Figure 1). Peak 1 was identified by retention time and mass spectrum as unreacted starting

peptide (abundant signal at *m/z* 660.0 corresponding to the protonated molecular ion, most intense peak at *m/z* 330.9, the doubly protonated molecule, data not shown). Peak 2 gave a mass spectrum with signals at *m/z* 614.5, 632.5, and 654.4. The most intense peak *m/z* 632.5 corresponds to the hydrated form of the aldehyde, $(HO)_2CHCO-$PVSEK-amide (**2**) with one proton, and *m/z* 654.4 corresponds to sodium cationization of the same species. The small signal at *m/z* 614.5 in the spectrum of peak 2 became the most intense peak in the spectrum of peak 3, where it was accompanied by *m/z* 636.6. These two signals correspond to O=CHCO−PVSEK-amide (i.e., the aldehyde) with one proton and with one sodium ion, respectively, although we show below that peak 3 is actually a cyclic isomer (**3**) of the aldehyde. Peak 2 material, upon storage in aqueous solution at pH 4.6 (sodium acetate buffer), was found by HPLC and mass spectrometry to transform to peak 3 material over a number of days, but was more stable in 0.1% TFA at pH 2 (not shown). Thus, the signal at *m/z* 614.5 in the spectrum of Peak 2 material could be due to dehydration of the hydrate within the mass spectrometer to give either the aldehyde itself or its isomer (**3**). Peaks 1, 2, and 3 were found to be stable for days in aqueous solution at pH 2 at room temperature, and for months as lyophilized powders at −20 °C (not shown).

Oximation of oxidized TPVSEK-amide (peaks 2 and 3) was studied at pH 4.6 and pH 7.0. It has previously been shown that oximation proceeds faster at lower pH, and very slowly indeed at neutral pH (*7*). Oximation of peak 2 (the hydrated aldehyde) with aminooxyacetic acid at pH 4.6 was found to proceed extremely rapidly. Figure 2a shows almost quantitative reaction after 130 min: reaction halftime was approximately 10 min judging by earlier time points (not shown). The expected oxime product was identified by mass spectrometry through its protonated molecular ion at *m/z* 687.7. A trace of peak 3 material is also formed, which elutes 2 min after the oxime (ox). Oximation of peak 3 (which has the mass of the aldehyde) proceeded extremely slowly at pH 4.6, with very little product formed after 130 min (Figure 2b). The oxime was nevertheless being formed (it elutes 2 min earlier than peak 3 and is just visible in Figure 2b), and it represented about 12% after 35 h (product confirmed by mass spectrometry, not shown).

At pH 7.0, almost exactly the same chromatograms were obtained during oximation of peak 2 (Figure 2c) and peak 3 (Figure 2d). After 10 min, both showed presence of peak 2 and peak 3, with virtually no oxime product. At this pH, peaks 2 and 3 clearly interconvert rapidly: equilibrium is almost attained after 10 min, but not quite since we notice that Figure 2c is slightly richer in the starting peak 2 whereas Figure 2d is still slightly richer in the starting peak 3. In both cases, oxime formation proceeded very slowly, reaching about 30% after 10 h (not shown). Thus, although oximation proceeded very slowly at pH 7.0 for both peaks 2 and 3, it nonetheless proceeded more rapidly than for peak 3 at pH 4.6 (but much less rapidly than for peak 2 at pH 4.6).

These results were difficult to understand. For years it has been known that small aliphatic aldehydes (such as heptanal), many peptides and proteins carrying a O=CH−CO−NH−CHR−CO− group (where R is the side chain of a genetically coded amino acid), many polypeptides carrying a $-NHCH_2CH=O$ group, and many peptides carrying a O=CH−CO− group attached to the side chain of Lys undergo rapid and almost quantitative oximation at mildly acid pH. In the case of the oxidized small synthetic peptide TPVSEK-amide, the hydrated aldehyde (peak 2) was able to undergo rapid oximation at pH 4.6, but the apparent aldehyde (peak 3) was not. This led us to investigate by NMR spectroscopy the structure of peaks 1, 2, and 3.

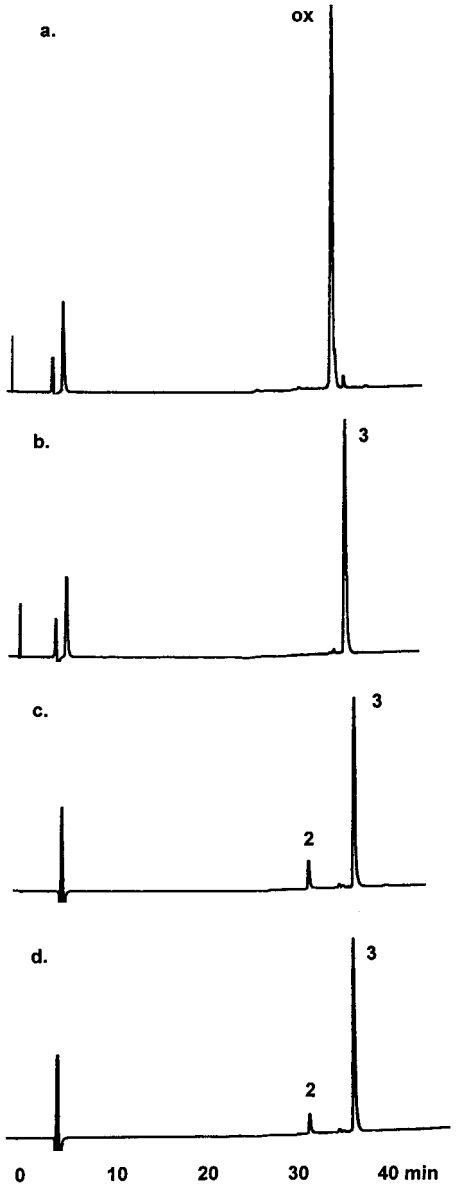


Figure 2. Analytical HPLC chromatograms of oximation reactions of peaks 2 and 3 of Figure 1. Remaining material is labeled 2 or 3, accordingly. Oxime product (ox) was identified by mass spectrometry. After a 5 min isocratic period at 100% A, a gradient of 1.17%/min solvent B was applied, monitoring at 214 nm. (a) Peak 2, pH 4.6, 130 min. (b) Peak 3, pH 4.6, 130 min. (c) Peak 2, pH 7, 10 min. (d) Peak 3, pH 7, 10 min.

NMR Analysis. The $^1H/^1H$-DQF−COSY spectra of compounds **1**, **2**, and **3** allowed assignment of all resonances of hydrogen atoms bound to carbon (*14*). Since the amino acid residues differ all in their spin systems, the assignment was straightforward and unambiguous. Data for ^1H chemical shifts are compiled in Table 1.

Comparison of the ^1H-spectra of **1** and **2** immediately confirmed the Thr residue as the site of oxidative cleavage. The three signals of Thr of **1** are missing in compound **2** and are replaced by a singlet at δ (ppm) 5.58. This is the resonance of the H−C(2) proton of the newly formed dihydroxyacetyl residue [the former H−C(α) of Thr]. That we were dealing with a hydrated aldehyde was corroborated by an HSQC-experiment (*15*−*17*) which correlates this proton to a ^{13}C signal at δ (ppm) 86.0 via

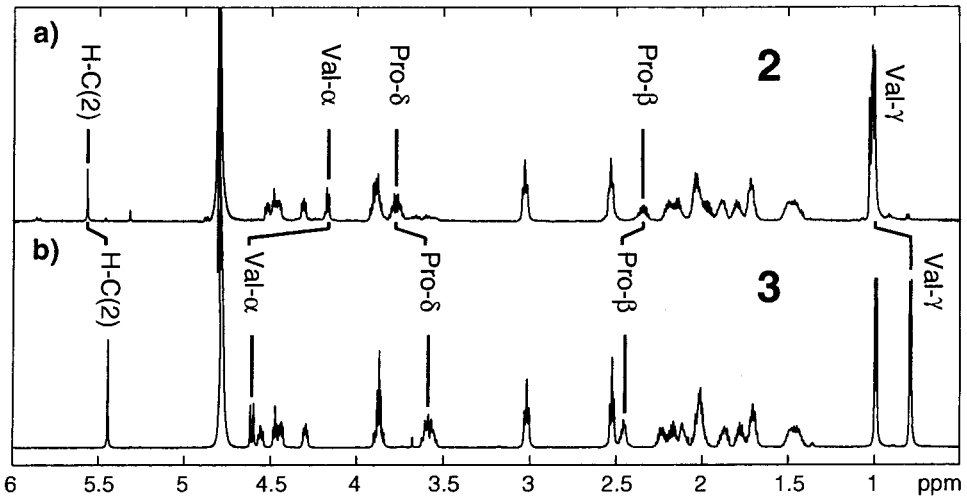


Figure 3. ^{1}H NMR spectra recorded at 600 MHz in D_2O of (a) compound **2** and (b) compound **3**, with assignment of those resonances which change significantly upon cyclization.

Table 1. ^{1}H Chemical Shifts for the Amino Acid Residues of Compounds 1, 2, and 3 at 600 MHz in D_2O (pD 4.7)

residue	position	1	2	3
Thr (T) or modified residue[a]	H−C(2)	4.26	5.58	5.46
	H−C(β)	4.20		
	$H_3C(\gamma)$	1.39		
Pro (P)	H−C(α)	4.58	4.52	4.58
	$H_2C(\beta)$	1.93/2.36	1.97/2.34	2.03/2.47
	$H_2C(\gamma)$	∼2.10	∼2.03	2.04/2.13
	$H_2C(\delta)$	3.72/3.83	3.75/3.77	3.57/3.61
Val (V)	H−C(α)	4.12	4.17	4.63
	H−C(β)	2.10	2.14	2.25
	$H_3C(\gamma)$	0.97/1.00	0.99/1.01	0.81/1.01
Ser (S)	H−C(α)	4.46	4.47	4.49
	$H_2C(\beta)$	3.86/3.88	3.86/3.88	3.89
Glu (E)	H−C(α)	4.45	4.44	4.45
	$H_2C(\beta)$	2.00/2.19	1.96/2.18	2.04/2.18
	$H_2C(\gamma)$	2.50	2.51	2.55
Lys (K)−(amide)	H−C(α)	4.30	4.30	4.31
	$H_2C(\beta)$	1.78/1.86	1.79/1.88	1.80/1.89
	$H_2C(\gamma)$	1.42/1.46	1.45/1.49	1.47/1.50
	$H_2C(\delta)$	1.70	1.70	1.72
	$H_2C(\epsilon)$	3.03	3.01	3.04

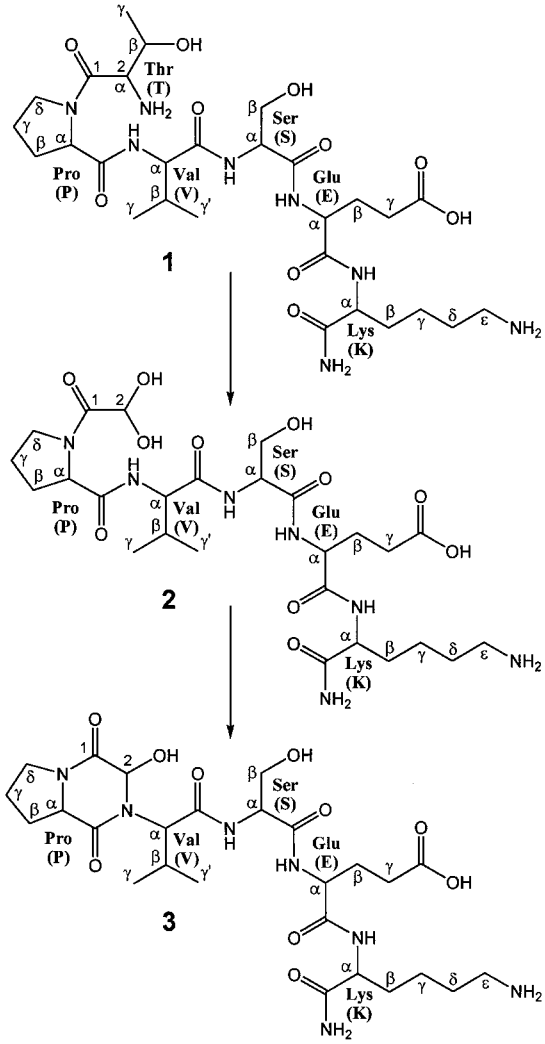
[a] Dihydroxyacetate for **2**, and H−C(2) of the new six-membered heterocycle for **3**.

^1J scalar coupling. The ^{1}H chemical shifts of the remaining five residues (Pro, Val, Ser, Glu, and Lys-amide) show a remarkable similarity between compounds **1** and **2**. Clearly, these amino acid residues were not altered.

However, when comparing compounds **2** and **3** (Table 1 and Figure 3), it was evident that the dehydration reaction resulted in significant changes of the Pro and Val resonances. One of the methyl groups of Val had undergone an upfield shift of 0.2 ppm, whereas H−C(α) of Val changed from 4.17 to 4.63. A significant change (5.58 → 5.46) was observed also for the H−C(2) resonance of the oxidized residue. The signals of the three remaining amino acid residues Ser, Glu, and Lys-amide are almost identical for **2** and **3**. These findings clearly show that only Val and Pro sense the new molecular environment in **3**. Bond formation between the nitrogen atom of Val and C(2) of the oxidized residue, i.e. the disguised aldehyde, best accounts for our observations (Scheme 1).

The conclusions found strong support by a HMBC experiment (*18, 19*), which unveiled scalar ^{1}H/^{13}C coupling between H−C(α) of Val and C(2) of the oxidized residue. The absolute value of this $^3J_{C/H}$ coupling is 4.6 Hz. The existence of the crucial C(2)−$N_{(Val)}$ bond was

Scheme 1. Structures of Unoxidized Peptide (1), Hydrated Glyoxylyl Peptide (2), and Cyclic Isomer of Glyoxylyl Peptide (3)



eventually ascertained by specific ^{15}N-labeling of compound **3** in the $N_{(Val)}$ position. The ^{13}C NMR spectrum of this labeled material [$^{15}N_{(Val)}$-**3**] shows $^1J_{C/N}$ coupling for three carbon atoms, which are C(2) [at δ = 79.9, $^1J_{C/N}$ = 7.6 Hz], $C(\alpha)_{(Val)}$ [at δ = 64.4, $^1J_{C/N}$ = 8.4 Hz], and $CO_{(Pro)}$ [at δ = 175.9, $^1J_{C/N}$ = 12.8 Hz]. In addition, $^{15}N_{(Val)}$ couples

Table 2. Ease of Oximation of Various Oxidized Polypeptides

N-terminal sequence	source	oximation after isolation of oxidized polypeptide
SAKELR.....	IL-8	easy
SLAADT.....	MIP-1α	easy
SQLHSG.....	GCSF fragment	easy
TPVSEK.....	β-lactamase	possible[a]
TPVSEK-amide	synthetic	difficult
SPYSSD.....	Rantes	difficult
TPQNIT.....	Cholera toxin B subunit	difficult

[a] After much optimization (*5*).

over two bonds with $C(\alpha)_{(Pro)}$ [at $\delta = 61.58$, $^2J_{C/N} = 5.4$ Hz]. These values are close to what is expected for **3** (*20*), and they leave no doubt that $N_{(Val)}$ is bound to three carbon atoms. The ring closure creates, with high stereoselectivity, a new center of chirality. We see a single epimer of **3**. The absolute configuration at H−C(2), however, is unknown.

The cyclization process **2** → **3** is entropically favored by the rigidity of the proline ring, which keeps the two reacting centers in proximity. This propensity to cyclize is probably responsible for the difficulty sometimes encountered to oximate a polypeptide which, by mass spectrometry, has the mass of the aldehyde. All of our difficult oximations have involved X-Pro sequences, where X is Thr or Ser (Table 2, where only a small selection of easily oximated polypeptides is shown).

Studying "glyoxylyl-Pro-Ile-Val-amide" made by treatment of diisopropylthioacetyl peptide with N-bromosuccinimide and isolation under acidic conditions, Qasmi et al. (*21*) found the mass of the aldehyde form (which is the same as that of the cyclic form) by isobutane CI mass spectrometry, but found evidence by NMR (in DMSO) and FAB mass spectrometry (thioglycerol matrix) that the polypeptide can also exist in hydrated form, as we found for our synthetic peptide. By proton NMR, they found no aldehydic proton at all for "glyoxylyl-Pro-Ile-Val-amide", but found a singlet at δ(ppm) 9.2−9.3 integrating 0.5 H for the aldehyde proton of "glyoxylyl-Phe-Pro-Ile-Val-amide" and "glyoxylyl-Asn-Phe-Pro-Ile-Val-amide".

Oxidation of CTB and oximation with the carrier molecule $NH_2OCH_2CO\text{-}Gly_3[Lys(Ser)]_5Gly\text{-}OH$ under the "one-pot" conditions described led to quantitative conversion (Figure 4a) to the expected oxime $CTB{=}NOCH_2CO\text{-}Gly_3[Lys(Ser)]_5Gly\text{-}OH$: relative molecular mass found by electrospray ionization mass spectrometry, 12 938 Da (theoretical mass, 12 937 Da). CTB normally exists as a noncovalent pentamer, but treatment with acid and organic solvents leads to the monomeric form exclusively. Oxidation of the side-chain Ser residues of the ligated carrier molecule followed by isolation of the oxidized protein possessing five aldehyde groups and oximation with the peptide $CH_3CO\text{-}DC(CH_2CONH_2)TLIDALLGDPH{-}K(COCH_2ONH_2)\text{-}NH_2$ (NH_2OCH_2CO-peptide) yielded 1 mg of product from 2 mg of starting CTB. Characterization by mass spectrometry showed this product (relative molecular mass, 21 102 Da, theoretical mass, 21 101 Da) to be the expected branched hybrid $CTB{=}NOCH_2CO\text{-}Gly_3[Lys(COCH{=}NOCH_2CO\text{-peptide})]_5Gly\text{-}OH$.

A similar product was made earlier (*22*) using the "one-pot" conditions and different form of the peptide, $CH_3CO\text{-}DC(SCH_2CH_2NHCOCH_2ONH_2)TLID\text{-}ALLGDPH{-}NH_2$. At that time, we did not know why it was necessary to use "one-pot" conditions for the first oximation step, while it was possible to isolate the oxidized protein prior to the second oximation step. By performing the "one-pot" oxidation-oximation at pH 6.5 instead of 7.0, and quenching after 2 min, it was possible to isolate four components from the reaction mixture (Figure 4b). Mass spectrometry identified peaks 1−4: peak 1 was the expected oxime (found, 12 938; calcd, 12 937); peak 2 was unoxidized CTB (found, 11 602; calcd, 11 604); peak 3 was hydrated glyoxylyl CTB $(HO)_2CHCO{-}CTB$ (found, 11 580; calcd, 11 577); and peak 4 had the mass expected for "glyoxylyl-CTB" but was most probably the cyclic isomer; found, 11 558; calcd, 11 559. Incubation of peak 3 material with $NH_2OCH_2CO\text{-}Gly_3[Lys(Ser)]_5Gly\text{-}OH$ led to formation of peak 1 material (oxime), while oximation of peak 4 material failed. Use of methanol, which leads to hemiacetal formation, in place of acetonitrile as cosolvent for electrospray ionization shifted the mass of peak 3 to, found, 11 589 and, calcd, 11591, but did not shift the other masses, in particular that of peak 4, providing further evidence of lack of a free aldehyde moiety for peak 4. Taken together with the mass spectrometric and NMR results obtained with the model peptide, it would seem that cyclization of glyoxylyl-Pro polypeptides to a cyclic isomer which oximate with difficulty may also occur with proteins.

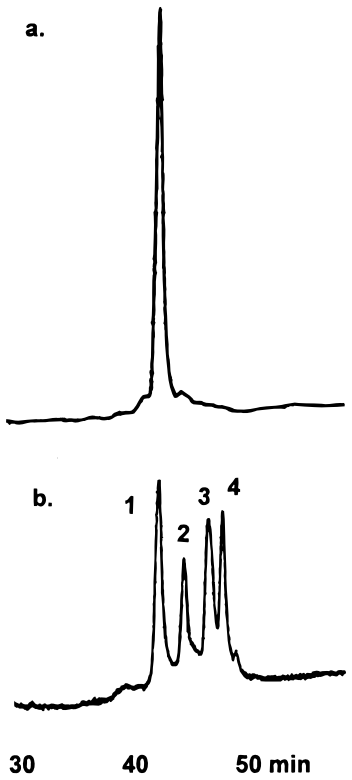


Figure 4. Analytical HPLC chromatograms of oximation reactions of oxidized CTB with $NH_2OCH_2CO\text{-}Gly_3[Lys(Ser)]_5\text{-}Gly\text{-}OH$. Compounds were identified by mass spectrometry. After a 5 min isocratic period at 35% B, a gradient of 0.2%/min solvent B was applied, monitoring at 214 nm. (a) "One-pot" oxidation-oximation under optimized conditions, showing quantitative conversion to the oxime. (b) "One-pot" reaction at suboptimal pH and time.

CONCLUSIONS

It is generally an advantage to isolate an oxidized (glyoxylyl-) polypeptide prior to oximation to avoid the necessity to use an excess of aminooxy component over the aldehydes coproduced during the oxidation reaction (formaldehyde from Ser, acetaldehyde from Thr, and formaldehyde from oxidation of the quenching agent ethyleneglycol). However, particularly when the N-ter-

minal Ser/Thr residue to be oxidized is followed by Pro, we recommend "one-pot" oxidation-oximation to avoid possible formation of the cyclic isomer of the aldehyde described here.

We have not studied the biological properties of the heterocyclic isomer of the aldehyde. It might be interesting as a scaffold for combinatorial chemistry of small (or even protein-sized) molecules, or for other purposes.

ACKNOWLEDGMENT

We are indebted to the Swiss National Science Foundation (Grants 31-50826.97 and 20-52905.97) and the Schmidheiny Foundation. We thank Marie-Laure Curchod, Irène Rossitto-Borlat, and Pierre-Olivier Regamey for expert technical assistance. The allocation of spectrometer time in the regional high-field NMR facilities in Lausanne-Dorigny is also gratefully acknowledged.

LITERATURE CITED

(1) Fields, R., and Dixon, H. F. (1968) A spectrophotometric method for the microdetermination of periodate. *Biochem. J. 108,* 883−887.

(2) Geoghegan, K. F., and Stroh, J. G. (1992) Site-directed conjugation of non-peptide groups to peptides and proteins via periodate oxidation of a 2-amino alcohol. (1992) *Bioconjugate Chem. 3,* 138−146.

(3) Gaertner, H. F., Rose, K., Cotton, R., Timms, D., Camble, R., and Offord, R. E. (1992) Construction of protein analogues by site-specific condensation of unprotected fragments. *Bioconjugate Chem. 3,* 262−268.

(4) Rose, K. (1994) Facile synthesis of homogeneous artificial proteins. *J. Am. Chem. Soc. 116,* 30−33.

(5) Mikolajczyk, S. D., Meyer, D. L., Starling, J. J., Law, K. L., Rose, K., Dufour, B., and Offord, R. E. (1994) High yield, site-specific coupling of N-terminally modified β-lactamase to a proteolytically derived single-sulfhydryl murine Fab′. *Bioconjugate Chem. 5,* 636−646.

(6) Zhang, L., and Tam, J. P. (1996) Thiazolidine formation as a general and site-specific conjugation method for synthetic peptides and proteins. *Anal. Biochem. 233,* 87−93.

(7) Rose, K., Zeng, W., Regamey, P.-O., Chernushevich, I. V., Standing, K. G., and Gaertner, H. F. (1996) Natural peptides as building blocks for the synthesis of large protein-like molecules with hydrazone and oxime linkages. *Bioconjugate Chem. 7,* 552−556.

(8) Nardin, E. H., Calvo-Calle, J. M., Oliveira, G. A., Clavijo, P., Nussenzweig, R., Simon, R., Zeng, W., and Rose, K. (1998) *Plasmodium falciparum* polyoximes: highly immunogenic synthetic vaccines constructed by chemoselective ligation of repeat B cell epitopes and a universal T-cell epitope of CS protein. *Vaccine 16,* 590−600.

(9) Melnyk, O., Bossus, M., David, D., Rommens, C., and Gras-Masse, H. (1998) Synthesis of lipopeptides using hydrazone chemical ligation. *J. Pept. Res. 52,* 180−184.

(10) Walker, R. I. (1994) New strategies for using mucosal vaccination to achieve more effective immunization. *Vaccine 12,* 387−400.

(11) Hathaway, L. J., Obeid, O. E., and Steward, M. W. (1998) Protection against measles virus-induced encephalitis by antibodies from mice immunized intranasally with a synthetic peptide immunogen. *Vaccine 16,* 135−141.

(12) Schnölzer, M., Alewood, P., Jones, A., Alewood, D., and Kent, S. B. H. (1992) *In situ* neutralization in Boc-chemistry solid phase peptide synthesis. Rapid, high yield assembly of difficult sequences. *Int. J. Pept. Protein Res. 40,* 180−193.

(13) Vilaseca, L. A., Rose, K., Werlen, R., Meunier, A., Offord, R. E., Nichols, C. L., and Scott, W. L. (1993) Protein conjugates of defined structure: synthesis and use of a new carrier molecule. *Bioconjugate Chem. 4,* 515−520.

(14) Cavanagh, J., Fairbrother, W. J., Palmer, A. G., III, Skelton, N. J. (1996) *Protein NMR Spectroscopy − Principles and Practice,* Academic Press, Inc., San Diego, CA.

(15) Palmer, A. G., III, Cavanagh, J., Wright, P. E., and Rance, M. (1991) Sensitivity improvement in proton-detected two-dimensional heteronuclear correlation NMR spectroscopy. *J. Magn. Reson. 93,* 151−170.

(16) Schleucher, J., Schwendinger M., Sattler, M., Schmidt, P., Schedletzky, O., Glaser, S. J., Sorensen, O. W., and Griesinger, C. (1994) A general enhancement scheme in heteronuclear multidimensional NMR employing pulsed field gradients. *J. Biomol. NMR 4,* 301−306.

(17) Kay, L. E., Keifer, P., and Saarinen, T. (1992) Pure absorption gradient enhanced heteronuclear single quantum correlation spectroscopy with improved sensitivity. *J. Am. Chem. Soc. 114,* 10663−5.

(18) Bax, A., Griffey, R. H., and Hawkins, B. L., (1983) Correlation of proton and nitrogen-15 chemical shifts by multiple quantum NMR. *J. Magn. Reson. 55,* 301.

(19) Willker, W., Leibfritz, D., Kerssebaum, R., and Bermel W., (1993) Gradient selection in inverse heteronuclear correlation spectroscopy. *Magn. Reson. Chem. 31,* 287−292.

(20) Berger, S., Braun, S., and Kalinowski, (1992) *^{15}N NMR-Spektroskopie,* Vol. 2 of *NMR−Spektroskopie von Nichtmetallen,* Georg Thieme Verlag, Stuttgart, Germany.

(21) Qasmi, D., de Rosny, E., René, L., Badet, B., Vergely, I., Boggetto, N., and Reboud-Ravaux, M. (1997) Synthesis of *N*-glyoxylyl peptides and their in vitro evaluation as HIV-1 protease inhibitors. *Bioorg. Med. Chem. 5,* 707−714.

(22) Rose, K., Zeng, W., Dragovic, M., Brown, L. E., and Jackson, D. C. (1996) Polyoxime artificial proteins as vaccines, in *Peptides: Chemistry, Structure, Biology* (P. T. P. Kaumaya and R. S. Hodges, Eds., Mayflower Scientific, Kingswinford, England, pp 767−769.

BC9900587

Surface Membrane Biotinylation Efficiently Mediates the Endocytosis of Avidin Bioconjugates into Nucleated Cells

Urszula Wojda, Paul Goldsmith,† and Jeffery L. Miller*

Laboratory of Chemical Biology, Building 10, Room 9N308, National Institute of Diabetes and Digestive and Kidney Diseases and Metabolic Disease Branch, National Institutes of Health, 9000 Rockville Pike, Bethesda, Maryland 20892. Received May 21, 1999; Revised Manuscript Received August 3, 1999

Here we demonstrate that biotin covalently attached to cell surface obligates existing receptors to endocytose avidin bioconjugates into nucleated cells. Incubation of fluorescein-labeled avidin with biotinylated cell lines resulted in uniform and rapid surface attachment and endocytosis compared with no detectable association of the avidin-conjugated dye with unbiotinylated cells. Uptake was detected within minutes with efficiencies approaching 100% in cell lines and freshly obtained peripheral blood mononuclear cells. After 24 h, avidin was barely detectable on the surface of the nucleated cells. In marked contrast, fluorescent avidin remained exclusively on the external membrane of erythrocytes after 24 h. To investigate biotin-mediated endocytosis for the delivery of DNA, we prepared polyethylenimine−avidin (PEI−avidin) conjugates. Surface biotinylation significantly increased the transfection efficiencies of PEI−avidin condensed plasmid DNA coding green fluorescent protein (GFP) to the level of transferrin-receptor targeted gene delivery (15−20% GFP positive cells in culture after 48 h). The increase in transfection efficiency was blocked by the addition of free avidin or biotin to the culture medium. Biotin covalently bound to cell surface membrane proteins efficiently mediates the entry of avidin bioconjugates into nucleated cells.

INTRODUCTION

Endocytosis describes the processes whereby eukaryotic cells internalize a wide range of extracellular materials including nutrients and toxins (*1*). Receptor-mediated endocytosis involves the attachment of extracellular molecules (ligands) to specified molecules (receptors) present on cell membranes and transport of those receptor−ligand complexes to the cell interior. The ligands are either then recycled to the cell surface, degraded within lysosomal compartments, or escape degradation and enter the cytoplasm. The endocytic process is responsible for a vast array of beneficial processes ranging from surface ligand clearance to nutrient uptake. In addition, some toxins and viruses require receptor-mediated endocytosis in order to access to the interior of cells (*2*, *3*).

Several factors determine the specificity and efficiency with which ligands present within the extracellular space enter cells after binding to cell surface receptors. The absolute number of receptors expressed on the cell surface largely determines the quantity of specific ligands permitted to enter individual cells. For instance, iron uptake is regulated by the number of transferrin receptors available on the cell surface (*4*). When cells proliferate, more transferrin receptors are expressed on the cell surface to enhance iron uptake. In the case of proliferating erythroid cells, exceedingly high levels of transferrin receptors are present due to the requirement of iron for hemoglobin synthesis, but the number of receptors decreases as iron requirements decrease and the cells mature (*4*). The affinity with which ligands bind to their receptors may also regulate entry into cells. Although receptors for interleukin-2 (IL-2R) exist in three forms: low, intermediate, and high affinity, only the high affinity form permits selective binding and uptake of the IL-2R targeted bioconjugates into cells (*5*). The entry of folic acid into cells is regulated both by the expression level of folate-binding receptors and the affinity of folate for those receptors (*6*).

It is well-known that conjugation of a receptor-specific ligand with molecules normally restricted to the extracellular space leads to their endocytosis into cells expressing the corresponding ligand-specific receptor. Examples include folate and transferrin conjugated to fluorescent dyes (*7*, *8*). Similarly, binding of specific monoclonal antibodies with affinities for individual cell surface receptors may result in their endocytosis (*9*). However, it remains unclear whether the modification of disparate receptors on the cell membrane by covalently bound molecules [defined here as receptor-adaptor(s)] is sufficient to mediate the endocytosis of adaptor-specific ligands. To test this hypothesis, biotin was covalently attached to proteins on the cell membranes to increase specifically the affinity of those biotin-modified proteins for avidin-containing molecules. Biotin was an ideal adaptor due to its small size, low toxicity in vivo (*10*, *11*) and the well recognized affinity of biotin for avidin (*12*). Remarkably, surface biotinylation resulted in fluorescein-tagged avidin entry into nearly 100% of cultured and primary cells tested compared with no detectable uptake by unbiotinylated cells. No evidence of exocytosis, surface recycling of the fluorescent probe, or growth inhibition was noted. A comparison of biotinylated-receptor and transferrin-receptor targeted polyethylenimine−DNA bioconjugates revealed equivalent transfection efficiencies. These data suggest that molecules covalently attached to proteins expressed on the cell membrane may be

* To whom correspondence should be addressed, Laboratory of Chemical Biology. Phone: (301) 402-2373. Fax: (301) 402-0101. E-mail: jm7f@nih.gov.

† Metabolic Disease Branch.

10.1021/bc990059z Not subject to U.S. Copyright. Published 1999 by American Chemical Society
Published on Web 09/21/1999

generally useful for mediating the endocytosis of ligands normally confined to the extracellular space.

EXPERIMENTAL PROCEDURES

Cells, Antibodies, and Plasmid DNA. K562 human chronic myelogenous leukemia, the human acute Jurkat T cell leukemia (clone E6-1), and HEL erythroleukemia cell lines were obtained from American Type Culture Collection and cultured in the recommended media supplemented with 10% fetal bovine serum (FBS; Biofluids, Rockville, MD) and with 25 μg/mL gentamicin (Life Technologies, Gaithesburg, MD). Primary hematopoietic cells were obtained from donated blood. Mononucleated cells and enucleated erythrocytes were isolated using Lymphocyte Separation Media (ICN Biomedicals, Aurora, OH) according to the manufacturer's protocol. Primary cells expressing transferrin receptor at high levels were obtained by flow cytometry (*13*). Staining of 10^5 K562 cells with mouse anti-avidin-FITC monoclonal antibody (clone WC19.10, IgG1, Sigma, St. Louis, MO) and control IgG1-FITC (Immunotech, Westbrook, ME) was performed by incubation with 4 μL of antibody in 100 μL of PBS for 30 min at 4 °C. The plasmid pGT encoding for green fluorescence protein was prepared and purified as described elsewhere (*14*). Briefly, pGT was subcloned from the 780 base pairs DNA *Eco*RI/*Not*I fragment encoding eGFP from pEGFP−N1 (Clontech, Palo Alto, CA) inserted into the pGreenLantern-1 vector (Life Technologies, Gaithersburg, MD) digested with *Eco*RI and *Not*I. All chemicals were purchased from Sigma (St. Louis, MO) unless otherwise stated in the text.

Biotinylation and Avidin−FITC Addition. Biotinylation of all cells was performed as follows: 10^6 cells were incubated in a final concentration of 0.5 ng of sulfo-NHS-biotin/cell (Pierce, Rockford, IL) in PBS for 30 min at 4 °C and washed twice with PBS. Avidin or avidin conjugated with fluorescein isothiocyanate (Av-FITC, 0.1 ng/cell) was incubated with the cells in 1 mL of PBS. In the time-course studies, cells labeled with Av-FITC were incubated at 37 °C, and at each time-point, cells were collected, fixed with 2% *p*-formaldehyde, and analyzed by flow cytometry and fluorescence microscopy.

Preparation of PEI−Avidin (PA) Conjugates. Polyethylenimine (PEI; Fluka, Switzerland) of MW 800 kDa was prepared as a 5% w/v hydrochloride salt solution (800 μL of commercial PEI, 7 mL of water, 200 μL of 36% hydrochloric acid). The pH of prepared PEI was 9.2, and the reagent was stored at 25 °C until used in conjugate preparation. Each avidin sample was prepared by dissolving 20 mg of lyophilized avidin in 2 mL of PBS, pH 7.4. To each sample of dissolved avidin was added 218 μL of 20 mg/mL sodium periodate solution, and the sample was wrapped with foil and incubated for 60 min at 25 °C. Since avidin is glycosylated, sodium periodate oxidation allows the introduction of aldehyde residues onto carbohydrates. Next the aldehyde residues can react with amine groups of PEI (Schiff base formation and reductive amination in the coupling buffer). Sodium periodate was dissolved in water (20 mg/mL) and stored at 25 °C protected from light. The reaction was quenched with glycerol followed by gel filtration on Sephadex G-25 superfine (PD10 Pharmacia) column. The resulting 3.5 mL fractions containing protein in PBS, pH 7.4, were used for conjugation with PEI. PEI was added to the avidin fractions at four different molar ratios: (A) 1: 2 (120 mg of PEI in 2.4 mL), (B) 1: 4 (60 mg of PEI in 1.2 mL), (C) 1: 8 (30 mg of PEI in 0.6 mL), and (D) 1: 16 (15 mg of PEI in 0.3 mL). The samples were mixed vigorously for 1 h at 25 °C, and 1 mL of coupling buffer (20 mM Na_3PO_4, pH 7.5, 0.2 M NaCl, and 3 mg/mL $NaCNBH_3$) was added to each sample followed by 1 h incubation. The addition of the coupling buffer was repeated twice at 1 h intervals with a total of 3 mL of coupling buffer added to each sample prior to overnight incubation. Glycine in molar excess quenched the avidin for 1 h at 25 °C. A 10 mm × 100 mm Macro-Prep High S support (Bio-Rad, Hercules, CA) cation-exchange column equilibrated at 20 mM Hepes, pH 7.5, containing 0.5 M NaCl was used to fractionate the samples with the 0.5−3 M NaCl gradient in 20 mM Hepes, pH 7.5, using Gilson HPLC system equipped with protein detection system at 280 and 214 nm. Some protein was eluted in the flow through. The main conjugate fraction of each sample was eluted between 1.3 and 3.0 M salt, pooled, concentrated to 6 mL by ultrafiltration, and dialyzed overnight against 3 × 1 L of PBS, pH 7.4. The avidin content of each conjugate preparation was determined at 280 nm and PEI content by ninhydrin assay (NIN-SOL ninhydrin reagent from Pierce) at 570 nm. The conjugate reactions yielded the following products: (A) 31.2 mg of PEI conjugated to 5.2 mg avidin at the molar ratio of 1:2.0, (B) 12 mg of PEI conjugated to 4.36 mg avidin at the molar ratio of 1:4.36 (PA4), (C) 3.32 mg of PEI conjugated to 2.30 mg of avidin at the molar ratio of 1:8.31 (PA8), and (D) 1.05 mg of PEI conjugated to 1.35 mg of avidin at a molar ratio of 1:15.46 (PA16). The overall yield of these conjugates based on PEI was (A) 26.0%, (B) 20.0%, (C) 11.7%, and (D) 7.0%; based on avidin, the yield was (A) 26.0%, (B) 21.8%, (C) 11.5%, and (D) 6.8%. The conjugates were aliquoted and stored at −80 °C. Gel retardation assay of the PEI conjugates was performed in 1.2% agarose gels as previously described (*15*).

Transfection of Cells. Transfection complexes of DNA with PEI or PEI−avidin (PA) conjugates were prepared as follows. Plasmid DNA was added and mixed gently with PEI or PA conjugates in PBS, in a total volume of 0.5 mL. PEI−DNA or PA−DNA complexes were formed at various molar ratios of PEI nitrogen to DNA phosphate (N:P) as indicated further in the text. Different N:P ratios were prepared by titrating DNA concentrations at a constant PEI concentration or by titrating PEI with the amount of DNA held constant. After 30 min of incubation in 25 °C, 0.5 mL of transfection mixture was added to the cells in 1.5 mL culture medium containing 10% FBS and gently mixed. Cells were biotinylated before transfection using standard procedure at 4 °C and washed with cold PBS. All transfections were performed in 24 well plates (Costar, Cambridge, MA) with 5 × 10^5 cells/well. After 4 h of incubation with the transfection complexes, 1 mL of fresh culture media containing 15% FBS was added to each well. Transfection was assessed based on GFP expression by fluorescence microscopy and flow cytometry 48 h later.

Transfection using Transferrin−PEI (TfPEI Kit, Bender MedSystems, Vienna, Austria) and with DMRIE-C Reagent (GIBCO BRL, Life Technologies, Grand Island, NY) was done according to manufacturer's instructions.

Flow Cytometry and Fluorescence Microscopy. Flow cytometry analyses were performed using an EPICS ELITE ESP flow cytometer (Coulter, Hialeah, FL). In each experiment, 10 000 cells were analyzed using argon laser excitation and 525 nm versus 575 nm band-pass emission filters for fluorescein (FITC), green fluorescent protein (GFP), and phycoerythrin (PE) detection. Fluo-

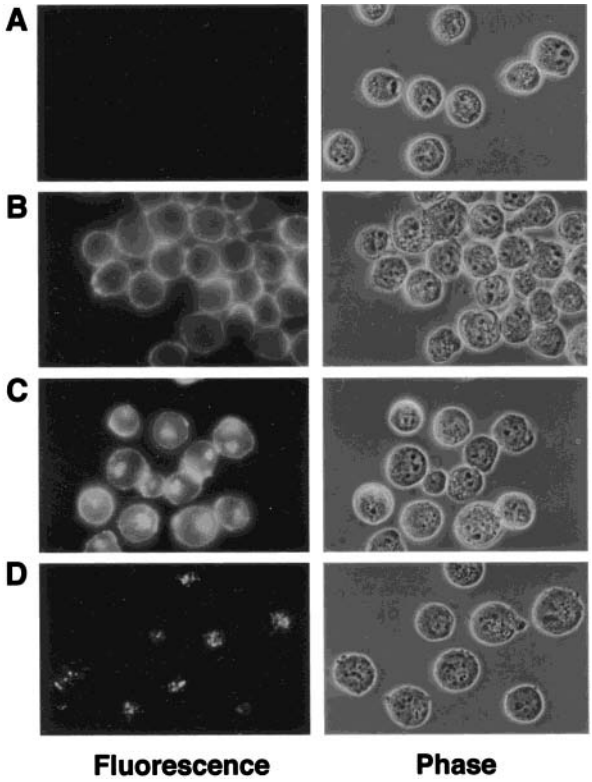


Figure 1. Addition of avidin-FITC to biotinylated K562 cells. Matching fluorescence (left panels) and phase (right panels) microscopy images of biotinylated cells incubated at 37 °C after addition of fluorescent avidin are shown (100× objective). Untreated biotinylated cells (A), and cells treated with avidin-FITC and observed immediately (B), after 30 min (C), and after 24 h (D) were compared. Each experiment was repeated several times with similar results.

rescence microscopy of cells was carried out using an Axiophot microscope and standard filter sets (Zeiss, Germany).

RESULTS

Entry of Fluorescein-Labeled Avidin into Cultured Cell Lines and Primary Hematopoietic Cells. Fluorescein-labeled avidin (Av-FITC) was used to examine kinetics of binding and possible internalization of avidin into biotinylated K562 leukemia cells. Untreated K562 cells showed very little autofluorescence or nonspecific binding of Av-FITC as assessed by flow cytometry and fluorescence microscopy (Figure 1A). When Av-FITC was added to biotinylated K562 cells, 100% of cells became fluorescently labeled. Av-FITC was well dispersed on the cell surfaces with several areas of increased fluorescence (Figure 1B). After 30 min, fluorescein was detected inside endosomal compartments in all the cells (Figure 1C). The fluorescence gradually shifted from the cell surface to the cell interior within the next 24 h as demonstrated by comparing the fluorescence and phase images of the same microscopic field (Figure 1D). Once endocytosed, the fluorescein remained inside the cells without evidence of recycling to the cell surface, and no exocytosis of fluorescent complexes was detected. Other biotinylated cell lines including HEL and Jurkat cells exhibited a nearly identical pattern and time-course of Av-FITC endocytosis under the same conditions, and no internalization was observed when the cells were incubated at 4 °C.

In the absence of biotinylation, incubation of freshly isolated peripheral blood cells with Av-FITC did not increase their fluorescence to detectable levels (Figure 2A). We next biotinylated separate pools of erythrocytes and mononuclear cells and examined Av-FITC uptake in those cells. Immediately upon the addition of Av-FITC and after 24 h, 100% of the biotinylated erythrocytes exhibited intense fluorescence evenly distributed only on their surfaces (Figure 2B). Unlike erythrocytes, after 24 h, the pattern of fluorescence among the biotinylated mononuclear peripheral blood cells was similar to that observed in cell lines with nearly 100% of nucleated cells internalizing the fluorescent label (compare Figure 2C and Figure 1D). A comparison of brightfield and fluorescent views of individual cells (Figure 2, bottom panels) revealed a punctuate cytoplasmic distribution consistent with endosomal localization of the fluorescein. The flourescent label was also retained at a low level on the plasma membrane of several nucleated blood cells compared with no surface label retained on the K562 cells after 24 h (Figure 1D).

Flow cytometry was used to examine whether avidin cross-linking affected the rate of avidin and biotin clearance from the cell surface or the growth of those cells. Untagged avidin was added to biotinylated cells at time = 0 and fluorescent anti-avidin antibodies were used to measure the amount of avidin remaining on the surface over time. The surface level decreased by 20% within 15 min, and only 50% of avidin-bound biotin remained after 2 h (Figure 3A, dotted line). In contrast, biotin was cleared from the cell surface at a much slower rate in the absence of avidin cross-linking (Figure 3A, solid line). Biotin-mediated endocytosis of the avidin caused no significant decrease in cell growth as measured by cell counts (Figure 3B), and no change in cell viability was detected by dye exclusion.

PEI−Avidin Conjugates Condense DNA and Transfect Biotinylated Hematopoietic Cells. We chose the model of DNA transfection to study the biotin-mediated endocytosis of more complex avidin bioconjugates designed for the delivery of biologically active molecules to the nucleus. Polyethylenimine (PEI), a DNA condensing agent that may enhance endosomal escape, was conjugated with avidin. Green fluorescent protein (GFP) encoded plasmid DNA provided a specific marker of endosomal escape and trafficking of plasmid DNA to the nuclear compartment. Another advantage of this transfection model for our study was the low transfection efficiency of PEI−DNA among hematopoietic cells unless the PEI−DNA complexes were delivered by receptor-mediated endocytosis (*15*). Four PEI−avidin conjugates were prepared with increasing content of avidin as described in the Experimental Procedures. PA2, PA4, PA8, and PA16 define conjugates with avidin to PEI molar ratios of 2, 4, 8, and 16, respectively. The gel retardation assay showed a similar profile of cationic binding for PEI and the PEI−avidin conjugates as a function of PEI nitrogen:DNA phosphate (N:P) molar ratios. Consistent with the p*K* profile of PEI, approximately one of six nitrogen atoms in PEI is protonated at physiological pH (*16*). Our gel retardation assay demonstrated that cationic binding of PEI or PEI−avidin completely neutralized the anionic charge of plasmid DNA and prevented electrophoretic mobility at N:P ratios above 3.

Gene-transfer efficiencies of PEI−avidin conjugates were measured in K562 cells by flow cytometry. GFP-expressing cells were defined as those cells having a fluorescence at levels at least 2 standard deviations above the negative control. Optimization of transfecting conditions was performed based on avidin content in the

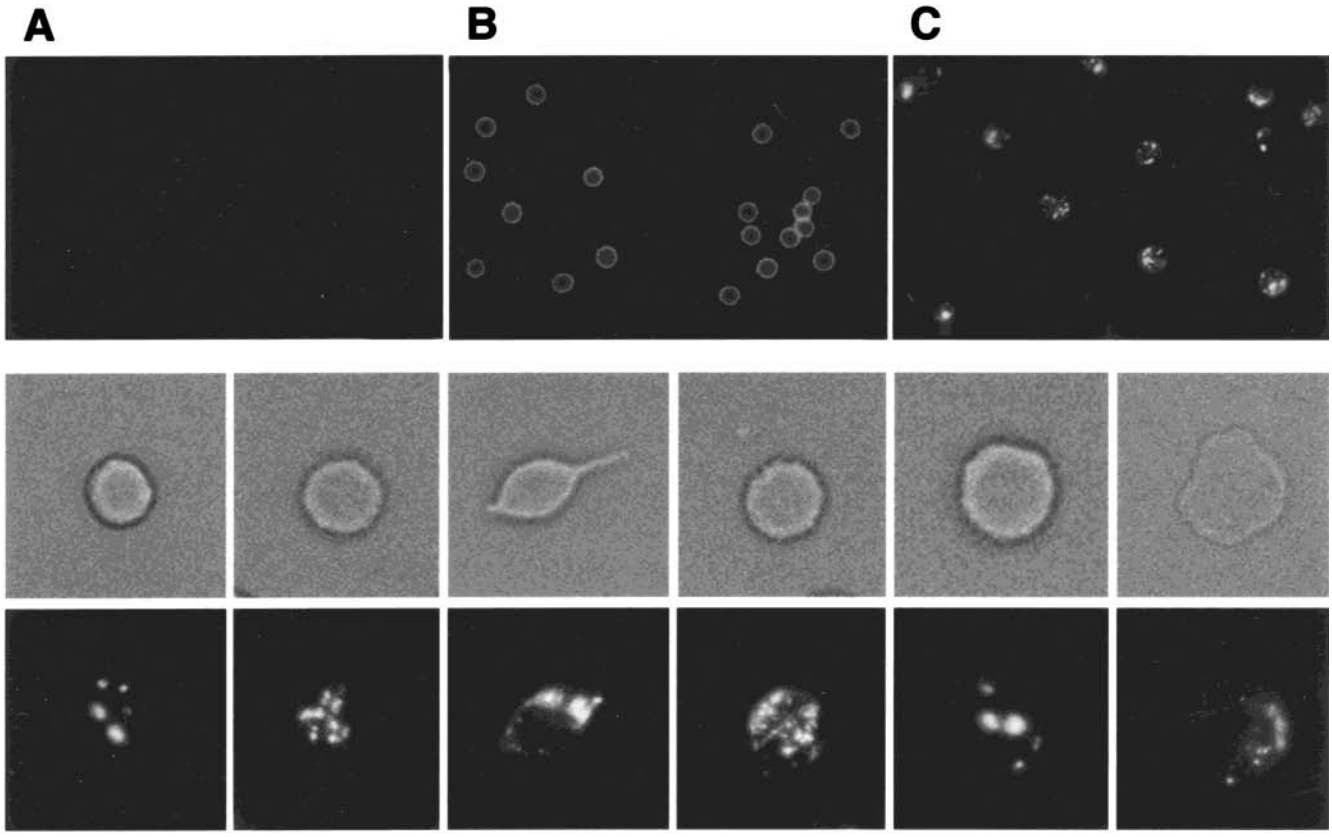


Figure 2. Examination of human peripheral blood cells. Cells were obtained from blood donations, biotinylated, and photographed 24 h after addition of avidin-FITC. Upper three panels show fluorescence microscopy of unbiotinylated, unseparated peripheral blood cells (A), biotinylated erythrocytes (B), and biotinylated mononuclear cells (C). (Lower panels) Enlargement of six individual mononuclear cells are shown in matching brightfield and fluorescent views for comparison.

conjugate, molar ratio of PEI nitrogen to DNA phosphate (N:P), cell number, and serum content. A comparison of gene-transfer efficiencies among the four conjugates was then performed. PA4 conjugates had the highest transfection efficiency when compared with PA2, PA8, and PA16 (Figure 4A). PA4 conjugates were most efficient at a N:P ratio of 6.4 (Figure 4B). At higher N:P ratios, increased cell toxicity was noted as a function of cation excess as reported elsewhere (*15, 16*). Reducing the amount of PA4−DNA added to cells resulted in a linear reduction in the transfection efficiency as measured by the percentage of cells expressing GFP after 48 h.

To determine the relative efficiency of biotin-mediated endocytosis for DNA transfection among hematopoietic cells, PA4 transfection efficiency was compared with unconjugated PEI and transferrin−PEI bioconjugates, as well as a lipid-based reagent DMRIE-C (Figure 5). Transfection of the cell lines with PA4 and trasferrin−PEI resulted in a significant increase in GFP expression when compared to PEI alone and a severalfold increase in transfection efficiency in comparison to lipid-based DMRIE-C. Incorporation of avidin into PEI significantly increased the transfection efficiency on biotinylated K562, Jurkat, and HEL cells to the level achieved with transferrin−PEI (15−20%). A significant increase in biotin-targeted transfection efficiency was detected among HEL cells (20 ± 1.9% PA4 versus 11.8 ± 1.0% transferrin−PEI). In contrast to the malignant cells, significant transfection of terminally differentiated or proliferating hematopoietic cells expressing the transferrin receptor at high levels was not demonstrable with any of the vectors (Figure 5, striped; dotted bars).

PEI−Avidin Mediated Gene Transfer into Biotinylated Cells Is Blocked by Free Avidin or Biotin. Free avidin or biotin was added to PA4 transfection mixtures in order to determine if PEI−avidin-mediated gene transfer required specific binding to the biotin-modified receptors. After formation of PA4−DNA complexes, 0.5 mg/mL biotin was added to the transfection mixture and incubated for 30 min. Alternatively, 10 μg/mL free avidin was added to the biotinylated cells before the addition of PA4−DNA complexes. As shown in Figure 6, free biotin or avidin significantly blocked PA4-mediated gene transfer in all the cell lines examined.

DISCUSSION

One mechanism cells use to determine which molecules are endocytosed is the expression of high-affinity receptors on their external membranes. In this way, nutrients such as iron, folic acid, and lipoproteins enter cells to meet metabolic needs while other molecules not useful to the cell are excluded. When a single receptor binds one or more ligands, the number of binding sites per receptor and the number of receptors per cell is limited in order to regulated ligand entry (*17, 18*). Receptor-binding specificity also plays a large role in restricting the tropism of several viruses (*19*). Here we have demonstrated that covalently added adaptor molecules can modify the cell surface in order to specifically mediate the endocytosis of extracellular elements. We used biotin as a receptor-adaptor due to the well-recognized interaction of biotin with avidin and the lack of avidin-specific receptors on human cells. The covalent addition of a sulfo-*N*-hydroxysuccinimide (sulfo-NHS) group to biotin permits conjugation to free amine groups, primarily the epsilon amine group of lysine residue in proteins. The receptor-mediated nature of avidin endocytosis was confirmed by the ability of free avidin or biotin to block

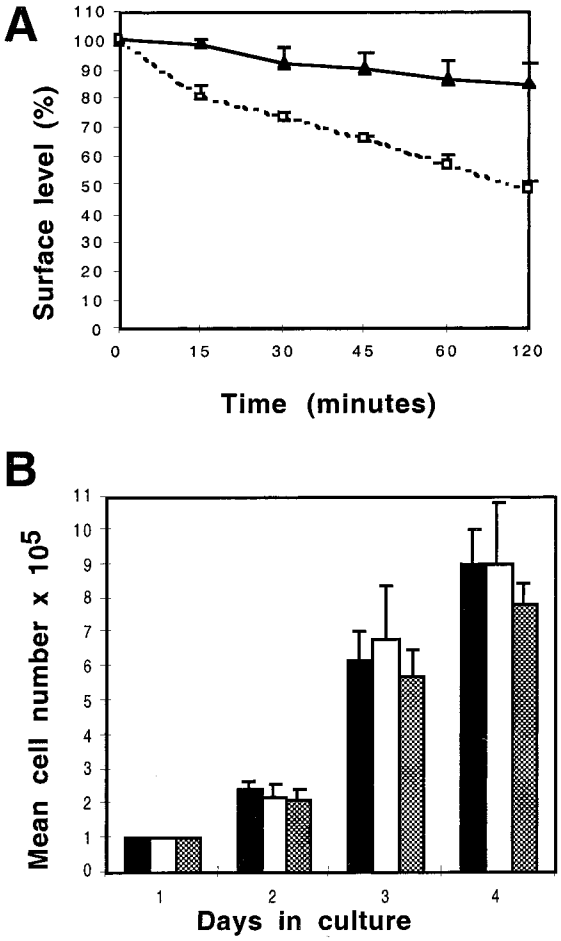


Figure 3. Kinetics of biotin and avidin clearance and cell growth before and after avidin addition. (A) Flow cytometry was used to measure the clearance of avidin and biotin from the cell surface. (solid line) K562 cells were biotinylated and the amount of biotin remaining on the cell surface was measured by relative fluorescence after the addition of avidin-FITC. (dotted line) Unlabeled avidin was added to biotinylated K562 cells at time = 0 and the clearance of avidin was measured using anti-avidin antibodies. The data points show the mean fluorescence values ± standard deviation of triplicate experiments with time = 0 representing 100%. (B) Following biotinylation and incubation with avidin-FITC, cell growth was measured on 3 successive days. Numbers of cells are means of triplicate experiments with standard deviation bars. (solid bars) control K562 cells, (open bars) biotinylated K562 cells, (hashed bars) biotinylated K562 cells incubated with avidin.

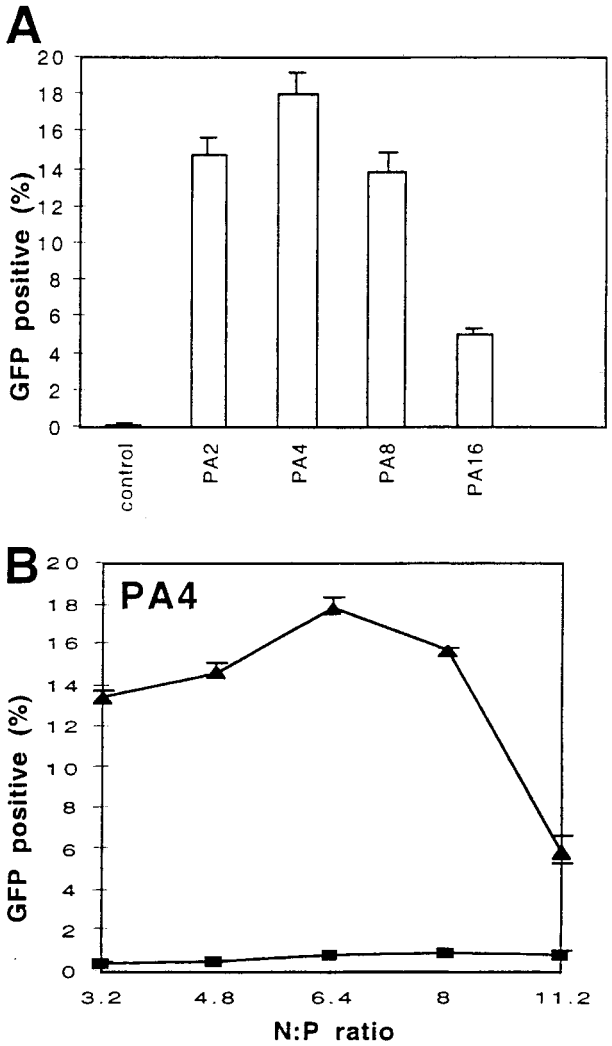


Figure 4. Transfection efficiency of PEI−avidin conjugate variants. (A) Transfection efficiency of PEI−avidin (PA) conjugates at increasing molar ratios of avidin: PA2, PA4, PA8, and PA16. (B) efficiency of PA4 in function of N:P ratio. PA4 was tested on biotinylated K562 cells (triangles) and compared to experiment with PEI alone on K562 cells (squares). The same experiment was performed for all PA conjugates. PEI or PA conjugates were mixed with 10 μg of DNA (pGT) in 0.5 mL of PBS at a growing N:P ratios as indicated on the figure and added to 5×10^5 cells/well in 1.5 mL culture medium (DMEM containing 10% serum), in a 24 well plate. After 4 h, 1 mL of DMEM containing 15% FBS was added to the cells. Flow cytometry was used to determine the percentage of cells expressing GFP 48 h after transfection. Values are shown as means ± standard deviation of triplicate transfections.

the process. The nonspecificity of the biotinylation reaction for free amines on the cell surface additionally suggests that membrane elements not classically associated with endocytosis may be adapted for this purpose. Avidin and biotin have been used extensively in the design of bioconjugates due to their remarkable affinity ($K_a = 10^{15}$ M^{-1}), low cost, and availability (*20*). Surface biotinylation of human red blood cells has been used in humans as an alternative to ^{51}Cr in labeling studies (*21*). Biotinylation has little effect on the stability of red blood cells in vivo, and surface biotinylation rarely modifies their antigenicity as measured by serological assays (*22*). However, internalization of the biotin molecules is prevented by the inability of erythrocytes to endocytose their membrane (*23*) (Figure 2B). The addition of avidin to biotinylated red blood cells also increases their immunogenicity due to their inability to clear bound avidin from the surface (*24*). In marked contrast with erythrocytes, nucleated cells rapidly endocytose the surface avidin as demonstrated here.

The dissociation constant of avidin−biotin is several powers of magnitude higher than that of naturally occurring receptor ligand pairs even at very low pH (*25*). Due to the high affinity and stability of the avidin−biotin bond, we expected a significant portion of the endocytosed avidin to be continuously recycled to the cell surface. However, within the limits of detection, the surface staining pattern of fluorescent avidin suggests most of the avidin was removed from the cell surface within 24 h (Figures 1 and 2).These findings probably reflect the ability of nucleated cells to redirect cross-linked receptors from the recycling pathway to the lysosomal compartment. This redirection away from recycling pathways and lysosomal retention of multivalent ligands has been demonstrated in the case of homodimerric cross-linking of Fc receptors (*26*) as well as oligomerization of transferrin receptors (*27*). The tetravalency of avidin for biotin

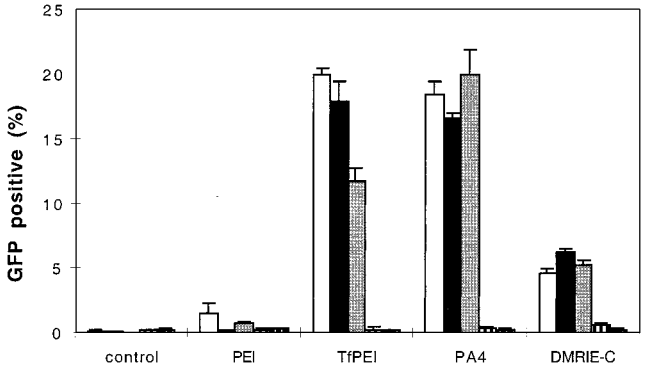


Figure 5. Comparison of PEI−avidin transfection efficiency in hematopoietic cells with other transfection reagents. Transfection efficiency using PEI, Transferrin−PEI, PEI−avidin (PA4), or DMRI-C with pGT plasmid was compared under similar conditions in K562 cells (open bars), Jurkat cells (solid bars), HEL cells (dashed bars), primary mononucleated cells from buffy coat (striped bars) and in proliferating primary erythroid cells demonstrating extremely high level transferrin receptor expression (dotted bars). Efficiency is represented as percentages of GFP expressing cells assessed by flow cytometry from three independent experiments done in duplicate.

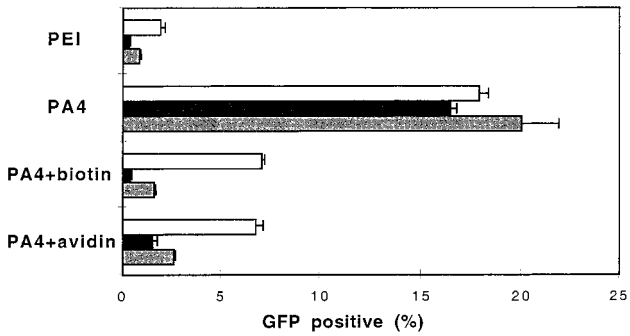


Figure 6. Transfection efficiency of PEI−avidin in biotinylated cells in the presence of excess free biotin or avidin. A total of 8 μg of PEI alone or in PEI−avidin (PA4) complexed with 10 μg of pGT (N:P ratio = 6.4) with and without addition of free biotin or avidin was used to transfect biotinylated K562 cells (open bars), Jurkat cells (solid bars) and HEL cells (dashed bars). Additional biotin was added to 0.5 mg/mL final concentration to preformed PEI−DNA or PA4−DNA complexes, the mixture was incubated for 30 min at 25 °C and used to transfect cells in the medium supplemented with 0.5 mg/mL biotin. Avidin was added to the 10 μg/mL concentration to cells in media and incubated for 30 min at 25 °C before transfection with PEI−DNA or PA4−DNA containing 10 μg/mL avidin. Forty-eight hours later, the percentage of GFP expressing cells was assessed by flow cytometry and is shown as means of triplicate studies ± standard deviation.

results in the clustering of biotinylated proteins on the cell surface (*28*). Therefore, trafficking of avidin−biotin protein complexes to lysosomal compartments may serve as a default pathway for the clearance of irreversibly clustered proteins from the cell surface. Endocytosis triggered by cross-linking of membrane domains containing glycosylphosphatidyinisitol-anchored receptors may also be involved in this process (*29*). Our study has not determined whether specific endocytic elements, such as clathrin, or specific signaling cascades are required for biotin-mediated endocytosis to occur.

In addition to the study of endocytosis itself, receptor adaptation on nucleated cells may be useful for targeting bioconjugates into cells. Immense efforts have recently been directed toward increasing the efficiency of gene transfer and other technologies by targeting membrane components classically associated with receptor-mediated endocytosis. Among nonviral vectors, folate-targeted conjugates (*30*), transferrin conjugates (*15*), galactose conjugates (*31, 32*), conjugates with integrin binding motifs (*33*), and antibody-coupled conjugates (*34*) have been developed for this purpose. Despite recent advances in targeting strategies, transfection of targeted nonviral vectors generally does not result in high-level gene expression in a majority of cells**.** Our data suggest the generally low transfection efficiency in this setting may be due to cell type specific barriers that are postendocytotic and not specifically related to the cell cycle. Additional explanations include the low sensitivity of GFP as a marker of gene transfection (*35*), and the physical state of the DNA−bioconjugate complexes (*32*). In the peripheral blood mononuclear cells studied here, little is known about the catabolism of transferred plasmid DNA, cytoplasmic trafficking after endosomal release, or nuclear localization. Despite the low level of effective gene transfer in these cells, the extremely high efficiency of biotin-mediated endocytosis in primary cells suggests receptor adaptation may prove useful for the entry of other therapeutic bioconjugates or the targeted clearance of extracellular toxins. Conceptually, receptor-adaptation should provide a generic means for delivering bioconjugates across tissue and species boundaries.

ACKNOWLEDGMENT

We thank Dr. A. Schechter for critical reading of the manuscript, Dr. A. Gubin for his assistance in the preparation of plasmid DNA, and J. Muthoni Njoroge for technical assistance with flow cytometry.

LITERATURE CITED

(1) Mukherjee, S., Ghosh, R. N., and Maxfield, F. R. (1997) Endocytosis. *Physiol. Rev. 77,* 759−803.

(2) Moya, M., Dautry-Varsat, A., Goud, B., Louvard, D., and Boquet, P. (1985) Inhibition of coated pit formation in Hep2 cells blocks the cytotoxicity of diphtheria toxin but not that of ricin toxin. *J. Cell Biol. 101,* 548−559.

(3) Treichel, U., Meyer zum Buschenfelde, K. H., Dienes, H. P., and Gerken, G. (1997) Receptor-mediated entry of hepatitis B virus particles into liver cells. *Arch. Virol. 142,* 493−498.

(4) Morgan, E. H. (1996) Cellular iron processing. *J. Gastroenterol. Hepatol. 11,* 1027−1030.

(5) Nichols, J., Foss, F., Kuzel, T. M., LeMaistre, C. F., Platanias, L., Ratain, M. J., Rook, A., Saleh, M., and Schwartz, G. (1997) Interleukin-2 fusion protein: an investigational therapy for interleukin-2 receptor expressing malignancies. *Eur. J. Cancer 33,* S34−S36.

(6) Wang, S., and Low, P. S. (1998) Folate-mediated targeting of antineoplastic drugs, imaging agents, and nucleic acids to cancer cells. *J. Controlled Release 53,* 39−48.

(7) Mayor, S., Sabharanjak, S., and Maxfield, F. R. (1998) Cholesterol-dependent retention of GPI-anchored proteins in endosomes. *EMBO J. 17,* 4626−4638.

(8) Sakai, T., Mizuno, T., Miyamoto, H., and Kawasaki, K. (1998) Two distinct kinds of tubular organelles involved in the rapid recycling and slow processing of endocytosed transferrin. *Biochem. Biophys. Res. Commun. 242,* 151−157.

(9) Wojda, U., Njoroge, J., and Miller, J. (1999) Protection of cells from complement mediated attack: CD59 receptor clustering for the entry of macromolecules into hematopoietic cells. *Immunol. Invest. 28,* 127−135.

(10) Suzuki, T., and Dale, G. L. (1987) Biotinylated erythrocytes: in vivo survival and in vitro recovery. *Blood 70,* 791−795.

(11) Hoffmann-Fezer, G., Trastl, C., Beisker, W., Berg, D., Obermaier, J., Kessler, W., Mysliwietz, J., Schumm, M., Filser, J., and Thierfelder, S. (1997) Preclinical evaluation of biotin labeling for red cell survival testing. *Ann. Hematol. 74,* 231−238.

(12) Savage, M. D., Mattson, G., Desai, S., Nielander, G. W., Morgensen, S., and Conklin, E. J. (1994) *Avidin−biotin Chemistry: A Handbook*, 2nd ed., Pierce Chemical Company, Rockford, IL.

(13) Miller, J. L., Njoroge, M., Gubin, A. N., and Rodgers, G. P. (1999) Prospective identification of erythroid elements in cultured peripheral blood. *Exp. Hematol.* (in press).

(14) Gubin, A. N., Koduru, S., Njioroge, J. M., Bathatnagar, R., and Miller, J. L. (1999) Stable expression of green fluorescent protein after liposomal transfection of K562 cells without selective growth conditions. *BioTechniques* (in press).

(15) Kircheis, R., Kichler, A., Wallner, G., Kursa, M., Ogris, M., Felzmann, T., Buchberger, M., and Wagner, E. (1997) Coupling of cell-binding ligands to polyethylenimine for targeted gene delivery. *Gene Ther. 4,* 409−418.

(16) Boussif, O., Lezoualc'h, F., Zanta, M. A., Mergny, M. D., Scherman, D., Demeneix, B., and Behr, J. P. (1995) A versatile vector for gene and oligonucleotide transfer into cells in culture and in vivo: polyethylenimine. *Proc. Natl. Acad. Sci. U.S.A. 92,* 7297−7301.

(17) Schwartz, A. L. (1995) Receptor cell biology: receptor-mediated endocytosis. *Pediatr. Res. 38,* 835−843.

(18) Willnow, T. E., Orth, K., and Herz, J. (1994) Molecular dissection of ligand binding sites on the low-density lipoprotein receptor-related protein. *J. Biol. Chem. 269,* 15827−15832.

(19) Douglas, J. T., Rogers, B. E., Rosenfeld, M. E., Michael, S. I., Feng, M., and Curiel, D. T. (1996) Targeted gene delivery by tropism-modified adenoviral vectors. *Nat. Biotechnol. 14,* 1574−1578.

(20) Diamandis, E. P., and Christopoulus, T. K. (1991) The biotin-(strept)avidin system: principles and applications in biotechnology. *Clin. Chem. 37,* 625−636.

(21) Franco, R. S., Lohmann, J., Silberstein, E. B., Mayfield-Pratt, G., Palascak, M., Nemeth, T. A., Joiner, C. H., Weiner, M., and Rucknagel, D. L. (1998) Time-dependent changes in the density and hemoglobin F content of biotin-labeled sickle cells. *J. Clin. Invest. 101,* 2730−2740.

(22) Cowley, H., Wojda, U., Cipolone, K., Procter, J., Stroncek, D., and Miller, J. (1999) Biotinylation modifies red cell antigens. *Transfusion 39,* 163−168.

(23) Schekman, R., and Singer, S. J. (1976) Clustering and endocytosis of membrane receptors can be induced in mature erythrocytes of neonatal but not adult humans. *Proc. Natl. Acad. Sci. U.S.A. 73,* 4075−4079.

(24) Muzykantov, V. R., Smirnov, M. D., and Samokhin, G. P. (1991) Avidin attachment to biotinylated erythrocytes induces homologous lysis via the alternative pathway of complement. *Blood 78,* 2611−2618.

(25) Linderman, J. J., and Lauffenburger, D. A. (1988) Analysis of intracellular receptor/ligand sorting in endosomes. *J. Theor. Biol. 132,* 203−245.

(26) Mellman, I., and Plutner, H. (1984) Internalization and degradation of macrophage Fc receptors bound to polyvalent immune complexes. *J. Cell Biol. 98,* 1170−1177.

(27) Marsh, E. W., Leopold, P. L., Jones, N. L., and Maxfield, F. R. (1995) Oligomerized transferrin receptors are selectively retained by a lumenal sorting signal in a long-lived endocytic recycling compartment. *J. Cell Biol. 129,* 1509−1522.

(28) Zaltzman, A. B., van den Berg, C. W., Muzykantov, V. R., and Morgan, B. P. (1995) Enhanced complement susceptibility of avidin−biotin-treated human erythrocytes is a consequence of neutralization of the complement regulators CD59 and decay accelerating factor. *Biochem. J. 307,* 651−656.

(29) Maxfield, F. R., and Mayor, S. (1997) Cell surface dynamics of GPI-anchored proteins. *Adv. Exp. Med. Biol. 419,* 355−364.

(30) Leamon, C. P., and Low, P. S. (1991) Delivery of macromolecules into living cells: a method that exploits folate receptor endocytosis. *Proc. Natl. Acad. Sci. U.S.A. 88,* 5572−5576.

(31) Zanta, M. A., Boussif, O., Adib, A., and Behr, J. P. (1997) In vitro gene delivery to hepatocytes with galactosylated polyethylenimine. *Bioconjugate Chem. 8,* 839−844.

(32) Perales, J. C., Grossmann, G. A., Molas, M., Liu, G., Ferkol, T., Harpst, J., Oda, H., and Hanson, R. W. (1997) Biochemical and functional characterization of DNA complexes capable of targeting genes to hepatocytes via the asialoglycoprotein receptor. *J. Biol. Chem. 272,* 7398−7407.

(33) Schneider, H., Harbottle, R. P., Yokosaki, Y., Kunde, J., Sheppard, D., and Coutelle, C. (1998) A novel peptide, PLAEIDGIELTY, for the targeting of alpha9beta1-integrins. *FEBS Lett. 429,* 269−273.

(34) Poncet, P., Panczak, A., Goupy, C., Gustafsson, K., Blanpied, C., Chavanel, G., Hirsch, R., and Hirsch, F. (1996) Antifection: an antibody-mediated method to introduce genes into lymphoid cells in vitro and in vivo. *Gene Ther. 3,* 731−738

(35) Zlokarnik, G., Negulescu, P. A., Knapp, T. E., Mere, L., Burres, N., Feng, L., Whitney, M., Roemer, K., and Tsien, R. Y. (1998) Quantitation of transcription and clonal selection of single living cells with beta-lactamase as reporter. *Science 279,* 84−88.

BC990059Z

Rapid Esterification of Nucleosides to Solid-Phase Supports for Oligonucleotide Synthesis Using Uronium and Phosphonium Coupling Reagents

Richard T. Pon,*,† Shuyuan Yu,† and Yogesh S. Sanghvi‡

Department of Molecular Biology and Biochemistry, University of Calgary, 3350 Hospital Drive N.W., Calgary, Alberta, Canada T2N 4N1, and Isis Pharmaceuticals, Development Chemistry Department, 2280 Faraday Avenue, Carlsbad, California 92008. Received May 24, 1999; Revised Manuscript Received August 4, 1999

Nucleosides can be esterified to solid-phase supports using uronium or phosphonium coupling reagents and a coupling additive, such as 1-hydroxybenzotriazole (HOBT), 7-aza-1-hydroxybenzotriazole (HOAT), *N*-methylimidazole (NMI), or 4-(dimethylamino)pyridine (DMAP). However, DMAP was far superior to other additives and high nucleoside loadings (up to 60 μmol/g) and rapid coupling reactions ($\leq$10 min) were possible. Hydroxyl-derivatized CPG was attached to nucleosides with 3′-succinyl or 3′-hydroquinone-*O*,*O*′-diacetic acid (HQDA or *Q-Linker*) carboxyl groups through a *primary* ester linkage. Alternatively, supports derivatized with succinic acid or the *Q-Linker* were attached directly to the 3′-OH group of nucleosides through a *secondary* ester linkage. Uronium reagents (HATU or HBTU) gave the best results with the HQDA linker arm, while the bromophosphonium (BrOP or PyBrOP) reagents were best with the succinyl linker arm. In all cases, the coupling reactions were much faster than previous methods using carbodiimide coupling reagents. The ease and speed of the reaction make this support derivatization procedure suitable for automated in situ couplings on DNA synthesizers.

INTRODUCTION

We have introduced a new dicarboxylic acid linker arm (*1*), hydroquinone-*O*,*O*′-diacetic acid (HQDA[1] or *Q-Linker*), which allows oligodeoxynucleotides to be cleaved from the support approximately 30 times faster than a traditional succinic acid linker arm (i.e., 2 min vs 60 min). We have also developed very fast ($\leq$60 s) and efficient (only 0.05 mmol of nucleoside required/g of support) coupling procedures for attaching the first nucleoside to amino derivatized solid-phase supports (*2*). Recently, we have used these improvements to recycle and reuse hydroxyl derivatized solid-phase supports multiple times, without having to remove the support from the synthesis column (*3, 4*).

The support recycling required *ester* attachments, which were more easily cleaved than the usual *amide* linkages. Coupling through ester linkages is also important when cellulose (*5, 6*), soluble poly(ethylene glycol) (*7*), poly(ethylene glycol)-polystyrene (*8, 9*), oxime (*10*), photolabile (*11*−*13*), or other hydroxyl (*14*) supports are used. There has also been interest in ester linkages for the synthesis of alcohol peptides (*15*−*17*), depsipeptides (*18, 19*), oligonucleotide−peptides (*20*), and combinatorial libraries (*21*). Unfortunately, the reduced nucleophilicity of hydroxyl groups relative to amino groups makes coupling through ester linkages more difficult, and so the coupling reactions are longer and often produce lower support loadings. This problem becomes even more pronounced when coupling must be made through a secondary alcohol (*22, 23*) such as the 3′-OH group in nucleosides. Therefore, we wanted to find coupling conditions which would form the required ester linkages faster and more efficiently than the carbodiimide coupling reagents previously used (*22*−*27*).

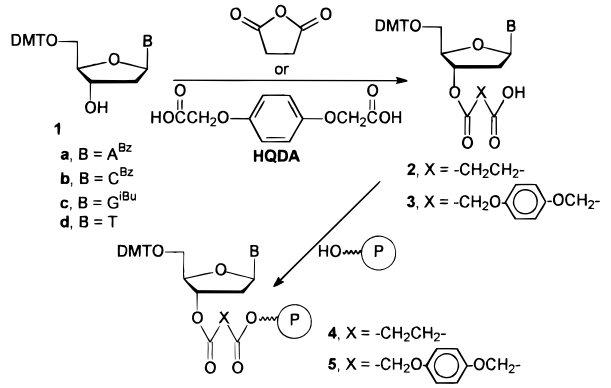
We investigated a number of commonly used uronium and phosphonium coupling reagents. These reagents have become very popular for peptide (*28, 29*) and PNA synthesis (*30*−*32*) because they are stable, nonhygroscopic, and easy to handle. Similar amide linkage formation in oligonucleotide synthesis has also been performed (*33*−*36*). Recently, PyBOP[1] and photolabile protecting groups have allowed functionalization of oligonucleotides while still immobilized on the support (*37*). Various phosphonium salt reagents have also been used to activate phosphate (*38*), phosphonate (*39, 40*) and phosphorothioate/dithioate compounds (*41, 42*). However,

* To whom correspondence should be addressed. Phone: (403) 220-4277. Fax: (403) 283-4907. E-mail: rtpon@ucalgary.ca.
† University of Calgary.
‡ Isis Pharmaceuticals.

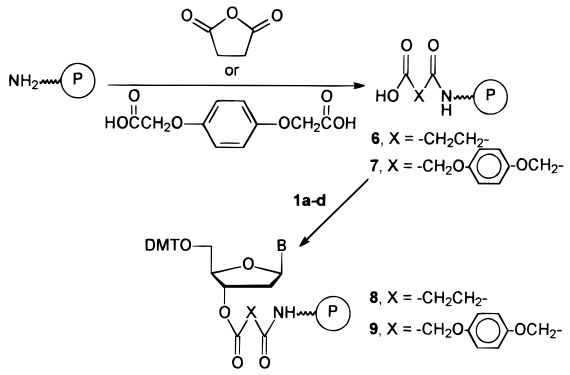
[1] Abbreviations: BOP, benzotriazol-1-yloxytris(dimethylamino)-phosphonium hexafluorophosphate; BrOP, bromotris(dimethylamino)phosphonium hexafluorophosphate; DEC, 1-(3-dimethylaminopropyl)ethylcarbodiimide; DIC, 1,3-diisopropylcarbodiimide; DIEA, diisopropylethylamine; DMAP,4-(dimethylamino)-pyridine; HATU, *O*-(7-azabenzotriazol-1-yl)-1,1,3,3-tetramethyluronium hexafluorophosphate; HBPipU, *O*-(1*H*-benzotriazol-1-yl)-1,1,3,3-bis(pentamethylene)uronium hexafluorophosphate; HBPyU, *O*-(1*H*-benzotriazol-1-yl)-1,1,3,3-bis(tetramethylene)-uronium hexafluorophosphate; HBTU, *O*-(benzotriazol-1-yl)-1,1,3,3-tetramethyluronium hexafluorophosphate; HOBT, *N*-hydroxybenzotriazole; HOAT, 7-aza-1-hydroxybenzotriazole; LCAA-CPG, long-chain alkylamine controlled pore glass; NMI, *N*-methylimidazole; PyBOP, benzotriazol-1-yloxytripyrrolidino-phosphonium hexafluorophosphate; PyBroP, bromotripyrrolidinophosphonium hexafluorophosphate; TBTU, 2-(1*H*-benzotrizol-1-yl)-1,1,3,3-tetramethyluronium tetrafluoroborate; TNTU, 2-(norbornen-2,3-dicarboximido)-1,1,3,3-tetramethyluronium tetrafluoroborate; TOTU, *O*-[(ethoxycarbonyl)cyanomethyleneamino]-1,1,3,3-tetramethyluronium tetrafluoroborate; TPTU, 2-(2-pyridon-1-yl)-1,1,3,3-tetramethyluronium tetrafluoroborate or *O*-(1,2-dihydro-2-oxo-1-pyridyl)-1,1,3,3-tetramethyluronium tetrafluoroborate.

10.1021/bc990063a CCC: $18.00 © 1999 American Chemical Society
Published on Web 09/10/1999

Scheme 1



Scheme 2



ester bond formation using these reagents has not been as common. BOP and PyBOP have been used to prepare primary, secondary, *tert*-butyl, or cyclic esters of amino acids (*43*−*45*), and 2,2,2-trihaloethyl esters have been converted into other esters by phosphonium salts generated in situ (*46*). Occasionally, HATU (*47*), HBTU (*48*), and TBTU (*49*) have also been used to attach amino acids to hydroxyl resins for peptide or PNA synthesis.

In this report, we describe conditions for efficient and rapid coupling of nucleosides, via succinyl or hydroquinone-*O*,*O*′-diacetyl ester linkages, to solid-phase supports using a number of commonly available uronium and phosphonium coupling reagents in acetonitrile solution. Conditions for coupling through both primary (Scheme 1) and secondary ester linkages (Scheme 2) have been developed using 1 equiv of DMAP as a coupling additive. These esterification reactions are much faster (1−60 min) than previous ester coupling reactions (*22, 23, 43*−*49*), yield excellent nucleoside loadings (up to ∼60 μmol/g), and can be readily implemented on automated DNA synthesizers.

MATERIALS AND METHODS

Materials and General Methods. LCAA-CPG (120−200 mesh, 500 Å, 90−120 μmol/g NH_2 groups) was obtained from CPG Inc. (Lincoln Park, NJ). Hydroxyl-CPG (*4*) and succinyl-CPG (*22*) were prepared as previously described. HBTU and HOBT were from Quantum Biotechnologies (Montreal, PQ, Canada), HATU and HOAT were from Perseptive Biosystems (Framingham, MA), BOP and HBPyU were from Sigma Chemical (St. Louis, MO), PyBOP, PyBrOP, TNTU, and TPTU were from Chem-Impex Intl. (Wood Dale, IL), BrOP and HBPipU were from Fluka Chemie (Buchs, Switzerland), and TOTU was from Aldrich Chemicals (Milwaukee, WI).

Caution. Precautions must be taken to avoid skin exposure to any coupling reagent since allergic sensitivity may develop in users.

Table 1. Automated Coupling of Nucleoside-3′-*O*-succinates to OH-CPG through Primary Ester Linkages Using Different Coupling Reagents and DMAP.

reagent	nucleoside[a]	nucleoside loading (μmol/g)[c]
BOP	2a	25
BrOP	2a	57
HATU	2a	30
HATU	2b	31
HATU	2c	33
HATU	2d[b]	18
HBTU	2a	23
HBTU	2b	18
HBTU	2c	19
HBTU	2d[b]	11
HBPipU	2a	21
HBPyU	2a	20
PyBOP	2a	20
PyBrOP	2a	47
TNTU	2a	2
TOTU	2a	26
TPTU	2a	2

[a] Nucleosides **2a**−**c**, coupling reagents, and coupling additives were used at a concentration of 0.05 M in acetonitrile with a wait step of 600 s during the coupling reaction. [b] Nucleoside **2d** required 1:1 acetonitrile/dichloromethane for solubility. [c] Loading determinations by trityl assay are ±5%.

Nucleoside-3′-*O*-succinates were purchased from Sigma Chemical and nucleoside-3′-*O*-hydroquinone-*O*,*O*′-diacetic acid hemiesters were prepared as previously described (*1*) and used as a mixture of both hemi- and diesters. DIEA was distilled and stored over molecular sieves and acetonitrile was freshly distilled from CaH_2. Quantitative analysis of dimethoxytrityl colors was performed using 5% dichloroacetic acid/1,2-dichloroethane (±5% accuracy). Synthesis, cleavage, and deprotection of trial oligonucleotides (data not shown) proceeded without modification.

Primary Esterification. OH-CPG (0.5 g), nucleoside **2** or **3** (0.1 mmol), HBTU (0.1 mmol), and coupling additive (DMAP, HOBT, HOAT, or NMI, 0.1 mmol) were combined in a septum-sealed 10 mL vial. DIEA (3 mmol, 520 μL) and acetonitrile (2.48 mL) were added, via syringe, and the reaction shaken at room temperature. Aliquots (∼10−20 mg) were removed at various intervals, washed with CH_2Cl_2, MeOH, and CH_2Cl_2, dried, and the progress of the reaction was determined by trityl analysis (*27*). The CPG was filtered off and washed with CH_2Cl_2, MeOH, and CH_2Cl_2. The results for nucleosides **2a**−**d**, using HBTU/HOBT and coupling times of either 10, 30, or 60 min were, for **2a**, 7, 14, and 20; for **2b**, 6, 12, and 16; for **2c**, 10, 20, and 22; and for **2d**, 13, 28, and 40 μmol/g. Other coupling results are shown in Figures 1 and 2.

Automated primary esterification reactions (see Table 1) were performed on a PE Biosystems 394 DNA synthesizer as previously described for primary amide coupling reactions (*2*). However, OH-CPG was used instead of LCAA-CPG, equal nucleoside and coupling reagents concentrations (0.05−2 M as described in the discussion), a 5 min capping step was included to acetylate unreacted hydroxyl groups on the support, and in the case of nucleoside **2d**, 1:1 acetonitrile/CH_2Cl_2 was required for solubility.

Preparation of HQDA-CPG 7. LCAA-CPG (1.0 g), HQDA (0.4 mmol, 90 mg), DMAP (0.38 mmol, 46 mg), and HBTU (0.38 mmol, 144 mg) were combined in a glass screw capped vial or flask and then DIEA (0.8 mmol, 140 μL) and acetonitrile (10 mL) were added via syringe. The reaction was shaken at room temperature (2 h). The support was filtered off and washed with acetonitrile, MeOH, and finally CH_2Cl_2. After drying, the amount of

Table 2. Automated Coupling of 5′-Dimethoxytritylthymidine 1d to Carboxyl Derivatized CPG through Secondary Ester Linkages.

		coupling time and nucleoside loading obtained (μmol/g)[a]			
coupling reagent[b]	support[c]	60 s	150 s	300 s	600 s
BrOP/DMAP	6	17	30	37	44
PyBrOP/DMAP	6	26	34	39	43
HATU/DMAP	6	10	14	20	28
HBTU/DMAP	6	9	12	15	24
BrOP/DMAP	7				13
HATU/DMAP	7	18	20	21	25
HBTU/DMAP	7	10	13	19	22
PyBrOP/DMAP	7				9
TOTU/DMAP	7	17	19	19	20

[a] Loading determinations by trityl assay are ±5%. [b] 0.05 M **1d** and DIEA solution was used with 0.05 M coupling reagent/DMAP solution. [c] The carboxyl loadings of the succinylated **6** and *Q-Linker* **7** supports were respectively, 90 and 40 μmol/g.

HQDA on the support (~40 μmol/g) was determined by derivatizing a small aliquot with *N*-monomethoxytrityl-6-amino-1-hexanol (*1*) followed by trityl analysis.

Secondary Esterification. 5′-Dimethoxytritylthymidine **1d** (0.1 mmol, 54 mg), HATU or HBTU (0.1 mmol), DMAP (12 mg), and carboxyl-CPG **6** or **7** (0.25 g) were combined in a 4 mL glass vial. Acetonitrile (1 mL) was added and the mixture shaken at room temperature. Aliquots (~10−20 mg) were removed at various intervals, washed with CH_2Cl_2, MeOH, and CH_2Cl_2, dried, and the progress of the reaction was determined by trityl analysis. The loadings obtained on succinylated support **6** after coupling times of 5, 15, 30, and 60 min were HATU/DMAP, 34, 47, 53, and 63; HBTU/DMAP, 45, 51, 61, and 59 μmol/g. The loading obtained on the *Q-Linker* support **7** after 2 h was 43 μmol/g.

The above reaction was also performed with succinylated support **6** using one-half the amount of nucleoside, and HATU/DMAP or HBTU/DMAP. The loadings obtained after coupling times of 5, 15, 30, and 60 min were, for HATU/DMAP, 17, 21, 22, and 23 and, for HBTU/DMAP, 15, 17, 18, and 19 μmol/g.

Automated secondary esterification reactions were performed as above, except a 0.05 M solution of **1d** and DIEA was used as the nucleoside reagent and carboxyl-CPG supports **6** and **7** were used instead of OH-CPG (see Table 2).

RESULTS AND DISCUSSION

Coupling through Primary Ester Linkages. The hydroxyl-derivatized solid-phase support (OH-CPG) was prepared from long-chain alkylamine controlled pore glass (LCAA-CPG), succinic anhydride, and 6-aminohexan-1-ol as previously described (*4*). Although, our initial experiments with this support, *Q-Linker* nucleosides **3a**−**d,** and an HBTU/HOBT coupling reagent were satisfactory, we found that this method did not work well with the 3′-O-succinylated nucleosides **2a**−**d**. For example, the *Q-Linker* nucleosides gave loadings of 30−50 μmol/g while the 3′-O-succinylated nucleosides produced only 6−13 μmol/g during a 10 min long coupling reaction.

Then we used DMAP as an additive, instead of HOBT, to improve coupling performance. A catalytic amount of DMAP is commonly used with carbodiimide coupling reagents (*22*−*27*), and recently, we found that DMAP greatly increases the speed and efficiency of amide formation with uronium or phosphonium coupling reagents (*2*). However, there have only been a few other reports of DMAP used with uronium (*47*−*50*) or phosphonium (*46*, *51*) coupling reagents. This is because DMAP is known to cause racemization during long amino acid couplings (*52*) as well as partial loss of base-sensitive Fmoc protecting groups (*45*). However, in oligonucleotide synthesis, these concerns are not an issue. Instead, it is important that the reagents not cause base modifications, such as those previously reported with sulfonic acid coupling reagents (*53*, *54*) or acetic anhydride/DMAP capping reagents (*55*). Although, only the first nucleoside and not subsequent bases are exposed to the uronium/phosphonium salt and DMAP coupling conditions, we looked for base modifications by treating nucleoside samples (**1c**−**d** or **3c**−**d)** with an excess (2 equiv) of coupling reagent (HBTU, BrOP, or PyBrOP) and DMAP in either the presence or absence of phenoxyacetic acid (2 equiv). Phosphorothioate oligonucleotide 20-mers made from supports derivatized with the HBTU/DMAP reagent were also analyzed by CE, AX-HPLC, and MS (*3*). In both cases, no unexpected products were detected (results not shown). It is also noteworthy that no base modifications have been reported in any previous applications of uronium or phosphonium coupling reagents in oligonucleotide synthesis (*33*−*35*, *38*, *40*−*42*) or PNA synthesis (*30*−*32*, *47*).

To evaluate the effect of DMAP as an additive, identical coupling reactions using the succinylated nucleosides **2a** and **2d** were setup with HBTU solutions (0.033 M) containing either HOBT or DMAP and samples were removed for trityl analysis at various times. In both cases, the DMAP coupling reactions were much better than the HOBT reactions (Figure 1a). The nucleoside

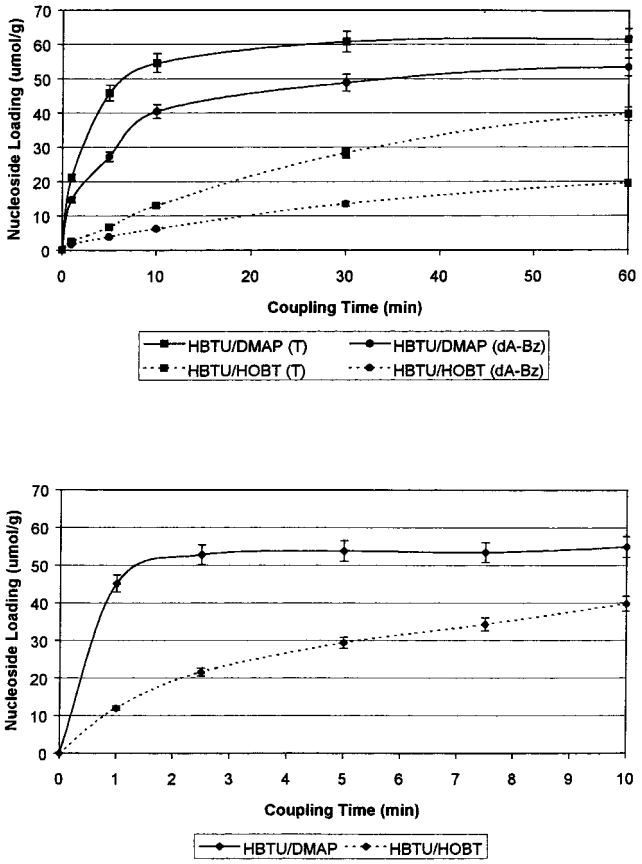


Figure 1. Comparison of HOBT (1 equiv) and DMAP (1 equiv) as additives in the coupling of nucleoside-3′-carboxylates to OH-CPG through primary ester linkages. 0.2 mmol/g of nucleoside and coupling reagent were used at a concentration of 0.033 M. (a) Nucleosides **2a** and **2d** with a 3′-succinyl linker arm. (b) Nucleoside **3d** with a 3′-HQDA linker arm.

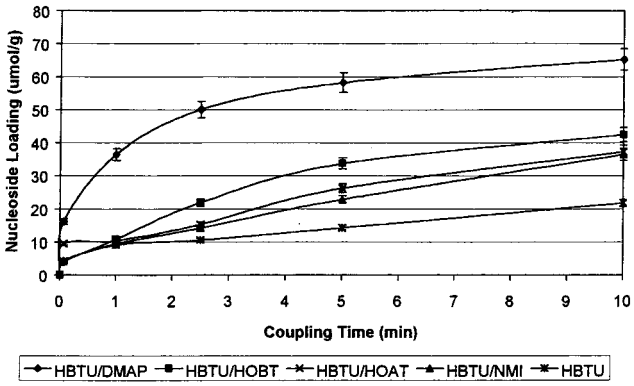


Figure 2. Comparison of different coupling additives in the coupling of 0.1 M nucleoside-3′-*O*-HQDA **3d** through a primary ester linkage to OH-CPG by HBTU.

loadings obtained with DMAP were 1.5−2 times greater than with HOBT and these loadings were obtained in only 10 min instead of 60 min.

A similar experiment with the *Q-Linker* nucleoside **3d** was also performed (Figure 1b). In this case, the *Q-Linker* nucleoside reacted much faster than the succinylated nucleosides using either HOBT or DMAP. However, the DMAP reaction was still much better. For example, after only a 1 min coupling, the respective loadings for the HOBT and DMAP reactions were 12 and 45 μmol/g.

The rapid couplings observed were ideal for implementation on an automated DNA synthesizer. Automation allows different coupling reagents and additives to be easily compared under identical conditions and allows inexpensive underivatized supports to be used for oligonucleotide synthesis (*2*). Therefore, an automated PE Biosystems 394 DNA synthesizer was programmed to fill a synthesis column with a mixture of nucleoside and coupling reagent solutions (4.0 s), wait a defined time for coupling (60−600 s), acetylate unreacted hydroxyl groups (300 s), and then continue with oligonucleotide synthesis. The nucleoside loading was determined by measurement of the trityl color released during detritylation (*27*).

In the first set of automated coupling experiments, the effect of different additives on the esterification of the *Q-Linker* nucleoside **3d** to OH-CPG using HBTU was investigated. Five identical sets of experiments were performed using either 0.1 M HBTU, HBTU/DMAP (1:1), HBTU/NMI (1:1) HBTU/HOBT/DIEA (1:1:1), or HBTU/HOAT/DIEA (1:1:1) and coupling times of up to 10 min. The results (Figure 2) showed that HBTU alone could produce some esterification (22 μmol/g) to the *Q-Linker* after 10 min. However, inclusion of 1 equiv of either NMI, HOAT, or HOBT with the HBTU almost doubled the nucleoside loading (37−42 μmol/g) within the same coupling time. However, a remarkable increase in the speed and amount of esterification was obtained when DMAP was used. Approximately the same nucleoside loading (37 μmol/g) was obtained using DMAP for 1 min, as produced in 10 min with either NMI, HOAT, or HOBT. Coupling for 10 min with DMAP produced more than three times the loading (65 μmol/g) as HBTU alone and ∼1.5 times the loading of the other three additives.

In a second set of experiments, the coupling efficiency of the four *Q-Linker* nucleosides **3a**−**d** with either 0.075 M HBTU/DMAP or 0.2 M HBTU/HOBT was compared (10 min coupling in each case). The average loading for the four nucleosides using 0.075 M HBTU/DMAP was 66 μmol/g, while the average loading using 0.2 M HBTU/HOBT was only 46 μmol/g. Therefore, even with more than twice the reagent concentration, the HBTU/HOBT coupling reagent was less satisfactory than HBTU/DMAP.

Coupling experiments were also performed with 0.075 M solutions of *Q-Linker* nucleoside **3d**, DMAP, and either HATU, HBTU, BrOP, or PyBrOP. These experiments showed that the uronium reagents were slightly better (69−71 μmol/g) than the bromophosphonium reagents (53−56 μmol/g) when used with a *Q-Linker* nucleoside.

Finally, the automated primary esterification experiments were performed using OH-CPG, and 0.05 M solutions of 3′-succinylated nucleosides **2a**−**d**, DMAP, and 11 coupling reagents (Table 1). When the results for the 3′-succinylated nucleoside **2a** were compared, the best coupling reagents were the bromophosphonium reagents BrOP and PyBrOP. These two reagents produced significantly higher nucleoside loadings (47−57 μmol/g) than the other coupling reagents, and the order of esterification efficiency was BrOP > PyBrOP > HATU > TOTU > BOP > HBTU > HBPipU ≈ HBPyU ≈ PyBOP ≫ TNTU ≈ TPTU. The only unsatisfactory results (2 μmol/g) were obtained using the last two reagents. Similar results were also obtained with nucleosides **2b**,**c** and HATU/DMAP or HBTU/DMAP. Poorer results were obtained with succinylated thymidine nucleoside **2d**, possibly because a 1:1 mixture of acetonitrile/dichloromethane instead of acetonitrile was required for solubility.

Coupling through Secondary Ester Linkages. We also investigated a scheme, which did not require prior synthesis of a separate nucleoside-3′-O-carboxylate (i.e., **2** or **3**) for each base. In this strategy, the dicarboxylic acid linker was first added to the support to produce carboxylic acid derivatized supports **6** and **7** (Scheme 2). The carboxyl supports were then coupled to a nucleoside's 3′-OH position via a secondary ester linkage. This strategy has three important advantages. First, the cost of nucleosides with free 3′-OH groups is less than the cost of nucleosides with 3′-carboxyl groups. Second, nucleosides, which may be rare or very expensive, do not need to be converted into 3′-carboxylic acid derivatives before being attached to the support. Finally, the strategy uses readily available amino-derivatized supports, instead of hydroxyl supports, as the starting materials. However, esterification to a secondary hydroxyl group is more difficult, and long coupling times (24 h) are required if carbodiimide coupling reagents (*22*, *23*) are used. Therefore, we were very interested to know if our faster coupling conditions could be used to improve this approach.

Succinylated-CPG **6** (90 μmol/g) was prepared from LCAA-CPG and succinic anhydride, (*22*) and HQDA-CPG **7** (40−45 μmol/g) was prepared by coupling HQDA to LCAA-CPG using HBTU/DMAP. Although, the carboxyl loading of support **7** was not as high as support **6**, the loading was still satisfactory for most purposes.

Nucleoside coupling was performed by shaking succinylated-CPG support **6** with either HATU/DMAP or HBTU/DMAP and either 0.2 or 0.4 mmol of nucleoside **1d** (0.05 and 0.1 M respectively) per gram of support. Unreacted carboxyl groups on the support were not blocked since carboxyl sites do not interfere with subsequent phosphoramidite synthesis (*56*). These initial experiments showed that nucleoside loadings within the range most commonly used (∼20−50 μmol/g) could be obtained within 15−30 min. A similar experiment, with HQDA-CPG **7** resulted in all the carboxyl groups (∼40 μmol/g) being derivatized with nucleoside **1d**. Thus, both the HATU/DMAP and HBTU/DMAP reagents were sig-

nificantly faster than the previously used carbodiimide reagents (*22, 23*).

Next, we adapted this coupling procedure to run on our automated DNA synthesizer. We examined coupling of 0.05 M **1d** to supports **6** or **7** using either BrOP, PyBrOP, HATU, HBTU or TOTU, and DMAP. Loadings were determined after coupling times of either 60, 150, 300, or 600 s **(**Table 2). Nucleoside loadings within the ideal range ~30−40 μmol/g were obtained on succinylated support **6** using either BrOP/DMAP or PyBrOP/DMAP and coupling times of 150−600 s. The nucleoside loadings obtained on the *Q-Linker* support **7** were lower (20−25 μmol/g), probably due to the lower (~40 μmol/g) carboxylic acid loading of the support, but still useful. Also, the uronium coupling reagents were more satisfactory for coupling to the *Q-Linker* than the bromophosphonium reagents. Finally, it should be noted that the thymidine compound **1d** with a free 3′-OH group was much more soluble than the thymidine compound **2d** with a 3′-succinyl group and so there were no solubility problems with any of the four 3′-OH nucleosides **1a**−**d**.

The above method is well-suited for automation on high-throughput oligonucleotide synthesizers (*57*) because the reagents are inexpensive, easy to handle, stable in solution, and fast enough to allow nucleoside attachment in about the same time period as a typical phosphoramidite coupling cycle. In particular, the cost savings obtained by using less expensive 3′-OH nucleosides and carboxyl derivatized supports is a significant improvement to our previous proposal to use nucleoside-3′-carboxylates and amino supports (*2*).

We believe that using automated on-line nucleoside attachment through amide or ester linkages is superior to adding the first base as a phosphoramidite derivative, as proposed for other "universal" supports (*58*−*60*). This is because our approach eliminates the need for either additional reagents or deprotection time to 3′-dephosphorylate the final product. There is also no possibility of 3′-phosphorylated impurities contaminating the final product if 3′-dephosphorylation is incomplete. Indeed, when the linker arm is the *Q-Linker*, the products can be very quickly removed (2 min) from the support with the desired 3′-OH terminus. Although, base deprotection must still be performed by conventional means, this can be done away from the synthesizer and the solid-phase support. This allows equipment to be reused sooner, allows easy separation of the final product from the support, and reduces any contamination from the support (i.e., dissolved silica).

In conclusion, we have found that uronium or phosphonium salt coupling reagents used with 1 equiv of DMAP are very efficient coupling reagents for both ester and amide couplings. The coupling reactions are very fast and both primary and secondary hydroxyl groups can form ester linkages to supports in 10 min or less. Esterification was obtained with a number of different reagents; however, the best reagents differed with the linker arm used. With the *Q-Linker*, the best results were obtained with uronium coupling reagents, while the best results with the succinyl linker were obtained with bromophosphonium reagents. Primary ester linkages, used to couple nucleoside-3′-carboxylates to OH-CPG, are best when short coupling times, high nucleoside loadings, and only the four common bases are required, i.e., the large-scale synthesis of antisense oligonucleotides (*3*). On the other hand, secondary ester couplings, used to attach nucleosides with free 3′-OH groups to carboxyl derivatized supports, are more suitable when the cost of the nucleosides is a concern, i.e., high volume, small-scale synthesis or use of rare or modified nucleosides.

Although our work has only used these conditions for coupling nucleosides to solid-phase supports, ester formation is of general synthetic interest. We hope the utility of the above coupling conditions will encourage others to use these reagents in the synthesis of other bioconjugates or combinatorial products.

LITERATURE CITED

(1) Pon, R. T., and Yu, S. (1997) Hydroquinone-*O,O′*-diacetic acid ('*Q-linker*') as a replacement for succinyl and oxalyl linker arms in solid-phase oligonucleotide synthesis. *Nucleic Acids Res. 25,* 3629−3635.

(2) Pon, R. T., and Yu, S. (1997) Rapid automated derivatization of solid-phase supports for oligonucleotide synthesis using uronium or phosphonium coupling reagents. *Tetrahedron Lett. 38,* 3331−3334.

(3) Pon, R. T., Yu, S., Guo, Z., Yang, X., and Sanghvi, Y. S. (1999) Reusable solid-phase supports for oligonucleotide synthesis using hydroquinone-*O, O′*-diacetic acid (Q-Linker). *Nucleosides Nucleotides* (in press).

(4) Pon, R. T., Yu, S., Guo, Z., and Sanghvi, Y. S. (1999) Multiple oligodeoxyribonucleotide syntheses on a reusable solid-phase CPG support via the hydroquinone-*O,O′*-diacetic acid *(Q-Linker*) linker arm. *Nucleic Acids Res. 27,* 1531−1538.

(5) Frank, R., Heikens, W., Heisterberg-Moutsis, G., and Blocker, H. (1983) A new general approach for the simultaneous chemical synthesis of large numbers of oligonucleotides: segmental solid supports. *Nucleic Acids Res. 13,* 4365−4377.

(6) Ott, J., and Eckstein, F. (1984) Filter disc supported oligonucleotide synthesis by the phosphite method. *Nucleic Acids Res. 12,* 9137−9142.

(7) Bonora, G. M. (1995) Poly(ethylene glycol). A high efficiency liquid phase (HELP) for the large scale synthesis of the oligonucleotides. *Appl. Biochem. Biotechnol. 54,* 3−17.

(8) Rapp, W. (1996) PEG grafted polystyrene tentacle polymers: Physicochemical properties and application in chemical synthesis. In *Combinatorial Peptide and Non-Peptide Libraries: A Handbook* (G. Jung, Ed.) pp 425−464, VCH, Weinheim.

(9) Gao, H. T., Gaffney, B. L., and Jones, R. A. (1991) H−Phosphonate Oligonucleotide Synthesis on a Polyethylene Glycol Polystyrene Copolymer. *Tetrahedron Lett. 32,* 5477−5480.

(10) Ohsima, S.-I., Morita, K., and Takaku, H. (1984) Solid-phase synthesis of deoxyribooligonucleotides by the phosphotriester method employing a new polymer support. *Chem. Pharm. Bull. 32,* 4690−4693.

(11) Peukert, S., and Giese, B. (1998) The pivaloylglycol anchor group: A new platform for a photolabile linker in solid-phase synthesis. *J. Org. Chem. 63,* 9045−9051.

(12) Greenberg, M. M. (1995) Photochemical release of protected oligonucleotides containing 3′-glycolate termini. *Tetrahedron 51,* 29−38.

(13) Yoo, D. J., and Greenberg, M. M. (1995) Synthesis of oligonucleotides containing 3′-alkyl carboxylic acids using universal, photolabile solid-phase synthesis supports. *J. Org. Chem. 60,* 3358−3364.

(14) Winter, M. (1996) Supports for solid-phase organic synthesis. In *Combinatorial Peptide and Non-Peptide Libraries: A Handbook* (G. Jung, Ed.) pp 465−510, VCH, Weinheim.

(15) Neugebauer, W., and Escher, E. (1989) Solid-Phase Synthesis of C−Terminal Peptide Amino Alcohols. *Helv. Chim. Acta 72,* 1319−1323.

(16) Swistok, J., Tilley, J. W., Danho, W., Wagner, R., and Mulkerins, K. (1989) A convenient preparation of C-terminal peptide alcohols by solid-phase synthesis. *Tetrahedron Lett. 30,* 5045−5048.

(17) Alsina, J., Chiva, C., Ortiz, M., Rabanal, F., Giralt, E., and Albericio, F. (1997) Active carbonate resins for solid-phase synthesis through the anchoring of a hydroxyl function. Synthesis of cyclic and alcohol peptides. *Tetrahedron Lett. 38,* 883−886.

(18) Crisma, M., Valle, G., Bonora, G. M., Toniolo, C., and Cavicchioni, G. (1993) Synthesis and conformational analysis

in solution and in the crystal state of depsipeptides containing α-hydroxyisobutyric acid. *Int. J. Pept. Protein Res. 41,* 553−560.

(19) Bianchi, E., Steinkühler, C., Taliani, M., Urbani, A., De Francesco, R., and Pessi, A. (1996) Synthetic depsipeptide substrates for the assay of human hepatitis C virus protease. *Anal. Biochem. 237,* 239−244.

(20) Truffert, J. C., Lorthioir, O., Asseline, U., Thuong, N. T., and Brack, A. (1994) On-Line Solid-Phase Synthesis of Oligonucleotide−Peptide Hybrids Using Silica Supports. *Tetrahedron Lett. 35,* 2353−2356.

(21) Henkel, B., and Bayer, E. (1998) 9-hydroxy-9-(4-carboxyphenyl)fluorene − A new linker for solid-phase synthesis. *Tetrahedron Lett. 39,* 9401−9402.

(22) Damha, M. J., Giannaris, P. A., and Zabarylo, S. V. (1990) An improved procedure for derivatization of controlled pore glass beads for solid-phase oligonucleotide synthesis. *Nucleic Acids Res. 18,* 3813−3821.

(23) Tong, G., Lawlor, J. M., Tregear, G. W., and Haralambidis, J. (1993) The synthesis of oligonucleotide polyamide conjugate molecules suitable as PCR primers. *J. Org. Chem. 58,* 2223−2231.

(24) Walsh, A. J., Clark, G. C., and Fraser, W. (1997) A direct and efficient method for derivatisation of solid supports for oligonucleotide synthesis. *Tetrahedron Lett. 38,* 1651−1654.

(25) Montserrat, F. X., Grandas, A., and Pedroso, E. (1993) Predictable and reproducible yields in the anchoring of DMT-nucleoside-succinates to highly loaded aminoalkyl-polystyrene. *Nucleosides Nucleotides 12,* 967−971.

(26) Markiewicz, W. T., Groger, G., Rosch, R., Zebrowska, A., Markiewicz, M., Klotz, M., Hinz, M., Godzina, P., and Seliger, H. (1997) A new method of synthesis of fluorescently labeled oligonucleotides and their application in DNA sequencing. *Nucleic Acids Res. 25,* 3672−3680.

(27) Pon, R. T., Usman, N., and Ogilvie, K. K. (1988) Derivatization of controlled pore glass beads for solid-phase oligonucleotide synthesis. *Biotechniques 6,* 768−775.

(28) Albericio, F., Bofill, J. M., Elfaham, A., and Kates, S. A. (1998) Use of onium salt-based coupling reagents in peptide synthesis. *J. Org. Chem. 63,* 9678−9683.

(29) Fields, C. G., Lloyd, D. H., Macdonald, R. L., Otteson, K. M., and Noble, R. L. (1991) HBTU activation for automated Fmoc solid-phase peptide synthesis. *Peptide Res. 4,* 95−101.

(30) Finn, P. J., Gibson, N. J., Fallon, R., Hamilton, A., and Brown, T. (1996) Synthesis and properties of DNA-PNA chimeric oligomers. *Nucleic Acids Res. 24,* 3357−3363.

(31) Bergmann, F., and Bannwarth, W. (1995) Solid phase synthesis of directly linked peptide-oligodeoxynucleotide hybrids using standard synthesis protocols. *Tetrahedron Lett. 36,* 1839−1842.

(32) Farese, A., Pairot, S., Patino, N., Ravily, V., Condom, R., Aumelas, A., and Guedj, R. (1997) Liquid-phase synthesis of peptide nucleic acid (or polyamide nucleic acid) dimers. *Nucleosides Nucleotides 16,* 1893−1906.

(33) Kahl, J. D., McMinn, D. L., and Greenberg, M. M. (1998) High-yielding method for on-column derivatization of protected oligodeoxynucleotides and its application to the convergent synthesis of 5′,3′-bis-conjugates. *J. Org. Chem. 63,* 4870−4871.

(34) Weiler, J., and Hoheisel, J. D. (1996) Combining the preparation of oligonucleotide arrays and synthesis of high-quality primers. *Anal. Biochem. 243,* 218−227.

(35) Wada, T., Mochizuki, A., Sato, Y., and Sekine, M. (1998) Functionalization of solid supports with N-unprotected deoxyribonucleosides. *Tetrahedron Lett. 39,* 5593−5596.

(36) Vu, H., Joyce, N., Rieger, M., Walker, D., Goldknopf, I., Hill, T. S., Jayaraman, K., and Mulvey, D. (1995) Use of phthaloyl protecting group for the automated synthesis of 3′-[(hydroxypropyl)amino] and 3′-[(hydroxypropyl)triglycyl] oligonucleotide conjugates. *Bioconjugate Chem. 6,* 599−607.

(37) Kahl, J. D., and Greenberg, M. M. (1999) Introducing structural diversity in oligonucleotides via photolabile, convertible C5-substituted nucleotides. *J. Am. Chem. Soc. 121,* 597−604.

(38) Hashmi, S. A. N., Adiraj, M., Kumar, A., and Katti, S. B. (1994) 6-Nitrobenzotriazol-1-yloxytris(dimethylamino)phosphonium hexafluorophosphate (NBOP): A new coupling reagent in oligonucleotide synthesis. *Nucleosides Nucleotides 13,* 1059−1067.

(39) Campagne, J. M., Coste, J., and Jouin, P. (1995) (1*H*-benzotriazol-1-yloxy)-tris(dimethylamino)phosphonium hexafluorophosphate- and (1*H*-benzotriazol-1-yloxy)-tripyrrolidinophosphonium hexafluorophosphate-mediated activation of monophosphonate esters: Synthesis of mixed phosphonate diesters, the reactivity of the benzotriazolyl phosphonic esters vs the reactivity of the benzotriazolyl carboxylic esters . *J. Org. Chem. 60,* 5214−5223.

(40) Wada, T., Sato, Y., Honda, F., Kawahara, S., and Sekine, M. (1997) Chemical synthesis of oligodeoxyribonucleotides using N-unprotected H−phosphonate monomers and carbonium and phosphonium condensing reagents: O-selective phosphonylation and condensation. *J. Am. Chem. Soc. 119,* 12710−12721.

(41) Kehler, J., Puschl, A., and Dahl, O. (1997) Solution phase synthesis of dithymidine phosphorodithioate using new S-protecting groups in combination with a chemoselective coupling reagent (PyNOP). *Nucleosides Nucleotides 16,* 23−32.

(42) Kehler, J., Puschl, A., and Dahl, O. (1997) Synthesis of oligodeoxynucleoside phosphoromonothioates and phosphorodithioates by a phosphotriester method. *Nucleosides Nucleotides 16,* 1633−1636.

(43) Coste, J., and Campagne, J. M. (1995) A propos de l′estérification des acides carboxyliques par le BOP ou le PyBOP. *Tetrahedron Lett. 36,* 4253−4256.

(44) Sliedregt, K. M., Schouten, A., Kroon, J., and Liskamp, R. M. J. (1996) Reaction of N-trityl amino acids with BOP: Efficient synthesis of *tert*-butyl esters as well as N-trityl serine- and threonine-β-lactones. *Tetrahedron Lett. 37,* 4237−4240.

(45) Kim, M. H., and Patel, D. V. (1994) "BOP" as a reagent for mild and efficient preparation of esters. *Tetrahedron Lett. 35,* 5603−5606.

(46) Hans, J. J., Driver, R. W., and Burke, S. D. (1999) One-pot synthesis of amides and esters from 2,2,2-trihaloethyl esters using phosphorus (III) reagents. *J. Org. Chem. 64,* 1430−1431.

(47) Bergmann, F., Bannwarth, W., and Tam, S. (1995) Solid-phase synthesis of directly linked PNA-DNA-hybrids. *Tetrahedron Lett. 36,* 6823−6826.

(48) Ambrosius, D., Casaretto, M., Gerardy-Schahn, R., Saunders, D., Brandenburg, D., and Zahn, H. (1989) Peptide analogues of the anaphylatoxin C3a; synthesis and properties. *Biol. Chem. Hoppe-Seyler 370,* 217−227.

(49) Harth-Fritschy, E., and Cantacuzene, D. (1997) Esterification of 9-fluorenylmethoxycarbonyl-glycosylated serine and cysteine derivatives with an hydroxymethyl resin. *J. Pept. Res. 50,* 415−420.

(50) Schmidt, R., and Neubert, K. (1991) Cyclization studies with tetra- and pentapeptide sequences corresponding to β-casomorphins. *Int. J. Pept. Protein Res. 37,* 502−507.

(51) Coste, J., Pantaloni, A., Dufour, M.-N., and Jouin, P. (1991) PyBOP and PyBroP: Two reagents for the difficult coupling of the α,α-dialkyl amino acid, Aib. *Tetrahedron 47,* 259−270.

(52) Atherton, E., Benoiton, N. L., Brown, E., Sheppard, R. C., and Williams, B. J. (1981) Racemization of activated, urethane-protected amino acids by *p*-(dimethylamino)pyridine: Significance in solid-phase peptide synthesis. *J. Chem. Soc., Chem. Commun.* 336−337.

(53) Efimov, V. A., Chakhmakhcheva, O. G., and Ovchinnikov, Y. A. (1985) Improved rapid phosphotriester synthesis of oligodeoxyribonucleotides using oxygen-nucleophilic catalysts. *Nucleic Acids Res. 13,* 3651−3666.

(54) Reese, C. B., and Ubasawa, U. (1980) Reaction between 1-arenesulphonyl-3-nitro-1,2,4-triazoles and nucleoside base residues. Elucidation of the nature of side-reactions during oligonucleotide synthesis. *Tetrahedron Lett. 21,* 2265−2268.

(55) Eadie, J. S., and Davidson, D. S. (1987) Guanine modification during chemical DNA synthesis. *Nucleic Acids Res. 15,* 8333−8349.

(56) Lyttle, M. H., Adams, H., Hudson, D., and Cook, R. M. (1997) Versatile linker chemistry for synthesis of 3′-modified DNA. *Bioconjugate Chem. 8,* 193−198.

(57) Lashkari, D. A., Hunickesmith, S. P., Norgren, R. M., Davis, R. W., and Brennan, T. (1995) An automated multiplex oligonucleotide synthesizer: Development of high-throughput, low-cost DNA synthesis. *Proc. Natl. Acad. Sci. U.S.A. 92,* 7912−7915.

(58) Scott, S., Hardy, P., Sheppard, R. C., and McLean, M. J. (1994) A universal support for oligonucleotide synthesis. In *Innovation and perspectives in solid-phase synthesis. Peptides, proteins, and nucleic acids, biological and biomedical applications* (R. Epton, Ed.) pp 115−124, Mayflower Worldwide Ltd., Birmingham.

(59) Azhayev, A. V. (1999) A new universal support for oligonucleotide synthesis. *Tetrahedron 55,* 787−800.

(60) Nelson, P. S., Muthini, S., Vierra, M., Acosta, L., and Smith, T. H. (1997) Rainbow universal CPG: A versatile solid support for oligonucleotide synthesis. *Biotechniques 22,* 752−756.

BC990063A

Molecular Necklaces. Cross-Linking Hemoglobin with Reagents Containing Covalently Attached Ligands

Sanda Crapatureanu, Ruxandra Serbanescu, Sharon Bisley Brevitt, and Ronald Kluger*

Lash Miller Laboratories, Department of Chemistry, University of Toronto, Toronto, Ontario, Canada M5S 3H6.
Received May 27, 1999; Revised Manuscript Received August 13, 1999

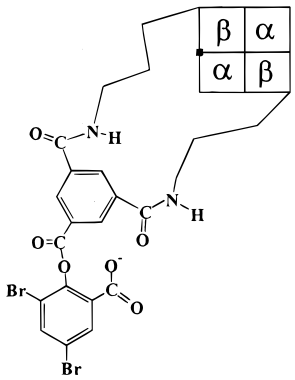
Hemoglobin can be cross-linked and converted to a bioconjugate in one step by a "molecular necklace", a reagent that contains two reacting sites and a pendant ligand. The compound to be conjugated is activated as an electrophile. The activated material is then combined with a reagent (3-aminoisophthalic acid) that contains a nucleophilic (amino) site and two latent (carboxyl) sites. The latent sites of the product are activated as 3,5-dibromosalicylates to produce the cross-linker. Illustrative examples of cross-linking are presented with pendant biotin [bis(3,5-dibromosalicyl) *N*-biotinyl-5-aminoisophthalate] and pendant *N*-trifluoroacetyl-L-isoleucylglycine [bis(3,5-dibromosalicyl) *N*-(*N*-trifluoroacetyl-L-isoleucylglycyl)-5-aminoisophthalate)]. The resulting modified hemoglobins contain two principal types of cross-link: (β-Lys-82−β'-Lys-82) and (α-Lys-99−α'-Lys-99). The functional properties of the modified hemoglobin containing biotin in a (β-Lys-82−β'-Lys-82) cross-link are (pH 7.4, 55 μM heme, 25 °C, 0.1 M chloride, and 50 mM Bis-Tris) $P_{50} = 4.9$ Torr, $n_{50} = 3.0$, values which are approximately the same as for native hemoglobin. The results of affinity chromatography of the biotinylated cross-linked hemoglobin using a column of immobilized avidin indicate that the pendant biotin is much less accessible than free biotin. We suggest that the results are consistent with the pendant species being strongly attracted into the hemoglobin environment.

INTRODUCTION

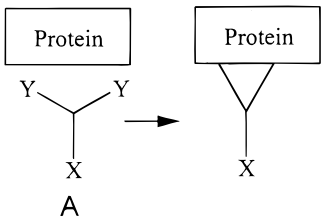
Human hemoglobin contains four subunits ($\alpha\alpha\beta\beta$) that dissociate spontaneously into $\alpha\beta$ dimers (*1*). The hemoglobin contained in red cell substitutes (for use in transfusions) must be altered to prevent its dissociation into dimers in order to avoid excretion via the kidney (*2*, *3*). Appropriate chemical cross-linking can prevent dissociation of the tetramer and has been used to create a wide variety of red cell substitutes. Site-directed reagents introduce cross-links and produce altered hemoglobins with defined structures (*4*−*7*).

The chemical alteration of hemoglobin that introduces a cross-link has potential utility beyond producing red cell substitutes: the entity created in the cross-link can serve as a site for tethering species with useful functions. In one potential application, the conjugated species can combine the properties of a red cell substitute with those of a drug-delivery agent (*8*−*10*). This complements an approach in which conjugation is achieved by de novo synthesis of mutants of hemoglobin containing additional cysteines that serve as linking points (*11*).

The existing method for producing conjugates on a cross-link (*9*) uses a trifunctional reagent [trimesyl tris(3,5-dibromosalicylate), TTDS], in which only two sites react with hemoglobin. The third site is available for addition to the resulting cross-linked hemoglobin. A schematic diagram of the cross-linked hemoglobin resulting from the reaction with TTDS is shown below. Substitution of the dibromosalicylate ester creates a novel adduct with a nucleophile.



Hydrolysis of the ester derived from TTDS in the cross-linked protein will compete with the desired substitution reaction that is used to produce a bioconjugate, reducing the potential yield of conjugated protein. Since hydrolysis and the desired ester substitutions compete in the necessarily aqueous medium, it is not likely that hydrolysis can be suppressed once the cross-linked ester has formed. An alternative approach can avoid the competition: form the bioconjugate with the reagent prior to cross-linking the protein. Such a reagent can be visualized as a "molecular necklace" with the bioconjugate materials contained in the unreactive portion of the cross-linking reagent. In the schematic diagram below, molecular necklace "A" has a pendant species "X" and two sites "Y" that react with the protein.



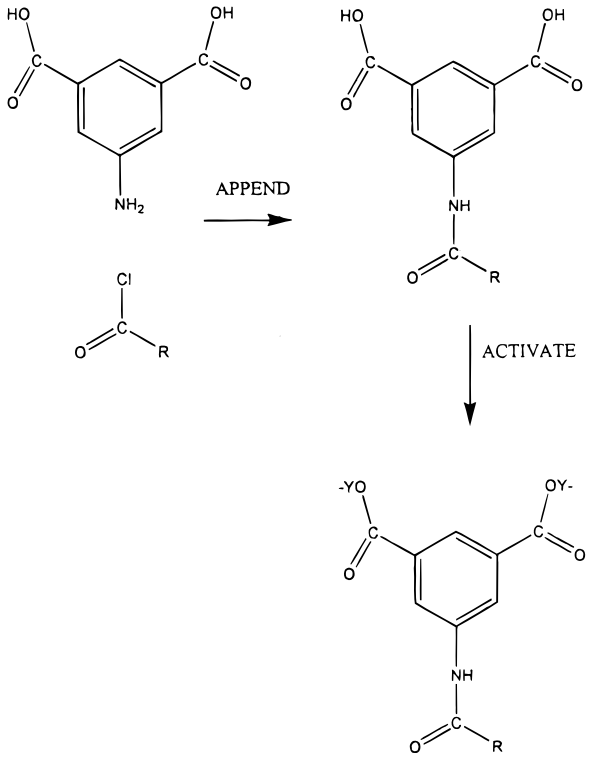
A

We have developed an efficient general route to produce compounds with the properties of "A". First, the compound to be conjugated (X) is activated as an elec-

* To whom correspondence should be addressed.

10.1021/bc990067f CCC: $18.00 © 1999 American Chemical Society
Published on Web 10/21/1999

Scheme 1



trophile. The activated material is then combined with a reagent that contains a nucleophilic site and two latent sites. The latent sites of the product are activated to produce the molecular necklace cross-linker. The general strategy is exemplified in Scheme 1, where the pendant ligand is added as an acid chloride and the carboxyls are activated as "OY-", which is an anionic ester group.

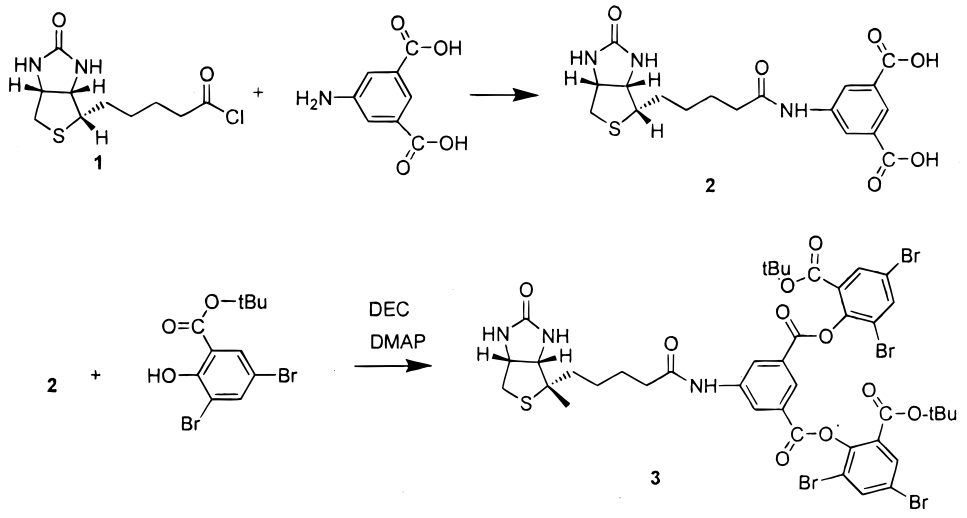
We illustrate the method by creating a cross-linking reagent with two examples of pendants, biotin (an affinity group) and a peptide, *N*-trifluoroacetyl-L-isoleucylglycine (for drug delivery or receptor activation). These react directly with hemoglobin, converting it into a cross-linked bioconjugated species.

EXPERIMENTAL PROCEDURES

Materials. D-Biotin, *N*-t-Boc-Ile-Gly, *N*-t-Boc-L-Phe, avidin, 3,5-dibromosalicylic acid, and 5-aminoisophthalic acid were obtained from commercial sources and used directly. Solutions of trypsin and endoproteinase Glu-C were freshly prepared. Human hemoglobin A was obtained in the carbonmonoxy form from Hemosol, Inc. All other materials were of the highest grade commercially available. The identity and purity of newly synthesized materials was assessed by NMR spectroscopy, mass spectrometry, infrared spectroscopy and thin-layer chromatography. Proton NMR spectra were recorded at 200 and 300 MHz. Carbon NMR and fluorine NMR spectra were recorded on multinuclear spectrometers whose proton resonance is 500 and 400 MHz. Melting points are uncorrected. Oxygen-binding analysis followed the automated method described originally by Imai (*12*−*14*). We developed a computer interface and program that enabled the data to be collected in an MS-DOS computer environment.

The structures of compounds in the descriptions of syntheses are numbered in Scheme 2. The synthesis of bis (3,5-dibromosalicyl) *N*-biotinyl-5-aminoisophthalate (**3**) involves addition of amino-isophthalic acid to the acid chloride of biotin (**1**) to form the dicarboxylic acid (**2**) followed by activation of the diacid to the bis-dibromosalicylate (**3**). Biotin (1.07 g, 4.38 mmol) was dissolved in 20 mL of distilled thionyl chloride at room temperature and stirred until it dissolved. After 20 min, excess thionyl chloride was distilled away. The residue, the acid chloride of biotin (**1**), was dried in vacuo. 5-Aminoisopthalic acid (0.99 g, 5.5 mmol) was dissolved in 25 mL of anhydrous *N*,*N*-dimethylacetamide and stirred for 20 min under nitrogen. 4-(Dimethylamino)pyridine (7.1×10^{-3} g, 0.58 mmol) was added to this solution and stirred until all material dissolved. The solution was cooled to 0 °C and then added to a solution of the biotin acid chloride. The reaction mixture was stirred at room temperature for 14 h. A light brown precipitate formed and was collected on a filter. The solid was dissolved in DMF and precipitated with water. This was collected by filtration, washed with hot methanol, and dried under vacuum (0.700 g, 1.72 mmol) to give bis(3,5-dibromosalicyl)-*N*-biotinyl-5-aminoisophthalate: mp 220−221 °C (decomposed); IR (KBr, cm^{-1}) 3391 (m), 2922 (m), 1696 (s), 1452 (m), 758 (m), 697 (s); ^{1}NMR (DMSO-d_6) δ 10.23(s, 1H, NH), 8.42(s, 2H, ArH), 8.12 (s, 1H, ArH), 6.43 (s, 1H, NH), 6.35 (s, 1H, NH), 4.25−4.29 (m, 1H), 4.11−4.15 (m, 1H), 3.10−3.12 (m, 1H), 2.77−2.80 (m, 1H), 2.58 (s, 1H), 2.32 (s, 2H), 1.34−1.61 (m, 6H); ^{13}C NMR (DMS0-d_6) δ 25.01, 28.11, 28.21, 36.26, 40.10, 55. 41, 59.20, 61.05, 123.4, 124.3,

Scheme 2



131.6, 139.9, 162.7, 166.5, 171.7; MS parent peak (CI) calcd, 407.4; found, 408 (MH^+).

Bis((1-*tert*-butoxycarbonyl)-3,5-dibromosalicyl) *N*-Biotinyl-5-amino-isophthalate (3). *N*-Biotinyl-5-aminoisophthalic acid (0.18 g, 0.43 mmol), *tert*-butyl 3,5-dibromosalicylate (0.340 g, 0.97 mmol), 1-(3-dimethylaminopropyl)-3-ethylcarbodiimide hydrochloride (0.334 g, 1.74 mmol), and 4-(dimethylamino)pyridine (0.0250 g, 0.200 mmol) were dissolved in 15 mL of anhydrous DMF and stirred at 4 °C for 20 h. The precipitated byproduct was removed by filtration. The filtrate was diluted with water and ethyl acetate. The aqueous layer was extracted several times with ethyl acetate. The organic layers were pooled, washed with water, saturated sodium bicarbonate, and water. The pooled organic extracts were dried over anhydrous magnesium sulfate and evaporated under vacuum (off-white solid). The product was purified by flash chromatography (silica gel 60; eluent, acetone). The product, bis((1-*tert*-butoxycarbonyl)-3,5-dibromosalicyl) *N*-biotinyl-5-amino-isophthalate was isolated, 0.19 g, 0.17 mmol: ^{1}H NMR (DMSO-d_6) δ 10.6 (s, 1H, NH), 8.83 (d, J = 1.5, 2H, ArH), 8.48 (t, J = 1.5, 1H, ArH), 8.35 (d, J = 2.4, 2H, ArH), 8.03 (d, J = 2.4, 2H, ArH), 6.46 (s, 1H, NH), 6.38 (s, 1H, NH), 4.31−4.27 (m, 1H), 4.15−4.12 (m, 1H), 3.13−3.10 (m, 1H), 2.79 (dd, J = 5, 1H), 2.58 (d, J = 12.3, 1H), 2.38 (t, J = 7.35, 1H), 1.66−1.59 (m, 1H), 1.31 (s, 18 H); ^{13}C (DMSO-d_6) δ 172.2, 162.7, 162.1, 161.5, 145.6, 141.1, 138.8, 133.0, 129.4, 128.6, 125.0, 124.9, 119.6, 119.1, 83.1, 61.0, 59.2,55.4, 40.0, 36.3, 28.2, 28.1, 24.8.

Bis(3,5-dibromosalicyl) *N*-Biotinyl-5-aminoisophthalate (4). Bis((1-*tert*-butoxycarbonyl)-3,5-dibromosalicyl) *N*-biotinyl-5-aminoisophthalate (0.18 g, 0.17 mmol) was dissolved in 15 mL of anhydrous trifluoroacetic acid (0 °C) and stirred 10 min at 0 °C, then for 30 min at room temperature. Diethyl ether was added to induce crystallization. The solution was left for 1 h at 4 °C. The resulting solid was collected by filtration, washed with diethyl ether, and dried under vacuum (0.16 g, 0.17 mmol): mp 235−236 °C (dec); IR (KBr, cm^{-1}) 3368 (m), 3025 (m), 2921 (s), 1708 (s), 1452 (s), 1198 (s), 697 (s); ^{1}H NMR (DMSO-d_6) δ 10.56 (s, 1H, NH), 8.77 (s, 2H, ArH), 8.41 (s, 1H, ArH), 8.34 (d, J = 2.1, 2H, ArH), 8.10 (d, J = 2.1, 2H, ArH), 6.47 (s, 1H, NH), 6.38 (s, 1H, NH), 4.31−4.27 (m, 1H), 4.15−4.10 (m,1H), 3.24−3.11 (m, 1H), 2.80 (dd, J = 5,1H), 2.58 (d, J = 12.6, 1H), 2.37 (t, J = 7.2, 2H), 1.65−1.40 (m, 6H); ^{13} C NMR (DMS0-d_6) δ 24.92, 28.15, 28.25, 36.34, 55.43, 59.26, 61.10, 119.36, 119.54, 124.8, 127.6, 129.5, 133.5, 139.05, 139.70, 140.90, 162.4, 162.8, 163.53. MS(ESI) calcd, 963.29; found: 963.4.

Bis(3,5-dibromosalicyl) *N*-(*N*-trifluoroacetyl-L-isoleucylglycyl)-5-aminoisophthalate (8). *N*-(*N*-*tert*-butyloxycarbonyl-L-isoleucylglycyl)-5-aminoisophthalic Acid Dimethyl Ester (5). *N*-t-Boc-Ile-Gly (2.88 g, 9.97 mmol), dimethyl 5-amino-isophthalate (2.11 g, 10.1 mmol) and 4-(dimethylamino)pyridine (0.125 g, 1.03 mmol) were dissolved in 60 mL of anhydrous DMF under nitrogen. DCC (2.05 g, 9.94 mmol) was dissolved in 30 mL of anhydrous DMF and added dropwise to the first solution. The reaction mixture was stirred for 3 days at room temperature under dry nitrogen. The precipitated *N*,*N*-dicyclohexylurea was removed by filtration. Ethyl acetate and water were added to the filtrate and the layers were separated. The aqueous layer was extracted three times with ethyl acetate. The organic layers were pooled, filtered to remove additional precipitate, and washed with 2 M hydrochloric acid (1.2 L), saturated salt solution (500 mL), saturated sodium bicarbonate solution (700 mL), and again with saturated salt solution (250 mL). The ethyl acetate solution was dried over magnesium sulfate, filtered, and concentrated under reduced pressure. The mixture was kept at 4 °C for 24 h. The resulting yellow precipitate was collected by filtration, washed with hexane, and dried under vaccuum (1.75 g, 3.65 mmol): mp 124−125 °C; IR (KBr) 3307 (m), 2967 (m), 1730 (s), 1555 (s), 1515 (s), 14 440 (s), 1343 (s), 1250 (s), 1168 (s), 1009 (m), 758 (s); ^{1}H NMR (DMSO-d_6) δ 10.2 (s, 1H, NH), 8.48 (d, J = 1.2, 2H, ArH), 8.34 (t, J = 5.4, 1H, NH), 8.14 (t, J = 1.5, 1H, ArH), 6.94 (d, J = 8.1, 1H, NH), 3.91−3.83 (m, 3H, masked), 3.87 (s, 6H), 1.71−1.69 (m, 2H), 1.35 (s, 9H), 1.16−1.11 (m, 1H), 0.86−0.78 (m, 6H); ^{13}C NMR (DMSO-d_6) δ 172.00 (s), 168.33 (s), 165.18 (s), 155.70 (s), 139.62 (s), 130.70 (s), 124.1 (s), 123.5 (s), 78.20 (s), 58.99 (s), 52.50 (s), 42.73 (s), 36.24 (s), 28.11 (s), 24.50 (s), 15.34 (s), 11.00 (s); MS (ESI) calcd, 479.5; found, 480.4 (MH^+).

***N*-[*N*-*tert*-butyloxycarbonyl-L-isoleucylglycyl]-5-aminoisophthalic Acid (6).** *N*-[*N*-*tert*-butyloxycarbonyl-L-isoleucylglycyl]-5-aminoisophthalic acid dimethyl ester (1.75 g, 3.65 mmol) was dissolved in 100 mL of methanol, 20 mL of 6 N sodium hydroxide was added, and the reaction mixture stirred under nitrogen for 2 h. After addition of water and 50 mL of 2 N HCl to the reaction mixture, a white precipitate formed, which was filtered, washed with water, and dried under vacuum (1.58 g, 3.50 mmol): mp 215−216 °C; IR (KBr, cm^{-1}) 3329 (m, br), 2970 (m), 1699 (s), 1558 (m), 1252 (m), 667 (w); ^{1}H NMR (DMSO-d_6) δ 10.15 (s, NH), 8.43 (d, J = 1.5, 2H, ArH), 8.33 (t, J = 5.7, 1H), 8.15 (t, J = 1.5, 1H, ArH), 6.90 (d, J = 8.1,1H, NH), 3.90−3.80 (m, 3H), 1.70−1.68 (m, 2H), 1.35 (s, 9H), 1.14−1.09 (m, 1H), 0.86−0.78 (m, 6H); ^{13}C NMR (DMSO-d_6) δ 172.04 (s), 168.24 (s), 166.45 (s), 155.74 (s), 139.35 (s), 131.87 (s), 124.69 (s), 123.56 (s), 78.24 (s), 59.04 (s), 42.78 (s), 36.31 (s), 28.20 (s), 24.57 (s), 15.40 (s), 11.07 (s); MS(ESI) calcd, 451.45; found, 452.4 (MH^+).

Bis((1-*tert*-butoxycarbonyl)-3,5-dibromosalicyl) *N*-[*N*-*tert*-butyloxycarbonyl-L-isoleucylglycyl]-5-aminoisophthalate (7). *N*-[*N*-*tert*-butyloxycarbonyl-L-isoleucyl-glycyl]-5-aminoisophthalic acid (1.58 g, 3.50 mmol), 4-(dimethylamino)pyridine (0.085 g, 0.7 mmol), and *tert*-butyl-3,5-dibromosalycilate (2.46 g, 7.00 mmol) were dissolved in 300 mL of anhydrous THF and cooled in an ice bath. 1-(3-dimethyl-aminopropyl)-3-ethylcarbodiimide hydrochloride (2.4 equiv, 1.61 g, 8.40 mmol) was dissolved in dry dichloromethane and added via a syringe, under nitrogen, dropwise to the solution. After stirring the mixture at 0 °C for 5 min and at room temperature for 48 h, the solvent was evaporated and the solid dissolved in ethyl acetate. The solution was washed successively with saturated sodium bicarbonate and water, evaporated under reduced pressure. The white solid product was used directly (1.40 g, 1.25 mmol).

Bis(3,5-dibromosalicyl) *N*-(*N*-trifluoroacetyl-L-isoleucylglycyl)-5-aminoisophthalate (8). Bis((1-*tertert*-butoxycarbonyl)-3,5-dibromosalicyl) *N*-[*N*-*tert*-butyloxycarbonyl-L-isoleucylglycyl]-5-aminoisophthalate (1.40 g, 1.25 mmol) was dissolved in a mixture of trifluoroacetic acid and trifluoroacetic acid anhydride and stirred under nitrogen at room temperature for 2 h. The solvent was removed under vacuum, leaving a clear oil as a residue. Addition of ether resulted in the formation of a white precipitate, which was filtered and identified as a decomposition product. Adding hexane to the filtrate precipitated the desired compound. The solid was collected by filtration and dried under vacuum (0.411 g, 0.410 mmol): mp 170−172 °C, IR (KBr, cm^{-1}) 3350 (m, br), 2923 (m), 1718 (s), 1558 (s), 1452 (s), 1199 (s), 697 (s);

^{1}H NMR (DMSO-d_6) δ 10.68 (s, 1H, NH), 9.59 (d, J = 8.4, 1H, NH), 8.75 (d, J = 1.5, 2H, ArH), 8.68 (t, J = 5.7, 1H, NH), 8.44 (t, J = 1.5, 1H, ArH), 8.36 (d, J = 2.4, 2H, ArH), 8.11 (d, J = 2.4, 2H, ArH), 4.08−3.89 (m, 3H), 1.92−1.88 (m, 2H), 1.46−1.40 (m, 1H), 0.83−0.78 (m, 6H); ^{13}C NMR (DMSO-d_6) δ 170.69 (s), 168.78 (s), 163.89 (s), 162.79 (s), 156.61 (q, J = 145), 146.95 (s), 140.94 (s), 139.42 (s), 133.90 (s), 130.10 (s), 128.04 (s), 125.51(s), 125.27 (s), 119.93 (s), 119.72 (s), 58.13 (s), 43.21 (s), 35.77 (s), 24.98 (s), 15.56 (s), 10.84 (s); ^{19}F NMR (DMSO-d_6) δ −74.07 (s, CF_3CO); MS (ESI) calcd, 1003.45; found, 1004.4 (MH^+).

Cross-Linking Procedures. Reactions were conducted in solutions of deoxyhemoglobin, which was prepared from carbonmonoxyhemoglobin. Stock solutions of carbonmonoxyhemoglobin (1.0 mL, 1.23 mM) in 50 mM bis-tris (pH 6.9) were passed through a Sephadex G-25 column at 4 °C equilibrated with 0.1 M sodium borate buffer (pH 9). Carbonmonoxyhemoglobin was converted to oxyhemoglobin by photoirradiation in a rotating flask under a stream of humidified oxygen for 3 h at 0 °C (*14*). Oxyhemoglobin was converted to deoxyhemoglobin by continuously flowing wet nitrogen through the rotating flask for 3 h at 37 °C. The cross-linking reagent (2 mol/mol of hemoglobin) was dissolved in 0.2−0.3 mL of peroxide-free dioxane and 0.3 mL of 0.1 M sodium borate buffer (pH 9). The reaction solution was deoxygenated under a stream of nitrogen for 1 h and then added to the hemoglobin solution via a syringe. The reaction mixture was kept rotating at 37° under slowly flowing nitrogen to maintain the hemoglobin in the deoxy state. The reaction was monitored by C-4 reversed-phase HPLC. The reaction was stopped when no more α- or β-chain modification was observed. At the end of the reaction period, the flask was cooled on ice, flushed with carbon monoxide, and passed through a Sephadex G-25 column equilibrated with 0.1 M borate buffer (pH 9) in order to remove unreacted cross-linking reagent.

Structural Characterization of Modified Hemoglobins. Chromatographic Analysis. Modified globin chains were identified by analytical reversed-phase HPLC (*15*) using a 330 Å pore size C-4 Vydac column (250 × 4.6 mm). The materials were then separated by preparative reversed-phase HPLC using the same column packing (250 × 12 mm). Developers contained 0.1% trifluoroacetic acid and gradients of acetonitrile in water from 20 to 60%. The effluent was monitored for absorbance at 220 nm. Analysis of the reaction mixture and isolation of modified hemoglobins was accomplished by analytical and semipreparative anion-exchange HPLC using a Synchropak AX-300 column (analytical, 250 × 4.5 mm; semipreparative, 250 × 10 mm) and a POROS column (from Perseptive Biosystems: 7000 Å pore, 10 μm particle). Developers for the AX-300 column contained 15 mM Tris, (pH 8) and gradients of sodium acetate in water starting at 10 mM and ending at 150 mM. The flow rate was 1 mL/min for the analytical analysis and 4 mL/min for the semipreparative separation. For the analysis using the POROS column, a pH gradient from pH 8.5 to 6.5 was used. The effluent was monitored at 420 nm.

Peptide fragments were separated by reversed-phase HPLC using a C-18 Vydac column (93 × 4.7 mm; 330 Å pore, 5 μm particle), with developers containing 0.1% trifluoroacetic acid. Gradients of acetonitrile in water ranged from 0 to 100%, pumped at 1 mL/min. The effluent was monitored at 220 and 280 nm (*14*).

The presence of cross-links between globin chains can be established by molecular mass bands that are multiples those of the 16 kDa monomers in SDS−PAGE (*16*). Polyacrylamide gels (12%) were run in a dual-slab cell apparatus at 200 mV. Prior to electrophoresis, the protein sample was dissolved in 0.5 M tris-HCl, pH 6.8, which contained 0.05% bromophenol blue, 4% v/v β-mercaptoethanol, 2% SDS, and 10% v/v glycerol. The sample was kept for 5 min in boiling water to denature it. Approximately 10 μg of protein was applied to each lane of the gel and subjected to electrophoresis for 35 min. Unmodified hemoglobin and molecular weight standards were used to estimate the molecular weight of the resulting bands after fixation followed by staining with Coomassie Brilliant Blue R.

The molecular masses of cross-linked hemoglobins were determined precisely by electrospray ionization mass spectrometry, coupled to reversed-phase HPLC, as described previously (*17*). Standard masses were taken from literature compilations (*18*).

Separation of peptides from tryptic digestion of partially acylated globin chains reveals the site of amide modification by comparison with the intensity of peaks of tryptic peptides from native globin chains (*14*). Native and cross-linked α and β chains were separated and collected using the reversed-phase HPLC procedure outlined above. Organic developers were evaporated under reduced pressure and water removed by lyophilization. The globin chains were then dissolved in 8 M urea to help denature the protein and promote complete hydrolysis. They were kept for 2 h at room temperature. The solution was diluted to 2 M urea with, pH 8.5, 0.8 M bicarbonate. Freshly prepared TPCK-treated trypsin solution (2 mg/mL, 4% of mass of total protein) was added and the digestion continued for 24 h at room temperature. The tryptic hydrolysate was heated in boiling water for 2 min and diluted to 1 M urea with 0.8 M bicarbonate buffer (pH 8.5). A solution of endoproteinase Glu-C (1 mg/mL, 2% of mass of total protein) was added and the mixture digested for 72 h at room temperature. The sample was clarified by filtration through a 0.45-μm filter before injection onto the C-18 reversed-phase HPLC column. Peptide fragments were separated according to the procedure described above. The modified peaks were identified by peptide pattern analysis. The tryptic-Glu-C peptide maps of modified α and β subunits were analyzed by comparison with the peptide maps of unmodified α and β subunits and by comparison with published standards (*14*).

Quantitative Affinity Chromatography. 4-Nitrophenyl chloroformate was use to activate Sepharose CL-4B. All steps in the activation procedure were performed in an ice bath according to the reported procedure (*19*). Sepharose Cl-4B (50 mL) was washed in batches through a sintered glass funnel with increasing concentrations of acetone in water, starting at 0% and ending at 100% absolute acetone. To the washed Sepharose gel, an acetone solution (50 mL) containing 4-nitrophenyl chloroformate (0.3 mmol/mL) was added. To this suspension, 50 mL of an acetone solution containing 4-dimethylaminopyridine (0.35 mmol/mL) was added dropwise with stirring, and the resin was stirred for 90 min. The activated Sepharose was then washed exhaustively with acetone (500 mL), acetone-2-propanol (1:1) (200 mL), 2-propanol (200 mL), 2-propanol-water (1:1) (200 mL), and distilled water until the solution remained clear in the presence of 0.2 N sodium hydroxide. The activated resin (0.737 mmol 4-nitrophenol/g resin) was dried by lyophilization and stored at 4 °C.

Avidin (3.8 mg) was dissolved in 6 mL of 0.1 M sodium bicarbonate (pH 8.5). To this solution, 2.73 g of activated Sepharose was added, and the reaction mixture stirred

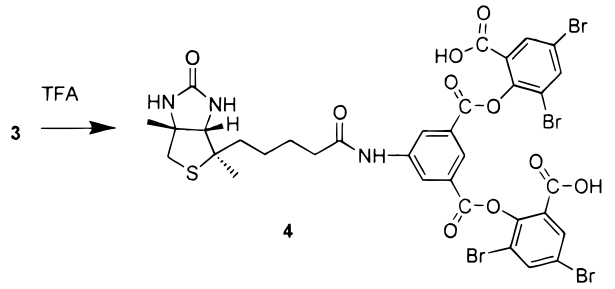
for 1 h at room temperature then overnight at 4 °C (*20*). The resin was then washed successively with water, 0.2 M acetic acid, water, and 0.01 M sodium hydroxide, followed by distilled water, 0.1 M sodium bicarbonate, and phosphate-buffered saline (PBS), pH 7.4. The immobilized avidin was stored at 4 °C in PBS.

Circular dichroism (CD) spectra of the native and modified hemoglobins were recorded on a Jasco J-710 instrument between 200 and 280 nm in, pH 9, 0.003 M sodium borate buffer. Circular dichroism (CD) spectra were recorded on a Jasco J-710 system between 200 and 280 nm (hemoglobin concentration 0.3 mM in sodium borate buffer, pH 9).

RESULTS AND DISCUSSION

We have been able to produce cross-linking reagents with appended molecules by a process that first adds the appendage to the amino group of amino isophthalic acid. We then activate the carboxylic acid groups by converting them to reactive esters. The resulting material has the potential to attach the pendant ligand while linking between two sites on the protein, functioning as a "molecular necklace". Producing the cross-linking reagent in this manner avoids hydrolysis of the activated ester, which occurs if the ester group is appended to the protein. The reaction sequence is presented in Scheme 2. Bis(3,5-dibromosalicyl) *N*-biotinyl-5-aminoisophthalate (DBBA, **4**) is a conjugation agent that adds a pendant molecule of biotin in the cross-linking process.

Addition of 5-aminoisophthalic acid to biotin acid chloride (**1**) gives *N*-biotinyl-5-aminoisophthalic acid (**2**). This is coupled with the substituted salicylate to give bis-[(1-*tert*-butoxycarbonyl)-3,5-dibromosalicyl] *N*-biotinyl-5-aminoisophthalate (**3**). Removal of the *tert*-butyl groups



gives the biotin-substituted cross-linker, bis(3,5-dibromosalicyl) *N*-biotinyl-5-aminoisophthalate (**4**, DBBA).

We used an analogous route to prepare a cross-linker with a pendant dipeptide derivative. The preparation of bis(3,5-dibromosalicyl) *N*-[*N*-trifluoroacetyl-L-isoleucylglycyl]-5-aminoisophthalate (DBTIA, **8**) is presented in Scheme 3. *N*-[*N*-*tert*-butyloxycarbonyl-L-isoleucylglycyl]-5-amino-isophthalic acid dimethyl ester (**5**) was prepared by coupling of *N*-t-Boc-Ile-Gly with dimethyl 5-aminoisophthalate. The diester was hydrolyzed to the diacid (**6**). This was coupled with the substituted salicylate to give the *tert*-butyl 3,5-dibromosalicylate ester (**7**). Removal of the *tert*-butyl group with trifluoroacetic acid and formation of trifluoroacetyl derivative of the terminal amino group with trifluoroacetic anhydride in a single step gave DBTIA (**8**).

In our experience, hemoglobin reacts with cross-linking reagents most readily and completely in its deoxy form (*21*). This is also the case with the reagents in the present study. Carbonmonoxyhemoglobin reacted very slowly with DBBA (pH 9, 37 °C). The reagent was much more reactive toward deoxyhemoglobin under the same conditions: combining 1 equiv of hemoglobin with 2 equiv of the reagent led to more than 75% conversion in 3 h. The solution contained two principal products. The larger fraction was the material cross-linked in the β subunits ($\alpha\alpha\beta82-82\beta'$), from acylation of the ϵ-amino groups of Lys-82 of each of the β subunits. The other major product is cross-linked between the ϵ-amino groups of Lys-99 of each of the α subunits ($\beta\beta\alpha99-99\alpha'$) (Figure 1). Increasing the reaction time to 14 h led to over 95% acylation of hemoglobin, with an increase in the extent of inter-α cross-linking and almost no further reaction of the β subunits. The details of the analysis follow.

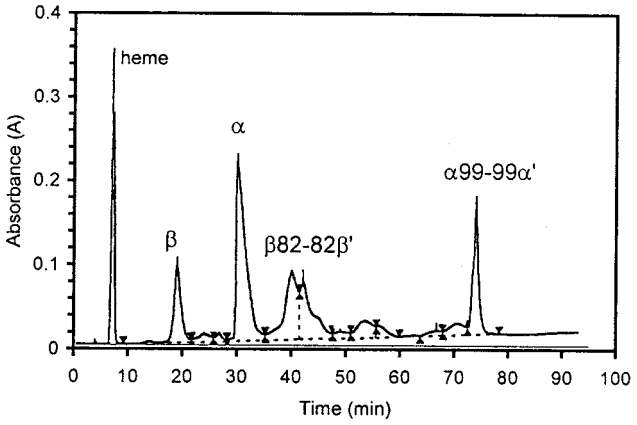


Figure 1. Globin chain separation after reaction of deoxyhemoglobin with DBBA (pH 9, 37 °C, 3 h).

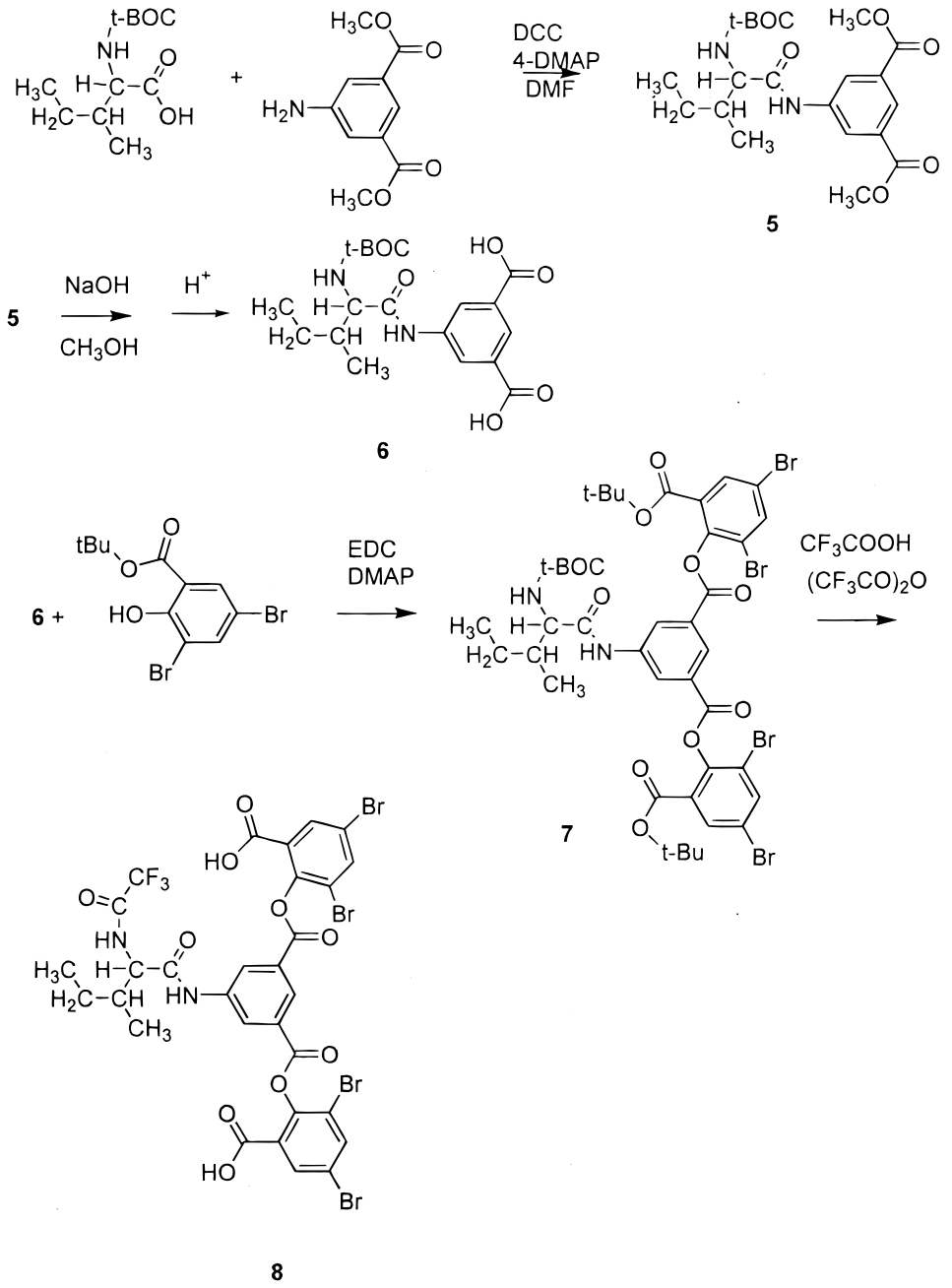
Product Structures. Products were analyzed as previously described (22). The C-4 reversed-phase HPLC chromatogram (Figure 1) has peaks for two cross-linked hemoglobin chains along with the peaks coincident with those of the native protein (heme, α and β subunits). The relative areas of the unreacted α and β chains compared to those from unreacted hemoglobin indicates that the chemical modification takes place predominantly in the β chains.

SDS−PAGE of the globin chains indicated the presence of covalent cross-links with 32 kDa bands corresponding to linked dimers from 16 kDa monomers. The mass of each globin chain was determined by HPLC-MS. The first major modified globin ($\beta82-82\beta'$ in Figure 1) has a mass of 32 093 Da, consistent with an inter-β cross-linked dimer containing *N*-biotinyl-5-aminoisophthalate (calculated mass, 32 093 Da). The second major modified globin ($\alpha99-99\alpha'$ in Figure 1) has a mass of 32 615 Da, consistent with an $\alpha-\alpha$ dimer containing *N*-biotinyl-5-aminoisophthalate (calculated mass, 32 619 Da). Two distinct peaks eluting at 43 and 45 min could not be distinguished by their molecular weight and peptide pattern analysis. Their different chromatographic behavior suggests that these could be stereoisomers, differing in the orientation of the biotin derivative with respect to the protein.

The intermediate chromatographic zones correspond to cross-linked globins having a second molecule of cross-linker attached to a third site with or without one leaving group hydrolyzed, as suggested by their HPLC-MS analysis. Since they made up only a small percentage of the other two products, they were not further analyzed.

The anion-exchange HPLC chromatogram of the reaction products is shown in Figure 2. The peaks were identified by comparison with the chromatogram of native hemoglobin run under the same conditions, separation of the main fractions, purification by chromatography on a POROS column and globin chain separation

Scheme 3



on a C-4 reversed-phase column of the purified hemoglobins. Retention times of globin chains separated on C-4 reversed-phase column from the purified hemoglobins were compared with those from the reaction mixture for which HPLC-MS analysis was performed. Peak A is unmodified hemoglobin. Peak B is the inter-α cross-linked hemoglobin. Regions C and D correspond to the $\alpha\alpha\beta 82-82\beta'$ hemoglobin conjugate. The inter-β cross-linked hemoglobin fraction (peak C) was concentrated and used for functional studies. Its C-4 chromatogram (Figure 3) indicates the presence of the heme, the α monomer and the $\beta-\beta'$ cross-linked dimer. Region E contains a mixture of modified hemoglobins corresponding to the minor globins in the C-4 chromatogram (Figure 2).

To determine the site of modification of the protein chain, the cross-linked dimers (peaks $\beta 82-82\beta'$ and $\alpha 99-99\alpha'$ in 1) were separated on a C-4 column and digested with trypsin followed by endoproteinase Glu-C. Peptide peaks were identified by comparison with the peptide pattern of the digest of native α and β globins. The patterns of tryptic peptides eluting at 43 and 45 min (Figure 1) are identical to one another (Figures 4 and 5). The peptide maps are characteristic of the β chain of human hemoglobin (*14*) with the exception of the absence of βT-9 and βT-10a′ peptide fragments and the presence of additional peaks at 93.8 and 94.3 min. These results are consistent with the selective acylation of the β-Lys-82. The peptide pattern for the peak eluting at 75 min in the C-4 chromatogram (Figure 1) is missing the αT-11 and αT-12 peak (Figure 6). A large peak elutes at 111.8 min. These results suggest the formation of an amide bond between the α-Lys-99 (on the C-terminus of αT-11) on each α subunit and the cross-linker. This newly formed amide bond prevents trypsin from hydrolyzing the peptide bond between αT-11 and αT-12 peptide fragments. These peptide pattern data along with the molecular masses determined experimentally by HPLC-MS

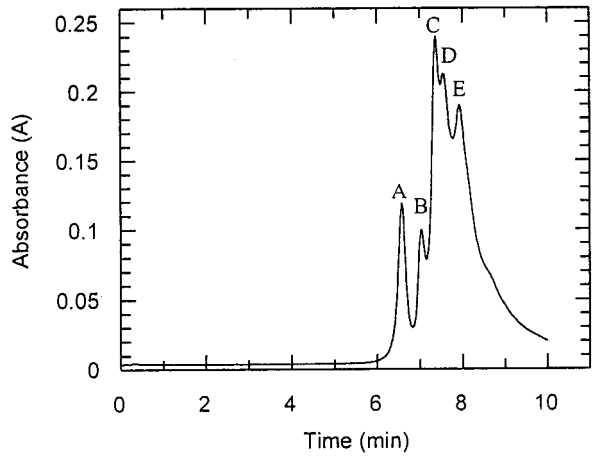


Figure 2. Anion-exchange HPLC profile on a POROS column for the reaction of DBBA with deoxyhemoglobin (37 °C, pH 9, sodium borate buffer, 3 h).

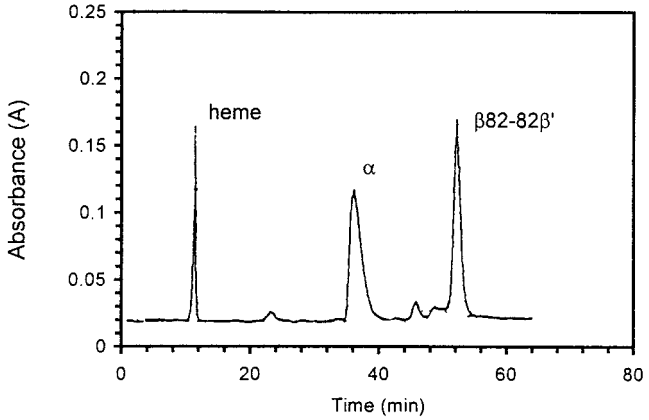


Figure 3. Globin chain separation on a C-4 column of the inter-β cross-linked Hb (peak C in Figure 2) purified on an AX-300 column.

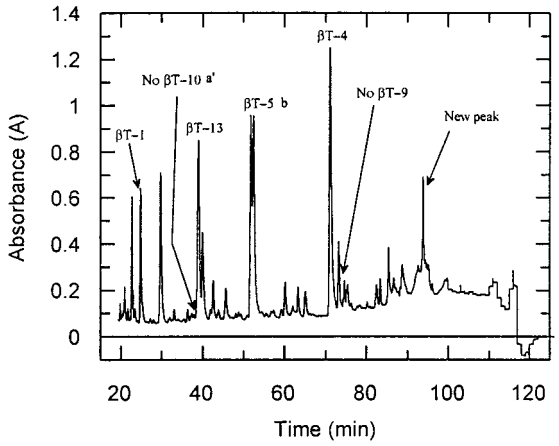


Figure 4. C-18 reversed-phase HPLC chromatogram of the β82−82β' globin dimer (peak eluting at 43 min in the C-4 chromatogram), after trypsin/Glu-C digestion, monitored at 200 nm.

for the globin dimers indicate that two β and two α chains are cross-linked by a *N*-biotinyl-5-aminoisophthalate moiety.

Affinity Chromatography of Cross-Linked Biotinylated Hemoglobin. Quantitative measurements of the accessibility to avidin on the column of biotin conjugated to hemoglobin followed the procedures described by Wilchek (*23*). The hemoglobin−biotin conjugate was applied to the avidin Sepharose column and

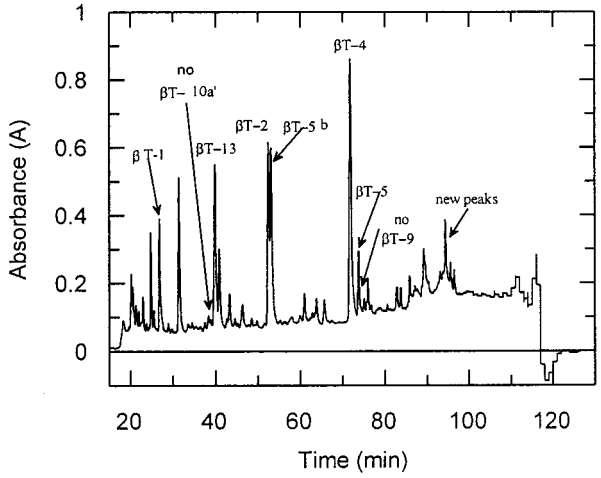


Figure 5. C-18 reversed-phase HPLC chromatogram of the β82−82β' globin dimer, after trypsin/Glu-C digestion, monitored at 200 nm.

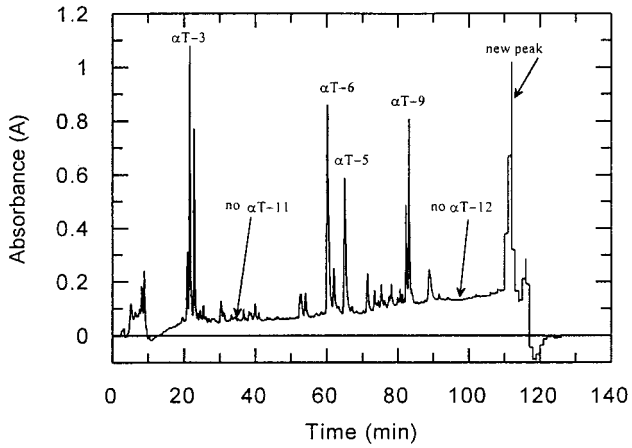


Figure 6. Tryptic digest separation on C-18 reversed-phase HPLC from cross-linked α99−99α′ globin dimer (obtained from reversed-phase HPLC of globin chains), monitored at 200 nm..

eluted with PBS, pH 7.4 (~4 mg avidin on the column; avidin:biotinylated hemoglobin 2:1, M:M).The column was eluted until absorbance at 420 nm was minimal. The ratio of absorption from hemoglobin (all as conjugate) in the effluent to absorption of total hemoglobin conjugate that had been applied was used to calculate the amount retained on the column:

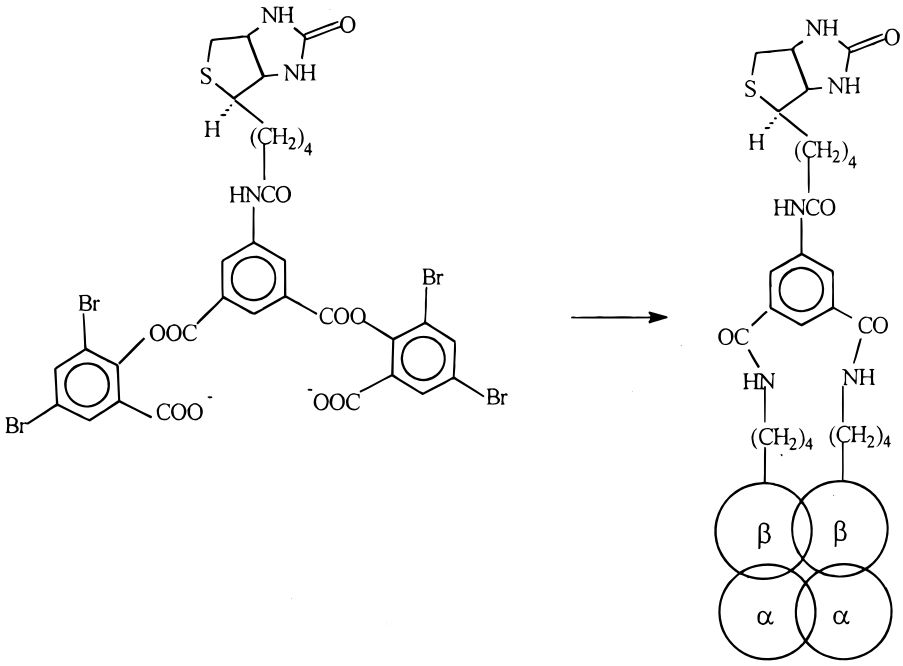
$$Hb_{total} - Hb_{effluent}/Hb_{total} = (A_{420applied} - A_{420effluent}/A_{420applied}) \times 100\%$$

These measurements indicate that only 17% of the modified hemoglobin adheres to the avidin column (which binds free biotin quantitatively) (*24*). It is likely that because of the relatively short tether, only part of the biotin species extends beyond the hemoglobin to which it is attached.

Reaction of hemoglobin with DBTIA. The materials, method, and analytical procedures are the same as for cross-linking hemoglobin with DBBA with a 2-fold molar excess of reagent to protein. The reaction was stopped after 3 h. C-4 HPLC analysis of the reaction mixture indicated formation of a reaction mixture in which the β-globin chains are all reacted while the α chains are mostly unreacted (Figure 7).

The material in each peak was identified by comparing the chromatogram with that for native protein combined

Scheme 4



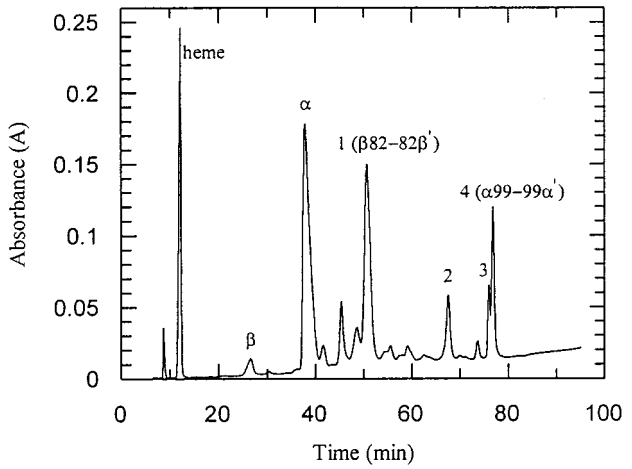


Figure 7. C-4 reversed phase HPLC chromatogram of separated subunits from the reaction of deoxyhemoglobin with DBTIA (pH 9, 37 °C, 3 h).

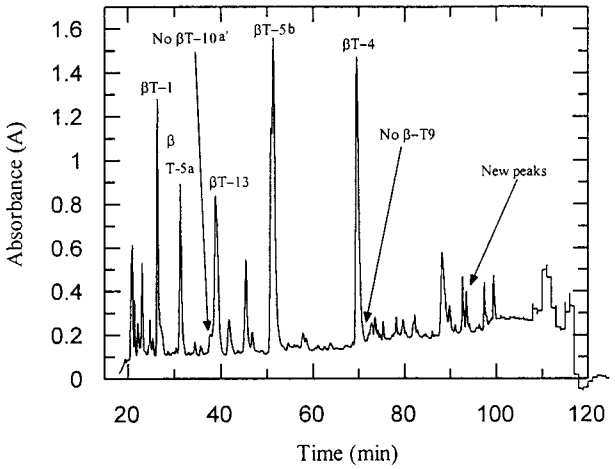


Figure 8. Tryptic-Glu-C peptide map of DBTIA-cross-linked β-chains (peak 1 in Figure 7).

with MS (ESI) analysis. The peaks designated "α" and "β" in Figure 7 are those of native globin chains. Peak 1 corresponds to a $\beta-\beta'$ dimer cross-linked by the isoleucylglycyl-5-aminoisophthalate (calculated, 32 133; found, 32 138). The molecular weight for the species in peak 2 is in the range expected for a $\beta-\beta$ cross-linked dimer that has a second molecule of cross-linker attached as a monoamine to the protein, with the second ester intact. This dimer is cross-linked between the same residues as 1, based on the peptide pattern analysis. The experimental mass for peak 3 is consistent with that of the α globin chain to with the reagent as a monoamide with the remaining ester intact (calculated, 15 832; found, 15 839). Peak 4 corresponds to an α−α cross-linked dimer (calculated, 30 661; found, 30 665). The reaction mixture was also analyzed by anion-exchange chromatography, which separates hemoglobin tetramers and modified tetramers, giving results consistent with the HPLC analysis.

To determine the site of modification of the protein chain, the cross-linked dimers (peaks 1, 2, and 4 in Figure 7) were collected and digested with trypsin followed by endoproteinase Glu-C. The peptide maps of native α and β chains obtained by C-18 reversed-phase HPLC were compared to those for the modified chains in order to identify the site of modification.

In the C-18 reversed-phase HPLC of peaks 1 and 2, the peptide fragments βT-9 and βT-10a′ are not present and new peaks elute at approximately 85−100 min (Figures 8 and 9). These two peptide fragments result from cleavage adjacent to Lys-82. In both chromatograms, the fragment β T-1 is unmodified. These results suggest that only the ϵ-amino groups of the β-Lys-82 residues have been blocked, the β-Val-1 residue [the amino group that is also modified by other reagents (*25*)] remaining unmodified. This is consistent with the formation of a bis-amide cross-link between the ϵ-amino group of the Lys-82 residue of one β chain and the ϵ-amino group of the Lys-82 residue of the other β chain. The peptide pattern for peak 4 in the C-4 chromatogram (Figure 7) is missing the αT-11 and the αT-12 peaks (Figure 10). These results, combined with the mass spectral data, suggest that a bis-amide cross-link between the ϵ-amino groups of two α-Lys-99 (the C-terminus of αT-11) has formed selectively.

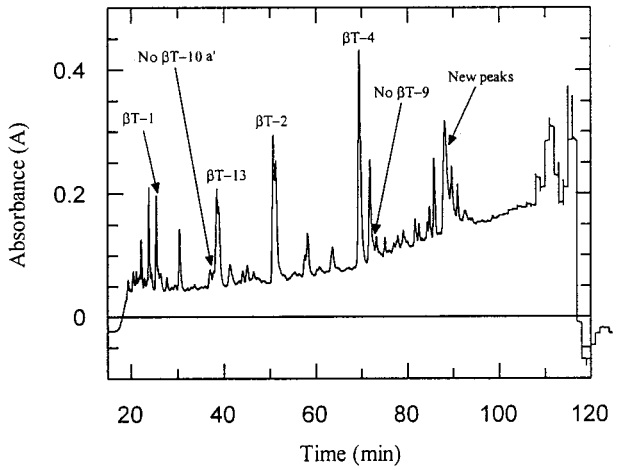


Figure 9. Tryptic-Glu-C peptide map of DBTIA-cross-linked β chains (peak 2 in Figure 7).

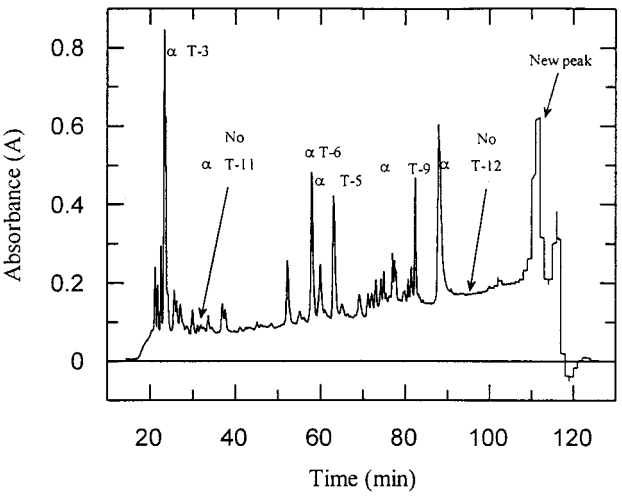


Figure 10. Tryptic-Glu-C peptide map of DBTIA-cross-linked α chains (peak 4 in Figure 7).

Table 1. Product Distributions (relative percentages ot total eluted) from Reaction of Deoxyhemoglobin with DBBA and with DBTIA (pH 9, 3 h: based on reversed phase HPLC analysis)

reagent	β82-X-82β'	α99-X-99α′	unreacted β	unreacted α
DBBA	21	10	7.4	23
DBTIA	14.3	4.9	0.7	13

On the basis of the structural analysis and quantitative measurement of products, we determined the yield of modified hemoglobin obtained in the reactions. The results are summarized in Table 1. The cross-linked hemoglobins are produced in sufficient yields to permit isolation of reasonable amounts of bioconjugates. The process is not efficient in terms of use of hemoglobin, but it does produce stable, modified species that are easily isolated. We made no attempt to optimize the process by varying reaction conditions.

The oxygen-binding properties of the biotinylated cross-linked hemoglobin [β82-(aminoisophthalylbiotintyl)-82β' (DBBA-Hb] were determined by a modification of the Imai method (*12*, *14*). The oxygen affinity (P_{50} = 5.0; pH 7.4, 25 °C, 0.1 M chloride and 50 mM bis-tris) is very close to that of native hemoglobin (P_{50} = 4.9) (*25*), and full cooperativity is maintained (n_{50} = 3.1). Previous work has established a linear correlation between the length of the cross-link span and the oxygen affinity of the hemoglobin conjugate (for common sites of modification) (*22*, *26*). The oxygen-binding properties of the DBBA-Hb conjugate fit this correlation for a span of ∼7 Å between the ϵ amino groups of the linked lysines (β82-X-82β'), the span of the isophthalyl cross-link. The cross-link is located on the 2-fold rotation axis of hemoglobin and does not introduce asymmetric distortion into the tetramer. Physical studies have shown that this cross-linking causes symmetrical perturbations in the structure of the protein (*27*), and related crystal structures show the retained symmetry (*28*). Thus, it is likely that the β82−82β' cross-link preserves the quaternary structure of the protein. The CD spectrum of the modified protein is essentially superimposable on that of the native protein, indicating that the modification does not alter the basic structure of the protein.

We have used sequential activation to produce the cross-linking reagents with pendant ligands. The ligand to be appended is activated to react with the amino group of 3-amino-isophthalic acid to form an amide. The two carboxylic acid groups are then activated as 3,5-dibromosalicylates to react with the protein. The reagents that we have produced, DBBA and DBTIA, have their reactive sites in the isophthalyl geometry that with other reagents produces a cross-link selectively between β-Lys-82 residues of hemoglobin. The data in Table 1 show that DBBA and DBTIA also give significant amounts of products with α-Lys-99-α′-Lys-99 connections as well as the expected β-Lys-82 products. Walder has shown that for reactions with fumaryl bis (3,5-dibromosalicylate), the α-Lys-99 amino groups are normally reactive if the β-Lys-82 sites are blocked (*29*). Thus, we propose that reaction at the α-Ly-99 probably occurs because a molecule of the reagent binds between the β subunits without reacting, directing a second reagent to the alternative site between the α subunits. A schematic representation of the primary cross-linking reaction leading to the product with biotin appended is shown in Scheme 4.

CONCLUSION

The procedures we have developed establish that molecular necklaces convert hemoglobin directly into cross-linked bioconjugates. Our method involves sequential activation, avoiding competition with hydrolysis in the final products. The method is general and should be applicable to generating a wide range of bioconjugates.

ACKNOWLEDGMENTS

We thank the Natural Sciences and Engineering Research Council of Canada for support. The program used to collect oxygenation data was written by Howard Feldman and revised by Bryan Keith.

LITERATURE CITED

(1) Guidotti, G. (1967) Studies on the chemistry of hemoglobin. II. The effect of salts on the dissociation of hemoglobin into subunits. *J. Biol. Chem. 242*, 3685−93.

(2) Winslow, R. M. (1995) *Hemoglobin-Based Red Cell Substitutes*, Johns Hopkins University Press, Baltimore.

(3) Keipert, P. E., Gomez, C. L., Gonzales, A., Macdonald, V. W., and Winslow, R. M. (1992) The role of the kidneys in the excretion of chemically modified hemoglobins. *Biomater., Artif. Cells, Immobilization Biotechnol. 20*, 737−45.

(4) Walder, J. A., Zaugg, R. H., Walder, R. Y., Steele, J. M., and Klotz, I. M. (1979) Diaspirins that cross-link beta chains of hemoglobin: bis(3,5-dibromosalicyl) succinate and bis(3,5-dibromosalicyl) fumarate. *Biochemistry 18*, 4265−70.

(5) Kluger, R. (1997) Chemical cross-linking and protein function. In *Protein Function a Practical Approach* (T. E. Creighton, Ed.) pp 185−214, IRL Press, Oxford.

(6) Arnone, A., Benesch, R. E., and Benesch, R. (1977) Structure of human deoxyhemoglobin specifically modified with pyridoxal compounds. *J. Mol. Biol. 115*, 627−642.
(7) Schumacher, M. A., Dixon, M. M., Kluger, R., Jones, R. T., and Brennan, R. G. (1995) Allosteric transition intermediates modelled by cross-linked haemoglobins. *Nature (London) 375*, 84−7.
(8) Kluger, R., Song, Y., Wodzinska, J., Head, C., Fujita, T. S., and Jones, R. T. (1992) Trimesoyl Tris(3,5-Dibromosalicylate): Specificity of reactions of a trifunctional acylating agent with hemoglobin. *J. Am. Chem. Soc. 114*, 9275−9.
(9) Kluger, R., and Song, Y. (1994) Changing a protein into a generalized acylating reagent. *J. Org. Chem. 59*, 733−6.
(10) Kluger, R., and Li, X. (1997) Efficient chemical introduction of a disulfide cross-link and conjugation site into human hemoglobin at beta-lysine-82 utilizing a bifunctional aminoacyl phosphate. *Bioconjugate Chem. 8*, 921−6.
(11) Trimble, S. P., Marquardt, D., and Anderson, D. C. (1997) Use of designed peptide linkers and recombinant hemoglobin mutants for drug delivery: in vitro release of an angiotensin II analogue and kinetic modeling of delivery. *Bioconjugate Chem. 8*, 416−23.
(12) Imai, K. (1981) Measurement of accurate oxygen equilibrium curves by an automatic oxygenation apparatus. *Methods Enzymol. 76*, 438−49.
(13) Imai, K. (1994) Adair fitting to oxygen equilibrium curves of hemoglobin. *Methods Enzymol. 232*, 559−76.
(14) Jones, R. T. (1994) Structural characterization of modified hemoglobins. *Methods Enzymol. 231*, 322−43.
(15) Shelton, J. B., Shelton, J. R., and Schroeder, W. A. (1984) High performance liquid chromatographic separation of globin chains on a large-pore C4 column. *J. Liq. Chromatogr. 7*, 1969−77.
(16) Laemmli, U. K. (1970) Cleavage of structural proteins during the assembly of the head of bacteriophage T-4. *Nature (London), 227*, 680−5.
(17) Kluger, R., Paal, K., and Adamson, J. G. (1999) An ether-linked tetrafunctional acylating reagent and its cross-linking reactions with hemoglobin. *Can. J. Chem. 77*, 271−80.
(18) Adamczyk, M., and Gebler, J. C. (1997) Electrospray mass spectrometry of alpha and beta chains of selected hemoglobins and their TNBA and TNB conjugates. *Bioconjugate Chem. 8*, 400−6.
(19) Bayer, E. A., Ben-Hur, H., and Wilchek, M. (1990) Isolation and properties of streptavidin. *Methods Enzymol. 184*, 80−9.
(20) Bayer, E. A., and Wilchek, M. (1990) Avidin- and streptavidin-containing probes. *Methods Enzymol. 184*, 174−87.
(21) Kluger, R., Jones, R. T., and Shih, D.-T. (1994) Cross-linking hemoglobin by design: lessons from using molecular clamps. *Artif. Cells, Blood Substitutes, Immobil. Biotechnol. 22*, 415−28.
(22) Kluger, R., Shen, L., Xiao, H., and Jones, R. T. (1996) Systematically cross-linked human hemoglobin: functional effects of 10 Å spans between beta subunits at lysine-82. *J. Am. Chem. Soc. 118*, 8782−6.
(23) Bayer, E. A., and Wilchek, M. (1990) Protein biotinylation. *Methods Enzymol. 184*, 138−60.
(24) Green, N. M. (1990) Avidin and streptavidin. *Methods Enzymol. 184*, 51−67.
(25) Dickerson, R. E., and Geis, I. (1983) *Hemoglobin: Structure, Function, Evolution, and Pathology*, The Benjamin/Cummings Publishing Co., Menlo Park, CA.
(26) Jones, R. T., Head, C. G., Fujita, T. S., Shih, D.-T., Wodzinska, J., and Kluger, R. (1993) Modification of human hemoglobin with methyl acyl phosphates derived from dicarboxylic acids. Systematic relationships between cross-linked structure and oxygen-binding properties. *Biochemistry 32*, 215−23.
(27) Shibayama, N., Imai, K., Hirata, H., Hiraiwa, H., Morimoto, H., and Saigo, S. (1991) Oxygen equilibrium properties of highly purified human adult hemoglobin cross-linked between 82β1 and 82β2 lysyl residues by bis(3,5-dibromosalicyl fumarate). *Biochemistry 30*, 8158−65.
(28) Schumacher, M. A., Zheleznova, E. E., Poundstone, K. S., Kluger, R., Jones, R. T., and Brennan, R. G. (1997) Allosteric intermediates indicate R2 is the liganded hemoglobin end state. *Proc. Natl. Acad. Sci. U.S.A. 94*, 7841−4.
(29) Snyder, S. R., Welty, E. V., Walder, R. Y., Williams, L. A., and Walder, J. A. (1987) HbXL99 alpha: a hemoglobin derivative that is cross-linked between the alpha subunits is useful as a blood substitute. *Proc. Natl. Acad. Sci. U.S.A. 84*, 7280−4.

BC990067F

New Class of Polymers for the Delivery of Macromolecular Therapeutics

Hector Gonzalez,† Sue Jean Hwang,† and M. E. Davis*

Division of Chemistry and Chemical Engineering, California Institute of Technology, Pasadena, California 91125. Received June 9, 1999; Revised Manuscript Received August 6, 1999

Cationic polymers show promise for the in vitro and in vivo delivery of macromolecular therapeutics. Known cationic polymers, e.g., poly(L)lysine (PLL) and polyethylenimine (PEI), have been employed in native and modified forms for the delivery of plasmid DNA (pDNA) and reveal varying levels of toxicity. Here, we report the preparation of a new class of cationic polymers that are specifically designed to deliver macromolecular therapeutics. Linear, cationic, β-cyclodextrin (β-CD)-containing polymers (CD-polymers) are synthesized by copolymerizing difunctionalized β-CD monomers (AA) with other difunctionalized comonomers (BB) such that an AABBAABB product is formed. The β-CD polymers are able to bind ~5 kbp pDNA above polymer to DNA (+/−) charge ratios of 1.5, compact the bound pDNA into particles of approximately 100−150 nm in size at charge ratios above 5+/−, and transfect cultured cells at charge ratios above 10+/−. In vitro transfections with the new β-CD-polymers are comparable to the best results obtained in our hands with PEI and Lipofectamine. Some cell line-dependent toxicities are observed for serum-free transfections; however, no toxicity is revealed at charge ratios as high as 70+/− in transfections conducted in 10% serum. Single IV and IP doses as high as 200 mg/kg in mice showed no mortalities.

INTRODUCTION

Methodologies currently under investigation for the in vivo delivery of macromolecular therapeutics, e.g., proteins, oligonucleotides, ribozymes, plasmid DNA, etc., include both viral and nonviral constructs. Viral transfection systems can produce efficient expression of transgenes within cells of interest. However, they have several disadvantages, e.g., adenoviruses have high immunogenicity, retroviruses produce random genomic integration, and both vectors have severely limiting capacities for the size of a foreign transgene. Additionally, scaled-up manufacture of replication-deficient viral constructs in the absence of recovered replication-competency is problematic (*1*). In contrast, nonviral transfection systems have low immunogenicity and the capacity to handle larger sizes of DNA than viruses and are amenable to large-scale manufacture. A recent review has appeared on nonviral gene delivery constructs (*2*). Despite the advantages of nonviral delivery systems, they reveal numerous problems such as substantially less gene expression than viral vectors and toxicity.

The goal of our work was to synthesize new nonviral vectors for the delivery of therapeutic macromolecules. Our approach was to construct a completely new family of materials specifically prepared for this application. We chose to work with polymeric materials and attempted to address the issue of toxicity. To this end, we synthesized a new class of cyclodextrin-containing polymers in the hope of creating a relatively nontoxic vector for the delivery of macromolecules since numerous cyclodextrins are known to have low toxicity (*3*).

* To whom correspondence should be addressed. Phone: (626) 395-4251. Fax: (626) 568-8743. E-mail: mdavis@cheme.caltech.edu.

† Equally contributing authors.

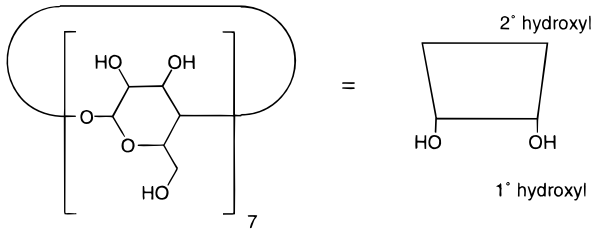


Figure 1. Schematic of β-cyclodextrin.

Cyclodextrins (CDs) are cup-shaped molecules formed by cyclic oligomers of glucose (see Figure 1). Cyclodextrins comprised of 6, 7, and 8 glucose units are called α-, β-, and γ-cyclodextrins, respectively. The three-dimensional structure of CDs is such that the cavity is relatively hydrophobic when compared to the exterior and thus can be used to imbibe hydrophobic compounds to form host−guest complexes. The ability of CDs to form inclusion complexes has been exploited in CD drug formulations throughout the world (including the U.S.; the first drug formulation to contain a CD, Sporanox, was approved by the FDA in 1997). Because of this, it is known that CDs have relatively low toxicity and lack immunogenicity (*3*). The question addressed here is whether these desirable features can be maintained in polymeric form in order to deliver macromolecules.

In this paper, the synthesis and characterization of a new family of β-CD-containing polymers is presented. Numerous polymers have been prepared (*4*), and here we provide several representative examples. It is shown that these polymers can bind and condense pDNA and transfect cells with a low level of toxicity.

MATERIALS AND METHODS

Monomers. 6A,6D-Dideoxy-6A,6D-diamino-β-cyclodextrin (**1**, Figure 2) and 6A,6D-dideoxy-6A,6D-di(2-

10.1021/bc990072j CCC: $18.00 © 1999 American Chemical Society
Published on Web 09/24/1999

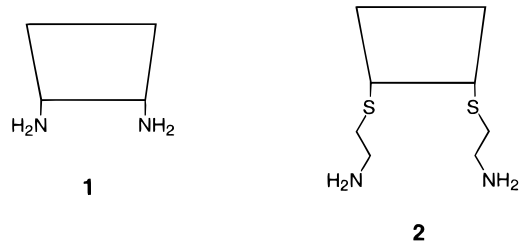


Figure 2. β-Cyclodextrin comonomers.

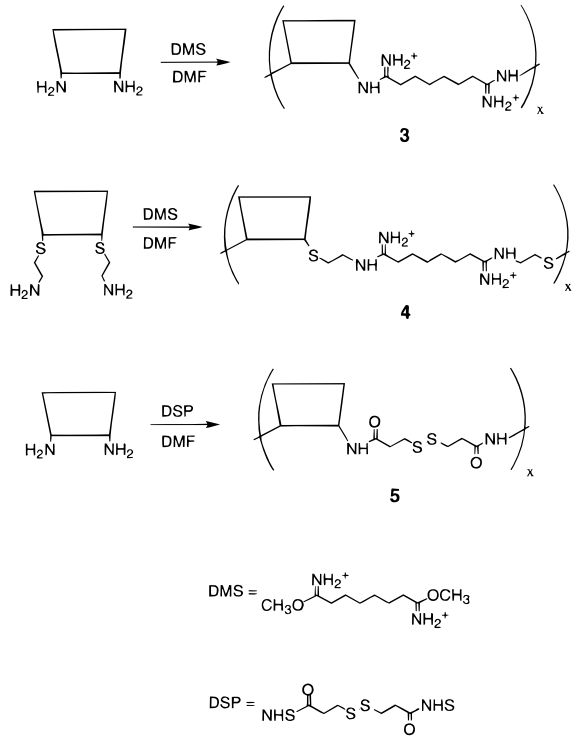


Figure 3. Schematic of β-cyclodextrin polymer (**3**−**5**) syntheses.

aminoethanethio)-β-cyclodextrin (**2**, Figure 2) were synthesized according to literature procedures (*4*) and had satisfactory NMR, mass spectral, and elemental analyses. All reagents were purchased from the Aldrich Chemical Co. (Milwaukee, WI) and used as received except for dimethylsuberimidate·2HCl (DMS) and dithiobis(succinimidyl propionate) (DSP), which were purchased from Pierce Chemical Co. (Rockford, IL), and used as received. The degree of hydration of the cyclodextrin samples was determined by measuring the weight loss on a TA Instruments TGA 951 thermogravimetric analyzer operating from 25 to 140 °C at a 5 °C/min heating rate.

Polymers Containing β-Cyclodextrin (3−5). β-CD copolymers **3**-**5** were prepared by the polymerization of a difunctionalized β-CD (AA) monomer with a difunctionalized comonomer (BB) to give an AABBAABB product (Figure 3). One procedure to form **4** is provided below. Additional synthetic methodologies can be found elsewhere (*4*). An 8 mL vial was charged with a solution of the bis(hydrogen carbonate) salt of 6A,6D-dideoxy-6A,-6D-di(2-aminoethanethio)-β-cyclodextrin hexahydrate (184.6 mg, 1.36×10^{-4} mol) dissolved in 0.5 M Na_2CO_3. DMS (37.0 mg, 1.36×10^{-4} mol) was added, and the solution was centrifuged briefly to dissolve the components. The resulting mixture was stirred at 25 °C for 15 h. The mixture was then diluted with ca. 10 mL of water and the pH brought to 4 with 10% HCl. This material was then dialyzed against a Spectra/Por 7 MWCO 3500 dialysis membrane (Spectrum, Houston, TX) in dH_2O for 24 h. The dialyzed solution was lyophilized to dryness yielding 51 mg (24%) of a white amorphous solid. Calcd for $C_{54}H_{94}N_4Cl_2O_{33}S_2 \cdot 7H_2O$: C, 40.83; H, 6.85; N, 3.53. Found: C, 40.77; H, 6.52; N, 3.46. ^{1}H NMR (500 MHz, D_2O) δ 1.39 (br, 4H), 1.69 (br, 4H), 2.49 (br, 4H), 2.92 (br, 4H), 3.16 (br, 4H), 3.5−4.0 (m, 42H), 5.05 (m, 7H). ^{13}C NMR (125 MHz, D_2O) δ 27.5, 28.6, 31.5, 33.8, 39.6, 42.6, 61.6, 73.2, 74.2, 82.7, 85.2, 103.2, 169.4. IR (KBr) 1652 (C═N).

Light Scattering and Molecular Weight Determination. The specific refractive index increment, d*n*/d*c*, was measured in 0.3 M NaCl using a Waters 2410 differential refractive index detector at a flow rate of 1.0 mL/min. The value of d*n*/d*c* for **4** in 0.3 M NaCl at λ = 930 nm and 25 °C was 0.155 mL/g. Polymer samples were then analyzed on a Hitachi D6000 HPLC system equipped with a ERC-7512 RI detector, a Precision Detectors PD2020/DLS light scattering detector and a Progel-TSK G2000 SWXL column using 0.3 M NaCl as eluant at a 0.7 mL/min flow rate. The weight average molecular weight, M_w, was determined to be 8800, with a polydispersity index, M_w/M_n of 1.10.

Cell Lines and Cell Culture. BHK-21 cells were purchased from ATCC (Rockville, MD) and maintained in Dulbecco's Modified Eagle Medium supplemented with 10% fetal bovine serum (FBS), 100 units/mL penicillin, 100 μg/mL streptomycin, and 0.25 μg/mL amphotericin. CHO-K1 cells were purchased from ATCC and maintained in Ham's F-12 medium with the above listed supplements. All cells were cultured at 37 °C in a 5% CO_2 humidified atmosphere and passaged every 4−5 days. Media and supplements were purchased from Gibco BRL (Gaithersberg, MD).

Plasmids. pGL3-Control Vector (pGL3-CV) plasmid, which contains the luciferase gene under the control of the SV40 promoter, was purchased from Promega (Madison, WI). Plasmids were amplified by *Escherichia coli* strain DH5α and purified using Qiagen's Endotoxin-free Megaprep Kit (Valencia, CA).

Preparation of DNA−Polymer Complexes and DNA Gel Retardation Assay. One microgram of pGL3-CV (0.1 μg/μL in distilled water) was mixed with an equal volume of polymer (10 μL in distilled water) at the appropriate charge ratios. After a 15−30 min incubation, the samples were pipetted with 1 μL of loading buffer into wells of a 0.6% agarose gel containing 6 μg of ethidium bromide/100 mL of TAE buffer (40 mM Tris-acetate, 1 mM EDTA) and electrophoresed.

Solid-Phase DNA Binding Assay. A 5′-amino-modified 50-mer oligonucleotide (5′-amino-AAA ACT GCT TAC CAG GGA TTT CAG TGC ATG TAC ACG TTC GTC ACA TCT CA-3′, "NMODSOL") and its complementary oligonucleotide ("COMPSOL") were synthesized by the Biopolymer Synthesis and Analysis Research Center at Caltech (Pasadena, CA). NMODSOL was covalently coupled to magnetic porous glass (MPG) supports according to manufacturer's instructions (Solid-Phase Oligo COUPLE-IT Kit, CPG. Inc, Lincoln Park, NJ). UV absorption analysis revealed successful coupling of 190 μg of oligo to 10 mg of MPG particles. The complementary oligo, COMPSOL, was then annealed to the coupled strand by heating a solution of COMPSOL in 45 mM NaCl with the MPG-coupled oligo in boiling water for 2 min and then allowing the solution to slowly cool to room temperature. UV analysis confirmed successful annealing of the complementary strand.

Primary amine-containing compounds to be analyzed for DNA-binding capability were added at a 1:5 (+/−) charge ratio in 1 mL of distilled water to the MPG-

supported DNA (dsDNA-MPG) and incubated with gentle rotation for 2 h. The particles were magnetically separated and the supernatant removed. Unbound molecules remaining in the supernatant were quantified by amine reaction with TNBS at pH 8.5 (*6*) and compared to amine quantification of the solution before exposure to dsDNA-MPG to determine extent of DNA binding.

Cell Transfections and Luciferase Assay. BHK-21 cells were plated at 60 000 cells/well in 24-well plates 24 h before transfection. Immediately prior to transfection, cells were rinsed once with PBS (pH 7.4) and 200 μL of Optimem (Gibco), for serum-free transfections, or complete media, for transfections in 10% serum, was added to each well. Polymer **4**−DNA complexes were prepared as described above. Lipofectamine (Gibco) and Superfect (Qiagen) complexes were prepared according to manufacturers' instructions. PEI (branched 25 kDa, Sigma) and polylysine (35 kDa, Sigma) complexes were prepared as described above, except in 150 mM NaCl at pH 7.0 instead of distilled water. Thirty minutes was allowed for complex formation before addition to cells. After 5 h, 800 μL of appropriate media with 10% FBS were added to cells. Twenty-four hours after transfection, the media in each well was replaced with 1 mL of culture media/well. After another 24 h, media was removed by aspiration, and cells were washed twice with PBS (pH 7.4) and lysed by one freeze−thaw cycle in 50 μL Cell Culture Lysis Buffer (Promega, Madison, WI). Cell lysates were analyzed for luciferase activity with Promega's luciferase assay reagent and for vector toxicity as described below. Light units were integrated over 10 s in duplicate with a luminometer (Monolight 2010, Analytical Luminescence Laboratory, San Diego, CA).

Toxicity. The amount of protein in cell lysates obtained 48 h after transfection was used as a measure of cell viability. Protein levels of transfected cells were determined by Bio-Rad's DC protein assay (Hercules, CA) and normalized with protein levels of cells transfected with naked DNA. A protein standard curve was run with various concentrations of bovine IgG (Biorad) in Cell Culture Lysis Buffer.

Physicochemical Characteristics of Polymer−DNA Composites. *Transmission Electron Microscopy.* Polymer−DNA complexes were prepared at different charge ratios as described above for the gel retardation assay. After 1 h of incubation, five microliters of sample was applied in duplicate to 400-mesh carbon-coated copper grids for 45 s, after which excess liquid was removed by blotting with filter paper. The 400-mesh carbon-coated copper grids were glow-discharged immediately prior to sample loading. One set of samples was then rotary shadowed at a 6° angle with a 3 cm tungsten wire while the duplicate set was negatively stained with 2% uranyl acetate for 45 s before blotting. Images were recorded using a Philips 201 electron microscope operated at 80 kV.

Dynamic Light Scattering (DLS) and ζ-Potential. For determination of particle size and charge, 2 μg of pGL-CV3 (0.1 μg/μL in dH_2O) was mixed with an equal volume of polymer (20 μL in dH_2O) and allowed to stand for 30 min before diluting with H_2O to a final volume of 1.3 mL for measurements. Particle size and ζ-potential of the complexes were measured using a ZetaPals dynamic light scattering detector (Brookhaven Instruments Corporation, Holtsville, NY). Three measurements were taken for each sample and data reported as average size and ζ-potential.

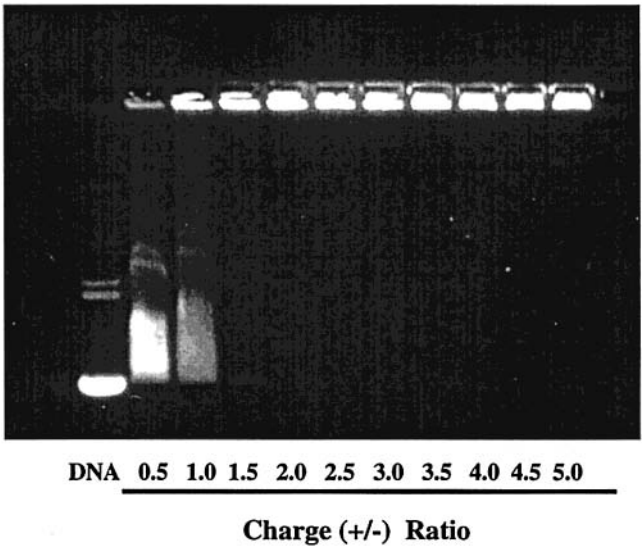


Figure 4. Determination of β-CD polymer **4**−DNA charge ratio necessary for complex formation by DNA retardation. DNA is visualized by ethidium bromide.

RESULTS

Binding of Functionalized CD Monomers 1 and 2 to DNA. DNA is not retarded in the electrophoresis assay by contact with the functionalized CD monomers **1** and **2** (data not shown), and this is most likely due to weak binding interactions that are disrupted by the presence of salts. Therefore, a solid-phase DNA-binding assay conducted in deionized water was developed as described in Materials and Methods. Using this assay, the CD-monomer **1** does not bind to DNA (0% binding), possibly due to the steric hindrance of the bulky cyclodextrin cups that are in very close proximity to the positive charge center. To test this hypothesis, **2** was prepared to specifically remove the amine further from the CD. CD-monomer **2** readily binds to DNA, with 88% binding. This binding compares favorably to other short polycations, such as spermine (19% binding).

DNA Binding of CD-Polymer. Although CD monomer **2** is not able to bind to DNA in the presence of salt, polymer **4** is able to completely bind DNA above polymer to DNA charge ratios of 1.5, as shown by DNA gel retardation (Figure 4). Binding is observed for complex formation in dH_2O, 150 mM NaCl, and complete media (data not shown). Polymer **3** does not bind to DNA even at polymer to DNA charge ratios as high as 50 (data not shown) and is likely due to the same reasons as mentioned previously with compound **1**.

In Vitro Transfection and Toxicity of DNA Complexes. One microgram of pGL3-CV, encoding for the luciferase gene under the control of the SV40 promoter, was complexed with **4** at various charge ratios in 10% serum and serum-free conditions and added to BHK−21 and CHO-K1 cells plated in 24-well plates. Transfection efficiencies of these complexes were determined by assaying for luciferase protein activity and reported in relative light units (RLU) per milligram of total cell protein. Luciferase protein activity in BHK-21 cells transfected in serum-free conditions reached a stable maximum at 30+/− with $\sim 1 \times 10^9$ RLU/mg of protein. The presence of 10% serum in the transfection media decreased luciferase activity at all charge ratios (Figure 5a). With CHO-K1 cells, increasing charge ratio also enhanced the transfection for all conditions tested. Ad-

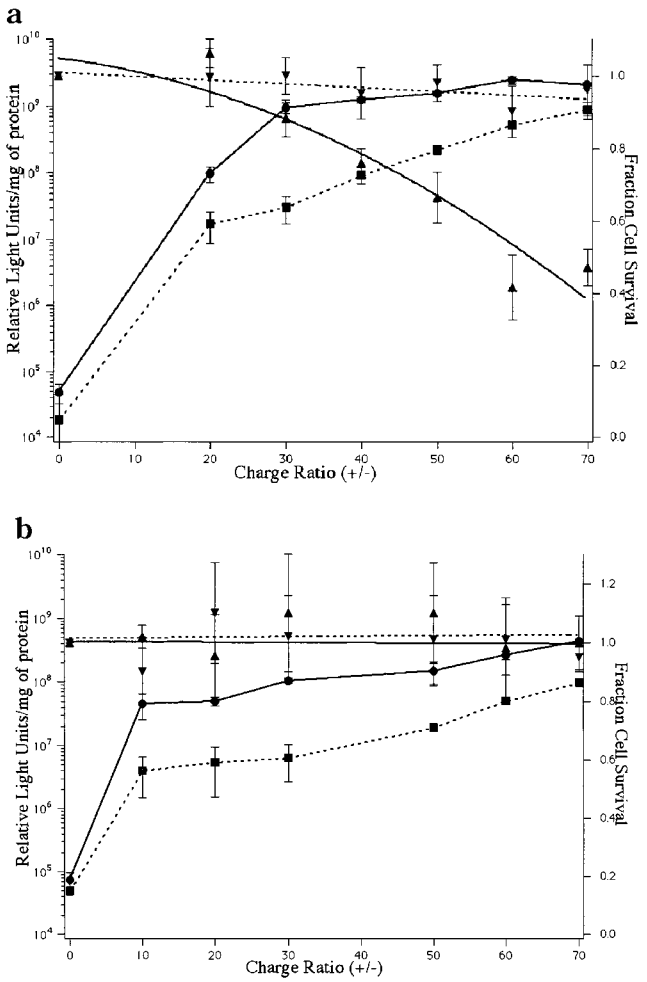


Figure 5. The effect of β-CD polymer **4** to DNA charge ratio and serum conditions on transfection efficiency (● and ■) and cell survival (▼ and ▲) in BHK-21 (a) and CHO-K1 (b) cells. Results from transfections in 10% serum and serum-free media are shown with the dotted and solid lines, respectively. Data are reported as the mean ± SD of three samples. Toxicity data are presented as best fit lines.

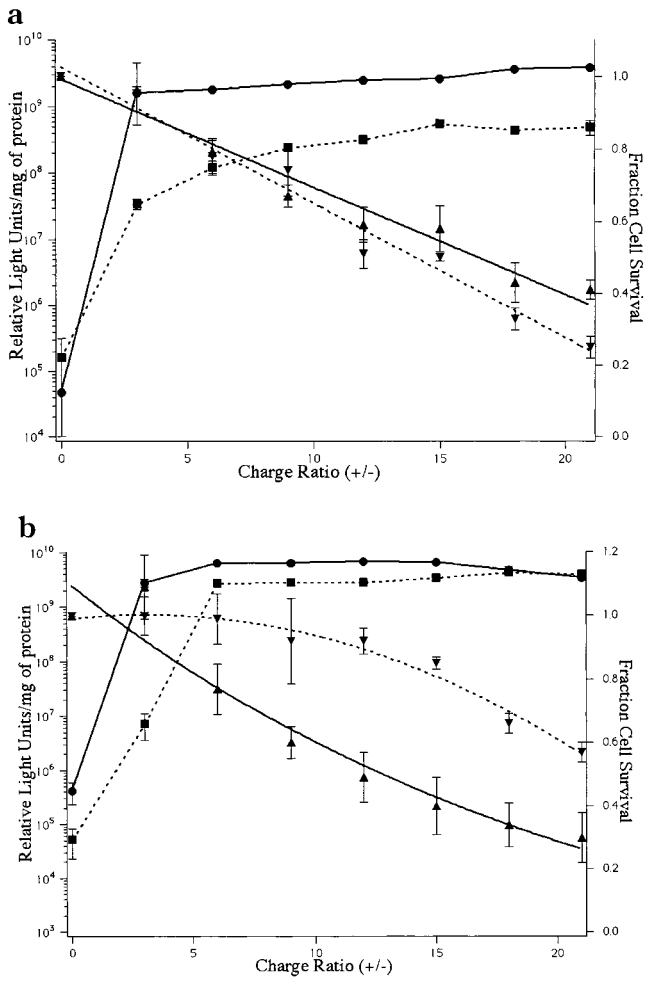


Figure 6. The effect of PEI to DNA charge ratio and serum conditions on transfection efficiency (● and ■) and cell survival (▼ and ▲) in BHK-21 (a) and CHO-K1 (b) cells. Results from transfections in 10% serum and serum-free media are shown with the dotted and solid lines, respectively. Data are reported as the mean ± SD of three samples. Toxicity data are presented as best fit lines.

ditionally, transfection in serum decreased light units by an order of magnitude (Figure 5b). The toxicity of the β-CD polymer to cells was measured by determining total cellular protein in the wells 48 h after transfection. Polymer **4** showed toxicity only to BHK-21 cells for transfections in the absence of serum. Toxicity was minimized with the presence of 10% serum during transfection (Figure 5a). No noticeable toxicity was observed from transfections to CHO-K1 cells (Figure 5b).

pGL3-CV was complexed with various commercially available transfection agents and exposed to BHK-21 and CHO-K1 cells under the same protocol as used with **4** for comparison. The transfection and toxicity results for PEI (branched 25 kDa) are shown in Figure 6. Maximum transfection was obtained at a charge ratio of 3+/− for BHK-21 cells and 6+/− for CHO-K1 cells. The presence of 10% serum decreased transfection efficiencies in both cell lines, although more dramatically for BHK-21 cells. Concentration-dependent toxicity was observed for both cell lines regardless of serum conditions.

pGL3-CV transfected with **4** gave RLUs that are 2 orders of magnitude higher than transfection with Superfect and on the same order of magnitude as transfection with PEI and Lipofectamine (Figure 7a). The toxicity of the vectors at conditions for maximum transfection are shown in Figure 7b. While transfection with some of the vectors resulted in less than 60% cell survival in one or both of the cell lines tested, transfection with **4** showed low toxicity.

Particle Characterization. Previously, it has been reported that negative staining with uranyl acetate may affect DNA condensation (*7*, *8*). Here, samples for electron microscopy were prepared by both rotary shadowing and negative staining. Electron microscopy of rotary-shadowed **4**−DNA samples showed discrete particles around 100−150 nm in diameter; however, these samples did not appear focused due to low electron density. Negatively stained samples revealed uniform structures at charge ratios of 5+/− and above (Figure 8), as observed by Tang et al. (*7*), that were not present in samples without polymer addition.

Particle size was also confirmed by dynamic light scattering and surface charge of the particles was determined by ζ-potential measurements (Figure 9a). Particle charge increased with increasing polymer addition, reaching neutrality between polymer to DNA charge ratios of 1 and 2. ζ-Potential of the particles approached +32 mV as charge ratios increased. Polymer **4** begins to condense DNA at a charge ratio of 1+/−, although the particles have a net negative charge. When the charge ratio is

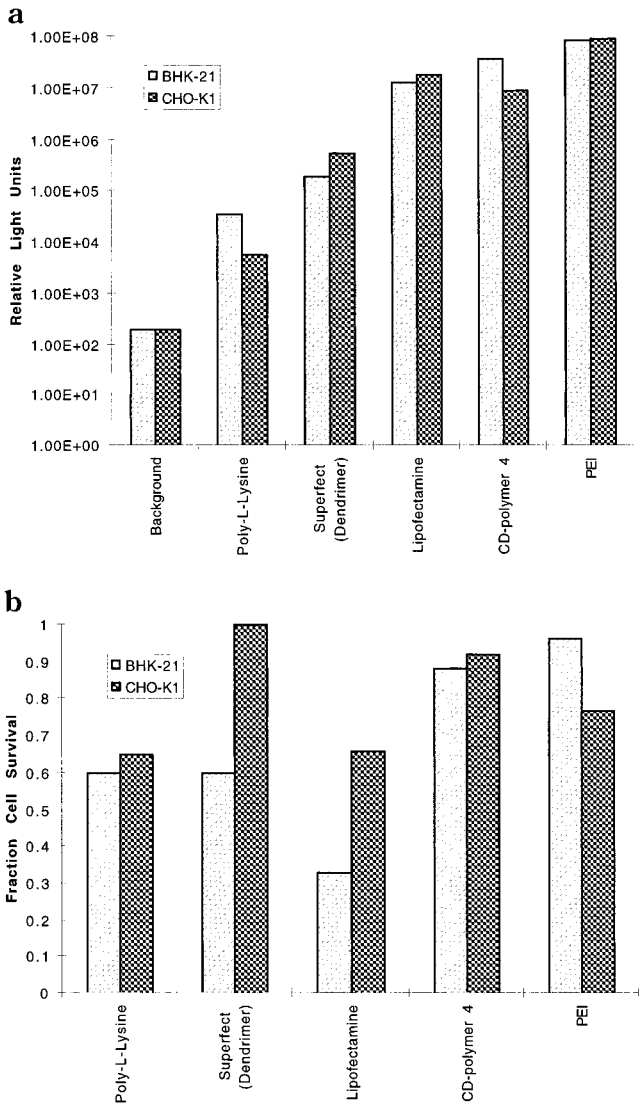


Figure 7. (a) Comparison of transfection efficiency of various nonviral vectors with BHK-21 cells. Cells were transfected with a range of vector/DNA charge ratios and starting cell densities for all vectors in serum-free media. The value reported here is obtained from the optimum transfection conditions found for each vector. (b) Comparison of the toxicities of various nonviral vectors to BHK-21 and CHO-K1 cells. Percent survival was determined by a modified Lowry protein assay at serum-free conditions giving the maximum transfection for each nonviral vector.

increased to 2+/−, the particles are near neutrality (ζ-potential = +5.8 mV) and particle aggregation occurs. The **4**−DNA particle diameter remains relatively constant at 150−180 nm above charge ratios of 10+/−. The particle size measured by DLS is slightly higher than that observed by TEM because the DLS measures the hydrodynamic diameter. Particles formed in water remained stable for several hours. Addition of 150 mM salt to the particles results in extensive aggregation that begins almost immediately. These results are consistent with those observed for peptide−DNA complexes (*9*).

A similar ζ-potential and particle diameter profile is observed for PEI−DNA complexes (Figure 9b). PEI begins to condense DNA at 1+/−. Neutral particles are formed around a charge ratio of 1.5+/− (+1.5 mV) as demonstrated by the aggregation of particles at this charge ratio. PEI also forms particles with pDNA of ca. 150 nm in diameter above charge ratios of 3+/−. The ζ-potential of the particles increases with charge ratio, reaching +40 mV at 21+/−.

DISCUSSION

The polyamidine-CD copolymer **4** prepared here is obtained with an overall yield of 24%. This yield is comparable to other synthetic, sugar-containing cationic polymers that are prepared via an AABB-type polymerization (*10*). The molecular weight, as determined by light scattering, was ca. 8800. This molecular weight corresponds to a degree of polymerization of 6, and an end-group analysis by ^{13}C NMR spectroscopy is consistent with this degree of polymerization. Polymers with pendent cyclodextrins of equivalent molecular weight have been prepared (*11*), but those reported here are the first to have the cyclodextrin as a part of the polymer backbone. Polymer **4** is found to be highly water soluble; solutions of at least 0.4 M concentration can be prepared. Thus, we were able to successfully incorporate a rather insoluble β-cyclodextrin moeity (1.6 mM) in a water-soluble polymer formulation.

The cationic nature of **4** allows for complexation to DNA. Plank et al. report that a minimum chain length of six to eight cationic amino acids is required to compact DNA into structures active in receptor-mediated gene delivery (*9*). Polymer **4** contains an average of 12 cationic charges and is able to condense plasmid DNA into discrete particles of 150 nm size in dH_2O. Although **4**−DNA particles aggregate under physiological salt conditions, there are methods of inhibiting particle aggregation by PEGylation (*12*) and we are currently exploring these and other techniques for preparing particle formulations that would be stable at physiological conditions.

The **4**−DNA complexes are also able to efficiently transfect cells in vitro. Transfection is observed for particles formed at and above +/− ratios of 10, which corresponds to an average ζ-potential of at least +24 mV. Increasing +/− ratios also increases transfection efficiency. Thus, particles are probably transfecting cells by proteoglycan-mediated entry (*13*). The presence of 10% serum during transfection decreases transfection efficiency in both BHK-21 and CHO-K1 cell lines.

Although positively charged **4**−DNA complexes of 150 nm diameter are formed by charge ratios of 5+/− (Figure 9a), transfection efficiencies continue to improve with increasing charge ratios despite little change in particle size and charge (Figure 5). It is possible that increasing the polymer to DNA ratio only serves to increase the concentration of free polymer in solution, which may in turn aid transfection by affecting the integrity of the cell membrane. To test this possibility, plasmid DNA was complexed with PEI under low charge ratio conditions which allow for complete DNA binding, but negligible transfection. Polymer **4** was then added to the transfection mixture at charge ratios up to 50+/−. Because PEI essentially binds irreversibly to pDNA, increases in transfection efficiency could be attributed to the effects of free **4** in the media. Instead, transfection efficiencies remained slightly above baseline at all concentrations of **4**. These results indicate that the increasing ratios of **4** to DNA aid transfection by affecting the properties of the **4**−DNA complexes. The nature of these phenomena are currently under investigation.

Initial trafficking studies with fluorescently labeled DNA (Gene Therapy Systems, San Diego, CA) show successful penetration of nearly 100% of cells; however, most of the complexes appear trapped in intracellular

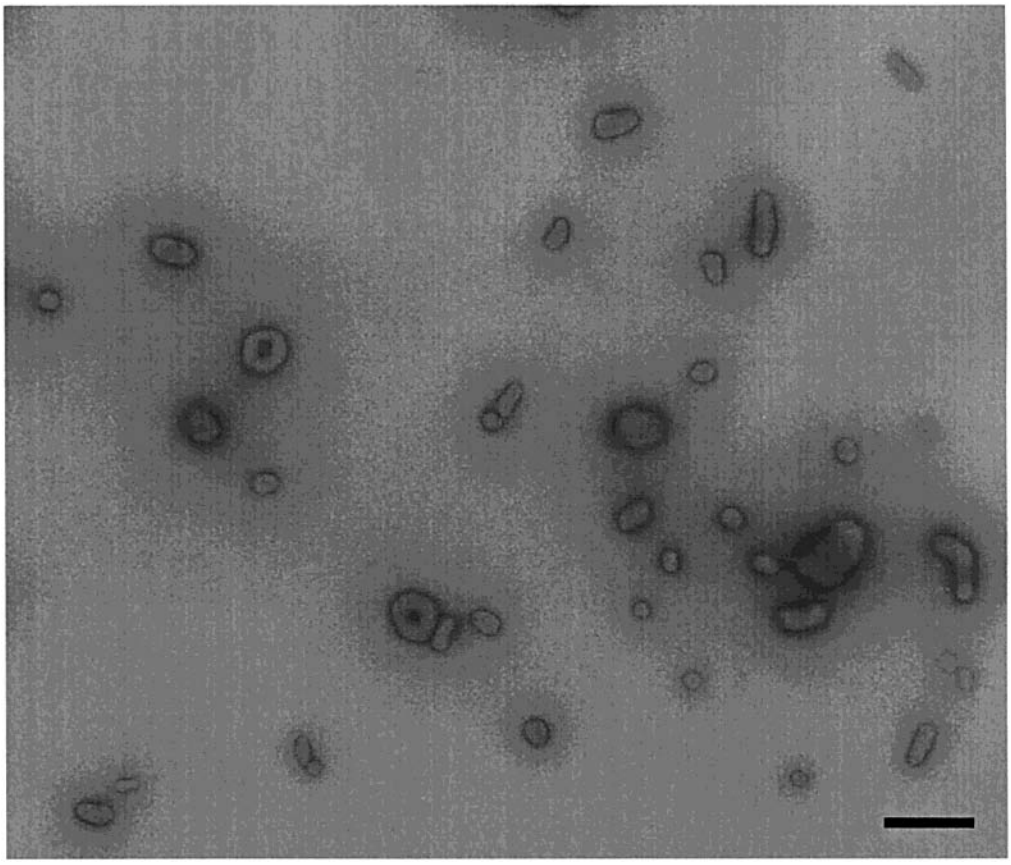


Figure 8. Electron micrographs of negatively stained complexes of polymer **4** complexed with DNA at 30+/− charge ratio in distilled water. Bar represents 200 nm.

vesicles, even 24 h after initial cell contact. The high percentage of cell transfection followed by subsequent vesicular entrapment has also been reported in lipid-based systems (*14*). Transfections at various charge ratios were, therefore, conducted in the presence of 25 μM chloroquine, an agent which delays lysosomal degradation of the pDNA by buffering the endosomal pH (*15*). The addition of chloroquine enhanced transfection efficiencies by over 2 orders of magnitude (an increase from 1×10^8 RLU/mg of protein to 7×10^{10} RLU/mg of protein at 20+/−). The transfection efficiency in the presence of chloroquine was also dependent on the polymer to DNA charge ratio; as seen before, increasing the polymer concentration also increases transfection efficiency. The transfection enhancement due to chloroquine addition confirms particle entry by endocytosis and the lack of efficient endosomal release. Nevertheless, the **4**−DNA complexes show transfection efficiencies comparable to vectors with endosome-escape mechanisms: PEI, that is speculated to act as a "proton sponge" to release complexes from endosomes by osmotic pressure (*16, 17*), and lipofectamine, which supposedly releases DNA by destabilizing endosomal membranes (*18*).

The cyclodextrin-based polymer **4** provides for efficient in vitro transfection of cells while remaining nontoxic under most conditions. Most cationic materials, such as lipid-based vectors and dendrimers have revealed some toxicity in in vitro studies (*17*). Polymer **4** showed toxicity to BHK-21 cells at increasing charge ratios in serum-free media (Figure 5a). However, no toxicity is observed with 10% serum for BHK-21 and CHO-K1 cell lines (Figure 5b), and in serum-free conditions for CHO-K1 cells, even up to charge ratios of 200+/− (data not shown).

Cytotoxicity of individual cyclodextrins is dependent upon type, e.g., α, β, and γ, and functionalization, e.g., native vs hydroxypropylated (*19*). Cyclodextrins can produce cell membrane solubilization by complexation with membrane components such as cholesterol (*19*). To test whether observed toxicity with **4** is from the polycationic nature of the polymer or from the cyclodextrin itself, BHK-21 and CHO-K1 cells were contacted with polymer **5** (no cationic charge), β-CD, and comonomer **2**. No toxicity was observed at β-CD monomer concentrations or monomer concentrations of **5** up to 700 μM, which is equivalent to the monomer concentration of **4** used for transfections at 200+/−. Finally, the cells were contacted with difunctionalized monomer DMS at concentrations up to 700 μM. Because DMS is a membrane permeable molecule, it is possible that the cell toxicity noted at high polymer concentrations is caused by the DMS end groups of the polymers. However, no cell toxicity was seen at the tested concentrations. These results indicate that the toxicity of **4** in BHK-21 cells is likely due to the polycationic nature of the polymer.

Preliminary in vivo toxicity studies have also been consistent with the in vitro findings. Single intravenous and intraperitoneal injections in mice of a cyclodextrin polymer similar to **4** at concentrations up to 200 mg/kg showed no mortalities. Macroscopic examinations at necropsy revealed no evidence of damage 5 days after polymer administration. For comparison, 22 kDa linear PEI has a LD_{50} of approximately 30 mg/kg in the presence of 5 mg/kg pDNA in mice (*20*) and a PEG-terminated copolymer of D-lysine/D-serine is lethal to mice within 30 min of i.v. administration at 200 mg/kg (*21*).

β-Cyclodextrin containing cationic polymers were synthesized in an effort to develop a delivery vehicle that would be nontoxic and would condense DNA to particles sufficiently small to enable efficient transfection. The polyamidine polymer **4** satisfies these criteria.

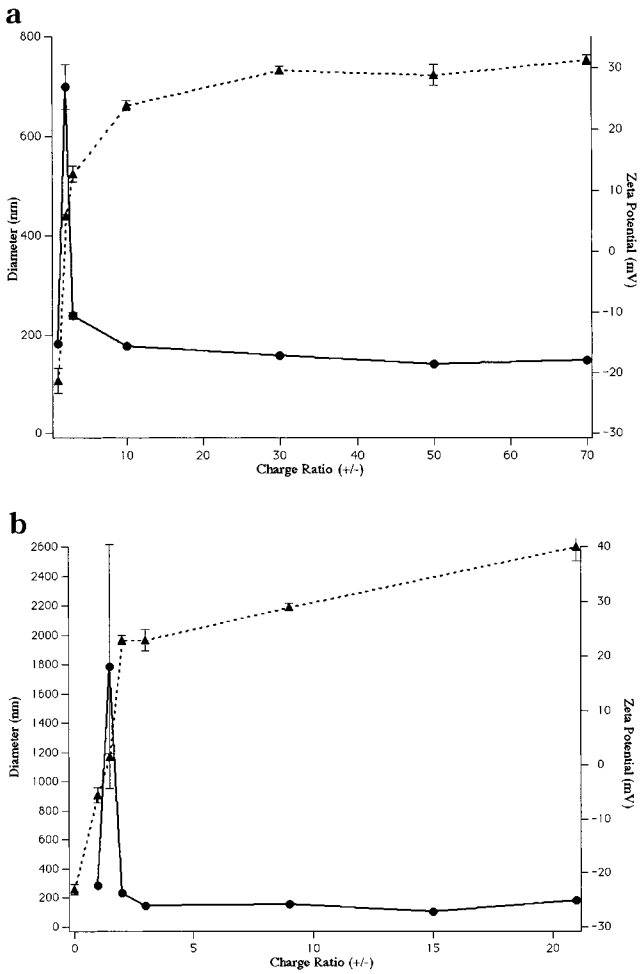


Figure 9. The effect of polymer **4** to DNA (a) and PEI to DNA (b) charge ratio on particle size (●), as determined by dynamic light scattering, and particle charge (▲), as estimated by ζ-potential measurements.

ACKNOWLEDGMENT

This work was partially supported by the Colvin Foundation and S.J.H. thanks the Whitaker Foundation for a doctoral fellowship. We also thank Pat Koen for his assistance with the transmission electron microscope.

LITERATURE CITED

(1) Zhu, J., Grace, M., Casale, J., Chang, A. T. I., Musco, M. L., Bordens, R., Greenberg, R., Schaefer, E., and Indelicato, S. R. (1999) Characterization of Replication-Competent Adenovirus Isolates from Large-Scale Production of a Recombinant Adenoviral Vector *Hum. Gene Ther. 10*, 113−121.

(2) Rolland, A. P. (1998) From Genes to Gene Medicines: Recent Advances in Nonviral Gene Delivery *Crit. Rev. Ther. Drug Carr. Sys. 15*, 143−198.

(3) Szejtli, J., and Osa, T., Eds. (1996) Cyclodextrins. *Comput. Supramol. Chem. 3*, Pergamon, U.K.

(4) Gonzalez, H., Hwang, S. J., and Davis, M. E. (1998) U.S. Patent Application.

(5) Tabushi, I., Shimokawa, K., and Fujita, K. (1977) Specific Bifunctionalization on Cyclodextrin *Tetrahedron Lett. 18*, 1527−1530.

(6) Hermanson, G. T. (1996) *Bioconjugate Techniques*, Academic Press, San Diego.

(7) Tang, M. X., and Szoka, F. C. (1997) The Influence of Polymer Structure on the Interactions of Cationic Polymers with DNA and Morphology of the Resulting Complexes. *Gene Ther. 4*, 823−832.

(8) Böttcher, C. Endisch, C., Fuhrhop, J.-H., Catterall, C., and Eaton, M. (1998) High-Yield Preparation of Oligomeric C-Type DNA Toroids and Their Characterization by Cryoelectron Microscopy. *J. Am. Chem. Soc. 120*, 12−17.

(9) Plank, C.. Tang, M. X., Wolfe, A. R., and Szoka, F. C. (1999) Branched Cationic Peptides for Gene Delivery: Role of Type and Number of Cationic Residues in Formation and in Vitro Activity of DNA Polyplexes. *Hum. Gene Ther. 10*, 319−322.

(10) Liu, X. C., and Dordick, J. S. (1999) Sugar-Containing Polyamines Prepared Using Galactose Oxidase Coupled with Chemical Reduction *J. Am. Chem. Soc. 121*, 466−467.

(11) Harada, A., Furue, M., Nozakura, S. (1976) Cyclodextrin-Containing Polymers. 1. Preparation of Polymers *Macromolecules 9*, 701−704.

(12) Ogris, M., Brunner, S., Schüller, S., Kircheis, R., and Wagner, E. (1999) PEGylated DNA/transferrin-PEI complexes: reduced interaction with blood components, extended circulation in blood and potential for systemic gene delivery. *Gene Ther. 6*, 595−605.

(13) Mislick, K. A., and Baldeschwieler, J. D. (1996) Evidence for the Role of Proteoglycans in Cation-Mediated Gene-Transfer. *Proc. Nat. Acad. Sci. 93*, 12349−12354.

(14) Tseng, W.-C., Haselton, F. R., and Giorgio, T. D. (1997) Transfection by Cationic Liposomes Using Simultaneous Single Cell Measurements of Plasmid Delivery and Transgene Expression. *J. Biol. Chem. 272*, 25641−25647.

(15) Stenseth, K., and Thyberg, J. (1989) Monensin and chloroquine inhibit transfer to lysosomes of endocytosed macromolecules in cultured mouse peritoneal macrophages. *Eur. J. Cell Bio. 49*, 326−333.

(16) Boussif, O. (1995) A Versatile Vector for Gene and Oligonucleotide Transfer into Cells in Culture and In-Vivo − Polyethylenimine. *Proc. Natl. Acad. Sci. 92*, 7297−7301.

(17) Demeneix, B. A., and Behr, J. P. (1996) The Proton Sponge: A Trick the Viruses Did Not Exploit. In *Artificial Self-assembling Systems for Gene Delivery* (P. Felgner, Ed.) pp 146−151, American Chemical Society, Washington D. C.

(18) Felgner, J. H., Kumar, R., Sridhar, C. N., Wheeler, C. J., Tsai, Y. J., Border, R., Ramsey, P., Martin, M., and Felgner, P. L. (1994) Enhanced Gene Delivery and Mechanism Studies with a Novel Series of Cationic Formulations. *J. Biol. Chem. 269*, 2550−2561.

(19) Irie, T., and Uekama, K. (1997) Pharmaceutical Applications of Cyclodextrins. III. Toxicological Issues and Safety Evaluation. *J. Pharm. Sci. 86*, 147−162.

(20) Goula, D., Benoist, C., Mantero, S., Merlo, G., Levi, G., and Demeneix, B. A. (1998) Polyethylenimine-based intravenous delivery of transgenes to mouse lungs. *Gene Ther. 5*, 1291−1295.

(21) Hisayasu, S., Miyauchi, M., Akiyama, K., Gotoh, T., Satoh, S., and Shimada, T. (1999) In vivo targeted gene transfer into liver cells mediated by a novel galactosyl-D-lysine/D-serine copolymer. *Gene Ther. 6*, 689−693.

BC990072J

Multicomponent DNA Carrier with a Vesicular Stomatitis Virus G-Peptide Greatly Enhances Liver-Targeted Gene Expression in Mice†

Martin J. Schuster, George Y. Wu, Cherie M. Walton, and Catherine H. Wu*

Department of Medicine, Division of Gastroenterology-Hepatology, University of Connecticut School of Medicine, Farmington, Connecticut 06030. Received June 9, 1999; Revised Manuscript Received September 10, 1999

Genes can be targeted to hepatocytes in vitro and in vivo by the use of asialoorosomucoid−polylysine conjugates. After systemic application, this nonviral vector is recognized by highly selective asialoglycoprotein (AsGP) receptors on the sinusoidal liver cell membrane and is taken up via receptor-mediated endocytosis. As most of the DNA is rapidly transferred to lysosomes where it is degraded, transfection efficiency is low and gene expression transient. To address this problem, we incorporated a pH-dependent synthetic hemolytic peptide derived of the G-protein of Vesicular Stomatitis Virus (VSV) into the gene transfer system, to increase endosomal escape of internalized DNA. The multicomponent carrier binds DNA in a nondamaging way, is still recognized by the AsGP receptor, and is targeted to the liver in vivo. Injection of DNA complexes containing a luciferase marker gene resulted in luciferase expression of 29 000 pg/g liver which corresponded to an increase of a factor of 10^3 overexpression after injection of DNA complexes without endosomolytic peptide. Furthermore, the amount of intact transgene within isolated liver cell nuclei was increased by a factor of 10^1−10^2 by the use of the multicomponent carriers. These results demonstrate that incorporation of a hemolytic peptide into a nonviral vector can greatly increase gene expression while retaining cell type targetability in vivo.

We have shown previously that DNA can be delivered specifically to the liver based on the presence of receptors on hepatocytes that recognize galactose-terminal (asialo)-glycoproteins (AsGP).[1] Binding of the soluble DNA−protein complex by the AsGP receptor results in internalization of the ligand into the endosomal compartment and ultimately degradation in lysosomes. In early studies, this strategy was used to deliver foreign genes to hepatocytes in vitro (*1*) as well as in vivo (*2*), resulting in short term, low level gene expression. Targeted transfer to hepatocytes by this technology was successfully applied to temporarily correct metabolic defects in animal models of human disease (*3*, *4*).

Subsequent experiments were performed to prolong the duration as well as to increase the efficiency of targeted gene expression. Partial hepatectomy immediately after intravenous injection of the complex resulted in extended persistence and expression of the transgene (*5*, *6*). The majority of the persisting DNA was shown to exist in cytoplasmic vesicles for many weeks (*7*, *8*). Disruption of the microtubule network, which is required for the translocation of endosomes to lysosomes (*9*) was shown to be responsible for this effect (*4*).

To circumvent the natural degradative process, in a noninvasive manner, we sought to imitate survival techniques of natural pathogens. We noted that vesicular stomatitis virus (VSV) has evolved a mechanism for survival that depends on release from endocytotic vesicles after cell entry. Membrane fusion is mediated by the VSV glycoprotein (G-protein) in a pH-dependent manner. After internalization within endosomes, the decrease in pH triggers a conformational change in the G-protein which results in insertion into the endosomal membrane and release of the virus from the endosome. It was demonstrated that G-protein-mediated fusion depends on an internal domain (*10*, *11*) as well as membrane anchoring (*12*) of the protein. A synthetic peptide corresponding to the amino-terminal 25 amino acids of VSV G-protein has been shown to be hemolytic at pH 5, but inactive at physiological pH, and thought to be the fusogenic domain (*13*, *14*). Although this peptide was later proven to be dispensable for G-protein membrane fusion (*15*), its properties appeared favorable for achieving release of endosomal contents following receptor mediated endocytosis.

In the following report, we demonstrate for the first time, that a hemolytic peptide corresponding to the amino-terminal 25 amino acids of the VSV G-protein (VSVG) increases the efficiency of receptor-mediated gene transfer in vivo. We found that this carrier was still highly liver selective and greatly enhanced receptor-mediated gene expression in vivo.

MATERIALS AND METHODS

Animals. Balb C female mice (∼20 g body weight) were obtained from Charles River Laboratory, Wilmington, MA, housed under controlled conditions of temperature and humidity, and fed normal chow ad libitum. All experimental procedures were performed in accordance with protocols approved by our Institutional Animal Care Committee.

† This work was presented, in part, at the annual American Association for the Study of Liver Diseases meeting in Chicago, IL, 7−11 November, 1997, and has been published in abstract form [*Hepatology* (1997) *26*, 129A].

* To whom correspondence should be addressed. Phone: (860) 679-3158. Fax: (860) 679-3159. E-mail: cwu@nso.uchc.edu.

[1] Abbreviations: AsGP, asialoglycoprotein; AsOR, asialoorosomucoid; OR, orosomucoid; VSV, vesicular stomatitis virus; VSVG, peptide derived from vesicular stomatitis virus G-protein; lysine-OMe, L-lysine-methyl ester; H and E, hematoxylin and eosin.

10.1021/bc990071r CCC: $18.00 © 1999 American Chemical Society
Published on Web 10/21/1999

Materials. A 878 bp *Bgl*II−*Hin*dIII fragment of pRc-CMV (Invitrogen, Carlsbad, CA) containing CMV immediate-early gene enhancer-promoter sequences was cloned into the *Bgl*II−*Hin*dIII sites of pGL3-Basic (Promega, Madison, WI) to create pGL3CMVluc. pEGFP-C1 was obtained from Clontech (Palo Alto, CA). Plasmid DNA was prepared as described previously (*16*). All chemicals used were of analytical grade (Sigma, St. Louis, MO), if not mentioned otherwise. DNA-modifying enzymes were obtained from Life Technologies (Gaithersburg, MD).

Preparation of DNA Carriers. Asialoorosomucoid (AsOR) was produced by acid hydrolysis (*17*) of orosomucoid isolated from pooled human serum (American Red Cross) (*18*) and covalently linked to L-lysine methyl ester (lysine-OMe) using 1-ethyl-3(3-dimethylaminopropyl) carbodiimide (EDC, Pierce, Rockford, IL) to incorporate positive charges for DNA binding. Ten milligrams of AsOR was dissolved in 1 mL of water and filtered through a 0.45 μm syringe-tip filter (Acrodisc, Gelman Sciences, Ann Arbor, MI). Fifty milligrams of lysine-OMe was dissolved in 1 mL of water and added to the AsOR, and the pH adjusted to 6.5 using NaOH at 0.1 N. To this mixture was added 4 mg of EDC, dissolved in 1 mL of water and incubated with stirring at 37 °C for 5 h, followed by dialysis of the reaction mixture through membranes with 12−14 kDa exclusion limits (Spectra/Por, Spectrum Medical Industries, Houston, TX) against 20 L of water at 4 °C for 24 h. The dialyzate was lyophilized and then redissolved in 0.15 M NaCl (10 mg/mL), filtered through a 0.45 μm syringe-tip filter, and applied on a Waters HPLC system using a Shodex KW-804 column (300 × 8 mm, Waters Corporation, Milford, MA). Samples of 250 μL were injected and eluted with 0.15 M NaCl at a flow rate of 0.12 mL/min. Samples 0.6 mL each were collected, and absorption was monitored at 280 nm. Samples of the two peaks in the effluent were analyzed by 12% SDS−PAGE. The second peak was used for further conjugation and corresponding samples were lyophilized.

Purified conjugates were hydrolyzed in constant boiling HCl and submitted for amino acid analysis to determine the ratios of components present. The total number of lysine residues minus the lysine residues expected from AsOR alone provided quantitation of the amount of lysine-OMe present. The number of aspartic acid residues was used to determine the amount of AsOR in each conjugate, and a lysine-OMe to AsOR molar ratio was calculated.

VSVG peptide (KFTIVFPHNQKGNWKNVPSNYHY-CP) was obtained from Immune Response Corporation (Carlsbad, CA) and shown to be hemolytic in a pH-dependent manner as described previously (*13*, *14*). The cysteine residue was used to couple peptides to AsOR-lysine-OMe with *N*-succinimidyl 3-(2-pyridyldithio) propionate (SPDP, Pierce). Five milligrams of purified AsOR-lysine-OMe was dissolved in 1 mL of PBS (pH 7.4), and 0.18 mL of freshly prepared SPDP (3.1 mg/mL in DMSO) was added to give a 30-fold molar excess of SPDP over AsOR-lysine-OMe. The mixture was incubated with stirring for 1 h at 25 °C. The reaction mixture was then dialyzed in membranes with 12−14 kDa exclusion limits against 20 L of water for 24 h at 4 °C and lyophilized. To remove any free SPDP, the conjugate was dissolved in water and applied to a Sephadex G25 column (Amersham Pharmacia Biotech, Piscataway, NJ), followed by elution with water. The eluate was checked for absorption at 280 nm and lyophilized. To determine the molar ratio of AsOR-lysine-OMe to SPDP, the absorption at 343 nm was measured with and without reduction using dithiothreitol (DTT) as described previously (*19*). To activate the sulfhydryl group, VSVG peptide was dissolved in PBS and incubated with a 10-fold molar excess of DTT for 60 min at 25 °C. Excess DTT was separated by HPLC using an Aquapore Cation Exchange CX-300 column (250 × 10 mm, Rainin Instrument) and elution with 0.3 M NaCl at a flow rate of 1 mL/min. VSVG was then conjugated to AsOR-lysine-OMe-SPDP. Two milligrams of AsOR-lysine-OMe-SPDP and 10 mg of activated VSVG peptide were each dissolved in 1 mL of water. VSVG was added in a 20-fold molar excess over AsOR to the conjugate. NaCl at 1.5 M was added to make a final concentration of 0.15 M, and the reaction mixture was passed through a 0.45 μm syringe-tip filter and incubated on a nutator at 25 °C for 18 h, followed by lyophilization. Five milligram samples were then dissolved in 0.5 mL of water, applied to a Sephadex G25 column, and eluted with water. The eluate was monitored for its absorbance at 280 nm, and the first peak was collected. The conjugates were analyzed on a 12% SDS−polyacrylamide gel with and without the addition of DTT as described previously (*19*). Amino acid analysis was performed to permit calculation of the molar ratio of VSVG to AsOR from tyrosine (present in AsOR and VSVG) and glutamic acid (present only in AsOR) content. AsOR-polylysine (26 kDa) was prepared as described (*2*), using poly-L-lysine, 26 kDa.

Formation of Protein Conjugate−DNA Complexes. Ethidium bromide exclusion was used to determine the DNA-binding capacity of protein conjugates. Sixty micrograms of pGL3CMVluc was dissolved in 2.5 mL of 0.15 M NaCl containing 2.5 μM ethidium bromide. Conjugates (0.6 mg/mL) were dissolved in 0.15 M NaCl and added in 50 μL increments to the DNA solution, while fluorescence was measured with excitation at 260 nm and emission at 591 nm on a fluorimeter. The minimum amount of protein conjugate resulting in maximum ethidium bromide exclusion was selected, and DNA complexation was confirmed by agarose gel retardation as described previously (*1*). DNA−protein conjugate complexes for injection were made starting with 40 μg/mL of DNA in 0.15 M NaCl. While continuously vortexing, 25 μL aliquots of protein conjugate were added over 30 min at 25 °C, followed by incubation for 30 min at 25 °C. Absorption was measured at 260, 340, and 400 nm to detect complexes. The purified products were filtered through a 0.22 μm syringe top filter (Gelman Sciences). Recovery of filtered complexes was measured by absorption at 260 nm and brought to a concentration of 10 μg with respect to DNA in 0.5 mL by adding sterile 0.15 M NaCl.

Dissociability and Stability of DNA−Protein Conjugate Complexes. To investigate dissociability, DNA was complexed with either AsOR-lysine-OMe, AsOR-lysine-OMe-VSVG, or AsOR-polylysine as described above and mixed with equal amounts of either 0.15 M NaCl, 8 M urea, or 0.15 M NaCl containing 200 units of heparin and incubated at 37 °C. Aliquots were withdrawn at 0, 10, and 30 min, respectively, transferred on ice, and analyzed on a 0.8% agarose gel containing 0.5 μg/mL EtBr. To determine if DNA complexed by protein conjugates were protected from degradation by serum nucleases, DNA complexes were incubated at 37 °C in the presence of 0.33 milliunits of DNase I (Boehringer Mannheim). Aliquots were withdrawn after 0, 2, 5, 10, and 30 min, respectively, and reactions stopped by adding Na_2EDTA up to 12.5 mM, followed by heat inactivation for 20 min at 75 °C. To release DNA from protein conjugates, 200 units of heparin (for AsOR-polylysine, AsOR-lysine-OMe) or an equal volume of 8 M urea (for

AsOR-lysine-OMe-VSVG) were added. Finally, all samples were analyzed on a 0.8% agarose gel containing 0.5 μg/mL EtBr. Following electrophoresis, DNA was visualized by UV transillumination (302 nm).

Organ Distribution of AsOR-Lysine-OMe-VSVG Conjugates. To determine whether the multicomponent carrier retained its ability to be recognized by hepatocyte AsGP receptors in vivo, conjugates were iodinated as described (*20*). Two micrograms of [^{125}I]AsOR-lysine-OMe-VSVG or AsOR-lysine-OMe-[^{125}I]VSVG with a specific activity of 10^6 cpm/μg, respectively, was injected intravenously into tail veins of mice. Animals were sacrificed after 10 min, and ^{125}I content of various organs was determined using a γ counter. Experiments were performed in triplicate, and results were expressed as means ± SEM. To determine whether the organ distribution of the radiolabeled carrier corresponded to luciferase expression found in the solid organs, liver, spleen, kidneys, and lungs were removed 24 h after injection, homogenized, and assayed for luciferase expression.

Assay for Targeted Gene Expression. Complexes containing 10 μg of pGL3CMVluc in 0.5 mL of 0.15 M NaCl were passed through 0.2 μm syringe-tip filters and immediately injected into the tail veins of mice over the course of 10−30 s. After 24 h and after 7 days, animals were sacrificed, and livers removed, washed with ice-cold PBS, and weighed. A liver section (~100 mg) was removed, weighed, and homogenized in lysis buffer (100 mg/mL, Luciferase Assay System, Promega), and liver luciferase activity determined by luminometry. A standard curve for luciferase using firefly luciferase (Analytical Luminescence Laboratory, Ann Arbor, MI) was performed along with the test samples. For each experiment, injections were performed under identical conditions in three animals in parallel, using free DNA, or DNA complexed by AsOR-lysine-OMe, AsOR-polylysine, or AsOR-lysine-OMe-VSVG, respectively. All experiments were performed at least in triplicate, and results were expressed as means ± SEM in units of picograms of luciferase per gram of liver tissue (1 pg corresponds to 200 000 LU/30 s). The remaining liver tissue was used for isolation of liver cell nuclei. Competition experiments were performed using AsOR or orosomucoid (OR) and mixed with the DNA−protein conjugates complexes in 100-fold molar excess immediately before injection.

To determine whether an adverse immune response could occur due to antigenicity of complexes, second injections of the identical complexes were performed 1 week after the first. Targeted gene expression was evaluated as described above for animals that received only single injections.

To determine the efficiency of liver cell transduction, immunohistochemical analysis for luciferase protein was performed 24 h after injection of DNA complexed with AsOR-lysine-OMe-VSVG. Animals were sacrificed, and livers were removed and frozen in Tissue Freezing Medium (Triangle Biomedical Medium, Durham, NC). Cryosections were fixed with 4% *p*-formaldehyde, incubated for 30 min with blocking solution (5% dry milk, 150 mM NaCl, 10 mM Tris Cl, pH 7.5, and 0.5% Tween 20), followed by incubation with anti-luciferase antibody (1:500, polyclonal, Cortex Biochemicals, San Leandro, CA) for 2 h, followed by washing and incubation with anti-rabbit-IgG Texas Red (1:5000, Amersham) for 30 min. Following treatment with antifade (Dabco, Sigma), samples were subjected to fluorescence laser scanning microscopy (Zeiss CLSM, Germany). For direct detection of green fluorescent protein (GFP) in liver sections from mice injected with pEGFP-C1 complexed with multicomponent carrier, cryosections were fixed with 4% *p*-formaldehyde, treated with antifade, and subjected to fluorescence laser scanning microscopy.

Assay for Acute Liver Toxicity. To investigate whether injection of DNA complexed by AsOR lysine-OMe-VSVG conjugates led to liver cell damage, blood samples were collected from the retroorbital plexus 24 h after injection, and serum was subjected to ALT analysis (kinetic ALT kit, Sigma). Liver sections were stained with H and E and examined by light microscopy to determine signs of liver cell necrosis or cellular infiltration.

Isolation of Nuclei and Extraction of Episomal DNA. Twenty four hours after injection of complexed DNA in the mice, livers were removed and homogenized in 4 mL of buffer (sucrose at 0.32 M, $CaCl_2$ at 3 mM, magnesium acetate at 2 mM, Na_2EDTA at 0.1 mM, Tris HCl, pH 8.0, at 10 mM, DTT at 1 mM, and NP40 at 0.5%) using a Dounce Tissue Grinder (Kontes) and applying five strokes with a loose, and then a tight-fitting pestle. The homogenate was loaded on a gradient consisting of four layers with 1.0, 1.4, 1.6, and 1.8 M sucrose, respectively, in buffer 2 (magnesium acetate at 5 mM, Na_2EDTA at 0.1 mM, Tris HCl, pH 8.0, at 10 mM, and DTT at 1 mM) and centrifuged for 40 min, 34000*g* at 4 °C (Beckmann SW28 rotor). The nuclei containing pellet was resuspended in 1 mL of buffer 1 (without NP40) and pelleted again by low-speed centrifugation (750*g*, 2 min). Finally, nuclei were resuspended in 1 mL of TE50/10 (Tris HCl, pH 7.5, at 50 mM and Na_2EDTA at 10 mM) and lysed with 1.5 mL of lysis buffer (SDS at 1% and NaOH at 0.2 N). To obtain episomal DNA, a modified Hirt extraction was performed by adding 1.25 mL of 3−5 M potassium acetate. After incubation for 15 min on ice, the precipitate was pelleted and the supernatant was extracted with phenol/chloroform. Following precipitation with ethanol, samples were resuspended in 100 μL of TE (Tris HCl, pH 7.5, at 10 mM and Na_2EDTA at 1 mM) and subjected to PCR analysis.

Semiquantitative PCR of Full-Length Luciferase Gene. A semiquantitative PCR assay was performed as described (*21*) to determine the amount of intact luciferase cDNA in isolated nuclei. Primers used were S1 (5′-3′) cat aaa gaa agg ccc ggc gcc att and AS1 caa aca caa ctc ctc cgc gca act, resulting in the amplification of a 1538 bp fragment, corresponding to nt 105−1642 of pGL3-Basic and comprising 93% of the luciferase coding sequence. As a competitive internal standard, a plasmid pLUC−*Kpn*I was constructed containing the 1538 bp luciferase PCR fragment cloned into pGEM-T vector (Promega) with an additional *Kpn*I restriction site at position 595 (with respect to the PCR product). The new *Kpn*I site was created by PCR site-directed mutagenesis, using S2 (5′-3′) ctg gat cta ctg ggg tac cta agg gtg tg and AS2 cac acc ctt agg tac ccc agt aga tcc ag as primers. After *Kpn*I digestion of PCR samples, PCR products generated from target sequences (1538 bp) or internal standard (596/942 bp), respectively, could be discriminated.

DNA amplification experiments were carried out with 2.5 units of Taq polymerase/reaction and 1.5 mM $MgCl_2$. A hot start protocol was used with annealing at 60 °C (45 s), elongation at 72 °C (3 min), and denaturation at 94 °C (45 s) for 35 cycles, followed by a final elongation at 72 °C for 10 min. For each sample of episomal DNA extracted from one animal, eight PCR reactions were performed in parallel, containing 5 μL of sample as template and an increasing amount (0−250 fg) of internal standard pLuc−*Kpn*I as competitive template. Fifteen microliters of each reaction was digested with *Kpn*I and loaded onto a 0.8% agarose gel containing 0.5 μg/mL EtBr

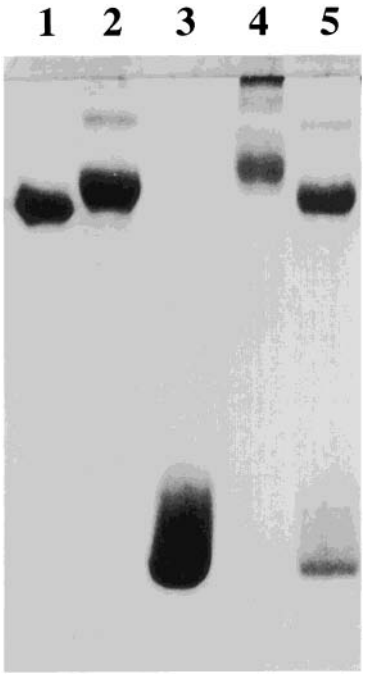


Figure 1. SDS−PAGE of AsOR-lysine-OMe-VSVG. Conjugates were analyzed with or without the addition of DTT to reduce disulfide bonds between peptides and AsOR-lysine-OMe. Lane 1, AsOR; lane 2, AsOR-lysine-OMe; lane 3, VSVG peptide (25 aa); lane 4, AsOR-lysine-OMe-VSVG; lane 5, AsOR-lysine-OMe-VSVG plus DTT.

and subjected to electrophoresis. DNA was visualized by UV transillumination (302 nm), and the intensity of bands was measured using IPLab Gel software. The PCR reaction with equal density of bands generated from internal standard and target sequences was used to calculate the relative increase of the amount of transgene in the isolated nuclei. Assays were performed in parallel for mice injected with either DNA alone or DNA complexed with AsOR-polylysine or AsOR-lysine-OMe-VSVG.

RESULTS

After covalently linking lysine-OMe to AsOR and purification by HPLC, the effluent fractions showed two peaks regarding absorbance at 280 nm. Analysis by SDS−PAGE demonstrated that the first peak contained aggregates and the second peak, which was used for further conjugation, was mostly monomeric conjugate. The molar ratio between linked lysine-OMe residues and AsOR was calculated to be 8:1 based on amino acid analysis of the purified material. AsOR-lysine-OMe migrated slightly slower on a 12% SDS−polyacrylamide gel compared to AsOR (Figure 1, lane 1 and 2). After conjugation of AsOR-lysine-OMe with SPDP and analysis of the product after reduction with DTT, the molar ratio of SPDP to AsOR-lysine-OMe was calculated to be 22−24:1. Conjugates of AsOR-lysine-OMe with VSVG were analyzed on a 12% SDS polyacrylamide gel and showed a single band that had no detectable free VSVG (Figure 1, lane 4). That the VSVG peptide was indeed linked by disulfide bonds was shown by reduction of the conjugates with DTT which resulted in the appearance of free peptide at the appropriate location (Figure 1, lane 5). On the basis of amino acid analysis, the ratio of AsOR:VSVG was calculated to be 1:8. The average minimum amount of conjugate resulting in maximum EtBr exclusion was approximately 1.6 μg/μg of DNA, with some variation between different batches. Binding of the DNA was confirmed by complete retardation on an agarose gel (Figure 2A), and complexes composed of this ratio were used in all subsequent experiments.

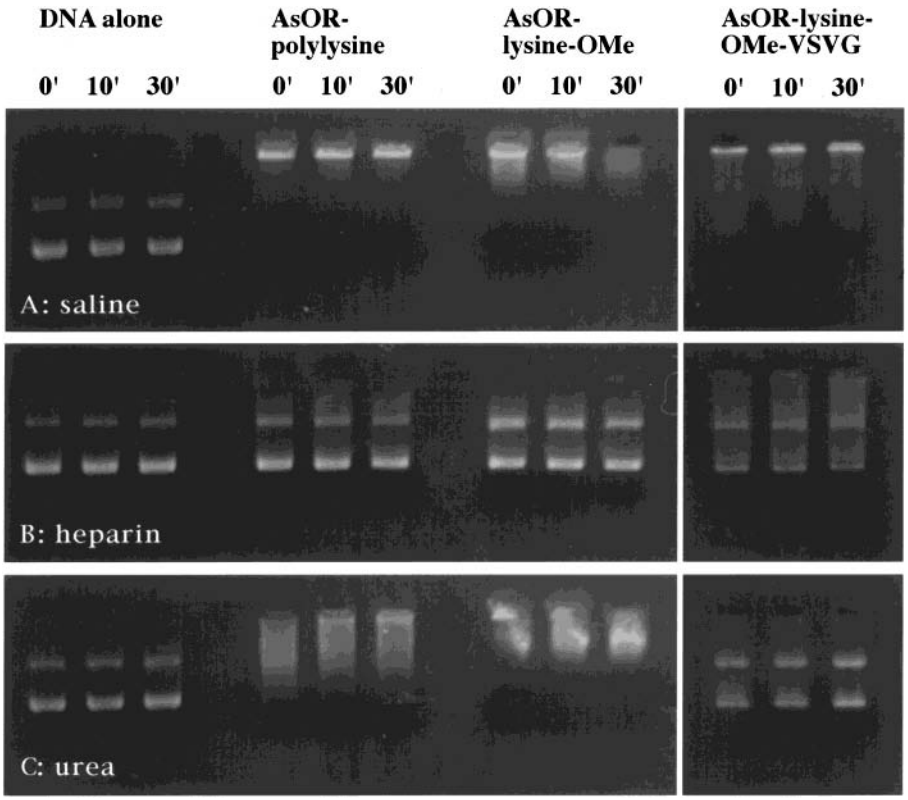


Figure 2. Agarose gel electrophoresis of DNA−protein conjugate complexes. Complexes were formed as described in the text containing 1 μg of DNA and incubated at 37 °C for the indicated time. (A) Incubation in saline; (B) Incubation with heparin; (C) Incubation with urea. Samples were analyzed on a 0.8% agarose gel containing 0.5 μg/mL EtBr and DNA was visualized by UV transillumination.

Table 1. Distribution of Radioactivity after Injection of ^{125}I-Labeled Protein Conjugates and Luciferase Expression in Different Organs[a]

organs	fraction of injected counts (%)			luciferase (pg/g tissue); pCMVluc AsOR-lysine-OMe-VSVG
	[^{125}I]AsOR (ref *2*)	[^{125}I]AsOR-lysine-OMe-VSVG	AsOR-lysine-OMe-[^{125}I]VSVG	
blood	8.5 ± 1.0	13.3 ± 4.1	12.3 ± 3.5	ND
liver	89 ± 3.5	78.6 ± 10.1	79 ± 8.0	15 351 ± 484
heart	0.1 ± 0.1	0.6 ± 0.4	0.7 ± 0.4	ND
spleen	0.5 ± 0.1	0.6 ± 0.3	2.7 ± 1.2	11.6 ± 6.2
lung	1.6 ± 0.1	5.1 ± 5.4	6.1 ± 4.4	9.7 ± 2.5
kidney	0.2 ± 0.1	1.9 ± 0.6	1.4 ± 0.9	11.3 ± 4.3

[a] Two micrograms of [^{125}I]AsOR, [^{125}I]AsOR-lysine-OMe-VSVG, or AsOR-lysine-OMe-[^{125}I]VSVG with a specific activity of 10^6 cpm/μg, respectively, was injected intravenously into mice. Animals were sacrificed after 10 min, and ^{125}I content of the organs was determined using a γ counter. Luciferase activity is shown in units of picograms per gram tissue 24 h after mice were injected with 10 μg of DNA complexed by AsOR-lysine-OMe-VSVG. Experiments were performed in triplicate, and results were expressed as means ± SEM (1 pg corresponds to 200 000 LU/30 s). ND, not done.

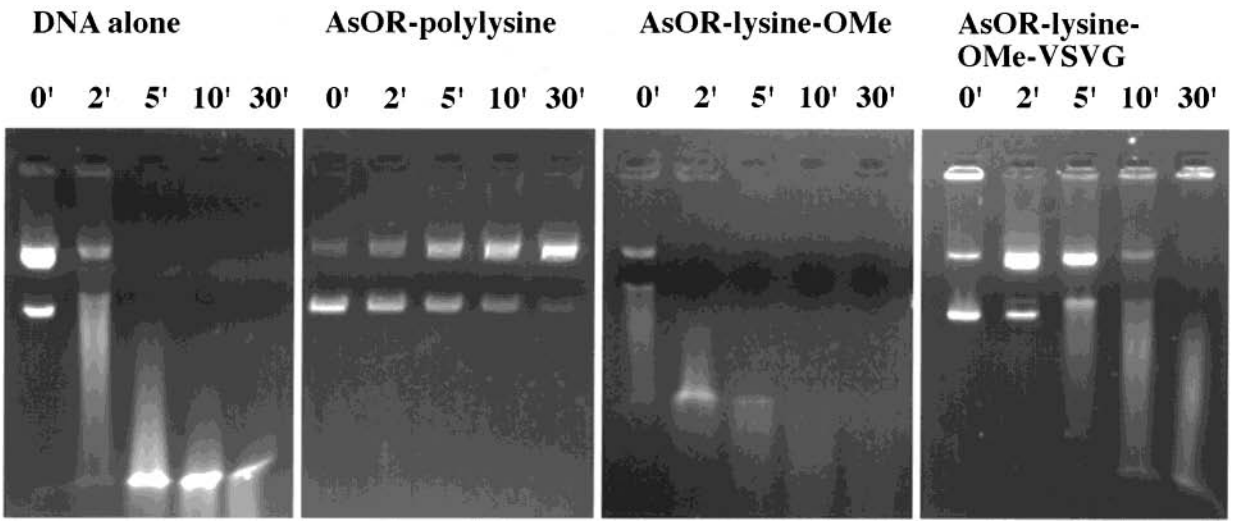


Figure 3. Protection of DNA complexed by protein conjugates against degradation. Complexes were formed as described in the text containing 1 μg of DNA and incubated at 37 °C in the presence of DNase I for the indicated time. After aliquots were withdrawn, reactions were stopped by adding Na_2EDTA up to 12.5 mM, followed by heat inactivation for 20 min at 75 °C. To release DNA from protein conjugates, 200 units of heparin (AsOR-polylysine, AsOR-lysine-OMe) or an equal volume of 8 M urea (AsOR-lysine-OMe-VSVG) was added. Samples were analyzed on a 0.8% agarose gel containing 0.5 μg/mL EtBr and DNA was visualized by UV transillumination.

The organ distribution of radioactivity after intravenous injection of iodinated AsOR-lysine-OMe-VSVG into mice showed a slight difference compared to the organ distribution of iodinated AsOR alone (*2*). When either AsOR or VSVG peptide was labeled with ^{125}I, about 80% of recovered radioactivity was found in the liver, while about 12−13% was still in the circulation (Table 1). An average of 96 ± 2% of total radioactivity injected was recovered. In accordance with the distribution of radioactivity, no substantial luciferase activity was detected in solid organs other than the liver (Table 1).

Dissociability of DNA from protein conjugates showed a notable difference between AsOR-polylysine, AsOR-lysine-OMe, and AsOR-lysine-OMe-VSVG conjugates. When incubated in the presence of heparin, DNA was dissociated from AsOR-polylysine conjugates completely, while DNA was only slightly released from AsOR-lysine-OMe-VSVG conjugates (Figure 2B). When incubated in the presence of 4 M urea, DNA was dissociated completely from the latter conjugate, but not from AsOR-lysine-OMe or AsOR-polylysine (Figure 2C). These differences suggest that interactions in addition to electrostatic ones between DNA and protein conjugates are likely involved with AsOR-lysine-OMe-VSVG conjugates. Figure 2 shows that DNA−protein conjugate complexes were stable when incubated at 37 °C in normal saline over 30 min, and DNA was completely retarded after agarose gel electrophoresis (Figure 2A). Incubation of AsOR-lysine-OMe-VSVG complexes in the presence of DNase I showed greater protection of DNA against degradation over 5 min, compared to DNA alone which was already completely degraded in the same incubation period (Figure 3). AsOR-polylysine provided greater protection to complexed DNA over 30 min, compared to AsOR-lysine-OMe (lacking VSVG peptide), which had no obvious protective effect (Figure 3).

Liver luciferase activity determined by luminometry performed 24 h after injection of pGL3CMVluc in the form of complexes is shown in Table 2. Luciferase activity after injection of DNA complexed with multicomponent protein conjugates was, on average, 3 orders of magnitude higher than luciferase activity after injection of AsOR-polylysine-DNA complexes containing the same amount of DNA, and more than 4 orders of magnitude increased over gene expression after injection of free DNA. Expression from multicomponent complexes was 99% blocked by competition with a 100-fold molar excess of AsOR, but essentially unaffected by coadministration of a 100-fold molar excess of OR, which has an identical amino acid sequence, but lacks exposed terminal galactose residues and, therefore, is not a ligand for the AsGP receptor (Table 2). The duration of gene expression was short, with only 1.0 ± 0.9% (n = 3) of luciferase activity remaining after 1 week. A second injection of DNA complexed by AsOR lysine-OMe-VSVG in the same animal, 1 week after the first injection, resulted in

Table 2. Luciferase Activity in Liver Tissue 24 h after Mice Were Injected with 10 μg of DNA Either Alone or Complexed by Protein Conjugates[a]

	luciferase (pg/g liver)				competition[c] (% inhibition)	
injection	mean	minimum	maximum	fold increase[b]	AsOR	OR
DNA alone	2.2 ± 1.9	0.1	5.5	NA	ND	ND
AsOR-lysine-OMe	2.2 ± 2.0	0.2	8.0	1.0	ND	ND
AsOR-polylysine	12.2 ± 11.4	0.7	29.7	11.1	ND	ND
AsOR-lysine-OMe-VSVG	29 000 ± 28 000	522	79 600	18 000	99.2 ± 0.9	3.0 ± 3.1

[a] For each experiment, injections were performed under identical conditions in three animals in parallel, using free DNA or DNA complexed by AsOR-lysine-OMe, AsOR-polylysine, or AsOR-lysine-OMe-VSVG, respectively. A standard curve for luciferase using firefly luciferase was performed along with the test samples. All experiments were performed at least in triplicate, and results were expressed as means ± SEM in units of picograms of luciferase per gram of liver tissue (1 pg corresponds to 200 000 LU/30 s). NA, not applicable. ND, not done. [b]Fold increase gives the average increase compared to the expression of luciferase after injection of free DNA. [c]Competition experiments were performed using AsOR or OR, mixed with the DNA−protein complexes in 100-fold molar excess immediately before injection. Results are shown as percent inhibition.

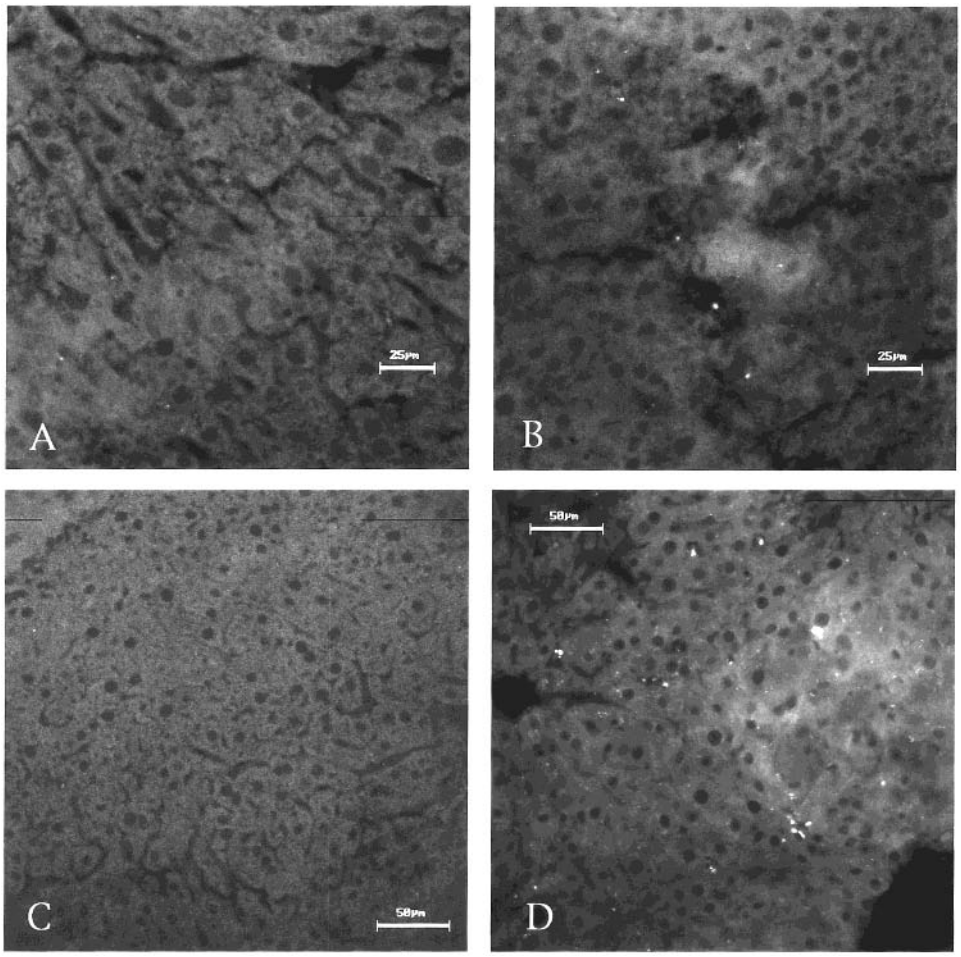


Figure 4. Immunohistochemical analyses of liver sections for luciferase gene expression (panels A and B) and green fluorescent protein gene expression (GFP, panels C and D). Twenty-four hours after injection of DNA (pCMVluc, panels A and B or pEGFP-C1, panels C and D) either alone (panels A and C), or complexed with AsOR-lysine-OMe-VSVG (panels B and D), animals were sacrificed and cryosections of the liver fixed, and treated as described in the the Materials and Methods. Representative sections of the liver are shown. Panels A and B show analyses of Texas Red signal for luciferase, and panels C and D show analyses for GFP expression.

luciferase expression of the same magnitude as the first injection (7695 ± 1777 pg of luciferase/g of liver, $n = 3$).

Immunohistochemical analysis of liver sections using anti-luciferase antibodies and laser scanning fluorescence microscopy showed a transfection efficiency of about 1.0% of cells. A representative section is shown in Figure 4B. Direct fluorescence analysis after delivery of a green fluorescent protein expression vector confirmed these results (Figure 4D). Animals injected with DNA alone, showed no expression of luciferase or GFP (Figure 4, panels A and C).

Injected animals showed no signs of acute toxicity, as shown by normal serum ALT values, and normal liver histology in H and E stained liver sections (data not shown).

The transgene could not be demonstrated in the episomal fraction of nuclear DNA 24 h after injection by Southern Blot analysis. However, semiquantitative competitive PCR assay, of which Figure 5 is a representative of six separate experiments, clearly demonstrated the presence of intact luciferase gene in liver cell nuclei after delivery by the various protein conjugates. The amount of DNA was approximately 1−2 orders of magnitude larger after injection of the multicomponent conjugate (panel D), compared to injection of the same amount of DNA in the form of AsOR−polylysine complexes (panel

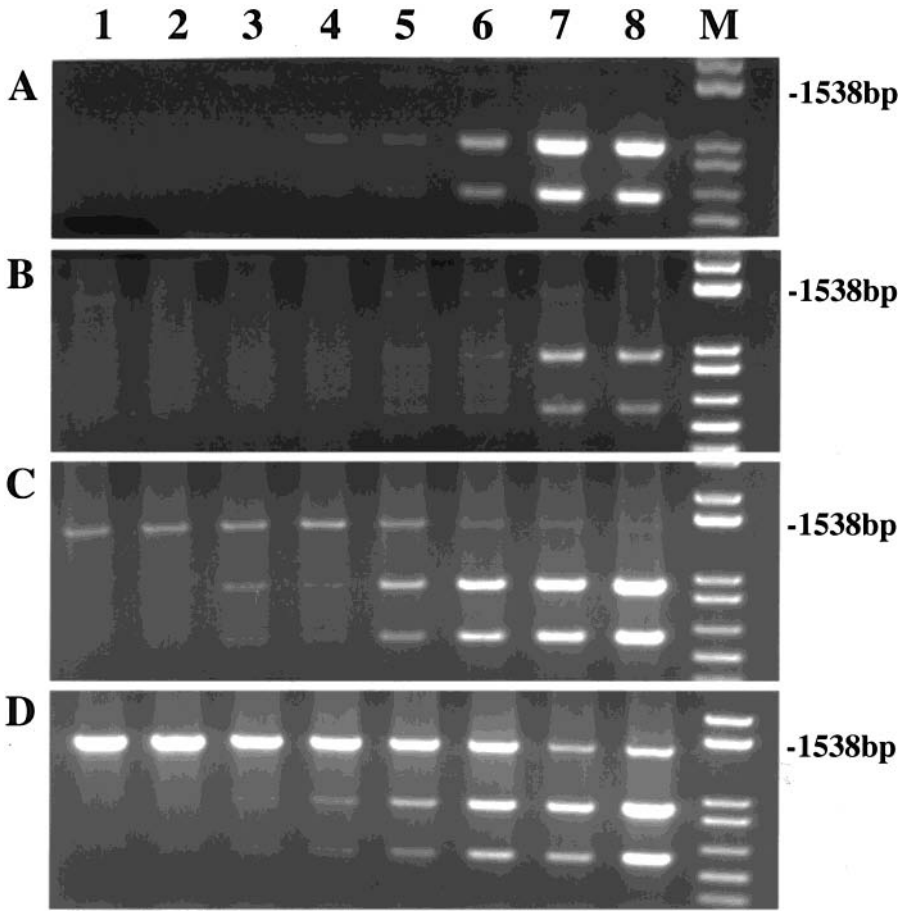


Figure 5. Semiquantitative competitive PCR analysis of episomal DNA extracted from isolated liver cell nuclei 24 h after injection of free DNA or DNA complexed with the various protein conjugates. (A) Negative control; (B) free DNA; (C) AsOR-polylysine; (D) AsOR-lysine-OMe-VSVG. Each PCR reaction contained the same amount of extracted episomal DNA (5 μL of a total of 100 μL) and an increasing amount of competitive template from lane 1 to lane 8 of 0, 0.25, 1.25, 2.5, 12.5, 25, 125, and 250 fg, respectively. After digestion with *Kpn*I, the PCR product amplified from wild-type luciferase DNA appeared as a band at 1538 bp. The PCR product amplified from competitive template sequences appeared as bands at 596 and 942 bp, respectively.

C). There was no intact luciferase gene present after injection of DNA alone (panel B).

DISCUSSION

In contrast to viral vectors, synthetic vectors resemble classical pharmaceutical agents in which defined compounds are produced by chemical means. A broad spectrum of genes in the form of plasmid DNA has been delivered to a large variety of cells by receptor-mediated endocytosis using nonviral vectors (*22*). So far, only a few studies have used this technique to successfully deliver polynucleic acids in vivo to the liver (*2*−*8*, *23*−*25*) and other organs (*26*−*29*). When linked to a target cell-specific ligand, the DNA is cointernalized by the target cell into the endosomal compartment, from which release is required into the cytoplasm in order to escape degradation in the lysosome. While disruption of the microtubular network, either through partial hepatectomy (*6*) or by administration of colchicine (*4*), has been used to increase and prolong gene expression, these methods are not likely to be practical clinically. In the current study, a DNA-binding component composed of lysine-OMe, and AsOR was used instead of polylysine for several reasons. First, it combines the cell-targeting component and DNA-binding component in a single molecule. Negatively charged amino acids on AsOR that react with lysine-OMe are converted into positively charged residues. For each lysine-OMe linked, there is a net increase of two positive charges per residue. Second, the dissociability of conjugate from DNA once inside the cells was hypothesized to be likely improved with a DNA carrier having dispersed positive charges rather than the concentrated multiple positive charges of polylysine-based carriers. Finally, it was possible that reproducibility of synthesis of conjugates might be improved by avoiding commercial polylysines that have substantial heterogeneity of chain length within the same batch, and especially from batch to batch (*30*).

Many viruses have evolved mechanisms to escape the degradative endosomal-lysosomal pathway. We and others have taken advantage of the endosomolytic property of whole viruses such as adenoviruses (*31*−*37*), rhinoviruses (*38*), or short synthetic fusogenic peptides derived from Influenza Virus hemagglutinin (*39*−*42*) to enhance DNA escape from endocytotic vesicles and augment gene expression after receptor-mediated gene transfer in vitro. The coadministration of endosomolytic viral particles, like adenoviruses, showed impressive enhancement of gene expression in vitro (*35*). Direct linkage between viral particle and the receptor ligand, substantially increased gene expression (*33*, *36*). The addition of VSVG protein partially purified from VSV-infected cells to cationic lipids enhanced gene transfer in vitro by a factor of 10 (*43*). The attachment of virus-derived or synthetic endosomolytic peptides to polylysine-based nonviral vectors has also been shown to be feasible in increasing gene expression in different cell types in vitro (*39*−*42*). However, until now, it has not been shown that viral peptides

can increase receptor-mediated gene delivery in vivo. While the incorporation of VSVG peptides into the DNA carrier was designed to enhance endosomal escape, the data on DNA stability of the complex suggest that the addition of the peptide also had the unexpected effect of increasing resistance to nuclease degradation compared to the AsOR-lysine-OMe parent conjugate, Figure 2. As there has not been described any inherent nuclease inhibitory activity for VSVG peptide, it is likely that the protective effect is related to the relative inaccessibility of the DNA when in the form of AsOR-lysine-OMe-VSVG complexes.

There was considerable variability in the liver assays particularly in Table 2. Different batches of conjugate were used for Table 1 and Table 2 experiments, which could account for the differences in the results between the values in the tables and the variability. As a result, there was no significant difference between the liver value in Table 1 (15 351 ± 484) and Table 2 (29 000 ± 28 000). Similarly, while the mean level of expression on reinjection was only approximately 25% (7695 ± 1777) of the initial value, because of the variability, this difference also did not reach statistical significance at the 0.05 level.

Our results demonstrate that it is possible to link a hemolytic peptide to nonviral vectors while retaining receptor recognition and internalization of the ligand. The present study demonstrates that this results in a large increase of gene expression and a higher amount of the intact transgene inside the liver cell nuclei. While increasing the level, the duration of gene expression was not extended and lasted not longer than 7 days. DNA delivered by asialoglycoprotein-targeting to the liver has been shown previously to remain episomal (*44*). The incorporation of the VSV peptide would not be expected to change the episomal status of the targeted DNA, and so an increase the duration of gene expression was not expected.

Although the data do not directly prove the mechanism of increased gene expression, the results are consistent with an improved endosomal release of delivered DNA by documented pH-dependent hemolytic properties of the VSVG peptide. Regarding the magnitude of increase of reporter gene expression, our results are in accordance with previously reported in vitro studies (*31*, *35*, *39*). The difference between the increase of nuclear transgene by a factor of 10^1-10^2 and the increase of gene expression can be explained by the fact that a single mRNA is translated into multiple copies of corresponding protein. In agreement with the pH-dependent hemolytic activity of the VSVG peptide (*13*, *14*), we neither observed physical distress in injected animals nor noticed any signs of hemolysis. Accordingly, neither elevations of serum ALT levels nor signs of liver cell necrosis or cellular infiltrates at the light microscopic level were found.

In conclusion, our results demonstrate, that DNA can be targeted to the liver in vivo using a multicomponent carrier. The protein conjugate−DNA complexes are taken up by receptor-mediated endocytosis via the AsGP receptor. The incorporation of a hemolytic peptide derived from VSV G-protein into an AsOR-based nonviral vector greatly increases gene expression in vivo. This concept could be extended to other DNA carriers based on other targeting ligands, which may permit enhanced DNA delivery and gene expression to a variety of nonhepatocytic cells.

ACKNOWLEDGMENT

We thank Dr. Ellen Carmichael for helpful advice. The technical assistance of Peili Zhan and the secretarial assistance of Mrs. Martha Schwartz is gratefully acknowledged. This work was supported in part by grants from the NIDDK: DK-42182 (G.Y.W.), the Immune Response Corporation (C.H.W.), and the Herman Lopata Chair in Hepatitis Research (G.Y.W.), and the Deutsche Forschungsgemeinschaft (Schu 1112/1-2 to M.J.S).

LITERATURE CITED

(1) Wu, G. Y., and Wu, C. H. (1987) Receptor-mediated in vitro gene transformation by a soluble DNA carrier system. *J. Biol. Chem. 262*, 4429−4432.

(2) Wu, G. Y., and Wu, C. H. (1988) Receptor-mediated gene delivery and expression *in vivo*. *J. Biol. Chem. 263*, 14621−14624.

(3) Wilson, J. M., Grossman, M., Wu, C. H., Roy Chowdhury N., Wu, G. Y., and Roy Chowdhury J. (1992) Hepatocyte-directed gene transfer in vivo leads to transient improvement of hypercholesterolemia in low-density lipoprotein receptor-deficient rabbits. *J. Biol. Chem. 26*, 963−967.

(4) Roy Chowdhury, N., Hays, R. M., Bommineni, V. R., Franki, N., Roy Chowdhury, J., Wu, C. H., and Wu, G. Y. (1996) Microtubular disruption prolongs the expression of human bilirubin-uridinediphosphoglucuronate-glucuronosyltransferase-1 gene transferred into Gunn rat livers. *J. Biol. Chem. 271*, 2341−2346.

(5) Wu, C. H., Wilson, J. M., and Wu, G. Y. (1989) Targeting genes: Delivery and persistent expression of a foreign gene driven by mammalian regulatory elements in vivo. *J. Biol. Chem. 264*, 16985−16987.

(6) Wu, G. Y., Wilson, J. M., Shalaby, F., Grossman, M., Shafritz, D. A., and Wu, C. H. (1991) Receptor-mediated gene delivery in vivo. Partial correction of genetic analbuminemia in Nagase rats. *J. Biol. Chem. 266*, 14338−14342.

(7) Roy Chowdhury N., Wu, C. H., Wu, G. Y., Yerneni, P. C., Bommineni, V. R., and Roy Chowdhury, J. (1993) Fate of DNA targeted to the liver by asialoglycoprotein receptor-mediated endocytosis in vivo. *J. Biol. Chem. 268*, 11265−11271.

(8) Bommineni, V. R., Roy Chowdhury, N., Wu, G. Y., Wu, C. H., Franki, N., Hays, R. M., and Roy Chowdhury, J. (1994) Depolymerization of hepatocellular microtubules after partial hepatectomy. *J. Biol. Chem. 269*, 25200−25205.

(9) Graham, W. (1990) Trawling for receptors. *Nature 346*, 318−319.

(10) Zhang, L., and Ghosh, H. P. (1994) Characterization of the putative fusogenic domain in vesicular stomatitis virus glycoprotein G. *J. Virol. 68*, 2186−2193.

(11) Fredericksen, B. L., and Whitt, M. A. (1995) Vesicular stomatitis virus glycoprotein mutations that affect membrane fusion activity and abolish virus infectivity. *J. Virol. 69*, 1435−1443.

(12) Odell, D., Wanas, E., Yan, J., and Ghosh, H. P. (1997) Influence of membrane anchoring and cytoplamic domains on the fusogenic activity of vesicular stomatitis virus glycoprotein G. *J. Virol. 71*, 7996−8000.

(13) Schlegel, R., and Wade, M. (1984) A synthetic peptide corresponding to the NH_2 terminus of vesiculo stomatitis virus glycoprotein is a pH-dependent hemolysin. *J. Biol. Chem. 259*, 4691−4694.

(14) Schlegel, R., and Wade, M. (1985) Biologically active peptides of the vesiculo stomatitis virus glycoprotein. *J. Virol. 53*, 319−323.

(15) Woodgett, C., and Rose, J. K. (1986) Amino-terminal mutation of the vesicular stomatitis virus glycoprotein does not affect its fusion activity. *J. Virol. 59*, 486-489.

(16) Sambrook, J., Fritsch, E. F., and Maniatis, T. (1989) *Molecular cloning. A laboratory manual*, 2nd ed. Cold Spring Harbor Laboratory Press, Plainview, NY.

(17) Schmidt, K., Polis, A., Hunziker, K., Fricke, R., and Yayoshi, M. (1967) Partial characterization of the sialic acid-free forms of α1-acid glycoprotein from human plasma. *Biochem. J. 104*, 361−368.

(18) Whitehead, P. H., and Sammons, H. G. (1966) A simple technique for the isolation of orosomucoid from normal and pathological sera. *Biochim. Biophys. Acta 12,* 209−211.
(19) Carlsson, J., Drevin, H., and Axen, R. (1978) Protein thiolation and reversible protein−protein conjugation. *Biochem. J. 173,* 723−737.
(20) Greenwood, F. C., Hunter, W. M., and Glover, J. S. (1963) The preparation of ^{131}I-labeled human growth hormone of high specific radioactivity. *Biochem. J. 89,* 114−119.
(21) Stieger, M., Demolliere, C., Ahlborn-Laake, L., and Mous, J. (1991) Competitive polymerase chain reaction assay for quantitation of HIV-1 DNA and RNA. *J. Virol. Methods 34,* 149−160.
(22) Zauner, W., Ogris, M., and Wagner, E. (1998 Polylysine-based transfection systems utilizing receptor-mediated delivery. *Adv. Drug. Delivery Rev. 30,* 97−113.
(23) Ferkol, T., Crawford, D. R., Lindberg, G. L., Ratnoff, O. D., Chen, J., Hanson, R. W., Perales, J. C. (1993) Regulation of the phosphoenolpyruvate carboxykinase/human factor IX gene introduced into the livers of adult rats by receptor-mediated gene transfer. *FASEB. 7,* 1081−1091.
(24) Perales, J. C., Ratnoff, O. D., Ferkol, T., Hanson, R. W., and Beegen, H. (1994) Gene transfer in vivo: sustained expression and regulation of genes introduced into the liver by receptor-targeted uptake. *Proc. Natl. Acad. Sci. U.S.A. 91,* 4086−4090.
(25) Perales, J. C., Ferkol, T., Grossmann, G. A., Harpst, J., Molas, M., Oda, H., Liu, G., and Hanson, R. W. (1997) Biochemical and functional characterization of DNA complexes capable of targeting genes to hepatocytes via the asialoglycoprotein receptor. *J. Biol. Chem. 272,* 7398−7407.
(26) Ferkol, T., Kaetzel, C. S., Perales, J. C., Hanson, R. W., Eckman, E., and Davis, P. B. (1995) Gene transfer into the airway epithelium of animals by targeting the polymeric immunoglobulin receptor. *J. Clin. Invest. 95,* 493−502.
(27) Ferkol, T., Trzaska, T., Pellicena-Palle, A., Tosi, M., Eckman, E., Redline, R., Perales, J. C., and Davis, P. B. (1996) Immunologic responses to gene transfer into mice via the polymeric immunoglobulin receptor. *Gene Ther. 3,* 669−678.
(28) Ferkol, T., Mularo, F., Perales, J. C., and Hanson, R. W. (1996) Receptor-mediated gene transfer into macrophages. *Proc. Natl. Acad. Sci. U.S.A. 93,* 101−105.
(29) Ferkol, T., Perales, J. C., Mularo, F., Ziady, A., Hilliard, J., Konstan, M., and Lodish, S. (1998) Transfer of the human Alpha1-antitrypsin gene into pulmonary macrophages in vivo. *Am. J. Respir. Cell. Mol. Biol. 18,* 591−601.
(30) Dolnik, V., and Novotny, M. V. (1993) Separation of amino acid homopolymers by capillary electrophoresis. *Anal. Chem. 65,* 563−567.
(31) Curiel, D. T., Agarwal, S., Wagner, E., and Cotten, M. (1991) Adenovirus enhancement of transferrin-polylysine-mediated gene delivery. *Proc. Natl. Acad. Sci. U.S.A. 88,* 8850−8854.
(32) Curiel, D. T., Wagner, E., Cotton, M., Birnstiel, M. L., Agarwal, S., Li, C. M., Loechel, S., and Hu, P. C. (1992) High-efficiency gene transfer mediated by adenovirus coupled to DNA−polylysine complexes. *Hum. Gene. Ther. 3,* 147−154.
(33) Wagner, E., Zatloukal, K., Cotten, M., Appos, H. K., Mechtler, K., Curiel, D. T., and Birnstiel, M. L. (1992) Coupling of adenovirus to transferrin-polylysine/DNA complexes greatly enhances receptor-mediated gene delivery and expression of transfected genes. *Proc. Natl. Acad. Sci. U.S.A. 89,* 6099−6103.
(34) Cotten, M., Wagner, E., Zatloukal, K., Phillips, S., Curiel, D. T., and Birnstiel, M. L. (1992) High-efficiency receptor-mediated delivery of small and large (48 kilobase) gene constructs using the endosome-disruption activity of defective or chemically inactivated adenovirus particles. *Proc. Natl. Acad. Sci. U.S.A. 89,* 6094−6098.
(35) Cristiano, R. J., Smith, L. C., and Woo, S. L. C. (1993) Hepatic gene therapy: Adenovirus enhancement of receptor-mediated gene delivery and expression in primary hepatocytes. *Proc. Natl. Acad. Sci. U.S.A. 90,* 2122−2126.
(36) Cristiano, R. J., Smith, L. C., Kay, M. A., Brinkley, B. R., and Woo, S. L. C. (1993) Hepatic gene therapy: Efficient gene delivery and expression in primary hepatocytes utilizing a conjugated adenovirus-DNA complex. *Proc. Natl. Acad. Sci. U.S.A. 90,* 11548−11552.
(37) Wu, G. Y., Zhan, P., Sze, L. L., Rosenberg, A. R., and Wu, C. H. (1994) Incorporation of adenovirus into a ligand-based DNA carrier system results in retention of original receptor specifity and enhanced targeted gene expression. *J. Biol. Chem. 269,* 11542−11546.
(38) Zauner, W., Blaas, D., Kuechler, E., and Wagner, E. (1995) Rhinovirus-mediated endosomal release of transfection complexes. *J. Virol. 69,* 1085−1092.
(39) Wagner, E., Plank, C., Zatloukal, K., Cotton, M., and Birnstiel, M. L. (1992) Influenza virus hemagglutinin HA-2 N-terminal fusogenic peptides augment gene transfer by transferrin-polylysine-DNA complexes: Toward a synthetic virus-like gene transfer vehicle. *Proc. Natl. Acad. Sci. U.S.A. 89,* 7934−7938.
(40) Plank, C., Zatloukal, K., Cotton, M., Mechtler, K., and Wagner, E. (1992) Gene transfer into hepatocytes using asialoglycoprotein receptor mediated endocytosis of DNA complexed with an artificial tetra-antennary galactose ligand. *Bioconjugate Chem. 3,* 533−539.
(41) Plank, C., Oberhauser, B., Mechtler, K., Koch, C., and Wagner, E. (1994) The influence of endosome-disruptive peptides on gene transfer using synthetic virus-like gene transfer systems. *J. Biol. Chem. 269,* 12918−12924.
(42) Midoux, P., Mendes, C., Legrand, A., Raimond, J., Mayer, R., Monsigny, M., and Roche, A. C. (1993) Specific gene transfer mediated by lactosylated poly-L-lysine into hepatoma cells. *Nucleic Acids. Res. 21,* 871−878.
(43) Abe, A., Miyanohara, A., and Friedmann, T. (1998) Enhanced gene transfer with fusogenic liposomes containing vesicular stomatitis virus G glycoprotein. *J. Virol. 72,* 6159−6163.
(44) Stankovics, J., Crane, A. M., Andrews, E., Wu, C. H., Wu, G. Y., and Ledley, F. D. (1994) Overexpression of human methylmalonyl CoA mutase in mice after in vivo gene transfer with asialoglycoprotein/polylysine/DNA complexes. *Hum. Gene. Ther. 5,* 1095−1104.

BC990071R

Comparison of Recombinant and Synthetically Formed Monoclonal Antibody-β-Lactamase Conjugates for Anticancer Prodrug Activation

David E. Kerr,[†] Vivekananda M. Vrudhula,[‡] Håkan P. Svensson,[§] Nathan O. Siemers,[||] and Peter D. Senter*

Bristol-Myers Squibb Pharmaceutical Research Institute, Seattle, Washington 98121. Received June 11, 1999; Revised Manuscript Received August 3, 1999

Conjugates of the L49 monoclonal antibody (binds to the p97 antigen on melanomas and carcinomas) were formed by attaching Enterobacter cloacae β-lactamase (bL) to the L49-Fab′ fragment using a heterobifunctional cross-linking reagent or by linking the enzyme to L49-sFv using DNA recombinant technology. The conjugates thus formed, L49-Fab′-bL and L49-sFv-bL, were designed to activate cephalosporin containing anticancer prodrugs at the surfaces of antigen positive tumor cells. Results from in vitro experiments using two lung carcinoma cell lines demonstrated that the conjugates were equally active in effecting the release of phenylenediamine mustard from the cephalosporin nitrogen mustard prodrug CCM. While treatment with either of the conjugates combined with the maximum tolerated doses of CCM led to cures of established SN12P renal cell carcinoma tumors in nude mice, only the L49-sFv-bL conjugate maintained its ability to do so at 1/4 the maximum tolerated dose of CCM. L49-sFv-bL was also superior to L49-Fab′-bL in the 1934J renal cell carcinoma tumor model and was shown to be quite active in two in vivo models of human lung carcinoma. These results demonstrate that the recombinant fusion protein leads to more pronounced therapeutic windows than the chemical conjugate and is active in an array of human tumor models.

INTRODUCTION

The use of antibody−enzyme conjugates for the activation of anticancer prodrugs has been the subject of a great deal of investigation (reviewed in refs *1*−*4*). This targeting strategy, commonly referred to as antibody-dependent enzyme prodrug therapy (ADEPT), is a form of pretargeting that involves two separate steps to achieve therapeutic efficacy. Initially, a nontoxic monoclonal antibody-enzyme (mAb−enzyme) conjugate is administered that diffuses into solid tumor masses and binds to cell-surface antigens. Once sufficiently high tumor to nontumor ratios are achieved, a relatively nontoxic prodrug is injected. Upon contact with the targeted enzyme, the prodrug is catalytically converted into a cytotoxic drug. There are now many examples demonstrating that this drug-targeting strategy results in high intratumoral drug concentrations, pronounced antitumor activities at well tolerated doses, and to positive responses in early clinical trials (*1*−*4*).

Several enzymes have been utilized for targeted prodrug activation (reviewed in refs *1*−*3*). We (*5*−*11*) and others (*12, 13*) have focused on the use of Enterbacter cloacae β-lactamase (bL) as an activating enzyme, due to its high specific activities on an array of cephalosporin containing anticancer prodrugs. Conjugates were formed by linking bL to the L49 and 96.5 mAbs (*9*−*11*) which recognize distinct epitopes on the p97 melanotransferrin antigen, present on the surfaces of most human melanoma tumors and on some carcinomas (*10, 14*). One of the advantages in using bL for prodrug activation is that there is no known human counterpart that can catalyze cephalosporin β-lactam hydrolysis. Consequently, the conjugated enzyme is the principal source of prodrug activation.

Therapy experiments in mice with melanoma xenografts have demonstrated that pronounced antitumor activities, including cures and complete regressions of established tumors, were obtained using the combination of 96.5-Fab′-bL with CCM (Figure 1), a prodrug from which phenylenediamine mustard (PDM) is released upon hydrolysis of the β-lactam bond (*9*). The prodrug in these experiments was injected 3 days post conjugate treatment, a period of time that allowed most of the nontargeted enzyme to clear from the systemic circulation. On the basis of these results, a recombinant L49-sFv-bL fusion protein was prepared and expressed in *Escherichia coli* (*11*). In contrast to the chemically produced L49-Fab′-bL conjugate, the fusion protein underwent very rapid intratumoral uptake and systemic clearance. It was therefore possible to safely administer the prodrug 12 h after conjugate administration, leading to pronounced therapeutic efficacy.

Although several mAb−enzyme fusion proteins have now been described for anticancer prodrug activation (*8, 11, 15*−*19*), their effects relative to chemically produced conjugates have not been reported. In this paper, we

* To whom correspondence should be addressed: Seattle Genetics, 22215 26th Avenue SE, Bothell, WA 98021. Phone: (425) 489-4993. Fax (425) 489-4798. E-mail: psenter@seagen.com.

[†] Present address: Biocontrol Systems, 12822 SE 32nd St., Bellevue, WA 98005.

[‡] Present address: Bristol-Myers Squibb Pharmaceutical Research Institute, Neuroscience and Genitourinary Chemistry, 5 Research Parkway, Wallingford, CT 06492.

[§] Present address: Xcyte Therapies, 2203 Airport Way South, Suite 300, Seattle, WA 98134.

[||] Present address: Bristol-Myers Squibb Pharmaceutical Research Institute, Department of Applied Genomics, Hopewell Building 3, PO Box 5400, Princeton, NJ 08543-5400.

10.1021/bc990075w CCC: $18.00 © 1999 American Chemical Society
Published on Web 09/09/1999

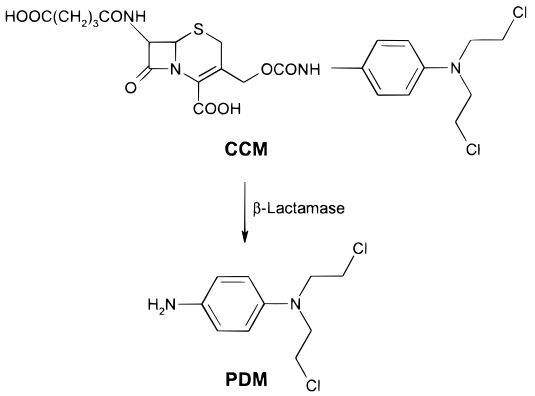


Figure 1. Structures of the cephalosporin mustard prodrug CCM and PDM, the drug released upon bL-catalyzed hydrolysis.

compare the antitumor activities obtained when L49-Fab′-bL/CCM and L49-sFv-bL/CCM combinations are administered in mice with renal cell carcinoma xenografts. We show that the fusion protein leads to better therapeutic windows in two renal cell carcinoma models. In addition, we demonstrate that the combination of the fusion protein with CCM is effective, both in vitro and in vivo, in treating models of p97 antigen positive human lung adenocarcinomas.

MATERIALS AND METHODS

Cell Lines and Reagents. The 3713 and 3754 lung carcinoma cell lines were developed at Bristol-Myers Squibb (Seattle, WA) from tumor biopsies obtained from patients with lung carcinoma. The SN12P and 1934J renal cell carcinoma lines have been reported earlier (*10*). The mAb L49 (IgG_1) binds to melanotransferrin (p97), a human melanoma associated antigen that is also expressed on a number of carcinomas (*10, 14*). P1.17 (IgG_{2a}) is a mouse myeloma protein that was used as a nonbinding control. L49-Fab′-bL was prepared as described earlier for other mAb−Fab′-bL conjugates (*20*). Briefly, the Fab'_2 fragment of the L49 mAb was reduced with dithiothreitol and combined with maleimide-substituted bL. The conjugate was subjected to purification on a boronic acid affinity column (hydrophilic type L), followed by gel filtration on Sepahacryl S-300. L49-sFv-bL, containing the r2-1 bL mutant (*21*), was expressed in *E. coli* and purified as reported earlier (*11*). Purification involved a combination of affinity chromatographic steps, first using immobilized p97, followed by immobilized boronic acid. PDM and CCM were synthesized as reported earlier (*5*).

Cell-Surface Expression of the p97 Antigen. The expression of melanotransferrin on SN12P and 1934J cells has been described previously (*10*). Fluorescein conjugates of L49 and P1.17 were used to assess antigen expression on the lung carcinoma cell lines. Cells were detached from monolayer cultures with trypsin, incubated in culture media with mAb−fluorescein conjugates at 10 μg/mL, washed, then subjected to fluorescence activated cell sorter analysis (FACScan, Becton-Dickinson). The L49/P1.17 binding ratios were determined from the ratios of the mean fluorescence intensities after incubation with the respective mAb−fluorescein conjugates.

In Vitro Cytotoxicity. A total of 3713 and 3754 lung adenocarcinoma cells were plated into 96-well microtiter plates (10^4 cells/well in 0.1 mL of IMDM with 10% fetal bovine serum, 0.06 mg/mL penicillin, and 0.1 mg/mL streptomycin) and allowed to adhere overnight. For blocking experiments, the cells were incubated with unconjugated whole L49 at 1 μM for 30 min prior to treatment with the L49 conjugates. The cells were then exposed to the L49-bL conjugates at 10 nM. After 30 min at 4 °C, the plates were washed three times with antibiotic free RPMI 1640 medium with 10% fetal bovine serum, and then various amounts of CCM were added. CCM and PDM were also added to cells that were not treated with the conjugates. After 1 h at 37 °C, the cells were washed with IMDM and incubated for approximately 18 h. The cells were then pulsed for 12 h with [^{3}H]thymidine (1 μCi/well) at 37 °C, detached by freezing and thawing, and were harvested onto glass fiber filter mats using a 96-well cell harvester. Radioactivity was counted using a β-plate counter.

In Vivo Therapy Experiments. Athymic nude mice from Harlan Sprague/Dawley (10 weeks old) were implanted with subcutaneous 3713 or 3754 tumors, and therapy experiments started 35 days later when tumors reached approximately 120 mm^3. Tumors from in vivo passages 3−8 were used. Groups of five mice were injected with L49-sFv-bL iv at 1 mg/kg (10 mL/kg in PBS). This was followed 15−18 h later by iv CCM treatment at various concentrations (10 mL/kg in 0.12 M sodium bicarbonate with 10% DMSO). Control mice were either untreated, or received iv PDM (10 mL/kg in saline) at the doses specified in the figures. This was repeated weekly for a total of three rounds. Tumor volume was computed using the following formula: 1/2[longest dimension × perpendicular dimension^2]. Mice were removed from the study before their tumor volumes reached 2000 mm^3, at which point the average tumor sizes from the remaining mice were no longer plotted. Maximum tolerated doses led to less than 20% sustained (≥2 weeks) weight loss, led to no treatment related deaths, and were within 50% of the dose where such events took place.

For the renal cell carcinoma experiments, mice (five per group) bearing subcutaneous 1934J or SN12P tumors were treated with 1.4 mg/kg L49-Fab′-bL or with 1.0 mg/kg L49-sFv-bL. The prodrug CCM was administered 3 days post-L49-Fab′-bL and 1 day post-L49-sFv-bL. Treatments were administered weekly for a total of three rounds.

RESULTS

Expression of the p97 Antigen on Carcinoma Cell Lines. The L49 mAb (IgG_1) has previously been shown to bind to the p97 melanotransferrin antigen with subnanomolar affinity (*11*) Almost all human melanomas tested have been reported to be strongly p97 positive (*14*). Antibodies against the p97 antigen also react with some carcinomas, although the antigen tends to be expressed at lower levels compared to melanomas (*10, 14*). The presence of the p97 antigen on a panel of 13 lung carcinoma cell lines was determined by fluorescence-activated cell sorter analysis using the L49 mAb conjugated to fluorescein. Binding was compared to that of P1.17-fluorescein, a nonbinding control conjugate. As shown in Table 1, most of the lung cell lines expressed the p97 antigen. Using a ratio of 1.3 as a cutoff for positive binding (*10*), 10 of the 13 lung carcinoma cell lines were p97 antigen positive. The average binding ratio among the positive cell lines was 3.0 ± 1.4, indicating generally low levels of p97 antigen expression. For comparison, the binding ratios for renal cell carcinoma and melanoma cell lines are shown, since L49-bL/CCM combinations have demonstrated pronounced in vivo

Table 1. L49 Binding to Cell Lines Relative to the Nonbinding P1.17 Control

cell line	tumor type	binding ratio[a]
2981	lung adenocarcinoma	1.5
2987	lung adenocarcinoma	1.0
3697	lung adenocarcinoma	1.1
3713	lung adenocarcinoma	4.9
3754	lung adenocarcinoma	4.4
3766	lung adenocarcinoma	1.0
3776	lung adenocarcinoma	1.5
3896	lung adenocarcinoma	1.6
3963	lung adenocarcinoma	3.5
4013	lung adenocarcinoma	2.2
4015	lung adenocarcinoma	2.7
4023	lung adenocarcinoma	5.0
4026	lung adenocarcinoma	2.5
3677	melanoma	4.2
SN12P	renal cell carcinoma	35[b]
1934J	renal cell carcinoma	1.8[b]

[a] Cells were incubated with L49-fluorescein or P1.17-fluorescein at 10 μg/mL, washed, and analyzed on a fluorescence activated cell sorter. Binding ratios are the ratios of mean fluorescence intensities of L49-fluorescein to P1.17-fluorescein. A ratio of greater than 1.3 is considered p97 antigen positive. [b] From ref *10*.

activities in these tumor models (*8*−*11*). A total of 7 of 13 of the lung carcinomas express relatively higher levels of the p97 antigen than the 1934J renal cell carcinoma, a tumor that underwent regression upon treatment with L49-sFv-bL/CCM.

In Vitro Studies. The L49-Fab′-bL conjugate was prepared according to previously described methods (*10*) by combining sulfhydryl-containing L49 Fab′, derived from reduction of L49 Fab'_2, with maleimide-substituted bL. After purification, SDS−PAGE analysis revealed a major protein band at approximately 90 kDa, and several minor bands at higher and lower molecular masses (*10*). The L49-sFv-bL fusion protein was expressed in *E. coli* and purified by affinity chromatography (*11*). In contrast to the chemically formed conjugate, the fusion protein was homogeneous according to SDS−PAGE analysis, and had a molecular mass of approximately 63 kDa (*11*). Both of these conjugates retained the enzymatic and binding activities of the proteins from which they were derived (*10*, *11*). The equilibrium dissociation constants (K_D) for the L49-Fab′-bL and L49-sFv-bL conjugates were 1.3 and 1.0 nM, respectively (*11*).

The cytotoxic activities of L49-Fab′-bL and L49-sFv-bL in combination with CCM were determined on the p97 positive 3713 and 3754 lung adenocarcinoma cell lines. The cells were exposed to the conjugates, washed to remove unbound material, and treated with varying concentrations of CCM. Cytotoxic activity was determined by measuring the incorporation of [^{3}H]thymidine into DNA relative to untreated cells. On 3713 cells, PDM was approximately 40 times more cytotoxic than the prodrug CCM (Figure 2, panels A and B). The L49-Fab′-bL and L49-sFv-bL conjugates both effectively activated the prodrug, leading to cytotoxicities that were equivalent to PDM. Prodrug activation by the conjugates was immunologically specific, since much lower levels of cytotoxic activity was obtained on cells that were saturated with unconjugated L49 prior to treatment with the conjugate/CCM combinations. Similar trends were obtained with the 3754 cells, but the differences in CCM and PDM cytotoxicity were only about 10-fold (Figure 2, panels C and D). These in vitro experiments demonstrate that L49-Fab′-bL and L49-sFv-bL bind equally well to the p97 antigen and are indistinguishable in their abilities to induce CCM activation on antigen positive cells.

In Vivo Therapeutic Activity. The relative antitumor activities of the L49-Fab′-bL and L49-sFv-bL conjugates in combination with CCM were compared in two models of human renal cell carcinoma. The tumors were implanted subcutaneously, and treatment was initiated at a point when they were well established (approximately 200 mm^3) and growing. The conjugates were injected iv at 1.0 mg/kg for L49-sFv-bL and 1.4 mg/kg for L49-Fab′-bL, and CCM was injected iv 24 and 72 h post-L49-sFv-bL and L49-Fab′-bL administration, respectively. These doses and schedules were considered nearly optimal, based on previously published in vivo efficacy and pharmacokinetic data (*7*−*13*), and led to comparable intratumoral conjugate levels (*11*). The intervals between conjugates and prodrug administrations were chosen since they allow sufficient time for the conjugates to localize in tumors and clear from the systemic circulation. This treatment protocol was repeated weekly for a total of three rounds of therapy. The therapeutic effects were compared to those of PDM at its maximum tolerated dose.

Treatment with either L49-sFv-bL (Figure 3A) or L49-Fab′-bL (Figure 3B) led to cures of all the SN12P tumors when combined with maximum tolerated doses (defined in Materials and Methods) of CCM. Most likely, the reason that more CCM could be administered to L49-sFv-bL (240 mg/kg/injection)- compared to L49-Fab′-bL (180 mg/kg/injection)-treated mice was that at the time of prodrug administration there were lower concentrations of the fusion protein compared to the chemical conjugate in the serum (*11*). Differences between the conjugates were evident when CCM was injected at levels significantly below the respective maximum tolerated doses. The antitumor effects of the L49-sFv-bL/CCM combination were maintained at 1/4 the maximum tolerated dose of CCM (60 mg/kg/injection), while this amount of CCM in L49-Fab′-bL treated mice (1/3 the maximum tolerated dose) resulted only in a delay of tumor outgrowth. PDM at the maximum tolerated dose had no antitumor activity.

Similar experiments were conducted in mice with 1934J renal cell carcinoma xenografts (Figure 3, panels C and D). This tumor model has previously been shown to have 1/4 the total p97 antigens/cell compared to SN12P, and accumulation of L49-Fab′-bL very poor (*10*). L49-sFv-bL treatment led to slightly better therapeutic efficacy than L49-Fab′-bL when each was combined with CCM. Cures were obtained at both 180 mg/kg CCM (two of five animals) and 120 mg/kg CCM (one of five animals) in the L49-sFv-bL treated mice, while all of the tumors in mice receiving L49-Fab′-bL/CCM eventually progressed. Again, PDM had no therapeutic activity.

The in vivo therapy results suggest that L49-sFv-bL effects a higher degree of intratumoral CCM activation compared to the chemical conjugate. To extend its utility, we explored the activities of L49-sFv-bL/CCM combinations in mice with p97 positive lung adenocarcinomas. Complete regressions and long-term growth delays were obtained in L49-sFv-bL/CCM treated animals bearing subcutaneous 3713 (Figure 4A) and 3754 (Figure 4B) tumors. The dosing regimens were well below the maximum tolerated doses, since there were no signs of toxicity or weight loss during and after treatment. The 3713 tumor model was insensitive to treatment with the maximum tolerated dose of PDM (3 mg/kg/injection), while 3754 tumor growth (maximum tolerated dose of

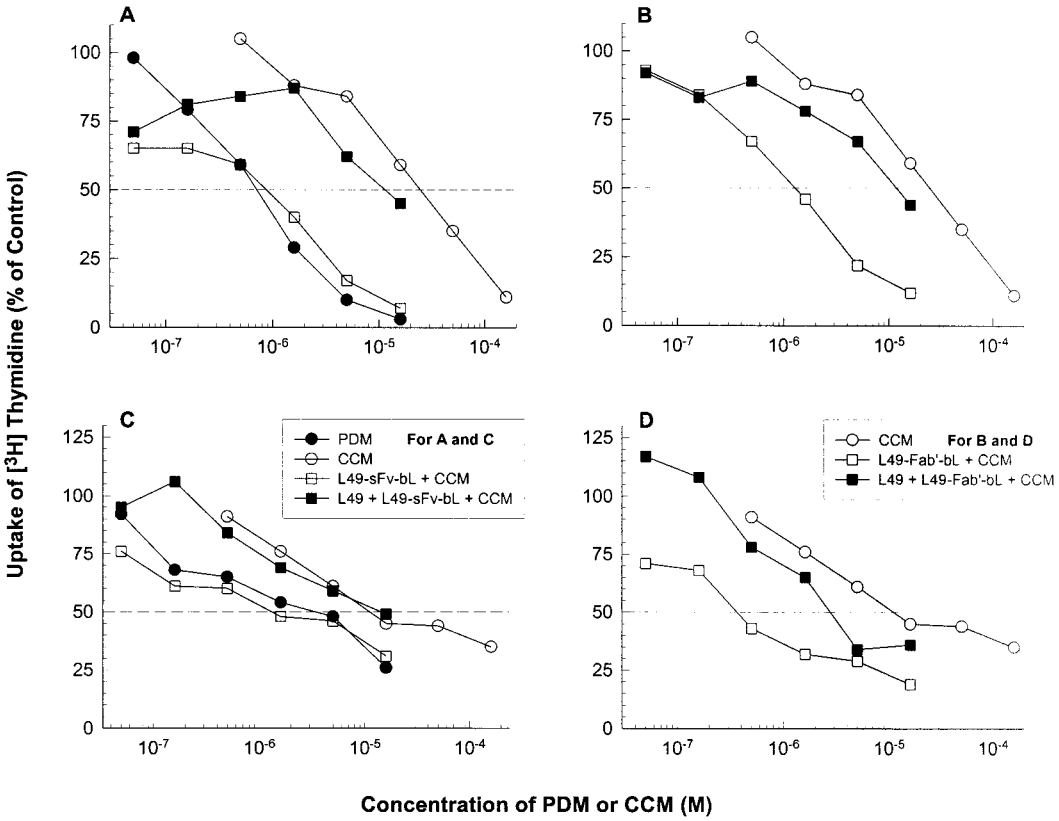


Figure 2. Cytotoxic effects of mAb−bL + CCM combinations on 3713 (A and B) 3754 and (C and D) human lung carcinomas. The cells were incubated with the mAb−bL conjugates, washed, and treated with CCM for 1 h. The effects were compared to cells treated with CCM or PDM for 1 h without prior conjugate exposure and to cells that were treated with saturating amounts of unconjugated L49 prior to conjugate treatment. The samples were run in triplicate, and the standard deviations were less than 10%.

PDM was 4 mg/kg/injection) was stable for 8 weeks before eventually growing out. The basis for this difference is unclear, but may be due to increased tolerance of PDM in mice with 3754 compared to 3713 tumor implants. These results provide the first evidence that L49-sFv-bL in combination with CCM may be efficacious for treating lung adenocarcinomas.

DISCUSSION

A number of recombinant mAb−enzyme fusion proteins are being explored and developed as tools in diagnostics and therapy. In contrast to nearly all chemically formed conjugates, such fusion proteins are molecularly defined, and after purification can consist of single molecular entities. An additional advantage in using recombinant technology for fusion protein production is the ease with which specific amino acid substitutions can be introduced in order to customize the proteins for their intended applications. A few examples of mAb−enzyme fusion proteins include mAb−alkaline phosphatase conjugates for immunoassays (*22*), mAb−toxin (*23*−*25*), and mAb−ribonuclease (*26*) conjugates for cancer and mAb−tissue plasminogen activator conjugates for dissolving blood clots (*27*). There are also several examples of recombinant mAb−enzyme fusion proteins for the activation of anticancer prodrugs. The first example, a mAb−β-glucuronidase conjugate, was reported by Bosslet and co-workers (*15*). A related molecule has since been reported by Haisma and co-workers that recognizes the CD20 antigen on lymphomas (*16*). Carter and co-workers have reported the development of a disulfide stabilized anti-p185HER2−Fv-*E. coli* bL conjugate for the activation of paclitaxel and doxorubicin prodrugs (*17, 18*). Our work with recombinant mAb−enzyme fusion proteins began with L6-*Bacillus cereus* bL for the activation of a doxorubicin prodrug (*19*) and has since shifted toward the construction of the L49-sFv-bL conjugate described here and elsewhere (*11*). The particular bL used was from *Enterobacter cloacae* but incorporated some mutations in one of the loops to enhance its ability to hydrolyze the β-lactams of nitrocefin and a doxorubicin prodrug (*21*). The L49 mAb was selected because of its ability to bind with high affinity to human melanomas and carcinomas (*10, 11*).

Prior to the studies reported here, there have been no published comparisons of chemical conjugates and recombinant fusion proteins for prodrug activation. Results from the in vitro studies shown in Figure 2 fail to distinguish between L49-Fab′-bL and L49-sFv-bL, which is not surprising since they have similar binding and enzymatic characteristics (*11*). In contrast, the in vivo studies show that L49-sFv-bL leads to better therapeutic efficacy compared to L49-Fab′-bL when each conjugate was combined with suboptimal doses of CCM (Figure 3). This is most likely due to differences in conjugate biodistribution at the time of prodrug administration. A detailed pharmacokinetic study in mice with subcutaneous melanoma tumors demonstrated that L49-sFv-bL treatment resulted in a tumor/blood ratio of 105 within 24 h of administration (*11*). Nontarget tissues took up very small amounts of the fusion protein. In contrast, specific intratumoral uptake of the L49-Fab′-bL chemical conjugate was not nearly as pronounced. L49-Fab′-bL cleared quite slowly from the blood, and reached a 5.6 tumor/blood ratio 72 h post conjugate administration. From these data, it can be predicted that fusion protein treatment leads to higher intratumoral drug concentrations compared to the chemically formed conjugate, since

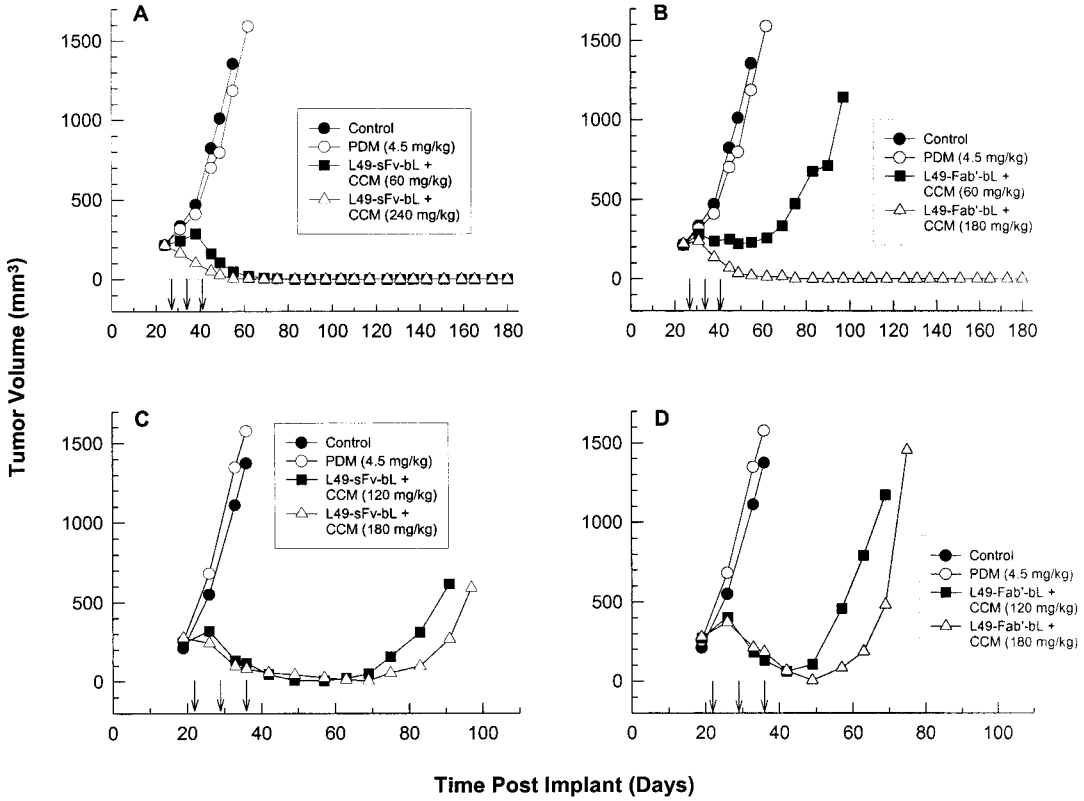


Figure 3. Therapeutic effects of L49-bL/CCM combinations in nude mice with SN12P (A and B) and 1934J (C and D) subcutaneous tumor xenografts. The L49-sFv-bL and L49-Fab′-bL conjugates were injected intravenously at 1.0 and 1.4 mg/kg/injection, respectively. CCM was administered intravenously 24 h after L49-sFv-bL and 3 days after L49-Fab′-bL on the days indicated by the arrows. The effects were compared to those of the maximum tolerated dose of PDM, which was administered on the days indicated by the arrows.

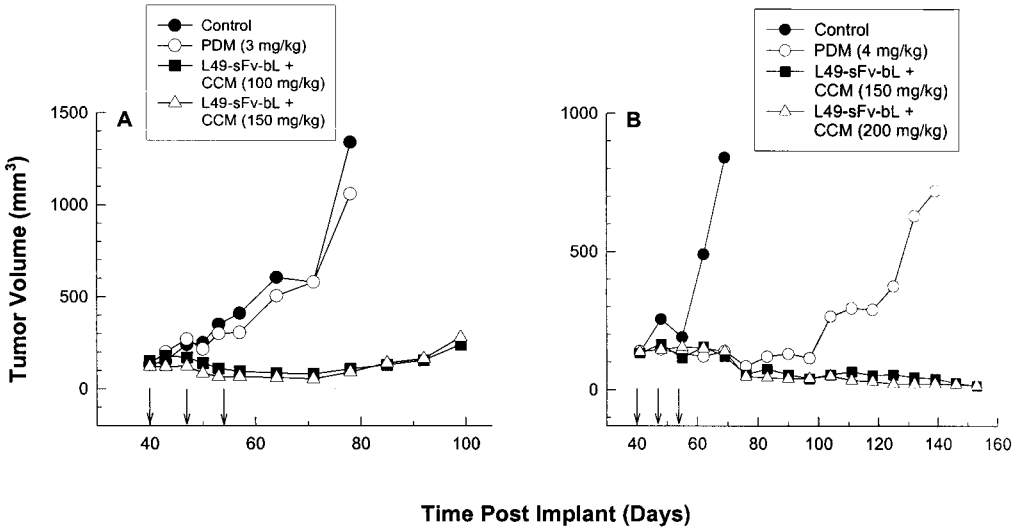


Figure 4. Therapeutic effects of L49-sFv-bL/CCM combinations in nude mice with (A) 3713 and (B) 3754 lung adenocarcinoma tumors. L49-sFv-bL was injected intravenously (1.0 mg/kg/injection). CCM, or PDM in previously untreated mice, was administered at the maximum tolerated dose intravenously 24 h later on the days indicated by the arrows.

more of the prodrug is activated in the tumor rather than in the blood. This might account for the improved activities of the fusion protein when the prodrug is administered well below the maximum tolerated dose. As with other mAb−enzyme/prodrug combinations (*7*, *28*−*30*), the intratumoral drug concentrations obtained are likely to be higher than that achieved from systemic drug administration.

In conclusion, the L49-sFv-bL fusion protein presents advantages over the chemically produced conjugate since it is more homogeneous in composition and leads to better therapeutic efficacy. It is significant that pronounced effects are obtained in lung tumor models that have low levels of antigen expression. The activities of the L49-sFv-bL/prodrug combinations in models of human melanoma (*8*, *11*), renal cell carcinoma (*10*; Figure 3), and lung adenocarcinoma (Figure 4) provide a compelling basis for clinical development.

ACKNOWLEDGMENT

We wish to thank Karl Erik and Ingegerd Hellström for their support throughout the course of this research and Joseph Francisco for his useful comments on the manuscript.

LITERATURE CITED

(1) Senter, P. D., and Svensson, H. P. (1996) A summary of monoclonal antibody-enzyme/prodrug combinations. *Adv. Drug Delivery Rev. 22*, 341−349.

(2) Niculescu-Duvaz, I., and Springer, C. J. (1995) Antibody-directed enzyme prodrug therapy (ADEPT): A targeting strategy in cancer chemotherapy. *Curr. Med. Chem. 2*, 687−706.

(3) Melton, R. G., and Sherwood, R. F. (1996) Antibody-enzyme conjugates for cancer therapy. *J. Natl. Cancer Inst. 88*, 153−165.

(4) Bagshawe, K. D. and Begent, R. H. J. (1996) First clinical experiment with ADEPT. *Adv. Drug Delivery Rev. 22*, 365−367.

(5) Vrudhula, V. M., Svensson, H. P., Kennedy, K. A, Senter, P. D., and Wallace, P. M. (1993) Antitumor activities of a cephalosporin prodrug in combination with monoclonal antibody-β-lactamase conjugates. *Bioconjugate Chem. 4*, 334−340.

(6) Vrudhula, V. M., Svensson, H. P., and Senter, P. D. (1995) Cephalosporin derivatives of doxorubicin as prodrugs for activation by monoclonal antibody-β-lactamase conjugates. *J. Med. Chem. 38*, 1380−1385.

(7) Svensson, H. P., Vrudhula, V. M., Emsweiler, J. E., MacMaster, J. F., Cosand, W. L., Senter, P. D., and Wallace, P. M. (1995) In vitro and in vivo activities of a doxorubicin prodrug in combination with monoclonal antibody β-lactamase conjugates. *Cancer Res. 55*, 2357−2365.

(8) Kerr, D. K., Li, Z., Siemers, N. O., Senter, P. D., and Vrudhula, V. M. (1998) Development and activities of a new melphalan prodrug designed for tumor-selective activation. *Bioconjugate Chem. 9*, 255−259.

(9) Kerr, D. E., Schreiber, G. J., Vrudhula, V. M., Svensson, H. P., Hellstrom I., Hellstrom, K. E., and Senter, P. D. (1995) Regressions and cures of melanoma xenografts following treatment with monoclonal antibody β-lactamase conjugates in combination with anticancer prodrugs. *Cancer Res. 55*, 3558−3563.

(10) Svensson, H. P., Frank, I. S., Berry, K. K., Vrudhula, V. M., and Senter, P. D. (1998) Therapeutic effects of monoclonal antibody-β-lactamase conjugates in combination with a nitrogen mustard anticancer prodrug in models of human renal cell carcinoma. *J. Med. Chem. 41*, 1507−1512.

(11) Siemers, N. O., Kerr, D. E., Yarnold, S., Stebbins, M., Vrudhula, V. M., Hellström, I., Hellström, K. E., and Senter, P. D. (1997) Construction, expression, and activities of L49-sFv-β-lactamase, a single chain antibody fusion protein for anticancer prodrug activation. *Bioconjugate Chem. 8*, 510−519.

(12) Meyer, D. L., Jungheim, L. N., Law, K. L., Mikolajczyk, S. D., Shepherd, T. A., Mackensen, D. G., Briggs, S. L., and Starling, J. J. (1993) Site-specific prodrug activation by antibody-β-lactamase conjugates: regressions and long-term growth inhibition of human colon carcinoma xenograft models. *Cancer Res. 53*, 3956−3963.

(13) Meyer, D. L., Law, L. L., Payne, J. K., Mikolajczyk, S. D., Zarrinmayeh, H., Jungheim, L. N., Kling, J. K., Shepherd, T. A., and Starling, J. J. (1995). Site-specific prodrug activation by antibody-β-lactamase conjugates: preclinical investigation of the efficacy and toxicity of doxorubicin delivered by antibody directed catalysis. *Bioconjugate Chem. 6*, 440−446.

(14) Woodbury, R. G., Brown, J. P., Yeh, M. Y., Hellström I., and Hellström K. E. (1980) Identification of a cell surface protein, p97, in human melanomas and certain other neoplasms. *Proc. Natl. Acad. Sci. U.S.A. 77*, 2183−2187.

(15) Bosslet, K., Czech, J., Lorenz, P., Sedlacek, H. H., Schuermann, M., and Seemann, G. (1992) Molecular and functional characterisation of a fusion protein suited for tumour specific prodrug activation. *Br. J. Cancer 65*, 234−238.

(16) Haisma, H. J., Sernee, M. F., Hooijberg, E., Brakenhoff, R. H., Meulen-Muileman, I. H., and Pinedo, H. M. (1998) Construction and characterization of a fusion protein of single-chain anti-CD20 antibody and human beta-glucuronidase for antibody-directed enzyme prodrug therapy. *Blood 92*, 184−190.

(17) Rodrigues, M. L., Presta, L. G., Kotts, C. E., Wirth, C., Mordenti, J., Osaka, G., Wong, W. L., Nuijens, A., Blackburn, B., and Carter, P. (1995) Development of a humanized disulfide-stabilized anti-p185HER2 Fv-beta-lactamase fusion protein for activation of a cephalosporin doxorubicin prodrug. *Cancer Res. 55*, 63−70.

(18) Rodrigues, M. L., Carter, P., Wirth, C., Mullins, S., Lee, A., and Blackburn, B. K. (1995) Synthesis and β-lactamase-mediated activation of a cephalosporin-taxol prodrug. *Chem. Biol. 2*, 223−227.

(19) Goshorn, S. C., Svensson, H. P., Kerr, D. E., Sommerville, J. E., Senter, P. D., and Fell, H. P. (1993) Genetic construction, expression, and characterization of a single-chain anti-carcinoma antibody fused to β-lactamase. *Cancer Res. 53*, 2123-2127.

(20) Svensson, H. P., Wallace, P. M., and Senter, P. D. (1994) Synthesis and characterization of monoclonal antibody-β-lactamase conjugates. *Bioconjugate Chem. 5*, 262−267.

(21) Siemers, N. O., Yelton, D. E., Bajorath, J., and Senter, P. D. (1996) Modifying the specificity and activity of the Enterobacter cloacae P99 β-lactamase by mutagenesis within an M13 phage vector. *Biochemistry, 35*, 2104−2111.

(22) Mousli, M., Goyffon, M., and Billiald, P. (1998) Production and characterization of a bivalent single chain Fv/alkaline phosphatase conjugate specfic for the hemocyanin of the scorpion *Androctonus australis*. *Biochim. Biophys. Acta 1425*, 348−360.

(23) Reiter, Y., and Pastan, I. (1996) Antibody engineering of recombinant Fv immunotoxins for improved targeting of cancer: disulfide-stabilized Fv immunotoxins. *Clin. Cancer Res. 2*, 245−252.

(24) Matthey, B., Engert, A., Klimka, A., Diehl, V., and Barth, S. (1999). A new series of pET-derived vectors for high efficiency expression of pseudomonas exotoxin-based fusion proteins. *Gene 229*, 145−153.

(25) Francisco, J. A., Gawlak, S. L., Miller, M., Bathe, J., Russell, D., Chace, D., Mixan, B., Zhao, L., Fell, H. P., and Siegall, C. B. (1997) Expression and characterization of bryodin 1 and a bryodin 1-based single-chain immunotoxin from tobacco cell culture. *Bioconjugate Chem. 8*, 708−713.

(26) Newton, D. L., Xue, Y., Olson, K. A., Fett, J. W., and Rybak, S. M. (1996) Angiogenin single-chain immunofusions: influence of peptide linkers and spacers between fusion protein domains. *Biochemistry 35*, 545−553.

(27) Runge, M. S., Bode, C., Haber, E., and Quertermous, T. (1991) Hybrid molecules: insights into plasminogen activator function. *Mol. Biol. Med. 8*, 245−255.

(28) Wallace, P. M., MacMaster, J. F., Smith, V. F., Kerr, D. E., Senter, P. D., and Cosand, W. L. (1994) Intratumoral generation of 5-fluorouracil mediated by an antibody-cytosine deaminase conjugate in combination with 5-fluorouracil. *Cancer Res. 54*, 2719−2723.

(29) Aboagye, E. O., Artemov, D., Senter, P. D., and Bhujwalla, Z. M. (1998) Intratumoral conversion of 5-fluorocytosine to 5-fluorouracil by monoclonal antibody-cytosine deaminase conjugates: noninvasive detection of prodrug activation by magnetic resonance spectroscopy and spectroscopic imaging. *Cancer Res. 58*, 4075−4078.

(30) Bosslet, K., Czech, J., and Hoffman, D. (1994) Tumor-selective prodrug activation by fusion-protein-mediated catalysis. *Cancer Res. 54*, 2151−2159.

BC990075W

Fluorescent Neoglycoproteins: Antibody-Aminodextran-Phycobiliprotein Conjugates

Olavi Siiman,*,† Julie Wilkinson,† Alexander Burshteyn,‡ Patricia Roth,† and Stephen Ledis†

Advanced Technology, and Reagents Applications & Development, Beckman Coulter, Inc., 11800 SW 147th Avenue, Miami, Florida 33196-2500. Received June 14, 1999; Revised Manuscript Received September 15, 1999

New, highly amino-substituted dextran or aminodextran (hereafter denoted Amdex) of various sizes between about 20 and 1000 kDa molecular mass and degrees of amino-substitution between 7 and 40% were prepared and characterized by elemental analyses and polyacrylamide gel electrophoresis. These aminodextrans together with others commercially available were shown by static light scattering, viscosity, and refractive index measurements to adopt a globular structure in aqueous salt solutions. Antibody and fluorescent protein dye, phycoerythrin, or its tandems with cyanin 5.1 and TEXAS RED, were covalently conjugated to the aminodextrans. The conjugates contained multiple dye molecules and were shown by dynamic light scattering and scanning electron microscopy to assume either globular structure or aggregates thereof. Streptavidin could be substituted for antibody to prepare streptavidin−aminodextran−PE conjugates, which were then used with biotinylated antibody to label subpopulations of white blood cells. The conjugates yielded up to 20-fold amplification of fluorescence intensity over direct antibody−dye conjugates in labeling white blood cells for flow cytometry.

INTRODUCTION

Water-soluble polysaccharides such as dextrans have enjoyed widespread use in the preparation of neoglycoproteins, the synthetic analogues of glycoproteins, as reviewed in ref *1*. Dextrans and other polysaccharides are inert to most direct reactions with proteins, and must be chemically activated to allow conjugation to proteins. The use of antibody-dextran-type substances as carriers for drugs, toxins, photoprobes, etc. has been previously described for ternary conjugates of antibody−polyaldehyde dextran−methotrexate (*2*), antibody−aminodextran−chlorin (*3*), and antibody−dextran hydrazide−Sn(IV) chlorin (*4*). Other conjugated and dextran-crosslinked species have been described in several texts and review articles (*5*−*9*). One of the primary methods of preparing protein−dextran conjugates first involves preparation of "aminodextran". Common practice for the introduction of amine groups at random positions in dextran has been to first cleave the sugar rings with periodate to form polyaldehyde−dextran. The second step is to react the cleaved rings with a diamine such as ethylenediamine or 1,3-diaminopropane to form a Schiffs' base, which is then stabilized by reduction with sodium borohydride. The "aminodextran" compounds as described in the literature cited above were not well characterized. Typically, they were not isolated as solid compounds and, thus, were not characterized by elemental analyses and average molecular mass determinations. Further, the periodate oxidation−diamine method of preparing aminodextrans was restricted to a low percentage of amino groups per molecule. The percentage was less than 4−5%. Higher degrees of amine substitution were not possible under the usual conditions because high diamine concentrations caused extensive aminolysis of the glucosidic linkages between the sugar rings in dextran which resulted in very low molecular mass fragments. As a result, the yields were low and decreased drastically as higher degrees of amine substitution were pursued.

An alternative method of producing aminodextrans without opening glucopyranose rings involves carboxymethylation of sugar residue hydroxyl groups by chloroacetic acid, followed by carbodiimide coupling of a diamine such as ethylenediamine. This method (*10*−*11*) has been used to produce an aminodextran having about one amine group per 67 glucose residues, which is then used to prepare anti-Ig antibody−aminodextran conjugates for use in inducing B cell activation and proliferation.

Other methods of preparing protein−dextran conjugates include the direct reaction of protein with polyaldehyde−dextran (*2*), the reaction of an oxidized oligosaccharide moiety in a monoclonal antibody (MCA) with dextran hydrazide (*4*), the coupling with cyanogen-bromide-activated dextran (*12*), the spontaneous Maillard reaction in controlled dry heating between the ϵ-amino groups in proteins and the reducing-end carbonyl groups in polysaccharides (*13*), and the selective reductive amination of the single terminal aldehyde group of dextran (*14*).

Protein−dextran conjugates possess certain advantageous properties. It has been shown that enzymes possess enhanced thermal stability, when they have been immobilized by covalent attachment to polymers. Examples include glucoamylase on various periodate oxidized polysaccharides (*15*, *16*) and trypsin on cyanogen-bromide-activated dextran (*12*). Other noted effects of protein conjugation to polysaccharides were improved emulsifying properties (*17*), improved solubility of insoluble gluten (*18*), enhanced antioxidant effect of ovalbumin (*19*), and broadened bactericidal effect of lysozyme (*20*). Our own work has been focused on the synthesis of new, highly substituted (7−40%) aminodextrans and their use as (1)

* To whom correspondence should be addressed. E-mail: olavi.siiman@coulter.com.
† Advanced Technology.
‡ Reagents Applications & Development.

10.1021/bc990077g CCC: $18.00 © 1999 American Chemical Society
Published on Web 10/26/1999

conjugates with anti-CD3 monoclonal antibody (*21*) for the activation and proliferation of T cells; (2) a locus for nucleation and growth of magnetic metal oxide (*22*) particles and luminescent II−VI metal sulfide semiconductor[1] nanoparticles; (3) a locus for nucleation and growth, and a reducing agent for preparation of colloidal metal particles (*23*−*24*); and (4) coatings (*25*, *26*) for colloidal particles.

Nevertheless, amplification of fluorescence by this method has not hithertofore been part of this success. Amplification of light signals for detection of species present in very low concentrations has been achieved in other ways, such as when enhanced light emission (*27*, *28*) was observed by indirect fluorescence staining of cell receptor sites with multiple layers of phycoerythrin−streptavidin attached to biotinylated antibody at cell receptor sites. However, enhanced light-induced photochemistry (*3*) was used in excitation of chlorin e_6 coupled through dextran to anti-T-cell monoclonal antibody to enhance singlet oxygen production. The common feature in these studies was the required increase in the number of probe molecules per targeted site.

This method applied to fluorescence amplification in organic dyes of low molecular mass does not work well. In one attempt, ca. 1978, described in refs *29* and *30*) at amplification of fluorescence signals, large numbers (several hundred) of fluorescein molecules were attached to a synthetic polymer, polyethylenimine, which was then conjugated with antibody. Since fluorescence emission from fluorescein molecules was quenched under these circumstances due to short nearest neighbor distances between fluorophores on the same polymer molecule, lack of control over fluorophore spatial orientation, and lack of control over the structure of the resultant conjugate, the method did not work. More than 100 fluorescent dextrans consisting of soluble dextrans (10−2000 kDa) conjugated with various fluorescent dyes such as fluorescein, dansyl, rhodamine, and TEXAS RED are commercially available (*31*). The degrees of substitution are 1−2 dyes/dextran of 10 kDa, 2−4 dyes/dextran of 40 kDa, 3−6 dyes/dextran of 70 kDa, ∼64 dyes/dextran of 500 kDa, and ∼134 dyes/dextran of 2000 kDa. Higher degrees of substitution than these may lead to quenching and nonspecific interactions. Most of the listed dextran conjugates are also available as so-called "lysine-fixable", i.e., have incorporated lysine residues, which can be used for further reaction such as covalent attachment of antibody molecules. Fluorescein isothiocyanate (FITC) derivatives of dextran and poly-L-lysine are also commercially available from sources such as Sigma Chemical Co. with degrees of substitution ranging 0.003−0.020 mol of FITC/mol of glucose and 0.003−0.01 mol of FITC/mol of lysyl residue. For the largest molecular mass dextran of 2000 kDa that is listed, 33−222 FITC molecules/molecule of dextran would be available. For a 70 kDa poly-L-lysine molecule, up to 5.5 FITCs are available. One molecule of phycoerythrin (PE) (*32*), however, contains 34 individual chromophoric groups, each of which exhibits about the same fluorescent intensity as one FITC unit. PE, isolated from phycobilisomes, the main light-harvesting pigment complexes in prokaryotes such as red algae and cyanobacteria, utilizes linear tetrapyrroles as chromophoric groups and is among the brightest fluorescent dyes currently available. On a molar basis, one molecule of PE has a fluorescence yield that is equivalent to at least 30 fluorescein or 100 rhodamine molecules at comparable wavelengths. Thus, the largest molecular mass FITC−dextran conjugate with the greatest degree of FITC substitution has the potential to yield a fluorescence enhancement factor of 222/30 = 7.4 over a single PE molecule. With so many FITC units per dextran carrier and a broad distribution in the molecular mass of each dextran, it would be difficult to synthetically mimic the monodisperse population of fluorescent groups that occurs naturally in molecules of PE. The spread in fluorescent intensities from one molecule of FITC−dextran complex to another will offset the large enhancement factor that may be numerically anticipated. No enhancement factor greater than one, relative to PE fluorescence, has hithertofore been reported for the above FITC derivatives of dextran or poly-L-lysine, and no direct fluorescent stain which has a net fluorescence intensity greater than a single PE molecule is currently known.

In phycoerythrin (PE) (*32*), there is a monodisperse population of fluorescent bilin groups naturally embedded in a protein through biosynthesis. PE exhibits maximal absorbance and fluorescence without susceptibility to either internal or external fluorescence quenching so that attachment of two or more PE molecules to a polymeric carrier should not quench PE fluorescence. The net fluorescence intensity from a PE−polymer complex should be the sum of fluorescence intensities from individual PE molecules. Only a single PE molecule (270 kDa) can normally be directly conjugated to an IgG antibody (160 kDa) and still retain antibody specificity (*33*, *34*). Polymeric carrier molecules such as aminodextran of sufficiently large molecular weight can accommodate multiple antibody molecules. Our previous experience, described in ref *21* in conjugating anti-CD3 (T3) monoclonal antibody to aminodextran (1×-Amdex, ∼1000 kDa, 7% diamine substitution; 5×-Amdex, ∼350 kDa, 25% diamine substitution) under saturating conditions of antibody on dextran gave a CD3 antibody:aminodextran molar ratio in the conjugates of 37:1 for CD3-1×-Amdex and 20:1 for CD3-5×-Amdex, thus showing that aminodextran can be effectively loaded with many large protein molecules. Similar methods can be used to prepare protein−aminodextran conjugates with two or more protein molecules per aminodextran molecule, the protein being of one type or several different types. Herein, we describe the preparation of such conjugates for immunofluorescent labeling applications in which one protein would be PE and the other would be an antibody. Aminodextrans and the ternary conjugates were characterized by light scattering and scanning electron microscopy (SEM). Triple detector (light scattering, viscosity, and refractive index) measurements for all aminodextrans derived from linear, water-soluble dextran showed that the product aminodextrans were also linear, even though analytical evidence for branching through intermolecular cross-linking was suggested for some preparations of highly substituted aminodextran. Previous work in the high-resolution transmission electron microscopy (TEM) of antibodies, polysaccharides, and phycobilisomes and their component pigments has revealed the ultrastructure of antibody shape, the branching of polysaccharide chains in proteoglycans (*35*, *36*), and the shape and size of R-phycoerythrin (*32*). Herein, moderate resolution SEM is used to determine the shape and size of ternary conjugates of MCA and PE with aminodextrans.

Enhanced phycoerythrin fluorescence intensities per marker in labeling white blood cells were obtained by substituting the direct conjugates with aminodextran-cross-linked conjugates, which results have been reported

[1] Matijevic, E., Sondi, I., Koester, S., and Siiman, O., unpublished results.

by us in meeting proceedings, and in issued and pending patents (*37*−*39*). The amplification of fluorescence was initially demonstrated for marked cells which usually showed dim fluorescence intensity (*37*, *38*) when their receptors for monoclonal antibodies (BB27, IL12Rβ.44, and BY55) were saturated with direct antibody−PE conjugates and their fluorescence intensity was measured by flow cytometry. PE-tandem dye molecules that can be excited with the same laser line, 488.0 nm Ar^+, as PE, were also incorporated into cross-linked conjugates to offer a set of six different markers using three colors, two intensity per color. One tandem dye is PC5 (PE-Cy5, phycoerythrin-cyanin 5.1) (*40, 41*), and a second tandem dye is ECD (phycoerythrin-TEXAS RED) (*42*, *43*). This allowed multiplex labeling (*39*) of cells for analysis of mixed cell populations by flow cytometry.

EXPERIMENTAL PROCEDURES

Materials. Dextran, T-2M, produced by *Leuconostoc mesenteroides*, strain B-512, was obtained from the Sigma Chemical Co., St. Louis, MO, as were other chemicals related to the preparation of aminodextrans. All inorganic chemicals were of reagent grade and were not further purified. Dextran, amino, nominally of 2 MDa M_r (molecular mass, was purchased from Molecular Probes, Inc., Eugene, OR, abbreviated as Amdex-M.P. Analytical data for lot 6551−3: 130 amines/mol. Measurement of the molecular mass of this lot of aminodextran by the Viscotek Corp. (Houston, TX) triple detection system (vide infra) gave ∼3 MDa. Therefore, there are (3 000 000 g/mol)/(162.1 g/mol glucose monomer) = 18 507 glucose units/dextran molecule or 130/18 507 = 0.007 02, i.e., ∼1/140 degree of substitution with single amine group per reacted glucose unit. The degree of substitution unless otherwise noted is defined as the total number of amino groups (primary and secondary) per monomeric glucose unit in the aminodextran molecule.

R-PE (catalog no. PB31), extracted and purified from red algae, was obtained from Prozyme, Inc., San Leandro, CA. Sulfosuccinimidyl 4-(*N*-maleimidomethyl) cyclohexane-1-carboxylate (sulfo-SMCC) was a Pierce product while 2-iminothiolane hydrochloride, L-cysteine, free base, and iodoacetamide were from Sigma. Column packing materials, G-25 or G-50 Sephadex and Bio-Gel A-5m and A-15m, were products of Pharmacia Biotech and Bio-Rad Laboratories, respectively. Phosphate-buffered saline, 1× PBS, pH 7.1−7.3, and conductivity, 13500−15500 $\mu\Omega^{-1}$ cm^{-1}, was prepared by dilution with distilled water from a 20× PBS stock solution, which contains 26.9 g dm^{-3} of K_2HPO_4, 6.4 g dm^{-3} of KH_2PO_4, and 170.0 g dm^{-3} of NaCl.

Desalting and purification of aminodextrans was carried out with hollow fiber (polysulfone, 9.9 ft^2 membrane surface area, 1 mm diameter fibers) cartridges, A/G Technology Corp. model UFP-5-E-35 (5 kDa MWCO) or model UFP-30-E-35 (30 kDa MWCO), with tubing adaptor kit, KA12-3P. Lyophilization of the final washed aminodextrans was accomplished with an FTS Systems, Inc. model TDS-00030-A, Dura-Dry microprocessor-controlled freeze-drier.

The CD4 antibody [CD4 clone SFCI12T4D11 (IgG1)] and CD8β antibody [CD8β clone 2ST8.5H7(IgG2a)] are products of Coulter Corp., Miami, FL. Anti-CD4-FITC, -PE, and -ECD are products of Coulter Corp. Streptavidin (catalog no. 15532-039) was obtained from Gibco Life Technologies, Inc., Gaithersburg, MD. Avidin, NeutraLite, R-phycoerythrin conjugate (catalog no. A-2660) was obtained from Molecular Probes, Inc.

Preparation of Aminodextrans. Aminodextrans were obtained commercially or were prepared by the following procedures. In a standard preparation of 1×-Amdex, 8.56 g of $NaIO_4$ in 100 mL of distilled water (DW) was added dropwise to 80 g of dextran (2 MDa) in 600 mL of DW over about 10 min with vigorous stirring, after which the mixture was stirred at room temperature for 3 h. The resulting viscous reaction mixture was then diluted to 2 L with DW and desalted using a hollow fiber cartridge and about 18−22 L of DW to obtain a solution having a final pH of 6.0−6.5. To the final, 800 mL volume of washed, oxidized dextran solution was slowly added 80 mL of colorless, liquid 1,3-diaminopropane (DAP) over about 10 min at room temperature. The resulting mixture was stirred for 3 h. Then, 3.2 g of $NaBH_4$ in 40 mL of 1 mM aqueous NaOH was added to the aminodextran reaction mixture over about 5 min with stirring. The resulting mixture was stirred for 1 h and then desalted using a 5 kDa MW cutoff hollow fiber cartridge and about 20−25 L of DW to reduce the specific conductance to about 3−4 $\mu\Omega^{-1}$ cm^{-1} and the pH to 6.0−6.5. The final volume of aminodextran solution was 400 mL. This solution was passed through a 0.2 μm sterile cellulose acetate filter unit and then freeze-dried to obtain 48 g of flaky, pale yellow solid, a 52% yield. Elemental analysis observed: C, 42.53; H, 6.52; N, 1.01; O (by difference), 49.94. Elemental analysis calcd for $C_{49}H_{84}NO_{40}\cdot 3H_2O$: C, 42.61; H, 6.57; N, 1.01; O, 49.81. The empirical formula $C_{49}H_{90}NO_{43}$ is very similar to the formula based on 31 units of glucose, 1 unit of fully diamine substituted sugar ring, and three units of water. The degree of substitution in dextran by diamine was 1/32. Other runs varied between 1/28 and 1/45 degree of substitution. Similar results were obtained for aminodextrans prepared from dextrans having average M_r of 10 kDa to 2 MDa with 1×−5×-diaminopropane substitution. Modifications were made to periodate oxidation, diamine addition, and borohydride reduction reactions. The first modification was to use only a 10% excess of diamine over the stoichiometric 2:1 diamine:periodate molar ratio previously used. Second, the diamine addition reaction was conducted at a temperature in the range of 5−10 °C. Third, the diamine addition reaction was spectroscopically monitored in the near-UV region for Schiffs' base formation, which was deemed completed when successive spectral analyses indicated a plateau was reached. These modifications reduced depolymerization and thus gave higher yield of product. Elemental analyses for 5×-Amdex, lot −11, which was prepared at a 500 g dextran scale and gave the best yield of conjugates were C , 44.45%; H, 7.20%; N, 3.79%, O (by difference), 44.56%. The empirical formula was $C_{13.7}H_{26.4}O_{10.3}N$, which is similar to the formula $C_{13}H_{24}O_9N\cdot H_2O$ based on 5 units of glucose/1 unit of 1.5 diaminopropane-substituted sugar ring ($C_{9.5}H_{21}O_2N_3$), or a degree of substitution in dextran of 1/6. Similar results were obtained for 5×-Amdex, lot −69 prepared at a 300 g dextran scale. High diamine concentrations caused depolymerization and thus gave significantly lower molecular weight aminodextrans than the starting dextran. β-Elimination and thereby depolymerization (*44*) has been previously noted in various oxidation reactions of cellulose and starch. The periodate oxidation of glucose units in dextran was shown (*45*, *46*) to release one mole of formic acid per mole of reacted glucose unit by 95% of the anhydroglucose residues. Thus, the overall redox equation requires 2 mol of periodate/1 mol of glucose unit or 2 mol of aldehyde for complete reaction. However, in 5×-Amdex preparations, 2 mol of periodate/5 mol of glucose units were used so

that the theoretical degree of substitution is 1/5. Thus, the maximum degree of substitution of dextran with DAP is also 1/5.

Partially cross-linked 5×-Amdex was prepared by a modified procedure. Dextran, T-2M, 500 g was blended in 4 L of DW to dissolve all solid. A solution of 267.5 g of sodium m-periodate in 2 L of DW was added to the dextran solution over a 5−15 min period using vigorous stirring. The reaction mixture was stirred for 4 h, over which 5−6 L of DW further was added to reduce the viscosity of the solution. The reaction mixture was then desalted using about 100 L of distilled water to obtain 6−9 L of washed, oxidized dextran solution having a specific conductance of about 6−20 $\mu\Omega^{-1}$ cm^{-1} and pH of 6.5−7.0. Then, the first portion of DAP, 70 mL of pure liquid, was added over about 5 min to the desalted, oxidized dextran solution. The resulting solution immediately began to show formation of a gel, which persisted for another 5−10 min before redissolving as a yellow solution. The reaction mixture was then put on an ice bath to maintain a reaction temperature of 8−10 °C and stirred vigorously before a second portion of 70 mL of DAP was added over a period of 5 min. After an additional 10 min of stirring, the third and final 70 mL portion of DAP was added to the reaction mixture. The total DAP addition and reaction time was 45 min. Then, 70 g of sodium borohydride in 700 mL of 1 mM aqueous KOH solution were added to the reaction mixture at 8−10 °C over about 10−15 min with overhead stirring. The reaction mixture was stirred for an additional 2 h until the yellow Schiffs' base color had disappeared. The reaction mixture was then desalted using a 5 kDa MW cutoff hollow fiber cartridge and about 80 L of DW to produce about 1.6 L of aminodextran solution having a specific conductance of 10−20 $\mu\Omega^{-1}$ cm^{-1} and pH of 7.0−8.0. The aminodextran solution was filtered through a 1.6 μm glass filter and lyophilized for a minimum of 72 h to produce 75−90 g (15−18% yield) of flaky, white to pale yellow crystals. Analyses for 5×-Amdex, lot 1−5, which gave a good yield of conjugates were C = 41.38%, H = 7.81%, N = 4.15%, O = 45.64%, I = 97 ppm, B = 590 ppm. The empirical formula was $C_{11.6}H_{26.1}O_{9.6}N$, which is similar to the formula $C_{11.2}H_{20.3}O_{7.3}N{\cdot}2H_2O$ based on 4 units of glucose/one unit of 1.5 diaminopropane-substituted sugar ring. Thus, the degree of diamine substitution in dextran was 1/5. Similar procedures were used in the preparation of 5×-Amdex, lot 2−2, except 1/3 x DAP was added in two portions and a 30 kDa MW cutoff hollow fiber cartridge was used for desalting to give a product which analyzed as C, 40.44%; H, 7.75%; N, 3.48%; O, 48.48% with a degree of substitution of 1/8.

Some 5×-Amdex lots require further description. The reaction mixture of the 5×-Amdex, lot 11−6, after addition of DAP and sodium borohydride, was adjusted to pH 8.5 with aqueous hydrochloric acid. It was then desalted, concentrated, and freeze-dried in the previously described manner. Elemental analyses for 5×-Amdex, lot 11−6, were C, 39.72%; H, 7.77%; N, 4.44%; Cl, 2.81%; O (by difference), 45.26%. The empirical formula based on actual analyses was $C_{10.4}H_{24.3}O_{8.9}NCl_{0.25}$. The chloride analysis showed that one of four total amine (primary and secondary) groups had a chloride counterion. As shown in the following section describing results of electrophoretic light-scattering experiments on suspensions of polystyrene latex beads coated with DAP or aminodextran, only primary amine groups are protonated near neutral pH to which the reaction mixture was desalted prior to lyophilization, this implies that 50% of the diaminopropane groups in aminodextran are bridging or cross-linking groups between dextran chains. A portion of the lyophilized aminodextran hydrochloride was dissolved in DW and deionized in batchwise fashion with mixed bed (H^+, OH^- form), Bio-Rad AG 501-X8 resin, until the specific conductivity of the supernatant was minimized. The resin was removed by filtration of the suspension through rayon cloth, and the aminodextran (∼50 mg/mL) in the filtrate was fractionated by precipitation with acetone (0−43% cut). The solid precipitate was washed with acetone and dried in a vacuum desiccator under silica gel. Elemental analyses of this deionized and fractionated material gave C, 45.55%; H, 7.03%; N, 3.82%; Cl < 0.5%, O (by difference), 43.60%, showing that chloride ion had been removed.

DELSA Results for DAP- and Amdex-Coated Polystyrene Latex Beads. 1,3-Diaminopropane (DAP) in aqueous solution is reported (*47*) to show acid dissociation constants, pK_{a1} = 10.94 and pK_{a2} = 9.03 at 10 °C. When either one of the primary amine groups of DAP is converted to a secondary amine in DAP derivatives, the pK_a of the secondary amine is expected to drop significantly. This was borne out when protonation of primary and secondary amines of DAP derivatives was observed (*48*) in Coulter DELSA (Doppler Electrophoretic Light Scattering Analyzer) 440 experiments with DAP−PS and 1×-Amdex-polystyrene (PS) latex beads dispersed in aqueous media. Multiangle Doppler electrophoretic light scattering measurements have been reviewed (*49*). Mobility versus pH data were obtained for PS aldehyde/sulfate beads, nominally of 2.0 μm diameter from Interfacial Dynamics Corp., and the same beads coated covalently with DAP or 1xAmdex at pH ∼10, followed by reduction of the Schiffs' base with sodium borohydride, and washing of the beads by centrifugation at 3000−4000*g*, discarding the supernatant, and redispersion of the residue in an equal volume of distilled water. The chemistry that was used in converting aldehyde PS beads to DAP−PS beads was the same as that used in the conversion of oxidized dextran to aminodextran. Note that any unreacted aldehyde in the reaction with DAP is converted to alcohol by borohydride reduction. Bead suspensions, 4 or 1% w/v solids, were diluted about 1000-fold with 0.01 M aqueous sodium nitrate solution, and pH was adjusted with either 0.1 M aqueous sodium hydroxide or 0.1 M aqueous sulfuric acid solutions.

The mobility of DAP−PS beads shows a relatively flat, −0.275 to −0.92 cm^2/V s, dependence from pH 7 to 9; but, a relatively steep rise from −0.275 to +4.87 cm^2/V s between pH 7.0 and 5.6. Raw PS aldehyde/sulfate beads show a highly negative mobility of −6.6 to −6.0 cm^2/V s between pH 9.9 and 5.6, and then a slight rise to −4.4 cm^2/V s at pH 4.3. The data for DAP−PS beads indicate nearly complete compensation of the negative sulfate group charge by protonated primary amine groups in the pH 9 to 7 range, and further protonation of secondary amine at acidic pH less than 7. A similar trend is observed in electrophoretic mobilities of 1×-Amdex-PS beads. An almost flat mobility versus pH dependence of −1.161 to −1.083 cm^2/V s from pH 7 to 9, but a rise from −1.161 to +0.567 cm^2/V s was observed between pH 7.0 and 5.6. 1×-Amdex-coated PS beads show less compensation for the negative sulfate charge due to less than saturation coverage of the bead surface by amine groups of the polymeric diaminopropane-dextran derivative and correspondingly fewer secondary amine groups protonated at acidic pH less than 7.

Preparation of Buffer-Exchanged Phycoerythrin (PE). In one run, four 2.5 mL portions of 20 mg/mL Prozyme PE concentrate (in 60% ammonium sulfate, 50

mM phosphate, and 5 mM sodium azide) were each pipetted into four 50 mL polypropylene centrifuge tubes. A total of 25 mL of PE storage buffer (50 mM phosphate and 2 mM EDTA, pH 7.0) was added to each of the four tubes. The tubes and contents were roller mixed for 30 min and then centrifuged for 30 min in a Beckman J6-B centrifuge at 3200 rpm. Residues were discarded. Supernatants were retained, and concentrated in CentriPrep-30 tubes (Amicon) by multiple centrifugations for about 20min each at 2000 rpm. The final 1−2 mL of PE concentrate was applied to the top of a 60 mL of G-50 Sephadex column, equilibrated, and eluted with PE storage buffer. The middle fraction, about 4 mL of total volume, was collected and retained. Absorbance readings for a 50-fold diluted sample at 565 nm gave a PE concentration in the concentrate of 35.050 mg/mL and a yield of 140.2 mg of PE. Further concentration of this fraction to 1−2 mL total volume gave a PE concentrate of 104.7 mg/mL.

Preparation of Antibody−Phycobiliprotein Conjugates. Direct monoclonal antibody (MCA)-fluorochrome (PE, PC5, and ECD) conjugates are commercially available for most antibodies from Coulter Corporation or Immunotech, as prepared by established procedures of conjugation reactions of 2-iminothiolane (IT) activated PE (or PC5; ECD) with sulfo-SMCC activated antibody or sulfo-SMCC activated PE (or PC5; ECD) with DTT (dithiothreitol) reduced antibody. The molar ratio of MCA:fluorochrome in these conjugates is about 1:1. Conjugation of IgG monoclonal antibody to PC5 was accomplished by sulfosuccinimidyl 4-[*N*-maleimidomethyl] cyclohexane-1-carboxylate (sulfo-SMCC) activation of PC5 and activation of antibody by reduction of disulfide bonds in the hinge region with DTT. As an example, a 100-fold dilution of the CD8β Antibody-PC5 conjugate pooled sample gave an $A_{565.5} = 0.4809$, yielding 20.31 mg of total PC5 in the CD8β−PC5 conjugate, and an $A_{280} = 0.1513$, giving 21.90 mg of total CD8β antibody in the CD8β−PC5 conjugate. The molar ratio of PC5/CD8β is, therefore, 0.618. A corrected *F*/*P* ratio based on the formula, MCA:PC5 = $[A_{280}/A_{565.5}$ (conjugate) − $A_{280}/A_{565.5}$ (dye)] × 8.77, is 0.864. Similar methods were used to prepare an CD4−ECD conjugate having an *F*/*P* ratio of 0.96.

Preparation of Antibody−Aminodextran−Phycobiliprotein Conjugates. The procedure was similar to the one previously (*21*) used to prepare conjugates of anti-CD3 antibody with aminodextran, either 1×-Amdex or 5×-Amdex. However, in the present work two different proteins, one, an iminothiolane-activated monoclonal antibody and the other, an iminothiolane-activated fluorescent protein, PE, PC5, or ECD, were conjugated simultaneously to the sulfosuccinimidyl 4-[*N*-maleimidomethyl] cyclohexane-1-carboxylate (sulfo-SMCC)-activated aminodextran. The IT to MCA and IT to PE (PC5 and ECD) molar ratios were maximized at 15 and 22.5, respectively, so as not to interfere with MCA activity (*7*) or with PE (PC5 and ECD) fluorescence intensity. Trials were typically done for new proteins at molar ratios of 7.5, 15, and 22.5. This is in accord with the exposure of CDR (complementary-determining or hypervariable region) and framework (or nonhypervariable region) residues in 34 human and murine antigen-binding regions of known three-dimensional structure (*50*). In 34 CDRs, of 78 total lys residues with an amine group which can react with IT, 60 are exposed to give an average of 2 exposed Lys/antibody, and of 3 total Cys residues, 0 are exposed, and 1 is partly buried. In 34 framework regions, of 296 total Lys residues, 237 are exposed to give an average of 7 exposed Lys/antibody, and of 136 total Cys residues, 0 are exposed, all are buried. Thus, the tested range 7.5−22.5 in IT:MCA molar ratio covers the maximum of about 9 Lys residues that can react with IT.

R-PE was further purified by centrifugation to remove high MW aggregates, followed by buffer exchange on G-50 Sephadex and concentration. Three protocols were used as follows.

(i) For 1×-Amdex conjugates, the molar ratio of reactants that were used was 4:1:4 = Dye:MCA:Amdex or the weight ratio was 25.713:4.287:10 = Dye:MCA:Amdex at the 10 mg Amdex scale.

(ii) For Amdex−Molecular Probes (hereafter denoted as Amdex or Amdex-M.P.), 50% less weight of dye, and MCA relative to Amdex was used so that molar ratio was 16:4:1 = Dye:MCA:Amdex and weight ratio was 12.856: 2.143:10 = Dye:MCA:Amdex at 10 mg Amdex scale.

(iii) For 5×-Amdex, the same dye:MCA:Amdex weight ratios as previously listed and as used in 1×-Amdex trials were adopted, but the molar ratio was 4:1:15 = Dye:MCA: Amdex.

Described below is the preparative procedure for Amdex-M.P.-cross-linked CD8β−PC5.

CD8β Antibody−Amdex−PC5 Conjugates. Conjugation was carried out with 50% less weight of dye and antibody relative to aminodextran so that molar ratio was 16:4:1 = PC5:CD8β antibody:Amdex and weight ratio was 12.856:2.143:10 at the 10 mg Amdex scale.

1. Activation of Aminodextran with sulfo-SMCC. A total of 0.340 mL of a 29.412 mg/mL solution of Amdex in distilled water, to which 0.018 mL of 20× PBS buffer solution was added to make a 1× PBS solution, was activated with 0.180 mL of 10 mg/mL sulfo-SMCC solution in 1× PBS, to which was added 0.462 mL of 1× PBS solution to make a total Amdex concentration of 10 mg/mL. The mixture was roller mixed for about 1 h at room temperature. After the mixing was completed, the reaction mixture was immediately applied to the top of a 60 mL (1.7 cm × 28 cm) G-50 Sephadex column equilibrated with 1× PBS. The sample was eluted using 1× PBS and collected in about 2 mL fractions. Fractions of the first band absorbing at 280 nm contained the high molecular weight activated Amdex as was verified by Tyndall scatter with a focused visible light beam (model 650, Cambridge Instruments, Inc., Buffalo, NY). These fractions were pooled to give about 5.8 mL of total sulfo-SMCC-activated Amdex.

2. Activation of Antibody. CD8β monoclonal antibody was activated by the addition of 0.033 mL of a 2 mg/mL solution of iminothiolane in 1× PBS and 0.219 mL of 1× PBS to 0.081 mL of CD8β concentrate (61.67 mg/mL). The resulting solution which had an antibody concentration of 15 mg/mL and an iminothiolane molar concentration 15-fold larger was mixed at ambient temperature for about 1 h. The reaction mixture was then chromatographed on a 60 mL (1.7 cm × 28 cm) G-50 Sephadex column equilibrated with 1× PBS, and the sample was eluted using 1× PBS. The first band peak fraction yielded about 4.2 mL of 1.113 mg/mL antibody solution, which contained a total of 4.67 mg of IT-CD8β antibody derivative.

3. Activation of PC5. PC5 was activated by the addition of 0.097 mL of a 2 mg/mL solution of iminothiolane in 1× PBS and 0.098 mL of 1× PBS to 0.179 mL of PC5 concentrate (83.625 mg/mL). The resulting solution which had a PC5 concentration of 40 mg/mL and an iminothiolane molar concentration 22.5-fold larger was mixed at room temperature for about 1 h. The reaction mixture

was then applied to the top of a 60 mL (1.7 cm × 28 cm) G-50 Sephadex column equilibrated with 1× PBS and the sample was eluted with 1× PBS. The first band peak fraction gave about 3.9 mL of 3.35 mg/mL PC5 at an A_{565}/A_{280} ratio of 6.2394, which contained a total of 13.065 mg of IT-PC5.

4. Conjugation of IT-CD8β and IT-PC5 to sulfo-SMCC-Amdex. For a 15 mg total protein, 10 mg Amdex weight ratio, 1.926 mL of 1.113 mg/mL IT-CD8β solution (about 2.143 mg antibody) was first mixed with 3.839 mL of 3.35 mg/mL IT-PC5 solution (about 12.86 mg IT-PC5), to which was added 5.8 mL of sulfo-SMCC−Amdex solution (about 10 mg Amdex), and the entire mixture was roller mixed overnight for 16−24 h.

After the mixing was completed, the total volume of the mixture was determined, and 0.120 times this volume of 5 mg/mL L-cysteine in 1× PBS was added to each conjugation mixture. The L-cysteine containing mixtures were then mixed for an additional 15 min to effect blocking of any unreacted sulfo-SMCC moieties. Last, 20 mg/mL iodoacetamide in 1× PBS in the amount of 0.120 times the total mixture volume and 1 M borate buffer solution, pH 9.8, in the amount of 0.020 times the total mixture volume were added to each mixture. The resulting mixtures were mixed for about 30 min to block any unreacted sulfhydryl groups.

5. Purification of CD8β-Amdex-PC5 conjugates. The total volume of conjugation mixture was reduced to about 2.5 mL by centrifuging an Amicon Centri-Prep 30 tube containing the sample for about 20 min at 2000 rpm using a refrigerated Beckman J-6B centrifuge. The sample was placed on the top of a Bio-Gel A-15m agarose column (2.5 cm × 48 cm) equilibrated with 1× PBS and chromatographed using 1× PBS as eluant. Eluant fractions of about 3.6 mL volume were collected using a Pharmacia LKB FRAC-100 collector operating in the drop collection mode. The fractions were monitored using a LKB 2138 Uvicord S monitor operating at 280 nm. The first narrow, intense band eluted from the column contained the CD8β−aminodextran−PC5 conjugate. A lower intensity shoulder of less than one-third the intensity of the first peak contained ∼1:1 PC5:aminodextran conjugate and excess PC5. A medium-to-low intensity well-separated third band was attributed to the low molecular weight excess blocking reagents.

The fractions collected for the CD8β−Amdex−PC5 conjugate were analyzed spectrophotometrically at 565.5 and 280 nm using a 1 mm path-length cell. The concentration of PC5 in mg/mL in the conjugate was derived from the absorbance at 565.5 nm by using the formula $A_{565.5}$/8.167. Data for fractions 19−24 under the first narrow peak gave 4.241 mg of total PC5 in the conjugate. Since 12.86 mg of IT-PC5 was used in conjugation, the yield was 33.32%.

6. Estimation of Molecular Masses of Antibody-Aminodextran-PE Conjugates. Blue dextran (Sigma, T-2M) was applied to an A-15m column that was used to purify the antibody−aminodextran−PE conjugates, eluted from the column with 1× PBS, monitored by A_{280}, and collected at the same drop count of 120 drops/fraction. The first narrow peak (about fraction 20) in the elution profile of antibody−aminodextran−dye conjugates occurred in the same fraction as the first narrow peak in the elution profile of blue dextran. Therefore, we estimate the conjugates to have a similar molecular mass of about 2 000 000 Da.

Trials with 5×-Amdex were run at a 4:1:15 molar ratio of Dye:MCA:Amdex or weight ratio of 25.713:4.287:10 at a 10 mg 5×-Amdex scale. Procedures for other aminodextrans were similar to the ones described above for Amdex-M.P., i.e., activation ratios were the same but amounts were doubled to reflect the 2× greater amount of dye and antibody. In trial 1 for CD8β antibody-5×-Amdex (lot −11)-PC5, purification of the conjugation mixture on Bio-Gel A-15m was carried out with collection of eluant fractions of 1.8 mL volume. A chromatogram showing the A_{280} versus fraction number recording is displayed in Figure 1. Data for fractions 36−46 under the first narrow peak containing the conjugate are listed in Table 1. The active CD8β antibody concentration was determined by an ELISA assay (*51*) for IgG1 antibody; however, assay results appeared to show interference from nonantibody parts of the conjugate. Thus, A_{280} values corrected for the PC5 contribution were used to obtain antibody concentrations. In another trial for CD8β antibody-5×-Amdex (lot 1−5)-PC5, the conjugation mixture gave an intense first band off the Bio-Gel A-15m column but the yield was low since the bulk of the blue−purple conjugate aggregated with the gel at the top of the column and could not be eluted. Fractions 20−25 collected at 3.6 mL/fraction gave 4.831 mg of conjugate, an 18.78% yield based on 25.724 mg of IT-PC5 used in the conjugation.

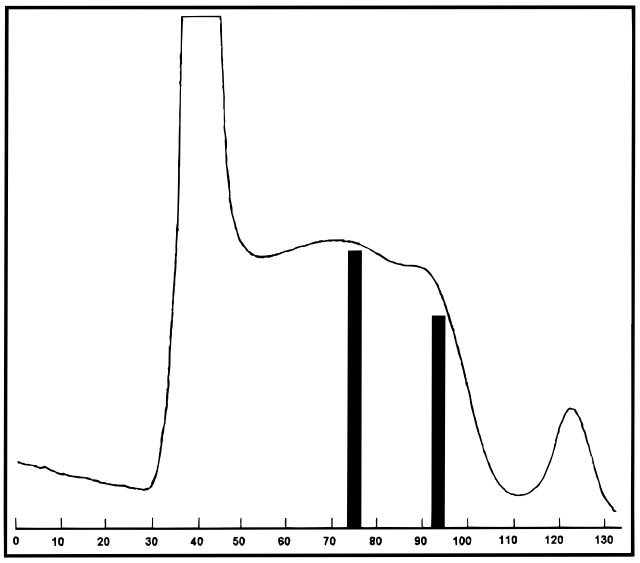


Figure 1. A_{280} versus fraction number trace for 2 mL of concentrate of CD8β−5×-Amdex−PC5 conjugate on Bio-Gel A 15 m column of 2.5 × 48 cm size. Run conditions: 1 mm/min chart speed; ∼1.3 mL/min elution with 1× PBS; 0−1 absorbance unit scale. Positions of A_{280} maxima for either PC5 or CD8β antibody alone on the column are indicated with bars in fractions 74−76, and 92−94, respectively.

Table 1. Fractionation Data for Trial 1, CD8β−5×-Amdex−PC5 Conjugate.

fraction	$A_{565.5}$	A_{280}	$A_{565.5}/A_{280}$	PC5 (mg/mL)	CD8β (mg/mL)
36	0.0891	0.0344	2.59	0.109	0.193
37	0.2661	0.0959	2.77	0.326	0.507
38	0.7280	0.2450	2.97	0.891	1.212
39	1.1681	0.3744	3.12	1.430	1.758
40	1.1810	0.3646	3.24	1.446	1.639
41	0.8906	0.2648	3.36	1.090	1.134
42	0.5169	0.1452	3.56	0.633	0.573
43	0.2720	0.0715	3.81	0.333	0.252
44	0.1637	0.0397	4.13	0.200	0.118
45	0.1160	0.0260	4.46	0.142	0.063
46	0.0915	0.0191	4.79	0.112	0.035

$A_{565.5}$ and A_{280} are absorbances measured at 565.5 and 280 nm with a 1 mm path length cell.

Table 2. Triple Detector System Data for Dextran and Various Aminodextrans.

sample	concentration (mg/mL)	d*n*/d*c* (mL/g)	M_w (kDa)	η (dL/g)	R_g (nm)	L (nm)	R_h (nm)
1. 5X-Amdex, lot −11	0.860	0.155	414	0.262	15.6	38.2	10.4
2. 5X-Amdex, lot −11	1.940	0.132	25.6	0.0602	3.79	9.28	2.52
3. 1X-Amdex, lot −75	0.940	0.155	1044	0.442	25.2	61.7	16.8
4. 1X-Amdex, lot −75	3.480	0.132	93.9	0.205	8.80	21.5	5.85
5. Dextran, T-2M	0.800	0.147	2,102	0.609	35.5	87.0	23.6
6. 5X-Amdex, lot 1−5	0.800	0.190	70.0	0.167	7.38	18.1	4.91
7. 5X-Amdex, lot 1−5	3.010	0.132	34.4	0.100	4.96	12.1	3.30
8. Amdex-M.P.	0.770	0.155	2999	0.674	41.3	101.2	27.5
9. 5X-Amdex, lot −69	2.400	0.132	69.95	0.141	7.06	17.3	4.69
10. 5X-Amdex, lot 11−6	2.610	0.132	44.5	0.0999	5.40	13.2	3.59
11. 5X-Amdex, lot 2−2	2.390	0.132	168.4	0.186	10.35	25.3	6.88
Dextran (*60*)			54 600		70.0		
Dextran (*63*)			65				12.5
Dextran (*63*)			20				10.0
Dextran (*63*)			500				22.5

CD4 Antibody−Amdex−ECD Conjugate. The procedures were the same as those outlined for the preparation of the anti-CD8β−Amdex−PC5 conjugate in Section II, except anti-CD4 antibody was activated with IT and used in the conjugation instead of CD8β antibody, and the tandem PE-Texas red or ECD fluorescent dye (*41, 42*) was used instead of PC5. In trial 2, IT-ECD (12.856 mg) and IT-CD4 (2.143 mg) were mixed with sulfo-SMCC−Amdex (10 mg) at concentrations of 1.10, 0.184, and 0.857 mg/mL, respectively, during conjugation. The IT-ECD ($A_{565.5}/A_{280}$) ratio was 5.424. The conjugation mixture was concentrated to about 1.5 mL and applied to the top of an A-15m column. Data for fractions 20−26, collected at about 3.6 mL/fraction under the first narrow peak in trial 2, gave 5.756 mg of total ECD in the conjugate. Since 12.858 mg of IT-ECD was used in conjugation, the yield was 44.77%.

CD4 Antibody−Amdex−PE Conjugates. Again, the procedures were the same as those outlined for the CD8β−Amdex−PC5 conjugate in section 2, except CD4 antibody of the IgG class and PE were activated with IT and used in the conjugation instead of CD8β antibody and PC5. In trial 3, the reactants, 3.896 mL of 3.30 mg/mL IT-PE (12.856 mg), were first mixed with 4.75 mL of sulfo-SMCC−Amdex (10 mg) solution, to which were then added 3.058 mL of 0.701 mg/mL IT-CD4 (2.143 mg). The IT-PE (A_{565}/A_{280}) ratio was 5.800. The conjugation mixture was concentrated to about 1.0 mL and applied to the top of an A-15m column. Data for fractions 18−24 collected at 3.6 mL/fraction under the first narrow peak in trial 3 gave 4.957 mg of total PE in the conjugate. Since 12.856 mg of IT-PE was used in conjugation, the yield was 38.56%.

Streptavidin−Amdex−PE Conjugates. The procedures were similar to those already described for CD8β−Amdex−PC5 and CD8β−5×-Amdex−PC5, except streptavidin was substituted for CD8β antibody and PE was substituted for PC5. To obtain concentrations of IT-streptavidin in milligrams per milliliter, the A_{280} values in two runs were divided by 2.5 [approximately the M_r ratio of IgG antibody/streptavidin = 160000/60000 Da = 2.67] in the 9−11 run and 3.0 in the 9−15 run. In both trials, 10 mg of Amdex (~30 mg/mL in 1× PBS) was activated with 0.180 mL of 10 mg/mL sulfo-SMCC, and the three purified fractions showing the most Tyndall scatter were pooled to give about 5−9 mL of sulfo-SMCC−Amdex solution. In run 9−11, 8.806 mg of IT-PE (8.30 mg/mL) and 2.143 mg IT-streptavidin (1.940 mg/mL) were mixed with 9 mL of sulfo-SMCC−Amdex−M.P., and 17.613 mg of IT-PE and 4.287 mg of IT-streptavidin were mixed with 9 mL of sulfo-SMCC−5×-Amdex (lot −11) overnight for 21 h. In run 9−15, 12.856 mg of IT-PE (8.85 mg/mL) and 2.143 mg of IT-streptavidin (1.202 mg/mL) were mixed with 8 mL of sulfo-SMCC−Amdex−M.P.; and 25.713 mg IT-PE and 4.287 mg IT-streptavidin were mixed with 5 mL of sulfo-SMCC−5×-Amdex (lot −11) overnight for 20 h. Blocking with L-cysteine free base and iodoacetamide was done for each run in the same way as previous conjugations. The concentrated reaction mixtures of about 1 mL of total volume were each individually purified on a Bio-Gel A-15m column. Fractions (about 3.6 mL) of the first band, peaking in protein and PE concentrations at fraction 21 for the Amdex-M.P. conjugate and at fraction 22 for the 5×-Amdex conjugate, were retained.

Triple Detector System Measurements. The Viscotek Corp. (Houston, TX) system consists of a model T-60 differential viscometer/light-scattering dual detector and a model LR40 differential laser refractometer with a 670 nm diode laser source. The principles of the method and analyses have been described (*52*). The responses of the three primary detectors are as follows: light scattering, $M(\mathrm{d}n/\mathrm{d}c)^2 \times c$; viscometer, ηc; refractometer, $\mathrm{d}n/\mathrm{d}c \times c$. Right-angle light-scattering gives the molecular weight when combined with viscometry detection. The 90° LS is corrected for angular dissymmetry using the Debye equation, together with the molecular size information provided by the viscometer. Viscometry yields the molecular density, which is related to conformation and branching. The refractometer measures sample concentration, providing a direct determination of the refractive index increment, d*n*/d*c*, of the polymer sample. The hydrodynamic volume of a polymer molecule in solution, related to the cube of its radius of gyration, R_g, is directly proportional to the intrinsic viscosity (η) and the weight average molecular weight (M_w), divided by Avogadro's number. The accuracy of R_g values determined by the triple detector system is claimed to be within 0.5 nm.

RESULTS

Light Scattering, Viscosity, Refractive Index Measurements. Molecular data for 11 samples, one dextran and 10 aminodextrans, determined from duplicate batch analyses by the triple detector system are summarized in Table 2. The samples were run at a concentration of 0.7−3.5 mg/mL in 0.2 M aqueous sodium nitrate solution through a column consisting of a 50 ft coil of 0.01 in. i.d. stainless steel tubing without any column packing in batch mode. Some lots of solid aminodextran resisted dissolution and needed a more extensive protocol to afford complete dissolution. Two dissolution protocols were followed: (1) by minimum heating at ~70−80 °C for 5−10 min for samples 1, 3, 5, 6, and 8; (2) by first soaking at

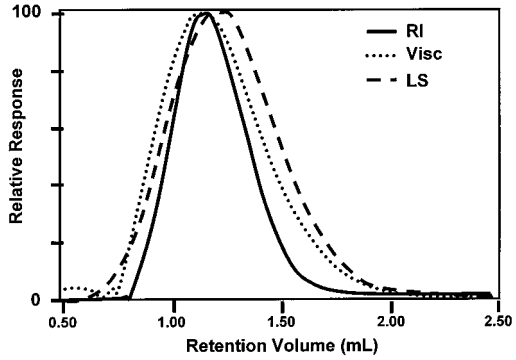


Figure 2. Triple chromatogram of Amdex-M.P. Run conditions: solvent, 0.05 M aqueous sodium sulfate; flow rate, 0.5 mL/min; injection volume, 50 μL; column temperature, ambient; concentration, 0.1 mg/mL. Traces of curves on RHS are for refractive index (RI), viscosity (Visc), and light scattering (LS) in order from left to right.

room temperature for 1−2 h and then heating at ∼70−80 °C for 30 min for samples 2, 4, 7, 9, 10, and 11. The latter dissolution protocol gave reproducible results. Comparison of relative responses of viscosity and light scattering versus retention time within each sample showed that peak positions and band shapes were similar to each other as shown for Amdex-M.P. in Figure 2, implying little or no branching in the dextran and aminodextran chains. Lots of 5×-Amdex prepared by the same 500 g dextran scale, the same molar ratio of DAP-to-sodium periodate, and the same mode of DAP addition in three equal portions consistently gave molecular mass figures in the 25−45 kDa range.

SDS−PAGE Gel Electrophoreses. SDS−PAGE of aminodextrans was run at 400 V (65 V h) on the Pharmacia Phast system, using a 4 to 15 gel gradient for the 30−300 kDa molecular mass range and SDS buffer strips. The use of this system for aminodextrans is made possible by the protonation and, thus, charging of primary amine groups at pH 8.1 of SDS buffer strips and the selective electrostatic interaction between negatively charged sulfonate groups of the widely used Coomassie blue stain (*53, 54*) and protonated, primary amine groups of aminodextrans. Electrophoresis, applied to the study of synthetic polyelectrolytes, has been shown (*55*) to provide a more detailed molecular mass distribution than size-exclusion chromatography. We obtained an accurate measure of the size distribution in aminodextrans from the spread of bands in the electrophoretograms. Both dissolution protocols 1 and 2 were used to prepare 1 mg/mL Amdex solutions in 1× PBS buffer, each mixed 1:1 with SDS buffer, which were then run together with a high molecular mass (200, 116, 97, 66, and 45 kDa) standards sample. Gel electrophoresis bands stained with Coomassie blue for the two runs are shown in Figure 3. All the aminodextrans showed well-stained SDS−PAGE gels, indicating the presence of abundant primary amine groups. Molecular weight ranges for the aminodextrans were estimated from the range of the heaviest blue stain in each lane of the gel referenced to the relatively narrow band positions of five standards in the same gel. The 5×-Amdex lots 1−5, 2−2, −11, and 11−6 and 1×-Amdex lot −75 gave molecular mass ranges of about 30−75, 60−190, 50−150, 35−250, and 150−250 kDa, respectively, for protocol 1 dissolution, and about 30−75, 55−175, 40−90, 30−110, and 150−250 kDa, respectively, for protocol 2 dissolution. The 5×-Amdex lots showed the largest change to lower molecular mass fragments with the more extensive protocol 2 dissolution procedure. Also, the 5×-Amdex lot 2−2, which was purified with a 30 kDa M_r cutoff membrane, showed a significantly higher starting M_r range than other 5×-Amdex lots which were purified with a 5 kDa M_r cutoff hollow fiber cartridge. Thus, other higher MWCO (100, 300, and 500 kDa) membranes that are available can be used to obtain narrower and higher size distributions of aminodextrans where they are required. The average molecular masses obtained from the triple detector system measurements, and the molecular mass ranges obtained from electrophoresis for 1×- and 5×-Amdex samples, both show the extensive depolymerization of dextran starting material (2−3 MDa) that occurred during the aminodextran preparation by the periodate oxidation-diamine addition route.

Dynamic Light Scattering. Hydrodynamic radii, R_h, were obtained from photon correlation spectroscopy (PCS), also known as quasi-elastic light-scattering (QELS), measurements (*56, 57*) on the COULTER N4MD analyzer. The N4MD contains a correlator and microprocessor which converts autocorrelator results using Provencher's program CONTIN to an intensity distribution. A second microprocessor then converts the intensity distribution by the exact Mie theory to give mass average molecular mass. Solutions of either PE, PC5, or ECD as well as their antibody−aminodextran−dye conjugates were measured at concentrations of 5 mg/mL or less in 1× PBS buffer, pH 7.2, with 632.8 nm He/Ne laser excitation. Measurements for freshly buffer-exchanged and purified PE at a concentration of 1.5 mg/mL in 50 mM phosphate, 2 mM EDTA buffer at pH 7.0 gave a mean diameter of 32.7 nm. The scattering angle was 22.8° instead of 90° to improve the intensity of scattered light by a factor of about 16, since PE is small and a poor scatterer which absorbs part of the incident laser light at 632.8 nm. PCS analyses of the peak chromatographic fraction for all three PE, PC5, and ECD conjugates with anti-CD4−Amdex-M.P. in 1× PBS gave the same mean diameter of 146 nm.

Scanning Electron Microscopy. More direct evidence for the structure of the conjugates was obtained from scanning electron microscope (SEM) photos taken with a Philips model XL40-FEG instrument. Samples were prepared by filtering about 0.5 mL of conjugate at 0.4 mg/mL in 1× PBS, pH 7.2, through an 0.2 μm polycarbonate membrane filter (Poretics Corp., Livermore, CA) and drying the filter in air in a sterile Petri dish for 3−4 h to overnight. Portions of the sample on the filter were cut and attached to double-sided carbon tape on an aluminum stub. All samples were gold-sputter-coated with a Cressington Model 108 auto coater at a 25 sec argon gas plasma cycle time and 7.5 cm platform-to-target distance for a thickness of 15−25 nm. Figure 4 shows images of four conjugate samples prepared in the above way for SEM. Note the globular shape of the conjugates, some of which are located inside the 0.2 μm pores of the membrane while others were retained on the surface of the filter. Hydrated samples, as shown in Figures 5 and 6 for CD4−Amdex-M.P.-PE (fraction 20) and CD8β−Amdex−M.P.−PC5 (fraction 19) conjugates, respectively, were measured within 1 day of sample preparation. This is necessary for retention of globular structure, especially for smaller conjugates with 5×- and 1×-Amdex; otherwise, the structures collapsed to varying degrees. The range of mean diameters from SEM photos is included in Table 3.

Flow Cytometry. CD8β−PC5 and fractions of CD8β−5×-Amdex−PC5 conjugates from trial 1 were titered with 3−0.5 μg of antibody in the conjugate per tube. Amounts

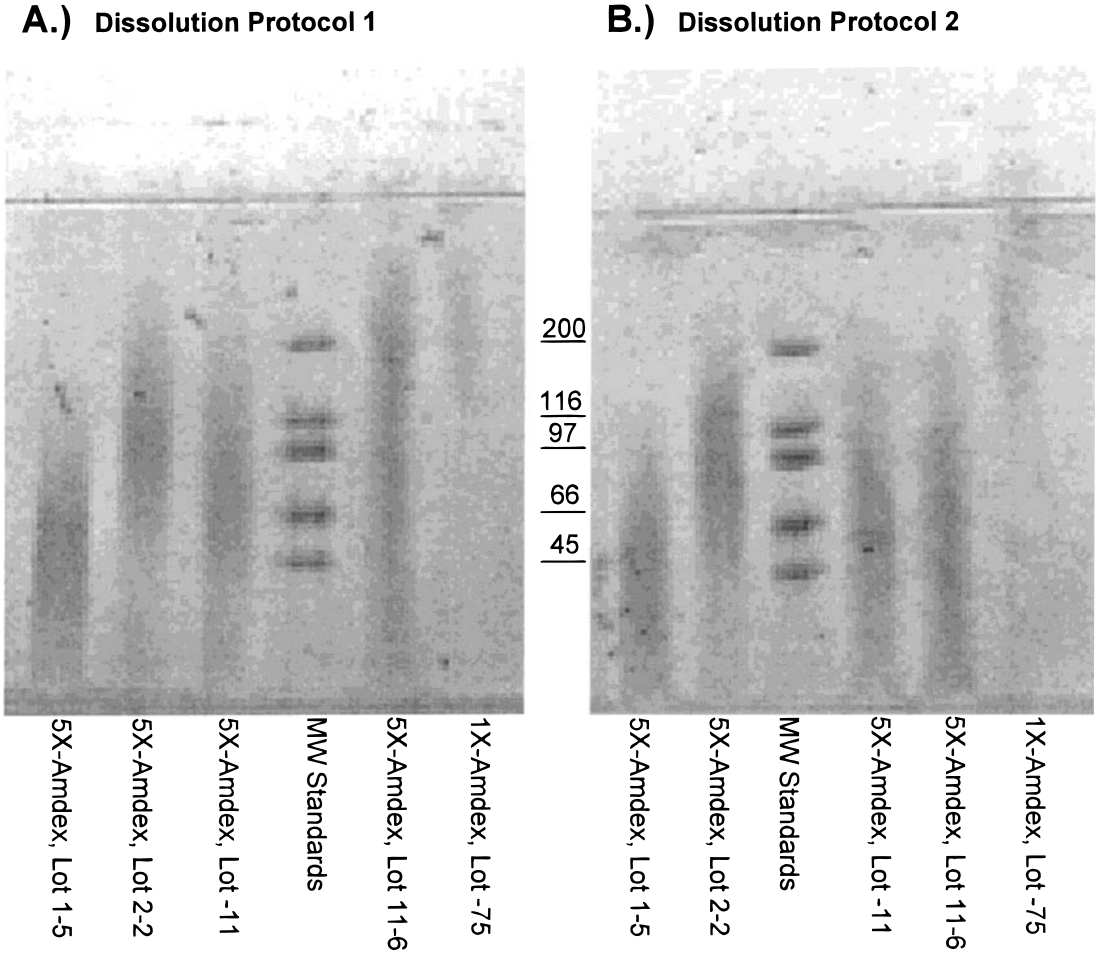


Figure 3. SDS−PAGE results for various aminodextran lots dissolved in 1× PBS buffer solution: (A) protocol 1 dissolution; (B) protocol 2 dissolution.

of antibody for the titers were determined from corrected A_{280} values for the conjugates. Dilutions were added to 100 μL of whole blood and incubated for 60 min at room temperature. For analysis on a flow cytometer (COULTER EPICS 4-color XL-MCL), the blood mixtures were lysed and quenched using the COULTER ImmunoPrep reagent system on the COULTER Q-Prep workstation, washed once with 1× PBS (addition of 2 mL of 1× PBS, centrifugation at 500 g for 5min, discarding supernatant), and the cell pellet was resuspended in 1 mL of 1× PBS. The lymphocyte cell population was distinguished with forward light scatter vs 90° light scatter, electronically gated, and displayed on single parameter histograms [*y*-axis = number of fluorescent events (count); *x*-axis = fluorescence intensity]. Flow cytometer instrument settings were adjusted to display the nonstaining negative lymphocyte subpopulation only within the first decade on the 4-decade log scale for fluorescence intensity. Figure 7 shows the ability of CD8β−5×-Amdex−PC5 conjugate as a fluorescent marker containing more than two PC5 molecules per dextran molecule, to enhance the mean channel PC5 fluorescence intensity (MFI) of the positive cell population over that obtained with the direct CD8β−PC5 conjugate which contains only 0.86 PC5/antibody. The histograms show that the cross-linked conjugate has 3.5-fold higher fluorescence intensity on CD8β+ lymphocytes. In another run, it was found that the mean channel fluorescence intensity of labeled T cells could be enhanced up to 8-fold by examining various fractions of trial 1, CD8β−5×-Amdex−PC5 conjugate as the fluorescent marker. Titers of the control, CD8β−PC5, and the sample, CD8β−5×-Amdex−PC5, with the same instrument settings were run and the results, mean channel PC5 fluorescence intensities and MFI ratios, sample fraction-to-control at same titers, are presented in Table 4 for another donor. MFI ratios corrected for the *F*/*P* ratio, 0.860, of the control, direct CD8β−PC5 conjugate, were about 16−17% higher than values listed in Table 4.

CD4−ECD and a single pooled sample of CD4−5×-Amdex−ECD conjugates were titered with 0.5−0.015 μg (based on the corrected A_{280} value for each conjugate) per tube in the same way as in the previous example. The results are shown in Figure 8 for the positive population mean channel ECD fluorescence intensities (MFI) for the $CD4^+$ lymphocytes with the direct and cross-linked antibody-ECD conjugates. The MFI ratios, maximizing at 9.7 were calculated from the mean channel positions of each 5×-Amdex sample compared to the saturating bottle product dose of CD4−ECD (0.5 μg). Using the *F*/*P* ratio of 0.96 for the CD4−ECD conjugate, the corresponding maximum MFI ratio is 10.1.

CD4 antibody conjugates were prepared to obtain an enhanced fluorescence standard with a narrow distribution of fluorescence intensities for positive lymphocytes. To 100 μL of whole blood from a single normal blood donor, 0.5 μg each of the CD4-PE control conjugate and the CD4−5×-Amdex−PE fraction samples were added and mixed for 30 min at room temperature. Concentrations of CD4 antibody in the conjugates were based on corrected A_{280} values. The samples were prepared for flow cytometric analyses (FCM) as before. The amplification

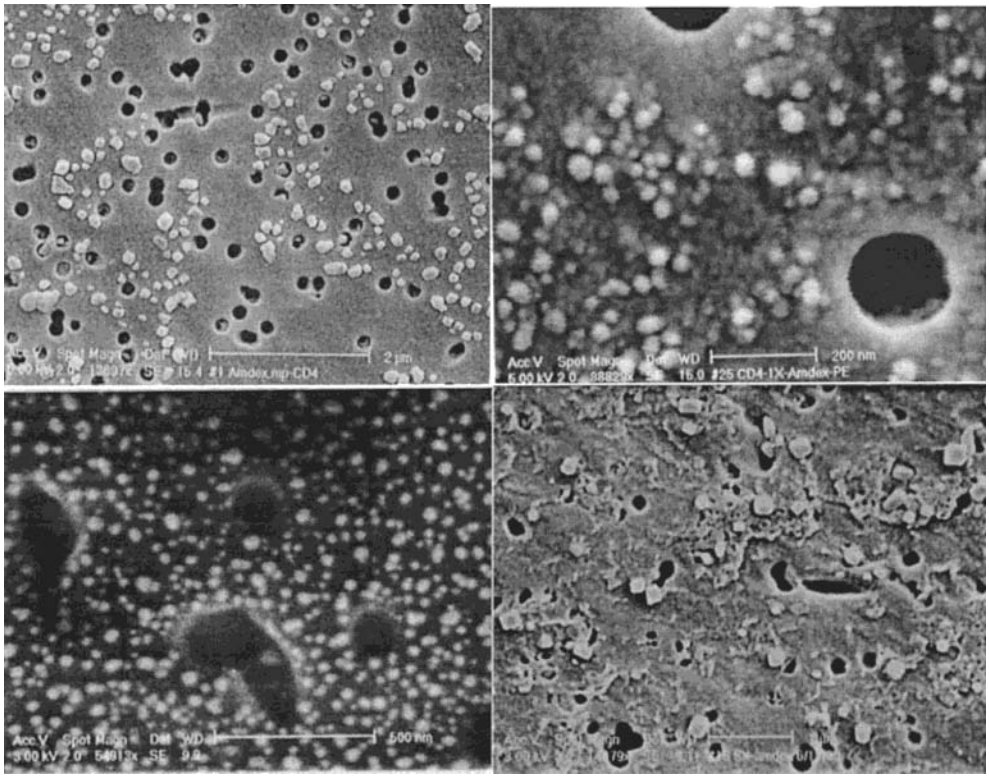


Figure 4. Scanning Electron Micrographs of CD4−Amdex, M.P.-PE, top, left; CD4-5×-Amdex(lot 1−5)-PE, bottom, left; CD4-1×-Amdex(lot−75), top, right; and CD8β−5×-Amdex(lot−11)-PC5 conjugates. The instrument was operated with the secondary emission detector and 3−5 kV electron beam intensity. Magnification was 13697×, 54913×, 88829×, and 14479×, respectively, on original photo, but should otherwise be determined from bar length.

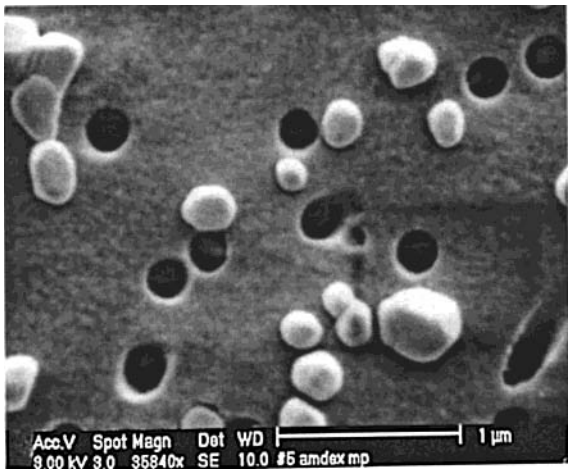


Figure 5. Scanning electron micrograph of CD4−Amdex, M.P.-PE conjugate, pooled and concentrated fractions 19 and 20.

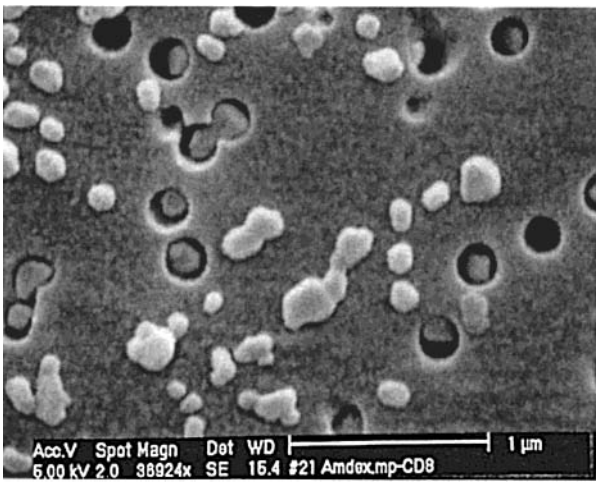


Figure 6. Scanning electron micrograph of CD8β−Amdex, M.P.-PC5 conjugate, fraction 19.

of the mean channel PE fluorescence intensities relative to the control, obtained at the same instrument settings, is shown in Table 5. The maximum positive amplification ratio was 4.7; however, the negative population of MFI was also amplified, although not to the same extent. The signal-to-noise (S/N) amplification, which encompasses both the positive and negative amplification ratios, was approximately 2.0. Both the amplified and nonamplified CD4 antibodies detected similar percentages of $CD4^+$ and $CD4^-$ lymphocytes.

Maximum amplification ratios of 8.5, 4.2, and 2.2 occurred in the CD4,PE; CD4,ECD; and CD8β,PC5 conjugates with Amdex-M.P. (fractions 19, 21, and 19, respectively) as shown in Tables 6-8. These fractions coincided with the lower fraction side (higher molecular mass) of the first intense band observed in chromatography of conjugation mixtures. The CD4−Amdex−PE conjugate demonstrated the highest amplification ratio ever obtained for a CD4, PE conjugate with any lot of aminodextran. Also, this ECD conjugate is the first one to show excellent yield in the first band as well as the highest amplification ratio of any ECD conjugate. Also notable in Tables 6−8 is that the Amdex M.P. gives low negative amplification ratio values, and thus higher S/N amplification ratios, as compared to the 5×-Amdex values in Table 5.

A degree of substitution of ~1/140 with a single amino group per reacted glucose unit was shown to be sufficient to obtain MCA−Amdex−PE (PC5, ECD) conjugates in good yields. For CD4−Amdex−PE conjugates, Amdex-M.P. has provided the highest amplification of fluorescence intensity over that obtained with direct CD4−PE

Table 3. Mean Diameters of PE and Its Conjugates and Molar Ratios of PE:Aminodextran

species	mean diameter by QELS (nm)	SEM diameter range (nm)	MW (kDa)	mole fraction [PE/(PE + Ab)]	PE/Amdex by packing	PE/Amdex by MW	PE/Amdex by flow cytometry
PE	27.7		270				
CD4-1X-Amdex-PE	90.2	36−71	2556	0.553	1.2	6.3	2.4
CD4-Amdex-PE	146	69−172	6697	0.488	23	8.4	8.2
CD4-5X-Amdex (lot −11)-PE	116		4227	0.401	0.16	7.8	4.2
CD4-5X-Amdex (lot 1−5) −PE	57.4	34−69	1035	0.560	0.39	2.6	4.4
CD8β-5X-Amdex(lot −11)-PC5	153	67−200					

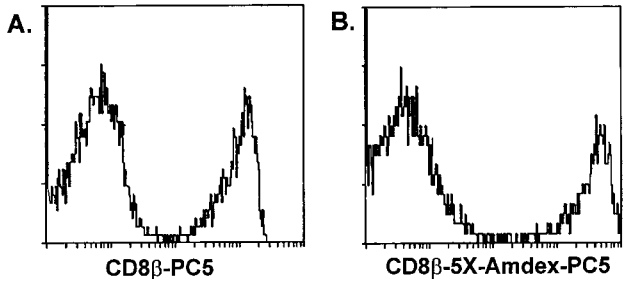


Figure 7. Flow cytometric histograms of CD8β−PC5 and CD8β−5×-Amdex−PC5 conjugates mixed with whole blood. 100 μL of whole blood from a normal donor was stained with 10 μL (2.5 μg) of CD8β monoclonal antibody either as (A) a CD8β−PC5 or (B) a CD8β−5×-Amdex−PC5 conjugate. The fluorescence intensity of a light scatter-gated lymphocyte sub-population is displayed as histograms where the *y*-axis represents the number of fluorescent events (count), and the *x*-axis shows fluorescence intensity. The nonstaining negative cell population is seen in the left quarter of the histogram.

Table 4. Flow Cytometric Data for CD8β−5×-Amdex−PC5 versus Control, CD8β−PC5

CD8β in sample/ control(μg)	sample: control CD8β-PC5	fraction no. CD8β-5X-Amdex-PC5: 36	37	38	39	40	41	42	43
Positive Mean Channel PC5 Fluorescence Intensities (MFI)									
3	53	265	325	379	419	376	377	381	
2.5	53	282	303	352	334	335	357	368	
2	55	236	266	302	293	293	319	320	
1.5	51	194	226	252	240	240	213	292	336
1	50	174	196	178	183	183	166	216	262
0.5	51	93	130	134	132	132	155	117	177
Positive MFI Ratios (Fraction/Control)									
3	1.0	5.0	6.1	7.1	7.9	7.1	7.1	7.1	7.1
2.5	1.0	5.3	5.7	6.6	6.3	6.3	6.7	6.9	
2	1.0	4.3	4.8	5.5	5.3	5.7	5.8	5.8	
1.5	1.0	3.8	4.4	4.9	4.7	4.2	5.2	5.7	6.6
1	1.0	3.5	3.9	3.6	3.7	3.3	4.0	4.3	5.3
0.5	1.0	1.8	2.5	2.6	2.6	3.0	2.2	2.3	3.5

conjugate in labeling CD4+ cells in whole blood. Flow cytometry histograms of the number of fluorescence events versus mean channel fluorescence intensity are shown in Figure 9 for CD4-PE versus various CD4−Amdex−PE-labeled lymphocytes of the same blood donor. Good separation between the direct conjugate and each Amdex-cross-linked conjugate was obtained. Also, no interference from CD4 negative populations ever was observed. Similar histograms for CD4−ECD versus CD4−Amdex−ECD are shown in Figure 10.

A graph comparing CD4,PE with carriers of various molecular masses is shown in Figure 11, and shows the direct, linear proportionality between amplified fluorescence intensity and molecular mass of carrier only for the direct conjugate and conjugates with 1×-Amdex and Amdex-M.P.

Both cross-linked, 5×-Amdex conjugates with CD4 antibody and PE show much higher amplification than predicted from the linear plot in Figure 11 for linear chain aminodextrans of low degree of amino substitution

μg CD4 /test	Mean Fluorescence Intensity (MFI) CD4-ECD	CD4-5X-Amdex-ECD	MFI Ratio, Sample/ Control
0.015	18	267	5.3
0.03	29	349	7.0
0.06	41	359	7.2
0.125	47	359	7.2
0.25	50	398	8.0
0.5	53	485	9.7

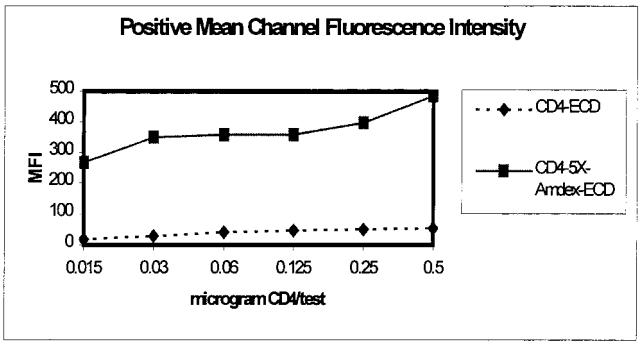


Figure 8. Flow cytometric results in tabulated and graphical form: positive population mean fluorescence intensity (MFI) data for direct CD4−ECD and CD4-5×-Amdex−ECD conjugates mixed with 100 μL whole blood at various titers of 0.015−0.5 μg of CD4.

and for the direct conjugate. Possibly, a more globular structure and higher degree of amino substitution in 5×-Amdex, albeit cross-linked, allows formation of multiply cross-linked complexes of the type -Amdex−MCA, PE−Amdex-, which, as a single unit in binding to antigenic sites on biological cells can yield greater amplification of fluorescence intensity. The broad range of yields of MCA−5×-Amdex−PE, PC5, or ECD conjugates and their much greater sensitivity to the nature of the antibody that was used in the conjugations, point to the formation of multimeric complexes.

Furthermore, several trials with aminodextran-cross-linked conjugates, streptavidin−Amdex−PE and streptavidin−5×-Amdex−PE, were used as indirect secondary reagents with biotinylated CD4 primary antibody to label and analyze for CD4+ cells in whole blood by flow cytometry. Titers between 0.25 and 5.0 μg of protein in the peak fraction 21 of lot 9−15, streptavidin−Amdex−PE conjugate with 100 μL of whole blood (previously stained with biotinylated CD4 antibody and washed once), were lysed, quenched, washed, and analyzed. These are shown in the overlaid histograms of Figure 12A. A plateau indicating saturation of CD4+ receptors in the sample was reached in mean channel fluorescence intensity at a titer of 2.5 μg. The Figure 12 histograms for different fractions of conjugates containing either (B) Amdex-M.P. or (C) 5×-Amdex, lot −11, showed that all fractions were equally good at providing fluorescence intensity, i.e., within each series of fractions the number of PE molecules per conjugate molecule was about the same. When compared against trials with 2.5 μg amounts

Table 5. Flow Cytometric Amplification Data for CD4-5×-Amdex−PE Conjugate Compared to Direct CD4-PE Conjugate[a]

							%	
fraction	neg. pop. MFI	pos. pop. MFI	*S*/*N*	*S*/*N* ampl. ratio	neg. ampl. ratio	pos. ampl. ratio	neg	pos
CD4-5X-Amdex-PE								
21	0.42	271	651	1.7	2.2	3.7	66	34
22	0.39	301	769	2.0	2.0	4.1	68	32
23	0.42	334	794	2.1	2.2	4.6	64	35
24	0.47	332	715	1.9	2.4	4.6	65	35
25	0.60	343	569	1.5	3.1	4.7	63	37
26	0.33	290	870	2.3	1.7	4.0	64	36
direct conjugate CD4-PE	0.19	73	376	1.0	1.0	1.0	64	36

[a] MFI = mean fluorescence intensity; positive (pos.) amplification (ampl.) ratio = pos. population (pop.) MFI Amdex conjugate:pos. pop. MFI direct conjugate; negative (neg.) amplification ratio = neg. pop. MFI Amdex conjugate:neg. pop. MFI direct conjugate; *S*/*N* = MFI pos. pop./MFI neg. pop.; *S*/*N* ampl. ratio = *S*/*N* Amdex conjugate:*S*/*N* direct conjugate; % neg. = percentage of negative nonstaining cells displayed on histogram; % pos. = percentage of positive cells displayed on histogram.

Table 6. Flow Cytometric Data for CD4−Amdex−PE Conjugate Compared to Direct CD4-PE Conjugate[a]

							%	
fraction	neg. pop. MFI	pos. pop. MFI	*S*/*N*	*S*/*N* ampl. ratio	neg. ampl. ratio	pos. ampl. ratio	neg	pos
CD4-Amdex-PE								
18	0.47	501	1072	3.6	1.9	6.9	46	54
19	**0.51**	**624**	**1226**	**4.1**	**2.1**	**8.5**	45	55
21	0.44	508	1168	3.9	1.8	7.0	45	55
22	0.37	426	1157	3.9	1.5	5.8	55	45
23	0.42	351	837	2.8	1.7	4.8	45	55
24	0.43	319	738	2.5	1.8	4.4	51	49
CD4-PE	**0.24**	**73**	**300**	**1.0**	**1.0**	**1.0**	**46**	**54**

[a] For headings, see footnote to Table 5.

Table 7. Flow Cytometric Data for CD4−Amdex−ECD Conjugate Compared to Direct CD4−ECD Conjugate[a]

							%	
fraction	neg. pop. MFI	pos. pop. MFI	*S*/*N*	*S*/*N* ampl. ratio	neg. ampl. ratio	pos. ampl. ratio	neg	pos
CD4-Amdex-ECD								
19	0.21	129	624	2	1.0	2.2	63	37
20	0.23	240	1032	4	1.1	4.1	63	37
21	**0.24**	**243**	**1016**	**4**	**1.1**	**4.2**	62	38
22	0.24	228	936	3	1.1	3.9	63	37
23	0.24	200	823	3	1.1	3.4	63	37
24	0.26	191	733	3	1.2	3.3	64	36
25	0.26	189	722	3	1.2	3.2	62	38
26	0.22	150	690	3	1.0	2.6	63	37
27	0.22	146	674	2	1.0	2.5	63	37
28	0.21	133	624	2	1.0	2.3	63	37
CD4-ECD	0.22	58	272	1	1.0	1.0	62	38

[a] For headings, see footnote to Table 5.

Table 8. Flow Cytometric Data for CD8*β*−Amdex−PC5 Conjugate Compared to Direct CD8*β*−PC5 Conjugate[a]

							%	
fraction	neg. pop. MFI	pos. pop. MFI	*S*/*N*	*S*/*N* ampl. ratio	neg. ampl. ratio	pos. ampl. ratio	neg	pos
CD8*β*-Amdex-PC5								
18	0.18	52	280	0.9	1.2	1.1	82	18
19	**0.20**	**102**	**519**	**1.7**	**1.3**	**2.2**	82	18
20	0.19	97	498	1.6	1.3	2.1	81	19
21	0.20	95	480	1.6	1.3	2.0	82	18
22	0.21	92	436	1.4	1.4	2.0	82	18
23	0.26	82	313	1.0	1.7	1.8	82	19
CD8*β*-PC5	0.15	47	307	1.0	1.0	1.0	83	17

[a] For headings, see footnote to Table 5.

of avidin in the direct conjugate, avidin, NeutraLite −PE, the streptavidin−Amdex−PE conjugates gave about 8−11-fold greater fluorescence intensity from labeled CD4+ lymphocytes as shown in Figure 13 for four runs.

DISCUSSION

Data from Table 2 were further used to construct a Mark−Houwink plot of log(η) versus log(M_w), shown in Figure 14. Linear regression analysis for all data gave a correlation coefficient of 0.976 and a slope of 0.451. The slope corresponds to the exponent in the equation, $[\eta] = KM^a$, where K is the proportionality constant. In the above samples, the value of the exponent is very similar to the $a = 0.50$ btained (*58*) for linear dextran (20−100 kDa) in water at 25° C. This value of the exponent has been established for linear, flexible polymers under "theta" temperature or solvent conditions, whereas the branched fraction of dextran of 800 kDa in water at 25° C gave $a = 0.20$. A similar plot of log(R_g) versus log(M_w) for all data gave a correlation coefficient of 0.998 and a

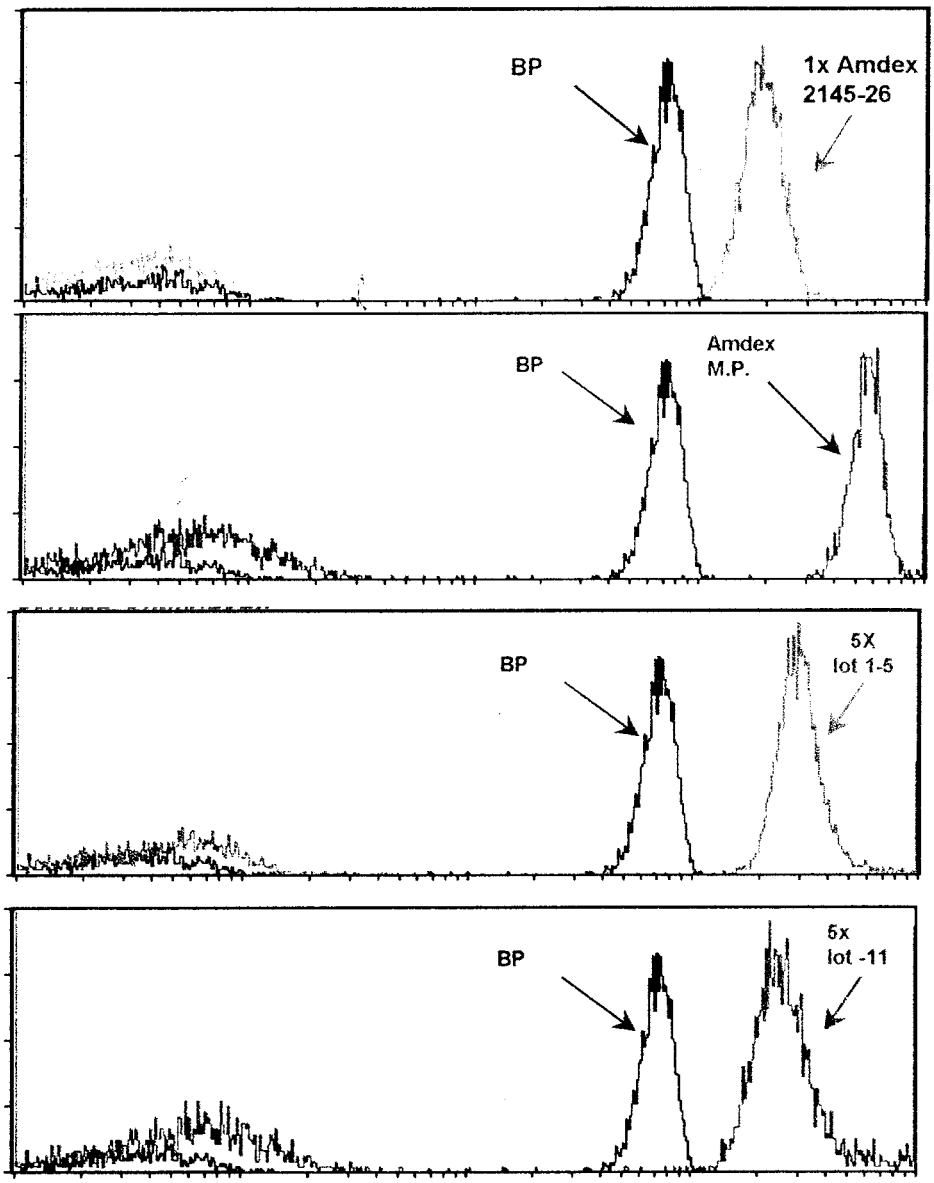


Figure 9. Comparison of flow cytometric histograms of direct CD4-PE and various CD4−Amdex−PE conjugates, 1X = 1×-Amdex, Amdex M.P., and two lots of 5×-Amdex, mixed with 100 μL of whole blood. The fluorescence intensity of a light scatter-gated lymphocyte subpopulation is displayed as histograms where the *y*-axis represents the number of fluorescent events (count), and the *x*-axis shows fluorescence intensity. The nonstaining negative cell population is seen in the left quarter of the histogram.

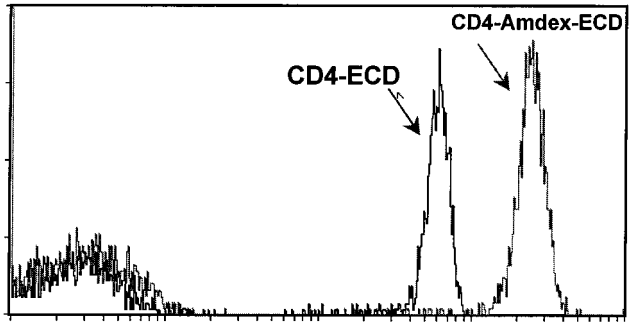


Figure 10. Comparison of flow cytometric histograms of direct CD4−ECD and CD4−Amdex, M.P.-ECD conjugates mixed with 100 μL of whole blood. The fluorescence intensity of a light scatter-gated lymphocyte subpopulation is displayed as histograms where the *y*-axis represents the number of fluorescent events (count), and the *x*-axis shows fluorescence intensity. The nonstaining negative cell population is seen in the left quarter of the histogram.

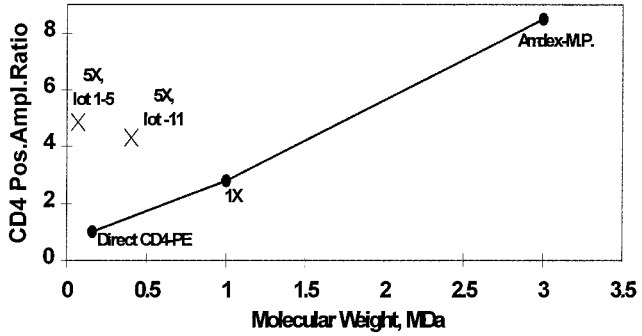


Figure 11. Graph of the positive amplification ratio [MFI (CD4−Amdex−PE)/MFI (CD4-PE)] for CD4 conjugates labeling CD4 positive lymphocytes in whole blood versus molecular mass for various aminodextrans.

slope of 0.481. We conclude, therefore, that the aminodextrans behave in aqueous sodium nitrate solution as flexible, linear chains arranged in a more relaxed, globular structure than the compact globular structures assumed by typical proteins. The positive charges of primary amino groups in 5×-Amdex are not sufficient to

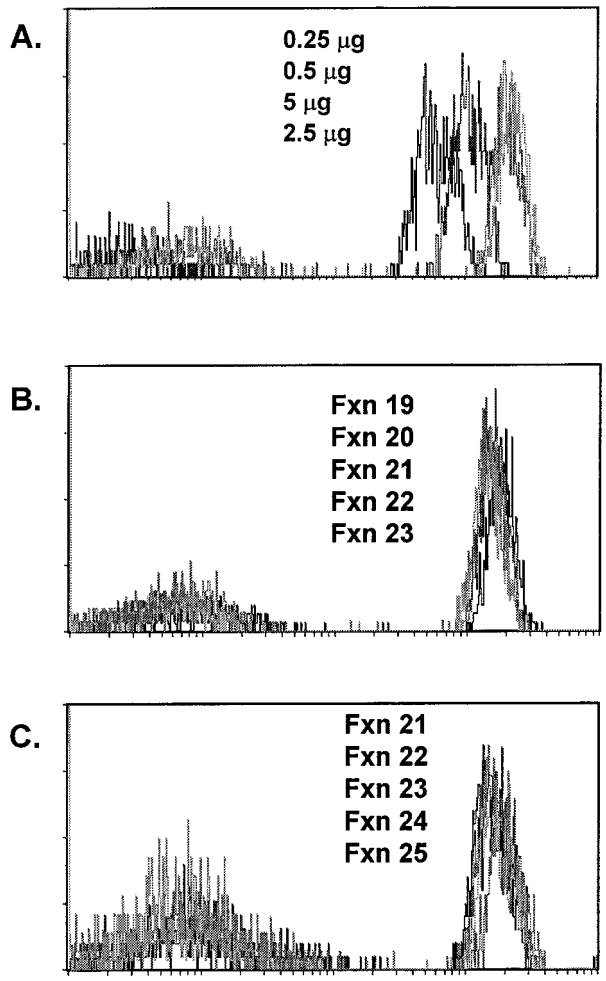


Figure 12. Flow cytometric histograms of streptavidin−Amdex−PE conjugates mixed with 100 μL of whole blood pretreated with biotinylated CD4 antibody. (A) Amdex, M.P. conjugate, lot 9−15, fraction 21 mixed in titers of 0.25, 0.5, 2.5, and 5 μg of protein. (B) Amdex, M.P. conjugate, lot 9−11, fractions 19, 20, 21, 22, and 23, all mixed individually at 2.5 μg of streptavidin. (C) 5×-Amdex conjugate, lot 9−15, fractions 21, 22, 23, 24, and 25, all mixed individually at 2.5 μg of streptavidin. The fluorescence intensity of a light scatter-gated lymphocyte subpopulation is displayed as histograms where the *y*-axis represents the number of fluorescent events (count), and the *x*-axis shows fluorescence intensity. The nonstaining negative cell population is seen in the left quarter of the histogram.

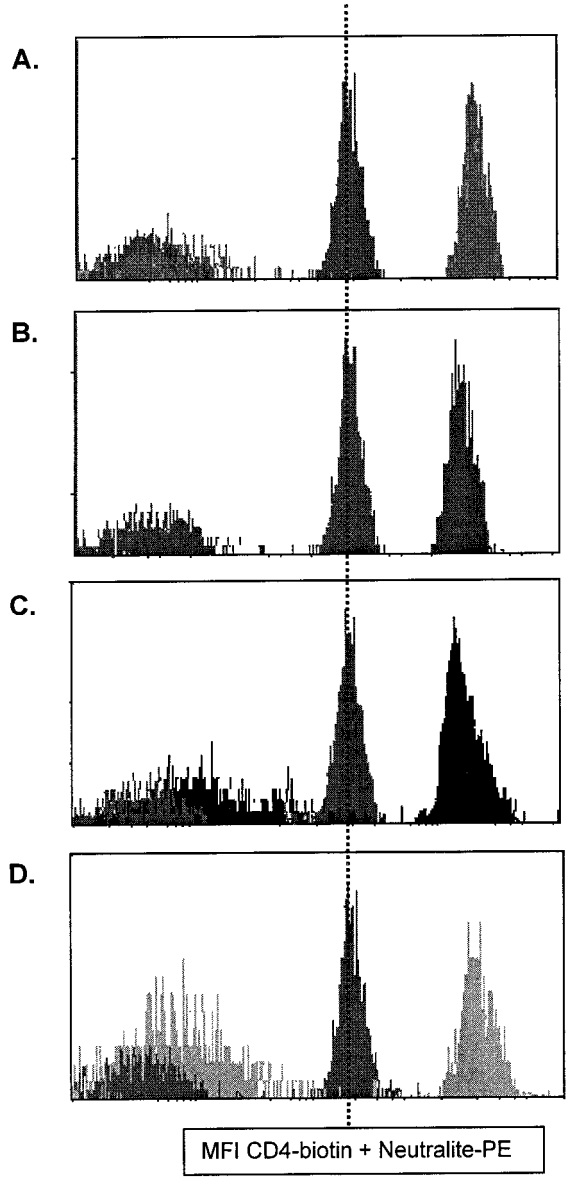


Figure 13. Comparison of flow cytometric histograms for avidin, NeutraLite-PE conjugate (vertical dotted line) and streptavidin−Amdex−PE conjugates, both individually mixed with 100 μL of whole blood pretreated with biotinylated CD4 antibody. (A) Amdex, M.P. conjugate, lot 9−15, fraction 21; (B) Amdex, M.P. conjugate, lot 9−11, fraction 21; (C) 5×-Amdex conjugate, lot 9−11, fraction 25; (D) 5×-Amdex conjugate, lot 9−15, fraction 26. Each sample contained 2.5 μg of avidin or streptavidin. The fluorescence intensity of a light scatter-gated lymphocyte sub-population is displayed as histograms where the *y*-axis represents the number of fluorescent events (count), and the *x*-axis shows fluorescence intensity. The nonstaining negative cell population is seen in the left quarter of the histogram.

force aminodextrans to assume an extended, straight chain structure.

The radius of gyration for a randomly coiled, linear, polymer molecule has been derived from random walk statistics as $R_g^2 = 1/6\ nl^2$, where n is the number of statistical segments in the polymer chain and l is the length of each statistical segment. Also, the mean square end-to-end distance, L^2, in a random coil is given by $L^2 = nl^2$, (*59*). Thus, the R_g and mass average molecular mass values obtained from light scatter and viscosity, and elemental analyses (empirical formulas and degree of substitution) can be used to calculate L and other parameters. Values of R_h, the hydrodynamic radius, were calculated from R_g values by using the relationship, $R_h = 0.665R_g$, derived for random polymer coils. Statistical segment lengths were 7.5−9.0 Å for the aminodextrans, compared to the length of a single unit of 1,6-linked glucose reported (*60*) as about 8 Å long. Free rotation about the methylene group between residues of 1,6-glucosyl units in aminodextran also confers extra flexibility on the polymer chain in contrast to the rigidity of the chain of 1,4-glucosyl units in cellulose nitrate in which glucose residues are joined only by an ether linkage. Light-scattering results and a Zimm plot for cellulose nitrate in acetone (*61, 62*) gave $M_w = 400$ kDa, a statistical segment length of 35 Å or about seven 1,4-glucosyl units, and a root-mean-square end-to-end distance, L, of 1500 Å. The longer statistical segment length and high L value confirm that cellulose nitrate has an unusually stiff and extended structure. The above data for randomly coiled polymer, dextran and aminodextrans, have shown them to assume much more tightly coiled and compact structures. Previous studies of dextran of molecular mass greater than 2000 Da also indicated a

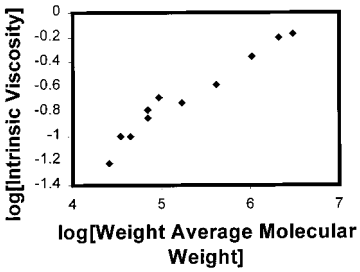


Figure 14. Mark−Houwink plot of log[intrinsic viscosity, η] versus log[molecular weight, M_w] for various aminodextrans and dextran as compiled in Table 2.

globular structure (*60*, *63*) in contrast to the open, extended structures of fiber and extracellular matrix polysaccharides such as cellulose (*61*, *62*) and proteoglycans (*35*, *36*). Dextran prepared by freeze fixation and detected by electron microscopy (*63*) showed dextran globules. Direct observation (*60*) of the polymerization reaction to form dextran in the cell of a light-scattering instrument followed by construction of Zimm plots for dextran solutions showed uniform spheres of 75−85 nm radii of gyration for molecular masses of 64−105 MDa; however, the process of purification of these high molecular mass dextrans invariably gave products insoluble in aqueous media. These results have made it easier to structurally visualize the formation of protein, antibody, and phycobiliprotein, conjugates of aminodextrans by constructing a working model of a central, loose, globular aminodextran core surrounded by a shell of protein molecules.

A direct proportionality between the total accessible surface area and molecular mass has been proposed (*64*) for large protein molecules. If this relationship, $4\pi R_h^2 \propto M$, is applied to the dextran and aminodextran data of Table 2 using the surface area of a sphere of radius R_h in angstroms, we find that $4\pi R_h^2 = 0.366$ M on the average for 11 measurements. This suggests that the total accessible surface area, $4\pi R_h^2/0.366$, of aminodextrans in random coil configurations is about 2.7 times greater than the surface area of a sphere of the same size. This figure is higher than the one for proteins for which the accessible surface area is quoted (*64*) as being nearly two times greater than that expected for a sphere of the same size.

In most 5×-Amdex samples, the average molecular mass determined from the triple detector system measurements fell in the middle of the range shown by SDS−PAGE results, even though the position of species in electrophoretograms depends strictly on their charge-to-size ratio. Two factors may have contributed to the high, apparent 150−250 kDa molecular range for 1×-Amdex. First, the molecular mass standards were globular proteins, which are more compact than aminodextrans of the same molecular mass, having a relatively open chain, random coil structure. The gel will be more effective in separating aminodextrans of somewhat lower molecular mass as compared with proteins. Second, aminodextrans of higher positive charge such as 5×-Amdex will travel more quickly through the gel compared to aminodextrans of low positive charge such as 1×-Amdex.

Several mechanisms for depolymerization of dextran dialdehyde by strongly alkaline media may be proposed. The mechanisms involve either of two acidic hydrogen atoms in the periodate cleaved, dialdehyde units of dextran dialdehyde polymer as shown in Figure 15 for each of the acidic hydrogen sites. Mechanism 1, β-carbonyl elimination, appears to be the more favored (*65*, *66*) one because of the presence of a carbonyl in β-position to a C-atom involved in the glycosidic linkage, which yields a conjugated C=O, C=C structure in the product.

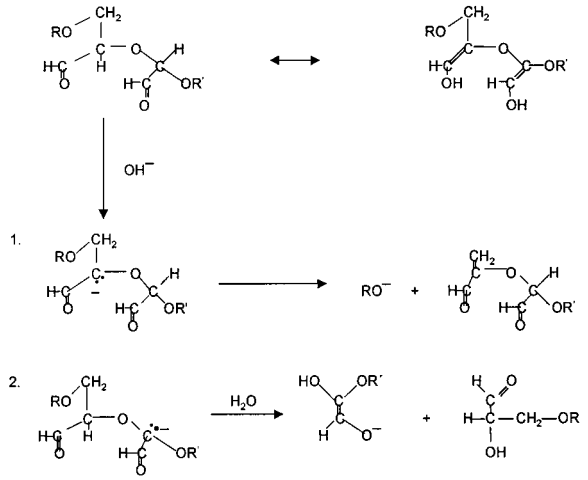


Figure 15. Schematic of the depolymerization mechanisms for dextran dialdehyde.

Mean hydrodynamic diameters of PE and conjugates were measured by PCS. Molar ratios, PE/Amdex, were obtained in three different ways (two, by model calculations, and one, from flow cytometry measurements): (1) by calculating the number of hard spheres of PE that can be arranged in a closest packed array around a hard sphere of aminodextran, i.e., surface area of sphere of aminodextran, $4\pi R_h^2$, divided by $d^2(\text{PE}) \times \sqrt{3}/2$, and then multiplying by the mole fraction of PE; (2) by subtracting the molecular mass of one aminodextran molecule from the molecular mass ($=4\pi R_h^2$) of the conjugate, then, dividing by the average of the molecular masses of IgG antibody (160 kDa) and PE (270 kDa), and finally multiplying by the mole fraction of PE; and (3) by taking the ratio of mean channel fluorescence intensity of the CD4−aminodextran−PE conjugate to the mean channel fluorescence intensity of the direct CD4−PE conjugate, both measured by flow cytometry at saturation of the receptor sites on the targeted CD4+ lymphocytes in whole blood.

Molecular masses (M) of the corresponding PE conjugates listed in Table 3 were calculated from hydrodynamic diameters determined from PCS measurements by assuming the relationship, $4\pi R_h^2 = M$ with radius R_h in angstroms, for large protein molecules (*64*). Estimates of the PE/Amdex ratios by packing and by molecular mass differ most widely from each other for 5×-Amdex conjugates. When the PE/Amdex ratio was less than 1 or close to 1 as with 5×-Amdex and 1×-Amdex conjugates, the size of the Amdex molecule was smaller than the size of either PE or antibody molecule. In these cases, the smaller Amdex (25−94 kDa) molecules will tend to pack around a larger, central PE (270 kDa) or antibody (160 kDa) molecule. Further, amplification factors exceed packing limits around a single, unassociated 5×-Amdex molecule for the CD4−5×-Amdex−PE conjugates and, thus, suggest that more than one 5×-Amdex molecule is part of the conjugate. This allows a network of 5×-Amdex−MCA, PE−5×-Amdex to form and contain additional PE molecules. The most consistent amplification ratios were obtained in conjugates with Amdex-M.P., which has a low degree of amine substitution and very large size.

The main criteria for success in obtaining good yields of antibody, fluorescent dye conjugates with aminodex-

tran, that produce large enhancements in fluorescence intensity of targeted cells appear to be the following: (1) use of the highest molecular mass possible for the aminodextran carrier while still retaining solubility in aqueous media; (2) a low degree of amine substitution (1/140) in dextran of 3 MDa still allows conjugation of antibody and phycobiliproteins; however, the percentage of saturation coverage of the aminodextran carrier may be low; (3) more highly substituted 5×-Amdex (1/5 to 1/8) allows a greater packing density of protein, and also the possibility of network structures containing even more aminodextran and phycobiliprotein.

With the advances now being made in microfluidics *(67*−*69)*, it will soon be possible to use these large conjugates to perform fluorescence-activated sorting of targeted molecules instead of just micron size objects such as biological cells and particles. Development of new detection and sequencing methods for nucleic acids could arise from using polymeric carriers such as aminodextrans with conjugated oligo and fluorescent dye.

LITERATURE CITED

(1) Lee, Y. C., and Lee, R. T. (1992) Synthetic Glycoconjugates. In *Glycoconjugates. Composition, Structure and Function* (H. J. Allen and E. C. Kisailus, Eds.) pp 121−165, Marcel Dekker, Inc., New York.

(2) Manabe, Y., Tsubota, T., Haruta, Y., Kataoka, K., Okazaki, M., Haisa, S., Nakamura, K., and Kimura, I. (1984) Production of a Monoclonal Antibody-Methotrexate Conjugate Utilizing Dextran T-40 and Its Biologic Activity. *J. Lab. Clin. Med. 104*, 445−454.

(3) Oseroff, A. R., Ohuoha, D., Hasan, T., Bommer, J. C., and Yarmush, M. L. (1986) Antibody-Targeted Photolysis: Selective Photodestruction of Human T-Cell Leukemia Cells Using Monoclonal Antibody-Chlorin e_6 Conjugates. *Proc. Natl. Acad. Sci. U.S.A. 83*, 8744−8748.

(4) Rakestraw, S. L., Tompkins, R. G., and Yarmush, M. L. (1990) Antibody-Targeted Photolysis: In Vitro Studies with Sn(IV) Chlorin e6 Covalently Bound to Monoclonal Antibodies Using a Modified Dextran Carrier. *Proc. Natl. Acad. Sci. U.S.A. 87*, 4217−4221.

(5) Wong, S. S. (1991) *Chemistry of Protein Conjugation and Cross-Linking*, p 279, CRC Press, Inc., Boca Raton, FL.

(6) Hermanson, G. T. (1996) *Bioconjugate Techniques*, pp 618−629, Academic Press, San Diego, CA.

(7) Aslam, M., and Dent, A. (1998) *Bioconjugation-Protein Coupling Techniques for the Biomedical Sciences*, Chap. 8, Grove's Dictionaries Inc., New York.

(8) Maeda, H., Seymour, L. W., and Miyamoto, Y. (1992) Conjugates of Anticancer Agents and Polymers: Advantages of Macromolecular Therapeutics in Vivo. *Bioconjugate Chem. 3*, 351−362.

(9) Brinkley, M. (1992) A Brief Survey of Methods for Preparing Protein Conjugates with Dyes, Haptens, and Cross-Linking Reagents. *Bioconjugate Chem. 3*, 2−13.

(10) Brunswick, M., Finkelman, F. D., Highet, P. F., Inman, J. K., Dintzis, H. M., and Mond, J. J. (1988) Picogram Quantities of Anti-Ig Antibodies Coupled to Dextran Induce B Cell Proliferation. *J. Immunol. 140*, 3364−3372.

(11) Mongini, P. K. A., Blessinger, C. A., Highet, P. F., and Inman, J. K. (1992) Membrane IgM-Mediated Signaling of Human B Cells. *J. Immunol. 148*, 3892−3901.

(12) Marshall, J. J., and Rabinowitz, M. L. (1976) Preparation and Characterization of a Dextran-Trypsin Conjugate. *J. Biol. Chem. 251*, 1081−1087.

(13) Kato, A. (1996) Preparation and Functional Properties of Protein-Polysaccharide Conjugates. In *Surface Activity of Proteins: Chemical and Physicochemical Modifications* (S. Magdassi, Ed.) Chap. 5, pp 115−129, Marcel Dekker, Inc., New York.

(14) Zhao, Q., Gottschalk, I., Carlsson, J., Arvidsson, L.-E., Oscarsson, S., Medin, A., Ersson, B., and Janson, J.-C. (1997) Preparation and Purification of an End to End Coupled mEGF-Dextran Conjugate. *Bioconjugate Chem. 8*, 927−934.

(15) Lenders, J.-P., and Crichton, R. R. (1988) Chemical stabilization of glucoamylase from *Aspergillus niger* against thermal inactivation. *Biotechnol. Bioeng. 31*, 267−277.

(16) Mosbach, K., ed. (1987) *Methods in Enzymology*, vol. 135, Academic Press, New York.

(17) Kato, A., Mifuru, R., Matsudomi, N., and Kobayashi, K. (1992) Functional Casein-Polysaccharide Conjugates Prepared by Controlled Dry Heating. *Biosci. Biotech. Biochem. 56*, 567−571.

(18) Kato, A., Shimokawa, K., and Kobayashi, K. (1991) Improvement of the Functional Properties of Insoluble Gluten by Pronase Digestion Followed by Dextran Conjugation. *J. Agric. Food Chem. 39*, 1053−1058.

(19) Nakamura, S., Kato, A., and Kobayashi, K. (1992) Enhanced Antioxidative Effect of Ovalbumin Due to Covalent Binding of Polysaccharides. *J. Agric. Food Chem. 40*, 2033−2037.

(20) Nakamura, S., Kato, A., and Kobayashi, K. (1991) New Antimicrobial Characteristics of Lysozyme-Dextran Conjugate. *J. Agric. Food Chem. 39*, 647−650.

(21) Bolton, W. E., Maples, J. A., Siiman, O., Kenyon, N. S., and Healy, C. G. *Anti-CD3 Antibody-Aminodextran Conjugates for Induction of T-Cell Activation and Proliferation*, U.S. Patents 5,527,713, issued June 18, 1996, and 5,658,741, issued August 19, 1997.

(22) Siiman, O., and Burshteyn, A. *In Situ Use of Gelatin or an Aminodextran in the Preparation of Uniform Ferrite Particles*, U.S. Patent 5,240,640, issued Aug. 31, 1993.

(23) Siiman, O., and Burshteyn, A. *Formation of Colloidal Metal Dispersions Using Aminodextrans as Reductants and Protective Agents*, U.S. Patent 5,248,772, issued September 28, 1993.

(24) Siiman, O., Burshteyn, A., and Cayer, M. *Immobilized Metal Colloids on Dispersed Polymer Microspheres*, U.S. Patent 5,552,086, issued September 3, 1996.

(25) Siiman, O., Burshteyn, A., and Gupta, R. *Biodegradable Gelatin-Aminodextran Particle Coatings and Processes for Making Same*, U.S. Patent 5,466,609, issued Nov. 14, 1995, and 5,707,877, issued January 13, 1998.

(26) Siiman, O., Burshteyn, A., and Gupta, R. *Polymeric Particles Having a Biodegradable Gelatin or Aminodextran Coating and Processes for Making Same*, U.S. Patent 5,639,-620, issued June 17, 1997, and 5,776,706, issued July 7, 1998.

(27) Cohen, J. H. M., Aubry, J. P., Jouvin, M. H., Wijdenes, J., Bancherau, J., Kazatchkine, M., and Revillard, J. P. (1987) *Enumeration of CR1 Complement Receptors on Erythrocytes using a New Method for Detecting Low-Density Cell Surface Antigens by Flow Cytometry*, *J. Immunol. Methods 99*, 53−58.

(28) Zola, H., Neoh, S. H., Mantzioris, B. X., Webster, J., and Loughnan, M. S. (1990) Detection of Immunofluorescence of Surface Molecules Present in Low Copy Numbers. *J. Immunol. Methods 135*, 247−255.

(29) Shapiro, H. M. (1995) *Practical Flow Cytometry*, 3rd ed., p 277, Wiley-Liss, New York.

(30) Hirshfeld, T. *Dye Tagged Reagent*, U.S. Patent 4,166,105, issued August 28, 1979.

(31) Haugland, R. P. (1996) *Handbook of Fluorescent Probes and Research*, 6th ed., Molecular Probes, Inc., Eugene, OR.

(32) MacColl, R., and Guard-Friar, D. (1983) *Phycobiliproteins*, CRC Press, Boca Raton, FL.

(33) Stryer, L., Glazer, A. N., and Oi, V. T. *Fluorescent Immunoassay Employing a Phycobiliprotein Labeled Ligand or Receptor*, U.S. Patent 4,520,110, issued May 28, 1985.

(34) Stryer, L., Glazer, A. N., and Oi, V. T. *Fluorescent Conjugates for Analysis of Molecules and Cells*, U.S. Patent 4,859,582, issued August 22, 1989.

(35) Rosenberg, L., Hellmann, W., and Kleinschmidt, A. K. (1975) Electron Microscopic Studies of Proteoglycan Aggregates from Bovine Articular Cartilage. *J. Biol. Chem. 250*, 1877−1883.

(36) Axelsson, I., Berman, I., and Pita, J. C. (1983) Proteoglycans from Rabbit Articular and Growth Plate Cartilage. *J. Biol. Chem. 258*, 8915−8921.

(37) Smith, C., Wilkinson, J., Roth, P., and Siiman, O. (1998) Detection of Low-Density Cell Surface Markers Using Novel Amplified Fluorochrome-Conjugated Antibodies. *Cytometry* (Suppl. 9), p 56, as presented at XIX Congress of International Society for Analytical Cytology, March 3−7, 1998, Colorado Springs, CO.

(38) Siiman, O., Smith, C., Roth, P., Burshteyn, A., and Raynor, R. *Antibody-Aminodextran-Phycobiliprotein Conjugates*, U.S. Patent 5,891,741, issued April 6, 1999.

(39) Mylvaganam, R., Wilkinson, J., Healy, C., Bolton, W., and Siiman, O. (1998) Seven Markers, Four Colors, Single Laser Flow Cytometry Using Amplified Fluorochrome Conjugated Antibodies. *Cytometry* (Suppl. 9), p 117, as presented at XIX Congress of the International Society for Analytical Cytology, March 3−7, 1998, Colorado Springs, CO.

(40) Waggoner, A. S., Ernst, L. A., Chen, C.-H., and Rechtenwald, D. J. (1993) A New Fluorescent Antibody Label for Three-Color Flow Cytometry with a Single Laser. *Ann. N. Y. Acad. Sci. 677*, 185−193.

(41) Gupta, R. K. *Method of Preferential Labeling of a Phycobiliprotein with a Second Dye for Use in a Multiple Color Assay and Product for Such Use*, U.S. Patent 5,171,846, issued December 15, 1992.

(42) Stryer, L., and Glazer, A. N. *Phycobiliprotein Fluorescent Conjugates*, U.S. Patent 4,542,104, issued September 17, 1985.

(43) Gupta, R. K. *Method of Preferential Labeling of a Phycobiliprotein with an Amine-Reactive Dye for Use in a Multiple Color Assay and Product for Such Use*, U.S. Patent 5,272,257, issued December 21, 1993.

(44) Besemer, A. C., de Nooy, A. E. J., and van Bekkum, H. Methods for the Selective Oxidation of Cellulose: Preparation of 2,3-Dicarboxycellulose and 6-Carboxycellulose. In *Cellulose Derivatives: Modification, Characterization, and Nanostructures* (T. J. Heinze and W. G. Glasser, Eds.) Chap. 5, pp 73−82, ACS Symposium Series 688, American Chemical Society, Washington, DC, 1998.

(45) Jeanes, A., and Wilham, C. A. (1950) Periodate Oxidation of Dextran. *J. Am. Chem. Soc. 72*, 2655−2657.

(46) Van Cleve, J. W., Schaefer, W. C., and Rist, C. E. (1956) The Structure of NRRL B-512 Dextran. *J. Am. Chem. Soc. 78*, 4435−4438.

(47) Weast, R. C., Astle, M. J., and Beyer, W. H., Eds. (1983−1984) *CRC Handbook of Chemistry and Physics*, 64th ed., p D-165, CRC Press, Inc., Boca Raton, FL.

(48) Siiman, O., Gordon, K., Rodriguez, C. M., Burshteyn, A., Maples, J. A., and Whitesell, J. K. *Protein-Colloidal Metal-Aminodextran Coated Particle and Methods of Preparation and Use*, U.S. Patent 5,945,293, issued August 31, 1999.

(49) Uzgiris, E. E. (1981) Laser Doppler Spectroscopy: Applications to Cell and Particle Electrophoresis. *Adv. Colloid Interface Sci. 14*, 75−171.

(50) Padlan, E. A. (1994) *Molecular Biology Intelligence Unit: Antibody−Antigen Complexes*, pp 27−27, R. G. Landes Co., Austin, TX.

(51) Maggio, E. T. (1985) *Enzyme-Immunoassay*, pp 181−196, CRC Press, Boca Raton, FL.

(52) Haney, M. A., Gillespie, D., and Yau, W. W. (1994) Viewing Polymer Structures Through the Triple 'Lens' of SEC^3. *Today's Chemist at Work 3* (11), 39−43.

(53) *Pierce Catalog and Handbook* (1994, 1995) Life Science & Analytical Research Products, Pierce Chemical Company, Rockford, IL.

(54) Congdon, R. W., Muth, G. W., and Splittgerber, A. G. (1993) The Binding Interaction of Coomassie Blue with Proteins. *Anal. Biochem. 213*, 407−413.

(55) Smisek, D. L., and Hoagland, D. A. (1989) Agarose Gel Electrophoresis of High Molecular Weight, Synthetic Polyelectrolytes. *Macromolecules 22*, 2270−2277.

(56) Provder, T., Ed. (1998) *Particle Size Distribution III: Assessment and Characterization*, ACS Symposium Series 693, American Chemical Society, Washington, DC.

(57) Weiner, B. B. (1992) Twenty Seven Years of QELS: A Review of the Advantages and Disadvantages of Particle Sizing with QELS. in *Particle Size Analysis* (N. G. Stanley-Wood and R. W. Lines, Eds.) pp 173−185, The Royal Society of Chemistry, Cambridge, England.

(58) Kurata, M., and Tsunashima, Y. (1989) Viscosity-Molecular Weight Relationships and Unperturbed Dimensions of Linear Chain Molecules. In *Polymer Handbook* (J. Brandrup and E. H. Immergut, Eds.) Chap. VII, pp 1−55, Wiley-Interscience, New York.

(59) Hiemenz, P. C., and Rajagopalan, R. (1997) *Principles of Colloid and Surface Chemistry*, 3rd ed., pp 94−98, Marcel Dekker, Inc., New York.

(60) Bovey, F. A. (1959) Enzymatic Polymerization. I. Molecular Weight and Branching During the Formation of Dextran. *J. Polym. Sci. 35*, 167−182.

(61) Doty, P., Schneider, N. S., and Holtzer, A. (1953) Molecular Dimensions of Cellulose Derivatives. *J. Am. Chem. Soc. 75*, 754.

(62) Holtzer, A. M., Benoit, H., and Doty, P. (1954) The Molecular Configuration and Hydrodynamic Behaviour of Cellulose Nitrate. *J. Phys. Chem. 58*, 624−634.

(63) Titova, E. F., Obolonkova, E. S., and Belavtseva, E. M. (1974) Electron-Microscopic Study of Dextran and Poly (vinyl alcohol) Solutions. *Farmatsiya 23* (5), 12−15.

(64) Creighton, T. E. (1983) *Proteins: Structures and Molecular Principles*, pp 241−242, W. H. Freeman, New York.

(65) Whistler, R. L., and BeMiller, J. N. (1958) Alkaline Degradation of Polysaccharides. In *Advances in Carbohydrate Chemistry* (M. L. Wolfrom and R. S. Tipson, Eds.) Vol. 13, pp 289−329, Academic Press, Inc., New York.

(66) Carubelli, R., Bhavanandan, V. P., and Gottschalk, A. (1965) Studies on Glycoproteins XI. The O-Glycosidic Linkage of N−Acetylgalactosamine to Seryl and Threonyl Residues in Ovine Submaxillary Gland Glycoprotein. *Biochim. Biophys. Acta 101*, 67−82.

(67) Chou, H.-P., Spence, C., Scherer, A., and Quake, S. A (1999) Microfabricated Device for Sizing and Sorting DNA Molecules. *Proc. Natl. Acad. Sci. U.S.A.* 96, 11−13.

(68) Weigl, B. H., and Yager, P. (1999) Microfluidic Diffusion-Based Separation and Detection. *Science 283*, 346−347.

(69) Freemantle, M. (1999) Downsizing Chemistry: Chemical Analysis and Synthesis on Microchips Promise a Variety of Potential Benefits. *Chem. Eng. News*, February 22, 27−36.

BC990077G

New Donor−Acceptor Pair for Fluorescent Immunoassays by Energy Transfer

Uwe Schobel,[†] Hans-Joachim Egelhaaf,[†] Andreas Brecht,[‡] Dieter Oelkrug,[†] and Günter Gauglitz*[,†]

Institute of Physical and Theoretical Chemistry, Auf der Morgenstelle 8, D-72076 Tübingen, Germany, DC-LCPPM, EPFL, CH-1014 Lausanne-Ecublens, Suisse. Received June 12, 1999; Revised Manuscript Received August 4, 1999

A novel Förster donor−acceptor dye pair for an immunoassay based on resonance energy transfer (RET) is characterized with respect to its photophysical properties. As donor and acceptor, we chose the long-wavelength excitable cyanine dyes Cy5 and Cy5.5, respectively. Due to the perfect spectral overlap, an exceptionally high R_0 value of 68.7 Å is obtained in solution. For biochemical applications, antibodies (IgG) are labeled with Cy5, while a tracer for competitive binding is synthesized by labeling bovine serum albumin (BSA) with an analyte derivative and Cy5.5. Binding the dyes to proteins at a low dye/protein ratio increases the fluorescence lifetimes and quantum yields, leading to an enhanced R_0 value of 85.2 Å. At higher dye/protein ratios, the formation of nonfluorescent dimeric species causes a decrease in the fluorescence lifetime and quantum yield due to RET from monomeric dyes to dimers within one protein molecule. The Förster distances could be calculated using the dimer absorption spectra to 83.9 and 83.6 Å for Cy5 and Cy5.5, respectively. Upon binding of the Cy5-labeled IgG to the tracer, efficient quenching of Cy5 fluorescence is observed. Steady-state and time-resolved measurements reveal that approximately 50% of the quenching results in Förster-type RET, while the residual quenching effect is caused by static quenching processes. The applicability of this dye pair is demonstrated in a homogeneous competitive immunoassay for the pesticide simazine.

INTRODUCTION

Immunoassays relying on fluorescence detection (fluoroimmunoassays, FIA) are known to be highly sensitive. They have the potential to replace the radioimmunoassay (RIA) technique (*1*) if the background signal arising from fluorescence of the biological matrix and light scattering can be effectively reduced (*2*−*4*). Two different approaches have been applied to minimize the background: (i) time-resolved fluorescent techniques (*5*−*9*) and (ii) methods using far-red excitable fluorescent dyes (*10*). The second approach takes advantage of reduced light scattering at longer wavelengths, and minimal tissue absorbance and autofluorescence, particularly above 600 nm (*10*, *11*). For excitation in the far-red wavelength region, inexpensive semiconductor laser diodes are available. Several classes of polymethine cyanine dyes, which are excitable in the far-red (635−1100 nm), including heptamethine cyanine dyes (*12*−*14*), squarine cyanine dyes (*15*), and sulfoindocyanine dyes (*16*−*21*), have been developed. Many of these have been successfully used as labels for analyte derivatives and/or antibodies in FIA-based applications (*22*−*25*). However, these dyes are known to aggregate (dimer formation) (*26*−*30*), particularly when present at high concentrations on protein surfaces. This leads to a drastic reduction in fluorescence intensity, since the dimers are essentially nonfluorescent. An accurate adjustment of the labeling ratio is therefore indispensable.

Several photophyiscal parameters of the labels are employed as observables in FIA to monitor the binding of the participating compounds, e.g., fluorescence polarization (*31*), fluorescence quenching (*32*, *33*) and enhancement (*34*), and resonant energy transfer (RET) (*35*). Among these FIA techniques, RET is the most versatile because of its little interference with different sample matrixes and the simple read-out technique (*36*). The efficiency of the RET process scales with the inverse 6th power of the distance R between the chromophores. The distances between donor and acceptor at which 50% of the excitation energy of the donor is transferred to the acceptor is the so-called Förster distance R_0. Typical R_0 distances are between 20 and 60 Å. So far, only four D−A pairs have been described with R_0 values between 60 and 70 Å (*37*). To achieve high-energy transfer efficiencies and thus high-intensity modulations in immunoassay-based applications, large R_0 values of the employed donor−acceptor pair are required.

In this paper, we present a new donor−acceptor pair with an exceptionally high R_0 value, comprising two commercially available long-wavelength excitable sulfoindocyanine dyes Cy5 and Cy5.5. The photophysical properties of the free and protein-bound dyes are determined. The effect of dimer formation of the protein-bound dyes on mean fluorescence lifetimes and quantum yields is investigated. To determine quantitatively the dependence of fluorescence intensity on the ratio of monomeric to dimeric dyes, the pure dimeric spectra are calculated. A homogeneous competitive RET immunoassay was set up with the optimized system. The fluorescence intensity modulation is investigated in detail, and the applicability of this immunoassay for the detection of the pesticide simazine is demonstrated.

EXPERIMENTAL PROCEDURES

N-Hydroxysuccinimidyl (NHS) esters of Cy5 (monofunctional) and Cy5.5 (bisfunctional) were purchased

* To whom correspondence should be addressed. E-mail: Guenter.Gauglitz@ipc.uni-tuebingen.de. Phone: [49] (7071) 2974667. Fax: [49] (7071) 295490.

[†] Institute of Physical and Theoretical Chemistry.

[‡] DC-LCPPM.

10.1021/bc990073b CCC: $18.00 © 1999 American Chemical Society
Published on Web 10/09/1999

from Amersham Life Science, Braunschweig/Germany. The triazine derivative 4-chloro-6-(isopropylamino)-1,3,5-triazine-2-(6'-amino)caproic acid (atrazine caproic acid, ACA) was synthesized and purified as described in ref *38*. Polyclonal anti-simazine antibody (IgG) was received as a present from Dr. Ram Abuknesha, GEC London. Solvents of analytical grade, Sephadex G-25 columns and all other common chemicals and biochemicals were purchased from Sigma Chemical Co., Deisenhofen/Germany and Fluka, Neu-Ulm/Germany.

Absorption spectra were recorded on a Perkin-Elmer λ 2 spectrophotometer. Fluorescence excitation and emission spectra were obtained with a Perkin-Elmer LS-50 B luminescence spectrometer equipped with a red-sensitive photomultiplier R928. Polarization spectra and anisotropies were determined using a Spex Fluorolog 222 spectrofluorometer. Fluorescence lifetimes were determined with a Spex Fluorolog 112. Single photon counting equipment was from EG & G ORTEC. The light source was a Hamamatsu laser diode at 653 nm. The emission was detected through a 670 nm cut-on filter. The emission monochromator was set to 680 and 705 nm for recording the decay of Cy5 and Cy5.5, respectively.

Fluorescence anisotropies r were calculated using the following equation:

$$r = \frac{I_{\parallel} - I_{\perp}}{I_{\parallel} + 2I_{\perp}} \tag{1}$$

where $I_{\parallel}$ and $I_{\perp}$ are the intensities observed parallel and perpendicular, respectively, to the axis of the vertically polarized excitation light (*39*). The excitation wavelength was set to the wavelength with the largest r_0 value in the excitation polarization spectra. To consider the effect of rotational diffusion on fluorescence anisotropies, we determined the rotational correlation time τ_R, which is given by the Perrin equation:

$$\tau_R = \frac{\tau}{(r_0/r) - 1} \tag{2}$$

where τ is the fluorescence lifetime and r_0 the anisotropy in the absence of depolarizing processes.

Time-resolved decays of fluorescence intensities $I(t)$ were fitted as a sum of exponentials

$$I(t) = \sum_i \alpha_i e^{-t/\tau_i} \tag{3}$$

where τ_i is the decay time and α_i the corresponding preexponential factor. The values of the parameters τ_i and α_i were determined using least-squares analysis software. Equation 3 was also used for fitting time-resolved fluorescence decays of protein-bound dyes which are additionally deactivated by RET. The assumption involved herein is that donor and acceptor are rather separated by a fixed distance than being randomly distributed. This situation is frequently encountered for labeled proteins (*39*).

The mean lifetime $\bar{\tau}$ was calculated according to

$$\bar{\tau} = \sum_i \alpha_i \tau_i^2 / \sum_i \alpha_i \tau_i \tag{4}$$

The Förster distance R_0 (*37*) was calculated using

$$R_0^6 = \frac{9000(\ln 10)\kappa^2 \phi_D J}{128\pi^5 n^4 N_{AV}} \tag{5}$$

Table 1. Molar Ratio of Reactive Dye and Protein Used in the Labeling Procedure in Comparison with the Obtained Dye/Protein Ratio of the Conjugates

protein	reactive dye	[reactive dye]/[protein] ratio	[attached dye]/[protein] ratio
IgG	Cy5-NHS	5	0.8
IgG	Cy5-NHS	20	3.7
IgG	Cy5-NHS	25	4.5
IgG	Cy5-NHS	35	8.7
BSA	Cy5.5-NHS	10	1.6
BSA	Cy5.5-NHS	20	2.9

where κ^2 is the orientation factor, ϕ_D is the donor quantum yield in the absence of acceptor molecules, J is the overlap integral, n is the refractive index of the medium, and N_{AV} is Avogadro's number. For the orientation factor κ^2, the average value of 2/3 for randomly oriented donors and acceptors in solution was assumed. The index of refraction n in PBS was assumed to be 1.33. The overlap integral J is defined as

$$J = \frac{\int \epsilon_A(\lambda) f_D(\lambda) \lambda^4 \, d\lambda}{\int f_D(\lambda) \, d\lambda} \tag{6}$$

where $f_D(\lambda)$ is the donor emission spectrum and $\epsilon_A(\lambda)$ is the extinction coefficient of the acceptor.

The fluorescence quantum yields ϕ_F(conjugate) of Cy5 monomers in the IgG−Cy5 conjugate (1:3.7) and Cy5.5 monomers in the BSA−Cy5.5 conjugate (1:1.6) were determined according to

$$\phi_F(\text{conjugate}) = \phi_F(\text{dye}) \frac{\tau_F(\text{conjugate})}{\tau_F(\text{dye})} \tag{7}$$

where ϕ_F(dye) is the fluorescence quantum yield of the free dye in solution and τ_F(conjugate) and τ_F(dye) are the experimental fluorescence lifetimes of the conjugate and of the corresponding dye, respectively.

The quantum yields of the IgG−Cy5 conjugates (1:0.8, 1:4.5, and 1:8.7) and BSA−Cy5.5 conjugate (1:2.9) were determined relative to the fluorescence quantum yields of the conjugates determined above by correcting the contribution of the nonfluorescent dimeric species to the absorbance at the excitation wavelength 649 nm and integration of the corrected emission spectra.

ACA−*N*-Hydroxysuccinimide Ester. A total of 3.76 mg (18 μmol) of dicyclohexylcarbodiimide (DCC) was added to a solution of 5 mg (16.5 μmol) of ACA and 2.1 mg (18 μmol) of *N*-hydroxysuccinimide (NHS) in 200 μL of absolute *N*,*N*-dimethylformamide (DMF) kept on ice. The mixture was stirred for 6 h at room temperature, filtered, and then used directly (without further purification) for conjugation to proteins.

Labeling of IgG and BSA with the Dyes. A total of 20 μL of reactive dye (for molar ratios see Table 1) in absolute DMF was added to a solution of 500 μg of protein (3.3 nmol of IgG or 7.2 nmol of BSA) in 250 μL of 0.1 M sodium carbonate-bicarbonate buffer, pH 9.7, and mixed thoroughly by gentle vortexing. The reaction was incubated at room temperature for 30 min. Unconjugated dye was separated from protein−dye conjugate by gel permeation chromatography over Sephadex G-25 using phosphate-buffered saline (PBS, 10 mM potassium dihydrogenphosphate, 150 mM sodium chloride, pH 7.4) as eluent. The dye-to-protein ratio was determined spectrophotometrically by measuring the absorbance at 653 nm (Cy5) or 681 nm (Cy5.5) and 278 nm (protein) in PBS: DMF (1:1, v/v) (*15*) and inserting the measured values

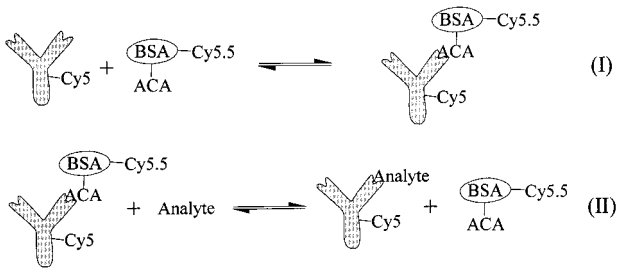


Figure 1. Schematic description of the competitive RET immunoassay. At low analyte concentrations (reaction I) the ACA-BSA-Cy5.5 conjugate is preferably bound to the antibody, at high analyte concentrations (reaction II) the ACA-BSA-Cy5.5 conjugate is displaced from the antibody binding sites.

into equation

$$[\text{attached dye}]/[\text{protein}] = \frac{A_{\text{dye}}\epsilon_{\text{protein}}}{(A_{278} - XA_{\text{dye}})\epsilon_{\text{dye}}} \quad (8)$$

The molar extinction coefficients of Cy5 and Cy5.5 (ϵ_{dye}) were assumed to be equal to their values in PBS (ϵ = 250 000 M^{-1} cm^{-1} and ϵ = 190 000 M^{-1} cm^{-1}, respectively), and the extinction coefficients of IgG and BSA ($\epsilon_{\text{protein}}$) were taken to be 201 700 M^{-1} cm^{-1} and 45 540 M^{-1} cm^{-1}, respectively. The factor X in the denominator accounts for dye absorption at 278 nm, which is 5 and 13% of the absorption of Cy5 (18) and Cy5.5 (20) at their maximum absorption (A_{dye}). The dye/protein ratios obtained are given in Table 1.

Labeling of BSA–Cy5.5 (1:1.6) Conjugate with ACA–NHS. A solution of 45 μg (150 nmol) of ACA–NHS in absolute DMF was added to a solution of 400 μg (5.8 nmol) of BSA–Cy5.5 conjugate in 250 μL of 0.1 M sodium carbonate-bicarbonate buffer, pH 9.7, and mixed thoroughly by gentle vortexing. The reaction condition and duration as well as the purification of the conjugate were the same as described above. The ACA concentration of the conjugates was determined by means of reflectometric interference spectroscopy (RIfS) (*40*). The ACA/BSA ratio was found to be 3.6:1, corresponding to a labeling efficiency of 15%.

RET Immunoassay. The principle of the competitive RET immunoassay is illustrated in Figure 1. The antibody (anti-simazine) was labeled with the donor Cy5 (IgG–Cy5). An analyte derivative (ACA) and the acceptor Cy5.5 were covalently linked by using bovine serum albumin (BSA) as carrier protein (ACA-BSA-Cy5.5). The immunoassay was performed by adding first 50 μL of IgG–Cy5 conjugate and then 50 μL of ACA-BSA-Cy5.5 conjugate to 400 μL standard solutions of simazine. The conjugates were dissolved in PBS, pH 7.4, containing 100 μg/mL chicken egg albumin (OVA) as background protein. The simazine standard solutions were diluted in PBS from a stock solution of c(simazine) = 1 mg/mL in DMF. After the addition of each conjugate, the solution was incubated for 10 min at 20 °C. After equilibration, the fluorescence intensity at 667 nm was measured. At low analyte concentrations the ACA-BSA-Cy5.5 conjugate is preferably bound to the antibody binding sites (reaction I). Due to the close proximity of Cy5.5 and Cy5 in the antigen–antibody complex, the IgG–Cy5 fluorescence is quenched by energy transfer. Higher analyte concentrations (reaction II) leads to a decreased occupation of the antibody binding sites by the ACA-BSA-Cy5.5 conjugate. This results in an increased IgG–Cy5 fluorescence.

The calibration curve was fitted to a four-parameter logistic equation according to the following formula (*41*):

$$y = \frac{A - B}{[1 + (x/C)^D]} + B \quad (9)$$

where y is the fluorescence intensity, x is the concentration of analyte, A and B are the upper and lower asymptotes, respectively, C is the concentration producing 50% of the maximal fluorescence intensity, and D is the slope at the inflection point of the sigmoidal curve.

RESULTS AND DISCUSSION

Photophysical Properties of the Free and Protein-Bound Dyes. The chemical structures of the sulfoindocyanine dyes Cy5 (donor) and Cy5.5 (acceptor) are shown in Figure 2. The absorption and fluorescence spectra of the two dyes are shown in Figure 3. There is an almost perfect spectral overlap between the Cy5 emission and the Cy5.5 absorption. The Förster distance (R_0) calculated for energy transfer from Cy5 to Cy5.5 (see eqs 5 and 6) is 68.7 Å, inserting a fluorescence quantum yield of $\phi_F^{Cy5} = 0.27$ for the donor (see Table 3) and an extinction coefficient of $\epsilon_{676nm}^{Cy5.5} = 190\,000$ M^{-1} cm^{-1} for the acceptor. The photophysical properties including absorption and emission maxima, extinction coefficients, fluorescence lifetimes, and rotational correlation times of the dyes are summarized in Table 2.

The photophysical properties of the IgG–Cy5 and BSA–Cy5.5 conjugates are also given in Table 2. The increase of the rotational correlation time τ_r indicates that the dyes are covalently attached to the proteins. Due to the higher polarizability of the environment, the absorption maxima shift toward longer wavelengths by 2 and 5 nm for Cy5 and Cy5.5, respectively. The fluorescence maxima of the conjugates are red-shifted by 2 and 10 nm.

Dimer Formation. The absorption spectra of the IgG–Cy5 and BSA–Cy5.5 conjugates (see Table 1) are shown in Figure 4A and Figure 5A, respectively. With increasing dye/protein ratio, the extinction coefficient of the absorption maximum is reduced and a new band appears, which is blue-shifted by 46 nm (Cy5) and 50 nm (Cy5.5), respectively. In addition, two isosbestic points appear, indicating that two colored species are in equilibrium. This effect is caused by attractive interactions between adjacent dye molecules, leading to the formation of dimeric species (*28*) at higher dye/protein ratios. The aggregated portion of the dyes in the conjugates is almost completely converted to the monomeric form by adding DMF to PBS solution of the conjugates (1:1, v/v) (*15*). Thus, the spectral positions of the isosbestic points could be determined accurately.

The fluorescence excitation spectra of these conjugates are superimposable on the monomer absorption spectra (see Figure 4A and Figure 5A). This indicates that the dimers are essentially nonfluorescent.

To calculate the proportion of the dimeric species on the protein conjugates, the molar extinction coefficients of the pure dimers at a given wavelength must be known. The dimer spectra can be calculated by applying the law of mass action to the monomer ⇌ dimer equilibrium of the free dyes in solution (*42*). If the fraction of the total molar concentration c of the dye in solution present as dimer is α, the association constant is

$$K = \frac{c_d}{{c_m}^2} = \frac{\alpha}{2(1 - \alpha)^2 c} \quad (10)$$

where c_d and c_m are the concentrations of the dimeric and monomeric dyes, respectively. In Figure 4B and Figure

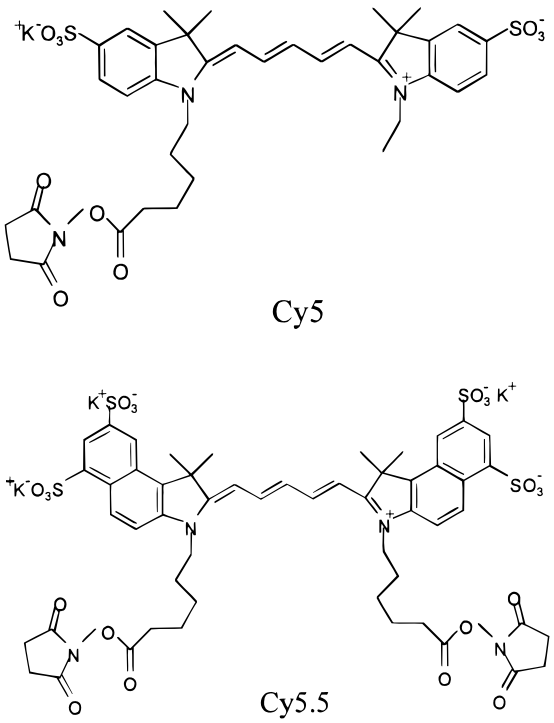


Figure 2. Chemical structures of the reactive NHS-esters of Cy5 (top) and Cy5.5 (bottom).

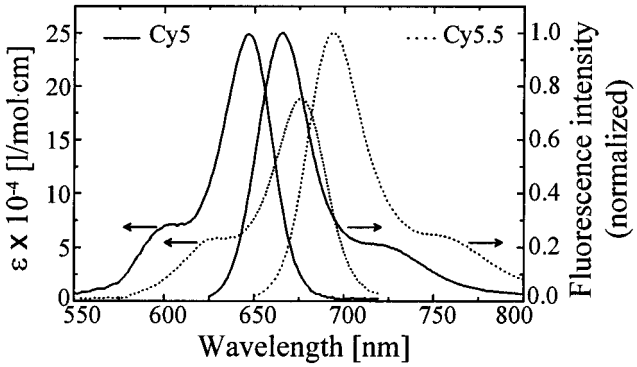


Figure 3. Absorption and emission spectra of Cy5 (—) and Cy5.5 (···) in PBS.

Table 2. Photophysical Properties of the Unbound and Protein-Bound Cy5 and Cy5.5 in PBS[a]

	Cy5	Cy5.5	IgG-Cy5	ACA-BSA-Cy5.5
λ_{max}(abs)[b] (nm)	647	676	649	681
λ_{max}(em)[b] (nm)	665	693	667	703
ϵ (L/mol cm)[b]	250 000[c]	190 000[d]	250 000	190 000
τ_1 (ns)	0.94	0.99	1.01 (0.12)[e]	1.17 (0.16)[f]
τ_2 (ns)			1.88 (0.1)[e]	1.94 (0.09)[f]
$\bar{\tau}$ (ns)			1.54[e]	1.53[f]
τ_r[b]	0.47	0.84	1.08[e]	1.27[f]

[a] The α_i values of the fitted fluorescence lifetimes τ_i are given in the brackets after the lifetimes. [b] Phosphate-buffered saline (PBS), [c] Values adopted from ref *18*. [d] Values adopted from ref *20*. [e] Values determined for IgG-Cy5 (1:3.7). [f] Values determined for ACA-BSA-Cy5.5 (3.6:1:1.6). The experimental error of τ and τ_r is typically ±5 and ±7%, respectively.

5B the absorption spectra of the pure monomeric dyes and the spectra of a 1×10^{-3} M and a 1×10^{-2} M solution of the dyes in PBS are shown together with the calculated dimeric spectra. Upon dimer formation, the main absorption band is split into two bands, one of high intensity at the high-frequency side of the monomeric maximum, and the other of lower intensity at the low-frequency side of the monomeric maximum. This splitting of the excited electronic state of the monomer into two states upon dimer formation is due to the interaction of obliquely oriented transition dipole moments, as explained by the exciton model (*29*).

Table 3. Quantum Yields of the Free and Protein-Bound Cy5 and Cy5.5 in PBS

	monomer (%)	ϕ_F[b]
Cy5	100	0.27[c]
IgG-Cy5 (1:0.8)	90	0.88
IgG-Cy5 (1:3.7)	74	0.44
IgG-Cy5 (1:4.5)	69	0.40
IgG-Cy5 (1:8.7)	52	0.14
Cy5.5	100	0.23[d]
BSA-Cy5.5 (1:1.6)	84	0.36
BSA-Cy5.5 (1:2.9)	76	0.21

[a] In the first column the percentage of monomer dye molecules present on the proteins are given. [b] Phosphate-buffered saline (PBS), [c] Value adopted from ref *18*. [d] Value adopted from ref *20*. The experimental error of ϕ_F is typically ±5%.

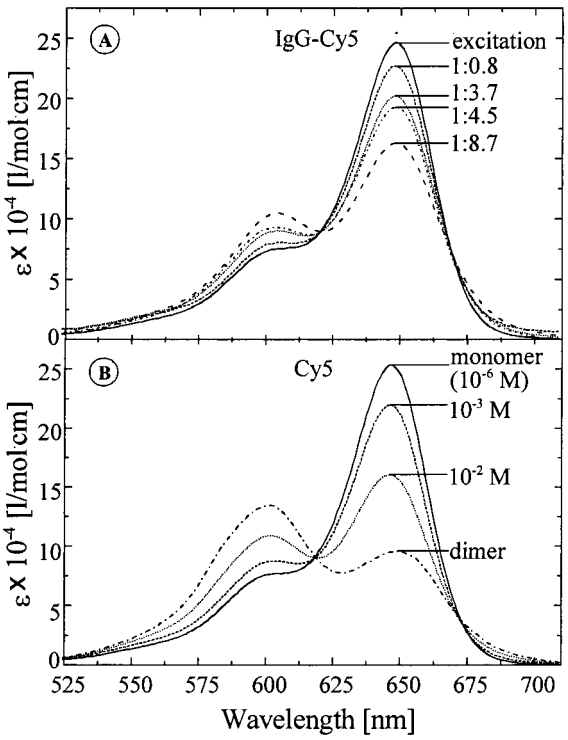


Figure 4. (A) Fluorescence excitation spectrum of the antibody conjugates in comparison with their absorption spectra in PBS. (B) Absorption spectra of different concentrations of the unbound Cy5 dye in PBS solution. The absorption spectrum of the monomer Cy5 dye is superimposable to its fluorescence excitation spectrum.

Using the dimeric spectra, we were able to calculate the monomer/dimer ratios of the employed protein conjugates. Table 3 shows the data obtained for the IgG−Cy5 as well as for the BSA−Cy5.5 conjugates. With increasing numbers of Cy5 and Cy5.5 molecules attached to the IgG (0.8−8.7) and BSA (1.6−2.9), the relative amounts of monomers are reduced from 0.9 to 0.52 and from 0.84 to 0.76.

Quantum Yields and Fluorescence Lifetimes. With the knowledge of the monomer/dimer ratio of the employed protein conjugates, it was possible to determine the fluorescence quantum yields of the protein-bound monomeric dyes. At low Cy5/IgG ratios, an enhancement of the fluorescence quantum yield of the monomeric Cy5, compared to that in solution, is observed (see Table 3).

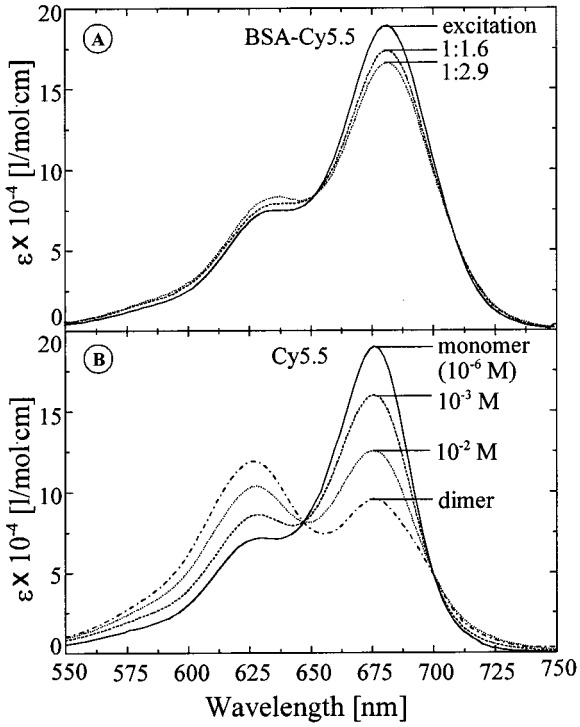


Figure 5. (A) Fluorescence excitation spectrum of the BSA conjugates in comparison with their absorption spectra in PBS. (B) Absorption spectra of different concentrations of the unbound Cy5.5 dye in PBS solution. The absorption spectrum of the monomer Cy5.5 dye is superimposable to its fluorescence excitation spectrum.

This enhancement, which goes along with the increase of the Cy5 fluorescence lifetime, is most likely due to the restricted torsional motion about the central methine bridge, a result obtained also for other cyanine dyes (*43*–*46*).

With increasing Cy5/IgG ratios, a decrease of the quantum yield is obtained. This decrease is due to RET from the fluorescent monomeric dye to increasing numbers of nonfluorescent dimer molecules on the antibody. The calculated Förster distance is $R_0 = 83.9$ Å, which results in very efficient fluorescence quenching by RET, if a radius of a spherical antibody molecule of approximately 6 nm is assumed. The maximum of fluorescence intensity per labeled antibody can be derived by multiplying the fluorescence quantum yield of Cy5 monomer with the number of monomeric Cy5 on the antibody. With rising Cy5/IgG ratios, the fluorescence increases, reaching a maximum at a Cy5/IgG ratio of approximately 4. At higher Cy5/IgG ratios, fluorescence quenching by RET begins to dominate, resulting in decreasing fluorescence intensity. This result is in good agreement with the value obtained in an earlier report (*19*) for a similar carboxymethylindocyanine dye (Cy5.12).

The fluorescence quantum yield for Cy5.5 shows a behavior similar to that of Cy5. An enhancement is observed when bound to BSA (Cy5.5/BSA ratio 1.6:1) (see Table 3), whereas a higher Cy5.5/BSA ratio (2.9:1) leads to a decrease in fluorescence quantum yield. The Förster distance for RET from the fluorescent monomeric Cy5.5 to nonfluorescent dimer molecules on the BSA is calculated to $R_0 = 83.6$ Å. Very efficient fluorescence quenching by RET results, if a radius of a spherical BSA molecule of approximately 3 nm is assumed.

Energy Transfer in the Antigen–Antibody Complex. The Förster distances for energy transfer from IgG–Cy5 (labeling ratio 1:3.7) to the BSA bound Cy5.5

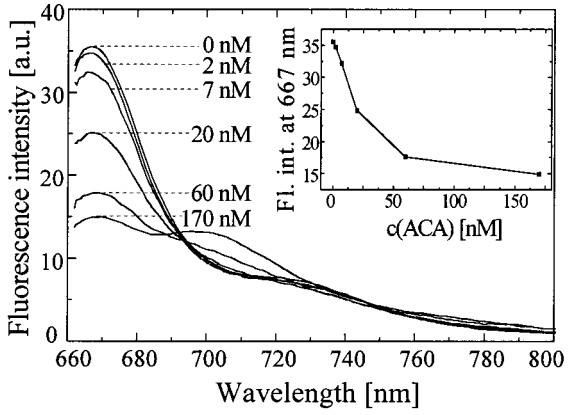


Figure 6. Titration of 67 nM IgG–Cy5 (1:3.7) with increasing amounts of ACA-BSA-Cy5.5 (3.6:1:1.6) [c(ACA) = 0–170 nM]. The quenching of the fluorescence signal of IgG–Cy5 [c(ACA) = 0 nM] amounts to 65% [c(ACA) = 170 nM].

monomers and dimers are calculated using the data in Table 2 and Table 3. Exceptionally high values of $R_0 = 75.9$ Å and $R_0 = 77.8$ Å are obtained for the monomeric and dimeric Cy5.5, respectively. This is the consequence of the increased overlap integral and the high fluorescence quantum yield of the fluorescent monomeric Cy5 compared to the free dyes in solution.

Emission spectra of 67 nM IgG–Cy5 (1:3.7) are shown in Figure 6. Additions of 0–170 nM ACA-BSA-Cy5.5 (3.6:1:1.6) (see Figure 1, reaction I) lead to a progressive decrease in the steady-state intensity of Cy5 emission (see inset of Figure 6). At 170 nM ACA-BSA-Cy5.5, a maximum quenching of the IgG–Cy5 fluorescence is achieved. The total quenching of IgG–Cy5 fluorescence (ΔI^{Cy5}_{quench}), calculated as the difference of the fluorescence intensities of IgG–Cy5 in absence (I_F^{Cy5}) and in the presence of 170 nM ACA-BSA-Cy5.5, equals to

$$\Delta I^{Cy5}_{quench} = 0.65 I_F^{Cy5} \tag{11}$$

In the following, we will show that two mechanisms are involved in the quenching of the IgG–Cy5 fluorescence in the antigen–antibody complex: (i) quenching due to RET from Cy5 to Cy5.5 and (ii) static quenching due to the close proximity of Cy5 and Cy5.5. Figure 7 shows the analysis of the quenching process. Negative values represent decrease of fluorescence intensity whereas increase of fluorescence intensity is plotted on the positive *y*-axis.

The fraction of fluorescence intensity of IgG–Cy5 which is quenched due to RET from Cy5 to Cy5.5 (ΔI^{Cy5}_{RET}) and thus leads to sensitized fluorescence of Cy5.5 ($\Delta I^{Cy5.5}_{RET}$) is given by

$$\Delta I^{Cy5}_{RET} = \Delta I^{Cy5.5}_{RET} \frac{\phi_F^{Cy5}}{\phi_F^{Cy5.5}} \tag{12}$$

and equals to

$$\Delta I^{Cy5}_{RET} = 0.53 \Delta I^{Cy5}_{quench} \tag{13}$$

$\Delta I^{Cy5.5}_{RET}$ has been corrected for directly excited fluorescence contributions, ϕ_F^{Cy5} is the fluorescence quantum yield of IgG bound monomeric Cy5, and $\phi_F^{Cy5.5}$ is the mean fluorescence quantum yield of BSA bound Cy5.5. To confirm the contribution of RET to the quenching process in the antigen–antibody complex, the IgG–Cy5

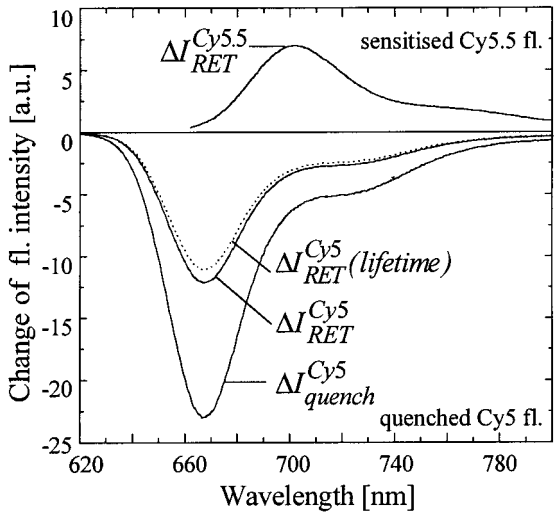


Figure 7. Plots of the sensitized ACA-BSA-Cy5.5 fluorescence (positive *y*-axis) and the quenching of IgG−Cy5 fluorescence (negative *y*-axis) which can be attributed to different quenching processes of IgG−Cy5 in the antigen−antibody complex. For details see text.

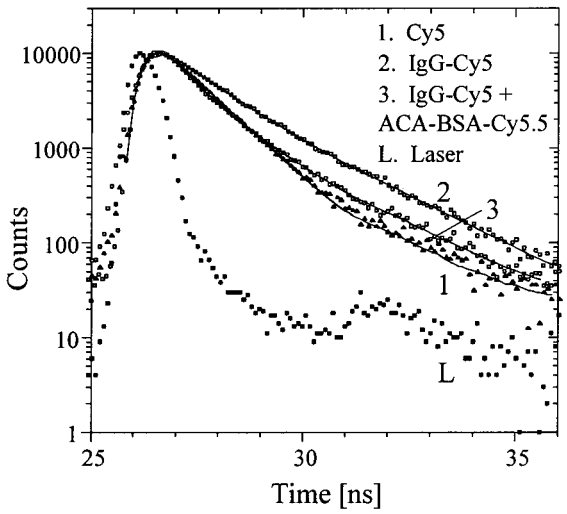


Figure 8. Fluorescence intensity decay of unbound Cy5 (1), 67 nM IgG−Cy5 in absence (2) and presence (3) of 170 nM ACA-BSA-Cy5.5.

fluorescence intensity decays were measured. Figure 8 shows the increase of the mean fluorescence lifetime of Cy5 upon binding to the antibody from 0.94 to 1.54 ns (see also Table 2) and the decrease of the mean fluorescence lifetime of Cy5 in the antigen−antibody complex from 1.54 to 1.06 ns, as it is expected for RET. From this it follows that a fraction of 0.31 of the donor excitation energy is deactivated by RET. The integral emission which corresponds to this quenching [ΔI_{RET}^{Cy5}(lifetime)] is also shown in Figure 7 (dashed line). It equals to

$$\Delta I_{RET}^{Cy5}(\text{lifetime}) = 0.48\Delta I_{quench}^{Cy5} \qquad (14)$$

The discrepancy between the fraction of fluorescence quenching by RET, which is derived from the steady-state (0.53) and the lifetime measurements (0.48), is within experimental error. Using the data from Table 3 the fraction of RET from IgG−Cy5 to the BSA bound Cy5.5 monomers and dimers can be calculated to $0.44\Delta I_{quench}^{Cy5}$ and $0.09\Delta I_{quench}^{Cy5}$, respectively. Table 4 summarizes the characteristical parameters which describe the energy transfer process, i.e., the Förster distance R_0,

Table 4. Analysis of Energy Transfer from IgG−Cy5 to ACA-BSA-Cy5.5

τ_D (ns)[a]	τ_{DA} (ns)[b]	R_0 (Å)	E_{RET}[c]	k_{RET} (1/s)[d]	R (Å)[e]
1.54	1.06	75.9	0.31	3×10^8	86.7

[a] Mean fluorescence lifetime of the donor in absence of the acceptor. [b] Mean fluorescence lifetime of the donor in the presence of the acceptor. [c] Efficiency of energy transfer. [d] Rate of energy transfer. [e] Average distance between the fluorophores.

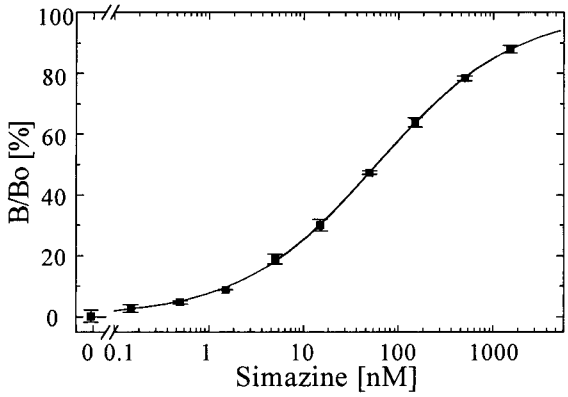


Figure 9. Calibration curve of simazine using an antibody concentration of 3 nM (450 ng/mL) and an ACA-BSA-Cy5.5 concentration of 10 nM (3 μg/L). Error bars are the standard errors of the mean from three replicate analyses.

the efficiency of energy transfer E_{RET}, the rate of energy transfer k_{RET} and the distance between the fluorophores R (*37*).

The fraction of the IgG−Cy5 quenching, which could not be ascribed to RET processes must be assigned to static quenching (ΔI_{static}^{Cy5})

$$\Delta I_{static}^{Cy5} = \Delta I_{quench}^{Cy5} - \Delta I_{RET}^{Cy5}(\text{lifetime}) = 0.47\Delta I_{quench}^{Cy5} \qquad (15)$$

The high fraction of static fluorescence quenching (47%) not resulting in sensitized acceptor fluorescence is favorable for energy-transfer immunoassays, because the signal modulation of Cy5 is enhanced.

Competitive Immunoassay. With the system described above, a competitive immunoassay for the analyte simazine has been performed (see Figure 1). The antibody concentration used was 3 nM (450 ng/mL). The ACA-BSA-Cy5.5 concentration was optimized by titration, to obtain the maximum quenching of the IgG−Cy5 fluorescence and thus a great dynamic range of the calibration curve. At a concentration of 10 nM (3 μg/L) ACA-BSA-Cy5.5, a quenching of 47.2% was achieved. A typical calibration curve for simazine, using these concentrations, is shown in Figure 9. The coefficients of variation are between 0.5 and 2%, the test midpoint is at 50 nM (10 μg/L) simazine, and the working range, defined as 10−90% B/B_0, is from 1.5 nM (0.3 μg/L) to 1000 nM (200 μg/L) simazine. The EU drinking water limit for a single pesticide of 0.1 μg/L cannot be achieved in this first assay. With further optimizations of the competitive analyte derivative with regard to the affinity of the antibody, the test midpoint and the limit of detection can be improved.

ACKNOWLEDGMENT

This work was supported by the German Ministry of Education, Science, Research and Technology under the "Mikrosystemtechnik 1994−1998" program (Project LINDAU/16SV541/VDI-VDE IT) and by the DFG (For-

schergruppe "Molekulare Mustererkennung..." and Graduiertenkolleg "Quantitative Analyse und Charakterisierung pharmazeutisch und biochemisch relevanter Substanzen" at the University of Tübingen).

LITERATURE CITED

(1) Yalow, R. S., and Berson, S. A. (1960) Immunoassay of endogenous plasma insulin in man. *J. Clin. Invest. 39*, 1157−1175.

(2) O'Donnell, C. M., and Suffin, S. C. (1979) Fluorescence Immunoassays. *Anal. Chem. 51*, 33A−40A.

(3) Chan, D. W. (1987) Fluorescence Immunoassay. *Immunoassay: a practical guide* (D. W. Chan, Ed.) pp 15−23, Academic Press Inc., San Diego.

(4) Christopoulos, T. K., and Diamandis, E. P. (1996) Fluorescence Immunoassay. *Immunoassay* (D. W. Chan, Ed.) pp 309−335, Academic Press Inc., San Diego.

(5) Siitari, H., Hemmilä, I., Soini, E., and Lövgren, T. (1983) Detection of hepatitis B surface antigen using time-resolved fluoroimmunoassay. *Nature 301*, 258−260.

(6) Youn, H. J., Terpetschnig, E., Szmacinski, H., and Lakowicz, J. R. (1995) Fluorescence Energy Transfer Immunoassay Based on a Long-Lifetime Luminescent Metal−Ligand Complex. *Anal. Biochem. 232*, 24−30.

(7) Yuan, J., and Matsumoto, K. (1998) A new Tetradentate *β*-Diketonate-Europium Chelate that can be Covalently Bound to Proteins for Time-Resolved Fluoroimmunoassay. *Anal. Chem. 70*, 596−601.

(8) Heyduk, E., and Heyduk, T. (1997) Thiol-Reactive Luminescent Europium Chelates: Luminescence Probes for Resonance Energy Transfer Distance Measurements in Biomolecules. *Anal. Biochem. 248*, 216−227.

(9) Gaillard, O., Kapel, N., Galli, J., Delattre, J., and Meillet, D. (1994) Time-resolved fluorometry: Principles and applications in clinical chemistry. *Ann. Biol. Clin. 52*, 751−755.

(10) Cullander, C. (1994) Imaging in the far-red with electronic light microscopy: requirements and limitations. *J. Microsc. 176*, 281−286.

(11) Wood, P. (1991) Heterogeneous fluoroimmunoassay. *Principles and practice of immunoassay* (C. P. Price and D. J. Newman, Eds.) pp 365−393, Stockton Press, New York.

(12) Narayanan, N., Strekowski, L., Lipowska, M., and Patonay, G. (1995) A New Method for the Synthesis of Heptamethine Cyanine Dyes: Synthesis of New Near-Infrared Fluorescent Labels. *J. Org. Chem. 60*, 2391−2395.

(13) Mason, J. C., and Patonay, G. (1996) Functionalization of Near-Infrared Cyanine Dyes. *J. Heterocycl. Chem. 33*, 1685−1688.

(14) Lee, L. G., Woo, S. L., Head, D. F., Dubrow, R. S., and Baer, T. M. (1995) Near-IR Dyes in Three-Color Volumetric Capillary Cytometrie: Cell Analysis With 633- and 785-nm Laser Excitation. *Cytometrie 21*, 120−128.

(15) Terpetschnig, E., Szmacinski, H., Ozinskas A., and Lakowicz, J. R. (1994) Synthesis of Squaraine-N−Hydroxysuccinimide Esters and Their Biological Application as Long-Wavelength Fluorescent Labels. *Anal. Biochem. 217*, 197−204.

(16) Ernst, L. A., Gupta, R. K., Mujumdar, R. B., and Waggoner, A. S. (1989) Cyanine Dye Labeling Reagents for Sulfhydryl Groups. *Cytometry 10*, 3−10.

(17) Mujumdar, R. B., Ernst, L. A., Mujumdar, S. R., and Waggoner, A. S. (1989) Cyanine Dye Labeling Reagents Containing Isothiocyanate Groups, *Cytometry 10*, 11−19.

(18) Mujumdar, R. B., Ernst, L. A., Mujumdar, S. R., Lewis C. J., and Waggoner, A. S. (1993) Cyanine Dye Labeling Reagents: Sulfoindocyanine Succinimidyl Esters. *Bioconjugate Chem. 4*, 105−111.

(19) Southwick, P. L., Ernst, L. A., Tauriello, E. W., Parker, S. R., Mujumdar, R. B., Mujumdar, S. R., Clever H. A., and Waggoner, A. S. (1990) Cyanine Dye Labeling Reagents−Carboxymethyl-indocyanine Succinimidyl Esters. *Cytometry 11*, 418−430.

(20) Mujumdar, S. R., Mujumdar, R. B., Grant, C. M., and Waggoner, A. S. (1996) Cyanine-Labeling Reagents: Sulfobenzindocyanine Succinimidyl Esters. *Bioconjugate Chem. 7 (3)*, 356−362.

(21) Soper, S. A., and Mattingly, Q. L. (1994) Steady-State and Picosecond Laser Fluorescence Studies of Nonradiative Pathways in Tricarbocyanine Dyes: Implications to the Design of Near-IR Fluorochromes with High Fluorescence Efficiencies. *J. Am. Chem. Soc. 116*, 3744−3752.

(22) Williams, R. J., Peralta, J. M., Tsang, V. C. W., Narayanan, N., Casay, G. A., Lipowska, M., Strekowski, L., and Patonay, G. (1997) Near-infrared heptamethine cyanine dyes: A new tracer for solid-phase immunoassays. *Appl. Spectrosc. 51* (6), 836−843.

(23) Chen, F. T., and Evangelista, R. A. (1994) Feasibility studies for simultaneous immunochemical multianalyte drug assay by capillary electrophoresis with laser-induced fluorescence. *Clin. Chem. 40* (9), 1819−1822.

(24) Wadkins, R. M., Golden, J. P., Pritsiolas, L. M., and Ligler, F. S. (1998) Detection of multiple toxic agents using a planar array immunosensor. *Biosens. Bioelectron. 13* (3−4), 407−415.

(25) Klotz, A., Brecht, A., Barzen, C., Gauglitz, G., Harris, R. D., Quigley, G. R., Wilkinson, J. S., and Abuknesha, R. A. (1998) Immunofluorescence sensor for water analysis. *Sens. Actuators, B 51*, 181−187.

(26) Li, Q., and Peng, B.-X. (1998) Benzimidazoloindocarbocyanines: Aggregation Behaviour, Redox Potential and Photographic Properties. *Dyes Pigment 36*, 323−337.

(27) Min, H., Park, J., Yu, J., and Kim, D. (1998) The Spectroscopic Studies on the Aggregation Behaviour of Cyanine Dyes. *Bull. Korean Chem. Soc. 19*, 650−654.

(28) West, W., and Pearce, S. (1965) The Dimeric State of Cyanine Dyes. *J. Phys. Chem. 69*, 1894−1903.

(29) Sundström, V., and Gillbro, T. (1985) Excited-state dynamics and photophysics of aggregated dye chromophores in solution. *J. Chem. Phys. 83*, 2733−2743.

(30) Sidorowicz, A., Pola, A., and Dobryszycki, P. (1997) Spectral properties of 3.3′-diethyloxadicarbocyanine included in phospholipid liposomes. *J. Photochem. Photobiol. B 38*, 94−97.

(31) Dandliker, W. B., and de Saussure, V. A. (1970) Fluorescence polarisation in immunochemistry. *Immunochemistry 7*, 799−828.

(32) Lin, M., and Nielsen, K. J. (1997) Binding of the Brucella abortus lipopolysaccharide O-chain fragment to a monoclonal antibody. Quantitative analysis by fluorescence quenching and polarization. *Bioconjugate Chem. 4*, 2821−2827.

(33) Chang, I. N., Lin, J.-N., Andrade, J. D., and Herron, J. N. (1995) Photoaffinity Labeling of Antibodies for Applications in Homogeneous Fluoroimmunoassays. *Anal. Chem. 67*, 959−966

(34) Smith, D. J. (1977) Enhancement fluoroimmunoassay of thyroxine. *FEBS. Lett. 77*, 25−27.

(35) Ullman, E. F., Schwarzberg, M., and Rubenstein, K. E. (1976) Fluorescent Excitation Transfer Immunoassays: A General Method for Determination of Antigens. *J. Biol. Chem. 251*, 4172−4178.

(36) Brecht, A., Schobel, U., and Gauglitz, G. (1998) Resonant Energy Transfer Detection for Low Volume Immunoassay in Environmental Applications. *Biosensors for Environmental Diagnostics* (Hock, Barceló, Camman, Hansen, and Turner, Eds.) pp 11−27, B. G. Teubner, Stuttgart.

(37) Van Der Meer, B. W., Coker, G., III, Chen, S.-Y. S. (1994) *Resonance Energy Transfer − Theory and Data*, Verlag Chemie, Weinheim.

(38) Weller, M., (1992) Strukturelle und kinetische Untersuchungen zur Entwicklung und Optimierung von Hapten-Enzymimmunoassays (ELISAs) am Beispiel der Bestimmung von Triazinherbiziden. Dissertation TU München, Fakultät für Chemie, Biologie und Geowissenschaften.

(39) Lakowicz, J. R. (1983) *Principles of Fluorescence Spectroscopy*, Plenum Press, New York.

(40) Piehler, J., Brecht, A., Giersch, T., Hock, B., and Gauglitz, G. (1997) Assessment of affinity constants by rapid solid-phase detection of equilibrium binding in a flow system. *J. Immunol. Methods 201*, 189−206.

(41) Dudley, R. A., Edwards, P., Ekins, R. P., Finney, D. J., McKenzie, I. G., Raab, G. M., Rodbard, D., and Rodgers, R. P. C. (1985) Guidelines for Immunoassay Data Processing. *Clin. Chem. 31*, 1264−1271.

(42) Förster, T., and König, E. (1957) Absorptionsspektren und Fluoreszenzeigenschaften konzentrierter Lösungen organischer Farbstoffe. *Z. Elektrochem. 61*, 344−348.

(43) Aramendia, P. F., Negri, R. M., and Román, E. S. (1994) Temperature Dependence of Fluorescence and Photoisomerisation in Symmetric Carbocyanines. Influence of Viscosity and Molecular Structure. *J. Phys. Chem. 98*, 3165−3173.

(44) Netzel, T. L., Nafisi, K., and Zhao, M. (1995) Base-Content Dependence of Emission Enhancements, Quantum Yields, and Lifetimes for Cyanine Dyes Bound to Double-Strand DNA: Photophysical Properties of Monomeric and Bichromophoric DNA Stains. *J. Phys. Chem. 99*, 17936−17947.

(45) Serpone, N., and Sahyun, M. R. V. (1994) Photophysics of Dithiacarbocyanine Dyes: Subnanosecond Relaxation Dynamics of a Dithia-2,2′-carbocyanine Dye and Its 9-Methyl-Substitued Meso Analogue. *J. Phys. Chem. 98*, 734−737.

(46) Carlsson, C., Larsson, A., Jonsson, M., Albinsson, B., and Nordén, B. (1994) Optical and Photophysical Properties of the Oxazole Yellow DNA Probes YO and YOYO. *J. Phys. Chem. 98*, 10313−10321.

(47) Doizi, D., and Mialocq, J. C. (1987) Photosensitized Electron-Transfer Reaction in the First Excited Singlet State of a Polymethine-Cyanine Dye. *J. Phys. Chem. 91*, 3524−3530.

BC990073B

Design of Dendritic Macromolecules Containing Folate or Methotrexate Residues

Kenji Kono,‡ Mingjun Liu, and Jean M. J. Fréchet*

Department of Chemistry, University of California, Berkeley, California 94720-1460. Received June 18, 1999; Revised Manuscript Received September 20, 1999

Polyether dendritic compounds bearing folate residues on their surface were prepared as model drug carriers with potential tumor cell specificity. Starting from ester-terminated polyether dendrimers, hydrazide groups were easily introduced to the surface of the dendrimers by reaction with hydrazine. Folate residues were then conjugated to the hydrazide chain ends of the dendrimers by direct condensation with folic acid in the presence of a condensing agent or by reaction with an active ester derivative of folic acid. Essentially complete functionalization of the terminal hydrazide groups was achieved for both the first and the second generation dendrimers with four and eight hydrazide groups. For the G-2 dendrimer with 16 hydrazide groups, an average number of only 12.6 folate residues were attached to each dendrimer. The conjugates are soluble in aqueous medium above pH 7.4. In addition, a similar conjugation of the antitumor drug methotrexate to the dendrimer was also investigated. Once optimized, these molecules may form the basis for a novel family of multivalent drug carriers.

Dendrimers are unique synthetic macromolecules that have attracted much interest due to their unique structures and properties since their introduction in the mid-1980s. Their highly branched and well-defined structure, globular shape, and controlled surface functionality are some of the important characteristics of dendrimers (*1*−*3*). While applications of dendrimers have been explored in a very broad range of fields, their use in drug delivery systems has remained largely unexplored.

The functional groups present at the surface of dendrimers have been utilized for the conjugation of various biologically active molecules. For example, antibody (*4*−*6*) and sugar moieties (*7*, *8*) have been conjugated to the chain ends of poly(amidoamine) dendrimers, and these modifications have afforded dendrimers that may possess site-specific properties via antibody−antigen binding or via interactions between sugars and their receptors on cell surfaces.

The interior of dendrimers has also been shown to be capable of encapsulating guest molecules. Meijer and coworkers have reported that guest molecules, such as Rose Bengal, may be physically entrapped into the internal "cavity" of high generation poly(propylene imine) dendrimers when an amino acid derivative was used to cap each end group of the dendrimer (*9*). Because the amino acid derivative used was bulky, sterically crowded, and subject to hydrogen bonding, the entrapped guest molecules could not diffuse out of the dense packed shell of the dendrimer into the surrounding solution. Yet another strategy for the encapsulation of guest molecules in dendrimers makes use of hydrophobic interactions. Thus, Newkome et al. have prepared dendritic macromolecules with hydrophobic interior and hydrophilic chain ends (*10*), and these molecules were shown to behave as unimolecular micelles capable of solubilizing various hydrophobic compounds in aqueous solution (*11*).

In early work, we have also reported that simple and well-characterized poly(aryl ether) dendrimers bearing carboxylic groups as chain ends were able to solubilize pyrene in water (*12*). More recently, we have explored the possibility of using more appropriately designed dendritic unimolecular micelles as drug delivery agents, and the result showed that ca. 11 wt % of a hydrophobic drug such as indomethacin could be easily entrapped inside the hydrophobic interior of dendritic micelles and released slowly into buffer solution (*13*, *14*). Another, yet less explored (*15*, *16*), approach to the use of dendrimers in drug delivery is to attach drug molecules to the chain ends of the dendrimers; therefore, a high concentration of drug may be carried by a simple well-defined molecule. If an appropriate ligand is conjugated to one of the terminal groups of the dendrimers, a targeting feature may eventually be added to these dendrimer−drug conjugates.

It is known that a membrane-associated folate receptor, folate binding protein, is overexpressed on the surface of a variety of human tumor cells (*17*−*19*). When folic acid molecules are covalently linked to proteins, the folate−protein conjugates are internalized into cells via receptor-mediated endocytosis (*20*). Therefore, folate has been used as a ligand for the targeting of proteins (*21*), liposomes (*22*, *23*), and other molecules (*24*, *25*) to tumor cells that express the folate-binding proteins. The folic acid molecule (see Figure 1) possesses two carboxyl groups, termed α- and γ-, and the latter exhibits a much higher reactivity in a carbodiimide-mediated coupling to amino groups (*26*). In addition, folate linked via its γ-carboxyl group retains a strong affinity toward its receptor (*26*).

In this study, we have designed and synthesized dendritic molecules containing folate residues as models

* To whom correspondence should be addressed. Phone: (510) 643-3077. Fax: (510) 643-3079. E-mail: Frechet@CChem.Berkeley.edu.

‡ Present address: Department of Applied Materials Science, College of Engineering, and Department of Applied Bioscience, Research Institute for Advanced Science and Technology, Osaka Prefecture University, Sakai, Osaka 599-8531, Japan.

10.1021/bc990082k CCC: $18.00 © 1999 American Chemical Society
Published on Web 10/21/1999

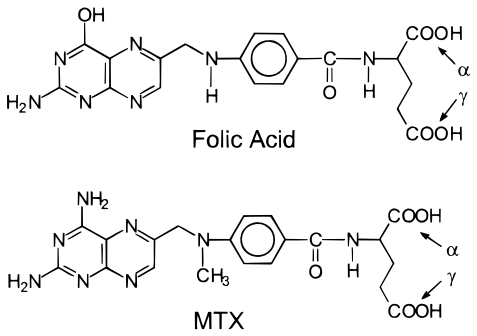


Figure 1. Structure of folic acid and MTX.

for drug carriers with tumor cell specificity. The synthesis is started from readily accessed ester-terminated dendrimers. After conversion of the ester groups to hydrazide groups, conjugation of folic acid to the dendrimers was accomplished by coupling the carboxylic groups of folic acid to the hydrazide groups of the dendrimers. The conjugation of methotrexate (MTX) (see Figure 1), an anti-cancer drug which has a structure similar to that of folic acid, to the dendrimer was also investigated.

EXPERIMENTAL PROCEDURES

General Methods. Folic acid and methotrexate (MTX) were purchased from Sigma. Poly(ethylene glycol) (PEG) monomethyl ether (M_n = 2000) was obtained from Shearwater Polymers, Inc. Other materials were obtained from Aldrich and used without further purification unless otherwise stated. DMSO was distilled under vacuum. ^{1}H NMR spectra were recorded on a Bruker AMX-300 (300 Hz) spectrometer and the solvent signals were used as the standard. Matrix-assisted laser desorption ionization time-of-flight (MALDI-TOF) mass spectra were recorded on a Voyager-DE PerSeptive Biosystems in a positive ion mode using 2,5-dihydroxybenzoic acid as the matrix.

Synthesis of Hydrazide-Terminated Dendritic Compounds. Diethyl isophthalate-terminated polyether dendrimers were synthesized according to the published procedure of Leon et al. (*27*). Hydrazide-terminated polyether dendrimers were prepared by reaction of ester-terminated dendritic precursors with hydrazine.

$(H_2NHNCO)_4$-[G-1]-OH (1). To a solution of $(EtO_2C)_4$-[G-1]-OH (0.50 g, 0.90 mmol) in DMF (10 mL) was added hydrazine (anhydrous, 1.5 mL), and the solution was stirred at 60 °C for 2 days under N_2 atmosphere. Methanol (50 mL) was added to the reaction mixture, and the white precipitate was collected by filtration. The crude product was redissolved in DMF and precipitated by addition of methanol. The precipitate was collected and dried under vacuum. Yield: 0.38 g, 84%. ^{1}H NMR δ 4.44 (s, 2 H, benzylic *H*), 4.53 (s, 8 H, NH_2), 5.15 (s, 5 H, benzylic *H* + O*H*), 6.59 (s, 1 H, aromatic *H*), 6.63 (s, 2 H, aromatic *H*), 8.00 (s, 4 H, aromatic *H*), 8.19 (s, 2 H, aromatic *H*), 9.84 (s, 4 H, CON*H*).

$(H_2NHNCO)_8$-[G-2]-OH (2). This was prepared via the same procedure from $(EtO_2C)_8$-[G-2]-OH and hydrazine. Yield: 66%. ^{1}H NMR δ 4.30−4.70 (m, 18 H, benzylic *H* and NH_2), 4.90−5.30 (m, 13 H, benzylic *H* + O*H*), 6.50−6.80 (m, 9 H, aromatic *H*), 8.01 (s, 8 H, aromatic *H*), 8.20 (s, 4 H, aromatic *H*), 9.84 (s, 8 H, CON*H*).

{$(H_2NHNCO)_8$-[G-2]}$_2$-[C] (3). This was prepared via the same procedure (except DMSO used as solvent instead of DMF) from {$(EtO_2C)_8$-[G-2]}$_2$-[C] and hydrazine. Yield: 94%. ^{1}H NMR δ 4.51 (s, 32 H, NH_2), 5.01 (s, 12 H, benzylic *H*), 5.14 (s, 16 H, benzylic *H*), 6.60−6.80 (m, 18 H, aromatic *H*), 7.00 (d, 4 H, J = 8.7 Hz, aromatic *H*), 7.46 (d, 4 H, J = 8.7 Hz, aromatic *H*), 7.98 (s, 16 H, aromatic *H*), 8.16 (s, 8 H, aromatic *H*), 9.79 (s, 16 H, CON*H*).

Conjugation of Folic Acid to Hydrazide-Terminated Dendritic Macromolecules. *Direct Condensation*. To a solution of folic acid (0.28 g, 0.63 mmol) and triethylamine (0.27 mL) dissolved in DMSO (10 mL) were added 1-hydroxybenzotriazole (0.19 g, 1.41 mmol) and EDC (0.27 g, 1.41 mmol), and the solution was stirred for 1 h at room temperature. Then, $(H_2NHNCO)_4$-[G-1]-OH **1** (0.040 g, 0.072 mmol) in DMSO (2 mL) was added and the mixture was stirred for 2 days at room temperature. Acetone was added to the reaction mixture, and a yellow precipitate formed. The precipitate was collected by filtration and dried under vacuum. The crude product was dissolved in water, and the pH was adjusted to ca. 9 using 1 N NaOH(aq) solution. The solution was loaded to a Sephadex G-25 column (40 cm × 2.5 cm) using water as effluent. Fractions containing the conjugate were collected, and the pH of the solution was adjusted to ca. 3 using 1 N HCl. The product precipitated out and was collected by filtration. The product was washed with water and dried under vacuum. Yield: 0.14 g.

Active Ester Method. The active ester of folic acid was prepared via the method reported by Lee and Low (*22*). To a solution of folic acid (0.30 g, 0.68 mmol) and triethylamine (0.10 g, 1.0 mmol) dissolved in DMSO (10 mL) was added DCC (0.14 g, 0.68 mmol), and the solution was stirred for 1 h at room temperature. Then, *N*-hydroxysuccinimide (0.12 g, 1.0 mmol) was added, and the mixture was stirred overnight at room temperature. The reaction mixture was filtered and the filtrate was precipitated into ether. The active ester of folic acid was collected by filtration, washed with dry THF, and dried under vacuum.

The active ester of folic acid was dissolved in DMSO (25 mg/mL), and the hydrazide-terminated dendrimers dissolved in DMSO (10 mg/mL) was added. The solution was stirred for 5 days (for **1** and **2**) and 10 days (for **3**) at room temperature. Acetone was added to the reaction mixture, and a yellow precipitate formed. The precipitate was collected by filtration and dried under vacuum. The product was purified using a Sephadex G-25 column as described above.

Conjugation of MTX to Hydrazide-Terminated Dendritic Macromolecule. To a solution of MTX (0.072 g) and triethylamine (0.050 mL) dissolved in DMSO (6 mL) was added DCC (0.066 g), and the mixture was stirred for 1 h at room temperature. Then, $(H_2NHNCO)_8$-[G-2]-OH (0.020 g) in DMSO (1 mL) was added, and the resulting mixture was stirred for 2 days. Ether was added to the reaction mixture, and a yellow precipitate formed. The precipitate was collected by filtration and dried under vacuum. The product was purified using a Sephadex G-25 column as described above. Yield: 0.028 g.

Synthesis of $(EtO_2C)_8$-[G-2]-PEG. To a dispersion of NaH (0.105 g) in dry THF (5 mL) was added PEG monomethyl ether (1.46 g) dissolved in THF (15 mL) dropwise at room temperature, and the solution was stirred for 2 h. Then, $(EtO_2C)_8$-[G-2]-Br (1.12 g) dissolved in THF (15 mL) was added and the reaction mixture was stirred for 2 h. The reaction mixture was filtered and the

[1] Abbreviation: MTX, methotrexate; MALDI-TOF, matrix-assisted laser desorption ionization time-of-flight; DCC, *N*,*N*′-dicyclohexylcarbodiimide; EDC, 1-[3-(dimethylamino)propyl]-3-ethylcarbodiimide, PEG, poly(ethylene glycol).

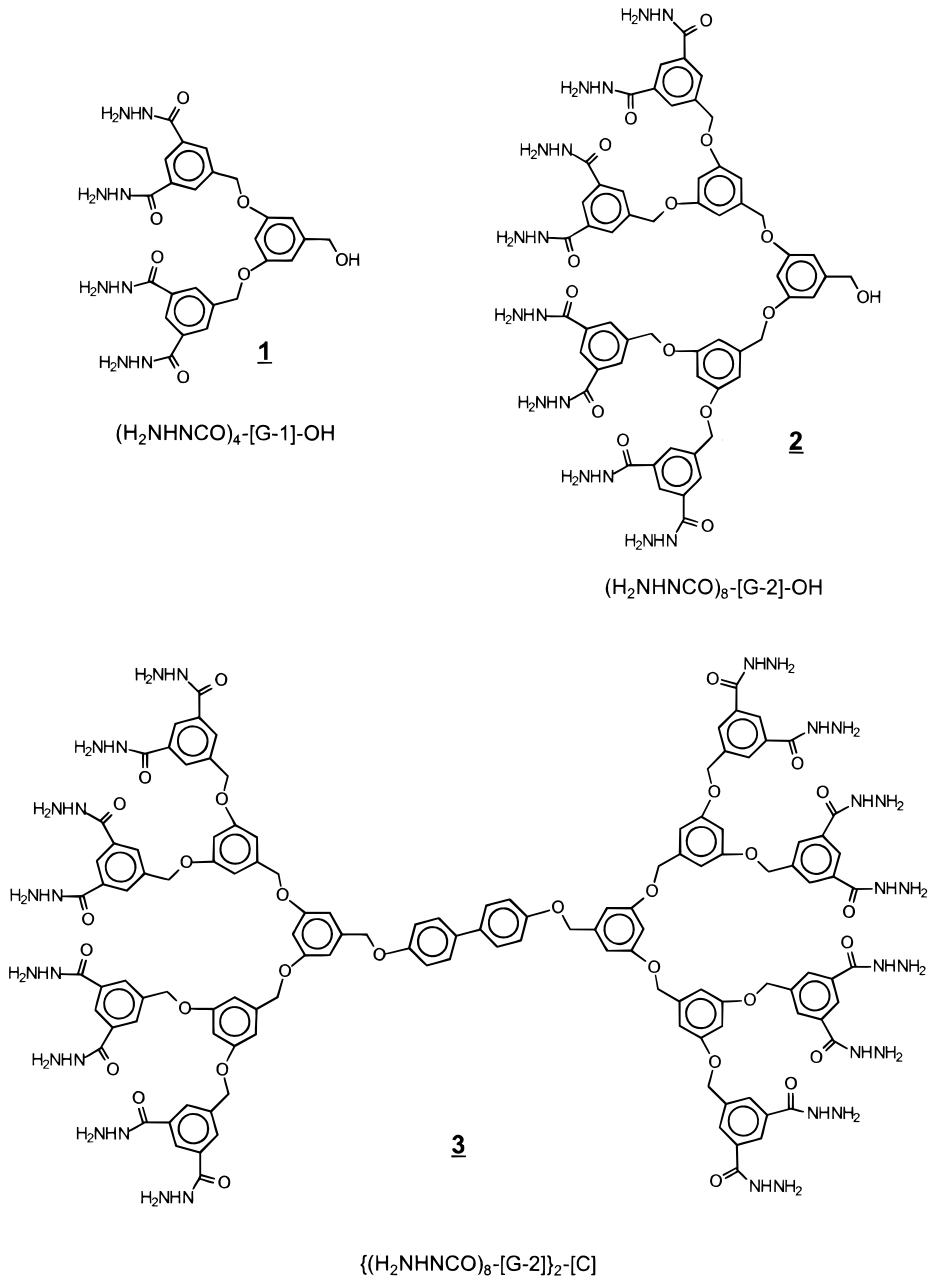


Figure 2. Structure of the hydrazide-terminated dendrimers.

crude product was precipitated by addition of ether to the filtrate. The crude product was loaded to silica gel column and washed with 15% THF/CH_2Cl_2. The eluent was changed to CH_2Cl_2, then 5% methanol/CH_2Cl_2. The product $(EtO_2C)_8$-[G-2]-PEG was eluted using 5% methanol/CH_2Cl_2. Yield: 0.58 g.

Synthesis of $(H_2NHNCO)_8$-[G-2]-PEG. $(EtO_2C)_8$-[G-2]-PEG (0.13 g) and hydrazine (2 mL) in DMSO (3 mL) were heated at 40 °C for 3 days. The product was precipitated by adding ether to the reaction mixture. The precipitate was dissolved in methanol, reprecipitated into ether, and dried under vacuum. Yield: 0.10 g.

Synthesis of Folate-[G-2]-PEG Conjugate. $(H_2NHNCO)_8$-[G-2]-PEG (0.040 g) was allowed to react with folic acid (0.132 g) in the presence of EDC (0.058 g) and triethylamine (0.092 mL) in DMSO (10 mL) for 4 days as described above. The conjugate was precipitated by addition of ether, collected by filtration, and purified using a Sephadex G-25 column eluted with water. Yield: 0.080 g.

Water-Solubility Measurement. The water solubility of the folate−dendrimer conjugates was examined by measuring the turbidity of their aqueous solutions. The conjugate sample (1.2 mg) was dissolved in 10 mM phosphate buffer solution containing 140 mM NaCl (3 mL) under an alkaline condition (pH 9−11). The pH of the solution was adjusted to a given value by the addition of 1 N HCl, and the optical density of the solution was measured using a spectrophotometer (JASCO V-560).

RESULTS AND DISCUSSION

1. Synthesis of Hydrazide-Terminated Dendritic Compounds. The selection of the functional groups used for conjugation of folic acid onto the dendrimer surface is important. In this work, we chose hydrazide groups because of their easy synthesis and high reactivity toward coupling with folic acid. Small dendritic polyvalent hydrazides have previously been used as cross-linkers for the preparation of hydrogels of hyaluronic acid (*28*). Starting from ester-terminated dendrimers, hydrazide

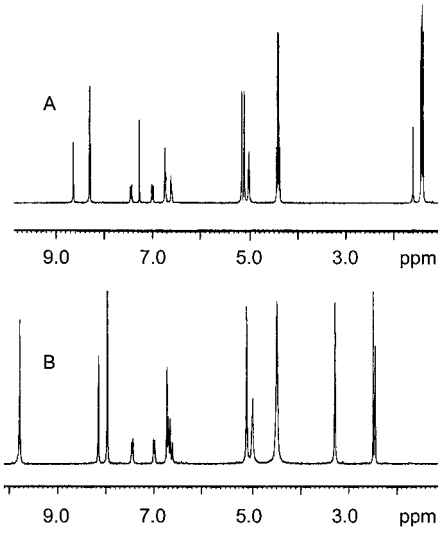


Figure 3. ^{1}H NMR spectra for the ester-terminated (A) and the hydrazide-terminated (B) $[G\text{-}2]_2$-[C] dendrimers.

groups could easily be introduced onto dendrimers by reaction with hydrazine. We prepared three different hydrazide-terminated dendritic compounds with 4, 8, and 16 hydrazide groups. Figure 2 shows the structure of the hydrazide-terminated dendritic compounds used in this work for the construction of conjugates. Characterization by ^{1}H NMR confirmed the complete transformation of ester groups to hydrazide groups. Figure 3 shows the ^{1}H NMR spectra for the precursor dendrimer $\{(EtO_2C)_8\text{-}[G\text{-}2]\}_2$-[C] and the corresponding hydrazide derivative $\{(H_2NHNCO)_8\text{-}[G\text{-}2]\}_2$-[C]. Signals for ethyl groups appear at 1.42 and 4.42 ppm in the spectrum for the ester-terminated dendrimer. In contrast, these signals disappeared completely after reaction with hydrazine, and a new signal corresponding to the protons from the hydrazide groups appeared at 4.50 and 9.78 ppm. The same changes in ^{1}H NMR spectra were also observed in the transformation of the precursor dendrimers, $(EtO_2C)_4$-[G-1]-OH and $(EtO_2C)_8$-[G-2]-OH, into the corresponding hydrazides, $(H_2NHNCO)_4$-[G-1]-OH and $(H_2NHNCO)_8$-[G-2]-OH.

2. Conjugation of Folic Acid to Dendrimers. Conjugation of folic acid to $(H_2NHNCO)_4$-[G-1]-OH was carried out via condensation between the γ carboxyl group of folic acid and the hydrazide groups of the dendrimer. Two methods were tested for this condensation (Scheme 1): direct condensation in the presence of the carbodiimide condensing agent EDC and reaction of the hydrazide groups with the active ester of folic acid as previously reported (*21*−*23*, *26*).

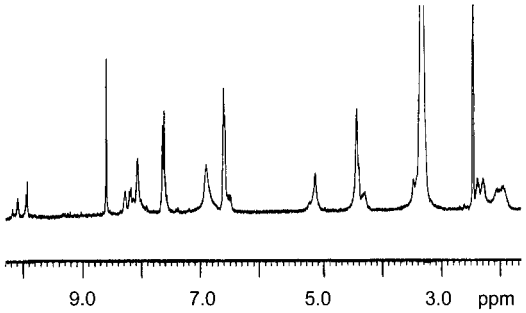
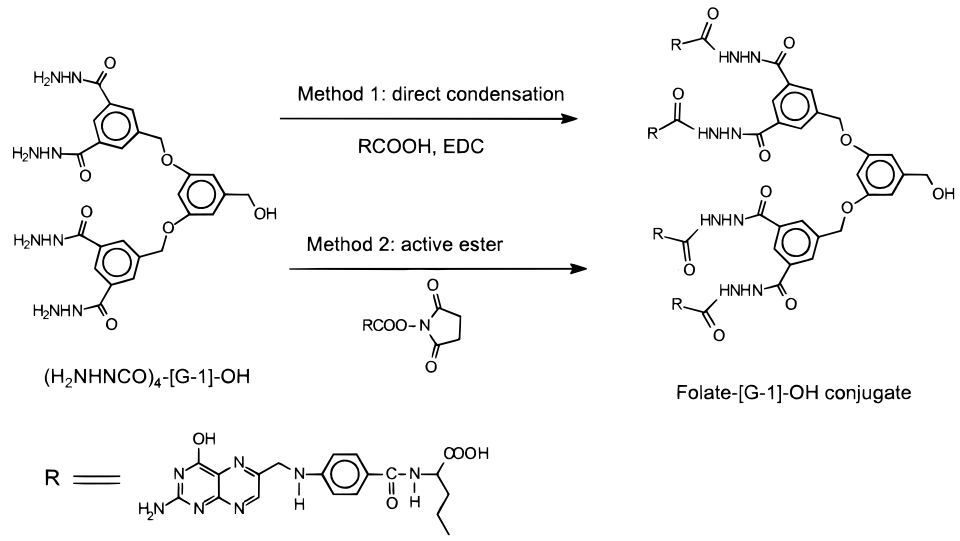


Figure 4. ^{1}H NMR spectrum for the folate-[G-1]-OH conjugate in DMSO-d_6.

The conjugates were characterized by ^{1}H NMR spectroscopy as shown in Figure 4. It is apparent that the spectrum of the conjugate contains signals originating from both folic acid and the dendrimer. From the integral ratio of the signal at 8.64 ppm, which corresponds to the proton at the 7-position of the pterin ring, to the signal at 5.15 ppm, which corresponds to the benzylic proton from the dendritic moiety, the average number of folate residues in the conjugate can be evaluated. By using excess of active ester of folic acid with the G-1 dendrimer, an average number of 3.6 folate molecules became attached to the dendrimer. However, when the conjugate was prepared via direct condensation, the average number of folate molecules per conjugate was 3.0. The lower number of folate per conjugate may be the result of reaction between the two carboxyl groups of one folic acid molecule and two hydrazide groups. Such coupling is possible since each of the two carboxyl groups of folic acid may be activated by EDC. After attachment of folic acid to the dendrimer by coupling between one carboxyl group and one hydrazide group, the other carboxyl group may react with second hydrazide groups on the same dendrimer, leading to a macrocyclic structure. Thus, the possibility of attachment of a folate residue via two hydrazide groups may be higher for the conjugation method involving carbodiimide-mediated direct conden-

Scheme 1



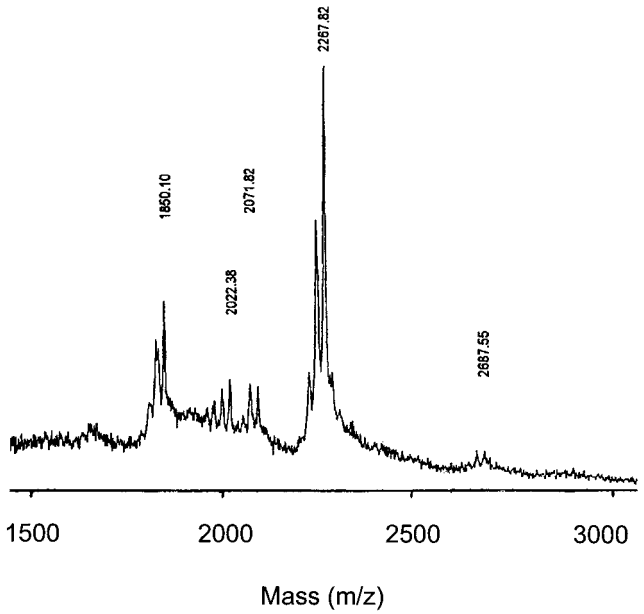


Figure 5. MALDI-TOF mass spectrum for the folate-[G-1]-OH conjugate.

Table 1. Syntheses of Folate-[G-2]-OH and Folate-[G-2]2-[C] Conjugates

conjugate	the ratio of folic acid/ dendrimer in reaction mixture	folate residues per conjugate
folate-[G-2]-OH	8.0	3.2
	15.2	7.3
	24.0	8.2
folate-[G-2]2-[C]	48.0	12.6

sation. Therefore, the active ester method was used in the construction of all of the conjugates described in this work.

The folate-[G-1]-OH conjugate was further characterized using MALDI-TOF mass spectrometry. Figure 5 depicts the MALDI-TOF mass spectrum for the conjugate prepared via the active ester method. The spectrum shows strong peaks at 2268 and 2247, which correspond to the $[M + Na]^+$ ion and the $[M + H]^+$ ion of the conjugate with four folate residues, respectively. In addition, relatively small peaks were observed at 1850 and 1826 corresponding to the $[M + Na]^+$ ion and the $[M + H]^+$ ion of the conjugate with three folate residues.

Conjugation of folic acid to $(H_2NHNCO)_8$-[G-2]-OH and $\{(H_2NHNCO)_8$-[G-2]$\}_2$-[C] using the active ester method was also examined. Preparation conditions and the average number of folate residues per conjugate are listed in Table 1. For folate-[G-2]-OH conjugate, the average number of folates per conjugate increases as the folic acid/ dendrimer ratio in the reaction mixture increases. Essentially complete functionalization of the hydrazide groups was achieved when 3 equiv of folic acid active ester were used for each hydrazide group. However, in the case of $\{(H_2NHNCO)_8$-[G-2]$\}_2$-[C] dendrimer with 16 hydrazide groups, only an average of 12.6 folate residues were found to be attached to the dendrimer even after 10 days of reaction. When the same reaction was carried out for 5 days, only 10.0 folate residues could be attached to the dendrimer. These findings suggest that the terminal hydrazide groups of the $\{(H_2NHNCO)_8$-[G-2]$\}_2$-[C] dendrimer are somewhat less accessible than those of the $(H_2NHNCO)_8$-[G-2]-OH, perhaps as a result of the increased steric congestion on the dendrimer surface, or due to reason intrinsic to this demanding carbodiimide-mediated coupling.

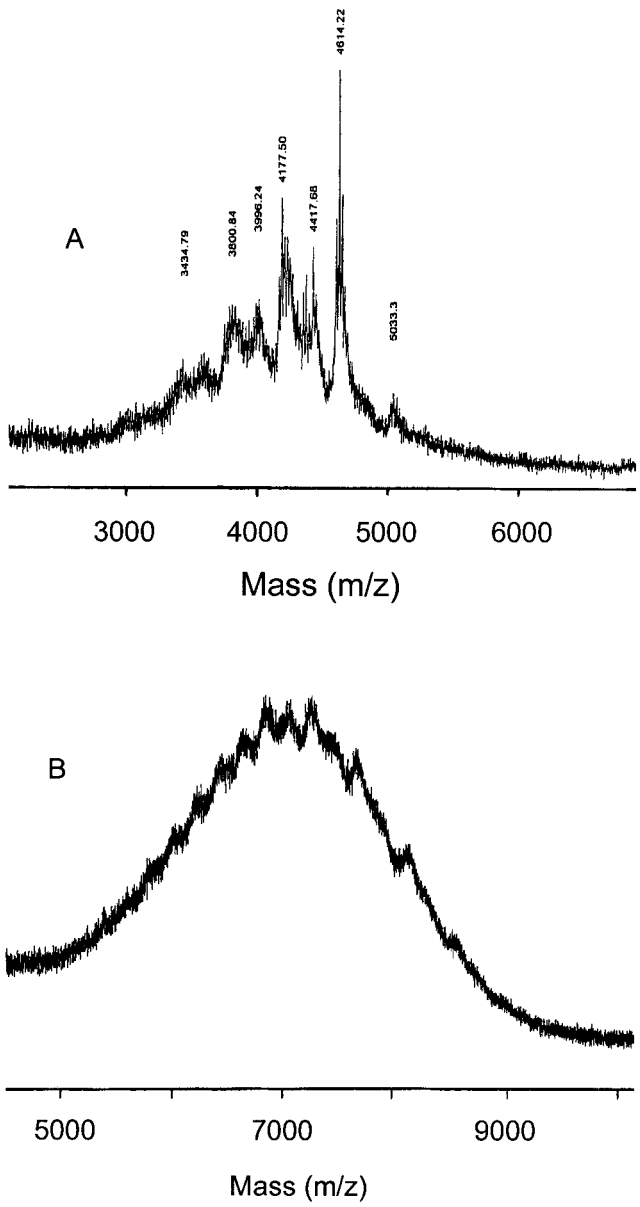


Figure 6. MALDI-TOF mass spectra for the folate-[G-2]-OH conjugate (A) and the folate-$[G-2]_2$-[C] conjugate (B).

The molecular weight of the conjugates was investigated by MALDI-TOF mass spectrometry. For the folate-[G-2]-OH conjugate (Figure 6A), strong peaks are observed at a mass of 4614, which corresponds to the $[M + Na]^+$ ion of the conjugate with eight folate residues. Also, several peaks were observed around 4177 that correspond to the conjugate with seven folate residues. The existence of peaks between those for conjugates with seven and eight folate residues suggests the occurrence of fragmentation of the conjugate residues during measurement. It has been reported that folate residues fragment readily with formation of pteridinyl radicals with a molecular mass of 176 Da (*26*). Therefore, peaks observed around 4417 are likely due to the molecular ions and Na adducts of the fragments of conjugates with eight folate residues that have lost a single pteridinyl radical. It is not unlikely that this kind of fragmentation could occur during the MALDI-TOF measurement since higher power is frequently used for such high MW compounds. Small peaks around 5033 correspond to the conjugate containing eight

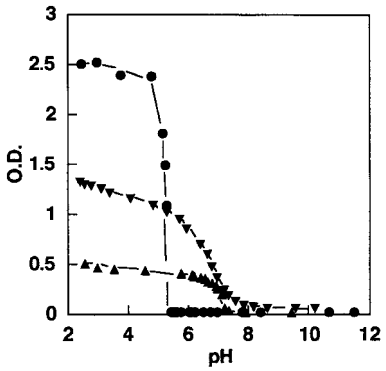


Figure 7. Turbidity of solutions of the folate-[G-2]-OH conjugate (▲); the folate-$[G\text{-}2]_2$-[C] conjugate (▼); and pure folic acid (●) in 10 mM phosphate-buffered solutions containing 140 mM NaCl at varying pH values. The ordinate shows the optical density of the solution at 550 nm.

folate residue at the chain ends plus one folate residue at the focal point. The MALDI-TOF spectrum for the folate-$[G\text{-}2]_2$-[C] conjugate with 12.6 folate residues as measured by NMR analysis is shown in Figure 6B. The conjugate gave a broad peak centered at a mass of 7100 that corresponds to a conjugate with an average of 10.7 folate residues.

3. Water Solubility of the Folate−Dendrimer Conjugates. Since the folate−dendrimer conjugates have carboxyl groups on their surface, they are expected to be soluble in water under conditions where these groups are charged. Thus, pH dependence of the water solubility of the conjugates was examined. Figure 7 shows the turbidity of the solutions of the conjugates and folic acid at varying pH values. The solution of folic acid was not turbid under either neutral or alkaline conditions. However, its turbidity increased drastically near pH 5.4, indicating precipitation of the folic acid. Potentiometric titration of an aqueous solution of folic acid at pH 8.3 using 10 mM HCl showed that 2 equiv of HCl was consumed to neutralize the folate anion near pH 5.4, indicating that both the α- and the γ-carboxyl groups of folic acid were neutralized at this pH value where precipitation is expected to take place. For the folate-[G-2]-OH conjugate, the solution was completely clear under alkaline conditions, showing that the conjugate is soluble in water under such conditions. However, an increase in turbidity was observed near pH 7.4. Similarly, an increase in turbidity was also seen for the solution of folate-$[G\text{-}2]_2$-[C] conjugate at the same pH. Agarose gel electrophoresis analysis of the folate-$[G\text{-}2]_2$-[C] conjugate showed that the conjugate was negatively charged at pH 8.0. Therefore, it is considered that these conjugates indeed acquired water solubility as a result of the presence of a negative charge on the remaining carboxylate group of the folate residues. Protonation of these carboxylate groups results in the precipitation of the conjugates. Precipitation of these conjugates took place at higher pH than observed for free folic acid, probably due to the hydrophobic nature of the dendritic moieties.

4. Conjugation of MTX. Because methotrexate (MTX), a widely used antitumor drug, is structurally similar to folic acid, coupling of MTX to the dendritic macromolecules is expected to occur through the same process. Conjugation of MTX to synthetic polymers has already been attempted and the MTX−polymer conjugates have shown antitumor activity or cell growth inhibitory activity (*29*, *30*). The conjugation of MTX to hydrazide terminated dendrimer $(H_2NHNCO)_8$-[G-2]-OH was examined briefly to demonstrate its feasibility. Using an

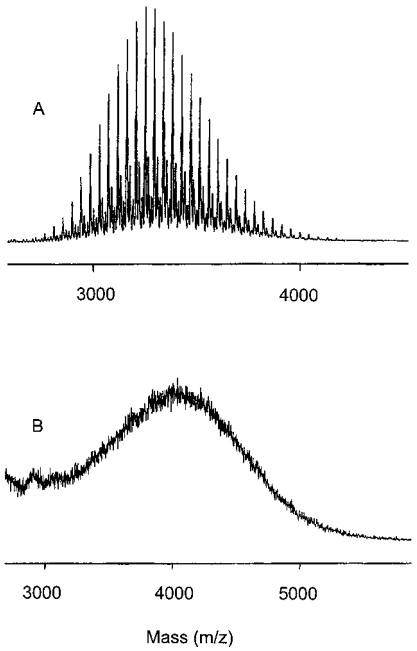


Figure 8. MALDI-TOF spectra of the ester-terminated [G-2]-PEG (A) and the folate-[G-2]-PEG conjugate (B).

MTX/dendrimer (mole/mole) ratio of 10.4, the ^{1}H NMR of the product showed that an average of 4.7 MTX residues/conjugate was bound.

5. Folate-dendron-PEG Conjugates. The G-2 dendron $(EtO_2C)_8$-[G-2]-OH possesses one hydroxyl group at the focal point, and this group may be used for the attachment of another molecule. This might be a targeting moiety or a solubilizing group. In a first exploration, we examined the introduction of a PEG chain at the focal point of the dendrimer since this PEG chain is expected to modify the behavior of the conjugate in the body and increase the overall water solubility of the conjugate (*31*, *32*). The hybrid molecule $(EtO_2C)_8$-[G-2]-PEG was prepared via a Williamson ether synthesis involving $(EtO_2C)_8$-[G-2]-Br and a PEG monomethyl ether with Mn 2000 and a polydispersity of 1.01. Figure 8A shows the MALDI-TOF spectrum of the resulting $(EtO_2C)_8$-[G-2]-PEG. A series of peaks centered at 3294 were observed. These correspond to the hybrid molecule with a PEG chain of MW 1968. The mass difference between two adjacent peaks in the MALDI spectrum is 44, which is the mass of one oxyethylene repeating unit. Unfortunately, the PEG sample is not monodisperse and its effect on broadening the dispersity of the dendrimer is quite significant. The hydrazide derivative of the hybrid and its subsequent folate conjugate were prepared via the same procedure as described above without optimization for complete coupling. The MALDI-TOF spectrum of the folate-[G-2]-PEG conjugate shown in Figure 8B consists of a broad peak centered at 4000, which corresponds to the conjugate with two folate residues only. This result demonstrates that the hydrazide groups of the dendrimer-PEG hybrid are still reactive and available for conjugation, although their reactivity appears to be reduced by the introduction of PEG chain. Further studies with optimized dendritic structure will focus on increased functionalization of such hybrid structures.

CONCLUSION

Our work has shown that folate residues could easily be conjugated to the chain ends of a hydrazide-terminated polyether dendrimer. The folate−dendrimer conju-

gates were soluble in phosphate buffer solution at physiological pH. The folate−dendrimer conjugates possess hydrophobic interior and hence might be useful to entrap hydrophobic drugs. Because these molecules have folate residues on their surface, they are expected to exhibit a strong affinity for tumor cells that overexpress folate receptor on the cell surface. Thus, these types of conjugates may potentially be useful as drug carriers with targeting specificity. In addition, the anticancer drug MTX has been successfully attached to a dendrimer. Although the toxicology of the polyether dendrimers remains to be clarified, these molecules or analogues thereof based on more biocompatible dendritic building blocks may be used in the design of a sophisticated type of multivalent drug carriers. Interactions of the conjugates with cells are currently under investigation.

ACKNOWLEDGMENT

Financial support of this research by the National Science Foundation (DMR-9816166) is acknowledged with thanks.

LITERATURE CITED

(1) Tomalia, D. A., Naylor, A. M., and Goddard, W. A., III (1990) Starburst dendrimers: molecular-level control of size, shape, surface chemistry, topology, and flexibility from atoms to macroscopic matter. *Angew. Chem., Int. Ed. Engl. 29*, 138−175.

(2) Newkome, G. R., Moorefield, C. N., and Vögtle, F. (1996) *Dendritic molecules: concepts, syntheses, perspectives*, VCH, Weinheim.

(3) Fréchet, J. M. J. (1994) Functional polymers and dendrimers: reactivity, molecular architecture, and interfacial energy. *Science 263*, 1710−1715.

(4) Roberts, J., Adams, Y. E., Tomalia, D., Mercer-Smith, J. A., and Lavallee, D. K. (1990) Using starburst dendrimers as linker molecules to radiolabel antibodies. *Bioconjugate Chem. 1*, 305−308.

(5) Singh, P., Moll, F., III, Lin, S. H., Ferzli, C., Kwok, S. Y., Koski, R. K., Saul, R. G., and Cronin, P. (1994) Starburst dendrimers: enhanced performance and flexibility for immunoassays. *Clin. Chem. 40*, 1845−1849.

(6) Barth, R. F., Adams, D. M., Soloway, A. H., Alam, F., and Darby, M. V. (1994) Boranated starburst dendrimer-monoclonal antibody immunoconjugates: evaluation as a potential delivery system for neutron capture therapy. *Bioconjugate Chem. 5*, 58−66.

(7) Aoi, K., Itoh, K., and Okada, M. (1995) Globular carbohydrate macromolecule "sugar balls". 1. Synthesis of novel sugar-persubstituted poly (amido amine) dendrimers. *Macromolecules 28*, 5391−5393.

(8) Zanini, D., and Roy, R. (1997) Synthesis of new α-thiosialodendrimers and their binding properties to the sialic acid specific lectin from *limax flavus*. *J. Am. Chem. Soc. 119*, 2088−2095.

(9) Jansen, J. F. G. A., de Brabander-van den Berg, E. M. M., and Meijer, E. W. (1994) Encapsulation of guest molecules into a dendritic box. *Science 266*, 1226−1229.

(10) Newkome, G. R., Moorefield, C. N., Baker, G. R., Johnson, A. W., and Behera, R. K. (1991) Alkane cascade polymers possessing micellar topology: micellanoic acid derivatives. *Angew. Chem., Int Ed. Engl. 30*, 1176−1178.

(11) Newkome, G. R., Moorefield, C. N., Baker, G. R., Saunders, M. J., and Grossman, S. H. (1991) Unimolecular Micelles. *Angew. Chem., Int. Ed. Engl. 30*, 1178−1180.

(12) Hawker, C. J., Wooley, K. L., and Fréchet, J. M. J. (1993) Unimolecular micelles and globular amphiphiles: dendritic macromolecules as novel recyclable solubilization agents. *J. Chem. Soc., Perkin Trans. 1*, 1287−1297.

(13) Liu, M., and Fréchet, J. M. J. (1999) Preparation of water-soluble dendritic unimolecular micelles as potential drug delivery agents. *Polym. Mater. Sci. Eng. 80*, 167−168.

(14) Liu, M., Kono, K., and Fréchet, J. M. J. (1999) Water-soluble dendritic unimolecular micelles: their potential as drug delivery agents. *J. Controlled Release* (in press).

(15) Zhuo, R. X., Du, B., and Lu, Z. R. (1999) In vitro release of 5-fluorouracil with cyclic core dendritic polymer. *J. Controlled Release 57*, 249−257.

(16) Liu, M., Kono, K., and Fréchet, J. M. J. (1999) Water-soluble dendrimer-poly(ethylene glycol) starlike conjugates as potential drug carriers. *J. Polym. Sci., Polym. Chem. 37*, 3492−3503.

(17) Garin-Chesa, P., Campbell, I., Saigo, P. E., Lewis, J. L., Old, L. J., and Lettig, W. J. (1993) Trophoblast and ovarian cancer antigen LK26. *Am. J. Pathol. 142*, 557−567.

(18) Buist, M. R., Molthoff, C. F. M., Kenemans, P., and Meijer, C. J. L. M. (1995) Distribution of OV-TL 3 and Mov18 in normal and malignant ovarian tissue. *J. Clin. Pathol. 48*, 631−636.

(19) Ross, J. F., Chaudhuri, P. K., and Ratnam, M. (1994) Differential regulation of folate receptor isoforms in normal and malignant tissues in vivo and established cell lines. Physiologic and clinical implications. *Cancer 73*, 2432−2443.

(20) Leamon, C. P., and Low, P. S. (1991) Delivery of macromolecules into living cells: A method that exploits folate receptor endocytosis. *Proc. Natl. Acad. Sci. U.S.A. 88*, 5572−5576.

(21) Cho, B. K., Roy, E. J., Patrick, T. A., and Kranz, D. M. (1997) Single-chain Fv/folate conjugates mediate efficient lysis of folate-receptor-positive tumor cells. *Bioconjugate Chem. 8*, 338−346.

(22) Lee, R. J., and Low, P. S. (1994) Delivery of liposomes into cultured KB cells via folate receptor-mediated endocytosis. *J. Biol. Chem. 269*, 3198−3204.

(23) Lee, R. J., and Low, P. S. (1995) Folate-mediated tumor cell targeting of liposome-entrapped doxorubicin in vitro. *Biochim. Biophys. Acta 1233*, 134−144.

(24) Mathias, C. J., Wang S., Lee, R. J., Waters, D. J., Low, P. S., and Green, M. A. (1996) Tumor-selective radiopharmaceutical targeting via receptor-mediated endocytosis of Gallium-67-deferoxamine-folate. *J. Nucl. Med. 37*, 1003−1008.

(25) Wiener, E. C., Konda, S., Shadron, A., Brechbiel, M., and Gansow, O. (1997) Targeting dendrimer-chelates to tumors and tumor cells expressing the high-affinity folate receptor. *Invest. Radiol. 32*, 748−754.

(26) Wang, S., Lee, R. J., Mathias, C. J., Green, M. A., and Low, P. S. (1996) Synthesis, purification, and tumor cell uptake of 67Ga-deferoxamine-folate, a potential radiopharmaceutical for tumor imaging. *Bioconjugate Chem. 7*, 56−62.

(27) Leon, J. W., Kawa, M., and Fréchet, J. M. J. (1996) Isophthalate ester-terminated dendrimers: versatile nanoscopic building blocks with readily modifiable surface functionalities. *J. Am. Chem. Soc. 118*, 8847−8859.

(28) Vercruysse, K. P., Marecak, D. M., Marecek, J. F., and Prestwich, G. D. (1997) Synthesis and in Vitro degradation of new polyvalent hydrazide cross-linked hydrogels of hyaluronic acid. *Bioconjugate Chem. 8*, 686−694.

(29) Przybylski, M., Fell, E., Ringsdorf, H., and Zaharko, D. (1978) Pharmacologically active polymers, 17: Syntheses and characterization of polymeric derivatives of the antitumor agent metnotrexate. *Makromol. Chem. 179*, 1719−1733.

(30) Ryser, H. J.-P., and Shen, W.-C. (1978) Conjugation of methotrexate to poly(L-lysine) increase drug transport and overcomes drug resistance in cultured cells. *Proc. Natl. Acad. Sci. U.S.A. 75*, 3867−3870.

(31) Abuchowski, A., McCoy, J. R., Palczuk, N. C., van Es, T., and Davis, F. F. (1977) Effect of covalent attachment of poly(ethylene glycol) on immunogenicity and circulating life of bovine liver catalase. *J. Biol. Chem. 252*, 3582−3586.

(32) Ashihara, Y., Kono, T., Yamazaki, S., and Inada, Y. (1978) Modification of E. coli L-asparaginase with poly(ethylene glycol), disappearance of binding ability to anti-asparaginase serum. *Biochem. Biophys. Res. Commun. 83*, 358−391.

BC990082K

Synthesis of Metallointercalator−DNA Conjugates on a Solid Support

R. Erik Holmlin, Peter J. Dandliker,† and Jacqueline K. Barton*

Division of Chemistry and Chemical Engineering, California Institiute of Technology, Pasadena, California 91125. Received June 21, 1999; Revised Manuscript Received August 26, 1999

Metallointercalator−DNA conjugates were prepared by amide bond formation between active esters on the nonintercalating ligands of transition metal complexes and primary amines presented at the 5′ or the 3′ termini of oligonucleotides attached to solid supports. The conjugates were liberated from the support by aminolysis and purified by HPLC on C18 or C4 stationary phases, which separates the two diastereomeric forms of the conjugates containing either the Λ or the Δ enantiomer of the octahedral metal complex. The coupling reaction proceeds with ∼75% conversion of the amino-terminated oligonucleotide into the conjugate; the isolated yield is ∼200 nmol for syntheses initiated on DNA-synthesis columns with a loading of 2 μmol. The conjugates were characterized by ultraviolet−visible and circular dichorism absorption spectroscopy, electrospray ionization mass spectrometry, enzymatic digestion, and polyacrylamide gel electrophoresis (PAGE). Oligonucleotides bearing $[Rh(phi)_2(bpy')]^{3+}$ (phi = 9,10-phenanthrene quinone diimine; bpy′ = 4-butyric acid-4′-methyl bipyridyl) form 1:1 duplexes with the complementary strand, and the electrophoretic mobility under nondenaturating PAGE of duplexes containing Δ-Rh is notably different from duplexes containing Λ-Rh. High-resolution PAGE of DNA photocleavage reactions initiated by irradiation of the tethered Rh complexes reveal intercalation of the complex only near the tethered end of the duplex. Analogous DNA-binding properties were observed with $[Rh(phi)_2(bpy')]^{3+}$ tethered to the 3′ terminus. By combining the 3′ and 5′ modification strategies, a mixed-metal DNA conjugate containing both $[Os(phen)(bpy')(Me_2\text{-}dppz)]^{2+}$ (Me_2-dppz = 7,8-dimethyldipyridophenazine) on the 3′ terminus and $[Rh(phi)_2(bpy')]^{3+}$ on the 5′ terminus was prepared and isolated. Taken together, these strategies for preparing metallointercalator−DNA conjugates offer a useful approach to generate chemical assemblies to probe long-range DNA-mediated charge transfer where the redox initiator is confined to and intercalated in a well-defined binding site.

INTRODUCTION

Investigations of long-range electron transfer (ET) reactions mediated by the stacked, heterocyclic bases of DNA are important to fundamental studies of ET, as well as the complete biochemical characterization of the genetic material. In our laboratories we employ transition metal complexes that bind to DNA by intercalation, metallointercalators, with well-defined redox properties to probe DNA-mediated electron transfer (*1*). Here we describe synthetic methods to prepare oligonucleotide conjugates in which a metallointercalator, $[Rh(phi)_2(bpy')]^{3+}$ (Figure 1; phi = 9,10-phenanthrene quinone diimine; bpy′ = 4-butyric acid-4′-methyl bipyridyl), is attached covalently to DNA at either the 5′ or 3′ terminus while the assembly is immobilized on a solid support.

Photoinduced ET between metallointercalators bound to DNA is remarkably fast and efficient (*2*−*5*). In titrations of electron acceptor (Δ-$[Rh(phi)_2(bpy)]^{3+}$) into solutions of electron donor (Δ-$[M(phen)_2(dppz)]^{2+}$) bound to DNA, 50% of the donors were quenched by just 1 equiv of Δ-$[Rh(phi)_2(bpy)]^{3+}$ on a time scale of <30 ps when the average donor−acceptor separation is 25 base pairs. These observations suggested that the DNA base stack could facilitate efficient ET over large separations of donor and acceptor. We (*2*) and others (*6*, *7*) also considered the possiblity that the metal complexes might preferentially intercalate in adjacent sites throughout the titration, which would result in only one donor−acceptor separation and explain the observation of a rate of recombination that was independent of the loading of acceptor on the helix.

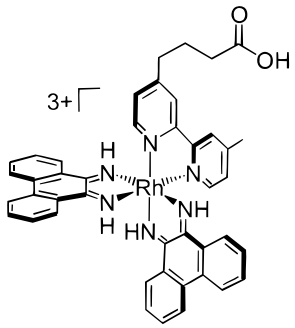


Figure 1. Schematic illustration of Δ-$[Rh(phi)_2(bpy')]^{3+}$.

In studies of oxidative damage to DNA at the 5′-guanine (G) of 5′-GG-3′ sequences, as well as oxidative repair of thymine dimer lesions in duplex DNA, we were unable to correlate the site of the chemical reaction on DNA with the site of intercalation by the metallointercalator (*8*, *9*). These observations again suggested the possiblity that the DNA base stack might facilitate electron transfer over long range.

To address unambiguously the question of whether long-range ET can occur on the DNA double helix, we

* To whom correspondence should be addressed.
† Current address: Abbott Laboratories, Abbott Park, IL, 60064.

10.1021/bc9900791 CCC: $18.00 © 1999 American Chemical Society
Published on Web 10/21/1999

sought to prepare DNA assemblies by covalently attaching the reactants to the terminus of oligonucleotides so as to confine intercalated donors and acceptors to well-defined binding sites. Murphy et al. tethered $[Ru(phen')_2(dppz)]^{2+}$ (phen′ = 5-amidoglutaricacid-1,10-phenanthroline) and Δ-$[Rh(phi)_2(phen')]^{3+}$ to opposite ends of a 15 bp duplex, and found that 100% of the ruthenium luminescence was quenched by the rhodium complex on a subnanosecond time scale (*10*). However, the synthetic methods used to generate these materials proved to be irreproducible and tedious, which impeded the systematic study of these assemblies. Other laboratories have now also developed methods to functionalize oligonucleotides with ruthenium complexes using solid-phase synthesis (*11*−*14*). These strategies have largely focused on the construction of ruthenium-modified nucleoside phosphoramidites for incorporation into oligonucleotides using automated techniques. While these methods offer the versality of incorporating a metal complex at any site along the oligonucleotide (*11*−*18*), methods of postmodification on the resin become valuable when the metallating species contains more sensitive functionality. In the particular applications we have been interested in addressing, we have, moreover, wanted to focus on modifying oligonucleotides with intercalators tethered to oligonucleotide termini, with tethers of sufficient length to ensure proper stacking in the helix. Therefore, we have developed a convenient and efficient strategy that permits the covalent attachment of a metallointercalator to an oligonucleotide either at the 3′ or 5′ terminus while the oligomer is attached to the solid support. This methodology allows the characterization of DNA-mediated ET reactions in molecular assemblies with well-defined separations beteween reactants.

EXPERIMENTAL SECTION

Materials. Solvents used in coupling chemistry were anhydrous (Fluka over molecular sieves). DNA synthesis reagents were supplied by Glen Research and chemicals for heterogeneous coupling reactions were obtained from Fluka, Aldrich, and Sigma and used as received.

Unmodified Oligonucleotides. Unmodified (native) oligonucleotides were prepared by the phosphoramidite method (*19*) on an ABI 394 DNA synthesizer. Purification was carried out on the 5′-DMT oligonucleotide by RP HPLC (C18; ammonium acetate/acetonitrile). The DMT group was removed by treatment with 400 μL of 80% (v/v) glacial acetic acid in water for 20 min, followed by precipitation by anhydrous ethanol. The alcoholic acid was removed under reduced pressure, and the 5′-OH strand purified a second time by RP HPLC.

Metal Complexes. $[Rh(phi)_2(bpy')]Cl_3$ and $[Os(phen)(bpy')(Me_2\text{-}dppz)]Cl_2$ (Me2-dppz = 7,8-dimethyldipyridophenazine) were synthesized as described previously (*20*, *21*).

Preparation of Conjugates: Aminoalkylation of the 5′ Terminus. This procedure followed closely the method of Wachter, with slight modification (*22*). The desired oligonucleotide was synthesized by automated DNA synthesis using the phosphoramidite approach (*19*) on CPG resin with 2000 Å pores (Glen Research). The synthesizer was programmed to leave the oligonucleotide on the resin with the DMT group off of the 5′ terminus. The DNA-coated beads (2 × 1 μmol loading) were removed from the synthesis columns and added to a 2.5 cm × 10 cm glass cylinder fitted with a course glass frit and stopcock at the bottom.

The oligonucleotide on the resin was washed three times with 3 mL of dry dioxane (Fluka; over molecular sieves), and a solution of carbonyl diimidazole (CDI) (Sigma) in dry dioxane (50 mg/1 mL) was added to the beads in the cylindrical reaction vessel. The suspension was agitated by bubbling dry Ar(g) through the glass frit. After 30 min of agitation the CDI solution was removed and the resin was washed five times with 3 mL of dry dioxane.

A solution of diaminononane in 9:1 dioxane/water (32 mg/1 mL) was added to the functionalized DNA on the resin and the suspension was agitated as above for 25 min. If this reaction proceeds for too long, the amino linker will hydrolyze the DNA from the resin. At the conclusion of the reaction time, the aminononane solution was washed from the resin and the beads were washed with excess dioxane and methanol. The methanol will dissolve unreacted diaminononane. At this point, the linker has been installed and the resin may be stored or reacted further.

Coupling $[Rh(phi)_2(bpy')]^{3+}$ to 5′-Aminoalkylated DNA on CPG. $[Rh(phi)_2(bpy')]Cl_3$ (10 mg) and *N*,*N*,*N*′,*N*′-tetramethyl-*O*-(*N*-succinimidyl)uronium tetrafluoroborate (TSTU) (8 mg; Aldrich) were dissolved in 0.5 mL of 1:1:1 $CH_3OH/CH_2Cl_2/CH_3CN$ along with *N*,*N*-diisopropyl ethylamine (DIEA) (6 μL) and stirred at ambient temperature for 1 h. The complete activation of the carboxylate was confirmed by thin-layer chromatography (TLC) on alumina (CH_3OH), where the R_f for the ester is much greater than the R_f for the acid. This solution of $[Rh(phi)_2(bpy')]^{3+}$-NHS ester was added to the DNA (aminoalkylated) coated beads in a 5 mL round-bottom (rb) flask (after wetting them with 1:1:1 $CH_3OH/CH_2Cl_2/CH_3CN$ and draining the excess solvent). DIEA (20 μL) was added and the resulting slurry was stirred for 12 h to effect coupling.

Liberating the Conjugate from the CPG Beads. Following the coupling reaction, the solution of metal complex was washed away from the beads on a glass frit, and the beads were washed with excess CH_3OH, CH_2Cl_2, and CH_3CN. At this stage, the beads are colored orange and the intensity of the color is strongly solvatochromic. The color appears darkest in CH_2Cl_2.

The beads were transferred into a 1.7 mL Eppendorf tube and combined with ∼500 μL of concentrated (37%) NH_3 (aq). The mixture was agitated to wet the beads and then incubated at 60 °C for 6 h. After 1 h of incubation, the solution is colored red and the intensity of color on the beads is reduced.

After 6 h of incubation, the mixture was cooled to room temperature (very important) and filtered on a centrifuge filter (nylon; Rainin). The ammonia solution was removed in vacuo on a speed vac evaporator.

After the sample was dried, it was redissolved in water (330 μL) and filtered to remove insoluble materials. The mixture was purified by reversed-phase HPLC on C4 or C18 stationary phases using 50 mM ammonium acetate (pH ∼6)/CH_3CN as the mobile phase. The extinction coefficient for Rh-modified oligonucleotides is taken as $1.9 \times 10^4\ M^{-1}\ cm^{-1}$ at 390 nm.

Synthesis of 3′-Rh-Modified Conjugates. CPG resin (Glen Research) functionalized with a hydroxyaminoalkyl linker protected at the amine with an Fmoc and at the hydroxyl group with DMT was used for DNA synthesis. A "dummy" base was incorporated at the 3′ terminus of the sequence so the DNA synthesizer would remove the DMT from the linker and build the DNA strand from that branching point. The DNA synthesizer was programmed to leave the oligonucleotide on the resin with the 5′ DMT group intact.

After the DNA synthesis was complete, the Fmoc was selectively removed by treatment of the beads with a solution of piperidine (20% v/v) in DMF (*23*) under Ar(g) for 30 min. The DMF solution was washed away from the beads, and the resin was transferred to a 5 mL round-bottom flask. A solution of $[Rh(phi)_2(bpy')]^{3+}$-NHS ester was added to the beads along with DIEA (20 μL), and the mixture was stirred for 12 h to effect coupling. For this procedure, we increased the concentration of the solution of NHS ester by reducing the volume to 250 μL and using the same amount of reagents. This modification of the procedure is necessary to accommodate the linker buried in the CPG and the fact that we are using 500 Å beads, which are smaller.

After the coupling reaction, we removed the DMT group before cleaving the conjugate from the resin by treatment with trichloroacetic acid in dichloromethane for 18 s on the DNA synthesizer. The conjugate was then liberated from the beads and purified as described above. In general, these conjugates are more hydrophilic than the 5′-modified analogues owing to an extra phosphate in the linker.

Synthesis of 3′,5′-bis-Heterometalated Oligonucleotides. A metal complex was introduced onto the 3′ terminus of an oligonucleotide using the procedure described above. After removing the DMT protecting group from the 5′-terminal hydroxyl by treatment with trichloroacetic acid in CH_2Cl_2, the oligonucleotide was 5′-aminoalkylated according to the standard procedure, and a second metallointercalator was coupled onto the 5′ terminus as described for singly modified strands. Liberation and purification procedures were the same as for the singly metalated DNA, however, higher concentrations of acetonitrile in the mobile phase were required to elute the product.

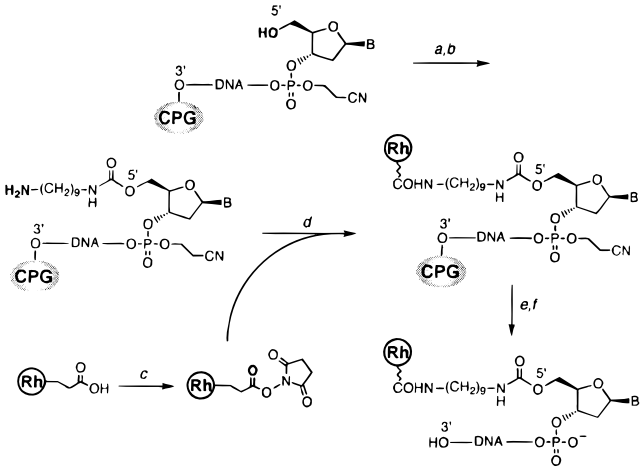
Methods. ESI data for oligonucleotides were provided by UC Riverside. CD spectroscopy was carried out on a Jasco 2500 spectrometer using 20 μM samples. Polyacrylamide gel electrophoresis (PAGE) and photocleavage assays were carried out using the methods described previously (*20*, *24*, *25*).

Enzymatic Digestion of Oligonucleotides. An aqueous solution of oligonucleotide containing ~1 nmol of strand was added to 10 μL of 1.0 M $MgCl_2$(aq), 10 μL of AP buffer (10× supplied with enzyme), 3 μL of SVP (Sigma), 3 μL of AP (Boehrringer Mannheim), and water in a 1.7 mL Eppendorf tube to give a volume of 100 μL. The cocktail was incubated at 37 °C for ~8 h.

Following incubation, the mixture was filtered on nylon (0.4 μm) centrifuge filters and analyzed by RP HPLC on a 100 Å, analytical (C18) column. The mobile phase consisted of 50 mM ammonium acetate, pH 5.5, and acetonitrile. The gradient started at 0% acetonitrile and went to 5% acetonitrile over 25 min. Some analyses required that the column be heated to 40 °C. The nucleotides elute from the column in the following order: 1-C, 2-G, 3-T, 4-A, as confirmed by co-injection of standard solutions.

The area under each peak (observation at 260 nm) was normalized to the extinction coefficient of the base (dC = 7.3 $mM^{-1}\,cm^{-1}$, dG = 11.7 $mM^{-1}\,cm^{-1}$, dT = 6.7 $mM^{-1}\,cm^{-1}$, dA = 15.0 $mM^{-1}\,cm^{-1}$; Glen Research). The fraction of normalized area for a given base was then multiplied by the total number of bases to indicate the number of that component present in the mixture. In general, we find the results for dG and dT to be slightly high (~10%; independent of the conjugation chemistry) and the results for dA to be slightly low, which probably reflects some error in the extinction coefficients used in the calculations.

Scheme 1. Multistep Heterogeneous Coupling of $[Rh(phi)_2(bpy')]^{3+}$ to the 5′ Terminus of Oligonucleotides Attached to a Solid Support[a,b]



[a] Reagents: (a) CDI, dioxane, 30 min, rt; (b) $H_2N(CH_2)_9NH_2$, dioxane/H_2O (9:1), 25 min, rt; (c) TSTU, DIEA, CH_3OH, CH_3CN, CH_2Cl_2 (1:1:1), rt, 1 h; (d) heterogeneous coupling, DIEA, rt, 12 h; (e) NH_3(aq), 60 °C, 6 h. [b]Abbreviations: CPG = controlled pore glass; Rh = $[Rh(phi)_2(bpy')]^{3+}$.

Hybridization of Complementary Oligonucleotides to Form Duplexes. Complementary DNA strands were dissolved in 5 mM sodium-phosphate buffer and 50 mM NaCl, pH 7.0, in a 1:1 ratio at the desired concentration. The sample was heated to 90 °C for 5 min and cooled to ambient temperature (20 °C) with a linear gradient over 180 min.

RESULTS AND DISCUSSION

Synthesis and Characterization of Oligonucleotide Conjugates with $[Rh(phi)_2(bpy')]^{3+}$ Attached to the 5′-Terminus. Several methods permit the synthesis of oligonucleotides with molecular probes attached to the terminal, 5′ hydroxyl (*26*, *27*). These strategies typically rely on amide bond formation between an activated carboxylate on the probe, and an amino-terminated linker attached to the oligonucleotide. We initiated our studies with $[Rh(phi)_2(bpy')]^{3+}$ (Figure 1) as a suitable complex for these studies since the nonintercalating ligand bears the carboxylate to be used in conjugation, which should preserve the DNA-binding properties of the intercalator.

(A) Synthetic Strategy. Scheme 1 outlines the multistep, hetereogeneous coupling method we developed to tether $[Rh(phi)_2(bpy')]^{3+}$ to the 5′ terminus of oligonucleotides. In this approach, the DNA is attached to the controlled pore glass (CPG) bead used for automated DNA synthesis. There are three principal advantages to this solid-phase approach. (i) Each reaction may be driven to completion by employing an excess of reagents since any unreacted material is simply washed away. (ii) The phosphate moieties of the DNA backbone are all protected as cyanoethyl esters so the oligonucleotide is uncharged and well solvated by organic solvents. (iii) The exocyclic amines on the DNA bases are masked with acyl protective groups. Thus, for our purposes, the only reactive functionality is the 5′-OH.

We employed the method of Wachter et al. (*22*) to introduce a flexible alkyl linker onto the 5′-OH through a carbamate linkage. This reaction proceeds in >85%

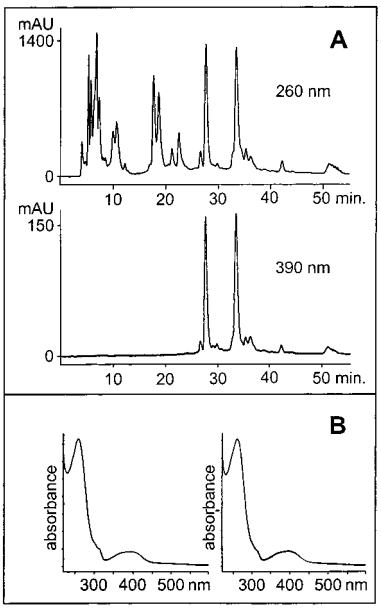


Figure 2. HPLC chromatogram of an Rh−DNA conjugate reaction mixture before purification (upper panel). UV−vis absorption spectra of the two rhodium-containing fractions at elution times of 28 min (left) and 34 min (right) (lower panel). The sequence of the oligonucleotide was as follows: 5′-Rh-ACG ATA TAC TAA CGT-3′.

yield and can be followed by reversed-phase HPLC (Supporting Information). At this stage, the oligonucleotide is poised for reaction with an electrophile.

We exploited simple, high-yield amide bond formation to tether the metal complex to the functionalized oligonucleotide on the solid support. The carboxylate of $[Rh(phi)_2(bpy')]^{3+}$ was converted to the NHS ester by treatment with TSTU. TSTU was used to synthesize an active ester with a derivative of $[Ru(phen)_3]^{2+}$ for conjugation to amino-modified DNA in solution (*28*−*30*), and in our work we favored TSTU because we could follow the activation of the carboxylate by TLC, and isolate the NHS ester for characterization. A matrix-assisted laser-desorption mass spectrum of the NHS ester of $[Rh(phi)_2(bpy')]^{3+}$ is provided in the Supporting Information.

We executed the coupling reaction by combining the solution of the NHS ester of $[Rh(phi)_2(bpy')]^{3+}$ (without isolation) and the CPG beads coated with the amino-modified DNA and stirring the slurry overnight. Owing to the tendency of the conjugate attached to the bead to be well solvated by organic solvents, we observed significant solvatochromism in the coloration of the CPG beads after the coupling reaction, which is consistent with incorporation of the transition metal chomophore.

The final step in this procedure is to liberate simultaneously the conjugate from the bead and remove the protecting groups by treatment with aqueous ammonia. The conjugates are purified by reversed-phase HPLC under the same conditions employed for purification of unmodified oligonucleotides. We estimate the yield of the coupling step to be ∼75% by comparing the amount of amino-modified DNA present (relative to the unmodified strand as an internal standard) before and after coupling. A similar procedure was employed to attach a metallointercalator containing ruthenium to the 5′ terminus of oligonucleotides in a study of long-range oxidative damage to guanine in DNA duplexes (*9*).

(B) Isolation of of 5′-Rh-Modified Oligonucleotides by HPLC. Figure 2 shows a typical chromatogram of an unpurified reaction mixture for the synthesis

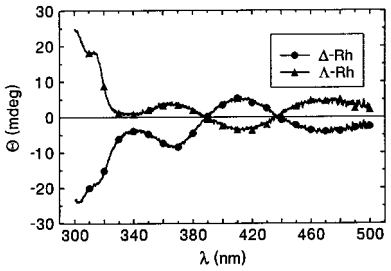


Figure 3. Circular dichroism of the two rhodium-containing products (Δ-Rh-151, Λ-Rh-151) isolated from the reaction mixture shown in Figure 2.

of 5′-Rh-modified DNA monitored at two wavelengths: 260 nm where everything in the mixture absorbs and 390 nm where only the rhodium complex absorbs. This reaction yields two products that contain rhodium. Owing to the hydrophobicity added by the metallointercalator, the conjugates elute with later retention times compared to the unmodified DNA, which simplifies their purification.

The absorption spectra of the two rhodium-containing products (Figure 2) are identical and consistent with expectation for Rh-modified DNA. The intense absorption centered at 260 nm reflects the contribution of the DNA bases, while the absorption centered at 390 nm corresponds to absorption of the metal complex. The transition centered at 390 nm is hypochromic compared to that for the metal complex free in solution. Such hypochromicity for the conjugate indicates that the metal complex interacts preferentially with the bases of the single-stranded DNA (*20*, *24*).

The HPLC chromatogram in this figure reveals several side products that do not contain a rhodium complex. Since we find that the amounts of these species vary considerably from one synthesis to the next, we suggest that they likely reflect side products and failed sequences in the DNA synthesis. It is important to note that the relative amount of these products is somewhat exaggerated by the fact that the Rh-modified DNA elutes as two peaks, so the relative height of the product peak is reduced by a factor of 2 while the height of the peaks due to the side products are constant.

(C) Circular Dichroism Spectroscopy of Rh-Modified DNA. To answer the question of why two products with identical absorption spectra are formed, we measured the circular dichroism (CD) spectra of each species (Figure 3). On the basis of the equal and opposite relationship of the spectra in this region where the metal complex absorbs and by comparison to CD spectra for the enantiomers of the parent $[Rh(phi)_2(bpy)]^{3+}$, we concluded that into one product we had incorporated the Δ enantiomer of $[Rh(phi)_2(bpy')]^{3+}$, while we introduced Λ-$[Rh(phi)_2(bpy')]^{3+}$ into the other. Remarkably, achiral HPLC was the only purification method required to separate these two diastereomeric Rh-DNA conjugates. Moreover, neither diastereomer was formed preferentially.

(D) Electrospray Ionization Mass Spectrometry of Rh−DNA Conjugates. We used electrospray ionization (ESI) MS to measure the mass of Rh-modified oligonucleotides. ESI MS can be used to confirm not only that the conjugate is intact, but also it confirms that all of the protecting groups have been eliminated (*31*).

Figure 4 shows the ESI MS of $[Rh(phi)_2(bpy')]^{3+}$ attached by a diaminononane linker to the 5′-hydroxyl of a 20 nt oligonucleotide. The data shown is a deconvoluted spectrum constructed from mass:charge (*m*/*z*) data for several charge states (*31*). The calculated mass for the

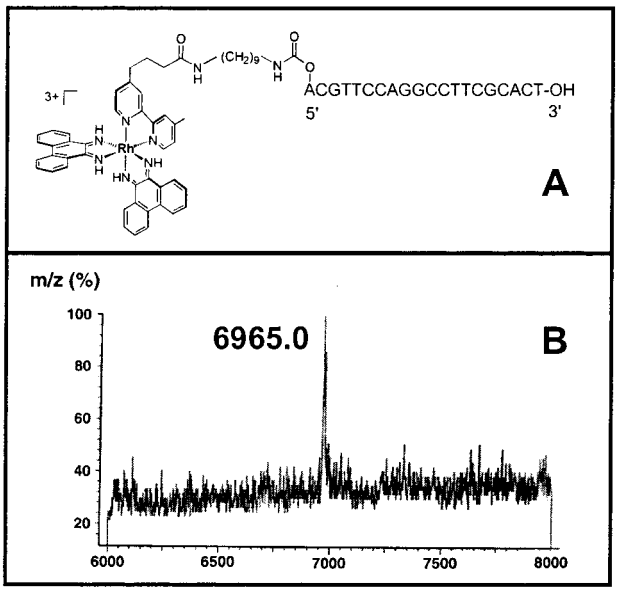
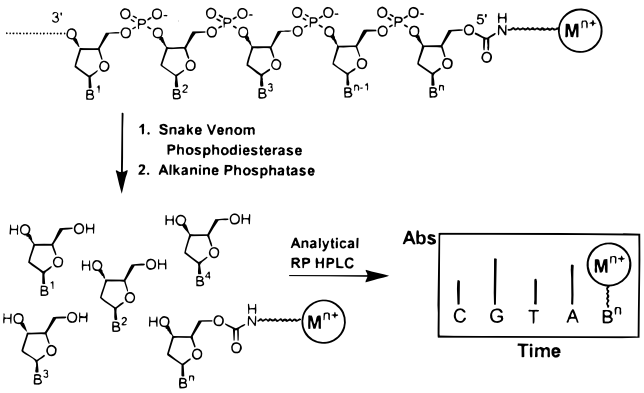


Figure 4. Electrospray ionization (ESI) mass spectrum of $[Rh(phi)_2(bpy')]^{3+}$ tethered to a 20-mer oligonucleotide. The calculated mass for this conjugate is 6964.8 amu and the observed mass is 6965.0.

Scheme 2. Schematic Illustration of the Enzymatic Digestion of Oligonucleotides by Snake Venom Phosphodiesterase To Give Nucleotide Monophosphates (NMPs)[a]



[a] Hydrolysis of NMPs by alkaline phosphatase gives the nucleotides. The 5′-terminal base remains attached to the metallointercalator because the enzymes do not hydrolyze the carbamate linkage. The products are separated by HPLC and the numbers of each base are counted.

conjugate is 6964.8, and the observed mass is 6965.0. From this spectrum we can say (i) the product is the desired conjugate and (ii) all of the protecting groups are remove upon treatment with aqueous ammonia without degredation of the metal complex or the DNA.

(E) Enzymatic Digestion of Rh-Modified DNA to Establish Base Content. To establish that covalent modification occurred at the targeted terminus as designed, we determined the base content of Rh-modified DNA and compared the results to data for unmodified DNA. The premise of this assay, outlined in Scheme 2, is to detect the modification of the 5′-terminal base. The oligonucleotide is treated with a cocktail of snake venom phosphodiesterase (SVP) and alkaline phosphatase (AP) (*32*). SVP cleaves the phosphodiester bonds of the oligonucleotide to release the nucleotide monophosphates (NMPs). AP then hydrolyzes the NMPs to give the neutral nucleotides, which are significantly more amenable to chromatographic separation. The reaction mixture is then analyzed by reversed-phase HPLC. Since the enzymes do not recognize the carbamate linkage that joins the nucleotide and the metal complex through an aliphatic linker, the modified DNA will appear to have lost one base in the HPLC analysis.

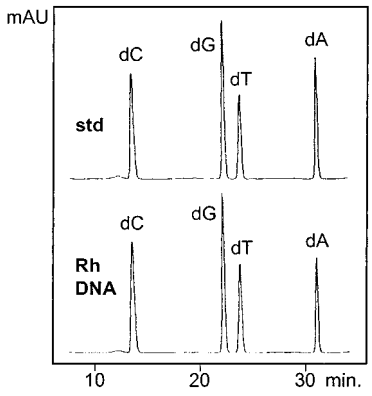


Figure 5. HPLC chromatograms monitored at 260 nm of the enzymatic digestion of an unmodified 14-mer (top) and a Rh-modified 14-mer (bottom). The area under the peak for dA is clearly reduced in the data for the conjugate. This loss of dA is consistent with the coupling of the metallointercalator to the 5′ terminus of this oligonucleotide.

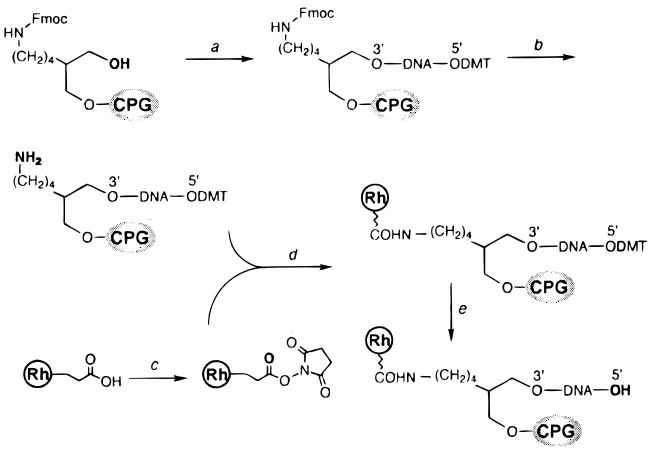
Figure 5 shows the results of the digestion of two oligonucleotides: an unmodified 14-mer and the corresponding Rh-modified 14-mer. For this conjugate, the rhodium complex is attached to a deoxyadenosine (dA). The quantity of each base, determined by integration of the chromatograms, is consistent with expectation based on the known sequence. The area under the peak corresponding to dA is clearly diminished for the conjugate compared to the unmodified strand. These results establish that the conjugation reaction is selective for the 5′ terminus and that no other bases are modified. Following the digestion, the metal complex attached to the 5′ terminal nucleoside adsorbs to the filter before analysis and therefore does not appear in the chromatogram in Figure 5.

Synthesis of Rh-Modified Oligonucleotides with the Metallointercaltor Attached to the 3′ Terminus. To generalize our method of generating metallointercalator−DNA conjugates, we developed a procedure to modify the 3′ terminus of oligonucleotides (Scheme 3). As with conjugation to the 5′-hydroxyl, this approach relies on derivatization of the strand on the CPG resin.

A commercially available CPG bead functionalized with a hydroxy aminoalkane masked with Fmoc and dimethoxy trityl (DMT) protecting groups was used as the support for automated DNA synthesis. Following selective removal of the DMT group, the DNA was synthesized by the standard phosphoramidite approach to give an oligonucleotide functionalized at the 3′ terminus with an Fmoc protected, alkylamine while the assembly remains attached to the solid support.

The amine is selectively unmasked by treatment with piperidine in DMF without affecting the protecting groups on the DNA bases or backbone (*23*). The oligonucleotide is then coupled to the NHS ester of $[Rh(phi)_2(bpy')]^{3+}$ as described for the 5′-modification strategy. Before removing the product from the bead, the DMT protecting group is removed from the 5′-hydroxyl by treatment with trichloroacetic acid in acetonitrile. Oligonucleotide conjugates prepared by this procedure are also purified by HPLC and can be resolved into the Δ- and Λ-rhodium-containing diastereomers (*33*).

Scheme 3. Coupling of $[Rh(phi)_2(bpy')]^{3+}$ to the 3′ Terminus of Oligonucleotides Attached to a Solid Support[a,b]



[a] Reagents: (a) Automated DNA synthesis (ABI 391 DNA synthesizer); (b) piperidine (20% v/v), DMF, rt, 30 min; (c) TSTU, DIEA, CH_3OH, CH_3CN, CH_2Cl_2 (1:1:1), rt, 1 h; (d) heterogeneous coupling, DIEA, rt, 12 h; (e) TCAA, CH_3CN, 18 s, rt. [b] Abbreviations: CPG = controlled pore glass; DMT = dimethoxy trityl; Rh = $[Rh(phi)_2(bpy')]^{3+}$.

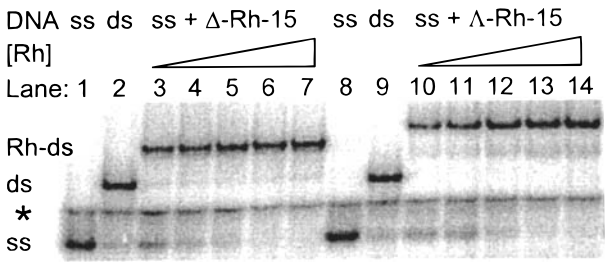


Figure 6. Nondenaturing polyacrylamide (20%) gel for following the hybridization of ^{32}P-end-labeled complement to Rh-modified DNA. Contents of lanes: (1) labeled complement (single stranded); (2) unmodified duplex (complement plus rhodium strand; 1:1); (3−7) labeled complement (8 μM) plus increasing concentrations of Δ-Rh-DNA (6, 7, 8, 9, 10 μM). Lanes 8−14 are the same as 1−7, with Λ-Rh substituted for the Δ isomer.

Characterization of Rh-Modified DNA Duplexes. (A) Monitoring the Hybridization of Rh-Modified Oligonucleotides to Their Complements by PAGE. We followed the hybridization of ^{32}P-end-labeled DNA to Rh-modified DNA on nondenaturing polyacrylamide gels (free of urea). Owing to the stiffness of duplex DNA relative to single strands, the duplexes are retarded relative to single stranded DNAs under electrophoresis on polyacrylamide gels.

Figure 6 illustrates a typical hybridization experiment for Λ-Rh-DNA and Δ-Rh-DNA (*25*). The first lane of each titration contains only the ^{32}P-end-labeled complement of the Rh-modified strand ([^{32}P]Rh-DNA-C). The second lane contains [^{32}P]Rh-DNA-C hybridized to 1 equiv of the unmodified rhodium strand. As expected for the formation of a 1:1 complex, a new band appears in the gel retarded relative to the single strand and there is no [^{32}P]-Rh-DNA-C remaining. The next five lanes contain [^{32}P]-Rh-DNA-C (8 μM) and increasing concentrations of Rh-DNA (6, 7, 8, 9, and 10 μM). As in the case of the unmodified duplex, a new band appears near the top of the gel. The intensity of this band increases with Rh-DNA until it reaches saturation at 8 μM. Similarly, the band for [^{32}P]Rh-DNA-C decreases in intensity until disappearing from the gel when the sample is fully duplexed. There is an exogenous source of radioactivity present at equal levels in the sample that is present in all lanes and migrates just above the single strand.

It is noteworthy that the Rh-modified duplexes migrate above the unmodified duplex. Such an observation is consistent with the positively charged metal complex reducing the total negative charge of the assembly and diminishing its attraction to the positive pole of the gel (*25*).

Upon comparison of migration profiles of the Δ and Λ-Rh-modified duplexes, the diastereomer containing Λ-Rh moves slower on the gel than the diastereomer containing Δ-Rh. Owing to the symmetry matching of the right-handed DNA duplex with the right-handed Δ-Rh, we expect the complex to be intercalated more deeply into the duplex than the Λ-isomer (*34*). The migration behavior observed in the gels is consistent with this notion, since a more compact structure should be less hindered by the gel, as is the duplex bearing Δ-$[Rh(phi)_2(bpy')]^{3+}$. In the lanes for duplexes with Δ-Rh, there is a faint band that migrates just ahead of the major band for the double-stranded conjugates; this species may reflect a small population of assemblies where the complex is intercalated at a site other than the predominant binding site. These experiments demonstrate that the presence of the rhodium complex does not preclude the stoichiometric formation of duplexes, and that the association of the Λ enantiomer of the metallointercalator with the duplex is different from the interactions of the Δ enantiomer.

(B) Establishing the Intercalation Site by Photocleavage in Rh-Modified DNA Duplexes. To apply Rh-modified oligonucleotides in studies of long-range charge transfer in DNA, it is critical that we know the site at which the reactants are bound to the DNA. Upon photoactivation with UV light ($\lambda \approx 313$ nm) in the presence of DNA, phi complexes of Rh(III) may abstract a hydrogen atom from the sugar residue at the base step of intercalation (*20*), which leads to direct strand scission and marks the site of intercalation. The products of the photochemical reaction with ^{32}P-labeled DNA are separated by PAGE and visualized by phosphorimagery (*25*). This experiment provides single-base resolution of the site of cleavage and permits the determination of the molecular distances that separate electron donors and acceptors during charge-transfer experiments.

Figure 7 shows the polyacrylamide gel used to reveal the site of intercalation in rhodium-modified DNA duplexes as a function of the length of the linker and the binding site. To clarify these results, the data are summarized schematically in Figure 8.

We examined photocleavage by the Δ and Λ enantiomers of $[Rh(phi)_2(bpy')]^{3+}$ tethered by diaminononane (C9) or diaminohexane (C6) linkers to a 15 base pair (bp) duplex (lanes 4−7; Figure 7). In lanes 8−11, the Rh-modified strand contains 16 nt, but it is hybridized to the 15 nt complement used for duplexes in lanes 4−7. This hybrid duplex has a thymine that extends the effective length of the linker joining the duplex and the C9 or C6 tether. These reactions were also compared to photocleavage by the parent complex $[Rh(phi)_2(dmb)]^{3+}$ (dmb = 4,4′-dimethyl bipyridine) bound noncovalently to the unmodified duplexes (lane 14). For the samples where the complex was bound noncovalently, the cleavage is distributed fairly evenly throughout the duplex, with some specificity for binding between the 5′-G(3) and 5′-A(4), as designed. In fact, the 5′-ACGA-3′ sequence was chosen to accommodate the tethered complex since this is a preferred binding sight of $[Rh(phi)_2(dmb)]^{3+}$. Cleavage by the tethered complex is only observed near the end of

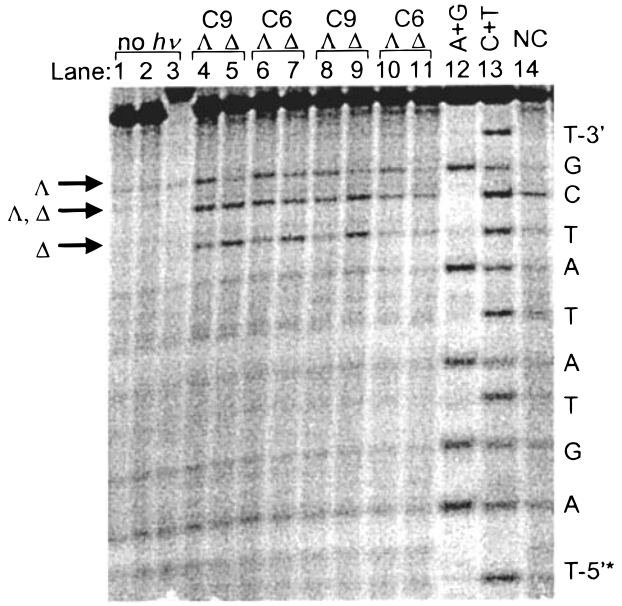


Figure 7. Phosphorimagery results depicting the products of the direct photocleavage of Rh-modified duplexes upon irradiation at 313 nm for 8 min. A schematic representation of these results is shown in Figure 8. The experiment measures the site of intercalation as a function of configuration about the metal center, linker length, and base sequence for a series of rhodium−DNA conjugates. All samples were 8 μM in duplex in 5 mM Na_3PO_4 and 50 mM NaCl, pH 7.0. The contents of each lane are as follows: **1**−**3**, 15 bp duplex, 16/15-mer hybrid duplex, 16 bp, duplex, respectively, no irradiation (dark control); **4**, **5**, Λ-Rh-15 bp duplex, and Δ-Rh-15 bp duplex with C9 linker; **6**, **7**, Λ-Rh-15 bp duplex, and Δ-Rh-15 bp duplex with C6 linker; **8**, **9**, Λ-Rh-16/15 hybrid duplex, and Δ-Rh-16/15 hybrid duplex with C9 linker; **10**, **11**, Λ-Rh-16/15 hybrid duplex, and Δ-Rh-16/15 hybrid duplex with C6 linker; **12**, **13**, Maxam−Gilbert sequencing lanes for 15-mer (A + G, 12; C + T, 13); **14**, Δ-$[Rh(phi)_2(dmb)]^{3+}$ bound noncovalently to 15 bp duplex.

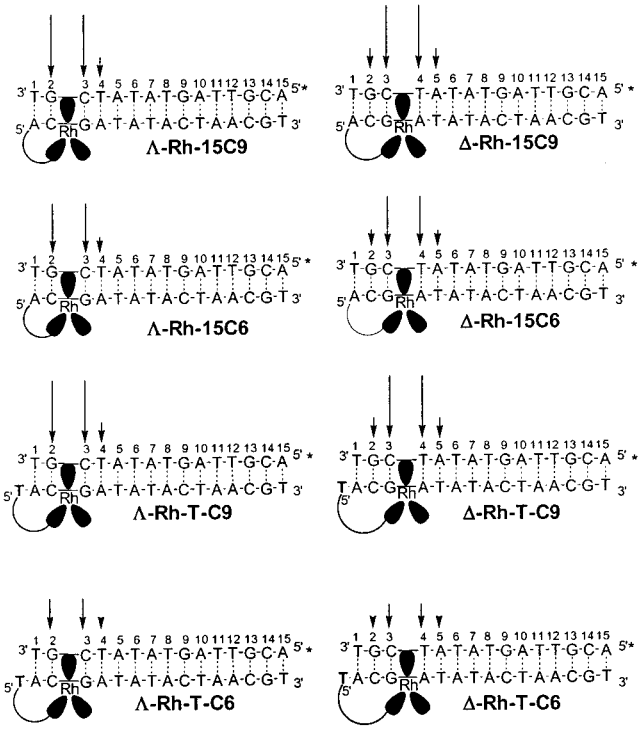


Figure 8. Summary of photocleavage of a 15 bp duplex by $[Rh(phi)_2(bpy')]^{3+}$ tethered to the 5′-ACGA terminus as indicated. The columns correspond to lane numbers in Figure 7 as follows: (left column, top to bottom) lane 4, lane 6, lane 8, lane 10; (right column, top to bottom) lane 5, lane 7, lane 9, lane 11. Arrows represent sites of cleavage and their height represents relative cleavage intensity.

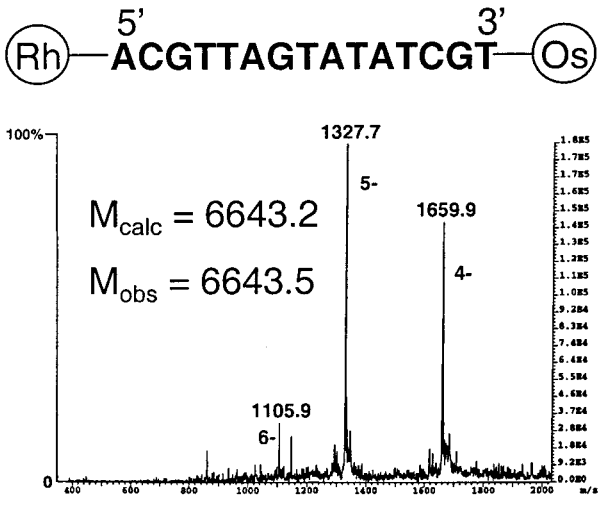


Figure 9. ESI mass spectrum of a 3′,5′-bis-heterometalated oligonucleotide. The calculated mass for the fully protonated species is M_{calc} = 6643.2. According to the distributions of ions present in the mass spectrum, the mass of the ion plus the appropriate number of hydrogens to achieve the targeted charge, leads to a mass of M_{obs} = 6643.5. This remarkable accuracy confirms that the material is the desired compound, and that all protecting groups have been removed.

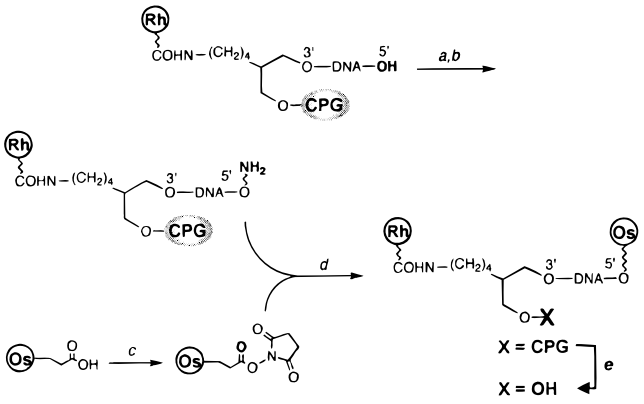
the duplex to which the metallointercalator is confined by the linker.

For modified duplexes bearing the C9 or C6 linkers, the Λ isomer binds primarily two bases in from the 5′-terminus and the Δ isomer binds three bases from the terminus. This observation has been made repeatedly for rhodium complexes tethered to the sequence 5′-ACGA-(T). In quantitative comparisons of cleavage intensities, it is apparent that there is a diminution in the amount of cleavage with the C6 linker, suggesting that this linker might not be long enough to permit efficient access of the preferred binding site. The presence of the overhanging thymine in the hybrid duplexes (Rh-16-mer hybridized to a 15 nt complement) does not seem to affect the site of intercalation, but the cleavage intensity does appear to decrease.

Synthesis of 3′,5′-bis-Hetereometalated Oligonucleotides. Scheme 3 outlines the preparation of oligonucleotides with a metallointercalator attached to the 3′-hydroxyl group. Over the course of these reactions, the 5′-hydroxyl is protected as the DMT ether (*19*). The last steps in that procedure involve deprotection of the 5′-hydroxyl group and liberation of the conjugate from the resin. We recognized that if we unmasked the 5′-hydroxyl of the 3′-modified oligonucleotide, left on the resin, we would be free to functionalize the 5′-hydroxyl as well (*26*, *27*). We could synthesize oligonucleotides that contain an electron donor, for example, at one terminus and an electron acceptor at the other.

We developed the strategy in Scheme 4, which permits the synthesis of so-called 3′,5′-bis-heterometalated oligonucleotides. The first phase of the synthesis consists of incorporating a metallointercalator onto the hydroxy aminoalkyl linker tethered to the 3′ terminus of the oligonucleotide according to the procedure developed for preparing 3′-modified DNA. Next, the DMT protecting group is removed from the 5′ hydroxyl by treatment with trichloroacetic acid in CH_2Cl_2. After coupling the appropriate diaminoalkyl linker to the 5′ hydroxyl, the second metallointercalator is coupled to the free amine

Scheme 4. Synthesis of 3′,5′-bis-Heterometallated Oligonucleotides on a Solid Support[a,b]



[a] Reagents: (a) CDI, dioxane, 30 min, rt; (b) $H_2N(CH_2)_9NH_2$, dioxane/H_2O (9:1), 25 min, rt; (c) TSTU, DIEA, CH_3OH, CH_3CN, CH_2Cl_2 (1:1:1), rt, 1 h; (d) heterogeneous coupling, DIEA, rt, 12 h; (e) NH_3(aq), 60 °C, 6 h. [b] Abbreviations: CPG = controlled pore glass; Os = $[Os(phen)(bpy')(Me_2\text{-}dppz)]^{2+}$.

according to the procedure established for modification of the 5′ terminus. Finally, the whole assembly is liberated from the conjugate and deprotected by treatment with NH_3(aq), and isolated by HPLC.

We executed this procedure to validate our method and isolated one major product. It is important to note that using racemic mixtures of each metallointercalator gives rise to eight possible isomers of the 3′,5′-bis-heterometalated oligonucleotide. The ESI MS of the product isolated in this reaction is shown in Figure 9. This methodology will be important in the application of DNA-mediated electron transfer for metallointercalator-DNA conjugates in sensing technology.

SUMMARY AND CONCLUSIONS

We have established methods to prepare oligonucleotides bearing metallointercalators on either the 5′, 3′, or both 5′ and 3′ termini. The procedures are based on a solid-phase approach in that the conjugates are prepared while the oligonucleotide is immobilized on the CPG bead used in automated DNA synthesis. This approach is attractive for three reasons: (i) excess reagents that drive reactions to completion can be easily washed away from the solid support following reactions; (ii) the phosphate groups are protected so the oligonucleotide is uncharged and well solvated; and (iii) all exocyclic amines on the DNA bases are protected so the only reactive functionality present is the desired point of attachment.

These protocols all provide a means to synthesize, in high, reproducible yields, a variety of conjugates that vary in the DNA sequence of the oligonucleotide as well as the length of the linker used to join the two species. We employed several methods to characterize the materials and establish the chemical composition of the conjugates as well as their ability to form duplexes with their complementary strands and the site of intercalation for the metallointercalator.

The methodology described in this paper has now been employed to prepare metallointercalator−DNA conjugates for investigations of the fundamental properties of DNA as a medium for charge transfer. Rh-modified oligonucleotides have been employed to demonstrate long-range oxidative DNA damage to 5′-GG-3′ sites (*8*), as well as to examine the effect of intervening bulges in the base stack (*35*). We have used Rh-modified DNA to effect the long-range repair of thymine-dimer lesions in DNA (*33*), and to compare long-range charge-transfer reactions in duplexes with 5′-GG-3′ and thymine dimer sites to those with either 5′-GG-3′ or thymine dimers (*36*). This work established for the first time that DNA damage and repair chemistry can be initiated from a remote site. Rh-DNA conjugates have also been useful, along with ethidium-modified DNA to characterize DNA-mediated electron-transfer chemistry using photophysical techniques (*37*). For future applications, these conjugates, including the 3′,5′-bis-heterometalated oligonucleotides, may provide the basis for developing novel DNA-based sensor technologies based on charge-transfer reactions involving the DNA base stack.

ACKNOWLEDGMENT

We are grateful to the NIH for their financial support. We also thank the Parsons Foundation (R.E.H.) and the Damon-Runyon Walter Winchell Cancer Fund (P.J.D.) for fellowship support.

Supporting Information Available: Illustration of the NHS ester of $[Rh(phi)_2(bpy')]^{3+}$, MALDI-TOF mass spectrum of $[Rh(phi)_2(bpy'\text{-NHS})]^{3+}$, and HPLC chromatograms. This material is available free of charge via the Internet at http://pubs.acs.org.

LITERATURE CITED

(1) Holmlin, R. E., Dandliker, P. J., and Barton, J. K. (1997) *Angew. Chem., Int. Ed. Engl. 36*, 2714−2730.

(2) Arkin, M. R., Stemp, E. D. A., Holmlin, R. E., Barton, J. K., Hörmann, A., Olson, E. J. C., and Barbara, P. F. (1996) *Science 273*, 475−480.

(3) Holmlin, R. E., Stemp, D. A., and Barton, J. K. (1996) *J. Am. Chem. Soc. 118*, 5236−5244.

(4) Murphy, C. J., Arkin, M. R., Ghatlia, N. D., Bossmann, S., Turro, N. J., and Barton, J. K. (1994) *Proc. Natl. Acad. Sci. U.S.A. 91*, 5315−5319.

(5) Arkin, M. R., Stemp, E. D. A., Turro, C., Turro, N. J., and Barton, J. K. (1996) *J. Am. Chem. Soc. 118*, 2267−2274.

(6) Lincoln, P., Tuite, E., and Nordén, B. (1997) *J. Am. Chem. Soc. 119*, 1454−1455.

(7) Olson, E. J. C., Hu, D., Hormann, A., and Barbara, P. F. (1997) *J. Phys. Chem. B. 101*, 299−303.

(8) Hall, D. B., Holmlin, R. E., and Barton, J. K. (1996) *Nature 382*, 731−735.

(9) Arkin, M. R., Stemp, E. D. A., Pulver, S. C., and Barton, J. K. (1997) *Chem. Biol. 4*, 389−400.

(10) Murphy, C. J., Arkin, M. R., Jenkins, Y., Ghatlia, N. D., Bossmann, S. H., Turro, N. J., and Barton, J. K. (1993) *Science 262*, 1025−1029.

(11) Hurley, D. J., and Tor, Y. (1998) *J. Am. Chem. Soc. 120*, 2194−2195.

(12) Khan, S. I., and Grinstaff, M. W. (1999) *J. Am. Chem. Soc. 121*, 4704−4705.

(13) Meggers, E., Kusch, D., and Giese, B. (1997) *Helv. Chim. Acta 80*, 640−652.

(14) Bannwarth, W., and Schmidt, D. (1989) *Tetrahedron Lett. 30*, 1513−1516.

(15) Manchanda, R., Dunham, S. U., and Lippard, S. J. (1996) *J. Am Chem. Soc. 118*, 5144−5145.

(16) Schliepe, J., Berghoff, U., Lippert, B., and Cech, D. (1996) *Angew. Chem., Int. Ed. Engl. 35*, 646−648.

(17) Mucic, R. C., Herrlien, M. K., Mirkin, C. A., and Letsinger, R. L. (1996) *Chem. Commun.* 555−557.

(18) Magda, D., Crofts, S., Lin, A., Miles, D., Wright, M., and Sessler, J. L. (1997) *J. Am. Chem. Soc. 119*, 2293−2294.

(19) Caruthers, M. H. (1985) *Science 230*, 281−285.

(20) Sitlani, A., Long, E. C., Pyle, A. M., and Barton, J. K. (1992) *J. Am. Chem. Soc. 114*, 2303−2311.

(21) Holmlin, R. E., Yao, J. A., and Barton, J. K. (1998) *Inorg. Chem. 38*, 174−189.
(22) Wachter, L., Jablonski, J.-A., and Ramachandran, K. L. (1986) *Nucleic Acids Res. 14*, 7985−7995.
(23) Früchtel, J. S., and Jung, G. (1996) *Angew. Chem., Int. Ed. Engl. 35*, 17−42.
(24) Sitlani, A., and Barton, J. K. (1994) *Biochemistry 33*, 12100−12108.
(25) Johann, T. W., and Barton, J. K. (1996) *Philos. Trans. R. Soc. London A. 354*, 299−324.
(26) Asseline, U., Thuong, N. T., and Helene, C. (1997) *New J. Chem. 21*, 5−17.
(27) Beaucage, S. L., and Iyer, R. P. (1993) *Tetrahedron 49*, 6123−6194.
(28) Bannwarth, W., and Knorr, R. (1991) *Tetrahedron Lett. 32*, 1157−1160.
(29) Knorr, R., Trzeciak, A., Bannwarth, W., and Gillessen, D. (1989) *Tetrahedron Lett. 30*, 1927−1930.
(30) Bannwarth, W., Schmidt, D., Stallard, R. L., Hornung, C., Knorr, R., and Müller, F. (1988) *Helvetica Chimica Acta 71*, 2085−2099.
(31) (a) Greig, M., and Griffey, R. H. (1995) *Rap. Comm. in Mass Spec. 9*, 97−102. (b) Nordhoff, E., Kirpekar, F., and Roepstorff, P. (1996) *Mass Spec. Rev. 15*, 67−138.
(32) Glen Research (1993) Technical Bulletin.
(33) Dandliker, P. J., Holmlin, R. E., and Barton, J. K. (1997) *Science 274*, 1465−1468.
(34) Barton, J. K. (1986) *Science 233*, 727−734.
(35) Hall, D. B., and Barton, J. K. (1997) *J. Am. Chem. Soc. 119*, 5045−5046.
(36) Dandliker, P. J., Nunez, M. E., and Barton, J. K. (1998) *Biochemistry 37*, 6491−6502.
(37) Kelley, S. O., Holmlin, R. E., Stemp, E. D. A., and Barton, J. K. (1997) *J. Am. Chem. Soc. 119*, 9861−9870.

BC9900791

© 1999 American Chemical Society, Bioconjugate Chem., Holmlin bc9900791 Supporting Info Page 1

SUPPLEMENTARY MATERIAL FOR:

Title: Synthesis of Metallointercalator-DNA Conjugates on a Solid Support

Authors: R. Erik Holmlin, Peter J. Dandliker, and Jacqueline K. Barton*

Affiliation: Division of Chemistry and Chemical Engineering

California Institiute of Technology

Pasadena, CA 91125

FIGURE CAPTIONS

Figure S1. (**A**) Schematic illustration of the N-hydroxysuccinimidyl (NHS) ester of $[Rh(phi)_2(bpy')]^{3+}$. (**B**) Matrix assisted laser desorption ionization (MALDI) time of flight (TOF) mass spectrum of $[Rh(phi)_2(bpy'\text{-}NHS)]^{3+}$.

Figure S2. HPLC chromatograms of an unmodified (upper trace) and an aminoalkylated (lower trace) 15-mer monitored at 260 nm. HPLC Conditions: C18 stationary phase; 50 mM ammonium acetate, pH 6.5/acetonitrile mobile phase; 0-15 % acetonitrile in 30 min. The aminoalkylated DNA shows a later retention time, consistent with increased hydrophobicity introduced by the linker.

Figure S3. HPLC chromatograms for the 3',5'-*bis*-heterometallated oligonucleotide pictured in Figure 9 monitored at 260 nm (top), 390 nm (middle), and 470 (nm) bottom. The 3',5'-*bis*-heterometallated oligonucleotide is the major product, and all eight diastereomers of this material coelute. HPLC Conditions: C18 stationary phase; 50 mM ammonium acetate, pH 6.5/acetonitrile mobile phase; 0-50 % acetonitrile in 75 min.

© 1999 American Chemical Society, Bioconjugate Chem., Holmlin bc9900791 Supporting Info Page 2

Supplementary Material

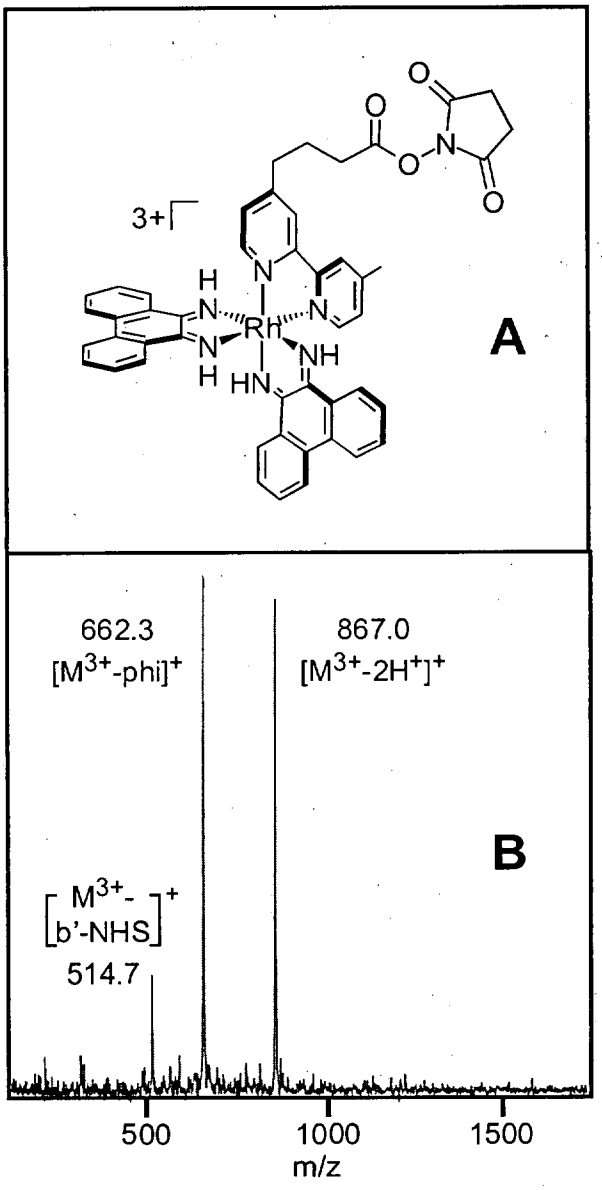


Figure S1

© 1999 American Chemical Society, Bioconjugate Chem., Holmlin bc9900791 Supporting Info Page 3

Supplementary Material

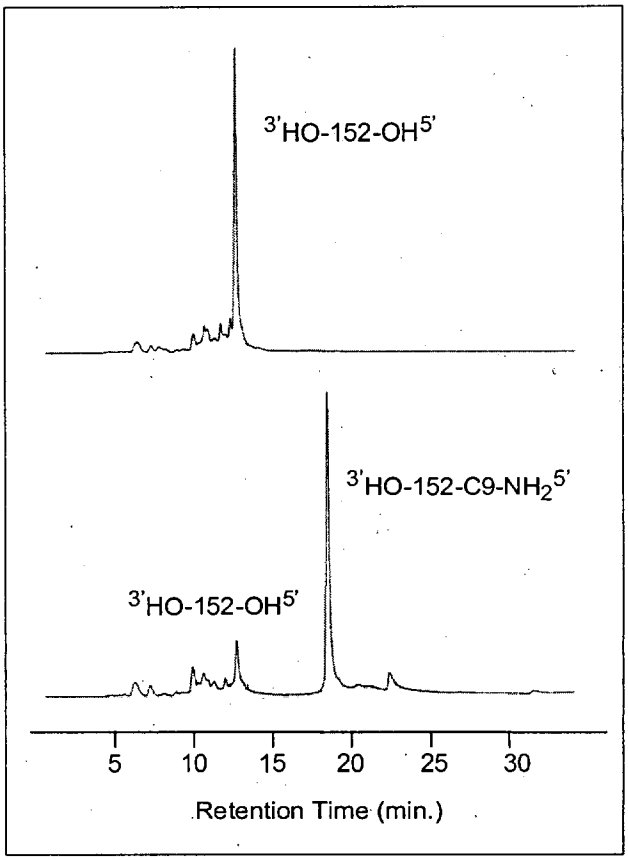


Figure S2

© 1999 American Chemical Society, Bioconjugate Chem., Holmlin bc9900791 Supporting Info Page 4

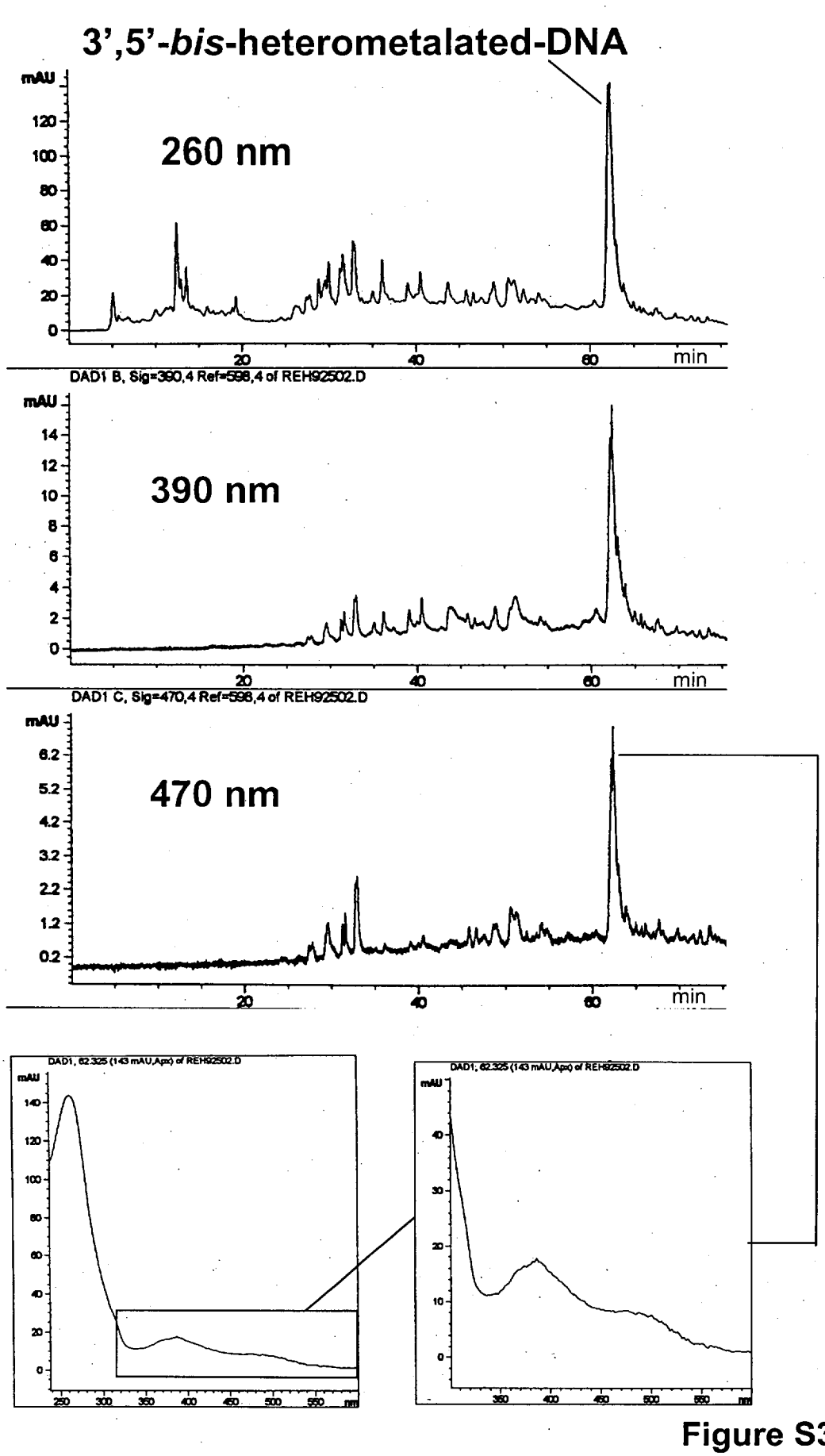


Figure S3

Synthesis and Biological Activity of Ribose-5′-Carbamate Derivatives of Vitamin B_{12}

J. F. McEwan,* H. S. Veitch, and G. J. Russell-Jones

Biotech Australia Pty Ltd., P.O. Box 20, Roseville, NSW 2069, Australia. Received June 23, 1999; Revised Manuscript Received August 23, 1999

Twelve biologically active derivatives of vitamin B_{12} (cyanocobalamin) have been synthesized in which spacers were attached to the ribose-5′-hydroxyl group of vitamin B_{12}. Their potential to act as oral delivery agents for proteins, nanospheres, or immunogens using the vitamin B_{12} uptake system was evaluated by determining their affinity for intrinsic factor (IF) and non-IF. The ribose-5′-hydroxyl group of vitamin B_{12} was activated through the use of 1,1′-carbonyldiimidazole (CDI), 1,1′-carbonyldi-(1,2,4-triazole) (CDT), or di(1-benzotriazolyl) carbonate (DBTC). Subsequent addition of an aminoalkane, diaminoalkane, or alkane diacid dihydrazide gave rise to vitamin B_{12} derivatives suitable for attachment to various proteins, peptides, or nanospheres to enable oral delivery utilizing the vitamin B_{12} uptake system. The ribose-5′-carbamate derivatives were found to possess similar affinity for intrinsic factor as that of the *e*-monocarboxylic acid of vitamin B_{12}. The affinity for non-IF was similar to cyanocobalamin or even higher for some of the smaller derivatives. Polysciences nanoparticles derivatized with vitamin B_{12} 5′-carbamate adipic dihydrazide into CaCo-2 cells showed significantly higher levels of transport of the particles, when compared to unmodified particles.

INTRODUCTION

The vitamin B_{12} uptake system possesses enormous potential as an absorption enhancing mechanism for orally administered proteins, peptides, and immunogens (*1*). Oral delivery of proteins, peptides, and immunogens is very inefficient due to the impenetrable barrier composed of the cells of the intestinal epithelium and because of proteolysis within the stomach and small intestine. Recent experiments on oral protein delivery have focused on the use of carrier molecules, such as lectins, bile salts, or vitamin B_{12} **1**, which are conjugated to the drug of choice, to utilize the receptor mediated endocytosis of the carrier molecule to provide co-absorption of the drug (*2*). Thus, Russell-Jones and co-workers have utilized this methodology in the generation of orally active conjugates of granulocyte colony stimulating factor (G-CSF), erythropoietin (EPO) (*3*), and luteinizing hormone releasing hormone (LHRH) (*4*) with vitamin B_{12}. Thus, intraduodenal infusion of the VB_{12}-G-CSF conjugates in rats resulted in highly elevated plasma levels of the conjugated protein (299 ± 160 ng/mL) as compared to nonconjugated G-CSF (1.94 ± 1.94 pg/ mL) (*5*). Similarly, the quantity of EPO reaching the systemic circulation when administered as a VB_{12} conjugate was 4-fold greater than the nonconjugated EPO. Conjugation to VB_{12} also seemed to reduce the susceptibility for proteolysis. Oral administration to rats of low doses of a D-Lys_6-ethylamide analogue of LHRH had no effect on serum LH levels, whereas administration of a conjugate with VB_{12} resulted in 20−45% systemic bioavailability, depending on the spacer used (*4*).

The above three examples all involved the attachment of spacers to the vitamin B_{12} *e*-monoacid. This molecule possesses 10-fold higher affinity for intrinsic factor (IF) and for transcobalamin II (TCII) than the alternative *b*- and *d*-monoacids (*6*). There are several other sites on vitamin B_{12} that are suitable for modification to form bioconjugates (*6*). The most readily derivatized position on vitamin B_{12} is the Co metal center; however, the bond so formed is photolabile (*7*, *8*). Conjugation can also occur through the 5′- and 2′-hydroxyl groups on the ribose moiety, the phosphate group, or through the use of appropriately substituted benzimidazoles. The work described herein concentrates on conjugation with the 5′-hydroxyl group of the ribose moiety.

Previous studies have examined the attack by the 5′-hydroxyl group on an acid anhydride, namely succinic anhydride (*9*) or glutaric anhydride (*10*), to provide a four or five carbon spacer possessing carboxylic acid functionality. While these derivatives were obtained in high yield, the methodology employed necessarily limits this procedure to the few anhydrides available. The route followed in this work examines the preactivation of the 5′-hydroxyl group on the ribose by the use of a reagent such as 1,1′-carbonyldiimidazole (CDI), 1,1′-carbonyldi(1,2,4-triazole) (CDT), or di(1-benzotriazolyl) carbonate (DBTC) followed by attack of a nucleophile to furnish the desired spacer. In particular, aminoalkanes, diaminoalkanes, and alkane diacid dihydrazides were employed as nucleophiles. Upon derivatization of the 5′-hydroxyl group, VB_{12} has been shown to retain most of its binding affinity for transcobalamin II (TCII) (*6*) whereas a marked decrease in affinity for diol dehydrase has been observed (*9*, *11*). Also, the 5′-succinic acid derivative did not inhibit the uptake of [^{13}H]cyanocobalamin by *Escherichia coli* (*9*). This work examines the binding affinity of the 5′-carbamate derivatives for non-IF (haptocorrin) (*12*) and IF and also the uptake and transport of nanoparticles, modified with various derivatives, by CaCo-2 cells.

EXPERIMENTAL PROCEDURES

Melting points were determined using an Electrothermal melting point apparatus and are uncorrected. Mass

* To whom correspondence should be addressed. Fax: (61-2) 9928 8899. E-mail: john_mcewan@mail.bioaust.com.au.

10.1021/bc990086p CCC: $18.00 © 1999 American Chemical Society
Published on Web 10/06/1999

spectra were recorded on a Mat LCQ detector using ESI with water/methanol (1:1) as solvent at 5 kV and a capillary temperature of 200 °C. Thin layer chromatography (TLC) was carried out on Merck precoated aluminum sheets coated with 0.2 mm silica gel 60 F_{254} and flash chromatography on Merck silica gel 60 (230−400 mesh ASTM). High-performance liquid chromatography (HPLC) was performed using Waters and Associates HPLC instrumentation fitted with a Waters μBondapak C18 column for **2**, **3**, and **7**−**15** and a Vydac 214TP C4 column for **4**, **5,** and **6**. All VB_{12} derivatives were purified to >95% purity as determined by analytical HPLC using a Waters 991 photodiode array detector. Products were eluted, after loading at 5% MeCN containing 0.1% TFA, using a gradient system at 1 mL/min comprising linear gradients to 18% MeCN at 2 min, 28% MeCN at 8.5 min, and 100% MeCN at 13 min.

General Procedure for Preparation of Alkane Derivatives. Solid 1,1′-carbonyldiimidazole (CDI, 260 mg) was added to cyanocobalamin (1.0 g, 0.74 mmol) previously dissolved in dimethyl sulfoxide (12 mL) at 30 °C, and the mixture was stirred for 25 min. Alkylamine (2.7 mmol) was added in one portion and stirring continued for a further for 24 h at room temperature. The mixture was extracted with phenol/dichloromethane (1:1, 2 × 20 mL) and back extracted with water (2 × 20 mL from 1:4 phenol/dichloromethane). The mixture was purified by phenyl sepharose (50 g) column chromatography, eluting the unmodified VB_{12} with 25% ethanol and the product with 60% ethanol. The solvent was removed at reduced pressure and the residue was sonicated for 5 min in acetone (50 mL). The mixture was filtered and the solid washed with acetone and air-dried.

Hexylamine derivative (**2**): yield, 60%; mp 213-215 °C (dec); MS (ESI) mass calcd for $C_{70}H_{101}N_{15}O_{15}CoP$ 1482, found 1505 $(M + Na)^+$; UV (H_2O) λ_{361} ($\epsilon = 10\,500$), HPLC retention time 16.0 min.

Dodecylamine derivative (**3**): yield, 52%; mp 215−218 °C (dec); MS (ESI) mass calcd for $C_{76}H_{113}N_{15}O_{15}CoP$ 1566, found 1589 $(M + Na)^+$; UV (H_2O) λ_{361} ($\epsilon = 16\,900$), HPLC retention time 19.6 min.

Tetradecylamine derivative (**4**): yield, 46%; mp 228−233 °C (dec); MS (ESI) mass calcd for $C_{78}H_{119}N_{15}O_{15}CoP$ 1595, found 1618 $(M + Na)^+$; UV (H_2O) λ_{361} ($\epsilon = 13\,000$), HPLC retention time 18.0 min.

Hexadecylamine derivative (**5**): yield, 48%; mp 223−227 °C (dec); MS (ESI) mass calcd for $C_{80}H_{121}N_{15}O_{15}CoP$ 1623, found 1646 $(M + Na)^+$; UV (H_2O) λ_{361} ($\epsilon = 20\,000$), HPLC retention time 18.4 min.

Octadecylamine derivative (**6**): yield, 66%; mp 220−223 °C (dec); MS (ESI) mass calcd for $C_{82}H_{125}N_{15}O_{15}CoP$ 1651, found 1674 $(M + Na)^+$; UV (H_2O) λ_{361} ($\epsilon = 17\,500$), HPLC retention time 18.8 min.

General Procedure for Preparation of Aminoalkane Derivatives. Solid 1,1′-carbonyldiimidazole (CDI, 260 mg) was added to cyanocobalamin (1.0 g, 0.74 mmol) previously dissolved in dimethyl sulfoxide (12 mL) at 30 °C, and the mixture stirred for 25 min. Diaminoalkane (2.7 mmol) was added in one portion, and the mixture stirred for 24 h at room temperature. The mixture was poured into ethyl acetate (30 mL) and left to stand. The supernatant was decanted and the residue sonicated for 5 min in acetone (50 mL). The resultant precipitate was filtered, and the solid washed with acetone. The product was purified by column chromatography (2-propanol 45%, *n*-butanol 30%, ammonia 2%, water 25%) then lyophilyzed.

1,2-Diaminoethane derivative (**7**): yield, 63%; mp 206−210 °C (dec); TLC (^{i}PrOH 30/*n*-BuOH 45/H_2O 25/NH_4OH 2) $R_f = 0.22$; MS (ESI) mass calcd for $C_{66}H_{94}N_{16}O_{15}CoP$ 1441, found 1441 $(M)^+$; UV (H_2O) λ_{361} ($\epsilon = 19\,900$), HPLC retention time 14.7 min.

1,4-Diaminobutane derivative (**8**): yield, 70%; mp 242−244 °C (dec); TLC (^{i}PrOH 30/*n*-BuOH 45/H_2O 25/NH_4OH 2) $R_f = 0.08$; MS (ESI) mass calcd for $C_{68}H_{98}N_{16}O_{15}CoP$ 1469, found 1469 $(M)^+$; UV (H_2O) λ_{361} ($\epsilon = 15\,500$), HPLC retention time 14.9 min.

1,6-Diaminohexane derivative (**9**): yield, 98%; mp 230−233 °C (dec); TLC (^{i}PrOH 30/*n*-BuOH 45/H_2O 25/NH_4OH 2) $R_f = 0.11$; MS (ESI) mass calcd for $C_{70}H_{102}N_{16}O_{15}CoP$ 1497, found 1497 $(M)^+$; UV (H_2O) λ_{361} ($\epsilon = 17\,000$), HPLC retention time 15.4 min.

1,12-Diaminododecane derivative (**10**): yield, 68%; mp 156−158 °C (dec); TLC (^{i}PrOH 30/*n*-BuOH 45/H_2O 25/NH_4OH 2) $R_f = 0.27$; MS (ESI) mass calcd for $C_{76}H_{114}N_{16}O_{15}CoP$ 1581, found 1581 $(M)^+$; UV (H_2O) λ_{361} ($\epsilon = 33\,000$), HPLC retention time 18.4 min.

General Procedure for Preparation of Hydrazidyl Derivatives. Solid 1,1′-carbonyldi(1,2,4-triazole) (CDT, 90 mg) was added to a solution of cyanocobalamin (500 mg, 0.37 mmol) in dimethyl sulfoxide (6 mL) at 30 °C, and the mixture stirred for 25 min. Acid dihydrazide (0.74 mmol) was added in one portion followed by triethylamine (100 μL), and the mixture stirred for a further 24 h at room temperature. The mixture was poured into ethyl acetate (30 mL) and left to stand. The supernatant was poured off and the residue sonicated for 5 min in acetone (20 mL). The mixture was filtered and the solid washed with acetone. The product was purified by RP HPLC then lyophilized.

Succinic dihydrazide derivative (**11**): yield, 68%; mp 206−208 °C (dec); TLC (^{i}PrOH 30/*n*-BuOH 45/H_2O 25/NH_4OH 2) $R_f = 0.36$; MS (ESI) mass calcd for $C_{68}H_{96}N_{18}O_{17}CoP$ 1581, found 1581 $(M)^+$; UV (H_2O) λ_{361} ($\epsilon = 15\,700$), HPLC retention time 11.8 min.

Adipic dihydrazide derivative (**12**): yield, 73%; mp 208−210 °C (dec); TLC (^{i}PrOH 30/*n*-BuOH 45/H_2O 25/NH_4OH 2) $R_f = 0.33$; MS (ESI) mass calcd for $C_{70}H_{100}N_{18}O_{17}CoP$ 1555, found 1555 $(M)^+$; UV (H_2O) λ_{361} ($\epsilon = 21\,100$), HPLC retention time 14.3 min.

Preparation of Gly Acid Derivative. Cyanocobalamin (1.0 g, 0.74 mmol) and 1,1′-carbonyldiimidazole (CDI, 260 mg) were added sequentially to dimethyl sulfoxide (12 mL) at 30 °C, and the mixture was stirred for 25 min. OMe-Gly (2.7 mmol) was added in one portion followed by triethylamine (200 μL), and the mixture stirred for 24 h at room temperature. The mixture was poured into ethyl acetate (30 mL) and left to stand. The supernatant was poured off, and the residue sonicated for 5 min in acetone (50 mL). The mixture was filtered, and the solid **13** washed with acetone. The residue was then dissolved in 0.1 M NaOH solution and stirred for 30 min. The crude acid was then purified on Dowex 1 × 4 resin eluting with 2% acetic acid.

Gly-acid derivative (**14**): yield, 95%; mp 239−242 °C (dec); TLC (^{i}PrOH 30/*n*-BuOH 45/H_2O 25/NH_4OH 2) $R_f = 0.41$; MS (ESI) mass calcd for $C_{66}H_{90}N_{15}O_{17}CoP$ 1456, found 1456 $(M)^+$; UV (H_2O) λ_{361} ($\epsilon = 19\,800$), HPLC retention time 15.3 min.

Binding of Cobalamin Derivatives with IF and Non-IF. A stock solution of [^{57}Co]VB_{12} was prepared containing 1 ng of [^{57}Co]VB_{12} and 250 ng of cold VB_{12} in 25 mL buffer (1 mg/mL BSA in 0.1 M potassium phosphate buffer, pH 7.5). A total of 100 μL of dilutions of cobalamin, or cobalamin analogues (in 10-fold dilutions from 10 μg to 0.1 ng) were added to 100 μL aliquots of [^{57}Co]VB_{12} solution. A total of 100 μL of a 10 IU/mL solution of porcine intrinsic factor (Sigma) was added and

the tubes incubated for 20 min. A total of 200 μL of a charcoal suspension (2.5% charcoal/0.5% BSA/pH 7.5) was then added, and the tubes were vortexed and centrifuged at 5000 rpm for 5 min. The amount of radioactivity in each fraction was determined in a γ-counter, and the 50% binding inhibition values were calculated for each derivative. A similar procedure was used for the non-IF binding study, in which non-IF (porcine gastric mucosa, Sigma) was substituted for IF in the above method.

Polysciences Particle Derivatives. To 1 mL of Polysciences YG 50 nm particles (25 mg/mL) was added adipic dihydrazide cobalamin derivative (10 mg) followed by 1-ethyl-3-(3-dimethylaminopropyl) carbodiimide (EDAC, 16 mg), and the mixture was stirred for 4 h. Glycine (100 mg) in 1 mL of 50 mM sodium carbonate solution was added, and the mixture stirred overnight. The nanoparticles were precipitated using 1.0 M $CaCl_2$ (300 μL) followed by centrifugation at 10 K for 5 min. The final pellet was resuspended in 1 M EDTA (1 mL) and rewashed three times. The pellet was resuspended in 1 M EDTA (1 mL) and dialyzed vs water overnight.

Cell Transport Studies. The Caco-2 cell line was obtained from the American Type Culture Collection. Cells were grown in Dulbecco's modified Eagle's medium (DMEM) containing 4.5 g/L glucose and 10% foetal bovine serum in an atmosphere of 5% CO_2. For transport experiments, cells were grown in T75 flasks until 80−100% confluent. Following washing with PBS, adherent cells were removed by treatment with 10 μg/mL trypsin in 10 mM EDTA. Cells were immediately diluted 15-fold into fresh culture medium and counted. Cultures were seeded at $(0.5-1.0) \times 10^5$ cells/mL in 24 well/plate transwells (Costar) and grown for 12−24 days. Costar transwells had a membrane insert size of 6.5 mm and a pore size of 0.4 μM, with an apical chamber volume of 0.25 mL and a basal chamber volume of 1 mL. Cells generally reached confluence within 10 days. Transepithelial resistance (TEER) measurements were made of monolayers and only cultures with greater than 250 ohms/cm^2 were used for experimentation. Prior to nanoparticle experiments, all cell cultures were checked for VB_{12} transport.

[^{57}Co]VB_{12} uptake experiments were conducted on 18−19 day old cultures. Briefly, medium was removed from both the apical and basal chamber, and then 1 mL of medium was added to the basolateral chambers. Cells in the apical chamber were washed once with PBS and a solution containing 2 μL of [^{57}Co]VB_{12}, 1 ng of cold VB_{12}, and 2 IU of IF in medium was added per apical well (250 μL). Cells were incubated overnight at 37 °C, and then apical and basal medium was removed and counted. Cells were washed once with PBS and fresh medium was added to the apical and basolateral wells. Cells were incubated overnight and the medium again removed and counted.

Preparation of VB_{12}-Modified Polysciences Nanoparticles. Fluorescent YG nanoparticles were obtained from Polysciences. These nanoparticles contain a fluorescein-like fluorophore and have surface carboxylic acids groups suitable for chemical modification and VB_{12}-derivatization. Unwashed Polysciences nanoparticles were modified with VB_{12} by activation with EDAC in the presence of **12** or an adipic dihydrazide derivative of eVB_{12} (*5*). Following derivatization, unreacted, EDAC-modified carboxyl groups were blocked by incubation with 50 mg/mL glycine in 0.1 M carbonate buffer, pH 9.5. Nanoparticles were washed 5 times by precipitation with 0.1 M $CaCl_2$, centrifugation (5′, 5K), and resuspension in 50 mM EDTA. After the fifth wash, the particles were dialyzed extensively against distilled water. Particles were analyzed for VB_{12} loading using visible absorption spectroscopy. Adipic eVB_{12} particles were coated at 11.5 μg of VB_{12}/mg particle and adipic 5′-VB_{12} particles were coated at 7.8 μg VB_{12}/mg particle.

Binding/Uptake and Transport of Nanoparticles by Caco-2 Cells. Apical and basal chambers of Caco-2 cell cultures (22−24 day old) which were shown to be positive for [^{57}Co]VB_{12} transport were washed once with buffer (PBS) and the basolateral wells were refed with 1 mL of complete medium. Dilutions of fluorescent Polysciences nanoparticles (0.25 mL) were added to the apical chamber of triplicate wells, and the cultures were incubated at 37 °C overnight. VB_{12}-coated particles, prepared as described previously, were then added to the wells.

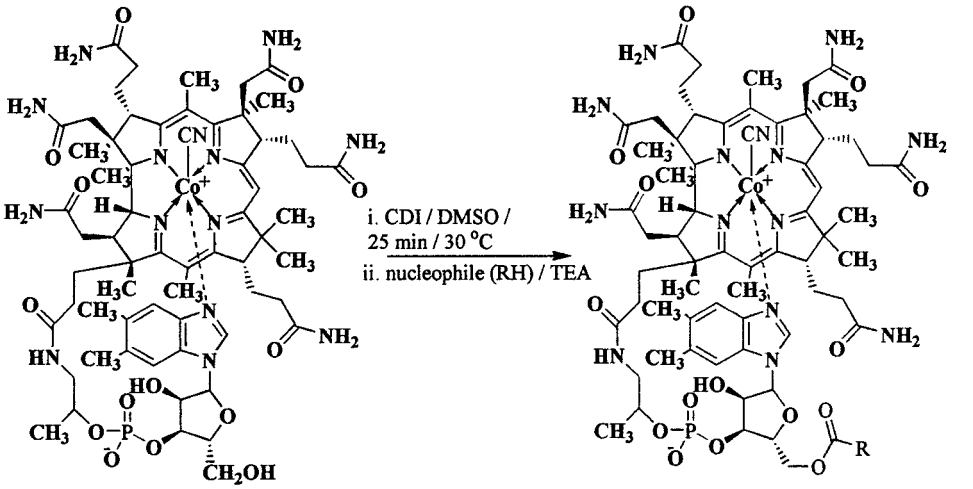
Following overnight incubation, apical and basal medium was removed from the wells and the cells washed with PBS (three times). The apical and basal chambers were assayed for bound, internalized, membrane associated, and transported fluorescence. Bound fluorescence was assessed by measuring the fluorescence release following incubation of the cultures with 5 mM EDTA, pH 5.0, for 15 min to release receptor-bound IF−VB_{12} or IF−VB_{12} nanoparticle complexes. Internalized fluorescence was determined following EDTA treatment (surface bound) and lysis of the cells by incubation with a solution of 2% SDS and 50 mM EDTA, pH 8.0, for ≥30 min at room temperature. Finally, the membrane inserts were excised from the transwell, and the fluorescence associated with the filter was assessed by lysis of the nanoparticles with 50% acetone to release the entrapped fluorochrome. All samples were adjusted to pH 8.0 with 1 M Tris·HCl, pH 9.0, prior to fluorescence measurement. Fluorescence was measured on a Bio-Tek Instruments Microplate Fluorescence Reader (FL500) at Ex_{485nm} and Em_{530nm} for YG nanoparticles. Data are expressed as the percentage of the total fluorescence added to the wells.

RESULTS AND DISCUSSION

Preparation of Cobalamin Derivatives. It was found that derivatives of vitamin B_{12} could readily be formed by first activating the ribose-5′-hydroxyl group using 1,1′-carbonyldiimidazole (CDI), 1,1′-carbonyldi-(1,2,4-triazole) (CDT), or di(1-benzotriazolyl) carbonate (DBTC) in dimethyl sulfoxide followed by addition of a nucleophile (Scheme 1). Use of hexylamine as nucleophile afforded **2** in 28% with DBTC, in 42% with CDI, and in 95% with CDT. Although CDT was found to be the most effective activating reagent, the cheaper CDI gave satisfactory yields of most derivatives made.

This functionalization of vitamin B_{12} is particularly useful in that a large variety of nucleophiles can potentially be employed to furnish novel cobalamin derivatives. In this work, alkylamines, diaminoalkanes, and acid dihydrazides were used as nucleophiles to provide a carbamate linkage to the cobalamin. Carbamates are only poorly cleaved by esterases; thus, the derivatives are stable in vivo. They are also suitable for oral delivery of drugs/proteins as the carbamate functionality is not cleaved in the stomach, being stable at pH 1 (>99% stability at 5 h). The derivatives are not stable, however, in a basic environment above pH 12 (71% stability at pH 13 after 2 h, compared with >98% stability at pH 12 after 5 h). We envisage that a carbonate linkage would be suitable in instances where a cleavable linkage is required as carbonates are more rapidly hydrolyzed by esterases and analogous carbonates could be prepared using the carbamate methodology developed here.

Scheme 1. Derivatization of Ribose-5′-Hydroxyl Group



1

2 R = $HN(CH_2)_5CH_3$
3 R = $HN(CH_2)_{11}CH_3$
4 R = $HN(CH_2)_{13}CH_3$
5 R = $HN(CH_2)_{15}CH_3$
6 R = $HN(CH_2)_{17}CH_3$
7 R = $HN(CH_2)_2NH_2$
8 R = $HN(CH_2)_4NH_2$
9 R = $HN(CH_2)_6NH_2$
10 R = $HN(CH_2)_{12}NH_2$
11 R = $HNNHCO(CH_2)_2CONHNH_2$
12 R = $HNNHCO(CH_2)_4CONHNH_2$
13 R = $HNCH_2COOMe$
14 R = $HNCH_2COOH$
15 R = CH_2CH_2COOH

Competitive Binding with IF and Non-IF. The cobalamin derivatives were evaluated for their binding to IF and non-IF in a competitive assay that measures the binding relative to cyanocobalamin. For use of the derivatives as oral delivery agents of proteins, peptides, and nanospheres, a high affinity for IF and non-IF is essential. A higher affinity for IF than the more commonly applied *e*-VB_{12} monoacid (30% or 3.3 pmol) would be desirable. The results of the binding studies are given in Figures 1−3 and summarized in Tables 1 and 2.

The smaller derivatives can be seen to retain much of the binding affinity for IF, particularly the 1,2-diaminoethane (45% or 2.2 pmol) and adipic dihydrazide (48% or 2.1 pmol) derivatives. A trend is observed in the alkylamine derivative series in that binding affinity decreases with increasing chain length. Nevertheless, high affinity is conserved until alkyl chains greater than C12 (dodecylamine) are used and the reduced IF affinity with longer chain length is most likely an artifact of the increased hydrophobicity. This is indicated by high IF affinities for lengthy conjugates determined in previous work (*3*). These levels of IF binding are similar in most cases to the *e*-monoacid cobalamin derivative (3.3 pmol) and are significantly higher than the *b*-monoacid (∼1% or ∼100 pmol) or the *d*-monoacid (∼0.1% or ∼1000 pmol).

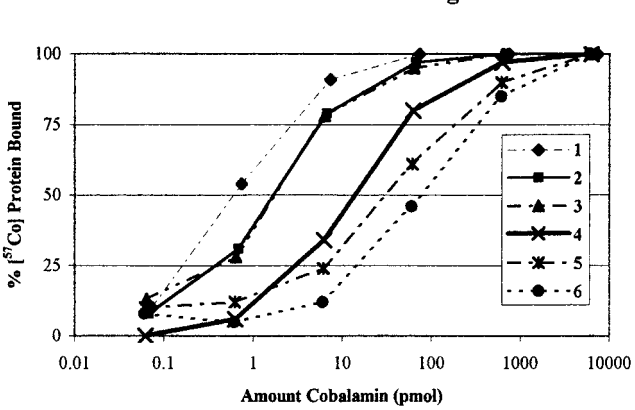


Figure 1. IF binding curve for alkylamine derivatives **2**−**6**. To obtain the data, a quantity of IF that would bind approximately 1 pmol of VB_{12} was mixed with 1 pmol of [^{57}Co]-VB_{12} and 0.01−10000 pmol of unmodified VB_{12} or VB_{12} derivative. The mixture was diluted with BSA/phosphate buffer and incubated at room temperature for 20 min. Free VB_{12} was adsorbed onto BSA-coated charcoal, and the protein-bound radioactivity in the supernatant fraction was measured.

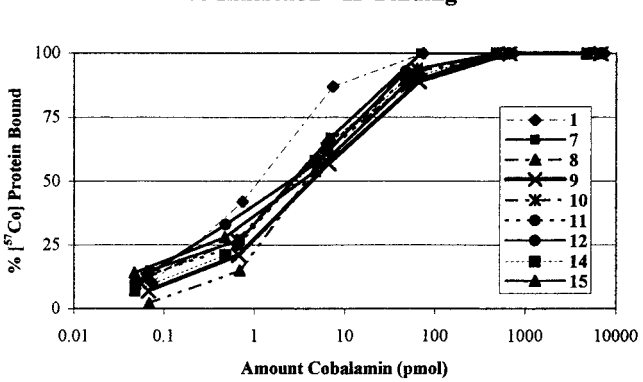


Figure 2. IF binding curve for cobalamin derivatives **7**−**15**. To obtain the data, a quantity of IF that would bind approximately 1 pmol of VB_{12} was mixed with 1 pmol of [^{57}Co]-VB_{12} and 0.01−10000 pmol of unmodified VB_{12} or VB_{12} derivative. The mixture was diluted with BSA/phosphate buffer and incubated at room temperature for 20 min. Free VB_{12} was adsorbed onto BSA-coated charcoal, and the protein-bound radioactivity in the supernatant fraction was measured.

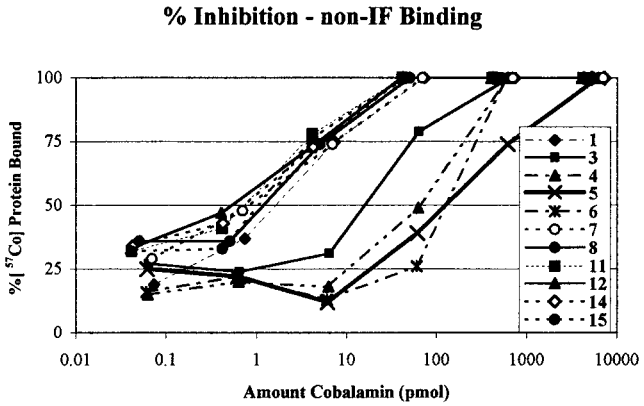


Figure 3. non-IF binding curve for cobalamin derivatives. To obtain the data, a quantity of non-IF that would bind approximately 1 pmol of VB_{12} was mixed with 1 pmol of [^{57}Co]-VB_{12} and 0.01−10000 pmol of unmodified VB_{12} or VB_{12} derivative. The mixture was diluted with BSA/phosphate buffer and incubated at room temperature for 20 min. Free VB_{12} was adsorbed onto BSA-coated charcoal, and the protein-bound radioactivity in the supernatant fraction was measured.

Table 1. Binding of VB_{12} Derivatives with IF Relative to Cyanocobalamin

derivative	50% binding inhibition for [^{57}Co]VB_{12}[a]	% relative IF binding[b]
1	1	100
2	2.8	36
3	2.9	34
4	22	4.5
5	48	2.1
6	134	0.75
7	2.2	45
8	3.3	30
9	3.8	26
10	2.3	43
11	2.4	42
12	2.1	48
14	2.5	40
15	2.8	36

[a] The binding inhibition quantity is that amount (pmol) of cobalamin derivative required to inhibit by 50% the binding of 1 pmol of [^{57}Co]VB_{12}. [b]The relative IF binding value (percent) is obtained by dividing 100 by the 50% binding inhibition quantity.

Table 2. Binding of VB_{12} Derivatives with Non-IF Relative to Cyanocobalamin

derivative	50% binding inhibition for [^{57}Co]VB_{12}[a]	% relative non-IF binding[b]
1	1	100
3	10	10
4	42	2.4
5	83	1.2
6	84	1.2
7	0.78	128
8	0.9	111
11	0.72	139
12	0.54	185
14	0.75	133
15	0.9	111

[a] The binding inhibition quantity is that amount (pmol) of cobalamin derivative required to inhibit by 50% the binding of 1 pmol of [^{57}Co]VB_{12}. [b]The relative Non-IF binding value (percent) is obtained by dividing 100 by the 50% binding inhibition quantity.

Since the yield of *e*-monoacid is low (∼6%), we therefore suggest that the ribose-5′-carbamate derivatives of cobalamin should be used for the production of bioconjugates for oral delivery in preference to a monoacid derivative.

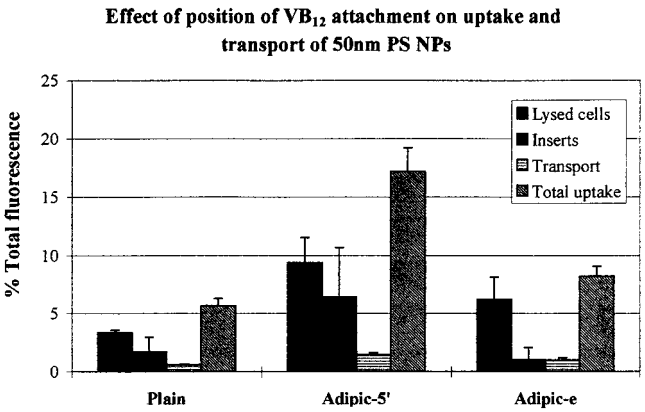


Figure 4. Uptake and transport of cobalamin derivatives in Caco-2 cells. To obtain the data, 625 μg of Polysciences nanoparticles coated with 625 ng VB_{12} were added to a monolayer of Caco-2 cells in 12 mm COSTAR Transwells (0.3 μm pore size) in triplicate. Cells were incubated with the particles overnight. The apical solution was removed, and the cell layer washed with PBS. The cell layer was lysed with SDS, and the inserts excised. The amount of nanoparticles present in the lysed cell layer, the inserts, and the basal chamber was determined by fluorescence measurement. Total uptake was calculated as the sum of all internalized and transported material.

Further, the shorter derivatives prepared possessed similar or even greater affinity for non-IF compared with cyanocobalamin, although the longer chain alkylamine derivatives again showed reduced affinity with increasing chain length.

Cell Transport Studies. In the cell transport studies, adipic acid dihydrazide derivatives of cobalamin were attached to 50 nm Polysciences particles using 1-ethyl-3-(3-dimethylaminopropyl) carbodiimide (EDAC) in water. The transport of the particles across Caco-2 cells was then investigated (Figure 4). Surface modification of the particles with either the 5′-O-adipic dihydrazide or the *e*-monoacid adipic dihydrazide cobalamin derivatives significantly enhanced transport of the nanoparticles when compared with the unmodified particles. The adipic dihydrazide-5′-O derivative was approximately twice as effective as the corresponding *e*-monoacid adipic dihydrazide derivative even though the particles had a lower degree of substitution.

SUMMARY

Twelve novel ribose-5′-O derivatives of vitamin B_{12} have been prepared and their bioactivity measured. The derivatives were obtained by activation of the hydroxyl group with CDI, CDT, or DBTC in moderate to high yield, with CDT giving the highest yield. This method of derivatization of cobalamin provides higher yields and greater scope than the traditional monoacid methodology. Furthermore, the 5′-O derivatives had similar or higher affinity for IF and non-IF compared with the corresponding *e*-monoacid derivatives.

Attachment of 5′-O-adipic dihydrazidyl cobalamin to 50 nm Polysciences nanoparticles dramatically enhanced uptake of the nanoparticles relative to unmodified particles. Use of 5′-O-adipic dihydrazidyl cobalamin as delivery agent for nanoparticles resulted in twice the level of transport as the use of the *e*-adipic dihydrazidyl cobalamin derivative.

Following this initial investigation, we intend to couple cobalamin to nanoparticles and peptides using various linkers on the 5′-OH position and investigate the oral activity of the resultant bioconjugates. Overall it appears that the employment of 5′-OH derivatives of cobalamin

in the preparation of bioconjugates provides a viable route to the successful oral delivery of proteins and peptides.

ACKNOWLEDGMENT

We would like to acknowledge Adventis Research & Technology for their financial support for these studies.

LITERATURE CITED

(1) Russell-Jones, G. (1996) Utilisation of the Natural Mechanism for Vitamin B_{12} Uptake for the Oral Delivery of Therapeutics. *Eur. J. Pharm. Biopharm. 42*, 241.
(2) Russell-Jones, G. J. (1996) The potential use of receptor-mediated endocytosis for oral drug delivery. *Adv. Drug Delivery Rev. 20*, 83.
(3) Habberfield, A., Jensen-pippo, K., Ralph, L., Westwood, S. W., and Russell-Jones, G. J. (1996) Vitamin B_{12}-mediated uptake of erythropoietin and granulocyte colony stimulating factor in vitro and in vivo. *Int. J. Pharm. 145*, 1.
(4) Russell-Jones, G. J., Westwood, S. W., Farnworth, P. G., Findlay, J. K., and Burger, H. G. (1995) Synthesis of LHRH Antagonists Suitable for Oral Administration via the Vitamin B_{12} Uptake System. *Bioconjugate Chem. 6*, 34.
(5) Russell-Jones, G. J., Westwood, S. W., and Habberfield, A. D. (1995) Vitamin B_{12} Mediated Oral Delivery Systems for Granulocyte-Colony Stimulating Factor and Erythropoietin. *Bioconjugate Chem. 6*, 459.
(6) Pathare, P. M., Wilbur, D. S., Heusser, S., Quadros, E. V., McLoughlin, P., and Morgan, A. C. (1996) Synthesis of Cobalamin-Biotin Conjugates That Vary in the Position of Cobalamin Coupling. Evaluation of Cobalamin Derivative Binding to Transcobalamin II. *Bioconjugate Chem. 7*, 217.
(7) Hogenkamp, H. P. C., Barker, H. A., and Mason, H. S. (1963) An Electron-Spin Resonance Study of Coenzyme B_{12}. *Arch. Biochem. Biophys. 100*, 353.
(8) Brady, R. O., and Barker, H., A. (1961) Recovery of Enzymatic Activity of Reduced Taka_Amylase A and Reduced Lysozyme by Air Oxidation. *Biochem. Biophys. Res. Commun. 4*, 373.
(9) Toraya, T., Ohashi, K., Ueno, H., and Fukui, S. (1975) Preparation, Properties and Biological Activities of Succinyl Derivatives of Vitamin B_{12}. *Bioinorg. Chem. 4*, 245.
(10) Habberfield, A. D., Kinstler, O. B., and Pitt, C. G. (1996) *Conjugates of Vitamin B_{12} and Proteins*. Patent 5,574,018, 11/1996.
(11) Toraya, T., and Fukui, S. (1980) The Synthesis of Several Immobilised Derivatives of Vitamin B_{12} Coenzyme and Their Use As Affinity Adsorbents for a Study of Interactions of Diol Dehydrase with the Coenzyme. *J. Biol. Chem. 255*, 3520.
(12) Castle, W. B. (1975) In *Cobalamin: Biochemistry and Pathophysiology* (B. M. Babior, Ed.) John Wiley & Sons, New York.

BC990086P

TECHNICAL NOTES

Preparation and Characterization of Domoic Acid−Protein Conjugates Using Small Amount of Toxin in a Reversed Micellar Medium: Application in a Competitive Enzyme-Linked Immunosorbent Assay

Philippe Branaa,[†] Jérôme Naar,[†] Mireille Chinain,[†] and Serge Pauillac*[,†,‡]

Unité d'Océanographie Médicale, Institut de Recherches Médicales Louis Malardé, PO Box 30, Papeete, Tahiti, French Polynesia, Unité d'Immunocytochimie, CNRS URA 359, Département d'Immunologie, Institut Pasteur, Paris, France. Received April 12, 1999; Revised Manuscript Received August 4, 1999

With the aim of producing novel antibodies to domoic acid (DA), an original, rapid, and simple procedure for preparing minute amount of hapten−protein conjugates was developed. The amide-bond-generating mixed anhydride method of Erlanger was performed using 0.32−0.64 μmol of DA in a reversed micellar medium allowing strong carrier haptenization as determined by spectrophotometric measurement. Bovine serum albumin (BSA) and ovalbumin (OVA) conjugates were, respectively, used for immunization of BALB/c mice and antibody screening by enzyme-linked immunosorbent assay (ELISA). Specific polyclonal antibodies were produced upon multiple injections of $(DA)_{17}$−BSA conjugate administered by three different routes: (i) intraperitoneal (i.p.), (ii) intraperitoneal + subcutaneous (i.p. + s.c.), (iii) footpad (f.p.). The i.p. route induced antisera of higher titer (1:350000) than did the other protocols (approximately 1:72900) and was selected throughout further experiments. Using a competitive ELISA format with a peroxidase immunoconjugate and a chromogenic substrate, no significant cross-reactivity was observed with glutamic acid, aspartic acid and kainic acid (KA), a structural analogue of DA. The sensitivity of this assay could be enhanced by 1 order of magnitude by using a β-galactosidase immunoconjugate with a fluorogenic substrate while preserving DA specificity. The calculated dissociation constant (K_D) for the interaction of the antibodies with free DA was 5×10^{-7} M (chromogenic assay) and 5×10^{-8} M (fluorogenic assay). Using the optimized assay the limit of detection (LOD) and the limit of quantitation (LOQ) in the ELISA buffer were 1.4 and 3 ng/mL, respectively. Moreover this assay was found applicable for measuring DA levels in spiked mussel extracts precleaned through a solid-phase extraction column, as a very good correlation ($r^2 = 0.96$) was observed between the actual amounts of DA added and amounts detected by ELISA. Thus, accurate determinations of DA in clean extracts could be achieved between 2 and 180 ng/mL in spiked samples which corresponds to 0.02−1.8 μg/g of original mussel tissue. Owing to the regulation limits of 20 μg DA/g of shellfish tissue, these extraction and assay procedures should provide a useful complement to the standard HPLC analytical technique currently employed in monitoring DA in shellfish tissue.

INTRODUCTION

Domoic acid (DA),[1] a naturally occurring amino acid produced by the marine diatom *Pseudonitzschia pungens*, is the most potent compound of a group of structurally related neurotoxins collectively referred to as kainoids after the name of the original member of the group, kainic acid (KA), isolated from the red macroalga *Digenea simplex* (Murakami et al., 1953). Since the first outbreak of food poisoning that occurred in Canada in 1987, DA has been found to accumulate in edible shellfish (Wright et al., 1989; Iverson et al., 1989; Quilliam and Wright, 1989), causing upon ingestion a human syndrome called Amnesic Shellfish Poisoning (ASP). The clinical picture is characterized by a gastrointestinal distress, followed by neurological symptoms such as headache, confusion, disorientation, and severe deficits in short-term memory (Teitelbaum et al., 1990; Perl et al., 1990). At the molecular level, kainoids have been found to exert

* To whom correspondence should be addressed. Phone: +689 41 64 69. Fax: +689 43 15 90. E-mail: spauillac@malarde.pf.
† Unité d'Océanographie Médicale.
‡ Unité d'Immunocytochimie.

[1]Abbreviations: AOT, aerosol OT or sodium bis(2-ethylhexyl) sulfosuccinate; BSA, bovine serum albumin; CFA, complete Freund's adjuvant; DA, domoic acid; DMSO, dimethylsulfoxyde; ELISA, enzyme-linked immunosorbent assay; f.p., footpad; GAM-βGZ, goat anti-mouse IgG heavy and light chain-β-galactosidase conjugate; GAM-PO, goat anti-mouse IgG heavy and light chain-horseradish peroxidase conjugate; IFA, incomplete Freund's adjuvant; i.p., intraperitoneal; i.p. + s.c., intraperitoneal + subcutaneous; KA, kainic acid; KLH, keyhole limpet hemocyanin; LOD, limit of detection; LOQ, limit of quantitation; 4-MUG, 4-methyl umbelliferyl β-D-galactoside; OPD, *o*-phenylenediamine; OVA, egg albumin; PBS, phosphate-buffered saline; PBS-M, 5% skim milk powder in PBS; PBS-T, PBS containing 0.1% Tween 20; PBS-TMB, PBS containing 0.1% Tween 20 plus 1% skim milk powder and 1% BSA; PL, poly-DL-lysine (average mol wt 77 000); TLC, thin-layer chromatography on silica gel.

10.1021/bc990041o CCC: $18.00 © 1999 American Chemical Society
Published on Web 10/08/1999

membrane depolarizing and neurodegenerative properties via the glutamatergic kainate receptor (Debonnel et al., 1989; Stewart et al., 1990).

Due to public health requirements and seafood industries interests, DA detection has been developed using the mouse bioassay (Iverson et al., 1989) and more specific assays based upon either instrumental method (gas or liquid chromatography coupled or not to mass spectrometry and capillary electrophoresis), or pharmacological and immunochemical techniques [see, for review, Wright and Quilliam (1995)]. Human toxicological data collected from the 1987 ASP Canadian incident have led to the establishment of generally admitted DA regulatory limits of 20 μg/g shellfish tissue. These safe limits, lower than the sensitivity of the mouse bioassay (Grimmelt et al., 1990), together with ethical and practical issues, contribute to exclude its routine use. Indeed routine monitoring of shellfish extracts requires high throughput sample screening with great specificity and sensitivity combined with simplicity, all requirements that only meet with automated binding assays or enzyme-linked immunosorbent assays (ELISA). However, in their present form, the disadvantage of receptor-binding assays is the use of radioactive tracers which imposes the purchase of expensive radiolabeled compounds and necessitates the disposal of radioactive waste. Although specific polyclonal antibodies have been produced (Newsome et al., 1991; Smith and Kitts, 1994, 1995; Osada et al., 1995; Garthwaite et al., 1998), until now there is no fully validated screening immunoassay commercially available for shellfish naturally contaminated with DA. Therefore, immunochemical techniques are to be most actively pursued in order to design a laboratory antibody-based assay that could be scaled up to fit the requirement of a routine cost-effective mass screening of shellfish prior to consumption.

This work describes the production of novel antibodies to DA using fully characterized DA−carrier conjugates obtained by a rapid and simple procedure we have recently designed (Pauillac et al., 1998). This paper is the first to document the production of antibodies to DA using very tiny amount of haptenic material (100−200 μg) in a reversed micellar medium. A preliminary application of these antibodies to competitive ELISA provides the basis to the development of a rapid, simple, specific, and sensitive assay for DA contaminated shellfish.

MATERIALS AND METHODS

Preparation of Conjugates. All chemical reagents, unless otherwise stated, were purchased from Sigma Chemicals Co. (St. Louis, MO). High-quality grade solvents obtained from Prolabo (France) were dried according to standard procedures.

Conjugates were prepared according to a modified version of the mixed anhydride coupling method of Erlanger et al. (1957) as recently described by Pauillac et al. (1998). Briefly, 0.321 or 0.642 μmol of DA were dissolved in 20 μL of dry dimethylsulfoxyde (DMSO), and then a 10-fold molar excess of tributylamine and isobutyl chlorocarbonate was added. The formation of the mixed anhydride was allowed to proceed for 30 min at room temperature. The reaction was monitored by thin-layer chromatography (TLC) run on silica gel 60 F_{254}-precoated plastic foils from Merck (Darmstadt, Germany) using CH_2Cl_2-MeOH (95:5) as developing solvent. UV illumination of the chromatogram showed conversion of DA, which remains at the origin ($R_f \approx 0$), to the mixed anhydride ($R_f = 0.77$) to an extent greater than 95%. The conjugation of activated DA to carriers was carried out in the system of reversed micelles of aerosol OT [AOT or sodium bis(2-ethylhexyl) sulfosuccinate] in heptane (Kabanov et al. 1989; Yatsimirskaya et al., 1993) with relevant modifications for miniaturization purpose and high haptenization yield (Pauillac et al., 1998). Three carriers were used throughout: bovine serum albumin (BSA), ovalbumin (OVA), and poly-DL-lysine (PL, average mol wt 77 000) providing an initial hapten/protein molar ratio around 100.

Control experiments run in parallel, consisting in carrier alone and carrier mixed with non-activated DA, were incubated in the reversed micellar medium under identical conditions.

All carriers in the vials (assay and control) were recovered by acetone precipitation. The precipitates were finally resuspended in 1 mL of distilled water, filter sterilized (0.22 μm), dispensed into sterile tubes, then freeze-dried overnight. Tubes were generally stored at −20 °C until use but some of them were kept at room temperature for subsequent analysis.

Conjugates Analysis. For analytical purpose, carriers from control and assay were resuspended in 1 mL of PBS. Carrier haptenization was assessed spectrophotometrically through a 1 cm light path quartz cuvette with a dual beam spectrophotometer (UV 160A, Shimadzu, Japan). Absorption spectra of all samples were recorded between 200 and 300 nm using a 1:3 (BSA and OVA conjugates) or 1:2 (PL conjugates) dilution in PBS. Concentrations of hapten (read at $\lambda_{max} = 242$ nm) and protein carriers (read at $\lambda_{max} = 280$ nm) were determined according to either standard curves with linear regression in the range 0−20 μg/mL of DA or previously reported extinction coefficients (DA, $\epsilon = 83.83$ mg^{-1} cm^2; BSA, $\epsilon = 0.66$ mg^{-1} cm^2; OVA, $\epsilon = 0.735$ mg^{-1} cm^2). After molar conversion, the degree of hapten conjugation was expressed by the hapten/carrier ratio of the samples, i.e., epitope density of the conjugates. For these calculations, total PL content was considered assuming complete recovery of the conjugate.

Mice Immunization. Three groups of two female BALB/c mice (6−8 weeks of age) were immunized by three different routes: intraperitoneal (i.p.), intraperitoneal + subcutaneous (i.p. + s.c.), and footpad (f.p.). All six animals received a total of six injections of 50 μg $(DA)_{17}$−BSA conjugate emulsified in 100 μL of PBS/adjuvant mixture (1:1). The first injection was made in Freund's complete adjuvant (FCA), and the following in Freund's incomplete adjuvant (FIA) at 3−4 week intervals. Mice were sequentially bled from the retroorbital venous system and pooled sera from each group were tested for anti-DA antibody activity.

Enzyme Immunoassays. The following buffers were used throughout ELISA experiments: phosphate-buffered saline (PBS, 0.01 M KH_2PO_4/K_2HPO_4−150 mM NaCl, pH 7.2) for coating, 5% skim milk powder in PBS as blocking buffer (PBS-M), PBS containing 0.1% Tween 20 (PBS-T) for washing steps, and this latter buffer supplemented with 1% skim milk powder and 1% BSA (PBS-TMB) for dilution of reagents (sera, immunochemicals, or DA standards). All immunochemical reagents, unless otherwise stated, were purchased from Boehringer Mannheim (Indianapolis, IN).

Flat-bottomed polystyrene 96-well Maxisorp Immunoplates (Nunc, Roskilde, Denmark) were coated with 100 μL of $(DA)_{10}$−OVA conjugate (20 ng/mL−1 μg/mL) in PBS by incubation for 1 h at 37 °C then overnight at 4 °C. They were then washed five times with PBS, and the

remaining active sites were blocked by addition of 250 μL of PBS-M. All subsequent incubation steps, unless otherwise stated, were carried out 1 h at 37 °C in precoated plates, which were thoroughly washed with PBS-T after each step.

Kinetics Experiments. For kinetics experiments, pooled sera collected at the indicated time from each 2-mice immunization group were diluted 1:2500 and applied to the plates at 100 μL/well. Bound antibodies were revealed by incubation with 100 μL of goat anti-mouse IgG peroxidase conjugate (GAM-PO) diluted 1:3000 followed by the addition of 100 μL of *o*-phenylenediamine (OPD) as a commercial substrate solution (FAST OPD, Sigma). After 30 min at 37 °C, the enzymatic reaction was terminated by adding 50 μL of 2 M H_2SO_4 and the absorbance at 492 nm was measured using a Multiskan Plus Titerteck (Flow Laboratories, Puteaux, France).

Titration Experiments. For titration experiments, serially diluted pooled immune sera collected after the last boost or control sera (1:300−1:1968300 dilutions) were applied to the plates at 100 μL/well. Bound antibodies were revealed by the successive incubations with GAM-PO and OPD, and the enzymatic reaction terminated as described above after 10 min at 37 °C.

Competitive Experiments. Competitive experiments were conducted using pooled sera collected one week after the last boost from mice immunized according to the i.p. protocol. Pooled sera (1:350000 final dilution) were first preincubated overnight at +4 °C with an equal volume of various concentrations of inhibitors (DA, KA, glutamic acid, and aspartic acid). Samples of these mixtures were transferred (100 μL/well) onto DA-OVA-precoated plates (250 ng/mL). After incubation and washing steps, the antibodies associated with the plates were revealed as described above. In another set of experiments, coating concentration was reduced to 20 ng/mL and bound antibodies were revealed using a fluorescence-based amplification signal by the successive addition of goat anti-mouse IgG−β-galactosidase conjugate (GAM−βGZ; 1:4000 dilution) and 4-methyl umbelliferyl β-D-galactoside (4-MUG) at saturation in 0.1 M phosphate buffer, pH 7.2. Following a 30 min incubation, fluorogenic substrate change was measured using a Dynatech Microfluor Reader with excitation at 365 nm and emission at 450 nm. Recorded values are expressed as relative fluorescence units.

Using both amplification systems, the signals obtained in the presence of various inhibitor concentrations and without inhibitor (maximal signal) are referred to as B and B_o, respectively. The limit of detection (LOD) of each format assay was therefore calculated assuming a decrease of 3 standard deviations from the mean value of B_o is significant ($n = 12$). Standard curves were generated by plotting the percentage of maximal signal (% B/B_o) against the log of free DA concentrations, using the four parameter logistic fitting model provided by the MultiCalc package program (EG & G−Wallac). The limit of quantitation (LOQ) was defined as the DA concentration necessary to produce a 80% decrease in B_o (IC_{80}).

Finally, the dissociation constant (K_D) of mice antibodies binding to DA was estimated by calculating the slope of the regression line obtained using the simplified mathematical equation of Klotz (1953) proposed by Friguet et al. (1985).

Measurement of DA Levels in Rapid Mussel Extracts. Rapid extraction of blue mussels (*Mytilus edulis*) was performed according to the method developed by Quilliam et al. (1998). Briefly 4 g of uncontaminated mussels was mixed with 16 mL of MeOH−H_2O (1:1) and homogenized thoroughly using a Brinkman Polytron. Particulate material was eliminated by centrifugation at 5000*g* for 10 min and the supernatant filtered through a dry methanol-compatible 0.5 μm filter unit. Five milliliter samples (1 g tissue equivalent) of this clear supernatant were either used without additional treatment (crude extract) or precleaned by passing it through a strong anion-exchange solid-phase extraction column (Supelclean LC−SAX, Supelco Inc., Bellefonte, PA). Following several washing steps, putative DA was eluted from the column using MeOH/H_2O/HCOOH (75:23:2). These precleaned extracts were evaporated to dryness under nitrogen atmosphere then reconstituted in 5 mL of MeCN/H_2O (1:9). Finally, 1 mL of this suspension (0.2 g tissue equivalent) and 1 mL of crude extract (0.2 g tissue equivalent) were spiked with 4 μg of DA analytical standard (DACS-1C, NRC−CNRC, Institute for Marine Biosciences, Halifax, Canada) to generate concentrations ranging from 4000 to 2 ng/mL by serial dilutions in MeCN/H_2O (1:9). The same dilutions of DA analytical standard were directly prepared in MeCN/H_2O (1:9) to serve as calibration solutions. These spiked samples or calibration solutions were mixed with an equal volume of pooled mice immune sera (1:400000 final dilution) and incubated overnight at +4 °C. DA levels were determined in triplicate 50 μL volumes of these mixtures, using the competitive ELISA format and the optimized fluorogenic amplification system as described above.

RESULTS AND DISCUSSION

Preparation and Analysis of the Conjugates. Conjugates were prepared in a reversed micellar medium according to the procedure described in the Materials and Methods. Their recovery and substitution ratio were carefully checked spectrophotometrically by incorporating controls in which carriers have been incubated under identical conditions with nonactivated hapten. DA is a chromophore with a unique absorption peak at 242 nm and a molecular extinction coefficient of 83.83 mg^{-1} cm^2 at pH 7 (Falk et al., 1989); therefore, proteins (BSA and OVA) but not the polyamino acid (PL) could be also estimated in the conjugates by UV absorbance at 280 nm (aromatic amino acids).

Consistent with former experiments (Pauillac et al., 1998), carrier protein recovery in control and assay tubes was found to be greater than 95%, hence, the whole carrier content (proteins or PL) was taken into account in the calculation of the hapten/carrier molar ratio (i.e., epitope density) of the samples. Another clue is provided by the demonstration that differential absorption spectra of the conjugates and carriers recovered from control experiments were quite similar to those of the free hapten (data not shown). Using a 100:1 hapten to carrier initial molar ratio, the epitope density of OVA, BSA, and PL conjugates was estimated to be around 10, 20, and 30, respectively. For these calculations the assumption was made that the extinction coefficient of DA is not altered by the conjugation process. This technique proceeding in a reversed micellar medium was initially set up for lipophilic carboxylic haptens (Pauillac et al., 1998) but proved to be likewise valuable for hydrophilic haptens (water solubility of DA is 7.6 mg/mL according to Falk et al., 1991). Compared to relatively high hapten quantities (1−12.4 mg of DA) used in previous studies (Newsome et al., 1991; Smith and Kitts, 1994, 1995; Garthwaite et al., 1998), a significant improvement in preparation of well-defined DA−protein conjugates was achieved by our method. Starting from 200 μg of DA, 435 μg of

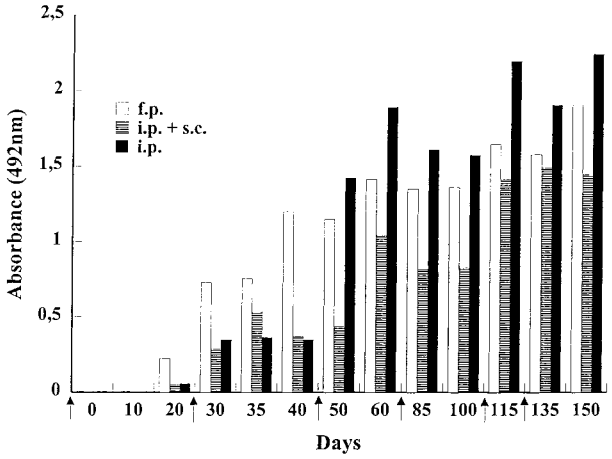


Figure 1. Kinetics of anti-DA antibodies production. Pooled sera from each group were diluted 1:2500 in PBS-TMB and tested for their reactivity onto microtiter plates coated with 1 μg/mL of $(DA)_{10}$−OVA conjugate in PBS. The reaction was developed following the successive incubations with GAM-PO and OPD. Each bar represents the mean of triplicate assays, which varied by no more than 5%. Mice immunization groups: f.p. (open bars), i.p.+ s.c.(hatched bars) and i.p.(black bars). Arrows indicate priming and subsequent boosts.

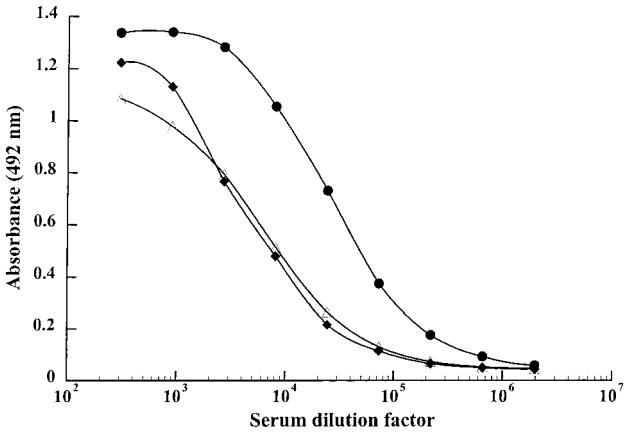


Figure 2. Titration of pooled mice antisera. Pooled sera were serially diluted (1:300−1:1968300) in PBS-TMB and added onto microtiter plates coated with 1 μg/mL of $(DA)_{10}$−OVA conjugate in PBS. The reaction was developed following the successive incubations with GAM-PO and OPD. Mice immunization groups: i.p. (●), i.p.+ s.c. (△), and f.p. (◆). Each value represents the mean of triplicate assays, which varied by no more than 5%.

DA−BSA conjugates were obtained from which 300 μg (six injections of 50 μg) were injected per mouse.

Comparison between the Three Different Routes of Immunization. To investigate the best immunization schedule, three groups of two mice were given a total of six injections of $(DA)_{17}$−BSA conjugates administered via three different routes (i.p., i.p. + s.c., and f.p.). Throughout experiments, mice injected by either route displayed no ill effects or symptoms typical of ASP. Animals were sequentially bled and their sera pooled according to the route of immunization. For each group, anti-DA antibodies production was tested by indirect ELISA using $(DA)_{10}$−OVA conjugate as target antigen. All preimmune sera were totally negative against a panel of coating antigens including the homologous (BSA) and heterologous (OVA) native carriers used (data not shown).

That all mice developed specific immune response upon immunization was clearly demonstrated by the antibody kinetics and level achieved but differences were observed according to the immunization schedule (Figure 1). For instance, the f.p. immunized group responded earlier (as soon as 3 weeks after priming), with a prolonged elevated antibody level attained approximately 3 weeks after the first boost. Consequently subsequent booster injections showed no clear efficacy on further antibody production. In contrast, a secondary immune response of normal magnitude and kinetics could be generated in the i.p. + s.c. and i.p. immunized groups after each injection, especially when the antibody levels had sufficiently decreased before. Nevertheless, the i.p. immunized group always exhibited a stronger specific response, whereas the i.p. + s.c. group tended to catch up with the f.p. one along the time course. These observations were later confirmed by titration experiments (Figure 2). Again, it can be seen that all pooled antisera dilutions exhibited DA specificity, and lower antibody concentrations yielded signals similar to background level (control without antibody). Moreover, it was observed that cross-absorbing anti-DA-BSA antisera with 1% BSA (PBS-TMB diluent buffer) completely neutralized the anti-carrier activity in the sera (data not shown). Therefore, titers estimated by the maximum serum dilution that allowed a 3-fold signal to target antigen, as compared to background level, were found to be 1:350000 for the i.p. mice group and around 1:72900 for the ip. + s.c. and f.p. groups. Consequently, all further reported ELISA experiments were conducted using pooled sera from the last bleeding of i.p. immunized mice.

It is noteworthy that $(DA)_{30}$−PL when used as target antigen yielded a high background noise and nonreproducible results.

Competitive Inhibition of Pooled Mice Antisera Binding to DA-OVA. To further assess the specificity of these anti-DA antibodies, competitive ELISA experiments were performed using various inhibitors (DA, KA, glutamic acid, and aspartic acid). The high specificity of anti-DA antibodies was again clearly demonstrated as all the other free haptens were essentially unrecognized in the concentration range 30−1000 μg/mL (data not shown). Figure 3 illustrates standard curves obtained by plotting the percentage of maximal signal (% B/B_o) against the log of free DA concentrations. These experiments also contributed to compare two amplification signals. The overall sensitivity of the GAM-βGZ/MUG (fluorogenic) amplification system over the GAM-PO/OPD (chromogenic) system is evident from the binding parameters of the standard curves. The working range covered by these assays was 3−245 ng/mL and 58−1437 ng/mL, respectively. Assuming that a difference of 3 standard deviations (n = 12) from the mean signal without inhibitor (B_o) is significant, the LOD of these assays was 1.4 ng/mL and 27 ng/mL using the fluorogenic and the chromogenic amplification systems, respectively. Finally, as can be expected, the K_D for the interaction of the antibodies with free DA was found to be lower using the fluorogenic assay (5×10^{-8} M) than the chromogenic one (5×10^{-7} M).

In the process of the analysis of sera from i.p. immunized mice, two antibody subpopulations were disclosed, which is in good agreement with an earlier observation (Nieto et al., 1984) that decreasing the coating antigen or/and antibody concentrations allowed different antibody subpopulations with increased affinities to be selected.

Recovery of DA from Spiked Samples. The optimized competitive fluorogenic assay has been used to measure DA levels in rapid mussels extracts spiked with DA calibration standards. The effect of matrixes was

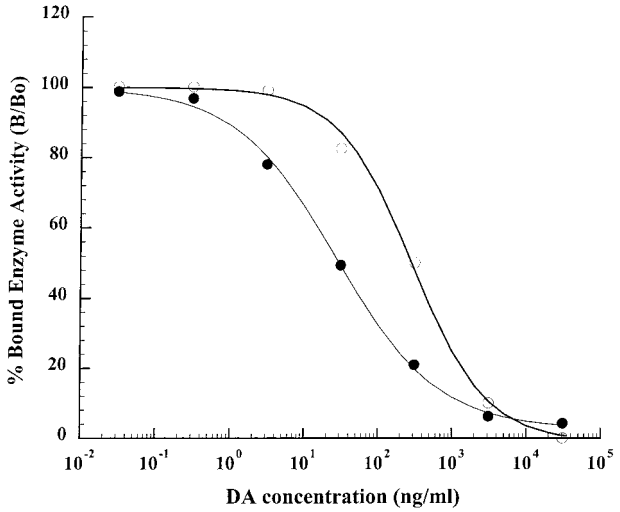


Figure 3. Competitive inhibition of pooled mice antisera binding to DA-OVA coated plates by free DA. $(DA)_{10}$−OVA coating concentration was 250 ng/mL and 20 ng/mL for the chromogenic and fluorogenic assays, respectively. The final antiserum dilution (i.p.-immunized group) was 1:350000 in PBS-TMB. The reaction was developed following the successive incubations of either GAM-PO and OPD (○) or GAM-βGZ and MUG (●) as reported in the Materials and Methods. Each value represents the mean of triplicate assays, which varied by no more than 5%.

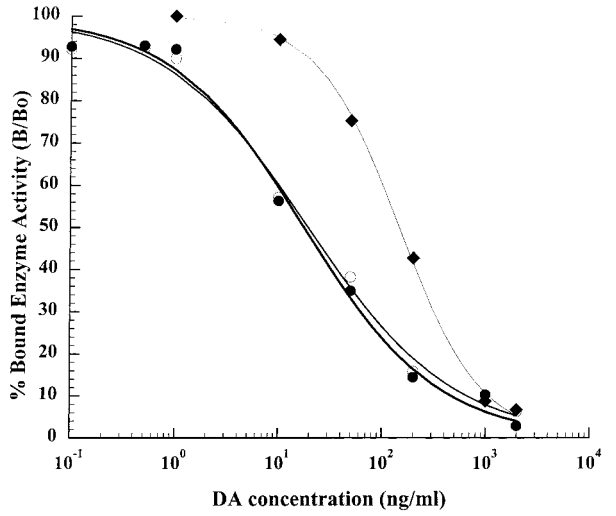


Figure 4. Effect of different biological matrixes on the DA calibration curve using the optimized ELISA format. See legend of Figure 3 for experimental conditions running the fluorogenic amplification system. DA calibration curves prepared in diluent buffer (●), in spiked mussel extracts: crude (◆) and pre-cleaned (○). Each value represents the mean of triplicate assays, which varied by no more than 3%.

investigated by comparing standard calibration curve obtained in diluent buffer with DA recovery from spiked mussel extracts (crude or precleaned). No significant matrix effect was observed for the precleaned extracts ($r^2 = 0.96$), as shown in Figure 4, whereas the use of crude extracts caused negative interferences (i.e., DA is less available for antibody interaction). Consequently, accurate determinations of DA in precleaned extracts could be achieved between 2 and 180 ng/mL in spiked samples, which corresponds to 0.02−1.8 μg/g of original mussel tissue. Owing to the regulation limits of 20 μg of DA/g of shellfish tissue, these extraction and assay procedures should provide a useful complement to the standard HPLC analytical technique currently employed in monitoring DA in shellfish tissue.

ACKNOWLEDGMENT

This work was supported by grants from the Government of French Polynesia (Tahiti) and Pasteur Institute (Paris, France).

LITERATURE CITED

Debonnel, G., Beauchesne, L., and de Montigny, C. (1989) Domoic acid, the alleged "mussel toxin", might produce its neurotoxic effect through kainic acid receptor activation: an electrophysiological study in the rat dorsal hyppocampus. *Can. J. Physiol. Pharmacol. 67*, 29−33.

Erlanger, B. F., Borek, F., Beiser, S. M., and Lieberman, S. (1957) Steroid-protein conjugates. I. Preparation and characterization of conjugates of bovine serum albumin with testosterone and with cortisone. *J. Biol. Chem. 228*, 713−727.

Falk, M., Walter, J. A., and Wiseman, P. W. (1989) Ultraviolet spectrum of domoic acid. *Can. J. Chem. 67*, 1421−1425.

Falk, M., Seto, P. F., and Walter, J. A. (1991) Solubility of domoic acid in water and nonaqueous solvents. *Can. J. Chem. 69*, 1740−1744.

Friguet, B., Chaffotte, A. F., Djavadi-Ohaniance, L., and Goldberg, M. (1985) Measurement of the true affinity constant in solution of antigen−antibody complexes by enzyme-linked immunosorbent assay. *J. Immunol. Methods 77*, 305−319.

Garthwaite, I., Ross, K. M., Miles, C. O., Hansen, R. P., Foster, D., Wilkins, A. L., and Towers, N. R. (1998) Polyclonal antibodies to domoic acid and their use in immunoasays for domoic acid in seawater and shellfish. *Nat. Toxins 6*, 93−104.

Grimmelt, B., Nijjar, M. S., Brown, J., Macnair, N., Wagner, S., Johnson, G. R., and Amend, J. F. (1990) Relationship between domoic acid levels in the blue mussel (*Mytilus edulis*) and toxicity in mice. *Toxicon* 28, 501−508.

Iverson, F., Truelove, J., Nera, E., Tryphonas, L., Campbell, J., and Lok, E. (1989) Domoic acid poisoning and mussel-associated intoxication: preliminary investigations into the response of mice and rats to toxic mussel extract. *Food Chem. Toxicol. 27*, 377−384.

Kabanov, A. V., Ovcharenko, A. V., Melik-Hubarov, N. S., Bannikov, A. I., Alakhov, V. Yu., Kiselev, V. I., Sveshnikov, P. G., Kiselev, O. I., Levashov, A. V., and Severin, E. S. (1989) Fatty acid acylated antibodies against virus suppress its reproduction in cells. *FEBS 250* (2), 238−240.

Klotz, I. M. (1953) *The Proteins* (H. Neurath and K. Baily, Eds.) Vol. 1, Academic Press, New York.

Murakami, S., Takemoto, T., and Shimizu, Z. (1953) Studies on the effective principles of Digenea simplex Aq. I. Separation of the effective fraction by liquid chromatography. *J. Pharm. Soc. Jpn. 73*, 1026−1028.

Newsome, H., Truelove, J., Hierlihy, L., and Collins, P. (1991) Determination of domoic acid in serum and urine by immunochemical analysis. *Bull. Environ. Contam. Toxicol. 47*, 329−334.

Nieto, A., Gaya, A., Jansa, M., Moreno, C., and Vives, J. (1984) Direct measurement of antibody affinity distribution by hapten-inhibition enzyme immunoassay. *Mol. Immunol. 21* (6), 537−543.

Osada, M., Marks, L. J., and Stewart, J. E. (1995) Determination of domoic acid by two different versions of a competitive enzyme-linked immunosorbent assay (ELISA). *Bull. Environ. Contam. Toxicol. 54*, 797−804.

Pauillac, S, Naar, J., Branaa, P., and Chinain, M. (1998) An improved method for the production of antibodies to lipophilic carboxylic hapten using small amount of hapten-carrier conjugates. *J. Immunol. Methods 220*, 105−114.

Perl, T. M., Bédard, L., Kosatsky, T., Hockin, J. C., Todd, E., and Remis, R. S. (1990) An outbreak of toxic encephalopathy caused by eating mussels contaminated with domoic acid. *New Engl. J. Med. 322*, 1775−1780.

Quilliam, M. A., and Wright, J. L. C. (1989) The amnesic shellfish poisoning mystery. *Anal. Chem. 61* (18), 1053A−1060A.

Quilliam, M. A., Thomas, K., and Wright, J. L. C. (1998) Analysis of domoic acid in shellfish by thin-layer chromatography. *Nat. Toxins* 6, 147−152.

Smith, D. S., and Kitts, D. D. (1994) A competitive enzyme-linked immunoassay for domoic acid determination in human body fluids. *Food Chem. Toxicol. 32*, 1147−1154.

Smith, D. S., and Kitts, D. D. (1995) Enzyme immunoassay for the determination of domoic acid in mussel extracts. *J. Agric. Food Chem. 43*, 367−371.

Stewart, G. R., Zorumski, C. F., Price, M. T., and Olney, J. W. (1990) Domoic acid: A dementia-inducing exitotoxic food poison with kainic acid receptor specificity. *Exp. Neurol. 110*, 127−138.

Teitelbaum, J. S., Zatorre, R. J., Carpenter, S., Gendron, D., Evans, A. C., Gjedde, A., and Cashman, N. R. (1990) Neurologic sequelae of domoic acid intoxication due to the ingestion of contaminated mussels. *New Engl. J. Med. 322*, 1781−1787.

Wright, J. L. C., and Quilliam M. A. (1995) Methods for domoic acid, the amnesic shellfish poisoning (ASP) toxin. In *Manual on Harmful Marine. IOC Manual and Guides* (G. M. Hallegraeff, D. M. Anderson, and A. D. Cembella, Eds.) vol. 33, pp 115−135, Paris, IOC-UNESCO.

Wright, J. L. C., Boyd, R. K., de Freitas, A. S. W., Falk, M., Foxall, R. A., Jamieson, W. D., Laycock, M. V., McCulloch, A. W., McInnes, A. G., Odense, P., Pathak, V., Quilliam, M. A., Ragan, M. A., Sim, P. G., Thibault, P., Walter, J. A., Gilgan, M., Richard, D. J. A., and Dewar, D. (1989) Identification of domoic acid, a neuroexcitatory amino acid, in toxic mussels from eastern Prince Edward Island. *Can. J. Chem. 67*, 481−490.

Yatsimirskaya, E. A., Gavrilova, E. M., Egorov, A. M., and Levashov, A. V. (1993) Preparation of conjugates of progesterone with bovine serum albumin in the reversed micellar medium. *Steroids 58* (11), 547−550.

BC990041O

An Improved Method for the Microscale Preparation and Characterization of Hapten−Protein Conjugates: The Use of Cholesterol as a Model for Nonchromophore Hydroxylated Haptens

Jérôme Naar,[†] Philippe Branaa,[†] Mireille Chinain,[†] and Serge Pauillac*[,†,‡]

Unité d'Océanographie Médicale, Institut de Recherches Médicales Louis Malardé, P.O Box 30, Papeete, Tahiti, French Polynesia. Received April 12, 1999; Revised Manuscript Received August 3, 1999

A minute amount (0.446 μmol) of cholesterol (Chol) was converted into an hemisuccinate derivative (Chol HS) using an excess of succinic anhydride. The optimal conditions for synthesis of Chol HS were explored by checkerboard experiments in which various succinic anhydride/Chol molar ratios ranging from 5:1 to 30:1 were assayed over a wide temperature range (50−85 °C) and for various incubation times (3−8 h). Total conversion was obtained at the higher reagent ratios, temperatures, and incubation times. Subsequently, this carboxylic derivative was first covalently linked to bovine serum albumin (BSA) then to various proteins (casein, ovalbumin, and hemocyanins) or to a synthetic homopolymer (poly-DL-Lysine) via a modified version of the mixed anhydride method of Erlanger, performed in a reversed micellar medium. The assessment of the number of haptenic groups per mole of BSA (epitope density) was achieved chromatographically by two methods according to a Chol standard curve established at 207 nm with linearity in the range 0−50 μg. These procedures involving an alkaline hydrolysis of a sample of either the conjugate (direct method) or the unreacted Chol HS (indirect method) yielded an acceptable level of agreement and concordant results in all cases. The influence of the activated hapten/BSA molar ratio on the coupling efficiency was investigated by the direct method within the range 10:1 to 250:1. Using the optimal conditions determined for Chol HS synthesis (a molar reagent ratio of 30:1 with incubation at 65 °C for 6 h) and for BSA haptenation (a 100-fold molar excess of activated hapten, with a carrier stock concentration of 5 mg/mL), epitope density of the conjugates lied between 23 and 27. By reacting the same amount of activated hapten (∼216 μg) with identical amounts of various carriers (300 μg), conjugation efficiency was found similar on a microgram of Chol bound per milligram of carrier basis. This simple and reproducible conjugation and analysis procedures should provide a general method applicable to poorly available and weakly immunogenic haptens bearing hydroxyl groups such as polyether-type marine toxins.

INTRODUCTION

Despite occasional reports that conjugates of cholesterol (Chol)[1] can be immunogenic (Bailey et al., 1964; Klopstock et al., 1964; Hara et al., 1979), Chol has long been considered as a poorly immunogenic hapten due to its ubiquitous distribution in the animal kingdom and important biological role. Nevertheless, specific antibodies have been generated using Chol-loaded liposomes containing lipid A as an adjuvant (Swartz et al., 1988). More recently, i.p. injections of silicone oil also have been found to induce specific antibodies through recruitment and adsorption of Chol at the injection site and potent immunostimulant properties (Alving et al., 1996). From all of these previous studies it can be concluded that production of antibodies to Chol may be readily achieved by utilizing a powerful adjuvant and/or a suitable Chol-carrier conjugate to help antigen presentation and recognition by the immune system. With the aim of developing new antibodies against lipophilic hydroxylated haptens such as polyether-type marine toxins [see, for review, Yasumoto and Murata (1993)], we have used Chol as a molecular model to investigate an improved method for the microscale preparation and characterization of hapten−protein conjugates. This choice was made considering Chol is a biologically relevant lipid hapten, is commercially available and inexpensive, possesses a unique secondary hydroxyl group, and has no useful absorption band suitable for detection, except the common absorption peak around 210 nm exhibited by most organic compounds.

In a preceding report (Pauillac et al., 1998), we have described a miniaturized procedure for the conjugation of lipophilic carboxylic haptens to carrier molecules and the production of specific antibodies. The key processes in this synthesis were an effective adaptation of the mixed anhydride method (Erlanger et al., 1957) and some relevant modifications of the reversed micellar system (Kabanov et al. 1989; Yatsimirskaya et al., 1993) for miniaturization purpose and high haptenization yield. In this previous study conducted with chromophoric carboxylic haptens, conjugate analysis could be readily performed spectrophotometrically.

* To whom correspondence should be addressed, Institut de Recherches Médicales Louis Malardé. Phone: +689 41 64 69. Fax: +689 43 15 90. E-mail: spauillac@malarde.pf.

[†] Unité d'Océanographie Médicale.

[‡] Unité d'Immunocytochimie, CNRS URA 359, Département d'Immunologie, Institut Pasteur, Paris, France.

[1]Abbreviations: AOT, aerosol OT or sodium bis(2-ethylhexyl) sulfosuccinate; BSA, bovine serum albumin; CAS, casein; Chol, cholesterol; Chol HS, cholesterol hemisuccinate; HPLC, high-performance liquid chromatography; KLH, keyhole limpet hemocyanin; LH, limulus polyphemus hemocyanin; OVA, egg albumin; PA, peak area; PBS, phosphate buffered saline; TLC thin-layer chromatography on silica gel; PL, poly-DL-lysine (MW 30000−70000); RT, retention time.

10.1021/bc990042g CCC: $18.00 © 1999 American Chemical Society
Published on Web 10/08/1999

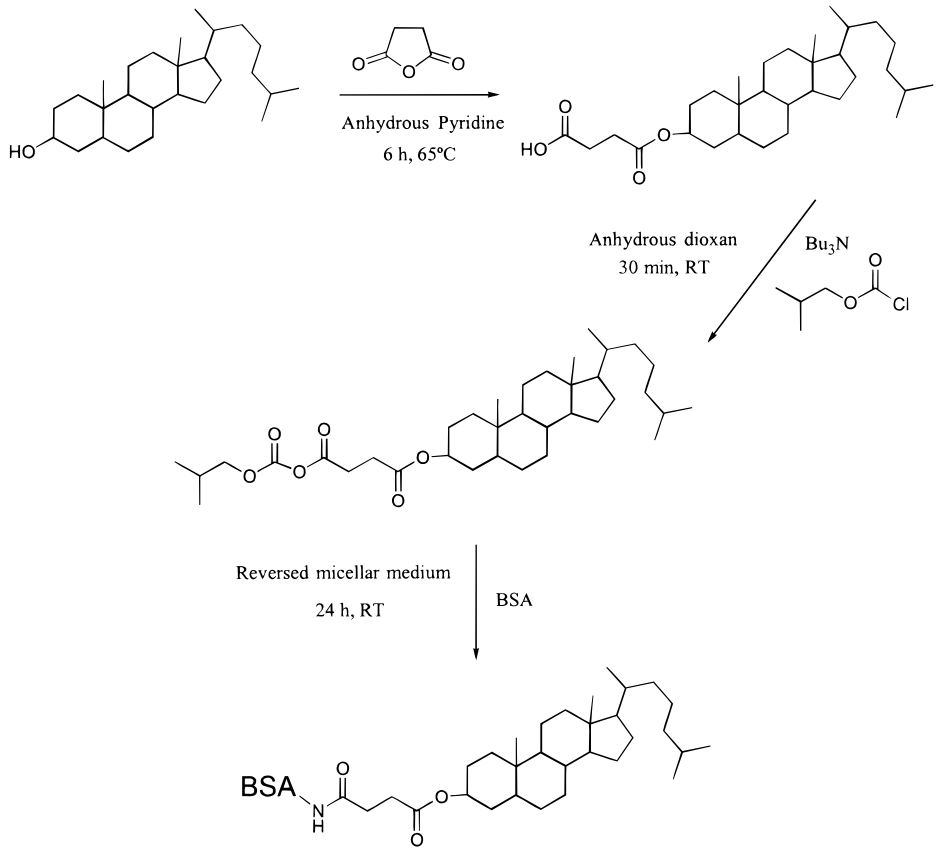


Figure 1. Chemical coupling of cholesterol to BSA in the reversed micellar medium.

Because Chol is a steroid with unique secondary hydroxyl group, the present paper deals first with the microscale preparation of a cholesterol hemisuccinate derivative (Chol HS) and its subsequent conjugation to carrier molecules in the reversed micellar medium, with emphasis on the elucidation of optimal conditions for both synthetic steps. Second, considering previous demonstrations that both the nature of the carrier protein (Fasciglione et al., 1996) and the epitope density of the conjugates (Klaus and Cross, 1974; Erlanger, 1980; Cooper et al., 1993, 1994) can greatly influence the induction of specific antibodies (amount, class, and affinity), the conjugation efficiency to various carrier proteins and a synthetic poly-amino acid has also been chromatographically evaluated. Conjugates immunogenicity has not been tested in this study.

MATERIALS AND METHODS

All chemical reagents, unless otherwise stated, were purchased from Sigma Chemicals Co (St. Louis, MO). High quality grade solvents from Prolabo (France) were dried according to standard procedures. Thin layer chromatograms (TLC) were run on silica gel 60 precoated aluminum foils from Merck (Darmstadt, Germany).

Synthesis and Purification of Cholesterol Hemisuccinate. The optimal conditions for synthesis of Chol HS were explored by checkerboard experiments in which various succinic anhydride/cholesterol molar ratios ranging from 5:1 to 30:1 were assayed over a wide temperature range (50−85 °C) for various incubation times (3−8 h). All reactions proceeding in a sealed vial, the most efficient condition, are described hereafter.

A 30-fold molar excess of succinic anhydride solubilized in 50 μL of anhydrous pyridine was added to 172 μg (0.446 μmol) of crystalline cholesterol in the internal cone of a 1 mL small reaction vial (Pierce, Rockford, IL). The vial was sealed and heated for 6 h at 65 °C, and the solvent evaporated under a stream of nitrogen. Finally, the residue was redissolved in 200 μL of CH_2Cl_2/MeOH (99:1) and succinylation was checked by TLC using CH_2Cl_2/MeOH (95:5) as developing solvent and 30% aqueous sulfuric acid as spray reagent. By heating, Chol and its derivative (Chol HS) appeared as pink spots with R_f values of 0.57 and 0.32, respectively.

Chol HS was purified by rapid chromatography technique on a Sep-Pak Plus silica gel cartridge (Waters-Millipore, Milford, MA) fitted with a 10 mL Luer-tipped syringe and conditioned with 5 mL of CH_2Cl_2. The 200 μL reaction mixture was loaded onto the cartridge, the vial was rinsed with 100 μL of CH_2Cl_2/MeOH (99:1) which was let to pass through the cartridge, and 5 mL of CH_2Cl_2 was added to induce sample stacking then elution was performed using a stepwise gradient beginning with 10 mL CH_2Cl_2-MeOH (90:10) and ending with 5 mL MeOH. The flow rate was maintained around 3 mL/min and 1 mL fractions were collected. Chol HS eluted in tubes 2−4 (10% MeOH) with a yield >95% whereas succinic anhydride was found in the pure MeOH fractions (tubes 12−14). Therefore, subsequent calculations were made on the basis of full recovery.

Preparation of Cholesterol−BSA Conjugates. Conjugates were prepared according to a modified version of the mixed anhydride coupling method of Erlanger et al. (1957) performed in a reversed micellar medium (Pauillac et al., 1998). The synthetic steps are outlined in Figure 1.

Following the rapid chromatographic procedure, fractions containing Chol HS were combined and dried under nitrogen atmosphere in a 1 mL small reaction vial. To this dry derivative, a 10-fold molar excess of tributyl-

amine (V_m = 254.94 μL/mmol) and isobutyl chlorocarbonate (V_m = 131.325 μL/mmol) were added as 1/12th dilutions in dry peroxide-free dioxane to provide a final volume of approximately 20 μL of reaction mixture. The tightly sealed vial was placed onto a mechanical stirrer, and the formation of the mixed anhydride was allowed to proceed for 30 min at room temperature. The reaction was monitored by TLC as described above. Sulfuric acid spraying and heating of the chromatogram showed conversion of Chol HS (R_f = 0.32) to the mixed anhydride (R_f = 0.96) to an extent greater than 95%. The conjugation of activated Chol HS to carriers, was carried out in the system of reversed micelles of aerosol OT [AOT or sodium bis(2-ethylhexyl) sulfosuccinate] in heptane (Kabanov et al. 1989; Yatsimirskaya et al., 1993) with relevant modifications for miniaturization purpose and high haptenization yield (Pauillac et al., 1998). Six carriers were used throughout: bovine serum albumin (BSA), ovalbumin (OVA), casein (CAS), poly-DL-Lysine (PL, average mol wt 77000), keyhole limpet, and *Limulus polyphemus* hemocyanins (KLH and LH, respectively).

During these experiments various activated hapten/carrier molar ratios were assayed in the range 10−250 using commercial Chol HS.

A typical experiment performed at room temperature with two BSA concentrations is described. Four volumes of a 0.5 M solution of AOT in heptane were added to 1 vol of BSA at 5 or 7.5 mg/mL in 0.1 M borate buffer, pH 10.2, under vigorous shaking. The formation of reversed micelles was achieved when the solution turned completely clear. Immediately after, volumes of these BSA micellar solutions corresponding to 300 μg (0.004 41 μmol) were poured into the vials containing the activated hapten and the mixtures were again vigorously shaken, providing for each reaction a hapten/protein molar ratio around 100:1. After a slight and transient turbidity was observed, the reactions were allowed to proceed overnight at room temperature.

Control experiments run in parallel, consisting in BSA alone and BSA mixed with nonactivated Chol HS, were incubated in the reversed micellar medium under identical conditions.

All proteins in the vials (assay and control) were precipitated 20 min at −20 °C in acetone (3 vol), and the whole content was transferred into 5 mL of borosilicate glass test tubes for centrifugation (6000*g* at +4 °C for 15 min). The resultants pellets were redissolved in PBS (250 μL at +4 °C), precipitated again, then thoroughly washed three times with cold acetone (−20 °C) to remove unbound Chol HS. The precipitates were generally resuspended in 1.2 mL of distilled water, filter sterilized, dispensed into 6 aliquots of 200 μL, freeze-dried overnight and stored at −20 °C until use. However, depending upon expected conjugation efficiency, either the whole conjugate (300 μg in 300 μL of distilled water) or a 200 μL aliquot (50 μg) and the pooled acetone supernatants were saved for analysis (see below**)**. Other fully characterized conjugates of Chol with OVA, CAS, PL, KLH, and LH were also obtained according to this procedure: 1 mg/mL of micellar carrier solutions were prepared and incubated with activated or nonactivated hapten under identical conditions as for BSA.

Characterization of Cholesterol−BSA Conjugates. Carrier haptenization was assessed chromatographically by two methods, both involving an alkaline hydrolysis of a sample of either the conjugate (direct method) or the unreacted Chol HS in the acetone phase (indirect method). Chol qualitative and quantitative analyses were performed using an HPLC system (Kontron Instrument, France) equipped with a UV monitor set at 207 nm and a chromatointegrator for calculation of peak areas (PA). The column was a 4.6 mm id × 150 mm Develosil ODS-HG-5 reversed-phase (Normora Chemical, Japan), and separation was carried out under isocratic conditions with pure MeOH at a flow rate of 1 mL/min. Chol content of each sample was determined according to a calibration curve with linear regression in the range 0−50 μg (150 μL/injection), obtained by serial dilutions of a stock solution of crystalline Chol in CH_2Cl_2/MeOH (1:99). After molar conversion, the epitope density of the conjugates (n) was expressed by the hapten/carrier ratio of the samples. For these calculations, according to previous results (Pauillac et al., 1998) the recovery of the conjugates was considered total.

Direct Method. A 200 μL aqueous sample containing 50 μg of Chol−BSA conjugate or the whole conjugate (300 μg in 300 μL distilled water) was mixed with 3 vol of 28% aqueous ammonia, and the mixture was allowed to stand overnight at room temperature. Afterward, the hydrolysis mixture was freeze-dried and the residue was extracted three times with 1 mL of CH_2Cl_2/anhydrous MeOH (20:80). The pooled organic fractions were evaporated under a stream of nitrogen, and the residue was redissolved in 150 μL of CH_2Cl_2/MeOH (1:99) and analyzed by HPLC as described above.

Indirect Method. The pooled acetone supernatant recovered from conjugate precipitation was evaporated to dryness, and the residue redissolved in 200 μL of CH_2Cl_2. Unreacted Chol HS was purified on a Sep-Pak Plus silica gel cartridge as described above. In this case, elution was performed using a stepwise gradient beginning with 10 mL of CH_2Cl_2/MeOH (97.5:2.5) and ending with 5 mL of MeOH. Again the flow rate was maintained around 3 mL/min and 1 mL fractions were collected. Chol HS eluted first (tubes 3−8) whereas AOT was found in the pure MeOH fractions (tubes 12−14). Chol HS containing fractions were combined, evaporated to dryness and redissolved in 200 μL of CH_2Cl_2/MeOH (5:95). Alkaline hydrolysis, freeze-drying, extraction, and solvent evaporation procedures were performed as described for the direct method. Finally, the residue was redissolved in 400 μL of CH_2Cl_2/MeOH (1:99), and a 100 μL sample was subjected to HPLC analysis as described above.

RESULTS

Chol-carrier conjugates were prepared in a reversed micellar medium according to the procedure described in Materials and Methods (Figure 1). Optimal conditions for their preparation were established at each step of the two stages involved. Their recovery and substitution ratio were carefully checked by incorporating controls in which carriers have been incubated in the same conditions with nonactivated hapten. The epitope density of the conjugates (*n*) was expressed by their hapten/carrier molar ratio considering a total recovery of the conjugates.

Chromatographic Quantitation of Cholesterol. Chol is a monohydroxylated, lipid-soluble compound with no characteristic peak absorption with respect to proteins, therefore a reversed-phase HPLC method employing UV detection at 207 nm has been set up for its quantitation (150 μL/sample run). Figure 2A illustrates a chromatogram obtained by injecting 25 μg of Chol, which eluted with a retention time (RT) varying from 9.6 to 10.13 min depending upon the ambient temperature. To assess the linearity of this method, a calibration curve with a working range of 0−50 μg was obtained by plotting peak areas (PA) expressed in millivolt minutes versus

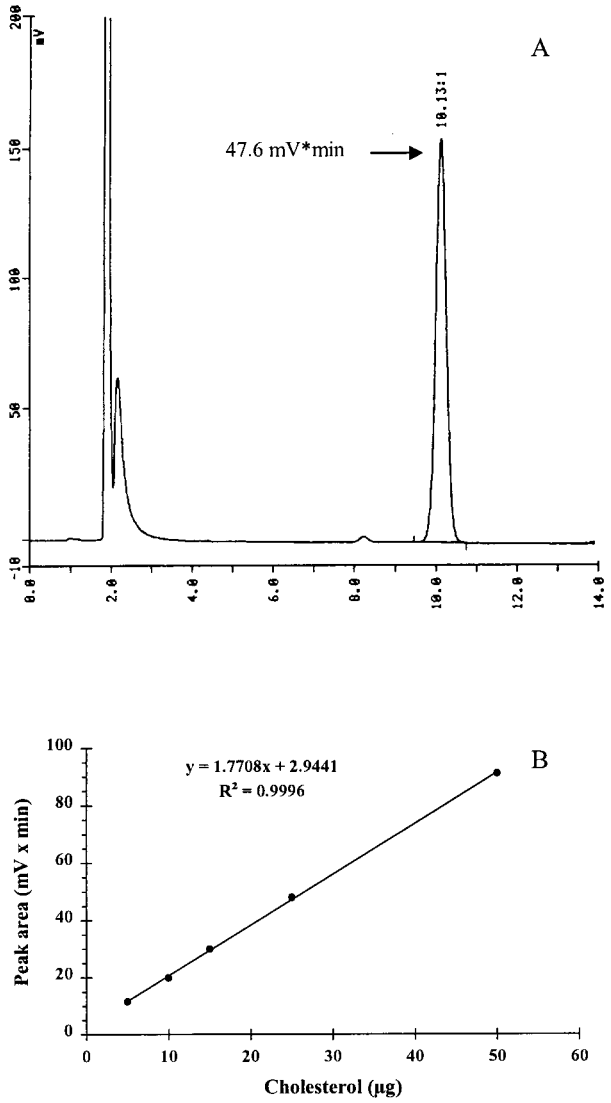


Figure 2. Chromatographic quantitation of cholesterol. chromatogram on a Develosil ODS-HG-5 reverse-phase column. Mobile phase 100% MeOH; flow rate 1 mL/min; detection UV at 207 nm; sample 25 μg of Chol applied in 150 μL of CH_2Cl_2/MeOH (1:99); Retention time, RT = 10.13 min; peak area, PA = 47.6 mV × min. Calibration curve. Increasing amounts of cholesterol solubilized in 150 μL of CH_2Cl_2/MeOH (1:99) were subjected to HPLC analysis. Corresponding peak areas (PA) are plotted versus amounts of injected sample. Values are the mean of two independent experiments (error bars are omitted because of symbol overlapping).

corresponding Chol amounts in micrograms (Figure 2B). All reported values are the means of two series of data obtained separately. The adequacy and high accuracy of this dosage is deduced from the value of the correlation coefficient which was very close to 1.

Optimization of the Succinylation Process. To optimize the succinylation process, the reaction was performed for 3−8 h at different temperatures (50−85 °C), using various succinic anhydride/Chol molar ratios (5:1 to 30:1). Regarding incubation time, in most cases it was found that 6 h was a good compromise because the reaction no longer progressed after this period. The reactions were monitored by TLC and accurately quantified by HPLC using an aliquot or the whole reaction mixture to evaluate remaining Chol amount. Appropriate factors were applied to restore the true value in the original reaction and a subtraction was made on a molar

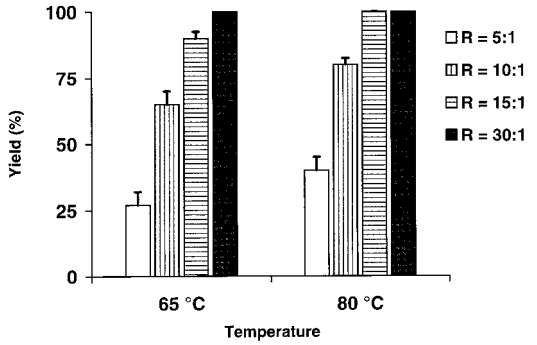


Figure 3. Determination of the optimal conditions for Chol HS synthesis. Effect of two temperatures (65 and 80 °C) and influence of the succinic anhydride/Chol molar ratio (5:1 to 30:1).

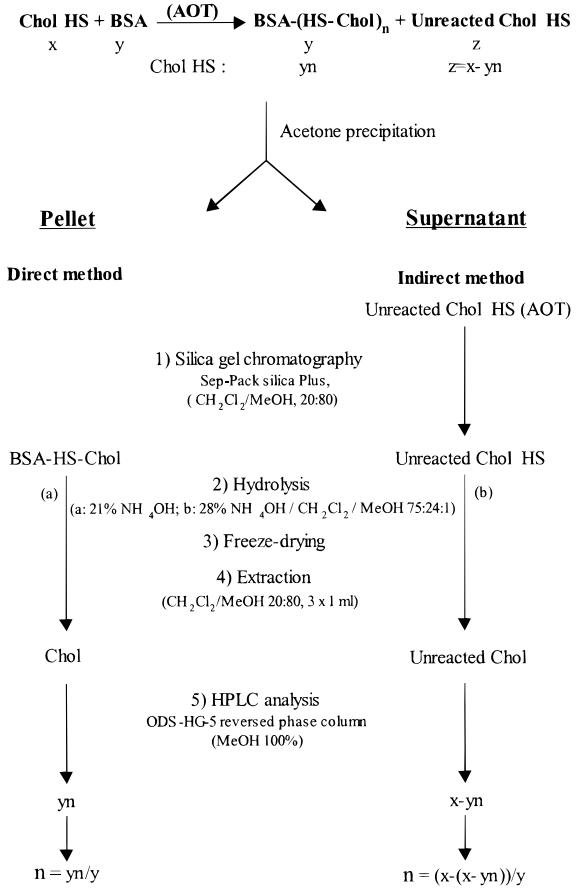


Figure 4. Outline of the two methods for the analysis of Chol-BSA conjugates. x and y are the number of moles of reagents and products; n (normal letter or subscript) is the number of haptenic residues per mole of BSA (epitope density). Calculations are made assuming a total recovery of the protein. The direct method determines bound Chol in the conjugate whereas the indirect method evaluates unreacted Chol in the acetone supernatant (other details in the text).

basis to estimate the amount of Chol HS synthesized. Reaction yield expressed as percentage of the molar ratio of Chol HS per total Chol are reported in Figure 3 for two temperatures (65 and 80 °C). These results clearly indicate that the yield is dependent upon the reagent ratio at both temperatures. However, at 80 °C, maximal yield (100%) can be reached with a 2-fold lower reagent ratio (15:1) compared to 30:1 necessary at 65 °C, thus highlighting also the temperature dependence of the reaction. In addition, temperatures below 60 °C were not favorable to provide yields greater than 40%, and the

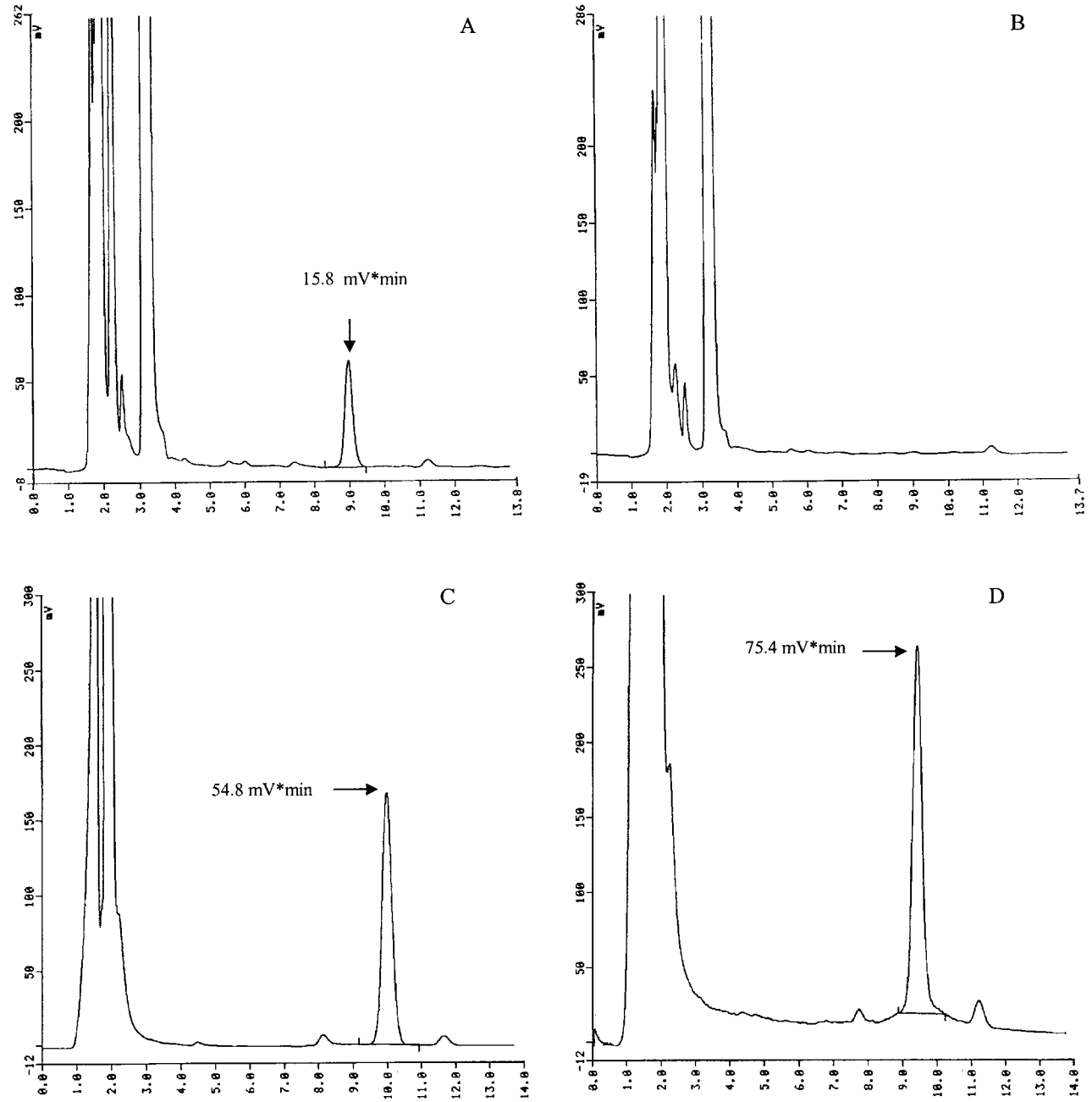


Figure 5. Chromatographic determination of the epitope density of Chol-BSA conjugates. BSA (300 μg) was reacted with either activated or nonactivated Chol HS in a 100-fold molar excess of hapten. Bound and unreacted Chol were evaluated chromatographically from an aliquot of the conjugate and the acetone supernatant, respectively (see Figure 4). Direct method (one-sixth of the original sample): (A) Chol-BSA conjugate; (B) control. Indirect method (one-fourth of the original sample): (C) Chol-BSA conjugate; (D) control.

influence of the reagent ratio was minimized in this temperature range (data not shown). Consequently, optimal conditions for this reaction were set at 65 °C for 6 h with a 30:1 molar reagent ratio.

Analysis of the Conjugates. Haptenation of the chemically activated Chol derivative (Chol HS) by the modified mixed anhydride method in the reversed micellar medium (Pauillac et al., 1998) yielded densely coated BSA carrier protein as revealed by chromatographic determination of bound Chol (direct method) or unreacted Chol HS (indirect method). These two methods are outlined in Figure 4 with the rationale for the determination of conjugates epitope density (n). Figure 5 illustrates these methods by chromatograms obtained with the same Chol-BSA conjugate and its control experiment (300 μg of BSA incubated under identical conditions with either 216.48 μg of activated or nonactivated Chol HS, respectively).

Using the direct method, the PA obtained for the conjugate sample (Figure 5A) corresponded to 7.26 μg of bound Chol (43.6 μg or 0.1127 μmol in the original reaction). Hence, n was found to be 26. It is noteworthy that no Chol was detected in control samples (Figure 5B) even up to a 500-fold molar excess of nonactivated Chol HS (data not shown).

By the indirect method, the PA obtained from the conjugate sample (Figure 5C) corresponds to 29.27 μg of unreacted Chol (117.08 μg in the original reaction). Considering the PA obtained from control sample (Figure 5D) equivalent to 40.93 μg of unreacted Chol, the maximum amount that could be recovered in the original reaction is 163.72 μg. Therefore, a good estimation of

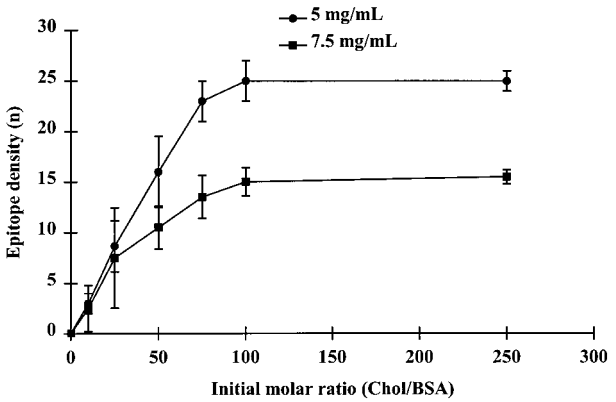


Figure 6. Optimization of cholesterol coupling to BSA. Dependency on hapten/protein molar ratio and influence of the concentration of the BSA stock solution (5 and 7.5 mg/mL). BSA (300 μg) was reacted with activated Chol HS in various molar excess (0−250). After purification, conjugates were solubilized in distilled water then analyzed for their epitope density according to the direct method.

Table 1. Determination of the Epitope Density of Various Chol-Carrier Conjugates

		conjugation efficiency	
carrier	mol wt	μg of Chol/ mg of carrier	n^b
BSA	68000	142	25
OVA	45000	125	14
KLH	ND[a]	112	ND
LH	ND[a]	139	ND
PL	70000	119	21
Casein	23000	151	9

[a] Not determined for the nonhomogeneous hemocyanins. [b] Epitope density, each value represents the average determination from three independent reactions, which varied by no more than 8% (direct method).

bound Chol in the conjugate is 46.64 μg (163.72−117.08), which gave $n = 27$. This value is very similar to that determined by the direct method (*26*). The adequacy and concordance of the direct and indirect method was further assessed by dual analyses of three BSA conjugates obtained using various hapten/carrier molar ratios. In all cases, the indirect method exhibited no more than 10% increase in *n* compared to the direct method and increase of bound Chol rigorously paralleled the decrease of unreacted Chol (data not shown).

Optimization of the Conjugates Preparation. Experiences aiming to investigate the influence of carrier concentration were designed using two BSA stock solutions (5 and 7.5 mg/mL) keeping the same hapten/carrier molar ratio. For convenience, these experiments were conducted using a commercial Chol HS activated at three concentrations (10, 20, and 40 mg/mL in dioxane), to keep approximately the same volume for the reaction mixtures. As shown in Figure 6, at the two stock BSA concentrations tested, the coupling rate is strongly dependent on the hapten/protein molar ratio up to a value of 100:1 but a plateau is eventually reached, indicating that conjugation no longer occurred for greater ratio values. Within the investigated reagent ratio range, the overall coupling efficiency of the assay using 5 mg/mL over the one using 7.5 mg/mL is clearly demonstrated. Maximal binding of Chol to BSA ($n \approx 25$) occurs using a 100-fold molar excess activated Chol HS with a 5 mg/mL protein stock concentration. Taking into account the above results, the optimized procedure was applied to the other carrier molecules and *n* was determined using the direct method (Table 1). For comparison purpose, the same amount of carrier (300 μg) was reacted with either activated or nonactivated Chol HS (∼216 μg), each value represents the average determination from three independent reactions, which varied by no more than 8%. Although *n* lies between 9 and 25, these results clearly show that conjugation efficiency is identical on a microgram of Chol bound per milligram of carrier basis.

DISCUSSION

To establish immunological reagents for the quantitation of haptens, there is a strict need for conjugation to appropriate carriers for preparing satisfactory material for immunization and antibody screening. Dealing with mice immunization, various immunogenic carriers have been successfully used; among them, BSA was the most widely assayed for many reasons. BSA is inexpensive and readily available, contains 60 amino groups of which ∼35 are exposed to the surface of the molecule under physiological conditions, in addition, this protein proved to be heterologous enough to provoke adequate mice immune response in most cases.

A simple conjugation reaction consists of a mixture of the protein, the hapten, and a coupling reagent in such a way that the yield of conjugate is maximal. Nevertheless, conjugation must not alter the antigenic properties of the hapten. To this goal, other practical aspects appear uppermost relevant, as the purity and concentration of the components, products yield, and finally conjugate recovery. Since all these critical factors can individually have a profound effect on the success of the procedure, optimal coupling conditions must be carefully checked.

Haptens bearing nonreadily reactive functional groups must be converted into more reactive derivatives using adequate chemical reagents (Erlanger, 1973, 1980; Wong, 1993). When hydroxyl groups are available, hemisuccinate derivatives are generally produced in the presence of an excess of succinic anhydride in pyridine, linkage to the amino groups of the carrier is subsequently accomplished through a reagent-mediated carboxyl activation. This process has the advantage of introducing a four-carbon spacer arm which exposes the hapten from the surface of the carrier, thus favoring its presentation and recognition by the immune system. However, it has been previously demonstrated that increasing the length of the chemical spacer can severely affect the production of hapten-specific antibodies (Beckett et al., 1978) since, as an artifact, it can also be part of the epitope recognized by the induced antibodies (Weyrer et al., 1990).

In this study, minute amount (0.446 μmol) of Chol was first entirely converted into an hemisuccinate (Chol HS), then the recently described conjugation technique proceeding in a reversed micellar medium (Pauillac et al., 1998) was successfully adapted to this carboxylic derivative as a one-pot synthesis method.

Because the degree of conjugation or epitope density is an essential attribute of a conjugate either as an immunogen (Klaus and Cross, 1974; Erlanger, 1980; Cooper et al., 1993, 1994) or a target antigen (Vyjayanthi et al., 1995), its assessment must be correctly addressed. For these reasons investigations were previously aimed (i) at the study of complete conjugate recovery (Pauillac et al., 1998) and (ii) at accurate determination of Chol on a reversed-phase HPLC column according to a calibration curve. The assessment of the Chol content of the conjugates either by the direct or indirect method gave consistent results. In the direct method, where covalently linked Chol is released by alkaline hydrolysis, corre-

sponding PA was linearly related to sample contents and a simple multiplication by 6 gave the Chol content in the whole conjugates. In the indirect method which measures unbound Chol, a 4-fold factor was applied to restore the true value in the whole supernatant and a subtraction from the total unreacted Chol recovered from control experiments was made to estimate bound Chol in the whole conjugates.

By reacting the same amount of activated hapten (~216 μg) with identical amounts of various carriers (300 μg), epitope density of the conjugates lied between 9 and 25, but on a microgram *o*f Chol bound per milligram of carrier basis, conjugation efficiency was identical. These values were found to fall within the optimal range to ensure hapten-specific antibody production (Erlanger, 1980).

As a matter of fact, using this procedure, PbTx-3 (400 μg; 0.446 μmol)—a member of the brevetoxin polyether-type toxins (Baden, 1989)—was totally converted into an hemisuccinate derivative (PbTx-3 HS) and covalently linked to BSA and OVA. Following mice immunization with $(PbTx\text{-}3)_{18}$—BSA conjugate, highly specific antibodies have been produced as revealed by ELISA on $(PbTx\text{-}3)_{10}$—OVA-coated plates (Naar et al., unpublished results).

In this study dealing with Chol, a hydroxylated lipid-soluble hapten, four major improvements have been achieved in the process of conjugates preparation and analysis: (1) Chol HS was produced with a 100% yield with as little as 172 μg of starting material; (2) the mixed anhydride method of Erlanger was successfully adapted to such minute hapten quantities with a moderate hapten/carrier molar ratio of 100:1; (3) quantitation of both bound Chol and unreacted Chol HS was accurately performed chromatographically; (4) no radioactive probe was required to monitor antigen preparation.

In conclusion, this simple conjugation procedure appears most valuable for poorly available and weakly immunogen haptens bearing hydroxyl groups such as polyether-type marine toxins through the specific induction of high-affinity antibodies.

ACKNOWLEDGMENT

The authors thank Philippe Cruchet for excellent technical assistancewith HPLC analyses. This work was supported by grants from the Government of French Polynesia (Tahiti) and Pasteur Institute (Paris, France).

LITERATURE CITED

(1) Alving, C. R., Wassef, N. M., and Potter, M. (1996) Antibodies to cholesterol: biological implications of antibodies to lipids. *Curr. Top. Microbiol. Immunol. 210*, 85−92.

(2) Baden, D. G. (1989) Brevetoxins: unique polyether dinoflagellate toxins. *FASEB J. 3*, 1807−1817.

(3) Bailey, J. M., Bright, R., and Tomar, R. (1964) Immunization with a synthetic cholesterol-ester antigen and induced atherosclerosis in rabbits. *Nature 201*, 407−408.

(4) Beckett, G. J., Hunter, W. M., and Percy-Robb, I. W. (1978) Investigation into the choice of immunogens, ligand, antiserum and assay conditions for radioimmunoassay of conjugated cholic acid. *J. Clin. Acta 88*, 257−266.

(5) Cooper, L. J., Shikhman, A. R., Glass, D. D., Kangisser, D., Cunningham, M. W., and Greenspan, N. S. (1993) Role of heavy chain constant domains in antibody−antigen interaction. Apparent specificity differences among streptococcal IgG antibodies expressing identical variable domains. *J. Immunol. 150* (6), 2231−2242.

(6) Cooper, L. J., Robertson, D., Granzow, R., and Greenspan, N. S. (1994) Variable domain-identical antibodies exhibit IgG subclass-related differences in affinity and kinetic constants as determined by surface plasmon resonance. *Mol. Immunol. 31* (8), 577−584.

(7) Erlanger, B. F. (1973) Principles and methods for the preparation of drug protein conjugates for immunological studies. *Pharmacol. Rev. 25*, 271−280.

(8) Erlanger, B. F. (1980) The preparation of antigenic hapten-carrier conjugates: a survey. *Methods Enzymol. 70*, 85−104.

(9) Erlanger, B. F., Borek, F., Beiser, S. M., and Lieberman, S. (1957) Steroid-protein conjugates. I. Preparation and characterization of conjugates of bovine serum albumin with testosterone and with cortisone. *J. Biol. Chem. 228*, 713−727.

(10) Fasciglione, G. F., Marini, S., Bannister, J. V., and Giardina, B. (1996) Hapten-carrier interactions and their role in the production of monoclonal antibodies against hydrophobic haptens. *Hybridoma 15* (1), 1−9.

(11) Hara, I., Muramatsu, T. Fukuda, T., and Sato, J. (1979) Immunochemical properties of phosphatidyl cholesterol and its homologue. *Chem. Phys. Lipids 23*, 2−12.

(12) Kabanov, A. V., Ovcharenko, A. V., Melik-Hubarov, N. S., Bannikov, A. I., Alakhov, V. Yu., Kiselev, V. I., Sveshnikov, P. G., Kiselev, O. I., Levashov, A. V., and Severin, E. S. (1989) Fatty acid acylated antibodies against virus suppress its reproduction in cells. *FEBS Lett. 250* (2), 238−240.

(13) Klaus, G. G. B., and Cross, A. M. (1974) The influence of epitope density on the immunological properties of hapten-protein conjugates. I. Characteristics of the immune response to hapten-coupled albumen with varying epitope density. *Cell. Immunol. 14*, 226−241.

(14) Klopstock, A., Pinto, M., and Rimon, A. (1964) Antibodies reacting versus steroid haptens. *J. Immunol. 92*, 515−519.

(15) Pauillac, S, Naar, J., Branaa, P., and Chinain, M. (1998) An improved method for the production of antibodies to lipophilic carboxylic hapten using small amount of hapten-carrier conjugates. *J. Immunol. Methods 220*, 105−114.

(16) Swartz, G. M., Jr., Gentry, M. K., Amende, L. M., Blanchette-Mackie, E. J., and Alving, C. R. (1988) Antibodies to cholesterol. *Proc Natl. Acad. Sci. U.S.A. 85*, 1902−1906.

(17) Vyjayanthi, V., Capoor, A. K., and Sashidhar, R. B. (1995) Binding characteristics of bovine serum albumin-aflatoxin B1 to polystyrene microtiter plates: importance of hapten to carrier protein molar ratio. *Indian J. Exp. Biol. 33* (5), 329−332.

(18) Weyrer, W., Most, J., Solder, B., Fuchs, D., Wachter, H., and Dierich, M. P. (1990) Production and characterization of a monoclonal antibody against neoptrin. *Hybridoma 9* (1), 71−79.

(19) Wong, S. S. 1993. Preparation of immunotoxins and other drug conjugates for targeting therapeutics. *Chemistry of protein conjugation and cross-linking*, Chapter 11, pp 267−290, CRC Press, Inc., Boston.

(20) Yasumoto, T., and Murata, M. (1993) Marine toxins. *Chem. Rev. 93*, 1897−1909.

(21) Yatsimirskaya, E. A., Gavrilova, E. M., Egorov, A. M., and Levashov, A. V. (1993) Preparation of conjugates of progesterone with bovine serum albumin in the reversed micellar medium. *Steroids 58* (11), 547−550.

BC990042G

Synthesis and Characterization of NVOC-DOPE, a Caged Photoactivatable Derivative of Dioleoylphosphatidylethanolamine

Zhi-Yi Zhang and Bradley D. Smith*

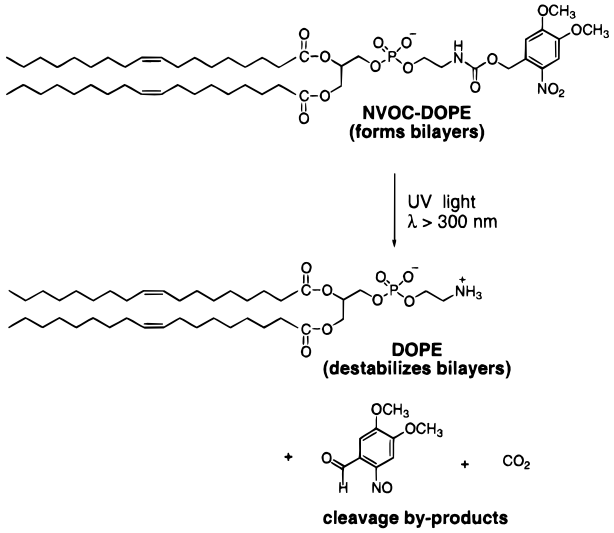
Department of Chemistry and Biochemistry, 251 Nieuwland Science Hall, University of Notre Dame, Notre Dame, Indiana 46556-5670. Received June 23, 1999; Revised Manuscript Received September 9, 1999

A caged, photocleavable derivative of dioleoylphosphatidylethanolamine (DOPE) called NVOC-DOPE was prepared by reaction of DOPE with 6-nitroveratryloxycarbonyl chloride. In contrast to egg phosphatidylethanolamine (EPE), NVOC-DOPE or its 1:1 mixture with EPE forms liposomes at both pH 7.4 and 5.0. Photolysis ($\lambda > 300$ nm) of aqueous liposomal dispersions of NVOC-DOPE at pH 9.0, 7.4, or 5.0 results in complete conversion to DOPE and subsequent release of entrapped calcein dye. The temporal and spatial control associated with the photorelease technique suggests that NVOC-DOPE can be used to study a range of important dynamic membrane processes such as membrane fusion and the action of membrane-associated enzymes.

INTRODUCTION

The presence of nonbilayer-forming lipids, such as phosphatidylethanolamine (PE), is known to activate important biological membrane processes such as bilayer fusion (Kinnunen, 1996b; Siegel, 1999) and the action of membrane-associated enzymes (Hunter et al., 1999; Kinnunen, 1996a; Stubbs and Slater, 1996; Williams, 1998). These dynamic supramolecular events are spatially localized and short-lived, which makes them hard to observe and characterize by physical methods (Chanturiya et al., 1997; Siegel and Epand, 1997; Siegel et al., 1994; Walter and Siegel, 1993). Thus, there is a need to develop triggered, biophysical characterization methods that have a short time frame. A classical photochemical approach is to synthesize an inert "caged" precursor of the active compound and use flash photolysis to rapidly release the compound in a spatially controlled manner (Adams and Tsien, 1993; Corrie and Trentham, 1993). Here we describe a caged version of 1,2-dioleoyl-*sn*-glycero-3-phosphoethanolamine (DOPE) called NVOC-DOPE and show that it is able to form stable liposomes. Upon irradiation, NVOC-DOPE is rapidly converted to DOPE (Scheme 1), which induces bilayer instability and liposome leakage.

Scheme 1



EXPERIMENTAL PROCEDURES

Reagents. 1,2-Dioleoyl-*sn*-glycero-3-phosphoethanolamine (DOPE) and egg phosphatidylethanolamine (EPE) were purchased from Avanti. Calcein, dithiothreitol (DTT), and 6-nitroveratryloxycarbonyl chloride (NVOC−Chloride, or 4,5-dimethoxy-2-nitrobenzyl chloroformate) were purchased from Aldrich.

Synthesis of NVOC-DOPE. DOPE (100 mg, 134 μmol) and 6-nitroveratryloxycarbonyl chloride (1.5 molar equivalents) were mixed in dry methylene chloride in the presence of triethylamine (4.0 molar equivalents). The mixture was stirred at 40 °C for 12 h under nitrogen in the dark. The reaction mixture was cooled to room temperature and washed successively with cold solutions of 4% Na_2CO_3, H_2O, 5% HCl, and H_2O. The organic layer was dried with Mg_2SO_4, and then evaporated. The residue was purified by column chromatography (silica gel) using $CHCl_3$ and subsequently $CH_3OH-CHCl_3$ (1:4, v/v) as eluant to give NVOC-DOPE as a yellow wax: yield 75%. ^{1}H NMR (300 MHz, CD_3OD) 7.74 (s, 1H), 7.20 (s, 1H), 5.46 (s, 2H), 5.34 (t, $J = 5.0$ Hz, 4H), 5.19 (m, 1H), 4.40 (dd, $J = 11.7$, 3.3 Hz, 1H), 4.15 (q, $J = 6.2$ Hz, 1H), 4.00−3.91 (m, 10H), 3.39 (t, $J = 5.4$ Hz, 2H), 2.33−2.26 (m, 4H), 2.02 (d, $J = 5.4$, 8H), 1.58 (m, 4H), 1.30 (m, 40H), 0.90 (t, $J = 6.6$ Hz, 6H) ppm; IR ($CHCl_3$ solution deposited on a NaCl plate) 1738, 1715, 1651, 1609, 1518 cm^{-1}; HRMS (FAB) observed *m/z* 1026.5579, calcd for $C_{51}H_{85}O_{14}N_2PNa_2$ [M + 2Na − 2H] 1026.5534; TLC $R_f = 0.37$ (silica gel/$CH_3OH-CHCl_3$, 1:4, v/v).

Liposome Preparation. A chloroform solution containing an appropriate amount of lipid was evaporated using a rotary evaporator (<30 °C), and the lipid film dried under vacuum for at least 1 h. The liposomes were dispersed in a solution of 50 mM calcein in either pH 5.0 buffer (100 mM NaCl/50 mM sodium acetate), pH 7.4 buffer [100 mM NaCl/5 mM *N*-tris(hydroxymethyl)-methyl-2-aminoethanesulfonic acid], or pH 9.0 buffer (100

* To whom correspondence should be addressed. Phone: (219) 631 8632. Fax: (219) 631 6652. E-mail: smith.115@nd.edu.

10.1021/bc990087h CCC: $18.00 © 1999 American Chemical Society
Published on Web 10/26/1999

mM NaCl/50 mM sodium carbonate) with the aid of vortex mixer. Pyrex glass beads were added before vortexing to facilitate removal of the lipid film from the sides of the flask (final lipid concentration: 10 mM). The resulting opaque dispersion was frozen in an ethanol/dry ice bath and then allowed to thaw in a water bath at 35−40 °C. This freeze−thaw cycle was repeated 10 times. The resulting mixture was extruded, at room temperature, 29 times through a 19 mm polycarbonate filter (Nucleopore) with 100 nm diameter pores using a hand-held Basic LiposoFast device purchased from Avestin. Untrapped calcein was separated by dialysis against isoosmotic buffer.

Photoinduced Calcein Release. A solution of NVOC-DOPE (300 μM, 300 μL) was placed in a 1 mL glass cuvette situated 20 cm from the output lens of a 150 W Xe lamp (filter cut off λ < 300 nm). The temperature was controlled by a thermostated cell holder. After irradiation, a 30 μL aliquot was diluted to 3.0 mL with isoosmotic buffer. The fluorescence intensity was measured at 25 °C. Excitation was set at 490 nm and fluorescence emission was measured at 520 nm. The fluorescence corresponding to 100% leakage was determined after addition of 75 μL of Triton X-100 (20% w/v). The fluorescence intensity for 100% leakage of a control dark sample was measured after liposome lysis with Triton. The percent leakage of calcein was calculated as $\{[I_t - (I_{100}/I_{100}^{dark})I_0]/[1.025\ I_{100} - (I_{100}/I_{100}^{dark})I_0]\} \times 100\%$ (Bondurant and O'Brien, 1998).

Extent of NVOC-DOPE Cleavage in Calcein-Filled Liposomes. The calcein loaded liposomes (300 μM, 300 μL) were lysed with excess ethanol. After removal of solvents and drying under vacuum, 3 mL of $CHCl_3$ was added to take up the lipids. The solution was passed through a 0.8 μm filter to remove the calcein particles and the absence of calcein was confirmed by UV. The extent of photoconversion was calculated from the decrease in absorbance at 350 nm and confirmed by TLC (silica gel; $CHCl_3$:CH_3OH:H_2O, 80:20:1; R_f NVOC-DOPE = 0.56, R_f DOPE = 0.46).

RESULTS AND DISCUSSION

PE does not form a bilayer membrane at physiological pH, but instead adopts inverse cubic and inverse hexagonal structures (Cullis and De Kruijff, 1976; Litzinger and Huang, 1992). Conversely, N-acylated PEs are negatively charged phospholipids and can form kinetically stable liposomes (Domingo et al., 1995; Shangguan et al., 1998). Triggered liposomal systems have been reported with chemically cleavable N-acyl PEs (Kirpotin et al., 1996; Pak et al., 1998), but to our knowledge there is no published example of a photocleavable N-acyl PE; however, polar lipids with caged headgroups (Tuchinsky and Zehavi, 1998) and hydrocarbon tails (Kusumi et al., 1989) are known. NVOC-DOPE is prepared in one step by reaction of DOPE with 6-nitroveratryloxycarbonyl chloride. After purification; NVOC-DOPE is stable to low-temperature storage in the dark. In contrast to pure DOPE, large unilamellar vesicles (LUVs) composed solely of NVOC-DOPE or a 1:1 mixture of EPE/NVOC-DOPE can be prepared at pH 7.4 or 5.0. Liposomes are not readily formed at neutral pH using a 7:3 mixture of EPE/NVOC-DOPE.

The photocleavage of NVOC-DOPE occurs readily in organic solvent, but an isosbestic point is not observed in the UV spectrum (Figure 1). Most likely, the released DOPE condenses with the 3,4-dimethoxy-2-nitrosobenzaldehyde byproduct, which is a common concern with this photocleavage method (Corrie and Trentham, 1993). The side reaction is not observed in aqueous solution, where reasonably concentrated aqueous dispersions of NVOC-DOPE LUVs (300 μM) at pH 9.0, 7.4, or 5.0 are completely converted to DOPE after irradiation with a 500 W Hg lamp (λ < 300 nm) for 4 min. TLC analysis shows that DOPE is liberated in a stoichiometric amount and that the presence of dithiothreitol, which acts as scavenger of 3,4-dimethoxy-2-nitrosobenzaldehyde (Corrie and Trentham, 1993), has no effect on the photocleavage reaction. A dynamic light scattering analysis of the NVOC-DOPE LUVs at pH 5 before photolysis indicated a mean size of 116 ± 47 nm. After photolysis, the dispersion was slightly turbid, and dynamic light scattering indicated a mean size of 495 ± 191 nm. Thus, concomitant with the photoconversion to DOPE, the vesicles undergo fusion and/or aggregation to form larger particles.

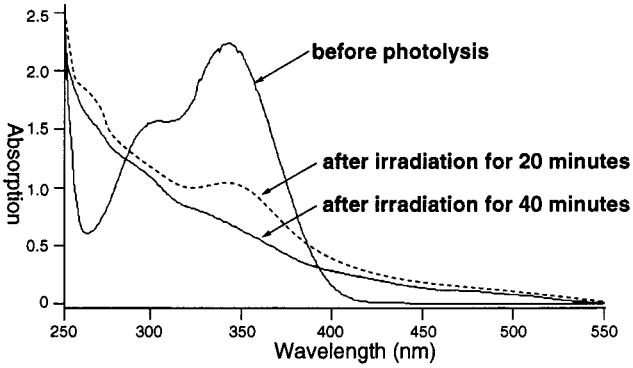


Figure 1. Absorption spectrum of NVOC-DOPE (300 μM) in chloroform.

Calcein leakage experiments show that increasing the fraction of DOPE in the liposomes by photolysis of NVOC-DOPE leads to liposome disruption. The fluorescence assay is hindered by two technical difficulties, the strongly absorbing calcein inhibits the photolysis of NVOC-DOPE, and the calcein emission is decreased due to photobleaching. For example, irradiation of calcein-containing LUVs made from 1:1 EPE/NVOC-DOPE with a 500 W Hg lamp results in rapid and complete leakage of all the calcein, but calcein photobleaching is extensive (~50%). Clearer mechanistic insight was gained using a less intense 150 W Xe lamp that required a longer irradiation time to complete the photocleavage, but produced a much smaller amount of calcein photobleaching and a slower leakage rate. As shown in Figure 2, a 20 min irradiation was needed to convert 90% of the NVOC-DOPE to DOPE, and the amount of escaped calcein initially increased in a slow, linear fashion. Initial calcein leakage rates were measured as a function of temperature, pH, and concentration. The results (Table 1) indicate that photoinduced leakage from 1:1 EPE/NVOC-DOPE LUVs increases with temperature (compare entries 1, 3, and 5), acidity (compare entries 3 and 7), and liposome concentration (compare entries 3 and 8). These trends are in agreement with previous studies of leakage from PE-containing liposomes (Litzinger and Huang, 1992) and show that leakage is promoted by experimental conditions that increase the amount of liposome-liposome contact.

In conclusion, caged derivatives of DOPE, such as NVOC-DOPE reported here, are likely to be useful as photochemical triggers of a range of dynamic membrane processes, especially membrane fusion and the action of

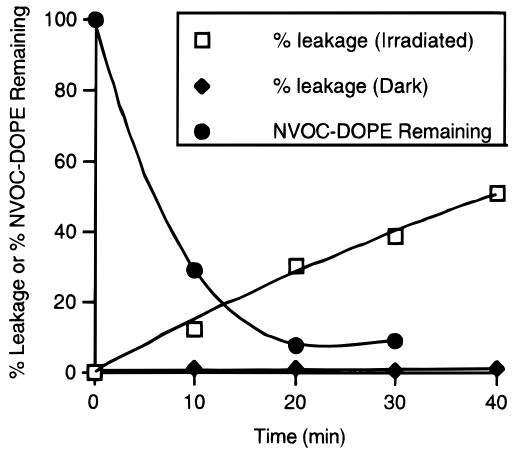


Figure 2. Photocleavage of NVOC-DOPE and calcein release from 1:1 EPE/NVOC-DOPE liposomes (300 μM) at pH 5 and 37 °C, upon irradiation with 150 W lamp.

Table 1. Photoinduced Calcein Leakage from 1:1 EPE/ NVOC-DOPE Liposomes[a]

entry	lipid concentrated (μM)	pH	temp (°C)	light (λ > 300 nm)	leakage rate[a] (% per min)
1	300	5.0	25	UV	0.65
2	300	5.0	25	dark	0
3	300	5.0	37	UV	1.5
4	300	5.0	37	dark	0.05
5	300	5.0	50	UV	2
6	300	5.0	50	dark	0.15
7	300	6.9	37	UV	0.9
8	100	5.0	37	UV	0.8

[a] Initial leakage rate is the extent of leakage after irradiating the sample with a 150 W lamp for 20 min which converted ~90% of the NVOC-DOPE to DOPE (see Figure 2 and Experimental Procedures).

membrane-associated enzymes. They can be employed in studies that require rapid, spatially controlled activation or where mechanical mixing is impractical. A technical drawback with NVOC-DOPE is that the UV light required to induce cleavage may interfere with some of the optical assays used to monitor the subsequent membrane process. The recent introduction of photolabile protecting groups that can be cleaved by two photon IR radiation, however, suggests that this potential problem can be overcome (Furata et al., 1999). Finally, we note that the development of photoactive liposomes for drug or reagent delivery is an active research area (Bondurant and O'Brien, 1998; Wymer et al., 1998) and that "caged" liposomes may be useful as general, triggered-release capsules for solutes (e.g., inorganic ions, peptides, and enzymes, etc.) that are difficult to modify by chemical methods (Morgan et al., 1995a,b).

ACKNOWLEDGMENT

This work was supported by the National Institutes of Health (GM 59078). We thank Professor G. Hartland for access to his DLS instrument.

Supporting Information Available: ^{1}H NMR spectrum of NVOC-DOPE. This material is available free of charge via the Internet at http://pubs.acs.org.

LITERATURE CITED

Adams, S. R., and Tsien, R. Y. (1993) *Annu. Rev. Physiol. 55*, 755−784.
Bondurant, B., and O'Brien, D. F. (1998) *J. Am. Chem. Soc. 51*, 13541−13542.
Chanturiya, A., Chernomordik, L. V., and Zimmerberg, J. (1997) *Proc. Natl. Acad. Sci. U.S.A. 94*, 14423−14428.
Corrie, J. E. T., and Trentham, D. R. (1993) In *Bioorganic Photochemistry* (H. Morrison, Ed.) pp 243−305, Wiley, New York.
Cullis, P. R., and De Kruijff, B. (1976) *Biochim. Biophys. Acta 436*, 523−540.
Domingo, J. C., Mora, M., and De Madriaga, M. A. (1995) *Chem. Phys. Lipids 75*, 15−25.
Furata, T., Wang, S. S.-H., Dantzker, J. L., Dore, T. M., Bybee, W. J., Callaway, E. M., Denk, W., and Tsien, R. (1999) *Proc. Natl. Acad. Sci. U.S.A. 96*, 1193−1200.
Hunter, G. W., Negash, S., and Squier, T. C. (1999) *Biochemistry 38*, 1356−1364.
Kinnunen, P. K. J. (1996a) *Chem. Phys. Lipids 81*, 151−166.
Kinnunen, P. K. J. (1996b) In *Handbook of Nonmedical Applications of Liposomes* (D. D. Lasic and Y. Barenholz, Eds.) Vol. 1, Chap. 6, CRC, Boca Raton.
Kirpotin, D., Hong, K., Mullah, N., Papahadjopoulos, D., and Zalipsky, S. (1996) *FEBS Lett. 388*, 115−118.
Kusumi, A., Nakahama, S., and Yamaguchi, K. (1989) *Chem. Lett.* 433−436.
Litzinger, D. C., and Huang, L. (1992) *Biochim. Biophys. Acta 1113*, 201−227.
Morgan, C. G., Bisby, R. H., Johnson, S. A., and Mitchell, A. C. (1995a) *FEBS Lett. 375*, 113−116.
Morgan, C. G., Yianni, Y. P., Sandhu, S., S., and Mitchell, A. C. (1995b) *Photochem. Photobiol. 62*, 24−29.
O'Brien, D. F., and Tirrell, D. A. (1993) In *Bioorganic Photochemistry* (H. Morrison, Ed.) pp 243−305, Wiley, New York.
Pak, C. C., Ali, S., Janoff, A. S., and Meers, P. (1998) *Biochim. Biophys. Acta 1372*, 13−27.
Shangguan, T., Pak, C. C., Ali, S., Janoff, A. S., and Meers, P. (1998) *Biochim. Biophys. Acta 1368*, 171−183.
Siegel, D. P. (1999) *Biophys. J. 76*, 291−313.
Siegel, D. P., and Epand, R. M. (1997) *Biophys. J. 73*, 3089−3111.
Siegel, D. P., Green, W. J., and Talman, Y. (1994) *Biophys. J. 66*, 402−414.
Stubbs, C. D., and Slater, S. J. (1996) *Chem. Phys. Lipids 81*, 185−195.
Tuchinsky, A., and Zehavi, U. (1998) *Chem. Phys. Lipids 92*, 91−97.
Walter, A., and Siegel, D. P. (1993) *Biochemistry 32*, 3271−3281.
Williams, E. E. (1998) *Am. Zool. 38*, 280−290.
Wymer, N. J., Gerasimov, O. V., and Thompson, D. H. (1998) *Bioconjugate Chem. 9*, 305−308.

BC990087H

© 1999 American Chemical Society, Bioconjugate Chem., Zhang bc990087h Supporting Info Page 1

